SFPE Handbook of Fire Protection Engineering

Third Edition

Editorial Staff

Philip J. DiNenno, P.E. (Hughes Associates, Inc.), Editor-in-Chief
Dougal Drysdale, PhD. (University of Edinburgh), Section 1
Craig L. Beyler, PhD. (Hughes Associates, Inc.), Section 2
W. Douglas Walton, P.E. (National Institute of Standards and Technology), Section 3
Richard L. P. Custer (Arup Fire USA), Section 4
John R. Hall, Jr., PhD. (National Fire Protection Association), Section 5
John M. Watts, Jr., PhD. (The Fire Safety Institute), Section 5

National Fire Protection Association
Quincy, Massachusetts

Society of Fire Protection Engineers
Bethesda, Maryland

Product Manager: Pam Powell
Developmental Editor: Robine Andrau
Editorial-Production Services: Omegatype Typography, Inc.
Interior Design: Omegatype Typography, Inc.
Composition: Omegatype Typography, Inc.
Cover Design: Twist Creative Group
Manufacturing Manager: Ellen Glisker
Printer: Courier/Westford

Published by the National Fire Protection Association
National Fire Protection Association, Inc.
One Batterymarch Park
Quincy, Massachusetts 02269

Notice Concerning Liability: Publication of this work is for the purpose of circulating information and opinion among those concerned for fire and electrical safety and related subjects. While every effort has been made to achieve a work of high quality, neither the NFPA nor the authors and contributors to this work guarantee the accuracy or completeness of or assume any liability in connection with the information and opinions contained in this work. The NFPA and the authors and contributors shall in no event be liable for any personal injury, property, or other damages of any nature whatsoever, whether special, indirect, consequential, or compensatory, directly or indirectly resulting from the publication, use of, or reliance upon this work.

This work is published with the understanding that the NFPA and the authors and contributors to this work are supplying information and opinion but are not attempting to render engineering or other professional services. If such services are required, the assistance of an appropriate professional should be sought.

NFPA No.: HFPE-01
ISBN: 087765-451-4
Library of Congress Control No.: 136232

Printed in the United States of America
03 04 05 06 5 4 3 2

Contents

SECTION THREE • HAZARD CALCULATIONS

SECTION FOUR • DESIGN CALCULATIONS

SECTION FIVE • FIRE RISK ANALYSIS

APPENDICES

Preface

The third edition of the *SFPE Handbook of Fire Protection Engineering* represents an update of existing material with the addition of some important new subject matter. The rapid assimilation of performance-based design in fire protection has underscored the importance of this handbook. While the process of performance-based design has been documented in detail, the fundamental knowledge base has remained fragmented. This handbook, as it has been from its inception, is a contribution toward documenting and integrating the theoretical and applied bases of fire safety engineering. The need for concise description of the theoretical basis of fire protection engineering in conjunction with material on engineering calculations and practice is clear. Significant effort was made to provide a more useful and direct link from some of the fundamental chapters to actual use in practice. Examples include a new chapter on calculation of heat fluxes to surfaces and new treatment of ignition phenomena.

The changes in many chapters reflect the incremental and slow progress made in improving the knowledge base in the area of fire dynamics. One notable exception to this slow change has been in the area of egress and human movement. Significant new material in this area was prepared by Guylène Proulx. The challenges and complexities of introducing a new fire suppression technology, water mist systems, are covered in a new chapter. The widespread use of field modeling as a practical tool in engineering design motivated the inclusion of a new chapter on that subject. Additional treatment of risk assessment methodologies, particularly as they are applied, is included as sectors of the profession move more quickly in that direction.

Another significant modification in this edition is the inclusion of new material in the chapter on radiation heat transfer calculations. This new material reflects, in part, the results of a technical committee of the SFPE directed toward developing consensus on engineering methods. It is anticipated that future editions will include the work of several engineering consensus groups directed at establishing a consensus-based standard of care in fire safety engineering. This, in turn, will provide a firmer technical basis for design while preserving the necessary level of public safety.

The generous contribution of the individual authors is gratefully acknowledged. Without their donation of time, energy, and expertise, this handbook would not be possible. While they are owed a debt that cannot be paid outright, we trust that the application of their work in solving fire safety engineering problems worldwide will serve as some reward for their efforts. As the fire protection engineering discipline expands, the need for additional authors and expertise will become a significant limitation in future editions.

This edition of the handbook is the first to be published without Jim Linville, who retired from NFPA during its preparation. Pam Powell has ably assumed the role of managing editor, providing guidance, encouragement, and the motivation necessary to complete and publish this edition.

The editors and the Society of Fire Protection Engineers welcome the comments and suggestions of readers as we seek to improve and expand this handbook in future editions.

Philip J. DiNenno, P.E.

Metrication

The editors of the *SFPE Handbook of Fire Protection Engineering* have worked toward expanded use of SI units for this third edition. In some instances, however, U.S. customary units have been retained. For example, when equations, correlations, or design methodologies have input variables or constants that have been developed from data originally in U.S. customary units, those units are retained. This is also the case for certain tables, charts, and nomographs. Where equations employing U.S. customary units are used in worked examples, the results are presented as SI units as well.

Section One
Fundamentals

Section 1 Fundamentals

CHAPTER 1

Introduction to Mechanics of Fluids

B. S. Kandola

Fluid Properties

A fluid is defined as a substance that has the capacity to flow freely and as a consequence deform continuously when subjected to a shear stress. A fluid can be either a liquid, a vapor, or a gas.

For the purposes of fluid flow studies, a very important distinction is made between compressible fluids and incompressible fluids. In general, the compressibility effects of liquids are so small that they can be regarded as incompressible, whereas gases and vapors can be either compressible or incompressible depending on the forces involved.

To simplify analytical investigation of fluid motion, the intermolecular forces of the fluids are ignored, and such a fluid is known as *inviscid* (i.e., zero viscosity).

An incompressible, inviscid fluid is called a *perfect fluid.* In reality no real fluid is a perfect fluid, but the effects of viscosity are so small in a perfect fluid that they can be ignored.

Density: The density of a fluid is defined as the mass of the fluid per unit volume. The density, ρ, is therefore defined as

$$\rho = \frac{\text{mass}}{\text{volume}} = \frac{m}{v}$$

where m is the mass of fluid of volume, v. If the units of mass are kilograms (kg) and the volume m^3, then the units of density are kg/m^3.

Specific volume: Specific volume is the reciprocal of density, that is, specific volume (m^3/kg)

$$v = \frac{1}{\rho}$$

Shear force: The component of total force, F, in a direction tangential to the surface of a body is called the shear force. Similarly, the component perpendicular to the tangent is called the normal force. Force is measured in newtons (N, or 1 kg m/s^2).

Shear stress: The shear stress, τ, at a point is defined as the limiting value of shear force per unit area as the area is reduced to a point, or

$$\tau = \frac{\text{shear force}}{\text{area}}$$

Pressure: The pressure, P, at a point in a fluid is defined as the limiting value of normal force to area as the area is reduced to the point, or

$$P = \frac{\text{normal force}}{\text{area}}$$

where the units are N/m^2, or pascals (Pa).

Physical Properties of Fluids

Viscosity: All real fluids offer some resistance, however small, to applied shear stresses. This resistance results from the property of the fluid called viscosity. According to Newton's law, the rate at which a fluid element deforms for a given shear stress is inversely proportional to the fluid viscosity.

For a two-dimensional flow between two parallel plates, the rate of deformation is the rate of change of x-component of velocity, u, with y-direction, that is, $\partial u/\partial y$. If τ is the frictional shearing stress, then according to the above definition

$$\tau \propto \frac{\partial u}{\partial y} \tag{1}$$

Dr. B. S. Kandola, formerly a member of the unit of fire safety engineering, Edinburgh University, and a senior consultant with AEA Technology and Lloyd's Register, is an independent safety and risk management consultant. He has worked on a range of research projects involving fire and smoke movement modeling on offshore oil and gas installations and for the nuclear industry. His current activities include risk assessment, consequence modeling, hazard analysis, and the development of safety cases for the petrochemical, offshore, and nuclear industries.

or

$$\tau = \mu \frac{\partial u}{\partial y} \tag{1a}$$

where μ is the coefficient of viscosity. The units of viscosity are Ns/m^2. In general, the viscosity of a gas increases with temperature, while the viscosity of a liquid decreases with temperature.

Kinematic viscosity: In all real fluid motions the frictional and inertia forces interact. The ratio of μ to ρ is important and is known as the kinematic viscosity, ν.

$$\nu = \frac{\mu}{\rho} \tag{2}$$

The units of ν are m^2/s.

The Equation of State

For a fluid in which the properties are the same at all points (i.e., uniform fluid) and having definite chemical composition, experimental evidence indicates that the fluid density, ρ, is a function only of the pressure, p, and temperature, T.

$$\rho = f(p, T) \tag{3}$$

According to this relation, any one property, that is, p, T, or ρ, is determined by any of the other two. For a gas at temperatures and pressures well away from liquefaction or dissociation, the following relationship holds with good approximation:

$$\frac{p}{\rho} = \frac{\overline{R}}{M} \cdot T \tag{4}$$

where

$\overline{R}$ = universal gas constant

M = molecular weight of the particular gas

T = absolute temperature (K)

The value of the universal gas constant, $\overline{R}$, is 8.315×10^3 m^2/s^2K (or $J/kg \cdot K$), and the molecular weights for various gases are shown in Table 1-1.1.

A gas that obeys Equation 4 is called a *perfect gas* (also sometimes referred to as *ideal gas*). With an acceptable degree of accuracy, this relationship is also assumed to apply for the calculation of air flows, although air is, in reality, a mixture of various gases. It is assumed that the equation of state holds when the gas is in motion as well as at rest.

Table 1-1.1 ***Molecular Weight of Gases***

Gas	Molecular Weight (M)
Hydrogen (H_2)	2.0
Carbon monoxide (CO)	28.0
Methane (CH_4)	16.0
Ethane (C_2H_6)	30.0
Propane (C_3H_8)	44.0
Air	28.9

Compressibility and Thermal Expansion

Equation 4 describes the compressibility of a gas. According to this equation, the volume is decreased with the increase in pressure, provided the process takes place under isothermal conditions.

If the volume changes from v to $v + \partial v$ due to the change in pressure from p to $p + \partial p$, the coefficient of compressibility is then defined as

$$\beta = \frac{1}{v}\left(\frac{\partial v}{\partial p}\right)_T \tag{5}$$

Similarly, at constant pressure

$$\beta_1 = \frac{1}{v}\left(\frac{\partial v}{\partial T}\right)_p \tag{6}$$

where β_1 is called the coefficient of thermal expansion. This equation describes the resulting change of volume due to any change in temperature occurring under isobaric conditions.

The compressibility of a liquid is described by its bulk modulus, K, which is the inverse of coefficient of compressibility, β;

that is,
$$K = \frac{1}{\beta} \tag{7}$$

For a perfect gas (i.e., a gas that obeys Equation 4)

$$\beta = \beta_1 = \frac{1}{T} \tag{8}$$

Specific heat: The specific heat of a substance (or gas) is defined as the quantity of heat required to raise the temperature of a unit mass of the substance by one degree. The specific heat depends on whether the process takes place under conditions of constant pressure, C_p, or constant volume, C_v. If q is the quantity of heat supplied per unit mass of gas, then

$$C_p = \left(\frac{\partial q}{\partial T}\right)_p \quad \text{constant pressure} \tag{9}$$

$$C_v = \left(\frac{\partial q}{\partial T}\right)_v \quad \text{constant volume} \tag{10}$$

Vapor pressure: When the temperature of a liquid increases, its molecular activity is also increased. With the sufficient rise in temperature, the molecules begin to escape from the surface of the liquid. The pressure exerted by these molecules just above the surface is called the vapor pressure of the liquid. The vapor pressure increases with the increase in temperature, and boiling occurs when the vapor pressure becomes equal to the pressure above the liquid surface.

Surface tension: The molecular attraction of liquids causes the free surface of a liquid to act as a stretched membrane in such a way that work is required to change the shape of its free surface.

The surface tension coefficient of a liquid is then defined as the force per unit length of any line on the free

surface of a liquid necessary to hold that surface together at that line

$$F = \int \sigma \, dl \tag{11}$$

The quantity σ is the surface tension coefficient and depends on the properties of the free surface of a liquid and its surroundings.

Fluid Statics and Buoyancy

When a fluid system is in motion, shear stresses develop in the fluid if one layer of fluid moves at a different velocity from an adjacent layer. These stresses are proportional to the velocity gradient. In the case of a static fluid (zero velocity), the shear stresses are zero.

Forces Acting on Fluid Systems

Forces acting on fluid systems are classified according to the geometry on which they act.

1. Body force is the force resulting from the total mass of the fluid system. For example, the body force of a solid object at rest equals its weight acting at its center of gravity.
2. Surface force (shear force) acts on a surface and is proportional to the extent of the surface. Such a force can be resolved into its normal and tangential components.
3. Line force (surface tension) depends on the extent of the line perpendicular to which the force acts.

Pressure at a Point

The pressure at a point is defined as the normal component of surface force acting on a unit area of the surface, or the limit of the ratio of normal force per unit area as the area approaches zero at the point. For a fluid system in equilibrium, the pressure is a scalar quantity, as it is independent of orientation.

For an imaginary wedge-shaped element in a static fluid, the forces acting on each side are due to body and surface forces, as shown in Figure 1-1.1.

Since the fluid is assumed to be in equilibrium, the sum of the horizontal forces and the vertical forces is zero, that is,

$$\sum F_x = 0 \tag{12}$$

$$\sum F_y = 0 \tag{13}$$

Resolving the forces shown in Figure 1-1.1, horizontally and vertically, it can be shown that in the limit as $\partial x \rightarrow 0$, $\partial y \rightarrow 0$

$$p_x = p_y = p_s \tag{14}$$

This result is sometimes referred to as Pascal's law, which states that for a fluid system in static equilibrium, the pressure at a point is the same in all directions.

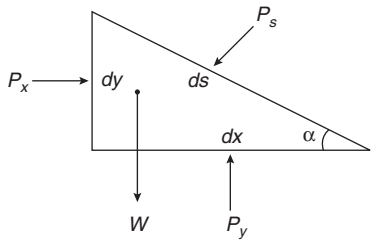

Figure 1-1.1. ***Wedge-shaped imaginary fluid element.***

Hydrostatic Equation

Within a static fluid, the rate of change of static pressure with height, z, from a datum level is given by

$$\frac{dp}{dz} = -\rho g \tag{15}$$

Integrating Equation 15 for constant ρ gives

$$p + \rho g z = C \tag{16}$$

where g is the acceleration due to gravity, and C is the constant of integration.

This equation is generally known as the hydrostatic equation or Torricelli's principle, which states that, at every elevation within a static, homogeneous, and incompressible fluid, the static pressure plus the head of fluid above a given datum line, $\rho g z$, is constant.

Forces on Submerged Surfaces

In numerous engineering design problems involving submerged surfaces (containers, offshore oil rigs, walls of a dam, the walls of a liquid-filled tank, etc.), it is necessary to know the magnitude of forces and the point of action of these forces that act on the surfaces. The total force acting on a submerged surface is obtained by integrating the pressure over the entire surface area.

$$F = \int_A p \, dA \tag{17}$$

If the pressure is constant, then the force on a submerged horizontal surface is given by

$$F = pA \tag{18}$$

where A is the total surface area.

The point on the surface at which this resultant force acts is called the center of pressure. It can be shown that the center of pressure for a horizontal submerged surface is at the centroid of the area. This result is arrived at by considering the moment of the distributed force about any axis through the center of pressure to be zero.

Forces on Plane-Inclined and Submerged Curved Surfaces

Consider an inclined plane surface, as shown in Figure 1-1.2.

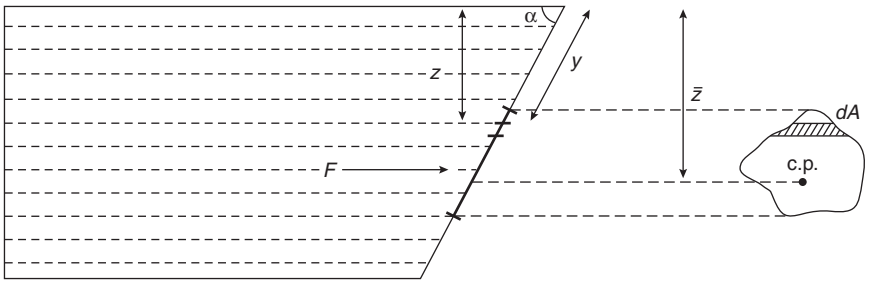

Figure 1-1.2. ***Plane-inclined surface.***

Force, dF, acting on elemental area, dA, at depth z from the free surface is given by

$$dF = \rho g z\, dA = \rho g y \sin \alpha\, dA \tag{19}$$

and the total force is given by

$$F = \rho g \sin \alpha \int_A y\, dA \tag{20}$$

If the y-coordinate of the centroid is defined as

$$\bar{y} = \frac{1}{A}\int_A y\, dA \tag{21}$$

then the total force can be written as

$$F = \rho g \bar{y} A \sin \alpha = \rho g \bar{z} A$$

or

$$F = p_{\bar{z}} A \tag{22}$$

This equation shows that for a plane-inclined surface the magnitude of the force on the surface is the product of the pressure at the centroid of the surface and its area.

For a curved surface, as shown in Figure 1-1.3, it can be shown that the horizontal and vertical components of force are

$$dF_x = \rho g y \sin \theta\, dA \tag{23}$$

$$dF_y = \rho g y \cos \theta\, dA \tag{24}$$

However, $\sin \theta\, dA$ is the projection of the elemental area, dA, onto a plane perpendicular to x-direction. Equation 23, therefore, shows that the horizontal component of pressure force on a curved surface is equal to the pressure force exerted on a projection of the curved surface.

The y-component of the force reduces to

$$F_y = \rho g \int_A dV \tag{25}$$

where $dV = y \cos \theta\, dA$.

Integration of Equation 25 gives

$$F_y = \rho g V \tag{26}$$

where V is the volume of fluid above the surface.

Equation 26 shows that the vertical component of pressure force on a curved surface is equal to the weight of liquid that is vertically above the curved surface extending up to free surface.

Buoyant Force on Submerged Bodies

As seen earlier in this chapter, a body submerged in a static fluid experiences a net force as a result of the pressure variation at its surface. The vertical component of this force is called the buoyant force and always acts vertically upward.

The magnitude of the buoyant force is expressed as the difference between the vertical component of the pressure force on the upper and the lower surfaces of the body. This fact is expressed in the form of Archimedes' principle, which states: "Any body submerged in a fluid experiences

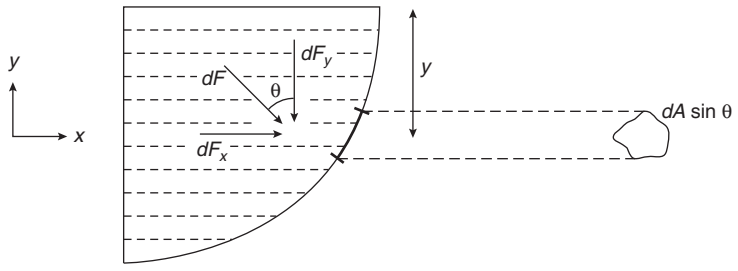

Figure 1-1.3. ***Submerged curved surface.***

a lift in a direction opposite to its weight and equal in magnitude to the weight of displaced volume of fluid."[1] If a submerged body is in equilibrium, it can be shown that

$$\rho = \rho_b \tag{27}$$

where ρ is the density of fluid and ρ_b is the density of body.

If the buoyant force is greater than the weight of the body, the body will float; but if the force is less, the body will sink.

Center of buoyancy: The center of buoyancy is the point on the body at which the buoyant force acts. The precise location of this point can be found by taking the integrated moments of the elementary buoyant forces and equating them to the moment of the total buoyant force or the weight of the displaced fluid.

It can be shown that the center of buoyany lies at the centroid of the displaced volume of fluid.

Stability of Floating and Submerged Bodies

From the previous text it is clear that a floating body in a static fluid is in equilibrium, provided (1) buoyant force is equal to the weight of the body and (2) center of buoyancy lies on the same vertical line as the center of gravity.

If a body is in such a stable equilibrium with respect to vertical displacement, then any upward or downward displacement sets up a force that tends to return the body to its original position.

In general, floating bodies are in a stable configuration if the center of gravity, *CG*, is lower than the center of buoyancy, *CB*. This relationship does not imply that stability may not exist when the opposite situation occurs.

Conversely, a completely submerged body is only rotationally stable if its center of gravity is below the center of buoyancy, as illustrated in Figure 1-1.4.

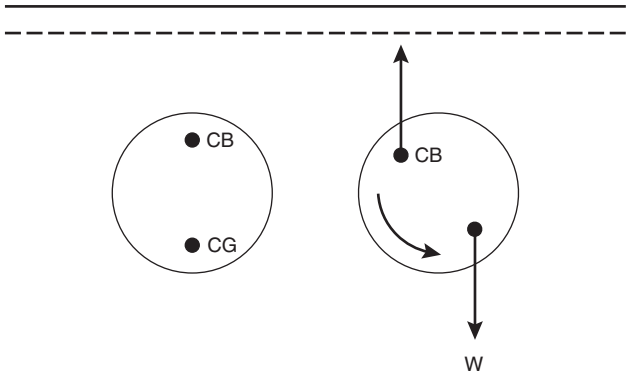

Figure 1-1.4. ***Rotationally stable submerged body.***

Kinematics of Fluid Motion

In general, kinematics of particle or fluid motion is concerned with the effects of motion on quantities derivable from displacement and time, such as velocity and acceleration. Although these motions are caused by external forces, they are studied in isolation from these forces.

In analyzing the motion of a rigid body or a fluid system, the space-time quantities are expressed in terms of a convenient coordinate system. The choice of this system is quite arbitrary and depends only on the nature of the problem investigated.

Two methods can be used to describe fluid motion: (1) the Langrangian method describing the motion of a particle in terms of a coordinate system that moves with the particle and (2) the Eulerian method describing the motion of a particle in terms of a fixed coordinate system. The Eulerian method is more commonly used to analyze fluid mechanics problems.

Classification of Fluid Motion

To simplify the analysis of fluid motion, various assumptions are made about the nature of fluid and its motion.

A *perfect fluid* is defined as that fluid which does not sustain shear stresses. A perfect fluid is inviscid ($\mu = 0$), and irrotational with constant density.

A *real fluid* is one in which the effects of viscosity are of paramount importance (i.e., $\mu \neq 0$). It is only in real fluids that a boundary layer is developed adjacent to a body over which the fluid flows.

Incompressible fluid motion is a motion in which the density remains unaltered (i.e., the time derivative of density is zero, $\partial\rho/\partial t = 0$).

With a *compressible fluid motion,* if the density of a fluid in motion is a function of time, the flow is termed as compressible (time derivative of density is nonzero, i.e., $\partial\rho/\partial t \neq 0$).

When a real fluid is in motion, two basic forces determine the nature of flow: (1) inertial forces, which arise as a result of the velocity of the fluid, and (2) viscous forces, which arise as a result of the viscosity of the fluid.

The ratio of inertial to viscous forces is known as the Reynolds number and is defined as

$$\mathrm{Re} = \frac{Vd}{\nu}$$

where

V = velocity

d = some characteristic length

ν = kinematic viscosity

For a fluid motion in which the value of Re is so small that the layers of flow are smooth and laminar, the flow is then referred to as laminar. As the velocity is increased (i.e., the inertial forces are increased), the layers start to break up and the flow is then said to be turbulent.

At a critical Reynolds number, the fluid flow becomes fully turbulent. For example, for a sharp-edged entry flow in a pipe, the critical Reynolds number is 2700.

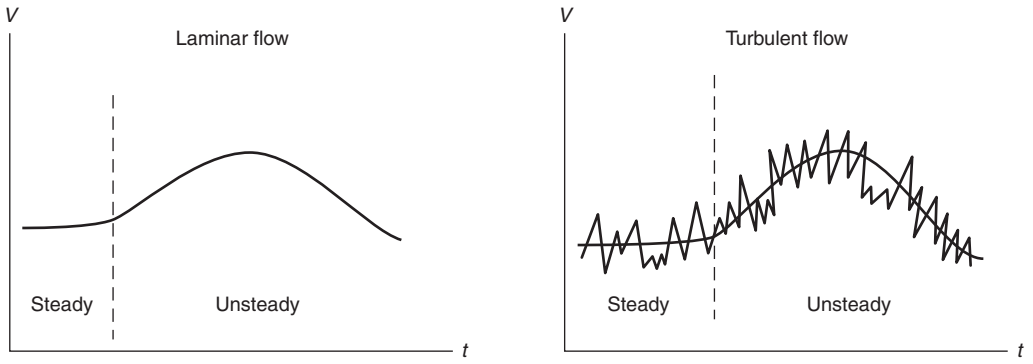

Figure 1-1.5. ***Steady and unsteady flows.***

Steady and unsteady motion: A flow in which the properties of the fluid do not vary with time is called the steady flow (i.e., $\partial V/\partial t = 0$). On the other hand, a flow regime in which these properties vary with time as well as space is characterized as unsteady (e.g., $\partial V/\partial t \neq 0$). A turbulent flow can either be steady or unsteady, as illustrated in Figure 1-1.5.

A turbulent flow is composed of the mean (average) component and a fluctuating component

$$u = \overline{u} + u' \tag{28a}$$

$$v = \overline{v} + v' \tag{28b}$$

where $\overline{u}$ and $\overline{v}$ are mean values of u and v, and u' and v' are the fluctuating components. The fluctuations u' and v' are such that their time average is zero.

Flow Concepts

Various flow concepts are used to make the mathematical analysis of fluid motion easier.

A *streamline* in a flow is defined as an imaginary curve in which the tangent at every point on this curve gives the direction of the fluid velocity at that point. Therefore there is no flow in the direction normal to the streamline. When the motion is steady, the streamlines are the same at all times.

Pathline is defined as a line in the flow field describing the path or trajectory of a given fluid element.

Streakline is defined as the locus in a flow field at a given time of all the fluid particles that have passed through a given point within the fluid. A smoke trail in the atmosphere at a given time is an example of a streakline.

For a steady motion the streamlines, streaklines, and pathlines are identical.

A stream filament is a group of neighboring streamlines forming a cylindrical passage with an infinitesimal cross section. A group of stream filaments is called a streamtube. The cross section of a streamtube is finite, and its surface across which there is no flow is called a stream surface. These concepts are illustrated in Figure 1-1.6.

Equation of Continuity

The flow through a streamtube (i.e., no flow through the stream surface) is shown in Figure 1-1.7.

Since there is no flow through the surface of the tube, and if the flow is steady, the mass of fluid flowing through area A_1 must equal the mass flowing through area A_2; that is, mass inflow equals mass outflow, or

$$\rho_1 A_1 u_1 = \rho_2 A_2 u_2 \tag{29}$$

For an incompressible flow, $\rho_1 = \rho_2$ and the previous equation then becomes

$$u_1 A_1 = u_2 A_2 \tag{30}$$

This relationship is known as the equation of continuity and, in general, can also be written as

$$\frac{\partial u}{\partial x} + \frac{\partial v}{\partial y} + \frac{\partial w}{\partial z} = 0 \tag{31}$$

where for an incompressible flow, u, v, and w are the velocity components in the x, y, and z directions.

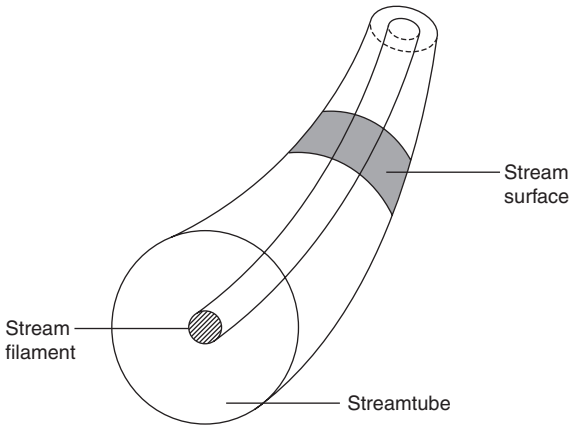

Figure 1-1.6. ***Basic concepts of stream filaments.***

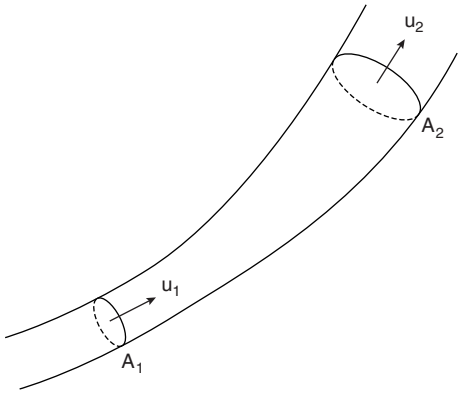

Figure 1-1.7. ***A streamtube.***

The Stream Function

Consider a two-dimensional incompressible flow in which the equation of continuity can be written as

$$\frac{\partial u}{\partial x} + \frac{\partial v}{\partial y} = 0 \tag{32}$$

From this equation it follows that there exists a function, ψ, such that

$$u = \frac{\partial \psi}{\partial y} \quad \text{and} \tag{33a}$$

$$v = \frac{\partial \psi}{\partial x} \tag{33b}$$

The function ψ is called the stream function, which satisfies the continuity equation. In cylindrical coordinates this relationship can be written as

$$v_r = \frac{1}{r}\frac{\partial \psi}{\partial \theta}, \quad v_\theta = -\frac{\partial \psi}{\partial r} \tag{34}$$

where v_r and v_θ are the velocity components in the r and θ directions.

Sources, Sinks, and Doublets

A point within a fluid from which fluid emanates and spreads radially outward in a uniform fashion is called a source. On the other hand, a sink is the opposite of a source, and the flow is inward into the point.

The strength of a source or sink is equal to the volume of fluid that issues from a source or to a sink per unit time. When a source-sink pair is separated by a distance, δx, such that $\delta x \rightarrow 0$, then this arrangement is called a doublet or a dipole.

Stream Function of a Two-Dimensional Source

Since the flow from a source is radially outward, the flux per unit time is the strength of the source. (See Figure 1-1.8.)

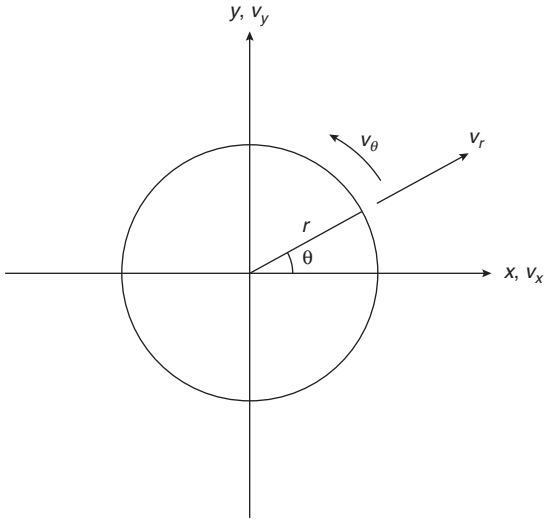

Figure 1-1.8. ***A two-dimensional source.***

If the flow is steady and incompressible, the strength, m, per unit length of cylinder is given by

$$m = 2\pi r v_r \tag{35}$$

where v_r is the radial velocity component.

Since the flow is completely radial, $v_\theta = 0$.

The radial component, v_r, is given by

$$v_r = \frac{1}{r}\frac{\partial \psi}{\partial \theta} = \frac{1}{r}\frac{d\psi}{d\theta} \tag{36}$$

Combining the two equations and integrating for ψ gives

$$\psi = \frac{m}{2\pi}\theta \tag{37}$$

This equation shows that the streamlines for a source are radial lines as shown in Figure 1-1.9.

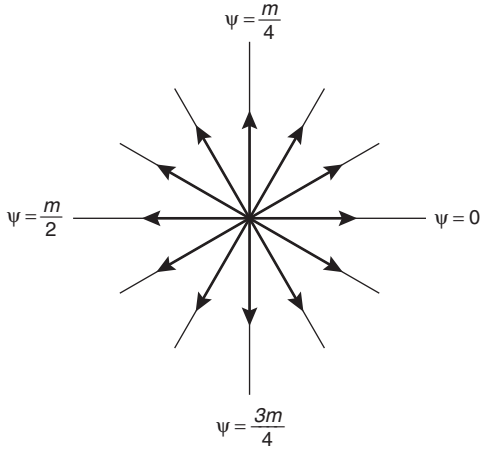

Figure 1-1.9. ***Streamlines of a two-dimensional source.***

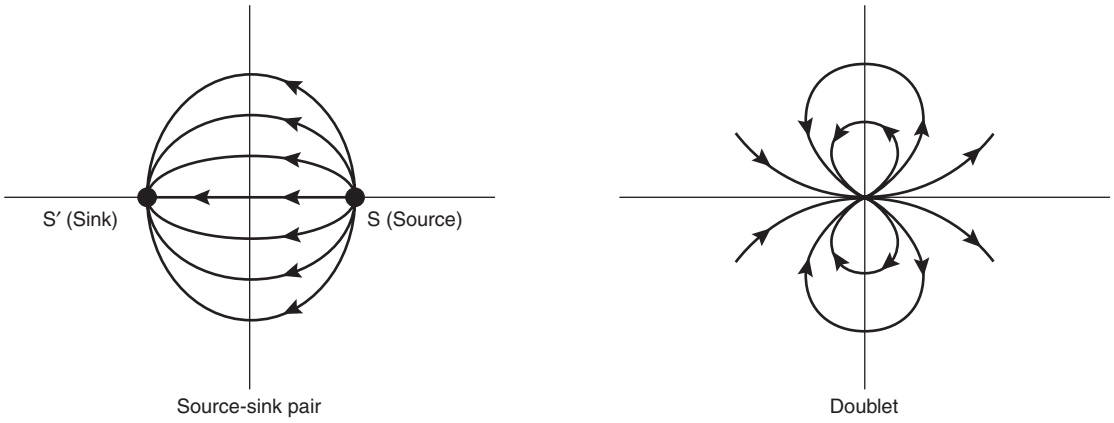

Figure 1-1.10. ***Streamlines of a source-sink pair and a doublet.***

Similarly, the streamlines for a two-dimensional source-sink pair and a two-dimensional doublet are shown in Figure 1-1.10.

Fluid Rotation

For a rigid body, if each particle of the body describes a circle about its axis of rotation, the body is said to be rotating.

But since in a fluid each particle is free to move in any direction, the fluid may not describe a perfect circle about the axis of rotation. Consequently, the rotation of a fluid element at a point is defined as the average angular velocity of the element.

An element of fluid is shown in Figure 1-1.11.

The average angular velocity of the element can be shown to be

$$2\omega_z = \frac{\partial v_y}{\partial x} - \frac{\partial v_x}{\partial y} \tag{38}$$

where $2\omega_z$ is called the *vorticity*, ζ_z.

The direction of the vorticity, by convention, is given by the right-hand screw rule. In this case ζ_z is positive in an upward direction, perpendicular to the plane of paper.

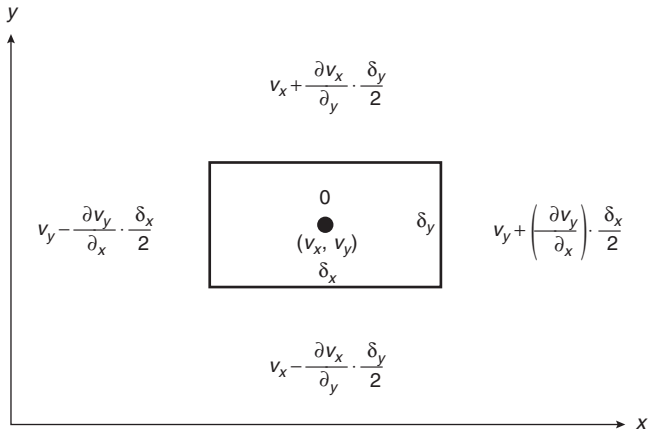

Figure 1-1.11. ***A fluid element.***

Similarly, the other components can be written as

$$\zeta_y = \frac{\partial v_x}{\partial z} - \frac{\partial v_z}{\partial x} \tag{39a}$$

$$\zeta_z = \frac{\partial v_z}{\partial y} - \frac{\partial v_y}{\partial z} \tag{39b}$$

The components of vorticity in cylindrical coordinates are

$$\zeta_z = \frac{1}{r}\left[\frac{\partial}{\partial r}\left(r v_\theta\right) - \frac{\partial v_\theta}{\partial \theta}\right] \tag{40a}$$

$$\zeta_\theta = \frac{\partial v_r}{\partial z} - \frac{\partial v_z}{\partial r} \tag{40b}$$

$$\zeta_r = \left(\frac{1}{r}\frac{\partial v_z}{\partial \theta}\right) - \frac{\partial v_\theta}{\partial z} \tag{40c}$$

The total vorticity of the fluid at a given point is obtained by vectorially adding the three components.

Irrotational fluid motion: If the vorticity at a given point within the fluid is zero, the fluid motion is said to be irrotational. For example, a uniform parallel flow with no velocity gradients is irrotational. The condition for irrotationality of flow in terms of stream function is

$$v_r = 0 \tag{41}$$

$$\frac{\partial^2 \psi}{\partial x^2} + \frac{\partial^2 \psi}{\partial y^2} = 0 \tag{42}$$

This equation is known as the Laplace equation.

Free Vortex

The type of motion in which the vorticity is zero and the peripheral velocity varies inversely with the radial distance is called the free vortex, that is,

$$v_r = 0 \tag{43a}$$

$$\zeta_z = 0 \tag{43b}$$

that is,

$$\frac{\partial v_\theta}{\partial r} + \frac{v_\theta}{r} = 0 \tag{43c}$$

This equation gives

$$v_\theta r = \text{constant} \tag{44}$$

From Equation 34

$$v_\theta = -\frac{\partial \psi}{\partial r} \tag{45}$$

Combining Equations 44 and 45 gives

$$\psi = k \ln r \tag{46}$$

where k is a constant.

The streamlines for a vortex, then, are circles as shown in Figure 1-1.12.

Velocity Potential

For an irrotational flow, all the components of vorticity are zero, that is,

$$\zeta_z = \zeta_y = \zeta_x = 0 \tag{47}$$

From Equations 38, 39a and 39b, and 47 it follows that there exists a function $\phi(x, y)$ such that

$$v_x = \frac{\partial \phi}{\partial x}, \quad v_y = \frac{\partial \phi}{\partial y}, \quad v_z = \frac{\partial \phi}{\partial z} \tag{48}$$

in cylindrical coordinates

$$v_r = \frac{\partial \phi}{\partial r}, \quad v_\theta = \frac{1}{r}\frac{\partial \phi}{\partial \theta} \tag{49}$$

These relationships generate

$$\frac{\partial^2 \phi}{\partial x^2} + \frac{\partial^2 \phi}{\partial y^2} = 0 \tag{50}$$

This equation shows that the velocity potential, ϕ, also satisfies Laplace's law.

It must be noted that the velocity components can only be expressed in terms of a velocity potential if the flow is irrotational. For ψ to exist continuity must be satisfied, and for ϕ to exist flow must be irrotational.

For a pure vortex

$$v_r = 0 \tag{51}$$

Therefore

$$v_\theta = \frac{1}{r}\frac{\partial \phi}{\partial \theta}$$

or

$$\phi = k\theta \tag{52}$$

where k is a constant.

The equipotential (constant ϕ) lines for a vortex are shown in Figure 1-1.13.

Circulation

The circulation around a closed contour within a flow field is defined as the sum of the product of the tangential velocity and the elemental length at every point on the contour. (See Figure 1-1.14.)

For a closed contour, C, the circulation is given by

$$\Gamma = \oint_c U \cos\theta \, ds \tag{53}$$

It can be shown that for an element of fluid $(\partial x, \partial y)$ the total circulation is given by

$$\Gamma = \int\int \zeta_z \, dx \, dy \tag{54}$$

This result is known as Stokes's theorem.

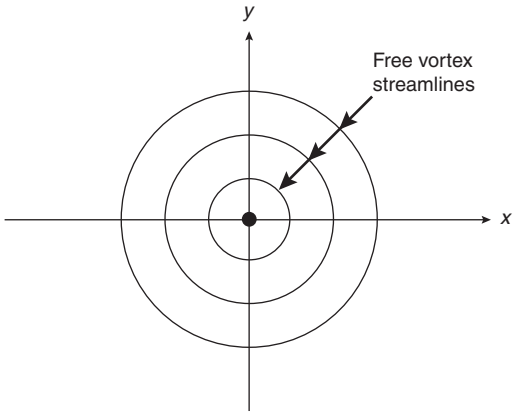

Figure 1-1.12. ***Free vortex streamlines.***

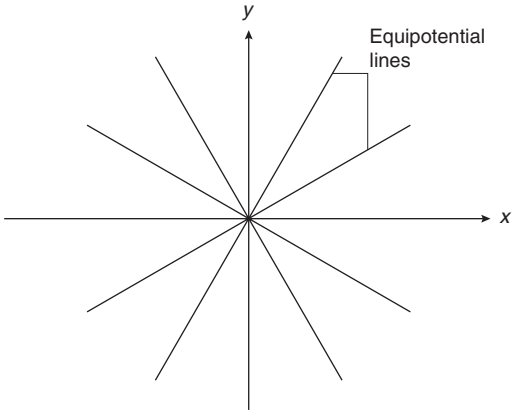

Figure 1-1.13. ***Equipotential lines for a vortex.***

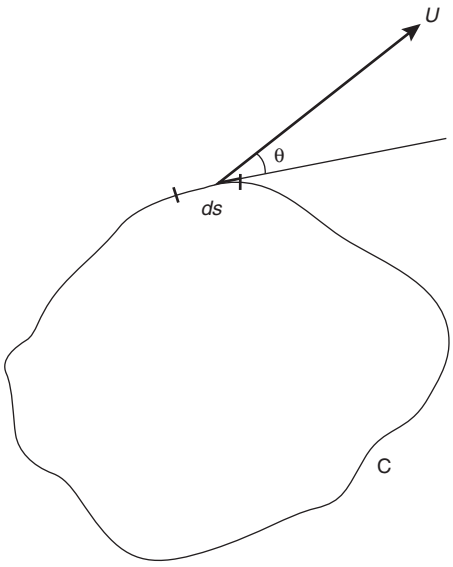

Figure 1-1.14. ***Circulation around a circuit, C.***

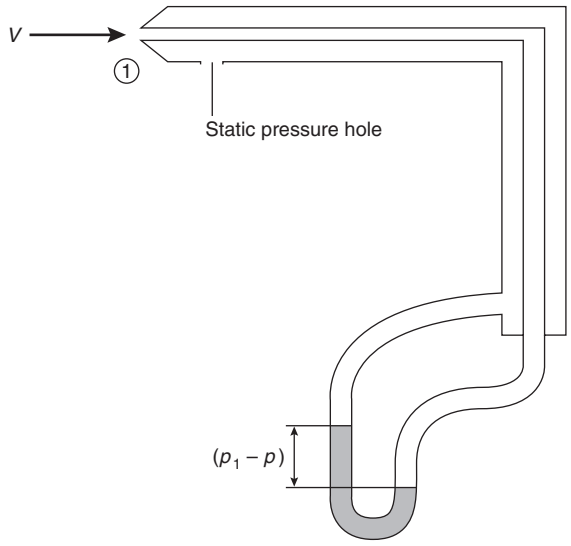

Figure 1-1.15. ***Pitot-static tube.***

Dynamics of Incompressible Fluids

Kinematics of fluid motion only deals with the general characteristics of flow of fluids. It does not answer the question of how fluids will move under given conditions (e.g., flow of real fluids over bodies of varying shapes). In other words, it is necessary to establish the relationship between the force and the resulting motion. This relationship is covered under the general heading of fluid dynamics.

The Bernoulli Equation

The Bernoulli equation expresses the relationship between the pressure and velocity within a fluid flow. The general form of the equation is

$$p + \frac{1}{2}\rho V^2 + \rho g z = \text{constant} \tag{55}$$

where

p = static pressure at the pressure head
$\frac{1}{2}(\rho V^2)$ = dynamic head
gz = position head

The constant is usually called the Bernoulli constant.

In some applications the position head term is considerably smaller, and therefore, the Bernoulli equation simplifies to

$$p + \frac{1}{2}\rho V^2 = \text{constant} \tag{56}$$

From Equation 56 it is clear that the static pressure, p, decreases with the increase in velocity, V. It should be remembered that the Bernoulli equation applies only to a streamline. It follows that this relationship enables the flow velocity to be calculated from the measurement of pressure. This application is the function of the pitot-static tube.

Figure 1-1.15 shows a typical arrangement of a pitot-static tube. When pointing in the direction of the flow, this tube allows the magnitude of the velocity to be determined through the measurement of pressures.

If V is the free stream velocity, then according to the Bernoulli equation

$$\frac{1}{2}\rho V^2 + p = \frac{1}{2}\rho V_1^2 + p_1 \tag{57}$$

At point 1 at the mouth of the tube the velocity $V_1 = 0$; that is, the stagnation point, and p_1 is the stagnation pressure at that point.

Equation 57 then becomes

$$V = \sqrt{\frac{2(p_1 - p)}{\rho}} \tag{58}$$

where $(p_1 - p)$ is pressure measured by the manometer.

Another application of the Bernoulli relation is to the flow of water under pressure from a tank. (See Figure 1-1.16.)

In Figure 1-1.16, p_1 is the atmospheric pressure.

Applying the Bernoulli equation at points 1 and 2 gives

$$p_1 + \frac{1}{2}\rho V_1^2 + \rho g z_1 = p_2 + \frac{1}{2}\rho V_2^2 + \rho g z_2 \tag{59}$$

If $V_1 \ll V_2$ then

$$\frac{1}{2}\rho V_2 = [p_2 - p_1 + \rho g(z_2 - z_1)] \tag{60a}$$

but $p_1 = p_2$ = atmospheric pressure.

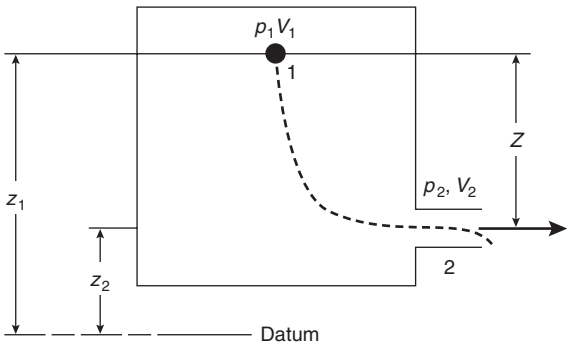

Figure 1-1.16. ***Efflux from a large tank.***

Therefore,

$$\frac{1}{2}\rho V_2^2 = \rho g(z_2 - z_1) = \rho g z \tag{60b}$$

or

$$V_2 = \sqrt{2gz} \tag{61}$$

This relationship is known as Torricelli's law for efflux from a container.

The Venturi meter, which measures the volume flow rate in a pipe, basically consists of a converging cone that merges into a parallel throat with a minimal cross-sectional area. (See Figure 1-1.17.) From the measurement of the static pressures in the parallel region and the converging region, the volume flow rate can be calculated as shown below.

Applying the Bernoulli equation at Points 1 and 2 gives

$$\frac{1}{2}\rho V_1^2 + p_1 = \frac{1}{2}\rho V_2^2 + p_2 \tag{62}$$

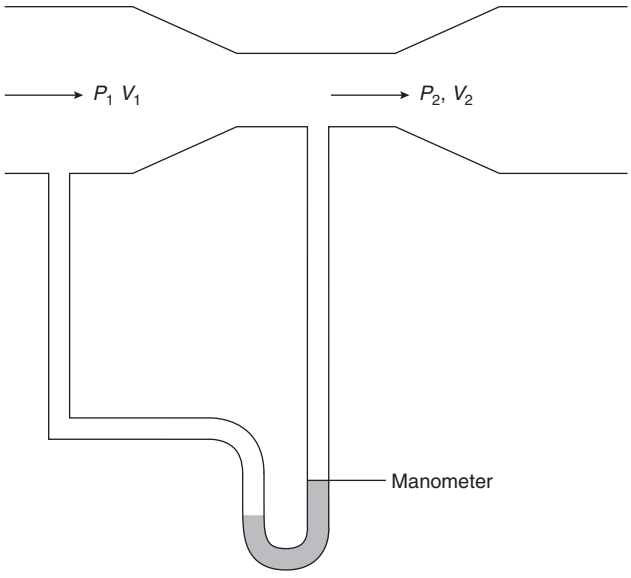

Figure 1-1.17. ***Venturi meter.***

But from continuity

$$\rho V_1 A_1 = \rho V_2 A_2 \tag{63}$$

Combining Equations 62 and 63 results in

$$V_2 = \sqrt{\frac{2}{\rho}\frac{A_1^2(p_2 - p_1)}{(A_2^2 - A_1^2)}} \tag{64}$$

Therefore the volume flow rate, Q, is given by

$$Q = V_2 A_2$$

or

$$Q = A_2\left[\frac{2A_1^2(p_2 - p_1)}{\rho(A_2^2 - A_1^2)}\right]^{1/2} \tag{65}$$

The Navier-Stokes Equations

The Navier-Stokes (N-S) equations are the exact equations describing the fluid motion. They are valid for both the laminar and turbulent flows. They are derived from Newton's second law of motion, which states that the sum of the external forces acting on a body is equal to the product of the mass and acceleration of the body. In the case of a fluid, this body is assumed to be a fixed control volume within which the fluid properties remain unchanged. To account for the fluid viscosity (i.e., stickiness of the fluid), it is further assumed that the instantaneous rate of strain (distortion) of the fluid element (body) is a simple linear function of the stresses (forces) in the fluid. Two types of forces are considered important: (1) the body forces (e.g., gravitation) and (2) the surface forces (e.g., pressure and friction).

The Navier-Stokes equations can be viewed as the transport equations that equate the net rate of transport of some quantity Q (momentum or enthalpy). For momentum transport the second law of motion is utilized, and for the enthalpy transport, the principle of first law of thermodynamics is used.

For momentum rate of transport, the general form of the N-S equations is

$$\frac{Du}{Dt} = X - \frac{1}{\rho}\frac{\partial p}{\partial x} + \nu\nabla^2 u \tag{66a}$$

$$\frac{Dv}{Dt} = Y - \frac{1}{\rho}\frac{\partial p}{\partial y} + \nu\nabla^2 v \tag{66b}$$

$$\frac{Du}{Dt} = Z - \frac{1}{\rho}\frac{\partial p}{\partial z} + \nu\nabla^2 w \tag{66c}$$

where

X, Y, Z = the body forces in the x, y, z directions
ρ = fluid density
p = pressure
ν = fluid kinematic viscosity
u, v, w = velocity components

D/Dt is the substantive derivative consisting of the non-steady and convective components.

For example

$$\frac{Du}{Dt} = \frac{\partial u}{\partial t} + u\frac{\partial u}{\partial x} + v\frac{\partial u}{\partial y} + w\frac{\partial u}{\partial z}$$

The Laplace's operator ∇^2 (also known as del squared) is defined as

$$\nabla^2 = \frac{\partial^2}{\partial x^2} + \frac{\partial^2}{\partial y^2} + \frac{\partial^2}{\partial z^2}$$

The Navier-Stokes equations, together with the continuity Equation 31, form four simultaneous differential equations from which the four unknowns (u, v, w, and p) could, in principle, be solved. However, the non-linear nature of these equations makes the task prohibitively complex. But for very simple cases of laminar flow, analytical solutions are possible, as demonstrated in Example 1. For more practical applications involving complex turbulent flows, the computer-based numerical techniques are used. In computational fire modeling, these computer codes are generally referred to as *field models.*

EXAMPLE 1: Flow in a Channel.

Consider the steady, incompressible viscous flow in an infinitely long two-dimensional stationary channel with two parallel flat plates. (See Figure 1-1.18.)

The flow everywhere is parallel to the x-axis. Since the flow is considered to be steady, the components of velocity in the y and z directions are zero; that is, $v = 0$, $w = 0$. The Navier-Stokes equations then become

$$-\frac{1}{\rho}\frac{\partial p}{\partial x} + \nu\frac{\partial^2 u}{\partial y^2} = 0 \tag{67}$$

$$-\frac{1}{\rho}\frac{\partial p}{\partial y} = 0 \tag{68}$$

From the continuity equation

$$\frac{\partial u}{\partial x} = 0 \tag{69}$$

These two equations are solved, subject to the boundary conditions

$$\begin{aligned} u &= 0, \quad y = b \\ u &= 0, \quad y = -b \end{aligned} \tag{70}$$

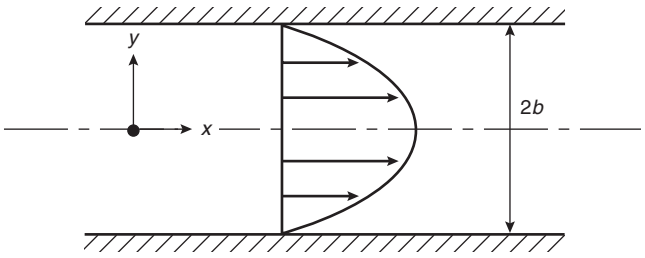

Figure 1-1.18. ***Flow in a channel.***

Equation 68 shows that the pressure, p, is a function of x only, while Equation 69 shows that u only varies with y.

Equation 67 therefore becomes

$$-\frac{1}{\rho}\frac{dp}{dx} + \nu\frac{d^2u}{dy^2} = 0$$

When solved for the given boundary conditions (Equation 70), the velocity component u becomes

$$\frac{dp}{dx} = \mu\frac{d^2u}{dy^2} \tag{71}$$

$$u = -\frac{1}{2\mu}\frac{dp}{dx}(b^2 - y^2) \tag{72}$$

Thus, the velocity profile is parabolic and the corresponding shear stress is given by

$$\tau = \mu\frac{du}{dy} = -\frac{1}{2\mu}\frac{dp}{dx}(b^2 - 2y) \tag{73}$$

The Energy Equation

As stated above, the N-S equations are basically the transport equations. As such, they apply to both the transport of momentum as well as the transport of heat (enthalpy). The transfer of heat between a solid body and a gaseous flow involves the conservation equations of motion and that of heat. In fire problems, the transfer of heat energy from a fire source and the resulting rise in temperature are of great importance, for example, the assessment of a fire barrier performance and fire detection. In the smoke transport problems, the temperature distribution throughout a building, contributing to the stack effect, is also of major importance. To calculate this distribution, it is necessary to solve the energy conservation equation along with the momentum transfer N-S equations.

For an incompressible fluid the energy balance is determined by the internal energy, the conduction of heat, the convection of heat and the generation of heat through friction, and by a heat source.

According to the First Law of Thermodynamics, the energy balance can be written as

$$\underset{\text{rate of heat input}}{\frac{dQ}{dt}} = \underset{\text{rate of change of internal energy}}{\frac{dE}{dt}} + \underset{\text{work done}}{\frac{dW}{dt}} \tag{74}$$

In Equation 74, the radiative heat transfer is neglected.

For a constant property fluid, the energy equation is given by

$$\frac{\partial\theta}{\partial t} + u\frac{\partial\theta}{\partial x} + v\frac{\partial\theta}{\partial y} + w\frac{\partial\theta}{\partial z} = \frac{k}{\rho c_p}\nabla^2\theta \tag{75}$$

where

θ = temperature rise above datum value (e.g., ambient)

k = thermal conductivity

c_p = specific heat at constant pressure

Turbulence

Randomness is the necessary and sufficient condition for turbulent motion. A fluid flow that is highly disordered, rotational, and three-dimensional has all the essential characteristics of turbulence. These features, at first glance, may point to the unpredictability of turbulent flow. Indeed, in reality, it is not possible either to define turbulence in precise terms or to predict precisely its flow characteristics. However, in practice, what is of importance is the effect of turbulence; that is, the way it manifests itself in the flow phenomenon. From this standpoint its definition in precise terms is neither essential nor desirable.

In nature, there is underlying order and regularity; that is, perpetual striving for local equilibrium (harmony). Instability is only a transition (intermediate stage) from one stable state to another. The macroscopic worldview of chaos and randomness pertains to human perception and is a consequence of human inability to relate the intrinsic stability at the infinitesimal scale to the finite world of the observed physical phenomena. It is for this reason that the empirical option of "lumped parameter" is the approach used for statistical descriptions.

On this basis and in order to make any meaningful progress in the treatment of turbulent flow, it is important to recognize that turbulent motion is effectively made up of (1) a mean component, which is intelligible, and (2) a fluctuating component, which is random. In terms of the mean flow, there are very little qualitative differences between the laminar and turbulent flows; that is, the mean motion is fully described. In contrast, fluctuations are based solely on statistical information.

One of the main observed features of turbulence is that it causes diffusion. In other words, it transports the fluid itself and any characteristic associated with it, such as the airborne pollution or smoke particles. In this respect, turbulence is a feature of the flow and not of the fluid. Experimental evidence shows that turbulent fluctuations result from the highly disordered array of eddies of widely different sizes that transport the fluid elements. These turbulent eddies, as they are swept along by the mean flow, undergo both the translational and rotational motion. During this process the larger eddies are distorted and stretched, and consequently break up into smaller ones.

As described, the turbulent motion can be broken down into mean and fluctuating components. Thus, the instantaneous value of a quantity, q, can be written as

$$q = \overline{q} + q'$$

where $\overline{q}$ is the mean with respect to time (time-average), defined as

$$\overline{q} = \frac{1}{\Delta t} \cdot \int_{t_0}^{t_0+\Delta t} q(t)\, dt$$

According to this definition, the time-average of all fluctuating quantities is equal to zero, that is,

$$\overline{q}' = 0$$

Accordingly, the instantaneous velocity and pressure components can be written as

$$u = \overline{u} + u', \quad v = \overline{v} + v', \quad w = \overline{w} + w', \quad p = \overline{p} + p'$$

By substituting these quantities into the continuity equation, it can readily be shown that

$$\frac{\partial \overline{u}}{\partial x} + \frac{\partial \overline{v}}{\partial y} + \frac{\partial \overline{w}}{\partial z} = 0$$

and

$$\frac{\partial u'}{\partial x} + \frac{\partial v'}{\partial y} + \frac{\partial w'}{\partial z} = 0$$

This result shows that the time-average velocity field and the fluctuating velocity components satisfy the same continuity equation as the actual velocity field.

Now, when the above definitions of the instantaneous velocity are substituted in the Navier-Stokes equations and the continuity equation is utilized, the x-direction turbulent form of the Navier-Stokes equation reduces to

$$\overline{u}\frac{\partial \overline{u}}{\partial x} + \overline{v}\frac{\partial \overline{v}}{\partial y} + \overline{w}\frac{\partial \overline{u}}{\partial z} = X - \frac{1}{\rho}\frac{\partial \overline{p}}{\partial x} + \nu\nabla^2\overline{u} - \left(\frac{\partial \overline{u}'^2}{\partial x^2} + \frac{\partial \overline{u}'\overline{v}'}{\partial y^2} + \frac{\partial \overline{u}'\overline{w}'}{\partial z^2}\right)$$

The y- and z-direction equations are of similar form.

From the comparison of the laminar and turbulent forms of these equations, it is clear that, in addition to the usual non-linearities, extra terms involving fluctuating velocity products ($\overline{u}'^2$, $\overline{u}'\overline{v}'$, $\overline{u}'\overline{w}'$) appear on the right-hand side. These terms, which account for the effects of turbulence, are generally known as the *Reynolds stresses* (also sometimes referred to as *apparent* or *virtual stresses*). These additional stresses arise from the turbulent fluctuations and have a similar influence as the viscous terms in the laminar flow case. It is for this reason they are often said to be caused by the *eddy viscosity.* In almost all turbulent flows of practical interest, Reynolds stresses are much larger than the viscous stresses. This relationship is one reason why turbulence is of such great practical importance.

The Navier-Stokes equations, as described, are the exact equations describing the fluid motion. However, in the solution of these equations a formidable mathematical difficulty arises due to the non-linearity of the relation between the velocity and momentum flux, as reflected in the Reynolds stress terms. An approach is therefore used that solves these equations over a numerical grid or mesh within the specified region having prescribed boundary conditions. The exact equations are averaged over a time scale. The Reynolds stresses are expressed in terms of known quantities under the framework of a "turbulence model." Appropriate turbulence models are selected depending on the nature and complexity of the flow phenomena. The so-called k-ε turbulence model is by far the most common and is shown to give the satisfactory answers for engineering applications. For fire applications,

this approach is referred to as "field modeling" in contrast to "zone modeling," which is purely an empirical approach. A detailed discussion of the numerical techniques and the turbulence models is beyond the scope of this text. However, a useful and comprehensive review of these models is given by Kumar.[2]

Flow Similarity and Dimensional Analysis

It is clear so far that the flow characteristics of any fluid flow system are determined not only by the properties of the fluid but also by the geometry of flow. For example, the flow through an open channel and tube will differ because the two flow regimes are not geometrically similar. This statement does not imply that any geometric similarity will produce flow similarity (i.e., dynamic similarity). For a process or physical system to be dynamically similar, the ratios of the forces involved, in addition to the geometrical similarity, must be equal.

In the experimental investigation of the underlying fluid flow phenomena, the small-scale "physical modeling" approach is often used. The basis of this approach relies on the hypothesis that the full-scale physical phenomena can be simulated in a model scale (i.e., small scale) experiment, provided certain non-dimensional parameters (or ratios) are preserved. In other words, provided the physical similarity (e.g., geometric, kinematic, and dynamic similarity) is maintained, the results of the small-scale experiments are assumed to be equally valid for the full-scale case. Table 1-1.2 outlines the physical significance of important dimensionless groups.

Kinematic similarity exists if the particle paths are geometrically similar. Dynamic similarity exists between two geometrically and kinematically similar systems if the ratios of all the forces are equal.

If F_p, F_μ, and F_u are denoted as the pressure, viscous, and inertial forces, respectively, for dynamic similarity

$$\frac{(F_p)_1}{(F_p)_2} = \frac{(F_\mu)_1}{(F_\mu)_2} = \frac{(F_u)_1}{(F_u)_2}$$

or

$$\left(\frac{F_p}{F_\mu}\right)_1 = \left(\frac{F_p}{F_u}\right)_2 = \text{constant}$$

or

$$\left(\frac{F_\mu}{F_u}\right)_1 = \left(\frac{F_\mu}{F_u}\right)_2 = \text{constant}$$

This relationship means that a flow over two spheres of different radii will be dynamically similar, provided

$$\left(\frac{F_u}{F_\mu}\right)_{\text{sphere 1}} = \left(\frac{F_u}{F_\mu}\right)_{\text{sphere 2}} = \text{Re}$$

where Re is a constant.

This constant is generally known as the Reynolds number and is defined as

$$\text{Re} = \frac{\rho V L}{\mu}$$

where

ρ = density of fluid
V = velocity
μ = viscosity
L = sphere diameter

If Re for two kinematically similar flows is the same, the flows are then said to be dynamically similar. Other similarity parameters are given in Table 1-1.2.

Dimensions and Units

There are three fundamental units of measure in fluid mechanics. These fundamental units are mass, *M;* length, *L;* and time, *T.* All the other quantities, such as force and pressure can be expressed in terms of these fundamental units.

If a quantity is capable of being expressed in these fundamental units, the resulting function of *M, L,* and *T* is then termed the dimensions of the quantity.

From Newton's second law of motion, force is given by $F = ma$, where m = mass and a = acceleration.

The dimensions of m are $[M]$ and are written as

$$[m] \triangleq [M]$$

the symbol $\triangleq$ means "has the dimensions of."

Table 1-1.2 ***Important Dimensionless Groups***

Name	Group	Physical Significance
Reynolds number	$\text{Re} = \frac{\rho u l}{\nu}$	Ratio of the inertia force to the friction force
Froude number	$\text{Fr} = \frac{u^2}{lg}$	Ratio of the inertia force to the gravity force—relevant to buoyant flows associated with fires
Grashof number	$\text{Gr} = \frac{gl^3\beta T}{\nu^2}$	Ratio of buoyancy to force to viscous forces, as in fire plumes
Prandtl number	$\text{Pr} = \frac{\mu c_p}{k}$	Ratio of momentum diffusivity to thermal diffusivity

Table 1-1.3 ***Measure Formula or Physical Dimensions of Quantities Occurring in Mechanics (based on mass, length, and time as fundamental units)***

Quantity	Measure Formula	Quantity	Measure Formula
Mass	M	Mass per unit area	ML^{-2}
Length	L	Mass moment	ML
Time	T	Moment of inertia and product of inertia	ML^2
Speed or velocity	LT^{-1}	Stress and pressure	$ML^{-1}T^{-2}$
Acceleration	LT^{-2}	Strain	$M^0L^0T^0$
Momentum and impulse	MLT^{-1}	Elastic modulus	$ML^{-1}T^{-2}$
Force	MLT^{-2}	Flexural rigidity of a beam E1	ML^3T^{-2}
Energy and work	ML^2T^{-3}	Torsional rigidity of a shaft GJ	ML^3T^{-2}
Power	ML^2T^{-2}	Linear stiffness (force per unit displacement)	MT^{-2}
Moment of force	ML^2T^{-2}	Angular stiffness (moment per radian)	ML^2T^{-2}
Angular momentum or moment of momentum	ML^2T^{-1}	Linear flexibility or receptance (displacement per unit force)	$M^{-1}T^2$
Angle	$M^0L^0T^0$	Vorticity	T^{-1}
Angular velocity	T^{-1}	Circulation (hydrodynamics)	L^2T^{-1}
Angular acceleration	T^{-2}	Viscosity	$ML^{-1}T^{-1}$
Area	L^2	Kinematic viscosity	L^2T^{-1}
Volume and first moment of area	L^3	Diffusivity of any quantity	L^2T^{-1}
Second moment of area	L^4	Coefficient of solid friction	$M^0L^0T^0$
Density	ML^{-3}	Coefficient of restitution	$M^0L^0T^0$

Similarly

$$[a] = \left[\frac{L}{T^2}\right] \triangleq [LT^{-2}]$$

and, therefore,

$$F \triangleq MLT^{-2}$$

A table of dimensions for other physical quantities is given in Table 1-1.3.

Dimensional Analysis

When a physical phenomenon is represented by an equation, it is absolutely necessary that all the terms in the equation have the same units, that is, that the equation be dimensionally homogeneous. A quick dimensional analysis of the parameters involved in an equation provides a powerful clue to the homogeneities of the equation.

EXAMPLE 2:

Find the expression for discharge, Q, through a horizontal capillary tube.

The discharge, Q, depends on the following parameters:

pressure drop per unit length	$\Delta p/\ell$
diameter of the tube	D
fluid viscosity	μ

These parameters have the following dimensions:

$$\frac{\Delta p}{\ell} \triangleq ML^{-2}T^{-2}, \qquad D \triangleq L$$

$$\mu \triangleq ML^{-1}T^{-1}$$

Therefore,

$$Q = k\left(\frac{\Delta p}{\ell}\right)^{\alpha} \cdot D^{\beta} \cdot \mu^{\gamma}$$

that is,

$$[L^3T^{-1}] = k[ML^{-2}T^{-2}]^{\alpha} \cdot [L]^{\beta} \cdot [ML^{-1}T^{-1}]^{\gamma}$$

From the principle of homogeneity and by comparing the exponents of each dimension

$$\gamma + \alpha = 0 \quad \text{from } [M]$$

$$\beta - 2\alpha - \gamma = 3 \quad \text{from } [L]$$

$$2\alpha + \gamma = 1 \quad \text{from } [T]$$

Solving these equations gives

$$\alpha = 1, \quad \gamma = 1, \quad \beta = 4$$

Therefore, the equation for discharge, Q, becomes

$$Q = k\left(\frac{\Delta p}{\ell}\right)^{1} \cdot D^4 \cdot \mu^{-1} = k\,\frac{\Delta p}{\ell} \cdot \frac{D^4}{\mu}$$

No information about the numerical value of the dimensionless constant k can be obtained from the equation. This information can be obtained, however, from the experiment.

Boundary Layers

When a fluid flows over a solid boundary (surface), the velocity at the surface is zero (no-slip condition). This

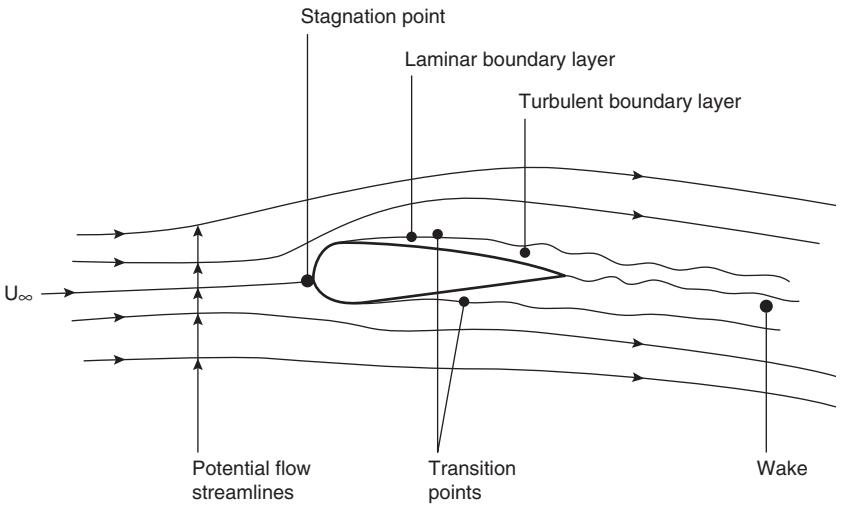

Figure 1-1.19. ***Flow over a two-dimensional aerofoil.***

velocity increases with the distance away from the surface and eventually becomes equal to the free stream velocity. Therefore, a region exists close to the surface of the body in which the velocity varies with distance. This region is called the boundary layer. Within this region each layer of fluid moves relative to the adjacent layer, and as a result large shear stresses are set up within the boundary layer. An important approximation can be made in solving the Navier-Stokes equations such that viscosity only plays a role within the boundary layer, while outside this layer the fluid can be treated as inviscid ($\mu = 0$).

Physics of Boundary Layers

The flow over a two-dimensional aerofoil is shown in Figure 1-1.19.

It can be observed that over the forward part, the flow is smooth and the streamlines are parallel to the surface. This region is known as the laminar boundary layer.

But as the flow progresses over the surface of the aerofoil toward the trailing edge, the streamlines break up, and there are random fluctuations in velocity, direction, and magnitude, even though the general mean motion remains roughly parallel to the surface. This region is called the turbulent boundary layer. As the flow leaves the surface behind the body, it merges to form a stream of relatively slow-moving fluid, which is known as the wake. Consequently, the velocity profiles in the turbulent and laminar boundary layers are quite different. The measurements of velocity profiles on a flat plate are shown in Figure 1-1.20.

This figure shows that the velocity gradient at the surface ($\partial u/\partial y$) is much greater in the turbulent boundary layer than in the laminar boundary layer. It follows that the frictional stresses, τ_w,

$$\tau_w = \mu\left(\frac{\partial u}{\partial y}\right)_{y=0} \tag{76}$$

at the wall surface, that is, the drag, are much greater for the turbulent than the laminar boundary layer.

As the pressure increases downstream along the surface, the velocity is decreased within the boundary layer. Thus, as $\partial p/\partial x$ increases, $\partial u/\partial y$ decreases. With any further increases in this pressure gradient a stage may be reached where $\partial u/\partial y$ at the wall is zero, and the fluid adjacent to the surface is then on the point of reversing its direction of flow. The boundary layer is then said to be on the point of separation, as illustrated in Figure 1-1.21.

Subsequently, the velocity gradient (du/dy) at the wall becomes negative downstream of separation, and an inner portion of the boundary layer then flows against the stream. This reversed flow forms a large eddy under the outer part of the boundary layer. These eddies carry a large amount of energy, which results in the increase of drag on the body.

A body with extensive boundary layer separation and a wake with large-scale eddies is referred to as a bluff body. In contrast, a body on which the boundary layer remains attached over the whole surface to the rearmost point and then merges smoothly into the wake without the formation of any large-scale eddies is referred to as a streamline body.

The nature and magnitude of drag on these two shapes of bodies are quite different. The drag of a bluff body is usually very large and is almost entirely due to the energy wasted in the castoff eddies. Drag can be determined fairly accurately from the pressure distribution acting normal to its surface. The drag of a streamline body is relatively small and is mainly due to the viscous or frictional stresses that act tangential to its surface.

Boundary Layer Thickness

The velocity within a boundary layer varies from zero at the surface to free-stream velocity just outside the boundary layer. The boundary layer thickness, δ, is defined as the distance from the wall at which the velocity reaches 99 percent of the free-stream velocity (at $y = \delta$, $u = 0.99U_\infty$).

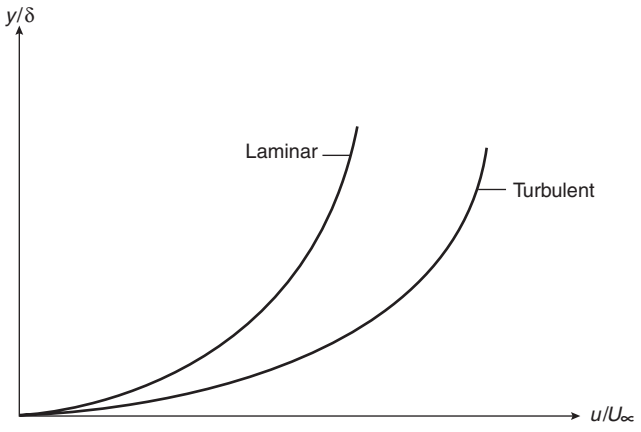

Figure 1-1.20. ***Velocity profiles over a flat plate.***

The displacement thickness, δ^*, is defined as that distance by which the external potential field of flow is displaced outward as a consequence of the decrease in velocity in the boundary layer. The precise form of displacement thickness is

$$\delta^* = \int_{y=0}^{\infty} \left(1 - \frac{u}{U_\infty}\right) dy \tag{77}$$

Momentum thickness, θ, is defined as

$$\theta = \int_{y=0}^{\infty} \frac{u}{U_\infty}\left(1 - \frac{u}{U_\infty}\right) dy \tag{78}$$

From this equation it is clear that $\rho U_\infty^2 \theta$ represents the defect in the rate of transport of momentum in the boundary layer as compared with the rate of transport of momentum in the absence of the boundary layer.

Energy thickness, δ_E, is defined as

$$\delta_E = \int_{y=0}^{\infty} \frac{u}{U_\infty}\left[1 - \left(\frac{u}{U_\infty}\right)^2\right] dy \tag{79}$$

The quantity $\rho U_\infty^3 \delta_E/2$ represents the defect in rate of transport of kinetic energy in the boundary layer when compared with the rate of transport in the absence of the boundary layer.

Flows in Pipes and Ducts

The flow in the inlet length of a circular pipe of constant cross section is shown in Figure 1-1.22. Initially, at distances very close to the inlet, the flow is uniform with a boundary layer of very small thickness forming very close to the wall surface.

The velocity profile across the pipe changes continuously downstream. As the boundary layer on the wall grows downstream, the velocity in the central region increases to compensate for this growth, since the equation of continuity must hold true. At some distance from the inlet the boundary layers merge and the flow becomes fully developed. Onward from this distance, the velocity profile remains the same. Since the velocity profile in the fully developed flow is constant, it follows that the force due to friction at the pipe wall exactly balances that force due to the pressure gradient down the pipe required to maintain the flow.

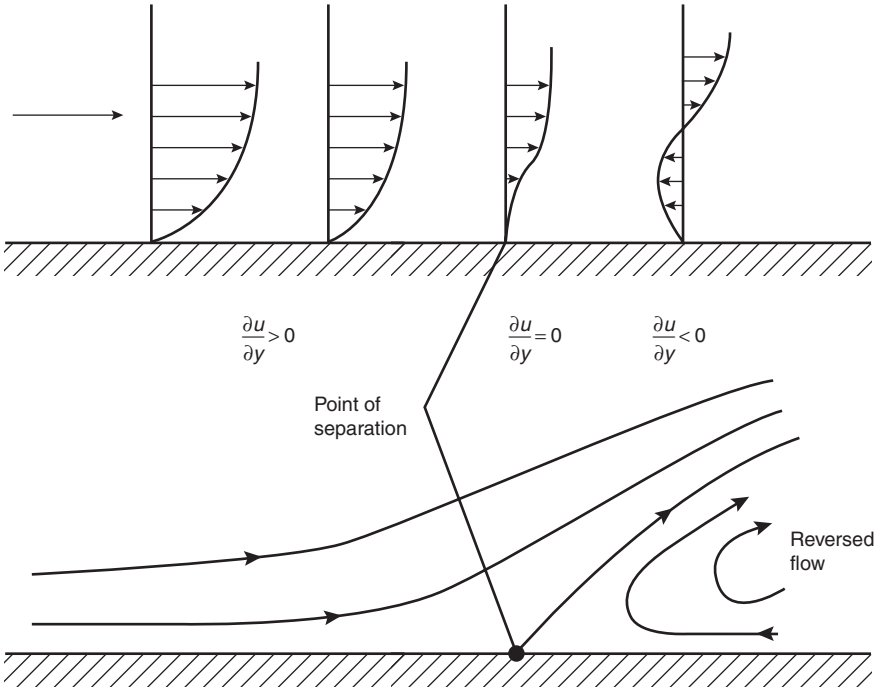

Figure 1-1.21. ***Point of separation and flow reversal.***

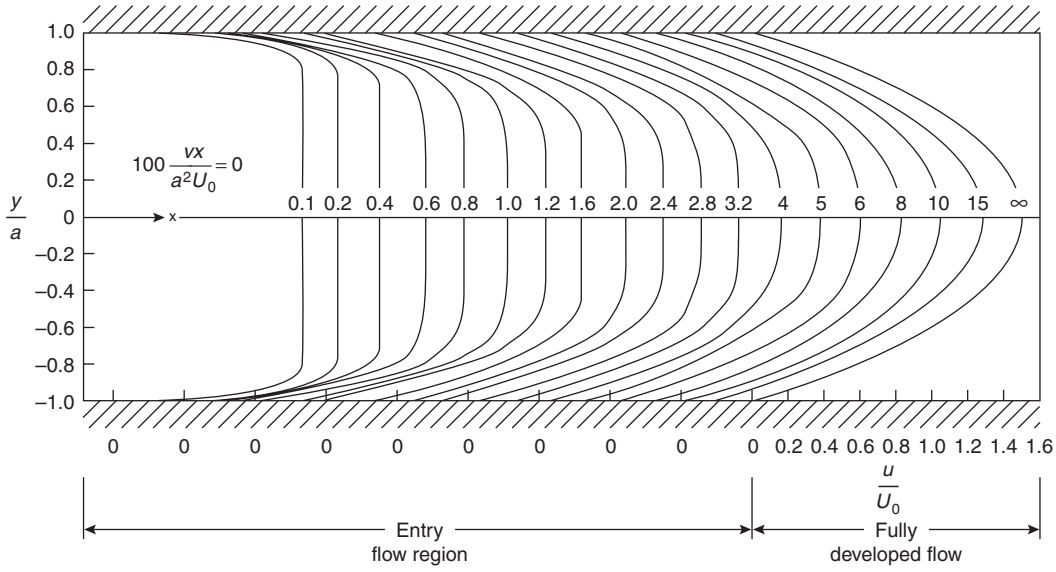

Figure 1-1.22. ***Development of laminar boundary layer in a pipe.***

Laminar Flow in a Pipe

With fully developed laminar flow in a smooth-walled pipe, the fluid moves under the influence of the pressure gradient and is retarded by the frictional forces acting on the wall surface. (See Figure 1-1.23.)

For equilibrium in the x-direction, the pressure force must balance the shear force, that is,

$$2\pi y\ell \cdot \tau = (p_2 - p_1)\pi y^2 \tag{80}$$

since

$$\tau = -\mu \frac{du}{dy} \tag{81}$$

Therefore,

$$\frac{du}{dy} = -\frac{p_2 - p_1}{\mu\ell} \cdot \frac{y}{2} \tag{82}$$

Integrating Equation 80 with 81 and 82 gives

$$u(y) = \frac{p_1 - p_2}{\mu\ell}\left(C - \frac{y^2}{4}\right) \tag{83}$$

The constant of integration, C, is obtained from the no-slip condition at the wall.

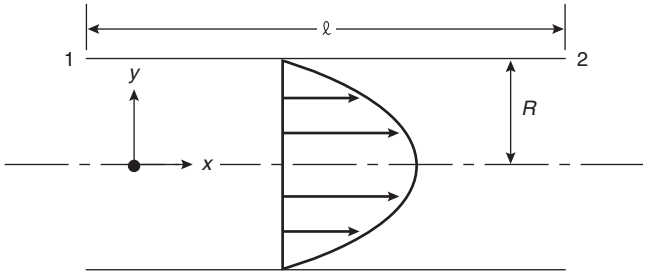

Figure 1-1.23. ***Fully developed laminar flow in a pipe.***

Thus, $u = 0$, $y = R$, so that $C = R^2/4$. Hence

$$u(y) = \frac{p_1 - p_2}{4\mu\ell}(R^2 - y^2) \tag{84}$$

This equation shows that the velocity is distributed parabolically over the radius. The same result is arrived at using the method of dimensional analysis (see the dimensional analysis example in this chapter) and also using the Bernoulli equation (Equation 55).

The maximum velocity on the pipe axis is

$$u_{\max} = \frac{p_1 - p_2}{4\mu\ell} R^2 \tag{85}$$

The volume of fluid passing in unit time is

$$Q = \frac{\pi}{2} R^2 U_{\max} = \frac{\pi R^4}{8\mu\ell}(p_1 - p_2) \tag{86}$$

The average velocity of flow is

$$\overline{u} = \frac{Q}{\pi R^2} \tag{87}$$

The expression for Q is known as the Hagen-Poiseuille equation of laminar flow through a pipe. This expression is only valid if the flow Reynolds number is less than the critical Reynolds number for a pipe (i.e., $\overline{u}d/\nu \leq 2300$, with $d = 2R$).

Turbulent Flow in a Pipe

Measurement of velocity profiles for a fully developed turbulent flow in a pipe shows that it is very different from the parabolic laminar profile just discussed. This difference results because in turbulent flow extra shear stresses are developed due to the turbulent momentum transfer from one layer to the other.

The shear stresses in the turbulent flow can be expressed as

$$\frac{\tau}{\rho} = \nu \frac{d\overline{u}}{dy} + \varepsilon \frac{d\overline{u}}{dy} \tag{88}$$

where

ν = kinematic viscosity

ε = eddy viscosity

$\overline{u}$ = mean velocity

For a smooth pipe, ε is very nearly equal to zero.

From the experimental measurements of turbulent flow in pipes conducted by Nikuradse,[3] three regions of flow can be identified. (See Figure 1-1.24.)

The profile is expressed in terms of the shearing or friction velocity, defined as

$$U_* = \left(\frac{\tau_w}{\rho}\right)^{1/2} \tag{89}$$

In a region very close to the surface, the velocity is proportional to the radial distance measured from the wall, y, and

$$\frac{u}{U_*} = \frac{yU_*}{v} \tag{90}$$

This region is called the laminar sublayer. In this region

$$\mu\left(\frac{d\overline{u}}{dy}\right) \gg \varepsilon\left(\frac{du}{dy}\right) \tag{91}$$

In the transition region the turbulent friction and the laminar friction are of the same order of magnitude. This result is true for the following range.

$$5 < \frac{yU_*}{v} < 70 \tag{92}$$

In the turbulent region the laminar contribution is negligible compared with the turbulent friction. This result occurs when

$$\frac{yU_*}{v} \geq 70 \tag{93}$$

For this region the following semi-empirical relation holds very well for the velocity profile. The contribution from eddy viscosity is also higher.

$$\frac{\overline{u}(y)}{U_\tau} = 5.75 \log_{10}\left(\frac{yU_\tau}{v}\right) + 5.5 \tag{94}$$

Duct Flows

In dealing with flow through noncircular cross section ducts, a parameter called the hydraulic radius, R_h, is defined as

$$R_h = \frac{2A}{C} \tag{95}$$

where A denotes the cross-sectional area and C is the wetted perimeter of the duct.

In the case of a circular cross section the hydraulic radius is equal to the radius of the circle.

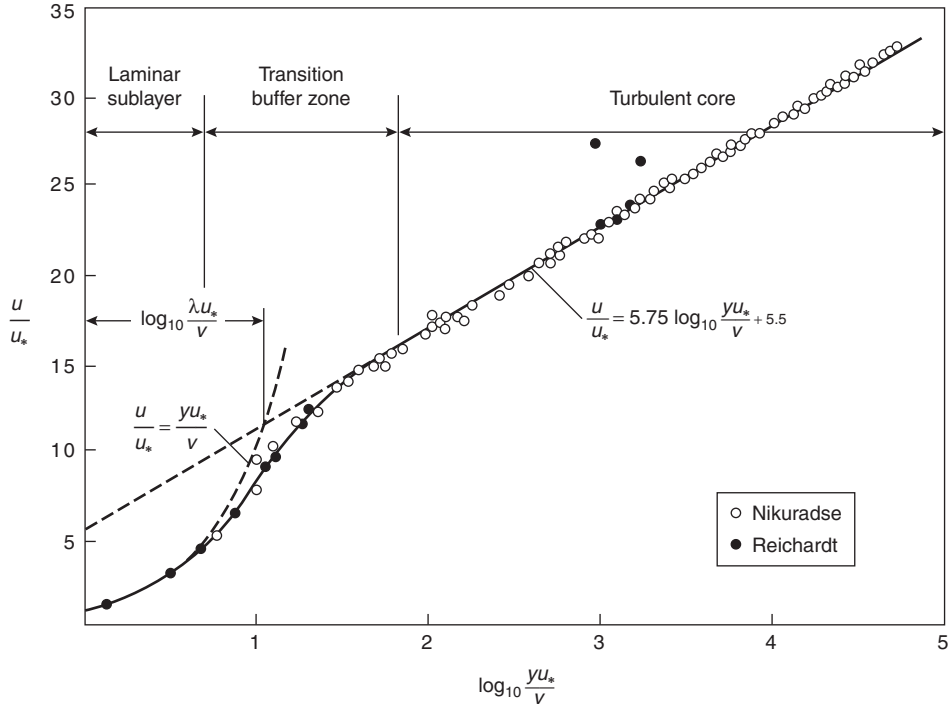

Figure 1-1.24. ***Measurement of turbulent velocity profile in a pipe.[1]***

Table 1-1.4 ***Laminar Flow Through Rectangular Ducts[4]***

a/*b* or *b*/*a*	C_1
0.00	1.50
0.05	1.40
0.10	1.32
0.12	1.28
0.16	1.23
0.25	1.14
0.40	1.02
0.50	0.97
0.75	0.90
1.00	0.89

Laminar flow: For a circular cross section pipe of diameter, d, of length, L, with pressure difference $(p_1 - p_2)$, the friction factor, λ, is defined as

$$\lambda = \frac{p_1 - p_2}{L} \cdot \frac{d}{1/2\rho\overline{u}^2} \tag{96}$$

Similarly, for noncircular cross section pipe, friction factor can be defined based on the hydraulic radius as

$$\lambda' = \frac{p_1 - p_2}{L} \cdot \frac{R_h}{1/2\rho\overline{u}^2} \tag{97}$$

For any noncircular shape the relationship between the friction factor and Reynolds number can be expressed in the form

$$\lambda' = \lambda C_1 \tag{98}$$

where C_1 is a function of geometry and λ is the friction factor for the flow in a circular pipe of the same Reynolds number, $\mathrm{Re} = uR_h/\nu$.

The values of C_1 for rectangular cross section ducts are given in Table 1-1.4.

Turbulent flow: Turbulent flow measurements show that for noncircular cross section ducts, the velocities at the corners are comparatively very large. This increase in velocity results because of secondary flows, which arise because all three components of the fluctuating velocity are nonzero. These flows are not present in the corresponding laminar motion because the fluctuating velocity components are not present. The secondary flows continually transport momentum from the center to the corners and generate high velocities there as shown in Figure 1-1.25.

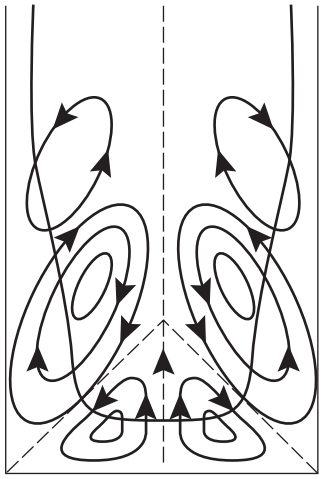

Figure 1-1.25. ***Secondary flows in the corners of a rectangular duct.[3]***

Turbulent velocity measurements in a rectangular duct made by Nikuradse are shown in Figure 1-1.26.

Building Aerodynamics and Applications to Fire Engineering

In general, building aerodynamics is concerned with the study of atmospheric wind flows and wind loading on buildings and structures. Such a study is important in building design, as large wind-induced loads may result in the instability and eventual collapse of a structure. Collapse of chimney stacks and suspension bridges are examples of such failures.

In fire engineering, obvious applications of such studies are in the problems relating to smoke control and buoyancy-driven roof vent design. Other applications may include the ingress of smoke and other contaminants from external sources and the effects of wind on fire spread.

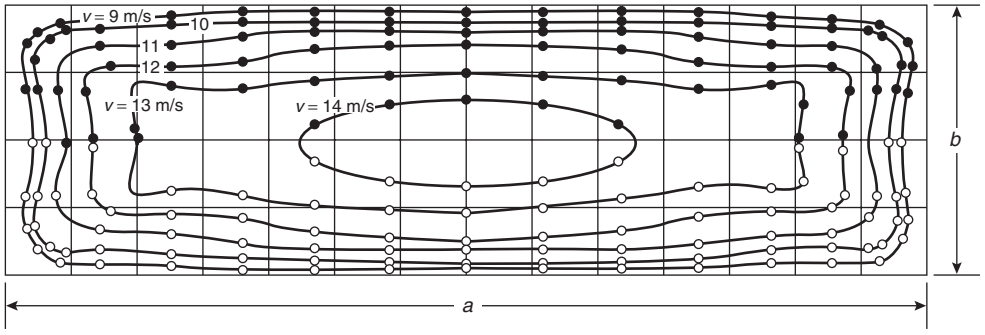

Figure 1-1.26. ***Axial turbulent contours in a rectangular duct.[3]***

Over the past two decades a large amount of experimental data, both in the wind-tunnel studies and full-scale measurements, has been collected for a wide range of building shapes and structures.[5–7] Initially, because of their immediate applications to structural design, most of the information was presented in the form of the wind loads. However, in recent years, attention has also been focused on the effects of wind on internal environment systems, such as ventilation and air conditioning. This research is important in controlling the spread of contaminants (such as smoke and other airborne particles generated by fire or explosion) to other parts of the building. Various smoke-control measures that are currently in use require the effects of wind to be taken into account in their design. It is essential that large pressure differentials do not hinder escape while serving to confine smoke to the fire areas. The design of a pressurization system, therefore, requires information on the flow field around, as well as inside, the building.

The wind-induced internal and external pressure distribution for a given building is determined not only by the building shape or size, but also by the wind characteristics. These characteristics include the wind velocity profile (which is terrain specific) and the level of turbulence (generated by the adjacent buildings) of the approaching wind.

Natural Wind Characteristics

On the global scale the movement of wind and weather systems is dependent on such factors as the location, vertical temperature gradient, the earth's rotation, etc.[8] In a region very close to the earth's surface the variation of wind velocity with height is considerable and is influenced by the surface roughness. This region is usually referred to as the terrestrial boundary layer. The height at which the velocity becomes independent of the surface roughness is called the gradient height (boundary layer thickness), Z_G, and the corresponding wind speed is called the gradient wind speed.

Figure 1-1.27 shows the terrestrial boundary layer velocity profile for a range of terrain (surface roughness) categories. Category 1 refers to plain areas such as deserts and the open sea, while Category 4 refers to the high-roughness city centers with numerous tall buildings. The other categories lie between these two limits.[9]

For the purposes of wind-tunnel investigations, the wind velocity profile is usually represented by a power law profile of the type,

$$\frac{\overline{V}_Z}{V_{Z_G}} = \left(\frac{Z}{Z_G}\right)^{\beta} \tag{99}$$

where $\overline{V}_Z$ is the mean wind speed at height Z and β is a constant, which varies for different terrain categories. For example, for Category 1, $\beta = 0.11$; and for Category 4, $\beta = 0.36$.

Wind Flow over Buildings

Wind-tunnel studies show that when buildings of rectangular cross section are subjected to a power law velocity profile, as shown in Figure 1-1.27, the windward surface of the building experiences positive pressures (i.e., higher than the atmospheric pressure) while all the other surfaces, including the roof, experience negative pressures (i.e., lower than the atmospheric pressure). These pressures are illustrated in Figure 1-1.28.

As the air flows toward the building it is slowed down and comes to rest at a point "*S*," called the stagnation point, on the windward surface. The total pressure increases with height up to the stagnation point and begins to decrease toward the roof. Below this point the pressure gradient down the face of the building causes air to flow down the building. At the ground level the flow

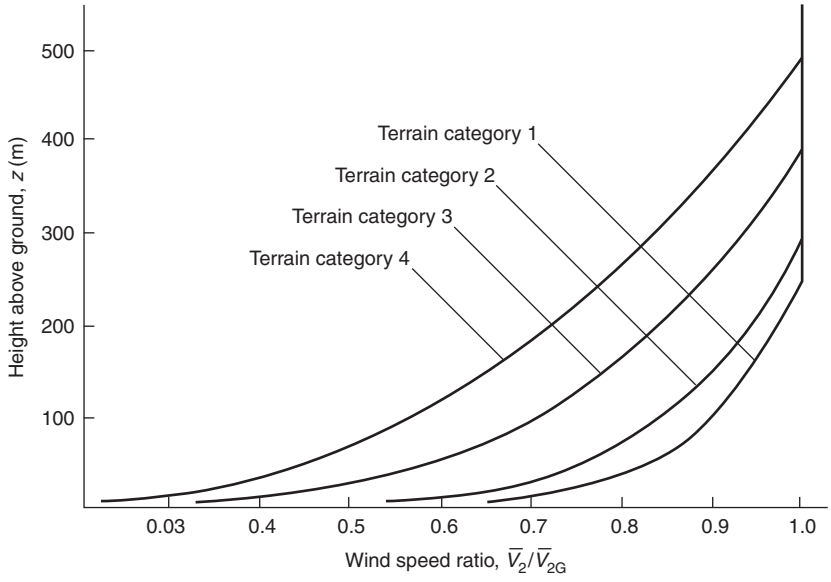

Figure 1-1.27. ***Velocity profile in the terrestrial boundary layer.[8]***

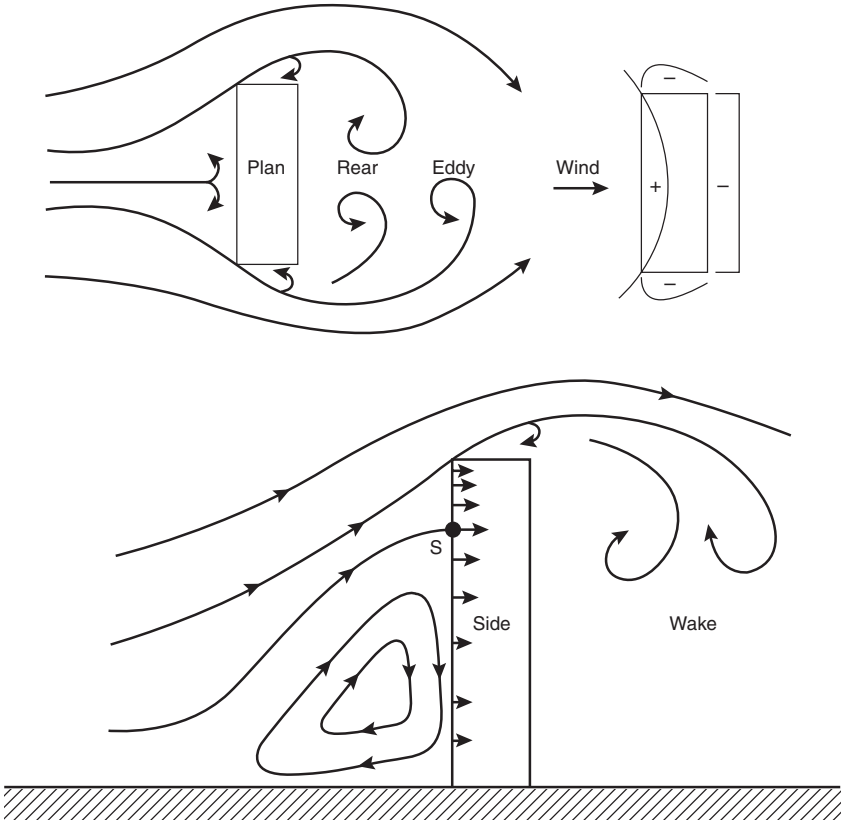

Figure 1-1.28. ***Flow over a tall building.***

turns and starts to flow upwind. At some distance from the building the flow is opposed by the oncoming wind and once again turns and starts to flow up toward the building. This way a vortex is set up in front of the building as illustrated in Figure 1-1.28.

The pressure measurements are usually expressed in terms of a pressure coefficient defined as

$$C_p = \frac{p - p_0}{1/2\rho V_H^2} \tag{100}$$

where

p = total pressure at a point
p_0 = static pressure at that point
V_H = wind speed at building height
ρ = air density

Figures 1-1.29(a) and 1-1.29(b) show wind-tunnel pressure measurements on the walls of a model building shown in Figure 1-1.29(c).[10] It is clear that, on the windward side [Figure 1-1.29(b)], the pressure is the highest at a point on the fourth-floor level (the stagnation point). This point usually occurs at about four-fifths the height of the building. On the rear wall (side R, for wind incidence $\alpha = 0$ degrees) the pressure distribution is negative but fairly constant. These negative pressures on the walls are caused by the eddies generated as a result of flow separation at the sharp corners of the building. Because of these marked pressure variations on the walls, internal flow patterns are set according to these variations.

Wind-Induced Internal Flows

For completely sealed buildings, the outside wind has no effect on the internal flow patterns in a building. The internal flows are greatly influenced by the outside wind for a building with outside doors and windows. The magnitude of internal pressure distribution is a function of wind speed, building geometry, and building leakage characteristics. Wind-tunnel experiments[11] show that the wind-induced internal pressures are determined by the outside pressures on the wall with highest leakage. The results are summarized in Figure 1-1.30, in which the leakage ratio, R, is defined as the ratio of the total leakage area of the windward wall to the total leakage area of the rear wall.

The curve for $\alpha = 0$ degrees clearly shows that as the windward wall leakage area is increased, the internal pressure is also increased. For the case of $\alpha = 90$ degrees, both the leaky walls are under negative outside pressure and the internal pressure is negative, as expected, and does not change very much with the leakage ratio.

Such a marked change in internal pressure due to the outside wind can have serious implications for the functioning of smoke extract vents used in these types of buildings.

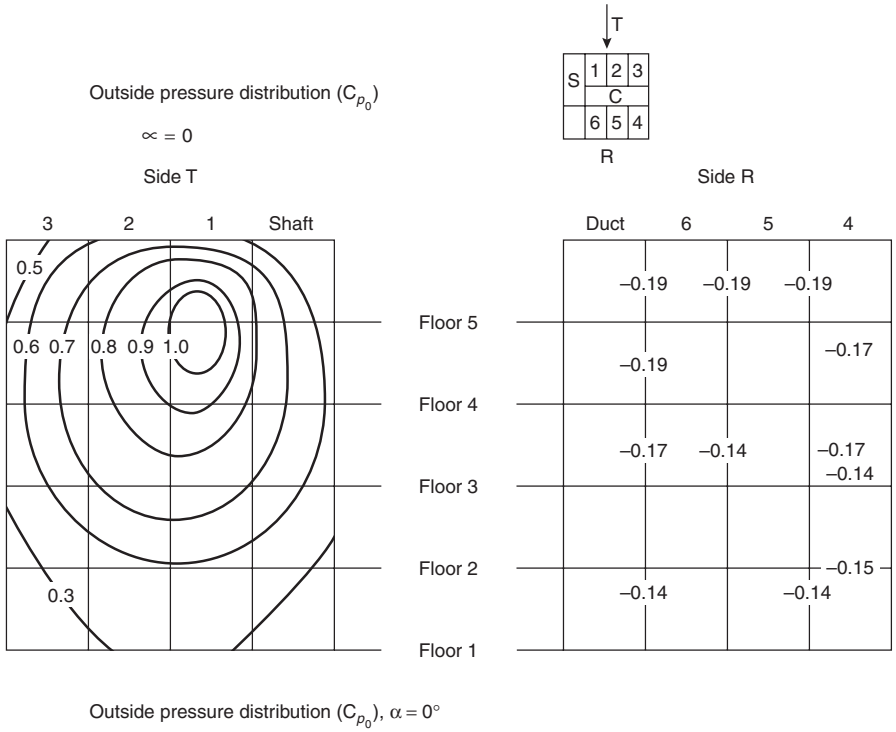

Figure 1-1.29(a). ***Outside pressure distribution (C_p), α = 0 degrees.***

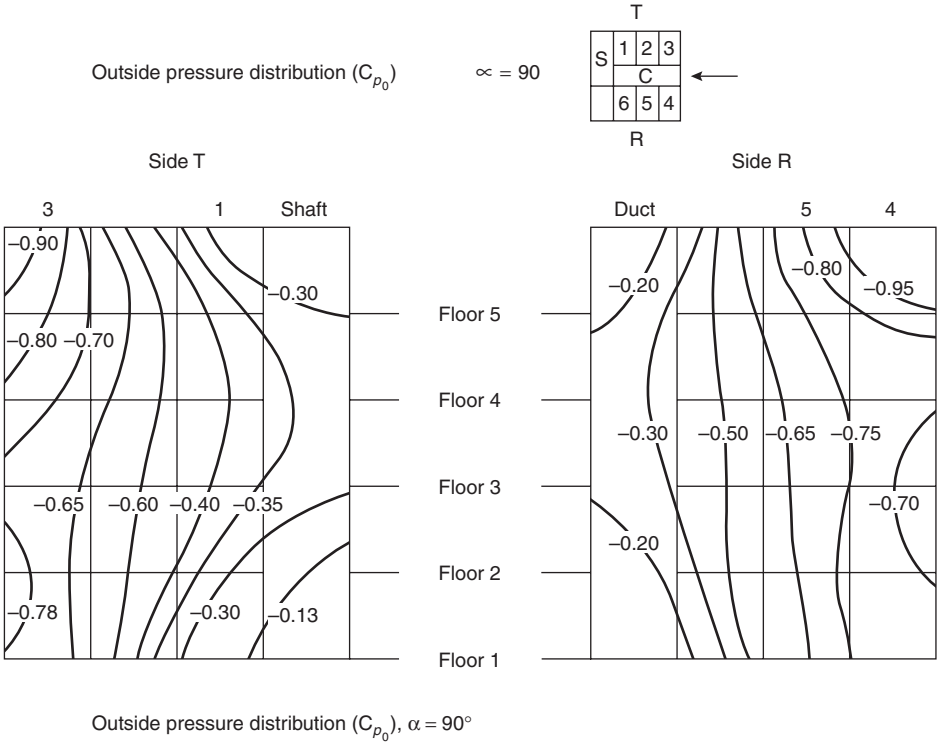

Figure 1-1.29(b). ***Outside pressure distribution (C_p), α = 90 degrees.***

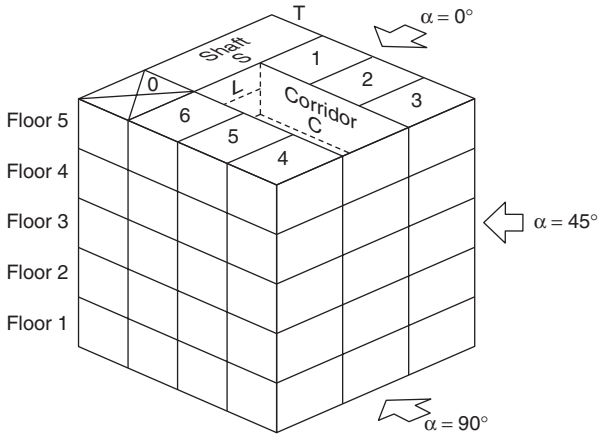

Figure 1-1.29(c). ***Five-story wind-tunnel model.[10]***

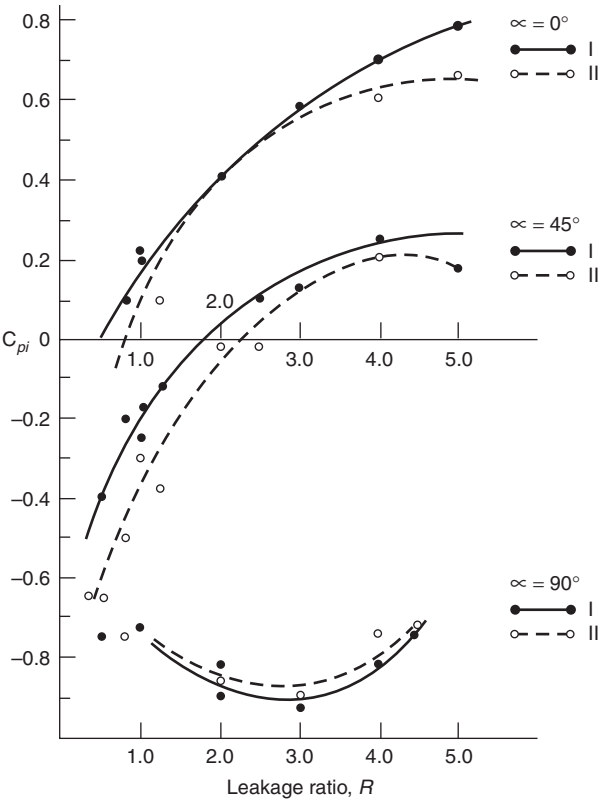

Figure 1-1.30. ***Variation of internal pressure, C_{pi}, with leakage ratio, R, for wind direction α = 0 degrees, 45 degrees, and 90 degrees.[11]***

Smoke Movement in Tall Buildings

When fire occurs in a building, smoke or toxic gases are carried to other parts of the building interior by the preexisting airflows. These flows are a function of the outside wind as well as the building leakage characteristics. For the example of a high-rise building (Figure 1-1.31), if fire occurs in a room that has window openings on a wall

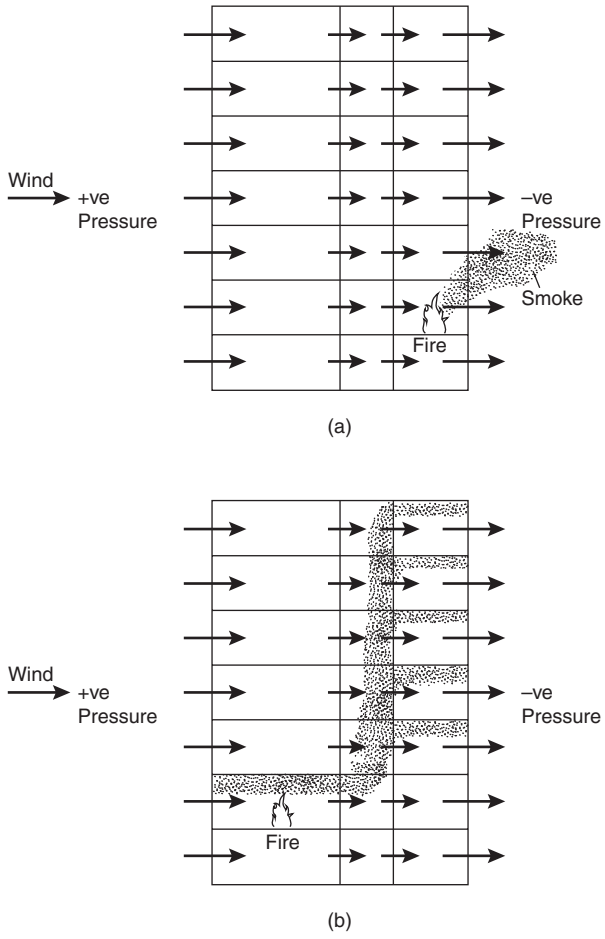

Figure 1-1.31. ***Smoke movement in a high-rise building.***

subjected to negative wind-induced pressures, most of the smoke will be drawn out of the building by the prevailing negative pressures on that wall. Smoke will be prevented from flowing into the building by the positive pressure there (Figure 1-1.31b).

However, the situation is reversed if the fire room has its window openings on the windward wall. The prevailing positive pressure on this wall will push the smoke into the building, where it will spread to other parts of the building, carried there by pre-existing flows.

If under such conditions a smoke control pressurization system is used, the design of such a system must account for the wind-induced pressures. Otherwise, the system may cause overpressure (preventing escape of occupants) or underpressure (rendering the system ineffective) within the building.

Roof Vent Design

For large single-space buildings (warehouses and factories, etc.), roof vents are used to extract smoke in fire situations. Usually, the design of these vents is based on the assumption that smoke buoyancy is the only force driving the smoke out. This assumption may not be true for very

tall buildings because the smoke cools very quickly as it moves up toward the ceiling. When this situation happens, the buoyant force of the smoke can be negligibly small, reducing the rate of flow through the vent.

If a sufficiently strong wind is blowing, the roof is subjected to considerable, high, wind-induced, negative pressures. These pressures can add to the buoyancy of the smoke with a subsequent increase in the extract flow velocity and mass rate. A situation may arise when the vent starts extracting clear air from underneath the hot layer. Under such conditions (Figure 1-1.32), the efficiency of the vent is decreased.

Therefore, a critical mass flow rate or cirtical vent area exists which must not be exceeded or the vent will be ineffective.[11] Figure 1-1.33 shows the variation of calculated critical vent area with leakage ration. These calculations were performed on the basis of roof pressure distribution shown in Figure 1-1.34.

Nomenclature

A	Area
b	Channel width (Figure 1-1.8)
C	A constant
C_p, C_p	Specific heat at constant pressure, or pressure coefficient
C_v	Specific heat at constant volume
d	Diameter, or characteristic length
E	Internal energy
F	Force
Fr	Froude number
g	Acceleration due to gravity
Gr	Grashof number
K	Bulk modulus
k	A constant, or thermal conductivity
L, l	Length, pipe length
m	Mass of fluid, or mass per unit length
M	Mass, or molecular weight
P, p	Pressure at a point

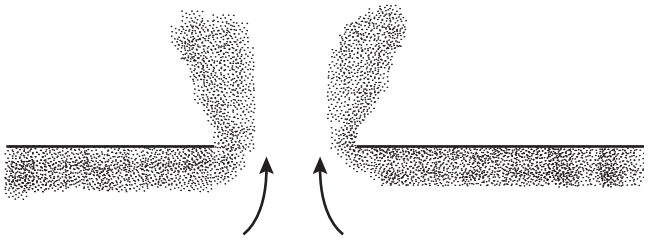

Figure 1-1.32. ***Operation of a roof vent.[12]***

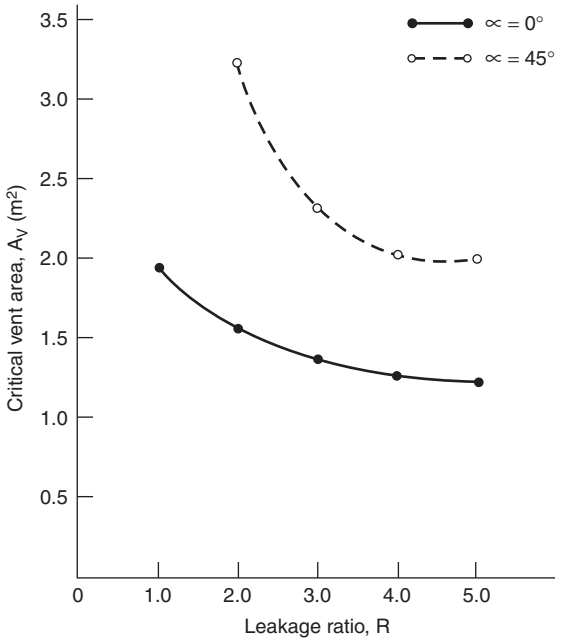

Figure 1-1.33. ***Variation of critical vent area (Av_{exit}) with leakage ratio R, for α = 0 degrees, 45 degrees.[11]***

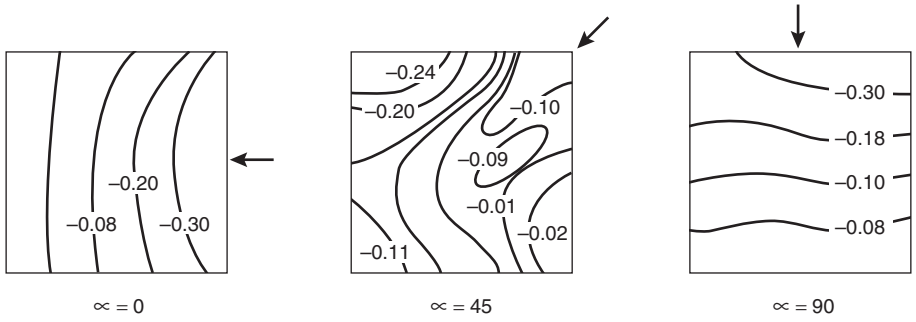

Figure 1-1.34. ***Pressure contours on the roof (C_{p0}) for wind directions α = 0 degrees, α = 45 degrees, and α = 90 degrees.[11]***

Pr	Prandtl number
q	Quantity of heat per unit mass
Q	Volume flow rate, or heat flux
R, r	Radius
R_L	Hydraulic radius
$\overline{R}$	Universal gas constant
Re	Reynold's number
T	Temperature
t, T	Time
u, v, w	Velocity components in the x, y, z direction, respectively
$\overline{u}, \overline{v}, \overline{w}$	Mean velocity components in the x, y, z direction, respectively
u', v', w'	Fluctuating velocity components in the x, y, z direction, respectively
U_∞	Free stream velocity
U_*	Friction velocity (Equation 89)
v	Volume of fluid
v_r, v_θ	Velocity components in the r and θ directions respectively
V	Volume of fluid (Equation 26), velocity (Equation 55)
V_H	Wind speed at building height
W	Work
x, y, z	Cartesian co-ordinates
$\overline{y}$	Position of centroid in the y direction
Z	Distance in the vertical direction
∇	Laplace's operator

Greek Symbols

α	Angle (Figure 1-1.2)
β	Coefficient of compressibility
β_1	Coefficient of thermal expansion
Γ	Circulation (Equation 53)
δ^*	Displacement thickness
δ_E	Energy thickness (Equation 79)
ε	Eddy viscosity
ϕ	Velocity potential
λ	Friction factor
μ	Coefficient of viscosity
ν	Kinematic viscosity
π	A constant (3.142)
θ	Angle (Figure 1-1.3)
ρ	Fluid density
σ	Surface tension coefficient
τ	Shear stress
ω	Angular velocity
ψ	Stream function
ζ	Vorticity

References Cited

1. E. Salamon, *Principles of Fluid Mechanics,* Allyn and Bacon, Boston (1963).
2. S. Kumar, "Mathematical Modeling of Natural Convection in Fire—A State-of-the-Art Review of the Field Modeling of Variable-Density Turbulent Flow," *Fire and Materials,* 7, 1 (1983).
3. H. Schlichting, *Boundary Layer Theory,* Pergamon, London (1955).
4. A.J. Ward-Smith, *Internal Fluid Flow,* Oxford University, Oxford, UK (1980).
5. T.W. Lawson, *Wind Effects on Buildings,* Applied Science, London (1980).
6. E. Naudascher (ed.), *Flow-Induced Structural Vibrations,* Symposium, Berlin (1972).
7. *Proceedings of the 3rd International Conference of Wind Effects on Buildings and Structures,* Saikon, Tokyo (1971).
8. R.S. Scorer, *Natural Aerodynamics,* Pergamon, London (1958).
9. R.M. Aynsley, W. Melbourne, and B.J. Vickery, *Architectural Aerodynamics,* Applied Science, London (1977).
10. B.S. Kandola, *F. Safety J.,* 10, p. 211 (1986).
11. B.S. Kandola, *J. of Indus. Aerodyn.,* 3, p. 267 (1978).
12. D.D. Drysdale, *Introduction to Fire Dynamics,* John Wiley and Sons, New York (1985).

CHAPTER 2

Conduction of Heat in Solids

John A. Rockett and James A. Milke

Introduction

There are three mechanisms by which heat (thermal energy) is transferred from one object to another: (1) radiation, (2) convection, and (3) conduction. This chapter addresses both heat conduction and the historic development of heat conduction theory.[1–5]

Before discussing heat conduction, it is useful to consider the heat content of an object; that is, the property of the object subject to movement by conduction. The heat content of an object, Q, and its temperature are closely linked. When the heat content of one gram of water at 0°C is increased by one calorie, its temperature increases one degree Celsius. Heat content is associated with the kinetic energy of vibration of the atomic particles of which an object is composed. Since at absolute zero temperature all motion stops, heat content is zero at zero (absolute) temperature. In metals, where there are free electrons (those electrons not localized on a particular atom, but free to move through the crystal lattice), some of the heat content is associated with this electron ''gas.'' In all materials the atoms vibrate about their average position in the crystal lattice. Atomic vibration within the crystal lattice (standing acoustic waves called "phonons") accounts for the remainder of the heat content. The hotter the object, the more violent is the vibration of the electrons and atoms. Thus the transfer of heat from one body to another, or from one part of a body to another part of the same body, is equivalent to transferring the kinetic energy of vibration from particles in one location to those in another, adjacent location.

Dr. John A. Rockett, formerly senior scientist, U.S. National Bureau of Standards, is a consultant based in Washington, DC. His research has focused on the growth and spread of fire and the development of analytic models for describing fire in buildings.

James A. Milke is associate professor of fire protection engineering at the University of Maryland. His recent research activities have included the impact of fires on the structural response of steel and composite members, as well as the design of smoke management systems.

The heat content of an object is expressed as the integral of the material's specific heat with respect to temperature from absolute zero to the temperature in question, that is,

$$q''' = \int_o^T \rho c \, dT$$

The inability to correctly calculate specific heat was one of the singular failures of classical physics. The roots of modern quantum physics lie in the work of Planck, Lorentz, and Einstein to resolve this problem. Building on their work, Debye, and (independently) Born and von Karman, published a theory of specific heat in 1912, which is still accepted today with only refinements in detail. According to this theory, the specific heat rises from zero at zero temperature and approaches a constant at high temperature. A temperature characteristic of the material, or the "Debye temperature," determines the region where transition from rising to constant specific heat occurs. At a point well above the Debye temperature, the specific heat is given by the classical, constant value; below it, quantum effects must be included. For heavy atoms the Debye temperature is well below room temperature, but it is higher for light atoms. Beryllium, for example, is light enough that its specific heat varies noticeably near room temperature. For aluminum at room temperature the specific heat is 93 percent of the classical value; for copper, 95 percent. For some minerals, however, the Debye temperature is quite high and the assumption of constant specific heat may lead to significant errors. Nevertheless, constant specific heat is generally assumed, usually without discussion, in heat conduction studies.

Heat conduction is observed when a hot object is brought in physical contact with a cold one: the hot object cools and the cold one is heated. This process was studied by Newton but, in the modern sense, first quantified by Fourier in 1812. Fourier's equation states that the quantity of heat transferred per unit time across an area, A, is pro-

portional to the area and the temperature gradient, dT/dx. The heat flows from the hotter to the cooler material, so

$$\dot{q} = -kA\frac{dT}{dx}$$

where

A = surface area across which heat is transferred (m^2)
d = differential operator
k = thermal conductivity of the solid (W/m·K)
$\dot{q}$ = the rate of heat flow across the area A (W)
T = temperature (K)
x = distance normal to the surface A (m)

A more modern and more precise statement of Fourier's law is

$$\frac{dQ}{dt} = -\int_A (k_{ij}T_{,j})n_i\, dA$$

where

Q = heat content (Joules) of the material inside the closed surface A
n_i = outward directed vector normal to the surface element dA
t = time
$T_{,j}$ = vector gradient of the temperature of the object
k_{ij} = thermal conductivity (written here in its most general form as a tensor)
A = integral taken over the entire surface

The thermal conductivity of a material, k, will play a central role in what follows. Wiedemann and Franz observed in 1853 that electrical and thermal conductivity were proportional for metals. This observation suggests that the kinetic energy of free electrons is primarily responsible for heat transfer. This is a good first approximation for good electrical conductors, where free electrons are abundant. Sommerfeld, in 1928, calculated the Wiedemann-Franz ratio (ratio of thermal to electrical conductivity) based on a quantum mechanical model for the free electron gas. He found

$$\frac{k}{T}\sigma = 2.45 \times 10^{-8}$$

where σ is electrical conductivity, and T is absolute temperature. This relation is obeyed (error less than about 10 percent) by gold, silver, copper, copper-silver alloys, tungsten, and molybdenum for absolute temperatures from 50 to 360 K.

If this were all that was involved, electrical insulators would conduct virtually no heat. Actually, although heat is poorly conducted by electrical insulators, the amount of heat conducted is orders of magnitude too great to be accounted for solely by free electron conduction. Thus, the ratio of electrical conduction of glass to that of gold is 1.44×10^{-19}, but the ratio of their thermal conduction is 2.5×10^{-2}. Phonons are present in all solids heated above absolute zero. However, if the crystal lattice were perfect, and the material perfectly pure, the material would conduct no heat because these standing, acoustic waves would experience no attenuation. But imperfections within the solid (e.g., missing atoms-vacancies, extra atoms-interstitials, and lattice imperfections-dislocations) scatter the phonons and free electrons when they are present. It is this scattering that diffuses the phonon energy to produce heat conduction in electrical insulators.

Because cold-working a metal increases dislocations and heat treatment (e.g., precipitation hardening), lattice imperfections, thermal conductivity, as well as physical properties, can be significantly altered by these treatments. In general, treatments that increase hardness will decrease thermal (and electrical) conduction.

For some materials, for example, some laminates and fibrous materials such as wood and reinforced plastics, the thermal conductivity differs depending on whether the heat flow is parallel or across the grain. For these materials, the thermal conductivity, in general, differs with the direction of the heat flow. This pattern is the most general case, and will be addressed in this chapter. For these materials (orthotropic solids), the conductivity is a diagonal matrix (its only nonzero elements are the diagonals, k_{ii}). These are normally written simply k_1, k_2, k_3. In other materials, most notably some types of crystals, the off-diagonal elements of the k matrix are nonzero. For these materials the conductivity must be expressed as a general matrix (tensor).

From this brief discussion it is clear that the theoretical basis for thermal analysis is comparatively recent. The mathematical analysis of heat conduction used today was, however, well-established by the end of the last century.

Equation of Heat Conduction

Fourier's equation of heat conduction (as given in the introduction to this chapter) has been generalized to the basic, modern statement of conductive heat transfer. To reproduce this, consider a small rectangular block of material with density, ρ, specific heat, c, thermal conductivity, k, and average temperature, T. This small block is a segment of a much larger solid. Let the small block be oriented parallel to a Cartesian coordinate system, x, y, z, and let its dimensions be dx, dy, and dz measured along the respective axes. The center of the block is at location x, y, z.

If the temperature within the solid varies nonuniformly, the heat flux entering the small block across the face with area $dydz$ located at $x - dx/2$ may be different from the heat leaving across the parallel face at $x + dx/2$. According to Fourier's law and using a Taylor-series expansion for k and T, the difference in heat flux would be

$$\begin{aligned}\dot{q}_{x-\text{net}} &= \left[\dot{q}''\left(x+\frac{dx}{2}\right) - \dot{q}''\left(x-\frac{dx}{2}\right)\right]dy\,dz \\ &= \left\{\left[\left(k_1 + \frac{\partial k_1}{\partial x}\frac{dx}{2}\right)\left(\frac{\partial T}{\partial x} + \frac{\partial^2 T}{\partial x^2}\frac{dx}{2}\right)\right]\right. \\ &\quad \left. - \left[\left(k_1 + \frac{\partial k_1}{\partial x}\frac{dx}{2}\right)\left(\frac{\partial T}{\partial x} - \frac{\partial^2 T}{\partial x^2}\frac{dx}{2}\right)\right]\right\} dy\,dz \end{aligned} \quad (1)$$

Expanding this and neglecting terms containing (dx^2), the result is

$$\dot{q}_x = \frac{\partial}{\partial x}\left(k_1 \frac{\partial T}{\partial x}\right) dx\, dy\, dz$$

Similarly,

$$\dot{q}_y = \frac{\partial}{\partial y}\left(k_2 \frac{\partial T}{\partial y}\right) dx\, dy\, dz$$

$$\dot{q}_z = \frac{\partial}{\partial z}\left(k_3 \frac{\partial T}{\partial z}\right) dx\, dy\, dz$$

The sum of these three terms is the net rate of heat gain by the small block. Dividing by the volume of the block, the net gain per unit volume is

$$\dot{q}''' = \frac{\partial}{\partial x}\left(k_1 \frac{\partial T}{\partial x}\right) + \frac{\partial}{\partial y}\left(k_2 \frac{\partial T}{\partial y}\right) + \frac{\partial}{\partial z}\left(k_3 \frac{\partial T}{\partial z}\right) \qquad (2)$$

As stated, the energy stored in a material at temperature, T, is

$$q''' = \int_0^T \rho c\, dT \qquad (3)$$

For temperatures well above the Debye temperature, this can be written as

$$q''' = q_0''' + \rho c(T - T_0) \qquad (4)$$

where

$$q_0''' = \int_0^{T_0} \rho c\, dT \qquad (5)$$

is the heat stored in the material as a result of raising its temperature from absolute zero to T_0, a temperature high enough that c, in Equation 4, can be assumed constant. T_0 may be conveniently assumed to be zero Celsius, 273.16 K. Further, since changes in energy are the concern, the reference energy, q_0''', can be dropped from further consideration. Thus, the rate of change of thermal energy stored in the block per unit volume can be written as

$$\dot{q}''' = \rho c \frac{dT}{dt} \qquad (6)$$

Sometimes it is required to analyze materials that undergo an internal change of state. For example, in heating porous materials, such as wood or gypsum plaster, absorbed water may evaporate in one part of the solid, diffuse to a cooler part, and condense. The evaporation will remove heat from the locality where it occurs due to the latent heat of vaporization of the moisture, and the condensation will add heat locally where it occurs. Let the rate of such local heat addition be $\dot{q}_i'''$.

Combining Equations 2 and 6 and accounting for heat addition due to chemical or physical changes in the material results in

$$\rho c \frac{\partial T}{\partial t} = \frac{\partial}{\partial x}\left(k_1 \frac{\partial T}{\partial x}\right) + \frac{\partial}{\partial y}\left(k_2 \frac{\partial T}{\partial y}\right) + \frac{\partial}{\partial z}\left(k_3 \frac{\partial T}{\partial z}\right) + \dot{q}_i''' \qquad (7)$$

Equation 7 is the basic equation describing heat conduction in a solid.

To solve the heat conduction equation, initial and boundary conditions must be provided. These conditions distinguish one problem of interest from another. The conditions that must be specified are:

1. The initial temperature throughout the solid, and
2. The temperature or heat flux at the surface of the solid for all times. Note that along any part of the surface, either the temperature or the heat flux (but not both) should be specified; temperature may be specified for some areas, and heat flux for others. The temperature and flux need not be constant in space or time.

In formulating Equations 2 and 7, it was assumed that the thermal conductivity might be different in each of the three directions and further, that each of these values might vary with position. There are cases where these variations are important.[6,7] However, for the remainder of this chapter (unless specifically mentioned) the solid will be assumed isotropic (i.e., k the same in each direction) and independent of temperature. Also, for simplicity, the heat addition term, $\dot{q}_i'''$, will be assumed zero, except for a few specific examples.

If a dimensionless time ($\tau = t/t_0$) and a dimensionless distance ($\xi = x/b$) are substituted into Equation 7, and t_0 is chosen as

$$t_0 = \frac{\rho c b^2}{k}$$

the equation contains no parameters (for the case of an isotropic solid without local heat addition). Since t_0 and b are related, the choice of b is significant. Normally b would be a dimension of the object in question, with the most useful dimension being that along the principal direction of heat transfer. The quantity ($k/\rho c$) is called the "thermal diffusivity" of the solid; it has dimensions (m^2/s) and is often represented by the Greek letter α.

Steady-State Solutions

If the thermal environment of a solid has been constant for a sufficient time (i.e., the boundary conditions have not changed in value), it will achieve a steady temperature distribution. In this case, the time derivative of T will vanish and the left side of Equation 7 will be zero. Five examples of steady-state heat conduction will be considered.

EXAMPLE 1: Flat, Rectangular Plate, Insulated along Its Edges, Heat Flowing from One Face to the Other.

In this case Equation 7 reduces to

$$\frac{\partial}{\partial x}\left(k \frac{\partial T}{\partial x}\right) = 0 \qquad (7a)$$

The first integral with respect to x yields

$$k \frac{\partial T}{\partial x} = -\dot{q}'' \qquad (7b)$$

where $\dot{q}''$ is the constant of integration; it is the heat flux per unit area through the plate. Equation 7b is a variation of Fourier's law. The constant heat flux is characteristic of the one-dimensional, steady-state problem. Consequently, dT/dx is also a constant for cases of uniform conductivity, yielding a linear temperature profile through the solid. Equation 7b, in turn, integrates to

$$T = T_0 - x\frac{\dot{q}''}{k} \tag{8}$$

T_0 is the second integration constant. Two integration constants, $\dot{q}''$ and T_0, have been introduced, but no boundary conditions used. The boundary conditions selected will fix the values of these two constants. If the thickness of the plate is b, T_0 is the temperature of the left face, and the heat flux, $\dot{q}''$, is specified, the temperature on the right face must be

$$T_b = T_0 - b\frac{\dot{q}''}{k}$$

Or, if the two surface temperatures are known, the heat flux through the plate will be

$$\dot{q}'' = (T_0 - T_b)\frac{k}{b} \tag{8a}$$

Figure 1-2.1 illustrates this example.

EXAMPLE 2: Flat, Rectangular, Laminated Plate, Insulated along I ts Edges.

Here Equation 8 is appropriate to each layer separately, but there may be different constants for each layer. For a two-layer laminate with layers of thickness b_1 and b_2, and thermal conductivities k_1 and k_2, the temperature at the interface will be

$$T_1 = T_0 - b_1\frac{\dot{q}''}{k_1} \tag{8b}$$

A key principle in the solution of this problem is that the heat flux is a constant across any plane parallel to the surface of the plate. (See first integration of the steady-state heat conduction, i.e., Equation 7b.) Thus the temperature of the rear face will be

$$T_2 = T_0 - \dot{q}''\left(\frac{b_1}{k_1} + \frac{b_2}{k_2}\right) \tag{8c}$$

See Figure 1-2.2.

EXAMPLE 3: Radial Heat Flow between Two Concentric Cylindrical Surfaces (heat loss through the wall of a pipe with inside radius, r_0, and thickness, b).

Rewriting Equation 7 in cylindrical coordinates and assuming radial symmetry yields

$$\rho c\frac{\partial T}{\partial t} = \frac{1}{r}\frac{\partial}{\partial r}\left(kr\frac{\partial T}{\partial r}\right) + \frac{\partial}{\partial z}\left(k\frac{\partial T}{\partial z}\right) + \dot{q}''' \tag{9}$$

For the present problem assume no heat addition, $\dot{q}''' = 0$, and no variation of T along the length of the pipe (z direction); hence the last two terms on the right vanish. For steady-state the left side also vanishes. Thus, for purely radial heat flow, Equation 9 can be integrated to

$$r\frac{\partial T}{\partial r} = -\frac{\dot{q}'}{2\pi k} \tag{9a}$$

where $\dot{q}'$ is a constant of integration whose significance will be discussed. A second integration yields

$$T = T_0 - \frac{\dot{q}'}{2\pi k}\left[\ln\left(\frac{r}{r_0}\right)\right] \tag{9b}$$

The integration constant, $\dot{q}'$, can be understood by considering a very thin-walled pipe, thickness b much less than r_0. Then $r_1 = r_0 + b$ and

$$\ln\left(\frac{r_1}{r_0}\right) = \ln\left(1 + \frac{b}{r_0}\right) \approx \frac{b}{r_0} + \frac{1}{2}\left(\frac{b}{r_0}\right)^2 + \cdots$$
$$\approx \frac{b}{r_0}$$

or, with this approximation and rewriting Equation 9b,

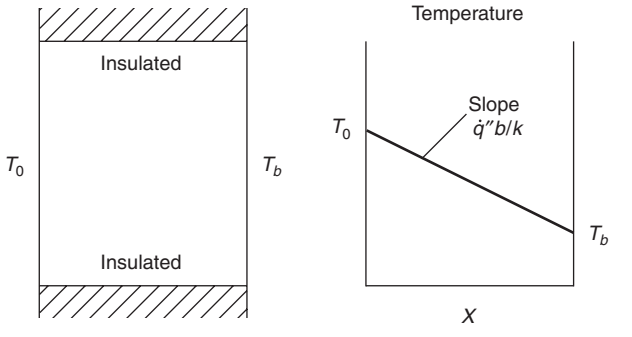

Figure 1-2.1. ***Flat plate of thickness b, insulated at its edges. Steady-state surface temperatures T_0 and T_b.***

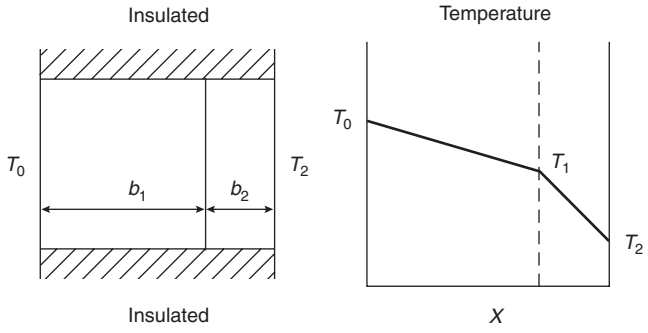

Figure 1-2.2. ***Two-layer, flat laminated plate insulated at its edges. Layer thickness b_1 and b_2. Layer 2 has the smaller thermal conductivity. Steady-state surface temperatures T_0 and T_2. Temperature of the interface between the plates, T_1.***

$$\frac{b}{r_0} = 2\pi k \frac{(T_0 - T_b)}{\dot{q}'}$$

$$\frac{\dot{q}'}{2\pi r_0} = k \frac{(T_0 - T_b)}{b}$$

Comparing this with Equation 8a it can be seen that

$$\dot{q}' = 2\pi r_0 \dot{q}''$$

or that $\dot{q}'$ equals the heat flux through the pipe per unit length. [See Figure 1-2.3(a).]

It can be verified that the heat flux per unit length of a pipe with conductivity k_1 and radii (r_0, r_1) surrounded by insulation, conductivity k_2, and radii (r_1, r_2) is

$$\dot{q}' = \frac{2\pi(T_0 - T_2)}{[(1/k_1)\ln(r_1/r_0) + (1/k_2)\ln(r_2/r_1)]} \qquad (9c)$$

where T_0 is the temperature at the inside of the pipe and T_2 the temperature of the outside of the insulation. [See Figure 1-2.3(b).] In this case integration of 9a gives the temperatures in the pipe and insulation. For the pipe, the integral 9b applies, but with $k = k_1$ and $\dot{q}'$ given by 9c, T_1, the temperature at the pipe-insulation interface, is given by this version of 9b with $r = r_1$. For the insulation, Equation 9b again applies with $\dot{q}'$ given by Equation 9c, and T_0 replaced by T_1, k by k_2, and r_0 by r_1.

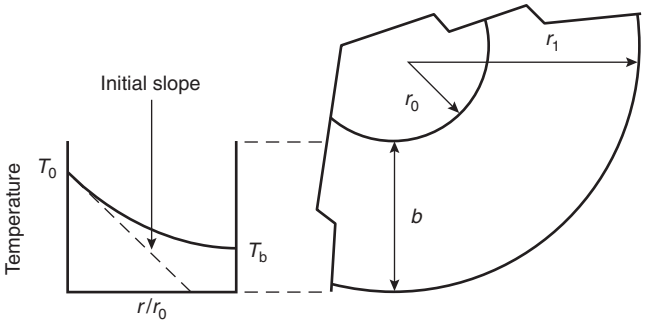

Figure 1-2.3(a). ***Steady-state radial heat flow through a thick-walled pipe, internal radius r_0, thickness b. The logarithmic curvature of the temperature vs. radius is shown by comparing the initial slope of the temperature curve with its final value.***

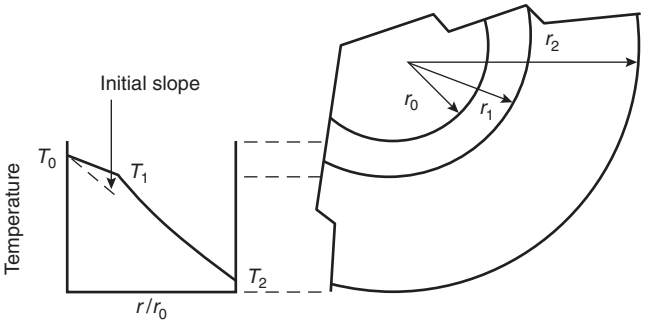

Figure 1-2.3(b). ***Steady-state radial heat flow through two concentric pipes or one pipe covered with insulation. The insulation has a lower conductivity than the pipe.***

EXAMPLE 4: Cavity Wall.

Many building walls consist of internal framing sheathed on both sides. For example, an interior wall of a residential building might be framed with wood 2″ × 4″ studs (41.3 × 92.1 mm), spaced 406 mm (16 in.) and sheathed with gypsum wallboard. An exterior wall might be similar except that the sheathing on the exterior side would be a weather-resistant material perhaps backed by insulation board. Between the two sheathing layers there will be a cavity unless the spaces between the studs are filled with insulation or other material.

For this example, assume that the two coverings are identical 15.9-mm ($^5/_8$ in.) gypsum board and the cavity is, for Case 1, filled with fiberglass insulation, and for Case 2, unfilled. The thermal conductivity of gypsum board is taken as 0.8 W/m·K, of wood 0.17 W/m·K, and of fiberglass 0.04 W/m·K.[8] Let the hot side wall surface temperature be 200°C and the cold side 20°C. [See Figure 1-2.4(a).]

Case 1: A correct calculation of this case requires solution of the two-dimensional steady-state heat flow equation (specialized from Equation 7). Either an analytical solution or numerical techniques (described later in this chapter) might be used. Here a small correction is anticipated for the studs. Equation 8 is used for the two layers of gypsum board and either the fiberglass insulation or the wood studs. An effective conductivity is calculated for the insulation or stud-filled cavity using an arithmetic average based on the space occupied by studs and insulation. The effective conductivity for the 92.1-mm deep by 406-mm wide cavity is

$$\frac{0.04 \cdot 0.3647 + 0.17 \cdot 0.0413}{0.406} = 0.0532 \text{ W/m·K}$$

Referring back to Example 2, the reader can verify that the heat conduction through the wall would be

$$\dot{q}'' = \frac{(200 - 20)}{(2 \times 0.0159/0.8 + 0.0921/0.0532)}$$

$$= \frac{180}{(0.0398 + 1.7312)}$$

$$= 0.1016 \text{ kW/m}^2$$

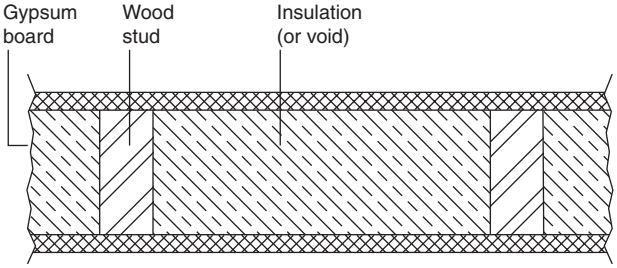

Figure 1-2.4(a). ***Geometry of the cavity wall.***

In spite of its low conductivity, the insulation in the cavity conducts the majority of the heat through the wall because of the large area occupied by it. The studs conduct about 30 percent of the heat for this particular case. Had the gypsum board not been present, the heat flow would have increased 2.3 percent for the same overall ΔT. Compared to the insulation, the gypsum board offers little resistance to the heat flow.

Had the steady-state, two-dimensional heat flow equation been solved for this case, the wood and insulation temperatures would reflect a small flow of heat from the insulation into the wood on the warm side of the cavity and an equal, reverse flow on the cool side. The temperature deviations (from one-dimensional heat flow) for the insulation are the larger, about 1.5°C, while those in the wood are less than 1°C. A small transverse heat flow in the gypsum board, toward the studs on the warm side of the cavity and away from the studs on the cool side, would be revealed. [See Figure 1-2.4(b).] In this figure, use has been made of symmetry about the center of the cavity.

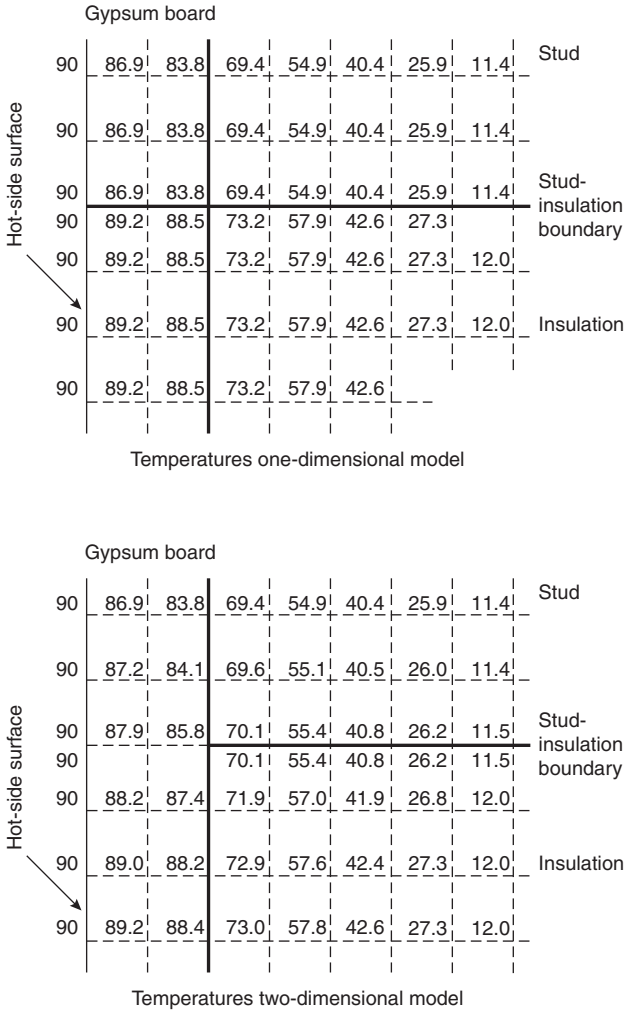

Figure 1-2.4(b). ***Comparison of wall and cavity temperatures—one- and two-dimensional models.***

The total 180°C temperature difference is divided in half: 90°C on the hot side and −90°C on the cool side. Only the area around the insulation-stud-gypsum board junction, on the hot side, is shown.

In the upper diagram in Figure 1-2.4(b), the stud and gypsum board opposite it are considered as one isolated unit, and the gypsum board and insulation as another. Each are separately analyzed using a one-dimensional model. There is a physically unrealistic temperature discontinuity within the gypsum board and between the stud and the insulation. The lower diagram is a two-dimensional treatment of the assembly. The temperatures at the interface between the insulation and the stud are now equal. There is a discontinuity in the slope of the temperature profile across the insulation-to-stud joint. This is expected, as the thermal conductivity of the stud and insulation are different. (See Example 2.)

Case 2: The two layers of gypsum board are treated as in Case 1. However, the cavity is empty and must be treated differently. With no insulation in the void, radiation across, and convection within it, will dominate the heat transfer. Again, conduction through the studs will yield a minor correction.

Radiation is addressed in Section 1, Chapter 4; the radiation exchange across the void is simple, but depends on the temperatures of the gypsum board on either side of the cavity, which must be approximated or found by an iterative calculation. Referring to Section 1, Chapter 4, the reader can verify that the effective conductivity of the cavity, if radiation alone were active and the emissivity of the gypsum board were 1.0, would be about 1.1723 W/m·K, more than 10 times that of the insulated cavity. (See Case 1.) If the wall were two sheets of gypsum board back to back (no cavity), about 4.5 kW/m^2 would be conducted. With the cavity present and only radiation active within it, this would be reduced to 1.52 kW/m^2.

Section 1, Chapter 3 addresses convection. In the absence of insulation to break up the buoyancy-induced flow in the cavity, air rises along the warmer side, crosses over, and descends along the cooler side. The calculation of the heat transferred by this circulation can be complex and is beyond the scope of this chapter. In a typical cavity, convective heat transfer is more than the heat transferred by radiation.

Is Case 2 consistent with what is known about vacuum bottles? The answer is yes. First, in the vacuum bottle, convective heat transfer is suppressed by removing the air. Second, the inner walls of the bottle are silvered and have a low emissivity. Had it been assumed that the cavity side of the gypsum board was aluminized and used an emissivity of 0.1 instead of 1.0, the radiative contribution to the heat transfer would have been comparable to that of the insulation.

EXAMPLE 5: Spherical Solid with Internal Heat Generation.

Rewriting Equation 7 in spherical polar coordinates and assuming spherical symmetry yields

$$\rho c \frac{\partial T}{\partial t} = \frac{1}{r^2} \frac{\partial}{\partial r} \left(k r^2 \frac{\partial T}{\partial r} \right) + \dot{q}''' \qquad (10)$$

For steady-state, purely radial heat flow, Equation 10 can be integrated to

$$-4\pi r^2 k \frac{\partial T}{\partial r} = \int_0^r \dot{q}''' \, 4\pi r^2 \, dr \tag{10a}$$

Here the term on the left is the outward heat flux across the spherical surface at r, while the term on the right is the total heat released inside the sphere bounded by this surface. A second integration yields

$$T = T_0 - \int_0^r \frac{1}{kr^2}\left(\int_0^r \dot{q}''' r^2 \, dr\right) dr$$

If $\dot{q}'''$ and k are constant and R is the outer radius of the sphere, the sphere's surface temperature will be

$$T_R = T_0 - \frac{\dot{q}''' R^2}{6k}$$

Conversely, the sphere is hottest at its center with temperature

$$T_0 = T_R + \frac{\dot{q}''' R^2}{6k} \tag{10b}$$

This analysis could be generalized to illustrate self-heating in a spherical object. However, it would involve a differential equation requiring more advanced mathematics than is desirable here. Instead, self-heating for a simpler, plane geometry is addressed later in this chapter.

One-Dimensional, Transient Equation

Thermally Thin Material

The simplest transient problem of interest is derived from the basic equation of heat conduction, Equation 7, in its one-dimensional form

$$\rho c \frac{\partial T}{\partial t} = \frac{\partial}{\partial x}\left(k \frac{\partial T}{\partial x}\right) \tag{11}$$

This is integrated once with respect to x. The result is

$$\rho c b \frac{\partial \overline{T}}{\partial t} = k \frac{\partial T}{\partial x}\bigg|_{x_1} - k \frac{\partial T}{\partial x}\bigg|_{x_0} \tag{12}$$

where $\overline{T}$ is the average plate temperature

$$\overline{T} = \frac{1}{b}\int_{x_0}^{x_1} T \, dx \tag{12a}$$

and $b = x_1 - x_0$.

The right side of Equation 12 is the net heat transferred into the plate; that is, the difference between the heat entering one side and that leaving by the other side. The left side of the equation is the rate of change of the average thermal energy stored in the plate.

For many problems it is sufficient to know only the average temperature (e.g., where thermal conduction within the plate is fast compared to the rate at which heat can be supplied to it). This will occur either for thin materials (small b) or ones of high thermal conductivity (large k).

As an example consider a plate with initial temperature of T_0, insulated on one face and suddenly exposed, at time $t = 0$, to a hot, moving air stream with temperature T_f. The heat transfer from such a hot stream is known, experimentally, to depend on the difference between the temperature of the air stream far from the plate (T_f) and the surface temperature of the plate ($\overline{T}$ in the present case, since it is assumed that the average temperature is a good approximation for the temperature anywhere in the plate). The constant of proportionality is the "convective heat transfer coefficient" and is usually designated with the letter h. (For more detail on convection, see Section 1, Chapter 3.) Thus, the heat transferred from the air to the plate is

$$h(T_f - \overline{T})$$

where h has units W/m²·K. Substituting this convective heating assumption for one term on the right of Equation 12 and zero (insulated rear face) for the other term yields the equation

$$\frac{\partial \overline{T}}{\partial t} = \frac{h}{\rho c b}(T_f - \overline{T})$$

This simple, first-order differential equation is easily integrated to give

$$\overline{T} = T_0 e^{-ht/\rho cb} + \frac{h}{\rho cb}\int_0^t T_f(\tau) e^{-(h/\rho cb)(t-\tau)} \, d\tau \tag{13}$$

The characteristic time for this solution is

$$t_c = \frac{\rho c b}{h} \text{ (seconds)}$$

It is noted that the transient heat flow equation, Equation 7, leads to the characteristic time

$$t_0 = \frac{\rho c b^2}{k}$$

Comparing these two characteristic times yields

$$\frac{t_0}{t_c} = \frac{hb}{k} = \text{Bi (Biot Number)}$$

When Bi is small (e.g., if thermal conductivity, k, is large or the sample thin) the material is thermally thin. Further, transient heat conduction within the solid is fast compared to heat transfer to its surface. Conversely, when Bi is large (e.g., if the surface heat transfer coefficient is large or the sample thick), it is not thermally thin and the above analysis would be inappropriate.

If T_f is a constant, the integral in Equation 13 can be evaluated. The result is

$$\overline{T} = T_0 e^{-t/t_e} + T_f(1 - e^{-t/t_c}) \tag{13a}$$

After a long time, $\overline{T} = T_f$.

The result, Equation 13a, can be recast in terms of the characteristic time mentioned above in the discussion of Equation 7. Recall that this time was

$$t_0 = \frac{\rho c b^2}{k}$$

Using this in Equation 13 gives

$$\frac{ht}{\rho cb} = \left(\frac{ht_0}{\rho cb}\right)\left(\frac{t}{t_0}\right)$$
$$= \left[\frac{h(\rho cb^2/k)}{\rho cb}\right]\left(\frac{t}{t_0}\right)$$
$$= \left(\frac{hb}{k_{\text{solid}}}\right)\left(\frac{t}{t_0}\right)$$
$$= \left(\frac{h\ell}{k_{\text{air}}}\right)\left(\frac{k_{\text{air}}}{k_{\text{solid}}}\right)\left(\frac{d}{\ell}\right)\left(\frac{t}{t_0}\right)$$

where ℓ is the length of the solid in the direction of the air flow. This length is needed to determine the value of h from published heat transfer data, such as McAdams.[9] The quantity, $\left(h\ell/k_{\text{air}}\right) = \text{Nu}$, is the Nusselt number, the ratio of the actual heat transferred under the given flow conditions to what would be conducted through still, stably stratified air, provided the temperature difference $(T_f - \overline{T})$ were applied over a distance ℓ. For natural convection, such as is often found in fire situations, the Nusselt number would be on the order of 100. For wood $(k_{\text{air}}/k_{\text{solid}})$ is about 0.1, and it may be supposed for the present that d/ℓ is also 0.1. Then the assumption that the sample is "thermally thin" would be true so long as t/t_0 were large compared to 1. For a metal, k_{solid} is 10^4 times that of wood, so the thermally thin assumption would hold for t/t_0 large compared to 10^{-3}.

A more interesting, but also more difficult problem arises if the hot air temperature is high enough that the plate begins to radiate significantly as it warms in response to the air's heating. This problem would arise if the heating were due to flames passing over the plate. For simplicity it can be assumed that the hot gas absorbs negligible radiant energy and all the radiation escapes to a distant, surrounding region, which is at the initial plate temperature, T_0. In this case, one must subtract the heat lost by radiation from the plate's surface from the heat transferred to the plate from the gas. (For more detail on radiation see Section 1, Chapter 4.) The re-radiation will be

$$\dot{q}_{RR} = \varepsilon\sigma(T^4 - T_0^4)$$

where σ = Boltzmann's constant = 5.6696×10^{-11} (kW/m²·K); ε = plate emissivity; and the equation to be integrated is

$$\rho cd\,\frac{\partial \overline{T}}{\partial t} = h(T_f - \overline{T}) - \varepsilon\sigma(\overline{T}^4 - T_0^4)$$

Because of the fourth power of $\overline{T}$ on the right side of the equation, this cannot be integrated in closed form. An approximate integral is obtained by linearizing the radiation term

$$(\overline{T}^4 - T_0^4) = \left(\frac{T_f^4 - T_0^4}{T_f - T_0}\right) \times (\overline{T} - T_0)$$

Linearized in this fashion, the equation can be integrated. After integration the result is

$$\overline{T} = T_0 + \left(\frac{h}{H}\right)(T_f - T_0)(1 - e^{-Ht/\rho cd})$$

where

$$H = h + \varepsilon\sigma\left(\frac{T_f^4 - T_0^4}{T_f - T_0}\right)$$

With significant effort, higher order analytic approximations can be obtained, or numerical methods used if a more accurate answer is needed. Note that, without the radiation loss, the plate temperature approaches the gas temperature, T_f (Equation 13a), but with the radiation loss, since $h/H < 1$, the final temperature is lower. (See Equation 14.) It also retains a dependence on the ambient temperature.

$$\overline{T} \rightarrow T_0 + \left(\frac{h}{H}\right)(T_f - T_0) \qquad (14)$$

Thick Plates

The theory of thick plates leads to much more involved analytic techniques than were needed for thermally thin plates. Only a brief outline of the theory will be given here; more complete treatments are available in such standard heat transfer texts as Carslaw and Jaeger.[10]

The most common approach to transient heating of thick plates uses the linearity of Equation 7. Equation 7 is linear only for the particular case where (1) the thermal diffusivity is either constant or a function of position, but not temperature, and (2) heat addition, if present, is a function of position and/or linear in temperature. These linearity restrictions can often be met while still giving useful results for practical problems. A linear equation can, of course, be solved by the linear superposition (sum) of primitive solutions. To use this technique, a suitable primitive solution is needed. Two ways to obtain and use primitive solutions will be discussed.

Separation of variables: A technique that may be used with Equation 7 for multidimensional problems is called "separation of variables."* Here the technique will be illustrated for only one dimension. The above linearity restrictions will be met by assuming constant density, specific heat, and thermal conductivity (more restrictive than just constant thermal diffusivity); and a heat addition term linear in temperature.

Consider a flat, rectangular plate of thickness $2b$, insulated along its edges, with heat generated within the plate at a rate that increases with temperature.

The following is a very simple example illustrating some aspects of self-heating. For an object to self-heat, it is necessary for an exothermic chemical reaction to occur within the solid. Further, the rate of this reaction should

*The method of separation of variables for solution of linear, partial differential equations is discussed in many graduate-level texts on mathematical methods of physics and chemistry. Recent texts tend to emphasize numerical methods to the exclusion of older, analytic ones. Texts predating the computer revolution may be more useful.

accelerate as the temperature rises. For a more complete discussion of self-heating see Thomas[11] or Section 2, Chapter 12 of this handbook.

The rate of chemical reactions typically increases exponentially with temperature, but to keep within the restrictions of the linear equation mathematics, it is assumed that the heat released per unit volume, $\dot{q}'''$, varies linearly with temperature

$$\dot{q}''' = C + DT$$

where C and D are presumably known and D is positive. For small temperature changes, this may be accepted as a valid linearization of an exponential increase. C may be eliminated by a suitable choice of reference temperature, $T_0 = -C/D$. It is assumed that the two surfaces of the plate are kept at the same temperature, T_s. The center of the plate is at $x = 0$. Because of the geometric symmetry, the boundary conditions are symmetric and T must be a symmetric function of x.

Using the separation of variables technique, assume that T can be written in the form

$$T = \theta(t)X(x)$$

Substituting this in the one-dimensional version of Equation 7, yields

$$\frac{X\partial\theta}{\partial t} = \frac{\alpha\theta\partial^2 X}{\partial x^2} + \left(\frac{D\alpha}{k}\right)\theta X$$

Dividing by θX yields

$$\frac{[\partial\theta(t)/\partial t]}{\theta(t)} = \alpha\frac{[\partial^2 X(x)/\partial x^2]}{X(x)} + \frac{D\alpha}{k} \tag{15}$$

The left side of the equation depends only on time while the right depends only on location, x. This can only be true if both sides are independently constant. Let this constant be λ and write two equations expressing the constancy of the two sides

$$\theta' + \lambda\theta = 0$$

$$X'' + \left(\frac{D}{k} + \frac{\lambda}{\alpha}\right)X = 0$$

If $\lambda = 0$ the first of these equations says θ = constant and the second that

$$\theta X = T = A\sin\left(\sqrt{\frac{D}{k}}\,x\right) + B\cos\left(\sqrt{\frac{D}{k}}\,x\right) \tag{15a}$$

Invoking the required symmetry and using the boundary condition $T = T_s$ at the surface, $x = b$, gives (remembering the reference temperature)

$$T = T_0 + (T_s - T_0)\frac{\cos\left(\sqrt{D/k}\,x\right)}{\cos\left(\sqrt{D/k}\,b\right)} \tag{15b}$$

This would be the steady-state (time-independent) solution, provided one exists.

If λ is not 0 the result is

$$T(x, t, \lambda) = e^{-\lambda t}\left[A(\lambda)\sin\left(\sqrt{\frac{D}{k} + \frac{\lambda}{\alpha}}\,x\right) + B(\lambda)\cos\left(\sqrt{\frac{D}{k} + \frac{\lambda}{\alpha}}\,x\right)\right] \tag{15c}$$

Equations 15a and 15c are the primitive solutions that are superimposed (summed). The separation parameter, λ, and the coefficients A and B are chosen to satisfy the initial and boundary conditions. The two major terms of Equation 15c decay exponentially with time (for positive λ), with those with the most rapid oscillation in x decaying most quickly. Clearly, this technique requires inclusion of many terms if the behavior for small time is needed. For hand calculations this is a serious drawback, but with the advent of very efficient "fast Fourier transform" numerical packages to evaluate the coefficients A_n and B_n, the separation of variables method has acquired some new appeal.

Combining Equation 15b (which is Equation 15a adjusted to satisfy the boundary conditions) with Equation 15c allows the evaluation of λ. Because the boundary conditions are already satisfied by Equation 15b, Equation 15c must be symmetric in X, and zero at $x = b$, hence $A_n = 0$ and

$$\sqrt{\frac{D}{k} + \frac{\lambda}{\alpha}} = \frac{(2n-1)\pi}{2b}$$

$$\lambda = \left\{\left[\frac{(2n-1)\pi}{2b}\right]^2 - \frac{D}{k}\right\}\alpha$$

and

$$T = T_0 + (T_s - T_0)\frac{\cos\left(\sqrt{D/k}\,x\right)}{\cos\left(\sqrt{D/k}\,b\right)} + \sum_{n=1}^{\infty} B_n\cos\left\{\left[\frac{(2n-1)\pi}{2}\right]\left(\frac{x}{b}\right)\right\} \times e - \left(\left\{\left[\frac{(2n-1)\pi}{2b}\right]^2 - \frac{D}{k}\right\}\alpha t\right) \tag{15d}$$

To satisfy the initial conditions, B_n are evaluated using the standard technique of multiplying both sides of Equation 15d, with $t = 0$, by the appropriate cosine and integrating with respect to x from 0 to b. To illustrate self-heating, however, this step is not necessary as long as it is realized that in general the B_n are nonzero. It will be assumed that the initial condition was almost the steady-state solution, Equation 15b (i.e., almost all the $B_n = 0$). But suppose that instead of the initial condition being exactly the steady-state distribution, a small perturbation away from the steady-state temperature distribution existed at $t = 0$. In other words, suppose that one of the B_n were a small, nonzero value. In this case Equation 15d

could show "thermal runaway"; that is, the temperature would grow exponentially with time, if D exceeded

$$D = k\left[\frac{(2n-1)\pi}{2b}\right]^2 \tag{15e}$$

In particular, if B_1 is nonzero, Equation 15e gives the critical value for D for which thermal runaway will occur. Where thermal runaway occurs, there is no steady-state solution. The use of Equation 15b is still valid, but its interpretation is altered—it describes a stable state if D is less than $k(\pi/2b)^2$; it is a metastable state if D is larger.

This example does not require evaluation of a large number of terms of the series. In fact, only one term is sufficient, since the lowest order term (smallest n) has the largest growth rate. Thus the separation of variables technique is particularly suited to this problem.

The analysis of self-heating involves many factors not considered in this simple calculation. One factor is determining the acceleration of the rate of chemical reaction as local temperature increases (i.e., determining the constant D for the material in question). Another factor is the effect of size. From the present simple example it is clear that for positive D, there is some thickness of material, $2b$, near which the potential for disastrous self-heating exists. The larger D, the smaller that b need be for self-heating runaway. Although the critical size is often large, materials, such as coal, wood chips, pelletized animal feeds, and so forth, are occasionally stored in piles large enough for self-heating to be important.

Integral (Duhammel's) method: Where a very large number of terms are needed to yield sufficient accuracy using the separation of variables technique, integral solutions may be more efficient. If an integral is considered as a special kind of sum, the technique is another type of superposition. Just as the separation of variables technique required a primitive solution, which could be summed, so the integral technique requires a suitable primitive solution. One such function is

$$f(x, t) = q_1'' 2\rho c\sqrt{\pi\alpha t}\,\exp\left(\frac{-x^2}{4\alpha t}\right) \tag{16}$$

where α is the thermal diffusivity referred to earlier. Also, $f(x, t)$ is the temperature response of the plate to an instantaneous heat addition per unit area of plate, q_1'' (units J/m^2) applied at time $t = 0$, and no heat is transferred to or from the plate at subsequent times. That f is a solution to the one-dimensional version of Equation 7 can be readily determined by differentiation. Note that at any time after the heat addition, the heat in the plate, assumed to extend to infinity in both directions from $x = 0$, will be

$$\begin{aligned}\rho c\int_{-\infty}^{\infty} f(x, t)\,dx &= q_1''\sqrt{\pi}\int_{-\infty}^{\infty}\exp\left(\frac{-x^2}{\sqrt{4\alpha t}}\right)d(x\sqrt{4\alpha t})\\ &= \frac{q_1''^2}{\sqrt{\pi}}\int_{-\infty}^{\infty}\exp(-\xi^2)\,d\xi\\ &= q_1''\end{aligned}$$

This equation shows that the quantity of heat added per unit area to the plate is just q'' which, with $q'' = 1$, gives 1 for the integral; that is, the total heat added to the plate is one Joule per unit area of plate.

Equation 16 yields a singular temperature at $x = 0$, $t = 0$. For all later times the temperature has a "Gaussian" profile with respect to x with a half width $\sqrt{4\alpha t}$. Thus the half width of the temperature distribution increases with time. The heat spreads out, so that, while the peak temperature drops, the heated part of the plate includes an ever thicker region adjacent to $x = 0$.

The principle of superposition, mentioned previously, is now used to construct a particular solution to the one-dimensional heat flow equation. Let

$$T(x, t) = T_0 + \int_{-\infty}^{\infty}\left[\frac{q'''(\xi)}{q_1''}\right] f_1(x - \xi, t)\,d\xi \tag{17}$$

where f_1 is used in place of the f of Equation 16 to emphasize the choice of $q_1'' = 1$ J per unit area. The quantity $q'''(\xi)d\xi/q_1''$ in Equation 17 is dimensionless. If q''' is chosen such that $q'''(-\xi) = q'''(\xi)$, the temperature at $x = 0$ will be T_0 and $[T(-x, t) - T_0] = -[T(x, t) - T_0]$, shifting from an infinite solid to a semi-infinite one. Further, writing $g = q'''/q_1''$ (g has dimension 1/m)

$$\begin{aligned}T(x, t) &= T_0 + \int_{-\infty}^{0} g(\xi) f_1(x - \xi, t)\,d\xi\\ &\quad + \int_{0}^{\infty} g(\xi) f_1(x - \xi, t)\,d\xi\\ &= T_0 - \int_{0}^{\infty} g(+\xi) f_1(x + \xi, t)\,d\xi\\ &\quad + \int_{0}^{\infty} g(\xi) f_1(x - \xi, t)\,d\xi\end{aligned}$$

Recalling the definition of f_1, substitute in the first integral

$$\xi = -x + 2\eta\sqrt{\alpha t}$$

and in the second

$$\xi = x + 2\eta\sqrt{\alpha t}$$

The result is

$$\begin{aligned}T(x, t) = T_0 + \frac{q_1''}{\rho c\sqrt{\pi}}\Bigg[&\int_{-x/2\sqrt{\alpha t}}^{\infty} g(x + 2\eta\sqrt{\alpha t})\exp(-\eta^2)\,d\eta\\ &-\int_{x/2\sqrt{\alpha t}}^{\infty} g(-x + 2\eta\sqrt{\alpha t})\exp(-\eta^2)\,d\eta\Bigg]\end{aligned} \tag{17a}$$

Finally, if g is constant,

$$T(x, t) = T_0 + \frac{q_1'' g}{\rho c}\left[2\sqrt{\pi}\int_0^{x/2\sqrt{\alpha t}}\exp(-\eta^2)\,d\eta\right] \tag{17b}$$

$T(x, t)$ is the temperature in a semi-infinite plate with initial temperature $T_0 + T_{c(x)}$ whose surface is brought to T_0 at

time zero and held there for all subsequent time.* If $x = 0$ the integral is zero and thus $T(0, t) = T_0$. The surface temperature of the plate is a constant for all time. Also, because of the t in the denominator of the limit of integration of the integral, it is clear that, for very small time, for any finite x, the integral tends to 1 and the result is $T_0 + q''\sqrt{\rho c} = T_0 + T_c$ (for simplicity). Thus Equation 17 is the temperature distribution in a solid, initially at temperature $(T_0 + T_c)$ which, at time 0, has its surface brought to temperature T_0 and held there for all future time. Figures 1-2.5(a) and (b) show the temperature in the plate according to Equation 17b.

What heat input to the material must be supplied in order to achieve this; that is, to bring the surface instantly from $(T_0 + T_c)$ to T_0 and hold it there? The heat input to the surface is just

$$-k\left.\frac{\partial T}{\partial x}\right|_{x=0} = kT_c\left(\frac{1}{\sqrt{\pi\alpha t}}\right)\exp\left(\frac{-x^2}{4\alpha t}\right)\Big|_{x=0} = kT_c\left(\frac{1}{\sqrt{\pi\alpha t}}\right) = T_c\left(\frac{k^2}{\pi\alpha t}\right)^{1/2} \tag{18}$$

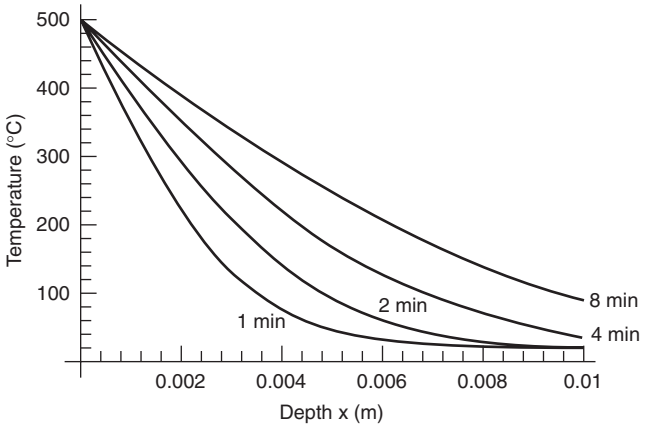

Figure 1-2.5(a). ***Equation 17b temperature vs. depth into the plate for four times.***

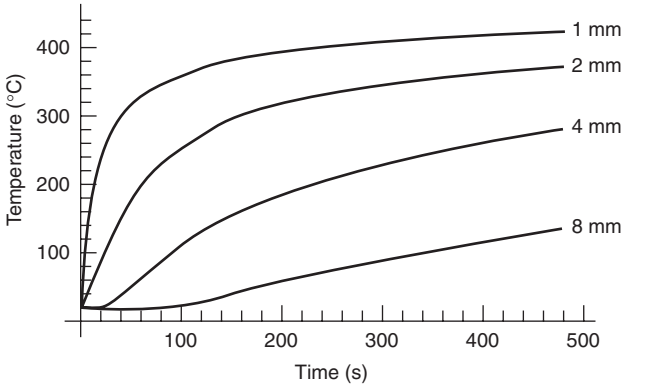

Figure 1-2.5(b). ***Equation 17b temperature vs. time for four depths into the plate.***

*The quantity within the square brackets is the "error function." Its value may be found in mathematical tables just as for the sine or cosine functions.

Thus the necessary heat flux to be applied at the surface is initially infinite (at $t = 0$) and for finite times, decreases as $1\sqrt{t}$.

This is a useful approximation for fire studies as many materials may be rapidly heated to a high temperature and their surface temperature stabilized there.

The quantity $k^2/\alpha = k\rho c$, which appears in Equation 18, is an important parameter of a material and is often referred to as the "thermal inertia." The ratio of the thermal inertia to the square of the convective heat transfer coefficient, h, has the units of time

$$\frac{k\rho c}{h^2}$$

$$(\text{W/m·K})(\text{gm/m}^3)(\text{J/gm·K})(\text{W/m}^2\text{·K})^2 = (\text{sec})$$

It is the characteristic time for the surface of a solid to respond to heating on exposure to a hot gas with film resistance h. With other modes of heating, an analogous ratio would be appropriate, and would have the same significance—the characteristic time for the solid to respond to the heating.

The next example of heat conduction in a solid is from thermal flame spread theory. The problem is to determine the temperature of the surface of a thick fuel as a function of time, as the fuel is heated from ambient conditions to its ignition temperature. This example of the thermally thick solid is analogous to the thermally thin case discussed earlier.

If heat is applied uniformly to the surface of a flat material (fuel), only one-dimensional heat conduction needs to be considered in calculating the surface temperature of the material. If the heat is applied nonuniformly, but in such a way that temperature gradients along the surface are small compared to those normal to the surface, lateral heat conduction in the fuel will be small compared to conduction normal to its surface, and a one-dimensional heat transfer model may still be adequate. For many cases this approach is indeed suitable. The principal exception is near extinction (very slow flame spread), where the flame spread rate is comparable to or less than the thermal penetration rate. Assuming that extinction is not a present concern, the one-dimensional approach may be adopted.

The analysis is complicated, but available in many standard heat transfer references, such as Carslaw and Jaeger.[10] It will not be repeated here. If the solid is exposed to a constant external heat flux, $\dot{q}''$, and loses heat by radiation and convection, its temperature will be given by

$$T(t) = T_0 + \frac{\dot{q}''}{H}\left[erfc\left(\frac{x}{2\sqrt{\alpha t}}\right) - e^{-\left(Hx/k + H^2t/\beta\right)}erfc\left(\frac{x}{2\sqrt{\alpha t}} + \sqrt{\frac{H^2t}{\beta}}\right)\right] \tag{19}$$

where *erfc* is the complementary error function $(1 - erf)$ and has a value of 1 for an argument of 0.

Figure 1-2.6 shows the temperature of the solid as given by Equation 19 for $x = 0$ (surface) and a depth of 1 mm below the surface $(x > 0)$. In preparing this plot, properties for oak were used.[8] The applied external flux

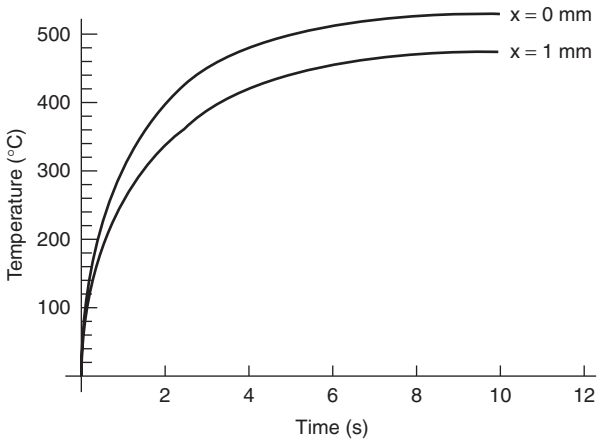

Figure 1-2.6. ***Transient heating of a solid exposed to a constant incident heat flux. The material loses heat to its surroundings by convection and a linearized approximation of radiation.***

was 30 kW/m^2. Ambient temperature was 20°C. When the surface of the sample reached the approximate ignition temperature of wood (420°C), the temperature 1 mm below the surface was 60°C cooler. The heat was diffusing into the sample, but was far from equilibrium conditions. [See Figure 1-2.5(a).] If pyrolysis products from the sample were exposed to a nonimpinging pilot flame, Equation 19 suggests that ignition would occur after about 3 sec exposure to the applied flux. If the applied flux were abruptly switched off as soon as ignition occurred, the sample would probably self-extinguish because of the heat loss to its interior. This would rapidly cool the surface to below its piloted ignition temperature. Conversely, Figure 1-2.6 illustrates that, to achieve sustained ignition, the surface must be: (1) heated to ignition temperature, but heating must continue until the bulk of the sample has been sufficiently heated and (2) that quenching will not occur due to heat conduction into the bulk material.

Many other integral solutions based on Equation 16, but satisfying other initial and boundary conditions, can be found in the heat conduction literature.[10] However, the solutions involve special mathematical functions and use more advanced analytic techniques than are appropriate to this text. The reader is urged to become acquainted with these powerful tools.

The above analysis is qualitatively correct, but, for fire problems, may not yield satisfactory quantitative results. The assumptions of constant material thermal properties and linearization of the convective/radiative heat transfer coefficient may not be valid for the temperature range encountered. In addition, for porous materials containing absorbed moisture (e.g., wood), thermal effects associated with migration of the moisture within the solid may lead to significant deviation from temperatures calculated on the assumption that heat conduction alone is occurring.

Considerable algebraic manipulation is required to get analytic solutions to heat conduction problems. The advantage of an analytic solution includes the insight that it gives about thermal behavior. However, even when this labor is completed, the solution may be limited by the necessity to linearize it. In many cases, numerical techniques, discussed next, may be the simplest route. A limitation of numerical methods is that, to understand the full thermal behavior, many solutions may be needed before a reasonable understanding of the behavior is attained.

Numerical Techniques

The heat conduction literature contains many analytic solutions to transient heat transfer problems for various geometries. However, rather than use the complex analytic forms, it is often easier to obtain solutions numerically, capitalizing on the recent increase in the availability of powerful, inexpensive microcomputers. Further, for solutions in which material properties vary significantly with direction or temperature, or heat addition within the solid is important, numerical methods are likely to be the most efficient approach. Two numerical formulations are available for solving heat conduction problems: (1) finite difference method and (2) finite element method. A comprehensive overview of numerical methods for heat transfer is available in Minkowycz.[12] An extensive review of the finite difference method is available in most introductory heat transfer texts. The finite element method is reviewed by Zienkiewicz.[13]

Both numerical formulations involve the *discretization* of the object being analyzed. *Discretization* divides the section into small segments using a set of nodes connected by lines referred to as grid or mesh. (See Figure 1-2.7.) Consequently, both methods approximate the geometry of the section being modeled.

Smaller grids provide increased accuracy, though extra nodes result in an increase in computation time. Grid spacing may vary through the assembly, being smallest where the temperature gradient is expected to be the greatest (e.g., near the heated boundary or in insulating materials). A variable grid spacing requires an additional amount of effort to formulate the governing equations for each node.

Generally, the finite difference method uses a "Taylor series" expansion to reformulate the partial differential equation, resulting in a set of algebraic equations. The finite difference form of Equation 7 for the case of transient

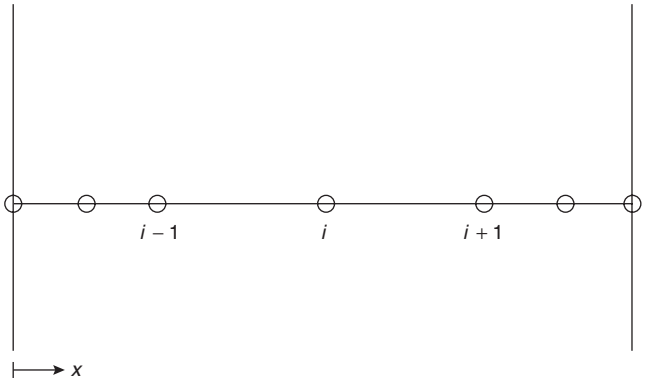

Figure 1-2.7. ***Nomenclature of finite difference grid.***

one-dimensional heat conduction with no internal heat addition is

$$C_i \frac{(T_i' - T_i)}{\Delta t} = \frac{k_m(T_{i+1} - T_i)/\Delta x - k_n(T_i - T_{i-1})/\Delta x}{\Delta x} \quad (20)$$

Equation 20 is applicable to cases where the grid spacing is the same on each side of node *i*. Alternative expressions can be readily developed for nonuniform grids. A version of Equation 20 must be developed for each node. Conditions at each node are assumed to represent the conditions in a small region around each node. In particular

T_i = temperature at node i at time t (at beginning of time step)

T_i' = temperature at node i after time step, Δt

where points $i + 1$, i, and $i - 1$ are all in the interior of the section, and

$$k_m = \frac{1}{2}(k_{i+1} + k_i)$$

$$k_n = \frac{1}{2}(k_i + k_{i-1})$$

$$C_i = \rho_i c_p \Delta x$$

Alternatively, for points on a surface, a heat balance needs to be formulated to develop the finite difference equation. Introductory heat transfer texts include finite difference equations for surface nodes exposed to a variety of conditions.

Equation 20 is expressed as an explicit formulation, that is, T_i', can be solved directly, as long as the nodal temperatures are known at the beginning of the time step. Consequently, the equations are uncoupled and can be readily solved. However, this formulation can provide numerically unstable results (computed temperatures may become greater than the exposure temperature or may decrease within an object even though it is being heated). Stability limits are based on the time step and grid size. For constant material properties, the stability limit for one-dimensional problems is expressed as

$$\frac{\alpha \Delta t}{(\Delta x)^2} < 0.5 \quad (21)$$

In order to satisfy the stability limit, a sufficiently small time step must be selected for a given grid spacing. As the grid spacing is decreased, the time step also needs to be decreased. The stability criterion is applied at each node, with the resulting time step for the analysis being less than the smallest time step required for stability.

Another formulation for the finite difference equation, referred to as the implicit formulation, is presented as

$$C_i \frac{(T_i' - T_i)}{\Delta t} = \frac{k_m(T_{i+1}' - T_i')/\Delta x - k_n(T_i' - T_{i+1}')/\Delta x}{\Delta x} \quad (22)$$

The implicit formulation has the characteristic of being numerically stable for any time step or grid size. In this formulation, the time step and grid size are selected solely based on concerns for accuracy. However, the disadvantage of the implicit formulation is that all of the equations are coupled as the right-hand side of the equation includes nodal temperatures at the end of the time step. Thus, all of the equations must be solved simultaneously.

EXAMPLE 6:

A 10-cm-thick wall is initially at a uniform temperature of 20°C. The properties of the wall are: conductivity = 25 W/m·K, density = 6000 kg/m^3, and the specific heat = 500 J/kg·K. Assume that the material properties are independent of temperature. The right side is suddenly exposed to a convective environment, with a coefficient of 10 W/m^2·K and a temperature of 500°C. The left side of the wall is maintained at 20°C. A grid size of 2.5 cm is selected. Determine the temperature within the wall after 5 min. (See Figure 1-2.8.)

Node 1 has a known temperature due to the maintained surface temperature. Thus, only the temperatures at the other nodes need to be determined.

The finite difference equation for the interior nodes (nodes 2 through 4), based on the formulation of Equation 20, is

$$6000 \cdot 500 \frac{(T_i' - T_i)}{\Delta t} = \frac{25(T_{i+1} - 2T_i + T_{i-1})}{(0.025)^2}$$

For node 5, the following equation is applicable

$$6000 \cdot 500 \frac{(T_i' - T_i)}{\Delta t} = \frac{10(500 - T_i) - 25(T_i - T_{i-1})/0.025}{0.025}$$

The stability criterion for nodes 2 through 4 is given as

$$\frac{[25/(6000 \cdot 500)]\Delta t}{0.025^2} < 0.5$$

According to this criterion, the time step must be less than 37 s. For node 5, the stability criterion is expressed as

$$\frac{(25/0.025 + 10)\Delta t}{(6000 \cdot 500 \cdot 0.025)} < 1.0$$

The maximum time step according to this criterion is 2970 s. Consequently, a time step of 30 s is selected, less than the smallest time step of 37 s determined for the wall. The resulting calculations are presented in Table 1-2.1.

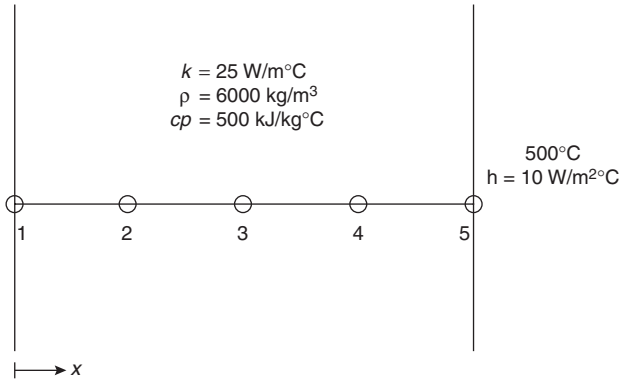

Figure 1-2.8. ***Finite difference grid, Example 6.***

Table 1-2.1 ***Temperatures within Wall Assembly (°C)***

Time (s)	Node 1	Node 2	Node 3	Node 4	Node 5
0	20.0	20.0	20.0	20.0	20.0
30	20.0	20.0	20.0	20.0	21.9
60	20.0	20.0	20.0	20.8	23.1
90	20.0	20.0	20.3	21.4	24.1
120	20.0	20.1	20.6	22.0	24.9
150	20.0	20.3	21.0	22.6	25.6
180	20.0	20.5	21.3	23.2	26.3
210	20.0	20.6	21.7	23.7	27.0
240	20.0	20.8	22.1	24.2	27.6
270	20.0	21.0	22.4	24.7	28.1
300	20.0	21.2	22.8	25.2	28.6

The finite element method also starts with a discretized object. However, one of the principal differences from the finite difference method is the use of the exact governing equation. Most finite element formulations use a polynomial fit of the temperature profile within an element to solve the equation. The partial differential equation is reformulated as an ordinary differential equation often using principles of variational calculus. Because an exact equation is used, and only the geometry is being approximated, the finite element method typically provides a more accurate analysis for course grids than the finite difference method. The equation is applied for each element, with the resulting set of equations assembled into a matrix.

$$[C]\{\dot{T}\} + [K]\{T\} = \{Q\}$$

where

C = capacitance matrix, accounting for ρc product associated with each element

K = conductivity matrix, accounting for conductivity of element

T = vector (column matrix), which represents temperature at each node

Q = vector (column matrix), which represents heat generation at each node

Determination of the temperature profile within the wall requires solving the matrix-based equations. Several typical matrix solutions can be used, such as Gaussian elimination, though such methods are not efficient due to the K matrix being sparsely populated. Consequently, advancements in finite element modeling are related to more efficient solution techniques.

As with finite difference models, explicit and implicit formulations can be developed. However, an elementary expression for the stability criterion for the explicit formulation is not available.

Numerous finite difference and finite element algorithms are available to analyze the heat conduction within a fire-exposed assembly. Even though recent publications refer more frequently to the application of finite element analyses, some recent applications of finite difference models have been described. Lie and Harmathy formulated a finite difference model to analyze the heating of circular reinforced concrete columns exposed to the standard fire.[14] In addition, finite difference models have been developed to examine the heating of fire-exposed concrete floor slabs, square reinforced concrete columns, and concrete-filled tubular steel columns.[15–17] Ahmed and Hurst have applied a one-dimensional, finite difference analysis of the coupled heat and mass transfer through carbonate and siliceous aggregate concrete slabs and multi-layered gypsum wallboard-and-stud assemblies.[18] Dehydration and evaporation phenomena and changes in porosity were considered in Ahmed and Hurst's model. Mehaffey and Takeda formulated a finite difference model to analyze the heating of wood stud walls exposed to the standard fire.[19] In Mehaffey and Takeda's model, dehydration and porosity of gypsum wallboard is accounted for through the use of effective properties. Milke and Vizzini developed a finite difference model to investigate the thermal response of fire-exposed anisotropic slabs, such as graphite-reinforced epoxy composites and glass-reinforced thermoplastic composites.[7,20] PATHOS-2 is a one-dimensional finite difference model developed principally for the evaluation of fire-exposed structures on offshore platforms.[21] In a recent review of thermal analysis programs by Sullivan et al.,[22] FIRETRANS and CEFICOSS were identified as contemporary finite difference models.[23,24] FIRETRANS can be used to address one-dimensional problems involving slabs exposed to fire. CEFICOSS is capable of addressing two-dimensional problems with one axis of symmetry perpendicular to the heating direction.

Several recently-documented examples can be found where finite element analyses have been applied to analyze the thermal response of fire-exposed building assemblies including steel beams, partially- and fully-protected steel columns, wall assemblies, and floor systems. Finite element models which have been specifically developed to address the thermal response of fire-exposed building assemblies include FIRES-T3, TASEF-2, SUPER-TEMPCALC, STABA-F, and a model by Terro.[25–29] All of the models can address two-dimensional problems except for FIRES-T3, which can address three-dimensional problems. FIRES-T3, TASEF-2, and SUPER-TEMPCALC can be used to evaluate the thermal response of assemblies with voids.

Some of the applications can only simulate conditions associated with the standard fire exposure associated with fire resistance tests, while others can address any specified exposure condition. Milke and Sullivan et al. provide reviews of five finite element models to evaluate thermal response from fire.[22,30]

FIRES-T3 and TASEF are of particular interest due to their capability to account for time-varying exposure conditions and temperature-dependent material properties.[25,26] Both codes were formulated to predict the temperature distribution in structural members resulting from exposure to a fire. Both models are based on the same principles and have virtually the same explicit formulation. They differ primarily in their input requirements. Some additional information on FIRES-T3 and TASEF is available in Section 4, Chapter 9 of this handbook. A comparison of FIRES-T3 and TASEF was provided elsewhere by Milke.[30] TASEF is available from Sterner and Wickström at

the Swedish National Testing Institute.[25] FIRES-T3 is available from Milke at the University of Maryland.

A typical diagram of a finite element mesh for a steel column with spray-applied, contour protection is presented in Figure 1–2.9. Element numbers are included within the circles, nodal numbers are encircled. Elements representing the steel are 1, 5, 9, and 13. As a result of symmetry, only one quadrant of the column needs to be modeled.

Limitations

This short summary of heat conduction has included only a few of the better known solutions of the heat conduction equation. It is very difficult to obtain analytic solutions for objects with complex geometric contours. Published analytic solutions all relate to simple geometric forms. Numerical methods can be used for more complex shapes, but coding the boundary conditions for complex shapes is awkward and tedious. It is seldom done unless there is strong economic motivation to do so.

For the temperature ranges found in fire studies, there are often significant changes in k, the thermal conductivity.[8] Where k is a function of T, the heat conduction equation becomes nonlinear and numerical methods are required. Using a variable k produces a quantitatively superior result, but usually not one that is qualitatively different than would be found with constant k.

Some materials, such as wood, are not isotropic and in these cases k is a tensor quantity. Although results calculated assuming a constant, scalar k may not differ qualitatively from more accurate calculations using a tensor k, in some cases (for example, flame spread), the difference may be important.[31]

Specific heat may also vary, though this is less often a problem than changes in k. When the specific heat appears to vary, it is well to suspect chemical changes, as they are more likely to occur than the Debye temperature being too high.

Transmission of heat in gases or liquids often plays a major role in fire analysis. Occasionally, conduction is important for these materials, but in making calculations, care must be taken that thermally induced convection or radiation does not dominate the heat transfer. If the hotter material is above the cooler it will be stable against convective motions, while in the reverse case, it will be unstable and convection will surely dominate. Radiation may be more important than conduction even in the thermally stable case because for many gases (e.g., air), conduction is low (since gases are electrical insulators), but they absorb radiation only weakly. The radiant energy passes directly through these gases. For example, near room temperature a layer of air 1 cm thick transmits about as much heat by radiation as by conduction.

Where liquids are involved, changes in surface tension with temperature have been shown to induce subsurface

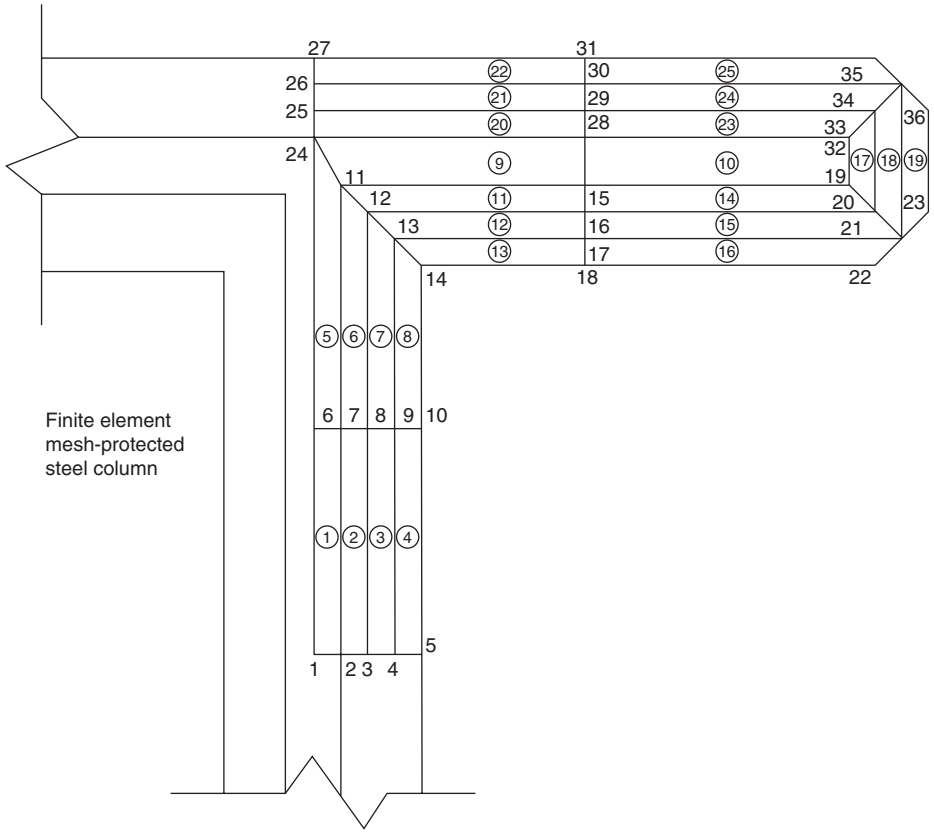

Figure 1-2.9. ***Finite element mesh—protected steel column.***

convective flows that dominate the heat transfer process. In this case, heat transfer calculations including only conduction (based on the assumption of a quiescent liquid) may be incorrect.[32]

An example where heat transmission in a "solid" may be influenced by convection is a large-pore, closed-cell cellular foam. When a temperature difference is imposed across the sides of a vertical slab, a small temperature difference is imposed across each cell. This results in small density differences in the gas in each cell. In the presence of gravity these differences will induce a convective circulation of the gas in each cell, which may transfer more heat across the cell than can be conducted through its thin walls.

Radiation may also be important in these materials. An example where radiation is an important mode of heat transfer within a "solid" is in a low-density porous, smoldering material or in porous char. The forward transmission of heat, which is necessary for the spread of smoldering combustion, against a thermally induced airflow through the porous material occurs almost entirely by radiation across the pores, not by conduction through the solid pore walls.[33]

One of the most serious problems in heat conduction calculations occurs when the material is not thermally stable. Changes in thermal conductivity may be important; but often more important, there may be the release or absorption of heat within the solid. This release or absorption is often accompanied by the release of material, which then migrates (diffuses) through the (porous) solid. The heat conduction equation allows for this release of heat, but the accompanying physical/chemical processes must be treated by separate, coupled, simultaneous equations. The total computation becomes complex (e.g., in the theoretical treatment of smoldering or the pyrolysis of wood). Theoretical studies of the fire performance of reinforced concrete require that the effect of adsorbed and chemically bound water be included, and today this is regularly done.[34,35] Similarly, the effect of moisture should be included in the analysis of the fire performance of gypsum wallboard. Unfortunately, this is not often done, although the same techniques that are used successfully with concrete apply.

There are two drawbacks to the applicability of numerical models to predict the thermal response of any building assembly to fire. One difficult aspect of applying a numerical model is associated with acquiring accurate input data. "Boundary conditions" associated with the exposure must be stipulated. Material properties need to be available as a function of temperature for all components of the object or assembly being analyzed.

The other difficult aspect involves material behavior. The existing heat transfer analysis algorithms are applicable primarily to inert materials. Where assemblies experience moisture migration, phase changes, dehydration, decomposition or changes in geometry, specific algorithms will need to be identified or developed to model the thermal response of such assemblies. Results for the available models often deviate appreciably from measured temperatures in the area of 100 to 200°C where concrete, gypsum, wood, and other moisture containing materials are included despite the use of effective properties to account for the change in enthalpy.[22] Ahmed and Hurst's model has much better predictive capabilities within this range of temperatures.[18]

Nomenclature

A	surface area across which heat is transferred (m^2)
A	constant
B	constant
b	plate thickness (m)
C	capacitance matrix
C_i	volumetric thermal capacitance of node i($J/m^3 \cdot K$)
c	specific heat ($J/gm \cdot K$)
D	rate of heat release parameter
H	convective heat transfer coefficient plus linearized radiation term ($W/m^2 \cdot K$) $h_c + \varepsilon\sigma[(T_s + T_a)^4 - (T_0 + T_a)^4]/[(T_s + T_a) - (T_0 + T_a)]$
h	convective film coefficient ($W/m^2 \cdot K$)
h_c	convective film coefficient ($W/m^2 \cdot K$)
K	conductivity matrix
k	thermal conductivity of the solid ($W/m \cdot K$)
k_i	thermal conductivity evaluated at temperature of node i($W/m \cdot K$)
$k_{m,n}$	average thermal conductivity ($W/m \cdot K$)
ℓ	length of plate in direction of airflow across its surface
Q	heat content (J)
$\dot{Q}$	heat generation vector
$\dot{q}''$	radiative heat flux per unit area to the surface (W/m^2)
T_a	ambient temperature (K)
T_i	temperature at node i(°C)
T_i'	temperature at node i at end of next time step (°C)
T_s	temperature of the material surface (K)
T	temperature (K)
T	temperature of the solid in Eq 19 (K)
T	temperature vector
T_0	reference temperature, T_0 (K)
t	time (s)
Δt	time step
x	distance normal to the surface (m)
x	coordinate normal to the fuel surface
Δx	grid spacing

Greek Letters

α	the material thermal diffusivity, $k/\rho c$ (m^2/s)
β	thermal inertia, $k\rho c$ ($W^2 s/m^4 \cdot K^2$)
ε	material surface emissivity
ξ	dimensionless distance
τ	dimensionless time
θ	temperature (K)
ρ	density (kg/m^3)
ρ_i	density evaluated at temperature of node i(kg/m^3)
σ	electrical conductivity (ohm)

σ Boltzmann's constant, $\sigma = 5.67 \times 10^{-11}$ (kW/m^2·K^4)
η dummy integration variable
μ dummy integration variable
∂ differential operator

References Cited

1. M. Born, *Atomic Physics,* Hafner, New York (1969).
2. H.L. Callendar, *Ency. Britannica,* 11th ed., 6, p. 890.
3. E.R.G. Eckert, *Heat and Mass Transfer,* McGraw-Hill, New York (1963).
4. F. Seitz, *The Modern Theory of Solids,* McGraw-Hill, New York (1940).
5. J.C. Slater, *Quantum Theory of Matter,* McGraw-Hill, New York (1951).
6. T. Handa, M. Morita, O. Sugawa, T. Ishii, and K. Hayashi, *Fire Sci. and Tech.,* 2 (1982).
7. J. Milke and A.J. Vizzini, "Thermal Response of Fire-Exposed Composites," in *Jour. of Composites Technology and Research*, 13, 3, pp. 145–151 (1991).
8. D. Gross, *NBSIR 85-3223,* National Bureau of Standards, Washington, DC (1985).
9. W.H. McAdams, *Heat Transmission,* McGraw-Hill, New York (1942).
10. H.S. Carslaw and J.C. Jaeger, *Conduction of Heat in Solids,* Oxford University, Oxford, UK (1959).
11. P.H. Thomas, *Special Technical Pub. No 502,* American Society of Testing and Materials, Philadelphia (1972).
12. W.J. Minkowycz, E.M. Sparrow, G.E. Schneider, and R.H. Pletcher, *Handbook of Numerical Heat Transfer,* John Wiley and Sons, New York (1988).
13. O.C. Zienkiewicz, *The Finite Element Method,* 3rd ed., McGraw-Hill, New York (1977).
14. T.T. Lie and T.Z. Harmathy, "A Numerical Procedure to Calculate the Temperature of Protected Steel Columns Exposed to Fire," Fire Study No. 28, NRCC 12535, Division of Building Research, National Research Council of Canada, Ottawa (1972).
15. T.T. Lie, "Calculation of the Fire Resistance of Composite Concrete Floor and Roof Slabs," *Fire Technology,* 14, 1, pp. 28–45 (1978).
16. T.T. Lie, "A Procedure to Calculate Fire Resistance of Structural Members," *Fire and Materials*, 8, 1, pp. 40–48 (1984).
17. T.T. Lie, T.D. Lin, D.E. Allen, and M.S. Abrams, "Fire Resistance of Reinforced Concrete Columns," *Technical Paper No. 378,* National Research Council of Canada, Division of Building Research, Ottawa (1984).
18. G.N. Ahmed and J.P. Hurst, "Modeling the Thermal Behavior of Concrete Slabs Subjected to the ASTM E119 Standard Fire Condition," *J. of Fire Protection Engineering,* 7, 4, pp. 125–132 (1995).
19. J.R. Mehaffey and H. Takeda, "Predicting Heat Transfer Through Wood Stud Walls Exposed to Fire," *International Conference on Fire Research and Engineering,* Society of Fire Protection Engineers (1995).
20. J.A. Milke and A.J. Vizzini, "Modeling and Evaluation of the Thermal Response of Fire Exposed Composites," *Proceedings of the 5th AIAA/ASME Thermophysical and Heat Transfer Conference,* Seattle, WA (1990).
21. PCL (Palm Computing Ltd.), *PATHOS 2 Manual,* Revision 2.01, Berkshire, UK (May 1992).
22. P.J.E. Sullivan, M.J. Terro, and W.A. Morris, "Critical Review of Fire Dedicated Thermal and Structural Computer Programs," *J. of Applied Fire Science,* 3, 2, pp. 113–135 (1994).
23. Ove Arup and Partners, "Large Panel Systems—Prediction of Behaviour in Fire Tests," A report submitted to the Building Research Establishment, Report No. 14404/JB/CW, Building Research Station (June 1985).
24. J.M. Frannsen, Étude du Comportement au Feu des Structures Mixtes Ancier-Béton, (CEFICOSS), (A Study of the Behaviour of Composite Steel-Concrete Structures in Fire), Ph.D. Dissertation, Université de Liège, Belgique (1987).
25. E.S. Sterner and U. Wickström, *TASEF—Temperature Analysis of Structures Exposed to Fire—Users Manual,* Report 1990:05, Swedish National Testing Institute, Borås, Sweden (1990).
26. R.H. Iding, Z. Nizamuddin, and B. Bresler, "Computer Program for the Fire Response of Structures—Thermal Three-Dimensional Version," University of California, Berkeley (1977).
27. Y. Anderberg, "Modeling Steel Behaviour," *Fire Safety J.,* 13, 1, pp. 17–26 (1988).
28. K. Rudolph, E. Richter, R. Hass, and U. Quast, Principles for Calculation of Load-Bearing and Deformation Behaviour of Composite Structural Elements under Fire Action (STABA-F)," *Proceedings of 1st International Symposium of Fire Safety Science* (1986).
29. M.J. Terro, "Numerical Modelling of Thermal and Structural Response of Reinforced Concrete Structures in Fire," Ph.D. Thesis, Department of Civil Engineering, Imperial College of Science, Technology and Medicine (1991).
30. J.A. Milke, "Temperature Analysis of Structures Exposed to Fire," in *Fire Technology,* 28, 2, pp. 184–189 (1992).
31. A. Atreya, *NBS-GCR-83-449,* National Bureau of Standards, Gaithersburg, MD (1984).
32. W.A. Sirignano and I. Glassman, *Comb. Sci. and Tech.,* 1, p. 307 (1974).
33. T. Ohlmiller, J. Bellan, and F. Rogers, *Comb. and Flame,* 36, p. 197 (1979).
34. B. Bressler, *F. Safety J.,* 9, pp. 103–117 (1985).
35. K. Harada and T. Terai, "Dependence of Thermal Responses of Composite Slabs Subject to Fire on Cross Sectional Shapes," in *Fire Safety Science—Proceedings of the 4th International Symposium, IAFSS,* pp. 1159–1170 (1994).

CHAPTER 3

Convection Heat Transfer

Arvind Atreya

Introduction

There are only two fundamental physical modes of energy transfer, conduction and radiation. In conduction, energy slowly diffuses through a *medium* from a point of higher temperature to a point of lower temperature, whereas in radiation, energy is transmitted with the speed of light by electromagnetic waves (or photons), and a transmitting medium is not required. Thus from a conceptual viewpoint, convection is not a basic mode of heat transfer. Instead, it occurs by a combined effect of conduction (and/or radiation) and the motion of the transmitting medium.

Nevertheless, convection plays a very important role in fires. It transports the enormous amount of chemical energy released during a fire to the surrounding environment by the motion of hot gases. This motion may be induced naturally by the fire itself (hot gases rise and cold air rushes to replace them) or by a source external to the fire, such as a prevailing wind. Based on this distinction, the subject of convective heat transfer is usually subdivided into *natural* (free) and *forced* convection. Obviously, both natural and forced convection may occur simultaneously, resulting in a mixed mode of convective heat transfer. A further subdivision based on whether the flow occurs inside (e.g., in a pipe) or outside the body under consideration is also often made. For application of convective heat transfer to fire science, natural convection around objects is clearly far more important than forced convection inside a pipe. Thus greater attention is devoted here to natural convective heat transfer and external flows.

The objective of this chapter is to provide a firm understanding of the physical mechanisms that underlie convective heat transfer, as well as to develop the means to perform convection heat transfer calculations. In the first section of the chapter, basic concepts and relations are developed, while calculation methods are illustrated with the help of examples in the second section. Tables of empirical and theoretical results (including their range of applicability) are also provided for quick reference.

Concepts and Basic Relations

A simple, everyday problem of drying a wet body in a stream of warm dry air is shown in Figure 1-3.1. From our knowledge of fluid mechanics, we expect the flow of air to slow down next to the surface of the wet body, thus transferring some of its momentum to the body. Conversely, the body will experience a drag force if it moves through stationary air. In addition to this exchange of momentum, the body also losses some of its moisture; that is, transfer of mass takes place from the wet surface to the warm air. Furthermore, for moisture to evaporate at the wet surface the necessary heat must also be transferred from the warm air to the wet body. Hence, the body experiences a simultaneous transfer of momentum, mass, and energy.

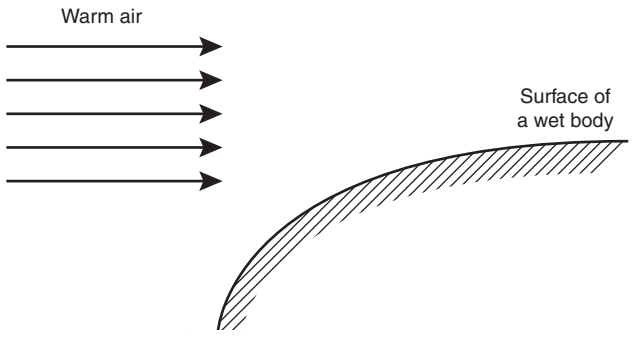

Figure 1-3.1. ***Drying of a wet body in a stream of warm air.***

Dr. Arvind Atreya is a professor of mechanical engineering at the University of Michigan. He has been actively involved in fire research since 1979. This chapter is respectfully dedicated to the author's father, Dr. Dharam Dev Atreya.

To obtain a quantitative description of the above process, note first that all the quantities (mass, momentum, and energy) being transported in the example are conserved, so conservation laws govern their rate of transfer.

These conservation laws need to be supplemented by basic or constitutive relations that relate the rate of transfer to the driving forces and fluid properties. These basic laws are: (1) Newton's law of viscosity, which relates the rate of change of momentum to velocity gradients; (2) Fourier's law of heat conduction, which relates the rate of heat transfer to temperature gradients; and (3) Fick's law of mass diffusion, which relates the rate of mass transfer to concentration gradients. With this framework of conservation and basic laws a majority of laminar convective heat transfer problems can be analyzed, at least in principle. For the turbulent case this framework provides guidance for developing useful empirical correlations.

This section covers the basic laws in the context of laminar flows and their relationships to the more familiar heat transfer coefficients. Later, we see how these heat transfer coefficients can be determined by the application of conservation laws. The effect of turbulence is also discussed and empirical correlations presented.

Basic Laws of Molecular Transfer

Newton's law of viscosity: An isothermal system is shown in Figure 1-3.2. It consists of a fluid trapped between two impervious flat plates that are infinite in extent and separated by a distance, δ. Experiments show that if the lower plate is fixed and the upper plate is moved at a constant velocity, u_∞, then the velocity of the fluid between the two plates varies from u_∞ near the top plate to zero at the fixed plate. Under steady laminar conditions, a linear velocity profile is established as shown in Figure 1-3.2. The fluid thus exerts a shear force on the stationary plate. Experiments also show that τ, the shear force exerted on the bottom plate per unit area, is directly proportional to u_∞ and inversely proportional to the separation distance, δ; that is,

$$\tau \alpha \frac{u_\infty}{\delta} \quad \text{or} \quad \tau = \mu \frac{u_\infty}{\delta}$$

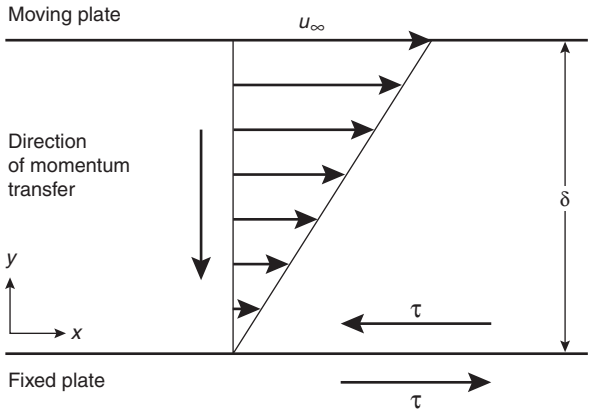

Figure 1-3.2. ***Steady-state velocity distribution in a Newtonian fluid.***

The constant of proportionality, μ, is called the dynamic viscosity of the fluid (units: $N \cdot s/m^2$) and the force per unit area, τ, is called the shear stress. (In some texts a negative sign is introduced to emphasize the direction of net momentum transfer, i.e., from the fluid at higher velocity to the fluid at lower velocity.) Note that the shear stress τ exerted by the fluid on the fixed plate is in the positive x-direction and that exerted by the fixed plate on the fluid is equal and opposite in direction.) In differential form this relationship expresses the shear stress at any location, y, in the fluid as

$$\tau = \mu \frac{du}{dy} \tag{1}$$

This is Newton's law of viscosity. Equation 1 states that the shear stress experienced by a fluid layer is directly proportional to the velocity gradient inside the fluid at that location.

Fluids that behave according to Equation 1 (i.e., τ is linearly related to the velocity gradient, du/dy, and μ is not a function of the velocity gradient) are called Newtonian fluids. Fortunately, all gases and most simple liquids such as water obey this simple law. For gases, μ roughly increases as the square root of temperature as predicted by the kinetic theory of dilute gases. Liquids, on the other hand, become "thinner" (less viscous), that is, μ decreases with increase in temperature. For non-Newtonian fluids (e.g., pastes, slurries, blood, etc.) the dynamic viscosity μ also depends on the velocity gradient or the rate of shear.

Fourier's law of heat conduction: Two stationary parallel plates separated by a distance, δ_t, are shown in Figure 1-3.3. Let the temperature of the upper plate be T_∞ and that of the lower plate be T_s. Under steady conditions and for temperature independent properties of the trapped fluid, a linear temperature distribution as shown in Figure 1-3.3 is obtained. Thus, as expected, heat is transferred by the stationary fluid from the hot to the cold plate. The heat flow per unit area per unit time through the fluid ($\dot{q}''$ J/m^2s) is found to be directly proportional to the temperature difference, $T_\infty - T_s$, and inversely proportional to the separation distance, δ_t; that is,

$$\dot{q}'' \alpha \frac{T_\infty - T_s}{\delta_t} = -k \frac{T_\infty - T_s}{\delta_t}$$

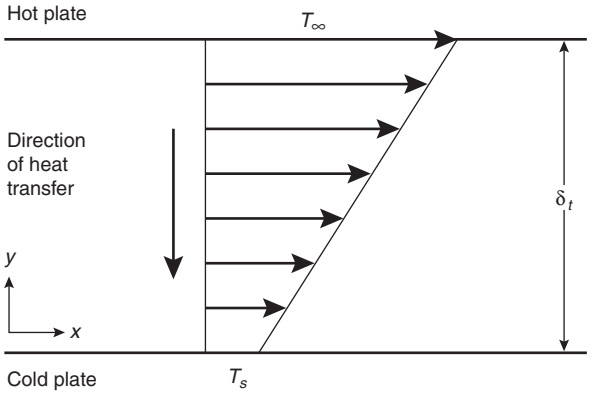

Figure 1-3.3. ***Steady-state temperature distribution.***

The constant of proportionality, k, is called the thermal conductivity (units: J/mKs). The minus sign is a consequence of the second law of thermodynamics, which requires the heat to flow in the direction of decreasing temperature. In differential form the heat across any fluid layer is given by

$$\dot{q}'' = -k\frac{dT}{dy} \tag{2}$$

This is known as Fourier's law of heat conduction, which states that the heat flux is directly proportional to the temperature gradient and the heat flux vector is oriented in the direction of decreasing temperature. The thermal conductivity, k, like viscosity, μ, is a physical property of the fluid. The thermal conductivity of gases at low densities increases with increasing temperature (roughly as $\sqrt{T}$ according to the kinetic theory of dilute gases) whereas the thermal conductivity of most liquids decreases with increasing temperature.

Fick's law of mass diffusion: Once again, consider the parallel plate example. This time, there are no temperature gradients and no directed motion of the plates. Instead, the top plate is maintained at a higher concentration of species A ($C_{A\infty}$, kg of A/m^3), assuming that it is wet, and the bottom plate is maintained at a fixed but lower concentration of species A (C_{AW}, kg of A/m^3). Then, under steady conditions a concentration profile, as shown in Figure 1-3.4, is established. This nonuniform concentration field is the driving force for species A to diffuse from the top to the bottom plate. The mass flux of species A, $\dot{m}''$ (units: kg/m^2s), leaving the top plate and arriving at the bottom plate through the fluid, B, is found to be directly proportional to the concentration difference and inversely proportional to the separation distance δ_d, that is,

$$\dot{m}''_A \alpha \frac{C_{A\infty} - C_{AW}}{\delta_d} = -D_{AB}\frac{C_{A\infty} - C_{AW}}{\delta_d}$$

The constant of proportionality, D_{AB}, is called diffusivity of species A through species B and has units of m^2/s. The negative sign once again indicates that the net mass transfer of species A occurs in the direction of decreasing concentration. In the differential form, the mass flux of species A across any layer of fluid B is given by

$$\dot{m}'' = -D_{AB}\frac{dC_A}{dy} \tag{3}$$

This is known as Fick's law of mass diffusion, which states that the mass flux across a fluid layer is directly proportional to the local concentration gradient. For binary gas mixtures, D_{AB} increases with increasing temperature roughly as three-halves power, as predicted by the kinetic theory of dilute gases.

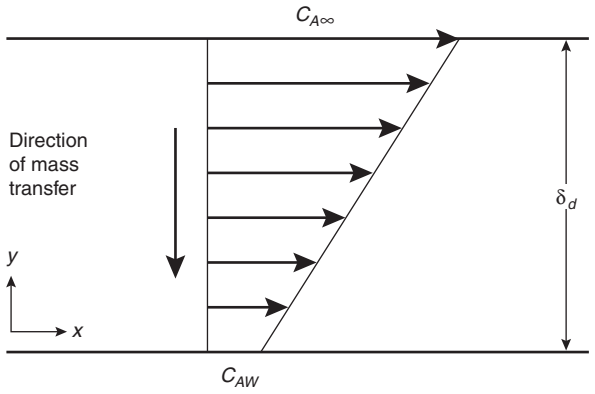

Figure 1-3.4. ***Steady-state concentration distribution.***

Discussion: Equations 1, 2, and 3 look very similar—they all relate the flux of the transported quantity to their respective local gradients. Actually, these equations may be considered definitions of the three macroscopic physical properties, μ, k, and D_{AB} of the fluid. In general, these properties are functions of temperature, pressure, and composition. As noted earlier, for low pressure binary gas mixtures (<10 atm) the pressure, temperature, and composition dependence of these properties can be approximately predicted by the kinetic theory of gases. In fact, the physical mechanism of all three transport processes is easily understood by considering the random motion of molecules in an ideal gas.

Molecules of a gas, even in the absence of bulk fluid motion, move around randomly at high speeds and bump into each other. Thus, a given molecule may be found anywhere between the two parallel plates. The problem, however, is how to distinguish one molecule from another. When the upper plate is moving relative to the bottom plate, the molecules adjacent to the upper plate attain a directed velocity over and above their random motion. Consequently, as the molecules near the upper plate find themselves in lower fluid layers (and vice versa) they exchange directed motion (or momentum) by bumping into each other. Similarly, the gas molecules near the hot upper plate are distinguished from those adjacent to the cold lower plate because they possess a higher kinetic energy. Once again, by virtue of random motion, these higher kinetic energy molecules find themselves near the cold plate and collide with low kinetic energy molecules (or vice versa), thus transporting energy. In the case of mass diffusion, the molecules are chemically labeled and their random motion results in mass transfer. Since increasing the gas temperature increases the random molecular motion, the transport processes become more efficient at higher gas temperatures. For gases, the macroscopic physical properties (viscosity, thermal conductivity, and diffusivity) that characterize momentum, heat, and mass transport must also increase with temperature.

Assuming constant properties, Equations 1 and 2 can be rewritten in the following forms:

$$\tau = \left(\frac{\mu}{\rho}\right)\frac{d(\rho u)}{dy} \tag{1a}$$

$$\dot{q}'' = -\left(\frac{k}{\rho c_p}\right)\frac{d(\rho c_p T)}{dy} \tag{1b}$$

Here, μ/p is known as the kinematic viscosity, ν, and has units of m^2/s. The product, ρu, has units of $(kg\ m/s)/m^3$; that is, momentum per unit volume. The quantity, $k/\rho c_p$, is known as the thermal diffusivity, α, and it too has units of m^2/s. The product, $\rho c_p T$, then becomes enthalpy per unit volume and has units of J/m^3. Comparing these with Equation 3, where the mass diffusivity, D_{AB}, also has units of m^2/s and C_A is expressed in kg of species A/m^3, we find that the fluxes are related to their corresponding gradients of volumetric concentration. Furthermore, the ratios of various physical constants yield the familiar nondimensional numbers. These are

$$\text{Prandtl number, Pr} = \nu/\alpha$$
$$\text{Schmidt number, Sc} = \nu/D_{AB}$$
$$\text{Lewis number, Le} = \alpha/D_{AB}$$

Here, the Prandtl number compares the relative magnitude of momentum transfer to heat transfer, the Schmidt number compares momentum transfer to mass transfer, and the Lewis number compares heat transfer to mass transfer. The significance of these nondimensional numbers will become obvious when we discuss boundary layer transfer processes. The balance of this section will discuss primarily heat transfer. The treatment of mass transfer is similar and will not be discussed. However, since fluid motion is central to convective heat transfer, it is necessary to understand momentum transport to solve convective heat transfer problems.

Relationship of Basic Laws to Transfer Coefficients

A flow condition is shown in Figure 1-3.5. A fluid of velocity, u_∞, and temperature, T_∞, flows over an arbitrarily shaped stationary surface of area, A_s. If the surface conditions are such that $T_s \neq T_\infty$, we know that convection heat transfer will occur. The convection heat transfer problem is to relate the local heat flux, $\dot{q}''$, to its driving force, $T_s - T_\infty$. By expressing the heat flux as

$$\dot{q}'' = h(T_s - T_\infty) \tag{4}$$

the problem is reduced to determining h, which is called the heat transfer coefficient. From Equation 2 it is clear that the heat transfer coefficient may be expressed as

$$h = \frac{-k(\partial T/\partial y)\Big|_{y=0}}{(T_s - T_\infty)} \left(\frac{\text{J}}{\text{m}^2\text{s K}}\right) \tag{5}$$

In Equation 5 the partial derivative is used because, in general, temperature is a function of x, y, z, and time. Thus, if the thermal conductivity of the fluid is known, the problem of determining the local heat transfer coefficient is reduced to that of determining the local temperature gradient in the fluid adjacent to the surface. This local temperature gradient can be experimentally measured or obtained theoretically from the solution of the conservation laws. Obviously, the temperature gradient will vary from point to point along the surface of the body. Often, such detail is not required and it may only be necessary to determine an average heat transfer coefficient, $\bar{h}$. This is obtained by integrating over the entire surface area, A_s. The total rate of heat transfer from the body to the fluid is given by

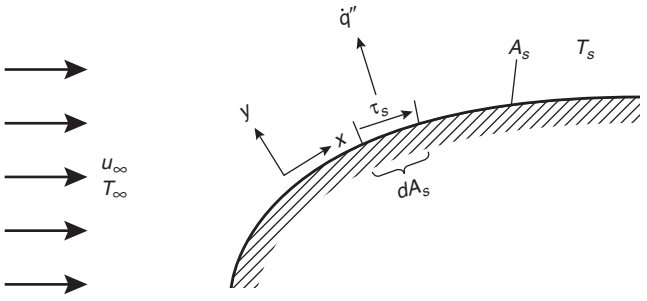

Figure 1-3.5. ***Example of the convection heat transfer problem.***

$$\dot{q}(\text{J/s}) = \int_{A_s} \dot{q}''(\text{J/m}^2\text{s}) \cdot dA_s(\text{m}^2) \tag{6}$$

Defining an average heat transfer coefficient, $\bar{h}$, as

$$\dot{q} = \bar{h} A_s (T_s - T_\infty) \tag{7}$$

The following is obtained from the use of Equations 4, 6, and 7

$$\bar{h} = \frac{1}{A_s(T_s - T_\infty)} \int_{A_s} h(T_s - T_\infty) dA_s \tag{8}$$

If the surface temperature, T_s, is held constant, then

$$\bar{h} = \frac{1}{A_s} \int_{A_s} h dA_s \left(\frac{\text{J}}{\text{m}^2\text{s K}}\right) \tag{9}$$

Similarly, the local shear stress at the surface, τ_s, can be related to its cause, the fluid velocity, u_∞. This relation is derived by defining a local nondimensional friction coefficient, C_f, according to the equation

$$\tau_s \equiv C_f \left(\frac{1}{2}\rho u_\infty^2\right) \tag{10}$$

Once again, the problem is reduced to the determination of C_f. Using Equation 1 we obtain

$$C_f = \frac{\mu(\partial u/\partial y)\Big|_{y=0}}{(1/2)\rho u_\infty^2} \tag{11}$$

Thus, the local friction coefficient can be evaluated from the knowledge of the local velocity gradient in the fluid adjacent to the surface. The average friction coefficient can easily be obtained by integrating the local shear stress, τ_s, over the entire surface area, A_s. The total drag force, D, experienced by the body is given by the product of average shear stress, $\bar{\tau}_s$, and the surface area, A_s. In other words,

$$D \equiv \bar{\tau}_s A_s = \int_{A_S} \tau_S dA_S \tag{12}$$

Assuming u_∞ to be the same at all locations

$$\bar{\tau}_s = \frac{(1/2\rho u_\infty^2)}{A_s} \int_{A_s} C_f A_s \tag{13}$$

Defining the average friction coefficient, $\overline{C}_f$, as

$$\overline{C}_f \equiv \frac{\bar{\tau}_s}{(1/2\rho u_\infty^2)} \tag{14}$$

we get

$$\overline{C}_f = \frac{1}{A_s} \int_{A_s} C_f \, dA_s \tag{15}$$

To obtain h, $\overline{h}$, C_f, and $\overline{C}_f$ a knowledge of fluid properties and temperature and velocity gradients in the fluid adjacent to the surface is required. To obtain these gradients it is necessary to be more specific about the surface geometry and the flow conditions. The governing conservation equations for an arbitrary surface geometry will be first derived and then applied to a flat plate to illustrate the methodology.

Conservation Equations for Convection Heat Transfer

It has been shown that to determine the heat transfer and friction coefficients, the temperature and velocity distributions in the flow are needed. In principle, these may be obtained from the solution of the conservation equations with appropriate boundary conditions. Although in practice it is difficult, the very knowledge of conservation equations and their solutions for simple cases (such as a flat plate) provide considerable insight about the parameters influencing the heat transfer and friction coefficients. Thus, the necessary equations will be first developed and then applied to a flat plate.

Consider the flow over the surface shown in Figure 1-3.6. To simplify the development assume two-dimensional flow conditions, for which x is the direction along the surface and y is normal to the surface. Extension of this to three-dimensional flows is available in the literature.[1–5]

Conservation of mass (continuity equation): The first conservation law that is pertinent to the problem is that matter is neither created nor destroyed. When applied to the differential control volume shown in Figures 1-3.6 and 1-3.7 it states that the net rate of mass flow entering the elemental control volume in the x-direction, plus the net rate of mass flow entering the elemental control volume in the y-direction equals the net rate of increase of mass stored in the control volume. Mass enters and leaves the control volume exclusively through gross fluid motions. Such a transport is often referred to as convective transport.

For a control volume of unit depth in the z-direction, mass entering the left face per unit time, $\dot{M}_x$, is given by

$$\dot{M}_x = \rho(\text{kg/m}^3) u(\text{m/s})\, dy(\text{m}) \cdot 1(\text{m})$$

Similarly, mass entering the bottom face per unit time, $\dot{M}_y$, is given by

$$\dot{M}_y = \rho \cdot v \cdot dx \cdot 1$$

where v is the fluid velocity in the y-direction.

Since ρu and ρv are continuous functions of x, y, and time, in general they will be different at different locations. To determine ρu at $(x + dx)$, expand ρu about the point x in the Taylor series as

$$\rho u(x + dx, y) = \rho u(x, y) + \left[\frac{\partial(\rho u)}{\partial x}\right]_{x,y} dx \tag{16}$$

Similarly,

$$\rho v(x, y + dy) = \rho v(x, y) + \left[\frac{\partial(\rho v)}{\partial y}\right]_{x,y} dy$$

Thus, mass leaving the right face per unit time, $\dot{M}_{x+dx}$, is given by

$$\dot{M}_{x+dx} = \left[\rho u + \frac{\partial(pu)}{\partial x} dx\right] \cdot dy \cdot 1 \tag{17}$$

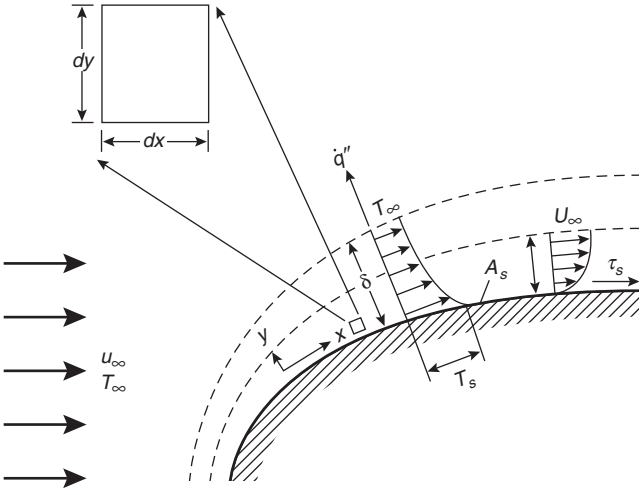

Figure 1-3.6. ***Velocity and temperature distributions inside the fluid for flow over a hot surface.***

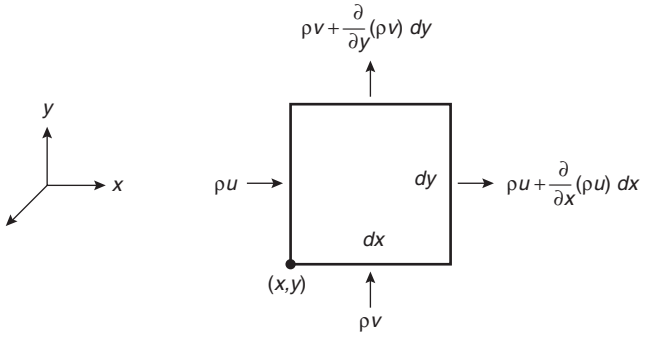

Figure 1-3.7. ***Differential control volume for mass conservation in a two-dimensional flow.***

and mass leaving the top face per unit time, $\dot{M}_{y+dy}$, is

$$\dot{M}_{y+dy} = \left[\rho v + \frac{\partial(\rho v)}{\partial y}\,dy\right] \cdot dx \cdot 1 \tag{18}$$

Finally, the rate of increase (or decrease) of mass stored in the control volume, $\dot{M}_s$, is of the form

$$\dot{M}_s = \frac{\partial}{\partial t}(\rho \cdot dx \cdot dy \cdot 1) = \frac{\partial \rho}{\partial t}\,dx\,dy \tag{19}$$

Thus, conservation of mass requirement may now be expressed as

$$\begin{aligned}(\rho u)\,dy + (\rho v)\,dx - \left[\rho u + \frac{\partial(\rho u)}{\partial x}\,dx\right]dy \\ - \left[\rho v + \frac{\partial(\rho v)}{\partial y}\,dy\right]dx = \frac{\partial \rho}{\partial t}\,dx\,dy\end{aligned} \tag{20}$$

After canceling terms and dividing by $dx\,dy$

$$\frac{\partial \rho}{\partial t} + \frac{\partial(\rho u)}{\partial x} + \frac{\partial(\rho v)}{\partial y} = 0 \tag{21}$$

This is the *continuity equation,* which is an expression of the overall mass conservation requirement and must be satisfied at every point in the flow. This equation applies for a single species fluid, as well as for mixtures in which species diffusion and chemical reactions may be occurring.

Conservation of momentum: The second conservation law pertinent to the convection heat transfer problem is Newton's second law of motion. For a differential control volume in a flow field, this requirement states that the sum of all forces acting on the control volume must equal the rate of increase of the fluid momentum within the control volume, plus the net rate at which momentum leaves the control volume (outflow-inflow).

The forces acting on the fluid may be categorized into *body forces* that are proportional to the volume, and *surface forces,* which are proportional to the area. Gravitational, centrifugal, magnetic, and electric fields are familiar examples of body forces. Of these, gravitational body force is the most important from the fire science point of view. The x- and y-components of this body force per unit volume of the fluid will be designated as F_{Bx} and F_{By}, respectively.

The surface forces, F_s, acting on the fluid are called stresses (force/area). These are due to fluid static pressure, p, and viscous stresses. Since pressure is always normal to the surface, the viscous stresses are also resolved into normal stresses, σ_{ii}, which act normal to the surface, and shear stresses, τ_{ij}, which act along or parallel to the surface. Figure 1-3.8 shows the various viscous stresses acting on the surface of a differential control volume. A double subscript notation is used to specify the stress components. The first subscript indicates the direction of the outward normal to the surface, and the second subscript indicates the direction of the force component. Accordingly, the stress τ_{xy}, acting on the left face, corresponds to the viscous shear force per unit area in the negative y-direction on a face whose normal is in the negative x-direction—resulting in a positive shear stress. All the viscous stresses shown in Figure 1-3.8 are positive according to the adopted convention. It should be noted that

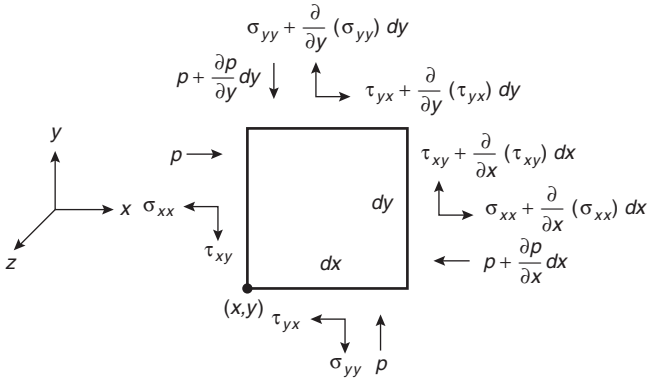

Figure 1-3.8. ***Static pressure, p, and normal and shear viscous stresses acting on a differential control volume in a two-dimensional flow.***

these forces act on the fluid inside the control volume and are caused by its interaction with the surrounding fluid. Thus, these viscous stresses will vanish if the fluid velocity, or more specifically the velocity gradient in the fluid, becomes zero. The normal viscous stresses shown in Figure 1-3.8 must not be confused with static pressure, p, which does not vanish for zero velocity. Since these stresses are continuous functions of x, y, and time, the customary Taylor's expansion is used to express the stresses on the top and right faces of the control volume shown in Figure 1-3.8. Thus, the net surface force in the x- and y-directions may be expressed as

$$F_{sx} = \left(\frac{\partial \sigma_{xx}}{\partial x} - \frac{\partial p}{\partial x} + \frac{\partial \tau_{yx}}{\partial y}\right)dx\,dy \tag{22}$$

$$F_{sy} = \left(\frac{\partial \sigma_{yy}}{\partial y} - \frac{\partial p}{\partial y} + \frac{\partial \tau_{xy}}{\partial x}\right)dx\,dy \tag{23}$$

To use Newton's second law, the time rate of change of momentum and the momentum influx and outflux must also be evaluated. To focus on the x-direction, the relevant momentum fluxes are shown in Figure 1-3.9. The mass flux through the left face is ρu and hence the corresponding momentum flux is $(\rho u)u$. Similarly, the x-momentum flux due to mass flow in the y-direction through the bottom face is $(\rho v)u$. Thus the net rate at which momentum leaves the control volume is given by (x-momentum outflow – inflow)

$$\frac{\partial}{\partial x}[(\rho u)u]\,dx\,dy + \frac{\partial[(\rho v)u]}{\partial y}\,dy\,dx$$

In addition, the time rate of change of x-momentum of the fluid within the control volume is given by

$$\frac{\partial}{\partial t}(\rho u)\,dx\,dy$$

Equating the total rate of change in the x-direction to the sum of forces in the x-direction, we obtain

$$\frac{\partial(\rho u)}{\partial t} + \frac{\partial[(\rho u)u]}{\partial x} + \frac{\partial[(\rho v)u]}{\partial y} = \frac{\partial \sigma_{xx}}{\partial x} - \frac{\partial p}{\partial x} + \frac{\partial \tau_{yx}}{\partial y} + F_{Bx} \tag{24}$$

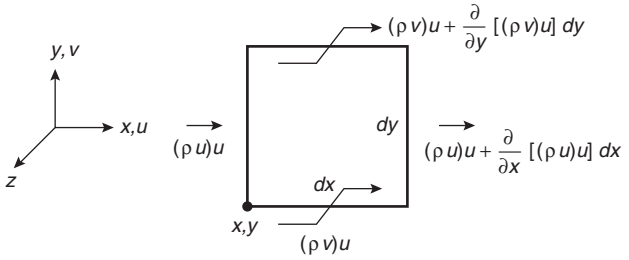

Figure 1-3.9. ***Influx and outflux of x-momentum in the control volume.***

By using Equation 21, Equation 24 may be expressed in a more convenient form as

$$\rho\left(\frac{\partial u}{\partial t} + u\frac{\partial u}{\partial x} + v\frac{\partial u}{\partial y}\right) = \frac{\partial}{\partial x}(\sigma_{xx} - p) + \frac{\partial \tau_{yx}}{\partial y} + F_{Bx} \qquad (25)$$

A similar expression is obtained for the y-direction. This is

$$\rho\left(\frac{\partial v}{\partial t} + u\frac{\partial v}{\partial x} + v\frac{\partial v}{\partial y}\right) = \frac{\partial}{\partial y}(\sigma_{yy} - p) + \frac{\partial \tau_{xy}}{\partial x} + F_{By} \qquad (26)$$

In Equations 25 and 26, the first term on the left side represents the increase in momentum of the fluid inside the control volume, and the remaining terms represent the net rate of momentum efflux from the control volume. The terms on the right side of the equations account for the net viscous, pressure, and body forces acting on the control volume. These equations must be satisfied at every point in the fluid. A solution of Equations 21, 25, and 26 along with appropriate boundary conditions yields the velocity field needed to determine the friction coefficient.

Before a solution to the above equations can be obtained, it is necessary to relate the viscous stresses to the velocity gradients. For a one-dimensional flow of a Newtonian fluid, Equation 1 relates the shear stress to the velocity gradient in the fluid. For a two-dimensional flow of Newtonian fluid,[2] the required stress-velocity gradient expressions are

$$\sigma_{xx} = 2\mu\frac{\partial u}{\partial x} - \frac{2}{3}\mu\left(\frac{\partial u}{\partial x} + \frac{\partial v}{\partial y}\right) \qquad (27)$$

$$\sigma_{yy} = 2\mu\frac{\partial v}{\partial y} - \frac{2}{3}\mu\left(\frac{\partial u}{\partial x} + \frac{\partial v}{\partial y}\right) \qquad (28)$$

$$\tau_{xy} = \tau_{yx} = \mu\left(\frac{\partial u}{\partial y} + \frac{\partial v}{\partial x}\right) \qquad (29)$$

On substituting Equations 27, 28, and 29 into Equations 25 and 26, the desired form of the x- and y-momentum equations is obtained. These are

x-momentum equation

$$\rho\left(\frac{\partial u}{\partial t} + u\frac{\partial u}{\partial x} + v\frac{\partial u}{\partial y}\right) = -\frac{\partial p}{\partial x} + \mu\left(\frac{\partial^2 u}{\partial x^2} + \frac{\partial^2 u}{\partial y^2}\right) + \frac{1}{3}\mu\frac{\partial}{\partial x}\left(\frac{\partial u}{\partial x} + \frac{\partial v}{\partial y}\right) + F_{Bx} \qquad (30)$$

y-momentum equation

$$\rho\left(\frac{\partial v}{\partial t} + u\frac{\partial v}{\partial x} + v\frac{\partial v}{\partial y}\right) = -\frac{\partial p}{\partial y} + \mu\left(\frac{\partial^2 v}{\partial x^2} + \frac{\partial^2 v}{\partial y^2}\right) + \frac{1}{3}\mu\frac{\partial}{\partial y}\left(\frac{\partial u}{\partial x} + \frac{\partial v}{\partial y}\right) + F_{By} \qquad (31)$$

For an isothermal system, Equations 21, 30, and 31 along with the equation of state ($p = \rho RT$ for an ideal gas) provide a complete set for determining the four dependent variables (u, v, p, and ρ) as a function of the three independent variables x, y, and t. However, for a non-isothermal system such as a fire, energy balance must also be considered.

Conservation of energy: The temperature field inside the fluid, $T(x, y, t)$, needed to determine the heat transfer coefficient is obtained by applying the first law of thermodynamics to the differential control volume shown in Figure 1-3.6. Before writing the energy balance for this control volume, it is necessary to identify the items that must be included in the energy budget. These are:

1. The stored energy. This includes the specific internal or thermal energy, e; J/kg, and the kinetic energy of the fluid per unit mass, $V^2/2 = (u^2 + v^2)/2$. Potential energy is neglected because for most problems in convective heat transfer it is substantially smaller than thermal and kinetic energy. Hence, the total energy content per unit volume is given by: $\rho(e + V^2/2)$.
2. Conduction of thermal energy across the surfaces of the control volume. Here, the rate of energy transported per unit area per unit time across the control surface is given by Equation 2 as $\dot{q}''_x = -k\partial T/\partial x$ for the x-direction, and $\dot{q}''_y = -k\partial T/\partial y$ for the y-direction.
3. Energy generated per unit volume per unit time inside the control volume (Q watts/m^3). This may be due to chemical reactions (endothermic or exothermic) or may be caused by the radiative loss of heat. Although the specific form of Q will depend upon the nature of the physical process, here we will treat it only as a rate of heat loss or gain per unit volume.
4. The rate of work done by surface or body forces. For surface forces, $\vec{F}_S$, it is given by: [$\vec{F}_S \cdot$ (velocity vector)] (surface area): and for the body forces, $\vec{F}_B$, it is given by: [$\vec{F}_B \cdot$ (velocity vector)](volume). Both these expressions have units of 'watts' or work done per unit time.

With these definitions, consider the control volume shown in Figures 1-3.6 and 1-3.10. The conservation of energy for this control volume can be simply stated as

$$\begin{pmatrix}\text{rate of increase}\\ \text{of energy inside}\\ \text{the control volume}\end{pmatrix} = \begin{pmatrix}\text{net rate of energy flow}\\ \text{into the control volume}\\ \text{by bulk fluid motion}\end{pmatrix} + \begin{pmatrix}\text{flow of heat through}\\ \text{the control surface}\\ \text{by conduction}\end{pmatrix} + \begin{pmatrix}\text{rate of work done by body}\\ \text{and surface forces}\end{pmatrix} + \begin{pmatrix}\text{energy generated inside}\\ \text{the control volume}\end{pmatrix} \qquad (32)$$

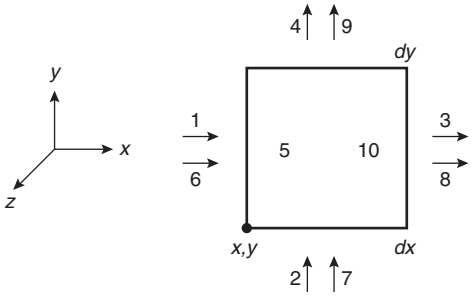

1. $\rho\left(e + \frac{V^2}{2}\right)u \cdot dy \cdot 1$
2. $\rho\left(e + \frac{V^2}{2}\right)v \cdot dx \cdot 1$
3. $\left\{\rho\left(e + \frac{V^2}{2}\right)u + \frac{\partial}{\partial x}\left[\rho u\left(e + \frac{V^2}{2}\right)\right]dx\right\} dy \cdot 1$
4. $\left\{\rho\left(e + \frac{V^2}{2}\right)v + \frac{\partial}{\partial x}\left[\rho v\left(e + \frac{V^2}{2}\right)\right]dy\right\} dx \cdot 1$
5. $\frac{\partial}{\partial t}\left[\rho\left(e + \frac{V^2}{2}\right)\right]dx \cdot dy \cdot 1$
6. $\dot{q}''_x \cdot dy \cdot 1$
7. $\dot{q}''_y \cdot dx \cdot 1$
8. $\left(\dot{q}''_x + \frac{\partial \dot{q}''_x}{\partial x}dx\right) dy \cdot 1$
9. $\left(\dot{q}''_y + \frac{\partial \dot{q}''_y}{\partial y}dy\right) dx \cdot 1$
10. Energy generated $\quad Q\,dx\,dy \cdot 1$

Figure 1.3-10. ***A control volume showing the energy conducted and convected through its control surfaces.***

In Equation 32 the rate of increase of energy inside the control volume is given by

$$\frac{\partial}{\partial t}\left[\rho\left(e + \frac{V^2}{2}\right)\right]dx\,dy$$

The net rate at which the energy enters the control volume by convection or bulk fluid motion is obtained by subtracting the energy going out from that coming in, to yield

$$-\frac{\partial}{\partial x}\left[\rho u\left(e + \frac{V^2}{2}\right)\right]dx\,dy - \frac{\partial}{\partial y}\left[\rho v\left(e + \frac{V^2}{2}\right)\right]dx\,dy$$

Similarly, the heat flowing into the control volume by conduction is given by

$$-\left(\frac{\partial \dot{q}''_x}{\partial x} + \frac{\partial \dot{q}''_y}{\partial y}\right)dx\,dy = \left[\frac{\partial}{\partial x}\left(k\frac{\partial T}{\partial x}\right) + \frac{\partial}{\partial y}\left(k\frac{\partial T}{\partial y}\right)\right]dx\,dy$$

Finally, the net rate at which work is done on the fluid inside the control volume (Figure 1-3.11) is given by the expression

$$(uF_{Bx} + vF_{By})\,dx\,dy - \left[\frac{\partial(pu)}{\partial x} + \frac{\partial(pv)}{\partial y}\right]dx\,dy + \left[\frac{\partial}{\partial x}(u\sigma_{xx}) + \frac{\partial}{\partial y}(v\sigma_{yy}) + \frac{\partial}{\partial y}(u\tau_{yx}) + \frac{\partial}{\partial x}(v\tau_{xy})\right]dx\,dy$$

On substituting these expressions into Equation 32, simplifying and using Equations 27 through 31, we obtain

$$\rho C_p\frac{\partial T}{\partial t} + \rho u C_p\frac{\partial T}{\partial x} + \rho v C_p\frac{\partial T}{\partial y} = \frac{\partial}{\partial x}\left(k\frac{\partial T}{\partial x}\right) + \frac{\partial}{\partial y}\left(k\frac{\partial T}{\partial y}\right) + \left(\frac{\partial p}{\partial t} + u\frac{\partial p}{\partial x} + v\frac{\partial p}{\partial y}\right) + \mu\Phi \tag{33}$$

In Equation 33, the thermodynamic definition of enthalpy ($i = e + p/\rho$ and $di = C_p dT$) has been used. Also, the term $u\Phi$ is called the viscous dissipation and is given by

$$u\Phi = 2\mu\left[\left(\frac{\partial u}{\partial x}\right)^2 + \left(\frac{\partial v}{\partial y}\right)^2\right] + \left(\frac{\partial u}{\partial y} + \frac{\partial v}{\partial x}\right)^2 - \frac{2}{3}\left(\frac{\partial u}{\partial x} + \frac{\partial v}{\partial y}\right)^2 \tag{34}$$

Equations 21, 30, 31, and 33, along with the equation of state ($p = \rho RT$, for an ideal gas), provide a complete set for determining the temperature and velocity field [$T(x, y, t)$,

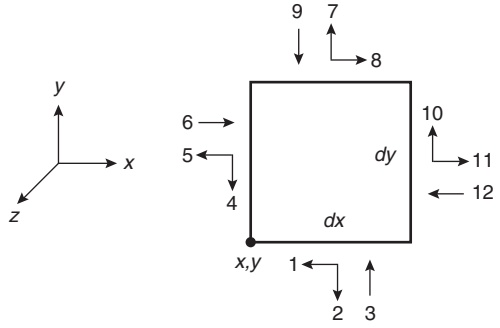

1. $-u\tau_{yx}\,dx$
2. $-v\sigma_{yy}\,dx$
3. $pv\,dx$
4. $-v\tau_{zy}\,dy$
5. $-u\sigma_{xx}\,dy$
6. $pu\,dy$
7. $\left[v\sigma_{yy} + \frac{\partial}{\partial y}(v\sigma_{yy})\,dy\right]dx$
8. $\left[u\tau_{yx} + \frac{\partial}{\partial y}(u\tau_{yx})\,dy\right]dx$
9. $\left[-pv - \frac{\partial}{\partial y}(pv)\,dy\right]dx$
10. $\left[v\tau_{xy} + \frac{\partial}{\partial x}(v\tau_{xy})\,dx\right]dy$
11. $\left[u\sigma_{xx} + \frac{\partial}{\partial x}(u\sigma_{xx})\,dx\right]dy$
12. $\left[-pu - \frac{\partial}{\partial x}(pu)\,dx\right]dy$

Figure 1-3.11. ***Control volume showing the rate of work done by various surface forces. All units are in watts.***

$u(x, y, t)$, $v(x, y, t)$] inside the fluid. However, it is not possible to solve the above set of coupled nonlinear partial differential equations. Therefore, several simplifying approximations are made. These are discussed below.

Simplifications:

1. *Low velocity:* For most problems encountered in convective heat transfer, the flow velocity is low enough (Mach number $< 1/3$) to ignore the contribution of viscous work in the energy equation. This allows the term $\mu\Phi$ in Equation 33 to be dropped.
2. *Incompressible flow:* Fluid density is assumed to be constant except in the buoyancy terms (F_{Bx}, F_{By}) of Equations 30 and 31. This is called the Boussinesq approximation and will be discussed later in greater detail.
3. *Steady flow:* This approximation allows all the time derivative terms in the above equations to be dropped.
4. *Constant properties:* Specific heat, thermal conductivity, and viscosity are all assumed to be constant; that is, independent of temperature and pressure.

With these simplifications and assuming that the body force is only due to gravity (i.e., $F_{Bx} = -\rho g_x$ and $F_{By} = -\rho g_y$), Equations 21, 30, 31, and 33 become

Continuity

$$\frac{\partial u}{\partial x} + \frac{\partial v}{\partial y} = 0 \tag{35}$$

x-momentum

$$u\frac{\partial u}{\partial x} + v\frac{\partial u}{\partial y} = -\frac{1}{\rho}\frac{\partial p}{\partial x} + \nu\left(\frac{\partial^2 u}{\partial x^2} + \frac{\partial^2 u}{\partial y^2}\right) - g_x \tag{36}$$

y-momentum

$$u\frac{\partial v}{\partial x} + v\frac{\partial v}{\partial y} = -\frac{1}{\rho}\frac{\partial p}{\partial y} + \nu\left(\frac{\partial^2 v}{\partial x^2} + \frac{\partial^2 v}{\partial y^2}\right) - g_y \tag{37}$$

Energy equation

$$u\frac{\partial T}{\partial x} + v\frac{\partial T}{\partial y} = \alpha\left(\frac{\partial^2 T}{\partial x^2} + \frac{\partial^2 T}{\partial y^2}\right) + \frac{1}{\rho C_p}\left(u\frac{\partial p}{\partial x} + v\frac{\partial p}{\partial y}\right) \tag{38}$$

Often, the energy equation is further simplified by assuming that the terms ($u\,\partial p/\partial x$) and ($v\,\partial p/\partial y$) are negligible. This assumption is justified since most processes of interest are nearly isobaric. Thus the energy equation becomes

$$u\frac{\partial T}{\partial x} + v\frac{\partial T}{\partial y} = \alpha\left(\frac{\partial^2 T}{\partial x^2} + \frac{\partial^2 T}{\partial y^2}\right) \tag{39}$$

Equations 35, 36, 37, and 39, along with the equation of state ($p = \rho RT$, for an ideal gas), provide a complete set for determining $u(x, y)$, $v(x, y)$, $T(x, y)$, $\rho(x, y)$, and $p(x, y)$. Once these dependent variables are known, the desired heat transfer coefficient and friction factor are obtained from Equations 5 and 11, respectively. However, the above equations are still too difficult to solve and a further simplification, known as the boundary layer approximation, is often made.

The Boundary Layer Concept

In 1904, Prandtl proposed that all the viscous effects are concentrated in a thin layer near the boundary and that outside this layer the fluid behaves as though it is inviscid. Thus, the flow over a body, such as the one shown in Figure 1-3.6, can be divided into two zones: (1) a thin viscous layer near the surface, called the boundary layer, and (2) inviscid external flow, which can be closely approximated by the potential flow theory. As will be seen later, the fact that the boundary layer is thin compared to the characteristic dimensions of the object is exploited to simplify the governing equations and obtain a useful solution. This boundary layer approximation plays an important role in convective heat transfer, since the gradients of velocity and temperature at the surface of the body are required to determine the heat transfer coefficient and the friction factor.

To illustrate these ideas, consider fluid flow over a flat plate as shown in Figure 1-3.12. The fluid particles in contact with the plate surface must assume zero velocity because of no slip at the wall, whereas the fluid particles far away from the wall continue to move at the free stream velocity, u_∞. The transition of fluid velocity from zero to u_∞ takes place in a small distance, δ, which is known as the boundary layer thickness and is defined as

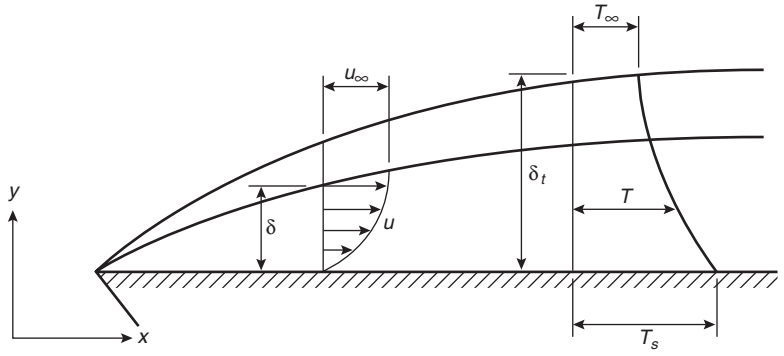

Figure 1-3.12. ***Velocity and thermal boundary layers on a flat plate.***

the value of y for which $u = 0.99\ u_\infty$. As is intuitively obvious, the thickness of the boundary layer increases with fluid viscosity and decreases with increasing free-stream velocity. By defining the Reynolds number, Re, as $\text{Re} = u_\infty L/\nu$, where L is the characteristic length of the plate, the boundary layer thickness decreases with increasing Re. For most flows of practical interest, the Reynolds number is large enough such that δ is much less than the characteristic length, L ($\delta \ll L$).

Just as a velocity boundary layer develops because of viscous effects near the surface, a thermal boundary layer develops due to heat transfer between the free stream and the surface if their temperatures are different. The fluid particles that come into contact with the plate surface achieve thermal equilibrium at the plate's surface temperature. In turn, these particles exchange energy with those in the adjoining fluid layer, and temperature gradients develop in the fluid. As shown in Figure 1-3.12, the region of the fluid in which these temperature gradients exist is the thermal boundary layer, and its thickness, δ_t, is defined as the value of y for which the ratio $[(T - T_S)/(T_\infty - T_S)] = 0.99$. The thermal boundary layer thickness increases with the thermal diffusivity, α, of the fluid and decreases with increasing free stream velocity. In other words, δ_t is inversely proportional to the product of Reynolds number and Prandtl number [$\text{Re Pr} = (u_\infty L/\nu)(\nu/\alpha) = u_\infty L/\alpha$]. For air, $\text{Pr} \approx 0.7$ and the Reynolds number is sufficiently large for flows of practical interest, consequently $\delta_t \ll L$.

Boundary layer approximation: The governing Equations 35 through 37 and 39 can be further simplified for the case when the Reynolds number is reasonably large [$\text{Re} \sim (L/\delta)^2$; that is, Re is of the order $(L/\delta)^2$] such that $\delta \ll L$. To compare the various terms in the governing equations, first normalize all the variables so that they are of the order of magnitude unity. By defining

$$x^* = \frac{x}{L} \quad y^* = \frac{y}{\delta} \quad u^* = \frac{u}{u_\infty}$$

and

$$T^* = \frac{T - T_S}{T_\infty - T_S} \tag{40}$$

variables that change from 0 to 1 inside the boundary layer are obtained. Substituting these into Equation 35 we find that

$$-\frac{\partial u^*}{\partial x^*} = \left(\frac{L}{\delta u_\infty}\right)\frac{\partial v}{\partial y^*}$$

This suggests that

$$v^* = \frac{Lv}{\delta u_\infty}$$

so that

$$\frac{\partial u^*}{\partial x^*} + \frac{\partial v^*}{\partial y^*} = 0 \tag{41}$$

Substituting x^*, y^*, u^*, and v^* into Equation 36 and simplifying

$$u^*\frac{\partial u^*}{\partial x^*} + v^*\frac{\partial u^*}{\partial y^*} = -\frac{\partial p^*}{\partial x^*} - g_x^* + \left(\frac{\nu}{Lu_\infty}\right)\left[\frac{\partial^2 u^*}{\partial x^{*2}} + \left(\frac{L}{\delta}\right)^2\frac{\partial^2 u^*}{\partial y^{*2}}\right] \tag{42}$$

where $p^* \equiv p/\rho u_\infty^2$ and $g_x^* \equiv g_x L/u_\infty^2$.

In Equation 42, the quantity ν/Lu_∞ is recognized as $1/\text{Re}$ which is of the order (δ/L^2). Thus all terms in Equation 42 are of order of magnitude unity except the term $[(\nu/Lu_\infty)\partial^2 u^*/\partial x^{*2}]$, which is much less than 1 and can be ignored. Thus, Equation 36 is simplified to

$$u\frac{\partial u}{\partial x} + v\frac{\partial u}{\partial y} = -\frac{1}{\rho}\frac{\partial p}{\partial x} - g_x + \nu\frac{\partial^2 u}{\partial y^2} \tag{43}$$

Similarly, Equations 37 and 39 reduce to

$$\frac{\partial p}{\partial y} \approx 0 \tag{44}$$

and

$$u\frac{\partial T}{\partial x} + v\frac{\partial T}{\partial y} = \alpha\frac{\partial^2 T}{\partial y^2} \tag{45}$$

Equation 44 simply implies that $p = p(x)$, that is, the pressure at any plane where x = constant does not vary with y inside the boundary layer and hence is equal to the free stream pressure. To summarize, the boundary layer approximation yields a simpler set of governing equations that are valid inside the boundary layer. These equations for steady flow of an incompressible fluid with constant properties are

Continuity

$$\frac{\partial u}{\partial x} + \frac{\partial v}{\partial y} = 0 \tag{35}$$

x-momentum

$$u\frac{\partial u}{\partial x} + v\frac{\partial u}{\partial y} = -\frac{1}{\rho}\frac{\partial p}{\partial x} - g_x + \nu\frac{\partial^2 u}{\partial y^2} \tag{43}$$

Energy

$$u\frac{\partial T}{\partial x} + v\frac{\partial T}{\partial y} = \alpha\frac{\partial^2 T}{\partial y^2} \tag{45}$$

To illustrate the use of these equations in determining the heat transfer coefficient, consider two classical examples: (1) laminar forced convection over a flat surface, and (2) laminar free convection on a vertical flat surface. Forced convection is chosen as a precursor to free convection because it is simpler and also allows us to illustrate the difference between them. A flat geometry is also chosen in both cases for simplicity.

Laminar forced convection over a flat surface: A schematic of this problem is presented in Figure 1-3.12, and the objective here is to obtain the gradients of temperature and velocity profile at $y = 0$. By applying the Bernoulli

Equation in the potential flow region outside the boundary layer we obtain

$$\frac{u_\infty^2}{2} + \frac{p}{\rho} + gh = \text{constant} \tag{46}$$

Since the free stream velocity, u_∞, is constant, for a given height $y = h$ above the flat surface we obtain that p = constant, that is, $p \neq p(x)$ outside the boundary layer in the potential flow region. From Equation 44 note that $p \neq p(y)$ inside the boundary layer. Hence, p = constant both inside and outside the boundary layer over a flat surface. This implies that the term $\partial p/\partial x$ equals zero in Equation 43. Also, since the flow is forced (i.e., generated by an external agent such as a fan, rather than by buoyancy) the gravitational force, g_x, in Equation 43 does not contribute to the increase in momentum represented by the left side of the equation, and $g_x = 0$. Thus Equation 43 becomes

$$u\frac{\partial u}{\partial x} + v\frac{\partial u}{\partial y} = \nu\frac{\partial^2 u}{\partial y^2} \tag{47}$$

Equations 35, 45, and 47 govern the temperature and velocity distributions inside the boundary layer shown in Figure 1-3.12. The associated boundary conditions are

no-slip

$$u = v = 0 \quad \text{at} \quad y = 0$$

and

$$T = T_S \quad \text{at} \quad y = 0 \tag{48}$$

also

$$u = u_\infty \quad \text{and} \quad T = T_\infty \quad \text{as} \quad y \to \infty$$

Nondimensionalizing Equations 35, 45, 47, and 48 according to Equation 40* we obtain

$$\frac{\partial u^*}{\partial x^*} + \frac{\partial v^*}{\partial y^*} = 0 \tag{49}$$

$$u^*\frac{\partial u^*}{\partial x^*} + v^*\frac{\partial u^*}{\partial y^*} = \frac{1}{\text{Re}_L}\frac{\partial^2 u^*}{\partial y^{*2}} \tag{50}$$

$$u^*\frac{\partial T^*}{\partial x^*} + v^*\frac{\partial T^*}{\partial y^*} = \frac{1}{\text{Re}_L \text{Pr}}\frac{\partial^2 T^*}{\partial y^{*2}} \tag{51}$$

*A more convenient definition of $y^* = y/L$ and $v^* = v/u_\infty$ has been used since we are no longer interested in quantities of order of magnitude unity; instead we are simply interested in eliminating units.

along with the boundary conditions

$$u^* = v^* = T^* = 0 \quad \text{at} \quad y^* = 0$$

and

$$u^* = T^* = 1 \quad \text{as} \quad y^* \to \infty \tag{52}$$

where

$$\text{Re}_L \equiv \frac{u_\infty L}{\nu}$$

is the Reynolds number based on length, L, and $\text{Pr} \equiv \nu/\alpha$ is the Prandtl number. Note that Equations 49 and 50 are sufficient for determining $u^*(x^*, y^*)$ and $v^*(x^*, y^*)$ and that once these are known, Equation 51 can be independently solved for $T^*(x^*, y^*)$. Also note that for Pr = 1, Equations 50 and 51 as well as their corresponding boundary conditions are identical. Thus for Pr = 1 only Equations 49 and 50 need to be solved.

A similarity solution of Equations 49 and 50 along with the boundary conditions (Equation 52) was obtained by Blasius.[2] Blasius observed that since the system under consideration has no preferred length, it is reasonable to suppose that the velocity profiles at different values of x have similar shapes; that is, if u and y are suitably scaled then the velocity profile may be expressed by a single function for all values of x. (See Figure 1-3.13.) An obvious choice is

$$\frac{u}{u_\infty} = \phi\left[\frac{y}{\delta(x)}\right]\phi \tag{53}$$

This choice, as it stands, is not very useful because $\delta(x)$ is not known. However, in accordance with the boundary layer approximation, $\text{Re}_x \equiv u_\infty x/\nu \sim (x/\delta)^2$. Therefore,

$$\delta \sim \sqrt{\frac{\nu x}{u_\infty}}$$

can be expected. Substituting into Equation 53 we obtain

$$u^* = \frac{u}{u_\infty} = \phi\left[\frac{y}{x}\sqrt{\text{Re}_x}\right] = \phi(\eta) \tag{54}$$

where

$$\eta \equiv \frac{y}{x}\sqrt{\text{Re}_x} = \left[\left(\frac{y^*}{\sqrt{x^*}}\right)\sqrt{\text{Re}_L}\right]$$

is the similarity variable. By introducing a stream function, ψ, such that

$$u^* = \frac{\partial \psi}{\partial y^*} \quad \text{and} \quad v^* = -\frac{\partial \psi}{\partial x^*} \tag{55}$$

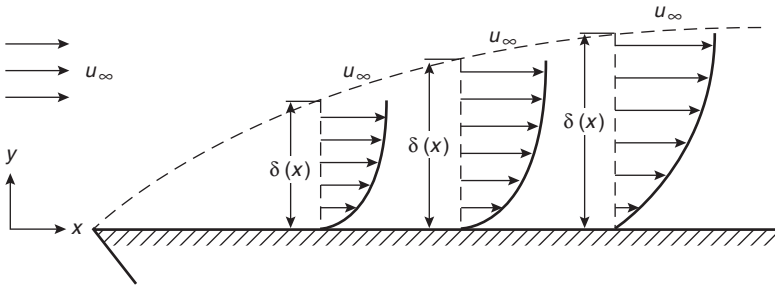

Figure 1-3.13. ***Observed velocity profiles at different values of x.***

Equation 49 is identically satisfied. Substituting Equation 54 into Equation 55 and integrating, we get

$$\psi = \int \phi(\eta)\, dy^* + f_1(x^*)$$
$$= \frac{\sqrt{x^*}}{\sqrt{\mathrm{Re}_L}} \int \phi(\eta)\, d\eta + f_1(x^*)$$

Since $v^* = 0$ at $y^* = 0, f_1(x^*)$ is at best an arbitrary constant which is taken as zero. Also, defining a new function $f(\eta) \equiv \int \phi(\eta)\, d\eta$, we obtain

$$\psi = \sqrt{x^*}\frac{f(\eta)}{\sqrt{\mathrm{Re}_L}} \tag{56}$$

therefore,

$$u^* = \left(\frac{\partial \psi}{\partial y^*}\right)_{x^*} = \left(\frac{\partial \psi}{\partial \eta}\right)_{x^*}\left(\frac{\partial \eta}{\partial y^*}\right)_{x^*} = f'(\eta) = \frac{df}{d\eta} \tag{57}$$

and

$$-v^* = \left(\frac{\partial \psi}{\partial x^*}\right)_{y^*} = \left(\frac{\partial \psi}{\partial x^*}\right)_{\eta} + \left(\frac{\partial \psi}{\partial \eta}\right)_{x^*}\left(\frac{\partial \eta}{\partial x^*}\right)_{y^*}$$
$$= \frac{1}{2}(f - \eta f')\sqrt{x^* \mathrm{Re}_L} \tag{58}$$

On substituting u^*, v^* into Equation 50 and simplifying we obtain

$$2f''' + ff'' = 0 \tag{59}$$

where primes represent differentiation with respect to η. Equation 59 is a third-order nonlinear ordinary differential equation. Recall that η was a combination of two independent variables, x^* and y^*, and it was assumed that $u^* = \phi(\eta)$. If this similarity assumption was incorrect, then the partial differential Equation 50 would not have reduced to an ordinary differential Equation 59—that is, x^* would not have completely disappeared from the governing equation. Note also that even though Equation 59 is nonlinear and has to be solved numerically, there are no parameters and therefore it needs to be solved only once. Boundary conditions corresponding to Equation 59 become

$$f = f' = 0 \quad \text{at} \quad \eta = 0, \quad \text{and} \quad f' = 1 \quad \text{as} \quad \eta \to \infty \tag{60}$$

A numerical solution of Equation 59 along with the boundary conditions, Equation 60 is shown in Figure 1-3.14. Note that for Pr = 1, the solution for T^* is the same as that for u^*. Also, once $T^*(x^*, y^*)$ and $u^*(x^*, y^*)$ are known the heat transfer coefficient and friction factor can easily be obtained from Equations 5 and 11. Furthermore, from the definition of thermal and velocity boundary layer thickness ($T^* = u^* = 0.99$), we find that $\eta = 5$.

Therefore,

$$\eta = \frac{y}{x}\sqrt{\frac{u_\infty x}{\nu}} = 5 \quad \text{for} \quad y = \delta = \delta_t$$

or for Pr = 1,

$$\delta = \delta_t = \frac{5x}{\sqrt{\mathrm{Re}_x}} \tag{61}$$

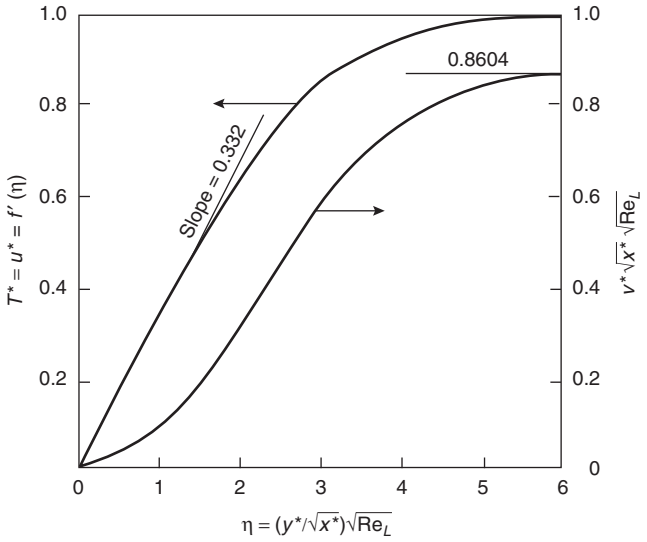

Figure 1-3.14. ***Nondimensional velocity profiles in laminar boundary layer over a flat plate.***

From Equation 61 it is clear that δ and δ_t increase with x but decrease with increasing u_∞ (the larger the free stream velocity, the thinner the boundary layer). Now, to determine the heat transfer coefficient and the friction factor we need $\partial T/\partial y\big|_{y=0}$ and $\partial u/\partial y\big|_{y=0}$. From Figure 1-3.14, we have

$$\left.\frac{\partial T^*}{\partial \eta}\right|_{\eta=0} = \left.\frac{\partial u^*}{\partial \eta}\right|_{\eta=0} = 0.332$$

Thus,

$$\tau_s = \mu \left.\frac{\partial u}{\partial y}\right|_{y=0} = 0.332 u_\infty \sqrt{\rho \mu u_\infty / x} \tag{62}$$

and

$$\dot{q}_s'' = -k \left.\frac{\partial T}{\partial y}\right|_{y=0} = 0.332(T_s - T_\infty)k\sqrt{\rho u_\infty / \mu x} \tag{63}$$

Hence the *local* friction and heat transfer coefficients are

$$C_f = \frac{0.664}{\sqrt{\mathrm{Re}_x}} \tag{64}$$

and

$$h = 0.332\frac{k}{x}\sqrt{\mathrm{Re}_x} \tag{65}$$

Equation 65 is often rewritten in terms of a nondimensional heat transfer coefficient called the Nusselt number, Nu, as

$$\mathrm{Nu} = \frac{hx}{k} = 0.332\sqrt{\mathrm{Re}_x} \tag{66}$$

All the above results are for the case when Pr = 1. When Pr $\neq$ 1, Equation 51 must also be solved with the help of the

solution just obtained for Equations 49 and 50. This solution does not change the expressions for δ and C_f given by Equations 61 and 64. However δ_t and Nu become[2]

$$\delta_t = \frac{5x}{\sqrt{\mathrm{Re}_x}}\,\mathrm{Pr}^{-1/3} = \delta \mathrm{Pr}^{-1/3} \tag{67}$$

and

$$\mathrm{Nu} = 0.332\sqrt{\mathrm{Re}_x}\mathrm{Pr}^{1/3} (\mathrm{Pr} \gtrsim 0.6) \tag{68}$$

Note that for $\mathrm{Pr} < 1$ (usually true for gases) $\delta_t > \delta$, that is, the thermal boundary layer is thicker than the momentum boundary layer. This is to be expected since $\mathrm{Pr} < 1$ implies that $\nu < \alpha$.

The results for the friction factor, C_f, and the Nusselt number, Nu, given by Equations 64 and 68 are for local values; that is, C_f and Nu change with x. This variation is shown in Figure 1-3.15. At $x = 0$, both C_f and h tend to infinity. This is physically incorrect and happens because near $x = 0$ the boundary layer approximation breaks down since δ is no longer much less than x.

For many applications, only average values of the heat transfer coefficient, $\overline{h}$, and friction factor, $\overline{C}_f$, are required. These are obtained by using Equations 9 and 15. In these equations $dA_s = dx \cdot$ (the unit width of the flat plate), and the average can be obtained from $x = 0$ to any length, L (which may be the total length of the plate). Simple integration leads to the following results:

$$\overline{C}_{fL} = 1.328\,\mathrm{Re}_L^{-1/2} = 2C_f\left(\begin{matrix}\text{evaluated}\\ \text{at } x = L\end{matrix}\right) \tag{69}$$

and

$$\overline{\mathrm{Nu}}_L \equiv \frac{\overline{h}_L L}{k} = 0.664\,\mathrm{Re}_L^{1/2}\mathrm{Pr}^{1/3} = 2\mathrm{Nu}\left(\begin{matrix}\text{evaluated}\\ \text{at } x = L\end{matrix}\right) \tag{70}$$

It is interesting to note that C_f and Nu are closely related. For example, from Equations 69 and 70 one can easily obtain

$$\overline{\mathrm{Nu}}_L = \frac{C_{fL}\,\mathrm{Re}_L\mathrm{Pr}^{1/3}}{2}$$

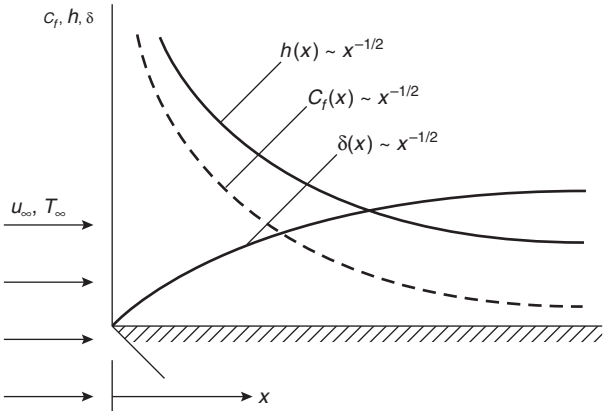

Figure 1-3.15. ***Variation of C_f, h, and δ with x for flow over a flat plate.***

or

$$\mathrm{St} \equiv \frac{\overline{\mathrm{Nu}}_L}{\mathrm{Re}_L\mathrm{Pr}} = \frac{\overline{C}_{fL}}{2}\,\mathrm{Pr}^{-2/3} \tag{71}$$

where St is known as the Stanton number.

This analogy between heat and momentum transfer is called the *Reynolds analogy* which is significant because the heat transfer coefficient can be determined from the knowledge of the friction factor. This analogy is especially useful for cases where mathematical solutions are not available.

Laminar free convection: In contrast with forced convection, where the fluid motion is externally imposed, for free convection the fluid motion is caused by the buoyancy forces. Buoyancy is due to the combined effect of *density gradients* within the fluid and a *body force* that is proportional to the fluid density. In practice the relevant body force is usually gravitational, although it may be centrifugal, magnetic, or electric. Of the several ways in which a density gradient may arise in a fluid, the two most common situations are due to (1) the presence of temperature gradients, and (2) the presence of concentration gradients in a multicomponent system such as a fire. Here, the focus will be on free convection problems in which the density gradient is due to temperature and the body force is gravitational. Note, however, that the presence of density gradients in a gravitational field does not ensure the existence of free convection currents. For example, the high temperature lighter fluid may be on top of a low temperature, denser fluid, resulting in a stable situation. It is only when the condition is unstable that convection currents are generated. An example of an unstable situation would be a denser fluid on top of a lighter fluid. In a stable situation there is no fluid motion and, therefore, heat transfer occurs purely by conduction. Here we will only consider the unstable situation that results in convection currents.

Free convection flow may be further classified according to whether or not the flow is bounded by a surface. In the absence of an adjoining surface, free boundary flows may occur in the form of a plume or a buoyant jet. A buoyant plume above a fire is a familiar example. However, here we will focus on free convection flows that are bounded by a surface. A classical example of boundary layer development on a heated vertical flat plate is discussed below.

Heated, vertical flat plate: Consider the flat plate shown in Figure 1-3.16. The plate is immersed in an extensive, quiescent fluid, with $T_s > T_\infty$. The density of the fluid close to the plate is less than that of the fluid that is farther from the plate. Buoyancy forces therefore induce a free convection boundary layer in which the heated fluid rises vertically, entraining fluid from the quiescent region.

Under steady-state laminar flow conditions, Equations 35, 43, and 45 describe the mass, momentum, and energy balances for the two-dimensional boundary layer shown in Figure 1-3.16. Assume that the temperature differences are moderate, such that the fluid may be treated as having constant properties. Also, with the exception of the buoyancy force term (g_x in Equation 43), the fluid can

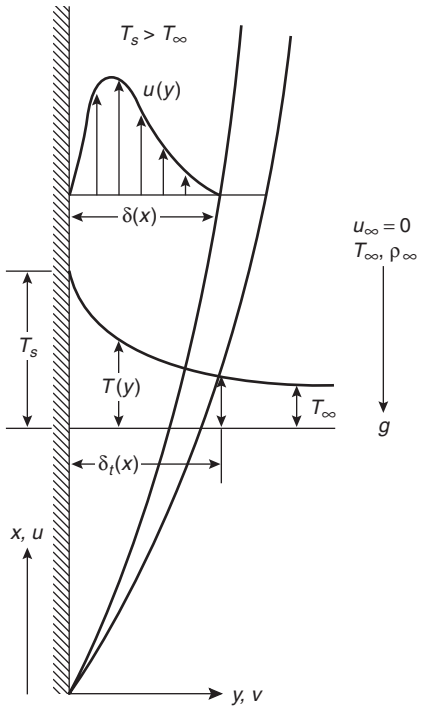

Figure 1-3.16. ***Boundary layer development on a heated vertical plate.***

be assumed to be incompressible. Outside the boundary layer, Equation 36 is valid, and since $u = v = 0$ outside the boundary layer we obtain: $\partial p/\partial x = -\rho_\infty g_x$. Since $\partial p/\partial y = 0$ because of the boundary layer approximation [i.e., $p \neq p(y)$ inside the boundary layer; Equation 44], $\partial p/\partial x$ inside the boundary layer must be equal to its corresponding value outside, that is, $\partial p/\partial x = -\rho_\infty g_x$.

Substituting this into Equation 43

$$u\frac{\partial u}{\partial x} + v\frac{\partial u}{\partial y} = g_x\frac{(\rho_\infty - \rho)}{\rho} + \nu\frac{\partial^2 u}{\partial y^2} \tag{72}$$

The first term on the right side of Equation 72 is the buoyancy force, and the flow originates because the density ρ is variable. By introducing the coefficient of volumetric thermal expansion, β,

$$\beta = -\frac{1}{\rho}\left(\frac{\partial \rho}{\partial T}\right)_\rho \approx -\frac{1}{\rho}\frac{(\rho_\infty - \rho)}{(T_\infty - T)} \tag{73}$$

it follows that

$$\frac{(\rho_\infty - \rho)}{\rho} = \beta(T - T_\infty) \tag{74}$$

Substituting Equation 74 into Equation 72 a useful form of the x-momentum is obtained as

$$u\frac{\partial u}{\partial x} + v\frac{\partial u}{\partial y} = g_x\beta(T - T_\infty) + \nu\frac{\partial^2 u}{\partial y^2} \tag{75}$$

From Equation 75 it is now apparent how buoyancy force is related to temperature difference. Note that the appearance of the buoyancy term in the momentum equation mathematically complicates the situation. The decoupling between the hydrodynamic and the thermal problems achieved in forced convection is no longer possible, since T appears in both Equations 45 and 75. The boundary conditions associated with the governing equations, Equations 35, 45, and 75, are

$$u = v = 0 \quad T = T_\infty \quad \text{as} \quad y \to \infty \tag{76}$$

Nondimensionalizing Equations 35, 45, 75, and 76 with $x^* = x/L$, $y^* \equiv y/L$, $u = u/u_0$, $v^* \equiv v/u_0$ and $T^* \equiv (T - T_\infty)/(T_s - T_\infty)$, we obtain

$$\frac{\partial u^*}{\partial x^*} + \frac{\partial v^*}{\partial y^*} = 0 \tag{77}$$

$$u^*\frac{\partial u^*}{\partial x^*} + v^*\frac{\partial u^*}{\partial y^*} = \frac{g\beta T^*(T_s - T_\infty)L}{u_0^2} + \frac{1}{\mathrm{Re}_L}\frac{\partial^2 u^*}{\partial y^{*2}} \tag{78}$$

and

$$u^*\frac{\partial T^*}{\partial x^*} + v^*\frac{\partial T^*}{\partial y^*} = \frac{1}{\mathrm{Re}_L\mathrm{Pr}}\frac{\partial^2 T^*}{\partial y^{*2}} \tag{79}$$

Note that u_0 in Equation 78 is an unknown reference velocity and not the free stream velocity as in the case of forced convection. Also, the dimensionless parameter

$$\frac{g\beta(T_s - T_\infty)L}{u_0^2}$$

is a direct result of buoyancy forces. To eliminate the unknown reference velocity, u_0 from the dimensionless parameter, we define

$$\text{Grashof Number, } \mathrm{Gr}_L \equiv \frac{g\beta(T_s - T_\infty)L}{u_0^2}\left(\frac{Lu_0}{\nu}\right)^2 = \frac{g\beta(T_s - T_\infty)L^3}{\nu^2}$$

Thus, the first term on the right side of Equation 78 becomes $\mathrm{Gr}_L/(\mathrm{Re}_L)^2$. The Grashof number plays the same role in free convection as the Reynolds number does in forced convection. Gr is the ratio of buoyancy and viscous forces. The governing equations now contain three parameters—the Grashof number, Reynolds number, and Prandtl number. For the forced convection case it is seen (Equation 68) that Nu = Nu (Re, Pr); thus for the free convection case, we expect Nu = Nu (Re, Gr, Pr). If the buoyancy term in Equation 79 is $\mathrm{Gr}/(\mathrm{Re})^2 \gg 1$, then we primarily have free convection; that is, Nu = Nu(Gr, Pr). For $\mathrm{Gr}/(\mathrm{Re})^2 \ll 1$, the forced convective case exists, where as has already been seen, Nu = Nu (Re, Pr). However, when $\mathrm{Gr}/(\mathrm{Re})^2 \sim 1$ a mixed (free and forced) convection case is obtained. For the present problem we will assume that $\mathrm{Gr} \gg (\mathrm{Re})^2$, thus, Nu must be a function of only Gr and Pr.

Since $\mathrm{Gr} \gg \mathrm{Re}^2$, it follows that buoyancy forces are much larger than inertia forces; in other words, the primary balance is between the buoyancy and viscous forces. Since the left side of Equation 78 represents the inertia forces, the primary balance is between the two terms on the right side, that is,

$$-\frac{g\beta T^*(T_s - T_\infty)L}{u_0^2} \approx \left(\frac{\nu}{u_0 L}\right)\frac{\partial^2 u^*}{\partial y^{*2}}$$

Crudely approximating the various terms, we have in dimensional variables

$$g\beta(T_\infty - T) \approx \nu \frac{u}{\delta^2} \tag{a}$$

Similarly approximating Equations 77 and 79 and expressing the result in dimensional form (it is more convenient to use Equations 35 and 45), we get from Equation 35 or 77

$$\frac{u}{x} \approx \frac{v}{\delta} \quad \text{or} \quad v \approx \frac{\delta u}{x} \tag{b}$$

and from Equation 79 or 45 along with relation (b)

$$u\frac{(T_\infty - T)}{x} \approx \alpha \frac{(T_\infty - T)}{\delta^2} \quad \text{or} \quad u \approx \frac{\alpha x}{\delta^2} \tag{c}$$

Combining (a) and (c) we obtain an expression for the boundary layer thickness, δ,

$$\delta \approx \left(\frac{\nu\alpha x}{g\beta(T_\infty - T)}\right)^{1/4}$$

Thus, we expect δ to scale with $x^{1/4}$ and u to scale with $x^{1/2}$. (Note that in the forced convective case we found that $\delta \sim x^{1/2}$; Figure 1-3.15.) Following a reasoning similar to the forced convective case, a similarity variable $\xi \approx y/\delta(x)$ or $\xi = Ay/x^{1/4}$ may be found, where A is an arbitrary constant. Also, motivated by Equation 57 for forced convection, it is hoped that $u = Bx^{1/2}f'(\xi)$, where B is an arbitrary constant. Expressing these in nondimensional variables, we get

$$\xi = Ay^*/x^{*1/4} \tag{80}$$

and

$$u^* = Bx^{*1/2}f'(\xi)$$

where $f'(\xi) = df/d\xi$. Note that the definitions of the arbitrary constants A and B have been changed during nondimensionalization. By introducing a stream function, ψ, as in Equation 55, Equation 77 is identically satisfied.

Thus,

$$\begin{aligned}\psi &= \int Bx^{*1/2}f'(\xi)\,dy^* + f_1(x^*) \\ &= \int \frac{B}{A}x^{*3/4}f'(\xi)\,d\xi + f_1(x^*) \\ &= \frac{B}{A}x^{*3/4}f(\xi) + f_1(x^*)\end{aligned} \tag{81}$$

Since $v^* = 0$ at $y^* = 0$ (or $\xi = 0$), $f_1(x^*)$ is at best an arbitrary constant which is taken to be zero without any loss of generality. From Equations 55 and 81 we get

$$v^* = -\frac{B}{4Ax^{*1/4}}[3f(\xi) - \xi f'(\xi)] \tag{82}$$

By using Equations 80 and 82, Equations 78 and 79 can be reduced to

$$f''' + 3ff'' - 2(f')^2 + T^* = 0 \tag{83}$$

and

$$T^{*\prime\prime} + 3\mathrm{Pr}fT^{*\prime} = 0 \tag{84}$$

where the following definitions of the arbitrary constants A and B have been used:

$$\begin{aligned}B &= \left[\frac{4g\beta(T_s - T_\infty)L}{u_\infty^2}\right]^{1/2} \\ A &= \left[\frac{g\beta(T_s - T_\infty)L^3}{4\nu^2}\right]^{1/4}\end{aligned} \tag{85}$$

Note that in Equation 84 it has been assumed that T^* is a function of ξ only. From Equation 85 it follows that

$$\xi = \frac{y^*}{x^{*1/4}}\left[\frac{g\beta(T_s - T_\infty)L^3}{4\nu^2}\right]^{1/4} = \frac{y^*}{x^{*1/4}}\left(\frac{\mathrm{Gr}_L}{4}\right)^{1/4} \tag{86}$$

The associated boundary conditions given by Equation 76 become

$$\begin{aligned} &f = f' = 0 \quad \text{and} \quad T^* = 1 \quad \text{when} \quad \xi = 0 \\ &\text{and} \quad f' = 0 \qquad\quad T^* = 0 \quad \text{at} \quad\ \xi = \infty\end{aligned} \tag{87}$$

A numerical solution of Equations 83 and 84 along with the boundary conditions given by Equation 87 is shown in Figure 1-3.17. Note that the nondimensional x-velocity component, u^*, may be readily obtained from Figure 1-3.17 part (a) through the use of Equations 80 and 85. Note also that, through the definition of the similarity variable, ξ, Figure 1-3.17 may be used to obtain values of u^* and T^* for any value of x^* and y^*. Once $u^*(x^*, y^*)$ and $T^*(x^*, y^*)$ are known, the heat transfer coefficient can easily be obtained from Equation 5. Thus, the temperature gradient at $y = 0$ after using Equation 86, becomes

$$\left.\frac{\partial T}{\partial y}\right|_{y=0} = \frac{(T_s - T_\infty)}{L}\left.\frac{\partial T^*}{\partial y^*}\right|_{y^*=0} = \frac{(T_s - T_\infty)}{Lx^{*1/4}}\left(\frac{\mathrm{Gr}_L}{4}\right)^{1/4}\left.\frac{dT^*}{d\xi}\right|_{\xi=0}$$

The *local* heat transfer coefficient is

$$h = \frac{-k}{Lx^{*1/4}}\left(\frac{\mathrm{Gr}_L}{4}\right)^{1/4}\left.\frac{dT^*}{d\xi}\right|_{\xi=0} \tag{88}$$

or

$$\mathrm{Nu} = \frac{hx}{k} = -x^{*3/4}\left(\frac{\mathrm{Gr}_L}{4}\right)^{1/4}\left.\frac{dT^*}{d\xi}\right|_{\xi=0} = \left(\frac{\mathrm{Gr}_x}{4}\right)^{1/4} g(\mathrm{Pr}) \tag{89}$$

As is evident from Figure 1-3.17, the dimensionless temperature gradient at $\xi = 0$ is a function of the Prandtl number. In Equation 89 this function is expressed as $-g(\mathrm{Pr})$. Values of $g(\mathrm{Pr})$ obtained from the numerical solution are listed in Table 1-3.1.

From Equation 88 for the local heat transfer coefficient the average heat transfer coefficient for a surface of length L is obtained by using Equation 9 as follows

$$\begin{aligned}\overline{h}_L &= \frac{1}{L}\int_0^L h(dx \cdot 1) = \frac{k}{L^{7/4}}\left(\frac{\mathrm{Gr}_L}{4}\right)^{1/4} g(\mathrm{Pr}) \times \int_0^L \frac{dx}{x^{1/4}} \\ &= \frac{4}{3}\frac{k}{L}\left(\frac{\mathrm{Gr}_L}{4}\right)^{1/4} g(\mathrm{Pr})\end{aligned} \tag{90}$$

Thus,

$$\overline{\mathrm{Nu}}_L = \frac{\overline{h}_L L}{k} = \frac{4}{3}\left(\frac{\mathrm{Gr}_L}{4}\right)^{1/4} g(\mathrm{Pr}) \tag{91}$$

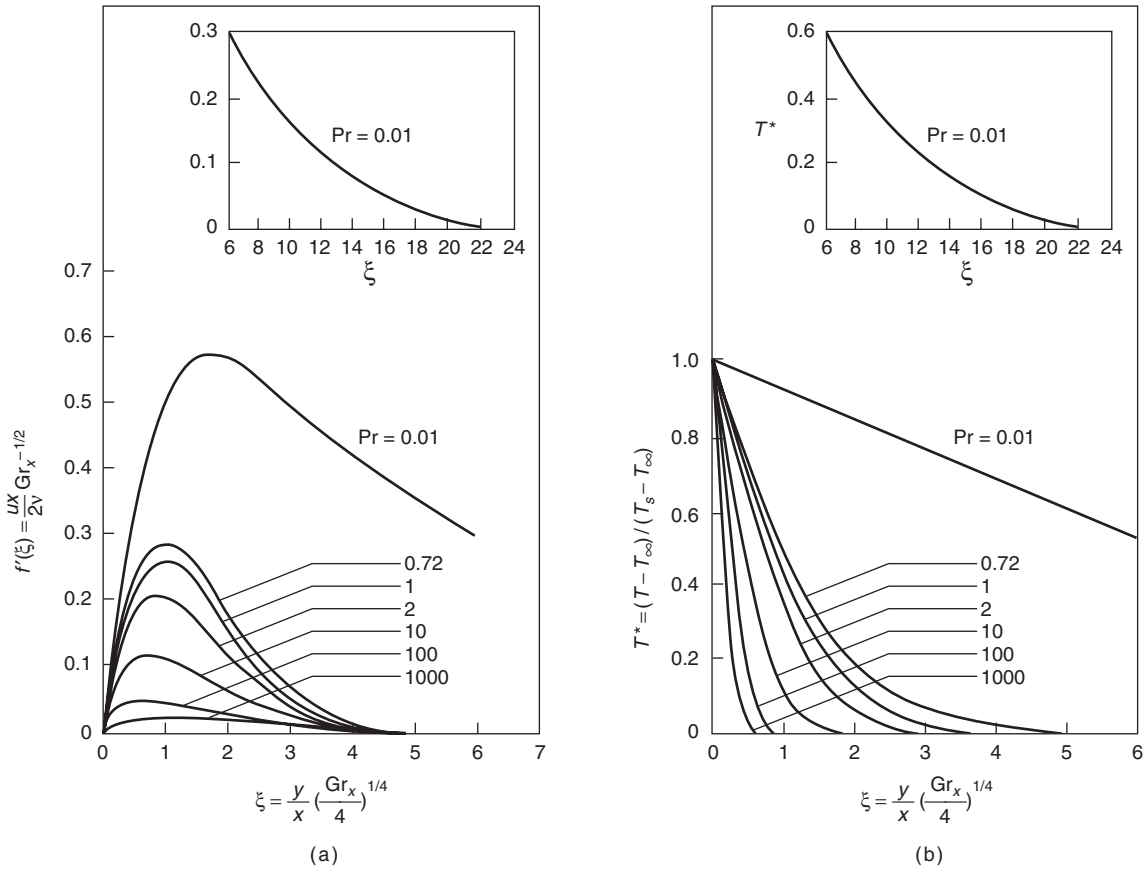

Figure 1-3.17. ***Laminar free convection boundary layer on an isothermal, vertical surface.***

or from Equation 89, with $x = L$ we get

$$\overline{\mathrm{Nu}}_L = \frac{4}{3}\mathrm{Nu}\left(\begin{matrix}\text{evaluated}\\ \text{at } x = L\end{matrix}\right) \tag{92}$$

It should be noted that the foregoing results apply irrespective of whether $T_s > T_\infty$ or $T_s < T_\infty$. If $T_s < T_\infty$, the conditions are inverted from those shown in Figure 1-3.16. The loading edge is on the top of the plate, and positive x is defined in the direction of the gravity force.

Complications in Practical Problems

In the previous section two relatively simple problems of laminar forced and free convection on a flat surface were solved. These solutions illustrate the methodology for determining the heat transfer coefficient and provide the necessary insight regarding the relationship between the various dimensionless parameters. Most practical situations are often more complex, and mathematical solutions, such as those presented in the previous section, are not always possible. Complexities arise due to more complex geometry, onset of turbulence, changes in fluid properties with temperature, and because of simultaneous mass transfer from the surface as illustrated in Figure 1-3.17. For such cases, empirical correlations are obtained. These correlations are discussed in the next section and the various complications are individually discussed below.

Table 1-3.1 ***Dimensionless Temperature Gradient for Free Convection on a Vertical Flat Plate***

Pr	0.01	0.72	1	2	10	100	1000
g(Pr)	0.081	0.505	0.567	0.716	1.169	2.191	3.966

Effect of turbulence: In both forced and free convective flows, small disturbances may be amplified downstream, leading to transition from laminar to turbulent flow conditions. These disturbances may originate from the free stream or be induced by surface roughness. Whether these disturbances are amplified or attenuated depends upon the ratio of inertia to viscous forces for forced flows (the Reynolds number), and the ratio of buoyancy to viscous forces for free convective flows (the Grashof number). Note that in both Reynolds and Grashof numbers, viscosity appears in the denominator. Thus for relatively large viscous forces or small Reynolds and Grashof numbers, the naturally occurring disturbances are dissipated, and the flow remains laminar. However, for sufficiently large Reynolds and Grashof numbers ($\mathrm{Re} > 5 \times 10^5$ and $\mathrm{Gr} > 4 \times 10^8$, for flow over a flat plate) disturbances are amplified, and a transition to turbulence occurs.

The onset of turbulence is associated with the existence of *random fluctuations* in the fluid, and on a small scale the flow is *unsteady*. As shown in Figure 1-3.18, there are sharp differences between laminar and turbulent flows. In the laminar boundary layer, fluid motion is highly ordered and it is possible to identify streamlines

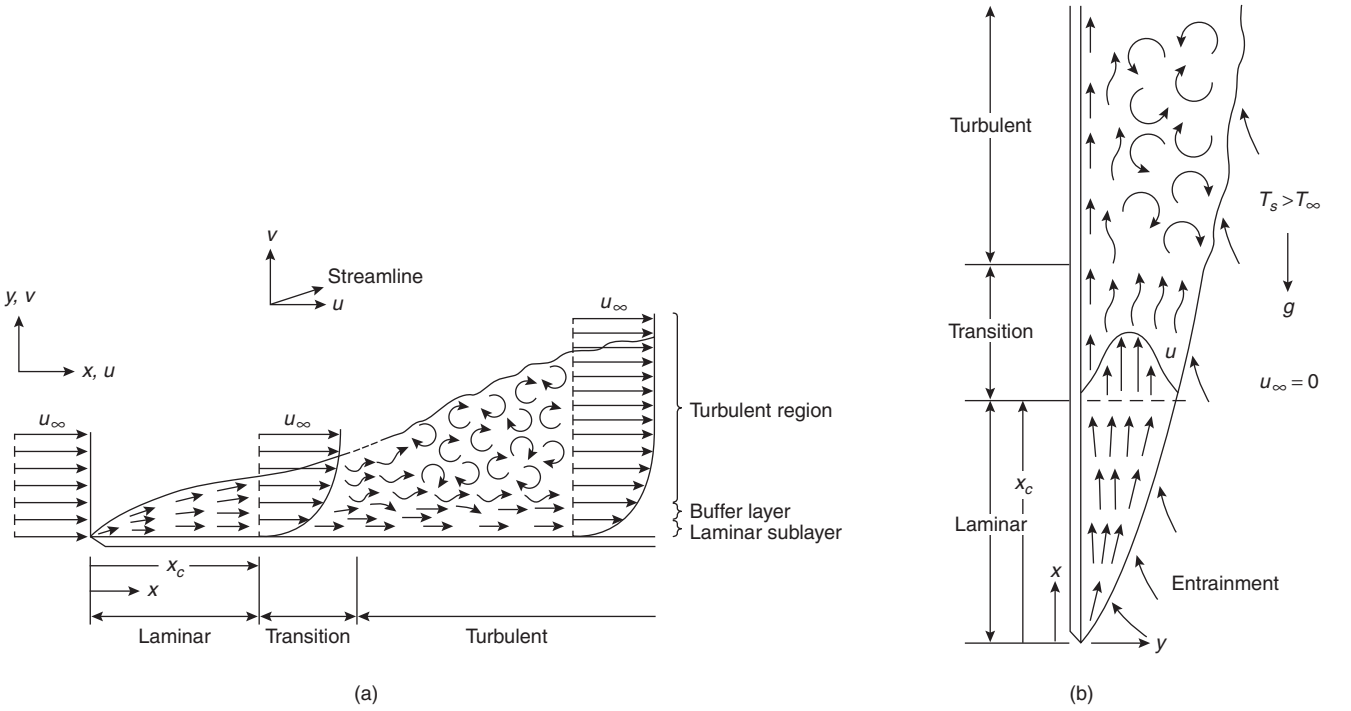

Figure 1-3.18. ***(a) Velocity boundary layer development on a flat plate for forced flow; (b) velocity boundary layer development on a vertical flat plate for free convective flow.***

along which fluid particles move. In contrast, fluid motion in the turbulent boundary layer is highly irregular and is characterized by velocity fluctuations. These fluctuations enhance the momentum and energy transfers and hence increase the surface friction and convection heat transfer rate. Also, due to the mixing of fluid resulting from the turbulent fluctuations, the turbulent boundary layer is thicker and the boundary layer profiles (of velocity, temperature, and concentration) are flatter than in laminar flow.

In a fully turbulent flow, the primary mechanism of momentum and heat transfer involves macroscopic lumps of fluid randomly moving about in the flow. Turbulent flow contrasts with the random molecular motion resulting in molecular properties discussed at the beginning of this chapter. In the turbulent region *eddy viscosity* and *eddy thermal conductivity* are important. These eddy properties may be ten times as large as their molecular counterparts.

If one measures the variation of an arbitrary flow variable, *P,* as a function of time at some location in a turbulent boundary layer, then the typical behavior observed is shown in Figure 1-3.19. The variable *P,* which may be a velocity component, fluid temperature, pressure, or species concentration, can be represented as the sum of a time-mean value, $\overline{P}$, and a fluctuating component, P'. The average is taken over a time interval that is large compared with the period of a typical fluctuation, and if $\overline{P}$ is time independent then the mean flow is steady. Thus, the instantaneous values of each of the velocity components, pressure, and temperature are given by

$$u = \overline{u} + u', \quad v = \overline{v} + v', \quad p = \overline{p} + p'$$
$$T = \overline{T} + T' \quad \text{and} \quad \rho = \overline{\rho} + \rho' \tag{93}$$

Substituting these expressions for each of the flow variables into the boundary layer equations (Equations 35, 43, and 45) and assuming the mean flow to be steady, incompressible (ρ = constant) with constant properties, and using the well established time averaging procedures,[1–4] the following governing equations are obtained:

Continuity

$$\frac{\partial \overline{u}}{\partial x} + \frac{\partial \overline{v}}{\partial y} = 0 \tag{94}$$

x-momentum

$$\rho\left(\overline{u}\,\frac{\partial \overline{u}}{\partial z} + \overline{v}\,\frac{\partial \overline{u}}{\partial y}\right) = \frac{\partial}{\partial y}\left(\mu\,\frac{\partial \overline{u}}{\partial y} - \rho\overline{u}'\overline{v}'\right) - \frac{\partial \overline{p}}{\partial x} - \rho g_x \tag{95}$$

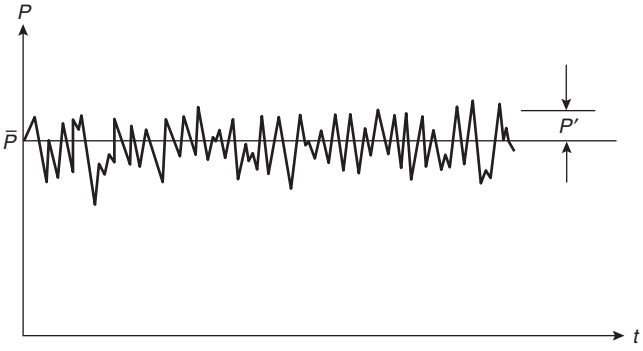

Figure 1-3.19. ***Variation in the variable P with time at some point in a turbulent boundary layer.***

Energy

$$\rho C_p\left(\overline{u}\frac{\partial \overline{T}}{\partial x}+\overline{v}\frac{\partial \overline{T}}{\partial y}\right)=\frac{\partial \overline{T}}{\partial y}\left(k\frac{\partial \overline{T}}{\partial y}-\rho C_p\overline{v}'\overline{T}'\right) \quad (96)$$

Equations 94 through 96 are similar to the laminar boundary layer equations expressed in mean flow variables, except for the presence of additional terms $\rho\overline{u}'\overline{v}'$ and $\rho C_p\overline{v}'\overline{T}'$. Physical arguments[2] show that these terms result from the motion of macroscopic fluid lumps and account for the effect of the turbulent fluctuations on momentum and energy transport.

On the basis of the foregoing result it is customary to speak of total shear stress and total heat flux, which are defined as

$$\tau_{\text{tot}} \equiv \left(\mu\frac{\partial \overline{u}}{\partial y}-\rho\overline{u}'\overline{v}'\right)$$

and

$$\dot{q}_{\text{tot}} \equiv -\left(k\frac{\partial \overline{T}}{\partial y}-\rho C_p\overline{v}'\overline{T}'\right) \quad (97)$$

The terms $\rho\overline{u}'\overline{v}'$ and $\rho C_p\overline{v}'\overline{T}'$ are always negative and so result in a positive contribution to total shear stress and heat flux. The term $\rho\overline{u}'\overline{v}'$ represents the transport of momentum flux due to turbulent fluctuations (or eddies), and it is known as the Reynolds stress. The notion of transport of heat and momentum by turbulent eddies has prompted the introduction of transport coefficients, which are defined as the eddy diffusivity for momentum transfer, ε_M, and eddy diffusivity for heat transfer, ε_H, and have the form

$$\begin{aligned}\varepsilon_M\frac{\partial \overline{u}}{\partial y} &\equiv -\overline{u}'\overline{v}'\\ \varepsilon_H\frac{\partial \overline{T}}{\partial y} &\equiv -\overline{v}'\overline{T}'\end{aligned} \quad (98)$$

Thus Equation 97 becomes

$$\tau_{\text{tot}} \equiv \rho(\upsilon+\varepsilon_M)\frac{\partial \overline{u}}{\partial y}$$

and

$$\dot{q}''_{\text{tot}} \equiv -\rho C_p(\alpha+\varepsilon_H)\frac{\partial \overline{T}}{\partial y} \quad (99)$$

As noted earlier, eddy diffusivities are much larger than molecular diffusivities, therefore the heat and momentum transfer rates are much larger for turbulent flow than for laminar flow. A fundamental problem in performing turbulent boundary layer analysis involves determining the eddy diffusivities as a function of the mean properties of the flow. Unlike the molecular diffusivities, which are strictly fluid properties, the eddy diffusivities depend strongly on the nature of the flow. They vary across the boundary layer and the variation can only be determined from experimental data. This is an important point, because all analyses of turbulent flow must eventually rely on experimental data. To date, there is no adequate theory for predicting turbulent flow behavior.

Complex geometry: In a previous section on the boundary layer concept, analysis was limited to the simplest possible geometry, that is, a flat plate. This provided considerable simplification because $dp/dx = 0$ in Equation 43 for the forced flow case. However, the situation is not as simple for fluid flow over bodies with a finite radius of curvature.

Consider a common example of flow across a circular cylinder shown in Figure 1-3.20. Boundary layer formation is initiated at the forward stagnation point, where the fluid is brought to rest with an accompanying rise in pressure. The pressure is a maximum at this point and decreases with increasing x, the streamline coordinate, and θ, the angular coordinate. (Note: In the boundary layer approximation, the pressure is the same inside and outside the boundary layer. This can be seen from Equation 44.) The boundary layer then develops under the influence of a favorable pressure gradient ($dp/dx < 0$). At the top of the cylinder (i.e., at $\theta = 90°$) the pressure eventually reaches a minimum and then begins to increase toward the rear of the cylinder. Thus, for $90° < \theta < 180°$, the boundary layer development occurs in the presence of an adverse pressure gradient ($dp/dx > 0$).

Unlike parallel flow over a flat plate, for curved surfaces the free stream velocity, u_∞, varies with x. [Note that in Figure 1-3.20 a distinction has been made between the fluid velocity upstream of the cylinder, V, and the velocity outside the boundary layer, $u_\infty(x)$.] At the stagnation point, $\theta = 0°$, $u_\infty = 0$. As the pressure decreases for $\theta > 0°$, u_∞ increases according to the Bernoulli equation, Equation 46, and becomes maximum at $\theta = 90°$. For $\theta > 90°$, the adverse pressure gradient decelerates the fluid, and conversion of kinetic energy to pressure occurs in accordance with Equation 46, which applies only to the inviscid flow outside the boundary layer. The fluid inside the boundary layer has considerably slowed down because of viscous friction and does not have enough momentum to overcome the adverse pressure gradient, eventually leading to boundary layer separation, which is illustrated more clearly in Figure 1-3.21. At some location in the fluid, the velocity gradient at the surface becomes zero and the boundary layer detaches or separates from the surface. Farther downstream of the separation point, flow reversal occurs and a wake is formed behind the solid. Flow in this region is characterized by vortex formation and is highly irregular. The separation point is defined as the location at which $(\partial u/\partial y)_{y=0} = 0$. If the boundary layer transition

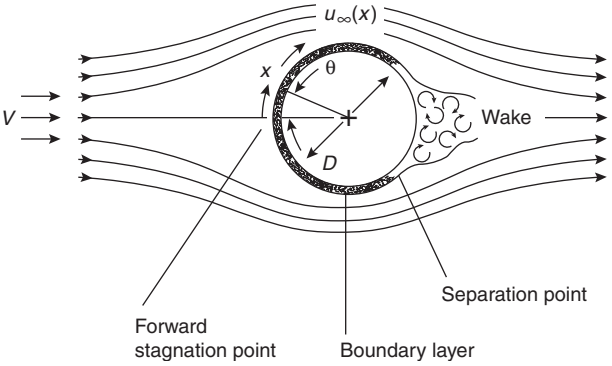

Figure 1-3.20. ***Boundary layer formation and separation on a circular cylinder in cross flow.***

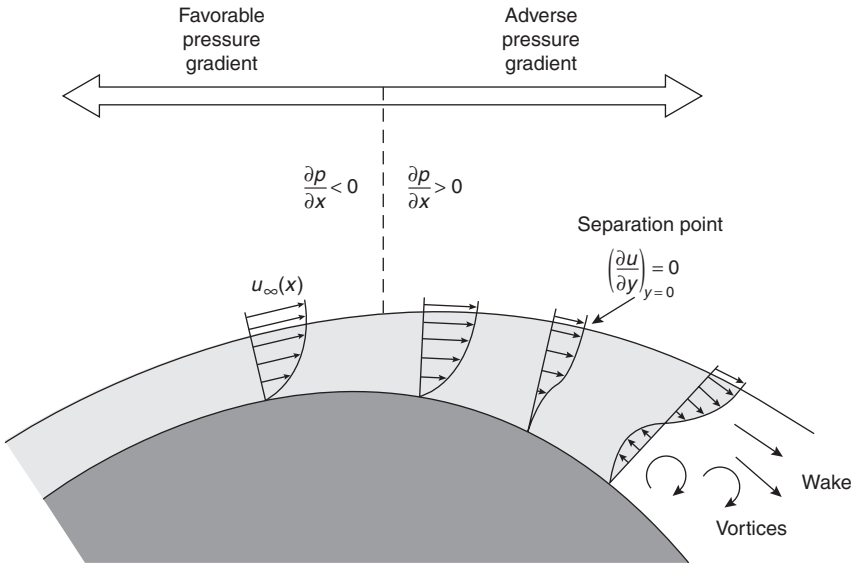

Figure 1-3.21. ***Velocity profiles associated with separation on a circular cylinder in cross flow.***

to turbulence occurs prior to separation, the separation is delayed and the separation point moves farther downstream. This happens because the turbulent boundary layer has more momentum than the laminar boundary layer to overcome the adverse pressure gradient.

The foregoing processes strongly influence both the rate of heat transfer from the cylinder surface and the drag force acting on the cylinder. Because of the complexities associated with flow over a cylinder, experimental methods are used to determine the heat transfer coefficient. Such experimental results for the variation of the local Nusselt number with θ are shown in Figure 1-3.22 for a cylinder in a cross flow of air. Consider the results for $Re_D \leq 10^5$ (note: Re_D is defined as VD/ν). Starting at the stagnation point, Nu_θ decreases with increasing θ due to the development of the laminar boundary layer. However, a minimum is reached at $\theta \approx 80°$. At this point separation occurs, and Nu_θ increases with θ due to the mixing associated with vortex formation in the wake. For $Re_D \geq 10^5$, the variation of Nu_θ with θ is characterized by two minima. The decline in Nu_θ from the value at the stagnation point is again due to laminar boundary layer development, but the sharp increase that occurs between 80° and 100° is now due to boundary layer transition to turbulence. With further development of the turbulent boundary layer, Nu_θ must again begin to decline. However, separation eventually occurs ($\theta \approx 140°$), and Nu_θ increases due to considerable mixing associated with the wake region.

The foregoing example clearly illustrates the complications introduced by nonplanar geometry. Heat transfer correlations for these cases are often based on experimental data. Fortunately, for most engineering calculations the local variation in the heat transfer coefficient such as that presented in Figure 1-3.22 is not required; only the overall average conditions are needed. Empirical correlations for

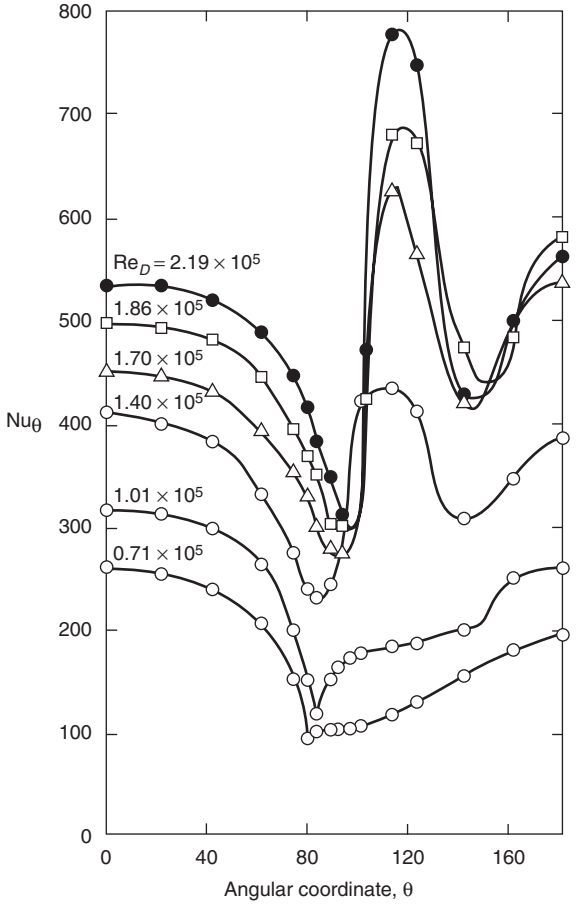

Figure 1-3.22. ***Local Nusselt number for airflow normal to a circular cylinder.***

average heat transfer coefficients will be presented in the next section.

Changes in fluid properties: In the analysis and discussion presented thus far, fluid properties were assumed to be constant. However, fluid properties vary with temperature across the boundary layer and this variation will have a significant impact on the heat transfer rate. In the empirical heat transfer correlations this influence is accounted for in one of two ways: (1) in correlating the experimental data all properties are evaluated at the mean boundary layer temperature, $T_f = (T_s + T_\infty)/2$, called the film temperature, and (2) alternatively, all properties are evaluated at T_∞ and an additional parameter is used to account for the property variation. This parameter is commonly of the form $(\mathrm{Pr}_\infty/\mathrm{Pr}_s)^r$ or $(\mu_\infty/\mu_s)^r$, where the subscripts ∞ and s designate evaluation of properties at the free stream and surface temperatures, respectively, and r is an empirically determined constant.

It is important to note that in the empirical correlations to be presented in the next section, the same method that is employed in deriving the correlation should be used when applying the correlation.

Effect of mass transfer: Special attention needs to be given to the effect that species mass transfer from the surface of the solid has on the velocity and thermal boundary layers. Recall that the velocity boundary layer development is generally characterized by the existence of zero fluid velocity at the surface. This condition applies to the velocity component v normal to the surface, as well as to the velocity component u parallel to the surface. However, if there is simultaneous mass transfer to or from the surface, it is evident that v can no longer be zero at the surface. Nevertheless, for the problems discussed in this chapter, mass transfer is assumed to have a negligible effect, that is, $v \approx 0$. This assumption is reasonable for problems involving some evaporation from gas-liquid or sublimation from gas-solid interfaces. For larger surface mass transfer rates a correction factor (often called the blowing correction) is utilized. This correction factor is simply stated here, and discussed in greater detail by Bird et al.[1] The correction factor is defined as $E(\phi) \equiv h^*/h$, where h^* is the corrected heat transfer coefficient and h is the heat transfer coefficient in the absence of mass transfer. According to film theory, $E(\phi)$ is given by

$$E(\phi) = \frac{\phi}{(e^{\phi} - 1)} \tag{100}$$

where

$$\phi = \frac{\dot{m}'' C_{pg}}{h}$$

$\dot{m}'' = \rho_s v_s$ is the mass flux coming out of the surface and C_{pg} is the specific heat of the gas.

Empirical Relations of Convection Heat Transfer

The analysis and discussion presented in the section on the boundary layer concept have shown that for simple cases the convection heat transfer coefficient may be determined directly from the conservation equations. In the previous section it was noted that the complications inherent to most practical problems do not always permit analytical solutions, and that it is necessary to resort to experimental methods. Experimental results are usually expressed in the form of either empirical formulas or graphical charts so that they may be utilized with maximum generality. Difficulties are encountered in the process of trying to generalize the experimental results in the form of empirical correlations. The availability of an analytical solution for a simpler but similar problem greatly assists in guessing the functional form of the results. Experimental data is then used to obtain values of constants or exponents for certain significant parameters, such as the Reynolds or Prandtl numbers. If an analytical solution for a similar problem is not available, it is necessary to rely on the physical understanding of the problem and on dimensional or order-of-magnitude analysis. In this section the experimental methods, the dimensionless groups, and the functional form of the relationships expected between them will be discussed; in addition the empirical formulas that will be used in the "Applications" section of this chapter will be summarized.

Functional form of solutions: The nondimensional Equations 49, 50, 51, and 78 are extremely useful from the standpoint of suggesting how important boundary layer results can be generalized. For example, the momentum equation, Equation 50, suggests that although conditions in the velocity boundary layer depend on the fluid properties, ρ and μ, the velocity, u_∞, and the length scale, L, this dependence may be simplified by grouping these variables in a nondimensional form called the Reynolds number. We therefore anticipate that the solution of Equation 50 will be of the form

$$u^* = f_1\left(x^*, y^*, \mathrm{Re}_L, \frac{dp^*}{dx^*}\right) \tag{101}$$

Note that the pressure distribution, $p^*(x^*)$, depends on the surface geometry and may be obtained independently by considering flow conditions outside the boundary layer in the free stream. Hence, as discussed in the section on complex geometry, the appearance of dp^*/dx^* in Equation 101 represents the influence of geometry on the velocity distribution. Note also that in Equation 50 the term dp^*/dx^* did not appear because it was equal to zero for a flat plate.

Similarly we anticipate that the solution of Equation 78 will be of the form

$$u^* = f_2(x^*, y^*, \mathrm{Gr}_L, \mathrm{Pr}) \tag{102}$$

Here, the Prandtl number is included because of the coupling between Equations 78 and 79. If the flow is mixed, that is, buoyant as well as forced, then the Reynolds number must also be included in the functional relationship expressed by Equation 102.

From Equation 1, the shear stress at the surface, $y^* = 0$, may be expressed as

$$\tau_s = \mu \left.\frac{\partial u}{\partial y}\right|_{y=0} = \left(\frac{\mu u_\infty}{L}\right) \left.\frac{\partial u^*}{\partial y^*}\right|_{y^*=0}$$

and from Equation 10 it follows that the friction coefficient is

$$C_f = \frac{\tau_s}{1/2\rho u_\infty^2} = \frac{2}{\mathrm{Re}_L}\left.\frac{\partial u^*}{\partial y^*}\right|_{y^*=0} \tag{103}$$

From Equation 101 it is clear that

$$\left.\frac{\partial u^*}{\partial y^*}\right|_{y^*=0} = f_3\left(x^*, \mathrm{Re}_L, \frac{dp^*}{dx^*}\right) \tag{104}$$

Hence, for a prescribed geometry (i.e., dp^*/dx^* is known from the free stream conditions) we have

$$C_f = \frac{2}{\mathrm{Re}_L} f_3(x^*, \mathrm{Re}_L) \tag{105}$$

Equation 105 is very significant because it states that the friction coefficient may be expressed exclusively in terms of a dimensionless space coordinate and the Reynolds number. For a prescribed geometry, the function that relates C_f to x^* and Re_L can be expected to be *universally* applicable. That is, it can be expected to apply to different fluids and over a wide range of values for u_∞ and L.

Similar results may be obtained for the heat transfer coefficient. Equation 51 suggests that the solution may be expressed in the form

$$T^* = f_4\left(x^*, y^*, \mathrm{Re}_L, \frac{dp^*}{dx^*}\right) \tag{106}$$

for forced flow, and

$$T^* = f_5(x^*, y^*, \mathrm{Gr}_L, \mathrm{Pr}) \tag{107}$$

for free convective flow. Here Re_L, Gr_L, and dp^*/dx^* originate from the influence of fluid motion (u^* and v^*) on Equation 51.

From the definition of the convection heat transfer coefficient, Equation 5, and Equation 40 with $y^* = y/L$ we obtain

$$h = -\frac{k(\partial T/\partial y)\big|_{y=0}}{(T_s - T_\infty)} = +\frac{k}{L}\left.\frac{\partial T^*}{\partial y^*}\right|_{y^*=0} \tag{108}$$

Thus

$$\mathrm{Nu} \equiv \frac{hL}{k} = \left.\frac{\partial T^*}{\partial y^*}\right|_{y^*=0}$$

Note that the Nusselt number, Nu, is equal to the dimensionless temperature gradient at the surface. From Equation 106 or 107 it follows that for a prescribed geometry, i.e., known dp^*/dx^*

$$\mathrm{Nu} = f_6(x^*, \mathrm{Re}_L, \mathrm{Pr}) \tag{109}$$

for forced flow, and

$$\mathrm{Nu} = f_7(x^*, \mathrm{Gr}_L, \mathrm{Pr}) \tag{110}$$

for free convective flow. The Nusselt number is to the thermal boundary layer what the friction factor is to the velocity boundary layer. Equations 109 and 110 imply that for a given geometry, the Nusselt number must be some *universal* function of x^*, Re_L, and Pr. If this function were known, it could be used to compute the value of Nu for different fluids and different values of u_∞, T_∞ and L. Furthermore, since the average heat transfer coefficient is obtained by integrating over the surface of the body, it must be independent of the spatial variable, x^*. Hence, the functional dependence of the average Nusselt number is

$$\overline{\mathrm{Nu}} = \frac{\bar{h}L}{k} = f_8(\mathrm{Re}_L, \mathrm{Pr}) \tag{111}$$

for forced flow, and

$$\overline{\mathrm{Nu}} = f_9(\mathrm{Gr}_L, \mathrm{Pr}) \tag{112}$$

for free convective flows.

Although it is very helpful to know the functional dependence of Nu, the task is far from complete, because the function may be any of millions of possibilities. It may be a sine, exponential, or a logarithmic function. The exact form of this function can only be determined by an analytical solution of the governing equations, such as Equations 70 and 91.

Experimental determination of heat transfer coefficient: The manner in which a convection heat transfer correlation may be obtained experimentally is illustrated in Figure 1-3.23. If a prescribed geometry, such as the flat plate in parallel flow, is heated electrically to maintain $T_s > T_\infty$ convection heat transfer occurs from the surface to the fluid. It would be a simple matter to measure T_s and T_∞ as well as the electrical power, $E \cdot I$, which is equal to the total heat transfer rate, $\dot{q}$. The average convection coefficient, $\bar{h}_L$, can now easily be computed from Equation 7. Also, from the knowledge of the characteristic length, L, and the fluid properties, the values of the various nondimensional numbers—such as the Nusselt, Reynolds, Grashof, and Prandtl numbers—can be easily computed from their definitions.

The foregoing procedure is repeated for a variety of test conditions. We could vary the velocity, u_∞, the plate length, L, and the temperature difference $(T_s - T_\infty)$, as well as the fluid properties, using, for example, fluids such as air, water, and engine oil, which have substantially different Prandtl numbers. Many different values of the Nus-

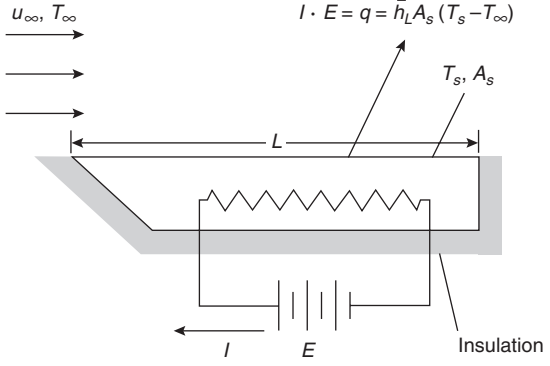

Figure 1-3.23. ***Experiment for measuring the average convection heat transfer coefficient, $\bar{h}_L$.***

selt number would result, corresponding to a wide range of Reynolds and Prandtl numbers. At this stage, an analytical solution to a similar but simpler problem proves very useful in guiding how the various nondimensional numbers should be correlated. For laminar flow over a flat plate it has been seen that in Equation 70 the relationship is of the form

$$\overline{\mathrm{Nu}} = C\,\mathrm{Re}_L^m \mathrm{Pr}^n$$

Thus, we plot the results on a log-log graph as shown in Figure 1-3.24 and determine the values of C, m, and n. Because such a relationship is inferred from experimental measurements, it is called an empirical correlation. Along with this empirical correlation it is specified how the temperature-dependent properties were determined for calculating the various nondimensional numbers. When such a correlation is used, it is important that the properties must be calculated in exactly the manner specified. If they are not specified, then the mean boundary layer temperature, T_f, called the film temperature, must be used.

$$T_f \equiv \frac{T_s + T_\infty}{2} \tag{113}$$

A summary of empirical and practical formulas: In this section selected dimensionless groups (Table 1-3.2) and a variety of convection correlations (Tables 1-3.3 and 1-3.4) for external flow conditions are tabulated. Correlations for both forced and free convection are presented along with their range of applicability. The contents of this section are more or less a collection of "recipes." Proper use of these recipes is essential to solving practical problems. The reader should not view these correlations as sacrosanct; each correlation is reasonable over the range of conditions specified, but for most engineering calculations one should not expect the accuracy to be much better than 20 percent.

For proper use of the foregoing correlations it is important to note that the flow may not be laminar or turbulent over the entire length of the plate under consideration. Instead, transition to turbulence may occur at a distance x_c ($x_c < L$, where L is the plate length) from the leading edge of the plate. In this mixed boundary layer situation, the average convection heat transfer coefficient for the entire plate is obtained by integrating first over the laminar region ($0 \le x \le x_c$) and then over the turbulent region ($x_c < x \le L$) as follows:

$$\overline{h}_L = \frac{1}{L}\left(\int_0^{x_c} h_{\mathrm{lam}}\,dx + \int_{x_c}^{L} h_{\mathrm{turb}}\,dx\right) \tag{114}$$

where x_c may be obtained from the critical Reynolds or Grashof numbers.

Also, several correlations given in Tables 1-3.3 and 1-3.4 are for the constant heat flux ($\dot{q}_s''$ = constant) boundary condition. Thus, the surface temperature of the object is unknown and yet the fluid properties are to be determined at $T_f = (T_s + T_\infty)/2$. For such cases an iterative procedure is employed and the average surface temperature can be determined as follows:

$$\dot{q}_s''(\text{known}) = \overline{h}(T_s - T_\infty) = \frac{\overline{\mathrm{Nu}}_L}{(L/k)}(T_s - T_\infty)$$

thus

$$T_s(\text{average}) = T_\infty + \frac{\dot{q}_s''(L/k)}{\overline{\mathrm{Nu}}_L} \tag{115}$$

The use of correlations given in Tables 1-3.3 and 1-3.4 is illustrated via examples in the next section.

Applications

This section briefly summarizes the methodology for convection calculations and then presents examples to illustrate the use of various correlations.

Methodology for convection calculations: The application of a convection correlation for any flow situation is facilitated by following a few simple rules:

1. Become immediately cognizant of the flow geometry. Does the problem involve flow over a flat plate, a sphere, a cylinder, and so forth? The specific form of the convection correlation depends, of course, on the geometry.

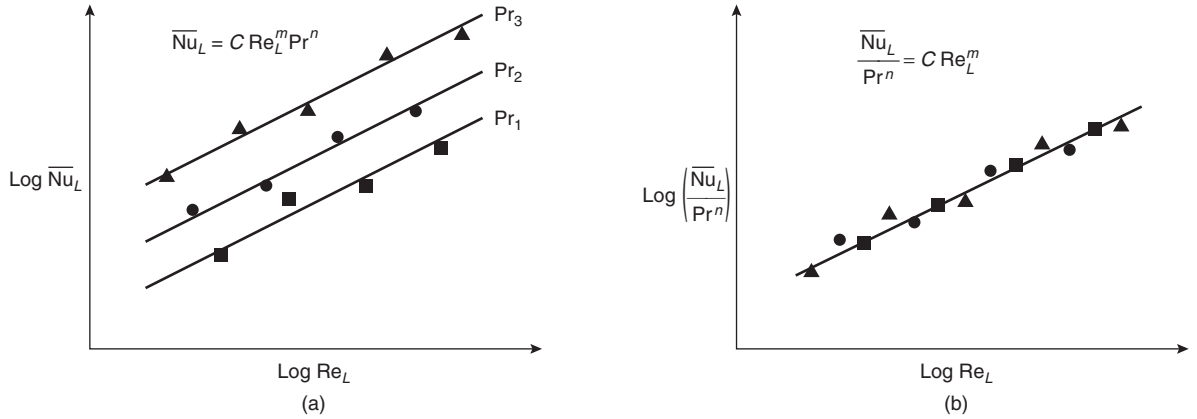

Figure 1-3.24. ***Dimensionless representation of convection heat transfer measurements.***

Table 1-3.2 ***Selected Dimensionless Groups***

Group		Definition	Interpretation
Friction coefficient	local	$C_f = \frac{\tau_2}{\rho u^{2}_{\infty}/2}$	Dimensionless surface shear stress
	average	$\bar{C}_f = \frac{\bar{\tau}_s}{\rho u^{2}_{\infty}/2}$	
Reynolds number	location x	$\mathrm{Re}_x = \frac{u_\infty x}{\nu}$	Ratio of inertia and viscous forces
	length L	$\mathrm{Re}_L = \frac{u_\infty L}{\nu}$	
	diameter D	$\mathrm{Re}_D = \frac{u_\infty D}{\nu}$	
Prandtl number		$\mathrm{Pr} = \frac{Cp\mu}{k} = \frac{\nu}{\alpha}$	Ratio or molecular momentum and thermal diffusivities
Grashof number	location x	$\mathrm{Gr}_x = \frac{g\beta(T_s - T_\infty)x^3}{\nu^2}$	Ratio of buoyancy to viscous forces
	length L	$\mathrm{Gr}_L = \frac{g\beta(T_s - T_\infty)L^3}{\nu^2}$	
	diameter D	$\mathrm{Gr}_D = \frac{g\beta(T_s - T_\infty)D^3}{\nu^2}$	
Rayleigh number	location x	$\mathrm{Ra}_x = \mathrm{Gr}_x\mathrm{Pr} = \frac{g\beta(T_s - T_\infty)x^3}{\nu\alpha}$	Product of Grashof and Prandtl numbers
		replace x by L and D to get Ra_L and Ra_D	
Nusselt number	location x	$\mathrm{Nu}_x = \frac{hx}{k}$	Ratio of convection heat transfer to conduction in a fluid slab of thickness x
		replace x by L and D to get Nu_L and Nu_D	
Modified Grashof number	location x	$\mathrm{Gr}^*_x = \mathrm{Gr}_x\mathrm{Nu}_x = \frac{g\beta\dot{q}''_s x^4}{k\nu^2}$	Product of Grashof and Nusselt numbers
Stanton number		$\mathrm{St} = \frac{h}{\rho u_\infty c_p} = \frac{\mathrm{Nu}}{\mathrm{Re}\,\mathrm{Pr}}$	Dimensionless heat transfer coefficient

2. Specify the appropriate reference temperature and then evaluate the pertinent fluid properties at that temperature. For moderate boundary layer temperature differences, it has been found that the film temperature may be used for this purpose. However, there are correlations that require property evaluation at the free stream temperature and include a property ratio to account for the nonconstant property effect.
3. Determine whether the flow is laminar or turbulent. This determination is made by calculating the Reynolds number and comparing the value with the appropriate transition criterion. For example, if a problem involves parallel flow over a flat plate for which the Reynolds number is $\mathrm{Re}_L = 10^6$ and the transition criterion is $\mathrm{Re}_{\mathrm{crit}} = 5 \times 10^5$, it is obvious that a mixed boundary layer condition exists.
4. Decide whether a local or surface average coefficient is required. Recall that the local coefficient is used to determine the flux at a particular point on the surface, whereas the average coefficient determines the transfer rate for the entire surface.

Having complied with the foregoing rules, sufficient information will be available to select the appropriate correlation for the problem.

EXAMPLE 1:

Electrical strip heaters are assembled to construct a flat radiant heater 1 m wide for conducting fire experiments in a wind tunnel. The heater strips are 5 cm wide and are independently controlled to maintain the surface temperature at 500°C. Construction details are shown in Figure 1-3.25. If air at 25°C and 60 m/s flows over the plate, at which strip is the electrical input maximum? What is the value of this input? The radiative heat loss is ignored.

Table 1-3.3 ***Summary of Forced Convection Correlations for External Flow Geometries***

Geometry/Flow	Type	Equation	Restrictions	Comments
Flat plate/laminar (T_s = constant)	Local:	$\mathrm{Nu}_x = 0.332\,\mathrm{Re}_x^{1/2}\mathrm{Pr}^{1/3}$	$\mathrm{Re}_x < 5 \times 10^5$	Properties evaluated at $T_f = (T_s + T_\infty)/2$
	Average:	$\overline{\mathrm{Nu}}_L = 0.664\,\mathrm{Re}_L^{1/2}\mathrm{Pr}^{1/3}$	$0.6 \le \mathrm{Pr} \le 50$	
	Boundary layer thickness:	$\frac{\delta}{x} = 5\,\mathrm{Re}_x^{-1/2}$		
Flat plate/laminar ($\dot{q}_s''$ = constant)	Local:	$\mathrm{Nu}_x = 0.453\,\mathrm{Re}_x^{1/2}\mathrm{Pr}^{1/3}$	$\mathrm{Re}_x < 5 \times 10^5$ $0.6 \le \mathrm{Pr} \le 50$	Properties evaluated at T_f. However, T_s is not known. Instead, q_s'' is known. Thus, $T_f = T_\infty + (\bar{T}_s - \bar{T}_\infty)/2$ where, $(\bar{T}_s - \bar{T}_\infty) = \frac{q_s L/K}{0.6795\,\mathrm{Re}_L^{1/2}\mathrm{Pr}^{1/3}}$
Flat plate/turbulent (T_s = constant)	Local:	$\mathrm{Nu}_x = 0.0296\,\mathrm{Re}_x^{4/5}\mathrm{Pr}^{1/3}$	$\mathrm{Re}_x < 10^8$	Properties evaluated at T_f.
	Boundary layer thickness:	$\frac{\delta}{x} = 0.37\,\mathrm{Re}_x^{-1/5}$	$0.6 \le \mathrm{Pr} \le 60$	
	Mixed average (laminar-turbulent):	$\overline{\mathrm{Nu}}_L = (0.037\,\mathrm{Re}_L^{4/5} - 871)\mathrm{Pr}^{1/3}$	Transition to turbulence at $\mathrm{Re}_{crit} = 5 \times 10^5$	
Flow across cylinders	Average:	$\overline{\mathrm{Nu}}_D = C\,\mathrm{Re}_D^m\mathrm{Pr}^{1/3}$	$0.4 < \mathrm{Re}_D < 4 \times 10^5$	Properties evaluated at T_f.
Circular cylinder		Re_D — C — m: $0.4 - 4$ — 0.989 — 0.330 $4 - 40$ — 0.911 — 0.385 $40 - 4000$ — 0.683 — 0.466 $4 \times 10^3 - 4 \times 10^4$ — 0.193 — 0.618 $4 \times 10^4 - 4 \times 10^5$ — 0.027 — 0.805		
Other Geometries Square 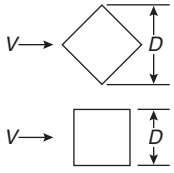		$5 \times 10^3 - 10^5$ — 0.246 — 0.588 $5 \times 10^3 - 10^5$ — 0.102 — 0.675		
Hexagon 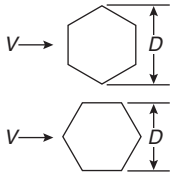		$5 \times 10^3 - 1.95 \times 10^4$ — 0.160 — 0.638 $1.95 \times 10^4 - 10^5$ — 0.0385 — 0.782		
Vertical Plate 		$5 \times 10^3 - 10^5$ — 0.153 — 0.638 $4 \times 10^3 - 1.5 \times 10^4$ — 0.228 — 0.731		
Flow across spheres	Average:	$\overline{\mathrm{Nu}}_D = 2 + (0.4\,\mathrm{Re}_D^{1/2} + 0.06\,\mathrm{Re}_D^{2/3})\mathrm{Pr}^{0.4}\left(\frac{\mu_\infty}{\mu_s}\right)^{1/4}$	$3.5 < \mathrm{Re}_D < 7.6 \times 10^4$ $0.71 < \mathrm{Pr} < 380$ $1.0 < \left(\frac{\mu_\infty}{\mu_s}\right) < 3.2$	Properties evaluated at T_∞.
Falling drop	Average:	$\overline{\mathrm{Nu}}_D = 2 + 0.6\,\mathrm{Re}_D^{1/2}\mathrm{Pr}^{1/3} \cdot \left(25\left(\frac{x}{D}\right)^{-.07}\right)$	where x is the falling distance measured from rest.	Properties evaluated at T_∞.

Table 1-3.4 ***Summary of Free Convection Correlations for External Flow Geometries***

Geometry/Flow	Type	Equation	Restrictions	Comments
Vertical Plates 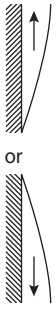 or	Local: (T_s = const)	$\mathrm{Nu}_x g(\mathrm{Pr})$ from Table 1-3.1 $= \left(\frac{\mathrm{Gr}_x}{4}\right)^{1/4} g(\mathrm{Pr})$	$\mathrm{Gr}_x \le 4 \times 10^8$ (Laminar)	Properties evaluated at $(T_f = T_s + T_\infty)/2$
	Average: (T_s = const)	$\overline{\mathrm{Nu}}_L = \frac{4}{3}\left(\frac{\mathrm{Gr}_L}{4}\right)^{1/4} g(\mathrm{Pr})$	$\mathrm{Gr}_x \le 4 \times 10^8$ (Laminar)	Properties at T_f
	Average: (T_s = const)	$\overline{\mathrm{Nu}}_L = \left\{0.825 + \frac{0.387\ \mathrm{Ra}_L^{1/6}}{[1+(0.492/\mathrm{Pr})^{9/16}]^{8/27}}\right\}^2$	none	Properties at T_f This correlation may be applied to vertical cylinders if $\left(\frac{D}{L}\right) \ge (35/\mathrm{Gr}_L^{1/4})$
	Local: ($\dot{q}_s''$ = const)	$\mathrm{Nu}_x = 0.6(\mathrm{Gr}_x^* \mathrm{Pr})^{1/5}$	$10^5 < \mathrm{Gr}_x^* 10^{11}$ (Laminar)	Properties at T_f
	Local: ($\dot{q}_s''$ = const)	$\mathrm{Nu}_x = 0.17(\mathrm{Gr}_x^* \mathrm{Pr})^{1/4}$	$2 \times 10^{13} < \mathrm{Gr}_x^* \mathrm{Pr} < 10^{16}$	Properties at T_f
	Average: ($\dot{q}_s''$ = const)	$\overline{\mathrm{Nu}}_L = 0.75(\mathrm{Gr}_L^* \mathrm{Pr})^{1/5}$	$10^5 < \mathrm{Gr}_x^* < 10^{11}$ (Laminar)	Properties at T_f
Horizontal plates (hot surface up or cold surface down) 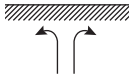	Average: (T_s = const)	$\overline{\mathrm{Nu}}_L = 0.54\ \mathrm{Ra}_L^{1/4}$ $\overline{\mathrm{Nu}}_L = 0.15\ \mathrm{Ra}_L^{1/3}$	$10^5 \le \mathrm{Ra}_L \le 10^7$ $10^7 \le \mathrm{Ra}_L \le 10^{10}$	Properties at T_f characteristic length L is defined as $L = A_s/P$ where A_s = plate surface area F = perimeter of the plate (1) All properties except β are evaluated at $T_e = T_s - \frac{1}{4}(T_s - T_\infty)$ β is evaluated at T_f.
	Average: ($\dot{q}_s''$ = const)	$\overline{\mathrm{Nu}}_L^{(1)} = 0.16\ \mathrm{Ra}_L^{1/3}$	$\mathrm{Ra}_L \le 2 \times 10^8$	
Horizontal plates (cold surface up or hot surface down) 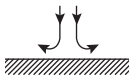	Average: (T_s = const)	$\overline{\mathrm{Nu}}_L = 0.27\ \mathrm{Ra}_L^{1/4}$	$10^5 \le \mathrm{Ra}_L \le 10^{10}$	
	Average: ($\dot{q}_s''$ = const)	$\overline{\mathrm{Nu}}_L^{(1)} = 0.16\ \mathrm{Ra}_L^{1/3}$	$2 \times 10^8 \le \mathrm{Ra}_L \le 10^{11}$	
Inclined plates 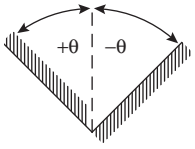 Hot Surface	Average: ($\dot{q}_s''$ = const)	$\overline{\mathrm{Nu}}_L = 0.56\ (\mathrm{Ra}_L \cos\theta)^{1/4}$ (hot surface facing down) For hot surface facing up $\overline{\mathrm{Nu}}_L = 0.14\ [(\mathrm{Gr}_L \mathrm{Pr})^{1/3} - (\mathrm{Gr}_c \mathrm{Pr})^{1/3}] + 0.56\ (\mathrm{Ra}_L \cos\theta)^{1/4}$ $\theta = -15^*$; $\mathrm{Gr}_c = 5 \times 10^9$ -30^*; 2×10^9 -60^*; 10^8 -75^*; 10^5	$\theta < 88''$ $10^5 < \mathrm{Ra}_L \cos\theta < 10^{11}$ $-15^* > \theta > -75^*$ $10^5 < \mathrm{Ra}_L \cos\theta < 10^{11}$	Properties evaluated at $T_e = T_s - \frac{1}{4}(T_s - T_\infty)$ Grashof number
Horizontal cylinders 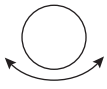	Average: (T_s = const)	$\overline{\mathrm{Nu}}_D = \left\{0.6 + \frac{0.387\ \mathrm{Ra}_D^{1/6}}{[1+(0.559/\mathrm{Pr})^{9/16}]^{8/27}}\right\}^2$	$10^{-5} < \mathrm{Ra}_D < 10^{12}$	Properties evaluated at T_f.
Spheres 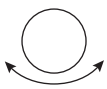	Average: (T_s = const)	$\overline{\mathrm{Nu}}_D = 2 + 0.43\ \mathrm{Ra}_D^{1/4}$ $\overline{\mathrm{Nu}}_D = 2 + 0.5\ \mathrm{Ra}_D^{1/4}$	$1 < \mathrm{Ra}_D < 10^5$ $\mathrm{Pr} \approx 1$ $3 \times 10^5 < \mathrm{Ra} < 8 \times 10^8$	Properties evaluated at T_f.

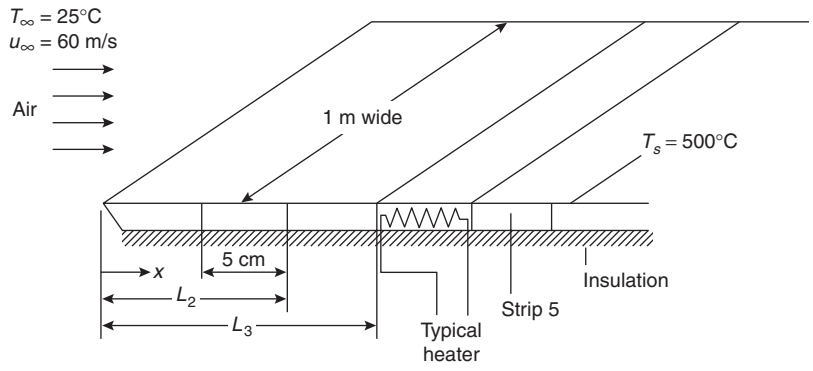

Figure 1-3.25. ***Construction details for wind tunnel experiments.***

SOLUTION:

Assumptions

Steady-state conditions, neglect radiation losses, and no heat loss through the bottom surface.

Properties

T_f = 535 K: ρ = 1 atm. From air property Table 1-3.5, k = 42.9 × 10^{-3} W/m K; ν = 43.5 × 10^{-6} m^2/s; Pr = 0.683.

Analysis

The strip heater requiring the maximum electrical power is that for which the average convection coefficient is the largest. From the knowledge of variation of the local convection coefficient with distance from the leading edge, the local maximum can be found. Figure 1-3.15 shows that a possible location is the leading edge on the first plate. A second likely location is where the flow becomes turbulent. To determine the point of boundary layer transition to turbulence assume that the critical Reynolds number is 5 × 10^5. It follows that transition will occur at x_c, where

$$x_c = \frac{\nu \, \mathrm{Re}_{\mathrm{crit}}}{u_\infty} = \frac{43.5 \times 10^{-6} \times 5 \times 10^5}{60} \, \mathrm{m}$$
$$= 0.36 \, \mathrm{m} \quad \text{or on the eighth strip}$$

Thus there are three possibilities:

1. Heater strip 1, since it corresponds to the largest local, laminar convection coefficient
2. Heater strip 8, since it corresponds to the largest local turbulent convection coefficient
3. Heater strip 9, since turbulent conditions exist over the entire heater

For the first heater strip

$$q_{\mathrm{conv},1} = \overline{h}_1 L_1 W (T_s - T_\infty)$$

where $\overline{h}_1$ is determined from the equation below (see also Table 1-3.3).

$$\overline{\mathrm{Nu}}_1 = 0.664 \, \mathrm{Re}_1^{1/2} \, \mathrm{Pr}^{1/3}$$
$$= 0.664 \left(\frac{60 \times 0.05}{43.5 \times 10^{-6}} \right)^{1/2} (0.683)^{1/3}$$
$$= 153.6$$

hence,

$$\overline{h}_1 = \frac{\overline{\mathrm{Nu}}_1 k}{L_1} = \frac{153.6 \times 42.9 \times 10^{-3}}{0.05}$$
$$= 131.8 \, \mathrm{W/m^2 \, K}$$

hence,

$$q_{\mathrm{conv},1} = (131.8)(0.05)(1 \, \mathrm{m})(500 - 25)$$
$$= 3129 \, \mathrm{W}$$

The power requirement for the eighth strip may be obtained by subtracting the total heat loss associated with the first seven heaters from that associated with the first eight heaters. Thus

$$q_{\mathrm{conv},8} = \overline{h}_{1-8} L_8 W (T_s - T_\infty) - \overline{h}_{1-7} L_7 W (T_s - T_\infty)$$

The value of $\overline{h}_{1-7}$ is obtained from the equation applicable to laminar conditions (Table 1-3.3). Thus

$$\overline{\mathrm{Nu}}_{1-7} = 0.664 \, \mathrm{Re}_7^{1/2} \, \mathrm{Pr}^{1/3}$$
$$= 0.664 \left(\frac{60 \times 7 \times 0.05}{43.5 \times 10^{-6}} \right)^{1/2} (0.683)^{1/3}$$
$$= 406.3$$
$$\overline{h}_{1-7} = \frac{\overline{\mathrm{Nu}}_{1-7} k}{L_7} = \frac{406.3 \times 42.9 \times 10^{-3}}{7 \times 0.05}$$
$$= 49.8 \, \mathrm{W/m^2 \, K}$$

By contrast, the eighth heater is characterized by mixed boundary layer conditions. Thus use the formula (Table 1-3.3).

$$\overline{\mathrm{Nu}}_{1-8} = (0.037\ \mathrm{Re}_8^{4/5} - 871)\ \mathrm{Pr}^{1/3}$$
$$\mathrm{Re}_8 = 8 \times \mathrm{Re}_1 = 5.52 \times 10^5$$
$$\overline{\mathrm{Nu}}_{1-8} = 510.5$$
$$\overline{h}_{1-8} = \frac{\overline{\mathrm{Nu}}_{1-8} k}{L_8} = 54.7\ \mathrm{W/m^2\ K}$$

The rate of heat transfer from the eighth strip is then

$$q_{\mathrm{conv},8} = (54.7 \times 8 \times 0.05 - 49.8 \times 7 \times 0.05)(500 - 25)$$
$$= 2113.8\ \mathrm{W}$$

The power requirement for the ninth heater strip may be obtained by either subtracting the total heat loss associated with the first eight from that associated with the first nine, or by integrating over the local turbulent expression, since the flow is completely turbulent over the entire width of the strip. The latter approach produces

$$\overline{h}_9 = \left(\frac{k}{L_9 - L_8}\right) 0.0296 \left(\frac{u_\infty}{v}\right)^{4/5} \mathrm{Pr}^{1/3} \int_{L_8}^{L_9} \frac{dx}{x^{1/5}}$$
$$\overline{h}_9 = \left(\frac{42.9 \times 10^{-3}}{0.05}\right) 0.0296 \left(\frac{60}{43.5 \times 10^{-6}}\right)^{4/5}$$
$$\times (0.683)^{1/3} \int_{L_8}^{L_9} \frac{dx}{x^{1/5}}$$
$$= 1825.22[(0.45)^{0.8} - (0.4)^{0.8}] = 86.7$$
$$q_{\mathrm{conv},9} = 86.7 \times 0.05 \times 1 \times (500 - 25) = 2059\ \mathrm{W}$$

hence

$$q_{\mathrm{conv},1} > q_{\mathrm{conv},8} > q_{\mathrm{conv},9}$$

and the first heater strip has the largest power requirement.

EXAMPLE 2:

A glass-door fire screen, shown in Figure 1-3.26, is used to reduce exfiltration of room air through a chimney. It has a height of 0.71 m, a width of 1.02 m, and reaches a temperature of 232°C. If the room temperature is 23°C, estimate the convection heat transfer rate from the fireplace to the room.

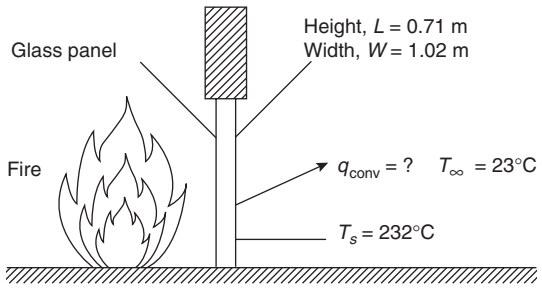

Figure 1-3.26. ***Glass panel fire screen.***

SOLUTION:

Assumptions

The screen is at a uniform temperature, T_s, and room air is quiescent.

Properties

$T_f = 400$ K, $P = 1$ atm. From air property table (Table 1-3.5):

$$k = 33.8 \times 10^{-3}\ \mathrm{W/m\ K}; \qquad \nu = 26.41 \times 10^6\ \mathrm{m^2/s};$$
$$\alpha = 38.3 \times 10^{-6}\ \mathrm{m^2/s};\ \ \mathrm{Pr} = 0.69;\ \ \beta = 1/T_f = 0.0025\ \mathrm{K^{-1}}$$

Analysis

The rate of heat transfer by free convection from the panel to the room is given by

$$q = \overline{h} A_s (T_s - T_\infty)$$

where $\overline{h}$ is obtained from the following equation from Table 1-3.4.

$$\overline{\mathrm{Nu}}_L = \left\{0.825 + \frac{0.387\ \mathrm{Re}_L^{1/6}}{[1 + (0.492/\mathrm{Pr})^{9/16}]^{8/27}}\right\}^2$$

here

$$\mathrm{Ra}_L = \frac{g\beta(T_s - T_\infty)L^3}{\alpha\nu}$$
$$= \frac{9.8 \times 0.0025 \times (232 - 23) \times (0.71)^3}{38.3 \times 10^{-6} \times 26.4 \times 10^{-6}}$$
$$= 1.813 \times 10^9$$

Since $\mathrm{Ra}_L > 10^9$, transition to turbulence will occur on the glass panel and the appropriate correlation from Table 1-3.4 has been chosen

$$\overline{\mathrm{Nu}}_L = \left\{0.825 + \frac{0.387(1.813 \times 10^9)^{1/6}}{[1 + (0.492/0.69)^{9/16}]^{8/27}}\right\}^2$$
$$= 147$$

Hence

$$\overline{h} = \frac{\overline{\mathrm{Nu}}_L \times k}{L} = \frac{147 \times 33.8 \times 10^{-3}}{0.71} = 7\ \mathrm{W/m^2\ K}$$

and

$$q = 7\ \frac{\mathrm{W}}{\mathrm{m^2\ K}}\ (1.02\ \mathrm{m} \times 0.71\ \mathrm{m}) \times (232 - 23)°\mathrm{C}$$
$$= 1060\ \mathrm{W}$$

Note: in this case radiation heat transfer calculations would show that radiant heat transfer is greater than free convection heat transfer.

Table 1-3.5 ***Thermophysical Properties of Air at Atmospheric Pressure***

T K	ρ kg/m³	c_p kJ/kg·K	$\mu \cdot 10^7$ N·s/m²	$\nu \cdot 10^6$ m²/s	$k \cdot 10^3$ W/m·K	$\alpha \cdot 10^6$ m²/s	Pr
100	3.5562	1.032	71.1	2.00	9.34	2.54	0.786
150	2.3364	1.012	103.4	4.426	13.8	5.84	0.758
200	1.7458	1.007	132.5	7.590	18.1	10.3	0.737
250	1.3947	1.006	159.6	11.44	22.3	15.9	0.720
300	1.1614	1.007	184.6	15.89	26.3	22.5	0.707
350	0.9950	1.009	208.2	20.92	30.0	29.9	0.700
400	0.8711	1.014	230.1	26.41	33.8	38.3	0.690
450	0.7740	1.021	250.7	32.39	37.3	47.2	0.686
500	0.6964	1.030	270.1	38.79	40.7	56.7	0.684
550	0.6329	1.040	288.4	45.57	43.9	66.7	0.683
600	0.5804	1.051	305.8	52.69	46.9	76.9	0.685
650	0.5356	1.063	322.5	60.21	49.7	87.3	0.690
700	0.4975	1.075	338.8	68.10	52.4	98.0	0.695
750	0.4643	1.087	354.6	76.37	54.9	109	0.702
800	0.4354	1.099	369.8	84.93	57.3	120	0.709
850	0.4097	1.110	384.3	93.80	59.6	131	0.716
900	0.3868	1.121	398.1	102.9	62.0	143	0.720
950	0.3666	1.131	411.3	112.2	64.3	155	0.723
1000	0.3482	1.141	424.4	121.9	66.7	168	0.726
1100	0.3166	1.159	449.0	141.8	71.5	195	0.728
1200	0.2902	1.175	473.0	162.9	76.3	224	0.728
1300	0.2679	1.189	496.0	185.1	82	238	0.719
1400	0.2488	1.207	530	213	91	303	0.703
1500	0.2322	1.230	557	240	100	350	0.685
1600	0.2177	1.248	584	268	106	390	0.688
1700	0.2049	1.267	611	298	113	435	0.685
1800	0.1935	1.286	637	329	120	482	0.683
1900	0.1833	1.307	663	362	128	534	0.677
2000	0.1741	1.337	689	396	137	589	0.672
2100	0.1658	1.372	715	431	147	646	0.667
2200	0.1582	1.417	740	468	160	714	0.655
2300	0.1513	1.478	766	506	175	783	0.647
2400	0.1448	1.558	792	547	196	869	0.630
2500	0.1389	1.665	818	589	222	960	0.613
3000	0.1135	2.726	955	841	486	1570	0.536

Nomenclature

A	area (m²)
A_s	surface area (m²)
B_i	Biot number
C	molar concentration (kmol/m³)
C_f	friction coefficient
c_p	specific heat at constant pressure (J/kg·K)
c_v	specific heat at constant volume (J/kg·K)
D	diameter (m)
D_{AB}	binary mass diffusion coefficient (m²/s)
D_h	hydraulic diameter (m)
e	Specific internal or thermal (sensible) energy (J/kg)
f	friction factor
Gr	Grashof number
g	gravitational acceleration (m/s²)
h	convection heat transfer coefficient (W/m²·K)
$\overline{h}$	average convection heat transfer coefficient (W/m²·K)
h_m	convection mass transfer coefficient (m/s)
h_{rad}	radiation heat transfer coefficient (W/m²·K)
k	thermal conductivity (W/m·K)
L	characteristic length (m)
Le	Lewis number
M	mass (kg)
$\dot{M}$	mass flow rate (kg/s)
$\dot{m}''$	mass flux (kg/m²·s)
$\dot{m}_i''$	mass flux of species i (kg/m²·s)
Nu	Nusselt number
P	perimeter (m)
Pe	Peclet number (RePr)
Pr	Prandtl number
p	pressure (N/m²)
Q	energy generation rate per unit volume (W/m³)
$\dot{q}'$	heat transfer rate per unit length (W/m)

$\dot{q}''$	heat flux (W/m^2)
R	universal gas constant
Ra	Rayleigh number
Re	Reynolds number
r, ϕ, z	cylindrical coordinates
r, θ, ϕ	spherical coordinates
Sc	Schmidt number
Sh	Sherwood number
St	Stanton number
T	temperature (K)
t	time (s)
U	overall heat transfer coefficient (W/m^2·K)
u, v, w	mass average fluid velocity components (m/s)
F_{BX}, F_{BY}, F_{BZ}	components of the body force per unit volume (N/m^3)
F_{SX}, F_{SY}, F_{SZ}	components of the surface force
x, y, z	rectangular coordinates (m)
$x_{fd,h}$	hydrodynamic entry length (m)
$x_{rd,t}$	thermal entry length (m)

Greek Letters

α	thermal diffusivity (m^2/s)
β	volumetric thermal expansion coefficient (K^{-1})
δ	hydrodynamic boundary layer thickness (m)
δ_t	thermal boundary layer thickness (m)
δ_d	mass transfer boundary layer thickness (m)
η	similarity variable
θ	zenith angle (rad)
ϕ	azimuthal angle (rad)
μ	viscosity (kg/s·m)
ν	kinematic viscosity (m^2/s)
ρ	mass density (kg/m^3)
σ_{ij}	components of the stress tensor (N/m^2)
ψ	stream function (m^2/s)
τ	shear stress (N/m^2)

Subscripts

A,B	species in a binary mixture
conv	convection
D	diameter; drag
f	fluid properties
fd	fully developed conditions
H	heat transfer conditions
h	hydrodynamic; hot fluid
L	based on characteristic length
max	maximum fluid velocity
s	surface conditions
sur	surroundings
t	thermal
x	local conditions on a surface
∞	free stream conditions

References Cited

1. R.B. Bird, W.E. Stewart, and E.N. Lightfoot, *Transport Phenomena,* Wiley, New York (1966).
2. H. Schlichting, *Boundary Layer Theory,* McGraw-Hill, New York (1979).
3. V.S. Arpaci and P.S. Larsen, *Convection Heat Transfer,* Prentice Hall, Englewood Cliffs, NJ (1984).
4. E.R.G. Eckert and R.M. Drake, *Analysis of Heat and Mass Transfer,* McGraw-Hill, New York (1973).
5. F.P. Imcropera and D.P. Dewitt, *Fundamentals of Heat Transfer,* Wiley, New York (1981).

CHAPTER 4

Radiation Heat Transfer

C. L. Tien, K. Y. Lee, and A. J. Stretton

Introduction

Researchers have become increasingly aware of the role of thermal radiation in fires, and a significant amount of recent research work has been published on the subject. An overview of the current understanding in this area can be found in the literature.[1–3] Human safety has made the assessment of fire hazard one of the most important concerns of fire protection engineers. Many fire research experiments in the past were performed in laboratories with very few attempts to simulate actual fire situations, due to the inherent expense and difficulty of controlling large fires. However, these experiments lacked information on thermal radiation, since reduced fire scales often reduce the proportion of radiation as compared to the other modes of heat transfer. It is now recognized that radiation is the dominant mode of heat transfer in flames with characteristic lengths exceeding 0.2 m, while convection is more significant in smaller flames.

Thermal radiation in fires involves energy exchange between surfaces (i.e., walls, ceilings, floors, furniture, etc.) as well as emission and absorption by various gases and soot particles. Among those gases of great practical importance to fire engineers are water vapor and carbon dioxide, which are strongly absorbing-emitting in the major thermal radiation spectrum of 1 to 100 μm (1 μm = 10^{-6} m). Many petroleum-based materials, such as plastics, evolve hydrocarbon gases upon heating, which are also strongly absorbing. In addition, the contribution of the soot particles is very important in evaluating the properties of the participating media and in most situations, soot radiation contributes more than gaseous radiation. Exact calculations of radiative exchanges in fire systems are often prohibitively expensive, even under idealized conditions, due to the dependence of the radiation properties of each material on geometry and wavelength. Many of the simplifying assumptions used in current analytical methods will be covered in this chapter.

This chapter will introduce the fundamentals of thermal radiation and offer simple methods of calculating radiant heat transfer in fires. The first section of the chapter, on basic concepts, deals with the theoretical framework for radiative heat transfer and is followed by the engineering assumptions and simple equations used for practical heat transfer calculations. The third section, on thermal radiation properties of combustion products, covers the properties of various gases and soot present in fires. The last section applies the preceding methods to several fire systems and shows some of the directions of current research.

Dr. C. L. Tien is professor of mechanical engineering at the University of California at Berkeley.

Dr. K. Y. Lee is Manager, New Engine Development, Daewoo Technical Center, Inchon, Korea.

A. J. Stretton is assistant professor of mechanical engineering at the University of Toronto.

Basic Concepts

Radiation Intensity and Energy Flux

Thermal radiation transport can be described by electromagnetic wave theory or by quantum mechanics. In the general quantum mechanical consideration, electromagnetic radiation is interpreted in terms of photons. Each photon possesses energy, $h\nu$, and momentum, $h\nu/c$, with h as the Planck constant (6.6256×10^{-34} J·s), ν the frequency of the radiation, and c the speed of light in the medium. A radiation field is fully described when the flux of photons (or energy) is known for all points in the field for all directions and for all frequencies. The net flow of thermal radiative energy for a single frequency, across a surface of an arbitrary orientation, is represented by the spectral radiative energy flux[4–6]

$$q_\nu = \int_0^{4\pi} I_\nu \vec{n} \cdot \vec{R}\, d\Omega = \int_0^{4\pi} I_\nu \cos\theta\, d\Omega \qquad (1)$$

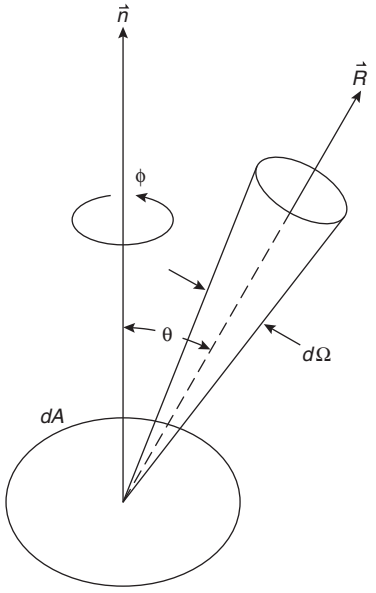

Figure 1-4.1. ***Coordinate system for radiation intensity.***

In Equation 1, Ω denotes solid angle ($d\Omega = \sin\theta\, d\theta\, d\phi$) and I_ν is the intensity of radiation expressed as energy per unit area per unit solid angle (Figure 1-4.1) within a unit frequency interval. Intensity is a useful measure for thermal radiation because the intensity of a radiant beam remains constant if it is traveling through a nonparticipating medium.

Planck's Law

The energy spectrum of the radiation given off by a surface that is a perfect emitter and absorber can be calculated by Planck's quantum theory. This theoretical surface is called a blackbody radiator, and is best simulated by a small opening into an enclosed cavity. The isotropic equilibrium radiation field within a uniform temperature enclosure is called blackbody radiation. The spectral (or monochromatic) intensity of blackbody radiation, $I_{b\nu}$, is often called the Planck function, illustrated in Figure 1-4.2, and is given by Equation 2.

$$I_{b\nu}(T) = \frac{2h\nu^3 n^2}{c_0^2[\exp(h\nu/kT) - 1]} \tag{2}$$

where

k = Boltzmann constant ($k = 1.3806 \times 10^{-23}$ J/K)

c_0 = speed of light in vacuum ($c_0 = 2.998 \times 10^8$ m/s)

n = index of refraction for the medium ($n = c_0/c$ is very close to one for most gases of interest in fires)

In many engineering applications and experimental measurements of thermal radiation properties, it is advantageous to use wavelength λ instead of ν. Equation 2 can then be expressed in the form

$$\frac{I_{b\lambda}}{T^5} = \frac{2hc_0^2}{n^2(\lambda T)^5[\exp(hc_0/n\lambda kT) - 1]} \tag{3}$$

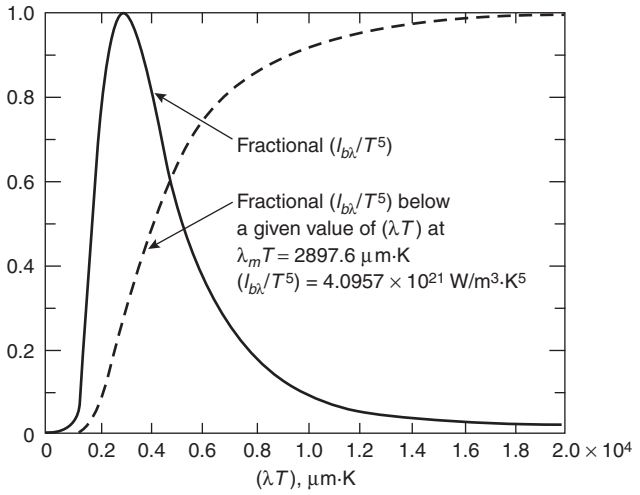

Figure 1-4.2. ***Planck's function.***

where the relations $\nu = c_0/n\lambda$ and $I_{b\lambda}d\lambda = -I_{b\nu}d\nu$ have been used. The wavelength at which radiation intensity becomes the maximum is readily obtainable by simple differentiation as

$$(n\lambda T)_{\max} = 2897.8\ \mu\text{m·K} \tag{4}$$

This relationship is known as Wien's displacement law, which shows that the maximum monochromatic emmisive power of a blackbody shifts to shorter wavelengths as its temperature increases. The total radiant intensity from a blackbody radiator can be obtained by integrating Equation 3 over the entire range of wavelengths, giving

$$I_b = \int_0^\infty I_{b\lambda}\, d\lambda = \frac{n^2\sigma T^4}{\pi} \tag{5}$$

where σ is the Stefan-Boltzmann constant (5.6696×10^{-8} W/m²·K⁴). The intensity of radiation from a blackbody is independent of direction, which allows integration of Equation 1 in a simple manner to give the total hemispherical emissive power per unit area of a blackbody

$$E_b = \int_0^{4\pi} I_b \cos\theta\, d\Omega \tag{6}$$

Kirchhoff's Law

If a fire in an isolated, uniform temperature enclosure that contains different media inside has reached its equilibrium state, the relation

$$\alpha_v + \rho_v + \tau_v = 1 \tag{7}$$

will hold at the interface between each medium, where α, ρ, and τ denote the fraction of energy absorbed by, reflected at, and transmitted through the interface, respectively. The assumption of the local thermodynamic equilibrium can be used to derive more extensive results and is used extensively in radiation heat transfer calculations. Kirchhoff's law states that in order to maintain

equilibrium, the spectral absorptivity and spectral emissivity must be related by

$$\alpha_v = \frac{I_v}{I_{bv}} = \varepsilon_v \tag{8}$$

More importantly, when Equation 8 is applied to total properties,

$$\alpha_t = \varepsilon_t \tag{9}$$

is valid for the special case when the incident radiation is independent of the incident angle and has the same spectral proportions as a blackbody radiator (i.e., a "gray body"). Fortunately, this is the case in many radiation heat transfer engineering models for participating media in fire applications. Although gas emissivity is only dependent on the state of the gas, the absorptivity is also a function of the source temperature of the incident beam of radiation, which may originate outside the gas body (e.g., wall temperature).

The Equation of Transfer

The equation of transfer describes the variation in intensity of a radiant beam at any position along its path in an absorbing-emitting-scattering medium. This equation is the foundation upon which detailed radiation analyses are based, and the source of approximate solutions when simplifying assumptions are made. For a given direction line in the medium, the equation of transfer is

$$\frac{1}{\kappa_\lambda(T, S)} \frac{dI_\lambda(S)}{dS} + I_\lambda(S) = I_{b\lambda}(T) \tag{10}$$

where S represents the physical pathlength and κ_λ represents the spectral extinction coefficient, which includes the effects of both absorption and scattering within the medium. The intensity, $I_\lambda(S)$, is coupled with the spatial distribution of the extinction coefficient and with temperature through conservation of energy in the medium. The contributions of intensity passing through an area must be integrated over all directions to calculate a net radiative energy flux. The integral nature of radiation makes analysis difficult and simplifications necessary for engineering practice.

Basic Calculation Methods

Energy Exchange in a Nonparticipating Medium

In this section, cases are examined where the surfaces are separated by a medium that does not emit, absorb, or scatter radiation. A vacuum meets this requirement exactly, and common diatomic gases of symmetric molecular structure such as N_2, O_2, and H_2 are very nearly nonparticipating media within the thermal radiation spectrum. The radiative energy transfer between the surfaces depends on the geometry, orientation, and temperature of the surfaces, while the material surface radiative properties are a function of temperature, bounding medium, direction, and polarization of radiation. In practice, most surfaces (either entire or subdivided) are assumed to be isothermal, surface radiation properties are approximated by those of ideal diffuse surfaces, and polarization effects are neglected. The geometry and orientation of each surface is commonly accounted for in calculations by one or more configuration factors, which are also known as view factors, shape factors, angle factors, and geometric factors.[5–8] A configuration factor is a purely geometrical relation between two surfaces, and is defined as the fraction of radiation leaving one surface which is intercepted by the other surface.

Configuration factors and their algebra: Consider the two arbitrarily oriented surfaces A_1 and A_2 in Figure 1-4.3. Assuming that the radiosity from dA_1 on A_1 is diffusely distributed, the configuration factor for the differential area dA_1 to the finite area A_2, F_{d1-2}, is given by

$$F_{d1-2} = \int_{A_2} \frac{\cos\beta_1 \cos\beta_2}{\pi |\vec{R}|^2} dA_2 \tag{11}$$

where

$|\vec{R}|$ = separation distance between the two surfaces

β = angle between the line of sight $\vec{R}$ and the surface normal $\vec{n}$

A_2 = area of surface 2

If the assumption of the radiosity distribution on surface A_1 is extended to include a uniform radiosity distribution over A_1 (physically, a uniform radiant heat flux from an isothermal surface), then the configuration factor for the finite area A_1 to A_2, F_{1-2}, is simply

$$F_{1-2} = \frac{1}{A_1} \int_{A_1} \int_{A_2} \frac{\cos\beta_1 \cos\beta_2}{\pi |\vec{R}|^2} dA_1 \, dA_2 \tag{12}$$

When the radiant fluxes from both surfaces are uniformly and diffusely distributed (a common engineering assumption), a reciprocity relation for the configuration factors for

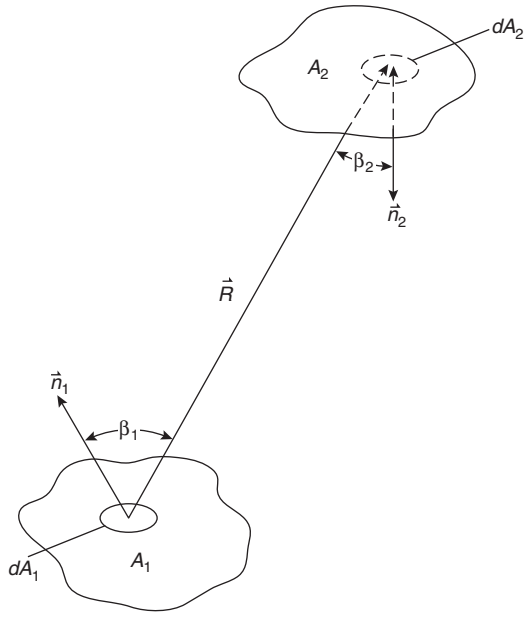

Figure 1-4.3. ***Coordinate system for shape factors.***

any given pair in a group of exchanging surfaces can readily be obtained to be

$$A_i F_{i-j} = A_j F_{j-i} \tag{13}$$

The summation rule is another useful relation for calculating unknown configuration factors

$$\sum_j F_{i-j} = 1 \tag{14}$$

where F_{i-j} relate to surfaces that subtend a closed system. Note that it is possible for a concave surface to "see" itself, which can make F_{i-i} important.

All configuration factors can be derived using the multiple integration of Equations 11 and 12, but this is generally very tedious except for simple geometries. A large number of cases have already been tabulated with the numerical results or algebraic formulas available in various references.[5–7] A catalog of common configuration factors is provided in Table 1-4.1. This data base can be extended to cover many other situations by the use of configuration algebra and the method of surface decomposition. In surface decomposition, unknown factors can be determined from known factors for convenient areas or for imaginary surfaces which can extend real surfaces or form an enclosure.[5,6]

Gray diffuse surfaces: For engineering purposes, the emittance from most surfaces is treated as having diffuse directional characteristics independent of wavelength and temperature. Real surfaces exhibit radiation properties that are so complex that information about these property measurements for many common materials is not available. The uncertainties associated with the property measurements, combined with the simplifying assumptions used in the calculations, usually reduce the knowledge of the radiative energy transfer to a simple overall flux. The gray diffuse surface is a useful model that alleviates many of the complexities associated with a detailed radiation analysis, while providing reasonably accurate results in many practical situations. The advantage of diffuse surface analysis is that radiation leaving the surface is independent of the direction of the incoming radiation, which greatly reduces the amount of computation required to solve the governing equations. Discussions for specularly reflecting surfaces and nongray surfaces can be found in the literature.[5,6]

A convenient method to analyze radiative energy exchange in an enclosure of diffuse gray surfaces is based on the concept of radiosity and irradiation. The irradiation, G_i, represents the radiative flux reaching the ith surface regardless of its origin

$$G_i = \sum_j F_{i-j} J_j \tag{15}$$

where J_j is the surface radiosity, defined as the total radiative flux leaving the jth surface (including both emission and reflection)

$$J_i = \varepsilon_i E_{bi} + \rho_i G_i \tag{16}$$

The net loss of radiative energy is then given by

$$Q_i = (J_i - G_i) A_i \tag{17}$$

It should be reemphasized that the radiosity-irradiation formulation is based on the assumption that each surface has uniform radiosity and irradiation (or equivalently, uniform temperature and uniform heat flux). Physically unrealistic calculations can result if each surface does not approximately satisfy this condition. Larger surfaces should be subdivided into smaller surfaces if necessary.

Resistance network method: The radiosity-irradiation formulation allows a more physical and graphic interpretation using the resistance network analogy. Eliminating the irradiation G_i from Equations 15 through 17, and substituting $\rho_i = 1 - \varepsilon_i$ gives

$$Q_i = \frac{E_{bi} - J_i}{(1 - \varepsilon_i)/(\varepsilon_i A_i)} = \sum_j \frac{J_i - J_j}{1/(A_i F_{i-j})} \tag{18}$$

The denominator in the last term of Equation 18 corresponds to resistance in electric circuits. As illustrated in Figure 1-4.4, the diffuse-gray surface has a radiation potential difference $(E_{bi} - J_i)$ and a resistance $(1 - \varepsilon_i)/\varepsilon_i A_i$. This simple example also illustrates that an adiabatic surface, such as a reradiating or refractory wall, exhibits a surface temperature that is independent of the surface emissivity or reflectivity.

Thermal Radiation in Participating Media

Spectral emissivity and absorptivity: From a microscopic viewpoint, emission and absorption of radiation are caused by the change in energy levels of atoms and molecules due to interactions with photons. A summary and discussion of these effects in gases from an engineering perspective has been written by Tien.[9] Consider a monochromatic beam of radiation passing through a radiating layer of thickness L; provided that the temperature and properties of the medium are uniform along the path, the intensity of radiant beam at point x is given by integration of Equation 10 as

$$I_\lambda(x) = I_\lambda(0) e^{-\kappa_\lambda x} + I_{b\lambda}\left(1 - e^{-\kappa_\lambda x}\right) \tag{19}$$

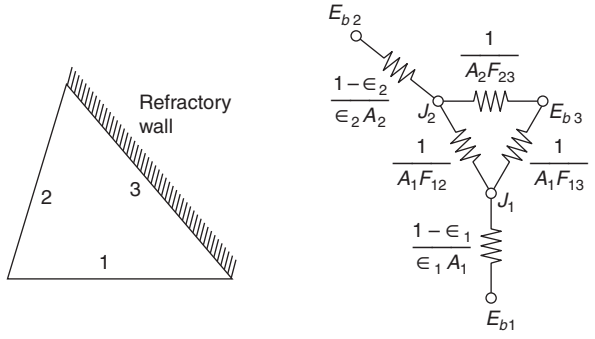

Figure 1-4.4. ***Network analogy for radiative exchange.***

Table 1-4.1 ***Common Configuration Factors***

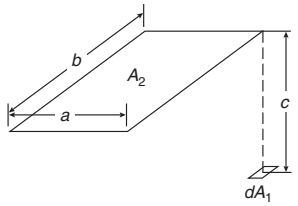

$$X = a/c \qquad Y = b/c$$

$$F_{d1-2} = \frac{1}{2\pi}\left[\frac{X}{\sqrt{1+X^2}}\tan^{-1}\left(\frac{Y}{\sqrt{1+X^2}}\right) + \frac{Y}{\sqrt{1+Y^2}}\tan^{-1}\left(\frac{X}{\sqrt{1+Y^2}}\right)\right]$$

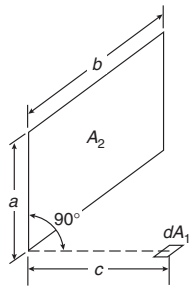

$$X = a/b \qquad Y = c/b \qquad A = 1/\sqrt{X^2+Y^2}$$

$$F_{d1-2} = \frac{1}{2\pi}\left[\tan^{-1}(1/Y) - AY\tan^{-1}A\right]$$

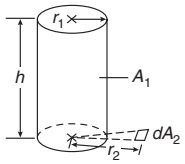

$$R = r_1/r_2 \qquad L = h/r_2 \qquad X = \sqrt{(1+L^2+R^2)^2 - 4R^2}$$

$$F_{d1-2} = \frac{1}{2\pi}\cos^{-1}R + \frac{1}{\pi}\left[\tan^{-1}\left(\frac{R}{\sqrt{1-R^2}}\right) - \frac{1+L^2-R^2}{X}\tan^{-1}\left(\frac{X\tan(0.5\cos^{-1}R)}{1+L^2+R^2-2R}\right)\right]$$

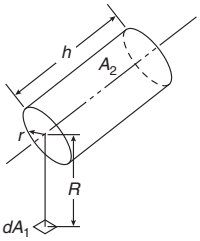

$$L = h/r \qquad H = R/r \qquad X = (1+H)^2 + L^2 \qquad Y = (1-H)^2 + L^2$$

$$F_{d1-2} = \frac{1}{\pi H}\tan^{-1}\left(\frac{L}{\sqrt{H^2-1}}\right) + \frac{L}{\pi}\left[\frac{X-2H}{H\sqrt{XY}}\tan^{-1}\sqrt{\frac{X(H-1)}{Y(H+1)}} - \frac{1}{H}\tan^{-1}\sqrt{\frac{H-1}{H+1}}\right]$$

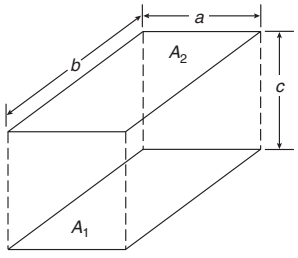

$$X = a/c \qquad Y = b/c$$

$$F_{1-2} = \frac{2}{\pi XY}\left[\ln\sqrt{\frac{(1+X^2)(1+Y^2)}{1+X^2+Y^2}} + X\sqrt{1+Y^2}\tan^{-1}\left(\frac{X}{\sqrt{1+Y^2}}\right) + Y\sqrt{1+X^2}\tan^{-1}\left(\frac{X}{\sqrt{1+X^2}}\right) - X\tan^{-1}X - Y\tan^{-1}Y\right]$$

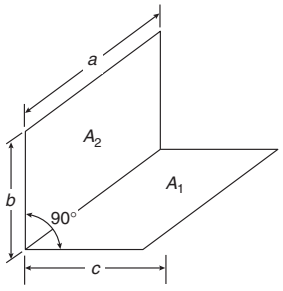

$$X = b/a \qquad Y = c/a$$

$$F_{1-2} = \frac{1}{\pi Y}\left(Y\tan^{-1}\left(\frac{1}{Y}\right) + X\tan^{-1}\left(\frac{1}{X}\right) - \sqrt{X^2+Y^2}\tan^{-1}\left(\frac{1}{\sqrt{X^2+Y^2}}\right) + \frac{1}{4}\ln\left\{\frac{(1+X^2)(1+Y^2)}{1+X^2+Y^2}\left[\frac{X^2(1+X^2+Y^2)}{(1+X^2)(X^2+Y^2)}\right]^{X^2}\left[\frac{Y^2(1+X^2+Y^2)}{(1+Y^2)(X^2+Y^2)}\right]^{Y^2}\right\}\right)$$

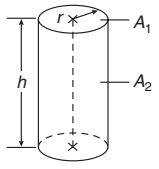

$$H = h2r$$

$$F_{1-2} = 2\left(\sqrt{1+H^2} - H\right)$$

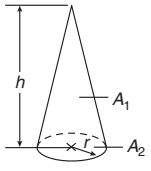

$$H = h/r$$

$$F_{1-2} = 1/\sqrt{1+H^2}$$

which accounts for the loss of intensity by absorption and the gain by emission, and where κ_λ denotes the extinction coefficient. The extinction coefficient is generally the sum of two parts: the absorption coefficient and the scattering coefficient. In many engineering applications, the effects of scattering are negligible and the extinction coefficient represents only absorption. The spectral emissivity for pathlength S in a uniform gas volume can be readily expressed by considering the case of no incident radiation (or $I_\lambda(0) = 0$)

$$\varepsilon_\lambda = \frac{I_\lambda}{I_{b\lambda}} = 1 - e^{-\kappa_\lambda S} \tag{20}$$

which compares the fraction of energy emitted to the maximum (blackbody) emission at the same temperature for the pathlength S through the material.

The term $\kappa_\lambda S$ in Equation 20, called the optical pathlength or opacity, can be defined more generally for nonhomogeneous media as

$$\tau_\lambda = \int_o^S \kappa_\lambda(x)\, dx \tag{21}$$

If $\tau_\lambda \ll 1$, the medium is optically thin at wavelength λ and the properties of the participating medium can generally be expressed with the very simple approximation $\varepsilon_\lambda \approx \tau_\lambda$. The medium is considered optically thick when $\tau_\lambda \gg 1$, which implies that the mean penetration distance is much less than the characteristic length of the medium. In optically thick media, the local radiant intensity results only from local emission and the equation of transfer can be approximated by a diffusion equation.

Total emissivity: Total emissivity is an average property over all wavelengths, defined by

$$\varepsilon_t = \frac{\pi}{\sigma T^4} \int_0^\infty \varepsilon_\lambda I_{b\lambda}\, d\lambda \tag{22}$$

At moderate temperatures up to about 2000 K (which is the range of interest for fire protection engineers), the total emissivity of combustion gases consists of contributions from discrete bands, with negligible contributions from wavelengths between the bands. It is thus convenient to use

$$\varepsilon\left(T, S, P_e\right) \approx \pi \sum_i \left(\frac{I_{\lambda bi}}{\sigma T^4}\right) \varepsilon_i\left(T, X, P_e\right) \tag{23}$$

where $I_{\lambda bi}$ is the blackbody intensity evaluated at the center of the ith band, and ε_i is the total band absorption defined by

$$\varepsilon_i = \int_{(\Delta\lambda)_i} \left(1 - e^{-\kappa_\lambda S}\right) d\lambda \tag{24}$$

Recent progress on band structure and absorption has made it possible to determine total emissivity information by both theoretical and experimental means. Engineers traditionally determine the total emissivity of a homogeneous gas by graphical interpolation from charts with temperature and pressure-pathlength as parameters. The total emissivity of a mixture of gases cannot be determined simply by adding the total emissivities of the various components, because the active spectral bands for a combination of gases will often overlap. The correction for band overlapping should be calculated from spectral information for each gas, which can be estimated from the wide-band model of Edwards.[10,11]

Mean absorption coefficient: The mean absorption coefficient is often useful when radiative energy transport theory must be used to describe the local state of a gas at various locations. The mathematical complexity involved in the calculations often dictates a solution based on the gray-gas assumption, where all radiation parameters are considered to be wavelength independent. Thus, solutions are given in terms of mean (gray-gas) absorption coefficients representing average properties over the whole spectrum of wavelengths. It has been well established that the appropriate mean absorption coefficients are the Planck mean, κ_P, for optically thin mediums, and the Rosseland mean, κ_R, for optically thick mediums.[4–6,9]

The Planck mean absorption coefficient is defined as

$$\kappa_P \equiv \frac{\int_0^\infty I_{b\lambda}\kappa_\lambda\, d\lambda}{\int_0^\infty I_{b\lambda}\, d\lambda} = \frac{\pi}{\sigma T^4} \int_0^\infty I_{b\lambda}\kappa_\lambda\, d\lambda \tag{25}$$

It is important to note that this form of the absorption coefficient is a function of temperature alone and is independent of pressure. The effect of the beam source temperature (e.g., a hot or cold wall) in the gas absorptivity is approximated by a simple ratio correction[9,11]

$$\kappa_m = \kappa_P(T_s)\frac{T_s}{T_g} \tag{26}$$

where T_s is the source temperature and T_g is the gas temperature. When the Planck mean absorption coefficient is used to estimate the emissivity of a gas, the source temperature is set equal to the gas temperature.

The formulation of radiative transfer becomes relatively simple when the medium is optically thick. In this case, the radiative transfer can be regarded as a diffusion process (the Rosseland or diffusion approximation), and the governing equation is approximated by

$$q_\lambda \approx -\frac{4}{3\kappa_\lambda}\frac{\partial e_{b\lambda}}{\partial S} \tag{27}$$

Evaluation of the total heat flux in an optically thick medium is simplified by defining an average absorption coefficient which is independent of wavelength

$$\frac{1}{\kappa_R} \equiv \int_0^\infty \frac{1}{\kappa_\lambda}\frac{de_{b\lambda}}{de_b} d\lambda \tag{28}$$

The Rosseland mean absorption coefficient is not well defined for gases under ordinary conditions, because astronomically long pathlengths are required to make the windows between the bands optically thick. The Rosse-

land limit is, however, useful when dealing with gases in the presence of soot particles, which are characterized by a continuous spectrum. The source temperature effect is accounted for by using Equation 26 in the same manner as for the Planck mean absorption coefficient.

The radiating gas in many actual fire systems is neither optically thin nor optically thick, so it is necessary to use band theory to calculate a mean absorption coefficient, κ_m. However, with a reasonable estimate of the mean absorption coefficient radiative transport calculations are much more convenient.

Mean beam length for homogeneous gas bodies: The concept of mean beam length is a powerful and convenient tool to calculate the energy flux from a radiating homogeneous gas volume to its boundary surface. It may also be used to approximate radiative energy flux for a nonhomogeneous gas, especially when more elaborate calculations are not feasible. Consider the coordinate system given in Figure 1-4.1, where dA is a differential area on the boundary surface of the gas body. The radiative heat flux from the gas body to dA is

$$q = \int_0^\infty \int_\Omega \varepsilon_\lambda(X) I_{b\lambda} \cos\theta \, d\lambda \, d\Omega \tag{29}$$

where the spectral emissivity, ε_λ, is a function of pressure pathlength

$$X \equiv \int_0^S P_a x(\xi) \, d\xi$$

which in turn varies with solid angle Ω according to the gas body geometry.

In practical situations, the calculation of q is more convenient in terms of total emissivity, which is often available in chart form. From the definition of total emissivity, Equation 29 can be expressed as

$$q = \frac{\sigma T^4}{\pi} \int_\Omega \varepsilon_t(X) \cos\theta \, d\Omega \equiv \sigma T^4 \varepsilon_t(L) \tag{30}$$

which gives the definition of mean beam length, L, for a gas body, where $\varepsilon_t(L)$ has the same functional form as $\varepsilon_t(X)$. Physically, the mean beam length represents the equivalent radius of a hemispherical gas body such that it radiates a flux to the center of its base equal to the average flux radiated to the boundary surface by the actual volume of gas. The determination of the mean beam length is considerably simplified when the gas is optically thin and only the geometry of the gas body enters the calculation. In the optically thin limit, it is convenient to define

$$L = L_0 \equiv \frac{1}{\pi} \int_\Omega X \cos\theta \, d\Omega \tag{31}$$

where L_0 is called the geometric mean beam length. In the optically thick limit, it has been found that the use of a simple correction factor provides reasonable radiative fluxes

$$L \approx C L_0 \tag{32}$$

In Table 1-4.2, L_0 and C have been provided for a variety of gas body shapes. For an arbitrarily shaped gas volume, the geometric beam length from the gas volume to the entire boundary surface can be estimated by

$$L_0 = \frac{4V}{A} \tag{33}$$

where V and A are the volume and the area of the boundary surface of the gas body, respectively. The correction factor C should be estimated as 0.9, which is close to the known values for a wide range of geometries.

Thermal Radiation Properties of Combustion Products

Radiation Properties of Gases

The emissivity of any gas is a strong function of wavelength, varying by as much as several orders of magnitude over minute changes in wave number. However, the level of accuracy required in engineering calculations, where many of the parameters are difficult to measure or estimate, seldom requires high resolution spectra of emissivity. Where wavelength dependence of the radiative heat flux is a concern, the properties of the gas may be calculated by means of the exponential wide-band model.[10] The uncertainties involved in estimating parameters to calculate radiative heat flux make average properties such as total emissivity a useful tool. The first comprehensive total emissivity charts were formulated by H. C. Hottel and coworkers to summarize work performed up to about 1945. Modern formulations for the emissivity of gases have been summarized by Edwards.[11]

New total emissivity charts for water vapor and carbon dioxide[11] have been provided in Figures 1-4.5 and 1-4.6, respectively. The gas emittance can be found from the charts by knowing the partial pressure and temperature of each gas and the mean beam length for the gas volume geometry. Correction factors for the chart emissivities are available in the literature for the pressure effect on water vapor emissivity,[12] the pressure effect on carbon dioxide emissivity,[4,6] and the band overlap for mixtures of the two gases.[13] For most fire protection engineering applications, the pressure correction factors are 1.0 and the band overlap correction is approximately $\Delta\varepsilon \approx 1/2\varepsilon_{CO_2}$ for medium to large fires. Assuming the carrier gas is transparent (e.g., air), the emittance is given by

$$\varepsilon_g = C_{H_2O}\varepsilon_{H_2O} + C_{CO_2}\varepsilon_{CO_2} - \Delta\varepsilon \approx \varepsilon_{H_2O} + \frac{1}{2}\varepsilon_{CO_2} \tag{34}$$

At temperatures below 400 K, the older charts by Hottel[4,6] may be more reliable than the new charts used in Figure 1-4.5 and Figure 1-4.6, and the use of wide-band models is advised to estimate the band overlap correction instead of using the correction charts at these lower temperatures.[14] For crucial engineering decisions, wide-band model block calculations as detailed by Edwards[11] are recommended over the graphical chart method to determine total emissivity.

Table 1-4.2 ***Mean Beam Lengths for Various Gas Body Shapes***

Geometry of Gas Body		Radiating to	Geometric Mean Beam Length L_0	Correction Factor C
Sphere	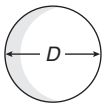	Entire surface	0.66 D	0.97
Cylinder $H = 0.5D$	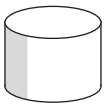	Plane and surface Concave surface Entire surface	0.48 D 0.52 D 0.50 D	0.90 0.88 0.90
Cylinder $H = D$	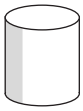	Center of base Entire surface	0.77 D 0.66 D	0.92 0.90
Cylinder $H = 2D$		Plane end surface Concave surface Entire surface	0.73 D 0.82 D 0.80 D	0.82 0.93 0.91
Semi-infinite cylinder $H \rightarrow \infty$	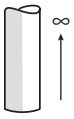	Center of base Entire base	1.00 D 0.81 D	0.90 0.80
Infinite slab	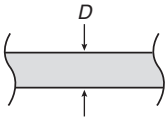	Surface element Both bounding planes	2.00 D 2.00 D	0.90 0.90
Cube $D \times D \times D$	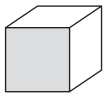	Single face	0.66 D	0.90
Block $D \times D \times 4D$		1 × 4 face 1 × 1 face Entire surface	0.90 D 0.86 D 0.89 D	0.91 0.83 0.91

Other gases such as sulphur dioxide, ammonia, hydrogen chloride, nitric oxide, and methane have been summarized in chart form.[4] The carbon monoxide chart by Hottel is not recommended for use according to recent measurements[15] and other theoretical investigations, probably due to traces of carbon dioxide in the original experiments. Recent results, including both spectral and total properties, have recently been published for some of the important hydrocarbon gases, for example, methane, acetylene, and propylene.[16–18] Mixtures of several hydrocarbon gases are subject to band overlapping, and appropriate corrections must be made to avoid overestimating total emissivity of a mixture of fuels.

The total emissivity for a gas in the optically thin limit can be calculated from the Planck mean absorption coefficient. Graphs of the Planck mean absorption coefficient for various gases that are important in fires are shown in Figure 1-4.7, which can be used with Equation 20 to estimate the total emissivity (by assuming that total properties represent a spectral average value).

Radiation Properties of Soot

In a nonhomogeneous (e.g., with soot) medium, scattering becomes an important radiative mechanism in addition to absorption and emission. The absorption and scattering behavior of a single particle can be described by solving the electromagnetic field equations; however, many physical idealizations and mathematical approximations are necessary. The most common assumptions include perfectly spherical particles, uniformly or randomly

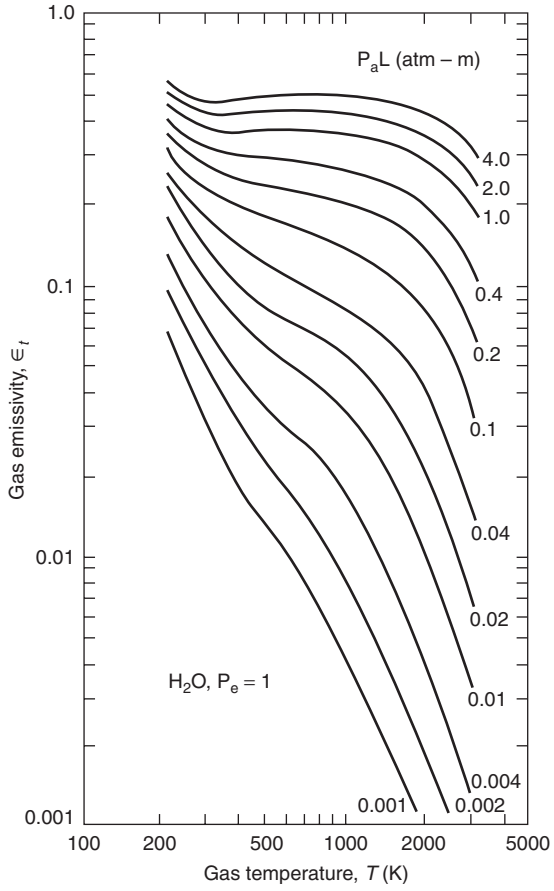

Figure 1-4.5. ***Total emittance of water vapor.***

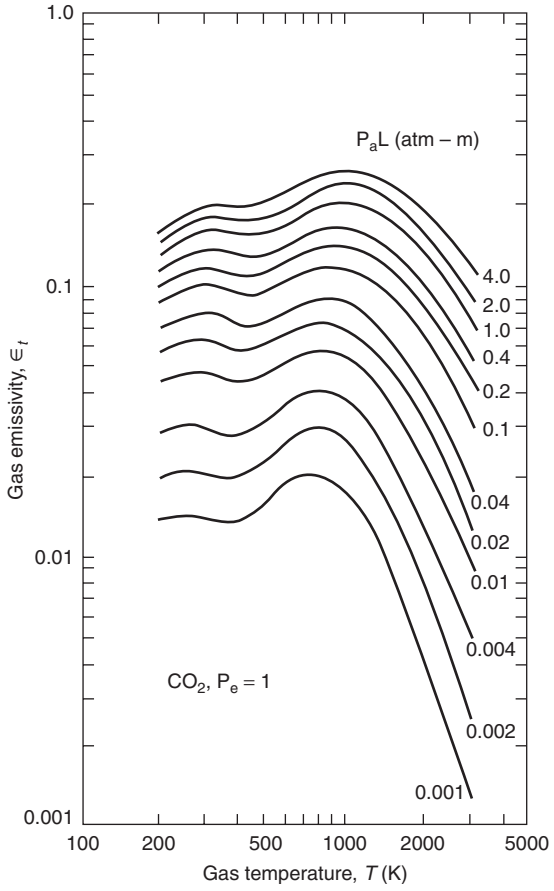

Figure 1-4.6. ***Total emittance of carbon dioxide.***

distributed particles, and interparticle spacing so large that the radiation for each particle can be treated independently.

Soot particles are produced as a result of incomplete soot combustion and are usually observed to be in the form of spheres, agglomerated chunks, and long chains. They are generally very small (50–1000 Å where 1 Å = 10^{-10} m = 10^{-4} μm) compared to infrared wavelengths, so that the Rayleigh limit is applicable to the calculation of radiation properties.[19,20] Soot particles are normally characterized by their optical properties, size, shape, and chemical composition (hydrogen-carbon ratio). From a heat transfer viewpoint, radiation from a soot cloud is predominantly affected by the particle size distribution and can be considered independent of the chemical composition.[19] Soot optical properties are relatively insensitive to temperature changes at elevated temperatures, but as shown in Figure 1-4.8, room temperature values representative of soot in smoke do show appreciable deviations. By choosing appropriate values of optical constants for soot, the solution for the electromagnetic field equations gives[21]

$$k_\lambda = \frac{C_0}{\lambda} f_v \tag{35}$$

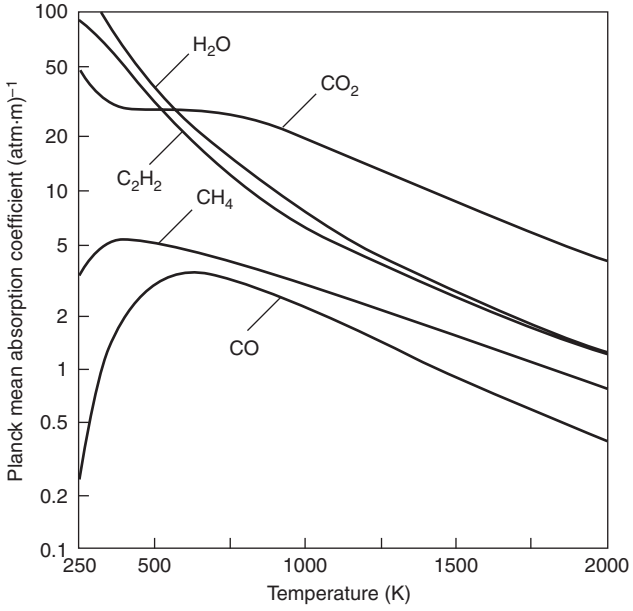

Figure 1-4.7. ***Planck mean absorption coefficient for various gases.***

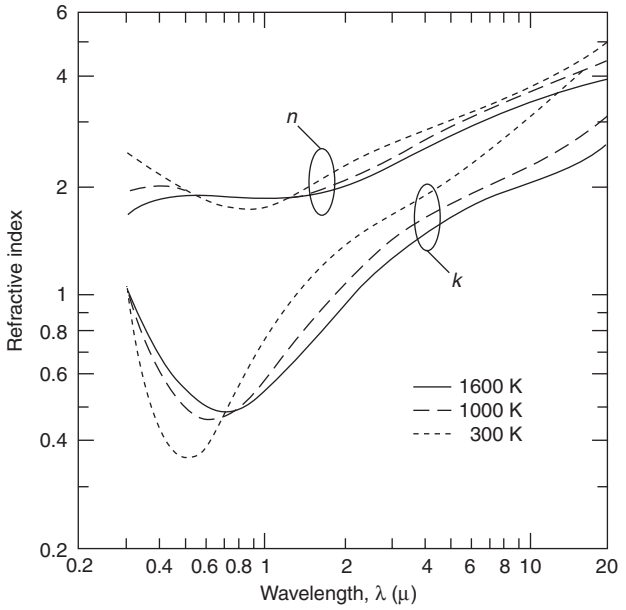

Figure 1-4.8. ***Optical constants for soot.***

where f_v is the soot volume fraction (generally about 10^{-6}), and C_0, a constant between 2 and 6 dependent on the complex index of refraction $m = n - ik$, is given by

$$C_0 = \frac{36\pi nk}{(n^2 - k^2 + 2)^2 + 4n^2k^2} \tag{36}$$

Equations 35 and 36 can be used to evaluate the Planck mean absorption coefficient in the optically thin limit,[22] giving

$$\kappa_P = 3.83 \frac{C_0}{C_2} f_v T \tag{37}$$

where C_2 is Planck's second constant (1.4388×10^{-2} m·K). The Rosseland mean absorption coefficient in the optically thick limit is

$$\kappa_R = 3.6 \frac{C_0}{C_2} f_v T \tag{38}$$

A mean coefficient that may be used for the entire range of optical thickness is suggested as

$$\kappa_m = 3.72 \frac{C_0}{C_2} f_v T \tag{39}$$

to be used in Equation 40 for the soot radiation calculations. Typical temperatures, volume fractions, and mean absorption coefficients for soot particles in the luminous flames of various fuels are tabulated in Table 1-4.3.[21,23]

Radiation Properties of Gas-Soot Mixtures

The calculation of the total emissivity of a gas-soot mixture requires information on basic flame parameters such as soot volume fraction, the absorption coefficient of the soot, the temperature and geometric length of the flame, and the partial pressure of the participating gas components.[24] These parameters can be estimated for various types of fuel when actual measurements are unavailable for a particular situation. Recent research to develop simple accurate formulas to predict total emissivities for homogeneous gas-soot mixtures has found the following equation to be an excellent approximation[23]

$$\varepsilon_t = (1 - e^{-\kappa S}) + \varepsilon_g e^{-\kappa_s S} \tag{40}$$

where

S = physical pathlength
ε_g = total emissivity of the gas alone
κ_s = effective absorption coefficient of the soot

The Planck mean absorption coefficients for gas-soot mixtures in luminous flames and smoke are shown in Figure 1-4.9. In situ measurements are currently the only way other than estimation to obtain the soot volume fraction in smoke, since the soot particle concentration can be either diluted or concentrated by the gas movements within the smoke region.

Table 1-4.3 ***Radiative Properties for Soot Particles***

	Fuel, Composition	κ_s (m^{-1})	$f_v \times 10^6$	T_s (K)
Gas fuels	Methane, CH_4	6.45	4.49	1289
	Ethane, C_2H_6	6.39	3.30	1590
	Propane, C_3H_8	13.32	7.09	1561
	Isobutane, $(CH_3)_3CH$	16.81	9.17	1554
	Ethylene, C_2H_4	11.92	5.55	1722
	Propylene, C_3H_6	24.07	13.6	1490
	n-butane, $(CH_3)(CH_2)_2(CH_3)$	12.59	6.41	1612
	Isobutylene, $(CH_3)_2CCH_2$	30.72	18.7	1409
	1,3-butadiene, $CH_2CHCHCH_2$	45.42	29.5	1348
Solid fuels	Wood, $\approx (CH_2O)_n$	0.8	0.362	1732
	Plexiglas, $(CH_5H_8O_2)_n$	0.5	0.272	1538
	Polystyrene, $(C_8H_8)_n$	1.2	0.674	1486

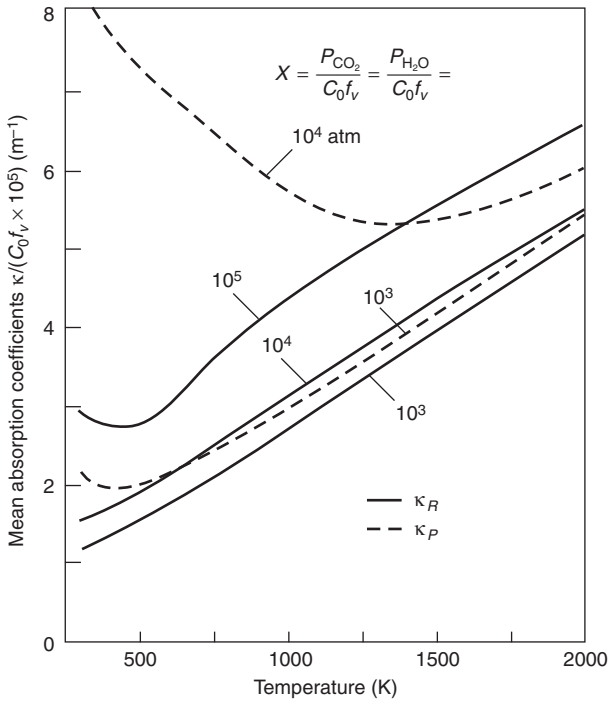

Figure 1-4.9. ***Mean absorption coefficients for luminous flames and smoke.***

Application to Flame and Fire

Heat Flux Calculation from a Flame

Prediction of the radiative heat flux from a flame is important in determining ignition and fire spread hazard, and in the development of fire detection devices. The shape of flames under actual conditions is arbitrary and time dependent, which makes detailed radiation analysis very cumbersome and uneconomical. In most calculations, flames are idealized as simple geometric shapes such as plane layers or axisymmetric cylinders and cones. A cylindrical geometry will be analyzed here and used in a sample calculation.

Assuming κ_λ is independent of pathlength, integration of the radiative transport of Equation 10 yields[25]

$$I_\lambda = I_{b\lambda}\left[1 - \exp\left(\frac{-2\kappa_\lambda}{\sin\theta}\sqrt{r^2 - L^2\cos^2\phi}\right)\right] \tag{41}$$

where θ, ϕ, r and L are geometric variables defined in Figure 1-4.10. The monochromatic radiative heat flux on the target element is given by

$$\frac{dq}{d\lambda} = \int_\Omega \frac{I_\lambda}{|\vec{R}|}(\vec{n}\cdot\vec{R})\,d\Omega \tag{42}$$

where $\vec{n}$ is a unit vector normal to the target element dA and $\vec{R}$ is the line-of-sight vector extending between dA and the far side of the flame cylinder. The evaluation of Equation 42 is quite lengthy, but under the condition of $L/r \gtrsim 3$, it can be simplified to[25]

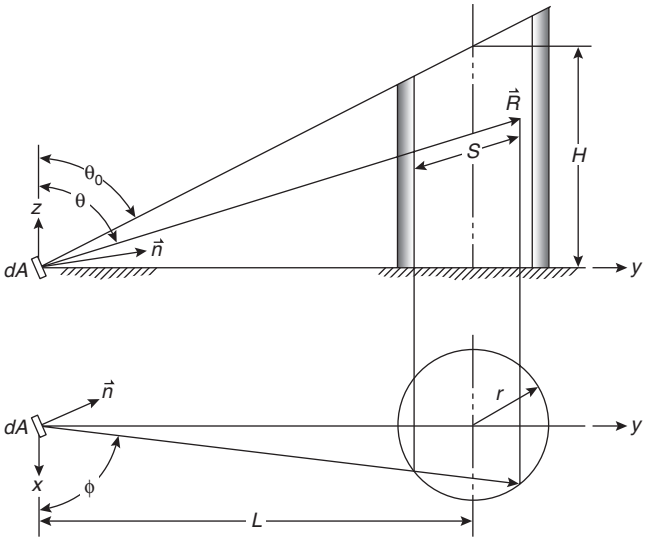

Figure 1-4.10. ***Schematic of a cylindrical flame.***

$$\frac{dq}{d\lambda} = \pi I_{b\lambda}\varepsilon_\lambda(F_1 + F_2 + F_3) \tag{43}$$

where the shape factor constants and emittance are defined as

$$F_1 = \frac{u}{4\pi}\left(\frac{r}{L}\right)^2[\pi - 2\theta_0 + \sin(2\theta_0)] \tag{44a}$$

$$F_2 = \frac{v}{2\pi}\left(\frac{r}{L}\right)[\pi - 2\theta_0 + \sin(2\theta_0)] \tag{44b}$$

$$F_3 = \frac{w}{\pi}\left(\frac{r}{L}\right)\cos^2\theta_0 \tag{44c}$$

$$\varepsilon_\lambda = 1 - \exp\left(-0.7\,\mu_\lambda\right) \tag{45}$$

The parameters in the definitions are given by

$$\theta_0 = \tan^{-1}\left(\frac{L}{H}\right) \tag{46a}$$

$$\mu_\lambda = 2r\,\frac{\kappa_\lambda}{\sin(1/2\theta_0 + 1/4\pi)} \tag{46b}$$

$$\vec{n} = u\vec{i} + v\vec{j} + w\vec{k} \tag{46c}$$

If the flame is considered to be homogeneous and Equation 43 is integrated over all wavelengths, the total heat flux is simply

$$q = \varepsilon_m E_b \sum_{j=1}^{3} F_j \tag{47}$$

EXAMPLE 1:

A fire detector is located at the center of the ceiling in a room (2.4 × 3.6 × 2.4 m) constructed of wood. (See

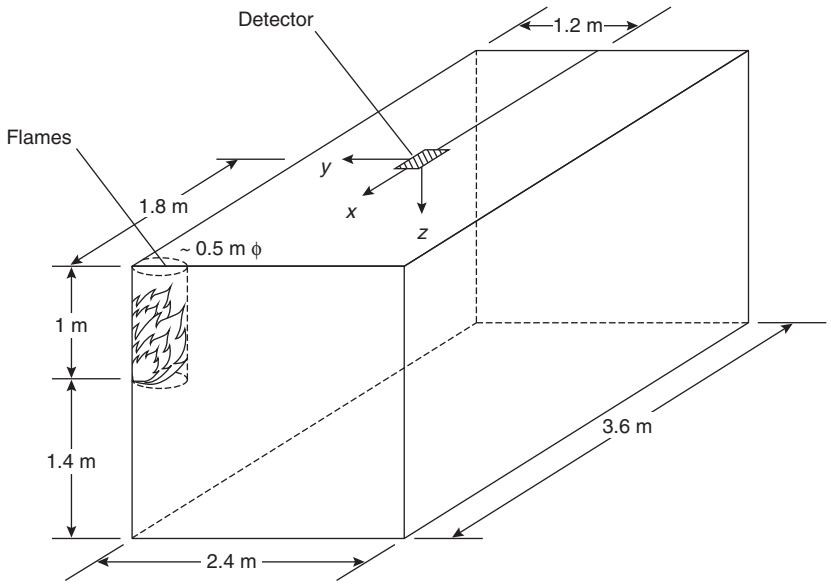

Figure 1-4.11. ***Example calculation for flux to target element from flame.***

Figure 1-4.11.) The sprinkler system is capable of extinguishing fires smaller than 0.5 m in diameter × 1.0 m high. For this example, determine the appropriate heat flux setting for the detector, using a worst case scenario of ignition in one of the upper ceiling corners.

SOLUTION:

First, the condition of $L/r \gtrsim 3$ should be checked to verify that the previous analysis is applicable.

$$\frac{L}{r} = \frac{\sqrt{(1.2^2) + (1.8^2)}}{0.25} = 8.65 > 3$$

The unit normal vector to the detector is given by $\vec{n} = \vec{k}$, the polar angle $\theta_0 = \tan^{-1}(1.818) = 1.068$ is determined from Equation 46a, and the shape factors are evaluated from Equations 44a, b, and c

$$F_1 = F_2 = 0.0$$
$$F_3 = \frac{1}{\pi}\left(\frac{0.25}{1.818}\right)\cos^2(1.068) = 0.0102$$

From Equation 47, the required heat flux can be obtained as

$$\begin{aligned} q &= \left(1 - e^{-\kappa_m S}\right)(\sigma T_f^4)F_3 \\ &= \left(1 - e^{0.8\times 0.5}\right)\left[5.67 \times 10^{-11} \times (1730)^4\right](0.0102) \\ &= 1.7 \text{ kW/m}^2 \end{aligned}$$

If the geometry of the example had been $L/r < 3$, it would have been necessary to interpolate between the $L/r = 3$ case and the $L/r = 0$ case, which has been obtained accurately.[6,25] If the detector is pointed directly at the burning corner in this example (i.e., $\vec{n} = 0.55\vec{i} + 0.83\vec{j}$), the calculated heat flux jumps to 9.0 kW/m², showing the strong influence of direction in calculations of radiation heat transfer.

Heat Flux Calculation from a Smoke Layer

Consider radiative heat transfer in a room fire situation where a smoke layer is built up below the ceiling. Typical smoke layers are generally at temperatures ranging up to 1100–1500 K, and are composed of strongly participating media such as carbon dioxide, water vapor, and soot particles. Heat flux from the smoke layer has been directly related to ignition of remote surface locations such as furniture or floor carpets. The schematic in Figure 1-4.12 will be considered in a radiative transport analysis and example calculation. The calculation is based on a considerably simplified formulation which provides reasonable results with only a small penalty in accuracy.

Integration of Equation 10 over the pathlength S through the smoke layer yields

$$I(S) = \frac{\sigma T^4}{\pi}\left\{1 - \left(\frac{T_w}{T}\right)^4\right\} e^{-\kappa S} \tag{48}$$

The monochromatic radiative heat flux on a differential target element is again given by Equation 42. However, for the present geometry of the ceiling layer and enclosure surface, integration of Equation 42 is quite time-consuming since the upper and lower bounds of the integral vary with the angle of the pathlength. The calculation can be simplified by assuming as a first order approximation that the lower face of the smoke layer is an isothermal surface. Using this assumption, the problem can be handled using the simple relations of radiative exchange in a nonparticipating medium between gray surfaces (the absorption of the clear air below the smoke layer is negligible). From basic

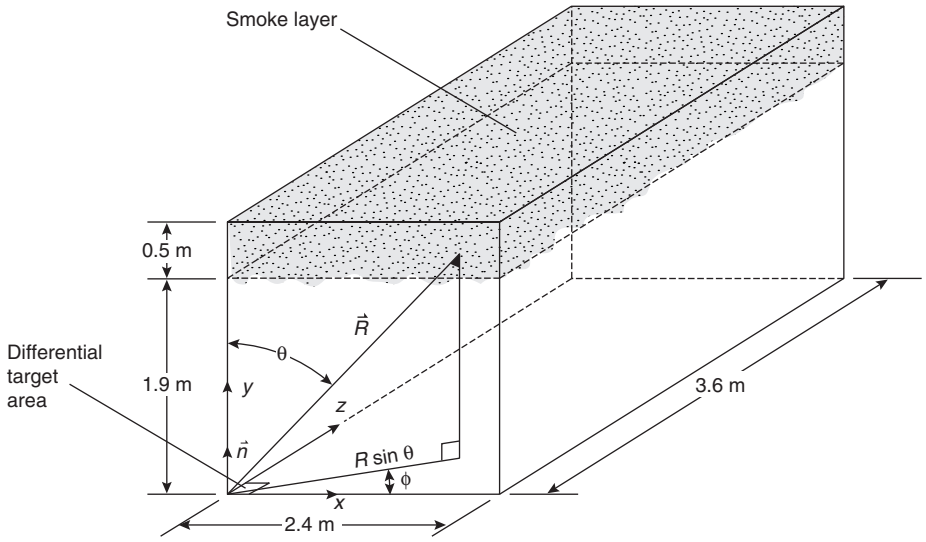

Figure 1-4.12. ***Example calculation for flux to target element from smoke layer.***

calculation methods we have the radiosity and the irradiation of each surface in the enclosure:

$$J_i = \varepsilon_i \sigma T_i^4 + (1 - \varepsilon_i) G_i \tag{49a}$$

$$G_i = \sum_j F_{i-j} J_j \tag{49b}$$

After solving the simultaneous equations for all J_i and G_i, the net heat flux on any of the surfaces can be calculated from

$$q_i = J_i - G_i \tag{50}$$

EXAMPLE 2:

A smoke layer 0.5 m thick is floating near the ceiling of a room with dimensions of 3.6 × 2.4 × 2.4 m. (See Figure 1-4.12.) The floor is made from wood, and the four side walls are concrete covered with zinc white oil paint. The calculation will determine the heat flux in a bottom corner of the room, assuming that each surface in the enclosure is kept at constant temperature: the smoke layer at 1400 K, the side walls at 800 K, and the floor at 300 K. Assume there is a differential target area 0.01 m² in one of the corners of the floor, and also at the floor temperature of 300 K.

SOLUTION:

The bottom of the smoke layer will be designated surface 1, the floor will be surface 2, and the differential target area in the bottom corner will be surface 3. Only four surfaces are required since the four side walls can be treated as a single surface 4. Shape factors F_{12} and F_{31} can be found in Table 1-4.1, and from these two factors, the remaining shape factors are determined by shape factor algebra:

$$F_{12} = 0.3242,$$
$$F_{31} = 0.1831,$$
$$F_{13} = \frac{A_3}{A_1} F_{31} = 0.0002,$$
$$F_{14} = 1 - F_{12} - F_{13} = 0.6756$$

Continuing in a similar fashion, the other shape factors are obtained as

$F_{21} = 0.3242$	$F_{31} = 0.1831$	$F_{41} = 0.2560$
$F_{22} = 0$	$F_{32} = 0$	$F_{42} = 0.2561$
$F_{23} = 0$	$F_{33} = 0$	$F_{43} = 0.0003$
$F_{24} = 0.6758$	$F_{34} = 0.8169$	$F_{44} = 0.4876$

The emissivity for wood and white zinc paint are 0.9 and 0.94, respectively,[6] and the emissivity for the smoke layer can be estimated from the mean absorption coefficient for a wood flame (Table 1-4.3) as

$$\varepsilon_1 = 1 - e^{-\kappa_m S} = 1 - e^{-0.8 \times 0.5} = 0.33$$

The blackbody emission flux from each surface is calculated by the simple relation of Equation 6, for example,

$$(\sigma T^4)_1 = 5.6696 \times 10^{-8} (1400)^4 = 217.8 \text{ kW/m}^2$$

From Equations 49a and 49b, the radiative fluxes to and from each surface are determined by solving the eight simultaneous equations

$J_1 = 88.7$ kW/m²	$G_1 = 17.7$ kW/m²
$J_2 = 4.7$ kW/m²	$G_2 = 43.3$ kW/m²
$J_3 = 3.9$ kW/m²	$G_3 = 34.8$ kW/m²
$J_4 = 23.9$ kW/m²	$G_4 = 34.3$ kW/m²

The net radiative heat flux on the target element from Equation 50 is

$$q_3 = J_3 - G_3 = -30.9 \text{ kW/m}^2$$

where the negative sign indicates that heat must be removed from the target element so it remains in equilibrium. This example also could have been solved by the resistance network method. (See Figure 1-4.13.)

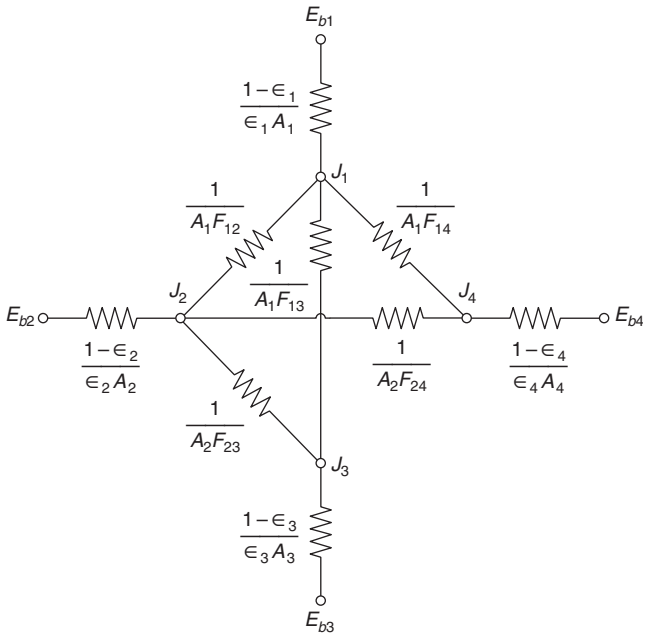

Figure 1-4.13. ***Equivalent resistance network for an enclosure problem.***

Fuel Pyrolysis Rate

Fuel pyrolysis is an important concern in the combustion of condensed fuels, which upon heating undergo gasification (sometimes preceded by liquefication for solid fuels) before combustion in the gaseous phase.[26] This process is often strongly influenced by radiative heat flux. Unlike an internal combustion engine or burner where the fuel is supplied externally, the fuel must be supplied by gasification of the material itself. The rate of gasification is sometimes called the pyrolysis rate or burning rate, and can serve as a measure of fire hazard since it is directly proportional to the growth rate of the fire. Because determination of the pyrolysis rate is based on conservation of energy and mass at the surface of the material, it is essential to know the total heat flux reaching the fuel surface. Assuming steady-state conditions, the energy balance can be expressed as

$$q_e + q_c + q_r + q_{rr} = \dot{m}''\Delta H \tag{51}$$

where

q = heat flux (the subscripts are external, convective, radiative, and reradiative, respectively)

$\dot{m}''$ = pyrolysis rate

ΔH = latent heat of gasification

The configuration of the fire and the thermophysical properties of the fuel are required to calculate the terms in the energy balance, with the exception of the external flux term, which represents heat exchanged with the environment away from the fire.

Analysis of turbulent combustion with radiation in three-dimensional systems has been an ultimate research goal in the field of combustion for many years. Despite recent progress, the current state of the art is capable of handling only very limited problems in laminar combustion and turbulent combustion in simple geometries. Thermal radiation has been included in only a few special cases such as analysis of stagnation point combustion in boundary layer type flows,[27,28] and empirical studies of pool fire configurations.[29] In this section two cases will outline incorporating radiation into modeling the fuel pyrolysis rate, which can be applied to fire growth rate estimates.

Some basic concepts of the combustion phenomenon should be reviewed. Flames are often categorized as either diffusion or premixed, depending on the dominant physical processes controlling the burning. In a diffusion flame, the characteristic time for transport of the species is much longer than that required for the chemical reaction. Flames in which the oxygen initially separated from the fuel are generally considered to be diffusion flames. In a premixed flame, the fuel and oxygen are mixed together before reaching the combustion zone, so the characteristic times for transport and reaction are comparable in magnitude. The details of the chemical reaction, which even for simple reactions often involve many intermediate reactions and species conservation of intermediate products, are usually simplified in radiation analysis to a one-step irreversible global relationship such as

$$\text{fuel} + \text{oxygen} \rightarrow \text{products} + \text{heat} \tag{52}$$

Another major simplification that is frequently used is the flame sheet approximation, where it is assumed that the fuel and oxygen react nearly instantaneously upon contact, thus forming an infinitely thin reaction zone. This approximation is quite useful in the study of flames where the chemical reaction kinetics are dominated by the physical process of diffusion, such as a typical room fire. The counterpart to the flame sheet approximation is the flame layer approximation, where the chemical reaction is assumed to take place at a finite rate and creates a reaction zone of finite thickness. The flame layer approximation is applicable to the study of ignition, extinction, flame stability, and other transient flame phenomena.

Pyrolysis rate in boundary layer combustion: Due to the complicated nature of radiative calculations, only one-dimensional radiation in the limit of an optically thin medium has been attempted in boundary layer analysis. Kinoshita and Pagni[27] analyzed stagnation point flow under the approximations of the flame sheet model, unity Lewis number, and film optical depth of less than 0.1. The net effect of radiation heat transfer on the pyrolysis process was small, which is to be expected in an optically thin convective environment; however, the relative importance of the dimensionless parameters governing pyrolysis was dramatically altered by the inclusion of radiation in the analysis. The pyrolysis rate and excess (unburned) pyrolyzed gases were strongly dependent on both the wall temperature and the heat of combustion, which had been of secondary importance in the nonradiative analysis. In general, the effect of radiation is to reduce the pyrolysis rate by compensatory surface emission and by radiative loss from the flame to the cold environment, which lowers the flame temperature and decreases the conduction heat flux.

Pyrolysis rate in a pool fire: Applying energy conservation to find the fuel pyrolysis rate in a pool fire has been difficult due to a lack of appropriate information on both convective heat transfer and radiative feedback. Prediction of the pyrolysis rate is still largely dependent on correlations of limited experimental data, but effort has been made to theoretically formulate the convective and radiative contributions.[29] The pyrolysis rate can be calculated from Equation 51, assuming that the external heat supply can be neglected and the radiation terms are given by

$$q_{rr} = \varepsilon_s \sigma (T_s^4 - T_\infty^4) \tag{53}$$

$$q_r = \sigma T_f^4 [1 - e^{\kappa_f L_m}] \tag{54}$$

where ε_s is the fuel surface emissivity (typically 1.0 for liquids and char) and T_f is the flame temperature as represented by a homogeneous isothermal gas volume. The accuracy of Equation 54 is dependent on the values chosen for the flame absorption coefficient, κ_f, and the mean beam length, L. Orloff and deRis[29] have proposed the use of

$$\kappa_f = \frac{-1}{L_m} \ln \left(1 - \frac{\chi r \dot{q}_a''' L_m}{36 \chi_a \sigma T_f^4} \right) \tag{55}$$

$$L_m = 3.6 \frac{V_f}{A_b} \tag{56}$$

where

χ_α = fractional measure of the completeness of combustion lying in the range 0.6 to 0.95 depending on the type of fuel[30]

χ_r = fraction of heat lost by radiation in the flame[1,29,30]

$\dot{q}_a'''$ = volumetric heat output of the flame (typically on the order of 1200 kW/m^3 in many flames)

V_f = flame volume

T_f = flame temperature

A_b = area of the pool of fuel

Orloff and deRis also proposed an expression for the convective heat flux

$$q_c = \frac{h_c}{C_p} \left[\frac{\Delta H (\chi_a - \chi_r) r}{x_a} - C_p (T_s - T_\infty) \right] \left(\frac{y}{e^y - 1} \right) \tag{57}$$

where y is defined to be

$$\left(\frac{m'' C_p}{h_c} \right)$$

and r is the stoichiometric mass ratio of fuel to air.

Large-scale fires are distinctly nonhomogeneous in both temperature and gas species concentrations, which makes single-zone flame models difficult to correlate to the available experimental data. A two-zone model has recently been proposed;[31] it successfully predicts the pyrolysis rate of large PMMA (Plexiglas) fires. The flame is modeled as two conical homogeneous layers: a lower cool layer of pyrolyzed fuel gases, and an upper hot layer of product gases and soot. More experimental data on large-scale pool fires is required to verify the model for fuels other than PMMA.

Ignition Applications

Ignition is a branch of flammability-limiting behavior concerned with the initiation of burning. Ignition is a rate-controlled mechanism in which chemical reaction kinetics play an important role. Prediction of ignition phenomena is largely dependent on the ignition criteria chosen in the analysis.[26] These criteria are currently the center of a vigorous controversy and far from being uniquely defined. Many practical applications of ignition theory are based on knowledge of the ignition temperature, which in turn makes the heat flux directed at the fuel surface the most important physical quantity. Fire prediction often requires the determination of the ignition delay time after the fuel surface is exposed to a given heat flux. The transient nature of ignition makes it necessary to consider full transient energy equations unless the quasi-steady assumption can be invoked, which makes radiation analysis extremely difficult for many ignition applications.

Pilot ignition and spontaneous ignition are two of the main classes in the broad category of ignition. Pilot ignition is generally achieved through localized heating such as a spark or pilot flame, and the flame then propagates into the rest of the fuel material. In contrast, spontaneous or self-ignition occurs as a result of raising the bulk temperature of a combustible gas mixture, and does not require any further external heat supply once combustion has started. Spontaneous ignition requires a higher temperature for the same material than pilot ignition. Radiation heat transfer has generally been neglected in analyses of these mechanisms due to a lack of physical understanding and practical calculation methods,[32] and more work is required in this area to make the radiation calculations worthwhile.

A somewhat different phenomenon occurs in enclosure fires, where excessive radiant heat supply from the fire ignites material away from the flames. This is called secondary or remote ignition and is of special interest to fire protection engineers as a significant source of flame propagation. Quasi-steady analysis, where the gas is treated with a steady analysis and the solid fuel is handled with a transient analysis, has been shown to yield reasonably accurate results.[33] The chemical reaction terms can be neglected for a first order analysis, although they often play an important role in higher order models.

The relatively simple geometry of a semi-infinite solid bounded by a gas can illustrate a one-dimensional radiative analysis.[34] Attention will be focused on the solid region near the interface, so that the transient energy conservation equation is expressed as

$$\frac{\partial T}{\partial t} = \alpha \frac{\partial^2 T}{\partial x^2} \tag{58}$$

where α is the thermal diffusivity of the solid. The boundary conditions for Equation 58 are given by

$$T = T_i \qquad \text{at } t = 0, \quad x \to \infty \tag{59a}$$

$$k \frac{\partial T}{\partial x} + \varepsilon_s q_r = h_c (T - T_i) \quad \text{at } x = 0 \tag{59b}$$

Equation 59b states that conduction, convection, and radiation will be balanced at the fuel surface, and Equation 59a dictates the temperature level. Solution of Equation 58

is straightforward with the Laplace transform technique, giving the result[35]

$$T(x,t) = \left(T_i + \frac{\varepsilon_s q_r}{h_c}\right)\left[\operatorname{erfc}\left(\frac{x}{2\sqrt{\alpha t}}\right) - \exp\left(h_c x + \alpha h_c^2 t\right)\operatorname{erfc}\left(\frac{x}{2\sqrt{\alpha t}} + \frac{h_c}{k}\sqrt{\alpha t}\right)\right] \quad (60)$$

The ignition delay time (from initial application of the heat flux) can be accurately calculated from Equation 60 if the radiant heat flux, q_r, is known. The ignition delay time calculation is significantly affected by changes in q_r, which is dependent on the radiation properties of the smoke layer beneath the ceiling flames and the relatively cool pyrolyzed gases near the fuel surface. This effect is called radiation blockage or radiation blanketing, and is a current area of attention in the field of flame radiation research.[36] The blockage effect can be accurately calculated if the composition and properties of the smoke layer are known.[34] Another form of thermal energy blockage to the fuel surface is the surface emissivity, ε_s, which can have strong wavelength dependence. For example, a fuel such as PMMA is a poor absorber of radiation in wavelengths below 2.5 μm, where the radiant intensity is strongest from typical flame and smoke temperatures, and is an excellent absorber at wavelengths above 2.5 μm. In addition, the total emissivity of a surface can change as the fuel surface liquefies or begins to char due to pyrolysis. Care should be taken when considering the radiative properties of the fuel surface, which can be strongly dependent on the surface conditions.

Nomenclature

A	area (m^2)
C	correction factor for mean beam length
C_0	soot concentration parameter
C_p	specific heat (J/kg·K)
C_2	Planck's second constant (1.4388×10^{-2} m·K)
c	speed of light in the medium (m/s)
c_0	speed of light in a vacuum (2.998×10^8 m/s)
E	radiative emmisive power (W/m^2)
F_{i-j}	configuration factor from surface i to surface j
f_v	soot volume fraction
G	irradiation or radiative heat flux received by surface (W/m^2)
H	height (m)
h	Planck's constant (6.6256×10^{-34} J·s)
h_c	convective heat transfer coefficient ($W/m^2 \cdot K$)
I	radiation intensity (W/m^2)
$\vec{i}, \vec{j}, \vec{k}$	Cartesian coordinate direction vectors
J	radiosity or radiative heat flux leaving surface (W/m^2)
k	Boltzmann constant (1.3806×10^{-23} J/K), or infrared optical constant of soot (imaginary component), or thermal conductivity (W/m·K)
L	mean beam length or distance (m)
L_0	geometrical mean beam length (m)
M_i	molecular weight of species i
m''	mass loss rate or pyrolysis rate ($kg/m^2 \cdot s$)
n	index of refraction (c_0/c) or infrared optical constant of soot (real component)
$\vec{n}$	unit normal vector
P_a	partial pressure of absorbing gas (Pa)
P_e	effective pressure (Pa)
Q	energy rate (W)
q	heat flux (W/m^2)
q_a'''	volumetric heat output (W/m^3)
$\vec{R}$	line of sight vector
r	radius of cylinder (m) or fuel/air stoichiometric mass ratio
S	pathlength (m)
T	temperature (K)
t	time (s)
u, v, w	Cartesian components of unit vector $\vec{n}$ volume (m^3)
X	Pressure pathlength, $\int_0^s P_a x(\xi)\, d\xi$ (atm·m)
x	spatial coordinate (m)
y	defined parameter, Equation 57

Greek Symbols

α	absorptivity or thermal diffusivity $k/\rho C_p$ (m^2/s)
β	angle from normal (radians)
ΔH	latent heat of gasification (J/kg)
ε	emissivity
θ	polar angle (radians)
κ	extinction coefficient or absorption coefficient (m^{-1})
λ	wavelength (m)
μ	micron (10^{-6} m)
μ_λ	defined parameter, Equation 46b
ν	frequency (s^{-1})
ξ	integration dummy variable
ρ	reflectivity or density (kg/m^3)
Ω	solid angle (steradians)
σ	Stefan-Boltzmann constant (5.6696×10^{-8} $W/m^2 \cdot K^4$)
τ	transmissivity or optical pathlength
ϕ	azimuthal angle (radians)
χ	fractional measure

Subscripts

a	actual
b	blackbody or base
c	convective
e	external
f	flame or fuel
g	gas
i	initial or ith surface

j	summation variable or jth surface
m	mean value
0	original
P	Planck mean
R	Rosseland mean
r	radiative
rr	reradiative
s	surface or soot
t	total
w	wall
λ	spectral wavelength
ν	spectral frequency
∞	ambient

References Cited

1. J. deRis, *17th Symposium (International) on Combustion,* 1003, Combustion Institute, Pittsburgh, PA (1979).
2. S.C. Lee and C.L. Tien, *Prog. Energy Comb. Sci.,* 8, p. 41 (1982).
3. G.M. Faeth, S.M. Jeng, and J. Gore, in *Heat Transfer in Fire and Combustion Systems,* American Society of Mechanical Engineers, New York (1985).
4. H.C. Hottel and A.F. Sarofim, *Radiative Heat Transfer,* McGraw-Hill, New York (1967).
5. E.M. Sparrow and R.D. Cess, *Radiation Heat Transfer,* McGraw-Hill, New York (1978).
6. R. Siegel and H.R. Howell, *Thermal Radiation Heat Transfer,* McGraw-Hill, New York (1981).
7. J.R. Howell, *A Catalog of Radiation Configuration Factors,* McGraw-Hill, New York (1982).
8. C.L. Tien, in *Handbook of Heat Transfer Fundamentals,* McGraw-Hill, New York (1985).
9. C.L. Tien, *Advances in Heat Trans.,* 5, p. 253 (1968).
10. D.K. Edwards, *Advances in Heat Trans.,* 12, p. 115 (1976).
11. D.K. Edwards, in *Handbook of Heat Transfer Fundamentals,* McGraw-Hill, New York (1985).
12. C.B. Ludwig, W. Malkmus, J.E. Reardon, and J.A.L. Thompson, *Handbook of Radiation from Combustion Gases,* NASA SP-3080, Washington, DC (1973).
13. T.F. Smith, Z.F. Shen, and J.N. Friedman, *J. Heat Trans.,* 104, p. 602 (1982).
14. J.D. Felske and C.L. Tien, *Comb. Sci. Tech.,* 11, p. 111 (1975).
15. M.M. Abu-Romia and C.L. Tien, *J. Quant. Spec. Radiat. Trans.,* 107, p. 143 (1966).
16. M.A. Brosmer and C.L. Tien, *J. Quant. Spec. Radia. Trans.,* 33, p. 521 (1985).
17. M.A. Brosmer and C.L. Tien, *J. Heat Trans.,* 107, p. 943 (1985).
18. M.A. Brosmer and C.L. Tien, *Comb. Sci. Tech.,* 48, p. 163 (1986).
19. S.C. Lee and C.L. Tien, *18th Symposium (International) on Combustion,* Combustion Institute, 1159, Pittsburgh, PA (1981).
20. C.L. Tien, in *Handbook of Heat Transfer Fundamentals,* McGraw-Hill, New York (1985).
21. G.L. Hubbard and C.L. Tien, *J. Heat Trans.,* 100, p. 235 (1978).
22. J.D. Felske and C.L. Tien, *J. Heat Trans.,* 99, p. 458 (1977).
23. W.W. Yuen and C.L. Tien, *16th Symposium (International) on Combustion,* Combustion Institute, 1481, Pittsburgh, PA (1977).
24. J.D. Felske and C.L. Tien, *Comb. Sci. Tech.,* 7, p. 25 (1977).
25. A. Dayan and C.L. Tien, *Comb. Sci. Tech.,* 9, p. 41 (1974).
26. A.M. Kanury, *Introduction to Combustion Phenomenon,* Gordon and Breach, New York (1975).
27. C.M. Kinoshita and P.J. Pagni, *18th Symposium (International) on Combustion,* Combustion Institute, 1415, Pittsburgh, PA (1981).
28. D.E. Negrelli, J.R. Lloyd, and J.L. Novotny, *J. Heat Trans.,* 99, p. 212 (1977).
29. L. Orloff and J. deRis, *19th Symposium (International) on Combustion,* Combustion Institute, 885, Pittsburgh, PA (1982).
30. A. Tewarson, J.L. Lee, and R.F. Pion, *18th Symposium (International) on Combustion,* Combustion Institute, 563, Pittsburgh, PA (1981).
31. M.A. Brosmer and C.L. Tien, *Comb. Sci. Tech.,* 51, p. 21 (1987).
32. I. Glassman, *Combustion,* Academic, New York (1971).
33. T. Kashiwagi, B.W. MacDonald, H. Isoda, and M. Summerfield, *13th Symposium (International) on Combustion,* 1073, Combustion Institute, Pittsburgh, PA (1971).
34. K.Y. Lee and C.L. Tien, *Int. J. Heat and Mass Trans.,* 29, p. 1237 (1986).
35. H.S. Carslaw and J.C. Jaeger, *Conduction of Heat in Solids,* Oxford University, Oxford, UK (1959).
36. T. Kashiwagi, *Comb. Sci. Tech.,* 20, p. 225 (1979).

CHAPTER 5

Thermochemistry

D. D. Drysdale

The Relevance of Thermochemistry in Fire Protection Engineering

Thermochemistry is the branch of physical chemistry that is concerned with the amounts of energy released or absorbed when a chemical change (reaction) takes place.[1,2] Inasmuch as fire is fundamentally a manifestation of a particular type of chemical reaction, viz., combustion, thermochemistry provides methods by which the energy released during fire processes can be calculated from data available in the scientific and technical literature.

To place it in context, thermochemistry is a major derivative of the first law of thermodynamics, which is a statement of the principle of conservation of energy. However, while concerned with chemical change, thermodynamics does not indicate anything about the rate at which such a change takes place or about the mechanism of conversion. Consequently, the information it provides is normally used in association with other data, for example, to enable the rate of heat release to be calculated from the rate of burning.

The First Law of Thermodynamics

It is convenient to limit the present discussion to chemical and physical changes involving gases; this is not unreasonable, as flaming combustion takes place in the gas phase. It may also be assumed that the ideal gas law applies, that is,

$$PV = n \cdot \mathrm{R}T \tag{1}$$

where P and V are the pressure and volume of n moles of gas at a temperature, T (in degrees Kelvin); values of the universal gas constant (R) in various sets of units are summarized in Table 1-5.1. At ambient temperatures, deviations from "ideal behavior" can be detected with most gases and vapors, while at elevated temperatures such deviations become less significant.

Internal Energy

As a statement of the principle of conservation of energy, the first law of thermodynamics deals with the relationship between work and heat. Confining our attention to a "closed system"—for which there is no exchange of matter with the surroundings—it is known that there will be a change if heat is added or taken away, or if work is done on or by "the system" (e.g., by compression). This change is usually accompanied by an increase or decrease in temperature and can be quantified if we first define a function of state known as the internal energy of the system, E. Any change in the internal energy of the system (ΔE) is then given by

$$\Delta E = q - w \tag{2}$$

where q is the heat transferred to the system, and w is the work done by the system. This can be expressed in differential form

$$dE = dq - dw \tag{3}$$

Table 1-5.1 ***Values of the Ideal Gas Constant,*** **R**

Units of Pressure	Units of Volume	Units of R	Value of R
Pa (N/m^2)	m^3	J/K·mol	8.31431
atm	cm^3	cm^3·atm/k·mol	82.0575
atm	ℓ	ℓ·atm/K·mol	0.0820575
atm	m^3	m^3·atm/K·mol	8.20575×10^{-5}

Dr. D. D. Drysdale is professor of fire safety engineering in the School of Civil and Environmental Engineering at the University of Edinburgh, Scotland. His research interests lie in fire science, fire dynamics, and the fire behavior of combustible materials.

Being a function of state, E varies with temperature and pressure, that is, $E = E(T, P)$.

According to the standard definition, work, w, is done when a force, F, moves its point of application through a distance, x, thus, in the limit

$$dw = F \cdot dx \tag{4}$$

The work done during the expansion of a gas can be derived by considering a cylinder/piston assembly (see Figure 1-5.1); thus

$$dw = P \cdot A \cdot dx = P\, dV \tag{5}$$

where

P = pressure of the gas

A = the area of the piston

dx = distance through which the piston is moved; the increment in volume is therefore $dV = A \cdot dx$

The total work done is obtained by integrating Equation 5 from the initial to the final state; that is,

$$w = \int_{\text{initial}}^{\text{final}} P \cdot dV \tag{6}$$

Combining Equations 3 and 5, the differential change in internal energy can be written

$$dE = dq - P \cdot dV \tag{7}$$

This shows that if the volume remains constant, as $P \cdot dV = 0$, then $dE = dq$; if this is integrated, we obtain

$$\Delta E = q_v \tag{8}$$

where q_v is the heat transferred to the constant volume system; that is, the change in internal energy is equal to the heat absorbed (or lost) at constant volume.

Enthalpy

With the exception of explosions in closed vessels, fires occur under conditions of constant pressure. Consequently, the work done as a result of expansion of the fire gases must be taken into account. At constant pressure, Equation 5 may be integrated to give

$$w = P \cdot (V_2 - V_1) \tag{9}$$

where V_1 and V_2 are the initial and final volumes, respectively. Equation 2 then becomes

$$\Delta E = E_2 - E_1 = q_p + PV_1 - PV_2 \tag{10}$$

or, rearranging,

$$q_p = (E_2 + PV_2) - (E_1 + PV_1) = H_2 - H_1 \tag{11}$$

where q_p is the heat transferred at constant pressure, and H is known as the enthalpy ($H \equiv E + PV$). The change in enthalpy is therefore the heat absorbed (or lost) at constant pressure (provided that only $P - V$ work is done), and consequently it is the change in enthalpy that must be considered in fire-related problems.

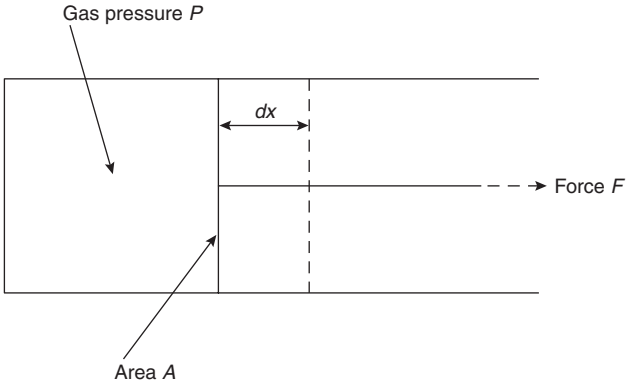

Figure 1-5.1. ***Cylinder/piston assembly.***

Specific Heat

Specific heat, or heat capacity, of a body or "system" is defined as the amount of heat required to raise the temperature of unit mass by one degree Celsius; the units are J/kg·K, although for most thermochemical problems the units J/mol·K are more convenient. The formal definition of the "mole" is the amount of a substance (solid, liquid, or gas) which contains as many elementary units (atoms or molecules) as there are carbon atoms in exactly 0.012 kg of carbon-12 (C^{12}). This number—known as Avogadro's number—is actually 6.023×10^{23}; in its original form, Avogadro's Hypothesis was applied to gases and stated that equal numbers of molecules of different gases at the same temperature and pressure occupy the same volume. Thus, the quantity of a substance which corresponds to a mole is simply the gram-molecular weight, but expressed in kilograms to conform with SI units. For example, the following quantities of the gases N_2, O_2, CO_2, and CO represent one mole of the respective gas and, according to Avogadro's Hypothesis, will each occupy 0.022414 m^3 at 273 K and 760 mm Hg (101.1 kPa):

0.028 kg nitrogen (N_2)
0.032 kg oxygen (O_2)
0.044 kg carbon dioxide (CO_2)
0.028 kg carbon monoxide (CO)
0.016 kg methane (CH_4)
0.044 kg propane (C_3H_8)

The concept of specific heat is normally associated with solids and liquids, but it is equally applicable to gases. Such specific heats are required for calculating flame temperatures, as described below. Values for a number of important gases at constant pressure and a range of temperatures are given in Table 1-5.2.

It is important to note that there are two distinct heat capacities; at constant pressure, C_p, and at constant volume, C_v. Thus, at constant pressure

$$dq_p = dH = C_p \cdot dT \tag{12}$$

Table 1-5.2 ***Heat Capacities of Selected Gases at Constant Pressure (101.1 kN/m²)***[5]

	C_p (J/mol·K)				
Temperature (K)	298	500	1000	1500	2000
Species					
CO	29.14	29.79	33.18	35.22	36.25
CO_2	37.129	44.626	54.308	58.379	60.350
H_2O(g)	33.577	35.208	41.217	46.999	51.103
N_2	29.125	29.577	32.698	34.852	35.987
O_2	29.372	31.091	34.878	36.560	37.777
He	20.786	20.786	20.786	20.786	20.786
CH_4	35.639	46.342	71.797	86.559	94.399

while at constant volume

$$dq_v = dE = C_v \cdot dT \tag{13}$$

For an ideal gas, $C_p = C_v + R$.

While the concept of specific heat is normally associated with solids and liquids, it is equally applicable to gases. Indeed, such specific heats are required for calculating flame temperatures. (See the section on calculation of adiabatic flame temperatures.)

Heats of Combustion

Chemical Reactions and Stoichiometry

When chemical reactions occur, they are normally accompanied by the release or absorption of heat. Thermochemistry deals with the quantification of the associated energy changes. This requires a definition of the initial and final states, normally expressed in terms of an appropriate chemical equation, for example,

$$C_3H_8 + 5O_2 \rightarrow 3CO_2 + 4H_2O \tag{R1}$$

in which the reactants (propane and oxygen) and products (carbon dioxide and water) are specified. This balanced chemical equation defines the *stoichiometry* of the reaction, that is, the exact proportions of the two reactants (propane and oxygen) for complete conversion to products (no reactants remaining). Note that the physical states of the reactants and products should also be specified. In most cases, the initial conditions correspond to ambient (i.e., 25°C and atmospheric pressure) so that there should be no doubt about the state of the reactants. In this case both are gaseous, but it is more common in fires for the "fuel" to be in a condensed state, either liquid or solid. As an example, the oxidation of n-hexane can be written

$$C_6H_{14} + 9.5O_2 \rightarrow 6CO_2 + 7H_2O \tag{R2}$$

but the fuel may be in either the liquid or the vapor state. The consequences of this will be discussed below.

Reaction 1 may be used to calculate the mass of oxygen or air required for the complete oxidation of a given mass of propane. Thus, we deduce that one mole of propane (44 g) reacts completely with five moles of oxygen (5 × 32 = 160 g); that is, 1 g propane requires 3.64 g oxygen. If the propane is burning in air, then the presence of nitrogen needs to be taken into account, although it does not participate to any significant extent in the chemical change. As the ratio of oxygen to nitrogen in air is approximately 21:79 (or 1:3.76), Reaction 1 can be rewritten

$$C_3H_8 + 5O_2 + 18.8N_2 \rightarrow 3CO_2 + 4H_2O + 18.8N_2 \tag{R3}$$

(where 18.8 = 5 × 3.76), showing that 44 g propane requires (160 + 18.8 × 28), or 686.4 g of "air" for complete combustion, that is, 15.6 g air/g propane. Calculations of this type are valuable in assessing the air requirements of fires.

Thus, on the assumption that wood has the empirical formula[3] $CH_{1.5}O_{0.75}$, it can be shown that its stoichiometric air requirement is 5.38 g air for each gram of fuel, assuming complete combustion of wood to CO_2 and H_2O. In this calculation no distinction is made of the fact that flaming combustion of wood involves oxidation of the volatile gases and vapors produced by the pyrolysis of wood, while the residual char burns much more slowly by surface oxidation.

Measurement of Heats of Combustion

The heat of combustion of a fuel is defined as the amount of heat released when unit quantity is oxidized completely to yield stable end products. In the present context, the relevant combustion processes occur at constant pressure so that we are concerned with an enthalpy change, ΔH_c. It should be remembered that as oxidation reactions are exothermic, ΔH_c is always negative, by convention.

Heats of combustion are measured by combustion bomb calorimetry in which a precise amount of fuel is burned in pure oxygen inside a pressure vessel whose temperature is strictly monitored. The apparatus is designed to reduce heat losses to a minimum so that the amount of heat released can be calculated from the rise in temperature and the total thermal capacity of the system; corrections can be made for any residual heat loss. Combustion bomb calorimetry has received a great deal of attention within physical chemistry[1] as the technique has provided a wealth of information relevant to thermochemistry. However, the experiment gives the heat re-

leased at constant volume; that is, the change in internal energy, ΔE (Equation 8). The change in enthalpy is given by

$$\Delta H = \Delta E + \Delta(PV) \quad (14)$$

where $\Delta(PV)$ is calculated using the ideal gas law

$$\Delta(PV) = \Delta(n\mathrm{R}T) \quad (15)$$

The method gives the gross heat of combustion; that is, in which the reactants and products are in their standard states. The net heat of combustion, on the other hand, refers specifically to the situation in which water as a product is in the vapor state. Net heat of combustion is less than the gross heat of combustion by an amount equal to the latent heat of evaporation of water (2.26 kJ/g) and is the value that should be used in fire calculations. It should be remembered that there is a heat of gasification associated with any condensed fuel (liquid or vapor); a correction must be made for this if the heat of combustion of the fuel vapor is required.

Table 1-5.3 contains the heats of combustion (ΔH_c) of a number of combustible gases, liquids, and solids, expressed in various ways, viz., kJ/mole (fuel), kJ/g (fuel), kJ/g (oxygen), and kJ/g (air). The first of these is the form normally encountered in chemistry texts and reference books, while the second is more commonly found in sources relating to chemical engineering and fuel technology and is more useful to the fire protection engineer. However, the third and, particularly, the fourth have very specific uses in relation to fire problems. It is immediately apparent from Table 1-5.3 that $\Delta H_c(O_2)$ and ΔH_c (air) are approximately constant for most of the fuels listed, having average values of 13.1 kJ/g and 3 kJ/g, respectively. (See the section on rate of heat release in fires.)

The data quoted in Table 1-5.3 refer to heats of combustion measured at ambient temperature, normally 25°C. These data will be satisfactory for virtually all relevant fire problems, but occasionally it may be necessary

Table 1-5.3 ***Heats of Combustion of Selected Fuels at 25°C (298 K)***[a]

Fuel	ΔH_c (kJ/mol)	ΔH_c (kJ/g)	ΔH_c[c] [kJ/g(O_2)]	ΔH_c [kJ/g(air)]
Carbon monoxide (CO)	283	10.10	17.69	4.10
Methane (CH_4)	800	50.00	12.54	2.91
Ethane (C_2H_6)	1423	47.45	11.21	2.96
Ethene (C_2H_4)	1411	50.53	14.74	3.42
Ethyne (C_2H_2)	1253	48.20	15.73	3.65
Propane (C_3H_8)	2044	46.45	12.80	2.97
n-Butane (n-C_4H_{10})	2650	45.69	12.80	2.97
n-Pentane (n-C_5H_{12})	3259	45.27	12.80	2.97
n-Octane (n-C_8H_{18})	5104	44.77	12.80	2.97
c-Hexane (c-C_6H_{12})	3680	43.81	12.80	2.97
Benzene (C_6H_6)	3120	40.00	13.06	3.03
Methanol (CH_3OH)	635	19.83	13.22	3.07
Ethanol (C_2H_5OH)	1232	26.78	12.88	2.99
Acetone (CH_3COCH_3)	1786	30.79	14.00	3.25
D-glucose ($C_6H_{12}O_6$)	2772	15.40	13.27	3.08
Cellulose[b]	—	16.09	13.59	3.15
Polyethylene	—	43.28	12.65	2.93
Polypropylene	—	43.31	12.66	2.94
Polystyrene	—	39.85	12.97	3.01
Polyvinylchloride	—	16.43	12.84	2.98
Polymethylmethacrylate	—	24.89	12.98	3.01
Polyacrylonitrile	—	30.80	13.61	3.16
Polyoxymethylene	—	15.46	14.50	3.36
Polyethyleneterephthalate	—	22.00	13.21	3.06
Polycarbonate	—	29.72	13.12	3.04
Nylon 6,6	—	29.58	12.67	2.94
Polyester	—	23.8	—	—
Wool	—	20.5	—	—
Wood (European Beech)	—	19.5	—	—
Wood volatiles (European Beech)	—	16.6	—	—
Wood char (European Beech)	—	34.3	—	—
Wood (Ponderosa Pine)	—	19.4	—	—

[a]Apart from the solids (d-glucose, etc.), the initial state of the fuel and of all the products is taken to be gaseous.

[b]Cotton and rayon are virtually pure cellulose and can be assumed to have the same heat of combustion.

[c]ΔH_c (O_2) = 13.1 kJ/g is used in the oxygen consumption method for calculating rate of heat release.

to consider the heat released when combustion takes place at higher temperatures. This requires a simple application of the first law of thermodynamics. If the reaction involves reactants at temperature T_0 reacting to give products at the final temperature T_F, the process can be regarded in two ways:

1. The products are formed at T_0, absorb the heat of combustion, and are heated to the final temperature T_F.
2. The heat of combustion is imagined first to heat the reactants to T_F, then the reaction proceeds to completion, with no further temperature rise.

By the first law, we can write

$$(\Delta H_c)^{T_0} + C_p^{\mathrm{Pr}} \cdot (T_F - T_0) = (\Delta H_c)^{T_F} + C_p^{\mathrm{R}} \cdot (T_F - T_0) \quad (16)$$

where C_p^{Pr} and C_p^{R} are the total heat capacities of the products and reactants, respectively. This may be rearranged to give

$$\frac{(\Delta H_c)^{T_F} - (\Delta H_c)^{T_0}}{T_F - T_0} = \Delta C_p \quad (17)$$

or, in differential form, we have Kirchoff's equation

$$\frac{d(\Delta H_c)}{dT} = \Delta C_p \quad (18)$$

where $\Delta C_p = C_p^{\mathrm{Pr}} - C_p^{\mathrm{R}}$. This may be used in integrated form to calculate the heat of combustion at temperature T_2 if ΔH_c is known at temperature T_1 and information is available on the heat capacities of the reactants and products, thus

$$(\Delta H_c)^{T_2} = (\Delta H_c)^{T_1} + \int_{T_1}^{T_2} \Delta C_p \cdot dT \quad (19)$$

where

$$\Delta C_p = \sum C_p(\text{products}) - \sum C_p(\text{reactants}) \quad (20)$$

and C_p is a function of temperature, which can normally be expressed as a power series in T, for example,

$$C_p = a + bT + cT^2 + \cdots \quad (21)$$

Information on heat capacities of a number of species and their variation with temperature may be found in References 4 and 5. Some data are summarized in Table 1-5.2.

Heats of Formation

The first law of thermodynamics implies that the change in internal energy (or enthalpy) of a system depends only on the initial and final states of the system and is thus independent of the intermediate stages. This is embodied in thermochemistry as Hess's Law, which applies directly to chemical reactions. From this, we can develop the concept of heat of formation, which provides a means of comparing the relative stabilities of different chemical compounds and may be used to calculate heats of chemical reactions which cannot be measured directly.

The heat of formation of a compound is defined as the enthalpy change when 1 mole of that compound is formed from its constituent elements in their standard state (at 1 atm pressure and 298 K). Thus, the heat of formation of liquid water is the enthalpy change of the reaction (at 298 K)

$$H_2(g) + 0.5O_2(g) \rightarrow H_2O(\mathrm{l})\ \Delta H_f = -285.8\ \mathrm{kJ/mol} \quad (R4)$$

so that ΔH_f (H_2O) (l) = −285.8 kJ/mole at 25°C. This differs from the heat of formation of water vapor [ΔH_f ($H_2O(g)$) = −241.84 kJ/mol] by the latent heat of evaporation of water at 25°C (43.96 kJ/mol).

By definition, the heats of formation of all the elements are set arbitrarily to zero at all temperatures. This then allows the heats of reaction to be calculated from the heats of formation of the reactants and products, thus

$$\Delta H = \Delta H_f(\text{products}) - \Delta H_f(\text{reactants}) \quad (22)$$

where ΔH is the heat (enthalpy) of the relevant reaction. However, most heats of formation cannot be obtained as easily as heats of combustion. The example given is unusual in that the heat of formation of water also happens to be the heat of combustion of hydrogen. Similarly, the heat of combustion of carbon in its most stable form under ambient conditions (graphite) is the heat of formation of carbon dioxide. Fortunately, combustion calorimetry can be used indirectly to calculate heats of formation.

The heat of formation of ethyne (acetylene), which is the enthalpy change of the reaction

$$2\mathrm{C(graphite)} + H_2 \rightarrow C_2H_2 \quad (R5)$$

can be deduced in the following way: the heat of combustion of ethyne has been determined by bomb calorimetry as −1255.5 kJ/mol at 25°C (298 K). This is the heat of the reaction

$$C_2H_2 + 2.5O_2 \rightarrow 2CO_2 + H_2O \quad (R6)$$

which, by Hess's Law (see Equation 22), can be equated to

$$(\Delta H_c)^{298}(C_2H_2) = 2(\Delta H_f)^{298}(CO_2) + (\Delta H_f)^{298}(H_2O) - (\Delta H_f)^{298}(C_2H_2) - 2.5(\Delta H_f)^{298}(O_2) \quad (23)$$

We know that

$$(\Delta H_c)^{298}(C_2H_2) = -1255.5\ \mathrm{kJ/mol}$$
$$(\Delta H_f)^{298}(CO_2) = -393.5\ \mathrm{kJ/mol}$$
$$(\Delta H_f)^{298}(H_2O) = -241.8\ \mathrm{kJ/mol}$$
$$(\Delta H_f)^{298}(O_2) = 0.0\ \mathrm{kJ/mol\ (by\ definition)},$$

so that by rearrangement, Equation 23 yields

$$(\Delta H_f)^{298}(C_2H_2) = +226.7\ \mathrm{kJ/mol}$$

This compound has a positive heat of formation, unlike CO_2 and H_2O. This indicates that it is an endothermic compound and is therefore less stable than the parent ele-

Table 1-5.4 ***Heats of Formation at 25°C (298 K)***

Compound	$(\Delta H_f)^{298}$ (kJ/mol)
Hydrogen (atomic)	+218.00
Oxygen (atomic)	+249.17
Hydroxyl (OH)	+38.99
Chlorine (atomic)	+121.29
Carbon Monoxide	−110.53
Carbon Dioxide	−393.52
Water (liquid)	−285.8
Water (vapor)	−241.83
Hydrogen Chloride	−92.31
Hydrogen Cyanide (gas)	+135.14
Nitric Oxide	+90.29
Nitrogen Dioxide	+33.85
Ammonia	−45.90
Methane	−74.87
Ethane	−84.5
Ethene	+52.6
Ethyne (Acetylene)	+226.9
Propane	−103.6
n-Butane	−124.3
iso-Butane[a]	−131.2
Methanol	−242.1

[a]Heats of formation of other hydrocarbons are tabulated in Reference 6.

ments. Under appropriate conditions, ethyne can decompose violently to give more stable species.

The heats of formation of a number of compounds are given in Table 1-5.4. The most stable compounds (CO_2 and H_2O) have the largest negative values, while positive values tend to indicate an instability with respect to the parent elements. While this can indicate a high chemical reactivity, it gives no information about the rates at which chemical changes might take place (i.e., kinetics are ignored). However, heats of formation have been used in preliminary hazard assessment to provide an indication of the risks associated with new processes in the chemical industry. It should be noted that the heats of combustion of endothermic compounds do not give any indication of any associated reactivity (compare Tables 1-5.3 and 1-5.4).

Rate of Heat Release in Fires

While thermochemistry can give information relating to the total amount of energy that can be released when a fuel is burned to completion, it is rarely (if ever) possible to use heats of combustion directly to calculate the heat released in "real" fires. However, it can be argued that the *rate* of heat release is more important than the total available.[7] When a single item is burning in isolation, the rate of burning and the rate of heat release in the flame are coupled. Nevertheless, it is convenient to express the rate of heat release in terms of the burning rate, which is expressed as a rate of mass loss, $\dot{m}$ (kg/s)

$$\dot{Q}_c = \dot{m} \cdot \Delta H_c \tag{24}$$

where ΔH_c is the net heat of combustion of the fuel (kJ/kg). However, this assumes that combustion is complete, although it is known that this is never so in natural fires. Even under conditions of unrestricted ventilation, the products of combustion will contain some species which are only partially oxidized, such as carbon monoxide, aldehydes, ketones, and particulate matter in the form of soot or smoke. Their presence indicates that not all the available combustion energy has been released. The "combustion efficiency" is likely to vary from around 0.3 to 0.4 for heavily fire-retarded materials to 0.9 or higher in the case of oxygen-containing products (e.g., polyoxymethylene).[8]

Fires burning in compartments present a completely different problem. In the first place, there is likely to be a range of different fuels present, each with a different stoichiometric air requirement. These will all burn at different rates, dictated not just by the nature of the fuel but also by the levels of radiant heat existing within the compartment during the fire. The rate of heat release during the fully developed stage of a compartment fire is required for calculating post-flashover temperature-time histories for estimating fire exposure of elements of structure, as in the method developed by Pettersson et al.[9] Calculating the rate of heat release is apparently complicated by the fact that not all of the fuel may burn within the compartment; some of the fuel volatiles can escape to burn outside as they mix with fresh air. The proportion of the heat of combustion that is effectively lost in this way cannot easily be estimated.

However, if it is assumed that the fire is ventilation controlled and that all of the air that enters the compartment is "burned" therein, then the rate of heat release within the compartment can be calculated from the expression

$$\dot{Q}_c = \dot{m}_{\text{air}} \cdot \Delta H_c(\text{air}) \tag{25}$$

where $\dot{m}_{\text{air}}$ is the mass flow rate of air into the compartment, and ΔH_c(air) is the heat of combustion per unit mass of air consumed (3 kJ/g, see Table 1-5.3). The mass flow rate of air can be approximated by the expression

$$\dot{m}_{\text{air}} = 0.52 A_w h^{1/2} \quad \text{(kg/s)} \tag{26}$$

where A_w is the effective area of ventilation (m^2) and h is the height of the ventilation opening (m).[10]

In this, it is tacitly assumed that the combustion process is stoichiometric, although in fact the rate of supply of air may not be sufficient to burn all the fuel vapors within the compartment. Indeed, if the equivalence ratio $\dot{m}_{\text{air}}/\dot{m}$ is less than the stoichiometric ratio, excess fuel will escape from the compartment and mix with air to give external flames whose length will depend *inter alia* on the equivalence ratio.[11] Furthermore, in using Equation 26 to calculate the temperature-time course of a fire, it is implied that the fire remains at its maximum rate of burning for its duration, the latter being controlled by the quantity of fuel present (the fire load). This method will overestimate the severity of fuel-controlled fires in which the ventilation openings are large.[12]

Much useful data on the fire behavior of combustible materials can be obtained by using the technique of "oxygen consumption calorimetry." This is the basis of the

"cone calorimeter," in which the rate of heat release from a small sample of material burning under an imposed radiant heat flux is determined by measuring the rate of oxygen consumption.[13] The latter can be converted into a rate of heat release using the conversion factor 13.1 kJ/g of oxygen consumed. (A small correction is required for incomplete combustion, based on the yield of CO.) This technique can be used on a larger scale to measure the rate of heat release from items of furniture, wall lining materials, and so on[14,15] and is now used routinely in both fire research and fire testing facilities.

Calculation of Adiabatic Flame Temperatures

In the previous sections, no consideration has been given to the fate of the energy released by the combustion reactions. Initially it will be absorbed within the reaction system itself by (1) unreacted reactants, (2) combustion products, and (3) diluents, although it will ultimately be lost from the system by various heat transfer processes. This is particularly true for natural fires in enclosed spaces. However, if we consider a premixed reaction system, such as a flammable vapor/air mixture, and assume it to be adiabatic, that is, there is no transfer of heat to or from the system, then we can calculate the maximum theoretical temperature, the adiabatic flame temperature.

Consider a flame propagating through a stoichiometric propane/air mixture of infinite extent (i.e., there are no surfaces to which heat may be transferred) and which is initially at 25°C. The appropriate equation is given by Reaction 7:

$$C_3H_8 + 5O_2 + 18.8N_2 \rightarrow 3CO_2 + 4H_2O + 18.8N_2 \qquad (R7)$$

This reaction releases 2044 kJ for every mole of propane consumed. This quantity of energy goes toward heating the reaction products, that is, 3 moles of carbon dioxide, 4 moles of water (vapor), and 18.8 moles of nitrogen for every mole of propane burned. The thermal capacity of this mixture can be calculated from the thermal capacities of the individual gases, which are available in the literature (e.g., JANAF).[5] The procedure is straightforward, provided that an average value of C_p is taken for each gas in the temperature range involved. (See Table 1-5.5.)

Table 1-5.5 ***Thermal Capacity of the Products of Combustion of a Stoichiometric Propane/Air Mixture***

		Thermal Capacity at 1000 K	
	No. of Moles	(J/mol·K)	(J/K)
CO_2	3	54.3	162.9
H_2O	4	41.2	164.8
N_2	18.8	32.7	614.8
Total thermal capacity (per mole of propane) =			942.5 J/K

As 2044 kJ are released at the same time as these species are formed, the maximum temperature rise will be

$$\Delta T = \frac{2044000}{942.5} = 2169 \text{ K}$$

giving the final (adiabatic) temperature as 2169 + 298 = 2467 K. In fact, this figure is approximate for the following reasons:

1. Thermal capacities change with temperature, and average values over the range of temperatures appropriate to the problem have been used.
2. The system cannot be adiabatic as there will be heat loss by radiation from the hot gases (CO_2 and H_2O).
3. At high temperatures, dissociation of the products will occur; as these are endothermic processes, there will be a reduction in the final temperature.

Of these, (2) and (3) determine that the actual flame temperature will be much lower than predicted. These effects can be taken into account. Thus, with propane burning in air, the final temperature may not exceed 2000 K.

If the propane were burning as a stoichiometric mixture in pure oxygen, then in the absence of nitrogen as a "heat sink," much higher temperatures would be achieved. The total thermal capacity would be (942.5 − 614.8) = 327.7 J/K. However, the amount of heat released remains unchanged (2044 kJ) so that the maximum temperature rise would be

$$\Delta T = \frac{2044000}{327.7} = 6238 \text{ K}$$

predicting a final temperature of 6263°C. Because dissociation will be a dominant factor, this cannot be achieved and the temperature of the flame will not exceed ~3500 K.

The occurrence of dissociation at temperatures in the region of 2000 K and above makes it necessary to take dissociation into account. Dissociation is discussed in Section 1, Chapter 6. However, the simple calculation outlined above can be used to estimate the temperatures of near-limit flames, when the temperature is significantly lower and dissociation can be neglected.

It is known that the lower flammability limit of propane is 2.2 percent. The oxidation reaction taking place in this mixture can be described by the following equation:

$$0.022C_3H_8 + 0.978(0.21O_2 + 0.79N_2) \rightarrow \text{products}$$

Dividing through by 0.022 allows this to be written

$$C_3H_8 + 9.34O_2 + 35.12N_2 \rightarrow 3CO_2 + 4H_2O + 4.34O_2 + 35.12N_2 \qquad (R8)$$

showing that the heat released by the oxidation of 1 mole of propane is now absorbed by excess oxygen (4.34 moles) and an increased amount of nitrogen. Carrying out the same calculation as before, it can be shown that the adiabatic flame temperature for this limiting mixture is 1281°C (1554 K). If the same calculation is carried out for the other hydrocarbon gases, it is found that the adiabatic limiting flame temperature lies in a fairly narrow band,

Table 1-5.6 ***Adiabatic Flame Temperature of Lower-Limiting Hydrocarbon/Air Mixtures***

Gas	Adiabatic Flame Temperature at Lower Flammability Limit (K)
Methane	1446
Ethane	1502
Propane	1554
n-Butane	1612
n-Pentane	1564
n-Heptane	1692
n-Octane	1632

1600 ± 100 K. (See Table 1-5.6.) This can be interpreted by assuming that the limit exists because heat losses (by radiation from the flame) exceed the rate of heat production (within the flame). As a consequence, flame cannot sustain itself. This concept can be applied to certain practical problems relating to the lower flammability limit.

EXAMPLE:

A mechanical engineering research laboratory contains a six-cylinder internal combustion engine which is being used for research into the performance of spark plugs. The fuel being used is methane, CH_4, and the fuel/air mixture can be adjusted at will. The combustion products are extracted from the exhaust manifold through a 30 cm square duct, 20 m long. It is found that the engine will continue to operate with a stoichiometric mixture when only three of the cylinders are firing. If under these conditions the average temperature of the gases entering the duct from the manifold is 700 K, is there a risk of an explosion in the duct?

SOLUTION:

The stoichiometric reaction for methane in air is

$$CH_4 + 2O_2 + 7.52N_2 \rightarrow CO_2 + 2H_2O + 7.52N_2 \qquad \text{(R9)}$$

If we consider that one mole of fuel passes through each of the six cylinders, but of the six moles only three are burned, we have overall

$$6CH_4 + 12O_2 + 45.12N_2 \rightarrow 3CH_4 + 3CO_2 + 6H_2O + 6O_2 + 45.12N_2 \qquad \text{(R10)}$$

Dividing through by 3 gives

$$2CH_4 + 4O_2 + 15.04N_2 \rightarrow CH_4 + 2O_2 + CO_2 + 2H_2O + 15.04N_2 \qquad \text{(R11)}$$

The mixture discharged into the exhaust manifold has the composition given by the right-hand side of Reaction 11. If this "burns" at 700 K, the final abiabatic flame temperature may be calculated on the basis of the reaction

$$CH_4 + 2O_2 + CO_2 + 2H_2O + 15.04N_2 \rightarrow 2CO_2 + 4H_2O + 15.04N_2 \qquad \text{(R12)}$$

The total thermal capacity of the product gases ($2CO_2 + 4H_2O + 15.04N_2$) (at 1000 K) can be shown to be 765.3 J per mole of methane burned. Using Kirchoff's Equation (Equation 19), $\Delta H_c(CH_4)$ at 700 K is calculated as 802.8 kJ/mol, giving $T = 802800/765.3 = 1049$ K. This gives a final temperature of 1749 K, which is significantly higher than the limiting flame temperature (1600 K) discussed above. This indicates that there is a risk of explosion, and measures should be applied to prevent this mixture being discharged into the duct.

It should be noted that at 700 K there will be a "slow" reaction between methane and the oxygen present, which could invalidate the tacit assumption that the duct becomes completely filled with the mixture described by the right-hand side of Reaction 10. However, slow oxidation of the methane will tend to make the mixture less flammable, and so the calculation gives a conservative answer.

Nomenclature

A	area (Equation 5)
A_w	area of ventilation opening
C_p	specific heat
E	internal energy
F	force (Equation 4)
h	height of ventilation opening
H	enthalpy
ΔH_c	heat of combustion
ΔH_f	heat of formation
$\dot{m}$	mass rate of burning
$\dot{m}_{\text{air}}$	mass flow rate of air
n	number of moles
P	pressure
q	energy
Q_c	rate of heat release
R	universal gas constant
T	temperature
V	volume
w	work

Subscripts

c	combustion
F	final
f	formation
o	initial
p	constant pressure
v	constant volume

Superscripts

Pr	products
R	reactants

References Cited

1. W.J. Moore, *Physical Chemistry,* 5th ed, Longman, London (1974).
2. D.D. Drysdale, *Introduction to Fire Dynamics,* 2nd ed., John Wiley and Sons, Chichester, UK (1998).
3. A.F. Roberts, *Comb. and Flame,* 8, p. 245 (1964).
4. R.A. Strehlow, *Combustion Fundamentals,* McGraw-Hill, New York (1984).
5. *JANAF Thermochemical Tables.* National Bureau of Standards. Washington, DC (1970).
6. R.C. Weast, *Handbook of Chemistry and Physics,* Chemical Rubber Co., Cleveland, OH (1973).
7. V. Babrauskas and R. Peacock, "Heat Release Rate: The Single Most Important Variable in Fire Hazard," in *Fire Safety Journal, 18,* pp. 255–272 (1992).
8. A. Tewarson, in *Flame Retardant Polymeric Materials* (M. Lewin, ed.), Plenum, New York (1982).
9. O. Pettersson, S.E. Magnusson, and J. Thor, *Fire Engineering Design of Structures,* Swedish Institute of Steel Construction, Publication, 50 (1976).
10. W.D. Walton and P.H. Thomas, "Estimating Temperatures in Compartment Fires," in *SFPE Handbook of Fire Protection Engineering,* 3rd ed. (P.J. Di Nenno et al., eds.) pp. 3.171–3.188 (Society of Fire Protection Engineers, Boston, 2002).
11. M.L. Bullen and P.H. Thomas, *17th Symposium (International) on Combustion,* Combustion Institute, Pittsburgh, PA (1979).
12. P.H. Thomas and A.J.M. Heselden, "Fully Developed Fires in Compartments," *CIB Report No. 20; Fire Research Note No. 923,* Conseil International du Batiment, France (1972).
13. V. Babrauskas, "The Cone Calorimeter," in *SFPE Handbook of Fire Protection Engineering,* 3rd ed. (P.J. Di Nenno et al., eds.) pp. 3.63–3.81 (Society of Fire Protection Engineers, Boston, 2002).
14. V. Babrauskas and S.J. Grayson (eds.), *Heat Release in Fires,* Elsevier Applied Science, London (1992).
15. M.L. Janssens, "Calorimetry," in *SFPE Handbook of Fire Protection Engineering,* 3rd ed. (P.J. Di Nenno et al., eds.) Society of Fire Protection Engineers, Boston, pp. 3.38–3.62 (2002).

CHAPTER 6

Chemical Equilibrium

Raymond Friedman

Relevance of Chemical Equilibrium to Fire Protection

The temperature of a flame must be known in order to calculate convective and radiative heat transfer rates, which control pool-fire burning rates, flame spread rates, remote ignitions, damage to exposed items (e.g., structural steel, wiring), and response of thermal fire detectors or automatic sprinklers.

Section 1, Chapter 5, "Thermochemistry," provides a simple technique for calculating flame temperature, based on ignoring the dissociations that occur at high temperature. This technique gives answers that are too high. For example, if propane (C_3H_8) burns in stoichiometric proportions with air at 300 K, and it is assumed that the only products are CO_2, H_2O, and N_2, then the simple thermochemical calculation yields a flame temperature of 2394 K. On the other hand, if chemical equilibrium is considered, so that the species CO, O_2, H_2, OH, H, O, and NO are assumed present in the products, then the flame temperature, calculated by methods described in this section, comes out to be 2268 K. Flame temperature measurements in laminar premixed propane-air flames agree with the latter value. (The discrepancy in flame temperature caused by neglecting dissociation would be even greater for fires in oxygen-enriched atmospheres.)

The chemical equilibrium calculation yields not only the temperature but the equilibrium composition of the products. Thus, the generation rate of certain toxic or corrosive products such as carbon monoxide, nitric oxide, or hydrogen chloride may be calculated, insofar as the assumption of equilibrium is valid.

For a fire in a closed volume, the final pressure as well as the temperature will depend on the dissociations and therefore require a calculation taking chemical equilibrium into account.

From a fire research viewpoint, there is interest in correlating flammability limits, extinguishment, soot formation, toxicity, flame radiation, or other phenomena; and chemical equilibrium calculations in some cases will be a useful tool in such correlations.

In a later part of this chapter, departure of actual fires from chemical equilibrium will be discussed.

Introduction to the Chemical Equilibrium Constant

Consider a chemical transformation, such as

$$2CO + O_2 \rightarrow 2CO_2 \tag{1}$$

If this process can occur, presumably the reverse process can also occur (principle of microscopic reversibility, or principle of detailed balancing):

$$2CO_2 \rightarrow 2CO + O_2 \tag{2}$$

If both processes occur at finite rates in a closed system, then, after a sufficient time, a condition of *chemical equilibrium* will be reached, after which no further change occurs as long as the temperature and pressure remain constant and no additional reactants are introduced. This condition of equilibrium can be expressed as a *mathematical constraint* on the system, which, for the gaseous reaction $2CO + O_2 \rightleftarrows 2CO_2$, can be written

$$K_3 = \frac{p_{CO_2}^2}{p_{CO}^2 p_{O_2}} \tag{3}$$

Dr. Raymond Friedman was with Factory Mutual Research from 1969 through 1993. During most of this time he was vice president and manager of their Research Division. Currently he is an independent consultant. He has past experience at Westinghouse Research Laboratories and Atlantic Research Corporation. He is a past president of The Combustion Institute, past vice chairman and current secretary of the International Association for Fire Safety Science, and an expert in fire research and combustion.

where the p_i are partial pressures (atm), and K_3 is the equilibrium constant. This expression can be rationalized by the following argument.

According to the chemical "law of mass action," first stated a century ago, the rate of the forward reaction (Equation 1) at a given temperature is given by $k_f p_{CO}^2 p_{O_2}$, while the rate of the reverse reaction (Equation 2) is given by $k_r p_{CO_2}^2$. At equilibrium, the forward rate must be equal to the reverse rate:

$$k_f p_{CO}^2 p_{O_2} = k_r p_{CO_2}^2 \tag{4}$$

which may be rearranged to

$$\frac{p_{CO_2}^2}{p_{CO}^2 p_{O_2}} = \frac{k_f}{k_r} = K_3 \tag{5}$$

While this appears to be a satisfactory explanation, research over the past hundred years has shown that chemical reactions in fact rarely proceed as suggested by the stoichiometric equation. For example, the three-body collision of two CO molecules and an O_2 molecule, resulting in the formation of two CO_2 molecules, simply does not happen. Rather, the reaction would occur as follows:

$$O_2 + M \rightarrow 2O + M \tag{6}$$

(where M is any molecule) followed by

$$O + CO + M \rightarrow CO_2 + M \tag{7}$$

Now, observe how Equation 3 can be obtained from this reaction sequence.

The reverse of $O_2 + M \rightarrow 2O + M$, namely $2O + M \rightarrow O_2 + M$, can also occur, and the equilibrium constant for this pair of reactions, which actually do occur, is $K_6 = p_O^2 p_M / p_{O_2} p_M = p_O^2 / p_{O_2}$. (The p_M term cancels.)

Similarly the reverse reaction $CO_2 + M \rightarrow O + CO + M$ can occur, and the equilibrium constant is $K_7 = p_{CO_2} / p_{CO} p_O$. If we now multiply K_7^2 by K_6, we obtain

$$K_7^2 K_6 = \left(\frac{p_{CO_2}}{p_{CO} p_O}\right)^2 \frac{p_O^2}{p_{O_2}} = \frac{p_{CO_2}^2}{p_{CO}^2 p_{O_2}} = K_3 \tag{8}$$

Thus, Equation 3 is perfectly valid, even if the "law of mass action" does not correctly describe the reaction process involving CO and O_2.

To get a further understanding of the validity of the equilibrium constant concept, consider the following facts: CO will not react with O_2—even by the above mechanism involving O atoms—unless first heated to quite high temperatures. However, at least a trace of moisture is usually present, and in such cases the reaction occurs by the following process, which can occur at lower temperatures. First, H and OH are formed by dissociation of H_2O. Then, the CO is converted by

$$CO + OH \rightleftarrows CO_2 + H \qquad K_9 = \frac{p_{CO_2} p_H}{p_{CO} p_{OH}} \tag{9}$$

while the O_2 reacts with H:

$$O_2 + H \rightleftarrows OH + O \qquad K_{10} = \frac{p_{OH} p_O}{p_{O_2} p_H} \tag{10}$$

If the quantity $K_9^2 K_{10}$ is now calculated,

$$K_9^2 K_{10} = \frac{p_{CO_2}^2}{p_{CO}^2 p_{O_2}} \frac{p_H p_O}{p_{OH}} \tag{11}$$

But, the reaction $H + O + M \rightarrow OH + M$ can occur, as well as its reverse, $OH + M \rightarrow H + O + M$. It does not matter if these reactions are actually important in the rate of oxidation of CO in the presence of H_2O. As long as these reactions can occur, then at equilibrium

$$k_f p_H p_O p_M = k_r p_{OH} p_M$$

and

$$\frac{k_f}{k_r} = K_{12} = \frac{p_{OH}}{p_H p_O} \tag{12}$$

Substituting this into Equation 11

$$\frac{p_{CO_2}^2}{p_{CO}^2 p_{O_2}} = K_9^2 K_{10} K^{12} = K_3 \tag{13}$$

Thus, the ratio $p_{CO_2}^2 / p_{CO}^2 p_{O_2}$ is a constant at equilibrium (at a given temperature) regardless of the reaction mechanism, even if other (hydrogen-containing) species are involved, because by the principle of microscopic reversibility, these other species (catalysts) affect the reverse reaction as well as the forward reaction.

Let us now consider the mathematical specification of the CO-CO_2-O_2 system at equilibrium. The system, at a given temperature and pressure, may be described by three variables, namely the partial pressures of the three species: p_{CO}, p_{O_2}, and p_{CO_2}. There are already two well-known constraints on the system: (1) The sum of the partial pressures must equal the total pressure, p

$$p_{CO} + p_{O_2} + p_{CO_2} = p \tag{14}$$

and (2) the ratio of carbon atoms to oxygen atoms in the system must remain at the original, presumably known, value of C/O:

$$\frac{C}{O} = \frac{p_{CO} + p_{CO_2}}{p_{CO} + 2p_{O_2} + 2p_{CO_2}} \tag{15}$$

A third constraint, that of chemical equilibrium, provides a third equation involving p_{CO}, p_{O_2}, and p_{CO_2}:

$$\frac{p_{CO_2}^2}{p_{CO}^2 p_{O_2}} = K_3 \tag{3}$$

Now the system is completely defined by the simultaneous solution of these three equations. The equilibrium constant varies with temperature but is independent of pressure (except at rather high pressures). It is also independent of the presence of other reactive chemical species.

Generalized Definition of Equilibrium Constant

For a generalized reaction

$$aX_1 + bX_2 \rightleftarrows cY_1 + dY_2$$

K would be given by

$$K = \frac{(p_{Y_1})^c (p_{Y_2})^d}{(p_{X_1})^a (p_{X_2})^b}$$

Notice that, instead of writing $2CO + O_2 \leftrightarrows 2CO_2$, one could equally well have written $CO + \frac{1}{2}O_2 \leftrightarrows CO_2$. The equilibrium constant for the latter formulation is

$$K_{16} = \frac{p_{CO_2}}{p_{CO} p_{O_2}^{1/2}} \tag{16}$$

By comparison of Equation 16 with Equation 3, it is clear that $K_{16} = \sqrt{K_3}$. Again, the equilibrium constant for the reaction, if written $2CO_2 \leftrightarrows 2CO + O_2$, would be equal to $1/K_3$.

Simultaneous Equilibria

In most real chemical systems, one must deal with a number of simultaneous chemical equilibria. For example, air at 2500 K will contain the species N_2, O_2, NO, and O. The following simultaneous equilibria may be considered

$$O_2 = 2O \qquad K_{17} = \frac{p_O^2}{p_{O_2}} \tag{17}$$

$$N_2 + O_2 = 2NO \qquad K_{18} = \frac{p_{NO}^2}{p_{N_2} p_{O_2}} \tag{18}$$

$$N_2 + 2O = 2NO \qquad K_{19} = \frac{p_{NO}^2}{p_{N_2} p_O^2} \tag{19}$$

It is easily seen from the above relations that $K_{19} = K_{18}/K_{17}$. Hence, Equations 17, 18, and 19 are not three independent equations, and any *two* of these equations may be used to describe the equilibrium condition; the third would be redundant. To determine the four unknowns, p_{N_2}, p_{O_2}, p_{NO}, and p_O, one would solve the selected two equilibrium relations plus the following two relations:

$$p_{NO} + p_{N_2} + p_{O_2} + p_O = p \tag{20}$$

and

$$\frac{p_{NO} + 2p_{N_2}}{p_{NO} + 2p_{O_2} + p_O} = 3.76 \tag{21}$$

where 3.76 is the ratio of nitrogen atoms to oxygen atoms in air.

If one knows the temperature, the equilibrium constants may be calculated from the thermodynamic properties of the reactants and products, as discussed in the next section. However, since the various equilibrium reactions release or absorb energy, and accordingly raise or lower the temperature of an adiabatic system, the determination of equilibrium composition of an adiabatic system must proceed simultaneously with the calculation of its temperature; that is, an energy balance must be satisfied as well as the equilibrium equations, the atom-ratio equations, and the $p = \sum p_i$ equation.

As a general rule, a gaseous chemical system *at a given temperature*, containing s kinds of chemical species involving e chemical elements, requires s-e equilibrium relations, e-1 atom-ratio relations, and a $p = \sum p_i$ equation, in order to specify it. If the temperature is unknown, an energy balance equation is also needed. (If the pressure is unknown but the volume is known, then the equation of state must be used in the pressure equation.)

In order to solve an actual problem, one must select the species to be considered. The more species one includes, the more difficult is the calculation. There is no need to include any species that will be present in very small quantity at equilibrium. Some guidelines can be provided.

For combustion of a C–H–O compound in air, it is usually sufficient to include the species CO_2, H_2O, N_2, O_2, CO, H_2, OH, H, O, and NO. These species are adequate if the air-fuel ratio is sufficiently large so that the O/C atomic ratio is greater than one. If the O/C atomic ratio is less than one, then solid carbon must be considered, as well as many additional gaseous species. If chlorine is present, then HCl, Cl_2, and Cl must be added. If sulfur is present, then SO_2 and SO_3 are the primary species, unless there is a deficiency of oxygen.

The Quantification of Equilibrium Constants

While a chemist might establish the numerical value of an equilibrium constant for $A \leftrightarrows 2B$ by direct measurement of the partial pressures of A and B in a system at equilibrium, this is rarely done because it is difficult to make such measurements in a high-temperature system, and it takes a long time to establish equilibrium in a low-temperature system. Instead, the equilibrium constant is generally determined from the thermodynamic relation first deduced by van't Hoff in 1886[1]

$$\Delta F^\circ = -RT \ln K \tag{22}$$

If this equation is applied to $A \leftrightarrows 2B$ at absolute temperature T, then $K = p_B^2/p_A$, and ΔF° is the free energy of two moles (mol) of B at 1 atm and temperature T, minus the free energy of 1 mol of A at 1 atm and temperature T. (The superscript o designates that each substance is in its "standard state," that is, an ideal gas at one atmosphere.) By definition

$$\Delta F^\circ = \Delta H^\circ - T\Delta S^\circ = \Delta E^\circ + \Delta(pV^\circ) - T\Delta S^\circ \tag{23}$$

Accordingly, if $\Delta S°$, the entropy difference, and either $\Delta H°$, the enthalpy difference, or $\Delta E°$, the energy difference, are known for the substances involved in an equilibrium at temperature T, then the equilibrium constant, K, may be calculated. It happens that $\Delta S°$, $\Delta H°$, and $\Delta E°$ are well known for almost all substances expected to be present at equilibrium in combustion gases at any temperature up to 4000 K, so the calculation of equilibrium constants is straightforward.

The variation of the equilibrium constant with temperature was shown by van't Hoff[1] to be given by

$$\frac{d \ln K}{dT} = \frac{\Delta H°}{RT^2} \left[= \frac{\Delta H}{RT^2} \text{ for ideal gases} \right] \tag{24}$$

Thus, for an exothermic reaction occurring at temperature T, ΔH is negative and K decreases as T increases. The converse is true for endothermic reactions.

It is appropriate to inquire about the underlying physical reason for the value of K to be governed by $\Delta F°$ (actually $\Delta H°$ and $\Delta S°$). An explanation is as follows: any chemical system being held at constant temperature will seek to reduce its energy, E, and to increase its entropy, S. The reduction of energy is analogous to a ball rolling downhill. The increase of entropy is analogous to shuffling a sequentially arranged deck of cards, yielding a random arrangement. These two tendencies will often affect the equilibrium constant in opposite directions.

Consider the equation

$$\ln K = \frac{\Delta S°}{R} - \frac{\Delta E°}{RT} - \Delta n \tag{25}$$

where Δn is the increase in the number of moles of product relative to reactant. Equation 25 is obtained by combining Equations 22 and 23 with the ideal gas law at constant temperature $\Delta(pV°) = \Delta nRT$. Inspection of Equation 25 shows that, if $\Delta S°$ is a large positive quantity and $\Delta S°/R$ dominates the other terms, K will be large, that is, the reaction is driven by the "urge" to increase entropy. Again, if the reaction is highly endothermic, then $-\Delta E°/RT$ will be a large negative number and can dominate the other terms to cause K to be small, that is, the reaction prefers to go in the reverse, or exothermic, direction and reduces the energy of the system. (Most spontaneous reactions are exothermic.) The Δn term is generally small compared with the other terms and represents the work done by the expanding system on the surroundings, or the work done on the contracting system by the surroundings.

In summary, Equation 25 represents the balance of these various tendencies and determines the relative proportions of reactants and products at equilibrium. Notice that the term $\Delta E°/RT$ becomes small at sufficiently high temperature, and the entropy term then dominates. In other words, all molecules break down into atoms at sufficiently high temperature, to maximize entropy. The important conclusion from this discussion is that there is no need to consider rates of forward and reverse processes to determine equilibrium.

Table 1-6.1 provides values of equilibrium constants for 13 reactions involving most species found in fire products at equilibrium, over a temperature range from 600 K to 4000 K. Equilibrium constants for other reactions involving the same species may be obtained by combining these constants, as in Equation 13, or as illustrated in the examples below.

Table 1-6.1 does not include the $\frac{1}{2}N_2 = N$ equilibrium, because fire temperatures are generally not high enough for significant N to form. Tables 1-6.2 and 1-6.3 present information on the degree to which various gases are dissociated at various temperatures.

In performing calculations, remember that even if a relatively small fraction of dissociation occurs, a rather large amount of energy may be absorbed in the dissociation, with a corresponding large increase in the energy of the system. For example, if water vapor initially at 2800 K is allowed to dissociate adiabatically at 1 atm, only 5.7 percent of the H_2O molecules will dissociate, but the temperature will drop from 2800 K to 2491 K; that is, the temperature relative to a 300 K baseline is lower by 12.4 percent.

Carbon Formation in Oxygen-Deficient Systems

Solid carbon (soot) may be expected to form in oxygen-deficient combustion products, under some conditions. Since solid carbon does not melt or boil until extremely high temperatures (~4000 K), we only need concern ourselves with solid carbon $C_{(s)}$, not liquid $C_{(l)}$ or gaseous carbon $C_{(g)}$.

Consider pure carbon monoxide at 2000 K. There are three conceivable ways in which it might form solid carbon:

$$\alpha: \quad CO \rightleftarrows \frac{1}{2} C_{(s)} + \frac{1}{2} CO_2 \qquad K_\alpha = \frac{(p_{CO_2})^{1/2}}{p_{CO}}$$

$$\beta: \quad CO \rightleftarrows C_{(s)} + \frac{1}{2} O_2 \qquad K_\beta = \frac{(p_{O_2})^{1/2}}{p_{CO}}$$

$$\gamma: \quad CO \rightleftarrows C_{(s)} + O \qquad K_\gamma = \frac{p_O}{p_{CO}}$$

Note that solid carbon does not appear in any of the equilibrium expressions. (By convention, a solid in equilibrium with gases is assigned a value of unity.)

From Table 1-6.1, we see that, at 2000 K,

$$K_\alpha = \frac{K_E^{1/2}}{K_F} = \text{antilog}_{10}\left[\left(\frac{10.353}{2} \right) - 7.469 \right]$$
$$= 5.1 \times 10^{-3}$$

$$K_\beta = \frac{1}{K_F} = \text{antilog}_{10}[0 - 7.469] = 3.4 \times 10^{-8}$$

$$K_\gamma = \frac{K_A}{K_F} = \text{antilog}_{10}[-3.178 - 7.469] = 2.2 \times 10^{-11}$$

Table 1-6.1 ***Values of Log_{10} K for Selected Reactions***

TEMP (K)	K_A $\frac{1}{2}O_2 = O$	K_B $\frac{1}{2}H_2 = H$	K_C $H_2 + \frac{1}{2}O_2 = H_2O$	K_D $\frac{1}{2}H_2 + \frac{1}{2}O_2 = OH$	K_E $C_{(S)} + O_2 = CO_2$	K_F $C_{(S)} + \frac{1}{2}O_2 = CO$	K_G $\frac{1}{2}N_2 + \frac{1}{2}O_2 = NO$	K_H $\frac{1}{2}F_2 = F$	K_I $\frac{1}{2}Cl_2 = Cl$	K_J $\frac{1}{2}Br_2 = Br$	K_K $\frac{1}{2}H_2 + \frac{1}{2}F_2 = HF$	K_L $\frac{1}{2}H_2 + \frac{1}{2}Cl_2 = HCl$	K_M $\frac{1}{2}H_2 + \frac{1}{2}Br_2 = HBr$
600	–18.574	–16.336	18.633	–2.568	34.405	14.318	–7.210	–3.814	–7.710	–5.641	24.077	8.530	5.036
700	–15.449	–13.599	15.583	–2.085	29.506	12.946	–6.086	–2.810	–6.182	–4.431	20.677	7.368	4.374
800	–13.101	–11.539	13.289	–1.724	25.830	11.914	–5.243	–2.053	–5.031	–3.522	18.125	6.494	3.876
900	–11.272	–9.934	11.498	–1.444	22.970	11.108	–4.587	–1.462	–4.133	–2.814	16.137	5.812	3.486
1000	–9.807	–8.646	10.062	–1.222	20.680	10.459	–4.062	–.988	–3.413	–2.245	14.544	5.265	3.173
1100	–8.606	–7.589	8.883	–1.041	18.806	9.926	–3.633	–.599	–2.822	–1.799	13.240	4.816	2.917
1200	–7.604	–6.707	7.899	–.890	17.243	9.479	–3.275	–.273	–2.328	–1.389	12.152	4.442	2.702
1300	–6.755	–5.958	7.064	–.764	15.920	9.099	–2.972	.003	–1.909	–1.059	11.230	4.124	2.520
1400	–6.027	–5.315	6.347	–.656	14.785	8.771	–2.712	.240	–1.549	–.775	10.438	3.852	2.364
1500	–5.395	–4.756	5.725	–.563	13.801	8.485	–2.487	.447	–1.236	–.527	9.752	3.615	2.229
1600	–4.842	–4.266	5.180	–.482	12.940	8.234	–2.290	.627	–.962	–.311	9.191	3.408	2.110
1700	–4.353	–3.833	4.699	–.410	12.180	8.011	–2.116	.788	–.720	–.119	8.420	3.225	2.006
1800	–3.918	–3.448	4.270	–.347	11.504	7.811	–1.962	.930	–.504	.053	8.147	3.062	1.913
1900	–3.529	–3.102	3.886	–.291	10.898	7.631	–1.823	1.058	–.310	.207	7.724	2.916	1.829
2000	–3.178	–2.790	3.540	–.240	10.353	7.469	–1.699	1.173	–.136	.346	7.343	2.785	1.754
2100	–2.860	–2.508	3.227	–.195	9.860	7.321	–1.586	1.277	.022	.472	6.998	2.666	1.686
2200	–2.571	–2.251	2.942	–.153	9.411	7.185	–1.484	1.372	.166	.587	6.684	2.558	1.625
2300	–2.307	–2.016	2.682	–.116	9.001	7.061	–1.391	1.459	.298	.692	6.396	2.459	1.568
2400	–2.065	–1.800	2.443	–.082	8.625	6.946	–1.305	1.539	.419	.789	6.134	2.368	1.517
2500	–1.842	–1.601	2.224	–.050	8.280	6.840	–1.227	1.613	.530	.879	5.892	2.285	1.469
2600	–1.636	–1.417	2.021	–.021	7.960	6.741	–1.154	1.681	.633	.962	5.668	2.208	1.425
2700	–1.446	–1.247	1.833	.005	7.664	6.649	–1.087	1.744	.729	1.039	5.460	2.136	1.384
2800	–1.268	–1.089	1.658	.030	7.388	6.563	–1.025	1.802	.818	1.110	5.268	2.070	1.347
2900	–1.103	–.941	1.495	.053	7.132	6.483	–.967	1.857	.900	1.178	5.088	2.008	1.311
3000	–.949	–.803	1.343	.074	6.892	6.407	–.913	1.908	.978	1.240	4.920	1.950	1.278
3100	–.805	–.674	1.201	.094	6.668	6.336	–.863	1.956	1.050	1.299	4.763	1.896	1.248
3200	–.670	–.553	1.067	.112	6.458	6.269	–.815	2.001	1.118	1.355	4.616	1.845	1.219
3300	–.543	–.439	.942	.129	6.260	6.206	–.771	2.043	1.182	1.407	4.478	1.798	1.192
3400	–.423	–.332	.824	.145	6.074	6.145	–.729	2.082	1.242	1.459	4.347	1.753	1.166
3500	–.310	–.231	.712	.160	5.898	6.088	–.690	2.120	1.299	1.503	4.224	1.710	1.142
3600	–.204	–.135	.607	.174	5.732	6.034	–.653	2.155	1.353	1.547	4.108	1.670	1.119
3700	–.103	–.044	.507	.188	5.574	5.982	–.618	2.189	1.404	1.589	3.998	1.632	1.098
3800	–.007	.042	.413	.200	5.425	5.933	–.585	2.220	1.452	1.629	3.894	1.596	1.077
3900	.084	.123	.323	.212	5.283	5.886	–.554	2.251	1.498	1.666	3.795	1.562	1.058
4000	.170	.201	.238	.223	5.149	5.841	–.524	2.280	1.541	1.703	3.700	1.529	1.039

Partial pressures of all gases are expressed in atmospheres (Pascals/101,325). Graphite, $C_{(S)}$, is assigned a value of unity in the equilibrium expressions for K_E and K_F.

Table 1-6.2 ***Temperature (K) at Which a Given Fraction of a Pure Gas at 1 atm Is Dissociated***

Fraction	CO_2	H_2O	H_2	O_2	N_2
0.001	1600	1700	2050	2200	4000
0.004	1800	1900	2300	2400	—
0.01	1950	2100	2450	2600	—
0.04	2200	2400	2700	2900	—
0.1	2450	2700	2900	3200	—
0.4	2950	3200	3350	3700	—

Table 1-6.3 ***Temperature at Which Air at Equilibrium Contains a Given Fraction of Nitric Oxide, at 1 atm***

Fraction	Temperature (K)
0.001	1450
0.004	1750
0.01	2100
0.04	2800

We see that K_α, K_β, and K_γ are all small compared with unity, so very little of the CO would decompose by any of these modes. However, K_α is much larger than either K_β or K_γ, so it is the dominant mode for whatever decomposition may occur.

Thus, from the expression $p_{CO_2} = (K_\alpha p_{CO})^2$, and taking p_{CO} as 1 atm, we calculate $p_{CO_2} = (5.1 \times 10^{-3})^2 = 2.6 \times 10^{-5}$ atm. Since, by process α, 2 mol of CO must decompose for each mole of CO_2 formed, we conclude that $2 \times 2.6 \times 10^{-5}$ or 5.2×10^{-5} mol of CO will decompose to $C_{(s)}$ plus CO_2, per mole of CO originally present, after which we will have reached an equilibrium state. In other words, about 1/20,000 of the CO will decompose.

If the original mixture had consisted of CO at 1 atm plus CO_2 at any pressure greater than 2.6×10^{-5} atm, at 2000 K, then we could conclude that no carbon whatsoever would form.

It can also be shown that addition of a trace of O_2 or H_2O to CO at 2000 K would completely suppress carbon formation. As a general statement, for a chemical system containing fewer carbon atoms than oxygen atoms, the equilibrium condition will favor CO formation rather than that of solid carbon.

For a carbon-containing system with little or no oxygen, carbon may or may not form, depending on the hydrogen partial pressure. For example, carbon may form according to $C_2H_2 \leftrightarrows C_{(s)} + H_2$. The equilibrium expression for this reaction is written

$$\frac{p_{H_2}}{p_{C_2H_2}} = K(=13.9 \text{ at } 3000 \text{ K})$$

Again, note that solid carbon does not appear in the expression. If we rewrite the expression in the form $p_{H_2} > 13.9\, p_{C_2H_2}$, it becomes the criterion for suppression of carbon formation at 3000 K. In other words, as long as p_{H_2} is more than 13.9 times as large as $p_{C_2H_2}$, no carbon will form at 3000 K and any carbon present will be converted to C_2H_2. On the other hand, pure C_2H_2 will decompose to $C_{(s)}$ plus H_2 until the H_2/C_2H_2 ratio reaches 13.9, after which no further decomposition will occur at 300 K.

Another way to view this is to say that H_2, C_2H_2, and solid carbon at 3000 K will be in a state of equilibrium if and only if the ratio $p_{H_2}/p_{C_2H_2} = 13.9$, and this is true regardless of the quantity of solid carbon present, and also regardless of the presence of other gases.

For a C–H–O–N system, the threshold conditions for equilibrium carbon formation are somewhat more complicated, but the trends are illustrated by the calculated values shown in Table 1-6.4 for carbon formation thresholds in carbon-hydrogen-air systems at 1 atm.

It must be noted that carbon forms more readily in actual flames than Table 1-6.4 indicates, because of nonequilibrium effects. In premixed laminar flames, incipient carbon formation occurs at a C/O ratio roughly 60 percent of the values shown in Table 1-6.4. See the next section for further comments on nonequilibrium.

Departure from Equilibrium

This procedure of specifying chemical systems by equilibrium equations will only yield correct results if the system is truly in equilibrium. If one prepares a mixture of H_2 and O_2 at room temperature and then ages the mixture for a year, it will be found that essentially nothing has happened and the system will still be very far from equilibrium. On the other hand, such a system at a high temperature characteristic of combustion will reach equilibrium in a small fraction of a second. For example, a hydrogen atom, H, in the presence of O_2 at partial pressure 0.1 atm will react so fast at 1400 K that its half-life is only about 2 microseconds. (At room temperature, the half-life of this reaction is about 300 days.)

Since peak flame temperatures are almost always above 1400 K, and sometimes as high as 2400 K, it would appear that equilibrium would always be reached in flames. However, luminous (yellow) flames rapidly lose heat by radiation, turbulent flames may be partially quenched by the action of steep velocity gradients, and flames burning very close to a cold wall may be partially quenched by heat conductivity to the wall. Thus, the equilibrium condition is only a limiting case that real flames may approach. The products of a nonluminous laminar flame more than a few millimeters from any cold surface will always be very nearly in equilibrium.

Table 1-6.4 ***Threshold Atomic C/O Ratios for Carbon Formation (Equilibrium at 1 atm, N/O = 3.76)***

Temperature (K)	1600	2000	2400	2800
Atomic H/C Ratio				
0	1.00	1.00	1.00	1.00
2	1.00	1.02	1.09	1.30
4	1.00	1.05	1.16	1.56

Sample Problems

EXAMPLE 1:

Given a mixture of an equal number of moles of steam and carbon monoxide, what will the equilibrium composition be at 1700 K and 1 atm?

SOLUTION:

We would expect the species CO, H_2O, CO_2, and H_2 to be present. From Table 1-6.2, we see that the equilibria $H_2 \leftrightarrows 2H$, $O_2 \leftrightarrows 2O$, and $H_2O \leftrightarrows \frac{1}{2}H_2 + OH$ can all be neglected at 1700 K, so the species H, O, and OH will not be present in significant quantities.

Since we have four species involving three chemical elements, we will require $4 - 3$, or 1, equilibrium relationship, for the equilibrium $H_2O + CO \leftrightarrows H_2 + CO_2$.

The relationship is

$$\frac{p_{H_2} \cdot p_{CO_2}}{p_{H_2O} \cdot p_{CO}} = K \tag{26}$$

In addition, we need $3 - 1$, or 2, atom-ratio relations, which are

$$\frac{H}{C}: \quad \frac{2p_{H_2} + 2p_{H_2O}}{p_{CO} + p_{CO_2}} = 2 \tag{27}$$

(because the original mixture of H_2O + CO contains two H atoms per C atom) and

$$\frac{O}{C}: \qquad \frac{p_{H_2O} + p_{CO} + 2p_{CO_2}}{p_{CO} + p_{CO_2}} = 2 \tag{28}$$

(because the original mixture of H_2O + CO contains two O atoms per C atom). Finally, the sum of the partial pressures equals 1 atm:

$$p_{H_2O} + p_{CO} + p_{H_2} + p_{CO_2} = 1 \tag{29}$$

We now have a well-set problem, four equations and four unknowns, which may be solved as soon as K is quantified.

We do not find the equilibrium $H_2O + CO \leftrightarrows H_2 + CO_2$ in Table 1-6.1. However, if we calculate $K_E/(K_FK_C)$ from Table 1-6.1, we see that

$$\frac{K_E}{K_FK_C} = \frac{p_{CO_2}}{(1)\cdot p_{O_2}} \cdot \frac{(1)\cdot (p_{O_2})^{1/2}}{p_{CO}} \cdot \frac{p_{H_2}\cdot (p_{O_2})^{1/2}}{p_{H_2O}}$$

$$= \frac{p_{CO_2}\cdot p_{H_2}}{p_{CO}\cdot p_{H_2O}} = K$$

From Table 1-6.1, $\log_{10}(K_E/K_FK_C)$ at 1700 K = 12.180 – 8.011 – 4.699 = –0.51, and K = antilog$_{10}$ (–0.51) = 0.309.

Upon substituting K = 0.309 into Equation 26, and then simultaneously solving Equations 26 through 29, we obtain

$$p_{CO_2} = p_{H_2} = 0.179 \text{ atm}$$

and

$$p_{H_2O} = p_{CO} = 0.321 \text{ atm}$$

EXAMPLE 2:

One mole of hydrogen is introduced into a 50-L vessel that is maintained at 2500 K. How much dissociation will occur, and what will the pressure be?

SOLUTION:

Let α be the degree of dissociation of the hydrogen defined by $\alpha = (p_H/2)/[p_{H_2} + (p_H/2)]$. Thus, α ranges from zero to one. One mole of H_2 partially dissociates to produce 2α mol of H, leaving $1 - \alpha$ mol of H_2. The total number of moles is then $2\alpha + 1 - \alpha$, or $\alpha + 1$. In view of the definition of α, the total number of moles present is $(p_H + p_{H_2})/[p_{H_2} + (p_H/2)]$.

By the ideal gas law, $PV = nRT$.

$$(p_H + p_{H_2})(50) = \frac{p_H + p_{H_2}}{p_{H_2} + (p_H/2)} \quad (0.08206)(2500) \tag{30}$$

which reduces to

$$p_{H_2} + \frac{p_H}{2} = 4.103 \tag{31}$$

The equilibrium equation is

$$\frac{p_H}{(p_{H_2})^{1/2}} = K_B \tag{32}$$

From Table 1-6.1, $\log_{10}K_B$ = –1.601 at 2500 K, and therefore K_B = 0.0251. Upon substitution into Equation 32 and elimination of p_{H_2} between Equations 31 and 32, one obtains

$$p_H^2 + 0.000315p_H - 0.00258 = 0 \tag{33}$$

This equation yields a positive and a negative root. The negative root has no physical significance. The positive root is p_H = 0.0506 atm. Then, Equation 32 yields p_{H_2} = 4.08 atm, and the total final pressure is 4.08 + 0.0506 = 4.13 atm. The degree of dissociation, α, comes out to be 0.0062. (This is less dissociation than indicated by Table 1-6.2 because the pressure is well above 1 atm.)

EXAMPLE 3:

Propane is burned adiabatically at 1 atm with a stoichiometric proportion of air. Calculate the final temperature and composition. The initial temperature is 300 K.

SOLUTION:

The problem must be solved by a series of iterations. The first step is to assume a final temperature, either based on experience or by selecting a temperature substantially below the value calculated by assuming that CO_2 and H_2O are the only products of combustion. The second step is to solve the set of equations that specify the equilibrium composition at the assumed final temperature. The third step is to consult an overall enthalpy balance equation, which will show that the assumed final temperature was either too high or too low. The fourth step is to assume an appropriate new final temperature. The fifth and sixth steps are repeats of the second and third steps. If the correct final temperature is now found to be bracketed between these two assumed temperatures, then an interpolation should give a fairly accurate value of the true final temperature. Additional iterations may be made to improve the accuracy of the results to the degree desired. As a guess, the final temperature is assumed to be 2300 K.

Now the equilibrium equations at 2300 K are set up. The species to be considered are three principal species: CO_2, H_2O, and N_2, and seven minor species: H_2, O_2, OH, H, O, CO, and NO. (Based on chemical experience, the following possible species may be neglected at 2300 K when stoichiometric oxygen is present: N, $C_{(g)}$, NH, CN, CH, C_2, HO_2, HCN, O_3, C_3, NO_2, HNO, C_2H, CH_2, C_2O, CHO, and NH_2.) Thus, we consider ten species involving four elements, so $10 - 4$, or 6, equilibrium equations are needed. Any six *independent* equilibria may be selected. We can assure independence by requiring that each successive equilibrium expression we write will introduce at least one new chemical species. Observe that this requirement is met in the following list:

$$CO + \frac{1}{2}O_2 = CO_2 \qquad \frac{p_{CO_2}}{p_{CO}\cdot (p_{O_2})^{1/2}} = K = \frac{K_E}{K_F} \tag{34}$$

$$\frac{1}{2}O_2 = O \qquad \frac{p_O}{(p_{O_2})^{1/2}} = K_A \tag{35}$$

$$\frac{1}{2}O_2 + \frac{1}{2}N_2 = NO \qquad \frac{p_{NO}}{(p_{O_2} \cdot p_{N_2})^{1/2}} = K_G \tag{36}$$

$$H_2 + \frac{1}{2}O_2 = H_2O \qquad \frac{p_{H_2O}}{p_{H_2}(p_{O_2})^{1/2}} = K_C \tag{37}$$

$$\frac{1}{2}H_2 + \frac{1}{2}O_2 = OH \qquad \frac{p_{OH}}{(p_{H_2} \cdot p_{O_2})^{1/2}} = K_D \tag{38}$$

$$\frac{1}{2}H_2 = H \qquad \frac{p_H}{(p_{H_2})^{1/2}} = K_B \tag{39}$$

Four additional equations are needed to determine the ten unknown partial pressures. These are three atom-ratio equations and a summation of the partial pressures to equal the total pressure. To obtain the atom ratios, we take air to consist of 3.76 parts of N_2 (by volume) per part of O_2, neglecting argon, and other species. Then, from stoichiometry, $C_3H_8 + 5O_2 + (5 \cdot 3.76)N_2 \rightarrow 3CO_2 + 4H_2O + 18.8N_2$.

$$\frac{H}{C}: \qquad \frac{8}{3} = \frac{p_H + p_{OH} + 2p_{H_2O} + 2p_{H_2}}{p_{CO_2} + p_{CO}} \tag{40}$$

$$\frac{H}{N}: \qquad \frac{8}{37.6} = \frac{p_H + p_{OH} + 2p_{H_2O} + 2p_{H_2}}{2p_{N_2} + p_{NO}} \tag{41}$$

$$\frac{O}{C}: \qquad \frac{10}{3} = \frac{p_O + p_{OH} + p_{NO} + p_{CO} + p_{H_2O} + 2p_{O_2} + 2p_{CO_2}}{p_{CO_2} + p_{CO}} \tag{42}$$

Finally,

$$p_{CO_2} + p_{H_2O} + p_{N_2} + p_{H_2} + p_{O_2} + p_{OH} + p_H + p_O + p_{CO} + p_{NO} = 1 \tag{43}$$

From Table 1-6.1 at 2300 K:

x	$\log_{10} x$	x
K_E	9.001	—
K_F	7.061	—
K_E/K_F	9.001–7.061	87.1
K_A	–2.307	0.00493
K_G	–1.391	0.0406
K_C	2.682	481
K_D	–0.116	0.766
K_B	–2.016	0.00964

We insert these K values into Equations 34 through 39, and then solve the set of 10 equations, Equations 34 through 43, for the equilibrium values of the 10 partial pressures at 2300 K. This solution may be obtained by a tedious set of successive approximations. The first approximation is obtained by solving for the three principal species N_2, CO_2, and H_2O, assuming the partial pressures of the remaining species are zero. Then, using this trial value of p_{CO_2}, solve for p_{CO} and p_{O_2}, using Equation 34 and assuming that $p_{CO} = 2\,p_{O_2}$. Next, using p_{H_2O} and p_{O_2} as determined, use Equation 37 to determine a trial value of p_{H_2}. Then, using all the foregoing partial pressures, determine p_O from Equation 35, p_{NO} from Equation 36, p_{OH} from Equation 38, and p_H from Equation 39. Thus, ten trial values of the partial pressures are found. However, upon substitution into Equations 40, 41, 42, and 43, none of these equations will be quite satisfied. The partial pressures of the principal species must then be adjusted so as to satisfy Equations 40 through 43, and then a second iteration with the equilibrium equations must be carried out to establish new values for the minor species. After four or five such iterations, the results should converge to a set of partial pressures satisfying all equations.

A faster method is to use a computer program to solve the equations. (See the following section.)

The equilibrium partial pressures at 2300 K will come out to be:

P_{N_2}	0.7195 atm
P_{H_2O}	0.1474 atm
P_{CO_2}	0.1006 atm
P_{CO}	0.0143 atm
P_{O_2}	0.0066 atm
P_{H_2}	0.0038 atm
P_{OH}	0.0037 atm
P_{NO}	0.0028 atm
P_H	0.0006 atm
P_O	0.0004 atm

Now, we must determine if 2300 K was too high or too low a guess, by writing the enthalpy balance equation. (See Section 1, Chapter 5 on thermochemistry).

As a basis for the enthalpy balance, we assume that we have exactly 1 mol of products, at 1 atm. Then, if $p_{CO_2} = 0.1006$ atm (see above), we must have 0.1006 mol of CO_2. Similarly, we have 0.0143 mol of CO. Since these are the only two carbon compounds in the products, and since 3 mol of CO_2 plus CO must form from each mole of C_3H_8 burned, it follows that $(0.1006 + 0.0143)/3 = 0.0383$ mol of C_3H_8 must have burned. Since the original C_3H_8-air mixture was stoichiometric, it follows that the reactants also consisted of $5 \times 0.0383 = 0.1915$ mol of O_2 and $3.76 \times 0.1915 = 0.7200$ mol of N_2. (Thus, a total of 0.9498 mol of reactant form 1 mol of product, if the product is indeed at equilibrium at 2300 K.)

The enthalpy balance equation is

$$\sum n_i H_{i,T_r} = \sum n_j H_{j,T_p} \tag{44}$$

where n_i and H_i are the number of moles and the enthalpy per mol of each reactant species at reactant temperature T_r, and n_j and H_j are the number of moles and the enthalpy per mol of each product species at product temperature T_p.

The enthalpy of each reactant or product species x at temperature T is given by

$$H_{x,T} = (\Delta H_f^\circ)_{298.15} + H^\circ - H_{298}^\circ \tag{45}$$

where $(\Delta H_{f,298.15}^\circ)_x$ is the enthalpy of formation of a mol of species x from its constituent elements in their standard

states at 298 K. These constituent elements are H_2, O_2, N_2, and $C_{(s)}$, so $\Delta H^\circ_{f,298.15}$ for each of these four species is zero, by definition.

Values of $(\Delta H^\circ_f)_{298.15}$ and $H^\circ - H^\circ_{298}$* for various species are contained in Table 1-6.5. Substitution of numerical values into Equation 44 yields:

Reactant Species	$(\Delta H^\circ_f)_{298.15}$ (kJ/mol)	$H^\circ_{300} - H^\circ_{298}$ (kJ/mol)	H°_{300} (kJ/mol)	n_i (mol)	$n_i H^\circ_{i,300}$ (kJ)
C_3H_8	–103.85	0.16	–103.69	0.0383	–3.971
O_2	0	0.05	0.05	0.1915	+0.010
N_2	0	0.05	0.05	0.7200	+0.036
					–3.925

*If $H^\circ - H^\circ_{298}$ is not available from a table, it may be evaluated from the equation $H^\circ - H^\circ_{298} = \int_{298}^{T} C_p dT$. For C_3H_8, $C_p = 0.09$ kJ/mol·K at 298 K.

and

Product Species	$(\Delta H^\circ_f)_{298.15}$ (kJ/mol)	$H^\circ_{2300} - H^\circ_{298}$ (kJ/mol)	H°_{2300} (kJ/mol)	n_i (mol)	$n_i H^\circ_{i,2300}$ (kJ)
N_2	0	66.99	66.99	0.7195	+48.199
H_2O	–241.83	88.29	–153.54	0.1474	–22.632
CO_2	–393.52	109.67	–283.85	0.1006	–28.555
CO	–110.53	67.68	–42.85	0.0143	–0.613
O_2	0	70.60	70.60	0.0066	+0.466
H_2	0	63.39	63.39	0.0038	+0.241
OH	38.99	64.28	103.27	0.0037	+0.382
NO	90.29	68.91	159.20	0.0028	+0.446
H	218.00	41.61	259.61	0.0006	+0.156
O	249.17	41.96	291.13	0.0004	0.116
					–1.794

Table 1-6.5 ***Enthalpies of Selected Combustion Products***

Species	N_2	O_2	O	NO	H_2	H	H_2O (g)	OH	CO_2	CO
$(\Delta H^\circ_f)_{298.15}$	0.00 kJ/mol	0.00 kJ/mol	249.17 kJ/mol	90.29 kJ/mol	0.00 kJ/mol	218.00 kJ/mol	–241.83 kJ/mol	38.99 kJ/mol	–393.52 kJ/mol	–110.53 kJ/mol
Temp (K)	$H^\circ - H^\circ_{298}$, kJ/mol	$H^\circ - H^\circ_{298}$, kJ/mol	$H^\circ - H^\circ_{298}$, kJ/mol	$H^\circ - H^\circ_{298}$, kJ/mol	$H^\circ - H^\circ_{298}$, kJ/mol	$H^\circ - H^\circ_{298}$, kJ/mol	$H^\circ - H^\circ_{298}$, kJ/mol	$H^\circ - H^\circ_{298}$, kJ/mol	$H^\circ - H^\circ_{298}$, kJ/mol	$H^\circ - H^\circ_{298}$, kJ/mol
100	–5.77	–5.78	–4.52	–6.07	–5.47	–4.12	–6.61	–6.14	–6.46	–5.77
200	–2.86	–2.87	–2.19	–2.95	–2.77	–2.04	–3.28	–2.97	–3.41	–2.87
298	0.00	0.00	0.00	0.00	0.00	0.00	0.00	0.00	0.00	0.00
300	.05	.05	.04	.05	.05	.04	.06	.05	.07	.05
400	2.97	3.03	2.21	3.04	2.96	2.12	3.45	3.03	4.01	2.97
500	5.91	6.08	4.34	6.06	5.88	4.20	6.92	5.99	8.31	5.93
600	8.90	9.24	6.46	9.15	8.81	6.28	10.50	8.94	12.92	8.94
700	11.94	12.50	8.57	12.31	11.75	8.35	14.18	11.90	17.76	12.02
800	15.05	15.84	10.67	15.55	14.70	10.43	17.99	14.88	22.82	15.18
900	18.22	19.24	12.77	18.86	17.68	12.51	21.92	17.89	28.04	18.40
1000	21.46	22.70	14.86	22.23	20.68	14.59	25.98	20.94	33.41	21.69
1100	24.76	26.21	16.95	25.65	23.72	16.67	30.17	24.02	38.89	25.03
1200	28.11	29.76	19.04	29.12	26.80	18.74	34.48	27.16	44.48	28.43
1300	31.50	33.34	21.13	32.63	29.92	20.82	38.90	30.34	50.16	31.87
1400	34.94	36.96	23.21	36.17	33.08	22.90	43.45	33.57	55.91	35.34
1500	38.40	40.60	25.30	39.73	36.29	24.98	48.10	36.84	61.71	38.85
1600	41.90	44.27	27.38	43.32	39.54	27.06	52.84	40.15	67.58	42.38
1700	45.43	47.96	29.46	46.93	42.84	29.14	57.68	43.50	73.49	45.94
1800	48.98	51.67	31.55	50.56	46.17	31.22	62.61	46.89	79.44	49.52
1900	52.55	55.41	33.63	54.20	49.54	33.30	67.61	50.31	85.43	53.12
2000	56.14	59.17	35.71	57.86	52.95	35.38	72.69	53.76	91.45	56.74
2100	59.74	62.96	37.79	61.53	56.40	37.46	77.83	57.25	97.50	60.38
2200	63.36	66.77	39.88	65.22	59.88	39.53	83.04	60.75	103.57	64.02
2300	66.99	70.60	41.96	68.91	63.39	41.61	88.29	64.28	109.67	67.68
2400	70.64	74.45	44.04	72.61	66.93	43.69	93.60	67.84	115.79	71.35
2500	74.30	78.33	46.13	76.32	70.50	45.77	98.96	71.42	121.93	75.02
2600	77.96	82.22	48.22	80.04	74.09	47.85	104.37	75.01	128.08	78.71
2700	81.64	86.14	50.30	83.76	77.72	49.92	109.81	78.63	134.26	82.41
2800	85.32	90.08	52.39	87.49	81.37	52.00	115.29	82.27	140.44	86.12
2900	89.01	94.04	54.48	91.23	85.04	54.08	120.81	85.92	146.65	89.83
3000	92.71	98.01	56.58	94.98	88.74	56.16	126.36	89.58	152.86	93.54
3100	96.42	102.01	58.67	98.73	92.46	58.24	131.94	93.27	159.09	97.27
3200	100.14	106.02	60.77	102.48	96.20	60.32	137.55	96.96	165.33	101.00
3300	103.85	110.05	62.87	106.24	99.96	62.40	143.19	100.67	171.59	104.73
3400	107.57	114.10	64.97	110.00	103.75	64.48	148.85	104.39	177.85	108.48
3500	111.31	118.16	67.08	113.77	107.55	66.55	154.54	108.12	184.12	112.22

(continued)

Table 1-6.5 ***Enthalpies of Selected Combustion Products (Continued)***

$C_{(s)}$	F_2	F	HF	Cl_2	Cl	HCl	Br_2	Br	HBr
0.00 kJ/mol	0.00 kJ/mol	78.91 kJ/mol	–272.55 kJ/mol	0.00 kJ/mol	121.29 kJ/mol	–92.31 kJ/mol	0.00 kJ/mol	111.86 kJ/mol	–36.44 kJ/mol
$H° - H°_{298}$, kJ/mol	$H° - H°_{298}$, kJ/mol	$H° - H°_{298}$, kJ/mol	$H° - H°_{298}$, kJ/mol	$H° - H°_{298}$, kJ/mol	$H° - H°_{298}$, kJ/mol	$H° - H°_{298}$, kJ/mol	$H° - H°_{298}$, kJ/mol	$H° - H°_{298}$, kJ/mol	$H° - H°_{298}$, kJ/mol
–.99	–5.92	–4.43	–5.77	–6.27	–4.19	–5.77	–21.72	–4.12	–5.77
–.67	–2.99	–2.23	–2.86	–3.23	–2.10	–2.86	–16.82	–2.04	–2.86
0.00	0.00	0.00	0.00	0.00	0.00	0.00	0.00	0.00	0.00
.02	.06	.04	.05	.06	.04	.05	.14	.04	.05
1.04	3.28	2.30	2.97	3.54	2.26	2.97	34.61	2.12	2.97
2.36	6.64	4.53	5.88	7.10	4.52	5.89	38.31	4.20	5.90
3.94	10.11	6.72	8.80	10.74	6.80	8.84	42.02	6.28	8.87
5.72	13.66	8.90	11.73	14.41	9.08	11.81	45.76	8.36	11.88
7.64	17.27	11.05	14.68	18.12	11.34	14.84	49.51	10.46	14.96
9.67	20.91	13.19	17.64	21.84	13.59	17.91	53.27	12.57	18.10
11.79	24.59	15.33	20.64	25.59	15.82	21.05	57.03	14.70	21.30
13.99	28.30	17.45	23.68	29.34	18.03	24.24	60.81	16.84	24.56
16.24	32.03	19.56	26.76	33.10	20.23	27.48	64.58	19.01	27.87
18.54	35.77	21.67	29.87	36.88	22.41	30.78	68.37	21.20	31.24
20.88	39.54	23.78	33.04	40.66	24.60	34.12	72.16	23.40	34.65
23.25	43.32	25.89	36.24	44.45	26.77	37.51	75.96	25.61	38.10
25.66	47.11	27.99	39.48	48.25	28.93	40.93	79.76	27.85	41.59
28.09	50.91	30.09	42.76	52.05	31.09	44.39	83.57	30.09	45.11
30.55	54.72	32.18	46.09	55.86	33.23	47.89	87.38	32.35	48.66
33.02	58.54	34.28	49.44	59.68	35.38	51.41	91.20	34.61	52.24
35.53	62.38	36.37	52.83	63.51	37.51	54.96	95.02	36.88	55.84
38.05	66.22	38.46	56.25	67.34	39.64	58.53	98.85	39.15	59.46
40.58	70.07	40.55	59.69	71.18	41.77	62.12	102.68	41.43	63.10
43.13	73.93	42.64	63.17	75.02	43.89	65.73	106.52	43.70	66.76
45.71	77.80	44.73	66.66	78.88	46.02	69.37	110.36	45.98	70.44
48.29	81.67	46.82	70.18	82.74	48.13	73.01	114.20	48.26	74.13
50.89	85.55	48.91	73.73	86.61	50.25	76.68	118.05	50.54	77.83
53.50	89.45	50.99	77.29	90.50	52.36	80.36	121.91	52.81	81.55
56.13	93.35	53.08	80.87	94.39	54.48	84.06	125.77	55.09	85.28
58.77	97.25	55.17	84.47	98.29	56.58	87.76	129.63	57.36	89.02
61.43	101.16	57.25	88.09	102.21	58.69	91.48	133.49	59.63	92.77
64.09	105.08	59.34	91.72	106.14	60.79	95.21	137.37	61.89	96.53
66.78	109.01	61.42	95.37	110.08	62.90	98.95	141.24	64.15	100.31
69.47	112.94	63.50	99.03	114.03	65.00	102.70	145.13	66.41	104.09
72.17	116.88	65.59	102.71	118.00	67.10	106.46	149.01	68.67	107.88
74.89	120.83	67.67	106.39	121.98	69.20	110.23	152.90	70.92	111.68

The enthalpy of the products (–1.794 kJ) is seen to be 2.131 kJ larger than the enthalpy of the reactants (–3.925 kJ). To put this 2.131 kJ difference in perspective, note that the heat of combustion of 0.0383 mol of propane at 298 K, to form 3 mol of CO_2 and 4 mol of H_2O per mole of propane, is $0.0383\ (3 \times 393.52 + 4 \times 241.83 - 103.85) = 78.29$ kJ. Thus, the 2.131 kJ discrepancy when compared with 78.29 kJ is rather small, showing that the 2300 K "first guess" was very close. Since the products, at 2300 K, are seen to have a slightly higher enthalpy than the reactants, the correct temperature must be slightly less than 2300 K.

To continue the calculation, the next step is to assume that the final temperature is 2200 K instead of 2300 K. The details will not be presented, but this will yield a new and slightly different set of values of the ten partial pressures of the products. Thus, a new enthalpy balance may be attempted, in the same manner as before. When this is done, the result will be that this time the enthalpy of the reactants will come out to be slightly higher than the enthalpy of the products, showing that the correct temperature is above 2200 K.

An interpolation may be made between the 2200 K enthalpy discrepancy and the 2300 K enthalpy discrepancy, which will show that the correct final temperature is 2268 K. Furthermore, the partial pressures of each product species may be obtained by interpolating between the 2200 K partial pressures and the 2300 K partial pressures, with results as follows:

$T = 2268$ K	P_{N_2}	0.7207 atm
	P_{H_2O}	0.1484 atm
	P_{CO_2}	0.1026 atm
	P_{CO}	0.0125 atm
	P_{O_2}	0.0059 atm
	P_{H_2}	0.0034 atm
	P_{OH}	0.0032 atm
	P_{NO}	0.0025 atm
	P_H	0.0005 atm
	P_O	0.0003 atm

Computer Programs for Chemical Equilibrium Calculations

In view of the extremely tedious calculations needed for determination of the equilibrium temperature and composition in a combustion process, a computer program for executing these calculations would be desirable. Fortunately, such programs have been developed.

However, the user of a computer program should be warned that thorough understanding of the material in this chapter is needed to avoid misinterpreting the computer output. Further, given such understanding, simple manual calculations can be performed to obtain independent checks of the computer output.

One program, entitled GASEQ, can be used with any computer using Windows. It can be downloaded from http://www.c.morley.ukgateway.net/gseqmain.htm. Alternatively, a program may be obtained from Reaction Design, 6440 Lusk Blvd, Suite D209, San Diego, CA 92121. Their e-mail address is <chemkin@Reaction.Design.com>.

These programs will calculate the final equilibrium conditions for adiabatic combustion at either constant pressure or constant volume, given the initial conditions. For the constant-pressure calculations, one specifies the initial temperature, the pressure, and the identities and relative proportions of the reactants. The computer programs contain the properties of selected reactants including: air, oxygen, nitrogen, hydrogen, graphite, methane, acetylene, ethylene, ethane, propane, butane, 1-butene, heptane, octane, benzene, toluene, JP-4, JP-5, methanol, ethanol, and polyethylene. If the fire only involves reactants from this list, no further input is necessary. If the fire involves a reactant not on this list, the input data must include the elemental composition and the enthalpy of formation of the reactant at 298 K, as well as enthalpy versus temperature data for the reactant over the temperature range from 298 K to the initial temperature. (If the initial temperature is 298 K, the last item is not needed.)

The computer programs can handle reactants containing any of the following elements: A, Al, B, Br, C, Cl, F, Fe, H, He, K, Li, Mg, N, Na, Ne, O, P, S, Si, and Xe. Data are included in the program on all known compounds, including liquids and solids, that can form at elevated temperatures from combinations of these elements. It is not necessary for the user to specify which product species to consider. The program can consider them all, and will print out all equilibrium species present with mole fractions greater than 5×10^{-6}, unless instructed to print out trace values down to some lower specified level.

The program can calculate Chapman-Jouguet detonation products as well as constant-pressure or constant-volume combustion products, if desired.

An addition to the program permits calculation of viscosity and thermal conductivity of gaseous mixtures, selected from 154 gaseous species, at temperatures from 300 K to 5000 K.

Nomenclature

C_p	heat capacity at constant pressure (kJ/mol·K)
$\Delta E°$	energy of products relative to energy of reactants, all at temperature T and 1 atm (kJ/mol)
$\Delta F°$	free energy of products relative to free energy of reactants, all at temperature T and 1 atm (kJ/mol)
$\Delta H°$	enthalpy of products relative to enthalpy of reactants, all at temperature T and 1 atm (kJ/mol)
K	equilibrium constant (based on partial pressures expressed in atmospheres)
K	degrees Kelvin
n	number of moles (e.g., a mole of oxygen is 32 g)
p_i	partial pressure of ith species (atm)
p	total pressure (atm)
R	gas constant (kJ/mol·K)
$\Delta S°$	entropy of products relative to entropy of reactants, all at temperature T and 1 atm (kJ/mol)
T	absolute temperature (K)

Reference Cited

1. J. van't Hoff, cf. G. Lewis, M. Randall, K. Pitzer, and L. Brewer, *Thermodynamics,* McGraw-Hill, New York (1961).

CHAPTER 7

Thermal Decomposition of Polymers

Craig L. Beyler and Marcelo M. Hirschler

Introduction

Solid polymeric materials undergo both physical and chemical changes when heat is applied; this will usually result in undesirable changes to the properties of the material. A clear distinction needs to be made between thermal decomposition and thermal degradation. The American Society for Testing and Materials' (ASTM) definitions should provide helpful guidelines. Thermal decomposition is "a process of extensive chemical species change caused by heat."[1] Thermal degradation is "a process whereby the action of heat or elevated temperature on a material, product, or assembly causes a loss of physical, mechanical, or electrical properties."[1] In terms of fire, the important change is thermal decomposition, whereby the chemical decomposition of a solid material generates gaseous fuel vapors, which can burn above the solid material. In order for the process to be self-sustaining, it is necessary for the burning gases to feed back sufficient heat to the material to continue the production of gaseous fuel vapors or volatiles. As such, the process can be a continuous feedback loop if the material continues burning. In that case, heat transferred to the polymer causes the generation of flammable volatiles; these volatiles react with the oxygen in the air above the polymer to generate heat, and a part of this heat is transferred back to the polymer to continue the process. (See Figure 1-7.1.) This chapter is concerned with chemical and physical aspects of thermal decomposition of polymers. The chemical processes are responsible for the generation of flammable volatiles while physical changes, such as melting and charring, can markedly alter the decomposition and burning characteristics of a material.

The gasification of polymers is generally much more complicated than that of flammable liquids. For most flammable liquids, the gasification process is simply evaporation. The liquid evaporates at a rate required to maintain the equilibrium vapor pressure above the liquid. In the case of polymeric materials, the original material itself is essentially involatile, and the quite large molecules must be broken down into smaller molecules that can vaporize. In most cases, a solid polymer breaks down into a variety of smaller molecular fragments made up of a number of different chemical species. Hence, each of the fragments has a different equilibrium vapor pressure. The lighter of the molecular fragments will vaporize immediately upon their creation while other heavier molecules will remain in the condensed phase (solid or liquid) for some time. While remaining in the condensed phase, these heavier molecules may undergo further decomposition to lighter fragments which are more easily vaporized. Some polymers break down completely so that virtually no solid residue remains. More often, however, not all the original fuel becomes fuel vapors since solid residues are left behind. These residues can be carbonaceous (char), inorganic (originating from heteroatoms contained in the original polymer, either within the structure or as a result of additive incorporations), or a combination of both. Charring materials, such as wood, leave large fractions of the original carbon content as carbonaceous residue, often as a porous char. When thermal decomposition of deeper layers of such a material continues, the volatiles produced must pass through the char above them to reach the surface. During this travel, the hot char may cause secondary reactions to occur in the volatiles. Carbonaceous chars can be intumescent layers, when appropriately formed, which slow down further thermal decomposition considerably. Inorganic residues, on the other hand, can form glassy lay-

Dr. Craig L. Beyler is the technical director of Hughes Associates, Fire Science and Engineering. He was the founding editor of the *Journal of Fire Protection Engineering* and serves on a wide range of committees in the fire research community.

Dr. Marcelo M. Hirschler is an independent consultant on fire safety with GBH International. He has over two decades of experience researching fire and polymers and has managed a plastics industry fire testing and research laboratory for seven years. He now serves on a variety of committees addressing the development of fire standards and codes, has published extensively, and is an associate editor of the journal *Fire and Materials.*

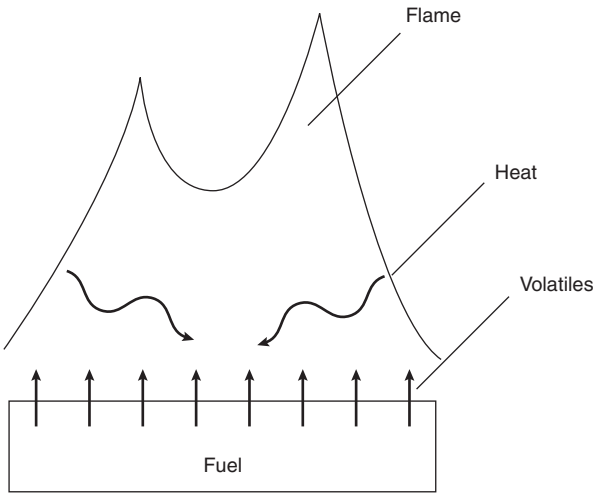

Figure 1-7.1. ***Energy feedback loop required for sustained burning.***

ers that may then become impenetrable to volatiles and protect the underlying layers from any further thermal breakdown. Unless such inorganic barriers form, purely carbonaceous chars can always be burned by surface oxidation at higher temperatures.

As this brief description of the thermal decomposition process indicates, the chemical processes are varied and complex. The rate, mechanism, and product composition of these thermal decomposition processes depend both on the physical properties of the original material and on its chemical composition.

Polymeric Materials

Polymeric materials can be classified in a variety of ways.[2] First, polymers are often classified, based on their origin, into natural and synthetic (and sometimes including a third category of seminatural or synthetic modifications of natural polymers). However, more useful is a classification based on physical properties, in particular the elastic modulus and the degree of elongation. Following this criterion, polymers can be classified into elastomers, plastics, and fibers. Elastomers (or rubbers) are characterized by a long-range extensibility that is almost completely reversible at room temperature. Plastics have only partially reversible deformability, while fibers have very high tensile strength but low extensibility. Plastics can be further subdivided into thermoplastics (whose deformation at elevated temperatures is reversible) and thermosets (which undergo irreversible changes when heated). Elastomers have elastic moduli between 10^5 and 10^6 N/m^2, while plastics have moduli between 10^7 and 10^8 N/m^2, and fibers have moduli between 10^9 and 10^{10} N/m^2. In terms of the elongation, elastomers can be stretched roughly up to 500 to 1000 percent, plastics between 100 to 200 percent, and fibers only 10 to 30 percent before fracture of the material is complete.

Polymers can also be classified in terms of their chemical composition; this gives a very important indication as to their reactivity, including their mechanism of thermal decomposition and their fire performance.

The main carbonaceous polymers with no heteroatoms are polyolefins, polydienes, and aromatic hydrocarbon polymers (typically styrenics). The main polyolefins are thermoplastics: polyethylene [repeating unit: $-(CH_2-CH_2)-$] and polypropylene {repeating unit: $-[CH(CH_3)-CH_2]-$}, which are two of the three most widely used synthetic polymers. Polydienes are generally elastomeric and contain one double bond per repeating unit. Other than polyisoprene (which can be synthetic or natural, e.g., natural rubber) and polybutadiene (used mostly as substitutes for rubber), most other polydienes are used as copolymers or blends with other materials [e.g., in ABS (acrylonitrile butadiene styrene terpolymers), SBR (styrene butadiene rubbers), MBS (methyl methacrylate butadiene styrene terpolymers), and EPDM (ethylene propylene diene rubbers)]. They are primarily used for their high abrasion resistance and high impact strength. The most important aromatic hydrocarbon polymers are based on polystyrene {repeating unit: $-[CH(phenyl)-CH_2]-$}. It is extensively used as a foam and as a plastic for injection-molded articles. A number of styrenic copolymers also have tremendous usage, for example, principally, ABS, styrene acrylonitrile polymers (SAN), and MBS.

The most important oxygen-containing polymers are cellulosics, polyacrylics, and polyesters. Polyacrylics are the only major oxygen-containing polymers with carbon–carbon chains. The most important oxygen-containing natural materials are cellulosics, mostly wood and paper products. Different grades of wood contain 20 to 50 percent cellulose. The most widely used polyacrylic is poly(methyl methacrylate) (PMMA) {repeating unit: $-[CH_2-C(CH_3)-CO-OCH_3]-$}. PMMA is valued for its high light transmittance, dyeability, and transparency. The most important polyesters are manufactured from glycols, for example, polyethylene terephthalate (PET) or polybutylene terephthalate (PBT), or from biphenol A (polycarbonate). They are used as engineering thermoplastics, as fibers, for injection-molded articles, and unbreakable replacements for glass. Other oxygenated polymers include phenolic resins (produced by the condensation of phenols and aldehydes, which are often used as polymeric additives), polyethers [such as polyphenylene oxide (PPO), a very thermally stable engineering polymer], and polyacetals (such as polyformaldehyde, used for its intense hardness and resistance to solvents).

Nitrogen-containing materials include nylons, polyurethanes, polyamides, and polyacrylonitrile. Nylons, having repeating units containing the characteristic group $-CO-NH-$, are made into fibers and also into a number of injection-molded articles. Nylons are synthetic aliphatic polyamides. There are also natural polyamides (e.g., wool, silk, and leather) and synthetic aromatic polyamides (of exceptionally high thermal stability and used for protective clothing). Polyurethanes (PU), with repeating units containing the characteristic group $-NH-COO-$, are normally manufactured from the condensation of polyisocyanates and polyols. Their principal area of application is as foams (flexible and rigid), or as thermal insulation.

Other polyurethanes are made into thermoplastic elastomers, which are chemically very inert. Both these types of polymers have carbon–nitrogen chains, but nitrogen can also be contained in materials with carbon–carbon chains, the main example being polyacrylonitrile [repeating unit: $-(CH_2-CH-CN-)$]. It is used mostly to make into fibers and as a constituent of engineering copolymers (e.g., SAN, ABS).

Chlorine-containing polymers are exemplified by poly(vinyl chloride) [PVC, repeating unit: $-(CH_2-CHCl)-$]. It is the most widely used synthetic polymer, together with polyethylene and polypropylene. It is unique in that it is used both as a rigid material (unplasticized) and as a flexible material (plasticized). Flexibility is achieved by adding plasticizers or flexibilizers. Through the additional chlorination of PVC, another member of the family of vinyl materials is made: chlorinated poly(vinyl chloride) (CPVC) with very different physical and fire properties from PVC. Two other chlorinated materials are of commercial interest: (1) polychloroprene (a polydiene, used for oil-resistant wire and cable materials and resilient foams) and (2) poly(vinylidene chloride) [PVDC, with a repeating unit: $-(CH_2-CCl_2)-$ used for making films and fibers]. All these polymers have carbon–carbon chains.

Fluorine-containing polymers are characterized by high thermal and chemical inertness and low coefficient of friction. The most important material in the family is polytetrafluoroethylene (PTFE); others are poly(vinylidene fluoride) (PVDF), poly(vinyl fluoride) (PVF), and fluorinated ethylene polymers (FEP).

Physical Processes

The various physical processes that occur during thermal decomposition can depend on the nature of the material. For example, as thermosetting polymeric materials are infusible and insoluble once they have been formed, simple phase changes upon heating are not possible. Thermoplastics, on the other hand, can be softened by heating without irreversible changes to the material, provided heating does not exceed the minimum thermal decomposition temperature. This provides a major advantage for thermoplastic materials in the ease of molding or thermoforming of products.

The physical behavior of thermoplastics in heating is dependent on the degree of order in molecular packing, that is, the degree of crystallinity. For crystalline materials, there exists a well-defined melting temperature. Materials that do not possess this ordered internal packing are amorphous. An example of an amorphous material is window glass. While it appears to be a solid, it is in fact a fluid that over long periods of time (centuries) will flow noticeably. Despite this, at low temperatures amorphous materials do have structural properties of normal solids. At a temperature known as the glass transition temperature in polymers, the material starts a transition toward a soft and rubbery state. For example, when using a rubber band, one would hope to use the material above its glass transition temperature. However, for materials requiring

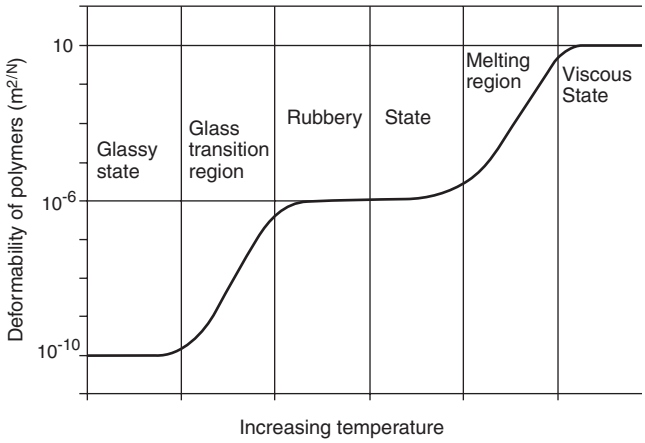

Figure 1-7.2. ***Idealized view of effect on deformability of thermoplastics with increasing temperature.***

rigidity and compressive strength, the glass transition temperature is an upper limit for practical use. In theoretical terms, this "deformability" of a polymer can be expressed as the ratio of the deformation (strain) resulting from a constant stress applied. Figure 1-7.2 shows an idealized view of the effect on the deformability of thermoplastics of increasing the temperature: a two-step increase. In practice, it can be stated that the glass transition temperature is the upper limit for use of a plastic material (as defined above, based on its elastic modulus and elongation) and the lower limit for use of an elastomeric material. Furthermore, many materials may not achieve a viscous state since they begin undergoing thermal decomposition before the polymer melts. Some typical glass transition temperatures are given in Table 1-7.1. As this type of physical transformation is less well defined than a phase transformation, it is known as a second order transition. Typically, materials are only partially crystalline, and, hence, the melting temperature is less well defined, usually extending over a range of 10°C or more.

Neither thermosetting nor cellulosic materials have a fluid state. Due to their structure, it is not possible for the original material to change state at temperatures below that at which thermal decomposition occurs. Hence, there are no notable physical transformations in the material before decomposition. In cellulosic materials, there is an important semi-physical change that always occurs on heating: desorption of the adsorbed water. As the water is both physically and chemically adsorbed, the temperature and rate of desorption will vary with the material. The activation energy for physical desorption of water is 30 to 40 kJ/mol, and it starts occurring at temperatures somewhat lower than the boiling point of water (100°C).

Many materials (whether cellulosic, thermosetting, or thermoplastic) produce carbonaceous chars on thermal decomposition. The physical structure of these chars will strongly affect the continued thermal decomposition

Table 1-7.1 ***Glass Transition and Crystalline Melting Temperatures***

Polymer	% Crystalline	Glass Transition Temperature (°C)	Crystalline Melting Temperature (°C)
Acetal	high		175–181
Acrylonitrile-butadiene-styrene	low	91–110	110–125
Cellulose	high		decomposes
Ethylene-vinyl acetate	high		65–110
Fluorinated ethylene propylene	high		275
High-density polyethylene	95	–125	130–135
Low-density polyethylene	60	–25	109–125
Natural rubber	low		30
Nylon 11	high		185–195
Nylon 6		75	215–220
Nylon 6-10		50	215
Nylon 6-6		57	250–260
Polyacrylonitrile	low	140	317
Poly(butene 1)		–25	124–142
Polybutylene		–26	126
Poly(butylene terephthalate)	high	40	232–267
Polycarbonate	low	145–150	215–230
Polychlorotrifluoroethylene	high	45	220
Poly(ether ether ketone)	high	143	334
Poly(ether imide)		217	
Poly(ethylene terephthalate)	high	70	265
Poly(hexene 1)			55
Poly(methylbutene 1)			300
Polymethylene	100		136
Poly(methyl methacrylate)	low	50	90–105
Polyoxymethylene	75–80	–85	175–180
Poly(pentene 1)			130
Poly(3-phenylbutene 1)			360
Poly(phenylene oxide)/polystyrene	low	100–135	110–135
Poly(phenylene sulphide)	high	88–93	277–282
Polypropylene	65	–20	170
Polystyrene	low	>80	230
Polysulphone	low	190	190
Polytetrafluoroethylene	100	125	327
Poly(vinyl chloride)	5–15	80–85	75–105 (212)
Poly(vinylidene chloride)	high	–18	210
Poly(vinylidene fluoride)	high	–30– –20	160–170
Poly(*p*-xylene)			>400
Styrene-acrylonitrile	low	100–120	120

process. Very often the physical characteristics of the char will dictate the rate of thermal decomposition of the remainder of the polymer. Among the most important characteristics of char are density, continuity, coherence, adherence, oxidation-resistance, thermal insulation properties, and permeability.[3] Low-density–high-porosity chars tend to be good thermal insulators; they can significantly inhibit the flow of heat from the gaseous combustion zone back to the condensed phase behind it, and thus slow down the thermal decomposition process. This is one of the better means of decreasing the flammability of a polymer (through additive or reactive flame retardants).[1,3,4] As the char layer thickens, the heat flux to the virgin material decreases, and the decomposition rate is reduced. The char itself can undergo glowing combustion when it is exposed to air. However, it is unlikely that both glowing combustion of the char and significant gas-phase combustion can occur simultaneously in the same zone above the surface, since the flow of volatiles through the char will tend to exclude air from direct contact with the char. Therefore, in general, solid-phase char combustion tends to occur after volatilization has largely ended.

Chemical Processes

The thermal decomposition of polymers may proceed by oxidative processes or simply by the action of heat. In many polymers, the thermal decomposition processes are accelerated by oxidants (such as air or oxygen). In that case, the minimum decomposition temperatures are lower in the presence of an oxidant. This significantly complicates the problem of predicting thermal decomposition rates, as the prediction of the concentration of oxygen at the polymer surface during thermal decomposition or combustion is quite difficult. Despite its importance to fire, there have been many fewer studies of thermal decomposition processes in oxygen or air than in inert atmospheres.

It is worthwhile highlighting, however, that some very detailed measurements of oxygen concentrations and of the effects of oxidants have been made by Stuetz et al. in the 1970s[5] and more recently by Kashiwagi et al.,[6–10] Brauman,[11] and Gijsman et al.[12] Stuetz found that oxygen can penetrate down to at least 10 mm below the surface of polypropylene. Moreover, for both polyethylene and polypropylene, this access to oxygen is very important in determining thermal decomposition rates and mechanisms. Another study of oxygen concentration inside polymers during thermal decomposition, by Brauman,[11] suggests that the thermal decomposition of polypropylene is affected by the presence of oxygen (a fact confirmed more recently by Gijsman et al.[12]) while poly(methyl methacrylate) thermal decomposition is not. Kashiwagi found that a number of properties affect the thermal and oxidative decomposition of thermoplastics, particularly molecular weight, prior thermal damage, weak linkages, and primary radicals. Of particular interest is the fact that the effect of oxygen (or air) on thermal decomposition depends on the mechanism of polymerization: free-radical polymerization leads to a neutralization of the effect of oxygen. A study on poly(vinylidene fluoride) indicated that the effect of oxygen can lead to changes in both reaction rate and kinetic order of reaction.[13]

Kashiwagi's work in particular has resulted in the development of models for the kinetics of general random-chain scission thermal decomposition,[14] as well as for the thermal decomposition of cellulosics[15] and thermoplastics.[16]

There are a number of general classes of chemical mechanisms important in the thermal decomposition of polymers: (1) random-chain scission, in which chain scissions occur at apparently random locations in the polymer chain; (2) end-chain scission, in which individual monomer units are successively removed at the chain end; (3) chain-stripping, in which atoms or groups not part of the polymer chain (or backbone) are cleaved; and (4) cross-linking, in which bonds are created between polymer chains. These are discussed in some detail under General Chemical Mechanisms, later in this chapter. It is sufficient here to note that thermal decomposition of a polymer generally involves more than one of these classes of reactions. Nonetheless, these general classes provide a conceptual framework useful for understanding and classifying polymer decomposition behavior.

Interaction of Chemical and Physical Processes

The nature of the volatile products of thermal decomposition is dictated by the chemical and physical properties of both the polymer and the products of decomposition. The size of the molecular fragments must be small enough to be volatile at the decomposition temperature. This effectively sets an upper limit on the molecular weight of the volatiles. If larger chain fragments are created, they will remain in the condensed phase and will be further decomposed to smaller fragments, which can vaporize.

Figure 1-7.3 shows examples of the range of chemical or physical changes that can occur when a solid polymer is volatilized. The changes range from simple phase transformations (solid going to liquid and then to gas, at the top of the figure), to complex combinations of chemical and physical changes (in the lower part of the figure). Water and many other liquids forming crystalline solids on freezing (e.g., most flammable liquids) undergo straightforward physical phase changes. Sublimation, that is, the direct phase change from a solid to a gas, without going through the liquid phase, will happen with materials such as carbon dioxide (e.g., CO_2, dry gas) or methenamine at normal temperatures and pressures. Methenamine is of interest in fires because methenamine pills are the ignition source in a standard test for carpets, ASTM D2859,[17] used in mandatory national regulations.[18,19] Thermoplastics can melt without chemical reaction to form a viscous state (polymer melt), but they often decompose thermally before melting. This polymer melt can then decompose into smaller liquid or gaseous fragments. The liquid fragments will then decompose further until they, too, are sufficiently volatile to vaporize. Some polymers, especially thermosets or cellulosics, have even more complex decomposition mechanisms. Polyurethanes (particularly flexible foams) can decompose by three different mechanisms. One of them involves the formation of gaseous isocyanates, which can then repolymerize in the gas phase and condense as a "yellow smoke." These iso-

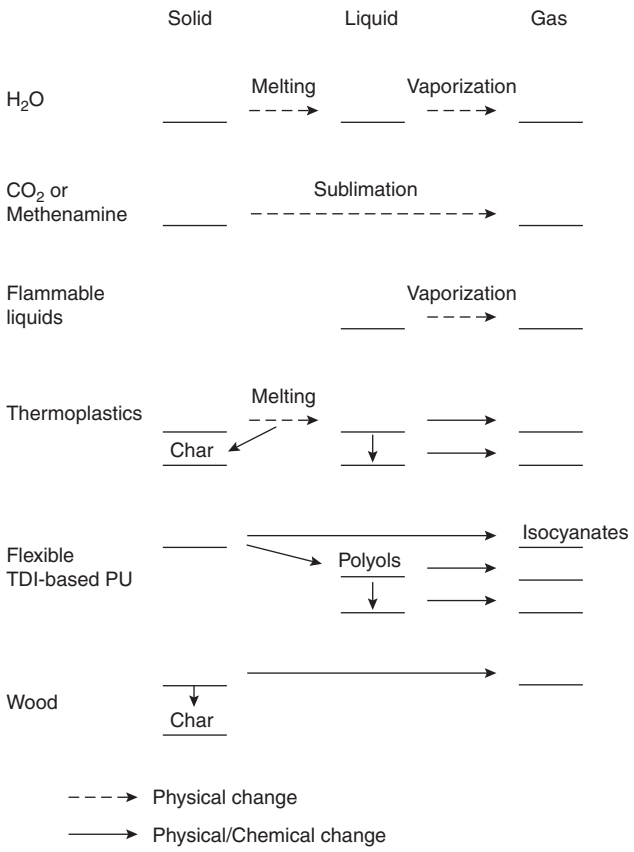

Figure 1-7.3. ***Physical and chemical changes during thermal decomposition.***

cyanates are usually accompanied by liquid polyols, which can then continue to decompose. Cellulosics, such as wood, decompose into three types of products: (1) laevoglucosan, which quickly breaks down to yield small volatile compounds; (2) a new solid, char; and (3) a series of high molecular weight semi-liquid materials generally known as tars. Figure 1-7.3 illustrates the complex and varied physicochemical decomposition pathways available, depending on the properties of the material in question. These varied thermal degradation/decomposition mechanisms have clear effects on fire behavior.

Experimental Methods

By far, the most commonly used thermal decomposition test is thermogravimetric analysis (TGA). In TGA experiments, the sample (mg size) is brought quickly up to the desired temperature (isothermal procedure) and the weight of the sample is monitored during the course of thermal decomposition. Because it is impossible in practice to bring the sample up to the desired temperature before significant thermal decomposition occurs, it is common to subject the sample to a linearly increasing temperature at a predetermined rate of temperature rise. One might hope to obtain the same results from one nonisothermal test that were possible only in a series of isothermal tests. In practice, this is not possible since the thermogram (plot of weight vs. temperature) obtained in a nonisothermal test is dependent on the heating rate chosen. Traditional equipment rarely exceed heating rates of 0.5 K/s, but modifications can be made to obtain rates of up to 10 K/s.[20,21] This dependence of thermal decomposition on heating rate is due to the fact that the rate of thermal decomposition is not only a function of the temperature, but also of the amount and nature of the decomposition process that has preceded it.

There are several reasons why the relevance of thermogravimetric studies to fire performance can be questioned: heating rate, amount of material, and lack of heat feedback are the major ones. For example, it is well known that heating rates of 10 to 100 K/s are common under fire conditions but are rare in thermal analysis. However, low heating rates *can* occur in real fires. More seriously, thermogravimetric studies are incapable of simulating the thermal effects due to large amounts of material burning and resupplying energy to the decomposing materials at different rates. However, analytical thermogravimetric studies do give important information about the decomposition process even though extreme caution must be exercised in their direct application to fire behavior.

Differential thermogravimetry (DTG) is exactly the same as TGA, except the mass loss versus time output is differentiated automatically to give the mass loss rate versus time. Often, both the mass loss and the mass loss rate versus time are produced automatically. This is, of course, quite convenient as the rate of thermal decomposition is proportional to the volatilization or mass loss rate. One of the main roles where DTG is useful is in mechanistic studies. For example, it is the best indicator of the temperatures at which the various stages of thermal decomposition take place and the order in which they occur as illustrated in Figure 1-7.4. Part (a) of this figure shows the DTG of a thermoplastic polymer, acrylonitrile-butadiene-styrene (ABS), and part (b) shows the same polymer containing 40 percent alumina trihydrate.[22] The polymer decomposes in two main stages. The addition of alumina trihydrate has a dual effect: (1) it makes the material less thermally stable, and (2) it introduces a third thermal decomposition stage. Moreover, the first stage is now the elimination of alumina trihydrate. A more complex example is shown in Figure 1-7.5, where the effects of a variety of additives are shown;[23] some of these additives are effective flame retardants and others are not: the amount of overlap between the thermal decomposition stages of polymer and additives is an indication of the effectiveness of the additive.

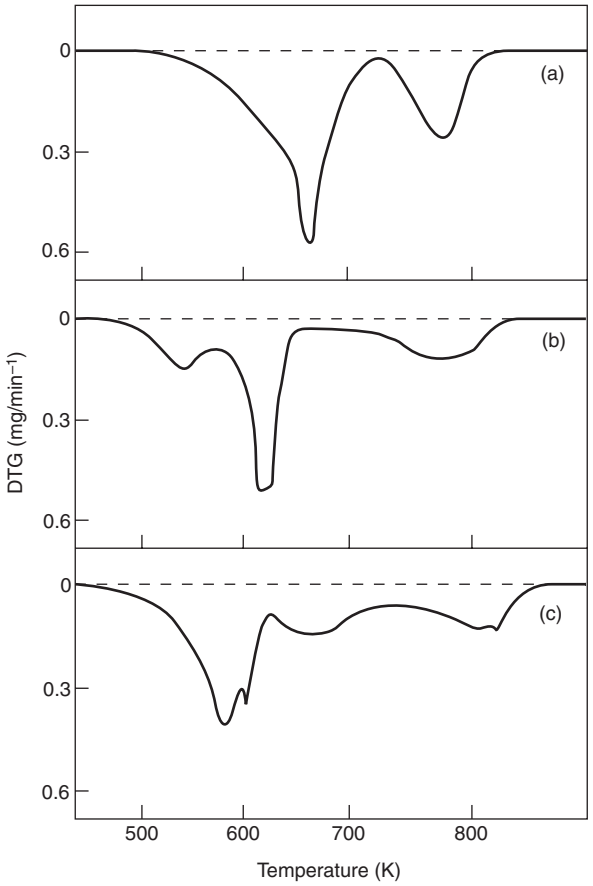

Figure 1-7.4. ***Effect of hydrated alumina and of antimony oxide-decabromobiphenyl (DBB) on DTG of ABS copolymer: (a) ABS; (b) ABS (60%) $A\ell_2O_3$, 3 H_2O (40%); (c) ABS (70%) + DBB (22.5%) + Sb_2O_3 (7.5%).***

Another method for determining the rate of mass loss is thermal volatilization analysis (TVA).[24] In this method, a sample is heated in a vacuum system (0.001 Pa) equipped with a liquid nitrogen trap (77 K) between the sample and the vacuum pump. Any volatiles produced will increase the pressure in the system until they reach the liquid nitrogen and condense out. The pressure is proportional to the mass volatilization rate, and a pressure transducer, rather

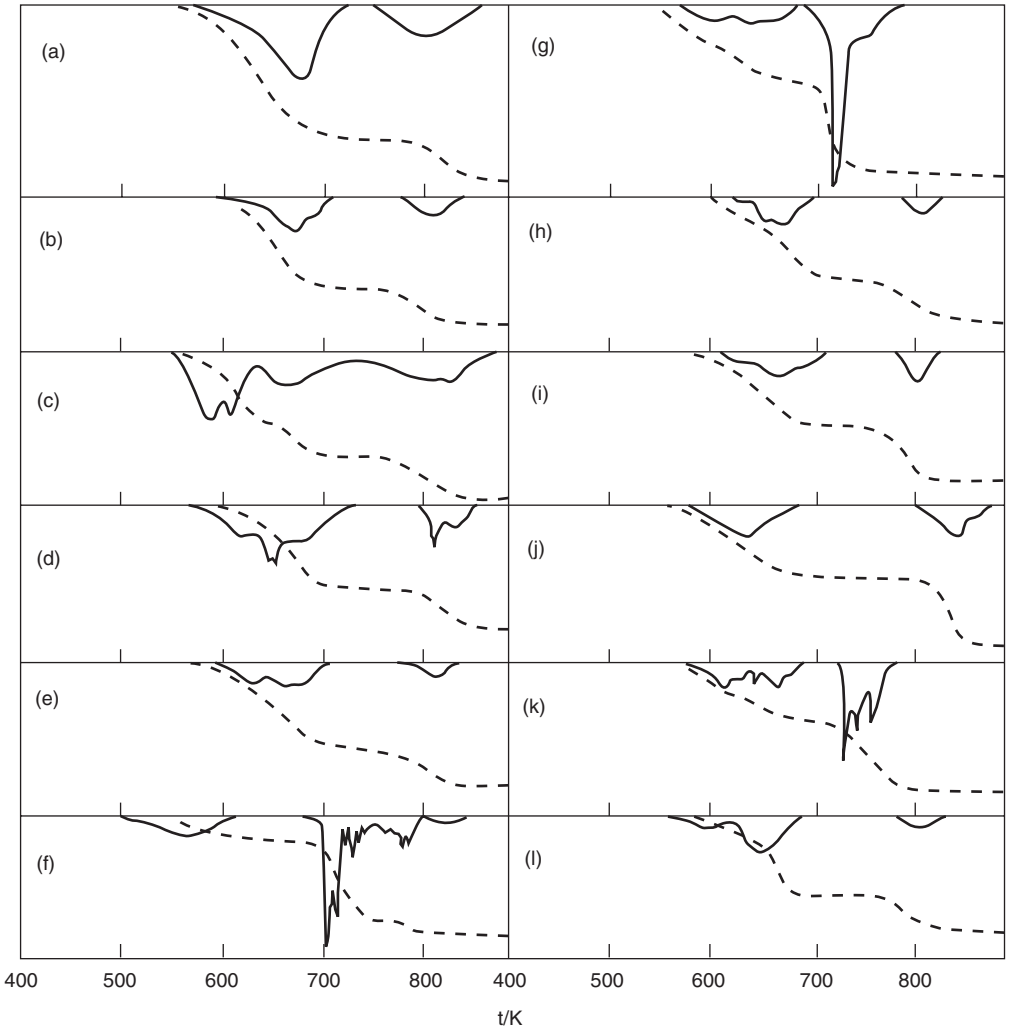

Figure 1-7.5. ***Thermal analyses of systems containing ABS, decabromobiphenyl (DBB), and one metal oxide, where DTG curves are indicated by a continuous line and TGA curves by a dashed line: (a) ABS; (b) ABS + DBB; (c) ABS + DBB + Sb_2O_3; (d) ABS + DBB + SnO; (e) ABS + DBB + $SnO_2 \cdot H_2O$; (f) ABS + DBB + ZnO; (g) ABS + DBB + Fe_2O_3; (h) ABS + DBB + AlOOH; (i) ABS + DBB + Al_2O_3; (j) ABS + DBB + $Al_2O_3 \cdot 3\,H_2O$; (k) ABS + DBB + ammonium molybdate; (l) ABS + DBB + talc. DTG (—); TGA (----).***

than a sample microbalance, is used to measure the decomposition rate.

In addition to the rate of decomposition, it is also of interest to determine the heat of reaction of the decomposition process. In almost all cases, heat must be supplied to the sample to get it to a temperature where significant thermal decomposition will occur. However, once at such a temperature, the thermal decomposition process may either generate or utilize additional heat. The magnitude of this energy generation (exothermicity) or energy requirement (endothermicity) can be determined in the following ways.

In differential thermal analysis (DTA), a sample and a reference inert material with approximately the same heat capacity are both subjected to the same linear temperature program. The sample and reference material temperatures are measured and compared. If the thermal decomposition of the sample is endothermic, the temperature of the sample will lag behind the reference material; if the decomposition is exothermic, the temperature of the sample will exceed the reference material temperature. Very often, the sample is held in a crucible, and an empty crucible is used as a reference. Such a test can be quite difficult to calibrate to get quantitative heats of reaction.

In view of the considerable importance of the exact process of thermal decomposition, it is advantageous to carry out simultaneously the measurements of TGA, DTG, and DTA. This can be achieved by using a simultaneous thermal analyzer (STA), which uses a dual sample/reference material system. In the majority of cases, polymeric materials are best represented by a reference material which is simply air, that is, an empty crucible. STA instru-

ments can then determine, at the same time, the amounts of polymer decomposed, the rates at which these stages/processes occur, and the amount of heat evolved or absorbed in each stage. Examples of the application of this technique are contained in References 20 and 21. Recently, STA equipment is often being connected to Fourier transform infrared spectrometers (FTIR) for a complete chemical identification and analysis of the gases evolved at each stage, making the technique even more powerful.

Another method, which yields quantitative results more easily than DTA, is differential scanning calorimetry (DSC). In this test procedure, both the sample and a reference material are kept at the same temperature during the linear temperature program, and the heat of reaction is measured as the difference in heat input required by the sample and the reference material. The system is calibrated using standard materials, such as melting salts, with well-defined melting temperatures and heats of fusion. In view of the fact that DSC experiments are normally carried out by placing the sample inside sealed sample holders, this technique is seldom suitable for thermal decomposition processes. Thus, it is ideally suited for physical changes, but not for chemical processes. Interestingly, some of the commercial STA apparatuses are, in fact, based on DSC rather than DTA techniques for obtaining the heat input.

So far the experimental methods discussed have been concerned with the kinetics and thermodynamics of the thermal decomposition process. There is also concern with the nature of the decomposition process from the viewpoints of combustibility and toxicity. Chemical analysis of the volatiles exiting from any of the above instruments is possible. However, it is often convenient to design a special decomposition apparatus to attach directly to an existing analytical instrument. This is particularly important when the heating rate to be studied is much higher than that which traditional instruments can achieve. Thermal breakdown of cellulosic materials, for example, has been investigated at heating rates as high as 10 K/s[25,26] or even more than 1000 K/s[27–29] in specialized equipment. The major reason this was done was in order to simulate the processes involved in "smoking," but the results are readily applicable to fire safety.

Given the vast numbers of different products that can result from the decomposition in a single experiment, separation of the products is often required. Hence, the pyrolysis is often carried out in the injector of a gas chromatograph (PGC). In its simplest but rarely used form, a gas chromatograph consists of a long tube with a well-controlled flow of a carrier gas through it. The tube or column is packed with a solid/liquid that will absorb and desorb constituents in the sample. A small sample of the decomposition products is injected into the carrier gas flow. If a particular decomposition product spends a lot of time adsorbed on the column packing, it will take a long time for it to reach the end of the column. Products with different adsorption properties relative to the column packing will reach the end of the column at different times. A detector placed at the exit of the gas chromatograph will respond to the flow rate of gases other than the carrier gas, and if separation is successful, the detector output will be a series of peaks. For a single peak, the time from injection is characteristic of the chemical species, and the area under the peak is proportional to the amount of the chemical species. Column packing, column temperature programming, carrier gas flow rate, sample size, and detector type must all be chosen and adjusted to achieve optimal discrimination of the decomposition products.

Once the gases have been separated, any number of analytical techniques can be used for identification. Perhaps the most powerful has been mass spectrometry (MS). Again speaking in very simple terms, in MS the chemical species is ionized, and the atomic mass of the ion can be determined by the deflection of the ion in a magnetic field. Generally, the ionization process will also result in the fragmentation of the molecule, so the "fingerprint" of the range of fragments and their masses must be interpreted to determine the identity of the original molecule. Gas chromatography and mass spectrometry are the subject of a vast literature, and many textbooks and specialized journals exist.

Useful physical data can be obtained by thermomechanical analysis (TMA). This is really a general name for the determination of a physical/mechanical property of a material subjected to high temperatures. Compressive and tensile strength, softening, shrinking, thermal expansion, glass transition, and melting can be studied by using TMA.

As displayed in Table 1-7.2, many of these tests can be performed *in vacuo,* in inert atmospheres, and in oxidizing atmospheres. Each has its place in the determination of the decomposition mechanism. Experiments performed *in vacuo* are of little practical value, but under vacuum the products of decomposition are efficiently carried away from the sample and its hot environment. Thus, secondary reactions are minimized so that the original decomposition product may reach a trap or analytical instrument intact. The practical significance of studies of thermal decomposition carried out in inert atmospheres may be

Table 1-7.2 ***Analytical Methods***

Method	Isothermal	Nonisothermal	In Vacuo	Inert	Air
Thermogravimetric analysis (TGA)	X	X	X	X	X
Differential thermogravimetry (DTG)	X	X	X	X	X
Thermal volatilization analysis (TVA)	X	X	X		
Differential thermal analysis (DTA)		X		X	X
Differential scanning calorimetry (DSC)		X		X	X
Pyrolysis gas chromatography (PGC)	X			X	
Thermomechanical analysis (TMA)	X	X		X	X

argued. However, when a material burns, the flow of combustible volatiles from the surface and the flame above the surface effectively exclude oxygen at the material's surface. Under these conditions, oxidative processes may be unimportant. In other situations, such as ignition where no flame yet exists, oxidative processes may be critical. Whether or not oxygen plays a role in decomposition can be determined by the effect of using air rather than nitrogen in thermal decomposition experiments.

The decomposition reactions in the tests of Table 1-7.2 are generally monitored by the mass loss of the sample. With the exception of charring materials (e.g., wood or thermosets), analysis of the partially decomposed solid sample is rarely carried out. When it is done, it usually involves the search for heteroatom components due to additives. Analysis of the composition of the volatiles can be carried out by a wide range of analytical procedures. Perhaps the simplest characterization of the products is the determination of the fraction of the volatiles that will condense at various trap temperatures. Typically, convenient temperatures are room temperature (298 K), dry-ice temperature (193 K), and liquid nitrogen temperature (77 K). The products are classified as to the fraction of the sample remaining as residue; the fraction volatile at the pyrolysis temperature, but not at room temperature, V_{pyr}; the fraction volatile at room temperature, but not at dry-ice temperature, V_{298}; the fraction volatile at dry-ice temperature, but not at liquid nitrogen temperature, V_{-193}; and the fraction volatile at liquid nitrogen temperature, V_{-77}. This characterization gives a general picture of the range of molecular weights of the decomposition products. The contents of each trap can also be analyzed further, perhaps by mass spectroscopy.

The residual polymer can be analyzed to determine the distribution of molecular weights of the remaining polymer chains. This information can be of great value in determining the mechanism of decomposition. The presence of free radicals in the residual polymer can be determined by electron spin resonance spectroscopy (ESR, EPR), which simplistically can be considered the determination of the concentration of unpaired electrons in the sample. Other techniques, like infrared spectroscopy (IR), can be usefully employed to detect the formation of bonds not present in the original polymer. Such changes in bonding may be due to double-bond formation due to chain-stripping or the incorporation of oxygen into the polymer, for example.

General Chemical Mechanisms

Four general mechanisms common in polymer decomposition are illustrated in Figure 1-7.6. These reactions can be divided into those involving atoms in the main polymer chain and those involving principally side chains or groups. While the decomposition of some polymers can be explained by one of these general mechanisms, others involve combinations of these four general mechanisms. Nonetheless, these categorizations are useful in the identification and understanding of particular decomposition mechanisms.

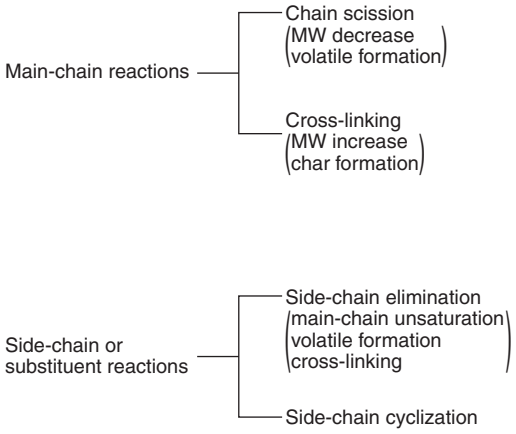

Figure 1-7.6. ***General decomposition mechanisms.***

Among simple thermoplastics, the most common reaction mechanism involves the breaking of bonds in the main polymer chain. These chain scissions may occur at the chain end or at random locations in the chain. End-chain scissions result in the production of monomer, and the process is often known as *unzipping*. Random-chain scissions generally result in the generation of both monomers and oligomers (polymer units with 10 or fewer monomer units) as well as a variety of other chemical species. The type and distribution of volatile products depend on the relative volatility of the resulting molecules.

Cross-linking is another reaction involving the main chain. It generally occurs after some stripping of substituents and involves the creation of bonds between two adjacent polymer chains. This process is very important in the formation of chars, since it generates a structure with a higher molecular weight that is less easily volatilized.

The main reaction types involving side chains or groups are elimination reactions and cyclization reactions. In elimination reactions, the bonds connecting side groups of the polymer chain to the chain itself are broken, with the side groups often reacting with other eliminated side groups. The products of these reactions are generally small enough to be volatile. In cyclization reactions, two adjacent side groups react to form a bond between them, resulting in the production of a cyclic structure. This process is also important in char formation because, as the reaction scheme shows, the residue is much richer in carbon than the original polymer as seen, for example, for poly(vinyl chloride):

$$-CH_2-CHCl-\Rightarrow -CH=CH-+HCl$$

which leads to a hydrogenated char or for poly(vinylidene chloride):

$$-CH_2-CCl_2-\Rightarrow -C\equiv C-+2HCl$$

which yields a purely carbonaceous char with an almost graphitic structure. These chars will tend to continue

breaking down by chain scission, but only at very high temperatures.

Chain-Scission Mechanisms

Decomposition by chain scission is a very typical mechanism for polymer decomposition. The process is a multistep radical chain reaction with all the general features of such reaction mechanisms: initiation, propagation, branching, and termination steps.

Initiation reactions are of two basic types: (1) random-chain scission and (2) end-chain scission. Both, of course, result in the production of free radicals. The random scission, as the name suggests, involves the breaking of a main chain bond at a seemingly random location, all such main chain bonds being equal in strength. End-chain initiation involves the breaking off of a small unit or group at the end of the chain. This may be a monomer unit or some smaller substituent. These two types of initiation reactions may be represented by the following generalized reactions:

$$P_n \Rightarrow R_r + R_{n-r} \qquad \text{(random-chain scission)}$$

$$P_n \Rightarrow R_n + R_E \qquad \text{(end-chain initiation)}$$

where P_n is a polymer containing n monomer units, and R_r is a radical containing r monomer units. R_E refers to an end group radical.

Propagation reactions in polymer decomposition are often called *depropagation reactions,* no doubt due to the polymer chemist's normal orientation toward polymer formation (polymerization) rather than decomposition. Regardless, there are several types of reactions in this class [see Figure 1-7.7, parts (a), (b), and (c)]:

$$R_n \Rightarrow R_{n-m} + P_m \qquad \text{(intramolecular H transfer, random-chain scission)}$$

$$P_m + R_n \Rightarrow P_{m-j} + P_n + R_j \qquad \text{(intermolecular H transfer)}$$

$$R_n \Rightarrow R_{n-1} + P_1 \qquad \text{(unzipping, depropagation, depolymerization)}$$

The first of these reactions involves the transfer of a hydrogen atom within a single polymer chain, that is, intramolecular hydrogen atom transfer. The value of m is usually between one and four as polymer molecules are often oriented such that the location of the nearest available H within the chain is one to four monomer units away from the radical site. The value of m need not be a constant for a specific polymer as the closest available hydrogen atom in the chain may vary due to conformational variations. Decomposition mechanisms based on this reaction are sometimes known as random-chain scission mechanisms. The second reaction involves the transfer of a hydrogen atom between polymer chains, that is, intermolecular hydrogen atom transfer. The original radical, R_n, abstracts a hydrogen atom from the polymer, P_m. As this makes P_m a radical with the radical site more often than not within the chain itself (i.e., not a terminal radical site), the newly formed radical breaks up into an unsaturated polymer, P_{m-j}, and a radical, R_j. In the final reaction, no hydrogen transfer occurs. It is essentially the reverse of the polymerization step and, hence, is called *unzipping, depropagation,* or *depolymerization.* Whether the decomposition involves principally hydrogen transfer reactions or unzipping can be determined by examining the structure of the polymer, at least for polymers with only carbon in the main chain. If hydrogen transfer is impeded, then it is likely that the unzipping reaction will occur.

Vinyl polymers, strictly speaking, are those derived from a vinyl repeating unit, namely

$$—[CH_2—CH_2]_n—$$

where n is the number of repeating monomers. Here, the hydrogen atoms can be substituted, leading to a repeating unit of the following form:

$$\begin{array}{c} W\ \ Y \\ |\ \ | \\ —[C—C]_n— \\ |\ \ | \\ X\ \ Z \end{array}$$

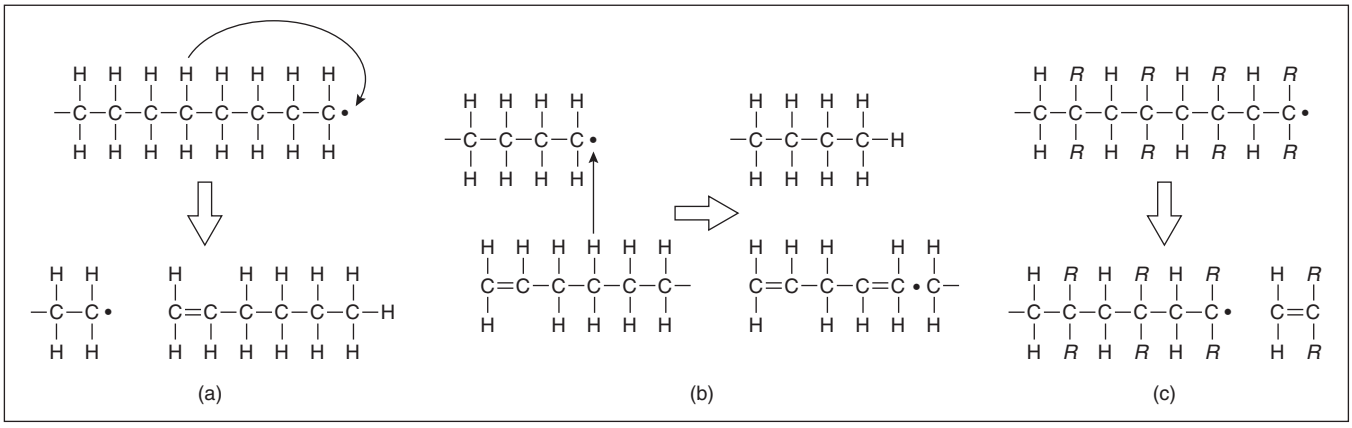

Figure 1-7.7. ***(a) Intramolecular H transfer, (b) intermolecular H transfer, (c) unzipping.***

where *W, X, Y,* and *Z* are substituent groups, perhaps hydrogen, methyl groups, or larger groups. Consider that the C–C bond connecting monomer units is broken and that a radical site results from the scission shown as

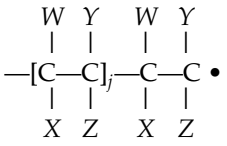

where the symbol • indicates an unpaired electron and, hence, a radical site. In order for a hydrogen atom to be transferred from the chain to the radical site, it must pass around either *Y* or *Z*. If *Y* and *Z* are hydrogens, this is not at all difficult due to their small size. However, if the alpha carbon has larger substituents bound to it (i.e., *Y* and *Z* are larger groups), the transfer of hydrogen to the radical site is more difficult. This type of interference with hydrogen transfer is known as *steric hindrance.* Table 1-7.3 shows this effect.[2] Polymers near the top of Table 1-7.3 have *Y* and *Z* substituents that are generally large, with a resulting high monomer yield, characteristic of unzipping reactions. Near the bottom of Table 1-7.3, where *Y* and *Z* are small, the polymers form negligible amounts of monomer as other mechanisms dominate.

While chain-branching reactions seem to be of little importance in polymer decomposition, termination reactions are required in all chain mechanisms. Several types of termination reactions are common.

$$R_m \Rightarrow P_m \qquad \text{(unimolecular termination)}$$

$$R_m + R_n \Rightarrow P_{m+n} \qquad \text{(recombination)}$$

$$R_n + R_m \Rightarrow P_m + P_n \qquad \text{(disproportionation)}$$

Table 1-7.3 ***Monomer Yield from Thermal Decomposition of Polymers of the General Form*** **[C*WX* – C*YZ*]$_n$**[2]

Polymer	*W*	*X*	*Y*	*Z*	Monomer Yield (wt. %)	Decomposition Mechanism[a]
PMMA	H	H	CH_3	CO_2CH_3	91–98	E
Polymethacrylonitrile	H	H	CH_3	CN	90	E
Poly (α-methylstyrene)	H	H	CH_3	C_6H_5	95	E
Polyoxymethylene[b]	—	—	—	—	100	E
Polytetrafluoroethylene	F	F	F	F	95	E
Poly (methyl atropate)	H	H	C_6H_5	CO_2CH_3	>99	E
Poly (*p*-bromostyrene)[c]	H	H	H	C_6H_4Br	91–93	E
Poly (*p*-chlorostyrene)[c]	H	H	H	C_6H_4Cl	82–94	E
Poly (*p*-methyoxystyrene)[c]	H	H	H	C_7H_7O	84–97	E
Poly (*p*-methylstyrene)	H	H	H	C_7H_7	82–94	E
Poly (*a*-deuterostyrene)	H	H	D	C_6H_5	70	E
Poly (*a*,β,β-trifluorostyrene)	F	F	F	C_6H_5	44	E/R
Polystyrene	H	H	H	C_6H_5	42–45	E/R
Poly (*m*-methylstyrene)	H	H	H	C_7H_8	44	E/R
Poly (β-deuerostyrene)	H	D	H	C_6H_5	42	E/R
Poly (β-methylstyrene)	H	CH_3	H	C_6H_5		E/R
Poly (*p*-methoxystyrene)[d]	H	H	H	C_7H_7O	36–40	E/R
Polyisobutene	H	H	CH_3	CH_3	18–25	E/R
Polychlorotrifluoroethylene	F	F	Cl	F	28	E/S
Poly (ethylene oxide)[b]	—	—	—	—	4	R/E
Poly (propylene oxide)[b]	—	—	—	—	4	R/E
Poly (4-methyl pent-1-ene)	H	H	H	C_4H_9	2	R/E
Polyethylene	H	H	H	H	0.03	R
Polypropylene	H	H	H	CH_3	0.17	R
Poly (methyl acrylate)	H	H	H	CO_2CH_3	0.7	R
Polytrifluoroethylene	F	F	H	F	—	R
Polybutadiene[b]	—	—	—	—	1	R
Polyisoprene[b]	—	—	—	—	5	R
Poly (vinyl chloride)	H	H	H	Cl	0–0.07	S
Poly (vinylidene chloride)	H	H	Cl	Cl	—	S
Poly (vinylidene fluoride)	H	H	F	F	—	S
Poly (vinyl fluoride)	H	H	H	F	—	S
Poly (vinyl alcohol)	H	H	H	OH	—	S
Polyacrylonitrile	H	H	H	CN	5	C

[a]R, random-chain scission; E, end-chain scission (unzipping); S, chain-stripping; C, cross-linking

[b]Not of general form [C*WX* – C*YZ*]$_n$

[c]Cationic polymerization

[d]Free-radical polymerization

The first of these reactions is, strictly speaking, not generally possible. Nonetheless, there are instances where the observed termination reaction appears to be first order (at least empirically). It is impossible to remove the radical site from a polymer radical without adding or subtracting at least one hydrogen atom while still satisfying the valence requirements of the atoms. What probably occurs is that the termination reaction is, in fact, second order, but the other species involved is so little depleted by the termination reaction that the termination reaction appears not to be affected by the concentration of that species. This is known as a pseudo first-order reaction. The recombination reaction is a classical termination step that is actually just the reverse of the random-chain scission initiation reaction. Finally, the disproportionation reaction involves the transfer of a hydrogen atom from one radical to the other. The hydrogen donor forms a double bond as a result of the hydrogen loss, and the acceptor is fully saturated. If this sort of reaction occurs immediately after an initiation reaction, no unzipping or other propagation reaction occurs, and the polymer decomposition is fully characterized by a random process of bond scissions.

There is a natural tendency to regard all materials with the same generic name, such as poly(methyl methacrylate), as being the same material with the same properties. As these are commercial products, the preparation methods (including the polymerization process) are dictated by the required physical and chemical properties of the material for normal use. Additives, both intentional and inadvertent, may be present, and the method of polymerization and the molecular weight of the polymer chains may vary. This is particularly important in the case of polymeric "compounds" (the actual polymeric material that is used commercially to fabricate a product of any kind) that contain a large fraction of additives. In some polyolefins, the fraction of polymer (known as *resin*) may be much less than half of the total mass of the compound, because of the presence of large amounts of fillers. In some compounds derived from poly(vinyl chloride), flexibility is introduced by means of *plasticizers.*

In this regard, it is interesting and important to note that polymers tend to be less stable than their oligomer counterparts. This results from several effects involved in the production and aging of polymers as well as simply the chain length itself. Initiation reactions in a polymer can lead to far more monomer units being involved in decomposition reactions, relative to the polymer's short-chain oligomeric analog. In the production and aging of polymers, there are opportunities for the production of abnormalities in the polymer chains due to the mode of synthesis and thermal, mechanical, and radiation effects during aging.

In the synthesis of the polymer, abnormalities may result from several sources. Unsaturated bonds result from chain termination by free-radical termination reactions. End-chain unsaturation results from second-order disproportionation reactions, and midchain unsaturation often occurs due to chain-transfer reactions with subsequent intramolecular hydrogen transfer. Chain branching may result from the formation of midchain radicals. During synthesis, chain transfer reactions may cause midchain radicals that then go on to react with monomers or polymers to create a branched polymer structure. Termination of the polymerization reaction may also result in *head-to-head linkages*; that is, monomer units are attached such that some of the monomers are oriented opposite to the remainder of the chain. Lastly, foreign atoms or groups may be incorporated into the polymer chain. This may occur due to impurities, polymerization initiators, or catalysts. Oxygen is often a problem in this regard.

The purity and the molecular weight of the polymer can markedly affect not only the decomposition rates, but also the mechanism of decomposition. An example of such a change might involve chain initiations occurring at the location of impurities in the chain of a polymer which, if pure, would principally be subject to end-chain initiation. Both the mechanism and the decomposition rate would be affected. Not all polymer "defects" degrade polymer thermal performance. In a polymer that decomposes by unzipping, a head-to-head linkage can stop the unzipping process. Thus, for an initiation that would have led to the full polymer being decomposed, only the part between the initiation site and the head-to-head link is affected. At least one additional initiation step is required to fully decompose the chain. This has been studied in detail by Kashiwagi et al.[6–10]

Kinetics

Eight generic types of reaction involved in simple decomposition processes have been addressed in the previous sections. Even if only a subset of these reaction types are required and the reaction rates are not a strong function of the size of the polymer chains and radicals, the kinetics describing the process can be quite complex. In engineering applications, such complex reaction mechanisms are not used. Rather, simple overall kinetic expressions are generally utilized if, in fact, decomposition kinetics are considered at all. The most common assumption is that the reactions can be described by an Arrhenius expression of first order in the remaining polymer mass. Often one goes even further and ignores any dependence of the reaction rate on the remaining polymer or the thickness of the decomposition zone and simply expresses the volatilization rate per unit surface area as a zero-order Arrhenius expression. This effectively assumes that the decomposition zone is of constant thickness and fresh polymer replaces the decomposed polymer by surface regression. Such an approach would clearly not be satisfactory for charring materials where decomposition is clearly not a surface phenomenon. As some of the work quoted earlier has indicated (e.g., Reference 13), it is also not suitable for many thermoplastic polymers.

Despite the fact that detailed kinetic models are not used in engineering calculations, it is instructive to consider some very simple cases, by the use of overall kinetic expressions, to indicate what is being lost. The effect of the initiation mechanism on decomposition kinetics can be easily demonstrated by considering either random- or end-chain initiation with propagation by unzipping and no termination reactions other than exhaustion of the

polymer chain by unzipping. The rate of weight loss for random-chain initiation can be expressed as

$$\frac{dW}{dt} = D_p \cdot k_{ir} \cdot W$$

where D_p, the degree of polymerization, is the number of monomer units per polymer chain; and k_{ir} is the rate constant for the random-chain initiation reaction. Notice that the rate constant of the propagation reaction is not included in the expression. A further assumption that the propagation rate is much faster than the initiation rate has also been made. The initiation reaction is said to be the *rate-limiting step.* The degree of polymerization arises in the equation since, for each initiation, D_p monomer units will be released; and the remaining weight, W, arises because the number of bonds available for scission is proportional to W. Since the polymer unzips completely, the molecular weight of all remaining polymer chains is the same as the initial molecular weight.

Considering end-chain initiation, the rate of mass loss is given by

$$\frac{dW}{dt} = D_p \cdot (2n) \cdot k_{ie}$$

where n is the number of polymer chains, and, hence, $2n$ is the number of chain ends, and k_{ie} is the rate constant for end-chain initiation. The number of polymer chains is simply the mass of the sample divided by the molecular weight of each chain, or

$$n = \frac{W}{D_p \cdot MW_m}$$

where MW_m is the molecular weight of the monomer. Using this expression yields

$$\frac{dW}{dt} = \frac{2 \cdot k_{ie} \cdot W}{MW_m}$$

Comparing this with the random initiation expression, one can see that, for random initiation, the rate is dependent on the original degree of polymerization; whereas for end-chain initiation the rate is independent of the degree of polymerization or, equivalently, the original molecular weight of the polymer. In both cases, however, the rate is first order in the mass of the sample. This derivation has been for a monodisperse polymer; that is, all chains have been considered to be the same length initially.

Returning to the random-chain initiation expression, it is clear that longer chains are decomposed preferentially. If the initial sample had a range of molecular weights, the longer chains would disappear more quickly than shorter chains, and the molecular weight distribution would change with time, unlike in the monodisperse case. It can be shown that in this case the reaction order is no longer unity, but is between one and two, depending on the breadth of the distribution.[30] Thus,

$$\frac{dW}{dt} \sim W^n$$

with

$$1 < n < 2$$

for random-chain initiation and complete unzipping of a polydisperse system.

This simple comparison illustrates some of the ways in which the details of the polymerization process, which control variables like the molecular weight distribution, can alter the decomposition process. For a particular polymer sample, no single initiation reaction need be dominant, in general. The activation energies for the different initiation steps may be quite different, leading to large variations in the relative rates with temperature. For instance, in PMMA, the dominant initiation step at low temperatures (around 570 K) is end-chain initiation. At higher temperatures (around 770 K), the random-chain initiation step dominates. In a single nonisothermal TGA experiment, this temperature range can easily be traversed, and overall interpretation of the results in terms of a single mechanism would be unsatisfactory and misleading.

Nonetheless, simple overall kinetic expressions are likely to be dominant in engineering for some time. The pitfalls with this approach simply serve to reinforce the need to determine the kinetic parameters in an experiment that is as similar to the end use as is practical. This is one of the major reasons why the use of TGA results has been brought into question. As stated before, the heating rates often are far less than those generally found in fire situations. The low heating rates in TGA experiments tend to emphasize lower-temperature kinetics, which may be much less important at the heating rates characteristic of most fire situations.

One interesting study worth presenting here is a theoretical analysis of thermal decomposition that presents a technique for calculating the temperature at the beginning and end of thermal decomposition, based on structural data from the polymer and on scission at the weakest bond, with considerable degree of success, particularly for successive members of a polymeric family.[31] A subsequent analysis has also been published that is much simpler, but it has not been validated against experimental data.[32]

General Physical Changes during Decomposition

The physical changes that occur on heating a material are both important in their own right and also impact the course of chemical decomposition significantly. The nature of the physical changes and their impact on decomposition vary widely with material type. This section addresses the general physical changes that occur for thermoplastic (glass transition, melting) and thermosetting (charring, water desorption) materials.

Melting and Glass Transition

On heating a thermoplastic material, the principal physical change is the transformation from a glass or solid to the fluid state. (See Figure 1-7.2.) If this transformation

occurs at temperatures well below the decomposition temperature, it becomes more likely that the material will drip and/or flow. While such behavior is a complication, in terms of fire safety it can either improve or degrade the performance of the material. In some configurations, flowing of the material can remove it from the source of heat and thus avoid ignition or further fire growth. In other situations, the flow of material may be toward the heat source, leading to a worsened fire situation. Many standard fire tests that allow materials to flow away from the heat source have been shown to be unsuitable for assessing the hazards of flowing or dripping materials. Care must be taken in the evaluation of standard test results in this regard. However, many thermoplastics do not show marked tendencies to flow during heating and combustion. Whereas polyethylene melts and flows readily, high-quality cast poly(methyl methacrylate) shows only slight tendencies to flow under fire conditions.

When designing a material, there are several techniques that can be utilized to increase the temperature at which physical transformations occur. These strategies are generally aimed at increasing the stiffness of the polymer or increasing the interactions between polymer chains. It is clear that increasing the crystallinity of the polymer increases the interaction between polymer chains. In the highly ordered state associated with crystalline materials, it is less possible for polymer chains to move relative to one another, as additional forces must be overcome in the transformation to the unordered fluid state. Crystallinity is enhanced by symmetric regular polymer structure and highly polar side groups. Regular structure allows adjacent polymer chains to pack in a regular and tight fashion. As such, isotactic polymers are more likely to crystallize than atactic polymers, and random copolymers do not tend to crystallize. Polar side groups enhance the intermolecular forces. Regular polar polymers, such as polyesters and polyamides, crystallize readily. Even atactic polymers with OH and CN side groups will crystallize due to polarity. The melting temperature of a polymer is also increased with increasing molecular weight up to a molecular weight of about 10,000 to 20,000 g/mol.

Melting temperatures can also be increased by increasing the stiffness of the polymer chain. Aromatic polyamides melt at much higher temperatures than their aliphatic analogs due to stiffness effects. Aromatics are particularly useful for chain stiffening, as they provide stiffness without bulk which would hinder crystallinity. At the opposite extreme, the increased flexibility of the oxygen atom links in polyethers is responsible for a lowering of the melting temperature of polyethers relative to polymethylene. Chain stiffening must be accompanied by suitable thermal stability and oxidation resistance in order to achieve increased service temperatures. Many aromatic polymers have melting temperatures in excess of their decomposition temperatures, making these materials thermosetting.

Cross-linking also increases the melting temperature and, like chain stiffening, can render a material infusible. Cross-links created in fabrication or during heating are also important in thermoplastics. The glass transition temperature can be increased in amorphous polymers by the inclusion of cross-links during fabrication. Random-chain scissions can quickly render a material unusable by affecting its physical properties unless cross-linking occurs. Such cross-linking in thermoplastics on heating may be regarded as a form of repolymerization. The temperature above which depolymerization reactions are faster than polymerization reactions is known as *ceiling temperature.* Clearly, above this temperature catastrophic decomposition will occur.

Charring

While char formation is a chemical process, the significance of char formation is largely due to its physical properties. Clearly, if material is left in the solid phase as char, less flammable gas is given off during decomposition. More importantly, the remaining char can be a low-density material and is a barrier between the source of heat and the virgin polymer material. As such, the flow of heat to the virgin material is reduced as the char layer thickens, and the rate of decomposition is reduced, depending on the properties of the char.[3] If the heat source is the combustion energy of the burning volatiles, not only will the fraction of the incident heat flux flowing into the material be reduced, but the incident heat flux as a whole will be reduced as well. Unfortunately, char formation is not always an advantageous process. The solid-phase combustion of char can cause sustained smoldering combustion. Thus, by enhancing the charring tendency of a material, flaming combustion rates may be reduced, but perhaps at the expense of creating a source of smoldering combustion that would not otherwise have existed.

Charring is enhanced by many of the same methods used to increase the melting temperature. Thermosetting materials are typically highly cross-linked and/or chain-stiffened. However, charring is not restricted to thermosetting materials. Cross-linking may occur as a part of the decomposition process, as is the case in poly(vinyl chloride) and polyacrylonitrile.

Implications for Fire Performance

As explained earlier, one of the major reasons why thermal decomposition of polymers is studied is because of its importance in terms of fire performance. This issue has been studied extensively.

Early on, Van Krevelen[33,34] showed that, for many polymers, the limiting oxygen index (LOI, an early measure of flammability)[35] could be linearly related to char yield as measured by TGA under specified conditions. Then, since Van Krevelen showed how to compute char yield to a good approximation from structural parameters, LOI should be computable; and for pure polymers having substantial char yields, it is fairly computable. Somewhat later, comparisons were made between the minimum decomposition temperature (or, even better, the temperature for 1 percent thermal decomposition) and the LOI.[2,22] The conclusion was that, although in general low flammability resulted from high minimum thermal decomposition

temperatures, no easy comparison could be found between the two. There were some notable cases of polymers with both low thermal stability and low flammability. This type of approach has since fallen into disrepute, particularly in view of the lack of confidence remaining today in the LOI technique.[36] Table 1-7.4 shows some thermal decomposition temperatures and limiting oxygen indices[22] as well as heat release rate values, the latter as measured in the cone calorimeter.[37,38] It is clear from the data in Table 1-7.4 that thermal decomposition is *not* a stand-alone means of predicting fire performance. Promising work in this regard is being made by Lyon,[39] who appears to be able to preliminarily predict some heat release information from thermoanalytical data.

However, mechanisms of action of fire retardants and potential effectiveness of fire retardants can be well predicted from thermal decomposition activity (for example, see Figures 1-7.4 and 1-7.5).[22,23] It is often necessary to have some additional understanding of the chemical reactions involved. In Figure 1-7.5, for example, the systems containing ABS, decabromobiphenyl, and either antimony oxide (c) or ferric oxide (g) have very similar TGA/DTG curves, with continuous weight loss. This indicates that the Sb system is effective but the iron one is not, because antimony bromide can volatilize while iron bromide does not. On the other hand, the system containing zinc oxide (f) is inefficient because the zinc bromide volatilizes too early, that is, before the polymer starts breaking down. Some authors have used thermal decomposition techniques via the study of the resulting products to understand the mechanism of fire retardance (e.g., Grassie[40]), or together with a variety of other techniques (e.g., Camino et al.[41,42]).

Whatever the detailed degree of predictability of fire performance data from thermal decomposition data, its importance should not be underestimated: *polymers cannot burn if they do not break down.*

Table 1-7.4 ***Thermal Stability and Flammability of Polymers***

Polymer	T_d[a] (K)	$T_{1\%}$[b] (K)	LOI[c]	Pk RHR[d] (kW/m²)
Polyacetal	503	548	15.7	360
Poly(methyl methacrylate)	528	555	17.3	670
Polypropylene	531	588	17.4	1500
Polyethylene (LDPE)	490	591	17.4	800[e]
Polyethylene (HDPE)	506	548	17.4	1400
Polystyrene	436	603	17.8	1100
ABS copolymer	440	557	18.0	950[e]
Polybutadiene	482	507	18.3	
Polyisoprene	460	513	18.5	
Cotton	379	488	19.9	450[e]
Poly(vinyl acohol)	337	379	22.5	
Wool	413	463	25.2	310[e]
Nylon-6	583		25.6	1300
Silicone oil	418	450	32	140[e]
Poly(vinylidene fluoride)	628	683	43.7	30[e]
Poly(vinyl chloride)	356	457	47	180
Polytetrafluoroethylene	746	775	95	13

[a] T_d: Minimum thermal decomposition temperature from TGA (10-mg sample, 10-K/min heating rate, nitrogen atmosphere)[22]

[b] $T_{1\%}$: Temperature for 1% thermal decomposition, conditions as above[22]

[c] LOI: Limiting oxygen index[22]

[d] Pk RHR: Peak rate of heat release in the cone calorimeter, at 40-kW/m² incident flux, at a thickness of 6 mm,[35] all under the same conditions

[e] Pk RHR: Peak rate of heat release in the cone calorimeter, at 40-kW/m² incident flux, from sources other than those in Footnote *d*

Behavior of Individual Polymers

The discussion, thus far, has been general, focusing on the essential aspects of thermal decomposition without the complications that inevitably arise in the treatment of a particular polymer. This approach may also tend to make the concepts abstract. Through the treatment of individual polymers by polymer class, this section provides an opportunity to apply the general concepts to real materials. In general, the section is restricted to polymers of commercial importance. More complete and detailed surveys of polymers and their thermal decomposition can be found in the literature.[2,30,43–52]

Polyolefins

Of the polyolefins, low-density polyethylene (LDPE), high-density polyethylene (HDPE), and polypropylene (PP) are of the greatest commercial importance because of their production volume. Upon thermal decomposition, very little monomer formation is observed for any of these polymers; they form a large number of different small molecules (up to 70), mostly hydrocarbons. Thermal stability of polyolefins is strongly affected by branching, with linear polyethylene most stable and polymers with branching less stable. The order of stability is illustrated as follows:

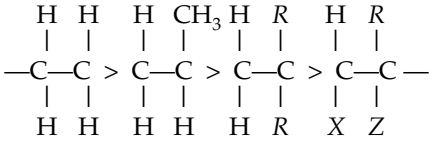

where *R* is any hydrocarbon group larger than a methyl group.

Polyethylene (PE): In an inert atmosphere, polyethylene begins to cross-link at 475 K and to decompose (reductions in molecular weight) at 565 K though extensive weight loss is not observed below 645 K. Piloted ignition of polyethylene due to radiative heating has been observed at a surface temperature of 640 K. The products of decomposition include a wide range of alkanes and alkenes. Branching of polyethylene causes enhanced intramolecular hydrogen transfer and results in lower thermal stability. The low-temperature molecular weight changes without volatilization are principally due to the scission of weak links, such as oxygen, incorporated into the main chain as impurities. Initiation reactions at higher temperatures involve scission of tertiary carbon bonds or ordinary carbon–carbon bonds in the beta position to tertiary carbons. The major products of decomposition are

propane, propene, ethane, ethene, butene, hexene-1, and butene-1. Propene is generated by intramolecular transfer to the second carbon and by scission of the bond beta to terminal $=CH_2$ groups.

The intramolecular transfer route is most important, with molecular coiling effects contributing to its significance. A broad range of activation energies has been reported, depending on the percent conversion, the initial molecular weight, and whether the remaining mass or its molecular weight were monitored. Decomposition is strongly enhanced by the presence of oxygen, with significant effects detectable at 423 K in air.

Polypropylene (PP): In polypropylene, every other carbon atom in the main chain is a tertiary carbon, which is thus prone to attack. This lowers the stability of polypropylene as compared to polyethylene. As with polyethylene, chain scission and chain transfer reactions are important during decomposition. By far, secondary radicals (i.e., radical sites on the secondary carbon) are more important than primary radicals. This is shown by the major products formed, that is, pentane (24 percent), 2 methyl-1-pentene (15 percent), and 2–4 dimethyl-1-heptene (19 percent). These are more easily formed from intramolecular hydrogen transfer involving secondary radicals. Reductions in molecular weight are first observed at 500 to 520 K and volatilization becomes significant above 575 K. Piloted ignition of polypropylene due to radiative heating has been observed at a surface temperature of 610 K. Oxygen drastically affects both the mechanism and rate of decomposition. The decomposition temperature is reduced by about 200 K, and the products of oxidative decomposition include mainly ketones. Unless the polymer samples are very thin (less than 0.25–0.30 mm or 0.010–0.012 in. thick), oxidative pyrolysis can be limited by diffusion of oxygen into the material. At temperatures below the melting point, polypropylene is more resistant to oxidative pyrolysis as oxygen diffusion into the material is inhibited by the higher density and crystallinity of polypropylene. Most authors have assumed that the oxidation mechanism is based on hydrocarbon oxidation, but recent work suggests that it may actually be due to the decomposition of peracids resulting from the oxidation of primary decomposition products.[12]

Polyacrylics

Poly(methyl methacrylate) (PMMA): PMMA is a favorite material for use in fire research since it decomposes almost solely to monomer, and burns at a very steady rate. Methyl groups effectively block intramolecular H transfer as discussed in the General Chemical Mechanisms section, leading to a high monomer yield. The method of polymerization can markedly affect the temperatures at which decomposition begins. Free-radical polymerized PMMA decomposes around 545 K, with initiation occurring at double bonds at chain ends. A second peak between 625 and 675 K in dynamic TGA thermograms is the result of a second initiation reaction. At these temperatures, initiation is by both end-chain and random-chain initiation processes. Anionically produced PMMA decomposes at about 625 K because the end-chain initiation step does not occur due to the lack of double bonds at the chain end when PMMA is polymerized by this method. This may explain the range of observed piloted ignition temperatures (550 to 600 K). Decomposition of PMMA is first order with an activation energy of 120 to 200 kJ/mol, depending on the end group. The rate of decomposition is also dependent on the tacticity of the polymer and on its molecular weight. These effects can also have a profound effect on the flame spread rate.

It is interesting to note that a chemically cross-linked copolymer of PMMA was found to decompose by forming an extensive char, rather than undergoing end-chain scission which resulted in a polymer with greater thermal stability.[53]

Poly(methyl acrylate) (PMA): Poly(methyl acrylate) decomposes by random-chain scission rather than end-chain scission, with almost no monomer formation. This results because of the lack of a methyl group blocking intramolecular hydrogen transfer as occurs in PMMA. Initiation is followed by intra- and intermolecular hydrogen transfer.

Polyacrylonitrile (PAN): PAN begins to decompose exothermically between 525 K and 625 K with the evolution of small amounts of ammonia and hydrogen cyanide. These products accompany cyclization reactions involving the creation of linkages between nitrogen and carbon on adjacent side groups. (See Figure 1-7.8.) The gaseous products are not the result of the cyclization itself, but arise from the splitting off of side or end groups not involved in the cyclization. The ammonia is derived principally from terminal imine groups (NH) while HCN results from side groups that do not participate in the polymerization-like cyclization reactions. When the polymer is not isotactic, the cyclization process is terminated when hydrogen is abstracted by the nitrogen atom. The cyclization process is reinitiated as shown in Figure 1-7.9.

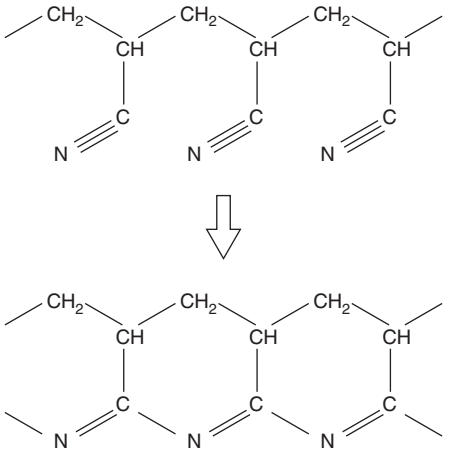

Figure 1-7.8. ***PAN cyclization.***

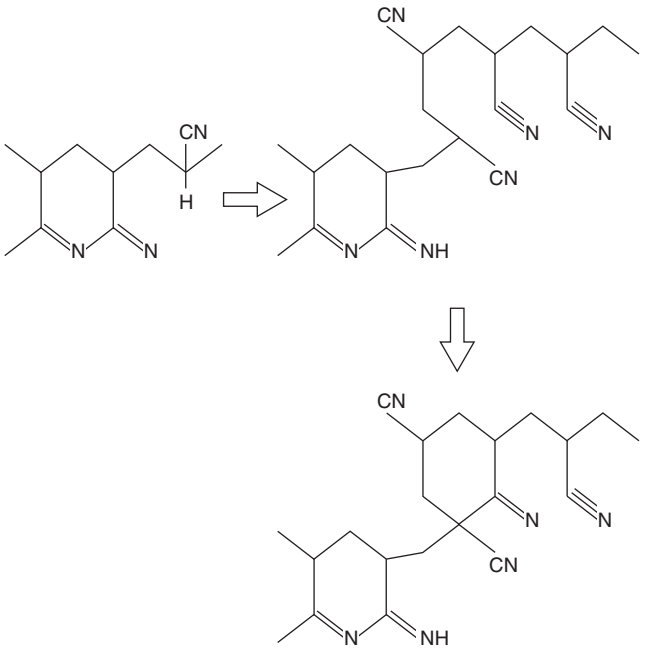

Figure 1-7.9. ***Reinitiation of PAN side-chain cyclization.***

This leaves CN groups not involved in the cyclization which are ultimately removed and appear among the products as HCN. Typically, there are between 0 and 5 chain polymerization steps between each hydrogen abstraction. At temperatures of 625 to 975 K, hydrogen is evolved as the cyclic structures carbonize. At higher temperatures, nitrogen is evolved as the char becomes nearly pure carbon. In fact, with adequate control of the process, this method can be used to produce carbon fibers. Oxygen stabilizes PAN, probably by reacting with initiation sites for the nitrile polymerization. The products of oxidative decomposition are highly conjugated and contain ketonic groups.

Halogenated Polymers

Poly(vinyl chloride) (PVC): The most common halogenated polymer is PVC; it is one of the three most widely used polymers in the world, with polyethylene and polypropylene. Between 500 and 550 K, hydrogen chloride gas is evolved nearly quantitatively, by a chain-stripping mechanism. It is very important to point out, however, that the temperature at which hydrogen chloride starts being evolved in any measurable way is heavily dependent on the stabilization package used. Thus, commercial PVC "compounds" have been shown, in recent work, not to evolve hydrogen chloride until temperatures are in excess of 520 K and to have a dehydrochlorination stage starting at 600 K.[54] Between 700 and 750 K, hydrogen is evolved during carbonization, following cyclization of the species evolved. At higher temperatures, cross-linking between chains results in a fully carbonized residue. The rate of dehydrochlorination depends on the molecular weight, crystallinity, presence of oxygen, hydrogen chloride gas, and stabilizers. The presence of oxygen accelerates the dehydrochlorination process, produces main-chain scissions, and reduces cross-linking. At temperatures above 700 K, the char (resulting from dehydrochlorination and further dehydrogenation) is oxidized, leaving no residue. Lower molecular weight increases the rate of dehydrochlorination. Dehydrochlorination stabilizers include zinc, cadmium, lead, calcium, and barium soaps and organotin derivatives. The stability of model compounds indicates that weak links are important in decomposition. The thermal decomposition of this polymer has been one of the most widely studied ones. It has been the matter of considerable controversy, particularly in terms of explaining the evolution of aromatics in the second decomposition stage. The most recent evidence seems to point to a simultaneous cross-linking and intramolecular decomposition of the polyene segments resulting from dehydrochlorination, via polyene free radicals.[54] Earlier evidence suggested a Diels-Alder cyclization process (which can only be intramolecular if the double bond ends up in a "cis" orientation).[55] Evidence for this was given by the fact that smoke formation (inevitable consequence of the emission of aromatic hydrocarbons) was decreased by introducing cross-linking additives into the polymer.[56] Thus, it has now become clear that formation of any aromatic hydrocarbon occurs intramolecularly. The chemical mechanism for the initiation of dehydrochlorination was also reviewed a few years ago.[57] More recently, a series of papers was published investigating the kinetics of chain stripping, based on PVC.[58]

Chlorinated poly(vinyl chloride) (CPVC): One interesting derivative of PVC is chlorinated PVC (CPVC), resulting from post-polymerization chlorination of PVC. It decomposes at a much higher temperature than PVC, but by the same chain-stripping mechanism. The resulting solid is a polyacetylene, which gives off much less smoke than PVC and is also more difficult to burn.[59]

Poly(tetrafluoroethylene) (PTFE): PTFE is a very stable polymer due to the strength of C–F bonds and shielding by the very electronegative fluorine atoms. Decomposition starts occurring between 750 and 800 K. The principal product of decomposition is the monomer, CF_4, with small amounts of hydrogen fluoride and hexafluoropropene. Decomposition is initiated by random-chain scission, followed by depolymerization. Termination is by disproportionation. It is possible that the actual product of decomposition is CF_2, which immediately forms in the gas phase. The stability of the polymer can be further enhanced by promoting chain transfer reactions that can effectively limit the zip length. Under conditions of oxidative pyrolysis, no monomer is formed. Oxygen reacts with the polymeric radical, releasing carbon monoxide, carbon dioxide, and other products.

Other fluorinated polymers are less stable than PTFE and are generally no more stable than their unfluorinated analogs. However, the fluorinated polymers are more stable in an oxidizing atmosphere. Hydrofluorinated polymers produce hydrogen fluoride directly by chain-stripping reactions, but the source of hydrogen fluoride by perfluorinated polymers, such as PTFE, is less clear. It is

related to the reaction of the decomposition products (including tetrafluoroethylene) with atmospheric humidity.

Other Vinyl Polymers

Several other vinyl polymers decompose by mechanisms similar to that of PVC: all those that have a single substituent other than a hydrogen atom on the basic repeating unit. These include poly(vinyl acetate), poly(vinyl alcohol), and poly(vinyl bromide), and result in gas evolution of acetic acid, water, and hydrogen bromide, respectively. While the chain-stripping reactions of each of these polymers occur at different temperatures, all of them aromatize by hydrogen evolution at roughly 720 K.

Styrenics: *Polystyrene (PS).* Polystyrene shows no appreciable weight loss below 575 K, though there is a decrease in molecular weight due to scission of "weak" links. Above this temperature, the products are primarily monomer with decreasing amounts of dimer, trimer, and tetramer. There is an initial sharp decrease in molecular weight followed by slower rates of molecular weight decrease. The mechanism is thought to be dominated by end-chain initiation, depolymerization, intramolecular hydrogen transfer, and bimolecular termination. The changes in molecular weight are principally due to intermolecular transfer reactions while volatilization is dominated by intramolecular transfer reactions. Depropagation is prevalent despite the lack of steric hindrance due to the stabilizing effect of the electron delocalization associated with the aromatic side group. The addition of an alpha methyl group to form poly(α-methylstyrene) provides additional steric hindrance such that only monomer is produced during decomposition while the thermal stability of the polymer is lessened. Free-radical polymerized polystyrene is less stable than anionic polystyrene with the rate of decomposition dependent on the end group.

Other styrenics tend to be copolymers of polsytyrene with acrylonitrile (SAN), acrylonitrile and butadiene (ABS), or methyl methacrylate and butadiene (MBS), and their decomposition mechanisms are hybrids between those of the individual polymers.

Synthetic Carbon–Oxygen Chain Polymers

Poly(ethylene terephthalate) (PET): PET decomposition is initiated by scission of an alkyl–oxygen bond. The decomposition kinetics suggest a random-chain scission. Principal gaseous products observed are acetaldehyde, water, carbon monoxide, carbon dioxide, and compounds with acid and anhydride end groups. The decomposition is accelerated by the presence of oxygen. Recent evidence indicates that both PET and PBT [poly(butylene terephthalate)] decompose via the formation of cyclic or open-chain oligomers, with olefinic or carboxylic end groups.[60]

Polycarbonates (PC): Polycarbonates yield substantial amounts of char if products of decomposition can be removed (the normal situation). If volatile products are not removed, no cross-linking is observed due to competition between condensation and hydrolysis reactions. The decomposition is initiated by scission of the weak O–CO_2 bond, and the volatile products include 35 percent carbon dioxide. Other major products include bisphenol A and phenol. The decomposition mechanism seems to be a mixture of random-chain scission and cross-linking, initiated intramolecularly.[61] Decomposition begins at 650 to 735 K, depending on the exact structure of the polycarbonate in question.

Blends of polycarbonate and styrenics (such as ABS) make up a set of *engineered thermoplastics.* Their properties are intermediate between those of the forming individual polymers, both in terms of physical properties (and processability) and in terms of their modes of thermal breakdown.

Phenolic resins: Phenolic resin decomposition begins at 575 K and is initiated by the scission of the methylene–benzene ring bond. At 633 K, the major products are C_3 compounds. In continued heating (725 K and higher), char (carbonization), carbon oxides, and water are formed. Above 770 K, a range of aromatic, condensable products are evolved. Above 1075 K, ring breaking yields methane and carbon oxides. In TGA experiments at 3.3°C/min, the char yield is 50 to 60 percent. The weight loss at 700 K is 10 percent. All decomposition is oxidative in nature (oxygen provided by the polymer itself).

Polyoxymethylene (POM): Polyoxymethylene decomposition yields formaldehyde almost quantitatively. The decomposition results from end-chain initiation followed by depolymerization. The presence of oxygen in the chain prevents intramolecular hydrogen transfer quite effectively. With hydroxyl end groups, decomposition may begin at temperatures as low as 360 K while with ester end groups decomposition may be delayed to 525 K. Piloted ignition due to radiative heating has been observed at a surface temperature of 550 K. Acetylation of the chain end group also improves stability. Upon blocking the chain ends, decomposition is by random-chain initiation, followed by depolymerization with the zip length less than the degree of polymerization. Some chain transfer occurs. Amorphous polyoxymethylene decomposes faster than crystalline polyoxymethylene, presumably due to the lack of stabilizing intermolecular forces associated with the crystalline state (below the melting temperature). Incorporating oxyethylene in polyoxymethylene improves stability, presumably due to H transfer reactions that stop unzipping. Oxidative pyrolysis begins at 430 K and leads to formaldehyde, carbon monoxide, carbon dioxide, hydrogen, and water vapor.

Epoxy resins: Epoxy resins are less stable than phenolic resins, polycarbonate, polyphenylene sulphide, and polytetrafluoroethelyne. The decomposition mechanism is complex and varied and usually yields mainly phenolic compounds. A review of epoxy resin decomposition can be found in Lee.[43]

Polyamide Polymers

Nylons: The principal gaseous products of decomposition of nylons are carbon dioxide and water. Nylon 6

produces small amounts of various simple hydrocarbons while Nylon 6–10 produces notable amounts of hexadienes and hexene. As a class, nylons do not notably decompose below 615 K. Nylon 6–6 melts between 529 and 532 K, and decomposition begins at 615 K in air and 695 K in nitrogen. At temperatures in the range 625 to 650 K, random-chain scissions lead to oligomers. The C–N bonds are the weakest in the chain, but the $CO–CH_2$ bond is also quite weak, and both are involved in decomposition. At low temperatures, most of the decomposition products are nonvolatile, though above 660 K main chain scissions lead to monomer and some dimer and trimer production. Nylon 6–6 is less stable than nylon 6–10, due to the ring closure tendency of the adipic acid component. At 675 K, if products are removed, gelation and discoloration begin.

Aromatic polyamides have good thermal stability, as exemplified by Nomex, which is generally stable in air to 725 K. The major gaseous products of decomposition at low temperatures are water and carbon oxides. At higher temperatures, carbon monoxide, benzene, hydrogen cyanide (HCN), toluene, and benzonitrile are produced. Above 825 K, hydrogen and ammonia are formed. The remaining residue is highly cross-linked.

Wool: On decomposition of wool, a natural polyamide, approximately 30 percent is left as a residue. The first step in decomposition is the loss of water. Around 435 K, some cross-linking of amino acids occurs. Between 485 and 565 K, the disulphide bond in the amino acid cystine is cleaved with carbon disulphide and carbon dioxide being evolved. Pyrolysis at higher temperatures (873 to 1198 K) yields large amounts of hydrogen cyanide, benzene, toluene, and carbon oxides.

Polyurethanes

As a class, polyurethanes do not break down below 475 K, and air tends to slow decomposition. The production of hydrogen cyanide and carbon monoxide increases with the pyrolysis temperature. Other toxic products formed include nitrogen oxides, nitriles, and tolylene diisocyanate (TDI) (and other isocyanates). A major breakdown mechanism in urethanes is the scission of the polyol–isocyanate bond formed during polymerization. The isocyanate vaporizes and recondenses as a smoke, and liquid polyol remains to further decompose.

Polydienes and Rubbers

Polyisoprene: Synthetic rubber or polyisoprene decomposes by random-chain scission with intramolecular hydrogen transfer. This, of course, gives small yields of monomer. Other polydienes appear to decompose similarly though the thermal stability can be considerably different. The average size of fragments collected from isoprene decomposition are 8 to 10 monomer units long. This supports the theory that random-chain scission and intermolecular transfer reactions are dominant in the decomposition mechanism. In nitrogen, decomposition begins at 475 K. At temperatures above 675 K, increases in monomer yield are attributable to secondary reaction of volatile products to form monomer. Between 475 and 575 K, low molecular weight material is formed, and the residual material is progressively more insoluble and intractable. Preheating at between 475 and 575 K lowers the monomer yield at higher temperatures. Decomposition at less than 575 K results in a viscous liquid and, ultimately, a dry solid. The monomer is prone to dimerize to dipentene as it cools. There seems to be little significant difference in the decomposition of natural rubber and synthetic polyisoprene.

Polybutadiene: Polybutadiene is more thermally stable than polyisoprene due to the lack of branching. Decomposition at 600 K can lead to monomer yields of up to 60 percent, with lower conversions at higher temperatures. Some cyclization occurs in the products. Decomposition in air at 525 K leads to a dark impermeable crust, which excludes further air. Continued heating hardens the elastomer.

Polychloroprene: Polychloroprene decomposes in a manner similar to PVC, with initial evolution of hydrogen chloride at around 615 K and subsequent breakdown of the residual polyene. The sequences of the polyene are typically around three (trienes), much shorter than PVC. Polychloroprene melts at around 50°C.

Cellulosics

The decomposition of cellulose involves at least four processes in addition to simple desorption of physically bound water. The first is the cross-linking of cellulose chains, with the evolution of water (dehydration). The second concurrent reaction is the unzipping of the cellulose chain. Laevoglucosan is formed from the monomer unit. (See Figure 1-7.10.) The third reaction is the decomposition of the dehydrated product (dehydrocellulose) to yield char and volatile products. Finally, the laevoglucosan can further decompose to yield smaller volatile products, including tars and, eventually, carbon monoxide. Some laevoglucosan may also repolymerize.

Below 550 K, the dehydration reaction and the unzipping reaction proceed at comparable rates, and the basic skeletal structure of the cellulose is retained. At higher temperatures, unzipping is faster, and the original structure of the cellulose begins to disappear. The cross-linked dehydrated cellulose and the repolymerized laevoglucosan begin to yield polynuclear aromatic structures, and graphite carbon structures form at around 770 K. It is well known that the char yield is quite dependent on the rate of heating of the sample. At very high rates of heating, no char is formed. On the other hand, preheating the sample at 520 K will lead to 30 percent char yields. This is due both to the importance of the low-temperature dehydration reactions for ultimate char formation and the increased opportunity for repolymerization of laevoglucosan that accompanies slower heating rates.

Wood is made up of 50 percent cellulose, 25 percent hemicellulose, and 25 percent lignin. The yields of gaseous products and kinetic data indicate that the decomposition may be regarded as the superposition of the

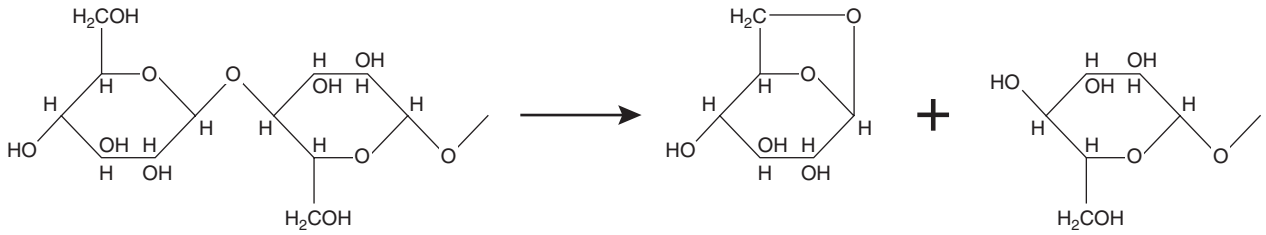

Figure 1-7.10. ***Formation of laevoglucosan from cellulose.***

individual constituent's decomposition mechanisms. On heating, the hemicellulose decomposes first (475 to 535 K), followed by cellulose (525 to 625 K), and lignin (555 to 775 K). The decomposition of lignin contributes significantly to the overall char yield. Piloted ignition of woods due to radiative heating has been observed at a surface temperature of 620 to 650 K.

Polysulfides and Polysulphones

Polysulfides are generally stable to 675 K. Poly(1, 4 phenylene sulfide) decomposes at 775 K. Below this temperature, the principal volatile product is hydrogen sulfide. Above 775 K, hydrogen, evolved in the course of cross-linking, is the major volatile product. In air, the gaseous products include carbon oxides and sulfur dioxide.

The decomposition of polysulphones is analogous to polycarbonates. Below 575 K, decomposition is by heteroatom bridge cleavage, and above 575 K, sulfur dioxide is evolved from the polymer backbone.

Thermally Stable Polymers

The development of thermally stable polymers is an area of extensive ongoing interest. Relative to many other materials, polymers have fairly low use temperatures, which can reduce the utility of the product. This probable improvement in fire properties is, often, counterbalanced by a decrease in processability and in favorable physical properties. Of course, materials that are stable at high temperatures are likely to be better performers as far as fire properties are concerned. The high-temperature physical properties of polymers can be improved by increasing interactions between polymer chains or by chain-stiffening.

Chain interactions can be enhanced by several means. As noted previously, crystalline materials are more stable than their amorphous counterparts as a result of chain interactions. Of course, if a material melts before volatilization occurs, this difference will not affect chemical decomposition. Isotactic polymers are more likely to be crystalline due to increased regularity of structure. Polar side groups can also increase the interaction of polymer chains. The melting point of some crystalline polymers is shown in Table 1-7.1.

The softening temperature can also be increased by chain-stiffening. This is accomplished by the use of aromatic or heterocyclic structures in the polymer backbone. Some aromatic polymers are shown in Figure 1-7.11. Poly(p-phenylene) is quite thermally stable but is brittle, insoluble, and infusible. Thermal decomposition begins at 870 to 920 K; and up to 1170 K, only 20 to 30 percent of the original weight is lost. Introduction of the following groups:

$$–O–,\ –CO–,\ –NH–,\ –CH_2–,\ –O–CO–,\ –O–CO–O–$$

into the chain can improve workability though at the cost of some loss of oxidative resistance. Poly(p-xylene) melts at 675 K and has good mechanical properties though it is insoluble and cannot be thermoprocessed. Substitution of halogen, acetyl, alkyl, or ester groups on aromatic rings can help the solubility of these polymers at the expense of some stability. Several relatively thermostable polymers can be formed by condensation of bisphenol A with a second reagent. Some of these are shown in Figure 1–7.12. The stability of such polymers can be improved if aliphatic groups are not included in the backbone, as the $–C(CH_3)_2–$ groups are weak links.

Other thermostable polymers include ladder polymers and extensively cross-linked polymers. Cyclized PAN is an example of a ladder polymer where two chains are periodically interlinked. Other polymers, such as rigid polyurethanes, are sufficiently cross-linked so that it becomes impossible to speak of a molecular weight or

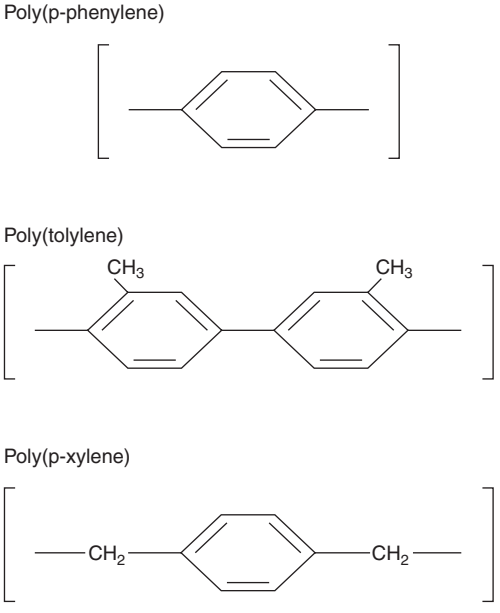

Figure 1-7.11. ***Thermostable aromatic polymers.***

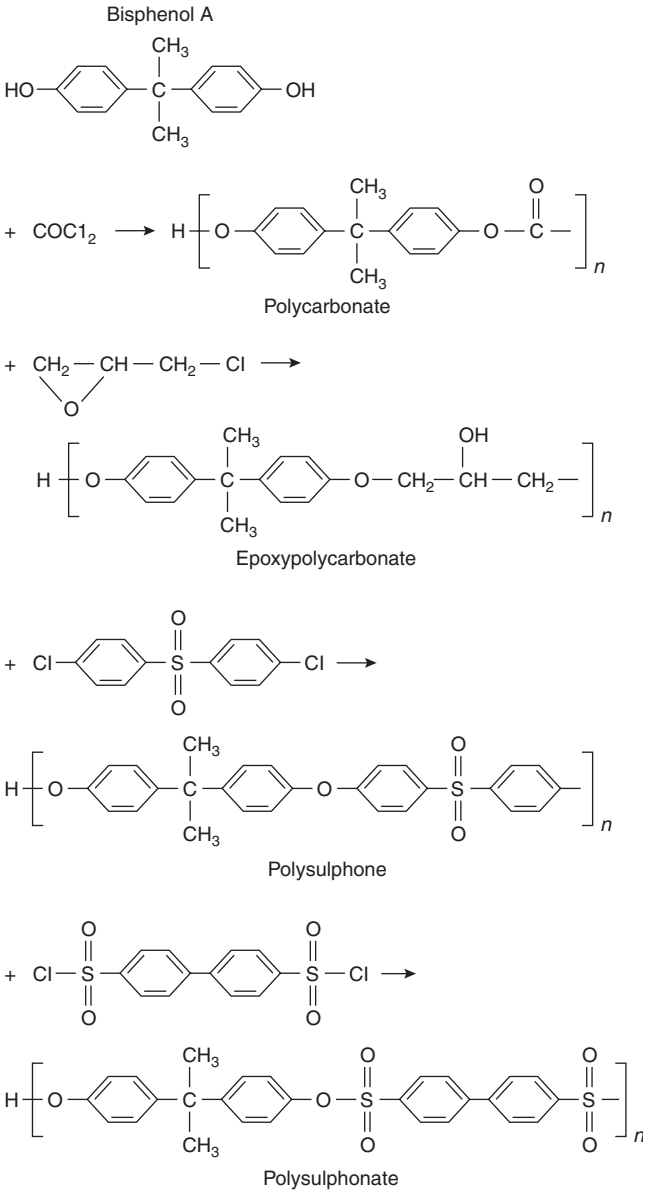

Figure 1-7.12. ***Bisphenol A polymers.***

definitive molecular repeating structure. As in polymers that gel or cross-link during decomposition, cross-linking of the original polymer yields a carbonized char residue upon decomposition, which can be oxidized at temperatures over 775 K.

References Cited

1. ASTM E176, "Standard Terminology of Fire Standards," in *Annual Book of ASTM Standards,* Vol. 4.07, American Society for Testing and Materials, West Conshohocken, PA.
2. C.F. Cullis and M.M. Hirschler, *The Combustion of Organic Polymers,* Oxford University Press, Oxford, UK (1981).
3. E.D. Weil, R.N. Hansen, and N. Patel, "Prospective Approaches to More Efficient Flame-Retardant Systems," in *Fire and Polymers: Hazards Identification and Prevention* (G.L. Nelson, ed.), ACS Symposium Series 425, Developed from *Symp.* at 197th. ACS Mtg. Dallas, TX. April 1989, Chapter 8, pp. 97–108, Amer. Chem. Soc., Washington, DC (1990).
4. M.M. Hirschler, "Recent Developments in Flame-Retardant Mechanisms," in *Developments in Polymer Stabilisation,* Vol. 5, (G. Scott, ed.), pp. 107–152, Applied Science Publ., London (1982).
5. D.E. Stuetz, A.H. DiEdwardo, F. Zitomer, and B.F. Barnes, "Polymer Flammability II," in *J. Polym. Sci., Polym. Chem. Ed.,* 18, pp. 987–1009 (1980).
6. T. Kashiwagi and T.J. Ohlemiller, "A Study of Oxygen Effects on Flaming Transient Gasification of PMMA and PE during Thermal Irradiation," in *Nineteenth Symp. (Int.) on Combustion,* Combustion Institute, Pittsburgh, PA, pp. 1647–1654 (1982).
7. T. Kashiwagi, T. Hirata, and J.E. Brown, "Thermal and Oxidative Degradation of Poly(methyl methacrylate), Molecular Weight," *Macromolecules,* 18, pp. 131–138 (1985).
8. T. Hirata, T. Kashiwagi, and J.E. Brown, "Thermal and Oxidative Degradation of Poly(methyl methacrylate), Weight Loss," *Macromolecules,* 18, pp. 1410–1418 (1985).
9. T. Kashiwagi, A. Inabi, J.E. Brown, K. Hatada, T. Kitayama, and E. Masuda, "Effects of Weak Linkages on the Thermal and Oxidative Degradation of Poly(methyl methacrylates)," *Macromolecules,* 19, pp. 2160–2168 (1986).
10. T. Kashiwagi and A. Inabi, "Behavior of Primary Radicals during Thermal Degradation of Poly(methyl methacrylate)," *Polymer Degradation and Stability,* 26, pp. 161–184 (1989).
11. S.K. Brauman, "Polymer Degradation during Combustion," *J. Polymer Sci.,* B, 26, pp. 1159–1171 (1988).
12. P. Gijsman, J. Hennekens, and J. Vincent, "The Mechanism of the Low-Temperature Oxidation of Polypropylene," *Polymer Degradation and Stability,* 42, pp. 95–105 (1993).
13. M.M. Hirschler, "Effect of Oxygen on the Thermal Decomposition of Poly(vinylidene fluoride)," *Europ. Polymer J.,* 18, pp. 463–467 (1982).
14. A. Inabi and T. Kashiwagi, "A Calculation of Thermal Degradation Initiated by Random Scission, Unsteady Radical Concentration," *Eur. Polym. J.,* 23, 11, pp. 871–881 (1987).
15. T. Kashiwagi and H. Nambu, "Global Kinetic Constants for Thermal Oxidative Degradation of a Cellulosic Paper," *Combust. Flame,* 88, pp. 345–368 (1992).
16. K.D. Steckler, T. Kashiwagi, H.R. Baum, and K. Kanemaru, "Analytical Model for Transient Gasification of Noncharring Thermoplastic Materials," in *Fire Safety Sci., Proc. Third Int. Symp.* (G. Cox and B. Langford, eds.), Elsevier, London (1991).
17. ASTM D2859, "Standard Test Method for Flammability of Finished Textile Floor Covering Materials," in *Annual Book of ASTM Standards,* Vol. 4.07, American Society for Testing and Materials, West Conshohocken, PA.
18. CFR 1630, 16 CFR Part 1630, "Standard for the Surface Flammability of Carpets and Rugs (FF 1-70)," in *Code of Federal Regulations, Commercial Practices, Subchapter D: Flammable Fabrics Act Regulations,* Vol. 16, Part 1602–1632, pp. 697–706 (2000).
19. CFR 1631, 16 CFR Part 1631, "Standard for the Surface Flammability of Small Carpets and Rugs (FF 2-70)," in *Code of Federal Regulations, Commercial Practices, Subchapter D: Flammable Fabrics Act Regulations,* Vol. 16, Parts 1602–1632, pp. 706–715 (2000).
20. L.A. Chandler, M.M. Hirschler, and G.F. Smith, "A Heated Tube Furnace Test for the Emission of Acid Gas from PVC Wire Coating Materials: Effects of Experimental Procedures and Mechanistic Considerations," *Europ. Polymer J.,* 23, pp. 51–61 (1987).

21. M.M. Hirschler, "Thermal Decomposition (STA and DSC) of Poly(vinyl chloride) Compounds under a Variety of Atmospheres and Heating Rates," *Europ. Polymer J.,* 22, pp. 153–160 (1986).
22. C.F. Cullis and M.M. Hirschler, "The Significance of Thermoanalytical Measurements in the Assessment of Polymer Flammability," *Polymer,* 24, pp. 834–840 (1983).
23. M.M. Hirschler, "Thermal Analysis and Flammability of Polymers: Effect of Halogen-Metal Additive Systems," *Europ. Polymer J.,* 19, pp. 121–129 (1983).
24. I.C. McNeill, "The Application of Thermal Volatilization Analysis to Studies of Polymer Degradation," in *Developments in Polymer Degradation,* Vol. 1 (N. Grassie, ed.), p. 43, Applied Science, London (1977).
25. C.F. Cullis, M.M. Hirschler, R.P. Townsend, and V. Visanuvimol, "The Pyrolysis of Cellulose under Conditions of Rapid Heating," *Combust. Flame,* 49, pp. 235–248 (1983).
26. C.F. Cullis, M.M. Hirschler, R.P. Townsend, and V. Visanuvimol, "The Combustion of Cellulose under Conditions of Rapid Heating," *Combust. Flame,* 49, pp. 249–254 (1983).
27. C.F. Cullis, D. Goring, and M.M. Hirschler, "Combustion of Cigarette Paper under Conditions Similar to Those during Smoking," in *Cellucon '84* (Macro Group U.K.), Wrexham (Wales), Chapter 35, pp. 401–410, Ellis Horwood, Chichester, UK (1984).
28. P.J. Baldry, C.F. Cullis, D. Goring, and M.M. Hirschler, "The Pyrolysis and Combustion of Cigarette Constituents," in *Proc. Int. Conf. on "Physical and Chemical Processes Occurring in a Burning Cigarette,"* R.J. Reynolds Tobacco Co., Winston-Salem, NC, pp. 280–301 (1987).
29. P.J. Baldry, C.F. Cullis, D. Goring, and M.M. Hirschler, "The Combustion of Cigarette Paper," *Fire and Materials,* 12, pp. 25–33 (1988).
30. L. Reich and S.S. Stivala, *Elements of Polymer Degradation,* McGraw-Hill, New York (1971).
31. A.A. Miroshnichenko, M.S. Platitsa, and T.P. Nikolayeva, "Technique for Calculating the Temperature at the Beginning and End of Polymer Thermal Degradation from Structural Data," in *Polymer Science* (USSR) 30, 12, pp. 2707–2716 (1988).
32. O.F. Shlenskii and N.N. Lyasnikova, "Predicting the Temperature of Thermal Decomposition of Linear Polymers," *Intern. Polymer Sci. Technol.,* 16, 3, pp. T55–T56 (1989).
33. D.W. Van Krevelen, "Thermal Decomposition" and "Product Properties, Environmental Behavior and Failure," in *Properties of Polymers,* 3rd ed., Elsevier, Amsterdam, pp. 641–653 and 725–743 (1990).
34. D.W. Van Krevelen, "Some Basic Aspects of Flame Resistance of Polymeric Materials," *Polymer,* 16, pp. 615–620 (1975).
35. ASTM D2863, "Standard Method for Measuring the Minimum Oxygen Concentration to Support Candle-like Combustion of Plastics (Oxygen Index)," in *Annual Book of ASTM Standards,* Vol. 8.02, American Society for Testing and Materials, West Conshohocken, PA.
36. E.D. Weil, M.M. Hirschler, N.G. Patel, M.M. Said, and S. Shakir, "Oxygen Index: Correlation to Other Tests," *Fire Materials,* 16, pp. 159–167 (1992).
37. ASTM E1354, "Standard Test Method for Heat and Visible Smoke Release Rates for Materials and Products Using an Oxygen Consumption Calorimeter," in *Annual Book of ASTM Standards,* Vol. 4.07, American Society for Testing and Materials, West Conshohocken, PA.
38. M.M. Hirschler, "Heat Release from Plastic Materials," Chapter 12a in *Heat Release in Fires* (V. Babrauskas and S.J. Grayson, eds.), Elsevier, London (1992).
39. R.E. Lyon, "Fire-Safe Aircraft Materials" in Fire and Materials, Proceeding 3rd Int. Conference and Exhibition, Crystal City, VA, Interscience Communications, pp. 167–177 (1994).
40. N. Grassie, "Polymer Degradation and Fire Hazard," *Polymer Degradation and Stability,* 30, pp. 3–12 (1990).
41. G. Camino and L. Costa, "Performance and Mechanisms of Fire Retardants in Polymers—A Review," *Polymer Degradation and Stability,* 20, pp. 271–294 (1988).
42. G. Bertelli, L. Costa, S. Fenza, F.E. Marchetti, G. Camino, and R. Locatelli, "Thermal Behaviour of Bromine-Metal Fire Retardant Systems," *Polymer Degradation and Stability,* 20, pp. 295–314 (1988).
43. L.H. Lee, *J. Polymer Sci.,* 3, p. 859 (1965).
44. R.T. Conley (ed.), *Thermal Stability of Polymers,* Marcel Dekker, New York (1970).
45. W.J. Roff and J.R. Scott, *Fibres, Films, Plastics, and Rubbers,* Butterworths, London (1971).
46. F.A. Williams, in *Heat Transfer in Fires,* Scripta, Washington, DC (1974).
47. C. David, in *Comprehensive Chemical Kinetics,* Elsevier, Amsterdam (1975).
48. S.L. Madorsky, *Thermal Degradation of Polymers,* reprinted by Robert E. Kreiger, New York (1975).
49. D.W. Van Krevelen, *Properties of Polymers,* Elsevier, Amsterdam (1976).
50. T. Kelen, *Polymer Degradation,* Van Nostrand Reinhold, New York (1983).
51. W.L. Hawkins, *Polymer Degradation and Stabilization,* Springer Verlag, Berlin (1984).
52. N. Grassie and G. Scott, *Polymer Degradation and Stabilisation,* Cambridge University Press, Cambridge, UK (1985).
53. S.M. Lomakin, J.E. Brown, R.S. Breese, and M.R. Nyden, "An Investigation of the Thermal Stability and Char-Forming Tendency of Cross-Linked Poly(methyl methacrylate)," *Polymer Degradation Stability,* 41, pp. 229–243 (1993).
54. G. Montaudo and C. Puglisi, "Evolution of Aromatics in the Thermal Degradation of Poly(vinyl chloride): A Mechanistic Study," *Polymer Degradation Stability,* 33, pp. 229–262 (1991).
55. W.H. Starnes, Jr., and D. Edelson, *Macromolecules,* 12, p. 797 (1979).
56. D. Edelson, R.M. Lum, W.D. Reents, Jr., W.H. Starnes, Jr., and L.D. Westcott, Jr., "New Insights into the Flame Retardance Chemistry of Poly(vinyl chloride)," in *Proc. Nineteenth (Int.) Symp. on Combustion,* Combustion Institute, Pittsburgh, PA, pp. 807–814 (1982).
57. K.S. Minsker, S.V. Klesov, V.M. Yanborisov, A.A. Berlin, and G.E. Zaikov, "The Reason for the Low Stability of Poly(vinyl chloride)—A Review," *Polymer Degradation Stability,* 16, pp. 99–133 (1986).
58. P. Simon et al., "Kinetics of Polymer Degradation Involving the Splitting off of Small Molecules, Parts 1–7," *Polymer Degradation Stability,* 29, pp. 155; 253; 263 (1990); pp. 35, 45; 157; 249 (1992); pp. 36, 85 (1992).
59. L.A. Chandler and M.M. Hirschler, "Further Chlorination of Poly(vinyl chloride): Effects on Flammability and Smoke Production Tendency," *Europ. Polymer J.,* 23, pp. 677–683 (1987).
60. G. Montaudo, C. Puglisi, and F. Samperi, "Primary Thermal Degradation Mechanisms of PET and PBT," *Polymer Degradation Stability,* 42, pp. 13–28 (1993).
61. G. Montaudo, C. Puglisi, R. Rapisardi, and F. Samperi, "Further Studies on the Thermal Decomposition Processes in Polycarbonates," *Polymer Degradation Stability,* 31, pp. 229–246 (1991).

CHAPTER 8

Structural Mechanics

Robert W. Fitzgerald

Introduction

Structural mechanics is the analysis of the external and internal force systems of structural members, as well as the behavior of those members under loading conditions. Before describing the different types of members and their structural characteristics, it is helpful to describe briefly the structural design process.

Structural design follows roughly the same stages of design as the architectural process. During the schematic stage when the building layout is being created, the structural engineer and the architect identify column locations. Then, a number of different framing schemes utilizing the different structural materials are considered. A design is made for each potential framing alternative for a part of the building that is representative of a major segment of the structure. Economic and functional analyses are made with the different alternatives. The architect and structural engineer select the framing system that is best for the specific building being designed.

After the schematic design has been completed and accepted, the detail design and contract documents stages are undertaken. During these stages, all of the structural members and the important details are designed. Critical design connections, significant construction details, and specifications are developed to ensure a complete and adequate structural system.

The structural design must conform to accepted professional practice at the time. Regardless of materials, this involves three major interrelated considerations. They are

1. The appropriate loading conditions and combinations
2. Structural mechanics
3. Control parameter limits

Dr. Robert W. Fitzgerald is professor of civil and fire protection engineering at Worcester Polytechnic Institute. His major activities are in structural engineering and in building design and technology for fire safety.

The objective of structural design is to select materials and dimensions so that economy is achieved and the building will perform satisfactorily. Performance here means that the structure is compatible with architectural needs and is free from excessive deflection and vibration. Prevention of collapse under expected or reasonably foreseen conditions is included in performance, and safety is a major part of the professional responsibility.

A major aspect of structural engineering is the recognition of conditions that can lead to failure. When these conditions are present, the designer must proportion the members or take other measures to ensure that failure under design conditions will not occur. The identification of loads, selection of engineering calculation models, and the establishment of control parameter limits are all interwoven. Figure 1-8.1 shows a schematic relationship of these components. Although each component may be addressed separately, their interrelationships comprise the unification of the design methodology. Together they allow performance to be monitored.

The loading conditions of Figure 1-8.1 are generally specified in the building code. They include live load values for floor systems, snow and ice, wind, and earthquake. The engineer also will include the dead load for

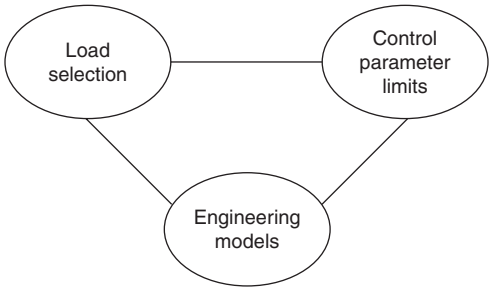

Figure 1-8.1. ***Components of the design methodology.***

the framing system and any special loading that may be expected for the structure being considered.

The engineering models involve two considerations. One is the mechanics of computing the internal forces that result from the loading, dimensions, and support conditions. The other is the relationship between these internal forces and the performance function. This performance function relates the internal forces to control parameters. Stress is the most convenient control parameter, although others, such as deflection, are used also.

Structural mechanics is the engineering science that enables the engineer to calculate the internal shear, moment, and axial force and the related stresses at any location in the structural member for any combination of loads. In addition, it describes the behavior of the member as loads are increased up to failure. This is dependent on the materials involved, the type of loading, and the geometric and support conditions of the member. The behavior includes deformations, vibrations, and failure modes. Structural mechanics may be considered as the "exact" analytical part of the design process.

Another consideration in Figure 1-8.1 involves the specific design requirements for the materials and assembly. These are developed by the different products industries. For example, the American Institute of Steel Construction (AISC) publishes its code of practice,[1] and the American Concrete Institute (ACI) publishes its building code.[2] These publications, often called *codes* by the engineers, give requirements on design and construction that will avoid failure for normal usage. The values for allowable stress are the most common limits. These values are empirically selected considering theoretical mechanical behavior for the material and practical applications. When a designer uses building code loadings with allowable stresses and other control criteria through the mechanism of the engineering models, one can have confidence that the member probably will not fail. The control performance consideration is normally deflection, even though the calculations usually involve stress. Stress and deformation are, of course, related.

The reliability of structural design has evolved through consideration of the entire process. Although individual parts can be examined by in-depth research, the process as a whole is considered in design. Values for loading and codified limits of the parameters are established by the end performance to be achieved.

Professional structural practice integrates the loadings, usually obtained from the local building code or from the conditions that may reasonably be expected by the engineer, with the structural (mechanical) analysis and the design procedures of the structural code. The structural codes are updated periodically, usually about every five to ten years. The literature of the profession can keep the engineer aware of new developments in the field.

With this brief discussion of the structural design process, we will now describe briefly the elements of structural mechanics. In general, this may be grouped as the calculation of external reactions and internal forces and the prediction of failure modes for different materials, geometry, support conditions, and loads.

Statical Analysis for Reactions

The calculation of external reactions of a defined structural element for a given loading condition is the first part of the statical analysis. For planar structures, the available equations of statics are $\sum F_x = 0$, $\sum F_y = 0$, and $\sum M = 0$. For three-dimensional structures, $\sum F_z = 0$, $\sum M = 0$, about the other axes are added. Therefore, for planar structures, one can calculate as many as three unknown reactions on each free body diagram by statical analysis. For three-dimensional structures, one can calculate as many as six unknowns. For this discussion, we will consider only planar structures.

EXAMPLE 1:

To illustrate this process, consider the beam *ABC* of Figure 1-8.2. The supports include a pin at *B* and a roller at *C*. Figure 1-8.2(b) shows the free body of this beam. The reactions are computed as follows:

$$\sum M_B = 0:$$

$$C_y(18) - (1)(24)(6) - \left(\frac{1}{2}\right)(2)(18)(12) + 6(6) = 0$$

$$C_y = 18 \text{ k}$$

$$\sum M_C = 0:$$

$$B_y(18) - (1)(24)(12) - \left(\frac{1}{2}\right)(2)(18)(6) - 6(24) = 0$$

$$B_y = 30 \text{ k}$$

$$\sum F_x = 0: \; B_x = 8 \text{ k}$$

Since there were only three reaction components, one could calculate all three by means of statics alone. The structure would be described as statically determinate. However, if an additional support were introduced, as shown in Figure 1-8.3, four reaction components would exist. Since only three equations of statics are available, all of these reactions cannot be calculated by means of statics alone. The structure of Figure 1-8.3 would be described as statically indeterminate. Means other than statics alone are needed to calculate the reactions. Generally, these techniques involve either superposition or relaxation methods of analysis.

Statical Analysis for Internal Forces

After the external reactions have been calculated, the characteristics of the internal shear, moment, and axial force are determined. This may be computed by cutting the member at the desired location and drawing a free body diagram of one segment.

EXAMPLE 2:

Figure 1-8.4 shows a free body diagram for a section a distance, *x*, between *B* and *C* of the beam of Figure 1-8.2. The internal forces are the shear, *V*; the bending moment,

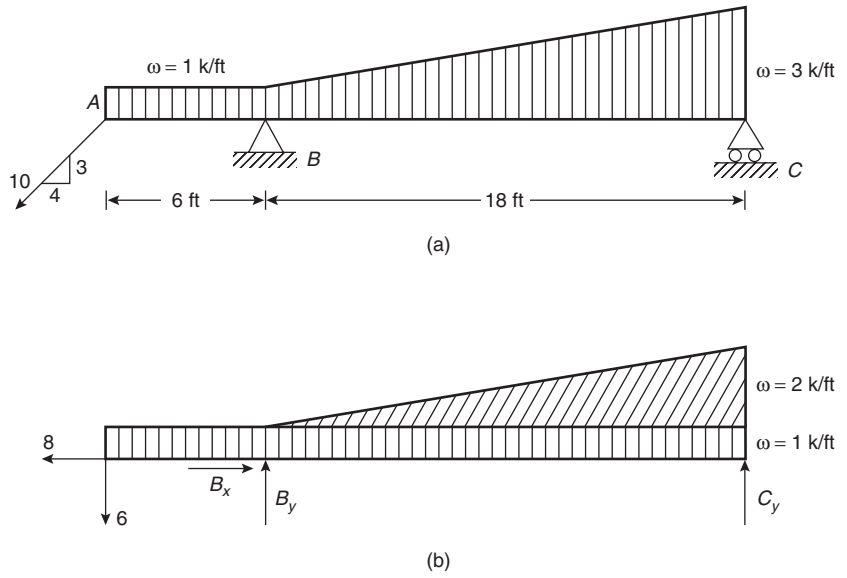

Figure 1-8.2. ***Statically determinate beam.***

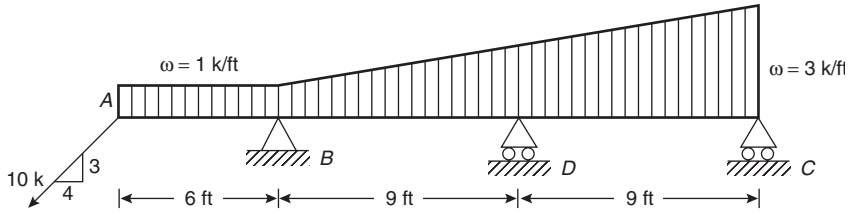

Figure 1-8.3. ***Statically indeterminate beam.***

M; and the normal force, N. These forces are calculated from the free body diagram of Figure 1-8.4 as follows:

$$\sum M_{cut} = 0: \quad M + \frac{1(6+x)(6+x)}{2} + \frac{1}{2}\left(\frac{x}{9}\right)(x)\left(\frac{x}{3}\right) + 6(x+6) - 30(x) = 0$$

$$M = -\frac{x^3}{54} - \frac{x^2}{2} + 18x - 54$$

$$\sum F_y = 0: \quad V + 1(x+6) + \frac{1}{2}\left(\frac{x}{9}\right)(x) + 6 - 30 = 0$$

$$V = -\frac{x^2}{18} - x + 18$$

$$\sum F_x = 0: \quad N = 8$$

The distribution of the internal forces may be plotted on diagrams that show the change in values throughout the length of the beam. Figure 1-8.5 shows the N, V, and M diagrams for the beam of Figure 1-8.2.

Failure Modes

Structural design consists of identifying all of the potential failure modes and providing resistance to avoid failure. Both safety and economy are considerations. A major part of the professional engineering services is the skill in identifying appropriate loading conditions and the associated failure modes for the construction conditions.

The ways in which members fail depend upon the materials, geometry, loading conditions, and support conditions. This section will describe the common structural forms and the failure modes generally associated with those forms.

Tension Members

Figure 1-8.6 illustrates tensile loading on a straight member. The stress in the member is defined as $\sigma = P/A$. The load must be applied through the centroid of the cross section for this equation to be valid. When loads are applied eccentrically to the cross section, a combined bending and axial condition exists. This will be described later.

Figure 1-8.7(a) shows relationship between unit stress, $\sigma = P/A$, and unit strain, $\varepsilon = \delta/L$, for a coupon of mild structural steel. This stress-strain diagram is obtained experimentally and depicts only mild structural steel loaded in tension. Stress-strain diagrams for other materials are also obtained experimentally and show distinctly different load-deformation characteristics.

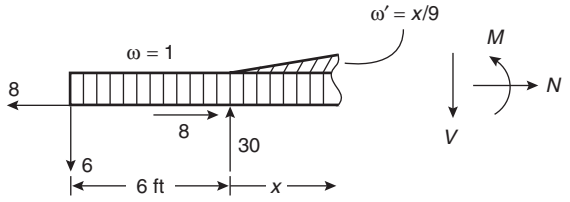

Figure 1-8.4. ***Free body diagram.***

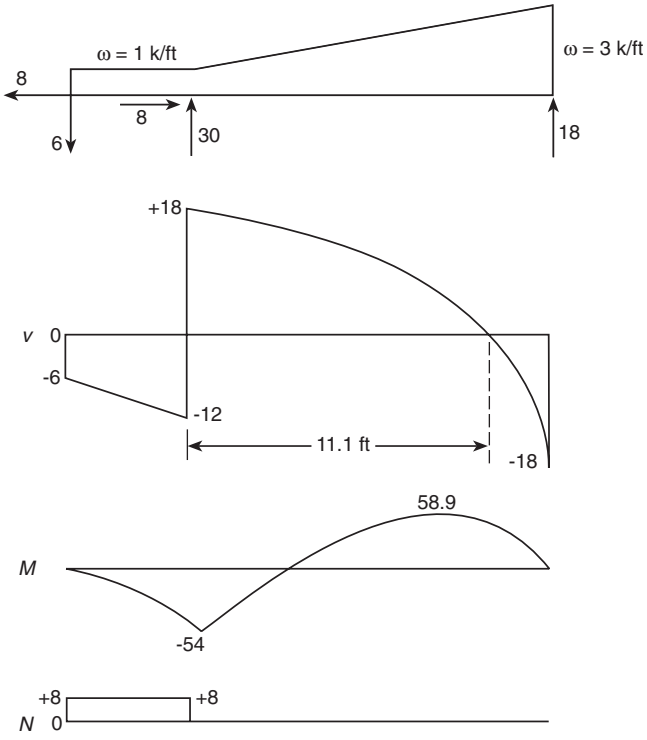

Figure 1-8.5. ***Shear, moment and normal force diagram.***

Figure 1-8.6. ***Tensile loading of a straight member.***

The stress-strain diagram provides an indication of the expected failure mode of the member. A ductile material, such as the mild steel in Figure 1-8.7(a), will elongate significantly under tensile loading. Frequently, the deformations are so great that the structure becomes unusable long before actual rupture. Rupture eventually will occur if loads are increased to the ultimate stress. Brittle materials, such as those shown in Figure 1-8.7(b), will fail by sudden rupture. Little or no warning of impending failure may be present with materials of this type.

There are situations in which a normally ductile material will exhibit a brittle type of failure. This occurs under conditions of low temperature or repeated, fatigue loading conditions.

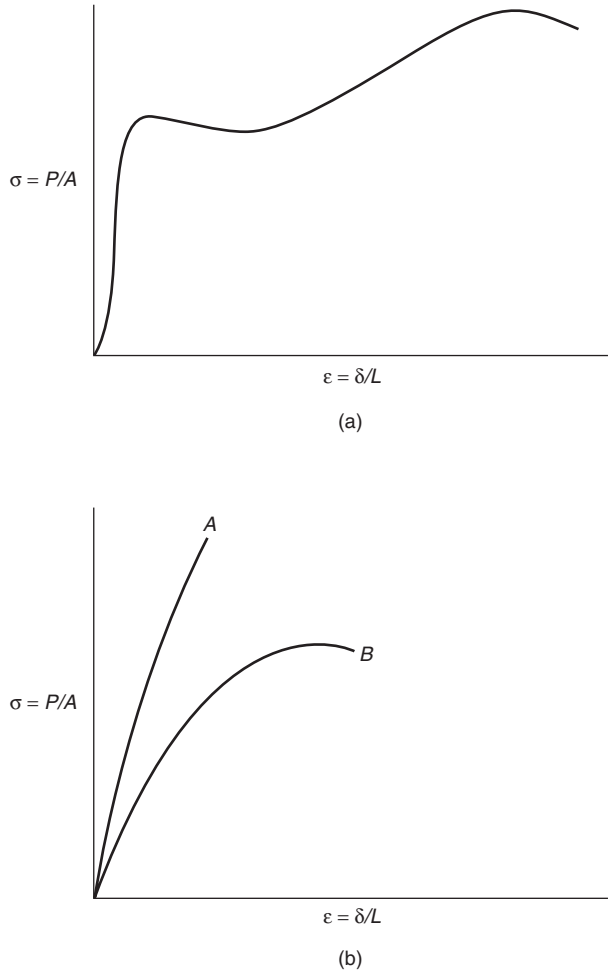

Figure 1-8.7. ***Stress-strain diagram for (a) ductile and (b) brittle materials.***

High temperatures, such as those present in building fires, will cause an increase in the elongation of tension members because of creep. Creep is the phenomenon in which a member will continue to deform after the applied load becomes steady. The magnitude of creep depends upon the material being loaded, the level of stress, the temperature, and the time duration.

Other potential failure modes for tension members include connection failures, excessive stress concentrations due to changes in cross sections, and twisting when unsymmetrical members are excessively long.

Compression Members

Figure 1-8.8 illustrates compressive loading on a member. When the loading is applied along the centroidal axis of the member, the stress may be calculated as $\sigma = P/A$. The importance of centroidal loading is even more critical for compressive forces than for tensile forces because of the magnification effect of eccentricity. This will be discussed more completely later.

Compression members, unlike tension members, have no single general failure mode, regardless of their

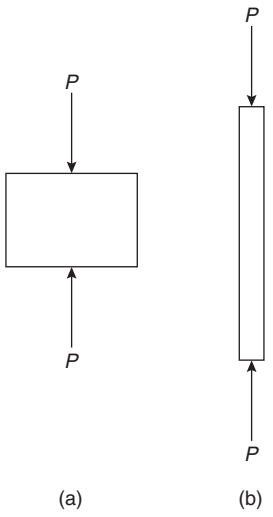

Figure 1-8.8. ***Compressive loading of (a) short and (b) long columns.***

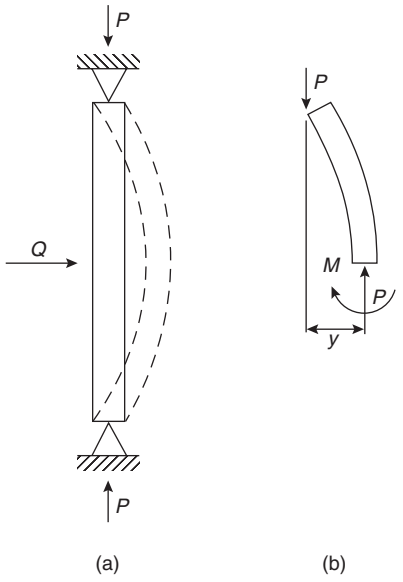

Figure 1-8.9. ***Column buckling.***

length. Short columns, as illustrated by Figure 1-8.8(a), fail by general yielding. Long columns, as illustrated by Figure 1-8.8(b), fail by buckling. Buckling is the rapid collapse of a compression member due to instability. To describe the nature of column behavior, the following discussion may be helpful.

Consider the column shown in Figure 1-8.8(b). Assume that the axial compressive load P starts at a low value and gradually increases in magnitude. Assume a small lateral force is applied, as shown in Figure 1-8.9(a). The bar will deflect laterally by a small amount. When Q is removed, the bar returns to its original position. When a particular value of P is reached, the bar will remain in the deflected position after Q is removed. That load for which the bar is indifferent to its position is defined as the critical buckling load, P_{cr}. If P were increased above P_{cr}, the bar would collapse. If P were decreased below P_{cr}, the bar would return to its straight P position. The critical buckling load is, therefore, the particular load at which neutral equilibrium occurs.

Considering the equilibrium condition when the bar is deformed, we may determine the bending moment from Figure 1-8.9(b), as

$$\sum M_{cut} = 0: \quad M = -Py$$

The equation of the elastic curve of a beam[3] is $d^2y/dx^2 = M/EI$. Substituting this for M above, we obtain

$$\frac{d^2y}{dx^2} + \frac{Py}{EI} = 0$$

Letting $\kappa^2 = P/EI$ and solving this differential equation yields $y = A \cos(\kappa x) + B \sin(\kappa x)$.

Using the boundary conditions of $y = 0$ at $x = 0$ and $y = 0$ at $x = L$, we obtain $A = 0$ and $B \sin(\kappa L) = 0$. Since B cannot be zero, $\sin(\kappa L) = 0$. This eigenvalue equation has solutions of

$$\kappa L = 0, \pi, 2\pi, 3\pi, \ldots, n\pi$$

Taking the general solution we obtain

$$\kappa L = n\pi, \qquad \frac{P}{EI} = \frac{n\pi}{L}$$

$$P = \frac{n^2\pi^2 EI}{L^2}$$

The n-term describes the number of modes of buckling. Since the first mode of buckling will cause failure unless special construction features exist, buckling will occur at $P_{cr} = \pi^2 EI/L^2$.

This column equation was originally described in 1757 by Leonhard Euler, a Swiss mathematician. Controversy about its validity for predicting column loads raged for sixty years. In 1820 it was recognized that the derivation incorporated the bending equation, $\sigma = Mc/I$. Consequently, all assumptions of elastic behavior are intrinsic to the use of the Euler column equation. Therefore, the limit of validity is the proportional limit of the material.

Two clearly identifiable compression failure conditions can exist. One is the yielding condition for short columns where $P = \sigma_y A$, as illustrated in Figure 1-8.8(a). The second is the buckling of long, slender columns, where $P_{cr} = \pi^2 EI/L^2$. This equation may be converted into one involving axial stress by recognizing that $I = Ar^2$, where r is the radius of gyration of the cross-section. Dividing both sides by A gives

$$\sigma_{cr} = \frac{\pi^2 E}{(L/r)^2}$$

The term L/r is defined as the slenderness ratio. Therefore, column slenderness is a function both of the length and the cross-sectional geometry, as described by the radius of gyration, *r.*

If the critical stress versus the slenderness ratio were plotted for columns, the graph of Figure 1-8.10 would result. The segment from *C* to *D* describes long columns in which the critical buckling load may be calculated from Euler's equation. The failure mode is pure buckling, and the limit of validity of the equation is the proportional limit of the material, σ_{PL}. The segment from *A* to *B* identifies short columns, which fail by yielding. The maximum load is $P = \sigma_y A$.

The segment from *B* to *C* is described as the intermediate column range where failure may be considered a combination of buckling and yielding.

Considerable controversy and research has been associated with attempts to relate theory and experimental validation in this intermediate range. While the history of these studies is fascinating, the major interest here relates to design equations. The importance of the intermediate column range is that, from a practical viewpoint, most columns have slenderness ratios within this range. Therefore, the readily derived and theoretically accurate Euler's equation, $P_{cr} = \pi^2 EI/L^2$, is inappropriate for slenderness ratios less than $(L/r)_{PL}$.

From a historical and practical viewpoint, intermediate column formulas have been obtained by curve fitting experimental results. Therefore, one obtains equations that are material dependent, rather than an equation analogous to $\sigma = Mc/I$ that may be valid for a variety of materials. Most column equations have been parabolic or straight-line expressions for ease of design calculations. These expressions may be used because a factor of safety is incorporated for design purposes. The material product industries publish equations appropriate for their materials. Therefore, one must be careful to select column equations that are appropriate to the materials and conditions for the construction.

The most prevalent failure mode for columns is due to general buckling, as described previously. It may be seen from Figure 1-8.10 that the load carrying capacity is reduced significantly as the slenderness ratio increases. Consequently, a long column will buckle at axial loads considerably lower than those for a shorter column of the same cross section. In addition to the slenderness ratio, the strength of columns is dependent upon the modulus of elasticity. In fire conditions, the modulus of elasticity is reduced. This reduction causes a loss in strength of columns.

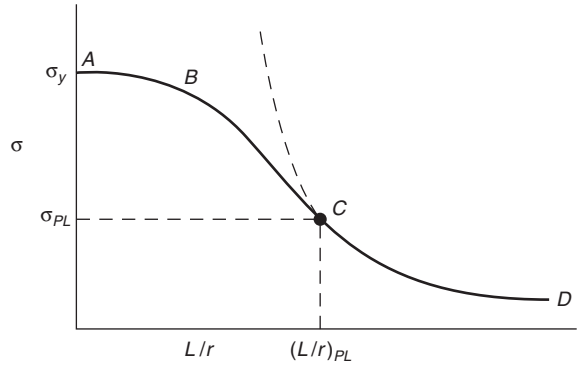

Figure 1-8.10. ***Critical stress of columns as a function of the slenderness ratio, L/r.***

Although general buckling is the most common type of failure, local buckling can occur on platelike elements in compression. This occurs when the plates are too thin for the applied load and premature localized buckling takes place. Because this type of behavior is also related to the modulus of elasticity, fire conditions can cause an earlier localized buckling to members, such as wide-flange steel shapes or angles that are made of thin-plate elements.

Flexural Members

The third type of structural loading is flexural. This occurs when loads are applied perpendicular to the longitudinal axis of the member. These members are described as being in flexure or bending. In structural use they are described as beams, girders, slabs, plates, and rigid frames. Although each of these types of members acts in flexure, their behaviors will differ.

Figure 1-8.11 shows flexural members with couples as the applied load. The top fibers of Figure 1-8.11(a) are in compression, and the bottom fibers are in tension. This is defined as positive bending. The opposite occurs in Figure 1-8.11(b), and this condition is described as negative bending.

Figure 1-8.3 showed a beam supporting transverse loads. The reactions of the beam were calculated in Example 1. The internal shear, moment, and axial forces were computed for a general distance *x* in Example 2. Diagrams that describe the change in vertical shear, *V,* and the change in internal moment, *M,* are constructed to show the distribution of these changes throughout the beam. These are called *shear and moment diagrams.* Every textbook on mechanics of materials and most texts on statics cover procedures for constructing *V* and *M* diagrams for beams. From these shear and moment diagrams the design values for those parameters are selected.

The relationship between the fiber stresses in the member and the internal resisting moment can be obtained in the following manner. Consider a homogeneous beam in pure bending as shown in Figure 1-8.12(a). Two lines, parallel before bending, would assume the position shown after the couples are applied. It is assumed that plane sections before bending remain plane after bending. Figure 1-8.12(b) shows the strain distribution of the fibers throughout the cross section. The top fibers have

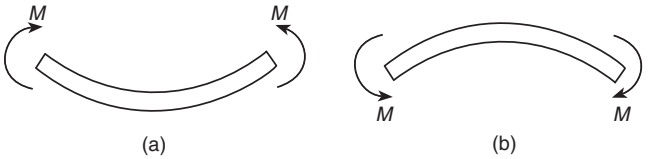

Figure 1-8.11. ***Deflection of flexural members under load.***

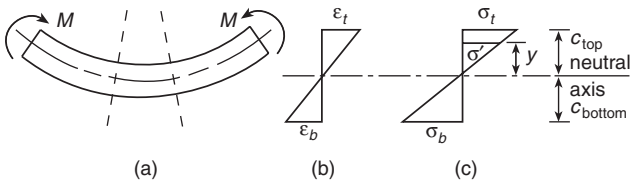

Figure 1-8.12. ***Homogeneous beam in (a) pure bending, and the resulting (b) strain distribution, and (c) stress distribution.***

shortened, and the bottom fibers have elongated. One layer of fibers has not changed in length. This plane is called the neutral plane of the member.

Hooke's law states that stress is proportional to strain. When the proportionality is linear, the stress distribution is as shown in Figure 1-8.12(c). The maximum stress, σ, will occur at the fibers located farthest from the neutral axis. The stress at the neutral axis is zero.

If we consider the stress, σ_1, in a single fiber of area, dA, at a distance, y, above the neutral axis, the force exerted by that fiber due to the stress is $dP = \sigma' dA$. This stress may be related to the stress, σ, in the extreme fibers, by the similar triangles of Figure 1-8.12(c).

$$\frac{\sigma'}{y} = \frac{\sigma'}{c}, \quad \text{or} \quad \sigma' = \sigma\left(\frac{y}{c}\right)$$

The force, dP, exerted by this fiber may be expressed as

$$dP = \sigma' dA = \sigma\left(\frac{y}{c}\right) dA$$

The moment of this force about the neutral axis is

$$dM = dPy = \sigma\left(\frac{y}{c}\right) dA(y)$$

$$dM = \frac{\sigma}{c} y^2\, dA$$

Summing the moments of each of the fibers of the member yields

$$\int_0^M dM = \int_{-c}^{+c} \frac{\sigma}{c} y^2\, dA = \frac{\sigma}{c} \int_{-c}^{+c} y^2\, dA$$

The moment of inertia, I, of the cross section is defined as

$$I = \int_{-c}^{+c} y^2\, dA$$

The flexure formula, therefore, may be expressed as

$$\sigma = \frac{Mc}{I} \tag{1}$$

where

σ = flexural stress at the extreme fibers

M = bending moment at the section of the beam being considered

c = distance from the neutral axis to the extreme fibers

I = moment of inertia of the cross section

Equation 1 has several limitations that have been incorporated into the assumptions of its derivation. These include (1) the beam is initially straight and of constant cross section; (2) all stresses are below the proportional limit, and Hooke's law applies; (3) the modulus of elasticity in compression is equal to that in tension; (4) loads are applied through the shear center so that torsion will not occur; and (5) the compression fibers are laterally restrained.

The design of flexural members for bending loads involves (1) determining the dead and live loading for the member; (2) calculating the maximum moment in the beam; (3) selecting the materials and obtaining the allowable stresses; (4) calculating a required section modulus; and (5) selecting a beam to provide for that section modulus efficiently and economically; and (6) ensuring that all other failure modes will not occur.

Because many beams have common loading and support conditions, it is possible to develop standard conditions to obtain the maximum shear and moment by formula. Figures 1-8.13 and 1-8.14 illustrate two common conditions. Most handbooks and mechanics of materials textbooks provide several additional cases. The maximum moment from Figure 1-8.13 is $M = 1/8\omega L^2$, and that from Figure 1-8.14 is $M = Pab/L$. Loading conditions may be combined by superposition. However, it is important to conform with the conditions where superposition is valid. For example, Figure 1-8.15 shows a beam with a uniformly distributed load, ω, and a concentrated load, P, at the center. Because the maximum moment of each load occurs at the same location, it is possible to compute the maximum moment as $M = \omega L^2/8 + PL/4$. However, if the concentrated load were at another location, as in Figure 1-8.16, superposition would not be valid. In those cases, the engineer must compute the maximum V and M by using the basic principles of statics. Example 2 illustrated that technique.

Statically Indeterminate Beams

It is common to construct beams with more reactions than are necessary for statical stability alone. These members are statically indeterminate because the calculation of reactions requires means in addition to statics alone. Figure 1-8.17 illustrates some statically indeterminate

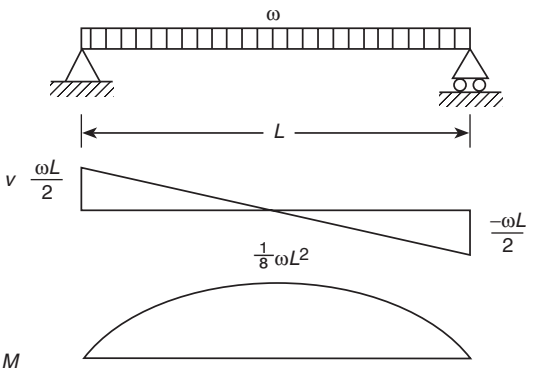

Figure 1-8.13. ***Shear and moment diagram for a simply supported beam under uniform loading.***

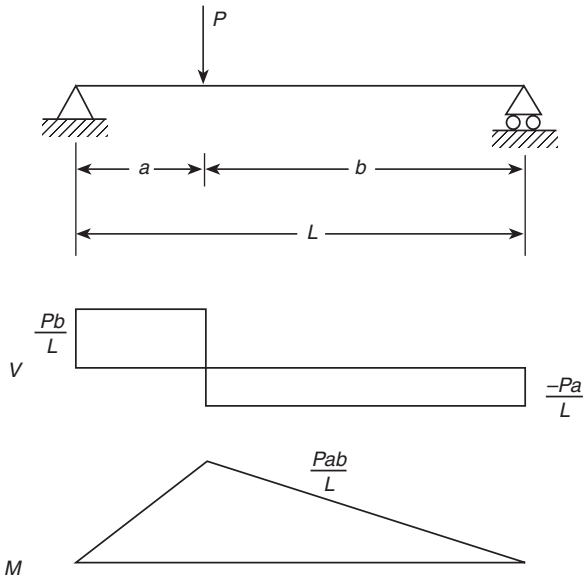

Figure 1-8.14. ***Shear and moment diagram for a simply supported beam under concentrated loading.***

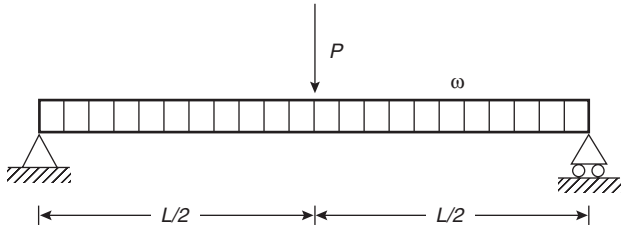

Figure 1-8.15. ***Uniformly distributed load with a concentrated load at the center.***

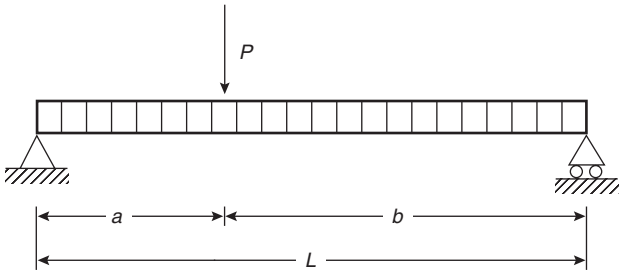

Figure 1-8.16. ***Nonsymmetric loading where superposition is not valid.***

beams, and Figure 1-8.18 shows some statically indeterminate frames.

The procedure for designing statically indeterminate beams is similar to that described for statically determinate beams. An increased complication arises, however, when determining the maximum shear and moment for a beam such as that shown in Figure 1-8.17(c). The dead load is applied over the entire span and is fixed. The live load is movable and may be applied to any or all spans. An integral part of the computation of the design shear and moment is to place the movable live load at positions that produce the most severe values. This may be done by constructing influence lines for the design functions. An influence line is a graph of the function as a unit load moves across the structure. The influence line shows where loads must be placed to produce the most severe conditions. To illustrate this concept, the loading condition shown in Figure 1-8.17(c) would be used to determine the maximum negative moment over support *E*, while the loading condition shown in Figure 1-8.17(d) would be used to determine the maximum positive moment at the midpoint of span *DE*.

Statically indeterminate structures are inherently stronger than statically determinate structures. This occurs because of the additional load-carrying capacity due to the redistribution of moments. The amount of this increased load capacity depends upon the type and location of load, the support conditions, the material properties, and the geometry and dimensions of the cross section.

To illustrate this concept, consider the simply supported beam of Figure 1-8.19. The maximum moment is $M = 1/8\omega L^2$. The stress may be computed as $\sigma = Mc/I$ as long as the fibers are stressed below the proportional limit. Figure 1-8.20(a) shows a wide flange cross section. Figure 1-8.20(b) shows a stress variation that is valid up to the value where the extreme fibers reach σ_y. The moment that causes that stress is M_y, the bending moment that will just cause yielding to be imminent at the extreme fibers. That value is the limit of validity for the flexure formula, $\sigma = Mc/I$.

The beam, however, has an increased load-bearing capacity beyond that value. Excessive deformation (i.e., collapse) will not occur until the entire cross section has yielded. The stress distribution for this condition is shown in Figure 1-8.20(c). The moment capacity at that point is called the fully plastic moment, M_p. The increase in moment is dependent upon the geometry of the cross section. The ratio of M_p/M_y is the shape factor. For steel wide-flange beams, the shape factor averages 1.14. The shape factor will be different for other geometrical shapes and dimensions.

If the simply supported beam of Figure 1-8.19 were a steel wide-flange shape, we would expect the collapse load to be 14 percent higher than the yield load. The design load usually has a factor of safety of 1.5 over the yield load. Therefore, the factor of safety for collapse above the design value is $1.50 \times 1.14 = 1.71$ for normal design conditions.

If the support conditions are fixed, as shown in Figure 1-8.21, the maximum moment occurs at the support. For elastic conditions, the moment at the support is $M = (1/12)\omega L^2$, and the moment at the center is $M' = (1/24)\omega L^2$. As the load is increased to the point where σ_y is first reached (at the ends), the value of $M_y = (1/12)\omega_y L^2$.

As the load continues to increase, the location of greatest stress (the ends) will reach their fully plastic value, M_p. However, the beam still has additional carrying capacity because a collapse mechanism will not occur until three hinges form. At the time M_p occurs at the ends, the other location of maximum moment, the center, is still

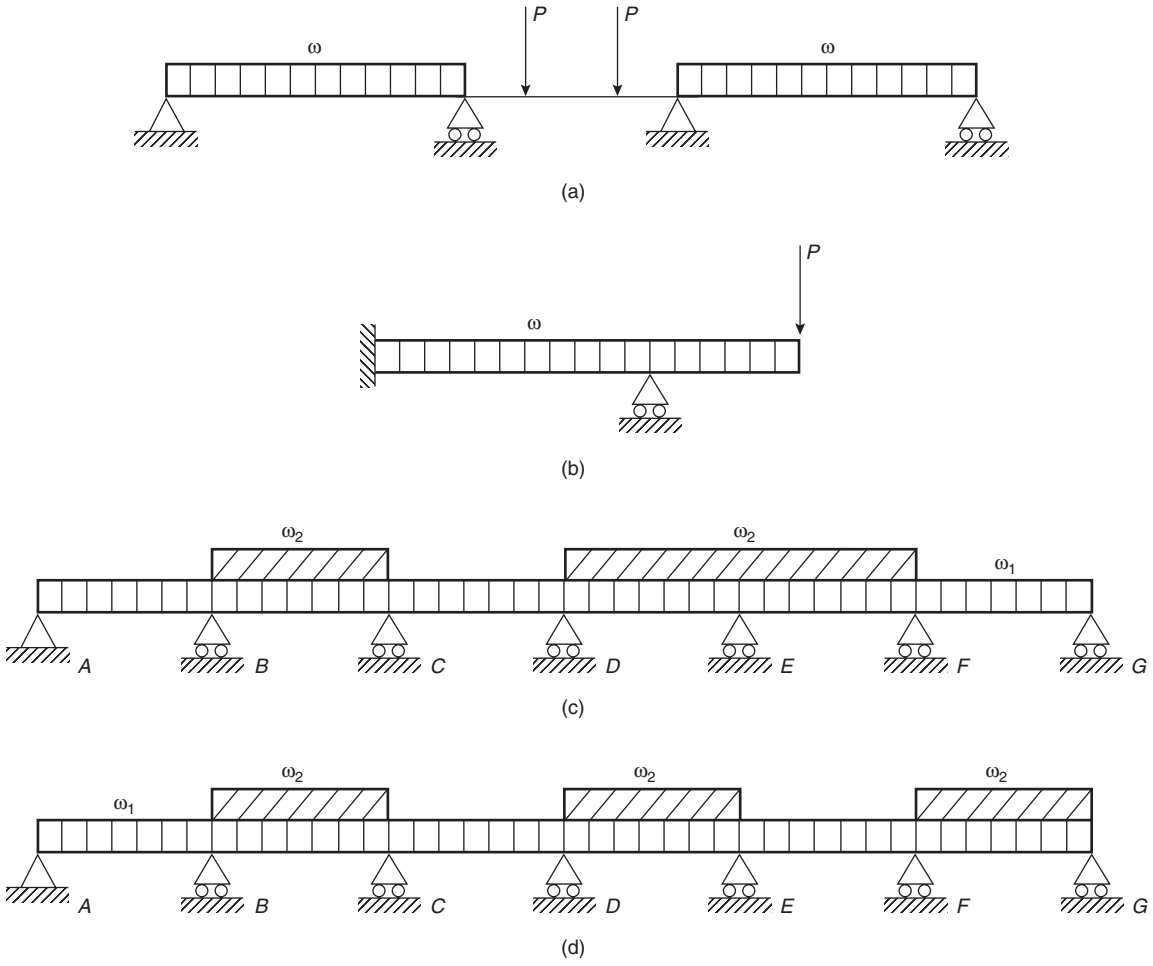

Figure 1-8.17. ***Statically indeterminate beams.***

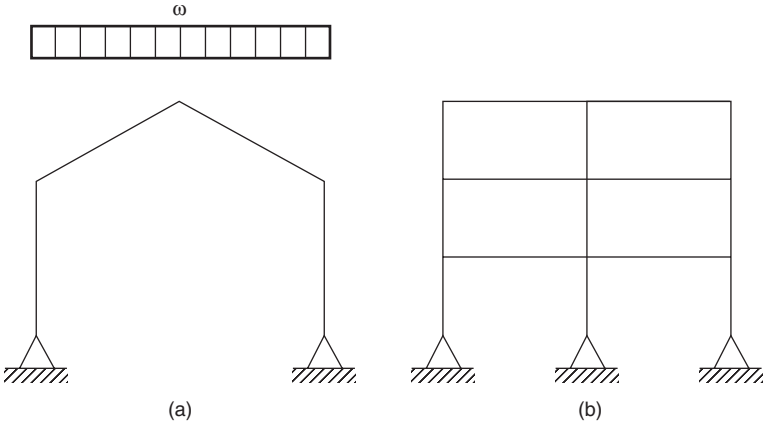

Figure 1-8.18. ***Statically indeterminate frames.***

in the elastic range. The value of M_p at the ends cannot increase. Therefore, any increase in load must be carried by the elastic portion. The moments redistribute, as illustrated by the dashed line of Figure 1-8.21(c). They will increase until M_p occurs at the center. At that time, collapse is imminent.

The collapse moment for the beam of Figure 1-8.21 is $2M_p = 1/8\omega_u L^2$; therefore $\omega_u = 16\ M_p/L^2$. The collapse

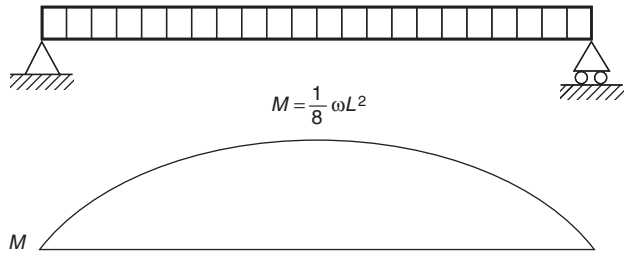

Figure 1-8.19. ***Uniformly loaded simply supported beam.***

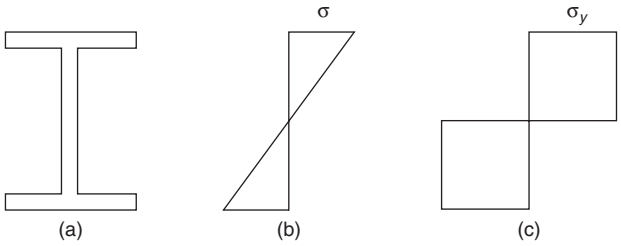

Figure 1-8.20. ***(a) Wide flange cross section and stress distributions, (b) prior to yielding of extreme fibers, and (c) after complete yielding.***

moment for the simply supported beam of Figure 1-8.19 is $M_p = 1/8\omega_u L^2$; therefore $\omega_u = 8\ M_p/L^2$. Therefore, the ultimate load-carrying capacity of the beam with fixed ends is twice that of a beam with simply supported ends.

This concept is sometimes described as limit state design, ultimate design, inelastic design, or plastic design. Limit state design seems more appropriate to a variety of materials.

The concept of ductility and its behavior is intrinsic to safe structural design because a ductile structure will deform considerably before collapse. This deformation warns occupants of impending danger before failure. Brittle design and elastic instability are not as desirable because failure can occur with relatively little warning. Therefore, structural engineers attempt to incorporate ductility into their designs as much as possible. This ductility is evident in most structural building materials.

Flexural Failure Modes

Depending upon the magnitude, type of loading, and support conditions, flexural members may exhibit different types of failure modes. The most evident type of failure is the overstress that contributes to the development of a plastic hinge. This was described in the previous section. A statically determinate structure will collapse when the first plastic hinge forms. A statically indeterminate structure requires two or three hinges to form before collapse. The support conditions determine the number of hinges needed for collapse.

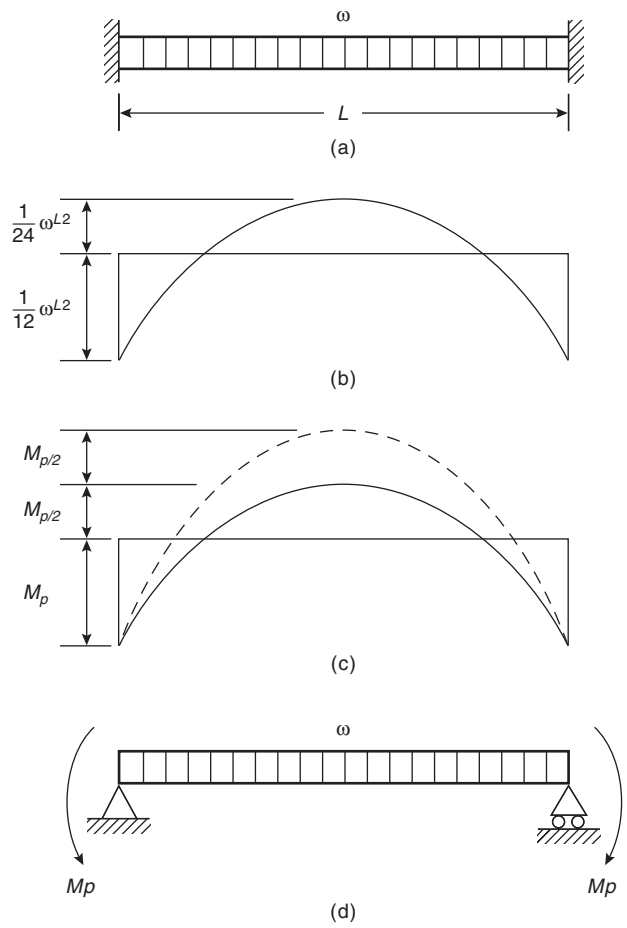

Figure 1-8.21. ***Moment redistribution in a fixed-ended beam.***

Another common mode of failure is lateral instability. The compression flange of the beam must be supported laterally at sufficient intervals to prevent lateral buckling. Lateral buckling is similar to column buckling, and it can occur when supports are spaced too far apart. When lateral supports are spaced farther apart than the distance needed to avoid lateral buckling, the allowable stress is reduced to compensate for the reduction in local carrying capacity.

A third mode of beam failure is through torsional loading. An open cross section is particularly weak when subjected to torsional loads. A torsional load exists whenever the line of action of the applied loads does not intersect the shear center of a beam. The shear center is a particular location on the cross section. For symmetrical members, such as that of Figure 1-8.22(a), the shear center coincides with the centroid. For unsymmetrical members, the shear center may be calculated. Figure 1-8.22(b) and (c) illustrate the location of the shear center for this type of cross section. Whenever loads do not pass through the shear center, construction features must be introduced to counterbalance the rotational effect of the loads.

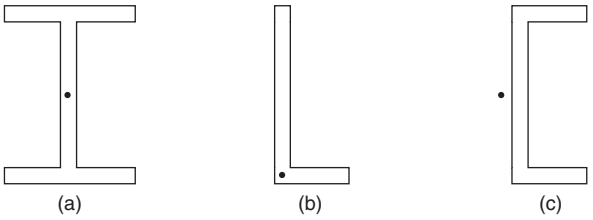

Figure 1-8.22. ***Location of shear center for (a) symmetrical and (b,c) unsymmetrical sections.***

Another mode of failure is excessive deflection. This can occur when the stiffness is insufficient and can occur at relatively low stresses. In addition to excessive deflection, unwanted vibrations or sway, such as wind loads on tall buildings, may occur.

It is not uncommon for members to be loaded with both axial and flexural forces. Rigid frames and chord members of trusses, where the load is applied directly to a chord, are common examples of this condition. Depending upon the construction conditions, failure may occur due to premature formation of plastic hinges or buckling of the compression flange.

Structural Design for Fire Conditions

The theory and procedures for structural analysis and design at normal temperatures have been well studied. Understanding of theoretical and empirical relationships, and the ability to predict performance for practical applications and conditions, is relatively clear to most practitioners. However, the understanding of the structural behavior for fire conditions becomes theoretically and practically a far more complex problem.

Structural analysis and design for fire conditions can take one of several forms. The simplest application can be described by the procedures used in most conventional building codes. In this case, a representative sample is tested in a standard fire endurance test, such as ISO 834 or ASTM E119, *Standard Test Methods for Fire Tests of Building Construction and Materials.* The length of time in the laboratory test before failure occurs produces a fire endurance time. Building codes specify the fire endurance required for structural members and barriers in identified occupancies and classifications of construction. The engineer or architect need only incorporate the standard construction features identified by the test results and published documentation to satisfy the code requirements.

This procedure requires no knowledge of fire or structural engineering by the practitioner. A catalog of construction assemblies and their fire endurance ratings are the only data needed to satisfy code compliance. Unfortunately, the actual structural performance in fires is not known or investigated. The sophisticated knowledge of the interrelationships that lead to an understanding of structural performance and economical design is submerged in the process. The increased structural strength achieved by continuity in construction is not a consideration in this procedure. The rated fire endurance of a beam and its value from the building code viewpoint is the same whether it is constructed as a statically determinate structure or as continuous construction, even though the performance may vary quite significantly.

Another procedure involves the calculation of structural fire endurance based on the standard ASTM E119 or ISO 834 fire test. Empirical and theoretical relationships are used to predict the fire endurance, based on the standard fire time-temperature relationship. Two advantages of this procedure are that (1) it allows the building codes to retain their present form and (2) it leaves undisturbed the interrelationship between construction classifications and other fire defense measures. Also, it provides more flexibility: fire endurance of different types of assemblies can be obtained by calculation rather than by test. However, the same limitations present in the traditional test procedure and code format remain.

A third procedure can be described as a rational approach to structural design for fire conditions. This approach is exemplified by the procedures for (1) structural steel design and (2) reinforced concrete design developed in Sweden. In these procedures, the design incorporates the structural performance at elevated temperatures in a manner analogous to design at normal temperatures. The mechanical properties of the structural materials at elevated temperatures are incorporated into the traditional structural theory to develop a rational analytical procedure for predicting structural behavior. Further, the natural room fire temperature-time relationship is used instead of the standard test time-temperature relationship, and the thermal properties and heat transfer through the insulating materials are incorporated into the analysis. The procedures follow more closely the traditional structural engineering methods for predicting structural behavior.

Summary

The ability of structural members to withstand failure of excessive deflection, insufficient strength, and instability is a major requirement of any structure. While the analysis and design process for normal loads and conditions is not particularly difficult, it does require care in application. The care relates to the type and validity of the assumptions made and to the form of construction used.

The anatomy of the entire structural system is an important aspect of the analysis and design process. Unless care is taken to specify clearly the construction details, inappropriate design calculations can result. To the lay person, one form of construction often appears to be the same as another. To the student who often has insufficient opportunity and training to recognize the construction details, analysis and design may appear to be an academic exercise. Normally, much of the ability to recognize the essential details is obtained through engineering practice with a professional engineer.

Fires in buildings create an added dimension of complexity to the analysis of the behavior of structural members at elevated temperatures. The fire design of structural members must include the same attention to details as the design of members at normal temperatures.

Nomenclature

A = area
c = distance from neutral axis to extreme fibers
E = modulus of elasticity
F = force
I = moment of inertia
L = length of beam or member
M = moment
P = concentrated or point load
r = radius of gyration
V = shear
x = space coordinate along the beam
y = space coordinate normal to the beam
ε = strain
δ = deformation
σ = stress
ω = uniform load density

References Cited

1. *Manual of Steel Construction,* American Institute of Steel Construction, Chicago (1980).
2. *ACI 318-83,* American Concrete Institute, Detroit (1983).
3. R.W. Fitzgerald, *Mechanics of Materials,* Addison-Wesley, Reading, MA (1982).

Additional Readings

ASTM E119, *Standard Test Methods for Fire Tests of Building Construction and Materials,* American Society for Testing and Materials, Philadelphia.

ISO 834, International Organization for Standardization, Geneva, Switzerland.

O. Pettersson, S. E. Magnusson, and J. Thor, "Fire Engineering Design of Structures," *Publication 50,* Swedish Institute of Steel Construction (1976).

CHAPTER 9

Premixed Burning

Robert F. Simmons

Introduction[1]

When a mixture of fuel vapor and oxidant burns on a cylindrical tube, as with a Bunsen burner, the resulting premixed flame has the characteristic structure of a luminous inner cone and an outer sheath of hot combustion gases.[1] This inner cone depicts the end of the primary reaction zone of the flame, in which a fast oxidation reaction occurs, so that in this part of the flame the temperature rises very rapidly. When the initial mixture of fuel and oxidant is fuel rich, that is, there is a deficiency of oxidant in terms of the stoichiometric conversion of the fuel to its oxidation products, the outer sheath is essentially a diffusion flame in which the hot combustion products from the primary reaction zone burn in the surrounding atmosphere. In contrast, with lean flames this outer sheath is indistinct as there is sufficient oxidant in the initial mixture for the complete combustion of the fuel, and the surrounding atmosphere is entrained into the burnt gases.

A stable premixed flame can only be obtained over a limited range of mixture compositions and flow rates, and the flow conditions for a given initial mixture can be seen from a consideration of an idealized flat flame, as shown in Figure 1-9.1. For such a flame, the flow of the initial combustible mixture is normal to the flame front. If the flow is too fast the flame is "blown off," while if it is too slow the flame "flashes back." A stable flame is only obtained when the flow velocity of the incident mixture is just equal to the *burning velocity* of the mixture. This fundamental parameter is defined as the velocity with which a premixed flame moves normal to its surface through the adjacent unburnt mixture. While a flat flame can only be stabilized over a narrow range of flow velocities, a conical flame can be established over a much wider range of flows, as the area of the inner cone can change to maintain the balance between the burning velocity and the flow velocity normal to the flame front. A typical flow pattern and temperature distribution in such a flame is shown in Figure 1-9.2.[2]

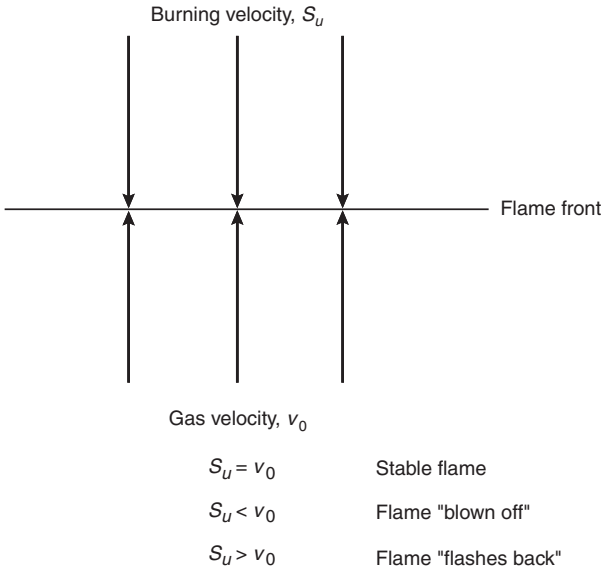

Figure 1-9.1. ***Diagrammatic representation of a flat premixed flame.***

The maximum temperature in the flame is usually reached a little downstream of the inner cone. If the flame is sufficiently large, the adiabatic flame temperature is reached in the middle part of the gas stream; thus, with the temperature distribution given in Figure 1-9.2, the calculated adiabatic flame temperature is nearly reached just

Dr. Robert F. Simmons has a Ph.D. in physical chemistry and his major research interests have centered around flame propagation, the chemistry of combustion reactions, and industrial safety. Until his retirement, he was a senior lecturer in chemistry at the University of Manchester Institute of Science and Technology, and he served as deputy editor of *Combustion and Flame.*

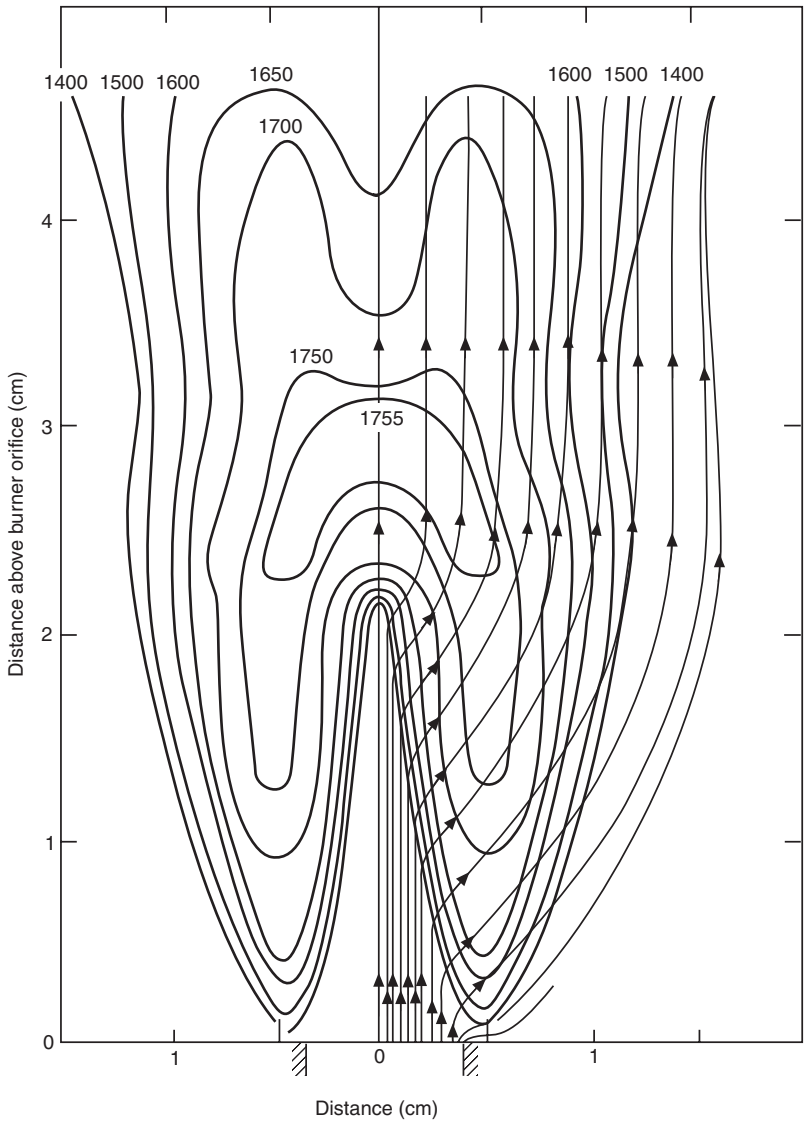

Figure 1-9.2. ***Temperature distribution and flow pattern in a premixed flame (7.5 percent natural gas and air burning on a rectangular burner 0.755 × 2.19 cm). The quoted temperatures are °C.[2]***

above the inner cone of the flame. Toward the outside of the flame, however, heat losses lead to a steep temperature gradient between the combustion products and surroundings. This *adiabatic flame temperature* is given by the balance between the heat released in the combustion reaction (ΔH_r^θ) at the initial temperature of the reactants (T_i) and the heat required to raise the temperature of the products to the final flame temperature (T_f), that is,

$$\Delta H_r^\theta = \int_{T_i}^{T_f} C_p \, dT$$

where C_p is the heat capacity of the combustion products. This calculation assumes that heat losses from the flame by radiation, thermal conduction, or diffusion to a wall can be neglected. Thus, small premixed flames and turbulent flames of all kinds normally fail to reach their adiabatic flame temperature as the heat loss from such flames is appreciable.

Calculation of the adiabatic flame temperature always assumes chemical equilibrium has been reached in the burnt gas. For lean flames with a relatively low adiabatic flame temperature, the calculation is relatively straightforward, in that the combustion products are given by the simple stoichiometry for the overall combustion process, but for temperatures above 1800 K allowance must be made for the heat used up in the dissociation of carbon dioxide, steam, oxygen, and so

forth. However, the composition of the products can only be calculated if the temperature is known, and the temperature depends on this composition. As a result, a method of successive approximations must be employed in the calculation, and this can most conveniently be done using a computer program, such as NASA SP-273.[3] Although the adiabatic flame temperature is only reached in a restricted region of a large premixed flame, it is a useful combustion parameter and especially useful in the calculation of limits of flammability. (See Section 1, Chapter 5, "Thermochemistry.")

All experimental determinations of burning velocity involve measuring the area of the flame front for a particular flow of unburnt mixture. Much of the discrepancy between different determinations can be ascribed to the method used to specify the position of the flame front; further, when burner flames have been used there is also the complication of quenching near the burner rim and the increase in burning velocity near the tip of the cone (because the heat flow in this region is strongly convergent). For example, the maximum values reported for the laminar burning velocity of propane-air mixtures mainly lie between 37 and 45 $cm \cdot s^{-1}$, but the majority of the values lie in the range of 41 ± 2 $cm \cdot s^{-1}$. All the saturated hydrocarbons have about the same maximum burning velocity, and Table 1-9.1 lists the maximum values for some other fuel-oxidant combinations.

The values in Table 1-9.1 refer to initial conditions of room temperature and atmospheric pressure. In general, hotter flames have higher burning velocities, and thus increasing the initial temperature of the mixture increases the burning velocity. For example, when the initial temperature of propane-air mixtures is increased from 300 to 480 K, the maximum burning velocity doubles.[4] The effect of pressure on burning velocity is simple and is frequently expressed as a simple power law

$$\frac{S_{u,a}}{S_{u,b}} = \left(\frac{p_a}{p_b}\right)^n \tag{1}$$

where $S_{u,a}$ and $S_{u,b}$ are the burning velocities with respect to the unburnt gas at pressures p_a and p_b, respectively, and n is a constant for the flame. Values of n have been reported for a number of flames ranging from 0.25 (for hot flames with oxygen as the oxidant) to -0.33 (for cooler flames supported by air).[5]

Table 1-9.1 ***Maximum Burning Velocities for Laminar Fuel-Oxidant Mixtures***

Mixture	Maximum Burning Velocity S_u/cm·s^{-1}	Reference
Propane-air	41	1
Ethene-air	68	1
Acetylene-air	175	1
Hydrogen-air	320	6
Propane-oxygen	360	7
Acetylene-oxygen	1120	6
Hydrogen-oxygen	1180	6

Another factor that affects the burning velocity is the degree of turbulence in the flame. In laminar flames the flow lines in any given volume are parallel, but for turbulent flow the velocities have components normal to the average flow direction. The state of flow is usually characterized in terms of the Reynolds number (Re) which is the dimensionless quantity

$$\mathrm{Re} = \frac{vd\rho}{\eta} \tag{2}$$

where

v = average gas velocity

d = diameter of the tube

ρ = density of the gas stream

η = viscosity of the gas stream

For $\mathrm{Re} < 2300$ the flow is always laminar, and for $\mathrm{Re} > 3200$ it is usually turbulent.[8] In the intermediate region the flow alternates between laminar and turbulent flow, the periods of each depending on whether Re is nearer the lower or higher value.

When the flow is laminar the flame front is sharply defined, but as the Reynolds number of the flow increases the flame front becomes progressively more and more blurred, so that the whole volume in which the primary reaction occurs has the appearance of a "brush." This arises because of the fluctuations in the local gas velocity. At points where the velocity is high the flame front moves away from the burner, while in regions of low velocity it moves toward the burner. Thus, the net effect of turbulence is to increase the effective area of the flame front, with a resulting increase in burning velocity. For example, with propane-air, ethene-air, and acetylene-air flames, the burning velocity approximately doubles as the Reynolds number is increased to 40,000.[9] A theoretical treatment of turbulent combustion suggests that the burning velocity can increase by a factor of five when the degree of turbulence in the flow is very high.[10]

The above discussion has been concerned with stationary flames burning on a burner; but if the local flow velocity in a tube or duct is too low to sustain a stationary flame, the flame propagates through the incident mixture provided it is flammable, that is, its composition lies within the *limits of flammability.* These are the limits of composition over which a self-sustaining flame can propagate and, as such, they are important parameters in any consideration of the fire and explosion risk associated with a particular fuel-oxidant system. They are normally measured for upward propagation of the flame (since this gives the widest limits) in a tube sufficiently wide to minimize quenching effects and sufficiently long to ensure that it is the self-propagation of the flame that is being studied, that is, the measured limits are independent of the energy input from the ignition source. The dimensions of the tube are typically 100-cm long × 5-cm inside diameter (ID); this is quite satisfactory for hydrocarbon fuels, but a larger diameter is necessary for fuels, such as ethyl chloride, that have a large quenching distance.[11]

It should be noted that if burning occurs in a closed vessel, the resulting temperature rise produces a corre-

sponding rise in pressure. For example, a stoichiometric hydrocarbon-air mixture at an initial temperature of 300 K has an adiabatic flame temperature of about 2200 K, so that the pressure can reach a little over 7 bar under adiabatic conditions. In practice, the maximum pressure is likely to be somewhat lower because of heat loss to the walls of the vessel; but unless the vessel has been designed to withstand such pressures it will rupture explosively. The situation is further complicated if connected vessels are involved, as burning in one vessel leads to an increased pressure in the connected vessel; if the flame then propagates into this second vessel, a correspondingly higher pressure is produced.

These limits of flammability widen as the temperature increases, but at sufficiently low temperatures the flammable range is limited by the vapor pressure of the liquid fuel, as shown in Figure 1-9.3. It follows that the *flash point* is the temperature at which the vapor pressure is just sufficient to give a lean limit mixture of the fuel vapor in air. However, a somewhat higher temperature (the *fire point*) is needed before the fuel is ignited by the burning gas above the surface of the material. At sufficiently high temperatures autoignition occurs and the minimum temperature at which this can happen is termed the *autoignition temperature.* (See Section 2, Chapter 8, "Ignition of Liquid Fuels.") Although the flame in a real fire is essentially a diffusion flame (addressed later in this chapter), the initial ignition of the combustible material, whether liquid or solid, involves the ignition of a mixture of fuel vapor and air in the boundary layer above its surface.

If the flame tries to propagate through a gap that is too small it is quenched. These limiting distances are usually measured using spark ignition at the center of a pair of parallel plates[12] or a rectangular burner,[13] and the *quenching distance* is the maximum distance that will just prevent the propagation of a flame through any mixture of the fuel-oxidant mixture. The quenching is probably due to a combination of heat loss to the walls and the removal of free radicals which are important for the propagation of the flame. These quenching effects are utilized in flame traps, but here it is also necessary that any hot gas forced through the trap must be sufficiently cooled so that it does not ignite any flammable mixture present on the other side.

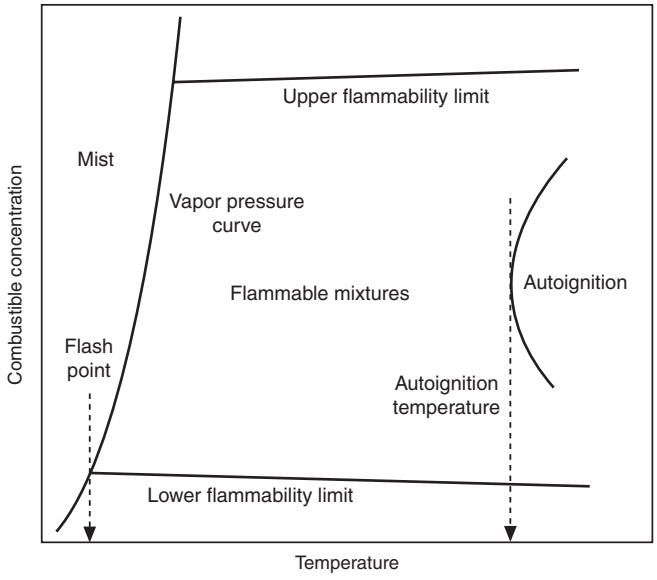

Figure 1-9.3. ***Effect of temperature on the limits of flammability of a combustible vapor in air at a constant initial pressure.[14]***

A flame propagating along a duct away from an opening usually proceeds, at first, at a fairly uniform speed which is controlled by the burning velocity of the mixture and the area of the flame front. This linear velocity, *V,* is related to the burning velocity through the relation

$$V = \frac{S_u A_f}{A_d} \tag{3}$$

where A_f and A_d are the areas of the flame front and the cross section of the duct, respectively. Since A_f is always greater than A_d (typically by a factor of two or three), it follows that the linear velocity of the flame is correspondingly larger than the burning velocity. This distinction is important when the design of automatic protection is considered.

If the hot combustion products cannot vent to maintain an approximately constant pressure in the system, they force the flame and the unburnt gases forward with increasing velocity. In turn, this induces increased turbulence ahead of the flame front with a consequential further increase in burning velocity. If the duct is sufficiently long and the resulting acceleration is sufficiently rapid, the flame front acts as an accelerating piston and a shock wave is formed ahead of the flame front. Under such conditions, the flame becomes a detonation propagating at supersonic velocity, typically between 1500 and 3000 m s^{-1}.[15] For gases initially at atmospheric pressure, the pressure immediately behind the detonation can be up to 20 bar, and up to 100 bar if it is reflected from the end of the duct. As a result, detonations are much more destructive than a propagating premixed flame.

Mechanism of Flame Propagation

The preceding discussion has been concerned with phenomena associated with the propagation of the flame and, while these are important from the practical viewpoint, they give no insight into how the flame propagates from one layer of gaseous mixture to the next. Such insight comes from using the continuity equations for flame propagation in a laminar flow[16] and, for convenience and simplicity, the following discussion is based on the equations for a flat flame.

First, there must be *conservation of mass* through the flame, so that

$$\rho v A = \rho_0 v_0 A_0 = M \tag{4}$$

where

ρ = density
v = gas velocity
A = cross-sectional area of the gas flow
M = mass burning rate (mass per unit time)

Conservation of energy requires that the heat conducted into a gaseous element of the flame plus the heat liberated by chemical reaction within the element is used up in raising its temperature, that is,

$$\frac{d(k \cdot dT/dz)}{dz} + Q \cdot R - \frac{d(c_p \cdot T \cdot \rho \cdot v)}{dz} = 0 \qquad (5)$$

where

k = thermal conductivity of the mixture
c_p = heat capacity
T = temperature at distance z
Q = heat of reaction
R = rate of reaction

There must also be *conservation of the individual atomic species* through the flame; that is, for a given chemical species i there must be a balance between its rate of production (or removal) in a given element of the flame and its transport by diffusion and convection. Thus,

$$R_i + \frac{d(D_i \cdot dn_i/dz)}{dz} - \frac{d(n_i \cdot v)}{dz} = 0 \qquad (6)$$

where D_i is its diffusion coefficient, and n_i its concentration. Equation 6 leads to the following expression for the rate of reaction of species i

$$R_i = \left(\frac{\rho_0 v_0}{M_i}\right)\left(\frac{dG_i}{dz}\right) \qquad (7)$$

where

M_i = molecular weight of species i
V_i = diffusion velocity
G_i = mass flux fraction

The latter is given by

$$G_i = \frac{M_i(v + V_i)}{v}$$

where the diffusion velocity, V_i is given by

$$V_i = \frac{-D_i}{X_i}\left(\frac{dX_i}{dz}\right) \qquad (8)$$

In principle, Equations 4 through 6 can be solved to give the burning velocity (v_0), plus the composition and temperature profiles through the flame, but it will be obvious that a detailed reaction mechanism is needed before this can be done. Dixon-Lewis has used the established mechanism for the hydrogen-oxygen reaction to do this for hydrogen-air flames,[17] and similar calculations have been carried out for other hydrocarbon-air flames, such as those presented by Warnatz[18]; such numerical computations for the structure of one-dimensional flames have now become quite commonplace.[19]

The present detailed understanding of the important chemical processes occurring in a premixed flame has come from an analysis of the experimental temperature and concentration profiles through a flat flame; some typical results for a lean propane-oxygen-argon flame are given in Figure 1-9.4.[20] Such analyses show that the flame can be divided up into a number of distinct regions, as shown at the top of Figure 1-9.4. In the initial *pre-heating zone* the temperature rise is that expected from conduction of heat back from the hotter parts of the flame, and chemical reaction does not start until the temperature has reached about 700 K. There is some depletion of fuel at lower temperatures than this, but it is the result of its forward diffusion to a higher temperature region of the flame and not chemical reaction. Similarly, there is back-diffusion of carbon monoxide, carbon dioxide, and water vapor into this region of the flame.

The reaction in the *primary reaction zone* is induced by the diffusion of free radical species, X, back from the hotter parts of the flame. These react with the fuel to give alkyl radicals in reaction (1). At the start of the primary reaction zone in lean flames, X is probably mainly the hydroxyl radical,[20] but in rich flames the hydrogen atom is likely to be the predominant species. It should be noted that the reaction of these alkyl radicals with oxygen is not important in flames,[21] and there is direct experimental evidence that octyl radicals (for example) break down into smaller fragments (mainly C_1 and C_2) in this region of the flame.[22] In the case of propane, both n-propyl and sec-propyl radicals are formed in reaction (1), and these react by reactions (2) and (3), respectively.

$$X + C_3H_8 = HX + C_3H_7 \qquad (R1)$$

$$n - C_3H_7 = C_3H_6 + H \qquad (R2)$$

$$sec - C_3H_7 = CH_3 + C_2H_4 \qquad (R3)$$

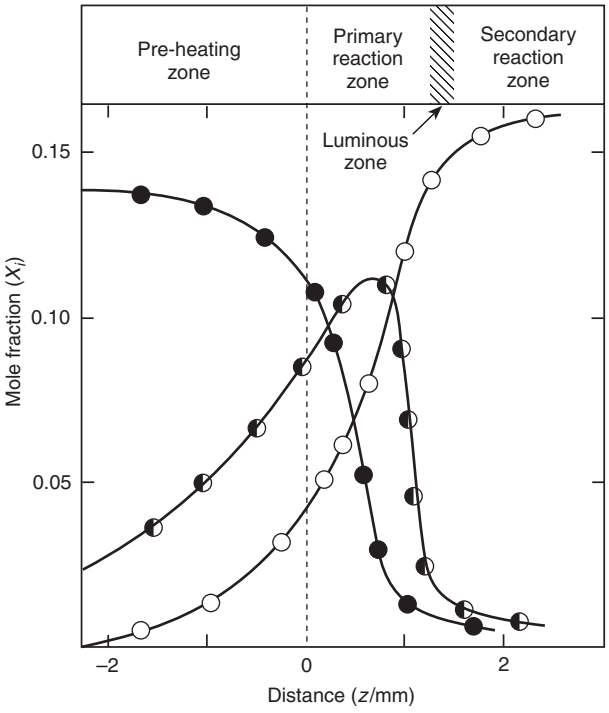

Figure 1-9.4. ***Typical composition profiles through a flat propane-oxygen-argon flame (1.38 percent propane; O_2:Ar = 15.85). Note: ⊙ 4 × CO_2; ● 10 × C_3H_8; ◐ 10 × CO.***[20]

Typical reaction rate profiles are given in Figure 1-9.5. This shows that the maximum rate of removal of propane and the maximum rate of formation of carbon monoxide both occur at about the same temperature (1160 K), and, at this temperature, about 90 percent of the original propane has been consumed. In this region of the flame, the ratio $R_{CO} + R_{CO_2}/-R_{C_3H_8}$ has a value of 3.1, which is reasonably close to the expected value of 3.0; such simple checks give confidence that the analysis of the experimental data is essentially correct. A detailed discussion of the chemistry involved in the formation of carbon monoxide from the hydrocarbon fragments is inappropriate for the present purposes, but it is generally agreed that one very important route is *via* the reaction of methyl radicals with oxygen atoms. This produces formaldehyde, which subsequently gives carbon monoxide by reactions such as (5) and (6).

$$CH_3 + O = HCHO + H \quad \text{(R4)}$$

$$X + HCHO = HX + CHO \quad \text{(R5)}$$

$$CHO = H + CO \quad \text{(R6)}$$

$$OH + CO = CO_2 + H \quad \text{(R7)}$$

Figure 1-9.5 shows that there is significant conversion of carbon monoxide to carbon dioxide in the primary reaction zone of lean flames, and this arises through reaction (7). Many researchers have used the experimentally measured rate of this formation in conjunction with the experimental local concentration and temperature (and, hence, known rate constant),[23] to derive a mole fraction profile for hydroxyl radicals. Such a profile is shown in Figure 1-9.6, together with the profile obtained for lower temperatures, assuming the removal of propane is due solely to its reaction with hydroxyl radicals. While the two profiles cover different parts of the flame, they are in excellent agreement where they overlap. A further indication that the removal of propane is *via* reaction with hydroxyl radicals comes from the temperature dependence of the rate of heat release in the early part of the flame; this is about 10 kJ mol^{-1}, which is close to that expected for the reaction of propane and hydroxyl radicals and much less than that expected for the reaction of propane with either hydrogen atoms or HO_2 radicals (37 and 78 kJ mol^{-1}, respectively). It must be stressed, however, that this conclusion comes from the analysis of data for very lean flames and that reaction with hydrogen atoms will become increasingly important as the mole fraction of propane in the initial mixture increases.

$$H + O_2 = OH + O \quad \text{(R8)}$$

$$H + O_2 + M = HO_2 + M \quad \text{(R9)}$$

Figure 1-9.5 shows that the maximum rate of removal of oxygen occurs somewhat later in the flame (at 1280 K) than the maximum rate of removal of propane (1160 K). It is instructive to examine the relative rates of reaction of hydrogen atoms with oxygen through the preheating and primary reaction zones of the flame. (See Table 1-9.2.) It can

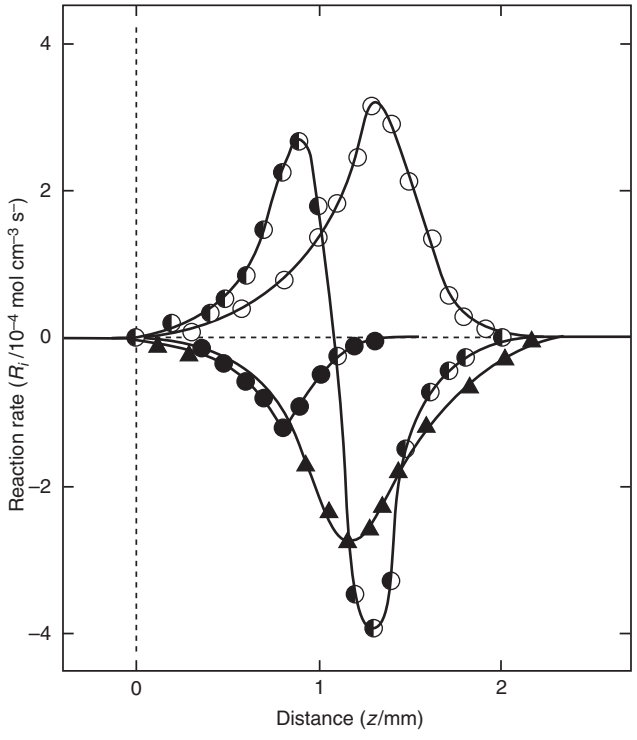

Figure 1-9.5. ***Reaction rate profiles through the flame of Figure 1-9.4. Note: ● C_3H_8; ▲ O_2; ◐ CO; ⊙ CO_2.[20]***

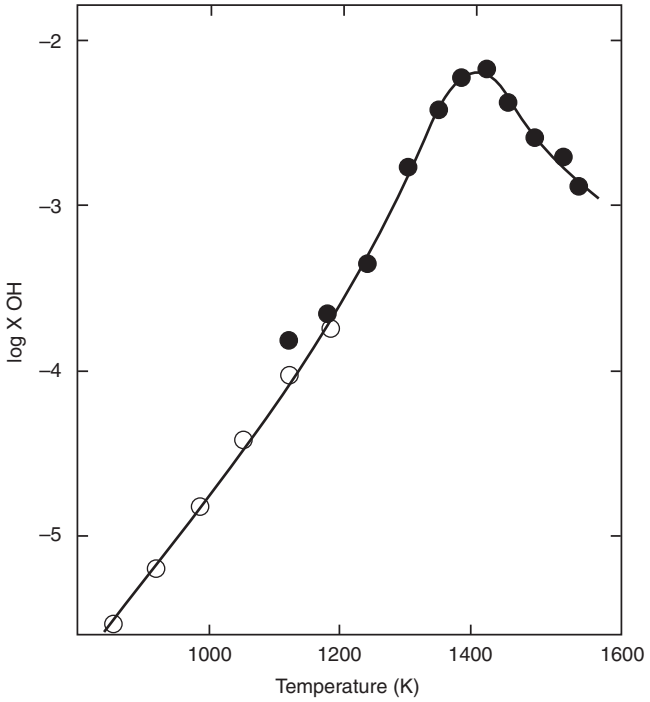

Figure 1-9.6. ***Variation in X_{OH} with temperature through the flame of Figure 1-9.4. Note: ● from R_{CO_2}; ⊙ from $-R_{C_3H_8}$.[20]***

Table 1-9.2 ***Relative Rates of Reaction of Hydrogen Atoms with Oxygen and Propane through a Premixed Propane-Oxygen-Argon Flame***

Initial mixture composition: 1.38 percent C_3H_8, 14.8 percent O_2, 83.82 percent Ar

Temp (K)	R_{H+O_2+M}/R_{H+O_2}	$R_{H+C_3H_8}/R_{H+O_2}$
600	450	38
800	12	7.5
1000	1.2	1.5
1200	0.25	0.4

k_{H+O_2} and k_{H+O_2+M} have been taken from Baulch et al.[24]
$k_{H+C_3H_8}$ has been taken from Walker.[25]

be seen that, at the lower temperatures, the termolecular reaction (9) predominates over the branching reaction (8); however, as the temperature rises above 1000 K, reaction (8) becomes increasingly important. Similarly, Table 1-9.2 also shows that, between 1000 and 1200 K, reaction (8) becomes faster than the removal of hydrogen atoms by reaction with propane. As a result, there is a rapid increase in the concentration of free atoms and radicals, that is, chain centers, toward the end of the primary reaction zone, so that the expected thermal equilibrium level can be exceeded by more than an order of magnitude.[26]

This rapid increase is in accordance with chain reaction theory.[27] This shows that, with a reaction involving linearly branched chains and linear chain termination, there is an exponential increase in the concentration of chain centers, even under isothermal conditions, as soon as the rate of chain branching exceeds the rate of chain termination. The situation is more complicated in the case of a hydrocarbon-air flame, as there has already been a major consumption of reactants by the time the branching reaction (8) becomes important. This consumption limits the concentration of chain centers, as shown in Figure A-1-9.1. In principle, another limiting factor to the growth in the concentration of chain centers in the flame is the occurrence of quadratic termination processes, such as reaction (10), which are known to be important in the secondary reaction zone of the flame. A combination of linearly branched chains and quadratic termination must lead to a stationary-state concentration.

$$H + OH + M = H_2O + M \qquad \text{(R10)}$$

This high concentration of chain centers produces the luminous flame front, that is, the characteristic inner cone of the Bunsen burner flame. The radiation from this region of the flame includes that from electronically excited hydroxyl radicals, which are believed to be formed partly by radical-radical reactions, such as reactions (11) and (12), and partly by reaction (13).[1]

$$O + H = OH^* \qquad \text{(R11)}$$

$$H + OH + OH = OH^* + H_2O \qquad \text{(R12)}$$

$$CH + O_2 = CO + OH^* \qquad \text{(R13)}$$

At this point in the flame all the fuel has effectively been consumed, some of the resulting carbon monoxide has been converted to carbon dioxide, and the radical concentration exceeds the corresponding thermal equilibrium level. Thus, in the *secondary reaction zone,* the important processes are the conversion of the major part of the carbon monoxide to carbon dioxide plus the decay in the concentration of radical species by recombination reactions. This leads to a further, but slower, rise in temperature until the final thermodynamic equilibrium has been reached with the burnt gas at the final flame temperature.

$$CH_4 + 2O_2 = CO_2 + H_2 + H_2O \qquad \text{(R14)}$$

$$CO + H_2O = CO_2 + H_2 \qquad \text{(R15)}$$

$$O_2 + 2H_2 = 2H_2O \qquad \text{(R16)}$$

The detailed computations for a one-dimensional laminar flame structure typically involve more than 120 elementary reaction steps for even simple hydrocarbon fuels; with more realistic fuels, the potential number can become very large. While this is practicable for such systems, it is out of the question for many engineering applications where three-dimensional and time-dependent effects arise (e.g., turbulent flames). Here, a substantial reduction in the number of reaction steps is needed before inclusion of the chemistry in the computations becomes practicable. The early attempts at producing a simplified global reaction scheme involved adjusting rate coefficients and reaction orders to fit the experimental observations, but this has too many unsatisfactory aspects. A much more satisfactory approach involves the systematic use of steady-state and partial-equilibrium approximations to reduce the number of independent reaction steps.[28] Under these circumstances, the rate constants for these global reaction steps can be expressed as a combination of the known rate constants of elementary reactions. For example, Peters and Williams have shown that the three-step mechanism comprising reactions (14) through (16) gives a good representation of a stoichiometric methane-air flame burning at atmospheric pressure and above.[28] Similar mechanisms have also been derived for methanol and propane flames.[29]

Effect of Additives on Flame Propagation

When inert diluents such as nitrogen, argon, and carbon dioxide are introduced into a premixed flame, they reduce the final flame temperature and, if the corresponding reduction in burning velocity is sufficiently large, the flame is extinguished. The limits of flammability data for propane[30] in Figure 1-9.7 show that the "peak" concentration of nitrogen is quite high [about 43 percent (by vol)], so that the oxygen content of an air-nitrogen mixture must be reduced to below 12 percent to ensure that no mixture of propane and air will burn. For such systems, the adiabatic flame temperature at the limit of flammability is not only remarkably constant, but this temperature is effectively the same all around the limit curve, so that the additive must act only as a diluent.

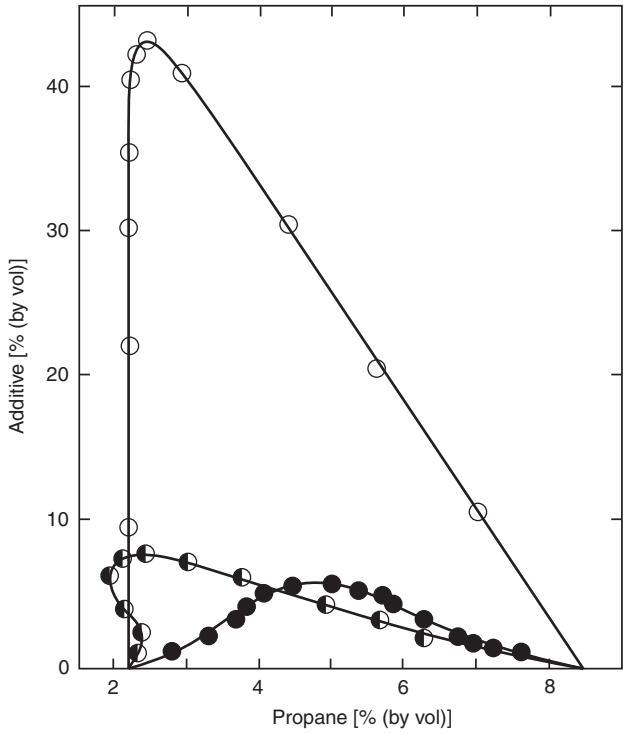

Figure 1-9.7. ***Effect of nitrogen, hydrogen bromide, and methyl bromide on the limits of flammability of propane in air (pressure 380 mmHg). Note: ⊙ N_2; ● HBr; ◐ CH_3Br.***

Hydrogen chloride must also act predominantly as an inert diluent as its effect on the limits of flammability of hydrogen-air mixtures is almost identical to that of nitrogen.[31] This arises because although the formation of chlorine atoms by reaction (17) is fast, the subsequent abstraction of a hydrogen atom by reaction (18) is also fast. However, the effective equilibrium position lies over on the side of hydrogen chloride, so that even though the additive is involved chemically, it has no overall chemical effect on the combustion process.

$$X + HCl = HX + Cl \quad \text{(R17)}$$

$$Cl + RH = HCl + R \quad \text{(R18)}$$

In contrast, bromine compounds are much more effective than the inert diluents in preventing flame propagation as they act as chemical inhibitors.[32,33] (See Figure 1-9.7.) Even a trace amount of such compounds in a premixed flame markedly reduces its burning velocity, and it is particularly striking that when sufficient compound has been added to extinguish a stoichiometric hydrocarbon-air flame, the adiabatic flame temperature of the resulting limit mixture is only slightly lower than that in its absence.[32] The action of such inhibitors can be illustrated by considering the action of hydrogen bromide in a hydrogen flame.[34] In this case, hydrogen atoms are removed by reaction (19) in preference to reacting in the chain branching reaction (8), so that the reactive hydrogen atoms are converted into relatively unreactive bromine atoms. Computations show that apart from in the very early stages of the flame, reactions (19) and (20) are effectively in equilibrium locally, with the equilibrium lying over on the side of bromine atoms. This produces some reduction in burning velocity, but it does not explain quantitatively the observed results. The inclusion of an additional chain-termination step, such as reaction (21), is required so that the rate of chain termination is increased relative to the rate of chain branching, in accord with the theory of chain reactions. (See Appendix A to this chapter.)

$$H + O_2 = OH + O \quad \text{(R8)}$$

$$H + HBr = H_2 + Br \quad \text{(R19)}$$

$$H + Br_2 = HBr + Br \quad \text{(R20)}$$

$$Br + Br + M = Br_2 + M \quad \text{(R21)}$$

Application to "Real" Fires

A basic understanding of premixed burning is an important prerequisite in a number of applications concerning "real fires," even though the latter are essentially diffusion flames by nature. In such systems, the rate-controlling process is normally the diffusion of fuel and oxygen from their respective sides of the flame and not the rate of chemical reaction (1) and, in the case of a jet of fuel gas burning in air, the stability of the flame depends on the burning of a pocket of premixed gas at the base of the flame. Immediately above the burner rim there is a region where the gas velocity is low and where the fuel and air mix; it is a combination of the burning velocity of this mixture and the local gas velocity that determines whether the diffusion flame is stable or is "blown off." Similarly, diffusion flames can be stabilized behind an obstruction in a gas stream, since the recirculation zone behind the obstruction produces a region of low gas velocity. Such stabilization has important practical implications concerning the extinction of fires where the source of the fuel lies behind an obstruction, since such flames can be highly stable.[35]

In a diffusion flame, the fuel and oxidant react overall in stoichiometric proportions, but the local stoichiometric ratio ranges from very fuel rich in the yellow carbon zone to excess oxygen in the hot blue zone on the air side of the flame. The basic chemistry of the combustion process in a hydrocarbon-air diffusion flame is essentially the same as in a premixed flame, but the detailed mechanism reflects the change in local conditions across the flame. Thus, on the fuel side of the flame, thermal decomposition reactions are the most important processes and, owing to the lack of oxygen in this region, this leads to carbon formation and the characteristic yellow color associated with such flames. The maximum temperature is reached in the main reaction zone on the air side of the flame. The oxygen consumption occurs mainly on the air side of this zone by reaction (8),[36] and diffusion of the resulting hydroxyl radicals toward the rich side of the flame leads to the conversion of carbon monoxide to carbon

dioxide by reaction (7). Since this latter reaction produces hydrogen atoms, reactions (7) and (8) constitute a self-sustaining sequence for this part of the combustion process. In addition, reaction (8) is also the source of the oxygen atoms required for the formation of carbon monoxide by reactions (4) through (6).

$$OH + CO = CO_2 + H \quad (R7)$$

$$H + O_2 = OH + O \quad (R8)$$

$$H + H_2O = H_2 + OH \quad (R22)$$

Many researchers have assumed that a state of quasi-equilibrium exists in the main reaction zone of a diffusion flame, but this is strictly true only for a limited region of the flame. For example, Mitchell et al. have shown that the water-gas reaction ($CO + H_2 = CO_2 + H_2$) approaches equilibrium on the fuel side of the main reaction zone of a methane-air flame, which implies that reactions (7) and (22) are effectively balanced in this part of the flame.[37] Similarly, comparison of experimental data for a propane flame with that expected from thermodynamic equilibrium shows that the situation is close to equilibrium around the stoichiometric plane of the flame.[36] On the rich side of the flame, however, the carbon dioxide and water vapor levels exceed their thermodynamic equilibrium values while the carbon monoxide level is much lower. On the air side, the conversion of carbon monoxide to carbon dioxide has not reached complete equilibrium. The final "burnout" of carbon monoxide to carbon dioxide on the air side of the flame is effectively stopped when the temperature falls below 1250 K provided a critical temperature gradient is also exceeded.[38] Since this conversion occurs by reaction (7), this quenching must reflect a correspondingly sharp drop in the concentration of hydroxyl radicals, as it has a low-temperature dependence with an activation energy of only 3 kJ mol^{-1}.[23]

As far as the elementary reactions are concerned, Bilger et al. has shown that reactions (23) and (24) are effectively balanced on the fuel side of a methane-air diffusion flame, and that reactions (8), (25), and (26) only approach equilibrium in a very narrow region of the flame.[39]

$$CH_4 + H = CH_3 + H_2 \quad (R23)$$

$$H + H_2O = H_2 + OH \quad (R24)$$

$$O + H_2O = 2OH \quad (R25)$$

$$O + H_2 = OH + H \quad (R26)$$

This lack of equilibrium is much more pronounced in turbulent diffusion flames, where it has long been recognized as a problem in the modeling of such systems from first principles. With "real fires" there is the added complication of the feedback mechanism responsible for the growth of the fire. Such modeling involves a highly complex interaction of chemistry, heat transfer, and fluid dynamics and, to date, such simulations have effectively ignored the chemistry by either concentrating on the steady-state situation or assuming an exponential rate of growth for the fire as observed experimentally. Since the flow is usually dominated by buoyancy, the rate of mixing (and, hence, chemical reaction) is controlled by the resulting turbulent motion. If it is also assumed that chemical equilibrium exists through the flame, the problem reduces to the solution of the classical equations for conservation of mass, momentum, heat, and species to obtain gas velocities and temperatures for discrete points in space and moments in time.

One promising way of avoiding the equilibrium assumption is the use of laminar flamelets, in which a given microscopic element in the turbulent flow is assumed to have the same composition as an element of the same overall stoichiometry in a laminar flame.[40,41] The advantage of this approach can be seen from the predictions for carbon monoxide for a turbulent methane-air diffusion flame; when thermodynamic equilibrium was assumed the peak mole fraction of carbon monoxide was about 2.5 times that observed experimentally, whereas when the laminar flamelet approach was used the agreement was within 10 percent.[42] Lack of appropriate experimental data may restrict the use of this approach, however, unless it can be shown experimentally that essentially the same variation in composition with stoichiometry is obtained for a range of fuels.

$$CH_4 + 2H + H_2O = CO + 4H_2 \quad (R27)$$

$$CO + H_2O = CO_2 + H_2 \quad (R15)$$

$$O_2 + 2H_2 = 2H_2O \quad (R16)$$

$$O_2 + 3H_2 = 2H + 2H_2O \quad (R28)$$

An alternative approach is to simplify the chemical component of the computation by using a reduced reaction mechanism.[38,43] Full calculations for a laminar methane-air diffusion flame shows that the steady-state approximation can be applied to the species

$$OH, O, HO_2, CH_3, CH_2O, \text{ and } CHO$$

Using this approximation enables the full mechanism to be reduced to four global reaction steps, for example,[39] reactions (27), (15), (16), and (28), whose rate can be represented by a combination of the rates of individual elementary reactions. The computational advantage of this approach comes from reducing the number of chemical species, since it is the number of species rather than the number of reaction steps that determines the complexity of the calculations.

Appendix A
Mathematical Treatment of Branching Chain Reactions

Linearly Branched Chains with Linear Gas-Phase Termination under Isothermal Conditions

With such a system, the rate of change of radical concentration can be represented by an equation of the form

$$\frac{dn}{dt} = \theta + fn - gn \quad \text{(A1)}$$

where

n = radical concentration
θ = rate of chain initiation
f = coefficient of linear branching
g = coefficient of linear termination

The classic example of such a system is the thermal reaction between hydrogen and oxygen, where the second explosion limit is controlled by a competition between the reactions

$$H + O_2 = OH + O \quad \text{(R8)}$$

$$H + O_2 + M = HO_2 + M \quad \text{(R9)}$$

In this case: $n = [H]$, $f = k_2[O_2]$, and $g = k_3[O_2][M]$, where i represents the concentration of species i.

Three cases can be distinguished:

1. $g > f$

In this case the rate of chain termination is greater than the rate of chain branching, and integration of Equation A1 gives

$$n = \frac{\theta}{(f-g)} \cdot [1 - \exp^{-(g-f)\cdot t}] \quad \text{(A2)}$$

When t is large $\exp^{-(g-f)\cdot t}$ approaches zero, so that n tends to the stationary state value

$$n = \frac{\theta}{(g-f)} \quad \text{(A3)}$$

2. $f = g$

In this case n increases linearly with time, that is,

$$n = \theta \cdot t \quad \text{(A4)}$$

3. $f > g$

In this case the rate of chain branching is always greater than the rate of chain termination, and so n grows exponentially with time. Integration of Equation A1 gives

$$n = \frac{\theta}{(f-g)} \cdot [\exp^{(f-g)\cdot t} - 1]$$

These three cases are represented graphically in Figure A-1-9.1 and, in the latter case, the exponential increase in the radical concentration must lead to explosion unless this is prevented by consumption of reactants.

In the case of the hydrogen-oxygen reaction, where the hydrogen atom is the slowest reacting species, it has been shown that the ratios [H]/[OH] and [H]/[O] maintain their stationary-state values even during the exponential growth in radical concentration which leads to explosion. As a result, with such systems the usual practice is to consider the change in concentration of the slowest reacting species and assume that the concentration of all other species is the corresponding stationary-state value.

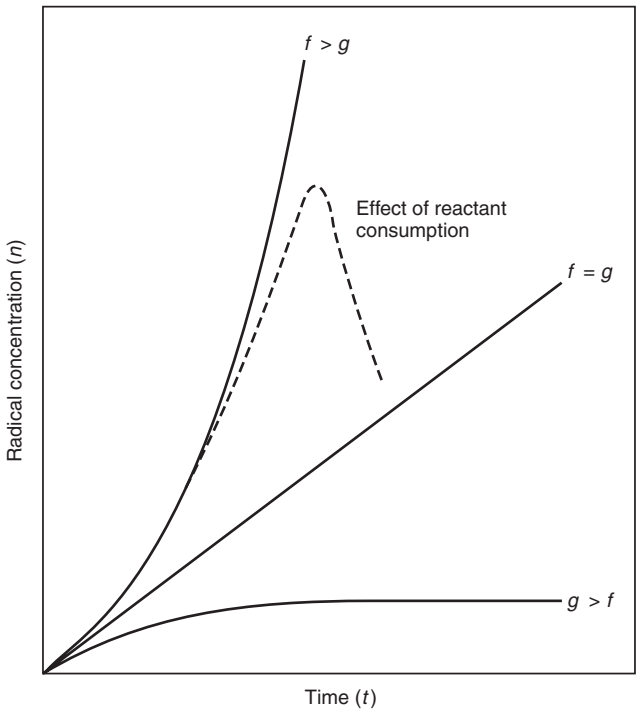

Figure A-1-9.1. ***Growth of free radical concentration, n, with time, t, in a linearly branched and terminated reaction. Boundary condition between a steady-state and exponential growth is f = g.***

References Cited

1. A.G. Gaydon and H.G. Wolfhard, *Flames: Their Structure, Radiation, and Temperature,* 4th ed., Chapman and Hall, London (1979).
2. B. Lewis and G. von Elbe, *Combustion, Flames, and Explosions of Gases,* 2nd ed., Academic Press, New York, p. 280 (1961).
3. S. Gordon and B.J. McBride, *NASA SP-273* (1971).
4. B. Lewis, *Selected Combustion Problems,* Butterworth, London, p. 177 (1954).
5. G.L. Dugger and S. Heimel, Data reported in Ref 1, *NACA Tech. Note 2624,* p. 82 (1952).
6. E. Bartholome, *Z. Elektrochem,* 54, p. 165 (1950).
7. J.M. Singer, J. Grumer, and E.B. Cook, Data reported in Ref 2, *Proc. Gas Dynamics Symposium on Aerothermochemistry*, p. 390 (1956).
8. H. Mache, *Forsch. Ing. Wes.*, 14, p. 77 (1943).
9. D.T. Williams and L.M. Bollinger, *Third Symposium on Combustion, Flames, and Explosion Phenomena,* Williams and Wilkins, Baltimore, p. 176 (1949).
10. B. Karlovitz, D.W. Denniston, and F.E. Wells, *J. Chem. Phys.*, 19, p. 541 (1951).
11. H.F. Coward and G.W. Jones, *Bulletin 503,* U.S. Bureau of Mines (1952).
12. M.V. Blanc, P.G. Guest, B. Lewis, and G. von Elbe, *J. Chem. Phys.*, 15, p. 798 (1947).
13. R. Freidman, *3rd Symposium on Combustion, Flames, and Explosion Phenomena,* Williams and Wilkins, Baltimore, p. 110 (1949).
14. M.G. Zabetakis, *Bulletin 627,* U.S. Bureau of Mines (1964).

15. B. Lewis and G. von Elbe, *Combustion, Flames, and Explosions of Gases,* 2nd ed., Academic Press, New York, p. 511 ff (1961).
16. R.M. Fristrom and A.A. Westenberg, *Flame Structure,* McGraw-Hill, New York (1965).
17. G. Dixon-Lewis, *Phil. Trans. Roy. Soc.,* A292, p. 45 (1979).
18. J. Warnatz, *Eighteenth Symposium on Combustion,* Combustion Institute, Pittsburgh, PA, p. 369 (1981).
19. N. Peters and J. Warantz (eds.), *Numerical Methods in Laminar Flame Propagation,* Vieweg, Braunschweig, Germany (1982).
20. S.J. Cook and R.F. Simmons, *Combust. and Flame,* 46, p. 177 (1982).
21. J. Warnatz, *Combust. Sci. & Tech.,* 34, p. 177 (1983).
22. E. Axelssohn and L.G. Rosengren, *Combust. and Flame,* 64, p. 229 (1986).
23. D.L. Baulch, D.D. Drysdale, J. Duxbury, and S.J. Grant, *Evaluated Kinetic Data for High Temperatures,* Vol. 3, Butterworths, London (1976).
24. D.L. Baulch, C.J. Cobos, R.A. Cox, P. Frank, G. Hayman, T.H. Jost, J.A. Kerr, T. Murrells, M.J. Pilling, J. Troe, R.W. Walker, and J. Warnatz, *Combust. and Flame,* 98, p. 59 (1994).
25. R.W. Walker, *Reaction Kinetics I,* The Chemical Society, London, p. 161 (1975).
26. E.M. Bulewicz and T.M. Sugden, *Proc. Roy. Soc.,* A277, p. 143 (1964).
27. F.S. Dainton, *Chain Reactions,* Methuen, London (1956).
28. N. Peters and F.A. Williams, *Combust. and Flame,* 68, p. 185 (1987).
29. G. Paczko, P.M. Lefdal, and N. Peters, *Twenty-first Symposium on Combustion,* Combustion Institute, Pittsburgh, PA, p. 739 (1986).
30. R.F. Simmons and N. Wright, Unpublished Results.
31. R.N. Butlin and R.F. Simmons, *Combust. and Flame,* 12, p. 447 (1968).
32. R.F. Simmons and H.G. Wolfhard, *Trans.* Faraday Soc., 51, p. 1211 (1955).
33. W.A. Rosser, H. Wise, and J. Miller, *Seventh Symposium on Combustion,* Butterworths, London, p. 175 (1959).
34. M.J. Day, D.V. Stamp, K. Thompson, and G. Dixon-Lewis, *Thirteenth Symposium on Combustion,* Combustion Institute, Pittsburgh, PA, p. 705 (1971).
35. R. Hirst and D. Sutton, *Combust. and Flame,* 5, p. 317 (1961).
36. S. Evans and R.F. Simmons, *Twenty-second Symposium on Combustion,* Combustion Institute, Pittsburgh, PA, p. 1433 (1988).
37. R.E. Mitchell, A.F. Sarofim, and L.A. Clomburg, *Combust. and Flame,* 37, p. 201 (1980).
38. C.P. Fenimore and J. Moore, *Combust. and Flame,* 22, p. 343 (1974).
39. R.W. Bilger, S.H. Starmer, and R.J. Kee, *Combust. and Flame,* 80, p. 135 (1990).
40. F.A. Williams, in *Turbulent Mixing in Non-Reactive and Reactive Flows* (S.N. Muthy, ed.), Plenum Press, p. 189 (1975).
41. R.W. Bilger, in *Turbulent Reacting Flows* (P.A. Libby and F.A. Williams, eds.), p. 65, Springer, New York (1980).
42. S.K. Liew, K.N.C. Bray, and J.B. Moss, *Combust. Sci. & Tech.,* 27, p. 69 (1981).
43. N. Peters and R.J. Kee, *Combust. and Flame,* 68, p. 17 (1987).

CHAPTER 10

Properties of Building Materials

V. K. R. Kodur and T. Z. Harmathy

Introduction

Building components are to be designed to satisfy the requirements of serviceability and safety limit states. One of the major safety requirements in building design is the provision of appropriate fire resistance to various building components. The basis for this requirement can be attributed to the fact that, when other measures of containing the fire fail, structural integrity is the last line of defense. In this chapter, the term *structural member* is used to refer to both load bearing (e.g., columns, beams, slabs) and non–load-bearing (e.g., partition walls, floors) building components.

Fire resistance is the duration during which a structural member exhibits resistance with respect to structural integrity, stability, and temperature transmission. Typical fire resistance rating requirements for different building components are specified in building codes.

In the past, the fire resistance of structural members could be determined only by testing. In recent years however, the use of numerical methods for the calculation of the fire resistance of various structural members is gaining acceptance since these calculation methods are far less costly and time consuming.

The fire performance of a structural member depends, in part, on the properties of the materials the building component is composed of. The availability of material properties at high temperature and temperature distributions permits a mathematical approach to predicting the performance of building components exposed to fire. When a structural member is subjected to a defined temperature-time exposure during a fire, this exposure will cause a predictable temperature distribution in the member. Increased temperatures cause deformations and property changes in the materials. With knowledge of the deformations and property changes, the usual methods of structural mechanics can be applied to predict fire resistance performance.

In recent years, significant effort has been undertaken to develop material properties of various construction materials at elevated temperatures. In this chapter, the characteristics of materials are outlined. The various properties that influence fire resistance performance, together with the methods used to develop these properties, is discussed. The trends on the variation of thermal, mechanical, and other material-specific properties with temperature of commonly used construction materials are presented.

Dr. V. K. R. Kodur is Research Officer at the Institute for Research in Construction, National Research Council of Canada. He has published over 75 papers in the structural and fire resistance areas. He is a member of the ACI 216 Committee and the ASCE Committee on Structural Fire Protection. His research interests are in the fire resistance of structural members, material behavior, and on the nonlinear design and analysis of structures.

Dr. T. Z. Harmathy was head of the Fire Research Section, Institute of Research in Construction, National Research Council of Canada, until his retirement in 1988. His research centered on materials science and the spread potential of compartment fires.

Material Characteristics

Classification

Materials, based on composition, can be classified as either a homogeneous or heterogeneous type. *Homogeneous* materials have the same composition and properties throughout their volume, and are rarely found in nature. *Heterogeneous* materials have different composition and properties. Most construction materials are heterogeneous, yet their heterogeneity is often glossed over when dealing with practical problems.

The heterogeneity of concrete is easily noticeable. Other heterogeneities related to the microstructure of materials, that is, their grain and pore structures, are rarely detectable by the naked eye. The microstructure depends greatly on the way the materials are formed. In general,

materials formed by solidification from a melt show the highest degree of homogeneity. The result of the solidification is normally a *polycrystalline* material, comprising polyhedral grains of crystals which, in general, are equiaxial and randomly oriented. Severe cold-working in metals may produce an elongated grain structure and crystals with preferred orientations.

Noncrystalline solids are called *amorphous* materials. Gels and glasses are amorphous materials. Gels are formed by the coagulation of a colloidal solution. Glasses (vitreous materials) are solids with a liquid-like, grainless submicroscopic structure with low crystalline order. On heating, they will go through a series of phases of decreasing viscosity.

Synthetic polymers (plastics) are made up of long macromolecules created by polymerization from smaller repeating units (monomers). In the case of *thermoplastic* materials, the mobility of the molecular chains increases on heating. Such materials soften, much like glass. In some other types of plastics, called *thermosetting* materials, polymerization also produces cross-bonds between the molecular chains. These cross-bonds prevent the loosening of the molecular structure and the transition of the material into a liquid-like state.

Some building materials (e.g., gypsum, brick) are formed from a wet, plastic mass or from compacted powders by firing. The resulting product is a polycrystalline solid with a well-developed pore structure.

Two important building materials, concrete and gypsum, are formed by mixing finely ground powders (and aggregates) with water. The mixture solidifies by hydration. The cement paste in a concrete has a highly complex microstructure, interspersed with very fine, elaborate pores.

Most building materials can be treated as *isotropic* materials, that is, as though they possessed the same properties in all directions. An exception to this is some of the advanced composite materials, such as fiber-reinforced polymers (FRP), which might possess varying properties in different directions and are classifed as *anisotropic* materials.

Among the material properties, those that are unambiguously defined by the current composition and phase are referred to as *structure-insensitive.* Some others depend on the microstructure of the solid or on its previous history. These properties are *structure-sensitive.*

Porosity and Moisture Sorption

The fire performance of a material is dependent on the chemical composition and atomic structure of the material. The presence of water in the material composition influences the properties of materials at elevated temperatures. The two commonly associated terms to describe the composition and the extent of water present in a material are porosity and moisture sorption.

What is commonly referred to as a solid object is actually all the material within its visible boundaries. Clearly, if the solid is porous—and most building materials are—the so-called solid consists of at least two phases: (1) a solid-phase matrix, and (2) a gaseous phase (namely, air) in the pores within the matrix. Usually, however, there is also a liquid or liquid-like phase present: moisture either absorbed from the atmosphere to the pore surfaces, or held in the pores by capillary condensation. This third phase is always present if the pore structure is continuous; discontinuous pores (like the pores of some foamed plastics) are not readily accessible to atmospheric moisture.

The pore structure of materials is characterized by two properties: *porosity, P* ($m^3 \cdot m^{-3}$), the volume fraction of pores within the visible boundaries of the solid; and *specific surface, S* ($m^2 \cdot m^{-3}$), the surface area of the pores per unit volume of the material. For a solid with continuous pore structure, the porosity is a measure of the maximum amount of water the solid can hold when saturated. The specific surface and (to a lesser degree) porosity together determine the moisture content the solid holds in equilibrium with given atmospheric conditions.

The *sorption isotherm* shows the relationship at constant temperature between the equilibrium moisture content of a porous material and the relative humidity of the atmosphere. A sorption isotherm usually has two branches: (1) an *adsorption branch,* obtained by monotonically increasing the relative humidity of the atmosphere from 0 to 100 percent through very small equilibrium steps; and (2) a *desorption branch,* obtained by monotonically lowering the relative humidity from 100 to 0 percent. Derived experimentally, the sorption isotherms offer some insight into the nature of the material's pore structure.[1,2]

For heterogeneous materials consisting of solids of different sorption characteristics (e.g., concrete, consisting of cement paste and aggregates), the sorption isotherms can be estimated using the simple mixture rule (with $m = 1$; see Equation 1).

Building materials, such as concrete (or more accurately, the cement paste in the concrete) and wood, because of their large specific surfaces, can hold water in amounts substantial enough to be taken into consideration in fire performance assessments.

Mixture Rules

Some properties of materials of mixed composition or mixed phase can be calculated by simple rules if the material properties for the constituents are known. The simplest mixture rule is[3]

$$\pi^m = \sum_i \nu_i \pi_i^m \tag{1}$$

where

π = material property for the composite

π_i = material property for the composite's ith constituent

ν_i ($m^3 \cdot m^{-3}$) = volume fraction of the ith constituent

m (dimensionless) = constant that has a value between -1 and $+1$

Hamilton and Crosser recommended the following rather versatile formula for two-phase solids:[4]

$$\pi = \frac{\nu_1 \pi_1 + \gamma \nu_2 \pi_2}{\nu_1 + \gamma \nu_2} \tag{2}$$

where

$$\gamma = \frac{n\pi_1}{(n-1)\pi_1 + \pi_2} \quad (3)$$

Here phase 1 must always be the principal continuous phase. n (dimensionless) is a function of the geometry of phase distribution. With $n \rightarrow \infty$ and $n = 1$, Equations 2 and 3 convert into Equation 1 with $m = 1$ and $m = -1$, respectively. With $n = 3$, a relation is obtained for a two-phase system where the discontinuous phase consists of spherical inclusions.[5]

By repeated application, Equations 2 and 3 can be extended to a three-phase system,[6] for example, to a moist, porous solid that consists of three essentially continuous phases (the solid matrix, with moisture and air in its pores).

Survey of Building Materials

There are burnable (combustible) and nonburnable (noncombustible) building materials. The reason for preferring the use of the words *burnable* and *nonburnable* has been discussed by Harmathy.[2] To a designer concerned with the structural performance of a building during a fire, the mechanical and thermal properties of these materials are of principal interest. Yet burnable building materials may become ignited, and thereby the positive role assigned to these materials by design (i.e., functioning as structural elements of the building) may change into a negative role—that is, becoming fuel and adding to the severity of fire. Those properties of burnable building materials that are related to the latter role are discussed in other chapters of this handbook.

From the point of view of their performance in fire, building materials can be divided into the following groups:

1. *Group L (load-bearing) materials.* Materials capable of carrying high stresses, usually in tension or compression. With these materials, the mechanical properties related to behavior in tension and/or compression are of principal interest.
2. *Group L/I (load-bearing/insulating) materials.* Materials capable of carrying moderate stresses and, in fire, providing thermal protection to Group L materials. With Group L/I materials, the mechanical properties (related mainly to behavior in compression) and the thermal properties are of equal interest.
3. *Group I (insulating) materials.* Materials not designed to carry load. Their role in fire is to resist the transmission of heat through building elements and/or to provide insulation to Group L or Group L/I materials. With Group I materials, only the thermal properties are of interest.
4. *Group L/I/F (load-bearing/insulating/fuel) materials.* Group L/I materials that may become fuel in fire.
5. *Group I/F (insulating/fuel) materials.* Group I materials that may become fuel in fire.

The number of building materials has been increasing dramatically during the past few decades. In the last decade or so, a number of high-performing materials, such as FRP and high-strength concrete (HSC), have been developed to achieve cost-effectiveness in construction. While many of these high-performing materials possess superior properties at ambient temperatures, the same cannot be said of their performance at elevated temperatures. In materials such as HSC, additional complexities such as spalling arise, which might severely impact the fire performance of a structural member.

By necessity, only a few of those materials that are commonly used will be discussed in this chapter in some detail. These materials are as follows: in Group L—structural steel, lightguage steel, and reinforcing/prestressing steel; Group L/I—concrete and brick (including fiber-reinforced concrete); Group L/I/F (or Group I/F and L/F)—wood and FRP; and Group I—gypsum and insulation.

Material Properties at Elevated Temperatures

The behavior of a structural member exposed to fire is dependent, in part, on the thermal and mechanical properties of the material of which the member is composed. While calculation techniques for predicting the process of deterioration of building components in fire have developed rapidly in recent years, research related to supplying input information into these calculations has not kept pace. The designer of the fire safety features of buildings will find that information on the properties of building materials in the temperature range of interest, 20 to 800°C, is not easy to come by. Most building materials are not stable throughout this temperature range. On heating, they undergo physicochemical changes ("reactions" in a generalized sense), accompanied by transformations in their microstructure and changes in their properties. For example concrete at 500°C is completely different from the material at room temperature.

The thermophysical and mechanical properties of most materials change substantially within the temperature range associated with building fires. In the field of fire science, applied materials research faces numerous difficulties. At elevated temperatures, many building materials undergo physicochemical changes. Most of the properties are temperature dependent and sensitive to testing method parameters such as heating rate, strain rate, temperature gradient, and so on. Harmathy[7] cited the lack of adequate knowledge of the behavior of building materials at elevated temperatures as the most disturbing trend in fire safety engineering. There has been a tendency to use "notional" (also called "typical," "proprietary," "empirical," etc.) values for material properties in numerical computations—in other words, values that ensure agreement between experimental and analytical results. Harmathy warned that this practice might lead to a proliferation of theories that lack general validity.

Clearly, the generic information available on the properties of building materials at room temperature is seldom applicable in fire safety design. It is imperative, therefore, that the fire safety practitioner know how to extend, based on a priori considerations, the utility of the scanty data that can be gathered from the technical literature. Also, knowledge of unique material-specific characteristics at

elevated temperatures, such as spalling in concrete or charring in wood, is critical to determine the fire performance of a structural member. These properties are discussed in the following sections.

Reference Condition

Most building materials are porous and therefore capable of holding moisture, the amount of which depends on the atmospheric conditions. Since the presence of moisture may have a significant and often unpredictable effect on the properties of materials at any temperature below 100°C, it is imperative to conduct all property tests on specimens brought into a moistureless "reference condition" by some drying technique prior to the test. The reference condition is normally interpreted as that attained by heating the test specimen in an oven at 105°C until its weight shows no change. A few building materials however, among them all gypsum products, may undergo irreversible physicochemical changes when held at that temperature for an extended period. To bring them to a reference condition, specimens of these materials should be heated in a vacuum oven at some lower temperature level (e.g., at 40°C in the case of gypsum products).

Mechanical Properties

The mechanical properties that determine the fire performance of structural members are strength, modulus of elasticity, and creep of the component materials at elevated temperatures.

Stress-Strain Relationships

The mechanical properties of solids are usually derived from conventional tensile or compressive tests. The strength properties are usually expressed in stress-strain relations, which are often used as input data in mathematical models calculating the fire resistance. Figure 1–10.1 shows, for a metallic material, the variation of stress, σ (Pa), with increasing strain (deformation), ε ($m \cdot m^{-1}$), while the material is strained (deformed) in a tensile test at a more or less constant rate (i.e., constant crosshead speed), usually of the order of 1 $mm \cdot min^{-1}$. Generally, because of a decrease in the strength and ductility of the material, the slope of the stress-strain curves decreases with increasing temperature.

Modulus of Elasticity, Yield Strength, Ultimate Strength

The modulus of elasticity is a measure of the ability of the material to resist deformation, and is expressed as the ratio of the deforming stress to the strain in the material. Generally, the modulus of elasticity of a material decreases gradually with increasing temperature.

The tensile or compressive strength of the material is generally expressed by means of yield strength and ultimate strength. Often the strength at elevated temperature is expressed as a percentage of the compressive (tensile) strength at room temperature. Figure 1-10.2 shows the variation of strength with temperature (ratio of strength at elevated temperature to that at room temperature) for concrete, steel, and wood. For all four materials, the strength decreases with increasing temperature; however, the rate of strength loss is different.

For materials such as concrete, compressive strength is of main interest since it has very limited tensile strength at higher temperatures. However, for materials such as steel, both compressive and tensile strengths are of equal interest.

Section 0-*e* of the curve in Figure1-10.1 represents the elastic deformation of the material, which is instantaneous and reversible. The modulus of elasticity, *E* (Pa), is the slope of that section. Between points *e* and *u* the deforma-

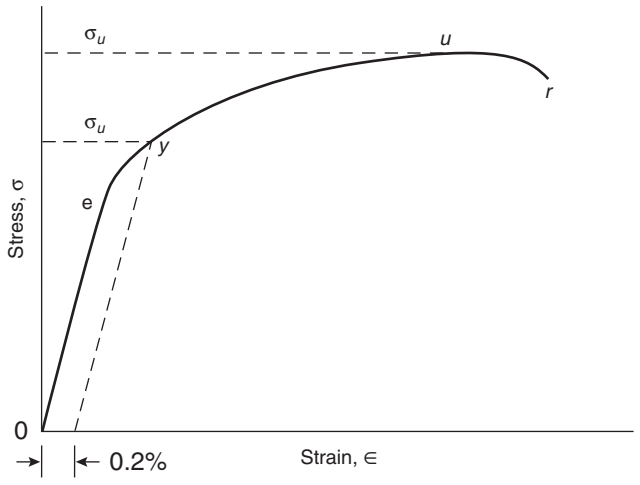

Figure 1-10.1. ***Stress-strain curve (strain rate is roughly constant).***

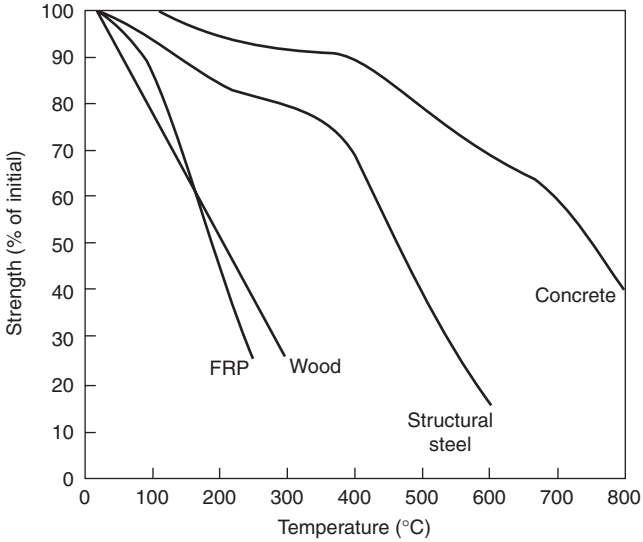

Figure 1-10.2. ***Variation of strength with temperature for different materials.***

tion is plastic, nonrecoverable, and quasi-instantaneous. The plastic behavior of the material is characterized by the yield strength at 0.2 percent offset, σ_y (Pa), and the ultimate strength, σ_u (Pa). After some localized necking (i.e., reduction of cross-sectional area), the test specimen ruptures at point *r*. The modulus of elasticity is more or less a structure-insensitive property.

For metals of similar metallurgical characteristics, the stress-strain curve can be reproduced at room temperature at a reasonable tolerance, and the shape of the curve does not depend significantly on the crosshead speed. At sufficiently high temperatures, however, the material undergoes plastic deformation even at constant stress, and the *e*-*r* section of the stress-strain curve will depend markedly on the crosshead speed.

Creep

Creep, often referred to as creep strain, is defined as the time-dependent plastic deformation of the material and is denoted by ε_t (m·m^{-1}). At normal stresses and ambient temperatures, the deformation due to creep is not significant. At higher stress levels and at elevated temperatures, however, the rate of deformation caused by creep can be substantial. Hence, the main factors that influence creep are the temperatures, the stress level, and their duration.

In a creep test the variation of ε_t is recorded against time, *t* (h), at constant stress (more accurately, at constant load) and at constant temperature *T* (K). A typical strain-time curve is shown in Figure 1-10.3(a). The total strain, ε (m·m^{-1}), is

$$\varepsilon = \frac{\sigma}{E} + \varepsilon_t \tag{4}$$

The 0-*e* section of the strain-time curve represents the instantaneous elastic (and reversible) part of the curve; the rest is creep, which is essentially nonrecoverable. The creep is fast at first [primary creep, section *e*-s_1 in Figure 1-10.3(a)], then proceeds for a long time at an approximately constant rate (secondary creep, section s_1-s_2), and finally accelerates until rupture occurs (tertiary creep, section s_2-*r*). The curve becomes steeper if the test is conducted either at a higher load (stress) or at a higher temperature.

Dorn's concept is particularly suitable for dealing with deformation processes developing at varying temperatures.[8] Dorn eliminated the temperature as a separate variable by the introduction of a new variable: the "temperature-compensated time," θ (h), defined as

$$\theta = \int_0^t e^{-\Delta H_c/RT}\, dt \tag{5}$$

where ΔH_c (J·kmol^{-1}) is the activation energy of creep, and *R* (J·kmol^{-1}·K^{-1}) is the gas constant.

From a practical point of view, only the primary and the secondary creeps are of importance. It has been shown that the creep strain in these two regimes can be satisfactorily described by the following equation[9]

$$\varepsilon_t = \frac{\varepsilon_{t0}}{\ln 2} \cosh^{-1}(2^{Z\theta/\varepsilon_{t0}}) \qquad (\sigma \simeq \text{constant}) \tag{6}$$

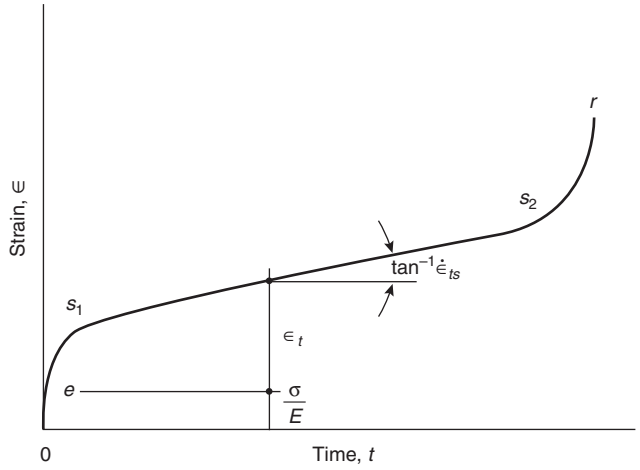

(a)

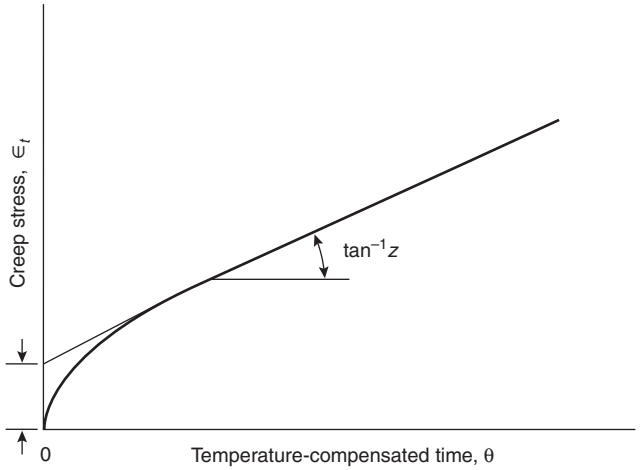

(b)

Figure 1-10.3. ***(a) Creep strain vs. time curve (T = constant; σ ≈ constant); (b) creep strain vs temperature-compensated time curve (σ ≈ constant).***

or approximated by the simple formula[10]

$$\varepsilon_t \approx \varepsilon_{t0} + Z\theta \qquad (\sigma \simeq \text{constant}) \tag{7}$$

where *Z* (h^{-1}) is the Zener-Hollomon parameter, and ε_{t0} (mm^{-1}) is another creep parameter, the meaning of which is explained in Figure 1-10.3(b). The Zener-Hollomon parameter is defined as[11]

$$Z = \dot{\varepsilon}_{ts} e^{\Delta H/RT} \tag{8}$$

where $\dot{\varepsilon}_{ts}$ (mm^{-1}·h^{-1}) is the rate of secondary creep at a temperature, *T*. The two creep parameters, *Z* and ε_{t0}, are functions of the applied stress only (i.e., they are independent of the temperature).

For most materials, creep becomes noticeable only if the temperature is higher than about one-third of the melting temperature (on the absolute scale).

The creep of concrete is due to the presence of water in its microstructure.[12] There is no satisfactory explanation for the creep of concrete at elevated temperatures. Anderberg and Thelandersson,[13] and Schneider[14] suggested techniques for the calculation of the deformation of concrete under conditions characteristic of fire exposure.

Thermal Properties

The material properties that influence the temperature rise and distribution in a member are its thermal conductivity, thermal expansion, specific heat, thermal diffusivity, and mass loss. These properties depend on the composition and characteristics of the constituent materials.

Thermal Expansion

The thermal expansion characterizes the expansion (or shrinkage) of a material caused by heating and is defined as the expansion (shrinkage) of unit length of a material when it is raised one degree in temperature. The expansion is considered to be positive when the material elongates and is considered negative when it shortens. In general, the thermal expansion of a material is dependent on the temperature. The dilatometric curve is a record of the fractional change of a linear dimension of a solid at a steadily increasing or decreasing temperature. With mathematical symbolism, the dilatometric curve is a plot of

$$\frac{\Delta \ell}{\ell_0} \quad \text{against} \quad T$$

where $\Delta \ell = \ell - \ell_0$ and ℓ (m) and ℓ_0 (m) are the changed and original dimensions of the solid, respectively, the latter usually taken at room temperature. $\Delta \ell$ reflects not only the linear expansion or shrinkage of the material, but also the dimensional effects brought on by possible physicochemical changes (i.e., "reactions").

The heating of the solid usually takes place at a predetermined rate, 5°C·min^{-1} as a rule. Because the physicochemical changes proceed at a finite rate and some of them are irreversible, a dilatometric curve obtained by heating rarely coincides with that obtained during the cooling cycle. Sluggish reactions may bring about a steady rise or decline in the slope of the dilatometric curve. Discontinuities in the slope indicate very fast reactions. Heating the material at a rate higher than 5°C·min^{-1} usually causes the reactions to shift to higher temperatures and to develop faster.

The coefficient of linear thermal expansion, β (m·m^{-1}·K^{-1}), is defined as

$$\beta = \frac{1}{\ell} \frac{d\ell}{dT} \tag{9}$$

Since $\ell = \ell_0$, the coefficient of linear thermal expansion is, for all intents, the tangent to the dilatometric curve. For solids that are isotropic in a macroscopic sense, the coefficient of volume expansion is approximately equal to 3β.

The thermal expansion is measured with a dilatometric apparatus, capable of producing curves that show the expansion of the materials with temperature in the range from 20°C to 1000°C. Harmathy,[7,15] using a horizontal dilatometric apparatus, recorded dilametric curves for various types of concrete and brick, some of which are presented in later sections. The sample was 76.2-mm-long and about 13 by 13 mm in cross section. It was subjected to a small spring load that varied during the test. Unfortunately, even this small load caused creep shrinkage with those materials that tended to soften at higher temperatures. Furthermore, since the apparatus did not provide a means for placing the sample in a nitrogen atmosphere, in certain cases oxidation may also have had some effect on the shape of the curves.

Mass Loss

The mass loss is often used to express the loss of mass at elevated temperatures. The thermogravimetric curve is a record of the fractional variation of the mass of a solid at steadily increasing or decreasing temperature. Again, with mathematical symbolism, a thermogravimetric curve is a plot of

$$\frac{M}{M_0} \quad \text{against} \quad T$$

where M and M_0 (kg) are the changed and original masses of the solid, respectively, the latter usually taken at room temperature. Generally a heating rate of 5°C·min^{-1} is used in the measurements.

A thermogravimetric curve reflects reactions accompanied by loss or gain of mass but, naturally, it does not reflect changes in the materials' microstructure or crystalline order. $M/M_0 = 1$ is the thermogravimetric curve for a chemically inert material. Again, an increase in the rate of heating usually causes those features of the curve that are related to chemical reactions to shift to higher temperatures and to develop faster.

The thermogravimetric curves to be shown were obtained by a DuPont 951 thermogravimetric analyzer,[16] using specimens of 10 to 30 mg in mass, placed in a nitrogen atmosphere.[7] The rate of temperature rise was 5°C·min^{-1}. Figure 1-10.4 shows the variation of mass loss for concrete in the temperature range from 20°C to 1000°C.

Density, Porosity

The density, ρ (kg·m^{-3}), in an oven-dry condition, is the mass of a unit volume of the material, comprising the solid itself and the air-filled pores. Assuming that the material is isotropic with respect to its dilatometric behavior, its density at any temperature can be calculated from the thermogravimetric and dilatometric curves.

$$\rho = \rho_0 \frac{(M/M_0)_T}{[1 + ((\Delta \ell)/(\ell_0))_T]^3} \tag{10}$$

where ρ_0 (kg·m^{-3}) is the density of the solid at the reference temperature (usually room temperature), and the T subscript indicates values pertaining to temperature T in the thermogravimetric and dilatometric records.

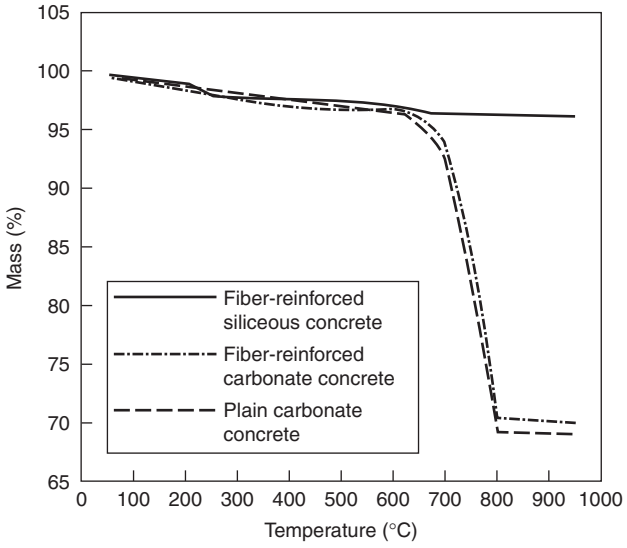

Figure 1-10.4. ***Mass loss of various concrete types as a function of temperature.[17]***

The density of composite solids at room temperature can be calculated by means of the mixture rule in its simplest form (Equation 1 with $m = 1$).

$$p = \sum_i \nu_i p_i \tag{11}$$

where the i subscript relates to information on the ith component. At elevated temperatures, the expansion of the components is subject to constraints, and therefore the mixture rule can only yield a crude approximation.

If, as usual, the composition is given in mass fractions rather than in volume fractions, the volume fractions can be obtained as

$$\nu_i = \frac{w_i/p_i}{\sum_i w_i/p_i} \tag{12}$$

where w_i is the mass fraction of the ith component (kg·kg^{-1}).

True density, ρ_t (kg·m^{-3}), is the density of the solid in a poreless condition. Such a condition is nonexistent for many building materials, and, therefore, ρ_t may be a theoretical value derived on crystallographic considerations, or determined by some standard technique, for example, ASTM C135.[18] The relationship between the porosity and density is

$$P = \frac{\rho_t - \rho}{\rho_t} \tag{13}$$

The overall porosity of a composite material consisting of porous components is

$$P = \sum_i \nu_i P_i \tag{14}$$

where, again, the i subscript relates to the ith component of the material.

Specific Heat

The specific heat of a material is the characteristic that describes the amount of heat required to raise a unit mass of the material at unit temperature. A calorimetric curve describes the variation with temperature of the apparent specific heat of a material at constant pressure, c_p (J·kg^{-1}·K^{-1}). The apparent specific heat is defined as

$$c_p = \frac{\delta h}{\delta T_p} \tag{15}$$

where h is enthalpy (J·kg^{-1}), and the p subscripts indicate the constancy of pressure. If the heating of the solid is accompanied by physicochemical changes (i.e., "reactions"), the enthalpy becomes a function of the reaction progress variable, ξ (dimensionless), that is, the degree of conversion at a particular temperature from reactant(s) into product(s). For any temperature interval where physicochemical change takes place,[2,6,19] $0 \le \xi \le 1$, and

$$c_p = \bar{c}_p + \Delta h \frac{d\xi}{dT} \tag{16}$$

where c_p (J·kg^{-1}·K^{-1}) is the specific heat for that mixture of reactants and (solid) products that the material consists of at a given stage of the conversion (as characterized by ξ), and Δh_p (J·kg^{-1}) is the latent heat associated with the physicochemical change.

As Equation 16 and Figure 1-10.5 show, in temperature intervals of physicochemical instability, the apparent specific heat consists of sensible heat and latent heat contributions. The latter contribution will result in extremities in the calorimetric curve: a maximum if the reaction is endothermic, a minimum if it is exothermic.

In heat flow studies, it is usually the ρc_p product (J·m^{-3}·K^{-1}) rather than c_p that is needed as input information. This product is referred to as volume specific heat.

Until the eighties, adiabatic calorimetry was the principal method to study the shape of the c_p versus T relationship. Since the eighties, differential scanning calorimetry

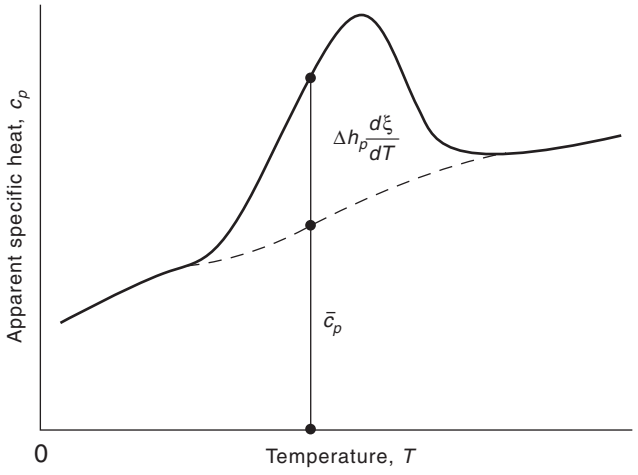

Figure 1-10.5. ***The apparent specific heat.***

(DSC) is the most commonly used technique for mapping the curve in a single temperature sweep at a desired rate of heating. Unfortunately, the accuracy of the DSC technique in determining the sensible heat contribution to the apparent specific heat may not be particularly good (sometimes it may be as low as ±20 percent). The rate of temperature rise was usually 5°C·min^{-1}. At higher heating rates, the peaks in the DSC curves tend to shift to higher temperatures and become sharper. For temperatures above 600°C, a high-temperature differential thermal analyzer (DTA) is also used. Harmathy, with the aid of a DuPont 910 differential scanning calorimeter, developed calorimetric curves for a number of materials by placing the samples, 10 to 30 mg in mass, in a nitrogen atmosphere.[7,20]

Materials that undergo exothermic reactions may yield negative values in the calorimetric curve. A negative value for c_p indicates that, at the applied (and enforced) rate of heating, the rate of evolution of reaction heat exceeds the rate of absorption of sensible heat by the material. In natural processes, the apparent specific heat can never be negative, because the heat evolving from the reaction is either scattered to the surroundings or, if absorbed by the material, causes a very fast temperature rise. If the heat of reaction is not very high, obtaining nonnegative values for c_p can be achieved by suitably raising the scanning rate. For this reason, some materials undergoing exothermic reactions must be tested at rates of heating higher than 5°C·min^{-1}, often as high as 50°C·min^{-1}.

If experimental information is not available, the c_p versus T relationship can be calculated from data on heat capacity and heat of formation for all the components of the material (including reactants and products), tabulated in a number of handbooks.[21,22] Examples of calculations are presented in References 2 and 6, where information is developed for the apparent specific heat versus temperature relation for a cement paste and four kinds of concrete.

Thermal Conductivity

The temperature rise in a member, as a result of heat flow, is a function of the thermal conductivity of the material. Heat transmission solely by conduction can occur only in poreless, nontransparent solids. In porous solids (most building materials), the mechanism of heat transmission is a combination of conduction, radiation, and convection. (If pore size is less than that about 5 mm, the contribution of pores to convective heat transmission is negligible.) The thermal conductivity of porous materials is, in a strict sense, merely a convenient empirical factor that makes it possible to describe the heat transmission process with the aid of the Fourier law. That empirical factor will depend not only on the conductivity of the solid matrix, but also on the porosity of the solid and the size and shape of the pores. At elevated temperatures, because of the increasing importance of radiant heat transmission through the pores, conductivity becomes sensitive to the temperature gradient.

Since measured values of the thermal conductivity depend to some extent on the temperature gradient employed in the test, great discrepancies may be found in thermal conductivity data reported by various laboratories. A thermal conductivity value yielded by a particular technique is, in a strict sense, applicable only to heat flow patterns similar to that characteristic of the technique employed.

Experimental data indicate that porosity is not a greatly complicating factor as long as it is not larger than about 0.1. With insulating materials, however, the porosity may be 0.8 or higher. Conduction through the solid matrix may be an insignificant part of the overall heat transmission process; therefore, using the Fourier law of heat conduction in analyzing heat transmission may lead to deceptive conclusions.

If the solid is not oven-dry, a temperature gradient will induce migration of moisture, mainly by an evaporation condensation mechanism.[23] The migration of moisture is usually, but not necessarily, in the direction of heat flow, and manifests itself as an increase in the apparent thermal conductivity of the solid. Furthermore, even oven-dry solids may undergo decomposition (mainly dehydration) reactions at elevated temperatures. The sensible heat carried by the gaseous decomposition products as they move in the pores adds to the complexity of the heat flow process. At present there is no way of satisfactorily accounting for the effect of simultaneous mass transfer on heat flow processes occurring under fire conditions.

The thermal conductivity of layered, multiphase solid mixtures depends on whether the phases lie in the direction of, or normal to, the direction of heat flow and is determined using the simple mixture rule.[4,24] At higher temperatures, because of radiative heat transfer through the pores, the contribution of the pores to the thermal conductivity of the solid must not be disregarded.[25]

The thermal conductivity of solids is a structure-sensitive property. For crystalline solids, the thermal conductivity is relatively high at room temperature, and gradually decreases as the temperature rises. For predominantly amorphous solids, on the other hand, the conductivity is low at room temperature and increases slightly with the rise of temperature. The conductivity of porous crystalline materials may also increase at very high temperatures because of the radiant conductivity of the pores.

The thermal conductivity of materials such as concrete or brick can be measured, in the temperature range between 20°C and 800°C, using a non-steady-state hot wire method.[26,27] The thermal conductivity values at discrete temperature levels can be plotted to obtain a curve. Unfortunately, no scanning technique exists for acquiring a continuous thermal conductivity versus temperature curve from a single temperature sweep.

Special problems arise with the estimation of the thermal conductivity for temperature intervals of physicochemical instability. Both the steady-state and variable-state techniques of measuring thermal conductivity require the stabilization of a pattern of temperature distribution (and thereby a certain microstructural pattern) in the test sample prior to the test. The test results can be viewed as points on a continuous thermal conductivity versus temperature curve obtained by an imaginary scanning technique performed at an extremely slow scanning rate. Since each point pertains to a more or less stabilized microstructural pattern, there is no way of knowing how the thermal conductivity would vary in the course of a

physicochemical process developing at a finite rate and varying microstructure.

On account of the nonreversible microstructural changes brought about by heating, the thermal conductivity of building materials (and perhaps most other materials) is usually different in the heating and cooling cycles. Open and solid circles are used in the figures to identify thermal conductivity values obtained by stepwise increasing and stepwise decreasing the temperature of the sample, respectively. Also, often the thermal conductivity of a material is taken as invariant with respect to the direction of heat flow.

Thermal Diffusivity

The thermal diffusivity of a material is defined as the ratio of thermal conductivity to the volumetric specific heat of the material. It measures the rate of heat transfer from an exposed surface of a material to the inside. The larger the diffusivity, the faster the temperature rise at a certain depth in the material. Similar to thermal conductivity and specific heat, thermal diffusivity varies with temperature rise in the material. Thermal diffusivity, α, can be calculated using the relation:

$$\alpha = \frac{k}{\rho c_p} \tag{17}$$

where

k = thermal conductivity
ρ = density
c_p = specific heat of the material

Special (Material-Specific) Properties

In addition to thermal and mechanical properties, certain other properties, such as spalling in concrete and charring in wood, influence the performance of a material at elevated temperature. These properties are unique to specific materials and are critical for predicting the fire performance of a structural member.

Critical Temperature

In building materials, such as steel and FRP, the determination of failure in a structural member exposed to fire is simplified to the calculation of critical temperature. The critical temperature is defined as the temperature at which the material loses much of its strength and can no longer support the applied load. When this temperature is reached, the safety factor against failure becomes less than 1.

North American standards (ASTM E119) assume a critical or failure temperature of 538°C (1000°F) for structural steel. It is a typical failure temperature for columns under full design load. This temperature is also regarded as the failure temperature in the calculation of fire resistance of steel members. If a load is applied to the member, the test is continued until the member actually fails, which, depending on the load intensity, may occur at a higher or lower steel temperature.

This concept of critical temperature is also used for reinforced and prestressed steel in concrete structural members for evaluating the fire resistance ratings. These ratings are generally obtained through the provision of minimum member dimensions and minimum thickness of concrete cover. The minimum concrete cover thickness requirements are intended to ensure that the temperature in the reinforcement does not reach its critical temperature for the required duration. For reinforcing steel, the critical temperature is 593°C, while for prestressing steel the critical temperature is 426°C.[28]

Spalling

Spalling is defined as the breaking of layers (pieces) of concrete from the surface of the concrete elements when the concrete elements are exposed to high and rapidly rising temperatures, such as those experienced in fires. Spalling can occur soon after exposure to heat and can be accompanied by violent explosions, or it may happen when concrete has become so weak after heating that, when cracking develops, pieces fall off the surface. The consequences may be limited as long as the extent of the damage is small, but extensive spalling may lead to early loss of stability and integrity due to exposed reinforcement and penetration of partitions.

While spalling might occur in all concretes, high-strength concrete (HSC) is believed to be more susceptible than normal-strength concrete (NSC) because of its low permeability and low water-cement ratio. In a number of test observations on HSC specimens, it has been found that spalling is often of an explosive nature.[29,30] Hence, spalling is one of the major concerns in the use of HSC and should be properly accounted for in evaluating fire performance. Spalling in NSC and HSC columns is compared in Figure 1-10.6 using the data obtained from full-scale fire tests on loaded columns.[31] It can be seen that the spalling is quite significant in the HSC column.

Spalling is believed to be caused by the buildup of pore pressure during heating. The extremely high water vapor pressure, generated during exposure to fire, cannot escape due to the high density (and low permeability) of HSC, and this pressure buildup often reaches the saturation vapor pressure. At 300°C, the pressure reaches approximately 8 MPa; such internal pressures are often too high to be resisted by the HSC mix having a tensile strength of approximately 5 MPa.[32] The drained conditions at the heated surface, and the low permeability of concrete, lead to strong pressure gradients close to the surface in the form of the so-called "moisture clog."[2,33] When the vapor pressure exceeds the tensile strength of concrete, chunks of concrete fall off from the structural member. The pore pressure is considered to drive progressive failure; that is, the greater the spalling, the lower the permeability of concrete. This falling off can often be explosive in nature, depending on the fire and concrete characteristics.

However, other researchers explain the occurrence of spalling on the basis of fracture mechanics and argue that the spalling results from restrained thermal dilatation close to the heated surface.[34] This leads to compressive stresses parallel to the heated surface, which are released by brittle fractures of concrete, in other words, spalling.

(a) (b)

Figure 1-10.6. ***Spalling in NSC and HSC columns after exposure to fire:[31] (a) normal-strength concrete column, and (b) high-strength concrete column.***

Spalling, which often results in the rapid loss of concrete during a fire, exposes deeper layers of concrete to fire temperatures, thereby increasing the rate of transmission of heat to the inner layers of the member, including the reinforcement. When the reinforcement is directly exposed to fire, the temperatures in the reinforcement rise at a very high rate, leading to a faster decrease in strength of the structural member. The loss of strength in the reinforcement, added to the loss of concrete due to spalling, significantly decreases the fire resistance of a structural member.

In addition to strength and porosity of concrete mix, density, load intensity, fire intensity, aggregate type, and relative humidity are the primary parameters that influence spalling in HSC. The variation of porosity with temperature is an important property needed for predicting spalling performance of HSC. Noumowe et al. carried out porosity measurements on NSC and HSC specimens, using a mercury porosimeter, at various temperatures.[35]

Charring

Charring is the process of formation of a layer of char at the exposed surface of wood members during exposure to fire. The charring process also occurs in other members, such as FRP and some types of plastics. When exposed to heat, wood undergoes thermal degradation (pyrolysis), the conversion of wood to char and gas, resulting in a reduction of the density of the wood. Studies have shown that the charring temperature for wood lies in the range of 280°C to 300°C.[28]

The charred layer is considered to have practically no strength. The fire resistance of the member depends on the extent of charring and the remaining strength of the uncharred portion.

The charring rate, a critical parameter in determining the fire resistance of a structural wood member, is defined as the rate at which wood is converted to char. In the standard fire resistance test, it has been noted that the average rate of charring transverse to the grain is approximately 0.6 mm/min.[28] The charring rate parallel to the grain of wood is approximately twice the rate when it is transverse to the grain. Detailed studies on the charring rates for several specimen and timber types are reported by various researchers[36–38] and are summarized in a report.[39] These charring rates were constant (in each study) and ranged from 0.137 to 0.85 mm/min. The assumption of a constant rate of charring is reasonable for thick wood members.

Charring is influenced by a number of parameters, the most important ones being density, moisture content, and contraction of wood. The influence of the moisture content and density of the wood on the charring rate is illustrated in Figure 1-10.7 for Douglas fir exposed to the standard fire.[28] It can be seen that the charring rate decreases with increasing density of the wood and also with increasing moisture content.

It is important to recognize that the charring rate in real fires depends on the severity of fire to which the wood is exposed. This depends on the fuel load and the ventilation factor of the compartment (for full details see Section 4, Chapter 8, "Fire Temperature-Time Relations" in this book). Detailed information on the charring of untreated wood—with expressions for charring rate in terms of the influencing factors of density, moisture con-

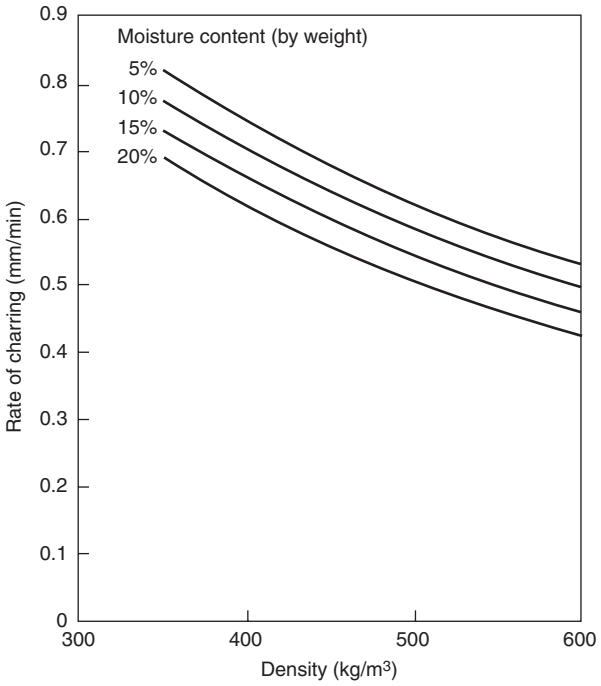

Figure 1-10.7. ***Rate of charring in Douglas fir as a function of its density (dry condition) for various moisture contents when exposed to ASTM standard fire.[28]***

tent, external heat flux, and oxygen concentration—when exposed to real fires is given by Hadvig[40] and Mikkola.[41]

Sources of Information

Information on the properties of building materials at elevated temperatures is scattered throughout the literature. There are a few publications, however, that may be particularly valuable for fire safety practitioners. A book by Harmathy[2] and the ASCE manual on structural fire protection[28] present a wealth of information on concrete, steel, wood, brick, gypsum, and various plastics. The thermal properties of 31 building materials are surveyed in an NRCC report.[7] The mechanical and thermal properties of concrete are discussed in an ACI guide,[42] and in reports by Bennetts[43] and Schneider.[44] Those of steel are surveyed in the ACI guide, in Bennetts's report, and in a report by Anderberg.[45] Information on the thermal conductivity of more than 50 rocks (potential concrete aggregates) is presented in a paper by Birch and Clark.[46] The relationships for thermal and mechanical properties, at elevated temperatures, for some building materials are listed in the ASCE structural fire protection manual.[28] In most cases these properties are expressed, in the temperature range of 0 to 1000°C, as a function of temperature and other properties at ambient temperature. These values can be used as input data in mathematical models for predicting the temperatures and fire performance of structural members.

Steel

Steel is a Group L material. The steels most often used in the building industry are either hot-rolled or cold-drawn. The structural steels and concrete-reinforcing bars are hot-rolled, low-carbon, ferrite-pearlite steels. They have a randomly oriented grain structure, and their strength depends mainly on their carbon content. The prestressing steel wires and strands for concrete are usually made from cold-drawn, high-carbon, pearlitic steels with an elongated grain structure, oriented in the direction of the cold work. In addition, light-gauge steel, made from cold-formed steel, finds wide applications in lightweight framing, such as walls and floors.

Information on the mechanical properties of two typical steels [a structural steel (ASTM A36) and a prestressing wire (ASTM A421)] is presented in Figures 1-10.8 through 1-10.10, and in Table 1-10.1.[47] Figures 1-10.8 and 1-10.9 are stress-strain curves at room temperature (24°C and 21°C, respectively) and at a number of elevated temperature levels. Figure 1-10.10 shows the effect of temperature on the yield and ultimate strengths of the two steels.

Table 1-10.1 presents information on the effect of stress on the two creep parameters, Z and ε_{t0} (see Equation 7). Since creep is a very structure-sensitive property, the creep parameters may show a substantial spread, even for steels with similar characteristics at room temperature. The application of the creep parameters to the calculation of the time of structural failure in fire is discussed in Reference 4.

The modulus of elasticity (E) is about 210×10^3 MPa for a variety of common steels at room temperature. Figure 1-10.11 shows its variation with temperature for struc-

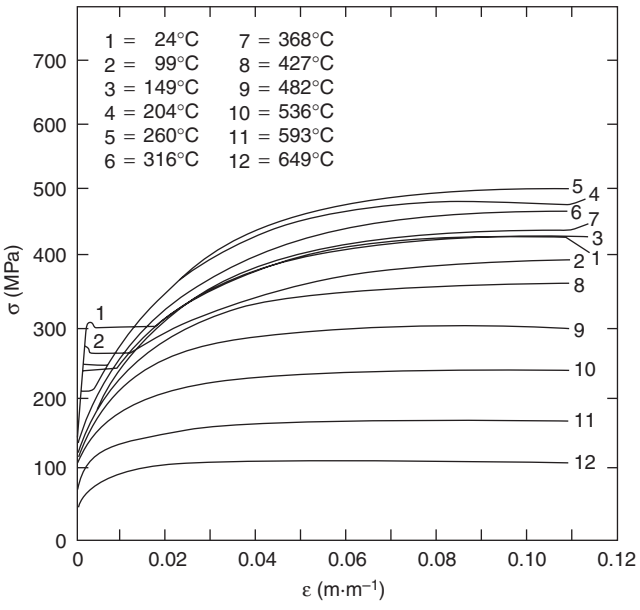

Figure 1-10.8. ***Stress-strain curves for a structural steel (ASTM A36) at room temperature and elevated temperatures.[47]***

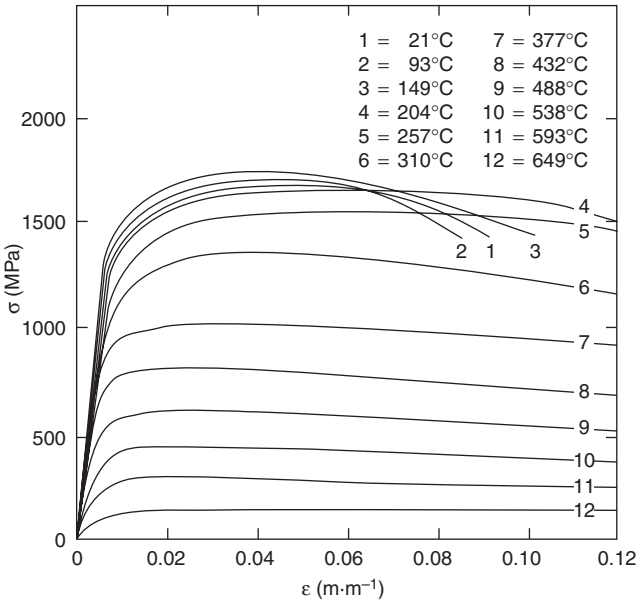

Figure 1-10.9. ***Stress-strain curves for prestressing steel (ASTM A421) at room temperature and elevated temperatures.[47]***

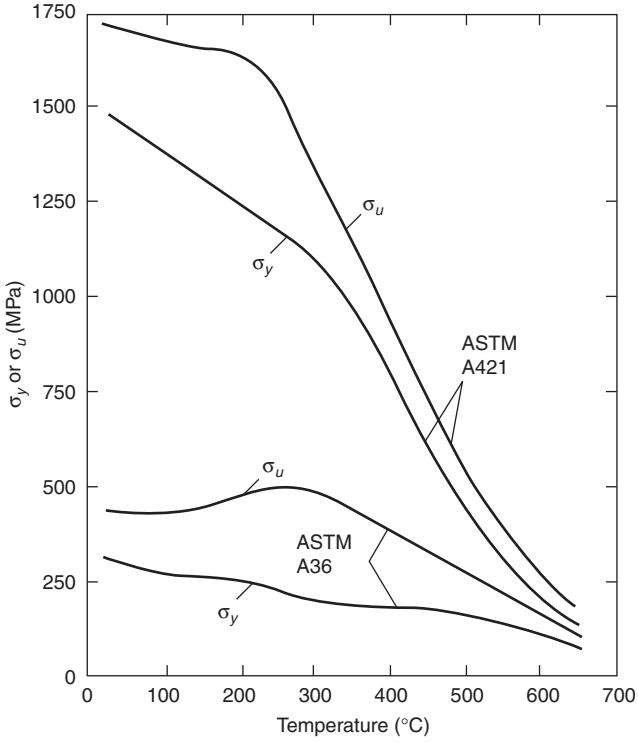

Figure 1-10.10. ***The ultimate and yield strengths for a structural steel (ASTM A36) and a prestressing steel (ASTM A421) at elevated temperatures.[47]***

tural steels[48] and steel reinforcing bars.[49] (E_0 in Figure 1-10.11 is the modulus of elasticity at room temperature.)

The density (ρ) of steel is about 7850 kg·m^{-3}. Its coefficient of thermal expansion (β) is a structure-insensitive property. For an average carbon steel, β is 11.4×10^{-6} m·m^{-1}·K^{-1} at room temperature. The dilatometric curve shown in Figure 1-10.12 is applicable to most of the common steels. The curve reveals substantial contraction of the material at about 700°C, which is associated with the transformation of the ferrite-pearlite structure into austenite.

Being a structure-sensitive property, the thermal conductivity of steel is not easy to define. For carbon steels it usually varies within the range of 46 to 65 W·m^{-1}·K^{-1}.

Equations for various properties of steel, as functions of temperature, are available in the ASCE structural fire protection manual[28] and in Eurocode 3.[50,51] In the ASCE manual, the same set of relationships is applicable for thermal properties of both structural and reinforcing steel. However, separate relationships for stress-strain and elasticity are given for the two steels with slightly conservative values for stuctural steel. Recently, Poh proposed a general stress-strain equation that expreses stress explicitly in terms of strain in a single continuous curve.[52]

The critical temperature of steel is often used as a bench mark for determining the failure of structural members exposed to fire. This ensures that the yield strength is not reduced to less than that of 50 percent of ambient value. The critical temperature for various types of steels is given in Table 1-10.2.

The properties of cold-formed light-gauge steel are slightly different from those of hot-rolled structural steel. Gerlich[53] and Makelainen and Miller,[54] based on steady-

Table 1-10.1 ***Creep Parameters for a Structural Steel and a Prestressing Steel[47]***

Steel	$\Delta H_c/R$ (k)	$\varepsilon_{t0}(\sigma)$ (m·m^{-1})	$Z(\sigma)$ (h^{-1})
ASTM A36	38,890	$3.258 \times 10^{-17\sigma 1.75}$	$2.365 \times 10^{-20\sigma 4.7}$ if $\sigma \le 103.4 \times 10^6$ $1.23 \times 10^{16} \exp(4.35 \times 10^{-8\sigma})$ if $103.4 \times 10^6 \le \sigma \le 310 \times 10^6$
ASTM A421	30,560	$8.845 \times 10^{-9\sigma\ 0.67}$	$1.952 \times 10^{-10\sigma 3}$ if $\sigma \le 172.4 \times 10^6$ $8.21 \times 10^{13} \exp(1.45 \times 10^{-8\sigma})$ if $172.4 \times 10^6 \le \sigma \le 690 \times 10^6$

σ is measured in Pa

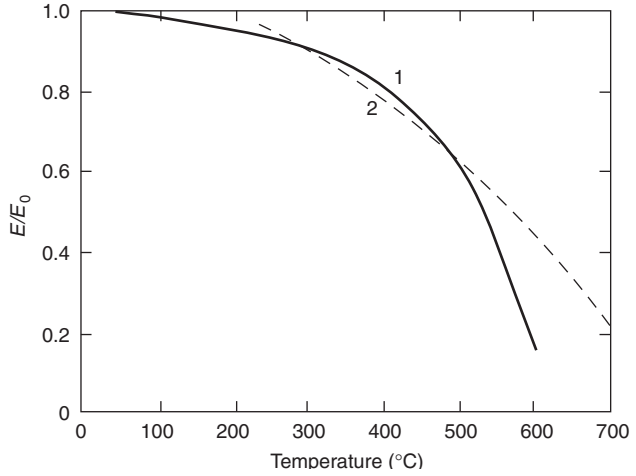

Figure 1-10.11. ***The effect of temperature on the modulus of elasticity of (1) structural steels and (2) steel reinforcing bars.[49]***

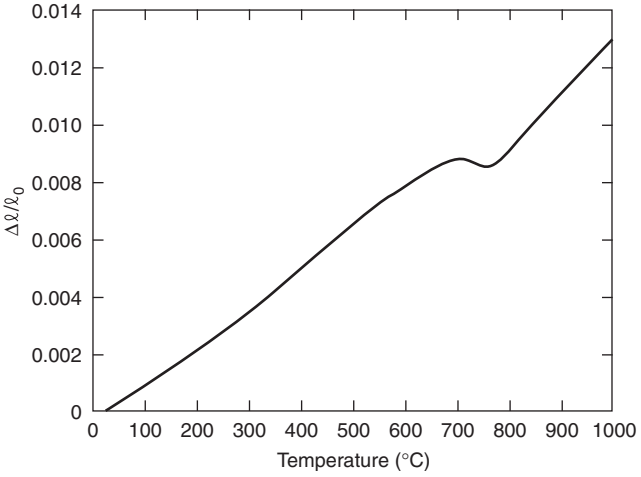

Figure 1-10.12. ***Dilatometric curve for steel.***

Table 1-10.2 ***Critical Temperature for Various Types of Steel***

Steel	Standard/Reference	Temperature
Structural steel	ASTM	538°C
Reinforcing steel	ASTM	593°C
Prestressing steel	ASTM	426°C
Light-gauge steel	EC 3[50]	350°C
	Gerlich et al.[55]	400°C

state and transient tests on cold-formed steel tension coupons (cut from studs) and galvanized sheets, proposed relationships for yield strength and modulus of elasticity. Figure 1-10.13 shows the variation of yield strength of light-gauge steel at elevated temperatures, corresponding to 0.5 percent, 1.5 percent, and 2 percent strains based on

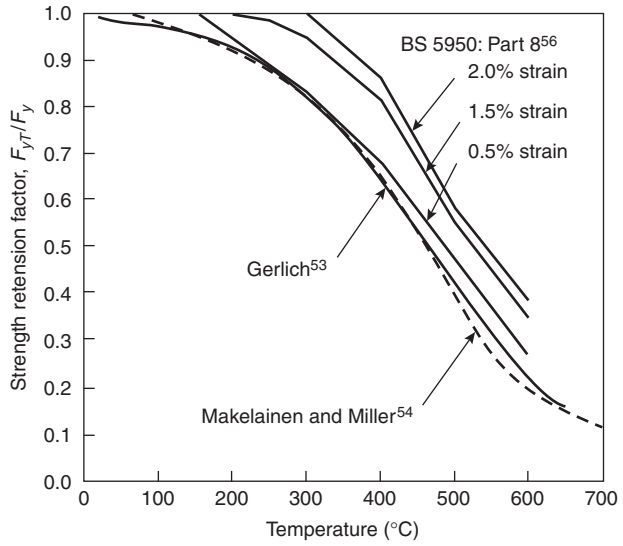

Figure 1-10.13. ***Reduction of the yield strength of cold-formed light-gauge steel at elevated temperatures.[53,54,56]***

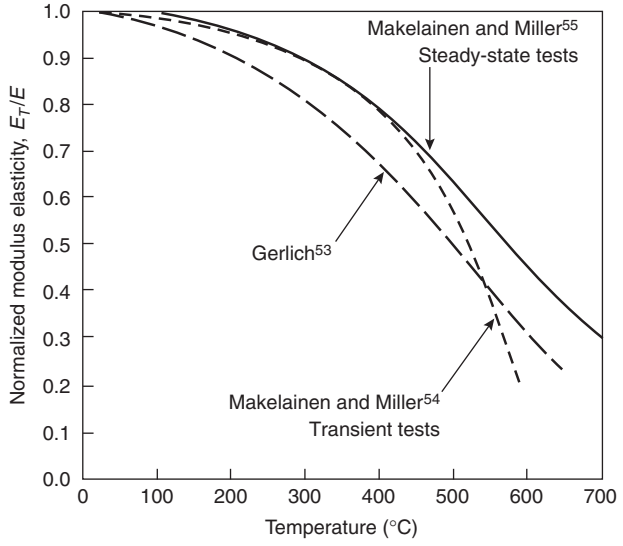

Figure 1-10.14. ***Modulus of elasticity of cold-formed light-gauge steel at elevated temperatures.[53,55]***

the proposed relationships and on the relationship in BS 5950.[56] The BS 5950 curves represent a conservative 95 percent confidence limit (i.e., a 5 percent chance that strength would fall below the curve), while the other two curves are representative of mean test data. Figure 1-10.14 shows the variation of modulus of elasticity of light-gauge steel at elevated temperatures. The modulus E_T represents the tangent modulus at low stress levels (or initial tangent modulus), because steel stress-strain relationships become increasingly nonlinear at elevated temperatures. The effect of zinc coating on the mechanical properties of steel is of little significance.

The light-gauge steel has somewhat lower thermal expansion when compared to similar expressions for other steels.[54] The other thermal properties of steel, such as specific heat and thermal conductivity, are of little importance for the thermal modeling of light-gauge steel because steel framing plays a minor role in the heat transfer mechanism. A review of some of these properties is presented in a review paper.[57]

The critical temperature of light-gauge steel is much lower than for other types of steels. While Eurocode 3 limits this to a conservative value of 350°C, in other cases a critical temperature of 400°C is used (see Table 1-10.2).

Concrete

Concrete is a Group L/I material. The word *concrete* covers a large number of different materials, with the single common feature that they are formed by the hydration of cement. Since the hydrated cement paste amounts to only 24 to 43 volume percent of the materials present, the properties of concrete may vary widely with the aggregates used.

Traditionally, the compressive strength of concrete used to be around 20 to 50 MPa, which is referred to as normal-strength concrete (NSC). In recent years, concrete with a compressive strength in the range 50 to 100 MPa has become widely used and is refered to as high-strength concrete (HSC). Depending on the density, concretes are usually subdivided into two major groups: (1) normal-weight concretes with densities in the 2150- to 2450-kg·m^{-3} range, and (2) lightweight concretes with densities between 1350 and 1850 kg·m^{-3}. Fire safety practitioners again subdivide the normal-weight concretes into silicate (siliceous) and carbonate aggregate concrete, according to the composition of the principal aggregate. Also, a small amount of discontinuous fibers are often added to the concrete mix to achieve superior performance; this concrete is referred to as fiber-reinforced concrete (FRC). In this section, the properties of concrete are discussed under three groups: namely, NSC, FRC, and HSC.

Normal-Strength Concrete

A great deal of information is available in the literature on the mechanical properties of various types of normal-strength concrete. This information is summarized in reports by Bennetts[43] and Schneider,[44] the ACI guide,[42] the ASCE fire protection manual,[28] and in Harmathy's book.[2] Figure 1-10.15 shows the stress-strain curves for a lightweight concrete with expanded shale aggregate at room temperature (24°C) and a few elevated temperature levels.[58] The shape of the curves may depend on the time of holding the test specimen at the target temperature level before the compression test.

The modulus of elasticity (E) of various concretes at room temperature may fall within a very wide range, 5.0×10^3 to 35.0×10^3 MPa, dependent mainly on the water-cement ratio in the mixture, the age of concrete, the method of conditioning, and the amount and nature of the aggregates. Cruz found that the modulus of elasticity decreases rapidly with the rise of temperature, and the fractional decline does not depend significantly on the type of aggregate.[59] (See Figure 1-10.16; E_0 in the figure is the modulus of elasticity at room temperature.) From other surveys,[2,43] it appears, however, that the modulus of elasticity of normal-weight concretes decreases faster with the rise of temperature than that of lightweight concretes.

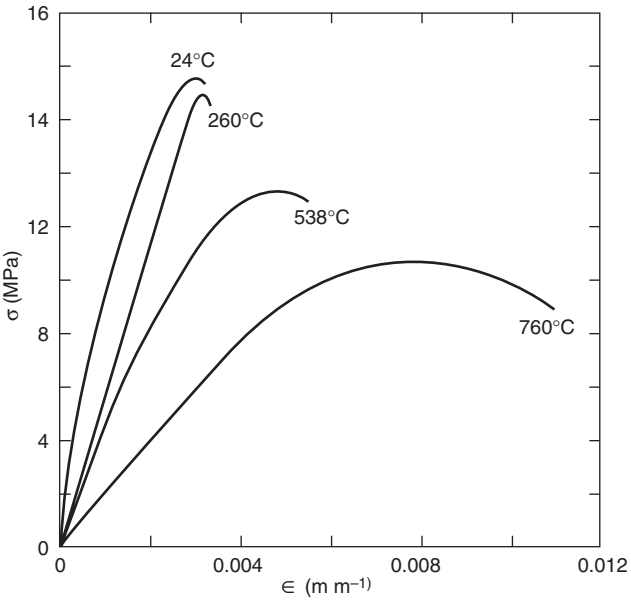

Figure 1-10.15. ***Stress-strain curves for a lightweight masonry concrete at room and elevated temperatures.[58]***

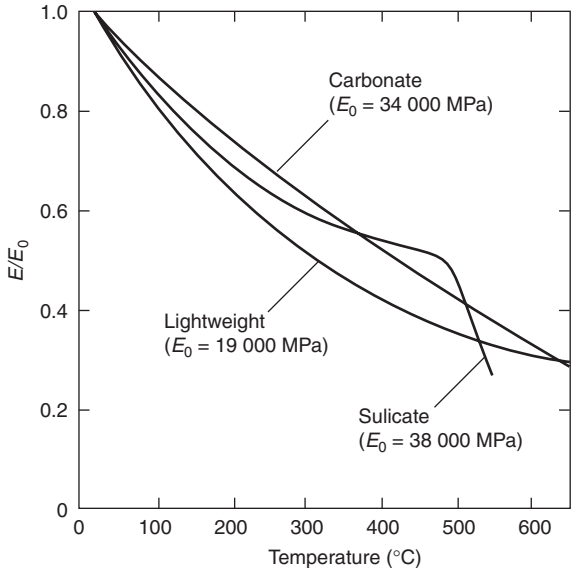

Figure 1-10.16. ***The effect of temperature on the modulus of elasticity of concretes with various aggregates.[59]***

The compressive strength (σ_u) of NSC may also vary within a wide range. Compressive strength is influenced by the same factors as the modulus of elasticity. For conventionally produced normal-weight concretes, the strength at room temperature is usually between 20 and 50 MPa. For lightweight concretes, the strength is usually between 20 and 40 MPa.

Information on the variation of the compressive strength with temperature is presented in Figure 1-10.17 (for a silicate aggregate concrete), Figure 1-10.18 (for a carbonate aggregate concrete), and Figure 1-10.19 (for two lightweight aggregate concretes, one made with the addition of natural sand).[60] [$(\sigma_u)_0$ in the figures stands for the compressive strengths of concrete at room temperature.] In some experiments, the specimens were heated to the test temperature without load (see curves labeled "unstressed"). In others they were heated under a load amounting to 40 percent of the ultimate strength (see curves labeled "stressed"). Again, in others they were heated to the target temperature without load, then cooled to room temperature and stored at 75 percent relative humidity for six days, and finally tested at room temperature (see curves labeled "unstressed residual").

Some information on the creep of concrete at elevated temperatures is available from the work of Cruz,[61] Mare-

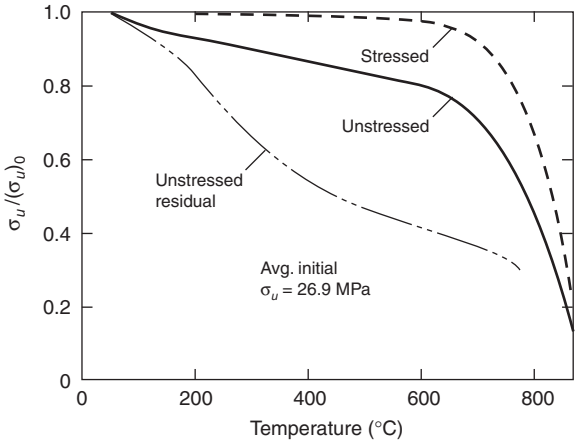

Figure 1-10.17. ***The effect of temperature on the compressive strength of a normal-weight concrete with silicate aggregate.[60]***

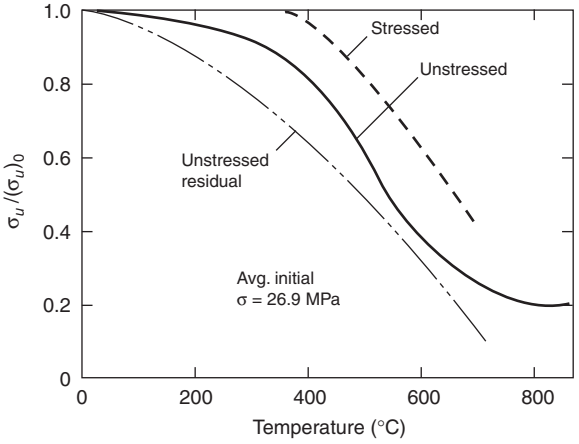

Figure 1-10.18. ***The effect of temperature on the compressive strength of a normal-weight concrete with carbonate aggregate.[60]***

Âchal,[62] Gross,[63] and Schneider et al.[64] The creep curves shown in Figure 1-10.20 are those recorded by Cruz for a normal-weight concrete with carbonate aggregates.

Since the aggregates amount to 60 to 75 percent of the volume of concrete, the dilatometric curve usually resembles that of the principal aggregate. However, some lightweight aggregates, for example, pearlite and vermiculite,

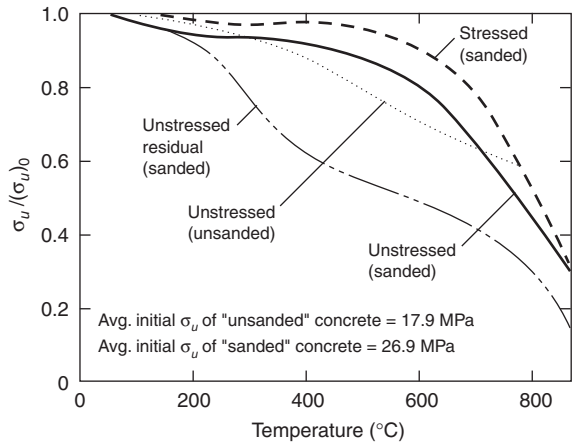

Figure 1-10.19. ***The effect of temperature on the compressive strength of two lightweight concretes (one with natural sand).[60]***

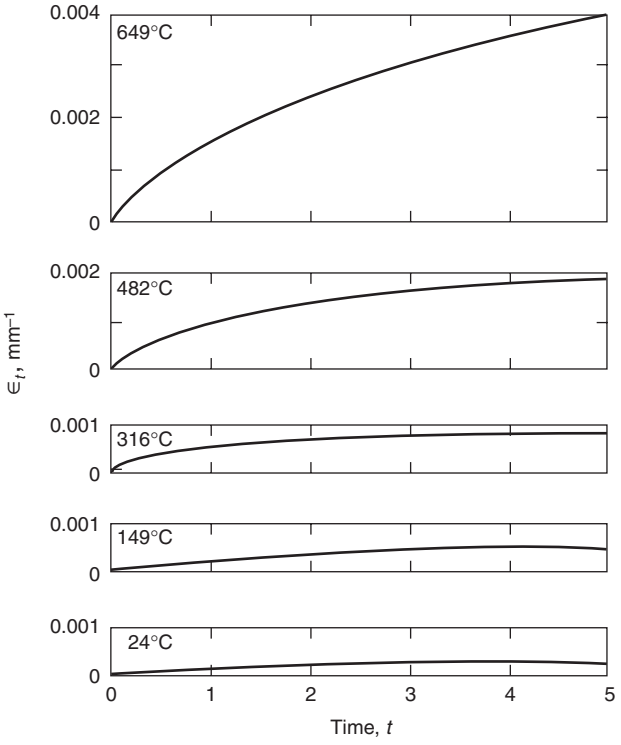

Figure 1-10.20. ***Creep of a carbonate aggregate concrete at various temperature levels (applied stress:12.4 MPa; compressive strength of the material at room temperature: 27.6 MPa).[61]***

are unable to resist the almost continuous shrinkage of the cement paste on heating, and therefore their dilatometric curves bear the characteristic features of the curve for the paste.

The dilatometric curves of two normal-weight concretes (with silicate and carbonate aggregates) and two lightweight concretes (with expanded shale and pumice aggregates) are shown in Figure 1-10.21.[19] These curves were obtained in the course of a comprehensive study performed on 16 concretes.

The results of dilatometric and thermogravimetric tests were combined to calculate the density (ρc_p) versus temperature relation for these four concretes, as shown in Figure 1-10.22. The partial decomposition of the aggregate is responsible for a substantial drop (above 700°C) in the density of concretes made with carbonate aggregate.

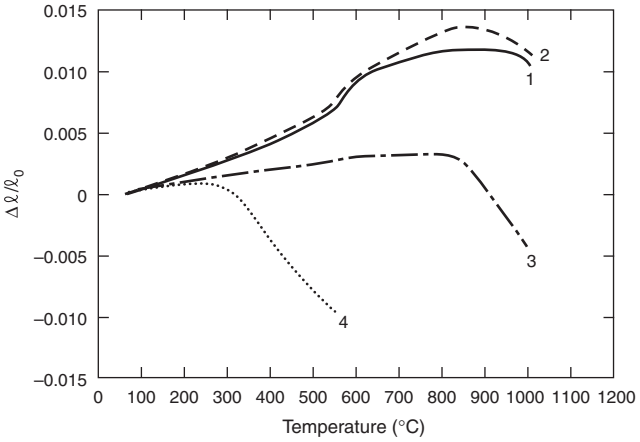

Figure 1-10.21. ***Dilatometric curves for two normal-weight and two lightweight concretes.[19] (1) normal-weight concrete with silicate aggregate, (2) normal-weight concrete with carbonate aggregate, (3) lightweight concrete with expanded shale aggregate, (4) lightweight concrete with pumice aggregate.***

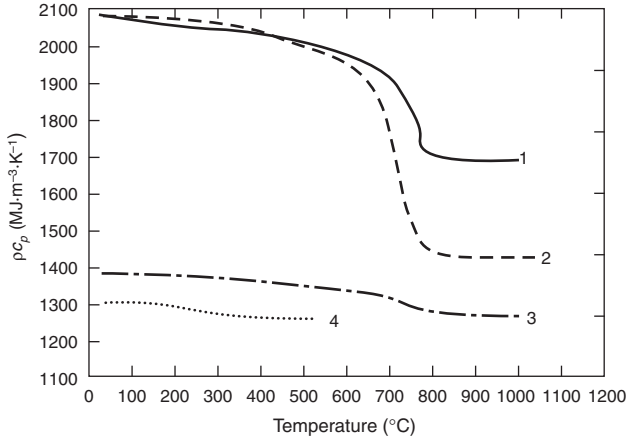

Figure 1-10.22. ***Density of two normal-weight and two lightweight concretes.[19] (1) normal-weight concrete with silicate aggregate, (2) normal-weight concrete with carbonate aggregate, (3) lightweight concrete with expanded shale aggregate, (4) lightweight concrete with pumice aggregate.***

The aggregate type and moisture content have significant influence on the specific heat of concrete. The usual ranges of variation of the volume-specific heat (i.e., the product ρc_p) for normal-weight and lightweight concretes is shown in Figure 1-10.23. This information, derived by combining thermodynamic data with thermogravimetric observations,[2,6] has since been confirmed by differential scanning calorimetry.[7] Experimental data are also available on a few concretes and some of their constituents.[2,7]

The thermal conductivity (k) of concrete depends mainly on the nature of its aggregates. In general, concretes made with dense, crystalline aggregates show higher conductivities than those made with amorphous or porous aggregates. Among common aggregates, quartz has the highest conductivity; therefore, concretes made with siliceous aggregates are on the whole more conductive than those made with other silicate and carbonate aggregates.

Derived from theoretical considerations,[6] the solid curves in Figure 1-10.24 describe the variation with temperature of the thermal conductivity of four concretes. In deriving these curves, two concretes (see curves 1 and 2) were visualized to represent limiting cases among normal-weight concretes, and the other two (see curves 3 and 4), limiting cases among lightweight concretes. The points in Figure 1-10.24 stand for experimental data. They reveal that the upper limiting case is probably never reached with aggregates in common use, and that the thermal conductivity of lightweight concretes may be somewhat higher than predicted on theoretical considerations.

Further experimental information on the thermal conductivity of some normal-weight and many lightweight concretes is available from the literature.[6,7,19]

Fiber-Reinforced Concrete

Steel and polypropylene discontinuous fibers are the two most common fibers used in the concrete mix to im-

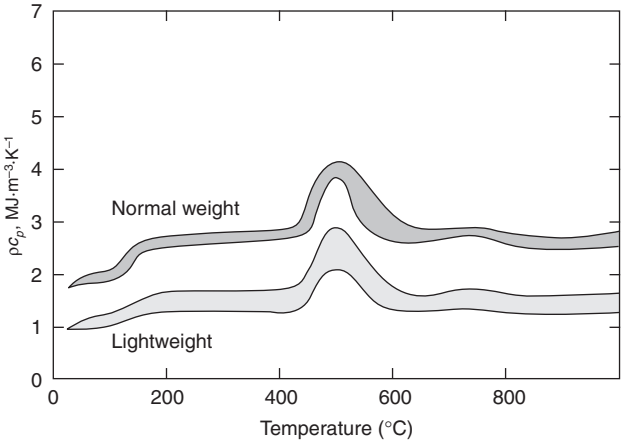

Figure 1-10.23. ***Usual ranges of variation for the volume-specific heat of normal-weight and lightweight concretes.[6]***

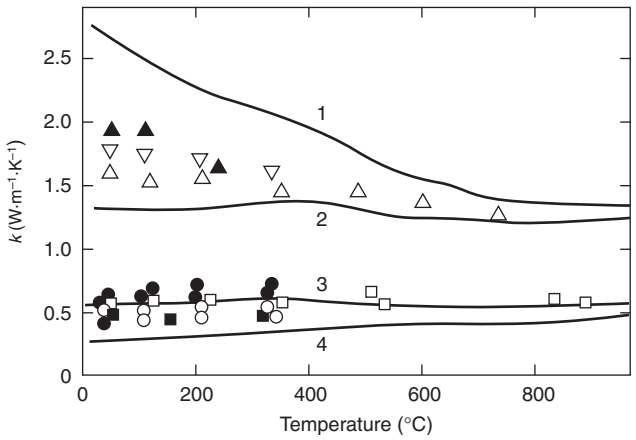

Figure 1-10.24. ***Thermal conductivity of four "limiting" concretes and some experimental thermal conductivity data.[6,19] Symbols: ▲, ▽—various gravel concretes; ●—expanded slag concretes; ■, □—expanded shale concretes; ○—pumice concrete.***

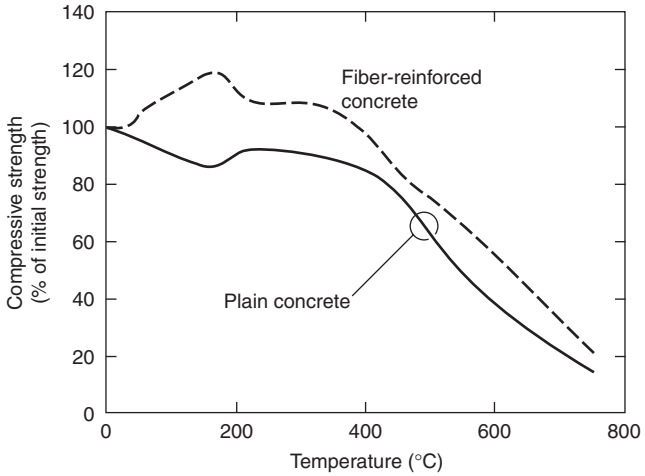

Figure 1-10.25. ***Effect of temperature on compressive strength of steel fiber–reinforced concrete.***

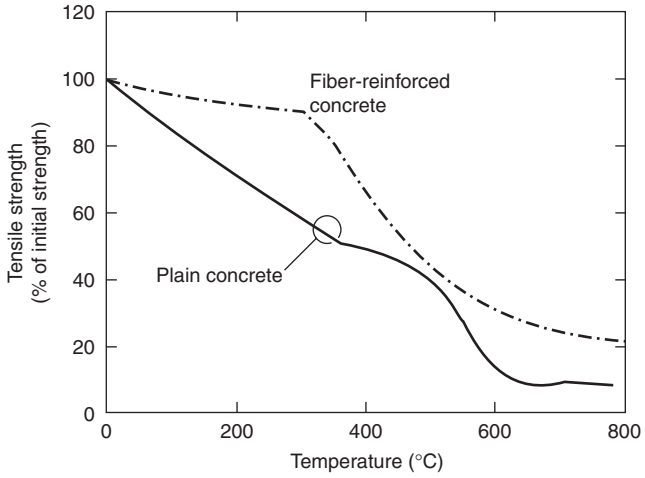

Figure 1-10.26. ***Effect of temperature on tensile strength of steel fiber–reinforced concrete.***

prove structural properties of concrete. Studies have shown that polypropylene fibers in a concrete mix are quite effective in minimizing spalling in concrete under fire conditions.[65,66] The polypropylene fibers melt at a relatively low temperature of about 170°C and create channels for the steam pressure in concrete to escape. This prevents the small explosions that cause the spalling of the concrete. Based on these studies, the amount of polypropylene fibers needed to minimize spalling is about 0.1 to 0.25 percent (by volume). The polypropylene fibers were found to be most effective for HSC made with normal-weight aggregate.

The addition of fibers improves certain mechanical properties, such as tensile strength, ductility, and ultimate strain, at room temperature. However, there is very little information on the high-temperature properties of this type of concrete.[67]

Steel fiber–reinforced concrete (SFRC) exhibits, at elevated temperatures, mechanical properties that are more beneficial to fire resistance than those of plain concrete. There is some information available on SFRC's material properties at elevated temperatures. The effect of temperature on the compressive strength for two types of SFRC is shown in Figure 1-10.25. The strength of both types of SFRC exceeds the initial strength of the concretes up to about 400°C. This is in contrast to the strength of plain concrete, which decreases slightly with temperatures up to 400°C. Above approximately 400°C, the strength of SFRC decreases at an accelerated rate.[68]

The effect of temperature on the tensile strength of steel fiber–reinforced carbonate concretes is compared to that of plain concrete in Figure 1-10.26.[69] The strength of SFRC decreases at a lower rate than that of plain concrete throughout the temperature range, with the strength being significantly higher than that of plain concrete up to about 350°C. The increased tensile strength delays the propagation of cracks in fiber-reinforced concrete structural members and is highly beneficial when the member is subjected to bending stresses.

The type of aggregate has a significant influence on the tensile strength of steel fiber–reinforced concrete. The decrease in tensile strength for carbonate aggregate concrete is higher than that for siliceous aggregate concrete.[69]

The thermal properties of SFRC, at elevated temperatures, are similar to those of plain concrete. Kodur and Lie[26,67] have carried out detailed experimental studies and developed dilatometric and thermogravimetric curves for various types of SFRC. Based on these studies, they have also developed expressions for thermal and mechanical properties of steel fiber–reinforced concrete, in the temperature range 0 to 1000°C.[70]

High-Strength Concrete

The strength of concrete has significant influence on the properties of HSC. The material properties of HSC vary differently with temperature than those of NSC. This

variation is more pronounced for mechanical properties, which is affected by these factors: compressive strength, moisture content, density, heating rate, percentage of silica fume, and porosity. The available information on the mechanical properties of HSC at elevated temperatures is presented in a review report by Phan.[29]

The loss in compressive strength with temperature is higher for HSC than that for NSC up to about 450°C. Figure 1-10.27 shows the comparison of strengths for NSC and HSC types, together with CEB and European design curves for NSC. The difference between compressive strength versus temperature relationships of normal-weight and lightweight aggregate concrete is not significant. However, HSC mixture with silica fume have higher strength loss with increasing temperature than HSC mixture without silica fume. The variation, with temperature, of modulus of elasticity and tensile strength of HSC is similar to that of NSC.

Kodur and Sultan have presented detailed experimental data on the thermal properties of HSC (for both plain and steel fiber–reinforced concrete types).[71] The type of aggregate has significant influence on the thermal properties of HSC at elevated temperatures. Figure 1-10.28 shows the thermal conductivity and specific heat of HSC, with siliceous and carbonate aggregates, as a function of temperature.

The variation of thermal expansion with concrete temperature for siliceous and carbonate aggregate HSC is similar to that of NSC, with the aggregate having a strong influence. Overall, the thermal properties of HSC, at elevated temperatures, are similar to those of NSC.

HSC, due to low porosity, is more susceptible to spalling than NSC, and explosive spalling may occur when HSC is exposed to severe fire conditions. Hence, one of the major concerns for the use of HSC is regarding its behavior in fire, in particular, the occurrence of spalling at elevated temperatures. For predicting spalling performance, knowledge of the variation of porosity with temperature is essential. Figure 1-10.29 shows the variation of porosity with temperature for NSC and HSC. The data in this figure are taken from the measurements of porosity after exposure to different temperatures.[35]

The spalling in HSC can be minimized by creating pores through which water vapor can be relieved before vapor pressure reaches critical values. This is usually done by adding polypropylene fibers to the HSC.[65,66,72]

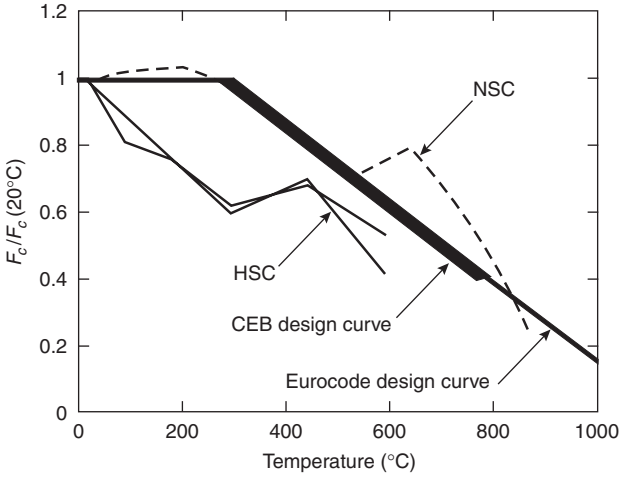

Figure 1-10.27. ***Comparison of design compressive strength and results of unstressed tests of lightweight aggregate concrete.[29]***

Brick

Building brick belongs in the L/I group of materials. The density (ρ) of bricks ranges from 1660 to 2270 kg·m^{-3}, depending on the raw materials used in the manufacture, and on the molding and firing technique. The true density

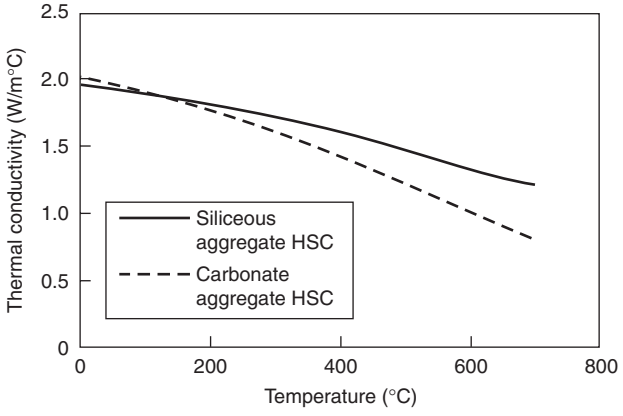

(a)

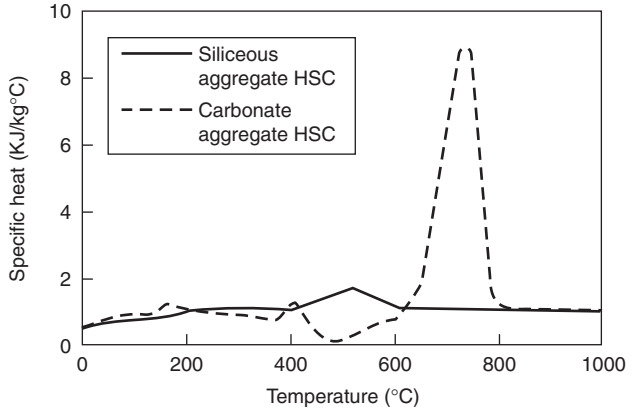

(b)

Figure 1-10.28. ***Thermal conductivity and specific heat capacity of HSC as a function of temperature:[71] (a) thermal conductivity of high-strength concrete, and (b) specific heat of high-strength concrete.***

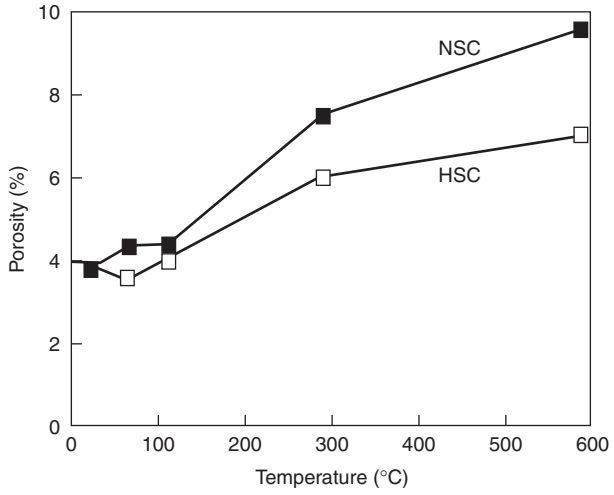

Figure 1-10.29. ***Porosity of HSC and NSC as a function of temperature.[35]***

of the material (ρ_t) is somewhere between 2600 and 2800 kg·m^{-3}.

The modulus of elasticity of brick (E) is usually between 10×10^3 and 20×10^3 MPa. Its compressive strength (σ_u) varies in a very wide range, from 9 to 110 MPa—50 MPa may be regarded as average.[73] This value is an order of magnitude greater than the stresses allowed in the design of grouted brickwork. Since brick is rarely considered for important load-bearing roles in buildings, there has been little interest in the mechanical properties of bricks at elevated temperatures.

At room temperature, the coefficient of thermal expansion (α) for clay bricks is about 5.5×10^{-6} m·m^{-1}·K^{-1}. The dilatometric and thermogravimetric curves for a clay brick of 2180 kg·m^{-3} density are shown in Figure 1-10.30.[7] The variation with temperature of the specific heat and the thermal conductivity of this brick is shown in Figures 1-10.31 and 1-10.32, respectively.[7]

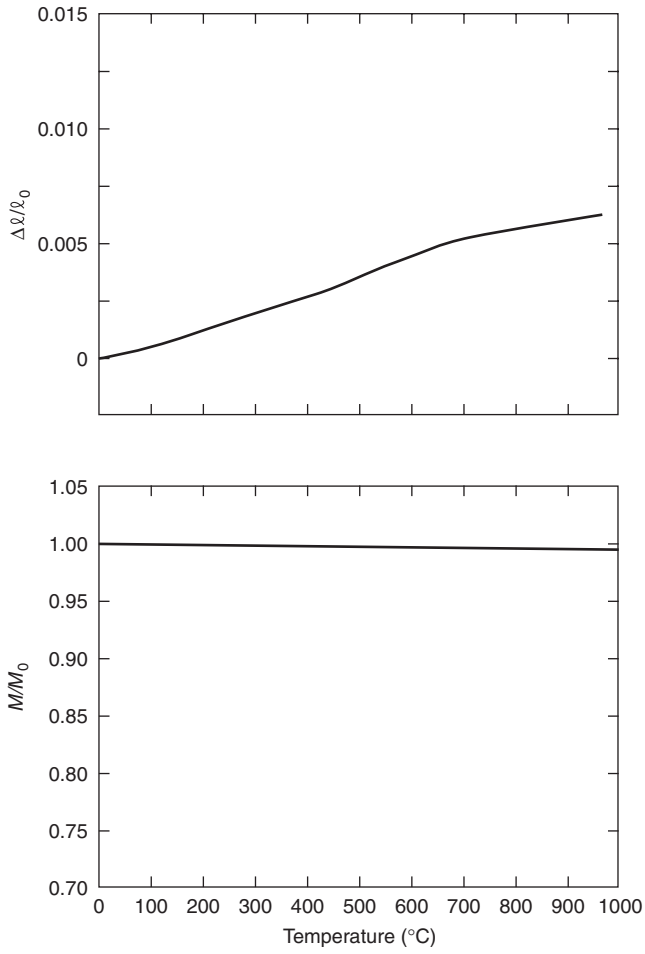

Figure 1-10.30. ***Dilatometric and thermogravimetric curves for a clay brick.[7]***

Wood

Wood is a Group L/I/F or I/F material. As structural members, wood is widely used in residential and low-rise constructions. Although about 180 wood species are commercially grown in the United States, only about 25 species have been assigned working stresses. The two groups most extensively used as structural lumber are the Douglas firs and the southern pines.

The oven-dry density (ρ) of commercially important woods ranges from 300 kg·m^{-3} (white cedar) to 700 kg·m^{-3} (hickory, black locust). The density of Douglas firs varies from 430 to 480 kg·m^{-3}, and that of southern pines, from 510 to 580 kg·m^{-3}. The true density of the solid material that forms the walls of wood cells (α_t) is about 1500 kg·m^{-3} for all kinds of wood. The density of wood decreases with temperature; the density ratio (ratio of density at room temperature to that at elevated temperature) drops to

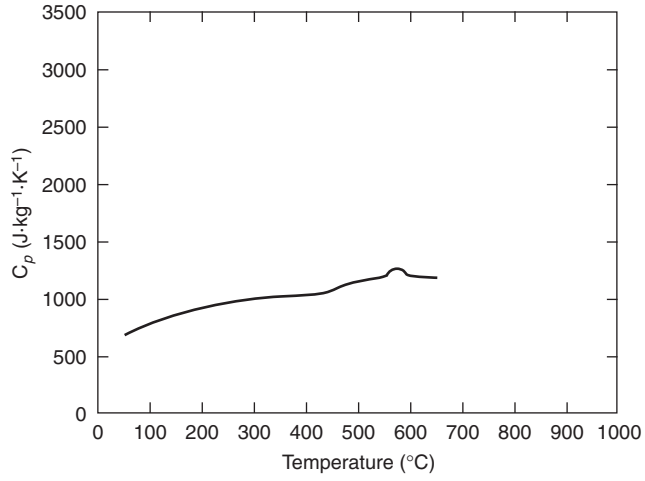

Figure 1-10.31. ***Apparent specific heat of a clay brick.[7]***

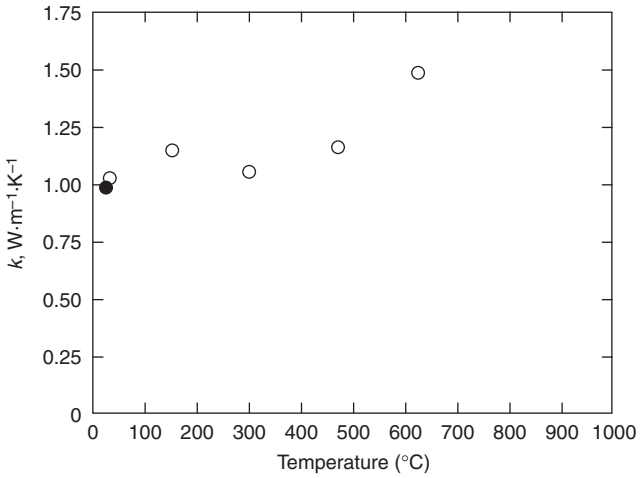

Figure 1-10.32. ***Thermal conductivity of a clay brick. Symbols: ○—heating cycle, ●—after cooling.[7]***

about 0.9 at 200°C and then declines sharply to about 0.2 at about 350°C.[39]

Wood is an orthotropic material, so the strength and stiffness in longitudinal and transverse directions are influenced by grain orientation. The mechanical properties of wood are affected by temperature and are influenced by moisture content, rate of charring, and grain orientation. The modulus of elasticity (E) of air-dry, clear wood along the grain varies from 5.5×10^3 to 15.0×10^3 MPa, and its crushing strength (σ_u) varies from 13 to 70 MPa. These properties are related and roughly proportional to the density, regardless of the species.[74]

Figure 1-10.33 shows the variation of the modulus of elasticity and compressive strength of oven-dry, clear wood with temperature.[75–77] [E_0 and $(\sigma_u)_0$ in the figure are modulus of elasticity and compressive strength at room temperature, respectively]. The modulus of elasticity decreases slowly with temperature up to about 200°C, when it reaches about 80 percent, and then the decline is more rapid. The compressive strength also drops linearly to about 80 percent at about 200°C, and then the drop is more rapid—to about 20 percent around 280°C.

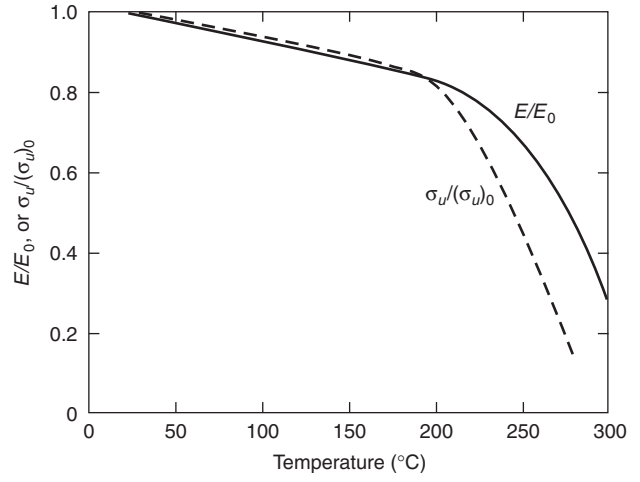

Figure 1-10.33. ***The effect of temperature on the modulus of elasticity and compressive strength of wood.[75–77]***

The tensile strength exhibits behavior similar to that of compressive strength, but the decline in tensile strength with temperature is less rapid. The moisture content plays a significant role in determining the strength and stiffness, with increased moisture content leading to higher reduction. There is very little information on stress-strain relationships for wood. The formulas for reduced stiffness and design strength can be found in Eurocode 5[78] (Part 1.2).

The coefficient of linear thermal expansion (β) ranges from 3.2×10^{-6} to 4.6×10^{-6} m·m^{-1}·K^{-1} along the grain, and from 21.6×10^{-6} to 39.4×10^{-6} m·m^{-1}·K^{-1} across the grain.[79] Wood shrinks at temperatures above 100°C, because of the reduction in moisture content. Lie[28] reported that the amount of shrinkage can be estimated as 8 percent in the radial direction, 12 percent in tangential direction, and an average of 0.1 to 0.2 percent in the longitudinal direction. The dilatometric and thermogravimetric curves of a pine with a 400 kg·m^{-3} oven-dry density are shown in Figure 1-10.34.[7]

The thermal conductivity (k) across the grain of this pine was measured as 0.86 to 0.107 W·m^{-1}·K^{-1} between room temperature and 140°C.[13] The thermal conductivity increases initially up to a temperature range of 150 to 200°C, then decreases linearly up to 350°C, and finally increases again beyond 350°C.

Figure 1-10.35 shows the apparent specific heat for the same pine, as a function of temperature.[7] The accuracy of the curve [developed by differential scanning calorimeter (DSC)] is somewhat questionable. However, it provides useful information on the nature of decomposition reactions that take place between 150 and 370°C.

Charring is one of the main high-temperature properties associated with wood and should be considered in predicting performance under fire conditions. The rate of charring is influenced by the radiant heat flux or, alternatively, the fire severity. Generally, a constant transverse-to-grain char rate of 0.6 mm/min can be used for woods subjected to standard fire exposure.[28] The charring rate parallel to the grain of wood is approximately twice the rate when it is transverse to the grain. These charring rates should be used only when attempting to model the performance of wood sections in the fire resistance furnace.

Charring is influenced by a number of parameters, the most important ones being density, moisture content, and contraction of wood. It is reasonable to modify the 0.6 mm/min to approximately 0.4 mm/min for moist dense wood, or to 0.8 mm/min for dry and light wood. The fire retardants, often used to reduce flame spread in wood on charring rate, may only slightly increase the time until ignition of wood.

Specific charring rates for different types of wood can be found in References 28 and 39. Eurocode[78] gives an expression for charring depth in a wood member exposed to standard fire.

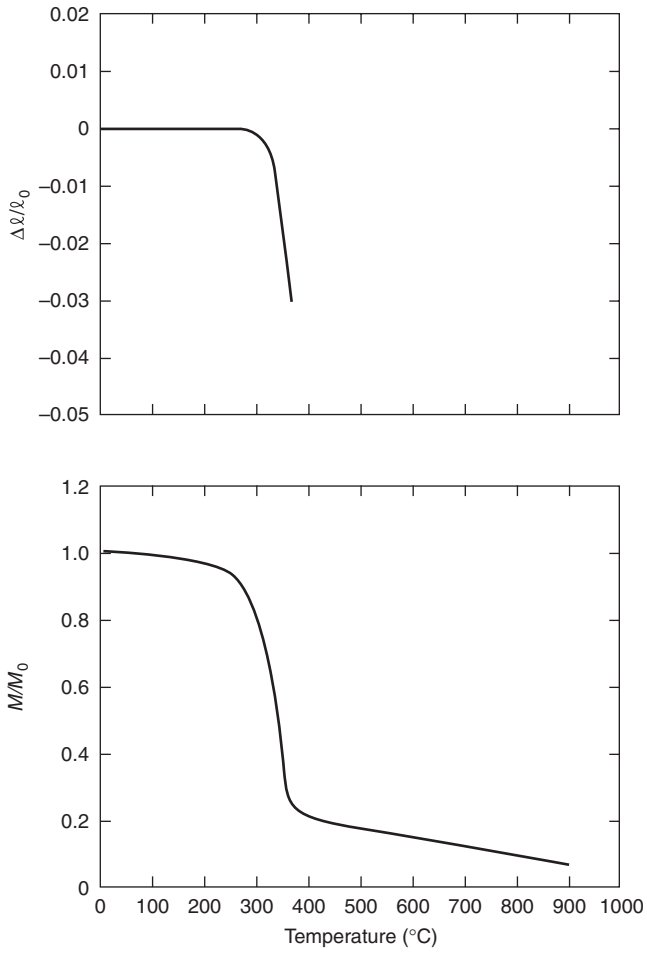

Figure 1-10.34. ***Dilatometric and thermogravimetric curves for a pine of 400 kg·m^{-3} density.***[7]

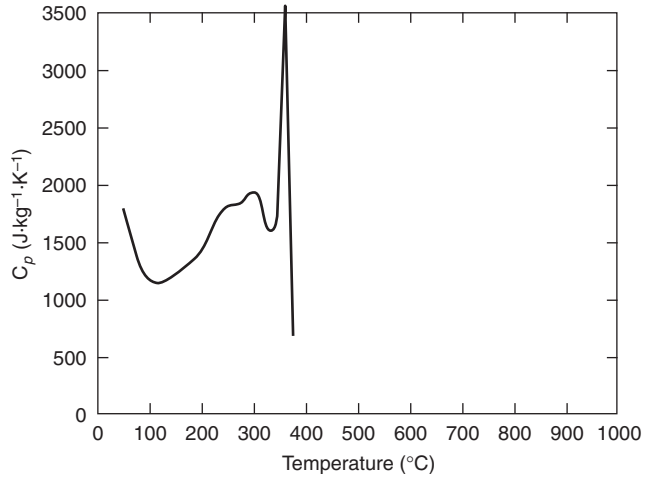

Figure 1-10.35. ***Apparent specific heat for a pine of 400 kg·m^{-3} density.***[7]

Fiber-Reinforced Polymers

In recent years, there has been a growing interest in the use of fiber-reinforced polymers (FRPs) in civil engineering applications due to the advantages, such as high strength and durability (resistance to corrosion), that FRP offers over traditional materials. FRP composites consist of two key elements, namely the fibers (glass, carbon, or aramid) and a thermosetting polymer matrix such as epoxy, vinyl ester, phenolic, or polyester resin. The commonly used types of FRP composite materials are glass fiber–reinforced plastic (GFRP), carbon fiber–reinforced plastic (CFRP), and aramid fiber–reinforced plastic (AFRP) composites. FRPs are similar to wood in that they will burn when exposed to fire and can be classifed as an L/I/F type material.

FRP is used as an internal reinforcement (reinforcing bars as an alternative to traditional steel reinforcement) and as external reinforcement in forms, such as wrapping and sheeting for the rehabilitation and strengthening of concrete members. One of the main impediments to using FRPs in buildings is the lack of knowledge about the fire resistance of FRP.[80,81]

There are some major differences associated with FRP as a material. The properties depend on the type and composition of FRP, and the availability of various types of FRP makes it difficult to establish the properties at elevated temperatures. The material properties are controlled by the fibers in the longitudinal direction, and by the matrix in the transverse direction. In addition to thermal and mechanical properties, factors such as burning, charring, evolution of smoke, and toxicity in fire also play a significant role in determining the fire performance. A summary of typical mechanical properties for various types of FRPs, in comparison to other commonly used construction materials, at room temperatures, is presented in Table 1-10.3.

There is very little information on the material properties of FRPs at elevated temperatures.[80] The impact of high temperatures on the behavior of FRP composites is severe degradation of its properties: reduction of strength and stiffness, and increase in deformability, thermal expansion, and creep. Above 100°C temperature, the degradation can be quite rapid as the glass transition temperature of the matrix is reached.

The glass transition temperature, which is often considered the upper use temperature, varies with the type of resin used and was found to be as low as 100°C in some resins and as high as 220°C in others. From the limited studies, it appears that as much as 75 percent of the GFRP strength and stiffness is lost by the time the temperature reaches 250°C.[80,82]

The stress-strain relationships, from the studies conducted by Gates,[82] for a CFRP composite (IM7/5260) are shown in Figure 1-10.36 for various temperatures. It can be seen that the tensile strength of IM7/5260 composite reduces to approximately 50 percent at about 125°C, and to about 75 percent at a temperature of 200°C. The strain level, for a given stress, is also higher with the increase in temperature.

Table 1-10.3 ***Properties of Various FRP Composites and Other Materials***

Material	Modulus of Elasticity E_1 (MPa)	Modulus of Elasticity E_2 (MPa)	Tensile Strength σ_{t1} (MPa)	Comp. Strength σ_{c1} (MPa)	Shear Modulus G (MPa)	Shear Strength S (MPa)	Poisson's Ratio ν	Tensile Strength σ_2 (MPa)	Comp. Strength σ_{c2} (MPa)
GFRP (glass/epoxy)	55,000	18,000	1,050	1,050	9,000	42	0.25	28	140
GFRP (glass/epoxy) unidirectional	42,000	12,000	700	—	5,000	72	0.30	30	—
CFRP (carbon/epoxy) unidirectional	180,000	10,000	1,500	—	7,000	68	0.28	40	—
CFRP (graphite/epoxy)	207,000	5,200	1,050	700	2,600	70	0.25	40	120
Boron/epoxy	207,000	21,000	1,400	2,800	7,000	126	0.30	84	280
ARP (aramid/epoxy) unidirectional	76,000	8,000	1,400	—	3,000	34	0.34	12	—
Mild steel	200,000	—	550	240	—	380	—	—	—
Concrete (normal strength)	31,000	—	~4	40	—	~7	0.15–0.20	—	—
Douglas fir	9,800	—	69	—	—	—	—	—	—

E_1 = modulus of elasticity in longitudinal direction
E_2 = modulus of elasticity in transverse direction

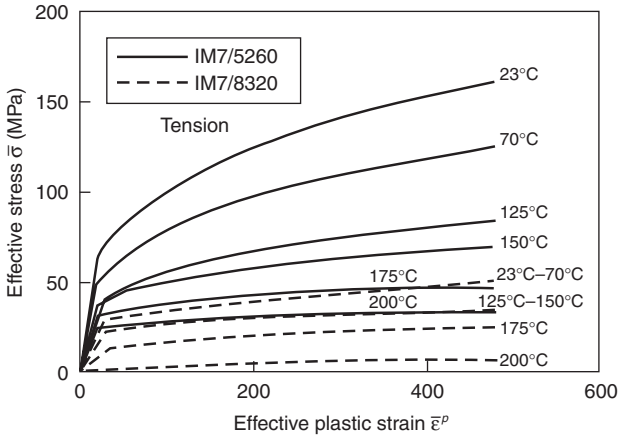

Figure 1-10.36. ***Tensile stress-strain curves for CFRP at various temperatures.[82]***

The variation of strength with temperature (ratio of strength at elevated temperature to that at room temperature) for FRP along with that of other traditional construction materials is shown in Figure 1-10.2. The curve showing the strength degradation of FRP is based on the limited information reported in the literature.[80,82] The rate of strength loss is much greater for FRP than for concrete and steel, resulting in a 50 percent strength loss by about 200°C.

The critical temperature of FRP is much lower than that for steel and depends on the composition of fibers and matrix. Kodur and Baingo have assumed a critical temperature of 250°C in modeling the behavior of FRP-reinforced concrete slabs.[80]

The variation of elastic moduli of FRP with temperature is different in each direction. Typical values for various types of FRP are given in Table 1-10.3.[80] The three values represent the longitudinal, transverse, and shear moduli, respectively, of different unidirectional FRPs. At high temperature, the elastic moduli of FRPs decreases at a faster rate than that for concrete or steel.

Similar to mechanical properties, the thermal properties of FRP are also dependent on direction, fiber type, fiber orientation, fiber volume fraction, and laminate configuration. Table 1-10.4 shows thermal properties for various types of FRP at room temperature. In the longitudinal direction, the thermal expansion of FRPs is lower than that of steel. However, in the transverse direction, it is much higher than that of steel. Some of the information available in the literature can be found in a review report by Kodur and Baingo.[80] At room temperatures, FRPs in general have low thermal conductivity, which makes them useful as insulation materials. With the exception of carbon fibers, FRPs have a low thermal conductivity.

Information on the thermal properties of FRP at elevated temperatures is very scarce, which is likely due to the fact that such information is proprietary to the composite materials' manufacturers. Also, there is not much information on evolution of smoke and toxins in FRP composites exposed to fire.

Gypsum

Gypsum (calcium sulfate dihydrate: $CaSO_4 \cdot 2H_2O$) is a Group I material. Gypsum board is produced by mixing water with plaster of paris (calcium sulfate hemihydrate: $CaSO_4 \cdot \frac{1}{2}H_2O$) or with Keene's cement (calcium sulfate an-

Table 1-10.4 ***Thermal Properties of Various FRPs and Other Materials at Room Temperature***

Material	Coefficient of Thermal Expansion (Unidirectional) (β: 10^{-6} m·m^{-1}·°C)		Thermal Conductivity k (W·m^{-1}·°C^{-1})	
	Longitudinal α_L	Transverse α_T	Longitudinal k_L	Transverse k_T
Glass/epoxy (S-glass)	6.3	19.8	3.46	0.35
Glass/epoxy (E-glass: 63% fiber)	7.13	—	—	—
Carbon/epoxy (high modulus)	–0.9	27	48.4–60.6	0.865
Carbon/epoxy (ultra-high modulus)	–1.44	30.6	121.1–129.8	1.04
Boron/epoxy	4.5	14.4	1.73	1.04
Aramid/epoxy (Kevlar 49)	–3.6	54	1.73	0.73
Concrete	6.16		1.36–1.90	
Steel	10.8–18		15.6–46.7	
Epoxy	—	54–90	—	0.346

hydrite: $CaSO_4$). The interlocking crystals of $CaSO_4 \cdot 2H_2O$ are responsible for the hardening of the material.

Gypsum products are used extensively in the building industry in the form of boards, including wallboard, formboard, and sheathing. The core of the boards is fabricated with plaster of paris, into which weight- and set-controlling additives are mixed. Furthermore, plaster of paris, with the addition of aggregates (such as sand, pearlite, vermiculite, or wood fiber) is used in wall plaster as base coat, and Keene's cement (neat or mixed with lime putty) is used as finishing coat.

Gypsum board, based on composition and performance, is classified into various types, such as regular gypsum board, type X gypsum board, and improved type X gypsum board. A gypsum board with naturally occurring fire resistance from the gypsum in the core is defined as regular gypsum. When the core of the gypsum board is modified with special core additives or with enhanced additional properties, to improve the natural fire resistance from regular gypsum board, it is classified as type X or improved type X gypsum board. There might be significant variation in fire performance of the gypsum board based on the type and the formulation of the core, which varies from one manufacturer to another.

Gypsum is an ideal fire protection material. The water inside the gypsum plays a major role in defining its thermal properties and response to fire. On heating, it will lose the two H_2O molecules at temperatures between 125 and 200°C. The heat of complete dehydration is 0.61×10^6 J per kg gypsum. Due to the substantial absorption of energy in the dehydration process, a gypsum layer applied to the surface of a building element is capable of markedly delaying the penetration of heat into the underlying load-bearing construction.

The thermal properties of the gypsum board vary depending on the composition of the core. The variation with temperature of the volume specific heat (ρc_p) of pure gypsum has been illustrated in Reference 83, based on information reported in the literature.[84,85] The thermal conductivity of gypsum products is difficult to assess, owing to large variations in their porosities and the nature of the aggregates. A typical value for plaster boards of about 700 kg·m^{-3} density is 0.25 W·m^{-1}·K^{-1}. Figures 1-10.37 and 1-10.38 illustrate the typical variation of the thermal conductivity and the specific heat, respectively, of the gypsum

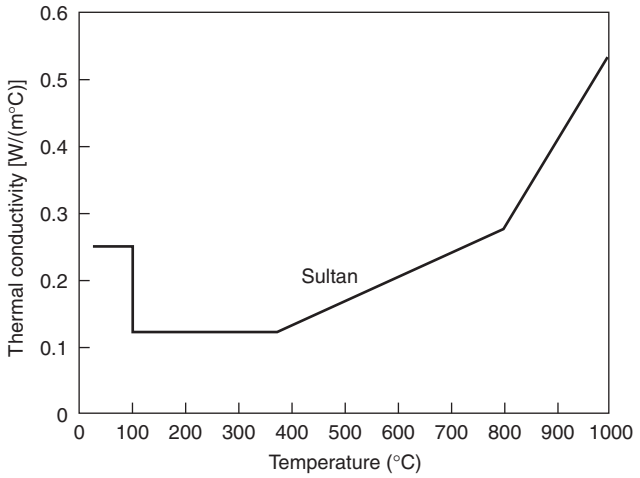

Figure 1-10.37. ***Thermal conductivity of type X Gypsum board core as a function of temperature.[86]***

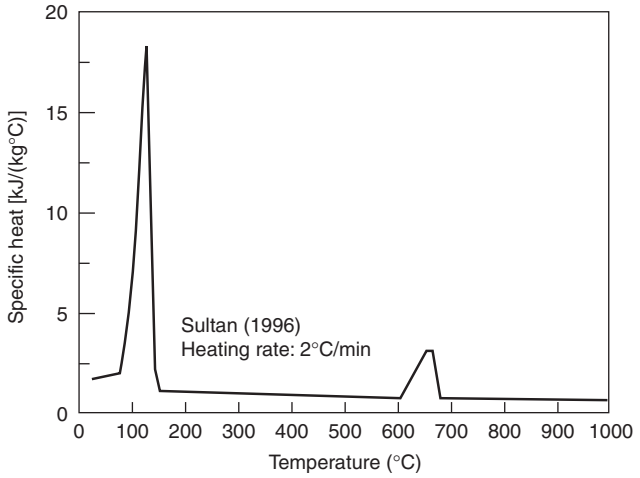

Figure 1-10.38. ***Specific heat of type X Gypsum board core as a function of temperature.[86]***

board core with temperature. The plots reflect the expressions proposed recently by Sultan,[86] based on tests conducted on type X gypsum board specimens. The specific heat measurements were carried out at a heating rate of 2°C/min. The dehydration of gypsum resulted in the two peaks that appear in the specific heat curve at temperatures around 100°C and 650°C. The peak values are slightly variant to those reported earlier by Harmathy;[14] this may be due to the differences in gypsum composition.

The coefficient of thermal expansion (β) of gypsum products may vary between 11.0×10^{-6} and 17×10^{-6} $m \cdot m^{-1} \cdot K^{-1}$ at room temperature, depending on the nature and amount of aggregates used. The dilatometric and thermogravimetric curves of a so-called fire-resistant gypsum board of 678 $kg \cdot m^{-3}$ density are shown in Figure 1-10.39.

There is not much information about the mechanical properties of the gypsum board at elevated temperatures because these properties are difficult to obtain experimentally. The strength of gypsum board at an elevated temperature is very small and can be neglected. The Gypsum Association[87] lists typical mechanical properties, at room temperature, for some North American gypsum board products. The attachment details (screw spacing, orientation of gypsum board joints, stud spacing, etc.) may have a noticeable effect on the fire performance of the gypsum board.

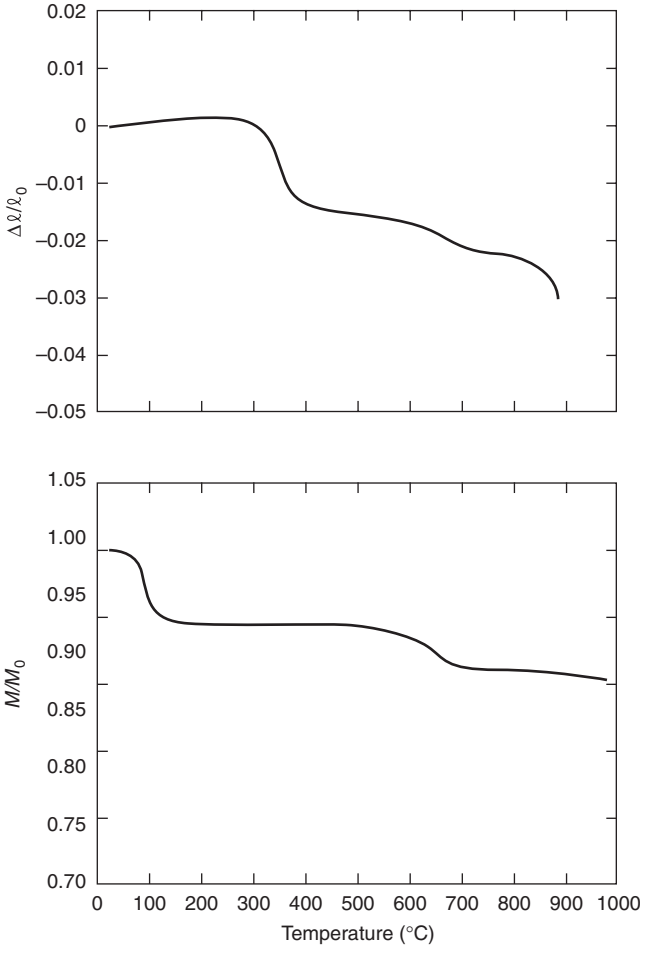

Figure 1-10.39. ***Dilatometric and thermogravimetric curves for a Gypsum board of 678 kg·m⁻³ density.[7]***

Insulation

Insulation is a Group I material and is often used as a fire protection material for both heavy structural members such as columns and beams, and for lightweight framing assemblies such as floors and walls. The insulation helps delay the temperature rise of structural members, thereby enhancing fire resistance. There are a number of insulation materials available in the market. Mineral wool and glass fiber are the two most widely used insulation materials in walls and floors.

The thermal properties of insulation play an important role in determining the fire resistance. However, there is not much information available on the thermal properties of various types of insulation. Figure 1-10.40 shows the variation of thermal conductivity with temperature for glass and rock fiber insulation types. The differences in thermal conductivity values at higher temperatures are mainly due to variation in the chemical composition of fiber.

Full-scale fire resistance tests on walls and floors have shown that the mineral fiber insulation performs better than glass fiber insulation. This is mainly because glass fiber melts in the temperature range of 700 to 800°C and cannot withstand direct fire exposure. The melting point for mineral fiber insulation is higher. The density of glass fiber is about 10 kg/m^3 and is much lower than that of rock fiber, which is about 33 kg/m^3.

The mineral wool insulation, when installed tightly between the studs, can be beneficial for the fire resistance of non-load-bearing steel stud walls because it acts as an additional fire barrier after the fire-exposed gypsum

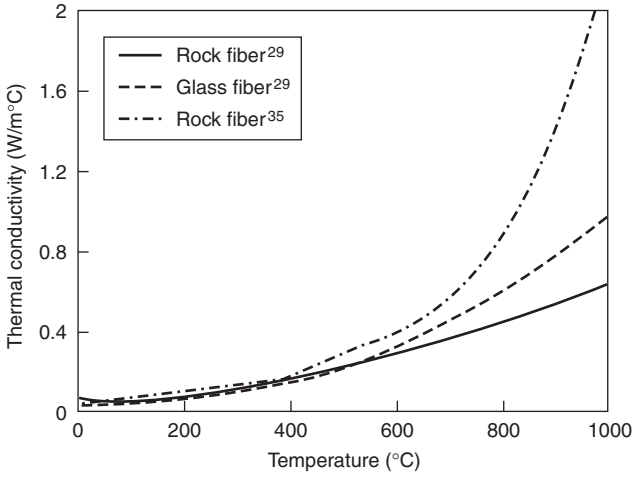

Figure 1-10.40. ***Thermal conductivity of insulation as a function of temperature.[39]***

board falls off.[88] On the other hand, cavity insulation slows down the flow of heat through the wall assembly and can cause an accelerated temperature rise in the fire-exposed gypsum board.

Other Miscellaneous Materials

Further information is available from the literature on the dilatometric and thermogravimetric behavior, apparent specific heat, and thermal conductivity of a number of materials in Group I, including asbestos cement board, expanded plastic insulating boards, mineral fiber fireproofing, arborite, and glass-reinforced cement board.[7] The properties of plastics and their behavior in fire are discussed in other chapters of this handbook and in Reference 2.

Summary

The use of numerical methods for the calculation of the fire resistance of various structural members is gaining acceptance. One of the main inputs needed in these models is the material properties at elevated temperatures. The thermal and mechanical properties of most materials change substantially within the temperature range associated with building fires.

Even to date, there is lack of adequate knowledge of the behavior of many building materials at elevated temperatures. While there is sufficient information available for some materials, such as normal-strength concrete and steel, there is a complete lack of information on certain properties for widely used materials, such as wood, insulation, and so on. Often, traditional materials are being modified (e.g., high strength concrete) to enhance their properties at room temperatures without giving due consideration to elevated temperatures. In many cases, these modifications will deteriorate the properties at elevated temperatures and introduce additional complexities, such as spalling in HSC.

In the field of fire science, applied materials research faces numerous difficulties. At elevated temperatures, many building materials undergo physicochemical changes. Most of the properties are temperature dependent and sensitive to testing method parameters such as heating rate, strain rate, temperature gradient, and so on. One positive note is that in the last two decades, there has been significant progress in developing measurement techniques and commercial instruments for measuring the properties. This will likely lead to further research in establishing material properties.

The review on material properties provided in this chapter is a broad outline of the available information. Additional details related to specific conditions on which these properties are developed can be found in cited references. Also, when using the material properties presented in this chapter, due consideration should be given to the material composition and other characteristics, such as fire and loading, since the properties at elevated temperatures depend on a number of factors.

Disclaimer: Certain commercial products are identified in this paper in order to adequately specify the experimental procedure. In no case does such identification imply recommendations or endorsement by the National Research Council, nor does it imply that the product or material identified is the best available for the purpose.

Nomenclature

a	material constant, dimensionless
b	constant, characteristic of pore geometry, dimensionless
c	specific heat ($J \cdot kg^{-1} \cdot K^{-1}$)
$\bar{c}$	specific heat for a mixture of reactants and solid products ($J \cdot kg^{-1} \cdot K^{-1}$)
E	modulus of elasticity (Pa)
h	enthalpy ($J \cdot kg^{-1}$)
Δh	latent heat associated with a "reaction" ($J \cdot kg^{-1}$)
ΔH_c	activation energy for creep ($J \cdot kmol^{-1}$)
k	thermal conductivity ($W \cdot m^{-1} \cdot K^{-1}$)
L_v	heat of gasification of wood
ℓ	dimension (m)
$\Delta \ell = \ell - \ell_0$	
m	exponent, dimensionless
M	mass (kg)
n	material constant, dimensionless
P	porosity ($m^3 \cdot m^{-3}$)
q_n	net heat flux to char front
R	gas constant (8315 $J \cdot kmol^{-1} \cdot K^{-1}$)
S	specific surface area ($m^2 \cdot m^{-3}$)
t	time (h)
T	temperature (K or °C)
ν	volume fraction ($m^{-3} \cdot m^3$)
w	mass fraction ($kg \cdot kg^{-1}$)
Z	Zener-Hollomon parameter (h^{-1})

Greek Letters

α	thermal diffusivity
β	coefficient of linear thermal expansion ($m \cdot m^{-1}$)
γ	expression defined by Equation 3, dimensionless
β_0	charring rate (mm/min)
δ	characteristic pore size (m)
ε	emissivity of pores, dimensionless
ε	strain (deformation) ($m \cdot m^{-1}$)
ε_{t0}	creep parameter ($m \cdot m^{-1}$)
$\dot{\varepsilon}_{ts}$	rate of secondary creep ($m \cdot m^{-1} \cdot h^{-1}$)
θ	temperature-compensated time (h)
ξ	reaction progress variable, dimensionless
π	material property (any)
ρ	density ($kg \cdot m^{-3}$)
σ	stress; strength (Pa)
σ	Stefan-Boltzmann constant (5.67×10^{-8} $W \cdot m^{-2} \cdot K^{-4}$)

Subscripts

a	of air
i	of the *i*th constituent
p	at constant pressure
s	of the solid matrix
t	true
t	time-dependent (creep)
T	at temperature *T*
u	ultimate
y	yield
0	original value, at reference temperature

References Cited

1. T.Z. Harmathy, *Technical Paper No. 242,* National Research Council of Canada, Ottawa (1967).
2. T.Z. Harmathy, *Fire Safety Design and Concrete,* Longman Scientific and Technical, Harlow, UK (1993).
3. D.A.G. Bruggeman, *Physik. Zeitschr.,* 37, p. 906 (1936).
4. R.L. Hamilton and O.K. Crosser, *I & EC Fundamen.,* 7, p. 187 (1962).
5. J.C. Maxwell, *A Treatise on Electricity and Magnetism,* 3rd ed., 1, Clarendon Press, Oxford, UK (1904).
6. T.Z. Harmathy, *J. Matls.,* 5, p. 47 (1970).
7. T.Z. Harmathy, *DBR Paper No. 1080, NRCC 20956,* National Research Council of Canada, Ottawa (1983).
8. J.E. Dorn, *J. Mech., Phys. Solids,* 3, p. 85 (1954).
9. T.Z. Harmathy, in *ASTM STP 422,* American Society for Testing and Materials, Philadelphia (1967).
10. T.Z. Harmathy, "Trans. Am. Soc. Mech. Eng.," *J. Basic Eng.,* 89, p. 496 (1967).
11. C. Zener and J.H. Hollomon, *J. Appl. Phys.,* 15, p. 22 (1944).
12. F.H. Wittmann (ed.), *Fundamental Research on Creep and Shrinkage of Concrete,* Martinus Nijhoff, The Hague, Netherlands (1982).
13. Y. Anderberg and S. Thelandersson, *Bulletin 54,* Lund Institute of Technology, Lund, Sweden (1976).
14. U. Schneider, *Fire & Matls.,* 1, p. 103 (1976).
15. T.Z. Harmathy, *J. Am. Concr. Inst.,* 65, 959 (1968).
16. *951 Thermogravimetric Analyzer (TGA),* DuPont Instruments, Wilmington, DE (1977).
17. T.T. Lie and V.K.R. Kodur, "Thermal and Mechanical Properties of Steel Fibre-Reinforced Concrete at Elevated Temperatures," *Canadian Journal of Civil Engineering,* 23, p. 4 (1996).
18. ASTM Test Method C135±86, *1990 Annual Book of ASTM Standards,* 15.01, American Society for Testing and Materials, Philadelphia (1990).
19. T.Z. Harmathy and L.W. Allen, *J. Am. Concr. Inst.,* 70, p. 132 (1973).
20. *910 Differential Scanning Calorimeter (DSC),* DuPont Instruments, Wilmington, DE (1977).
21. J.H. Perry (ed.), *Chemical Engineers' Handbook,* 3rd ed., McGraw-Hill, New York (1950).
22. W. Eitel, *Thermochemical Methods in Silicate Investigation,* Rutgers University, New Brunswick, Canada (1952).
23. T.Z. Harmathy, *I & EC Fundamen.,* 8, p. 92 (1969).
24. D.A. DeVries, in *Problems Relating to Thermal Conductivity,* Bulletin de l'Institut International du Froid, Annexe 1952–1, Louvain, Belgique, p. 115 (1952).
25. W.D. Kingery, *Introduction to Ceramics,* John Wiley and Sons, New York (1960).
26. T.T. Lie and V.K.R. Kodur, "Thermal Properties of Fibre-Reinforced Concrete at Elevated Temperatures," *IR 683,* IRC, National Research Council of Canada, Ottawa (1995).
27. *Thermal Conductivity Meter (TC-31), Instruction Manual,* Kyoto Electronics Manufacturing Co. Ltd., Tokyo, Japan (1993).
28. ASCE, "Structural Fire Protection: Manual of Practice," No. 78, American Society of Civil Engineers, New York (1993).
29. L.T. Phan, "Fire Performance of High-Strength Concrete: A Report of the State-of-the-Art," National Institute of Standards and Technology, Gaithersburg, MD (1996).
30. U. Danielsen, "Marine Concrete Structures Exposed to Hydrocarbon Fires," Report, SINTEF—The Norwegian Fire Research Institute, Trondheim, Norway (1997).
31. V.K.R. Kodur and M.A. Sultan, "Structural Behaviour of High Strength Concrete Columns Exposed to Fire," *Proceedings, International Symposium on High Performance and Reactive Powder Concrete,* Concrete Canada, Sherbrooke, Canada (1998).
32. U. Diederichs, U.M. Jumppanen, and U. Schneider, "High Temperature Properties and Spalling Behaviour of High Strength Concrete," in *Proceedings of Fourth Weimar Workshop on High Performance Concrete,* HAB, Weimar, Germany (1995).
33. Y. Anderberg, "Spalling Phenomenon of HPC and OC," in *International Workshop on Fire Performance of High Strength Concrete, NIST SP 919,* NIST, Gaithersburg, MD (1997).
34. Z.P. Bazant, "Analysis of Pore Pressure, Thermal Stress and Fracture in Rapidly Heated Concrete," in *International Workshop on Fire Performance of High Strength Concrete, NIST SP 919,* NIST, Gaithersburg, MD (1997).
35. A.N. Noumowe, P. Clastres, G. Debicki, and J.-L. Costaz, "Thermal Stresses and Water Vapor Pressure of High Performance Concrete at High Temperature," *Proceedings, 4th International Symposium on Utilization of High-Strength/High-Performance Concrete,* Paris, France (1996).
36. J.A. Purkiss, *Fire Safety Engineering Design of Structures,* Butterworth Heinemann, Bodmin, Cornwall, UK (1996).
37. E.L. Schaffer, "Charring Rate of Selected Woods—Transverse to Grain," *FPL 69,* US Department of Agriculture, Forest Service, Forest Products Laboratory, Madison, WI (1967).
38. B.F.W. Rogowski, "Charring of Timber in Fire Tests," in *Symposium No. 3 Fire and Structural Use of Timber in Buildings,* HMSO, London (1969).
39. N. Bénichou and M.A. Sultan, "Fire Resistance of Lightweight Wood Frame Assemblies: State-of-the-Art Report," *IR 776,* IRC, National Research Council of Canada, Ottawa (1999).
40. S. Hadvig, *Charring of Wood in Building Fires—Practice, Theory, Instrumentation, Measurements,* Laboratory of Heating and Air-Conditioning, Technical University of Denmark, Lyngby, Denmark (1981).
41. E. Mikkola, "Charring of Wood," *Report 689,* Fire Technology Laboratory, Technical Research Centre of Finland, Espoo (1990).
42. *Guide for Determining the Fire Endurance of Concrete Elements, ACI-216–89,* American Concrete Institute, Detroit, MI (1989).
43. I.D. Bennetts, *Report No. MRL/PS23/81/001,* BHP Melbourne Research Laboratories, Clayton, Australia (1981).
44. U. Schneider (ed.), *Properties of Materials at High Temperatures—Concrete,* Kassel University, Kassel, Germany (1985).
45. Y. Anderberg (ed.), *Properties of Materials at High Temperatures—Steel,* Lund University, Lund, Sweden (1983).
46. F. Birch and H. Clark, *Am. J. Sci.,* 238, p. 542 (1940).

47. T.Z. Harmathy and W.W. Stanzak, in *ASTM STP 464,* American Society for Testing and Materials, Philadelphia (1970).
48. "European Recommendations for the Fire Safety of Steel Structures," *European Convention for Construction Steelwork, Tech. Comm. 3,* Elsevier, New York (1983).
49. Y. Anderberg, "Mechanical Properties of Reinforcing Steel at Elevated Temperatures," *Tekniska Meddelande,* 36, Sweden (1978).
50. *Eurocode 3—Design of Steel Structures, Part 1–2: General Rules—Structural Fire Design,* European Committee for Standardization (CEN), Brussels, Belgium (1995).
51. T. Twilt, "Stress-Strain Relationships of Reinforcing Structural Steel at Elevated Temperatures, analysis of various options and European Proposal," *TNO-Rep. BI-91-015,* TNO Build. and Constr. Res., Delft, Netherlands (1991).
52. K.W. Poh, "General Stress-Strain Equation,"*ASCE—Journal of Materials in Civil Engineering,* Dec. (1997).
53. J.T. Gerlich, "Design of Loadbearing Light Steel Frame Walls for Fire Resistance," Fire Engineering Research Report 95/3, University of Canterbury, New Zealand (1995).
54. P. Makelainen and K. Miller, *Mechanical Properties of Cold-Formed Galvanized Sheet Steel Z32 at Elevated Temperatures,* Helsinki University of Technology, Finland (1983).
55. J.T. Gerlich, P.C.R. Collier, and A.H. Buchanan, "Design of Light Steel-Framed Walls for Fire Resistance," *Fire and Materials,* 20, 2 (1996).
56. BS 5950, "Structural Use of Steelwork in Building," Part 8, in *Code of Practice for Fire Resistant Design,* British Standards Institution, London (1990).
57. F. Alfawakhiri, M.A. Sultan, and D.H. MacKinnon, "Fire Resistance Of Loadbearing Steel-Stud Walls Protected With Gypsum Board: A Review," *Fire Technology,* 35, 4 (1999).
58. T.Z. Harmathy and J.E. Berndt, *J. Am. Concr. Inst.,* 63, p. 93 (1966).
59. C.R. Cruz, *J. PCA Res. Devel. Labs.,* 8, p. 37 (1966).
60. M.S. Abrams, in *ACI SP 25,* American Concrete Institute, Detroit, MI (1971).
61. C.R. Cruz, *J. PCA Res. Devel. Labs.,* 10, p. 36 (1968).
62. J.C. MareÂchal, in *ACI SP 34,* American Concrete Institute, Detroit, MI (1972).
63. H. Gross, *Nucl. Eng. Design,* 32, p. 129 (1975).
64. U. Schneider, U. Diedrichs, W. Rosenberger, and R. Weiss, *Sonderforschungsbereich 148,* Arbeitsbericht 1978–1980, Teil II, B 3, Technical University of Braunschweig, Germany (1980).
65. V.K.R. Kodur, "Fibre-Reinforced Concrete for Enhancing the Structural Fire Resistance of Columns," ACI-SP (2000).
66. A. Bilodeau, V.M. Malhotra, and G.C. Hoff, "Hydrocarbon Fire Resistance of High Strength Normal Weight and Light Weight Concrete Incorporating Polypropylene Fibres," in *Proceedings, International Symposium on High Performance and Reactive Powder Concrete,* Sherbrooke, Canada (1998).
67. V.K.R. Kodur and T.T. Lie, "Fire Resistance of Fibre-Reinforced Concrete," in *Fibre Reinforced Concrete: Present and the Future,* Canadian Society of Civil Engineers, Montreal (1997).
68. U.-M. Jumppanen, U. Diederichs, and K. Heinrichsmeyer, "Materials Properties of F-Concrete at High Temperatures," *VTT Research Report No. 452,* Technical Research Centre of Finland, Espoo (1986).
69. J.A. Purkiss, "Steel Fibre-Reinforced Concrete at Elevated Temperatures," *International Journal of Cement Composites and Light Weight Concrete,* 6, 3 (1984).
70. T.T. Lie and V.K.R. Kodur, "Effect of Temperature on Thermal and Mechanical Properties of Steel Fibre-Reinforced Concrete," IR 695, *IRC,* National Research Council of Canada, Ottawa (1995).
71. V.K.R. Kodur and M.A. Sultan, "Thermal Properties of High Strength Concrete at Elevated Temperatures," *CANMET-ACI-JCI International Conference, ACI SP-170,* Tokushima, Japan, American Concrete Institute, Detroit, MI (1998).
72. V.K.R. Kodur, "Spalling in High Strength Concrete Exposed to Fire—Concerns, Causes, Critical Parameters and Cures," in *Proceedings: ASCE Structures Congress,* Philadelphia (2000).
73. J.W. McBurney and C.E. Lovewell, *ASTM—Proceedings of the Thirty-Sixth Annual Meeting,* Vol. 33 (II), p. 636, American Society for Testing and Materials, Detroit, MI (1933).
74. *Wood Handbook: Wood as an Engineering Material,* Agriculture Handbook No. 72, Forest Products Laboratory, U.S. Gov. Printing Office, Washington, DC (1974).
75. C.C. Gerhards, *Wood & Fiber,* 14, p. 4 (1981).
76. E.L. Schaffer, *Wood & Fiber,* 9, p. 145 (1977).
77. E.L. Schaffer, *Res. Paper FPL 450,* U.S. Dept. of Agric., Forest Products Lab., Madison, WI (1984).
78. "Structural Fire Design," Part 1.2, in *Eurocode 5,* CEN, Brussels, Belgium (1995).
79. F.F. Wangaard, Section 29, in *Engineering Materials Handbook,* C.L. Mantell (ed.), McGraw-Hill, New York (1958).
80. V.K.R. Kodur and D. Baingo, "Fire Resistance of FRP Reinforced Concrete Slabs," *IR 758,* IRC, National Research Council of Canada, Ottawa (1998).
81. V.K.R. Kodur, "Fire Resistance Requirements for FRP Structural Members," *Proceedings—Vol I, 1999 CSCE Annual Conference,* Canadian Society of Civil Engineers, Regina, Saskatchewan (1999).
82. T.S. Gates, "Effects of Elevated Temperature on the Viscoelastic Modeling of Graphite/Polymeric Composites," *NASA Technical Memorandum 104160,* NASA, Langley Research Center, Hampton, VA (1991).
83. T.Z. Harmathy, in *ASTM STP 301,* American Society for Testing and Materials, Philadelphia (1961).
84. R.R. West and W.J. Sutton, *J. Am. Ceram. Soc.,* 37, p. 221 (1954).
85. P. Ljunggren, *J. Am. Ceram. Soc.,* 43, p. 227 (1960).
86. M.A. Sultan "A Model for Predicting Heat Transfer Through Noninsulated Unloaded Steel-Stud Gypsum Board Wall Assemblies Exposed to Fire," *Fire Technology,* 32, 3 (1996).
87. "Gypsum Board: Typical Mechanical and Physical Properties," *GA-235–98,* Gypsum Association, Washington, DC (1998).
88. M.A. Sultan, "Effect of Insulation in the Wall Cavity on the Fire Resistance Rating of Full-Scale Asymmetrical (1×2) Gypsum Board Protected Wall Assemblies," in *Proceedings of the International Conference on Fire Research and Engineering, Orlando, FL,* SFPE, Boston (1995).

CHAPTER 11

Probability Concepts

John R. Hall, Jr.

Introduction

This chapter introduces the basic definitions and methods of probability theory, which is the foundation for all work on statistics, fire risk evaluation, reliability analysis, and the other topics of this section. With increased availability of sizeable quantities of reliable data on a whole range of topics related to fire protection engineering, it is essential that the analysis of this data be based on sound mathematical principles from probability theory.

Basic Concepts of Probability Theory

Probability Theory

Probability theory is a branch of mathematics dealing with the modeling of uncertainty through measures of the relative likelihood of alternative occurrences, whether specifically or generally defined.

Set

A set is a collection of elements; to be well-defined it must be possible, for any object that can be defined or described, to say with certainty whether that object is or is not an element or part of the set.

Set Theory

The theory of sets is the most fundamental branch of mathematics and is relevant to probability theory, because all probabilities are built up from sets.

Dr. John R. Hall, Jr., is assistant vice president for fire analysis and research at the National Fire Protection Association. He has been involved in studies of fire experience patterns and trends, models of fire risk, and studies of fire department management experiences since 1974 at NFPA, the National Bureau of Standards, the U.S. Fire Administration, and the Urban Institute.

Subsets

A set, A, that consists entirely of elements that all are also contained in set B is called a subset of B. Each element in a set may also be considered a subset of that set.

Set Operators

There are three basic operators essential to the algebraic manipulation of sets:

Complement ($\sim$): The complement operator applies to a single set A and produces the set of all elements that are *not* in A. Such an operator is always applied relative to some specification of the set of all elements, which is called the *universal set*, ($\cup$). The complement of the universal set is the *null set* (ϕ) or *empty set*, the set with no elements.

Union ($\cup$): The union operator is applied to two sets, as in $A \cup B$. It produces the set consisting of all elements that are members of *either* A or B or both.

Intersection ($\cap$): The intersection operator is applied to two sets, as in $A \cap B$. It produces the set consisting of all elements that are members of *both* A and B.

Relationships among the Operators

$$\sim (A \cup B) = \sim A \cap \sim B$$

$$\sim (A \cap B) = \sim A \cup \sim B$$

$$(A \cup B \cap C = (A \cap C) \cup (B \cap C)$$

$$(A \cap B) \cup C = (A \cup C) \cap (B \cup C)$$

$$(A \cup B) \cup C = A \cup (B \cup C)$$

$$(A \cap B) \cap C = A \cap (B \cap C)$$

Venn diagrams: Venn diagrams are a graphical technique for displaying relationships among sets (represented by circles) and operators, within a rectangle that represents the universal set, ∪. (See Figures 1-11.1 through 1-11.3.)

Sample Space

Sample space is a set of mutually exclusive elements, each representing a possible outcome or occurrence and collectively representing all possible outcomes or occurrences for the experiment or problem under consideration. A sample space must also have the property that the set operators defined previously, if applied to the subsets of the sample space in any combination, will always produce subsets of the sample space. Subsets of a sample space are called *events.*

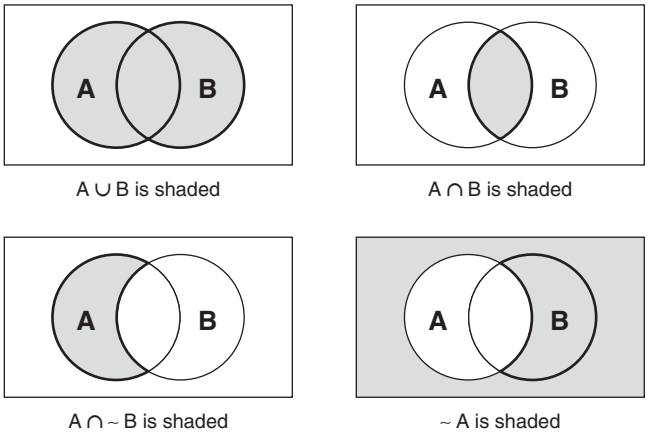

Figure 1-11.1.

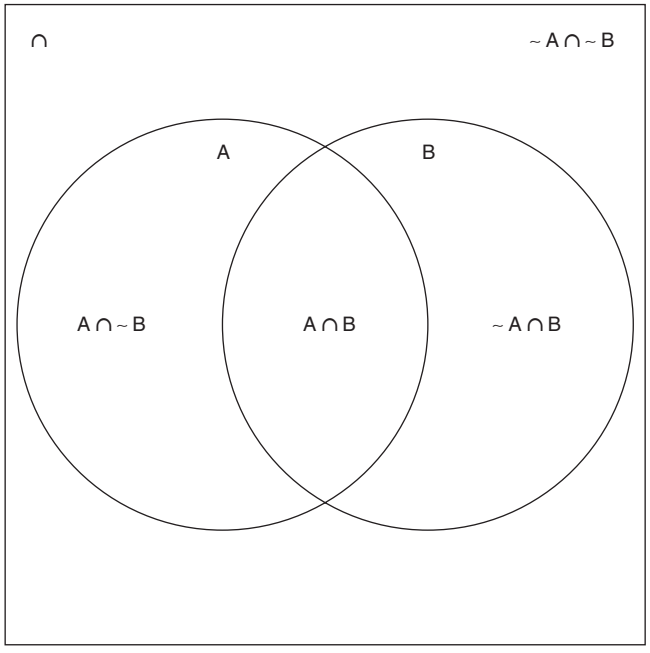

Figure 1-11.2.

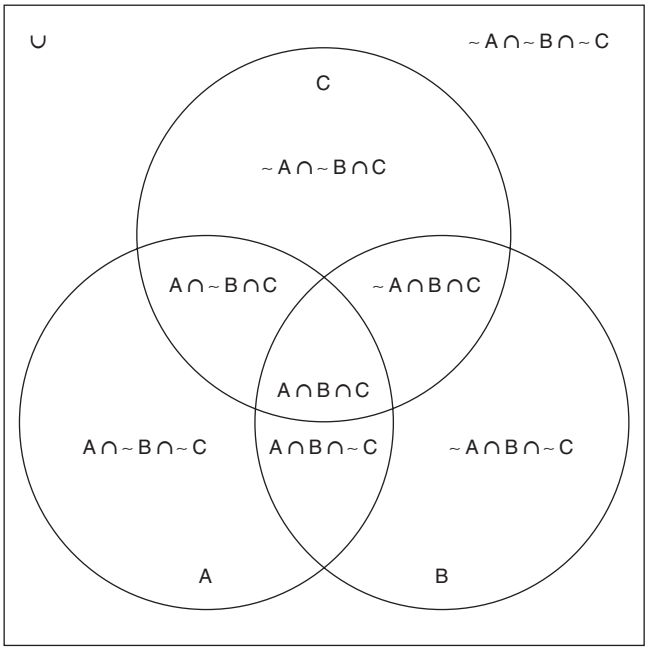

Figure 1-11.3.

Probability Measure

A probability measure is a mathematical function, *P,* defined on the subsets (events) of a sample space, *U,* and satisfying the following rules:

1. $P(A) \geq 0$ for any A, where A is an event subset of U.
2. $P(\phi) = 0$.
3. $P(U) = 1$.
4. If $A \cap B = \phi$, then $P(A \cup B) = P(A) + P(B)$.

In the classical theory of probability, it was assumed that all probability measures must be based on experiments (actual or at least imaginable) which could be run repeatedly, so that for each outcome e (an element of the sample space of possible outcomes), $P(e)$ would be given asymptotically as the ratio between the number of times outcome e occurs and the number of times the experiment is performed. This interpretation is called the *frequency interpretation of probability.* More recently, theorists associated with the Bayesian school of statistical inference have argued for the interpretation of probability only as a measure of the individual's strength of belief in the likelihood of an outcome. This interpretation is called *subjective probability.* Each of these two schools represents both an underlying conceptual model and an approach that makes practical sense in some but not all situations. In assigning probabilities to the outcomes of heads and tails for a single coin, for example, a relatively brief frequency experiment is easy to conduct. In assigning probabilities to the possible values of the annual inflation rate for next year,

the requisite experiment cannot be performed repeatedly. The mathematics of probability theory applies regardless of the source of the probability measure.

Probability Formulas Related to Set Operators

1. $P(A \cup B) = P(A) + P(B) - P(A \cap B)$
2. $P(\sim A) = 1 - P(A)$

These two formulas state, respectively, that (1) the probability that either (inclusive version) of two events will occur is equal to the sum of the probabilities that each event will occur minus the probability that both will occur; and (2) the probability that an event will not occur is equal to one minus the probability that it will occur.

Independence and Conditionality

The two events, A and B, are called *independent* if $P(A \cap B) = P(A) \times P(B)$. Two events that are not independent are called *dependent.*

The *conditional probability of A given B,* $P(A \mid B)$, is defined as $P(A \cap B)/P(B)$. It is normally interpreted to mean the probability that A will occur, given that B has occurred or will occur. If A and B are independent, then $P(A \mid B) = P(A)$ and $P(B \mid A) = P(B)$; in other words, the occurrence of A does not affect the likelihood of B, and vice versa.

It is important to note that two events may be dependent without either being the cause of the other and without any apparent logical connection. A common phenomenon involves two apparently unrelated variables (e.g., annual fire department expenditures on gasoline, annual sales revenue from plastics and petrochemicals) that are dependent because each is related in an understandable way to a third variable (e.g., price per barrel of oil).

Bayes's law (also called *Bayes's theorem* and *Bayes's formula)* states that

1. If B_i, $i = 1, \ldots, N$, are sets (events), and
2. If $B_1 \cup B_2 \cup \ldots \cup B_N = U$, and
3. If $B_i \cap B_j = \phi$ for all $i \neq j$ between 1 and N, and
4. If $P(B_i) \neq 0$, $i = 1, 2, \ldots, N$,

then

$$P(B_i|A) = \frac{P(B_i) \times P(A|B_i)}{[P(B_1) \times P(A|B_1) + P(B_2) \times P(A|B_2) + \cdots + P(B_N) \times P(A|B_n)]}$$

Bayes's law is a particularly powerful consequence of the laws of conditional probability and is the foundation for modern statistical decision theory. What makes it so powerful is this application. Suppose $P(B_1), \ldots, P(B_N)$ represent the current best estimates of the probabilities of various events of interest prior to the performance of an experiment (or the collection of some data on experience). These are called *prior probabilities.* Suppose A is a possible outcome of that experiment whose probability of occurrence, given each of the events $B_1, \ldots, B_N$, can be derived. Then Bayes's law can be used to develop a new set of probabilities, $P(B_1 \mid A), \ldots, P(B_N \mid A)$, that incorporate the information provided by the experiment. These are called *posterior probabilities* because they are probabilities calculated *after* the gathering of information (e.g., through an experiment).

EXAMPLE:

Suppose you have ten coins, nine of which are fair (0.5 probability of heads) and one of which is fixed (1.0 probability of heads). Choose one coin. With no other information, the probability that you have a fair coin (B_1) is 0.9 and the probability that you have the fixed coin (B_2) is 0.1. Suppose you flip the coin once.

If it comes up tails, you know it is a fair coin and Bayes's law confirms this. Let A be the event of getting tails on the one coin flip. Then

$$P(A \mid B_1) = 0.5 \quad \text{and} \quad P(A \mid B_2) = 0$$

Therefore,

$$P(B_1 \mid A) = \frac{(0.5)(0.9)}{(0.5)(0.9) + (0)(0.1)} = 1$$

If the coin comes up heads, you still do not know whether it is the fixed or a fair coin. Since heads is more likely with the fixed coin, the evidence points slightly in that direction. Let A' be the event of getting heads on the single coin flip. Then

$$P(A' \mid B_1) = 0.5 \quad \text{and} \quad P(A' \mid B_2) = 1$$

Therefore,

$$P(B_1 \mid A') = \frac{(0.5)(0.9)}{(0.5)(0.9) + (1.0)(0.1)} = 0.82$$

Thus the result of flipping the coin once and obtaining heads has lowered the estimate of the probability that you hold a fair coin from 0.9 to 0.82; correspondingly, your estimate that you hold the fixed coin has risen from 0.1 to 0.18.

Random Variables and Probability Distributions

A *random variable* is a real-number-valued function defined on the elements of a sample space. In some cases, the elements of a sample space may lend themselves to association with a particular random variable (e.g., the sample space consists of outcomes of tossing a die; the random variable is the number of spots on the exposed face). In other cases, the random variable may be only one of many that could easily have been associated with the sample space (e.g., the sample space consists of all citizens of the United States; the random variable is the weight to the nearest pound).

Each value of a random variable corresponds to an event subset of the sample space consisting of all elements for which the random variable takes on that value. The *probability of a value of the random variable,* then, is the probability of that event subset.

A *discrete probability distribution* is one for which the random variable has a finite or countably infinite number

of possible values (e.g., values can be any integer from 0 to 10; values can be any integer).

A *continuous probability distribution* is one for which the random variable can take on an uncountably infinite number of possible values (e.g., values can be any real number from 0 to 10; values can be any real number).

A *probability distribution function* (also called *probability density, probability density function,* and *probability distribution*) is a mathematical function, *f,* that gives the probability associated with each value of a random variable, $f(y) = P(x = y)$. The term *density* is usually reserved for random variables that can take on an uncountably infinite range of values, so that the probability of a range of values of the variable must be computed through integral calculus.

Because each value, *y,* of a random variable, *x,* is associated with a subset of the sample space, $f(y) \geq 0$ for all *y.*

Because no element of a sample space can take on two or more values of a random variable and each element must take on some value, the values of the random variable collectively correspond to a set of mutually exclusive subsets that exhaust all elements of the sample space, and so

$$\sum_{\text{all } x} f(x) = 1$$

for discrete probability distributions, and

$$\int_{\text{all } x} f(x)\,dx = 1$$

for continuous probability distributions.

A *cumulative distribution* is a mathematical function that, for each value of a random variable, gives the probability that the random variable will take on that value or any lesser value

$$F(y) = P(x \leq y) = \sum_{x \leq y} f(x)$$

for discrete probability distributions, and

$$F(y) = \int_{x \leq y} f(x)\,dx$$

for continuous probability distributions.

Note that some references use the term "probability distribution" to refer to the cumulative distribution function, *F,* of a continuous probability distribution, while referring to the probability density function, *f,* only as a probability density function.

A *survival function* is a mathematical function that, for each value of a random variable, gives the probability that the random variable will exceed that value

$$S(y) = P(x > y) = \sum_{x > y} f(x)$$

for discrete probability distributions, and

$$S(y) = \int_{x > y} f(x)\,dx$$

for continuous probability distributions.

Therefore, for any probability distribution function $P(x)$ and any value *y,* the cumulative distribution and the survival function based on $P(x)$ sum to one for all values of *y.*

$$F(y) + S(y) = 1$$

A *multivariate probability distribution* gives the probability for all combinations of values of two or more random values, for example, $f(u, v) = P(x = u \text{ and } y = v)$.

Key Parameters of Probability Distributions

Certain key parameters of probability distributions are of use because (1) they help to provide essential summary information about the random variable and its probability distributions and (2) they are included in the functional forms of certain probability distributions that are of use in many practical situations.

The mean, μ, of a random variable (also called its *expected value* or *average*) is defined as

$$\mu = \sum_{\text{all } x} xf(x)$$

for discrete probability distributions, and

$$\mu = \int_{\text{all } x} xf(x)\,dx$$

for continuous probability distributions.

It is also written as $E(x)$, which stands for *expected value of x.* This is the most commonly used of several parameters that relate to some concept of the most typical or average value of a random variable.

The expected value can also be calculated for a function of the random variable, as follows:

$$E[g(x)] = \sum_{\text{all } x} g(x)f(x)$$

for discrete probability distributions, and

$$E[g(x)] = \int_{\text{all } x} g(x)f(x)\,dx$$

for continuous probability distributions.

The *variance,* σ^2, of a random variable is a measure of the likelihood that a random variable will take on values far from its mean value. It is a parameter used in the functional form of some commonly occurring probability distributions.

$$\sigma^2 = \sum_{\text{all } x} (x - \mu)^2 f(x)$$

for discrete probability distributions, and

$$\sigma^2 = \int_{\text{all } x} (x - \mu)^2 f(x)\,dx$$

for continuous probability distributions.

The variance can also be expressed as the expected value of a function of the random variable, as follows:

$$\sigma^2 = E[(x-\mu)^2] = E(x^2) - \mu^2 = E(x^2) - [E(x)]^2$$

The variance is expressed as σ^2 because most calculations use the square root of the variance, which is called the *standard deviation*, σ.

The *moments* of a probability distribution are defined as the expected values of powers of the random variable. The nth moment is $E(x^n)$. Thus, the mean is the first moment, and the variance is the second moment minus the square of the first moment. The value given by $E[(x-\mu)^n]$ is defined as the nth moment about the mean.

The function defined by $E[e^{\theta x}]$ is called the moment generating function because it is equivalent to an infinite series whose terms consist of, for all k, the kth moment of x times $(\theta^k/k!)$.

For continuous probability distributions, the *median* is that value, y, for which the cumulative distribution, $F(y)$, is equal to 0.5. For discrete probability distributions, the median is that value, y, for which $f(x<y) = f(x>y)$. If the random variable can take on only a finite number of values, the median may not be uniquely defined. The median is less sensitive than the mean to extreme values of the random variable and is the "average" of choice for certain kinds of analyses.

Skewness refers to the symmetry of a probability distribution function around its mean. The median is not equal to the mean in a skewed distribution. An age distribution of fire department uniformed personnel will be skewed, for example, because the small number of personnel in their 50s and 60s will raise the average (mean) age well above the typical age (middle to late 20s). The term is used more frequently than is any specific measure of it. A symmetric distribution has a skewness of zero, no matter how skewness is measured.

Kurtosis is a rarely used term for the relative flatness of a distribution.

The *failure rate* or *hazard rate*, $r(x)$, is defined as: $r(x) = f(x)/S(x)$

When $f(x)$ is a probability density function for the time to failure, then $r(x)$ will give the conditional probability of time to failure, given survival to time x.

Degrees of freedom is the term given to certain parameters in many commonly used distributions (e.g., Student's t, chi-square, F). The distributions that use these parameters are used in tests of the variance of samples. In those tests the parameters always correspond to positive integer values based on the size of the sample (e.g., $n, n-1, n-2$). Since increasing sample size gives the sample more freedom to vary, it is natural to call those parameters measures of the "degrees of freedom" to vary in the sample.

Commonly Used Probability Distributions

Uniform and Rectangular Distributions

These distributions give equal probability to all values. The term *rectangular distribution* is reserved for the continuous probability distribution case.

1. $f(x) = 1/N$, for $x_1, \ldots, x_N$, if $f(x)$ is a discrete probability distribution over N values of a random variable.
2. $f(x) = 1/(b-a)$, for $a \le x \le b$, if $f(x)$ is a continuous probability distribution over a finite range.

Multivariate versions of the uniform distribution can be readily constructed for both the discrete and the continuous cases.

The uniform and rectangular distributions are used when every outcome is equally likely. As such, they tend to be useful, for example, as a first estimate of the probability distribution if nothing is known; that is, if nothing is known, treat every possibility the same.

EXAMPLE 1:

One of the 30 fire protection engineers in a firm is to be selected at random to accompany the local fire department on a fire code inspection. Each engineer is assigned a playing card, the reduced deck of 30 cards is shuffled and cut several times, and the top card is selected. Here, N is 30, so $f(x) = 1/30$, for each engineer.

EXAMPLE 2:

When the winning engineer arrives at the fire department, a random procedure is used to select one point on the city map. Whatever point is selected, they will inspect the buildings on the property of which that point is part.

Suppose A is the total area of the city. Then $f(x) = 1/A$, for every point in the city. For a given occupancy B, whose lot has area a, the probability of the event of choosing B (which corresponds to choosing any point on B's property) is equal to

$$\int_{\text{all points in } B} \left(\frac{1}{A}\right) dx = \frac{a}{A}$$

Note that while this is a uniform (rectangular) distribution over all *area* in the city, it is not a uniform distribution over all occupancies of the city, because an occupancy's probability of being chosen will be proportional to the size of its lot. In any analysis, there may be several different, incompatible ways of treating all possibilities "equally."

Normal Distribution (also called Gaussian Distribution)

The normal distribution, the familiar bell-shaped curve, is the most commonly used continuous probability density function in statistics; its density is a function of its mean, μ, and standard deviation, σ, as follows:

$$f(x) = \frac{1}{\sigma\sqrt{2\pi}} \exp\left[-\frac{1}{2}\left(\frac{x-\mu}{\sigma}\right)^2\right], \quad \text{for } -\infty < x < +\infty$$

The *Central Limit Theorem* establishes that for *any* probability density function, the distribution of the sample mean, $\bar{x}$, of a sample from that density asymptotically approaches a normal distribution as the size of the sample increases. This means that the normal distribution can be used validly to test hypotheses about the means of any population, even if nothing is known or can be assumed

about the population's underlying distribution. Also, the *Law of Large Numbers* establishes that the standard deviation of the distribution of the sample mean is inversely proportional to the square root of the sample size, which means that larger samples always produce more precise estimates of the sample mean. These two results are the cornerstones of sample-based statistical inference.

In addition to proving a valid distribution for sample *means* in all situations, the normal distribution also directly characterizes many *populations* of interest, including experimental measurement errors and quality control variations in materials properties.

A sample size of at least 30 should be used to obtain an acceptable fit of the sample mean distribution to the normal distribution.

The standard tables of the normal distribution are for a random variable with mean 0 and variance 1. They can be used for values from any normal distribution by subtracting the mean, then dividing the result by the standard deviation.

The multivariate form of the normal distribution is also commonly used. Its parameters are given by a vector of the means of all the variables and a matrix with both the variances of all the variables and the covariances of pairs of variables (which are functions of the variances and the correlation coefficients).

EXAMPLE 1:

The promotional examination for lieutenant is taken by 100 fire fighters, whose test scores, shown in Table 1-11.1 below, fit a normal distribution with mean score of 50 and standard deviation of 15. The fit is not exact because strictly speaking, the 100 scores comprise a discrete distribution, not a continuous distribution, and the possible scores are bounded by 0 and 100. Also, with only 100 scores, the fit to a normal distribution can be seen in this grouped data but might not be apparent if every score had its own frequency entered separately. (See Figure 1-11.4.)

EXAMPLE 2:

Suppose the widths of U.S. adults, fully clothed (including overcoats), at their widest points are normally distributed with mean 0.5 m and standard deviation of 0.053 m. Then, a door width equal to the mean (0.5 m) would accommodate 50.0 percent of the population [$F(x \leq \mu) = 0.50$]. A door width equal to the mean plus one standard deviation (0.553 m) would accommodate

Table 1-11.1 ***Normal Distribution Sample Test Scores***

Score	Number of Fire Fighters Receiving That Score
0–9	1
10–19	2
20–29	7
30–39	15
40–49	25
50–59	25
60–69	15
70–79	7
80–89	2
90–100	1

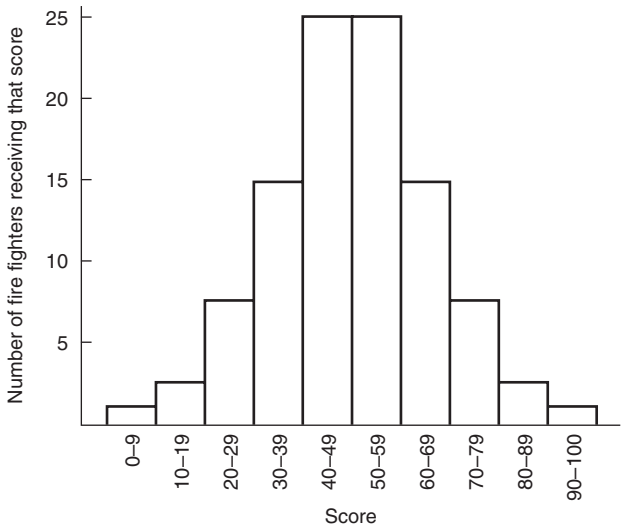

Figure 1-11.4.

84.1 percent of the population [$F(x \leq \mu + \sigma) = 0.841$]. A door width equal to the mean plus two standard deviations (0.606 m) would accommodate 97.7 percent of the population [$F(x \leq \mu + 2\sigma) = 0.977$].

But some buildings hold 10,000 persons, so suppose it is desired to construct a door width that will be too narrow for only one of every 20,000 persons. Then the value of a is desired, such that $F(x \leq \mu + a\sigma) = 0.99995$. That value of a is 3.87, which translates to a door width of 0.705 m, or more than 40 percent wider than the door width that sufficed for one-half the population.

All basic statistics texts contain tables of the cumulative distribution function for the normal distribution.

Log-Normal Distribution

It is not unusual to deal with random variables whose logarithms (to any base) are normally distributed. In such cases, the original variables are said to be log-normally distributed. For example, fire load density (i.e., mass of combustibles per unit floor area) typically has a log-normal distribution.

Student's t Distribution

For small samples, the distribution of the sample mean is not well approximated by the normal distribution. Even for somewhat larger samples, the population variance is typically not known, and the sample variance must be used instead. The Student's t distribution may be used instead of the normal distribution, but it does assume that the population is normally distributed. Its distribution is a function of its degrees of freedom, m.

$$f(t) = \frac{[\Gamma(m + 1/2)][(1 + t^2/m)^{-(m+1)/2}]}{\sqrt{\pi m}[\Gamma(m/2)]} \quad \text{for } -\infty < t < +\infty$$

where

$$\Gamma(u) = \int_0^\infty y^{u-1} e^{-y}\, dy$$

Expressed in this standard form, the t distribution has a mean of zero and a variance of $m/(m-2)$. Since the Student's t distribution is used primarily in statistical testing, an example of its use is included in Section 4, Chapter 3.

Chi-Square Distribution

Whereas the normal and t distributions may be used to test hypotheses about means, the chi-square distribution may be used to test hypotheses about variances or entire distributions. Its density is a function of its degrees of freedom, m.

$$f(x) = \frac{x^{(m-2)/2}e^{-x/2}}{2^{m/2}\Gamma(m/2)}, \quad \text{for } x \geq 0$$

where

$$\Gamma(u) = \int_0^\infty y^{u-1}e^{-y}\,dy$$

Expressed in this standard form, the chi-square distribution has its mean equal to m, the number of degrees of freedom, and its variance equal to $2m$.

F Distribution

Whereas the normal distribution may be used to test hypotheses about the means of samples of a single random variable, the F distribution permits simultaneous testing of hypotheses about the means of samples reflecting several random variables, each with its own variance, and each pair of variables correlated to some unknown degree. Its density is a function of two noninterchangeable degrees-of-freedom parameters, m_1 and m_2.

$$f(x) = \frac{(m_1/m_2)^{m_1/2}x^{(m_1-2)/2}\{\Gamma[(m_1+m_2)/2]\}}{[\Gamma(m_1/2)][\Gamma(m_2/2)][(1+m_1x/m_2)^{(m_1+m_2)/2}]}$$

where

$$\Gamma(u) = \int_0^\infty y^{u-1}e^{-y}\,dy$$

The mean of the F distribution is $m_2/(m_2-2)$, and the variance is given by

$$\sigma^2 = \frac{2m_2^2(m_1+m_2-2)}{m_1(m_2-2)^2(m_2-4)} \quad \text{if } m_2 > 4$$

Exponential Distribution

The exponential distribution is the simplest distribution for use in reliability analysis, where it can be used to model the time to failure. Its density is a function of a parameter, θ, that is equal to its mean and its standard deviation.

$$f(x) = \left(\frac{1}{\theta}\right)e^{-x/\theta} \quad \text{for } x \geq 0$$

Its hazard rate is a constant, $1/\theta$, so the exponential distribution is the one to use if the expected time to failure is the same, regardless of how much time has already elapsed. This distribution also is commonly used to represent the time required to serve customers waiting in a queue.

EXAMPLE:

A smoke detector is installed in a private home and is powered by a battery from a lot with average life of six months. Suppose the time until the battery dies can be represented by an exponential distribution. (In practice, retailed batteries have a more complex failure rate function.) Then the time until failure might look like that shown in Table 1-11.2.

Note that there is a high probability of failure in the first month and a high probability of survival past one year.

Poisson Distribution

If a system has exponentially distributed time to failure with mean time θ, then the distribution of the total number of failures, n, in time, t, has a Poisson distribution. Its distribution is given by a parameter, λ, that is equal to both its mean and its variance.

$$f(n) = \frac{\lambda^n e^{-\lambda}}{n!}$$

for

$$n = 0, 1, 2, \ldots, +\infty$$

where

$$\lambda = \frac{t}{\theta} \quad \text{and} \quad n! = n(n-1)(n-2)\cdots(3)(2)(1)$$

This distribution also is commonly used to represent the number of customers entering a queue for service in a unit of time. It assumes that the expected number of arriving customers in any short interval of time is proportional to the length of time.

EXAMPLE:

Using the smoke detector scenario in the previous example, suppose each time the battery fails, it is detected immediately and immediately replaced with a new battery of similar expected life. Then the number of times the batteries will fail in the first year is given by a Poisson dis-

Table 1-11.2 ***Example of Exponential Distribution (detector batteries)***

Months Old	Probability of Failure by This Age (i.e., this soon or sooner)
0–1	0.154
1–2	0.283
2–3	0.393
3–4	0.487
4–5	0.565
5–6	0.632
6–7	0.689
7–8	0.736
8–9	0.777
9–10	0.811
10–11	0.840
11–12	0.865
Over 12	1.000

Table 1-11.3 *Poisson Distribution*

Number of Times Detector Will Have Dead Batteries in One Year	Probability
0	0.135
1	0.271
2	0.271
3	0.181
4	0.090
5	0.036
6 or more	0.016

tribution. (See Table 1-11.3.) Here t is 12 months and θ is 6 months, so λ is 2.

Gamma Distribution (also called Erlang Distribution)

The gamma distribution is also commonly used to represent time to failure for a system, particularly in a situation where m independent faults, all with identical exponential distributions of time to occur, are required before the system fails. Its density is a function of two parameters, m and θ, which must both be greater than zero; m need not be an integer.

$$f(x) = \frac{x^{m-1}e^{-x/\theta}}{[\theta^m \Gamma(m)]} \quad \text{for } x \geq 0$$

where

$$\Gamma(m) = \int_0^\infty y^{m-1}e^{-y}\,dy$$

The mean is $m\theta$ and the variance is $m\theta^2$.

Weibull Distribution

Another distribution commonly used in reliability studies to represent time to failure, the Weibull distribution is flexible enough to permit failure rates that increase or decrease with system age. Its density is a function of two parameters, a and b, which must both be greater than zero.

$$f(x) = abx^{b-1}e^{-ax^b}, \quad \text{for } x \geq 0$$

$$\mu = a^{-(1/b)}\Gamma\left(\frac{b+1}{b}\right)$$

$$\sigma^2 = a^{-(2/b)}\left\{\left[\Gamma\left(\frac{b+2}{b}\right)\right] - \left[\Gamma\left(\frac{b+1}{b}\right)\right]^2\right\}$$

where

$$\Gamma(u) = \int_0^\infty y^{u-1}e^{-y}\,dy$$

The cumulative distribution can be expressed in closed form, as follows:

$$F(x) = 1 - e^{-ax^b}$$

Therefore, the failure rate has a simple form

$$h(x) = abx^{b-1}$$

The failure rate increases with x (e.g., system age) if $b > 1$ and decreases if $b < 1$. If $b = 1$, the Weibull distribution becomes an exponential distribution, with $\theta = 1/a$.

EXAMPLE:

Suppose the example in Table 1-11.2 is modified to show the time to failure for the detector batteries as having a Weibull distribution. Suppose $\alpha = 1/6$. Then if $b = 1$, the Weibull distribution will be the same exponential distribution shown in Table 1-11.2. If $b < 1$, early failures are less likely, and if $b > 1$, early failures are more likely. Some examples are shown in Table 1-11.4. Note that it is not necessary to reduce b in order to make early failures unlikely. An exponential distribution with a higher θ (or Weibull distribution with a lower α) will also make early failures unlikely.

Pareto Distribution

The Pareto distribution is not as commonly used but does provide a simple form for a distribution whose failure rate decreases with system age. Its density is a function of two parameters, a and b, which must both be greater than zero.

$$f(x) = ab^a x^{-(a+1)} \quad \text{for } x > b$$

$$\mu = ab/(a-1)$$

$$\sigma^2 = ab^2/[(a-1)^2(a-2)]$$

$$F(x) = 1 - b^a x^{-a}$$

$$h(x) = a/x$$

The parameter a must be greater than 2 for the mean and variance to converge to the values shown above. In general, a must be greater than k for the kth moment to converge.

Table 1-11.4 *Weibull Distribution (detector batteries)*

	Probability of Failure by This Age (i.e., this soon or sooner)			
Months Old	$b = 1$	$b = 2$	$b = 0.5$	$b = 0.1$
0–1	0.154	0.154	0.154	0.154
1–2	0.283	0.487	0.210	0.164
2–3	0.393	0.777	0.251	0.170
3–4	0.487	0.931	0.283	0.174
4–5	0.565	0.984	0.311	0.178
5–6	0.632	0.998	0.335	0.181
6–7	0.689	1.000	0.357	0.183
7–8	0.736	1.000	0.376	0.186
8–9	0.777	1.000	0.393	0.187
9–10	0.811	1.000	0.410	0.189
10–11	0.840	1.000	0.425	0.191
11–12	0.865	1.000	0.439	0.192
Over 12	1.000	1.000	1.000	1.000

Bernoulli Distribution

The Bernoulli distribution is the most basic of the discrete probability distributions and it represents a single trial or experiment in which there are only two possible outcomes—success (with probability p) and failure. The random variable is the number of successes.

$$f(x) = p^x(1-p)^{(1-x)} \quad \text{for } x = 0, 1$$

Therefore $f(x) = p$ if $x = 1$ and $f(x) = (1-p)$ if $x = 0$. The mean is p and the variance is $p(1-p)$.

EXAMPLE:

Suppose there are 100 fire fighters in a department, 15 of whom are minorities. If all fire fighters are equally qualified, the probability that a minority fire fighter will be chosen as the next lieutenant is give by a Bernoulli distribution, with $p = 15/100 = 0.15$.

Binomial Distribution

The binomial distribution is the probability distribution for the number of successes in n independent Bernoulli trials, all having the same probability of success.

$$f(x) = \binom{n}{x} p^x(1-p)^{(n-x)} \quad \text{for } x = 0, 1, \ldots, n$$

where

$$\binom{n}{x} = \frac{n!}{x!(n-x)!}$$

and

$$x! = x(x-1)(x-2)\ldots(3)(2)(1)$$

The mean is np and the variance is $np(1-p)$.

The use of *factorials* (e.g., $x!$) can lead to time consuming calculations. It is possible for large values of n to approximate the binomial distribution by a normal distribution [with $\mu = np$ and $\sigma^2 = np(1-p)$]. This approximation will work acceptably if $np \geq 5$ and $n(1-p) \geq 5$. For small values of p, μ, and σ^2 become very close, and one can approximate the binomial distribution by a Poisson distribution (with $\lambda = np$). This works acceptably if $n > 100$ and $p < 0.05$.

EXAMPLE:

Suppose in the fire fighter promotion example just used, five lieutenants have been selected sequentially. Also suppose that each time a fire fighter is promoted to lieutenant, that slot is filled with another fire fighter of the same race before the next lieutenant is selected. Under these conditions, the five promotions represent five Bernoulli trials, all having the same probability that a minority fire fighter will be promoted. The number of minority fire fighters promoted will then be governed by a binomial distribution, as shown in Table 1-11.5.

Table 1-11.5 ***Example of Binomial Distribution***

Number of Minority Fire Fighters Promoted	Probability
0	0.444
1	0.392
2	0.138
3	0.024
4	0.002
5	0.000

Geometric Distribution

In the case of a potentially unlimited number of independent Bernoulli trials with identical probabilities of success, the geometric distribution gives the distribution of the trial on which the first success will occur.

$$f(x) = p(1-p)^{(x-1)}, \quad \text{for } x = 1, 2, 3, \ldots, +\infty$$

The mean is $(1/p)$ and the variance is $(1-p)/p^2$.

EXAMPLE:

Continuing the example of serial promotions in which each open slot is filled by a new fire fighter of the same race, the geometric distribution would give the probability of which of the promotions will be the first to involve a minority fire fighter. (See Table 1-11.6.)

Note the high probability that chance alone will delay the first minority promotion past the tenth promotion.

Negative Binomial Distribution (also called Pascal Distribution)

This generalization of the geometric distribution gives the probability distribution for the trial on which the kth success will occur.

$$f(x) = \binom{x-1}{k-1} p^k(1-p)^{-(x-1)}$$
$$\text{for } x = k, k+1, k+2, \ldots, +\infty$$

where

$$\binom{x-1}{k-1} = \frac{(x-1)!}{(k-1)!(x-k)!}$$

and

$$x! = x(x-1)(x-2)\ldots(3)(2)(1)$$

Table 1-11.6 ***Geometric Distribution with Serial Promotion Example***

First Promotion to Involve a Minority Fire Fighter	Probability
First	0.150
Second	0.128
Third	0.108
Fourth	0.092
Fifth	0.078
Sixth	0.067
Seventh	0.057
Eighth	0.048
Ninth	0.041
Tenth	0.035
Later than tenth	0.196

Hypergeometric Distribution

The hypergeometric distribution is a variation on the binominal distribution that applies to cases where the initial probability of success, p, reflects a fixed number of total successes and failures, N, available for selection so that each trial reduces either the number of successes remaining or the number of failures remaining. (For example, imagine an urn filled with balls of two different colors. If each trial consists of removing a ball, then replacing it in the urn, the binomial distribution applies. If each trial consists of removing a ball and keeping it out, the hypergeometric distribution applies.)

$$f(x) = \frac{\binom{Np}{x}\binom{N(1-p)}{n-x}}{\binom{N}{n}} \quad \text{for } x = 0, 1, 2, \ldots, n$$

where

N is the total number of successes and failures possible, $n \leq N$ Np and $N(1-p)$ are integers

$$\binom{m}{y} = \frac{m!}{y!(m-y)!}$$

and

$$y! = y(y-1)(y-2)\ldots(3)(2)(1)$$

The mean is np and the variance is $np(1-p)[(N-n)/(N-1)]$. For very large values of N (relative to n), the hypergeometric distribution asymptotically approaches the binomial distribution.

EXAMPLE:

Continuing the fire fighter promotion example, suppose five promotions are carried out all at once. (See Table 1-11.7.) The hypergeometric distribution then gives the probability distribution for the number of minorities promoted; note how its probabilities differ from those generated by the binomial distribution.

For example,

$$0.436 = \frac{\binom{15}{0}\binom{85}{5}}{\binom{100}{5}} = \frac{[15!/(15!0!)][85!/(80!5!)]}{[100!/(95!5!)]}$$
$$= \frac{(85)(84)(83)(82)(81)}{(100)(99)(98)(97)(96)}$$

Table 1-11.7 ***Example of Hypergeometric Distribution***

Number of Minority Fire Fighters Promoted	Probability
0	0.436
1	0.403
2	0.138
3	0.022
4	0.001
5	0.000

Multinomial Distribution

The multinomial distribution is a generalization of the binomial distribution that addresses the case where there are more than two possible outcomes. Given k possible outcomes, such that the probability of the ith outcome is always p_i and the p_i collectively sum to unity, then for a series of n independent trials

$$f(x_1, \ldots, x_k) = \frac{n!}{x_1!x_2!\ldots x_k!} p_1^{x_1} p_2^{x_2} \ldots p_k^{x_k}$$

for all cases of $x_1 = 0, 1, 2, \ldots, n$, for $i = 1, 2, \ldots, k$, subject to

$$\sum_{i=1}^{k} x_i = n$$
$$\mu_i = np_i$$
$$\sigma_i^2 = np_i(1-p_i)$$

EXAMPLE:

Continuing the fire department example, suppose that the department's 100 fire fighters include 15 black fire fighters and 5 female fire fighters, none of whom is black. Suppose two promotions are made, and the slot vacated for the first promotion is filled by a fire fighter of the same race and sex before the second promotion is made. Then the multinomial distribution (Table 1-11.8) describes the possible outcomes of interest.

For example, this is the probability that the promotions will go to one white male and one white female:

$$0.080 = \frac{2!}{0!1!1!}(0.15)^0(0.05)^1(0.80)^1 = 2 \times 0.05 \times 0.80$$

Beta Distribution

In Bayesian statistical inference, if the phenomenon of interest is governed by a Bernoulli distribution, then one needs a probability distribution for the parameter, p, of that Bernoulli distribution, and a Beta distribution is typically used.

$$f(p) = \frac{\Gamma(a+b)}{[\Gamma(a)][\Gamma(b)]} p^{a-1} 1 - p^{(b-1)}$$

where

$$\Gamma(u) = \int_0^\infty y^{u-1} e^{-y}\, dy$$

Table 1-11.8 ***Example of Multinomial Distribution***

Number of Fire Fighters Promoted			Probability
Minority Males	Female	White Males	
0	0	2	0.640
0	1	1	0.080
0	2	0	0.002
1	0	1	0.240
1	1	0	0.015
2	0	0	0.023

The mean is $a/(a + b)$ and the variance is given by

$$\Gamma^2 = \frac{ab}{(a+b)^2(a+b+1)}$$

If a = b = 1, this becomes a *uniform distribution.* Larger values of b correspond to smaller variances, hence tighter confidence bands around the mean estimate of the parameter.

Additional Readings

J.R. Benjamin and C.A. Cornell, *Probability, Statistics and Decision for Civil Engineers,* McGraw-Hill, New York (1970).

W. Feller, *An Introduction to Probability Theory and Its Applications,* John Wiley and Sons, New York (1957).

J.E. Freund and F.J. Williams, *Dictionary/Outline of Basic Statistics,* McGraw-Hill, New York (1966).

N.A.J. Hastings and J.B. Peacock, *Statistical Distributions: A Handbook for Students,* Butterworths, London (1975).

M.R. Spiegel, *Probability and Statistics,* McGraw-Hill, New York (1975).

R.E. Walpole and R.H. Myers, *Probability and Statistics for Engineers and Scientists,* Macmillan, New York (1972).

CHAPTER 12

Statistics

John R. Hall, Jr.

Introduction

Statistical analysis is basic to all aspects of fire protection engineering that involve abstracting results from experiments or real experience. Statistical analysis is the applied side of the mathematics of probability theory.

Basic Concepts of Statistical Analysis

Statistic

A statistic is (a) any item of numerical data, or (b) a quantity (e.g., mean) computed as a function on a body of numerical data, or the function itself.

Statistical Analysis

Statistical analysis is the use of mathematical methods to condense sizeable bodies of numerical data into a small number of summary statistics from which useful conclusions may be drawn.

Statistical Inference

Statistical inference is statistical analysis that consists of using methods based on the mathematics of probability theory to reason from properties of a body of numerical data, regarded as a sample from a larger population, to properties of that larger population.

In *classical statistical inference*, a single best estimate of each statistic of interest is developed from available data, the uncertainty of that statistic is estimated, and hypotheses are tested and conclusions drawn from those bases.

Dr. John R. Hall, Jr. is assistant vice president for fire analysis and research at the National Fire Protection Association. He has been involved in studies of fire experience patterns and trends, models of fire risk, and studies of fire department management experiences since 1974 at NFPA, the National Bureau of Standards, the U.S. Fire Administration, and the Urban Institute.

In *Bayesian statistical inference*, a probability distribution for each statistic of interest is developed, using a form that permits new information, when it is acquired, to be used to adjust that distribution. Bayes's law, which was described in Section 1, Chapter 11, "Probability Concepts," is used to adjust the distribution in light of the new information.

EXAMPLE:

Suppose there are 100 fire fighters in a department, 15 of them black, and in a group of 5 recent promotions, all the promotions were given to whites. How likely is it that the department never selects blacks for promotions?

A Bayesian analysis uses (a) a prior estimate of the probability that the department discriminated, made before considering the evidence of the recent promotions; (b) a computed probability that the promotions would have had this pattern if the department never selects blacks; and (c) a computed probability that the promotions would have had the result if promotions are random with respect to race. For (b), the probability is 1.0, because an all white promotion list is the only possible outcome under the hypothesis that blacks are never selected. For (c), the probability is given by the hypergeometric distribution

$$\frac{\binom{15}{0}\binom{85}{5}}{\binom{100}{5}} = 0.44.$$

By Bayes's law, then, given a prior probability, q, that blacks are never selected, the posterior probability is $q/(0.56q + 0.44)$. The new evidence produces some shift in the estimated likelihood of prejudice. If prejudice was considered an even proposition before ($q = 0.5$), then the new estimate is 0.69. If prejudice was considered certain ($q = 1.0$) or impossible ($q = 0.0$) before, no new evidence will alter those estimates. If prejudice was considered very unlikely before (say, $q = 0.01$), then it will still be considered very unlikely (new value of 0.022).

Suppose in the same example there had been 25 promotions with no blacks selected. This more extensive evidence would have produced a more dramatic shift in the estimated probability. Instead of 0.44, the probability of this outcome (given no prejudice) would be 0.009. If the prior probability was 0.5, the posterior probability would be 0.991. Even if the prior probability is 0.01, the posterior probability would be 0.529. In other words, the new evidence changes the estimate of the likelihood that the department never selects blacks from one chance in a hundred to a better than even chance.

In more sophisticated Bayesian statistical analysis, the prior probability is given not as a single probability but as a probability distribution, which permits the analyst to reflect the strength of the evidence that went into choosing the prior probability distribution.

Exploratory Data Analysis

Exploratory data analysis is the development of *descriptive statistics,* that is, statistical analysis that does not make inferences to a population.

Key Parameters of Descriptive Statistics

The *mean, median, variance,* and *standard deviation,* as described in the previous chapter, can all be applied here, using the relative frequency of occurrence of each value in the body of data to define a discrete probability distribution.

The *mode* is the value that occurs most frequently, that is, the value of x for which $f(x) > f(y)$ for all $y \neq x$.

A body of data is called *unimodal* if $f(z) < f(y)$ in all cases where $|z - x| > |y - x|$, that is, if the probability distribution function steadily decreases as one moves away from the mode.

A body of data is called *multimodal* if it is not unimodal. In such cases there will be two or more values of x for which $f(x) > f(y)$ for all $y \neq x$ and $|y - x| < \varepsilon$, where ε is some small value. Although there may be only one mode in the sense of a most frequently occurring value, the existence of local maximums in the probability distribution function is sufficient to make the distribution multimodal. Multimodal data usually occur when data are combined from two or more populations, each having an underlying unimodal distribution. For example, if data were collected on the lengths of fire department vehicles, it probably would be multimodal, having one peak each for automobiles, ambulances/vans, engines, and ladders.

A *geometric mean* is another type of average:

$$\text{G.M.} = (x_1 x_2 x_3 \ \ldots \ x_n)^{1/n}$$

The geometric mean is useful in averaging index numbers reflecting rates of change. For example, suppose a, b, and c are annual rates of increase in the fire department budget for three successive years. Then $A = 1 + a$, $B = 1 + b$, and $C = 1 + c$ would be index numbers reflecting those three rates. The index number, D, reflecting the cumulative increase over all three years, would be given by $D = ABC$, and so an index number yielding an "average" rate of inflation for the three-year period would be given by $(ABC)^{1/3}$, or the geometric mean of the index numbers. This geometric mean is the index number that could be compounded over the three years to obtain the actual cumulative increase. Note that the geometric mean is equivalent to computing the arithmetic mean of the logarithms of the data values, then exponentiating the result, that is, using the result as an exponential power to be applied to the base used in computing the logarithms.

The *harmonic mean* is a less commonly used average that consists of the reciprocal of the arithmetic mean of the reciprocals of the data values. For example, suppose $V_1, \ldots, V_n$ are a set of n values of the speed achieved by an engine company on a set of test runs from the firehouse to a single location. Then these speeds can also be represented as $d/t_1, d/t_2, \ldots, d/t_n$, where d is the constant distance and $t_1, \ldots, t_n$ are the times of the n runs. The average speed would be given by $nd/(t_1 + t_2 + \cdots + t_n)$, or total distance divided by total time. That value will also be given by the harmonic mean of the speed values. This example also helps illustrate why the harmonic mean is rarely used. It is likely that anyone who had access to the speed values would also have access to time values, $t_1, \ldots, t_n$, and could compute the average more quickly by using them directly.

The *range* is the difference between the highest and lowest values, or the term may be used to refer to those two values and the interval between them.

Quartiles, deciles, and *percentiles* are useful measures of the dispersion of the data. If the data are arranged in ascending or descending order, the three quartiles, Q_1, Q_2, and Q_3, are the values that mark off 25 percent, 50 percent, and 75 percent, respectively, of the data set. In other words,

Q_1 is chosen so that $F(Q_1) = 0.25$

Q_2 is chosen so that $F(Q_2) = 0.50$; Q_2 is also the median

Q_3 is chosen so that $F(Q_2) = 0.75$

Deciles and percentiles are defined analogously so as to divide the data set into tenths or hundredths, respectively, rather than fourths. Like the second quartile, the fifth decile equals the median. The *interquartile range,* or $Q_3 - Q_1$, is an alternative to the full range that is less sensitive to extreme values.

A *histogram* is a technique of exploratory data analysis for displaying the frequency of occurrence of a finite set of data. The data values are arrayed along the x-axis of a graph, and the y-axis is used to plot the frequency, usually as number of occurrences or percentage of total occurrences.

A *scatter plot* or *scatter diagram* is a technique of exploratory data analysis for displaying the patterns of a finite set of bivariate data. Each pair of data values is plotted on an (x, y) graph. This technique works best if both dimensions of the data are continuous so that the same pair of values does not occur more than once.

The *coefficient of variation* is given by the standard deviation divided by the mean. When the result is multiplied by 100, it gives the scatter about the mean in percentage terms relative to the mean.

Correlation, Regression, and Analysis of Variance

Correlation

In qualitative terms, correlation refers to the degree of association between two or more random variables. (Random variables with discrete and continuous probability distributions were defined in the previous chapter.)

The most common quantitative measure of correlation specifically addresses the extent to which two random variables are linearly related.

Correlation Coefficient (also called the Pearson product-moment correlation coefficient)

Let two discrete random variables, X and Y, have a joint probability distribution given by $f(x_i, y_j)$ = probability $(X = x_i \text{ and } Y = y_j)$.

Then the correlation coefficient of X and Y is given by

$$\rho_{XY} = \frac{[\sum_{i=1}^{\infty}\sum_{j=1}^{\infty}(x_i - \mu_X)(y_j - \mu_Y)f(x_i, y_j)]}{\sqrt{\sum_{i=1}^{\infty}\sum_{j=1}^{\infty}[(x_i - \mu_X)^2 f(x_i, y_j)]}\sqrt{\sum_{i=1}^{\infty}\sum_{j=1}^{\infty}[(y_i - \mu_Y)^2 f(x_i, y_j)]}}$$

where

$$\mu_X = \sum_{i=1}^{\infty}\sum_{j=1}^{\infty} x_i f(x_i, y_j)$$

and

$$\mu_Y = \sum_{i=1}^{\infty}\sum_{j=1}^{\infty} y_i f(x_i, y_j)$$

Let two continuous random variables, X and Y, have a joint probability density function given by $f(x, y)$ such that

$$\int_{-\infty}^{y}\int_{-\infty}^{x} f(u, v)\, du\, dv = \text{probability } (X \le x \text{ and } Y \le y)$$

Then the correlation coefficient of X and Y is given by

$$\rho_{XY} = \frac{\left[\int_{-\infty}^{\infty}\int_{-\infty}^{\infty}(x - \mu_X)(y - \mu_Y)f(x, y)\, dx\, dy\right]}{\sqrt{\int_{-\infty}^{\infty}\int_{-\infty}^{\infty}(x - \mu_X)^2 f(x, y)\, dx\, dy}\sqrt{\int_{-\infty}^{\infty}\int_{-\infty}^{\infty}(y - \mu_Y)^2 f(x, y)\, dx\, dy}}$$

where

$$\mu_X = \int_{-\infty}^{\infty}\int_{-\infty}^{\infty} x f(x, y)\, dx\, dy$$

and

$$\mu_X = \int_{-\infty}^{\infty}\int_{-\infty}^{\infty} y f(x, y)\, dx\, dy$$

If $y = ax + b$, then $\rho = 1$ if $a > 0$ and $\rho = -1$ if $a < 0$.

It is possible for one variable to be a function of another, yet have zero correlation with it (e.g., $y = x$ for $x \ge 0$ and $y = -x$ for $x < 0$).

If two random variables are independent, they will have zero correlation. However, zero correlation can occur without independence.

Even if two variables are highly correlated, it is not necessary for either to be the cause of the other. Many so-called spurious correlations occur. An example is a case of two variables (e.g., sales of fire extinguishers, sales of chewing gum) that are both strongly influenced by a third variable (e.g., disposable income) and so will be highly correlated with each other because each is correlated with the third variable.

In the case of a multimodal joint probability distribution, the correlation may be quite different at a macro- and a microlevel. Consider the variables of fire rate per household and average income per household with regard to census tracts in a city. A small number of tracts typically will have high fire rates and low incomes; the rest will have low fire rates and high incomes. The two variables will be highly correlated if all census tracts are considered together, but if the two relatively homogeneous areas are analyzed separately, there may be little correlation.

If a sample of size n consists of pairs of values (x_i, y_i), then the sample correlation coefficient is

$$r_{XY} = \frac{\sum_{i=1}^{\infty}(x_i - \bar{x})(y_i - \bar{y})}{\sqrt{\sum_{i=1}^{n}(x_i - \bar{x})^2}\sqrt{\sum_{i=1}^{n}(y_i - \bar{y})^2}}$$

EXAMPLE:

Suppose the scores of ten fire fighters on a promotional exam are compared to their numbers of years with the fire service, with results shown in Table 1-12.1 and in Figure 1-12.1.

Then the mean age is 23.7 and the mean score is 72. The correlation coefficient is 0.67, indicating moderate correlation. If the second individual's score, which is the farthest from the group pattern, were changed from 85 to 60, the correlation coefficient would rise to 0.89, indicating high correlation.

The *coefficient of determination* (also called the *percentage of variation explained*) is given by the square of the correlation coefficient.

Table 1-12.1 *Distribution of Test Scores*

Age	Score
18	54
20	85
20	62
20	60
22	66
25	70
25	75
28	88
29	70
30	90

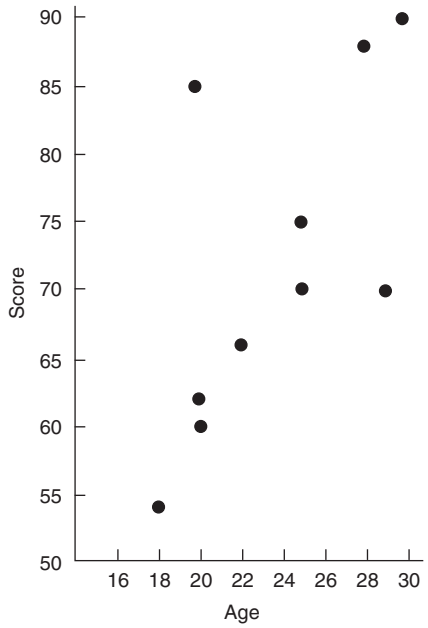

Figure 1-12.1. ***Distribution of test scores.***

Regression

Regression analysis consists of fitting a relationship, usually a linear relationship ($Y = aX + b$), to two random variables, X and Y. The term "regression" is left over from one of the findings in one of the earliest applications of the theory, where it was discovered that heights of parents are good predictors of heights of children but that heights of children tend to "regress" toward the mean. (In other words, for this problem, the best fit was $Y = a(X - \mu_x) + \mu_y$, where $a < 1$.)

Method of Least Squares

The method of least squares assumes that the best fit is obtained by minimizing the weighted sum of the squared differences between predicted and observed values of Y. In other words:

For two discrete random variables, X and Y, with joint probability distribution $f(x_i, y_j)$, choose a and b to minimize

$$\sum_{i=1}^{\infty} \sum_{j=1}^{\infty} (y_i - ax_i - b)^2 f(x_i, y_j)$$

For two continuous random variables, X and Y, with joint density function $f(x, y)$, choose a and b to minimize

$$\int_{-\infty}^{\infty} \int_{-\infty}^{\infty} (y - ax - b)^2 f(x, y)\, dx\, dy$$

For a sample of size n of pairs of values (x_i, y_i), choose a and b to minimize

$$\sum_{i=1}^{n} (y_i - ax_i - b)^2$$

The method of least squares is the best method if the deviations between observed and expected values of Y are themselves normally distributed, independent random variables. This condition would be satisfied, for example, in most experiments if the only source of deviation was error in reading a measuring device. The deviations are also called *residuals.*

Analysis of patterns in residuals can be done to confirm the normality assumptions cited above. Also, data points may be selected with extremely large residuals and studied for common characteristics as a means of trying to identify other factors that may be correlated to the outcomes, y. These results, in turn, may lead to a more sophisticated, multivariate regression analysis.

Regression Coefficients

The least-squares fit of a relationship of the form $Y = aX + B$ will be given by

$$a = \frac{\rho_{xy}\sigma_y}{\sigma_x}$$

$$b = \mu_y - a\mu_x$$

For a sample of size n of pairs (x_i, y_i), the formulas are

$$a = \frac{(n\sum_{i=1}^{n} x_i y_i) - [(\sum_{i=1}^{n} x_i)(\sum_{i=1}^{n} y_i)]}{(n\sum_{i-1}^{n} x_i^2) - [(\sum_{i=1}^{n} x_i)^2]}$$

$$b = \frac{[(\sum_{i=1}^{n} x_i^2)(\sum_{i=1}^{n} y_i)] - [(\sum_{i=1}^{n} x_i)(\sum_{i=1}^{n} x_i y_i)]}{(n\sum_{i=1}^{n} x_i^2) - [(\sum_{i=1}^{n} x_i)^2]}$$

EXAMPLE:

Reexamine the case of age versus test score examined earlier under the discussion of correlation. In that case, as noted, the correlation coefficient was 0.67, the mean age was 23.7, and the mean score was 72. The ratio of standard deviations can be calculated as 2.87. Therefore, a = 1.92 and b = 26.5. This means that the predicted score for age 20 would be 64.9, compared to the 60, 62, and 85 scored by persons of that age, while the predicted score for age 30 would be 84.1, compared to the 90 scored by the person of that age.

This regression line tends to overpredict scores for younger persons because the line is tipped as it tries to accommodate the 85 score achieved by one 20 year old. If that score had been a 60, then as noted the correlation coefficient would be 0.89; also, the mean score would be 69.5 and the ratio of standard deviations would be 2.78. Therefore, a would be 2.47 and b would be 11.0. The predicted score for age 20 would change from 64.9 to 60.4, and the predicted score for age 18 would change from 61.1 to 55.5, much closer to the score actually achieved by the 18 year old.

While it is theoretically possible to fit any relationship, not just a linear one, between X and Y, it is rarely possible to develop least-square formulas for a and b if the relationship is not linear. Accordingly, the analyst will usually want to try to transform problems into linear regression problems. For example, if the true relationship is believed to be of the form $y = c^{(x+d)}$, one would set up a linear regression of log y versus x. Then $d \log c = b$ and $\log c = a$.

Hypothesis Testing in Classical Statistical Inference

Hypothesis and Test

A statistical *hypothesis* is a well-defined statement about a probability distribution or, more frequently, one of its parameters. A classical *test* of a statistical hypothesis is based on the use of several concepts to organize the uncertainty inherent in any probabilistic situation.

The hypothesis being considered is called the *null hypothesis* and implies a probability distribution. Classical statistical inference asks whether the probability of having obtained the statistics actually collected, given the null hypothesis, is so low that the null hypothesis must be rejected.

The test works on the basis of a statistic computed from a sample. That statistic is compared to a reference value. If the statistic falls to one side of the reference value, then the null hypothesis is rejected; if the statistic falls to the other side, then the null hypothesis is not rejected.

For the reasons given above, a statistical test resolves doubts in favor of the null hypothesis. Therefore, an analyst may choose to say that the null hypothesis was "not rejected" rather than say it was "accepted." The analogy is to a criminal trial, which may find a defendant "not guilty" but does not make findings of "innocent."

A *Type I error* occurs when the null hypothesis is really true, but the test says that it should be rejected. A *Type II error* occurs when the null hypothesis is really false, but the test says it should not be rejected. (Informally, many analysts use the term *Type III error* to refer to analyses that set up the initial problem incorrectly, thereby producing results that, however precise, are irrelevant to the real issue.)

A *confidence coefficient*, or measure of the *degree of confidence*, is used to indicate the maximum acceptable probability of Type I error. In most cases, the null hypothesis corresponds to a single, well-defined probability distribution. Therefore, the probability of the sample statistic falling on the reject side of the reference value can be calculated precisely, and the reference value can be selected so as to set that probability equal to the confidence coefficient.

One way of using the confidence coefficient is to set *confidence limits* or define a confidence interval. These limits or internal boundaries are set so that if the null hypothesis is true, then the probability of obtaining a sample whose test statistic is outside the limits (or interval) is equal to the confidence coefficient. These confidence limits indicate to the user how precisely the probability distribution or its parameter can be defined, given the size of the sample and its variability.

The value of the confidence coefficient can be set at any of certain standard levels (90 percent, 95 percent, and 99 percent are often used), or it can be derived from an analysis that seeks to balance Type I and Type II errors. The latter approach is more comprehensive, but it is much more difficult because the alternative(s) to the null hypothesis rarely correspond(s) to a single probability distribution. In a typical case, the null hypothesis states a single value for a population parameter ($\mu = a$) and the alternative corresponds to all other values ($\mu \neq a$). Each specific alternative defines a specific probability distribution with a specific probability of Type II error. The *power function of the test* is that function which gives the probability of *not* committing a Type II error for each parameter value covered by the alternative(s) to the null hypothesis.

As the parameter value approaches the value in the null hypothesis (e.g., $\mu \rightarrow a$), the power of the test drops toward the confidence coefficient.

Test of Mean—z Test

If a sample has been collected from a population with known standard deviation σ, the central limit theorem indicates that the sample mean has an approximately normal distribution about the true population mean μ_0.

Let

$$z = (\sqrt{n})(\bar{x} - \mu_0)\sigma$$

where

n = sample size

μ_0 = hypothesized true value of μ

$\bar{x}$ = sample mean

Let z_α be the value for which $F(z_\alpha) = 1 - \alpha$, where F is the cumulative distribution function of a normal distribution with mean zero and variance one. (Note that $z_{1-\alpha} = -z_\alpha$.)

A *two-sided test* presumes that, if the true population mean is not μ_0, then it is equally likely to be greater than or less than μ_0. In that case, positive and negative values of z are treated the same and the confidence coefficient must be divided between the two sides of the confidence interval. Then if α is the confidence coefficient, the two-sided test says accept the null hypothesis if

$$-z_{\alpha/2} \leq z \leq z_{\alpha/2}$$

A *one-sided test* presumes that if the true population mean is not μ_0, then it must be greater than (or less than) μ_0. If α is the confidence coefficient, then the one-sided test says accept the null hypothesis if

$$z \geq -z_\alpha \quad \text{if the alternative to } \mu = \mu_0 \text{ is } \mu < \mu_0$$

or

$$z \leq z_\alpha \quad \text{if the alternative to } \mu = \mu_0 \text{ is } \mu > \mu_0$$

The value

$$\frac{\sigma}{\sqrt{n}}$$

is called the *standard error of the mean.*

Test of Difference between Two Means—z Test

If two samples from populations with known standard deviations, σ_1 and σ_2, have been collected, a null hypothesis might be that they are from the same population, which

means their means would be the same ($\mu_1 = \mu_2$). Then a two-sided test is applied, using the following statistic:

$$z = \frac{(\bar{x}_1 - \bar{x}_2)}{\sqrt{\sigma_1^2/n_1 + \sigma_2^2/n_2}}$$

where $\bar{x}_i$, σ_i^2, and n_i are the sample mean, population variance, and sample size, respectively, of the ith sample.

Test of Proportion—z Test

If a sample has been drawn from a population governed by a binominal distribution, then the normal approximation gives the following statistic, to be used in one- or two-sided tests

$$z = \frac{n(\bar{p} - p_0)}{\sqrt{p_0(1 - p_0)}}$$

where p_0 is the hypothesized true proportion and p is the sample proportion.

Test of Difference between Two Proportions—z Test

Again the normal approximation to the binomial distribution gives the test statistic

$$z = \frac{(\bar{p}_1 - \bar{p}_2)}{\sqrt{[\bar{p}_1(1 - \bar{p}_1)/n_1] + [\bar{p}_2(1 - \bar{p}_2)/n_2]}}$$

Test of Mean—t Test

The z tests assume known variance(s), so if variances are not known, a test based on Student's t distribution must be used. Let $t_{\alpha,m}$ be defined such that $F(t_{\alpha,m}) = 1 - \alpha$, where F is the cumulative distribution function for a Student's t distribution with m degrees of freedom. Note that $t_{(1-\alpha),m} = -t_{\alpha,m}$. Then

$$t = \frac{\sqrt{n}(\bar{x} - \mu_0)}{s}$$

where

n = sample size
μ_0 = hypothesized population mean
s = sample standard deviation

A two-sided test says accept the null hypothesis if

$$-t_{(\alpha/2),(n-1)} \leq t \leq t_{(\alpha/2),(n-1)}$$

Note that the number of degrees of freedom is one less than the sample size. An informal method of remembering this is that one degree of freedom is used to estimate the standard deviation.

A one-sided test says accept the null hypothesis if

$$t \geq -t_{\alpha,(n-1)} \quad \text{if the alternative to } \mu = \mu_0 \text{ is } \mu < \mu_0$$

or

$$t \leq -t_{\alpha,(n-1)} \quad \text{if the alternative to } \mu = \mu_0 \text{ is } \mu > \mu_0$$

A test of differences between two means is constructed analogously.

EXAMPLE:

This example will illustrate all the tests described thus far. Suppose there are two fire departments, each of which has given promotional tests to 100 fire fighters. Scores can range from 0 to 100, and the passing score is 70. The actual distributions of scores are shown in Table 1-12.2 and Figure 1-12.2.

Suppose that nationwide the standard deviation for this test is 17.45, the mean score is 50, and the proportion who pass is 0.17. Is Department A an average department? This suggests a two-sided test of the mean score, using the z test because the standard deviation is known. Let α be 0.05, so $z_{\alpha/2} = 1.96$. The z statistic for the test is

$$\frac{(\sqrt{100})(53.2 - 50)}{17.60} = 1.83$$

which is between -1.96 and $+1.96$, so the null hypothesis is accepted. Department A is average.

Table 1-12.2 ***Distribution of Test Scores***

Score	Number of Fire Fighters with That Score in Department A	Department B
10	0	5
20	6	5
30	5	10
40	20	20
50	29	25
60	20	20
70	9	10
80	5	3
90	3	2
100	3	0
Total	100	100
Sample mean	53.2	48.2
Sample standard deviation	17.54	17.34
Proportiion of sample passing	0.20	0.15

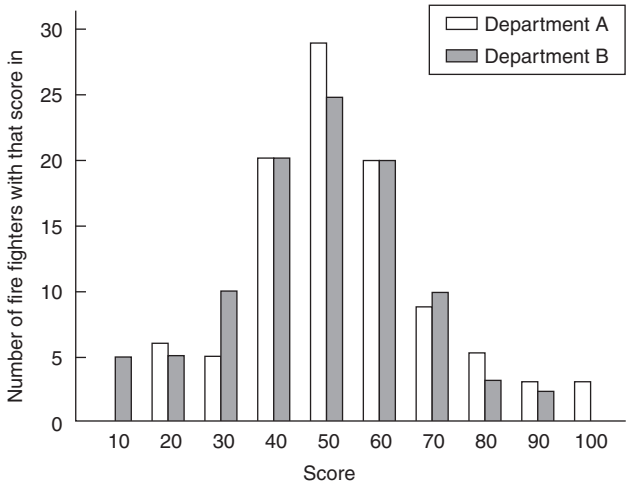

Figure 1-12.2. ***Distribution of test scores in two fire departments.***

Suppose it is asked instead whether Department A is a better-than-average department. This formulation suggests a one-sided test of the mean score, again using the z test because the standard deviation is known. Again, let $\alpha = 0.05$, so $Z_{\alpha/2} = 1.64$. The z statistic for the test is again 1.83, which is greater than 1.64, so we reject the null hypothesis and conclude that Department A is above average.

The results for these two tests seem contradictory because one concludes that Department A is average and the other concludes that Department A is above average. Such discrepancies are inherent to statistical tests. They can be sensitive to the choice of α. (If α were 0.10, both null hypotheses would be rejected, while if α were 0.01, both null hypotheses would be accepted. In either case, the two tests would give consistent results.) They can be sensitive to how the alternatives were posed, as was true here.

Suppose it is asked whether Departments A and B have significantly different mean scores. This formulation suggess a z test of the difference between two means. In this case the standard deviations are the same and the sample sizes are the same, so the z statistic reduces to

$$\frac{53.2 - 48.2}{\sqrt{2 \times 17.45/100}} = 8.46$$

The two-sided test reference value of 1.96, calculated earlier, is easily exceeded, and we conclude that the two departments do have statistically significant differences in their mean scores.

Suppose it is asked whether Department A's proportion of students passing (0.20) is statistically significantly greater than the overall average of 0.17. This formulation calls for a z test of a proportion, and the z statistic is

$$\frac{(\sqrt{100})(0.20) - 0.17}{\sqrt{(0.17)(0.83)}} = 0.80$$

This result is not statistically significant under either a one-sided or a two-sided test.

Are the proportions passing in Departments A and B different? This formulation suggests a z test of the difference between two proportions, and the z statistic is

$$\frac{0.20 - 0.15}{\sqrt{[(0.20)(0.80)/100] + [(0.15)(0.85)/100]}} = 0.93$$

Even though the average scores for Departments A and B were found to be different by a statistically significant margin, their percentage of test takers passing were not found to be significantly different.

Suppose the value of the overall standard deviation for the test was not known, or it was not known whether it applied to these departments, but it was known that the overall average score was 50. Is Department A's score significantly better? This formulation suggests a one-sided t test. The t statistic is

$$\frac{\sqrt{100}(53.2 - 50.0)}{17.54} = 1.82$$

For a one-sided t test with a 0.05 confidence level and 99 degrees of freedom, the reference value is the same as for a one-sided z test with a 0.05 confidence level, namely 1.64. Because the sample standard deviation is also nearly equal to the overall standard deviation used earlier, the test results are virtually the same, and the null hypothesis is rejected. This would not have been the case if the sample size had been considerably smaller, leading to a larger reference value. The smaller the difference you are examining, the larger the sample size required to be sure that difference is real and not just the result of random variation.

Test of Variance—Chi-Square Test

Assuming a normal population, one can test the hypothesis $\sigma = \sigma_0$ with the following:

$$\psi_2 = \frac{(n-1)s^2}{\sigma_0^2}$$

where n is the sample size and s^2 is the sample variance.

A two-sided test accepts the null hypothesis if

$$\psi^2_{(1-\alpha/2),(n-1)} \leq \psi^2 \leq \psi^2_{(\alpha/2),(n-1)}$$

where $\psi^2_{\alpha,m}$ is the value such that $F(\psi^2_{\alpha,m}) = 1 - \alpha$, where F is the cumulative distribution function of a chi square distribution with m degrees of freedom. Note that the degrees of freedom used in the test are one less than the sample size. One-sided tests can be constructed analogously.

Test of Goodness of Fit to a Distribution—Chi-Square Test

A special use of the test of variance is to test how well a set of experimental data fit a presumed theoretical probability distribution. Suppose the distribution in question is represented as a set of k values or ranges of values for the random variable. Let $p_i, \ldots, p_k$ be the hypothesized probabilities for those k values or ranges; let $p_i, \ldots, p_k$ be the sample estimates of those probabilities; and let n be the sample size. Then the statistic is

$$\psi^2 = \sum_{i=1}^{k} \left\{ \frac{[u(p_i, \overline{p}_i, n)]^2}{np_i} \right\}$$

where

$$u(p_i, \overline{p}_i, n) = \begin{Bmatrix} 0 & \text{if } -\frac{1}{2} \leq np_i - n\overline{p}_i \leq \frac{1}{2} \\ np_i - n\overline{p}_i - \frac{1}{2} & \text{if } np_i - n\overline{p}_i > \frac{1}{2} \\ n\overline{p}_i - np_i - \frac{1}{2} & \text{if } n\overline{p}_i - np_i > \frac{1}{2} \end{Bmatrix}$$

This process of reducing the gap between np_i and $n\overline{p}_i$ by ½ is called the *Yates continuity correction*, and it compensates for the fact that the chi-square distribution, a continuous function, is being used to approximate a discrete probability distribution. Also, to apply this test validly, one must make sure that the k classes are grouped sufficiently that $np_i \geq 5$ for all $i = 1, \ldots, k$.

The null hypothesis says this sample came from the distribution represented by $p_i, \ldots, p_k$. That hypothesis is accepted if

$$\psi^2 \leq \psi^2_{\alpha,j}$$

where j is at most $k - 1$ and may be less if the p_i are based in part on the sample.

For example, suppose an analyst wishes to test goodness of fit to a binomial distribution but has no prior estimate of which binomial distribution should be used. The analyst would select the particular binomial distribution that has p equal to the sample proportion. In that case one parameter has been estimated from the sample, and j would be reduced by one to $(k - 2)$. If the analyst were testing goodness of fit to a normal distribution and estimated both mean and variance from the sample, then j would drop by two to $(k - 3)$.

Contingency Test of Independence—Chi-Square Test

A special case of the goodness of fit test is a test of the hypothesis that two random variables are independent, in which case the goodness of fit test is displayed in a *contingency table,* as follows:

Let $X_1, \ldots, X_m$ be the m values or subranges of a random variable, X; and let $Y_1, \ldots, Y_k$ be the k values or subranges of a random variable, Y.

Let p_i be the estimated probability of X_i, for $i = 1, \ldots, m$, and let q_j be the estimated probability of Y_j, for $j = 1, \ldots, k$.

Let n be the size of a sample such that, for each sample entry, a value of X and a value of Y are provided. (Be sure $np_iq_j \geq 5$ for all i and j.)

Let r_{ij} be the number of sample entries for which $X = X_i$ and $Y = Y_j$.

Therefore

$$\sum_{i=1}^{m} \sum_{j=1}^{k} r_{ij} = n$$

Then the sample will provide estimated values of p_i and q_j as follows

$$p_i = \frac{\left(\sum_{j=i}^{k} r_{ij}\right)}{n}$$

and

$$q_j = \frac{\left(\sum_{i=i}^{m} r_{ij}\right)}{n}$$

If the two random variables are independent, then the expected values for r_{ij} are given by np_iq_j.

The test statistic, therefore, is given by

$$\psi^2 = \sum_{i=1}^{m} \sum_{j=1}^{k} \left\{ \frac{[u(r_{ij}, p_i, q_j, n)]^2}{np_iq_j} \right\}$$

where

$$u(r_{ij}, p_i, q_j, n) = \begin{Bmatrix} 0 & \text{if } -\frac{1}{2} \leq r_{ij} - np_iq_j \leq \frac{1}{2} \\ r_{ij} - np_iq_j - \frac{1}{2} & \text{if } r_{ij} - np_iq_j > \frac{1}{2} \\ np_iq_j - r_{ij} - \frac{1}{2} & \text{if } np_iq_j - r_{ij} > \frac{1}{2} \end{Bmatrix}$$

The null hypothesis of independence is accepted if

$$\psi^2 \leq \psi^2_{\alpha,[(m-1)(k-1)]}$$

The number of degrees of freedom comes from the formula given for goodness-of-fit tests. One begins with $mk - 1$ degrees of freedom. There are m values of p_i, but they sum to one, so only $m - 1$ need be estimated from the sample, and similarly $(k - 1)$ values of q_j must be estimated. Therefore the degrees of freedom for the test equal $(mk - 1) - (m - 1) - (k - 1) = (m - 1)(k - 1)$.

Nonparametric Tests

There are a large number of nonparametric tests, so called because they use no sample or population parameters and make no assumptions about the type of probability distribution that produced the sample.

Sampling Theory

A *random sample* is a sample chosen in accordance with a well-defined procedure that assures (a) each equal item (e.g., each person) has an equal chance of being selected; or (b) each value of a random variable (e.g., height) has a likelihood of being selected that is the same as its probability of occurrence in the full population. A sample that is selected with no conscious biases still may not be truly random; the burden of proof is on the procedure that claims to produce a random sample. A random sample may not be as representative as a sample that is chosen to be representative, but a sample chosen to be representative on a few characteristics may not be random and may not be representative with respect to other important characteristics.

In addition to requiring that each item have an equal chance of being selected, a random sample must assure that every combination of items also has an equal chance of being selected. For example, a random sample of currently married couples would not be a random sample of currently married persons, because spouses would be either selected or not selected together in the former but not necessarily in the latter.

A *sampling frame* is a basis for reaching any member of a population for sampling in a way that preserves the randomness of selection. An example would be a mailing list, although if it had missing names or duplicate names it would be deficient as a sampling frame, because each equally likely name would not have an equal chance at selection. A *sample design* is a procedure for drawing a sample from a sampling frame so that the desired randomness properties are achieved.

A *simple random sample* is a sample that is drawn by a procedure assuming complete randomness from a population all of whose elements are equally likely. If they are not all equally likely, a procedure that assures complete randomness is called a *probability sample.*

A *stratified random sample* is a sample that achieves greater precision than a simple random sample by taking advantage of existing knowledge about the variance structure of subpopulations. By concentrating a dispro-

portionate share of the sample in subpopulations that account for disproportionate shares of the total variance, a stratified random sample produces lower total variance for a given sample size. The annual National Fire Protection Association survey of fire departments that produces the annual estimates of total U.S. fire loss is a stratified random sample.

A *cluster sample* is a sample that randomly selects certain subpopulations, then samples only them. This approach often involves subpopulations that consist of geographical areas, in which case it is also called an *area sample.* The purpose of cluster sampling is to hold down the cost of sampling. It is not as statistically acceptable as a simple or stratified random sample.

A *systematic sample* begins with a listing of the population, then random selection of the first sample member, and finally selection of the remaining members at fixed intervals (e.g., every *k*th name on the list). This approach is simpler than true random sampling but not as acceptable.

A *representative sample* is one chosen to guarantee representation from each of several groups. If properly designed, it is a special case of stratified random sampling, but often the term is used for samples where the need for representation is the only part of the procedure specified. If the size of the representation is also specified, it is called a *quota sample.* The statistical properties of a sample constructed in this way cannot be determined, and nothing useful can be said about its accuracy or precision. That is also true of a *judgment sample,* in which the only rules governing sample selection are the statistician's judgments.

Characterization of Data from Experimentation or Modeling

Data Variability

Any data source is subject to variability for reasons other than those with substantive importance. Results of a test of burning behavior of a material may vary because of the ambient temperature or humidity. Such variation can be virtually eliminated through careful experimental controls. Results may vary because of naturally occurring variations in the composition of the material or human variability in the production process. Such variation can be reduced through careful controls, and it may be possible to measure the variation that cannot be eliminated. Test results may vary because of moment-to-moment variations in air flow or in the heat output of the heating apparatus or in many other physical conditions and characteristics. Such variation can be reduced through careful controls, but residual variation may be difficult or impossible to measure. And because test results may vary as a result of standardization and care, or the lack thereof, it is also true that test results may vary with the laboratories, organizations, and people conducting the tests.

Interpretation of test results—or of modeling results based on input test data—must take account of data variability from causes other than those of interest. Such variability is often called "error" in statistical terminology, where the term "error" is used to refer to all deviations between predicted and actual results, not just to deviations involving improper human behavior. Standards for test methods typically have sections for what is called *precision* and *bias* information. Precision refers to the magnitude of error. Bias refers to the symmetry of error. Precision asks, "Are large differences possible even if there is no difference in the characteristics we intended to test for?" Bias asks, "Are we more likely to err in one direction than in another?"

Precision and bias sections are often lacking in test method documentation—or at least lacking in detail. For laboratory testing the principal source of precision and bias information is interlaboratory studies. Through reported experiments at each of several laboratories under what are intended to be identical testing conditions, one can quantify the magnitude of variation from one run to the next in a single laboratory (called *repeatability*) and of variation between laboratories (called *reproduceability*).

There are standard statistical methods for assessing such variation, but the work is expensive, which accounts for the scarcity of such data. Also, the results, when published, are attached to a test method but may show more precision than a user will obtain in another application (e.g., different material) or in a laboratory without the heightened attention to precise controls that one expects in an interlaboratory evaluation. (No laboratory wishes to be found less precise, or less capable generally, than its competitors, but in most day-to-day work, there is no expectation of such calibration of performance, and people may relax.)

One might think that inherently statistical databases—such as fire incident databases—would be easier to assess, and it is true that precision can be readily calculated based on sample size. However, bias depends on the adequacy of the sampling—is the sample truly random and so representative of its universe?—and most statistical databases are not truly random. The National Fire Incident Reporting System (NFIRS) captures nearly a million fire incidents a year, typically close to half the total fires reported to fire departments. The precision of NFIRS is outstanding, on that basis. However, national estimates of specific fire problems project and calibrate NFIRS using a smaller database, the NFPA annual fire experience survey, and so reflect that smaller database's lesser (though still excellent) precision. More importantly, NFIRS is not a true random sample (although the NFPA survey is), and so its bias cannot be calculated from any standard statistical methods. Instead, NFIRS users note the large share of total fires it represents and the absence of any obvious sources of significant bias. (For example, NFIRS is believed to be less represented in rural or large urban areas but is well represented in both.)

In the end, engineering analysis must consider and address data variability issues but typically cannot hope to fully quantify or resolve them.

Testing Models for Goodness of Fit

Earlier in this chapter, the use of the chi-square test to assess goodness of fit was described for a statistical distribution. The same method can be used to assess goodness of fit between any set of model predictions and laboratory

data. In essence, this statistical test assumes that each laboratory data point is equally likely. If there are n data points, then the test is based on

$$\psi^2 = \sum_{i=1}^{n} \frac{(x_{i,\,\text{measured}} - x_{i,\,\text{predicted}})^2}{x_{i,\,\text{predicted}}}$$

This method is a one-sided test using $n - 1 - k$ degrees of freedom, where k is equal to the number of model parameters estimated from the data. (The more the data is used indirectly to predict itself, the less variation one would expect to see.)

The more common practice in assessing goodness of fit is to "eyeball" the two curves, that is, be guided by an impression of proximity. This can be highly misleading. The eye tends to measure distances between two curves as the shortest distance between the curves, whereas accuracy of prediction is based on differences in predicted versus actual y-axis values for given x-axis values. These differences can be very large between two curves with steep slopes that look close together, and steep slopes are commonplace in curves for variables that describe fire development and related environmental conditions.

On the other hand, sometimes the most relevant and appropriate measures of the correspondence between two curves lies in the correspondence between key summary measures and not in the exactness of the correspondence between the full curves. For example, the timing of the transition from smoldering to free burning is not well described by any model and is subject to enormous variability. However, this should not be allowed to obscure the agreement of model with empirical data during the free-burning stage.

One way to adjust the comparison so that it excludes the smoldering phase is through recalibration of the curve. Set the timing and fire conditions at the onset of free burning for the model equal to the timing and fire conditions from the lab data. Then, use formal statistical methods to assess how well the model predicts the data from that point on. Note, however, that the steepness of the curves makes it quite possible that calculated agreement will be poor even with this adjustment.

Another way to adjust the comparison is to compare the timing of transition points (also called *inflection points* in calculus), such as time from the onset of free burning to flashover; and appropriate maximums (e.g., peak heat release rate) and minimums (e.g., oxygen concentration). The problem with this approach is that there may not be simple statistical tests, such as the chi-square test for goodness of fit of whole curves, that will indicate how much difference in timing of transition points or in other summary measures can be expected statistically due to measurement error or other normal variability and how much difference is significant. There needs to be an extended dialogue between fire protection engineers and statisticians to determine which statistical bases for evaluating goodness of fit of models to empirical data are both executable as statistical tests and meaningful to the modelers.

Propagation of Uncertainty

The procedures just described form a basis for describing the readily quantifiable uncertainty associated with input data and modeling components for engineering analysis. Additional statistical procedures are needed to calculate how these component uncertainties translate into a combined measure of error or uncertainty in the output data. This is typically called *propagation of uncertainties* because the procedures measure how uncertainty at the early steps of the calculation is propagated—modified or passed through—the later steps of the calculation to affect the final result.

There is no general guidance possible for these procedures because they are highly dependent upon the functional forms and mathematical relationships linking the uncertain variables. The only practical guidance is cautionary. The step of propagating uncertainties and estimating cumulative uncertainty is a necessary step that is almost never performed in fire protection engineering analysis. A reasonable expectation is that uncertainties will accumulate, producing more uncertainty in the output data than in any of the components along the way, but uncertainties are rarely additive, even if the underlying variables are combined linearly, and it is possible for uncertainties to be reduced in the propagation analysis, due to interdependencies or mathematical transformations implied by the models, rather than to cumulate.

The issue of uncertainty propagation is another area where much more dialogue is needed between fire protection engineers and statisticians to identify or develop statistical assessment procedures that are soundly based and practical for routine use.

Additional Readings

R. Baldwin, *Some Notes on the Mathematical Analysis of Safety,* Fire Research Note 909, Joint Fire Research Organization, Borehamwood, UK (1972).

J.R. Benjamin and C.A. Cornell, *Probability, Statistics and Decision for Civil Engineers,* McGraw-Hill, New York (1970).

M.H. DeGroot, *Optimal Statistical Decisions,* McGraw-Hill, New York (1970).

J.E. Freund, *Mathematical Statistics,* Prentice Hall, Englewood Cliffs, NJ (1962).

J.E. Freund and F.J. Williams, *Dictionary/Outline of Basic Statistics,* McGraw-Hill, New York (1966).

G.J. Hahn and S.S. Shapiro, *Statistical Models in Engineering,* John Wiley and Sons, New York (1966).

N.A.J. Hastings and J.B. Peacock, *Statistical Distributions: A Handbook for Students,* Butterworths, London (1975).

P.G. Hoel, *Introduction to Mathematical Statistics,* John Wiley and Sons, New York (1962).

D. Huff, *How to Lie with Statistics,* Penguin, Middlesex, UK (1973).

K.C. Kapur and L.R. Lamberson, *Reliability in Engineering Design,* John Wiley and Sons, New York (1977).

A.M. Mood and F.A. Graybill, *Introduction to the Theory of Statistics,* McGraw-Hill, New York (1963).

D.T. Phillips, *Applied Goodness of Fit Testing,* American Institute of Industrial Engineers, Atlanta (1972).

S. Siegel, *Nonparametric Statistics for the Behavioral Sciences,* McGraw-Hill, New York (1956).

M.R. Spiegel, *Probability and Statistics,* McGraw-Hill, New York (1975).

R.E. Walpole and R.H. Myers, *Probability and Statistics for Engineers and Scientists,* Macmillan, New York (1972).

Section Two
Fire Dynamics

Section 2 Fire Dynamics

CHAPTER 1

Fire Plumes, Flame Height, and Air Entrainment

Gunnar Heskestad

Introduction

Practically all fires go through an important, initial stage in which a coherent, buoyant gas stream rises above a localized volume undergoing combustion into surrounding space of essentially uncontaminated air. This stage begins at ignition, continues through a possible smoldering interval, into a flaming interval, and may be said to end prior to flashover. The buoyant gas stream is generally turbulent, except when the fire source is very small. The buoyant flow, including any flames, is referred to as a fire plume.

Combustion may be the result of pyrolysis of solid materials or evaporation of liquids because of heat feedback from the combustion volume, or of pressurized release of flammable gas. Other combustion situations may involve discharge of liquid sprays and aerosols, both liquid and solid, but these will not be discussed here. In the case of high-pressure releases, the momentum of the release may be important. Flames in these situations are usually referred to as *diffusion flames,* being the result of combustible vapor or gas mixing or diffusing into an ambient oxidant, usually air, as opposed to being premixed with an oxidant.

The properties of fire plumes are important in dealing with problems related to fire detection, fire heating of building structures, smoke filling rates, fire venting, and so forth. They can also be important in fire suppression system design.

This chapter deals with axisymmetric, turbulent fire plumes and reviews some relations for predicting the properties of such plumes. It is assumed throughout the chapter that the surrounding air is uncontaminated by fire products and that it is uniform in temperature, except where specifically treated as temperature stratified. Release of gas from a pressurized source is assumed to be vertical. The relations cease to be valid at elevations where the plume enters a smoke layer.

Main topics are flame heights, plume temperatures and velocities, virtual origin, air entrainment, and effects of ambient temperature stratifications. At the end of the chapter, a few additional aspects of diffusion flames are touched on briefly, including flame pulsations, wall/corner effects, and wind effects.

Dr. Gunnar Heskestad is principal research scientist at Factory Mutual Research, specializing in fluid mechanics and heat transfer of fire, with applications to fire protection.

Fire Plume Features

Figure 2-1.1 shows a schematic representation of a turbulent fire plume originating at a flaming source, which may be solid or liquid. Volatiles driven off from the combustible, by heat fed back from the fire mix with the surrounding air and form a diffusion flame. Laboratory simulations often employ controlled release of flammable gas through a horizontal, porous surface. The mean height of the flame is *L.* Surrounding the flame and extending upward is a boundary (broken lines) that confines the entire buoyant flow of combustion products and entrained air. The air is entrained across this boundary, which instantaneously is very sharp, highly convoluted, and easily discernible in smoky fires. The flow profile could be the time-averaged temperature rise above the ambient

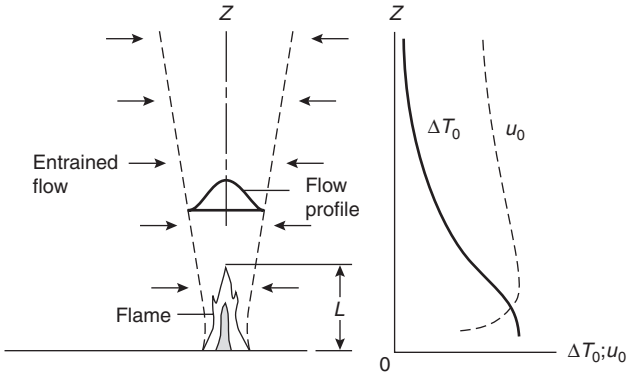

Figure 2-1.1. ***Features of a turbulent fire plume, including axial variations on the centerline of mean excess temperature, ΔT_0, and mean velocity, u_0.[34]***

temperature, or the concentration of a gas (such as CO_2) generated by the fire, or the axial velocity in the fire plume.

Figure 2-1.1 suggests qualitatively, based on experimental observations,[1–5] how the temperature rise on the centerline, ΔT_0, and the velocity on the centerline, u_0, might behave along the plume axis. In this example of a relatively tall flame, the temperatures are nearly constant in the lower portion of the flame. Temperatures begin to decay in the intermittent, upper portion of the flame as the combustion reactions trail off and air entrained from the surroundings cools the flow. The centerline velocities, u_0, tend to have their maxima slightly below the mean flame height and always decay toward higher elevations. If the combustible is porous and supports internal combustion, there may not be as pronounced a falloff in the gas velocity toward the top of the combustible, as suggested in Figure 2-1.1.[3]

The total heat release rate of a fire source, $\dot{Q}$, is either convected, $\dot{Q}_c$, or radiated, $\dot{Q}_r$, away from the combustion region. In a fire deep in a porous combustible pile (e.g., a stack of wood pallets), some of the total heat generated is trapped by and stored in the not yet burning material; the rest escapes from the combustible array as either convective or radiative energy flux. If most of the volatiles released undergo combustion above the fuel array, as in pool fires of liquids and other horizontal-surface fires, and even in well-developed porous pile fires, then the convective fraction of the total heat release rate is rarely measured at less than 60 to 70 percent of the total heat release rate.[6,7] The convective flux, $\dot{Q}_c$, is carried away by the plume above the flames, while the remainder of the total heat liberated, $\dot{Q}_r$, is radiated away in all directions.

The total heat release rate, $\dot{Q}$, is often assumed to be equal to the *theoretical* heat release rate, which is based on complete combustion of the burning material. The theoretical heat release rate in kW is evaluated as the mass burning rate in kg/s multiplied by the lower heat of complete combustion in kJ/kg. The ratio of the total heat release rate to the theoretical heat release rate, which is the combustion efficiency, is indeed close to unity for some fire sources (e.g., methanol and heptane pools),[6] but may deviate significantly from unity for others (e.g., a polystyrene fire, for which the combustion efficiency is about 45 percent,[7] and a fully involved stack of wood pallets, for which the combustion efficiency is 63 percent[6]).

Calculation Methods

Flame Heights

The visible flames above a fire source contain the combustion reactions. Tamanini[8] has investigated the manner in which combustion approaches completion with respect to height in diffusion flames.

Typically, the luminosity of the lower part of the flaming region appears fairly steady, while the upper part appears to be intermittent. Sometimes vortex structures, more or less pronounced, can be observed to form near the base of the flame and shed upward.[9,10]

Figure 2-1.2 helps to define the mean flame height, L.[10] It shows schematically the variation of flame intermittency, I, versus distance above the fire source, z, where $I(z)$ is defined as the fraction of time that at least part of the flame lies above the elevation, z. The intermittency decreases from unity deep in the flame to smaller values in the intermittent flame region, eventually reaching zero. The mean flame height, L, is the distance above the fire source where the intermittency has declined to 0.5. Objective determinations of mean flame height according to intermittency measurements are fairly consistent with (although tending to be slightly lower than) flame heights that are averaged by the human eye.[10]

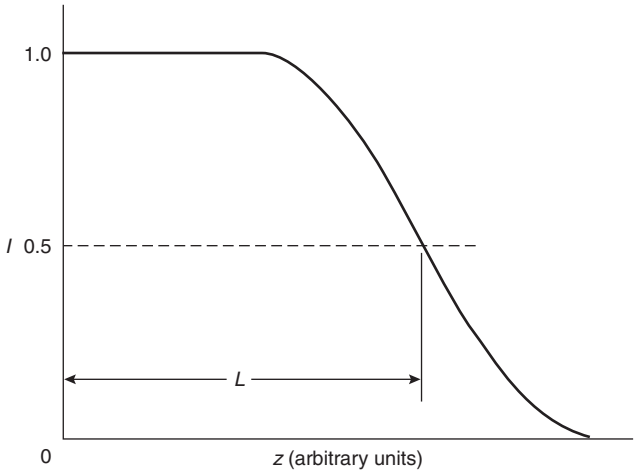

Figure 2-1.2. ***Definition by Zukoski et al.[10] of mean flame height, L, from measurements of intermittency, I.***

The mean flame height is an important quantity that marks the level where the combustion reactions are essentially complete and the inert plume can be considered to begin. Several expressions for mean flame height have been proposed. Figure 2-1.3, taken from McCaffrey,[11] shows normalized flame heights, L/D, as a function of a Froude number, $\dot{Q}^*$ (represented as $\dot{Q}^{*2/5}$ to compress the horizontal scale), from data correlations available in the literature. This Froude number is defined

$$\dot{Q}^* = \frac{\dot{Q}}{\rho_\infty c_p T_\infty \sqrt{gD} D^2} \tag{1}$$

where

$\dot{Q}$ = total heat release rate (given in terms of the mass burning rate, $\dot{m}_f$, as $\dot{m}_f H_c$)

ρ_∞ and T_∞ = ambient density and temperature, respectively

c_p = specific heat of air at constant pressure

g = acceleration of gravity

D = diameter of the fire source

Quoting McCaffrey with respect to this figure: "On the left are pool-configured fires with flame heights of the same order of magnitude as the base dimension D. In the middle is the intermediate regime where all flames are similar and the $\dot{Q}^{2/5}$ is seen as a 45-degree line in the figure. Finally, in the upper right is the high Froude number, high-momentum jet flame regime where flame height ceases to vary with fuel flow rate and is several hundred times the size of the source diameter."

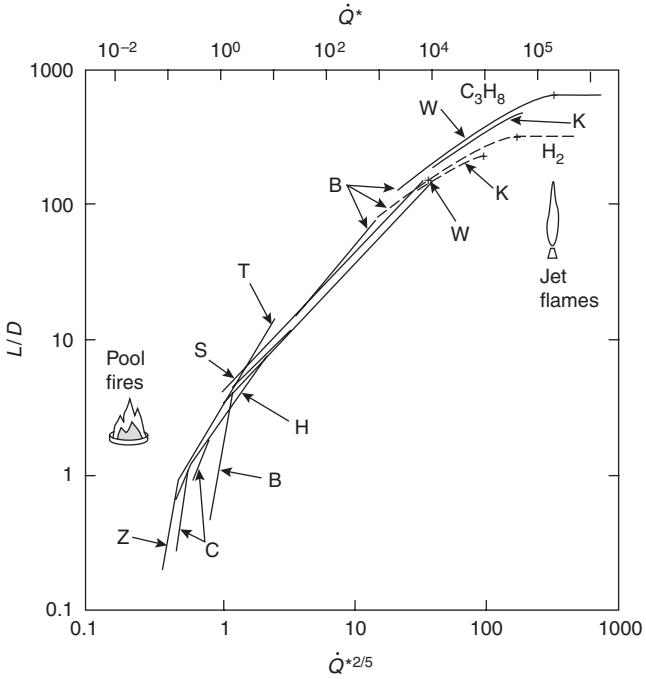

Figure 2-1.3. ***Flame height correlations compiled by McCaffrey.[11] Capital letters without subscripts correspond to various researchers as follows: B = Becker and Liang,[12] C = Cox and Chitty,[13] H = Heskestad,[14] K = Kalghatgi,[15] S = Steward,[16] T = Thomas,[17] W = Hawthorne et al.,[18] and Z = Zukoski.[19] Capital letters with subscripts represent chemical formulae.***

Buoyancy regime: The correlation by Heskestad (*H*) represented in Figure 2-1.3 covers the entire $\dot{Q}^*$ range except the momentum regime and has the following form given by McCaffrey:[11]

$$\frac{L}{D} = -1.02 + 3.7\dot{Q}^{*2/5} \tag{2}$$

Actually, this correlation was originally presented in the form:[14]

$$\frac{L}{D} = -1.02 + 15.6N^{1/5} \tag{3}$$

As before, D is the diameter of the fire source (or effective diameter for noncircular fire sources such that $\pi D^2/4$ = area of fire source) and N is the nondimensional parameter defined by

$$N = \left[\frac{c_pT_\infty}{g\rho_\infty^2(H_c/r)^3}\right]\frac{\dot{Q}^2}{D^5} \tag{4}$$

where H_c is the actual lower heat of combustion and r is the actual mass stoichiometric ratio of air to volatiles.

It is readily shown that N and $\dot{Q}^*$ are related as follows:

$$N = \left(\frac{c_pT_\infty}{H_c/r}\right)^3\dot{Q}^{*2} \tag{5}$$

This equation, combined with Equation 3, leads to Equation 2 when typical values are substituted for the environmental and fuel variables.

The parameter N was derived specifically by consideration of the flaming region,[14] whereas $\dot{Q}^*$ was originally derived by Zukoski[20] from analysis of the nonreacting turbulent plume. In a recent paper, Heskestad[21] presented results of flame height measurements at widely varying ambient temperatures. The parameter $\dot{Q}^*$ did not account correctly for the observed variations in flame height (increasing flame height with increasing ambient temperature), while the parameter N did. For that reason, N is considered the more appropriate scaling parameter.

Equation 3 is based on liquid pool fires, other horizontal-surface fires, and jet flames (but excluding high momentum jet discharge corresponding to values N well beyond 10^5). Subsequent to its derivation, the equation was found also to represent large, deep storages when the flames extended above the storage and flame heights were measured above the base of the fire (bottom of storage in the experiments).[22] The storages investigated included 4.5-m-high palletized storage of different commodities, 3 to 6 m high rack storage of two different commodities, and wood pallets stacked 0.3 to 3.3 m high. In these cases the fire diameter was calculated as the diameter of a fire area equal to the ratio of heat release rate to heat release rate per unit area.

A convenient form of Equation 3 can be developed. Let

$$A = 15.6\left[\frac{c_pT_\infty}{g\rho_\infty^2(H_c/r)^3}\right]^{1/5} \tag{6}$$

Then Equation 3 can be written in the dimensional form

$$L = -1.02D + A\dot{Q}^{2/5} \tag{7}$$

The coefficient, A, varies over a rather narrow range, associated with the fact that H_c/r, the heat liberated per unit mass of air entering the combustion reactions, does not vary appreciably among various combustibles. For a large number of gaseous and liquid fuels, H_c/r remains within the range of 2900 to 3200 kJ/kg, for which the associated range of A under normal atmospheric conditions (293 K, 760 mmHg) is 0.240 to 0.226 (m $kW^{-2/5}$), with a typical value of $A = 0.235$. Hence, under normal atmospheric conditions

$$L = -1.02D + 0.235\dot{Q}^{2/5} \tag{8}$$

(L and D in m; $\dot{Q}$ in kW).

Fairly common fuels that deviate significantly from the cited range 0.240 to 0.226 for A include acetylene, hydrogen (0.211), and gasoline (0.200). In general, the coefficient $A = 0.235$ in Equation 8 may be considered adequate unless actual values of H_c and r are known that indicate otherwise, and/or atmospheric conditions deviate significantly from normal.

Referring to any of the flame-height relations in Equations 3, 7, and 8, it can be seen that negative flame heights are calculated for sufficiently small values of the heat release rate. Of course, this situation is unphysical and the correlation is not valid here. For pool fires, there are indications that a single flaming area breaks down

into several zones when heat release rates decrease to the point where negative flame height (L) is calculated.[23]

EXAMPLE 1:

Consider a 1.5-m-diameter pan fire of methyl alcohol with a heat release intensity of 500 kW/m^2 of surface area. Normal atmospheric conditions prevail (760 mm Hg, 293 K). Calculate the mean flame height.

SOLUTION:

Available values of the lower heat of combustion (H_c = 21,100 kJ/kg) and stoichiometric ratio (r = 6.48) give H_c/r = 3260 kJ/kg. With this value for H_c/r substituted in Equation 6, together with c_p = 1.00 kJ/kg K, T_∞ = 293 K, g = 9.81 m/s^2 and ρ_∞ = 1.20 kg/m^3, the coefficient A is calculated as 0.223 (m kW$^{-2/5}$). The total heat release rate is $\dot{Q} = 500\pi 1.5^2/4 = 884$ kW. Equation 7 gives a mean flame height of $L = -1.02 \cdot 1.5 + 0.223 \cdot 884^{2/5} = 1.83$ m.

EXAMPLE 2:

This example is similar to Example 1, except for new atmospheric conditions representative of Denver, Colorado, on a hot day: 630 mm Hg pressure and 310 K temperature.

SOLUTION:

Using Equation 6, the new coefficient, A, increases from 0.223 to 0.249 [most readily calculated from $(310/293)^{3/5}$ $(760/630)^{2/5}$ 0.223 = 0.249, where the equation of state for a perfect gas has been used]. Using Equation 7, the new flame height is L = 2.23 m, increased from 1.83 m for normal atmospheric conditions.

Example 3:

One 1.2-m high stack of wood pallets (1.07 × 1.07 m) burns at a total heat release rate of 2600 kW under normal atmospheric conditions. Calculate the mean flame height above the base of the pallet stack.

SOLUTION:

The square flaming area can be converted to an equivalent diameter: $\pi D^2/4 = 1.07^2$, which gives the equivalent diameter, D, of 1.21 m. Since the combustion efficiency of wood is considerably less than 100 percent, it is difficult to select reliable and consistent values for H_c and r to form the ratio H_c/r. Instead, it can be assumed that A = 0.235, the typical value. Using Equation 7, the mean flame height above the base of the pallet stack is calculated as $L = -1.02 \cdot 1.21 + 0.235 \cdot 2600^{2/5} = 4.22$ m.

Momentum regime: In Figure 2-1.3 it is seen that at high values of $\dot{Q}^*$ the normalized flame heights begin to level off and eventually attain constant values, but not at the same value of $\dot{Q}^*$ and not at the same normalized flame height.

Flame heights of vertical turbulent jet flames have been studied by a number of investigators reviewed by Blake and McDonald,[24,25] who proposed a new correlation of normalized flame heights versus a "density-weighted Froude number." Although an improvement over previous work, the correlation still exhibits significant scatter. At about the same time, Delichatsios[26] proposed an alternative approach. Previously, other authors had proposed flame height relations, including Becker and coworkers,[12,27] and Peters and Göttgens.[28] More recently, Heskestad[29] also considered the high-momentum regime, especially with respect to defining an unambiguous transition to momentum control and flame heights in this regime.

Heskestad's work[29] was based on an extension of the author's correlation for buoyancy-controlled turbulent diffusion flames. A momentum parameter is defined, R_M, which is the ratio of gas release momentum to the momentum generated by a purely buoyant diffusion flame:

$$R_M = 1.36\left[\left(\frac{T_\infty}{T_L}\right)\left(\frac{c_p \Delta T_L}{(H_c/r)}\right)^{4/5}\right]\left(\frac{\rho_\infty/\rho_s}{r^2}\right)N^{2/5} \qquad (9)$$

Here, T_L and ΔT_L are the plume centerline temperature and excess temperature (above ambient), respectively, at the mean flame height of purely buoyant diffusion flames, and ρ_s is the density of the source gas in the discharge stream. A value of 500 K is assigned[29] to ΔT_L. Note that the first two sets of parentheses are nearly constant for normal ambient temperatures and fuels with comparable values of (H_c/r). Under these circumstances, the momentum parameter is closely linked to the parameter N, but is affected quite significantly by the source gas density at the discharge conditions as well as the mass stoichiometric ratio. If the gas discharge is sonic or choked, the density of the source gas can be considerably higher than is the case at atmospheric pressure.

Figure 2-1.4 presents flame heights of jet diffusion flames in the form L/L_B versus R_M, where L is the flame height reported by various investigators and L_B is the buoyancy-controlled flame height according to Equation 3. The data scatter about a value L/L_B = 1.2, approximately, for $R_M < 0.1$. At higher values of R_M, the flame height ratio approaches an asymptotic slope of –1/2, indicated by a dashed line. The associated values of N are so large that we can take $L_B/D \propto N^{1/5}$ (see Equation 3), which together with Equation 9 imply that L/D is constant when the slope

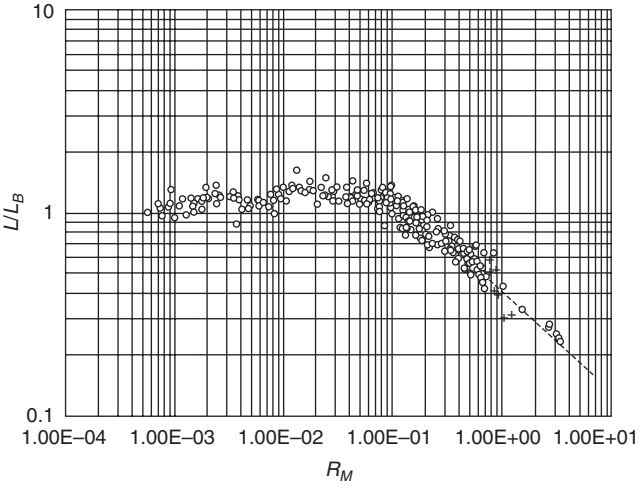

Figure 2-1.4. ***Data on flame heights of turbulent jet diffusion flames in ratio to the corresponding buoyancy-controlled flame heights, plotted versus the ratio of gas release momentum to buoyancy momentum (from Reference 29). Data plotted as + pertain to choked discharge of hydrogen.***

is equal to –1/2 (for constant source gas and discharge density). Constant slope and constant L/D (for a given gas and density) appear to be achieved reasonably quickly above $R_M = 0.1$.

The fact that the low-R_M flame height ratios in Figure 2-1.4 tend to scatter about a level higher than unity has been attributed to several possible factors.[29] One of the two most important may be the working definition of mean flame height employed by some investigators, producing greater values than the 50 percent flame-intermittency height. Another may be retinal retention of flame images in visual averaging of rapidly pulsating flames (typical of the scales of the experiments), tending to make an observer exaggerate the mean flame height.

Above $R_M = 0.1$, adopting the dashed line in Figure 2-1.4 as representative of the momentum regime, the normalized flame height is

$$\frac{L_M}{D} = \left[5.42\left(\frac{T_m}{T_\infty}\right)^{1/2}\left(\frac{H_c/r}{c_p\Delta T_m}\right)^{2/5}\right]\left(\frac{\rho_s}{\rho_\infty}\right)^{1/2} r \qquad (10)$$

where L_M is the flame height in the momentum regime. For $H_c/r = 3100$ kJ/kg (many common gases), $\Delta T_m = 500$ K, and $T_\infty = 293$ K, Equation 10 becomes

$$\frac{L_M}{D} = 18.5\left(\frac{\rho_s}{\rho_\infty}\right)^{1/2} r \qquad (11)$$

In this case the nondimensional flame height in the momentum regime depends in a simple manner on the mass stoichiometric ratio and the source gas density at discharge.

It should be pointed out that the transition to the momentum regime, $R_M = 0.1$, and the flame height in the momentum regime, Equations 10 and 11, differ significantly from previously proposed relations, as discussed in Reference 29.

EXAMPLE 4:

Calculate the normalized height of a hydrogen jet flame from a 5-mm diameter nozzle connected to a reservoir (tank, pipe, etc.) at ambient temperature of 293 K and a pressure above ambient of either (a) 150 kPa or (b) 300 kPa.

SOLUTION:

(a) The ratio of ambient pressure (101 kPa) to the reservoir pressure (150 kPa) is 0.673, corresponding to subsonic discharge (sonic discharge occurs at a pressure ratio of 0.528, as for air). The mass flow of hydrogen from the nozzle is calculated with the aid of a compressible flow formula (e.g., Shapiro[30]) as 1.74 g/s, using a ratio of specific heats $k = 1.4$ (as for air). Based on a heat of combustion of 120,000 kJ/kg, the heat release rate is $\dot{Q} = 209$ kW. The source gas density in the discharge stream, ρ_s, is calculated from the source gas density at ambient temperature and pressure, $\rho_{s\infty}$, as follows: $\rho_s = (\rho_s/\rho_{s\infty})\rho_{s\infty} = (\rho_s/\rho_{s0})(\rho_{s0}/\rho_{s\infty})\rho_{s\infty}$, where ρ_{s0} is the source gas density in the gas reservoir. The density ratios can be expressed in terms of pressure ratios, with the result: $\rho_s = (p_s/p_{s0})^{1/k}(p_{s0}/p_\infty)\rho_{s\infty}$, where p_s is the pressure in the discharge stream (ambient pressure for subsonic discharge) and p_{s0} is the pressure of the gas reservoir. Finally we obtain $\rho_s = (101/150)^{1/1.4}(150/101)\rho_{s\infty} = 1.12 \times 0.083 = 0.093$ kg/m^3, where 0.083 (kg/m^3) is the density of hydrogen at ambient temperature and pressure. Now the momentum parameter can be calculated from Equation 9, taking $\Delta T_L = 500$ K, $H_c = 120{,}000$ kJ/kg, $r = 34.3$, and $\rho_s = 0.093$ kg/m^3, yielding $R_M = 1.16 \times 10^{-3}N^{2/5}$. The parameter N is calculated from Equation 4, with the result $N = 6.76 \times 10^6$, which results in $R_M = 0.62$ and places the flame in the momentum regime. The normalized flame height is calculated from Equation 10 as $L_M/D = 185$. NOTE: The calculated height may include the visual-averaging bias toward somewhat higher than actual values built into the data base.

(b) The ratio of ambient pressure (101 kPa) to reservoir pressure (300 kPa) is 0.337, corresponding to sonic, or choked discharge. The mass flow of hydrogen from the nozzle is calculated with the aid of an appropriate compressible flow formula for choked discharge (e.g. Shapiro[30]) as 3.65 g/s, corresponding to a heat release rate of 436 kW. The source gas density for choked flow is calculated as in (a), except the ratio (p_s/p_{s0}) is set equal to the value for a Mach number of unity, 0.528, that is, $\rho_s = 0.528^{1/k}(p_{s0}/p_\infty) \times 0.083 = 0.634(300/101) \times 0.083 = 0.156$ kg/m^3. The parameter N is calculated from Equation 4 as 2.94×10^7 and the momentum parameter from Equation 9 as $R_M = 6.93 \times 10^{-4}N^{2/5} = 0.67$, indicating the flame is in the momentum regime as in (a). The normalized flame height is calculated from Equation 10 as $L_M/D = 239$, somewhat higher than for the lower discharge pressure in (a).

NOTE: If the nozzles of cases (a) and (b) are sharp-edged holes or openings instead, it is recommended that the source diameter be multiplied by (discharge coefficient)$^{1/2}$; see, for example, Shapiro[30] for values of the discharge coefficient of sharp-edged orifices in compressible flow (varying from 0.60 near incompressible flow conditions to 0.77 for choked flow).

Plume Temperatures and Velocities

The first plume theories assumed

1. A point source of buoyancy
2. That variations of density in the field of motion are small compared to the ambient density
3. That the air entrainment velocity at the edge of the plume is proportional to the local vertical plume velocity, and
4. That the profiles of vertical velocity and buoyancy force in horizontal sections are of similar form at all heights

Morton et al.[31] developed an integral formulation on the further assumption that the profiles are uniform "top hat" profiles. The mean motion is then governed by the following three conservation equations for continuity, momentum, and buoyancy:

Continuity $$\frac{d}{dz}(b^2u) = 2\alpha bu \qquad (12)$$

Momentum $$\frac{d}{dz}(b^2u^2) = b^2g\frac{\rho_\infty - \rho}{\rho_\infty} \qquad (13)$$

Buoyancy $$\frac{d}{dz}\left(b^2ug\frac{\rho_\infty - \rho}{\rho_\infty}\right) = 0 \qquad (14)$$

In these equations, z is the elevation above the point source of buoyancy; b is the radius to the edge of the plume; u is the vertical velocity in the plume; α is the entrainment coefficient (the proportionality constant relating the inflow velocity due to entrainment at the edge of the plume to u); ρ is the density in the plume; and ρ_∞ is the ambient density. Equation 14 can be integrated immediately to

$$b^2 u g \frac{\rho_\infty - \rho}{\rho_\infty} = B = \text{constant} \tag{15}$$

Here, B is the buoyancy flux in the plume which remains constant at all heights. The flux can be related to the convective heat in the plume, $\dot{Q}_c$, by noting

$$\dot{Q}_c = \rho u \pi b^2 c_p (T - T_\infty) = \pi u b^2 c_p (\rho_\infty - \rho) T_\infty \tag{16}$$

where the ideal gas law has been used. In this equation, T is the plume temperature and T_∞ is the ambient temperature. Combining Equations 15 and 16 gives

$$B = g(\pi c_p T_\infty \rho_\infty)^{-1} \dot{Q}_c \tag{17}$$

Solutions to Equations 12, 13, and 15 can be determined[31] in the form (expressing B in terms of $\dot{Q}_c$ using Equation 17)

$$b = \frac{6\alpha}{5} z \tag{18}$$

$$u = \frac{5}{6}\left(\frac{9}{10\pi\alpha^2}\right)^{1/3} g^{1/3} (c_p \rho_\infty T_\infty)^{-1/3} \dot{Q}_c^{1/3} z^{-1/3} \tag{19}$$

$$\frac{\Delta\rho}{\rho_\infty} = \frac{5}{6}\left(\frac{9\pi^2\alpha^4}{10}\right)^{-1/3} g^{-1/3} (c_p \rho_\infty T_\infty)^{-2/3} \dot{Q}_c^{2/3} z^{-5/3} \tag{20}$$

Equations 18 through 20 are the weak plume (small density deficiency) relations for point sources. To account for area sources, a virtual source location or virtual origin, z_0, is introduced[31,32] and z in Equations 18 through 20 is replaced by $z - z_0$. In addition, to accommodate large density deficiencies as are present in fire plumes, Morton's extension of the weak-plume theory[33] leads to the result that $\Delta\rho/\rho_\infty$ in Equation 20 should be replaced by $\Delta\rho/\rho$ [$= \Delta T/T_\infty$ using the ideal gas law]. Also, Equation 18 for growth in plume radius should incorporate the additional factor $(\rho_\infty/\rho)^{1/2}$ [$= (T/T_\infty)^{1/2}$ using the ideal gas law] on the right side of the equation. Relaxing the assumption that the flow profiles are uniform renders the numerical coefficients in the resulting equations in doubt.

Measurements in fire plumes above the flames have to a large extent supported the theory. The plume radius and centerline values of mean excess temperature and mean velocity have been found[34] to obey the following relations:

$$b_{\Delta T} = 0.12\left(\frac{T_0}{T_\infty}\right)^{1/2} (z - z_0) \tag{21}$$

$$\Delta T_0 = 9.1\left(\frac{T_\infty}{g c_p^2 \rho_\infty^2}\right)^{1/3} \dot{Q}_c^{2/3} (z - z_0)^{-5/3} \tag{22}$$

$$u_0 = 3.4\left(\frac{g}{c_p \rho_\infty T_\infty}\right)^{1/3} \dot{Q}_c^{1/3} (z - z_0)^{-1/3} \tag{23}$$

Here, $b_{\Delta T}$ is the plume radius to the point where the temperature rise has declined to $0.5\Delta T_0$; T_0 is the centerline temperature, $\dot{Q}_c$ is the convective heat release rate, z is the elevation above the fire source, and z_0 is the elevation of the virtual origin above the fire source.* (If z_0 is negative, the virtual origin lies below the top of the fire source.)

The virtual origin is the equivalent point source height of a finite area fire. This origin is usually located near the fuel surface for pool fires and may be assumed coincident with the fuel surface when the plume flow is predicted at high elevations. Near the fire source, however, it is important to know the location of the virtual origin for accurate predictions. Calculation of the virtual origin is discussed in the following section for both pool fires and three-dimensional storage arrays.

Equations 21 through 23 are known as the *strong plume relations.* The numerical coefficients for the relations have been determined from data sets for which the locations of the virtual origin, z_0, have been established and the convective heat release rates, $\dot{Q}_c$, are known.[4,35]

We may compare the experimentally derived numerical coefficients in Equations 21 through 23 to the theoretical coefficients indicated in Equations 18 through 20, which are based on the integral theory of Morton et al.[31] for weak plumes, point sources, and top hat profiles. Forcing equality between the coefficients for ΔT_0 in Equation 22 and $\Delta\rho/\rho_\infty$ in Equation 20, we obtain a value for the entrainment coefficient of $\alpha = 0.0964$. With this value for α, the theoretical coefficient for centerline velocity in Equation 19 becomes 2.61, compared to the experimental value 3.4 in Equation 23. The theoretical coefficient for plume radius in Equation 18 becomes 0.116, compared to the experimental value 0.12 in Equation 21. There is good consistency between the theoretical and experimental coefficients. However, the theoretical expression for mass flow rate in a weak plume, generated from the product $\rho_\infty u(\pi b^2)$ (using Equations 18 and 19) and the value for α above, produces a numerical coefficient that is only 56 percent of the coefficient based on experiments (see discussion of Equation 40 later in the chapter).

In addition to the temperature radius of a plume, $b_{\Delta T}$, a velocity radius, b_u, can also be defined. The velocity radius is the plume radius to the point where the gas velocity has declined to 0.5 u_0. The most reliable measurements[35] indicate that b_u is perhaps 10 percent larger than $b_{\Delta T}$. Other measurements indicate ratios $b_u/b_{\Delta T}$ of 0.86,[36] 1.00,[37] 1.08 and 1.24,[38] 1.31,[5] 1.05,[1] and 1.5.[2] The widely differing results can probably be attributed to the difficulty of positioning the measuring probes accurately with respect to the plume centerline, and to different, intrinsic errors associated with the diverse types of anemometers used (pitot tube, bidirectional flow probe, hot wire, vane anemometer, cross-correlation techniques, laser Doppler anemometer).

*For normal atmospheric conditions ($T_\infty = 293$ K, $g = 9.81$ m/s^2, $c_p = 1.00$ kJ/kg K, $\rho_\infty = 1.2$ kg/m^3), the factor $9.1[T_\infty/(g c_p^2 \rho_\infty^2)]^{1/3}$ has the numerical value 25.0 K m$^{5/3}$ kW$^{-2/3}$, and the factor $3.4[g/(c_p \rho_\infty T_\infty)]^{1/3}$ has the numerical value 1.03 m$^{4/3}$s^{-1}kW$^{-1/3}$.

Often, profiles of temperature rise and velocity are represented as Gaussian in shape, although there is no theoretical foundation for this distribution.

$$\Delta T = \Delta T_0 \exp\left[-\left(\frac{R}{\sigma_{\Delta T}}\right)^2\right] \tag{24}$$

$$u = u_0 \exp\left[-\left(\frac{R}{\sigma_u}\right)^2\right] \tag{25}$$

Here, ΔT and u are the local values, at the radius, R, in the plume of temperature rise and gas velocity. The quantities $\sigma_{\Delta T}$ and σ_u are measures of the plume width, corresponding to the radii where local values of temperature rise and velocity are $e^{-1} = 0.368$ multiplied by the centerline values. For Gaussian profiles, the plume radii $\sigma_{\Delta T}$ and σ_u are 1.201 multiplied by the plume radii, $b_{\Delta T}$ and b_u, discussed previously.

Equations 21 through 23 cease to be valid at and below the mean flame height. However, it is possible to represent ΔT_0 such that a general plot of experimental temperature variations is produced throughout the length of the plume, including the flames. The method is based on the observation that $\dot{Q}_c^{2/3}(z - z_0)^{-5/3}$ in Equation 22 can be written as $[(z - z_0)/\dot{Q}_c^{2/5}]^{-5/3}$. This result suggests plotting ΔT_0 versus $(z - z_0)/\dot{Q}_c^{2/5}$. Figure 2-1.5 shows the result in logarithmic coordinates for normal atmospheric conditions. For values of the abscissa greater than 0.15 to 0.20 (m/kW$^{2/5}$), the centerline temperature rise falls off with the $-\frac{5}{3}$ power of the abscissa, in accordance with the plume law for temperature (Equation 22). Abscissa values in the 0.15 to 0.20 range correspond to the mean flame height; an associated temperature rise of about 500 K is indicated in Figure 2-1.5. At smaller abscissa values, the experimentally observed temperature rise increases more slowly, approaching a value deep in the flame of approximately $\Delta T_0 = 900$ K. When closer to the fuel surface than represented in Figure 2-1.5, the temperatures on the plume axis tend to decrease again.[1,2,5]

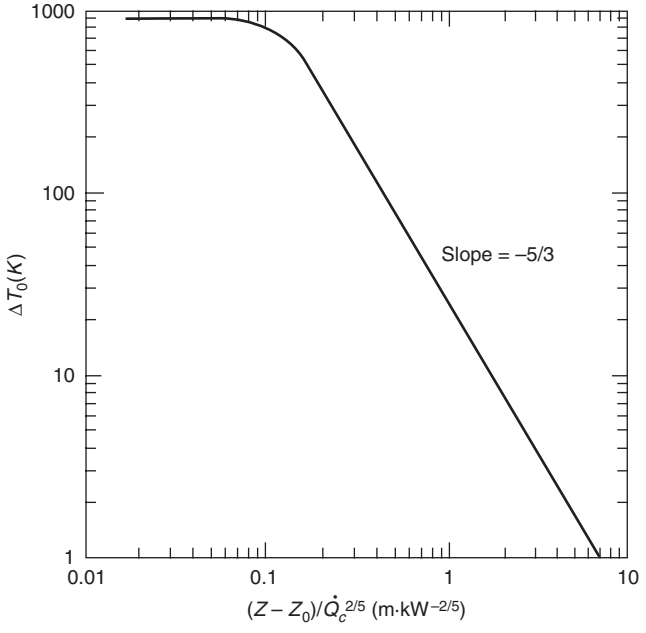

Figure 2-1.5. ***Temperature rise on the plume centerline of pool fires for normal atmospheric conditions[34] in a form attributable to McCaffrey,[1] and Kung and Stavrianidis.[4]***

The plume law for velocity, Equation 23, may be combined with the plume law for temperature, Equation 22, to produce the following useful nondimensional parameter[3]

$$\xi = \left[\frac{T_\infty^{2/5}(c_p\rho_\infty)^{1/5}}{g^{2/5}}\right]\frac{u_0}{(\Delta T_0 \dot{Q}_c)^{1/5}} \tag{26}$$

In the plume region where Equations 22 and 23 are valid, their numerical coefficients correspond to a constant value $\xi = 2.2$. This value has been confirmed for a number of test fires,[3] at heights as low as the mean flame height and even somewhat lower. Equation 26 with $\xi = 2.2$ is a useful relation for determining the maximum velocity in the plume, which occurs slightly below the mean flame height where the temperature rise may be taken at approximately $\Delta T_0 = 650$ K. For normal atmospheric conditions and the value $\xi = 2.2$, Equation 26 becomes

$$\frac{u_0}{(\Delta T_0 \dot{Q}_c)^{1/5}} = 0.54 \tag{27}$$

The maximum velocity just under the mean flame height, u_{0m}, is obtained by setting $\Delta T_0 = 650$ K

$$u_{0m} = 1.97 \dot{Q}_c^{1/5} \tag{28}$$

Fires with low flame height-to-diameter ratios have not been investigated extensively and may require special consideration. For one particular fire with very low flame height[4] in which a proprietary silicone transformer fluid was burned in a 2.44-m diameter pool, a flame height ratio of $L/D = 0.14$ was measured* at a convective heat release rate of $\dot{Q}_c = 327$ kW. Using the results in the next section, the virtual origin is calculated at $z_0 = -1.5$ m, assuming $\dot{Q}_c/\dot{Q} = 0.7$. With respect to the abscissa in Figure 2-1.5, the lowest possible value is $-z_0/\dot{Q}_c^{2/5}$ corresponding to the fuel surface, $z = 0$. For the present case, $-z_0/\dot{Q}_c^{2/5} = 1.5/327^{2/5} = 0.15$ (m kW$^{-2/5}$). At this abscissa value, a centerline temperature rise of 580 K is indicated in Figure 2-1.5. From the experiment,[4] a near surface ΔT_0 of 440 K can be determined by slight extrapolation, fairly close to the prediction from Figure 2-1.5. Fires with very low flame height-to-diameter ratios may generally be expected to produce lower maximum mean temperatures than other fires. However, it is not yet clear whether the type of prediction attempted here for a particular low L/D fire is generally valid.

*A ratio $L/D = 0.02$ can be calculated from Equation 7 assuming $H_c/r = 3470$ kJ/kg, an average for silicone oils from values reported by Tewarson[39] and assuming a convective heat fraction $\dot{Q}_c/\dot{Q} = 0.7$. If a value of H_c/r near the bottom of the reported range[39] is selected, 3230 kJ/kg, the observed value $L/D = 0.14$ is reproduced; slight changes in the assumed convective fraction will also reproduce the measured value.

There is also uncertainty associated with assuming that ξ in Equation 26 remains completely constant down to the flame level in low *L/D* fires. It may be found that ξ still remains approximately constant down to the height where the maximum gas velocity occurs, although this maximum will probably occur above the flames. The associated temperatures at this height cannot as yet be predicted. Consequently, the relation in Equation 28 becomes somewhat uncertain as *L/D* decreases (ΔT_0 is overestimated, resulting in u_{0m} being overestimated, although the effect is probably not very large because of the slow, $\frac{1}{5}$th power dependence on ΔT_0).

The turbulence intensities in a fire plume are quite high. On the axis, George et al.[35] report an intensity of temperature fluctuations of approximately $T'/\Delta T_0 = 0.38$, where T' is the root mean square (rms) temperature fluctuation. Centerline values of the intensity of axial velocity fluctuations were measured near $u'/u_0 = 0.27$ by George et al.[35] and near $u'/u_0 = 0.33$ by Gengembre et al.,[5] where u' is the rms velocity fluctuation in the axial direction.

EXAMPLE 5:

Example 1 concerned a 1.5-m-diameter methyl alcohol fire burning under normal atmospheric conditions, generating $\dot{Q} = 884$ kW with a calculated mean flame height of 1.83 m. For an elevation of 5 m and given a virtual origin $z_0 = -0.3$ m (from Example 7), calculate the temperature radius, $b_{\Delta T}$, as well as the centerline value of temperature rise, ΔT_0, and gas velocity, u_0. Also calculate the maximum gas velocity in the flame.

SOLUTION:

Assume* $\dot{Q}_c = 0.8\dot{Q}$ and first calculate the temperature rise, using Equation 22 and properties for normal atmospheric conditions ($T_\infty = 293$ K, $g = 9.81$ m/s^2, $c_p = 1.00$ kJ/kg K, $\rho_\infty = 1.20$ kg/m^3)

$$\Delta T_0 = 9.1\left(\frac{293}{9.81 \cdot 1.00^2 \cdot 1.20^2}\right)^{1/3}(0.8 \cdot 884)^{2/3}(5 + 0.3)^{-5/3}$$
$$= 123 \text{ K}$$

The temperature radius can now be calculated from Equation 21

$$b_{\Delta T} = 0.12\left(\frac{123 + 293}{293}\right)^{1/2}(5 + 0.3)$$
$$= 0.76 \text{ m}$$

The velocity is calculated from Equation 23

$$u_0 = 3.4\left(\frac{9.81}{1.00 \cdot 1.20 \cdot 293}\right)^{1/3}(0.8 \cdot 884)^{1/3}(5 + 0.3)^{-1/3}$$
$$= 5.3 \text{ m/s}$$

Instead of Equation 23, the velocity can also be calculated from Equation 26 in this case, since ΔT_0 is already known. Actually, because normal ambient conditions prevail, Equation 27 can be used

$$u_0 = 0.54(123 \cdot 0.8 \cdot 884)^{1/5} = 5.3 \text{ m/s}$$

Finally, the maximum velocity in the flame is given by Equation 28

$$u_{0m} = 1.97(0.8 \cdot 884)^{1/5} = 7.3 \text{ m/s}$$

EXAMPLE 6:

Recalculate the quantities called for in Example 5 using ambient conditions representative of Denver, Colorado, on a hot day: 630 mm Hg pressure and 310 K temperature.

SOLUTION:

Changed ambient variables entering the equations include $T_\infty = 310$ K and $\rho_\infty = 0.78$ kg/m^3. From Equation 22, the new temperature rise is

$$\Delta T_0 = 167 \text{ K (versus 123 K in Example 4)}$$

The new velocity from Equation 23 is

$$u_0 = 6.0 \text{ m/s (versus 5.3 m/s)}$$

For the new ambient conditions, the relation analogous to Equation 28 is calculated as

$$u_{0m} = 2.10\dot{Q}_c^{1/5}$$

from which the new maximum velocity in the flame is

$$u_{0m} = 7.8 \text{ m/s (versus 7.3 m/s)}$$

Plumes in Temperature-Stratified Ambients

When a buoyant, turbulent plume rises, it cools by entrainment of ambient air. If the ambient air increases in temperature with height, which is normal in buildings, and the fire source is weak, the temperature difference between the plume and the ambient, which gives the plume buoyancy, may vanish and actually reverse in sign. Eventually the plume ceases to rise.

The maximum height achieved by plumes in temperature-stratified space has been given by Heskestad,[40] based on pioneering theoretical and experimental work by Morton et al.[31]

$$z_m = 3.79\left[\frac{T_{a1}}{g(\rho_{a1}c_p)^2}\right]^{1/8}\dot{Q}_c^{1/4}\left(\frac{dT_a}{dz}\right)^{-3/8} \qquad (29)$$

Here, dT_a/dz is the ambient temperature gradient, T_{a1} and ρ_{a1} are the ambient temperature and density, respectively, at the level of the fire source, and the constant 3.79 traces to experiments using dyed light liquid injected into a density stratified salt solution.[31] Other results are presented in Figure 2-1.6, which shows the ratio on the plume centerline of stratified value versus unstratified value for

*Without specific knowledge, $\dot{Q}_c/\dot{Q}$ may usually be assumed at 0.7. However, methyl alcohol produces a fire of low luminosity and radiation, for which $\dot{Q}_c/\dot{Q} = 0.8$ is a good estimate.

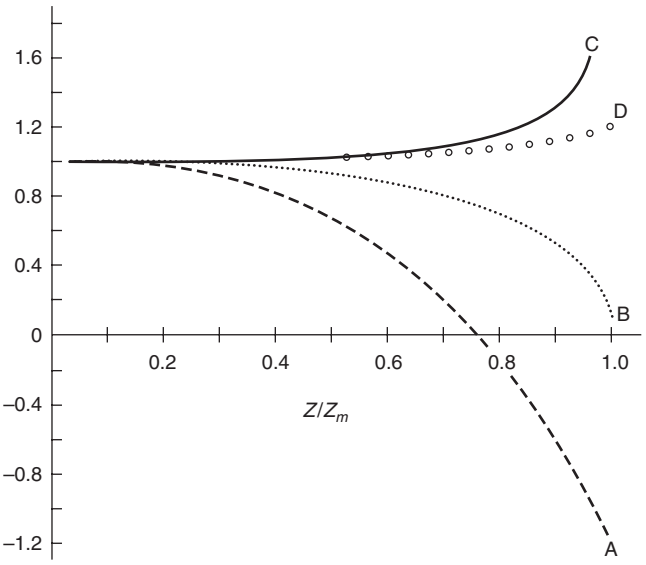

Figure 2-1.6. ***Theoretical behavior of centerline plume variables in linearly temperature-stratified ambients. From Heskestad,[40,64] traceable to Morton et al.[31] Curve A: ratio of temperature rises (stratified versus unstratified), Curve B: ratio of axial velocities. Curve C: ratio of plume radii. Curve D: ratio of volumetric species concentrations.***

various plume variables: temperature rise relative to the pre-existing value at each level (curve A), axial velocity (curve B), plume radius (curve C), and volume concentration of a combustion species (curve D). The ratios are plotted against the fraction of maximum elevation achieved by the plume, z/z_m. By definition, the stratified velocity (B) decreases to zero at $z/z_m = 1$. The stratified temperature rise (A) becomes negative below the maximum reach. The stratified plume radius (C) grows rapidly in approach to the maximum plume reach. However, there is little effect of the stratification on the centerline variation of concentration of a combustion species.

Fire experiments in temperature stratified space[41] have largely supported the validity of Figure 2-1.6 for temperature rise (A) and volume concentrations (D), except that the experimental values needed an incremental height, roughly equal to 25 percent of the theoretical plume reach, to return to zero.

The maximum plume reach can be interpreted in terms of a critical ambient temperature rise from the source level to an elevated observation plane, just strong enough to prevent plume fluid from penetrating the plane. Experiments[41] show that the critical ambient temperature rise for a linear profile is *7.4 times the centerline temperature rise at the level of the observation plane which results from a fire source in a uniform environment*. Furthermore, the critical temperature rise is surprisingly insensitive to the shape of the stratification profile. For a profile where one-half of the ambient temperature rise to the observation plane occurred higher than 75 percent of the elevation of the observation plane above the source, the critical ambient temperature rise was only 12 percent greater than that for the linear profile.

EXAMPLE 7:

Consider a 20-m high atrium where the temperature rise, floor to ceiling, is 5 K. What heat release rate is required of a floor-level fire to drive the plume to the ceiling? What would be the effect of doubling the ceiling height?

SOLUTION:

The temperature rise in unstratified space is required as a reference and is calculated from Equation 22, taking $z_0 = 0$ for simplicity since deviations of the virtual origin from the level of the fire can be assumed to be inconsequential in this case. We have

$$\Delta T_0 = 25.0 \dot{Q}_c^{2/3} z^{-5/3} \tag{30}$$

The temperature rise of the stratification, 5 K, is 7.4 times the value of ΔT_0 for this associated, unstratified-space fire, which will just drive the plume to the ceiling. Solving Equation 30 for $\dot{Q}_c$, setting $\Delta T_0 = 5/7.4$ K and $z = 20$ m, we get $\dot{Q}_c = 7.9$ kW. Assuming a ratio of 0.7 for convective in ratio to the total heat release rate, the latter is $\dot{Q} = 11.4$ kW. If the ceiling height is doubled to 40 m, the new result is $\dot{Q} = 64$ kW.

Virtual Origin

Pool fires: As pointed out earlier in this chapter, knowledge of the virtual origin of fire plumes is important for predicting the near source plume behavior. The virtual origin is a point source from which the plume above the flames appears to originate.

The virtual origin of a test fire is most conveniently determined from temperature data above the flames along the plume axis. According to Equation 22, a plot of $\Delta T_0^{-3/5}$ versus z should produce a straight line which intercepts the z-axis at z_0. Despite this apparent simplicity of obtaining z_0, the task is very difficult in practice. Slight inaccuracies in the determinations of centerline temperatures have large effects on the intercept, z_0; such inaccuracies may be associated with off-axis placement of sensors, radiation-induced errors in the temperature signal, or inadequate averaging of the signal.

Data obtained in this manner on the virtual origin for pool fires varying in diameter from 0.16 to 2.4 m,[1,3,4] were examined for consistency with a theoretical model by Heskestad.[42] The model relied heavily on the flame-height correlation represented by Equation 3 and led to the prediction

$$\frac{z_0}{D} = -1.02 + F \frac{\dot{Q}^{2/5}}{D} \tag{31}$$

where F is a rather complex dimensional function of environmental variables c_p, T_∞, ρ_∞, g; H_c/r for the combustible, the fraction of the total heat release carried away by convection,[42] and the mean centerline temperature at the mean flame height, T_L. It appeared that F could be considered a constant for wide variations in ambient temperature and pressure, but might be affected by wide swings in the fuel variables, H_c/r and convective fraction. The available data did not reflect any sensitivity to fuel identity within their scatter, and led to the determination $F = 0.083$ m kW$^{-2/5}$, with Equation 31 becoming

$$\frac{z_0}{D} = -1.02 + 0.083 \frac{\dot{Q}^{2/5}}{D} \quad (\dot{Q} \text{ in kW}, D \text{ in m}) \tag{32}$$

Later, Hasemi and Tokunaga[43] analyzed their temperature measurements in plumes from gas burners of diameters in the 0.2 to 0.5 m range and established alternative correlations for the virtual origin. In terms of the nondimensional parameter $\dot{Q}^*$ defined in Equation 1, their correlations are

$$\begin{aligned} \frac{z_0}{D} &= 2.4(\dot{Q}^{*2/5} - 1) && \dot{Q}^* \geq 1.0 \\ \frac{z_0}{D} &= 2.4(\dot{Q}^{*2/3} - \dot{Q}^{*2/5}) && \dot{Q}^* < 1.0 \end{aligned} \tag{33}$$

For normal ambient conditions, these correlations can be written in terms of the variable $\dot{Q}^{2/5}/D$ (cf. Equation 32)

$$\begin{aligned} \frac{z_0}{D} &= -2.4 + 0.145\frac{\dot{Q}^{2/5}}{D} && \frac{\dot{Q}^{2/5}}{D} \geq 16.5 \\ \frac{z_0}{D} &= 0.0224\left(\frac{\dot{Q}^{2/5}}{D}\right)^{5/3} - 0.145\frac{\dot{Q}^{2/5}}{D} && \frac{\dot{Q}^{2/5}}{D} < 16.5 \end{aligned} \tag{34}$$

Cetegen et al.[44] have proposed correlations for the virtual origin on the basis of their air entrainment measurements in fire plumes and attempts to apply entrainment theory for a point source to the laboratory fires. Their experiments involved gas burners (natural gas) with diameters of 0.10, 0.19, 0.30, and 0.50 m. The experiments were performed with and without a floor mounted flush with the upper surface of the burners located some distance above the floor of the laboratory. Their correlations for the virtual origin are

$$\begin{aligned} \frac{z_0}{D} &= c + 1.09\dot{Q}^{*2/5} && \dot{Q}^* > 1 \\ \frac{z_0}{D} &= c + 1.09\dot{Q}^{*2/3} && \dot{Q}^* \leq 1 \end{aligned} \tag{35}$$

where $\dot{Q}^*$ has been defined by Equation 1, and where $c = -0.50$ with a flush floor around the burners and $c = -0.80$ without a flush floor. Using Equation 1, Equation 35 can be written in terms of $\dot{Q}^{2/5}/D$ yielding

$$\begin{aligned} \frac{z_0}{D} &= c + 0.0659\frac{\dot{Q}^{2/5}}{D} && \frac{\dot{Q}^{2/5}}{D} > 16.5 \\ \frac{z_0}{D} &= c + 0.01015\left(\frac{\dot{Q}^{2/5}}{D}\right)^{5/3} && \frac{\dot{Q}^{2/5}}{D} \leq 16.5 \end{aligned} \tag{36}$$

where $c = -0.50$ and $c = -0.80$ with and without a flush floor, respectively.

Figure 2-1.7 is a composite plot of the various correlations for the virtual origin of pool fires, plotted as z_0/D versus $\dot{Q}^{2/5}/D$. Despite the diverse approaches, the overall correlations are surprisingly similar. Precise measurements are not yet available to clearly identify an optimal correlation. In the meantime, curve 1 in Figure 2-1.7 (i.e., Equation 32) is recommended for its simplicity, clear foundation in theory,[42] and central position among the other correlations.

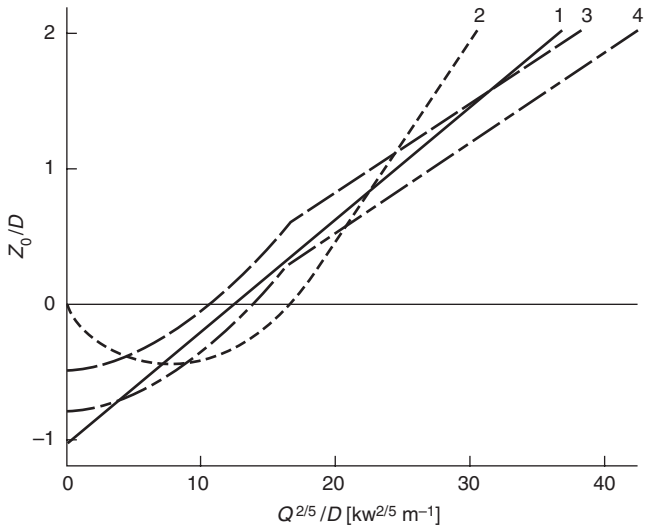

Figure 2-1.7. ***Correlations for the virtual origin of pool fires. Curve 1—Equation 32; Curve 2—Equation 34; Curve 3—Equation 36 with floor; Curve 4—Equation 36 without floor.***

Other fire types: The original derivation of Equation 31 for pool fires[42] includes the following expression:

$$z_0 = L - 0.175\dot{Q}_c^{2/5} \qquad (L \text{ and } z_0 \text{ in m; } \dot{Q}_c \text{ in kW}) \tag{37}$$

In addition to representing pool fires, Equation 37 has also been verified to represent deep storage fires,[22] allowing the location of the virtual origin to be calculated from knowledge of the mean flame height and the convective heat release rate. As discussed earlier, mean flame heights above the base of a fire in storages can be determined from Equation 3 when the flames extend above the storage, which implies that values of z_0 calculated refer to the distance above the base of the fire (usually the base of the storage). Equation 37 may also be assumed to be valid for turbulent jet fires.

EXAMPLE 8:

Example 1 concerned a 1.5-m diameter methyl alcohol fire generating $\dot{Q} = 884$ kW. Calculate the virtual origin.

SOLUTION:

In this example, $D = 1.5$ m. Direct substitution into Equation 32 gives

$$\begin{aligned} \frac{z_0}{D} &= -1.02 + \frac{0.083(884)^{2/5}}{1.5} \\ &= -1.02 + 0.83 = -0.19 \end{aligned}$$

from which

$$z_0 = -0.19 \cdot 1.5 = -0.29 \text{ m}$$

This is the value for z_0 (rounded off) used in Example 1.

EXAMPLE 9:

Negative values for z_0 are often calculated for low heat release fires and sufficiently large fire diameters, as in Example 7. Positive virtual origins are often found for high heat release fires. Substituting heptane for methyl alcohol in Example 7 (2500 kW/m^2 rather than 500 kW/m^2 measured for methyl alcohol),[6] calculate the new virtual origin.

SOLUTION:

The new heat release rate is

$$\dot{Q} = \frac{\pi 1.5^2}{4} 2500 = 4420 \text{ kW}$$

From Equation 32,

$$\frac{z_0}{D} = -1.02 + 0.083 \cdot \frac{4420^{2/5}}{1.5} = 0.57$$

from which

$$z_0 = 0.57 \cdot 1.5 = 0.85 \text{ m}$$

EXAMPLE 10:

A 3-m deep storage is known to produce a heat release rate per unit floor area of 4000 kW/m^2 when fully involved. At a stage of fire development in such a storage, a heat release rate of 1500 kW is reached. What is the location of the virtual origin?

SOLUTION:

First determine the flame height. Evaluate the effective fire diameter from $\pi D^2/4 = 1500/4000 = 0.375$ m^2, which gives $D = 0.69$ m. From Equation 7, calculate the flame height as 3.67 m (above base of storage), which is 0.67 m above the top of the storage. The height of the virtual origin above the base of the storage is calculated from Equation 37, assuming $\dot{Q}_c = 0.7\dot{Q} = 1050$ kW, yielding $z_0 = 3.67 - 0.175 \times 1050^{2/5} = 0.84$ m.

Entrainment

After ignition, the fire plume carries fire products diluted in entrained air to the ceiling. A layer of diluted fire products, or smoke, forms under the ceiling, which thickens and generally becomes hotter with time. The fire environment is intimately tied to the behavior of this layer which, in turn, depends to a major extent on the mass flow rate of plume fluid into the layer. Consequently, it is important to be able to predict the mass flow rate that may occur in a fire plume.

The mass flow at a particular elevation in a fire plume is almost completely attributable to air entrained by the plume at lower elevations. The mass flow contributed by the fire source itself is insignificant in comparison.

For a weak plume, the mass flow rate at a cross section can be written

$$\dot{m}_{\text{ent}} = E\rho_\infty u_0 b_u^2 \tag{38}$$

where E is a nondimensional constant of proportionality. With the aid of Equation 23 and the equivalent of Equation 21 written for b_u (setting $T_0/T_\infty = 1$ because of the weak plume assumption), Equation 38 becomes

$$\dot{m}_{\text{ent}} = E\left(\frac{g\rho_\infty^2}{c_p T_\infty}\right)^{1/3} \dot{Q}_c^{1/3}(z - z_0)^{5/3} \tag{39}$$

Early measurements by Yih[45] indicated a value $E = 0.153$.

Cetegen et al.[44,46] concluded from theoretical analysis that Equation 39 also applies to strongly buoyant plumes. From extensive entrained-flow measurements for natural gas burners of several diameters, these authors proposed a coefficient $E = 0.21$ based on the total heat release rate, corresponding to $E = 0.24$ based on the convective heat release rate as in Equation 39 (assuming a convective fraction of 0.7). However, the plume flow rates at large heights were somewhat overpredicted and those at low heights, approaching the flames, were somewhat underpredicted.

Heskestad[47] reconsidered the entrainment problem for strong plumes, assuming self-preserving density deficiency profiles instead of self-preserving excess temperature profiles as traditionally assumed. This approach led to the following extension of Equation 39

$$\dot{m}_{\text{ent}} = E\left(\frac{g\rho_\infty^2}{c_p T_\infty}\right)^{1/3} \dot{Q}_c^{1/3}(z - z_0)^{5/3} \cdot \left[1 + \frac{G\dot{Q}_c^{2/3}}{(g^{1/2}c_p\rho_\infty T_\infty)^{2/3}(z - z_0)^{5/3}}\right] \tag{40}$$

Equation 40, with $E = 0.196$ and $G = 2.9$, was found to represent the data of Cetegen et al.[44,46] very well over the entire nonreacting plume for all their fire diameters, ranging from 0.10 m to 0.50 m.[47] At large heights, the bracketed term involving G approaches unity, and at levels approaching the flame tip (Equation 3), this term approaches 1.5, approximately. Equation 40, with $E = 0.196$ and $G = 2.9$, is the recommended relation for calculating mass flow rates in plumes, at and above the mean flame height.

The entrained flow at the mean flame height, $\dot{m}_{\text{ent},L}$, follows from setting $z - z_0 = L - z_0$ in Equation 40 (with $E = 0.196$ and $G = 2.9$), taking L from Equation 3 and z_0 from Equation 31 (with substitution of full expression for F), with the result,

$$\dot{m}_{\text{ent},L} = 0.878\left[\left(\frac{T_L}{T_\infty}\right)^{5/6}\left(\frac{T_\infty}{\Delta T_L}\right) + 0.647\right]\frac{\dot{Q}_c}{c_p T_\infty} \tag{41}$$

The numerical values are linked to the experimental calibration coefficient for F (based on $F = 0.083$ m kW$^{-2/5}$ at normal atmospheric conditions as indicated under Equation 31) and taking $\Delta T_L = 500$ K. Interestingly, $\dot{m}_{\text{ent},L}$ is independent of the acceleration of gravity, g.

Mass flow rates in fire plumes at levels below the flame tip have been found to increase linearly with height for fire diameters of 0.3 m and greater,[47] where the flames are substantially turbulent, from zero (essentially) at the fire base to the flame-tip value in Equation 41, that is,

$$\dot{m}_{\text{ent}} = \dot{m}_{\text{ent},L} z/L \tag{42}$$

Measurements in the flaming region for fire diameters *smaller* than 0.30 m do not show a linear variation of mass flow rate with height, including data by Cetegen et al.[44,46] (fire diameters of 0.10 and 0.19 m) and Beyler[48] (0.19 m and 0.13 m). (It is important to note, however, that all these data are consistent with an approach to the mass flow rate at the mean flame height given by Equation 41.[47]) Neither do the mass flow measurements in turbulent jet flames by Delichatsios and Orloff[49] show a linear variation with height (estimated values of N in range 50–6300 and momentum parameter R_M in range 0.0015–0.010); in fact, these measurements indicate a 5/2 power dependence, within the flames, of mass flow rate on height above the nozzle exit. As a guide to entrainment estimates in the flaming region for sources smaller than 0.30 m in diameter, it appears that a second power variation of mass flow rate with height is quite representative of the fire sources referred to above of diameters 0.13 and 0.10 m, in which case Equation 42 is replaced by

$$\dot{m}_{\text{ent}} = \dot{m}_{\text{ent},L}\left(\frac{z}{L}\right)^2 \tag{43}$$

The 0.19-m diameter sources generated scattered results between the linear and second power variation.[47] Delichatsios[50] as well as Quintiere and Grove[51] have also analyzed mass flow rates in the flaming region.

We digress briefly on the appropriateness of relating entrainment behavior to the diameter of the fire source. The governing parameters for fire plumes from horizontal, circular sources have been considered so far to be the parameter N and the momentum parameter R_M. However, for small fire sources it is common to see a laminar flame sheet preceding transition to turbulence around the rim of the fire source, and the degree to which such laminar regions and effects exists will depend on the flame Reynolds number. A flame Reynolds number can be formulated as $u_{0m}b_{um}/\nu_m$, where u_{0m} is the characteristic gas velocity in the flame, proportional to $\dot{Q}^{1/5}$ according to Equation 28; b_{um} is the associated characteristic flame radius, proportional to[52] $\dot{Q}^{2/5}$; and ν_m is the kinematic viscosity evaluated at the mean maximum flame temperature, which can be considered constant. Hence, the flame Reynolds number can be considered proportional to $\dot{Q}^{3/5}$. Assuming the discharge momentum is not important (small R_M), the flame entrainment behavior should be a function of N and $\dot{Q}$. When the entrainment behavior is represented on N, $\dot{Q}$ coordinates for the various test fires indicated above, it is found that the fires with linear increase of mass flow rate with height in the flame plot above a line $\dot{Q} \propto N^{1/2}$, with some uncertainty about the precise level. With the aid of Equation 4 it becomes clear that this relation implies an equivalent limit line $D = constant$, which justifies relating the entrainment behavior to the source diameter.

For normal atmospheric conditions Equations 40 through 42 can be written as follows for the plume mass flow rate at various heights:

Above the mean flame height, L ($\dot{Q}_c$ in kW, z and z_0 in m):

$$\dot{m}_{\text{ent}}\,(\text{kg/s}) = 0.071\dot{Q}_c^{1/3}(z - z_0)^{5/3} \cdot [1 + 0.027\dot{Q}_c^{2/3}(z - z_0)^{-5/3}] \tag{44}$$

At the mean flame height, L ($\Delta T_L = 500$ K):

$$\dot{m}_{\text{ent},L}\,(\text{kg/s}) = 0.0056\dot{Q}_c\,(\text{kW}) \tag{45}$$

At and below the mean flame height, L, for fire source diameters of 0.3 m and greater:

$$\dot{m}_{\text{ent}}\,(\text{kg/s}) = 0.0059\dot{Q}_c\,(\text{kW}) \cdot \frac{z}{L} \tag{46}$$

Under the prevailing assumptions, and the further assumption $\dot{Q}_c/\dot{Q} = 0.7$ and $H_c/r \approx 3100$ kJ/kg, Equation 45 implies that the mass flow at the flame tip is 13 times the mass stoichiometric requirement of the fuel.[47]

Fires with very low flame height-to-diameter (L/D) ratios have not been investigated extensively. It is not clear to what L/D limit the entrained-flow relations presented here apply, but this limit is smaller than 0.9, the lowest L/D ratio associated with the data of Cetegen et al.[44,46] For plume mass flows above the flames, there is no L/D limit for predictions at the higher elevations, but predictions of mass flows at levels just above the flames may begin to deteriorate before $L/D = 0.14$ is reached, as seems to be implied in the observations following Equation 28.

Further, mention should be made of a plume mass flow formula often used because of its simplicity, originally developed for the flaming region of large fires by Thomas et al.[53]

$$\dot{m}_{\text{ent}} = 0.096(g\rho_\infty\rho_{f\ell})^{1/2}W_f z^{3/2} \tag{47}$$

Here $\rho_{f\ell}$ is the gas density in the flames and W_f is the fire perimeter. This formula has also been tested against mass flow data above the flames by Hinkley,[54] who claims it is very satisfactory for heights up to 10 times the linear dimension (or diameter) of a fire, although there is little theoretical justification for its use above the flames. The following version of Equation 47 is often used[54] (based on normal atmospheric conditions and an assumed flame temperature):

$$\dot{m}_{\text{ent}}(\text{kg/s}) = 0.188W_f\,(\text{m})\,z\,(\text{m})^{3/2} \tag{48}$$

It is instructive to compare the predictions of Equations 44 and 48 for plume regions above the flames. In a number of comparisons for heat release rates in the range 1000 to 8000 kW, heat release rates per unit area in the range 250 to 1000 kW/m^2, and heights varying from the flame level to 128 m, the predictions of Equation 48 range from 0.64 to 1.38 times the predictions of Equation 44.

Cetegen et al.,[44,46] whose data have contributed most to the mass flow recommendations in this text, have carefully pointed out that their fire plumes were produced in as quiet an atmosphere as could be maintained in their laboratory. They report that small ambient disturbances could provide 20 to 50 percent increases in the measured plume mass flows. Clearly, there is need for further research.

EXAMPLE 11:

Calculate plume mass flow rates for the methyl alcohol fire of Examples 1, 5, and 7.

SOLUTION:

From Example 1, $\dot{Q} = 884$ kW and $L = 1.83$ m; from Example 5, $\dot{Q}_c = 0.8\dot{Q} = 707$ kW; from Example 7, $z_0 = -0.29$ m. At the mean flame height, 1.83 m, the mass flow rate follows from Equation 45

$$\dot{m}_{\text{ent},L} = 0.0059 \cdot 707 = 4.2 \text{ kg/s}$$

Mass flow rates in the flaming region are calculated using Equation 46

$$\dot{m}_{\text{ent}} \text{ (kg/s)} = 4.2 \cdot \frac{z}{1.83} = 2.3z \text{ (m)}$$

Mass flow rates above the flames are obtained from Equation 44; for example, at a height of 3.66 m (twice the flame height)

$$\begin{aligned}\dot{m}_{\text{ent}} &= 0.071 \cdot 707^{1/3}(3.66 + 0.29)^{5/3} \\ &\quad \cdot [1 + 0.027 \cdot 707^{2/3}(3.66 + 0.29)^{-5/3}] \\ &= 6.24(1 + 0.22) \\ &= 7.6 \text{ kg/s}\end{aligned}$$

Illustration

In addition to the previous examples, it is instructive to work through a somewhat larger problem to illustrate handling of the equations and their limitations. Units used throughout this section are kW for heat release rate, m for length, s for time, K for temperature, and m/s for velocity.

The example can be used of a large building that will allow clear, uncontaminated air to exist around a particular growing fire for at least 10 minutes before smoke begins to recirculate into the region. Normal atmospheric conditions prevail. Wood pallets are stored in a large, continuous array on the floor to a height of 1.2 m. This array is ignited locally at an interior point, and the fire spreads in a circular pattern at constant radial speed (as predicted and observed for wood cribs),[55] such that the heat release rate grows with the second power of time

$$\dot{Q} \text{ (kW)} = 1000\left(\frac{t}{t_g}\right)^2 \tag{49}$$

Here, t is time and t_g is the so-called growth time. When t_g is 60 s, the fire grows through a magnitude of 1000 kW in 60 s. When t_g is 600 s, the fire grows through a magnitude of 1000 kW in 600 s, a much slower growth rate. In this illustration, it is assumed that the growth time is $t_g = 140$ s.[56] It is also assumed that the fully involved pallet storage generates a total heat release rate of 2270 kW/m^2 of floor area.[6] The objective is to determine flame height as a function of time, as well as the variation of plume centerline temperature, plume centerline velocity, and plume width at an elevation of 5 m above the base of the fuel array where a structural member may cross and be heated by the plume.*

*In addition to convective heating, which depends on gas temperature and velocity, radiative heating would also be important in such cases and might even dominate over convective heating if the structure is immersed in flames.

For the assumed growth time, $t_g = 140$ s, the variation of total heat release rate with time comes from Equation 49

$$\dot{Q} = 5.10 \times 10^{-2} t^2 \tag{50}$$

The convective heat release rate is assumed at 70 percent of the total heat release rate

$$\dot{Q}_c = 3.57 \times 10^{-2} t^2 \tag{51}$$

The instantaneous fire diameter, D, is determined as follows. Since the heat release rate per unit floor area is 2270 kW/m^2

$$\dot{Q} = 2270 \frac{\pi D^2}{4} \tag{52}$$

Upon eliminating $\dot{Q}$ between Equations 50 and 52, the following can be obtained:

$$D = 5.35 \times 10^{-3} t \tag{53}$$

First, the behavior of flame height may be calculated using Equation 8. Substitution of Equations 50 and 53 into Equation 8 gives the following relation of flame height as a function of time

$$L = -5.46 \times 10^{-3} t + 7.15 \times 10^{-2} t^{4/5} \tag{54}$$

This relation is plotted in Figure 2-1.8 for the 10-min (600-s) fire interval and is labeled L. The fire diameter, D, is also plotted in Figure 2-1.8, based on Equation 53.

The virtual origin, z_0, is determined from Equation 32, with substitutions for $\dot{Q}$ a from Equation 50 and for D from Equation 53

$$z_0 = -5.46 \times 10^{-3} t + 2.52 \times 10^{-2} t^{4/5} \tag{55}$$

The curve labeled z_0 in Figure 2-1.8 represents the virtual origin according to Equation 55. It is seen that z_0 nearly levels off in the time interval plotted in the figure; actually, z_0 begins to decrease again at somewhat larger times.

With this foundation, there is sufficient information to calculate gas temperatures, velocities, and plume widths at the 5-m height above the base of the fuel array.

The temperature rise on the plume centerline at the selected height is determined from Equation 22 by substituting $z = 5$ (m), z_0 from Equation 55; $\dot{Q}_c$ from Equation 51, and values of T_∞, g, c_p, and ρ_∞ for the normal atmosphere, yielding

$$\Delta T_0 = \frac{2.71 t^{4/3}}{(5 + 5.46 \times 10^{-3} t - 2.52 \times 10^{-2} t^{4/5})^{5/3}} \tag{56}$$

This relation is valid up to the time that a temperature rise associated with the flame tip, $\Delta T_0 = 500$ K, is felt at the selected height, which occurs at $t = 303$ s. The plot of ΔT_0 in Figure 2-1.9 is according to Equation 56 up to the time $t = 303$ s. At larger times, ΔT_0 is determined from Figure 2-1.5 in the following manner: at each selected time, $z - z_0$ is calculated using Equation 55; $\dot{Q}_c$ is calculated from Equation 51; the quantity $(z - z_0)/\dot{Q}_c^{2/5}$ is determined and ΔT_0 is read from Figure 2-1.5. The resulting extension of the ΔT_0 curve is seen in Figure 2-1.9.

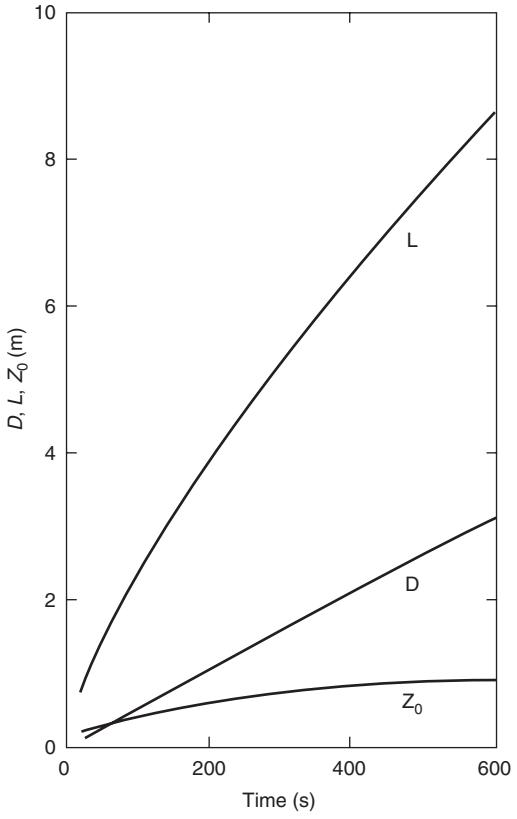

Figure 2-1.8. ***Growing fire illustration: fire diameter, D, flame height, L, and virtual origin, z_0.***

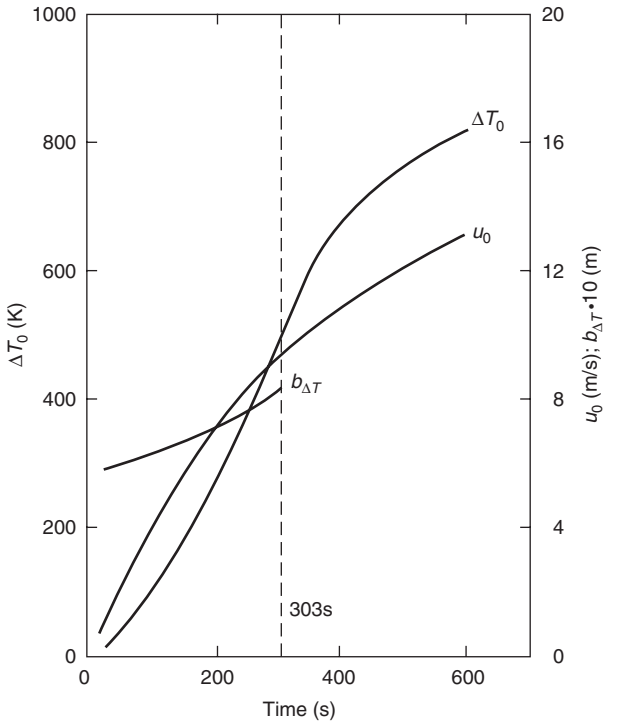

Figure 2-1.9. ***Growing fire illustration: plume width, $b_{\Delta T}$, and centerline values of temperature rise, ΔT_0, and velocity, u_0, at 5 m above the base of the fuel.***

The centerline gas velocity at the 5-m height above the base of the fuel array can then be considered. Equation 23 can be used up to the moment that the flame tip reaches the 5-m height; that is, at $t = 303$ s. After substitution of $z = 5$ (m), z_0 from Equation 55, $\dot{Q}_c$ from Equation 51, and normal ambient conditions, Equation 23 becomes

$$u_0 = \frac{0.339t^{2/3}}{(5 + 5.46 \times 10^{-3}t - 2.52 \times 10^{-2}t^{4/5})^{1/3}} \qquad (57)$$

The u_0 curve in Figure 2-1.9 follows Equation 57 to the limit, $t = 303$ s. As stated in conjunction with Equation 27, the maximum velocity (for a given size fire) occurs just below the mean flame height where $\Delta T_0 = 650$ K, which corresponds to $(z - z_0)/\dot{Q}_c^{2/5} = 0.135$ according to Figure 2-1.5. Using $z = 5$ (m), z_0 and $\dot{Q}_c$ from Equations 55 and 51, the 0.135 limit is found to correspond to a time of $t = 385$ s, where Equation 28 gives the centerline velocity in terms of $\dot{Q}_c$. In fact, it appears that Equation 28 can be used with good accuracy to even larger times, at least to times associated with a lower limit of $(z - z_0)/\dot{Q}_c^{2/5} = 0.08$, according to available measurements.[1,5] Since the largest time in Figure 2-1.9 corresponds to $(z - z_0)/\dot{Q}_c^{2/5} = 0.092$, Equation 28 has been used to calculate the entire extension of the u_0 curve in Figure 2-1.9.

The temperature radius of the plume at the 5-m height above the fuel array is calculated from Equation 21, which can be written

$$b_{\Delta T} = 0.12\left(1 + \frac{\Delta T_0}{T_\infty}\right)^{1/2}(z - z_0) \qquad (58)$$

With substitution of $z = 5$ (m), ΔT_0 from Equation 56 and z_0 from Equation 55, Equation 58 becomes

$$b_{\Delta T} = 0.12\left[\frac{1 + 9.25 \cdot 10^{-3}t^{4/3}}{(5 + 5.46 \cdot 10^{-3}t - 2.52 \cdot 10^{-2}t^{4/5})^{5/3}}\right]^{1/2} \cdot (5 + 5.46 \cdot 10^{-3}t - 2.52 \cdot 10^{-2}t^{4/5}) \qquad (59)$$

This equation is plotted in Figure 2-1.9 up to the time the flames reach the 5-m height at $t = 303$ s. The temperature radius at the 5-m height is seen to vary from 0.59 m early in the fire to 0.83 m at 303 s. Plume fluid will reach a minimum of twice the temperature radius, $b_{\Delta T}$; hence, the total width of the plume in this example will be at least four times $b_{\Delta T}$, growing from a minimum of 2.4 m early in the fire to a minimum of 3.3 m as the flames reach the 5-m height.

Additional Flame Topics

Flame Pulsations

Flame pulsations have been studied by a number of investigators, tracing at least as far back as Rashbash et al.[56] and reviewed in conjunction with a recent study reported by Cetegen and Ahmed.[57] The two latter authors

summarize the published data on pulsation frequency in a single plot for burner or pool diameters ranging from 0.03 to 20 m and propose the simple curve fit

$$f(Hz) = 1.5[D(m)]^{-1/2} \quad (60)$$

As a measure of the data scatter it is noted that measured frequencies near a given diameter differ by a factor of up to two.

Wall/Corner Effects

McCaffrey[11] has reviewed effects on flame height of placing fire sources next to a wall or in a corner, referring to experiments by Hasemi and Tokunaga,[58] Back et al.,[59] Mizuno and Kawagoe,[60] and Kokkala.[61] The effects are generally reported to be small.

Windblown Flames

The main effect of wind is to bend or deflect the flames away from the vertical. Another effect, observed in wind tunnel studies by Welker and Sliepcevich[62] is "flame trailing," in which the flames trail off the burner along the floor in the downwind direction for a significant distance. Flame trailing was thought to be associated primarily with fuel vapors of greater density (higher molecular weight) than air, as was the case with all the various liquid fuels used in the experiments.

Wind tunnel measurements of flame deflection angle,[63] involving fire diameters in the range 0.10–0.60 m, and large scale data for square LNG pools in the effective diameter range 2–28 m, obtained by Attalah and Raj,[63] have been found to correlate well against the ratio of wind velocity to the maximum velocity in the flame according to Equation 28.[64] The relationship indicates that a flame deflection angle of approximately 25 degrees can be expected for a velocity ratio of 0.10. Effects of wind on flame length were minor for velocity ratios up to 0.35 (flame deflection angle of approximately 60 degrees). Data by Huffman et al.[65] indicate that at the considerably higher velocity ratio of 1.0, flame lengths are approximately 30 percent greater than under quiescent conditions.

Data Sources

NFPA 204M, *Guide for Smoke and Heat Venting*,[66] was referenced in this chapter for tables of heat release rate per unit floor area, kW/m^2, and growth times, t_g, of a number of fuel arrays. The same information has been incorporated by Alpert and Ward,[67] together with additional data.

In Section 3, Chapter 4 by Tewarson, tables are included to estimate combustion efficiencies as well as total and convective heat release rates per unit exposed area of materials under full-scale burning conditions.

Nomenclature

A	defined in Equation 6 (m·kW$^{-2/5}$)
B	buoyancy flux defined in Equation 15 (m^4·s^{-3})
b	plume radius (m)
$b_{\Delta T}$	plume radius to point where $\Delta T/\Delta T_0 = 0.5$ (m)
b_u	plume radius to point where $u/u_0 = 0.5$ (m)
b_{um}	b_u at level of maximum gas velocity near flame tip (m)
c	adjustable constant, Equation 35
c_p	specific heat of air at constant pressure (kJ/kg·K)
D	diameter (m)
F	function (c_p, T_∞, ρ_∞, g); see Equation 31 (m·kW$^{-2/5}$)
f	frequency (s^{-1})
g	acceleration due to gravity (m/s^2)
H_c	actual lower heat of combustion (kJ/kg)
I	intermittency
k	ratio of specific heats, constant-pressure versus constant-volume
L	mean flame height (m)
L_B	buoyancy controlled flame height (m)
L_M	momentum controlled flame height (m)
$\dot{m}_{ent}$	entrained mass flow rate in plume (kg/s)
$\dot{m}_{ent,L}$	$\dot{m}_{ent}$ at the mean flame height, L (kg/s)
$\dot{m}_f$	mass burning rate (kg/s)
N	nondimensional parameter defined in Equation 4
p_s	pressure in source gas discharge stream (Pa)
p_{s0}	pressure in source gas reservoir (Pa)
$\dot{Q}$	$\dot{m}_f H_c$, total heat release rate (kW)
$\dot{Q}_c$	convective heat release rate (kW)
$\dot{Q}_r$	radiative heat release rate (kW)
$\dot{Q}^*$	nondimensional parameter defined in Equation 1
R	radius (m)
r	actual mass stoichiometric ratio, air to fuel volatiles
R_M	momentum parameter defined in Equation 8
T	mean temperature (K)
T_0	mean centerline temperature in plume (K)
T_∞	ambient temperature (K)
T'	rms temperature fluctuation (K)
$T_a(z)$	ambient temperature at level z (K)
T_{a1}	ambient temperature at source level (K)
T_L	T_0 at mean flame height (K)
ΔT	$T - T_\infty$, mean temperature rise above ambient (K)
ΔT_0	value of ΔT on plume centerline (K)
ΔT_L	$T_L - T_\infty$ (K)
t	time (s)
t_g	growth time; see Equation 38 (s)
u	mean axial velocity (m/s)
u_0	mean axial velocity on centerline (m/s)
u_{0m}	maximum value of u_0, near flame tip (m/s)
u'	rms velocity fluctuation in axial direction (m/s)
W_f	fire perimeter (m)
z	height above top of combustible (m)
z_0	height of virtual origin above top of combustible (m)
z_m	maximum vertical penetration of plume fluid in stratified ambient (m)

α entrainment coefficient
ξ nondimensional parameter defined in Equation 26
ν_m kinematic viscosity of flame gases at maximum flame temperature ($m^2 \cdot s^{-1}$)
ρ mean density (kg/m^3)
ρ_{a1} ambient density at source level (kg/m^3)
$\rho_{f\ell}$ mean density in flames (kg/m^3)
ρ_s density of source gas discharge stream (kg/m^3)
ρ_{s0} density of source gas in reservoir (kg/m^3)
$\rho_{s\infty}$ density of source gas at ambient temperature and pressure (kg/m^3)
ρ_∞ ambient density (kg/m^3)
$\Delta\rho$ $\rho_\infty - \rho$, mean density deficiency (kg/m^3)
$\sigma_{\Delta T}$ plume radius to point where $\Delta T/\Delta T_0 = e^{-1}$ (m)
σ_u plume radius to point where $u/u_0 = e^{-1}$ (m)

References Cited

1. B.J. McCaffrey, *NBSIR 79-1910,* National Bureau of Standards, Washington, DC (1979).
2. G. Cox and R. Chitty, *Comb. and Flame,* 39, p. 191 (1980).
3. G. Heskestad, *18th Symposium on Combustion,* Combustion Institute, Pittsburgh, PA (1981).
4. H.C. Kung and P. Stavrianidis, *19th Symposium on Combustion,* Combustion Institute, Pittsburgh, PA (1983).
5. E. Gengembre, P. Cambray, D. Karmed, and J.C. Bellet, *Comb. Sci. and Tech.,* 41, p. 55 (1984).
6. G. Heskestad, *Report OC2E1.RA,* Factory Mutual Research Corp., Norwood, MA (1981).
7. A. Tewarson, *NBS-GGR-80-295,* National Bureau of Standards, Washington, DC (1982).
8. F. Tamanini, *Comb. and Flame,* 51, p. 231 (1983).
9. E.E. Zukoski, T. Kubota, and B. Cetegen, *F. Safety J.,* 3, p. 107 (1980–81).
10. E.E. Zukoski, B.M. Cetegen, and T. Kubota, *20th Symposium on Combustion,* Combustion Institute, Pittsburgh, PA (1985).
11. B. McCaffrey, *The SFPE Handbook of Fire Protection Engineering,* 2nd ed., Society of Fire Protection Engineers and National Fire Protection Association, Quincy, MA (1995).
12. H.A. Becker and D. Liang, *Comb. and Flame,* 32, p. 115 (1978).
13. G. Cox and R. Chitty, *Comb. and Flame,* 60, p. 219 (1985).
14. G. Heskestad, *F. Safety J.,* 5, p. 103 (1983).
15. G.T. Kalghatgi, *Comb. Sci. and Tech.,* 41, p. 17 (1984).
16. F.R. Steward, *Comb. Sci. and Tech.,* 2, p. 203 (1970).
17. P.H. Thomas, *Ninth Symposium on Combustion,* Combustion Institute, Pittsburgh, PA (1963).
18. W.R. Hawthorne, D.S. Weddel, and H.C. Hottel, *Third Symposium on Combustion,* Williams and Wilkins, Baltimore (1949).
19. E.E. Zukoski, *Fire Safety Science—Proceedings of the First International Symposium,* Hemisphere, New York (1984).
20. E.E. Zukoski, "Convective Flows Associated with Room Fires," *Semi-annual Progress Report to National Science Foundation,* California Institute of Technology, Pasadena (1975).
21. G. Heskestad, *F. Safety J.,* 30, p. 215 (1998).
22. G. Heskestad, *Fire Safety Science—Proceedings of the Fifth International Symposium,* International Association for Fire Safety Science (1998).
23. G. Heskestad, *Comb. And Flame,* 83, p. 293 (1991).
24. T.R. Blake and M. McDonald, *Comb. and Flame,* 94, p. 426 (1993).
25. T.R. Blake and M. McDonald, *Comb. and Flame,* 101, p. 175 (1995).
26. M.A. Delichatsios, *Comb. and Flame,* 33, p. 12 (1993).
27. H.A. Becker and S. Yamazaki, *Comb. and Flame,* 33, p. 12 (1978).
28. N. Peters and J. Göttgens, *Comb. and Flame,* 85, p. 206 (1991).
29. G. Heskestad, *Comb. and Flame,* 118, p. 51 (1999).
30. A.H. Shapiro, *The Dynamics and Thermodynamics of Compressible Fluid Flow,* Vol. 1, The Ronald Press Company, New York (1953).
31. B.R. Morton, G.I. Taylor, and J.S. Turner, *Proc. Roy. Soc.,* A234, 1 (1956).
32. B.R. Morton, *J. Fluid Mech.,* 5, p. 151 (1959).
33. B.R. Morton, *10th Symposium on Combustion,* Combustion Institute, Pittsburgh, PA (1965).
34. G. Heskestad, *F. Safety J.,* 7, p. 25 (1984).
35. W.K. George, R.L. Alpert, and F. Tamanini, *Int. J. Heat Mass Trans.,* 20, p. 1145 (1977).
36. H. Rouse, C.S. Yih, and H.W. Humphreys, *Tellus,* 4, p. 201 (1952).
37. S. Yokoi, *Report No. 34,* Building Research Institute, Japan (1960).
38. G. Heskestad, *Report 18792,* Factory Mutual Research Corp., Norwood, MA (1974).
39. A. Tewarson, in *Flame-Retardant Polymeric Materials,* Plenum, New York (1982).
40. G. Heskestad, *F. Safety J.,* 15, p. 271 (1989).
41. G. Heskestad, *Comb. Sci. and Tech.,* 106, p. 207 (1995).
42. G. Heskestad, *F. Safety J.,* 5, p. 109 (1983).
43. Y. Hasemi and T. Tokunaga, *Fire Sci. and Tech.,* 4, p. 15 (1984).
44. B.M. Cetegen, E.E. Zukoski, and T. Kubota, *Comb. Sci. and Tech.,* 39, p. 305 (1984).
45. C-S Yih, *Proc. U.S. National Cong. App. Mech.,* New York (1952).
46. B.M. Cetegen, E.E. Zukoski, and T. Kubota, *Report G8-9014,* California Institute of Technology, Daniel and Florence Guggenheim Jet Propulsion Center, Pasadena (1982).
47. G. Heskestad, *21st Symposium on Combustion,* Combustion Institute, Pittsburgh, PA (1986).
48. C.L. Beyler, *Development and Burning of a Layer of Products of Incomplete Combustion Generated by a Buoyant Diffusion Flame,* Ph.D. Thesis, Harvard University, Cambridge, MA (1983).
49. M.A. Delichatsios and L. Orloff, *20th Symposium on Combustion,* Combustion Institute, Pittsburgh, PA (1985).
50. M.A. Delichatsios, *The SFPE Handbook of Fire Protection Engineering,* 2nd ed., Society of Fire Protection Engineers and National Fire Protection Association, Quincy, MA (1995).
51. J.Q. Quintiere and B.S. Grove, *27th Symposium on Combustion,* Combustion Institute, Pittsburgh, PA (1998).
52. G. Heskestad and T. Hamada, *F. Safety J.,* 21, p. 69 (1993).
53. P.H. Thomas, P.L. Hinkley, C.R. Theobald, and D.L. Sims, *Fire Technical Paper No. 7,* H. M. Stationery Office, Joint Fire Research Organization, London (1963).
54. P.L. Hinkley, *F. Safety J.,* 10, p. 57 (1986).
55. M.A. Delichatsios, *Comb. and Flame,* 27, p. 267 (1976).
56. D.J. Rasbash, Z.W. Rogowski, and G.W.V. Stark, *Fuel,* 35, p. 94 (1956).
57. B.M. Cetegen and T.A. Ahmed, *Comb. and Flame,* 23, p. 157 (1993).
58. Y. Hasemi and T. Tokunaga, *Com. Sci. and Tech.,* 40, p. 1 (1984).

59. J. Back, C. Beyler and P. DiNenno, *Comb. Sci. and Tech.,* 40, p. 1 (1984).
60. T. Mizuno and K. Kawagoe, *Fire Safety Science—Proceedings of the First International Symposium,* Hemisphere, New York (1984).
61. M.A. Kokkala, *Interflam 1993,* Interscience Communications Limited, London (1993).
62. J.R. Welker and C.M. Sliepcevich, *Technical Report No. 2,* NBS Contract XST 1142 with University of Oklahoma, Norman (1965).
63. S. Attalah and P.K. Raj, *Interim Report on Phase II Work,* Project IS-3.1 LNG Safety Program, American Gas Association, Arlington, VA (1974).
64. G. Heskestad, *Phil. Trans. Roy. Soc. Lond. A,* 356, p. 2815 (1998).
65. K.G. Huffman, J.R. Welker and C.M. Sliepcevich, *Technical Report No. 1441-3,* NBS Contract CST 1142 with University of Oklahoma, Norman (1967).
66. NFPA 204M, *Guide for Smoke and Heat Venting,* National Fire Protection Association, Quincy, MA (1998).
67. R.L. Alpert and E.J. Ward, *F. Safety J.,* 7, p. 127 (1984).

CHAPTER 2

Ceiling Jet Flows

Ronald L. Alpert

Introduction

Much of the hardware associated with detection and suppression of fire, in commercial, manufacturing, storage, and modern residential buildings is located near the ceiling surfaces. In case of a fire, hot gases in the fire plume rise directly above the burning fuel and impinge on the ceiling. The ceiling surface causes the flow to turn and move horizontally under the ceiling to other areas of the building remote from the fire position. The response of smoke detectors, heat detectors, and sprinklers installed below the ceiling so as to be submerged in this hot flow of combustion products from a fire provides the basis for building fire protection.

Studies quantifying the flow of hot gases under a ceiling resulting from the impingement of a fire plume have been conducted since the 1950s. Studies at the Fire Research Station in Great Britain,[1,2] Factory Mutual Research Corporation,[3–7] the National Institute of Standards and Technology (NIST),[8,9] and at other research laboratories[10,11] have sought to quantify the gas temperatures and velocities in the hottest portion of the flow produced by steady fires beneath smooth, unconfined horizontal ceilings.

Ceiling jet refers to the relatively rapid gas flow in a shallow layer beneath the ceiling surface that is driven by the buoyancy of the hot combustion products from the plume. Figure 2-2.1 shows an idealization of an axisymmetric ceiling jet flow at varying radial positions, r, beneath an unconfined ceiling. In actual fires within buildings, the simple conditions pictured—a hot, rapidly moving gas layer sandwiched between the ceiling surface and tranquil, ambient-temperature air—exist only at the beginning of a fire, when the quantity of combustion gases produced is not sufficient to accumulate into a stagnant, heated gas layer in the upper portion of the compartment. Venting the ceiling jet flow through openings in the ceiling surface or edges can retard the accumulation of this heated gas layer.

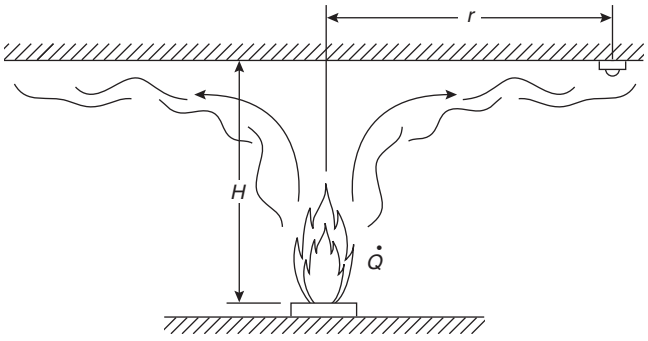

Figure 2-2.1. ***Ceiling jet flow beneath an unconfined ceiling.***

As shown in Figure 2-2.1, the ceiling jet flow emerges from the region of plume impingement on the ceiling, flowing radially away from the fire. As it does, the layer grows thicker by entraining room air at the lower boundary. This entrained air cools the gases in the jet and reduces its velocity. As the hot gases move out across the ceiling, heat transfer cools the portion adjacent to the ceiling surface.

Steady Fires

Weak Plume-Driven Flow Field

A generalized theory to predict gas velocities, gas temperatures, and the thickness (or depth) of a steady fire-

Dr. Ronald L. Alpert received his undergraduate and graduate education at the Massachusetts Institute of Technology, where he majored in mechanical engineering. He is manager of the Flammability Technology Research Program at Factory Mutual Research. Dr. Alpert currently chairs the ASTM subcommittee on Fire Safety Engineering and the U.S. Technical Advisory Group to ISO TC92/SC4 (Fire Safety Engineering). He has published numerous papers in refereed journals and technical reports.

driven ceiling jet flow has been developed by Alpert[4] for the case of a weak plume, when flame height is much less than the height, H, of the ceiling above the burning fuel. This work involves the use of several idealizations in the construction of the theoretical model, but results are likely to provide reasonable estimates over radial distances of one or two ceiling heights from the point of fire plume impingement on the ceiling.

Ceiling jet thickness: Alpert defined the thickness of the ceiling jet, ℓ_T, as the distance below the ceiling where the excess of gas temperature above the ambient value, ΔT, drops to $1/e$ (1/2.718 …) of the maximum excess temperature. Based on this definition, measurements obtained with a liquid pool fire 8 m beneath a ceiling show that ℓ_T/H is about 0.075 at an r/H of 0.6, increasing to a value of 0.11 for r/H from about 1 to 2. These results are in good agreement with detailed measurements and analysis for the region $r/H < 2$ performed by Motevalli and Marks[12] during their small-scale (0.5- and 1.0-m ceiling heights) experiments. The following correlation for ℓ_T/H developed by Motevalli and Marks from their temperature data confirms the predicted constancy of ceiling jet thickness (at about 10 to 12% of H) for $r/H > 1$ from Alpert's theory:

$$\frac{\ell_T}{H} = 0.112\left[1 - \exp\left(-2.24\,\frac{r}{H}\right)\right] \qquad \text{for } 0.26 \le \frac{r}{H} \le 2.0 \tag{1}$$

Additional measurements of ceiling jet thickness, for steady flows induced by strong plumes and for transient flows, are discussed later.

Within the ceiling jet flow, the location of maximum excess temperature and velocity are predicted[4] to be highly scale dependent, even after normalization by the ceiling height. Measurements of the distance below the ceiling at which these maxima occur have been made mainly for 1-m scale experiments.[12,15] Results show distances below the ceiling ranging from about 1 to 2 percent of the ceiling height for r/H from less than 1 to 2, with predicted reductions in the percent of ceiling height at larger scales.

Much of the discussion below deals with predictions and correlations of the maximum excess temperature and velocity in the ceiling jet flow, which occur, as already noted, relatively close to the ceiling surface. Often fire detectors or sprinklers are placed at ceiling standoff distances that are outside of this region and therefore will experience cooler temperatures and lower velocities than predicted. In facilities with very high ceilings, the detectors could be closer to the ceiling than 1 percent of the fire source-to-ceiling separation and will fall in the ceiling jet thermal and viscous boundary layers. In low-ceiling facilities, it is possible for sprinklers or detectors to be placed outside of the ceiling jet flow entirely if the standoff is greater than 12 percent of the fire source-to-ceiling height. In this case, response time could be drastically increased.

Ceiling jet temperature and velocity: Alpert[3] has developed easy-to-use correlations to quantify the maximum gas temperature and velocity at a given position in a ceiling jet flow produced by a steady fire. These correlations are widely used in hazard analysis calculations. Evans and Stroup[13] have employed the correlations in the development of a generalized program to predict heat detector response for the case of a detector totally submerged in the ceiling jet flow. The correlations are based on measurements collected during fire tests involving fuel arrays of wood and plastic pallets, empty cardboard boxes, plastic materials in cardboard boxes, and liquid fuels. Heat release rates for these fuels range from 668 kW to 98 MW while total ceiling heights range from 4.6 to 15.5 m. In SI units, Alpert's[3] correlations for maximum ceiling jet temperatures and velocities are as follows:

$$T - T_\infty = 16.9\,\frac{\dot{Q}^{2/3}}{H^{5/3}} \qquad \text{for } r/H \le 0.18 \tag{2}$$

$$T - T_\infty = 5.38\,\frac{\dot{Q}^{2/3}/H^{5/3}}{(r/H)^{2/3}} \qquad \text{for } r/H > 0.18 \tag{3}$$

$$U = 0.96\left(\frac{\dot{Q}}{H}\right)^{1/3} \qquad \text{for } r/H \le 0.15 \tag{4}$$

$$U = 0.195\,\frac{(\dot{Q}/H)^{1/3}}{(r/H)^{5/6}} \qquad \text{for } r/H > 0.15 \tag{5}$$

where temperature, T, is in °C; velocity, U, is in m/s; total heat release rate, $\dot{Q}$, is in kW; and radial position and ceiling height (r and H) are in m.

Data from these fire tests are correlated using the total rate at which heat is actually released in the fire. Even though it is the convective component of this total heat release rate that is directly related to the buoyancy of the fire, most available data are correlated using the total heat release rate. For the liquid alcohol pool fires that constitute the primary basis of the correlation developed by Alpert, the total heat release rate is roughly the same as the convective heat release rate, $\dot{Q}_c$. However, for the remaining solid commodities and pallets, the convective heat release rate is about 60 percent of the total rate at which heat is actually released. Hence, for general commodities, it may be inaccurate to assume that convective heat release rate is always equal to the total heat release rate, $\dot{Q}$.

The correlations for both temperatures and velocities (Equations 2, 3, 4, and 5) are broken into two parts. One part applies for the ceiling jet in the area of the impingement point where the upward flow of gas in the plume turns to flow out beneath the ceiling horizontally. These correlations (Equations 2 and 4) are independent of radius and are actually axial plume-flow temperatures and velocities calculated at the ceiling height above the fire source. The other correlations apply outside of this turning region as the flow moves away from the impingement area.

Certain constraints should be understood when applying these correlations in the analysis of fire flows. The correlations apply only during times after fire ignition when the ceiling flow may be considered unconfined; that is, no accumulated warm upper layer is present. Walls close to the fire affect the temperatures and velocity in the ceiling jet independent of any effect on the fire-burning rate due to radiant heat received from the walls. The correlations were developed from test data to apply in cases

where the fire source is at least a distance 1.8 times the ceiling height from the enclosure walls. For special cases where burning fuel is located against a flat wall surface or two wall surfaces forming a 90-degree corner, the correlations are adjusted based on the method of reflection. This method makes use of symmetry to account for the effects of the walls in blocking entrainment of air into the fire plume. For the case of a fire adjacent to a flat wall, $2\dot{Q}$ is substituted for $\dot{Q}$ in the correlations. For a fire in a 90-degree corner, $4\dot{Q}$ is substituted for $\dot{Q}$ in the correlations.[3]

Experiments have shown that unless great care is taken to ensure that the fuel perimeter is in contact with the wall surfaces, the method of reflection used to estimate the effects of the walls on ceiling jet temperature will be inaccurate. For example, Zukoski et al.[14] found that a circular burner placed against a wall so that only one point on the perimeter contacted the wall, behaved almost identically to a fire far from the wall with plume entrainment only decreasing by 3 percent. When using Equations 2, 3, 4, and 5, this fire would be represented by replacing $\dot{Q}$ with $1.05\dot{Q}$ and not $2\dot{Q}$ as would be predicted by the method of reflections. The value of $2\dot{Q}$ would be appropriate for a semicircular burner with the entire flat side pushed against the wall surface.

Consider the following calculations, which demonstrate typical uses of the correlations Equations 2, 3, 4, and 5.

(a) The maximum excess temperature under a ceiling 10 m directly above a 1.0-MW heat-release-rate fire is calculated using Equation 2 as

$$T - T_\infty = \frac{16.9(1000)^{2/3}}{10^{5/3}}$$

$$= \frac{16.9(100)}{46.42}$$

$$\Delta T = 36.4\ ^\circ C$$

(b) For a fire that is against noncombustible walls in a corner of a building and 12 m below the ceiling, the minimum heat release rate needed to raise the temperature of the gas below the ceiling 50°C at a distance 5 m from the corner is calculated using Equation 3 and the symmetry substitution of $4\dot{Q}$ for $\dot{Q}$ to account for the effects of the corner as

$$T - T_\infty = 5.38\,\frac{(4\dot{Q})^{2/3}/H^{5/3}}{(r/H)^{2/3}}$$

$$50 = 5.38\,\frac{(4\dot{Q})^{2/3}}{12^{5/3}(5/12)^{2/3}}$$

$$\dot{Q} = \frac{5}{4}\left[\frac{50(12)}{5.38}\right]^{3/2}$$

$$\dot{Q} = 1472\ \text{kW} = 1.472\ \text{MW}$$

(c) The maximum velocity at this position is calculated from Equation 5, modified to account for the effects of the corner as

$$U = 0.195\,\frac{(4\dot{Q}/H)^{1/3}}{(r/H)^{5/6}}$$

$$= \frac{0.195(5888)^{1/3}}{(5/12)^{5/6}12^{1/3}}$$

$$U = 3.2\ \text{m/s}$$

Nondimensional ceiling jet relations: Heskestad[7] developed correlations* for maximum ceiling jet excess temperature and velocity based on alcohol pool-fire tests performed at the U.K. Fire Research Station in the 1950s. These correlations are cast in the following heat-release-rate, excess temperature, and velocity variables that are nondimensional (indicated by the superscript asterisk) and applicable to steady-state fires under unconfined ceilings (indicated by the subscript 0):

$$\dot{Q}_0^* = \frac{\dot{Q}}{\rho_\infty c_p T_\infty g^{1/2} H^{5/2}} \tag{6}$$

$$\Delta T_0^* = \frac{\Delta T/T_\infty}{(\dot{Q}_0^*)^{2/3}} \tag{7}$$

$$U_0^* = \frac{U/\sqrt{gH}}{(\dot{Q}_0^*)^{1/3}} \tag{8}$$

Figure 2-2.2 shows a plot of the Heskestad correlation for excess temperature and velocity data as solid line curves. The correlations developed by Alpert[3] are plotted as broken curves, using the same dimensionless parameters with assumed ambient temperature of 293 K (20°C), normal atmospheric pressure, and convective heat release rate equal to the total heat release rate, $\dot{Q}_c = \dot{Q}$. Generally, the results of Heskestad[7] predict slightly higher excess temperatures and substantially greater gas velocities than Alpert's[3] results. Another curve shown in Figure 2-2.2 is a fit to the mean ceiling jet velocity predicted by the generalized theory of Reference 4, which also predicts that the turning-region boundary should be at $r/H = 0.17$. This predicted velocity is reasonably close to Heskestad's[7] experimental correlation for velocity. Based on the results shown in Figure 2-2.2, the nondimensional excess temperature from the Heskestad[7] correlation and the nondimensional velocity from Alpert's theory,[4,15] are recommended for the prediction of steady ceiling jet flows beneath unobstructed ceilings. The Heskestad correlation and the Alpert theory are adequately fit, respectively, by the following expressions:

$$\Delta T_0^* = \left(0.225 + 0.27\,\frac{r}{H}\right)^{-4/3} \qquad \text{for } 0.2 \le r/H < 4.0 \tag{9}$$

$$\Delta T_0^* = 6.3 \qquad \text{for } r/H \le 0.2 \tag{10}$$

$$U_0^* = 1.06\left(\frac{r}{H}\right)^{-0.69} \qquad \text{for } 0.17 \le r/H < 4.0 \tag{11}$$

$$U_0^* = 3.61 \qquad \text{for } r/H \le 0.17 \tag{12}$$

*Originally developed by G. Heskestad and C. Yao in "A New Approach to Development of Installation Standards for Fired Detectors," *Technical Proposal No. 19574,* prepared for The Fire Detection Institute, by Factory Mutual Research Corporation, Norwood, MA (1971).

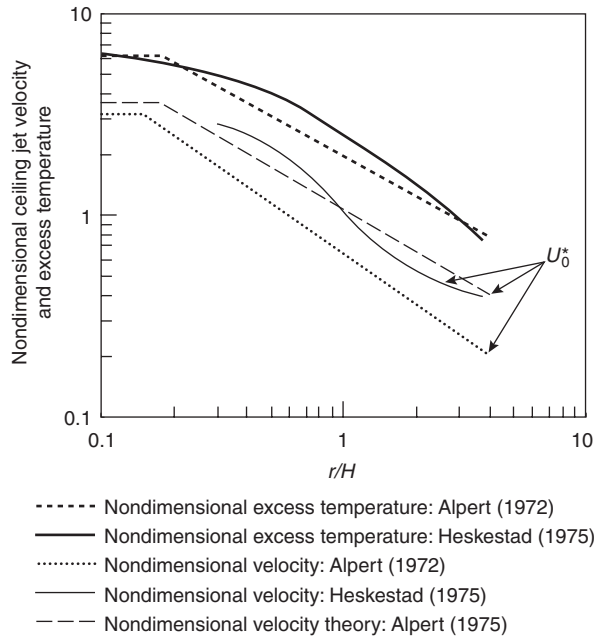

Figure 2-2.2. ***Dimensionless correlations for maximum ceiling jet temperatures and velocities produced by steady fires. Solid line: Heskestad;[7] dotted line: Alpert.[3]***

Heskestad and Delichatsios[24] examined the original data from Reference 7 and concluded that nondimensional velocity and temperature could be related by the following equation:

$$\frac{U_0^*}{\sqrt{\Delta T_0^*}} = 0.68\left(\frac{r}{H}\right)^{-0.63} \qquad \text{for } r/H \geq 0.3 \qquad (13)$$

The preceding relation has been found applicable to a much wider range of conditions than just steady-state alcohol pool fires having weakly buoyant plumes. For example, this relationship between ceiling jet velocity and excess temperature is consistent with measurements[24] for time-dependent fires having strong plumes.

Other methods used to calculate ceiling jet velocity and maximum possible (when the ceiling is adiabatic) ceiling jet temperatures are reported by Cooper and Woodhouse.[9] A critical review of correlation formulas for excess temperature and velocity in the ceiling jet under a variety of conditions has been assembled by Beyler.[16] To apply these and the preceding expressions to realistic burning situations, it is recommended that the convective heat release rate should be used.

Strong Plume-Driven Flow Field

Ceiling jet temperature: When the flame height of a fire plume is comparable to the height of the ceiling above the burning fuel, the resultant ceiling jet is driven by a strong plume. Heskestad and Hamada[6] measured ceiling jet temperatures for ratios of free flame height (in the absence of a ceiling, obtained from existing knowledge of flame heights) to ceiling height ranging from 0.3 up to 3. A correlation of excess temperatures could be achieved by using the plume radius, b, at the ceiling as a normalizing length scale, rather than the ceiling height used for the case of a weak plume. This correlation takes the form:

$$\frac{\Delta T}{\Delta T_p} = 1.92\left(\frac{r}{b}\right)^{-1} - \exp\left[1.61\left(1 - \frac{r}{b}\right)\right] \qquad \text{for } 1 \leq \frac{r}{b} \leq 40 \qquad (14)$$

where ΔT_p is the excess temperature on the plume centerline at the level of the ceiling (obtained from Equations 2 or 10 or other fire-plume relations) and b is the radius where the velocity of the impinging plume is one-half the centerline value. The expression for this characteristic plume radius is given by

$$b = 0.42[(c_p\rho_\infty)^{4/5} T_\infty^{3/5} g^{2/5}]^{-1/2} \frac{T_p^{1/2} \dot{Q}_c^{2/5}}{\Delta T_p^{3/5}} \qquad (15)$$

The Heskestad and Hamada[6] correlation is derived from measurements made with propane burner fires having heat release rates from 12 to 764 kW and beneath ceilings up to 2.5 m in height. This correlation is found to be accurate for ratios of free flame height to ceiling height less than or equal to about 2.0. At greater flame-height ratios, significant heat released in the ceiling jet itself appears to be the cause for a lack of agreement with the correlation.

Flame lengths in the ceiling jet: It is very interesting to note an often-overlooked finding of Heskestad and Hamada.[6] When there is flame impingement on the ceiling (flame-height ratio > 1), the mean flame radius along the ceiling from the plume centerline is observed to be about equal to the difference between the free flame height and the ceiling height. Hence, Heskestad and Hamada find that the total average length of flame from the burning fuel to the flame tip under the ceiling is virtually the same as the free flame height.

In an earlier study involving small (0.36 to 8 kW) pool fires beneath ceilings up to 0.336 m in height, Yu (You)* and Faeth[10] measure the mean flame radius along the ceiling. Their results yield a flame radius about one-half the difference between the free flame height and the ceiling height, or one-half that of Heskestad and Hamada, perhaps due to the smaller scale of their experiment.

Ceiling jet thickness: For strong plumes, Atkinson and Drysdale[17] demonstrate that much of the plume kinetic energy is lost (possibly 75 percent of that in the incident plume) during the process of ceiling impingement. As a result of this kinetic energy loss, the initial ceiling jet thickness after the turning region may be twice that expected for the case of weak plumes, about 11 percent of the ceiling height at $r/H = 0.2$. Measurements made by Atkinson and Drysdale and by Yu[5] show that the ceiling jet thickness may reach a minimum of 8 percent of ceiling height at $r/H = 0.5$ and then increase up to 12 percent of ceiling height at large radial distances, as for weak plumes.

*H. Z. Yu formerly published under the spelling *You.*

Convective Heat Transfer to the Ceiling

Convection is the dominant mode of heat transfer for the case of weak plumes impinging on ceilings. This heat-transfer regime is important for the prediction of activation times for detection devices and the prediction of damage for objects, such as cables or pipes, suspended below the ceiling. However, damage to the ceiling structure itself will much more likely be the result of strong plume (flame) impingement, for which heat transfer due to thermal radiation will be just as important or more important than convection. The maximum convective heat flux to a ceiling occurs when the ceiling surface is at or near ambient temperature, T_∞, before there has been any significant heating of the ceiling material. This maximum convective flux is the subject of the following discussion. For additional discussion of ceiling heat loss, see Section 2, Chapter 14.

Weak Plume Impingement (Turning) Region

Quantification of convective heat transfer from weak fire plumes impinging on ceiling surfaces has been an area of research activity for many years. In the turning region, a widely used correlation is derived by Yu and Faeth, from experiments with small pool fires (convective heat release rates, $\dot{Q}_c$, from 0.05 to 3.46 kW; ceiling heights, H, less than 1 m). This correlation gives convective heat flux to the ceiling, $\dot{q}''$, as

$$\frac{\dot{q}''H^2}{\dot{Q}_c} = \frac{31.2}{\mathrm{Pr}^{3/5}\,\mathrm{Ra}^{1/6}} = \frac{38.6}{\mathrm{Ra}^{1/6}} \tag{16}$$

where Pr is the Prandtl number, and the plume Rayleigh number, Ra, is given by

$$\mathrm{Ra} = \frac{g\dot{Q}_c H^2}{3.5 p \nu^3} = \frac{0.027\dot{Q}_c H^2}{\nu^3} \tag{17}$$

for gases similar to air, having ambient absolute pressure, p, and kinematic viscosity, ν. It is recommended that when these expressions are applied to actual heat-transfer problems, the ceiling height be corrected for the location of the virtual point source for the plume.

Note that the heat-flux parameter on the left side of Equation 16 is proportional to the classic heat-transfer Stanton number and that the Rayleigh number is proportional to the cube of the plume Reynolds number, Re (defined in terms of centerline velocity, characteristic plume diameter, $2b$, and kinematic viscosity at the plume centerline temperature).

Equation 16 has been established for mainly weak plumes with Rayleigh numbers from 10^9 to 10^{14}. Kokkala[18] has verified this impingement zone heat-transfer correlation, using up to 10 kW natural gas flames, for flame heights up to 70 percent of the ceiling height. For greater flame height to ceiling height ratios, Kokkala[18] finds that heat-transfer rates are many times higher than predicted, partly due to thermal radiation.

Alpert[19] performed small-scale (0.3-m ceiling height) experiments at elevated air pressures, which allow Rayleigh numbers greater than 2×10^{15} to be achieved while maintaining somewhat better control of ambient disturbances than in 1-atm experiments. Results of these experiments essentially confirm the predictions of the correlation in Equation 16, as well as an expression recommended for the plume impingement region by Cooper.[8] The latter expression yields nondimensional ceiling heat transfer, in terms of the plume Reynolds number defined by Alpert,[19] as follows:

$$\frac{\dot{q}''H^2}{\dot{Q}_c} = 49 \times \mathrm{Re}^{-1/2} = 105\left(\frac{\dot{Q}_c^{1/3}H^{2/3}}{\nu}\right)^{-1/2} \tag{18}$$

Although Equations 16 and 18 have identical dependence of impingement heat flux on fire heat release rate and ceiling height, heat-flux values from Equation 18 are about 50 percent higher, since this expression is derived from data on turbulent jets.

Ceiling Jet Region

Outside of the turning region, the convective flux to the ceiling is known to drop off sharply with increasing radial distance from the plume axis. The experiments of Yu and Faeth[10] described in the preceding section were also used to determine this radial variation in ceiling jet convective flux. Their own data, as well as data from small-scale experiments (ceiling heights of 0.5 to 0.8 m) by Alpert[15] and by Veldman[11] are all consistent with the following correlation that is given in Reference 10:*

$$\frac{\dot{q}''H^2}{\dot{Q}_c} = 0.04\left(\frac{r}{H}\right)^{-1.3} \qquad \text{for } 0.2 \le \frac{r}{H} < 2.0 \tag{19}$$

An alternate derivation of Equation 19 can be obtained by using Alpert's correlation for ceiling jet excess temperature (Equation 3) and Alpert's theory for average ceiling jet velocity (Equation 11) with the Reynolds/Colburn analogy, as discussed in References 10 and 11. From the Reynolds/Colburn analogy, the heat-transfer coefficient at the ceiling, h, should be related to ceiling jet average velocity and density as follows:

$$\frac{h}{\rho_\infty U c_p} = \mathrm{Pr}^{-2/3}\frac{f}{2} \tag{20}$$

where Pr is the Prandtl number and f is the ceiling friction factor. By using Equation 11 for average ceiling jet velocity, U, the ceiling heat-transfer coefficient becomes

$$h = 0.246\, f\left(\frac{\dot{Q}_c}{H}\right)^{1/3}\left(\frac{r}{H}\right)^{-0.69} \qquad \text{for } 0.17 \le \frac{r}{H} < 4.0 \tag{21}$$

With $f = 0.03$, Equation 21 is identical to the simplified expression listed in Beyler's extensive compilation.[16] The nondimensional heat flux to a ceiling at ambient temperature can then be expressed as follows, since $\dot{q}'' = h\Delta T$, with ΔT given by Equation 3:

$$\frac{\dot{q}''H^2}{\dot{Q}_c} = 1.323f\left(\frac{r}{H}\right)^{-1.36} \qquad \text{for } 0.2 \le \frac{r}{H} < 4.0 \tag{22}$$

*Note that there is a typographical error in the exponent of r/H in Equation 17 of this reference.

Equations 19 and 22 are in good agreement for a friction factor of 0.03, which is comparable with the value of 0.02 deduced from the theory of Reference 4.

Sloped Ceilings

There have been very few studies of the ceiling jet flow that results from plume impingement on a flat ceiling that is not horizontal, but is inclined at some angle, θ, to the horizontal. One such study, by Kung et al.,[20] obtained measurements showing pronounced effects in the velocity variation along the steepest run from the point of impingement of a strong plume, both in the upward and downward directions. In the upward direction, the rate of velocity decrease with distance, r, from the intersection of the plume vertical axis with the ceiling was reduced significantly as the ceiling slope increased. In the downward direction, the flow separated from the ceiling and turned upward at a location, $-r$, denoted by Kung et al.[20] as the penetration distance. These results were the outcome of experiments with 0.15- and 0.228-m-diameter pan fires located 0.279 to 0.889 m beneath an inclined 2.4-m square ceiling and were limited to convective heat release rates in the range of 3 to 13 kW.

Following Heskestad and Hamada,[6] Kung et al. developed correlations by scaling near-maximum excess temperature and velocity, as well as radial distance along the ceiling, in terms of the quantities in the undeflected plume at the impingement point. These correlations take the following form:

$$\frac{\Delta T}{\Delta T_p} = \exp\left[(0.12\sin\theta - 0.42)\left(\frac{r}{b} - 1\right)^{0.7}\right] \quad (23)$$

$$\frac{U}{V_p} = \exp\left[(0.79\sin\theta - 0.52)\left(\frac{r}{b} - 1\right)^{0.6}\right] \quad (24)$$

for $r/b \geq 1$ (upward direction from the impingement point) and $\theta = 0 - 30°$;

$$\frac{\Delta T}{\Delta T_p} = (0.15\sin\theta + 0.11)\left(\frac{r}{b}\right) + 0.97 - 0.06\sin\theta \quad (25)$$

$$\frac{U}{V_p} = (0.21\sin\theta + 0.10)\left(\frac{r}{b}\right) + 0.99 - 1.17\sin\theta \quad (26)$$

for $r/b < 0$ (downward direction from the impingement point), valid only for $\theta = 10 - 30°$, and for ΔT and $U \geq 0$.

In Equations, 23, 24, 25, and 26, the characteristic plume radius is proportional to that defined in Equation 15 but with a slightly different magnitude, namely,

$$b = 0.548[(c_p\rho_\infty)^{4/5}T_\infty^{3/5}g^{2/5}]^{-1/2}\frac{T_p^{1/2}\dot{Q}_c^{2/5}}{\Delta T_p^{3/5}} \quad (27)$$

Equation 26 shows that the ceiling jet velocity first becomes zero in the downward direction at values of r/b equal to -5.6, -3.5, and -2.0 for ceiling slopes of 10°, 20°, and 30°, respectively.

Time-Dependent Fires

Quasi-Steady Assumption

For time-dependent fires, all estimates from the previous section may still be used, but with the constant heat release rate, $\dot{Q}$, replaced by an appropriate time-dependent $\dot{Q}(t)$. In making this replacement, a "quasi-steady" flow has been assumed. This assumption implies that when a change in heat release rate occurs at the fire source, full effects of the change are immediately felt everywhere in the flow field. In a room-size enclosure, under conditions where the fire is growing slowly, this assumption is reasonable. However, in other cases, the time for the heat release rate to change significantly may be comparable to or less than the time, $t_f - t_i$, for gas to travel from the burning fuel to a detector submerged in the ceiling jet. The quasi-steady assumption may not be appropriate in this situation, unless the following condition is satisfied, depending on the accuracy desired:

$$\frac{\dot{Q}}{d\dot{Q}/dt} > t_f - t_i \quad (28)$$

where t_i is an ignition reference time.

The quasi-steady assumption, together with the strong plume-driven ceiling jet analysis of Heskestad and Hamada,[6] has been used by Kung et al.[21] to correlate ceiling jet velocity and temperature induced by growing rack-storage fires. Although gas travel times for these large-scale experiments may amount to many seconds, Equation 28 shows that a sufficiently small fire-growth rate allows a quasi-steady analysis to be used.

Testing has shown that the heat release rate during the growth phase of many fires can often be characterized by simple time-dependent polynomial or exponential functions. The most extensive research and analysis have been performed with heat release rates that vary with the second power of time.

Power-Law Fire Growth

The growth phase of many fires can be characterized by a heat release rate increasing proportionally with a power, p, of time measured from the ignition reference time, t_i, as follows:

$$\dot{Q} = \alpha(t - t_i)^p \quad (29)$$

Figure 2-2.3 shows one case where the heat release rate for a burning foam sofa during the growth phase of the fire, more than 80 s (t_i) after ignition,[22] can be represented by the following equation:

$$\dot{Q} = 0.1736(t - 80)^2 \quad (30)$$

Heskestad[23] used the general power-law behavior given by Equation 29 to propose a set of theoretical modeling relations for the transient ceiling jet flow that would result from such a time-varying heat release rate. These relations were validated in an extensive series of tests conducted by Factory Mutual Research Corporation,[24,25] where measurements were made of maximum ceiling jet

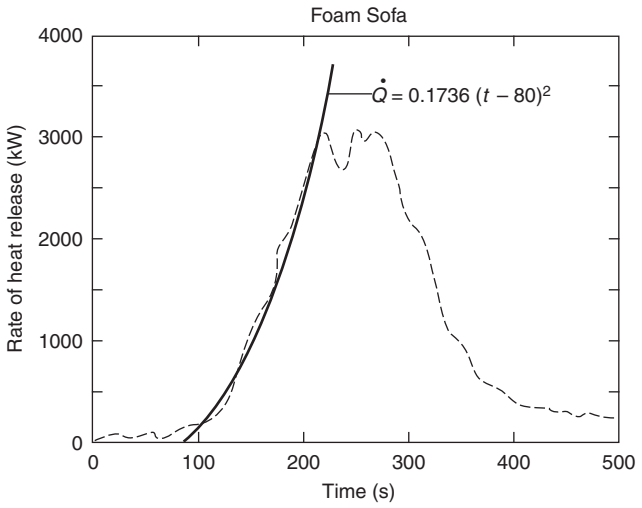

Figure 2-2.3. ***Heat release rate history for a burning foam sofa.[22]***

temperatures and velocities during the growth of fires in three different sizes of wood crib. Subsequent to this original experimental study, Heskestad and Delichatsios[26] corrected the heat release rate, $\dot{Q}$, computed for the crib tests and also generalized their results to other types of fuels by using the more relevant, convective heat release rate, $\dot{Q}_c$. The resulting dimensionless correlations for maximum ceiling jet temperatures and velocities are given by

$$\Delta T_2^* = 0 \qquad t_2^* \le (t_2^*)_f \tag{31}$$

$$\Delta T_2^* = \left(\frac{t_2^* - (t_2^*)_f}{0.126 + 0.210 r/H} \right)^{4/3} \qquad t_2^* > (t_2^*)_f \tag{32}$$

$$\frac{U_2^*}{\sqrt{\Delta T_2^*}} = 0.59 \left(\frac{r}{H} \right)^{-0.63} \tag{33}$$

where

$$t_2^* = \frac{t - t_i}{(A\alpha_c H^{-4})^{-1/5}} \tag{34}$$

$$U_2^* = \frac{U}{(A\alpha_c H)^{1/5}} \tag{35}$$

$$\Delta T_2^* = \frac{(T - T_\infty)/T_\infty}{(A\alpha_c)^{2/5} g^{-1} H^{-3/5}} \tag{36}$$

$$A = \frac{g}{\rho_\infty c_p T_\infty} \tag{37}$$

$$\alpha_c = \frac{\dot{Q}_c}{(t - t_i)^2} \tag{38}$$

$$(t_2^*)_f = 0.813 \left(1 + \frac{r}{H} \right) \tag{39}$$

and where dimensionless variables are indicated with the superscript asterisk.

Notice that in Equation 32 the dimensionless time, t_2^*, has been reduced by the time $(t_2^*)_f$. This reduction accounts for the gas travel time, $t_f - t_i$, between the fire source and the location of interest along the ceiling at the specified r/H. For dimensionless times after ignition less than $(t_2^*)_f$, the initial heat front has not yet arrived at r/H, so the gas temperature is still at the ambient value, as shown in Equation 31. In dimensional terms, the gas travel time is given by the following, after using the definition of t_2^* in Equation 39:

$$t_f - t_i = H^{4/5} \frac{0.813(1 + r/H)}{(A\alpha_c)^{1/5}} \tag{40}$$

Substitution of Equation 29 into Equation 28 shows that for power-law fire growth, the quasi-steady assumption will always be valid beginning at a sufficiently long time after ignition. For the specific case of t^2 fire growth, substitution of Equation 38 and the expression for the gas travel time, Equation 40, into Equation 28 results in the following requirement if a quasi-steady analysis is to be appropriate:

$$\frac{t - t_i}{2} > H^{4/5} \frac{0.813(1 + r/H)}{(A\alpha_c)^{1/5}} \tag{41}$$

In the limit of very large values of $t - t_i$, Equation 41 will always be satisfied and a quasi-steady limit is achieved, as shown by an alternative method in Reference 24. The value of the quasi-steady excess temperature, $(\Delta T_2^*)_{qs}$, in this limit of $t_2^* \gg (t_2^*)_f$ becomes, from Equation 32

$$(\Delta T_2^*)_{qs} = \left(\frac{t_2^*}{0.126 + 0.210 r/H} \right)^{4/3} \tag{42}$$

The preceding correlations of ceiling jet temperatures and velocities are the basis for the calculated values of fire detector spacing found in NFPA 72®, *National Fire Alarm Code®*, Appendix B, "Engineering Guide for Automatic Fire Detector Spacing."[27] In NFPA 72, three or four selected fire heat release rates assumed to increase proportionally with the square of time are used as the basis for the evaluation. These fire heat release rate histories are chosen to be representative of actual fires involving different commodities and geometric storage arrangements. The chosen release-rate histories are as follows:

Slow, $\dot{Q} = 0.00293 t^2$ (43)

Medium, $\dot{Q} = 0.01172 t^2$ (44)

Fast, $\dot{Q} = 0.0469 t^2$ (45)

Ultrafast, $\dot{Q} = 0.1876 t^2$ (46)

where $\dot{Q}$ is in kW and t is in s.

EXAMPLE:

Sofa fire: Consider how the following calculation demonstrates a use of the correlation (Equations 32 and 33) for calculating the ceiling jet maximum temperature and velocity produced by a t^2 fire growth.

A foam sofa, of the type analyzed in Figure 2-2.3, is burning in a showroom 5 m below a suspended ceiling. The showroom temperature remote from the fire remains at 20°C at floor level as the fire begins to grow. Determine the gas temperature and velocity at the position of a ceiling-mounted fire detector submerged in the ceiling jet flow 4 m away from the fire axis when the convective heat release rate (assumed to equal the total heat release rate) first reaches 2.5 MW.

Figure 2-2.3 shows that the heat release rate from the sofa first reaches 2.5 MW (2500 kW) at about 200 s after ignition. Using the analytic formula for the time-dependent heat release rate, Equation 30, the time from the virtual ignition of the sofa at 80 s to reach 2500 kW is

$$2500 = 0.1736(t - 80)^2$$
$$(t - 80) = 120 \text{ s}$$

In this problem, the low-level heat release rate up to 80 s after actual ignition of the sofa is ignored. Thus, the sofa fire can be treated as having started at $t = 80$ s and grown to 2.5 MW in the following 120 s. Equations 34 through 39 are used to evaluate parameters of the problem, using the dimensionless correlations for ceiling jet temperature and velocity.

For the sofa fire in the showroom example, $T_\infty = 293$ K, $\rho = 1.204$ kg/m^3, $c_p = 1$ kJ/kg·K, $g = 9.8$ m/s^2, $\alpha_c = 0.1736$ kW/s^2, $A = 0.0278$ m^4/kJ·s^2, $r = 4$ m, $H = 5$ m, $(t_2^*)_f = 1.46$, $t - t_i = 120$ s, and $t_2^* = 11.40$. For the conditions of interest, $t_2^* > (t_2^*)_f$, so the correlation (Equation 32) is used to evaluate the dimensionless ceiling jet temperature:

$$\Delta T_2^* = \left[\frac{11.40 - 1.46}{0.126 + 0.210(4/5)}\right]^{4/3}$$
$$\Delta T_2^* = 109.3$$

Equation 33 is used to calculate the dimensionless ceiling jet velocity

$$U_2^* = 0.59(4/5)^{-0.63}\sqrt{109.3}$$
$$= 7.10$$

The dimensional excess temperature and velocity are calculated using Equations 36 and 35, respectively, to yield

$$\Delta T = 147 \text{ K}$$
$$T = 147 \text{ K} + 293 \text{ K} = 440 \text{ K} = 167°\text{C}$$
$$U = 3.37 \text{ m/s}$$

The corresponding gas temperature calculated with the quasi-steady analysis of Equation 42 instead of the t^2 fire analysis is 197°C.

EXAMPLE:

Rack storage: Yu and Stavrianidis[28] were interested in predicting activation times of quick-response sprinklers protecting high rack storage of plastics. Since the sprinklers are activated typically in less than 1 min by the ceiling jet flow, information on flow temperature and velocity shortly after ignition is required. The objective was to correlate properties of the ceiling jet induced by fires in 2- to 5-tier-high rack storage, consisting of polystyrene cups packaged in corrugated paper cartons on pallets. When this fuel array is ignited at its base, the initial growth period ($t - t_i \approx 25$ s) can be characterized as heat release rates increasing by the third power of time, as follows:

$$\dot{Q}_c = \alpha_c(t - t_i)^3 \tag{47}$$

where $\alpha_c = 0.0448$. Because of upward and lateral flame propagation during the transient rack-storage fire, the virtual origin elevation, z_o, of the plume changes during the course of fire growth, as follows:

$$z_o = -2.4 + 0.095\dot{Q}_c^{2/5} \tag{48}$$

thereby complicating the effort to correlate ceiling jet properties. Nevertheless, Yu and Stavrianidis were able to develop correlations based on the following dimensional temperature and velocity variables, which are similar to those first proposed by Heskestad[23] for power-law fire growth:

$$\Delta\hat{T}_m = \alpha_c^{-1/3}(H - z_o)^{1/3}\frac{\Delta T_m}{T_\infty} \tag{49}$$

$$\hat{U}_m = \alpha_c^{-1/6}(H - z_o)^{-1/3}U_m \tag{50}$$

where the maximum ceiling jet excess temperature, $\Delta\hat{T}_m$, and velocity, $\hat{U}_m$, variables depend on the following heat release rate and radial distance parameters, respectively:

$$X = \alpha_c^{-1/6}(H - z_o)^{-2/3}\dot{Q}_c^{1/3} \tag{51}$$

$$\hat{R} = \frac{r}{H - z_o} \tag{52}$$

The exact form of the preceding correlations, in terms of detailed formulas, is provided in Reference 28.

In addition to maximum excess gas temperature and velocity, Yu and Stavrianidis[28] also measured the depth of the ceiling jet, in terms of the distance below the ceiling where the velocity and excess temperature are $1/e$ of the respective maximum values. Results show the ceiling jet depth based on velocity to be very similar to that based on excess temperature and both depths to be fairly insensitive to the transient fire growth process. Typical values for the ratio of ceiling jet temperature depth to effective ceiling height, $\ell_T/(H - z_o)$, for radial positions, $r/(H - z_o)$ of 0.217, 0.365, 1.75, and 4.33 are about 0.07, 0.1, 0.14, and 0.2, respectively.

Confined Ceilings

Channel Configuration

Previous discussions of ceiling jets in this chapter have all dealt with unconfined radial spread of the gas flow away from a ceiling impingement point. In practice this flow may be interrupted by ceiling beams, or corridor walls, creating a long channel that partially confines the

flow. Knowledge of the resultant ceiling jet flows is important in determining fire detector response times. For the channel configuration, the flow near the impingement point will remain radial (i.e., axisymmetric), but after spreading to the walls or beams that bound the ceiling, the flow will become generally parallel with the confining boundary. Delichatsios[29] has developed correlations for steady-state ceiling jet temperature and velocity, which apply to the channel flow between beams and down corridors. In the case of corridors, the correlations apply when the corridor half-width, ℓ_b, is greater than 0.2 times the ceiling height, H, above the fire source. Note that this value of ℓ_b corresponds approximately to the outer radius of the ceiling jet turning region. In the case of beams, the flow must also be contained fully so that only a flow in a primary channel results, without spillage under the beams to the adjoining secondary channels. For the latter condition to be satisfied, the beam depth, h_b, must be greater than the quantity $(H/10)(\ell_b/H)^{-1/3}$. Downstream of where the ceiling jet flow is parallel to the beams or corridor walls and in the absence of spillage, Delichatsios[29] determined that the average excess ceiling jet temperature and velocity within the primary channel are given by the following:

$$\frac{\Delta T}{\Delta T_p} = \mathrm{a}\left(\frac{H}{\ell_b}\right)^{1/3} \exp\left[-6.67\,\mathrm{St}\,\frac{Y}{H}\left(\frac{\ell_b}{H}\right)^{1/3}\right] \tag{53}$$

$$U = 0.102\sqrt{H\Delta T}\left(\frac{H}{\ell_b}\right)^{1/6} \tag{54}$$

under the conditions:

$$Y > \ell_b$$

$$h_b/H > 0.1(\ell_b/H)^{-1/3}$$

$$\ell_b/H > 0.2$$

$$0.5 < \frac{Y}{H}\left(\frac{\ell_b}{H}\right)^{1/3} < 3.0$$

where

ΔT_p = excess temperature on the plume centerline defined previously in Equation 14

Y = distance along the channel measured from the plume impingement point

St = Stanton number, whose value is recommended to be 0.03

Based on the minimum value of $\ell_b/H = 0.2$, the limit on h_b/H implies that the beam depth to ceiling height ratio must be at least 0.17 for the fire gases to be restricted to the primary channel. The constant a in Equation 53 is determined by Delichatsios to be in the range 0.24 to 0.29. This equation is based on the concept that the channel flow has undergone a hydraulic jump, which results in greatly reduced entrainment of cooler, ambient air from below. Reductions in ceiling jet temperature or velocity are then mainly due to heat losses to the ceiling and would thus be dependent on ceiling composition to some extent.

Additional detailed measurements of the ceiling jet flow in a primary beamed channel have been obtained by Koslowski and Motevalli.[30] Their data generally validate the Delichatsios beamed ceiling correlation (Equation 53) and ceiling jet flow behavior, but additional measurements for a range of beam depth to ceiling height ratios has allowed the correlation to be generalized. Furthermore, Koslowski and Motevalli recast the correlation in terms of the nondimensional heat release rate defined by Heskestad and Delichatsios (Equations 6 and 7), instead of centerline plume conditions at the ceiling, with the following result:

$$\Delta T_0^* = \mathrm{C}\left(\frac{H}{\ell_b}\right)^{1/3} \exp\left[-6.67\,\mathrm{St}\,\frac{Y}{H}\left(\frac{\ell_b}{H}\right)^{1/3}\right] \tag{55}$$

where Stanton number is recommended to be 0.04, rather than 0.03, and the constant, C, has the following dependence on the ratio of beam depth, h_b, to ceiling height, H:

$$\mathrm{C} = -25.38\left(\frac{h_b}{H}\right)^2 + 13.58\,\frac{h_b}{H} + 2.01 \quad \text{for } 0.5 \le \frac{Y}{H} \le 1.6 \tag{56}$$

To derive Equation 56, Koslowski and Motevalli vary the h_b/H ratio from 0.07 up to 0.28. In so doing, they note that C increases steadily with this ratio until leveling off near h_b/H equals 0.17, determined by Delichatsios as the condition for the fire gases to be restricted to the primary channel. Between values of h_b/H of 0.07 (or even much less) and 0.17, spillage from the primary channel to adjacent secondary channels is steadily reduced, thereby increasing temperatures in the primary channel. Characteristics of the ceiling jet flow in the secondary channels, as well as the primary channel, have also been studied by Koslowski and Motevalli.[31]

General Enclosure Configurations

The analyses in preceding sections for unconfined ceiling jet flows may be sufficient for large industrial or commercial storage facilities. In smaller rooms, or for very long times after fire ignition in larger industrial facilities, a quiescent, heated layer of gas will accumulate in the upper portion of the enclosure. This heated layer can be deep enough to totally submerge the ceiling jet flow. In this case, temperatures in the ceiling jet can be expected to be greater than if the ceiling jet were entraining gas from a cooler, ambient-temperature layer. It has been shown by Yu and Faeth[10] that the submerged ceiling jet also results roughly in a 35 percent increase in the heat transfer rate to the ceiling.

There are analytical formulas to predict temperature and velocity in such a two-layer environment, in which the ceiling jet is contained in a heated upper layer and the fire is burning in a lower, cool layer. This type of prediction, which has been developed by Evans,[32,33] Cooper,[34] and Zukoski and Kubota,[35] can best be used to check the proper implementation of readily available numerical

models (e.g., zone or field/CFD) of fire-induced flows in enclosures. An example of a zone model to predict activation of thermal detectors by a ceiling jet submerged in a heated layer is the algorithm developed by Davis.[36] This model, which assumes that thermally activated links are always located below the ceiling at the point of maximum ceiling jet temperature and velocity, is based partly on a model and thoroughly documented software developed by Cooper.[37]

Formulas to predict the effect of the heated upper layer in an enclosure are based on the assumption that the ceiling jet results from a fire contained in a uniform environment at the heated upper-layer temperature. This substitute fire has a heat release rate, $\dot{Q}_2$, and location below the ceiling, H_2, differing from those of the real fire. Calculation of the substitute quantities $\dot{Q}_2$ and H_2, depends on the heat release rate and location of the real fire, as well as the depths and temperatures of the upper and lower layers within the enclosure.

Following the development by Evans,[33] the substitute source heat release rate and distance below the ceiling are calculated from Equations 57 through 60. Originally developed for the purpose of sprinkler and heat detector response time calculations, these equations are applicable during the growth phase of enclosure fires.

$$\dot{Q}^*_{l,2} = \left(\frac{1 + C_T \dot{Q}^{*\,2/3}_{l,1}}{\xi C_T - 1/C_T} \right)^{3/2} \tag{57}$$

$$Z_{l,2} = \left\{ \frac{\xi \dot{Q}^*_{l,1} C_T}{\dot{Q}^{*\,1/3}_{l,2} \left[(\xi - 1)(\beta^2 + 1) + \xi C_T \dot{Q}^{*\,2/3}_{l,2} \right]} \right\}^{2/5} Z_{l,1} \tag{58}$$

$$\dot{Q}_{c,2} = \dot{Q}^*_{l,2} \rho_{\infty,2} c_{p\infty} T_{\infty,2} g^{1/2} Z^{5/2}_{l,2} \tag{59}$$

$$H_2 = H_1 - Z_{l,1} + Z_{l,2} \tag{60}$$

Further explanation of variables is contained in the nomenclature section.

Cooper[34] has formulated an alternative calculation of substitute source heat release rate and distance below the ceiling that provides for generalization to situations in which portions of the time-averaged plume flow in the lower layer are at temperatures below the upper-layer temperature. In these cases, only part of the plume flow may penetrate the upper layer sufficiently to impact on the ceiling. The remaining portion at low temperature may not penetrate into the hotter upper layer. In the extreme, when the maximum temperature in the lower-layer plume flow is less than the upper-layer temperature, none of the plume flow will penetrate significantly into the upper layer. This could be the case during the decay phases of an enclosure fire, when the heat release rate is small compared to earlier in the fire growth history. In this calculation of substitute fire-source quantities, the first step is to calculate the fraction of the plume mass flow penetrating the upper layer, m^*_2, from Equations 61 and 62.

$$m^*_2 = \frac{1.04599\sigma + 0.360391\sigma^2}{1 + 1.37748\sigma + 0.360391\sigma^2} \tag{61}$$

where

$$\sigma = \left(\frac{\xi}{\xi - 1} \right) \left[\frac{1 + C_T (\dot{Q}^*_{l,1})^{2/3}}{\xi} - 1 \right] \tag{62}$$

Then, analogous to Equations 58, 59, and 60 of the previous method:

$$Z_{l,2} = Z_{l,1} \xi^{3/5} (m^*_2)^{2/5} \left(\frac{1 + \sigma}{\sigma} \right)^{1/3} \tag{63}$$

$$\dot{Q}_{c,2} = \dot{Q}_{c,1} \left(\frac{\sigma m^*_2}{1 + \sigma} \right) \tag{64}$$

$$H_2 = H_1 - Z_{l,1} + Z_{l,2} \tag{65}$$

The last step is to use the substitute source values of heat release rate and distance below the ceiling, as well as heated upper-layer properties for ambient conditions, in the correlations developed for ceiling jet flows in uniform environments.

To demonstrate the use of the techniques, the previous example in which a sofa was imagined to be burning in a showroom may be expanded. Let all the parameters of the problem remain the same except that at 200 s after ignition ($t - t_i = 120$ s), when the fire heat release rate has reached 2.5 MW, a quiescent heated layer of gas at a temperature of 50°C is assumed to have accumulated under the ceiling to a depth of 2 m. For this case, the two-layer analysis is needed to determine the ceiling jet maximum temperature at the same position as calculated previously (a radial distance of 4 m from the plume impingement point on the ceiling).

All of the two-layer calculations presented assume quasi-steady conditions. From Equation 41 with the values of parameters in the single-layer calculation, it can be shown that the time after sofa ignition must be at least 31 s for a quasi-steady analysis to be acceptable. Since the actual time after ignition is 120 s, such an analysis is appropriate. It will be assumed that this finding will carry over to the two-layer case.

Using Equations 57 through 60 from the work of Evans,[33] values of the heat release rate and position of the substitute fire source that compensates for the two-layer effects on the plume flow can be calculated. The dimensionless heat release rate of the real fire source evaluated at the position of the interface between the upper and lower layers is as follows:

$$\dot{Q}^*_{l,1} = \frac{\dot{Q}}{\rho_\infty c_{p\infty} T_\infty g^{1/2} Z^{5/2}_{l,1}} \tag{66}$$

For an actual heat release rate of 2500 kW, ambient temperature of 293 K, and distance between the fire source and the interface between the lower and upper layers of 3 m, Equation 66 becomes

$$\dot{Q}^*_{l,1} = \frac{2500}{1.204 \times 1 \times 293 \times 9.8^{1/2} \times 3^{5/2}} = 0.1452$$

Using the ratio of upper-layer temperature to lower-layer temperature, $\xi = 323/293 = 1.1024$ and the constant, $C_T = 9.115$, the dimensionless heat release rate for the substitute fire source is

$$\dot{Q}^*_{I,2} = 0.1179$$

Using the value for the constant $\beta^2 = 0.913$,, the position of the substitute fire source relative to the two-layer interface is

$$Z_{I,2} = 3.161$$

Now, from Equations 59 and 60, the dimensional heat release rate and position relative to the ceiling are found to be

$$\dot{Q}_2 = 2313 \text{ kW} \qquad H_2 = 5.161 \text{ m}$$

The analogous calculations for substitute fire-source heat release rate and position following the analysis of Cooper,[34] Equations 61 through 65, are

$$\sigma = 23.60$$
$$m^*_2 = 0.962$$
$$Z_{I,2} = 3.176$$
$$\dot{Q}_2 = 2308 \text{ kW}$$
$$H_2 = 5.176 \text{ m}$$

These two results are essentially identical for this type of analysis.

Since it has been shown that the quasi-steady analysis is appropriate for this example, the dimensionless maximum temperature in the ceiling jet flow, 4 m from the impingement point, can now be calculated from $(\Delta T^*_2)_{qs}$ in Equation 42. Using the ceiling height above the substitute source, this equation yields the result:

$$(\Delta T^*_2)_{qs} = \left[\frac{11.40}{0.126 + 0.210(4/5.161)}\right]^{4/3} = 134.4$$

For the given time after ignition of 120 s and the assumed t^2 fire growth, the calculated $\dot{Q}_2$ value implies that α equals 0.1606, instead of the original sofa fire growth factor of 0.1736. Substitution of this new α in Equation 36, along with H_2 and the upper-layer temperature as the new ambient value, yields the following dimensional excess temperature at the 4-m radial position in the ceiling jet:

$$\Delta T = \frac{134.4 \times 323 \times (0.0278 \times 0.1606)^{2/5}}{9.8 \times 5.161^{3/5}}$$
$$\Delta T = 190 \text{ K}$$
$$T = 190 \text{ K} + 323 \text{ K} = 513 \text{ K} = 240°\text{C}$$

This is 73°C above the temperature calculated previously using the quasi-steady analysis and a uniform 20°C ambient, demonstrating the effect of flow confinement on gas temperature.

Ceiling Jet Development

At the beginning of a fire, the initial buoyant flow from the fire must spread across the ceiling, driven by buoyancy, to penetrate the cooler ambient air ahead of the flow. Research studies designed to quantify the temperatures and velocities of this initial spreading flow have been initiated.[38] At a minimum, it is useful to become aware of the many fluid mechanical phenomena embodied in a description of the ceiling jet flow in a corridor up to the time when the ceiling jet is totally submerged in a quiescent, warm upper layer. Borrowing heavily from a description of this flow provided by Zukoski et al.,[38] the process is as follows.

A fire starts in a small room with an open door to a long corridor having a small vent near the floor at the end opposite the door. As the fire starts, smoke and hot gases rise to form a layer near the fire room ceiling. The layer is contained in the small room by the door soffit [see Figure 2-2.4(a)]. As the fire continues, hot gas from the room begins to spill out under the soffit into the hallway. The fire grows to a relatively constant heat release rate.

The outflowing gas forms a short, buoyant plume [see Figure 2-2.4(b)] that impinges on the hallway ceiling, producing a thin jet that flows away from the fire room in the same manner that the plume within the room flows over the interior ceiling. The gas flow in this jet is supercritical, analogous to the shooting flow of liquids over a weir. The velocity of the gas in this flow is greater than the speed of gravity waves on the interface between the hot gas and the cooler ambient air. The interaction of the leading edge of this flow with the ambient air ahead of it produces a hydraulic, jumplike condition, as shown in Figure 2-2.4(c). A substantial amount of ambient air is entrained at this jump. Downstream of the jump, the velocity of the gas flow is reduced and mass flow is increased due to the entrainment at the jump. A head is formed at the leading edge of the flow. Mixing between this ceiling-layer flow and the ambient cooler air occurs behind this head.

The flow that is formed travels along the hallway ceiling [see Figures 2-2.4(c) and 2-2.4(d)] with constant velocity and depth until it impinges on the end wall [see Figure 2-2.4(e)]. A group of waves are reflected back toward the jump near the fire room, traveling on the interface. Mixing occurs during the wall impingement process [see Figure 2-2.4(f)], but no significant entrainment occurs during the travel of the nonbreaking reflected wave. When these waves reach the jump near the fire room door, the jump is submerged in the warm gas layer, eliminating the entrainment of ambient lower-layer air at this position [see Figure 2-2.4(g)].

After several wave reflections up and down the corridor along the interface, the wave motion dies out, and a ceiling layer uniform in depth is produced. This layer slowly grows deeper as the hot gas continues to flow into the hallway from the fire room.

It is clear from the preceding description that quantification of effects during development of a submerged ceiling jet flow is quite complex.

Analysis and experiments have been performed to understand better the major features of a developing ceil-

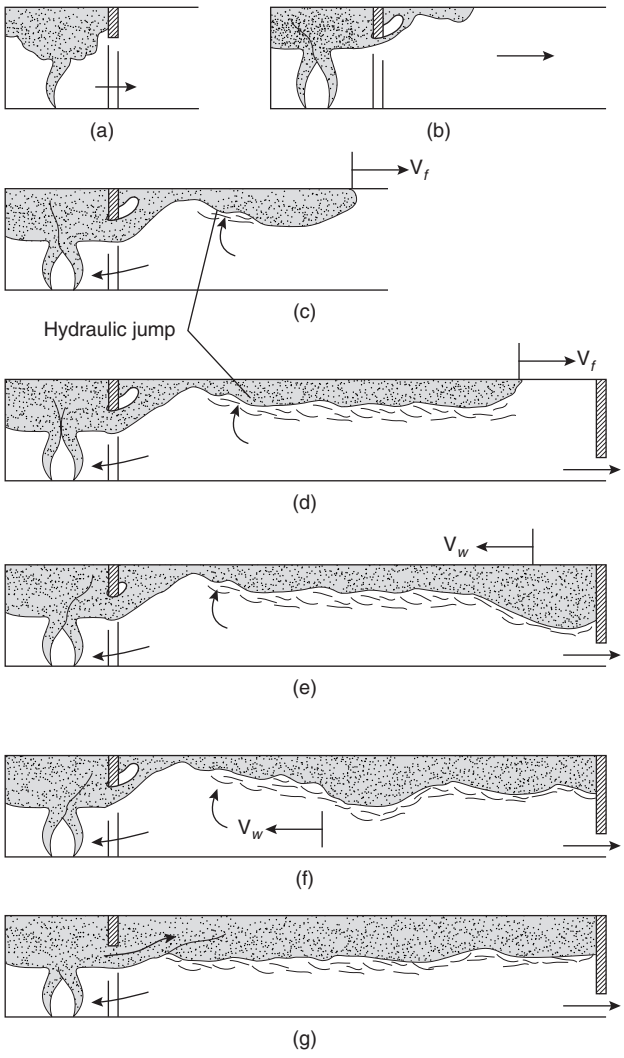

Figure 2-2.4. ***Transient ceiling jet flow in a room and corridor.[38]***

ing jet flow in a corridor.[39,40] One such study[41] contains a description somewhat different from that already given.

Summary

Reliable formulas are available to predict maximum gas temperatures and velocities and approximate temperature/velocity profiles in fire-driven ceiling jet flows beneath unobstructed ceilings for both steady and power-law fire growth. These predictive formulas, which also apply to certain situations where the ceiling jet flow is confined by beams or corridor walls, are very useful for verifying that detailed, numerical enclosure fire models have been implemented properly. The predictive techniques are the basis for acceptable design of fire detection systems, as exemplified by Appendix B of NFPA 72, *National Fire Alarm Code*.[27]

Nomenclature

A	$g/(\rho_\infty c_p T_\infty)$ (m^2/kg)
a	constant in Equation 53, equal to 0.24 to 0.29
b	effective plume radius at the intersection with the ceiling elevation (m)
C_T	constant, related to plume flow, equal to 9.115 (Reference 14)
c_p	heat capacity at constant pressure (J/kg·K)
f	ceiling friction factor
g	gravitational acceleration (m/s^2)
H	ceiling height above fire source (m)
h	heat transfer coefficient ($kW/m^2 \cdot K$)
h_b	depth of beams in a primary beam channel (m)
ℓ_b	half-width for corridor or primary beam channel (m)
ℓ_T	ceiling jet thickness based on $1/e$ depth of excess temperature profile (m)
m_2^*	fraction of fire-plume mass flux penetrating upper layer
p	ambient air pressure (Pa); also, as exponent of time for general power-law fire growth
Pr	Prandtl number
$\dot{Q}$	total heat release rate (kW)
$\dot{Q}_c$	convective heat release rate (kW)
$\dot{Q}_0^*$	$\dot{Q}/(\rho_\infty c_p T_\infty \sqrt{g} H^{5/2})$
$\dot{q}''$	rate of heat transfer per unit area (heat flux) to the ceiling surface (kW/m^2)
R	radial distance to detector (m)
$\hat{R}$	$r/(H - z_o)$
Ra	Rayleigh number
Re	Reynolds number
r	radial distance from axis of fire plume (m)
St	Stanton number, $h/(\rho U c_p)$
T	ceiling jet gas temperature (K)
T_∞	ambient air temperature (K)
T_p	peak gas temperature in plume at the intersection with ceiling elevation (K)
ΔT	excess gas temperature, $T - T_\infty$ (K) or (°C)
t	time (s)
U	ceiling jet gas velocity (m/s)
V_p	maximum plume velocity at the intersection with ceiling elevation (m/s)
Y	distance along channel or corridor, measured from plume axis (m)
Z_I	distance of layer interface above the real or substitute fire source (m)
z	distance above top surface of fire source (m)
z_o	position of virtual point-source origin of plume with respect to fire source (m)
$d\dot{Q}/dt$	rate of change of heat release rate with time (kW/s)

Greek

- α growth parameter for t^2 fires (kW/s^2)
- β^2 constant related to plume flow, equal to 0.913 (Reference 14)
- ν kinematic viscosity (m^2/s)
- θ angle of inclination of the ceiling with respect to the horizontal (degrees)
- ρ gas density (kg/m^3)
- σ parameter defined in Equation 62
- ξ ratio of temperatures, $T_{\infty,2}/T_{\infty,1}$

Subscripts

- 0 based on steady-state fire source
- 1 associated with lower layer
- 2 associated with upper layer; or parameter associated with t^2 fire growth
- ∞ ambient, outside ceiling jet or plume flows
- c convective fraction
- f associated with gas travel time delay
- I value at the interface position between the heated upper layer and cool lower layer
- i reference value at ignition
- p associated with plume flow
- q_s quasi-steady flow condition

Superscripts

- * dimensionless quantity
- ^ quantity related to transient rack-storage fire

References Cited

1. R.W. Pickard, D. Hird, and P. Nash, "The Thermal Testing of Heat-Sensitive Fire Detectors," *F.R. Note 247,* Building Research Establishment, Borehamwood, UK (1957).
2. P.H. Thomas, "The Distribution of Temperature and Velocity Due to Fires beneath Ceilings," *F.R. Note 141,* Building Research Establishment, Borehamwood, UK (1955).
3. R.L. Alpert, *Fire Tech.,* 8, p. 181 (1972).
4. R.L. Alpert, *Comb. Sci. and Tech.,* 11, p. 197 (1975).
5. H.Z. Yu (You), *Fire and Matls.,* 9, p. 46 (1985).
6. G. Heskestad and T. Hamada, *F. Safety J.,* 21, p. 69, (1993).
7. G. Heskestad, "Physical Modeling of Fire," *J. of Fire & Flammability,* 6, p. 253 (1975).
8. L.Y. Cooper, "Heat Transfer from a Buoyant Plume to an Unconfined Ceiling," *J. of Heat Trans.,* 104, p. 446 (1982).
9. L.Y. Cooper and A. Woodhouse, "The Buoyant Plume-Driven Adiabatic Ceiling Temperature Revisited," *J. of Heat Trans.,* 108, p. 822 (1986).
10. H.Z. Yu (You) and G.M. Faeth, *Fire and Matls.,* 3, p. 140 (1979).
11. C.C. Veldman, T. Kubota, and E.E. Zukoski, "An Experimental Investigation of the Heat Transfer from a Buoyant Gas Plume to a Horizontal Ceiling—Part 1: Unobstructed Ceiling," *NBS-GCR-77–97,* National Bureau of Standards, Washington, DC (1977).
12. V. Motevalli and C.H. Marks, "Characterizing the Unconfined Ceiling Jet under Steady-State Conditions: A Reassessment," *Fire Safety Science, Proceedings of the Third International Symposium* (G. Cox and B. Langford, eds.), Elsevier Applied Science, New York, p. 301 (1991).
13. D.D. Evans and D.W. Stroup, *Fire Tech.,* 22, p. 54 (1986).
14. E.E. Zukoski, T. Kubota, and B. Cetegen, *F. Safety J.,* 3, p. 107 (1981).
15. R.L. Alpert, "Fire Induced Turbulent Ceiling-Jet," *Technical Report Serial No. 19722-2,* Factory Mutual Research Corporation, Norwood, MA, p. 35 (1971).
16. C.L. Beyler, "Fire Plumes and Ceiling Jets," *F. Safety J.,* 11, p. 53 (1986).
17. G.T. Atkinson and D.D. Drysdale, "Convective Heat Transfer from Fire Gases," *F. Safety J.,* 19, p. 217 (1992).
18. M.A. Kokkala, "Experimental Study of Heat Transfer to Ceiling from an Impinging Diffusion Flame," *Fire Safety Science, Proceedings of the Third International Symposium* (G. Cox and B. Langford, eds.), Elsevier Applied Science, New York, p. 261 (1991).
19. R.L. Alpert, "Convective Heat Transfer in the Impingement Region of a Buoyant Plume," *ASME J. of Heat Transfer,* 109, p. 120 (1987).
20. H.C. Kung, R.D. Spaulding, and P. Stavrianidis, "Fire Induced Flow under a Sloped Ceiling," *Fire Safety Science, Proceedings of the Third International Symposium* (G. Cox and B. Langford, eds.), Elsevier Applied Science, New York, p. 271 (1991).
21. H.C. Kung, H.Z. Yu (You), and R.D. Spaulding, "Ceiling Flows of Growing Rack Storage Fires," *21st Symposium (International) on Combustion,* Combustion Institute, Pittsburgh, PA, p. 121 (1986).
22. R.P. Schifilliti, *Use of Fire Plume Theory in the Design and Analysis of Fire Detector and Sprinkler Response,* Thesis, Worcester Polytechnic Institute, Worcester, MA (1986).
23. G. Heskestad, "Similarity Relations for the Initial Convective Flow Generated by Fire," *ASME Paper No. 72-WA/HT-17,* American Society of Mechanical Engineers, New York (1972).
24. G. Heskestad and M.A. Delichatsios, "The Initial Convective Flow in Fire," *17th International Symposium on Combustion,* Combustion Institute, Pittsburgh, PA (1978).
25. G. Heskestad and M.A. Delichatsios, "Environments of Fire Detectors," *NBS-GCR-77-86* and *NBSGCR-77-95,* National Bureau of Standards, Washington, DC (1977).
26. G. Heskestad and M.A. Delichatsios, "Update: The Initial Convective Flow in Fire," Short Communication, *F. Safety J.,* 15, p. 471 (1989).
27. NFPA 72®, *National Fire Alarm Code®,* National Fire Protection Association, Quincy, MA (1999).
28. H.Z. Yu and P. Stavrianidis, "The Transient Ceiling Flows of Growing Rack Storage Fires," *Fire Safety Science, Proceedings of the Third International Symposium (*G. Cox and B. Langford, eds.), Elsevier Applied Science, New York, p. 281 (1991).
29. M.A. Delichatsios, *Comb. and Flame,* 43, p. 1 (1981).
30. C. Koslowski and V. Motevalli, "Behavior of a 2-Dimensional Ceiling Jet Flow: A Beamed Ceiling Configuration," *Fire Safety Science, Proceedings of the Fourth International Symposium (*T. Kashiwagi, ed.), International Association of Fire Safety Science, Bethesda, MD, p. 469 (1994).
31. C.C. Koslowski and V. Motevalli, "Effects of Beams on Ceiling Jet Behavior and Heat Detector Operation," *J. of Fire Protection Eng.,* 5, 3, p. 97 (1993).
32. D.D. Evans, *Comb. Sci. and Tech.,* 40, p. 79 (1984).
33. D.D. Evans, *F. Safety J.,* 9, p. 147 (1985).

34. L.Y. Cooper, "A Buoyant Source in the Lower of Two Homogeneous, Stably Stratified Layers," *20th International Symposium on Combustion,* Combustion Institute, Pittsburgh, PA (1984).
35. E.E. Zukoski and T. Kubota, "An Experimental Investigation of the Heat Transfer from a Buoyant Gas Plume to a Horizontal Ceiling—Part 2: Effects of Ceiling Layer," *NBS-GCR-77-98,* National Bureau of Standards, Washington, DC (1977).
36. W.D. Davis, "The Zone Fire Model Jet: A Model for the Prediction of Detector Activation and Gas Temperature in the Presence of a Smoke Layer," *NISTIR 6324,* National Institute of Standards and Technology, Gaithersburg, MD (1999).
37. L.Y. Cooper, "Estimating the Environment and the Response of Sprinkler Links in Compartment Fires with Draft Curtains and Fusible Link-Actuated Ceiling Vents—Theory," *F. Safety J.,* 16, pp. 137–163 (1990).
38. E.E. Zukoski, T. Kubota, and C.S. Lim, "Experimental Study of Environment and Heat Transfer in a Room Fire," *NBS-GCR-85-493,* National Bureau of Standards, Washington, DC (1985).
39. H.W. Emmons, "The Ceiling Jet in Fires," *Fire Safety Science, Proceedings of the Third International Symposium* (G. Cox and B. Langford, eds.), Elsevier Applied Science, New York, p. 249 (1991).
40. W.R. Chan, E.E. Zukowski, and T. Kubota, "Experimental and Numerical Studies on Two-Dimensional Gravity Currents in a Horizontal Channel," *NIST-GCR-93-630,* National Institute of Standards and Technology, Gaithersburg, MD (1993).
41. G. Heskestad, "Propagation of Fire Smoke in a Corridor," *Proceedings of the 1987 ASME/JSME Thermal Engineering Conference,* Vol. 1, American Society of Mechanical Engineers, New York (1987).

CHAPTER 3

Vent Flows

Howard W. Emmons

Introduction

Fire releases a great amount of heat which causes the heated gas to expand. The expansion produced by a fire in a room drives some of the gas out of the room. Any opening through which gas can flow out of the fire room is called a *vent.*

The most obvious vents in a fire room are open doors and open or broken windows. Ventilation ducts also provide important routes for gas release. A room in an average building may have all of its doors and windows closed and if ventilation ducts are also closed, the gas will leak around normal closed doors and windows and through any holes made for pipes or wires. These holes will act as vents. (If a room were hermetically sealed, a relatively small fire would raise the pressure in the room and burst the window, door, or walls.)

Gas will move only if it is pushed. The only forces acting on the gas are the gas pressure and gravity. Since gravity acts vertically, it might seem that gas could only flow through a hole in the floor or ceiling. Gravity, however, can produce horizontal pressure changes, which will be explained in detail below. A gas flow that is caused directly or indirectly by gravity is called a *buoyant flow.*

When a pressure difference exists across a vent, fluid (liquid or gas) will be pushed through. Precise calculation of such flows from the basic laws of nature can only be performed today by the largest computers. For fire purposes, and all engineering purposes, calculations are carried out with sufficient precision using the methods of hydraulics. Since these formulas are only approximate, they are made sufficiently accurate (often to within a few percent) by a flow coefficient. These coefficients are determined by experimental measurements.

Dr. Howard W. Emmons was professor emeritus of mechanical engineering at Harvard University. His research has focused on heat transfer, supersonic aerodynamics, numerical computation, gas turbine compressors, combustion, and fire. Dr. Emmons died in 1998.

Calculation Methods for Nonbuoyant Flows

If a pressure drop, $\Delta p = p_1 - p_2$, exists across a vent of area, A, with a fluid density, ρ, the flow through the vent has (see Figure 2-3.1)[1]

Velocity $$V = \sqrt{\frac{2\Delta p}{\rho}} \quad (1)$$

Volume flow $$Q = CA\sqrt{\frac{2\Delta p}{\rho}} \quad (2)$$

and

Mass flow $$\dot{m} = CA\sqrt{2\rho\Delta p} \quad (3)$$

In these formulas the SI units are Δp = (Pa) = (N/m^2), A = (m^2), ρ = (kg/m^3), V = (m/s), Q = (m^3/s), $\dot{m}$ = (kg/s).

If the flow of water from a fire hose or sprinkler (Figure 2-3.2) is to be calculated and the pressure, p_g, is read on a gauge (in lb/in^2) at the entrance to the nozzle where

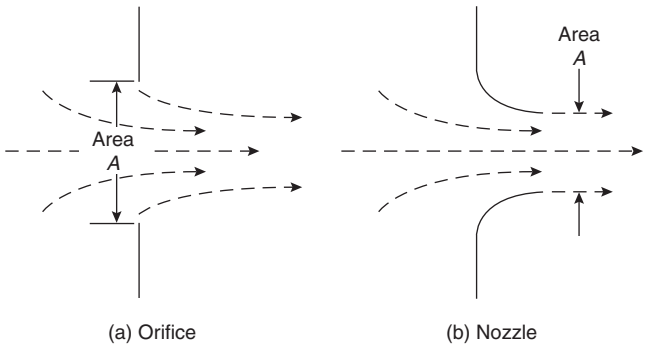

Figure 2-3.1. ***Most fire vents are orifices.***

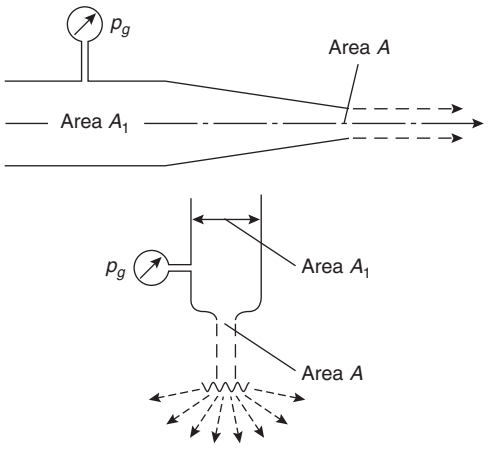

Figure 2-3.2. ***A hose nozzle and a sprinkler nozzle.***

the area is A_1, the previous formulas provide the velocity, volume flow, and mass flow by using

$$\Delta p = \frac{6895 p_g}{1 - (A/A_1)^2} \tag{4}$$

where A = area of vent and A_1 = area of supply pipe.

The factor 6895 converts pressure in lb/in^2 to Pascals while the factor $[1 - (A/A_1)^2]$ corrects Δp for the dynamic effect of the inlet velocity in the supply hose or pipe.

In the atmosphere, the pressure at the ground is p_a, which is just sufficient to support the weight of the air above. If the air density is ρ_a, the pressure, p, at height, h, is less than p_a by the weight of the air at height, h. Thus the pressure difference is

$$\Delta p = p_a - p = \rho_a g h \tag{5}$$

It is sometimes convenient when considering fire gases to use $h = \Delta p/\rho_a g$, the pressure head, in meters of ambient air, in the velocity and flow rate formulas given above.

The previous discussion supposes that the flowing fluid is of constant density. For liquids this is true for all practical situations. The density of air or fire gases will not change significantly during the flow through the vent so long as the pressure change is small, so they can also be treated as constant density fluids.

If the pressure drop is large, the equations become more complicated.[2] If the pressure and density upstream of the vent are p_1, ρ_1 while the pressure after the vent is p_2, the equations for velocity and mass flow become

$$V = \sqrt{\frac{2p_1}{\rho_1}} \left\{ \frac{\gamma}{\gamma - 1} \left(\frac{p_2}{p_1} \right)^{2/\gamma} \left[1 - \left(\frac{p_2}{p_1} \right)^{(\gamma-1)/\gamma} \right] \right\}^{1/2} \tag{6}$$

$$\dot{m} = CA\sqrt{2\rho_1 p_1} \left\{ \frac{\gamma}{\gamma - 1} \left(\frac{p_2}{p_1} \right)^{2/\gamma} \left[1 - \left(\frac{p_2}{p_1} \right)^{(\gamma-1)/\gamma} \right] \right\}^{1/2} \tag{7}$$

where $\gamma = c_p/c_v$.

The value of γ depends upon the complexity of the molecules of the flowing gas. For fire gases (which always contain a large amount of air) the value of γ will fall between 1.33 and 1.40. For most fire purposes the diatomic gas value (air) of 1.40 is sufficiently accurate.

The mass flow given by the previous equation has a maximum at

$$\frac{p_2}{p_1} = \left(\frac{2}{\gamma + 1} \right)^{\gamma/(\gamma-1)} \tag{8}$$

For $\gamma = 1.40$, the maximum flow is reached for a downstream pressure $p_2 = 0.528 p_1$. For all lower back pressures the flow remains constant at its maximum

$$\dot{m} = CA\sqrt{\rho_1 p_1} \left[\gamma \left(\frac{2}{\gamma + 1} \right)^{(\gamma+1)(\gamma-1)} \right]^{1/2} \tag{9}$$

With these equations, the mathematical description of the rate of flow of liquids and gases through holes is complete as soon as the appropriate flow coefficients are known. The coefficients, found by experiment, correct the formulas for the effect of the fluid viscosity, the nonuniformity of the velocity over the vent, turbulence and heat transfer effects, the details of nozzle shape, the location of the pressure measurement points, and so forth. The corrections also depend upon the properties and velocity of the fluid. The most important coefficient corrections for any given vent geometry is the dimensionless combination of variables which is called the Reynolds number, Re, and

$$\mathrm{Re} = \frac{VD\rho}{\mu} \tag{10}$$

where

V = velocity of the fluid given by the previous equations

D = diameter of the nozzle or orifice

ρ = density of the fluid approaching the vent

μ = viscosity of the fluid approaching the vent

A door or window vent is almost always rectangular, not circular. The D to be used in the Reynolds number should be the hydraulic diameter

$$D = \frac{4A}{P} \tag{11}$$

where

A = area of the vent

P = perimeter of vent

For a rectangular vent, a wide and b high, $A = ab$, $P = 2(a + b)$.

$$D = \frac{2ab}{(a + b)} \tag{12}$$

The experimental values of the flow coefficients for nozzles and orifices are given in Figure 2-3.3.[2] Flow coefficients for nozzles are near unity while for orifices are approximately 0.6; the reason for this can be seen from

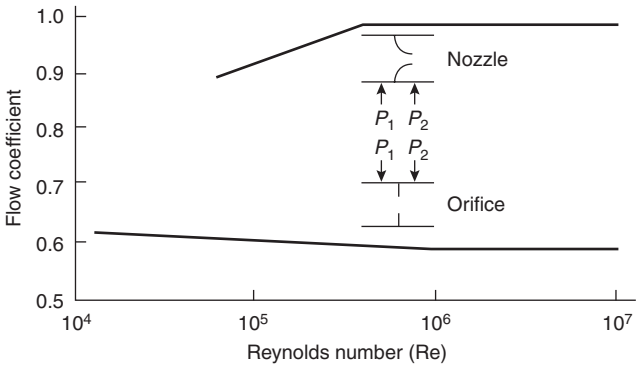

Figure 2-3.3. ***Orifice and nozzle flow coefficients.***

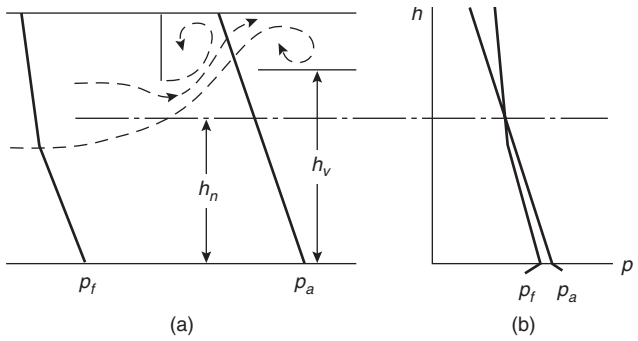

Figure 2-3.4. ***Pressure gradients: (a) each side of a door; (b) superimposed on a pressure versus height graph.***

Figure 2-3.1, wherein the flow from an orifice separates from the edge of the orifice and decreases to a much smaller area, in fact about 0.6 of the orifice area.

For most fire applications the Reynolds number will be about 10^6. Sprinklers and fire nozzles are small but the velocity is quite high. Conversely, ventilation systems of buildings are larger but have a lower velocity. Finally, doors and windows in the areas of a building not too near the fire are still larger but the velocity is still smaller. For most purposes the flow coefficient can be set as $C = 0.98$ for a nozzle and $C = 0.60$ for an orifice.

Buoyant Flows through Vertical Vents

A fire in a room causes gases to flow out through a vent by two processes. The heating of the air in a room causes the air to expand, pushing other air out through all available vents and hence throughout the entire building. At the same time, the heated air, with products of combustion and smoke, rises in a plume to the ceiling. When the hot layer of gas at the ceiling becomes deep enough to fall below the top of a vent, some hot gas will flow out through the vent. As the fire grows, the buoyant flow out will exceed the gas expansion by the fire. Thus the pressure in the fire room at the floor will fall below atmospheric, and outside air will flow in at the bottom. A familiar sight develops, where smoke and perhaps flames issue out the top of a window while fresh air flows in near the bottom. This buoyant flow mechanism allows a fire to draw in new oxygen so essential for its continuation.

For these buoyantly driven flows to occur, there must be a pressure difference across the vent. Figure 2-3.4 illustrates how these pressure differences are produced. The pressure difference at the floor is

$$\Delta p_f = p_f - p_a \tag{13}$$

where

p_f = pressure at the floor inside the room in front of the vent

p_a = pressure at the floor level outside of the room just beyond the vent

The pressure at height y is less than the pressure at the floor and can be found by the following hydrostatic equations:

Inside
$$p_1 = p_f - \int_0^y \rho_1 g \, dy \tag{14}$$

Outside
$$p_2 = p_a - \int_0^y \rho_2 g \, dy \tag{15}$$

The pressure difference at height, h, is

$$\Delta p = p_1 - p_2 = \Delta p_f + \int_0^h (\rho_2 - \rho_1) g \, dy \tag{16}$$

Since the outside density, ρ_2, is greater than the inside density, ρ_1, the integral is positive so that Δp is often positive (outflow) at the top of the vent and negative (inflow) at the bottom. The flow properties at the elevation, h, are the same as previously given.

$$V = \sqrt{\frac{2\Delta p}{\rho}} \tag{17}$$

$$\frac{Q}{A} = C\sqrt{\frac{2\Delta p}{\rho}} \tag{18}$$

$$\frac{\dot{m}}{A} = C\sqrt{2\rho\Delta p} \tag{19}$$

Since they are not the same at different heights in the vent, the volume and mass flow are given as flow per unit area.

Measuring Vent Flows in a Fire Experiment

Sufficient measurements must be made to evaluate ρ and Δp to allow use of Equation 19. There are four different available methods which differ in simplicity, accuracy, and cost.

Method 1: The dynamic pressure distribution can be measured in the plane of the vent. This measurement re-

quires a sensitive pressure meter. The pressure difference is almost always less than the atmospheric pressure difference between the floor, p_f, and the ceiling, p_c. For a room 2.5 m in height the atmospheric pressure difference is

$$p_f - p_c = \rho_a g H = 1.176 \times 9.81 \times 2.5$$
$$= 28.84 \text{ Pascals} \quad (3.0 \text{ mm } H_2O)$$

This is only

$$\frac{p_f - p_c}{p_a} = \frac{28.84}{101{,}325}$$
$$= 0.00028 \quad \text{fraction of atmospheric pressure}$$

Thus the buoyantly driven flow velocities induced by a room fire could be as high as

$$V = \sqrt{\frac{2\Delta p}{\rho}} = \sqrt{\frac{2 \times 28.84}{1.176}} = 7.00 \text{ m/s} \quad (23 \text{ ft/s})$$

Since the pressure varies with height and time, a series of pressure probes are required and each should have its own meter or a rapid activation switch. Although standard pitot tubes are the most accurate dynamic pressure probes, they are sensitive to flow direction and would have to be adjusted at each location for the direction of the local flow, especially for outflow and inflow. The probe orientation would need to be continually changed as the fire progressed.

A single string of fixed orientation pressure probes arranged vertically down the center of the door increases convenience of the measurement but forces a decrease in accuracy. The out-in flow problem is avoided by use of bidirectional probes in place of pitot tubes.[3] (See Figure 2-3.5.) These probes give velocities within 10 percent over an angular range of ±50 degrees of the probe axis in any direction.

Determination of the local velocity also requires the measurement of the local gas density. The density of fire gases can be determined from measured gas temperatures with sufficient accuracy by the ideal gas law

$$\rho = \frac{Mp}{RT} \tag{20}$$

where

M = avg. molecular weight of flowing gas

$R = 8314 \dfrac{\text{J}}{\text{kg mol K}}$ = universal gas constant

As noted previously, the pressure changes only by a very small percentage throughout a building so its effect on gas density is negligible.

Fire gases contain large quantities of nitrogen from the air and a variety of other compounds. The average molecular weight of the mixture will be close to but somewhat larger than that of air. Incomplete knowledge of the actual composition of fire gas prevents high accuracy calculations. For most fire calculations, it is accurate enough

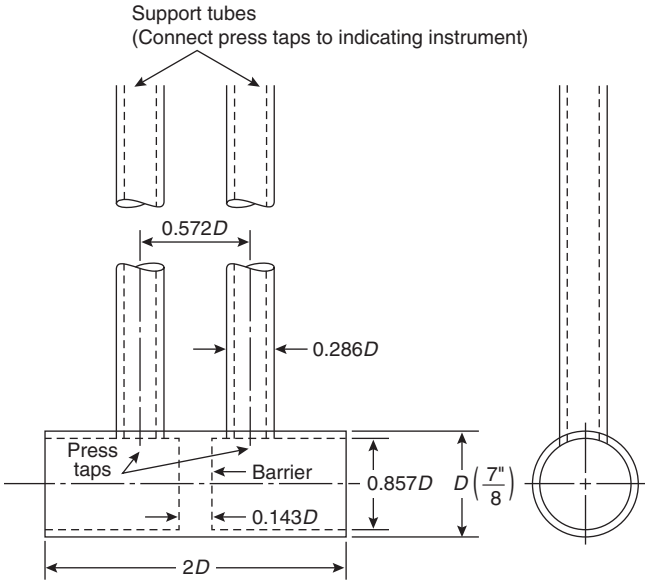

Figure 2-3.5. ***A bidirectional flow probe.***

to neglect the effect of the change of molecular weight from that of air ($M_a = 28.95$). Density of gas is determined primarily by its temperature (which may vary by a factor of 4 in a fire). Thus

$$\rho = \frac{352.8}{T} \frac{\text{kg}}{\text{m}^3} \tag{21}$$

where T = temperature in Kelvin (= °C + 273)

A string of thermocouples must be included along with the bidirectional probes to measure vent flows. For higher accuracy, aspirated thermocouples must be used or a correction made for the effect of fire radiation.[3] The temperature, and hence the gas density, will vary over the entire hot vent outflow. To determine the temperature distribution so completely would require an impracticably large number of thermocouples. Fortunately the temperature in the vent is a reflection of the temperature distribution in the hot layer inside the room, which normally is stratified, and hence varies most strongly with the distance from the ceiling. Thus a string of thermocouples hanging vertically on the centerline of the vent is usually considered to be the best that can be done in a practical fire test. Special care must be exercised to keep the test fire some distance away from the entrance to the vent. Since a fire near a vent has effects at present unknown, fire model calculations of real fire vent flows under such conditions will be of unknown accuracy. The velocity distribution vertically in the vent is given by

$$V = 0.93\sqrt{\frac{2\Delta p}{\rho}} \tag{22}$$

where ρ follows from Equation 21 using the temperature distribution *in the vent* with a calibration factor of 0.93 for

the bidirectional probes.[4] Using ρ from Equation 21 gives the directly useful forms

$$\begin{aligned} V &= 0.070\sqrt{T\Delta p} \qquad \Delta p\left(\frac{\text{N}}{\text{m}^2}\right) \\ V &= 5.81\sqrt{T\Delta p} \qquad \Delta p\left(\frac{\text{lb}}{\text{in}^2}\right) \end{aligned} \quad \text{pressure measured with bidirectional probe} \tag{23}$$

where

V is in (m/s) $\qquad \left[V\left(\frac{\text{ft}}{\text{s}}\right) = 3.281 V\left(\frac{\text{m}}{\text{s}}\right) \right]$

T is in (K)

Except for very early stages of a room fire, there will be flow out at the top ($V, \Delta p > 0$) and flow in at the bottom ($V, \Delta p < 0$).* Thus there is a position in the vent at which $V = 0$; this is the vertical location where the pressure inside is equal to that outside. This elevation, h_n, is called the neutral axis. Defining the elevation of the vent sill as h_b ($h_b = 0$ for a door) and the elevation of the soffit as h_t, the flows are given by

$$\text{Flow out} \qquad \dot{m}_u = C\int_{h_n}^{h_t} \rho V b \, dy \tag{24}$$

$$\text{Flow in} \qquad \dot{m}_d = C\int_{h_b}^{h_n} \rho V b \, dy \tag{25}$$

where

b = width of the vent

C = experimentally determined flow coefficient (= 0.68)[7]

These equations in the most convenient form are

$$\text{Flow out} \qquad \dot{m}_u = 16.79\int_{h_n}^{h_t} b\sqrt{\frac{\Delta p}{T_V}}\, dy \quad \text{(kg/s)} \tag{26}$$

$$\text{Flow in} \qquad \dot{m}_d = 16.79\int_{h_b}^{h_n} b\sqrt{\frac{\Delta p}{T_V}}\, dy \quad \text{(kg/s)} \tag{27}$$

where

Δp = pressure drop in Pascals measured with bidirectional probe as a function of y

b = width of the vent in m

T_V = vertical distribution of temperature (K) in the vent

If the bidirectional probe pressures are measured in psi, the coefficient 16.79 must be replaced by 1394.

Method 2: A somewhat simpler but less accurate procedure to measure vent flows requires the measurement of the pressure difference at the floor (or some other height). One pressure difference measurement together with the vertical temperature distribution measurement, T_1, *inside the room* (about one vent width in from the vent) and T_2, *outside the vent* (well away from the vent flow) provides the density information required to find the pressure drop at all elevations (Equation 16).

$$\Delta p = \Delta p_f + 3461\int_0^y \left(\frac{1}{T_2} - \frac{1}{T_1}\right) dy \tag{28}$$

For most fires, Δp_f will be negative; that is, the pressure at the floor inside the fire room will be less than the pressure outside. This is only true for a fire room with a normal size vent (door, window). For a completely closed room the inside pressure is well above the outside pressure. Since the temperature inside the fire room is higher than that outside, Equation 28 gives a Δp which becomes less negative, passes through zero at the neutral axis, h_n, and becomes positive at higher levels in the fire room. The vertical location of the neutral axis is therefore readily found from Equation 28.

The calculation of the pressure distribution requires measurement of the temperature distribution both inside, T_1, and outside, T_2, of the vent. However, calculation of the flow requires a knowledge of the density distribution in the vent itself. Thus a third thermocouple string is required to measure the temperature distribution, T_V, in the vent. The desired flow properties[6] are

Velocity

$$V = \sqrt{\frac{2\Delta p}{\rho}} = 4.43\sqrt{T_V\int_{h_n}^{y}\left(\frac{1}{T_2} - \frac{1}{T_1}\right) dy} \quad \text{(m/s)} \tag{29}$$

Flow out

$$\begin{aligned} \dot{m}_u &= C\int_{h_n}^{h_t} \rho b V \, dy \\ &= 1063\int_{h_n}^{h_t} b\left[\frac{1}{T_V}\int_{h_n}^{y}\left(\frac{1}{T_2} - \frac{1}{T_1}\right) dy\right]^{1/2} dy \end{aligned} \tag{30}$$

Flow in

$$\begin{aligned} \dot{m}_d &= C\int_{h_b}^{h_n} \rho b V \, dy \\ &= 1063\int_{h_b}^{h_n} b\left[\frac{1}{T_V}\int_{h_b}^{y}\left(\frac{1}{T_2} - \frac{1}{T_1}\right) dy\right]^{1/2} dy \end{aligned} \tag{31}$$

where

b = width of the vent at height y

Δp = calculated from Equation 16 using the temperatures (and thus densities) *inside and outside of the room*

ρ = density computed from the temperature *in the vent*

(Note that for inflow Δp is negative. Therefore the equation takes the square root of the magnitude $|\Delta p|$ while its sign gives the flow direction.)

*Equation 23 should be written $V = (\text{sign}\ \Delta p)K\sqrt{T|\Delta p|}$ since when $\Delta p < 0$ the absolute value must be used to avoid the square root of a negative number and the sign of the velocity changes since the flow is in and not out.

Method 3: The use of a sensitive pressure meter can be avoided entirely by visually (or better, photographically) locating the bottom of the outflow *in the vent* during the test. This is at the position of the neutral axis, h_n, where $\Delta p = 0$. Method 3 is the same as Method 2 except that the neutral axis location is found directly by experiment, rather than being deduced from the pressures. The distribution of pressure drop across the vent is found by integrating Equation 16 above ($\Delta p > 0$) and below ($\Delta p < 0$) h_n using the density distribution *inside,* ρ_1, and *outside,* ρ_2, *the room.* The flow properties are computed as before from Equations 29 through 31.

Method 4: A simpler but less accurate method uses the fair assumption that the gas in the fire room soon separates into a nearly uniform hot layer of density, ρ, with a nearly uniform cold layer below density, ρ_d. This separation with appropriate notation is shown in Figure 2-3.6. In this approximation the appropriate flow formulas[7] are

$$\text{Outflow} \qquad V_u = \left(2g\frac{\rho_a - \rho}{\rho}y\right)^{1/2} \tag{32}$$

where y is distance above the neutral plane

$$\dot{m}_u = \frac{\sqrt{8}}{3}Cb\sqrt{g\rho(\rho_a - \rho)}(h_v - h_n)^{3/2} \tag{33}$$

The inflow by this two-layer method depends upon d, which is small and cannot be determined with sufficient accuracy because of the effect of gas motions in the fire room.

The neutral axis may be found in several ways:

1. It may be located visually or photographically during the test.
2. It may be found from the vent temperature distribution by locating [visually on a plot of $T_V(y)$] the position just below the most rapid temperature rise from bottom to top of the vent.

The low temperature, T_d, of the two-layer model is taken as the gas temperature just above the vent sill. The high temperature, T_u, is chosen so that the two-layer model has the same total mass (i.e., the same mean density) in the vent as the real flow.*

$$\left(\frac{1}{T}\right) = \frac{1}{h_v}\int_0^{h_v}\frac{dy}{T} = \frac{h_n}{h_v T_d} + \frac{h_v - h_n}{h_v T_u} \tag{34}$$

The densities ρ_a and ρ are found using Equation 21 from the temperatures T_a and T_u, respectively.

The outflow velocity and mass flow are found from Equations 32 and 33.

An estimate of the air inflow rate can be found if the test has included the measurement of the oxygen concentration in the gases leaving the fire room. The gas outflow rate is equal to the inflow rate plus the fuel vaporized, except for the effect of transient variations in the hot layer depth. Thus

$$\dot{m}_d = \dot{m}_u\left(\frac{1 + y_{O_2}\lambda}{1 + 0.23\lambda}\right) \tag{35}$$

where λ = effective fuel-air ratio.

The flow coefficient to be used for buoyant flows is 0.68 as determined by specific experiments designed for the purpose. For nonbuoyant flows (nozzles and orifices), the flow coefficients are determined to better than 1 percent and presented as a function of the Reynolds number as in Figure 2-3.3. This accuracy is possible because the fluid can be collected and measured (by weight or volume).

For buoyant flows the experiments are much more difficult because the hot outflow and cold inflow cannot be collected and weighed. The best fire-gas vent flow coefficient measurements to date[5,6] have ±10 percent accuracy with occasional values as bad as ±100 percent (for inflow). The most accurate buoyant flow coefficients were measured not for fire gases but for two nonmiscible liquids (kerosene and water).[7] In this case the two fluids could be separated and measured, and the value 0.68 was found except for the very low flow rates (near the beginning of a fire). When buoyant flow coefficients can be measured within a few percent accuracy, they will be a function of the Reynolds number, $\text{Re} = Vh_v\rho/\mu$; the Froude number, $\text{Fr} = V^2\rho_a/gh_v(\rho - \rho_a)$; and the depth parameter, h_n/h_v.

The best option now available is to use $C = 0.68$ and expect ±10 percent errors in flow calculations.

Note that all of the above four methods require a knowledge of h_n, the dividing line between outflow above and inflow below. It would be useful to have a simple formula by which h_n could be calculated without any special measurements. What determines h_n?

The fire at the start sends a plume of heated gas toward the ceiling and, by gas expansion, pushes some gas out of the vent. The hot plume gases accumulate at the ceiling with little, if any, flowing out the vent. After a

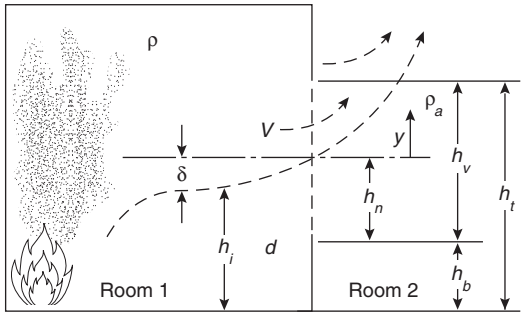

Figure 2-3.6. ***Buoyant flow out of the window of a fire room.***

*Sometimes the mean temperatures, $\overline{T}$, of the two-layer model and the real flow are also used and both h_n and T_u are determined (using T_d as above). The requirement of identical $\overline{T}$ is arbitrary, sometimes leads to impractical results, and is not recommended.

time, dependent on the size of the room, the hot layer depth becomes so large that its lower surface falls below the top of the vent. Hot gas begins to flow out.

When a fire has progressed to a second room, there is a hot layer on each side of a connecting vent. Thus, (with two layers on each side) there are as many as four different gas densities: $\rho_{d_1} > \rho_1$, densities below and above in room 1, and $\rho_{d_2} > \rho_2$, densities below and above in room 2. There are also four pertinent levels: h_b, sill height (0 if the vent is a door); h_t, soffit height; h_{i_1}, interface height in room 1; h_{i_2}, interface height in room 2. There are many different flow situations possible depending upon these eight values.

The pressure variation from floor to ceiling in each room depends upon the densities and layer heights in that room. In addition, the pressure difference between the two rooms (at the floor, for example) may have any value depending upon the fire in each room, all the room vents, and especially the vent (or vents) connecting the two rooms. Figure 2-3.7 shows a few of the possible pressure distributions. The pressure distribution in room 1 is shown with a dotted line while that in room 2 is shown as a solid line.

In Figure 2-3.7(a), there are no hot layers, the pressure in room 1 at every level is higher than that in room 2, and the flow is everywhere out (positive) (room 1 to room 2).

In Figure 2-3.7(b), a common situation exists. The density in room 2 is uniform (perhaps the outside atmosphere). Room 1 has a hot layer and a floor pressure difference such that there is outflow at the top, inflow at the bottom, and a single neutral axis somewhat above the hot-cold interface in the room.

In Figure 2-3.7(c), the flow situation is similar to that in Figure 2-3.7(b), although there are hot layers in both rooms (but with a neutral axis above the interface in room 1 and below the interface in room 2).

In Figure 2-3.7(d), the densities (slopes of pressure distribution lines) are somewhat different than those in Figure 2-3.7(c) (the hot layer in room 2 is less deep but hotter than that in room 1). Consequently there are two neutral axes with a new small inflow layer at the top, three flow layers in all—two in and one out.

In Figure 2-3.7(e), the densities and floor level pressure difference are such that there are four flow layers, two out and two in, with three neutral axes.

These five cases do not exhaust the possible vent flow situations.

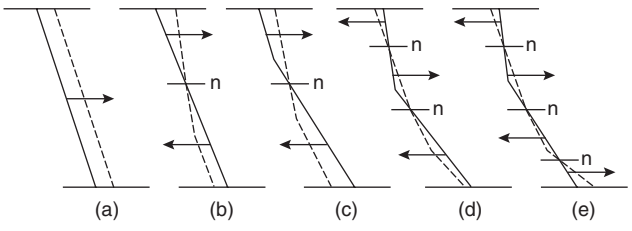

Figure 2-3.7. ***Some selected two-layer vent pressure drop distributions. Dotted line is pressure distribution in room 1; solid line is pressure distribution in room 2.***

Figure 2-3.7(a, b) account for all cases early in a fire and all cases of vents from inside to outside of a building. They are also the only cases for which experimental data is available. The case illustrated in Figure 2-3.7(c) is common inside a building after a fire has progressed to the point that hot layers exist in the two rooms on each side of a vent. The cases illustrated in Figures 2-3.7(d, e) have not been directly observed but probably account for an occasional confused flow pattern. (In fact, the above discussion assumes two distinct layers in each room.) The layers are seldom sharply defined and in this case there may be many neutral axes, or regions, with a confusing array of in-out flow layers. These confused flow situations are probably not of much importance in a fire since they seldom occur and when they do they don't last very long.

The previous discussion of the possible two-layer flow situation is very important for the zone modeling of a fire. Fire models to date are all two-layer models (a three- or more layer model will present far more complex vent flows than those pictured in Figure 2-3.7). In fire computation by a zone model, such as cases (d) and (e) in Figure 2-3.7 will be unimportant to fire development. However, since these situations can arise, they should be handled via fire computation; that is, by computing the flow layer by layer. Each layer has a linear pressure variation from sill, interface, or neutral axis up to the next interface, neutral axis, or soffit.

By use of the pressure drop at the floor and the room densities on each side of the vent in Equation 16, the position, h_i, of all layers and the sill, interfaces, neutral axes, and soffit will be known. Thus, for each layer (defined as j) the pressure drop at the bottom, Δp_j, and at the top, Δp_{j+1}, will be known. Since the room densities are constant in each room for each layer, the vent pressure drop will vary linearly from Δp_j to Δp_{j+1}. The flow in each layer from room 1 to room 2, found by integration,[8] is given by

$$\dot{m}_i = (\text{sign } \alpha) C \frac{\sqrt{8}}{3} b (h_{j+1} - h_j) \sqrt{\rho} \times \left(\frac{|\Delta p_j| + \sqrt{|\Delta p_j \Delta p_{j+1}|} + |\Delta p_{j+1}|}{\sqrt{|\Delta p_j|} + \sqrt{|\Delta p_{j+1}|}} \right) \qquad (36)$$

where

$\alpha = \left(\frac{\Delta p_j + \Delta p_{j+1}}{2} \right)$ whose sign determines the in-out direction of the flow

ρ = density of the gas flowing in the flow layer i

Thus

$$\rho = \begin{cases} \text{density in room 1 at height } h_j^+ & \text{if } \alpha > 0 \\ \text{density in room 2 at height } h_j^+ & \text{if } \alpha < 0 \end{cases}$$

This flow calculation appears complex but can be coded quite easily for computer use and then used to calculate all the possible cases.

Although all vent flows can now be calculated, the path of each layer of gas flow when it enters a room is still needed for fire modeling. If the two-layer model is to be

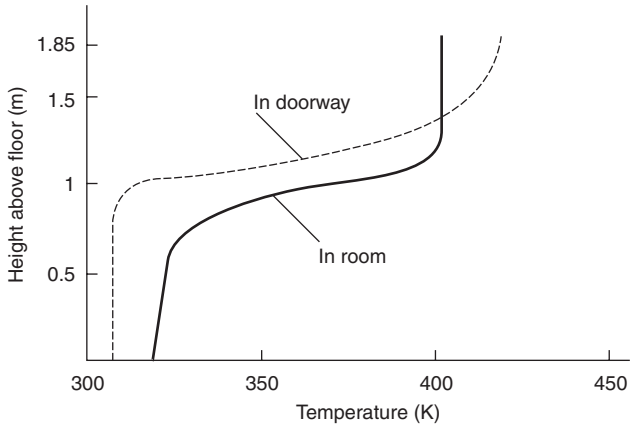

Figure 2-3.8. ***Sample fire room and doorway temperature distributions.***

preserved, each inflow must mix with the hot layer or the cold layer, or be divided between them. No information is yet available as to the best solution of this problem.

To illustrate these various methods of flow calculation, some test data from a steady burner fire in a room at the U.S. Bureau of Standards[6] is used. Some typical data are shown in Figure 2-3.8. Accurate results, even in a steady-state fire, are difficult to obtain and questions about the data in this figure will be noted as appropriate. The vent temperatures were measured by small diameter bare thermocouples for which there is some unknown radiation correction. This unknown correction may account for the top vent temperature being higher than that in the fire room.

The vent was 1.83 m high, 0.737 m wide and the outflow measured with bidirectional probes (not corrected for flow angle) was 0.588 kg/sec for a fire output of 0.63 kW. The ambient temperature was 21.3°C (= 294.3 K). This flow was determined by using Method 1.

Method 2 uses the known location of the neutral axis and requires the integration of Equations 30 and 31. In this way the data of Figure 2-3.8 gives outflow of 0.599 kg/s, 1.8 percent higher compared to Method 1 and inflow of 0.652 kg/s. A measured (by bidirectional probes) inflow is not given, but it seems odd that the inflow is greater than the outflow since inflow must be smaller than the outflow by the mass rate of fuel burned at steady state.

Data for use of Method 3 are not available.

Method 4 requires the selection from Figure 2-3.8, of a neutral axis location and inlet temperature. In the figure the rapid temperature rise *in the vent* begins at about 1 m. Hence this height is chosen as the neutral axis. The lowest inlet temperature is T_d = 308 K. By computing $(1/T_V)$ the average value was found to be $(1/T_V) = 2.875 \times 10^{-3}$. Now by Equation 34

$$2.875 \times 10^{-3} = \frac{1.00 - 0}{1.83 \times 308} + \frac{1.83 - 1.00}{1.83 T_u}$$

Thus T_u = 411.9 K. The corresponding density is ρ = 352.8/411.9 = 0.8565 kg/m^3. From the ambient temperature, T_a, we find ρ_a = 352.8/294.3 = 1.199 kg/m^3. Thus the outflow by Equation 33 is

$$\dot{m}_u = \frac{\sqrt{8}}{3} 0.68 \times 0.737 [9.81 \times 0.8565 (1.199 - 0.8565)]^{1/2} \times (1.83 - 1)^{3/2} = 0.607 \text{ kg/s}$$

This value is 3.2 percent higher compared to Method 1.

Buoyant Flows through Horizontal Vents

Unlike nonbuoyant flows through orifices or flow through vents in a vertical wall, very little quantitative work has been done on flow through vents in horizontal (floors or flat roofs) or slightly sloped (inclined roofs) surfaces. The following discussion is included to clarify the present status of our knowledge and to provide flow calculation formulas of unknown accuracy in lieu of nothing.

Consider the flow through a hole in a horizontal surface. The velocity and flow rate are determined by the pressure drop from the upstream side of the vent to the *vena contracta.* Therefore, the buoyancy of the fluid from the vent to the *vena contracta* influences the flow. Thus, for upward flow of the lower fluid the velocity is given by

$$v_H = \left[\frac{2}{\rho_H} (gh\Delta\rho + \Delta p) \right]^{1/2} \tag{37}$$

where

$\Delta\rho = \rho_c - \rho_H$

$\Delta p = p_H - p_c$ measured at the vent's lower and upper surfaces

h = the vertical distance from the vent lower surface to the *vena contracta* (about equal to the orifice diameter D)

If the unidirectional flow were down, the velocity would be

$$v_c = -\left[\frac{2}{\rho_c} (gh\Delta\rho - \Delta p) \right]^{1/2} \tag{38}$$

The magnitude of the buoyancy effect is 8.6 Pascals (for a fire density ratio of 4 to 1 and a 1-m diameter horizontal vent), and a buoyant velocity of 4 m/s (about 1/6 of the velocity) is produced by the fire room buoyancy. The plume above the *vena contracta* stirs the fluid on the upper surface but does not influence the flow.

As the flow nears zero, the interface between the lower (hot) and upper (cold) gases becomes flat and is unstable. The unidirectional flow is replaced by simultaneous up and down flows usually oscillating in time and location.

At present there are no measurements of effective values of *h.* There are only a couple of quantitative studies of horizontal vent flows in which the pressure drop-flow information has been adequately measured.[9,10] These are for very small holes (a diameter of 2 in. or less), and in many cases the holes were fitted with a short pipe. Ceiling or roof holes in fires are usually irregular in shape and have

a length to "diameter" ratio of 0.13 or less. There are a number of studies[11,12,13] of rooms with a ceiling hole with a fire either under the hole or on a wall. These supply interesting fire data but are not useful as horizontal vent studies, since the results do not include adequate orifice pressure and flow measurements. Epstein and Kenton[9] have measured the transfer of fluid from the lower to the upper chambers using water below and a brine above (density ratio 1.1 or less). They found that, at zero net volume flow (the lower chamber was closed except for a ceiling hole 2 in. in diameter or less), the fluid transfer to the upper chamber was

$$\frac{Q_H}{[D^5 g(\Delta\rho/\bar{\rho})]^{1/2}} = 0.055 \tag{39}$$

while the unidirectional volume flow, q, that just prevented reverse flow was

$$\frac{q}{[D^5 g(\Delta\rho/\bar{\rho})]^{1/2}} = 0.20 \tag{40}$$

The unidirectional volume flows that follow from the velocity Equations 37 and 38 are

$$\frac{Q_H}{[D^5 g(\Delta\rho/\rho_H)]^{1/2}} = \frac{\pi}{8} C_D \left(\frac{h}{D} + \frac{\Delta p}{\Delta\rho g D}\right)^{1/2} \tag{41}$$

$$\frac{Q_C}{[D^5 g(\Delta\rho/\rho_c)]^{1/2}} = \frac{\pi}{8} C_D \left(\frac{h}{D} - \frac{\Delta p}{\Delta\rho g D}\right)^{1/2} \tag{42}$$

If we assume that when $Q_H = q$, the flooding value, then $\Delta p/\Delta\rho g D$ has the value for which $Q_C = 0$. Then $\Delta p/\Delta\rho g D = h/D$, and by Equations 40 and 41

$$\frac{\Delta p}{\Delta\rho g D} = 0.045 \tag{43}$$

With this value as the limit of unidirectional flow, $-.045 < \Delta p/\Delta\rho g D < .045$ is the pressure range in which flows occur simultaneously in both directions. There is no current theory nor measurements to compute these low flows so each flow squared up and down are assumed to vary linearly in this range. The resultant flows are

$$\dot{m} = cD[2\rho_H(\Delta\rho g D + \Delta p)]^{1/2} \quad \text{for } \Delta p > .045\Delta\rho g D \tag{44}$$

$$\left.\begin{aligned} \dot{m}_u &= cD[23.22\rho_H(.045\Delta\rho g D + \Delta p)]^{1/2} \\ \dot{m}_D &= -cD[23.22\rho_c(.045\Delta\rho g D - \Delta p)]^{1/2} \end{aligned}\right\} \begin{array}{l}\text{simultaneous} \\ \text{up-down} \\ \text{flow for} \\ -.045\Delta\rho g D \\ < \Delta p < \\ .045\Delta\rho g D\end{array} \tag{45}$$

$$\dot{m} = -cD[2\rho c(\Delta\rho g D - \Delta p)]^{1/2} \quad \text{for } p < -.045\Delta\rho g D \tag{46}$$

Note: The use of the dimensionless form $\Delta p/\Delta\rho g D$ has been changed in Equations 44 thru 46 so that numerical computations when there is no density change ($\Delta\rho = 0$) does not encounter division by zero.

Equations 44 through 46 describe the positive upward flow through a horizontal vent over the entire pressure range from $-\infty$ inflow to $+\infty$ outflow. This theory is shown in Figure 2-3.9 for a density ratio of 2 with coordinates using the average density.

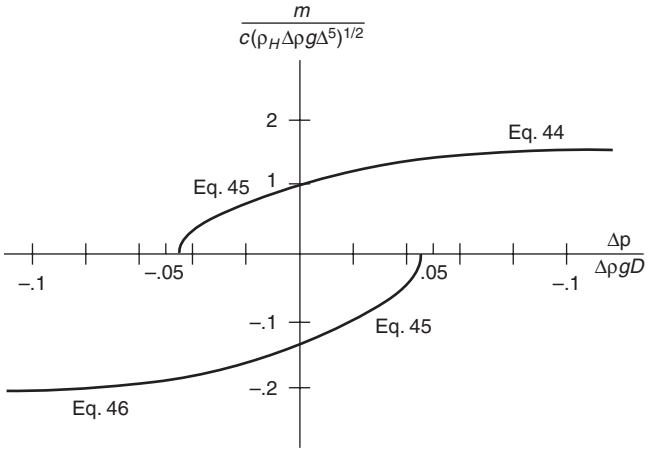

Figure 2-3.9. ***Theory of flow based on Equations 44 through 46.***

The theory of Cooper[14] omitted the buoyancy effect on the vertical flow and was developed before the Epstein flood data were available. However, in view of present horizontal vent data uncertainty, it is a useful alternative.

Accuracy of Vent Flow Calculations

For nonbuoyant flows (using nozzles or orifices in a straight run of pipe made and calibrated with a specific geometry over a known Reynolds number range) one easily obtains 2 percent accuracy. Thus, Equations 1 through 9 are capable of high accuracy.

For vents in vertical walls with limited internal room fire circulations, the best methods of measurement may get 5 percent accuracy. However, in real fires, induced circulations are often severe and unknown. Thus, errors of 10 percent or higher must be expected. Even if flow instrumentation is located in the vent itself, there is never enough to really account for variations over the vent surface and time fluctuations originating in the fire phenomena inside the fire room.

For vents in a horizontal surface, the accuracy is completely unknown. Equations 45 through 48 reproduce the water-brine experiments in small holes. The experimental accuracy is 10 percent. However, for a real fire, the errors are probably much higher. A typical case is a hole in the ceiling burned through by the flames from below. The hole geometry is very irregular and is completely unknown. Furthermore, a fire directly below the hole supplies hot gas with a considerable vertical velocity. Also, the ceiling jet flow often provides considerable cross flow.

Full-scale experimental results determining the effects of fire circulation, large density ratios, and large Reynolds numbers are needed. The present formulas are given as "better than nothing."

Vents as Part of the Building Flow Network

A building is an enclosed space generally with floors, walls that divide the space both vertically and horizontally into rooms, corridors, and stairwells. A fire that starts at any place in the building causes gas expansion, which raises the local pressure and pushes air throughout the building through all pathways leading to the outside. If a window is open in the room of fire origin, and there is little or no wind, little flow moves through the remainder of the building. If there is no open window, the flow will move toward cracks and leaks wherever they may be in the building. All these flows are initially nonbuoyant. The flow through the building is simply flow through a complex system of pipes and orifices. As the fire grows larger, hot gas flows buoyantly out of the place of origin, while cold gas flows in below. Thus, while the net flow (out-in) is just sufficient to accommodate the fire gas expansion, the actual volumetric hot gas outflow may be 2.5 times larger than the inflow. A layer of hot gas moves along the ceiling of connected spaces and at the first opportunity proceeds up a stairwell or other ceiling (roof) opening into regions above.[15] The accumulating hot gas will help spread the fire while the newly created hot fire gases build a new hot layer in the adjacent spaces. The flow and pressure drop across each vent will then progress through a succession of situations as previously discussed. The flow throughout the building is therefore determined by the vent and flow friction drops along *all* of the available flow paths from the fire to the outside of the building.

The vent flow calculation procedures described in this section are sufficiently accurate and general to compute the required flow-pressure drop relations for building flow networks (except slow buoyant flows through horizontal vents).

Nomenclature

A	area (m^2)
a	length (m)
b	width (m)
C	flow coefficient
D	orifice diameter (m)
Fr	Froude number
g	gravity constant (m/s^2)
h	height (m)
M	molecular weight (kg/kg mol)
$\dot{m}$	mass flow rate (kg/s)
P	perimeter (m)
p	pressure (Pa)
Q	volume flow rate (m^3/s)
R	gas constant (J/kg mol K)
Re	Reynolds number
T	temperature (K)
V	velocity (m/s)
y	vertical coordinate (m)
Δ	increment of
δ	depth (see Figure 2-3.6) (m)
$\gamma = c_p/c_v$	isentropic exponent
ρ	density (kg/m^3)
μ	viscosity ($N \cdot s/m^2$)

Subscripts

a	atmosphere
b	sill of vent
c	ceiling of room
d	lower
f	floor
g	gauge
i	hot-cold interface
j	index of layer
n	neutral axis
O_2	oxygen
t	soffit of vent
u	upper
v	in the vent
1	upstream of orifice
2	downstream of orifice

References Cited

1. H. Rouse, *Fluid Mechanics for Hydraulic Engineers,* McGraw-Hill, New York (1938).
2. *Mark's Mechanical Engineers Handbook,* McGraw-Hill, New York (1958).
3. J.S. Newman and P.A. Croce, *Serial No. 21011.4,* Factory Mutual Research Corp., Norwood, MA (1985).
4. D.J. McCaffrey and G. Heskestad, *Comb. and Flame,* 26, p. 125 (1976).
5. J. Quintiere and K. DenBraven, *NBSIR 78-1512,* National Bureau of Standards, Washington, DC (1978).
6. K.D. Steckler, H.R. Baum, and J. Quintiere, *20th Symposium on Combustion,* Pittsburgh, PA (1984).
7. J. Prahl and H.W. Emmons, *Comb. and Flame,* 25, p. 369 (1975).
8. H.E. Mitler and H.W. Emmons, *NBS-GCR-81-344,* National Bureau of Standards, Washington, DC (1981).
9. M. Epstein and M.A. Kenton, *Jour. of Heat Trans.,* 111, p. 980 (1989).
10. Q. Tan and Y. Jaluria, *NIST-G&R-92-607,* National Institute of Standards and Technology, Gaithersburg, MD (1992).
11. C.F. Than and B.J. Savilonis, *Fire Safety Jour.* 20, p. 151 (1993).
12. J.L. Bailey, F.W. Williams, and P.A. Tatum, *NRL Report 6811,* Naval Research Lab., Washington, DC (1991).
13. R. Jansson, B. Onnermark, and K. Halvarsson, *FAO Report C 20606-D6,* Nat. Defense Research Inst., Stockholm (1986).
14. L.Y. Cooper, *NISTIR 89-4052,* National Institute of Standards and Technology, Gaithersburg, MD (1989).
15. T. Tanaka, *Fire Sci. and Tech.,* 3, p. 105 (1983).

CHAPTER 4

Visibility and Human Behavior in Fire Smoke

Tadahisa Jin

Background

This chapter presents the scientific basis for establishing safety evacuation countermeasures, that is, evacuation plans, escape signs, and so forth in case of fire. The data were obtained in Japan, but should provide more general guidance internationally. In particular, issues of physical and physiological effects of fire smoke on evacuees are addressed. The chapter consists of three sections: (1) visibility, (2) characteristics of human behavior, and (3) development of an intensive system for escape guidance in fire smoke.

In Japan, since the 1960s, an increasing number of people have been killed by smoke in fire-resistant buildings. Toxic gases and/or depletion of oxygen in fire smoke are the final causes of death of those victims. However, many evacuees are trapped in an early stage of fire by relatively thin smoke, and loss of visibility is an indirect but fatal cause of death. For this reason, the relations between the visibility and optical density of fire smoke were examined experimentally, and practical equations were proposed.

For further understanding of human behavior in fire smoke, many investigations were conducted by interviewing evacuees and analyzing questionnaires. Also, experimental research was carried out with subjects under limited fire smoke conditions and the threshold of fire smoke density for safe evacuation was examined.

Through many field investigations of fires, it is found that an effective guidance sign system is required for safe evacuation in fire smoke. Development of conspicuous exit signs, using a flashing light source was one means of improving evacuation in smoke-filled conditions.

A new type of escape guidance in fire smoke by continuously traveling, flashing light sources was developed, and its effectiveness was examined in a smoke-filled corridor. These innovative technologies for safe evacuation are now in practical use in Japan. A form of this is already found in floor lighting of passenger aircraft cabins.

Tadahisa Jin was born in 1936 in Japan. He received his doctor of engineering degree from Kyoto University in 1975. He joined the Fire Research Institute in 1962 and has worked in the field of visibility and human behavior in fire smoke. In 1996, he joined the Fire Protection Equipment and Safety Center of Japan and is technical advisor for the improvement of new fire protection equipment.

Visibility in Fire Smoke

Introduction

There has been much research on visibility in fog in the past, whereas relatively little research has been carried out on visibility in fire smoke. This difference is due mainly to the physical characteristics of these composite particles. Fog is composed of water mist and the individual particles are spherical. The particle size is also relatively stable in time and space. These simple characteristics enable a visibility model in fog to be developed. On the other hand, the characteristics of fire smoke, that is composition, shape, and size of the particles, depend on the combustible materials involved and the conditions of combustion. These characteristics are also highly dependent on surrounding flow and temperature fields and vary with time.

Figure 2-4.1 shows the result of measuring the relationship between visibility and smoke density on the extinction coefficient obtained from experiments performed in Japan.[1] A large difference is shown in data though the correlation is roughly between both. There are two reasons for the decrease in visibility through smoke: (1) luminous fluxes from a sign and its background are interrupted by smoke particles and reduce its intensity when reaching the eyes of a subject, and (2) luminous flux scattered from the general lighting of corridors or rooms by smoke particles

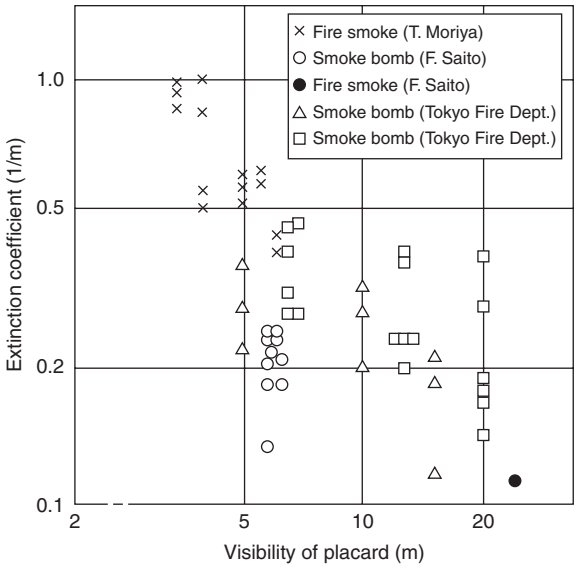

Figure 2-4.1. ***Relation between visibility of the placard-type signs and extinction coefficient by the experiments performed in Japan.***

in the direction of a subject's eyes is superimposed on the reduced flux mentioned in (1).

The human eye can distinguish a sign from the background in smoke only when the difference of intensity between the flux from the sign and that from the background is larger than some threshold value, that is, when the following equation can be established between the intensity of luminous flux from a sign (including scattered flux) B_e, the intensity of luminous flux (including scattered flux) from the background B_b, and the threshold value δ_c:

$$\left| \frac{B_e - B_b}{B_b} \right| \geq \delta_c$$

The value (the threshold contrast of signs) varies depending on the intensity of luminous flux from the background and the properties of smoke, but particularly when discussing the visibility in a meteorological fog, a constant value $\delta_c = 0.02$ is normally employed for both day and night.

Smoke Density and Visibility

Development of a mathematical visibility model based on physical parameters has attracted some researchers, but it is very complicated and tends to be of little practical use. A simple visibility model for signs seen through fire smoke is proposed by Jin as Equation 1:[2]

$$V \approx \frac{1}{C_s} \ln\left(\frac{B_{EO}}{\delta_c k L}\right) \quad (1)$$

where

V = visibility of signs at the obscuration threshold (m)

C_s = smoke density expressed by the extinction coefficient (1/m)
(hereafter, smoke density will be expressed by the extinction coefficient in 1/m)*

B_{EO} = brightness of signs (cd/m^2)

δ_c = contrast threshold of signs in smoke at the obscuration threshold (0.01 ~ 0.05)

$k = \sigma_s/C_s$ (0.4 ~ 1.0) and $C_s = \sigma_S + \sigma_{ab}$ (σ_S: scattering coefficient; σ_{ab}: absorption coefficient)

L = 1/π of mean illuminance of illuminating light from all directions in smoke (1 m/m^2)

For placard-type (reflecting) signs, Equation 1 can be modified to

$$V \approx \frac{1}{C_s} \ln\left(\frac{\alpha}{\delta_c k}\right) \quad (2)$$

where

α = reflectance of sign.

The signs in a smoke-filled chamber were observed from outside through a glass window. The results are shown in Figure 2-4.2. This shows the relation between the visibility of self-illuminated signs at the obscuration threshold and the density of smoldering smoke (white) or flaming smoke (black). In the range of the visibility of 5 to 15 m, the product of the visibility, V, at the obscuration threshold and the smoke density, C_s, is almost constant.

The visibility in black smoke is somewhat better than in white smoke of the same density; this remarkable difference in visibility is not recognized among smokes from various materials. For reflecting signs, the product of the visibility and smoke density is almost constant, too. The product depends mainly on the reflectance of the sign and the brightness of illuminating light. The visibility, V, at the obscuration threshold of signs is found to be

$$V = \frac{(5 \sim 10)}{C_s} \text{ (m)} \quad \text{for a light-emitting sign} \quad (3)$$

and

$$V = \frac{(2 \sim 4)}{C_s} \text{ (m)} \quad \text{for a reflecting sign} \quad (4)$$

The visibility of other objects such as walls, floor, doors, stairway, and so forth in an underground shopping mall or a long corridor varies depending on the interior and its contrast condition; however, the minimum value for reflecting signs may be applicable.

---

*Note that the extinction coefficient (C_s) can be obtained by the following equation:

$$C_s = \frac{1}{L} \ln\left(\frac{I_o}{I}\right)$$

where

I_o = the intensity of the incident light

I = the intensity of light through smoke

L = light path length (m)

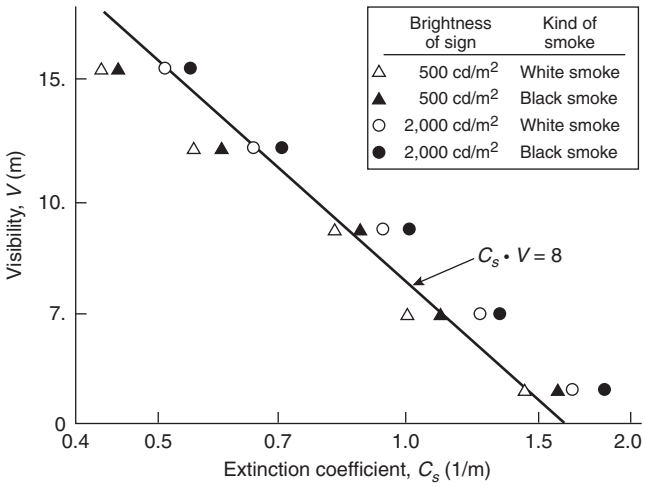

Figure 2-4.2. ***Relation between the visibility of self-illuminated signs at the obscurity threshold and smoke density (extinction coefficient).***

Visibility of Signs through Irritant Smoke and Walking Speed

A 20-m-long corridor was filled with smoke corresponding to an early stage of fire; a highly irritant white smoke was produced by burning wood cribs with narrow spacing between the sticks, and a less irritant black smoke was produced by burning kerosene. The subjects were instructed to walk into the corridor from one end, or to record the places where they saw a lighted FIRE EXIT sign (previous signs before 1982) at another end, or to read the words on the signs.[2,3]

For the obscuration threshold of the sign, the following relation can be found $C_S \cdot V \cong$ constant. However, for visibility at the legible threshold of words, this relation can only apply to nonirritant smoke, as shown in Figure 2-4.3.

The visibility in irritant smoke decreases sharply at a smoke density exceeding a certain level. In thick irritant smoke, the subjects could only keep their eyes open for a short time and tears ran so heavily that they could not see the words on the signs. However, in this case when the exit signs are very simple or sufficiently familiar to the occupants to be recognized at a glance, this irritant effect of smoke may not cause so much trouble in locating the exits.

The smoke irritation reduces the visibility for evacuees and consequently there will be a possibility of needless unrest or panic. The smoke hazards of concern are found not only in such psychological reactions, but also in evacuees' actions, especially walking speed.[4,5]

In this experiment, walking speed in the smoke was determined as shown in Figure 2-4.4. Both smoke density and irritation appear to effect the walking speed. This figure shows that the walking speed in nonirritant smoke decreases gradually as the smoke density increases. However, in the irritant smoke, the speed decreases very rapidly in the same range of smoke density levels. From this observation, the sharp drop in walking speed is explained by the subjects' movements: they could not keep their eyes open and they walked inevitably zigzag or step by step along the side wall.

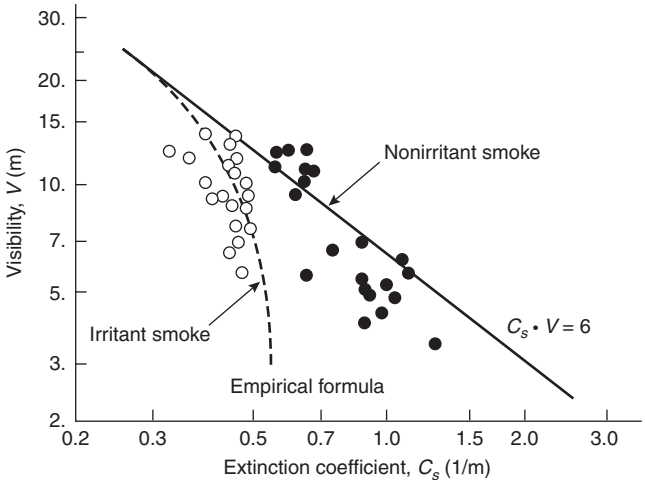

Figure 2-4.3. ***Visibility of the FIRE EXIT sign (signs of the type used before 1982) at the legible threshold of the words in irritant and nonirritant smoke.***

Decrease of Visual Acuity in Irritant Smoke

Further laboratory studies were conducted to determine the relationship between visual acuity and the smoke irritant effect in a room filling with a high irritant smoke.[3] Visual acuity indicates the ability of the human eye to distinguish two points very close together. A visual acuity of 1.0 is defined as the conditions under which a 1.5 mm gap between two points can be distinguished from a distance of 5 m. The visual acuity is 0.5 when the gap can be distinguished from only 2.5 m. Usually, visual acuity is obtained from the Landolts ring test chart. This has been an international standard since 1909 when it was established by the International Association for Ophthalmology.

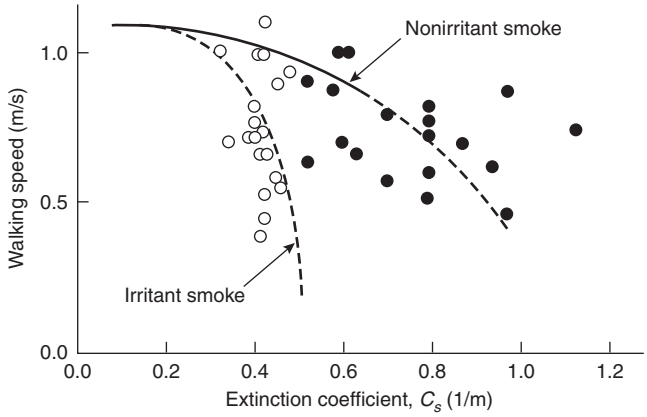

Figure 2-4.4. ***Walking speed in fire smoke.***

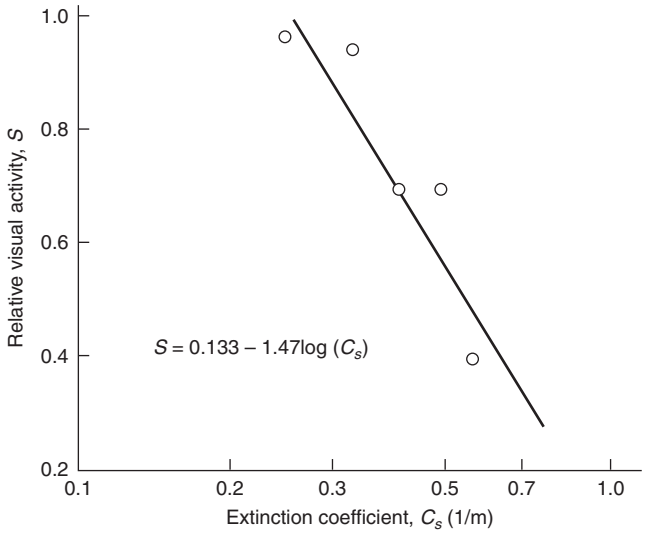

Figure 2-4.5. ***Decrease of relative visual acuity due to smoke irritant effect.***

Weber-Fechner's law gives the relationship between an impact on human sensitivity and its response; the response of human sensitivity is logarithmically proportional to the impact intensity.[6] This well-known theory is applied to the series of experiments, that is,

$$S = A - B \log C_S$$

where

S = relative visual acuity as the response
C_S = extinction coefficient as the impact
A, B = experimental constants

The relative visual acuity, S, and C_S data are plotted on a semi–log chart as shown in Figure 2-4.5 in the region of $C_S > 0.25$ 1/m. The data plotted in this figure indicate an approximately linear relationship, then the decrease of visual acuity due to the smoke irritant effect is expressed as

$$S = 0.133 - 1.47 \log C_S \quad (5)$$

The drop of visual acuity through smoke seems to be caused mainly by two factors. One is the apparent decrease of the visual acuity due to the physical effect of smoke particles obscuring the object. The other is the physiological irritant effect of smoke. Thus the visibility through smoke is expressed by the next approximations:

$$V_1 = C/C_S \qquad (0.1 \leq C_s < 0.25 : \text{in nonirritant region}) \quad (6)$$

$$V_2 = (C/C_S)(0.133 - 1.47 \log C_S) \quad (C_S \geq 0.25: \text{in irritant region}) \quad (7)$$

The empirical constant C in the equations depends on several experimental conditions; the brightness of objects and their surroundings, the contrast between them, and the kinds of objects present. The obtained relationships Equations 6 and 7 are applied to the series of experiments on visibility through smoke, and the results are presented in Figure 2-4.3 with dash-dotted line. The theoretical curves approximately agree with the experimental data when the constant is set to be 6.0. The visibility through other kinds of smoke besides the irritant white smoke from smoldering wood may be considered to vary in the intermediate region between Equations 6 and 7.

Visibility of Colored Signs

Measurement of spectral extinction properties of smoke: Figure 2-4.6 shows the change of the relative spectral extinction coefficient (ratio of spectral extinction coefficient to that at a wavelength of 700 μm) with time for smoldering wood smoke. It indicated that reduction of the longer wavelength (red light) is small compared with the shorter wavelength (blue light) in fire smoke. However, this reduction (gradients of the curve in the figure) changes with time. The inversion results from change in the size of smoke particles.

The relative spectral extinction properties have also been measured for the smoldering smoke from polystyrene foam and polyvinyl chloride. Compared with the properties of wood, the time for the gradient inversion is longer for the smoke of these materials. The relative spectral extinction properties of flaming wood smoke are shown in Figure 2-4.7. There is no inversion of the gradient of these curves. There is little or no change in the spectral extinction with time for smoke from flaming PVC, polystyrene, or kerosene.

Ratio visibility of red light to that of blue light: Let us assume that the smoke density at which fire escape is still possible is 0.5/m, and that the time for such smoke density to develop in a building is about 10 min after ignition.

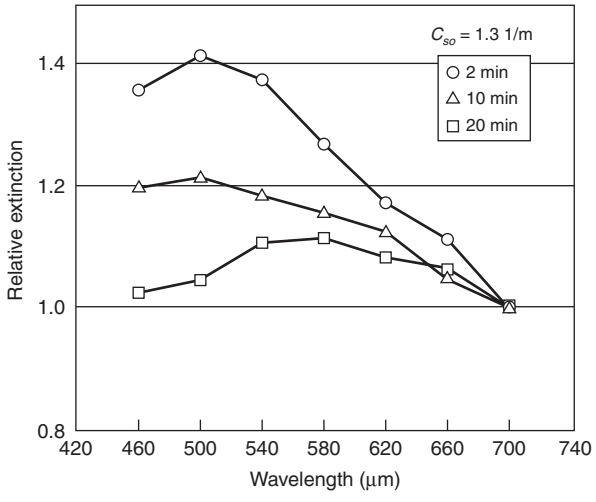

Figure 2-4.6. ***The change of the relative spectral extinction coefficient with time for smoldering smoke from wood.*** C_{s0} ***= Initial smoke density.***

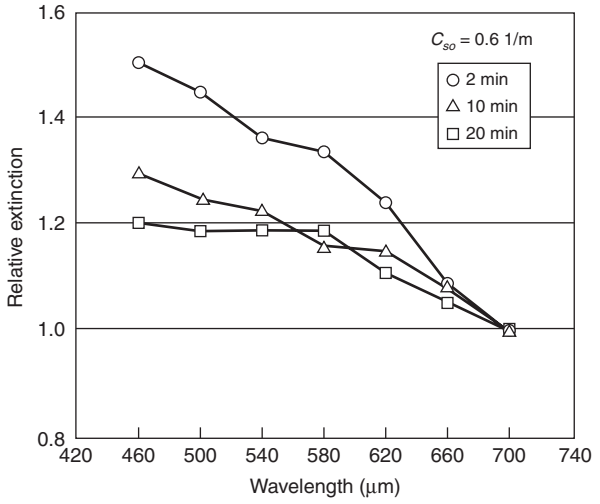

Figure 2-4.7. ***The change of the relative spectral extinction with time for flaming wood smoke. C_{s0} = initial smoke density.***

The visibilities of blue light through smoke will be compared with that of red using a calculation with the following assumptions:

1. The wave length is 657 nm for red light and 483 nm for blue light.
2. The same brightness can be obtained for both lights with a luminance meter with spectral luminous efficiency.
3. The contrast threshold at the obscuration threshold is the same for both red and blue lights.

Under the above assumptions, the ratio of visibility of a red-lighted sign, V_{red}, to that of a blue-lighted sign, V_{blue}, can be expressed by

$$\frac{V_{red}}{V_{blue}} \approx \frac{C_{s,blue}}{C_{s,red}}$$

where $C_{s,blue}$, $C_{s,red}$ are the extinction coefficients for blue light and red light, respectively.

The ratios of sign, V_{red} to V_{blue} for various smokes (10 min after generation and for the initial extinction coefficient, $C_{s0} \approx 0.5$ 1/m) are given in Table 2-4.1. This table shows that the visibilities of red-lighted signs are 20 to 40 percent larger for smoldering smoke and 20 to 30 percent larger for flaming smoke than those of blue-lighted signs. This fact indicates that visibility varies by only a few tens of percent at the most by changing the color while keeping the brightness constant. If we require to double the visibility of a conventional sign, there is no other way but to increase the brightness by a significant factor (see Equation 1).

Table 2-4.1 ***Values of V_{red}/V_{blue} for Fire Smoke***

Smoldering Smoke	V_{red}/V_{blue}	Flaming Smoke	V_{red}/V_{blue}
Wood	1.3	Wood	1.2
Polystyrene	1.4	Polystyrene	1.2
Polyvinyl chloride	1.2	Polyvinyl chloride	1.2
		Kerosene	1.3

Human Behavior in Fire Smoke

Emotional State in Fire Smoke

An attempt was made to monitor the subjects' emotional state of mind when exposed to fire smoke using a steadiness tester that is often employed in psychological studies.[4] A test chamber was used that has a floor area of 5 × 4 m, no windows, and floor-level illumination averaging 30 lx at the start of the experiment. White smoke was produced by placing wood chips in an electric furnace. The smoke generation rate was adjusted such that the extinction coefficient increased at the rate of 0.1 1/m per minute.

One subject sat at a table in the enclosure and manipulated the steadiness tester that was located on the table. The tester is faced with a metal plate in which four holes have progressively graded diameters as shown in Figure 2-4.8. The subject was told to thrust a metal stylus into holes in a specified order, trying not to touch the hole edges with the stylus. The smaller the hole size, the more concentration the subject needs to avoid contact. As the smoke density in the test room increased, fear of smoke and irritations to his or her eyes and throat hampered concentration more seriously, causing an increasing frequency of contact between the stylus and hole edges. About half of the 49 subjects subjected to the test consisted of researchers from the Fire Research Institute (former name of National Research Institute of Fire and Disaster): most of the remainder were housewives.

Figure 2-4.9 is the result of an attempt to determine the subjects' emotional variations on the basis of the num-

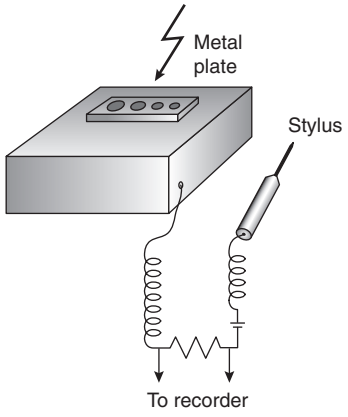

Figure 2-4.8. ***Sketch of a steadiness tester to monitor the subjects' emotional fluctuation.***

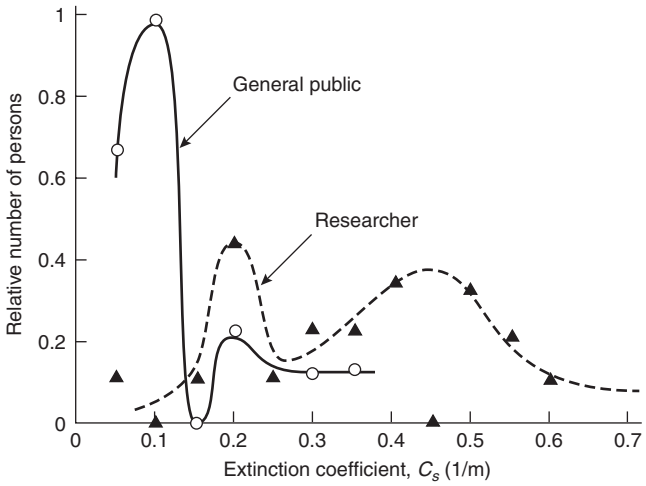

Figure 2-4.9. ***Number of emotionally affected subjects versus smoke density at the point of rapid increase in the number of contacts in the steadiness tester.***

ber of stylus contact on the steadiness tester. Curves with two peaks as shown were obtained for both groups of subjects. These peaks seem to attest to the following facts: other than the Institute researchers, most subjects began to be emotionally affected when the smoke density reached 0.1 1/m, but in a few others, emotional fluctuations did not begin to be pronounced until the smoke reached an extinction coefficient of $0.2 \sim 0.4$ 1/m. In contrast, most researchers began to show emotional fluctuations only when the smoke density reached $0.35 \sim 0.55$ 1/m although a small number of them responded at the lower smoke density of 0.2 1/m.

Interviews with some subjects were held after the experiment. Comments by many of the subjects representing the general public could be generalized like this: "Smoke itself didn't scare me much when it was thin, but irritation to my eyes and throat made me nervous. When I thought of the smoke still getting thicker and thicker, I was suddenly scared of what was going to happen next." In other words, these subjects were more afraid of what was going to happen next than they were physiologically unable to withstand the smoke.

Hence, the author believes that the data obtained from these subjects could reasonably be treated as equivalent to those that would be obtained from a group of unselected people who are unfamiliar with the internal geometry of a building on fire. The smoke density of 0.15 1/m, at which most of the subjects analyzed in Figure 2-4.9 began to feel uneasy, could be determined as the maximum smoke density for safe evacuation of a building to which the public have access.

In contrast, the Institute researchers who served as subjects said in the interview, "Irritation to my eyes was rather acute but the smoke didn't scare me because I had heard in the pretest briefing that it was harmless. But as the smoke grew denser, I began to feel more acute irritation in my eyes and throat, and when I got the signal to end the test (smoke extinction coefficient $0.5 \sim 0.7$ 1/m), irritation and suffocation were near the limit I could physiologically withstand. Toward the end of the test, visibility in the test room was so limited that I saw only a small floor area around my feet, and this made me a little nervous when I walked through the smoke."

Even though these researchers had some knowledge of smoke from the pretest briefing and were well informed of the geometry in the test room, most of them began to be emotionally affected when the smoke density exceeded 0.5 1/m. It could be reasoned that emotional instability of these subjects during the test resulted from physiological rather than psychological reasons.

These facts led the author to believe that the results of this experiment using Institute researchers as the subjects can be treated as data relevant to people who are well informed of the inside geometry of a building on fire. This means that the smoke density of 0.5 1/m, at which Figure 2-4.9 indicates most of the researchers began to lose steadiness, can be determined as the threshold where escape becomes difficult even for persons who are well familiar with the escape route in the building.

Visibility at these smoke densities is listed in Table 2-4.2, which indicates that those who know the inside geometry of the building on fire need a visibility of 4 m for safe escape while those who do not need a visibility of 13 m.

In Table 2-4.3, a comparison is made between some of the values of acceptable visibility or allowable smoke density proposed by researchers who have conducted many experiments on escape through fire smoke.[2] Wide variations in the proposed values are probably due to differences in the geometry of the places and the composition of the group escaping from fire.

Table 2-4.2 ***Allowable Smoke Densities and Visibility That Permits Safe Escape***

Degree of Familiarity with Inside Building	Smoke Density (extinction coefficient)	Visibility
Unfamiliar	0.15 1/m	13 m
Familiar	0.5 1/m	4 m

Table 2-4.3 ***Values of Visibility and/or Allowable Smoke Density for Fire Safe Escape Proposed by Fire Researchers***

Proposer	Visibility	Smoke Density (extinction coefficient)
Kawagoe[7]	20 m	0.1 1/m
Togawa[8]	—	0.4 1/m
Kingman[9]	4 ft (1.2 m)	—
Rasbash[10]	15 ft (4.5 m)	—
Los Angeles Fire Department[11]	45 ft (13.5 m)	—
Shern[12]	—	0.2 1/m
Rasbash[13]	10 m	0.2 1/m

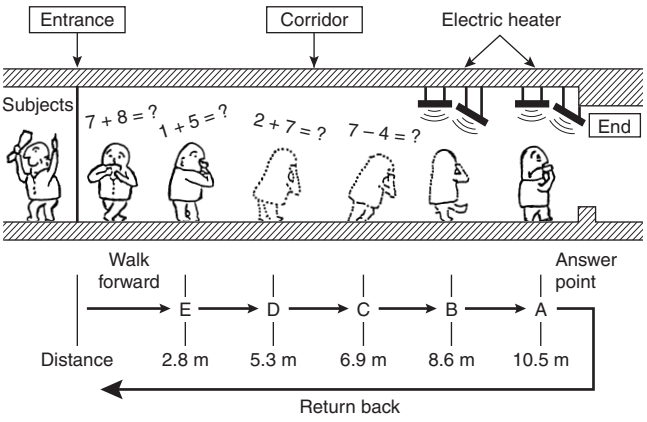

Figure 2-4.10. ***Outline of experiment.***

Correct Answer Rate and Emotional Instability in Thick Fire Smoke

An experimental study was conducted in order to obtain data on emotional instability in thick, hot smoke (see Figure 2-4.10). Mental arithmetic and walking speed were adopted as indicators and the subjects were asked to complete a questionnaire to allow their response to smoke and heat to be assessed.[14]

The corridor was filled with white smoke generated by wood chips that were allowed to smolder in an electric furnace before each experiment. At the start of each experiment, the smoke density was adjusted to 1.2 1/m and 2 or 3 subjects entered into the corridor individually at the same smoke density condition. The temperature inside the corridor was about 20°C. At the inner positions A and B, subjects were exposed to radiant heat from an electrical radiator (12 kW at A and 3 kW at B) installed at ceiling level. The maximum heat fluxes at positions A and B, 1.5 m above the ground, were 2.4 kW/m² and 1.6 kW/m² respectively. The mean radiant temperature measured with a glove thermometer was about 82°C at A and 75°C at B.

In this experiment, a mental arithmetic test was adopted to estimate the degree of emotional instability under thick and hot smoke condition. The rate of correct answers to simple arithmetic questions was expected to decrease with increasing human emotional instability. This rate was adopted as an index of emotional instability. The mental arithmetic questions were recorded in an endless tape and 10 questions were put to the subject by a loudspeaker at each five answer positions (A to E). Thirty-one adults aged 20 to 51 (14 male, 17 female) participated in this experiment. The females were mainly housewives and the males were undergraduate students.

The smoke density was not the same at the beginning of each experiment. The values varied in the range of $C_S = 0.92 \pm 0.21$ 1/m. In the first experimental trials with thicker smoke, 17 subjects (6 male and 11 female) could reach the furthest position A, but the other 14 subjects (8 male and 6 female) turned back. The solid line in Figure 2-4.11 shows how the relative correct answer rate varied with distance reached from the entrance. The average rate of the 17 subjects who were able to reach position A fell to the lowest level just after entering the corridor (at position E) but tended to increase as they walked further into the corridor.

The subjects pointed out afterwards that they felt uneasy as they were walking forward. The results showed that the walking speed decreased in proportion to distance from the entrance. From these observations, the extent of the decrease in the relative correct answer rate which is due to psychological factors as the subjects walk forward is not known, but may be illustrated by the dashed line in Figure 2-4.11. The abrupt decrease in the correct answer rate just after entering the corridor can be explained by the physiological effect of the smoke on the subjects' eyes and throat. This discomfort eases with lapse of time due to conditioning and the correct answer rate can rise as the subject walks further into the corridor. This is illustrated in Figure 2-4.11 by the dashed and dotted line. The effect of radiant heat is apparent in the experimental data at positions A and B.

The experimental data obtained and shown in Figure 2-4.11 with the solid line appear to be composed of two kinds of smoke effect, physiological and psychological. The relation between these two effects, for example, whether a simple algebraic addition can explain the data or not, is a task for further investigations.

Figure 2-4.12 presents the mental arithmetic results in the absence of smoke. The data at position A drop to 10 percent below those at the other positions. This decrease is caused by the heat radiation from electric heat radiators installed at the ceiling. The same drop at position A is also apparently recognized under the smoke condition presented with a normal line in Figure 2-4.11. Nevertheless, there is no fall at position B. The maximum heat flux intensity was 2030 kcal/m²h (2.47 kW/m²) at 1.5 m above the floor at A and 1370 kcal/m²h (1.60 kW/m²) at B. This suggests that there is a threshold value of heat flux be-

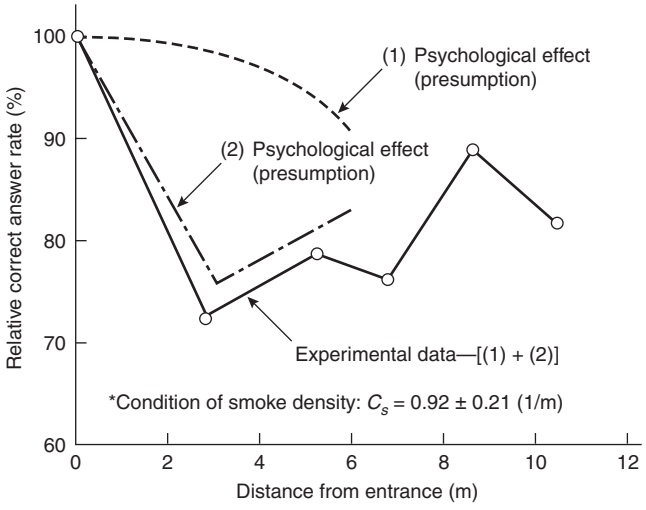

Figure 2-4.11. ***Relation between distance from entrance and correct answer rate: 17 subjects (6 males, 11 females) reached at the end of the corridor in the first trial.***

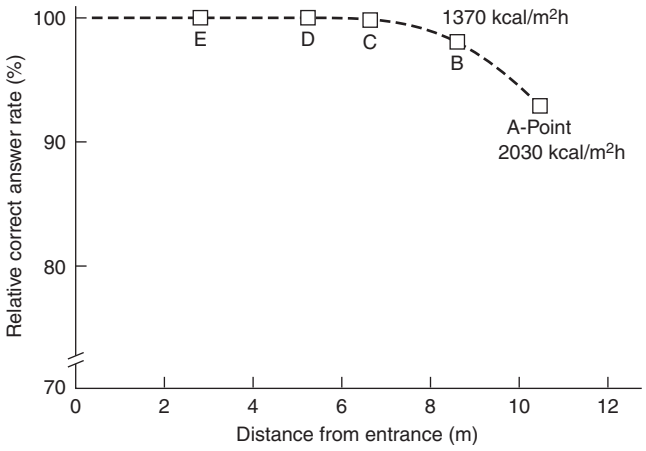

Figure 2-4.12. ***Relation between distance from entrance and correct answer rate with electric heater and without smoke: the electric heater is installed at positions A and B.***

tween 1.6 and 2.4 kW/m² above which decision making may be affected.

Some questions were asked of each subject after the experiment. One was related to the subject's response to the smoke: "What are the uncomfortable factors of smoke? Select three factors concerned with fire smoke from the following items." The result is shown in Table 2-4.4. Some variances between male and female were found. Physiological factors were mainly selected by males. Irritation of the eyes and/or throat was the first or the second selected item. Difficulty in breathing was selected as the second or the third uncomfortable factor. In comparison with the above answers from males, females tended to feel psychological discomfort. As well as physiological annoyance, the reduction in visibility was selected as the first cause of discomfort of females along with irritation and inhalation problems. The reduction in visibility was also cited as the second cause.

These experimental results indicate that the emotional instability in thick fire smoke is not necessarily caused by the same factors for males and females. Under thin smoke conditions, the smoke irritation and heat flux are selected as the first or the second factor, regardless of sex.

Table 2-4.4 ***Uncomfortable Factors of Fire Smoke***

	Male (n = 14)			Female (n = 18)		
Selection Items	First	Second	Third	First	Second	Third
Foul smell	1 (7%)	2 (14%)	3 (21%)	1 (6%)	0 (0%)	1 (7%)
Smoke irritation	8 (57%)	4 (29%)	1 (7%)	7 (41%)	6 (35%)	2 (13%)
Difficulty in breathing	5 (36%)	4 (29%)	5 (36%)	4 (24%)	3 (18%)	6 (40%)
Reduction in visibility	0 (0%)	3 (21%)	3 (21%)	5 (29%)	6 (35%)	5 (33%)
Heat	0 (0%)	1 (7%)	0 (0%)	0 (0%)	1 (6%)	0 (0%)
Feeling of isolation	0 (0%)	0 (0%)	1 (7%)	0 (0%)	1 (6%)	1 (7%)
Others	0 (0%)	0 (0%)	1 (7%)	0 (0%)	0 (0%)	0 (0%)

Intensive System for Escape Guidance

Improvement of Conspicuousness of Exit Sign by Flashing Light Source

An emergency exit sign, which indicates a location and/or direction of emergency exit and leads evacuees to a safe place swiftly, is important in case of fire or other emergencies. In Japan, three sizes of emergency exit sign are currently being used [40 cm(h) × 1200 cm(w); 20 cm(h) × 60 cm(w); and 12 cm(h) × 36 cm(w)]. However, the conspicuousness of an exit sign in a location where there are many other light sources was not known. In the first experiments, the conspicuousness of an "ordinary" exit sign in an underground shopping mall was measured during business hours. The experimental variables were the observation distance, size, and luminance of the sign. In the second series of experiments, the conspicuousness of a self-flashing type exit sign (flashing the lamp in the sign) was compared with that of an ordinary exit sign.[15] The type of emergency exit sign currently in use in Japan is shown in the photo in Figure 2-4.13.

Visibility and conspicuousness of exit sign: Prior to this study, another experimental study on visibility of exit signs had been carried out. In that experiment, the original type of exit sign was observed in a background without other light sources. Figure 2-4.14 shows one of the results concerned with the relation between visibility expressed by visual angle (defined by the height of the pictograph) and surface luminance. In this figure, visibility is represented on two discrimination levels; one is the level at which a person can distinguish the details of the pictograph and the other is the level at which only the direction

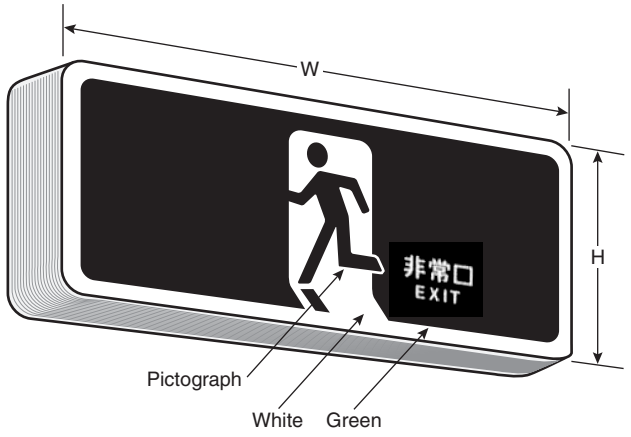

Figure 2-4.13. ***Emergency exit sign currently used in Japan.***

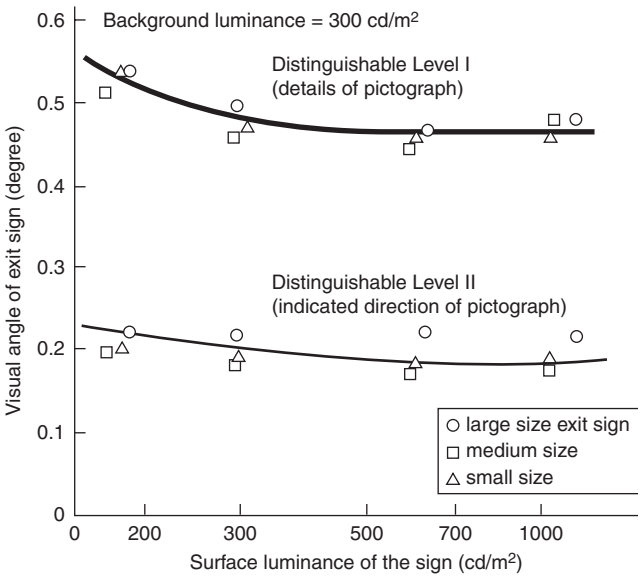

Figure 2-4.14. ***Relation between surface luminance of ordinary exit sign and visual angle associated with visibility.***

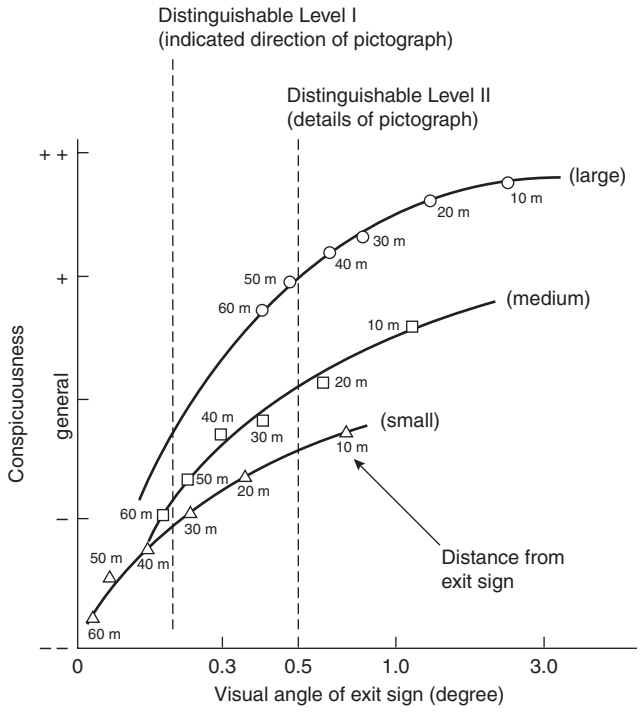

Figure 2-4.15. ***Relation between conspicuousness of ordinary type exit sign and visual angle.***

of the running person in the pictograph is distinguishable. This result indicates that visibility is almost constant when the luminance of the white part of the exit sign is more than 300 cd/m^2. This observation is true for every size of the exit sign. It is independent of the size of the sign when visibility is expressed in terms of the visual angle.

Figure 2-4.15 shows the relation between conspicuousness of ordinary exit signs and the visual angle according to the evaluation categories given in Table 2-4.5.[16] The larger-size exit sign is more conspicuous than the smaller one when the visual angle is the same. This indicates that conspicuousness depends on the relative scale of exit sign against the size of surrounding lights. In this sense, the visibility expressed in terms of visual angle does not always correspond rationally to conspicuousness.

Table 2-4.5 ***Categories for Evaluating Conspicuousness of Ordinary Type Exit Sign***

Evaluation Categories	(Marks in Fig. 2-4.15)
1. The exit sign is fairly conspicuous	(++)
2. The exit sign is slightly conspicuous	(+)
3. The exit sign is similar to the general level	(general)
4. The exit sign is less conspicuous	(–)
5. The exit sign is not conspicuous at all	(––)

Improvement of conspicuousness by flashing the light sources: Figure 2-4.16 shows the relation between conspicuousness of an ordinary exit sign and that of the self-flashing type exit sign using the categories for evaluation given in Table 2-4.6. In this figure the vertical interval between the dash-dotted line and the curves corresponds to the improvement of conspicuousness by the flashing light in the sign. For the medium-size exit sign, a self-flashing type sign is more effective to improve conspicuousness. However, the small-size exit sign of self-flashing type is not conspicuous enough when observed from a distance more than 20 m in the background with many other lights, because the exit sign is too small to be recognized as an exit sign, even though the flashing was expected to be much more conspicuous. The large exit sign is big enough to have sufficient conspicuousness without flashing even in the background with many competing light sources. Conspicuousness of the sign could also be improved by adding a flashing light source the same as a flashing-type sign.

In addition to the improvement achieved by adding a flashing light, the author has suggested the development of an acoustic guiding exit sign. Adding a speaker and voice recorded IC chip to the flashing exit sign can provide an announcement such as "Here is an Emergency Exit" when fire is detected by, for example, smoke detectors.[17]

Effect of Escape Guidance in Fire Smoke by Traveling Flashing of Light Sources

An escape guidance system has been developed for safe evacuation. This system indicates the appropriate escape directions by creating a row of flashing lights leading away from a hazardous area such as a fire in a

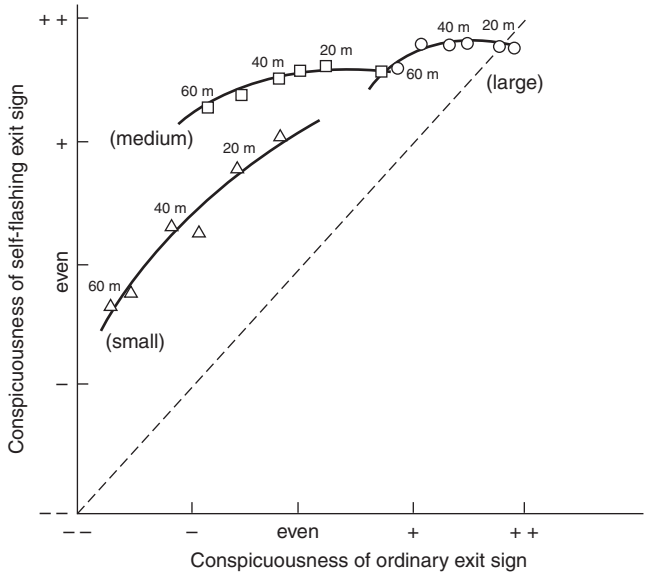

Figure 2-4.16. ***Relation between the conspicuousness of a self-flashing exit sign and that of an ordinary one.***

Table 2-4.6 ***Categories for Evaluating Conspicuousness of Self-Flashing Exit Signs***

Evaluation Categories *(as compared with the ordinary-type exit sign)*	(Marks in Fig. 2-4.16)
1. The flashing exit sign is fairly conspicuous	(++)
2. The flashing exit sign is slightly conspicuous	(+)
3. The flashing exit sign has similar conspicuousness	(general)
4. The flashing exit sign is less conspicuous	(–)
5. The flashing exit sign is not conspicuous	(– –)

building. A form of this is already found in the floor lighting of passenger aircraft cabins.

An experiment was carried out to evaluate this system using a portion of passageway (1.4 m wide, 6.3 m long, and 2.5 m high) filled with smoke. As lighting for the passageway, fluorescent lamps are provided under the ceiling, giving about 200 lx at the center of the passage in the absence of smoke. The flashing light unit boxes are set on the floor along the side of the right-hand wall at intervals of 0.5 m, 1.0 m, and 2.0 m as a test guidance system.[18]

The effectiveness of the escape guidance was evaluated by 12 subjects who walked in a line at a side of a row of flash-traveling green light sources located on the floor under various conditions, that is, the spacing and the traveling speed of flashing lights and smoke concentration. Under each condition, subjects walk along the system successively; however, only two or three subjects are inside the passageway at a time to maintain free walking speed.

The degree of effectiveness of escape guidance is classified into seven steps as follows, and the evaluations are made by filling one score from seven points into an observation sheet directly after each test run. These categories are adopted as a semantic differential scale for escape guidance.

Score	Effectiveness
7 point	very effective for escape guiding
5 point	fairly effective
3 point	a little effective
1 point	not effective

(Points 2, 4, and 6 correspond to the middle point between 1 and 3, 3 and 5, and 5 and 7 respectively.) In general, the effectiveness decreases with increasing smoke. The evaluation value of 4 point stands for less effective than fairly effective and more effective than a little effective, so we consider the value a threshold where practical effectiveness of escape guidance is secured.

The correlation between smoke concentration and the effect of escape guidance is shown in Figure 2-4.17. This indicates that this system is useful for evacuees to escape in thick smoke (up to an extinction coefficient of 1.0

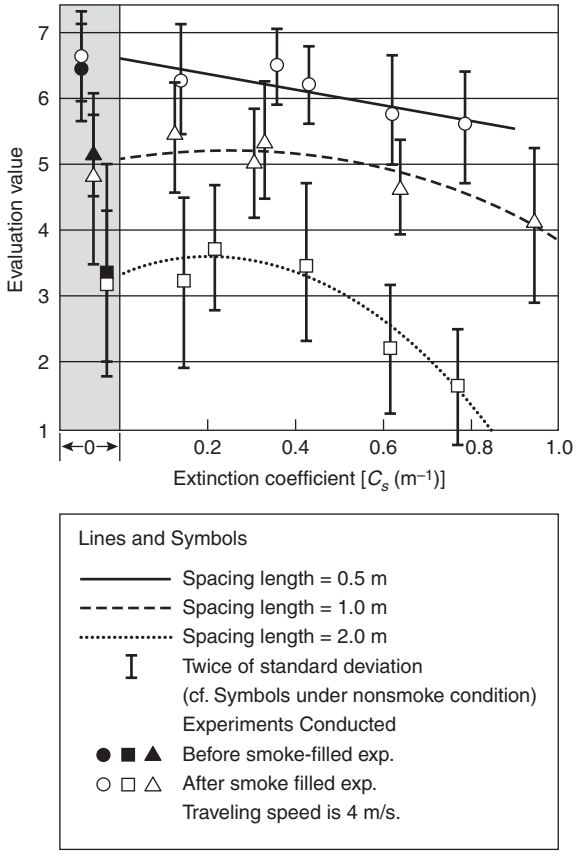

Figure 2-4.17. ***Relation between smoke density and the effect of escape guidance with variation of flashing light sources under a smoke condition.***

per meter) when the spacing length is 0.5 m and the flashing speed is 4 m/s. When the spacing length is set to be 1.0 m, the effectiveness decreases but it is still useful in smoke under 0.8 1/m. However, when the spacing is greater than 2.0 m, less effectiveness is expected even under a no-smoke condition and it decreases as the smoke density increases. The evaluation values in the meshed area to the left in Figure 2-4.17 were obtained before and after smoke inhalation, but under conditions of no smoke. This area shows stability of the evaluation, and no assimilation effects are observed.

From Figure 2-4.17, the effectiveness of flashing traveling signs in an ambient atmosphere is maintained up to a smoke density of 0.4 1/m. This result is very important for evaluating the escape guidance system from the viewpoint of safe evacuation. Visibility (observable distance) of normal exit signs drops rapidly from more than 10 m to 5 m, and the guidance effectiveness is also lost over the same range of smoke densities.[2] This relation between the visibility of ordinary exit signs and the smoke density is expressed in Figure 2-4.18.

Compared with the decrease in visibility of ordinary exit signs, the decrease in the effectiveness of the guidance system with increasing obscuration seems to be small, so that the new system is expected to maintain high and stable effectiveness of guidance escape, even in relatively dense smoke. It is known that the threshold of smoke density for safe evacuation of a building without emergency signs is under 0.5 1/m for evacuees who are familiar with the building and 0.15 1/m for strangers.[4]

The effectiveness of this escape guiding system is also illustrated by previous experimental observations mentioned in the section headed Correct Answer Rate and Emotional Instability in Thick Fire Smoke, that is, 7 subjects out of 31 participants could not proceed beyond 2.8 m from the exit, 3 subjects were stopped at 5.3 m, 3 subjects at 6.9 m, and 1 subject at 8.6 m in the corridor filled with thick smoke ($C_S = 0.92 \pm 0.21$). Many evaluation values at 0.2 1/m smoke density give higher values than those under a nonsmoke condition. It is considered that interference by the background lighting is weakened by the smoke and the evacuees are able to concentrate more on the flashing light. Therefore, in thinner smoke at the very beginning of fire, this type of guidance system can be expected to have a high effectiveness for safety evacuation, as well as in thick smoke.

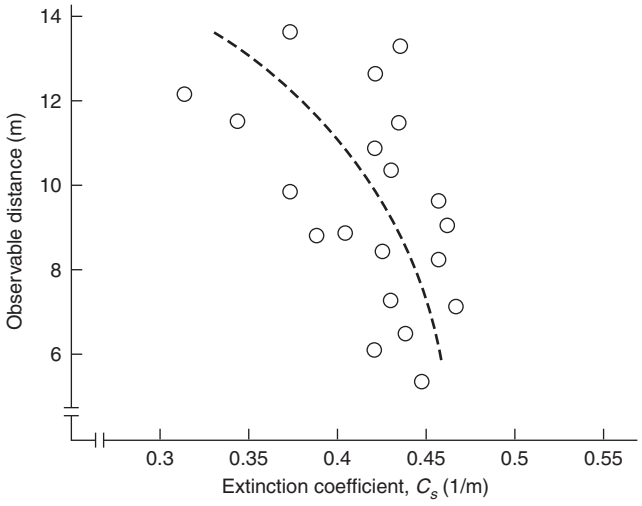

Figure 2-4.18. ***Relation between smoke density and visibility of exit sign.***

Clearly, the spacing between flashing light sources is a very important factor to maintain effectiveness. High effectiveness is expected, especially, when the spacing is less than 1 m. The relation between effectiveness and flashing light conditions in the presence of smoke is found to be almost the same as the relation under a nonsmoke condition.

Conclusion

The following are the major conclusions derived from these research activities:

1. Relation between smoke density and visibility in fire smoke was examined under various kinds of smoke, and simple equations were proposed for practical use.
2. The visibility in fire smoke depends on its irritating nature as well as the optical density of the smoke. Increasing irritating effect causes a rapid drop of visual acuity. A modification due to irritating effect was made for the visibility versus smoke density equation.
3. Evacuees begin to feel emotional instability in relatively thin smoke; however the threshold of smoke density varies with the subject. Through experiments and investigations, it was found that the level depended on the degree of evacuees' familiarity of the internal geometry of a building on fire. Evacuees in unfamiliar buildings tend to feel emotional instability in thinner smoke.
4. Ability of evacuees to think clearly when exposed to fire smoke decreases with increasing smoke density. Generally, this is caused by both psychological and physiological effects on evacuees. Also, in due course, hot smoke causes a further decrease of thinking ability.
5. Conspicuousness of the ordinary exit sign was improved by a flashing light source sign or by adding a flashing light source in conditions where there were many other light noises.
6. A new type of escape guidance in fire smoke by traveling flashing light sources toward exits was developed, and the effectiveness was examined in a smoke-filled corridor. This new system is expected to maintain high and stable escape guidance, even in relatively thick smoke.

References Cited

1. T. Jin, "Visibility through Fire Smoke," *Bull. of Japanese Assoc. of Fire Science & Eng.*, 19, 2, pp. 1–8 (1970).
2. T. Jin, "Visibility through Fire Smoke," *J. of Fire & Flammability,* 9, pp. 135–157 (1978).
3. T. Jin and T. Yamada, "Irritating Effects of Fire Smoke on Visibility," *Fire Science & Technology,* 5, 1, pp. 79–89 (1985).

4. T. Jin, "Studies of Emotional Instability in Smoke from Fires," *J. of Fire & Flammability,* 12, pp. 130–142 (1981).
5. T. Jin, "Studies on Decrease of Thinking Power and Memory in Fire Smoke," *Bull. of Japanese Assoc. of Fire Science & Eng.,* 32, 2, pp. 43–47 (1982).
6. A. Weber, T. Fischer, and E. Grandjean, *Int. Archives of Occupational and Environmental Health,* 43, pp. 183–193 (1979).
7. K. Kawagoe and F. Saito, *Journal of Japanese Society for Safety Engineering,* 6, 2, p. 108 (1967).
8. K. Togawa, unpublished manuscript.
9. F.E.T. Kingman, *J. Appl. Chem.,* 3, p. 463 (1953).
10. D.J. Rasbah, *Fire,* 59, 735, p. 175 (1966).
11. Los Angeles Fire Department, Operation School Burning (1961).
12. J.H. Shern, *Sixty-ninth Annual Meeting of the ASTM* (1966).
13. D.J. Rasbash, *International Seminar on Automatic Fire Detection,* Aachen, Germany (1975).
14. T. Jin and T. Yamada, "Experimental Study of Human Behavior in Smoke Filled Corridor," *Proceedings of the Second International Symposium of Fire Safety Science,* International Association for Fire Safety Science, Boston, pp. 511–519 (1989).
15. T. Jin, T. Yamada, S. Kawai, and S. Takahashi, "Evaluation of the Conspicuousness of Emergency Exit Signs," *Proceedings of the Third International Symposium of Fire Safety Science,* International Association for Fire Safety Science, Boston, pp. 835–841 (1991).
16. Illumination Engineering Institute of Japan, *The Report of Basic Research on Visibility of Exit Sign,* 1 (1984).
17. T. Jin and K. Ogushi, "Acoustic Evacuation Guidance," *Bull. of Japanese Assoc. of Fire Science & Eng.,* 36, 1, pp. 24–29 (1986).
18. T. Jin and T. Yamada, "Experimental Study on Effect of Escape Guidance in Fire Smoke by Travelling of Light Source," *Proceedings of the Fourth International Symposium of Fire Safety Science,* International Association of Fire Safety Science, Boston, pp. 705–714 (1994).

CHAPTER 5

Effect of Combustion Conditions on Species Production

D. T. Gottuk and B. Y. Lattimer

Introduction

A complete compartment fire hazard assessment requires a knowledge of toxic chemical species production. Although combustion products include a vast number of chemical species, in practical circumstances the bulk of the product gas mixture can be characterized by less than ten species. Of these, carbon monoxide (CO) represents the most common fire toxicant. (See Section 2, Chapter 6.) Over half of all fire fatalities have been attributed to CO inhalation.[1,2] Concentrations as low as 4000 ppm (0.4 percent by volume) can be fatal in less than an hour, and carbon monoxide levels of several percent have been observed in full-scale compartment fires. A complete toxicity assessment should not only include the toxicity of CO but also include the synergistic effects of other combustion products, such as elevated CO_2 and deficient O_2 levels.

The transport of combustion products away from the room of the fire's origin is of the utmost importance, because nearly 75 percent of the fatalities due to smoke inhalation occur in these remote locations.[3] However, conditions close to the compartment of origin will govern the levels that are transported to remote locations. The research in this area has focused on characterizing species levels produced under a variety of conditions, both inside and nearby the compartment of fire origin.

Species product formation is affected by the compartment geometry, ventilation, fluid dynamics, thermal environment, chemistry, and mode of burning. The mode of burning and ventilation are two of the key conditions that dictate product formation. These conditions can be used to classify fires into three general categories (1) smoldering, (2) free- (or open-) burning fires, and (3) ventilation-limited fires. Smoldering is a slow combustion process characterized by low gas temperatures and no flaming. Under these conditions, high levels of CO can be generated. Section 2, Chapters 6 and 9, and Section 3, Chapter 4, discuss this mode of burning in detail; thus, it will not be discussed further here. Free-burning fires are flaming fires that have an excess supply of air. These well-ventilated fires (discussed in Section 3, Chapter 4) are generally of little concern in terms of generating toxic species. This chapter focuses primarily on the third category, ventilation-limited flaming fires. These fires consist of burning materials inside an enclosure, such as a room, in which airflow to the fire is restricted due to limited ventilation openings in the space. As a fire grows, conditions in the space will transition from overventilated to underventilated (fuel rich). It is normally during underventilated conditions that formation of high levels of combustion products, including CO, creates a major fire hazard.

This chapter discusses the production of species within a compartment fire and the transport of these gases out of the fire compartment to adjacent areas. Engineering correlations are presented along with brief reviews of pertinent work on species production in compartment fires. These sections provide the background and basis for understanding the available engineering correlations and the range of applicability and limitations. An engineering methodology is presented to utilize the information given in this chapter.

This chapter is organized according to the following outline:

- Basic Concepts
- Species Production within Fire Compartments
  - Hood Experiments
  - Compartment Fire Experiments

Dr. Daniel T. Gottuk is a senior engineer at the fire science and engineering firm of Hughes Associates, Inc. He received his Ph.D. from Virginia Tech in the area of carbon monoxide generation in compartment fires. He continues to work in the area of species generation and transport in compartment fires.

Dr. Brian Y. Lattimer is a research scientist at Hughes Associates, Inc. His research has focused on species formation and transport in building fires, fire growth inside compartments, flame spread, and heat transfer from flames.

Chemical Kinetics
Fire Plume Effects
Transient Conditions
Species Transport to Adjacent Spaces
Engineering Methodology

Basic Concepts

In a typical compartment fire, a two-layer system is created. The upper layer consists of hot products of combustion that collect below the ceiling, and the lower layer consists of primarily ambient air that is entrained into the base of the fire. (See Figure 2-5.1a.) Initially, the fire plume is totally in the lower layer, and the fire burns in an overventilated mode similar to open burning. Due to excess air and near-complete combustion, little CO formation is expected in this mode. (See Section 3, Chapter 4 for yields.) As the fire grows, ventilation paths in the room restrict airflow, creating underventilated (fuel-rich) burning conditions. It is generally under these conditions that products of incomplete combustion are created. Typically, the fire plume extends into the upper layer, such that layer gases recirculate through the upper part of the plume.

Depending on both the size of the room and the size of the fire, it is possible to have a fire plume that cannot be contained within the room, resulting in flame extension out of windows or doors. Flame extension can occur when the fire plume impinges on the ceiling and the ceiling jets are longer than the distance from the plume to outside vent openings (See Figure 2-5.1b). Flame extension is different from a second burning phenomenon outside of the fire compartment, called external burning, which is discussed below. The main point to understand is that flame extension outside of the fire compartment is a result of a fire that is too large to be contained in the room. Flame extension can occur during both over- and underventilated burning conditions. To estimate when flame extension may occur, the maximum heat release rate that can be supported by the compartment ventilation needs to be determined. Flame length correlations can then be used to determine whether flames will extend outside of the compartment.

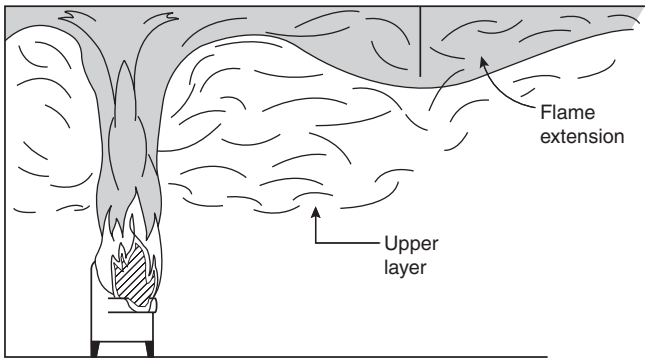

Figure 2-5.1b. ***A fire compartment with flame extension out of the doorway.***

As a fire progresses and the upper layer descends, the layer will spill below the top of doorways or other openings into adjacent areas. The hot, vitiated, fuel-rich gases flowing into adjacent areas can mix with air that has high O_2 concentrations to create a secondary burning zone outside of the compartment. (See Figure 2-5.1c.) This is referred to as external burning. External burning can also be accompanied by layer burning. Layer burning is the ignition of fuel-rich upper layer gases at the interface between the upper and lower layers. External burning and layer burning occur due to the buildup of sufficient fuel in an atmosphere that is able to mix with available oxygen. These phenomena can only occur during underventilated burning conditions. In some circumstances, external burning can decrease human fire hazard through the oxidation of CO and smoke leaving the fire compartment. (See the section in this Chapter on species transport to adjacent spaces.).

The occurrence of external burning has been predicted using a compartment layer ignition model developed by Beyler.[4] (See Section 2, Chapter 7.) Beyler derived a relationship called the ignition index to predict the ignition of gases at the interface of the upper and

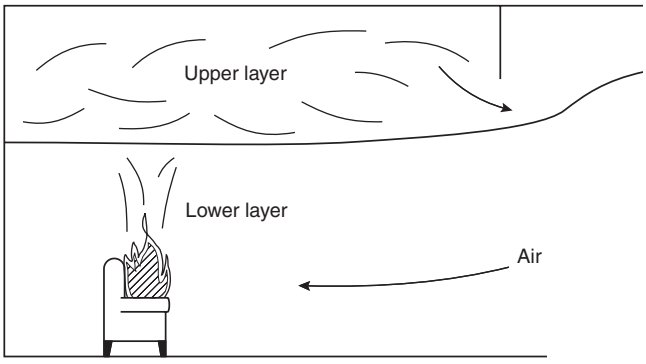

Figure 2-5.1a. ***An overventilated compartment fire with the fire plume below the layer interface.***

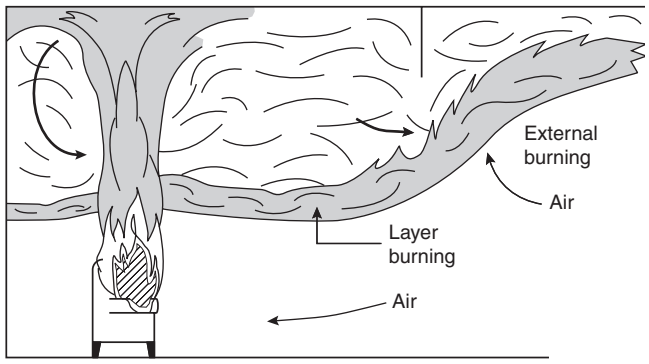

Figure 2-5.1c. ***An underventilated compartment fire with external burning of fuel-rich upper layer gases.***

lower layers inside a compartment. The ignition index, I, is defined as

$$I = \sum_j \frac{\left(C_j/100\right)\Delta H_{c,j}}{\int_{T_o}^{T_{SL,j}} n_{prod} C_p dT} \geq 1.0 \quad (1)$$

where

j = fuel species of interest
C_j = volume concentration of fuel j when fuel stream is stoichiometrically mixed with oxidant stream
$\Delta H_{c,j}$ = heat of combustion of the species j (kJ/g·mol)
$T_{SL,j}$ = adiabatic flame temperature at the stoichiometric limit for fuel species j (K)
T_o = temperature of the gas mixture prior to reaction (K)
n_{prod} = number of moles of products of complete combustion per mole of reactants (stoichiometric mixture of fuel and oxidant streams)
C_p = heat capacity of products of complete combustion (kJ/g·mol K)

The use of the ignition index is discussed in detail in Section 2, Chapter 7 of this book. An ignition index greater than 1.0 indicates that ignition is expected if the mixture contains sufficient fuel.

Species Yields

The generation of fire products in compartment fires can be quantified in terms of species yields, Y_i, defined as the mass of species i produced per mass of fuel burned (g/g):

$$Y_i = \frac{m_i}{m_f} \quad (2)$$

Similarly, oxygen is expressed as the depletion of O_2, (i.e., D_{O_2}), which is the grams of O_2 consumed per gram of fuel burned:

$$D_{O_2} = \frac{m_{O_2}}{m_f} \quad (3)$$

The normalized yield, f_i, is the yield divided by the theoretical maximum yield of species i for the given fuel, k_i. For the case of oxygen, f_{O_2} is the normalized depletion rate, where k_i is the theoretical maximum depletion of oxygen for the given amount of fuel. As a matter of convenience, the use of the term yield throughout this chapter will also include the concept of oxygen depletion. As in Section 3, Chapter 4, the normalized yield is also aptly referred to as the "generation efficiency" of compound i. By definition, the normalized yields range from 0 to 1, and are thus good indicators of the completeness of combustion. For example, under complete combustion conditions the normalized yields of CO_2, H_2O and O_2 are 1. As a fire burns more inefficiently, these yields decrease. The use of normalized yields is also useful for establishing mass balances. The conservation of carbon requires that

$$f_{CO} + f_{CO_2} + f_{THC} + f_{resid.C} = 1 \quad (4)$$

where f_{THC} is the normalized yield of gas-phase total hydrocarbons and $f_{resid.C}$ is the normalized yield of residual carbon, such as soot in smoke, or high molecular weight hydrocarbons that condense out of the gas sample.

For two-layer systems the yield of all species except oxygen can be calculated as follows:

$$Y_i = \frac{X_{i_{wet}}(\dot{m}_f + \dot{m}_a)M_i}{\dot{m}_f M_{mix}} \quad (5)$$

where

$X_{i_{wet}}$ = the wet mole fraction of species i
$\dot{m}_a$ = the mass air entrainment rate into the upper layer
$\dot{m}_f$ = the mass loss rate of fuel
M_i = the molecular weight of species i
M_{mix} = the molecular weight of the mixture (typically assumed to be that of air)

The depletion rate of oxygen is calculated as

$$D_{O_2} = \frac{0.21\dot{m}_a M_{O_2}/M_a - X_{O_2\,wet}(\dot{m}_f + \dot{m}_a)M_{O_2}/M_{mix}}{\dot{m}_f} \quad (6)$$

The normalized yield, f_i, is simply calculated by dividing the yield by the maximum theoretical yield

$$f_i = \frac{Y_i}{k_i} \quad (7)$$

Typical operation of common gas analyzers requires that water be removed from the gas sample before entering the instrument. Consequently, the measured gas concentration is considered dry and will be higher than the actual wet concentration. Equation 8 can be used to calculate the wet mole fraction of species i, $X_{i_{wet}}$, from the measured dry mole fraction, $X_{i_{dry}}$. As can be seen from Equation 8, the percent difference between $X_{i_{dry}}$ and $X_{i_{wet}}$ is on the order of the actual H_2O concentration which, depending on conditions, is typically 10 to 20 percent by volume.

$$X_{i_{wet}} = (1 - X_{H_2O_{wet}})X_{i_{dry}} \quad (8)$$

Reliable water concentration measurements are difficult to obtain. Therefore, investigators have calculated wet species concentrations using the above relationship with the assumption that the molar ratio, C, of H_2O to CO_2 at any equivalence ratio is equal to the calculated molar ratio at stoichiometric conditions.[5,6] Based on this assumption, Equation 9 can be used to calculate wet species concentrations from dry concentration measurements.

$$X_{i_{wet}} = \frac{X_{i_{dry}}}{1 + CX_{CO_{2_{dry}}}} \quad (9)$$

Equivalence Ratio

The concept of a global equivalence ratio (GER) can be used to express the overall ventilation of a control volume, such as a fire compartment. However, due to the complex interaction between the plume and the upper

and lower layers, as well as the potential extension of the fire beyond the initial compartment, a unique definition for the GER does not exist. Therefore, if one uses the term GER, it must be associated with a defined control volume.

The first efforts in developing the GER concept were based on hood experiments[7–11] (e.g., as in Figure 2-5.2) in which the idea of a plume equivalence ratio was introduced. The plume equivalence ratio, ϕ_p, is the ratio of the mass of fuel burning, m_f, to the mass of oxygen entrained, m_a, into the fire plume (below the upper layer) normalized by the stoichiometric fuel-to-oxygen ratio, r_{O_2}.

$$\phi_p = \frac{m_f/m_{O_2}}{r_{O_2}} \tag{10a}$$

Since oxygen is typically entrained into a fire plume via air, ϕ_p is commonly defined as

$$\phi_p = \frac{m_f/m_a}{r} \tag{10b}$$

where m_a is the mass of air entrained into the plume (in the lower layer) and r is the stoichiometric mass fuel-to-air ratio. As discussed in the section on species production within fire compartments, this simple characterization of the equivalence ratio well represented the global conditions that existed in the first hood and compartment fire experimental configurations.

In order to more accurately describe the time integrated conditions within the upper layer, a second equivalence ratio was defined for this control volume.[7,10,11] The upper layer equivalence ratio, ϕ_{ul}, is the ratio of the mass of the upper layer that originates from fuel sources, to the mass of the upper layer that originates from any source of air into the upper layer, divided by the stoichiometric fuel-to-air ratio.

The two equivalence ratios (ϕ_p and ϕ_{ul}) are not necessarily the same. As a fire grows, the upper layer composition represents a collective time history of products. In an ideal two layer fire, where all air enters the upper layer through the plume, ϕ_{ul} is the same as ϕ_p only during steady burning conditions. If the burning rate of the fire changes quickly compared to the residence time of the gases in the upper layer, the upper layer equivalence ratio lags behind the plume equivalence ratio. The residence time, t_R, can be defined as the time required for a unit volume of air to move through the upper layer volume, and can be characterized according to Equation 11.

$$t_R = \frac{V_{ul}\rho_{ul}}{\dot{m}_{exhaust}} \tag{11}$$

where

$\dot{m}_{exhaust}$ = mass flow rate of gases out of the layer
ρ_{ul} = density of the upper layer gases
V_{ul} = volume of the upper layer

For example, consider a compartment fire burning with a plume equivalence ratio of 0.5 with upper layer gases that have a residence time of 20 seconds. If the fire grows quickly such that ϕ_p increases to a value of 1.5 in about 5 seconds, ϕ_{ul} would now lag behind (less than 1.5). The fuel rich (ϕ_p = 1.5) gas mixture from the plume is effectively diluted by the upper layer gases since there has not been sufficient time (greater than 20 seconds) for the layer gases to change over. The result is that ϕ_{ul} will have a value between 0.5 and 1.5. Another instance when ϕ_{ul} can differ from ϕ_p is when additional fuel or air enters the upper layer directly. An example of this would be the burning of wood paneling in the upper layer.

The calculation of ϕ_{ul} can be a complex task. Either a fairly complete knowledge of the gas composition is needed[7] or time histories of ventilation flows and layer residence times are needed, to be able to calculate ϕ_{ul}. Toner[7] and Morehart[12] present detailed methodologies for calculating ϕ_{ul} from gas composition measurements. Equation 12 can be used to calculate ϕ_{ul} if the mass flow rates can be expressed as a function of time.

$$\phi_{ul} = \frac{1\int_{t-t_R}^{t} \dot{m}_f(t')\,dt'}{r\int_{t-t_R}^{t} \dot{m}_a(t')\,dt'} \tag{12}$$

Although termed the upper layer equivalence ratio, ϕ_{ul} actually represents the temporal aspect of the equivalence ratio no matter what the control volume. For instance, the control volume may be the whole compartment, as shown in Figure 2-5.1. In this case, the compartment equivalence ratio, ϕ_c, is defined as the ratio of the mass, m_f, of any fuel entering or burning in the compartment to the mass, m_a, of air entering the compartment normalized by the stoichiometric fuel-to-air ratio.

In a compartment fire, air is typically drawn into the space through a door or window style vent. If all of the air drawn into the compartment is entrained into the lower layer portion of the plume, then the plume equivalence ratio can be an adequate representation of the fire environment. However, if layer burning occurs, or multiple vents cause air to enter the upper layer directly, the use of

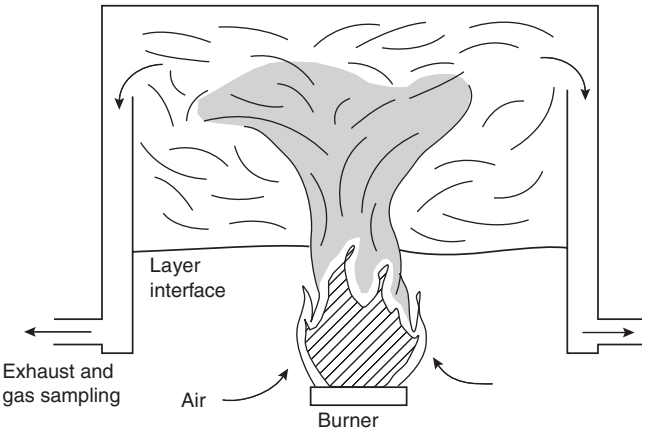

Figure 2-5.2. ***Schematic of the two-layer system created in the hood experiments of Beyler.[8,9]***

a compartment equivalence ratio is more appropriate. As a practical note, for fires within a single compartment, the equivalence ratio is calculated (and experimentally measured) based on the instantaneous fuel mass loss rate, $\dot{m}_f$, and air flow rate, $\dot{m}_a$, into the compartment (Equation 13a).

$$\phi = \frac{\dot{m}_f/\dot{m}_a}{r} \tag{13a}$$

As noted previously, r is defined as the stoichiometric fuel-to-air ratio. Unfortunately, the ratio r is sometimes defined as the air-to-fuel ratio, r_a. Therefore, consideration must be given to values obtained from tabulated data. Keeping with the nomenclature of this chapter, the equivalence ratio can also be expressed as

$$\phi = \frac{\dot{m}_f}{\dot{m}_a} \cdot r_a = \frac{\dot{m}_f}{\dot{m}_a} \frac{r_o}{Y_{O_{2,air}}} \tag{13b}$$

where

r_a = mass air-to-fuel ratio
r_o = oxygen-to-fuel mass ratio
$Y_{O_{2,air}}$ = mass fraction of oxygen in air (0.23)

The formulation of Equation 13b allows direct use of r_o values tabulated for various fuels in Table C-2 of this handbook. Another useful expression for ϕ can be derived from Equation 13b by multiplying the numerator and denominator by the fuel heat of combustion, Δh_c, and recognizing that the heat release per mass of oxygen consumed, E, is equal to Δh_c over r_o, yielding

$$\phi = \frac{\dot{Q}}{\dot{m}_a} \cdot \frac{1}{EY_{O_{2,air}}} = \frac{\dot{Q}}{\dot{m}_a} \cdot \frac{1}{3030} \tag{13c}$$

where

$\dot{Q}$ = ideal heat release rate of the fire (kW)
$\dot{m}_a$ = air flow rate, (kg/s)
$E \approx$ 13,100 kJ/kg (Reference 33)

Note that Q is the ideal heat release rate, which is determined by multiplying the mass loss rate by the heat of combustion, and is not limited by the amount of air flowing into the compartment or control volume. To date, Equation 13c has not been utilized in the literature and therefore has not been well established. However, it offers a convenient means to calculate the equivalence ratio without the need to know the fuel chemistry.

The equivalence ratio is an indicator of two distinct burning regimes, overventilated (fuel lean) and underventilated (fuel rich). Overventilated conditions are represented by equivalence ratios less than one, while underventilated conditions are represented by equivalence ratios greater than one. An equivalence ratio of unity signifies stoichiometric burning which, in an ideal process, represents complete combustion of the fuel to CO_2 and H_2O with no excess oxygen. During underventilated conditions there is insufficient oxygen to completely burn the fuel; therefore, products of combustion will also include excess fuel (hydrocarbons), carbon monoxide, and hydrogen. It follows that the highest levels of CO production in flaming fires is expected when underventilated conditions occur in the compartment on fire. This basic chemistry also suggests that species production can be correlated with respect to the equivalence ratio. Although the not-so-ideal behavior of actual fires prevents accurate theoretical prediction of products of combustion, experimental correlations have been established.

A simple model for the most complete combustion of a fuel can be represented by the following expressions:[8]

$$f_{CO_2} = f_{O_2} = f_{H_2O} = 1 \qquad \text{for } \phi < 1 \tag{14a}$$
$$f_{CO_2} = f_{O_2} = f_{H_2O} = 1/\phi \qquad \text{for } \phi > 1 \tag{14b}$$
$$f_{CO} = f_{H_2} = 0 \qquad \text{for all } \phi \tag{14c}$$
$$f_{THC} = 0 \qquad \text{for } \phi < 1 \tag{14d}$$
$$f_{THC} = 1 - 1/\phi \qquad \text{for } \phi > 1 \tag{14e}$$

These expressions assume that for $\phi > 1$, all excess fuel can be characterized as unburned hydrocarbons. Since compartment fire experiments have shown that significant levels of both CO and H_2 are produced at higher equivalence ratios, Expression 14c is not always representative, and reveals a shortcoming of assuming this simple ideal behavior. However, for the products of complete combustion (CO_2, O_2 and H_2O), this model serves as a good benchmark for comparison of experimental results.

EXAMPLE 1:

Consider a piece of cushioned furniture to be primarily polyurethane foam. The nominal chemical formula of the foam is $CH_{1.74}O_{0.323}N_{0.07}$. Calculate the stoichiometric fuel-to-air ratio, the maximum yields of CO, CO_2, and H_2O, and the maximum depletion of O_2.

SOLUTION:

For complete combustion of the fuel to CO_2 and H_2O, the following chemical equation can be written

$$CH_{1.74}O_{0.323}N_{0.07} + 1.2735(O_2 + 3.76N_2) \rightarrow 1.0CO_2 + 0.87H_2O + 4.823N_2$$

The molecular weight of the fuel, M_f, = 1(12) + 1.74(1) + 0.323(16) + 0.07(14) = 19.888.

The stoichiometric fuel-to-air ratio is

$$r = \frac{(1\text{mole fuel})(M_f)}{(\text{moles of air})(M_a)} = \frac{19.888}{1.2735(4.76)(28.8)}$$
$$r = 0.1139$$

The stoichiometric air-to-fuel ratio is

$$\frac{1}{r} = 8.78$$

The maximum yield of CO (i.e., k_{CO}), is calculated by assuming that all carbon in the fuel is converted to CO. Therefore, the number of moles of CO formed, n_{CO},

equals the number of moles of carbon in one mole of fuel. For the polyurethane foam, $n_{CO} = 1$.

$$k_{CO} = \frac{n_{CO}(M_{CO})}{n_f(M_{fuel})} = \frac{(1)(28)}{(1)(19.888)} = 1.41$$

Similarly, k_{CO_2} and k_{H_2O} are calculated as

$$k_{CO_2} = \frac{(1)(44)}{19.888} = 2.21$$

$$k_{H_2O} = \frac{(0.87)(18)}{19.888} = 0.787$$

The maximum depletion of oxygen, k_{O_2}, refers to the mass of oxygen needed to completely combust one mole of fuel to CO_2 and H_2O. This is the same as the stoichiometric requirement of oxygen.

$$k_{O_2} = \frac{n_{O_2}(M_{O_2})}{n_f M_f} \frac{(1.2735)(32)}{(1)19.888} = 2.05$$

EXAMPLE 2:

The fuel specified in Example 1 is burning at a rate of 9 g/s and entraining air at a rate of 56 g/s. Measurements of the upper layer gas composition reveal dry concentrations of 3.7 percent by volume CO, 14.3 percent CO_2, and 0.49 percent O_2. Correct the concentrations for the water removed during the gas analysis process (i.e., calculate the wet concentrations).

SOLUTION:

In order to use Equation 9 to calculate the wet mole fractions, the stoichiometric molar ratio of H_2O to CO_2 for *C* needs to be calculated. This ratio is simply obtained from the stoichiometric chemical equation in Example 1.

$$C = \frac{n_{H_2O}}{n_{CO_2}} = \frac{0.87}{1} = 0.87$$

Once *C* is obtained, the wet mole fractions can be calculated as

$$X_{CO_{wet}} = \frac{0.037}{1 + 0.87(0.143)} = 0.033$$

$$X_{CO_{2wet}} = \frac{0.143}{1 + 0.87(0.143)} = 0.127$$

$$X_{O_{2wet}} = \frac{0.0049}{1 + 0.87(0.143)} = 0.0044$$

The estimated mole fraction of water is

$$X_{H_2O} = CX_{CO_{2wet}} = 0.87(0.127) = 0.11$$

Therefore, the corrected gas concentrations on a percent volume basis are 3.3 percent CO, 12.7 percent CO_2, and 0.44 percent O_2.

EXAMPLE 3:

Continuing from Example 2, calculate the yields and normalized yields for each species measured. The wet mole fractions are $X_{CO_{wet}} = 0.033$, $X_{CO_{2wet}} = 0.127$, and $X_{O_{2\,wet}} = 0.0044$.

SOLUTION:

Using Equations 5 and 7, the yield and normalized yield of CO, CO_2, and H_2O can be calculated. The maximum yields calculated in Example 1 are $k_{CO} = 1.41$, $k_{CO_2} = 2.21$, $k_{H_2O} = 0.787$, and $k_{O_2} = 2.05$.

$$Y_{CO} = \frac{X_{CO_{wet}}(\dot{m}_f + \dot{m}_a)M_{CO}}{\dot{m}_f M_a} = \frac{(0.033)(9 + 56)(28)}{9(28.8)} = 0.23$$

$$f_{CO} = \frac{Y_{CO}}{k_{CO}} = \frac{0.23}{1.41} = 0.16$$

$$Y_{CO_2} = \frac{(0.127)(9 + 56)(44)}{9(28.8)} = 1.40$$

$$f_{CO_2} = \frac{1.40}{2.21} = 0.63$$

$$Y_{H_2O} = \frac{(0.11)(9 + 56)(18)}{9(28.8)} = 0.50$$

$$f_{H_2O} = \frac{0.50}{0.787} = 0.63$$

The depletion of oxygen is calculated using Equation 6, assuming the molecular weight of the gas mixture, M_{mix}, to be approximately that of air.

$$D_{O_2} = \frac{0.21\dot{m}_a M_{O_2}/M_a - X_{O_{2wet}}(\dot{m}_f + \dot{m}_a)M_{O_2}/M_{mix}}{\dot{m}_f}$$

$$D_{O_2} = \frac{0.21(56)32/28.8 - 0.0044(9 + 56)32/28.8}{9}$$

$$D_{O_2} = 1.42$$

The normalized yield is calculated as

$$f_{O_2} = \frac{D_{O_2}}{k_{O_2}} = \frac{1.42}{2.05} = 0.69$$

Species Production within Fire Compartments

Hood Experiments

Beyler[8,9] was the first to publish major species production rates in a small-scale two-layer environment. The experiments performed consisted of situating a burner under a 1-m diameter, insulated collection hood. The result was the formation of a layer of combustion products in the hood similar to that found in a two-layer compartment fire. (See Figure 2-5.2.) By varying the fuel supply rates and the distance between the burner and layer interface, and, consequently, the air entrainment rate, a range of equivalence ratios was obtained. Layer gases were exhausted at a constant, metered flow rate from the periphery of the hood at a depth of 15 cm below the ceiling. The general procedure was to allow steady-state burning

conditions to develop, so the layer maintained a constant depth below the exhaust flow location. Tests revealed a reasonably well-mixed uniform layer both in temperature and chemical composition during the steady-state conditions. Gas analysis was performed on samples taken from the exhaust stream. Table 2-5.1 shows the physicochemical properties of the fuels tested.

Beyler's results show that species yields correlate very well with the plume equivalence ratio. Figure 2-5.3 shows normalized yields of major species for propane fires plotted against the plume equivalence ratio. The trends seen in these plots for propane are fairly representative of the other fuels tested. For overventilated conditions, the yield of CO_2 and H_2O and depletion of O_2 are at a maximum, and there is virtually no production of CO, H_2, or unburned hydrocarbons (*THC*). As underventilated burning conditions ($\phi \geq 1$) are approached, products of incomplete combustion (CO, H_2, and *THC*) are generated.

For comparison, the expressions for ideal complete combustion (Equations 14a through 14e) are shown on each plot in Figure 2-5.3. The CO_2 yield departs from Equation 14b as CO production increases at higher equivalence ratios. This departure, which is fairly independent of ϕ for $\phi > 1$, has been described by the yield coefficient.[5] The ratios of the normalized yield of CO_2, H_2O or normalized depletion of O_2 to the theoretical maximums expressed by Equations 14a through 14e are defined as the yield coefficients, B_{CO_2}, B_{H_2O} and B_{O_2}, respectively.[5]

$$B_{CO_2} = \frac{f_{CO_2}}{1} \qquad \text{for } \phi < 1 \qquad (15a)$$

$$B_{CO_2} = \frac{f_{CO_2}}{1/\phi} \qquad \text{for } \phi > 1 \qquad (15b)$$

$$B_{H_2O} = \frac{f_{H_2O}}{1} \qquad \text{for } \phi < 1 \qquad (16a)$$

$$B_{H_2O} = \frac{f_{H_2O}}{1/\phi} \qquad \text{for } \phi > 1 \qquad (16b)$$

$$B_{O_2} = \frac{f_{O_2}}{1} \qquad \text{for } \phi < 1 \qquad (17a)$$

$$B_{O_2} = \frac{f_{O_2}}{1/\phi} \qquad \text{for } \phi > 1 \qquad (17b)$$

These terms are useful in discussing characteristics of the combustion efficiency. For example, an O_2 yield of one indicates complete utilization of available O_2. In the case of CO_2 and H_2O, deviation from the model (as indicated by B_{CO_2} or $B_{H_2O} < 1$) is a measure of the degree of incomplete combustion. It can be seen from Figure 2-5.3 that the production of CO is primarily at the expense of CO_2 (i.e., B_{O_2} and B_{H_2O} remain nearly 1, while B_{CO_2} is about 0.8). Table 2-5.2 shows average yield coefficients for underventilated fires.

Figure 2-5.4 shows unnormalized CO yields plotted against the plume equivalence ratio for fuels tested by Beyler.[8,9] The correlations agree quite well for all fuels. Below an equivalence ratio of 0.6, minimal CO production is observed. Above ϕ_p equal to 0.6, carbon monoxide yield increases with ϕ_p and, for most fuels, tends to level out at equivalence ratios greater than 1.2. Toluene, which creates large amounts of soot, is anomalous compared to the other fuels studied. As can be seen in Figure 2-5.4, the CO yields from toluene fires remain fairly constant at about 0.09 for both overventilated and underventilated burning conditions.

It should be noted that Beyler originally presented all correlations with normalized yields, f_{CO}. However, better agreement is found between unnormalized CO yield-equivalence ratio correlations for different fuels, Y_{CO} (shown in Figure 2-5.4), rather than normalized yields. One point of interest though, is that when CO production is correlated as normalized yield, a more distinct separation of the data occurs for $\phi_p > 1$. The degree of carbon monoxide production (represented as f_{CO}) during underventilated conditions can be ranked by chemical structure

Table 2-5.1 ***Physicochemical Data for Selected Fuels***

Fuel	Empirical Chemical Formula of Volatiles	Empirical Molecular Weight	Maximum Theoretical Yields				
			k_{CO}	k_{CO_2}	k_{O_2}	k_{H_2O}	$1/r^c$
Acetone	C_3H_6O	58	1.45	2.28	2.21	0.93	9.45
Ethanol	C_2H_5OH	46	1.22	1.91	2.09	1.17	8.94
Hexane	C_6H_{14}	86	1.95	3.07	3.53	1.47	15.1
Isopropanol	C_3H_7OH	60	1.40	2.20	2.40	1.20	10.3
Methane	CH_4	16	1.75	2.75	4.00	2.25	17.2
Methanol	CH_3OH	32	0.88	1.38	1.50	1.13	6.43
Propane	C_3H_8	44	1.91	3.00	3.64	1.64	15.6
Propene	C_3H_6	42	2.00	3.14	3.43	1.29	14.7
Polyurethane foam	$CH_{1.74}O_{0.323}N_{0.0698}$	20	1.41	2.21	2.05	0.79	8.78
Polymethylmethacrylate	$C_5H_8O_2$	100	1.40	2.20	1.92	0.72	8.23
Toluene	C_7H_8	92	2.13	3.35	3.13	0.78	13.4
Wood (ponderosa pine[a])	$C_{0.95}H_{2.4}O$	30	0.89	1.40	1.13	0.73	4.83
Wood (spruce[b])	$CH_{3.584}O_{1.55}$	40	0.69	1.09	0.89	0.80	3.87

[a]Reference 9, chemical formula estimated from $\phi < 1$ yield data

[b]Reference 5

[c]r = stoichiometric fuel to air ratio

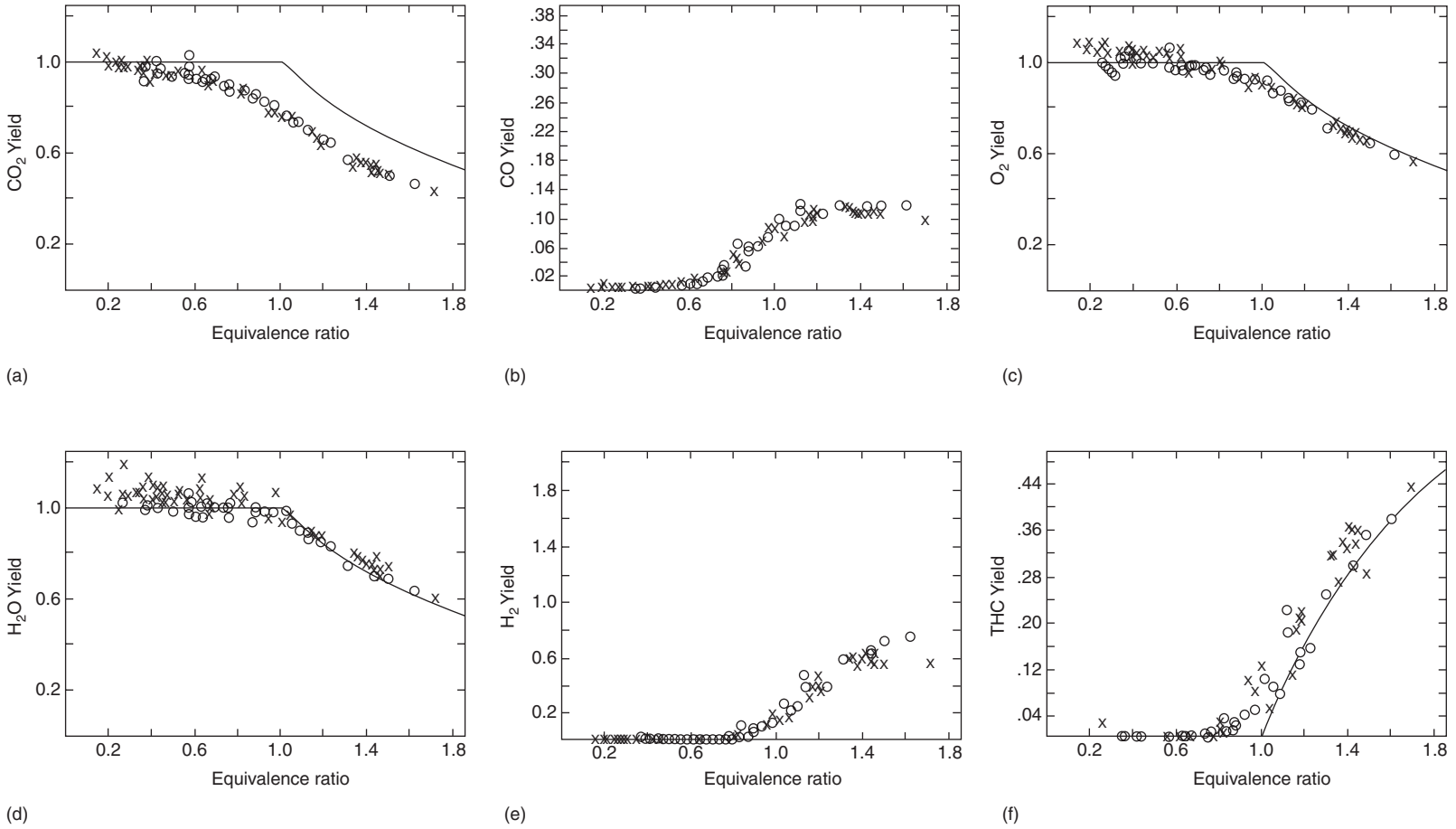

Figure 2-5.3. ***Normalized yields of measured chemical species as a function of the equivalence ratio for propane experiments using a 13-cm (o) or 19-cm (x) burner with supply rates corresponding to 8 to 32 kW theoretical heat release rate.[8]***

Table 2-5.2 ***Average Yield Coefficients and Upper Layer Temperatures for Underventilated Fires[a] (Values in parenthesis are standard deviations)***

Fuel	B_{CO_2}	B_{O_2}	B_{H_2O}	Temperature (K)	Reference
Acetone	0.78 (0.03)	0.92 (0.04)	0.99 (0.04)	529 (76)	8
Ethanol	0.79 (0.01)	0.97 (0.01)	1.00 (0.04)	523 (72)	8
Hexane	0.61 (0.10)	0.82 (0.02)	0.87 (0.03)	529 (25)	8
Hexane	0.83 (0.05)	0.96 (0.06)	NA	1038 (62)	5
Isopropanol	0.75 (0.01)	0.89 (0.01)	0.96 (0.01)	513 (33)	8
Methane	0.80 (0.05)	1.00 (0.04)	1.01 (0.03)	713 (101)	7
Methane	0.69 (0.03)	0.87 (0.07)	0.86 (0.06)	547 (12)	12
Methanol	0.79 (0.03)	0.99 (0.00)	0.94 (0.02)	566 (53)	8
Propane	0.78 (0.05)	0.97 (0.03)	1.05 (0.04)	557 (62)	8
Propene	0.77 (0.08)	0.92 (0.08)	1.02 (0.10)	629 (51)	8
Polyurethane foam	0.87 (0.04)	0.97 (0.02)	NA	910 (122)	5
Polymethylmethacrylate	0.77 (0.06)	0.92 (0.19)	0.72 (0.04)	525 (37)	9
Polymethylmethacrylate	0.93 (0.04)	0.98 (0.04)	NA	1165 (126)	5
Toluene	0.57 (0.04)	0.62 (0.05)	0.78 (0.03)	509 (23)	8
Wood (ponderosa pine)	0.85 (0.05)	0.89 (0.03)	0.79 (0.10)	537 (37)	9
Wood (spruce)	0.90 (0.00)	0.95 (0.00)	NA	890 (0)	5

[a]Values have been calculated from data found in the cited references. Values for References 7–9 and 12 are from hood experiments, and values for Reference 5 are for a reduced-scale enclosure.

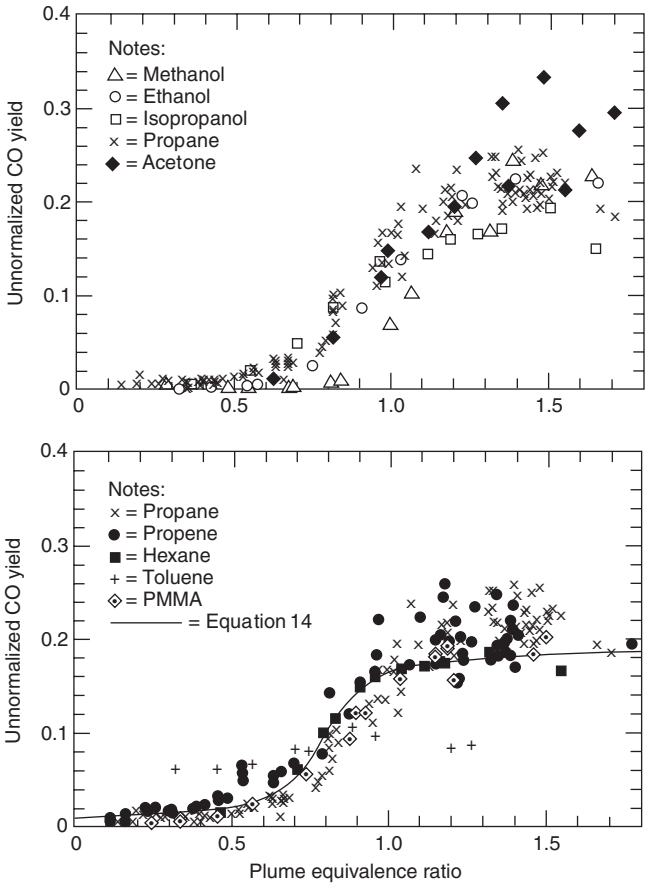

Figure 2-5.4. ***Unnormalized carbon monoxide yields as a function of the plume equivalence ratio for various fuels studied by Beyler in a hood apparatus.[8,9]***

according to oxygenated hydrocarbons > hydrocarbons > aromatics. This ranking is not observed for unnormalized yield correlations.

Toner et al.[7] and Zukoski et al.[10,11] performed similar hood experiments with a different experimental setup. The hood used was a 1.2 m cube, insulated on the inside with ceramic fiber insulation board. The layer in the hood formed to the lower edges where layer gases were allowed to spill out. Gas sampling was done using an uncooled stainless-steel probe inserted into the layer. Detailed gas species measurements were made using a gas chromatograph system. The upper layer equivalence ratio was determined from conservation of atoms using the chemical species measurements, the measured composition of the fuel, and the metered fuel flow rate. Natural gas flames with heat release rates of 20 to 200 kW on a 19-cm-diameter burner were studied. The layer in the hood was allowed to form and reach a steady-state condition before gas sampling was performed.

It was concluded that species concentrations were well correlated to the upper layer equivalence ratio, ϕ_{ul}, and insensitive to temperatures for the range studied (490 to 870 K). Since these experiments were conducted during steady-state conditions, with mean upper layer residence times of about 25 to 180 s, it can be concluded that ϕ_p and ϕ_{ul} were equal.

The data of Toner et al.[7] have been used to plot CO and CH_4 yields versus upper layer equivalence ratio in Figures 2-5.5 and 2-5.6, respectively. The correlations are qualitatively similar to the correlations obtained by Beyler for different fuels. An analysis of these test results also showed that normalized CO_2 and O_2 yield versus equivalence ratio data is represented reasonably well by Equations 15–17. Similar to Beyler's propane results, the average B_{O_2} value is about 1 and B_{CO_2} is 0.8 for underventilated burning conditions (the use of yield coefficients is discussed further in the section on engineering correlations).

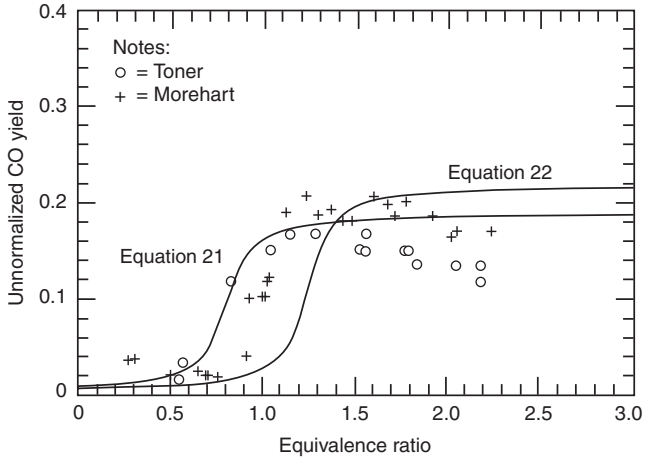

Figure 2-5.5. ***Unnormalized carbon monoxide yields as a function of equivalence ratio for methane fires studied by Toner et al.[7] and Morehart et al.[12] in hood experiments. Yields were calculated from data in References 7 and 12.***

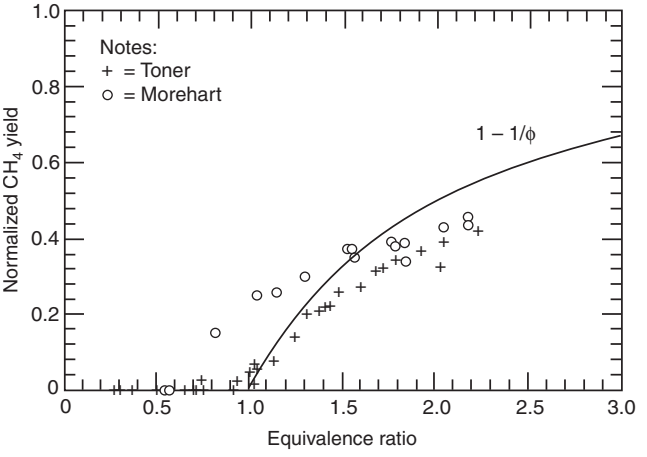

Figure 2-5.6. ***Normalized yields as a function of equivalence ratio for methane fires studied by Toner et al.[7] and Morehart et al.[12] in hood experiments. Yields were calculated from data in References 7 and 12.***

Toner compared the measured species concentrations to the calculated equilibrium composition of the reactants at constant temperature and pressure. The layer composition was modeled quite well by the chemical equilibrium composition for very overventilated conditions but not for underventilated conditions. His observance of CO production for near-stoichiometric and underventilated fires, at the expense of CO_2 production, led them to suggest that the oxidation of CO was "frozen out" before completion. (At low temperatures, there is insufficient energy for CO to chemically react to CO_2.)[7] Since the results showed that species production was independent of temperature for the range studied (490 to 870 K), Toner et al. concluded that, if a freeze-out temperature existed, it must be higher than 900 K. Work by Pitts[13] and by Gottuk et al.,[14] discussed later, shows that a freeze-out temperature does exist in the range of 800 to 900 K, depending on other factors.

Zukoski, Morehart, et al.[11] performed a second series of tests similar to that described above for Zukoski et al.[10] and Toner et al. Much of the same apparatus was used except for a different collection hood. The hood, 1.8 m square by 1.2 m high, was larger than that used by Toner et al. and was uninsulated.

Morehart et al.[12] experiments consisted of establishing steady-state burning conditions such that the burner-to-layer interface height was constant. A constant ϕ_p was maintained based on this constant interface height in conjunction with the fact that the mass burning rate of fuel was metered at a constant rate. Additional air was then injected into the upper layer at a known flow rate until a new steady-state condition was achieved. This procedure established a ϕ_{ul} that was lower than the ϕ_p, since ϕ_p was based on the ratio of the mass burning rate to the mass of air entrained into the plume from room air below the layer interface. By increasing the air supply rate to the upper layer, a range of ϕ_{ul} was established while maintaining a constant ϕ_p.

Although similar, the correlations obtained by Morehart et al. deviated from those obtained by Toner et al. Figures 2-5.5 and 2-5.6 compare the CO and CH_4 yields calculated from the data of Morehart et al. with the yields calculated from the data of Toner et al. For overventilated conditions, Morehart et al. observed higher CO and CH_4 yields, signifying that the fires conducted by Morehart et al. burned less completely. For underventilated methane fires, Morehart et al. observed lower CO, CO_2, and H_2O and higher CH_4 and O_2 concentrations than Toner et al. The only apparent differences between experiments was that Morehart found layer temperatures were 120 to 200 K lower for fires with the same equivalence ratio as those observed by Toner, that is, they ranged from 488 to 675 K. Due to the similarity in experimental apparatus, except for the hood, Morehart concluded that the temperature difference resulted from having a larger uninsulated hood.

Morehart studied the effect of increasing temperature on layer composition by adding different levels of insulation to the hood. Except for the insulation, the test conditions (e.g., ϕ of 1.45 and layer interface height) were held constant. Residence times of layer gases in the hood were in the range of 200 to 300 s. For the range of temperatures studied (500 to 675 K), substantial increases in products of complete combustion (i.e., CO_2 and H_2O) and decreases in fuel and oxygen occurred with increasing layer temperature. Upper layer oxygen mass fraction was reduced by approximately 70 percent and methane was reduced by 25 percent.[11,12] Excluding one outlier data point, CO concentrations increased by 25 percent. This is an important result. Although the gas temperatures were well below 800 K, an increase in the layer temperature resulted in more fuel being combusted to products of complete combustion and additional CO. (See section on chemical kinetics.)

Compartment Fire Experiments

The hood experiments performed by Beyler and Zukoski et al. differ from actual compartment fires in several ways. The hood setup allowed considerable radiation to the lab space below. Conversely, a real compartment would contain most of the radiation, thus resulting in higher wall and upper layer temperatures. Consequently, higher fuel mass loss rates for pool fires would be expected for an actual compartment fire. Also, the hood setup results in a lower layer that has an infinite supply of air which is neither vitiated nor heated. In a real compartment fire, the air supply is limited by ventilation openings (doors, windows, etc.) and the depth of the upper layer. The air that is entrained into the lower layer of an actual compartment fire can be convectively heated by hot compartment surfaces prior to fire plume entrainment. The hood experiments did not include any significant ceiling and wall flame jets. These dynamic flame structures enhance mixing of the upper layer in actual compartment fires and extend the flame zone beyond the plume. Lastly, the hood experiment correlations were developed from sustained steady-state burning conditions. Actual fires of interest are usually in a continual growth stage, and, thus, more transient in nature.

Tewarson reported that CO and CO_2 yields and O_2 depletion were correlated well by the air-to-fuel stoichiometric fraction (i.e., the reciprocal of the equivalence ratio) for wood crib enclosure fires.[15] Enclosure fire data was taken from previous work in the literature for cellulosic-base fiberboard and pine wood cribs burned in various compartment geometries, 0.21 to 21.8 m^3 in volume, with single and dual horizontal and vertical openings centered on the end walls. Additional data were obtained for pine wood cribs burned in a small-scale flammability apparatus that exposed the samples to variable external radiant heat fluxes with either natural or forced airflow from below.

The characteristics of the correlations presented by Tewarson are similar to the correlations developed by Beyler. The CO_2 yield and O_2 depletion are relatively constant for low equivalence ratios and decrease sharply as the equivalence ratio increases for underventilated conditions. The CO yield correlates with the equivalence ratio but with a fair amount of scatter in the data.

Due to the lack of measurements, the air entrainment rate used to calculate the mass air-to-fuel ratio was estimated from the ventilation parameter, $Ah^{1/2}$, where A is the cross-sectional area and h is the height of the vent. Although the general shape of the correlations are valid, the use of the ventilation parameter assumption causes the equivalence ratio data to be suspect. In addition, the elemental composition of the fuel volatiles for the wood was not corrected for char yield. A correction of this sort would tend to decrease the calculated equivalence ratio and increase the CO and CO_2 yields.

Gottuk et al.[5,16] conducted reduced-scale compartment fire tests specifically designed to determine the yield-equivalence ratio correlations that exist for various fuels burning in a compartment fire. A 2.2 m^3 (1.2 m × 1.5 m × 1.2 m high) test compartment was used to investigate the burning of hexane, PMMA, spruce, and flexible polyurethane foam. The test compartment was specially designed with a two-ventilation path system that allowed the direct measurement of the air entrainment rate and the fuel volatilization rate. The setup created a two-layer system by establishing a buoyancy-driven flow of air from inlet vents along the floor, up through the plume, and exhausting through a window-style exhaust vent in the upper layer. There was no inflow of air through the exhaust vent. The upper layer gas mixture was sampled using an uncooled stainless steel probe placed into the compartment through the center of the exhaust vent. This location for the probe was chosen after species concentration and temperature measurements, taken at several locations in the upper layer, showed a well-mixed, uniform layer.

Table 2-5.1 shows the physicochemical properties used for the four fuels. It should be noted that in determining properties of a fuel, such as maximum yields or the stoichiometric fuel-to-air ratio, the chemical formula must characterize the volatiles, not necessarily the base fuel. For liquid fuels or simple polymers, such as PMMA, the composition of the volatiles is the same as the base fuel. However, more complex fuels can char or contain nonvolatile fillers, as found in polyurethane foams. As a result, the composition of the volatiles differs from that of the base material. As an example, the composition of the wood volatiles used in this study was obtained by adjusting the analyzed wood composition for an observed average of 25 percent char.[5]

The results of these compartment tests showed similarities to Beyler's hood experiments. However, some significant quantitative differences exist. Figure 2-5.7 compares the CO yield correlations from Beyler's hood study and that of these compartment tests for hexane fires. This plot illustrates the primary difference observed between the hood and compartment hexane and PMMA fire test results. An offset exists between the rise in CO yield for the two studies. For the hood experiments, higher CO pro-

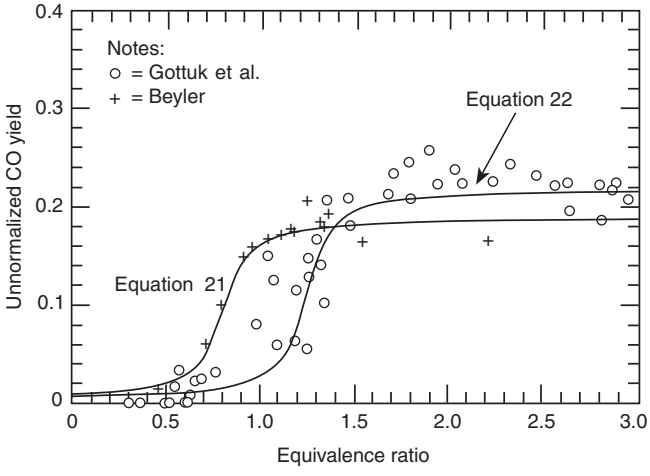

Figure 2-5.7. ***Comparison of unnormalized CO yield correlations for hexane fires in a compartment and under a hood apparatus. (Figure taken from Reference 5.)***

duction was observed for overventilated ($\phi_p < 1$) and slightly underventilated burning conditions. For the compartment fire experiments, negligible CO was produced until underventilated conditions were reached. Consistent with the increased CO production and the conservation of carbon, CO_2 yields were lower for the hood experiments compared to the compartment fires. The spruce and polyurethane compartment fires produced similar CO yield-equivalence ratio correlations to those observed by Beyler in hood experiments (i.e., high CO yields were observed for overventilated fires).

The differences in CO formation can be explained in terms of temperature effects. For the region of discrepancy between equivalence ratios of 0.5 and 1.5, upper layer temperatures in Beyler's hood experiments and the spruce and polyurethane compartment fire experiments were typically below 850 K, whereas temperatures for the hexane and PMMA fires were above 920 K (temperatures typically associated with postflashover fires).[17]

As is detailed in the section on chemical kinetics, the temperature range between 800 and 900 K is a transition range over which the oxidation of CO to CO_2 changes from a very slow to a fast reaction. That is, for upper layer temperatures below 800 K, the conversion of CO to CO_2 does not occur at an appreciable rate to affect CO yields. Since the oxidation of a fuel first results in the production of CO, which then further reacts to form CO_2, the low temperatures (< 800 K) prevent CO from oxidizing. This results in high CO yields. For temperatures greater than 900 K, the reactions that convert CO to CO_2 occur faster as temperature increases. Therefore, for the overventilated conditions discussed above, the high temperatures associated with the hexane and PMMA compartment fires resulted in virtually all CO being oxidized to CO_2 for $\phi_p < 1$.

Overall, the compartment fire test results revealed that the production of CO is primarily dependent on the compartment flow dynamics (i.e., the equivalence ratio) and the upper layer temperature.

The National Institute of Standards and Technology, (NIST) Building and Fire Research Laboratory, has also performed reduced-scale compartment fire experiments using a natural gas burner for the heat source.[6] The compartment (0.98 m $\times$ 1.46 m $\times$ 0.98-m-high) had a single ventilation opening consisting of a 0.48-m wide by 0.81-m-high doorway. A large number of tests were conducted covering a range of heat release rates from 7 to 650 kW. Fires greater than 150 kW resulted in upper layer temperatures greater than 870 K and flames 0.5 to 1.5 m out of the door. This single ventilation opening and the large fires (up to 650 kW) produced non-uniform upper layer conditions. For fires with heat release rates greater than about 250 kW ($\phi > 1.5$), carbon monoxide concentrations in the front of the compartment were approximately 30 to 60 percent higher than in the rear. Temperature gradients of 200 to 300°C were observed from the back to the front of the compartment. Due to the nonuniform air entrainment at the base of the fire and possible mixing of additional air near the front, it is difficult to determine the local equivalence ratio for each region. The concentration gradient from front to rear of the compartment may have been due to differences in the local equivalence ratios. Nonetheless, plots of concentration measurements in the rear of the compartment versus equivalence ratio are quite similar to the data of Zukoski et al. and Toner et al. Yield data for these results have not yet been reported.

A second set of experiments was performed by NIST to investigate the generation of CO in wood-lined compartments.[18] Douglas fir plywood (6.4 mm thick) was lined on the ceiling and on the top 36 cm of the walls of the compartment described above. Natural gas fires ranging from 40 to 600 kW were burned in the compartment. The results showed that, for tests in which wood pyrolysis occurred, increased levels of CO were observed compared to burning the natural gas alone. Carbon monoxide concentrations (dry) reached levels of 7 percent in the front and 14 percent in the rear of the compartment. These are extremely high concentrations compared to the peak levels of 2 to 4 percent observed in the unlined compartment fire tests with the methane burner only. Typical peak CO concentrations observed for a range of fuels (including wood) in hood experiments[8–11] and the compartment fire experiments of Gottuk et al.[5] also ranged from 2 to 4 percent. However, concentrations greater than 5 percent have also been reported for cellulosic fuels burning in enclosures.[15,19]

Since wood is an oxygenated fuel, it does not require additional oxygen from entrained air to form CO. This enhances the ability of the wood to generate CO in a vitiated atmosphere. Therefore, there are two reasons that high CO concentrations can result in fires with oxygenated fuels in the upper layer. First, the fuel-bound oxygen allows the fuel to generate CO during pyrolysis. Second, due to preferential oxidation of hydrocarbons over CO, the limited oxygen in the upper layer reacts with the pyrolizing wood to form additional CO. Aspects of this chemistry are discussed in the next section.

These initial test results for fires with wood on the walls and ceiling emphasized the importance of adding additional fuel to the upper layer. The practical implications are significant, as many structures have cellulosic-based wall coverings and other combustible interior finishes. Because of the initial studies by NIST, Lattimer et al.[20] conducted a series of tests to evaluate the effect on species production from the addition of wood in the upper layer of a reduced-scale enclosure fire. The enclosure was the same as used by Gottuk et al.,[5] measuring 1.5 m wide, 1.2 m high and 1.2 m deep. Two primary sets of tests were conducted for cases with and without Douglas fir plywood suspended below the ceiling 1) with a 0.12 m^2 window vent opening and 2) with a 0.375 m^2 doorway opening, both leading to a hallway.

In the compartment with a window opening and wood burning in the upper layer, Lattimer et al. measured CO concentrations of 10 percent on average, which is nearly three times greater than the levels measured without the wood. Peak concentrations were as high as 14 percent, the same as measured by Pitts et al.[18] CO concentrations were similarly high when the doorway opening was used. In this case, the quasi-steady state average CO concentrations were 8 percent with peaks greater than 10.6 percent with wood compared to approximately 5.7 percent average levels with a doorway vent and no wood. Regardless of the vent opening, these tests

showed that wood in the upper layer resulted in CO concentrations increasing dramatically (10.1 percent, vs. 3.2 percent without wood) with only small increases in the CO_2 concentrations (11.6 percent, vs. 10.4 percent without wood). These trends are summarized in Table 2-5.3, which presents the average upper layer species concentrations for tests with and without wood for both window and doorway vent conditions. For comparison, the data from the NIST research has also been included.

The compartment equivalence ratio was calculated for both the tests with and without wood in the upper layer when the window vent was used. Figures 2-5.8 through 2-5.10 show the corresponding calculated yields of CO_2, O_2, and CO plotted as a function of equivalence ratio. Also included in these plots are the data from the compartment fires of Gottuk et al.[5] The results show that the global equivalence ratio concept is capable of predicting the CO_2, O_2, and CO yields, although somewhat fortuitous, in a compartment with wood pyrolyzing in the hot, vitiated upper layer. These tests also indicate that the correlations hold to fairly high equivalence ratios of about 5.5, as observed for the tests with wood. More work is needed to determine whether the global equivalence ratio concept can predict species levels when non-oxygenated fuels are in the upper layer. It is also unclear whether other oxygenated fuels will follow the correlations as well as the available wood fire data.

The data in Table 2-5.3 should provide an assessment of the effect of the ventilation opening on species generation. However, it is uncertain whether the differences are due more to differences in sampling locations relative to the flame regions. In the tests with a doorway vent, the larger opening resulted in larger air flow rates and, thus, larger fires in the compartment (approximately 500 kW vs. 220 kW with the window vent). The larger fires increased the flame zone within the compartment. Consequently, the sampling probe was probably within the flame zone at times, which would yield higher CO and lower CO_2 concentrations than measurements from the window vent tests in which the sampling probe was not

Table 2-5.3 ***Summary of Quasi-Steady State Average Species Concentrations (percent volume dry) for Underventilated Reduced-Scale Compartment Fire Tests with and without Wood in the Upper Layer[20,21]***

Window Vent Tests[20]	No Wood in Upper Layer	Wood in Upper Layer
CO	3.2	10.1
CO_2	10.3	11.6
O_2	0.2	0.04
Doorway Vent Test[20]		
CO	5.7	8.0
CO_2	8.7	9.6
O_2	0.2	0.1
NIST Results[21]		
Doorway Vent		
CO	2.6–1.8[a]	5.5–11.5[a]
CO_2	6.5–7.5[a]	10–15.5[a]
O_2	0.1–0[a]	0–0.5[a]

[a]Front and back, respectively

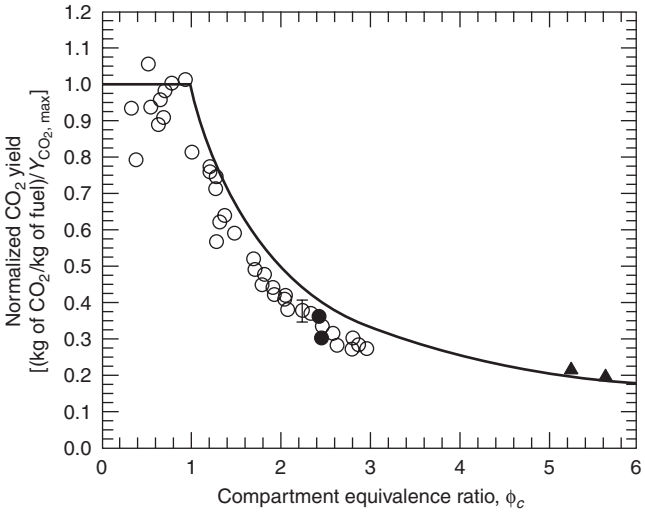

Figure 2-5.8. ***The normalized CO_2 yield data of Gottuk et al.[5] (○), data from Lattimer et al.[20] with no wood in the compartment upper-layer (●), and data from Lattimer et al.[20] with wood in the upper-layer (▲). Also shown in this plot is the normalized CO_2 yield estimated using the complete combustion model of Equation 14 (—).***

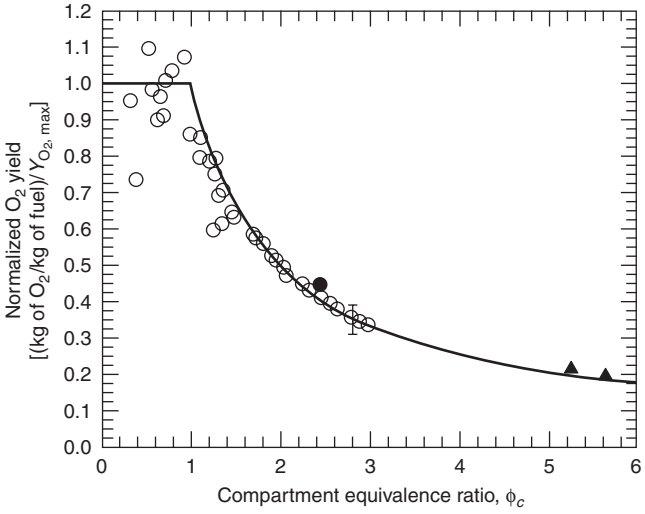

Figure 2-5.9. ***The normalized O_2 yield data of Gottuk et al.[5] (O), data from Lattimer et al.[20] with no wood in the compartment upper-layer (●), and data from Lattimer et al.[20] with wood in the upper-layer (▲). Also shown in this plot is the normalized O_2 yield estimated using the complete combustion model of Equation 14 (—).***

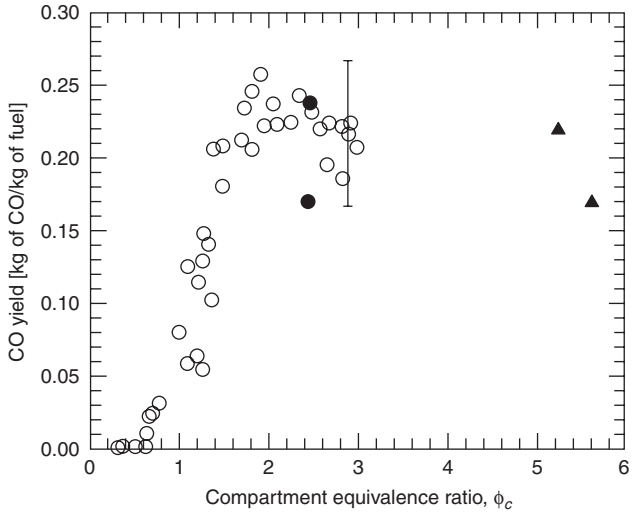

Figure 2-5.10. ***The unnormalized CO yield data of Gottuk et al.[5] (○), data from Lattimer et al.[20] with no wood in the compartment upper-layer (●), and data from Lattimer et al.[20] with wood in the upper-layer (▲).***

sampling from a flame zone. With the window vent, the fires were small enough such that there was no ceiling jets at the level of the sampling probe.

The research discussed thus far has concentrated on reduced-scale enclosures. Limited full-scale studies have been reported in the literature to date. One study by NIST systematically examined the production of species in light of the global equivalence ratio concept. NIST conducted a set of tests using a standard enclosure (as defined by ISO 9705) to compare the results from the NIST reduced-scale enclosure tests to fires conducted in a full-scale enclosure.[22–25] The enclosure measured 2.44 m wide, 3.67 m deep and 2.44 m tall, with a door (0.76 m by 2 m) centered at one end of the compartment. The fires consisted of a 35-cm-diameter natural gas burner centered in the enclosure. The burner was scaled to provide the same exit gas velocities as in the reduced-scale enclosure tests. Twelve tests were conducted, with fires ranging in size from 0.5 to 3.4 MW. In one test, the ceiling and upper portions of the walls were lined with 12.7 mm thick plywood.

In the full-scale enclosure, fires greater than 1250 kW created underventilated conditions. The NIST researchers concluded that although the reduced-scale and full-scale enclosures were geometrically similar, with good agreement between predicted mass flows, the differences in measured gas concentrations indicated that the generation of combustion products is not entirely controlled by the ventilation within the compartment. CO concentrations (upwards of 6 percent by volume) were as much as two times higher in the full-scale enclosure than in the reduced-scale tests. These results also coincided with higher upper layer temperatures, approaching 1400 to 1500 K. The variation in CO concentrations from front to back in the enclosure was reversed in the full-scale enclosure compared to the reduced-scale enclosure. In the full-scale enclosure, higher CO concentrations were observed in the back of the compartment. In the reduced-scale enclosure, higher concentrations were measured in the front. Pitts primarily associates the higher CO concentrations with the high layer temperatures that are in the range that strongly favor the formation of CO toward equilibrium concentrations (values can approach 16 percent at ϕ of 3).[25]

One full-scale enclosure test was conducted with wood in the upper layer. This test resulted in high CO concentrations of 8 percent in the front and 12 percent in the rear for a 2 MW fire. The temperatures were lower than those observed in the full-scale tests without wood. These results are similar to those observed in the NIST reduced-scale enclosure.

Chemical Kinetics

The field of chemical kinetics can be used to describe the changes in gas composition with time that result from chemical reactions. The kinetics of actual combusting flows are dependent on the initial species present, temperature, pressure, and the fluid dynamics of the gases. Due to the inability to adequately characterize the complex mixing processes and the significant temperature gradients in turbulent flames, the use of kinetic models is restricted to simplified combusting flow processes. Consequently, the fire plume in a compartment fire is beyond current chemical kinetics models. However, the reactivity of the upper layer gas composition can be reasonably modeled if one assumes that the layer can be characterized as a perfectly stirred reactor, or that the layer gases flow away from the fire plume in a plug-flow-type process.[13,14] Pitts has shown that no significant differences between results exist for either modeling approach when applied to these upper layers.[13]

Several kinetics studies have been performed to examine aspects of the reactivity of upper layer gases.[12,13,14] Comparisons between different hood experiments and between hood and compartment fire experiments have indicated that upper layer temperatures have an effect on CO production. The results of these chemical kinetics studies provide insights into CO generation in compartment fires, which also serve to explain the differences in CO yields between experiments with respect to temperature effects. These studies primarily focused on the question "What would the resulting composition be if the upper layer gases in the hood experiments existed at different isothermal conditions (constant temperature)?" A particular focus was to examine the resulting compositions for cases modeled under the high temperatures characteristic of compartment fires. Chemical kinetics models calculate the change in species concentrations with respect to time. Calculations are dependent on the reaction mechanism (i.e., the set of elementary reactions and associated kinetic data) and the thermodynamic data base used.

Thermodynamic data is fairly well known and introduces little uncertainty into the modeling. However, reaction mechanisms do vary, and this is an area of active research. Pitts presents a comparison of the use of various

mechanisms in the literature.[13] The comparison indicates that reaction kinetics for high temperatures (greater than 1100 K) are fairly well understood. However, the elementary reactions for the range of 800 to 1000 K are not as certain; therefore, quantitative modeling results in this range may be suspect. Nevertheless, the general trends presented below are valid despite any uncertainty associated with the mechanisms used.

Chemical kinetics modeling shows that significantly different trends occur for overventilated and underventilated burning conditions. This can be seen in Figures 2-5.11 and 2-5.12, which present major species concentrations with respect to time for an overventilated and underventilated condition, respectively. Figure 2-5.11 shows a modeled case for ϕ equal to 0.91 and a temperature of 900 K. The initial composition is taken from Beyler's data for a fire with a layer temperature of 587 K. The temperature of 900 K corresponds to the temperature observed by Gottuk et al. for a hexane compartment fire at the same global equivalence ratio. For overventilated conditions, increased temperatures cause CO concentrations to initially increase. As can be seen in Figure 2-5.11, this is due to the incomplete oxidation of hydrocarbons (modeled as C_2H_4). Once the hydrocarbons are consumed, available O_2 is used in the oxidation of CO to CO_2. Since overventilated conditions indicate excess oxygen, CO concentrations are reduced to zero given sufficient time. This is representative of the case of the overventilated hexane and PMMA compartment fires studied by Gottuk et al., in which the higher compartment temperatures, compared to the hood tests of Beyler, resulted in near-zero CO yields for $\phi < 1$.

Figure 2-5.12 shows an underventilated case for ϕ equal to 2.17 and a temperature of 1300 K. The initial composition is taken from Morehart et al. for a methane hood experiment.[12] Similar to the overventilated conditions, CO increases due to the oxidation of hydrocarbons (CH_4).

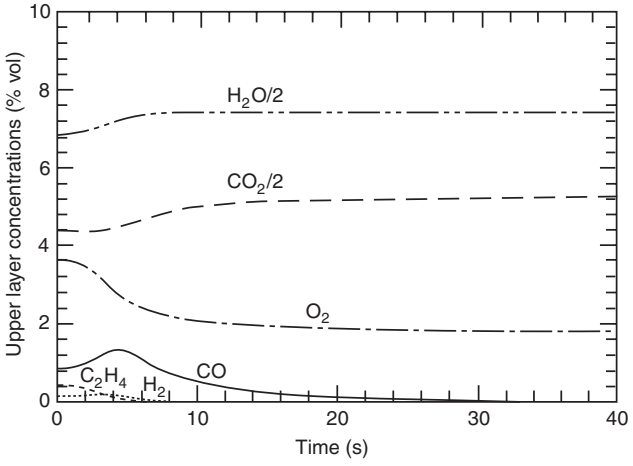

Figure 2-5.11. ***Chemical kinetics model calculated species concentrations versus time for an overventilated (ϕ = 0.91) burning condition with an upper layer temperature of 900 K. (Figure taken from Reference 14.)***

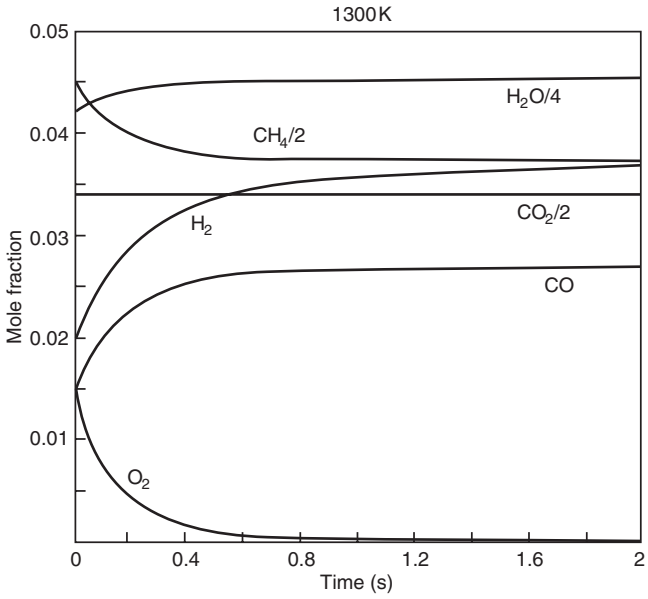

Figure 2-5.12. ***Chemical kinetics model calculated species concentrations versus time for an underventilated (ϕ = 2.17) burning condition with an upper layer temperature of 1300 K. (Figure taken from Reference 13.)***

However, the available oxygen is depleted before the hydrocarbons are fully oxidized. The resulting composition consists of higher levels of CO and H_2 and decreased levels of unburned fuel. Carbon dioxide levels remain virtually unchanged. The much higher temperature studied in this case results in much quicker reaction rates, as is reflected in the 2 s time scale for Figure 2-5.12 compared to 30 s for Figure 2-5.11.

It is clear from Figures 2-5.11 and 2-5.12 that hydrocarbon oxidation to CO and H_2 is much faster than CO and H_2 oxidation to CO_2 and H_2O, respectively. This is a result of the preferential combination of free radicals, such as OH, with hydrocarbons over CO. Carbon monoxide is oxidized almost exclusively by OH to CO_2.[26] Therefore, it is not until the hydrocarbons are consumed that free radicals are able to oxidize CO to CO_2.

The formation and consumption of CO in a reactive gas mixture is dependent on both the temperature of the mixture and the amount of time over which the mixture reacts. This point is illustrated in Figure 2-5.13 which shows the resulting CO concentrations at different isothermal conditions from an initial gas mixture taken from an underventilated fire (ϕ = 2.17). Pitts noted that there are three distinct temperature regimes. At temperatures under 800 K, the gas mixture is unreactive and the CO to CO_2 reactions are said to be "frozen out." As the temperature increases in the range of 800 to 1000 K, the mixture becomes more reactive and CO is formed at faster rates, due to the oxidation of unburned hydrocarbons. For the time period shown, it is interesting to note that the ultimate concentra-

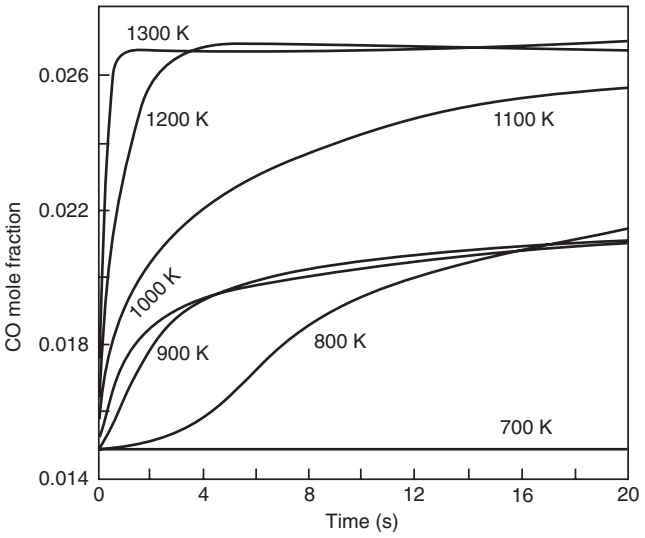

Figure 2-5.13. ***Carbon monoxide concentrations as a function of time for a range of isothermal conditions. Initial concentrations from a methane hood fire at ϕ = 2.17.[13]***

tion is approximately constant* for each case in this temperature range. The third regime of high temperatures above 1100 K is characterized by fast reaction rates and much higher CO production for the 20 s reaction time shown. With sufficient time, the ultimate CO concentration for the 800 to 1000 K conditions would approach the same value as that seen for the higher temperatures.

Results of Zukoski et al.[10] and Gottuk et al.[14] indicated that layer temperatures of 850 to 900 K or higher are needed for the layer gases to be reactive. Considering that the minimum (freeze out) temperature above which a gas mixture is reactive is dependent on the time scale evaluated. These values are consistent with the results shown in Figure 2-5.10. In terms of compartment fires, the time over which the gases react can be taken as the residence time of the gases in the upper layer, which is calculated according to Equation 11. In many practical cases of high-temperature compartment fires, it would be reasonable to assume that the residence time of layer gases would be longer than the time needed for the gas mixture to react fully.

Fire Plume Effects

Although a fire plume is too complex to adequately model the chemistry, the hood experiments discussed earlier provide significant insights with respect to the fire plume and species production in compartment fires. Results of Beyler's hood experiments suggest that the production of upper layer gases is independent of the structure and fluid dynamics of the flame.

Beyler modified a 19 cm propane burner by including a 2.8 cm lip to enhance turbulence and the large-scale structure of the flame.[8] Compared to the no-lip burner, the flame was markedly changed, and air entrainment was increased by 30 percent. Yet, the upper layer species-equivalence ratio correlations were the same for both burners. Additionally, as shown in Figure 2-5.3, correlations for different size burners are also identical.

The insensitivity of species yields to the details of the flame structure is also suggested by the compartment fire hexane results of Gottuk et al.[5] The correlations include data from fires utilizing various size burn pans and with a wide range of air entrainment rates. In several cases, nearly equal steady-state equivalence ratio fires were obtained with quite different burning rates and air entrainment rates. Although the conditions varied significantly, the positive correlation between yields and equivalence ratio suggests that the yields are not sensitive to the details of the flame structure.

The temperature of the fire plume has a significant effect on species production from the fire plume. It is reasonable to assume that differences in upper layer temperature are also reflective of a similar trend in the average temperature of the fire plume gases. An increase in the upper layer temperature can increase the fire plume temperature in two ways. For plumes that extend into the upper layer, entrainment of hotter upper layer gases will result in increased plume temperatures compared to plumes in layers with lower temperature gases. Secondly, an increase in the surrounding temperature (both gases and compartment surfaces) reduces the radiant heat loss from the plume, thus resulting in a higher plume temperature.

The effect of temperature on species generation in a fire plume can be found in the methane hood experiments of Morehart et al.[12] and Zukoski et al.[11] Morehart studied the effect of increasing temperature on layer composition by adding different levels of insulation to his hood. Except for the insulation, the test conditions (e.g., ϕ of 1.45 and layer interface height) were held constant. For the range of temperatures studied (500 to 675 K), substantial increases in products of complete combustion and decreases in fuel and oxygen occurred with increasing layer temperature. Upper layer oxygen mass fraction was reduced by approximately 70 percent and methane was reduced by 25 percent. Excluding one outlier data point, CO concentrations increased by 25 percent. The temperatures of the Morehart et al. upper layer were well below 700 K. Therefore, based on kinetics modeling, these layers were unreactive at these low temperatures. It follows that the change in layer composition must have been due to changes in the plume chemistry. The more complete combustion can be attributed to an extension of the flammability limits (or reaction zone) in the plume due to raising the flame temperature. The above discussion demonstrates that increasing the plume temperature substantially increases the consumption of O_2 and fuel, and primarily increases the levels of products of complete combustion.

*Note that although the ultimate CO concentration is roughly constant, the value of 2.1 percent for this illustration is not to be taken as a universal limit for this temperature range. In general, the resulting CO concentration will depend on the initial gas composition and the time to which the mixture is allowed to react.

The effect of changing temperature on a compartment fire upper layer composition is twofold (1) the generation of species in the fire plume is changed, and (2) oxidation of post-flame gases in the layer is affected. Elevated compartment temperatures correlate with increased fire plume temperatures and more complete oxidation of the fuel to CO_2 and H_2O within the fire plume. The layer temperature dictates post-flame oxidation in the upper layer.

Upper layer temperatures below about 800 K indicate chemically unreactive layers. As such, combustion within the fire plume controls the final CO levels that would be measured in the upper layer. At these low temperatures significant levels of CO can be generated even for some overventilated conditions ($0.5 < \phi < 1$). The yield of CO is inversely proportional to temperature for overventilated conditions and directly proportional to temperature for underventilated conditions.

Upper layer temperatures of about 900 K and higher indicate chemically reactive layer gases. As such, reactions in the layer dictate final CO production. Temperatures above 900 K allow nearly complete oxidation of CO to CO_2 for overventilated conditions. For underventilated fires, chemical kinetics modeling indicates that higher temperature environments may result in slightly higher CO yields due to preferentially accelerated hydrocarbon oxidation compared to CO oxidation.

During underventilated conditions, two mechanisms affecting net CO formation compete (i.e., CO and hydrocarbon oxidation). Increasing gas temperatures above 900 K depletes CO by accelerating the CO to CO_2 conversion. However, incomplete oxidation of unburned hydrocarbons increases the CO production. Since hydrocarbon oxidation is much faster than CO oxidation, net CO levels increase until all available oxygen is consumed.

Transient Conditions

Transient conditions cause the upper layer equivalence ratio to differ from the plume equivalence ratio. A fast-growing fire will tend to have a ϕ_{ul} that is less than ϕ_p. Conversely, a fire that is dying down quickly, such that ϕ_p is decreasing rapidly, will have a ϕ_{ul} that is higher than ϕ_p. These trends result due to the upper layer being a temporary collection reservoir for the gases from the fire plume.

In an effort to characterize transient conditions, Gottuk et al. defined a steady-state time ratio, τ_{SS}, as the ratio of the residence time, t_R, to a characteristic growth time of the fire. Since fire growth is directly related to the fuel volatilization rate, a representative growth time of the fire was defined as the ratio of the fuel mass loss rate, $\dot{m}_f$, to the derivative of the fuel volatilization rate, $\ddot{m}_f$. An increase in τ_{SS} is indicative of more transient conditions.

$$\tau_{SS} = \frac{t_R}{\dot{m}_f/\ddot{m}_f} \tag{18}$$

An analysis of the transient nature of the compartment fires studied by Gottuk et al. showed that values well below 1 indicated near steady-state conditions, such that the plume and upper layer equivalence ratios could be considered equal. Investigation of individual fires showed that the steady-state time ratio decreased below 1.0 at very early times in the fire. Typically, the ratio was 0.1 or less for the quasi-steady-state periods over which data was averaged. For some fires, during the highly transient transition from overventilated to underventilated conditions, the τ_{SS} increased quickly, approaching a value of 1.

The correlations presented in the engineering methodology represent data that have been averaged over steady-state (hood experiments) or quasi-steady-state (compartment fires) periods. For the purpose of modeling fires with respect to time it is of interest to know how the species yields correlate with the equivalence ratio during transient conditions (i.e., as the fire is growing). Determining this correlation was accomplished by plotting the yield to equivalence ratio data for individual fires from the time of ignition to the steady-state period. These transient correlations were compared to the steady-state correlations obtained from steady-state averaged data from all tests (e.g., the CO yield correlation shown in Figure 2-5.7). An example of one comparison is shown in Figure 2-5.14. Figure 2-5.14 shows the steady-state hexane CO yield correlation along with the transient yield vs. equivalence ratio data for a hexane compartment fire that obtained a steady-state average ϕ_p of 3. The solid dots in Figure 2-5.14 represent the steady-state time ratio data, τ_{SS}. For this example, τ_{SS} remained fairly constant at about 0.1 for the entire fire. And as can be seen, the agreement between the transient and steady-state correlations is quite good, even for the transition to underventilated conditions. Good agreement between transient and steady-state data was also observed for CO_2 and O_2 yield correlations.

Although more transient in nature than the hood experiments, the compartment fires are characterized as primarily quasi-steady and, therefore, do not differ significantly from Beyler's hood experiments in this respect. This analysis also shows that the species yield correla-

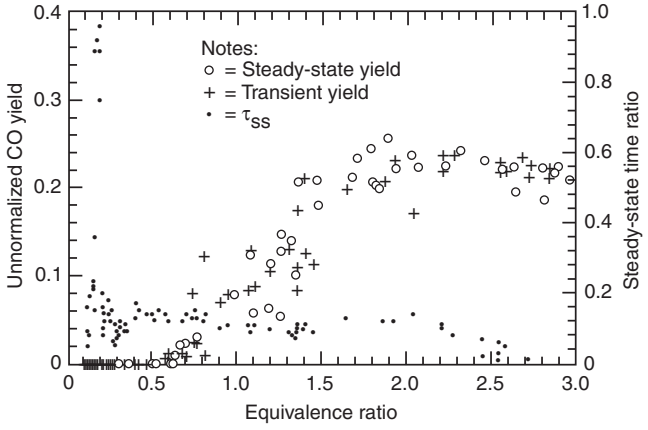

Figure 2-5.14. ***Comparison between a transient, unnormalized CO yield correlation for a hexane fire with an average steady-state ϕ_p of 3 and the steady-state correlation for all hexane fires studied by Gottuk et al. The steady-state time ratio, τ_{SS}, data are shown as solid dots. (Figure taken from Reference 16.)***

tions developed for steady-state conditions are representative of the transient growth periods of these fires.

In terms of full-scale application, these results suggest that ϕ_p and ϕ_{ul} are approximately equal for compartment fires characterized by relatively slow growth compared to the upper layer residence time (i.e., $\tau_{SS} \ll 1$). However, the low τ_{SS} values observed in the reduced-scale compartment fires may not always be representative of full-scale fires. The reduced-scale compartment fires had residence times typically between 4 and 20 s. These short residence times were a result of having relatively large fires compared to the compartment volume. Until flashover conditions are approached, a full-scale compartment fire will most likely have smaller fires compared to the volume of the space. As a result, the residence time of gases in the upper layer of a full-scale fire may be much longer. Times on the order of 5 to 10 min. may not be unrealistic in some cases. Therefore, in the case of a fast-growing full-scale fire, values of ϕ_p could increase relative to ϕ_{ul}. The application point is that the control volume used for the equivalence ratio must be considered with respect to the residence time of gases in the upper layer.

Species Transport to Adjacent Spaces

The species levels transported from a compartment depend on a variety of conditions produced during the course of the fire. As compartment fire gases exit the compartment, they entrain the gases present in the adjacent space. (See Figure 2-5.15.) If a fuel-rich mixture is produced in the compartment, the gases flowing out may ignite, causing burning in the adjacent space. This burning is an indication that oxidation reactions are taking place, which ultimately affects the species levels transported to remote areas. As the gases continue to flow through the adjacent space, they are cooled by mixing with surrounding gases and heat losses to the boundaries. Eventually, gases are cooled to a temperature below which oxidation reactions do not readily occur. At this point the reactions are said to be frozen. The amount of combustion products that exist at this point will continue to flow throughout the rest of the structure. As a result, combustion product levels in the overall structure will accumulate as the fire inside the compartment persists and/or additional items in the structure begin to burn.

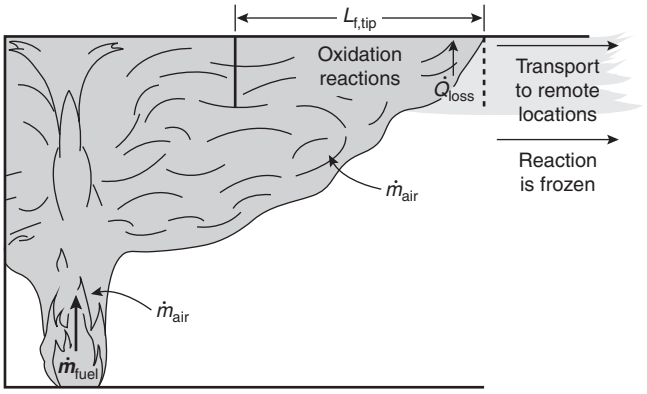

Figure 2-5.15. ***Phenomena controlling species transport to remote locations.***

Conditions inside the fire compartment and in the directly adjacent space will govern the species levels transported to remote locations. The primary consideration is the conditions that develop inside the compartment. If burning outside of the fire compartment occurs due to either flame extension or external burning, gases will continue to react outside of the compartment influencing the species levels transported to remote areas. The degree to which gases react outside the compartment depends on the mixing of oxygen with the fuel-rich gases flowing out the compartment, and the addition of fuel to the gases flowing along the adjacent space.

General Effects of Burning Outside the Compartment

Species levels transported to remote locations will be equivalent to those formed inside the compartment unless burning occurs outside. Chemical kinetics indicate that oxidation reactions cannot occur efficiently outside the compartment unless gas temperatures are near those produced at the onset of flashover (775–875 K). (See the section in this chapter on chemical kinetics.) In the presence of oxygen, hydrocarbons begin to react efficiently when temperatures are above 700 K.[13] Perhaps more importantly, the oxidation of CO to CO_2 does not readily occur until temperatures rise above 800 K. The occurrence of burning outside the compartment, either from flame extension or the onset of flashover, will result in local temperatures in excess of 1300 K.[4] At these temperatures, oxidation reactions for both hydrocarbons and CO occur in the presence of available oxygen.

The occurrence of burning outside the compartment has been shown, in most situations, to reduce the incomplete combustion products (including smoke and CO levels) transported to remote locations.[5,27–29] The burning in unconfined adjacent areas (e.g., surroundings) has been measured to decrease incomplete combustion products more efficiently than burning in confined adjacent areas (e.g., a corridor). In addition, the consumption of incomplete combustion products during burning in confined areas was found to be sensitive to the air entrainment into the plume/ceiling jet flow. This entrainment is a function of the mass flow from the compartment, the geometry of the opening between the compartment of fire origin and the adjacent space, and the geometry of the adjacent space itself. Smoke layers that develop in confined adjacent spaces can cause lower oxygen levels to be entrained into the plume/ceiling jet flow in the adjacent space, increasing the incomplete combustion product levels transported to remote areas.

Burning in Unconfined Adjacent Areas

Unconfined adjacent areas are those areas where the flame extending from the compartment of origin is not redirected by the boundaries of the adjacent area, and the

gases are allowed to burn as a buoyant plume. Examples of unconfined adjacent areas include surroundings, atriums, and corridors with high ceilings relative to the door height of the burning compartment. Gottuk et al.[14,30] investigated the impact of external burning on combustion products downstream of an unconfined jet. The compartment was connected to its surroundings through a window opening. Tests were performed with compartment fires with and without external burning. In these tests, a compartment equivalence ratio of 1.6 was the lowest ϕ_c where external burning was noted to occur. The effects of external burning on the CO levels downstream of the fire are shown in Figure 2-5.16. With a compartment equivalence ratio greater than 1.6, CO levels were measured to decrease below the fire compartment levels. The CO yield is shown to decrease to a minimum of 0.02 at ϕ greater than 2.0. The decrease in CO represents a 75 to 90 percent reduction of the CO generated in the fire compartment.

Burning in Confined Adjacent Areas

Burning in a confined adjacent area, such as a corridor or room, causes the external flame to impinge on a ceiling, and possibly on walls. Compared with flow in an unconfined area, the ceiling and walls in the confined area will reduce the amount of air entrainment into the gas jet exiting the fire compartment. The effects of burning in confined areas on species transport have been investigated by Ewens et al.[27,31] and Lattimer et al.[28,29] using the same fire compartment design in the unconfined external burning study (Figures 2-5.17a and b).[16,30] The transport of species to remote locations is geometry dependent and can be affected by smoke layers that develop in the confined area. However, species levels transported to remote areas can be predicted by defining an equivalence ratio for a control volume involving both the fire compartment and the burning in the adjacent space.

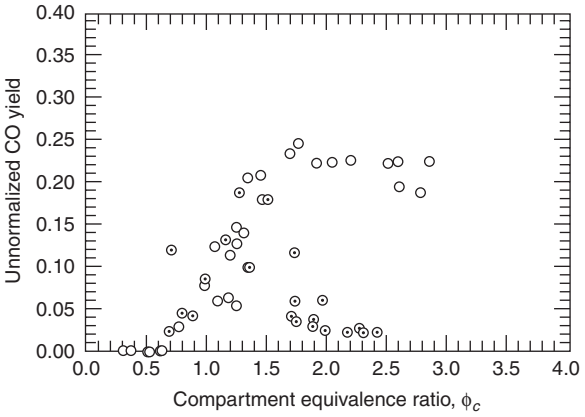

Figure 2-5.16. ***Effect of external burning on CO levels downstream of an unconfined adjacent area. CO yield versus compartment equivalence ratio for hexane compartment fires with an exhaust jet to the open atmosphere through a window opening; (○) compartment levels, (⊙) downstream levels. (Data taken from References 16 and 30.)***

Species transport has been evaluated for two common compartment-hallway configurations. Ewens[27] and Lattimer et al.[29] evaluated species transport in a configuration with the fire compartment on the end of a hallway. (See Figure 2-5.17a.) Lattimer et al.[28,29] performed a study with the fire compartment on the side of a hallway. (See Figure 2-5.17b.) In both studies, most tests were performed with a window connecting the compartment and hallway.

Using the apparatus shown in Figure 2-5.17a, Ewens[27] evaluated the effects of different geometric variables and compartment stoichiometry on CO levels (in addition to other species) downstream of the external burning where reactions were considered frozen. As shown in Figure 2-5.18, Ewens[27] demonstrated that burning in confined areas outside the compartment decreases incomplete combustion product levels, but not always to the same extent as when the fire gases spill into an unconfined space. The degree of oxidation was found to be dependent on both air entrainment into the gases exiting the compartment and the fuel flowing out of the compartment. The data of Ewens shows that both fire size and geometric parameters will impact species production. The two important results to understand are that geometries which increase air entrainment in the adjacent space (e.g., an inlet soffit vs. no soffit), or reduce the layer depth in the adjacent space, will enhance the oxidation reactions and result in lower levels of incomplete combustion products, such as CO.

Fire gases flowing into and through the adjacent space entrain surrounding gases as they flow away from the fire compartment. These gases can undergo chemical reactions, particularly as they are within the flaming region. A sample plot of the species variation along the flame length in the hallway is shown in Figure 2-5.19.[27] Results shown in Figure 2-5.19 are from post-flashover hexane fire tests with an average compartment equivalence ratio of $\phi = 2.0$, a 0.12 m^2 opening (0.50 m wide $\times$ 0.24 m high) connecting the compartment and adjacent space, and no inlet soffit above the opening in the hallway. These data represent time-averaged conditions 0.025 m below the ceiling along the hallway during the quasi-steady state period of the fire, when external burning was occurring.

Gases entered the adjacent space as a ceiling jet, but were allowed to expand horizontally until intersecting the walls of the hallway. For this geometry, the largest increase in the total mass flow rate was during the first half of the flame length, which was 2.7 m (on average) from the compartment. By $x/L_{f,\text{tip}} = 0.75$, the total mass flow rate had reached a maximum. This indicated that all of the entrainment into the ceiling jet flow occurred by $x/L_{f,\text{tip}} = 0.75$. The majority of the oxidation reactions had also occurred by $x/L_{f,\text{tip}} = 0.75$. The mass flow rates of CO, CO_2, and O_2 were essentially constant downstream of $x/L_{f,\text{tip}} = 0.75$. This indicates that the oxidation of CO to CO_2 was frozen by an $x/L_{f,\text{tip}} = 0.75$. Small amounts of total hydrocarbons (THC) continued to react from $0.75 < x/L_{f,\text{tip}} < 1.0$; however, this was not measured to significantly increase CO levels.

Analysis of data in Figure 2-5.19, as well as other data by Ewens et al.[27,31] and Lattimer et al.,[28,29] indicates that by the flame tip all of the oxidation reactions have oc-

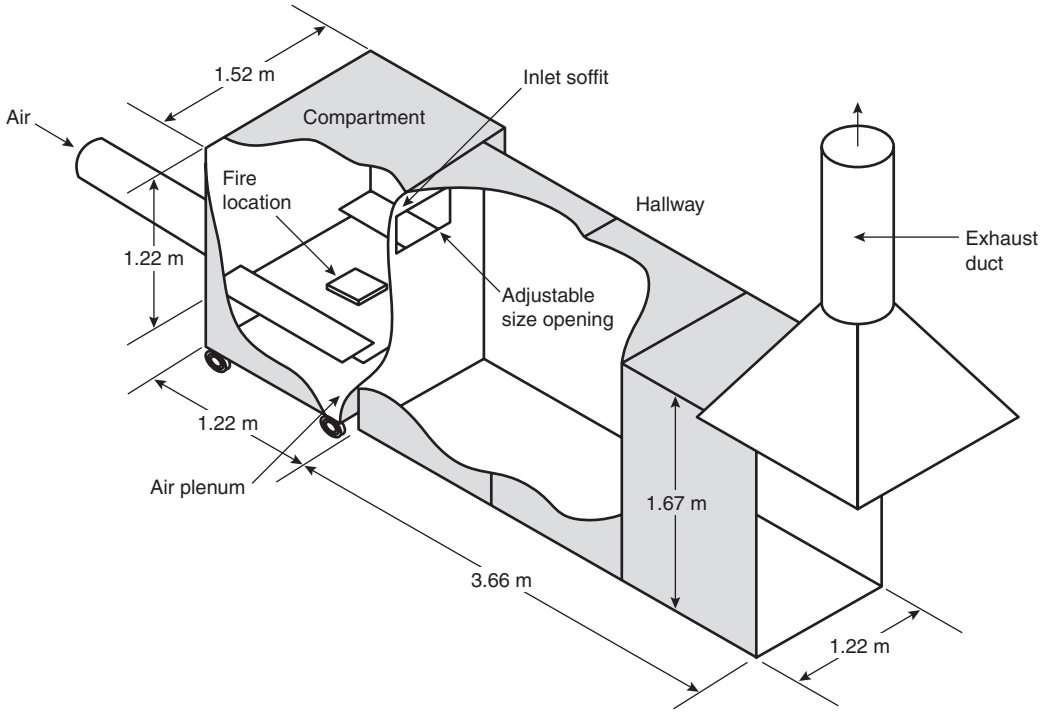

Figure 2-5.17a. ***Compartment on the end of a hallway.***[27,29,31]

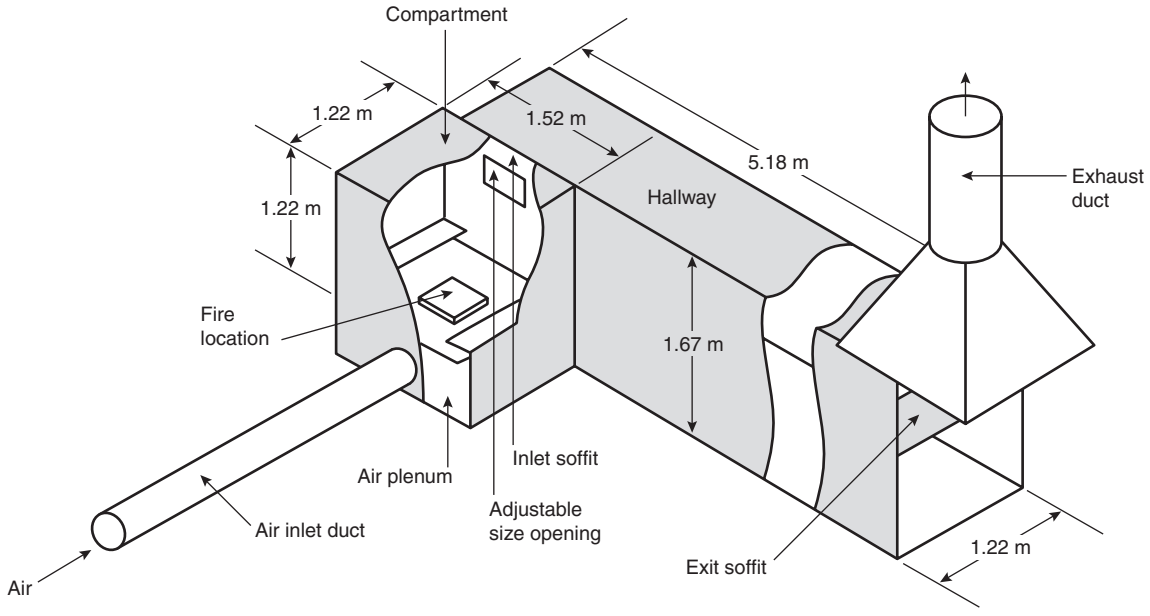

Figure 2-5.17b. ***Compartment on the side of a hallway.***[28,29]

curred. As a result, the mass flow rates of the major combustion products beyond the flame tip will be transported to remote locations. The mass flow rate levels will be influenced by the oxygen availability in the flaming region. Based on test results from Ewens et al.[27,31] and Lattimer et al.,[28,29] mixing near the compartment has been shown to have the most significant influence on the combustion products transported to remote areas.

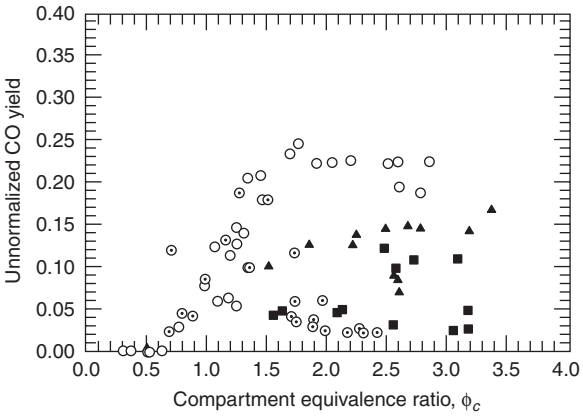

Figure 2-5.18. ***Effect of external burning on CO levels downstream of a post-flashover compartment fire. Adjacent hallway with a (▲) 0 m inlet soffit and (■) 0.20 m inlet soffit. (⊙) Unconfined area and (○) inside the compartment. (Data taken from References 16, 27, 30, 31.)***

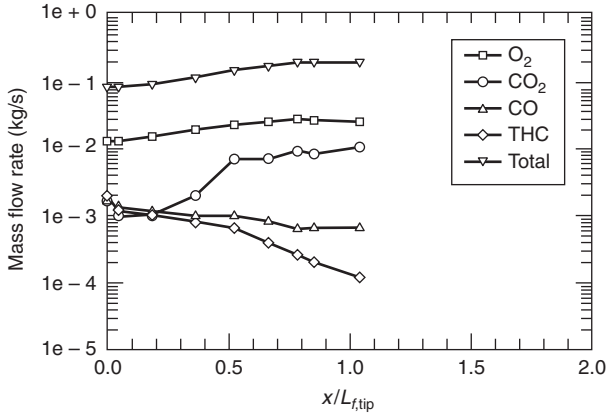

Figure 2-5.19. ***The mass flow rates in a space adjacent to a post-flashover fire with external burning plotted versus the ratio of the distance down the hall, x, to the length of the flame to its tip, $L_{f,tip}$. Opening of 0.12 m², no inlet soffit above the opening, and an average compartment ϕ = 2.0. (Data taken from Reference 27.)***

Predicting Species Levels

Lattimer[32] performed additional analysis on Ewens' data to develop a correlation between species transported and ϕ for a control volume consisting of part of the area in the adjacent space where burning occurred. In this set of data, the mixing in the adjacent space (hallway) was varied by using windows with different areas and aspect ratios to connect the compartment to the adjacent space, and by adding a 0.20 m soffit above the window. The equivalence ratio in this analysis was calculated using a control volume that extended to the sampling point located in the adjacent space. Using this control volume, the mass flow rate of air for the ϕ_{cv} calculation in Equation 13 was the air flow rate into the compartment plus the air entrainment into the plume/ceiling jet flow in the adjacent space, up to the sampling location. In these experiments, gas sampling was always performed in or just downstream of the flame within the hallway.

The species yields are plotted in Figures 2-5.20 through 2-5.23 vs. the control volume equivalence ratio, ϕ_{cv}. Note that CO yields are not normalized because for various fuels unnormalized CO yields were found to correlate best with ϕ. The line in the normalized O_2 depletion, and CO_2 and THC yield plots, represents the results from the complete combustion model presented in Equation 14. Due to limited data near the compartment, there are few data points at high ϕ_{cv}.

The trends in the species data were similar to those observed in the hood experiments by Beyler[8,9] and in the compartment experiments by Gottuk et al.[5] The normalized O_2 depletion is approximately unity at ϕ_{cv} less than

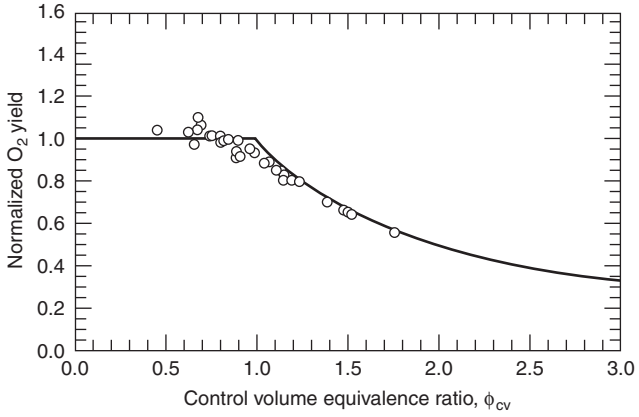

Figure 2-5.20. ***Normalized O_2 depletion of gases in a space adjacent to a post-flashover compartment fire. Control volume includes fire compartment and a portion of the adjacent space where burning occurs.***

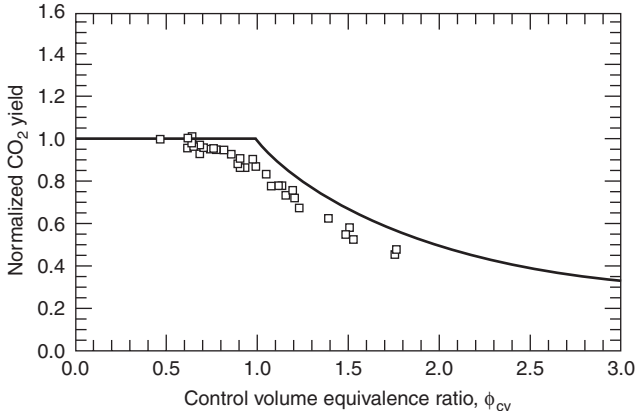

Figure 2-5.21. ***Normalized CO_2 yields of gases in a space adjacent to a post-flashover compartment fire.***

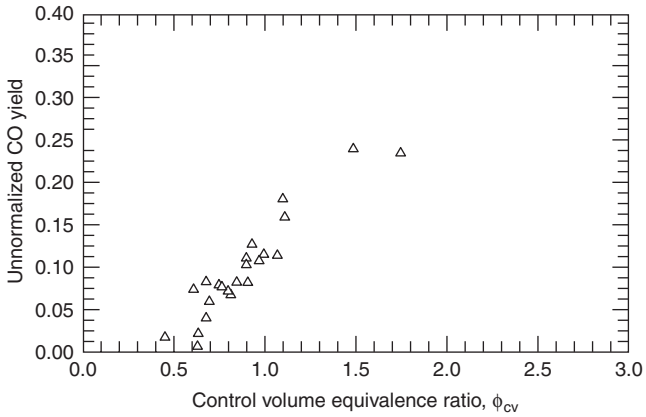

Figure 2-5.22. ***Unnormalized CO yields of gases in a space adjacent to a post-flashover compartment fire.***

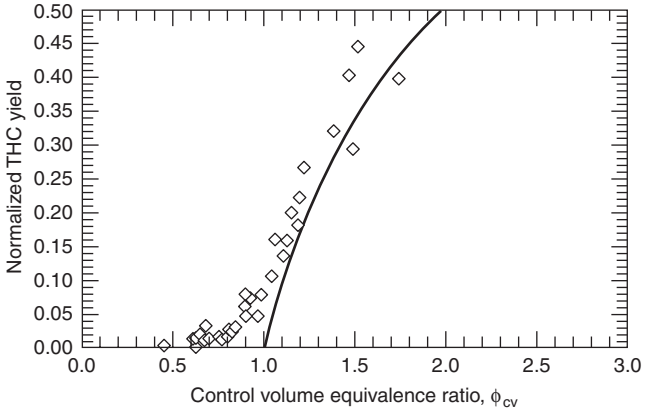

Figure 2-5.23. ***Normalized THC yields of gases in a space adjacent to a post-flashover compartment fire.***

1.0 and decays at the rate prescribed by the complete combustion model at higher ϕ_{cv}. CO_2 normalized yields are near unity up to a ϕ_{cv} of approximately 0.8. At $\phi_{cv} > 0.8$, the CO_2 levels begin to decay and are consistently less than the level predicted by the complete combustion model. This behavior is consistent with the rise in incomplete combustion products, such as CO and THC, at ϕ_{cv} ranging from 0.6–0.8. These results indicate that species levels in adjacent spaces can be adequately correlated by the same global equivalence ratio correlations obtained for species production in fire compartments as long as ϕ_{cv} is calculated using the appropriately defined control volume. ϕ_{cv} accounts for the effects of external burning on species levels and can be used with Equations 19–25 to estimate species transported to remote areas.

Effects of Oxygen Deficient Smoke Layers in Adjacent Spaces

The development of hot, oxygen deficient smoke layers in the adjacent space affects both the entrainment into the plume-ceiling jet and the amount of oxygen mixing with the fuel-rich gases flowing from the fire compartment.

Ewens et al.[27,31] demonstrated that layers as thin as 0.20 m may have an impact on incomplete combustion products being transported to adjacent areas. Lattimer et al.[28,29] performed a series of tests with different oxygen deficient layer depths in the space directly adjacent to a post-flashover fire. (See Figure 2-5.17b.) Tests were performed with three different opening sizes connecting the compartment to the adjacent space, but the compartment stoichiometry was approximately the same in all tests. In each test, the layer depth was kept at a constant level by the use of an exit soffit. In order to change the layer depth from test to test, the height of the exit soffit was adjusted for each test.

Except for cases with a deep smoke layer in the adjacent space, external burning occurred in all tests. Figure 2-5.24 contains a plot of time to ignition for tests with different layer depths. Layer depth is represented as a dimensionless depth, $\gamma = \delta/z$, which relates the distance between the ceiling and the bottom of the visible smoke layer, δ, to the distance between the ceiling and the bottom of the gases flowing out of the compartment, z. (For a window configuration, z is measured to the bottom of the window.) As shown in Figure 2-5.24, the smoke layer did not affect the time to ignition until the visible smoke layer was nearly deep enough to prevent ignition altogether (indicated by the infinite time to ignition). At layer depths greater than $\gamma = 1.7$, external burning did not occur since the exiting fire gases were not able to entrain sufficient fresh air to provide the necessary oxygen for combustion. Rather, the gases exiting the fire compartment entrained primarily vitiated gases in the upper layer of the adjacent space.

The CO, CO_2 and THC yields measured at a remote location (in the exhaust duct) for the different window opening sizes are shown plotted in Figures 2-5.25a to 2-5.25c with respect to the smoke layer depth. Each data point is the time-averaged yield during the quasi-steady

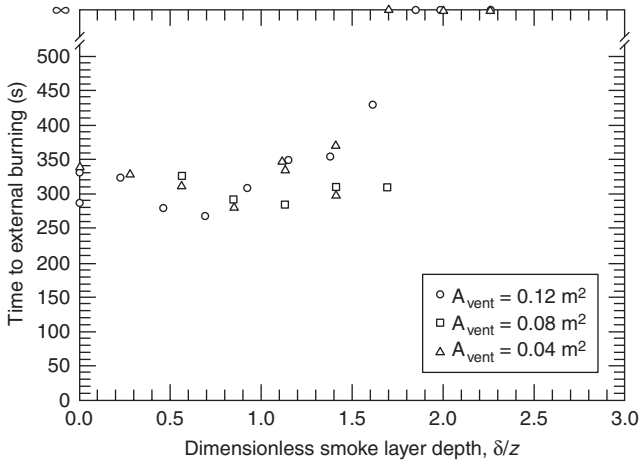

Figure 2-5.24. ***Time for external burning in tests with a range of layer depths in the adjacent space with a 6.32 m² floor plan area.[29]***

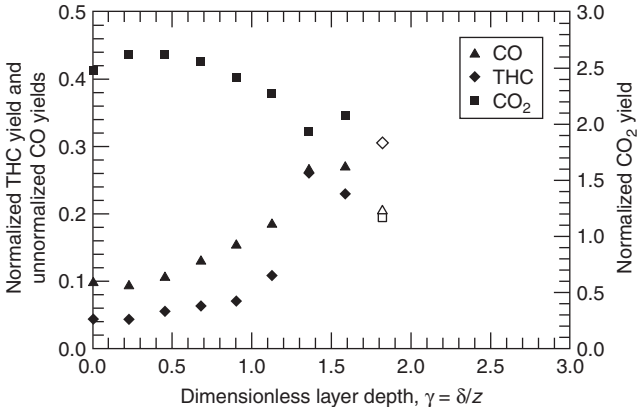

Figure 2-5.25a. ***The effect of an oxygen deficient upper-layer on downstream species yields from a post-flashover fire extending into a hallway. Opening of 0.12 m², 0.20 m soffit above the opening, and an average ϕ_c = 3.1. Open symbols are tests with no external burning. $\gamma > 1$ indicates layer is below the bottom of the vent.[28,29]***

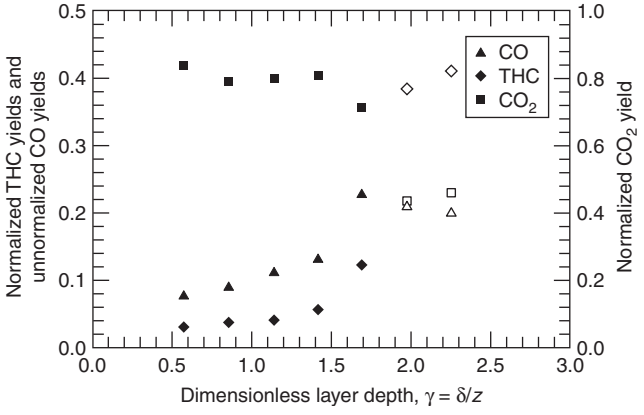

Figure 2-5.25b. ***The effect of an oxygen deficient upper-layer on downstream species yields from a post-flashover fire extending into a hallway. Opening of 0.08 m², 0.20 m soffit above the opening, and an average ϕ_c = 2.8. Open symbols are tests with no external burning.[29]***

state part of the fire. For this geometry, combustion product levels were not significantly affected by the smoke layer until it fell below the bottom of the opening ($\gamma > 1.0$). As the layer depth increased from $\gamma = 1.0$ to 1.8, the burning outside the compartment became increasingly less efficient. This resulted in an increase in CO and THC yields and a decrease in the CO_2 yield. The increase in CO and THC yields was attributed to reducing the oxygen available to oxidize the combustion products. When the smoke layer was increased to a dimensionless layer depth of $\gamma = 1.7$–1.8, external burning was not observed and downstream species yields were consistent with levels inside the fire compartment.

External burning in some tests with deep oxygen deficient upper-layers actually caused additional CO formation in the adjacent space. As shown in Figure 2-5.25a, in tests with the largest opening, 0.12 m², and a dimensionless layer depth of $\gamma = 1.3-1.5$, CO yields increased to approximately 0.27 kg/kg, which is approximately 0.05 kg/kg higher than compartment levels. In addition, corresponding normalized THC yields were on average 0.06 kg/kg lower than compartment levels. These results indicate that available oxygen is being used to preferentially oxidize THC instead of CO. This oxidation of THC forms additional CO, causing an increase in CO levels transported to remote locations. The exact conditions in the adjacent space necessary to produce these results have not been fully established.

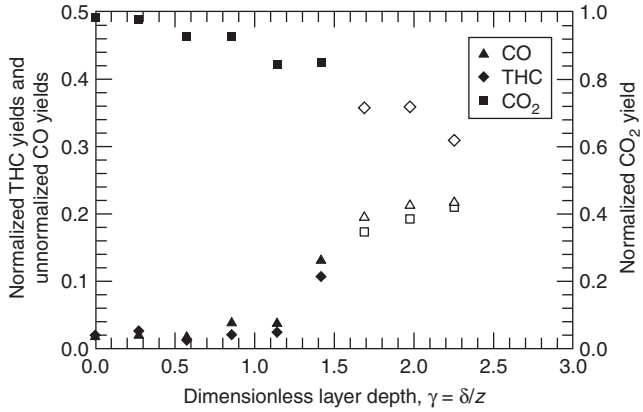

Figure 2-5.25c. ***The effect of an oxygen deficient upper-layer on downstream species from a post-flashover fire extending into a hallway. Opening of 0.04 m², 0.20 m soffit above the opening, and an average ϕ_c = 2.8. Open symbols are tests with no external burning.[28,29]***

Other Considerations

There are other variables that may influence the combustion product levels being transported to remote locations that have not been fully explored. These variables include the effects of air addition through forced ventilation, additional fuel decomposition in the adjacent space, and heat losses to the ceiling and walls.

The addition of air to the system through forced ventilation may have an influence on species levels, depending on where the air is added relative to the external burning. Forced ventilation in the region where external burning is occurring will introduce additional oxygen into the flow, and possibly induce additional mixing. This may result in better oxidation of incomplete combustion products, such as CO. Addition of air to the system downstream of the external burning will dilute the gases, but will not reduce the amount (in terms of mass) of incomplete combustion products being transported to remote location.

Decomposition of fuel in the adjacent space may affect species levels transported to remote locations. This effect may be sensitive to the location of the decomposing fuel, the type of fuel, whether it is flaming or smoldering, and the conditions surrounding the fuel.

Heat losses to the ceiling and walls can cause gas temperatures in the adjacent space to decrease more readily for some materials, compared to well insulated boundaries. An example of this may be steel decks and bulkheads on ships. A decrease in gas temperature may cause temperatures to reach levels where no reactions can occur sooner than those observed in well-insulated cases. As a result, higher heat loss to the boundaries may result in higher incomplete combustion products, including CO, to be transported to remote areas.

Species concentrations may not always be transported away from the compartment in a uniform manner. In experiments performed by Lattimer et al.,[28,29] with the compartment located on the side of a hallway, the bulk flow from the compartment was measured to flow across the hallway and down the side of the hallway opposite the fire compartment. This resulted in higher CO, CO_2, and THC levels (and lower O_2) flowing along the side of the hallway opposite the fire compartment. For example, CO levels were measured to be as high as 1.9 percent along the side of the hallway opposite the fire compartment, while on the side of the hallway with the fire compartment the maximum CO level was measured to be 1.0 percent. As these gases flow further from the compartment, they are expected to become more uniform across the hallway. However, the distance away from the compartment where mostly uniform flow occurs was not quantified.

Engineering Methodology

In light of the experimental work and chemical kinetics considerations discussed previously, several correlations can be used as guidelines for fire protection engineering. The production of chemical species in compartment fires has been shown to be correlated with the control volume equivalence ratio, ϕ_{cv}. For most purposes, the equivalence ratio can be calculated using instantaneous fuel burning rates and air mass flow rates assuming quasi-steady state conditions. The following methodology presents a guide to determining bounds on species production as well as comments on the limits of this approach.

The methodology for estimating species transported to remote locations is provided in Figure 2-5.26. This approach considers the occurrence of external burning outside the compartment. In general, the primary steps in the analysis are

1. Determine the compartment equivalence ratio, ϕ_c.
2. If $\phi_c < 1$, estimate species levels using the global equivalence ratio-yield correlations presented in Equations 19–25 with the ϕ_c.
3. If $\phi_c > 1$, determine whether external burning will occur outside of the compartment. External burning can be assumed to occur at a ϕ_c (plume or compartment) of 1.6, or by calculating the ignition index using Equation 1.
4. If there is no external burning, use the ϕ_c and Equations 19–25 to calculate the species transported.
5. If external burning is occurring, determine the effect of the smoke layer using the dimensionless smoke depth, $\gamma = \delta/z$, where δ is the depth of the layer below the ceiling and z is the lowest elevation of gases exiting the compartment.
6. If $\gamma > 1.0$, and external burning is predicted, the smoke layer can be assumed to inhibit oxidation in the adjacent space. CO and other incomplete-combustion products are not reduced. The ϕ_c and Equations 19–25 can be used to estimate the species transported to remote locations.
7. If $\gamma < 1.0$, and external burning is predicted, the smoke layer does not inhibit the oxidation in the adjacent space and incomplete-combustion products, such as CO will be reduced. The species transported can be estimated using Equations 19–22 and the equivalence ratio for a control volume, ϕ_{cv}, that incorporates the compartment and the adjacent space out to the flame tip. (See Figure 2-5.15.)

It should be noted that this methodology may not provide the maximum levels of incomplete combustion products that can be produced in a fire. Equations presented in this methodology for species yields as a function of equivalence ratio have been shown to provide good correlations even for wood as a secondary fuel pyrolyzing in the hot upper layer. However, it is not clear whether these correlations will hold for non-oxygenated fuels in the upper layer or how well they will represent other oxygenated fuels.

Several empirical correlations have been developed to predict species levels at a range of equivalence ratios. Different correlations are given in the following paragraphs to accommodate analyses of various levels of complexity.

Due to its toxicity, CO production is of primary importance. Four correlations (see Equations 19–22) are presented, representing varying degrees of complexity. In each case, the correlations basically represent a lower bound for the yield of CO. Equation 19 (parts a and b) represents a "zeroth order" correlation between CO yield and equivalence ratio. For overventilated burning conditions, there is no CO production and for underventilated conditions CO is produced at a yield of 0.2 grams per gram of fuel burned. This correlation applies best to fires with average upper layer temperatures greater than 900 K.

$$f_{CO} = 0 \qquad \text{for } \phi < 1 \tag{19a}$$

$$f_{CO} = 0.2 \qquad \text{for } \phi > 1 \tag{19b}$$

Equation 20 (parts a, b, and c) accounts for some of the temperature effect by including a linear rise in CO yield over the transition region from ϕ of 0.5 to 1.5.

$$f_{CO} = 0 \qquad \text{for } \phi < 0.5 \tag{20a}$$

$$f_{CO} = 0.2\phi - 0.1 \qquad \text{for } 0.5 < \phi < 1.5 \tag{20b}$$

$$f_{CO} = 0.2 \qquad \text{for } \phi > 1.5 \tag{20c}$$

The temperature effect on CO production is best represented in the following two correlations. Equation 21, which represents a fit to the hexane data of Beyler's hood experiments, is suggested for compartment fires with

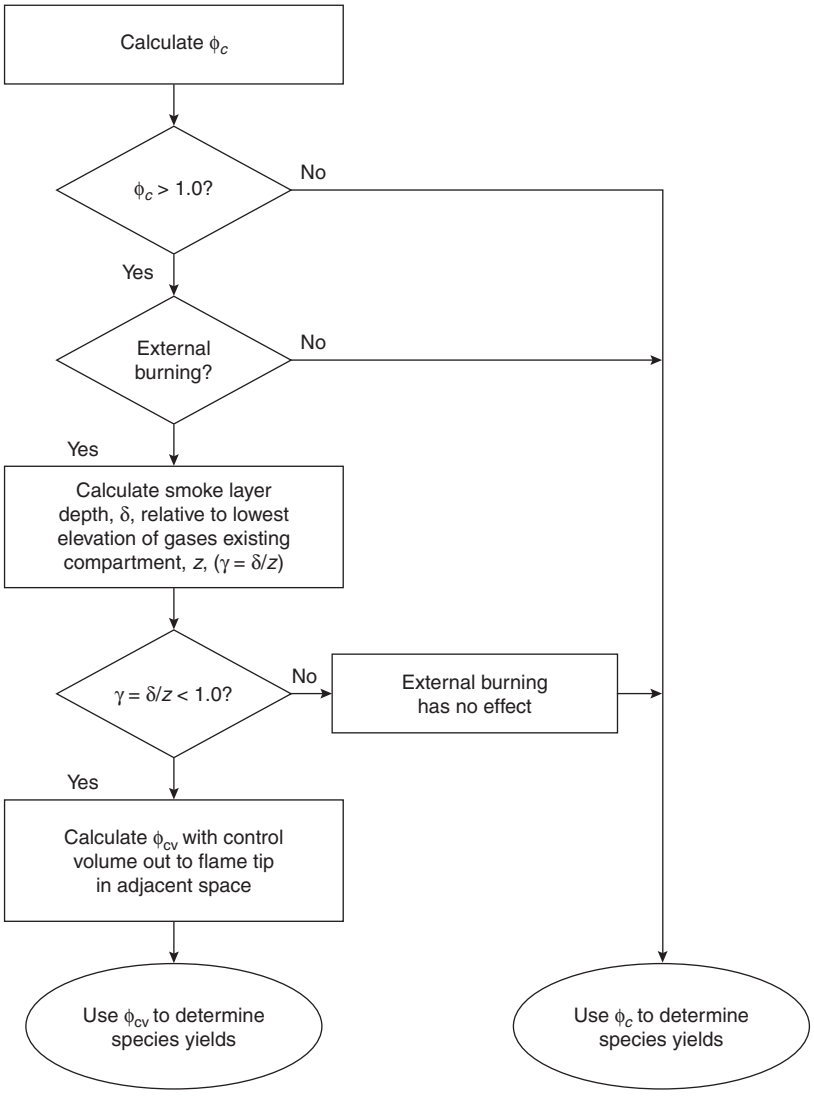

Figure 2-5.26. ***General methodology for predicting species levels transported to remote locations from a fire compartment.***

average upper layer temperatures below 800 K. Equation 22 is used for fires with upper layer temperatures above 900 K. Equation 15 is an approximate fit to the compartment fire hexane data of Gottuk et al. For the most part, CO yields from hexane fires represent lower limits observed for the fuels studied to date.[5,8] Therefore, these equations provide a *minimum* CO production that can be used for hazard analysis.

$$Y_{CO} = (0.19/180)\ \tan^{-1}(X) + 0.095 \qquad \text{for } T < 800\ \text{K} \quad (21)$$

where $X = 10(\phi - 0.8)$ in degrees

$$Y_{CO} = (0.22/180)\ \tan^{-1}(X) + 0.11 \qquad \text{for } T > 900\ \text{K} \quad (22)$$

where $X = 10\ (\phi - 1.25)$ in degrees

The figures presented earlier of CO yield versus equivalence ratio also show plots of Equations 21 and 22. Figure 2-5.5 shows the CO yield data for methane hood experiment fires in which upper layer temperatures ranged from 490 to 870 K. The CO yield data of Zukoski et al. and Toner et al. lies between the curves of Equation 21 and 22, particularly for slightly overventilated and stoichiometric conditions. This is consistent with the fact that these fires had temperatures that were higher than those represented by Equation 14 and some were within the transition range of 800 to 900 K.

The simple model presented as Equation 14 (parts a through e) with the inclusion of the empirically determined yield coefficients, is fairly adequate for predicting CO_2, O_2, and H_2O normalized yields. (See Equations 23–25.) Suggested average yield coefficients for compartment fires of elevated temperatures ($T > 900$ K) are 0.88

for B_{CO_2} and 0.97 for B_{O_2}.[5] Suggested values for low upper layer temperatures ($T < 800$ K) are 0.77 for B_{CO_2}, 0.92 for B_{O_2}, and 0.95 for B_{H_2O}. Average yield coefficients for underventilated fires are shown in Table 2-5.2.

$$f_{CO_2} = 1 \quad \text{for } \phi < 1 \tag{23a}$$
$$f_{CO_2} = B_{CO_2}/\phi \quad \text{for } \phi > 1 \tag{23b}$$
$$f_{O_2} = 1 \quad \text{for } \phi < 1 \tag{24a}$$
$$f_{O_2} = B_{O_2}/\phi \quad \text{for } \phi > 1 \tag{24b}$$
$$f_{H_2O} = 1 \quad \text{for } \phi < 1 \tag{25a}$$
$$f_{H_2O} = B_{H_2O}/\phi \quad \text{for } \phi > 1 \tag{25b}$$

As presented in Equations 23–25, normalized chemical species yields, f, can be correlated quite well by the global equivalence ratio. This is true for a wide range of fuel types. However, it is worthwhile to point out that for different fuels, the CO_2, O_2, and H_2O yields to equivalence ratio correlations only collapse down to a single curve when the yields are normalized by the maximum possible yield for a given fuel (i.e., presented as f rather than Y). Although complete combustion does not occur, combustion efficiencies with respect to equivalence ratio are similar enough between fuels that the stoichiometry of a particular fuel will dictate the generation of CO_2 and the depletion of O_2. Therefore, the species associated with complete combustion (CO_2, O_2, and H_2O) are not expected to have equal yields for different fuels, since varying fuel compositions will dictate different limits of CO_2 and H_2O that can be generated and O_2 that can be consumed for a gram of fuel burned. By normalizing the yields, the variability of fuel composition is removed.

On the other hand, carbon monoxide production is best correlated by the equivalence ratio when represented as a simple yield, Y_{CO}, rather than a normalized yield, f_{CO}. This is one indicator that CO production is not strongly dependent on fuel type, as is production of CO_2 and O_2. The reason for this is believed to be due to the fact that CO is effectively an intermediate product that depends more on the elementary chemistry than on fuel composition which determines products of complete combustion.

Once yields are determined using the above correlations, species gas concentrations can be calculated. Equation 26 can be used to calculate the concentration of species i for all species except oxygen. Oxygen concentrations can be calculated from the depletion of oxygen using Equation 27.

$$X_{i_{wet}} = \frac{Y_i \dot{m}_f M_{mix}}{(\dot{m}_f + \dot{m}_a) M_i} \tag{26}$$

$$X_{O_{2\,wet}} = \frac{0.21 \dot{m}_a M_{O_2}/M_a - D_{O_2} \dot{m}_f}{(\dot{m}_f + \dot{m}_a) M_{O_2}/M_a} \tag{27}$$

The yield-equivalence ratio correlations shown in Figure 2-5.7, which are also represented by Equations 21 and 15, have been replotted as CO concentration vs. equivalence ratio in Figure 2-5.27a. As indicated previously, the yield correlations in Figure 2-5.7 (and thus, the concentrations in Figure 2-5.27a) represent a reasonable lower bound for a range of typical fuels. Higher concentrations of CO can be created, particularly when additional fuel is added to a vitiated upper layer. Corresponding to 2-5.27a, CO_2 and O_2 concentrations for hexane compartment fires are shown in Figures 2-5.27b and c, respectively. Even though the peak concentrations of CO_2 will be dependent on the fuel type, the oxygen concentration as a function of ϕ will be similar for most hydrocarbons.[5]

The ratio of CO to CO_2 concentrations can be used as an indicator of the combustion mode. Higher combustion efficiency is obtained as more fuel is burned completely to CO_2 and H_2O and is indicated by a ratio of CO to CO_2 near zero. Since CO is a product of incomplete combustion, the ratio of CO to CO_2 concentrations will increase as fires burn less efficiently. The ratio increases with equivalence ratio even for underventilated conditions, as evidenced by experimental data [e.g., Reference 5] and the engineering correlations presented above.

EXAMPLE 4:

Consider that the piece of furniture described in Example 1 is burning in a room such that a two-layer system develops. The only ventilation to the room is an open doorway through which 217 g/s of air is being entrained. The material is burning at a rate of 37 g/s, and the average temperature of the upper layer is 700°C. Calculate the plume equivalence ratio and determine the yield of CO and depletion of O_2.

SOLUTION:

The plume equivalence ratio is calculated using Equation 10b. The stoichiometric fuel-to-air ratio, r, has already been calculated in Example 1.

$$\phi_p = \frac{\dot{m}_f/\dot{m}_a}{r} = \frac{37/217}{0.1139} = 1.5$$

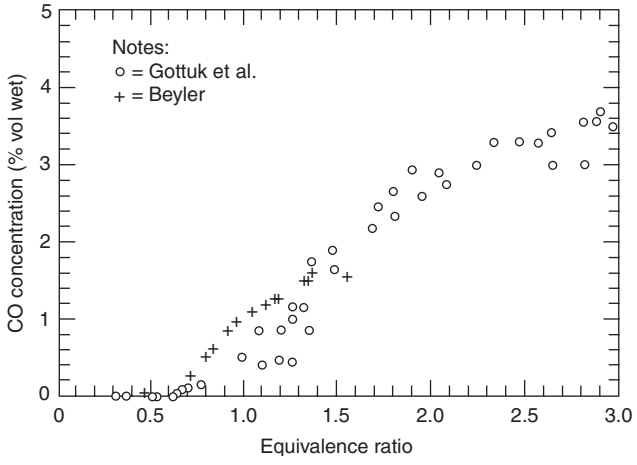

Figure 2-5.27a. ***Carbon monoxide concentrations as a function of equivalence ratio for hexane fires in a compartment (•) and under a hood (+). Data represent the same tests shown in Figure 2-5.7 as unnormalized yields.***

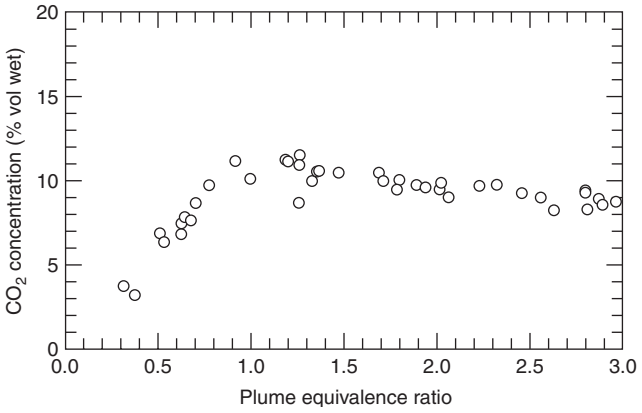

Figure 2-5.27b. ***CO_2 concentrations as a function of equivalence ratio for hexane compartment fires. (Data taken from Reference 5.)***

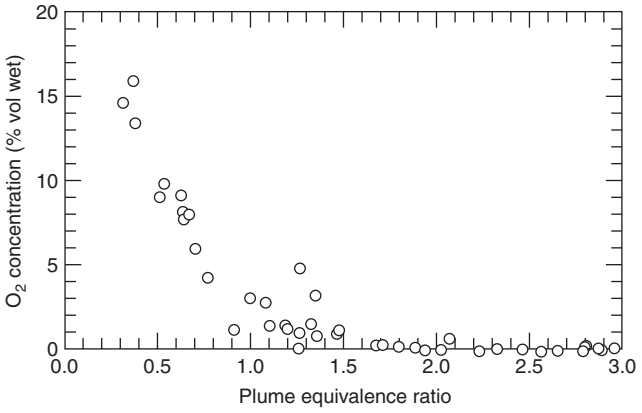

Figure 2-5.27c. ***O_2 concentrations as a function of equivalence ratio for hexane compartment fires. (Data taken from Reference 5.)***

Since the average upper layer temperature (700°C + 273 = 973 K) is above 900 K, Equation 22 is used to calculate the yield of CO. The argument, X, of the inverse tangent is

$$X = 10(\phi_p - 1.25) = 10(1.5 - 1.25) = 2.5$$

$$Y_{CO} = \left(\frac{0.22}{180}\right)\tan^{-1}(X) + 0.11$$

$$Y_{CO} = \left(\frac{0.22}{180}\right)\tan^{-1}(13.75) + 0.11$$

$$Y_{CO} = 0.19$$

Therefore, 0.19 grams of CO are produced for every gram of polyurethane foam that burns. The production rate of CO is equal to that yield, Y_{CO}, multiplied by the fuel burning rate (0.19 × 37 g/s = 7.0 g/s).

The normalized yield of oxygen is determined using Equation 24, and the recommended yield coefficient, B_{O_2}, of 0.97.

$$f_{O_2} = \frac{B_{O_2}}{\phi} = \frac{0.97}{1.5} = 0.65$$

From Example 1, we obtain the maximum theoretical depletion of oxygen, k_{O_2}, and calculate the depletion of oxygen as

$$D_{O_2} = f_{O_2} k_{O_2} = 0.65 \quad (2.05)$$
$$= 1.33\text{g of } O_2 \text{ per gram of fuel burned}$$

The depletion rate of oxygen is 49.2 g/s (1.33 × 37 g/s).

EXAMPLE 5:

For the piece of furniture burning in Example 4, calculate the CO and O_2 concentrations in the upper layer.

Gas concentrations can be calculated from the yields determined in Example 4 using Equation 26 for CO and Equation 27 for O_2.

$$X_{CO_{wet}} = \frac{Y_{CO}\dot{m}_f M_{mix}}{(\dot{m}_f + \dot{m}_a)M_{CO}} = \frac{0.19(37)(28.8)}{(37 + 217)(28)} = 0.028$$

$$X_{O_2} = \frac{0.21\dot{m}_a M_{O_2}/M_a - D_{O_2}\dot{m}_f}{(\dot{m}_a + \dot{m}_f)M_{O_2}/M_a}$$

$$= \frac{0.21(217)32/28.8 - 1.33(37)}{(32 + 217)32/28.8}$$

$$X_{O_2} = 0.005$$

The resulting concentrations of CO and O_2 are 2.8 and 0.5 percent by volume, respectively.

EXAMPLE 6:

A fire is burning in a room that has one door open and no other ventilation. The room is 7 m wide and 4 m deep with a 2.43 m high ceiling. The door measures 0.76 m wide and 2.05 m high (area = 1.56 m²). The peak heat release rate of the fire has been estimated to be 4.5 MW. Determine how much CO can be transported to other rooms in the building.

SOLUTION:

The first step is to calculate the compartment equivalence ratio, ϕ_c. Since details of the fire are not provided, the mass burning rate of the fuel is not known. Therefore, ϕ_c is estimated via Equation 13c using the heat release rate, Q, of 4.5 MW

$$\phi_c = \frac{Q}{\dot{m}_a} \cdot \frac{1}{3030} = \frac{4500\text{ kW}}{\dot{m}_a \cdot 3030}$$

The mass flow rate of air, $\dot{m}_a$, into the room is estimated using the ventilation parameter[33] as follows:

$$\dot{m}_a = 0.5A\sqrt{h} = 0.5 \cdot 1.56\sqrt{2.05} = 1.12\text{ kg/s}$$

Substituting $\dot{m}_a$ into the equation above for the compartment equivalence ratio yields a ϕ_c of 1.3. Since $\phi_c > 1$, the occurrence of external burning must be considered. However, using the criteria that $\phi_c < 1.6$, it is assumed that no external burning will occur. Species levels inside the room are calculated by Equations 19–25 using ϕ_c. The yield of

CO is calculated using Equation 21 or 22, depending on the temperature of the upper layer. The upper layer temperature can be estimated using the McCaffrey, Quintiere, and Harkleroad (MQH) correlation[34] that is presented in Section 3, Chapter 6 of this book. According to the MQH correlation, the upper layer gas temperatures exceed 900 K for fires above 1100 kW. For temperatures above 900 K, Equation 22 is used to calculate the CO yield as

$$Y_{CO} = (0.22/180) \cdot \tan^{-1}(10(\phi - 1.25)) + 0.11 = 0.14$$

Since there is no external burning, the CO generated in the compartment (0.14 kg of CO per kg of fuel burned) will flow to other parts of the building. Before dilution occurs away from the fire compartment, the initial concentration of CO in the gases from the fire compartment can be calculated using Equation 26

$$X_{CO_{wet}} = \frac{Y_{CO}\dot{m}_f M_{mix}}{(\dot{m}_f + \dot{m}_a)M_{CO}} = \frac{0.14(\dot{m}_f)28.8}{(\dot{m}_f + 1.12)28}$$

Since there is no information on the contents burning in the room, an accurate assessment of the fuel mass burning rate, $\dot{m}_f$, cannot be obtained. An estimate of $\dot{m}_f$ can be made using Equation 13a, with an assumed value of r, the stoichiometric fuel-to-air ratio. Values of r are presented in Table 2-5.1 for various fuels as $1/r$. In order to bound the possible CO concentrations, values of $1/r$ of 4 to 15 are chosen to represent a reasonable range of hydrocarbon fuels that may be burning in the room. The following shows an example of the $\dot{m}_f$ calculation using Equation 13a and $1/r = 4$:

$$\dot{m}_f = \frac{\phi \cdot \dot{m}_a}{1/r} = \frac{1.3(1.12 \text{ kg/s})}{4} = 0.36 \text{ kg/s}$$

The corresponding calculation for $1/r$ of 15 yields a $\dot{m}_f$ of 0.097 kg/s. Substituting the values for $\dot{m}_f$ into the above equation for $X_{CO_{wet}}$ results in CO concentrations of 3.5 and 1.1 percent, respectively.

Nomenclature

B_i	yield coefficients of species i
C	stoichiometric molar ratio of water to carbon dioxide
C_j	volume concentration of fuel j when fuel stream is stoichiometrically mixed with oxidant stream
C_p	heat capacity of products of complete combustion, (kJ/g·mol K)
D_{O_2}	mass depletion of oxygen per gram of fuel burned (g/g)
E	energy released per kg of oxygen consumed
f	normalized yield or generation efficiency
$\Delta H_{c,j}$	heat of combustion of the species j, (kJ/g·mol)
j	fuel species of interest
k	maximum theoretical yield
$L_{f,tip}$	Length of flame tip for flame extending down a corridor ceiling
M	molecular weight
m_a	mass of air
$\dot{m}_a$	mass flow rate of air
m_f	mass of fuel
$\dot{m}_f$	mass loss rate of fuel
$\ddot{m}_f$	the derivative of the fuel mass loss rate
$\dot{m}_{exhaust}$	mass flow rate out of the layer
n	molar quantity
n_{prod}	number of moles of products of complete combustion per mole of reactants (stoichiometric mixture of fuel and oxidant streams)
Q	ideal heat release rate
r	stoichiometric fuel-to-air ratio
r_a	stoichiometric air-to-fuel ratio
r_{O_2}	stoichiometric fuel-to-oxygen ratio
T	temperature
$T_{SL,j}$	adiabatic flame temperature at the stoichiometric limit for fuel species j, (K)
T_o	temperature of the gas mixture prior to reaction, (K)
t	time
t_r	residence time of gases in the upper layer
τ_{SS}	steady-state time ratio
V_{ul}	volume of the upper layer
X	mole fraction
$X_{i_{dry}}$	dry mole fraction of species i (H_2O removed from sample)
$X_{i_{wet}}$	wet mole fraction of species i
Y	yield (g/g) also refers to D_{O_2}
$Y_{O_2,air}$	mass fraction of oxygen in air
z	distance between the bottom of the compartment outflow and the ceiling in the adjacent space
γ	dimensionless layer depth in adjacent space ($\gamma = \delta/z$)
δ	layer depth in the adjacent space
ϕ	equivalence ratio
ϕ_c	compartment equivalence ratio
ϕ_{cv}	equivalence ratio defined per a specified control volume
ϕ_p	plume equivalence ratio
ϕ_{ul}	upper layer equivalence ratio
ρ_{ul}	density of the upper layer

Subscripts

a	air
f	fuel
CO	carbon monoxide
O_2	oxygen
CO_2	carbon dioxide
H_2O	water
H_2	hydrogen
THC	total unburned hydrocarbons
resid,C	residual carbon

wet gas concentration including with water in the mixture

dry gas concentration with no water in the mixture

References Cited

1. R.A. Anderson, A.A. Watson, and W.A. Harland, "Fire Deaths in the Glasgow Area: II The Role of Carbon Monoxide," *Med. Sci. Law,* 21, pp. 289–294 (1981).
2. B. Harwood and J.R. Hall, "What Kills in Fires: Smoke Inhalation or Burns?" *Fire Journal,* 83, pp. 29–34 (1989).
3. R.J. Gann, V. Babrauskas, and R.D. Peacock, "Fire Conditions for Smoke Toxicity Measurements," *Fire and Materials,* 18, 3, pp. 193–199 (1994).
4. C.L. Beyler, "Ignition and Burning of a Layer of Incomplete Combustion Products," *Combustion Science and Technology,* 39, pp. 287–303 (1984).
5. D.T. Gottuk, R.J. Roby, M.J. Peatross, and C.L. Beyler, "Carbon Monoxide Production in Compartment Fires," *J. of Fire Prot. Engr.,* 4, pp. 133–150 (1992).
6. N.P. Bryner, E.L. Johnsson, and W.M. Pitts, "Carbon Monoxide Production in Compartment Fires—Reduced-Scale Enclosure Test Facility," *NISTIR 5568,* National Institute of Standards and Technology, Gaithersburg, MD (1995).
7. S.J. Toner, E.E. Zukoski, and T. Kubota, "Entrainment, Chemistry, and Structure of Fire Plumes," *NBS-GCR-87-528,* National Institute of Standards and Technology, Gaithersburg, MD (1987).
8. C.L. Beyler, *Fire Safety Journal,* 10, pp. 47–56 (1986).
9. C.L. Beyler, *Fire Safety Science—Proceedings of First International Symposium,* Hemisphere, Washington, DC, pp. 430–431 (1986).
10. E.E. Zukoski, S.J. Toner, J.H. Morehart, and T. Kubota, *Fire Safety Science—Proceedings of the Second International Symposium,* Hemisphere, Washington, DC, pp. 295–304 (1989).
11. E.E. Zukoski, J.H. Morehart, T. Kubota, and S.J. Toner, *Combustion and Flame,* 83, pp. 324–332 (1991).
12. J.H. Morehart, E.E. Zukoski, and T. Kubota, "Species Produced in Fires Burning in Two-Layered and Homogeneous Vitiated Environments," *NBS-GCR-90-585,* National Institute of Standards and Technology, Gaithersburg, MD (1990).
13. W.M. Pitts, *24th Symposium (International) on Combustion,* Combustion Institute, Pittsburgh, PA (1992).
14. D.T. Gottuk, R.J. Roby, and C.L. Beyler, "The Role of Temperature on Carbon Monoxide Production in Compartment Fires," *Fire Safety Journal,* 24, pp. 315–331 (1995).
15. A. Tewarson, "Fully Enveloped Enclosure Fires of Wood Cribs," *20th Symposium (International) on Combustion,* Combustion Institute, Pittsburgh, PA, p. 1555 (1984).
16. D.T. Gottuk, "The Generation of Carbon Monoxide in Compartment Fires," *NBS-GCR-92-619,* National Institute of Standards and Technology, Gaithersburg, MD (1992).
17. W.D. Walton and P.H. Thomas, "Estimating Temperatures in Compartment Fires," *The SPFE Handbook of Fire Protection Engineering,* National Fire Protection Association, Quincy, MA, 1988, Ch. 2-2.
18. W.M. Pitts, E.L. Johnsson, and N.P. Bryner, "Carbon Monoxide Formation in Fires by High-Temperature Anaerobic Wood Pyrolysis," presented at the *25th Symposium (International) on Combustion,* Combustion Institute, Pittsburgh, PA (1994).
19. D. Gross and A.F. Robertson, *10th Symposium (International) on Combustion,* Combustion Institute, Pittsburgh, PA, pp. 931–942 (1965).
20. B.Y. Lattimer, U. Vandsburger, and R.J. Roby, "Carbon Monoxide Levels in Structure Fires: Effects of Wood in the Upper Layer of a Post-Flashover Compartment Fire," *Fire Technology,* 34, 4 (1998).
21. W.M. Pitts, "The Global Equivalence Ratio Concept and the Prediciton of Carbon Monoxide Formation in Enclosure Fires," *NIST Monograph 179,* National Institute of Standards and Technology, Gaithersburg, MD (1994).
22. N.P. Bryner, E.L. Johnsson, and W.M. Pitts, "Carbon Monoxide Production in Compartment Fires: Full-Scale Enclosure Burns," in *Proceedings of the Annual Conference on Fire Research, NISTIR 5499,* National Institute of Standards and Technology, Gaithersburg, MD (1994).
23. W.M. Pitts, N.P. Bryner, and E.L. Johnsson, "Combustion Product Formation in Under and Overventilated Full-Scale Enclosure Fires," in *Proceedings of Combustion Fundamentals and Applications, Joint Technical Meeting,* San Antonio, TX (1995).
24. N.P. Bryner, E. L. Johnsson, and W.M. Pitts, "Scaling Compartment Fires—Reduced- and Full-Scale Enclosure Burns," in *Proceedings, International Conference on Fire Research and Engineering,* (D.P. Lund and E.A. Angell, eds.,) Society of Fire Engineers, Boston (1995).
25. W.M. Pitts, "An Algorithm for Estimating Carbon Monoxide Formation in Enclosure Fires," *Fire Safety Science—Proceedings of the Fifth International Symposium,* International Association of Fire Safety Science," pp. 535–546 (1997).
26. J. Warnatz, in *Combustion Chemistry,* (W.C. Gardiner, ed.,) Springer-Verlag, New York, pp. 224–232 (1984).
27. D.S. Ewens, "The Transport and Remote Oxidation of Compartment Fire Exhaust Gases," M.S. Thesis, Virginia Polytechnic Institute and State University, Department of Mechanical Engineering, Blacksburg, VA (1994).
28. B.Y. Lattimer, U. Vandsburger, and R.J. Roby, "The Transport of Carbon Monoxide from a Burning Compartment Located on the Side of a Hallway," *26th Symposium (International) on Combustion,* Combustion Institute, Naples, Italy, pp. 1541–1547 (1996).
29. B.Y. Lattimer, U. Vandsburger, and R.J. Roby, "The Transport of High Concentrations of Carbon Monoxide to Locations Remote from the Burning Compartment," *NIST-GCR-97-713,* U.S. Department of Commerce, 315 pp. (1997).
30. D.T. Gottuk, R.J. Roby, and C.L. Beyler, "A Study of Carbon Monoxide and Smoke Yields from Compartment Fires with External Burning," *24th Symposium (International) on Combustion,* Combustion Institute, Pittsburgh, PA, pp. 1729–1735 (1992).
31. B.Y. Lattimer, D.S. Ewens, U. Vandsburger, and R.J. Roby, "Transport and Oxidation of Compartment Fire Exhaust Gases in Adjacent Corridor," *Journal of Fire Protection Engineers,* 6, 4 (1994).
32. B.Y. Lattimer, unpublished data (2000).
33. D. Drysdale, *An Introduction to Fire Dynamics,* 2nd ed., John Wiley and Sons, Chichester, UK (1999).
34. B.J. McCaffery, J.G. Quintiere, and M.F. Harkleroad, "Estimating Room Fire Temperatures and the Likelihood of Flashover Using Fire Test Data Correlations," *Fire Technology,* 17, 2, pp. 98–119 (1981).

CHAPTER 6

Toxicity Assessment of Combustion Products

David A. Purser

Introduction

It has long been recognized that exposure to toxic smoke products is one of the hazards confronting people in fires. There was a considerable increase in concern in this area during the 1970s and 1980s. In the United States, attention has been focused on the toxicity problem by a number of large fire disasters where victims have died from exposure to toxic smoke products.[1] Although this is also true to some extent for the United Kingdom, a major impetus for work in this area followed statistical surveys of fire casualties carried out in the mid-1970s. These surveys of casualties from all fires, and particularly from fires in domestic dwellings, revealed that not only were a large proportion of fatal and nonfatal fire casualties being reported in the category "overcome by smoke and toxic gases" rather than "heat and burns," but also that there was a fourfold increase in the former category between 1955 and 1971[2] (Figures 2-6.1 and 2-6.2). This increasing trend has continued into the 1980s, so that now approximately half of all fatal casualties and a third of all nonfatal casualties of dwelling fires (the majority caused by fires in furniture and bedding) were reported as being "overcome by smoke and toxic gases."[3] This has occurred despite the fact that the total numbers of fires have remained approximately constant. During the 1990s there was some reduction in total annual numbers of fire deaths in the United Kingdom (and in the United States), but smoke deaths in the United Kingdom are still running at

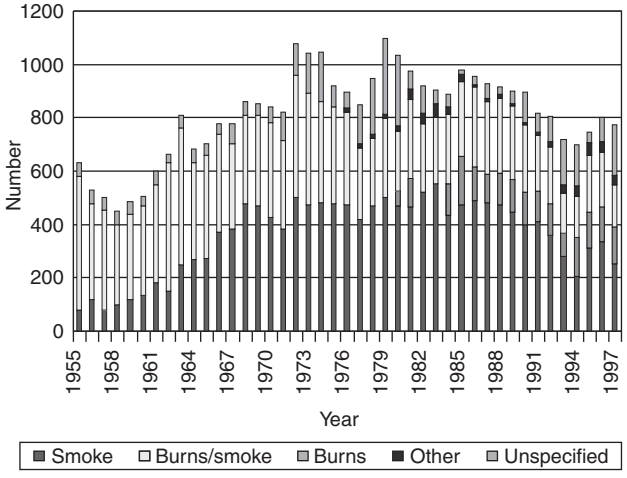

Figure 2-6.1. ***U.K. fire deaths.[3]***

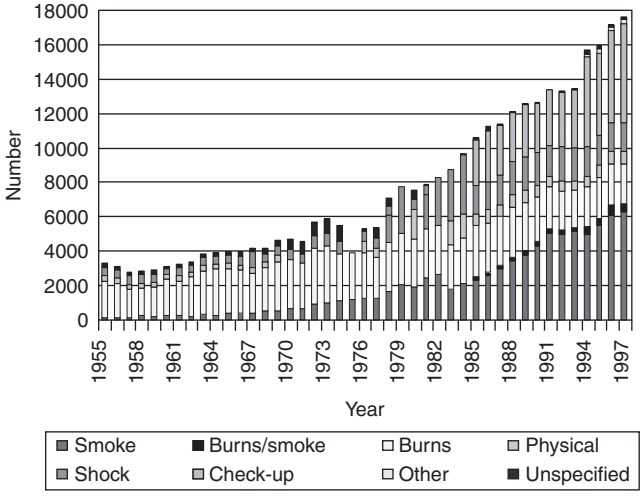

Figure 2-6.2. ***U.K. nonfatal fire injuries.[3]***

Professor David A. Purser has a Ph.D. in neurophysiology, and a diploma in toxicology from the Royal College of Pathologists. As former director of combustion toxicology research at Huntingdon Research Centre, England, and, currently, as associate director of the Fire Safety Engineering Centre in the Fire and Risk Sciences Division at BRE Ltd., Watford, England, he has worked on fire toxicology and life assessment for 30 years, and serves as an expert for the International Organization for Standardization (ISO) fire hazard and fire safety engineering working groups.

approximately four times the levels during the 1950s. Injuries from smoke and toxic fumes have increased continuously from an annual rate of approximately 1000 to more than 6000 during the late 1990s.

A number of possible reasons have been suggested for this increase in smoke-related casualties. They have been linked with the increased use of modern synthetic materials in furnishings. Another view is that the increase may not be directly related to modern materials but to changes in living styles over the period which have led to more furnishing and upholstery material being used in the average British home, and, therefore, a greater fire load. It has also been suggested that the increase is not real, but a statistical anomaly resulting from an increased awareness by the emergency services of toxic effects on victims. Epidemiological data are often difficult to interpret, but many of those working in this area are convinced that the increase in smoke-related casualties is real. The situation in the United States is difficult to interpret since it contains a larger and more diverse population, and statistics may not have been collected to reveal such a trend. The U.S. fire death rates were around twice those in the United Kingdom, western Europe in general and Japan 20 years ago, but have improved steadily up to the 1990s so that they are currently close to the U.K. and European death rates of approximately 14 per million inhabitants.[4–5] However in the United States and the United Kingdom, toxic smoke products are recognized as being the major cause of death in fires.[6] A possible difference between the pattern of fire deaths in the United Kingdom and United States is that in the United Kingdom the majority of fatalities occur in the room of fire origin (mainly in domestic dwellings) for fires that have not spread beyond the room of fire origin (65 percent of deaths). For 50 percent of deaths the fire spread is restricted to less than one third of the room area.[3] In the United States more than 50 percent of deaths are reported to occur remote from the room of origin, from fires that have spread beyond the room of origin (mostly post-flashover fires).[7] Although deaths remote from the room of origin involving spreading fires are also common in the United Kingdom, these differences indicate that cultural differences and differences in building styles can be important.

Materials-Based and Combustion Product-Based Approaches to Toxicity Assessment

There are two main views as to why smoke toxicity appears to be an increasing problem, which in turn have led to two rather different approaches to the evaluation of toxicity.

1. One view held that smoke from modern synthetic materials contained new toxic products that were not present previously, and that in some cases these products (the so-called "supertoxicants") might be very potent, exerting novel toxic effects at very low doses. Such effects could therefore be detected by means of simple, small-scale toxicity tests which could be used for regulatory purposes.[8–10] To some extent this approach followed the discovery that two materials, a flexible polyurethane foam containing a phosphorus-based fire retardant, and polytetrafluoroethylene (PTFE), could under certain laboratory conditions evolve products with a very high toxic potency.[8,9] This led to the use of rather simplistic materials-based toxicity tests, where the toxicity of materials is ranked in terms of the rodent LC_{50} (the concentration of combustion products expressed in terms of mg of material per liter of air causing the deaths of 50 percent of animals exposed).[10,11] This approach implies that the engineer should design by using those materials with the better performance in toxicity tests and that are consistent with good performance in other types of small-scale fire tests.
2. The other main view was that the basic toxic products of fires were much the same as always, but that in many modern fires the rate of fire growth and the rate of evolution of the common toxic products were much greater than they had been previously. Therefore, the best way to mitigate toxic hazard in fires was to control such factors as ignition, flame spread, and rate of smoke evolution rather than the qualitative nature of toxic products. For this approach, which is favored in the United Kingdom, there is more interest in estimating toxicity by making a chemical determination of the main toxic products given off by materials. This can be achieved by carrying out large-scale fire tests. Alternatively data on the yields of the main toxic products can be obtained from suitable small-scale tests and used as input to calculation of full-scale fire behavior using engineering calculation models such as those described in Chapters 2-5[12] and 3-4.[13] These data are then used to estimate time to incapacitation and death. In this context the main function of small-scale toxic potency tests (other than to provide data on yields of the main toxic gases) would be to confirm that the toxicity associated with particular burning materials was indeed due to the common toxic fire products via chemical atmosphere analysis in conjunction with animal exposures, and to identify those cases where unusual toxic effects occurred. This approach enables a firesafety engineer to design to a set of fire scenarios in a system (for example, a hotel bedroom or an aircraft cabin) and, by a simple chemical analysis of atmospheres produced during small- and large-scale fire tests, predict likely toxic hazard. The difficulty with these models is that they are often based on simplistic and erroneous assumptions concerning the effects and interaction of toxic products.

In practice there is a need for both small-scale materials-based toxicity tests and for profile modeling based on a few major toxic fire products. Existing information is often inadequate and misleading, and a better standard of research and testing is needed if data are to be produced for practical use. This chapter will give the reader an understanding of what is known about combustion product toxicity, the extent to which effects can be predicted from a knowledge of common fire products, and how small-scale tests should be performed and the results interpreted and used.

The Significance of Toxicity as Part of Total Fire Hazard

For scenarios involving the escape of occupants from a fire, survival depends upon the outcome of two parallel processes.

1. *The developing hazard from the fire.* This process incorporates ignition, fire growth, and the spread of fire and fire effluent. These depend upon a range of variables, such as the nature and disposition of the fire load, potential ignition sources, the reaction to fire properties of the lining materials and contents, the height and ventilation of the compartment, and the nature of the fire effluent. The actions of occupants and the provision of passive containment and active smoke extraction or suppression systems also affect the rate of development and extent of the hazard from a fire.

   Assessment of these processes for any particular scenario is aimed at calculating the time when an occupant would receive an incapacitating exposure to fire effluent.
2. *The process by which occupants escape.* This depends upon detection, the provision of warnings, response to warnings (premovement time), occupant profile (such as age and physical and mental ability, sleeping or waking, and population density) subsequent preegress behavior (such as seeking information, collecting belongings, choosing an exit, and other activities), egress (including wayfinding, movement towards an exit, crowd flow, and other factors), design of escape routes, exit numbers and widths, and the psychological and physiological influence of exposure to heat and smoke on escape behavior.

   Assessment of these processes for any particular fire scenario is aimed at calculating the time required for escape.

Once a fire has started, the outcome of the situation depends upon the outcome of these two processes. If the occupants have escaped before the fire becomes hazardous, with a reasonable margin of safety, then the design can be considered to have succeeded, but if the fire growth processes result in the fire becoming hazardous before the occupants have escaped, or within a narrow margin of safety, the design may be considered to have failed.

It is evident from this list of parameters that when all the needs of building occupants are considered, there is no single answer to fire safety or fire hazard, and that any practical system involves some compromise between all of these parameters. Fire safety can be improved or compromised in a number of different ways, while the occupants are involved in a number of ways, both in terms of their physiology and their behavior.

It is possible to consider the effects of fires on victims in three phases.

1. The first phase consists of the period when the fire is growing, but before the victim is affected by heat or smoke. During this phase the important factors influencing escape and ultimate survival are largely psychobehavioral or logistical factors, such as how the victim is alerted to the fire and reacts to that knowledge, whether he/she responds to alarms, attempts to leave or stays to fight the fire, interacts with other individuals, and how the person responds to the geography of the fire environment in effecting an escape.
2. The middle phase is the period when the victim is exposed to smoke, heat and toxic products, and where physiological factors such as irritancy and asphyxiation affect the victim's escape capability. During this phase such factors as the toxic nature of fire products and the dynamics of their production become critically important to escape.
3. The third phase is death in the fire, which may be caused by the major factors of toxicity and burns or a number of other factors.

The toxic effects of fire products are therefore most important during the second and third phases of fire growth. Most studies of fire toxicity have been confined to aspects of lethality. The ultimate causes of death in fires have been studied through pathological investigations of fire fatalities such as the Strathclyde study in the United Kingdom.[14] Also, the majority of combustion toxicity studies on laboratory animals have been used to measure lethality, principally in terms of the LC_{50} for individual fire products such as carbon monoxide (CO) or hydrogen chloride (HCl), or mixtures of thermal decomposition products from individual materials.[15]

The middle phase, of incapacitation in fires, can be studied either by animal experimentation or by investigations of the circumstances surrounding real fire casualties, particularly survivors of serious smoke exposure. However, this crucial area of toxicity has been largely neglected.

One particular series of studies has been carried out on the sublethal effects of combustion atmospheres on animals, mainly primates, to examine the mechanisms whereby people become incapacitated in fires.[16] Incapacitation rather than death has been studied because most fires are potentially lethal due to heat or CO if the victim is exposed to these for sufficient time. The two major determinants of whether a potential victim escapes are (1) the point at which incapacitation by toxic products is reached, and (2) how these products affect escape capability during the window of time available for escape between ignition and the development of lethal conditions.

The physiological effects of exposure to toxic smoke and heat in fires result in varying degrees of incapacitation which may also lead to death or permanent injury. Incapacitating effects include

1. Impaired vision resulting from the optical opacity of smoke and from the painful effects of irritant smoke products and heat on the eyes
2. Respiratory tract pain and breathing difficulties or even respiratory tract injury resulting from the inhalation of irritant smoke which may be very hot. In extreme cases this can lead to collapse within a few minutes from asphyxia due to laryngeal spasm and/or bronchoconstriction. Lung inflammation may also occur, usually after some hours, which can also lead to varying degrees of respiratory distress

3. Asphyxia from the inhalation of toxic gases, resulting in confusion and loss of consciousness
4. Pain to exposed skin and the upper respiratory tract followed by burns, or hyperthermia, due to the effects of heat preventing escape; this can lead to collapse

All of these effects can lead to permanent injury, and all except item 1 can be fatal if the degree of exposure is sufficient.

With regard to hazard assessment the major considerations are

1. The time when partially incapacitating effects are likely to occur which might delay escape
2. The time when incapacitating effects are likely to occur which might prevent escape, compared with the time required for escape
3. Whether exposure is likely to result in permanent injury or death

Up to a certain level of severity, the hazards listed in items 1 through 4 under physiological effects cause a partial incapacitation, by reducing the efficiency and speed of escape. These effects lie on a continuum from little or no effect at low levels to relatively severe incapacitation at high levels, with a variable response from different individuals. It is important to make some estimate of effects that are likely to delay escape, which may result in fewer occupants being able to escape during the short time before conditions become so bad that escape is no longer possible. Most important in this context is exposure to optically dense and irritant smoke, which tends to be the first hazard confronting fire victims. For more severe exposures a moment may be reached when incapacitation is predicted to be sufficiently bad as to prevent escape. For some forms of incapacitation, such as when asphyxia leads to a rapid change from near normality to loss of consciousness, this moment is relatively easy to define. For other effects a defining moment is less easily characterized; for example, when smoke becomes so irritant that pain and breathing difficulties lead to the cessation of effective escape attempts, or when pain and burns prevent movement. Nevertheless it is considered important to attempt some estimate of the moment when conditions become so severe in terms of these hazards that effective escape attempts are likely to cease, and when occupants are likely to suffer severe incapacitation or injuries. In the following text the mechanisms whereby these various factors cause incapacitation and death, and how they are likely to produce partial incapacitation and affect escape capability, are examined in detail. Toxicological and physiological data and models are presented to enable calculations to be made of time (or exposure dose) to incapacitation and death.

Basic Toxicity Patterns of Fire Products

As a result of chemical studies of large- and small-scale experimental fires[17] and animal exposures to the thermal decomposition products from a wide range of materials,[16] two important basic points have emerged concerning the nature of fire product toxicity.

1. Atmospheres of thermal decomposition products, even from single materials, contained large numbers of potentially toxic products. The chemical composition of the products could vary considerably depending upon the different conditions of temperature and oxygen supply under which they were decomposed.[16] When animals were exposed to these atmospheres, similar variations in toxicity were observed. In many cases, however, similar basic ranges of products were evolved from quite different materials.[17]
2. Despite the great complexity in chemical composition of smoke atmospheres, the basic toxic effects were relatively simple. For each individual smoke atmosphere the toxicity was dominated either by an asphyxiant gas (CO or HCN) or by irritants. Also, interactions between individual asphyxiant gases or, between asphyxiants and irritants, were found to be approximately additive, so that a reasonably good predictive model for incapacitation could be developed by summing the effects of each individual toxic component as acting separately.[16]

This work and that done by others using rodents[15] seems to indicate that the theory that smoke casualties have increased because new, highly toxic products are formed from modern materials is unlikely to be correct. Also, the finding that a small number of basic products are particularly important leads to the possibility of predicting toxic effects from a relatively simple chemical analysis of fire products. (This is not to say that unusual highly toxic products cannot occur, as at least two examples have been discovered in the laboratory;[8,9] and this is one important reason that the toxicity of thermal decomposition products from materials should be submitted to an animal screen.)

Dose/Response Relationships and Dose Estimation in the Evaluation of Toxicity

Before considering the particular effects of individual toxic fire products it is necessary to determine the basic parameters required to quantify exposure. Ultimately, the degree of toxicity is determined by such factors as the concentration of toxic product in the target organ of the body, and the time period for which a toxic concentration is maintained. For an asphyxiant product, the most important criterion is the concentration in the cerebral blood supply or inside the brain cells, while for an irritant product the most important factor is the concentration in the lining of the nose, throat, or lung. In some cases it is important and feasible to measure such parameters directly. For CO it is not the concentration in the smoke that directly determines how someone will be affected, but the concentration that has accumulated in the blood in the form of carboxyhemoglobin, and this can be determined relatively simply from a drop of blood.[18,19]

In practice, however, it is often not feasible to measure the amount of toxic product directly accumulated in the subject. Also, relating observed toxic effects to measurements of toxic products in the smoke itself is preferable, since it enables predictions of toxicity to be made based on chemical measurements of fire atmospheres without necessarily exposing animals. A series of useful

secondary measurements can, therefore, be made that can be related to toxic effects in animals, but it must be remembered that these indirect measurements of exposure always involve some degree of error or uncertainty.

The Relationships between Concentration Inhaled, Duration of Exposure, and Toxicity

In inhalation toxicology two parameters that are always measured and reported are the actual analyzed concentration of the test material per unit volume of air in the animals' exposure chamber, and the duration of exposure. For droplet aerosols or dusts the particle size range in the atmosphere is also measured so the respirable fraction (the part capable of entering the body) can be calculated. Where toxic effects can occur rapidly, as with the asphyxiant gases, it is also important to measure the rate of uptake of the toxicant. This can be estimated by measuring the volume of air breathed by the animal per minute (the respiratory minute volume, or RMV), although for accurate calculation of uptake and dose, further measurements, such as of blood levels, must be made. Variations in RMV can have dramatic effects on toxicity as will be described in the following section.

Although such parameters as respiration and particle size of aerosols are important, the most basic parameters reported are the concentration of the toxicant and the duration of exposure, which enables a rudimentary estimation of the dose. Thus the product of concentration and time (*Ct* product) gives an estimate of the dose available to the animal. In general safety evaluation of novel chemicals for an acute exposure, a standard single 4-hr exposure time is used and toxicity is expressed in terms of the concentration of test material causing the death of 50 percent of the animals during exposure or within 14 days after exposure. This is known as the 4-hr LC_{50} concentration.

In practice, however, it may be necessary to predict what will happen to a subject exposed to a higher concentration for a shorter period of time, or a lower concentration for longer time. Although this can be done by carrying out more LC_{50} experiments using different exposure durations, as an approximation toxicologists often resort to Haber's rule, which states that the toxicity depends upon the dose accumulated, and that the product of time and concentration is a constant,[20] so that

$$W = C \times t \tag{1}$$

where W is a constant dose, specific for any given effect. In practice, dose in inhalation toxicology is often expressed in terms of Ct product. In the case of the LC_{50}, the effect is death of 50 percent of the animals and

$$W = LC \cdot t_{50} \tag{2}$$

expressed in mg·min/liter (i.e., the product of the concentration and the duration of exposure causing lethality). This relationship implies a linear uptake of the toxic substance with time. (See Figure 2-6.3.) It holds true for many substances where the primary target organ is the lung; in the context of combustion toxicology this relationship can be applied to estimates of the dose of a lung irritant likely

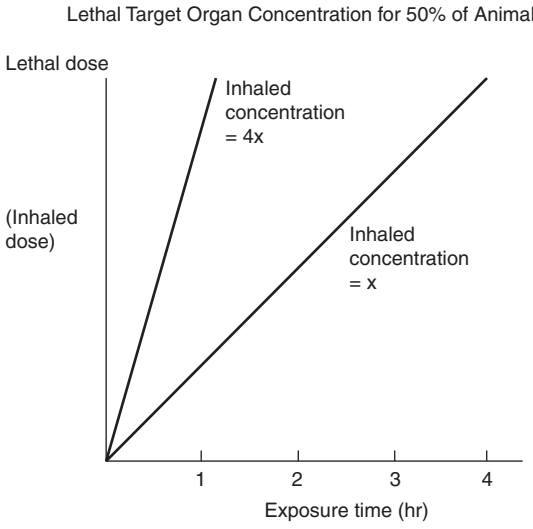

Figure 2-6.3. ***Uptake of a substance obeying Haber's rule (i.e., with a long halflife of detoxification or excretion), where the rate of uptake is directly proportional to the inhaled concentration, so that 1-hour LC_{50} is four times the 4-hour LC_{50}. The lethal represents a lethal target organ concentration for 50 percent of the animals.***

to cause postexposure fire deaths from lung inflammatory responses. An example of such an irritant is carbonyl fluoride, a highly toxic lung irritant produced during the thermal decomposition of PTFE, which has a 1-hr LC_{50} of 0.990 mg/L, which is exactly four times the 4-hr LC_{50} of 0.248 mg/L.[21]

Unfortunately, this simple principle does not always hold true. In particular, some volatile substances (such as CO) are both taken up and excreted via the lungs. In this case the rate of uptake depends upon the difference between the concentration inhaled and that in the body, giving an exponential uptake so that

$$W = C(1 - e^{-tk}) \tag{3}$$

which is the basis for the Coburn-Forster-Kane (CFK) equation[22,23] describing the uptake of CO in humans. This relationship approaches the linear Haber's rule (Equation 1) when the concentration, C, in the atmosphere is high with respect to the concentration in the body required to cause incapacitation or death (Figure 2-6.4), and for short exposures to high CO concentrations, uptake is approximately linear. This is illustrated by the results from CO exposure experiments in primates. At a constant level of activity, and thus respiration, the animals became unconscious when exposed to approximately 27,000 ppm·min of CO at concentrations between 1000 and 8000 ppm (Figure 2-6.5). For such situations it is therefore possible to use linear models for CO uptake without serious error.

Some toxic effects, however, are not dependent upon a dose acquired over a period of time, but are concentration related. Thus the irritant effects of smoke products on the eyes and upper respiratory tract (sensory irritation) occur immediately upon exposure, with the severity depending upon the exposure concentration. In fact, far

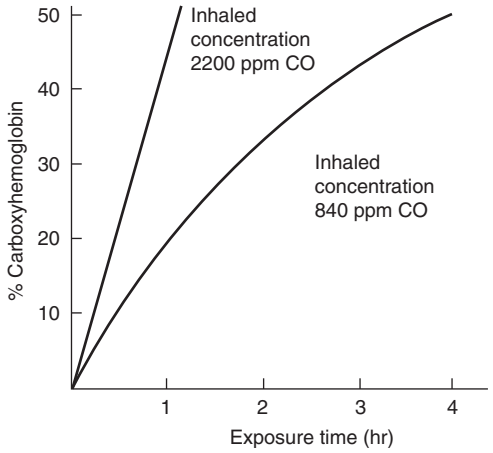

Figure 2-6.4. ***Uptake of a substance (carbon monoxide) which is both absorbed and excreted via the lungs, and where the rate of uptake depends upon the difference between the concentration inhaled and that in the body. For short exposures at high concentrations, uptake to a lethal dose is almost linear, obeying Haber's rule. For longer exposure times, uptake follows a curve so that the inhaled concentration necessary to achieve a lethal dose (50 percent carboxyhemoglobin) at four hr (840 ppm), is 0.38 times that required for deaths at one hr, as opposed to 0.25 times (550 ppm) as predicted by Haber's rule. Uptake was calculated for a 70 kg human at rest (RMV 8.5 L/min) using the CFK equation.***

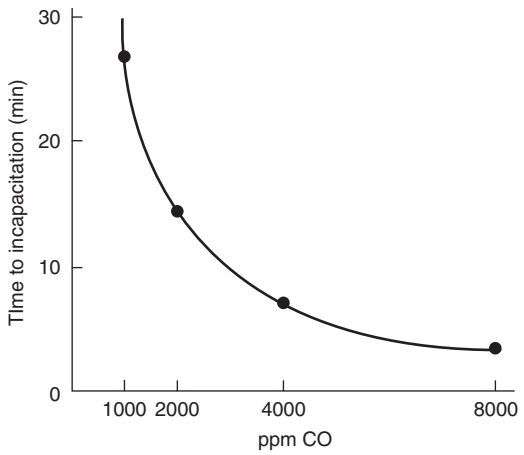

Figure 2-6.5. ***Relationship between time to incapacitation and carbon monoxide concentration in active monkeys. 1000 ppm Ct = 26,600 ppm·min; 2000 ppm Ct = 28,097 ppm·min; 4000 ppm Ct = 26,868 ppm·min; 8000 ppm Ct = 26,086 ppm·min.***

from increasing as exposure continues, the effects usually lessen, as the subject adapts to the painful stimulus even though the dose is increasing.[24]

Other cases where concentration is an important determinant of toxicity as well as duration of exposure are the asphyxiant effects of hypoxic hypoxia (oxygen lack) and hypercapnia (high CO_2 concentrations). If a subject is exposed suddenly to a low oxygen concentration, a finite time is required for the air in the lungs and gases in the blood to equilibrate to the new conditions, so to some extent a "dose" of hypoxia is acquired over a period of time. Once equilibrium is established, usually within a few minutes, the severity of the effects depend upon the oxygen concentration and do not then change appreciably with time.[25,26] This also applies to high CO_2 concentrations. Equilibrium is established within a few minutes and concentration related effects then determine the pattern of toxicity.[25]

For the other main asphyxiant gas in smoke, hydrogen cyanide (HCN), although accumulation of a dose is one factor, the most important determinant of toxicity appears to be the rate of uptake, which in turn depends upon the concentration. Thus as shown in Figure 2-6.6 incapacitation occurs rapidly (after 2 min) at the high concentration of 180 ppm (*Ct* product 400 ppm·min), but at the lower concentration of 100 ppm, incapacitation occurs only after approximately 20 min, requiring a much higher *Ct* product dose (2000 ppm·min). This effect leads to the unusual kinked HCN time/concentration curve shown in Figure 2-6.6 compared to the smooth curve for CO.

In attempting to predict what will happen to a subject exposed to a smoke atmosphere containing all these products it is therefore important to allow for these different concentration/time/effect relationships.

Ct Product and Fractional Effective Dose

The basic concept established in the previous section is that for the majority of toxic products in a fire atmosphere a given toxic endpoint such as incapacitation or death occurs when the victim has inhaled a particular *Ct* product dose of toxicant. In order to make some estimate of the likely toxic hazard in a particular fire it is therefore necessary to determine at what point in time during the course of the fire exposure the victim will have inhaled a toxic dose. This can be achieved by integrating the area under the fire profile curve for the toxicant under consideration. When the integral is equal to the toxic dose the victim can be assumed to have received a dose capable of producing that toxic effect.

A practical method for making this calculation is the concept of *fractional effective dose* (FED).[27] The *Ct* product doses for small periods of time during the fire are divided by the *Ct* product dose causing the toxic effect. These fractional effective doses are then summed during the exposure until the fraction reaches unity, when the toxic effect is predicted to occur. Thus

$$\text{FED} = \frac{\text{dose received at time } t(Ct)}{\text{effective } Ct \text{ dose to cause incapacitation or death}} \qquad (4)$$

For substances obeying Haber's rule the denominator of the equation is a constant for any particular toxic effect. For substances deviating from Haber's rule the denominator for each time segment during the fire is the *Ct* product dose at which incapacitation or death would occur at the concentration during that time segment. For

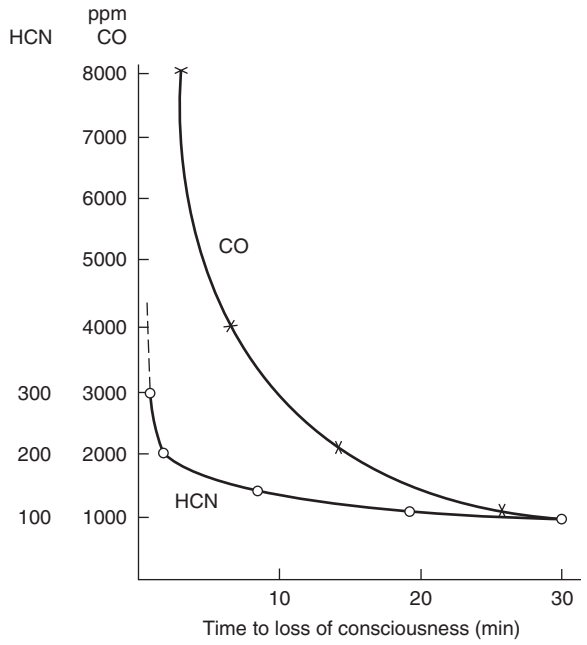

Figure 2-6.6. ***Comparison of the relationship between time to incapacitation and concentration for HCN and CO exposures in primates. Time and concentration are equivalent for CO; for HCN, a small increase in concentration causes a large decrease in time to incapacitation.***

the hazard model presented in this chapter the denominator is presented in the form of equations giving the required *Ct* product doses predicted for man, which have been derived for each toxic gas and are presented in the following sections. Special cases of the fractional effective dose are referred to as the *fractional incapacitating dose* (FID) and the *fractional lethal dose* (FLD).

For sensory irritation—a toxic effect which depends upon the immediate concentration of an irritant to which a subject is exposed, rather than the dose—a concept of *fractional irritant concentration* (FIC) has been developed, where

$$\text{FIC} = \frac{\text{concentration of irritant to which subject is exposed at time } (t)}{\text{concentration of irritant required to cause impairment of escape efficiency}} \quad (5)$$

The Nominal Atmosphere Concentration

There are occasions in combustion toxicology when it may be desirable to relate the toxic effects of an exposure to the material being decomposed rather than to its individual toxic products. This applies particularly to small-scale test results, where, for example, the LC_{50} of wood when decomposed in a particular way might be considered. This is a somewhat unsatisfactory approach, since it cannot be predicted that any material will evolve the same products with the same yields in a large-scale fire as in a small-scale test, and therefore exhibit the same degree of toxicity. However, this parameter does have some value when calculated in conjunction with measurements of the actual toxic products. This approach is related to another concept used in inhalation toxicology, that of the nominal atmosphere concentration, NAC. This theoretical concentration of test material in the test atmosphere is calculated from the amount of material produced from the atmosphere generation system each minute, divided by the diluent airflow rate. This concept is not strictly applicable in combustion toxicology since the test material is decomposed in the fire or furnace system, but two analagous concepts are very useful with regard to small-scale test methods since they enable some relationship to be established between the test material and the degree of toxicity. These are the nominal atmosphere concentration in terms of mass charged into the furnace, and the nominal atmosphere concentration in terms of mass decomposed, as follows:

1. Nominal atmosphere concentration (mass charge) equals mass of material placed in the furnace system divided by volume of air into which it is dispersed.
2. Nominal atmosphere concentration (mass loss) equals mass lost by material during decomposition divided by volume of air into which it is dispersed.

In practice the calculation of these parameters depends upon the particular decomposition system used (see the section of this chapter on small-scale test methods) and a shortcoming of some systems is that these parameters cannot easily be estimated.

If predictions of toxicity are to be made from large-scale fire test atmospheres, or if toxicity data from animals are to be interpreted, the following data should be available:

1. The nominal atmosphere concentration(s) of the test material(s) mass charge ($g \cdot m^{-3}$) (NAC mass charge)
2. The nominal atmosphere concentration of the test material mass loss ($g \cdot m^{-3}$) (NAC mass loss)
3. The concentration of each major toxic product in the atmosphere and the anticipated duration of exposure, that is, the concentration/time profile
4. The rate of uptake of the atmosphere, or RMV
5. Measurement of the blood concentration of certain toxicants
6. Particle size range. This is also important in determining the respirability and site of deposition of atmospheric products. However, smoke from nonflaming decomposition in small-scale tests is usually highly respirable
7. The nature of the effects of toxic products and the time/concentration relationships of these effects

Allowance for Margins of Safety and Variations in Susceptibility of Human Populations

The methods for assessing the effects of toxic gases were originally developed to predict the exposure concentrations or exposure doses that would be expected to cause serious effects such as impairment of escape capability, incapacitation, or death in a building occupant.

When they are used for design purposes, the main consideration is to predict not a serious effect level, but a maximum safe level. When used in this context, it is necessary to use some degree of conservatism in applying tenability endpoints for two reasons. One reason is to allow for uncertainties in the predictability of the endpoints. This is mainly because the endpoints cannot be fully quantified within narrow limits without performing experimental human exposures to a variety of complex and dangerous toxic effluent mixtures. This obviously cannot be done for ethical reasons. Another reason is the wide range of sensitivities to toxic effects in a heterogeneous human population.

The physiological algorithms are based partly upon experimental data and reported effects in humans, and partly upon animal studies. These methods involve either the exposure dose or concentration predicted to produce a given effect on humans exposed to fire effluent. However, the effects are based upon data for healthy young adult animals or humans. The exposure dose or concentration therefore represents the maximum in a statistical distribution of subjects' responses surrounding that exposure dose or concentration, that is, the mode, or most frequently expected exposure dose for an exposed population. Individual exposure doses or concentrations for the response would, in practice, be statistically distributed around the mode in a probability curve. The overall human population contains a number of subpopulations, which exhibit greater sensitivity to various fire effluent toxicants, principally due to compromised cardiovascular and pulmonary systems.

Two of the largest such subpopulations are the elderly and the approximately 15 percent of children and 5 percent of adults who are asthmatic.[28] The elderly, and particularly those with impaired cardiac perfusion, are particularly susceptible to asphyxiant gases. Thus the average lethal carboxyhaemoglobin (COHb) concentration in adults dying in fires or from accidental CO exposure is lower in the elderly.[29] Figure 2-6.7 shows the distribution of postmortem carboxyhaemoglobin concentrations in human fire and non-fire CO fatalities in the United States.[29] The results show that some individuals died at COHb concentrations below 30 percent while other survived long enough to obtain blood concentrations above 90 percent COHb. Many fire fatalities occur at lower COHb concentrations than for cases of CO poisoning alone. This may partly reflect the influence of other toxic gases in addition to CO in fire atmospheres. Also it has been shown in experimental studies that as little as 2 percent COHb significantly reduces the time to the onset of pain in an exercise test of angina sufferers.[30] This could be very important when attempting to escape from a fire. Asthmatics, and sufferers of other lung conditions such as chronic bronchitis and reactive airways dysfunction syndrome, are particularly susceptible to bronchoconstriction upon even brief exposure to very low concentrations of irritants, with distress, severely reduced aerobic work capacity, collapse and death resulting, depending upon the sensitivity of the individual and the severity of the exposure.

It is the objective of fire safety engineering to ensure that essentially all occupants, including the sensitive subpopulations, should be able to escape safely without experiencing or developing serious health effects. Thus, safe levels for exposure of the human population to fire effluent toxicants must be significantly lower than those determined from experiments with uniformly healthy animal or even human surrogates.

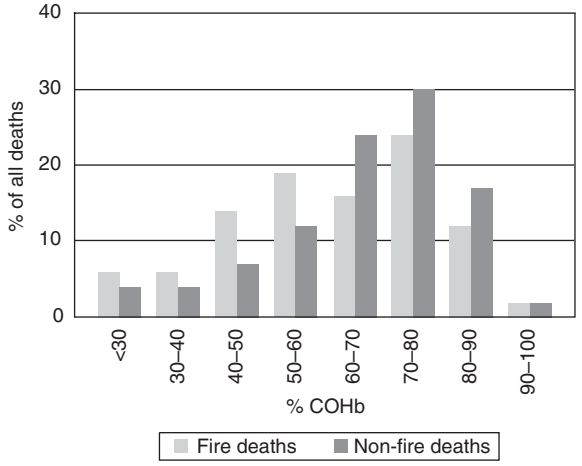

Figure 2-6.7. ***Range of lethal sensitivity to carbon monoxide in humans (after Nelson[29]).***

Fractional Effective Dose Hazard Assessments and Toxic Potency

In the context of fire safety, toxicity information is useful only to the extent that it can be used to assess toxic hazard in a full-scale fire scenario. There are a number of reasons for carrying out such an assessment. It may be needed in order to carry out a fire safety engineering assessment of a building design. In this context a particular set of fire scenarios may be run in order to assess probable outcomes in terms of the relationship between time available for escape compared to time required for escape. Time available for escape depends on the fire dynamics and time to incapacitation for building occupants exposed to toxic smoke. Time required for escape may also depend partly on the effect of toxic smoke on escape behavior. Another reason for modeling time to incapacitation may be the investigation of fire incidents in order to evaluate effects on fire victims. Another reason may be for a manufacturer to evaluate and compare potential toxic fire hazards from different materials of products, or for specifiers to determine the applicability of particular materials or products to particular design applications. In this situation a range of full-scale fire scenarios can be considered in order to evaluate product performance.

A difficulty with carrying out toxic-hazard assessments is that toxic products exert a range of different effects on building occupants, and toxicity information may be presented in a number of different forms. Confusion also often arises in relation to toxic potency data and its application to toxic-hazard assessment.

The toxic potency of a substance depends upon how much is required for a given toxic effect. The smaller the

amount needed, the more potent the toxic substance. For example, in fires, hydrogen cyanide is about 20 to 40 times more potent than carbon monoxide, because the amount needed to be inhaled to cause collapse is a much smaller exposure dose for hydrogen cyanide than for carbon monoxide.

Toxic hazard in a fire depends upon the extent to which toxic products in that fire scenario present a danger to building occupants. Put simply it depends upon how quickly and how much toxic products are produced, and how potent the products are.

Toxic Potency

Toxic potency can be considered in terms of

- An individual toxic gas such as carbon monoxide or hydrogen chloride
- A mixture of toxic products occurring in a fire (for example, the asphyxiant toxic potency of a CO and HCN mixture, or the irritant potency of a mixture, of acid gases)
- The mixture of toxic products evolved from the thermal decomposition under defined conditions of a particular material or product (such as wood, polyethylene, or a length of electrical cable)

The Toxic Potency of Individual Fire Gases and Gas Mixtures

In fires three major toxic effects are important.

1. The concentrations of irritant gases likely to impair escape efficiency or cause incapacitation (sensory irritation)
2. The exposure doses (*Ct* product doses) of asphyxiant gases likely to cause incapacitation through confusion and loss of consciousness (or to cause death)
3. The exposure doses of irritants likely to cause death through lung edema and inflammation after the fire

For sensory irritants the main criteria are the time during the course of a fire when the concentrations of irritants are sufficient to impair escape efficiency, and the time when they are likely to cause incapacitation through pain and respiratory distress. This is evaluated using the concept of fractional irritant concentration (FIC), by which the fractions of an irritant concentration for each irritant present are summed. When FIC = 1 a tenability endpoint (escape impairment) is predicted. Incapacitation is predicted at higher concentrations (FIC ~ 3–5). The sensory irritant potencies of different individual irritants occurring in fire atmospheres cover an enormous range spanning six orders of magnitude. More than 20 irritant compounds are considered to contribute to the overall sensory irritancy of fire atmospheres. The most important irritants identified are acid gases (hydrogen fluoride, hydrogen chloride, hydrogen bromide, nitrogen oxides, phosphoric acid, and sulphur dioxide) and organic irritants (such as acrolein, formaldehyde, and crotonaldehyde). Detailed guidance on the assessment of sensory irritancy of fire effluent is presented in the section on irritant fire products.

For asphyxiant gases the main criterion is the time during the course of a fire when a sufficient exposure dose (*Ct* product dose) of asphyxiants has been inhaled to cause incapacitation through confusion and loss of consciousness. This is evaluated using the FED concept, incapacitation being predicted at FED = 1. The gases important in causing asphyxiation are carbon monoxide, hydrogen cyanide, and reduced oxygen concentration. Carbon dioxide is important mainly because it increases the rate of uptake of CO and HCN. The toxic potencies of asphyxiant gases are less simple to define, because for cyanide (and reduced oxygen concentration) the incapacitating exposure dose is not a constant. However, the exposure doses lethal to rats over a 30-min exposure period are approximately 5700 ppm for CO and 164 ppm for HCN. The evaluation of asphyxiants is described in detail in the section on asphyxiants.

Another aspect of irritants that needs to be considered is the time during the course of a fire when a sufficient exposure dose of mixed irritants had been inhaled to cause potentially lethal lung inflammation. The toxic potencies of different lung irritants occurring in fire effluent cover a very wide range of approximately five orders of magnitude (see Table 2-6.1). Detailed guidance on the evaluation of lethal lung irritation is given in the section on irritants.

Toxic Potencies of Individual Materials

When individual materials are decomposed in full-scale fires or small-scale combustion toxicity tests, they produce a range of individual irritant and asphyxiant toxic products. The overall toxic potency of the resultant effluent mixture will depend on the yields of individual toxic products and their toxic potencies. For any particular material the yields of individual toxic products depend upon the thermal decomposition conditions (non-flaming oxidative, well-ventilated flaming, or vitiated flaming). In general, materials produce high yields of toxic products under nonflaming oxidative and vitiated flaming conditions, and lower yields under well-ventilated flaming conditions. This is described in detail in the sections on chemical composition and toxicity of combustion product atmospheres and the section on fire scenarios and victim incapacitation.

For any individual material decomposed under a particular decomposition condition in a small-scale test, it is possible to evaluate the toxic potency of the effluent mixture in terms of sensory irritation, asphyxiation or potential for lung inflammation. The toxic potency is then expressed in terms of the nominal concentration of the decomposed material rather than in terms of individual toxic products. Table 2-6.2 shows examples of the sensory irritant potency of fire effluent from materials, expressed in terms of the mouse RD_{50} concentration of the material decomposed (expressed as the mass loss concentration). The RD_{50} is the concentration causing a 50 percent decrease in respiration rate in mice during a short exposure. A reasonably good relationship has been found between the mouse RD_{50} concentrations for a range of irritant vapors and the concentrations reported as being painfully irritant to humans[93] (see section on

Table 2-6.1 ***Sensory and Pulmonary Irritancy of Combustion Products***

Irritant	RD_{50} (ppm) Mouse[b]	Severe Sensory Irritancy in Humans (ppm)	30-Min LC_{50} (ppm) Mammal[c]	LC_{50}/RD_{50}
	0.1–1.0			
Toluene diisocyanate	0.20	1.0[21]	100[21]	500
O-chlorobenzylidene -malonitrile (CS)[a]	0.52	0.5[24]	150–400[89,90]	529
α-chloroacetophenone (CN)[a]	0.96	6–50[17]	300–400[82,91]	365
	1.0–10			
Acrolein	1.7	1–5.5[21,82]	140–170[82,85,91]	91
Formaldehyde	3.1	5–10[21,82]	700–800[84,91]	242
Chlorine[1]	9.3	9–20[82]	100[84]	11
	10–100			
Crotonaldehyde		4–45[21]	200–1500[21,91,92]	
Acrylonitrile		>20[21]	4,000–4,600[91]	
Penteneone			1,000[91]	
Phenol		>50[21]	400–700[91]	
	100–1,000			
SO_2	117	50–100[21,82]	300–500[84,91]	3
NH_3	303	700–1700[88]	1,400–8,000[84,91]	16
HF		120[21]	900–3,600[91]	
HCl	309	100[21,82]	1,600–6,000[84,85,91]	12
HBr		100[21]	1,600–6,000[91]	
NO_2	349	80[21,82]	60–250[84,91]	0.4
Styrene	980	>700[21]	10,000–80,000[91]	46
	1,000–10,000			
Acetaldehyde	4946	>1,500[21]	20,000–128,000[91]	15
	10,000–100,000			
Ethanol	27,314	>5,000[21]	400,000[91]	15
Acetone	77,516	>12,000[21]	128,000–250,000[21,91]	2

The potential for causing sensory irritation spans six orders of magnitude, while that for causing death spans approximately three orders of magnitude. For substances down to NO_2 death is likely to be due to lung irritation, while for the remainder from styrene to acetone death is likely to be due to asphyxiation.

[a]Substances not detected in combustion atmospheres

[b]RD_{50} from Alarie,[93] where no data exist substances have been ranked according to their reported irritancy in man

[c]LC_{50} concentrations have been normalized to a 30-min exposure time according to Haber's rule.

irritancy). The table shows the mouse RD_{50} for a number of materials, some of which occur in aircraft, when decomposed under the thermal decomposition conditions indicated, using the BRE tube furnace method.[32] The majority of experiments were conducted under nonflaming oxidative decomposition conditions, but a small number of experiments were conducted under flaming decomposition conditions. The results show that the majority of materials have RD_{50} values lying between 0.05 and 0.5 g/m^3 under nonflaming oxidative decomposition conditions. This means that if the products of decomposition of between 0.05 and 0.5 g of material are dispersed into each cubic meter of air, then the resultant atmosphere is predicted to be painfully irritant to the eyes and respiratory tract. However, under flaming decomposition conditions the smoke irritancy decreases by a factor of 10 or more. For use in a hazard analysis for humans the RD_{50} mass loss concentration should be regarded as producing a total FIC_{irr} of approximately 0.5 for the effluent from the material in question.

Although it is therefore possible to measure or calculate the sensory irritant toxic potency of the fire effluent from materials decomposed under specific decomposition conditions, traditionally, toxic potencies for materials have been expressed in terms of overall lethal toxic potency to rats. This information was originally obtained by exposing groups of rats to thermal decomposition atmospheres from materials in small-scale tests and establishing the exposure concentrations causing the deaths of half the exposed animals (LC_{50} concentrations) during or within 14 days after a 30-minute exposure period. These data can also be expressed in terms of an exposure dose (*Ct* product dose) by multiplying the LC_{50} concentration by 30 to give an LCt_{50} exposure dose. Animal experiments of this kind have now largely been replaced by chemical measurements used in conjunction with appropriate calculation models as a method for estimating the rat LC_{50}. For this method the same small-scale tests may be used and the composition of the fire effluent is measured in terms of the major toxic fire gases. The data are then used as input to a

Table 2-6.2 ***Mass Loss Concentrations of Thermal Decomposition Products Predicted to Be Painfully Irritant (mouse RD_{50} g/m³)[32]***

Material	Temp. (°C)	NF/F*	RD_{50} g/m³ Mass Loss	95% Confidence Limits
General materials:				
acrylonitrile butadiene styrene	500	NF	0.11	0.07–0.17
as above	600	F	~1	
low density polyethylene	500	NF	0.05	0.03–0.07
nylon-6	480	NF	0.47	0.29–1.10
as above	600	F	~20	
polyvinylchloride (PVC) (rigid)	400	NF	0.17	0.12–0.25
polyvinylchloride (plasticized)	380	NF	0.19	0.09–0.28
as above	600	NF	0.17	0.12–0.22
as above	650	F	~2.6	
Thermoplastic polyurethane	425	NF	0.20	0.14–0.96
as above	600	F	~3	
Cable materials:				
PVC insulation (plasticized)	550	NF	0.56	0.39–1.00
PVC jacket (plasticized)	550	NF	0.34	0.27–0.47
cross-linked polyethylene (insul.)	550	NF	0.12	0.09–0.17
as above XLPE (jacket)	550	NF	0.32	0.20–0.32
Aircraft materials:				
phenolic fiberglass	600	NF	>9.1	
PVC decorative laminate	600	NF	0.10	
polycarbonate	600	NF	0.25	
phenolic oil fiberglass insulation	600	NF	0.05	
aluminized PVF/paper covering	600	NF	0.37	
Redux adhesive	600	NF	0.10	0.06–0.16
silicone rubber	600	NF	0.06	0.01–0.29
jointing compound JC5V	600	NF	0.18	0.07–0.32
Viton sealant	600	NF	0.21	0.15–0.27
Berger elastomer	600	NF	1.38	1.12–1.80

*NF = nonflaming
F = flaming

special type of FED calculation designed to predict lethal toxic potency in rats. (This should not be confused with the FED calculation methods used to predict incapacitation and death of humans exposed to full-scale fire atmospheres). Details of these FED calculations for rat lethality are presented in the section on the relationship between toxic potencies of materials in small-scale tests and full-scale fires. Standard methods have been published in British[33] and International[34] standards.

The lethal exposure concentrations or exposure doses expressed in this way represent the overall lethal toxic potency of the effluent from both asphyxia and lung irritation. Sensory irritation is not considered. The lethal toxic potency to rats is considered to be similar to that expected to occur in humans. It can therefore be used to represent an exposure dose of effluent from a material under defined fire conditions predicted to be lethal to humans. Incapacitation would be predicted at around a third of this exposure dose. In this context the toxic potency is expressed in terms of the nominal atmosphere concentration of the material (e.g., $g \cdot m^{-3} \cdot min$ mass loss of wood). This obviously provides a very crude estimate of the toxic potency of effluent to humans, since it does not take into account different toxic endpoints such as sensory irritancy and asphyxiation, it does not allow for deviations from Haber's rule known to be important with asphyxiant gases, it does not differentiate between effects occurring during exposure and afterwards, and it does not allow for differences between rodents and humans or the range of different sensitivities occurring within the human population.

The lethal toxic potencies of materials tend to be dominated by toxic gases evolved at high yields such as carbon monoxide, hydrogen cyanide, and acid gases when the relevant anions are present as a significant part of the elemental composition of the material. Under some conditions organic irritants or other compounds, including irritant ultrafine particulates, can be important. Figure 2-6.8 illustrates the range of lethal toxic potencies from individual compounds occurring in fire atmospheres and for individual materials decomposed under different combustion conditions.[35,36] The acute lethal toxic potencies of individual toxic products occurring in fire atmospheres range over more than five orders of magnitude. The most acutely toxic substance so far identified in the thermal decomposition product atmosphere is the ultrafine fluoropolymer particulate evolved when perfluorinated polymers such as polytetrafluoroethylene (PTFE) are decomposed under nonflaming conditions at temperatures of 400–650°C.[36] The LC_{50} of this particulate is $< 0.017\ g \cdot m^{-3}$. This toxic particulate has a short half life and is unlikely to present a hazard in most fire scenarios. It is not formed at high temperatures or when the fluoropolymer is flaming. Other compounds with a high acute lethal toxic potency evolved during fires are perfluoroisobutylene, carbonyl fluoride, and carbonyl chloride. Hydrogen cyanide and nitrogen dioxide, and some low molecular weight carbonyl compounds are also highly toxic in the 0.1–~1 g/m^3 range. Carbon monoxide and common acid gases such as hydrogen chloride lie in the 1.0–10 g/m^3 range, while a range of organic products with varying toxic potencies occupy higher ranges up to some with very low acute toxic potencies such as methane and other aliphatic compounds.

When the range of toxic potencies of these individual toxic products is compared with the acute lethal toxic potencies of effluent mixtures from particular materials or classes of materials expressed in terms of NAC mass loss (g/m^3), then a similar range of approximately four to five orders of magnitude occurs, ranging from fluoropolymers decomposed in such a way as to evolve ultrafine particulate (~0.017 g/m^3) to cellulosic materials decomposed under well-ventilated conditions in such a way that very low yields of toxic products are formed (>100 g/m^3). In practice, the lethal toxic potency of perfluorinated polymers covers a very wide range from

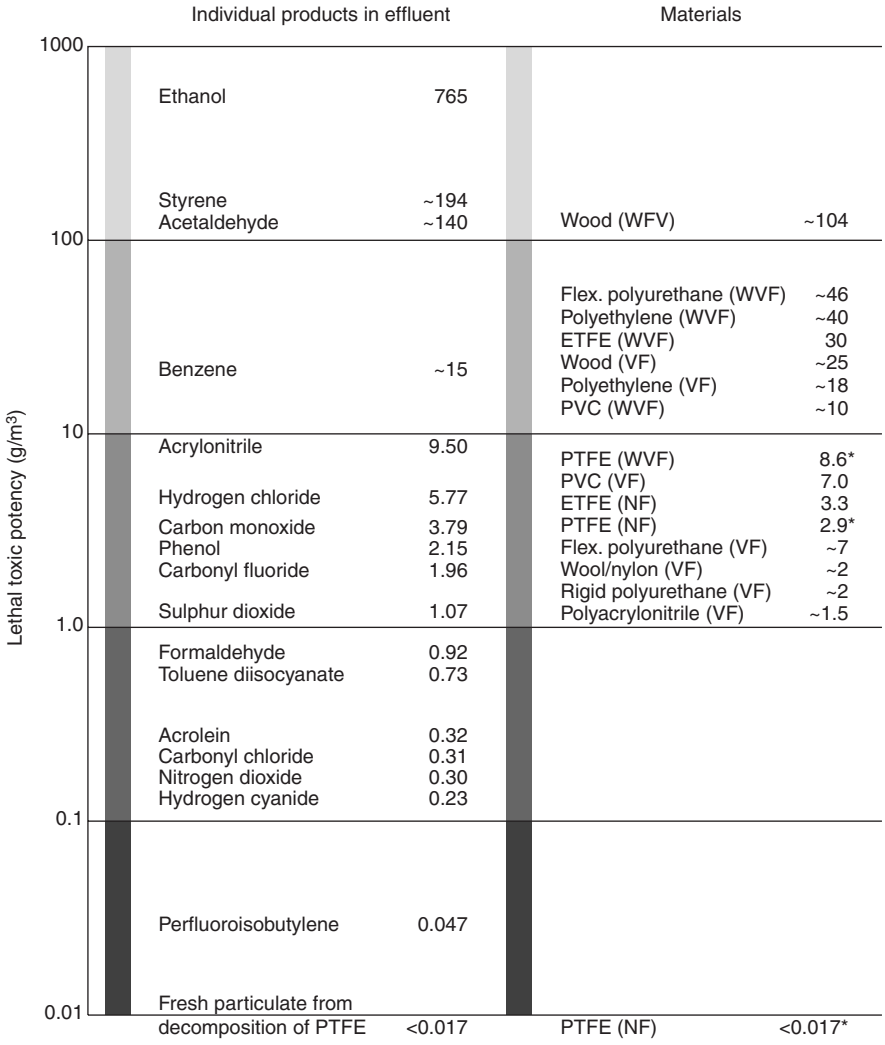

Figure 2-6.8. ***Lethal toxic potencies (g/m³) of individual compounds and the combustion products from various materials.***

NF = Nonflaming, WVF = well-ventilated flaming, VF = vitiated flaming

*The toxic potency of particulates evolved from fluoropolymers (and therefore the toxic potency of fluoropolymers themselves) varies considerably with the decomposition conditions and the age of the particulates. Extreme toxic potencies have not been observed for fluoropolymers under full-scale fire conditions.

approximately 0.017–8.6 g/m³, depending upon the decomposition conditions.[36] For most materials, the worst case conditions for producing high toxic potencies are nonflaming or vitiated flaming conditions, particularly for materials containing nitrogen or halogens. Many materials show toxic potencies in the range 1–10 g/m³ under these conditions. Well-ventilated flaming tends to destroy toxic products such as CO, HCN, and organic irritants, so that for polymers containing carbon, hydrogen, and oxygen the toxic potencies are low, with LC_{50} in the 10–100 g/m³ range. These aspects are discussed in more detail in later sections (see Tables 2-6.3 and 2-6.4), but the figure illustrates that for most materials under most fire conditions (including fluoropolymers) the lethal toxic potencies (30-min LC_{50}) fall within a range of approximately two orders of magnitude.

Despite the limitations of lethal toxic potency data for individual materials, they can be used for simple estimations of toxic hazard in full-scale fires. This represents one of a number of different approaches that can be used for the assessment of toxic hazard in full-scale fires, with varying degrees of sophistication and validity. The different methods are summarized in the next section.

Basic Requirements for Toxic Hazard Assessments of Full-Scale Fires

A key step in the process of toxic hazard assessment is to describe the growth of the fire, the production of toxic effluent, and its spread. A number of methods can be used to achieve this, but the main elements are as follows:

Table 2-6.3 ***Lethal Toxicity Data for Combustion Products from a Range of Materials***

Author	*n*	Test Method	30-Min LC_{50} (mg/l mass loss) Mean	Range	Wood	$L(Ct_{50})$ (mg·min/l mass loss) Mean	Range
Levin[9]		NBS (NF)	24	5–40	25	720	150–1200
	11	(F)	27	4–57	49	810	120–1710
Kimmerle and Prager[42]	18	DIN (NF)	23	6–60	20–50	690	180–1500
Alexeev and Packham[43]	46	UPIT (mixed)	19	4–88	68	580	117–2648
Average			23	5–61	42	700	142–1765

NF = nonflaming
F = flaming

1. Obtain the mass loss curve for the fire and the dispersal volume of the effluent, either by conducting a simple large-scale test (measuring mass loss or heat release), by using a design fire, or by modeling
2. Determine the time-concentration curves for the main toxic fire gases, smoke optical density, and temperature of the fire either by
   a. direct measurement in a full-scale fire test
   b. calculation from the yields of toxic products, smoke and heat from the materials involved in item (1), measured in small-scale tests performed under appropriate fire conditions
   c. calculation from a knowledge of the composition of the materials involved in item (1) and fire decomposition chemistry
3. As an alternative to item (2), calculate the mass loss concentrations and mass loss exposure doses for materials involved in the fire

Once the growth of the fire and the spread of the fire and effluent has been described it is possible to proceed to quantify hazardous effects and estimate time to incapacitation and death. This can be done in two main ways.

Table 2-6.4 ***Approximate Lethal Exposure Doses (LCt_{50} g·m^{-3}·min), LC_{50} (g·m^{-3}), and Toxic Potency Factors for Common Materials under Different Fire Conditions***

Material	Nonflaming			Early Flaming			Post-Flashover		
Cellulosics	730	24	(0.7)	3120	104	(0.2)	750	25	(0.7)
C, H, O plastics	500	17	(1.0)	1200	40	(0.4)	530	18	(0.9)
PVC	500	17	(1.0)	300	10	(1.6)	200	7	(2.5)
Wool/nylon (low N_2)	500	17	(1.0)	920	31	(0.5)	70	2	(7)
Flexible polyurethane	680	23	(0.7)	1390	46	(0.4)	200	7	(2.5)
Rigid polyurethane	63	2	(8)	100	3	(5)	54	2	(8)
Modacrylic/PAN	160	5	(3)	140	5	(3.6)	45	1.5	(11)

Toxic potency factors are calculated from the LCt_{50} based upon a "normal" potency of 500 g·m^{-3}·min. LC_{50} is for a 30-min exposure time with 14 days observation period.

1. Time to incapacitation and death can be estimated using physiological FIC and FED calculation models for smoke, irritant, and asphyxiant fire gases in conjunction with time-concentration curves for toxic fire gases as input data. This method calculates
   a. Time at which concentrations of smoke and sensory irritants are likely to impair or reduce the efficiency of egress due to psychological or physiological effects
   b. Time at which exposure concentrations or doses are likely to cause incapacitation or prevent egress due to psychological or physiological effects
   c. Time at which a lethal exposure dose has been inhaled
2. Alternatively, lethal toxic potency data for the materials involved in the fire can be obtained from small-scale combustion toxicity test atmospheres using animal exposures or using chemical analysis of the key toxic gases measured in such tests in conjunction with rat lethality FED calculations. These data can then be used with mass loss exposure dose curves (from method (3) to estimate time to incapacitation or death.

The Application of Small-Scale Tests for the Determination of Toxic Product Yields, and Time Concentration Curves, to Toxic Hazard Assessment

Where time concentration curve data are obtained from full-scale fire tests it is possible to proceed directly to an assessment of time to incapacitation using physiological FED algorithms. This method is described in the section on the prediction of time to incapacitation. Where full-scale fire data are unavailable, it is necessary to use modeling and small-scale test data obtained from performance-based tests to estimate the full-scale fire and the time-concentration curves of the main fire gases. In order to do this, it is necessary to use some form of fire growth curves (such as a t^2 fire growth curve or curves derived from heat release rate data) and a zone or computational fluid dynamics model to calculate the distribution and concentration of fire effluent (expressed in terms of fuel mass loss concentration) with time within the building enclosures. It is then necessary to obtain data for the yield of toxic fire products per unit mass of fuel decomposed, from which the concentrations of smoke and

toxic gases in the fire can be calculated. As described in Section 2, Chapter 5 and Section 3, Chapter 4, for particular fuels, the yields of CO and other toxic gases are dependent upon the equivalence ratio (ϕ) and particular characteristics of the fuels (such as the organic structure and the presence of oxygen or fire retardant additives [such as nitrogen, halogens, or phosphorus]).

As with all fire parameters the yields of toxic gases in full-scale fires can be variable and difficult to measure, while the equivalence ratio can be expressed in several different ways on a global or local basis within a fire enclosure. In practice, it is not practical to carry out full-scale tests to evaluate most hazard scenarios, so it is necessary to rely on modeling using reaction to fire data from small-scale tests or standardized fire curves, although these represent a further abstraction from the full-scale scenario, and need to be used with caution. One way of obtaining data on the relationship between ϕ and the yields of toxic products is to decompose the material in a small-scale toxicity test designed to combust materials under defined equivalence ratios. If the mass loss and product dispersal curve for the full-scale fire and the full-scale equivalence ratios are calculated, it is then possible to estimate the concentrations of toxic products by reference to the small-scale data. One example of such a small-scale test is the Factory Mutual apparatus, data from which are shown in Section 3, Chapter 4.[13] Another is the tube furnace method developed at the U.K. BRE Fire and Risk Sciences.[37–39] These methods have been used to examine the relationship between ϕ and toxic products yields, and the results obtained appear to be reasonably similar to those obtained in full-scale tests.[12,40] The apparatus is described in the section on second generation test methods. The following section gives a simple theoretical example of the application of this method.

Using small-scale toxic product yield data in toxic hazard assessments: Figure 2-6.9 shows the relationship between ϕ and CO yield for two fuels comprised of carbon and hydrogen only. Large-scale data using hexane and fuel are reproduced from Gottuk.[12,40] The small-scale data are taken from Hull et al.[39] and Purser[38] for polyethylene and PVC using the FRS Tube furnace. As the figure shows, CO yield is very low for these fuels at ϕ values > 1 and peaks at ϕ values of around 2 at approximately 0.2 g/g. Similar relationships occur for other toxic products and an inverse relationship for CO_2 (see Tewarson Chapter 3.4[13]). As a simple example, a full-scale fire is estimated as a medium growth rate t^2 fire, with a theoretical fuel decomposing with the same CO and CO_2 yields as were obtained from the tube furnace tests at ϕ values of 0.5 (well ventilated) and 1.5 (vitiated). The fire is in an enclosed room ($2.44 \times 3 \times 2.44$ m) with a 1 m $\times$ 0.3 m vent at floor level. The fire growth rate, heat release rate, and upper zone filling rate are modeled using CFAST. The mass loss rate is calculated from the heat release rate. The CO yield and CO_2 yields are taken from the tube furnace experiments as

well-ventilated:	0.007 CO	2.54 CO_2	g/g fuel mass loss
vitiated:	0.149 CO	1.57 CO_2	g/g fuel mass loss

The FED for human incapacitation from CO and CO_2 is calculated, using Equations 7 and 18. (Figure 2-6.10) Three cases were calculated. For one it was assumed that the CO and CO_2 yields remained fixed at the well-ventilated levels. For the second it was assumed that the yields changed linearly with time from the start to the peak of the fire, and for the third it was assumed that the yields remained constant throughout at those obtained under vitiated conditions. In reality, the yields would be expected to change with ϕ, which could be calculated for the full-scale fire case. The results of the exercise for the variable yields illustrate that the yields of CO and CO_2 during the early, well-ventilated phase of the fire produce only a small increase in FED for asphyxiation. This is partly because the smoke layer is above the occupant's head for some of the time, but mainly because the fire is small and producing only small amounts of effluent. During the later parts of the simulation the fire is larger, producing effluent at a much greater rate. It is also becoming vitiated so that both the mass and yield of CO are increasing. After 200 seconds the FED is predicted to reach 1 and incapacitation is predicted to occur. If the CO and CO_2 yields are assumed to remain constant at the well-ventilated levels throughout, then the increasing toxic hazard is seriously underestimated, reaching only an FED value of only 0.1 after 200 seconds. When the CO and CO_2 yields are assumed to remain constant at the vitiated yield values, then the increasing FED is slightly earlier than, but very similar to, that obtained when continuously varying yields were assumed. This illustrates the importance of obtaining toxic product yield data under the correct fire conditions and the extent to which the toxic hazard is driven by the later stages when the fire is larger and the CO yields greater. In this example the error obtained by assuming a constant high yield of CO throughout is small.

It is then possible to consider what outcome might have occurred if the polyethylene was substituted by a polymer treated with a fire retardant such as phosphorus or halogen additives. When these materials burn they tend

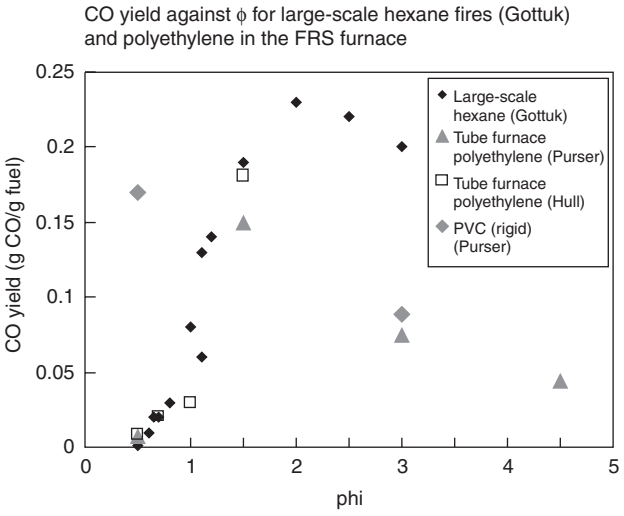

Figure 2-6.9. ***CO yield against ϕ.***

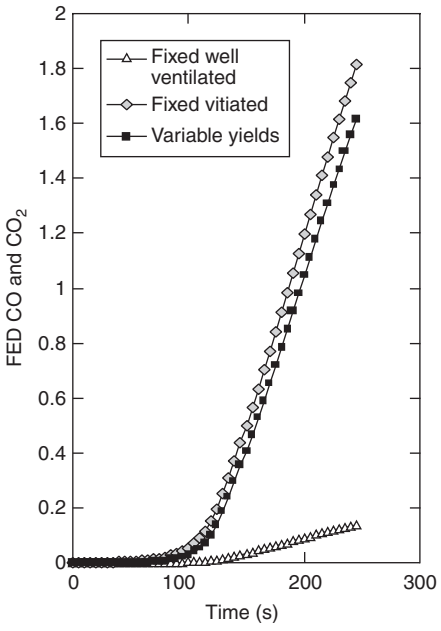

Figure 2-6.10. ***FED for human incapacitation due to CO and CO_2 during a theoretical enclosed room fire involving a polymeric material such as polyethylene. CO and CO_2 yields obtained using the FRS tube furnace, fire modeled using CFAST.[38]***

to produce high yields of CO even under well-ventilated conditions, and so might be considered to present a toxic hazard in some fires. For the example shown here, it is possible to examine the potential toxic hazard from CO and CO_2 if a halogenated polymer such as PVC was burned and the yields were as obtained in the tube furnace. Assuming that initially the fire growth rate of PVC was the same as for polyethylene (while in practice it is likely to be much slower) and the yields of CO were as obtained in the tube furnace, then it is possible to consider the effects on FED development for asphyxiant gases. As Figure 2-6.9 shows, the yield of CO from PVC under both well-ventilated and vitiated conditions was very similar to that obtained from polyethylene under vitiated combustion conditions. It can therefore be estimated that the FED for PVC would follow the case calculated for a constant high CO yield. If the toxic potency of PVC (in terms of asphyxiants) under well-ventilated combustion conditions was the only item considered, then it might be estimated that PVC was a much more hazardous material than polyethylene, because the CO yield under these conditions is more than 20 times greater than for polyethylene. However, as the hazard modeling shows, the differences in CO yield during the well-ventilated phase of the fire have very little influence on the hazard development, so that, at least for this example, very little difference in time to incapacitation from asphyxiation would be expected between either fuel. In practice it would be expected that the fire growth curve for the PVC would be much slower than for polyethylene (assuming flaming ignition occurred) with a consequently slower growing FED curve. However an additional hazard from a PVC fire would be the evolution of hydrogen chloride and other irritants, which would also need to be considered in the model. For all such hazard analysis it must be remembered that it is the concentration of toxic products at the breathing zone of a building occupant that is important. Depending upon the positions of the occupants and the time during the fire development it is likely that concentrations of acid gases in particular will be diluted relative to those near the fire and further reduced by losses to building surfaces.

Using Mass Loss Lethal Toxic Potency Data for a Simple Toxic Hazard Assessment

Another method for making a simple hazard assessment is to make use of lethal toxic potency data for materials obtained from a small-scale toxicity test. One way of performing a preliminary simple hazard analysis for a fire is to consider what exposure in terms of a single criterion, the mass loss concentration profile of products in a fire, is likely to be lethal to a victim. For such a calculation use can be made of mass loss lethality data from small-scale rodent toxicity test data for the material or materials involved in the fire. This makes the assumption that the lethal concentration to a human would be similar to that in a rat, but this is standard practice in toxicology for making approximate classifications of hazard for the acute effects of industrial chemicals. It is also necessary to make the assumption that mass loss lethality data follow Haber's rule, but any inaccuracies introduced by deviations from ideal behavior should not be important in such an approximate analysis. The three items of data needed for such an assessment are

1. The basic fire condition (smoldering, early flaming, or post-flashover)
2. The mass loss/dispersal volume-time curve for the fire
3. The rodent LCt_{50} concentrations for the materials involved in the fire in terms of the mass loss concentration for a quoted exposure time, determined under the same conditions as those in the fire

LCt_{50} data for common materials have been derived using a number of small-scale test methods under a variety of decomposition conditions. Most published data relate to nonflaming oxidative decomposition conditions, well-ventilated flaming, or mixed flaming and nonflaming conditions. Very few data are available for post-flashover fire decomposition conditions. Table 2-6.3 shows examples of data sets obtained using three well-known test methods. The range of LC_{50} for the references quoted (shown in Table 2-6.3) was approximately 5 to 60 $g \cdot m^{-3}$ mass loss for a 30-minute exposure, which is equivalent to an LCt_{50} dose range of approximately 150 to 1800 $g \cdot m^{-3} \cdot min$, with an average value of 23 $g \cdot m^{-3}$ (690 $g \cdot m^{-3} \cdot min$). Allowing for a small margin of safety, it has been suggested within British standards that, for a simple hazard assessment, a single figure of 500 $g \cdot m^{-3} \cdot min$ might be considered as a single average figure for the approximate toxic potency of the thermal decomposition products from common materials. For the purpose of carrying out hazard calculations, the toxic potency of any individual material can then be expressed in terms of a potency factor relating the actual LCt_{50} to 500, as follows:

Toxic potency factor for a material under a defined fire condition = $500/LCt_{50}$ g·m^{-3}·min

General Pattern of Toxic Potency for Common Materials under Three Fire Conditions

Using a wider database than that for Table 2-6.3, a survey of the toxic potency data for common materials in nonflaming, early flaming, and post-flashover fire conditions revealed an inadequate database, but it was possible to derive approximate LCt_{50} for common materials.[35] The results for individual materials range over approximately two orders of magnitude from 20 to 3750 g·m^{-3}·min; but when the data are reduced to basic types of materials under each decomposition condition, a relatively simple pattern can be described, as presented in Table 2-6.4. The table shows the approximate average lethal exposure doses (LCt_{50}) for classes of materials, the LC_{50} for 30-minute exposures, and a potency factor (based upon a figure of 500 g·m^{-3}·min for the "normal" lethal potency for combustion products), respectively. The findings are as follows:

Under nonflaming oxidative decomposition conditions at >400°C, most materials have a similar potency close to 500 g·m^{-3}·min, that is, potency factor of approximately 1, due mainly to the effects of carbon monoxide and irritants. The main exceptions are nitrogen-containing materials releasing significant HCN at low temperatures (e.g., polyacrylonitrile, modacrylic, and rigid polyurethane foam), which have toxic potency factors of 3 to 8.

Under early well-ventilated flaming conditions most nonfire-retarded materials are substantially less toxic than under nonflaming conditions. Cellulosics (wood and cotton) are the least toxic with LCt_{50} of >3000 g·m^{-3}·min (potency factor 0.2). Plastics containing carbon, hydrogen, or oxygen are somewhat more toxic with a potency factor of 0.4 ($LCt_{50} \sim 1200$), and those containing low percentages of nitrogen (e.g., flexible polyurethanes, wool, and nylon) also fall into this area. PVC and fire-retarded materials have a similar toxic potency factor to that under nonflaming conditions of approximately 1. Rigid polyurethanes and nitrogen-containing acrylics have high potencies similar to those under nonflaming conditions.

Under post-flashover conditions (and pre-flashover vitiated combustion conditions), the potency of all materials increases due to the increased yields of HCN and CO. More smoke and irritants are also present than under early flaming conditions, which may add somewhat to the potency, particularly of the non-nitrogen-containing materials. For cellulosic materials and hydrocarbon plastics, the potency is similar to that under nonflaming conditions (potency factor close to 1). For all nitrogen-containing materials, the toxic potency is high, ranging from approximately 2.5 for flexible polyurethane foam to approximately 11 for modacrylic and polyacrylonitrile. It is suggested that PVC would have a potency factor of approximately 2.5 under these conditions.

It is suggested that the data in Table 2-6.4 provide a mechanism whereby small-scale toxicity test data, obtained under appropriate decomposition conditions, can be applied in fire engineering calculations. A simple, first estimate could be based upon a single lethal toxic potency figure of 500 g·m^{-3}·min for all materials, using total fire load or heat release as the source of the mass term. In order to assess an incapacitating exposure dose (and to allow for possible greater sensitivities between rats and average humans) this should be multiplied by 0.3 to give an incapacitating dose of 150 g·m^{-3}. A further factor of 0.3 could then be applied to allow for the range of sensitivities in the human population, giving a figure of 45 g·m^{-3}·min to allow for escape of the majority of the occupant population. When more detailed information on the nature of the materials likely to be involved in a fire is known, the calculations for particular fire scenarios can be based upon the predicted mass loss rate for each material, adjusted by the appropriate toxic potencies. The range of toxic potencies of common materials decomposed under conditions occurring in flaming fires is approximately two orders of magnitude. Data obtained so far that relate to nonflaming fires show a relatively narrow range of potencies around 500 g·m^{-3}·min. Early flaming, well-ventilated fires show toxic potency to be generally low where combustion is efficient, ranging from approximately 75 to 3750 g·m^{-3}·min, while data obtained so far that relate to vitiated, post-flashover fires show that potencies are generally higher, due to increased yields of CO and HCN, ranging from approximately 21 to 3000 g·m^{-3}·min.

Difficulties in making estimates of the specific toxicities and toxic potencies of common materials arise from the very poor database of both small- and large-scale tests conducted under appropriate conditions. This is particularly true of the vitiated post-flashover condition, which is not well simulated by existing test methods, except possibly the DIN and FRS methods, for which very few data are available.

Theoretical Example of the Application of the Mass Loss Lethal Toxic Potency Data for a Simple Toxic Hazard Assessment[33]

Consideration is being given to replacing the floor covering material in a hotel bedroom. There is a concern that if the material is ignited by a small ignition source the rate of development of a toxic hazard from the new material (material B) should not be worse than that from the old material (material A). It is considered that the most likely scenario would involve a closed room, so that rapid smoke filling would occur and the effluent can be considered as evenly mixed throughout the room volume (i.e. layering effects can be considered very transient, and can be ignored). A problem is that the toxic potency of material B is twice that of material A, although it burns more slowly once ignited.

Information available: The volume of the room is 40 m^3. The floor covering materials are 1 cm thick with an area density of 1 kg/m^2. Horizontal burning tests have shown that both materials burn through rapidly so that a front of complete combustion spreads from the point of ignition. For material A the rate of flame spread is 10 cm/min while for material B the rate of flame spread is only 5 cm/min. However, small-scale toxicity tests have shown that, under well-ventilated flaming conditions, the toxic potency of material B (LC_{50} 10 g·m^{-3}, lethal exposure dose 300 g·m^{-3}·min) is twice that of material A (LC_{50} 20 g·m^{-3}, lethal exposure dose 600 g·m^{-3}·min).

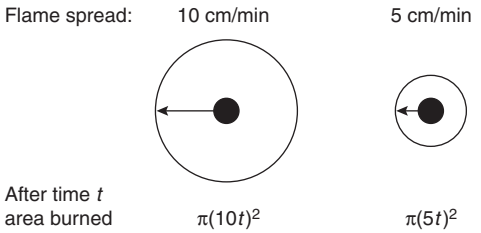

Figure 2-6.11. ***Flame spread rate for two materials.***

Hazard analysis: Assuming a small point ignition source, both materials will burn through, and a circle of burned area will spread out from the point of ignition (Figure 2-6.11). Since material A burns twice as quickly as material B, the area of material A consumed will be four times that of material B at any time during the early stages of the fire.

Table 2-6.5 shows how the FED calculations are made using material A as an example. The FED for each point in time is the exposure dose divided by the lethal exposure dose for that material. The FEDs for each time interval are them summed throughout the fire until the FED reaches unity, at which point the toxicological endpoint, in this case lethality, is predicted.

Figure 2-6.12 shows the results of the FED calculations for materials A and B in the 40-m^3 room. The analysis shows that lethal conditions are attained after approximately 6 min for material A, and approximately 1.5 min later for material B. It can therefore be concluded that material B presents less of a toxic hazard than material A in this scenario, despite the fact that material B has twice the toxic potency of material A.

Incapacitation

This rather crude method could be used to give an approximate indication of when conditions in a fire are likely to be lethal, but in practice the effects of fires on exposed victims are not so simple. In many cases death is not due to the immediate toxic effects of exposure, but results from the victim being trapped in the fire, either because irritant and optically-obscuring smoke prevents escape, or because asphyxiant gases cause incapacitation, so that the victim remains in the fire to die either from a fatal dose of toxic products acquired during the prolonged exposure, or from burns. One way of taking these factors into account would be to determine the *Ct* product dose at which effects such as incapacitation due to asphyxia occur in small-scale toxicity tests. These could then be applied to the fire hazard analysis to estimate the fractional incapacitating dose, rather than the fractional lethal dose. However, because of differences in generating small-scale fire test atmospheres similar to those occurring in large-scale fires, a potentially much more effective way of predicting toxic hazard would be to measure the concentration/time profiles of the important toxic products in the fire and to determine their effects from toxicity data derived from experiments in man and primates (and to a lesser extent also from rodents). In the following sections the characteristics of the major asphyxiant and irritant fire products are described, together with methods for calculating their uptake and predicting their toxic effects.

Table 2-6.5 ***Example FED Calculation Data for Materials A and B***

Time (min)	Area Burned (cm^2)	Mass Consumed (g)	Mass Loss Concentration (averaged for each time interval) (g•cm^{-3})	Exposure Dose (g•cm^{-3}• min)	FED
Material A	(LC_{50} 20 g•m^{-3}; LCt_{50} 600 g•m^{-3}•min)				
0	0	0	0	0	0
0.5	79	79	1.0	0.5	0.001
1.0	314	314	4.9	2.9	0.005
at 5 min	7854	7854	177.7	328.9	0.548
Material B	(LC_{50} 10 g•m^{-3}; LCt_{50} 300 g•m^{-3}•min)				
0	0	0	0	0	0
0.5	20	20	0.25	0.12	0.000
1.0	79	79	1.2	0.74	0.002
at 5 min	1963	1963	44.4	82.2	0.274

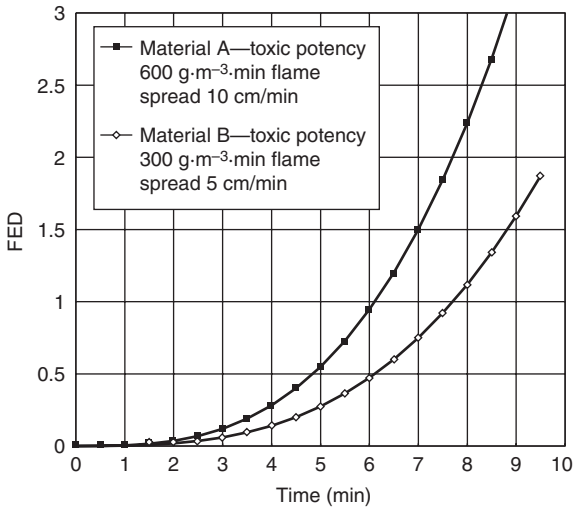

Figure 2-6.12. ***Relative toxic hazard from two materials calculated according to the mass loss lethal exposure dose method (time to lethality when FED = 1).[33]***

Asphyxiation by Fire Gases and Prediction of Time to Incapacitation

Asphyxiant gases cause incapacitation mainly by effects on the central nervous system and to some extent, the cardiovascular system.[25] In general, time to incapacitation and its severity are predictable in that usually a short period of intoxication is followed by a relatively sharp decline into severe incapacitation (i.e., loss of consciousness).[16,44] Most asphyxiant gases produce their effects by causing brain tissue hypoxia.[25,26] Since the body

possesses powerful adaptive mechanisms designed to maximize oxygen delivery to the brain, it is usually possible to maintain normal body function up to a certain dose of asphyxiant, and the victim is often unaware of the impending intoxication. Once a point is reached where normal function can no longer be maintained, however, deterioration is rapid and severe—beginning with signs similar to the effects of severe alcohol intoxication, consisting of lethargy or euphoria with poor physical coordination, and followed rapidly by unconsciousness and death if exposure continues.[26,44]

Asphyxiant Fire Products

The two major asphyxiant gases in fires are: (1) carbon monoxide (CO) and (2) hydrogen cyanide (HCN). Carbon monoxide is always present to some extent in all fires, irrespective of the materials involved or the stage (or type) of fire, so that there is almost always some degree of risk of asphyxia from CO exposure.[17] Hydrogen cyanide is always present to some extent when nitrogen-containing materials are involved in fires. These include materials such as acrylics, polyurethane foams, melamine, nylon and wool, which are likely to be involved to some extent in most fires in buildings. Hydrogen cyanide is likely to be present at high concentrations in large, post-flashover fires. Unlike carboxyhemoglobin, which is routinely measured in the blood of fire victims, blood cyanide is often not measured. However, it has been detected at high concentrations in the blood of some fire victims, particularly when blood samples have been taken immediately after exposure.[14] In addition, low concentrations of oxygen (less than 15 percent)[45] and very high concentrations of carbon dioxide, CO_2, (greater than 5 percent) can have asphyxiant effects.[46]

Carbon Monoxide

Carbon monoxide combines with hemoglobin in the blood to form carboxyhemoglobin (COHb), which results in a toxic asphyxia because it reduces the amount of oxygen supplied to the tissues of the body, particularly brain tissue. Tissue oxygen supply is reduced because the amount of hemoglobin available for the carriage of oxygen (in the form of oxyhemoglobin) is reduced, and also because the ability of the remaining oxyhemoglobin to release oxygen to the tissues is impaired (due to a leftward shift of the oxygen dissociation curve).

The affinity of hemoglobin for CO is extremely high, so that the proportion of hemoglobin in the form of carboxyhemoglobin increases steadily as CO is inhaled. The toxicity of CO therefore depends upon the accumulated dose of carboxyhemoglobin, which is expressed in terms of the percentage of total hemoglobin in the form of carboxyhemoglobin, (% COHb).[19]

There is little doubt that CO is the most important asphyxiant agent formed in fires. In the Strathclyde pathology study[10] lethal levels (>50 percent COHb) were found in 54 percent of all fatalities, while some 69 percent of fatalities had carboxyhemoglobin levels capable of causing incapacitation (>30 percent COHb). Incapacitating levels of carboxyhemoglobin are also common in victims surviving immediate fire exposure. Carbon monoxide is therefore particularly important because

1. It is always present in fires, often at high concentrations.
2. It causes confusion and loss of consciousness, thereby impairing or preventing escape.
3. It is the major ultimate cause of death in fires.

To understand the effects of CO exposure on fire victims and to predict the likely consequences of a particular exposure, it is essential to know a number of features of CO intoxication. (To some extent these apply to an evaluation of the toxicity of any fire product.) It is necessary to

1. Determine which types of toxic effects occur at different dose levels.
2. Determine the concentration/time relationships of these toxic effects, whether they occur immediately or some time after exposure, and whether the effects of a short high concentration exposure are the same as those of a longer, low concentration, exposure.
3. Quantify the parameters that determine the rate of uptake and removal of CO from the body.

Some information on these points is available from accidental exposures and low-level experimental exposures in humans,[19] and data are available on the symptoms experienced in humans at various carboxyhemoglobin concentrations at rest.[19,45,47] Loss of consciousness is predicted at approximately 40 percent COHb, but can occur at lower levels (~30 percent COHb), and lower levels can be dangerous for subjects with compromised cardiac function.[19] Death is predicted at COHb concentrations of 50 to 70 percent COHb,[45,48,49] but it has been suggested that death can occur at lower concentrations in susceptible subjects.[19,50] The severe incapacitation caused by high-level exposures, such as those encountered in fires, has been studied experimentally in animals.[25,44] The effects of experimental exposures on cynomolgus monkeys are shown in Figure 2-6.13 in terms of physiological parameters (respiration, cardiovascular parameters, and brain electroencephalogram or EEG) monitored in sedentary animals sitting in chairs, and in Figure 2-6.5, where free-moving animals were trained to perform a behavioral task designed to simulate some aspects of the escape maneuvers of human fire victims (i.e., tasks involving bodily movements with a certain amount of exercise, requiring the use of coordinated movements and the application of psychomotor skills).

The first important characteristic of CO poisoning illustrated by these experiments is that CO uptake and intoxication are extremely insidious. During the early stages as the carboxyhemoglobin concentration builds up gradually in the blood the effects are minimal. Thus Figure 2-6.13 shows no detectible changes in physiological parameters until the end of the exposure when the COHb concentration approached 40 percent. In active animals the first minor signs of behavioral performance deficits did not occur until concentrations of 15 to 20 percent COHb were achieved. Similar results have been obtained in humans, where O'Donnel et al.[51] could find no effects upon psychomotor performance at levels of up to 12 per-

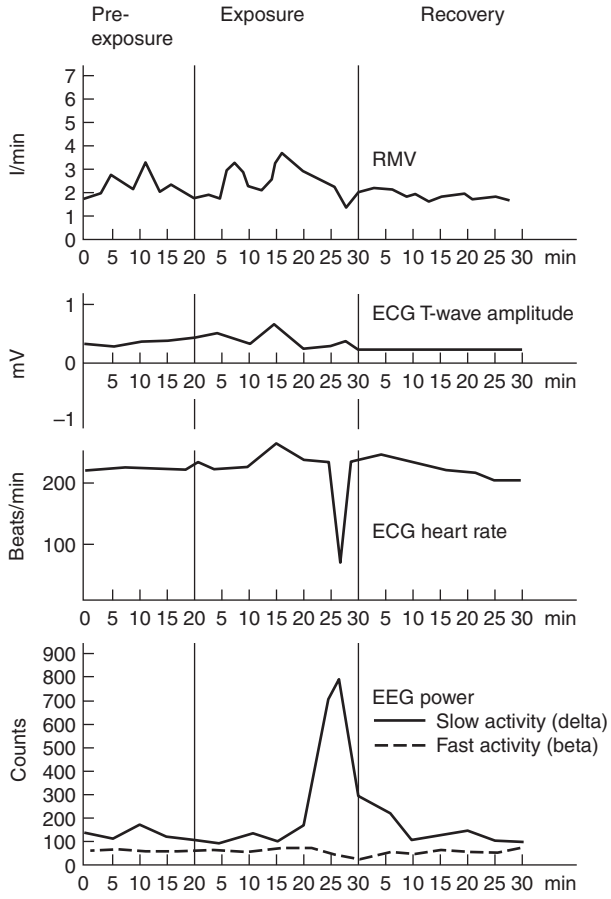

Figure 2-6.13. ***Physiological effects of an atmosphere containing CO (1850 ppm)—wood pyrolyzed at 900°C. From Purser and Woolley.[16]***

cent COHb, and Stewart et al.[47] reported the first symptoms (consisting of a headache) to occur at 15 to 20 percent COHb, while objective tests at these levels showed only minor deficits in behavioral performance.

Another major characteristic of asphyxia shown clearly by the animal experiments is that when significant effects do occur, their onset is sudden and the degree of incapacitation rapidly becomes severe, so that by the time a victim is aware that he or she is affected effective action is probably not possible. Thus Figure 2-6.13 shows the physiology of a monkey passing from a normal state to unconsciousness within a few minutes after 25 minutes of exposure, with decreased respiration, a severe decrease in heart rate, and greatly increased slow-wave EEG activity (indicative of cerebral depression). For active animals there was a sudden rapid decline in behavioral task performance accompanied briefly by signs similar to severe alcohol intoxication, which led rapidly to a state of deep coma.

These findings may explain why deaths from CO derived from defective heating appliances are so common. Survivors of such situations often report that they, or other victims that died, experienced headaches or nausea, but had no idea of the cause, so they did not attempt to leave the area until overcome by fumes.[52]

During the early stages of incapacitation the main effects appear to be on motivation and psychomotor ability, with a tendency for the victim to sleep if left undisturbed.[44] Under these conditions one might expect a subject, if alerted by a sudden noise such as of breaking glass (often reported by fire survivors), to "sober up" and awake sufficiently to make an escape attempt. However, such a victim is likely to fail for three reasons.

1. This stage is rapidly followed by unconsciousness and coma.
2. Active subjects are seriously affected by carboxyhemoglobin concentrations that have only minor effects on sedentary subjects. Thus, while sedentary primates were often unaffected at carboxyhemoglobin levels of up to 40 percent, those engaged in light activity were seriously affected at carboxyhemoglobin levels in the 25 to 35 percent range.[44] Similarly, in one study of humans, although a sedentary subject could perform such tasks as writing, even at the exceptionally high level of 55 percent carboxyhemoglobin, the subject collapsed and became unconscious immediately when attempting to rise and walk.[53] Therefore, a victim in a bed or chair attempting to escape not only would be in danger of a rapid collapse due to continued CO uptake, but even if no further uptake occurred the ability to perform even light work or exercise would be severely impaired. Even the simple act of rising from a horizontal to an upright position could precipitate loss of consciousness.
3. The rate of uptake of CO depends on the respiration (respiratory minute volume) and hence the activity of the subject. When the subject becomes active the blood carboxyhemoglobin is therefore likely to increase rapidly to an incapacitating level.

A Model for the Prediction of Time to Incapacitation by CO in Fires

Incapacitation by CO depends upon a dose accumulated over a period of time until a carboxyhemoglobin concentration is reached where compensatory mechanisms fail and collapse occurs. To predict time to incapacitation of fire victims due to CO it is necessary to know the carboxyhemoglobin concentrations at which incapacitation is likely to occur, and the rate of uptake of CO so that the time to achieve this concentration can be calculated. The carboxyhemoglobin concentrations likely to cause incapacitation depend upon the activity of the victim and should be similar to the concentrations causing incapacitation in primates at similar levels of activity.[44]

Since CO is both inhaled and excreted via the lungs, the rate of uptake depends upon the difference between the CO concentration in the blood, W, and that in the inhaled air, C, and is an exponential function described by the general equation (Equation 3):

$$W = C(1 - e^{-tk}) \tag{3}$$

where t is the time exposed and k is a constant determined by a number of factors, so that uptake is rapid initially, but gradually levels off as uptake and removal from the blood reach equilibrium. This relationship is described fully by the Coburn-Forster-Kane (CFK) equation,[22,23] which takes into account a whole range of variables, including RMV, body size, exposure duration, and parameters related to lung and blood physiology (see Appendix 2-6A). When all these various factors are known, this equation enables accurate predictions of CO uptake to be made that agree well with experimental data.[23,54] The uptake pattern for CO is illustrated in Figure 2-6.4, which predicts time to achieve a potentially lethal blood CO concentration (50 percent COHb) for a 70 kg human at rest (RMV 8.5 L/min) at two CO concentrations, 2200 and 840 ppm.

When the inhaled concentration is high compared to that in the blood as during short duration, high concentration exposures such as those that occur in flaming fires, the departure from linear uptake is not great as shown in Figure 2-6.4, and the deviation from Haber's rule ($W = C \times t$) is small. However, over long periods at lower concentrations, as equilibrium is approached, uptake deviates considerably from linearity. For short exposures at high concentrations when the blood concentration is well below saturation level, an approximate prediction of COHb concentration can therefore be made assuming a linear relationship. Such an equation is derived from experimental human exposures by Stewart et al.[48]

$$\%\text{COHb} = (3.317 \times 10^{-5})(\text{ppm CO})^{1.036}(\text{RMV})(t) \qquad (6)$$

where

ppm CO = CO concentration (ppm)
RMV = volume of air breathed (L/min)
t = exposure time (min)

Thus, for the examples shown in Figure 2-6.4, which were calculated using the CFK equation, a concentration of 50 percent COHb is predicted following a 1-hr exposure to 2200 ppm CO, while the Stewart equation predicts 49 percent COHb. However, for a 4-hr exposure the CFK equation predicts 50 percent COHb from 840 ppm, while the Stewart equation would predict 50 percent COHb from 550 ppm over 4 hr, or a concentration of 72 percent COHb from 840 ppm.

Justification of the linear uptake relationship under high concentration/short exposure duration circumstances is illustrated by a series of primate exposures carried out over a 1000 to 8000 ppm concentration range. These experiments were performed using an active behavioral model,[44] with the endpoint being loss of consciousness, which occurred at approximately 34 percent COHb. The results are illustrated in Figure 2-6.5, which shows time to incapacitation for different inhaled CO concentrations. At each concentration the inhaled dose (Ct product) required to produce incapacitation in ppm CO·minutes is constant, as predicted by the linear uptake model of Haber's rule.

As stated, it is possible to make accurate predictions of CO uptake for a range of situations by using the CFK equation, provided that a number of variables are taken into account. For a particular individual the most important variable is the RMV, which varies considerably depending upon the level of activity of the subject. Figures for this and other variables can be obtained from standard reference data.[55] Figure 2-6.14, generated from these data, shows the probable time to incapacitation (loss of consciousness) for a 70 kg human exposed to different CO concentrations at three levels of activity. The figure shows that the degree of activity can have a major effect on time to incapacitation. It must also be remembered that RMV per kilogram of body weight is greater for small subjects, which means that children will take up CO much more rapidly than adults and succumb much earlier, while uptake in small laboratory animals is even more rapid. An assumption made in these calculations is that the level of activity and hence the RMV remain constant during the exposure. In practice there is a tendency for the level of activity and ventilation to decrease slightly as the point of incapacitation is approached. It is considered that with a model for predicting time to incapacitation (unconsciousness), errors due to reduced ventilation will be minor, since the primate experiments demonstrate that there is little change in RMV until the point of incapacitation. Once the subject becomes unconscious, the RMV and hence the rate of CO uptake will be considerably reduced, particularly if the subject was previously engaged in heavy work. It is therefore possible that for calculating time to death allowance could be made for a low RMV (~6 L/min) once incapacitation has occurred. Not making this allowance does err slightly on the side of safety.

The Stewart[48] and CFK[22] equations enable reasonably good predictions of time to incapacitation or death for short (less than one hour) or long (greater than one hour)

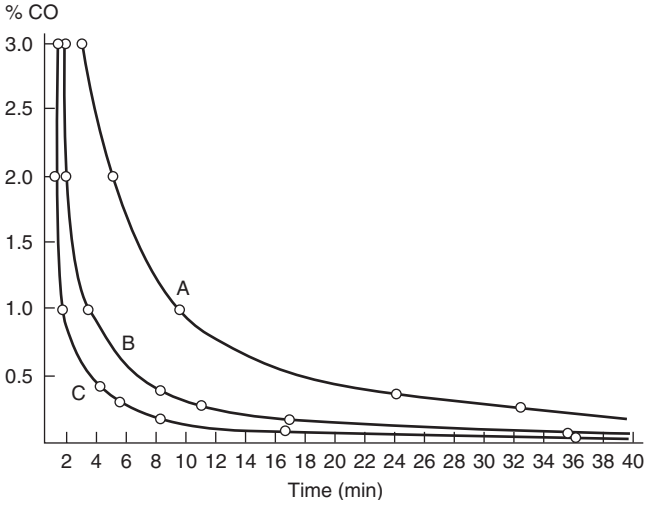

Figure 2-6.14. ***Time to incapacitation by carbon monoxide for a 70 kg human at different levels of activity. Curve A—40 percent carboxyhemoglobin RMV 8.5 L/min at rest sitting; Curve B—30 percent carboxyhemoglobin RMV 25 L/min, light work (e.g., walking 6.4 km/h); Curve C—20 percent carboxyhemoglobin RMV 50 L/min, heavy work (e.g., slow running 8.5 km/h) (or for walking 5.6 km/h up a 17 percent gradient).***

exposures, respectively, to constant concentrations of CO in air. In fires, however, victims are exposed to concentrations of CO which change during the course of the fire. For smoldering fires the CO concentration may grow slowly and remain fairly constant over long periods, but for early flaming fires and many fully developed fires where the victim is in a remote location, the CO concentration may increase rapidly over a short period of time as in Figure 2-6.15. It is therefore necessary to be able to apply the uptake models to situations where the CO concentration is not constant. For most situations, fluctuations in CO concentration do not present a problem since incapacitation depends upon the total dose of CO inhaled, in the form of COHb, and is not affected by the immediate CO concentration. The COHb concentration is thus dependent upon the average CO concentration over the period of exposure, and significant errors will not occur even if the CO concentration falls somewhat at certain stages of the exposure. Errors in predicting the COHb concentration are possible if the CO concentration drops dramatically toward the end of an exposure, or if it decreases moderately during a prolonged exposure of several hours duration, when COHb concentrations can approach equilibrium with the inhaled CO concentration. In this case a fall in CO may result in a decrease in COHb concentration. The basic rule to apply is that fluctuations are unlikely to cause the COHb concentration to deviate from that predicted by assuming the constant average concentration throughout, providing the CO concentration is on a rising trend, is stable, or is well above the equilibrium concentration with the blood COHb.

Ct Product and Fractional Incapacitating Dose

Although the average CO concentration during a fire exposure can be used to predict COHb concentration and time to incapacitation, another useful concept for predicting incapacitation or death is the relationship with concentration-time (*Ct*) product, which is a representation of CO "dose." In changing fire conditions the *Ct* product may be obtained by integrating the CO concentration/time curve. The dose inhaled may then be related to the dose required to cause incapacitation, and the fraction of an incapacitating dose at any time, *t*, may be calculated, incapacitation occurring when the fractional dose reaches 1.0. Since the *Ct* "dose" actually represents the COHb concentration, the fractional dose would be better represented by the ratio of the COHb concentration at time, *t*, with the COHb concentration known to cause incapacitation or death, rather than by simple *Ct* product ratios. The Stewart equation[48] can be rewritten in the form of COHb ratios, requiring only a knowledge of the CO concentration and the exposure time, as follows:

$$F_{I_{co}} = \frac{K(\text{ppm CO}^{1.036})(t)}{D} \tag{7}$$

where

$F_{I_{co}}$ = fraction of incapacitating dose
t = exposure time (min)
K = 8.2925×10^{-4} for 25 L/min RMV (light activity)
D = COHb concentration at incapacitation (30 percent for light activity)

This concept of *Ct* product fractional dose is also useful for predicting incapacitation and death from other fire products, and combinations of products, as will be discussed later in this chapter.

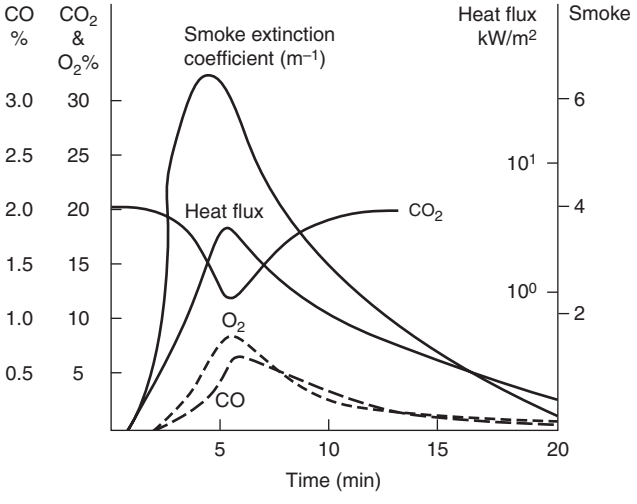

Figure 2-6.15. ***Smoke, heat, and gases during single armchair room burn. Armchair is polystyrene with polyurethane cushions and covers. Room is 39 m³ with open doorway. Gases measured in doorway at 2.1 m height.[56]***

Hydrogen Cyanide

Hydrogen cyanide (HCN) has been measured in the blood of both fatal[57] and nonfatal[58] fire victims. However, in the Strathclyde fire fatality study high concentrations of hydrogen cyanide in the blood of victims were usually associated with lethal levels of carboxyhemoglobin, so that the role of hydrogen cyanide as a cause of incapacitation was difficult to determine.[57] It is also difficult to relate blood cyanide levels from samples collected after a fire to likely HCN exposure, since the dynamics of HCN uptake and removal from the blood are poorly understood.[59,60]

Although the ultimate effects of HCN exposure (consisting of unconsciousness with cerebral depression) are similar to those produced by CO, the pattern of toxicity during the early stages is very different. While the onset of CO intoxication is slow and insidious, HCN intoxication tends to be rapid and dramatic. The physiological signs of incapacitation produced in monkeys by an atmosphere containing HCN are shown in Figure 2-6.16.[59] As with CO the immediate effects were relatively minor, consisting of a slightly raised ventilation, but at some time during a 30-minute exposure period there was a marked increase in respiration (hyperventilation), the RMV increasing up to four times. Within one to five minutes of the start of this episode of hyperventilation the animals lost consciousness. This was accompanied by EEG signs of severe cerebral depression; loss of muscle tone; and marked effects upon the heart and circulation, including a significant

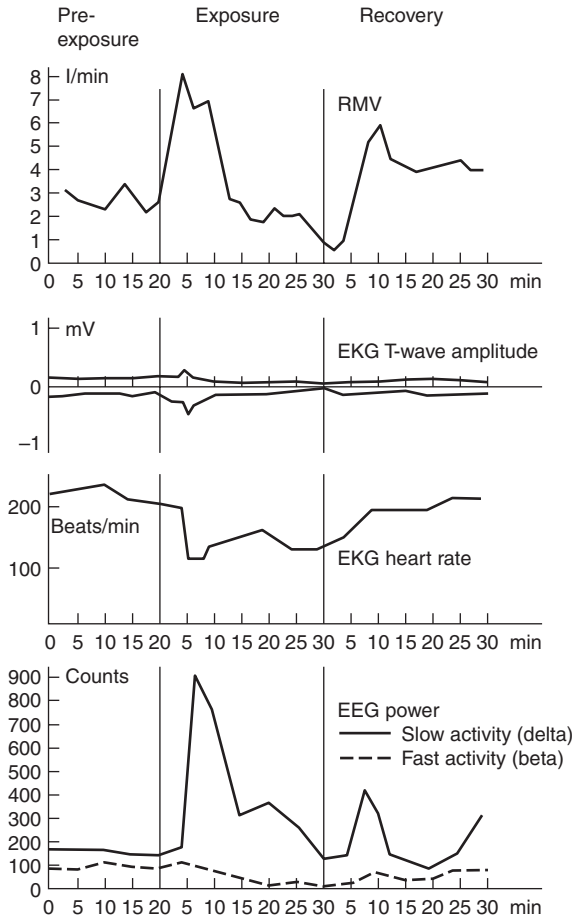

Figure 2-6.16. ***Physiological effects of an atmosphere of HCN gas (147 ppm) on monkeys.[59]***

decrease in heart rate, arrhythmias and changes in the EKG waveform indicative of cardiac hypoxia. This hyperventilatory episode was caused by the stimulatory effects of cyanide upon respiration. Since the cyanide was taken in via inhalation, a positive feedback situation resulted, and inhaled cyanide caused hyperventilation which increased the rate of HCN uptake and in turn provided a stronger hyperventilatory stimulus. Once the animals became unconscious the hyperventilation subsided and they went into a slow decline for the remainder of the exposure. This led eventually to a cessation of breathing in some cases, which would have proved fatal if exposure had not been terminated. It was therefore possible for an animal to survive a continuous HCN exposure for some time after the point of incapacitation. Once exposure was terminated the recovery was rapid and almost complete within five to ten minutes.

The pattern of incapacitation for HCN is somewhat different from that produced by CO in that the effects occur more rapidly, as unlike CO, HCN is not held almost exclusively in the blood, but is carried rapidly to the brain.[61] Although the accumulation of a dose is one factor, the most important determinant of incapacitation with HCN appears to be the rate of uptake, which in turn depends upon the HCN concentration in the smoke and the subjects' respiration. Thus in the animal experiments,[25,59] it was found that at HCN concentrations below approximately 80 ppm the effects were minor over periods of up to one hour, with mild background hyperventilation. At concentrations above 80 ppm up to approximately 180 ppm, an episode of hyperventilation with subsequent unconsciousness occurred at some time during a 30-minute period; there was a loose linear relationship between HCN concentration and time to incapacitation. Above 180 ppm the hyperventilatory episode began immediately with unconsciousness occurring within a few minutes. Data on human exposures to HCN are limited but Kimmerle[45] does quote some approximate data showing a similar effect in humans, with incapacitation occurring after 20 to 30 minutes at 100 ppm HCN and after 2 minutes at 200 ppm, death occurring rapidly at concentrations exceeding approximately 300 ppm.

Other data suggest that human victims might be able to survive higher concentrations of HCN for shorter periods. McNamara[62] suggests 539 ppm as the 10-minute LC_{50} for humans, and there is a report of a survival from an accidental exposure to 444 ppm.[63] An experimental human exposure to 530 ppm HCN was survived without immediate symptoms for 1.5 minutes, although a dog exposed at the same time suffered respiratory arrest.[64] Dogs are known to be particularly susceptible to cyanide poisoning,[62] but it does seem likely that, to some extent, with HCN (as with CO) body size influences time to incapacitation, and that a human would be able to tolerate exposure to a given concentration longer than a cynomolgus monkey. With HCN and CO, physical activity would be likely to cause more rapid uptake in adults, and uptake would be more rapid in children because of their smaller body size. The primate data therefore seem to provide a reasonable model for humans, possibly erring slightly on the side of safety.

The differences between CO and HCN in terms of the relationship between inhaled concentration and time to incapacitation are illustrated in Figure 2-6.6. While CO gives a smooth curve with incapacitation occurring at a constant *Ct* product of approximately 27,000 ppm·min for all CO concentrations, the almost linear portion of the HCN curve results in a *Ct* product of approximately 2000 ppm·min at 100 ppm HCN and 400 ppm·min at 200 ppm, with very rapid incapacitation at higher HCN concentrations. This deviation from Haber's rule (which predicts a constant *Ct* product) was recognized by Haber himself in 1924, when he stated that the *Ct* product for HCN depended upon the exposure concentration.[20] The exact reason for this is not known, but appears to be related to relationship between the rate of uptake of HCN and the dynamics of its distribution between different body fluid compartments.[60] The effect is to render concentrations in the range greater than 150 ppm more toxic than would be predicted from the effects of longer exposures to lower concentrations.

A Model for the Prediction of Time to Incapacitation by HCN in Fires

From these results it is possible to predict that HCN concentrations below a threshold concentration of ap-

proximately 80 ppm will have only minor effects over periods of up to 1 hour.

From 80 to 180 ppm the time to incapacitation (unconsciousness) t_{Icn} will be between 2 and 30 minutes approximately, according to the relationship

$$t_{I_{CN}}(\text{min}) = \frac{(185 - \text{ppm HCN})}{4.4} \quad (8)$$

For concentrations above approximately 180 ppm incapacitation will occur very rapidly (within two minutes). This linear expression gives a reasonably good fit with the primate data over the range 80–180 ppm, but it would be preferable to derive a more general expression to include the effects of higher and lower concentrations for making fractional dose estimations. An exponential expression has therefore been derived which also gives a reasonably good fit with the data (regression coefficient 0.984) as follows:

$$t_{I_{CN}}(\text{min}) = \exp(5.396 - 0.023 \times \text{ppm HCN}) \quad (9)$$

HCN could be particularly dangerous in fires due to its rapid "knockdown" effect, and low HCN levels in the 100 to 200 ppm range could cause fire victims to lose consciousness rapidly and consequently to die later as a result of accumulation of CO or some other factor. A small change in HCN concentration could also cause a large decrease in time to incapacitation; for example, doubling the concentration from 100 to 200 ppm could bring the incapacitation time down from approximately 20 min to approximately 2 min.[45,59]

Although this relationship should enable reasonable predictions to be made of time to unconsciousness for subjects exposed continuously to HCN, especially over the critical range between 180 ppm (above which incapacitation will be rapid) and 80 ppm (below which incapacitation is unlikely over periods of up to 1 hour), real fires will involve exposures to changing concentrations. One method of predicting time to incapacitation or death would be to take the average concentration over the period of exposure. Although approximate times to incapacitation can be estimated with this method it is prone to error because of the departure from Haber's rule. In practice, since short exposures to high concentrations are more likely to cause incapacitation than longer exposures to lower concentrations, and averaging the concentration tends to give longer estimates of time to incapacitation than would be expected. This method also does not include the concept of fractional dose. A better model would include some degree of weighting to allow for the enhanced effect of high concentration exposure, and also enable incapacitation to be estimated in terms of *Ct* product fractional dose.

A method for estimating fractional dose to incapacitation has been developed for the rat by Hartzell et al.,[27] based on this concept. In that model the *Ct* product over short periods of time is expressed as a fraction of the *Ct* product required to cause incapacitation or death at that concentration. The fractions for each short time interval are summed until the fraction reaches unity, which indicates incapacitation.[27] This approach should enable reasonable predictions of time and dose to incapacitation and death to be made, provided that the HCN concentration is stable or increasing (Hartzell et al. have found a good correspondence between calculated predictions and experimental data in rats). This approach can be used to derive a fractional dose model for humans based upon the time to incapacitation equation (Equation 9), derived from primate and human data, as follows:

For a constant HCN concentration

$$t_{I_{CN}} = \exp(5.396 - 0.023 \times \text{ppm HCN})$$

Dose to incapacitation = (ppm HCN)($t_{I_{CN}}$)
Therefore, for a short exposure time, t, to a given HCN concentration

$$F_{I_{CN}} = \frac{(\text{ppm HCN})(t)}{(\text{ppm HCN})(t_{I_{CN}})}$$

where $F'_{I_{CN}}$ = fraction of an incapacitating dose.
Taking t = 1 minute, this simplifies to

$$F_{I_{CN}} = \frac{1}{t_{I_{CN}}} \quad (10)$$

If the fractional doses per minute, $F'_{I_{CN}}$ are summed throughout the exposure, the dose and time to incapacitation can be predicted.

EXAMPLE:
A subject is exposed to 90 ppm HCN for 15 minutes, then to 180 ppm HCN for 2 minutes.

$$t_{I_{CN}} \text{ for 90 ppm} = \exp(5.396 - 0.023 \times 90) = 27.83$$
$$t_{I_{CN}} \text{ for 180 ppm} = 3.51 \text{ min}$$
$$F_{I_{CN}} = (1/27.83) \times 15 + (1/3.51) \times 2$$
$$= 1.111$$

Incapacitation is therefore predicted at between 17 and 18 minutes.

The $F_{I_{CN}}$ equation has since been simplified to

$$F_{I_{CN}} = \frac{\exp([\text{CN}]/43)}{220} \quad (11)$$

where [CN] represents the concentration of cyanide (ppm) corrected for the presence of other nitriles besides HCN and for the protective effect of NO_2. [CN] can be calculated as

$$[\text{CN}] = [\text{HCN}] + [\text{total organic nitriles}] - [\text{NO}_2]$$

Cyanide in Blood

The importance of HCN as a cause of incapacitation and death in fires can be underestimated, due to poor understanding of the dynamics of cyanide uptake, dispersal and metabolism in the body, and the inadequate database of blood cyanide measurements from both injured and dead fire victims. Carboxyhemoglobin is the only blood toxin routinely measured in fire victims, and when blood

cyanide is measured (usually post mortem), the sample and measurement are often taken a day or more after exposure.

Evidence from the primate experiments reported above, and from further experiments where measurements were made of arterial blood cyanide during and after exposure,[60] shows that when HCN is inhaled for short periods at air concentrations above approximately 150 to 200 ppm, loss of consciousness results from a transient high plasma cyanide concentration. HCN uptake rate is then greatly reduced when the subject loses consciousness (or dies) and the cyanide in the plasma disperses throughout the body fluids, leaving a low immediate post-exposure plasma concentration. Also, cyanide decomposes rapidly in cadavers,[65] by approximately 50 percent in 1 to 2 days, and may subsequently decrease further, or even increase slightly in stored blood. For these reasons, blood cyanide concentrations measured in fire victims are often relatively low, but when blood samples are obtained immediately after exposure,[66] higher, toxicologically significant or life-threatening levels are detected. It is suggested that, in freshly obtained whole blood samples, levels of 2.0 to 2.5 μg CN/ml should be considered capable of causing incapacitation and 3.0 μg CN/ml should be considered lethal, while for samples not taken and analyzed immediately after exposure, these concentrations/effect ranges should be at least halved, depending upon the time of storage.

Hypoxia

Apart from the tissue hypoxia caused by CO and HCN, hypoxia in fires can also be caused by exposure to low oxygen concentrations. To some extent, a lowered oxygen concentration in the inspired air or a lowered oxygen concentration in the lungs (during exercise for example) is a normal physiological occurrence, and there are compensatory mechanisms that tend to maximize the supply of oxygen to the brain. When a subject is placed in a hypoxic situation, there is a reflex increase in cerebral blood flow and also, up to a point, the unloading of oxygen from the blood is more efficient at lower arterial and venous blood oxygen concentrations.[67] These factors compensate to a large degree for any decrease in the oxygen concentration of the inspired air. When cynomolgus monkeys were exposed to atmospheres containing 15 percent oxygen no deleterious effects occurred beyond a slight increase in heart rate.[25]

However, a time is reached where these compensatory mechanisms fail; a 10 percent oxygen atmosphere produced a marked cerebral depression in monkeys.[25] In humans hypoxia due to lack of oxygen (hypoxic hypoxia) has been studied extensively, particularly hypoxia that occurs at high altitudes.[26,67] As in monkeys there is little effect down to 15 percent O_2, beyond a slightly reduced exercise tolerance, but at approximately 10 percent O_2 effects suddenly become severe. It is possible, however, to identify a number of degrees of physiological and behavioral decrement, and for low-oxygen hypoxia certain signs can be related to particular exposure concentrations. From experiments in humans the effects have been classified into four phases as follows,[26,45] the appropriate altitude ranges and equivalent sea-level oxygen concentrations being given for each phase:

1. Indifferent phase (sea level–3,000 m or 20.9–14.4 percent O_2): Minor effects on visual dark adaptation and beginnings of effects on exercise tolerance toward 15 percent O_2
2. Compensated phase (3,000–4,500 m or 11.8–14.4 percent O_2): Slightly increased ventilation and heart rate, slight loss of efficiency in performance of complex psychomotor tasks and short term memory, some effects on judgment. Maximal exercise work capacity is reduced
3. Manifest hypoxia (4,500–6000 m or 9.6–11.8 percent O_2): Degradation of higher mental processes and neuromuscular control, loss of critical judgment and volition, with dulling of the senses. Emotional behavior may vary from lethargy and indifference to excitation with euphoria and hallucinations. Marked increase in cardiovascular and respiratory activity. This is the region likely to be particularly dangerous during fire exposures, representing the catastrophe point as a victim passes from this stage into the fourth stage at approximately 10 percent O_2 (or COHb or blood cyanide concentrations producing an equivalent degree of brain hypoxia)
4. Critical hypoxia (6000–7,600 m or 7.8–9.6 percent O_2): Rapid deterioration of judgment and comprehension leading to unconsciousness followed by cessation of respiration and finally of circulation at death

If a subject is suddenly placed into a low-oxygen environment, a finite time elapses before the blood gas concentration equilibriates with the new conditions, and a certain degree of physiological effect then occurs, depending upon the equilibrium blood concentration attained. The time-to-effect functions described in the next section have been based on the concept of a certain "dose" of hypoxia being taken up over a period of time to reach equilibrium at the chosen endpoint of severe incapacitation (the catastrophe point). The concept of the catastrophe point relates to observations, mainly during exposures of primates to the asphyxiant gases CO, HCN and low-oxygen hypoxia,[25,44] that due to physiological compensatory mechanisms there is very little decrement in physiological status or behavioral task performance as the severity of an exposure increases, until a certain point is reached when tissue hypoxia becomes critical and deterioration becomes very marked and very rapid, usually leading to unconsciousness. This endpoint therefore marks the sudden change in a potential fire victim from a condition of near normality to a condition in which escape would not be possible.

A Model for the Prediction of Time to Incapacitation by Hypoxia in Fires

Incapacitation due to oxygen lack, consisting of loss of consciousness, occurs when the oxygen supply to cerebral tissue falls below a certain critical value, which in turn occurs when the partial pressure of oxygen in the cerebral venous blood falls below 20 mmHg.[26] Due to the effects of the compensatory mechanisms, to residual oxygen in the lungs, and to oxygen stores available from the

blood, a certain period of time elapses before the oxygen tension of venous blood declines to this critical level when a subject is suddenly faced with a reduced oxygen atmosphere after breathing normal air.[26] The time taken for this depletion depends upon the level to which the oxygen concentration falls, but also on the activity of the subject (which affects oxygen demand) and the RMV. It is therefore possible to plot time to loss of consciousness against oxygen concentration. Studies of this kind have been performed on human subjects, principally for hypoxia caused by exposure to reduced atmospheric pressures simulating the effects of high altitudes, which has similar effects to those of exposure to reduced oxygen concentrations at sea level. Figure 2-6.17 shows such a plot of time of useful consciousness for humans at rest following sudden decompression (less than one second transition time) to a range of simulated altitudes. The data are adapted from Luft,[26] and are expressed in terms of altitude. The equivalent sea-level oxygen concentrations have been added to the figure, and also the percentage oxygen vitiation (i.e., the equivalent decrease in percentage oxygen concentration at sea level below the normal concentration of 20.9 percent oxygen).

From this curve it is possible to derive an equation that should give a reasonable prediction of time to loss of consciousness (t_{I_O}) for a victim exposed to a hypoxic fire environment, as follows

$$(t_{I_O})\ \text{min} = \exp\,[8.13 - 0.54(20.9 - \%O_2)] \qquad (12)$$

where $(20.9 - \%\ O_2) = \%\ O_2\text{Vit}$ (percent oxygen vitiation)

As with exposure to HCN, time to incapacitation for exposure to low oxygen concentrations does not follow Haber's rule, since short exposures to severe hypoxia cause incapacitation very rapidly, and long exposures to modest hypoxia have little effect (e.g., at 17 percent O_2Vit, $Ct = 17 \times 0.33 = 5.61$ percent·min, while at 11.3 percent O_2Vit, $Ct = 11.3 \times 7.73 = 87.3$ percent·min). In attempting

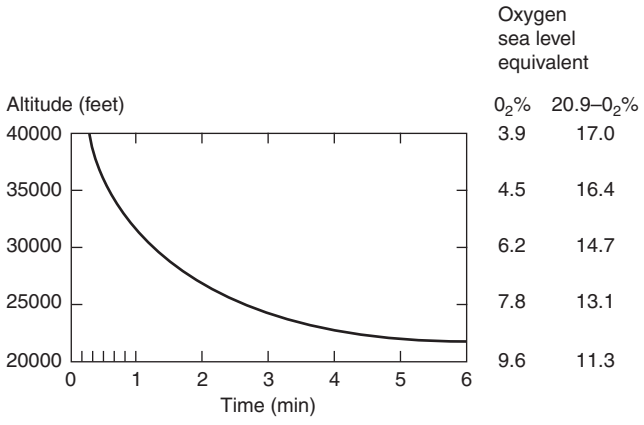

Figure 2-6.17. ***Time of useful consciousness on sudden exposure to high altitudes (less than 1 s transition time). Scales also show equivalent sea-level percent oxygen concentration and percent oxygen vitiation (decrease below 20.9 percent O_2).[26]***

to predict time or dose to incapacitation or death for a subject exposed to changing oxygen concentrations, it is therefore necessary to apply a weighting factor to allow for these deviations from ideal behavior. As with HCN this may be achieved by using the fractional effective dose concept as follows:

For a constant level of hypoxia, the time to incapacitation due to oxygen depletion is given by

$$t_{I_O} = \exp[8.13 - 0.54(20.9 - \%\ O_2)]$$

Dose to incapacitation $= (20.9 - \%\ O_2)(t_{I_O})$
Therefore, for a short exposure time, t, to a given level of oxygen vitiation

$$F_{I_O} = \frac{(20.9 - \%O_2)(t)}{(20.9 - \%O_2)(t_{I_O})}$$

Where F_{I_O} = fraction of an incapacitating dose of hypoxia, and where $t = 1$ min this simplifies to

$$F'_{I_O} = 1/t_{I_O} \qquad (13)$$

If the fractional doses per each minute are summed throughout the exposure, the dose and time to incapacitation can be predicted.

EXAMPLE:

A subject is exposed to a concentration of 10 percent oxygen for 5 min followed by 7.8 percent oxygen for 1.5 min. For 10 percent O_2 (10.9% O_2Vit)

$$t_{I_O} = \exp\,[8.13 - 0.54(20.9 - 10)]$$
$$1/t_{I_O} = 0.106$$

For 7.8% O_2 (13.1% O_2Vit)

$$t_{I_O} = 2.8748$$
$$1/t_{I_O} = 0.3478$$
$$F_{I_O} = 0.106 \times 5 + 0.3478 \times 1.5$$
$$= 1.05$$

Therefore loss of consciousness is predicted at 6.5 minutes.

A Model for the Prediction of Hyperventilation and Time to Incapacitation by Carbon Dioxide

Carbon dioxide (CO_2), like carbon monoxide, is universally present in fires. Although carbon dioxide is not toxic at concentrations of up to 5 percent it stimulates breathing, so that at 3 percent the RMV is approximately doubled, and at 5 percent tripled.[25] This hyperventilation, apart from being stressful, can increase the rate at which other toxic fire products (such as CO) are taken up.

For asphyxiant gases such as CO or HCN it is likely that the increased uptake resulting from carbon dioxide induced hyperventilation will significantly reduce time to incapacitation and death. The ventilatory response to carbon dioxide varies among individuals and reported data also vary. An average curve has been constructed from

data given in three sources[68–70] and is presented in Figure 2-6.18, giving the following regression equation

$$\text{RMV(L/min)} = \exp(0.2496 \times \%CO_2 + 1.9086) \quad (14)$$

From this expression a multiplication factor (VCO_2) can be calculated for the enhanced uptake of other asphyxiant gases as follows

$$VCO_2 = \frac{\exp(0.2496 \times \%CO_2 + 1.9086)}{6.8} \quad (15)$$

Where 6.8 L/min is a suggested figure for the resting RMV at the background CO_2 concentration. This has been simplified to

$$VCO_2 = \exp\left(\frac{[CO_2]}{4}\right) \quad (16)$$

Upon further examination of this relationship it is considered that, although it provides a reasonable estimate of the change in VCO_2, it gives an exaggerated value for the increase in uptake rate for other gases. This is primarily because the efficiency of uptake decreases as ventilation increases. A modified expression has therefore been derived, based upon that used in the CFK equation,[22] which gives a somewhat lower prediction for the increase in uptake rate of other gases. A slightly higher figure has also been used for the resting RMV. The modified equation is as follows:

$$VCO_2 = \frac{\exp(0.1903 \times \%CO_2 + 2.0004)}{7.1} \quad (17)$$

This has been simplified to

$$VCO_2 = \exp\left(\frac{[CO_2]}{5}\right) \quad (18)$$

At concentrations of approximately 5 percent and above carbon dioxide is itself an asphyxiant, but for elevated CO_2 concentrations (hypercapnia) the change in degree of incapacitation with exposure concentration is more gradual than with hypoxia. From approximately 3 percent up to 6 percent there is a gradually increasing degree of respiratory distress. This becomes severe at approximately 5 to 6 percent, with clinical comments from subjects such as "breathing fails to satisfy intense longing for air" or "much discomfort, severe symptoms impending," with headache and vomiting also occurring.[71] Although due to the gradual equilibration process these signs tend to worsen during exposure, it seems unlikely that they would proceed as far as loss of consciousness over the course of a 30- or even a 60-min exposure period. However, once the concentration of carbon dioxide is in the 7 to 10 percent plus range, a new set of signs consisting of dizziness, drowsiness, and unconsciousness is superimposed on the severe respiratory effects. A time factor does enter here due to gradual uptake, with loss of consciousness being more certain, and occurring earlier (over a period of a few minutes) as the exposure concentration approaches and exceeds 10 percent.[45,46,71,72] Approximate tolerance times for the distressing effects on breathing and the onset of asphyxia for humans are shown in Figure 2-6.18. The effects are perceptible to subjects from 3 percent as increasingly rapid breathing, and at approximately 6 percent become intolerable within 20 minutes. Symptoms of dizziness, headache, and fatigue start to occur at concentrations above 7 percent, with danger of unconsciousness occurring within a few minutes increasing from 7 to 10 percent. Loss of consciousness is likely within 2 minutes at 10 percent CO_2 in humans.[71]

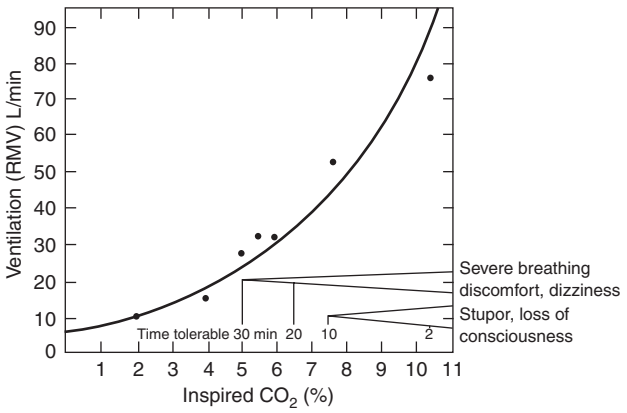

Figure 2-6.18. ***Ventilating response to carbon dioxide.[68–71]***

As with HCN and low-oxygen hypoxia, intoxication by carbon dioxide does not follow Haber's rule (Ct for 10 percent CO_2 = 20 percent·min, Ct for 5 percent CO_2 = 175 percent·min). From the approximate data in Figure 2-6.18 an expression predicting approximate time to incapacitation $t_{I_{CO_2}}$ has been derived as follows:

$$t_{I_{CO_2}} = \exp(6.1623 - 0.5189 \times \%CO_2) \quad (19)$$

Using the fractional-dose concept previously described for HCN and hypoxia, it is possible to predict approximate dose to incapacitation, provided that the CO_2 concentration is stable or increasing, as follows:

For a constant CO_2 concentration

$$t_{I_{CO_2}} = \exp(6.1623 - 0.5189 \times \%CO_2)$$

Dose to incapacitation = $(\%CO_2)(t_{I_{CO_2}})$

Therefore, for a short exposure time, t, to a given CO_2 concentration

$$F_{I_{CO_2}} = \frac{(\%CO_2)(t)}{(\%CO_2)(t_{I_{CO_2}})}$$

Where $F_{I_{CO_2}}$ = fraction of an incapacitating dose, and where t = 1 min. This simplifies to

$$F_{I_{CO_2}} = \frac{1}{t_{I_{CO_2}}} \quad (20)$$

If the fractional doses per minute are summed throughout the exposure, the dose and time to incapacitation can be predicted.

EXAMPLE:

A subject is exposed to a concentration of 5 percent CO_2 for 20 minutes, followed by 9 percent CO_2 for 2 min.

For 5% CO_2, $t_{l_{CO_2}} = 35.44$; $1/t_{l_{CO_2}} = 0.0282$

For 9% CO_2, $t_{l_{CO_2}} = 4.45$; $1/t_{l_{CO_2}} = 0.2247$

$$F_{l_{CO_2}} = 0.0282 \times 20 + 0.2247 \times 2 = 1.01$$

Severe incapacitation with probable loss of consciousness is therefore predicted at approximately 22 minutes.

Interactions between Toxic Fire Gases

Although data on the concentration/time/dose relationships of the dangerous and lethal asphyxiant effects in humans of individual fire gases are necessarily limited, they are adequate for the construction of a usable incapacitation model. However, the effect of interactions between combinations of these gases on time to incapacitation in fires is an area that requires further investigation, as very little information is currently available. The best that can be done currently is to suggest likely degrees of interaction based on physiological data from individual gases and on such experimental data for gas combinations as do exist.

Effect of Carbon Dioxide on Effects of CO, HCN, and Low-Oxygen Hypoxia

The interaction likely to be most important is that hyperventilation due to carbon dioxide exposure will increase the rate of uptake of other toxic gases and thus decrease the time to incapacitation (or the time taken to inhale a lethal dose), in proportion to the increase in ventilation. This is likely to be most important with respect to CO intoxication, particularly for a subject at rest, and also to some extent for active subjects. An expression for calculating the increase in RMV resulting from exposure to different carbon dioxide concentrations is given in the section on CO_2, but as an approximation it should be assumed that there would be little effect below 3 percent CO_2, while at 3 percent CO_2, RMV would be doubled, so time to incapacitation by CO should be halved. At 5 percent CO_2, RMV would be approximately tripled and time to incapacitation would be approximately one-third of that in the absence of carbon dioxide. There is a possibility that the effects on time to incapacitation would not be as dramatic as this, since there is evidence that the presence of carbon dioxide may counteract the leftward shift in the oxygen dissociation curve caused by carbon monoxide, somewhat counteracting its deleterious effects.[73] However, in the absence of experimental data on combination exposures it is best to ignore this possible beneficial effect, since the effect on uptake rate is likely to be dominant. A similar effect on uptake may also occur with HCN. With regard to low oxygen, carbon dioxide has been shown to have a marked beneficial effect on resistance to incapacitation. This is partly due to the hyperventilatory effect that increases the rate of oxygen uptake, and partly due to the rightward shift in the oxygen dissociation curve caused by carbon dioxide. This improves the delivery of oxygen to the tissues, counteracting the respiratory alkalosis that otherwise occurs.[74,75] New evidence is currently being obtained from experiments on the effects of combinations of asphyxiant gases with CO_2 in rodents, that with severe exposures, postexposure lethality is increased by the presence of CO_2. When animals are severely affected and suffering from a hypoxia-induced metabolic acidosis, this appears to be enhanced by the further acidotic effect of CO_2 inhalation, and the animals then fail to recover after exposure under conditions when they would otherwise be expected to do so. It is also to be expected that hyperventilation induced by CO_2 would increase the uptake of substances that irritate the lung, which also tend to cause toxic effects some time after exposure, and recent experiments in rodents are providing evidence that this is so, with increased deaths possibly caused by postexposure acidosis and increased lung damage. Exercise also causes a CO_2-driven hyperventilation, and there is new evidence that this may also cause deaths when rodents are exposed to irritants at normally sub-lethal concentrations.[76]

Interactions between CO and HCN

Some studies have been made of interactions between CO and HCN, with varying results.[77] On theoretical grounds little interaction is to be expected, since CO diminishes the carriage of oxygen in the blood and its delivery to the tissues, while HCN diminishes the ability to use oxygen once delivered to the tissues. It is therefore to be expected that either one or the other gas would constitute the rate-limiting step in oxygen supply and utilization. However the consensus view is that there is at least some additive effect between these two gases. Experiments in primates have shown that time to incapacitation by HCN is slightly reduced by the presence of near-toxic concentrations of CO;[77] also, the rate of uptake of CO may be increased by the hyperventilatory effect of HCN. In these circumstances it is probably safest to assume that these gases are additive in terms of time to incapacitation and dose to death, and that incapacitation or death will occur when the fraction of the toxic dose of each one adds up to unity.

Interactions between CO and Low-Oxygen Hypoxia

The most likely interaction between CO and low-oxygen hypoxia would be some degree of addition, since both reduce the percentage oxygen saturation of arterial blood, and CO also impairs the delivery of oxygen to the tissue by causing a leftward shift of the oxygen dissociation curve.[73] It is possible that during the early stages of CO exposure in hypoxic subjects the CO occupies the upper, oxygen-free part of the oxygen dissociation curve, and therefore has little effect. Von Leggenhager[53] reports that subjects at rest at altitude remain symptom free at low levels of CO saturation. However, it is likely that the effect of more severe exposure to CO in a hypoxic subject would be additive to some extent, as reported by Heim[78] and McFarland et al.[79]

An important point is the possible interaction between irritant smoke products and asphyxiant gases. This effect is particularly strong when rats and mice are exposed to smoke, since the rodent response to irritation of the upper respiratory tract is a marked decrease in respiratory rate and RMV. Thus if CO is present in the smoke, the rate of uptake will be considerably reduced if the smoke is irritant. This sometimes leads to misleading results in combustion product toxicity tests, where a material producing irritant smoke will have an apparently low LC_{50}, although high CO concentrations are present in the atmosphere.

This marked, prolonged decrease in respiratory rate does not occur in humans or nonhuman primates; indeed, in primate smoke experiments, irritant products tend to increase rather than decrease ventilation (although not sufficiently to increase CO toxicity).[16,25]

In summary, data on interactions between the asphyxiant gases CO, HCN, low oxygen, and CO_2 are limited, but where deleterious interactions are likely it would be prudent to include them in the incapacitation model, if only to err on the side of safety. For this reason it is proposed that the interactions should be quantified in the incapacitation model as follows:

1. Assume that CO and HCN are directly additive (1:1) on a fractional dose basis (the evidence suggests that they are additive, but that the additive interaction may actually be less than unity).
2. Assume that the rates of uptake of CO and HCN and their fractional doses are increased in proportion to any increase in ventilation (RMV) caused by carbon dioxide.
3. Assume that the fractional doses of CO and HCN, adapted for carbon dioxide, are additive with the fractional dose of low-oxygen hypoxia.
4. Assume that asphyxia by carbon dioxide is independent of that induced by CO, HCN, and hypoxia.
5. Assume that irritancy is independent of asphyxia, but that uptake of irritants is increased by carbon dioxide (see next section of this chapter).

Implications of Interactions for Predicting Time to Incapacitation in Smoke Atmospheres

In general, there is evidence for some possible interactions between toxic fire gases, but whether these are likely to be important in practice depends upon the composition of actual fire atmospheres, which is discussed in a later section of this chapter. For most practical situations, the composition of fire atmospheres will be such that for asphyxiant effects CO will be the most important toxic product, and that the most important interaction will be an increased rate of CO uptake due to hyperventilation caused by CO_2. The additional effects of HCN and low-oxygen hypoxia will contribute to the effects of CO-induced asphyxia, and may significantly reduce time to incapacitation in some situations.

On this basis the fractional dose equation for asphyxiation would be*

$$F_{IN} = [(F_{I_{CO}} + F_{I_{CN}} + FLD_{irr}) \times V\mathrm{CO}_2 + \mathrm{FED}_{I_O}] \text{ or } F_{I_{CO_2}} \quad (21)$$

where

F_{IN} = fraction of an incapacitating dose of all asphyxiant gases

$F_{I_{CO}}$ = fraction of an incapacitating dose of CO

$F_{I_{CN}}$ = fraction of an incapacitating dose of HCN (and nitriles, corrected for NO_2)

FLD_{irr} = fraction of an irritant dose contributing to hypoxia (This term represents a correction for the effects of irritants on lung function and is developed in the section on irritants. This term may be omitted if the effects of asphyxiant gases only are under consideration)

$V\mathrm{CO}_2$ = multiplication factor for CO_2-induced hyperventilation

FED_{I_O} = fraction of an incapacitating dose of low-oxygen hypoxia

$\mathrm{FED}_{I_{CO_2}}$ = fraction of an incapacitating dose of CO_2

Each individual term in the FED equation is itself the result of the following equations, which give the FED for incapacitation for each gas and the multiplication factor for CO_2, where t is the exposure time at a particular concentration in minutes. The FED acquired over a each period of time during the fire are summed until the total FED_{IN} reaches unity, at which point incapacitation (loss of consciousness) is predicted. In order to allow for differences in sensitivity and to protect susceptible human subpopulations a factor of 0.1 FED should allow for safe escape of nearly all exposed individuals. Death is predicted at approximately two to three times the incapacitating dose.

For a 1-minute exposure to each gas at a concentration C

$$F'_{I_{CO}} = \frac{8.2925 \times 10^{-4} \times \mathrm{ppm\ CO}^{1.036}}{30}$$

$$F'_{I_{CN}} = \frac{(\exp([\mathrm{CN}]/43))}{220} \quad (11)$$

where CN represents the concentration of cyanide corrected for the presence of other nitriles besides HCN and for the protective effect of NO_2. CN can be calculated as [CN] = [HCN] + [total organic nitriles] − [NO_2]

$$V\mathrm{CO}_2 = \exp\frac{[\mathrm{CO}_2]}{5}$$

$$\mathrm{FLD}_{irr} = \mathrm{FLD}_{HCl} + \mathrm{FLD}_{HBr} + \mathrm{FLD}_{HF} + \mathrm{FLD}_{SO_2} + \mathrm{FLD}_{NO_2} + \mathrm{FLD}_{CH_2CHO} + \mathrm{FLD}_{HCHO} + \Sigma\mathrm{FLD}_x \quad (22)$$

*The effect of CO_2-induced hyperventilation will be to increase the rate of uptake of inhaled gases as a function of the increase in ventilation. Another approach to the quantification of this effect would be to multiply the concentration of each gas by $V\mathrm{CO}_2$ in the FED expression for that gas rather than in Equation 21. This would produce a similar result to Equation 21, except for the effect of HCN inhalation, for which a greater value of $F_{I_{CN}}$ corrected for $V\mathrm{CO}_2$ would result. This may represent a more correct approach and is currently under consideration.

where ΣFLD_x = FLDs for any other irritants present

$$F'_{I_O} = \frac{1}{\exp\,[8.13 - 0.54(20.9 - \%O_2)]}$$

$$F'_{I_{CO_2}} = \frac{1}{\exp\,[6.1623 - 0.5189 \times \%O_2]}$$

Figure 2-6.19 shows an expanded detail of asphyxiant gas profiles during the first 10 minutes of the single armchair room burn that is presented in more detail in Figure 2-6.15. The histograms show the average concentrations of each gas at minute intervals during the first 6 min of the fire, the figures for which are given in Table 2-6.6. The HCN concentration was not measured in this fire, but it is likely to have been present as a major toxic product. Possible HCN concentrations have therefore been suggested for inclusion in the model and are shown in a histogram.

Applying the expressions for the fractional incapacitating dose of each gas to the data in Table 2-6.6, the total fractional dose of all asphyxiant gases for each minute during the fire (F_{IN}) has been calculated according to Equation 21, and summed for each successive minute during the fire, as shown in Table 2-6.7. Incapacitation (loss of consciousness) is predicted at 5 min when the fractional incapacitating dose exceeds unity ($F_{IN} = 1.2$).

Irritant Fire Products

Unlike the incapacitating effects of asphyxiants, which are clear-cut and well understood, the incapacitative effects of irritants are much more difficult to determine. Irritant fire products produce incapacitation during and after exposure in two distinct ways. During exposure the most important form of incapacitation is sensory irritation, which causes painful effects to the eyes and upper respiratory tract, and to some extent also the lungs. Although exposure may be painful and thus incapacitating, it is unlikely to be directly lethal during exposure unless exceptionally high concentrations of irritants are present. However, the second effect of irritants penetrating into the lungs is an acute pulmonary irritant response, consisting of edema and inflammation which can cause respiratory difficulties and may lead to death 6 to 24 hr after exposure.[80,81] The effects do not show the sharp cut off of asphyxiation, but lie on a continuum from mild eye irritation to severe pain, depending upon the concentration of the irritant and its potency.[24,82,83] For sensory irritation the effects do not depend upon an accumulated dose but occur immediately upon exposure, and usually lessen somewhat if exposure continues.[16,24] For the later inflammatory reaction the effect does depend upon an accumulated dose, approximately following Haber's rule, and there seems to be a threshold below which the consequences are minor, but when this dose is exceeded severe respiratory difficulties and often death occur, usually 6 to 24 hr after exposure. However, for most sensory irritants the ratio between the concentration producing severe irritation and

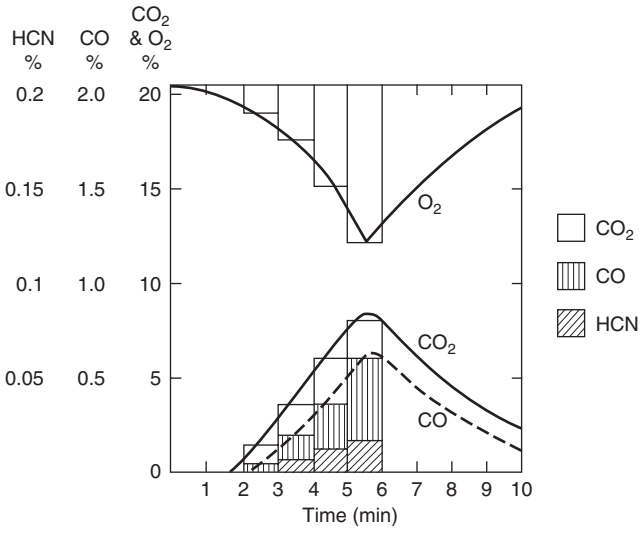

Figure 2-6.19. ***Expanded detail from Figure 2-6.15—average concentrations of asphyxiant gases each minute (histograms) from gas profiles (curves) measured during the first 10 min of a single armchair (polystyrene with polyurethane cushions and covers) room burn.[56] Since HCN was not measured, but was likely to have been present as an important toxic product, possible concentrations have been suggested for inclusion in the model.***

Table 2-6.6 ***Average Concentrations of Asphyxiant Gases Each Minute during the First Six Minutes of the Single Armchair Room Burn Shown in Figure 2-6.19***

Time (min)	1	2	3	4	5	6
CO ppm	0	0	500	2000	3500	6000
HCN ppm	0	0	0	75	125	174
CO_2%	0	0	1.5	3.5	6	8
O_2%	20.9	20.9	19	17.5	15	12

Table 2-6.7 ***Fractions of an Incapacitating Dose of Asphyxiant Gases Calculated from the Data in Table 2-6.6 According to Equation 21 for One-Minute Intervals during the Single Armchair Room Burn Shown in Figure 2-6.19***

Time (min)	1	2	3	4	5
F'_{Ico}	0	0	0.017	0.074	0.130
$+ F'_{Icn}$	0	0	0.000	0.025	0.080
$\times VCO_2$	0	0	1.442	2.376	4.434
$=$	0	0	0.025	0.233	0.931
$+ F_{Io}$	0	0	0.001	0.002	0.007
$=$ Total	0	0	0.026	0.235	0.938
Running total (F_{IN})	0	0	0.026	0.261	1.199
or:					
F'_{Ico_2}	0	0	0.005	0.013	0.047
Running total (F_{IN})	0	0	0.005	0.018	0.065

F_{IN} = 1.2 at 5 minutes due to the combined effects of CO, HCN, and low-oxygen hypoxia, the uptake of which was increased by CO_2, and incapacitation is predicted at between 4 and 5 minutes. Although carbon dioxide was present at concentrations sufficient to have caused significant hyperventilation, the fractional incapacitating dose for asphyxiation by carbon dioxide was only 0.065 at 5 min, and this is therefore unlikely to have had any effect.

the dose causing death is usually large (15 to 500 times)[84,85] for 30-min exposure times. (See Table 2-6.1.)

The effects of low concentrations of irritants can best be considered as adding to the obscurational effects of smoke by producing mild eye and upper respiratory tract irritation. In this situation irritants may have some effect by impairing the speed of an individual's movement through a building (as would simple visual obscuration), but the combined effects of eye irritation and direct visual obscuration may be more serious, and it has been shown that human volunteers moved more slowly through irritant smoke than through nonirritant smoke.[86] The limitation of escape capability may not be simply restricted to direct physiological effects, but also to psychological and behavioral effects such as the willingness of an individual to enter a smoke-filled corridor.[86]

At the other end of the scale, when irritants are present at high concentrations, there is some disagreement about the likely degree of incapacitation. Some investigators believe that the painful effects on the eyes and upper respiratory tract would be severely incapacitating, so that, for example, escape from a building would be rendered extremely difficult.[87] Others believe that the effects peak at moderate concentrations, and that although the effects may be very unpleasant they would not significantly impair the ability to escape from a building, and would provide a strong stimulus to escape that might almost be beneficial.[85]

One of the main difficulties in attempting to predict the consequences of exposure to irritants is the poor quality of data available on humans. Obviously very few controlled studies have been made of the effects of severe irritancy in humans, so that most data are anecdotal, derived from accidental industrial exposures, with only a vague knowledge of exposure concentrations. Reports of the severity of the effects also tend to be very subjective, so that the term "severe irritation" could cover a wide range of sensations with varying degrees of actual incapacitation. Another problem is that since sensory irritation covers a continuous range from mild eye and upper respiratory tract irritation to severe pain, there are no simple objective end points or thresholds. The most extensive studies of the effects of severe irritancy in humans have been performed on volunteers exposed to riot-control agents such as CS (o-chlorobenzylidine malonitrile) or CN (α-chloroacetophenone). Even these studies do not really show how the ability to escape from a building might be affected, but they do to some extent convey the severity of the effects.

The effects of CS, which are probably similar to those of any severe sensory irritant, have been described by Beswick et al.[24] They consist of an almost instantaneous severe inflammation of the eyes accompanied by pain, excessive lacrimation (tearing), and blepharospasm (spasm of the eyelids). There is irritation and running of the nose with a burning sensation in the nose, mouth, and throat, and a feeling of intense discomfort during which the subjects cough, often violently. If the exposure continues, the discomfort spreads to the chest and there is difficulty in breathing. Many subjects describe a tightness of the chest or chest pain as the worst symptom of CS exposure. The respiration pattern is irregular and the breath is held for short periods. Attempts to avoid the irritation by breath-holding, followed eventually by fairly deep breaths, are reported as being extremely unpleasant. At this stage most individuals are acutely apprehensive and highly motivated to escape from the smoke. However, if exposure continues there is some remission of signs and symptoms. When subjects were exposed to 0.08 ppm CS, they found the immediate effects very unpleasant but after 4 to 5 min were able to play cards. Another finding with CS, perhaps related to the development of tolerance, was that subjects could endure a relatively high concentration (~0.8 ppm CS) if it was achieved gradually even over as short a period as 10 min (as is likely to occur in fires) while they were totally unable to bear an immediate exposure to the same concentration.[24,83]

Reports are conflicting among fire victims. Some persons say they went through dense smoke without experiencing any great discomfort, while others say that respiratory difficulties prevented them from entering smoke-filled areas.[94] This seems to depend upon the type of fire. For example, the smoke from some well-ventilated fires involving primarily cellulosic materials has been reported as irritant but not seriously incapacitating, while that from some plastic materials (e.g., the interior of a burning car) was found to cause severe effects when only a small amount of smoke was inhaled. Anyone who has had bonfire smoke in their eyes will know the pain of the experience. However, the effects can be mitigated by blinking or shutting the eyes, and the effects on the nose can be mitigated by mouth breathing and breath-holding. Also, it is known that people in emergency situations are often unaware of painful stimuli.[95] It is therefore likely that irritant smoke products do have some severe effects on the escape capability of fire victims, but it is difficult at present to predict accurately the likely degree of incapacitation.

Animal Models for the Assessment of Irritancy and Their Extrapolation to Humans

Having established that irritancy is likely to be a major cause of incapacitation in fires, it is important to find some way of assessing the potential of fire atmospheres for causing irritancy. The basic effects, consisting of an acute inflammatory reaction of the tissues accompanied by stimulation of pain receptors, are common to all mammals, so that animals can realistically be used to assess the potential for irritancy in humans.

The characteristic response to eye irritation is stimulation of trigeminal nerve endings in the cornea leading to pain, blepharospasm (reflex, or more or less involuntary closure of the eyelids), and lacrimation. Severe damage may also lead to corneal opacity.

The effects of irritants on the upper respiratory tract have been studied in a number of species, including humans, for a wide range of airborne irritants including atmospheres of combustion products.[96,97] The characteristic physiological response (also due to trigeminal nerve stimulation), is a reflex decrease in respiratory rate accompanied by a prickling or burning sensation in the nose, mouth, and throat, often accompanied by mucus secre-

tion. At very high concentrations rapidly developing inflammatory reactions in the upper respiratory tract and laryngeal spasm may cause death during or soon after exposure, but in humans the lung is likely to be the more seriously affected target organ.

In contrast to these effects, the characteristic response to irritants penetrating into the lung is an increase in respiratory rate, generally accompanied by coughing and a slight decrease in tidal volume. There may also be bronchial constriction and increased pulmonary flow resistance, particularly if the victim is hypersensitive to the irritant.[84,96] This is accompanied by tissue inflammation and edema, which at very high concentrations can cause death during, or more often after, exposure.[14,80]

The effect (upper respiratory tract or lung irritancy) that predominates depends upon a number of factors such as the physical characteristics of the aerosol, the aqueous solubility of the irritant, the animal species, and the duration of the insult. An important difference between mice and rats (which are often used to measure irritancy) and primates, including humans, is that in rodents the nasal passages are complex in structure and have a large surface area, so that soluble gases are readily taken up and particulates are readily deposited. A decrease in respiratory rate in the upper respiratory tract is the major response in rodents, which tends to protect them from exposure. Their great tolerance to hypoxia (and possible circulatory adaptations similar to the diving reflex) also enables them to maintain greatly reduced breathing for long periods. In humans and other primates the nasal passages are simply structured with a relatively small surface area, and in humans particularly, mouth breathing is common. Thus, although upper respiratory tract irritation occurs initially and is accompanied by some respiratory rate decrease, a greater proportion of the inhaled irritant is carried into the lungs, so that lung irritation is generally a more pronounced effect. In primates, including humans, a transient respiratory rate depression is followed rapidly by the increased respiratory rate characteristic of lung irritation.[16,79] (See Figures 2-6.20 and 2-6.21.)

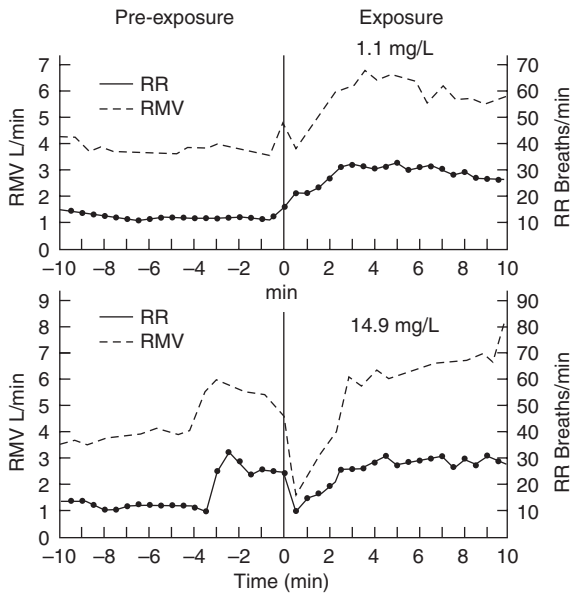

Figure 2-6.20. ***Respiratory effects of polypropylene decomposed under nonflaming oxidative conditions—cynomolgus monkey.***

Rodent Respiratory Rate Depression Test

The method most commonly used to quantify upper respiratory tract irritancy both for pedigree chemicals and combustion products is the mouse respiratory rate depression test.[97,98] The basic method involves measurement of the percentage decrease in respiratory rate during exposure over a range of different atmosphere concentrations. From this measurement the RD_{50} (the concentration required to produce a 50 percent decrease in respiratory rate) is calculated. Since the basic irritant mechanisms are the same in all mammals, it is certainly possible to identify an individual substance, or mixture (such as a combustion atmosphere), that is likely to be irritant to humans; however, it may also be possible to predict the degree of irritation in humans. As a result of comparisons of data from humans with results from mice, Alarie[93] has demonstrated a relationship between the potency of known sensory irritants in humans and a derivative of the mouse RD_{50}. When the log of the TLV (often based on symptoms of irritancy in man) is plotted against the log of 0.03 multiplied by the RD_{50} in ppm, most chemicals known to be sensory irritants in humans fall into a linear relationship with the respiratory effects in mice. Chemicals that are highly irritant in humans such as acrolein or chlorine have low RD_{50} measures in mice while mild irritants such as ethanol have a high mouse RD_{50}.[93] (See Table 2-6.7.)

Such methods appear to give good predictions of irritancy at low levels that are suitable for fixing hygiene standards, but for the high concentrations occurring in fires it is necessary to predict which concentrations will produce sufficient incapacitation to cause serious impairment of escape capability, and also which concentrations will cause serious lung damage after exposure. As stated previously, such predictions of incapacitation in humans are difficult because of the variable and subjective nature of irritancy. However, Alarie states that a human exposed at the mouse RD_{50} concentration of any substance would find the atmosphere severely irritating and would be seriously incapacitated within 3 min.[87] Certainly this seems to be justified in terms of some individual chemicals. For example, the work with CS[24,83] shows that, although it is very difficult to measure intolerable irritancy in humans, there does seem to be a reasonable agreement between the human and mouse data. Thus the mouse RD_{50} (4 mg/m^3, 0.52 ppm) is very close to the concentration found to be immediately intolerable when humans were exposed for up to 12 min (5 mg/m^3, 0.6 ppm), and the list of RD_{50} levels and concentrations reported as highly irritant in humans[21] given in Table 2-6.1 shows a reasonable correspondence, particularly for the irritants commonly found in fires.

However, these apparent irritancy correlations between rodents and humans still do not enable the exact

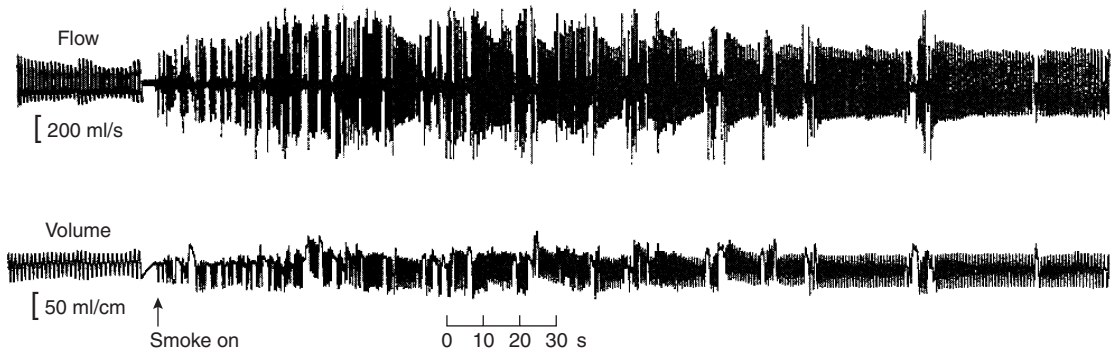

Figure 2-6.21. ***Effects upon respiration of exposure to an irritant smoke atmosphere; wood pyrolyzed at 300°C. When the smoke reaches the primate there is an initial sensory irritant response consisting of a decrease in respiratory rate with pauses between breaths. This rapidly gives way to a pulmonary irritant response consisting of an increase in respiratory rate and volume, which is maintained for the duration of the exposure.[16]***

prediction of the degree of incapacitation likely in humans, and in some cases there is evidence that the mouse model does not even give a good prediction of the degree of sensory irritation, although it can be used to demonstrate when sensory irritation is likely to occur in humans. Three experiments, two involving nonhuman primates and the other involving humans may illustrate the difficulties of extrapolating from the RD_{50} and physiological effects in mice to the degree of irritancy, incapacitation, and physiological effects in primates. In a series of experiments the irritant effects of smoke produced by the nonflaming oxidative decomposition of polypropylane were evaluated in cynomolgus monkeys.[16,31] The effects of breathing smoke through a face mask were mild at concentrations (NAC mass charge) of up to 4 mg polypropylene/L, consisting of a transient decrease in respiratory rate lasting approximately 30 seconds (a sensory irritant response), followed by an increased respiratory rate (lung irritant response) with a slight increase in RMV. (See Figure 2-6.20.) The respiratory response pattern is illustrated in Figure 2-6.21, where similar effects occurred during exposure to pyrolysis products from wood. For polypropylene the lung irritant response was the most sensitive effect with a threshold of 1 mg polypropylene/L. At concentrations above 6 mg/L the irritant effects were more marked, and although recovery appeared complete immediately after exposure, signs of nasal and pulmonary inflammation occurred some hours later. One animal died following an exposure of 30 minutes at 8 mg polypropylene/L. When free-moving monkeys trained to perform a behavioral task were exposed, there was evidence of some eye irritation and mild disruption of behavioral performance at a concentration of 1.85 mg polypropylene/L, the effects of exposure at 0.92 mg/L being very slight. However, the mouse RD_{50} for the same polypropylene atmosphere was found to be 0.1 mg/L. According to the model this concentration should have been highly irritant to the monkey, and yet in practice only the mildest of signs occurred at concentrations more than an order of magnitude higher. Similarly, in another study Potts and Lederer[99] exposed mice and humans simultaneously to smoke from the pyrolysis of red oak (mouse RD_{50} 0.37 mg/L). At this concentration the smoke was barely visible and all human subjects stated that although the smoke was unpleasant and irritating, in no sense were they physically incapacitated, and they were quite capable of performing tasks such as threading nuts and bolts of various sizes.

The third experiment was performed on two pedigree substances, hydrogen chloride and acrolein, often regarded as important irritants in smoke. In these experiments baboons were trained to press a lever in order to escape from a chamber after a 5-min exposure.[85] It was found that the animals could perform this task efficiently even at the incredibly high concentrations of 2780 ppm acrolein or 16,570 ppm HCl, although in both cases the animals died from lung inflammation after exposure. These concentrations compare with mouse RD_{50}s of 1.68 ppm for acrolein and 309 ppm for HCl, and at these concentrations both substances are highly irritant in humans. (See Table 2-6.8.)

As a result of this work on irritants in rodents, nonhuman primates, and humans, it would seem that the rodent models are good methods for identifying smoke atmospheres or individual substances likely to be irritant to humans and even for ranking irritants in order of potency and setting hygiene standards. However, when predicting concentrations of smoke atmospheres that would seriously impair the ability to escape from a fire, there is a need for more work to establish the effects of known irritants in humans and to establish the relationship between the rodent response and human incapacitation.

Lung Inflammatory Reactions

Just as it is difficult to predict the degree of incapacitation from sensory irritation likely to occur in victims during fire exposure, it is also difficult to predict concentrations likely to cause death in humans from lung inflammatory reactions, although experiments in rodents should enable some estimates to be made from postex-

Table 2-6.8 ***Irritancy Data***

Acrolein[a]

Mouse $RD_{50} = 1.68$ ppm[87]

Marked irritation of eyes and nose in humans—1 ppm[21]

Severe irritation of eyes and nose in humans—5.5 ppm[21]

Henderson and Haggard[21] state that 10 + ppm is lethal in humans within a short time due to pulmonary irritation. However 10 ppm for 3.5 hr in cats was nonlethal[21]

Kaplan[85] has reported that baboons can escape from a chamber after 5 min exposure at up to 2780 ppm. One animal died due to pulmonary effects following exposure at 1025 ppm, and another following 2780 ppm. No signs of pulmonary effects were observed following exposure at 505 ppm and below

A case has been reported of a man dying following exposure to 153 ppm for 10 min[91]

The 6-hr mouse LC_{50} is 66 ppm[91]

The 30-min rat LC_{50} is 135 ppm[91]

Hydrogen chloride[b]

Mouse $RD_{50} = 309$ ppm[87]

Strongly irritant to humans at 50 to 100 ppm for 1 hr[21]

Brief exposure at 1,000 to 2000 ppm is regarded as dangerous to lethal in humans[82]

Humans LCLO 1300 ppm for 30 min[91]

Kaplan exposed baboons for 5 min to concentrations of up to 16,570 ppm and found that they were able to perform escape maneuvers. One animal suffered permanent lung damage at 11,400 ppm and two died at approximately 17,000 ppm (≃2830 ppm for 30 min).

[a]From these rather variable data the concentration lethal to humans following a 20-min exposure would be 80 to 260 ppm. A severe irritant effect on the upper respiratory tract would be expected at around 5 ppm, but from Kaplan's work[85] this may not be unbearable, even up to several hundred ppm.

[b]Therefore, anything over 100 ppm is likely to be highly irritant and over a 20-min period approximately ten times this concentration may cause permanent lung damage or endanger life.

posure LC_{50} data. When rodents are exposed to smoke atmospheres in small-scale combustion toxicity experiments, death occurs principally either during exposure due to asphyxiant gases (CO, HCN) or some time after exposure, due to lung irritation. In cases where the majority of deaths occur after exposure and are accompanied by signs of lung irritation, measurements of the concentration causing postexposure deaths give some indication of concentrations likely to be hazardous to humans.

Since the effects of asphyxiant gases can be predicted without animal exposure, while the potential for causing sensory irritation and lung inflammation cannot, measurements of sensory irritancy by the respiratory depression test (RD_{50}) and measurements of the concentrations causing postexposure deaths (LC_{50}) are important uses for small-scale toxicity tests. It is also important to stress that whereas sensory irritation occurs immediately upon exposure, and is concentration related, the inflammatory reactions resulting from lung irritancy are dose related and depend approximately upon the product of exposure concentration and duration (Ct product). When an LC_{50} concentration is quoted, it is also important to quote the exposure duration. For combustion toxicity experiments exposure times are usually 10 or 30 min, and the 30 min LC_{50} should be approximately one third of the 10 min LC_{50} when postexposure irritancy is the cause of death. It is also important to know the time over which the deaths were scored. Thus some studies quote LC_{50} levels only in terms of animals dying during exposure (which will be due to asphyxia or very high concentrations of irritants). Other studies include deaths occurring both during or up to 24 hours after exposure, while other studies use the standard method for inhalation toxicology studies which includes deaths during exposure and for up to 14 days after. For the assessment of toxic hazard in possible fire scenarios, it is important to take all these factors into account when considering different building designs or applications of materials.

Irritant Components of Thermal Decomposition Product Atmospheres

If mathematical models are to be constructed to predict the potential for sensory irritancy and later lung inflammation of exposures in fires, it is important to attempt to identify the main irritant chemical species occurring in fires and to measure their potency individually and in combination. This is an area where knowledge is still inadequate, but large numbers of known irritant chemicals have been found to occur in fire atmospheres.[16,17] (See Table 2-6.1.) The irritant chemicals released in fires are formed during the pyrolysis and partial oxidation of materials, and the combinations of products from different materials are often remarkably similar.[17] Some materials release irritant components simply upon pyrolysis, such as HCL from PVC, isocyanates from flexible polyurethanes, and various substances from natural materials such as wood. However, for all organic materials and particularly for simple hydrocarbon polymers such as polypropylene or polyethylene, the main pyrolysis products, which consist of various hydrocarbon fragments, are innocuous. Thus when polypropylene is pyrolyzed in nitrogen the products listed in Table 2-6.9 are produced, and such an atmosphere was found to have no effect upon primates.[16,80] However when these products are oxidized during nonflaming decomposition in air, some are converted to highly irritant products as shown in the table, and such atmospheres were indeed found to be highly irritant to both mice and primates.[31]

Table 2-6.9 ***Pyrolytic and Oxidative Decomposition Products of Polypropylene at 500°C Showing Percentage Yields of Major Irritants as Indicated, and Threshold Limit Values (TLVs) Where Available from American Conference of Governmental Industrial Hygienists[21]***

MS Interpretation	Pyrolysis Yield[b] (%) ($\times 10^{-1}$)	Oxidation Yield[b] (%) ($\times 10^{-1}$)	TLV (ppm)
Ethylene	10.4	8.1	
Ethane	3.7	2.1	
Propene	18.6	18.4	
Cyclopropane	0.5	0.3	
Formaldehyde[a]	—	33.2	2
Propyne	0.2	—	
Acetaldehyde[a]	—	35.0	100
Butene	9.6	20.1	
Cyclobutene	0.3	0.8	
Methyl vinyl ether[a]	—	10.4	
Acetone[a]	—	38.4	750
Butane	1.2	—	
Methyl propane	0.4	—	
Methyl butane	4.0	—	
Butenone[a]	—	1.3	
Methyl butene	29.7	12.9	
Pentanol[a]	—	12.5	
Cyclopentane	0.5	1.4	
Pentadiene	1.3	—	
Crotonaldehyde[a]	—	7.7	2
Ethylcyclopropane	0.1	—	
Methyl vinyl ketone[a]	—	2.8	
Methyl ethyl ketone[a]	—	4.7	200
Hexane	0.9	1.2	
Cyclohexane	32.2	19.3	
Hexadiene	3.7	2.2	
Hexyne	—	1.3	
Benzene	6.7	5.1	
Methyl propyl ketone[a]	—	1.9	
Pent-2-ene-4-one[a]	—	7.5	
Phenol[a]	—	11.6	5
Toluene	2.4	16.1	
Methyl cyclohexadiene	2.1	0.1	
Xylene	6.1	0.2	
Styrene	5.6	4.0	

[a]Oxygen-containing products

[b]Weight percentage conversion of polymer

These atmospheres produced by the nonflaming oxidative decomposition of materials are always the "worst case" for any material in terms of irritant potency. Both the chemical profile and the irritant potency as determined by the mouse RD_{50} test are often similar for different materials, the majority lying within a range of approximately one order of magnitude.[32] However, when materials flame, these organic irritants are destroyed in the flame to produce CO_2 and water, so that the irritancy of the atmosphere depends upon how much irritant escapes the actual flame zone and the efficiency of combustion. Thus "clean," smoke-free flames, involving efficient combustion such as those that occur in a gas burner or well-ventilated fire, are relatively nonirritant, whereas "dirty," smoky flames resulting from inefficient combustion may contain high concentrations of irritants, and produce these irritants at a greater rate than under smoldering or nonflaming conditions. In primates the atmosphere produced by flaming polypropylene was found to retain some irritancy, although considerably less than under nonflaming conditions.[16] In mouse experiments, some fire retardant materials, which could be induced to flame only intermittently, with considerable smoke production, were found to produce atmospheres up to 300 times more irritant than the same polymer in its non-fire retardant state, which burned cleanly.[100]

The picture is again confused regarding the role of specific chemical products in smoke. Table 2-6.1 shows some irritants identified in smoke atmospheres in order of their sensory irritancy, and includes data on the LC_{50}, due principally to lung inflammation, where these were obtainable from the literature. In some cases there was a considerable range of estimates for both sensory irritancy and lethality, and these are indicated. The lethality data are mostly for rodents, and have been normalized to a 30-min exposure period assuming that lethality is dose-related according to Haber's rule. Table 2-6.8 gives more detailed data for the effects in humans and animals of the best known fire irritants, hydrogen chloride and acrolein. One point to note from Table 2-6.1 is that irritants vary enormously in their potency, over five orders of magnitude. The most important irritants are probably the ones near the top of the list, including isocyanates (from polyurethanes), the unsaturated aledehydes acrolein and crotonaldehyde, and the first of the saturated aldehyde series—formaldehyde (which is produced by nearly all materials when decomposed). Irritants with a moderate potency, such as phenol and the halogen acid gases HCl, HF, HBr may be important in some fires if they are present in high concentrations, while it is difficult to conceive of any product with an RD_{50} of more than 1000 ppm, such as acetaldehyde, methanol, or any hydrocarbon, being of significance as a smoke irritant.

A difficulty in predicting the irritancy potential of fire atmospheres is that it is not known exactly how the various irritant components of an atmosphere interact, although there are indications that some degree of additive effect occurs. However, a more serious problem is that where comparisons have been made between the mouse RD_{50} of combustion atmospheres and their chemical composition as revealed by GC-MS analysis, the atmospheres in most cases turn out to be much more irritant than can be accounted for by a knowledge of their components. It is possible that small amounts of short-lived reactive chemical species with a very high irritant potency ($RD_{50} < 1$ ppm) are responsible, and more work is needed in this area.[105]

Prediction of Incapacitation Due to Sensory and Lung Irritation

In previous sections a model for the prediction of asphyxia in fires has been presented. This model is realistic because it is based on the following facts:

1. Asphyxiation in fires gives two well-defined endpoints, loss of consciousness and death, both of which are likely to occur during the fire exposure.
2. Time and dose to these endpoints can be predicted from established data.
3. Asphyxiation in fires can be shown to depend upon a few known products.
4. The effects of each product are well known, and so to some extent are their interactions, so that predictions of asphyxia based on gas profile measurements show a good agreement with observations of animal exposures.

However, it is very difficult to develop a predictive model for irritancy because

1. Sensory irritation does not have a clear endpoint, but lies on a continuum of increasing eye and respiratory tract pain. Although this pain may be considered incapacitating, sensory irritation does not cause obvious incapacitative effects such as loss of consciousness, and it is not lethal, except under extreme conditions.

   Lung inflammation appears to cause relatively minor effects until near lethal levels of exposure are reached, so the main predictable endpoint is death, although this does not usually occur until several hours after exposure.
2. The identity and number of the irritant products important in fires are unknown. There is also a poor correlation between the composition of experimental fire atmospheres in terms of known irritants and their actual irritant effects on animals.
3. The concentration/time/dose effects of irritants and the degree of interaction between different irritants are also unknown.

For these reasons it is currently possible only to develop an approximate mathematical model to predict irritant effects from a knowledge of fire profiles in terms of known irritant products. An alternative is to base a model empirically on the effects on animals of smoke atmospheres produced in small-scale tests (which are described in a later section of this chapter).

To use small-scale test data, it is first necessary to ensure that the test fire model reasonably represents the decomposition conditions in the type of fire of interest (smoldering, early flaming, or post-flashover). The concentration of irritants may then be represented in terms of mass charge or mass loss of the test material per liter of diluent air.

Sensory irritation may then be measured in terms of the mouse RD_{50} test. Although this test relates primarily to upper respiratory tract irritation, the results also show some correlation with eye irritation;[93] sensory irritation may also be assessed directly if required in terms of the severity of eye lesions occurring in the mice (ranging from lacrimation through chromodacryorrhoea to ocular opacity).

Lung edema and inflammation may be measured in terms of the mouse or rat LC_{50} where deaths occur principally after exposure and are accompanied by signs of inflammation such as increased lung weights or histopathological lung lesions.

Attempts may then be made to relate the RD_{50} and LC_{50} to possible effects in humans, but as described there are difficulties with these extrapolations. Fortunately, for most different materials the rodent RD_{50} and LC_{50} levels cover relatively narrow ranges (approximately one order of magnitude) under some given thermal decomposition conditions. For these reasons it is difficult with current knowledge to give guidance on irritancy for hazard modeling. Rough, general tenability limits can be presented, based upon observations of the sensory and lethal lung irritant effects of exposures of rodents and primates (and humans) to combustion product atmospheres from a range of materials decomposed under a range of conditions. It is therefore suggested that irritancy should be treated as follows:

1. Sensory irritation occurs immediately on exposure and is primarily concentration-related, not increasing with exposure duration.
2. All fire atmospheres are likely to be highly irritant, and at low concentrations the irritant effects should be regarded as adding to the obscurational effects of smoke through eye irritation, and possibly causing mild behavioral disruption by effects on the respiratory tract. At higher concentrations the disruptive effects of severe sensory irritation on vision and breathing may seriously limit escape capability, and as a rough approximation nonflaming atmospheres are likely to cause severe sensory irritation at a nominal atmosphere concentration (mass loss) of around 1 mg material/L air. This may occur when the optical density of the smoke is very low (<0.01/m) or even where there is no detectable smoke. It is therefore proposed that an NAC (mass loss) of 1 mg/L should be used as a tenability limit, although this may be modified in the light of RD_{50} or other data on the particular material and fire condition of interest.
3. Lung edema and inflammation are most likely to occur some hours after fire exposure, and severity of these is basically dose-related, approximately following Haber's rule.
4. Dangerous lung edema and inflammation are likely to occur following a 30-min exposure to an NAC (mass loss) of approximately 10 mg material/L, representing a Ct product of approximately 300 mg/L min. This figure may be replaced by LCt_{50} data on the materials involved in individual fires.
5. These exposure limits for sensory and lung irritation are based largely on exposures to nonflaming atmospheres. Flaming atmospheres may be somewhat less of an irritant, depending upon the efficiency of combustion and the severity of the fire.
6. Data for some common fire irritants are shown in Tables 2-6.1 and 2-6.8.

A Model for the Prediction of the Effects of Optically Dense, Irritant Smoke on the Eyes and Respiratory Tract

Although it is difficult to make precise predictions of the effects exposure to irritant smoke has on escape behavior, the degree of incapacitation, and the post-exposure

effects on lungs, it is important to consider these effects in engineering design, and to be able to make some estimates of the likely effects of exposure. Herein is presented a current "best estimate" model for likely effects.

Evaluation of the Effects of Optically Dense, Irritant, Smoke on Visibility

Optically dense smoke affects exit choice and escape decisions, as well as wayfinding ability and the speed of movement of occupants. These effects depend upon the concentration (optical density) of the smoke and its irritancy to the eyes and upper respiratory tract. Fundamental work on this subject was carried out by Professor Jin in Japan. In experiments where people were asked to walk down a smoke-logged corridor, Jin found that for nonirritant smoke, walking speed decreased with smoke density, and that at an optical density of 0.5/m (extinction coefficient 1.15) walking speed decreased from approximately 1.2 m/s (no smoke) to 0.3 m/s (Figure 2-6.22).[101] Under these conditions people behaved as if they were in total darkness, feeling their way along the walls. When people were exposed to irritant smoke, made by heating wood chippings, movement speed was reduced to that in darkness at a much lower optical density (optical density 0.2 OD/m, extinction coefficient 0.5), and the experience was found to be more distressing.

In addition to these effects upon movement speed, there is the problem of deciding whether people will move at all. In a number of studies of fires in buildings, a proportion of people (approximately 30 percent) were found to turn back rather than continue through smoke-logged areas[41,102] (see Section 3, Chapter 12[103]). The average density at which people turned back was at a "visibility" distance of 3 m (0.33 OD/m, extinction coefficient 0.76), and women were more likely to turn back than men. These effects are summarized in Table 2-6.10. A difficulty with this kind of statistic is that in many fires in buildings there is a choice between passing through smoke to an exit or turning back to take refuge in a place of relative safety such as a closed room. In some situations people have moved through very dense smoke when the fire was behind them, while in other cases people have failed to move at all. Behavior may also depend on whether layering permits occupants to crouch down to levels where the smoke density is lower, and if low-level lighting is used to improve visibility. However it is likely that some people will not move through dense smoke.

Based upon considerations such as those described above for the optical density and irritancy of the smoke it is possible to set tenability limits for smoke density appropriate to particular fire scenarios, in relation to the physiological effects on the ability of occupants to see sufficiently well to escape efficiently, and possible psychological effects on their escape behavior. Appropriate limits will depend upon the building and occupant characteristics. For example, for small spaces with short travel distances to exits, it may be possible to set less stringent tenability criteria if occupants are familiar with the building. For large spaces it may be necessary to set more stringent tenability limits, particularly if occupants are likely to be unfamiliar with the building and need to be able to see much further in order to orient themselves to find exits. With regard to the effects of irritancy on the ability to see, it may be necessary to use more stringent smoke density tenability criteria for scenarios where the smoke evolved is likely to be highly irritant to the eyes. Other factors to be taken into consideration would be the complexity of the space, the lighting, and the visibility of the signage. Suggested tenability limits are presented in Table 2-6.10. Jin[86] suggests tenability limits of extinction coefficient 0.15/m (OD/m = 0.06) for subjects familiar with an escape route or 0.5/m (OD/m = 0.2) for subjects unfamiliar with the escape route. Rasbash[160] suggests a 10-m visibility limit (equivalent to OD/m = 0.08), while Babrauskas[56] suggested a tenability limit of extinction co-

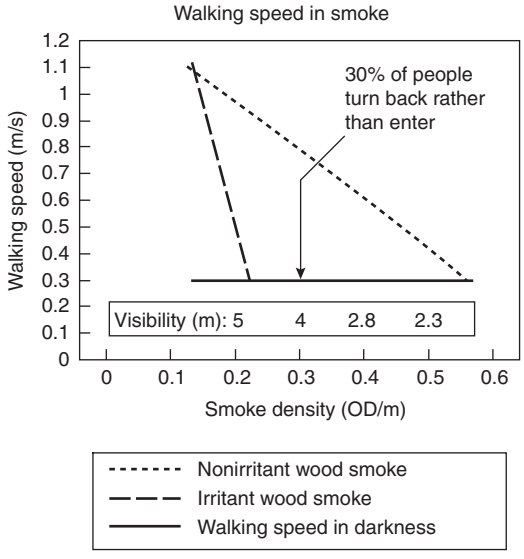

Figure 2-6.22. ***Walking speeds in nonirritant and irritant smoke.[101]***

Note: Visibility distance scale relates to opacity of non-irritant smoke and does not allow for physiological effects of irritants on vision.

Table 2-6.10 ***Reported Effects of Smoke on Visibility and Behavior***

Smoke Density and Irritancy OD/m (extinction coefficient)	Approximate Visibility (diffuse illumination)	Reported Effects
none	Unaffected	Walking speed 1.2 m/s
0.5 (1.15) nonirritant	2 m	Walking speed 0.3 m/s
0.2 (0.5) irritant	reduced	Walking speed 0.3 m/s
0.33 (0.76) mixed	3 m approx.	30% people turn back rather than enter
Suggested tenability limits for buildings with:		
—Small enclosures and travel distances:		OD/m 0.2 (visibility 5 m)
—Large enclosures and travel distances:		OD/m 0.08 (visibility 10 m)

efficient 1.2/m (OD/m = 0.5) in the context of domestic fires. In order to assess the visual obscuration effects of smoke, a concept of fractional effective concentration (FEC) has been developed, whereby the smoke concentration is expressed as a fraction of the concentration considered to significantly affect escape efficiency. If the total FEC_{smoke} reaches unity, then it is predicted that the level of visual obscuration would be sufficient to seriously affect escape attempts.

$$FEC_{smoke} = [OD/m]/0.2 \text{ for small enclosures or } [OD/m]/0.08 \text{ for large enclosures} \quad (23)$$

Setting Tenability Criteria for Sensory/Upper Respiratory Tract and Lung Irritancy

The work by Jin and others does provide some possibility to determine the effects of smoke obscuration on escape speed and efficiency, but a problem remains in determining the likely irritancy of the smoke and the likely severity of the effects of the irritants. It seems from the experience of people exposed in fires that there is a considerable variation in irritant severity between different types of fire effluent. Some fires produce large amounts of sooty smoke that is optically obscuring but relatively nonirritant. Other fires produce smoke that is both optically obscuring and irritant, while in some cases a highly irritant fire atmosphere has been reported when there was little or no visible smoke. From work at BRE Ltd., Fire Research Station (FRS), it has been found that smoke irritants consist of inorganic acid gases (such as hydrogen chloride) and organic compounds, particularly low molecular weight aldehydes (formaldehyde and acrolein). More than twenty irritant substances have been detected in smoke and it is considered that others remain to be identified (see section on irritants). The yields of inorganic acid gases in fires depend mainly on the elemental composition of the materials being burned, while the yields of smoke and organic irritants depends mainly upon the decomposition conditions in the fire. In general, smoldering or vitiated flaming fires (fires burning inefficiently) tend to produce irritant smoke while well-ventilated flaming fires, if burning efficiently, tend to produce nonirritant smokes.

The first effect of exposure to smoke irritants is sensory irritation, which consists of painful stimulation of the eyes, nose, throat, and lungs. Sensory irritation depends on the immediate concentration of irritants to which the subject is exposed, rather than a dose acquired over a period of time, with the effects lying on a continuum from mild eye irritation to severe eye and respiratory tract pain. Most people are familiar with the effects of smoke with a high irritant potency from exposure to bonfire smoke in the garden. The effects can be temporarily incapacitating with severe eye pain, closure of the eyes and tears. If the smoke is inhaled, coughing and breathing difficulties occur. It is easy to imagine how difficult it must be to find one's way through the escape routes in a building under such conditions. One of the best scientific descriptions of the effects of exposure to a sensory irritant is in a paper on the effects of experimental exposures of human volunteers to a substance designed to cause incapacitation due to sensory irritation, CS riot control gas.[24] The effects described consisted of an almost instantaneous severe inflammation of the eyes, accompanied by pain, excessive lacrimation (tearing), and blepharospasm (involuntary closure of the eyes due to spasm of the eyelids). There is irritation and running of the nose with a burning sensation in the nose, mouth, and throat, and a feeling of intense discomfort during which the subjects cough, often violently. If the exposure continues, the discomfort spreads to the chest and there is difficulty in breathing. Many subjects describe a tightness of the chest or chest pain as the worst symptom. The breathing is irregular and the breath is held for short periods. Attempts to avoid the irritation by breath-holding, followed eventually by fairly deep breaths, are reported as being extremely unpleasant. At this stage most individuals are acutely apprehensive and highly motivated to escape from the smoke.

In evaluating this aspect of irritancy in fires, the aim is to predict what concentration of mixed irritant products is likely to cause such pain and difficulty in breathing that escape attempts would be slowed or rendered less efficient, and what concentration is likely to seriously disrupt or prevent escape (a degree of incapacitation approximately equivalent to that at the point of collapse resulting from exposure to asphyxiant). For example, with regard to hydrogen chloride it is considered that concentrations from approximately 100 to 500 ppm would be painfully irritant, producing effects similar to those described for the CS experiments, and that the effects may slow escape but probably would not prevent it. However, at approximately 1000 ppm and above it is suggested that the effects might be so severe as to prevent escape.[104] The effects of exposure to different concentrations of an acid gas irritant (HCl), detailed in Table 2-6.8, are shown in Table 2-6.11. Figure 2-6.23 shows the respiratory depression response of mice to exposure to a sensory irritant atmosphere from PVC decomposed under nonflaming oxidative conditions.

Table 2-6.11 ***Example of the Effects of Exposure to an Acid Gas Irritant—Hydrogen Chloride***

No Odor ppm	
<5	Minor nasal irritation can be detected below 5 ppm (the OEL)
10–50	Perceived as irritant, but work is possible at up to approximately 50 ppm
50–100	Strongly irritant, and some people report exposure to 100 ppm as being excruciatingly painful to the eyes and respiratory tract
309	Mouse RD_{50}
1000–2000	Brief exposure regarded as being dangerous to lethal to humans
3800	Lethal exposure dose to rats for a 30-min exposure, representing an exposure dose of 114,000 ppm·min
15,000	5-min lethal exposure concentration in rats and baboons is around 15,000 ppm

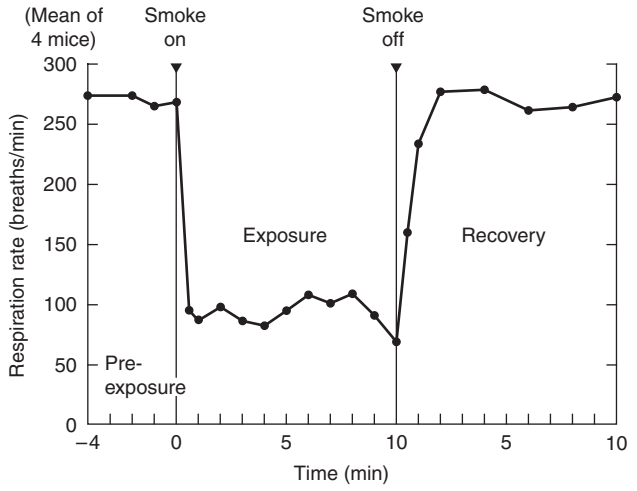

Figure 2-6.23. ***Concentration-effect relationships for sensory irritants: effect of exposure on mouse breathing rate of thermal decomposition products from PVC-J (0.72 g·m^{-3}).[105]***

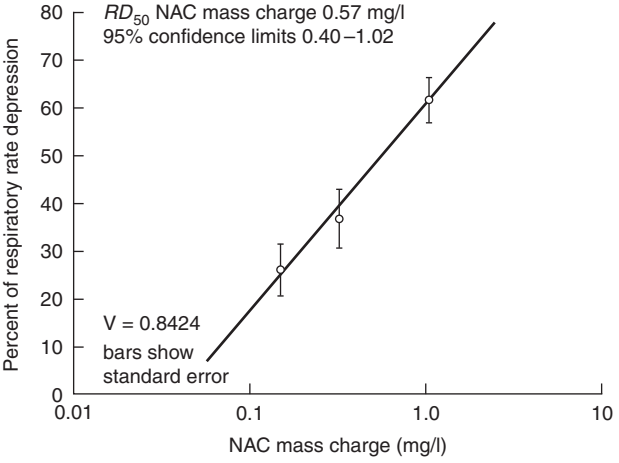

Figure 2-6.24. ***Concentration-effect relationships for sensory irritants percent breathing rate depression in mice is proportional to log concentration.[105] RD_{50} PVC-I 0.57 g·m^{-3}.***

Figure 2-6.24 shows the logarithmic concentration–effect relationship. In the absence of detailed information on irritant mixtures it is assumed that all irritants would be additive in their effects, since they are all capable of causing damage to lung tissue. In large-scale fire tests it is possible to measure inorganic irritants directly, but it is difficult to assess the degree of irritancy from organic products, which form a very important component. In general, the effects of organic irritants depend on the concentration of partially oxidized organic species in the smoke. For example, smokes from smoldering wood or polyolefines decomposed under smoldering or vitiated flaming conditions have a high organic content and are highly irritant, and are characterized by low CO_2/CO ratios and high smoke yields. Under well-ventilated flaming conditions, the organic content of the effluent is low, and irritancy is low. In general, it is predicted that smoke from a mixed fuel source with an optical density/meter of 0.5 would be strongly irritant to the eyes and respiratory tract. However, for a given smoke density, there are differences between different types of fires.

It is difficult to quantify these irritant effects exactly because the database on the effects of individual irritants or irritant mixtures on escape behavior in humans is poor, and, because the effects lie on a continuum of severity, there are no precise endpoints. Assessment has to be based upon a small number of human experimental exposures, usually at relatively low concentrations, accidental exposures, and the results of bioassay studies. For ethical reasons it is never going to be possible to obtain direct data for effects on humans so that estimates of this important parameter must be based on existing data and the judgment of physiologists. Further details of data from human and animal exposure to HCl and other irritants are given in reference[104] and the section on irritants.

Another concern is the range of susceptibility in the human population. Some individuals, particularly those with respiratory diseases, are likely to be more susceptible than others, while others, particularly fit individuals or those used to working in irritant environments, are likely to be more resistant. It is also likely that the subjective irritancy of an exposure is on a log scale of sensitivity for humans, as it is in rodents. Figure 2-6.25 shows a suggested likely distribution of sensitivity for a human population for HCl, in terms of the proportion of the population likely to suffer severe irritancy, to have impaired escape efficiency at different concentrations, and to suffer incapacitation. This is based upon existing human and animal data, and the judgment of the author. While most individuals are considered to be likely to be affected at around 200 ppm, some may be affected by low concentrations of around 100 ppm, but some may be able to tolerate exposure to very high concentrations of over 500 ppm without suffering serious effects on escape capability.

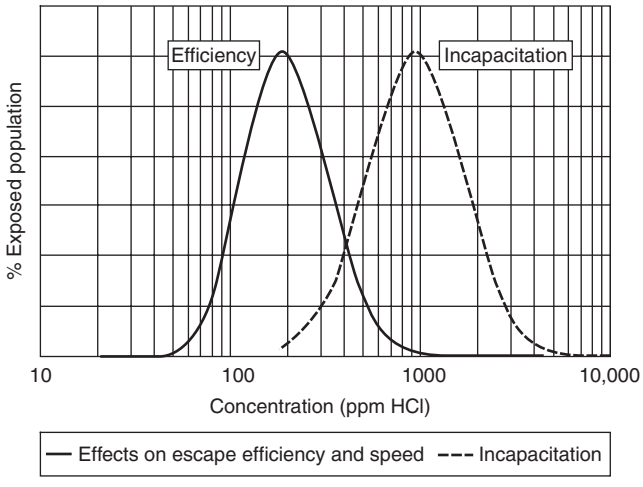

Figure 2-6.25 ***Estimated sensitivity distribution for human population to HCl exposure.[106]***

In order to assess the combined effects of irritants, a concept of fractional irritant concentration (FIC) has been developed, whereby the concentration of each irritant present is expressed as a fraction of the concentration considered to be severely irritant. The FICs for each irritant are then summed to give a total FIC. If the total FIC reaches unity, then it is predicted that the smoke atmosphere would be highly irritant, sufficient to slow escape attempts. If the total exceeds unity by a factor of approximately four or more, then it is likely that escape would be prevented, and possible that collapse might occur due to static hypoxia from bronchoconstriction or laryngeal spasm. On the basis of available data, current estimates of the concentrations of each gas likely to be highly irritant are as shown in Table 2-6.12.

It is predicted that each gas at the above concentrations is likely to be sufficiently irritant to affect escape efficiency in the majority of subjects and may cause incapacitation in susceptible individuals. A factor of 0.3 FEC for escape impairment should allow for safe escape of nearly all exposed individuals.

On the basis of the assumption that all irritants capable of damaging lung tissue are additive in their effects the overall irritant concentration FIC is then given by Equation 24:

$$\begin{aligned} FIC = {} & FIC_{HCl} + FIC_{HBr} + FIC_{HF} + FIC_{SO_2} \\ & + FIC_{NO_2} + FIC_{CH_2CHO} + FIC_{CH_2O} + \sum FIC_x \end{aligned} \quad (24)$$

where $\sum FIC_x$ = FICs for any other irritants present.

Current Concerns Regarding Effects of Sensory Irritants

In the preceding sections, the background data and considerations from which guidance on the effects of irritant have been derived have been presented in some detail. The proposed tenability limits can never be precisely verified since the human experiments needed cannot be performed, but by the same token it is not possible to determine accurate lower safety limits. For this reason the best guidance can only be given by toxicologists familiar with the background human and animal data. The figures presented have been derived in this way, and are very similar to those proposed by an expert panel of toxicologists in an International Standards Committee (ISO/TC992/SC3). Concerns have been expressed from some quarters that the proposed limits are too low for application to practical fire safety engineering and provide too wide a limit of safety. An important point to consider in this context is that the proposed tenability limits are designed to be applied at the breathing zone of a potential building occupant and not at the fire source. In a fire scenario, it is likely that some time will elapse from ignition to the time these tenability limits are breached in the breathing zone of a building occupant some distance from the fire source. With regard to the actual limits used, these have been chosen in the context of escape and survival in an emergency situation, and are considerably in excess of hygiene levels. Even with regard to emergency situations, other expert groups of toxicologists have proposed similar or even lower tenability limits. One set of limits developed for dangerous acute exposures in an industrial context by the American Industrial Hygiene Association is the Emergency Response Planning Guidelines (ERPG). These are expressed in term of three limit levels, two of which are relevant to survival in emergencies such as fires. These are

ERPG-3: maximum levels designed to prevent death

ERPG-2: maximum levels below which nearly all individuals could be exposed for up to one hour without experiencing or developing irreversible or other serious health effects or symptoms that could impair an individual's ability to take protective action

For irritant gases, there are two issues: concentrations at which individuals are likely to experience serious health effects or symptoms likely to impair escape or ability to take protective action, and exposure doses which might cause life threatening health effects. For example, with respect to hydrogen chloride:

ERPG-2 set at 20 ppm on the basis that >20 <100 ppm would be expected to cause serious eye and respiratory tract irritation (which might impair an individual's ability to take protective action). This reflects the immediate effect of exposure concentration.

ERPG-3 set at 100 ppm on the basis that exposure exceeding this level for one hr may be expected to produce severe health effects such as pulmonary edema and possibly death in a heterogeneous human population. This reflects the effect of an exposure dose. The same principle applies to the other irritant gases.

In the context of ability to escape from a fire, the ERPG-2 level would therefore represent the appropriate tenability limit. This is, in fact, an order of magnitude more stringent than the design tenability limit proposed here for fire engineering design. It is considered that although 20 ppm HCl would be sufficiently irritant to adversely affect most people, it is unlikely that concentrations as low as this would seriously inhibit the ability of most people to perform the actions necessary to escape from a fire. On this

Table 2-6.12 ***Irritant Concentrations of Common Fire Gases***

Gas	Concentration Predicted to Impair Escape in Half the Population (ppm)	Concentration Predicted to Cause Incapacitation in Half the Population (ppm)
HCl	200	900
HBr	200	900
HF	200	900
SO_2	24	120
NO_2	70	350
CH_2CHO (acrolein)[a]	4	20
HCHO (formaldehyde)[a]	6	30

[a]Where the concentrations of acrolein and formaldehyde (or other important irritants) are unknown, a term derived from smoke density 0.5 OD/meter may be used as an indication of irritancy likely to impair escape efficiency.

basis, the higher concentration of 200 ppm is proposed as a tenability limit for the average person, although it is likely that a proportion of the population might suffer some degree or impairment at lower concentrations as indicated in Figure 2-6.25. Table 2-6.13 shows the ERPG levels for some sensory irritants commonly occurring in fire atmospheres.[107]

The other important effect of irritants is that a proportion of those inhaled penetrate into the deep lung. If a sufficient dose is inhaled over a period of time, a lung inflammatory response can occur, usually some hours after exposure. The deep-lung effects of irritants may be increased by the presence of smoke particulates. This may cause respiratory failure and death, or permanent lung damage in survivors. The 30-min exposure doses (30-min exposure LC_{50} concentrations multiplied by 30) likely to be lethal for each irritant gas are as shown in Table 2-6.14.

The effects depend upon the exposure dose, which can be quantified approximately in terms of the product of concentration (c) and exposure time (t) to give the ct product exposure dose (ppm·min). During a fire, when the concentrations of the toxic products vary with time, it is possible to predict when an incapacitating or lethal dose has been received by using the FED method. For this method the ct product doses for small periods of time during the fire are expressed as a fraction of the dose causing a toxic effect, and these FEDs are summed until the fraction reaches unity, when the toxic effect is predicted. The fraction of a lethal dose (FLD) for each irritant is calculated as the ct product exposure dose during a period in the fire (for example in ppm·min) expressed as a fraction of the lethal exposure dose. The lethal effects of the different irritants are assumed to be additive on the same basis as the irritant effects, so that the total FLD_{irr} for each time period is given by Equation 22:

$$FLD_{irr} = FLD_{HCl} + FLD_{HBr} + FLD_{HF} + FLD_{SO_2} + FLD_{NO_2} + FLD_{CH_2CHO} + FLD_{HCHO} + \Sigma FLD_x \quad (22)$$

where ΣFLD_x = FLDs for any other irritants present.

The FLD_{irr} for short periods of time during the fire are summed until the FLD_{irr} reaches unity, when it is predicted that a lethal dose has been inhaled.

Table 2-6.13 ***Emergency Response Planning Guidelines for Common Fire Irritants***

Definition	HCN	HCl	HF	Acrolein	Formaldehyde
ERPG-3 (ppm) The maximum airborne concentration below which is believed that nearly all individuals could be exposed for up to 1 hr without experiencing or developing life threatening health effects	25	100	50	3	25
ERPG-2 (ppm) The maximum airborne concentration below which is believed that nearly all individuals could be exposed for up to 1 hr without experiencing or developing irreversible or other serious health effects or symptoms that could impair an individual's ability to take protective action	10	20	20	0.5	10
ERPG-1 (ppm) The maximum airborne concentration below which is believed that nearly all individuals could be exposed for up to 1 hr without experiencing other than mild, transient adverse health effects or without perceiving a clearly defined objectionable odor	na	3	5	0.1	1

Table 2-6.14 ***Lethal Exposure Doses of Irritants Contributing to Asphyxia and Lung Damage[106]***

Gas	Exposure Doses Predicted to Be Lethal to Half the Population (ppm·min)
HCl	114,000
HBr	114,000
HF	87,000
SO_2	12,000
NO_2	1,900
CH_2CHO (acrolein)[a]	4,500
HCHO (formaldehyde)[a]	22,500

[a]where the concentrations of acrolein and formaldehyde (or other important irritants) are unknown, a term derived from smoke density and time of 90 OD/m·min may be used as an indication of lethal organic irritant exposure dose

Chemical Composition and Toxicity of Combustion Product Atmospheres

In the preceding sections the effects of individual asphyxiant gases and irritant chemical products known to occur in fires have been described together with their interactions. In this section the occurrence of these products in large-scale fires and laboratory-scale thermal decomposition experiments and the extent to which the toxicity can be interpreted in terms of these common products will be examined. In the next section the application of these data to fire scenarios and the interpretation of fire victim statistics will be examined.

From the point of view both of product composition and toxic hazard, it is possible to distinguish four basic types of fire situations.

1. Nonflaming thermal decomposition/smoldering fires
2. Early/developing flaming fires
3. Small oxygen vitiated flaming fires
4. Fully developed or post-flashover fires

The work of Woolley and his colleagues at the U.K. Fire Research Station[17] has shown that at midrange temperatures (400 to 700°C) such as those found in smoldering fires or in the vicinity of early flaming fires, materials are decomposed into pyrolysis products and oxidation fragments containing a mixture of asphyxiant and irritant gases and particulates. Under these conditions the highest yields of a variety of potentially toxic products are formed (Tables 2-6.9 and 2-6.15), and since incomplete oxidation is favored, CO yields are high with CO_2:CO ratios approaching unity. For many materials the product mix remains fairly constant over this temperature range, although the yields may increase somewhat with temperature.

Once flaming occurs, the high-temperature well-oxygenated flames of early flaming fires consume most of these combustion products to form simple, mostly innocuous products such as carbon dioxide and water. The CO_2 to CO ratios are very high initially, even up to the 500 to 1000 range. Since CO is only approximately 10 to 50 times as toxic as CO_2, it is conceivable that in this type of fire CO_2 could present more of a toxic hazard than CO. However, as the CO_2 concentration in the fire compartment approaches 5 percent and the O_2 concentration decreases towards 15 percent, the combustion becomes less efficient and the CO_2 to CO ratios decrease to the region of 50 to 100, CO becoming a more important toxic factor. Nevertheless, as Figure 2-6.15 shows, the atmosphere obtained in a rapidly growing fire can contain asphyxiant concentrations of CO_2 (>5 percent), CO (>1000 ppm) and low oxygen (<15 percent O_2). With such flaming fires, the yields of irritant, oxidized fragments and of CO are generally lower than under nonflaming conditions. However, due to the rapid growth and development of such fires the rate of production of these toxic products is often very high. Another factor that has been found to influence the yield and rate of production of toxic products (at least in small-scale experiments)[37,106,108] is the efficiency of combustion. When materials burn with efficient, nonsmoky flames, most CO, HCN, and organic irritants are consumed so the resultant atmosphere is relatively nontoxic. However immediately after ignition, and during intermittent flaming of some materials when combustion is inefficient and smoke production tends to be high, it has been found that high yields of CO, HCN, and irritants are produced, giving highly toxic atmospheres.

Under the severe conditions found in high temperature postflashover fires (exceeding 800°C) where oxygen concentrations are low, there is a major qualitative change in decomposition in that the main pyrolysis products break down into low molecular weight fragments and can contain high concentrations of asphyxiant substances such as CO and HCN, with low CO_2 to CO ratios. (See Table 2-6.15.)

Chemical product formation and the resultant toxicity can vary in different types and stages of fires,[16] as shown in a series of experiments. In the experiments, a number of materials were decomposed under a range of temperatures and oxygen supplies designed to simulate some of the conditions described previously. In one series of experiments, a study was made of the effects of temperature on the pyrolysis of three materials—polyacrylonitrile, flexible polyurethane foam, and wood. These were decomposed at 300, 600, and 900°C to cover as far as possible the full temperature range known to occur in fires, simulating conditions where oxygen supply might be limited. Another set of experiments were then carried out on a further range of polymers to examine the effects of nonflaming and flaming oxidative decomposition on toxicity over midrange temperatures (440 to 700°C). These conditions were chosen to embrace the conditions known to give the greatest complexity of products, particularly with polymers that are known to be sensitive to oxidation in product formation. In this series the test materials were rigid polyurethane foam, polypropylene, polystyrene,

Table 2-6.15 ***Classification of Toxic Hazards in Fires as Revealed by Large-Scale Fire Simulation Tests***

Fire	Rate of Growth	CO_2/CO	Toxic Hazard	Time to Incapacitation	Escape Time Available
1. Smoldering/nonflaming: victim in room of origin or remote	Slow	≃1	CO 0 to 1500-ppm low O_2 15 to 21% irritants, smoke	Hours	Ample if alerted
2. Flaming: victim in room of origin	Rapid	1000 decreasing toward 50	CO 0 to 1% CO_2 0 to 10% low O_2 10 to 21% irritants, heat, smoke	A few minutes	A few minutes
3. Small vitiated flaming: victim in room of origin or remote	Rapid, then slow	<10	CO 0.2 to 4% CO_2 1 to 10% O_2 < 12% irritants, heat, smoke	A few minutes	A few minutes
4. Fully developed: (Post-flashover) victim remote	Rapid	<10	CO 0 to 3%[a] HCN 0 to 500 ppm some irritants, smoke, and possibly heat	<1 min near fire, elsewhere depends on degree of smoke dilution	Escape may be impossible, or time very restricted. More time at remote locations

[a]Concentrations depend on position relative to fire compartment.

and nylon. In all cases, the sublethal toxic effects of exposure were evaluated using primates.

With the series of pyrolysis experiments, it was found that up to midrange temperatures a rich product mix occurred, while at 900°C clear atmospheres containing high yields of simple, low molecular weight products occurred. Thus for wood, which contains oxygen in its structure, the principal products at lower temperatures were oxidized organics, which caused upper respiratory tract and lung irritancy. There was a relatively low CO yield with wood, causing signs of asphyxia at sufficiently high wood nominal atmosphere concentrations. Polyacrylonitrile produced relatively low yields of HCN and other nitriles, causing signs of cyanide intoxication.[16] With the flexible polyurethane foam, the lower-temperature atmospheres consisted principally of a dense yellow isocyanate smoke which was a powerful lung irritant capable of causing severe pulmonary inflammation after exposure.[16,80,109,110] Low yields of CO and HCN resulted with this foam.

At 900°C, the isocyanate smoke from flexible polyurethane foam was destroyed, giving a clear atmosphere consisting mainly of HCN and CO, the main signs being of cyanide poisoning. Polyacrylonitrile also produced high yields of HCN, causing cyanide intoxication, and wood produced clear atmospheres consisting principally of CO.

An example of the effects of oxidation on product formation and toxicity is given by the effects of polypropylene decomposition products. Under pyrolytic conditions, polypropylene decomposed to give a nontoxic atmosphere consisting of hydrocarbon fragments. (See Table 2-6.9.) Under nonflaming oxidative conditions, some of these fragments are oxidized to form a highly irritant atmosphere that caused upper respiratory tract and lung irritation during exposure and severe pulmonary inflammation after exposure.[16,80] There were also minor signs of CO-induced asphyxia. Under flaming conditions the pyrolysis and oxidation products were partially destroyed, with the most important products being carbon monoxide, carbon dioxide, water, and some irritants. The principal toxic effect of this atmosphere was CO intoxication with some signs of irritancy. With flaming atmospheres, however, the nature and degree of toxicity depends upon the efficiency of combustion. By varying the decomposition conditions it is possible to substantially alter the toxicity.

From the animal exposures to these thermal decomposition and combustion product atmospheres, the major findings were that despite the great complexity in chemical composition of the test atmospheres, the basic toxic effects were relatively simple. For each individual atmosphere, the toxicity was always dominated either by a asphyxiant gas (CO or HCN) or by irritants. The toxicity of each atmosphere was therefore basically that of the major component that was present at its most toxic concentration. For asphyxia, the effects of individual atmospheres were virtually identical to those of either CO or HCN as individual gases at the same concentrations as they were present in the smoke atmosphere.

There were some minor exceptions. For those atmospheres containing HCN, the asphyxia appeared to be marginally less than that for an equivalent HCN/air atmosphere. However, the asphyxiant effects of atmospheres containing CO were identical to those of equivalent CO/air mixtures. The presence of low concentrations of hydrocarbons (which are potentially asphyxiant at high concentrations) and of CO_2 in the 1000 to 7000 ppm range did not contribute to the asphyxia. The effects of irritant products on respiratory patterns for primates did not affect the pattern of CO or HCN asphyxia. There may have been a marginal additive effect of CO on HCN toxicity, but in these cases the pattern of asphyxia and times to incapacitation were very similar to those produced by equivalent HCN/air mixtures. Irritant effects did, of course, occur in these exposures in conjunction with asphyxia, but there was no interaction between them, in that irritancy did not affect the progress of asphyxia, and asphyxiant gases did not affect the response to irritants.

Implications for Human Asphyxiation Models for Fire Exposures

As a result of this work, it can be stated with some confidence that the asphyxiant effects of fire atmospheres should be predictable on the basis of the common asphyxiant gases CO, HCN, low O_2, and CO_2, and that the models derived from the work on individual gases should be valid. It is not possible with current knowledge to predict exactly the potential of a fire atmosphere to cause sensory irritation or lung inflammation from a chemical analysis of the product composition, but the model presented is considered a reasonable best estimate.

Smoke

Smoke comprises the total effluents from a fire and consists of two parts: the invisible vapor phase and the visible particulate phase. From a toxicological standpoint, all of the asphyxiant fire products occur in the vapor phase, while irritant products may occur in both phases. The particulate phase consists of solid and liquid particles covering a wide range of particle sizes, depending upon the nature and age of the smoke. These particles may contain condensed liquid or solid irritant products; or irritant products including gaseous ones may be dissolved in liquid particles (as in acid mists), or be absorbed onto the surface of solid, carbonaceous particles. Particle size is of great toxicological importance since it determines how "deeply" particles penetrate into the respiratory tract and the patterns of subsequent deposition. Particles with a mean aerodynamic diameter of less than 5 μm are capable of penetrating deep into the lung, while larger particles tend to deposit in the nasal passages and upper airways. Generally speaking, the smoke from smoldering or nonflaming decomposition tends to consist mainly of small particles (less than 1 μm mean aerodynamic diameter, as in cigarette smoke) which are highly respirable. Smoke from flaming fires contains larger particles, particularly as it ages and the particles agglomerate; however, reports on fire victims usually record smoke penetration well into

the lung.[49] At very high concentrations, smoke deposits may physically clog the airways. This could occur even with biologically inert particles at concentrations in excess of 5 mg/L, and is more probable with irritant smoke particles that are likely to acutely inflame tissues. Apart from the toxic effects of these particles on the lung, they may also be important in increasing the thermal capacity of the smoke and increasing the likelihood of lung burns (see next section of this chapter).

The Exposure of Fire Victims to Heat

There are three basic ways in which exposure of fire victims to heat may lead to incapacitation and death: by (1) heat stroke, (2) body surface burns, and (3) respiratory tract burns.

Heat Stroke (Hyperthermia)

If a subject is exposed to a hot environment, especially if the humidity is high and the subject is active, there is a danger of incapacitation and death due to hyperthermia. The time to effect and the type of hyperthermia depend principally upon the heat flux to which the subject is exposed, and are greatly affected by factors such as the amount and type of clothing and degree of work performed. A detailed analysis of the parameters that determine heat transfer to subjects over a range of environmental conditions and levels of activity, and the protective effects of different types of clothing, is given by Berenson and Robertson,[111] and Simms and Hinkley.[112]

Simple hyperthermia involves prolonged exposure (approximately 15 minutes or more) to heated environments at ambient temperatures too low to cause burns. Under such conditions, where the air temperature is less than approximately 120°C for dry air or 80°C for saturated air, the main effect is a gradual increase in the body core temperature.[113] Increases above the normal core temperature of 37°C up to approximately 39°C are within the physiological range and can occur at normal ambient temperatures during hard exercise, but once 40°C is reached consciousness becomes blurred and the subject becomes seriously ill. Further increase causes irreversible damage, with temperatures above 42.5°C being fatal unless treated within minutes.[111,114] The time taken to reach such a state depends upon a number of variables including those mentioned. Figure 2-6.26, adapted from Blockley,[80] shows approximate tolerance times for unclothed subjects at rest, under conditions of low air movement (30 m/min). At temperatures below 120°C tolerance is limited by hyperthermia, whereas above this temperature pain followed by burns become important. The data points A to D (for clothed subjects) were taken from various authors, and are added for comparison. At temperatures below 120°C evaporative cooling from sweat is important, so that humidity has a considerable influence on tolerance time. Clothing, therefore, offers some immediate protection at temperatures above 120°C, but at lower temperatures may reduce tolerance time by impeding heat loss due to evaporative cooling. Details of the data points and authorship are given in Table 2-6.16.

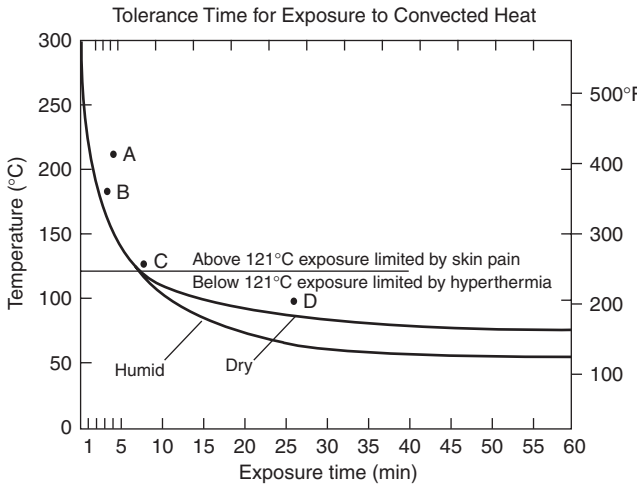

Figure 2-6.26. ***Thermal tolerance for humans at rest, naked skin exposed, with low air movement (less than 30 m/min). Adapted from Blockley.[113] See text and Table 2-6.16 for discussion of data points A to D.[112,115,116]***

Experiments conducted with pigs by Moritz et al.[118] confirm the basic signs of hyperthermia, with death occurring principally due to circulatory collapse associated with severe cardiac irregularities (ventricular tachycardia).

A second situation described by Moritz et al.[118] involves exposure to high temperatures for short periods (less than 15 minutes), and here hyperthermia is accompanied by cutaneous burns (in pigs at temperatures above 120°C). When deaths occurred soon after exposure to severe heat (within 30 minutes) the cause was considered to be due not to burns but to a rise in blood temperature. In

Table 2-6.16 ***Reported Tolerance Times for Exposures to Hot Air***

	Temperature (°C)	Time (min)		Reference	Letter in Figure 2.6.26
Dry air					
	110	25		112	D
	180	3		112	B
	205	4	Bare headed, protected	115	A
	126	7		116	C
Humid air	32 at 100% RH	32	Men working	117	

this situation the exposure duration was insufficient to raise the body core temperature greatly, but if the temperature of the blood in the heart reached 42.5°C, the animal died within a few minutes from circulatory collapse.

It therefore seems that a victim exposed for more than a few minutes to high temperatures and heat fluxes (exceeding 120°C) in a fire is likely to suffer burns and die either during or immediately after exposure, due principally to hyperthermia. Victims surviving the hyperthermia phase may die later due to burns of the upper respiratory tract, particularly the larynx, or due to the secondary effects of skin burns. A victim or fire fighter exposed to temperatures unlikely to cause burns (less than 120°C) may also suffer heat stroke after a prolonged exposure (exceeding 15 min), especially if the humidity is high and the person is working hard.

Skin Burns

According to Buettner,[119] pain from the application of heat to the skin occurs when the skin temperature at a depth of 0.1 mm reaches 44.8°C, which agrees with the finding of Lawrence and Bull[120] that discomfort was experienced when the interface between a hot handle and the skin of the hand reached 43°C. The sensation of pain is followed soon afterward by burns, causing incapacitation, severe injury, or death depending upon their severity. The time from the application of heat to the sensation of pain, and from pain to the occurrence of burns of various degrees of severity, depends upon the temperature, or more properly, the heat flux to which the skin is exposed. The effects of heating the skin are essentially the same whether the heat is supplied by conduction from a hot body, convection from air contact, or by direct radiation.[119,121] Curves for the relationship between time and effect have been published for conducted heat from a "hot handle"[121] and radiant heat. The relationship between time and effect is exponential. (See Figure 2-6.27.) Thus for conduction from heated metal at 60°C, pain occurs after 1 s and a burn after 10 s, while at 80°C pain occurs at 100 ms and a burn after 1 s contact.

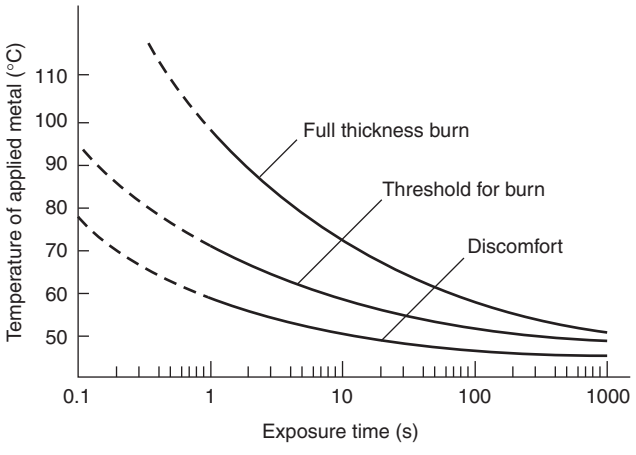

Figure 2-6.27. ***The relation between time and the temperature of metal to cause thermal injury to skin (values below 1 s are extrapolated).[121]***

Pain therefore occurs when the difference between the rate of supply of heat to the skin surface exceeds the rate at which heat is conducted away by an amount sufficient to raise the skin temperature to 44.8°C. The thermal inertia of human skin is similar to that of water[119] or wood[121] with a value of $k\rho c$ for the surface (depth 0.1 mm) of 1.05 W/m·K. For the skin surface the rate of heat removal is not considered to be affected by blood supply[119] except for the fingertips, where blood flow may be sufficient to remove a significant amount of heat.[119] However, blood supply may have some effect on the occurrence of burns, especially to the deeper layers of the skin.[121] Obviously, rates of heating and the occurrence of pain and burns are greatly affected by the extent and type of clothing,[112,118,122] but only effects on naked skin are considered here. The temperature increase of the skin for the situation in which constant radiant heat is absorbed by the upper surface of the skin, or heat from a hot air current is applied to the skin, may be calculated as follows:[119]

$$T - T_0 = \frac{2Q\sqrt{t}}{\sqrt{\pi k\rho c}} \tag{25}$$

where

T = final temperature of skin at 0.1 mm depth
T_0 = starting temperature of skin at 0.1 mm depth
Q = heat supply (W/m²)
$k\rho c$ = 1.05 W/m·k
t = time (s)

Conducted heat: The effect of conducted heat is related to the temperature of the hot object and its thermal inertia, depending upon the interface temperature between the object and the body tissue at the skin surface,[121,122] as illustrated by the examples in Table 2-6.17.

A skin temperature of 43°C causes pain and some cellular damage, while a temperature of 60°C coagulates tissue protein. A brass block heated to 60°C will produce a partial thickness skin burn within 10 s, pain within 1 s and a full thickness burn after approximately 100 s.[121] The time/temperature relationships for these effects of conducted heat are shown in Figure 2-6.27.

Convected heat: For a victim attempting to escape from a fire, the most important sources of heat exposure are ra-

Table 2-6.17 ***Theoretical Contact Temperatures between Skin at 35°C and a Selection of Hot Bodies at 100°C[121]***

Material of Hot Body	Contact Temperature (°C)
Mild steel	98
Glass	82
Wood	65
Cork	46

diation from hot areas and convection from hot gases. Pain and the likelihood of skin burns occur at air temperatures above approximately 120°C. The rate of heat transfer from hot air to the skin depends upon the rate of ventilation, humidity, and the protective value of clothing as well as air temperature. The effects of these parameters are described by Berenson and Robertson,[111] and Simms and Hinkley.[112] However, for unprotected areas such as the head, data on naked skin are relevant, and the data shown in Figure 2-6.26 for temperatures above 120°C provide limits for tolerance to the painful effects of contact with hot air.

Apart from the problem of hyperthermia, dry air has been tolerated by humans as shown in Table 2-6.16. Moritz et al.[118] state that dry air at 300°C injured unprotected skin within 30 s in pigs and dogs. Pigs also suffered burns at 150°C after 100 s and after 400 s at 100°C. However, it was considered that humans would be more resistant to burns, especially at temperatures below 120°C, due to the protective effect of sweating. Air with a high level of humidity not only reduces or prevents heat loss through sweat, but also delivers more heat to the skin. Thus Moritz et al.[123] found that steam at 100°C destroyed the epidermis of dogs within a few seconds.

Figure 2-6.26 shows curves for tolerance time of convected heat for both dry and humid air. A search for the original data used to produce these curves has not been successful, but upon careful consideration it seems likely that the humid curve must represent air that was humid (perhaps saturated) at *room* temperature, which was then heated subsequently, and was therefore nowhere near saturated with water vapor at higher temperatures. This must be the case because the capacity of air for water vapor increases dramatically at temperatures above 60°C, so that the amount of deliverable latent heat also increases. In practice, 60°C has been found to be the highest temperature at which 100 percent water-vapor saturated air can be breathed. Since all fires produce a considerable amount of water from combustion, it is possible that the presence of water vapor may be an important neglected hazard in fires.

Radiant heat: For radiant heat, clothing also greatly influences tolerance times, but again, data on naked skin are relevant to exposure of unprotected areas such as the head. Figure 2-6.28,[111] shows the relationship between time to skin pain and radiant heat flux. Data points A to E, taken from a number of authors (detailed in Table 2-6.18) have been added for comparison. Points B through E agree with the curve presented by Berenson, but data from one source (Perkins et al.)[124] (points labeled A) deviate somewhat from the rest. From Perkins's data (which were produced by experiments where thermal injury was caused by exposing subjects to radiant heat from a searchlight), the heat fluxes for erythema (reddening of the skin said to coincide with pain[121]) appear rather higher than the heat flux limits for pain supplied by the other authors. This is possibly due to differences in the wavelength, and thus degree of penetration, of the radiation.[119] The searchlight data do, however, show the relationship between time to erythema, time to partial skin burn, and time to full thickness skin burn. The shape of the radiant heat tolerance curve suggests a fairly obvious tolerance limit for exposure to radiant heat of 0.25 W/cm² (2.5 kW/m²) which is that suggested by Babrauskas.[56]

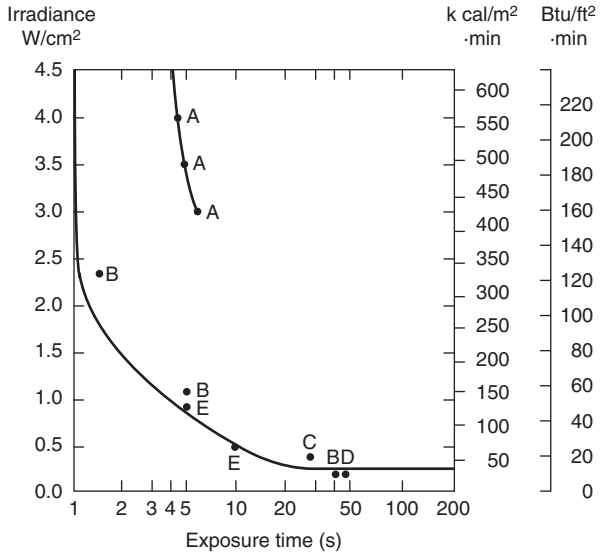

Figure 2-6.28. ***Time to severe skin pain from radiant heat. Adapted from Berenson and Robertson.[111] See text and Table 2-6.18 for discussion of data points A to E.[56,112,115,118,124,125]***

Table 2-6.18 ***Data on the Effects of Exposure to Radiant Heat***

Reference Source	Heat Flux W/cm²	Time to Effect(s) Erythema (or pain)	Burn	Full Burn	Letter in Figure 2-6.28
Perkins et al.[124]	15	1	2.5	4	
	10	2	4	6	
	5	4	7	>15	
	4	4.5	9	>15	A
	3.5	5	9.5	>15	A
	3	6	10	>15	A
Buettner[119]	2.35	1.6			B
	1.05	5			B
	0.25	40			B
Veghte[115]			Blisters		
	0.42		30		C
Simms and Hinkley[112]		Unbearable pain			
	0.126	600			
	0.252	30 to 60			D
Dinman[125]	0.24	Lower limit for pain after a long period			
	0.82	5			E
	0.48	10			E
Berenson and Robertson[111]	0.34	Limit for blood to carry away heat			
Babrauskas[56]	0.25	Tenability limit			

Consequences of body surface burns: Apart from the immediate pain caused by exposure to heat and by skin burns, as well as the accompanying psychological shock and fear, incapacitation may result from body surface burns during or after a fire due to physiological shock. In this situation loss of body fluids into the burn results in circulatory failure and a fall in blood pressure, which may lead to collapse and even loss of consciousness.[14,118] The immediate effect of burns and the later chances of recovery depend upon a number of factors such as the site and extent of the burn, the depth of the burn, the age of the victim, and the treatment received.[121] While victims may continue to function for some time with severe burns, and survivals have occurred with up to 80 percent body surface area burns,[121] in general, if 35 percent or more of the body surface area is burned the chances of survival are low. Young adults generally have the best chance of survival, with a 50 percent chance of surviving a 50 percent body surface area burn, while children and old people are the most vulnerable, with a 50 percent chance of surviving a 20 percent body surface area burn in the elderly.[14,121] The depth of burn is classified on a scale of six degrees. First-, second-, and third-degree burns involve damage to the skin from which it can recover, while fourth-degree burns require skin grafts. Fifth- and sixth-degree burns involve destruction of muscle and/or bones, respectively.[14] Another scheme classifies burns as partial thickness skin burns, which will heal, or full thickness burns, which require grafts.[121]

If the victim survives the initial period of shock, death may occur over a period of up to a few weeks due to secondary effects on the brain, heart, lungs, liver, and kidneys.[14] The most common secondary effect and cause of death involves the lungs,[14,126–128] consisting of pulmonary edema resulting from effects on the circulatory system secondary to shock and metabolic acidosis. Post-exposure treatment to replace body fluids and control acidosis are important in improving the prognosis for survival. If the victim survives the respiratory distress resulting from edema during the first week after exposure, pneumonia may then develop as a further, possibly fatal complication.[14,129–131]

This fatal damage to the lungs may occur following body surface burns when there has been no inhalation of heat or toxic gases. In many fire victims, however, damage to the respiratory tract and lungs results from a combination of all three causes.[14,129–131]

Thermal Damage to the Respiratory Tract

Thermal (as opposed to chemical) burns to the respiratory tract never occur in the absence of burns to the skin of the face.[81,131] Heat damage to the respiratory tract is even more dependent upon the humidity of inhaled hot gases than are skin burns. As a result of the low thermal capacity of dry air and the large surface area of the airways, which are lined with a wet surface and good blood supply, thermal burns are not induced by dry air below the top of the trachea. However, steam at around 100°C is capable of causing severe burns to the entire respiratory tract down to the deep lung, due to its higher thermal capacity and the latent heat released during condensation. These effects of inhaled hot gases are demonstrated by the work of Moritz et al.[118] in which anesthetized dogs and pigs breathed hot air, flame from a burner, or steam, supplied through a cannula to the larynx. Dry air at 350°C and flame from a blast burner at 500°C caused damage to the larynx and trachea, but had no effect on the lung, while steam at 100°C caused burns at all levels. In these experiments the most important site of damage was the larynx, and death resulted from obstructive edema of the laryngopharynx within a few hours of exposure. This work was taken further by Zikria[131] using steam burns in dogs, induced by a 15 s application of steam at 100°C via an endotracheal tube. The animals survived the initial effects and a number of phases of reaction were observed. The first phase consisted of necrosis and edema in the tracheobronchial airway, and early lung parenchymal edema within one hour. This was followed by increasing parenchymal edema, sloughing of the mucosa, and collapse of lung segments. The next phase after 24 hours consisted of bronchopneumonia behind respiratory tract obstructions.

All these features occur in fire victims, but it is difficult to separate the effects of thermal inhalation burns from edema and inflammation due to burns caused by irritant chemical smoke products, or edema secondary to body surface burns, all of which may be involved.[14,129–131] Thus fire victims with facial burns subjected to endoscopy have been found to have burns well into the respiratory tract.[81] If these lesions are caused by heat, it would imply that fire atmospheres resemble steam rather than dry air in terms of their thermal capacity. However, it is possible that such lesions are caused by chemical smoke irritants, which have been shown to produce fatal pulmonary edema and inflammation in the absence of heat.[80] Unfortunately, data on the thermal capacity and latent heat of actual fire atmospheres are not readily available, although it may be possible to calculate probable values from a knowledge of fire atmosphere temperature and composition.

The situation is therefore complicated, but from a fire engineering standpoint a number of basic points may be useful.

1. Thermal burns to the respiratory tract will not occur unless the air temperature and/or humidity are sufficient to cause facial skin burns.
2. Dry air at around 300°C may cause burns at the larynx after a few minutes. This may result in life-threatening obstructive edema of the larynx within an hour if not treated, although damage to the deeper structures of the lung is unlikely. It is possible that such laryngial burns may occur at lower temperatures down to approximately 120°C depending upon the duration of exposure, and breathing dry air at these temperatures would be painful. Laryngial burns followed by obstructive edema are common findings in fire victims, and are important causes of incapacitation and death during and immediately after fires.[14,129–131]
3. Humid air, steam, or smoke with a high thermal capacity or latent heat (due to vapor content or suspended liquid or solid particles) may be dangerous at temperatures of around 100°C, causing burns throughout the respiratory tract. It may be possible to predict the likely effects of hot-smoke atmospheres if thermal capacity or latent heat were measured.

4. In practice, fire victims may be affected by the inhalation of chemically irritant smoke, by hot humid gases, and by the secondary effects on the lung of body surface burns, all of which may combine to cause fatal respiratory tract lesions during the hours, days, or weeks following the fire exposure. However, these effects are probably less likely to be fatal during exposure to the fire atmosphere over periods of less than 30 minutes.
5. Heat flux and temperature tenability limits designed to protect victims from incapacitation by skin burns should be adequate to protect them from burns to the respiratory tract.

Model of the Prediction of Time to Incapacitation by Exposure to Heat in Fires

There are three basic ways in which exposure to heat may lead to incapacitation: through heat stroke (hyperthermia), skin pain and burns, or respiratory tract burns. Thermal burns to the respiratory tract from air containing less than 10% by volume water vapor do not occur in the absence of burns to facial skin. Therefore, tenability limits with regard to skin pain and burns are normally lower than for thermal burns to the respiratory tract. Thermal burns to the respiratory tract may occur upon inhalation or air above only 60°C when saturated with water vapor, as may occur when water is used for fire extinguishment.

The tenability limit for exposure of skin to radiant heat is approximately 2.5 kW/m^2, below which exposure can be tolerated for at least several minutes. Radiant heat at this level and above causes skin pain followed by burns within a few seconds, but lower fluxes can be tolerated for more than 5 min. For situations where occupants are required to pass under a hot smoke layer in order to escape, this radiant flux corresponds approximately to a hot layer temperature of 200°C. Above this threshold, time (minutes) to incapacitation due to radiant heat $t_{I\text{rad}}$, at a radiant flux of q kW/m^2, is given by Equation 26.[132,133]

$$t_{I\text{rad}} = \frac{133}{q^{1.33}} \tag{26}$$

The effects of heat on an occupant response may depend upon the situation. The threshold for pain occurs at approximately 1.333–1.667 (kW·m^{-2})$^{4/3}$ min, second degree burns at 4–12.17 (kW·m^{-2})$^{4/3}$ min and third degree burns at approximately 16.667 (kW·m^{-2})$^{4/3}$ min. Radiant heat tends to be directional in fires, so that the main problem tends to be local heating of particular areas of skin. The air temperature, and hence that of the air breathed and that in contact with other parts of the body, may be relatively low, even when the radiant flux is high. For this reason the main hazard is pain and burns to the skin, rather than hyperthermia. Skin temperature depends upon the relationship between the rate of heat supply to the skin surface and the removal of heat from inner layers by the blood. There is, therefore, a threshold radiant flux below which significant heating of the skin is prevented, but above which rapid heating of the skin occurs.

For exposures of up to two hours to convected heat from air containing less than 10% by volume of water vapor, the time (min) to incapacitation $t_{I\text{conv}}$ at a temperature T (°C) is calculated from Equation 27, which is derived from Figure 2-6.26.

$$t_{I\text{conv}} = 5 \times 10^7\, T^{-3.4} \tag{27}$$

As with toxic gases, the body of a fire victim may be regarded as acquiring a "dose" of heat over a period of time during exposure, with short exposure to a high radiant flux or temperature being more incapacitating than a longer exposure to a lower temperature or flux. The same fractional incapacitating dose model as with the toxic gases may be applied and, providing that the temperature in the fire is stable or increasing, the fractional dose of heat acquired during exposure can be calculated by summing the radiant and convected fractions using Equation 28:

$$\text{FED} = \sum_{t_1}^{t_2} \left(\frac{1}{t_{I\text{rad}}} + \frac{1}{t_{I\text{conv}}} \right) \Delta t \tag{28}$$

Note: $t_{I\text{rad}}$ will tend to zero as q tends to <2.5 kW/m^2

Thermal tolerance data for unprotected skin of humans suggest a limit of about 120°C for convected heat, above which considerable pain is quickly incurred along with the production of burns within a few minutes. Depending upon the length of exposure, convective heat below this temperature may still result in incapacitation due to hyperthermia. Examples of tolerance times to different radiant fluxes and air temperatures are shown in Table 2-6.19. Conducted heat is physiologically important only when skin is in contact with hot surfaces, such as door handles. A 1-s contact with metal at 60°C can cause burns.

Example of a Calculation of Time to Incapacitation for Physical Fire Parameters and Irritancy

In a previous section the single armchair room burn shown in Figure 2-6.15 was used to illustrate how the model for prediction of asphyxiation could be applied to a practical fire scenario. To complete the incapacitation model it is necessary to include calculations for the effects of physical parameters (heat, smoke optical density), and mass loss concentration as an indication of irritancy. The curves for radiant heat, air temperature, smoke extinction

Table 2-6.19 ***Limiting Conditions for Tenability Caused by Heat[106]***

Mode of Heat Transfer	Intensity	Tolerance Time
Radiation	<2.5 kW·m^{-2}	>5 min
	2.5 kW·m^{-2}	30 s
	10 kW·m^{-2}	4 s
Convection	<60°C 100% saturated	>30 min
	100°C <10% H_2O[a]	12 min
	120°C <10% H_2O	7 min
	140°C <10% H_2O	4 min
	160°C <10% H_2O	2 min
	180°C <10% H_2O	1 min

[a] v/v

coefficient, and mass loss during the first ten minutes of the armchair burn are shown in Figure 2-6.29.

Of the physical factors likely to affect a victim during the fire exposure, the majority are basically concentration or intensity-related rather than dose-related, and for these factors tenability limits have been set (radiant heat, smoke optical density, and sensory irritancy). The other two factors, convected heat and lung irritancy, are primarily dose-related, but lung irritant effects are likely to be relatively minor until after exposure. This leaves the fractional incapacitating dose of convected heat to be calculated. The average temperatures per minute during the first minutes of the fire are shown as histograms in Figure 2-6.29 with Table 2-6.20 showing the fractional incapacitating dose calculation.

Convected heat: The effects of exposure to convected heat increase dramatically in this type of fire as shown in Figure 2-6.29. Incapacitation, mainly due to skin pain and burns, is predicted sometime during the fourth minute, when the air temperature is 220°C. The situation then rapidly worsens, and it would seem likely that severe and probably fatal burns or fatal hyperthermia would be sustained by any victim remaining in the fire during the fifth minute. Even if the victims were protected to some extent by clothing, they would sustain burns to the face and probably fatal burns to the larynx. The occurrence of lung burns would depend on the thermal capacity (principally the latent heat) of the smoke.

Radiant heat: From Figure 2-6.29, it would seem that the effects of radiant heat would be relatively minor in this fire compared to the effects of convected heat. The radiant heat peaks at just above 3kW/m^2 during the sixth minute, and therefore just exceeds the tenability limit. Nevertheless, the radiation alone would probably be sufficient to cause some burns and seriously inhibit escape during the sixth minute, and there would almost certainly be some degree of additive effect with convected heat.

Smoke: From the point of view of its obscurational effects, incapacitation by smoke is concentration-related rather than dose-related. For this series of chair burns, Babrauskas sets a tenability limit of extinction coefficient 1.2/m (OD/m 0.52).[56] This would give approximately 2 m visibility, which should be adequate for escaping from a room, and could be used as a tenability limit for input into the model. Incapacitation due to visual obscuration would occur at the end of the second minute. The smoke curve is rising very steeply at this point, with an OD/m of 1 at the beginning of the third minute. Escape would therefore become extremely difficult, and certainly slow during the third minute, unless the victim was fa-

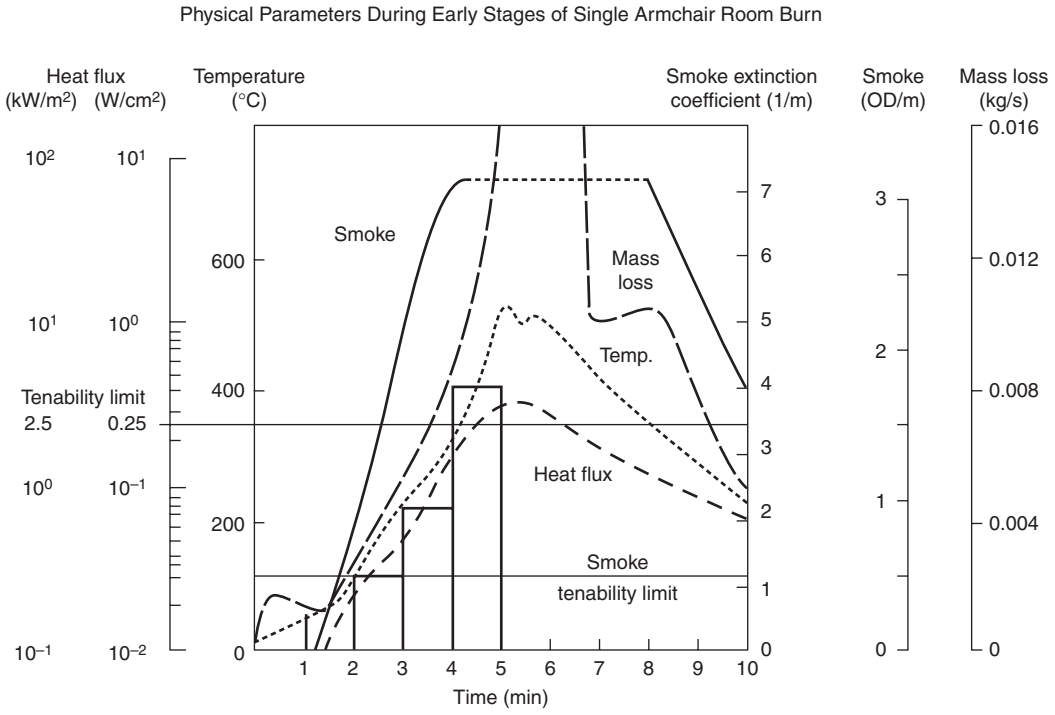

Figure 2-6.29. ***Profiles for heat (radiant flux and temperature), smoke and mass loss rate during the first 10 min of a single armchair (polystyrene, with polyurethane cushions and covers) room burn.[56] (Expanded detail from Figure 2-6.15.) Histogram shows average temperature each minute during the first five minutes.***

Table 2-6.20 ***Calculation of Fractional Incapacitating Accumulation of Convected Heat for the Single Armchair Room Burn Data Shown in Figure 2-6.29. (Calculated According to Equation 34.)***

Time (min)	1	2	3	4	5	6
Average temp. (°C)	20	65	125	220	405	510
F_{lh}	0	0.033	0.170	2.273	355	6236
Cumulative F_{lh}			0.203	2.476		

Incapacitation occurs when $F_{lh} = 1$, and is therefore predicted during the fourth minute of exposure.

miliar with the surroundings and able to find the exit in the dark.

Irritancy: As stated in the section of this chapter on irritancy, there are two factors to consider: the immediate incapacitation due to the painful effects of sensory irritation of the eyes and respiratory tract, adding to the obscurational effects of smoke and disrupting escape behavior, and the later inflammatory effects on the lung which may cause death after exposure.

The first consideration is whether the victim would be able to escape from the fire. In this context, sensory irritation is the most important. This is concentration-related; to predict the irritancy of the smoke, it is necessary to know the RD_{50} concentration of the atmosphere produced by the materials involved under the particular decomposition conditions existing in the fire. Most importantly, it is necessary to know the concentration/time profile of the fire products in terms of mass loss per liter of air (NAC mass loss). Although the mass loss curve for the armchair is shown in Figure 2-6.29, there are no data on the volume of air into which this mass was dispersed during the fire; so for the purposes of this example it will be necessary to make an estimate of possible mass loss concentration. Also, since the RD_{50} of the polyurethane and polystyrene components of the chair under flaming conditions are unknown, it will be necessary to use estimated values.

In the discussion of irritancy, a general tenability limit for severe sensory irritation was set at a concentration of 1 mg/L NAC mass loss, and an incapacitating dose for serious postexposure lung inflammation was set at 10 mg/L NAC mass loss for 30 minutes (a Ct product of 300 mg·min/L). From the general conditions, the smoke curve, and the CO concentration curve, it is estimated that the tenability limit for sensory irritancy would be exceeded during the third minute, greatly adding to the deleterious effects of smoke on vision and escape behavior.

With regard to lung irritation, it is estimated that the average mass loss concentration over the first five minutes of the fire would be approximately 10 mg/L. If so, this would represent a fractional incapacitating dose of 50 mg·min/L, which would probably be insufficient to cause significant lung damage after exposure, compared to the more serious effects of heat exposure. However, if the average mass loss concentration over the first five minutes should reach 60 mg/L, serious effects on the lung would likely occur after and probably during exposure.

Interactions: In terms of physiological effects, it is likely that there would be some degree of interaction between asphyxia and several of these physical factors, but it is likely that most would be relatively minor during the fire, except for some possible enhancement of pulmonary irritation due to the hyperventilatory effect of CO_2 during the fourth to sixth minute of the fire. A reasonable model can be used in which asphyxia, sensory irritancy, and the effects of heat and visual obscuration can be treated separately. Interactions may be more important at the behavioral level. The interaction between sensory irritation and visual obscuration has been mentioned and there is some experimental evidence for such an interaction in humans.[86] After exposure, as mentioned in the section on heat, the effects of skin burns, respiratory tract burns, and chemical irritation (and even possibly CO asphyxia) all combine to increase the probability of fatal pulmonary edema and inflammation.

Summary: From the analyses performed, the effects on a victim exposed to the conditions in the armchair room burn (Figure 2-6.15) are predicted as follows:

1. Toward the end of the second minute and beginning of the third minute, the smoke optical density and mass loss/liter would sufficiently exceed the tenability limits for visual obscuration and sensory irritancy to severely inhibit escape from the room.
2. During the fourth minute, the average temperature was 220°C, and sufficient heat would be accumulated in the skin surface to cause skin burns resulting in incapacitation.
3. During the fifth minute, a victim is likely to lose consciousness due to the combined effects of the accumulated doses of asphyxiant gases.
4. It is predicted that a victim escaping or rescued after the fourth minute would suffer severe postexposure effects due to skin burns, plus pulmonary edema and inflammation which might well be fatal (due to the combined effects of inhaled hot gases, chemical irritants, and the pulmonary secondary effects of skin burns). After the sixth minute, it is likely that a rescued victim would die at some time between a few minutes and one hour due to the effects of asphyxia and circulatory shock.

It is unlikely that an otherwise healthy adult would be able to escape from a fire such as this if he or she remained longer that three minutes after ignition. However, three minutes is a long time in which to leave a room, so that providing the victim is awake and aware of the fire, is not otherwise incapacitated, and does not stay after two minutes in an attempt to fight the fire or rescue belongings, it is likely that he or she would be able to escape without serious injury. In the next section, data on real fire victims is examined in an attempt to relate fire conditions to actual injury and death statistics.

Worked Example of a Simplified Life Threat Hazard Analysis

In the previous sections, the various elements of a physiological FED model for predicting time to incapacitation of occupants during full-scale fires have been developed. The following section consists of a worked example including tenability calculations for all toxic and physical hazards: time-to-escape efficiency impairment from the effects of optical obscuration by smoke, time-to-escape efficiency impairment from sensory irritation, time to incapacitation by asphyxiant gases, time to incapacitation due to skin pain and burns from radiant and convected heat, and time to inhale a lethal exposure dose of lung irritants. Table 2-6.21 shows the input data and calculation results for the life threat hazard analysis cal-

Table 2-6.21 ***Illustration of Life Threat Analysis for the First Six Minutes of a Furniture Fire Based upon a Single Armchair Room Burn. (The armchair is polystyrene with polyurethane cushions and covers. The room is 39 m^3 with open doorway. CO, CO_2, O_2, smoke, temperature, and radiant flux are as measured in doorway at 2.1-m height. Other gases are estimates to illustrate calculation method.)[106]***

Gas Concentrations Each Minute	1	2	3	4	5	6
Smoke (OD/m)	0.1	0.2	0.5	1.5	3.0	3.5
HCl (ppm)	10	50	150	200	250	200
acrolein (ppm)	0.4	0.8	2.0	6.0	12.0	14.0
formaldehyde (ppm)	0.6	1.2	3.0	9.0	18.0	21.0
CO (ppm)	0	0	500	2000	3500	6000
HCN (ppm)	0	0	50	150	250	300
CO_2 (%)	0	0	1.5	3.5	6.0	8.0
O_2 (%)	20.9	20.9	19.0	17.5	15.0	12.0
Temp (°C)	20	65	125	220	405	405
Heat flux (kW/cm^2)	0	1.0	4.0	10.0	25.0	25.0
Fractional smoke concentration FEC_{smoke}	0.50	**1.00**	2.50	7.50	15.00	17.50
Fractional irritant concentration						
FIC_{HCl}	0.06	0.28	0.83	1.11	1.39	1.11
$FIC_{acrolein}$	0.10	0.20	0.50	1.50	3.00	3.50
FIC_{form}	0.10	0.20	0.50	1.50	3.00	3.50
Σ FIC	0.26	0.68	**1.83**	4.11	7.39	8.11
Fractional lethal dose (irritants)						
FLD_{HCl}	0.00	0.00	0.00	0.00	0.00	0.00
$FLD_{acrolein}$	0.00	0.00	0.00	0.00	0.00	0.00
FLD_{form}	0.00	0.00	0.00	0.00	0.00	0.00
Σ FEC_{irr}	0.00	0.00	0.00	0.00	0.00	0.00
Fractional asphyxiant dose						
$FED_{I_{CO}}$	0.00	0.00	0.02	0.07	0.13	0.23
$FED_{I_{CN}}$	0.00	0.00	0.01	0.15	1.52	4.87
FLD_{irr}	0.00	0.00	0.00	0.00	0.01	0.04
VCO_2	1.00	1.00	1.35	2.01	3.32	4.95
$FED_{I_{O_2}}$	0.00	0.00	0.00	0.00	0.01	0.04
FED_{IN} (asphyxiants)	0.00	0.00	0.04	0.45	5.50	25.29
Σ FED_{IN}	0.00	0.00	0.04	0.50	**6.00**	31.29
Fractional heat doses						
FED_{rad}	0.00	0.00	0.00	0.00	2.54	2.54
FED_{conv}	0.00	0.03	0.27	1.84	14.67	14.67
FED_{heat}	0.00	0.03	0.27	1.84	17.21	17.21
Σ FED_{heat}	0.00	0.03	0.30	**2.14**	19.35	36.55

The endpoint, escape impairment (for smoke obscuration and irritancy), or incapacitation (for heat and asphyxiant gases) is reached when the FIC or FED value reaches 1.

Limiting values are emboldened. Lethal values are approximately 2–3 times incapacitating levels for dose related parameters, and incapacitation 5–10 times the FIC.

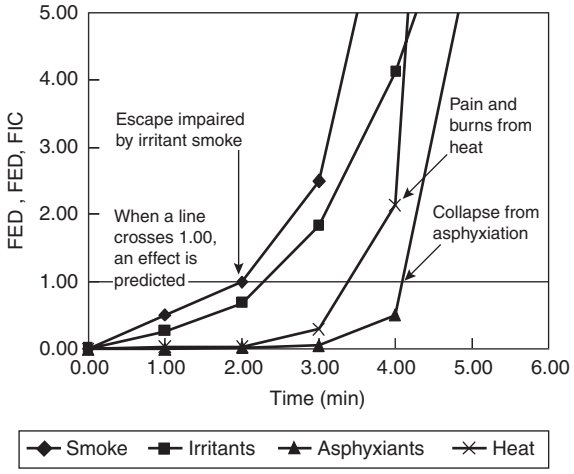

Figure 2-6.30. ***Example of an FED analysis.***[106]

culation using the methods described. The results of the analysis are presented in Figure 2-6.30. This figure shows plots of the FED for smoke, FIC for sensory irritation and FED values for each hazard parameter as they increase with time. The endpoints of escape impairment or loss of tolerability (for smoke obscuration and irritants) and incapacitation (for heat and asphyxiant gases) are reached when the line for each parameter crosses 1. Higher FECs and FEDs indicate more severe effects. For irritancy, incapacitation is predicted at FEC_{irr} values of approximately 5–10 and for asphyxiation death is predicted at FED_{in} values of approximately 2–3.

The analysis is designed to predict the severity of each hazard and the time during the fire at which it becomes significant. The toxic gas concentrations, smoke optical density, temperature, and radiant heat flux have been averaged over each of the first six minutes of a theoretical furniture fire, but are generally similar to conditions obtained in the smoke layer at head height in some experiments performed in ISO room tests. The analysis shows that the smoke obscuration is the first hazard confronting a room occupant. The level of obscuration exceeds the tenability limit for irritant smoke in a small enclosure after the second minute, with an FEC of 1. The second hazard to confront the occupant is irritancy. This becomes significant during the third minute, reaching an FIC of 1 at 3 minutes. The tenability limit designed to protect vulnerable individuals (FIC 0.3) is exceeded approximately one minute earlier. It is therefore predicted that after the second minute the level of obscuration and the irritancy of the smoke would be sufficient to impair and possibly prevent escape from the room due to difficulty in seeing and increasing pain in the eyes and respiratory tract. The effects of radiant and convected heat then become significant, crossing the tenability limit during the fourth minute and reaching an FED_{heat} value of 2.14, so that it is predicted that a room occupant would suffer severe skin pain and burns due to the effects of convected heat, which would be lethal during the fourth or fifth minutes.

During the fifth minute the radiant flux reaches the tenability limit of 2.5 kW/m^2, so that skin pain would be predicted within seconds due to radiation alone, were it not that the temperature has already exceeded the limiting exposure dose. Also during the fifth minute the FED_{IN} reaches 5.5, predicting that anyone breathing the smoke would lose consciousness due to asphyxia, and might die after six minutes. The level for exposure to asphyxiants considered to provide protection for vulnerable subpopulations (FED_{IN} of 0.1) is crossed at approximately 3.5 minutes, half a minute before the FED_{IN} reaches 1. The exposure dose of irritants is very small during the first six minutes of the fire, so that there should be little danger of post-exposure lung damage. An important point about all these parameters is that the FIC and FED curves are rising very steeply after the tenability threshold (FIC or FED of 1) is crossed. This means that even if the true exposure concentrations or exposure doses required to cause incapacitation were higher than the tenability limits chosen there would be little effect on predicted time to incapacitation.

The overall prediction is that for this fire, escape would become difficult during the third minute and incapacitation could occur due to the effects of irritant smoke. A person remaining in the room after this time would suffer severe pain and burns after 4 minutes, which would probably be lethal. In this analysis it is assumed that the head of a room occupant would be in the smoke at all times. In practice, if the room doorway was open, the hot, effluent-rich layer would descend from the ceiling to a level probably between 1 and 1.2 m above the floor as the chair reached its peak burning rate. A more sophisticated analysis could allow for the possibility that a room occupant might be at, or move to, a lower level in the room. If the height of the smoke layer with time is measured then it is possible to allow for this in the calculation.

Fire Scenarios and Victim Incapacitation

From the point of view of both product composition and toxic hazard, it is possible to distinguish four basic types of fire situations (see Table 2-6.15).

1. Smoldering fires where the victim may be in the room of origin of the fire or a remote location
2. Early flaming fires where the victim is in the room of origin
3. Small oxygen vitiated fires in poorly ventilated enclosures where the victim may be in the room of origin or a remote location
4. Fully developed or postflashover fires where the victim is remote from the fire

In the U.K., 80 percent of fire deaths and injuries occur in domestic dwellings, and in most cases the casualties occur in the compartment or origin of the fire. This class of fire is responsible for the highest incidence of deaths (60 percent) and a high incidence of injuries (39 percent). These fires occur mostly in living rooms or bedrooms, and in upholstery or bedding.[3] In these cases, fire is often confined to the material first ignited. The toxic hazard in such fires depends upon whether there is a long period of smoldering or a rapidly growing flaming fire.

Smoldering Fires

With smoldering fires, the decomposition temperatures are relatively low (~400°C) and materials are decomposed into a mixture of pyrolysis and oxidation fragments containing mixtures of asphyxiant and irritant gases and particulates. Under these conditions, the highest yields of a great variety of products are formed, many of which are irritant.[16,17] Incomplete oxidation is favored and CO_2 to CO ratios approach unity, so CO is likely to be an important toxic factor. The formation of high yields of HCN is, however, not normally favored.[17]

Although toxic products are formed under these conditions, the rate of evolution is slow, smoke is seldom dense, and room temperatures are relatively low. A potential victim therefore has ample time to escape if alerted sufficiently early, but may be overcome by fumes after a long period of time if unaware of the danger, particularly if asleep. The main danger here is almost certainly asphyxia by CO, with possibly a small contribution from low oxygen if the victim is in a room with a poor air supply.[16,106,134,135] It is not possible from fire statistics to determine how often this type of fire occurs, since in many cases smoldering fires become flaming fires before they are detected. However, it is likely that fires estimated to have burned for 30 min or more before discovery have involved long-term smoldering, and it may be relevant that for victims in the 19–49 age group, deaths are 20 times more likely in this situation than for fires discovered within 5 min of ignition, which are often rapidly growing flaming fires.[3]

The ability of smoldering fires to build up concentrations of CO capable of causing incapacitation and death in potential victims has been shown in large-scale fire tests.[136] A good example of such a situation is presented by a series of tests carried out at NIST,[137,138] where two armchair types made from a standard and a fire-retarded polyurethane foam with cotton covers (combustible mass 5.7 kg) were burned in a simulated small apartment (volume 101 m^3) consisting of a burn room (11.8 m^3), connected via a corridor 12 m long to a target room (volume 12.08 m^3). (See Tables 2-6.22 and 2-6.23.) The armchairs were tested by flaming ignition of the seat back, and also by smoldering caused by one or two cigarettes placed in the seat angle for approximately 1 hour, followed either by spontaneous flaming or ignition from a flaming source. Under smoldering conditions, approximately 1 kg of foam was decomposed in just over 1 hour. The smoke layer had reached the floor after 1 hour, but there was a concentration gradient for smoke and toxic gases between the burn room and the target room. The major asphyxiant gas present was CO, which gradually increased in concentration in the burn room from 180 ppm during the first 13 min to 1000 ppm between 67 to 75 min. This was sufficient to have caused incapacitation (i.e., loss of consciousness) in just over 1 hour in the burn room, but probably not in the target room where the concentration was lower. When flaming ignition occurred the armchair burned very rapidly, and produced high concentrations of asphyxiant gases that would have been almost immediately fatal in the burn room. Within the target room an occupant would have become unconscious within less than 1 min and received a fatal dose within 2 min. The smoke in the system was also very irritant, and it is likely that anyone spending more than 1 hr in the burn room would have suffered serious and possibly fatal lung damage, even if that person had been rescued. This example illustrates the dangers of smoldering conditions, which can continue for several hours and spread lethal products throughout a building, creating danger for the sleeping, trapped, or otherwise incapacitated occupant. Since such fires often change to flaming before they are discovered, it is difficult to know the true incidence of incapacitation and death occurring during the nonflaming phase of fires.

Table 2-6.22 ***Concentrations of Toxic Gases and FEDs in Burn Room for Smoldering Followed by Flaming Ignition of Standard Foam Armchairs***

Fractional effective doses of narcotic gases								
Time (min)	0–13	13–27	27–40	40–53	53–67	67–75	75–76	76–77
Gas concentrations—burn room								
CO ppm	180	300	360	700	700	1000	10000	
HCN ppm	0	0	0	0	0	0	1320	
CO_2%	0.11	0.16	0.18	0.30	0.30	0.40	15.00	
O_2%	21	21	21	21	21	21	3	
Fractional effective doses for incapacitation								
FED_{CO}	0.006	0.010	0.012	0.024	0.024	0.035		
FED_{HCN}	0	0	0	0	0	0	Immed.	
VCO_2	1.019	1.032	1.037	1.069	1.069	1.096	fatal	
FED_O	0	0	0	0	0	0		
FED/min	0.006	0.010	0.013	0.026	0.026	0.039		
Σ FED	0.078	0.218	0.387	0.725	**1.089**	1.401		

By 71 min the mass loss exposure dose of irritants was approximately 600 g·m^3·min, which may cause fatal lung damage.

Table 2-6.23 ***Concentrations of Toxic Gases and FEDs in Target Room for Smoldering Followed by Flaming Ignition of Standard Foam Armchairs***

Fractional effective doses of narcotic gases								
Time (min)	0–13	13–27	27–40	40–53	53–67	67–75	75–76	76–77
Gas concentrations—target room								
CO ppm	0	0	100	270	550	800	2700	2000
HCN ppm	0	0	0	0	0	0	125	120
CO_2%	0.04	0.04	0.08	0.15	0.20	0.30	9.00	8.50
O_2%	21	21	21	21	21	21	13	14
Fractional effective doses for incapacitation								
FED_{CO}			0.003	0.009	0.019	0.028	0.099	0.073
FED_{HCN}			0	0	0	0	0.080	0.072
VCO_2			1.012	1.030	1.042	1.069	5.772	5.248
FED_O			0	0	0	0	0.021	0.012
FED/min	0	0	0.003	0.009	0.020	0.030	1.054	0.773
Σ FED	0	0	0.039	0.156	0.436	1.676	**1.730**	2.503

By 71 min the mass loss exposure dose of irritants was approximately 300 g·m3·min, which may cause some lung damage.

For this example, both the standard and FR chairs would have caused incapacitation after 1 hr in the burn room, but due to its higher yield of CO and irritants, the FR chair would also cause incapacitation in the target room soon after, and death in the burn room after 1.5 hrs of smoldering. The standard foam death at both locations would occur within 1 min of the spontaneous transition to flaming after 75 min. These dangers can be overcome by the provision of detection and warnings, but the siting of detectors can be important for effective operation.

Flaming Fires

For flaming fires where the victim is in the room of origin, the hazard relates to the early stages of fire growth. Such fires often grow quickly, but even the most rapidly growing flaming fires take approximately 3 min to reach levels of heat and gases hazardous to life,[56] which should allow ample time to escape from a room, and of course most people do escape. As Figure 2-6.15 shows, the hazard in this situation relates to a number of factors, all of which may reach life-threatening levels simultaneously as the fire reaches the rapid phase of exponential growth. As stated previously, in the high temperature, well-oxygenated flames of early flaming fires, much of the thermal decomposition products are consumed to form simple, comparatively innocuous products such as CO_2 and water, the CO_2 to CO ratios being high initially and then decreasing to the region of 50 to 100 as the oxygen concentration decreases toward 15 percent. The yields and relative rates of production of CO_2, CO, and irritant smoke depend upon the rate and efficiency of combustion. As Figure 2-6.15 and Table 2-6.15 show, the atmospheres obtained in a rapidly growing fire can contain asphyxiant concentrations of CO_2 (greater than 5 percent), CO (greater than 1000 ppm), and low oxygen (less than 15 percent O_2), as well as dense irritant smoke from products escaping the flame zone. A victim in this situation is therefore likely to be confronted simultaneously by high temperatures and heat radiation, smoke, and high concentrations of CO and CO_2 accompanied by low O_2, any one of which could incapacitate and prevent escape.

The inability of victims to escape from such fires seems to depend upon a number of factors. Casualties include a higher proportion of young children and the elderly than does the general population. (In 1978, fatalities in bedding fires for those over 65 were seven times those expected from the distribution in the 1978 population.)[3,14] People who are incapacitated by a previous period of smoldering or by some other infirmity (such as a physical disability or alcohol or drug intoxication) are obviously more at risk.[14] However, there seem to be two other factors of importance: (1) the behavior of the victim and (2) the exponential rate of fire development.

In many cases, the victim has a short period in which to carry out the correct actions enabling escape, after which he or she is rapidly trapped. Some victims may be asleep during this critical escape "window," but there are also reports of situations where the victim was aware of the fire from time of ignition, but remained in an attempt to extinguish the fire, or for some other reason failed to leave before the phase of very rapid fire growth when heat and asphyxiant gases rapidly reach life-threatening levels. Another, perhaps surprising, finding is that victims often appear to be unaware of the fire, and are discovered in a burned out chair or bed where they have remained. The insidious nature of CO intoxication has been described; it also seems that irritant smoke products often fail to wake sleeping victims, although a sudden noise such as of breaking glass may do so. It may seem odd that acrid fumes may fail to alert sleeping victims, but a possible explanation may lie in the adaptation to sensory irritation during continuous exposure reported for the experiments with CS gas.[24] In smoldering fires, the concentration buildup of irritants is slow, allowing time for adaptation to occur. There may be no subsequent

response to a high concentration which, if presented suddenly (as, for example, with smelling salts), would rouse the subject. Other victims appear to have roused themselves at some stage of the fire but have been overcome, again probably by CO or HCN, before they are able to escape, and are found behind a door. There are also cases reported by survivors where a victim has attempted to extinguish a rapidly growing flaming fire, but failed to leave in time and is discovered near the fire having been overcome by fumes.[108,134] Unfortunately, reports of such effects on victims are largely anecdotal, and systematic studies of fire victim experience are lacking. The apparent anomaly of why so many casualties occur in the room of fire origin when theoretically there should be ample time to escape would seem to be a particular area that needs further investigation. The following pilot study has therefore been made of this problem.

Pilot Study of Room-of-Origin Deaths

As stated, the results of large-scale fire tests suggest that even in a worst-case situation there should be a period of at least three minutes before conditions in a rapidly growing flaming fire become untenable, and in many cases fire growth will take considerably longer. From a knowledge of the toxicity of fire products, it would therefore seem that a normal, healthy, waking individual should be able to escape from such situations without much difficulty, while a sleeping or otherwise incapacitated victim may be overcome by a smoldering or slowly growing fire, as well as by a rapidly growing fire. To test this hypothesis, an examination was made of the 1981 U.K. statistics, specifically for textile fires in dwellings for casualties in the 19 to 49 year age group, a group most likely to be active and able bodied. The data are summarized in Table 2-6.24 for fires estimated to have been discovered within 5 min of ignition (most likely to have been rapidly growing flaming fires) and for fires where the time to discovery is estimated to have been 30 min or more (most likely to have involved a period of prolonged smoldering before severe flaming).

The preliminary data show that there were 23,082 fires in the first category, but only 4 fatalities, while for the second category there were fewer fires (5,870) but 20 fatalities, a ratio per fire of 1:20. Obviously, a number of interpretations could be put on these data, but it does seem that people in this active age group are able to escape from rapidly growing fires in domestic-sized compartments. Fatalities are much more likely in fires that have undergone a period of prolonged smoldering, when victims may have been overcome by prolonged, low level exposure to asphyxiant fumes. If this is the case, perhaps there should be more concern about the ability of materials to continue smoldering, with toxic gas buildup over a long period of time, at least in the context of this class of fire.

Table 2-6.24 ***Fatal Casualties in Room of Fire Origin (Textile Fires in Dwellings for 1981,[3] Age Group 19–49 Years)***

Time to Discovery (min)	Number of Fires	Number of Fatalities
< 5	23,082	4
> 30	5,870	20
		Ratio 1:20

Small Restricted Ventilation Fires in Closed Compartments

Closed-room fires are hazardous situations, wherein a smoldering, or especially a flaming, fire quickly uses up the available oxygen, and as the oxygen concentration falls after a minute or so of burning the combustion becomes inefficient, producing a dense smoke rich in carbon monoxide and other toxic products. These, together with the lowered oxygen concentration in a room, can produce a rapidly lethal atmosphere. An example is a recent fire involving an adult and a four-year-old child. Both were in a small bedroom for a short time during which the adult went to sleep and the child is thought to have ignited a small piece of foam using a cigarette lighter. The fire was discovered after a few minutes, when the door was opened by a family member, who extinguished the very small fire with a bucket of water. Both the adult and child were dead, with blood carboxyhemoglobin concentrations of about half a lethal level. Based upon the dimensions of the room, it is calculated that the decomposition of approximately 0.5 kg of material would be sufficient to lower the oxygen concentration to 10 percent and give carbon monoxide concentrations of approximately 1 percent or more, which together with other toxic products would cause incapacitation and death within a few minutes. With such small fires it would seem that early detection and warning, coupled with materials giving a slow fire growth, would greatly increase the probability of escape and survival.

During the period when most occupants are at risk, the majority of fires in small enclosed buildings (such as houses, flats, hotels, boarding houses, cellular offices, and small shops) are likely to be restricted ventilation (vitiated) pre-flashover fires. However if external windows or doors are open, or (as often happens) are opened at a later stage of the event, then flashover may occur. The characteristics of restricted ventilation fires are that there are three main regions at which combustion reactions occur. One is at the interface between the solid (or liquid) fuel and the base of the flame, where fuel materials are decomposed and partially oxidized by heat to form the gaseous fuel for the fire. The second is in the lower part of the flame zone, where air and fuel gases combine to produce heat and primary products. The third is in the vitiated hot zone in the upper part of the flame and beyond where hot, partially combusted fuel gases react in a restricted oxygen atmosphere to produce high yields of irritant and asphyxiant smoke products. These conditions occur when the upper layer has filled down to a low level above the fire in the fire enclosure and where partially combusted fire effluent may be recycled into the fire from outside the fire enclosure. Such fires are usually relatively small, often being limited to the item first ignited, sometimes involving some decomposition (nonflaming or vitiated flaming) of combustible materials at high levels in

the room (such as paint, coving or objects placed on cupboards or the upper levels of bookcases or racks).

The main hazards from such fires during the critical stages are likely to be from irritant smoke and asphyxiant gases. Inefficient combustion leads to high yields of these toxic smoke products. Apart from the immediate vicinity of the fire, the temperatures in the fire enclosure and beyond are not particularly high, so that heat is usually not the primary hazard.

These descriptions of fire scenarios illustrate that fire hazards, particularly the toxic hazards, vary considerably depending upon the combustion conditions. In buildings, the majority of fires hazardous to occupants are likely to involve vitiated flaming combustion conditions to some extent, either pre- or post-flashover depending upon the scenario. This is likely to be especially true of fires in domestic dwellings, which account for the vast majority of injuries and deaths. Most fire deaths in the United Kingdom (61 percent in 1992)[3] result from small fires when the victim is in the room of fire origin. In order to study the development of hazardous conditions in typical domestic fires and to develop a series of realistic design fires for smaller enclosures with restricted ventilation, a series of 23 fires had been carried out at the Fire Research Station over a number of years. These fires were carried out in three experimental rigs (Figure 2-6.31), consisting of a room corridor–rig, a room–corridor–room rig, and a typical domestic two story house. The first rig simulates conditions for a fire in a small enclosure connected via a corridor to a source of ventilation, such as an open door or window, or a much large interior space. The second rig simulates conditions in a small single story apartment, while the third simulates conditions for house fires. For all these experiments the fire was in one room and the developing fire conditions were measured in the fire room and other locations throughout the experimental rigs. The majority of fires involved single items of upholstered furniture (armchairs).

In order to give an example of the developing conditions in a typical fire in a domestic house and the likely hazards faced by occupants, one of these experiments is described. This experiment involved a common situation in which a fire was started in the seat of an armchair. The armchair was typical of modern furniture, upholstered with combustion modified foam and fire retardant back coated acrylic covers. A flaming ignition source was used, consisting of a No. 7 wood crib, which is approximately equivalent to two sheets of newspaper. The armchair was placed in the downstairs lounge with the door to the hallway open. Upstairs, the front bedroom door was open and the back bedroom door shut. The kitchen and bathroom doors were also shut. Figures 2-6.32 and 2-6.33 show the developing conditions in the lounge and bedroom, with estimates of the developing hazards faced by occupants of the lounge and open bedroom. For each of Figures 2-6.32 and 2-6.33 the lower graphs show the gas and smoke concentrations, while the upper graphs show the hazard development at head height for a standing occupant. The hazard development is expressed in terms of the FEC (smoke), FIC (fractional irritant concentration), or FED (fractional effective dose) for each hazard parameter. This means that for each parameter a tenability limit is

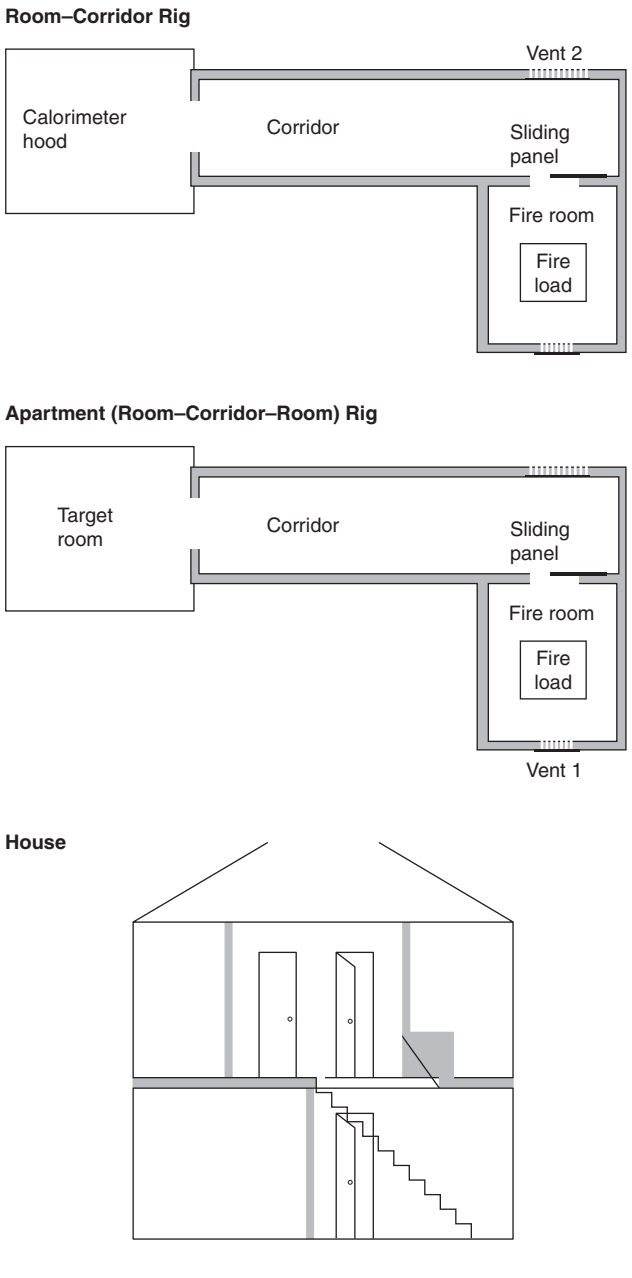

Figure 2-6.31. ***Full-scale fire test rigs.***[106]

reached when the line crosses 1 on the *Y* axis. The graphs for the fire gases show that in the lounge the fire grows slowly at first producing some smoke, but then grows more rapidly after about 4 min. From about 5 min the oxygen concentration in the fire room starts to decrease so that at around 9 min the fire self-extinguishes. The peak temperature at the ceiling in the hottest region above the fire was 350°C. The peak carbon monoxide concentration was 1.1% and the peak hydrogen cyanide concentration 1100 ppm. The ionization smoke detector in the lounge was triggered at 0.5 min and the optical detector at 1.5 min. The first hazard confronting an occupant of the

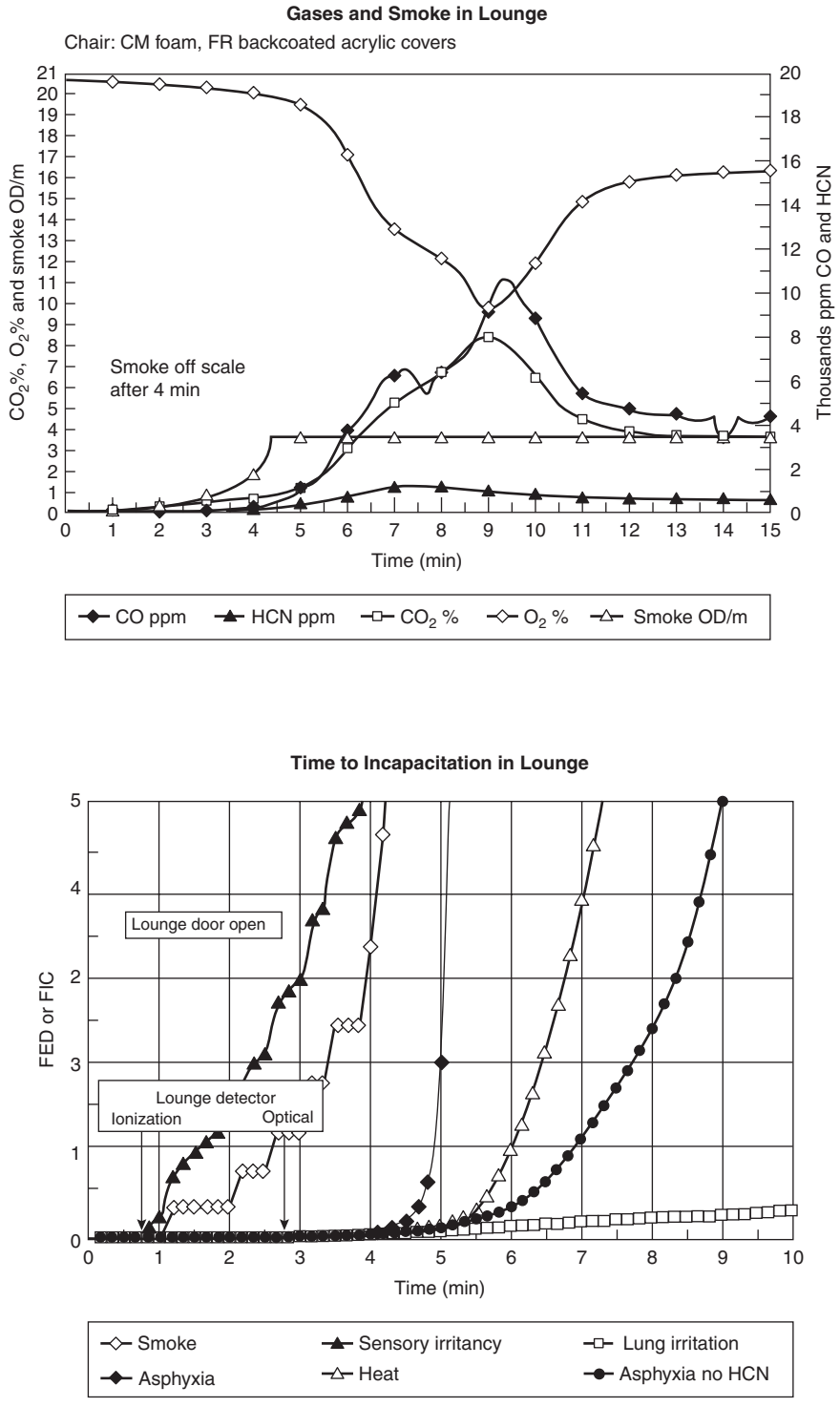

Figure 2-6.32. ***Gases, smoke, and hazard analysis in lounge for armchair fire in house.[106]***

lounge would be smoke, and from the smoke analysis it is considered that the smoke would be irritant. The line for irritant smoke crosses the tenability limit at around 1.5 min in the lounge. From this point, a room occupant would experience difficulties in seeing due to painful eye irritation and the presence of smoke, and breathing difficulties. It is likely that these effects would hamper, but probably not prevent, a room occupant from finding their

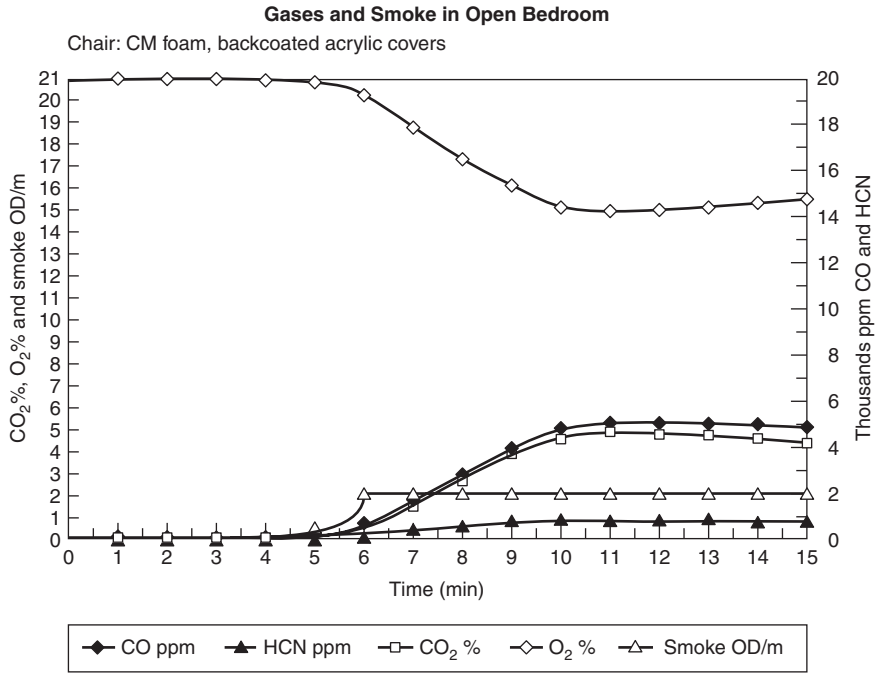

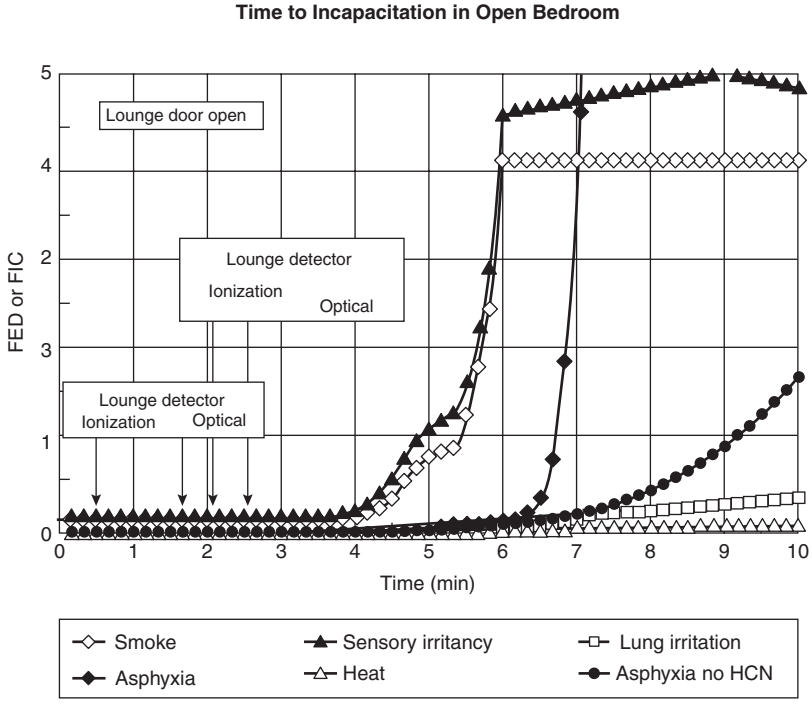

Figure 2-6.33. ***Gases, heat, and hazard analysis in open bedroom for armchair fire in house.***

way out of the room to the front door. One minute later, the purely visual obscuration effects of the smoke (i.e. assuming the smoke was non-irritant) reach the tenability limit of 2 m visibility. If an occupant was still in the room at 5 min, it is predicted that they would collapse unconscious due to the effects of asphyxiant gases. This collapse is largely due to the presence of hydrogen cyanide. If there was no cyanide present, it is predicted that collapse

would not occur for a further 2 min (at 7 min). At 8 min it is predicted that an occupant would be overcome by heat, suffering burns to unprotected skin.

Figure 2-6.33 shows the conditions in the open upstairs bedroom. The smoke and gases start to increase significantly from around 4 min, but there was sufficient smoke on the upstairs landing to trigger the ionization smoke detector at around 2 min and the optical detector at around 2.5 min. The gas and smoke concentrations increase more gradually than in the lounge, since they are well mixed by the time they reach the bedroom. From around 11 min the smoke and gas concentrations are similar throughout the house. The temperature in the bedroom peaked at around 60°C after 9 min. The hazard analysis shows that irritant smoke is predicted to be a problem from around 4.5 min. After this time a bedroom occupant might experience some difficulties in finding their way out of the room and down the stairs. They would also have to decide whether it would be better to close the bedroom door and stay in the room until the fire brigade arrived, or to attempt to escape via the door or window. Analysis of the conditions in the closed bedroom showed protection for some 20 min or so if the door was closed throughout. If an open bedroom occupant was still in the room after approximately 5.5 min, it is predicted that they would collapse unconscious from the effects of asphyxiant gases. As with the lounge, this is predominantly due to the effects of hydrogen cyanide, conditions remaining tenable for around 9.5 min if this gas is absent. The temperature in the bedroom is insufficient to cause incapacitation.

This example shows how typical flaming furniture fires are likely to develop and threaten the occupants of a domestic house. The main hazards are firstly irritant smoke and secondly asphyxiant gases, particularly hydrogen cyanide and carbon monoxide. The fires are often small, being limited to the item first ignited, and self extinguish when the oxygen concentration decreases. In practice, many domestic fires begin by a variable period of nonflaming/smoldering before flaming ignitions occurs. This may last for several hours. Depending upon the nature of the smoldering materials, a hazard may develop, primarily from carbon monoxide. The house fills with a slowly thickening and irritant smoke, which may trigger detectors before the situation becomes dangerous. Another possibility is that the fire will grow rapidly, possibly to flashover. This is particularly likely if external doors or windows are open (or if windows break and fall out). Such large fires commonly develop when occupants are roused during the early stages and open external doors or windows during the fire to affect escape or rescue. The conditions rapidly become fatal, due to the large amounts of heat and toxic smoke produced, and there is often considerable damage resulting from fire spread throughout the building. All data from the 23 fire tests have been placed on a CD-ROM database. Further details of the fire loads and results of tests are given in Purser et al.[139] Table 2-6.25 shows examples of four fires in terms of times to alarm and different tenability limits. Figures 2-6.34 and 2-6.35 illustrate the times between ignition, detection and the various tenability criteria in the lounge and bedroom for these and other fires.[106,139]

For all fires except Experiment CDT 16, the fire room door was open to the remainder of the apartment or house. Figure 2-6.34 shows similar results in the apartment rig to those in the two story house for the same type of chair (Experiments CDT 11, 21, and 23), but when fire retarded covers were used, the tenability times for asphyxia are increased by approximately 1.5 min (Experiments CDT 17 and 18). The importance of HCN as a primary cause of incapacitation in these fires is shown by comparing the asphyxia with HCN bar with asphyxia without HCN bar. If no HCN were present, the time to asphyxia is increased by up to 2.5 min. For flaming fires in the fire room, ionization detectors triggered 1–2 min earlier than optical detectors, although optical detectors would be expected to trigger earlier if the fires had been initiated by a nonflaming source. Times in Figure 2-6.34 are for optical detectors on the upstairs landing ceiling. For this location there was only a small difference between ionization and optical triggering times as shown in Figure 2-6.35. Figure 2-6.35 shows the situation in the open upstairs bedroom. In this situation the results are similar to those from the fire room, in that times to loss of tenability from asphyxia are several minutes longer for the chairs with fire retarded covers.

Hazardous situations in fires develop as a result of a complex interaction between the building, the burning contents, and the occupants. When evaluating materials, it is important to consider not just the toxic potency of the combustion products, but the overall fire risk and burning behavior of the item. Although some modern materials and fire retardant systems may present possible toxic potency and environmental problems, they give rise to considerable overall benefits if they reduce the number of fires occurring. It is also obvious that slow fire development, buying time for occupants to escape, is beneficial, particularly when linked with efficient detection and warning systems. It is likely that a combination of these factors has led to recent reductions in fire deaths compared with the early 1980s. Although the majority of fires and toxic effluent derive mainly from building contents rather than the structure, it is evident that the building and its systems are very important factors in the development of the fire and its hazards. In the domestic context, the type, maintenance, and placement of smoke alarm systems are likely to be important in the provision of early warnings to occupants. The simple expedient of closing doors and windows on unoccupied rooms is also likely to considerably reduce fire hazards while providing a tenable escape route. The use of sprinklers and smoke venting systems are other important strategies, particularly in nondomestic buildings.

Fully Developed Fires

The third scenario involves large, fully developed fires where casualties occur remote from the source of the fire. This type of fire has progressed beyond the stage of local growth and has spread from the material first ignited to others. The fire may still be largely confined to the compartment or area of origin, but large amounts of toxic smoke are formed, which spread throughout build-

Table 2-6.25 ***Apartment and House Fires—Times to Alarm and Tenability Limits***

Parameter	Times (min:sec) to Effect							
Test	CDT11 CM Non-FR Acrylic		CDT16 CM FR Cotton		CDT17 CM FR Cotton		CDT23 CM Non-FR Acrylic Fully Furnished	
Conditions: Building/Fire Room Door	Apartment Door 630 mm		2-Story House, Door Shut		2-Story House, Door 750 mm		2-Story House, Door 750 mm	
Alarm lounge								
Ion optical			1:00	3:00	1:00	3:00	0:50	1:25
Alarm landing								
Ion optical	1:50	1:55	4:30	4:35	2:50	3:35	1:20	1:30
Smoke								
Lounge bedroom	2:50	3:20	2:35	7:10	3:35	5:50	2:20	3:50
Irritants								
Lounge bedroom	2:50	3:20	2:35	7:10	3:30	5:50	2:10	3:35
Asphyxia + HCN								
Lounge bedroom	3:00	4:20	4:40	6:50	4:35	6:50	2:25	3:55
Asphyxia − HCN								
Lounge bedroom	4:30	5:30	6:00	>10	6:50	8:00	2:35	4:45
Heat								
Lounge bedroom	3:40	>10	5:30	>10	5:50	>10	3:30	>10
Time available lounge								
Smoke: ion optical	1:00	0:55	–1:55	–2:00	0:40	0:00	1:00	0:50
Asphyxia: ion optical	1:10	1:05	0:10	0:05	1:45	1:00	1:05	0:55
Time available bedroom								
Smoke: ion optical	1:30	1:25	2:40	2:05	3:00	2:15	2:30	2:20
Asphyxia: ion optical	2:30	2:25	>5:30	>5:25	4:00	3:25	2:35	2:25

ings, giving rise to lethal atmospheres remote from the actual fire. Apart from being a common occurrence in domestic dwellings, such situations often occur in public buildings where there may be major loss of life in a single incident. Materials in such fires are subjected to substantial external heat flux and in some cases to oxygen deficient environments. Under the severe conditions found in such high temperature, postflashover fires with low oxygen concentrations, the basic pyrolysis products break down into low molecular weight fragments and can contain high concentrations of asphyxiant substances such as CO and HCN, with CO_2 to CO ratios of less than 10.[17]

Under such conditions, a building can fill rapidly with a lethal smoke capable of causing incapacitation and death within minutes. Fires where the victim is remote from the compartment of origin are responsible for the highest incidence of nonfatal casualties (48 percent) and a large proportion of deaths (37 percent) in the United Kingdom.[3] The victim is five times more likely to be killed by smoke than by burns, and is often unaware of the fire during the crucial early phase, so that the gases may not penetrate to the victim until the fire has reached its rapid growth phase and the victim is already trapped. The major causes of incapacitation and death in this type of fire are almost certainly asphyxiant gases, particularly CO, which can build rapidly to high concentrations (although the role of irritants in causing incapacitation and impeding escape attempts may be crucial to victim survival).

An example of such a fire is provided by some studies of the effects of the penetration of a large external fuel fire into the cabin of an airplane, as happened in the Manchester Airtours fire.[140] Table 2-6.26 shows the results obtained inside the cabin of a Boeing 707 containing a few rows of seats opposite an open doorway, outside which was 50 gal of burning aviation fuel.[137] The rapid involvement of the cabin contents gave rise to a dense smoke containing large amounts of carbon monoxide and hydrogen cyanide at a measurement point half way down the fuselage. Incapacitation is predicted just after 2 min followed rapidly by death, mainly from the effects of hydrogen cyanide (high concentrations of which were found in the blood of the Manchester victims).

Although in many large fires the original fuel and the major source of heat and toxic products may be the contents, a significant contribution may be made by construction products. Of great importance in some cases are surface coverings or components with a large surface area, such as doors or partitions. Surface coverings may contribute to flashover spread (as in the Dublin Stardust disco fire) and may release a bolus of toxic products very quickly, which may have a serious incapacitating effect on victims. An example would be vinyl wall coverings or the

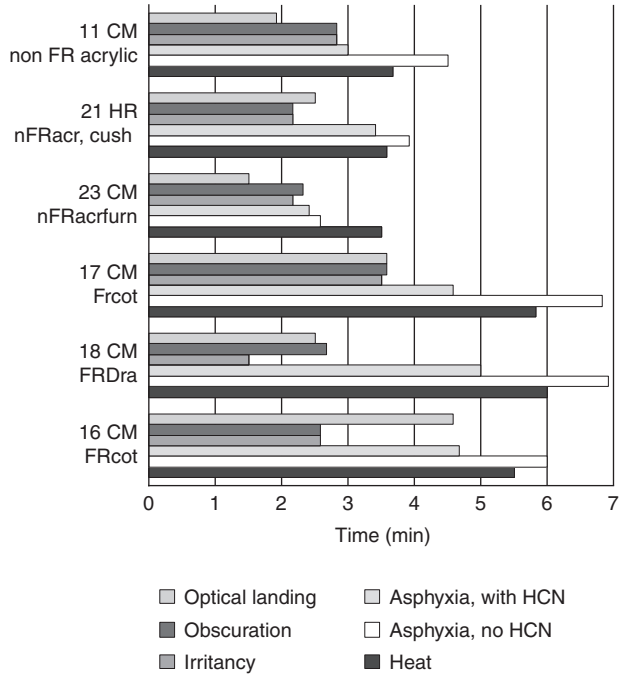

Figure 2-6.34. ***Time to detection and effect for armchair fire in the lounge (fire room).***

Key:

11 CM non FR acrylic (armchair, non-fire-retarded acrylic covers, combustion modified foam—apartment rig)
21 HR nFRacr, cush (nonFR acrylic covers, combustion modified foam, foam scatter cushions—house)
23 CM nFRacrfurn (nonFR acrylic covers, combustion modified foam, fully furnished room—house)
17 CM FRcot (FR back-coated cotton covers, combustion modified foam—house)
18 CM FRDra (FR back-coated acrylic covers, combustion modified foam—house)
16 CM FRcot (same as for 17, but fire room door closed)

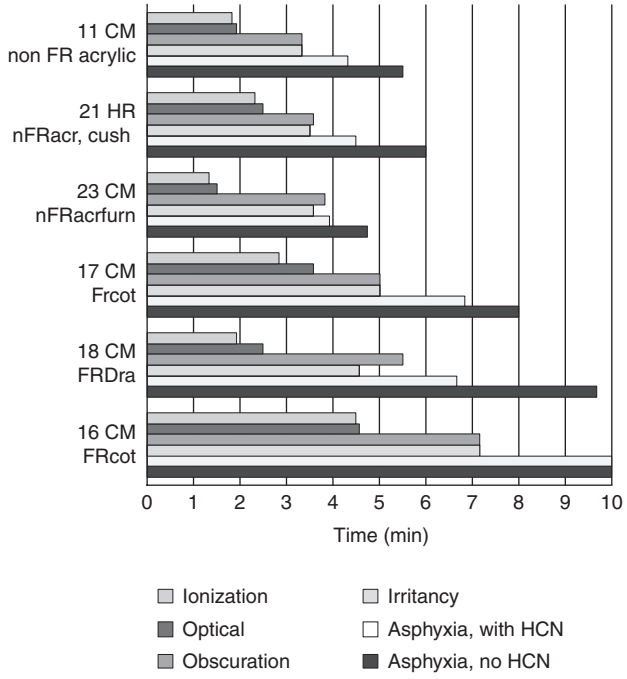

Figure 2-6.35. ***Time to detection and effect for armchair fire in the bedroom (fire in the lounge). Key as for Figure 34.***

vinyl laminates used in aircraft cabins. PVC releases all its hydrogen chloride at a low temperature (approximately 250 to 300°C), so that, as a fire develops and the hot layer reaches this temperature, HCl may be suddenly released. In another aircraft fire test conducted by the FAA, high concentrations of HCl and HF occurred in the cabin atmosphere before other gases reached toxic levels.[104]

In general, although in some cases fire and heat may eventually kill victims, this is usually preceded by dense, highly toxic smoke that can spread rapidly throughout a space or a building, and it is this that is usually responsible for the initial incapacitation of occupants, as well as being the cause of many deaths.

A common feature in many major fire disasters is a failure in early detection and effective warnings. In many cases the fire was detected at an early stage, and some attempts were made to deal with the fire, but often there was a failure to instruct people to leave while the fire was small and a failure to realize that a small fire grows with exponential speed into a life-threatening one. For example, in Summerland[141] the initial fire was considered nonthreatening, and occupants were encouraged to remain seated rather than to leave. At the Manchester Woolworth's fire[142] people continued to eat in the restaurant area while the fire was growing on the other side of the sales floor. At the Bradford stadium fire people watched the early fire development at the end of the stand and did not begin to move until a late stage. At the Dupont Plaza hotel, the fire began in an unoccupied furniture storage area, but was discovered and fought at an early stage; however, mass evacuation of the hotel did not occur until after the fire went to flashover and started to spread. At the Beverly Hills Supper Club fire,[141] 20 min elapsed between discovery and evacuation instructions. At the Kings Crossing fire,[141] the escalator fire was burning for some time before attempts were made to close the station. At the Dublin Stardust disco, the fire grew unnoticed behind a partition. It could be said that when a person is able to perceive a fire as a possible threat to their life, it may already be too late to escape. In the majority of these cases, evacuation occurred at a late stage and there were failures in the provision of accurate, authoritative, and informative evacuation instructions.

General Comment

The severe asphyxiant incapacitation and subsequent death of many fire victims are almost certainly due to the common asphyxiant gases. However, the importance of irritants in impeding escape is an important consideration, and it is not obvious from asphyxiant gas profiles why so many fatalities occur in the room of fire origin.

Table 2-6.26 ***Average Concentrations of Toxic and Physical Hazards and Fractional Incapacitating Doses over 30-s Periods during Aircraft Cabin Fire***

Fractional effective doses of asphyxiant gases							
Time (min)	0.5	1.0	1.5	2.0	2.5	3.0	3.5
Gas concentrations							
CO ppm	8	34	282	1157	3326	8410	19490
HCN ppm	0	10	38	143	340	740	1380
CO_2%	0.0	0.0	0.4	1.2	2.8	4.1	6.0
O_2%	21	21	21	20	18	16	13
Fractional incapacitating doses							
FED_{CO}	0.00	0.00	0.00	0.02	0.06	0.16	0.38
FED_{HCN}	0.00	0.00	0.01	0.06	5.65	>10	>10
VCO_2	1.00	1.00	1.12	1.31	1.77	2.27	3.26
FED_O	0.00	0.00	0.00	0.00	0.00	0.00	0.01
FED/30s	0.00	0.00	0.00	0.10	10.10	>10	>10
Σ FED	0.00	0.00	0.00	0.11	11.10	>10	>10
Fractional effective doses of convected heat							
Temp °C	12	14	28	81	156	274	408
FED/30s	0.00	0.00	0.01	0.03	0.20	4.96	>10
Σ FED	0.00	0.00	0.01	0.04	0.24	5.20	>10
Radiant heat flux							
W/cm²	0.10	0.12	0.14	0.18	0.23	0.28	0.57

Time to exceed smoke tenability limit: 1 min 40 sec

Time to incapacitation by asphyxiant gases: 2 min 15 sec

Time to incapacitation by convected heat: 2 min 45 sec

Time to tenability limit for radiant heat: 2 min 45 sec

Effects of irritants:

Over period between 1 and 4 min: average respirable particulates 6.7 mg/l
average total particulates 11.6 mg/l
average HCl concentration 1027 ppm
average HBr concentration 1228 ppm

It is considered that the oily, organically rich, particulate collected, with its very high acid gas content, would be highly irritant and extremely painful to eyes and breathing, causing incapacitation and impairing escape attempts. It is considered likely that these irritants reached high concentrations (approaching 1000 ppm total acid gases) early in the fire at approximately 1 to 1.5 min, from which time escape capability would be significantly impaired. It is likely that sufficient irritants would be inhaled up to 4 min to cause life-threatening post-exposure lung damage.

Useful information may be obtainable from survivors who have experienced exposure to dense, irritant smokes, and from case studies of room of origin fires.

Possible Routes to Mitigation of Toxic Hazard

For smoldering fires it would be advantageous if materials were designed to self-extinguish, and if the formation of products other than CO during decomposition (such as oxidized hydrocarbon fragments or CO_2) could be encouraged. Early audible warning by smoke alarms may be particularly advantageous, as sound often appears to alert victims where the presence of irritant smoke or heat fails.

For early flaming fires where the victim is in the room of origin, any measure that limits the rate of growth once ignition has occurred will give a victim more time to extinguish a small fire or escape from a growing one.

For fully developed fires where the victim is remote from the point of origin, the most important mitigating factors are probably early warning and containment of the fire and gases within the original fire compartment.

The development of hazardous situations in a fire involves a whole range of factors, including fire development from ignition to the post-flashover spread of fire and smoke, toxicity, and the interaction of the fire with the structure and with passive and active fire protection, as well as escape-related factors, including detection, warnings, the provision of escape routes, wayfinding, physiological and behavioral impairment, and escape movements or rescue. In designing a system to be safe in fire, all these factors should be considered, and the ultimate evaluation of safety depends upon whether it is possible to ensure, by performing a life-threat hazard and risk assessment, that the occupants can reasonably be expected to have escaped before they are exposed to

levels of heat and smoke that may endanger health and threaten life.

The Use of Small-Scale Combustion Product Toxicity Tests for Estimating Toxic Potency and Toxic Hazard in Fires

Essential Criteria for Test Methods

The evolution of toxic products in large-scale fires is determined essentially by two sets of parameters.

One set of parameters relates to the large-scale structure and development of fire scenarios that determine the growth and spread of the fire, the decomposition conditions under which products are formed, and their rate of evolution. It is not possible to model these features in a single small-scale test, although they are the most important factors determining the toxic hazard in a fire. This is the main reason why it has not been possible for experts to agree on standard test methods suitable for regulatory control of materials.

The other set of parameters that contributes to the determination of toxic hazard, and that can be modeled using small-scale fire tests (albeit only in a general way) is the set of thermal decomposition conditions encountered by materials at different stages or in different types of fires. Basically, the thermal decomposition products given off by any material depend upon the temperature and oxygen supply to which it is subjected, and whether it is flaming or nonflaming. Although it is possible to identify a number of subsets, there are three basic thermal decomposition conditions, namely:

1. Nonflaming oxidative/smoldering decomposition at mid-range temperatures
2. Flaming decomposition in a local environment at mid-range temperatures
3. High temperature/low oxygen conditions encountered in fully developed or postflashover fires

If it can be demonstrated that a particular small-scale test method can model one or more of these conditions, then it has the potential, if used with a suitable bioassay procedure, to produce toxicity information that can be used as one item in a toxic hazard evaluation. To produce such information, a number of essential test criteria must be fulfilled.

1. The most important criterion for any small-scale fire model is that it should be capable of producing atmospheres with broadly similar compositions to those formed in one or more of the basic stages of a fire.
2. Following from this, it is essential that measurements should be made of the temperature and/or radiant flux to which the sample is subjected, the air/fuel ratio, the smoke optical density, and whether the sample is flaming or nonflaming. The chemical composition of the atmosphere must also be characterized as fully as possible, the minimum being in terms of CO, CO_2 (with calculation of the CO_2 to CO ratio), O_2, and HCN (if the material contains nitrogen), or hydrogen halides (if F, Cl, or Br are present). These measurements are important for two reasons: first, because they define whether one of the basic fire conditions is being adequately simulated; and second, because they should enable the key products responsible for the animal toxicity to be identified, or at least make it possible to decide if unusual toxic products are present.

   The time/concentration profiles of the key toxic products can then be measured in large-scale fire tests, or predicted by mathematical fire modeling. Estimates of likely toxic hazard in realistic fire scenarios can then be attempted.

   If possible, a fuller product analysis including GC-MS measurements of the profiles of organic products should be made for more accurate correlations with the observed toxicity. In addition, comprehensive measurements of product composition in small-scale tests enable comparisons to be made with product profiles in large-scale fire tests, and a judgment of how well the small-scale decompositions are able to reproduce the chemical "cocktails" present in different large-scale fire conditions.[17]
3. The bioassay method must be capable of detecting and measuring the particular types of toxic effects experienced by human fire victims. It must also be possible to make a reasonable extrapolation from the toxic effects in the animal model to those likely to occur in humans. It is therefore essential to determine both the qualitative and quantitative aspects of toxicity, and the time during or after exposure when they occur. People in fires experience incapacitating effects that may crucially impair their ability to escape, causing them to remain in the fire to be killed later by heat or CO, so a simple body count (LC_{50}) animal test without any description of preterminal toxicity is of very limited usefulness for input to toxic hazard models.
4. Some estimate of dose must be made. This should be reported in terms of concentration and duration of exposure as mass charged and mass consumed of material per liter of diluent air, and concentrations of basic toxic products as described previously. By carrying out tests at different concentrations, estimates should then be made of dose/time/response relationships.

Practical Methods for Toxic Hazard Assessment

There are essentially two ways in which toxic hazard in fire can be assessed.

1. From large-scale fire tests that include measurements of the concentration/time profiles of the major toxic gases, and existing knowledge of the toxic effects of these gases
2. From a battery of small-scale tests and mathematical models, or simple large-scale tests. The essential components are
   (a) the toxic potency data for materials [lethal mass loss exposure dose ($g \cdot m^{-3} \cdot min$)] obtained from small-scale tests using animal exposures or analytical methods
   (b) the mass loss/concentration curve for the fire

Of these, full-scale simulations and large-scale tests are the most valuable, since they enable the first two major parameters (fire growth and product yield) to be measured directly. For the third parameter (toxicity), an algorithm for calculating times to incapacitation and death for humans from toxic gases, heat, and smoke obscuration from large-scale fire data has been developed, and a simplified version is presented in ISO/IEC TR 9122-5.[143] Full-scale tests are already in use for a number of purposes (such as the furniture calorimeter and room calorimeter used for heat release measurements). With the addition of a few simple gas measurements, they can be extended to provide the data for full-scale hazard assessment. Although the use of full-scale tests for regulating fire performance has been criticized on grounds of cost, this approach has been used successfully in California.

The other notable method is to make use mainly of small-scale test data. Small-scale tests suffer from the difficulty that they are several steps removed from a full-scale fire, so that it is important to determine the validity of the parameters measured with respect to real fire conditions.

It has been claimed that some small-scale tests can be used to give a direct indication of the toxic hazard presented by a material in a full-scale fire, including elements of ignitability, fire growth and toxic potency. The UPITT test and the NIBS test are claimed to be usable in this way to produce hazard rankings for materials. However, small-scale tests cannot successfully model the complex growth and development of a full-scale fire, so that such methods are considered invalid. It may however be possible to extract a number of characteristics of the fire behavior of a material from a single test protocol, and use these as inputs to mathematical models for making hazard assessments. An example is the use of the cone calorimeter for measurement of both heat release and toxic gas yield from a material.

Nevertheless, the main job of small-scale toxicity tests is to provide data on the toxic *potency* of the combustion products from materials so that the data can be used as input to toxic hazard analysis in conjunction with fire growth data obtained from other sources.

The lethal toxic potency of combustion products from materials can be measured in small-scale tests in terms of the LCt_{50}, the lethal exposure dose to rodents. This is expressed in terms of the mass loss concentration of products (the mass of material decomposed in the test) divided by the volume of air into which they are dispersed (g/m^3) and multiplied by the time for which the animals were exposed, to give the exposure dose ($g \cdot m^{-3} \cdot min$). It is possible to quote the toxic potencies of materials in these terms for most small-scale test protocols, so that the results from different tests can be compared directly and so that the data can be used in conjunction with mass loss data from full-scale fire tests or model calculations to make toxic hazard assessments. The toxic hazard presented by the materials in full-scale fires can then be estimated in terms of the time during a fire when a victim will have received a lethal exposure dose, provided that the decomposition conditions in the small-scale test are the same as those in the full-scale fire. This is done by the fractional effective dose (FED) method, in which the mass loss exposure dose generated each minute during the full-scale fire (either measured or calculated) is expressed as a fraction of the lethal mass loss exposure dose for the material, obtained from the small-scale toxicity tests. When the integrated fractions during the fire reach unity, death is predicted. This method has been developed for use in toxic hazard assessments in British Standards[144] and in ISO/IEC.[143]

Examples of Small-Scale Test Methods

A variety of different methods have been used to generate combustion product atmospheres and evaluate their toxicity, and it is not possible here to describe these methods or the results obtained from them in detail. There are, however, three test methods that are in relatively wide use in the United States and in Europe—the NBS test method,[9,145] the DIN test method,[42,146,147] and the University of Pittsburgh test method.[98] An excellent description of these and other methods, and of the results obtained from them, is given in Kaplan et al.[15] A brief description of the principles of these three methods and their validity in predicting effects of exposure to large-scale fire environments follows. The methods are illustrated diagramatically in Figure 2-6.36(a) and (b).

National Bureau of Standards (NBS) Test Method

The NBS test method[9,145] is the simplest of the three. The test apparatus consists of a sealed rectangular polymethylmethacrylate chamber (200-L volume) containing a cup furnace set into the floor at one end. The animals (rats) are exposed nose only and placed in restraining tubes that are plugged into the sides of the chamber. Exposures are carried out under nonflaming conditions 25°C below the ignition temperature of the sample and under flaming conditions 25°C above the ignition temperature. The sample is placed into the preheated cup with the animals already in position, and they are exposed to the atmosphere in the chamber for 30 minutes. For this test there is thus an initial period when the concentration of decomposition products in the box increases as the sample decomposes, followed by a period when the atmospheric composition remains relatively constant for the remainder of the exposure. The concentration of products in the chamber is varied by placing different amounts of sample in the cup. This type of method is referred to as a "static" method, since there is no forced airflow over the sample and no ventilation of the chamber. It is possible to characterize the atmosphere approximately in terms of mass charge per liter of air by assuming a constant composition for the duration of the test. The atmosphere also can be characterized in terms of mass loss by weighing the residue after the test, or by placing the cup on a load cell. Measurements are also made of the chemical composition of the atmosphere in terms of the principle products. The animal toxicity is usually quoted in terms of the LC_{50} concentration of mass charge/L, but it is also common to monitor the asphyxiant effects on the animals by means of the leg flexion test. Effects upon respiration (such as irritant effects) could be monitored if desired.

(a) University of Pittsburg Apparatus

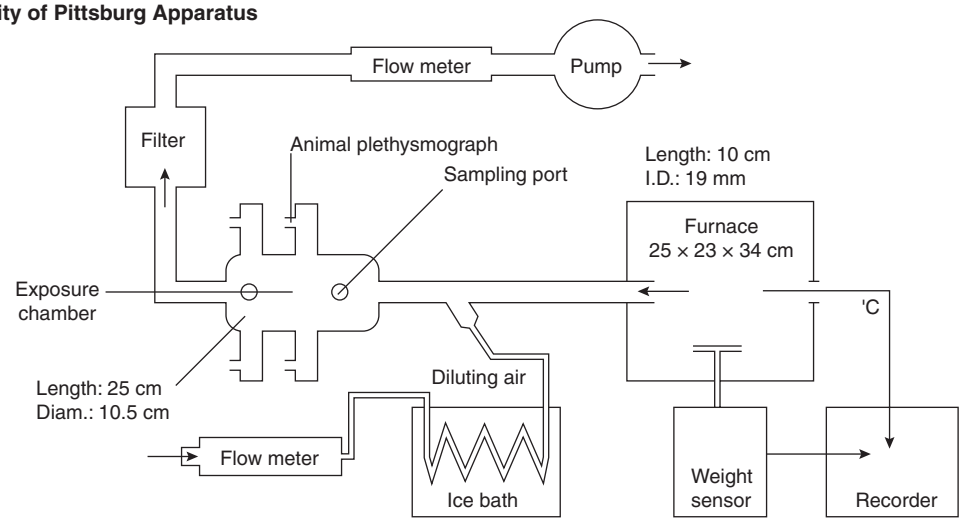

(b) National Bureau of Standards (NBS) Apparatus.[9]

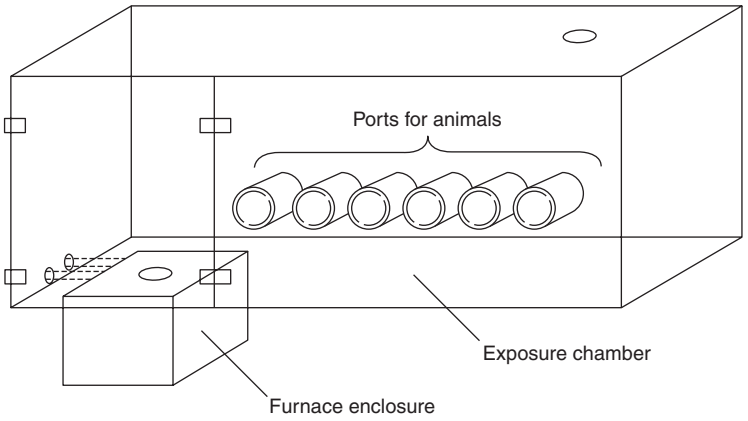

(c) DIN 53436 Apparatus.[148]

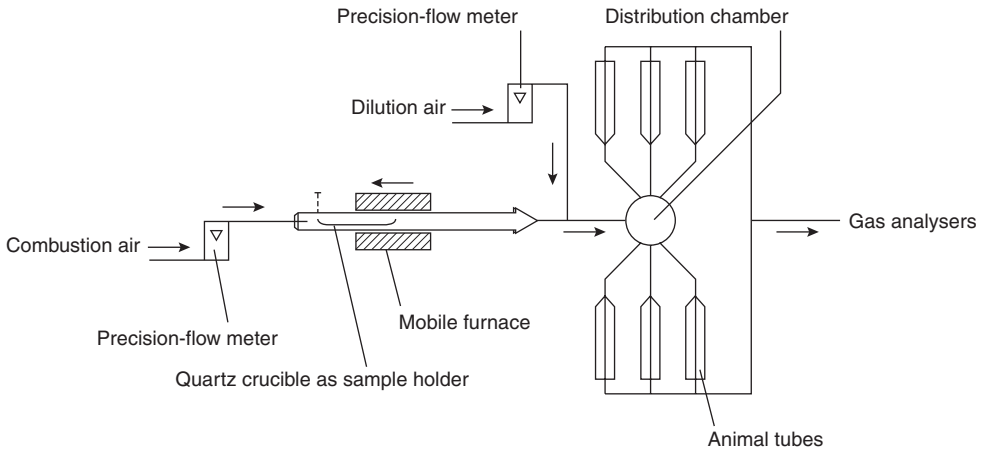

Figure 2-6.36. ***Laboratory-scale combustion toxicity test methods.***

The main advantage of this method is its simplicity, but it has the disadvantage that there is little control over the decomposition conditions. Another disadvantage is that the composition of the atmosphere does not remain constant, since there is a variable period during which the sample is decomposing, followed by a period when the smoke is aging and some products may condense onto the chamber walls. In tests where the decomposition product atmosphere has been compared to that produced in large-scale tests,[17] it has been found that the method gives a reasonably good simulation of the products from a smoldering or nonflaming fire, and also of the conditions during the early stages of a flaming fire. However, it was not possible to model the decomposition conditions of a high-temperature, fully developed fire, since when the cup is heated to high temperatures the pyrolysis products tend to escape from the cup before they are fully decomposed. In general, it should therefore be possible to use data from this method as one item in a toxic hazard assessment for nonflaming or early flaming fires.

University of Pittsburgh Test Method

In this method[98] the sample is also heated statically in a cylindrical furnace (early versions of the test used a tube furnace). However, in this case a flow of air is maintained over the sample and then mixed with diluent air before being passed through the animal (mouse) exposure chamber. In this way fresh products are continually passed to the animals under dynamic airflow conditions as they are generated over a 30-min exposure period. The unique feature of this method is that the sample is not maintained at a constant temperature, but is heated by means of a ramped temperature profile, the temperature increasing at 20°C/min. The animal exposure starts when the sample begins to decompose and lose weight as indicated by a load cell. The mice are exposed in the head-only configuration, as with the NBS method. In the University of Pittsburgh method the composition of the atmosphere changes continuously throughout the 30-minute animal exposure, and the atmosphere usually changes from nonflaming to flaming at some stage. The concentration of the decomposition products can be varied by changing the mass of material placed in the furnace (although presumably this could also be achieved by altering the flow of diluent air). It is possible to measure the changing profile of products to which the animals are exposed throughout the test, and also to monitor toxic effects such as asphyxia or irritancy, mainly from recordings of respiratory pattern. However, in its more recent application, the results of the test are usually expressed in terms of the LC_{50} in grams of material charged, which is used to rank different materials.

The main advantage of this method is that it theoretically covers a number of different decomposition conditions within a single test run, ranging from low-temperature nonflaming to high-temperature flaming. It is also said that this situation mimics the conditions in a real fire where materials begin by being cold, and are then heated up until they pyrolize and eventually flame. A feature of the test is that the time/temperature increase taken from the start of the decomposition run to the occurrence of the evolution of smoke, toxic effects, and flaming may be used as criteria for judging materials. Thus a material that flames early or produces smoke early may be judged more hazardous than one that does not start to decompose until a high temperature is attained.

Although ramped heating of a sample may provide a useful model for the specific situation where a material is subjected to a slowly rising temperature, it cannot be said to mimic the changing conditions in a fire. In a fire, a material or its immediate pyrolysis products may be subjected to any of a variety of conditions of temperature or oxygen supply under nonflaming or flaming conditions, and the way in which these conditions change is governed by the nature of the large-scale fire scenario. In order to model these various conditions, it is necessary to subject separate samples of test material to a range of different temperatures (or radiant fluxes) and oxygen supplies. The main problem with ramped heating of a sample is that it does not submit the whole material to the necessary range of conditions, since it causes fractional decomposition of the material. Products evolved at relatively low temperatures will not therefore be present at a later stage to be involved in flame; neither will they be subjected to high temperatures, since they will have left the furnace before higher temperatures are achieved. This may have a profound effect upon the kind of products evolved and hence the toxicity.

Another disadvantage of this test method is the difficulty of characterizing dose, since the composition of the atmosphere changes throughout the test. For comparison with other methods, it would be possible to calculate a very approximate nominal atmospheric concentration in terms of mass charged/L if it is assumed that the decomposition averages out over the duration of the test. A better estimate may be made of the atmosphere concentration in terms of mass loss/L if the mass loss as measured by a load cell is integrated over the exposure period. This might give a reasonable measure of dose to enable an LC_{50} to be calculated, but other estimates of toxicity are complicated by the changing nature of the atmosphere. Thus, if death or asphyxia were to occur at 30 min, for example, it is not possible to determine whether this would be due to the delayed effect of a product evolved at 5 min or an immediate effect of a product from 29 min.

There are thus some difficulties with this method, both as a fire model and as a toxicity assay. But, if the method is backed by a full profile of material mass loss and product concentrations, plus qualitative and quantitative estimates of toxic effects throughout and after the exposure, it may be possible to apply the data in certain special situations.

German DIN 53 436 Test Method

This method[42,146,147] is widely used both in the United States and in Europe. It employs a fully dynamic system in that fresh material is decomposed at a constant rate throughout the test and fresh atmosphere is supplied continuously to the animals. The method has been used with rats, mice, and primates; rats being the principal test animals. The principle of the method is that a strip of test

material is placed in a silica tube under a current of air (or nitrogen for studies of pyrolysis) and a traveling annular furnace is moved along the outside of the tube at a constant rate, thereby continuously decomposing the sample. The products are expelled from the silica tube, whereupon they are mixed with diluent air and passed through the animal exposure chamber for 30 min. The rats are exposed in the head-only manner as with the other methods. The sample weight and volume, the primary air supply to the sample, the diluent air, the decomposition temperature, and the concentrations of products in the exposure chamber are measured. The test may be repeated over a range of temperatures under nonflaming or flaming conditions, and the concentration of the products is varied principally by changing the diluent airflow. This has the advantage that the decomposition conditions remain constant as the product concentration is changed, which is not necessarily the case with the other two methods. However, it is also possible to change the product concentration by altering the furnace load, if necessary. The animal toxicity is usually reported in terms of the LC_{50}, which is expressed in terms of mass charged (mass entering the furnace/min)/L diluent air. It is also possible to calculate the concentration in terms of mass loss from the mass of residue remaining after the test run, since the rate of decomposition is constant. Sometimes the results are expressed in terms of the volume of material consumed. In addition, it is possible to monitor the toxic effects on the animals during and after the test as with the other methods.

The great advantage of this method is its versatility, and in theory it can model any of the three basic fire conditions: nonflaming, flaming, and high temperature, as well as variations on them. It is also possible to carry out static ramped temperature decompositions similar to the Pittsburgh method, if required. In practice the method has been found to provide a good correlation with large-scale nonflaming decomposition conditions, and at high temperatures it provides a reasonable model for the conditions of a fully developed flaming or nonflaming fire (high temperature-low oxygen).[17] However, under standard conditions it does not provide a good model for an early flaming fire (which is reasonably modeled by the NBS method) as the oxygen concentration in the furnace tube tends to be low. Another problem is that the flame tends to travel along the sample more rapidly than the furnace, giving an uneven decomposition. These problems can be overcome by varying the fuel-to-air ratio in the furnace tube and by altering the rate of travel of the furnace.

On balance, the DIN method is reasonably good, and the data obtained could be applied to a number of stages of a fire as one item in a hazard assessment. However, like all small-scale tests it cannot mimic the changing and developing conditions of a large-scale fire; neither can it test materials or objects in their end-use configuration, all of which can have an enormous impact on a developing toxic hazard.

Second Generation Test Methods

Since these small-scale test methods were developed, there has been considerable progress in understanding of how toxic hazard develops in fires, and in particular that hazard depends to a large extent on the general fire properties of materials (in terms of ignitibility, flame spread, rate of fire growth, and smoke evolution), as well as the specific toxicity of the combustion products. Also, critical examination of the fire models used for toxicity test methods (and for small-scale tests for other fire properties such as smoke) has led to the recognition that the models are somewhat inadequate, particularly for the main fire condition of flaming. Another difficulty is that toxicity data are of little value unless they can be related to a range of physical and chemical parameters necessary to characterize the thermal decomposition process, as described in the previous section of this chapter.

There is, therefore, a case for arguing that for many material-based fire properties, a good small-scale test method depends upon a decomposition model that can be convincingly related to the essential features of large-scale decomposition conditions. If such a model could be developed, it could be used to measure simultaneously a number of material-based fire performance parameters ranging from ease of ignition, through growth and heat release characteristics, to smoke and toxicity.

A second generation of small-scale fire test methods is being developed, incorporating, hopefully, some of the best features of existing methods, and designed to measure a range of parameters.

Cone calorimeter: A second generation small-scale test method currently under development is the National Bureau of Standards (NBS—now NIST) cone calorimeter,[149] which has been developed primarily as a heat release apparatus, but which may also offer the possibility of measuring ignitibility, smoke evolution, and toxicity. This would not only enable a range of parameters to be measured simultaneously, but would enable the separate parameters to be related, hopefully providing a more comprehensive data set for comparison with, and inputs for modeling of, large-scale fire conditions.

In practice the cone calorimeter has not proved to be very suitable for measuring toxic potency. It is capable only of reproducing the decomposition conditions in very well-ventilated fires, and the products are subjected to a very large dilution, so that measurement of toxic species is difficult. Attempts are being made to enlarge the range of fire types and stages addressed by modification of the apparatus.

NIST radiant method: A second generation version of the NABS cup furnace method has been developed in which the cup furnace was replaced by a radiant panel heater unit. This method has been developed to address the conditions in post-flashover fires, but as with the cup furnace version, and the cone calorimeter, the combustion process tends to be too well ventilated to reproduce the conditions typical of these fires, which are usually rather vitiated.

Tube furnace method developed at the U.K. Fire Research Station:[37] The most recently developed method intended to address some of the deficiencies of older methods is a tube furnace method based upon the same

concept as the DIN tube furnace method. The new method employs a strip of sample being advanced through a standard tube furnace under a stream of air. (See Figure 2-6.37.) The products are expelled into a chamber where they are diluted with secondary air, and analytical measurements are made or animals can be exposed nose-only. By using a range of different temperatures and airflow rates it is possible to reproduce all the different fire stages and types defined by ISO (and others), including low-temperature non-flaming oxidative decomposition, well-ventilated flaming, and high-temperature vitiated (post-flashover) flaming decomposition conditions. The method also provides stable flaming conditions, solving the problem of mixed, intermittent periods of flaming and nonflaming common with the original DIN method.

Relationship between Toxic Potencies of Materials in Small-Scale Tests and Full-Scale Fires

When the toxic potency of the combustion products from a material are expressed empirically in mass loss terms, the data relate to the toxic effects of the total mixed combustion product evolved. This depends upon the type of toxic products evolved and their yields. The most difficult problem in estimating the toxic potency of a material in a fire is that the yields of toxic products depend very much upon the decomposition conditions, which vary considerably at different stages and between different types of fires. If small-scale test data are to be used as estimates of the likely toxic potency of products evolved in full-scale fires, it is essential that the decomposition conditions in the test be shown to be the same as those in the type or stage of full-scale fire being modeled, otherwise the small-scale test data are not valid.

The decomposition conditions and yields of toxic products evolved from materials in full-scale fires depend mainly upon whether or not the fuel is flaming, the fuel/air ratio (equivalence ratio), and the upper layer temperature. In ISO/IEC TR 9122-4[150] an attempt has been made to define the major categories of fire in these terms, the type of decomposition for flaming fires being expressed in terms of the CO_2/CO ratio. A revised scheme is shown in Table 2-6.27. The six fire types shown in the table contain three major categories: (1) nonflaming, (2) well-ventilated flaming, where the fire size is small in relation to the size of the compartment, the flames are below the base of the hot layer, and fire size is fuel controlled, and (3) less well-ventilated flaming, where the fire size may be large in relation to the size of the compartment, the flames are partly above the base of the hot layer, and fire size is ventilation controlled. The third case includes small vitiated fires in enclosed or poorly ventilated compartments and post-flashover fires in large or well-ventilated compartments. In ISO/IEC TR 9122-4 small-scale toxicity test protocols are judged by the extent to which the test conditions are relatable to one of these categories in terms of temperature or radiant heat flux, oxygen concentration, and CO_2/CO ratio. If they are to be considered useful to measure the toxic potency of

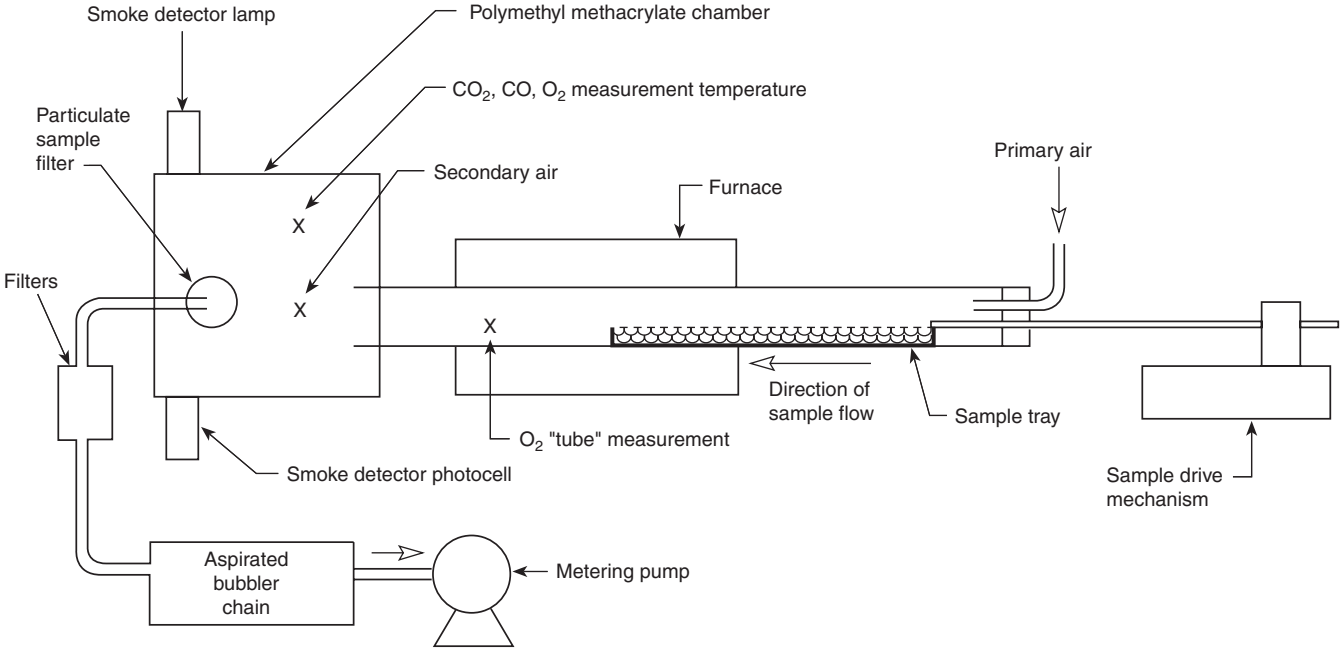

Figure 2-6.37. ***Improved tube furnace method.***

Table 2-6.27 ***Revised Classification of Fire Types***[33]

Fire Stage or Type	Temperature (°C)		Fire Effluents		
	Fire	Hot Layer	Oxygen to Fire (%)	Oxygen from Fire (%)	CO_2/CO (v/v)
1. Nonflaming					
a. Self-sustaining	450–600	RT	21	>20	1–5
b. Oxidative pyrolysis from externally applied radiation	300–600	<50	21	>20	1–5
c. Nonoxidative pyrolysis from externally applied radiation	300–600	<50	0	0	<5
2. Well-ventilated flaming where the fire size is small in relation to the size of the compartment, the flames are below the base of the hot layer and fire size is fuel controlled	>700	RT to 500	>15	5–21	>20[a]
3. Less well-ventilated flaming where the fire size may be large in relation to the size of the compartment, the flames are partly above the base of the hot layer and fire size is ventilation controlled:					
a. Small vitiated fires in closed compartments	>700	RT to 500	<15	0–12	2–20
b. Post-flashover fires in large or open compartments	>700	500 to 1000	<15	0–12	2–20

[a]May be lower if the burning materials contain fire retardants. In order to determine whether flaming decomposition conditions in a particular apparatus fall into category 2 or category 3, it is necessary to use a nonfire-retarded reference material capable of efficient combustion.

the combustion products from materials, the decomposition conditions must relate to one of these fire stages or types, and the results of any small-scale test are then only valid for the particular category being modeled. Based upon the results of full-scale fire tests, and fire death statistics, it is suggested here that the most important toxic hazard situations that should be assessed for all materials are

1. Nonflaming oxidative/smoldering decomposition at low/mid-range temperatures where the potential hazard relates mainly to victims in the compartment of fire origin
2. Early/well-ventilated flaming conditions at mid-range temperatures, and later small vitiated fires in closed compartments, where the potential hazard relates mainly to victims in the compartment of fire origin
3. Fully developed/post-flashover, vitiated decomposition at high temperatures, where the potential hazard relates mainly to victims remote from the fire

In the United Kingdom just over half of all fire deaths in buildings occur in the room of fire origin and most result from exposure to toxic smoke evolved from small fires (which may involve periods of nonflaming and both early and later flaming decomposition). The other major category, particularly related to deaths from smoke exposure, consists of victims in remote locations following fully developed fires. It is this second category that has been identified as the major problem in the United States, particularly in relation to fires in multi-occupation buildings.

Unfortunately, many existing small-scale test protocols do not cover the necessary range of decomposition conditions found in full-scale fires, especially the third category of the fully developed, high-temperature, oxygen vitiated fire. However, a new technique is presented here whereby certain predictions about the toxicity of combustion product atmosphere can be made, based entirely upon analytical data. This enables use of data both from small-scale experiments and full-scale fire tests.

It is considered that the major toxic effects of fire effluents can be explained in terms of a small number of well-known fire gases, so that the effects of fire gases on human fire victims can be predicted to a large extent if the concentrations of these gases during a fire are known. In a similar way, it is now possible to a large extent to predict the exposure dose of combustion products generated in small-scale tests that would be lethal to rodents, if the concentrations of the major toxic gases are measured. If necessary, it is then possible to verify the prediction by carrying out the animal exposures. Experiments of this kind, carried out by Hartzell et al.[151] and Levin et al.,[152] have shown that toxic gases are basically additive in their effects, so that, for example, an exposure to an atmosphere containing half a lethal dose of carbon monoxide mixed with half a lethal dose of hydrogen cyanide constitutes a lethal mixed atmosphere.

The toxic effects of combustion products result mainly from asphyxia and irritancy. Asphyxiation is caused by carbon monoxide, hydrogen cyanide, low-oxygen hypoxia, and carbon dioxide, and so can be quite well predicted if the concentrations of these gases are known. Irritancy is somewhat harder to predict because many irritant organic products and inorganic acid gases occur in fire atmospheres. Where acid gases are present

the concentrations can be measured and their effects added to those of the asphyxiant gases. In small-scale tests where both chemical analysis and animal exposures are used it is possible to calculate the contribution to the overall toxicity made by the measured asphyxiant gases and acid gas irritants. Any residual lethal toxicity can then be reasonably considered to be due to the effects of organic irritants, except in very rare cases where unusual toxic effects occur. For small-scale tests, or even large-scale fires, where analytical data only are available it is possible to calculate a theoretical LCt_{50} in terms of the main asphyxiant fire gases and acid gases. This then represents the *highest* estimate of what constitutes a lethal dose for that atmosphere (i.e., the smoke atmosphere must be at least as toxic as this, and could be somewhat more toxic if substantial amounts of organic irritants are present, or if unusual toxic effects are present. In small-scale tests there is little oxygen vitiation, so this effect can be ignored. On this basis an equation has been developed to predict the lethal FED to rats of a combustion product atmosphere as follows:

$$\text{fractional effective dose (FED)} = [(\text{CO ppm}/LC_{50}\,\text{CO} + \text{HCN ppm}/LC_{50}\,\text{HCN} + \text{ppm each acid gas}/LC_{50}\,\text{each gas} + \text{ppm each organic irritant}/LC_{50}\,\text{each organic irritant}) \times V\text{CO}_2] + A \quad (29)$$

where

$V\text{CO}_2$ is a multiplication factor for CO_2-driven hyperventilation $= 1 + \exp\dfrac{(0.14 \times [\text{CO}_2\%]) - 1}{2}$

A is an acidosis factor $= [\text{CO}_2\%] \times 0.05$

LC_{50} is the lethal exposure concentration for a 30-min exposure for the material in mass loss terms

Currently generally accepted 30-minute LC_{50} concentrations for exposure of rats to common fire effluent gases are given in Table 2-6.28.[33,106]

When the FED for this equation equals unity, then death is predicted, and the mass loss exposure dose for the material producing these gas concentrations is then equal to the LCt_{50} for that material decomposed under the conditions of the test. If the concentrations of the irritants present and their lethal exposure doses are known, then the equation can be solved fully (e.g., the LCt_{50} for HCl is 112,980 ppm·min).[153,154] Where unknown irritants are present, the equation enables the maximum LCt_{50} to be predicted based upon the asphyxiant gases and any known irritants.

This is a powerful technique because it enables a number of things to be done, as follows:

1. Where a material is tested in a small-scale test using only chemical atmosphere analysis, it enables an estimate to be made of the likely approximate toxic potency of the combustion products from the material, without the use of animal exposures.
2. Where a material is tested in a small-scale test using both chemical atmosphere analysis and animal exposures, then it is possible to determine the extent to which the toxicity of the combustion products can be accounted for in terms of the common toxic gases, or if additional toxicants are present.
3. If the toxic effects are almost entirely accountable in terms of the common toxic gases (as is often the case), then it enables the toxic effects of full-scale test atmospheres to be predicted with confidence, without animal exposures, if these gases are measured.
4. Where the LCt_{50} in a small-scale test is estimated from analytical data, or where it is measured using animals, it enables estimates of toxic potency of full-scale fires to be made simply from the mass loss rate and dispersal of products in the fire, provided the full-scale fire is of the same type as the small-scale test decomposition.
5. Where analytical data are available from full-scale tests, they enable some estimates to be made of the toxic potencies of the materials involved.

Table 2-6.28 ***Currently Accepted 30-min LC_{50} Concentrations for Common Fire Gases***

Gas	Concentration (ppm)
CO	5700
HCN	165
HCl	3800
HBr	3800
HF	2900
SO_2	400–1400[a]
NO_2	170
acrolein	150
formaldehyde	750

[a]Range or results from a number of studies

The following examples show how this technique can be applied, using data from experiments with wood. When samples of Douglas fir were decomposed under flaming conditions in the NABS cup furnace, the LCt_{50} for a 30-min exposure of rats was 1194 $g \cdot m^{-3} \cdot min$. In the test, the CO concentration was 3400 ppm and the CO_2 concentration 3.71 percent, a CO_2/CO ratio of 11/1. According to the FED equation given above, this represents a FED of 1.0. It can therefore be concluded that in this test the observed toxic potency can be fully accounted for in terms of CO and CO_2, and that there was little or no contribution from irritants or other toxic products on lethality. This result is to be expected, since the NBS cup furnace method generally simulates reasonably well-ventilated early flaming conditions where combustion is usually efficient, so that the yield of organic irritants would be expected to be low. However, in this test it is surprising that the CO_2/CO ratio is so low, and more representative of somewhat vitiated burning conditions.

It is now possible to examine some full-scale test data on wood fires of this type, in the knowledge that CO and CO_2 are the main toxic products to consider. Such a test was performed at the U.K. Fire Research Station, where a 5-kg wood crib (Scotch pine) was burned in a closed 26 m^3 room. At 6 min into this fire the CO_2/CO ratio in the smoke was 60/1. Based upon a 44 percent carbon content

for wood, and assuming that all carbon in the mass lost was converted to carbon oxides (CO_2 + CO), it is now possible to calculate what mass loss of wood in a small-scale test would be required for a 50 percent rodent lethality at a CO_2/CO ratio of 60/1. It is to be expected that under these conditions the wood smoke would be less toxic than in the reported NBS test, since the major toxicant is the CO, and the CO yield is low at this moment in the fire. This is indeed likely to be the case, since the FED equation predicts an LCt_{50} of 3750 g·m^{-3}·min under these decomposition conditions, approximately three times less toxic than in the small-scale test.

Major Determinants of Toxicity in Fires and Small-Scale Tests

The toxicity of the combustion products from individual materials in fire, in terms of the type and yields of the major asphyxiant, irritant, and other toxic products depends principally upon three factors.

1. The elemental composition of the material
2. The organic composition of the material
3. The decomposition conditions

The most important toxic products from fires are usually carbon monoxide and hydrogen cyanide, so that the most important elemental determinants of toxic potency are normally the carbon and nitrogen content of the fuel, with the halogen content being important to a lesser extent in some cases, and organic irritants in others.

Nonflaming Oxidative/Smoldering Fires

Nonflaming decomposition is slow, so that a long time is required for the development of hazardous conditions. However, of the small masses of materials decomposed during nonflaming oxidative decomposition, the yield of CO can be quite high, and these conditions generally provide the highest yields or organic products, including irritants, the identity of which is often unknown. In small-scale tests conducted under these conditions, only a small proportion of the observed toxic potency can be accounted for in terms of the common toxic gases. Table 2-6.29 shows two examples of this type, from experiments using the NBS cup furnace method to decompose Douglas fir and a flexible polyurethane foam under nonflaming oxidative conditions. The results show that at the LCt_{50} of wood to rats of 684 g·m^{-3}·min, only 0.47 of the observed toxicity could be accounted for in terms of common toxic gases, and for the flexible polyurethane foam only 0.29 of the observed toxicity could be accounted for. This means that for these (and many other) materials decomposed under nonflaming oxidative conditions, a large part of the toxic potency is due to products other than those normally measured, almost certainly organic irritants, so that the FED method tends to underestimate the toxicity, unless allowance is made for irritancy (such as assuming that approximately half of the toxic potency is likely to be due to irritants for most common materials under these decomposition conditions).

However, the nonflaming condition is adequately replicated by a number of small-scale test methods, and there is a large toxicity data base available for many materials, since by far the greatest amount of published test results are obtained under these conditions.

From a recent review of published toxic potency data from common materials[35] including data from a number of small- and large-scale test methods it is possible to make some general observations regarding the toxic potencies of the decomposition products from materials under a range of fire conditions. For nonflaming oxidative decomposition conditions, the range of LCt_{50} for individual materials covers approximately a factor of 12 from 63 to 767 g·m^{-3}·min.

Early or Well-Ventilated Flaming Fires

In flaming fires, the yields of carbon oxides and nitrogen compounds depend mostly upon the decomposition conditions, particularly the air/fuel ratio. With regard to carbon, the main consideration is the CO_2/CO ratio, which not only determines the toxic potency of the smoke, since CO is approximately 20 times more toxic than CO_2, but to a large extent defines the fire type. In early well-ventilated fires combustion is usually efficient, and the CO_2/CO ratio may be as high as 200/1, although in practice somewhat lower ratios around 60/1 are more

Table 2-6.29 ***Toxic Potency Analysis of Materials Decomposed under Nonflaming Oxidative Conditions in the NBS Cup Furnace***

	Douglas Fir 440°C		Flexible Polyurethane Foam 400°C	
	Concentration	FED	Concentration	FED
Carbon monoxide	2700 ppm	0.47	1261 ppm	0.22
Hydrogen cyanide	0 ppm	0.00	11 ppm	0.07
Carbon dioxide	0.69%	× VCO_2 1.0	0.4%	× VCO_2 1.0
Total FED asphyxiants		0.47		0.29
FED presumed due to irritants		0.53		0.71
LCt_{50} calculated	1455 g·m^{-3}·min		3621 g·m^{-3}·min	
LCt_{50} observed	684 g·m^{-3}·min		1050 g·m^{-3}·min	

typical. Under these conditions the yield of organic irritants is usually low, since combustion is efficient, and the yield of CO is so low that the overall toxic potency of materials containing principally hydrogen and carbon can be expected to be low. The exceptions tend to be fire-retardant materials, "naturally" fire-retardant materials such as PVC, and some largely aromatic materials such as polystyrene, all of which tend to burn inefficiently and give low CO_2/CO ratios even under well-ventilated conditions. This results in high yields of CO and usually of irritants, and somewhat higher toxic potencies than for more easily and cleanly burning materials.

With nitrogen-containing materials, the situation is somewhat analogous to that with carbon, since in well-ventilated, early flaming fires, most nitrogen in materials is oxidized to nitrogen oxides and N_2. The yield of HCN is generally low (with the exception of acrylic materials, and to some extent rigid polyurethanes). Although NO_2, which is a potent lung irritant, can be expected to be present at high yields under these conditions, the general effects seems to be that, since the HCN yield is low, toxic potency tends to be low. With materials like PVC, almost all the chloride is released as HCl under almost all decomposition conditions, including flaming conditions.

The general picture then is that the toxic potency of combustion products from most materials is lowest under early, well-ventilated flaming conditions. Materials that tend to perform comparatively less well under these conditions are FR-materials, and materials like PVC, where the halogen acid gases cannot be destroyed by the flames.

Small-Scale Tests Replicating Well-Ventilated Flaming Conditions

To study the toxic potencies of materials under the decomposition conditions similar to those during the early stages of flaming fires it is necessary to use a test method that provides flaming combustion throughout the test until the material is fully decomposed. The test method must also provide good ventilation of nonvitiated air to the specimen, and have a general temperature environment of around 400 to 700°C (or equivalent radiant flux). Most important, however, it must produce high CO_2/CO ratios (in the range approximately 200/1 to 50/1) from normally combustible (i.e., non-FR) materials.

NBS cup furnace test: Of the small-scale test methods commonly in use, a number perform well in this area. The one for which the most toxicity data are available is the NBS cup furnace test. In this test the material specimen is decomposed in a crucible furnace, and the products are evolved into a 200-L box. The key feature of this test is that it is normally used with quite small specimens, so that the oxygen concentration in the box is not significantly lowered during the test, and studies of the combustion process have shown that air circulates rapidly down into the cup furnace during decomposition, so that combustion tends to be reasonably efficient. The CO_2/CO ratios typically produced in tests are in the 40/1 to 60/1 region, so that, although perhaps not representing the most efficient combustion, they are generally a reasonable model for the results obtained in small, well-ventilated full-scale fire tests.

NIST U.S. radiant (NIBS) test: A more recent development of the NBS cup furnace test is the NIBS test or NIST radiant test. The two versions of the test use the same apparatus, but somewhat different test protocols. For this test a radiant heating unit is placed in a cavity under the NBS chamber, and connected to it by a slit-shaped chimney. Investigations of the combustion mode of this test[21] have also shown that under flaming combustion conditions the circulation of air is such that the specimen is very well ventilated, so that CO_2/CO ratios are generally reasonably high. Data from this test method suggest that it may best represent the decomposition conditions in a well-ventilated fully developed (possibly post-flashover) fire. However, in its present form it does not appear to generate the very low CO_2/CO ratios and high CO and HCN yields found in typical post-flashover fires in compartments.

Cone calorimeter: The cone calorimeter has not been used very successfully with animal exposures, but using the FED model presented in this chapter, it is possible to make some useful estimates of likely toxic potency based on the toxic gas yields and the mass loss of the specimen. The cone calorimeter gives the most efficient combustion conditions of any test method, typically producing CO_2/CO ratios in the 200/1 to 100/1 range for non-FR materials. It can also therefore be used as representative of the decomposition conditions during very early and very well-ventilated fires. So far, attempts to modify the combustion process and decrease the combustion efficiency to model other stages of fire have not proved very successful.

DIN method: For the DIN 53 436 method, decomposition occurs in a tube furnace, the furnace passing over a strip of sample, with decomposition achieved by passing a stream of air through the furnace and over the sample. The products from the tube furnace may then be diluted with secondary air for animal exposures, if required. The atmosphere produced is in a "dynamic steady state," in that the concentrations of decomposition products remain constant because the test material is decomposed at a constant rate throughout the test. The epithet "DIN" has come to represent a number of tube furnace methods based upon the same principle, generally accepted as DIN test results, the important point being to demonstrate that the decomposition atmosphere generated is relatable to real fire conditions, rather than that the apparatus design is standard.

The important feature of this design is its versatility, since the decomposition conditions can be varied over a wide range by varying the sample load, air supply, and furnace temperature. This contrasts with the other methods described, which are very restricted in the range of conditions that can be modeled. The improved tube furnace method, recently developed at the UK Fire Research Station (FRS),[37] is based upon the DIN method concept, and is the only one developed so far that can simulate the decomposition conditions for all fire types, including

nonflaming, early flaming, and fully developed fires with restricted ventilation, particularly post-flashover fires. (See Figure 2-6.37.) A limitation with the official method, in regard to flaming combustion, is that the decomposition conditions tend to be rather vitiated, giving low CO_2/CO ratios, and flaming is unstable. However, this is remedied in the FRS method by increasing the air/fuel ratio in the furnace tube, and the rate of sample advance. In a recent series of experiments it has been possible to increase the ratios to those occurring in early, well-ventilated, full-scale fires, while achieving stable flaming conditions.

UPITT method: The University of Pittsburgh method is considered to give a poor representation of actual fire conditions, and it is considered that it is not possible to relate it to any of the fire conditions shown in Table 2-6.27. For this reason (and others), UPITT data are considered unsuitable for the assessment of toxic potency of materials involved in fires, except in very special cases where the conditions can be shown to be similar to the sequence of events occurring in the UPITT apparatus.

Toxic Potency Data Obtained from Tests under Early, Well-Ventilated Flaming Conditions

Because well-ventilated flaming conditions tend to destroy compounds such as organic irritants, it is to be expected that the toxic potency will be more completely due to the common toxic gases than for the nonflaming fires shown in Table 2-6.29. Table 2-6.30 illustrates this with some examples taken from NBS cup furnace test data. The data for Douglas fir shown that, unlike the nonflaming situation illustrated in Table 2-6.29, the toxic potency can be fully accounted for in terms of carbon oxides, and an LCt_{50} for wood calculated on this basis would be very close to the observed value. For flexible polyurethane (FPU) foam it was not possible to obtain a lethal concentration in the cup furnace under flaming conditions due to limits on the capacity of the apparatus for the size of sample required, but in other experiments a mixture of polyester and FPU were tested. With this mixture of materials it was possible to obtain lethal exposure conditions, and the data are also shown in Table 2-6.30. As with the wood, it was possible to account fully for the observed toxic potency on the basis of carbon oxides and hydrogen cyanide.

For materials that burn less efficiently under these conditions, or which produce inorganic acid gases, the data analyses indicate contributions to lethality from irritants. For example, Table 2-6.31 shows data on PVC and a FR polyurethane foam obtained using the NBS cup furnace method. For the PVC test, the contribution to the total FED from carbon oxides was only 0.19, so that the major cause of death had to be some other factor. Unfortunately the HCl concentration was not measured, but from the mass of PVC decomposed, it can be estimated at approximately 5000 ppm. As the analysis shows this would have been more than enough to have accounted for the observed lethality. With regard to the FR FPU, the yield of common toxic gases was significantly greater than that from the untreated foam, so that it was possible to obtain an LCt_{50} using the cup furnace. The concentrations of carbon oxides and hydrogen cyanide were sufficient to account for approximately 0.7 of the observed toxic potency, but it is possible that the remaining 0.3 represents the effects of unidentified irritants evolved due to the less efficient combustion occurring from this foam compared to an untreated foam.

Based upon available published small- and large-scale test data, it is possible to make some general observations regarding the early, well-ventilated, flaming condition. The basic finding is that the published database is very poor, there being only a few tests or none on quite common materials. The only materials for which a reasonable number of tests have been performed under flaming conditions are wood, flexible polyurethanes, and PVC. Needless to say, these involve a variety of wood species and polymer formulations. Based upon this inadequate database, the pattern that emerges is that the range of toxic potencies of common materials covers approximately a factor of 50, with LCt_{50} exposure doses of from approximately 75 to 3750 $g \cdot m^{-3} \cdot min$. As could be predicted, the least toxic materials are the cellulosics and simple hydrocarbon polymers, such as polypropylene. Flexible polyurethanes are of low to intermediate toxic potency within this range. The most toxic materials are the acrylonitriles, which release quite large amounts of

Table 2-6.30 ***Toxic Potency Analysis of Materials Decomposed under Early, Well-Ventilated Flaming Conditions in the NBS Cup Furnace***

	Douglas Fir 485°C		Flexible Polyurethane Foam and Polyester 525°C	
	Concentration	FED	Concentration	FED
Carbon monoxide	3400 ppm	0.60	2270 ppm	0.40
Hydrogen cyanide	0 ppm	0.00	63 ppm	0.38
Carbon dioxide	3.71%	$\times\ VCO_2\ 1.4 + 0.2$	3.36%	$\times\ VCO_2\ 1.25 + 0.1$
Total FED asphyxiants		1.04		1.08
FED presumed due to irritants		0		0
LCt_{50} calculated	1148 $g \cdot m^{-3} \cdot min$		1038 $g \cdot m^{-3} \cdot min$	
LCt_{50} observed	1194 $g \cdot m^{-3} \cdot min$		1170 $g \cdot m^{-3} \cdot min$	

Table 2-6.31 ***Toxic Potency Analysis of Materials Decomposed Less Efficiently under Early, Well-Ventilated Flaming Conditions in the NBS Cup Furnace***

	PVC 625°C		FR Flexible Polyurethane Foam 425°C	
	Concentration	FED	Concentration	FED
Carbon monoxide	1100 ppm	0.19	1040 ppm	0.18
Hydrogen cyanide	5000 ppm	1.33	86 ppm	0.52
Carbon dioxide	0.55%	$\times$ VCO_2 1	2.1%	$\times$ VCO_2 1
Total FED asphyxiants		0.19		0.70
FED presumed due to irritants		1		0.30
LCt_{50} calculated	341 g·m^{-3}·min		1157 g·m^{-3}·min	
LCt_{50} observed	519 g·m^{-3}·min		810 g·m^{-3}·min	

HCN even under well-ventilated flaming conditions. PVCs are generally somewhat more toxic than the cellulosic materials under these conditions, due to their relatively low combustion efficiency and high HCl yield.

Small-Scale Tests Replicating Fully Developed Fire Conditions—Especially Post-Flashover Fires

The decomposition conditions in fully developed fires depend very heavily upon the conditions in fire compartments and in particular the air supply. A general principle would be that in the common situation of a fire in a building, which would typically contain large amounts of combustible fuel, the fire growth will depend upon the rate of involvement of the fuel in the early stages, with efficient combustion and high CO_2/CO ratios (100/1 to 200/1). Then as the fire grows, combustion becomes increasingly ventilation controlled, so that fully developed fires tend to be oxygen vitiated, with low CO_2/CO ratios ($<$10/1). However, it is possible to have fully developed, well-ventilated fires with high CO_2/CO ratios (up to 100/1), as indicated in Table 2-6.27. These conditions can commonly occur during some stages of test fires in large-scale test rigs. Such large-scale tests usually have a relatively small amount of fuel (such as a single chair), and have a rig with an open side or doorway or window openings, which are, in turn, supplied freely with air from outside or from a large test facility building. Another factor that may provide high CO_2/CO ratios in the effluents from a primarily vitiated post-flashover fire is secondary combustion outside the fire compartment, where the products mix with air and are sufficiently hot to support further combustion. This effect has been observed at the DIN furnace outlet when attempting to simulate post-flashover decomposition conditions.

Accidental fires in real occupied buildings often have access to a much larger amount of fuel than test fires, and often have access to a more restricted air supply (such as air from inside the building). Thus in the Boston Fire Department study of accidental fires,[155] 50 percent had CO_2/CO ratios of less than 10/1 and a further 22 percent had ratios of approximately 10 to 20/1. Only 17 percent fell into the well-ventilated category, with ratios above 40/1. When full-scale tests are more closely related to real buildings or contents, then low ratios occur. For example, a simulation of a fire in a fully furnished hotel bedroom, opening on an open corridor with a side room attached, gave CO_2/CO ratios of 2/1 in the burn room and 3/1 in the side room at the fire peak.[138]

Once a fire has passed beyond the very early, well-ventilated stage, there are basically two paths for continued development, depending largely on the type of fire compartment. First, where the fire occurs in a room-sized compartment, and the room doors and windows are shut, the combustion becomes vitiated from a very early stage, since a typical domestic room will not support complete combustion of more than approximately 1 kg of fuel before the oxygen concentration in the room is reduced to approximately 10 percent and the fire extinguishes or dies down. Fires of this type, involved in many deaths, tend not to develop beyond a small size as long as the compartment is closed, but the CO_2/CO ratio decreases from a very early stage. An example is a burning 5-kg wood crib in a closed room. Table 2-6.32 shows the gas concentrations in the room during this fire, the atmosphere becoming progressively more vitiated and the CO_2/CO ratio decreasing as the fire progresses. The last column shows the influence this process has on the toxic potency of wood, assuming that carbon oxides are the only important toxic products (and also ignoring any toxic effects of low-oxygen hypoxia). The data show that, if a sample of wood was decomposed in a number of runs of a small-scale test under conditions giving the range of CO_2/CO ratios recorded at different stages of the full-scale fire, then the toxic potency of the wood would increase from very low levels as shown.

The other common situation is where a window or door is open, or where the compartment is large, so that there is sufficient ventilation to support a much bigger fire before the air supply becomes the controlling factor. Such fires, typically the cause of smoke deaths in locations remote from the fire, become both hot and vitiated, and constitute the post-flashover situation that chiefly needs to be simulated in small-scale tests, with a temperature of 800°C or more, and CO_2/CO ratios of less than 10/1, and as low as 2/1. The lower part of Table 2-6.32 illustrates this with data from the developed stage of larger (44 kg) wood fires run in the same rig as the 5-kg test. These fires were run

Table 2-6.32 ***Toxic Gas Concentrations and Calculated Toxic Potencies during Full-Scale Wood Fires in a Room-Corridor Test Rig***

1. Fire of 5-kg wood in a closed room—total mass loss 3.5 kg; room temperature approximately 200°C

Time (min)	CO ppm	CO_2 ppm	CO_2/CO Ratio	O_2%	LCt_{50}[a] for COx g·m^{-3}·min
6	750	45,000	60	18	3,750
8	1,500	75,000	50	13.5	3,461
10	2,500	88,500	35	11	2,857
12	4,000	95,000	24	10	2,222
20	9,000	75,000	8.3	11.5	1,034

2. Fires of 44-kg wood in open room with high and low ventilation; room temperature approximately 800°C

High vent.	10,000	150,000	15	9	1,800
Low vent.	50,000	150,000	3 to 1.5[b]	4	750

[a] LCt_{50} calculated in terms of mass loss concentration of wood, assuming carbon oxides to be only toxic products of importance.

[b] Second figure shows ratio in corridor, all other figures in room.

with high and low ventilation from the corridor, to simulate well-ventilated and oxygen-vitiated fully developed (post-flashover) fires. The results show that both fires become vitiated when fully developed, the poorly ventilated fire giving very low CO_2/CO ratios of 3/1 in the room and 1.5/1 in the corridor.

If the typical post-flashover fire is hot, and oxygen vitiated, with low CO_2/CO ratios, the next consideration is what effects these decomposition conditions have on the toxic potency of the products. The most obvious effect is that the toxic potency is increased compared to well-ventilated fires due to the higher concentrations of CO produced as the CO_2/CO ratio falls. The series of room-corridor fires performed at the Fire Research Station using 44-kg wood cribs provides a good example. When these were burned with restricted ventilation, the CO_2/CO ratio fell to the low values mentioned, of 3/1 in the room and 1.5/1 in the corridor after 3.5 min, with very high concentrations of CO (5 percent) in the room. Assuming as before that toxicity would be due solely to carbon oxides, then the theoretical LCt_{50} would be 750 g·m^{-3}·min, which is approximately 5 times more toxic than that in the well-ventilated, early flaming fire, and is similar to results obtained for pine and sipo wood in the DIN apparatus at 850°C.[20] Table 2-6.33 shows the toxic potency analysis for this fire.

A very important aspect of post-flashover fire conditions is the fate of nitrogen in materials. Under hot, vitiated conditions the yield of HCN from all nitrogen-containing materials increases dramatically. Hydrogen cyanide can, therefore, be an important toxic product in post-flashover fires where the fuel has a high nitrogen content. Another problem with such fires is the yield of organic irritants. Vitiated post-flashover fires produce large quantities of smoke, and recent experiments with some common materials decomposed under these conditions in a DIN-style tube furnace have shown that the dense smoke is rich in organic products, which are irritant to mice. With regard to inorganic irritants, such as HCl, these are produced at the same high yield as with early flaming fires, except that their effects are less prominent in the fully developed fire in comparison with the high yields of other toxic products.

Results from DIN and Other Tube Furnace Methods and Full-Scale Tests

If the database of small-scale toxicity test results on materials tested under early flaming conditions is poor, that on materials tested under post-flashover conditions is almost nonexistent. The only small-scale apparatus that can be used to replicate these conditions is the DIN tube furnace, when it is run at high temperatures. A small amount of rodent lethality data is available from tests run using this method at temperatures above 800°C. Apart from this, other data are from a number of small-scale and large-scale tests where analytical measurements were made, from which it is possible to make toxic potency as-

Table 2-6.33 ***Toxic Potency Analysis of Materials Decomposed under High-Temperature, Vitiated Conditions in Large-Scale Fires and in the DIN Apparatus***

	Scotch Pine 850°C Room Corridor Low Ventilation		Wool 700°C DIN	
	Concentration	FED	Concentration	FED
Carbon monoxide	5515 ppm	0.97	379 ppm	0.07
Hydrogen cyanide	0 ppm	0	153 ppm	0.93
Carbon dioxide	1.7%	$\times \frac{VCO_2}{1}$	0.17%	$\times \frac{VCO_2}{1}$
Total FED asphyxiants		0.97		1
FED presumed due to irritants		0		0
LCt_{50} calculated	750 g·m^{-3}·min		81 g·m^{-3}·min	
LCt_{50} observed (DIN test under similar conditions)	876 g·m^{-3}·min		no data	

sessments, assuming that toxic effects were due only to carbon oxides and HCN. In such vitiated post-flashover conditions, it is to be expected that carbon monoxide and hydrogen cyanide would be the dominant toxic species, since carbon monoxide will be present at high yields in all fires and hydrogen cyanide can also be expected at high yields if the materials being burned contain nitrogen. Added to this will be an uncertain contribution from organic irritants, and a contribution from inorganic irritants if these are present. While recent work suggests that organic irritants may be more important under these conditions than was thought previously, it is considered likely that they are less important than under nonflaming conditions, and are unlikely to be the dominant factor in the toxic potency.

Table 2-6.33 shows some examples of toxic potency analyses for this fire condition. The table shows analytical data from a large-scale wood fire, compared with animal data from a DIN test on wood for which no analytical data are available, and data from a small-scale (DIN) furnace test on a nitrogen-containing material (i.e., wool). Rats were exposed in the test at an exposure dose of 18 $g \cdot m^{-3} \cdot min$, and all died. The data shown are projected gas concentrations at the calculated LCt_{50}. For the wood data, the point illustrated is that, based upon the measured carbon oxide concentrations, the toxic potency is likely to be dominated by CO, and on this basis the potency of wood is greater than under well-ventilated flaming conditions. That this projection is reasonable is supported by the results of DIN work on Scotch pine, carried out under nominally similar conditions. This work gave a rat LCt_{50} of 875 $g \cdot m^{-3} \cdot min$, which is similar to the predicted figure for wood decomposed under these general conditions. Unfortunately, no analytical data were published for the DIN test results. For the wool data, the main point illustrated is that even at 700°C, which is somewhat below what would be considered a post-flashover temperature, the toxicity is likely to be dominated by the high HCN yield, and this is also considered to be true for most other nitrogen-containing materials. The other point made strongly by these examples is the paucity of available data for this type of fire.

Based upon the available data it is estimated that the toxic potency range for common materials decomposed under vitiated post-flashover conditions covers an LCt_{50} range from approximately 21 $g \cdot m^{-3} \cdot min$ for materials with a high nitrogen content decomposed at temperatures around 1000°C, up to 3000 $g \cdot m^{-3} \cdot min$ for certain cellulosic or hydrocarbon-based polymers, a range of more than two orders of magnitude for the small sample of published data.

Adaptation of Data from Other Small-Scale Tests

It has been recognized that tests other than the DIN, such as the cone calorimeter and the U.S. radiant method, are incapable of simulating post-flashover decomposition conditions, producing the wrong yields of CO and the wrong CO_2/CO ratios. However, since it is also considered in the U.S. that this fire condition is the most important to study, suggestions have been made that a calculation method can be applied to cone and U.S. radiant data toxicity data to allow for the low CO yield in the tests, relative to those in post-flashover fires. This is obviously not a realistic suggestion, since even if a calculation factor could be used to correct the CO data, the result would still be wrong if no factor were used to correct for the differences in the yields of HCN and other nitrogen-containing products, and for the yields of the many other organic irritants. Rather, if it is wished to study the behavior of materials under vitiated, high-temperature post-flashover conditions, small-scale tests should be used that create such decomposition conditions, so that the chemistry and toxicity of the decomposition products evolved under these conditions can be studied. Since tube-furnace methods similar to the DIN are cheap and very effective means of simulating this fire condition, it is recommended that this method be used, under appropriate conditions of temperature and airflow, for this purpose. Where calculation methods are to be used, it is better to base them on the elemental composition of the material and knowledge of full-scale fire conditions rather than on small-scale tests conducted under inappropriate conditions.

General Pattern of Toxic Potency for Common Materials under Three Fire Conditions

The survey of the toxic potency data for common materials under three fire conditions, (1) non-flaming, (2) early flaming, and (3) post-flashover, has revealed an inadequate database, but it has been possible to derive approximate LCt_{50} for common materials. The results for individual materials range over approximately two orders of magnitude from 20 to 3750 $g \cdot m^{-3} \cdot min$, but when the data are reduced to basic types of materials under each decomposition condition a relatively simple pattern can be described. (See Table 2-6.4.) The table shows the approximate average lethal exposure doses (LCt_{50}) for classes of materials, the LC_{50} for 30-min exposures, and a potency factor (based upon a figure of 500 $g \cdot m^{-3} \cdot min$ for the "normal" lethal potency for combustion products). The findings are as follows.

Under nonflaming oxidative decomposition conditions at >400°C most materials have a similar potency close to 500 $g \cdot m^{-3} \cdot min$ (i.e., a potency factor of approximately 1) due mainly to the effects of carbon monoxide and irritants. The main exceptions are nitrogen-containing materials releasing significant HCN at low temperatures (e.g., polyacrylonitrile, modacrylic, and rigid polyurethane foam), which have toxic potency factors of 3 to 8.

Under early flaming conditions most non-fire-retardant materials are substantially less toxic than under nonflaming conditions. Cellulosics (e.g., wood and cotton) are the least toxic with LCt_{50} of >3000 $g \cdot m^{-3} \cdot min$ (potency factor 0.2). Plastics containing carbon, hydrogen, or oxygen are somewhat more toxic with a potency factor of 0.4 (LCt_{50} ~1200), and those containing low percentages of nitrogen (e.g., flexible polyurethanes, wool, and nylon) also fall into this area. Both PVC and fire-retardant materials have toxic potencies similar to those under nonflaming conditions of approximately 1. Rigid polyurethanes and nitrogen-containing acrylics have high potencies similar to those under nonflaming conditions.

Under post-flashover conditions the potency of all materials increases due to the increased yields of HCN or CO. More smoke and irritants are also present than under early flaming conditions, which may add somewhat to the potency, particularly of the non-nitrogen-containing materials. For cellulosic materials and hydrocarbon plastics, the potency is similar to that under nonflaming conditions (potency factor close to 1). For all nitrogen-containing materials the toxic potency is high, ranging from approximately 2.5 for flexible polyurethane foam to approximately 11 for polyacrylonitrile and modacrylic. It is suggested that PVC would have a potency of approximately 2.5 under these conditions.

The Conduct and Application of Small-Scale Tests in the Assessment of Toxicity and Toxic Hazard

Small, laboratory-scale toxicity tests are of necessity capable only of investigating materials. Investigation of toxic fire hazard associated with actual items such as furnishings can be investigated only in large-scale tests, although it may be possible to a limited extent to study some composite materials using small-scale tests. The potential usefulness of these tests is then to examine the toxicity of the decomposition products from materials. This information can be used in conjunction with other small-scale test data on such characteristics of materials as ease of ignition, rate of flame spread, heat release, and smoke production to judge the suitability of one material versus another for a particular application, and ideally as a prelude to large-scale fire tests. From these it should be possible to draw some conclusions as to likely fire scenarios as well as the toxic and general fire hazards involved. A sensible approach to the use and application of such toxicity tests should involve the following steps:

1. Decide what kinds of fire scenarios are of interest and likely to involve the material under investigation, and what types of fire conditions it may be subjected to—smoldering/overheat, small flaming fire, or fully developed/post flashover.
2. Choose a small-scale test method or methods capable of simulating these conditions.
3. Run the test without animals and measure as many as possible of the common fire products important with respect to toxicity. A minimum that should be measured include CO, CO_2, O_2, HCN (if nitrogen present in material), HCl (or other appropriate acid gases if likely to be present), smoke optical density, and particulate concentration. All tests should be characterized in terms of NAC mass charge, NAC mass loss, decomposition temperature, and whether the decomposition is flaming or nonflaming. Calculate an approximate LCt_{50} at this point for use in hazard modeling. If more information is required, proceed to carry out animal experiments.
4. Set up a test atmosphere at a concentration that should be just sublethal for the known toxic atmosphere constituents (in most cases the determining factor will be the CO concentration). Then, expose a group of animals and measure the toxic effects in terms of type (asphyxiant or irritant), time of onset, severity, and duration, noting in particular the degree of incapacitation and the occurrence of any deaths. In the first instance this should involve a 30-min exposure followed by a 14-day observation period.
5. Decide from this whether the observed effects are consistent with the toxicity due to common fire products, or whether there were any unusual or severe toxic effects. If the toxicity can be interpreted in terms of the common asphyxiant products CO and HCN, then it should be possible to attempt modeling of toxic hazard on the large scale. However, if the products are irritant, as in most cases they will be, or if some unexpected toxic effect should occur, then further investigations are indicated.
6. If some unexpected toxic effect should occur, attempt to identify the toxic product or products responsible, and the conditions under which they are likely to be formed. The minimum necessary is to establish the 30-min exposure LC_{50} concentration to give some indication of the possible toxic potency of the material when decomposed in a fire. However, if the identity of the toxic product and the conditions of its formation are not understood, it is unwise to assume that small-scale tests will adequately predict of what might happen in a large-scale fire. A good example is PTFE (teflon). In one small-scale test method (the NBS method), PTFE decomposes to form a highly toxic lung irritant which causes death at concentrations of two to three orders of magnitude less than that of other polymeric materials.[9] In the Pittsburgh method the material is approximately 20 percent less toxic,[156] and in a tube furnace method similar to the DIN method a further three times less toxic,[157] although still somewhat more toxic than most other materials. However, when decomposed in a way different from any of these tests, the high toxic potency is lost,[158] and it is possible that under real fire conditions the products may not be significantly more toxic than those of other materials, although this is yet to be established.
7. Assess the irritancy potential of a material by measuring the effects of its thermal decomposition and combustion products in animals. With regard to the assessment of irritancy, although many known irritants have been identified in combustion product atmospheres, it is still not possible to predict the irritancy of an atmosphere from an analysis of its composition. The potential for causing upper respiratory tract and eye irritation (sensory irritancy) should be assessed by measuring the mouse RD_{50} concentration of the material. The potential for causing lung irritation with serious or lethal lung inflammation should be assessed by examining postexposure lethality in rats or mice. Thus if carbon monoxide concentrations are relatively low in relation to irritant products, a concentration of decomposition products may occur when the animals die either during, or in most cases after, exposure due to lung inflammation. An LC_{50} concentration for these nonasphyxiant deaths should then be determined to indicate the potency of the material in terms

of causing lung inflammation under specific decomposition conditions. If it is not possible to identify the product or products responsible for these irritant effects, it will be necessary to use the material RD_{50} and LC_{50} data in an attempt to predict likely large-scale toxic hazard. Although this measurement is only approximate, there are indications that both the RD_{50} and LC_{50} levels of most materials fall into relatively narrow bands, each effect spanning approximately one order of magnitude, with one to two orders of magnitude between the effects, at least under nonflaming conditions. Under nonflaming conditions it is likely that most materials may cause potentially serious lung inflammation following a 30-min exposure at an NAC mass loss of approximately 10 mg/L, and severe sensory irritation at somewhat lower concentrations, possibly around 1 mg/L, although tenability limits for humans are difficult to estimate. Under flaming conditions the degree of irritancy is likely to be less, sometimes considerably so, depending upon the efficiency of combustion.

8. Having evaluated the toxicity of the combustion products from the material in this way, it should be possible to use the data in conjunction with other information from small- and large-scale fire tests, or mathematical models, to assess potential toxic hazard for the material or materials in question in their end use configuration.

Misuse of Toxicity Test Data

Another way of using toxicity test results is to rank materials in order of toxicity and choose the least "toxic" material, as if toxic hazard were an inherent property of the material. This is not a realistic approach, since the toxic hazard associated with any material is not an inherent property but depends upon how the material is used and how it may be decomposed in a real fire scenario. Indeed, it is very easy to alter the toxicity of a material in a small-scale fire test simply by altering the test conditions, particularly with respect to CO and HCN yields. Thus, when wood or most other hydrocarbon polymers are decomposed under flaming conditions with restricted oxygen, the CO_2 to CO ratio in the products can be lowered (to around a value of 4)[16,17] and the toxic potency is high. However, under well-oxygenated efficient combustion conditions, the CO_2 to CO ratios in a fire may be as high as 1000, and under such conditions the toxic potency of the products is very low. Although such anomalies can be overcome to some extent by careful control of the small-scale decomposition conditions and by relating them to conditions known to occur in large-scale fires, it is still difficult to predict the CO concentration profile, and hence the toxic hazard, for a large-scale fire from the small-scale fire model in a toxicity test. For this reason, ranking materials in order of their performance in small-scale toxicity tests does not have much meaning or usefulness. The best use of small-scale toxicity tests is to identify the products responsible for the major toxic effects so that the concentration/time profiles of these products in large-scale fires can be measured or modeled, and the likely toxic hazard can be assessed.

Summary of Toxic and Physical Hazard Assessment Model

Having identified the main toxic products evolved in particular fire scenarios in terms of the main types of fire conditions—smoldering/nonflaming, early flaming, and fully developed/post flashover—estimates of potential toxic hazard can be made by a consideration of two sets of information.

1. The concentration/time profiles of the major toxic products in the full-scale fire
2. The time/concentration/toxicity relationships for these toxic products when they occur individually and in combination

From these two data sets, it is possible to construct a model to predict probable time to incapacitation or death due to toxicity for a victim exposed in such a fire.

The first data set, the large-scale fire profile, may be determined by a combination of small- and large-scale fire tests and mathematical modeling. A guide to the general characteristics of fires is shown in Table 2-6.15, and an example of a fire profile in Figure 2-6.15.

The fire profile should be characterized in terms of the following minimum range of parameters, measured or estimated at the breathing zone of a potential victim:

1. Mass loss of material divided by the volume of air into which the material is dispersed
2. Carbon monoxide concentration
3. Hydrogen cyanide concentration (if materials containing nitrogen are present)
4. Carbon dioxide concentration
5. Oxygen concentration
6. Radiant heat flux
7. Air temperature
8. Smoke optical density

Ideally, some measure should also be made of

9. Mass charge concentration of material divided by the volume of air into which the products are dispersed
10. Acid gas concentrations (HF, HCl, HBr, SO_2, or NO_2)
11. Organic product profile, particularly oxidized organic species (especially acrolein, formaldehyde, and crotonaldehyde)

Any properly conducted large-scale fire test or practical fire model should be able to provide concentration (or intensity)/time profiles for all of the first eight parameters. These can then be used as input data for the toxic and physical hazard assessment model.

The aim of the hazard assessment model is to determine the point in time during exposure when potential victims are predicted to become incapacitated, such that they would be unable to escape or their ability to escape would be severely compromised. The model also determines the point where the exposure would be sufficient to cause death either during the fire or later, as a result of the injuries sustained. The hazard assessment is based on a "step through" approach whereby the degree of hazard is calculated for each successive minute (or other appropriate time interval) during the fire, until a point is reached when incapacitation or death is predicted.

For some fire parameters the occurrence of incapacitation (or death) is related primarily to the concentration or intensity of the agent to which the victim is exposed (e.g., radiant heat, smoke optical density, or sensory irritation). Tenability limits have been set for these parameters, and incapacitation is predicted to occur rapidly at the point where the limits are met.

For other parameters (e.g., carbon monoxide, hydrogen cyanide, carbon dioxide, low-oxygen hypoxia, convected heat, and lung irritants) a dose accumulated over a period of time is the primary concern. For these parameters, the fraction of an incapacitating dose acquired each minute is calculated, and the fractions added for each successive minute until the fractional dose reaches unity, when incapacitation is predicted.

Preliminary Rough Estimate of Toxic Hazard

Although it is strongly recommended that a hazard assessment for any particular fire scenario be based on all of the eight major parameters previously listed, it is possible to make a very crude assessment of the existence of a serious toxic hazard by reference to a single parameter, the mass loss/volume dispersed profile. The three items of data needed for such an assessment are

1. The basic fire condition (smoldering, early flaming, or fully developed)
2. The mass loss/dispersal volume time curve for the fire
3. The rodent LC_{50} concentrations for the materials involved in the fire in terms of NAC mass loss, determined from small-scale tests performed under the same decomposition conditions as those in the fire

The dose of products available in the fire per minute in terms of mg min/L of mass loss is expressed as a fraction of the rodent LC_{50} dose in mg·min/L. The fractions of a lethal dose available each minute are added until the fraction reaches unity, when it is predicted that a human fire victim would probably have inhaled a lethal dose of toxic products.

Since the toxic potencies of combustion products from most materials fall into a relatively narrow range of approximately one order of magnitude,[9,42,156] (Table 2-6.2) it is possible to use a single toxic potency figure in simple hazard models. The range of LC_{50} for the preceding references quoted was 5 to 61 mg/L NAC mass loss for a 30-min exposure, which is equivalent to a dose range of approximately 150 to 1800 mg·min/L, with an average value of approximately 30 mg·min/L. Allowing for a margin of safety and for the possibility (derived from primate data)[80] that humans may be more sensitive than rodents to lung damage from fire products, it is recommended that a figure of 300 mg·min/L should be used as a probable lethal dose of combustion products in man for preliminary modeling purposes.

Main Toxic and Physical Hazard Assessment Model

Asphyxiation: The first task is to assess the point at which a victim is likely to become incapacitated by loss of consciousness due to the effects of asphyxiant (narcotic) gases. For this assessment, it is necessary to calculate the fractional incapacitating doses of each asphyxiant gas (CO, HCN, O_2, and CO_2) individually, and interactions between them, for each successive minute of the fire.

Carbon monoxide: The most important toxic fire product is CO. Toxic effects occur when a certain dose in the form of carboxyhemoglobin (COHb) has been inhaled. Time to achieve a COHb concentration causing incapacitation (unconsciousness) for a 70-kg human engaged in three levels of activity is shown in Figure 2-6.14 and calculated from primate incapacitation data and the Coburn-Forster-Kane equation.

For short exposures to high concentrations of CO, COHb concentration can be calculated approximately using the Stewart equation (Equation 6)

$$\%\text{COHb} = (3.317 \times 10^{-5})(\text{ppm CO})^{1.036}(\text{RMV})(t) \quad (6)$$

where

CO = CO concentration (ppm)
RMV = volume of air breathed (L/min)
t = exposure time (min)

From this equation, the expression for the fractional incapacitating dose each minute for a 70-kg human engaged in light activity over periods of up to one hour is derived

$$F_{I\text{co}} = \frac{K(\text{ppm CO}^{1.036})(t)}{D} \quad (7)$$

where

$F_{I_{\text{CO}}}$ = fraction of incapacitating dose
t = exposure time (min)
$K = 8.2925 \times 10^{-4}$ for 25 L/min RMV (light activity)
D = COHb concentration at incapacitation (30 percent for light activity)

For a 70-kg human engaged in light work, an RMV of approximately 25 L/min can be expected with loss of consciousness at around 30 percent COHb. Therefore, this equation predicts incapacitation after approximately 5.3 minutes at a concentration of 5000 ppm CO. For a subject at rest, the RMV will be approximately 8.5 L/min giving a value for K of 2.8195×10^{-4}, and incapacitation is likely at approximately 40 percent COHb. Thus, at 5000 ppm, time to incapacitation will be approximately 21 min.

For smaller adults and especially for children, or for CO concentrations below approximately 2000 ppm and exposure durations above one hour, or also for estimating time to death (at approximately 50 percent COHb), the rate of uptake departs significantly from the Stewart equation and predictions should be based on the CFK equation. (See Appendix 2-6A.) Time to incapacitation and death for small children may be one-half that for adults.

Hydrogen cyanide: Hydrogen cyanide is the next most important toxic gas causing incapacitation by asphyxia in fires. Time to incapacitation depends partly on rate of uptake and partly on dose. (See Figure 2-6.6.) Below a threshold of approximately 80 ppm HCN only minor ef-

fects should occur over periods of up to one hour. From 80 to 180 ppm, time to incapacitation $t_{I_{CO}}$ (loss of consciousness) will be between 2 and 30 min approximately according to the relationship (Equation 8).

$$(t_{I_{CN}})(\text{min}) = \frac{(185 - \text{ppm HCN})}{4.4} \quad (8)$$

For concentrations above approximately 180 ppm, incapacitation will occur rapidly (0 to 2 min).

Deriving an exponential expression for the data gives

$$(t_{I_{CN}})(\text{min}) = \exp\,(5.396 - 0.023 \times \text{ppm HCN}) \quad (9)$$

From Equation 8, the fractional incapacitating dose per minute equation for HCN is derived

$$F'_{I_{CN}} = \frac{1}{\exp\,(5.396 - 0.023 \times \text{ppm HCN})}$$

This has been simplified to

$$F'_{I_{CN}} = \frac{\exp\,([CN]/43))}{220} \quad (11)$$

where [*CN*] represents the concentration of cyanide corrected for the presence of other nitriles besides HCN and for the protective effect of NO_2. [*CN*] can be calculated as [*CN*] = [HCN] + [total organic nitriles] – [NO_2].

Low-oxygen hypoxia: The effects of low-oxygen hypoxia are partly concentration-related and partly dose-related. When a subject reaches equilibrium with respect to different oxygen concentrations, the effects are approximately as follows:

20.9–14.4 percent—no significant effects, slight loss of exercise tolerance
14.4–11.8 percent—slight effects on memory and mental task performance, reduced exercise tolerance
11.8–9.6 percent—severe incapacitation, lethargy, euphoria, loss of consciousness
9.6–7.8 percent—loss of consciousness, death

The time taken to achieve a blood oxygen concentration causing incapacitation depends on the dose of hypoxia acquired over that period. For input into the model, time to loss of consciousness is given by

$$(t_{I_O})\text{min} = \exp\,[8.13 - 0.54(20.9 - \%O_2)] \quad (12)$$

where 20.9 – $\%O_2$ = $\%O_2$ Vit (percent oxygen vitiation)

From this the expression for fractional incapacitating dose per minute is derived

$$F'_{I_O} = \frac{1}{\exp\,[8.13 - 0.54(20.9 - \%O_2)]} \quad (13)$$

Carbon dioxide: As with hypoxia, the effects of carbon dioxide are partly concentration-related, but it is also possible to calculate the time taken to acquire a dose capable of causing loss of consciousness. The concentration-related effects of carbon dioxide are approximately

3–6 percent—respiratory distress, increasing with concentration
6–7 percent—severe respiratory distress, dizziness, bordering on loss of consciousness
7–10 percent—loss of consciousness

There are, therefore, two important considerations with respect to carbon dioxide: (1) it greatly increases the RMV, which will increase the rate of uptake of other toxic gases, and (2) it is itself a asphyxiant.

It is therefore necessary to calculate a multiplication factor ($V\text{CO}_2$) to allow for the effect of the increased RMV caused by carbon dioxide on the rate of uptake of other toxic gases. The expression for this is

$$\text{VCO2} = \exp\left(\frac{[CO_2]}{5}\right) \quad (18)$$

It is also necessary to calculate the fractional incapacitating dose of carbon dioxide. Time to unconsciousness by carbon dioxide is given by

$$t_{I_{CO_2}} = \exp[6.1623 - 0.5189 \times \%CO_2) \quad (19)$$

From this the fractional incapacitating dose per minute expression is derived

$$F'_{I_{CO_2}} = \frac{1}{\exp\,(6.1623 - 0.5189 \times \%CO_2)} \quad (15)$$

Interactions between asphyxiant gases: For the purposes of the hazard model, the following interaction factors are used:

1. CO and HCN are considered to be directly additive.
2. CO_2 increases the rate of uptake of CO and HCN in proportion to its effect on the RMV.
3. The asphyxiant effect of low oxygen hypoxia is considered to be directly additive to the combined effects of CO and HCN.
4. The asphyxiant effect of CO_2 is considered to act independently of the effect of the other gases.

On this basis, it is possible to derive a fractional incapacitating dose equation for asphyxia (Equation 21)

$$F_{in} = [(F_{I_{CO}} + F_{I_{CN}} + \text{FLD}_{\text{irr}}) \times V\text{CO}_2 + \text{FED}_{I_O}] \text{ or } F_{I_{CO_2}} \quad (21)$$

where

F_{in} = fraction of an incapacitating dose of all asphyxiant gases
$F_{I_{CO}}$ = fraction of an incapacitating dose of CO
$F_{I_{CN}}$ = fraction of an incapacitating dose of HCN (and nitriles, corrected for NO_2)
FLD_{irr} = fraction of an irritant dose contributing to hypoxia
$V\text{CO}_2$ = multiplication factor for CO_2-induced hyperventilation
F_{I_O} = fraction of an incapacitating dose of low oxygen hypoxia
$F_{I_{CO_2}}$ = fraction of an incapacitating dose of CO_2

for a 1-min exposure to each gas concentration, C,

$$F_{I_{CO}} = \frac{(8.2925 \times 10^{-4} \times \text{ppm CO}^{1.036})}{30}$$

$$F_{I_{CN}} = \frac{(\exp([CN]/43))}{220}$$

where [CN] represents the concentration of cyanide corrected for the presence of other nitriles besides HCN and for the protective effect of NO_2. [CN] can be calculated as [CN] = [HCN] + [total organic nitriles] – [NO_2].

$$\begin{aligned} \text{FLD}_{\text{irr}} = {} & \text{FLD}_{\text{HCl}} + \text{FLD}_{\text{HBr}} + \text{FLD}_{\text{HF}} + \text{FLD}_{\text{SO}_2} \\ & + \text{FLD}_{\text{NO}_2} + \text{FLD}_{\text{CH}_2\text{CHO}} + \text{FLD}_{\text{HCHO}} + \Sigma\text{FLD}_x \end{aligned} \quad (22)$$

$$V\text{CO}_2 = \exp\left(\frac{[\text{CO}_2]}{5}\right)$$

$$F_{I_O} = \frac{1}{\exp[8.13 - 0.54(20.9 - \%\text{O}_2)]}$$

$$F_{I_{CO_2}} = \frac{1}{\exp(6.1623 - 0.5189 \times \%\text{CO}_2)}$$

An example using data obtained from a large-scale fire test (the single armchair room burn shown in Figures 2-6.15 and 2-6.19) is given in Table 2-6.6. The histograms in Figure 2-6.19 show the average concentrations of asphyxiant gases each minute for the first six minutes of the fire, which are shown numerically in Table 2-6.6. Using the equations given above, the fractional incapacitating dose for each asphyxiant gas is calculated for each minute and these data are shown in Table 2-6.7. The first two rows give the fractional doses for CO and HCN, which are added together and multiplied by the carbon dioxide hyperventilation factor $V\text{CO}_2$. The fractional dose of low-oxygen hypoxia is added to give a total fractional dose for asphyxia for each minute. The running total summed each minute exceeds unity during the fifth minute, giving a figure of 1.199, and indicating the onset of incapacitation (loss of consciousness). Alternatively, asphyxia may occur due to the effects of carbon dioxide, but the cumulative dose of this gas is only 0.065 during the fifth minute, which is insufficient to have any asphyxiant effect.

Physical factors and irritancy: Having calculated the effects of asphyxiant gases the next steps are to assess the effects of radiant and convected heat, smoke obscuration, sensory irritation, and lung irritation.

Radiant heat: As shown in Figure 2-6.28, there is a fairly obvious intensity limit for tolerance of radiant heat at 0.25 W/cm² (2.5 kW/m²). Below this intensity, radiant heat can be tolerated for at least several minutes, but above this intensity for a few seconds only. The curves of radiant heat flux and of the other physical parameters for the first ten minutes of the armchair fire are shown in Figure 2-6.29. The tenability limit is exceeded for approximately one minute during the sixth minute of the fire, and it is predicted that some degree of pain and skin burns might be sustained during that minute due solely to the effects of radiant heat.

The tenability limit for exposure of skin to radiant heat is approximately 2.5 kW/m², below which exposure can be tolerated for at least several minutes. Radiant heat at this level and above causes skin pain followed by burns within a few seconds, but lower fluxes can be tolerated for more than 5 min. For situations where occupants are required to pass under a hot smoke layer in order to escape, this radiant flux corresponds approximately to a hot layer temperature of 200°C. Above this threshold, time (seconds) to incapacitation due to radiant heat $t_{I\text{rad}}$, at a radiant flux of q kW/m² is given by Equation 26 (see Hockey and Rev[132] and Purser[157]).

$$t_{I\text{rad}} = \frac{80}{q^{1.33}} \quad (26)$$

Radiant heat tends to be directional in fires, so that the main problem tends to be local heating of particular areas of skin. The air temperature, and hence that of the air breathed and that in contact with other parts of the body, may be relatively low, even when the radiant flux is high. For this reason the main hazard is pain and burns to the skin, rather than hyperthermia. Skin temperature depends upon the relationship between the rate of heat supply to the skin surface and the removal of heat from inner layers by the blood. There is, therefore, a threshold radiant flux below which significant heating of the skin is prevented, but above which rapid heating of the skin occurs.

Convected heat: For exposures of up to one hour to convected heat from air containing less than 10 percent by volume of water vapor, the time (min) to incapacitation, $t_{I\text{conv}}$ at a temperature T (°C) is calculated from Equation 27:

$$t_{I\text{conv}} = 5 \times 10^7 T^{-3.4} \quad (27)$$

As with toxic gases, the body of a fire victim may be regarded as acquiring a "dose" of heat over a period of time during exposure, with short exposure to a high radiant flux or temperature being more incapacitating than a longer exposure to a lower temperature or flux. The same fractional incapacitating dose model as with the toxic gases may be applied and, providing that the temperature in the fire is stable or increasing, the fractional dose of heat acquired during exposure can be calculated by summing the radiant and convected fractions using Equation 28.

$$\text{FED} = \sum_{t_1}^{t_2} \left(\frac{1}{t_{I\text{rad}}} + \frac{1}{t_{I\text{conv}}}\right)\Delta t \quad (28)$$

Note: $t_{I\text{rad}}$ will tend to zero as q tends to <2.5 kW/m².

Thermal tolerance data for unprotected skin of humans suggest a limit of about 120°C for convected heat, above which considerable pain is quickly incurred along with the production of burns within a few minutes. Depending upon the length of exposure, convective heat below this temperature may still result in incapacitation due to hyperthermia. Examples of tolerance times to different radiant fluxes and air temperatures are shown in Table 2-6.19.

Conducted heat is physiologically important only when skin is in contact with hot surfaces, such as door handles. A 1-s contact with metal at 60°C can cause burns.

The average temperature each minute during the fire and the fractional incapacitating dose of heat are shown in Table 2-6.20. The cumulative fractional dose exceeds unity during the fourth minute (2.273) as the temperature exceeds 220°C, and then continues to increase dramatically during the fifth and sixth minutes. There will also be some degree of added effect from the radiant heat which would further increase the fractional dose. Incapacitation due to skin pain and burns is therefore predicted during the fourth minute, with severe and probably fatal burns of the skin and upper respiratory tract being a strong possibility, particularly after the fourth minute.

Smoke: Visual obscuration by smoke is obviously concentration-related, and a tenability limit of extinction coefficient 1.2/m (OD/m = 0.5) has been set. As Figure 2-6.29 shows, this limit is exceeded during the second minute of the armchair fire, and an extinction coefficient 2.4/m (OD/m = 1.0), or approximately 1 m visibility, is exceeded at the beginning of the third minute, at which point the smoke curve rises very steeply.

The FEC for smoke is given by

$$\text{FEC}_{\text{smoke}} = [\text{OD/m}]/\,0.2 \text{ for small enclosures or } [\text{OD/m}]/0.08 \text{ for large enclosures} \quad (23)$$

Sensory and lung irritancy: As stated in the section on irritancy, there are two factors to consider: (1) the immediate incapacitation due to the painful effects of sensory irritation of the eyes and respiratory tract, adding to the obscurational effects of smoke and disrupting escape behavior, and (2) the later inflammatory effects on the lung which may cause death after exposure.

The FIC for sensory irritatancy is given by

$$\text{FIC} = \text{FIC}_{\text{HCl}} + \text{FIC}_{\text{HBr}} + \text{FIC}_{\text{HF}} + \text{FIC}_{\text{SO}_2} + \text{FIC}_{\text{NO}_2} + \text{FIC}_{\text{CH}_2\text{CHO}} + \text{FIC}_{\text{CH}_2\text{O}} + \Sigma\text{FIC}_x \quad (24)$$

where ΣFIC_x = FICs for any other irritants present.

The FLD for lung inflammation is given by

$$\text{FLD}_{\text{irr}} = \text{FLD}_{\text{HCl}} + \text{FLD}_{\text{HBr}} + \text{FLD}_{\text{HF}} + \text{FLD}_{\text{SO}_2} + \text{FLD}_{\text{NO}_2} + \text{FLD}_{\text{CH}_2\text{CHO}} + \text{FLD}_{\text{HCHO}} + \Sigma\text{FLD}x \quad (25)$$

where ΣFLD_x = FLDs for any other irritants present.

Alternatively the sensory irritancy can be assessed in terms of the RD_{50} of a fire effluent mixture evolved from a material under defined decomposition conditions in a small-scale combustion toxicity test. Lung inflammation can be assessed in terms of late rodent death (postexposure) in a small-scale combustion toxicity test.

With regard to the worked example, the first consideration is whether the victim would be able to escape from the fire. In this context sensory irritation is most important. This is concentration-related, and in order to predict the irritancy of the smoke, it is necessary to know the RD_{50} concentration of the atmosphere produced by the materials involved under the particular decomposition conditions existing in the fire. Most importantly, it is necessary to know the concentration/time profile of the fire products in terms of mass loss per liter of air (NAC mass loss). Although the mass loss curve for the armchair is shown in Figure 2-6.29, there are no data on the volume of air into which this mass was dispersed during the fire. For the purposes of this example it will be necessary to make an estimate of possible mass loss concentration. Also, since the RD_{50} of the polyurethane and polystyrene components of the chair under flaming conditions are unknown, it will be necessary to use estimated values.

In the section on irritancy, a general tenability limit for severe sensory irritation was set at a concentration of 1 mg/L NAC mass loss, and an incapacitating dose for serious postexposure lung inflammation was set at 10 mg/L NAC mass loss for 30 min (a *Ct* product of 300 mg·min/L). From the general conditions, the smoke curve, and the CO concentration curve, it is estimated that the tenability limit for sensory irritancy would be exceeded during the third minute, greatly adding to the deleterious effects of smoke on vision and escape behavior.

With regard to lung irritation, it is estimated that the average mass loss concentration over the first five minutes of the fire would be approximately 10 mg/L. If so, this would represent a fractional incapacitating dose of 50 mg·min/L, which would probably be insufficient compared with the more serious effects of heat exposure, to cause significant lung damage after exposure. However, if the average mass loss concentration over the first five minutes should reach 60 mg/L, then serious effects on the lung would likely occur after, and probably during, exposure.

Interactions: In terms of physiological effects, it is likely that there would be some degree of interaction between asphyxia and several of these physical factors, but it is likely that most would be relatively minor during the fire, and a reasonable model can be used in which asphyxia, sensory irritancy, and the effects of heat and visual obscuration can be treated separately (with the possible exception of the effects of CO_2-induced hyperventilation on the uptake of irritants). At the behavioral level, interactions may be more important. The interaction between sensory irritation and visual obscuration has been mentioned and there is some experimental evidence for such an interaction in humans.[86] After exposure, as mentioned in the section of this chapter on heat, the effects of skin burns, respiratory tract burns, and chemical irritation (and even possibly CO asphyxia) all combine to increase the probability of fatal pulmonary edema and inflammation.

Summary of Model Predictions for Armchair Fire

From the analysis, the effects on a victim exposed to the conditions in the armchair room burn (Figure 2-6.15) are predicted as follows:

1. Toward the end of the second minute and the beginning of the third minute, the smoke optical density and mass loss/liter would exceed the tenability limits for

visual obscuration and sensory irritancy sufficiently to severely inhibit escape from the room.
2. During the fourth minute, the average temperature is 220°C, and sufficient heat would be accumulated in the skin surface to cause skin burns resulting in incapacitation.
3. During the fifth minute, a victim is likely to lose consciousness due to the combined effects of the accumulated doses of asphyxiant gases.
4. It is predicted that a victim escaping or rescued after the fourth minute would suffer severe postexposure effects due to skin burns, possible laryngeal burns with accompanying edema and danger of obstructive asphyxia, and also pulmonary edema and inflammation which might well be fatal (due to the combined effects of inhaled hot gases, chemical irritants, and the pulmonary secondary effects of skin burns). After the sixth minute, it is likely that a victim would die at some time between a few minutes and one hour due to the effects of asphyxia, circulatory shock, and possibly hyperthermia.

It is unlikely that an otherwise healthy adult would be able to escape from a fire such as this if he or she remained longer than three minutes after ignition. Three minutes is a long time in which to leave a room, however, so providing the victim is awake and aware of the fire, is not otherwise incapacitated, and does not stay after two minutes in an attempt to fight the fire or rescue belongings, it is likely that he or she would be able to escape without serious injury. Tenability limits for some 5- and 30-minute exposures to common toxic fire products in terms of time to incapacitation and death are shown in Appendix 2-6B.

Appendix 2-6A

Coburn-Forster-Kane Equation for the Uptake of Carbon Monoxide in Man

The Coburn-Forster-Kane (CFK) equation[22] provides an accurate method for predicting the blood carboxyhemoglobin concentration in humans (or various animal species) resulting from exposure to a given concentration of carbon monoxide. The theoretical predictions of the equation have been validated for humans by experimental human exposures to carbon monoxide.[23,54] The strength of the equation is that it is based upon numerical values for all the main constants and variables that determine the uptake of CO into the blood; it is therefore not based on a simple empirical fit to observed uptake data in individuals, as are other CO uptake equations.[19,27] The result is a powerful equation that can be used to predict CO uptake over wide ranges of concentrations and time scales, and can accommodate variables such as the degree of activity of the subject, body size (for men, women, or children), blood volume, hemoglobin concentration, and lung function status, all of which can affect CO uptake and therefore time to incapacitation or death for a given subject. The equation should be equally applicable to animals, providing of course that data for the various constants and variables are available. The disadvantage of the CFK equation is its complexity. In particular, several of the variables need to be calculated from other equations, which in turn contain variables which must be calculated from further equations. The data in the text and figures in this chapter are all based on CO uptake for a 70-kg human, either at rest [RMV approximately 8.5 L/min, engaged in light work (e.g., walking 6.4 km/h—RMV approximately 25 L/min)] or engaged in heavy work (e.g., slow running 8.5 km/h or walking 5.6 km/h up a 17 percent gradient—RMV approximately 50 L/min).[55] In this Appendix, data for necessary constants and equations for the derivation of all variables, with their sources, have been provided to enable uptake calculations to be made for any particular situation.

The basic form of the CFK equation[22] is as follows:

$$\frac{A[\mathrm{HbCO}]_t - BV_{\mathrm{CO}} - PI_{\mathrm{CO}}}{A[\mathrm{HbCO}]_0 - BV_{\mathrm{CO}} - PI_{\mathrm{CO}}} = e^{-tAV_bB}$$

where

$$A = \frac{\overline{P}_{\mathrm{C,O_2}}}{M[\mathrm{HbO_2}]}$$

$$\overline{P}_{\mathrm{C,O_2}} = PI_{\mathrm{O_2}} - 49$$

$$PI_{\mathrm{O_2}} = 148.304 - 0.0208 \times PI_{\mathrm{CO}}$$

$$M = 218$$

$$[\mathrm{HBO_2}] = 0.22 - [\mathrm{HbCO}]_t$$

$$[\mathrm{HbCO}]_t = [\mathrm{COHb\%}t] \times 0.0022$$

$$B = 1/DL_{\mathrm{CO}} + PL/VA$$

$$DL_{\mathrm{CO}} = 35V\mathrm{O_2} \times e^{0.33} \quad \text{Reference 159}$$

$$V\mathrm{O_2} = \frac{\mathrm{RMV}}{22.274} - 0.0309 \quad \text{Reference 55}$$

$$PL = 713$$

$$V_A = 0.933V_E - 132f$$

$$f = \exp\,[0.0165 \times \mathrm{RMV} + 2.3293] \quad \text{Reference 159}$$

where

$[\mathrm{HbO_2}]$ = mL of O_2 per mL of blood

$[\mathrm{HbCO}]_t$ = mL of CO per mL of blood at time of t

$[\mathrm{HbCO}]_0$ = mL of CO/mL blood at the beginning of the exposure. Can be taken as 0.8 percent COHb = 0.00176 mL CO/mL blood for a nonsmoker[21]

M = ratio of the affinity of blood for CO to that for O_2

$P_{\mathrm{C,O_2}}$ = average partial pressure of oxygen in lung capillaries, mmHg

$\dot{V}_{\mathrm{CO}}$ = rate of endogenous CO production, mL/min very small set at 0.007 mL/min[23]

DL_{CO} = diffusivity of the lung for CO, mL/min·mmHg

PL = barometric pressure minus the vapor pressure of water at body temperature, mmHg

V_b = blood volume, mL; 74 mL/kg body weight (approximately 5,500 mL for a 70 kg human)[23]

PI_{CO} = partial pressure of CO in inhaled air, mmHg
V_A = alveolar ventilation rate, mL/min
t = exposure duration, min
e = 2.7182
PI_{O_2} = partial pressure of oxygen in inspired air
COHb%t = percent carboxyhemoglobin at time of t
V_{O_2} = oxygen consumption, L/min
RMV = respiratory minute volume (volume of air breathed/min, liters)
V_E = RMV, mL
f = respiratory frequency, breaths/min

Appendix 2-6B

Tenability Limits

Asphyxiants: Concentrations at which there would be danger of incapacitation (loss of consciousness) and death after approximately 5 and 30 minutes exposure in a person engaged in light activity are shown in Table 2-6B(a).

Irritants: The initial painful effects of irritants (sensory irritation) are mainly upon the eyes and upper respiratory tract. These effects do not worsen with prolonged exposure and may even lessen. The toxic effects on the lungs increase with prolonged exposure, are often most serious some hours after exposure, and may cause death.

For sensory irritation two levels are presented: level a represents unpleasant and quite severely disturbing eye and upper respiratory tract irritation; and level b represents severe eye and upper respiratory tract irritation with severe pain, blepharospasm, copious lacrymation, and mucus secretion accompanied by chest pain. For deaths, the levels represent concentrations at which there is danger of death occurring during or immediately after exposure.

In general, smokes are irritating when they contain oxidized organic products.[16] The most irritating of these substances known to occur commonly in smokes from a number of different materials is acrolein. Another well-known irritant is the acid gas hydrogen chloride, which is evolved during the thermal decomposition of polyvinyl chloride (PVC). Data on these two products are presented in Table 2-6B(b) as examples of irritant effects.

Appendix 2-6C

Glossary of Terms

Acidosis: A condition in which the pH of the blood is lowered (i.e., becomes more acidic). Respiratory acidosis in fire exposures results from excess carbon dioxide uptake. Metabolic acidosis results from impaired tissue respiration (due to tissue hypoxia) caused by burns or asphyxia. (See alkalosis.)

Addition: Two or more toxic substances are considered to exert an additive effect when they act in concert, such that the effect in combination is greater than the effect of either substance acting alone, but not greater than the sum of the effects of either substance acting alone (when they may be said to be directly additive). (See also synergism.)

Aerodynamic diameter: The aerodynamic diameter of a particle is an expression of particle size, and represents the diameter of a spherical particle of unit density with the same aerodynamic properties as the particle under consideration.

Aerosol: Solid or liquid particles dispersed in air.

Alkalosis: Respiratory alkalosis occurs when the pH of the blood is increased (i.e., becomes more alkaline). It is caused by excess removal of carbon dioxide from the blood via the lungs during hyperventilation, and may cause a loss of consciousness.

Asphyxia: Suffocation, decrease in the oxygen content, and increase in the carbon dioxide content of the blood. This may occur due to laryngeal spasm caused by burns or irritant gases, or to impairment of breathing or gas exchange in the lung. The term has been extended to include all causes of tissue hypoxia, including exposure to asphyxiant gases (low oxygen concentration due to the excess of any other gas, or exposure to the asphyxiant gases carbon monoxide and hydrogen cyanide, which produce asphyxia chemically).

Atmosphere (Fire atmosphere or Test atmosphere): The total airborne medium to which a victim or experimental animal is exposed, consisting of solid and liquid particles and vapors dispersed in air.

Behavioral effects/incapacitation: The extent to which exposure to fire products affects the ability or willingness of a subject or experimental animal to perform coordinated movements or tasks, particularly movements or

Table 2-6B(a) ***Tenability Limits for Incapacitation or Death from Exposures to Common Asphyxiant Products of Combustion***

	5 min		30 min	
	Incapacitation	Death	Incapacitation	Death
CO	6000–8000 ppm	12,000–16,000 ppm	1400–1700 ppm	2500–4000 ppm[44,45]
HCN	150–200 ppm	250–400 ppm	90–120 ppm	170–230 ppm[45,59]
Low O_2	10–13%	<5%	<12%	6–7%[21,25,45]
CO_2	7–8%	>10%	6–7%	>9%[21,25,45]

Table 2-6B(b) ***Tenability Limits for Sensory Irritation or Death from Irritant Substances***

	Sensory irritation		Death (minutes)		
	a	b	5	10	30
Acrolein (ppm)	1–5[21,84]	5–95[84,85]	500–1000[85]	150–690[84,91]	50–135[84,91]
HCl (ppm)	75–300[21]	300–11,000[84,85]	12,000–16,000[84,85]	10,000[84]	2000–4000[21]

tasks similar to those required to escape from a fire. (See incapacitation.)

Bioassay: Originally a term reserved for the use of a biological system to detect or measure the amount of a biologically active material. In the fire context, it refers to the use of animal exposures rather than chemical analysis to determine the toxicity of a combustion product atmosphere.

Blepharospasm: Involuntary and sustained closure (spasm) of the eyelids. In fires this is due to the painful stimulation of the cornea by combustion products that are sensory irritants.

Bronchoconstriction: Constriction of the conducting airways in the lung due to the contraction of smooth muscle in the airway walls in response to an agonist or to stimulation of irritant receptors acting through the vagus nerve.

Burn: Tissue lesion caused by heat or chemicals. For description of burn types and degrees, see text.

Carboxyhemoglobin (COHb): Combination of carbon monoxide with hemoglobin in the blood, which limits the combination of hemoglobin with oxygen (oxyhemoglobin), and therefore the carriage of oxygen in the blood.

Cerebral depression: Condition in which the electrical activity of the cerebral cortex as revealed in the electroencephalogram consists mainly of slow wave (or delta wave) activity. This is typical of a semiconscious or unconscious state.

Combustion products: Strictly speaking, this means the products of flaming decomposition, and is used in this sense when contrasted with thermal decomposition products. However, in general usage, the term "combustion products" may be taken to include all fire products, whether produced by flaming or nonflaming thermal decomposition.

Concentration: The amount of a contaminant in the atmosphere per unit volume of the atmosphere, usually quoted as mass/volume (mg/L or mg/m^3) or volume/volume (ppm or percent). (See nominal atmosphere concentration.)

Dose: The amount of a toxicant to which a fire victim or test animal is exposed. The simplest estimation of dose for inhalation toxicology is to multiply the atmosphere concentration by the duration of exposure (Ct product). A lethal dose may be expressed in terms of the LCt_{50}. However, other factors may affect the amount of toxicant actually entering the body, and for fires it may be necessary to express dose in terms of the material in the fire. (See nominal atmosphere concentration.)

Edema: Accumulation of an excessive amount of fluid in cells, tissues, or body cavities. Pulmonary edema occurs when a fluid exudate leaks out of blood vessels as a result of inflammation or circulatory insufficiency, and the lung tissues become swollen and waterlogged. Further development results in a fluid exuded within the alveolar spaces. This fluid accumulation seriously affects gas exchange in the lung and may be fatal.

Electroencephalogram: Waves of electrical activity in the cerebral cortex recorded from the surface of the head, which give an indication of the physiological state of the brain and the degree of alertness of the subject. A preponderance of fast (beta and alpha) activity indicates a conscious and normal state, whereas a preponderance of slow (theta and delta) activity signifies a physiologically depressed or unconscious state.

Erythema: Reddening of the skin in response to heat. This change coincides with pain and just precedes a skin burn.

Fire profile: Record of the changes with time of the concentrations of important fire products and intensities of physical parameters during the course of a fire.

Flaming fire: In the context of this chapter, this refers to the early stages of fire growth (pre flashover), when the fire is still confined to burning items within a well-defined area.

Flashover: Point in growth of a flaming fire where the flames are no longer confined to burning items, but also occur within the fire effluent, remote from the seat of the fire.

Fractional incapacitating dose: The dose of a toxic product acquired during a short period of time, expressed as a fraction of the dose required to cause incapacitation at the average exposure concentration during that time interval. The fractional incapacitating doses acquired during each short time period are summed throughout the exposure, incapacitation occurring when the fraction reaches unity.

Fully developed fire: A fire that has reached its maximum extent of growth, usually extending throughout the fire compartment.

Haber's rule: Principle that toxicity in inhalation toxicology depends on the dose available and that the product of concentration and exposure time is a constant.

Hazard: A toxic fire hazard exists when a toxic product is present at a sufficient concentration and over a sufficient period of time to cause a toxic effect. A physical fire hazard exists when a physical fire parameter (heat or

smoke), is present at an intensity and over a period sufficient to cause injury or seriously inhibit the ability to escape from a fire.

Hypercapnia: Increased blood carbon dioxide concentration.

Hyperthermia (heat stroke): An increase in body temperature above 37°C. Hyperthermia is life-threatening if the body core temperature, or temperature of the blood entering the heart, exceeds 42.5°C.

Hyperventilation: Increased rate and depth of breathing (increased respiratory minute volume, or RMV), in response to increased carbon dioxide, hypoxic hypoxia, hydrogen cyanide, exercise, heat, or stimulation of pulmonary irritant receptors.

Hypoxia: A reduction in the amount of oxygen available for tissue respiration. This can occur in the following four ways:

Anemic hypoxia: The arterial PO_2 is normal, but the amount of hemoglobin available to carry oxygen is reduced and the ability to release oxygen to the tissues is impaired. For fire exposures this results mainly from the formation of carboxyhemoglobin following exposure to CO, but an anemic subject would be at increased risk.

Histotoxic hypoxia: The amount of oxygen delivered to the tissues is adequate, but due to the action of a toxic agent such as HCN, the tissue cells cannot make use of the oxygen supplied to them.

Hypoxia hypoxia (low-oxygen hypoxia): The PO_2 of the arterial blood is reduced as a result of a low atmospheric oxygen concentration or impairment of gas exchange in the lung, due to bronchoconstriction or respiratory tract damage or disease.

Ischemic hypoxia: Blood flow to a tissue is so low that adequate oxygen is not delivered to it despite a normal PO_2 and hemoglobin concentration. This occurs during shock following burns and in cerebral tissue due to alkalosis, or briefly during postural hypotension.

Incapacitation: An inability to perform a task (related to escape from a fire) caused by exposure to a toxic substance or physical agent in a fire. A distinction is sometimes made between severe physiological incapacitation, in which the subject is unable to move normally, such as might occur in an unconscious or badly burned victim, and the more behavioral incapacitation, such as that caused by visual obscuration or eye irritation from smoke, in which the victim is more or less intact, but still unable to escape from the fire.

Inflammation: A complex of reactions occurring in blood vessels and adjacent tissues around the site of an injury. The initial reaction is congestion (engorgement of local blood vessels), exudation of fluid into the tissues (edema), and pain. This is followed by a phase of destruction and removal of injured tissue by inflammatory cells, and then a phase of repair.

Intensity: Level of a harmful physical fire parameter (such as radiant heat flux, air temperature, or smoke optical density).

Intoxication: A state in which a subject is adversely affected by a toxic substance. Specifically, the time at which a subject has taken up sufficient of an asphyxiant (narcotic) gas that he or she behaves like someone severely affected by alcohol.

Irritation and irritancy: Irritation is the action of an irritant substance, irritancy is the response. This response takes the following two forms:

Pulmonary (lung) irritant: Response occurs when an irritant penetrates into the lower respiratory tract. This may result in breathing discomfort (dyspnea), bronchoconstriction, and an increase in respiratory rate during the fire exposure. In severe cases it is followed after a period (usually of a few hours) by pulmonary inflammation and edema, which may be fatal.

Sensory irritant: Response occurs when an irritant substance comes in contact with the eyes and upper respiratory tract (and sometimes the skin), causing a painful sensation accompanied by inflammation with lacrimation or mucus secretion. At low concentrations, this adds to the visual obscuration caused by smoke, but at high concentrations the severe effects may cause behavioral, and to some extent physiological, incapacitation. Sensory irritation causes a decrease in respiratory rate which is transient in humans, but continuous in rodents.

Lacrimation: The production of tears in response to sensory irritation of the eyes.

LC_{50}: Lethal concentration—50 percent. The concentration statistically calculated to cause the deaths of one half of the animals exposed to a toxicant for a specified time. It may be expressed as volume/volume (ppm, percent) or mass/volume (mg/L). Care must be taken in comparing LC_{50}s of both the exposure duration and the postexposure period over which deaths were scored. In combustion toxicology, the LC_{50} may be related to the test material rather than its products, and expressed in terms of the nominal atmosphere concentration of material either of mass charge or mass loss. (See nominal atmosphere concentration.)

LCt_{50}: The product of exposure concentration and duration causing the deaths of 50 percent of animals.

Narcosis: Literally "sleep induction," but used in combustion toxicology to describe central nervous system depression causing reduced awareness, intoxication, and reduced escape capability, leading to loss of consciousness and death in extreme cases. The asphyxiant gases CO, HCN, and CO_2 cause asphyxia, as does lack of oxygen due to the inhalation of an atmosphere low in oxygen, an impairment of breathing, or an impairment of gas exchange in the lung. The terms "narcosis" and "narcotic gases" are used synonymously with the terms "asphxia" and "asphyxiant gases."

Nominal Atmosphere Concentration (NAC): The theoretical concentration of test substance in a test atmosphere, calculated from the mass of test substance produced from the atmosphere generation system each minute divided by the air volume into which it is generated. This concept is not directly applicable to combustion toxicology since

the test material is decomposed in the fire or furnace system, but two derivative concepts are used to relate the test material to the degree of toxicity as follows:

Nominal Atmosphere Concentration mass charge (NAC mass charge): The mass of material placed in the furnace system per volume of air into which it is dispersed (mg material/liter).

Nominal Atmosphere Concentration mass loss (NAC mass loss): The mass loss of material during decomposition per volume of air into which it is dispersed (mg material/liter).

Physiological effects: Effects of chemical fire products or physical fire parameters on the functioning of the body, as opposed to parameters affecting the mind. Thus, a physiological effect of smoke is that it obscures vision, which might have a psychological effect on the willingness of a victim to enter a smoke-filled corridor.

Pneumonia (Pneumonitis): Inflammation of the lungs, in fire victims due to the direct effects of inhaled chemicals or hot gases, or secondarily to skin burns. The initial inflammatory phase may be followed by infection. As it passes through different phases, pneumonia may be life-threatening at any time from one hour after exposure in a fire to several weeks after exposure.

Potency: The toxic potency is a measure of the amount of a toxic substance required to elicit a specific toxic effect—the smaller the amount required, the greater the potency.

Psychological effects: Psychological effects of exposure to fire scenarios are on the mind of the victim, and may result in a variety of behavioral effects. These are distinct from physiological effects on body function (see above). A fire victim is likely to suffer both types of effects at various stages of a fire, and interactions between psychological and physiological effects are likely.

Psychomotor: Psychomotor skills are required to perform behavioral tasks involving a series of coordinated movements of the type required to escape from a fire in a compartment (such as a building).

Pyrolysis: In this chapter, the term "pyrolysis" is restricted to the thermal decomposition of materials without oxidation. In small-scale tests pyrolysis may be achieved by heating the material in a stream of nitrogen.

RD_{50}: Respiratory depression 50 percent—statistically calculated concentration of a sensory irritant required to reduce the breathing rate of laboratory rodents (usually mice) by 50 percent.

Respiratory Minute Volume (RMV): Volume of air breathed each minute (liters/minute). RMV = TV × RR.

Respiratory Rate (RR): Respiratory frequency (i.e., number of breaths per minute).

Respiratory tract: The nose, pharynx, larynx, trachea, and large bronchi are termed the upper respiratory tract, and the bronchioli, alveolar ducts, and alveoli are termed the lower respiratory tract.

Shock: A reduction in the circulating blood volume with a fall in blood pressure.

Smoke: Total fire effluents, consisting of solid and liquid particles and vapors.

Smoldering/Nonflaming Oxidative Decomposition: Thermal decomposition in which there is partial oxidation of the pyrolysis products, but no flame. This may result from overheating of materials by means of an external heat source, or from self-sustained smoldering.

Specific toxicity: A particular adverse effect caused by a toxicant (e.g., asphyxia, irritancy).

Supertoxicant: A term used to describe a toxicant with an unusual specific toxicity not usually associated with fire effluents, often with a high potency.

Synergism: Situation where the toxic potency of two or more substances acting in concert is greater than the sum of the potencies of each substance acting alone.

Tenability limit: Maximum concentration of a toxic fire product or intensity of a physical fire parameter that can be tolerated without causing incapacitation.

Thermal decomposition: Chemical breakdown of a material induced by the application of heat.

Tidal Volume (TV): Volume of air exhaled in each breath.

Toxicity: The nature and extent of adverse effects of a substance upon a living organism.

Ventilation (lung): The volume of air breathed each minute (synonymous with respiratory minute volume).

References Cited

1. NFPA, *The Reconstruction of a Tragedy, the Beverly Hills Supper Club Fire.* National Fire Protection Association, Quincy, MA (1978).
2. P.C. Bowes, *Ann. Occup. Hyg.*, 17, p. 143 (1974).
3. *United Kingdom Fire Statistics 1983,* Home Office, London (1983).
4. B.F. Clarke, in *Fire Deaths, Causes and Strategies for Control,* Technomic, Lancaster, PA (1984).
5. J.R. Hall and A.E. Cote, in *Fire Protection Handbook,* 18th ed. (A.E. Cote, editor-in-chief), NFPA, Quincy, MA, 1997, Ch. 1-1.
6. V. Berl and B. Halpin, *NBS Grant Contract Report NBS-GCR 168,* National Bureau of Standards, Washington, DC (1979).
7. J. Hall, personal communication.
8. J.H. Petajan, K.L. Voorhees, S.C. Packham, R.C. Baldwin, I.N. Einhorn, M.L. Grunnet, B.G. Dinger, and M.M. Birky, *Sci.,* 187, p. 742 (1975).
9. B.C. Levin, A.J. Fowell, M.M. Birky, M. Paabo, S. Stolte, and D. Malek, *NBSIR 82-2532,* National Bureau of Standards, Washington, DC (1982).
10. R.C. Anderson, P.A. Croce, F.G. Feeley, and J.D. Sakura, *Reference 88712,* Arthur D. Little, Cambridge, MA (1983).
11. C.J. Hilado, *Mod. Plastics,* July (1977).
12. D.T. Gottuk and B.Y. Lattimer, in *SFPE Handbook of Fire Protection Engineering,* 3rd ed., NFPA, Quincy, MA, pp. 2-54–2-82 (2002). Ch. 2-5.

13. A. Tewarson, in *SFPE Handbook of Fire Protection Engineering,* 3rd ed., NFPA, Quincy, MA, pp. 3-82–3-161 (2002). Ch. 3-4.
14. R.A. Anderson, A.A. Watson, and W.A. Harland, *Med. Sci. Law,* 21, p. 175 (1981).
15. H.L. Kaplan, A.F. Grand, and G.E. Hartzell, *Combustion Toxicology: Principles and Test Methods,* Technomic, Lancaster, PA (1983).
16. D.A. Purser and W.D. Woolley, *J. Fire Sci.,* 1, p. 118 (1983).
17. W.D. Woolley and P.J. Fardell, *F. Safety J.,* 5, p. 29 (1982).
18. B.T. Commins and P.J. Lawther, *Br. J. Ind. Med.,* 22, p. 139 (1965).
19. R.D. Stewart, *J. Comb. Toxicol.,* 1, p. 167 (1974).
20. F. Haber, *Funf Vortrange aus den jaren 1920–1923,* Verlag von Julius Springer, Berlin (1924).
21. "Documentation of the Threshold Limit Values for Substances in Workroom Air," *American Conference of Governmental Industrial Hygienists,* Cincinnati (1980).
22. R.F. Coburn, R.E. Forster, and P.B. Kane, *J. Clin. Invest.,* 44, p. 1899 (1965).
23. J.E. Peterson and R.D. Stewart, *J. Appl. Physiol.,* 39, p. 633 (1975).
24. F.W. Beswick, P. Holland, and K.H. Kemp, *Br. J. Ind. Med.,* 29, p. 298 (1972).
25. D.A. Purser, *J. Fire. Sci.,* 2, p. 20 (1984).
26. U.C. Luft, in *Handbook of Physiology,* American Physiology Society, Washington, DC (1965).
27. G.E. Hartzell, D.N. Priest, and W.G. Switzer, *J. Fire Sci.,* 3, p. 115 (1985).
28. L. Brodie, National Asthma Audit (Press Release), National Asthma Campaign, London (1996).
29. G.L. Nelson, "Carbon Monoxide and Fire Toxicity: A Review and Analysis of Recent Work," *Fire Technology,* 34, pp. 38–58 (1998).
30. A.L. Hinderliter, K.F. Adams, C.J. Price, M.C. Hebst, G. Koch, and D.S. Sheps, "Effects of Low-Level Carbon Monoxide Exposure on Resting and Exercise-Induced Ventricular Arrhythmias in Patients with Coronary Artery Disease and No Baseline Ectopy." *Arch. Environ. Health,* 44, pp. 89–93 (1989).
31. D.A. Purser, "Combustion Toxicity Research and Animal Models," *Society of Plastics Industry Meeting,* Hilton Head, SC (1983).
32. D.A. Purser, *Toxicology,* 115, p. 25 (1996).
33. "British Standard Code of Practice for Assessment of Hazard to Life and Health from Fire. Part 2: Guidance on Methods for the Quantification of Hazards to Life and Health and Estimation of Time to Incapacitation and Death in Fires," *BS 7899-2,* British Standards, London (1999).
34. "Determination of the Lethal Toxic Potency of Fire Effluents," *ISO 13344* (1996).
35. D.A. Purser, *Proceedings of First International Fire and Materials Conference,* Interscience Communications, London (1992).
36. D.A. Purser, *Fire and Materials,* 16, p. 67 (1992).
37. D.A. Purser, in *Proceedings of Flame Retardants 1994 Conference,* Interscience Communications, London (1994).
38. D.A. Purser, "Recent Developments in the Use of a Tube Furnace Method for Evaluating Toxic Product Yields under a Range of Fire Conditions," *Fire Protection Research Association 2000 Fire Risk and Hazard Research Application Symposium,* Atlantic City (June 28–30, 2000).
39. T.R. Hull, J.M. Carmen, and D.A. Purser, *Polymer International,* 49, p. 1256 (2000).
40. W.M. Pitts, *Prog. Energy Combust. Sci.,* 21, p. 197 (1995).
41. P.G. Wood, "The Behavior of People in Fires," *Fire Research Note 953,* Fire Research Station, Watford, UK (1972).
42. G. Kimmerle and F.C. Prager, *J. Comb. Toxicol.,* 7, p. 54 (1980).
43. G.V. Alexeev and S.C. Packham, *J. Fire Sci.,* 2, p. 362 (1984).
44. D.A. Purser and K.R. Berrill, *Arch. Environ. Hlth.,* 38, p. 308 (1983).
45. G. Kimmerle, *J. Comb. Toxicol.,* 1, p. 4 (1974).
46. J.S. Haldane, in *Respiration,* Yale University, New Haven (1922).
47. R.D. Stewart, J.E. Peterson, E.D. Baretta, H.C. Dodd, and A.A. Herrmann, *Arch. Environ. Hlth.,* 21, p. 154 (1970).
48. R.D. Stewart, J.E. Peterson, T.N. Fisher, M.J. Hosko, E.D. Baretta, H.C. Dodd, and A.A. Herrmann, *Arch. Environ. Hlth.,* 26, p. 1 (1973).
49. R.A. Anderson, A.A. Watson, and W.A. Harland, *Med. Sci. Law,* 21, p. 175 (1981).
50. Consumer Product Safety Commission, *Federal Register,* 45-182, 61925 (1980).
51. R.D. O'Donnel, P. Miluka, P. Heinig, and J. Theodorem, *Toxicol. App. Pharmacol.,* 18, p. 593 (1971).
52. "Carbon Monoxide Poisoning Due to Faulty Gas Water Heaters in British Holidaymakers on the Algarve," *Sunday Times,* London (1983).
53. K. Von Leggenhager, *Acta. Med. Scand.,* 196/suppl. 563, p. 1 (1974).
54. H. Hauck and M. Neuberger, *Eur. J. Appl. Physiol.,* 53, p. 186 (1984).
55. *Handbook of Respiration,* Saunders, Philadelphia (1958).
56. V. Babrauskas, *Technical Note 1103,* National Bureau of Standards, Washington, DC (1979).
57. R.A. Anderson, I. Thompson, and W.A. Harland, *Fire and Matls.,* 3, p. 91 (1979).
58. C.J. Clark, D. Campbell, and W.H. Reid, *Lancet,* 1332 (June 20, 1981).
59. D.A. Purser, P. Grimshaw, and K.R. Berrill, *Arch. Environ. Hlth.,* 39, p. 394 (1984).
60. D.A. Purser, "Determination of Blood Cyanide and Its Role in Producing Incapacitation in Fire Victims," *Royal Society of Chemistry Meeting,* Huntingdon (1984).
61. B. Ballantyne, *Fund. Appl. Toxicol.,* 3, p. 400 (1983).
62. B.P. McNamara, *EA-TR-76023,* Edgewood Arsenal, Aberdeen Proving Ground, MD (1976).
63. J.L. Bonsall, *Human Toxicol.,* 3, p. 57 (1984).
64. J. Barcroft, *J. Hyg.,* 31, p. 1 (1931).
65. B. Ballantyne, in *Forensic Toxicology,* Wright, Bristol (1974).
66. F.J. Baud, P. Barriot, V. Toffis, et al., *New Eng. J. Med.,* 325, p. 1761 (1991).
67. L.C. Luft, in *Clinical Cardiopulmonary Physiology,* Grune and Stratton, Orlando, FL (1969).
68. C.J. Lambertson, *Anaesthesiology,* 21, p. 642 (1960).
69. J.H. Comroe, R.E. Forster, A.B. Dubois, W.A. Briscoe, and E. Carlsen, in *The Lung,* Year Book Medical Publishers, Chicago (1962).
70. *Environmental Biology, (*P. Altman and D.S. Ditter, eds.), Federation of American Societies for Experimental Biology, Bethesda, MD (1966).
71. B.G. King, *J. Ind. Hyg. Toxicol.,* 31, p. 365 (1949).
72. J.E. Schulte, *Arch. Environ. Hlth.,* 8, p. 427 (1964).
73. W.S. Root, in *Handbook of Physiology,* American Physiology Society, Washington, DC (1985).
74. F.A. Gibbs, E.L. Gibbs, W.G. Lennox, and L.F. Nims, *J. of Aviation Med.,* 14, p. 250 (1943).

75. A.A. Karl, G.R. McMillan, S.L. Ward, A.T. Kissen, and M.E. Souder, *Aviation, Space, and Environ. Med.*, 49, p. 984 (1978).
76. G.E. Hartzell, B.C. Levin, and Y. Alarie, *Personal Communications* (1988).
77. D.A. Purser and P. Grimshaw, *Fire and Matls.*, 8, p. 10 (1984).
78. J.W. Heim, *J. Aviation Med.*, 10, p. 211 (1939).
79. R.A. McFarland, F.J. Roughton, M.H. Halperin, and J.I. Niven, *J. Aviation Med.*, 15, p. 381 (1944).
80. D.A. Purser and P. Buckley, *Med. Sci. Law,* 23, p. 142 (1983).
81. D. Campbell, *Respiratory Tract Trauma in Burned Patients,* Colloquium, Borehamwood, UK (1985).
82. L. Kane, C.S. Barrow, and Y. Alarie, *Am. Ind. Hyg. Assoc. J.*, 40, p. 207 (1979).
83. C.L. Punte, E.J. Owens, and P.J. Gutentag, *Arch. Environ. Hlth.*, 6, p. 366 (1963).
84. Y. Alarie, *Proceedings of the Inhalation Toxicology Symposium, Upjohn Company,* Ann Arbor Science (The Butterworth Group), Ann Arbor, MI (1980).
85. H.L. Kaplan, A.F. Grand, W.R. Rogers, W.G. Switzer, and G.C. Hartzell, *DOT/FAA/CT-84/16,* Federal Aviation Administration, Washington, DC (1984).
86. T. Jin, *J. Fire Flamm.*, 12, p. 130 (1981).
87. Y. Alarie, *CRC Crit. Rev. Toxicol.*, 2, p. 299 (1973).
88. T.J. Cole, J.E. Cotes, G.R. Johnson, H. deV. Martin, J.W. Reed, and M.J. Saunders, *Q. J. Exp. Physiol.*, 62, p. 130 (1977).
89. C.L. Punte, J.T. Weimer, T.A. Ballard, and J.L. Wilding, *Toxicol. Appl. Pharmacol.*, 4, p. 656 (1962).
90. B. Ballantyne and S. Calloway, *Med. Sci. Law,* 12, p. 43 (1972).
91. *Registry of Toxic Effects of Chemical Substances,* National Institute for Occupational Safety and Health, Washington, DC (1982).
92. H. Salem and H. Cullumbine, *Toxicol. Appl. Pharmacol.*, 2, p. 183 (1960).
93. Y. Alarie, *Fd. Cosmet. Toxicol.*, 19, p. 623 (1981).
94. D. Canter, *Studies of Human Behavior in Fire: Empirical Results and Their Implications for Education and Design,* University of Surrey, UK (1983).
95. R. Melzack and P.D. Wall, *Sci.*, 150, p. 971 (1965).
96. D.G. Clark, S. Buch, J.E. Doe, H. Frith, and D.H. Pullinger, *Pharmacol. Ther.*, 5, p. 149 (1979).
97. C.S. Barrow, H. Lucia, M.F. Stock, and M.F. and Y. Alarie, *Am. Ind. Hyg. Assoc. J.*, 40, p. 408 (1979).
98. Y. Alarie and R.C. Anderson, *Toxicol. Appl. Pharmacol.*, 51, p. 341 (1979).
99. W.J. Potts and T.S. Lederer, *J. Comb. Toxicol.*, 5, p. 182 (1978).
100. D.A. Purser, in *Fire Retardant Materials* (A.R. Horrocks and D. Price, eds.), CRC Press, Boca Raton, FL, p. 92 (2000).
101. T. Jin, "Visibility through Fire Smoke—Part 5, Allowable Smoke Density for Escape from Fire." *Report No. 42,* Fire Research Institute of Japan, p. 12 (1976).
102. J.L. Bryan, "Smoke As a Determinant of Human Behavior in Fire Situations (Project People)," *NBS-GCR-77-94,* U.S. Department of Commerce, National Bureau of Standards, Washington, DC (1977).
103. J.L. Bryan, in *SFPE Handbook of Fire Protection Engineering,* 3rd ed., NFPA, Quincy, MA, pp. 3-315–3-341 (2002).
104. D.A. Purser, "Modeling Time to Incapacitation and Death from Toxic and Physical Hazards in Aircraft Fires," In *Conference Proceedings No. 467, Aircraft Fire Safety, NATO-AGARD,* Sintra, Portugal, pp. 41-1–41-13 (May 22–26, 1989).
105. M.M. Hirschler and D.A. Purser, *Fire and Materials,* 17, p. 7 (1993).
106. D.A. Purser, *Polymer International,* 47, p. 1232 (2000).
107. *Emergency Response Planning Guidelines,* American Industrial Hygiene Association, Akron, OH (1989).
108. D.A. Purser, unpublished data (1982–85).
109. W.D. Woolley, *Br. Polym. J.*, 4, p. 27 (1972).
110. W.D. Woolley, S.A. Ames, and P.J. Fardell, *Fire Matls.*, 3, p. 110 (1979).
111. P.J. Berenson and W.G. Robertson, in *Bioastronautics Data Book,* Biotechnology, Virginia (1972).
112. D.L. Simms and P.L. Hinkley, *Fire Research Special Report No. 3,* Her Majesty's Stationary Office, London (1963).
113. W.V. Blockley, in *Biology Data Book,* Federation of American Societies for Experimental Biology, Bethesda, MD (1973).
114. D.C. Edholm, in *A Companion to Medical Studies,* Blackwell, Oxford, UK (1968).
115. J.H. Veghte, *F. Service Today,* 49, p. 16 (1982).
116. H. Elneil, in *A Companion To Medical Studies,* Blackwell, Oxford, UK (1968).
117. C.S. Leithead and A.R. Lind, in *Heat Stress and Heat Disorders,* Cassel and Co., London (1963).
118. A.R. Moritz, F.C. Henriques, F.R. Dutra, and J.R. Weisiger, *Arch. Pathol.*, 43, p. 466 (1947).
119. K. Buettner, *J. Appl. Physiol.*, 3, p. 703 (1951).
120. J.P. Lawrence and J.C. Bull, *Eng. Med.*, 5, p. 61 (1976).
121. J.P. Bull and J.C. Lawrence, *Fire Matls.*, 3, p. 100 (1979).
122. *PD 6504,* British Standards Institution, London (1983).
123. A.R. Moritz, F.C. Henriques, and R. McLean, *Am. J. Path.*, 21, p. 311 (1945).
124. J.B. Perkins, H.E. Pearse, and H.D. Kingsley, *UR217 Atomic Energy Project,* University of Rochester, New York (1952).
125. B.D. Dinman, *J. Am. Med. Assoc.*, 235, p. 2874 (1976).
126. Y. Enson, R.M. Harvey, M.L. Lewis, W.B. Greenough, K.M. Ally, and R.A. Panno, *J. Ann. NY Acad. Sci.*, 150, p. 577 (1968).
127. W.E. Zimmermann, *J. Ann. NY Acad. Sci.*, 150, p. 584 (1968).
128. S.M. Rosenthal and R.C. Millican, *J. Ann. NY Acad. Sci.*, 150, p. 604 (1968).
129. B.C. Zawacki, R.C. Jung, J. Joyce, and E. Rincon, *Ann. Surg.*, 185, p. 100 (1977).
130. H.N. Harrison, *J. Ann. NY Acad. Sci.*, 150, p. 627 (1968).
131. B.A. Zikria, W.O. Sturner, N.K. Astarjian, C.L. Fox, Jr., and J.M. Ferrer, *J. Ann. NY Acad. Sci.*, 150, p. 618 (1968).
132. S.M. Hockey and P.J. Rew, "Human Response to Thermal Radiation," Contract Research Report No. 97/1996, HSE Books, Sudbury Suffolk, UK (1996).
133. D.A. Purser, "Review of Human Response to Thermal Radiation," *Fire Safety Journal,* 28, pp. 290–291 (1997).
134. A. Silcock, D. Robinson, and N.P. Savage, *Current Paper CP80/78,* Building Research Establishment, Borehamwood, UK (1978).
135. D.A. Purser, unpublished experimental data (1985).
136. J.G. Quintiere, M.M. Birky, F. Macdonald, and B. Smith, *Fire Matls.*, 6, p. 99 (1982).
137. D.A. Purser, in *Proceedings of Interflam '93,* Interscience Communications, London (1993).
138. D.A. Purser, "The Development of Toxic Hazard in Fires from Polyurethane Foams and the Effects of Fire Retardants," in *Proceedings of Flame Retardants 90, (*British Plastics Federation, ed.), Elsevier, London, pp. 206–221 (1990).
139. D.A. Purser, J.A. Rowley, P.J. Fardell, and M. Bensilum, "Fully Enclosed Design Fires for Hazard Assessment in Relation to Yields of Carbon Monoxide and Hydrogen Cyanide," *Interflam '99. Eighth International Fire Science and Engineering Conference,* Edinburgh, Proceedings pp. 1163–1169, Interscience Communications, London (June–July 1999).

140. D.F. King, "Aircraft Accident Report 8/88," *Air Accidents Investigation Branch,* Her Majesty's Stationery Office, London (1989).
141. J. Sime, "Crowd Safety Design, Communications and Management: The Psychology of Escape Behavior," *Easinwold Papers No. 4,* pp. 16–29, Home Office Emergency Planning College, York, UK (1992).
142. *The Fire at Woolworth's, Piccadily, Manchester, on 8 May 1979,* Home Office, London (1980).
143. "Toxicity Testing of Fire Effluents—Part 5. Prediction of Toxic Effects of Fire Effluents," *ISO/IEC TR 9122-5* (1993).
144. "Code of Practice for Assessment of Hazard to Life and Health from Fire—Part 2. Guidance on Methods for the Quantification of Hazards to Life and Health and Estimation of Time to Incapacitation and Death in Fires, B57899-2 (1999).
145. W.J. Potts and T.S. Lederer, *J. Comb. Toxicol.,* 4, p. 113 (1977).
146. *DIN 53 436.*
147. H. Klimisch, H.W. Hollander, and J. Thyssen, *J. Comb. Toxicol.,* 7, p. 209 (1980).
148. C. Herpol and P. Vandevelde, *F. Safety J.,* 4, p. 271 (1981).
149. V. Babrauskas, *NBSIR 82-2611,* National Bureau of Standards, Washington, DC (1982).
150. "Toxicity Testing of Fire Effluents—Part 4, The Fire Model." *ISO/IEC TR 9122-4* (1993).
151. G.E. Hartzell, W.G. Switzer, and D.N. Priest, "Modeling of Toxicological Effects of Fire Gases," *J. Fire Sci.,* 3, pp. 330–342 (1985).
152. B.C. Levin, M. Paabo, J.L. Gurman, and S.C. Harris, "Effects of Exposure to Single or Multiple Combinations of the Predominant Toxic Gases and Low-Oxygen Atmospheres Produced in Fires," *Fund. Appl. Toxicol.,* 9, pp. 236–250 (1987).
153. G.E. Hartzell, S.C. Packham, A.F. Grand, and W.G. Switzer, "Modeling of Toxicological Effects of Fire Gases: III. Quantification of Post-Exposure Lethality of Rats from Exposure to HCI Atmospheres," *J. Fire Sci,* 3, pp. 196–207 (1985).
154. G.E. Hartzell, A.F. Grand, and W.G. Switzer, "Modeling of Toxicological Effects of Fire Gases VI. Further Studies on the Toxicity of Smoke Containing Hydrogen Chloride," *Advances in Combustion Toxicology, Vol. II,* (G.E. Hartzell, ed.), Technomic, Lancaster, PA, pp. 285–308 (1989).
155. W.A. Burgess, R.D. Trietman, and A. Gold, "IR Contaminants in Structural Firefighting," *Final Report to the National Fire Prevention and Control Administration and the Society of Plastics Industry Inc.,* Harvard School of Public Health, Cambridge, MA (1979).
156. R.C. Anderson and Y.C. Alarie, *J. Comb. Toxicol.,* 5, p. 54 (1978).
157. W.E. Coleman, L.D. Scheel, R.E. Kupel, and R.L. Larkin, *Am. Ind. Hyg. Assoc. J.,* 29, p. 33 (1968).
158. S.J. Williams and F.B. Clarke, *Fire Matls.,* 6, p. 161 (1982).
159. T.E. Bernard and J. Duker, *Am. Ind. Hyg. Assoc. J.,* 42, p. 271 (1981).
160. D.J. Rasbah, *Fire International,* 5, 40, p. 30 (1975).

Additional Reading

V. Babrauskas, B.C. Levin, R.G. Gann, et al., *Toxic Potency Measurement for Fire Hazard Analysis,* NIST Special Publication 827 (1991).

CHAPTER 7

Flammability Limits of Premixed and Diffusion Flames

Craig Beyler

Introduction

It is well known that not all fuel/oxidant/diluent mixtures can propagate flame. There exist limits definable in terms of fuel/oxidant/diluent composition outside which normal flame-type combustion cannot be sustained. Definition of these limits has received a great deal of attention in premixed combustion conditions, that is in systems where the fuel and oxidant are mixed prior to combustion. Despite scientific interest in the subject dating back to the nineteenth century, the mechanism responsible for flammable limits is not yet understood. Nonetheless, a great deal has been learned that has practical application.

Much less investigation into the nature and cause of limits in diffusion flames has been undertaken. Empirically, clear parallels exist between diffusion and premixed limits, and these will be explored in the latter portion of this chapter.

Premixed Combustion

Premixed flame fronts can only propagate within a range of compositions of fuel and oxidant. The composition limits within which a flame can propagate are known as the upper and lower flammable limits, and are expressed as concentrations of the fuel in a specified oxidant/diluent mixture at a specified temperature and pressure. For instance, the lower flammable limit (LFL) of methane in air at normal temperature and pressure is 5 percent by volume, and the upper flammable limit (UFL) is 15 percent by volume. As such, only methane/air mixtures with methane concentrations between 5 and 15 percent methane will support propagation of flame. For most simple hydrocarbons, the lower and upper flammable limits in air correspond to an equivalence ratio of approximately 0.5 and 3, respectively. The lower flammable limit concentrations for these fuels is approximately 48 g/m^3. (See Figure 2-7.1[1])

The most widely used method of measuring flammable limits was developed by the U.S. Bureau of Mines.[2] The apparatus consists of a 1.5 m-long, 0.05 m-diameter vertical tube which is filled with the fuel/oxidant/diluent mixture to be tested. The top of the tube is closed, and the base of the tube can be closed until the start of the test to prevent diffusion of the mixture from the tube. With the base of the tube open, the mixture is ignited by a spark or small pilot flame at the base of the tube, and the travel of the flame front up the tube is observed. The mixture is deemed to be within the flammable limits if the flame can propagate halfway up the 1.5 m tube. The test is designed

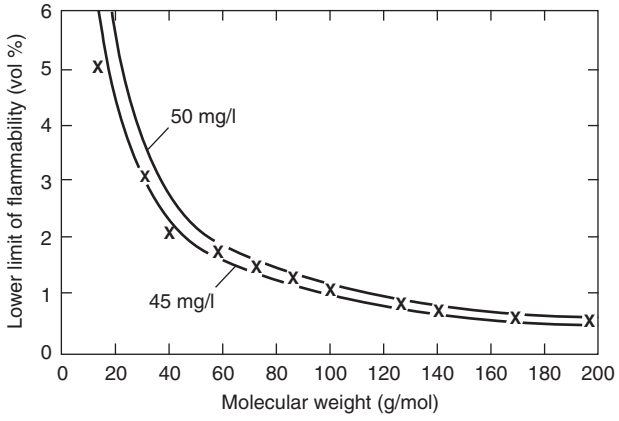

Figure 2-7.1. ***Effect of molecular weight on lower limits of flammability of alkanes at 25°C.[1]***

Dr. Craig Beyler earned a Ph.D. in engineering science at Harvard University under the direction of Professor Howard Emmons and served on the faculty of Worcester Polytechnic Institute's Center for Firesafety Studies. Dr. Beyler is currently technical director of Hughes Associates, Inc., Fire Science and Engineering.

to identify the range of mixture compositions capable of flame propagation remote from the ignition source.

The apparatus can be used with ignition at the top of the tube, but the flammable limits determined for downward propagation are narrower than for upward propagation. The 0.05-m diameter of the tube was chosen as the smallest diameter at which the heat losses from the flame to the tube wall had minimal effect on the flammable limits determined. (See Figure 2-7.2[3]) Several other methods for determining flammable limits are available.[4–7] While some methods are designed for use in special conditions, others simply reflect national differences. While each method gives substantially similar results, some variations in results do exist (see, for example, References 8 and 9).

Mixtures are capable of combustion outside the flammable limits, but external energy must be provided throughout the mixture volume in order to allow propagation of a flame.[10] An example of this behavior is shown in Figure 2-7.3. A small hydrogen diffusion flame is used as a pilot source in a lean methane/air mixture. At methane concentrations less than 5 percent, combustion occurs only in the wake of the pilot flame. Above 5 percent, the flame can propagate away from the pilot flame, regardless of the orientation of the pilot flame.

Flammable limits are a function of the oxygen and inert concentrations, as well as the mixture temperature and pressure. As the concentration of inerts is reduced and the

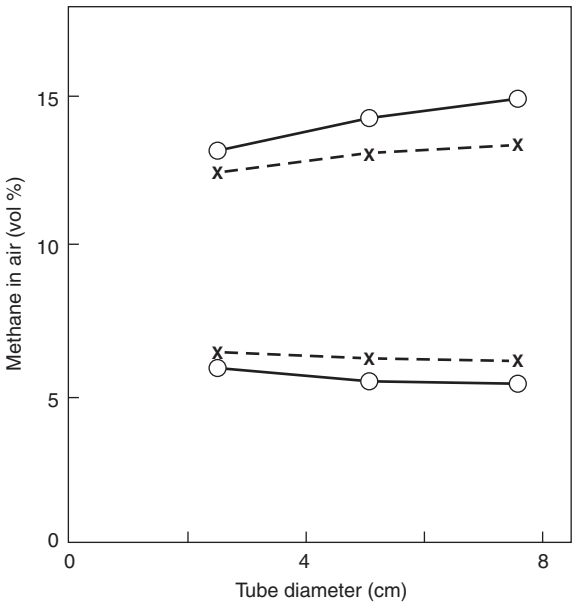

Figure 2-7.2. ***Upper and lower flammable limits of methane as determined in a vertical tube apparatus for upward propagation (circles), and for downward propagation (crosses).[3]***

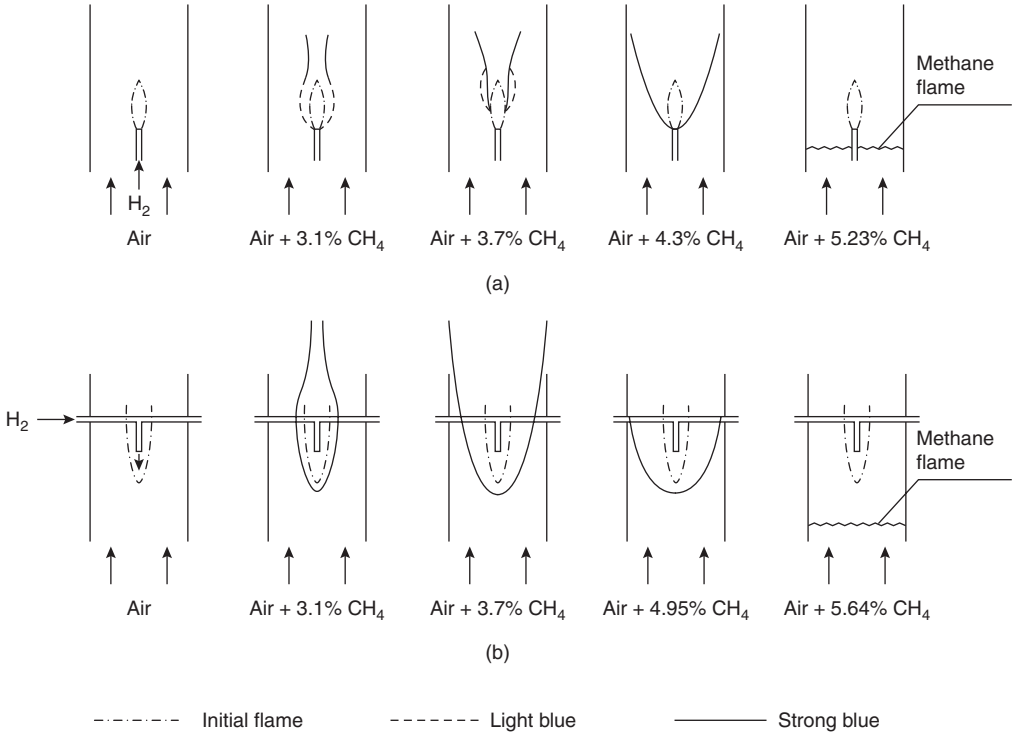

Figure 2-7.3. ***A small jet diffusion flame in a coflowing (a) and contraflowing (b) stream as the concentration of the fuel in the stream is gradually increased up to ignition. The stream velocity is 0.222 m/s, and the hydrogen jet diameter is 1.52 mm.[10]***

oxygen concentration is increased, the upper flammable limit is increased, while the lower limit is relatively unchanged. This result can be understood by observing that at the lower flammable limit there is always more than enough oxygen present for complete combustion, while at the upper limit less than the stoichiometrically required oxygen is present. Hence, at the upper limit the additional oxygen participates in the combustion process, while at the lower limit the additional oxygen simply replaces inert gas.

The lower flammable limit is also insensitive to the pressure, except at pressures well below atmospheric. The upper limit shares this insensitivity at subatmospheric pressures, but the upper limit increases with increasing pressure above atmospheric. (See Figure 2-7.4.)[1]

The flammable limits widen with increases in mixture temperature as illustrated in Figure 2-7.5;[1] this aspect will be discussed further later in this chapter. Figure 2-7.5 also relates flammable limits with the saturation vapor curve and the autoignition temperature (AIT). The flashpoint of a liquid is given in the figure as T_L. At that temperature, the vapor pressure at the liquid surface is at the lower flammable limit. The corresponding upper limit temperature is given as T_U. If a liquid is contained within a closed vessel and the vapors are allowed to come into equilibrium at temperatures above the upper limit temperature, the vapors in the vessel will be above the upper flammable limit. This result typically occurs in an automobile gas tank. If the liquid is not enclosed fully, there will be a location above from the surface of the liquid where the fuel/air mixture will be diluted below the upper flammable limit and will ignite if an ignition source is present.

Predicting Lower Flammable Limits of Mixtures of Flammable Gases (Le Chatelier's Rule)

Based on an empirical rule developed by Le Chatelier in the late nineteenth century, the lower flammable limit

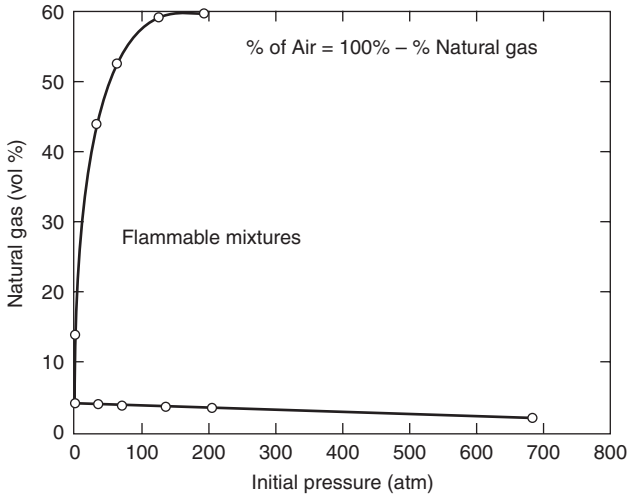

Figure 2-7.4. ***Effect of pressure on the limits of flammability of natural gas in air at 28°C.[1]***

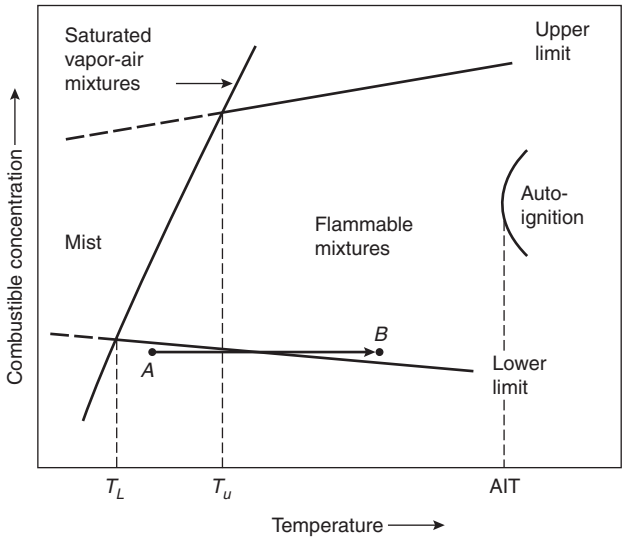

Figure 2-7.5. ***Effect of temperature on limits of flammability of a combustible vapor in air at constant initial pressure.[1]***

of mixtures of multiple flammable gases in air can be determined. A generalization of Le Chatelier's rule was given by Coward et al.[11]

$$\sum_{i=1}^{n} \frac{C_i}{\mathrm{LFL}_i} \geq 1 \tag{1}$$

where C_i is the volume percent of fuel gas, i, in the fuel/air mixture, and LFL_i is the volume percent of fuel gas, i, at its lower flammable limit in air alone. If the indicated sum is greater than unity, the mixture is above the lower flammable limit. This relationship can be restated in terms of the lower flammable limit concentration of the fuel mixture, LFL_m, as follows:

$$\mathrm{LFL}_m = \frac{100}{\sum_{i=1}^{n} (C_{f_i}/\mathrm{LFL}_i)} \tag{2}$$

where C_{f_i} is the volume percent of fuel gas i in the fuel gas mixture.

EXAMPLE 1:

A mixture of 50 percent methane, 25 percent carbon monoxide, and 25 percent hydrogen is mixed with air. Calculate the lower flammmable limit of this fuel gas mixture.

SOLUTION:

Referring to Table 2-7.1, LFLs of methane, carbon monoxide, and hydrogen are 5.0 percent, 12.5 percent, and 4.0 percent by volume, respectively. Using Equation 2 we find

$$\mathrm{LFL}_m = \frac{100}{50/5 + 25/12.5 + 25/4} = 5.48\%$$

Table 2-7.1 ***Summary of Limits of Flammability, Lower Temperature Limits (T_L), and Minimum Autoignition Temperatures (AIT) of Individual Gases and Vapors in Air at Atmospheric Pressure[1]***

Combustible	Limits of Flammability (vol %)		T_L (°C)	AIT (°C)	Combustible	Limits of Flammability (vol %)		T_L (°C)	AIT (°C)
	LFL[y]	UFL[y]				LFL[y]	UFL[y]		
Acetal	1.6	10	37	230	Cumene	0.88[a]	6.5[a]	—	425
Acetaldehyde	4.0	60	—	175	Cyanogen	6.6	—	—	—
Acetic acid	5.4[a]	—	40	465	Cycloheptane	1.1	6.7	—	—
Acetic anhydride	2.7[b]	10[c]	47	390	Cyclohexane	1.3	7.8	—	245
Acetanilide	1.0[d]	—	—	545	Cyclohexanol	1.2[d]	—	—	300
Acetone	2.6	13	—	465	Cyclohexene	1.2[a]	—	—	—
Acetophenone	1.1[d]	—	—	570	Cyclohexyl acetate	1.0[d]	—	—	335
Acetylacetone	1.7[d]	—	—	340	Cyclopropane	2.4	10.4	—	500
Acetyl chloride	5.0[d]	—	—	390	Cymene	0.85[a]	6.5[a]	—	435
Acetylene	2.5	100	—	305	Decaborane	0.2	—	—	—
Acrolein	2.8	31	—	235	Decalin	0.74[a]	4.9[a]	57	250
Acrylonitrile	3.0	—	–6	—	*n*-Decane	0.75[l]	5.6[m]	46	210
Acetone-cyanohydrin	2.2	12	—	—	Deuterium	4.9	75	—	—
Adipic acid	1.6[d]	—	—	420	Diborane	0.8	88	—	—
Aldol	2.0[d]	—	—	250	Diesel fuel (60 cetane)	—	—	—	225
Allyl alcohol	2.5	18	22	—	Diethyl amine	1.8	10	—	—
Allyl amine	2.2	22	—	375	Diethyl analine	0.8[d]	—	80	630
Allyl bromide	2.7[d]	—	—	295	1,4-Diethyl benzene	0.8[a]	—	—	430
Allyl chloride	2.9	—	–32	485	Diethyl cyclohexene	0.75	—	—	240
o-Aminodiphenyl	0.66	4.1	—	450	Diethyl ether	1.9	36	—	160
Ammonia	15	28	—	—	3,3-Diethyl pentane	0.7[a]	—	—	290
n-Amyl acetate	1.0[a]	7.1[a]	25	360	Diethyl ketone	1.6	—	—	450
n-Amyl alcohol	1.4[a]	10[a]	38	300	Diisobutyl carbinol	0.82[a]	6.1[j]	—	—
tert-Amyl alcohol	1.4[d]	—	—	435	Diisobutyl ketone	0.79[a]	6.2[a]	—	—
n-Amyl chloride	1.6[e]	8.6[a]	—	260	2-4,Diisocyanate	—	—	120	—
tert-Amyl chloride	1.5[f]	—	–12	345	Diisopropyl ether	1.4	7.9	—	—
n-Amyl ether	0.7[d]	—	—	170	Dimethyl amine	2.8	—	—	400
Amyl nitrite	1.0[d]	—	—	210	2,2-Dimethyl butane	1.2	7.0	—	—
n-Amyl propionate	1.0[d]	—	—	380	2,3-Dimethyl butane	1.2	7.0	—	—
Amylene	1.4	8.7	—	275	Dimethyl decalin	0.69[a]	5.3[j]	—	235
Aniline	1.2[g]	8.3[g]	—	615	Dimethyl dichlorosilane	3.4	—	—	—
Anthracene	0.65[d]	—	—	540	Dimethyl ether	3.4	27	—	350
n-Amyl nitrate	1.1	—	—	195	*n,n*-Dimethyl formamide	1.8[a]	14[a]	57	435
Benzene	1.3[a]	7.9[a]	—	560	2,3-Dimethyl pentane	1.1	6.8	—	335
Benzyl benzoate	0.7[d]	—	—	480	2,2-Dimethyl propane	1.4	7.5	—	450
Benzyl chloride	1.2[d]	—	—	585	Dimethyl sulfide	2.2	20	—	205
Bicyclohexyl	0.65[a]	5.1[h]	74	245	Dimethyl sulfoxide	—	—	84	—
Biphenyl	0.70[i]	—	110	540	Dioxane	2.0	22	—	265
2-Biphenylamine	0.8[d]	—	—	450	Dipentene	0.75[h]	6.1[h]	45	237
Bromobenzene	1.6[d]	—	—	565	Diphenylamine	0.7[d]	—	—	635
Butadiene (1,3)	2.0	12	—	420	Diphenyl ether	0.8[d]	—	—	620
n-Butane	1.8	8.4	–72	405	Diphenyl methane	0.7[d]	—	—	485
1,3-Butandiol	1.9[d]	—	—	395	Divinyl ether	1.7	27	—	—
Butene-1	1.6	10	—	385	*n*-Dodecane	0.60[d]	—	74	205
Butene-2	1.7	9.7	—	325	Ethane	3.0	12.4	–130	515
n-Butyl acetate	1.4[e]	8.0[a]	—	425	Ethyl acetate	2.2	11	—	—
n-Butyl alcohol	1.7[a]	12[a]	—	—	Ethyl alcohol	3.3	19[k]	—	365
sec-Butyl alcohol	1.7[a]	9.8[a]	21	405	Ethyl amine	3.5	—	—	385
tert-Butyl alcohol	1.9[a]	9.0[a]	11	480	Ethyl benzene	1.0[a]	6.7[a]	—	430
tert-Butyl amine	1.7[a]	8.9[a]	—	380	Ethyl chloride	3.8	—	—	—
n-Butyl benzene	0.82[a]	5.8[a]	—	410	Ethyl cyclobutane	1.2	7.7	—	210
sec-Butyl benzene	0.77[a]	5.8[a]	—	420	Ethyl cyclohexane	2.0[n]	6.6[n]	—	260
tert-Butyl benzene	0.77[a]	5.8[a]	—	450	Ethyl cyclopentane	1.1	6.7	—	260
n-Butyl bromide	2.5[a]	—	—	265	Ethyl formate	2.8	16	—	455
Butyl cellosolve	1.1[h]	11[j]	—	245	Ethyl lactate	1.5	—	—	400
n-Butyl chloride	1.8	10[a]	—	—	Ethyl mercaptan	2.8	18	—	300
n-Butyl formate	1.7	8.2	—	—	Ethyl nitrate	4.0	—	—	—
n-Butyl stearate	0.3[d]	—	—	355	Ethyl nitrite	3.0	50	—	—
Butyric acid	2.1[d]	—	—	450	Ethyl propionate	1.8	11	—	440
α-Butryolactone	2.0[h]	—	—	—	Ethyl propyl ether	1.7	9	—	—
Carbon disulfide	1.3	50	—	90	Ethylene	2.7	36	—	490
Carbon monoxide	12.5	74	—	—	Ethyleneimine	3.6	46	—	320
Chlorobenzene	1.4	—	21	640	Ethylene glycol	3.5[d]	—	—	400
m-Cresol	1.1[h]	—	—	—	Ethylene oxide	3.6	100	—	—
Crotonaldehyde	2.1	16[k]	—	—	Furfural alcohol	1.8[o]	16[p]	72	390

[a] T = 100°C. [e] T = 50°C. [i] T = 110°C. [m] T = 86°C. [q] T = 125°C. [u] T = 43°C. [x] T = 96°C. [aa] T = 247°C.
[b] T = 75°C. [f] T = 85°C. [j] T = 175°C. [n] T = 130°C. [r] T = 200°C. [v] T = 195°C. [y] T = 70°C. [bb] T = 30°C.
[c] T = 75°C. [g] T = 140°C. [k] T = 60°C. [o] T = 72°C. [s] T = 78°C. [w] T = 160°C. [z] T = 29°C. [cc] T = 203°C.
[d] Calculated. [h] T = 150°C. [l] T = 53°C. [p] T = 117°C. [t] T = 122°C.

Table 2-7.1 ***Summary of Limits of Flammability, Lower Temperature Limits (T_L), and Minimum Autoignition Temperatures (AIT) of Individual Gases and Vapors in Air at Atmospheric Pressure (Continued)***[1]

Combustible	Limits of Flammability (vol %) LFL[y]	UFL[y]	T_L (°C)	AIT (°C)
Gasoline:				
100/130	1.3	7.1	—	440
115/145	1.2	7.1	—	470
Glycerine	—	—	—	370
n-Heptane	1.05	6.7	–4	215
n-Hexadecane	0.43[d]	—	126	205
n-Hexane	1.2	7.4	–26	225
n-Hexyl alcohol	1.2[a]	—	—	—
n-Hexyl ether	0.6[d]	—	—	185
Hydrazine	4.7	100	—	—
Hydrogen	4.0	75	—	400
Hydrogen cyanide	5.6	40	—	—
Hydrogen sulfide	4.0	44	—	—
Isoamyl acetate[1]	1.1	7.0[a]	25	360
Isoamyl alcohol[1]	1.4	9.0[a]	—	350
Isobutane	1.8	8.4	–81	460
Isobutyl alcohol	1.7[a]	11[a]	—	—
Isobutyl benzene	0.82[a]	6.0[j]	—	430
Isobutyl formate	2.0	8.9	—	—
Isobutylene	1.8	9.6	—	465
Isopentane	1.4	—	—	—
Isophorone	0.84	—	—	460
Isopropylacetate	1.7[d]	—	—	—
Isopropyl alcohol	2.2	—	—	—
Isopropyl biphenyl	0.6[d]	—	—	440
Jet fuel:				
JP-4	1.3	8	—	240
JP-6	—	—	—	230
Kerosene	—	—	—	210
Methane	5.0	15.0	–187	540
Methyl acetate	3.2	16	—	—
Methyl acetylene	1.7	—	—	—
Methyl alcohol	6.7	36[k]	—	385
Methyl amine	4.2[d]	—	—	430
Methyl bromide	10	15	—	—
3-Methyl butene-1	1.5	9.1	—	—
Methyl butyl ketone	S51.2	8.0[a]	—	—
Methyl cellosolve	2.5[q]	20[g]	—	380
Methyl cellosolve acetate	1.7[h]	—	46	—
Methyl ethyl ether	2.2[d]	—	—	—
Methyl chloride	7[d]	—	—	—
Methyl cyclohexane	1.1	6.7	—	250
Methyl cyclopentadiene	1.3[a]	7.6[a]	49	445
Methyl ethyl ketone	1.9	10	—	—
Methyl ethyl ketone peroxide	—	—	40	390
Methyl formate	5.0	23	—	465
Methyl cyclohexanol	1.0[d]	—	—	295
Methyl isobutyl carbinol	1.3[d]	—	40	—
Methyl isopropenyl ketone	1.8[e]	9.0[e]	—	—
Methyl lactate	2.2[a]	—	—	—
α-Methyl naphthalene	0.8[d]	—	—	530
2, Methyl pentane	1.2[d]	—	—	—
Methyl propionate	2.4	13	—	—
Methyl propyl ketone	1.6	8.2	—	—
Methyl styrene	1.0[d]	—	49	495
Methyl vinyl ether	2.6	39	—	—
Methylene chloride	—	—	—	615
Monoisopropyl bicyclohexyl	0.52	4.1[r]	124	230
2-Monoisopropyl biphenyl	0.53[j]	3.2[r]	141	435
Monomethylhydrazine	4	—	—	—
Naphthalene	0.88[s]	5.9[t]	—	526
Nicotine	0.75[a]	—	—	—
Nitroethane	3.4	—	30	—
Nitromethane	7.3	—	33	—
1-Nitropropane	2.2	—	34	—
2-Nitropropane	2.5	—	27	—
n-Nonane	0.85[u]	—	31	205
n-Octane	0.95	—	13	220
Paraldehyde	1.3	—	—	—
Pentaborane	0.42	—	—	—
n-Pentane	1.4	7.8	–48	260
Pentamethylene glycol	—	—	—	335
Phthalic anhydride	1.2[g]	9.2[v]	140	570
3-Picoline	1.4[d]	—	—	500
Pinane	0.74[w]	7.2[w]	—	—
Propadiene	2.16	—	—	—
Propane	2.1	9.5	–102	450
1,2-Propandiol	2.5[d]	—	—	410
β-Propiolactone	2.9[c]	—	—	—
Propionaldehyde	2.9	17	—	—
n-Propyl acetate	1.8	8	—	—
n-Propyl alcohol	2.2[k]	14[a]	—	440
Propyl amine	2.0	—	—	—
Propyl chloride	2.4[d]	—	—	—
n-Propyl nitrate	1.8[q]	100[q]	21	175
Propylene	2.4	11	—	460
Propylene dichloride	3.1[d]	—	—	—
Propylene glycol	2.6[x]	—	—	—
Propylene oxide	2.8	37	—	—
Pyridine	1.8[k]	12[y]	—	—
Propargyl alcohol	2.4[e]	—	—	—
Quinoline	1.0[d]	—	—	—
Styrene	1.1[z]	—	—	—
Sulfur	2.0[aa]	—	247	—
p-Terphenyl	0.96[d]	—	—	535
n-Tetradecane	0.5[d]	—	—	200
Tetrahydrofurane	2.0	—	—	—
Tetralin	0.84[a]	5.0[h]	71	385
2,2,3,3-Tetramethyl pentane	0.8	—	—	430
Tetramethylene glycol	—	—	—	390
Toluene	1.2[a]	7.1[a]	—	480
Trichloroethane	—	—	—	500
Trichloroethylene	12[bb]	40[y]	30	420
Triethyl amine	1.2	8.0	—	—
Triethylene glycol	0.9[g]	9.2[bb]	—	—
2,2,3-Trimethyl butane	1.0	—	—	420
Trimethyl amine	2.0	12	—	—
2,2,4-Trimethyl pentane	0.95	—	—	415
Trimethylene glycol	1.7[d]	—	—	400
Trioxane	3.2[d]	—	—	—
Turpentine	0.7[a]	—	—	—
Unsymmetrical dimethylhydrazine	2.0	95	—	—
Vinyl acetate	2.6	—	—	—
Vinyl chloride	3.6	33	—	—
m-Xylene	1.1[a]	6.4[a]	—	530
o-Xylene	1.1[a]	6.4[a]	—	465
p-Xylene	1.1[a]	6.6[a]	—	530

[a] T = 100°C. [b] T = 75°C. [c] T = 75°C. [d] Calculated. [e] T = 50°C. [f] T = 85°C. [g] T = 140°C. [h] T = 150°C. [i] T = 110°C. [j] T = 175°C. [k] T = 60°C. [l] T = 53°C. [m] T = 86°C. [n] T = 130°C. [o] T = 72°C. [p] T = 117°C. [q] T = 125°C. [r] T = 200°C. [s] T = 78°C. [t] T = 122°C. [u] T = 43°C. [v] T = 195°C. [w] T = 160°C. [x] T = 96°C. [y] T = 70°C. [z] T = 29°C. [aa] T = 247°C. [bb] T = 30°C. [cc] T = 203°C.

The composition of the lower flammable limit fuel/air mixture is 2.74 percent methane, 1.37 percent carbon monoxide, 1.37 percent hydrogen, and 94.5 percent air.

Critical Adiabatic Flame Temperature at the Lower Flammable Limit

As early as 1911, Burgess and Wheeler[12] noted the constancy of the potential heat release rate per unit volume of normal alkane/air lower flammable mixtures at room temperature. Since the heat capacity of the products of complete combustion are nearly the same for all hydrocarbons, their observation also implies that the adiabatic flame temperature at the lower flammable limit is a constant. Examination of a wide range of C,H,O-containing fuels indicates that the adiabatic flame temperature at the LFL is approximately 1600 K (±150K) for most C,H,O-containing fuels, with the following notable exceptions: hydrogen, 980 K; carbon monoxide, 1300 K; and acetylene, 1280 K. This result indicates that the adiabatic flame temperature at the lower flammable limit is an indication of the reactivity of the fuel. The lower the adiabatic flame temperature, the more reactive the fuel.

The utility of the concept of a critical adiabatic flame temperature at the lower flammable limit goes beyond that outlined above. It has been demonstrated that the adiabatic flame temperature at the lower flammable limit is relatively insensitive (±100 K) to the diluent used and to the initial temperature of the mixture.[13–15]

The adiabatic flame temperature at the limit is insensitive to initial temperature only so long as significant preflame combustion reactions do not occur. As such, for a mixture near or above its autoignition temperature (AIT) for a significant length of time, the adiabatic flame temperature at the limit is not expected to be constant. Weinberg[15] has shown that a mixture of 1 percent methane (LFL = 5 percent at 293 K) in air can burn if it is preheated to 1270 K, even though the flame only increases that temperature by about 250 K, in accordance with the expected adiabatic flame temperature. This result was achieved by mixing the methane and air just before the flame so that preflame reactions were not allowed to proceed significantly.

Due to the constancy of the adiabatic flame temperature at the lower limit, the concept can be utilized to predict the effect of variable mixture temperature and diluents on the flammable limits of a mixture. Coward and Jones[2] have examined variable oxygen/diluent ratios, using nitrogen, carbon dioxide, water, argon, and helium as diluents. Their work shows that the limit temperature is insensitive to the oxygen/diluent ratio. Figure 2-7.6, adapted from Reference 16, illustrates the change in adiabatic flame temperature at the lower flammable limit as additional nitrogen is added to decrease the oxygen/nitrogen ratio. The figure shows an increase in the adiabatic flame temperature at the lower flammable limit from 1550 K to over 1700 K as we move from normal air to the stoichiometric limit. Beyond the stoichiometric limit, no fuel-lean mixture can burn. The region beyond the stoichiometric limit can be best understood in the context of flammability diagrams and upper flammable limits. We will examine these later in the chapter.

The insensitivity of the limit temperature to the chemical structure of C,H,O-containing fuels contributes significantly to the utility of the concept of a critical adiabatic flame temperature at the lower flammable limit. No systematic evaluation of the limit temperature concept for fuels containing sulfur, nitrogen, or halogens has been undertaken. Existing data indicates that halogen-containing fuels have limit temperatures several hundred degrees higher than C,H,O fuels. Since halogens are combustion inhibitors, this conclusion is consistent with the idea that the adiabatic flame temperature at the lower flammable limit is indicative of the reactivity of the fuel. Thus, possible exceptions to the generalization that the adiabatic flame temperature at the lower flammable limit is approximately 1600 K may be identifiable by considering the reactivity of the fuel gas.

Egerton and Powling[17] have shown that the limit temperatures at the upper flammable limit for hydrogen and carbon monoxide are equal to their limit temperatures at the lower flammable limit. Stull[18] has reported the same result for methane. However, it is not generally possible to calculate the adiabatic flame temperature for other fuels, since the products of combustion under fuel-rich conditions include a mixture of products of combustion and pyrolysis, which cannot be predicted by assuming chemical equilibrium is achieved or by detailed chemical kinetics calculations. Equilibrium calculations indicate that the only carbon-containing species that should be produced are CO, CO_2, CH_4, and solid carbon. This conclusion is not generally a good approximation under fuel-rich conditions.

EXAMPLE 2:

The lower flammable limit of propane at 20°C is 2.1 percent by volume. Find the lower flammable limit at 200°C.

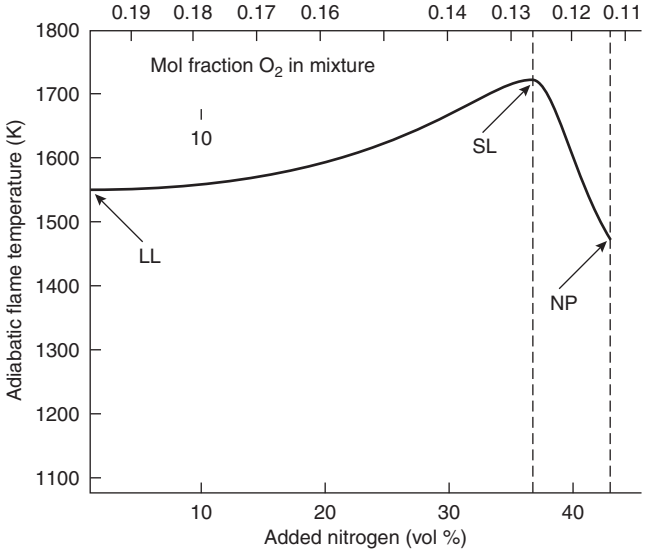

Figure 2-7.6. ***Computed adiabatic flame temperature along the lower branch of the flammability limits of propane (adapted from Reference 16). SL and NP are defined in Figure 2-7.9.***

SOLUTION:

For adiabatic combustion, all the heat released is absorbed by the products of combustion:

$$\left(\frac{\text{LFL}}{100}\right)\Delta H_c = \int_{T_0}^{T_{f,\text{LFL}}} nC_p dT \tag{3}$$

where

ΔH_c = heat of combustion of the fuel
LFL/100 = mole fraction of fuel
n = number of moles of products of combustion per mol of fuel/air mixture
C_p = heat capacity of the products of combustion
T_0 = initial temperature of the fuel/air mixture
$T_{f,\text{LFL}}$ = adiabatic flame temperature of a lower flammable limit mixture

This equation is a utilization of concepts developed in the chapter on thermochemistry. For the present purposes, it is suitable to use an average value of the heat capacity. This adjustment reduces Equation 3 to

$$\left(\frac{\text{LFL}}{100}\right)\Delta H_c = nC_p(T_{f,\text{LFL}} - T_0) \tag{4}$$

We know that $T_{f,\text{LFL}} = 1600$ K, and for $T_0 = 20$°C, we also know that LFL = 2.1 percent. Rearranging Equation 4 yields

$$\frac{\Delta H_c}{nC_p} = \frac{(T_{F,\text{LFL}} - T_0)}{\text{LFL}/100}$$
$$= \frac{1600\text{ K} - 293\text{ K}}{2.1/100}$$
$$= 6.22 \times 10^4\text{ K}$$

Both the heat of combustion and the heat capacity are weak functions of temperature, and these effects will be ignored. As such we can use the above expression to predict the lower flammable limit for an initial temperature of 200°C.

$$\frac{T_{F,\text{LFL}} - T_0}{\text{LFL}/100} = \frac{1600\text{ K} - 473\text{ K}}{\text{LFL}/100}$$
$$= 6.22 \times 10^4\text{ K}$$
$$\text{LFL} = 1.8\text{ percent}$$

Flammability Diagrams

While the flammable limits of a fuel in air can be characterized by the lower and upper flammable limits, it is necessary to represent flammable limits of more general fuel/oxidant/inert mixtures, using flammability diagrams. Examples of flammability diagrams for methane/oxygen/nitrogen mixtures are shown in Figures 2-7.7(a) and (b). Based on an extensive series of tests with a range of mixture compositions, a flammability diagram can be constructed indicating the regions of mixture compositions within the flammable limits.

Two types of flammability diagrams are often used: (1) diagram utilizes three axes in which each of the three constituent gases is explicitly represented, and (2) diagram utilizes only two axes in which the third gas concentration is determined by the difference between the sum of the other two gases and 100 percent. Both types give the same information.

Shown in Figures 2-7.7(a) and (b) are the air and limit lines. Anywhere along the air line the ratio of oxygen to

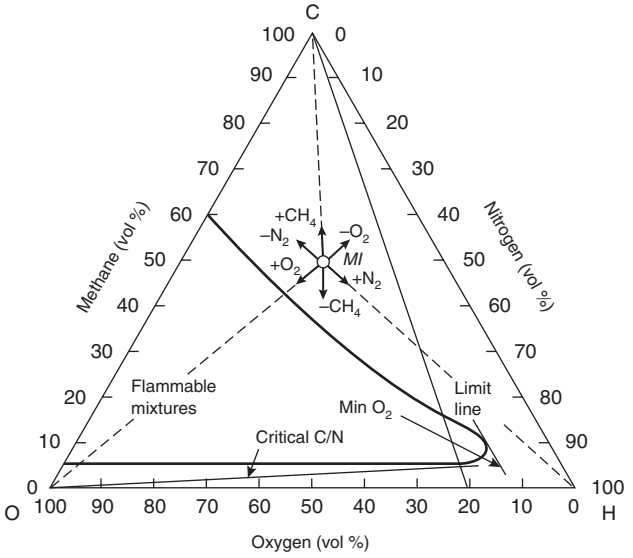

Figure 2-7.7a. ***Three-axis flammability diagram for the system methane/oxygen/nitrogen at atmospheric pressure and 26°C.[1]***

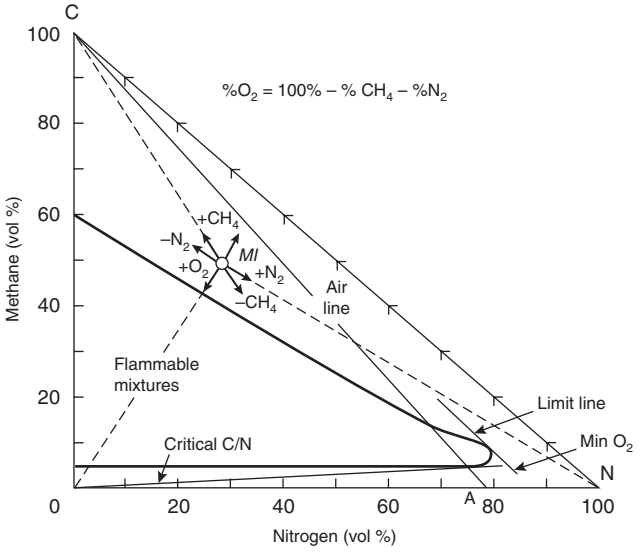

Figure 2-7.7b. ***Two-axis flammability diagram for the system methane/oxygen/nitrogen at atmospheric pressure and 26°C.[1]***

nitrogen is the same as in air. The limit line represents a range of mixtures with a fixed oxygen-to-nitrogen ratio which is tangent to the flammable region. Any oxygen/nitrogen mixture with an oxygen-to-nitrogen ratio less than that of the limit line will not support flame propagation when mixed with any amount of methane. This condition is known as the limiting oxygen concentration (LOC).

The LOC is an important concept in inerting. If the oxygen concentration can be maintained below the LOC, then premixed burning can be prevented. The LOC is a function of the temperature, pressure, fuel, and inert gas. Table 2-7.2 shows the LOC[19–23] of a wide range of fuels with nitrogen and carbon dioxide as the inert diluents. The tabulated values apply to diluted air/fuel mixtures at normal temperature and pressure. Like flammable limits, the dynamics of the LOC can generally be understood using the AFT concepts.

As can be seen in Table 2-7.2 with nitrogen diluent, the LOC is generally in the 10 to 12 percent range. Fuels like carbon monoxide and hydrogen have lower LOCs, and chlorinated fuels have higher values. These trends are expected based on AFT concepts at the LFL. For carbon dioxide as a diluent, the LOCs are generally 2 to 3 percent higher than for nitrogen diluent. Again this is expected based on AFT concepts due to the higher molar heat capacity of carbon dioxide.

Figure 2-7.8 is yet another representation of the flammable limits of fuel/oxidant/inert mixtures. The dilution of a fuel/air mixture is given by the percent of inert gas in excess of the nitrogen present in air. Figure 2-7.8 includes only mixtures that lie to the right of the air line, and as such is a magnification of a portion of the region included in Figures 2-7.7(a) and (b). Also shown in Figure 2-7.8 are several lines and points of specific interest. The highest concentration of nitrogen that will allow propagation of a flame is known as the nitrogen point (NP). Of course, this concept can be generalized to any inert (IP). If the concentration of the inert is greater than that at the inert point, no mixture of fuel and oxidant will propagate a flame remote from the ignition source.

As shown in Figure 2-7.8, the stoichiometric line passes through the flammable region. The point at which the stoichiometric line intersects the boundary of the flammable region is known as the stoichiometric limit (SL). The SL limit is the most dilute stoichiometric mixture that will propagate a flame remote from the ignition source. In the case of methane, the peak of the flammable region occurs near the stoichiometric limit. (See Figure 2-7.9.) For longer chain alkanes, the peak shifts to the rich side of the stoichiometric line. (See Figure 2-7.8.) For C_5 and higher hydrocarbons, the peak of the flammable region is bisected by the stoichiometric line defined by combustion to CO rather than to products of complete combustion. This shift has been attributed to incomplete combustion[16] and to preferential diffusion of reactants.[24] A similar shift of the maximum burning velocity to the rich side of stoichiometry is also observed. In this case, preferential diffusion of reactants has been shown to be the responsible factor.

Flammability diagrams are useful not only in determining the flammability of a given mixture, but also in

TABLE 2-7.2 ***Limiting Oxygen Concentrations at Normal Temperature and Pressure***

Gas or Vapor	Limiting Oxidant Concentration N_2/Air (volume % O_2 above which deflagration can take place)	Limiting Oxidant Concentration CO_2/Air (volume % O_2 above which deflagration can take place)	Reference
Ethane	11	13.5	19
Propane	11.5	14.5	19
n-Butane	12	14.5	19
Isobutane	12	15	19
n-Pentane	12	14.5	19
Isopentane	12	14.5	20
n-Hexane	12	14.5	19
n-Heptane	11.5	14.5	20
Ethylene	10	11.5	19
Propylene	11.5	14	19
1-Butene	11.5	14	19
Isobutylene	12	15	20
Butadiene	10.5	13	19
3-Methyl-1-butene	11.5	14	22
Benzene	11.4	14	19
Gasoline			
(73/100)	12	15	20
(100/130)	12	15	20
(115/145)	12	14.5	20
Kerosene	10 (150°C)	13 (150°C)	23
JP-1 fuel	10.5 (150°C)	14 (150°C)	20
JP-3 fuel	12	14.5	20
JP-4 fuel	11.5	14.5	20
Natural gas			
(Pittsburgh)	12	14.5	19
n-Butyl chloride	14	—	21
	12 (100°C)	—	21
Methylene chloride	19 (30°C)	—	21
	17 (100°C)	—	21
Ethylene dichloride	13	—	21
	11.5 (100°C)	—	21
1,1,1-trichloroethane	14	—	21
Trichloroethylene	9 (100°C)	—	21
Acetone	11.5	14	22
n-Butanol	—	16.5 (150°C)	22
Carbon disulfide	5	7.5	22
Carbon monoxide	5.5	5.5	22
Ethanol	10.5	13	22
2-Ethyl butanol	9.5 (150°C)	—	22
Ethyl ether	10.5	13	22
Hydrogen	5	5.2	22
Hydrogen sulfide	7.5	11.5	22
Isobutyl formate	12.5	15	22
Methanol	10	12	22
Methyl acetate	11	13.5	22
Methyl ether	10.5	13	22
Methyl formate	10	12.5	22
Methyl ethyl ketone	11	13.5	22

Data were determined by laboratory experiment conducted at atmospheric temperature and pressure. Vapor-air-inert gas samples were placed in explosion tubes and ignited by electric spark or pilot flame.

Source: Adapted from Table C-1, NFPA 69, *Explosion Prevention Systems.*

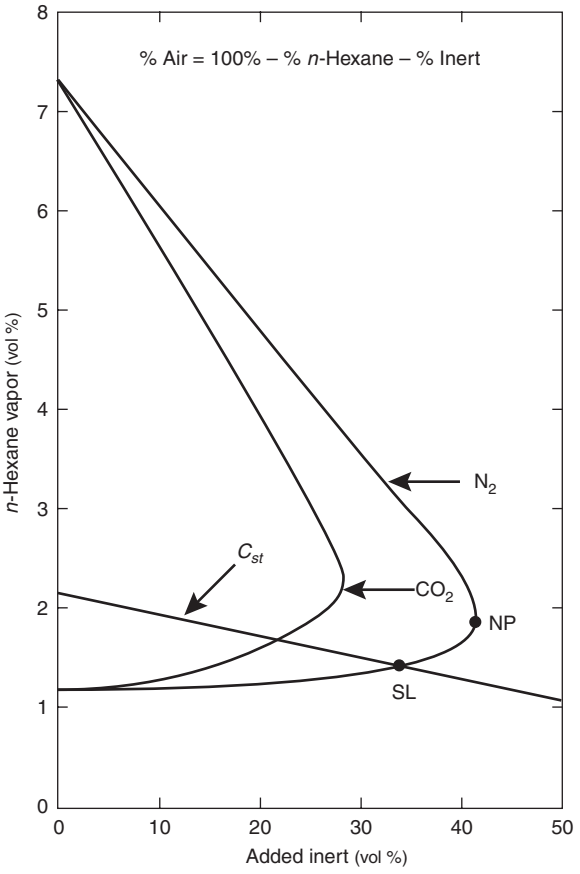

Figure 2-7.8. ***Limits of flammability of various n-hexane/inert gas/air mixtures at 25°C and atmospheric pressure.[1]***

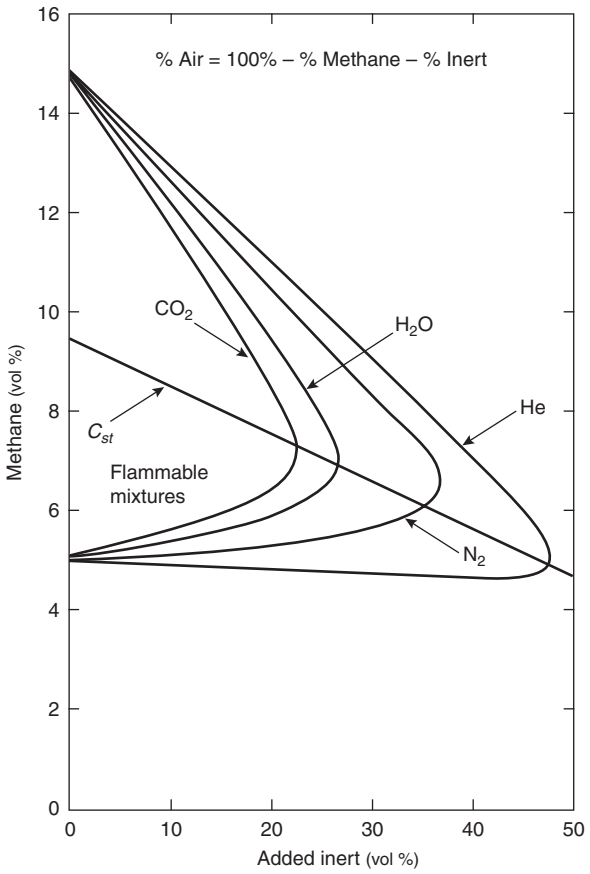

Figure 2-7.9. ***Limits of flammability of various methane/inert gas/air mixtures at 25°C and atmospheric pressure.[1]***

developing strategies for avoiding flammable mixtures while diluting fuel-rich mixtures. In order to make use of the diagrams in this fashion, we must examine the change in position on the diagram when fuel, oxygen, or inert gas is added to the mixture. Consider a mixture given by point *MI* in the three-axis diagram, Figure 2-7.7(a). The arrows indicate the change in the mixture composition with the addition or removal of each gas species. In the three-axis diagram, moving toward the vertex corresponding to 100 percent of any one of the gases corresponds to the addition of that gas, since adding an infinite amount of a single gas will reduce the concentrations of the other gases to zero. Adding air corresponds to moving toward the point on the air line at which there is no fuel. Clearly, following these examples, the effect of adding any gas or gas mixture can be plotted in the three-axis diagram. In the two-axis diagram, moving toward the vertex with 0 percent inert, 0 percent fuel corresponds to the addition of oxygen. In Figure 2-7.8 moving toward the 0 percent inert, 0 percent fuel vertex corresponds to adding air.

Figure 2-7.9 shows the effect of various inert diluents on the flammable region. As indicated by the critical adiabatic flame temperature concept, the lower flammable limit is increased in proportion to the heat capacity of the diluent. (See Section 1, Chapter 5.)

EXAMPLE 3:

A methane leak fills a 200 m^3 room until the methane concentration is 30 percent by volume. Calculate how much nitrogen must be added to the room before air can be allowed in the space.

SOLUTION:

The initial mixture in the room is given by the point B in Figure 2-7.10. Adding nitrogen moves along the line toward pure nitrogen (the N point). Drawing the line from the air point, A, tangent to the flammable region defines the mixture C: the mixture with the least nitrogen added that, on mixing with air, will not form a flammable mixture. Referring to Figure 2-7.10 we see that point C corresponds to a methane concentration of 13 percent. In order to reduce the methane concentration from 30 percent to 13 percent, an as yet unknown amount of nitrogen must be added. If we could remove only the initial mixture and replace it with nitrogen, the amount of nitrogen would simply be

$$\frac{30 - 13}{30} \times 200 \text{ m}^3 = 113 \text{ m}^3$$

However, there is generally no way to prevent mixing of the initial mixture to be exhausted and the nitrogen being

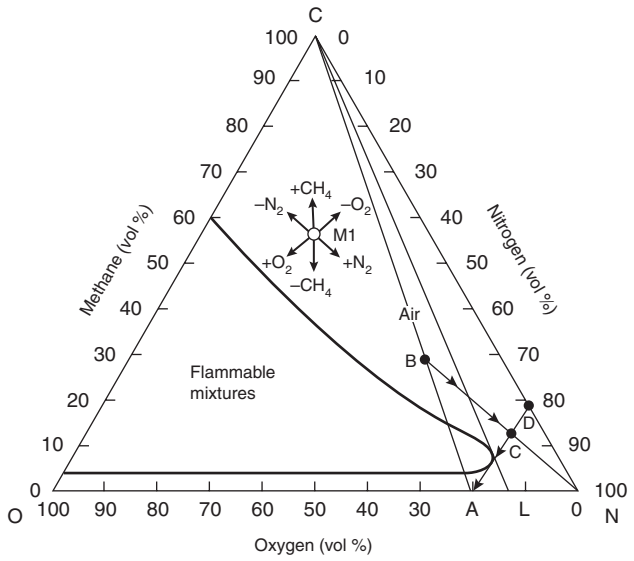

Figure 2-7.10. ***Graphic solution of Example 3 (adapted from Reference 1).***

introduced to replace it. As such, inerting nitrogen is also lost. We can model this occurrence by assuming that the room is well mixed during nitrogen injection so that the concentrations are uniform everywhere. Under these conditions the methane concentration, C, is given by

$$C = C_0 \exp\left(\frac{-V_N}{V}\right)$$

where

C_0 = initial methane concentration
V_N = volume of nitrogen added
V = volume of the room

Rearranging this equation we find

$$V_N = -V \ln\left(\frac{C}{C_0}\right) = -200\ \text{m}^3 \ln\left(\frac{13}{30}\right) = 167\ \text{m}^3$$

Of course, the flow of gases out of the room contains methane and may burn on mixing with air. Mixing air and the initial gases in the room results in mixtures along the line AB (see Figure 2-7.10), some of which are clearly flammable. As such, ignition sources must be excluded near the room exhaust, or the exhaust also needs to be inerted.

EXAMPLE 4:

A 1 kg/s flow of methane is being dumped into the atmosphere. How much nitrogen must be mixed with methane to avoid a flammable mixture in the open?

SOLUTION:

In order to make the methane nonflammable, it needs to be diluted with enough nitrogen so that on further addition of air the flammable region is missed. Such a mixture of methane and nitrogen is given by extrapolating the line AC back to zero oxygen; that is, point D on Figure 2-7.10, where the mixture is 82 percent nitrogen, 18 percent methane. The ratio of the flow rates of nitrogen to methane must equal the ratio of the concentrations of nitrogen and methane. Since concentrations expressed as volume percent are directly related to mole fractions, the flow rates of nitrogen and methane must be expressed as molar flow rates, $\dot{n}$,

$$\frac{\dot{n}_{N_2}}{\dot{n}_{CH_4}} = \frac{C_{N_2}}{C_{CH_4}}$$

The molar flow rate of methane is given by

$$\dot{n}_{CH_4} = \frac{\dot{m}_{CH_4}}{MW_{CH_4}}$$

where MW is the molecular weight and $\dot{m}$ is the mass flow rate.

$$\begin{aligned}
\dot{n}_{N_2} &= \left(\frac{\dot{m}_{CH_4}}{MW_{CH_4}}\right)\left(\frac{C_{N_2}}{C_{CH_4}}\right) \\
&= \left(\frac{1000\ \text{g/s}}{16\ \text{g/mol}}\right)\left(\frac{82\%}{18\%}\right) \\
&= 285\ \text{mol/s} \\
\dot{m}_{N_2} &= \dot{n}_{N_2} MW_{N_2} \\
&= (285\ \text{mol/s})(28\ \text{g/mol}) \\
&= 7970\ \text{g/s or } 7.97\ \text{kg/s}
\end{aligned}$$

Ignition Energies and Quenching Diameters

The energy required to ignite flammable mixtures is generally quite low, on the order of a few tenths of a millijoule (mJ) for near-stoichiometric mixtures in air and as low as a few thousandths of a millijoule in oxygen. Here again, preferential diffusion causes the minimum to occur for rich mixtures for fuels with molecular weights greater than that of air.[24] As the flammable limits are approached, the ignition energy increases sharply.

Several methods exist for preventing the initiation of an explosion. These include avoiding flammable mixtures, excluding ignition sources whose energy is greater than the minimum ignition energy, and enclosing any ignition sources in an enclosure that will not allow the propagation of the flame to the outside. We have already discussed the first of these. Some low-power electrical equipment can be designed such that the worst fault condition cannot produce the minimum ignition energy for a specified gas. Such equipment is termed "intrinsically safe" and may be used where there is a risk of a flammable atmosphere being formed.

Where this method is not feasible, the electrical equipment may be housed in an "explosion-proof" enclosure, which will not allow propagation of the flame out of the enclosure. This situation is accomplished by making the size of the openings small enough that sufficient heat is lost by the flame as it passes through the opening that it is quenched. The quenching distance is most often

determined by placing a pair of flanged electrodes in a gas mixture and attempting to ignite the gases. The flanges are parallel plates, and if the mixture can be ignited in the presence of the plates, the separation of the plates is greater than the quenching distance. The quenching distance with parallel plates, $d_{\parallel}$, is 65 percent of the quenching diameter in circular tubes. Figure 2-7.11[25] shows the relation of the quenching distance to the minimum ignition energy for a number of hydrocarbon/air mixtures. The relation can be expressed as $E_{min} = 0.06 d_{\parallel}^2$, where E_{min} is the minimum ignition energy in air given in mJ and $d_{\parallel}$ is the quenching distance in air given in mm.

Because the hot quenched flame gases in an enclosure will expand through the opening, they may autoignite outside the enclosure. It has been found that the minimum experimental safe gap (MESG) for most hydrocarbons is approximately half the quenching distance.[25]

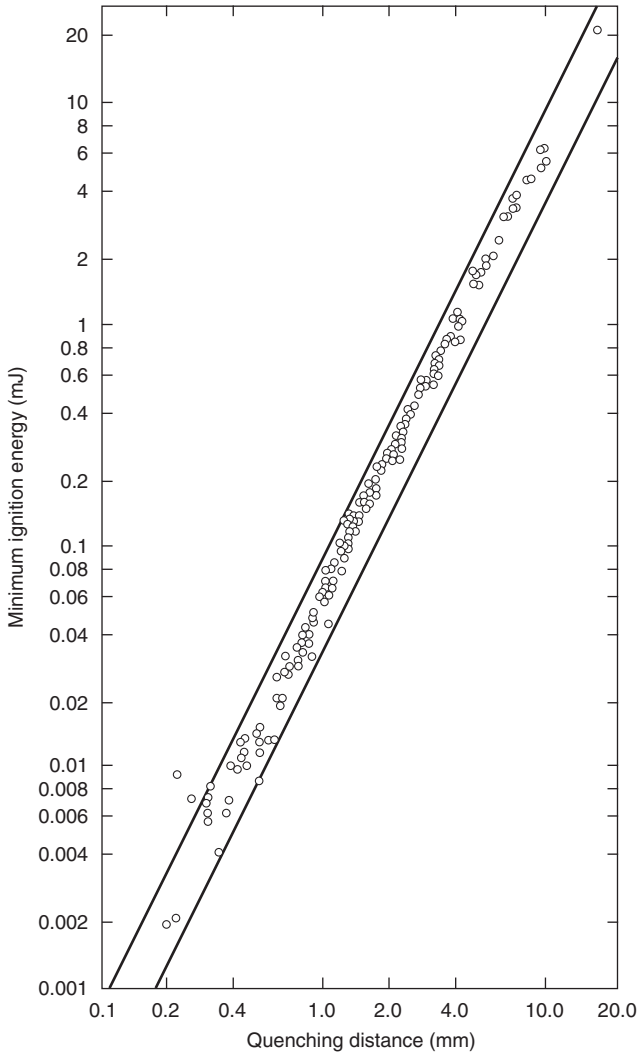

Figure 2-7.11. ***The relation between flat-plate quenching and spark minimum ignition energies for a number of hydrocarbon-air mixtures.[25]***

Dusts and Mists

The lower flammable limit of dusts and mists would be expected to be higher than their gaseous counterparts due to the need to volatilize the dust or mist. For very small particles with high surface-area-to-volume ratios, the lower flammable limit is independent of particle diameter, and the limit concentrations are approximately the same as the analogous gaseous fuel for fuels that volatilize completely. Hertzberg et al.[26] have shown that bituminous coal dusts with particle diameters of 50 μm or less and polyethylene dusts with particle diameters of 100 μm or less have lower flammable limits in air which are independent of particle diameter. Figure 2-7.12 shows the measured lower flammable limit concentration for Pittsburgh bituminous coal as a function of average particle diameter and oxygen concentration. Notice that the lower flammable limit in the small-particle limit is a function of the oxygen concentration, unlike gaseous fuels. Also note that the lower flammable limit concentration is much higher than 48 g/m^3, typical of gaseous hydrocarbons. These effects are due to the fact that not all the coal dust is volatilized. The fraction of dust which is volatilized is a function of the particle diameter and the oxygen concentration. As the oxygen concentration affects the maximum flame temperature and, hence, the heat flux to the particle, both the ability of heat to penetrate the particle and the rate of heating are affected. It is well known that the fraction of the material volatilized increases with the rate of heating. It is not expected that the lower flammable limit can be reduced below 50 g/m^3, even at 100 percent oxygen.

As the particle size increases, it would be expected that the lower flammable limit would also increase due to the difficulty of getting the fuel into the gas phase where combustion will take place. This result does in fact occur, but depending on the geometry of the test, the apparent

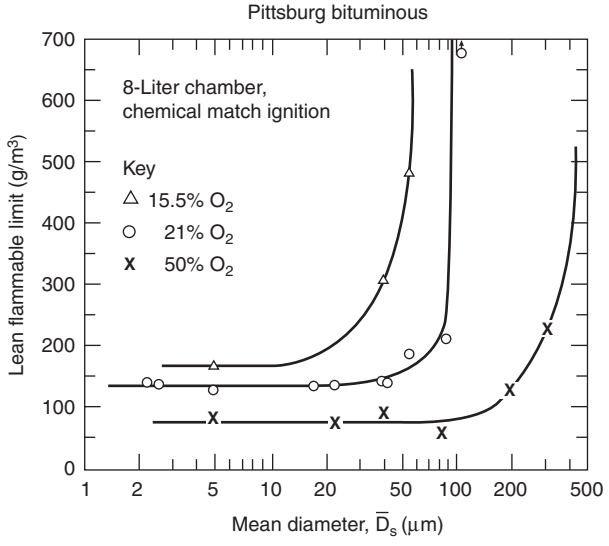

Figure 2-7.12. ***Lean flammability limit data for Pittsburgh bituminous coal as a function of particle size for three oxygen concentrations.[26]***

lower flammable limit of mists can actually decrease with increasing particle diameter due to the effects of gravity.[27] If the ignition source is at the bottom of the container and the aerosol is not kept well mixed, the particles can begin to settle out, causing the local concentration in the lower portions of the apparatus to be higher. This laboratory effect can also be expected to operate under actual conditions, depending on the degree of mixing of the aerosol.

While it is in principle possible for flame propagation to occur as a result of heterogeneous combustion of particles, this appears not to be an important mechanism for organic materials. Lower flammable limits of anthracite coal dusts with only a 20 percent volatile yield can be explained solely on the basis of gas-phase combustion.[28] Flame propagation by heterogeneous combustion is important for metal and graphite dusts.

Diffusion Flame Limits

The limits of flammability for diffusion flames were first examined by Simmons and Wolfhard.[29] In their experiments, they determined the minimum level of dilution of the oxidant stream necessary to prevent the stabilization of a diffusion flame for a variety of gas and liquid fuels. The oxygen mole fraction, X_{O_2}, of the oxidant stream at the flammability limit is known as the limiting oxygen index (LOI), or simply the oxygen index (OI). Simmons and Wolfhard's results are included in Table 2-7.3. They observed that the oxygen index of their diffusion flames equaled the ratio, $X_{O_2}/(X_{O_2} + X_{\text{diluent}})$, found in a premixed stoichiometric-limit mixture involving the same fuel. This result implies that the adiabatic flame temperature for the limit diffusion flame, calculated on the basis of stoichiometric combustion of the fuel and oxidant streams, is equal to the adiabatic flame temperature at the stoichiometric limit of a premixed system involving the same fuel, oxidant, and diluent.

Figure 2-7.13 graphically illustrates the relationship of the adiabatic flame temperatures at the lean, premixed limit in air, at the stoichiometric limit (premixed), and at the oxygen index (premixed). As the figure shows, the adiabatic flame temperature at the stoichiometric limit and the oxygen index are essentially equal, and the adiabatic flame temperature at the lower flammable limit in air is approximately 150 K less. Ishizuka and Tsuji[30] verified Simmons and Wolfhard's results for methane and hydrogen, and showed that the adiabatic flame temperature at the limit is the same whether dilution is of the fuel or oxidizer stream.

The information in Figure 2-7.13 forms the basis of a method for the evaluation of diffusion flame limits for fuel mixtures. In essence, the ability of a fuel and oxidant pair to react in a diffusion flame is evaluated by examining the flammability of a premixed stoichiometric mixture of the fuel and oxidant.

To do this, we assume that Le Chatelier's rule holds at the stoichiometric limit; that is,

$$\sum_{i=1}^{n} \left(\frac{C_i}{\text{SL}_i} \right) \geq 1 \tag{5}$$

Table 2-7.3 ***Thermodynamic Equilibrium Properties at Extinction (adapted from References 16 and 25)***

Fuel	LFL (vol %)	T(LFL) (K)	X(SL)[a]	T(SL) (K)	X(NP)[a]	T(NP) (K)	OI[a]	X(OI)[a]	T(OI) (K)
CH_4	5.0	1480	0.123	1720	0.117	1610	0.139	0.130	1780
C_2H_2	2.7						0.085		1540
C_2H_4	2.7						0.105		1610
C_2H_6	3.0	1530	0.114	1620	0.111	1540	0.118	0.114	1630
C_3H_8	2.1	1540	0.125	1730	0.114	1470	0.127	0.124	1720
n-C_4H_{10}	1.8	1640	0.134	1830	0.121	1490	—	—	—
n-C_5H_{12}	1.4	1590	0.135	1810	0.115	1410	0.1325	0.130	1760
n-C_6H_{14}	1.2	1610	0.135	1800	0.117	1420	0.1335	0.132	1770
n-C_7H_{16}	1.05	1620	0.134	1770	0.118	1430	—	—	—
n-C_8H_{18}	0.90	1650	0.134	1770	0.118	1440	0.134	0.133	1780
n-$C_{10}H_{22}$							0.1345	0.133	1780
CH_3COCH_3	2.6						0.1285		1730
CH_3OH	6.7	1550	0.112	1690	0.085	1430	0.111	0.103	1530
C_2H_5OH	3.3	1490	0.118	1700	0.106	1430	0.126	0.121	1670
n-C_3H_7OH	2.2	1490					0.128	0.124	1700
n-C_4H_9OH	1.7	1510					0.129	0.126	1710
n-$C_5H_{11}OH$	1.4	1550					0.130	0.128	1730
n-$C_6H_{13}OH$	1.2	1490					0.1315	0.130	1740
n-$C_8H_{17}OH$							0.1315	0.130	1750
C_6H_6	1.3						0.133		1810
C_6H_{12}	1.2						0.134		1770
H_2	4.0						0.054		1080
CO	12.5						0.076		1450

[a]Expressed as mole fraction of oxygen.

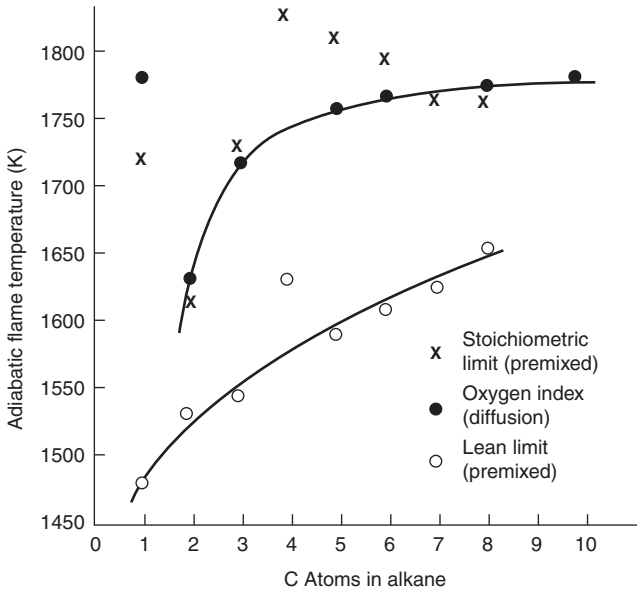

Figure 2-7.13. ***Computed adiabatic flame temperatures at flammability limits for n-alkanes (adapted from Reference 16).***

and that the adiabatic flame temperature at the stoichiometric limit for each fuel is a constant. These lead to the expression

$$\sum_{i=1}^{n} \frac{(C_i/100)\Delta H_{c,i}}{\int_{T_0}^{T_{f,\mathrm{SL},i}} n_p C_p dT} \geq 1 \qquad (6)$$

where

C_i = volume percent of fuel species, i, when the fuel stream is mixed stoichiometrically with the oxidant stream

$T_{f,\mathrm{SL},i}$ = adiabatic flame temperature of the stoichiometric limit mixture for fuel species i
- = 1700 K for most hydrocarbons
- = 1450 K for carbon monoxide
- = 1080 K for hydrogen

T_0 = temperature of the stoichiometric mixture prior to reaction

$\Delta H_{c,i}$ = heat of combustion of fuel species
- = 620 kJ/mol for hydrocarbons (per carbon, assuming $H/C = 2$)
- = 283 kJ/mol for carbon monoxide
- = 242 kJ/mol for hydrogen

n_p = number of moles of products of combustion per mole of reactants (stoichiometric mixture of the fuel and oxidant streams)

C_p = heat capacity of the products of combustion

This approach has been successfully used to predict the flammability of the hot gas layer formed in enclosure fires.[31]

While the hot gas layer formed in enclosure fires can become flammable, under some conditions the oxygen concentration in the hot layer can cause extinction of flames fully immersed in the hot layer. Based upon the analogies between premixed and diffusion flames, one would expect the oxygen concentration in the layer at extinction to be approximately equal to the premixed LOC. In fact, comparing the nitrogen diluent in Table 2-7.2 with Table 2-7.3, one can see a very close correspondence between the LOC and the LOI.

Morehart, Zukoski, and Kubota[32] examined the oxygen concentration at extinction of flames by dilution of air with combustion products. They found that flames were extinguished at oxygen concentrations of 12.4 to 14.3 percent, with the lower value occurring for a 50-cm-diameter pool burner and the higher value occurring for a 9-cm pool burner. These results are consistent with diesel pan fire tests (0.62 m and 0.84 m diameters) conducted by Peatross and Beyler[33] in which oxygen concentrations below 14 percent could not be achieved during pool burning in a compartment. It is also consistent with the results of Back et al.[34] Back et al. measured oxygen concentrations at extinction in water mist extinguishment tests in obstructed machinery space fires. They found an average oxygen concentration of 14.5 percent for heptane spray fires and 13.5 percent for pool fires at extinction. Since the molar heat capacity of water vapor is midway between nitrogen and carbon dioxide, one would expect water mist and combustion product extinction limits to be between nitrogen and carbon dioxide.

All of the above results are for relatively quiescent conditions. It is well known that at higher strain rates, the oxygen concentration at extinction increases. This phenomenon can most easily be seen in counterflow diffusion flame extinction experiments such as Hamins et al.[35]

EXAMPLE 5:

As part of a hazard analysis of a particular room fire, the composition of the hot layer during fire development has been estimated. The results of the analysis indicate that the following composition represents the highest concentration of fuel gases expected:

Hot layer—700 K, 10 percent total hydrocarbons (THC), in the form of CH_2, 2 percent CO, 1 percent H_2, 15 percent CO_2, 2 percent O_2, 70 percent N_2

Cold layer—300 K, 21 percent O_2, 79 percent N_2

Will the hot layer burn?

SOLUTION:

The working equation is Equation 6. The first step is to write a balanced chemical equation for stoichiometric burning:

$$0.1CH_2 + 0.02CO + 0.01H_2 + 0.02O_2 + 0.7N_2 + 0.15CO_2 + x(O_2 + 3.78N_2) \rightarrow 0.27CO_2 + 0.11H_2O + (0.7 + 3.78X)N_2$$

We can find x by requiring that both sides of this equation have the same amount of oxygen:

$$\begin{array}{cccccccc} \mathrm{CO} & & \mathrm{O_2} & \mathrm{CO_2} & \text{air} & \mathrm{CO_2} & \mathrm{H_2O} \\ \frac{0.02}{2} & + & 0.02 & + & 0.15 + x & = & 0.27 + \frac{0.11}{2} \end{array} \rightarrow x = 0.145$$

The concentrations in the stoichiometric mixture can be determined from the balanced chemical equation:

$$\begin{aligned} C_i &= \left(\frac{n_i}{n_T}\right) \times 100\% \\ n_T &= 0.1 + 0.02 + 0.01 + 0.02 + 0.7 + 0.15 \\ &\quad + 0.145 + 0.145(3.78) = 1.693 \\ C_{\mathrm{THC}} &= \left(\frac{0.1}{1.693}\right) \times 100\% = 5.9\% \\ C_{\mathrm{CO}} &= \left(\frac{0.02}{1.693}\right) \times 100\% = 1.2\% \\ C_{\mathrm{H_2}} &= \left(\frac{0.01}{1.693}\right) \times 100\% = 0.6\% \end{aligned}$$

Similarly, the number of moles of products per mole of reactants can be determined from the chemical equation

$$n_p = \frac{[0.27 + 0.11 + 0.7 + 0.145(3.78)]}{1.693} = 0.962$$

This result is lower than typical values of 1 to 1.1, because the unknown hydrocarbon mixture is taken as CH_2. This choice is not an error, since CH_2 has been consistently used for the heat release and heat capacity as well. For convenience, we will use constant average specific heats taken from Drysdale:[3]

	C_p (J/mol·K)	C (%)[a]
CO_2	54.3	16.2
H_2O	41.2	6.6
N_2	32.7	77.2

[a]Calculated by the same method as the fuel gas concentrations.

$$\begin{aligned} n_p C_p &= n_p \sum \left(\frac{C_i}{100}\right) C_{p,i} \\ &= 0.96[(0.162)(54.3) + (0.066)(41.2) + (0.772)(32.7)] \\ &= 35.3 \text{ J/mol·K} \end{aligned}$$

Notice that the average specific heat is near that of nitrogen, since it is the major constitutent of the mixture. In calculating T_0, the initial temperature of the mixture, we will ignore variations in C_p between the hot and cold layers.

$$\begin{aligned} T_0 &= \frac{n_h Th + n_c Tc}{n_h + n_c} \quad n_h + n_c = n_T \\ &= \frac{(1)(700 \text{ K}) + (0.69)(300 \text{ K})}{1.69} = 537 \text{ K} \end{aligned}$$

where n_h and n_c are the number of moles originating in the hot and cold layers, respectively. Substituting into Equation 5,

$$\sum_{i=1}^{n} \frac{(C_i/100)\Delta H_{c,i}}{C_p(T_{f,\mathrm{SL},i} - T_0)} = \frac{(0.059)(620)10^3}{35.3(1700 - 537)} + \frac{(0.012)(283)10^3}{35.3(1450 - 537)} + \frac{(0.006)(242)10^3}{35.3(1080 - 537)} = 1.07 \tag{7}$$

Since the result is greater than one, the hot layer *will* ignite and burn.

While the approach to the onset of layer burning used in Example 5 has a great deal of generality, it requires a very detailed characterization of the upper and lower layers. It has been shown by Beyler[31] that a much simpler method can be used to evaluate the conditions required for layer burning.

The method[31] is based on the very simple chemical model

$$\text{Fuel} + \text{Oxidizer} \rightarrow \begin{cases} \text{Products} + \text{Excess Oxidizer for } \phi < 1 \\ \text{Products} + \text{Excess Fuel for } \phi > 1 \end{cases} \tag{8}$$

where the equivalence ratio, ϕ, is given by

$$\begin{aligned} \phi &= \frac{\dot{m}_f}{\dot{m}_{\text{air}} \cdot r} \\ r &= \left(\frac{m_f}{m_{\text{air}}}\right)_{\text{Stoichiometric}} \end{aligned} \tag{9}$$

According to this model, the fuel mass fraction in the upper layer is

$$\begin{aligned} Y_f &= 0 && \text{for } \phi < 1 \\ Y_f &= \frac{1 - 1/\phi}{1 + 1/\phi r} && \text{for } \phi > 1 \end{aligned} \tag{10}$$

Equation 6 can be expressed on a mass basis for this application as

$$\frac{Y_f \Delta H_c}{m_p C_p (T_{\mathrm{SL}} - T_0)} \geq 1 \tag{11}$$

where ΔH_c is the heat of combustion of the fuel, and m_p is the mass of products resulting from burning a unit mass of upper layer gases.

Substituting the $\phi > 1$ relationship for Y_f into Equation 6, expressing the heat release in terms of oxygen consumed using

$$\Delta H_c = \frac{\Delta H_{O_2} Y_{O_2}}{r} \tag{12}$$

and recognizing that

$$m_p = 1 + \frac{Y_f}{r} \tag{13}$$

yields

$$\left(\frac{1-1/\phi}{1+r}\right)\left[\frac{\Delta H_{O_2} Y_{O_2}}{C_p(T_{SL}-T_0)}\right] \geq 1 \qquad (14)$$

Equation 14 can be solved for the equality condition to give the equivalence ratio at which layer burning begins, ϕ_{ig},

$$\phi_{ig} = \frac{k}{k-r-1} \qquad (15)$$

where

$$k = \frac{\Delta H_{O_2} Y_{O_2}}{C_p(T_{SL}-T_0)}$$

T_0 is the precombustion temperature resulting from stoichiometric mixing of the air and fuel streams. Here, the upper layer contains the fuel and the lower layer contains the air. T_0 can be expressed as

$$T_0 = \frac{T_u + (Y_f/r)T_1}{1 + Y_f/r} \qquad (16)$$

Using Equations 15 and 16, a relationship between the critical ignition equivalence ratio and the layer temperatures can be developed. Using normal values for the semi-universal constants, $\Delta H_{O_2} = 13.4$ MJ/kg, $C_p = 1.1$ kJ/kg K, $T_{SL} = 1700$ K. Using air properties for the lower layer, $Y_{O_2} = 0.233$ and $T_1 = 300$ K. Using a typical $r = 0.07$ yields the relationship between ϕ_{ig} and T_u shown in Figure 2-7.14. The results shown in Figure 2-7.14 are consistent with the measurements of Beyler,[31] where ϕ_{ig} was found to be 1.7 for T_u of 500 to 600 K. Gottuk[36] found that external burning was first observed in flashes at $\phi = 1.4 \pm 0.4$, and sustained external burning was first observed at $\phi = 1.9 \pm 0.3$ when T_u was in the range 900 to 1100 K. While in Gottuk's[36] experiments it was difficult to observe burning at the layer interface due to soot deposits on the viewing ports, layer interface burning was generally observed shortly after the initiation of flashes in the exhaust. Because the exhaust flow was isolated from the inflow in the experiment, there is some issue of the availability of a pilot flame which does not arise in normal two-directional vents found in most fires. Thus, Gottuk's work is generally consistent with Figure 2-7.14.

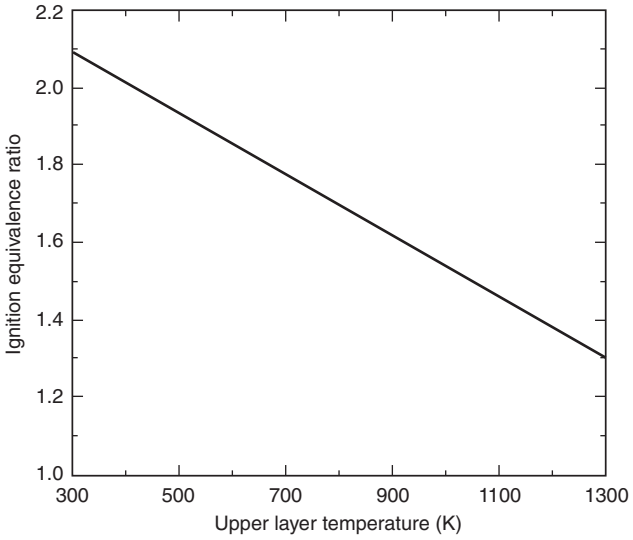

Figure 2-7.14. ***Equivalence ratio required for upper layer ignition as a function of the upper layer temperature determined using Equations 15 and 16 with typical properties. Using normal values for the semi-universal constants, $\Delta H_{O_2} = 13.4$ MJ/kg, $C_p = 1.1$ kJ/kg K, $T_{SL} = 1700$ K. Using air properties for the lower layer, $Y_{O_2} = 0.233$, $T_1 = 300$ K. Using a typical $r = 0.07$ yields the relationship between ϕ_{ig} and T_u.***

Oxygen Index Test Method

The original oxygen index test method, used to determine the oxygen index of liquid and gas fuels, utilizes a counterflow diffusion flame formed at the stagnation region of a porous cylinder or sphere through which fuel vapors are fed. A low-velocity oxidant stream passes over the porous body. This arrangement yields the most favorable aerodynamic conditions for flame stabilization. As such, fuel and oxidant streams that can burn in the low-velocity counterflow system may not burn under less favorable aerodynamic conditions characterized by higher velocities and shear.

It is also important to point out the difference between the oxygen index as measured for gas and liquid fuels and the oxygen index of solids as measured using a candle-type test.[37,38] The oxygen indexes of the gas and liquid fuels as tested by Simmons and Wolfhard[29] were governed by gas-phase effects. In the American Society for Testing and Materials test[33] for solids, the extinction can be caused by gas- and solid-phase effects. As such, the oxygen index of a solid fuel is not directly relevant to gas-phase diffusion flame limits and should not be used to calculate adiabatic flame temperature at the limit for use in the expressions presented here.

Nomenclature

AIT	autoignition temperature (C or K)
C	concentration (volume percent)
C_p	heat capacity (J/kg K)
LFL	lower flammable limit (volume percent)
M	mass (kg)
n	moles
r	stoichiometric fuel/air ratio
SL	stoichiometric limit (volume percent)
T	temperature (C or K)
V	volume (m^3)
X	mole fraction
Y	mass fraction
ΔH_c	heat of combustion (J/kg)
ϕ	equivalence ratio

Subscripts

c	combustion
i	species
ig	ignition
f	flame, or fuel
l	lower layer
L	liquid
m	mixture
N	nitrogen
NP	nitrogen point
O	initial or ambient
OI	oxygen index
p	products of combustion
SL	stoichiometric limit
U	upper layer

References Cited

1. M.G. Zabetakis, *Bulletin No. 627,* U.S. Bureau of Mines, Washington, DC (1965).
2. H.F. Coward and G.W. Jones, *Bulletin, No. 503,* U.S. Bureau of Mines, Washington, DC (1952).
3. D.D. Drysdale, *An Introduction to Fire Dynamics,* John Wiley and Sons, New York (1999).
4. ASTM E681-94, *Standard Test Method for Concentration Limits of Flammability of Chemicals,* American Society for Testing and Materials, Philadelphia (1994).
5. ASTM E918-83, *Standard Test Method for Concentration Limits of Flammability of Chemicals,* American Society for Testing and Materials, Philadelphia (1993).
6. DIN 51 649 Teil 1, *Bestimmung der Explosionsgrenzen von Gasen and Gasgemischen in Luft,* Deutsches Institute fur Normung, Berlin, Germany (1986).
7. VDI 2263 Part 1, *Test Methods for the Determination of the Safety Characteristics of Dusts,* Verein Deutscher Ingenieure (1990).
8. G. Smedt, F. Corte, R. Notele, and J. Berghmans, "Comparison of Two Standard Test Methods for Determining Explosion Limits of Gases at Atmospheric Conditions," *J. of Haz. Mat.,* A70, pp. 105–113 (1999).
9. M. Goethals, B. Vanderstraeten, J. Berghmans, G. Smedt, S. Vliegen, and E. Van't Oost, "Experimental Study of the Flammability Limits of Toluene–Air Mixtures at Elevated Pressure and Temperature," *J. of Haz. Mat.,* A70, pp. 99–104 (1999).
10. G.A. Karim, I. Wierzba, M. Metwally, and K. Mohon, in *18th Symposium (International) on Combustion,* Combustion Institute, Pittsburgh, PA.
11. H.F. Coward, C.W. Carpenter, and W. Payman, *J. Chem. Soc.,* 115, 27 (1919).
12. M.J. Burgess and R.V. Wheeler, *J. Chem. Soc.,* 99, 2013 (1911).
13. A.G. White, *J. Chem. Soc.,* 127, 672 (1925).
14. M.G. Zabetakis, S. Lambiris, and G.S. Scott, *Seventh Symposium (International) on Combustion,* Combustion Institute, Pittsburgh, PA.
15. F.J. Weinberg, *Nature,* 283, 239 (1971).
16. A. Macek, *Comb. Sci. and Tech.,* 21, 43 (1979).
17. A. Egerton and J. Powling, *Proc. Roy. Soc.,* 193, London (1948).
18. D.R. Stull, *F. Res. Abst. and Rev.,* 13, 161 (1971).
19. H.F. Coward and G.W. Jones, "Limits of Flammability of Gases and Vapors," *Bulletin 503,* U.S. Bureau of Mines, Washington, DC (1952).
20. G.W. Jones, M.G. Zabetakis, J.K. Richmond, G.S. Scott, and A.L. Furno, "Research on the Flammability Characteristics of Aircraft Fuels," *Technical Report 52-35, Supplement I,* Wright Air Development Center, Wright-Patterson AFB, OH (1954).
21. J.M. Kuchta, A.L. Furno, A. Bartkowiak, and G.H. Martindill, "Effect of Pressure and Temperature on Flammability Limits of Chlorinated Combustibles in Oxygen-Nitrogen and Nitrogen Tetroxide-Nitrogen Atmospheres," *Journal of Chemical and Engineering Data,* 13, 3, p. 421 (1968).
22. M.G. Zabetakis, "Flammability Characteristics of Combustible Gases and Vapors," *Bulletin 627,* U.S. Bureau of Mines, Washington, DC (1965).
23. M.G. Zabetakis and B.H. Rosen, "Considerations Involved in Handling Kerosene," *Proceedings AP1,* 37, p. 296 (1957).
24. B. Lewis and G. Von Elbe, *Combustion, Flame, and Explosions of Gases,* Academic, New York (1961).
25. R.A. Strehlow, *Combustion Fundamentals,* McGraw-Hill, New York (1984).
26. M. Hertzberg, K. Cashdollar, and R. Conti, *19th Symposium (International) on Combustion,* Combustion Institute, Pittsburgh, PA.
27. J.H. Burgoyne and L. Cohen, *Proc. Roy. Soc.,* A225, 375 (1954).
28. M. Hertzberg, K. Cashdollar, and C. Lazzara, *18th Symposium (International) on Combustion,* Combustion Institute, Pittsburgh, PA.
29. R.F. Simmons and H.G. Wolfhard, *Comb. and Flame,* 1, 155 (1957).
30. S. Ishizuka and H. Tsuji, *18th Symposium (International) on Combustion,* Combustion Institute, Pittsburgh, PA (1981).
31. C.L. Beyler, *Comb. Sci. and Tech.,* 39, 287 (1984).
32. J. Morehart, E. Zukoski, and T. Kubota, "Characteristics of Large Diffusion Flames Burning in a Vitiated Atmosphere," in *Third International Symposium on Fire Safety Science,* Elsevier Science Publishers, UK, pp. 575–583 (1991).
33. M. Peatross, and C. Beyler, "Ventilation Effects on Compartment Fire Characterization," in *Fifth International Symposium on Fire Safety Science,* Elsevier Science Publishers, UK, pp. 403–414 (1997).
34. G. Back, C. Beyler, R. Hansen, "A Quasi Steady-State Model for Predicting Fire Suppression in Spaces Protected by Water Mist Systems," *Fire Safety Journal,* 35, pp. 327–362.
35. A. Hamins, D. Trees, K. Seshadri, H. Chelliah, "Extinction of Nonpremixed Flames with Halogenated Fire Suppressants," *Combustion and Flame,* 99, pp. 221–230 (1994).
36. D.T. Gottuk, "The Generation of Carbon Monoxide in Compartment Fires," Ph.D. Dissertation, Virginia Polytechnic and State University, Blacksburg, VA (1992). [Also in NIST-GCR-92-619, National Institute of Standards and Technology, Gaithersburg, MD (1992).]
37. C.P. Fenimore and F.J. Martin, *Comb. and Flame,* 10, 135 (1966).
38. ASTM D2863-97, *Standard Test Method for Measuring the Minimum Oxygen Concentration to Support Candle-Like Combustion of Plastics (Oxygen Index),* American Society for Testing and Materials, Philadelphia (1997).

CHAPTER 8

Ignition of Liquid Fuels

A. Murty Kanury

Introduction

This chapter introduces the topic of liquid fuel ignition in air. A qualitative description of the physical and chemical steps leading to ignition makes possible a systematic identification of the factors of concern. Different measures of liquid fuel ignitibility are defined, and a comprehensive collection of data is presented. Simple mechanistic models are formulated for the piloted ignition (i.e., flash point) of liquids as well as for the autoignition of vapor and air mixtures. The results of these models are employed to highlight (1) the manner in which physics and chemistry play a complicated role to culminate in ignition, (2) the resultant dependency of the measurements on the specific apparatus test method, and (3) a number of dependencies of the measured ignition temperature on experimental conditions. These predicted dependencies are found to be consistent with the trends in reported data.

Liquid combustibles are ever-present in the context of mobile and stationary power plants as well as in an innumerable array of industrial processes. A variety of physical forms in which they arise can be identified. Dip tanks of paints or solvents, sprays, spills from a storage tank, flowing or creeping films, and pools in open pits are but a few examples. In almost all situations, air is in contact, or readily comes into contact, with the fuel to make the associated fire hazard obvious. The following questions arise in relation to fire safety in these situations:

1. Under what circumstances is ignition possible?
2. Under the conditions of possible ignition, what is the external impulse required to produce ignition within a given time? Alternately stated, given a set of conditions under which ignition is possible, how long an exposure is required to produce ignition?

The first of these questions is addressed here along with some cursory observations on the second question.

Ignition is defined as the onset or initiation of combustion, usually flaming. As such, ignition is indicated by the oxidation reaction attaining a rapidly increasing rate. The rapidity often makes the ignition phenomenon an abrupt event. In practice, ignition is noted by the appearance of a flame, by a significant increase in oxidative energy release, or by a corresponding large rise in temperature.

Three sets of conditions have to be fulfilled to ignite a condensed-phase material. First, sufficient quantities of combustible vapors and gases have to be emanated as a result of preheating the solid or liquid. Second, these vapors and gases have to be mixed with the oxidant in the gas phase. Third, the mixture has to be either at a high enough temperature to induce self-accelerative oxidation (i.e., *spontaneous* or *autoignition)* or to be provided with a pilot source (e.g., a small ignitor flame, a heated wire, or an electric spark) to locally heat a minimum quantity of the mixture to a temperature approaching the adiabatic flame temperature (i.e., *piloted* or *forced ignition*). These three sets of conditions enable a systematic enumeration of the factors influencing the ignition process.

Vaporization: A Contrast between Liquid and Solid Combustibles

All condensed-phase materials release vapors and gases in response to heating. As related to the first of the three steps mentioned above, this response is dramatically different between solids and liquids.

Liquids generally* vaporize in the sense of a thermodynamic phase change in which the chemical structure of vapor remains the same as that of liquid. Such a vaporization is usually a surface mass transfer phenomenon,

Dr. A. Murty Kanury is professor of mechanical engineering at Oregon State University. His professional activities are centered around teaching thermal science and research in fire and combustion.

*Some high molecular weight liquids are exceptional in that they exhibit a chemical breakdown in response to heating.

although intense (and internal) heating may produce bubbles within the liquid. In contrast, heating of solids generally* results in complicated destructive distillation (also known as thermochemical degradation or *pyrolysis*) to yield a complex combustible mixture of gases and vapors. Known also as pyrolyzate, this mixture is produced *within* the solid at a rate dependent upon the local instantaneous density and temperature. The pyrolysis process, thus, is volumetric and chemical rather than superficial and physical.

Pyrolysis of most solids leaves a carbon-rich porous residue, known as char, behind. Vaporization of most common liquids, in contrast, leaves no residue behind.

Upon heating a liquid body, internal convective currents develop with an intensity dependent on the heating rate, viscosity, surface tension, gravity, and geometry of the body. The heating of a solid, by definition, does not invoke the same sort of bulk flows. There does arise, however, an internal convection process associated with the outflow of the pyrolyzates through the partially or totally degraded porous solid. The temperature distribution within a liquid body can be made artificially uniform by mixing with a stirrer; the same is not possible within a solid body.

The ease with which vapors can be produced by heating a liquid is known as its volatility. A liquid is said to be highly volatile if its vapor pressure at a given temperature is high (i.e., its boiling point at a given pressure is low), and its *latent heat* (i.e., enthalpy of vaporization) is low.

Mixing of Vapors with Air

The vapors emanating from the surface of a heated liquid mix with the ambient gas, which is usually air at normal pressure. This mixing is dependent on such factors as whether the air is quiescent or in motion, whether the liquid reservoir is closed or open, the geometry relative to the gravity vector, the temperature of the liquid surface relative to the ambient, the molecular weight of the vapors relative to that of air, and the height and nature of the lip of the vessel containing the liquid.

Ignition of the Mixture

The mixture thus formed has to be rich enough in combustible content to be over the so-called *lean limit of flammability* to make a propagable flame possible from a localized pilot source. The location and nature of the pilot is of obvious importance. Generally, when ignition is possible, the flame would simply flash through the mixture, consume the combustibles in its sweep, and then go out. Only if the vaporization is copious enough, due to a higher bulk temperature of the liquid, does the flame become self-sustained. These flashing and self-sustainment concepts are central to the liquid fuel ignition process.

If the gaseous mixture temperature is sufficiently high, ignition may occur even without a pilot source. This is known as auto- or spontaneous ignition.

*Some solids, such as waxes, are exceptional in that they melt and vaporize in the manner of a simple liquid. Some other exceptional solids, such as camphor and sulfur, sublime to a gas phase.

Figure 2-8.1, the rudiments of which were first formulated by Zabetakis,[1] indicates the essence of the previous descriptions. Part (a) of Figure 2-8.1, familiar from elementary thermodynamics, exhibits the exponential dependency of equilibrium vapor pressure on the liquid temperature. The normal melting and boiling point temperatures are also shown in this figure. Part (b) shows that as the temperature is gradually raised, the vapor pressure of the combustible liquid gradually rises to yield, at a limit temperature, T_L, a lean limit mixture capable of supporting a propagable flame. At a higher temperature, the partial pressure may become too high and make the mixture too rich to support a flame. Furthermore, at relatively high temperatures exceeding T_a, ignition can occur even in the absence of a pilot source. As indicated, the lean and rich limits, as well as the autoignition limits, are generally temperature dependent. Part (c) shows that the features of ignition of a pyrolyzing combustible solid are similar to those of a combustible liquid, except for the fact that the pyrolyzates are evolved due to degradation over a range of temperatures.

Some Experimental Techniques and Definitions

Piloted ignition data are mostly measured in a number of American Society for Testing and Materials (ASTM) tests.[2] These tests involve either an open-cup (e.g., ASTM D1310 open-cup test or D92 Cleveland Test) or a closed-cup test (e.g., ASTM D56 Tag Closed Tester and D93 Pensky-Martens test) to hold the fuel to a prescribed level. This cup is then heated either directly by a prescribed, Bunsen-type laboratory flame, or indirectly by a water (or water and glycol mixture) bath. There are similar international tests under a variety of names, including Engler and Haass, Danish open, Tagliabue, Elliot, Luchaire, Treumann, Albrecht, Abel, Saybolt, and Parish, among others.

Mullins[3] presents a comprehensive review of a variety of methods by which the spontaneous ignition temperature, T_a, of combustible liquids is experimentally determined. A number of variations, in which the reaction vessel is a crucible, flask, furnace, bomb, or a compression device, are employed to precisely control the experimental conditions, to observe whether or not ignition will occur, and to measure the time to ignition (i.e., the ignition delay). Flow methods, as well as heating of the liquid by hot surfaces, are also frequently employed. The ASTM test standard D2155 holds the liquid in a flask, which is heated in a furnace to determine the autoignition temperature and ignition delay.

The finer details of these tests are not materially relevant to the scope of this chapter. Zabetakis[1] and the ASTM standards[2] do an excellent job of giving these details. It is important, however, to define certain measures of the volatility and ignitibility of liquid fuels as obtained from these experimental techniques.

The *bubble point (R : 1)* of a liquid fuel[4] is the temperature at which equilibrium exists between the wholly condensed fuel and an infinitesimal quantity of its vapor mixed with air in the ratio of 1 : R. When R is zero, the bubble point is the same as the normal boiling point.

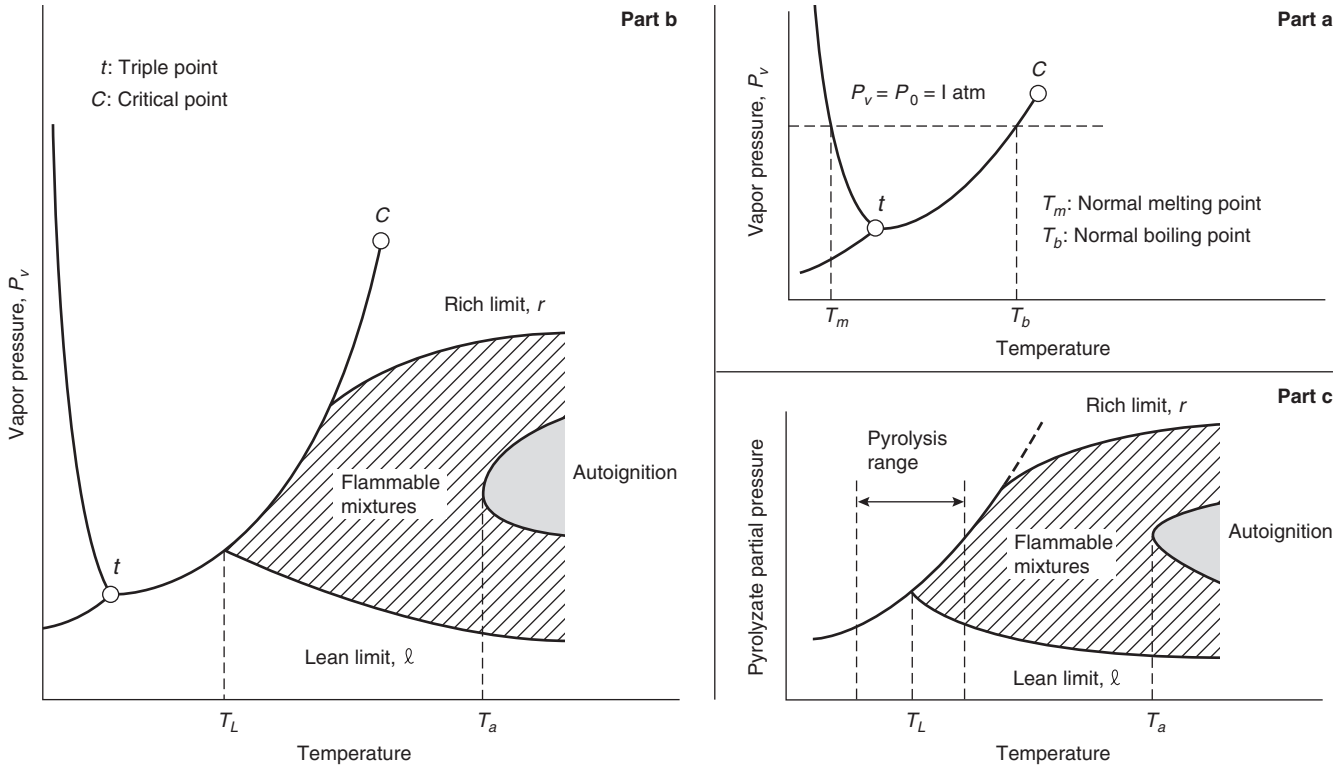

Figure 2-8.1. ***Phase-change diagram for: (a) an inert liquid; (b) a combustible liquid; and (c) a combustible solid.***

The *flash point* of a liquid fuel is its temperature (presumed to be uniform) at which the vapor and air mixture lying just above its vaporizing surface is capable of supporting a momentarily flashing propagation of a flame when prompted by a quick sweep of a small gas flame pilot near the surface. It is expected that the flash point is somehow related to the minimum temperature, T_L, for piloted ignition indicated in Figure 2-8.1(b).

The *fire point* of a liquid fuel is very similar in definition to the flash point, except that the flame does not merely flash and cease but must also be self-sustained, so as to continue burning the liquid.

The *autoignition temperature,* T_a, of a vapor (or gas) and air mixture is the minimum temperature at which the mixture is self-igniting.

Another property relevant in interpreting the significance of flash point is the *lean limit of flammability,* defined as the lowest *volume* percentage of fuel vapor (or gas) in the mixture with air (or oxygen) that will support propagation of a flame away from a pilot ignition source.

Example Data

The most extensive flash point and fire point data sources are the *International Critical Tables*[5] and the *Loss Prevention Handbook*.[6] Tables 2-8.1, 2-8.2, and 2-8.3 are excerpted from these two sources to note the typical values and to make several important observations.

Table 2-8.1 shows the flash points of a number of liquids in air measured by various test methods to indicate that the measurements depend quite strongly upon the apparatus employed. Although, as expected, the closed-cup tests (e.g., Pensky-Martens) produce flashing at a lower temperature than the open-cup tests (e.g., Cleveland). Other differences are neither small nor systematic.

Table 2-8.2 gives open- and closed-cup flash and fire points for a number of real-world combustibles of varying specific gravity. Two points are noteworthy: the fire point consistently exceeds the flash point by about 20 to 40°C, and heavier fuels tend to have higher flash points. Recalling that a higher flash point implies a lower saturation pressure and, hence, a lower volatility, this second observation is reasonable.

Table 2-8.3, adapted from *ICT*,[5] shows the closed-cup flash points as well as the minimum autoignition temperatures for a number of real liquids. The decrease in T_a due to high pressure is noteworthy.

Table 2-8.4, is a comprehensive collection of the flash points, lean limits, and autoignition temperatures for a host of liquid fuels in air at a nominal pressure of 1 atm. A number of other properties, useful in the following section, are also included. Besides serving as a practical reference dictionary, Table 2-8.4 also indicates a number of trends that are often vague or weak. Most of these trends are conceptually unsubstantiated to date. For example, in a given family of fuels, an increase in fuel molecular weight generally (but not always) indicates (1) a marked increase in the normal boiling point T_b°, (2) a slight decrease in the normal enthalpy of vaporization h_{fg}°, (3) an apparent increase in the flash point T_F°, (4) a modest and erratic decrease in the lean limit ℓ, and (5) a noticeable decrease in the minimum temperature for autoignition, T_a.

Table 2-8.1 ***Flash Points of Several Combustible Liquids Measured by Several Different Tests in Air***

	Flash Point (°C) as Measured in						
	Abel	Tagliabue	Elliot	Pensky-Martens	Cleveland	Luchaire	Open Cup
Naphtha	34.4	39.4	36.4	40.6	46.1	50.0	
Kerosene	52.8	54.4	53.3	57.2	60.0	58.9	
Petrolite	61.1	59.4	60.0	65.6	68.3	62.2	
Gas oil				90.6	93.3	92.2	
300 oil				123.9	129.4	130.0	
Straw oil				157.2	162.8	161.1	
Engine oil				221.1	226.7	221.1	
Heavy oil				265.6	293.3	265.5	
Mexican crude				19.0			35.0
Petrol				26.5			33.5
Tar oil				87.0			92.5

Source: Excerpted from the *International Critical Tables*[5]

Theory and Discussion

Theoretical models are required in order to substantiate and understand these and other trends that may lie buried in elaborate data. The mechanisms culminating in the global effects of flashing and autoignition also elicit the way in which the measured properties depend on the apparatus used and the testing procedure followed. However, the physics and chemistry involved in open- or closed-cup flash point and autoignition testers is much too complicated, with numerous interacting thermodynamic, fluid mechanical, heat and mass transport, and chemical kinetic processes. Complete mathematical models capable of predicting the outcome of a specific test do not exist and are nearly impossible. Simple syntheses of the essential physical and chemical processes of the tests, are not only possible but enlightening.

Table 2-8.2 ***Flash and Fire Points of Some Hydrocarbon Liquids in Air***

Liquid	Flash Point (°C)	Fire Point (°C)	Specific Gravity
Fuel oil[a]	133	164	0.921
Crude[a]	125	155	0.923
Light fuel[a]	187	220	0.900
Black oil[a]	144	172	0.928
Refined oil[a]	122	135	0.904
Texas solar oil[a]	92	97	0.862
Shale oil[a]	130	150	0.862
Gas oil[a]	90	109	1.067
Neutral oils[a]	135	163	0.843
	216	252	0.878
Paraffin oils[a]	163	193	0.870
	216	254	0.912
Paraffin oil[b]	98	112	0.916
Naphthene base oil[a]	196	227	0.937
Diesel fuel[b]			
Russia	53–138	78–180	0.876–0.950
N. America	82–166	103–200	0.865–0.950
India	92–150	120–174	0.890–0.950
Tar oil for diesels[b]			
Coke oven	90–135	108–166	1.14–1.18
Water gas	34–91	50–155	0.97–1.13
Oil gas	18–69	20–89	1.05–1.07
Coal tar oil	66–121	84–160	1.00–1.11

[a] = Open cup

[b] = Pensky closed cup

Source: Extracted from the *International Critical Tables*[5]

Flash Point and Lean Flammability Limit

In principle, the problem involves transient analysis of heat and mass transfer with oxidative reactions in the gas phase lying above the liquid surface. In cup tests, the boundaries of the three-dimensional space of interest are the vaporizing liquid surface at the bottom, the open or closed top, and the side walls, which are probably cylindrical and therefore impervious to mass but conductive to heat. (The flash points and autoignition temperatures measured in cups or flasks whose walls are highly conductive are known to be higher.) If the cup were open, airflow and drafts in the room would be expected to alter the heat and mass transport processes of concern, and hence, the measurement. A closed cup minimizes these alterations by allowing air to stealthily leak into the region of interest.

Table 2-8.3 ***Autoignition Temperatures at Two Pressures and Closed-Cup Flash Points for a Number of Liquid Fuels in Air***

Fuel	Flash Point (K)	Autoignition Temp. T_a (K)	
		P° = 1 atm	P° = 33 atm
Sperm oil	509	581	413
Lard oil	513	546	417
Castor oil	536	598	426
Glycerine	—	685	478
Kerosene	328	528	448
Spindle oil	467	521	451
Turbine oils	—	—	526–564
Compressor oil, A	—	582	461
Compressor oil, B	469	546	460
Compressor oil, C	489	559	430

Source: Adapted from the *International Critical Tables*[5]

Table 2-8.4 ***Selected Ignition, Flammability, and Autoignition Properties of Some Fuels in Air[3–8]***

Fuel	Formula	Weight (kg/kmol)	T_b° (K)	h_{fg}° (kJ/kg)	h_c (MJ/kg)	T_k° (K) Closed	T_k° (K) Open	Fl. Limits by Vol. Lean	Fl. Limits by Vol. Rich	T_a° (K)	h_{fg}°/RT_b°
Alkanes:											
Methane	CH_4	16	111	509	50.2	—	—	0.053	0.150	910	8.81
Ethane	C_2H_6	30	184	489	47.6	—	138	0.030	0.125	745	9.57
Propane	C_3H_8	44	231	426	46.4	—	169	0.022	0.095	723	9.76
n-Butane	C_4H_{10}	58	273	386	45.9	—	213	0.019	0.084	561	9.88
i-Butane			263	366	—	156	—	0.018	0.084	735	9.71
n-Pentane	C_5H_{12}	72	309	365	45.5	—	224	0.014	0.078	516	10.22
i-Pentane			286	371	—	—	222	0.014	0.076	693	11.23
n-Hexane	C_6H_{14}	86	342	365	45.2	251	—	0.012	0.074	498	11.04
i-Hexane			—	—	—	244	—	0.010	0.070	—	—
n-Heptane	C_7H_{16}	100	371	365	45.0	269	—	0.012	0.067	477	11.83
i-Heptane			—	—	—	255	—	0.010	0.060	—	—
n-Octane	C_8H_{18}	114	398	298	44.9	286	—	0.008	0.032	479	10.26
i-Octane			—	—	—	261	—	0.010	0.060	—	—
n-Nonane	C_8H_{20}	128	424	288	44.8	304	—	0.007	0.029	478	10.46
n-Decane	$C_{10}H_{22}$	142	447	360	44.7	317	—	0.006	0.054	474	13.76
n-Undecane	$C_{11}H_{24}$	156	469	308	44.6	—	338	0.007[a]	0.123	—	12.32
n-Dodecane	$C_{12}H_{26}$	170	489	293	44.6	345	—	0.006	0.123	476	12.25
Kerosene ~	$C_{14}H_{30}$	198	505	291	44.0[a]	322	—	0.006	0.056	533	13.72
Alkenes:											
Ethylene	C_2H_4	29	169	516	47.3	152	—	0.027	0.286	763	10.28
Propene	C_3H_6	42	225	437	45.9	165	—	0.021	0.111	728	9.81
1-Butene	C_4H_8	56	267	398[a]	45.4	193	—	0.016	0.099	658	10.04
1-Pentene	C_5H_{10}	70	303	314	46.9	—	255	0.014	0.097	548	8.72
Hexelene	C_6H_{12}	84	340[a]	388	47.5	—	—	—	—	518	11.53
Cycloparaffins:											
CycloPropane	C_3H_6	42	239	588	46.3	178	—	0.024	0.104	771	12.43
CycloButane	C_4H_8	56	286	483	44.8	208	—	0.011[a]	—	483	11.38
CycloPentane	C_5H_{10}	70	322	443	44.3	236	—	0.020[a]	—	634	11.58
CycloHexane	C_6H_{12}	84	354	358	43.9	253	—	0.013	0.078	518	10.22
CycloHeptane	C_7H_{14}	99	392	376	43.7	282[a]	—	0.012[a]	—	—	11.31
Dimethyl-cycloHexane	C_8H_{16}	112	392	300	46.3[a]	284	—	—	—	505	10.31
Aromatics:											
Benzene	C_6H_6	78	353	432	40.7	262	—	0.012	0.071	771	11.48
Toluene	C_7H_8	92	383	362	41.0	277	280	0.013	0.068	753	10.46
m-Xylene	C_8H_{10}	106	412	343	41.3	298	—	0.011	0.070	801	10.61
o-Xylene			414	347	41.3	290	297	0.010	0.060	737	10.69
p-Xylene			410	339	41.3	298	—	0.011	0.070	802	10.54
bi-Phenyl	$C_{12}H_{10}$	154	527	—	40.6	386	397	—	—	813	—
Naphthalene	$C_{10}H_8$	128	491	316[a]	40.3	352	361	0.009	0.059	799	9.91
Anthracene	$C_{13}H_{10}$	166	613	310[a]	40.0[a]	394	469	0.006	—	813	10.10
EthylBenzene	C_8H_{10}	106	409	320[a]	43.1	288	297	0.010	—	705	9.98
ButylBenzene	$C_{10}H_{14}$	134	446	277[a]	43.7	322	336	0.008	0.059	683	10.01
Alcohols:											
Methanol	CH_3OH	32	337	1101	20.8	285	289	0.067	0.365	658	12.57
Ethanol	C_2H_5OH	46	351	837	27.8	286	295	0.033	0.190	636	13.19
n-Propanol	C_3H_7OH	60	370	686	31.3	288	302	0.022	0.135	705	13.38
i-Propanol			355	667	33.1	285	—	0.020	0.118	672	13.56
n-Butanol	C_4H_9OH	74	390	621	36.1	302	316	0.014	0.113	616	14.17
i-Butanol			380	578	36.1	301	—	0.017	—	678	13.54
2-Pentanol	$C_5H_{11}OH$	88	392	575	—	—	314	0.012	—	616	15.52
i-Amyl alcohol	$C_5H_{11}OH$	88	403	501	35.3	316	319	0.012	0.100	573	13.16
3-Pentanol			391	575[a]	—	307	312	0.012[a]	—	708	15.56
n-Hexanol	$C_6H_{13}OH$	102	430	458	36.4	318	347	0.012[a]	—	—	13.07
Cyclohexanol			434	460[a]	36.6	341	—	0.012[a]	—	573	13.00
n-Heptanol	$O_7H_{15}OH$	116	449	439	39.8	—	344	—	—	—	13.64
1*n*-Octanol	$C_8H_{17}OH$	130	469	408	40.6	354	—	—	—	—	13.60
2*n*-Octanol			453	419	—	347	355	—	—	—	14.46
Nonanol	$C_9H_{19}OH$	144	487	403	40.3	—	—	—	—	—	14.33
i-Decanol	$C_{10}H_{21}OH$	158	508	373	—	—	—	—	—	561	14.12

Table 2-8.4 *(Continued)*

Fuel	Formula	Weight (kg/kmol)	T_b° (K)	h_{fg}° (kJ/kg)	h_c (MJ/kg)	T_k° (K) Closed	T_k° (K) Open	Fl. Limits by Vol. Lean	Fl. Limits by Vol. Rich	T_a° (K)	h_{fg}°/RT_b°
Carbonyls:											
Formaldehyde	CH_2O	30	370	826	18.7	366	—	0.070	0.73	703	8.05
37% in H_2O		—	370[a]	826[a]	—	327	366	0.070[a]	—	697	8.05
Acetaldehyde	C_2H_4O	44	294	570	25.1	235	—	0.040	0.570	477	10.26
Allyl alcohol	C_3H_6O	58	368	684	31.9	294	297	0.025	0.180	651	12.93
i-Butyraldehyde	C_4H_8O	72	334	444[a]	33.8	233	249	0.025	—	503	11.51
Crotonaldehyde	C_4H_6O	70	375	490[a]	34.8	286	—	0.021	0.155	505	11.00
Diethyl Acetaldehyde	$C_4H_{12}O$	76	391	500[a]	—	294	—	—	—	—	11.70
Ethyl Hexaldehyde	$C_8H_{16}O$	128	436	325[a]	39.4	—	325	—	—	—	11.48
Paraldehyde	$C_6H_{12}O_3$	132	397	328	—	290	309	0.013	—	511	13.11
Salicyl aldehyde	$C_7H_6O_2$	122	469s	396	—	351	—	—	—	—	12.39
Benzaldehyde	C_7H_6O	106	452	362	—	337	347	—	—	465	10.21
Ketones:											
Acetone	C_3H_6O	58	329	521	29.1	255	264	0.026	0.128	738	11.05
2-Butanone	C_4H_8O	72	353	443	33.8	271	274	0.018	0.095	677	10.87
Diethyl ketone	$C_5H_{10}O$	86	374	380	33.7	—	286	—	—	723	10.51
Methyl *i*-Butyl ketone	$C_6H_{12}O$	100	389	345[a]	35.2	296	297	0.014	0.076	806	10.66
Dipropyl ketone	$C_7H_{14}O$	114	417	317	38.6	—	—	—	—	806	10.42
Methyl *n*-Propyl ketone	$C_5H_{10}O$	86	375	376[a]	33.7	280	289	0.015	0.082	613	10.37
Methyl vinyl ketone	C_4H_6O	70	354	440[a]	—	266[a]	—	—	—	—	10.46
Acids:											
Formic acid	CH_2O_2	46	374	502	5.7	342	—	—	—	813	7.42
Acetic acid	$C_2H_4O_2$	60	391	405	14.6	313	330	0.054	—	737	7.48
Benzoic acid	$C_7H_6O_2$	122	523s	270[a]	24.4	394	—	—	—	843	7.58
Miscellany:											
Camphor	$C_{10}H_{16}O$	152	477s	265[a]	38.8	339	366	0.006	0.035	739	10.16
Carbon disulfide	CS_2	76	320s	—	13.6	303	—	0.013	0.500	398	—
m-Creosol	C_7H_8O	108	476	—	34.6	359	—	0.011	—	832	—
o-Creosol			464	—	34.1	354	—	0.013	—	872	—
p-Creosol			475	—	34.1	359	—	0.010	—	832	—
Furan	C_4H_4O	68	304	399	—	238	—	0.023	0.143	—	10.73
Pyridine	C_5H_5N	79	387	449	35.0	293	—	0.018	0.124	755	11.02
Aniline	C_6H_7N	93	456	434	36.5	349	364	0.013	—	890	10.64
Acetal	$C_6H_{14}O_2$	118	376	277	31.8	252	—	0.016	0.104	503	10.46
p-Cymene	$C_{10}H_{14}$	134	449	283	43.9	320	336	0.007	0.056	709	10.16
o-Dichloro Benzene	$C_6H_4Cl_2$	146	453	—	19.3	339	347	0.022	0.092	921	—
1.1-Dichloro Ethylene	$C_2H_2Cl_2$	96	310	—	—	—	263	0.056	0.114	733	—
1.2-Dichloro Ethylene			334	—	—	279	—	0.097	0.128	—	—
Monochloro Benzene	C_6H_5Cl	112	405	—	—	305	311	0.018	—	947	—
Resorcinol	$C_6H_6O_2$	110	549	—	26.0	400	—	0.014	—	881	—
EthylFormate	$C_3H_6O_2$	74	327	—	22.5	253	261	0.027	0.164	728	—
EthylAcetate	$C_4H_8O_2$	88	350	—	25.9	269	272	0.022	0.114	700	—
Methyl Propionate	$C_4H_8O_3$	104	353	—	22.2	271	—	0.024	0.130	742	—
Acrolein	C_3H_4O	56	326	—	29.1	—	247	0.028	0.310	508	—
Acrylonitrile	C_3H_3N	53	350	—	24.5	—	273	0.030	0.170	754	—
n-Amyl Acetate	$C_7H_{14}O_2$	130	422	—	33.5	297	300	0.011	0.075	633	—
1-Amyl Acetate			416	—	—	298	311	0.010	0.075	652	—
1,3-Butadiene	C_4H_6	54	269	—	—	197	—	0.020	0.115	693	—
n-Butyl Acetate	$C_6H_{12}O_2$	116	400	—	30.0	295	305	0.014	0.076	694	—
n-Butyl Ether	$C_8H_{18}O$	130	414	—	39.7	298	311	0.015	—	467	—
Dimethyl Ether	C_2H_6O	46	249	—	31.6	232	—	0.034	0.267	623	—
Divinyl Ether	C_4H_4O	70	312	—	—	243[a]	—	0.017	0.270	633	—
Diethyl Ether	$C_4H_{10}O$	74	308	—	37.4	228	—	0.019	0.365	433	—
Gasoline ~	—	—	306	—	44.1	228	—	0.014	0.068	644[a]	—
Naptha ~	—	—	450	—	—	314	—	0.008	0.050	519	—
Petroleum Ether	—	—	351	—	—	255	—	0.014	0.059	561	—

[a]Estimate; ~ approximate line; — unavailable; $R = \bar{R}/M$; $\bar{R} = 8.314$ kJ/kmol K.

If the vapor were to be released at a constant rate at the hot liquid surface, beginning with time, t, equal to zero, it would transiently diffuse in the vertical direction, leading to a concentration profile* with the highest vapor concentration at the fuel surface and the least at the mouth of the cup. In the initial stages, the concentration everywhere is too low to support a flame. As time progresses, however, the temperature of the gas mixture near the surface rises beyond the minimum temperature limit T_L. (See Figure 2-8.1.) Equally important, the vapor concentration also increases to, and beyond, the lean limit. Later still, the thickness of the mixture layer that is beyond the lean limit increases due to diffusion. (If a pilot source were presented to this layer, a propagable flame could be generated. Thus, it is evident that the location and time at which a pilot is introduced are important in a test seeking the conditions of a propagable flame.) With continued time, the mixture at the surface becomes much too fuel-rich (oxygen-poor) to permit generation of a propagable flame with a pilot source. After longer periods of time, the spatial belt containing mixtures between the lean and rich limits broadens and propagates away from the surface.

This description of transient diffusion of vapor issued at a constant rate at the surface also holds, qualitatively, to a situation of a temporally variable vapor release rate, as in a typical flash point test.

As pointed out by Burgoyne and Williams-Leir[9] and Kanury,[10] the vapor release boundary condition is quite crucial in the flash point phenomenon. For a flame to flash over the surface of liquid fuel when presented with an ignition source, the vapor and air mixture (at the location and instant of the ignition source) has to contain sufficient fuel to be above the lean limit of flammability, ℓ. The partial pressure of the vapor in the mixture at the liquid surface is approximately equal to the saturation pressure, P_v, of the fuel at the surface temperature, T. The error associated with the assumption of thermodynamic equilibrium (at the surface across which mass transfer occurs at a nonnegligible rate) is known to be quite small. The $P_v(T)$ relation is given by the integrated form of the well-known[11] Clausius-Clapeyron equation of state†

$$\frac{P_{vs}}{P^\circ} = \exp\left[\left(\frac{h^\circ_{fg}}{RT^\circ}\right)\left(1 - \frac{T^\circ}{T_s}\right)\right] \tag{1}$$

where T° and P° are reference temperature and pressure. The subscript s denotes the surface. When T° is equal to the normal boiling point temperature, T°_b, of the liquid, the reference vapor pressure, P°, will become equal to the atmospheric total pressure. Equation 1 is generally written in the form $\ln P_{vs} = -\alpha/T_s + \beta$, where $\alpha \equiv h^\circ_{fg}/R$ and $\beta \equiv \ln P^\circ + \alpha/T^\circ$ are constants of the liquid. The *CRC Handbook of Physics and Chemistry*[7] gives extensive $P_v(T)$ tabulations for hundreds of liquids.

For many nonpolar liquids, the molar specific entropy of vaporization is found to be a universal constant, a consequence of the observed invariance of the ratio of normal boiling point to the critical temperature, so that

$$\frac{h^\circ_{fg}}{RT^\circ_b} \approx \text{a constant} = 10.18$$

Known as *Trouton's rule*,[13] this powerful relation enables one to estimate the normal enthalpy of vaporization h°_{fg} from a knowledge of the normal boiling point T°_b and the liquid molecular* weight, M. The last column of Table 2-8.4 indicates the validity of Trouton's rule; in general, Trouton's constant is larger than 10.18 for alcohols and smaller for acids.

Due to noninfinite diffusion effects, the molar (or volume) fraction, $X_v \equiv P_v/P^\circ$, of fuel vapor at stations away from the surface will be smaller than that at the surface, given by Equation 1. The solution of the diffusion equation, with Equation 1 serving as one of the boundary conditions, gives the following distribution. With y denoting the distance in the gas phase from, and normal to, the surface and t denoting time, let $g(y, t)$ be a distribution solution such that

$$\frac{P_v(y,t)}{P^\circ} = g(y,t)\,\frac{P_{vs}}{P^\circ} \tag{2}$$

The function $g(y, t)$ is dimensionless and smaller than unity in magnitude.

Suppose that a large enough pilot source is introduced at a height, y_p, and time, t_p. Recalling the definition of the lean limit, ℓ, the flame would then flash if the local instantaneous mole fraction, $P_v(y_p, t_p)/P^\circ$, is even marginally in excess of the lean limit, ℓ. Thus, the flash point and the lean limit are related by

$$g(y_p, t_p)\exp\left[\left(\frac{h^\circ_{fg}}{RT^\circ}\right)\left(1 - \frac{T^\circ}{T_F}\right)\right] \geq \ell \tag{3}$$

Taking the total pressure to be 1 atm, $T^\circ = T^\circ_b$, the normal boiling point. We denote the flash point in 1 atm air by T°_F. The inequality sign in this equation is quite close to an equality. Noting that g and ℓ are smaller than unity, Equation 2 can be rewritten as

$$\ln\left(\frac{1}{\ell}\right) \approx \left(\frac{h^\circ_{fg}}{RT^\circ_b}\right)\left(\frac{T^\circ_b}{T^\circ_F} - 1\right) + \ln\frac{1}{g(y_p, t_p)} \tag{4}$$

*The steady-state, one-dimensional diffusion version of this problem is known as the *Stefan problem* and can be found in Bird, Stewart, and Lightfoot.[12]

†With its genesis in the Maxwell relation $(\partial P/\partial T)_v = (\partial s/\partial v)_T$, Equation 1 arises from the facts: (1) equilibrium evaporation is a reversible process of constant pressure and temperature; (2) the heat addition in a constant temperature reversible process is equal to $T\Delta s$; and (3) the constant pressure heat addition is equal to Δh; and the assumptions: (1) the enthalpy change associated with the change of phase from saturated liquid to saturated vapor is independent of temperature so that $\Delta h = h^\circ_{fg}$, a constant; (2) the vapor volume far exceeds the liquid volume; and (3) the vapor behaves nearly as an ideal gas. The basic constraint of equilibrium, of course, is the equality of Gibbs' free energy of the saturated liquid and that of the saturated vapor.

*Recall that the gas constant R is related to the universal gas constant $\bar{R} = 8.314$ (kJ/kmol K) through the molecular weight M (kg/kmol) by $R \equiv \bar{R}/M$ (kJ/kg K).

The following comments can be made of Equation 4:

1. The lean limit of flammability, ℓ, as listed in the literature and in Table 2-8.4, is itself an apparatus-dependent property. The most notable factor influencing it is gravity (causing buoyancy in the limit mixtures and inhomogeneity of the fuel-air mixture). The approximate equality sign in Equation 4 is meant to highlight this point.
2. Most of the flash point data seldom point out explicitly that they have been determined in air and nominally at 1 atm total pressure.
3. If the ambient total pressure, $P°$, is higher than 1 atm, the flash point is expected to be higher also. A plot of $\ln P°$ versus $1/T_F^\circ$ is known to be a straight line, apparently parallel to the boiling point line for the same liquid. Thus, correction for the flash point dependency on pressure can be made the same way as for the boiling point dependency. Leslie and Geniesse refer in *ICT*[5] (p. 161) to a method by which the flash point is calculated as the temperature at which the liquid's vapor pressure is equal to $P°/kN$, where $P°$ is the total pressure, N is the number of moles of oxygen stoichiometrically required for complete combustion of 1 mole of the liquid, and k is an apparatus constant of about 8. The stoichiometry ratio, N, apparently is introduced through the lean limit, ℓ.
4. The question of the dependency of lean limit on whether the ambient gas is normal air or pure oxygen is a complicated one. If the oxygen/fuel ratio at the lean limit is assumed to be the same for both cases, then ℓ is expected to be numerically larger in pure oxygen than in air. Lewis and von Elbe[8] report a few values to confirm this expectation. A consensus exists in combustion literature that the percent of fuel in the limit mixtures is, more or less, independent of the presence of nitrogen. This, too, leads to a larger value of ℓ in pure oxygen than in air. Both these arguments, coupled with Equation 4, lead to the conclusion that the flash point of a liquid will be higher (and closer to the boiling point) in pure oxygen than in air.

   This conclusion is, however, contrary to common sense. Ignition is expected to occur more easily in the absence of the impeding inert nitrogen. Experience indicates that in pure oxygen atmospheres, the minimum ignition energies of combustible mixtures are lower, quenching distances are smaller, and flame temperatures and speeds are larger. Based on this experience, it is logical to surmise that the chemical kinetics of oxidation and thermochemistry underlying the concept of the lean limit are far more complex than mere mass conservation. The paper of Mullins[14] on combustion in vitiated air and the tome of Lewis and von Elbe[8] serve well as starting points for a much-needed research investigation into this important unresolved issue of limit mixtures.
5. When the cup is closed, the escape of the fuel vapor to the environment is prevented or minimized. Appearing as the second boundary condition in the diffusion equation, this results in a higher value of $g(y, t)$ at any location and time. For a given lean limit, Trouton's constant, and normal boiling point, Equation 4 indicates that the observed flash point will be lower than if the cup were open.
6. The effects of the cup being open and the air being in a state of motion due to gravity or due to disturbance are in the direction of increasing the observed flash point, all due to reduced $g(y, t)$.
7. Burgoyne and Williams-Leir[9] assume the dispersion function $g(y_p, t_p)$ to be unity to use a variant form of Equation 4 to predict the flash point from given ℓ, h_{fg}°, and T_b°.
8. Such a use of Equation 4 as a predictive tool is probably premature for several reasons. First, the transient convective-diffusion process underlying the g-function has a crucial role to play in determining T_F°. Second, even if one works out the solution to obtain $g(y, t)$, the flash point experiments do not clearly stipulate the $y = y_p$ and $t = t_P$ values; that is, they do not state the time and location at which the pilot is introduced. Thus, the estimates of $g(y_p, t_p)$ require subjective judgments. Last, as discussed in item 4, the lean limit, ℓ, is still an empirical extrinsic parameter whose dependence on fundamental properties of the system is not quantitatively known.

   Notwithstanding these reasons, by merely noting that the last term in Equation 4 is always positive, one concludes that

$$\ln\left(\frac{1}{\ell}\right) \geq \left(\frac{h_{fg}^\circ}{RT_b^\circ}\right)\left(\frac{T_b^\circ}{T_F^\circ} - 1\right)$$

   A plot of $\ln(1/\ell)$ on the y-axis and $(T_b^\circ/T_F^\circ - 1)$ on the x-axis should then yield all experimental points lying above a straight line of slope $(h_{fg}^\circ/RT_b^\circ) \approx 10.18$ and intercept zero. Figure 2-8.2 shows most of the data of Table 2-8.4 thus plotted. It is obvious that the hypothesis underlying Equation 4 bears merit. The general trend of data (especially for each family of fuels) indicates that Trouton's constant (or a like one) holds to describe the slope. The intercept, expected to be zero if diffusional effects are absent, indicates that $g(y_p, t_p)$ lies in the approximate range of 0.07 to 0.25, substantially smaller than unity, indicating the need for consideration of diffusion.
9. All through this discussion energy conservation has not been considered, although it may be important.

Autoignition Temperature

Whereas the piloted ignition in flash point tests involves a localized initiation of the flame and observation to see if it would propagate away from the ignitor, the autoignition is a self-induced initiation of the flame in a relatively larger volume of the reacting gases. As such, the autoignition is perhaps amenable to an easier description than the forced ignition. At the outset, it should be noted that the autoignition process pertains to the vapor (or gas) and air mixture, irrespective of the source of the vapor or gas. Figure 2-8.1, part (b), indicates that by the time the autoignition process becomes evident, the liquid fuel will be vaporizing vigorously and even boiling.

Consider the oxidation reaction in a vessel of known geometry. The initial temperature and mixture composition

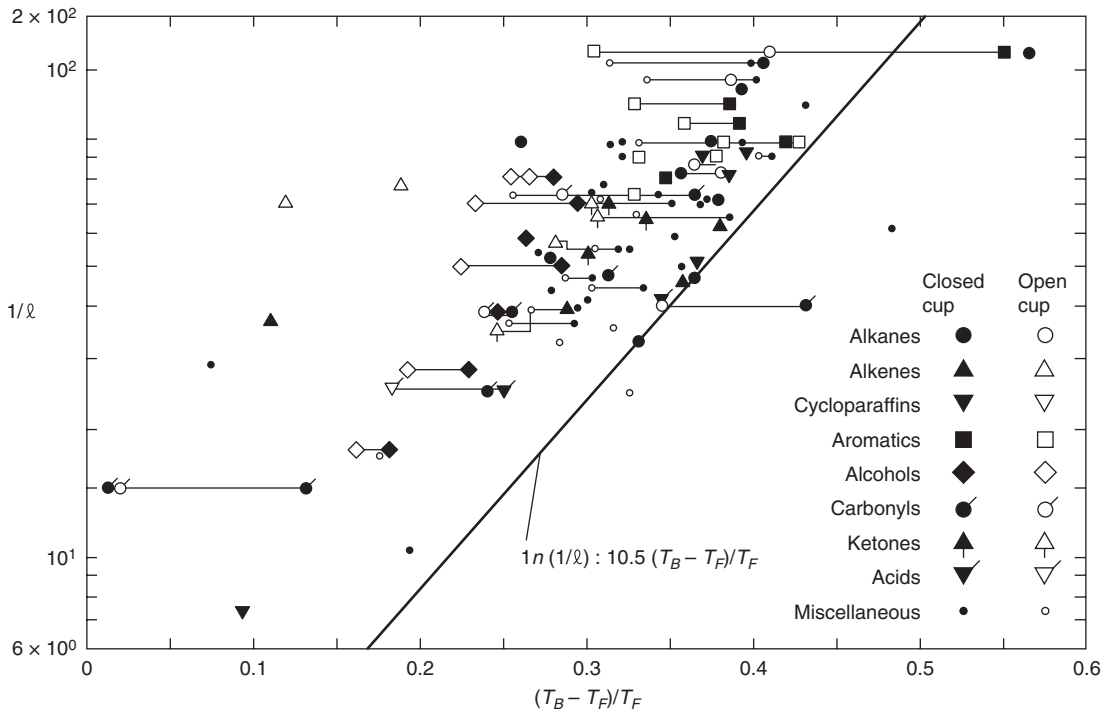

Figure 2-8.2. ***A relation between the lean limit, flash point, and boiling point.[10]***

are usually known. The mechanism of heat exchange between the reactive medium and the vessel walls constitutes the most important of the boundary conditions. Although the oxidation mechanism is probably composed of a complex set of elementary reaction steps, a global rate law for the fuel consumption rate generally suffices.

$$-\dot{W}_A''' = k_0 Y_A^n Y_B^m \exp\left(\frac{-E}{\overline{R}T}\right) \tag{5}$$

The quantity on the left side of Equation 5 is fuel consumption rate in kg/m³·s. The empirical kinetic constants k_0, n, m, and E are, respectively, the collision factor, orders with respect to the fuel (A) and oxygen (B), and activation energy (kJ/kmol). In principle, then, the equations of conservation of mass, momentum, energy, and species can be solved to obtain the transient fields of velocity, temperature, and composition. According to thermal theory,[15,16] ignition is inferred to have occurred at the instant when the temperature (usually, in the middle of the reactor) increases rapidly. Known as *thermal runaway*, this event also marks the onset of a rapid decrease in the reactant mass fractions, Y_A and Y_B. If the reactant consumption in the preignition period is ignored, then the autoignition is called a *thermal explosion.*

Solutions are available in the literature for this problem, with and without reactant depletion, for a number of geometries of the reactant mass and of boundary conditions. When the reactant depletion is ignored, the species equations become unnecessary. The convective mixing in gaseous mixtures is usually taken into account by defining an effective, augmented, thermal conductivity so as to obviate the momentum conservation and reduce the problem to one involving merely transient, reactive conduction. By considering the effective conductivity to be large (due to good mixing) and the heat loss from the reacting mixture to the vessel boundaries to be by convection, Semenov[15] solves the resultant transient, uniform reaction problem to predict thermal runaway conditions as

$$\frac{E(T_a - T_w)}{\overline{R}T_w^2} = 1$$
$$\mathrm{Da}_0 \equiv \frac{[h_c V(-\dot{W}_A''')_0]}{[hS(T_a - T_w)]} \geq 1/e \tag{6}$$

where

T_a = (critical) temperature of the reactive mass at the instant of explosion (see Figure 2-8.1)
T_w = vessel wall temperature
h_c = enthalpy of combustion (kJ/kg fuel)
h = heat transfer coefficient between the mixture and the walls (kW/m² K)
V/S = volume-to-surface ratio of the reactive mass
$(-\dot{W}_A''')_0$ = reaction rate given by Equation 5 at the initial conditions $T = T_0$, $Y_A = Y_{A0}$, and $Y_B = T_{B0}$
e = Naperian constant

Two points are immediately notable from Equation 6. First, the critical temperature T_a is quite close to T_w, since $\overline{R}T_w^2/\mathrm{E}$ is, generally, quite small. Thus, $T_a \approx T_w$. Second, due to the mixture being well mixed, the precise geometry of the reacting body is irrelevant; its V to S ratio suffices; $V/S = a/(j+1)$, where $j = 0$, 1, and 2, respectively, for an infinite plane slab geometry of thickness, $2a$, for an

infinitely long cylinder of diameter, $2a$, and a sphere of diameter, $2a$. Other implications of Equation 6 will be discussed later.

Frank-Kamenetskii[16] solves the problem by assuming that the effective conductivity, K, is small and seeks the conditions under which steady-state solutions are impossible. Thermal runaway is found to occur pursuant to the following critical conditions:

$$\frac{E(T_a - T_w)}{\overline{R}T_w^2} \qquad \begin{matrix} j=0 & j=1 & j=2 \\ 1.20 & 1.37 & 1.60 \end{matrix} \quad (7)$$

$$\mathrm{Da}_\infty \equiv \frac{a^3 h_c k_0 Y_{A0}^n Y_{B0}^m \exp(-E/\overline{R}T_w)}{a^2 K(T_a - T_w)/a} \qquad 0.88 \quad 2.00 \quad 3.32$$

This solution, as does Equation 6, indicates that $(T_a - T_w) \approx \overline{R}T_w^2/E$ is small. Vessels with a geometry resulting in a larger surface-to-volume ratio (e.g., a sphere) exhibit a larger critical temperature, T_a.

The nondimensional parameters Da_0 and Da_∞ of Equations 6 and 7, respectively, are known as Damköhler numbers. A Damköhler number is the ratio of the characteristic rate of energy release due to chemical reaction to that of physical dissipation (by convection in the Semenov problem and by conduction in the Frank-Kamenetskii problem).

The Semenov problem corresponds to the zero Biot number limit, while the Frank-Kamenetskii problem deals with the infinite Biot number situation. The finite Biot number problem has been solved by Thomas[17] and Kanury and Gandhi.[18] (An excellent review of this subject is presented by Gray and Lee.[19]) Equations 6 and 7 can be seen to be in mutual agreement if one notes that the heat transfer coefficient, h, is linearly proportional to the ratio of gas conductivity, K, to the vessel half-size, a.

Even more importantly, the pressure dependency of the collision factor is given by

$$k_0 \equiv k_0' M_A^{(1-n)} M_B^{-m} \left(\frac{PM}{\overline{R}T}\right)^{(n+m)} \quad (8)$$

where

k_0' = function only of the molecular collisional nature of species A and B

M_A and M_B = molecular weights, respectively, of the fuel (A) and oxygen (B)

M = mean molecular weight of the mixture

P = total pressure of the reacting mixture

The Damköhler number, Da_∞, from the criterion for explosion given by Equation 7 can then be recast to the form

$$\mathrm{Da}_\infty \equiv \left(\frac{k_0' \overline{R} M_B^{-m} M^{(n+m)} Y_{A0}^n Y_{B0}^m}{E^{(1+n+m)}}\right)\left(\frac{a^2 h_c P^{(n+m)} M_A^{1-n}}{K} f(T_a)\right) \quad (9)$$

where $f(T_a) \equiv [\exp(-E/\overline{R}T_a)]/(\overline{R}T_a/E)^4$. If the initial mixture composition (Y_{A0}, Y_{B0}) is kept fixed, the first bracketed quantity of Equation 9 is, more or less, a constant. For typical hydrocarbons reacting with air, $n \approx 0.5$, $m \approx 1.5$, and $E/\overline{R} \approx 15{,}000$ K. The function $f(T_a)$ monotonically increases with $(\overline{R}T_a/E)$, as indicated in Figure 2-8.3. The second bracketed term of Equation 9 and the explosion criterion constant of Equation 7 thus give the influence of a, h_c, P, M_A, and K on the minimum temperature for autoignition, T_a. Specifically, it is clear that the autoignition temperature is lower if the vessel size is larger, heat of combustion is larger, pressure is higher, fuel molecular weight is larger, or the mixture conductivity is smaller. This predicted pressure dependency is in excellent quantitative agreement with the data in Table 2-8.3. The influence of molecular weight appears corroborated by the data in Table 2-8.4. Not so evident from Table 2-8.4 is the effect of the heat of combustion, mainly due to the relatively minor variance of h_c within a family of fuels.

Ignition Delay

The discussion so far has centered on the threshold conditions below which ignition is not possible (i.e., question 1 of the Introduction). So far as the flash point and fire point are concerned, a more detailed analysis is required to go further. Concerning autoignition, however, a few further steps can be taken related to question 2 of the Introduction. First, note that the critical temperature T_a from Equations 6, 7, and 9 and Table 2-8.4 is the minimum temperature of the mixture that can produce autoignition, but marginally. This marginality implies that time to ignition at T_a is infinite. Any temperature greater than T_a will result in ignition within a finite time. The larger the temperature, the sooner the ignition.

Furthermore, as indicated in Figure 2-8.1, there exist upper and lower composition limits to autoignition at any $T > T_a$. The most quickly ignitible mixture at any T

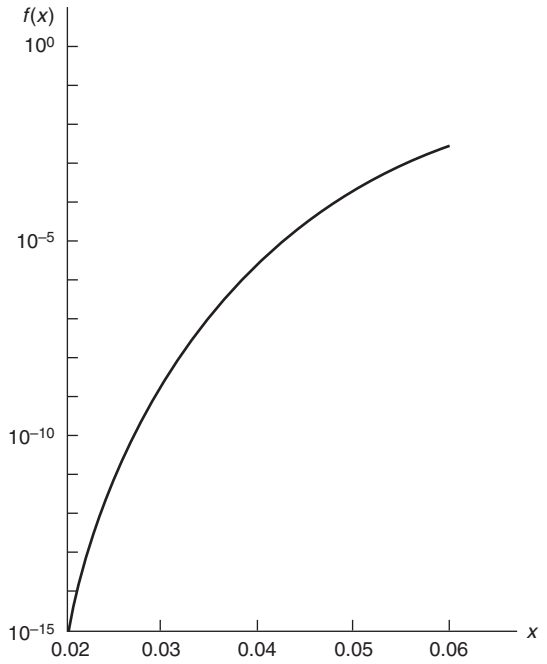

Figure 2-8.3. ***The monotonic nature of f(x) = [exp(–1/x)]/x⁴.***

will perhaps be near stoichiometric in composition. Thus, energy balance on the reacting mixture leads to the approximate ignition delay, t_i, of

$$t_i \approx \frac{(\rho C_p)(T - T_0)}{h_c(-W_A''')_{\text{ref}}} \tag{10}$$

where (ρC_p) is mixture volumetric heat capacity (kJ/m^3 K), T_0 is initial temperature of the mixture, and the reaction rate is estimated at the reference conditions of 0 for the Semenov (Biot number = 0) problem and w for the Frank-Kamenetskii (Biot number = ∞) problem. This rate also accounts for the mixture composition Y_{A0} and Y_{B0}. The Arrhenius dependency of the reaction rate on temperature makes the ignition delay, t_i, proportional to $\exp(-E/\overline{R}T_{\text{ref}})$. Thus, measurement of t_i at various T_{ref} values leads to determination of the activation energy, E. In the light of Equation 8, t_i will be approximately proportional to the inverse of the mixture pressure and to the square root of the molecular weight of the fuel. Since Da_0 and Da_∞ are about unity, the denominator of Equation 10 is proportional to $K(T - T_w)/a^2$ so that ignition delay is longer for higher conductivity mixtures, if all else is kept fixed.

If the consumption of reactants in the preignition reactions is significant, the problem becomes more difficult. The outcome, however, is that reactant consumption makes the limit temperature, T_a, somewhat higher than the estimates from Equations 6, 7, and 9, and the ignition delay is longer than that given by Equation 10.

Concluding Remarks

The concepts of piloted ignition of liquid fuels and the spontaneous ignition of their vapors mixed with air are examined in this chapter. Starting with a physical description of the ignition process and definitions, a number of experimental techniques were alluded to, and typical data were presented. The empirical trends were shown to be consistent with the predictions based on simple mechanistic models.

Although the flash point concept is useful in rating the volatility and ease of ignition of a variety of liquid combustibles, it must be noted that many practical situations involve heating of the liquid by a heat flux imposed on the evaporating surface. The heating process itself might then become a major topic of study to estimate the liquid surface temperature before examining whether this temperature is above or below the flash point at a given instant.

Nomenclature

a	vessel half-size (m)
C_p	specific heat (kJ/kg·K)
Da_0	Semenov's Damköhler number
Da_∞	Frank-Kamenetskii's Damköhler number
E	activation energy (kJ/kmol)
e	Naperian constant
g	dispersion function
h	heat transfer coefficient (W/m^2·K)
h_c	enthalpy of combustion (kJ/kg)
h_{fg}°	enthalpy of vaporization (kJ/kg)
j	geometry index
K	mixture thermal conductivity (W/m·K)
k	apparatus constant
k_0	collision factor (kg/m^3·s)
k_0'	collision parameter
ℓ	lean limit of flammability
M	molecular weight (unsubscripted for the mixture) (kg/kmol)
m	a reaction order
N	Stoichiometric molar O_2/fuel ratio
n	reaction order
P	pressure (atm)
P°	total pressure (atm)
P_v	vapor pressure (atm)
R	gas constant (kJ/kg·K)
$\overline{R}$	universal gas constant (kJ/kmol K)
S	surface area (m^2)
s	specific entropy (kJ/kg K)
T	temperature (K)
T_a	the least autoignition temperature (K)
T_b°	normal boiling point (K)
T_F°	flash point in air at 1 atm (K)
t	time (s)
V	volume (m^3)
v	specific volume (m^3/kg)
$\dot{W}'''$	reaction rate (kg/m^3 s)
Y	mass fraction
y	distance into gas phase from, and normal to, the vaporizing surface (m)

Greek

α	property constant (K)
β	property constant
ρ	density (kg/m^3)

Subscripts

A	fuel
a	autoignition
B	oxygen
b	boiling point
c	combustion
F	flash point
i	ignition
0	initial
p	pilot
s	liquid surface
v	vapor
w	vessel wall surface

References Cited

1. M.G. Zabetakis, *Bulletin No. 627,* U.S. Bureau of Mines, Pittsburgh, PA (1965).
2. ASTM, *Standard, Vol. 17, 20, and 22,* American Society for Testing and Materials, Philadelphia (1972).
3. B.P. Mullins, *Spontaneous Ignition of Liquid Fuels,* Butterworths, London (1955).
4. B.P. Mullins, in *Combustion Researches and Reviews,* Butterworths, London (1957).
5. *International Critical Tables of Numerical Data, Physics, Chemistry, and Technology,* McGraw-Hill, New York (1927).
6. Factory Mutual Research Corp., *Factory Mutual Handbook of Loss Prevention,* McGraw-Hill, New York (1967).
7. *CRC Handbook of Physics and Chemistry,* Chemical Rubber Co., Cleveland (1973).
8. B. Lewis and G. von Elbe, *Combustion, Flames and Explosions of Gases,* 3rd ed., Academic, New York (1987).
9. J.H. Burgoyne and G. Williams-Leir, *Fuel,* 28–7, p. 145 (1949).
10. A.M. Kanury, *Comb. Sci. and Tech.,* 31, p. 297 (1983).
11. W.C. Reynolds and H.C. Perkins, *Engineering Thermodynamics,* McGraw-Hill, New York (1977).
12. R.B. Bird, W.E. Stewart, and E.N. Lightfoot, *Transport Phenomena,* Wiley, New York (1960).
13. F. Daniels and R.A. Alberty, *Physical Chemistry,* Wiley, New York (1967).
14. B.P. Mullins, in *Selected Combustion Problems,* Butterworths, London (1954).
15. N. Semenov, *Chemical Kinetics and Chain Reactions,* Oxford, London (1935).
16. D.A. Frank-Kamenetskii, *Diffusion and Heat Exchange in Chemical Kinetics,* Princeton University, Princeton (1955).
17. P.H. Thomas, *Trans. Faraday Soc.,* 54, 421, p. 60 (1958).
18. A.M. Kanury and P.D. Gandhi, *Theory of Spontaneous Heating and Thermal Ignition: A Review,* unpublished manuscript (1989).
19. P. Gray and P.R. Lee, in *Oxidation and Combustion Reviews,* Elsevier, Amsterdam (1967).

CHAPTER 9

Smoldering Combustion

T. J. Ohlemiller

Introduction

Smoldering is a slow, low-temperature, flameless form of combustion, sustained by the heat evolved when oxygen directly attacks the surface of a condensed-phase fuel. Smoldering constitutes a serious fire hazard for two reasons. First, it typically yields a substantially higher conversion of a fuel to toxic compounds than does flaming (though this occurs more slowly). Second, smoldering provides a pathway to flaming that can be initiated by heat sources much too weak to directly produce a flame.

The term *smoldering* is sometimes inappropriately used to describe a non-flaming response of condensed-phase organic materials to an external heat flux. Any organic material, when subjected to a sufficient heat flux, will degrade, gasify, and give off smoke. There usually is little or no oxidation involved in this gasification process, and thus it is endothermic. This process is more appropriately referred to as forced pyrolysis, not smoldering.

A burning cigarette is a familiar example of true smoldering combustion. It is also one of the most common initiators of smoldering in other materials, especially upholstery and bedding.[1] A cigarette also has several characteristics common to most materials that smolder. The finely divided fuel particles provide a large surface area per unit mass of fuel, which facilitates the surface attack by oxygen. The permeable nature of the aggregate of fuel particles permits oxygen transport to the reaction site by diffusion and convection. At the same time, such particle aggregates typically form fairly effective thermal insulators that help slow heat losses, permitting sustained combustion despite low heat release rates.

The physical factors that favor smoldering must be complemented by chemical factors as well. Like virtually all other cellulosic materials, tobacco in a cigarette, when degraded thermally, forms a char. A char is not a well-defined material, but typically it is considerably richer in carbon content than the original fuel; its surface area per unit mass is also enhanced. This char has a rather high heat of oxidation and is susceptible to rapid oxygen attack at moderate temperatures (≥670 K). The attack of oxygen (to form mainly carbon monoxide and carbon dioxide) is facilitated not only by the enhanced surface area but also by alkali metal impurities (present in virtually all cellulosic materials derived from plants) which catalyze the oxidation process.[2] Char oxidation is the principal heat source in most self-sustained smolder propagation processes; the potential for smoldering combustion thus exists with any material that forms a significant amount of char during thermal decomposition. (Char oxidation is not always the only heat source and it may not be involved at all in some cases of smolder initiation.)[3]

Various quantitative combinations of these physical and chemical factors can produce a material that will undergo sustained smoldering in some conditions. The enormous range of factors results in materials that will only smolder when formed into fuel aggregates many meters across, at one extreme, to materials that smolder when formed into aggregates only a few tens of microns across. Unfortunately, a theory that allows for the calculation of materials and conditions that are conducive to smoldering has been developed only for certain types of smolder initiation. (See Section 2, Chapter 10.) Conditions sufficient to yield smolder initiation, especially near an external heat source, are not necessarily sufficient to assure self-sustained smolder spread away from the initiation region. The potential transition of the smolder process into flaming combustion is even less correlated with factors determining smolder initiation.

This chapter is restricted to consideration of post-initiation behavior of smoldering. There are several models of smoldering combustion in the literature, but they are mostly numerical in nature, and do not shed much light on the practical aspects of the problem. Smolder

Dr. T. J. Ohlemiller is a member of the research staff of the National Institute of Standards and Technology, Building and Fire Research Laboratory. He has investigated a variety of solid fuel combustion problems, specializing in smoldering and the flammability of solid fuels.

modeling has been reviewed by Ohlemiller,[4] but the reader should be aware that there has been substantial activity since that review. Readers wishing to pursue the literature on modeling of one-dimensional smolder propagation should refer to References 5–16. Two-dimensional propagation models can be found in References 17–20. Distinctive features peculiar to one- and two-dimensional smolder propagation modes are described later. Lacking any definitive theoretical description, this chapter is largely restricted to examining typical experimentally determined behavior. In this overview of smoldering, an attempt is made to convey some of the qualitative interplay of processes that determines overall behavior, together with specific experimental results.

Self-Sustained Smolder Propagation

The smolder initiation process is dominated by the kinetics of the oxidation of the solid. Subsequent propagation of smolder is controlled to a large degree, however, by the rate of oxygen transport to the reaction zone. The control via transport rate occurs because the heat evolved during smolder initiation raises the local temperature and thus the local reaction rate, until all of the neighboring oxygen is consumed. Subsequently, the reaction continues to consume oxygen as fast as it reaches the reaction zone, yielding a very low oxygen level locally, which limits the reaction rate.

The subsequent evolution of the smoldering zone away from the initiation region is heavily influenced by oxygen supply conditions. If initiation occurs deep within a layer of fine particles (sawdust, coal dust), for example, it will slowly work its way to the nearest free surface at a rate dictated by oxygen diffusion through the particle layer. (The more coarse and loosely packed the particles, the greater the influence of buoyant flow through the fuel leading to predominant upward spread.) When the smolder zone reaches the free surface region, it will spread more rapidly over this region in response to local convective and diffusive oxygen supply conditions. As will be seen, when smolder spread over the surface region of a fuel layer is forced by airflow, its response also depends on heat transfer considerations.

In examining self-sustained smolder propagation and its response to oxygen supply conditions, dimensionality is important. It is necessary to distinguish one-dimensional from multi-dimensional configurations. Further, it is necessary to discern whether the smolder zone is spreading in the same or opposite direction as the net movement of oxygen.

One-Dimensional Smolder Spread

One-dimensional smolder spread is an idealized situation that is sometimes approximated in real fires. For example, the spread outward or upward from deep in a layer of fuel particles approaches this one-dimensional limit when oxygen diffusion dominates convection and any curvature of the reaction front is small compared to the reaction zone thickness. In practice, this curvature requirement would likely be met by spread about 0.10 to 0.20 m away from the ignition source. One-dimensional smolder can be characterized by the direction of smolder propagation relative to the direction of oxygen flow—forward and reverse propagation.

Reverse propagation: When oxygen diffuses to the reaction zone from the outer surface of the fuel layer, through the unburned fuel and toward the reaction front, it is moving opposite to the direction of smolder propagation. Such a case of relative movement is called reverse smolder.

Palmer[21] examined this diffusive reverse smolder case using layers of wood sawdust of various depths. The configuration was only roughly one-dimensional. Some of his results are shown in Figure 2-9.1. Note that the time scale is in hours. The time to smolder up through a layer 1-m deep is about two weeks, a surprisingly long time. Palmer

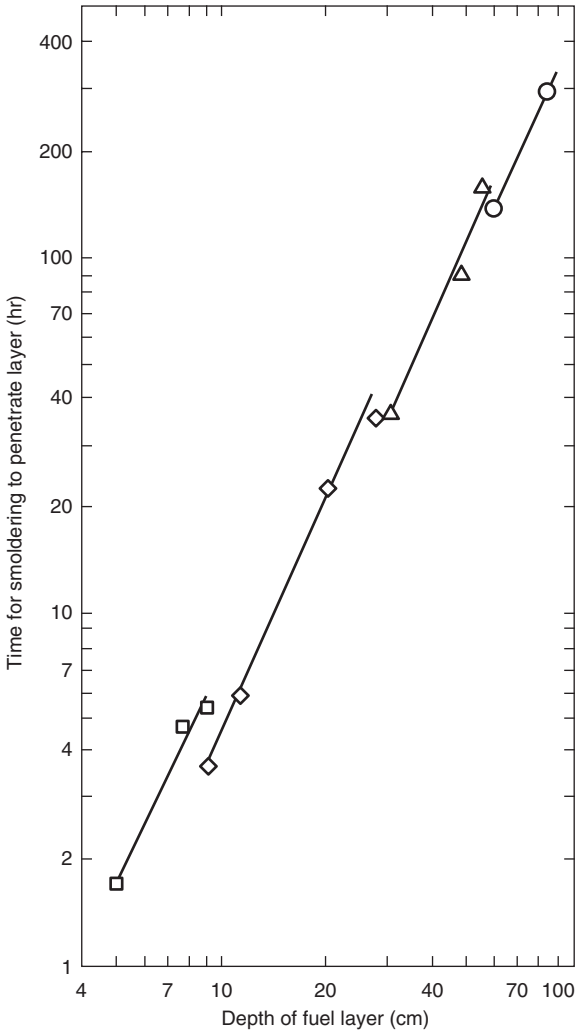

Figure 2-9.1. ***Smoldering upward from bottom within thick layers of mixed wood sawdust.[21] Squares: initiating layer 0.025 m deep, 0.3-m square box; diamonds: initiating layer 0.052 m deep, 0.3-m square box; triangles: initiation layer 0.052 m deep, 0.6-m square box; circles: initiating layer 0.052 m deep, 0.9-m square box.***

noted that in this configuration the smoldering process gave little hint of its presence until it was close to the surface of the fuel layer.

The slope in Figure 2-9.1 indicates that the time for smolder to penetrate a fuel layer in this mode is nearly proportional to the square of the layer depth.[21] Palmer showed that a second power dependence on layer depth would be expected if it is assumed that the smolder reaction zone propagation velocity is proportional to the one-dimensional diffusion rate of oxygen from the surroundings, through the unburned fuel, to the reaction zone. This results in

$$t_L = AL^2 \tag{1}$$

where t_L is the time for the smolder zone to penetrate the layer of thickness, L; and A is a constant that can, at present, only be determined by experimental measurement of at least one layer thickness.

This relation and Figure 2-9.1 imply that a 10-m fuel layer, such as might be encountered in a landfill or coal mine tailing pile, would require more than four years for smolder penetration. Such a deep layer is unlikely to be uniform in practice and the smolder front movement would be dominated by buoyant convective flow in regions of lesser flow resistance. However, this does illustrate how very slow some smolder processes can be.

A well-insulated reaction zone is a key factor in the existence of stable, self-sustaining smolder at such extremely low rates. The heat loss rate cannot exceed the heat generation rate. In this case, the same factor that is slowing the oxygen supply rate, and therefore the heat generation rate (i.e., the thick layer of wood particles over the reaction zone) is also slowing the heat loss rate.

In the previous example, the smolder propagation process is inherently unsteady because of the time-dependent oxygen supply process. If oxygen is instead continually supplied by a forced convective flow *through* the fuel layer, nearly steady propagation occurs. Such a configuration is encountered in some incinerators and coal burners but rarely in a smoldering fire. This configuration has been examined experimentally[8,9,22] and modeled,[5,6,8–12] and is a relatively well-understood smolder mode with underlying mechanisms qualitatively similar to the transient case just discussed.

In this mode of reverse smolder propagation, oxygen surrounds the fuel particles as they are heated by the advancing smolder reaction zone. Thermal degradation of some fuels in the presence of oxygen is exothermic. This exothermic degradation is particularly true of cellulosic materials and this heat can be sufficient to drive the smolder wave without any char oxidation.[22] In flexible polyurethane foams, the presence of oxygen during degradation plays another key role. Without oxygen many foams do not form any char,[23] although char oxidation is a necessary source of heat for these materials. In the reverse smolder mode, the net oxidation rate and net heat release rate are again directly proportional to the oxygen supply rate. The smolder zone spreads to adjacent material as fast as this generated heat can be transferred and radiated to it. An increased oxygen supply rate causes a greater rate of heat release and increased peak temperature in the reaction zone which, in turn, increases the heat transfer rate to adjacent fuel, thus accelerating the smolder spread rate. This sequence implies that the smolder reaction zone may well move through a layer of fuel without fully consuming the solid at any point. This unconsumed material, in fact, acts like an insulator for the reaction zone, increasing its stability. On the other hand, Dosanjh et al.,[6] point out that this mode of smolder propagation can achieve a steady-state only if, as a minimum, the energy released is sufficient to heat the incoming air supply; otherwise it will extinguish.

Figure 2-9.2 shows measured reverse smolder velocities for several types of fuel as a function of airflow velocity through the fuel bed. The bulk densities of the fuel bed are all low but typical for these types of materials. Note that the airflow velocity range is also quite low, although higher flows are sufficient to move the fuel particles in the bed (i.e., an upward flow higher than approximately 0.01 to 0.02 m/s would fluidize the fuel bed).

Despite the considerable variation in the chemical nature of these fuels, the smolder velocity is always of order 10^{-4} m/s. For the same air supply rate, the smolder velocities do not vary much more than a factor of 2. This is consistent with the idea that the oxygen supply rate, not reaction kinetics, dominates the propagation process. (If the oxidizer flow rate is forced upward sufficiently in circumstances where bed fluidization is prevented, the smolder velocity begins to drop as cooling effects dominate. See Reference 8 for an example.) The differences with fuel nature that do exist mainly appear to reflect variations in available heat and effective thermal conductivity.

Only limited information is available on toxic gas production from this mode of smoldering. The molar percentage of carbon monoxide in the evolved gases has been examined for two of the fuels in Figure 2-9.2. For the flexible polyurethane foam, the carbon monoxide was 6 to 7 mole percent for an air velocity of 1.5×10^{-3} m/s. The flow rate dependency was not examined.[23] For the cellulosic insulation material,[24] the carbon monoxide mole fraction varied from about 10 to 22 percent from the lowest to the highest air flow velocity in Figure 2-9.2. The mass flux of carbon monoxide from such a smoldering process (grams of CO/m^2 of smolder front/second) then is estimated as follows:

$$Y_{CO}(\dot{m}_{\text{air}} + \dot{m}_{GS}) \tag{2}$$

or

$$Y_{CO}[\rho_{\text{air}} v_{\text{air}} + (1 - \phi)\Delta\rho_s v_s] \tag{3}$$

Here Y_{CO} is the mass fraction of carbon monoxide in the evolved product gases (approximately equal to the mole fraction); m_{air} is the mass flux of air entering the smolder zone; m_{GS} is the mass flux of gaseous material evolved from the solid fuel; ρ_{air} is the density of the air at the point where its velocity, v_{air}, is measured; ϕ is the initial void fraction of the fuel bed; $\Delta\rho_s$ is the change in density of the fuel bed (for reverse smolder, typically 65 to 95 percent of the original mass is gasified); and v_s is the smolder front velocity.

Limited information is also available on the aerosol emitted by a reverse smolder source.[25] This is pertinent to

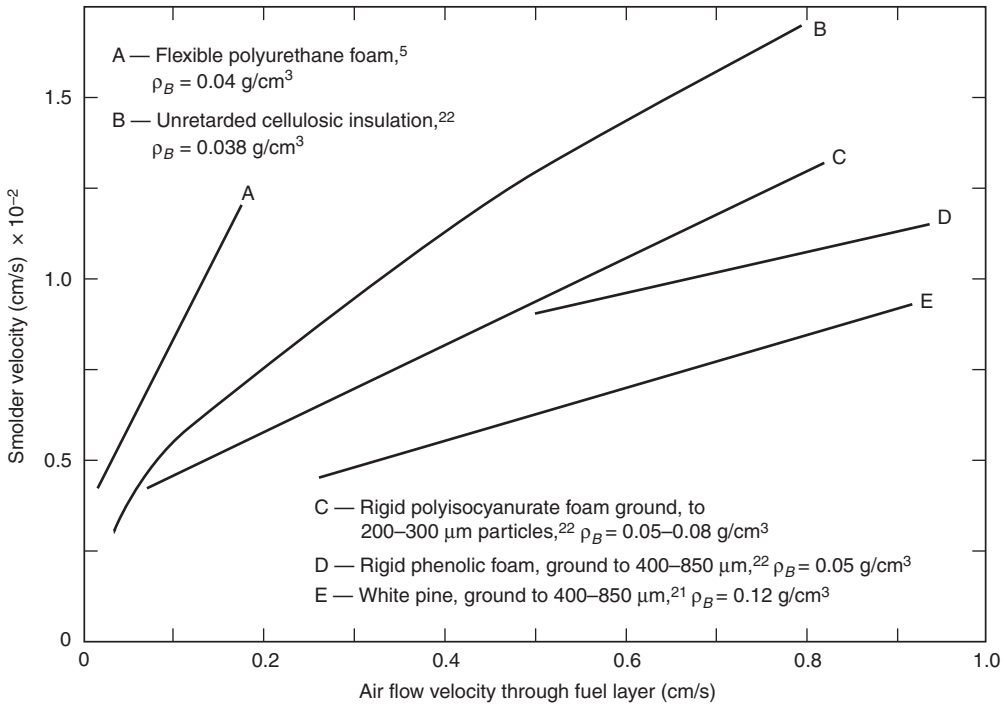

Figure 2-9.2. ***Smolder velocity versus airflow velocity into reaction zone for nearly one-dimensional reverse smolder. ρ_B is bulk density.***

detection of a smoldering fire. The source studied was essentially identical to that used to obtain the data for curve B in Figure 2-9.2. The fuel again was an unretarded cellulosic insulation. The mass mean particle size of the aerosol was 2 to 3 μm; this is about 5 times larger than cigarette smoke, and 50 to 200 times larger than the sooty particulate produced by flaming combustion. This large size explains the relatively poor sensitivity of ionization smoke detectors to realistic smolder sources. The residual solid left in the smolder wave and the original fuel both were found to be effective filters for this aerosol. This finding helps explain the observation by Palmer[21] that smoldering in a thick layer of fuel was not detectable until it neared the surface exposed to the ambient atmosphere.

The rate of heat release for this mode of smolder can be estimated from the total mass flux of products and their heat content (gas temperature typically 670 to 970 K). The result is a few kW/m^2 of smolder front. This translates to a few hundredths of a kW for a reverse smolder source 0.1 to 0.15 m in diameter. The strength of the heat source has a bearing on the behavior of the buoyant plume. (See Section 2, Chapter 1.) Sources as weak as those considered here generate plumes that may not reach the ceiling of a room.[26]

Forward propagation: The second limiting case of one-dimensional smolder propagation is called forward smolder. In this case the oxygen flow is in the same direction as the movement of the smolder front. The most familiar example (though not one-dimensional) of forward propagation is a cigarette during a draw. This limiting case is encountered in some industrial combustion processes but is unlikely to be found in its pure, one-dimensional form in a fire context (some elements of this mode are encountered in realistic cases, however). An approximate model of this process (in one dimension) has been presented by Dosanjh and Pagni.[7] They point out that this smolder mode will die out if the heat generated by char oxidation is insufficient to drive the drying and fuel pyrolysis reactions that precede char formation in the reaction zone. Other modeling studies of forward smolder propagation can be found in References 13–16. It is shown in Reference 14 that one-dimensional forward smolder is, in principle, capable of four differing modes of propagation depending on the oxygen concentration and supply rate. Two of these are limited by oxygen supply rate and two by reaction kinetics. Further experimental studies of forward smolder propagation through polyurethane foam can be found in References 27–28. A transient study of the requirements for the initiation of this smolder rate in polyurethane foam can be found in Reference 29.

Some characteristics of forward propagation are briefly mentioned here to describe the major effects that reversing the direction of oxygen flow can have on smolder propagation characteristics.

Forward and reverse smolder propagation have been compared experimentally.[22,24] The fuel was an unretarded cellulosic insulation. Forward smolder through this same fuel at the same air supply rate is about ten times slower than reverse smolder. The carbon monoxide mole fraction is independent of air supply rate and is about 0.09. Forward smolder also allows for more complete combustion

of the fuel. These and other differences between the two smolder modes can be explained in terms of the differing wave structures.[22]

An interesting aspect of a propagating, one-dimensional smolder wave is that the counterflowing materials (gas and solid, as viewed from the moving smolder front) form a system that retains the reaction heat and preheats the reactants with that heat.[13] This effect implies that the internal peak temperature can rise above the adiabatic reaction temperature. In Reference 16 an expression is given for limiting temperature in the reaction wave for the case in which there is only a single, net exothermic reaction. Whether this feature of forward smolder plays a role in the potential for transition into flaming has not been explored.

Frandsen[30] investigated the downward propagation of smoldering in horizontal layers of peat as a model fuel for the complex duff layer found on the floor of a forest. No external flow was imposed. This is essentially a diffusion-driven forward smolder process forced to be one-dimensional in this study; it normally is multidimensional in character. The influence of both moisture and inorganic diluents on the limits of smolder propagation was measured. At extremes, it was found that this cellulosic fuel will just smolder when it contains 50 percent water by weight and no inorganic diluents. When dry, it will just smolder when the mix contains 80 percent inorganic diluents. These results should be roughly indicative of the limits for other cellulosic fuels in the absence of a cross-flow over the fuel layer.

Multi-Dimensional Smolder Spread

Factors such as ignition source geometry, fuel geometry, and the strong influence of buoyant flow on oxygen supply usually interact to assure that a smolder reaction zone has significant gradients of temperature and species in two or three dimensions. The number of possible configurations becomes virtually limitless. The practical configurations that have been studied are few and they are usually two-dimensional; they do shed some light on most cases likely to be of practical interest.

Horizontal fuel layer: The configuration that has been studied most extensively is two-dimensional smolder propagation in a uniform horizontal layer of particles or fibers. Ohlemiller examined the structure of the smolder zone[31] in a thick (0.18-m) horizontal layer of cellulosic insulation in the absence of any forced airflow over the fuel layer. In these conditions, the flow induced by the buoyant plume rising above the smolder zone assures a constant supply of oxygen to the space above the layer. Oxygen penetrates the layer largely by diffusion.

If such a layer is ignited uniformly on one end, the smolder reaction zone soon evolves into a new shape dictated by oxygen supply rates.[31] The uppermost elements of the reaction zone, being closest to the free surface, and hence, ambient air, spread away from the ignition source the fastest. Successively deeper elements spread in the same direction but more slowly. The result is a smolder reaction zone that (viewed in vertical cross section) slopes upward from the bottom of the layer to the top, in the direction of movement. The steady-state length of this inclined smolder front is roughly twice the depth of the original fuel layer. This inclined reaction zone is several centimeters thick, and across this thickness there is a smooth transition from unburned fuel to ash. On the ash side (the free surface adjacent to air) oxygen diffuses down and inward in the same direction as the smolder front is moving and attacks the charred fuel; this is analogous to forward smolder discussed earlier. On the unburned fuel side of the inclined smolder front, oxygen diffuses in from the region ahead of the front to react with the fuel as it is thermally degraded by heat conducted from the char oxidation region. Oxygen here is moving opposite to the direction of smolder propagation, so this aspect of the overall reaction zone is analogous to reverse smolder. Remember that in cellulosic materials, this oxidative/thermal degradation is exothermic. Thus the two-dimensional horizontal smolder zone incorporates features of both forward and reverse smolder and is driven forward by the combined heat release from char oxidation and oxidative/thermal degradation.

The participation of oxidative/thermal degradation in driving the smolder process requires that oxygen have free access to the thermal degradation region. For a low-permeability fuel such as solid wood, this is not the case. Even though solid wood has basically the same reaction chemistry as cellulosic insulation (which consists mostly of wood fibers) and smolders with a qualitatively similar inclined reaction zone, it must be driven solely by char oxidation.

The low permeability and corresponding high density of solid wood has another consequence with regard to smolder. The self-insulating quality of the reaction zone is much less than with a low-density layer of fuel particles or fibers. A single layer of wood will not sustain smolder unless it is subjected to an additional heat input of about 10 kW/m^2.[36] This heat could come from some external radiant source or from another piece of smoldering wood that has an adequate radiative view factor with respect to the first piece.

In view of the strong role of oxygen supply rate in shaping the smolder process in a horizontal fuel layer, it is not surprising that smolder also accelerates in response to an increased oxygen supply rate produced by an airflow over the top of the smoldering layer. As with the one-dimensional propagation situation, two possibilities again exist: the airflow can travel in the same direction as the smolder front (again called forward smolder) or in the opposite direction (reverse smolder). Note, however, that now the actual fluxes of oxygen *within* the smoldering fuel bed may go in various directions. They are no longer constrained to being parallel to the smolder wave movement, as in the one-dimensional cases.

Palmer[21] examined both of the flow direction possibilities for relatively thin horizontal layers (3×10^{-3} to 5.7×10^{-2} m) of various cellulosic particles (cork, pine, beech, grass). Figure 2-9.3 shows some typical results. Note that the smolder velocities are less than or equal to those in Figure 2-9.2, despite the much higher air velocities. This is probably due to differing rates of actual oxygen delivery to the reaction zone, and to the fact that the near-surface region, which receives the best oxygen supply, is also subjected to the highest heat losses.

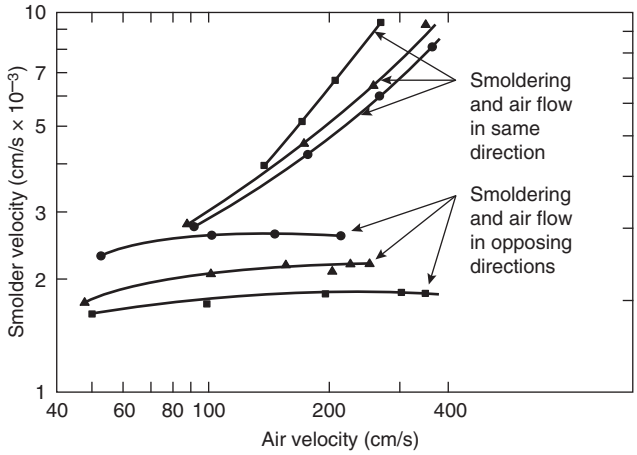

Figure 2-9.3. ***Dependence of smolder propagation rate through horizontal layers of beech sawdust on air velocity over top of layer.[21] Circles: 120 μm mean particle size; triangles: 190 μm mean particle size; squares: 480 μm mean particle size.***

The influence of two factors, fuel particle size and relative direction of airflow and smolder propagation is shown in Figure 2-9.3. Particle size has a relatively weak effect on smolder velocity but its effect depends on whether the smolder configuration is forward or reverse. The configuration itself (i.e., the relative direction of airflow and smolder propagation) has a much greater effect.

Ohlemiller[37] obtained comparable smolder velocities and dependence on configuration for 0.10- to 0.11-m thick layers of cellulosic insulation. It was found that the configuration dependence cannot be explained solely on the basis of oxygen supply rates. The mass transfer rate to the surface of the fuel bed was measured for forward and reverse configurations. It differed by only 20 to 30 percent (these differences were caused by changes in the bed shape due to shrinkage during smolder). It was pointed out that the observed dependence on relative direction of the airflow was consistent with there being a prominent role for convective heat transfer along the top surface of the fuel layer. This dependence occurs only if part of the smolder wave, that is, the region near the leading edge, is kinetically limited (and therefore highly temperature sensitive) rather than oxygen supply rate limited. This phenomenon explains the qualitative impact of both relative airflow direction and combustion retardants on smolder velocity. It also explains why forward smolder is faster than reverse smolder in the horizontal layer configuration, whereas the opposite was true for one-dimensional propagation. The role played by fuel particle size may be implicit in this view, but a quantitative model is not yet available.

In contrast to the monotonic enhancement of forward smolder velocity with increased airflow rate found by Palmer and by Ohlemiller, Sato and Sega[38] observed more complex behavior with thin (0.004 to 0.01-m) layers of a cellulosic mixture. Smolder velocity increased up to freestream air velocities of about 3 m/s and then remained constant to the highest air velocity examined (6 m/s). This plateau correlated with erratic behavior at the leading edge of the smolder reaction zone involving both periodic extinctions and mechanical disruptions. These authors also examined the thermal structure of their forced smolder waves. The results were qualitatively similar to those of Ohlemiller for buoyant smolder,[31] but the peak temperatures were appreciably higher due to the enhanced oxygen supply rates.

There is a minimum thickness below which a horizontal fuel layer will not undergo self-sustained smolder propagation. As the thickness of a fuel layer decreases, its surface-to-volume ratio increases (inversely with thickness to the first power). The ratio of the rate of heat loss to the rate of heat generation also varies in this manner so that ultimately the losses are overwhelming and extinction occurs. The exact thickness will depend on factors such as bulk density, fuel type and particle size, rate of oxygen supply, and so forth, influencing the heat generation per unit volume at a given thickness. The same considerations apply to other thin layers of fuel such as fabrics on upholstery and sheets of paper, wood, or particle board. Palmer[21] found that the minimum depth for sustained smolder in still air increased linearly with particle size for beech, pine and cork. For cork this dependence ceased above 2 mm, apparently because more complete oxidation of the char stabilized the process in the layers of larger particles. For very small particles, ($<$100 μm), the minimum depth dropped as low as 1 mm for cork dust, while 0.01 m was typical of small particles of beech or pine sawdust. Ohlemiller and Rogers[39] found the minimum depth in still air for an unretarded cellulosic insulation to be 0.035 m; a heavy loading of the smolder retardant boric acid roughly doubled this value. Since the insulation has a very small effective particle size and essentially the same chemistry as Palmer's sawdusts, most of the difference in minimum depth (for the unretarded material) probably lies in the bulk density, which is about four to five times less for the insulation compared to the sawdusts (40 kg/m^3 versus 180 kg/m^3). Palmer found that the minimum depth dropped rapidly with increased airflow over the sawdust layers, in keeping with the idea that a greater rate of heat release per unit volume stabilizes the smolder process.

Beever[32,40] has addressed a problem at the opposite extreme of layer thickness, that of underground fires in land fills, peat deposits, and mine tailings. These tend to be smoldering fires in roughly horizontal layers where the principal mode of oxygen access is from the top surface. Beever[32] studied this process on a laboratory scale using mixtures of fine sawdust or charcoal with an inert diluent, that is, diatomaceous earth, in a trough that was insulated on the sides and bottom but open to quiescent air on the top. The trough was 0.13 m by 0.38 m in cross section and 0.14 m deep. A deeper trough was used in separate experiments in which pure layers of the inert diluent were placed atop the combustible layer. Local ignition near the top of a layer yielded steady propagation over a limited depth at rates that varied only weakly with inert content. However, while 25 percent fuel content yielded smolder spread, 10 percent fuel content did not. (Frandsen[30] diluted peat moss and Douglas Fir duff with

powdered silica in his downward smolder propagation studies. He found sustained smolder in dry material at up to 80 percent inorganic loading, but the allowable inorganic level decreased strongly as moisture level was increased.) The depth to which Beever's spreading smolder zone reached increased with the cross-sectional dimensions of the fuel bed. Material below this depth, having been heated and partially decomposed by the smoldering zone above, could itself subsequently propagate a second wave moving in the opposite direction. It was pointed out that such behavior can make it possible for a landfill or similar fire to spread under a barrier intended to stop it. Similarly, inert covering layers may simply slow but not stop such fires. The true key to stopping a smoldering fire is getting the heat out of the fuel, but this can prove to be extraordinarily difficult. Oxygen removal is insufficient unless it is sustained until the fuel cools to a point where oxygen readmission will not cause reignition. For a landfill fire, the cooling period can be impractically large.

The duff layer on a forest floor was mentioned previously. This porous layer of decaying organic material is frequently ignited to smoldering by the passage of a forest fire. Smoldering in this layer is highly spatially irregular in extent. In addition to posing a threat of reignition of a flaming fire, this smoldering also has broad implications about the viability of dormant seeds and forest regeneration. This subject is reviewed in Reference 41.

Smolder propagation data on a few other fuels (including some that are inorganic) in horizontal layers can be found.[42] Unfortunately, no data are currently available on the yield of evolved products of horizontal layer smolder. For crude estimates on cellulosic materials the previous results for reverse smolder are adequate, but they should be applied here with caution.

The propagation of smoldering through a porous, horizontal fuel layer has been modeled numerically to a limited extent.[17] The predicted smolder wave shape was in qualitative agreement with experiment. The effects of variations in the reaction rate parameters on this wave structure and on the smolder propagation velocity were examined.

Other fuel configurations: Data on a few other multidimensional smolder configurations are summarized in Table 2-9.1. Again there is little more information available than the rate of smolder propagation. An exception to this is the smoldering cigarette, which has been extensively studied,[43–45] albeit usually in a manner most pertinent to its peculiar mode of cyclicly forced air supply. The cigarette smolder propagation process has also been numerically modeled one-[13] and two- dimensionally.[17,18] (Other two-dimensional and numerical smolder propagation models can be found in References 19 and 20.)

All the materials in Table 2-9.1 are fairly porous. As noted previously, solid wood, a low-porosity fuel, also smolders, given a configuration that limits heat losses.[36,52,53]

Ohlemiller[52,53] examined smolder spread along the interior surface of a three-sided channel constructed of either white pine or red oak. A controlled flow of air was introduced at one end of the channel; the products evolved from the other end were monitored as was the rate of smolder spread. For both types of wood, stable smolder was observed for only a narrow range of inlet air velocities, 0.05 to 0.20 m/s. (From limited data this appeared true for both forward and reverse smolder.) Below this range the smolder process extinguished and above it flaming eventually erupted. Both of these limits, but particularly the lower limit, are probably dependent on the specific conditions of the tests. Carbon monoxide typically comprised 2 to 3 percent of the gases leaving the channel or about 10 to 15 percent of the gases leaving the surface of the wood. The rate of heat release during smoldering was estimated from the oxygen consumption rate, correcting for carbon monoxide. This rate ranged from about 0.5 to 2 kW or roughly 10 to 30 kW/m^2, based on the approximate area visibly glowing.

The last type of smolder configuration referenced in Table 2-9.1 is quite pertinent to the scenario that makes smoldering a major contributor to residential fire deaths, that is, upholstery and bedding fires initiated by cigarettes. This is frequently a composite problem, with the smoldering tendency of both the fabric and the substrate (polyurethane foam, cotton batting) pertinent to the overall smolder behavior of the combined assembly.[54] Ortiz-Molina et al. have shown that the combination of a cellulosic fabric plus a polyurethane foam can smolder over a substantially wider range of conditions than can the foam alone.[55] The fabric smolder process supplies added heat to the foam smolder zone while simultaneously competing for oxygen. The full complexity of this interaction is yet to be explored. A considerable amount of empirical data on the tendency of cigarettes to initiate this type of smolder is available.[49,56–63] The factors influencing the smolder tendency of upholstery fabrics have been examined as well.[64–69]

The life hazard posed by smoldering bedding or upholstery within a closed room has been studied to some extent.[70–72] Data have been presented[70] on the buildup of carbon monoxide (near the ceiling) in a 2.4-m room on a side due to cigarette-initiated smolder in a cotton mattress. The smolder front was reported to spread radially at a rate of 6.3 10^{-5} m/s independent of the size of the smoldering area. In two out of five tests the smolder process underwent a transition to flaming combustion after 65 to 80 minutes, which is close to the time at which total carbon monoxide exposure was estimated to be lethal. Similar data are reported[71] for a greater variety of bedding and upholstery materials; these were ignited by cigarettes (and by flaming sources) in a room 4.3 $\times$ 3.6 $\times$ 2.4 m. Carbon monoxide and several other gases were sampled at three locations. Flaming developed from smoldering in several of the tests; this usually required 2 to 3 hours of smoldering first. Again, the total exposure to carbon monoxide from the smolder smoke approached or exceeded lethal levels. Lethal conditions due to carbon monoxide were reached in much shorter times in some cases.

All available data on the hazards of smoldering in a closed room were evaluated.[72] It was concluded that the probability of a lethal carbon monoxide dose and of transition to flaming are comparable for a period from 1 to 2½ hours after cigarette initiation of smoldering. A model is presented for buildup of carbon monoxide due to a smoldering fire;[72] the results generally show reasonable

Table 2-9.1 ***Data on Multi-Dimensional Smolder in Various Fuels***

Fuel	Fuel/Smolder Configuration	Air Supply Condition/Rate	Smolder Velocity (cm/sec)	Maximum Temp. (°C)	Reference	Comment
Pressed fiber insulation board, 0.23–0.29 g/cc	1.3 cm thick, horizontal strips, width large compared to thickness	Natural convection/ diffusion	$1.3–2.2 \cdot 10^{-3}$	NA	21	Smolder velocity increased ≈ 50% for strips with width ≈ thickness
Pressed fiber insulation board, 0.23–0.29 g/cc	1.3 cm × 1.3 cm strips varied angle to vertical	Natural convection/ diffusion	$2.7–4.7 \cdot 10^{-3}$	NA	21	Smolder velocity highest for upward spread; lowest for horizontal spread
Pressed fiber insulation board, 0.23–0.29 g/cc	1.3 cm × 5 cm strips forward smolder	Forced flow, 20 to 1500 cm/s	$3.5 \cdot 10^{-3}$ cm/s (20 cm/s air) $13.0 \cdot 10^{-3}$ cm/s (1400 cm/s air)	770°C (200 cm/s) 790°C (900 cm/s)	21	Some samples extinguished due to air cooling at air velocity > 1450 cm/s
Pressed fiber insulation board, 0.23–0.29 g/cc	1.3 cm × 5 cm strips reverse smolder	Forced flow, 80–700 cm/s	$2.8–3.5 \cdot 10^{-3}$ cm/s	NA	21	Extinguishment indicated above 900 cm/s
Pressed fiberboard (pine or aspen) 0.24 g/cc	1.3 cm × 30 cm sheets, horizontal, forward smolder	Forced flow, 10–18 cm/s	$0.7 \cdot 10^{-3}$ cm/s	NA	46	
Cardboard	Vertical rolled cardboard cylinder, downward propagation, varied dia. 0.19–0.38 cm	Natural convection, diffusion	$5.0–8.4 \cdot 10^{-3}$ cm/s	NA	47	Small dia. ≈ 2 × faster than large dia.; ambient temp. effect measured
Shredded tobacco	0.8 cm dia. cigarette, horizontal, in open air	Natural convection, diffusion	$3.0–5.0 \cdot 10^{-3}$ cm/s	820°C	48	
Cellulose fabric + 3% NaCl	Double fabric layer, 0.2 cm thick, horizontal, forward smolder	Forced flow, ≈ 10 cm/s	$\approx 1.0 \cdot 10^{-2}$ cm/s	770°C	49	Smolder behavior dependent on alkali metal content
Cellulosic fabric on substrates	Various weight fabrics horizontal on fiberglass, PU foam, cotton batting	Natural convection, diffusion	$\approx 3.0–75 \cdot 10^{-3}$ cm/s dependent on substrate and fabric	Reported values suspiciously low	50, 51	Smolder fastest on inert fiberglass substrate

agreement with experiment, though some of the input parameters must be forced slightly.

In contrast to the above result, a more recent study of the fire risks associated with upholstered furniture implied that the toxic exposure from a smoldering chair in an average house was rarely fatal; transition to flaming brought with it death due to thermal causes.[73] The methodology was indirect, and involved using the Hazard I smoke movement and tenability models in a reasonably successful effort to reproduce national fire statistics for upholstery fires. There are not as yet sufficient data on the toxicity hazards of smoldering upholstery materials to definitively resolve this issue.

A relatively common practical problem in smolder extinguishment occurs in grain silos.[74] Here the smoldering must be completely extinguished before emptying the silo, to avoid the possibility of a dust explosion. The practical problems are considerable due to the tendency of any extinguishing agent to follow higher permeability channels and thereby miss significant smolder zones. In Reference 74 a number of extinguishing agents were tested in small-scale tests. Gaseous CO_2, fed from the bottom, was found to be the most effective.

Transition to Flaming

The transition process from smolder to flaming in the above bedding and upholstery fires is essentially spontaneous. At room conditions both smoldering and flaming are possible in many such systems. Sato and Sega[33] explored the domain of overlapping smolder and flaming potential for cellulosic materials and noted a hysteresis in the spontaneous transition between these two combustion modes. The mechanism of such a spontaneous transition has not been investigated in detail. It has been suggested on the basis of small mock-up studies that a

chimneylike effect develops in the crevice between the horizontal and vertical cushions of a smoldering chair.[62] The enhanced air supply presumably accelerates local char oxidation, heating the char to the point where it can ignite pyrolysis gases. Such a mechanism is plausible but it has not been demonstrated to be operable in real upholstery or bedding, where the chimney effect may not develop so readily.

Transition to flaming (fast exothermic gas-phase reactions) requires both a mixture of gases and air that are within their flammability limits and a sufficient heat source to ignite this mixture. Furthermore, these two requirements must be realized at the same locus in space and at the same time. Any factor that either enhances the net rate of heat generation or decreases the net rate of heat loss will move the smoldering material toward flaming ignition by increasing both local temperature and rate of pyrolysis gas generation. Such factors include an enhanced oxygen supply, an increase in scale (which usually implies lesser surface heat losses per unit volume of smoldering material), or an increasingly concave smolder front geometry, which reduces radiative losses to the surroundings and enhances gaseous fuel concentration buildup. All of these factors may be operating simultaneously in the case of upholstery and bedding smolder. Sequential photos of smolder initiation, growth, and transition to flaming in an upholstered chair appear consistent with this idea.[62,75]

A further factor in this and in other systems involving cellulosic materials is secondary char oxidation. This process is quite similar to the afterglow seen in cellulosic chars left by flaming combustion. Intense, high-temperature (probably greater than 1070 K) reaction fronts propagate intermittently in seemingly random directions through the fibrous low-density char left by the main lower temperature smolder front. In charred fabrics, these glowing fronts can sometimes progress in a stable manner along the charred residue of a single fiber, despite very high heat losses per unit volume of fuel. Such a process requires the catalytic action of alkali metals that are frequently found naturally in cellulosics or left there during manufacture.[63–65,69,76] While in a very hot smolder front the size of a single fiber is unlikely to be sufficiently energetic to ignite flammable gases, the larger fronts (10^{-3} to 10^{-2} m in scale) may well be. An analogous process has been found to cause occasional flaming ignition of smoldering, unretarded cellulosic insulation.[31]

Babrauskas and Krasny[77] surveyed the available literature data on the buoyant smolder in upholstered chairs and beds. They found that about two-thirds of the tested items underwent a transition into flaming combustion. The reported times for this to occur varied from 22 min to 306 min after the initiation of the smoldering process.

The transition from smolder to flaming can also be induced, for example, by a forced increase in oxygen supply rate to the smolder reaction zone.[21,23,33,34,78] This effect was first studied quantitatively by Palmer[21] for airflow over horizontal layers of wood sawdust. This process, of course, is familiar to anyone who has started a camp fire from tinder and sparks. Transition to flaming was noted by Palmer only for airflow in the same direction as smolder propagation (forward smolder). Depending on the material, the transition occurred at airflow velocities from about 0.9 to 1.7 m/s. For these materials, flaming did not develop when the mean particle size was less than 1 mm. Ohlemiller[37,78] did obtain transition to flaming in layers of fibrous insulation materials of very small diameter (~25 μm) but again only with forward smolder. This result occurred at air velocities of about 2 m/s for unretarded insulation. Leisch[34] utilized ignition sources placed midway along the length of grain and wood particle fuel layers so that forward and reverse smolder zones were simultaneously obtained. Flaming was noted at 4 m/s air velocity only after the smoldering process produced a substantial depression or cavity in the surface of the fuel layer.

Ohlemiller[37,78] explained the weak response and lack of flaming transition in reverse smolder on the basis of heat transfer effects influencing the leading edge of the smolder reaction zone. These heat transfer effects intensify the smolder in the leading edge region for forward smolder. In the case of cellulosic insulation, the intensification leads to random development of small (a few cm) cavities near the leading edge which act as flame initiation regions and flame holders.

Ohlemiller[78] also found that both boric acid (a smolder retardant) and borax (a flame retardant) could each eliminate the transition to flaming when the retarded cellulosic insulation was the only fuel. However, the effectiveness of the acid and borax was substantially reduced if the smoldering fuel abutted unretarded wood (as it typically does in residential housing). Heat transferred from the smolder zone readily ignited the wood. Palmer[79] noted similarly that layers of fine dust that would not themselves undergo transition to flaming readily ignited adjacent flammable materials.

Smoldering solid wood undergoes a transition to flaming readily in a configuration that minimizes heat losses.[52,53] It was inferred that the limiting variable in the transition is the surface temperature of the smoldering wood, with the transition occurring when that temperature reached about 950 to 1000 K.

The transition from two-dimensional, forced flow smolder propagation, to flaming in polyurethane foam was investigated by Tse, et al.[80,81] The configuration involved a contained slab of foam with forced air across its outer surface. No fabric was involved. Smoldering ignition was on the upstream end so this was two-dimensional forward smolder propagation. A unique ultrasonic technique was used to follow the density distribution of the foam during the tests along with schlieren imaging of the gas flow near the foam surface. It was inferred that the transition to flaming in this system occurred not at the foam/air interface, but rather within the depth of the char left by the smolder front. Continued reactions there opened holes which allowed the onset of vigorous gas phase reactions. This is not greatly dissimilar to the mechanism found for the onset of flaming in a horizontal layer of cellulosic insulation subjected to an air flow over its top surface.[37] In a study of smoke explosions in a reduced-scale enclosure containing a smoldering wood crib, the transition from smoldering to flaming was hypothesized as the trigger of this explosion.[82] The evidence was indirect and not entirely unambiguous.

Conclusion

Smoldering is a branch of solid fuel combustion quite distinct in many aspects from flaming, but equally diverse and complex. Unfortunately it has not been studied nearly to the same extent as flaming. This is quite apparent in the lack of quantitative guidelines that can be provided here for estimating the behavior of realistic smolder propagation processes, smolder detection, toxic gas production, and the transition to flaming. The experimental data provided can be readily used for closely analogous situations. They must be used cautiously for dissimilar conditions. The reader should always bear in mind the strong role that the oxygen supply rate has on the smolder process. The other very important factor is the relative direction of movement of oxygen supply and smolder propagation. This can be somewhat obscure in many realistic configurations. The actual chemical nature of the fuel is relatively secondary, at least with regard to smolder rate. It may be important for toxic gas production rates, but the data here are quite limited.

References Cited

1. K. Rohr, "U.S. Home Product Report, 1992–1996: Forms and Types of Materials First Ignited in Fires," National Fire Protection Association, Quincy, MA (1999).
2. R. McCarter, "Smoldering Combustion of Cotton and Rayon," *J. Cons. Prod. Flamm.,* 4, p. 346 (1977).
3. P. Bowes, *Self-Heating: Evaluating and Controlling the Hazards,* Elsevier, New York, Chap. 7 (1984).
4. T. Ohlemiller, "Modeling of Smoldering Combustion Propagation," *Prog. in Energy and Comb. Sci.,* 11, p. 277 (1985).
5. T. Ohlemiller, J. Bellan, and F. Rogers, "A Model of Smoldering Combustion Applied to Flexible Polyurethane Foams," *Comb. and Flame,* 36, p. 197 (1979).
6. S. Dosanjh, P. Pagni, and C. Fernandez-Pello, "Forced Cocurrent Smoldering Combustion," *Comb. and Flame,* 68, p. 131 (1987).
7. S. Dosanjh, and P. Pagni, *Proc. of the 1987 ASME/JSME Thermal Engineering Joint Conference—Volume 1,* (P. Marto and I. Tanasawa, eds.) American Society of Mechanical Engineers, New York (1987).
8. M. Fatehi and M. Kaviany, "Adiabatic Reverse Combustion in a Packed Bed," *Comb. Flame,* 116, pp. 1–17 (1994).
9. D. Walther, C. Fernandez-Pello, and D. Urban, "Space Shuttle Based Microgravity Smoldering Combustion Experiments," *Comb. Flame,* 116, pp. 398–414 (1999).
10. A. Aldushin, B. Matkowsky, and D. Schult, "Downward Buoyant Filtration Combustion," *Comb. Flame,* 107, pp. 151–175 (1996).
11. S. Leach, J. Ellzey, and O. Ezekoye, "A Numerical Study of Reverse Smoldering," *Comb. Sci. Tech.,* 130, p. 247 (1997).
12. C. Fernandez-Pello, B. Matkowsky, D. Schult, and V. Volpert, "Propagation and Extinction of Forced Opposed Flow Smolder Waves," *Comb. Flame,* 101, pp. 461–470 (1995).
13. M. Summerfield, T. Ohlemiller, and H. Sandusky, "A Thermophysical Mathematical Model of Steady-Draw Smoking and Predictions of Overall Cigarette Behavior," *Comb. Flame,* 33, pp. 263–279 (1978).
14. C. Fernandez-Pello, B. Matkowsky, D. Schult, and V. Volpert, "Forced Forward Smolder Combustion," *Comb. Flame,* 104, pp. 1–26 (1996).
15. J. Buckmaster and D. Lozinski, "An Elementary Discussion of Forward Smoldering," *Comb. Flame,* 104, pp. 300–310 (1996).
16. A. Aldushin, L. Rumanov, and B. Matkowsky, "Maximal Energy Accumulation in a Superadiabatic Filtration Combustion Wave," *Comb. Flame,* 118, pp. 76–90 (1999).
17. M. Muramatsu, "Studies on the Transport Phenomena in Naturally Smoldering Cigarettes," *Japan Tobacco Monopoly Research Report No. 123* (1981).
18. H. Mitler and G. Walton, "Modeling the Ignition of Soft Furnishings by a Cigarette," *Report SP 852,* National Institute of Standards and Technology, Gaithersburg, MD (1993).
19. M. Moallemi, H. Zhang, and S. Kumar, "Numerical Modeling of Two-Dimensional Smoldering Processes," *Comb. Flame,* 95, pp. 170–182 (1993).
20. C. DiBlasi, "Mechanisms of Two-Dimensional Smoldering Propagation through Packed Fuel Beds," *Comb. Sci. Tech.,* 106, pp. 103–124 (1995).
21. K. Palmer, "Smoldering Combustion in Dusts and Fibrous Materials," *Comb. and Flame,* 1, p. 129 (1957).
22. T. Ohlemiller and D. Lucca, "An Experimental Comparison of Forward and Reverse Smolder Propagation in Permeable Fuel Beds," *Comb. and Flame,* 54, p. 131 (1983).
23. F. Rogers and T. Ohlemiller, "Smolder Characteristics of Flexible Polyurethane Foams," *J. Fire Flamm.,* 11, p. 32 (1980).
24. D. Lucca, *An Investigation of Co-Current and Counter-Current Smoldering Combustion in Particulated Fuel Beds,* M.S.E. Thesis, Princeton University, Princeton (1979).
25. G. Mulholland and T. Ohlemiller, "Aerosol Characterization of a Smoldering Source," *Aero. Sci. and Tech.,* 1, p. 59 (1982).
26. H. Hotta, Y. Oka, and O. Sugawa, "Interaction between Hot Layer and Updraft from a Smoldering Source. Part 1. An Experimental Approach," *Fire Sci. and Technol.,* 7, p. 17 (1987).
27. J. Torero and C. Fernandez-Pello, "Upward Smolder of Polyurethane Foam," *Fire Safety J.,* 24, pp. 35–52 (1995).
28. J. Torero and C. Fernandez-Pello, "Forward Smolder of Polyurethane Foam in a Forced Air Flow," *Comb. Flame,* 106, pp. 89–109 (1996).
29. R. Anthenien and C. Fernandez-Pello, "A Study of Forward Smolder Ignition of Polyurethane Foam," *Proceedings 27th Symposium (International) on Combustion, Vol. 2,* Combustion Institute, Pittsburgh, PA, pp. 2683–2690 (1998).
30. W. Frandsen, "The Influence of Moisture and Mineral Soil Content on the Combustion Limits of Smoldering Forest Duff," *Can. J. For. Res.,* 17, p. 1540 (1987).
31. T. Ohlemiller, "Smoldering Combustion Propagation through a Permeable Horizontal Fuel Layer," *Comb. and Flame,* 81, p. 341 (1990).
32. P. Beever, "Initiation and Propagation of Smouldering Reactions," Ph.D. Dissertation, University of Leeds, (1986).
33. K. Sato and S. Sega, "The Mode of Burning Zone Spread along Cylindrical Cellulosic Material," *J. Fire Sci.,* 3, p. 26 (1985).
34. S. Leisch, *Smoldering Combustion in Horizontal Dust Layers,* Ph.D. Dissertation, University of Michigan, Ann Arbor (1983).
35. J. Jones, T. Goh, and M. Dijanosic, "Smouldering and Flaming Combustion in Packed Beds of Casuarina Needles," *J. Fire Sciences,* 12, pp. 442–451 (1994).
36. T. Ohlemiller, unpublished test results.
37. T. Ohlemiller, "Forced Smolder Propagation and the Transition to Flaming in Cellulosic Insulation," *Comb. and Flame,* 81, p. 354 (1990).
38. K. Sato and S. Sega, *Fire Safety Science—Proceedings of the Second International Symposium,* Hemisphere Publishing Corp., New York, p. 87 (1989).

39. T. Ohlemiller and F. Rogers, "Cellulosic Insulation Material II. Effect of Additives on Some Smolder Characteristics," *Comb. Sci. and Tech.,* 24, p. 139 (1980).
40. P. Beever, "Subterranean Fires in the UK—the Problem," *Paper IP 3/89,* Building Research Establishment (1989).
41. E. Johnson and K. Miyanishi (eds.), *Forest Fires: Behavior and Ecological Effects,* Academic Press, New York (2000).
42. L. Cohen and N. Luft, "Combustion of Dust Layers in Still Air," *Fuel,* 34, p. 154 (1955).
43. R. Baker, "Temperature Distribution inside a Burning Cigarette," *Nature,* 247, p. 405 (1974).
44. R. Baker and K. Kilburn, "The Distribution of Gases within the Combustion Coal of a Cigarette," *Beitrage zur Tabakforschung,* 7, p. 79 (1973).
45. R. Baker, *Beitrage zur Tabakforschung,* 11, p. 1 (1981).
46. J. Brenden and E. Schaffer, "Wavefront Velocity in Smoldering Fiberboard," *Research Paper FPL 367,* U.S. Forest Products Laboratory (1980).
47. T. Kinbara, H. Endo, and S. Sega, *Proceedings 11th Symposium (International) on Combustion,* Combustion Institute, Pittsburgh, PA, p. 525 (1967).
48. A. Egerton, K. Gugan, and F. Weinberg, "The Mechanism of Smouldering in Cigarettes," *Comb. Flame,* 7, p. 63 (1963).
49. R. Gann, R. Harris, J. Krasny, R. Levine, H. Mitler, and T. Ohlemiller, "The Effect of Cigarette Characteristics on the Ignition of Soft Furnishings," *Technical Note 1241,* National Bureau of Standards, Gaithersburg, MD (1988).
50. D. Donaldson and D. Yeadon, "Smolder Characteristics of Cotton Upholstery Fabrics," *Textile Res. J.,* March, p. 196 (1981).
51. D. Donaldson and D. Yeadon, "Smoldering Phenomena Associated with Cotton," *Textile Res. J.,* March, p. 160, (1983).
52. T. Ohlemiller and W. Shaub, "Products of Wood Smolder and Their Relation to Wood-Burning Stoves," *NBSIR 88-3767,* National Bureau of Standards, Washington, DC (1988).
53. T. Ohlemiller, *Fire Safety Science—Proceedings of the Third International Symposium,* Elsevier, New York, p. 565 (1991).
54. G. Tesoro and T-Y. Toong, *Smoldering in Cotton Upholstery Fabrics and Fabric/Cushioning Assemblies,* Massachusetts Institute of Technology, Cambridge (1981).
55. M. Ortiz-Molina, T-Y. Toong, N. Moussa, and G. Tesoro, *17th Symposium (International) on Combustion,* Combustion Institute, Pittsburgh, PA (1979).
56. G. Damant, "A Survey of Upholstery Fabrics and Their Flammability Characteristics," *J. Cons. Prod. Flamm.,* 2, p. 2 (1975).
57. G. Damant, "Cigarette Induced Smoldering of Uncovered Flexible Polyurethane Foams," *J. Cons. Prod. Flamm.,* 2, p. 140 (1975).
58. G. Damant, "Home Furnishings Fire Retardant Requirements: The California Experience," *J. Cons. Prod. Flamm.,* 6, p. 95 (1979).
59. K. Palmer and W. Taylor, "Fire Hazards of Plastics in Furniture and Furnishings: Ignition Studies," *J. Cons. Prod. Flamm.,* 1, p. 186 (1974).
60. J. Loftus, *NBSIR 78-1438,* National Bureau of Standards, Washington, DC (1978).
61. J. Krasny, "Cigarette Ignition of Soft Furnishings—A Literature Review with Commentary," *NBSIR 86-3509,* National Bureau of Standards, Washington, DC (1986).
62. R. Salig, *Smoldering Behavior of Upholstered Polyurethane Cushioning and Its Relevance to Home Furnishings Fires,* Master's Thesis, Massachusetts Institute of Technology, Cambridge (1981).
63. A. Ihrig, A. Rhyne, V. Norman, and A. Spears, "Factors Involved in the Ignition of Cellulosic Upholstery Fabrics by Cigarettes," *J. Fire Sci.,* 4, p. 237 (1986).
64. K. Yeh, Z. Song, J. Reznichenko, and K. Jang, "Alkali Metal Ions and Their Effects on Smoldering of Cotton Upholstery Fabric—A Literature Review," *J. Fire Sciences,* 11, pp. 351–367 (1993).
65. A. Ihrig and S. Smith, "The Role of Alkaline Earth Metal Ions in Cellulosic Smoldering," *J. Fire Sciences,* 12, pp. 357–375 (1994).
66. L. Lewis, M. Morton, V. Norman, A. Ihrig, and A. Rhyne, "The Effects of Upholstery Fabric Properties on Fabric Ignitabilities by Smoldering Cigarettes," *J. Fire Sciences,* 13, pp. 445–471 (1995).
67. D. Kellogg, B. Waymack, D. McRae, and R. McGuire, "Smolder Rates of Thin Cellulosic Materials," *J. Fire Sciences,* 15, pp. 390–403 (1997).
68. A. Dyakanov and D. Grider, "Smolder of Cellulosic Fabrics. I. Development of a Framework," *J. Fire Sciences,* 16, pp. 297–322 (1998).
69. A. Dyakanov and D. Grider, "Smolder of Cellulosic Fabrics. II. Alkali and Inner Oxygen as Variables," *J. Fire Sciences,* 17, pp. 71–85 (1999).
70. K. Sumi and G. Williams-Leir, *Research Paper No. 402,* National Research Council, Ottawa (1969).
71. C. Hafer and C. Yuill, *Characterization of Bedding and Upholstery Fires,* Southwest Research Institute, San Antonio (1970).
72. J. Quintiere, M. Birky, F. McDonald, and G. Smith, "An Analysis of Smoldering Fires in a Closed Compartment and Their Hazard due to Carbon Monoxide," *Fire and Matls.,* 6, p. 99 (1982).
73. W. Stiefel, R. Bukowski, J. Hall, and F. Clarke, "Fire Risk Assessment Method: Case Study 1, Upholstered Furniture in Residences," *NISTIR 90-4243,* National Institute of Standards and Technology, Gaithersburg, MD (1990).
74. M. Tuomisaari, D. Baroudi, and R. Latva, "Extinguishing Smouldering Fires in Silos," *Publication 339,* VTT Technical Research Centre of Finland, Espoo, Finland (1998).
75. R. Ogle and J. Schumacher, "Fire Patterns on Upholstered Furniture. Smoldering Versus Flaming Combustion," *Fire Technol.,* 34, pp. 247–265 (1998).
76. R. McCarter, "Smoldering Combustion of Cotton and Rayon," *J. Cons. Prod. Flamm.,* 4, p. 346 (1977).
77. V. Babrauskas and J. Krasny, "Upholstered Furniture Transition from Smoldering to Flaming," *J. Forensic Sci.,* Nov., pp. 1029–1031 (1997).
78. T. Ohlemiller, *NBSIR 85-3212,* National Bureau of Standards, Washington, DC (1985).
79. K. Palmer, *Dust Explosions and Fires,* Chapman and Hall, London (1973).
80. S. Tse, C. Fernandez-Pello, and K. Miyasaka, *Proceedings 26th Symposium (International) on Combustion,* Combustion Insitute, Pittsburgh, PA, pp. 1505–1513 (1996).
81. S. Tse, C. Fernandez-Pello, and K. Miyasaka, *Proceedings Eighth International Symposium on Transport Phenom. in Combustion,* Francis & Taylor, Washington, DC, pp. 689–700 (1995).
82. B. Sutherland, "Smoke Explosions," *Fire Engineering Research Report 99/15,* University of Canterbury, Christchurch, New Zealand (1998).

CHAPTER 10

Spontaneous Combustion and Self-Heating

Brian Gray

Introduction

The term *spontaneous combustion* will be used here to refer to the general phenomenon of an unstable (usually oxidizable) material reacting with the evolution of heat, which to a considerable extent is retained inside the material itself by virtue of either poor thermal conductivity of the material or its container. Under some circumstances this process can lead to flaming combustion and overt fire in which case it is properly called *spontaneous ignition* and is regarded here as a special case of spontaneous combustion. This phenomenon has been responsible for significant losses of life and enormous losses of property.

Fire loss statistics from many sources show that spontaneous ignition is quoted as the cause in a much greater proportion of cases with multimillion-dollar losses than in smaller fires. Of course one should also note that the proportion of results having an unknown cause follows a similar trend, probably due to the greater degree of destruction and hence lost evidence in larger fires. In other circumstances, clearly delineated from the former, only relatively mild self-heating occurs. This occurrence may be referred to as *self-heating*, *spontaneous combustion*, or by research scientists as *subcritical* behavior. By the same token, spontaneous ignition would be referred to as *supercritical* behavior. The well-defined boundary between the two types of behavior is referred to as the *critical condition* and it plays an absolutely central role, both conceptually and pedagogically. It can crudely but pictorially be thought of as a watershed.

The critical condition is actually a whole set of combinations of parameters that affect the behavior. The most important of these are the ambient (surrounding) temperature, and the size and shape of the body of material involved. Thus for a given body of a particular material we would normally talk about the *critical ambient temperature (CAT)*. If we were dealing with a situation where the size of the body was always fixed by commercial practice, for instance, this term would be the normal statement of the critical condition. However, in the case of storage of a variable amount of material in a constant temperature environment, one would talk about the *critical size* or the *critical diameter* of the body for a given fixed temperature. The CAT is the most commonly used and stated critical condition.

For both fire prevention and fire cause investigation, it is essential to be able to identify the critical condition if spontaneous ignition is a possibility either before or after the event. It is also important to be aware of other possible factors operating in particular cases, such as solar irradiation in outdoor storage and preheating if recently manufactured or processed goods are involved. In cases such as hot laundry; hot new chipboard; hot, oily, porous food products (instant noodles, fried fish scraps); bagasse* the temperature of the material itself is a most important parameter affecting criticality in addition to the usual ones. In such cases we have to deal with and determine a critical stacking temperature (CST), which refers to the temperature of the material itself, not the ambient temperature. The CST is dependent on the CAT and the size of the body so such cases are a degree more complicated than the traditional ones involving, usually, agricultural materials stacked at ambient temperature. In addition, in such cases with preheated materials, the time to ignition (defined precisely later) is usually very much shorter than it is where the material is stacked at ambient temperature.

Since the basic processes competing with each other in spontaneous combustion are heat generation by chem-

Emeritus Professor Brian Gray has published extensively on spontaneous combustion and ignition of gases and solids, gas ignition, flame propagation, and related topics for many years. He now runs a combustion consulting company in Sydney, Australia, and was Professor of chemistry at Macquarie University, Sydney, from 1976 to 1998.

*Bagasse is the remainder of sugar cane after the extraction of sugar. It is cellulosic in nature and usually contains 50 percent water.

ical reaction and heat loss to the surroundings mainly by conduction, it is easy to see qualitatively why both a larger body and higher ambient temperature will favor ignition rather than subcritical behavior as they both decrease the rate of heat loss. Generally the temperature profile across the body itself is roughly parabolic in shape, with a peak at the center. Most chemical reaction rates increase almost exponentially with temperature whereas heat loss processes such as conduction increase only linearly. Thus the center of the body where the temperature is highest is the region where ignition, or *thermal runaway,* will commence if it is going to take place at all. Many bodies that have undergone spontaneous ignition show this telltale signature of charring or complete destruction to ash in the center while retaining almost pristine appearance on the outside, sometimes presenting rather dangerous situations for fire fighters in large-scale examples such as bagasse, woodchip, or peat piles. Similarly, the deep-seated nature of the burning started by spontaneous ignition can be difficult to extinguish completely, often reigniting days after apparent extinction.

The purpose of this article is to expound the detailed nature of the situations described above in a manner that approaches the relevant principles and minimizes mathematical formulation as far as is reasonable. The subject will involve relevance to fire cause and fire investigation and as such will refer mainly to solid systems. Many of the basic principles used were actually clarified by experimental work on gaseous systems; such systems still play a central role in current research on this topic, particularly ones where the chemical kinetics are simple and well understood in their own right.

A closely related aspect to be discussed here is the subject of *runaway reaction,* or *thermal runaway.* In the past two decades this topic has developed a literature of its own[1] and threatened to lose contact with the extensive literature on spontaneous combustion. These two terms, which can be taken as synonymous, are applied to supercritical conditions as defined above but only in the context of a chemical reactor. The reactor may be of batch, semibatch, or continuous flow type, but it will almost invariably be well stirred either mechanically or by deliberate turbulent mixing. Therein lies the attraction of such studies from a pedagogical point of view since the main difficulties in mathematical modeling of solid spontaneous combustion arising from spatial temperature variation and gradually decreasing concentration of reacting material are not present. Thus a mathematical theory describing such processes exactly serves as a first approximation, and a tractable one at that, to the more complex topic of solid spontaneous combustion. In addition, the difficult and messy "corrections" to the simplest possible theories due to Semenov[2] and Frank-Kamenetskii[3] are often impossible to apply in practical situations due to the dearth of data and/or their numerical uncertainties.

In addition, in the rare event that precise input data are available and detailed chemical kinetics are known, it is now entirely feasible for particular cases to invoke directly numerical integration of the relevant equations without use of the empirical and semiempirical curve fits involved in the classical corrections to the simplest theories. At the time of writing, average laptop computers were quite capable of such calculations for all but the most irregularly shaped bodies where finite element methods need to be invoked and custom written.

Accordingly we will spend some time here expounding the simplest possible theory (Semenov), which contains all the essential concepts for the understanding of criticality, the tangency between heat release and heat loss curves, and the existence (or otherwise) of stable and unstable steady states. We then move on briefly to the application of such ideas to more complex chemistry and the idea of thermal runaway in continuous stirred tank reactors (CSTR).

We then discuss the Frank-Kamenetskii version of thermal explosion theory, which considers temperature gradients within the self-heating body (thereby generalizing Semenov) and often gives better agreement with experiment for solid bodies with low thermal conductivity. For this reason it is much used in fire investigations, particularly when it is necessary to predict the CAT for a large-scale industrial body from small-scale laboratory tests. However this type of extrapolation requires great care in its application to all but the simplest chemistry.

We then present some ways in which corrections can be made to the predictions of the Frank- Kamenetskii theory occurring under conditions where some of its assumptions are not too accurate. This occurs when the heat of reaction is relatively small and/or when the resistance to heat flow in the boundary of the body (or container wall) is relatively large compared to that inside the body itself (case of small Biot number). Corrections are also necessary when more than one chemical reaction generates heat and when oxygen diffusion into the interior of the body is rate limiting.

All these factors are difficult to handle quantitatively, but fortunately none of them really alter the *qualitative* conceptual nature of what is going on. It is important in gaining an understanding of spontaneous combustion *not* to be confused by these corrections although in certain cases they can be quite large.

We will then move on to discuss experimental testing methods, both on a laboratory and a larger scale where possible. A large array of calorimetric methods can be used to obtain relevant information, but not all of them, particularly differential scanning calorimetry (DSC) and differential thermal analysis (DTA), can give other than very general information. Nevertheless such methods have their purpose when material of unknown origin and composition is involved. Sometimes one needs to know whether the unknown is capable of exothermic reaction at all as postulation of spontaneous ignition because a fire cause looks rather silly in its absence (this happens!).

A characteristic of fires where spontaneous ignition is suspected as the cause is that they often occur on premises that have been closed up or unoccupied for a significant period of time. A question of very great interest in such a context is, What is the time scale expected for a body of a given size in a given ambient temperature to reach ignition, that is, the appearance of overt flame? As one would expect, by application of Murphy's law, this question is very difficult to answer with confidence except in the simplest cases. The time to ignition is a parameter that is not only extremely sensitive to many factors,

which are often unknown, but also extremely sensitive to the degree of supercriticality, that is, how far the body is from the watershed. Not only does it depend on how far the body is from the watershed, but it depends sensitively on the direction as well. In other words, the term *degree of supercriticality* needs to be refined before any idea of time to ignition can be properly formulated.

A number of investigations of this problem have been carried out, and it is essential to recognize that most of the earlier ones addressed the question of time to ignition for the initial temperature of the body equal to the ambient temperature—such as would be the case in the building of a haystack. Hot, stacked material requires totally different considerations for the evaluation of times to ignition, and classical formulae cannot be used in such situations. Such bodies can ignite in times that may be an order of magnitude shorter than predicted by uncritically using classical formulae.

In the penultimate section of this article, we move on to discuss the actual fire where spontaneous ignition has been the cause, or suspected cause, of the fire. We discuss factors that would be either positive or negative indicators of spontaneous ignition, and also the appropriate examination of the aftermath of the fire for pointers as to whether or not spontaneous ignition was the cause. We then proceed to illustrate all the above with a number of case histories, some of them common and illustrative of the basic principles expounded here, others of a novel nature involving quite subtle and detailed investigations that nevertheless can give very definite results.

The Literature

There is a large and varied literature on this topic ranging from sophisticated mathematical theory to technical measurements on industrial and agricultural products. It is scattered over a very wide range of journals, magazines, and disciplines. The most comprehensive publication is probably the book written by Bowes,[4] *Self-Heating: Evaluating and Controlling the Hazards.* This book was published in 1984 and contains references to work published up to 1981, so at the present time it is in need of updating. However, it is the most useful reference available for those working, or commencing work, in the field, either from an academic or technical viewpoint.

Although much of the understanding of spontaneous combustion has come from the basic study of gas phase reactions, where it is generally referred to as *autoignition*, this article will be limited to spontaneous combustion of solid materials generally. Many advances have been made in the field of gaseous autoignition over the last decade or so, stemming from accurate and detailed kinetic measurements and considerable advances in computing power. The critical condition for gaseous systems is a very complex locus in the parameter space characterized by ambient temperature (as for solids), pressure, and composition. Many organic materials, such as hydrocarbons, exhibit more than one autoignition temperature and many also exhibit the phenomenon of igniting on *decreasing* ambient temperature. Many older tabulations of autoignition temperatures do not recognize these peculiarities and should be used with great caution. A detailed description of the reasons for such complexities and their importance in a hazard context is given by Griffiths and Gray[5] in the twenty-fourth Loss Prevention Symposium of the American Institute of Chemical Engineers (1990). A comprehensive list of references up to 1990 can be found in this article.

Reference to liquid reactions and related spontaneous ignitions and thermal instabilities will be given later in this article in the section on spatially homogeneous, or "well-stirred," systems. Otherwise references will be given at points throughout this text resulting in a reasonably complete bibliography.

The Concept of Criticality

During the last two decades the concept of criticality, which has been present in the thermal context for many years,[6] has been recognized as a branch of bifurcation theory,[7] an area of nonlinear applied mathematics that has grown rapidly and proven to be extremely powerful in solving nonlinear problems. In our case the nonlinearity comes from the temperature dependence of the chemical reaction (and therefore heat production) rate. The Arrhenius form for this for a single reaction is $Ze^{-E/RT}$ where E is the activation energy and R is the universal gas constant. T is the absolute temperature, of course. At temperatures rather less than E/R (which can typically be 10,000 K or more), the Arrhenius function is very convex; that is, it curves upward rather rapidly with temperature. In contrast, the rate of heat loss from a reacting body is generally only a linear function of temperature, for example, conduction. Although radiation losses are nonlinear functions of temperature, they are much more weakly nonlinear than the Arrhenius function and also generally rather small at the low temperatures involved in solid spontaneous combustion even though they are important in flame extinction. Typical heat generation and heat loss loci are shown in Figure 2-10.1.

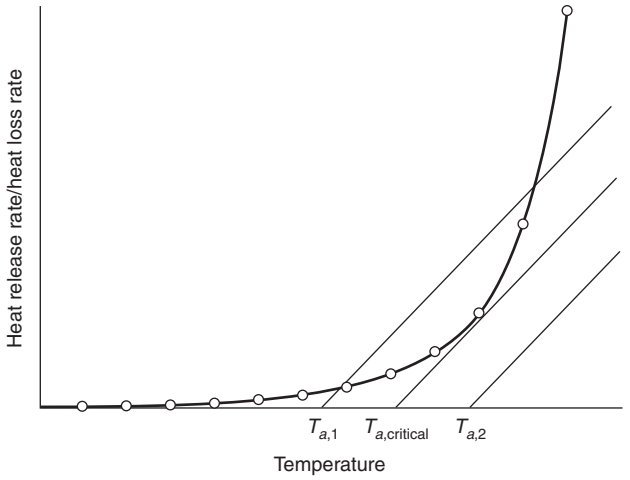

Figure 2-10.1. ***Typical Arrhenius heat-release and loss curves.***

The low temperature range of the Arrhenius curve is seen here to be rather convex and rapidly increasing with temperature. The three straight lines represent the rate of heat loss from a body of fixed given size at various ambient temperatures $T_{a,1}$, $T_{a,\text{critical}}$, and $T_{a,2}$.

At $T_{a,1}$ it can be seen that the heat production and loss curves intersect at two points. At $T_{a,2}$ they do not intersect at all and at $T_{a,\text{critical}}$ they intersect at only one point and, in fact, touch tangentially.

Since intersections represent conditions where heat production and loss balance exactly, we expect them to represent some sort of "equilibrium" or stationary point where the temperature of the body remains constant in time. It is important to remember that they do not represent equilibrium in any thermodynamic sense.

In the region of the lower intersection at $T_{a,1}$ it can be seen from the diagram that the temperature of the body will increase up to the balance point from below as heat release is greater than heat loss in this region. On the other hand, just above this balance point the temperature of the body will move down to it since the heat release is lower than the heat loss in this region. Thus the lower balance point occurring at ambient temperature $T_{a,1}$ is recognized as a *stable* balance, or stationary point. Small perturbations from it will be nullified and the body in this region will tend to stay at the balance point. Note that the temperature of the balance point is not $T_{a,1}$ but slightly above it, usually by 5–20°C. It represents subcritical self-heating and can cause loss of the material, but not by overt ignition or fire. It can appear as degradation or discoloration of many materials, making them useless for their required purpose. For example woodchips degraded in this way are not suitable for paper or cardboard production, and dried milk powder when discolored is unacceptable.

The second balance point at the ambient temperature $T_{a,1}$ can be seen by a similar simple analysis to be *unstable* in the sense that in the temperature region just below it, the heat production is *lower* than the heat loss, so the temperature tends to drop. In the temperature region just above it, the converse is true, so the body temperature tends to rise and leave the balance point. The latter acts as a watershed between two totally distinct types of behavior, that is, the temperature of the body dropping to the lower balance point or running away to the right of the diagram and much higher temperatures, representing ignition.

Here the temperature at the higher balance point would actually be the CST or *critical stacking temperature* for this particular body when stored at ambient temperature $T_{a,1}$. We can immediately see that if the ambient temperature is increased, that is, the straight line is moved to the right with fixed slope (which is determined by the size and shape of the body as we shall see later), the CST will *decrease*, a physically reasonable and intuitive result.

Thus this oversimplified but extremely useful model gives a simple understanding of what Bowes refers to as *thermal ignition* of the second kind, that is, what is probably better referred to as the *hot stacking problem*, a much more descriptive term. Not only that, but it also gives us a qualitatively correct picture of the more common or "normal" type of thermal ignition when the body self-heats from ambient to ignition without any preheating. At $T_{a,1}$ if we very slowly increase the ambient temperature after the steady state has been reached, we can see that the now "quasi-steady state" will also slowly increase until at $T_{a,\text{critical}}$ the quasi-steady state and the CST merge at the point of tangency. Beyond this ambient temperature there is no balance point, and in this temperature region the heat-release curve is now *always above the loss line* and therefore the temperature can only increase. Subsequent ignition will then occur. It will occur after some delay since the rate of temperature increase in this simple model is proportional to the imbalance between heat production and loss (i.e., the vertical distance between the two curves). This is initially quite small, increasing as the temperature rises. In this observation lie the seeds of the calculation of the *ignition delay* or *time to ignition (tti)* to be examined later.

Even more insights can be obtained from this simple type of reasoning. As we shall see later, the slope of the heat loss line is dependent on the surface area/volume ratio of the body in question. Thus for a body of given shape, the surface/volume ratio increases as the body gets smaller and decreases as the body gets larger. In Figure 2-10.2 we can see the effect of increasing the size of a body at a fixed ambient temperature. For this fixed ambient temperature we can speak of subcritical, critical, and supercritical sizes for the body, depending on whether any balance points exist.

Thus for a body with characteristic dimension r_{sub} we see the existence of both a CST and a balance point. For a larger body with dimension r_{super} we see that neither exist and we expect temperature rise to ignition. The critical condition, in this case expressed as a radius or body dimension, is given again by the tangency condition. This critical condition of course is identical with that obtained by thinking of quasi-static variation of the ambient temperature as well. The critical radius for a given ambient temperature will be identical with the CAT for a body of that same radius. How we describe it is simply a matter of where we are coming from.

Of course we do not usually continuously vary the size of a body, but we *do* often stack bodies together, for ex-

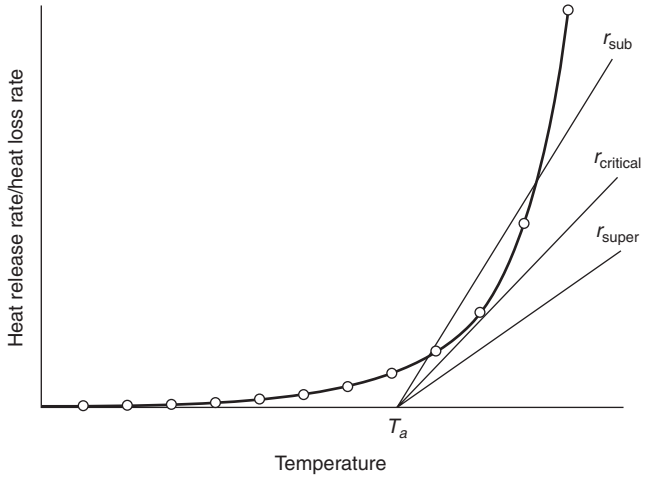

Figure 2-10.2. ***Disappearance of balance points with body size increase.***

ample, bales of cotton, bales of hay, and so forth, and allow larger than normal quantities to accumulate, for example, coal stockpiles. Even from the point of view of this very rudimentary theory, it is obvious that the CAT of two bales in contact will be considerably less than that for a single bale. Thus tests of the CATs of single bodies that are going to be stacked in groups either for transport or storage are useless unless a theory is available enabling calculation of the dependence of CAT on body size. The theory allowing this is thus extremely useful in relating practical tests on small bodies to be applied to storage of large numbers of them (with certain caveats to be discussed later).

To conclude this section it remains to show a convenient method of representing the behavior of the stable balance point and the unstable CST as a control parameter is varied (i.e., the ambient temperature or size of the body). This method enables a quick and convenient representation of the discussion given above on a single diagram (a bifurcation diagram) and also gives us a useful link to the mathematical developments of bifurcation theory.

Figure 2-10.3 shows what happens to the balance point temperature and the CST when T_a is varied continuously from below its critical value to above it. This takes place at constant body size. In this case the ambient temperature is known as the bifurcation parameter. We should note that even at very low ambient temperatures, the CST tends to a finite limit. In fact it becomes very insensitive to the ambient temperature, and no matter how cold the ambient temperature, there is no corresponding *rise* in the CST. Storing hot products in a cold warehouse does not help the problem much!

Conversely Figure 2-10.4 shows how the CST rises indefinitely as the size of the body decreases at fixed ambient temperature. Regardless of ambient temperature it does pay to keep hot stored bodies small! Figure 2-10.4 also shows how for sizes above the critical dimension there is no alternative but ignition. Of course the critical dimension depends on the ambient temperature, and as the latter goes down the critical dimension goes up. It is sometimes very useful to draw a critical dimension ver-

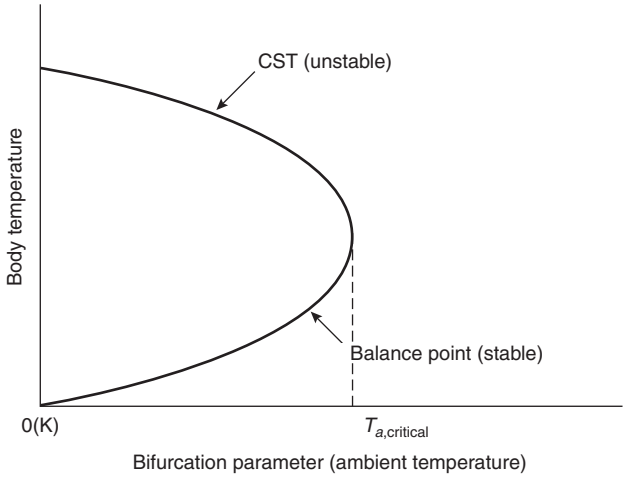

Figure 2-10.3. ***Variation of CST and stable subcritical temperature with ambient temperature, fixed body size.***

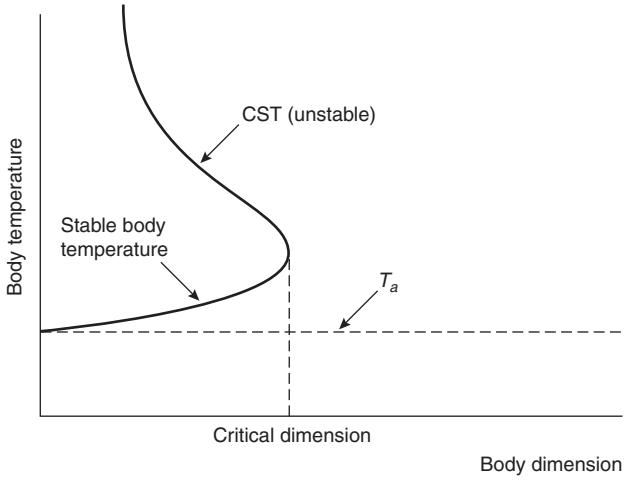

Figure 2-10.4. ***Variation of CST and stable subcritical temperature with body dimension, fixed ambient temperature.***

sus critical ambient temperature graph, and we will see how to do this later.

The whole discussion above assumes that we are dealing with a given material so that the thermal and chemical properties do not vary. The effects of varying thermal conductivity, heat-transfer coefficients, and density on the critical condition are also important but only when comparing different materials. The dependence of the critical condition on these properties will be enunciated in a later section.

One final point needs to be mentioned here. The Arrhenius function does actually level out to an asymptote at very high temperatures, which are off the scale in Figures 2-10.1 and 2-10.2. Thus, theoretically there is another balance point at very high temperature, but in fact this point is not physically significant as it usually occurs at many thousands of degrees, well beyond the region where the assumptions of the model are valid. It also gives rise to a high temperature branch of the curves in Figures 2-10.3 and 2-10.4, which is disjoint from the curves shown. Again it can be ignored from the point of view of low-temperature spontaneous ignition.

The Semenov (Well-Stirred) Theory of Thermal Ignition

The Semenov Theory represents the simplest mathematical formulation of the ideas presented above in qualitative form. As such it is a valuable introduction to quantitative aspects of spontaneous ignition without introducing the technical difficulties associated with more elaborate forms of theory where spatial variations of temperature and reaction rate within the body are considered. The assumptions for this theory follow.

1. The temperature within the reacting body is spatially uniform: A spatially uniform temperature implies either that the material of the body is well stirred (i.e., it would

have to be liquid or gas) or the resistance to heat flow within the body is so low compared to that within the container or boundary that it can all be assumed to be concentrated within the boundary. The latter results in a temperature discontinuity at the boundary of the material and is a good approximation in deliberately stirred fluids.[8]

It is not a good approximation for materials of vegetable origin where thermal conductivities of materials such as cellulose are low and of the order of 0.05 W/mK. Nevertheless, even for such materials semiquantitative conclusions can be drawn from this theory if the spatially averaged temperature of the body is used.

2. The heat generation is assumed to be due to a single chemical reaction of simple integral order: This assumption is often a reasonably good approximation, particularly when a "lumped" or empirically determined rate law has been measured independently. It does not mean that the chemical reaction taking place is only a single step reaction. In fact this empirical approximation works quite well in many cases that are not single step reactions.

3. Both the heat of reaction and activation energy are assumed to be sufficiently large to support ignition behavior: The reasons for these assumptions will become clearer later, but it is intuitively obvious that if there is zero heat of reaction, ignition cannot occur. Likewise with zero activation energy (acceleration of reaction rate with temperature increase), ignition cannot occur either.

With these assumptions we can write down two equations that determine the temperature and fuel concentration as functions of time (but uniform in space). These are simply the conservation of energy and the kinetic rate law respectively. They are

$$C_v \rho V \frac{dT}{dt} = VQf(c)e^{-E/RT} - S\chi(T - T_a) \tag{1}$$

$$\frac{dc}{dt} = -f(c)e^{-E/RT} \tag{2}$$

where

C_v = heat capacity at constant volume
ρ = density
V = volume
T = temperature of the reacting material (in K)
T_a = ambient temperature of the surroundings (assumed constant in time)
Q = heat of reaction per unit concentration of fuel
$f(c)$ = kinetic rate law
c = concentration of fuel
E = activation energy of the reaction
R = universal gas constant
S = surface area of the interface across which heat is lost to the surroundings
χ = heat transfer coefficient

The independent variable is time.

The first term on the right side of Equation 1 represents the rate of heat generation by the self-heating reaction. The second term represents the heat lost to the surroundings. The left side represents the difference between these two. Equation 2 simply expresses the fact that as the reaction proceeds, the concentration c decreases as the fuel is used up. The commonest and simplest form for $f(c)$ is Zc where Z is known as the preexponential factor, a constant. This case is known as a first-order reaction. These two terms are shown graphically in Figure 2-10.1 for any particular value of c.

Despite their apparent simplicity these two equations are not soluble by classical methods, so we cannot write down their solution. Nevertheless, we can in fact write down the critical condition exactly (and other important quantities) using bifurcation theory. We will illustrate this for the simplest possible case only, remembering that it can also be done for more realistic and complicated cases as well as within the confines of the Semenov theory.

First we write Equations 1 and 2 in dimensionless form (see nomenclature for details):

$$\frac{du}{d\tau} = \nu e^{-1/u} - \ell(u - u_a) \tag{3}$$

$$\frac{d\nu}{d\tau} = \varepsilon\nu e^{-1/u} \tag{4}$$

where u and ν are dimensionless temperature and fuel concentration, respectively, and ε is a dimensionless version of the ratio C_v/Q; that is, it is a measure of the amount of fuel decomposition required to produce a temperature rise of 1°C. τ is a dimensionless time and ℓ is a dimensionless heat transfer coefficient.

The most frequently used version of this theory, without fuel consumption, corresponds to taking the limit $\varepsilon \to 0$, thus maintaining ν at its initial value ν_0. We have only a single equation to deal with now, that is,

$$\frac{du}{d\tau} = \nu_0 e^{-1/u} - \ell(u - u_a) \tag{5}$$

Even this much-simplified equation is not analytically soluble. However, it relates exactly to Figure 2-10.1 and can be used to calculate the critical condition readily. We first note that the balance points in Figure 2-10.1 must satisfy the equation

$$\nu_0 e^{-1/u_s} - \ell(u_s - u_a) = 0 \tag{6}$$

For subcritical values of the ambient temperature, this equation will have three solutions for a given set of parameter values, ν_0, u_a, and ℓ. From Figure 2-10.1 it can be seen that at the critical condition ($T_{a,\text{critical}}$ corresponding to $u_{a,\text{cr}}$) not only do the two terms of Equation 6 balance, but their *slopes* also balance at this condition. Mathematically this means that their differential coefficients with respect to temperature must also be equal, that is,

$$\left[\frac{\partial(\nu_0 e^{-1/u})}{\partial u}\right]_{u=u_s} = \frac{\nu_0 e^{-1/u_s}}{u_s^2} = \ell \tag{7}$$

The critical value of u_s is then obtained by solving Equations 6 and 7 simultaneously, which interestingly can be done in closed form simply by eliminating the exponential, leaving a quadratic equation:

$$u_{s,\mathrm{cr}}^2 - u_{s,\mathrm{cr}} + u_{a,\mathrm{cr}} = 0 \tag{8}$$

From our definition of $u = RT/E$ and the general knowledge that $R/E \cong 0.0001$ for most combustion reactions, we can see that at normal ambient temperatures for ignition we will have $u_{a,\mathrm{cr}} \cong 0.02$, or in any case $u_{a,\mathrm{cr}} \ll 1$. Using the standard formula for the solution of a quadratic equation and expanding the radical occurring, we can derive

$$u_{s,\mathrm{cr}} = u_{a,\mathrm{cr}} + u_{a,\mathrm{cr}}^2 + \cdots \tag{9}$$

which is the lower of the two roots (the upper one is unphysical).

If we substitute this back into either Equation 6 or 7, we get a relationship between the parameters of the problem *which holds at criticality only.* Thus if we use Equation 6, we obtain, after some rearrangement,

$$\ell_{\mathrm{cr}} = \frac{\nu_0 e^{-1/u_{a,\mathrm{cr}}(1+u_{a,\mathrm{cr}})}}{u_{a,\mathrm{cr}}^2(1+u_{a,\mathrm{cr}})^2} \tag{10}$$

We can interpret this equation in a number of ways. Since ℓ_{cr} involves the size of the body as the only physically variable parameter, and ν_0 is proportional to the bulk density of the material, we can take this equation to give us the critical size body for a given ambient temperature and bulk density. $u_{a,\mathrm{cr}}$ is the only parameter here that cannot easily be made the argument of the equation.

Converting Equation 9 into dimensional form quickly gives us the relationship:

$$T_{s,\mathrm{cr}} - T_{a,\mathrm{cr}} \equiv \Delta T_{\mathrm{cr}} \cong \frac{RT_{a,\mathrm{critical}}^2}{E} \tag{11}$$

at the critical condition. ΔT_{cr} would typically be 20–30°C for ambient temperatures around 30–40°C. Not surprisingly, it is independent of the body shape, being dependent only on the total surface area through which heat is lost. Nevertheless, even this oversimplified result can be very useful in an emergency situation. If E is not known, it is a useful rule of thumb (especially for agricultural cellulosic materials) that self-heating of more than 30°C above ambient, that is, typically a body temperature of more than 60–70°C, represents imminent spontaneous ignition whereas an internal body temperature of 35–40°C represents subcritical heating that is unlikely to run away but quite likely to lead to degradation of the material.

Two further points need to be made before leaving this simplified model. First, in order that Equation 8 has real roots, it is necessary to require that

$$E \geq 4RT_{a,\mathrm{critical}} \tag{12}$$

Physically this means that the chemical heat generation rate is sufficiently accelerative to produce the phenomenon of criticality. If it is not satisfied, there is only a single stable balance point for all conditions and no abrupt change in behavior can occur.

Second, if we examine Equation 10, the critical condition, we should note that where the concentration ν_0 appears, in the case of gases we would normally convert this to pressure. Thus in this case Equation 10 gives a relationship between ambient temperature and pressure at the critical condition. This relationship is the familiar explosion limit curve extensively used in the study of gaseous explosions.

Inclusion of Fuel Consumption

If we do not make the assumption $\varepsilon \to 0$ in Equation 4, the clear distinction between subcritical and supercritical behavior no longer exists. We can no longer define the critical condition as the disappearance of two balance points. Equations 3 and 4 possess only a single balance point, $u = u_a$, and $c = 0$ for all possible parameter values, and this refers to the equilibrium state when all fuel has been exhausted and nothing is happening—clearly a condition of no interest. For the definition of criticality in such a case, it is helpful to examine the *experimental* or *phenomenological* definition. The experimentalist determines the critical condition by performing various tests at differing ambient temperatures (we will outline the details of test procedure in a later section) and by measuring the temperature/time history at the center of the sample. They will plot the maximum temperature attained against ambient temperature and will find there is a steep increase in slope over a narrow region of ambient temperature. The result is illustrated in Figure 2-10.5.

The distinction between points 1 and 2 is very clear both in terms of the maximum temperature attained and the physical condition of the material itself after the test is finished. Typically, at point 2 the material is hardly different visually from the initial condition, whereas at point 1 there is usually no more than a small amount of ash remaining. The temperature attained at point 1 is often of

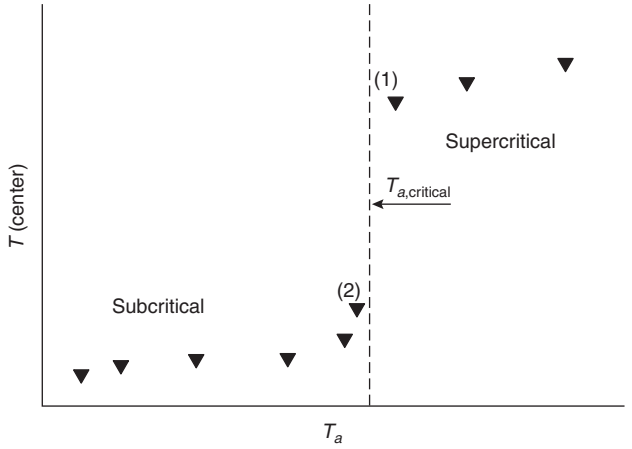

Figure 2-10.5. ***Typical experimental results for criticality tests.***

the order of hundreds of degrees above ambient compared with probably 30 degrees above ambient at point 2.

It is impossible to get points between 1 and 2 experimentally without wasting a great deal of time due to the extreme sensitivity in this region, so the convention is to define the CAT as the arithmetic mean of $T_{a,\ell}$ and $T_{a,2}$. With good equipment these will only be 3 or 4 degrees apart at the most.

From the point of view of theoretical calculation of the CAT in this case, we note that the points in Figure 2-10.5 can be joined by a smooth curve with a very steep region around an inflection point. It has been shown[9] that this definition of the CAT, when fuel consumption is significant, leads to a relation between the usual parameters, and this relation passes over smoothly to the one derived from the tangency condition as $\varepsilon \to 0$. For $\varepsilon \cong 0.05$ or less, which is the case for most practically important materials, the corrections arising from fuel consumption are not usually significant. This result is especially the case in fire investigations where a posteriori numerical knowledge of parameter values is rather limited, and this correction (and others) is not justified.

Extensive discussion of earlier work on the fuel consumption correction is given in Bowes's book.[4] Many empirical and semiempirical corrections were devised based on approximated integration of Equations 3 and 4. These corrections will not be discussed here since the advent of powerful PC and laptop computational capabilities has rendered them irrelevant. Equations 3 and 4 can be integrated with great speed and precision if accurate parameter values are available. Even so, it is necessary to have a definition of criticality when a computed or experimental version of Figure 2-10.5 has been obtained. With the definition given in Reference 9, allied with numerical integration, the problem can be regarded as solved for all practical purposes.

Extension to Complex Chemistry and CSTRs

Complex Chemistry

Other than elementary gas phase reactions, very few examples of chemical change occur via a single step as assumed above. As already remarked, the simple theory is more useful than might be expected because many complex chemical reactions behave as if they were a single step, over limited temperature ranges. This is usually because a single step does dominate the heat production rate, for example, when two reactions occur in parallel. If the activation energies are rather different, they will each in turn dominate the heat generation in two different temperature ranges and in each of these ranges the simple theory will hold. Of course, it will not hold in the changeover region.

Another case where the simple theory can hold unexpectedly is when a number of reactions are in series and one is particularly slow. The slow reaction will determine the overall heat generation rate and its parameters will dominate the critical condition. If none of the above conditions hold, it is still possible to derive a generalization of the theory that is conceptually very closely related. It is possible to prove[10] that if the heat release rate is defined as the sum of the heat release rates of all reactions taking place in the system, then the critical condition can be defined as the tangency of this quantity with the heat loss line. Thus a diagram like Figure 2-10.1 can be drawn and the same constructions used, provided the total heat release curve for all the reactions is used.

The heat release curve in this case can have a complex shape, and thus *more than one* critical condition can occur. This state of affairs is extremely important in the ignition of most organic vapors, particularly hydrocarbons[5] where some critical conditions occur on *decreasing* the ambient temperature. Also in the ignition of some commonly occurring solids, particularly when wet, more than one heat-generating reaction can be important, for example, in the spontaneous ignition of moist bagasse.[11] In this case there are two critical conditions, one where a jump from virtually no self-heating to self-heating of ~35°C occurs, and a second critical condition where this intermediate state jumps to full-fledged ignition. Modeling of such situations is possible but beyond the scope of this chapter; however, similar behavior is likely to occur in other moist cellulosic materials, including hay, chipboard, and so forth.

At this stage it is worth pointing out that for bagasse at least, microbial "heat production" is not a factor in these phenomena. Although natural bagasse contains large numbers of microorganisms, sterilization by various methods *does not affect heat production or self-heating* at all, as measured by Dixon[12] and predicted on the basis of bacterial microcalorimetric data by Gray.[13] Similar work on hay is under way.

CSTRs and Thermal Runaway

Strangely, this topic has become uncoupled from work on spontaneous ignition over recent years even though the basic principles and mathematical methods used are similar. It is a huge problem in the chemical process industry and receives much attention. For example, in 1998 the Joint Research Centre of the European Commission, Institute for Systems Informatics and Safety, produced a book describing the proceedings of a European Union seminar held in Frankfurt in 1994 that managed to avoid almost completely any reference to the fundamentals of the problem or related material. *Risk analysis* appears to have replaced fundamental scientific understanding in some aspects of this problem.

We will confine ourselves here to writing down the basic equations governing a single exothermic chemical reaction taking place in a CSTR (continuously stirred tank reactor) to exhibit their similarity to the equation describing a spontaneously ignitable material, that is, Equations 3 and 4.

The appropriate equations for this case are in fact 3 and 4 with terms representing inflow and outflow of reactants and products, that is,

$$V\rho C_v \frac{dT}{dt} = QVf(c)e^{-E/RT} - S\chi(T - T_a) - FC_v\rho(T - T_f) \tag{13}$$

$$V\frac{dc}{dt} = -Vf(c)e^{-E/RT} + F(c_f - c) \tag{14}$$

F is a volumetric flow rate and the subscript f refers to feed values. These equations can be cast in dimensionless form also. Here we simply note that they possess steady-state (balance point) solutions without making any approximations at all (such as neglect of fuel consumption) and Figure 2-10.1 can be applied directly in slightly modified form. The critical condition referred to earlier occurs here also, but it can now be stated in terms of the CAT or a critical feed temperature or, indeed, a critical flow rate.

A critical size also occurs and is particularly prominent in CSTR considerations where "scaleup" from prototype size to commercially viable size has resulted in exceeding the critical condition. Some references to scaleup are given in Reference 1, and there are many more in the chemical engineering literature and the study of self-heating in catalyst particles. See Aris[14] for an excellent discussion of this area.

The Frank-Kamenetskii Theory of Criticality

In its original form the Frank-Kamenetskii theory included a more realistic model of heat transfer within the reacting solid, that is, by incorporating the heat conduction law of Fourier. This law allows a calculation of the variation of temperature within the self-heating body itself and allows comparison of measured and calculated self-heating to take place. However, it sacrifices the simple description of time-dependent behavior given by the Semenov model because such considerations involve the solution of partial differential equations. This is now much faster than even a few years ago, in terms of numerical computation, and improving day by day. Nevertheless, such numerical solutions do not lend themselves to simple interpretation even with the use of rapidly developing file visualization techniques. Construction of appropriate meshes for finite element computation, necessary for practically occurring three-dimensional shapes, is also far from trivial.

As a result, the Frank-Kamenetskii theory is still mainly used for interpretation of testing experiments on self-heating and subsequent evaluation of parameters for individual systems. This is a viable proposition for materials with sufficiently large heats of reaction and activation energies. In such cases we shall see that the stationary (in time) conditions assumed in the Frank-Kamenetskii theory are indeed well approximated for the duration of typical tests in practical cases. In its original form this theory also neglects fuel consumption, as does the Semenov theory, with similar consequences. With these assumptions the equation describing the theory is

$$\kappa\nabla^2 T + Qf(c_0)e^{-E/RT} = 0 \tag{15}$$

with the boundary condition $T = T_a$ on the wall(s) of the body. T_a is the ambient temperature of the surroundings. This boundary condition assumes instantaneous transfer of heat from the surface of the body to the surrounding medium (usually air). When this is not approximately correct, very important consequences follow, as we shall see in a later section on the interaction of self-heating bodies with each other. In this formulation the shape of the body and its size both enter the mathematical formulation through the boundary condition only.

As usual, Equation 15 is not analytically soluble. However, by using an approximation to the Arrhenius function (Frank-Kamenetskii[3]), the modified equation can be solved analytically for a one-dimensional infinite slab of material. This same approximation was later shown to be analytically soluble for an infinite cylinder by Chambre.[15]

With this approximation, Equation 15 takes the form:

$$\nabla^2\theta + \delta e^{\theta} = 0 \tag{16}$$

with $\theta = 0$ on the boundary. θ is a dimensionless temperature defined by

$$\theta = \frac{E(T - T_a)}{RT_a^2} \tag{17}$$

that is, it is a measure of the temperature excess within the body at various points. The dimensionless parameter δ is defined by Equation 18:

$$\delta = \frac{QEr^2 f(c_0)e^{-E/RT_a}}{\kappa RT_a^2} \tag{18}$$

where the symbols are already defined apart from r, which is usually one-half of the smallest dimension of the body, that is, the radius of a cylinder, the radius of a sphere, or the half-width of a slab. Mathematical treatment of Equation 16, whether it is exactly soluble or not, indicates that a solution satisfying the boundary conditions exists only when $\delta \leq \delta_{\text{critical}}$ where δ_{critical} is some number depending on the shape of the body only. For an infinite slab of material $\delta_{\text{critical}} = 0.878$ and for an infinite cylinder it has the value 2.000. For other shape bodies the critical value has to be obtained either numerically or by semiempirical methods outlined in some detail by Bowes.[4] For convenience, a few of the values are listed in Table 2-10.1.

The tabulation of figures for infinite slab or infinite square rod is useful in so far as they are often rather good approximations for real bodies, provided one or more of their dimensions are much larger than the others. Thus for the rectangular box, if we take $r = l = 1$, $m = 10$, we get

Table 2-10.1 ***Values of $\delta_{critical}$ for Various Geometries***

Geometry	Dimensions	δ_{critical}
Infinite plane slab	Width $2r$	0.878
Rectangular box	Sides $2l$, $2r$, $2m$; $r < l, m$	0.873 $(1 + r^2/l^2 + r^2/m^2)$
Cube	Side $2r$	2.52
Infinite cylinder	Radius r	2.00
Equicylinder	Height $2r$, radius r	2.76
Sphere	Radius r	3.32
Infinite square rod	Side $2r$	1.700

$\delta_{critical} = 1.75$ compared to 1.700 for the infinite square rod. If we now look at Equation 18 for the particular case of a cube as an example, we get

$$\frac{QEf(c_0)r^2e^{(-E/RT_{a,\text{critical}})}}{\kappa RT^2_{a,\text{critical}}} = 2.52 \qquad (19)$$

at the critical condition. We have a number of choices as to interpretation of this equation depending on which parameter can be made the argument. If r is chosen as the argument, then the equation would be interpreted as giving a critical size for the body at a fixed ambient temperature T_a. Since c_0 depends on the density of the material, Equation 19 could be rearranged to give a critical density for that particular size body at ambient temperature T_a. What is not possible is isolation of T_a as the argument of the equation, and this is often the most easily varied parameter in a typical test oven.

This complex dependence of the critical condition on T_a is dealt with by rearranging Equation 18 and taking natural logarithms as follows:

$$\ln\left[\frac{\delta_{\text{critical}}T^2_{a,\text{critical}}}{r^2}\right] = \ln\left[\frac{QEf(c_0)}{R\kappa}\right] - \frac{E}{RT_{a,\text{critical}}} \qquad (20)$$

from which it can be seen that a plot of $\ln(T^2_{a,\text{critical}}/r^2)$ against $1/T_{a,\text{critical}}$ will be a straight line with slope $-E/R$ and intercept $\ln[QEf(c_0)/\kappa R\delta_{\text{critical}}]$. The traditional and recommended test protocol for spontaneous ignitions makes explicit use of this logarithmic form of the critical condition. Not only does it yield the activation energy from the slope, but the occurrence of a straight line plot assures us that the assumption of an Arrhenius temperature dependence for the heat-generating reaction is correct over the temperature range investigated.

Equation 20 can also be regarded as a scaling law, in principle enabling the prediction of CATs for large-scale bodies from measured CATs for much smaller laboratory-sized samples. However, as we shall see, it is necessary to ensure that the same chemical kinetics applies over the whole temperature range involved. Finally if it becomes necessary to estimate the CAT for a complex shape, not included in Table 2-10.1, an excellent and comprehensive discussion of approximation methods is given by Boddington, Gray, and Harvey.[16]

Experimental Testing Methods

Experimental testing methods are traditionally based on the scaling relationship (Equation 20). Appropriate containers (usually stainless steel gauze baskets) of various dimensions are used, being limited only by the size and heating capability of an accurately thermostatted oven, which must also have a spatially homogeneous ambient-temperature distribution (±1°C is recommended). The gauze containers may be any convenient shape, equicylindrical or cubic being preferred due to ease of construction. The gauze does not restrict oxygen ingress through the boundary, nor does it restrict egress of carbon dioxide and other product gases during combustion. If the air inside the oven is sufficiently turbulent, usually the boundary conditions of the Frank-Kamenetskii theory will hold quite well.

The boundary condition is easier to satisfy when the thermal conductivity of the material inside the gauze baskets is relatively low, as it is with many agricultural materials containing cellulose ($\kappa \sim 0.05$ W/mK). The efficacy of the boundary condition is determined by the heat transfer rate from the gauze to the oven air relative to the conduction rate within the material itself. This ratio ($\chi r/\kappa$) is known as the Biot number, and the larger it gets, the more accurate the Frank-Kamenetskii boundary condition ($T = T_a$) becomes. In practice a Biot number greater than 30 is effectively infinite as the CAT becomes extremely insensitive to it. We will return to this topic in a later section where the dependence of the critical condition on the Biot number is outlined.

The test procedure involves starting with the smallest basket and a trial oven temperature. The sample is equipped with one or more fine thermocouples placed at the center of the sample and, if desired, at various places along a radius if a spatial profile is wanted (this is generally not necessary). The sample is placed in the preheated oven and the center temperature followed as a function of time. If the oven temperature is well below the CAT, the sample will simply approach the oven temperature asymptotically. If it is slightly below, but getting close, it will cross above the oven (ambient) temperature and attain a maximum of the order of 1–30°C above ambient before declining. This oven temperature represents the subcritical condition.

The sample is discarded and replaced with a fresh, similar one. If the previous run was subcritical, the oven temperature will be increased usually by 20°C or less depending on the experience of the operator. The run is then repeated. If it is still subcritical, the procedure is again repeated until a supercritical oven temperature is attained. The arithmetic mean of the lowest supercritical temperature and the highest subcritical temperature is taken as the first estimate of the CAT. The uncertainty may be quite large at this stage, so the process is usually continued by testing at the estimated CAT. The process is repeated, halving the difference between highest subcritical and lowest supercritical temperatures each time until the desired errors are obtained. Typical temperature/time plots showing the critical separation are shown in Figure 2-10.6.

This reaction is an exothermic decomposition evolving oxygen. From these measurements one would conclude that the CAT was 55.2 ± 1.34°C. For greater accuracy the next test would be run at an ambient temperature of 55.2°C. After at least four or five such sets of runs have been carried out in differently sized containers, giving four or five CATs at various radii, then the next step is to construct the Frank-Kamenetskii plot of the scaling Equation 20. A typical plot is shown in Figure 2-10.7.

This plot shows a range of CATs for cylinders ranging in radius from 0.191 m down to 0.026 m, the larger radii corresponding to commercial containers. From the slope of this line, E/R can be read off directly and from the intercept; so can the dimensionless group occurring in the scaling equation. Sometimes components of this group may be known from independent measurements, for example, Q from calorimetry, κ from direct measurement, or $f(c_0)$ from kinetic measurements, in which case all the parameters can be obtained.

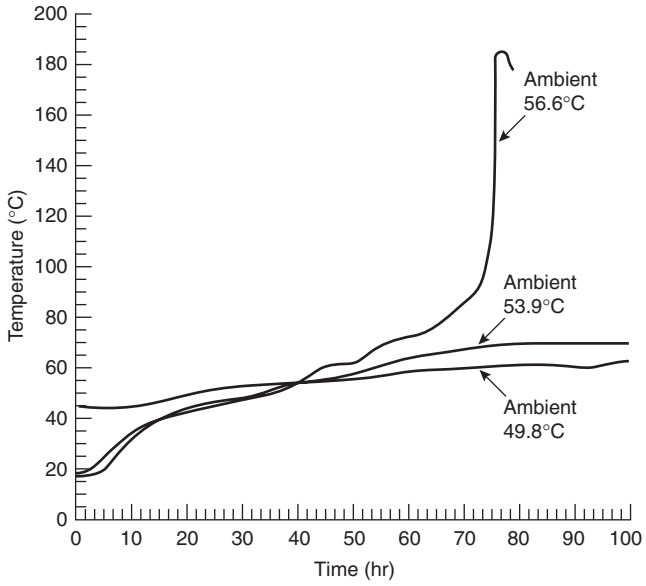

Figure 2-10.6. ***Two subcritical and one supercritical center temperature/time traces for a 0.175-m-radius equicylinder of hydrated calcium hypochlorite.[17]***

Special Cases Requiring Correction

The Presence of Water

When water is present in spontaneously combustible material, special considerations apply. First it is necessary to note that endothermic evaporation would be expected to partly offset some of the heat generation by the exothermic reactions taking place. While this expectation is true, it is often the case that at the high oven temperatures used in testing small samples, the low activation energy for evaporation (~40 kJ/mol) leads to rapid evaporation before the exothermic process has got fully under way. Many spontaneous combustion reactions have activation energies around 100 kJ/mol, particularly the group of reactions of cellulosic materials.

As a result, the high temperature CATs reflect the properties of the dry material, in particular the thermal conductivity. Consequently, extrapolations to temperatures well below 100°C will be questionable for this reason alone. In the lower temperature range the heat transfer will be significantly affected by the presence of water and its transport from the hotter to the cooler regions of the body by evaporation, diffusion, and condensation.

Many cellulosic materials are known to exhibit a "wet reaction"[19,20] in addition to the dry exothermic reaction. This reaction involves liquid water as a reactant and further complicates the picture as far as high-temperature testing is concerned. Simultaneous evaporation, diffusion, condensation, and reaction involving water have been modeled recently in connection with bagasse,[21,22] using an experimentally measured rate law for the wet reaction[23] giving results that are in good agreement with measured results for commercial-size piles of this material (minimum dimension 5–10 m).

The detailed nature of the wet reaction with a rate maximum around the 50–60°C mark has led to false identification with microbial activity. In bagasse at least it has been shown[24,25] that microbial activity does not contribute to self-heating to any significant degree. Piles sterilized by various methods showed self-heating rates indistinguishable from those of nonsterile piles. Microbial counts were carried out in all cases and large decreases did not affect the self-heating rates. It would be rather surprising if similar results were not obtained from tests on hay and straw where microbiological activity (but not necessarily heating) are known to occur, and it is surprising that such tests have not yet been carried out.

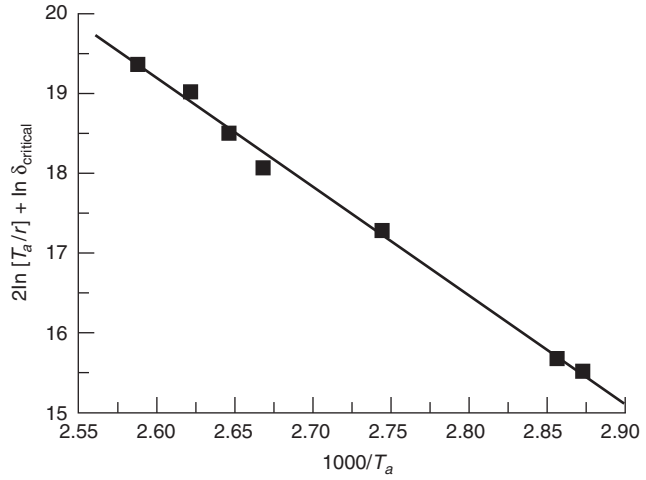

Figure 2-10.7. ***Typical Frank-Kamenetskii plot for anhydrous calcium hypochlorite from Uehara et al.[18]***

Parallel Reactions

If more than one exothermic reaction can take place in the material, and these reactions have rather different activation energies, then each will dominate in its own temperature range. Thus the higher activation energy reaction will cut in at higher temperatures and be insignificant at lower temperatures when the low activation energy reaction will dominate the heat generation. The wider the divergence in activation energies, the sharper the discontinuity in slope, that is, the narrower the temperature range over which both will contribute. Hydrated calcium hypochlorite shows a clear example of this, and it is reflected in a sharp break in the slope of the Frank-Kamenetskii plot where the changeover occurs. Figure 2-10.8 shows this plot. The low temperature activation energy for this system is about 48 kJ/mol while that of the higher temperature reaction is around 125 kJ/mol, the transition temperature being around 120°C.[17] Extrapolation of the high temperature line in this case gives CATs for large commercial-size containers that are seriously in error; that is, they are predicted to be much higher than they actually are. In the general case of two reactions with different activation energies, this will always be the case as the high activation energy is "frozen out" at low temperatures and the low activation energy reaction is "swamped" at higher temperatures.

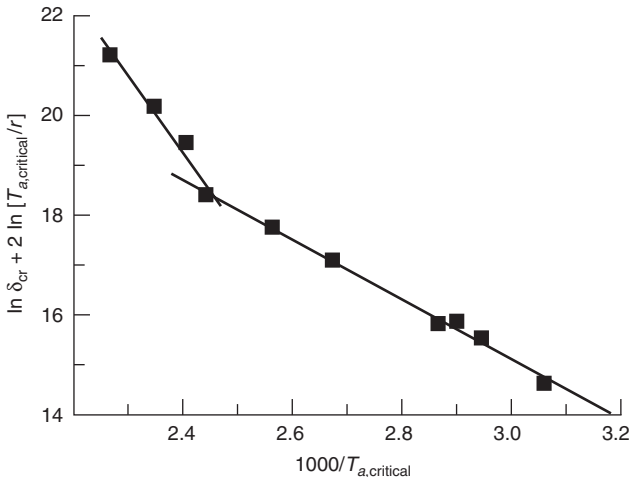

Figure 2-10.8. ***Frank-Kamenetskii plot for hydrated calcium hypochlorite with reaction mechanism change.***

Other examples of mechanism change are known and discussed by Bowes.[4] In such cases accurate predictions of CATs can still be made within each temperature range. This type of example emphasizes the need for tests covering as wide a range of temperatures as possible. Recent methods put forward as viable alternatives to the standard method, for example, Jones[26] and Chen,[27] are restricted to either measurement at a single temperature or over a limited temperature range and can give dangerously flawed results. Empirical tests such as the Mackey test[28] and the crossover test[29] are not reliable and cannot be properly related to the basic principles of spontaneous ignition theory.

Finite Biot Number

The Biot number is defined as

$$\mathrm{Bi} = \frac{\chi r}{\kappa} \tag{21}$$

where

χ = surface heat-transfer coefficient

r = smallest physical dimension of the body

κ = thermal conductivity of the material

It is the dimensionless measure of the ratio of the resistance to heat transfer within the body to that from the surface to the surroundings. Thus the Semenov theory is often referred to as *zero Biot number* and the Frank-Kamenetskii theory as *infinite Biot number.* They are both special cases of a more general (and more exact) formulation, as was originally pointed out by Thomas.[30,31]

In general the boundary condition at the edge of a self-heating body has the form of a *continuity condition,* which refers to the energy flux across the boundary. It states that the energy flux within the body (given by Fourier's law) and the energy flux from the body surface to the surrounding air must be equal, that is,

$$\kappa \frac{dT}{dn} = \chi(T - T_a) \tag{22}$$

In dimensionless form this becomes

$$\frac{du}{dn} = \mathrm{Bi}(u - u_a) \tag{23}$$

This boundary condition does not hold if there exist any heat sources on the boundary of the body itself, as can occur when there is incidence of radiation or when there is heat generated by friction during pulverization of materials capable of self-heating. Such cases (in the shape of an infinite cylinder) have been treated and the modified critical condition obtained.[32,33]

The values of the critical parameter δ quoted for the Frank-Kamenetskii theory are all for the limiting case $\mathrm{Bi} \to \infty$, and both Thomas and Barzykin have given semi-empirical functions exhibiting the dependence of $\delta_{\mathrm{critical}}$ on Bi, which are detailed in the book by Bowes. As the Biot number decreases, so does $\delta_{\mathrm{critical}}$ and hence so does the CAT, all compared with the standard Frank-Kamenetskii theory. For Biot numbers >30, the correction is rather small but is significant for smaller values. Typical heat transfer coefficients from smooth solid surfaces to rapidly stirred air (in a test oven for example) are of the order of 20 $\mathrm{W/m^2{\cdot}K}$, and thermal conductivities of typical cellulosic materials (such as sawdust) are around 0.05 W/m·K, giving a ratio of 400/m. Clearly for laboratory-size test bodies ($r \sim 0.1$ m), the Biot number is rather large.

For this reason a significant amount of work has simply *assumed* a sufficiently large Biot number without investigation of its actual numerical value. Sometimes the assumption is not justified, particularly where inorganic materials are involved, as their thermal conductivities can be quite large. For example, typical, inorganic salt thermal conductivities lie in the range of 0.2–3.0 W/m·K, giving for the ratio (χ/κ) a value of 7–100/m. Clearly for test bodies with $r \sim 0.1$ m, the Biot number will be only 0.7–10. The effect of the small Biot number on $\delta_{\mathrm{critical}}$ is to reduce it by a factor ranging from 0.21 to 0.83, respectively. Clearly for such materials, the more general boundary condition suggested by Thomas must be used, and it is good practice for all but the most strongly insulating materials to estimate the thermal conductivity (particularly in the presence of water) independently of the standard testing regime.

A further important feature of self-heating bodies with finite Biot number is that their CATs will be sensitive to the heat-transfer coefficient from their surface to the surrounding air. Thus the value of the CAT obtained may well be test-oven sensitive and be strongly influenced by air movement. For example, it has been shown for hydrated calcium hypochlorite[17] that in stirred air in a typical test oven the CAT is 60°C for a 0.175-m-radius container, but in still air the CAT is 55°C.

This observation raises serious questions about the value of empirical testing methods such as the SADT test for shipping self-heating materials[34] that determines

criticality-related parameters under vaguely defined conditions of forced airflow in a test oven. The results are then used to determine "safe" conditions for shipping such materials in *still air* inside, for example, a shipping container. Almost invariably many self-heating bodies are stacked inside the same still air inside a container, and they will interact with each other to a very significant extent if the transfer of heat through the container wall is not very rapid. In practice such transfer is rather slow, involving two successive air/metal transfers. As a result the self-heating bodies collectively heat the air inside the container and produce a "cooperative CAT," which can be tens of degrees lower than the CAT of a single body. The Semenov-type theory for this collective ignition has been formulated by Gray.[35] A more accurate version, where the individual bodies are assumed to obey the general boundary condition put forward by Thomas, has also been formulated (in preparation). The predictions of this theory have been compared to the experimental CAT for 18 14-kg equicylinders packed in a rectangular steel box with good agreement.[36] The CAT was reduced from 62.5°C for a single keg in still air to 54°C for 18 kegs in still air.

Times to Ignition (Induction Periods)

The terms *times to ignition* and *induction periods* tend to be used synonymously. Here we will abbreviate to *tti.* This represents the most difficult area of spontaneous combustion in so far as prediction is concerned. There are three principal reasons for this:

1. The theoretical treatment is much more difficult than that of criticality itself.
2. The actual definition has been greatly confused from case to case.
3. The *tti,* however defined, can be extremely sensitive to quantities that have hardly any effect on the position of the critical condition.

Theoretical Treatment

We refer the reader to Bowes[4] for discussion of earlier treatments. For illustrative purposes we will initially follow Bowes and define *tti* from Equation 5 by integration from ambient temperature to some value u_1, say,

$$\tau_i = \int_{u_a}^{u_1} [\nu_0 e^{-1/u} - \ell(u - u_a)]^{-1}\, du \qquad (24)$$

The equation is of course in dimensionless form. Our present interest is the implicit use of u_a as the lower limit; that is, it is the time for the sample to go from ambient temperature to some predetermined arbitrary figure, possibly the maximum temperature attained (it turns out that the integral is not sensitive to this limit, provided it is sufficiently high).

While the maximum temperature attained is a meaningful figure for laboratory tests under some circumstances, it does not always correspond to practical large-scale circumstances. For example, it requires recording the time taken for the center of the sample to heat up in a test oven to ambient temperature and using this as the reference time for *tti.* Unfortunately, when the center has reached this point, other parts of the body have often attained rather higher temperatures,[37] and the subsequent *tti* will be reduced compared to a large-scale body that may well have been built at ambient temperature and be quite uniform initially. Extrapolations of such laboratory tests will not then be reliable since the initial condition will not be appropriate.

The *tti* for the hot stacking problem is qualitatively different from that in which the body is formed uniformly at ambient temperature. Generally this time is *much shorter* than the *tti* for the more common case of initially ambient temperature throughout the body. The reasons have been given, with a comparison of the two cases, by Gray and Merkin.[38] Similar considerations apply when part of the body is at a high temperature (hot spot) and this case has been discussed in detail by Thomas.[39]

With the ready availability of powerful and fast numerical techniques, it is now feasible to integrate routinely the time-dependent heat conduction equation for this problem, which is probably the best solution. Zinn and Mader[40] were early participants in this effort, and more recently Gray, Little, and Wake[37] have noted that such numerical results can be usefully used to predict a very good lower bound to the *tti.* These results are desirable as they err on the side of safety.

Very close to criticality, perturbation treatments have been formulated,[41–45] but these are mainly of theoretical interest. At the critical condition the *tti* becomes infinite, and close to this condition it is extremely sensitive to the degree of criticality, so unless this is known accurately (hardly ever the case), use of such formulae is not advised.

In addition to the difficulties discussed above, which apply even when only a single simple reaction is assumed, there are others that are largely chemically kinetic. It has long been known that chain reactions, whether branching or not, can exhibit very long induction periods followed by very rapid onset of (sometimes non-explosive) reaction. Many exothermic, spontaneous ignition reactions do possess some chain characteristics even though these do not manifest themselves once the reaction is well underway. Thus it is feasible for complex chain mechanisms to determine the details of the *tti* but not be at all important in determining the critical condition where gross heat balance considerations are crucial. In many cases this leads to extremely irreproducible *tti*s without similar variation of CATs or other properties. In case this list of difficulties leads to an overly pessimistic view of the topic of *tti,* there are some things which can generally be relied on as far as the practical situation of fire investigation is concerned.

Very crudely speaking, notwithstanding the above discussion, the larger the body, the longer the *tti* will usually be. Thus a fire thought to have been caused by spontaneous ignition of a pile of linseed oil–contaminated rags contained in a wastepaper basket will usually appear within a few hours of the rags being placed there. On the other hand, a fire resulting from spontaneous ignition of thousands of metric tons of woodchips would only occur after some months of assembly, assuming the pile was

assembled at ambient temperature. For such bodies it is generally true that the *tti* increases with size in this manner. Accordingly haystacks tend to ignite (if they are supercritical) after a few weeks and coal stockpiles after a few months. However the *tti* can decrease dramatically if the body is very far beyond the CAT.

For hot stacked bodies on the other hand, times are generally much shorter and not particularly sensitive to the ambient temperature. Thus stacks of freshly manufactured chipboard with a volume of a few cubic meters can ignite much more quickly, that is, hours rather than days, than a similarly sized body self-heating from ambient. Beyond these general comments one has to treat each separate case on its merits with a careful eye for exceptions to any general rules. For example, the presence of any catalytic material, such as rusty metal (a common contaminant of many materials), can dramatically decrease the *tti.* This indicates the presence of free-radical or chain reactions and is fairly common, although the CATs and CSTs are only slightly affected.

In summary, in fire cause investigation, where spontaneous ignition is suspected, it is wise to be circumspect about time factors without a thorough investigation and detailed knowledge of the initial conditions likely to have existed when the body was put in place. Even the traditional linseed-oil rag example can be thrown out of the normal pattern by the presence of mineral turpentine, a very common diluent for oil-based stains. The evaporation of this from the rags can greatly prolong the *tti* by virtue of the consequent cooling effect and also the exclusion of air by the vapor. Depending on the circumstances, these factors could add two or three days to a *tti* that would normally be no more than a few hours.

Investigation of Cause of Possible Spontaneous Ignition Fires

From the investigative point of view it is well to list the practical factors which enhance the possibility of spontaneous ignition as a possible fire cause.

The size of the body of material: The larger the size of the body of material, the greater the likelihood of spontaneous ignition. By *size of the body* we mean the parts that are in thermal contact. A large pile of cotton bales with aisles through it would not necessarily be a large body in the thermal sense used here. This classification would be true even if (as often happens), once ignited, fire could spread easily from one section to the next.

High ambient temperatures: Since the air around the body in question has to act as a heat sink, the higher the ambient temperature, the more inefficient is the air as a coolant. Also, direct placement underneath a metal roof or adjacent to a northwest- (southern hemisphere) or southeast- (northern hemisphere) facing wall is a positive factor.

Thermal insulation: Sometimes spontaneously ignitable materials are stored in chemical warehouses or elsewhere packed against inert solids that prevent free airflow over the surface, thus reducing heat losses. This effect is evidenced by the appearance of maximum charring or self-heating that is off center and closer to the insulated side of the body. It also results in a reduced CAT.

Fibrous nature and porosity of material: Fibrous or porous materials allow greater access of air than otherwise (solid wood is not subject to spontaneous ignition at normal ambient temperatures, but woodchips and sawdust certainly are!). The concept that packing such porous materials by compression will increase the CAT by oxygen exclusion is badly flawed. This procedure increases the density (thus *lowering* the CAT) and has virtually no effect on the availability of oxygen. During the preflame development, the oxygen requirement is very low; by the time overt flame is observed, there are usually broad channels of destroyed material (chimneys) that will allow ready access.

Pure cotton in a test oven with a nitrogen atmosphere has been shown to undergo spontaneous ignition but with a longer induction period than in the presence of air.[46] This could be due to adsorbed oxygen on the cellulose fibers or due to exothermic decomposition of the cellulose in the absence of air.[47]

Otherwise "harmless" materials (i.e., liquids with very high flashpoints) can undergo spontaneous ignition at temperatures more than a hundred degrees below either their flashpoints or their so-called autoignition temperatures. The familiar drying oils (flashpoints around 230°C) spread on cotton afford such an example, igniting sometimes at room temperature under the appropriate conditions. In bulk such oils pose little threat of fire causation.

Similarly, hydraulic fluids, specifically designed for nonflammability and with extremely high flashpoints, can undergo spontaneous ignition if allowed to leak onto thermal lagging, such as mineral wool, fiberglass, and so forth, which are characterized by having particularly high surface area. Practical cases of this and experimental tests have been reported by Britton,[48] with particular reference to ethylene oxide fires. More recently a modeling project has been carried out[49,50] based on adaptation of the Semenov theory of ignition to a porous solid that was wetted with combustible liquid.

Temperature of stacking: The factor of temperature of stacking is simple—the hotter the worse! The main question is, How hot? The CST (critical stacking temperature) is only weakly dependent on the ambient temperature at low ambient temperatures, but it is sensitive to the size of the hot body. This situation arises with freshly manufactured products such as foodstuffs (milk powder, flour, instant noodles, fried batter, etc.), synthetic materials such as chipboard, cotton bales straight from the ginning process, bagasse straight from the sugar mill, fresh laundry (usually in commercial quantities), and so on.

To evaluate the CST requires full testing to obtain the parameters for the material (such as E, Q, κ, etc.) and then application of one of the methods in the literature for its calculation. Thomas[39] has given a method for hot spots of material, and Gray and Scott[51] have given a generaliza-

tion of this, removing the approximation to the Arrhenius function made by Thomas. A simpler method of calculation of the CST has been given by Gray and Wake.[52] It uses a spatially averaged temperature in the Arrhenius function and then obtains exact results for this simplified problem.

Length of time undisturbed: Material that has been in place for longer than usual is reason to suspect spontaneous ignition as a fire cause. Many industrial procedures involve the temporary storage of materials that are *normally* above their CAT but that are not left undisturbed for a period longer than or equal to their *tti.* Thus under normal circumstances fire does not occur even though the *tti* is regularly exceeded. If processes are slowed down for some reason, or storage is prolonged due to vacation, fire can occur even though no other parameters have been changed.

The Aftermath

There are very often characteristic signs of spontaneous ignition even after it has been the cause of a very large fire. Internal charring and ash is very characteristic in cellulose materials. Combustion starts in the well-insulated internal areas of the body, and warm or hot combustion products rise by convection through the path of least resistance (which is not always vertically upward) forming a "chimney" of discolored and partially combusted material. Since large bodies of material are rarely uniform in density or porosity, there can be more than one chimney formed and this is the norm. The occurrence of multiple chimneys and consequent discovery of more than one heavily charred or ashed area inside the body has led to erroneous charges of arson on the basis of the myth that more than one fire seat means the fire was deliberately lit. When a chimney reaches the edge of the body, smoke first becomes visible, then ingress of air causes flame. The latter may engulf more flammable materials in the building, and the whole structure can be destroyed while the spontaneously combusting material may well be chugging away slowly throughout most of its volume. This can even be the case after the fire has been extinguished. The result is then plenty of evidence as to the cause and origin of the fire. The author has measured temperatures as high as 200°C in buried, spontaneously ignited material more than two weeks after the extinction of the fire!

The internal burning of large piles or stacks of material can cause mechanical instability, and often the body collapses inward in the later stages of ignition. This inward collapse can cause some confusion in excavations, which should always be carried out if spontaneous ignition is suspected along with photographic and thermocouple temperature probe records at all stages.

It should be emphasized that the occurrence of significant amounts of unconsumed, spontaneously ignitable material does not mean that spontaneous ignition was not the cause of the fire. Frequently, oily rags are recovered almost intact from the bottom of waste bins that have been the seat of very large fires. The lower rags tend to be protected from incineration by a layer of char and also by lack of oxygen in the lower reaches of the bin.

Case Histories and Examples

Cottonseed Meal—Living Dangerously

A transit warehouse temporarily storing cottonseed meal to a depth of about 3 m burned down and was completely destroyed. The length and breadth of the building were much larger than the depth of the meal so the relevant physical dimension (for substitution into the formula for $\delta_{critical}$) was 3 m. Spontaneous ignition was suspected because of the known presence of unsaturated fatty acids prone to this. Standard CAT tests for small laboratory samples were carried out, and the extrapolation to lifesize was expected to be reasonably accurate since only small amounts of water were present and wet reaction was not suspected.

The body of meal in the warehouse turned out to be supercritical for the average ambient temperature in the area. The unusual factor in this particular case was the fact that the meal had been left undisturbed for much longer than usual due to a transport strike. It remained in place for longer than the *tti* although under normal circumstances it would have been moved on to customers well before significant self-heating could take place.

In this case an enlightened management installed underfloor ducting to produce a high-pressure air blast capable of rearranging the meal substantially from time to time. A similar solution has long been practiced for coal stockpiles, although in that case the disturbance is usually caused by a front-end loader.

Flaming Instant Noodles

Some years ago an instant noodle factory burned down soon after new management had taken over. New management was not satisfied with the throughput of the production line and wanted higher productivity. The latter was dependent on the speed of a single conveyer belt that conveyed the raw noodles through a hot oil bath, then under a number of powerful fans to remove excess oil and cool the cooked noodles for packing and palleting. Increasing the speed of the conveyer certainly increased the throughput in proportion, but the smaller length of time the noodles spent in the hot oil resulted in incomplete cooking. Thus the oil-bath temperature was increased substantially to compensate for this and again produce fully cooked noodles. However, the faster moving belt was now conveying cooked noodles to the packing area in a shorter time than before *and* they were also coming out of the fryer hotter than before. The result was that they were packed and palleted at a significantly higher temperature than under previous management.

Although the scientific and technological literature contained no reference to spontaneous ignition of noodles, their porous and oily nature indicated a possibility that this could occur. The suspicion was confirmed by

laboratory tests obtaining the CAT for a particular size noodle block. On this basis a full series of tests was carried out, and the parameters for the noodles obtained from the Frank-Kamenetskii plot in the usual way. With these parameters available it was possible to calculate the CST for a pallet full of noodle packages as these were shrink wrapped onto the pallets and completely encased in plastic, that is, the whole pallet full of noodles was in fact the body in question. The calculated CSTs (for a range of feasible ambient temperatures) turned out all to lie above the temperatures reached with the old process parameters but well below the temperatures reached with the new high-productivity parameters. The "bean counters" managed to achieve a productivity of zero until the factory was rebuilt.

Bagasse Storage—Some Complex Chemistry

The sugar industry in Australia wished to use bagasse containing the usual 50 percent moisture as a biomass for cogeneration of electricity as large excess tonnages are produced biannually. Removal of moisture increases the calorific (and hence monetary) value of the material as a fuel, provided it can be removed at no energy cost. At the same time it has been known for some time that large piles of bagasse are prone to spontaneous ignition and self-heating with consequent loss of value and also considerable pollution from the combustion products. An obviously desirable aim would be to create piles of bagasse that are not large enough to be supercritical but nevertheless large enough to self-heat significantly and hence drive off some of the moisture at no cost. Thus one would turn a dangerous energy release into a benefit. Clearly the balance would have to be just right. Consequently, a major research project was undertaken, both experimental and theoretical.

Application of the standard laboratory test methods to bagasse[52] results in a prediction of critical dimension for a pile at ambient temperature 30°C, which is an order of magnitude greater than the observed value. This is now known to be due to the fact that laboratory test CATs are above 100°C and simply drive off the moisture before the self-heating can get underway. The extrapolated results are therefore only good predictors for dry piles of material. In practice the water content of bagasse is close to 50 percent on a dry-weight basis, and this has recently been shown to be instrumental in partaking in a heat-producing reaction in addition to the one predominating in the dry material at higher temperatures.[19,20] This wet reaction has been characterized in isothermal calorimetric measurements over the temperature range 30°C to 90°C, and in this range the high-activation-energy dry reaction is almost completely shut down by the negative exponential in the Arrhenius function.

The wet reaction does not follow an Arrhenius temperature dependence at all, rather having a maximum rate at about 55–60°C. It also has a sharp, almost discontinuous dependence on water concentration, cutting out completely below 20 percent moisture. These characteristics are probably responsible for its occurrence being mistaken for microbiological activity. Inclusion of such complex chemistry in a generalization of the Frank-Kamenetskii theory for distributed temperatures, as well as the evaporation, condensation, and diffusive movement of water vapor through the pile, results in probably the most complex modeling yet of ignition phenomena.

Nevertheless this model describes quantitatively the behavior of real bagasse piles and answers the questions that led to its creation, that is, How does one choose a pile size in order to maximize the water removal without losing the pile to spontaneous ignition? The modeling is described in a number of publications (e.g., see Reference 11) and shows that present-day computing power coupled with appropriate knowledge of physical parameters enables quantitative or at worst semiquantitative modeling of spontaneous ignition situations with input of realistic chemistry and transport processes. Such developments have also taken place in the modeling of realistic chemistry in gas phase ignition of hydrocarbons and related organic materials dating back to the early work at the Shell Research Laboratories by Quinn et al.[53] and pursued by a number of workers, including Westbrook et al.[54]

It seems that we are not far from a situation where the simplified theories that have been useful tools for so long (with their empirical corrections) will be superseded by more detailed calculation of required properties such as CATs and CSTs. Nevertheless, the simplified theories will never lose their pedagogical value and will remain a firm conceptual foundation for more sophisticated models.

Milk Powder—A Numerical Example

The following example was given by Beever.[55] In a milk-drying plant air entering the spray dryer was heated to 200°C, and it was thought that surfaces in the region of the inlet may also reach this temperature. Any collection of powder on hot surfaces could cause spontaneous ignition, that would not only spoil the product but act as a source of ignition for a dust explosion. These have occurred in milk-drying plants with devastating consequences. Further down the dryer where there was deemed to be a greater likelihood of powder accumulation, surface temperatures of 80°C occurred. Three laboratory basket sizes were tested with half side-lengths of 0.025, 0.0375, and 0.050 m. The CATs of these were 171°C, 156°C, and 141.5°C, respectively. For a cube we can substitute the value 2.52 for δ_{critical} in Equation 20:

$$\ln\left(\frac{\delta_{\text{critical}} T_{a,\text{critical}}^2}{r^2}\right) = 41.85 - \frac{9497}{T_{a,\text{critical}}}$$

We can make r the argument of this equation and then substitute for $T_{a,\text{critical}}$ as required. If we require the critical temperature for a layer of material, we would use the value for δ_{critical} appropriate to an infinite slab, that is, 0.88. For such a flat layer with ambient temperature on each side of 200°C, a critical thickness of 0.017 m is obtained. For the cooler regions of the dryer at 80°C, a critical thickness of 0.4 m is obtained. It was decided that these critical thicknesses were sufficiently realistic to require regular cleaning inside the dryer to remove buildup. This problem is actually more complicated than indicated here since the critical parameters are rather sen-

sitive to moisture content, the critical thickness increasing significantly with moisture content, which can be up to 4 percent.[56]

Nomenclature

C_v	heat capacity at constant volume per unit mass (J/K·mol)
c	concentration (mol/m^3)
c_f	feed concentration in CSTR (mol/m^3)
CAT	critical ambient temperature (K)
CST	critical stacking temperature (K)
E	activation energy (J/mol)
F	feed rate in CSTR (m^3/s)
$f(c)$	chemical reaction rate (mol/m^3·s)
Q	heat of reaction (J/mol)
R	universal gas constant (J/mol·K)
r	characteristic radius
S	surface area (m^2)
T	temperature (K)
T_a	ambient temperature (K)
$T_{a,\text{critical}}$	critical ambient temperature (CAT) (K)
T_f	feed temperature in CSTR (K)
tti	time to ignition(s)
u	dimensionless temperature (RT/E)
u_a	dimensionless ambient temperature
V	volume of self-heating body (m^3)
ν	dimensionless concentration (c/c_0)
δ	Frank-Kamenetskii parameter
θ	Frank-Kamenetskii dimensionless temperature
ρ	bulk density (mol/m^3)
κ	thermal conductivity (W/m·K)
χ	heat-transfer coefficient (W/m^2·K)
ε	inverse dimensionless heat of reaction
τ	dimensionless time
ℓ	dimensionless heat transfer coefficient
Bi	Biot number ($\chi r/\kappa$)
$\partial(\,)/\partial n$	differential coefficient in a direction normal to the boundary of the body

References Cited

1. *Safety and Runaway Reactions,* Institute for Systems Informatics and Safety, Joint Research Centre European Commission, EUR 17723 EN (1998).
2. N.N. Semenov, *Z. Phys. Chem.,* 48, p. 571 (1928).
3. D.A. Frank-Kamenetskii, *Diffusion and Heat Transfer* in *Chemical Kinetics,* Plenum, New York (1969).
4. P.C. Bowes, *Self-Heating: Evaluating and Controlling the Hazards,* HMSO, London (1984).
5. J.F. Griffiths and B.F. Gray, *Twenty-Fourth Loss Prevention Symposium,* American Institute of Chemical Engineers, San Diego (1990).
6. J. Taffanel and M. Le Floch, *Compt. Rendus,* 156, p. 1544; 157, p. 469 (1913).
7. G.C. Wake, J.B. Burnell, J.G. Graham-Eagle, and B.F. Gray, 25–37, *Reaction Diffusion Equations,* (K.J. Brown and A.A. Lacey, eds.) Oxford, UK (1990).
8. J.F. Griffiths and J.A. Barnard, *Flame and Combustion,* Blackie, Glasgow, Scotland (1995).
9. B.F. Gray, *Combustion and Flame,* 24, p. 43 (1975).
10. B.F. Gray, *Transactions Faraday Society,* 65, p. 1603 (1969).
11. C. Macaskill, M.J. Sexton, and B.F. Gray, *J. Aust. Math. Soc.,* Series B (2001).
12. T. Dixon, *Proc. Aust. Sugar Cane Tech.,* 53 (1988).
13. B.F. Gray, unpublished.
14. R. Aris, *The Mathematical Theory of Diffusion and Reaction in Permeable Catalysts,* Oxford (1975).
15. P.L. Chambre, *J. Chem. Phys.,* 20, p. 1795 (1952).
16. T. Boddington, P. Gray, and I Harvey, *Phil. Trans. Roy. Soc.,* A270, p. 467 (1971).
17. B.F. Gray and B. Halliburton, *Fire Safety Journal* 35, pp. 223–241 (2000).
18. Y. Uehara, H. Uematsu, and Y. Saito, *Combustion and Flame,* 32, p. 85 (1978).
19. I.K. Walker, W.J. Harrison, and F.H. Jackson, *NZ J. Science,* 21, p. 487 (1978).
20. R.A. Sisson, A. Swift, G.C. Wake, and B.F. Gray, *IMA J. Applied Math.,* 50, p. 285 (1993).
21. R.A. Sisson, A. Swift, G.C. Wake, and B.F. Gray, *IMA J. Applied Math.,* 49, p. 273 (1992).
22. B.F. Gray and G.C. Wake, *Combustion and Flame,* 79, p. 2 (1990).
23. B. Halliburton, Ph.D. Dissertation, Macquarie University, Sydney, Australia (in press).
24. T. Dixon and N. Ashbolt, Sugar Research Institute, Mackay, Queensland, Australia, (1985).
25. B.F. Gray and B. Halliburton, *J. Chem. Tech. Biotech.* (in press) (2000).
26. J.C. Jones, *J. Loss Prevention in the Process Industries,* 12, p. 331 (1999).
27. X.D. Chen and L.V. Chong, *Trans. I. Chem. E.,* 76B, p. 90 (1998).
28. Mackey, W., *J. Soc. Chem. Ind.,* 15, p. 90 (1896).
29. N. Kirov, *CSIRO Technical Note,* Chatswood, Australia (1954).
30. P.H. Thomas, *Transactions Faraday Society,* 54, p. 60 (1958).
31. P.H. Thomas, *Transactions Faraday Society,* 56, p. 833 (1960).
32. B.F. Gray and G.C. Wake, *Combustion and Flame,* 55, p. 23, (1984).
33. B.F. Gray, A. Gomez, and G.C. Wake, *Combustion and Flame,* 61, p. 177 (1985).
34. "Transport of Dangerous Goods," *Manual of Tests and Criteria,* 2nd ed., United Nations, New York (1995).
35. B.F. Gray, *J. Aust. Math. Soc.,* Series B (in press) (2001).
36. B.F. Gray and B. Halliburton, *Fire Safety Science* (in preparation).
37. B.F. Gray, S.G. Little, and G.C. Wake, *24th International Combustion Symposium,* Combustion Institute, Pittsburgh, PA (1992).
38. B.F. Gray and J.H. Merkin, *Math. Engng. Ind.,* 4, p. 13 (1993).
39. P.H. Thomas, *Combustion and Flame,* 21, p. 99 (1973).
40. J. Zinn and L. Mader, *US J. App. Physics,* 31, p. 323 (1960).
41. T. Boddington, C. Feng, and P. Gray, *J. Chem. Soc. Faraday Trans. 2,* 79, p. 1299 (1983).
42. T. Boddington, C. Feng, and P. Gray, *J. Chem. Soc. Faraday Trans. 2,* 80, p. 1155 (1984).
43. T. Boddington, C. Feng, and P. Gray, *Proc. Roy. Soc.,* A385, p. 289 (1983).

44. T. Boddington, C. Feng, and P. Gray, *Proc. Roy. Soc.,* A391, p. 269 (1984).
45. B.F. Gray and J.H. Merkin, *J. Chem. Soc. Faraday Trans. 2,* 86, p. 597 (1990).
46. S.G. Little, "Spontaneous Ignition Studies," Masters Thesis, Macquarie University, Sydney, Australia (1991).
47. Y.I. Rubtsov, A.I. Kazakov, L.P. Andrienko, and S.B. Manelis, *Comb. Exp. and Shock,* 29, p. 710 (1993).
48. L.G. Britton, *Twenty-Fourth Loss Prevention Symposium,* American Institute of Chemical Engineers, San Diego (1990).
49. A.C. McIntosh and B.F. Gray, *Comb. Sci. and Technology,* 113, p. 503 (1996).
50. A.C. McIntosh, B.F. Gray, and G.C. Wake, *Proc. Roy. Soc.,* A453, p. 281 (1997).
51. B.F. Gray and S.K. Scott, *Comb. and Flame,* 61, p. 227 (1985).
52. B.F. Gray, J.F. Griffiths, and S.M. Hasko, *J. Chem. Tech. and Biotech.,* 34A, p. 453 (1984).
53. M.P. Halstead, A. Prothero, and C.P Quinn, *Comb. and Flame,* 20, p. 211 (1973).
54. C.K. Westbrook, J. Warnatz, and W.J. Pitz, *22nd Symposium (International) on Combustion,* Combustion Institute, Pittsburgh, PA (1988).
55. P.F. Beever, "Self Heating and Spontaneous Combustion," in *SFPE Handbook of Fire Protection Engineering,* 2nd ed. (P.J. diNenno et al., eds.), pp. 2-180–2-189 (1988).
56. C.M. Rivers, "Numerical Studies in Spontaneous Ignition," Master's Thesis, Massey University, Palmerston North, New Zealand (1994).

CHAPTER 11

Flaming Ignition of Solid Fuels

A. Murty Kanury

Introduction

This chapter concerns flaming ignition of solid combustibles that are heated by either thermal radiation or convection. Different kinds of ignitions encountered in practice are defined. The existing empirical knowledge is highlighted by describing Martin's map of spontaneous ignition of radiantly heated cellulosic solids. The various physical and chemical processes that culminate in ignition of a heated solid are identified through a qualitative description and a simplified mathematical model. The typical assumptions underlying a theoretical model are systematically enumerated to point out the complexities involved in the ignition problem.

A number of existing criteria for ignition are examined. Limiting case models are demonstrated to increase understanding of the ignition process. Analysis of the solid-conduction-controlled case, for example, leads to a prediction of the main features of Martin's map. A thumbnail sketch of the gas phase problem, in another limit, confirms the observed influences of the gas phase properties on ignition. Finally, a brief summary is given of the comprehensive analysis of Gandhi. Many existing fragments of knowledge on the ignition problem can now be synthesized into a coherent quantitative description.

The Process of Ignition

A number of aspects of unwanted combustion, in which an understanding of the ignition process is required, can be readily enumerated.

1. An obvious first step in all fire prevention strategies is the ignition-hardening of materials of construction, finishings, and furnishings.
2. Fire spread over combustibles is often viewed as a process of continuous ignition of the successively upstream material.
3. Room fire flashover is believed by many to be a process in which the contents of the room experience a nearly simultaneous ignition.
4. The jump of a forest fire across a firebreak is generally viewed to be a radiant ignition process.
5. Fire growth over noncontiguous surfaces in arrays of combustibles, such as buildings in a city, involves radiant heating to ignition.

Most of the natural and synthetic organic (and some inorganic) solids in air will become ignited in response to an externally imposed heating source. The subtleties of the ignition process—the definition and delineation of different sorts of ignitions, and the qualitative and quantitative understanding of the influence of various physical and chemical factors on ignition—are not always familiar. Kanury[1] and Steward[2] have presented comprehensive reviews of this subject. The global objective of this chapter is to develop a concise description of the ignition process to achieve enough familiarity with the concepts involved, existing literature and implications of this knowledge in such real-world problems as enumerated above.

Ignition of a heated combustible body marks a stage beyond which the associated fuel/oxidant system is capable of supporting a sustained exothermic reaction. It is necessary to clarify this definition to develop a qualitative picture of the technical problem addressed here and to define the scope of this chapter.

The heated body (i.e., the target) is taken here to be a piece of a cellulosic solid (e.g., wood, paper, cloth, etc.). The concepts are generally adaptable[3] to synthetic solids (e.g., the numerous modern polymers popularly known as *plastics*) as well. The physical and chemical characteristics of the body are assumed to be known. Thermophysical (conductivity, density, specific heat, etc.) and geometrical (dimensions, shape, and configuration) properties are

Dr. A. Murty Kanury is professor of mechanical engineering at Oregon State University. His professional activities are centered around teaching thermal science and research in fire and combustion.

physical. The intrinsic thermochemical properties (e.g., pyrolysis kinetics and energetics) are chemical.

Heating is presumed to be externally imposed. It can be radiative (as from a heat lamp, a bank of electrically heated incandescent tungsten filaments, a gas-fired radiant panel, or a nearby flame) and/or convective (as from a hot gas flowing about the body). These two modes of heating will be considered individually to note certain commonalities and differences, although many practical situations involve simultaneous convective and radiative heating.

When a porous reactive solid body is kept immersed in an ambient medium, a runaway self-heating may become possible if the rate of internal reactive energy release exceeds the rate of energy loss from the body to the ambient medium. This sort of self-heating is known to arise in connection with contaminated sawdust, oily shop rags, grain silos, and certain unstable solid propellant storages. The energy loss mechanism is generally conductive and convective. While an enhanced convective transport tends to increase the energy loss rate, it also increases the oxygen mass transfer to the surface and the net effect is quite complex. This type of self-heating problem is addressed in Section 2, Chapter 10.

Smoldering, a familiar fire phenomenon, is defined as a relatively low temperature combustion process within a porous fuel bed. Its inception usually involves a localized ignition source (such as an overheated electrical conductor or a steam pipe) within the fuel bed. The fuel bed porosity plays an important role in smoldering. A highly porous solid (1) implies finely divided, thermally thin fuel elements that are more easily heated conductively, and (2) offers an effective diffusion of the oxidant gas into the interior of the bed. Furthermore, high porosity makes the overall thermal conductivity of a solid quite low and, hence, ignition is easier. Once smoldering ignition begins, the smolder combustion wave propagates into the fresh fuel at a rate governed by thermal conduction in the porous solid and oxidant gas diffusion. It is possible for convection to intrude into this propagation process. The intensity with which this occurs is dependent upon such factors as the porosity itself; if the bounding surfaces are sealed or unsealed; and the direction of propagation relative to the sealed surfaces and to the gravity vector. Under certain suitable conditions, a smolder may suddenly flare into flame. The ignition and propagation of the smoldering combustion and its transition to flaming are addressed in Section 2, Chapter 9.

The combustible may be supplied to the reaction system in a gaseous, liquid, or solid state. It is solids we are concerned with here. All cellulosic and some synthetic solids undergo thermal degradation to yield char and fuel gases. Some other synthetic solids, known as thermoplastics, melt, depolymerize and decompose to yield fuel vapors. Some depolymerization reactions proceed in a manner remarkably similar to the simple physical vaporization of pure liquids.

Because the focus here is on gas phase ignition of charring type solids, there arises a possibility of surface ignition of the char. This type of an ignition marks the inception of glowing combustion of the carbonaceous solid (such as that encountered in carbon and charcoal combustion). The glowing ignition problem is not covered in this chapter.

As an event, ignition occurs at a certain pronounced instant in the history of the exposure. The time to ignition in a given situation depends upon three broadly grouped factors: (1) the degradative thermal response of the solid to yield the combustible gases, (2) the mixing of these gases with the oxidant gas (generally the oxygen of the normal air), and (3) the induction of the temperature- and composition-dependent rate of the combustion reaction to a sufficiently high level to be measurable and self-supporting. Sustainment of the reaction implies that the reaction can self-perpetuate even if the external heating is removed, and can even self-accelerate to grow in space or in intensity at a fixed size. An *exothermic reaction* refers to the combustive oxidation reaction itself. This reaction is called smoldering if it is situated within the subsurface layers of the solid, glowing if at the solid-gas interface, and flaming if in the gas phase.

Ignition in the absence of a pilot source is known as spontaneous, or autoignition. Ignition in the presence of a pilot source (such as a small flame, a heated wire, or an electric spark) in the reactive fuel/air mixture flow is called piloted, or forced ignition. A pilot source is not meant to heat the solid to generate the fuel gases nor to enhance the mixing of the fuel gases with air, but to locally induce the combustion reaction which would propagate into the mixture.

Finally, a distinction should be made between transient and persistent ignitions. Ignition can be produced with a minimum required heating, but the flame would not sustain itself if the external heating is removed. This is transient ignition, akin to the flash point phenomenon in liquid fuel ignition. Substantially longer heating is required to make a flame that would self-sustain, self-perpetuate, or persist even after the external heating is removed. This distinction becomes clearer in the next section of this chapter.

Conduction-Controlled Spontaneous Ignition of Cellulose Due to Radiant Heating—Martin's Map

The large number of experiments on spontaneous ignition of radiantly heated cellulosic solids (insulated back face) has been synthesized by Martin.[4] (See Figure 2-11.1.) The x-axis is the quantity $i_0\ell/K_s$ where i_0 is the exposure irradiance, ℓ is the target thickness and K_s is the target solid conductivity. Martin calls this quantity normalized irradiance, and its units are those of temperature (K). The y-axis, termed normalized exposure, is $i_0 t/\rho_s C_s \ell$ (where t is exposure time and $\rho_s C_s$ is the volumetric heat capacity of the solid); its units are K.

This ignition map shown in Figure 2-11.1 can be delineated into four distinct regions. The lowermost boundary indicates the minimum exposure intensity and time required to produce ignition. When intensity is low and exposure is long, glowing ignition of a thermally thin body is accomplished. In the upper left region of the map, the thickness of the target specimen is noted to be of

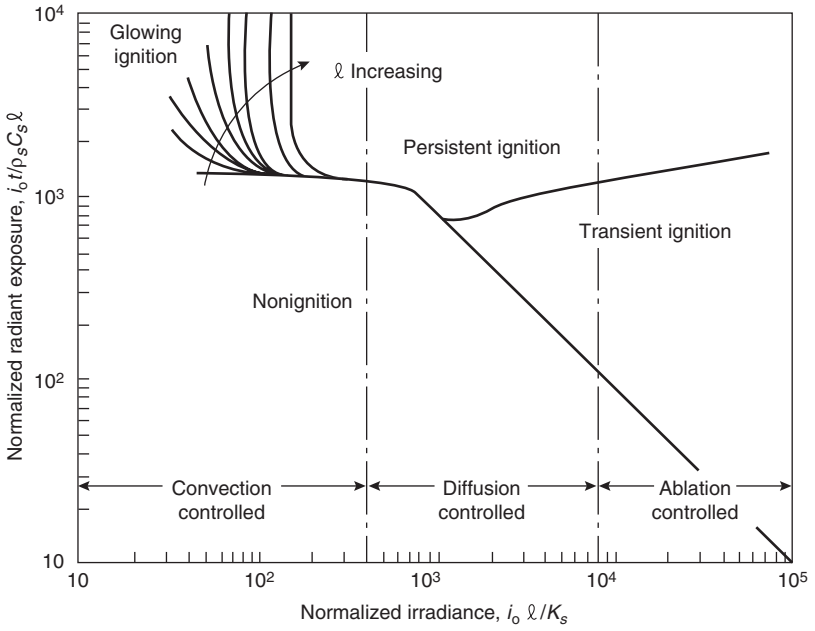

Figure 2-11.1. ***Ignition behavior of cellulose, showing areas controlled by convective cooling, diffusion of heat into the solid, and ablation of the exposed surface. Martin's map.[4]***

consequence—the thinner the specimen, the quicker the ignition. Furthermore, these thin bodies ignite not to yield a flame but to yield glowing combustion of the solid residue. The pyrolyzates not only are limited in quantity but are also released at a rate and time unsuitable for flame evolution.

The middle right region of the map deals with heating of thick targets with moderately high exposure intensities. Flaming ignition will occur within a moderate exposure time but will not persist to yield a self-supporting flame, presumably due to excessive conductive drain of energy into the thick solid and inadequate production of the pyrolyzates. At even higher exposure intensities, the surface is found to experience ablation without ignition.

For the ignition of thick bodies to persist into a flame, significantly longer exposures are required which are nearly independent of the exposure intensity. Martin considered many tests, which led him to draw the boundary line between the transient and persistent ignition regions. The persistence of flames is expected to depend on a purely physical cause such as the sustained evolution of pyrolyzates due to attainment of a certain minimum relaxed temperature by the entire body. Further discussion of Martin's work is presented later in this chapter.

A Qualitative Description

The initial uniform temperature of a vertical cellulosic slab (of known dimensions standing in a quiescent atmosphere of normal air) is perhaps the same as the temperature of the ambient air. (See Figure 2-11.2.) Orientation, geometry, the kind of solid, and the composition and motion of the atmosphere are chosen to consolidate a picture of the physical and chemical processes leading to ignition. The concept elicited in this qualitative description can be adapted, in principle, to other situations.

The front face of the solid is exposed to a radiant flux from time $t = 0$. In reality, this flux is generally unsteady in the period of exposure, nonuniform over the target surface, and composed of a spectrum of wavelengths. However, it is assumed that the incident flux is steady and uniform, and that the target surface is a diffuse, gray absorber/emitter. Furthermore, the incident flux is radiative

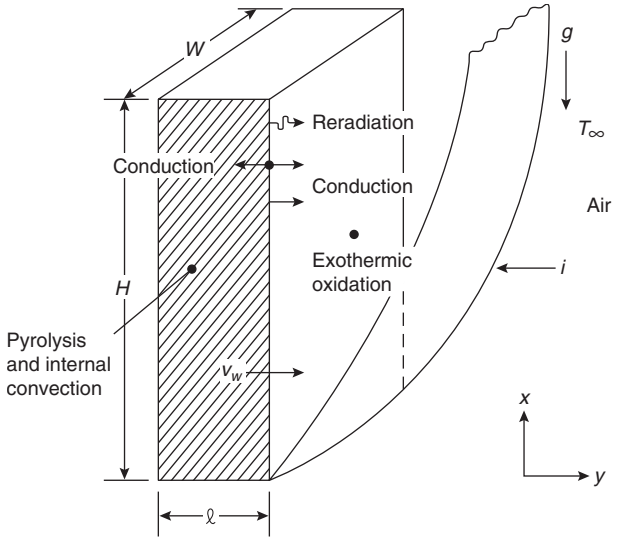

Figure 2-11.2. ***Schematic representation of the component processes.***

alone; the back face of the solid and its edges are taken to be impervious to both heat and mass flows.

Once the exposure is triggered, the interior of the solid is heated by transient conduction. The now hotter surface commences to reradiate energy to the surroundings. Energy is also imparted by the hot surface by transient conduction to the infinite, initially quiescent, adjacent, ambient gas. This heated gas soon responds to buoyancy and forms a transient natural convective boundary layer.

The incident radiant energy is thus partitioned into three components: conduction into the interior of the solid, reradiation to the surroundings, and natural convection to the adjacent gas. All these three components are transient. The energy conducted into the solid initially raises the solid temperature within a progressively thickening "conductive penetration layer." Any free moisture in the solid will be driven away from a layer when it attains a temperature of approximately 100°C. While most of the water vapor released in this manner flows out of the solid, some vapor may migrate towards the cooler interior to augment the heat flux by both convection and condensation. Subsequent evaporation will not only introduce a distinct heat sink but also physically and chemically modify the original solid, which is yet to experience pyrolysis.

There would soon ensue an instant at which layers of the solid near its surface would become sufficiently hot to undergo pyrolysis, leaving a carbonaceous residue (char) behind. With continued heating, progressively deeper layers of the solid become pyrolyzed so that the release of the gas mixture is distributed in space and time. The gas mixture, thus originating at different rates at different depths and time, flows predominantly out through the porous char. This flow introduces an outwardly convective heat flux in the char. The outward flux opposes the inward conductive flux and tends to retard the heating.

Integration of the pyrolysis rate over the thickness of the entire solid yields the total pyrolyzate mass flux issuing at the solid surface into the gas phase. This transpiration tends to thicken the instantaneous boundary layer. The boundary layer flow is generally expected to be laminar since the target size is usually small. This flow will cause mixing of the pyrolyzates with the ambient air.

If the pyrolyzates are either absent or inert, the boundary layer continues to receive heat from the bounding hot solid surface by conduction. The gas temperature profile will then be a monotonically decreasing function of the distance normal to the surface into the gas. If the pyrolyzates are combustible, however, oxidative energy release alters the boundary layer temperature profile to such an extent as to exhibit a temperature maximum in the gas phase at some finite distance from the surface. This nonmonotonic gas temperature profile, at later times, indicates a gas phase conductive heat flux to, rather than from, the solid surface. As the oxidation reaction develops in the boundary layer, the nature of the temperature profile is drastically changed. Spontaneous ignition can be presumed to have occurred in the reactive boundary layer at the instant when the sign of the gas temperature gradient at the surface is reversed. This time to ignition obviously depends upon factors governing the surface temperature, pyrolyzate transpiration rate and composition, air induction rate into the boundary layer, mixing of air and pyrolysis gases and gas-phase reactions.

This qualitative description applies to spontaneous ignition in the boundary layer, which is defined as a situation where the boundary layer mixture is not only within the flammability limits of composition but also at such a thermal condition that it can react on its own in an accelerating manner and lead to a flame. This description can also be extended to piloted ignition, that is, ignition in the presence of an ignition source such as a small flame, an electrical filament or spark, or an incandescent particle. A boundary layer mixture within the flammability limits of composition is a sufficient condition for piloted ignition. The required energetic strength of the ignition source is a function of several thermochemical and physical properties of the mixture in addition to its composition and temperature. Generally, the pilot source is so small that its contribution to heating and pyrolyzing the solid can be ignored. Changes brought by the pilot source in the boundary layer of the chemical environment can also be ignored. It is customary to consider the ignition source as a localized initiator of the combustion reaction whereupon the reaction wave propagates into the mixture. The ignition theory of premixed gases, however, dictates that the pilot source cannot be infinitely small. The source must exceed the approximate characteristic quenching distance of the ignited mixture.

Mixing of the transpired pyrolyzates with the induced air is a necessary condition for ignition. Turbulence in the boundary layer is obviously desirable to produce this mixing. Spontaneous ignition sometimes occurs in the wake of the target with the (so initiated) flame propagating down into the boundary layer. While mixing the fuel gases and air is a prerequisite for ignition, mixing may also result in thermal dilution (i.e., lowering of the mean boundary layer temperature) which is contrary to the requirements of spontaneous ignition.

The possibility also exists that the pyrolyzate plus air mixture in the boundary layer can selectively attenuate the incoming radiant beam so that the irradiance actually experienced by the exposed surface is substantially less than the level calibrated without the absorbing gas. This phenomenon has implications yet to be understood. First, attenuation is expected to retard the rate of heating and pyrolysis of the solid, and consequently to delay the attainment of an ignitable boundary layer mixture. Second, the attenuation in the boundary layer is expected to become significant only after vigorous pyrolysis of the solid is established to furnish the boundary layer with the attenuating species. Third, the attenuation and absorption is expected to raise the local temperature in the reactive boundary layer to accelerate the oxidation reaction leading to ignition. Finally, this attenuation is expected to occur selectively in certain distinct wavelength regions and hence to depend on the emission characteristics of the radiation source.

It is evident from the present qualitative description of flaming ignition that the total problem is complex and involves difficult features such as: (1) unsteady development of physical and chemical processes, (2) conjugate coupling of the solid and gas phases, (3) chemical kinetics and the associated strong nonlinearities of pyrolysis in the

solid phase and oxidation in the gas phase, (4) moving boundaries, (5) coupling of conservation equations, (6) strongly variable properties. When the lack of well-established input databases for the transport, thermodynamic (and thermochemical), and reaction kinetic properties is superimposed on this complexity, it is imminently clear that all attempts to solve the problem theoretically and apply the predictions to experimental data are prone to extensive approximation. Some of these attempts will be described in a subsequent section of this chapter.

Conservation Equations

In this section, the preceding qualitative description is cast into a mathematical form to identify the assumptions involved. For example, consider a vertical slab of a solid fuel of thickness, ℓ, height, H, and width, W, standing in a quiescent air atmosphere. The solid will occupy $0 \le y \le \ell$ and the gas phase, $\ell \le y < \infty$. (See Figure 2-11.2.) For time $t \ge 0$, the front face $y = \ell$ of the solid is exposed to an irradiance, i. While a part, i_0, of this flux is absorbed by the solid, the rest of the irradiance is reflected. The absorbed flux is partially conducted into the solid, partially reradiated by the surface to the surroundings, and the rest of the flux is imparted by gaseous conduction to the gaseous boundary layer. These three processes are highly transient. The heated solid undergoes transient pyrolysis, and the pyrolyzates flow out of the solid to mix with air in the boundary layer. At the instant when the mixture composition and temperature are suitable, flaming ignition will occur in the boundary layer. This section of the chapter will describe the estimation of this time to ignition.

A number of simplifying assumptions make the problem formulation easier. The initial temperature of the solid is usually uniform and equal to the temperature of the ambient air. The back face, $y = 0$, as well as all edges of the solid slab, are assumed to be impervious to both heat and mass. The solid surface is taken to be grey and diffuse with uniform radiosity. The imposed irradiance is considered to be constant with respect to time, and uniform over the entire exposed surface. The transient gas boundary layer problem is simpler to deal with in two dimensions, that is, $W \gg \ell$ and H. The transient solid conduction problem is taken to be one-dimensional in the direction of y. The solid is taken here to be initially dry. Absorption of radiation is taken to occur only at the solid surface and not in the layers beneath the surface; that is, diathermancy of the solid is taken to be zero. The char and virgin solid properties are considered to be different but independent of temperature.

A single-step Arrhenius rate law with reaction order equal to unity is generally sufficient to describe the pyrolysis kinetics. The pyrolyzates are viewed to flow through the char with no resistance. Thermal equilibrium between the pyrolyzates and the porous matrix is assumed. Secondary chemical transformation of the pyrolyzates flowing through the char is negligible, as is migration of the pyrolyzates into the cooler interior of the solid.

The air, pyrolyzates, and products of oxidation are taken to behave as radiatively nonparticipating ideal gases. The gas phase density is considered to be constant in all respects except in producing the buoyancy force (in other words, the Boussinesq approximation is made). Boundary layer approximations are made for the transient free convective gas flow in the vicinity of the heated surface. All gas properties are taken in this discussion to be constants, independent of both the temperature and composition. (This appears to be an overly crude approximation but leads to reasonable results.) Viscous dissipation in the boundary layer is ignored. Cross-diffusion effects in the gas phase are assumed to be absent.

The gas phase oxidation reaction is assumed to follow a simple, single step, second order, Arrhenius rate law. (Since the pyrolyzate composition is known to vary not only with time but also with the heating conditions and precise chemical constituency of the target solid, any further sophistication of these kinetics appears to be unwarranted at present.) Simple stoichiometry relates the sources and sinks of energy, fuel pyrolyzate, oxygen, and the products.

The conservation equations describing this problem follow. For the solid phase, the continuity and energy equations suffice, while the momentum equation is obviated by the assumption of no resistance to flow. Thus,

$$\frac{\partial \rho_s}{\partial t} + \frac{\partial \dot{m}''_p}{\partial y} = 0 \tag{1}$$

$$\frac{\partial}{\partial t}(\rho_s C_s T_s) + \frac{\partial}{\partial y}(\dot{m}''_p C_p T_s) = \frac{\partial}{\partial y}\left(K_s \frac{\partial T_s}{\partial y}\right) + \dot{q}'''_p \tag{2}$$

where

s = solid
p = pyrolyzate gas mixture
ρ = density
$\dot{m}''$ = mass flux
C = specific heat
T = temperature
K = thermal conductivity
t = time
y = depth normal to the exposed surface

Equation 1 says that the local spatial gradient of the pyrolyzate mass flux $\dot{m}''_p$ is equal in magnitude to the local and instantaneous rate of pyrolysis. The terms in the energy equation represent the unsteady energy accumulation rate, internal convective excess flux, conductive excess flux, and the pyrolysis sink, respectively. The constitutive equations for this part of the problem are given by the pyrolysis rate equation and the definition of the energy sink.

$$-\frac{\partial \rho_s}{\partial t} = Z_s(\rho_s - \rho_c)\exp\left(\frac{-E_s}{\overline{R}T_s}\right) \tag{3}$$

$$\dot{q}'''_p = h_p\left(-\frac{\partial \rho_s}{\partial t}\right) \tag{4}$$

Here ρ_s is the instantaneous, local solid density while ρ_c is the ultimate char density, Z_s is the pre-exponential factor, E_s is the activation energy of the pyrolysis reaction, and h_p is the pyrolysis enthalpy of reaction. The boundary and initial conditions will be discussed later in the chapter.

Let v and u denote the gas velocity components in the normal (y) and longitudinal (x) directions, respectively. With the enumerated assumptions the gas phase mass, momentum, energy, and species conservation equations then take the following forms:

$$\frac{\partial u}{\partial x} + \frac{\partial v}{\partial y} = 0 \tag{5}$$

$$\frac{\partial u}{\partial t} + u\frac{\partial u}{\partial x} + v\frac{\partial u}{\partial y} = \nu_g \frac{\partial^2 u}{\partial y^2} + \frac{(\rho_\infty - \rho_g)}{\rho_g} g \tag{6}$$

$$\frac{\partial P}{\partial y} = 0 \tag{6a}$$

$$\frac{\partial T_g}{\partial t} + u\frac{\partial T_g}{\partial x} + v\frac{\partial T_g}{\partial y} = \alpha_g \frac{\partial^2 T_g}{\partial y^2} + \frac{\dot{q}_g'''}{\rho_g C_g} \tag{7}$$

$$\frac{\partial Y_i}{\partial t} + u\frac{\partial Y_i}{\partial x} + v\frac{\partial Y_i}{\partial y} = D_{ig}\frac{\partial^2 Y_i}{\partial y^2} + \frac{\dot{m}_i'''}{\rho_g} \tag{8}$$

Here, subscript g is the gas mixture, ∞ the ambient conditions, and ν, α, D_{ig} are momentum, heat and species-i-mass diffusivities, respectively; P is pressure, Y_i is the ith species mass fraction with $i = F$ for the fuel pyrolyzate gas (O for oxygen, P for product and I for the inert). The respective volumetric source-sink strength due to the oxidation reaction is $\dot{m}_i'''$. The corresponding energy source strength is $\dot{q}_g'''$. While the energy and species equations indicate a balance between the unsteady accumulation, convection, diffusion and reaction rates, Equation 6 shows that momentum is conserved under the balance of accelerative, inertial, viscous, and buoyant forces. The constitutive relations to complement Equations 5 through 8 are

$$\sum Y_i = 1 \tag{9}$$

$$P = \rho_g(\overline{R}/M_g)T_g \tag{10}$$

$$\dot{m}_F''' = -Z_{gF}\rho_g^2 Y_F Y_O \exp(-E_g/\overline{R}T_g) \tag{11}$$

$$-\dot{m}_F'''/f = -\dot{m}_O'''/1 = +\dot{m}_P'''/(1+f) = +\dot{q}_g'''/fh_c \tag{12}$$

$$\dot{m}_I''' = 0 \tag{12a}$$

where

Z_{gF} = pre-exponential factor
E_g = activation energy
f = fuel pyrolyzate to oxygen stoichiometric mass ratio
h_c = enthalpy of oxidation

Besides the fact that all the edges of the solid are sealed for both mass and heat, the initial and boundary conditions are quite straightforward. In the solid $0 \le y \le \ell$, $0 \le x \le H$; for $t < 0$, $T_s = T_{s0}$ ($= T_\infty$) and $\rho_s = \rho_{s0}$, both uniform in space. At the back face of the solid $y = 0$, at all times $t \ge 0$, $\partial T_s/\partial y = 0$ as well as $\dot{m}_p'' = 0$. In the gas, at $t < 0$, $\ell \le y < \infty$, all x, and at $t \ge 0$, as $y \to \infty$, for all x, $u = v = 0$, $T_g = T_\infty$, $Y_F = Y_P = 0$ and $Y_O = Y_{O\infty}$.

The boundary conditions at the gas-solid interface ($y = \ell$, subscript w) play an important role in the physics of the problem. To avoid slip for the momentum equation, $u = 0$. The time-dependent normal transpiration velocity $v = v_w(t)$ is given by the transpiration mass flux of pyrolyzates $\dot{m}_{pw}''(t)$ [given by integration of the pyrolysis rate over the entire solid (Equation 1)] divided by the local gas density. The species balance at the interface indicates that the flux of species i arriving from within the solid is carried away into the gas phase by combined convection and diffusion. This balance, known as the Dankwert boundary condition, is given by

$$\dot{m}_{pw}'' Y_{iR} = \rho_g \nu_w Y_{iw} + (-\rho_g D_{ig}\partial Y_i/\partial y)_w \tag{13}$$

where Y_{iR} is the mass fraction of species i in the pyrolyzate mixture prior to any dilution with air. The energy interface condition states that the absorbed irradiance, i_0, is conducted into the solid and the gas or reradiated.

The problem is now fully formulated. Relaxation of any of the simplifying assumptions can be done by appropriately reworking the model equations. The intention here is to present the skeletal model which can reasonably easily be adapted to suit special needs. The solution is straightforward in principle, although implementation is not. The transience, conjugate nature, the radiation nonlinearity, and the presence of the Arrhenius exponential prevent these coupled equations from possessing similarity solutions. It is possible to obtain some approximate solutions which are useful in understanding the ignition process.

Ignition Criteria

Based upon experimental observations and intuition, attempts to identify the instant of ignition have led to the development of a number of criteria for ignition. The experiments of Bamford[5] with wood suggest that ignition can be expected when the pyrolyzate outflow rate reaches 2.5×10^{-4} g/cm^{2}s. Martin,[4] Akita,[6] and others[7,8] advocate that the event of ignition can be described simply by the attainment of a critical temperature of the exposed surface. Martin[4] postulates that persistent ignition is possible only when the entire solid attains an average temperature that exceeds a critical value. All these criteria presumably have something to do with the ease of heating the solid to cause sufficiently intense combustible gas generation by pyrolysis, and with the thermal conditions of the boundary layer conducive to flame inception. Experimental evidence developed by Alvares[9] suggests that the surface temperature and the pyrolyzate efflux rate at ignition are not constants but depend upon the exposure flux and other factors.

Deverall and Lai[10] showed theoretically that for solids that undergo ignition through gas-phase exother-

mic oxidation reactions, a reversal in the sign of the boundary layer gas temperature gradient at the solid-gas interface was a definite indication of ignition. Consistent with some experimental data for premixed gases ignited by a heated wire,[11] the transition of the gas-phase boundary layer to flaming justifies the gradient reversal criterion. Employing high-speed motion picture photography, Simms[7] observed that the flame is indeed initiated in the relatively well-mixed wake of the finite height vertical target, and that this flame quickly propagates down into the boundary layer, altering the nature of the gas temperature distribution so as to reverse the gradient at the interface. Sauer's correlations[12] on thick slabs of wood showed that a certain minimum char depth was required before ignition could occur. The method of estimating the instantaneous char thickness, however, is experimentally subjective and analytically difficult.

Intuition suggests that a rapid rise of gas temperature is a sure sign of ignition. Since this abrupt rise is due to the oxidation reaction, the phenomenon of ignition should be associated somehow with the reaction rate in the gas boundary layer. In pursuing this line of thought, Kashiwagi[13] suggested that ignition occurs when the reaction rate in the boundary layer exceeds an arbitrary value of approximately 10^{-5} g/cm^{3}s. This type of criterion is consistent with ideas employed in solid propellant ignition studies,[14] in which a surface reaction rate greater than a prescribed critical value is taken to ensure ignition of the exothermic surface reactions.

The ignition criteria utilized by various investigators can thus be summarized:

1. $T_{sw} \geq T_1^*$—critical surface temperature (Simms, Martin)
2. $\overline{T}_s \geq T_2^*$—critical average solid temperature (Simms, Martin)
3. $\dot{m}''_{pw} \geq R_t^*$—critical pyrolyzate mass flux rate (Bamford)
4. $\delta_c \geq \delta_c^*$—critical char depth (Sauer)
5. $\partial T_g/\partial t \geq R_3^*$—critical local gas temperature increase rate
6. $\int_0^\infty$(Reaction rate) $\geq R_4^*$—critical total reaction rate in the boundary layer (Kashiwagi)
7. $(\partial T_g/\partial y)_{\hat{y}=0} = 0$—gas temperature gradient reversal at the solid-gas interface (Deverall and Lai)

Kashiwagi demonstrated that if arbitrary but "reasonable" values were selected for the critical condition, the ignition delay was not sensitive to any particular ignition criterion employed. This is fully expected, for each of Numbers 1 through 6 above indicates a feature of the incipient flame and none excludes or contradicts another. Number 7 is a trivial, although powerful, indicator of the arrival of the flame.

If it is accepted that flaming ignition is merely the onset of significant gas oxidation reactions in the boundary layer, then it is evident that Numbers 5 through 7 would not only necessarily but also sufficiently address the ignition process mechanistically by accounting for the gas oxidation reaction as well as its prerequisite, namely, the solid decomposition rate. The question of which of these three criteria is more desirable may be answered if the sequence of events that lead to ignition is followed qualitatively.

The previous section on conduction-controlled spontaneous ignition indicates that the transiently heated solid conducts heat to the gas phase in the early stages of ignition. As the solid pyrolyzes, oxidation reactions begin in the gas phase. The reaction rate at any time is a function of distance normal to the slab surface. The composition distribution dictates that the reaction rate be zero at the edge of the boundary layer, and maximum somewhere within it. Therefore, a shift in the temperature profile occurs such that the deviation from the inert temperature profile at any point in the boundary layer reflects the oxidation reaction rate at that point. If the exothermic gas reactions persist, the gradient at the wall will eventually become zero. Beyond that point the solid begins to receive energy from the hotter gas, and the pyrolysis and gas oxidation rates increase until flaming occurs. Upon flaming, the gas temperature increases from the solid surface to the flame and then decreases from the flame to the ambient. Hence, attainment of a zero gradient of gas temperature at the wall is not only an important event leading to ignition but also a necessary indicator of the evolution of the flame. It must be recognized, however, that the gas temperature gradient reversal criterion is conservative in that it estimates the time to ignition equal to or less than the actual measured time.

Employing an integral solution approach, Gandhi[15] solves the ignition model of the preceding section of this chapter, paying full attention to simultaneous developments in both the solid and gas phases. A comparison[15,16] is made of the ignition criteria one, three, and six in the framework of criterion seven to note that the surface temperature, pyrolyzate efflux rate, and the total extent of gas phase reaction at ignition will all strongly depend upon such factors as the exposure intensity, target height and thickness, reradiant loss, and the chemical kinetics of both the pyrolysis and oxidation reactions. Alvares' experiments[9] are thus explained with the conclusion that the critical temperature, pyrolyzate efflux, and gas reaction criteria are not generally acceptable, although they are valid in narrowly defined circumstances.

Solid Conduction-Controlled Ignition

The complex problem of heterogeneous ignition has been tackled by various investigators to identify two limiting cases. When the intensity of exposure is relatively low and the pyrolyzate production is relatively slow, the time to ignition is found to be 10^{-1} second or longer and mainly governed by characteristics of the solid phase thermal response. Higher heating rates, higher fuel volatility, and low gas pressures are found to result in a short time to ignition (of the order of 10^{-2} second or shorter) and are mainly governed by the gas phase phenomena.

In the solid phase-controlled limit, the solid is approximated to be inert. Its ignition is presumed to occur when the exposed surface attains a prescribed critical temperature, a property of the substance. As discussed in

the preceding section of this chapter, this criterion is simple although limited in the range of validity.

Let the inert slab of thickness, ℓ, conductivity, K_s, density, ρ_s, specific heat, C_s, and initial uniform temperature, T_{s0}, experience heating at the front face $y = \ell$ by a calibrated constant uniform absorbed irradiance, i_o, while the back face $y = 0$ is insulated. (The solution will later be extended to ignition by convective heating.) As heating occurs, the front face is permitted to lose heat to the surroundings at T_∞ by convection. The convection loss coefficient, h, is assumed to be constant and uniform; the reradiative loss is ignored.

The solid phase continuity equation (Equation 1), the pyrolysis terms in the solid energy conservation (Equation 2), the gas-phase species conservation (Equation 3), and the energy source term (Equation 7) all become unnecessary. The gas phase continuity and the momentum and energy equations also become unnecessary because their combined outcome is embodied in the prescribed heat loss transfer coefficient, h. The interface boundary condition is simplified by ignoring the reradiative loss term and setting the gas conduction flux equal to the convective loss flux, $h(T_{sw} - T_\infty)$. The resulting simple one-dimensional transient conduction problem has a well-known closed-form solution. Adapted from Carslaw and Jaeger[17] the solution is

$$\frac{T_s - T_{s0}}{(i_o/h) + T_\infty - T_{s0}} = 1 - \sum_{n=1}^{\infty} \frac{2\text{Bi}\sec(a_n)\cos(a_n y/\ell)}{\text{Bi}(\text{Bi}+1) + a_n^2} \exp\left(\frac{-a_n^2 \alpha_s t}{\ell^2}\right) \tag{14}$$

where $\text{Bi} \equiv h\ell/K_s$ is the Biot number, indicating the characteristic ratio of convective and conductive fluxes. The constants a_n, $n = 1, 2, \cdots \infty$, are the positive roots of $a \tan(a) = \text{Bi}$; the first six of these roots are presented in Table 2-11.1. It is important to note that Equation 14 is applicable to (1) heating by irradiation in conjunction with surface heat loss by convection to the surrounding gas at T_∞ (which may be equal to the initial temperature of the solid, T_{s0}), (2) heating (or cooling) by convection alone (i_o is set equal to zero and T_∞ equal to the hot ambient gas temperature), and (3) heating by combined radiation and convection. The limiting form of Equation 14 when $h \rightarrow 0$ (i.e., radiant heating without the convective loss) is available explicitly as given in the final section of this chapter along with the versions of Equation 14 corresponding to thermally thin and semi-infinitely thick bodies.

Integration of Equation 14 over the space $0 \le y \le \ell$ leads to the determination of the average temperature, $\overline{T}_s$, of the solid at any point in time. The result[17] is

$$\frac{\overline{T}_s - T_{s0}}{(i_o/h) + T_\infty - T_{s0}} = 1 - \sum_{n=1}^{\infty} \frac{2(\text{Bi}/a_n)^2}{\text{Bi}(\text{Bi}+1) + a_n^2} \exp\left(\frac{-a_n^2 \alpha_s t}{\ell^2}\right) \tag{15}$$

Other inert transient conduction solutions involving two- and three-dimensional effects, a variety of geometries, and boundary conditions can be found in a number of treatises. Equations 14 and 15 are sufficient for the present purposes.

Equations 14 and 15 are shown plotted in Figure 2-11.3, taking $T_\infty = T_{s0}$. The solid curves show the surface temperature while the dashed curves indicate the mean temperature. The coordinates used in this figure are related to those obvious from

$$x\text{-coordinate: } \frac{i_o \ell}{K_s(T_s - T_{s0})} \equiv \frac{\text{Bi}}{(T_s - T_{s0})/[(i_o/h) + T_\infty - T_{s0}]}$$

$$y\text{-coordinate: } \frac{i_o \alpha_s t}{K_s(T_s - T_{s0})\ell} \equiv \frac{\alpha_s t}{\ell^2} \cdot x\text{-coordinate}$$

The x-coordinate is the intensity of radiant exposure normalized with the instantaneous characteristic conduction flux. The y-coordinate has the meaning of the radiant fluence, $i_o t$, nondimensionalized with the appropriate instantaneous conduction quantities. A quick comparison of Figures 2-11.1 and 2-11.3 points to the reasons underlying the choice of presenting Equations 14 and 15 in these coordinates. The following observations can be made from Figure 2-11.3.

The surface temperature is shown in Figure 2-11.3 for six different convective loss Biot numbers. The effect of convective heat loss is most pronounced when the specimen thickness is small, intensity of irradiance is low, and duration of exposure is long (i.e., in the top left region of the graph). The thin body limit solution is given by Equation 22 which shows the reason, in that convective loss

Table 2-11.1 ***The First Six Roots[17] of the Transcendental Equation a tan a = Bi***

Bi	a_1	a_2	a_3	a_4	a_5	a_6	a_n
0	0	3.1416	6.2832	9.4248	12.5664	15.7080	$(n-1)\pi$
10^{-3}	0.0316	3.1419	6.2833	9.4249	12.5665	15.7080	
10^{-2}	0.0998	3.1448	6.2848	9.4258	12.5672	15.7086	
10^{-1}	0.3111	3.1731	6.2991	9.4354	12.5743	15.7143	
10^{0}	0.8603	3.4256	6.4373	9.5293	12.6453	15.7713	
10^{1}	1.4289	4.3058	7.2281	10.2003	13.2142	16.2594	
10^{2}	1.5552	4.6658	7.7764	10.8871	13.9981	17.1093	
∞	1.5708	4.7124	7.8540	10.9956	14.1372	17.2788	$(n-1/2)\pi$

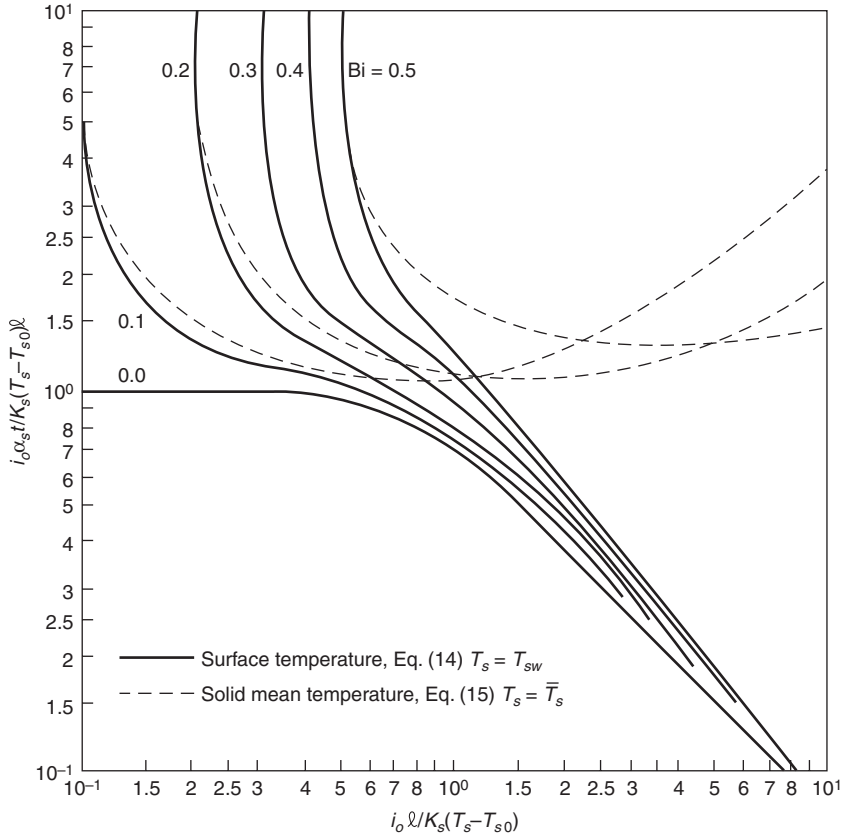

Figure 2-11.3. ***Surface and solid mean temperature histories for a slab heated by radiation and cooled by convective loss. Solid lines: surface temperature, Equation 14, $T_s = T_{sw}$. Dashed lines: solid mean temperature, Equation 15, $T_s = \bar{T}_s$. Numbers on curves are values of Bi.***

plays an equally prominent role with the radiant heating of the solid.

As the slab thickens (i.e., in the lower right region of the graph), the convective loss exerts a less significant effect, compared to the effect of conduction, on the surface temperature history. In this thick regime, the semi-infinite solid solution without surface heat loss given by Equation 25 results in a surface temperature history of

$$\frac{i_o \alpha_s t}{K_s(T_s - T_{s0})\ell} = \frac{\pi/4}{i_o \ell/[K_s(T_s - T_{s0})]} \tag{16}$$

where the length, ℓ, is used to depict this limiting solution on the same plane as the thin and finitely thick slab solutions. The Bi = 0 line of Figure 2-11.3 in the lower right region is, in fact, Equation 16 indicating a slope of -1.

Expectedly, the mean temperature of a heated solid is always lower than its surface temperature. When the solid is thin, internal gradients become negligible, and the mean and surface temperatures are equal and relatively low. Convective loss obviously makes the surface temperature always lower than it is without losses. This is not always true, however, for the mean temperature. A complex compromise between the exposure irradiance and the histories of conductive drain and convective loss results in a minimum in the exhibited mean temperature curves.

Consider now the premise that spontaneous ignition of a radiantly heated organic solid is primarily a consequence of heat conduction in the solid and convective loss to the gas phase, and that all other physical and chemical processes occur promptly without exerting any resistance. Additionally, the symptom of the incipient ignition is the attainment of a prescribed critical temperature at the exposed surface. Then, setting $T_{sw} = T^*_{sw}$, the solid curves of Figure 2-11.3 should give the time to ignition $t = t^*$. It may be postulated further that persistent flaming of thick bodies will occur only when the mean temperature of the body becomes sufficiently high to promise a continuous pyrolysis at an adequately high rate. Then the mean temperature curves of Figure 2-11.3 are expected to indicate the minimum required exposure for persistent flaming. With this framework of an ignition criterion, a remarkable similarity between Figures 2-11.1 and 2-11.3 can be recognized. This similarity perhaps endorses the prescribed critical temperature criterion for ignition and the cumulative outcome of the numerous assumptions underlying the development of Figure 2-11.3. The limitations of this success will be discussed later in this chapter.

There is a particular physical meaning of the coordinates chosen for Figure 2-11.3. As mentioned earlier, the x-coordinate, $i_o\ell/K_s(T_s - T_{s0})$, is a ratio of the imposed flux, i_o, to the instantaneous characteristic conductive flux, $K_s(T_s - T_{s0})/\ell$. The x-coordinate can also be viewed as a ratio of the physical thickness, ℓ, to the thermal length characteristic, $K_s(T_s - T_{s0})/i_o$, which is approximately the depth to which the thermal wave would penetrate into the solid in the time taken by the surface to raise its temperature from T_{s0} to T_s. If the ratio $i_o\ell/K_s(T_s - T_{s0}) \ll 1$, the solid may be considered thermally thin. On the other hand, if this ratio is much greater than unity, either because the solid is in fact physically thick or because the thermal length is small, then the body behaves as thermally thick. Large temperature gradients then exist near the exposed surface, and the relatively well-insulated interior of the solid results in the surface temperature being much higher than the average temperature.

The y-axis, $i_o\alpha_s t/K_s(T_s - T_{s0})\ell = i_o t/\rho_s C_s \ell(T_s - T_{s0})$, can also be viewed in different ways. It can be seen as a ratio of total energy incident on a unit area within the time, t (known as the *fluence*), to the characteristic enthalpy rise of the mass lying within this area. It is equally interesting to view the y-axis as a ratio of the elapsed time, t, to the heating time $\rho_s C_s \ell(T_s - T_{s0})/i_o$ taken by the flux, i_o, to raise the temperature of the involved solid mass from T_{s0} to T_s. The y-axis is also recognizable as the product of the x-axis and the traditional Fourier modulus, $\alpha_s t/\ell^2$. It is thus clear that when the intensity and duration of exposure are low, ignition of the solid is impossible.

Where possible, ignition can be one of three kinds

1. Thin bodies exposed to low intensity ignite, but only after a long exposure. The convective losses and the specimen thickness have a strong effect on this thin body ignition. In fact, experiments indicate that these thin bodies yield their small pyrolyzate content to the gas phase rather abruptly at a high rate. This happens so quickly that the gas phase thermal and mixture conditions are mutually out of phase to exclude the development of a flame. By the time the surface reaches a sufficiently high temperature, the solid is already converted to char. This char experiences the observed thin body glowing ignition. Martin's experiments confirm the strong influence of the specimen thickness on this glowing ignition. While this description is valid for isolated single thin fuel elements, it should not imply that beds of shredded paper and clouds of minute fuel particles will fail to flame. Such beds or clouds will have to be considered to be the global fuel element with low conductivity and large thickness, belonging at moderate to high values of the x-axis of Figure 2-11.3. Consideration of the volumetric absorption of radiation may become crucial in such a scenario.
2. Ignition occurs at moderate values of the exposure and fluence parameters, yielding only a transient flame. If the externally controlled exposure were then interrupted, the flame would cease, presumably due to large conductive and convective losses and inadequately established pyrolyzate production.
3. At moderate values of exposure intensity and long exposure time, the flaming will persist even if the external irradiance is cut off. The longer exposure will raise the entire solid to a sufficient temperature, at which sustained production of the pyrolyzate is possible. Martin's experiments confirm that the effect of specimen thickness on this persistent flaming ignition is relatively weak.

Figures 2-11.1 and 2-11.3 also show that as the irradiant intensity is gradually reduced, a threshold (a lower limit of i_o) is approached below which ignition is impossible even with infinitely long exposure. While both the theory based on prescribed critical temperature criterion and the related experiments appear to adequately predict the nature of and time to ignition, they do not address the ignition threshold. A scrutiny of the gas phase reaction dynamics is required to gain an understanding of this issue. In fact, sufficient evidence exists[9] to indicate that the ignition temperature increases with decreasing irradiance.

This is not the first time the essence of Figure 2-11.1 has been developed by inert conduction theory. Kanury[1] and Steward[2] independently obtained plots similar to Figure 2-11.3. The present Figure 2-11.3 is special because it is based on a single equation (Equation 14) rather than a patching of several solutions.

Martin's collection of experimental data, when examined in the perspective of Figure 2-11.3, indicate that for spontaneous ignition of radiantly heated thick cellulose, the critical surface temperature is in the vicinity of 900 K. These findings are in keeping with the measurements of Alvares[9] and Akita.[6] A comparison of the presently predicted and Martin's experimental results for persistent ignition leads to an estimation of the required mean solid temperature to be between 800 and 1200 K. Using physical reasoning, this temperature should be near, and slightly above, the temperature at which cellulose would pyrolyze profusely. Pyrolysis literature indicates this to be about 600 K. The present overestimation may be a consequence of the ignored reradiative heat loss from the surface.

Koohyar[18] demonstrates that the present concepts are valid also for a variety of woods exposed to radiation from flames, provided corrections are made for the surface absorptivity differences. Koohyar[18] and Wesson[19] demonstrate that the ignition of radiantly heated wood in the presence of a small pilot flame in the reactive boundary layer also obeys the essence of the inert conduction theory. The critical surface temperature for this situation is about 600 K, near the pyrolysis temperature. This is consistent with the conclusions reached earlier by Akita.[6] It thus appears that two conditions have to be met for spontaneous ignition: first, heating has to be sufficiently intense and long to produce sufficient pyrolyzates, which would result in a boundary layer mixture of fuel content exceeding the lean limit of flammability; and second, the boundary layer has to become sufficiently hot enough to support significant oxidation reaction. For piloted ignition, the first condition is adequate.

Hallman[3] demonstrates that the inert conduction theory can be used to predict piloted ignition time for a variety of synthetic materials (i.e., plastics) as well. Smith[20] experimentally found that edges and corners of pieces of pine blocks exposed to irradiation from a quartz lamp ignite sooner but require a higher surface temperature than

that required for surface ignition. Multidimensional conduction and the effect of orientation on the reactive boundary layer characteristics are the two most relevant factors here.

Equations 14 and 15 indicate that if i_o is replaced by $h(T_\infty - T_{s0})$, Figure 2-11.3 can describe ignition by convective heating[21] as well. The x- and y-coordinates then are

$$\mathrm{Bi}\cdot\frac{T_\infty - T_{s0}}{T_s - T_{s0}} \quad \text{and} \quad \mathrm{Bi}\cdot\frac{T_\infty - T_{s0}}{T_s - T_{s0}}\cdot\frac{\alpha_s t}{\ell^2}$$

respectively, with the same physical meaning as before. Several points should be noted

1. The Biot number stands to represent the convective losses in radiant ignition. In convective ignition, however, it stands to represent the heating itself.
2. In practice, convective heating generally occurs as a result of flowing hot flame gases adjacent to the target surface. These gases are either devoid of, or diminished in, the oxygen content. Such a heating may produce pyrolytic damage to the target without ever producing ignition and flame. If the oxygen content of these heating gases is sufficiently high, potential ignition may be piloted by the hot gas flame itself. To avoid these real-world complexities, application of Figure 2-11.3 to convective heating should be made only when the convective heat source is hot air.
3. It may seem desirable to sort out the framework of the ignition map such that the heating Biot number is removed from the coordinates and made to appear only as a parameter in the curves. If this occurs, however, all the physical interpretations must be revised as well. (No substantial improvement in understanding seems to be gained.)
4. Akita's[6] experiments indicate that spontaneous and piloted ignition temperatures[1] of convectively heated wood are about 765 and 725 K, respectively.

Role of the Gas Phase Processes

Alvares and Martin[22] reported experiments in which cellulose was radiantly and spontaneously ignited in an atmosphere of oxygen-enriched air at high pressures. Eliciting a number of interesting gas phase processes that influence heterogeneous ignition, this work indicates that the time to ignition is dramatically reduced by an increase in the ambient oxygen mass fraction and/or ambient gas pressure, and by a reduction in its thermal conductivity. The surface temperature at ignition is also found to substantially decrease with an increase in the oxygen content and in the pressure of the ambient gas. A simple analysis can be made to predict these observations and attempt to develop an understanding of the activity in the gas phase.

Consider a situation in which attention is focused only on the gas phase. Assume, accordingly, that the solid phase problem furnishes to the boundary layer a pyrolyzate content corresponding to a mass fraction of Y_F and the ambient gas furnishes oxygen such that its mass fraction is Y_O. Let the solid surface at $T_g = T_{sw}$ and the edge of the boundary layer at $T_g = T_\infty < T_{sw}$ constitute two large parallel plates separated by a distance, δ. Assume further that the reactive fluid mixture in this layer is stagnant so that energy transfer from the hot to cold boundary occurs only by conduction. Additionally, let the problem be steady state. Then, all equations become irrelevant, except for Equation 7, simplified. This simplification is

$$K_g\frac{d^2T_g}{d\hat{y}^2} + h_c\left[Z_{gF}\rho_g^2 Y_F Y_O \exp\left(\frac{-E_g}{\bar{R}T_g}\right)\right] = 0 \qquad (17)$$

with the boundary conditions: $\hat{y} = 0$, $T_g = T_{sw}$ and $\hat{y} = \delta$, $T_g = T_\infty$. Recall that the square-bracketed term in this equation is the volumetric fuel consumption rate due to oxidation, whose kinetics are taken to exhibit an order of unity with respect to both the pyrolyzate fuel and the oxygen.

For an inert gas mixture with constant conductivity, steady-state conduction would occur across the gas layer with a linear temperature profile. On the other hand, if the mixture is reactive in a strongly temperature dependent way, the energy source prevalent in the proximity of the hot wall will locally reduce the temperature gradient. The stronger this energy source becomes, the greater is this gradient reduction. In fact, if the source is strong and T_{sw} is sufficiently high, the gradient near the hot wall will even be reversed in sign, signifying that heat would flow from the reacting gas to the hot wall as well as to the cold wall. Ignition is thus conceivably accomplished when T_{sw} is just high enough to result in a zero temperature gradient at the hot wall. This critical T_{sw} will depend upon the kinetics and energetics of the exothermic reaction and the gas thermal conductivity. To determine the critical T_{sw}, the energy conservation problem of Equation 17 must be solved, in which the preignition reactant consumption is ignored and the mixture conductivity is assumed constant. Upon defining

$$\theta \equiv \frac{E_g(T_{sw} - T_g)}{\bar{R}T_{sw}^2} \qquad \eta = \frac{\hat{y}}{\delta}$$

and

$$D = \frac{E_g\delta^2 h_c\rho_g^2 Z_{gF} Y_F Y_O \exp\left(-E_g/\bar{R}T_{sw}\right)}{\bar{R}T_{sw}^2 K_g}$$

Equation 17 reduces to $d^2\theta/d\eta^2 - D\exp(-\theta) = 0$ with the boundary conditions $\theta(0) = 0$ and $\theta(1) = \theta_\infty$. Integration of this equation is quite straightforward, although somewhat tedious. One integration gives

$$\frac{d\theta}{d\eta} = \sqrt{[4C_1^2 - 2D\exp(-\theta)]} \qquad (18)$$

relating local temperature to its gradient. With one additional integration and application of the boundary conditions, $\theta = \theta(\eta; D, \theta_\infty)$ can be found and the conditions of $D = D^*(\theta_\infty)$ surrounding the ignition indicated by the zero temperature gradient at the hot wall can be deduced.

There is a simple approximation by which this ignition result can be obtained relatively easily. The temperature profile of a marginally igniting system is given by Equation 18 in which the constant, C_1, is evaluated by setting θ and $d\theta/d\eta$ equal to zero at $\eta = 0$. Thus, for the

temperature profile in the system at ignition, $4C_1^2 = 2D$, so that $d\theta/d\eta = \{2D[1 - \exp(-\theta)]\}^{1/2}$. Change in this gradient at ignition from zero to a nearly constant value of $\{2D[1 - \exp(-\theta_\infty)]\}^{1/2} \approx (2D)^{1/2}$ occurs within a remarkably small distance from the hot wall. If one assumes that the linearity of the temperature profile holds in the entire range $0 \le \xi \le 1$, the gradient is noted to be equal to θ_∞. Thus, ignition by the hot surface is expected if $(2D)^{1/2} \ge \theta_\infty$; that is, if

$$D \ge \frac{\theta_\infty^2}{2}$$

Written in physical terms, ignition would occur if

$$\frac{2\delta^2 \overline{R} T_{sw}^2 \rho_g^2 h_c Z_{gF} Y_F Y_O \exp(-E_g/\overline{R}T_{sw})}{K_g E_g (T_{sw} - T_\infty)^2} \ge 1 \qquad (19)$$

If T_∞ is small, the hot wall temperature appears only in the Arrhenius term. Therefore, it is easy to see that a small gas layer thickness requires a higher T_{sw} to produce ignition.

If the reactive gas were to be flowing over a hot plate, Equation 19 can be adapted by viewing δ, the boundary layer thickness, as the average thermal boundary layer thickness and the ratio (K_g/δ) as the average heat transfer coefficient, h. Inasmuch as both the boundary layer thickness and the heat transfer coefficient depend upon the flow dynamics and the nature of the fluid, ordinary heat transfer results may be incorporated into Equation 19. With $\delta = H/\mathrm{Nu}$ where H is the flow characteristic length and Nu is the average Nusselt number (which depends on the Grashof or Reynolds number of the flow and the Prandtl number of the fluid), ignition occurs if

$$\frac{2H^2 \overline{R} T_{sw}^2 h_c \rho_g^2 Z_{gF} Y_F Y_O \exp(-E_g/\overline{R}T_{sw})}{\mathrm{Nu}^2 K_g E_g (T_{sw} - T_\infty)^2} \ge 1 \qquad (20)$$

If all else is kept fixed, longer hot plates are capable of producing ignition with lower wall temperatures. Faster moving gas streams are not as likely to be ignited by the same T_{sw} hot plate as are the slower moving ones. This ignition-retarding effect of flow speed is more pronounced for laminar flows than for turbulent flows. (This deduction is, of course, based on the fact that $\mathrm{Nu} \propto \mathrm{Re}^b$, where $b \approx 1/2$ for laminar flow and $b \approx 1/5$ for turbulent flow.) Note also that Equation 20 can be adapted to hold for combustible gas flows over a variety of geometries.

Equations 19 and 20 are entirely consistent with the observations of Alvares and Martin.[22] As the surface temperature, T_{sw}, develops slowly due to the solid phase conductive response to heating, the gas phase responds quickly. It is eminently clear from Equations 19 and 20 that taller targets in a slow-moving, poorly conducting, low viscosity, high pressure, oxygen-enriched ambient gas will ignite sooner at a lower surface temperature. Although the present analysis is only approximate, it powerfully depicts how gas phase oxidation reactions are induced by the composition and thermal conditions.

Gandhi[15] solved the comprehensive set of the conservation equations, accounting for the full unsteady, reactive, conjugate heat and mass transfer problem with reradiant heat loss at the surface of the target, which is vertical and subjected to external irradiance. An integral technique is employed to obtain the characteristics of the transiently developing, reactive, natural convective boundary layer averaged over the target height. The gas temperature gradient reversal at the gas-solid interface is used as the criterion for spontaneous ignition. This solution yielded valuable information on the ignition criterion as discussed previously. Additionally, it is possible to predict such radiant spontaneous ignition phenomena as the time to ignition and ignition thresholds.

Figure 2-11.4 indicates Gandhi's predicted influence of exposure irradiance and the target thickness on the time to ignition for fixed values of the plate height, H, and kinetics of oxidation and pyrolysis. The general characteristics of Figures 2-11.1 and 2-11.3 obviously appear to be captured. (Recall that the surface reradiant energy loss has been ignored in deducing Figure 2-11.3.) Typical agreement of the predictions with measurements is shown in Figure 2-11.5. Further details of this predictive model are available.[15,16,23]

Most importantly, Gandhi predicts the lower limit exposure flux below which ignition of a given solid in a given situation is impossible. These limiting conditions, known as ignition thresholds, are difficult to measure experimentally. The threshold minimum flux is found to depend on the slab height and thickness, gas and solid phase reaction kinetics, and reradiant loss as well as the heat of combustion of the pyrolyzates. One typical prediction is indicated in Figure 2-11.6, where the threshold flux is plotted as dependent on the heat of combustion and the slab height for given reradiant loss and kinetics. Ignition will not occur in the area lying below the curve, while it will occur elsewhere. Taller targets will experience ignition even if the pyrolyzate is less combustible; for a fixed heat of combustion of the pyrolyzates, taller targets exhibit a lower threshold flux. The minima in these curves indicate that when the heat of combustion is very low, ignition is impossible irrespective of the exposure flux level. At enthalpies of combustion that are close to but slightly larger than the limiting value (which depends on the target height), two roots of the threshold flux exist between which ignition is possible. These are

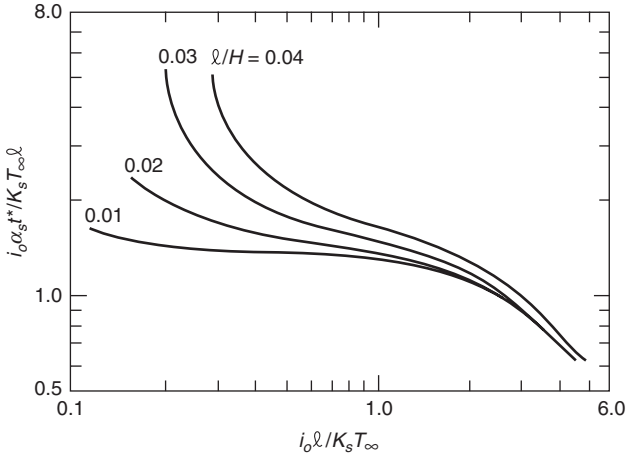

Figure 2-11.4. ***Influence of slab thickness on time of ignition. $gH^3/\nu_g^2 = 10^6$; $E_g/\overline{R}T_\infty = 30$; $Z_{gF}\rho_g \ell^2/\alpha_s = 10^8$; $E_s/\overline{R}T_\infty = 50$; $Z_s \ell^2/\alpha_s = 10^7$.***

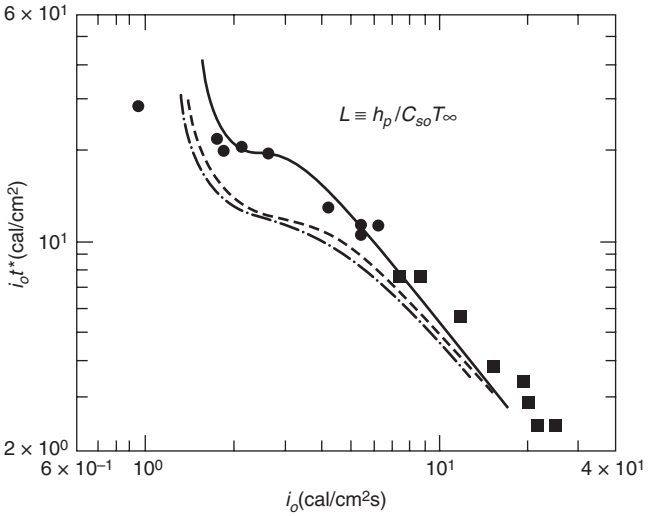

Figure 2-11.5. ***Comparison with Martin's data for α-cellulose. ■ and ●: data[24] solid line: theory[15] (L = –1); dashed line: theory[15] (L = 1); dash-dotted line: theory[15] (Cp = 0).***

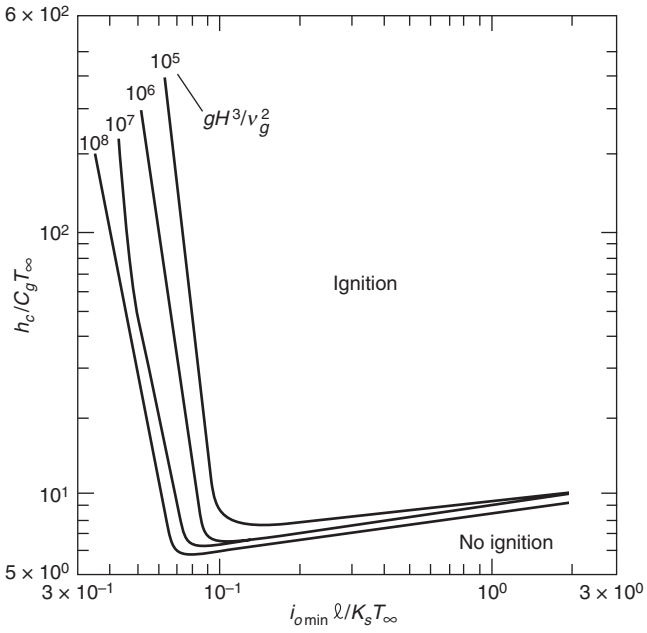

Figure 2-11.6. ***Influence of slab height on threshold flux. $E_s/\bar{R}T_\infty = 50$. $E_g/\bar{R}T_\infty = 30$. $\sigma\varepsilon_{sw}T_\infty^3\,\ell/K_s = 10^{-3}$.***

important findings and must be further studied for use in fire safety. While Figure 2-11.6 is presented here only as an example of Gandhi's predictions, much similar information is available.[15]

Some Practical Issues

The understanding of the ignition process developed earlier in this chapter is useful in a number of practical fire safety problems, including those cited in the Introduction. These problems fall broadly into two groups: those pertaining to the very initiation of the fire, and those pertaining to the spatial (or temporal) growth of fire in combustible ensembles. A number of questions arise in attempts to assess the ignition hazard on the basis of the existing simple viewpoints. These questions point out the need for care and for a comprehensive model of ignition through which the assessment can be made with some confidence.

The possibility of ignition of an object under a given set of conditions is presently judged by evaluating whether or not the exposed surface would attain a critical ignition temperature, T^*, construed as a property (albeit, extrinsic) of the material. T^* for transient ignition of a broad range of natural and synthetic organic solids is taken to be approximately as follows: for spontaneous ignition, 600°C for radiant exposure and 500°C for convective exposure; for piloted ignition, 300 to 410°C for radiant exposure and 450°C for convective exposure. Note that these are approximate values, mostly deduced from experiments on small vertical specimens. Measurements of this temperature on ignition of horizontal surfaces are also available in the recent literature.

Persistent ignition would require heating of the solid, over a minimum thickness near its exposed surface, to a mean temperature in excess of the material's characteristic pyrolysis temperature to ensure continued pyrolysis. This would presumably mean higher surface temperatures than those just cited. It is noteworthy in this context that in spite of significant physical and chemical differences in structure and composition, most organic solids undergo pyrolysis in a rather narrow temperature range of 325 ± 50°C.

It is also important to note here that the size of the specimen and its orientation are expected to exert an influence on T^* by altering the convective patterns and rates of heat loss and gas mixing. The mechanisms involved in this influence are not straightforward. Reduction of heat loss from the surface of a radiantly heated solid will obviously tend to increase its heating and pyrolysis. It is, therefore, expected to result in a hastened ignition. This expectation, however, is not always valid since the gas phase ignition requires mixing of the pyrolyzates with air and heating of the mixture so as to induce the preignition oxidation reaction. These mixing and heating processes of the gas phase require a certain optimal boundary layer flow. Thus, while mixing and heating of the boundary layer gases is a condition required for ignition, excessive mixing will dilute the reactant mixture and deprive the solid from its energy demand for sustained production of pyrolyzate.

These ideas are also important from another practical viewpoint. Traditional strategies to delay or prevent ignition involve a physical and/or chemical alteration of the materials. One goal of such an alteration is usually to make the pyrolysis difficult, for example, by increasing the associated activation energy or endothermicity. If the heating were convective, however, an easy pyrolysis with

an increased rate may be more desirable, for then the copious production of the pyrolyzate is expected to retard the convective heating rate by thickening the boundary layer.

Another material alteration that can delay or prevent ignition (irrespective of the radiative or convective heating mode) is to chemically tamper with the composition of the pyrolyzate mixture, rendering it abundant in such inert species as water vapor and carbon dioxide. Means of accomplishing this can be found in organic chemistry, wherein even trace quantities of certain additives are known to profoundly alter both the rate of production and composition of the pyrolyzate. However, complications arise due to the dependency of the action of these additives on the rate of heating of the sample.

The differences between spontaneous and piloted ignitions, and between radiant and convective heating to ignition, should be noted here. Spontaneous ignition requires (1) sufficient heating of the solid to produce enough pyrolyzates continuously, (2) mixing of these pyrolyzates with air to produce a mixture above the lean limit, and (3) heating of this boundary layer mixture to a temperature sufficiently high to result in a thermochemical runaway to the state of flame. Requirement 3 is not necessary for piloted ignition, wherein an external ignition energy source is available to initiate the flame. If the heating were by irradiation of the specimen, the exposed surface of the solid would be at the highest temperature, invoking a transient natural convective boundary layer in which the induced air mixes with the effluent pyrolyzates. If forced blowing of air over a radiantly heated solid surface were involved, the surface then would be cooled more intensely than due to natural convection. This would likely diminish the pyrolysis rate within the solid while enhancing the mixing in the boundary layer and its heating. The resultant ignition behavior would be rather complicated.

If the heating were by convection, drastic differences would arise, depending upon the nature of the convecting hot gas. Heating by hot air is conducive to quick ignition. Heating by hot (nonflaming) combustion gases can result in copious pyrolysis, but ignition in the mixing layer is thwarted by the poor oxygen content. If the convective heating were by hot flames, the flames themselves would become extended in space due to the added pyrolyzate fuel. In these circumstances, the very idea of ignition becomes vague.

The multitude of complexities and ambiguities involved in assessing the ignition hazard of a practical situation, even with the simple critical surface temperature criterion, is obvious. Care is therefore required in drawing quick conclusions from current simplified practices. The surface temperature at ignition is not a cause but an effect, and as such, depends on the conditions of an experiment (so, also, are most of the other known ignition criteria). A comprehensive quantitative model of physical chemistry of ignition, such as that presented by Gandhi for spontaneous ignition of radiantly heated vertical cellulosic solids, seems to be needed for piloted radiant ignition, for (spontaneous and piloted) ignition due to convective heating, and for a number of specimen orientations.

A Practical Illustration

Great advances have been made in understanding the fundamental mechanisms involved in flaming ignition of radiantly and/or convectively heated solids—natural as well as synthetic—with and without the presence of a pilot source. The current practice of ignition hazard assessment employs such simplified concepts as a prescribed critical ignition temperature of the solid. This practice is prone to ambiguities and difficulties. Physicochemical models of ignition are available and can be used to examine the ignition process in a broader and more complete perspective. Quantitative assessment of the conditions that differentiate between possible and impossible ignition is now feasible from these models. The time to ignition and energy required for ignition can be estimated with reasonable accuracy. The present understanding can be refined by relaxing most of the assumptions enumerated in the section of this chapter on conservation equations; but the degree of and the need for the necessary refinement must first be addressed.

To illustrate the practical utility of Figure 2-11.3, consider a firwood target 1 cm thick and 2 cm in height initially at 300 K in normal air, also at 300 K. Will spontaneous ignition occur if this target is exposed to an absorbed radiant flux of 2 W/cm^2 continuously for 1000 seconds? Will the ignition, if possible, be transient or sustained?

Approximate answers to such questions can be given using Figure 2-11.3. First, the conductivity, specific heat, density, and diffusivity of fir, respectively, are found to be 0.17 W/m·K, 2500 J/kg·K, 600 kg/m^3, and $11.3 \times 10^{-8} m^2/s$. From convection literature, the heat transfer coefficient, h, is estimated to be about 15 $W/m^2 \cdot K$. Then the Biot number and x, y-coordinates for Figure 2-11.3 are calculated with the given exposure flux and duration.

$$\mathrm{Bi} \equiv \frac{h\ell}{K_s} \approx \frac{15(\mathrm{W/m^2K})1(\mathrm{cm})}{0.17(\mathrm{W/mK})} \approx 0.88$$

$$x \equiv \frac{i_o \ell}{K_s(T^* - T_0)} \approx \frac{2(\mathrm{W/cm^2})1(\mathrm{cm})}{0.17(\mathrm{W/mK})(873-300)(\mathrm{K})} \approx 2.05$$

$$y \equiv \frac{i_o \alpha_s t}{K_s(T^* - T_0)\ell} \approx \frac{2(\mathrm{W/cm^2})11.3 \times 10^{-8}(\mathrm{m^2/s})1000(s)}{0.17(\mathrm{W/mK})573(\mathrm{K})1(\mathrm{cm})} \approx 2.32$$

The critical temperature $T^* = 873$ K comes from the summary in the previous section and corresponds to spontaneous ignition due to radiant heating. Entering these values of Bi, x, and y on Figure 2-11.3, sustained spontaneous ignition is concluded to be possible with the given exposure and duration. If the exposure duration were shorter, say 400 seconds, the y-coordinate would be 0.93, indicating that the ignition would be transient. With even shorter exposure (less than 260 seconds), y will be less than approximately 0.6 and ignition would not occur.

Repeating the example but with a thinner target of thickness $\ell = 0.1$ cm, and keeping all else unchanged, the Bi, x, and y coordinates are estimated to be 0.088, 0.205, and 23.2, respectively. Sustained spontaneous ignition is obviously ensured on this thin body. With 400 seconds of exposure, $y \approx 9.28$, sustained ignition continues to be possible. The minimum exposure required of this thin body

to produce ignition is 40 seconds, which is substantially shorter than the exposure of 260 seconds needed for transient ignition of the thicker body considered above.

If a pilot source were available, the appropriately lower critical temperature from the previous section of this chapter would enable similar estimates to be made of whether ignition would occur with a given exposure duration, whether the possible ignition would be transient or sustained, and of the minimum required exposures.

If convective heating from a hot gas flow at a temperature T_∞ were involved rather than radiant heating, the x- and y-coordinates of Figure 2-11.3 would be estimated by the definitions given at the end of the section of this chapter on solid conduction-controlled ignition. Throughout this example it should be remembered that Figure 2-11.3 has been developed on the basis of a greatly simplified view of the ignition process. The very concept of the prescribed critical temperature involves an oversimplification and limited validity. Detailed models, such as those underlying Figures 2-11.4 through 2-11.6, are more reliable, although considerably more difficult to apply.

Mathematical analyses lead to a predictive capability which is limited only by the accuracy and detail of such input data as the pyrolysis and combustion kinetic and thermodynamic properties, values of transport properties and their variability with temperature and composition, and so forth. Many real-world complexities exist: (1) materials are often encountered in practice as composites with glues, stitches, and bonds; (2) practical geometries of targets are seldom simple; (3) aging and durability of a solid alter its physical and chemical characteristics; (4) surfaces are almost always multicolored; and so forth. An adherence to fixed sets of physical and chemical properties or to voluminous dictionaries of property values under different circumstances may not be wise for use in a predictive model. It may be more prudent to seek only a fundamental conceptual or mechanistic understanding of a phenomenon such as flaming ignition from a mathematical model.

Even more importantly, mathematical models suggest useful ways of correlating the experimental measurements. Meaningful correlations lead one to maximize the value of limited experiments, generalize the observations, and to postulate, interpret, and exploit the basic mechanisms of chemistry and physics.

Conclusion

A qualitative, comprehensive map of flaming ignition has been developed in the work presented here. The nature of the problem and the component processes are well identified, and the global physicochemical behavior appears to be clear. Employing this understanding, it must be possible to draw some conclusions on the effects of such nonidealities as the edges and corners that reflect in three-dimensional conduction and in complicated boundary layer flows, surface roughness and color in conjunction with the nature of the radiation source, convective heating by vitiated hot gases, leakage of energy and mass through the backface and edges, and others.

Explicit Forms of Equation 14 for Some Limiting Cases

1. *Explicit form of Equation 14 as convective losses tend to zero:* The transcendental equation becomes $\sin a = 0$ so that $a_n = n\pi$, $n = 1, 2, \ldots, \infty$. This solution[17] is given as

$$\frac{K_s(T_s - T_{s0})}{i_o \ell} = \frac{\alpha_s t}{\ell^2} + \frac{y^2}{2\ell^2} - \frac{1}{6} - \sum_{n=1}^{\infty} \frac{2(-1)^n}{\pi^2 n^2} \cos\left(\frac{n\pi y}{\ell}\right) \exp\left(-\frac{n^2\pi^2\alpha_s t}{\ell^2}\right) \tag{21}$$

2. *Thermally thin slab:* If the solid were either physically so thin and/or so highly conductive that the temperature gradients within the solid are promptly relaxed by the rapid conduction, then the solid temperature is a function of time alone. The energy equation for this case is obtainable by integrating Equation 2 as $\rho_s C_s (V/S)\, dT_s/dt = i_o - h(T_s - T_\infty)$ along with the initial condition $T_s = T_{s0}$ at time $t = 0$. The ratio (V/S) is the solid volume over its surface area, equal to the thickness, ℓ, for a slab. The solution is easily obtained:

$$\frac{T_s - T_{s0}}{(i_o/h) + T_\infty - T_{s0}} = 1 - \exp\left(-\frac{hSt}{\rho_s C_s V}\right) \tag{22}$$

which in fact is a limiting form of Equation 14. In the further limit $h \to 0$, as in Item (1) above, Equation 22 reduces to

$$\frac{\rho_s C_s V (T_s - T_{s0})}{i_o S t} = 1 \tag{23}$$

for pure radiant heating of a thin body without any convective loss.

3. *Semi-infinite slab:* If the slab were physically so thick and/or so poor a conductor that the back face does not realize the effect of thermal exposure at the front face within the time period of interest, the slab then can be considered as a semi-infinite solid. A high front face exposure flux and a low conductivity will tend to make even a physically thin sheet of a slab behave as though it is thermally infinitely thick. With radiant heating and convective loss at the only face, we know that $y' = 0$ (with y' measured into the interior from the surface), and the temperature-time-space distribution corresponds to the small time limit of Equation 14. This solution is given explicitly as

$$\frac{T_s - T_{s0}}{(i_o/h) + T_\infty - T_{s0}} = \operatorname{erfc}\left(\frac{y'}{2\sqrt{\alpha_s t}}\right) - \left[\operatorname{erfc}\left(\frac{y'}{2\sqrt{\alpha_s t}} + \frac{h\sqrt{\alpha_s t}}{K_s}\right) \exp\left(\frac{hy'}{K_s} + \frac{h^2\alpha_s t}{K_s^2}\right)\right] \tag{24}$$

(The manner in which the unavailability of a physical reference length, ℓ, is handled can be observed from Equation 24.) Heating by radiation alone without any

Table 2-11.2 ***The Error Function and Its Derivative***

ϕ	erfϕ	erfcϕ = 1 – erfϕ	$\frac{d}{d\phi}$ erfϕ = $(2/\sqrt{\pi})\exp(-\phi^2)$
0	0	1.0	1.1284
0.05	0.05637	0.9436	1.1256
0.1	0.1125	0.8875	1.1172
0.2	0.2227	0.7773	1.0841
0.3	0.3286	0.6714	1.0313
0.4	0.4282	0.5716	0.9615
0.5	0.5205	0.4795	0.8788
0.6	0.6039	0.3961	0.7872
0.7	0.6778	0.3222	0.6913
0.8	0.7421	0.2579	0.5950
0.9	0.7969	0.2031	0.5020
1.0	0.8427	0.1573	0.4151
1.5	0.9661	0.0339	0.3568
2.0	0.9953	0.00468	0.0827
2.5	0.9996	0.00041	0.0109
3.0	0.99998	0.00002	0.0008

convective loss calls for the limit of Equation 24 as $h \to 0$. This limit solution[17] is given to be

$$\frac{K_s(T_s - T_{s0})}{2i_o\sqrt{\alpha_s t}} = \frac{1}{\sqrt{\pi}}\exp\left(-\frac{y'^2}{4\alpha_s t}\right) - \left(\frac{y'}{2\sqrt{\alpha_s t}}\right)\mathrm{erfc}\left(\frac{y'}{2\sqrt{\alpha_s t}}\right) \tag{25}$$

where erfc is the complementary error function. This and other related functions are tabulated in Table 2-11.2.

Nomenclature

a_n constants, $n = 1, 2, \ldots, \infty$
b index
Bi Biot number
C specific heat (kJ/Kg·K)
D Damköhler number
D_{ig} species i mass diffusivity through the gas mixture (m^2/s)
E activation energy (kJ/kmol)
f fuel pyrolyzate/oxygen stoichiometric mass ratio (kg F/kg O)
g standard acceleration of gravity (m/s^2)
H height of the solid target slab (m)
h heat transfer coefficient ($W/m^2 \cdot K$)
h_c enthalpy of combustion of fuel pyrolyzate (kJ/kg)
h_p enthalpy of pyrolysis (kJ/kg)
i incoming exposure irradiance (W/m^2)
i_o absorbed exposure irradiance (W/m^2)
K thermal conductivity (W/m·K)
ℓ thickness of the solid target slab (m)
M molar mass (kg/kmol)
$\dot{m}''$ mass flux ($kg/m^2 \cdot s$)
$\dot{m}_i'''$ species i source-sink strength ($kg/m^3 \cdot s$)
Nu Nusselt number
P pressure (Pa)
$\dot{q}'''$ energy source-sink strength (W/m^3)
Re Reynolds number
$\overline{R}$ universal gas constant (kJ/kmol·K)
S surface area (m^2)
T temperature (K)
$\overline{T}_s$ mean temperature of the solid (K)
t time (s)
u x-directional velocity component (m/s)
V volume (m^3)
v y-directional velocity component (m/s)
W width of the solid target slab (m)
x coordinate along the surface (m)
Y_i species i mass fraction
y coordinate normal to the surface (m)
$\hat{y}$ $(y - \ell)$ (m)
y' $(\ell - y)$ (m)
Z pre-exponential (or collision) factor (1/s for solid pyrolysis, and $m^3/kg \cdot s$ for gas oxidation)

Greek Symbols

α thermal diffusivity (m^2/s)
δ reactive boundary layer thickness (m)
ε_s solid surface emissivity
η nondimensional y
θ nondimensional temperature
ν kinematic viscosity (m^2/s)
ρ density (kg/m^3)

Subscripts

c char
F fuel pyrolyzate
g gas
I inert
O oxygen
0 initial
P products
p pyrolysis or fuel pyrolyzate
R reservoir
s solid
w interface
∞ ambient

Superscript

* ignition

References Cited

1. A.M. Kanury, *Fire Res. Abst. and Rev.,* 14, p. 24 (1971).
2. F.R. Steward, in *Heat Transfer in Fires,* Scripta, Washington, DC, p. 379 (1974).
3. J.R. Hallman, J.R. Welker, and C.M. Sliepcevich, "Ignition of Polymers," *Proceedings of 30th Annual Conference,* Soc. Plastics Engineers, p. 283 (1972).
4. S.B. Martin, "Diffusion-Controlled Ignition of Cellulosic Materials by Intense Radiant Energy," *10th Symposium (International) on Combustion,* Combustion Institute, Pittsburgh, PA, p. 877 (1965).
5. C.H. Bamford, J. Crank and D.H. Malan, *Proc. Cambridge Phil. Soc.,* 42, p. 166 (1946).
6. K. Akita, *Report Fire Res. Inst.,* Tokyo, 9 (1959).
7. D.L. Simms, *Comb. and Flame,* 4, p. 293 (1960).
8. C.C. Ndibizu and P. Durbetaki, *Fire Res.,* 1, p. 281 (1977–78).
9. N.J. Alvares, *Tech. Report 735,* U.S.N.R.D.L., San Francisco (1964).
10. L.I. Deverall and W. Lai, *Comb. and Flame,* 13, p. 8 (1969).
11. G. Adomeit, "Ignition of Gases at Hot Surfaces Under Nonsteady State Conditions," *10th Symposium (International) on Combustion,* Combustion Institute, Pittsburgh, PA, p. 237 (1965).
12. F.M. Sauer, *Interim Technical Report AFSWP-868,* U.S. Department of Agriculture/Forest Service, Berkeley, CA (1956).
13. T. Kashiwagi, *Comb. Sci. and Tech.,* 8, p. 225 (1974).
14. E.W. Price, H.H. Bradely, Jr., and G.L. Dehority, *AIAA J.,* 4, p. 1153 (1966).
15. P.D. Gandhi, "Spontaneous Ignition of Organic Solids by Radiant Heating in Air," Ph.D. dissertation, University of Notre Dame, Notre Dame, IN (1984).
16. P.D. Gandhi and A.M. Kanury, *Comb. Sci. and Tech.,* 50, p. 233 (1986).
17. H.S. Carslaw and J.C. Jaeger, *Conduction of Heat in Solids,* Oxford University, London (1959).
18. A.N. Koohyar, J.R. Welker, and C.M. Sliepcevich, *Fire Tech.,* 4, p. 284 (1968).
19. H.R. Wesson, J.R. Welker, and C.M. Sliepcevich, *Comb. and Flame,* 16, p. 303 (1971).
20. W.K. Smith, *Ignition of Edges and Corners of Wood,* WAM Paper No. 72-WA/HT-20, ASME, New York (1972).
21. W.D. Weatherford and D.M. Sheppard, "Basic Studies of the Mechanics of Ignition of Cellulosic Materials," *10th Symposium (International) on Combustion,* Combustion Institute, Pittsburgh, PA, p. 897 (1965).
22. N.J. Alvares and S.B. Martin, "Mechanism of Ignition of Thermally Irradiated Cellulose," *13th Symposium (International) on Combustion,* Combustion Institute, Pittsburgh, PA, p. 905 (1971).
23. P.D. Gandhi and A.M. Kanury, in *Dynamics of Reactive Systems, Part I: Flames and Configurations,* AIAA, New York, p. 208 (1986).
24. S.B. Martin and N.J. Alvares, *Tech. Report 1007,* U.S.N.R.D.L., San Francisco (1968).

CHAPTER 12

Surface Flame Spread

James G. Quintiere

Introduction

This chapter covers both opposed flow and wind-aided flame spread over solids. Approximate formulas are developed using simple assumptions in order to illustrate the role of the relevant physical and chemical variables. The relationship between these approximate formulas and more exact results and data is discussed. Although an extensive review is not presented, an attempt is made to illustrate the extent of knowledge and opportunities for application. Flame spread over liquid fuels, in the forest, and in microgravity is also briefly discussed.

This chapter has been entitled "Surface Flame Spread" to ensure its distinction from flame propagation in premixed fuel and air systems. In the context here, flame spread applies to the phenomenon of a moving flame in close proximity to the source of its fuel originating from a condensed phase, (i.e., solid or liquid). As in the premixed case, the flame propagates in the gas phase, with its front associated with the lower flammability limit mixture. The fuel in the mixture is the vaporized condensed-phase fuel. The vaporization process is caused by heat transfer from the advancing flame itself and is necessary to sustain the spreading flame. Thus, two advancing fronts are present (1) the flame in the gas phase, and (2) the evaporation or pyrolysis region in the condensed phase. The former is easily perceived by the casual observer, while the evaporation front is actually a measure of the surface flame spread for the condensed phase. This front is not easily measured, but its rate of movement is defined as the *flame spread velocity.* These processes are illustrated in Figures 2-12.1 and 2-12.5.

In natural fires, it is the flame-spread process that is critical to the fire's destiny. This applies whether the fire is an urban conflagration or is the first growth after ignition of a room's draperies. The process of growth is unstable, with the time for flame spread competing with the time for burning. If the spread time is small compared to the burn time, fire growth is likely to accelerate. Conversely, fire growth could decelerate and stop if the spread time is large compared to the burn time.

An example might illustrate the significance of flame spread in fire growth. Consider the ignition of an upholstered chair over a region 6 cm in diameter. Typical unenhanced spread rates are of the order of magnitude 1 mm/s, so in one minute the pyrolyzing region would be 18 cm in diameter, since the front would have grown 6 cm. This is nearly a tenfold increase in the pyrolyzing region, and, for sufficient fuel (long burn time), the increased rate of energy release will provide enhanced heat transfer to increase the flame spread rate. The fire growth is manifested by the size of the evaporation region over the condensed phase, and the rate of movement of its boundary is the flame spread velocity. Thus, surface flame spread plays a significant role in natural fire growth.

Premixed flame propagation can also occur in natural fires, provided that, in the gas phase, fuel and air are within their flammable limits over an extended region. This might result from a combustible gas leak, or could also arise under sufficient heating or restrictive ventilation conditions during the development of a fire in a confined space. In such cases, a sufficient energy source would initiate the propagation of flames in the gas phase at velocities of the order of magnitude 1 m/s compared to 1 mm/s associated with representative surface spread velocities. These values suggest the plausible limits of flame propagation in natural fires, but it is the lower end of the scale that governs the early development of fires on solid and liquid fuels. Subsequently, the nature and controlling variables can be described for such flame spread over solids and liquids. Table 2-12.1 gives the relative rates of flame spread for several fire phenomena, including horizontal surface spread and gas phase phenomena.

Dr. James G. Quintiere is the John L. Bryan Professor in the Department of Fire Protection Engineering at the University of Maryland, College Park. His research has focused on fire growth and flame spread.

Table 2-12.1 ***Relative Flame Spread Rates (order of magnitude)***

Phenomenon	Rate (cm/s)
Smoldering	10^{-3} to 10^{-2}
Lateral or downward spread on thick solids	$\sim 10^{-1}$
Upward spread on thick solids	1 to 10^2
Horizontal spread on liquids	1 to 10^2
Forest and urban fire spread	1 to 10^2
Pre-mixed flame speeds	
Laminar deflagration	10 to 10^2
Detonation	$\sim 3 \times 10^5$

Background

In recent years, research has focused on methods applying fundamental aspects of flame spread to real problems. Fundamental theory has provided a foundation for application, and formulas have been developed for practical use. However, these formulas are still limited by the lack of material data and phenomenological information about the fire conditions. For solid materials, the development of the cone calorimeter[1] and the lateral ignition and flame spread (LIFT)[2] tests has provided a basis for the needed material data. Attempts have been made to include configuration effects on flame spread, such as fire spread in vertical corners and ceilings. These attempts have not led to fully established methods, but have shown promise in replacing old flammability indices with more meaningful measures of flammability.

It is not possible to describe completely in a brief chapter all the research on flame spread. Hence, comprehensive reviews should be sought elsewhere. Recent reviews include Quintiere[3] on wall fire spread, and Hirano[4] on fundamental studies. A good source of material property data for wood species and products can be found from Janssens study.[5] Other noteworthy recent reviews on flame spread can also be found in the literature. For example, Fernandez-Pello and Hirano[6] give a detailed review of progress in flame spread over solids. Current knowledge on flame spread over liquid fuels is brought into focus by a critical review conducted by Glassman and Dryer.[7] For a more tutorial discussion, one might read the presentation by Drysdale[8] in the book, *An Introduction to Fire Dynamics.*

An excellent review and tutorial on flame spread was presented by Williams[9] in 1976. It organized the subject in terms of the nature of the fuel's configuration and the mechanisms controlling flame spread. Its clarity in describing these mechanisms in simple terms is valuable reading for any serious student of flame spread. It describes each type of flame spread by physical arguments and expressions based upon the "fundamental equation of flame spread." That equation considers the net energy (heat) transferred (per unit area per unit time), $\dot{q}''$, ahead of the advancing flame to heat the medium from its initial temperature, T_s, to its ignition temperature, T_{ig}. This energy is equated to the change in enthalpy (per unit area per unit time) that the medium experiences for an observer on the moving flame front. For steady conditions

$$\rho V \Delta h = \dot{q}'' \tag{1}$$

where

ρ = density of the medium

V = spread rate

Δh = change in enthalpy per unit mass of medium in going from T_s to T_{ig}

The concept of an ignition temperature here represents the solid or liquid surface temperature that would cause sufficient production of fuel in the gas phase to sustain piloted ignition. For liquid fuels, this temperature is called the firepoint, and for solids it would depend on the kinetics of thermal degradation. Usually, it is assumed that the condensed phase is heated to the ignition temperature as a constant-property homogeneous medium; therefore, we can write

$$\Delta h = c(T_{ig} - T_s) \tag{2}$$

where c is the specific heat of the solid or liquid. Thus, a conceptual formulation has been established for the flame spread speed, V. It is interesting to observe that, for a given flame heat flux, V will increase as the fuel density decreases, and will increase without bound as T_s approaches T_{ig}. Thus, low-density solids could pose a potential flame-spread hazard; and, as T_s ahead of the advancing flame is increased by far-field convective and radiative effects of the fire, the spread will accelerate.

Flame Spread over Solids

In this section, some theoretical aspects will be sketched to illustrate the nature of flame spread on solids. In general, flame spread can occur in the presence of an ambient wind, such that the spread is upwind (opposed flow flame spread) or downwind (wind-aided flame spread). The wind might be due to external causes, which could be meteorological in nature, or due to a fire-induced (natural convection) flow created by the spreading flame or an associated fire. These two categories will be treated subsequently. Also, flame spread on solids will depend on geometrical orientation, that is, vertical or horizontal, facing upward or downward. All of these factors will affect the heat transfer ($\dot{q}''$) indicated in Equation 1. Indeed, the complex problem of computing $\dot{q}''$ from first principles has limited our ability to predict flame spread. Thus, issues of heat transfer pertaining to laminar and turbulent flow and flame radiation all play a role. Ultimately, chemical kinetic factors that control flame temperature, and indeed the survival of the flame itself, come into play. Hence, only the form of simple theoretical expressions will be derived. For more details and for the inclusion of other variables, specific references should be examined.

Opposed Flow Spread

Following the concept of using an energy conservation principle to describe flame spread (i.e., Equation 1), some simple analyses will be described. Although these analyses will be heuristic, their final results will be consistent with more formal analyses found in the literature. First, opposed flow spread will be considered for a solid whose thickness is sufficiently small so that the temperature is uniform across its thickness. In all cases, the spread rate is assumed steady and the reference frame is fixed to the pyrolysis front, that is, the position where the solid (surface) temperature is T_{ig}. This is illustrated in Figure 2-12.1.

Thermally thin case: For this *thermally thin case* of physical thickness, δ, and no heat loss from the bottom face, the energy equation for the control volume is developed. The control volume has been selected to extend from the region at the onset of pyrolysis, T_{ig}, to the region unaffected by the energy transported into the solid from the flame. This region is a distance Δ from the pyrolysis region to the position of initial solid temperature, T_s. The heat flux from the flame, $\dot{q}''$, will be assumed constant over Δ. It follows that for the solid moving steadily through the flame-fixed control volume at the flame spread speed, V,

$$\rho c \delta (T_{ig} - T_s) V = \dot{q}'' \Delta \tag{3}$$

Equation 3 is a more complete version of Equation 1, with the length scales δ and Δ explicitly included. The net forward flame heat flux characterized as conduction in the gas phase suggests

$$\dot{q}'' \approx k_g \left(\frac{T_f - T_r}{\Delta} \right) \tag{4}$$

where

k_g = gas phase conductivity

T_f = flame temperature

T_r = reference temperature for the solid—either T_{ig} or T_s would suffice

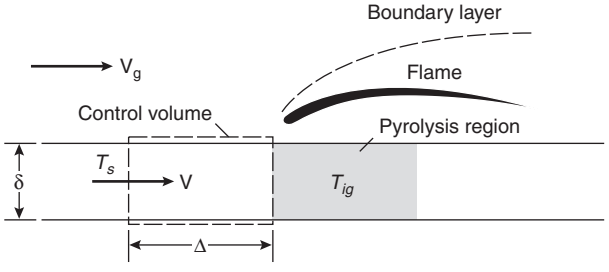

Figure 2-12.1. ***Energy conservation analysis in opposed flow spread.***

Combining Equations 3 and 4 yields an expression nearly identical to that more formally derived by deRis[10] for thermally thin solids

$$V = \frac{\sqrt{2} k_g (T_f - T_s)}{\rho c \delta (T_{ig} - T_s)} \tag{5}$$

The flame temperature, T_f, here should ideally be taken as that due to adiabatic stoichiometric combustion but, in general, could be thought of as less due to heat losses and chemical kinetic effects. Under these ideal theoretical considerations, it can be shown[11] that

$$T_f - T_{ig} = \frac{(T_\infty - T_{ig}) + (Y_{ox,\infty}/r c_g)(\Delta H - L)}{1 - Y_{ox,\infty}/r} \tag{6}$$

where

ΔH = heat of combustion of the solid fuel

L = heat of gasification

T_∞ = gas phase ambient temperature

$Y_{ox,\infty}$ = gas phase ambient oxygen concentration

r = stoichiometric mass ratio of oxygen to fuel

c_g = specific heat of the gas phase

Because ΔH and $Y_{ox,\infty}/r$ are relatively large, and $\Delta H_{ox} = \Delta H/r$ is nearly a constant for most hydrocarbons (13 kJ/g), Equation 6 suggests that

$$T_f - T_{ig} \sim Y_{ox,\infty} \Delta H_{ox} / c_g \tag{7}$$

Thus, the flame temperature for many solids is primarily only sensitive to the ambient oxygen concentration. This fact suggests that flame spread over a ceiling in a room would be reduced as the oxygen near the ceiling was reduced. Substitution of Equation 7 into 5, essentially yields the results of Magee and McAlevy;[12] however, they considered pressure effects as well. Incidentally, their early work in flame spread[12] contains extensive data on factors affecting flame spread.

Up to now, no mention of the opposed flow speed, V_g, has been made, and the flame spread velocity appears to be independent of it. Independence is only the case as long as chemical effects are unimportant. Chemical kinetic effects become important when the time for chemical reactions to be completed in the flame (t_{chem}) becomes long compared to the fluid flow transit time (t_{flow}) through the flame. If the flow is too fast, chemical reaction would be incomplete. The Damköhler number (D) is a parameter used to express these effects and may be represented as Equation 8

$$D \sim \frac{t_{\text{flow}}}{t_{\text{chem}}} \sim \frac{1}{V_g^2} \tag{8}$$

As a consequence, the flame heat transfer or theoretical flame temperature in Equation 5 is then modified by some function of D. The dependence of D measured spread rates over thin paper sheets has been correlated by Fernandez-Pello et al.[13] in forced flow conditions and by Altenkirch et al.[11] under buoyant flow downward spread

conditions. A recent theoretical analysis by Wichman[14] offers some explanation for these correlations. Each investigator defined a slightly different Damköhler number and selected different chemical kinetic property data. But in qualitative terms, Figure 2-12.2 represents the results given, with the measured spread velocity normalized with the ideal theoretical velocity Equation 5 plotted against D. The results show that the flame spread decreases with D, and therefore decreases as the opposed flow velocity is increased for the thermally thin solid.

For flame-induced flows in pure natural convection, the ambient flow velocity is characteristically given as[11]

$$(V_g)_{\substack{\text{natural}\\ \text{convection}}} \sim \left(\frac{\nu_g g \Delta H Y_{ox,\infty}}{c_g r T_\infty}\right)^{1/3} \tag{9}$$

where ν_g is the gas phase kinematic viscosity. But since $\Delta H/r = \Delta H_{ox}$, approximately constant at 13 kJ/g, V_g induced by buoyancy is primarily a function of $Y_{ox,\infty}$ to the 1/3 power.

In summary, for thermally thin solids, the flame spread speed under an opposed flow velocity, V_g, with an ambient oxygen concentration, $Y_{ox,\infty}$, is from Equation 5

$$V = V_{\text{ideal}} f(D) \tag{10}$$

where V_{ideal} is given by Equation 5 and the general behavior of $f(D)$ is shown in Figure 2-12.2. At some critical value of D, no further flame spread is possible and extinction occurs. For a given material, D depends on V_g and $Y_{ox,\infty}$, and, from Equation 7 the theoretical flame temperature depends only on $Y_{ox,\infty}$. Therefore, from Equations 5 and 10, the general form of the relationship in opposed flow flame spread on thin materials is

$$V = \frac{\phi(V_g, Y_{ox,\infty}, \text{material properties})}{\rho c \delta (T_{ig} - T_s)} \tag{11}$$

where the function ϕ depends on such factors as the gas velocity, the local oxygen concentration, and the properties of the material. For common combustible solids, it has been reasoned[10] that the above analysis holds for $\delta \leq$ 1 mm, approximately. In particular, Fernandez-Pello and Hirano[6] concluded that for polymethyl methacrylate (PMMA), downward flame spread could be considered thermally thin for $\delta < 2$ mm and thermally thick for $\delta >$ 2 cm. In between, the solid would have a nonuniform but finite temperature rise throughout flame spread.

Except for items like paper, garments, or draperies, most solids in practice will behave as thermally thick under flame spread conditions. It might appear, for engineering purposes, to regard solids with $\delta > 1$ mm as thermally thick. Up to a thickness of 1 to 2 cm, flame spread could depend on thickness and on the substrate material adjacent to the solid. Based on these factors, it is apparent that the thermally thick case is more significant, and it will be derived below.

Thermally thick case: The analysis based on Figure 2-12.1 still applies, except that for the *thermally thick case,* δ must be considered as the thermal penetration depth, which depends on time. From heat conduction theory, it can be reasoned that

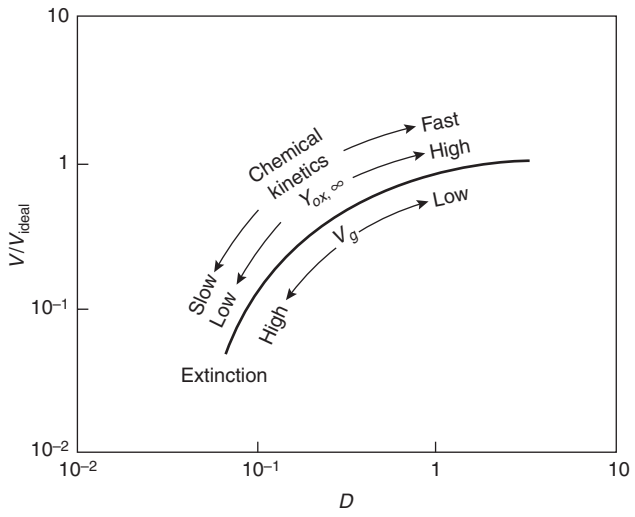

Figure 2-12.2. ***Qualitative dependence of opposed flow flame speed with Damköhler number, D.***

$$\delta \approx \sqrt{\frac{k}{\rho c} t} \tag{12}$$

where t is the time for the flame's pyrolysis front to traverse the heating length, Δ, of the control volume in Figure 2-12.1

$$t = \frac{\Delta}{V} \tag{13}$$

Substitution of Equations 12 and 13 into Equation 3 yields

$$V = \frac{(\dot{q}'')^2 \Delta}{k \rho c (T_{ig} - T_s)^2} \tag{14}$$

The length scale, Δ, depends on the nature of the forward heat transfer. In opposed flow spread, when forward conduction in the gas phase is the dominant mode of heat transfer, it can be reasoned that forward conduction must be balanced *with* convection, that is,

$$\rho c V_g \frac{\partial T}{\partial x} \sim k \frac{\partial^2 T}{\partial x^2}$$

in the gas phase.

As a consequence,

$$\Delta \sim \left(\frac{k}{\rho c}\right)_g / V_g \tag{15}$$

and, on combining with Equations 4 and 14 yields

$$V = \frac{V g (k \rho c)_g (T_f - T_{ig})^2}{k \rho c (T_{ig} - T_s)^2} \tag{16}$$

as the flame speed for the thermally thick case—identical to the formally derived by deRis.[10] This expression should

be termed the *ideal value*, with T_f given by its adiabatic stoichiometric value. With this viewpoint, the chemical kinetic effects enter through the Damköhler number, as in the thin case, with the actual velocity given as

$$\frac{V}{V_{\text{ideal}}} = F(D) \tag{17}$$

Figure 2-12.2 applies, as well. But, for the thick case, because the "ideal" flame speed (Equation 16) depends on the opposed velocity, V_g, directly as well as through the Damköhler number, D, the actual flame spread speed may either increase or decrease with V_g, depending on $Y_{ox,\infty}$. Fernandez-Pello et al.[13] show for PMMA that V is insensitive to V_g for $V_g \leq 30$ cm/s at normal ambient oxygen levels ($Y_{ox,\infty} = 0.233$) and decreases as V_g is increased. These results are sketched in Figure 2-12.3. At higher-than-normal oxygen levels for air, the dependence of V on V_g is more complicated. Thus, the Damköhler number dependence is required to fully understand the effect of V_g on V for thick fuels. One consolation, at least for PMMA, is that under normal fire conditions (e.g., downward spread on a wall), the buoyancy-induced flow speed is roughly 30 cm/s. For this air speed or less, V is primarily dependent on $Y_{ox,\infty}$ only.

In previous studies, the opposed flow has been laminar. The effects of turbulence have been investigated by Zhou and Fernandez-Pello[15] who found that the spread rate decreased in air flows as the opposed turbulent intensity increased for thin paper, but had a maximum for thick PMMA at approximately 0.5 m/s.

A complete numerical simulation, including the effects of solid- and gas-phase kinetics, has been attempted by Di Blasi et al.[16] with qualitative success. Such models will provide useful insight into the fundamental mechanisms, provided these effects can be computationally resolved.

A practical test procedure has been developed by Quintiere and Harkleroad[17] that allows one to determine the essential parameters needed to describe opposed-flow flame spread on thick materials burning in air under natural convection conditions. As done for the thin case in Equation 11, Equation 17 is rewritten as follows:

$$V = \frac{\Phi}{k\rho c(T_{ig} - T_s)^2} \tag{18}$$

where Φ depends on V_g and $Y_{ox,\infty}$, in general, for a given material. By measuring the flame spread laterally on a vertical sample exposed to an external radiant heat flux, the parameters Φ, $k\rho c$, and T_{ig} are deduced by analysis. A wide range of tests indicated that T_{ig} ranged from 280°C for PMMA to 570°C for the paper on gypsum wallboard. The parameter, Φ, for these conditions in air ranged from about 1 to 15 $(\text{kW})^2/\text{m}^3$. Also, a critical surface temperature was determined below which continued spread was not possible ($T_{s,min}$). Table 2-12.2 illustrates these deduced parameters for a range of materials. Results obtained in this lateral mode were shown to be similar to downward spread, except for materials with excessive melting and dripping,[17] and were shown to be similar to axisymmetric spread from a small (pool) fire on a horizontal surface.[18] Other data for wood products are given by Janssens.[5]

In these analyses, the ignition temperature has been assumed constant for each material, and its name implies a relationship between ignition and flame spread. It is interesting to illustrate this relationship by showing the behavior of spread velocity and time to ignite as a function of radiant heating. Consider downward or lateral spread on a vertical surface at various levels of irradiation, $\dot{q}''_e$. For each $\dot{q}''_e$ the surface is allowed to heat to a steady temperature, T_s, before flame spread is initiated. Thus, there is a unique T_s for a given $\dot{q}''_e$. Consider, also, piloted ignition of this same material under sufficiently high values of $\dot{q}''_e$. Such experiments have been done for a wide range of materials[17] and the results all have the same characteristics. These trends are shown for a 1.27-cm-thick Douglas fir particleboard in Figure 2-12.4. It might be termed a "flammability diagram" for the material, since it shows at a glance its ease of ignition and its propensity for spread. Moreover, the minimum irradiance for ignition, $\dot{q}''_e(T_{ig})$, marks a critical condition for spread; and T_{ig} can be inferred from a knowledge of $\dot{q}''_e(T_s)$. This procedure has been adopted in the standard test known as LIFT (lateral ignition and flamespread test).[2]

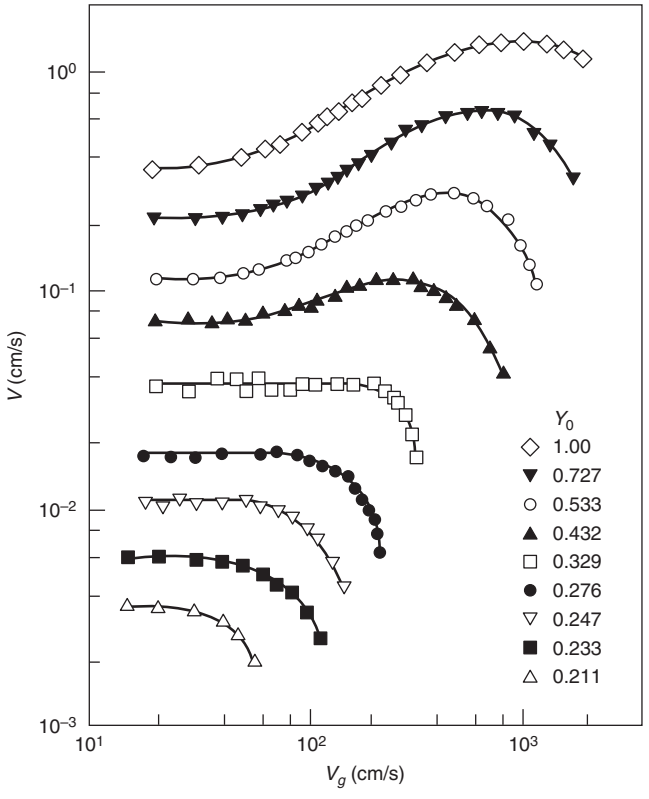

Figure 2-12.3. ***Effect of opposed velocity and oxygen concentration of flame spread speed for thick PMMA. (Taken from Fernandez-Pello et al.)[13]***

Wind-Aided Spread

Flame spread in the same direction as the ambient flow is much different from opposed flow spread. This classification of spread could result from an external wind

Table 2-12.2 ***Effective Flame Spread Properties (based on experimental correlations[17])***

Material	T_{ig} (°C)	$k\rho c$ (kW^2s/m^4K^2)	Φ (kW^2/m^3)	$T_{s,min}$ (°C)	$\Phi/k\rho c$ (mK^2/s)
PMMA polycast (1.59 mm)	278	0.73	5.4	120	8
Polyurethane (S353M)	280	—	—	105	82
Hardboard (6.35 mm)	298	1.87	4.5	170	2
Carpet (acrylic)	300	0.42	9.9	165	24
Fiberboard, low density (S119M)	330	—	—	90	42
Fiber insulation board	355	0.46	2.2	210	5
Hardboard (3.175 mm)	365	0.88	10.9	40	12
Hardboard (S159M)	372	—	—	80	18
PMMA type g (1.27 cm)	378	1.02	14.4	90	14
Asphalt shingle	378	0.70	5.3	140	8
Douglas fir particle board (1.27 cm)	382	0.94	12.7	210	14
Wood panel (S178M)	385	—	—	155	43
Plywood, plain (1.27 cm)	390	0.54	12.9	120	24
Chipboard (S118M)	390	—	—	180	11
Plywood, plain (0.635 cm)	390	0.46	7.4	170	16
Foam, flexible (2.54 cm)	390	0.32	11.7	120	37
GRP (2.24 mm)	390	0.32	9.9	80	31
Mineral wool, textile paper (S160M)	400	—	—	105	34
Hardboard (gloss paint) (3.4 mm)	400	1.22	3.5	320	3
Hardboard (nitrocellulose paint)	400	0.79	9.8	180	12
GRP (1.14 mm)	400	0.72	4.2	365	6
Particle board (1.27 cm stock)	412	0.93	4.2	275	5
Gypsum board, Wallpaper (S142M)	412	0.57	0.79	240	1
Carpet (nylon/wool blend)	412	0.68	11.1	265	16
Carpet #2 (wool, untreated)	435	0.25	7.3	335	30
Foam, rigid (2.54 cm)	435	0.03	4.0	215	141
Polyisocyanurate (5.08 cm)	445	0.02	4.9	275	201
Fiberglass shingle	445	0.50	9.0	415	18
Carpet #2 (wool, treated)	455	0.24	0.8	365	4
Carpet #1 (wool, stock)	465	0.11	1.8	450	17
Aircraft panel epoxy Fiberite	505	0.24	[a]	505	[a]
Gypsum board, FR (1.27 cm)	510	0.40	9.2	300	23
Polycarbonate (1.52 mm)	528	1.16	14.7	455	13
Gypsum board, (common) (1.27 mm)	565	0.45	14.4	425	32
Plywood, FR (1.27 cm)	620	0.76	[a]	620	[a]
Polystyrene (5.08 cm)	630	0.38	[a]	630	[a]

Values are only significant to two places.

[a]Flame spread was not measureable.

or the buoyancy-induced flow as a flame spreads up a wall or under a ceiling. Wind-aided spread can be accelerator and, therefore, appears more rapid than opposed flow spread. Despite their distinct differences, the previous simplified analyses can still be used to explain wind-aided spread.

The illustration in Figure 2-12.1 can be used here with the control volume of interest selected downstream of the pyrolysis zone. This is shown in Figure 2-12.5, where the length of the control volume, Δ, is selected to span the heat transfer from the adjacent flame and hot combustion products in the boundary layer. Here, Δ is of the order of the flame length and could be in the range of 0.1 to 10 m as compared to Δ in opposed flow flame spread in the range of 1 to 3 mm. The control volume is fixed to the leading edge of the pyrolysis zone where the temperature has achieved the ignition temperature, T_{ig}. A distance Δ away, the solid is still at its initial temperature, T_s, and moves through the control volume at the flame spread speed V. An energy balance applied to this control volume will lead to the same equations as developed in the opposed flow analyses, but with a different interpretation for the terms $\dot{q}''$ and Δ. From Equations 3 and 14, those results are given as follows for the thermally thin case:

$$V = \frac{dx_p}{dt} = \frac{\dot{q}''\Delta}{\rho c \delta (T_{ig} - T_s)} \tag{19}$$

and for the thermally thick case:

$$V = \frac{dx_p}{dt} = \frac{(\dot{q}'')^2\Delta}{k\rho c (T_{ig} - T_s)^2} \tag{20}$$

These results should be taken as qualitatively illustrative, especially since $\dot{q}''$ has been assumed constant over Δ. Actually the heat flux distribution will vary, in general, with

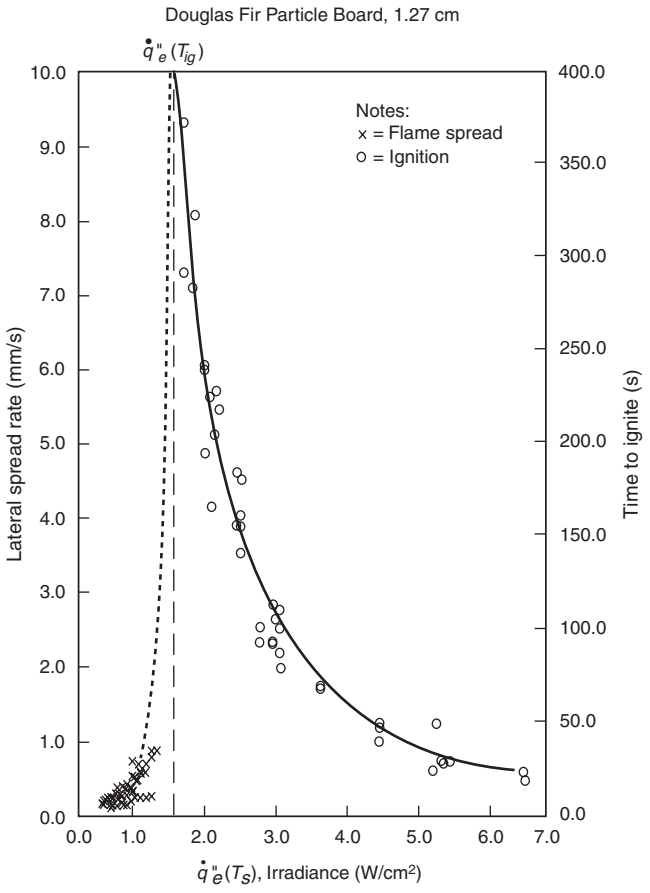

Figure 2-12.4. ***Relationship between piloted ignition and flame spread velocity.[17]***

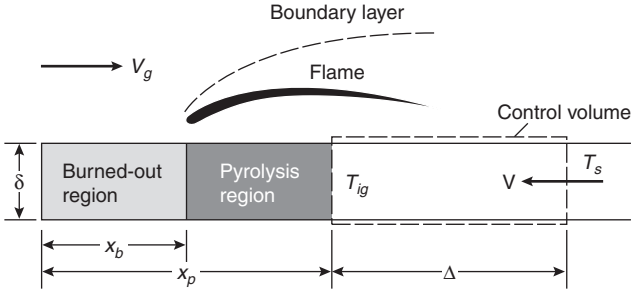

Figure 2-12.5. ***Energy conservation in wind-aided flame spread.***

the downstream coordinate (x) in accordance with the convective boundary layer and flame radiative characteristics. Also, Δ would be intimately related to the nature of the heat flux distribution.

Alternatively, Equations 19 and 20 can be written as

$$V = \frac{dx_p}{dt} = \frac{x_f - x_p}{\tau} \tag{21}$$

where τ is an ignition time associated with the flame heat flux. Wichman and Agrawal[19] more carefully show the basis of this formulation for wind-aided spread. Here, x_f is the flame length measured from $x = 0$, and the flame heat flux is assumed constant over this region Δ. Saito et al.[20] use this formulation to examine upward (or, in general, wind-aided) spread. From the definition of x_p,

$$x_p = x_p(0) + \int_0^t V(s)ds \tag{22}$$

It is postulated that x_f is directly related to energy released per unit width, $\dot{Q}'$, so that

$$x_f - x_b = K[\dot{Q}']^n \tag{23a}$$

where

$$\dot{Q}' = \int_{x_b}^{x_p} \dot{Q}''(\xi)d\xi \tag{23b}$$

with $\dot{Q}''$ the energy release per unit area. It should be noted that the cone calorimeter[1] can potentially provide data to derive $\dot{Q}''$. However, this depends on the heat flux appropriate to the flame spread configuaraton, not necessarily on the cone test irradiance. For example, for upward spread on a flat wall and under turbulent conditions, $K = 0.067\ \mathrm{m}^{5/3} \cdot \mathrm{kW}^{-2/3}$ and $n = 2/3$.[21] It can be shown[20] that

$$\dot{Q}' = x_p(0)\dot{Q}''(t) + \int_0^t \dot{Q}''(t-s)V(s)ds \tag{24}$$

for the case of $x_b = 0$. Substituting Equations 22 through 24 yields an integral equation for V. This formulation gives a framework for solving particular wind-aided spread problems, provided that the flame heat flux and flame length can be expressed for that configuration. Also, material data are needed to express τ and $\dot{Q}''$. Variations on this formulation have been applied successfully to predict upward turbulent flame spread.[22–25]

Fundamental studies have given us some limited results. A simpler result for V can be derived. The heat flux, $\dot{q}''$, could be reasoned to depend on the flame temperature, T_f, (Equation 7) and on the boundary layer thickness. The extent of heating, Δ, is related to flame length, and this has been shown to depend on the energy release rate to some power n (e.g., n is believed to be 1/2 to 1 in upward turbulent spread). Since the energy release rate depends on the extent of the pyrolyzing region, $(x_p - x_b)$, then it suggests that

$$V = \frac{dx_p}{dt} \propto (x_p - x_b)^n \tag{25}$$

provided $\dot{q}''$ is not sensitive to position. Thus, depending on n and the relationships governing burnout (i.e., $x_b(t)$), the flame speed can accelerate to a limit or without bound if $n > 0$. Markstein and deRis[26] found for thin textiles that n varied from 0.5 to 0.7, with $x_p - x_b$ approaching an asymptotic steady-state limit after some time. The nature of their experiments was upward turbulent burning conditions. Under laminar upward spread, Fernandez-Pello[27] derived $n = 3/4$ for the thermally thin case, $n = 1/2$ for the thermally thick case, and $x_b \equiv 0$. Orloff et al.[28]

found that upward turbulent spread on thick PMMA followed Equation 25, with $n = 0.964$ and $x_b \equiv 0$. After spread extended over approximately 1 m of the PMMA, the speed was measured at roughly 0.5 cm/s. Note, for $n = 1$ and $x_b = 0$, the speed grows exponentially in time. This growth marks the potential hazard of wind-aided spread. It should be clear that the outcome depends on flame length, which is controlled by configuration and flow conditions, and on burnout, which is controlled by the material.

There are several notable wind-aided studies. Atreya and Mekki[29] have studied laminar flame spread on a ceiling-mounted sample. Di Blasi et al.[30] mathematically modelled this spread problem, including unsteady and kinetic effects. They found that the spread speed reaches steady state at a given flow velocity, and also kinetic effects were only important at extinction. A turbulent flow study by Zhou and Fernandez-Pello[31] for ceiling- and floor-mounted PMMA (0.3 m in length) found flow speeds of 0.25 to 4.5 m/s with turbulent intensities 1 percent to 15 percent. They also found that the spread rate is steady at a given flow, but increases with flow speed. For their range of flow conditions, they found that Equation 20 agrees with a numerical coefficient of $1.4(4/\pi)$. At larger scales, radiation and buoyancy effects become important, especially for floor-mounted materials. Studies by Apte et al.[32] for 2.4-m-long PMMA and by Perzak and Lazzara[33] for 9.8-m-long PMMA at flow speeds of 0.8 to 3.8 m/s show higher spread rates due to flame radiation effects. They measure rates of 1 to 6 cm/s, compared to approximately 0.01 to 0.3 cm/s for smaller samples.[31]

The ASTM E84 Steiner tunnel test is the primary flammability test used in the United States. It represents a complex form of wind-aided spread on a ceiling-mounted material in a duct under forced flow conditions. Although that test is not capable of measuring x_p (nor x_b), a recent correlation showed its sensitivity to energy release rate.[34] It was found that tunnel ratings were low and insensitive to energy release rate per unit area, $\dot{Q}''$, for values less than approximately 70 kW/m² and highly sensitive and increasing above that value. In other words, some critical energy release rate appears to be required to permit sustained spread. It is likely that the ASTM E-84 Steiner tunnel test can be successfully modelled using Equation 20, provided tunnel relationships are developed for $\dot{q}''$ and Δ.

For upward turbulent flame spread on a vertical surface, it has been found that the flame heat flux ahead of the pyrolysis zone is approximately 25 kW/m² for moderate fires ($x_f < 1.4$ m), and approximately independent of material. This is shown in Figure 2-12.6 where the sketched region represents the data of Quintiere et al.[3,35] It also displays the laminar and turbulent results of Ahmed and Faeth[36] without radiation effects, the large-scale PMMA results of Orloff et al.,[37] and power-law correlations of the data by Hasemi.[38] It is seen that both laminar and large fires can exceed 25 kW/m². More recent data by Kulkarni et al.[24] generally confirm this heat flux distribution, with some exceptions, possibly due to measurement difficulties for melting materials. Figure 2-12.7 shows results of a study by Ito and Kashiwagi[39] using interferometry to examine the temperature distributions at the leading edge of spreading flames on PMMA at orientations

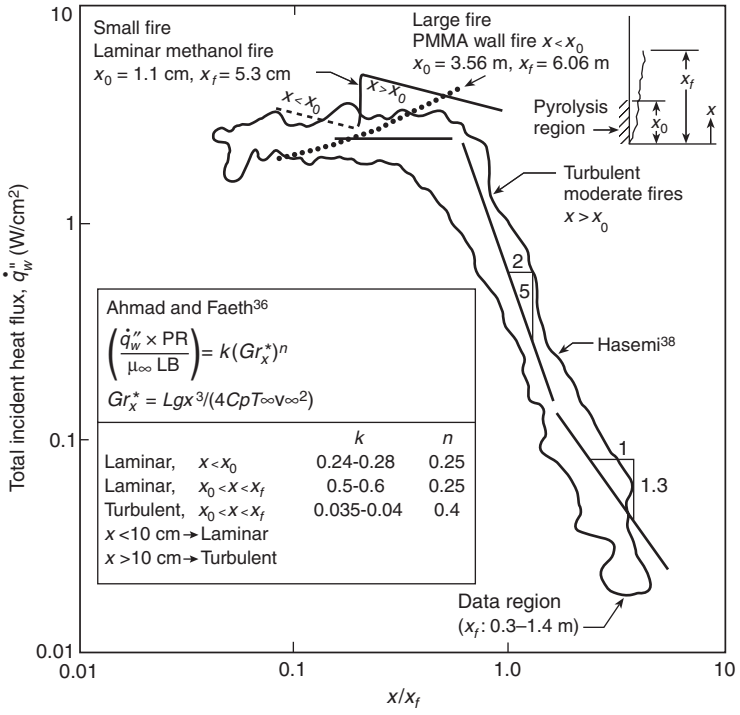

Figure 2-12.6. ***Wall flame incident heat flux for materials,[35] for laminar flames,[36] and for a large PMMA wall fire.[37]***

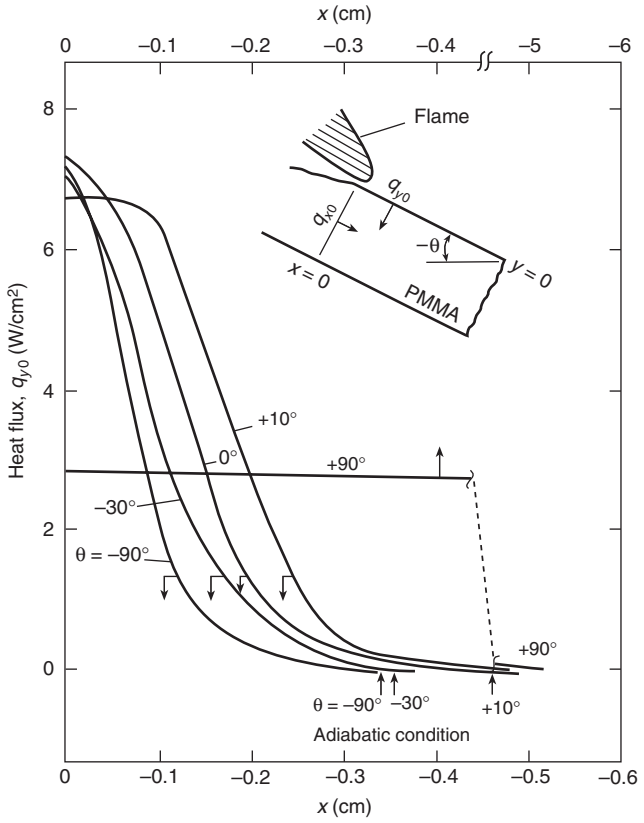

Figure 2-12.7. ***Distributions of normal heat flux at the surface along the distance ahead of the vaporization front, from Ito and Kashiwagi.[39]***

ranging from +90 degrees (upward vertical) to –90 degrees (downward vertical). Note the constant heat flux of approximately 25 kW/m² for upward spread, and a maximum of 70 kW/m² for downward spread. A notable orientation effect was found in the London King's Cross fire involving spread up a wooden escalator. The sidewalls of the escalator caused the flames to "hug" the steps.[40]

The room-corner test has been developed as a realistic testing protocol for the flammability of interior finish materials. Several investigators have had good success at predicting the results of this configuration using data from the cone calorimeter test and the flame spread equations discussed above.[41–45] It appears that accurate simulation models for fire growth can be developed using the flame spread theories outlined here along with relevant data.

Flame Spread over Liquids

Flame spread over horizontal pools of liquid fuels differs from flame spread over solids, due to convective flows within the liquid that enhance spread. Also, whereas solid decomposition is more complex, involving kinetically driven pyrolysis, the liquid fuel evaporates under thermodynamic principles. The liquid temperature, T_s, controls the rate of spread relative to a critical (ignition) temperature that corresponds to that necessary to produce a lean flammability limit over the fuel surface. This temperature is usually referred to as the flash point for liquid fuels, and several methods exist for its measurement. Glassman and Dryer[7] discuss the implications of its measurement and its relationship to mechanisms associated with flame spread on liquids.

The convective phenomenon generated in the liquid is due to surface tension effects. The surface tension increases inversely with temperature and, thus, can pull the flame toward the unheated liquid. This is illustrated in Figure 2-12.8 for a thin liquid layer, δ. Under steady conditions, the viscous forces on the control volume are balanced by the surface tension forces. Thus, the shear stress, τ, at the bottom surface equals the surface tension gradient ($d\sigma/dx$) along the free surface

$$\tau = \frac{d\sigma}{dx} = \left(\frac{d\sigma}{dT}\right)\left(\frac{\partial T}{\partial x}\right) \tag{26}$$

For a thin liquid layer, the surface tension effect results in nearly a Couette flow (constant shear) over the layer thickness, δ. Hence, it can be approximated that

$$\tau = \left(\mu \frac{\partial u}{\partial y}\right)_{y=0} \approx \mu \frac{V}{\delta} \tag{27}$$

where μ is the liquid viscosity. By further approximating the surface tension gradient as a difference over length Δ, the flame speed can be estimated as

$$V = \frac{[\sigma(T_s) - \sigma(T_{ig})]\delta}{\mu\Delta} \tag{28}$$

provided $\sigma(T)$, the surface tension, is known as a function of temperature for the liquid, and Δ can be estimated for the conditions of spread. Also, δ, as in the thermally thick case for solids, is only the physical liquid depth for pools less than about 1 mm, and, therefore, must be reinterpreted for pools of larger depth.[9] For example, one might estimate δ as

$$\sqrt{\left(\frac{\mu}{\rho}\right)\left(\frac{\Delta}{V}\right)}$$

for the deep-pool case.

Typical flame spread characteristics over a liquid fuel are sketched in Figure 2-12.9 for liquid methanol from the data of Akita.[46] Below the flash point, $T_s < T_{ig} \approx 11°C$, the spread is governed by transport phenomena within

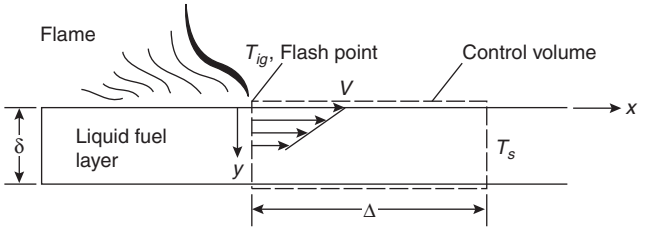

Figure 2-12.8. ***Enhanced flame spread speed in liquids due to surface-tension induced flow.***

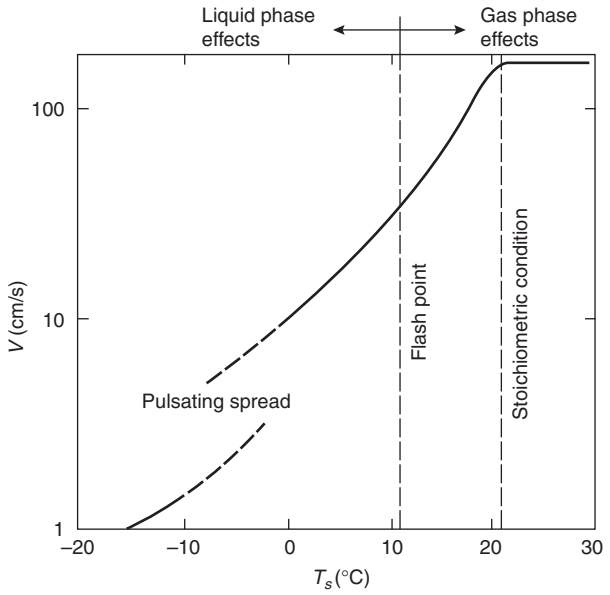

Figure 2-12.9. ***Results sketched for flame spread over liquid methanol, based on Akita.[3]***

the liquid fuel. For initial liquid bulk temperatures above the flash point, a flammable mixture always exists everywhere above the surface so that propagation is governed by gas phase effects. Above a liquid temperature, which corresponds to stoichiometric conditions above the surface, the flame speed remains constant and usually above the normal premixed laminar flame speed. A recent study by Ito et al.[47] used holographic interferometry to examine the liquid phase for subflash point liquid bulk temperatures. They examined the pulsating region depicted in Figure 2-12.9 and the adjacent uniform region of spread just below the flashpoint. They found that both a surface tension flow and a gravity-induced circulation flow in the liquid below the flame are present; both appear to contribute to flame spread rate in the uniform region. See Section 2, Chapter 15, for additional information on liquid flame spread.

Flame Spread in Forests

Flame spread in a forest has many characteristics related to fuel type and configuration, terrain, wind conditions, and humidity. Much research has been done, and no effort here will be made to describe that work. In recent years, based on its research, the Forest Service of the U.S. Department of Agriculture has implemented practical methods for estimating flame spread in forests under a variety of field conditions.[48]

Rothermel[49] presents a thorough review of the theory and models available for forest fire danger rating and behavior prediction. He also discusses a computer model (BEHAVE) that is based on the instructional format previously presented.[48]

Flame spread in a forest depends on radiant heat transfer and convective heating due to wind or the slope of the terrain. In most cases, the porous brush along the floor of the forest is involved, but for severe fires the crowns of the trees also, or exclusively, become involved. In addition, wind currents can transport large embers (fire brands) great distances from the fire to start spot fires at other locations. Breaks in the fuel array can be used to control the spread, but the size of a break sufficient to interrupt the fire will depend on the size of the fire and its heat transfer characteristics. Albini[50] gives an excellent discussion of forest fire phenomena in conceptual terms. Many of these cases have been addressed, and the Forest Service and others have developed analytical models and data for their treatment.

An approximate formula applicable to wildland fires, wood cribs, and urban conflagration is given by Thomas[51] as

$$V\rho_b = k(1 + V_\infty)$$

where

ρ_b is the bulk density of the fuel (kg/m^3)

V is the wind speed (concurrent) (m/s)

k = 0.07 for wildland fires (kg/m^3)
0.05 for wood cribs
0.046 for the Great Fire of London (V = 4.5 m/s)

Figure 2-12.10 shows the results for urban fires in Japan in relationship to this approximate formula.

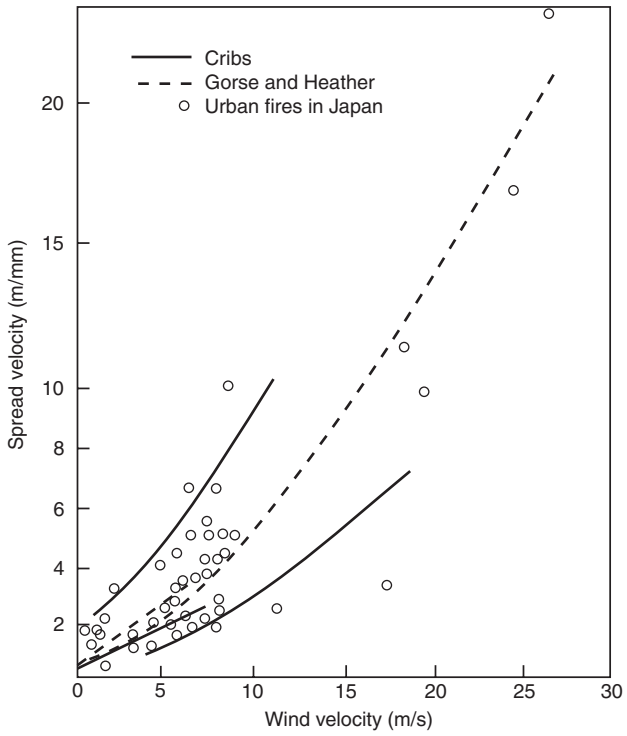

Figure 2-14.10. ***Comparison of rates of fire spread for urban and wildland fires as a function of wind speed.[51]***

Flame Spread in Microgravity

Because of an increased activity in space, flame spread research has been conducted under microgravity conditions. Research has been done in drop towers and in the space shuttle Discovery, as reported by Bhattacharjee and Altenkirch.[52] They examined flame spread over filter paper at 50 percent oxygen in nitrogen in a quiescent atmosphere. The spread rate was measured at 0.44 cm/s compared to a predicted value of 0.42 cm/s. Opposed flow theory applies, but the inclusion of gas-phase radiation was an essential mechanism. A study of flame spread over liquid fuels was conducted by Miller and Ross.[53] They found similar results between microgravity and 1-g conditions, except that opposed flow appears to lower the limiting oxygen concentration at extinction for microgravity. Forced-flow wind-aided flame spread would not be expected to be significantly affected by gravity.

Concluding Remarks

This chapter has provided some insight into the nature of fire spread over materials for the practicing engineer. In general, flame spread depends on the heat transfer processes at the flame front. These transport processes depend not only on the fuel, but also the fuel's configuration and orientation, and on ambient environment conditions. Thus, estimates of flame spread require complex analysis and specific material data. The current state of knowledge does provide limited formulas and material data to make some estimates. In this chapter, the full scope of flame spread phenomena has not been addressed. For example, flame spread in enclosures, mines, ducts, and buildings presents an entirely new complex array of conditions. Thus, flame spread on materials must be evaluated in the context of their use, and appropriate data must be made available for proper assessments of materials.

Nomenclature

c	specific heat
δ	fuel thickness
D	Damköhler number, Equation 8
Δh	enthalpy change
ΔH	heat of combustion
ΔH_{ox}	$\Delta H/r$
k	conductivity
μ	viscosity
ρ	density
Φ	numerator in Equation 18
ϕ	numerator in Equation 11
$\dot{q}''$	heat flux
Q	energy release
r	reference
r	stoichiometric mass ratio oxygen/fuel
t	time
T	temperature
V	spread velocity
V_g	gas velocity
x,y	coordinates
Y	mass fraction
Δ	length of flame heating
v	kinematic viscosity, μ/ρ
σ	surface tension

Superscripts

$\cdot$	per unit time
$'$	per unit length
$''$	per unit area

Subscripts

b	burnout
f	flame
g	gas phase
i	ignition
ox	oxygen
p	pyrolysis
r	reference
s	surface
∞	ambient

References Cited

1. ASTM E1354-90, *Standard Test Method for Heat and Visible Smoke Release Rates for Materials and Products Using an Oxygen Consumption Calorimeter,* American Society for Testing and Materials, West Conshohocken, PA (1990).
2. ASTM E1321-90, *Standard Method for Determining Material Ignition and Flame Spread Properties,* American Society for Testing and Materials, West Conshohocken, PA (1990).
3. J.G. Quintiere, "Application of Flame Spread Theory to Predict Material Performance," *Journal of Research of the National Bureau of Standards,* 93, 1, pp. 61–70 (1988).
4. T. Hirano, "Physical Aspects of Combustion in Fires," in *Proceedings 3rd International Symposium,* (G. Cox and B. Langford, eds.), Elsevier Applied Science, New York, pp. 27–44 (1991).
5. M.L. Janssens, "Fundamental Thermophysical Characteristics of Wood and Their Role in Enclosure Fire Growth," National Forest Product Assoc., Washington, DC, p. 492 (Sept. 1991).
6. A.C. Fernandez-Pello and T. Hirano, *Comb. Sci. and Tech.,* 32, p. 1 (1983).
7. I. Glassman and F.L. Dryer, *F. Safety J.,* 3, p. 123 (1980).
8. D.D. Drysdale, *An Introduction to Fire Dynamics,* 2nd ed., John Wiley and Sons, New York (2000).
9. F.A. Williams, "Mechanisms of Fire Spread (Invited Review)," in *16th Symposium (International) on Combustion,* Combustion Institute, Pittsburgh, PA, pp. 1281–1294 (1976).
10. J.N. de Ris, "Spread of a Laminar Diffusion Flame," in *12th Symposium (International) on Combustion,* Combustion Institute, Pittsburgh, PA, pp. 241–252 (1969).
11. R.A. Altenkirch, R. Eichhorn, and P.C. Shang, *Comb. and Flame,* 37, p. 71 (1980).
12. R.S. Magee and R.F. McAlevy III, *J. Fire and Flamm.,* 2, p. 271 (1971).
13. A.C. Fernandez-Pello, S.R. Ray, and I. Glassman, in *18th Symposium (International) on Combustion,* Pittsburgh, PA (1981).
14. I.S. Wichman, *Comb. Sci. and Tech.,* 40, p. 223 (1984).

15. L. Zhou, A.C. Fernandez-Pello, and R. Cheng, "Flame Spread in an Opposed Turbulent Flow," *Journal Combustion and Flame,* 81, 1, pp. 40–495 (July 1990).
16. C. DiBlasi, G. Continillo, S. Crescitelli, and G. Russo, "Numerical Simulation of Opposed Flow Flame Spread Over a Thermally Thick Solid Fuel," *Journal Combustion Science and Technology,* 54, 1-6, pp. 25–36 (1987).
17. J.G. Quintiere and M. Harkleroad, in *Fire Safety Science and Engineering,* American Society for Testing and Materials, West Conshohocken, PA (1985).
18. A. Atreya, C. Carpentier, and M. Harkleroad, in *Fire Safety Science, Proceedings of the First International Symposium on Fire Safety Science,* Hemisphere, New York (1984).
19. I.S. Wichman and S. Agrawal, "Wind-Aided Flame Spread Over Thick Solids," *Journal Combustion and Flame,* 83, 1-2, pp. 127–145 (1991).
20. K. Saito, J.G. Quintiere, and F.A. Williams, "Upward Turbulent Flame Spread," in *Fire Safety Science, Proceedings, 1st International Symposium,* Hemisphere Publishing Corp., New York, (C.E. Grant and P.J. Pagni, eds.), pp. 75–86 (1986).
21. K.-M. Tu and J.G. Quintiere, "Wall Flame Heights with External Radiation," *Fire Technol.,* 27 (3) pp. 195–203 (1991).
22. Y. Hasemi, M. Yoshida, A. Nohara, and T. Nakabayashi, "Unsteady-State Upward Flame Spreading Velocity along Vertical Combustible Solid and Influence of External Radiation on the Flame Spread," in *Fire Safety Science, Proceedings, 3rd International Symposium,* Elsevier Applied Science, New York, (G. Cox and B. Langford, eds.) pp. 197–206 (1991).
23. M.M. Delichatsios, M.K. Mathews, and M.A. Delichatsios, "Upward Fire Spread and Growth Simulation," in *Fire Safety Science, Proceedings, 3rd International Symposium,* Elsevier Appl. Science, New York, (G. Cox and B. Langford, eds.), pp. 207–216 (1991).
24. A.K. Kulkarni, C.I. Kim, and C.H. Kuo, "Turbulent Upward Flame Spread for Burning Vertical Walls Made of Finite Thickness," *NIST-GCR-91-597,* National Institute of Standards and Technology, Gaithersburg, MD (May 1991).
25. D. Baroudi and M. Kokkala, "Analysis of Upward Flame Spread," Project 5 of the EUREFIC Fire Research Program, VTT-Technical Research Center of Finland, Espoo Report, VTT Publications, 89, p. 50 (Feb. 1992).
26. G.H. Markstein and J. deRis, "Upward Fire Spread Over Textiles," in *14th Symposium (International) on Combustion,* Combustion Institute, Pittsburgh, PA, pp. 1085–1097 (1973).
27. A.C. Fernandez-Pello, *Comb. and Flame,* 31, p. 135 (1978).
28. L. Orloff, J. deRis, and G.H. Markstein, "Upward Turbulent Fire Spread and Burning of Fuel Surfaces," in *15th Symposium (International) on Combustion,* Combustion Institute, Pittsburgh, PA, pp. 183–192 (1975).
29. A. Atreya and K. Mekki, "Heat Transfer During Wind-Aided Flame Spread on a Ceiling-Mounted Sample," in *24th Symposium (International) on Combustion,* Combustion Institute, Pittsburgh, PA, pp. 1677–1684 (1992).
30. C. DiBlasi, S. Crescitelli, and G. Russo, "Near-Limit Flame Spread Over Thick Fuels in a Concurrent Forced Flow," *Journal Combustion and Flame,* 72, 2, pp. 205–212 (1988).
31. L. Zhou and A.C. Fernandez-Pello, "Turbulent, Concurrent, Ceiling Flame Spread: The Effect of Buoyancy," *Journal Combustion and Flame,* 92, 1–2, pp. 45–59 (1993).
32. V.B. Apte, R.W. Bilger, A.R. Green, and J.G. Quintiere, "Wind-Aided Turbulent Flame Spread and Burning Over Large-Scale Horizontal PMMA Surfaces," *Journal Combustion and Flame,* 85, 1-2, pp. 169–184 (1991).
33. F.J. Perzak and C.P. Lazzara, "Flame Spread Over Horizontal Surfaces of Polymethylmethacrylate," in *24th Symposium (International) on Combustion,* Combustion Institute, Pittsburgh, PA, pp. 1661–1668 (1992).
34. J. Quintiere, *Fire and Matls.,* 9, p. 65 (1985).
35. J.G. Quintiere, M.F. Harkleroad, and Y. Hasemi, "Wall Flames and Implicatons for Upward Flame Spread, Final Report," *Proceedings, Journal Combustion, Science and Technology,* 48, 3 & 4, pp. 191–222 (1986).
36. T. Ahmad and G.M. Faeth, in *17th Symposium (International) on Combustion,* Combustion Institute, Pittsburgh, PA, pp. 1149–1160 (1979).
37. L. Orloff, A.T. Modak, and R.L. Alpert, in *16th Symposium (International) on Combustion,* Combustion Institute, Pittsburgh, PA, 1345 (1976).
38. Y. Hasemi, "Thermal Modeling of Upward Wall Flame Spread," in *Proceedings of the 1st International Symposium on Fire Safety Science,* (C.E. Grant and P.J. Pagni, eds.) Hemisphere Publishing Corp., New York, 87 (1985).
39. A. Ito and T. Kashiwagi, "Characterization of Flame Spread Over PMMA Using Holographic Interferometry Sample Orientation Effects," *Proceedings Journal,* National Technical Information Services Combustion and Flame, 71, pp. 189–204 (1988).
40. D.D. Drysdale, A.J.R. Macmillan, and D. Shilitto, "King's Cross Fire: Experimental Verification of the 'Trench Effect'," *Fire Safety Journal,* 18, 1, pp. 75–82 (1992).
41. ASTM, "Proposed Method for Room Fire Test of Wall and Ceiling Materials and Assemblies," in *ASTM Annual Book of Standards Pt. 18,* American Society for Testing and Materials, West Conshohocken, PA, pp. 1618–38 (1982).
42. B. Karlsson and S.E. Magnusson, "Combustible Wall Lining Materials: Numerical Simulation of Room Fire Growth and the Outline of a Reliability Based Classification Procedure," in *Fire Safety Science, Proc. of the 3rd Int. Symp.,* (G. Cox and B. Langford, eds.), Elsevier Applied Science, London (1991).
43. T.G. Cleary and J.G. Quintiere, "A Framework for Utilizing Fire Property Tests," in *Fire Safety Science, Proceedings of the 3rd International Symposium,* (G. Cox and B. Langford, eds.), Elsevier Applied Science, London (1991).
44. U. Wickström and U. Göransson, "Prediction of Heat Release Rates of Surface Materials in Large-Scale Fire Tests Based on Cone Calorimeter Results," *ASTM J. Testing and Evaluation,* 15(6), pp. 364–370 (1987).
45. J.G. Quintiere, "A Simulation Model for Fire Growth on Materials Subject to a Room-Corner Test," *Fire Safety Journal* 20, pp. 313–339 (1993).
46. K. Akita, in *14th Symposium (International) on Combustion,* Combustion Institute, Pittsburgh, PA, p. 1075 (1975).
47. A. Ito, D. Masuda, and K. Saito, "Study of Flame Spread Over Alcohols Using Holographic Interferometry," *Journal Combustion and Flame,* 83, 3 & 4, pp. 375–389 (1991).
48. R.C. Rothermel, *Gen. Tech. Report INT-143,* Department of Agriculture/Forest Service, Madison, WI (1983).
49. R.C. Rothermel, "Modeling Fire Behavior," in *International Conference on Forest Fire Research,* Coimbra, Portugal (Nov. 1990).
50. F.A. Albini, "Dynamics and Modeling of Vegetation Fires: Observations," in *Fire in the Environment* (P.J. Crutzen and J.G. Goldhammer, eds.), John Wiley and Sons, New York, pp. 39–52 (1992).
51. P.H. Thomas, "Rates of Spread for Some Wind-Driven Fires," *Forestry,* XLIV, p. 2 (1971).
52. S. Bhattacharjee and R.A. Altenkirch, "Comparison of Theoretical and Experimental Results in Flame Spread Over Thin Condensed Fuels in a Quiescent, Microgravity Environment," in *24th Symposium (International) on Combustion,* Combustion Institute, Pittsburgh, PA, pp. 1669–1676 (1992).
53. F.S. Miller and H.D. Ross, "Further Observations of Flame Spread over Laboratory-Scale Alcohol Pools," in *24th Symposium (International) on Combustion,* Combustion Institute, Pittsburgh, PA, pp. 1703–1711 (1992).

CHAPTER 13

Smoke Production and Properties

George W. Mulholland

Introduction

The term *smoke* is defined in this chapter as the smoke aerosol or condensed phase component of the products of combustion. This differs from the American Society for Testing and Materials (ASTM) definition of smoke, which includes the evolved gases as well. Smoke aerosols vary widely in appearance and structure, from light colored, for droplets produced during smoldering combustion and fuel pyrolysis, to black, for solid, carbonaceous particulate or soot produced during flaming combustion. A large fraction of the radiant energy emitted from a fire results from the blackbody emission from the soot in the flame. The subject of radiant heat transfer is of such importance that it is treated in a separate chapter. This chapter focuses on smoke aerosols outside the combustion zone.

The effects of the smoke produced by a fire depend on the amount of smoke produced and on the properties of the smoke. The following section presents experimental results on smoke emission for a variety of materials. The smoke emission, together with the flow pattern, determines the smoke concentration as smoke moves throughout a building.

The most basic physical property of smoke is the size distribution of its particles. Results on size distribution for various types of smoke and techniques used for measuring particle size are presented in the section "Size Distribution." The section "Smoke Properties" focuses on those properties of greatest concern to the fire protection community: light extinction coefficient of smoke, visibility through smoke, and detectability of smoke. These properties are primarily determined by the smoke concentration and the particle size distribution. References for other smoke aerosol properties, such as diffusion coefficient and sedimentation velocity, are also provided.

Dr. George W. Mulholland is head of the Smoke Dynamics Research Group in the Center for Fire Research at the National Bureau of Standards. His research has focused on smoke aerosol phenomena and the development of accurate particle size standards.

Smoke Production

Smoke emission is one of the basic elements for characterizing a fire environment. The combustion conditions under which smoke is produced—flaming, pyrolysis, and smoldering—affect the amount and character of the smoke. The smoke emission from a flame represents a balance between growth processes in the fuel-rich portion of the flame and burnout with oxygen. While it is not possible at the present time to predict the smoke emission as a function of fuel chemistry and combustion conditions, it is known that an aromatic polymer, such as polystyrene, produces more smoke than hydrocarbons with single carbon-carbon bonds, such as polypropylene. The smoke produced in flaming combustion tends to have a large content of elemental (graphitic) carbon.

Pyrolysis occurs at a fuel surface as a result of an elevated temperature. This may be due to a radiant flux heating the surface. The temperature of a pyrolyzing sample, 600 to 900 K, is much less than the gas phase flame temperature, 1200 to 1700 K. The vapor evolving from the surface may include fuel monomer, partially oxidized products, and polymer chains. As the vapor rises, the low vapor pressure constituents can condense, forming smoke droplets appearing as light-colored smoke.

Smoldering combustion also produces smoke droplets, but in this case the combustion is self-sustaining, whereas pyrolysis requires an external heat source. While most materials can be pyrolyzed, only a few materials, including cellulosic materials (wood, paper, cardboard, etc.) and flexible polyurethane foam, are able to smolder. The temperature during smoldering is typically 600 to 1100 K.

In Table 2-13.1 the smoke conversion factor, ε, is given for a variety of materials commonly found in build-

Table 2-13.1 ***Smoke Production for Wood and Plastics***

Type	Smoke Conversion Factor, ε	Combustion Conditions	Fuel Area, m^2	Reference
Douglas fir	0.03–0.17	Pyrolysis	0.005	1
Douglas fir	< 0.01–0.025	Flaming	0.005	1
Hardboard	0.0004–0.001	Flaming[a]	0.0005	2
Fiberboard	0.005–0.01	Flaming[a]	0.0005	2
Polyvinylchloride	0.03–0.12	Pyrolysis	0.005	3
Polyvinylchloride	0.12	Flaming	0.005	1
Polyurethane (flexible)	0.07–0.15	Pyrolysis	0.005	3
Polyurethane (flexible)	< 0.01–0.035	Flaming	0.005	1
Polyurethane (rigid)	0.06–0.19	Pyrolysis	0.005	1
Polyurethane (rigid)	0.09	Flaming	0.005	1
Polystyrene	0.17 (m_{O_2} = 0.30)[b]	Flaming	0.0005	4
Polystyrene	0.15 (m_{O_2} = 0.23)	Flaming	0.07	5
Polypropylene	0.12	Pyrolysis	0.005	1
Polypropylene	0.016	Flaming	0.005	1
Polypropylene	0.08 (m_{O_2} = 0.23)	Flaming	0.007	5
Polypropylene	0.10 (m_{O_2} = 0.23)	Flaming	0.07	5
Polymethylmethacrylate	0.02 (m_{O_2} = 0.23)	Flaming	0.07	5
Polyoxymethylene	~0	Flaming	0.007	5
Cellulosic insulation	0.01–0.12	Smoldering	0.02	6

[a]Sample smoldered for a period of time after the pilot flame was extinguished.

[b]m_{O_2} refers to mol fraction of O_2.

ings. The quantity ε is defined as the mass of smoke produced/mass of fuel burned.

The references cited in Table 2-13.1 should be consulted regarding the detailed description of the combustion conditions. In many instances,[1,3] ε was measured for a range of radiant fluxes, oxygen concentrations, sample orientations, and ambient temperatures. It is seen in Table 2-13.1 that ε has a greater range for flaming combustion, with values in the range 0.001 to 0.17, compared to pyrolysis and smoldering, with values in the range 0.01 to 0.17. The following factors should be taken into account when using this table for smoke emission estimates:

1. Most of the measurements reported in Table 2-13.1 were made on small-scale samples.
2. Most experiments were for free burning at ambient conditions; reduced ventilation can strongly affect the smoke production.
3. In transport, the smoke may coagulate, partially evaporate, and deposit on surfaces through diffusion and sedimentation. Also, additional smoke may be formed through condensation.

Size Distribution

Smoke particle size distribution, together with the amount of smoke produced, primarily determines the properties of the smoke. A widely used representation of the size distribution is the geometric number distribution, $\Delta N/\Delta \log d$, versus $\log d$, where d represents the particle diameter. The quantity ΔN represents the number of particles per cm^3, with diameter between $\log d$ and $\log d + \Delta \log d$. As an example, the particle size distribution of

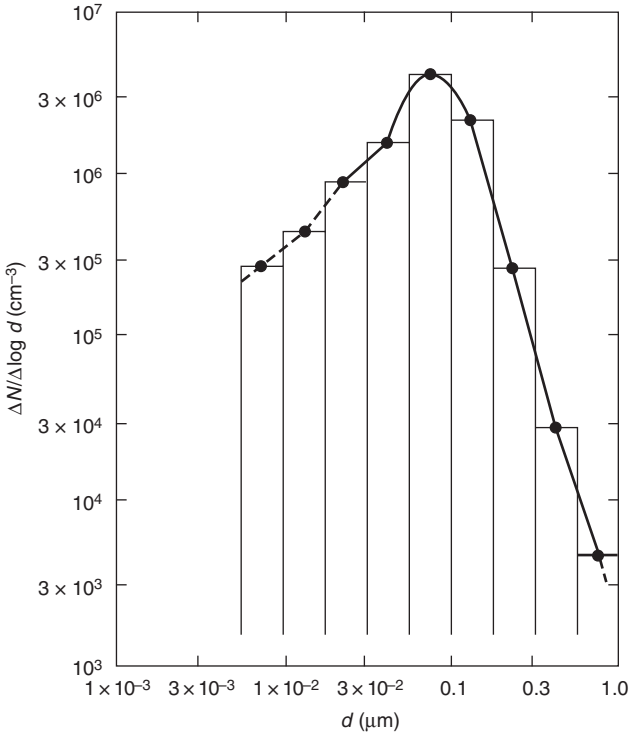

Figure 2-13.1. ***Size distribution of incense smoke as measured by an electrical aerosol analyzer. There is a large uncertainty in the dashed portion of the curve.***

smoke produced by a smoldering incense stick is plotted in Figure 2-13.1, where $\Delta \log d$ for each discrete size range equals 0.25. In this case, the total number concentration for a given size range equals $0.25(\Delta N/\Delta \log d)$. It is seen that the logarithmic scale is necessitated by the wide range in particle size and concentration.

For many applications, the most important characteristics of a size distribution are the average particle size and the width of the distribution. A widely used measure of the average size is the geometric mean number diameter, d_{gn}, defined by

$$\log d_{gn} = \sum_{i=1}^{n} \frac{N_i \log d_i}{N} \tag{1}$$

where

N = total number concentration

N_i = number concentration in the ith interval

log is to the base 10

For the size distribution plotted in Figure 2-13.1, $d_{gn} = 0.072$ μm.

The corresponding measure of the width of the size distribution is the geometric standard deviation, σ_g,

$$\log \sigma_g = \left[\sum_{i=1}^{n} \frac{\left(\log d_i - \log d_{gn}\right)^2 N_i}{N} \right]^{1/2} \tag{2}$$

For the size distribution plotted in Figure 2-13.1, $\sigma_g = 1.75$. A perfectly monodisperse distribution would correspond to $\sigma_g = 1$. The parameters d_{gn} and σ_g are useful because actual size distributions are observed to be approximately log-normal, which is the same as a normal or Gaussian distribution, except that $\log d$ is normally distributed instead of d. An important characteristic of the log-normal distribution is that 68.3 percent of the total particles are in the size range $\log d_{gn} \pm \log \sigma_g$; for $d_{gn} = 0.072$ μm and $\sigma_g = 1.75$, this corresponds to the size range of 0.041 to 0.126 μm.

EXAMPLE 1:

Compute d_{gn} and σ_g for the data given below:

Interval, μm	d_i	N_i, cm^{-3}	log d_i	$N_i \times$ log d_i, cm^{-3}
0.0056–0.01	0.0078	6×10^4	−2.11	-1.27×10^5
0.010–0.018	0.014	2×10^5	−1.85	-3.7×10^5
0.018–0.032	0.025	4×10^5	−1.60	-6.40×10^5
0.032–0.056	0.044	9×10^4	−1.36	-1.22×10^5
0.056–0.10	0.078	3×10^4	−1.11	-3.33×10^4
0.10–0.18	0.14	1×10^3	−0.85	-0.85×10^3
		7.81×10^5		-1.30×10^6

SOLUTION:

$$d_{gn} = 10^{(-1.30 \times 10^6 / 7.81 \times 10^5)} = 0.022 \text{ μm}$$

Compute the geometric standard deviation:

N_i	log d_i	log d_i − log d_{gn}	N_i(log d_i − log d_{gn})^2
6×10^4	−2.11	−0.45	1.22×10^4
2×10^5	−1.85	−0.19	7.2×10^3
4×10^5	−1.60	0.06	1.4×10^3
9×10^4	−1.36	0.30	8.1×10^3
3×10^4	−1.11	0.55	9.1×10^3
1×10^3	−0.85	0.81	6.5×10^2
7.81×10^5			3.87×10^4

SOLUTION:

$$\sigma_g = 10^{(3.87 \times 10^4 / 7.81 \times 10^5) 0.5} = 1.67$$

The size distribution plotted in Figure 2-13.1 is based on electrical mobility analysis of the smoke aerosol. Figures 2-13.2 and 2-13.3 show size distributions of droplet smoke produced by smoldering cellulosic insulation, as measured by an optical particle counter and by two cas-

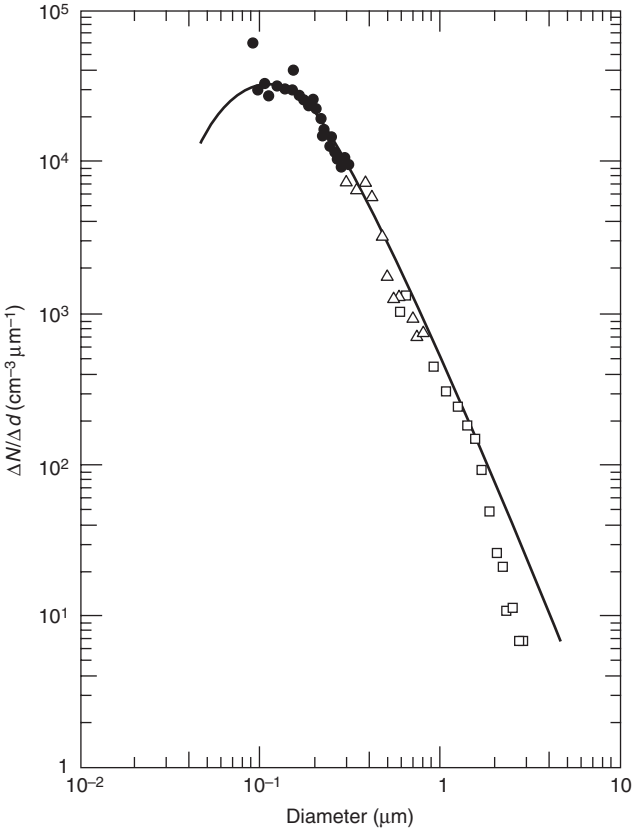

Figure 2-13.2. ***The number size distribution of smoke generated by smoldering cellulosic insulation as measured by an optical particle counter. The symbols correspond to the particle size range settings of the instrument, and the smooth curve is an exponentially truncated power law distribution fit to the data.***

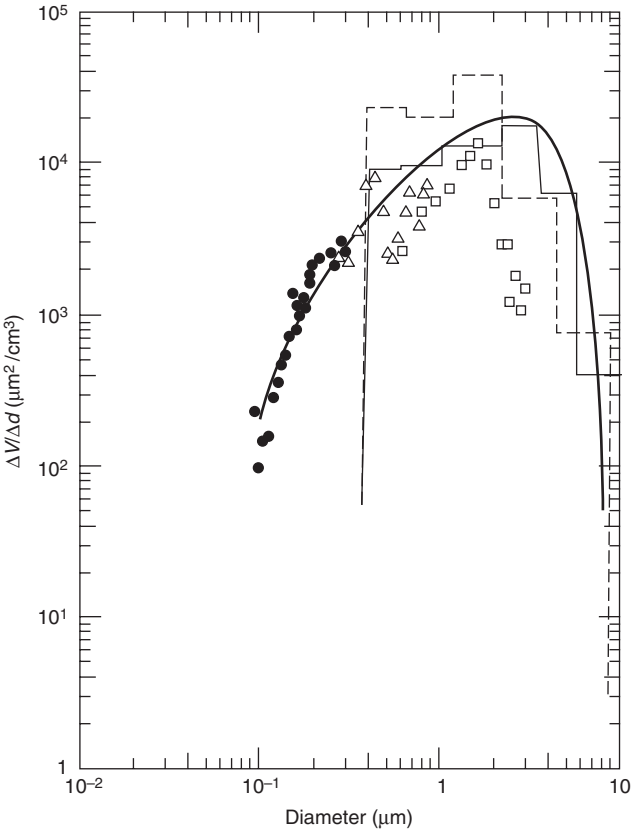

Figure 2-13.3. ***The volume size distribution of smoke obtained from the optical particle counter, quartz crystal microbalance cascade impactor (dashed histogram), and Andersen impactor (solid histogram). The smooth curve represents the exponentially truncated power law distribution.***

cade impactors.[6] The smoke volume distribution plotted in Figure 2-13.3 for the optical particle counter is obtained from the number distribution, using the following relation:

$$V_i = N_i \frac{1}{6} \pi d_i^3 \tag{3}$$

For particles sized above 1 μm, impactors provide more reliable information on the smoke volume distribution than optical particle counters. An optical particle counter is the preferred instrument for the number distribution measurement.

To correlate the smoke volume/particle size distribution, the geometric mean volume diameter, d_{gv}, is a convenient measure of average particle size:

$$\log d_{gv} = \frac{\sum_{i=1}^{n} V_i \log d_i}{V_T} \tag{4}$$

where V_T is the total volume concentration of the smoke aerosol. For a log-normal distribution, there is the following relationship between the geometric mean volume diameter, d_{gv}, and the geometric mean number diameter, d_{gn}:

$$\log d_{gv} = \log d_{gn} + 6.9(\log \sigma_g)^2 \tag{5}$$

In the case of smolder smoke, σ_g is above 2.4. This large value of σ_g results in a large difference between d_{gn} and d_{gv}, 0.2 μm versus 2 μm, respectively. Some devices, such as an ionization-type smoke detector, have an output depending primarily on d_{gn}, while others, such as light-scattering-type detectors, have an output depending more on d_{gv}. More than one instrument is necessary for a complete characterization of the smoke size distribution, because it is typically quite wide.

A list of commercially available instruments for measuring smoke aerosol concentration and particle size distribution is given in Table 2-13.2. Smoke measurements pose special problems because of the high concentration, wide particle size range, and sometimes high temperature. In selecting an instrument it is important to make the following considerations:

1. Will the instrument respond to the smoke of interest? For example, the piezoelectric mass monitor does not respond well to soot.
2. Will dilution of the smoke be required?
3. Is the measurement size range of the instrument adequate?
4. Is a mass or number distribution measurement appropriate?
5. What is the particle size resolution needed?
6. Is real-time measurement capability needed?
7. Will the instrument perform at the temperature of the smoke environment?

In Table 2-13.3, average particle size and the width of the size distribution are presented for smoke generated by a variety of materials. The results are most meaningful for smoke droplets produced during pyrolyzing and smoldering combustion. In the case of flaming combustion, complex soot agglomerates are formed as shown in Figure 2-13.4. For soot agglomerates, unlike for spherical smoke droplets, the apparent particle size depends on the measurement technique.

Smoke aerosols are dynamic with respect to their particle size distribution function. Smoke particles or droplets undergoing Brownian motion collide and stick together. The result of this behavior is that, in a fixed volume of smoke-laden gas, the number of particles decreases while the total mass of the aerosol remains unchanged. This process is known as coagulation. The fundamental parameter for describing coagulation is the coagulation coefficient, Γ, the rate constant for the coagulation equation

$$\frac{dN}{dt} = -\Gamma N^2 \tag{6}$$

Γ was found to be about 4×10^{-10} cm³/s for smoke produced from incense sticks and about 1×10^{-9} cm³/s for

Table 2-13.2 ***Operational Characteristics of Commercially Available Instruments for Smoke Characterization***

Instrument Type	Function/Range	Advantage/Limitation for Smoke Measurements
Filter-collection	Mass conc.	Accurate, slow
Piezoelectric mass monitor	Mass conc. $0.01 < d < 5$ μm	Real-time output, but dilution required if >20 mg/m^3; does not respond well to soot
Tapered element oscillating microbalance	Mass conc. <5 μm	Real time, 0.1–1000 mg/m^3; replace filter after 3–100 mg deposit
Condensation nuclei counter	Number conc. $0.005 < d < 2$ μm	$<3 \times 105$ particles/cm^3
Photometer	Scattered light 0.1–10 μm	1.1–1000 mg/m^3
Nephelometer	Total light scattered	<5 mg/m^3
Electrical aerosol analyzer	Size distribution $0.01 < d < 0.3$ μm	$<5 \times 10^5$ particles/cm^3; 2 min/scan
Cascade impactor	Mass size distribution[a] $0.5 < d < 10$ μm	No dilution needed, can be used at high temp., large sample required
Optical particle counter	Number distribution[b] $0.5 < d < 10$ μm	Highest resolution, $<10^3$ particles/cm^3, large dilution

[a]Low-pressure impactor extends size range down to 0.05 μm.

[b]Laser model extends size range down to 0.1 μm and concentration up to 10^4 particles/cm^3.

smoke produced from flaming α-cellulose.[7] The coagulation process has a more pronounced effect on the number distribution than the mass distribution as small particles collide to form larger particles.

EXAMPLE 2:

Calculate the change in the number concentration over a 5-min time interval for a uniformly distributed smoke, generated from flaming α-cellulose given an initial concentration of 1×10^7 particles/cm^3.

Integrating Equation 6 yields

$$N = \frac{N_0}{1 + \Gamma N_0 t} = \frac{1 \times 10^7}{1 + (10^{-9})(10^7)(300)} = \frac{10^7}{1 + 3}$$

$$N = 2.5 \times 10^6 \text{ particles/cm}^3$$

So in this example, there is a fourfold reduction in number concentration due to coagulation.

The effect of the decrease in number concentration on the size distribution is treated by Mulholland et al.[25] A

Table 2-13.3 ***Particle Size of Smoke from Burning Wood and Plastics***

Type	d_{gm}, μm[a]	d_{32}, μm[b]	σ_g	Combustion Conditions	Reference
Douglas fir	0.5–0.9	0.75–0.8	2.0	Pyrolysis	1, 3
Douglas fir	0.43	0.47–0.52	2.4	Flaming	1, 3
Polyvinylchloride	0.9–1.4	0.8–1.1	1.8	Pyrolysis	3
Polyvinylchloride	0.4	0.3–0.6	2.2	Flaming	3
Polyurethane (flexible)	0.8–1.8	0.8–1.0	1.8	Pyrolysis	3
Polyurethane (flexible)		0.5–0.7		Flaming	3
Polyurethane (rigid)	0.3–1.2	1.0	2.3	Pyrolysis	3
Polyurethane (rigid)	0.5	0.6	1.9	Flaming	3
Polystyrene		1.4		Pyrolysis	1
Polystyrene		1.3		Flaming	1
Polypropylene		1.6	1.9	Pyrolysis	1
Polypropylene		1.2	1.9	Flaming	1
Polymethylmethacrylate		0.6		Pyrolysis	1
Polymethylmethacrylate		1.2		Flaming	1
Cellulosic insulation	2–3		2.4	Smoldering	6

[a]d_{gm} is analogous to d_{gv} but with mass replacing volume in Equation 4. Values of d_{gm} less than about 0.5 μm are probably overestimates arising from the minimum size resolution of the impactor at about 0.4 μm.

[b]The quantity d_{32} is obtained by optical measurements

$$d_{32} = \frac{\sum_{i=1}^{n} N_i d^3_i}{\sum_{i=1}^{n} N_i d^2_i}$$

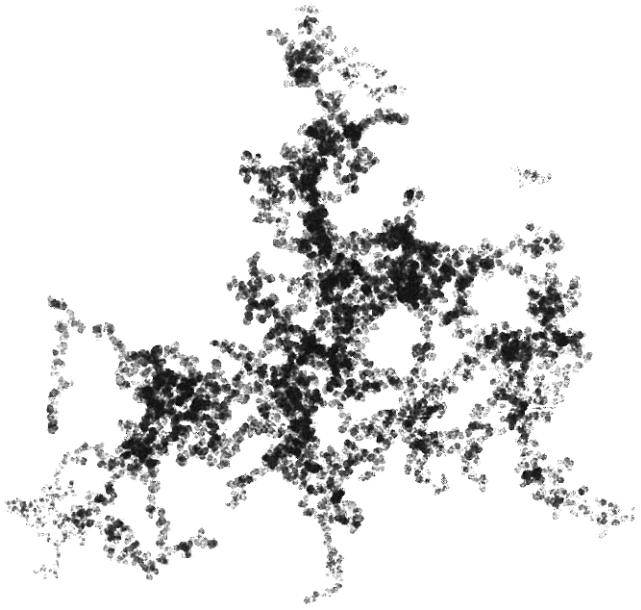

Figure 2-13.4. ***Transmission electron micrograph of a soot particle. The overall size of the agglomerate is about 6 μm, and the diameter of the individual spherules is about 0.03 μm.***

general discussion of coagulation phenomena in aerosols is given by Friedlander.[8] In addition to coagulation, other smoke-aging processes, including condensation of vapor onto existing particles and evaporation of the volatile component of the smoke, can also take place. There is relatively little information on these processes. Also, smoke particles can be lost to the walls, ceiling, and floor of an enclosure through a variety of processes, including diffusion, sedimentation, and thermophoresis.

Smoke Properties

The smoke properties of primary interest to the fire community are light extinction, visibility, and detection. For completeness, a list of other smoke aerosol properties and references is given in Table 2-13.4.

Table 2-13.4 ***Smoke Aerosol Properties***

Property	Reference
Diffusion coefficient	8
Sedimentation velocity	9
Thermophoretic velocity	10
Aerodynamic diameter	9
Electrical mobility	9
Thermal charging	9
Scattering coefficient	8
Extinction coefficient	8
Condensation/evaporation	8

The most widely measured smoke property is the light extinction coefficient. The physical basis for light extinction measurements is Bouguer's law, which relates the intensity, I_0^λ, of the incident monochromatic light of wavelength λ and the intensity of the light, I_λ, transmitted through the pathlength, L, of the smoke:

$$\frac{I_\lambda}{I_\lambda^0} = e^{-KL} \tag{7}$$

where K is the light extinction coefficient. When Equation 7 is expressed in terms of base 10,

$$\frac{I_\lambda}{I_\lambda^0} = 10^{-DL} \tag{8}$$

The quantity D is defined as the optical density per meter, and $D = K/2.3$.

The extinction coefficient, K, is an extensive property and can be expressed as the product of an extinction coefficient per unit mass, K_m, and mass concentration of the smoke aerosol, m.

$$K = K_m m \tag{9}$$

The specific extinction coefficient, K_m, depends on the size distribution and optical properties of the smoke through the relation

$$K_m = \frac{3}{2\rho m}\int_{d_{\min}}^{d_{\max}} \frac{1}{d}\frac{\Delta m}{\Delta d} Q_{\text{ext}}\left(\frac{d}{\lambda}, n_r\right) \delta d \tag{10}$$

In Equation 10 the symbol $\Delta m/\Delta d$ represents the mass size distribution. The single particle extinction efficiency, Q_{ext}, is a function of the ratio of particle diameter to wavelength of light, d/λ, and of the complex refractive index of the particle, n_r.[8] The quantity ρ represents the particle density.

Seader and Einhorn[11] obtained K_m values of 7.6 m^2/g for smoke produced during flaming combustion of wood and plastics and a value of 4.4 m^2/g for smoke produced during pyrolysis of these materials. The experiments were small scale, utilizing samples of about 50 cm^2, and the value of K_m represents an integrated result for the entirety of the test. The light source used in the measurements was polychromatic, while Bouguer's law is strictly valid only for monochromatic light. Foster[12] predicted a 22 percent deviation from Bouguer's law over the mass concentration range from 0.06 to 2.8 g/m^3 as a result of using a polychromatic light source with wood smoke. Still, it is useful to use the Seader and Einhorn[11] result as a rough guide if more detailed optical data on the smoke of interest is not available.

Mulholland[13] has described the general design of a light extinction instrument that satisfies Bouguer's law. Two key features are the use of monochromatic light and the elimination of forward scattered light at the detector.

The specific optical density, D_s, is measured in a standard laboratory smoke test[14] for assessing the amount of visible smoke produced in a fire. The dimensionless quantity D_s is defined by

$$D_s = \frac{DV_c}{A} \tag{11}$$

where V_c is the volume of the chamber, and A is the area of the sample. D_s is a convenient quantity to measure if the decomposed area is well defined. Since D_s depends on the sample thickness, the same thickness should be used for relative rating of materials tested. Table 2-13.5 includes results for D_s based on small-scale experiments with wood and plastics by Gross et al.,[14] Seader and Chien,[15] and Breden and Meisters.[16] Lopez[17] demonstrated a correlation for D_s between small- and large-scale fires with aircraft interior construction materials.

Table 2-13.5 ***Specific Optical Density and Mass Optical Density for Wood and Plastics***

Type (Sample #)	Maximum D_s	D_m (m^2/g)[a]	Combustion Conditions	Sample[b] Thickness (cm)	Reference
Hardboard	6.7×10^1		Flaming	0.6	14
Hardboard	6.0×10^2		Pyrolysis	0.6	14
Plywood	1.1×10^2		Flaming	0.6	14
Plywood	2.9×10^2		Pyrolysis	0.6	14
Polystyrene	$>6.6 \times 10^2$		Flaming	0.6	14
Polystyrene	3.7×10^2		Pyrolysis	0.6	14
Polyvinylchloride	$>6.6 \times 10^2$		Flaming	0.6	14
Polyvinylchloride	3.0×10^2		Pyrolysis	0.6	14
Polyurethane foam	2.0×10^1		Flaming	1.3	14
Polyurethane foam	1.6×10^1		Pyrolysis	1.3	14
Nylon carpet	2.7×10^2		Flaming	0.8	14
Nylon carpet	3.2×10^2		Pyrolysis	0.8	14
Acrylic	1.1×10^2		Flaming	0.6	14
Acrylic	1.6×10^2		Pyrolysis	0.6	14
Plywood	5.3×10^2	0.29	Pyrolysis	0.6	15
Polymethylmethacrylate	7.2×10^2	0.15	Pyrolysis	0.6	15
Polyvinylchloride	1.8×10^2	0.12	Pyrolysis	0.6	15
Polyvinylchloride (with plasticizer)	3.5×10^2	0.64	Pyrolysis	0.6	15
Neoprene	8.8×10^2	0.55	Pyrolysis	0.6	15
Douglas fir	6.2×10^2	0.28	Pyrolysis	0.6	15
Polypropylene	4.0×10^2	0.53	Flaming[c]	0.4	16
Polyethylene	2.9×10^2	0.29	Flaming[c]	0.4	16
Paraffin wax	2.3×10^2	0.23	Flaming[c]	0.4	16
Polystyrene		1.4	Flaming[c]	0.4	16
Styrene		0.96	Flaming[c]	0.4	16
Polyvinylchloride		0.34	Flaming[c]	0.4	16
Polyoxymethylene		$\sim$0	Flaming[c]	0.4	16
Polyurethane (7A)	2.1×10^2		Flaming	1.3	17
Polyurethane (7A)	1.5×10^2		Flaming[d]	1.3	17
Wool (8A)	$>5.5 \times 10^2$		Flaming	0.9	17
Wool (8A)	2.2×10^2		Flaming[d]	0.9	17
Acrylic (9B)	5.8×10^1		Flaming	0.14	17
Acrylic (9B)	1.2×10^2		Flaming[d]	0.14	17
Polyurethane (MO1)		0.33	Flaming[c]		18
Polyurethane (MO1)		0.22	Flaming[e]		18
Cotton (MO3)		0.17	Flaming[c]		18
Cotton (MO3)		0.12	Flaming[e]		18
Latex (MO4)		0.65	Flaming[c]		18
Latex (MO4)		0.44	Flaming[e]		18
Neoprene (MO8)		0.40	Flaming[c]		18
Neoprene (MO8)		0.20	Flaming[e]		18
Polystyrene (7)		0.79	Flaming[c]		19
Polystyrene (7)		1.0	Flaming[f]		19
Polystyrene foam (16)		0.79	Flaming[c]		19
Polystyrene foam (16)		0.82	Flaming[f]		19
ABS (18)		0.52	Flaming[c]		19
ABS (18)		0.54	Flaming[f]		19

[a]The value of D_m is computed by Quintiere,[20] based on data in Babrauskas.[18]

[b]Sample area is 0.005 m^2 in vertical configuration, unless stated otherwise.

[c]Sample is in horizontal configuration (0.005 m^2).

[d]0.09 m^2 sample size.

[e]The sample is a mattress.

[f]The sample is a plastic utility table.

If the mass loss of the sample is measured, then the mass optical density, D_m, is the appropriate measure of visible smoke.

$$D_m = \frac{DV_c}{\Delta M} \tag{12}$$

This technique requires an accurate measurement of the mass loss of the sample, ΔM, in addition to a light extinction measurement. Table 2-13.5 includes results for D_m for a variety of materials studied by Seader and Chien,[15] Breden and Meisters,[16] Babrauskas,[18] and Evans.[19] The results of Babrauskas' study were expressed in terms of D_m by Quintiere.[20]

In two of the studies,[18,19] a comparison was made between D_m measured in small-scale tests and D_m measured in large-scale tests. The large-scale tests involved mattresses[18] in one case and plastic utility tables[19] in the other. In these two cases, there appeared to be a qualitative correlation between D_m measured for small- and large-scale tests. Quintiere[20] has made an extensive investigation of the correlation between small- and large-scale studies in terms of D_m and D_s and finds that the correlation breaks down as fires become more complex. From his review of the literature, Quintiere[20] suggests that heat flux and ventilation conditions can have a major effect on smoke production.

In most cases of practical interest, an important goal is to be able to predict the extinction coefficient based on information regarding D_s or D_m. The extinction coefficient, in turn, is related to visibility through the smoke, as discussed below.

Visibility

Visibility of exit signs, doors, and windows can be of great importance to an individual attempting to survive a fire. To see an object requires a certain level of contrast between the object and its background. For an isolated object surrounded by a uniform, extended background, contrast, C, can be defined as[21]

$$C = \frac{B}{B_0} - 1 \tag{13}$$

where B is the brightness or luminance of the object, and B_0 is the luminance of the background. For daylight conditions, with a black object being viewed against a white background, a value of $C = -0.02$ is often used as the contrast threshold at which an object can be discerned against the background. The visibility of the object, S, is the distance at which the contrast is reduced to -0.02. Most visibility measurements through smoke have relied on test subjects to determine the distance at which the object was no longer visible rather than the actual measurement of C with a photometer.

Visibility depends on many factors, including the scattering and the absorption coefficient of the smoke, the illumination in the room, whether the sign is light emitting or light reflecting, and the wavelength of the light. Visibility also depends on the individual's visual acuity and on whether the eyes are "dark-" or "light-adapted." Nevertheless, a fair correlation between visibility of test subjects and the extinction coefficient of the smoke has been obtained in an extensive study by Jin[22] as illustrated in Figure 2-13.5. The visibility of light-emitting signs was found to be two to four times greater than light-reflecting signs. The following expressions were found to correlate the data:

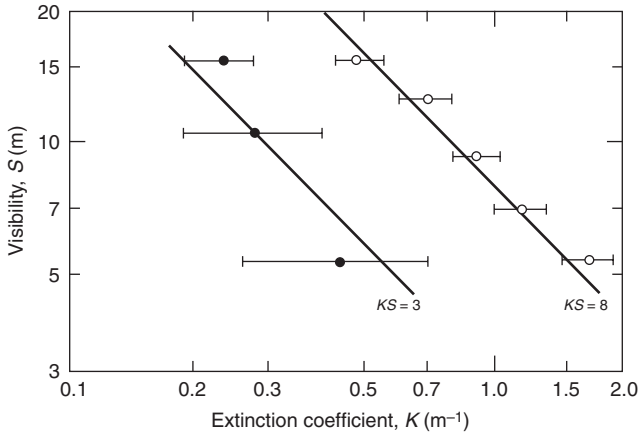

Figure 2-13.5. ***Visibility versus extinction coefficient for a light-emitting sign (○) and light-reflecting sign (●). The range bars include data for both flame- and smolder-generated smoke and sign illumination levels varying by about a factor of 4.***

$$KS = 8 \quad \text{light-emitting sign} \tag{14}$$

$$KS = 3 \quad \text{light-reflecting sign} \tag{15}$$

The data is based on subjects viewing smoke through glass so that the irritant effect of the smoke was eliminated. Jin and Yamada[23] have studied the visual acuity and eyeblink rate for highly irritant white smoke produced by burning wood cribs. They found that the ratio of visual acuity without goggles to acuity with goggles decreases markedly for smoke extinction coefficient, K, greater than 0.25 m^{-1}.

EXAMPLE 3:

Estimate the visibility of a light-reflecting exit sign in a 6-m square room with a 2.5-m height, as a result of flaming combustion of a 200-g polyurethane foam pillow.

The smoke yield for flexible polyurethane, according to Table 2-13.1, is about 0.03 for flaming combustion. This implies a smoke emission, M_s, given by

$$M_s = (0.03)(200) = 6 \text{ g}$$

The corresponding mass concentration in the room, m, is

$$m = \frac{6}{(6)^2(2.5)} = 0.067 \text{ g/m}^3$$

Taking K_m to be 7.6 m^2/g for flaming combustion, one obtains K using Equation 9,

$$K = (7.6)(0.067) = 0.51 \text{ m}^{-1}$$

The visibility is next estimated using Equation 15,

$$S = \frac{3}{K} = \frac{3}{0.51} = 5.9 \text{ m}$$

It is important to point out the approximations made in this analysis.

1. The smoke is confined to the room and is well mixed. Actually the concentration will be higher near the ceiling and decrease abruptly below the flame.
2. The value of 0.03 for the smoke conversion factor, ε, is an estimated value in the upper part of the range (0.01 to 0.035) for generic flexible polyurethane foams measured in small-scale experiments and may not be appropriate for a pillow. In a realistic case, the pillow would probably smolder before flaming, and ε is much larger in the smolder mode.
3. The value of K_m is based on a limited number of small-scale experiments with a polychromatic light source.
4. The range of validity of Equation 15 has not been widely studied.

An alternative method for estimating the visibility is based on using the mass optical density data in Table 2-13.5. The quantity D_m for the pillow is estimated to be 0.22 m^2/g based on Babrauskas' results[18] given in Table 2-13.5 for polyurethane (MO1). On rearranging Equation 12, the following result is obtained:

$$D = \frac{D_m \Delta M}{V_c} = \frac{(0.22)(200)}{(6)^2(2.5)} = 0.49 \text{ m}^{-1}$$

The smoke extinction coefficient, K, is 1.12 m^{-1} or 2.3 times D. Using Equation 15, we obtain S = 2.7 m compared to 5.9 m obtained by the first method. In principle, the second method is more reliable, because it is more direct.

Detection

In addition to their utility for estimating visibility, light extinction measurements are also widely used in characterizing smoke detector performance. Underwriters Laboratories' (UL) acceptance testing of smoke detectors[24] is based in part on a minimum sensitivity based on optical density per meter, D, of 0.06 (4 percent obscuration per ft for a 5 ft beam length) for gray (cellulosic) smoke and 0.14 (10 percent per ft) for black smoke (kerosene).

The electrical output of a detector, P, from a light-scattering or ionization-type smoke detector can be represented as an integrated product of the size distribution function and the basic response of the detector, $R(d)$.

$$P = \int_{d_{\min}}^{d_{\max}} R(d) \frac{\delta N}{\delta d} \delta d \qquad (16)$$

The response functions for two smoke detectors are plotted in Figure 2-13.6. It is seen that the ionization-type smoke detector is more sensitive to smoke particles smaller than about 0.3 μm, and the light-scattering type more sensitive to particles larger than 0.3 μm.

The basic principle of ionization detectors is the interception of gaseous ions by smoke particles, reducing the ion current in the detector until a preset alarm point is reached. The detector response function is approximately proportional to the product of the number concentration and particle diameter.[25,26] For one detector[25] the response function is given by

$$R(d) = cd \qquad (17)$$

where c has a value of 7 in units of μV per particle concentration per μm (μV $cm^3/\mu m$). Such detectors tend to be most sensitive to high concentrations of small particles, such as those produced by flaming paper and wood fires, and least sensitive to the low concentration of large smoke droplets produced in smoldering fires.

Light-scattering smoke detectors have a high sensitivity to smoke particles with diameters approximately equal to λ, the wavelength of light, and low sensitivity to

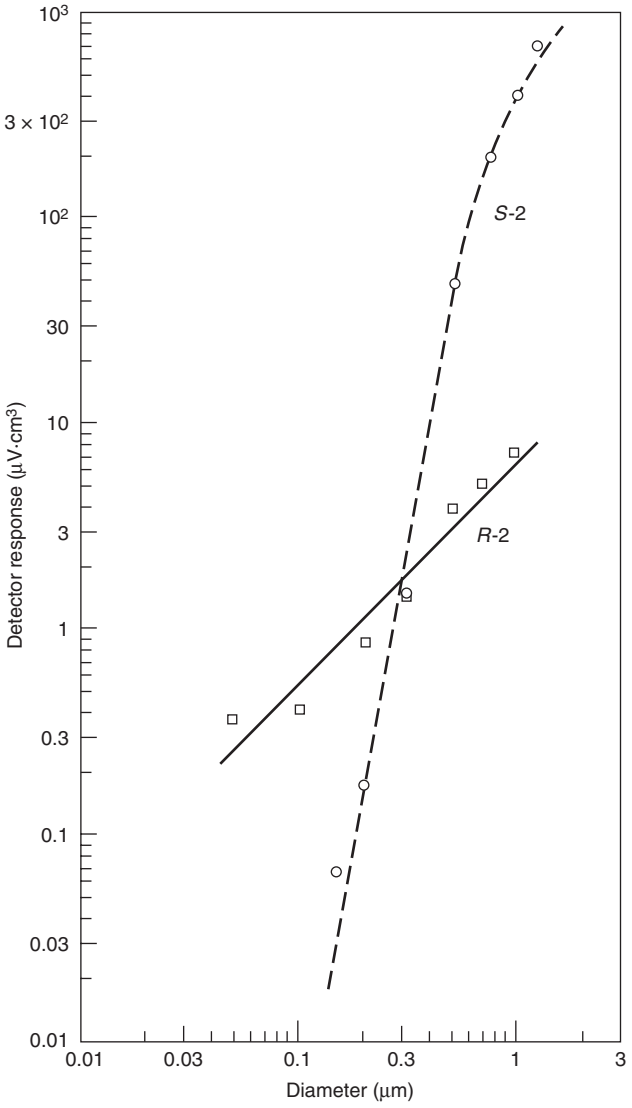

Figure 2-13.6. ***The detector response function, R(d), is plotted versus particle size for detectors S-2 (light-scattering) and R-2 (ionization).***

particles much smaller than λ. The response function, *R(d)*, depends on the wavelength of the light source in the smoke detector, the scattering angle, and the scattering volume. For smoke particles with diameter greater than about 0.3 μm, the output of several light-scattering smoke detectors was found to be approximately proportional to the mass concentration of the smoke.[25] Light-scattering detectors complement ionization detectors in that they have high sensitivity to smoldering fires and low sensitivity to low-smoking flaming fires, such as paper and wood fires.

The purpose of smoke detectors is to give the occupants of a room adequate warning to escape a developing fire. The final examples of this chapter illustrate how to utilize all the concepts discussed above to estimate escape time.

EXAMPLE 4:

Suppose the pillow in the preceding example is burning at a steady rate of 50 g/min. How long would it take for an ionization detector with response function given by Equation 17 to alarm? Assume an alarm voltage of 2.5 V above background. How much time would an individual have before the visibility decreased to an unsafe level?

SOLUTION:

First consider a first principle analysis based on the size distribution of the smoke. From Equations 16 and 17,

$$P = c\int_{d_{\min}}^{d_{\max}} d\,\frac{\delta N}{\delta d}\,\delta d$$

The following three identities[9] for the log-normal distribution are needed:

$$\int_0^\infty d\,\frac{\delta N}{\delta d}\,\delta d = N_0 d_{gn}\exp\left(\frac{1}{2}\ln^2\sigma_g\right) \qquad \text{(I-1)}$$

$$\int_0^\infty d^3\,\frac{\delta N}{\delta d}\,\delta d = N_0 d_{gn}^3\exp\left(\frac{9}{2}\ln^2\sigma_g\right) \qquad \text{(I-2)}$$

Here N_0 refers to the number concentration. Taking $(\delta N/\delta d)$ to be log-normal and using Equation I-1,

$$P = cN_0 d_{gn}\exp\left(\frac{1}{2}\ln^2\sigma_g\right)$$

Estimating σg to be 2.0, d_{gn} to be 0.1 μm for flexible polyurethane, and c to be 7 μV·cm³/μm, the following expression is obtained for *P:*

$$P = cN_0\left(d_{gn}\right)\exp\left(\frac{1}{2}\ln\sigma_g^2\right) = 7N_0(0.10)\exp\left[\frac{1}{2}(0.69)^2\right]$$

$$P = 0.89N_0\ \mu\text{m/cm}^3$$

The final task is to estimate N_0 based on the mass generation rate of smoke. In one minute, 50 g of the pillow are consumed and 1.5 g of smoke are produced. This corresponds to a mass concentration, *m*, given by

$$m = \frac{1.5}{(6)^2(2.5)} = 0.0167\ \text{g/m}^3 = 1.67\times10^{-8}\ \text{g/cm}^3$$

The quantity *m* is the third moment of the size distribution,

$$m = \int_0^\infty \frac{1}{6}\pi\rho d^3\,\frac{\delta N}{\delta d}\,\delta d$$

Using Equation I-2,

$$m = \frac{1}{6}\pi\rho N_0 d_{gn}^3\exp\left(\frac{9}{2}\ln^2\sigma_g\right)$$

Finally, solving for N_0,

$$N_0 = \frac{6m}{\pi\rho d_{gn}^3}\exp\left(-\frac{9}{2}\ln^2\sigma_g\right)$$

$$= \frac{(6)(1.67\times10^{-8})}{(3.14)(2)(1.0\times10^{-5})^3}\exp\left[-\frac{9}{2}\ln^2(2.0)\right]$$

$$N_0 = 1.8\times10^6\ \text{particles/cm}^3\ \text{(assuming }\rho = 2\ \text{g/cm}^3\text{)}$$

Substituting in the expression for *P,*

$$P = (0.89)(1.8\times10^6) = 1.6\times10^6\ \mu\text{V} = 1.6\ \text{volts}$$

This represents the voltage after 1 min. The estimated time to reach the alarm point, 2.5 V, will be 1.6 min. By the time the entire pillow is consumed in 4 min, the visibility has deteriorated to the point where escape is becoming less likely (visibility 5.9 m, according to Example 3, for a room 6 m across). So the individual's escape time is as follows:

$$\text{escape time} = \text{time to unsafe condition minus time to detector alarm}$$
$$= 4 - 1.6 = 2.4\ \text{min}$$

Example 4 is intended to illustrate the complete method for estimating the alarm time of smoke detectors. However, there is not adequate information at this time to implement the method in a realistic manner. Information on the size distribution and on the detector response functions is lacking for smoke agglomerates. The time for the smoke to reach the detector and the time lag for the smoke to enter the sensing zone of the detector are not included in this example, but should be included in a full analysis of the problem.

A simpler method for estimating the alarm time is to calculate the time at which the optical density per meter of the smoke exceeds the value of 0.06 (gray smoke) or 0.14 (black smoke), which correspond to the U.L. minimum sensitivity values. The limitation of this procedure is that a detector set to alarm at a particular optical density for one type of smoke may not respond in the same manner to another with a different size distribution and refractive index.

EXAMPLE 5:

Estimate the alarm time for the conditions given in Example 4, using the simpler method described above.

SOLUTION:

In Example 3, the optical density was estimated to be 0.49 m^{-1}, based on D_m measured for polyurethane. This

value corresponds to the burning of the entire pillow. Assuming a steady smoke generation rate, the alarm time [the time at which the minimum detector sensitivity value is exceeded (0.14 for black smoke)] is estimated to be given by

$$t = \frac{0.14}{0.49}(4) = 1.1 \text{ minutes}$$

This is comparable to the estimated 1.6 minutes in Example 4.

Nomenclature

ε	smoke conversion factor
d	particle diameter (μm)
d_i	midpoint of the ith particle size channel (μm)
d_{gn}	geometric mean number diameter (μm)
d_{gv}	geometric mean volume diameter (μm)
d_{32}	volume surface mean diameter (μm)
σ_g	geometric standard deviation
N	number concentration (particles/cm^3)
m	mass concentration of smoke (mg/m^3 or g/m^3)
V_T	volume concentration of smoke (cm^3/m^3 or μm^3/cm^3)
$\frac{\Delta N}{\Delta d}$ or $\frac{dN}{dd}$	number size distribution function cm^{-3}·μm^{-1}
$\frac{\Delta N}{\Delta \log d}$ or $\frac{dN}{d \log d}$	geometric number size distribution function (cm^{-3})
$\frac{\Delta m}{\Delta d}$ or $\frac{dm}{dd}$	mass size distribution function (mg·μm^{-1}·m^{-3})
Q_{ext}	extinction efficiency
λ	wavelength of light (μm)
n_r	complex refractive index of smoke particles
K	extinction coefficient (m^{-1})
D	optical density per meter (m^{-1})
K_m	specific extinction coefficient (m^2/g)
D_s	specific optical density
D_m	mass optical density (m^2/g)
I_λ	intensity of light at wavelength λ
B	luminance
C	contrast
s	visibility range (m)
L	pathlength
Γ	coagulation coefficient (cm^3/s)
t	time
ΔM	mass loss of sample (g)
P	detector output (V)
$R(d)$	detector size response function (μv cm$^{3)}$
V_c	volume of chamber (m^3)
A	area of sample (m^2)
M_s	mass of smoke (g)

References Cited

1. C.P. Bankston, B.T. Zinn, R.F. Browner, and E.A. Powell, *Comb. and Flame,* 41, p. 273 (1981).
2. C.J. Hilado and A.M. Machado, *J. Fire and Flamm.,* 9, p. 240 (1978).
3. C.P. Bankston, R.A. Cassanova, E.A. Powell, and B.T. Zinn, *NBS-GCR G8-9000,* National Bureau of Standards, Washington, DC (1978).
4. S.K. Brauman, N. Fishman, A.S. Brolly, and D.L. Chamberlain, *J. Fire and Flamm.,* 6, p. 41 (1976).
5. A. Tewarson, J.L. Lee, and R.F. Pion, *18th Symposium (International) on Combustion,* Pittsburgh, PA (1981).
6. G.W. Mulholland and T.J. Ohlemiller, *Aerosol Sci. and Tech.,* 1, p. 59 (1982).
7. G.W. Mulholland, T.G. Lee, and H.R. Baum, *J. Colloid Interface Sci.,* 62, p. 406 (1977).
8. S.K. Friedlander, *Smoke, Dust and Haze,* John Wiley and Sons, New York (1977).
9. P.C. Reist, *Introduction to Aerosol Science,* Macmillan, New York (1984).
10. T. Waldman and K.H. Schmitt, in *Aerosol Science,* Academic Press, New York (1966).
11. J.D. Seader and I.N. Einhorn, *16th Symposium (International) on Combustion,* Combustion Institute, Pittsburgh, PA (1976).
12. W.W. Foster, *Br. J. App. Phys.,* 10, p. 416 (1959).
13. G.W. Mulholland, *Fire and Matls.,* 6, p. 65 (1982).
14. D. Gross, J.J. Loftus, and A.F. Robertson, *ASTM STP 422,* American Society for Testing and Materials, West Conshohocken, PA (1967).
15. J.D. Seader and W.P. Chien, *J. Fire and Flamm.,* 5, p. 151 (1974).
16. L.H. Breden and M. Meisters, *J. Fire and Flamm.,* 7, p. 234 (1976).
17. E.L. Lopez, *J. Fire and Flamm.,* 6, p. 405 (1975).
18. V. Babrauskas, *J. Fire and Flamm.,* 12, p. 51 (1981).
19. D.D. Evans, *NBSIR 81-2400,* National Bureau of Standards, Washington, DC (1981).
20. J.G. Quintiere, *Fire and Matls.,* 6, p. 145 (1982).
21. E.J. McCartney, *Optics of the Atmosphere,* Wiley and Sons, New York (1976).
22. T. Jin, *J. Fire and Flamm.,* 9, p. 135 (1978).
23. T. Jin and T. Yamada, *Fire Sci. and Tech.,* 5, p. 79 (1985).
24. UL 217, *Standard for Single and Multiple Station Smoke Detectors,* Underwriters Laboratories, Northbrook, IL (1993).
25. G.W. Mulholland and B.Y.H. Liu, *J. Res. NBS,* 85, p. 223 (1979).
26. C. Helsper, H. Fissan, J. Muggli, and A. Scheidweiler, *Fire Tech.,* 14 (1983).

CHAPTER 14

Heat Fluxes from Fires to Surfaces

Brian Y. Lattimer

Introduction

The heat transfer from fires to adjacent surfaces is an important consideration in many fire analyses. Some example applications that may require knowledge of the heat transfer from a flame include heating and failure of structural beams, heat transfer through walls and ceilings, and the ignition and flame spread along combustible surfaces.

Flames transfer heat to adjacent surfaces primarily through convection and radiation. Techniques for efficiently modeling the heat transfer from flames are still being developed; however, experimental data and empirical correlations have been generated to predict flame heat transfer for a number of common geometries. This chapter will focus on the data and empirical correlations that have been developed.

Empirical correlations for predicting heat transfer from flames are typically simple to use; however, their use is usually limited to a particular type of fire or the geometry of the surface being heated. The types of fires considered in this chapter include

- Exposure area fires (burning objects)
- Wall and ceiling fires
- Window flames

Exposure area fires are burning objects located adjacent to or near the surface being heated. Wall and ceiling fires are those fires produced by a burning wall or ceiling. Window flames are flames extending outside a compartment containing a fire.

The heat transfer from fires has been characterized for a range of different surface geometries. The geometries included in this chapter are

- Flat vertical wall
- Flat unconfined and confined ceilings
- Parallel flat vertical walls
- Corner walls at 90°
- Corner walls at 90° with a ceiling
- Horizontal I-beams beneath a ceiling

Dr. Brian Y. Lattimer is a research scientist at Hughes Associates, Inc. His research has focused on species formation and transport in building fires, fire growth inside compartments, flame spread, and heat transfer from flames.

General Topics

The majority of the data reported in this chapter are total heat flux measurements made using water-cooled heat flux gauges. The total incident heat flux to the gauge is comprised of both radiative and convective heat transfer,

$$q''_{\text{inc},m} = q''_{\text{conv}} + q''_{\text{rad}} \tag{1}$$

where the radiative heat transfer to the gauge can include heating (or heat loss) effects of the environment if the flame is optically thin. Heat flux gauges are typically painted black to produce a high emissivity surface (~0.95) over the infrared spectrum. The gauge surface is usually cooled to a temperature ranging from 20–80°C, which can be much lower than the surface temperature of the material of interest. The low surface temperature, T_s, will increase the convective and radiative heat transfer incident on the surface. As a result, the total heat flux measured using water-cooled gauges will be a conservative estimate of the incident heat flux to most surfaces. The measured heat flux can be corrected for the actual heat flux on the surface if the heat transfer coefficient, surface emissive properties, and surface temperature are known.

EXAMPLE 1:

A water-cooled heat flux gauge is mounted onto a flat vertical wall located in a laboratory environment (300 K). The water running through the gauge is at a temperature of 300 K. When a fire with an optically thin flame is placed next to the wall, the heat flux gauge ($\varepsilon = 0.95$) measures the total heat flux to be 30 kW/m^2. A nearby thermocouple measures the wall material surface ($\varepsilon = 0.88$) temperature to be 600 K, while a second thermocouple measures the flame temperature to be 1300 K. Assuming a heat transfer coefficient to the wall of $h = 0.010$ kW/(m·K), how much of the measured heat flux is due to radiation?

SOLUTION:

An energy balance at the surface of the heat flux gauge can be used to develop an expression for the measured incident heat flux (see Figure 2-14.1). Note that there is no radiation exchange between the heat flux gauge and the lab environment since they are at the same temperature, making the measured heat flux the incident flux on the gauge.

$$q''_{\text{inc},m} = q''_{\text{conv}} + q''_{\text{rad}}$$

Solving for the radiation heat flux,

$$q''_{\text{rad}} = q''_{\text{inc},m} - h(T_g - T_s) - q''_{\text{inc},m}$$

$$q''_{\text{rad}} = 30 - 10 = 20 \text{ kW/m}^2$$

EXAMPLE 2:

For the problem stated in Example 1, what is the actual incident heat flux onto the material?

SOLUTION:

To determine the actual incident heat flux on the material, the reradiation from the surface to the surroundings must be accounted for in the calculations.

$$q''_{\text{inc}} = q''_{\text{conv}} + q''_{\text{rad}} - q''_{rr}$$

or

$$q''_{\text{inc}} = h(T_g - T_s) + q''_{\text{rad}} - \varepsilon\sigma T_s^4$$

Using the radiative heat flux from the flame determined above, the material surface temperature, and the material surface properties, the incident heat flux on the actual material was determined to be

$$q''_{\text{inc}} = 0.010(1300 - 600) + 20 - (0.88)(5.67 \times 10^{-11})(600)^4$$

$$q''_{\text{inc}} = 7.0 + 20 - 6.5 = 20.5 \text{ kW/m}^2$$

Therefore, for this case the incident heat flux onto the surface is approximately 9.5 kW/m^2 lower than that measured using the water-cooled heat flux gauge.

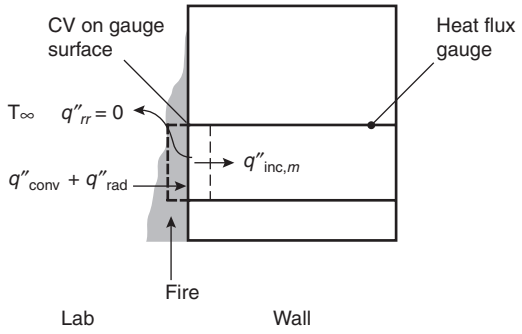

Figure 2-14.1. ***Energy balance at heat flux gauge surface.***

The heat transfer from a flame to an adjacent surface or object has historically been characterized with respect to the flame length. Many of the heat flux correlations developed in the literature are based on flame length data taken in that study. Measured flame lengths can vary depending on the measurement technique, definition, and surrounding geometry. For the studies considered in this chapter, the data was nondimensionalized with either the average (50 percent intermittent) flame length or the flame tip length. Therefore, heat flux correlations should be applied using either the flame length correlation developed in the study or with one that has been demonstrated to predict the flame length in that study.

Exposure Fires

Fires Adjacent to Flat Walls

Heat fluxes from exposure fires adjacent to flat walls have been experimentally studied using propane sand burners and characterized for various burning objects. The experimental study provides a systematic approach of calculating heat fluxes for this geometry.

An extensive experimental study was performed by Back et al.[1] to characterize the heat transfer from a fire to an adjacent wall. In this study, fires were generated using square propane sand burners with edge lengths of 0.28, 0.37, 0.48, 0.57, and 0.70 m. Heat flux fields were measured for fires ranging from 50 to 520 kW.

A plot of the peak heat fluxes measured for each type of fire evaluated is shown in Figure 2-14.2. Peak heat fluxes for the different fires evaluated were determined to be a function of fire heat release rate. This dependence was attributed to the larger fires resulting in thicker boundary layers, which is related to the radiation pathlength. Based on gray-gas radiation theory, the authors found that the following relation adequately represented the data:

$$q''_{\text{peak}} = 200[1 - \exp(-0.09Q^{1/3})] \qquad (2)$$

where q''_{peak} is in kW/m^2 and Q is in kW.

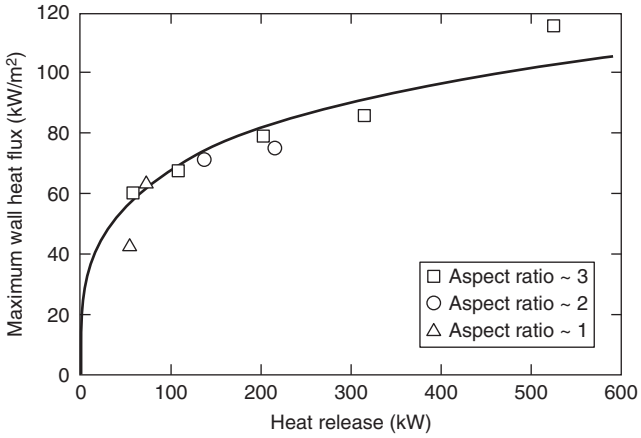

Figure 2-14.2. ***Peak heat release rates measured in square propane burner fires against a flat wall.[1]***

These peak heat fluxes were measured in the lower part of the fire ($z/L_f \leq 0.4$) along the centerline, with the flame length taken from Heskestad:[2]

$$L_f = 0.23Q^{2/5} - 1.02D \tag{3}$$

where L_f and D are in (m) and Q is in (kW)

Above this region, the heat fluxes were measured to decrease with distance above the fire. The heat flux data measured along the centerline is shown in Figure 2-14.3. Lines in this plot are a general correlation of the centerline data:

$$q''_{cl} = q''_{\text{peak}} \qquad z/L_f \leq 0.4 \tag{4a}$$

$$q''_{cl} = q''_{\text{peak}} - \frac{5}{3}(z/L_f - 2/5)(q''_{\text{peak}} - 20) \qquad 0.4 < z/L_f \leq 1.0 \tag{4b}$$

$$q''_{cl} = 20(z/L_f)^{-5/3} \qquad z/L_f > 1.0 \tag{4c}$$

Heat fluxes were measured to decrease with horizontal distance from the centerline, as shown in Figure 2-14.4. The normalized lateral heat flux distribution data shown in Figure 2-14.4 was found to be half-Gaussian in shape over the half-width of the burner. The line in the plots is a fit to the data in Figure 2-14.4(a):

$$q'' = q''_{cl} \exp\left[-\left(\frac{x}{0.5D}\right)^2\right] \qquad \frac{x}{0.5D} \leq 1.0 \tag{5a}$$

$$q'' = 0.38 q''_{cl}\left(\frac{x}{0.5D}\right)^{-1.7} \qquad \frac{x}{0.5D} > 1.0 \tag{5b}$$

Heat fluxes from burning objects to an adjacent wall have been measured for a variety of items; however, limited data has been published on this work.[3,4] Heat fluxes at the rim of wastebasket fires was reported by Gross and Fang.[3] At the rim, heat fluxes as high as 50 kW/m^2 were measured; however, the authors noted that peak heat fluxes for these fires occurred approximately 0.22 m above the rim.

Mizuno and Kawagoe[4] performed experiments with upholstered chair fires against a flat wall. In these tests, Mizuno and Kawagoe measured heat fluxes to the wall of 40 to 100 kW/m^2 over the continuous flaming region ($\sim z/L_f < 0.4$). All these tests were performed using foam-padded chairs.

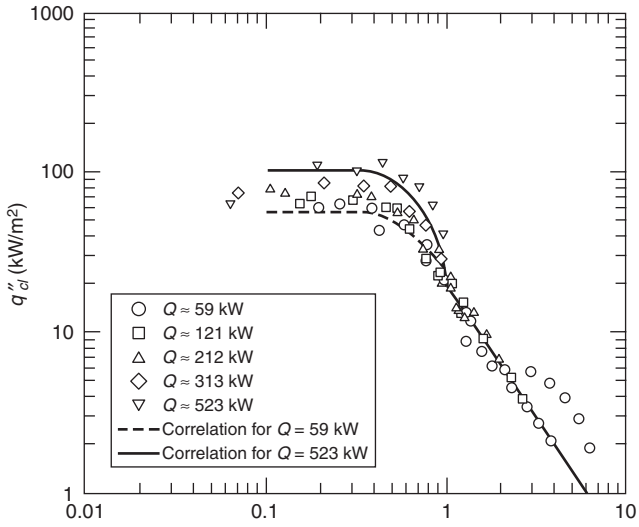

Figure 2-14.3. ***Vertical heat flux distribution along the centerline of a square propane burner fire adjacent to a flat wall.[1]***

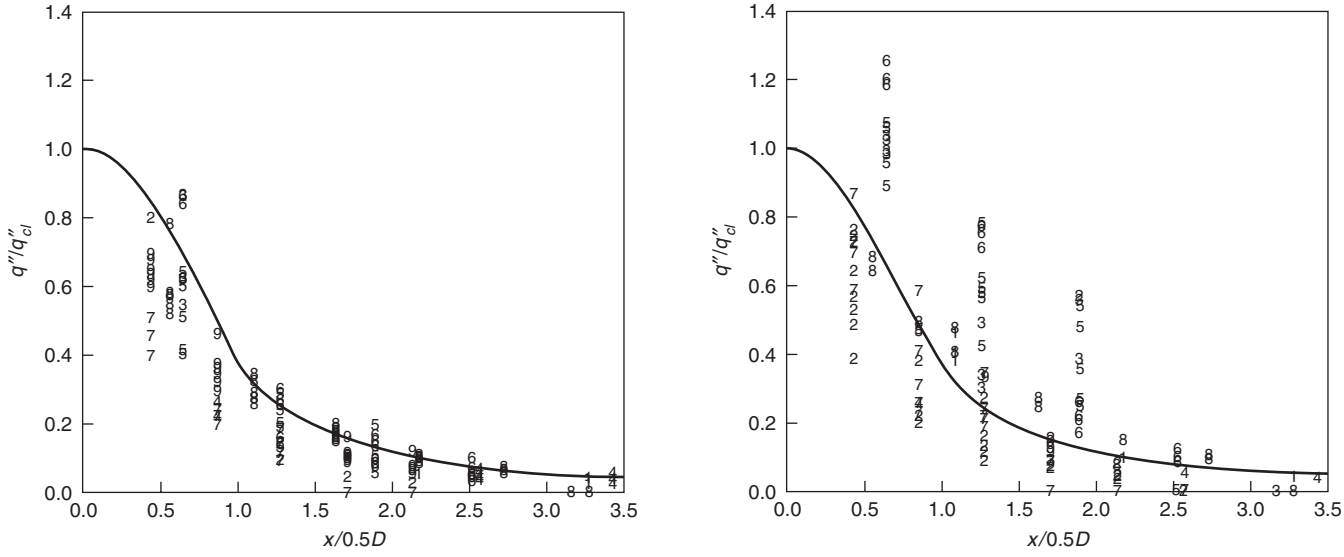

Figure 2-14.4. ***Lateral heat flux distribution with distance from the centerline of square propane burner fires against a flat wall[1] (a) in the flaming region and (b) in the plume.***

Fires in a Corner

Fires in a corner of a room lined with a combustible material have been shown to cause more rapid flame spread and growth to flashover compared to cases with fires in other locations within the room. For these reasons, a significant amount of work has been performed to characterize the heat fluxes produced by corner fires. Heat flux measurements have been performed both in an open environment to quantify the heat flux due to the exposure fire alone and within rooms to measure the heat flux due to the exposure fire and the room environment.

The heat flux from exposure fires have been quantified in several studies performed in an open laboratory environment.[5–10] All the studies were performed in a noncombustible corner with a ceiling except the study of Kokkala,[7] which was performed in a noncombustible corner without a ceiling. A comparison of the heat flux fields measured in the study with a ceiling[10] and the study without a ceiling[7] is shown in Figure 2-14.5. Note that the contour plot of Lattimer et al. is relative to the floor, while the plot of Kokkala is relative to the top of the burner. Lattimer et al. used a burner 0.15 m high.

Up to approximately 1.8 m above the floor, the heat flux distributions are similar. In the case with the ceiling, the ceiling jet and the radiation from the fire flowing along the ceiling was heating the top part of the wall. This resulted in higher heat fluxes further out from the corner along the top part of the wall.

A series of fire tests were performed by Lattimer et al.[10] to develop empirical correlations to estimate heat fluxes from an exposure fire to the walls and ceiling of a corner. Tests were performed using 0.17-, 0.30-, and 0.50-m square propane burners placed directly against the corner. Heat flux fields were measured for fires ranging from 25–300 kW.

Correlations were developed for three regions in the corner: along the height of the walls in the corner, along the top of the walls near the ceiling, and along the ceiling. The region containing the walls in the corner extended from the top of the fire to approximately 1.8 m above the floor, which is approximately the ceiling height minus twice the ceiling jet thickness ($\delta = 0.1H$). Correlations for the top part of the walls, which are heated by the ceiling jet, were developed using data at locations greater than 1.8 m above the floor.

Along the height of the walls in the corner, the peak heat fluxes were typically measured near the base of the fire. The peak heat fluxes along the height of the walls in the corner were measured to be a function of the fire diameter, as shown in Figure 2-14.6. The curve in Figure 2-14.6 is a correlation of the data and is expressed using the following relation:

$$q''_{\text{peak}} = 120\left[1 - \exp(-4.0D)\right] \tag{6}$$

The vertical distribution in the maximum heat flux along the walls near the corner is shown in Figure 2-14.7 plotted with the vertical distance normalized with respect to the flame tip,

$$L_{f,\text{tip}}/D = 5.9Q_D^{*1/2} \tag{7}$$

with

$$Q_D^* = \frac{Q}{\rho_\infty C_p T_\infty \sqrt{g} D^{5/2}} \tag{8}$$

Peak heat flux levels were measured in the lower part of the flame ($z/L_{f,\text{tip}} \le 0.4$), and decreased with distance above $z/L_{f,\text{tip}} = 0.4$. A general correlation to represent this behavior is

$$q''_{\text{max}} = q''_{\text{peak}} \qquad z/L_{f,\text{tip}} \le 0.4 \tag{9a}$$

$$q''_{\text{max}} = q''_{\text{peak}} - 4\left(\frac{z}{L_{f,\text{tip}}} - \frac{2}{5}\right)\left(q''_{\text{peak}} - 30\right) \qquad 0.4 < z/L_{f,\text{tip}} \le 0.65 \tag{9b}$$

$$q''_{max} = 7.2\left(\frac{z}{L_{f,\text{tip}}}\right)^{-10/3} \qquad z/L_{f,\text{tip}} \le 0.65 \tag{9c}$$

This is similar to the form used by Back et al.[1] to correlate heat fluxes from an exposure fire to a wall (see Equations 4a–4c), except the constants are different.

The horizontal distribution in the heat flux along the wall is shown in Figure 2-14.8 to best correlate with actual distance from the corner (in meters).[10] This was attributed to air being entrained in the corner, pushing the fire into the corner. Near the corner the shape is half-Gaussian; however, heat fluxes outside of this decrease more slowly. The trend in the data, which is shown as the line in Figure 2-14.8, can be represented using the following relations:

$$q'' = q''_{\text{max}} \exp\left[-7.5x^2\right] \qquad x \le 0.4 \tag{10a}$$

$$q'' = 0.058 q''_{\text{max}} x^{-1.8} \qquad x > 0.4 \tag{10b}$$

It has not been established whether this correlation holds for fire sources larger than 0.50 m in length on a single side.

Along the top part of the wall the maximum heat fluxes were measured at locations less than 0.15 m below the ceiling. The maximum heat fluxes are shown in Figure 2-14.9 plotted against the normalized distance along the flame $(x + H)/L_{f,\text{tip}}$, where x is the distance from the corner. These heat fluxes can be estimated using the following relations:

$$q''_{\text{max}} = 120 \qquad \left(\frac{x+H}{L_{f,\text{tip}}}\right) \le 0.52 \tag{11a}$$

$$q''_{\text{max}} = 13.0\left(\frac{x+H}{L_{f,\text{tip}}}\right)^{-3.5} \qquad \left(\frac{x+H}{L_{f,\text{tip}}}\right) > 0.52 \tag{11b}$$

The assumed plateau in the correlation was based upon the maximum heat flux expected from a flame according to Equation 6.

The heat fluxes to the ceiling were determined to be a function of normalized distance along the flame length, $(r + H)/L_{f,\text{tip}}$. All of the ceiling heat flux data taken in the study with a square burner in the corner is shown in Figure 2-14.10. Heat fluxes along the ceiling due to the exposure fire were similar to those measured along the top of

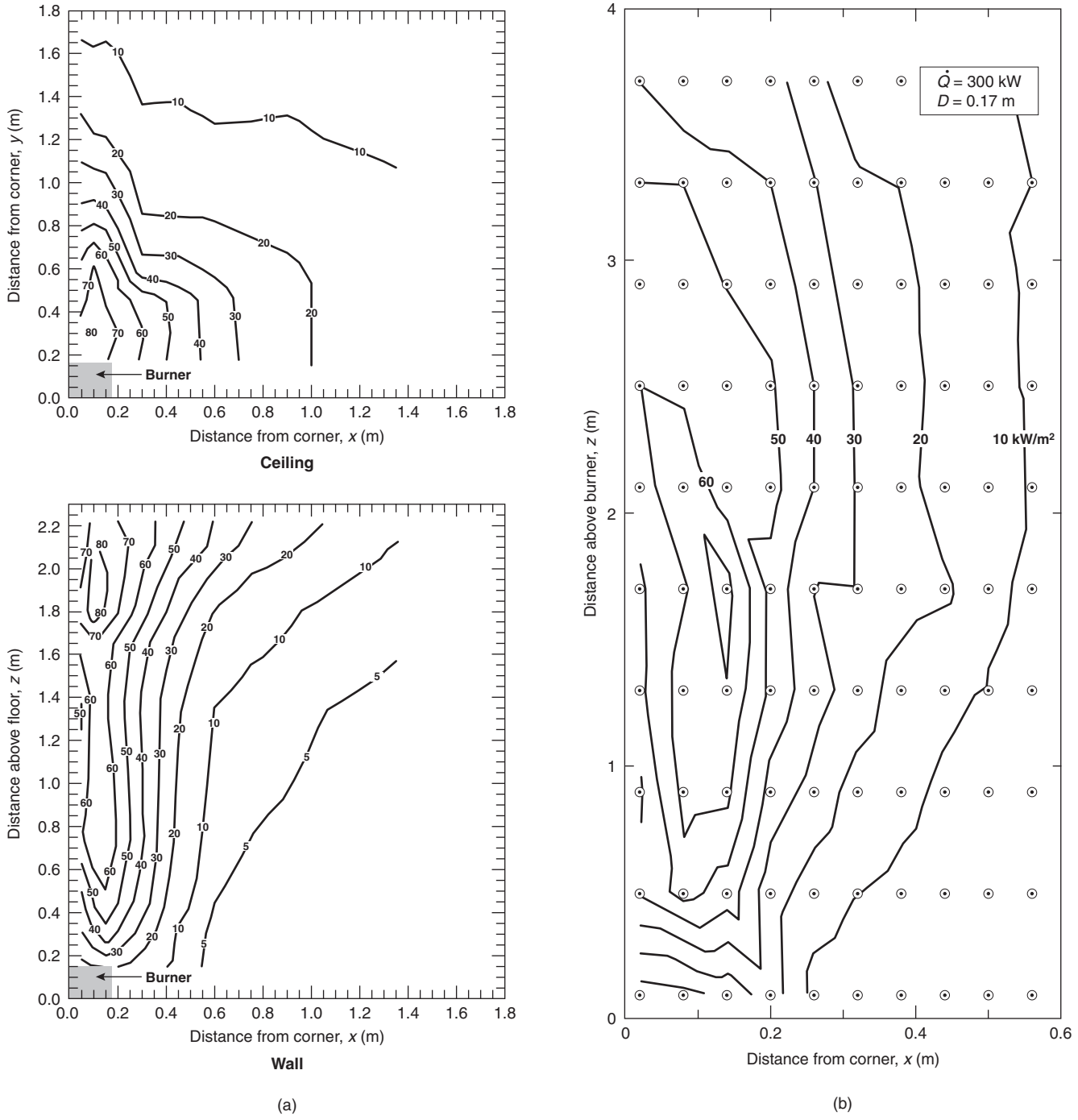

Figure 2-14.5. ***A comparison of the heat flux fields produced in a corner (a) with a ceiling[10] and (b) without a ceiling.[7] The fire was produced by a 0.17 m square propane burner with a heat release rate of 300 kW. Note that the data of Lattimer et al. are plotted relative to the floor and the data of Kokkala are plotted relative to the top of the burner.***

the wall. This resulted in similar correlations to estimate the heat flux to the ceiling:

$$q'' = 120 \qquad \left(\frac{r+H}{L_{f,\text{tip}}}\right) \le 0.52 \qquad (12a)$$

$$q'' = 13.0\left(\frac{r+H}{L_{f,\text{tip}}}\right)^{-3.5} \qquad \left(\frac{r+H}{L_{f,\text{tip}}}\right) > 0.52 \qquad (12b)$$

Again, the assumed plateau in the correlation was based upon the maximum heat flux expected from a flame, according to Equation 6.

Similar levels were measured by Hasemi et al.[6] with an exposure fire in the corner, simulated burning corner walls, and an exposure fire and simulated burning corner walls in the corner.

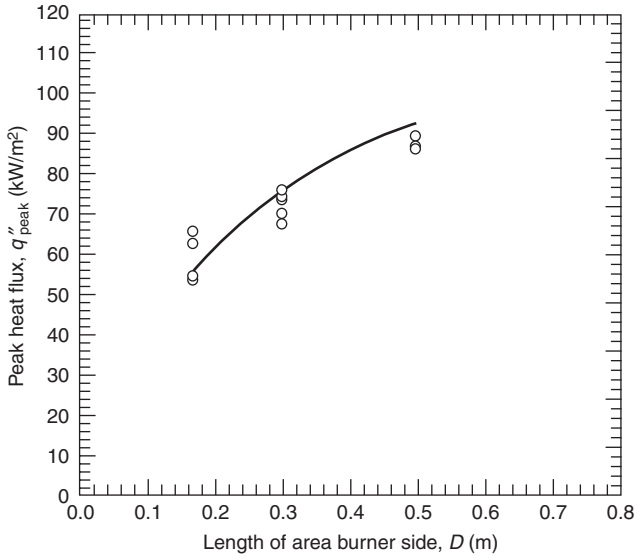

Figure 2-14.6. ***Peak heat flux along the height of the walls in the corner.[10]***

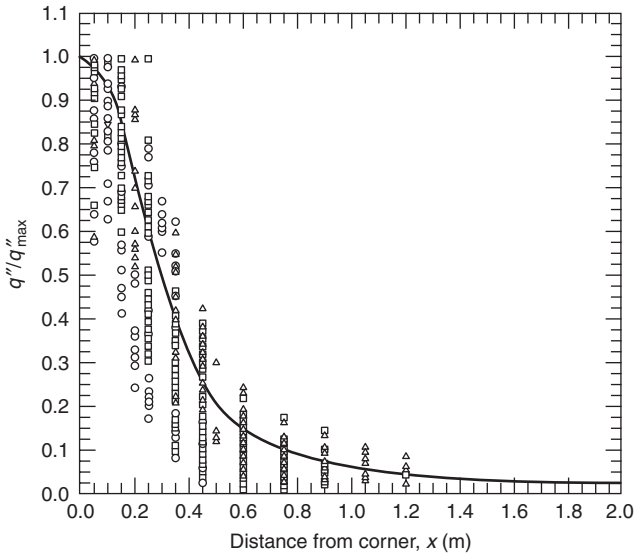

Figure 2-14.8. ***Lateral distribution in the heat flux along the walls with distance from the corner with square burner sides of 0.17 m (○), 0.30 m (△), 0.30 m (elevated) (▽), and 0.50 m (□) and fire sizes ranging from 50–300 kW.[10]***

Room environment effects: Corner fires are currently used to evaluate fire growth potential of a combustible lining material. As such, several studies have been conducted to characterize the heat flux from an exposure fire inside a room.[11–14] In these cases, the heat flux to the surface will be due to both the exposure fire and the room environment.

The effect of the room environment on the heat fluxes was clearly demonstrated through the work performed by Dillon[14] in an ISO 9705 room.[15] The incident heat fluxes from the fire were determined by measuring the temperature rise at several locations on an insulated steel plate. Heat fluxes were calculated using a two-dimensional heat balance on the plate. Heat fluxes included contributions from both the exposure fire and the room environment. Using the surface temperature measurements and initial heat flux measurements after the burner was ignited, the heat fluxes to the hot steel plate were corrected for both reradiation from surfaces in the room and heating by the hot gas layer.

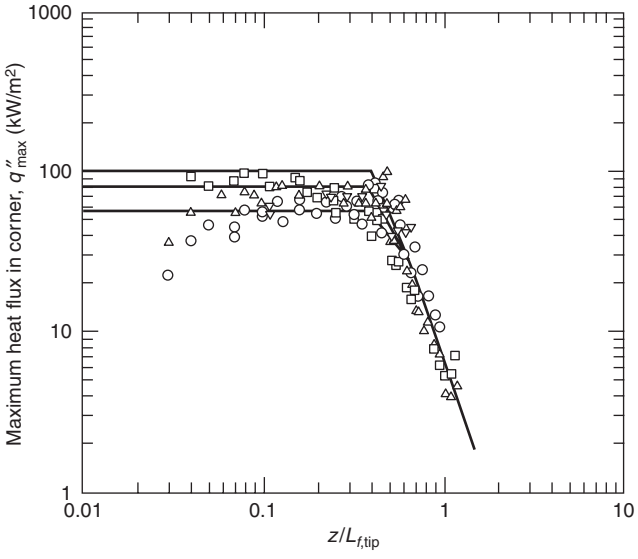

Figure 2-14.7. ***Maximum heat fluxes to the walls near the corner with square burner sides of 0.17 m (○), 0.30 m (△), 0.30 m (elevated) (▽), and 0.50 m (□) and fire sizes ranging from 50–300 kW.[10]***

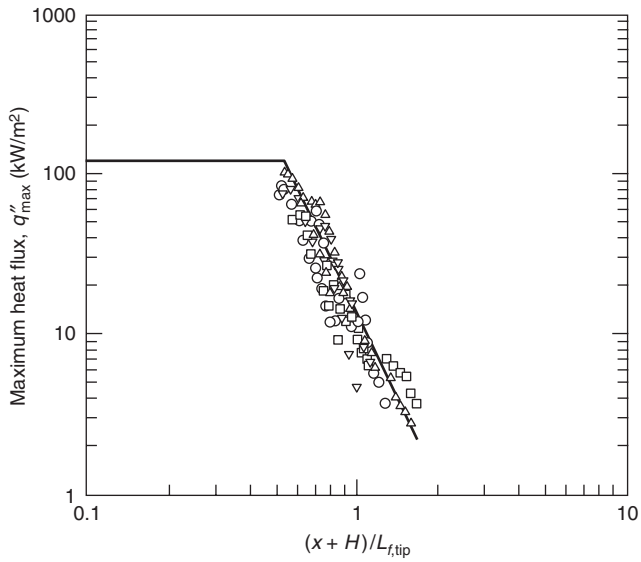

Figure 2-14.9. ***Maximum heat flux along the top of the walls during a corner fire test with square burner sides of 0.17 m (○), 0.30 m (△), 0.30 m (elevated) (▽), and 0.50 m (□) and fire sizes ranging from 50–300 kW.[10]***

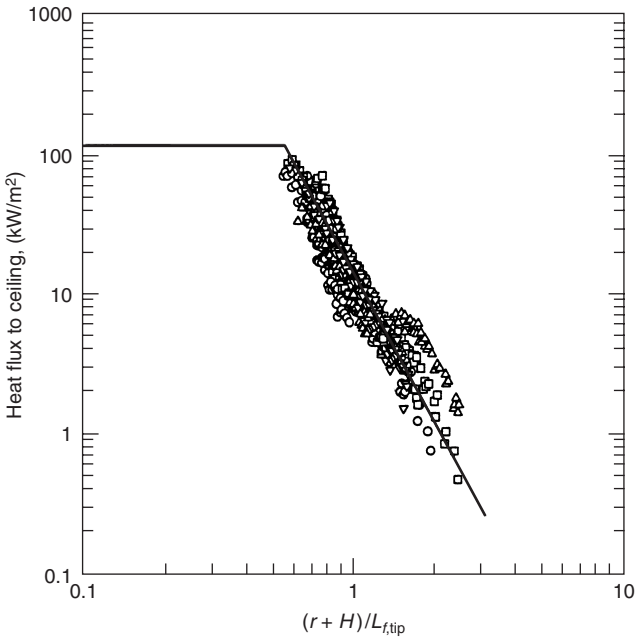

Figure 2-14.10. ***Heat flux along the ceiling above a fire located in a corner for tests with square burner sides of 0.17 m (○), 0.30 m (△), 0.30 m (elevated) (▽), and 0.50 m (□) and fire sizes ranging from 50–300 kW.[10]***

The effects of the room environment on the heat fluxes to the corner boundaries is discussed here for the case with a 300-kW fire in the corner, produced using a 0.17-m square burner. The heat fluxes shown in Figure 2-14.11(a) represent the heat flux from the fire only, as measured using a heat flux gauge (i.e., cold surface). Note that the top of the burner is 30 cm above the floor. In general, the heat fluxes in Figure 2-14.11(a) compare well with the total heat flux data shown in Figure 2-14.5(a).

Heat fluxes shown in Figure 2-14.11(b) correspond to heat fluxes due to the fire and the room environment (i.e., hot gas layer and reradiation from walls), as measured using a heat-flux gauge. For this room environment, the heat fluxes including the room environment were higher than the heat fluxes from the exposure fire to a cold wall. The magnitude of the increase depends on the elevation inside the room. Measurements in the lower part of the room showed less of an increase compared with those near the ceiling. Heat fluxes in the upper part of the room increased by as much as 20 kW/m^2, an increase largely attributed to the hot gas layer that forms inside the room during the fire. For the 300-kW fire inside the ISO 9705 compartment, average gas temperatures in the upper part of the room were measured to be approximately 680 K. Note that the heat flux due to the room environment is dependent on the gas layer temperature, which is dependent on the fire size, room geometry, ventilation, and thermal properties of the boundaries. A room or fire different from that used to produce the data in Figure 2-14.11(b) may result in a different gas layer temperature, which will result in a different heat flux contribution due to the room environment.

Heat fluxes due to the hot layer environment inside a room were measured by Tanaka et al.[16] In tests conducted in a 3.3-m-wide, 3.3-m-deep, 2.35-m-high room with the propane fire in the center of the room, heat fluxes were measured at different locations on one of the side walls. The average heat flux measured in the upper layer formed inside of the room is shown in Figure 2-14.12 versus the layer temperature for different compartment door widths. The line in the plot represents the black body heat flux using the layer gas temperature, $q'' = \sigma T_{gas}^4$. As seen in Figure 2-14.12, the black body heat flux using the layer gas temperature provides a reasonable estimate of the incident heat flux to the walls inside a compartment.

Effects of fire standoff distance: Several researchers have investigated the effects of moving the exposure fire away from the corner (i.e., standoff distance).[5,11,17] As one might expect, moving the fire away from the corner decreases the heat fluxes to the room boundaries. Tests were performed by Williamson et al.[11] in a full-scale ISO 9705 room using a 0.30-m-diameter burner. Heat fluxes to the wall were strongly dependent on whether the flame was attached to the corner walls or burned freely near the wall. At a heat release rate of 40 kW, with the burner against the corner walls, the flame was attached to the walls and heat fluxes were measured to be as high as 50 kW/m^2. When the fire was moved 50 mm from the walls, the flames were observed to be detached from the walls with the highest heat fluxes measured to be approximately 25 kW/m^2. In tests with a heat release rate of 150 kW, the fire was observed to be attached to the walls and heat fluxes of 40–60 kW/m^2 were measured at the walls. Additional work needs to be performed to investigate distances at which fires attach to nearby surfaces, such as a flat wall or walls in a corner.

Fires beneath Unconfined Ceilings

There have been several experimental and theoretical studies performed on fires impinging on an unbounded ceiling.[18–25] Total heat fluxes from fires and fire plumes impinging on the ceiling were measured by Hasemi et al.,[18] You and Faeth,[20,21] and Kokkala.[23,24]

Hasemi et al.[18] conducted a series of fire tests using propane gas burners located at different distances beneath a noncombustible ceiling. Fires as large as 400 kW (approximated) were considered in the study. Heat flux gauges were used to measure the incident heat flux along the ceiling at different distances away from the fire centerline, or stagnation point. The measured heat flux at the stagnation point is shown in Figure 2-14.13 to plateau at approximately 90 kW/m^2. In order to collapse the data, the unconfined flame tip length was normalized with respect to the distance between the ceiling and the fire, H, plus the virtual source location, z'. The virtual source location for this geometry was determined using the following relations:

$$z' = 2.4D\left(Q_D^{*2/3} - Q^{*2/5}\right) \qquad Q_D^* < 1.0 \tag{13a}$$

$$z' = 2.4D\left(1 - Q_D^{*2/5}\right) \qquad Q_D^* \geq 1.0 \tag{13b}$$

where Q_D^* is defined as in Equation 8, with D being the diameter of the exposure fire, z' is in meters and D is in

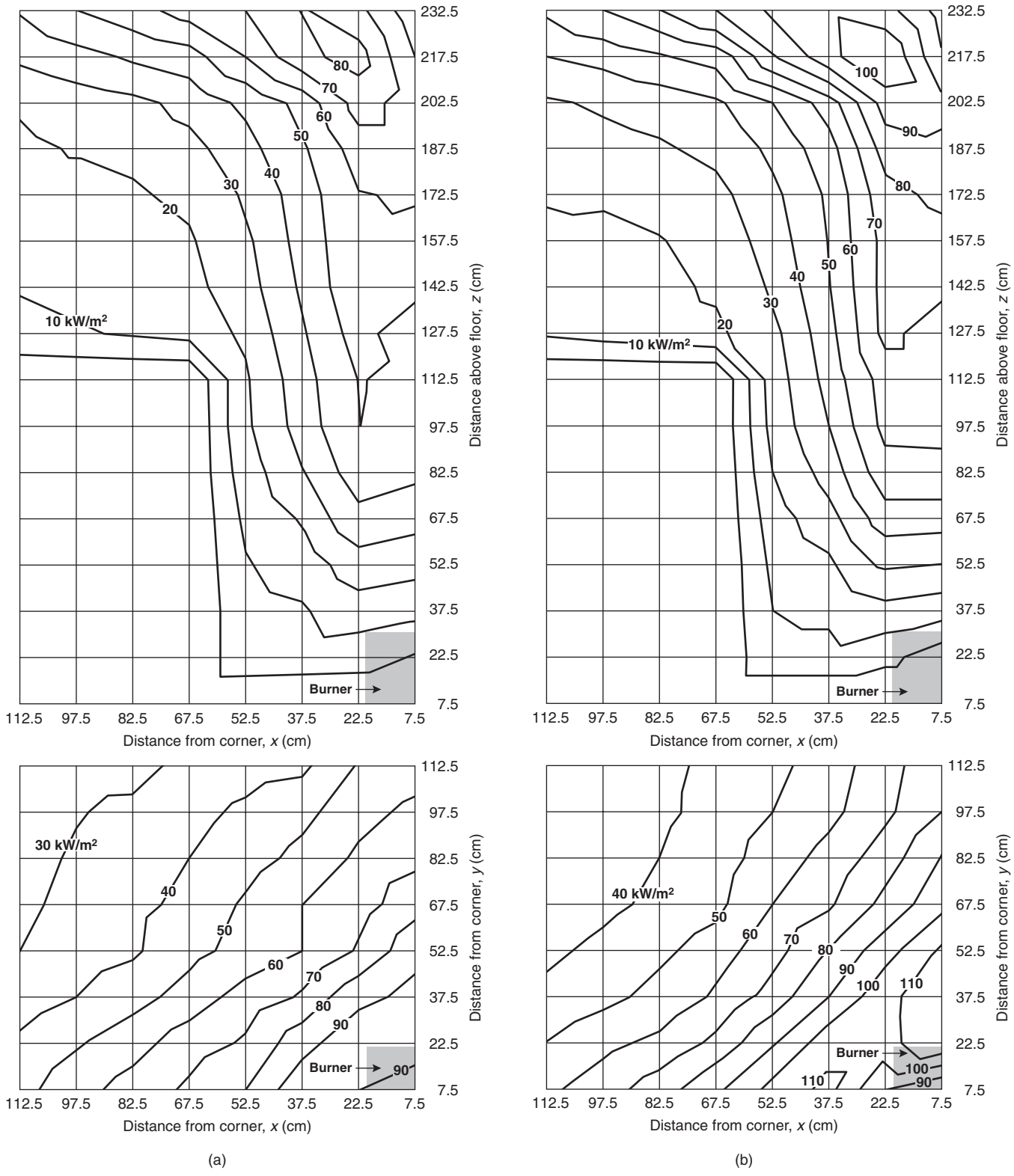

Figure 2-14.11. ***Heat fluxes to corner boundaries from (a) 300-kW, 0.17-m square propane sand burner exposure fire alone to a cold surface and from (b) the 300-kW exposure fire and the room environment.[14]***

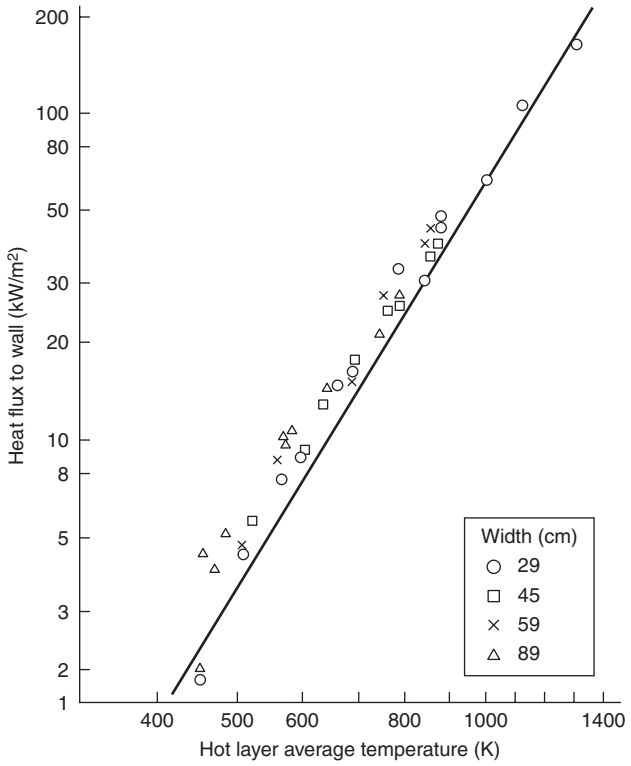

Figure 2-14.12. ***Heat flux to the walls inside a compartment containing a hot gas layer.[16]***

meters. The unconfined flame tip length was calculated using $L_f = 3.5Q_D^{*n} \cdot D$, where $n = 2/5$ for $Q_D^{*n} \geq 1.0$ and $n = 2/3$ for $Q_D^* < 1.0$, with L_f and D in meters. The length of the flame, $L_{f,\text{tip}}$, in this geometry is defined as the distance between the fire and the ceiling, H, plus the radial extension of the flame out from the center of the fire, L_H. The location of the flame tip in this geometry was found to correlate with Q_H^*, which is defined the same as in Equation 8 except D is replaced by H. The flame tip correlation was determined to be

$$\frac{(L_H + H)}{H} = \frac{L_{f,\text{tip}}}{H} = 2.89Q_H^{*1/3} \tag{14}$$

The heat flux was measured to decrease with distance from the fire stagnation point. Figure 2-14.14 contains a plot of the heat flux to the ceiling as a function of location within the flame. The correlation recommended by Wakamatsu[26] can be used to predict the heat fluxes:

$$q'' = 518.8e^{-3.7w} \tag{15a}$$

where

$$w = (r + H + z')/(L_H + H + z') \tag{15b}$$

Heat flux measurements with smaller fires (<11 kW) beneath a ceiling were made by Kokkala[23,24] and You and Faeth.[27] Kokkala used natural gas as a fuel and measured heat fluxes to plateau at 60 kW/m² at the stagnation point (see Figure 2-14.15). Due to the small burners used in this study (D = 0.064 m), Kokkala's data collapsed without applying a virtual source origin correction. Heat fluxes measured in the natural gas fire tests were lower than those measured by Hasemi et al.,[18] an effect that can partly be attributed to the higher radiation levels from the

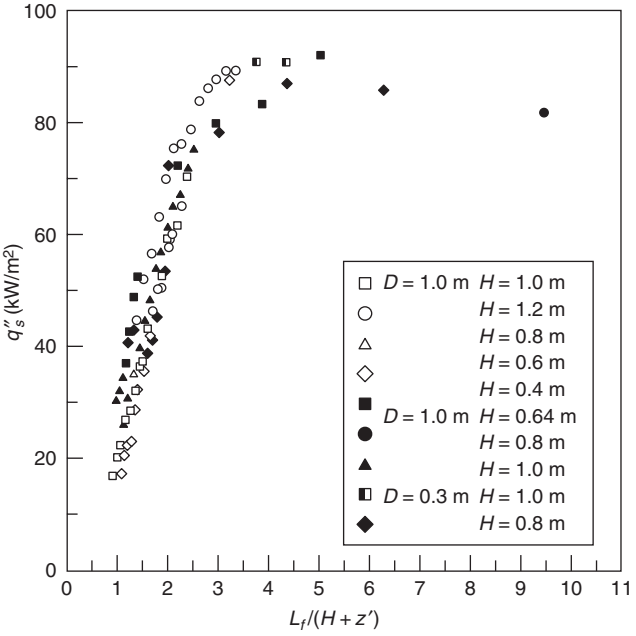

Figure 2-14.13. ***Stagnation point heat fluxes on an unbounded ceiling with a fire impinging on it.[18]***

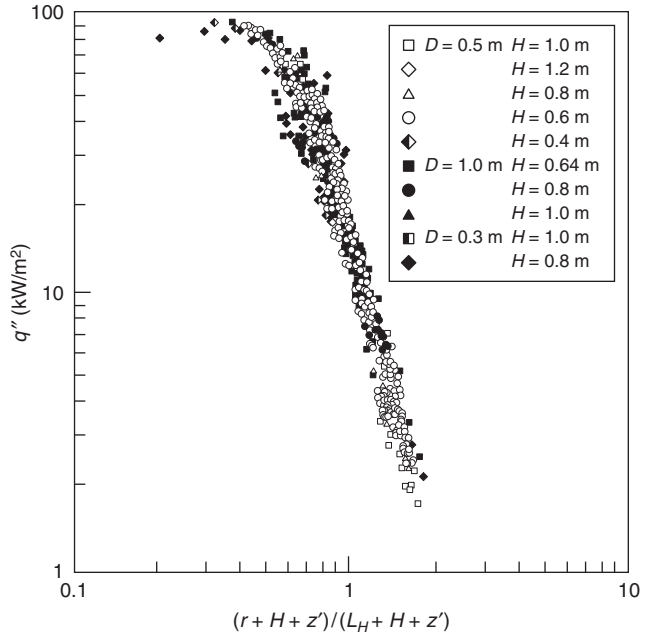

Figure 2-14.14. ***Heat fluxes to a ceiling due to a propane fire impinging on the surface.[18]***

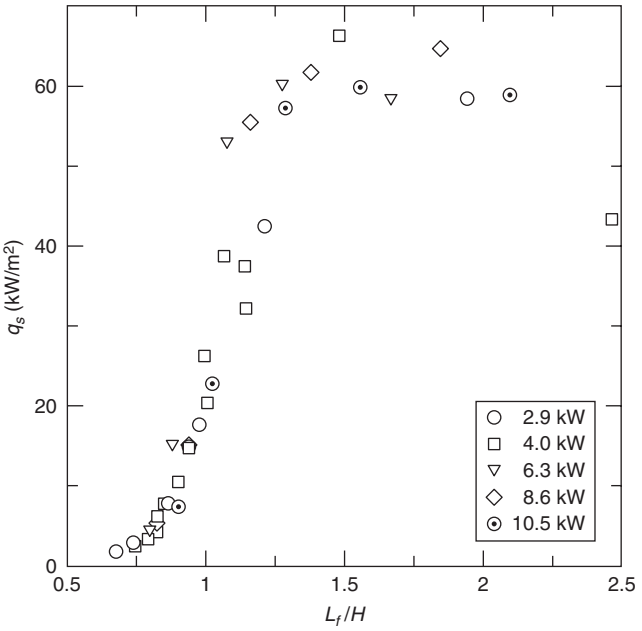

Figure 2-14.15. ***Heat fluxes at the stagnation point on a ceiling for tests with natural gas fires impinging on the ceiling.[23]***

propane flames. The heat fluxes measured by Kokkala[23] at different locations from the stagnation point are plotted in Figure 2-14.16. The distribution in the heat flux along the ceiling radially out from the stagnation point was measured to be similar to that measured by Hasemi et al.[28] with larger propane gas fires.

Fires in Corridors

There are few reported studies that have measured heat fluxes to the ceiling or walls of a corridor. Hinkley et al.[29–31] performed experiments with a town gas burner located at the end of a hallway. In tests with a noncombustible ceiling, tests were performed in a 1.2-m-wide hallway using a range of heat release rates (170–600 kW) with the burner at various distances (0.37–1.20 m) below the ceiling. Heat fluxes were determined through temperature measurements on exposed and unexposed sides of the ceiling material.

The heat fluxes determined in these experiments are provided in Figure 2-14.17, plotted as a function of $(x + x')/L$, where x' is the virtual source and L is the flame length from the virtual source. This plot indicates that heat fluxes as high as 140 kW/m² can exist in these types of scenarios. The increase in the heat flux over the unconfined ceiling data of Hasemi et al.,[18] where peak heat fluxes of approximately 90 kW/m², may be in part due to the thicker layer of flames formed in the corridor. However, due to the method used to develop the heat fluxes, the accuracy of the heat flux data reported by Hinkley et al. is uncertain.[29,30] Additional work needs to be performed to validate these results. In addition, heat fluxes in corridor geometries may also depend on the width of the corridor since this will affect the flame thickness. No work has been performed to evaluate this, but wider hallways should be expected to begin to provide results closer to the unconfined ceiling data.

Fires beneath I-Beams

Three studies have evaluated the heat flux incident onto an I-beam mounted to a ceiling with an exposure fire impinging upon the beam.[18,32,33] These studies all measured the heat flux to the four surfaces shown in Figure 2-14.18 on the I-beam: downward face of the lower flange, upward face of the lower flange, the web, and

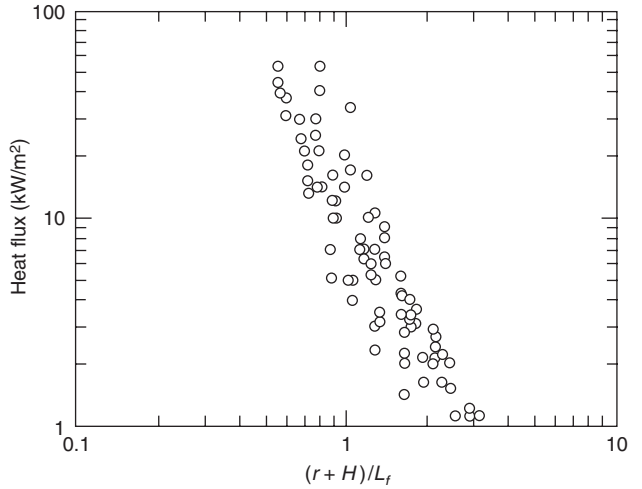

Figure 2-14.16. ***Heat fluxes to a ceiling due to a natural gas fire impinging on the surface.[23]***

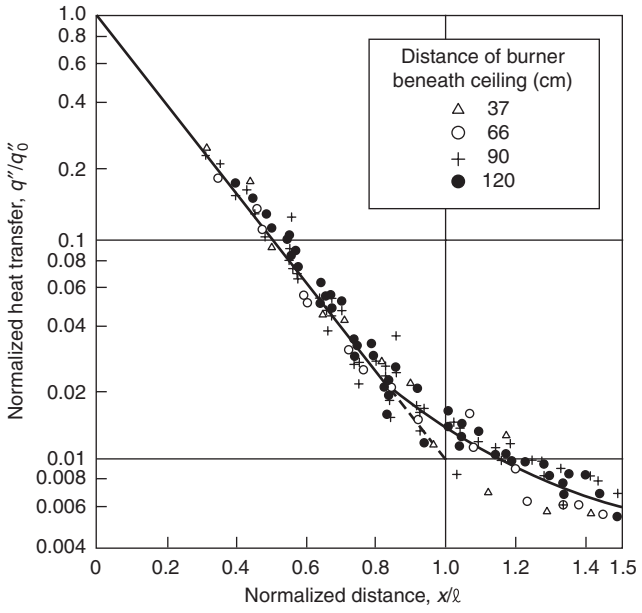

Figure 2-14.17. ***Heat fluxes to the ceiling in a corridor with an exposure fire at the closed end.[30]***

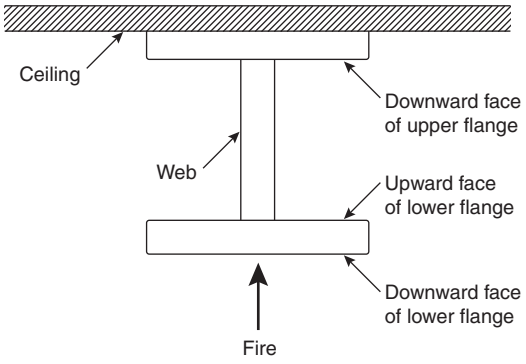

Figure 2-14.18. ***Location of heat flux measurements on I-beams.***

downward face of the upper flange. For each of these surfaces, heat fluxes were measured from the stagnation point of the fire (centerline of the fire) past the location of the flame tip.

The study by Wakamatsu et al.[32] provides a framework for determining heat fluxes to different parts of the I-beam. The I-beam evaluated in the study was 3.6 m long, a web 150 mm high and 5 mm thick, and flanges 75 mm wide and 6 mm thick. Tests were performed using fires from 0.5- or 1.0-m propane burners with heat release rates ranging from 100–900 kW. The distance between the fire source and I-beam was also varied.

When the fire impinges on the I-beam, the flame length is different on the lower flange compared to the flame length on the upper flange (see Figure 2-14.19). Flame lengths along the lower flange, L_B, were shorter than those observed near the upper flange, L_C. Heat fluxes along the lower flange were taken to be a function L_B while heat fluxes to other surfaces were related to L_C. Flame lengths were related to the dimensionless Q^* as defined in Equation 8 with D being replaced by the appropriate distance between the fire and the flange,

$$Q^*_{H_B} = \frac{Q}{\rho_\infty C_p T_\infty \sqrt{g} H_B^{5/2}} \tag{16}$$

$$Q^*_{H_C} = \frac{Q}{\rho_\infty C_p T_\infty \sqrt{g} H_C^{5/2}} \tag{17}$$

Correlations were developed to predict the flame tip length along the lower and upper flanges:

$$\frac{(L_B + H_B)}{H_B} = 2.3 Q^{*0.3}_{H_B} \tag{18a}$$

$$\frac{(L_C + H_C)}{H_C} = 2.9 Q^{*0.4}_{H_C} \tag{18b}$$

The heat flux measured at the stagnation point on the downward face of the lower flange was found to be the same as that measured for a fire beneath a ceiling, see Figure 2-14.20. The location of the virtual origin, z', was determined using Equation 13. The variation in the heat flux

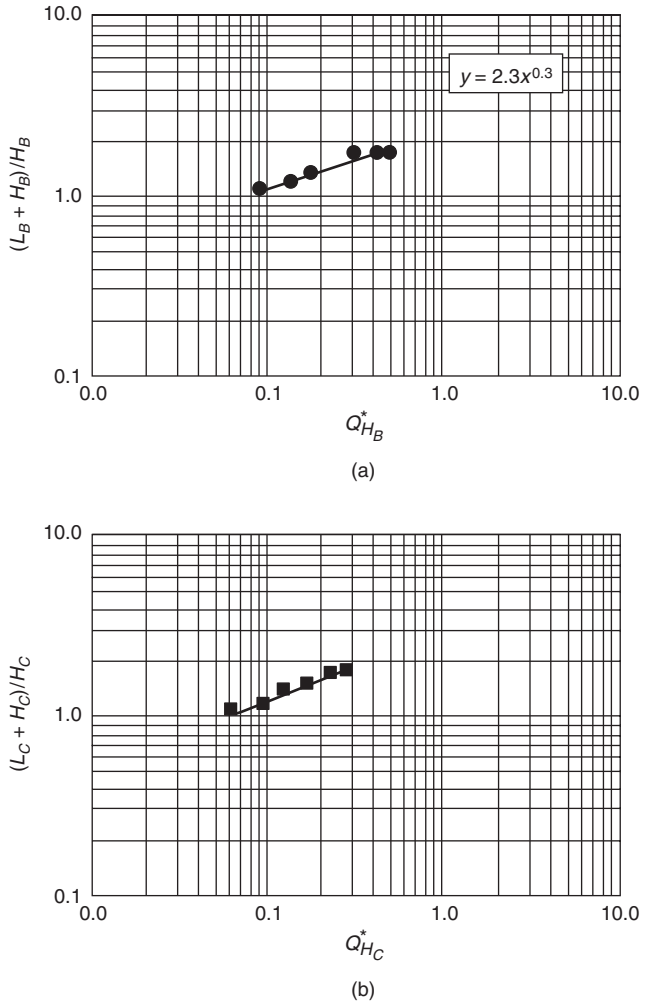

Figure 2-14.19. ***Flame lengths (a) along the lower flange (Equation 18a) and (b) along the upper flange (Equation 18b) in I-beam tests performed by Wakamatsu et al.[32]***

along the downward face of the lower flange with horizontal distance r from the stagnation point is shown in Figure 2-14.21. The data appears to fall between the range of the data measured in the unconfined ceiling tests, which are represented by the dashed and solid lines. These heat fluxes were the highest measured on the I-beam assembly and can be estimated using the following correlation:

$$q'' = 518.8 e^{-3.7w} \tag{19a}$$

where

$$w = (r + H_B + z')/(L_B + H_B + z') \tag{19b}$$

The heat fluxes to the upward face of the lower flange and the web are shown in Figures 2-14.22 and 2-14.23 to be lower than those on the downward face of the lower

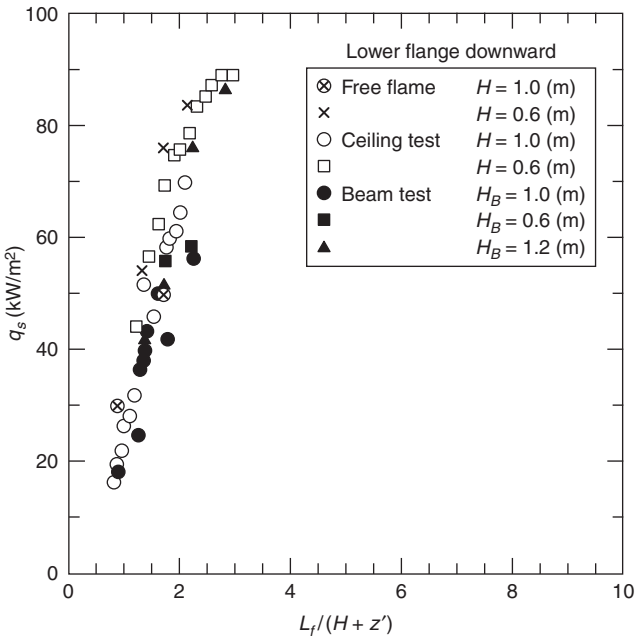

Figure 2-14.20. ***Heat flux at the stagnation point on the downward face of the lower flange.[32]***

flange. This was attributed to the lower flange shielding these parts of the I-beam from radiative and convective heat transfer. These data can be represented by the following expression:

$$q'' = 148.1e^{-2.75w} \tag{20a}$$

where

$$w = \frac{(r + H_C + z')}{(L_C + H_C + z')} \tag{20b}$$

The lowest heat fluxes on the I-beam were measured on the downward facing part of the upper flange. As seen in Figure 2-14.24, heat fluxes to this part of the I-beam are slightly less than those measured on an unconfined ceiling. Heat fluxes to the downward face of the upper flange can be estimated using the following fit to the data:

$$q'' = 100.5e^{-2.85w} \tag{21a}$$

where

$$w = \frac{(r + H_C + z')}{(L_C + H_C + z')} \tag{21b}$$

Myllymaki and Kokkala[33] evaluated the use of the approach and data of Wakamatsu et al.[32] to estimate heat fluxes onto I-beams exposed to fires as large as 3.9 MW. They found that for fires over 2.0 MW, the correlations suggested for the upward face of the lower flange, web, and downward face of the upper flange underestimate the heat flux to these areas on the I-beam. For these large fires, the I-beam becomes completely engulfed in fire. As a result, heat fluxes on all parts of the I-beam follow the correlation suggested for the downward face of the lower flange provided in Equation 19. Heat fluxes to the downward face of the lower flange, the upper flange, and the web are shown in Figure 2-14.25, along with the correlations recommended by Wakamatsu.[26] The highest heat fluxes measured in the tests performed by Myllymaki and Kokkala[33] were approximately 130 kW/m² and were along the downward face of the upper flange. To predict conditions along the web, Myllymaki and Kokkala[33] normalized the data with respect to the flame length along the center of the web,

$$L_{\text{web}} = H_{\text{web}}(2.9Q^{*0,4}_{\text{web}} - 1)$$

where

$$Q^*_{\text{web}} = \frac{Q}{\rho_\infty C_p T_\infty \sqrt{g} H^{5/2}_{\text{web}}}$$

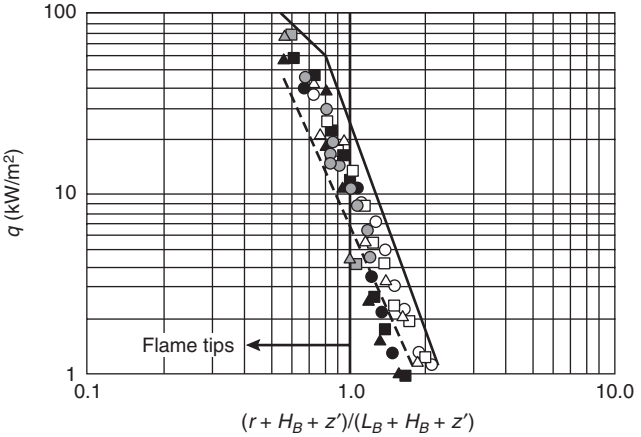

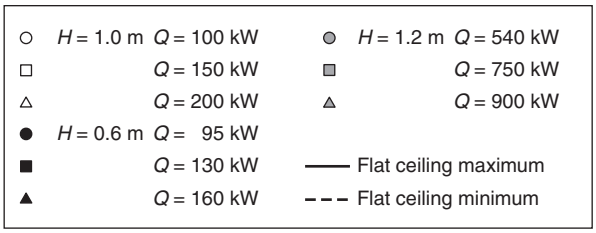

Figure 2-14.21. ***Heat flux along the downward face of the lower flange.[32]***

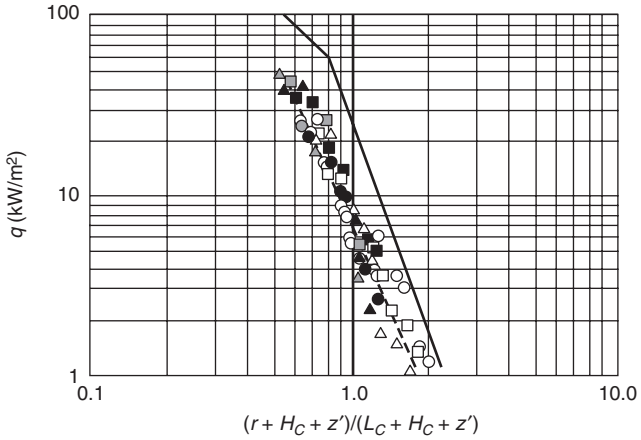

Figure 2-14.22. ***Heat flux along the upward face of the lower flange (key same as in Figure 2-14.21).[32]***

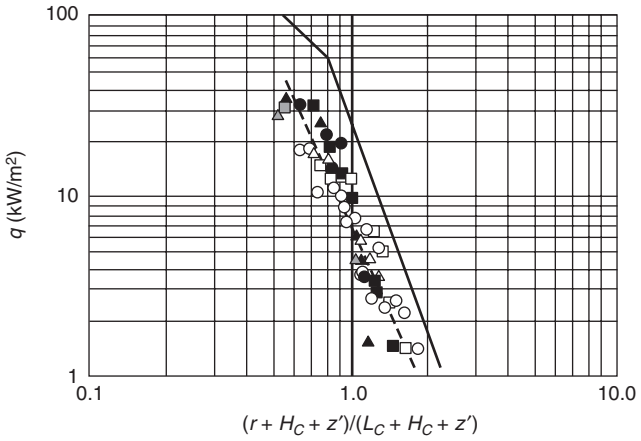

Figure 2-14.23. ***Heat flux along the web (key same as in Figure 2-14.21).[32]***

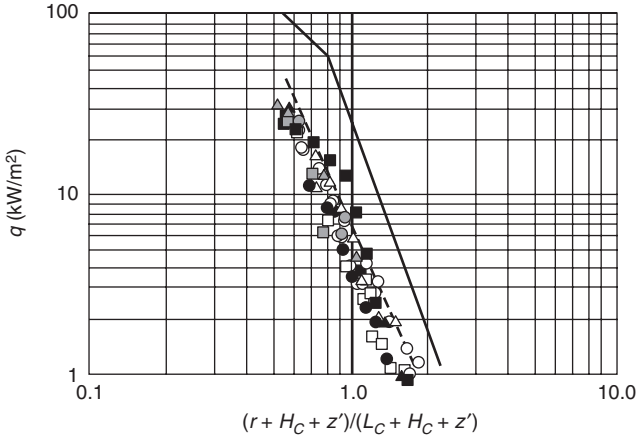

Figure 2-14.24. ***Heat flux along the downward face of the upper flange (key same as in Figure 2-14.21).[32]***

Burning Walls and Ceilings

Fires from burning boundaries typically produce thinner flames than those generated by exposure fires. As a result, heat fluxes from burning boundary flames are typically lower than those measured for exposure fires in a similar geometry. As was the case with heat fluxes from exposure fires, heat fluxes from burning boundaries are dependent on the geometry of the burning surfaces.

Wall Fires

Heat fluxes from a burning wall flame back to the surface has been studied fairly extensively. Most of the work in this area has been performed with smaller fires. Though the data indicates that these heat fluxes are dependent both on fire size and smoke production, no reported study has fully characterized this behavior.

Much of the detailed heat flux measurements for fires produced by burning flat surfaces have been done with smaller-scale fires (<100 kW). Through this work, the heat fluxes from flames produced by a variety of different burning materials have been characterized.[34–37] All these studies were conducted with fires over flat, solid surfaces except the study of Ahmad and Faeth,[34,35] which was performed using wicks soaked in different alcohols. Ahmad and Faeth performed flat wall fire experiments using a 0.66-m-wide, 0.81-m-high flat wall test apparatus, with the lower part of the wall being an alcohol-soaked wick. Different wick heights and different types of alcohol were included in the study. Data from Quintiere et al.[36] was performed using samples 0.28 m by 0.28 m exposed to different external heat fluxes to generate different heat release rate fires from the same sample. Experiments performed by Orloff et al.[37] were conducted using a 0.41-m-wide, 1.57-m-high sample of PMMA.

Data from the studies of Ahmad and Faeth[34,35] and Quintiere et al.[36] are shown in Figure 2-14.26. Heat fluxes are approximately 20–30 kW/m^2 in the lower part of the flame ($z = 0.5L_f$) for a wide range of fuels. Peak heat fluxes measured by Orloff et al.[37] (22 kW/m^2) were also in this 20–30-kW/m^2 range. The value of L_f can be determined by using a flame height correlation for a line fire, such as that proposed by Delichatsios:[38]

$$L_f = 0.052Q'^{2/3} \tag{22}$$

where Q' is the heat release rate per unit length of burning wall (kW/m) and L_f is in (m).

Several empirical correlations have been proposed in the literature[39–42] to predict heat fluxes to walls. All correlations assume a constant heat flux in the lower part of the fire and a power law decay above this. The difference in these correlations is the peak heat flux over the bottom part of the fire and the empirical constants that govern the decay. Similar to that proposed by Hasemi,[39] the line in the plot is an average fit to the data:

$$q'' = 25 \qquad (z/L_f) \le 0.5 \tag{23a}$$

$$q'' = 4.4(z/L_f)^{-2.5} \qquad (z/L_f) > 0.5 \tag{23b}$$

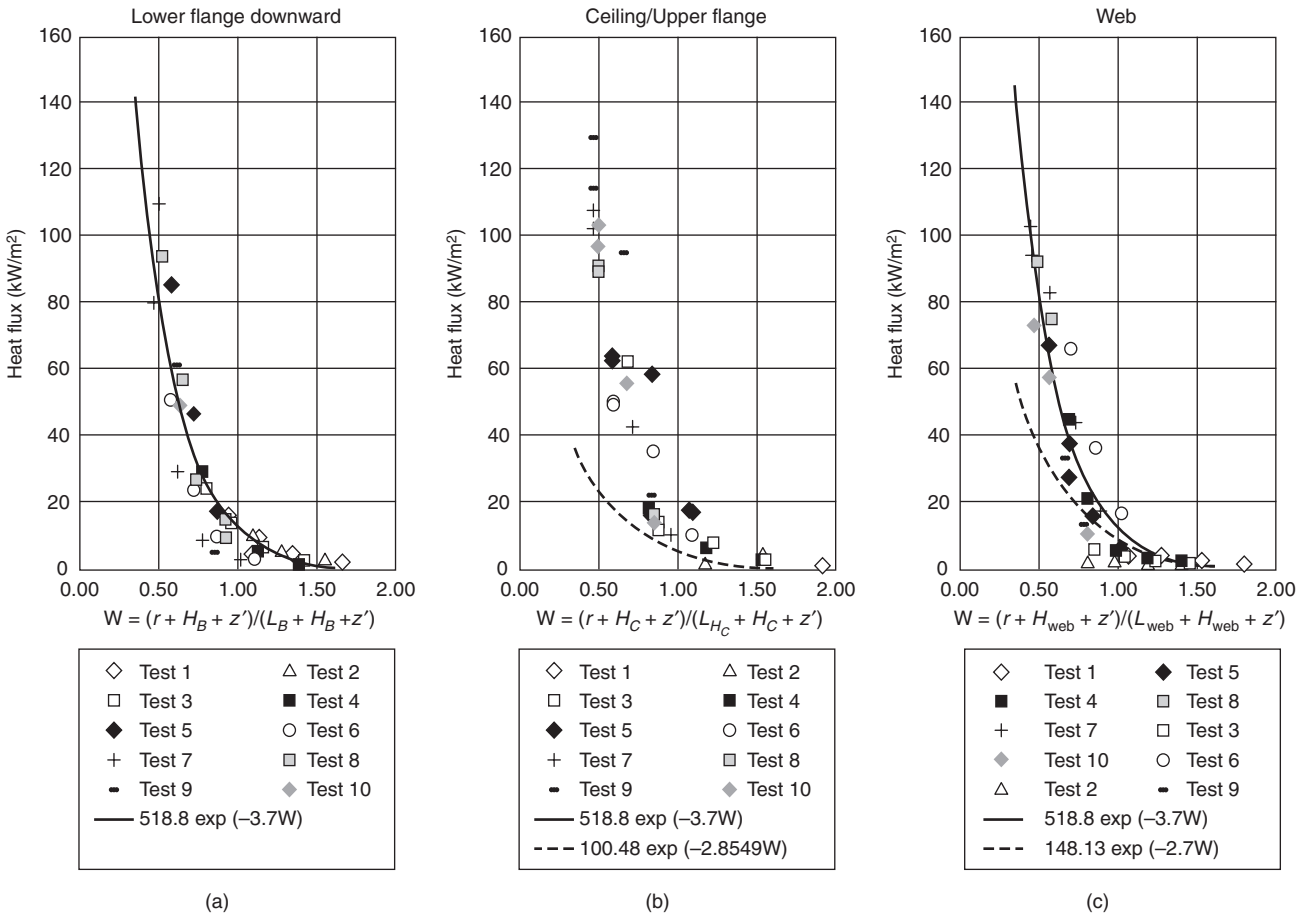

Figure 2-14.25. ***Heat fluxes measured at the (a) downward face of the lower flange, (b) upper flange, and (c) the web on an I-beam in the study by Myllymaki and Kokkala,[33] with fires as large as 3.9 MW.***

A more conservative fit that bounds this data set was developed:

$$q'' = 30 \qquad (z/L_f) \leq 0.7 \qquad (24a)$$

$$q'' = 12.3(z/L_f)^{-2.5} \qquad (z/L_f) > 0.7 \qquad (24b)$$

Line burners have been used by some researchers to simulate a fire produced by a burning surface such as a wall. Hasemi[39,43,44] measured the heat flux from a methane line burner fire to an incombustible wall. In this study, the fire heat release rate per unit length of burner (0.30 m) was varied from 16.7–218.2 kW/m and two different line burner widths (0.037 m and 0.082 m). For the test conditions considered, the heat fluxes along the flame are seen in Figure 2-14.26 to be similar for each test condition. In addition, heat fluxes measured in this study are shown in Figure 2-14.27 to be similar to those shown in Figure 2-14.26. The correlations presented in Equations 23 and 24 adequately bound the data. Line burner experiments using propane as fuel have resulted in higher heat fluxes than those measured with methane as the fuel. In tests using propane with Q' = 83 – 167 kW/m, Kokkala et al.[45] and Lattimer[10] both measured heat fluxes of approximately 45 kW/m² in the lower half of the flame ($z = 0.5L_f$). Though not shown on the plot, Foley and Drysdale[46] measured 40–50 kW/m² from propane line burners with Q' = 11.6 and 20.9 kW/m. These data indicate that the radiation from the fire to the surface is dependent on fuel smoke production.

Slightly larger-scale fire tests were performed by Kulkarni et al.[47,48] In this study, heat flux measurements were made along the lengths of different 0.3-m-wide, 1.2-m-high samples of solid combustibles. Fires were initiated using a line burner at the bottom of the sample, and heat fluxes were continuously measured during the test. Heat fluxes and flame lengths were continuously monitored as the fire spread along the combustible material. These transient heat flux and flame length measurements were averaged over particular time periods and plotted to determine the heat flux at different locations along the flame length.

Figure 2-14.28 provides the heat flux data for the different materials included in the study. Peak heat fluxes measured for the different materials ranged from 25–60 kW/m². Heat fluxes from burning masonite board, card-

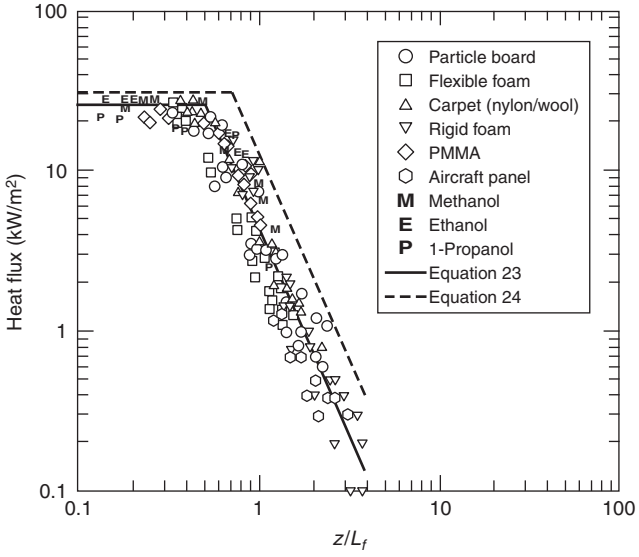

Figure 2-14.26. ***Heat fluxes from burning flat surfaces for fires less than 100 kW.[34–36]***

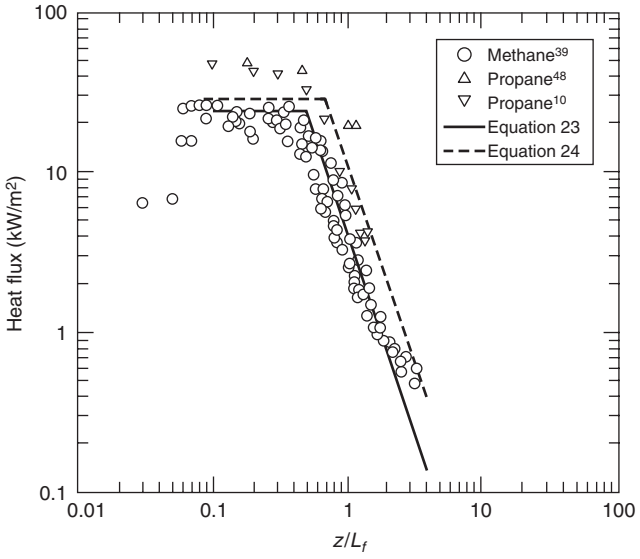

Figure 2-14.27. ***Heat fluxes from methane line burners against a flat wall.[10,39,48]***

board, and white pine board were in the 20–30-kW/m² range, similar to that measured in experiments by Ahmad and Faeth[34,35] and Quintiere et al.[36] However, fires involving PMMA, polyurethane foam, and velour fabric were all measured to produce heat fluxes greater than 30 kW/m². The PMMA and polyurethane foam had the highest flame lengths of all the materials (~1.75 m), which is comparable to the flame lengths reported by Quintiere et al.[36] for similar materials (PMMA and flexible foam). This indicates that the heat release rates for the PMMA and polyurethane foam is comparable in the two studies. The reason for the differences in the peak heat fluxes (e.g., 30–60 kW/m² in tests by Kulkarni et al.[48] with PMMA while 20–26 kW/m² in tests by Quintiere et al.[36]) is not known.

Less detailed heat flux measurements have been reported in the literature for larger fires. Orloff et al.[49] and Delichatsios[38] reported data on heat fluxes from flames produced by a 3.6-m-high burning PMMA wall. Total heat fluxes incident on the PMMA were calculated using theory and mass loss rate data. Heat fluxes are shown in Figure 2-14.29 to increase with height. All the data in this plot were at positions where $z/L_f < 0.5$. This behavior is

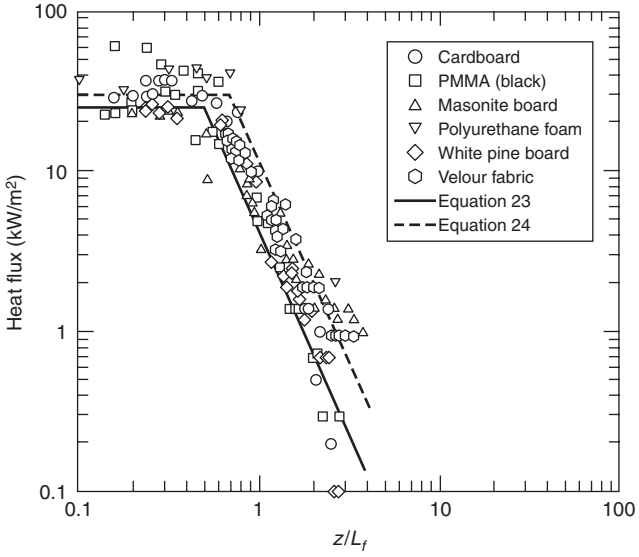

Figure 2-14.28. ***Heat fluxes for different materials.[47,48]***

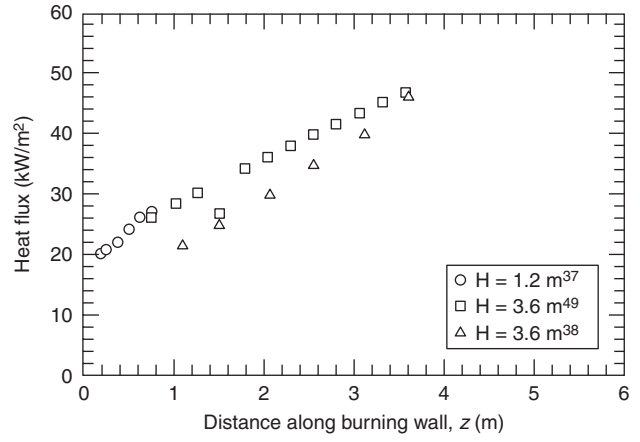

Figure 2-14.29. ***Heat flux from a PMMA wall flame back to the fuel surface.[37,38,49]***

different than that observed with smaller fires, where heat flux is relatively constant over this region.

Markstein and DeRis[50] also explored the effects of larger fire size and soot production on the heat flux incident on the burning surface. The apparatus used in the study was 0.38 m wide and 1.98 m high, with the bottom 0.79 m of the wall being a sintered metal gas burner. Heat flux data for methane, ethane, ethylene, and propylene fires were reported. The impact of fire size on the heat flux distribution along the height of the panel is shown in Figure 2-14.30. Similar to the PMMA results, the heat fluxes were measured to increase with height in the test with the higher heat release rate (816 kW/m).

The heat flux from the flame is shown in Figure 2-14.31 to also be a function of fuel smoke production rate. Methane and ethane have low smoke yields (less than 0.013 g/g)[51] and are measured to produce heat fluxes as high as 35–38 kW/m^2. The smoke yield of ethylene (0.043)[51] is less than that of propylene (0.095), but similar heat fluxes were measured with height along the apparatus. Peak heat fluxes of 59 kW/m^2 were measured for the largest propylene fire considered in the study.

Heat fluxes were measured in tests on large (2.4-m-high, 0.60-m-wide) plywood walls.[52] The peak heat fluxes measured in these tests are provided in Table 2-14.1 for various preheat levels. As the heat release rate per unit width increases, the heat flux from the fire to the wall increases. Though heat fluxes are not as high as those measured for a burning PMMA wall, the heat flux is 3–9 kW/m^2 higher than the 30-kW/m^2 peak level measured in the smaller-scale tests after the radiant part of the exposure was removed.

Similar experiments were performed by Ohlemiller and Cleary[53] on composite panels. The peak heat fluxes measured in this study are provided in Table 2-14.2. Similar to the results of Delichatsios et al.,[52] heat fluxes were measured to increase with an increase in heat release rate (i.e., increase in external heat flux).

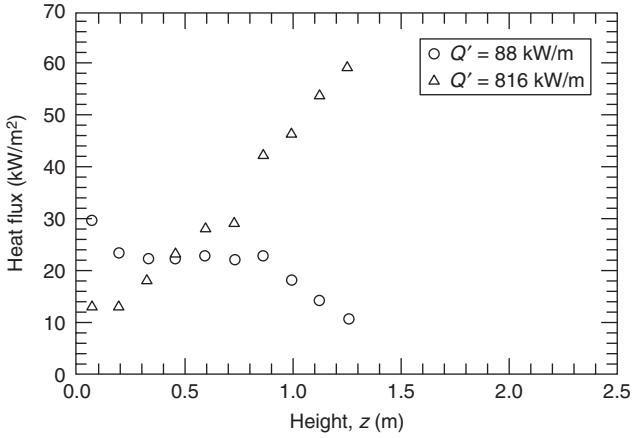

Figure 2-14.30. ***Heat fluxes along a propylene gas wall fire at different heat release rates per unit width.[50] Burning wall height was 0.79 m.***

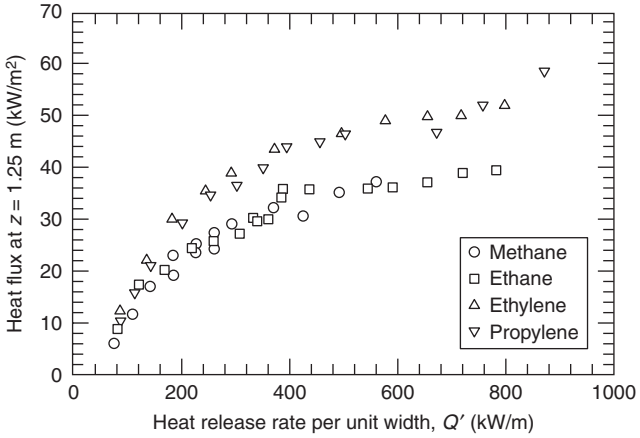

Figure 2-14.31. ***Heat flux at a height of z = 1.25 m for different fire sizes and different fuels.[50] Burning wall height was 0.79 m.***

Data presented in this section demonstrates that both heat release rate and smoke production rate of the fuel can influence the heat flux levels produced by wall flames back onto the burning surface. Larger fires with high smoke production rates can result in heat fluxes to the walls of approximately 60 kW/m^2. Additional research needs to be performed to better quantify the transition between the smaller-fire experiments and the large-fire results.

Table 2-14.1 ***Peak Heat Flux from Flames Measured in 2.4 m High, 0.60 m Wide Plywood Wall Experiments[52] (measurements up to 1.8 m above floor)***

Fuel	Radiant Exposure (kW/m^2)	Heat Release Rate per Unit Width Q′ (kW/m)	Peak Heat Flux (kW/m^2)
Plywood	4.8	175	38
(finished side	5.2	197	40
exposed)	7	292	45
Plywood	7.5	217	45
(unfinished	11	417	50
side exposed)			

Table 2-14.2 ***Heat Fluxes from 1.2 m High, 0.3 m Wide Composite Panel Fires[53]***

Fuel	Radiant Exposure (kW/m^2)	Heat Release Rate per Unit Width Q′ (kW/m)	Peak Heat Flux (kW/m^2)
Fire retarded	2.5	N/A	35
vinyl ester	7.5	N/A	48
	11	N/A	52
Polyester	0	N/A	35

Corner Wall Fires

Limited work has been performed to quantify the heat fluxes from burning boundaries in a corner. In general, the heat fluxes produced by burning corner walls are higher than those produced by a wall flame.

Qian et al.[54,55] measured heat fluxes produced in a corner of burning PMMA walls beneath an incombustible ceiling. In these experiments, a 1.6-m-high corner was lined with 12.7-mm-thick PMMA that was 0.20 m in width. During the tests, the walls were ignited using a torch at the bottom of the corner and were allowed to burn until flames had spread to the top of the walls. The peak heat release rate of the fire was estimated to be 80 kW. Heat fluxes measured during the growing fire are shown in Figure 2-14.32. In the lower half of the flame, heat fluxes were measured to be, on average, 33 kW/m^2. Above this, heat fluxes were measured to decay similarly to heat fluxes measured for wall fires (see Equations 25 and 26).

A series of experiments were conducted by Hasemi et al.[28] using L-shaped, sintered metal burners mounted to the walls of a corner to simulate burning corner walls. Using propane gas as fuel, experiments were conducted using two different burner sizes (0.23 m wide by 0.45 m high, and 0.23 m wide by 0.90 m high) mounted to an open corner of walls with no ceiling. The heat fluxes above the burners in these fires are provided in Figure 2-14.33 for fire heat release rates of 15–60 kW. The line on the plots represents the decay in the heat flux of a wall fire. Peak heat fluxes in the lower part of the flame were measured to range from 28–38 kW/m^2, and were constant up to approximately half the flame length. Above this, heat fluxes were measured to decay in a manner similar to that determined for burning walls.

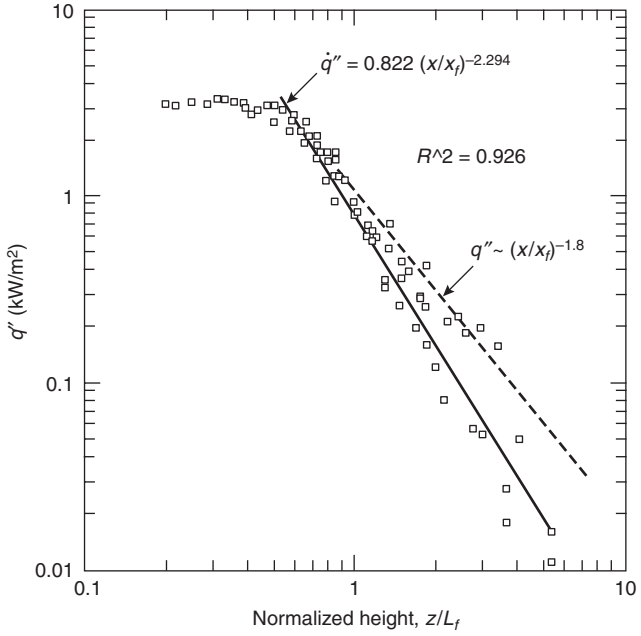

Figure 2-14.32. ***Heat flux from burning PMMA corner walls (1.6 m high and 0.20 m wide).[55]***

Hasemi et al.[28] also performed tests in a 1.8-m-high corner with a ceiling. Tests were performed with the top 1.35 m of the corner lined with 0.23-m-wide sintered metal burners and with the top 0.45 m of the corner lined with sintered metal burners. Heat fluxes to the ceiling were measured to be as high as 40 kW/m^2, while heat fluxes as high as 60 kW/m^2 were measured along the top of the walls near the ceiling.

Lattimer et al.[10] performed a detailed study using L-shaped propane line burners in the corner. Burners were placed in a 2.4-m-high corner with a ceiling, with all surfaces constructed of noncombustible materials. In this study, heat fluxes were measured for different burner sizes (single side length of 0.17 m, 0.30 m, and 0.50 m) and various heat release rates (50–300 kW).

Similar to the approach used to develop the heat flux correlations for area burners, burning boundary correlations were developed for three regions in the corner: along the height of the walls in the corner, along the top of the walls near the ceiling, and along the ceiling. The region containing the walls in the corner extended from the top of the fire to approximately 1.8 m above the fire. Above 1.8 m was considered to be the region along the top of the wall, or the wall-ceiling interface region.

Heat flux data for these fires was normalized with respect to the flame tip location. The flame tip was the furthest distance at which flaming was visually observed. In cases where the fire impinged and flowed along the ceiling, the flame tip length was taken to be the corner height plus the flame extension along the ceiling. Lattimer et al.[10] developed the following correlation to predict the flame tip of a burning boundary fire:

$$\frac{L_{f,\text{tip}}}{d} = 5.9 Q_d^{*1/2} \tag{25}$$

where, dimensionless Q_d^* is

$$Q_d^* = \frac{Q}{\rho_\infty C_p T_\infty \sqrt{g} d^{5/2}} \tag{26}$$

Equations 25 and 26 are similar to those used in predicting flame heights from area burners in a corner except the length scale is d, which is the width of the burning area on the wall or the side of a single L-shaped burner. In the L-shaped line burner tests, d is the length of a single side; however, in a burning corner, d was found to be the average width of the burning on the walls. For fires in a 2.4-m-high corner, the width of the burning 0.90 m above the floor was found to represent the average burning width.[10]

The vertical distribution in the maximum heat flux along the walls near the corner is shown in Figure 2-14.34 plotted with the vertical distance normalized with respect to the flame tip. Peak heat fluxes were measured over the initial half of the flame length. Above this, heat fluxes decayed in a fashion similar to that observed for wall fires. The line in the plot represents a fit to the data and are described by the following expressions:

$$q''_{\max} = 70 \qquad (z/L_f) < 0.5 \tag{27a}$$

$$q''_{\max} = 10.0(z/L_f)^{-2.8} \qquad (z/L_f) > 0.5 \tag{27b}$$

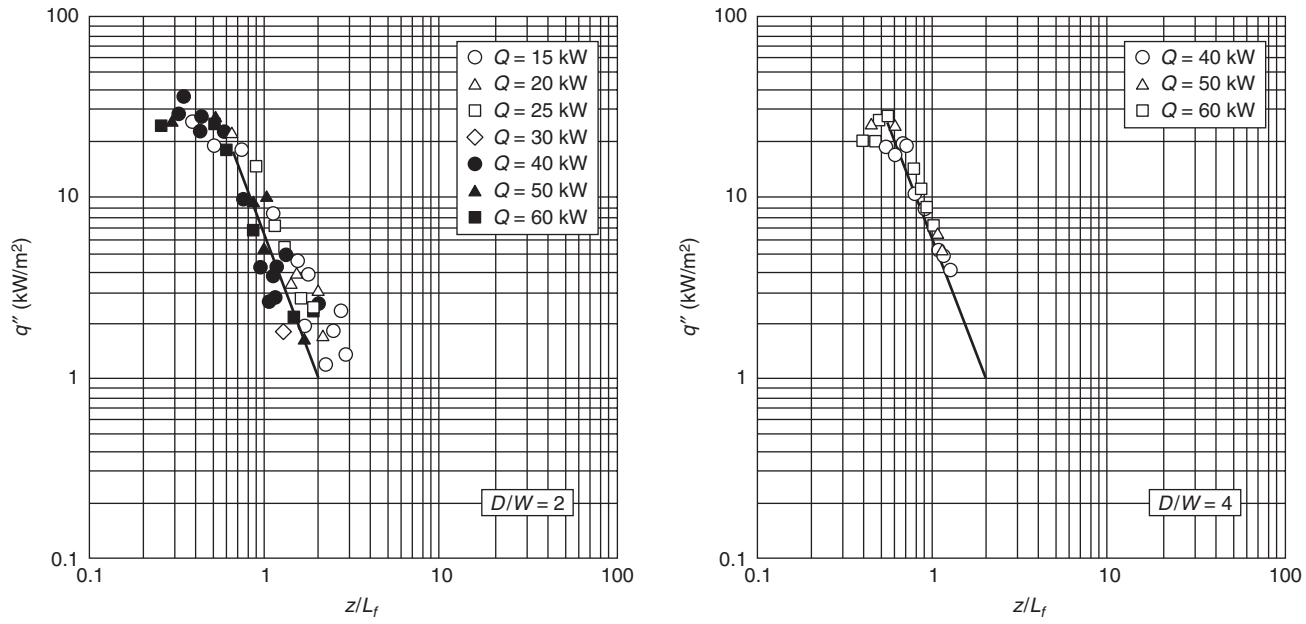

(a) $W = 0.225$ m, $D = 0.45$ m

(b) $W = 0.225$ m, $D = 0.90$ m

Figure 2-14.33. ***Heat fluxes to a corner from a simulated burning corner fire using propane as fuel.[6]***

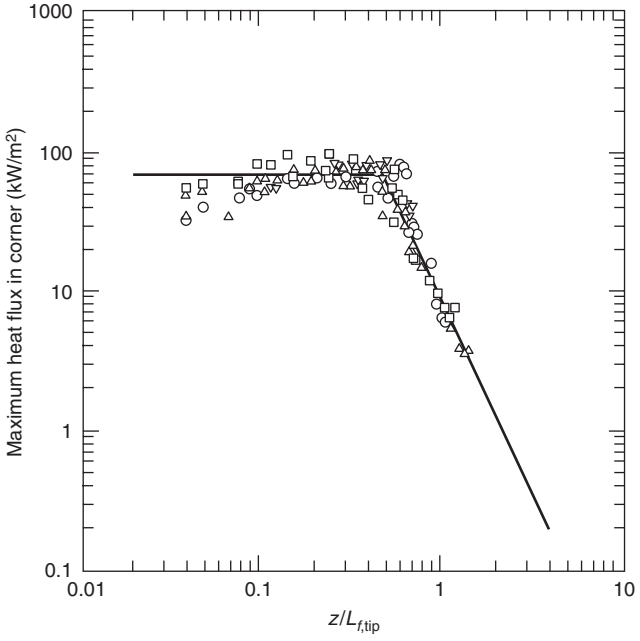

Figure 2-14.34. ***Heat flux from simulated corner wall fires back to the corner walls at a height less than 1.8 m above the floor. L-shaped line burner with single side lengths of 0.17 m (○), 0.30 m (△), 0.30 m (elevated) (▽), and 0.50 m (□) and fire sizes ranging from 50–300 kW.[10]***

Heat fluxes in the decay region $(z/L_f) > 0.5$ decrease with dimensionless height raised to the -2.8 power, which is a slightly lower power than the decay for wall fires (-2.5).

Peak heat fluxes in the corner are shown in Figure 2-14.35 to have some dependence on the heat release rate of the fire. The increase in the peak heat flux with increase in fire size was attributed to an increase in radiative pathlength. Assuming the gases to be gray, the following curve fit was developed:

$$q''_{\text{peak}} = 120\left[1 - \exp(-0.1Q^{1/2})\right] \tag{28}$$

Based on Equation 28, a more conservative fit to the data in Figure 2-14.34 was developed:

$$q''_{\max} = q''_{\text{peak}} \qquad \left(\frac{z}{L_f}\right) \le 0.5 \tag{29a}$$

$$q''_{\max} = q''_{\text{peak}} - 5\left(\frac{z}{L_f} - 0.5\right)(q''_{\text{peak}} - 27) \qquad 0.5 < \left(\frac{z}{L_f}\right) \le 0.7 \tag{29b}$$

$$q''_{\max} = 10.0\left(\frac{z}{L_f}\right)^{-2.8} \qquad \left(\frac{z}{L_f}\right) > 0.7 \tag{29c}$$

The maximum heat fluxes along the height of the corner shown in Figures 2-14.34 and 2-14.35 were measured approximately 0.05–0.10 m outside of the corner. Heat fluxes decrease with horizontal distance from the corner. The horizontal heat flux distributions at heights less than 1.8 m below the ceiling are shown in Figure 2-14.36 to be

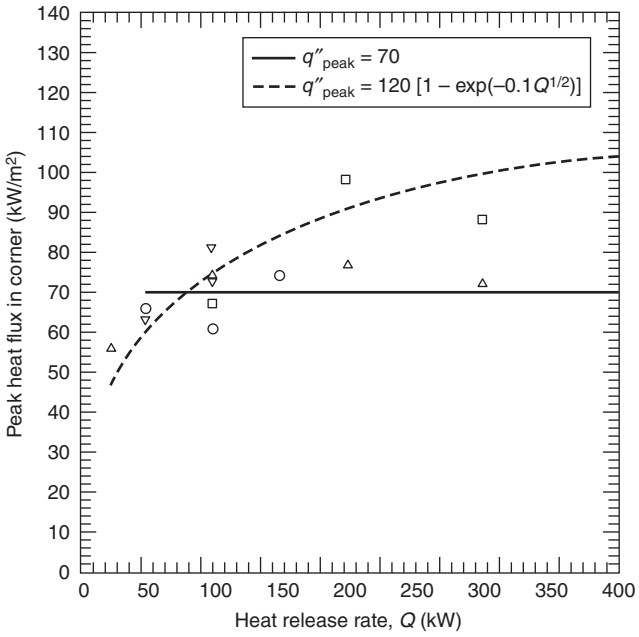

Figure 2-14.35. ***Peak heat flux to the walls in the corner as a function of wall heat release rate less than 1.8 m above the floor. L-shaped line burner with single side lengths of 0.17 m (○), 0.30 m (△), 0.30 m (elevated) (▽), and 0.50 m (□) and fire sizes ranging from 50–300 kW.[10]***

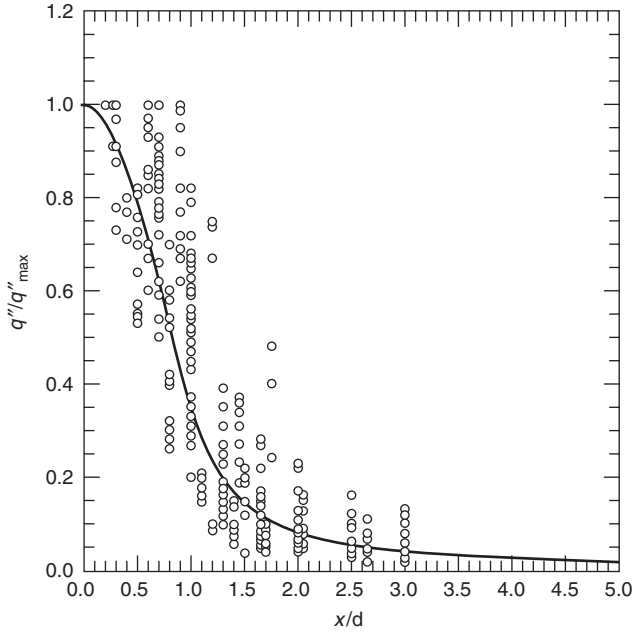

Figure 2-14.36. ***Horizontal heat flux distribution on the walls out from the corner at a height less than 1.8 m above the floor.[10]***

half-Gaussian in shape over the flame, but decays slower than predicted by a half-Gaussian curve outside the flaming region. The line in this plot is a fit to the data, which can be represented by the following expressions:

$$\frac{q''}{q''_{max}} = \exp\left[-1.0\left(\frac{x}{d}\right)^2\right] \qquad \frac{x}{d} < 1.3 \qquad (30a)$$

$$\frac{q''}{q''_{max}} = 0.30\left(\frac{x}{d}\right)^{-1.8} \qquad \frac{x}{d} \geq 1.3 \qquad (30b)$$

Burning boundary beneath a ceiling will form a ceiling jet that will heat the top part of the walls and the ceiling. The maximum heat flux along the top part of the walls is shown in Figure 2-14.37. The line in the plot represents a fit to the data, which can be represented by the following expressions:

$$q''_{max} = 120 \qquad \left(\frac{x+H}{L_{f,tip}}\right) \leq 0.52 \qquad (31a)$$

$$q''_{max} = 13.0\left(\frac{x+H}{L_{f,tip}}\right)^{-3.5} \qquad \left(\frac{x+H}{L_{f,tip}}\right) > 0.52 \qquad (31b)$$

The assumed plateau in the correlation is based upon the maximum heat flux expected from a flame in this configuration. This correlation is the same as that determined for area fires in a corner.

The heat flux to the ceiling was correlated to the dimensionless distance away from the burner, $(r + H)/L_{f,tip}$.

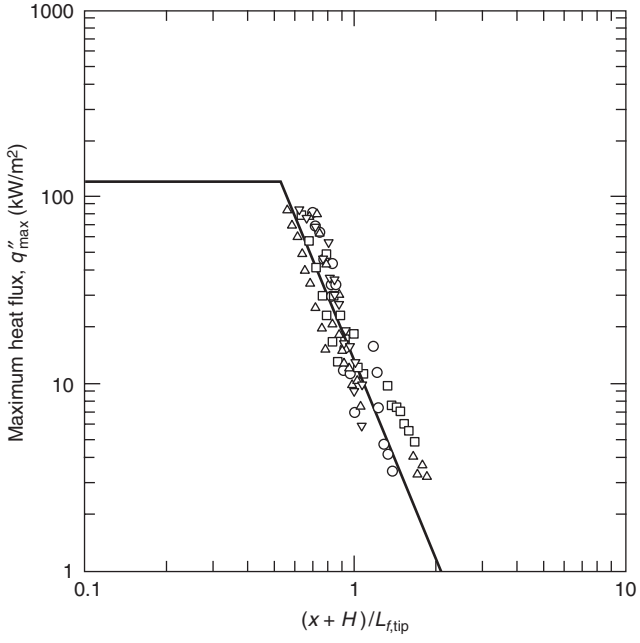

Figure 2-14.37. ***Maximum heat flux along the top of the walls with a simulated burning boundary fire in the corner. L-shaped line burner with single side lengths of 0.17 m (○), 0.30 m (△), 0.30 m (elevated) (▽), and 0.50 m and fire sizes ranging from 50–300 kW (□).[10]***

A plot of the heat flux versus this dimensionless parameter is shown in Figure 2-14.38. The line in this plot is a fit to the data, which is represented through the following relations:

$$q'' = 120 \qquad \left(\frac{r+H}{L_{f,\text{tip}}}\right) \le 0.52 \tag{32a}$$

$$q'' = 13.0\left(\frac{r+H}{L_{f,\text{tip}}}\right)^{-3.5} \qquad \left(\frac{r+H}{L_{f,\text{tip}}}\right) > 0.52 \tag{32b}$$

This is the same relation used for the top of the corner walls, except the length scale in the overhead data is r. In addition, this is the same relation determined using the ceiling heat-flux data from tests with an area burner.

Ceiling Fires

Heat fluxes from burning ceilings have been evaluated for both unconfined ceilings and ceilings in a corridor. Due to buoyancy effects, flames from burning ceilings tend to be relatively thin. As a result, peak heat fluxes from burning ceilings range from 20–30 kW/m^2, which is similar to those measured for small wall fires.

Unconfined ceiling fires: Heat fluxes from unconfined ceiling fires were measured by Hasemi et al.[56] using different sizes of sintered metal propane gas burners mounted to a 1.8-m square incombustible ceiling. Using two different circular burner sizes (D = 0.09 and 0.16 m), heat flux to the ceiling was measured for fire heat release rates of 2.5–38 kW.

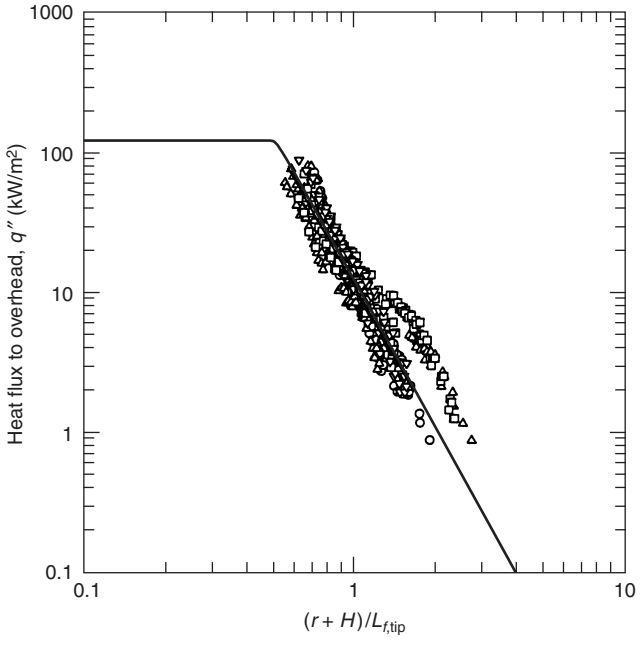

Figure 2-14.38. ***Heat flux along the ceiling with a simulated burning boundary fire in the corner. L-shaped line burner with single side lengths of 0.17 m (○), 0.30 m (△), 0.30 m (elevated) (▽), and 0.50 m and fire sizes ranging from 50–300 kW (□).[10]***

The radius of the flame (intermittent) measured using the two burners is shown in Figure 2-14.39 to be slightly dependent on burner size, with the larger burner having a lower radius. However, as the fires become larger, the dependence on burner diameter becomes small. Flame lengths are proportional to the heat release rate raised to the one-half power.

Hasemi et al.[56] also measured the heat fluxes as a function of distance from the center of the burner. The measured heat fluxes are shown in Figure 2-14.40 to be at peak levels in the first $0.4L_f$ and then decay with distance from the burner. Peak heat fluxes were measured to range from 16–27 kW/m^2, with the smaller burner producing higher heat fluxes. These peak heat fluxes were similar to those measured for burning ceilings in a corridor (i.e., one-

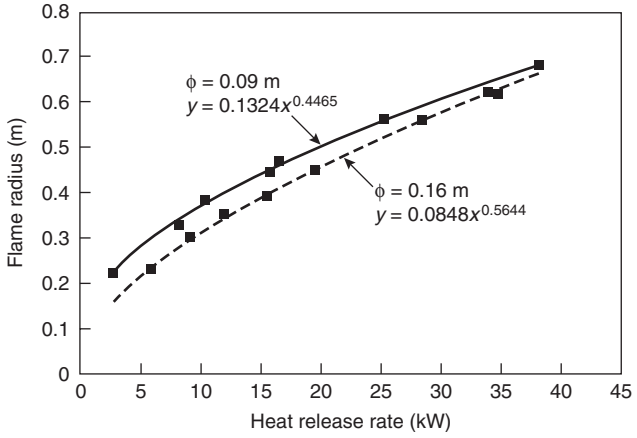

Figure 2-14.39. ***Flame radius produced by a simulated burning ceiling in an unconfined area.[56]***

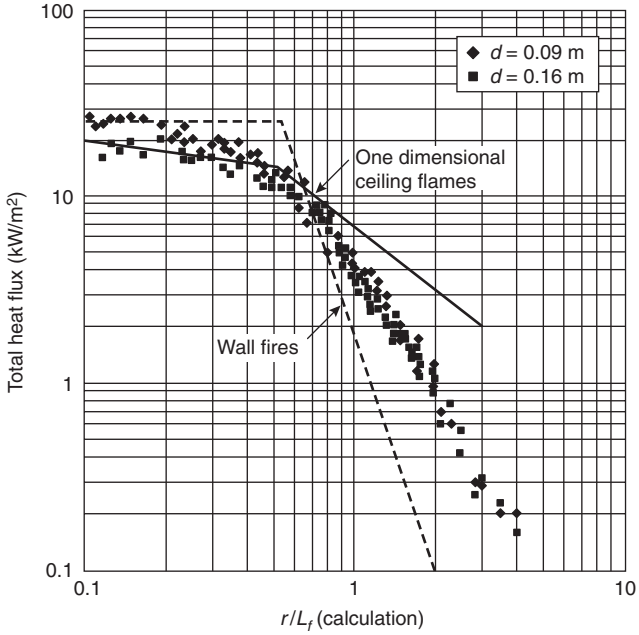

Figure 2-14.40. ***Heat flux from fires beneath an unconfined ceiling.[56]***

dimensional ceiling flames) and for small wall fires. Heat fluxes from the unconfined ceiling fires were measured to decay at a rate between that measured for wall fires and that observed for a burning ceiling in a corridor.

Ceiling fires in a corridor: Heat fluxes from flames produced by burning ceilings in a corridor were investigated by Hasemi et al.[28] Tests were performed beneath a 2.73-m-long ceiling with two 0.10-m-high soffits mounted along the length of the ceiling to form a 0.30-m-wide channel. At the closed end of the channel, a 0.30-m-wide, 0.04-m-long porous propane burner was mounted in the ceiling. Heat flux distributions along the corridor were measured for fire heat release rates ranging from 10–50 kW (33–166 kW per meter of corridor width).

The intermittent flame lengths from these fires are seen in Figure 2-14.41 to increase linearly with heat release rate per unit hallway width. A fit to this data produced the following relation to predict flame length due to a burning ceiling in a corridor:

$$L_f = 0.0122Q' \tag{33}$$

The heat fluxes distributions along the center of the corridor are shown in Figure 2-14.42 for the different fires considered in the study. The line in the plot represents a best fit to the methane line burner data of Hasemi.[39] Heat fluxes were measured to be constant at approximately 20 kW/m^2 up to $0.4L_f$. Above this, heat fluxes were measured to decay at a slower rate than that previously measured for wall fires. Heat fluxes along a flame from a burning ceiling in a corridor (not shown in the figure) can be determined using the following expressions:

$$q'' = 20 \qquad (x/L_f) \le 0.4 \tag{34a}$$

$$q'' = 6.36(x/L_f)^{-5/4} \qquad (x/L_f) > 0.4 \tag{34b}$$

Burning Parallel Vertical Surfaces

A common configuration encountered when commodities are being stored in rooms or warehouses is parallel vertical surfaces. As a result, several studies have focused on both experimentally and analytically characterizing this configuration.[45,57,58] Ingason and DeRis[59] also performed experiments in a rack storage configuration with a fire between four equally spaced storage towers.

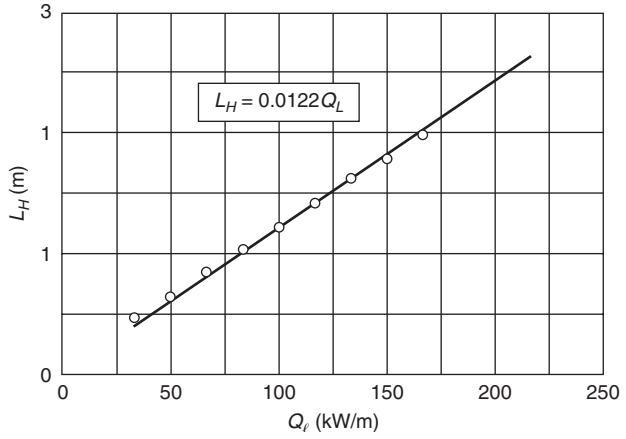

Figure 2-14.41. ***Flame length produced by a burning ceiling in a corridor.[28]***

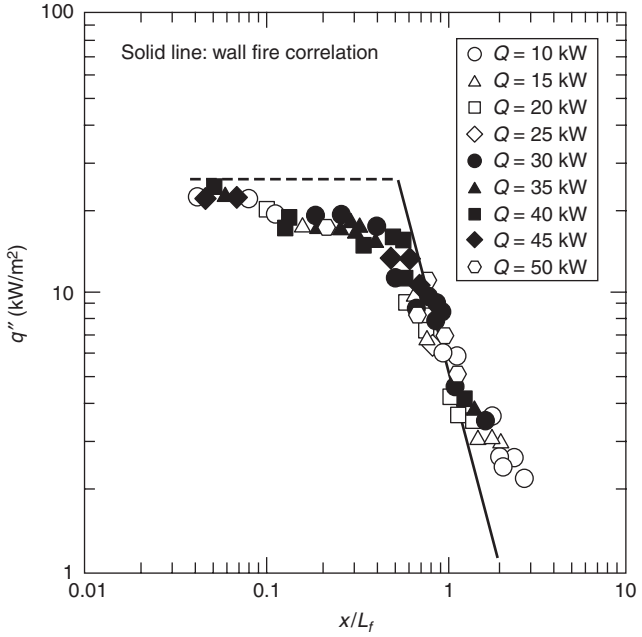

Figure 2-14.42. ***Heat fluxes to the ceiling of a corridor.[28]***

Part of the work by Tamanini[57,58] investigated the effects of wall spacing on the fuel mass loss rate of combustible parallel vertical walls. Walls were 0.94 m high and 0.460 m wide with the spacing varying from 0.470–0.025 m and no floor at the base of the walls. The average fuel mass loss rate was measured to increase (i.e., the average heat flux to the wall increased) with an increase in spacing until the spacing was less than 0.076 m. At a spacing of 0.038 m or less, the average mass loss rate was less than that measured with no parallel wall. At a spacing of 0.038 m (or wall height divided by spacing of 25 with a fire size of approximately 180 kW), the flames from the two burning surfaces were observed to merge together approximately two-thirds the distance up the walls. Though not evaluated in this study, the presence of a floor may cause the flames to merge together at larger spacings.

Heat fluxes due to a fire between two parallel vertical surfaces were measured by Foley and Drysdale.[46] The study was performed using two 0.61-m-wide, 0.81-m-high walls separated by a gap of 0.06, 0.10, or 0.14 m. The fire was a 0.60-m-long propane line burner that had either a 11.6-kW/m or a 20.9-kW/m heat release rate per unit length. One of the walls was instrumented with four heat flux gauges that could be moved to measure the heat flux distribution on the walls. Heat fluxes were measured as far as 0.150 m from the centerline of the wall. For the different gap and heat-release rate fires, heat fluxes were measured with the burner against the instrumented wall and with the fire in the center of the gap between the two walls. The effect of air entrainment flow path was also evaluated by performing tests with and without a floor

between the panels. Results were correlated using a/d where the spacing between the walls, a, is divided by the burner length, d, and the dimensionless quantity Q_d^*, as defined in Equation 26, with d being the burner length.

The heat flux distributions measured with the fire against the instrumented wall are shown in Figure 2-14.43. As seen in Figure 2-14.43(a), heat fluxes reached as high as 80 kW/m^2 with an open base (no floor between the walls). Heat fluxes on the panel can be estimated using the following expression:

$$q'' = 67.38\{z(a/d)^{0.36}/[Q_d^{*2/3}d(y'/d)^{0.38}]\}^{-1.47} \qquad (35)$$

where $y' = 0.5d - y$ with y being the horizontal distance from the burner centerline.

With the base of the walls closed (a floor between the walls) and the fire against the instrumented wall, the heat flux data in Figure 2-14.43(b) were seen to be as high as 70 kW/m^2. Heat fluxes for this case are slightly lower than the open-base case. A similar expression to that in Equation 35 was developed by Foley and Drysdale to predict heat fluxes with the base of the walls closed:

$$q'' = 23.31\{z(a/d)^{0.905}/[Q_d^{*2/3}d(y'/d)^{2/3}]\}^{-1.2} \qquad (36)$$

Heat fluxes were also measured with the fire in the center of the gap between the two walls. In the case with an open base (no floor), the heat fluxes were measured to be 50 percent lower than those measured with the fire against the instrumented wall. As seen in Figure 2-14.44(a), the peak heat flux was measured to be approximately 30 kW/m^2. This decrease was attributed to the air being drawn up at the base of the walls, preventing the fire from attaching to the instrumented wall. The line in the figure is the best fit to the data, which is given by the following expression:

$$q'' = 22.71\{z(a/d)^{1.04}/[Q_d^{*}d(y'/d)^{0.806}]\}^{-0.797} \qquad (37)$$

The case with the base closed and the fire in the center of the gap resulted in the highest heat fluxes measured in the study. As seen in Figure 2-14.44(b), heat fluxes greater than 100 kW/m^2 were measured in this case. In the tests with the high heat fluxes, the flames were observed to occupy the width of the gap. This behavior was attributed to only allowing air to be entrained into the fire through the sides of the gap. The following expression can be used to estimate the heat flux to the walls for this case:

$$q'' = 23.94\{z(a/d)^{1.7}/[Q_d^{*}d(y'/d)^{1.34}]\}^{-1.04} \qquad (38)$$

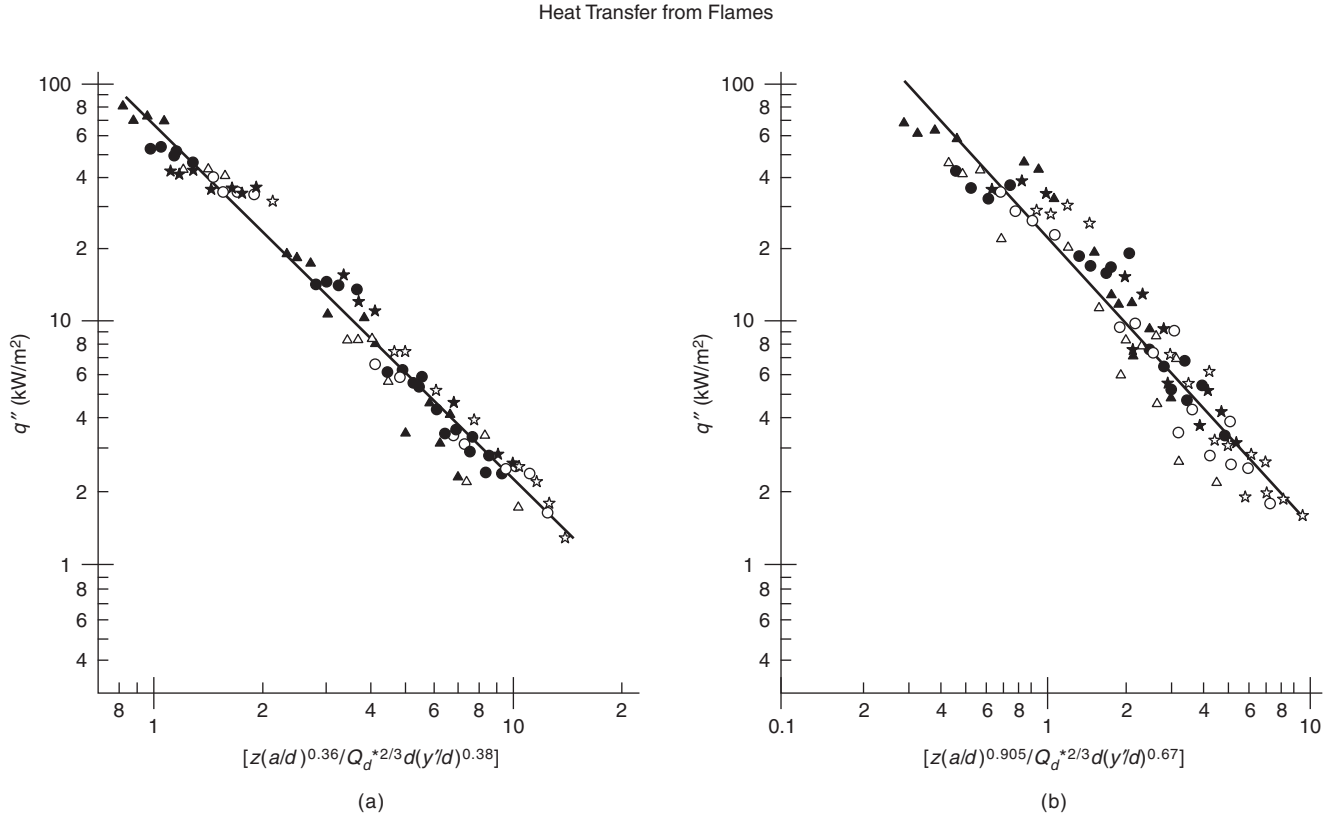

Figure 2-14.43. ***Heat fluxes measured with the fire against the instrumented wall with (a) an open base (no floor in the gap) and (b) a closed base (a floor in the gap): 0.140-m spacing (☆), 0.10-m spacing (○), 0.060-m spacing (□); open symbols, Q' = 11.6 kW/m; closed symbols, Q' = 20.9 kW/m.[45]***

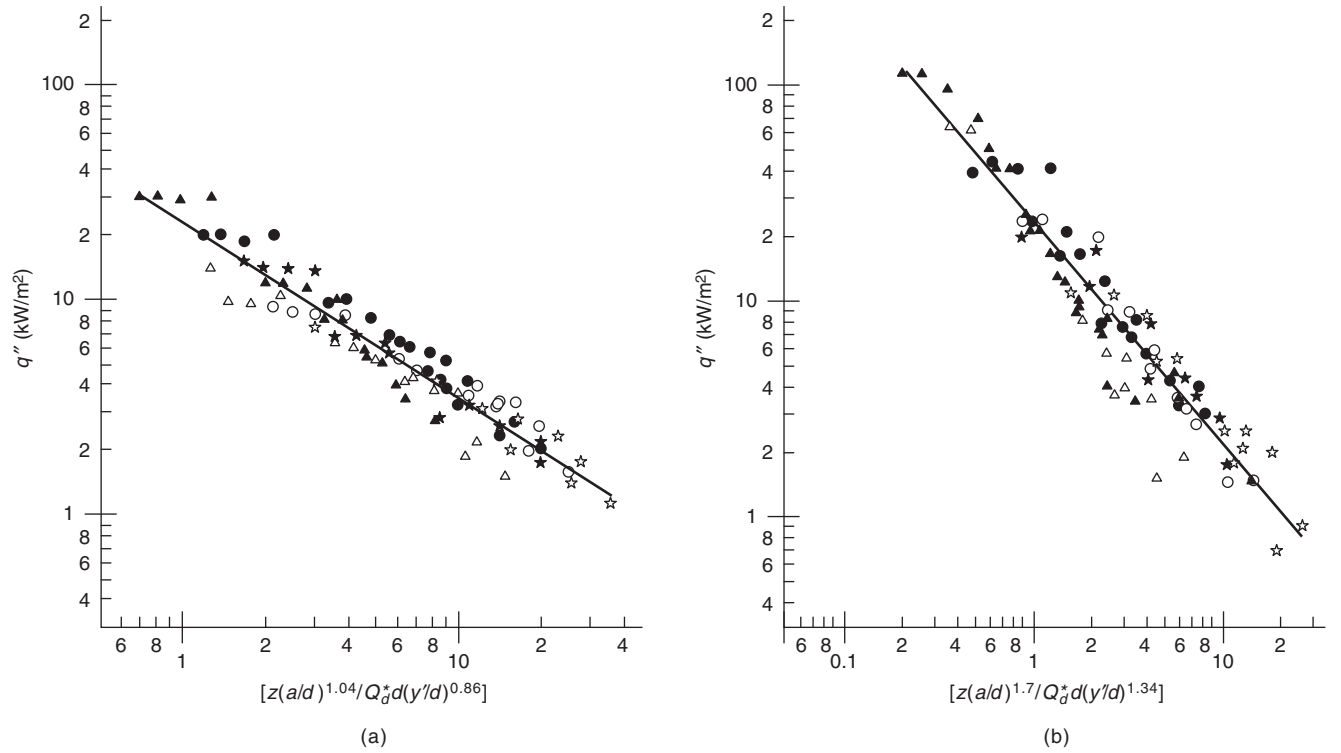

Figure 2-14.44. ***Heat fluxes measured with the fire in the center of the gap with (a) an open base (no floor in the gap) and (b) a closed base (a floor in the gap): 0.140-m spacing (☆), 0.10-m spacing (○), 0.060-m spacing (△); open symbols, Q' = 11.6 kW/m; closed symbols, Q' = 20.9 kW/m.[46]***

Additional research needs to be performed with this configuration to further validate the results. Larger-scale tests need to be conducted to verify the results of Foley and Drysdale. In addition, the transition from wall fire heat fluxes to gap fire heat fluxes needs to be identified. Heat fluxes produced by area fires between parallel walls also need to be quantified.

Exposure Fires and Burning Walls and Ceilings

A series of tests were performed by Lattimer et al.[10] to investigate the use of steady-state heat flux correlations, developed using burners and noncombustible boundaries, for estimating the heat fluxes in growing fires. Three tests were performed in a 2.4-m-high, 2.0-m-wide open corner lined with a combustible material. A single test was performed on three different lining materials: 12-mm-thick Douglas fir plywood, 12-mm-thick E-glass fire-retarded vinyl ester, and 88-mm-thick sandwich composite (76-mm-thick balsa wood with 6-mm-thick E-glass fire-retarded vinyl ester facings). The initiating fire in the test was a 0.17-m square propane sand burner with a heat release rate of 100 kW for 10 min followed by 300 kW for 10 min, total test time of 20 min. Total heat release during the test was measured by performing oxygen calorimetry on the gases collected in an exhaust hood, and flame lengths were measured through visual observation. Heat fluxes were measured 0.075 m from the corner along at eight different elevations, 0.15 m below the ceiling along the top of the wall, and along the ceiling on a 45° diagonal out from the corner. Due to mounting the heat flux gauges along the top of the wall too far below the ceiling, no comparison between predicted and measured heat fluxes was done for the region along the top of the wall.

Transient data was averaged every 30 s to generate a reasonable amount of data to compare to the developed correlations. A comparison of the flame length predicted using Equations 7 and 25 and the measured flame length is shown in Figure 2-14.45. The dimensionless length used in this calculation was the width of the burner, D, while the burning had spread laterally less than the width of the burner. When the lateral flame spread 0.9 m above the floor exceeded the burner width, the dimensionless length was taken to be the horizontal flame front location 0.9 m above the floor. The flame front at 0.9 m above the floor was approximately the average flame front on the wall.

Heat fluxes to the walls near the corner are provided in Figure 2-14.46. Measured heat fluxes were slightly higher than values predicted by both the initiating fire correlation and the burning boundary correlation (assuming the heat flux is independent of wall heat release rate). Inspection of the data indicates better agreement between the data and the correlations can be achieved using the initiating fire correlation up to when ignition occurs in the corner. After

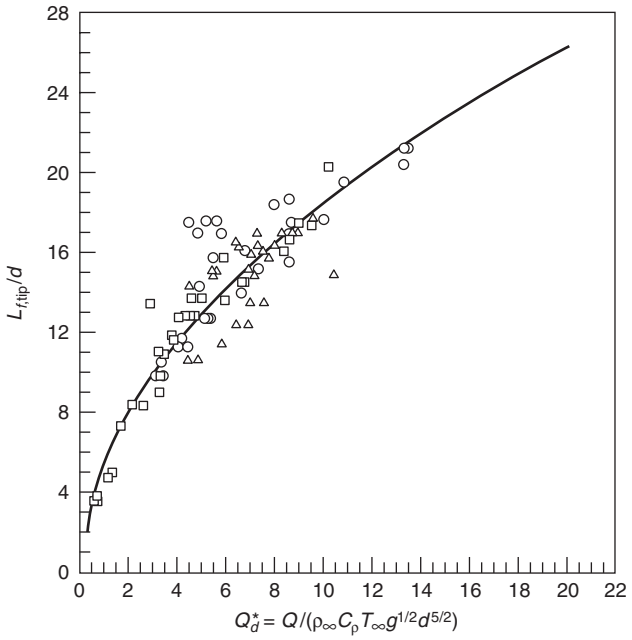

Figure 2-14.45. ***Flame lengths measured in combustible corner fire tests compared with the flame length correlations developed for initiating and burning boundary fires in Equations 7 and 25: plywood (□), E-glass FR vinyl ester (○), sandwich composite (△).[10]***

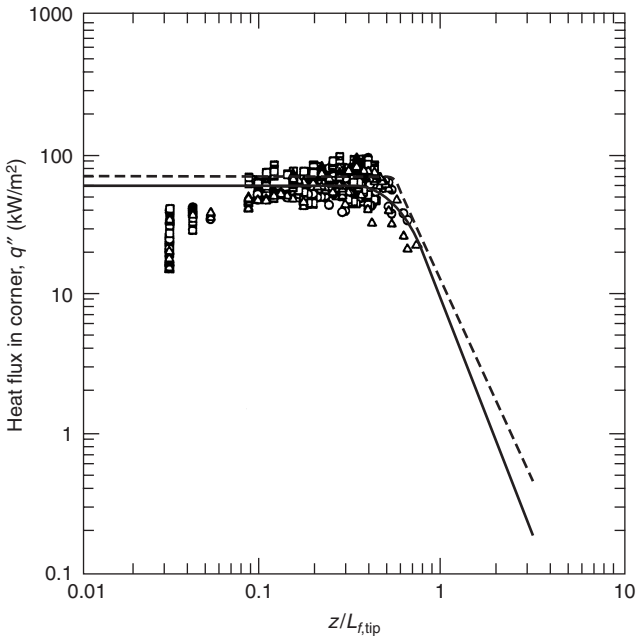

Figure 2-14.46. ***Heat fluxes along the height of the corner in tests with different combustible boundaries compared with the heat flux predicted using Equation 27 (—) and Equation 9 (---): plywood (□), E-glass FR vinyl ester (○), sandwich composite (△).[10]***

this, the corner wall heat flux correlations in Equations 28 and 29 can be used to estimate heat fluxes in the corner.

A comparison of the heat fluxes along the ceiling and the heat fluxes predicted using Equation 32 is shown in Figure 2-14.47. In general, heat fluxes are adequately predicted by the correlation, with heat fluxes as high as 130 kW/m^2 measured during a test. This indicates that Equation 32 can be used to estimate heat fluxes to the ceiling near the corner containing the fire.

Fires from Windows

Fires that have reached flashover conditions typically result in burning outside of the actual burn room. Flames from postflashover fires extending out of a building through a window will buoyantly rise along the exterior of the building. Experiments characterizing the heat fluxes to the wall above the window of a postflashover compartment fire have been performed by Oleszkiewicz,[60,61] Bullen and Thomas,[62] and Beitel and Evans.[63] In these studies, heat fluxes as high as 200 kW/m^2 have been measured.

Experiments performed by Oleszkiewicz[60,61] were conducted using two differently sized full-scale rooms with a wall above the window that extended as much as two stories above the burn room (see Figure 2-14.48). The effects of window size, window aspect ratio, and fire size inside the compartment were evaluated in the study. Heat fluxes from the flames extending outside the burn room for different door sizes and different fires sizes are shown in Figure 2-14.49 and Figure 2-14.50 for propane gas fires.

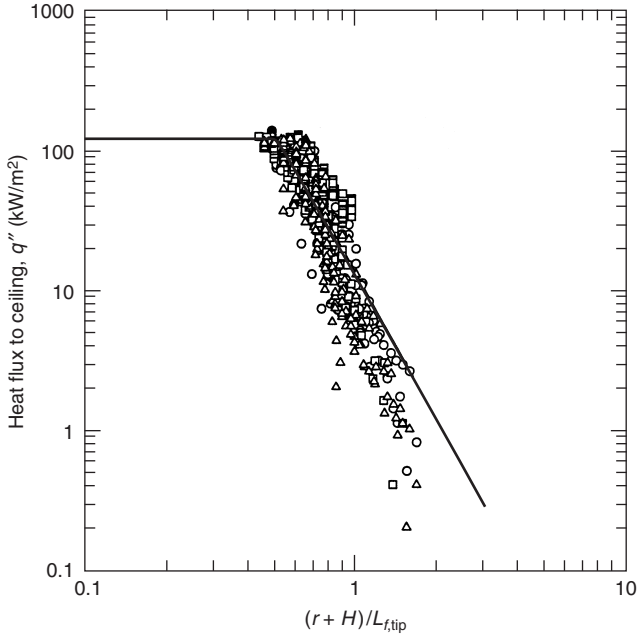

Figure 2-14.47. ***Heat fluxes to the ceiling during open corner tests with corner lined with a combustible material compared with the heat flux predicted using Equation 32: plywood (□), E-glass FR vinyl ester (○), sandwich composite (△).[10]***

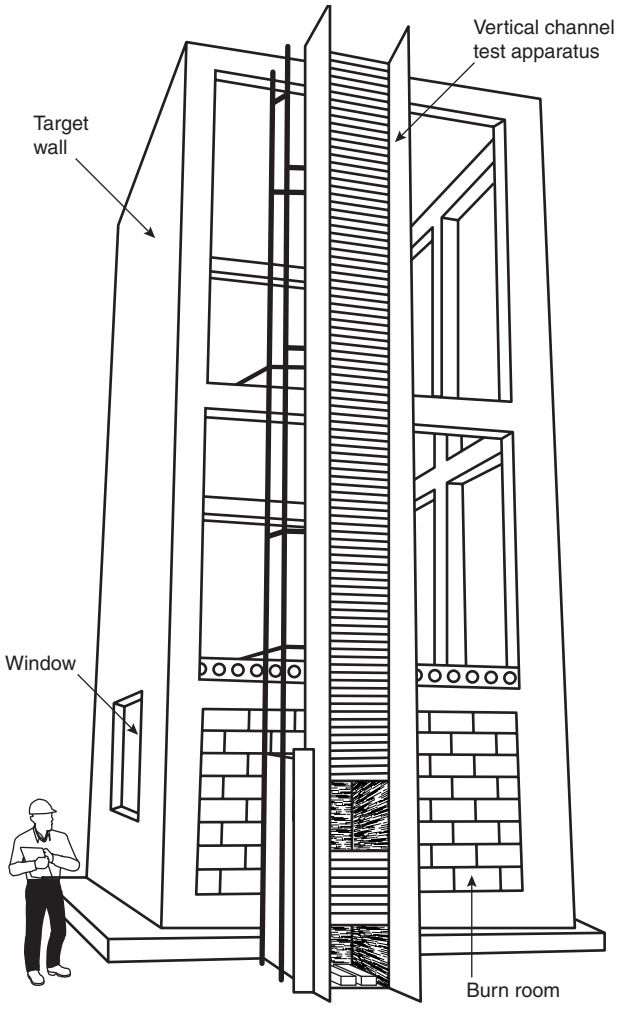

Figure 2-14.48. ***Exterior wall fire test facility used by Oleszkiewicz.[61]***

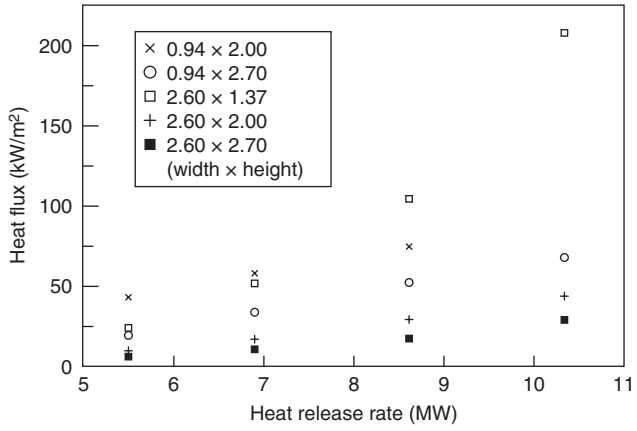

Figure 2-14.49. ***Heat fluxes from a window flame 0.5 m above the top of the window for different propane fire sizes inside the compartment.[61]***

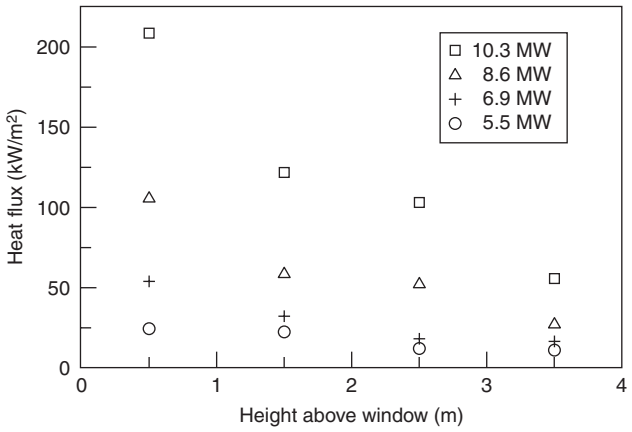

Figure 2-14.50. ***Heat fluxes from window flames along the exterior wall above a 2.6-m-wide, 1.37-m-high window.[61]***

Note that the heat release rate of the fires stated in Figures 2-14.49 and 2-14.50 is the ideal heat release rate of the compartment fire, which was determined from the gas flow rate and the heat of combustion for propane. Data in Figure 2-14.49 show the effect of fire heat release rate and window size on the heat flux 0.5 m above the window. The distribution in the heat flux along the height of the exterior wall is shown in Figure 2-14.50 for the case with a window 2.6 m wide and 1.37 m high.

Quintiere and Cleary[13] found that flame lengths for this situation can be estimated using the relation developed by Yokoi.[64] With L_f being the distance from the bottom of the opening to the average flame height, the heat release rate outside the compartment, Q, and the effective diameter of the window, D, can be used to predict the flame length above the window with the following expression:

$$L_f = 0.0321\left(\frac{Q}{D}\right)^{2/3} \tag{39a}$$

where

$$D = 2\sqrt{\frac{H_o W_o}{2\pi}} \tag{39b}$$

Effects of Other Variables

The environment in which a fire is burning can affect the heat flux levels incident on the surface. Studies have been conducted by Atreya and Mekki,[65] Santo and Tamanini,[66] Mekki et al.,[67] and Chao and Fernandez-Pello[68] to evaluate the impact of oxygen concentration on the heat fluxes transferred by flames to surfaces. In tests with methane fires, Atreya and Mekki[65] found that flame radiation (and the total heat flux to the surface) was increased by increasing the oxygen concentration.

More important for most problems with fire is the effect of decreasing the oxygen concentration on heat fluxes from the flame. Santo and Tamanini found that decreasing the surrounding oxygen concentration from 20.9 percent to 18.0 percent decreased the radiative flux to an external

target by 40 percent.[66] This decrease was attributed to a decrease in lower soot concentrations in flames in lower oxygen environments. Chao and Fernandez-Pello[68] found that this reduction in heat transfer to the surface reduces the flame spread rate along combustible panels.

Nomenclature

a spacing between parallel walls (m)
C_p specific heat capacity of air at 300 K [998 kJ/(kg·K)]
d length of single side on L-shape burner, length of line burner, width of burning area on corner wall (m)
D length of single side of square burner, diameter (m)
g acceleration of gravity (9.81 m/s^2)
H distance between fire and ceiling (m)
H_B distance between fire and lower flange of I-beam (m)
H_C distance between fire and upper flange of I-beam (m)
H_o height of room window (m)
H_{web} distance between fire and center of web on I-beam (m)
h convective heat transfer coefficient [kW/(m·K)]
L_B flame tip length along lower flange of I-beam (m)
L_C flame tip length along upper flange of I-beam (m)
L_{web} flame tip length along center of web on I-beam (m)
L_f average flame length (m)
$L_{f,\text{tip}}$ flame tip length (m)
L_H flame extension along ceiling away from stagnation point (m)
Q fire heat release rate (kW)
Q' fire heat release rate per unit width (kW/m)
Q^* dimensionless parameter, $Q_D^* = \dfrac{Q}{\rho_\infty C_p T_\infty \sqrt{g} D^{5/2}}$, with D being length scale
r distance from corner or stagnation point to measurement location (m)
q'' heat flux (kW/m^2)
T_g room gas temperature (K)
T_s material surface temperature (K)
T_∞ ambient temperature (300 K)
W_o width of room window (m)
w dimensionless distance along ceiling or I-beam, $w = (r + H_B + z')/(L_B + H_B + z')$
x horizontal coordinate (m)
y horizontal coordinate (m)
y' distance from center of line burner, $y' = 0.5d - y$ (m)
z' vertical coordinate (m)
z' virtual source location (m)

Greek

ε material surface emissivity (dimensionless)
ρ_∞ ambient density of air (1.2 kg/m^3)
π constant (3.14159)
σ Stefan-Boltzman constant [5.67×10^{-11} kW/(m^2·K^4)]

Subscripts

cl centerline
conv convective
d defined using *d* as length scale
D defined using *D* as length scale
H defined using *H* as length scale
B defined using H_B as length scale
C defined using H_C as length scale
web defined using H_{web} as length scale
inc incident
m measured
max max level
net net
peak peak
rad radiative
rr reradiated

References Cited

1. G. Back, C.L. Beyler, P. DiNenno, and P. Tatem, "Wall Incident Heat Flux Distributions Resulting from an Adjacent Fire," in *Fire Safety Science—Proceedings of the Fourth International Symposium,* International Association of Fire Safety Science, Ottawa, Canada, pp. 241–252 (1994).
2. G. Heskestad, "Luminous Heights of Turbulent Diffusion Flames," *Fire Safety Journal,* 5, pp. 103–108 (1983).
3. D. Gross and J.B. Fang, "The Definition of a Low Intensity Fire," in *NBS Special Publication 361, Volume 1: Performance Concept in Buildings, Proceeding of the Joint RILEM-ASTM-CIB Symposium,* National Bureau of Standards, Washington, DC, pp. 677–686 (1972).
4. T. Mizuno and K. Kawagoe, "Burning Behaviour of Upholstered Chairs, Part 2: Burning Rate of Chairs in Fire Tests," *Fire Science and Technology,* 5, 1, pp. 69–78 (1985).
5. M. Daikoku and K. Saito, "A Study of Thermal Characteristics of Vertical Corner Wall in Room Fire," in *Proceedings of the ASME/JSME Thermal Engineering Joint Conference* Book No. H0933C-1995 (L.S. Fletcher and T. Aihara, eds.), Hilton Head, SC, pp. 83–90 (1995).
6. Y. Hasemi, M. Yoshida, S. Takashima, R. Kikuchi, and Y. Yokobayashi, "Flame Length and Flame Heat Transfer Correlations in Corner-Wall and Corner-Wall-Ceiling Configurations," in *Proceedings of INTERFLAM '96,* (Franks and Grayson, eds.), Interscience Communications Ltd., London, pp. 179–188 (1996).
7. M. Kokkala, "Characteristics of a Flame in an Open Corner of Walls," in *Proceedings from INTERFLAM '93,* Interscience Communications Ltd., London, pp. 13–24 (1993).
8. T. Ohlemiller, T. Cleary, and J. Shields, "Effect of Ignition Conditions on Upward Flame Spread on a Composite Material in a Corner Configuration," *Fire Safety Journal,* 31, pp. 331–344 (1998).
9. T.J. Ohlemiller and J.R. Shields, "The Effect of Surface Coatings on Fire Growth over Composite Materials in a Corner Configuration," *Fire Safety Journal,* 32, 2, pp. 173–193 (1999b).
10. B.Y. Lattimer, S.P. Hunt, H. Sorathia, M. Blum, T. Gracik, M. McFarland, A. Lee, and G. Long, "Development of a Model for Predicting Fire Growth in a Combustible Corner," *NSWCCD-TR-64-99/07,* U.S. Navy, West Bethesda, MD (1999).
11. R.B. Williamson, A. Revenaugh, and F.W. Mowrer, "Ignition Sources in Room Fire Tests and Some Implications for Flame

Spread Evaluation," in *Fire Safety Science—Proceedings of the Third International Symposium,* Elsevier Applied Science, New York, pp. 657–666 (1991).
12. H. Tran and M. Janssens, "Modeling the Burner Source Used in the ASTM Room Fire Test," *Journal of Fire Protection Engineering,* 5, 2, pp. 53–66 (1993).
13. J.G. Quintiere and T.G. Cleary, "Heat Flux from Flames to Vertical Surfaces," *Fire Technology,* 30, 2, pp. 209–231 (1994).
14. S.E. Dillon, "Analysis of the ISO 9705 Room/Corner Test: Simulations, Correlations and Heat Flux Measurements," *NIST-GCR-98-756,* U.S. Department of Commerce, National Institute of Standards and Technology, Washington, DC (1998).
15. International Standards Organization, ISO 9705:1993(E), *International Standard for Fire Tests—Full-Scale Room Test for Surface Products,* International Organization for Standardization (ISO), Geneva, Switzerland (1993).
16. T. Tanaka, I. Nakaya, and M. Yoshida, "Full Scale Experiments for Determining the Burning Conditions to Be Applied to Toxicity Tests," *Fire Safety Science—Proceedings of the First International Symposium,* Hemisphere Publishing, Gaithersburg, MD, pp. 129–138 (1986).
17. W. Takashi et al., "Flame and Plume Behavior in and Near a Corner of Walls," in *Fire Safety Science—Proceeding of the Fifth International Symposium* (Y. Hasemi, ed.), International Association for Fire Safety Science, Melbourne, Australia, pp. 261–271 (1997).
18. Y. Hasemi, S. Yokobayashi, T. Wakamatsu, and A. Ptchelintsev, "Fire Safety of Building Components Exposed to a Localized Fire—Scope and Experiments on Ceiling/Beam System Exposed to a Localized Fire," in *Proceedings from ASIAFLAM,* Kowloon, Hong Kong, pp. 351–361 (1995).
19. R.L. Alpert, "Convective Heat Transfer in the Impingement Region of a Buoyant Plume," *Transactions of ASME,* 109, pp. 120–124 (1987).
20. H.Z. You and G.M. Faeth, "Ceiling Heat Transfer during Fire Plume and Fire Impingement," *Fire and Materials,* 3, 3, pp. 140–147 (1979).
21. H.Z. You and G.M. Faeth, "An Investigation of Fire Impingement on a Horizontal Ceiling," NBS-GCR-79-188, U.S. Department of Commerce, Washington, DC (1979).
22. H.Z. You, "An Investigation of Fire-Plume Impingement on a Horizontal Ceiling 2—Impingement and Ceiling-Jet Regions," *Fire and Materials,* 9, 1, pp. 46–56 (1985).
23. M. Kokkala, "Heat Transfer to and Ignition of Ceiling by an Impinging Diffusion Flame," *VTT Research Report 586,* Technical Research Centre of Finland, Espoo, Finland (1989).
24. M. Kokkala, "Experimental Study of Heat Transfer to Ceiling from an Impinging Diffusion Flame," *Fire Safety Science—Proceedings of the Third International Symposium,* Elsevier Applied Science, New York, pp. 261–270 (1991).
25. L.Y. Cooper, "Heat Transfer from a Buoyant Plume to an Unconfined Ceiling," *ASME Journal of Heat Transfer,* 104, pp. 446–452 (1982).
26. T. Wakamatsu, personal communication (September, 1999).
27. H.Z. You and G.M. Faeth, "An Investigation of Fire Impingement on a Horizontal Ceiling," *NBS-GCR-79-188,* U.S. Department of Commerce, Washington, DC (1979).
28. Y. Hasemi, M. Yoshida, Y. Yokobayashi, and T. Wakamatsu, "Flame Heat Transfer and Concurrent Flame Spread in a Ceiling Fire," in *Fire Safety Science—Proceedings from the Fifth International Symposium* (Y. Hasemi, ed.), International Association for Fire Safety Science, Melbourne, Australia, pp. 379–390 (1997).
29. P.L. Hinkley, H.G.H. Wraight, and C.R. Theobald, "The Contribution of Flames under Ceilings to Fire Spread in Compartments," *Fire Safety Journal,* 7, pp. 227–242 (1984).
30. P.L. Hinkley, H.G.H. Wraight, and C.R. Theobald, "The Contribution of Flames under Ceilings to Fire Spread in Compartments, Part I: Incombustible Ceilings," *Fire Research Note No. 712,* Fire Research Stations, Borehamwood, Herts, UK (1968).
31. P.L. Hinkley, H.G.H. Wraight, and C.R. Theobald, "The Contribution of Flames under Ceilings to Fire Spread in Compartments, Part II: Combustible Ceiling Linings," *Fire Research Note No. 743,* Fire Research Stations, Borehamwood, Herts, UK (1969).
32. T. Wakamatsu, Y. Hasemi, Y. Yokobayashi, and A.V. Ptchelintsev, "Experimental Study on the Heating Mechanism of a Steel Beam under Ceiling Exposed to a Localized Fire," in *Proceedings from INTERFLAM '96* (Franks and Grayson, eds.), Interscience Communications Ltd., London, pp. 509–518 (1996).
33. J. Myllymaki and M. Kokkala, "Thermal Exposure to a High Welded I-Beam above a Pool Fire," *First International Workshop on Structures in Fires,* Copenhagen, pp. 211–226 (2000).
34. T. Ahmad and G.M. Faeth, "Fire Induced Plumes along a Vertical Wall, Part III: The Turbulent Combusting Plume," *NBS Report for Grant No. 5-9020,* U.S. Department of Commerce, Washington, DC (1978).
35. T. Ahmad and G.M. Faeth, "Turbulent Wall Fires," in *17th Symposium (International) on Combustion,* Combustion Institute, Pittsburgh, PA, pp. 1149–1160 (1979).
36. J.G. Quintiere, M. Harkelroad, and Y. Hasemi, "Wall Flames and Implications for Upward Flame Spread," *AIAA-85-0456,* American Institute of Aeronautics and Astronautics, Reno, NV (1985).
37. L. Orloff, J. De Ris, and G.H. Markstein, "Upward Turbulent Fire Spread and Burning of Fuel Surface," in *15th Symposium (International) on Combustion,* Combustion Institute, Pittsburgh, PA, pp. 183–192 (1975).
38. M.A. Delicatsios, "Flame Heights in Turbulent Wall Fires with Significant Flame Radiation," *Combustion Science and Technology,* 39, pp. 195–214 (1984).
39. Y. Hasemi, "Experimental Wall Flame Heat Transfer Correlations for the Analysis of Upward Wall Flame Spread," *Fire Science and Technology,* 4, 2, pp. 75–90 (1984).
40. H. Mitler, "Predicting the Spread Rates on Vertical Surfaces," in *23rd Symposium (International) on Combustion,* Combustion Institute, Pittsburgh, PA, pp. 1715–1721 (1990).
41. C.L. Beyler, S.P. Hunt, N. Iqbal, and F.W. Williams, "A Computer Model of Upward Flame Spread on Vertical Surfaces," in *Fire Safety Science—Proceedings of the Fifth International Symposium* (Y. Hasemi, ed.), International Association for Fire Safety Science, Melbourne, Australia, pp. 297–308 (1997).
42. F.W. Williams, C.L. Beyler, S.P. Hunt, and N. Iqbal, "Upward Flame Spread on Vertical Surfaces," NRL/MR/6180—97-7908, Navy Technology for Safety and Survivability, Chemistry Division (1997).
43. Y. Hasemi, "Thermal Modeling of Upward Wall Flame Spread," in *Fire Safety Science—Proceedings of the First International Symposium,* Hemisphere Publishing, Gaithersburg, MD, pp. 87–96 (1986).
44. Y. Hasemi, "Deterministic Properties of Turbulent Flames and Implications on Fire Growth," *INTERFLAM '88,* John Wiley and Sons, Cambridge, UK, pp. 45–52 (1988).
45. M. Foley and D.D. Drysdale, "Heat Transfer from Flames between Vertical Parallel Walls," *Fire Safety Journal,* 24, pp. 53–73 (1995).
46. M. Kokkala, D. Baroudi, and W.J. Parker, "Upward Flame Spread on Wooden Surface Products: Experiments and Numerical Modelling," in *Fire Safety Science—Proceedings of the*

Fifth International Symposium, International Association for Fire Safety Science, Melbourne, Australia, pp. 300–320 (1997).

47. A.K. Kulkarni, C.I. Kim, and C.H. Kuo, "Heat Flux, Mass Loss Rate and Upward Flame Spread for Burning Vertical Walls," *NIST-GCR-90-584,* U.S. Department of Commerce, Washington, DC 1990.
48. A.K. Kulkarni, C.I. Kim, and C.H. Kuo, "Turbulent Upward Flame Spread for Burning Vertical Walls Made of Finite Thickness," *NIST-GCR-91-597,* U.S. Department of Commerce, Washington, DC (1991).
49. L. Orloff, A.T. Modak, and R.L. Alpert, "Burning of Large-Scale Vertical Surfaces," in *16th Symposium (International) on Combustion,* Combustion Institute, Pittsburgh, PA, pp. 1345–1354 (1977).
50. G.H. Markstein and J. DeRis, "Wall-Fire Radiant Emission, Part 2: Radiation and Heat Transfer from Porous-Metal Wall Burner Flames," in *24th Symposium (International) on Combustion,* Combustion Institute, Pittsburgh, PA, pp. 1747–1752 (1992).
51. Tewarson, "Generation of Heat and Chemical Compounds in Fires," Section 3/Chapter 4, The SFPE Handbook of Fire Protection Engineering, 2nd ed. (P.J.D. Nenno, ed.), NFPA, Quincy, MA, pp. 3-53–3-124 (1995).
52. M.M. Delichatsios, P. Wu, M.A. Delichatsios, G.D. Lougheed, G.P. Crampton, C. Qian, H. Ishida, and K. Saito, "Effect of External Radiant Heat Flux on Upward Flame Spread: Measurements on Plywood and Numerical Predictions," *Fire Safety Science—Proceedings of the Fourth International Symposium,* International Association of Fire Safety Science, pp. 421–432 (1994).
53. T.J. Ohlemiller and T.G. Cleary, "Upward Flame Spread on Composite Materials," *Fire Safety Journal,* 32, pp. 159–172 (1999).
54. C. Qian, H. Ishida, and K. Saito, "Upward Flame Spread along PMMA Vertical Corner Walls, Part II: Mechanism of *M* Shape Pyrolysis Front Formation," *Combustion and Flame,* 99, pp. 331–338 (1994a).
55. C. Qian and K. Saito, "An Empirical Model for Upward Flame Spread over Vertical Flat and Corner Walls," in *Fire Safety Science—Proceedings from the Fifth International Symposium* (Hasemi, ed.), Melbourne, Australia, pp. 285–296 (1997).
56. Y. Hasemi, M. Yoshida, and R. Takaike, "Flame Length and Flame Heat Transfer Correlations in Ceiling Fires," poster at Fire Safety Science *Sixth International Symposium,* International Association for Fire Safety, Poitiers, France (1999).
57. F. Tamanini, "Calculations and Experiments on the Turbulent Burning of Vertical Walls in Single and Parallel Configurations," *FMRC J. I> OAOE7.BU-2,* FMRC Technical Report, Factory Mutual Research Corporation, Norwood, MA, (1979).
58. F. Tamanini and A.N. Moussa, "Experiments on the Turbulent Burning of Vertical Parallel Walls," *Combustion Science and Technology,* 23, pp. 143–151 (1980).
59. H. Ingason and J. De Ris, "Flame Heat Transfer in Storage Geometries," *Fire Safety Journal,* 31, pp. 39–60 (1998).
60. I. Oleszkiewicz, "Heat Transfer from a Window Fire Plume to a Building Façade," *ASME HTD,* 23, pp. 163–170 (1989).
61. I. Oleszkiewicz, "Fire Exposure to Exterior Walls and Flame Spread on Combustible Cladding," *Fire Technology,* 26, 4, pp. 357–375 (1990).
62. P.H. Thomas and M.L. Bullen, "Compartment Fires with Non-Cellulosic Fuels," in *17th Symposium (International) on Combustion,* Combustion Institute, Pittsburgh, PA, pp. 1139–1148 (1979).
63. J.J. Beitel and W.R. Evans, "Multi-Story Fire Evaluation Program," *SwRI Project 01-6112,* Final Report, Volume 1, Southwest Research Institute, San Antonio, TX, and Society of the Plastics Industry, Inc., New York (1980).
64. S. Yokoi, "Study on the Prevention of Fire Spread Caused by Hot Upward Current," *Report No. 34* Building Research Institute, Tokyo, Japan (1960).
65. A. Atreya and K. Mekki, "Heat Transfer during Wind-Aided Flame Spread on a Ceiling Mounted Sample," in *24th Symposium (International) on Combustion,* Combustion Institute, Pittsburgh, PA, pp. 1677–1684 (1992).
66. G. Santo and F. Tamanini, "Influence of Oxygen Depletion on the Radiative Properties of PMMA Flames," in *18th Symposium (International) on Combustion,* Combustion Institute, Pittsburgh, PA, pp. 619–631 (1981).
67. K. Mekki, A. Atreya, S. Agrawal, and I. Wichman, "Wind-Aided Flame Spread over Charring and Non-Charring Solids: An Experimental Investigation," in *23rd Symposium (International) on Combustion,* Combustion Institute, Pittsburgh, PA, pp. 1701–1707 (1990).
68. Y.H. Chao and A.C. Fernandez-Pello, "Flame Spread in a Vitiated Concurrent Flow," Heat Transfer in Fire and Combustion Systems, *ASME HTD,* 199, pp. 135–142 (1992).

CHAPTER 15

Liquid Fuel Fires

D. T. Gottuk and D. A. White

Introduction

Liquid fuel spill and pool fires represent potential hazards in many applications ranging from accidents at industrial plants, using combustible liquids, to arson fires with flammable fuels. A pool is characterized by a confined body of fuel that typically has a depth greater than 1 cm. A pool can result due to a liquid fuel release that collects in a low spot, such as a trench, or can exist as a result of normal storage of fuels in tanks and containers. A fuel spill is generally associated with thin fuel layers resulting from an unconfined release of fuel. The nature of a spill fire is highly variable, depending on the source of the release, surface features of the substrate (e.g., concrete, ground, water) on which the fuel is released, and the point and time of ignition. The ability to characterize fuel spills and the resulting fires in a consistent and conservative manner is required for many engineering analyses. This chapter provides an overview of the most relevant factors and methodology for evaluating a liquid fuel spill or pool fire in terms of fire growth and size.

The chapter is organized in three major sections corresponding to the three primary steps of evaluating the development of a liquid fuel spill or pool fire: (1) Spill or Pool Size, (2) Fire Growth, and (3) Fire Size. The first section deals with the process of estimating the physical size of any given fuel release or pool of fuel. Both static (fixed quantity of liquid) and continuously flowing spill fires have been considered. Once a liquid fuel spill or pool has occurred, ignition of the fuel will lead to a transient fire growth period. This transient period of a liquid fuel fire is dictated by the flame spread rate across the surface of the liquid. The second section of the chapter addresses the assessment of fire growth rate by providing an overview of flame spread on liquid fuels. The third section discusses the available data and correlations that can be used to evaluate the size of the fire in terms of heat-release rate and flame height.

The heat release rate of a fire is the primary parameter used in determining the impact of a fire on its surroundings. The impact of a fire is dealt with in other chapters of this handbook. The heat transfer from liquid fuel spill or pool fires is addressed by Beyler.[1]

Spill or Pool Size

The first step in analyzing a liquid fuel fire is to characterize the physical dimensions of the fuel spill or pool. The area of the initial body of fuel will correlate to the size of the resulting fire. A confined fuel release or existing open container of fuel will result in a pool fire of a known area. A pool fire represents a body of fuel that is confined by physical boundaries. In other words, the walls of a room or obstructions on a floor will limit a fuel release to a smaller area than the potential unconfined spill area. In almost all cases, a confined fuel release will create a pool that has a greater depth than the depth of an unconfined spill. When fuel is released onto a surface, it will spread laterally based on several factors, including the initial momentum of the fluid, the fluid surface tension, and the features of the substrate onto which it spilled. Some substrate features that need to be considered are porosity of material and surface roughness. Porous materials, such as sand or even some floor coverings like carpet, can result in different spill sizes and different fuel burning rates.

In general, fuel spills can be characterized as either continuously flowing or instantaneous (static). These characterizations are considered with respect to when the spill is ignited. In the case of a continuously flowing spill, ignition has occurred while the fuel is moving away from

Dr. D. T. Gottuk is a senior engineer at Hughes Associates, Inc. He has a Ph.D. in mechanical engineering from Virginia Polytechnic Institute. His research interests lie in fire dynamics and fire detection.

D. A. White, P.E., is a senior engineer at the fire science and engineering firm of Hughes Associates, Inc. He has been actively involved in fire hazard analyses for special situations as well as performance-based engineering projects for high-tech industrial facilities.

the source. For a static spill, the fuel nominally spreads to a maximum area and then is ignited, such that the flame spreads across the fuel surface. For a continuously flowing spill fire, the flame may spread across the fuel surface initially, but the flame front is ultimately controlled by the spread of the fuel over the substrate until steady-state burning conditions occur.

The spill area of a continuously flowing spill that is not burning will continue to increase until a physical boundary is reached. A continuous spill that is burning will have a steady-state spill size based on a balance between the volumetric flow rate and the volumetric burning rate of the fuel. This concept is developed later in the section Fire Size.

For a confined pool, the area, A, is dictated by the boundaries, and the pool depth, δ, can be simply calculated based on the volume, V, of liquid:

$$\delta = \frac{V}{A} \tag{1}$$

For an unconfined spill, the area has typically been determined via Equation 1 with an estimate of the fuel depth. There has been little compiled data for establishing appropriate fuel depths or spill areas of various fuels on solid substrates. In the past, engineers have conservatively estimated spill depths based on the minimum depth required to support flame spread (see Fire Growth Rate section). The use of a minimum depth will result in the largest possible spill area that can support a flame, therefore, the largest possible fire.

Literature results along with recently conducted tests provide a basis for estimating spill depths. Figure 2-15.1 shows a plot of spill depths for both noncombustible liquids and combustible fuel spill fires as a function of the amount of liquid released on an unconfined surface. Table 2-15.1 summarizes the details of the data in Figure 2-15.1, with other notable references. The figure shows that JP-8 and JP-4 spill fires occurred with initial spill depths as low as 0.7 mm and 1.0 mm, respectively. It is also interesting to note that both Chambers[2] and Gottuk et al.[3] observed increases in burning fuel spill areas after the liquid spill was ignited. Fires increased the initial fuel spill area by 22 to 89 percent for fuel releases ranging from 2 to 190 l. This increase in area corresponds to a similar decrease in fuel depth, below those reported in Figure 2-15.1. The practical implication of this increase in spill area is that the fires may be substantially larger than would be predicted per the initial fuel spill areas based on Figure 2-15.1. However, the larger area would also result in much shorter burning times before the fuel is consumed. When it is necessary to determine the maximum fire size of an unconfined spill, it is suggested (based on the limited data available) that the area of the fire, A, be equivalent to approximately 155 percent of the initial spill area:

$$A = 1.55A_S \tag{2}$$

The data in Figure 2-15.1 for water and AFFF were obtained by Gottuk et al.[3] for unconfined spill experiments in order to provide bounding data for estimating fuel spill depths and areas. The surface tensions of water and 6 percent AFFF solution bound those of most fuels; water has a surface tension of 73 dynes/cm and the AFFF has a value of approximately 15 to 16 dynes/cm at temperatures of 15 to 32°C.[4] As can be seen in Figure 2-15.2, the surface tension of different fuels from 10°C to 50°C ranges from 16 to 27 dynes/cm. Though surface tension is not the sole variable dictating spill area, the data in Figure 2-15.1 shows that spill depths for water and solutions of 6 percent AFFF appear to provide bounding values for the available fuel spill fires.

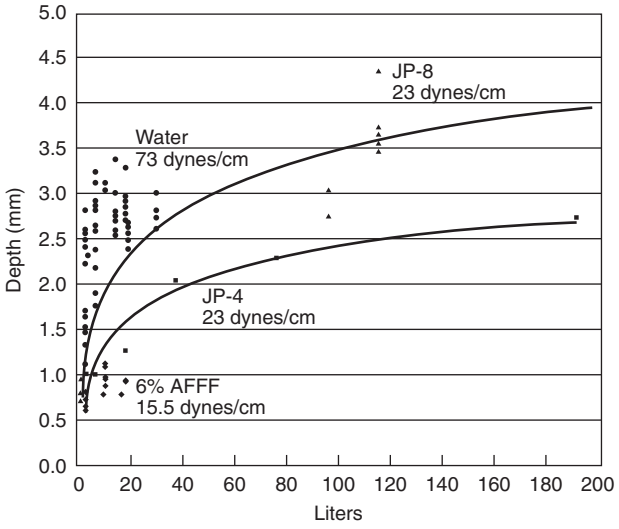

Figure 2-15.1. ***Liquid spill depths as a function of the amount of liquid released. The lines represent curve fits to the JP-8 and JP-4 data.***

The data of Figure 2-15.1 is presented in an alternate form in Figure 2-15.3, which shows the spill area per unit volume of liquid as a function of the amount of liquid released. Similar to Figure 2-15.1, the data shows quite a bit of variability [0.3 to 1.6 m^2/l (12 to 65 ft^2/gal)] for small quantities of fluid, particularly $\leq$7.6 l (2 gal). However, with increasing quantities of fluid, the spill area per volume appears to approach a common minimum value of approximately 0.3 m^2/l (12 ft^2/gal). This minimum value corresponds to the spill depths in Figure 2-15.1 of approximately 2.8 to 4 mm for fuel releases of 95 l (25 gal) or more.

The larger variability of spill depths for releases of ~8 l or less is attributed to the greater dependency on multiple variables, such as the initial spill height, surface features, and fluid properties. Though not fully understood, some of these factors are not as prevalent when larger quantities of liquid are spilled. An example of the variability in spill depths is shown in Figure 2-15.4, which presents the same 6 percent AFFF solution and water data of Figure 2-15.1 on an enlarged scale plot. For the water, depths varied for releases at different heights and of different quantities. However, this effect was not observed for releases of the 6 percent AFFF solution. Figure 2-15.4 also shows that similar water spills on vinyl tile floor produced the same spill depths as released on smooth concrete. Modak[5] reported that for very small spills of various oils (see Table 2-15.1) on steel and epoxy-coated

Table 2-15.1 ***Summary of Fixed-Quantity, Unconfined Liquid Spill Data***

Reference	Fuel	Quantity of Fuel	Spill Depth	Spill Area	Surface
Chambers[2]	JP-4	4–189 l (1–50 gal) from 1-ft height	0.7–2 mm after ignition	4–102 m^2	Concrete runway
Gottuk[3]	Water	3.8–30 l (1–8 gal)	1.1–3.4 mm	1–11 m^2	Smooth, unfinished concrete and tile floor
Gottuk[3]	6% AFFF	3.8–19 l (1–5 gal)	0.6–1.1 mm		Smooth, unfinished concrete
Gottuk[3]	JP-8	2–3 l (0.5–0.8 gal)	0.7–1.1 mm	2.1–3.1 m^2	Smooth concrete with polyurethane coating
Hill[22]	JP-8	95–114 L (25–30 gal)	2.8–4.4 mm	26–33 m^2	Smooth, unfinished concrete
Putorti[48]	Gasoline	0.25–1 l	0.5–0.7 mm	0.4–1.8 m^2	Wood parquet and vinyl tile
Modak[5]	#2 Fuel oil	0.005–0.030 l	0.22 mm	0.0075–0.0400 m^2	Both epoxy-coated concrete and steel
	Mobil DTE 797 turbine-lubricating oil		0.34 mm		(Spill depths were the same for both surfaces and were independent of the volume of liquid spilled.)
	Pennzoil 30-HD motor oil		0.75		
	Fyrquel 220 hydraulic control oil		0.84		

concrete, the spill areas (and depths) were the same for both substrate materials. However, spill areas were smaller for untreated concrete due to fuel absorption into the substrate surface.

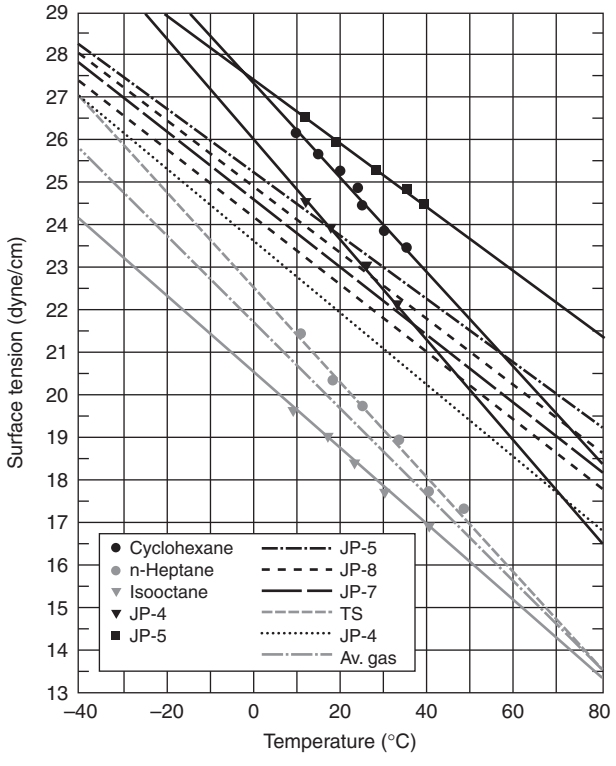

Figure 2-15.2. ***The effect of temperature on surface tension of hydrocarbon liquids (data taken from References 4 and 48).***

Based on the JP-8 spill fire data from Gottuk et al.,[3] as well as the bounding spills of 6 percent AFFF solution, the minimum spill depth can be assumed to be 0.7 mm. If an analysis warrants a more accurate assessment for the applicable conditions, the data presented in Figures 2-15.1, 2-15.3, and 2-15.4 can be used to provide guidance.

In summary, spill depths for liquid spill fires can range from 0.7 mm to 4 mm, depending primarily on the initial quantity of fuel released. Based on the data available, the

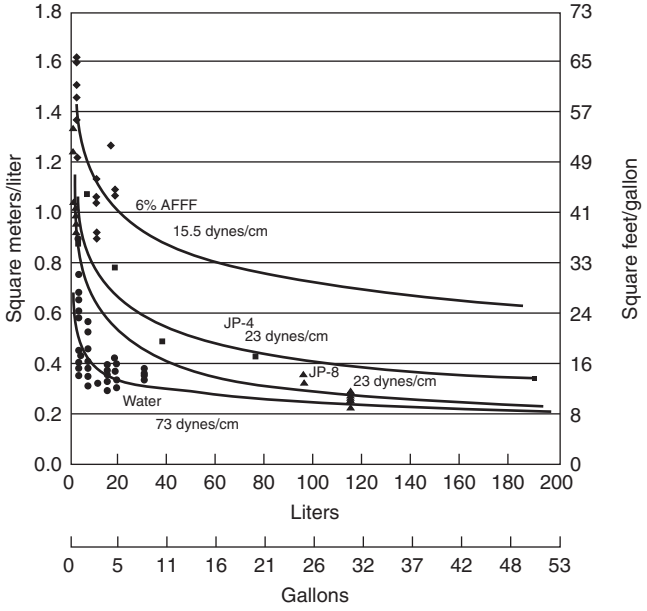

Figure 2-15.3. ***Spill area per volume of liquid released for the same data presented in Figure 2-15.1.[3]***

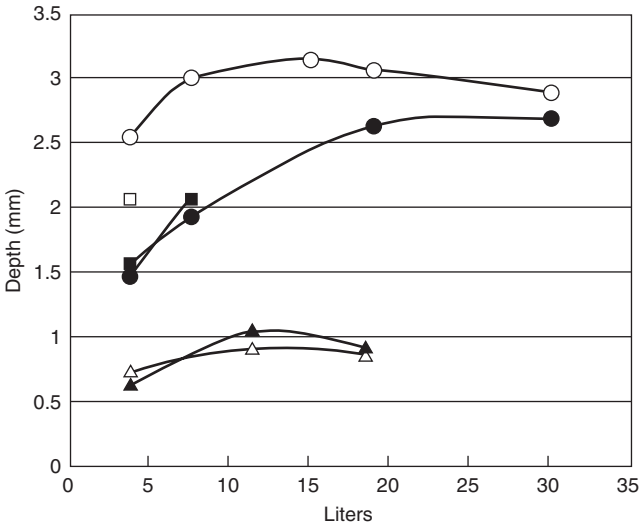

Figure 2-15.4. ***Spill depths for 6 percent AFFF solution and water releases on smooth concrete and tile floors for various fuel volumes and release heights:[3] AFFF on concrete from 0.6 m (△), AFFF on concrete from 1.0 m (▲), water on concrete from 0.6 m (○), water on concrete from 1.0 m (●), water on tile floor from 0.15 m (□), and water on tile floor from 0.9 m (■).***

following rules provide conservative minimum depths that will yield the maximum spill area:

$$\text{Spill} < 95\ \text{l (25 gal)} \qquad \delta = 0.7\ \text{mm} \qquad (3a)$$

$$\text{Spill} > 95\ \text{l (25 gal)} \qquad \delta = 2.8\ \text{mm} \qquad (3b)$$

Alternatively, the criteria can be stated as the reciprocal of the depth to yield the spill area per volume of fuel:

$$\text{Spill} < 95\ \text{l (25 gal)} \qquad A/V = 1.4\ \text{m}^2/\text{l}\ (57\ \text{ft}^2/\text{gal}) \qquad (4a)$$

$$\text{Spill} \geq 95\ \text{l (25 gal)} \qquad A/V = 0.36\ \text{m}^2/\text{l}\ (14.5\ \text{ft}^2/\text{gal}) \qquad (4b)$$

If a less conservative and potentially more accurate estimate is needed, then Figures 2-15.1, 2-15.3, and 2-15.4 should be used to provide guidance.

Fire Growth Rate

The temperature of the spilled liquid relative to its flash point is the single most important factor in identifying the flame spread rate over the surface of the liquid. The flame spread rate, in turn, determines the heat release rate history of the growing fire. Other factors also affect the flame spread rate, including the depth of the spilled liquid, size of the spill, type of liquid, and the substrate.

Generally, hazard assessments involving flammable, liquid pool fires require a conservative characterization of the fire growth rate history, peak burning rate, and fire duration. The purpose of the hazard assessment often defines that only a subset of these parameters are required. Peak burning rate and maximum burning duration at the peak burning rate are typically relevant to fire effects such as fire exposure to building elements, ignition of other fuel targets, or general environmental conditions that result from the fire.

The characterization of the spill or pool fire heat release rate history from ignition to peak burning rate (full involvement of pool fuel surface area) is important when dealing with time-related concerns or events. Examples of time-dependent concerns include egress or life safety conditions, activation of detection or suppression systems, spread of fire to other fuel packages, or failure of building elements. Presuming that one is interested in the pool fire heat release rate growth history, this can be defined as the integration of the flame spread rate for the particular geometry in question (e.g., circular for unconfined pools, rectangular for trenches) multiplied by the burning rate per unit surface area for the given liquid. Estimating the flame spread rate over the surface of the flammable/combustible liquid spill becomes critical in characterizing the fire growth history.

The majority of ignited, flammable liquid fuels results in flame spread that can be characterized by one of two major flame spread mechanisms for liquid fuels: liquid phase–controlled flame spread or gas phase–controlled flame spread. Flame spread rates for these two regimes can be grossly benchmarked: 1 to 12 cm/s for liquid phase–controlled flame spread and 130 to 220 cm/s for gas phase–controlled flame spread. A third regime for flammable liquid spills on porous surfaces can be defined where flame spread rates are measured in terms of cm/min. For some hazard analyses, identifying the appropriate flame spread region may sufficiently characterize the flame spread rate in a conservative fashion. The primary driver of the flame spread regime is the temperature of the spilled liquid relative to its flash point.

Basic Theory of Flame Spread on Liquids

Flame spread on liquid fuels has been widely studied in small-scale experiments and theoretical studies.[6–24] The flame spread rates are known to be dependent on fuel temperature and fuel flash point. Below the flash point temperature, the flame spreads by way of surface tension–induced flow of hot fuel ahead of the advancing flame. Above the flash point, the flame spread is by way of gas phase spread, which can be as rapid as 2 m/s. The majority of liquid flame spread studies have been limited to pure fuels, and most of the studies have used alcohol fuels in trays <10 cm wide. The majority of liquid flame spread studies have been focused on pure fuels with heavy emphasis on alcohol fuels in trays less than 10 cm wide. This chapter includes empirical data from nonpure hydrocarbon fuels[25] as well as data from large-scale studies.[26,27]

Flame spread regimes: Several flame spread regimes have been identified in the literature. These flame spread regimes are most notably a function of the liquid temperature. The dependence of flame spread rates on liquid temperature has been studied by a number of investigators.[6–22] The most extensive work has been done with nar-

row pans of alcohol fuels with fuel depths of 2–5 mm. These investigations indicate that the flame spread velocity is a strong function of fuel temperature, even when the fuel temperature is well below the flash point. Figure 2-15.5 shows the extensive work that Akita[9] conducted using methanol in a 2.6-cm-wide pan. Akita observed a number of different flame spread regimes. Above the flash point, spread was via the gas phase. Below the flash point, he observed regions of uniform, pulsating, and pseudo-uniform spread. The mechanistic explanations for these phenomena below the flash point are not widely agreed upon. A more detailed discussion of flame spread regimes and their mechanisms can be found in the review article by Ross.[28]

Semilog plots of flame spread rate as a function of liquid temperature have a characteristic shape with three regions: the liquid-controlled region, the gas phase–controlled region, and the asymptotic gas phase–controlled region. The slopes of the curve are different in each of these regions, and these differing slopes serve to define the regions. The transition from liquid to gas phase–controlled burning occurs at a temperature T_{go}; the transition from gas phase control to asymptotic gas phase spread occurs at a temperature T_{gm}. Figure 2-15.6 graphically portrays these temperatures with respect to flame spread rates. Figure 2-15.6 is intended as a conceptual depiction and the omission of units on the axes is intentional.

Figure 2-15.6 is conceptually the same as a figure first described by Glassman and Hansel.[29] In their paper, they identified the temperature at which gas phase–controlled flame spread begins as the fire point of the liquid; they also identified the temperature at which the maximum flame spread rate occurs as the stoichiometric temperature (the liquid temperature at which the vapor concentration at the surface is stoichiometric). While this interpretation is consistent with the interpretation of data for multicomponent fuels, in light of Glassman and Dryer,[14] it is not practical to define a fire point temperature for a multicomponent fuel. The difficulties are due to the need to model evaporation of many high-volatility components in a multicomponent fuel during the open heating that is required in the determination of a fire point. Determination of the fire point of a multicomponent fuel would require closed-cup heating of a fuel to a test temperature, exposing the liquid surface, and applying an ignition source. If the fire does not continue, the test temperature is below the fire point. Additional temperature tests would be required until the firepoint temperature is bracketed to the desired accuracy. This process is not practical. Similarly, for a multicomponent fuel it is not always practical to define the stoichiometric temperature, since determination of the vapor pressure of each component is, at the least, tedious and often impossible. Thus, while Glassman and Hansel's definitions are not easily generalized to multicomponent fuels, their pure fuel concepts can still provide guidance and motivation for the interpretation of multicomponent, liquid fuel flame spread results.

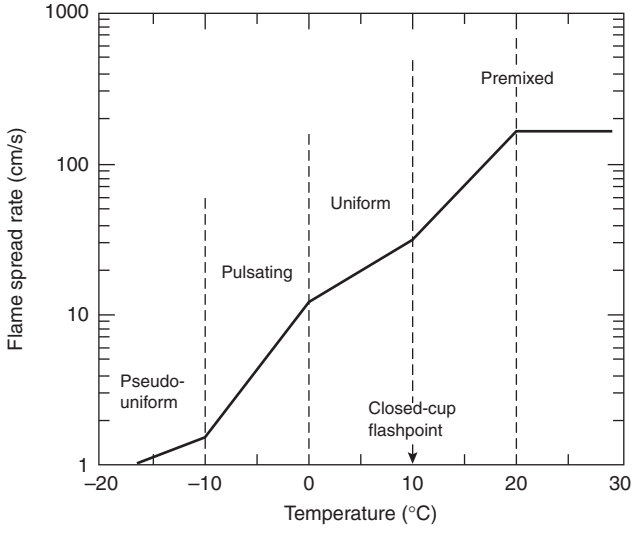

Figure 2-15.5. ***Flame spread rate on 1-cm-deep methanol as a function of fuel temperature in a 2.6-cm-wide pan.[9]***

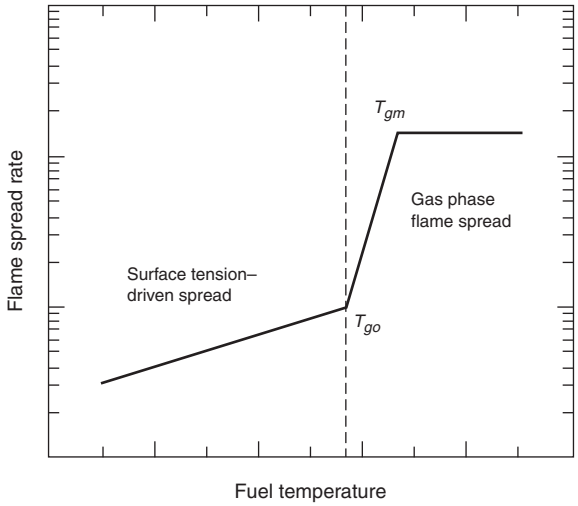

Figure 2-15.6. ***Graphic representation of the definitions of T_{go} and T_{gm}.***

Pool dimensions: The physical dimensions of a liquid fuel spill or pool influences the flame spread rate, assuming an ignition source is present. The primary factors of importance are pool depth and characteristic width of the pool, as discussed below.

Pool dimensions, including fuel depth, have no effect on the flame spread rate for situations where the flame spread mechanism is considered gas phase–controlled. However, the depth of a flammable liquid does have a significant impact on the flame spread rate for liquid phase–controlled burning. In general, the average flame spread velocity for liquid phase–controlled spread increases with fuel depth. The fuel depth is primarily governed by the type of fuel release, confined versus unconfined.

Scientific study of liquid flame spread can be traced back as far as the 1930s.[6] Most of the early work was done on relatively small-scale test setups, much of the work having been done with pans only 1–6 cm wide, using alcohol fuels at depths of 2–5 mm.[7–9] Work by Mackinven, Hansel, and Glassman[10] at Princeton is especially relevant here because it involved extensive experiments with decane, a pure fuel with similar characteristics to aviation fuels and other low–flash point, multicomponent hydrocarbon fuels that are common to fire hazard assessments. These workers documented the effects of pan width and fuel thickness on the observed flame spread rates.[10]

Several investigators have performed experiments in order to characterize the impact of fuel depth on liquid-controlled flame spread. Mackinven et al.[10] demonstrated the systematic variation of flame spread rates with fuel depth. They investigated decane fuel depths from 1 mm to 2 cm and found the flame spread rate to increase with fuel depth as shown in Figure 2-15.7. This increase can be attributed to the retarding effect of small fuel depths on liquid recirculation flows that cause flame spread. Calculations by Torrance[11,12] are in excellent agreement with Mackinven et al.'s experimental data shown in Figure 2-15.7. These calculations indicate that decane flame spread rates increase with pool depth up to 3 cm. Increases in fuel depth beyond this no longer increase the flame spread rate. Of course, fuel depths for unconfined fuel spills will always be far less than 3 cm. Investigations by Mackinven et al.[10] as well as Burgoyne and Roberts[7,8] indicate that flames do not spread away from the ignition source in liquid pools $\leq$1.5 mm deep. More recent work by Burelbach, Epstein, and Plys[30] demonstrated that the limiting fuel thickness for flame spread was 2.0 mm for decane and 2.3 mm for dodecane. Minimum fuel depths for flame spread are for the liquid-controlled spread regime. There is no evidence for fuel depth or pan width effects on gas phase flame spread.[7,9,13,15,18,20]

Mackinven et al.[10] found that for pan widths up to 20 cm the flame spread rates on decane are a strong function of pan width. At pan widths from 20 to 80 cm, the maximum width they studied, they observed only slight increases in flame spread rate. Their results are shown in Figure 2-15.8. Both aluminum and glass pan walls were used. While there are small differences between these two wall materials, which may be attributed to heat conduction effects, the major dependence at pan widths $<$20 cm is independent of wall material and has been attributed to a momentum reduction associated with viscous drag on the walls. The relative independence of pan width above 20 cm indicates that flame radiation is not a pivotal mechanism in determining liquid phase–controlled flame spread. The results were confirmed by Mackinven et al. by shielding the liquid ahead of the flame from flame radiation during flame spread experiments (20–80-cm-wide pans). They observed modest changes in flame spread rates between the shielded and unshielded experiments.

Temperature effects: The work of Burgoyne and Roberts[7] showed that at small pan widths the temperature dependence of the flame spread rate is a function of the pan width as shown in Figure 2-15.9. Unfortunately, their work extends only from 2.5- to 6.3-cm widths. The dependence on pan width disappears above 41°C, the flash point of isopentanol. Given the work of Mackinven et al.[10] using varying pan widths (see Figure 2-15.8) with decane 21°C below the closed-cup flash point (44°C) and the work of Burgoyne and Roberts,[7] the prior work indicates that pan width ceases to have an impact on the temperature dependence of the flame spread rate at pan widths $>$20 cm.

Flame spread experiments above the flash point indicate that the flame spread is via the gas phase. The flame spread rate increases rapidly from the flash point to the liquid temperature at which a stoichiometric fuel-air

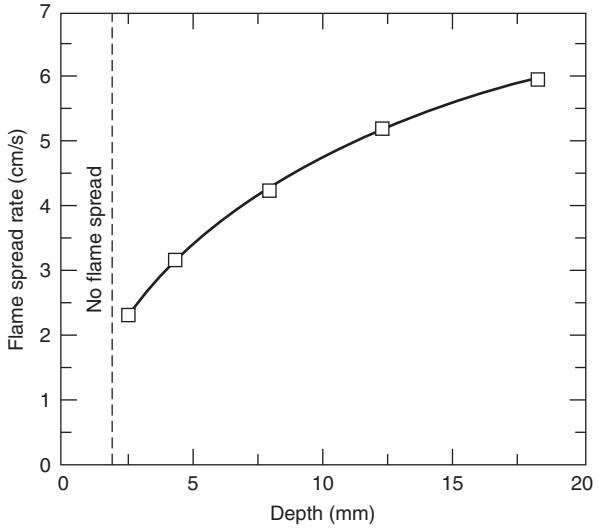

Figure 2-15.7. ***Flame spread rate on decane as a function of fuel depth.[10]***

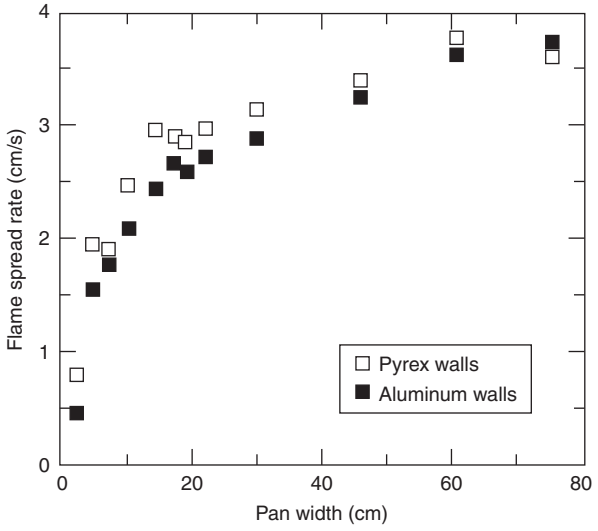

Figure 2-15.8. ***Flame spread rate on decane as a function of pan width.[10]***

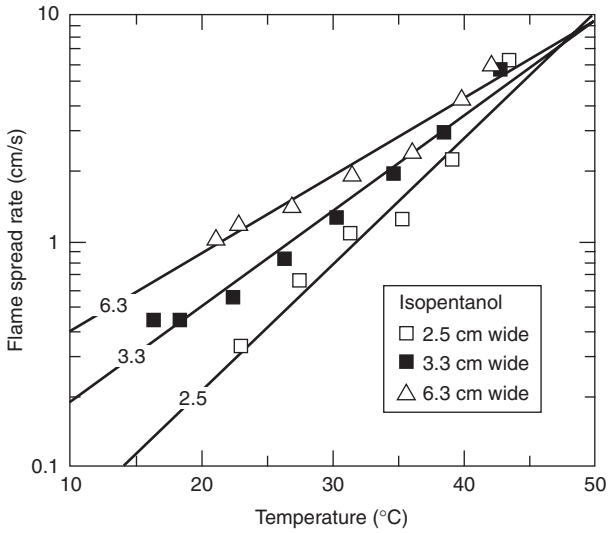

Figure 2-15.9. ***Effect of pan width on the temperature dependence of flame spread rate on isopentanol.[7]***

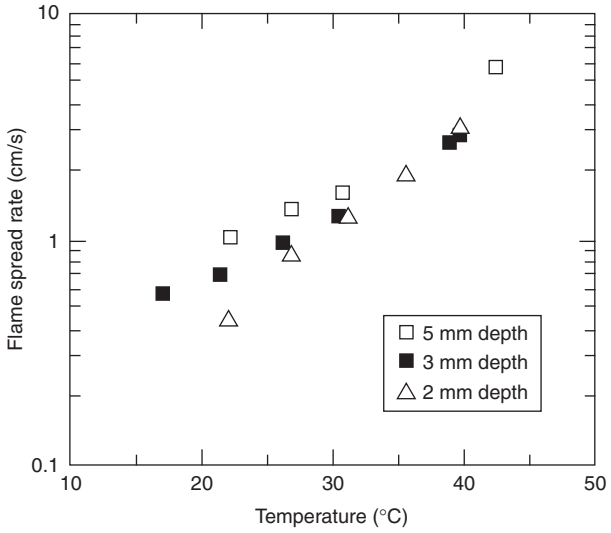

Figure 2-15.10. ***Effect of fuel depth on the temperature dependence of flame spread rate on isopentanol.[7]***

mixture exists above the liquid surface. Above this temperature, the flame spread rate is no longer temperature dependent. The flame spread velocities measured by Burgoyne and Roberts,[7] Akita,[9] Nakakuki,[15] and Hirano et al.[20] in this temperature region are from 1.3 to 2.2 m/s depending on the fuel. These velocities are similar to flame spread rates measured in stratified fuel-air mixtures found near ceilings of mine tunnels.[31–33]

The work of Burgoyne and Roberts also indicates that the temperature dependence of the flame spread rate is a function of the fuel depth.[7] They investigated isopentanol at fuel depths of 2 to 5 mm and their results are shown in Figure 2-15.10. Their results indicate that variations in flame spread rate with fuel temperature below the flash point (41°C) are lessened by increasing fuel depth.

Empirical Data

An overview of the experimental results for flame spread velocities follows. The overview includes alcohol fuels, multicomponent hydrocarbon fuels, and blends of multicomponent hydrocarbon fuels. While the bulk of the data is for laboratory-scale pools, there is limited data for large-scale pools of hydrocarbon fuels as well as some data for large-scale spills of jet fuel (hydrocarbon).

White, Beyler, Fulper, and Leonard[25] measured flame spread rates for aviation fuels, mixtures of these multicomponent hydrocarbon fuels, as well as 1-pentanol (alcohol). These measurements were made over a range of fuel temperatures in a pan with dimensions of 20 cm in width by 163 cm in length. The results for pure JP-5 and JP-8 are shown in Figures 2-15.11 and 2-15.12. The flame spread rates range from 3 to 140 cm/s over a temperature range of 10–90°C. The solid symbols indicate liquid-controlled flame spread and the open symbols indicate gas phase flame spread. JP-5 is a high–flash point kerosene used by the U.S. Navy that has a specified minimum flash point of 60°C.[34] JP-8 is a newer U.S. Air Force fuel, very similar to commercial Jet A-1, that is a kerosene with a lower specified minimum flash point of 38°C.[35] The flame spread rates in the liquid-controlled regime for JP-8 are 0.5 to 2 cm/s greater than for JP-5. At temperatures ~12–20°C above the closed-cup flash point, flame spread rates increase very rapidly to >100 cm/s. The major difference in flame spread characteristics of JP-5 and JP-8 is the temperature at which the flame spread rate rapidly increases: 68°C for JP-5 and 58°C for JP-8.

Figure 2-15.12 shows several data points where the application of the ignition source was systematically var-

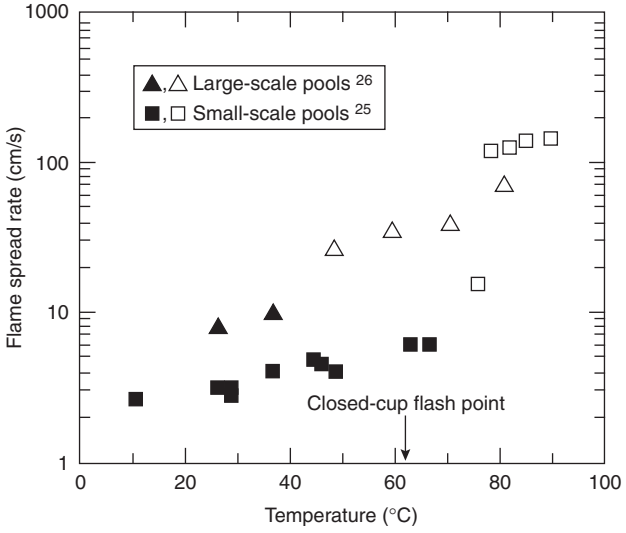

Figure 2-15.11. ***Flame spread rate for JP-5 as a function of temperature. Solid symbols denote liquid-controlled flame spread and open symbols denote gas phase flame spread for small-scale data only.***

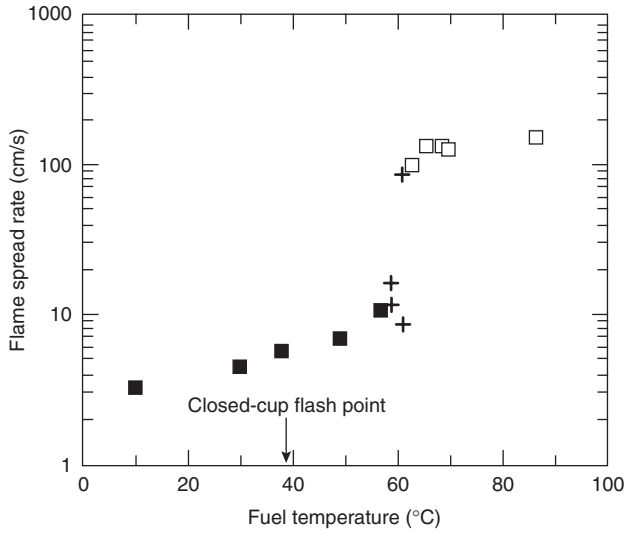

Figure 2-15.12. ***Flame spread rate for JP-8 as a function of temperature. Solid symbols denote liquid-controlled flame spread and open symbols denote gas phase flame spread; + indicates variable times to ignition of 3, 160, 240, and 460 s. The normal time to ignition is 35 s. Longer ignition times reduce the flame spread rate.[25]***

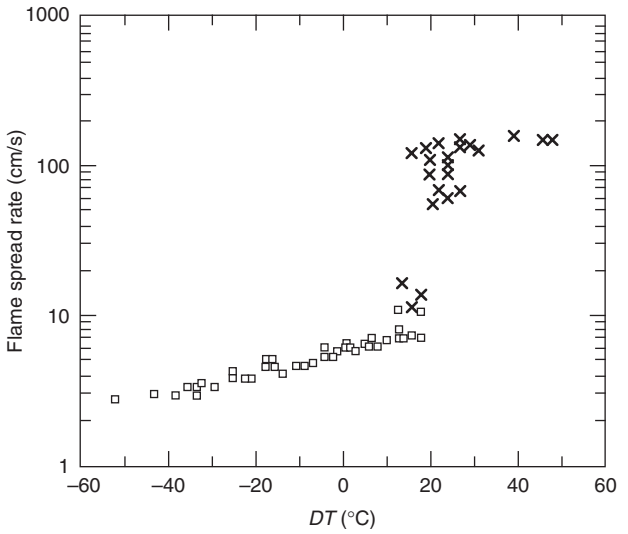

Figure 2-15.13. ***Flame spread rate for all JP fuels as a function of DT ($T_l - T_{fl}$).[25]***

ied from 3 to 460 s in the most sensitive temperature region (the transition between liquid controlled and gas phase–controlled flame spread). At higher and lower temperatures such ignition delays have little or no effect on the observed flame spread rate. Assuming that the flame spread rate is a function of the liquid temperature relative to the flash point temperature, the results are consistent with an increase in the flash point of ~10°C during the 3 to 460 s between fuel discharge and ignition. No systematic study of flash point variations with time for multicomponent fuels appears elsewhere in the literature.

The flame spread results for JP-5 and JP-8 indicate that the single most important determinant of flame spread is the initial temperature of the liquid prior to ignition relative to the fuel's flash point. Hillstrom[13] also observed this correlation and found that plotting the flame spread rate as a function of the temperature difference between the closed-cup flash point, T_{fl}, and the liquid fuel temperature, T_l, correlated data for a number of hydrocarbon fuels. Figure 2-15.13 shows flame spread rate data for pure JP-5, pure JP-8, and mixtures of the two fuels plotted as a function of DT ($T_{fl} - T_l$). In Figure 2-15.13 square symbols represent liquid-controlled flame spread and the X symbols indicate gas phase flame spread. The treatment of the data effectively correlates all of the jet fuel data over a range of DT from −50°C to +50°C. This representation of the data clearly shows the importance of DT ($T_{fl} - T_l$) in determining flame spread rate. Figure 2-15.13 also shows excellent consistency in the transition from liquid-controlled flame spread to gas phase spread at $DT = 18$°C.

Leonard et al.[26] performed large-scale flame spread experiments as part of an effort to evaluate the fire hazards of mixed jet fuels on aircraft carrier flight decks. The experiments, which evaluated pure JP-5, pure JP-8, and mixtures of these two jet fuels, were carried out in a large-scale pan measuring 1.52 m in width and 12.2 m in length. The Leonard et al. experiments are the largest pool fire flame spread experiments reported in the literature. The jet fuels were evaluated over a range of temperatures by introducing heated fuel into the large pan, which was also temperature controlled by circulation of water through chambers on the underside of the pan bottom. The results for JP-5 are presented in Figure 2-15.11. The results for JP-8 are illustrated in Figure 2-15.14.

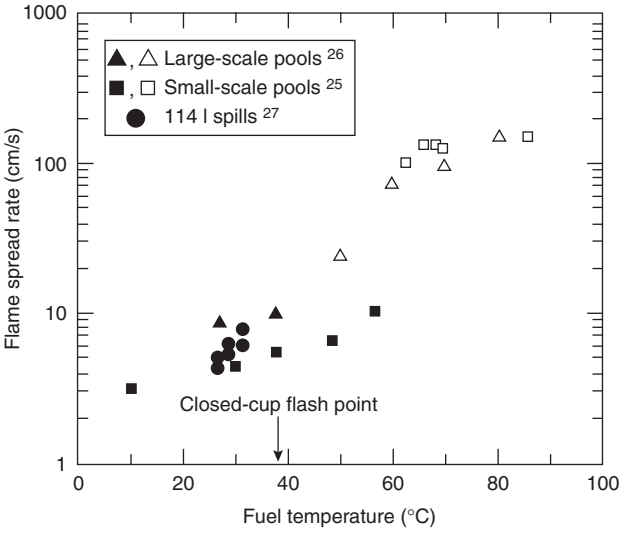

Figure 2-15.14. ***Flame spread rate for JP-8 as a function of temperature. Solid symbols denote liquid-controlled flame spread and open symbols denote gas phase flame spread.***

The large-scale results can easily be compared with the small-scale results in both Figures 2-15.11 and 2-15.14. This comparison yields identical qualitative results. The flame spread rates for the large-scale tests are notably higher for both the JP-5 and JP-8 liquid-controlled flame spread tests. Data for the JP-8 tests indicate that the liquid-controlled flame spread rate is 10 to 11.6 cm/s while that of the JP-5 tests show 8.2 to 10 cm/s in this regime. As with the small-scale tests, there is approximately 1.5- to 1.8-cm/s difference between the two jet fuels, with the JP-8 fuel being slightly faster. The transition to gas phase flame spread appears to occur at a lower temperature for both fuels. Similar gas phase flame spread velocities are obtained between small- and large-scale tests. The disparity between the small-scale and large-scale tests for these two fuels cannot be attributed to a single factor. It is speculated that the difference in flame spread behavior of the two experimental data sets may be due, in part, to width effects and flame radiation effects. Further work is necessary to identify the specific mechanisms responsible for this observed difference.

A recent set of experiments evaluating aircraft hangar fire detection technologies[27] included large-scale jet fuel spill fires. Hill, Scheffey, Walker, and Williams[27] evaluated alternative fire protection methods for U.S. Air Force aircraft hangars. Their work represents the largest spill fires evaluated in the literature for flame spread. A volume of 114 l (30 gal) of JP-8 was spilled on a concrete pad. While the main focus of this research was fire suppression systems, one important aspect was evaluated: the impact of various suppression systems on the flame spread rate after system activation. The experiments measured the flame spread rate over the large spill area, which covered approximately 30 m^2 at the time of ignition, both before and after operation of the suppression system. The full free-burn spill size was on the order of 37 m^2. Time for complete burn-out for the free-burn spill scenario was roughly 2 min. Measured flame spread rates for the JP-8 spills prior to suppression system activation have been identified in Figure 2-15.14. The temperature of the JP-8 fuel was approximately 25°C ± 2°C. These flame spread rates fall close to the data points from the small-scale tests. The Hill et al. data points show a 1.5- to 3.5-cm/s increase over the small-scale data for the liquid-controlled flame spread results. The large-scale spill data show higher flame spread rates in comparison to the small-scale pool experiment data.

Although there are depth issues associated with the comparison of pool experiments to spill experiments, the trend appears to be that larger scale flame spread experiments yield higher flame spread rates for the liquid-controlled flame spread regime with a transition to gas phase spread occurring at a lower temperature than observed in the small-scale pool experiments. While these differences may not be fully explainable, it is important to note that irrespective of the experiment scale, peak flame spread rates for the liquid-controlled flame spread regime is approximately 10 cm/s for JP-5 and 12 cm/s for JP-8. Furthermore, although the transition to gas phase spread seems to occur at a lower temperature, the maximum gas phase flame spread rates are maintained in the 120- to 200-cm/s range for both JP-5 and JP-8. Support for using a maximum flame spread velocity of 10 cm/s for liquid-controlled flame spread over hydrocarbon fuels can be drawn from Figure 2-15.15. Figure 2-15.15 shows a comparison of the jet fuel data from White et al.[25] and other hydrocarbon data from the literature. The results of the jet fuels were consistent with those of Hillstrom[13] and Mackinven et al.,[10] which show a very modest variation in flame spread rate below the flash point temperature. Figure 2-15.15 shows a comparison between the jet fuel data of White et al.,[25] the decane data from Hillstrom,[13] the diesel fuel data from Hillstrom,[13] and the decane data from Mackinven et al.[10] The decane results show a rise in the flame spread rate at a smaller value of DT than for the JP fuels. Also, below the closed-cup flash point, the decane shows lower flame spread rates. This variation may be due to the effect of using a water substrate in the decane tests rather than steel as used in the jet fuel work. All the data in Figure 2-15.15 were collected in 20-cm-wide pans.

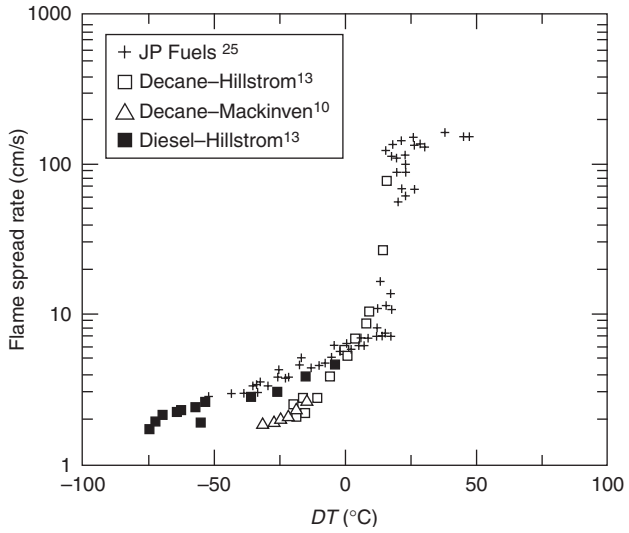

Figure 2-15.15. ***Comparison of JP fuel data with other hydrocarbon flame spread data from the literature.***

Empirical data for flame spread over alcohol pools consists of small-scale test data with White et al.[25] performing the largest experiments utilizing a 20-cm-wide pan. White et al.[25] evaluated 1-pentanol as part of their study. Results from these 1-pentanol flame spread tests are illustrated in Figure 2-15.16. These tests were performed to assess the effect of fuel type on flame spread for an alcohol fuel that had a similar flash point to the jet fuels primarily under study in this specific piece of work. Pentanol was chosen, in part, due to the previous pentanol flame spread work performed by Burgoyne and Roberts.[7]

Liquid-controlled flows were observed at temperatures <52°C. The change from liquid-controlled flame spread to gas phase flame spread occurred at ~4°C above the closed-cup flash point. Figure 2-15.16 illustrates a comparison of the 1-pentanol results from White et al.[20] with the alcohol data from Burgoyne and Roberts.[2] The 1-pentanol results take on the same characteristic dependence on *DT*, with the Burgoyne and Roberts data showing rapid rise in the flame spread rate at somewhat lower

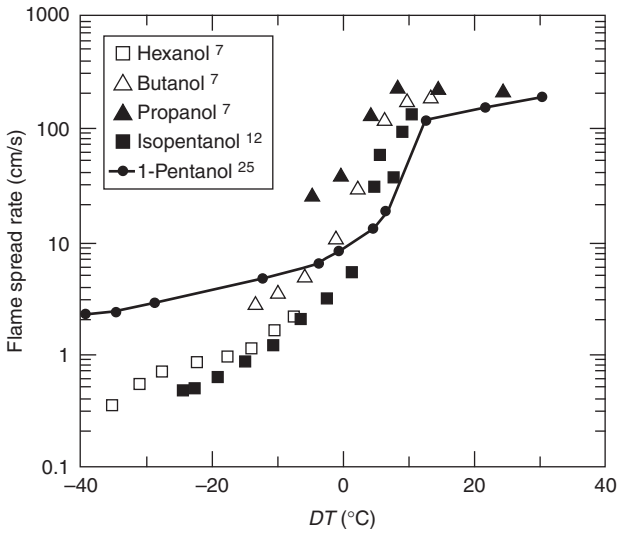

Figure 2-15.16. ***Comparison of the 1-pentanol data with the alcohol data of Burgoyne and Roberts.[7]***

values of DT than the 1-pentanol data. The slope difference between the Burgoyne and Roberts data and the 1-pentanol data for the liquid-controlled flame spread regime can be attributed to the effect of pan width on the temperature dependence of flame spread rate in this regime. It is very interesting to note that the data reflected in Figure 2-15.16 for alcohol flame spread are similar to the hydrocarbon data with respect to the maximum liquid-controlled flame spread rates on the order of 10 cm/s while the gas phase flame spread rates fall between 150 and 200 cm/s.

Table 2-15.2, reproduced from White et al. shows the closed-cup flash point, T_{fl}, the transition from liquid to gas phase–controlled burning, T_{go}, and the transition from gas phase control to asymptotic gas phase spread, T_{gm}, for the small-scale jet fuel data, the 1-pentanol data, and the decane data from Hillstrom.[13] The difference $T_{go} - T_{fl}$ averages 15°C for the hydrocarbon fuels. The difference $T_{gm} - T_{go}$ averages 6°C and the overall difference $T_{gm} - T_{fl}$ averages 21°C. These results may be expected to represent general properties for small hydrocarbon pools, but should not be used for alcohol fuels.

Glassman and Dryer[14] have pointed out some discrepancies in the measurement of flash points and fire-points of alcohols versus hydrocarbons, and the relevance of flash points with regard to the hazards of liquid fuels. While each of the standard flash point/fire point testing methods has its own difficulties, it is clear from the work of Glassman and Dryer that none of the standard flash point testing methods correlate with the onset of gas phase flame spread for all fuels. Glassman and Dryer point out major differences between alcohol and hydrocarbon flash points and point to the large quenching diameter for these two classes of fuels. Based on Glassman and Dryer's observations, transition to gas phase flame spread would be expected at temperatures near the closed-cup flash point for alcohol fuels, as observed for the 1-pentanol test results.

However, there are differences in $T_{go} - T_{fl}$ between jet fuels and decane. The more volatile aviation fuels are characterized by $T_{go} - T_{fl} \sim 18$°C while decane and JP-5 are characterized by $T_{go} - T_{fl} \sim 12$°C. This 6°C difference may be due to the loss of light ends from the more volatile hydrocarbon mixtures. This difference is consistent with the variations in the flame spread rate with ignition time delay represented in Figure 2-15.12. White et al. point out that it appears that the actual flash point of the JP-8 may have increased by ~6°C during the discharge and ignition delay period. While this deduction seems reasonable, a more systematic study of this issue is warranted. The important consideration for hazard analyses is that multicomponent hydrocarbon fuels can incur a reduction in effective flash point depending on the volatility of the fuel and the time period between the fuel release and ignition. The conservative approach would be to assume instantaneous ignition of the released fuel.

Fuel-soaked beds of porous media (e.g., small beads of glass or metal) have been used in flame spread experiments to simulate a fuel spill onto a porous surface. Flame spread over porous media generally has flame spread rates on the order of 1 to 8 cm/min, which are of similar magnitude to those measured for flame spread over the surface of relatively thick solids. Takeno and Hirano[36] have experimentally evaluated several parameters important to characterizing the flame spread rate over porous media soaked with fuel. Figure 2-15.17 represents the results from their study. Table 2-15.3 identifies the conditions of each experiment portrayed in Figure 2-15.17.

These tests used a steel tray 3.5 cm wide and 60 cm long that was filled with either glass or lead beads. Four observations can be made from this data: (1) the flame

Table 2-15.2 ***Critical Temperatures (°C) for Flame Spread***

Fuel	T_{fl}	T_{go}	$(T_{go} - T_{fl})$	T_{gm}	$(T_{gm} - T_{go})$	$(T_{gm} - T_{fl})$
JP-8	39	57	18	62	5	23
25/75 JP-8/5	42	60	18	66	6	24
50/50 JP-8/5	48	65	17	72	7	24
75/25 JP-8/5	54	68	14	74	6	20
JP-5	63	76	13	79	3	16
Decane[8]	44	56	12	62	6	18
Average 1–6	—	—	15	—	6	21
1-Pentanol	48	52	4	62	10	14

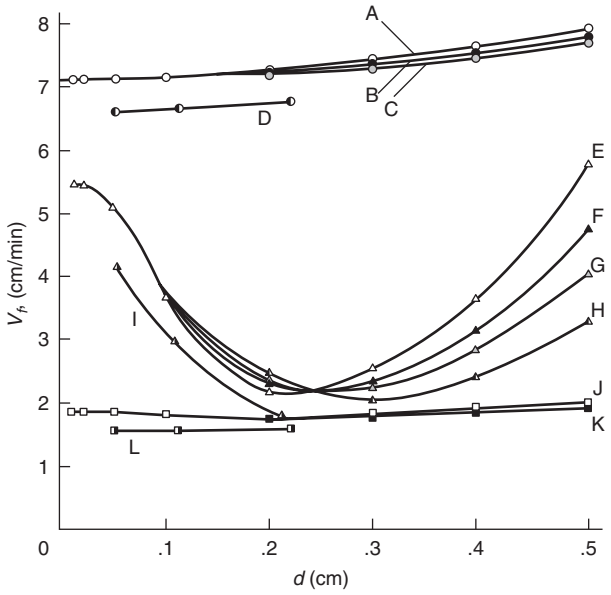

Figure 2-15.17. ***Variations of flame spread rate with bead diameter.[29] Table 2-15.3 lists conditions.[62]***

spread velocity increases slightly as the diameter of the beads, d, increases and there appears to be little dependence on the liquid viscocity (see Figure 2-15.17, conditions A, B, C) for 90 percent by volume of decane and 10 percent hexane; (2) the flame spread for pure decane is a function of the bead diameter and the viscosity (conditions E, F, G, H) where the flame spread velocity decreases with the increase of d for smaller values of d, a minimum flame spread rate occurs at approximately $d = 0.25$ cm, from this point the flame spread velocity increases with d and fuel viscosity effects are more pronounced with flame spread rate decreasing as the viscosity of the fuel increases; (3) for situations where the liquid level is below the top surface of the bead bed (conditions J, K), flame spread velocities are reduced and depend little on bead diameter or fuel viscosity; (4) when the glass beads are replaced with lead beads (conditions D, I, L), similar variations are observed as with the glass beads; however, the flame spread rates are reduced by approximately 10 percent. In general, the flame spread rates for pure decane ranged from 2 to 6 cm/min while the mixtures of 90 percent decane/10 percent hexane spanned 7 to 8 cm/min.

Ishida[37] has also investigated fire growth on fuel-soaked ground with a rectangular pan using central ignition. The shallow square steel tray measured 50 cm × 50 cm × 2 cm deep. The tray was filled with glass beads. Radial flame spread rates were measured for decane fuel over varying bead diameters. Figure 2-15.18 reproduces Ishida's results. Figure 2-15.18 demonstrates that the average flame spread velocity decreases as the bead diameter increases. It is also interesting to note that the flame spread rate accelerates as the fire size increases. The average flame spread rate over the duration from a 2-cm flame diameter to a 30-cm diameter ranges from 6 to 10 cm/min for the bead diameters investigated.

Using Flame Spread Velocities to Characterize the Rate of Involvement of a Pool or Spill

Characterizing the fire growth rate history of a fuel release fire is dependent on describing the time-dependent history of the area involved with fire. The flame spread rate must be placed in context of the fuel release geometry as well as the location of the ignition point. Thus, the geometry of the released fuel and the relative location of the ignition source define the framework for characterizing the area of involvement.

An example for a circular pool of fuel follows. A circular pool with the ignition source in the center yields the most rapid involvement of the entire fuel release. Assuming that uniform spread occurs, a circular fire will develop and the area of the pool involved will be a function of the fire radius:

$$A_{\text{fire}} = \pi r^2 \tag{5}$$

Table 2-15.3 ***Experimental Conditions of Fuel-Soaked Beds Presented in Figure 2-15.17***

	Combustible Liquid	Viscosity μ (cp)	Material of Beads	Initial Liquid Level y_s (cm)	Symbol
A	90% decane + 10% hexane	0.846 (normal)	Glass	0.0	○
B	90% decane + 10% hexane	2.617	Glass	0.0	●
C	90% decane + 10% hexane	4.552	Glass	0.0	●
D	90% decane + 10% hexane	0.846	Lead	0.0	◑
E	Pure decane	0.846	Glass	0.0	△
F	Pure decane	2.617	Glass	0.0	▲
G	Pure decane	4.552	Glass	0.0	▲
H	Pure decane	6.872	Glass	0.0	▲
I	Pure decane	0.846	Lead	0.0	▲
J	Pure decane	0.846	Glass	–0.5	□
K	Pure decane	4.552	Glass	–0.5	■
L	Pure decane	0.846	Lead	–0.5	◨

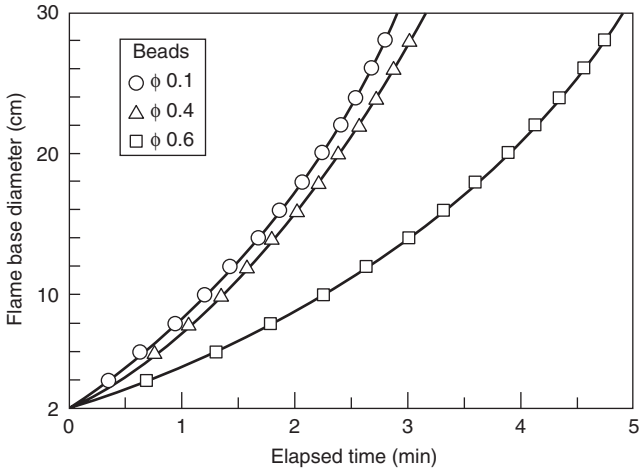

Figure 2-15.18. ***Diameter of flame pillar base as a function of eclipsed time.[37]***

where A_{fire} is the area of the fire in m^2 and r is the radius of the fire in m at any given time, t (s). Assuming a constant flame spread velocity, the radius of the burning area can be defined as

$$r = vt \tag{6}$$

where v is the flame spread velocity in m/s. Substituting Equation 6 into Equation 5:

$$A = \pi v^2 t^2 \tag{7}$$

In this manner, Equation 7 can be used to identify the area of the spill involved at any time subsequent to the ignition. Assuming that the mass burning rate per unit area is at a constant value ($\dot{m}'' = \dot{m}''_{max}$) and does not change as a function of time, a t^2 fire develops. Of course the time limit is defined when the fire involves the maximum area of the spill and this limit can be defined as follows:

$$t_{A,max} = \frac{r_{A,max}}{v} \tag{8}$$

where $t_{A,max}$ is the time the entire pool surface becomes involved with fire, and $r_{A,max}$ is the maximum radius of the fuel release.

A similar approach can be applied to a rectangular trench. Assuming an ignition source at one end of the trench, an alternative example can be developed. For the trench geometry the area is defined as

$$A = wl \tag{9}$$

where w is the width of the trench in m and l is the length of the trench involved with fire in m. Assuming w is small compared to l and that the ignition source at one end of the trench spans the width of the trench, and that the flame spread rate is constant, the length of trench involved is

$$l = vt \tag{10}$$

Substituting Equation 10 into Equation 9 yields the time-dependent area of the trench involved:

$$A = wvt \tag{11}$$

In this manner, Equation 11 can be used to identify the area of the trench involved at any time subsequent to the ignition at one end. Assuming that the mass burning rate per unit area is at a constant value ($\dot{m}'' = \dot{m}''_{max}$) and does not change as a function of time, a t^1 fire develops. Of course the time limit is defined when the fire involves the maximum area of the trench and this limit can be defined as follows:

$$t_{A,max} = \frac{l_{max}}{v} \tag{12}$$

where l_{max} is the maximum length of the trench.

This type of approach can be used for other fuel release configurations and ignition source locations. The heat release rate is then the area of the fuel release involved multiplied by the burning rate per unit area as well as the heat of combustion. This relationship is explained in more detail in the following section.

Fire Size

The fire size is primarily characterized by the heat release rate and the flame height. The heat release rate, $\dot{Q}$, is calculated as

$$\dot{Q} = \dot{m} \cdot \Delta h_c \tag{13}$$

where $\dot{m}$ is the mass burning rate of the fuel and Δh_c is the fuel heat of combustion. The fuel mass burning rate can be calculated via Equation 14 or 15 as follows:

$$\dot{m} = A \cdot \dot{m}'' \tag{14}$$

where A is the spill fire area and $\dot{m}''$ is the mass burning rate per unit area (kg/m^{2}s),

$$\dot{m} = A \cdot \dot{y} \cdot \rho \tag{15}$$

where $\dot{y}$ is the fuel burning regression rate (m/s) and ρ is the density of the fuel. The regression rate is the rate at which the fuel surface descends in a vertical direction as it burns; values are often reported in units of mm/min and therefore must be converted to m/s for the above calculations. Both, $\dot{m}''$ and $\dot{y}$ are empirically based values that are related per Equation 16:

$$\dot{m}'' = \dot{y} \cdot \rho \tag{16}$$

Data in the literature has been presented for both parameters and both are presented below. The most commonly referenced data was developed by Blinov and Khudiakov[38] for pool fires and presented by Hottel[39] as shown in Figure 2-15.19. Figure 2-15.19 shows the regression rate and flame height results for various fuels burning in a broad range of pan sizes, 0.004 to 23 m in diameter. The data indicates that the fuel regression rate is approxi-

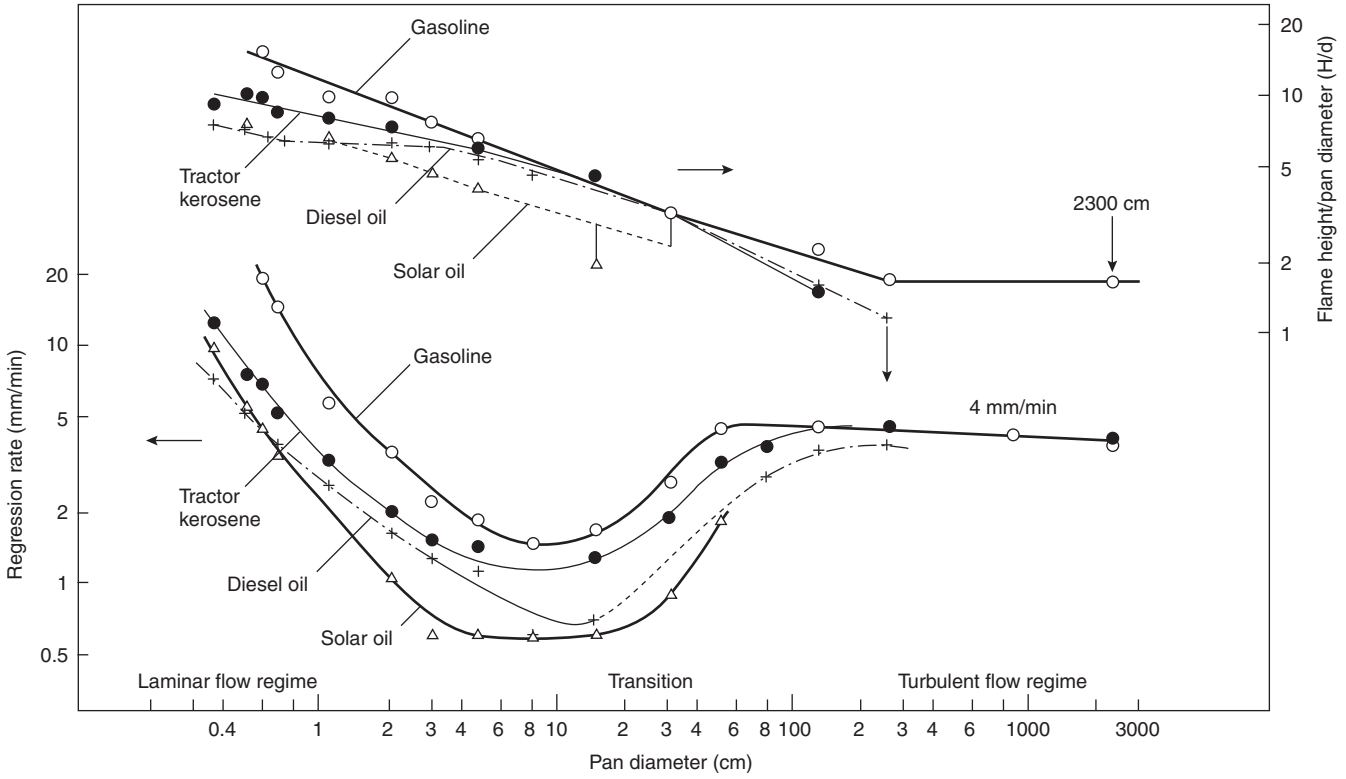

Figure 2-15.19. ***Regression rate and flame height data for liquid pools from Blinov and Khudiakov.[38]***

mately constant at 4 mm/min for all fuels tested burning as confined pool fires with diameters greater than 1 m. For smaller diameter fires, there is considerable difference in regression rates for the fuels presented. Hottel[39] discusses the trends in the burning rate data based on the balance of heat transfer to the fuel.

For fire sizes greater than about 1 m in diameter, the dominant mode of heat transfer to the liquid is via radiation from the plume. For smaller sizes, heat conduction from the pan (walls) or the substrate and convective heat transfer will constitute a larger fraction of the heat transferred to the liquid, thus having a larger effect on the burning rate of the fuel. Hottel,[39] Burgess, Strasser, and Grumer,[40] and Burgess, Grumer, and Wolfhard[41] present detailed discussions on these heat-transfer effects. At larger diameters (typically 1 to 2 m), the burning fuel regression rate tends to level out at a constant maximum value, $\dot{y}_{\max}$. For these pools in the radiation dominant region, Burgess et al.[40] with the U.S. Bureau of Mines accurately correlated the maximum regression rates of various single-component, burning fuels (pan fires) based on the thermochemistry of the liquids as follows:

$$\dot{y}_{\max} = 1.27 \times 10^{-6} \frac{\Delta h_c}{\Delta h_{v,\text{sen}}} \text{ (m/s)} \tag{17}$$

where Δh_c is the heat of combustion and $\Delta h_{v,\text{sen}}$ is the sensible heat of vaporization, calculated as

$$\Delta h_{v,\text{sen}} = \Delta h_v + \int_{T_o}^{T_b} C_p \, dt \tag{18}$$

where

Δh_v = heat of vaporization at the boiling point, T_b
C_p = specific heat of the liquid fuel
T_o = initial temperature of the liquid

The use of the sensible heat of vaporization accounts for the temperature dependence of the regression rate, which will vary appreciably (up to tens of percent) from the value calculated using only Δh_v. As the correlation expressed by Equation 17 suggests, the fuel regression rate is not constant for all fuels at larger diameters as indicated for the limited fuels in Figure 2-15.19. Based on a broad range of hydrocarbon pan fires, Zabetakis and Burgess[42] fit Equation 17 to the data shown in Figure 2-15.20. The fit is quite good except for the cryogenic fuels, liquefied natural gas and liquefied propane gas. It is noted that the data applies to single-component fuel fires burning in unvitiated air under calm conditions (e.g., no wind).

Further work by the Bureau of Mines researchers, Grumer et al.,[43] suggested that the regression rate for blended fuels can be represented by the same correlation (Equation 17) when the heats of combustion and vaporization are presented as shown in Equation 19 for each component of the fuel.

$$\dot{y}_{\max} = 1.27 \times 10^{-6} \left[\frac{\sum_{i=1}^{N} n_i \Delta h_{c_i}}{\sum_{i=1}^{N} n_i \Delta h_{vi} + \sum_{i=1}^{N} m_i \int_{T_o}^{T_b} C_p(T) dt} \right] \tag{19}$$

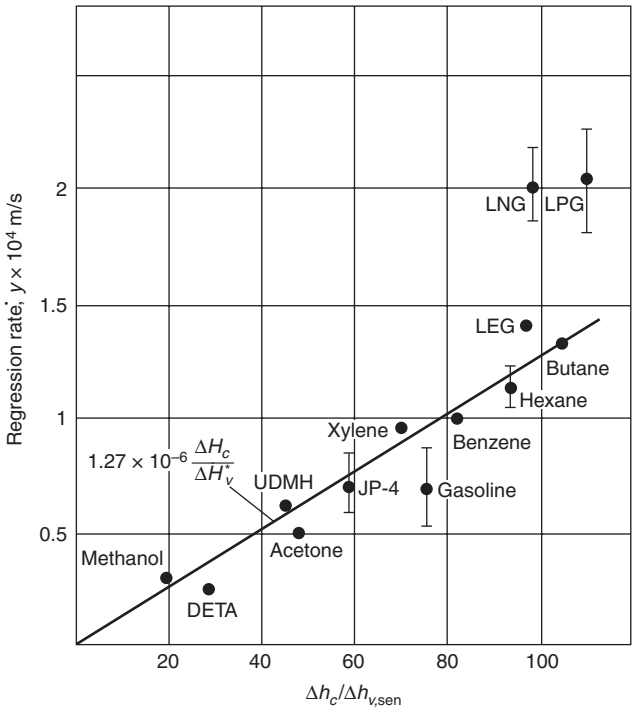

Figure 2-15.20. ***Burning fuel regression rate plotted versus thermochemical properties of fuels burning as pan fires (taken from Mudan[56]).***

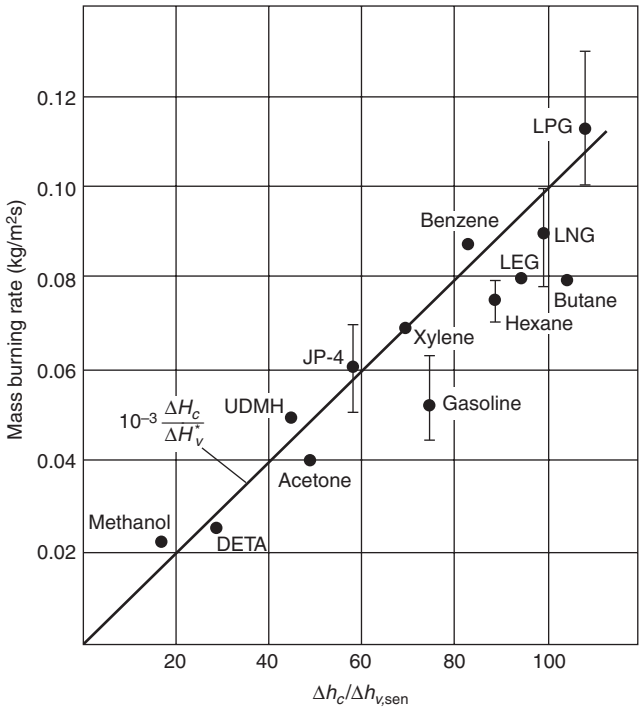

Figure 2-15.21. ***Mass burning rate per unit area versus the thermochemical property of fuels burning as pan fires (taken from Mudan[56]).***

where n_i and m_i are the mole fraction composition in the vapor and liquid phases, respectively.

A blended fuel with components of widely varying volatility will not burn at a uniform rate. Initially, the high volatile components will burn, and as time proceeds the burning will become more characteristic of the remaining lower volatile components. For blends, such as gasoline, that have components with similar heats of combustion and heats of vaporization and $n_i \approx m_i$, Equation 19 can be represented by

$$\dot{y}_{\max} = n_1\dot{y}_1 + n_2\dot{y}_2 + \cdots \tag{20}$$

Equation 20 has been reported to yield good estimates of the regression rate for multicomponent fuel blends.[43] Even for blends with widely varying boiling points, Equation 20 provides rough estimates except for the initial and final stages of the fire.

Converting the regression rate data of Figure 2-15.20 via Equation 16 allows the corresponding maximum mass burning rate per unit area, $\dot{m}''_{\max}$, to be plotted against the ratio of the heat of combustion to the heat of vaporization (see Figure 2-15.21). The fit to the data is represented by

$$\dot{m}''_{\max} = 1 \times 10^{-3} \frac{\Delta h_c}{\Delta h_{v,\text{sen}}} = \text{kg/m}^2\text{s} \tag{21}$$

The fit of Equation 21 to the burning rate data is not as good as Equation 17 to the regression rate data. However, Equation 21 does cover a wider range of fuels, including the liquefied gases.

The regression rate is particularly useful for confined pool fires of significant depth. For many spills, particularly continuously flowing fuels, the more useful quantity is the mass burning rate per unit area. As noted in the previous discussion, the burning rate of pool fires with diameters greater than 0.2 m (see Figure 2-15.19) increases with increasing diameter. Zabetakis and Burgess (1961) developed the following relationship to represent the burning rate per unit area as a function of pool diameter, D:

$$\dot{m}'' = \dot{m}''_{\max}[1 - \exp(-k\beta D)] \tag{22}$$

where the product kβ is represented as a single value. k is the extinction coefficient (m^{-1}) and β is the mean-beam-length correction. The maximum burning rate per unit area, $\dot{m}''_{\max}$, is also referred to in the literature by Babrauskas[44] as $\dot{m}''_{\infty}$, the mass burning rate for an infinite-diameter pool. If a confined pool is not circular, D is equal to the effective diameter, expressed as

$$D = \left(\frac{4A}{\pi}\right)^{1/2} \tag{23}$$

where A is the area of the pool.

Other than the data presented in Figure 2-15.21, the most comprehensive collection of burning rate data has been compiled by Babrauskas[44] and is presented in Table 3-1.13 in Section 3, Chapter 1. The correlation pre-

sented by Equation 22 agrees extremely well with the experimental data of some fuels, such as gasoline. The greatest disagreement occurs for alcohol fuels for which Babrauskas proposes a set of constant values for different diameter ranges (see *SFPE Handbook,* Section 3, Chapter 1[45]). Due to difficulties in experimentally evaluating the cryogenic fuels, there tends to be more scatter in the data, and thus not as good of a correlation with Equation 22 as seen for other hydrocarbon fuels.

The use of Equation 22 applies to confined pool fires burning in the open, under still-air conditions and in a vessel (e.g., pan or tank) without an excessive lip height.[44] The burning rate correlations presented have been developed from confined pool fire experiments. There is very limited data available for burning rates of unconfined fuel spill fires. Gottuk et al.[46] conducted a series of JP-8 and JP-5 fuel spill fires on a smooth polyurethane-coated concrete slab, as used in Navy aircraft hangars. The spill fires consisted of both continuously flowing fuel releases (~0.4, 0.8, and 1.7 lpm) and 1 to 3 l of fixed quantities of fuel that were poured onto the concrete, allowed to spread to nearly a maximum size, and then ignited at the edge of the spill.

The burning rate per unit area data for the unconfined spill fires are presented in Figures 2-15.22 and 2-15.23 for both JP-8 and JP-5, respectively. Figures 2-15.22 and 2-15.23 show the experimentally measured $\dot{m}''$ for each test versus the measured diameter of the spill fires. Also included for comparison are the curves for burning rate for pool fires as calculated per Equation 22, using the data of Table 3-1.13. A curve for JP-8 does not appear in Figure 2-15.22, due to a lack of experimental pool fire data. However, it is expected, based on fuel property data, that the burning rate curve for JP-8 is bounded by the curves for JP-4 and JP-5.

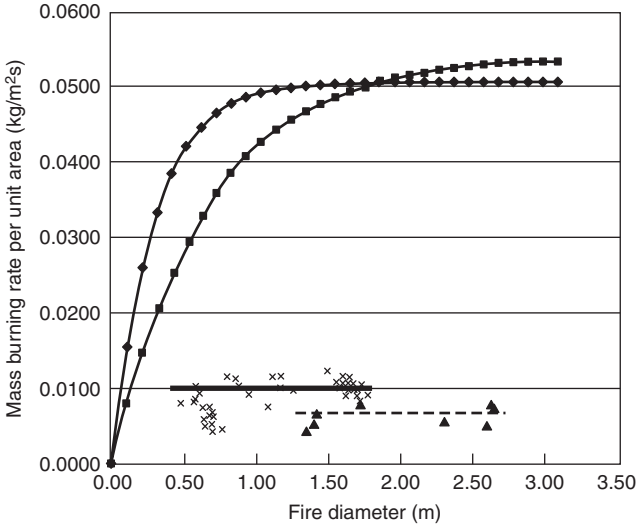

Figure 2-15.22. ***Mass burning rates for unconfined JP-8 spill fires on concrete[46]: (x) denote 0.4- to 1.7-lpm, continuous spill fires with an average value (——) for diameters >1.5 m; (▲) denote 1- to 3-l fixed-quantity spills with an average value (---) for diameters >1.5 m; the calculated pool fire burning rates per Equation 22 are shown for JP-4 (--◆--) and JP-5 (--■--).***

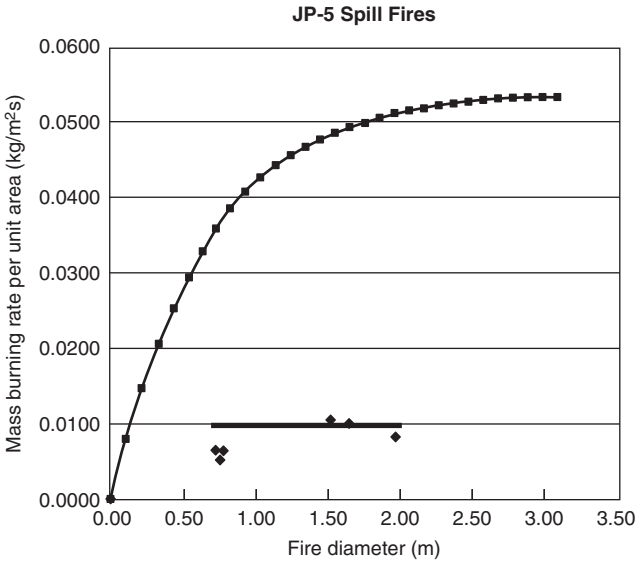

Figure 2-15.23. ***Mass burning rates for 0.4- to 1.7-lpm, unconfined JP-5 spill fires on concrete (◆).[46] The average value for diameters >1.5 m is shown as (——); the calculated pool fire burning rate per Equation 22 is shown as (—■—).***

The comparison between the spill fire data and the calculated pool fire $\dot{m}''$ values shows that the unconfined spill fire burning rates are remarkably lower than those for pool fires with the same diameter. For diameters greater than about 1 m, the burning rates for unconfined spill fires are approximately one-fifth of the maximum burning rates of confined pool fires. The results of the spill tests are summarized in Table 2-15.4. The lower burning rate is attributed to greater heat losses from the fuel to the concrete substrate in the spill fires than in the deeper pool fires, which have typically been conducted in pans. The spill fires had fuel depths on the order of 1 mm whereas most pan fire tests have been conducted with fuel depths of 1 to several centimeters. Since concrete has a higher thermal

Table 2-15.4 ***Unconfined Fuel Spill Burning Rates***

Description	Mass Burning Rate per Area (kg/m²s)	Standard Deviation	Reference
JP-8			
1–3-l spills	0.007[a]	0.0014	46
0.4–1.7-lpm spills	0.010[a]	0.0009	46
JP-5			
0.4–1.7-lpm spills	0.010[a]	0.0008	46
Gasoline	0.011	—	49

[a]Represents average for fires with diameters greater than 1.5 m

conductivity (~1.4 W/mK)[47] than a thick fuel layer (~0.11 W/mK),[48] more heat is lost to the substrate, which would otherwise contribute to heating the fuel. In other words, the deep fuel layer of a pool serves as a better insulator to the top fuel surface than does the concrete, resulting in the fuel surface heating up more quickly, and in turn vaporizing and burning at a higher rate.

Figures 2-15.22 and 2-15.23 also show that the spill fire burning rates do not increase significantly over the range of spill sizes evaluated (0.5- to 2.5-m diameter). The data suggest that the use of Equation 22 for the burning rate for spill fires is inappropriate. As illustrated in the figures, it is proposed that the average value for spill diameters greater than 1.5 m be used as the expected burning rate for all diameters.

Putorti et al.[49] provide burning rates for unconfined gasoline spills on wood parquet, vinyl tile, and various carpets. Consistent with the results for the JP-8 and JP-5 spill fire data noted above,[46] the burning rates for gasoline on the nonabsorbing materials were found to be one-fifth that of the maximum rate for pool fires. Therefore, based on the limited, fuel spill fire data, it is suggested that burning rates for unconfined liquid fuel spills be estimated as one-fifth of the maximum pool burning rate. The large difference between pool fire and unconfined spill fire burning rates illustrates the need for more experimental work to characterize accurately spill fire sizes, particularly at larger diameters.

As presented in Equations 13 and 14, the heat release rate of an unconfined spill or confined pool fire can be calculated per Equation 24 once the area of the fire is determined and an appropriate mass burning rate per area is identified.

$$\dot{Q} = \dot{m}'' \cdot A \cdot \Delta h_c \tag{24}$$

However, in the case of an unconfined, continuously flowing spill fire, the area is neither known a priori, nor can it be calculated per any fuel depth correlations as with a fixed quantity spill. As fuel flows from a continuous source, the size of the resulting spill will continue to increase indefinitely until a physical boundary is reached or the fuel is ignited and burns. The transient nature of a continuous spill fire is very dependent on the timing of the fuel ignition and the flame spread rate relative to the fuel flow rate and size of the spill at the time of ignition. For example, if a continuously flowing spill is immediately ignited at the source, the fire size will be equal to the spill size if the flame spread rate is faster than the fuel spill spread rate. However, if the fuel spill spread rate is faster than the flame spread rate, the spill will continue to spread out ahead of the flame front.

As discussed below, a continuously flowing spill fire will reach a steady-state burning size, characterized by the equivalent steady-state diameter, D_{ss}. It is possible for a fuel spill to reach a diameter that is larger than D_{ss} before it is ignited. In this case, the flame will spread across the fuel surface to the larger diameter and then the spill fire will reduce in size until D_{ss} is reached. These examples are only several of multiple scenarios that can occur. Currently, complete and accurate models of burning fuel spills do not exist. In order to estimate the transient nature of a continuous fuel spill fire, the engineer must consider the fuel spill rate, the relative time of ignition, and the steady-state burning spill area.

The steady-state burning spill area, A_{ss}, results due to a balance between the volumetric flow rate of the liquid release, $\dot{V}_L$ (m^3/s), and the volumetric burning rate of the fire as described by

$$\dot{V}_L = A_{ss} \cdot \dot{y} = \frac{\pi D_{ss}^2}{4} \dot{y} \tag{25a}$$

or, alternatively in terms of the mass burning rate as

$$\dot{V}_L = A_{ss} \frac{\dot{m}''}{\rho} = \frac{\pi D_{ss}^2 \dot{m}''}{4\rho} \tag{25b}$$

The steady-state size of the spill can be explicitly solved by rearranging Equations 25a and 25b in terms of D_{ss} (m):

$$D_{ss} = \left(\frac{4\dot{V}_L}{\pi \dot{y}} \right)^{1/2} \tag{26a}$$

$$D_{ss} = \left(\frac{4\dot{V}_L \rho}{\pi \cdot \dot{m}''} \right)^{1/2} \tag{26b}$$

The calculation of the spill size per Equation 26 assumes that all fuel is burned from the spill; that is, there are no other losses of fuel from the spill, such as into a porous substrate. As noted by the examples above, D_{ss} does not necessarily correspond to the maximum fire size, but equals the size of the fire once the burning rate becomes constant and equilibrium conditions are reached.

Empirical correlations can also be used to calculate the equivalent diameter of a continuous spill fire. Mansfield and Linley[50] developed a correlation for the burning spill diameter as a function of fuel flow rate for large release rate fires on concrete. The following correlation was developed for 568- to 2271-lpm (150- to 600-gpm), continuous spill fires of JP-5 ranging in size from 15 to 24 m in diameter:

$$D_{ss} = 134(\dot{V}_L)^{1/2} \tag{27a}$$

$$D_{ss} = 3.5(\dot{V}_L)^{1/2} \tag{27b}$$

where 1 m^3/s = 15,852 gpm.

The tests of Mansfield and Linley[50] were conducted outside with 2.2- to 12.5-m/s (5- to 28-mph) winds and ambient temperatures ranging from 7 to 32°C. Using Equation 25b with the diameter and spill rate data of Mansfield and Linley,[50] the mass burning rate per unit area of the large JP-5 continuous spill fires is calculated to be in the range of 0.055 $kg/m^2 \cdot s$, which agrees with the pool fire burning rate data reported by Babrauskas[45] in Table 3-1.13. The data are contrary to the smaller spill fire data of Gottuk et al.[46] and Putorti.[49] As a conservative approach to estimating the size of continuous spill fires, it is recommended that pool burning rates, as reported in Table 3-1.13, be used for large fuel release rates (~ >10 lpm) and that spill burning rates equal to one-fifth of the pool rates be used for smaller fuel release rates. Until further testing is performed to identify the actual criteria, 10

lpm is suggested since it is slightly larger than the flow rates for which experimental data is available.

As typically conducted in practice, the above discussions have suggested the use of steady-state or peak burning rates for pool fires and for unconfined spill fires. It is also frequently assumed that the peak burning rate occurs throughout the entire duration of the fire. This approach is intended to provide a conservative method for evaluating the largest possible fire given the particular pool or spill. In reality for unconfined spill fires, the peak burning rate will occur over a relatively short period of time. Therefore, a more realistic fire would burn for a longer period of time at a lower, time-averaged heat release rate compared to the assumption that the spill fire burns at the peak burning rate during the entire fire.

Liquid pool fires also demonstrate a similar transient behavior in that although the entire fuel surface may be fully involved, the burning rate per area (or regression rate) will increase over time until the maximum steady-state value is reached.[42] The transient time period may be tens of seconds to minutes, depending on the type of fuel, the fuel depth, and the bounding materials (e.g., building walls or metal tank). During this transient period, the temperature gradient in the fuel is being established. Once the fuel surface reaches the boiling temperature, the burning rate approaches the steady-state value. If a transient analysis of a fire is required, further consideration must be given to the mass burning rate (or regression rate) that is selected. The use of the maximum value may not be appropriate for the entire burning duration.

Other Factors and Limitations

The spill areas and burning rates of liquid spill or pool fires presented in this chapter have been developed from experimental data of fires on level surfaces. In many applications, fuel spills will occur on inclined and/or cluttered surfaces. Under these conditions, fuel spread will ultimately be dependent on the geometry of the surface, which may lead to pooling of the fuel, channeling, and/or larger wetted areas than would occur on a level surface. Fuel flowing on an inclined surface can result in faster and wider spread of fire. No published studies have evaluated the impact of three-dimensional fuel flow on spill fire burning rates.

This chapter has addressed the burning of liquid fuel fires that occur in the open. Fires occurring in enclosures may exhibit different burning rates as a hot upper layer develops and air becomes restricted. The development of a hot upper layer and hot compartment boundaries can lead to increased burning rates. The burning rates presented in this chapter apply to fuels burning in overventilated conditions. If a liquid fuel fire is burning in vitiated conditions, oxygen entrainment to the fire becomes restricted and the radiant feedback from the fire plume to the fuel can be decreased, resulting in lower burning rates.

Babrauskas[44] and Zabetakis and Burgess[42] have reported that burning rates of pool and spill fires both increase and decrease under increased wind speeds. Burgess and Hertzberg[51] reported that wind speeds increased the burning rate for small-diameter fires; however, burning rates never exceeded the maximum burning rate in still air corresponding to larger diameter fires. High wind speeds can cause fuel to spill out of contained areas or cause unconfined spill fires to move in the direction of the wind. At higher wind speeds, flames can also be blown off.

For pool fires in pans or tanks, the lip height can impact the burning rate of the fuel. There is limited data on this topic and experimental results show both an increase and decrease in the burning rate with larger lip heights.[44] Much of the experimental data has been for small pan diameters (<1 m) (e.g., Emmons, 1961[52]).

Flame Height

The flame height of a liquid spill or pool fire can be calculated based on a number of experimental correlations.[53] The following correlation developed by Heskestad[53] has been shown to be quite robust for different fuels over a wide range of pool fire sizes:

$$L_f = 0.23\dot{Q}^{2/5} - 1.02D \tag{28}$$

where

L_f = the 50 percentile intermittent flame height (m)

$\dot{Q}$ = the heat-release rate (kW)

D = the diameter of the fire (m)

The use of Equation 28 to characterize unconfined spill fire heights was evaluated by Gottuk[46] for JP-8 and JP-5 spill fires on concrete. The results of the comparison are shown in Figures 2-15.24 and 2-15.25, which present measured intermittent flame heights (50 percentile) and predicted flame height values plotted versus the spill diameter. For comparison, the predicted flame heights of pool fires are also plotted as a curve in each figure. The predicted pool

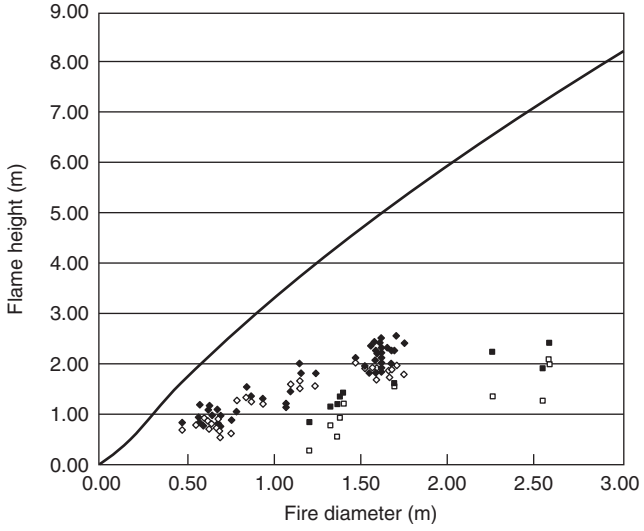

Figure 2-15.24. ***Comparison of measured and predicted flame heights for unconfined JP-8 spill fires[46]: measured (◆) and predicted (◇) 0.4- to 1.7-lpm, continuously flowing spill fires; measured (■) and predicted (□) 1- to 3-l fixed-quantity spill fires; and predicted pool fires (——).***

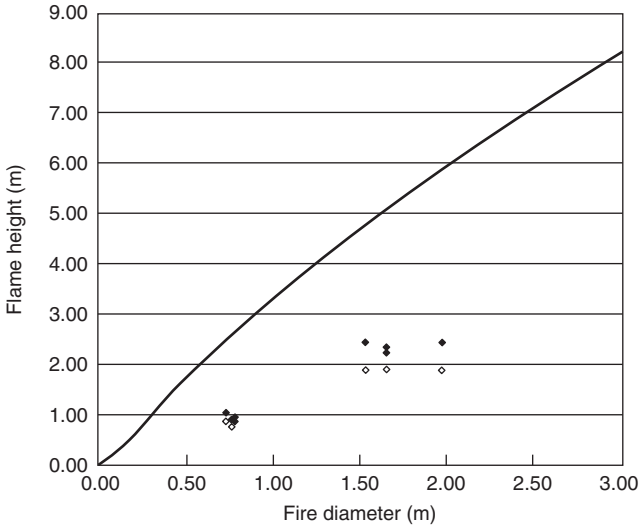

Figure 2-15.25. ***Comparison of measured and predicted flame heights for unconfined JP-5 spill fires[46]: measured (◆) and predicted (◇) 0.4- to 1.7-lpm, continuously flowing spill fires; and predicted pool fires (——).***

fire heights are based on Equation 28 and pool burning rate data of Table 3-1.13. Consistent with the difference in the mass burning rates between spill and pool fires, the spill flame heights are considerably shorter than those for pool fires of the same diameter. Using the Heskestad flame height correlation (Equation 28) with the spill fire data yields predicted heights that are approximately 17 percent low compared to the measured spill fire flame heights. For most engineering applications, the Heskestad flame height correlation (Equation 28) provides satisfactory predictions for both liquid pool and spill fires.

EXAMPLE 1:

A 208-l (55-gal) drum of gasoline is suddenly ruptured during a warehouse accident. The fuel is released quickly across the floor of the warehouse and is ignited when it comes in contact with a piece of faulty equipment. Determine the size of the resulting fire.

SOLUTION:

First the size of the spill is estimated using Equation 4b, assuming that the release occurs instantaneously (i.e., the spill is nearly at its maximum diameter at the time of ignition) and is allowed to spread freely.

$$A_S = (0.36\ \text{m}^2/\text{l})V = (0.36\ \text{m}^2/\text{l})(208\ \text{l}) = 75\ \text{m}^2$$

Per Equation 2, the maximum possible fire size is estimated using a fuel burning area, A, of

$$A = 1.55A_S = 1.55(75\ \text{m}^2) = 116\ \text{m}^2$$

The corresponding diameter of the burning spill is 12.2 m. The heat release rate for the fire is calculated per Equation 24 as

$$\dot{Q} = \dot{m}'' \cdot A \cdot \Delta h_c$$

From Table 3-1.13, the heat of combustion of gasoline is found to be 43.7 MJ/kg, the density is 740 kg/m^3, and the maximum mass burning rate per unit area for a pool of gasoline, $\dot{m}''_{\max}$, is 0.055 kg/m^{2}s. The maximum mass burning rate for the spill fire is estimated to be one-fifth of the maximum pool burning rate, thus yielding 0.011 kg/m^{2}s. The resulting heat release rate is

$$\dot{Q} = (0.011\ \text{kg/m}^2\text{s})(116\ \text{m})(43.7\ \text{MJ/kg}) = 56\ \text{MW}$$

The intermittent flame height is calculated per Equation 28 as

$$L_f = 0.23\dot{Q}^{2/5} - 1.02D$$
$$= 0.23(56{,}000\ \text{kW})^{2/5} - 1.02(12.2\ \text{m}) = 5.8\ \text{m}$$

If it is assumed that the fuel spill burns at the maximum rate for the duration of the fire, the burn time, t_b, for the fuel spill fire will be only 2 min:

$$t_b = \frac{m_f}{\dot{m}''A} = \frac{V \cdot \rho}{\dot{m}''A} = \frac{0.208\ \text{m}^3 \cdot 740\ \text{kg/m}^3}{0.011\ \text{kg/m}^2\text{s} \cdot 116\ \text{m}^2} = 121\ \text{s}$$

As illustrated in Example 2, the predicted burn time of 2 min is most likely too short. In reality, the fire will last longer due to the fact that the flame takes time to spread across the spill.

EXAMPLE 2:

Consider the situation in Example 1. What is the time required for the entire spill to become involved in the fire? The temperature in the warehouse is 20°C.

SOLUTION:

The most critical step in determining the time for the entire spill to become involved in the fire is to identify both the temperature of the liquid fuel spill and the flash point of the fuel. The flash point of gasoline is indicated to be −45°C as documented in Kanury's[54] table in the *SFPE Handbook*, "Selected Ignition, Flammability, and Autoignition Properties of Some Fuels in Air." Assuming that the gasoline is at the same temperature as the warehouse, 20°C, the spill temperature is well above the closed-cup flash point. The elevated temperature indicates that gas phase flame spread will occur if the spill is ignited. A reasonable and generally conservative approximation of the upper, gas phase, flame spread velocity is 200 cm/s.

The problem statement does not specify the location of the ignition source relative to the spill. The most conservative posture would be to assume that the ignition source is in the center of a circular spill. Using Equation 8 for circular spills will define the time for full involvement:

$$t_{A,\max} = \frac{r_{A,\max}}{v}$$

where $r_{A,\max}$ is 6.1 m and v is 2.0 m/s. The time for full involvement becomes

$$t_{A,\max} = \frac{6.1\ \text{m}}{2.0\ \text{m/s}}$$

$$t_{A,\max} = 3\ \text{s}$$

If the ignition source was located at the perimeter of the gasoline spill, it would take approximately 6 s to travel the full 12-m diameter of the pool to involve the spill completely. Irrespective of the ignition location, the time to involve the entire spill is small in the context of most hazard analyses time scales. Therefore, when gas phase flame spread is governing the involvement of a spill or pool of flammable liquid, it is often acceptable to assume instantaneous ignition of the entire fuel surface. This assumption may not be valid for extremely large spills (e.g. tanker spills) or when there are short time-scale concerns.

The difference between gas phase flame spread and liquid-controlled flame spread can be illustrated by assuming that the drum of gasoline in the foregoing example contained diesel fuel. The flash point of diesel fuel ranges from 52–96°C according to NFPA 325.[55] Since the warehouse is at 20°C, substantially below the flash point of diesel fuel, flame spread would be governed by liquid-controlled mechanisms. A conservative upper bound of the liquid-controlled flame spread in this case would be 10 cm/s. Assuming that the area of the diesel spill was identical to the gasoline spill and that there was a strong enough ignition source present to ignite the spill, a time to full ignition of the spill can be estimated. Assuming that the ignition source was in the center of the spill, Equation 8 would be used again, where the maximum radius of the spill is 6.1 m and the flame spread velocity is 0.1 m/s. The time for full involvement becomes

$$t_{A,\max} = \frac{6.1 \text{ m}}{0.1 \text{ m/s}}$$

$$t_{A,\max} = 61 \text{ s}$$

The conservative estimation of the time for full involvement of the diesel fuel is significantly greater than for the gas phase spread over gasoline.

Nomenclature

A	area (m^2)
A_s	area of spill (m^2)
A_{ss}	steady-state area of continuously flowing burning fuel spill (m^2)
C_p	specific heat of liquid fuel
D	diameter (m)
D_{ss}	steady-state area of diameter of burning fuel spill (m)
DT	$T_{fl} - T_l$
Δh_c	heat of combustion (kJ/kg)
$\Delta h_{v,\text{sen}}$	sensible heat of vaporization (kJ/kg)
k	extinction coefficient (m^{-1})
l	length of a trench involved with fire
$l_{\max}$	maximum length of trench (m)
L_f	flame height (m)
$\dot{m}''$	fuel-mass burning rate per unit area (kg/m^2s)
$\dot{m}''_\infty$	fuel-mass burning rate per unit area for infinite size pools (kg/m^2s)
$\dot{m}''_{\max}$	maximum fuel-mass burning rate per unit area (kg/ m^2s)
m_i	mole fraction of fuel in liquid phase
n_i	mole fraction of fuel in vapor phase
$\dot{Q}$	heat release rate (kW)
r	radius of the fire
$r_{A,\max}$	maximum radius of the fire for complete involvement of fuel release
t	time
$t_{A,\max}$	time at which fuel release becomes completely involved
T_b	boiling point temperature of liquid fuel
T_{fl}	closed-cup flash point temperature of fuel
T_{gm}	minimum liquid temperature at which asymptotic gas phase spread occurs
T_{go}	liquid temperature at the transition from liquid to gas phase–controlled burning
T_l	liquid fuel temperature
T_o	initial temperature of liquid fuel
v	flame spread velocity (cm/s)
V	volume (m^3)
$\dot{V}_L$	volumetric flow rate of liquid fuel (m^3/s)
w	width of a trench (m)
$\dot{y}$	regression rate (m/s)
$\dot{y}_{\max}$	maximum regression rate (m/s)

Greek

β	mean-beam-length correction
ρ	density (kg/m^3)
δ	spill depth (m)

References Cited

1. C. Beyler, "Fire Hazard Calculations for Large Open Hydrocarbon Fires," *The SFPE Handbook of Fire Protection Engineering,* NFPA, Quincy, MA, Chapter 3-11 (2002).
2. G.D. Chambers, "Flight Line Extinguisher Evaluation," U.S. Air Force Report DOD-AGFSRS-76-9 (1977).
3. D.T. Gottuk, et al., "Estimating Liquid Fuel Spill Areas," submitted to *Fire Technology* (2001).
4. H.E. Moran, J.C. Burnett, and J.T. Leonard, "Suppression of Fuel Evaporation by Aqueous Filmes of Fluorochemical Surfactant Solutions," *NRL Report 7247,* Naval Research Laboratory, Washington, DC (1971).
5. A.T. Modak, "Ignitability of High-Fire-Point Liquid Spills," *EPRI NP-1731,* Factory Mutual Research Corporation, Norwood, MA (1981).
6. T. Kinbara, *Bull. Inst. Phys. Chem. Res. Japan,* 9, p. 561 (1932).
7. J.H. Burgoyne and A.F. Roberts, "The Spread of Flame across a Liquid Surface, II. Steady-State Conditions," *Proc. Roy. Soc. A,* 308, pp. 55–68 (1968).
8. A.F. Roberts, Ph.D. Thesis, University of London (1959).
9. K. Akita, "Some Problems of Flame Spread along a Liquid Surface," in *14th Symposium (International) on Combustion,* Combustion Institute, Pittsburgh, PA, pp. 1075–1081 (1973).
10. R. Mackinven, J.G. Hansel, and I. Glassman, "Influence of Laboratory Parameters on Flame Spread across Liquid Fuels," *Combustion Science and Technology,* 1, pp. 293–306 (1970).

11. K.E. Torrance, "Subsurface Flows Preceding Flame Spread over a Liquid Fuel," *Combustion Science and Technology,* 3, pp. 133–143 (1971).
12. K.E. Torrance and R.L. Mahajan, "Fire Spread over Liquid Fuels: Liquid Phase Parameters," in *15th Symposium (International) on Combustion,* Combustion Institute, Pittsburgh, PA, pp. 281–287 (1975).
13. W.W. Hillstrom, "Temperature Effects on Flame Spreading over Fuels," *Paper to Eastern Section,* Combustion Institute, Pittsburgh, PA (1975).
14. I. Glassman and F.L. Dryer, "Flame Spreading across Liquid Fuels," *Fire Safety Journal,* 3, pp. 123–128 (1980).
15. A. Nakakuki, "Flame Spread over Solid and Liquid Fuels," *J. Fire & Flammability,* 7, pp. 19–40 (1976).
16. K. Akita and O. Fujiwara, "Pulsating Flame Spread along the Surface of Liquid Fuels," *Combustion and Flame,* 17, pp. 268–269 (1971).
17. H. Ishida, "Flame Spread over Fuel-soaked Ground," *Fire Safety Journal,* 10, pp. 163–171 (1986).
18. H. Ishida, "Flame Spread over Ground Soaked with Highly Volatile Liquid Fuel," *Fire Safety Journal,* 13, pp. 115–123 (1988).
19. W.A. Sirignano and I. Glassman, "Flame Spreading above Liquid Fuels: Surface-Tension-Driven Flows," *Combustion Science and Technology,* 1, pp. 307–312 (1970).
20. T. Hirano, T. Suzuki, I. Mashiko, and N. Tanabe, "Gas Movements in Front of Flames Propagating Across Methanol," *Combustion Science and Technology,* 22, pp. 83–91 (1980).
21. A. Ito, D. Masuda, and K. Saito, "A Study of Flame Spread over Alcohols Using Holographic Interferometry," *Combustion and Flame,* 83, pp. 375–389 (1991).
22. F. Miller and H. Ross, "Further Observations of Flame Spread over Laboratory-Scale Alcohol Pools," *24th Symposium (International) on Combustion,* Combustion Institute, Pittsburgh, PA, pp. 1703–1711 (1992).
23. W.A. Sirignano, "A Critical Discussion of Theories of Flame Spread across Solid and Liquid Fuels," *Combustion Science and Technology,* 6, pp. 95–105 (1972).
24. D.D. Cline and L.N. Koenig, "The Transient Growth of an Unconfined Pool Fire," *Fire Technology,* 19, 3, pp. 149–162 (1983).
25. D. White, C.L. Beyler, C. Fulper, and J. Leonard, "Flame Spread on Aviation Fuels," *Fire Safety Journal,* 28, pp. 1–31 (1997).
26. J.T. Leonard, C.R. Fulper, R. Darwin, G.G. Back, R.E. Burns, and R. Ouelette, "Fire Hazards of Mixed Fuels on the Flight Deck," *Naval Research Laboratory Memorandum Report 6975* (1992).
27. S.A. Hill, J.L. Scheffey, F. Walker, and F.W. Williams, "Tests of Alternative Fire Protection Methods for USAF Hangars," *Naval Research Laboratory Memorandum Report 8337* (1999).
28. H.D. Ross, "Ignition of and Flame Spread Over Laboratory-Scale Pools of Pure Liquid Fuels," *Prog. Energy Combust. Sci.,* 20, pp. 17–63 (1994).
29. I. Glassman and J. Hansel, "Some Thoughts and Experiments on Liquid Fuel Spreading, Steady Burning, and Ignitability in Quiescent Atmospheres," *Fire Research Abstracts and Reviews,* 10, 3, pp. 297–322 (1948).
30. J.P. Burelbach, M. Epstein, and M.G. Plys, "Brief Communication—Initiation of Flame Spreading on Shallow Subflash Fuel Layers," *Combustion and Flame,* 114, 1/2, pp. 280–282 (1998).
31. I. Liebmann, J. Corry, and H.E. Perlee, "Flame Propagation in Layered Methane-Air Systems," *Combustion Science and Technology,* 1, pp. 257–267 (1970).
32. C.C. Feng, S.H. Lam, and I. Glassman, "Flame Propagation through Layered Fuel-Air Mixtures," *Combustion Science and Technology,* 10, pp. 59–71 (1975).
33. H. Phillips, "Flame in a Buoyant Methane Layer," *10th Symposium (International) on Combustion,* Combustion Institute, Pittsburgh, PA, pp. 1277–1283 (1965).
34. Military Specification, "Turbine Fuel, Aviation, Grades JP-4, JP-5, and JP-5/JP-8 ST," *MIL-T-5624N* (1989).
35. Military Specification, "Turbine Fuel, Aviation, Grades JP-8," *MIL-T-83133B,* (1988).
36. K. Takeno and T. Hirano, "Behavior of Combustible Liquid Soaked in Porous Beds during Flame Spread," in *22nd Symposium (International) on Combustion,* Combustion Institute, Pittsburgh, PA, pp. 1223–1230 (1988).
37. H. Ishida, "Initiation of Fire Growth on Fuel-Soaked Ground," *Fire Safety Journal,* 18, pp. 213–230 (1992).
38. V.I. Blinov and G.N. Khudiakov, "Diffusion Burning of Liquids," U.S. Army Translation, *NTIS No. AD296762* (1961).
39. H.C. Hottel, "Certain Laws Governing Diffusive Burning of Liquids," *F. Res. Abs. and Rev.,* 1, p. 41, (1959).
40. D.S. Burgess, A. Strasser, and J. Grumer, "Diffusive Burning of Liquid Fuels in Open Trays," *F. Res. Abs. and Rev.,* 3, p. 177, (1961).
41. D.S. Burgess, J. Grumer, and H.G. Wolfhard, "Burning Rates of Liquid Fuels in Large and Small Open Trays," *Internation Symposium on the Use of Models in Fire Research, Publication 786,* National Academy of Sciences—National Research Council, Washington, DC, pp. 68–75 (1961).
42. M.G. Zabetakis and D.S. Burgess, "Research on Hazards Associated with the Production of and Handling of Liquid Hydrogen," *U.S. Bureau of Mines Report, RI 5705* (1961).
43. J. Grumer, A. Strasser, T.A. Kubala, and D.S. Burgess, "Uncontrolled Diffusive Burning of Some New Liquid Propellants," *Fire Res. Abs. and Rev.,* 3, p. 159 (1961).
44. V. Babrauskas, "Estimating Large Pool Fire Burning Rates," *Fire Tech.,* 19, p. 251 (1983).
45. V. Babrauskas, "Heat Release Rates," *The SFPE Handbook of Fire Protection Engineering,* 3rd edition, NFPA, Quincy, MA (2001).
46. D.T. Gottuk, J. Gott, and F.W. Williams, "Fuel Spill Fire Dynamics," submitted to *Fire Technology* (2001).
47. F.P. Incropera and D.P. DeWitt, *Fundamentals of Heat and Mass Transfer,* 2nd ed., John Wiley and Sons, New York (1985).
48. Coordinating Research Council, *Handbook of Aviation Fuel Properties,* (1983).
49. A.D. Putorti, Jr., J.A. McElroy, and D. Madrzykowski, "Flammable and Combustible Liquid Spill/Burn Patterns," *NIJ Report 604-00,* National Institute of Justice, Washington, DC (2001).
50. J.A. Mansfield and L.J. Linley, "Measurement and Statistical Analysis of Flame Temperatures from Large Fuel Spill Fires," *NWC TP 7061,* Naval Weapons Center, China Lake, CA (1991).
51. D.S. Burgess and M. Hertzberg, "Radiation from Pool Flames," *Heat Transfer in Flames,* Chapter 27, (N.H. Afgan and J.M. Beer, eds) Scripta Book Co., Washington, DC (1974).
52. H.W. Emmons, "Some Observations on Pool Burning," *The Use of Models in Fire Research,* Publication 786 NAS-NRC, Washington, DC, pp. 50–67 (1961).
53. G. Heskestad, "Luminous Heights and Turbulent Diffusion Flames," *Fire Safety Journal,* 5, pp. 103–108 (1983).
54. A.M. Kanury, "Ignition of Liquid Fuels," *SFPE Handbook of Fire Protection Engineering,* NFPA, Quincy, MA (1995).
55. NFPA 325, *Guide to Fire Hazard Properties of Flammable Liquids, Gases, and Volatile Solids,* NFPA, Quincy, MA (1994).
56. K.S. Mudan, "Thermal Radiation Hazards from Hydrocarbon Pool Fires," *Prog. Energy Combust. Sci.,* 10, pp. 59–80 (1984).

Section Three
Hazard Calculations

Section 3 Hazard Calculations

CHAPTER 1

Heat Release Rates

Vytenis Babrauskas

Introduction

Calculations of fire behavior in buildings are not possible unless the heat release rate of the fire is known. This chapter on heat release rates provides both theoretical and empirical information. The chapter is organized so that theory and basic effects are considered first, then a compendium of product data is provided, which is arranged in alphabetic order.

Definitions

The essential characteristic that describes quantitatively "How big is the fire?" is the heat release rate (HRR). This is so important that it has been described as the single most important variable in fire hazard.[1] The heat release rate of a burning item is measured in kilowatts (kW). It is the rate at which the combustion reactions produce heat. The term *burning rate* is also often found. This is a less specific term and it may denote either the HRR or the mass loss rate. The latter is measured in units of $kg \cdot s^{-1}$. It is best to reserve the term *burning rate* for nonquantitative fire descriptions and to use either HRR or mass loss rate, as appropriate. The relationship of these two quantities can be expressed as

$$HRR = \Delta h_c \times MLR \quad (1)$$

where h_c is the effective heat of combustion ($MJ \cdot kg^{-1}$) and MLR is the mass loss rate ($kg \cdot s^{-1}$). Such an equation implies that HRR and MLR are simply related by a constant. This is not in general true. Figure 3-1.1 shows the results obtained from a test on a 17-mm sample of Western red cedar. It is clear that the effective heat of combustion is not a constant; it is roughly 12 $MJ \cdot kg^{-1}$ for the first part of the test, but increases to around 30 $MJ \cdot kg^{-1}$ during the charring period at the end of the test.

In principle, the effective heat of combustion can be determined by theory or by testing. In practice, if the effective heat of combustion is not a constant, then experimental techniques normally involve directly measuring the HRR, rather than using Equation 1.

Measuring the HRR, Full Scale

The simplest case is when full-scale HRR can be directly measured. This can be grouped into two types of techniques: (1) open-burning HRR calorimeters and (2) room fire tests. Open-burning HRR calorimeters were developed in the early 1980s at NIST by Babrauskas and colleagues[2] and at FMRC by Heskestad.[3] The operating principles of these calorimeters are described in Section 3, Chapter 2. Based on this work, a large number of different test standards have been issued. The NORDTEST furniture calorimeter[7] is shown in Figure 3-1.2. Open-burning HRR measurements are simpler to make since a test room does not need to be constructed. The HRR within a room and under open conditions are, clearly, identical at very low HRR. What happens at higher values of HRR depends on the situation at hand. If the fire is so large that room flashover can be reached (about 1.5–1.75 MW if ventilation is through a single normal-sized door opening), then actual room HRR values postflashover can be drastically different from their open-burning rates. This is due primarily to additional radiant heat flux contribution from the hot gas layer and the hot room surfaces, although ventilation effects can also play a role.

For upholstered chairs, extensive studies have shown that room effects are only at the 20 percent level up to a 1-MW fire.[10] The same study, however, showed that for mattresses, a room presence effect shows up at much lower HRR values. For liquid pools, the HRR is extremely

Dr. Vytenis Babrauskas is the president of Fire Science and Technology, Inc., Issaquah, Washington, a company specializing in fire safety research, fire testing issues, and fire science applications to fire investigations and litigations.

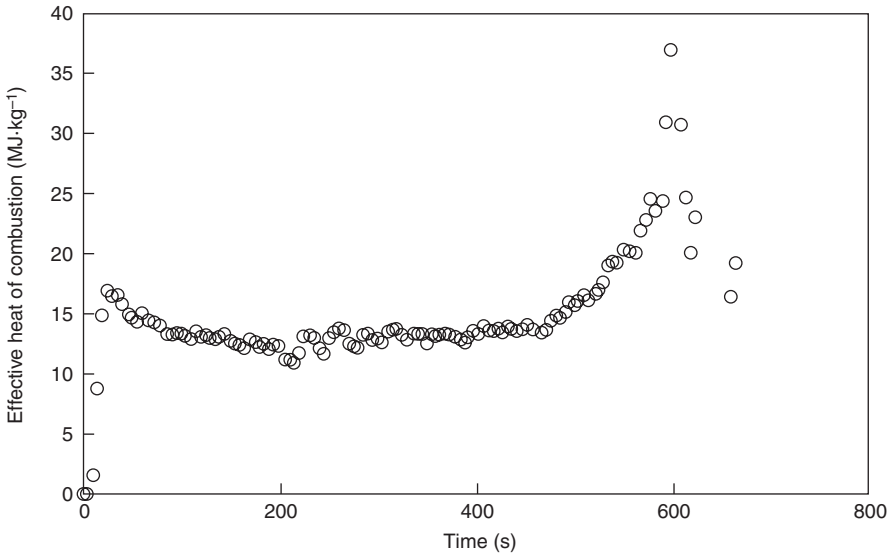

Figure 3-1.1. ***Effective heat of combustion for 17 mm thick Western red cedar, tested at an irradiance of 65 kW·m⁻².***

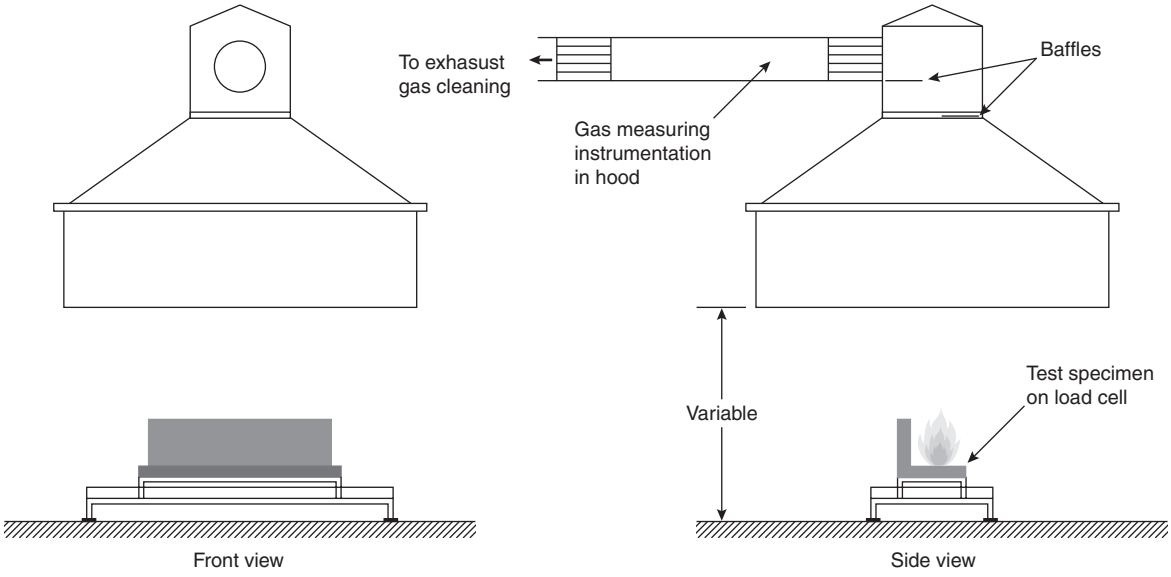

Figure 3-1.2. ***NORDTEST NT FIRE 032 calorimeter.***

strongly affected by the surrounding room.[11] For most other commodities, this issue has not been studied. The degree by which the room affects the HRR is largely determined by how "open" the fuel package itself is. A liquid pool on the floor has a view factor of 0 to itself and 1.0 to the room. By contrast, the reason that chairs tend to be little affected by the room is that the chair "sees" its own surfaces to a significant extent, rather than being fully exposed to the room. Some useful error analyses of large open calorimeter measurements have been reported;[12] a theoretical discussion of the ideal large-scale calorimeter has also been presented.[13]

Room fire tests should be commissioned when room effects are anticipated to be strong, or when a more precise estimate is needed. Apart from cost, there is a drawback to room fire testing. This is because the HRR measured in a room fire cannot be extrapolated to any rooms with larger ventilations. Open-burning HRR data could, by contrast, be applicable to such well-ventilated rooms.

The development of the modern room HRR test took place at several institutions, including Fisher and Williamson at the University of California,[14] Lee at NIST,[15] and Sundström at the Swedish National Testing and Research Institute.[16] Room test standards can be found in NT FIRE 025[17] and ISO 9705[18] and the room test portions of ASTM E1537[4] and ASTM E1590.[5] A typical standard room fire test, ISO 9705 is shown in Figure 3-1.3. This test equipment is available for commercial testing in North America, Europe, and other places also.

Measuring the HRR, Bench Scale

To measure the HRR in a bench-scale test is nowadays an easy task. Most commonly, the cone calorimeter[19] developed at NIST by Babrauskas will be used (Figure 3-1.4). These instruments are available at commercial and research laboratories worldwide. The procedures for conducting cone calorimeter tests are described in ASTM E1354[20] and ISO 5660.[21] (See Section 3, Chapter 3.) Other HRR calorimeters, such as the Ohio State University apparatus or the Factory Mutual Research Corporation Flammability Apparatus are also in use at some laboratories. A textbook is available that discusses many of the details of HRR measuring technology.[22] Thus, the modeler can assume that if at least enough material is available to run several small samples (100 mm × 100 mm, in the case of the cone calorimeter), an empirical HRR curve can be obtained by running bench-scale tests.

Measuring the HRR, Intermediate Scale

The newest experimental technology for determining the HRR is intermediate-scale calorimetry. Various earlier efforts have been made, but the first instrument to receive standards support is the ICAL, developed at Weyerhaeuser[23] (Figure 3-1.5). It has been standardized as ASTM E1623.[24] This test method accommodates 1.0-m by 1.0-m specimens, which allows for complex or highly nonhomogenous constructions to be tested. However, since the data are still not of full scale, some additional analysis is needed to be able to utilize the test data in fire modeling.

Modeling Implications for Using Full-Scale HRR Data

If access is available to full-scale HRR data, then the task of defining the fire is on a solid basis. Even here, however, there are a number of problems and caveats. Apart from the obvious issue that the available full-scale data must be known to describe the specific fuel source in question (and not some possibly very differently performing similar item), there are some additional concerns. Supposing one finds full-scale test results on one's exact commodity, can the data simply be used unquestioningly? The answer, of course, is no. There are two main issues:

1. The available data may be open-burning calorimetry data. One must then determine whether an enclosure effect needs to be accounted for.
2. The available data may be room fire data, but the test enclosure may not correspond to the room for which modeling is to be done.

The first of these issues was briefly touched on previously. The availability of quantitative guidance is not reassuring. For upholstered chair fires in a room of about the size of the ISO 9705 room, one can estimate a 20 percent augmentation over the open-burn rates when considering fires in the 100- to 1000-kW range. For mattresses, the effect is large and without adequate guidance. For liquid pools, a pool submodel must be specifically present in the fire model used, since no simple approximation is adequate. For wood cribs, there are formulas for guidance,[25] although of course wood cribs are hardly a

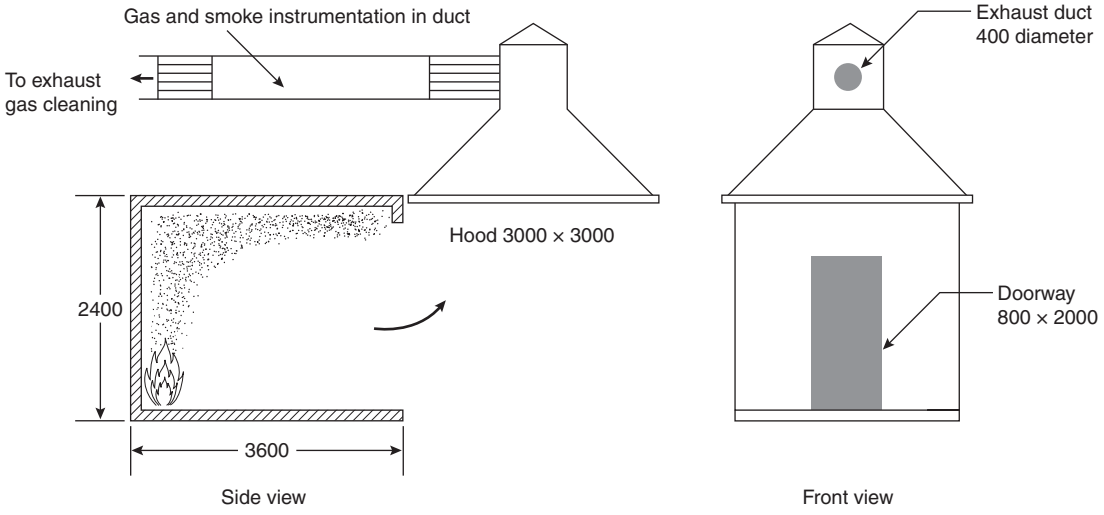

Figure 3-1.3. ***ISO 9705 room HRR test.***

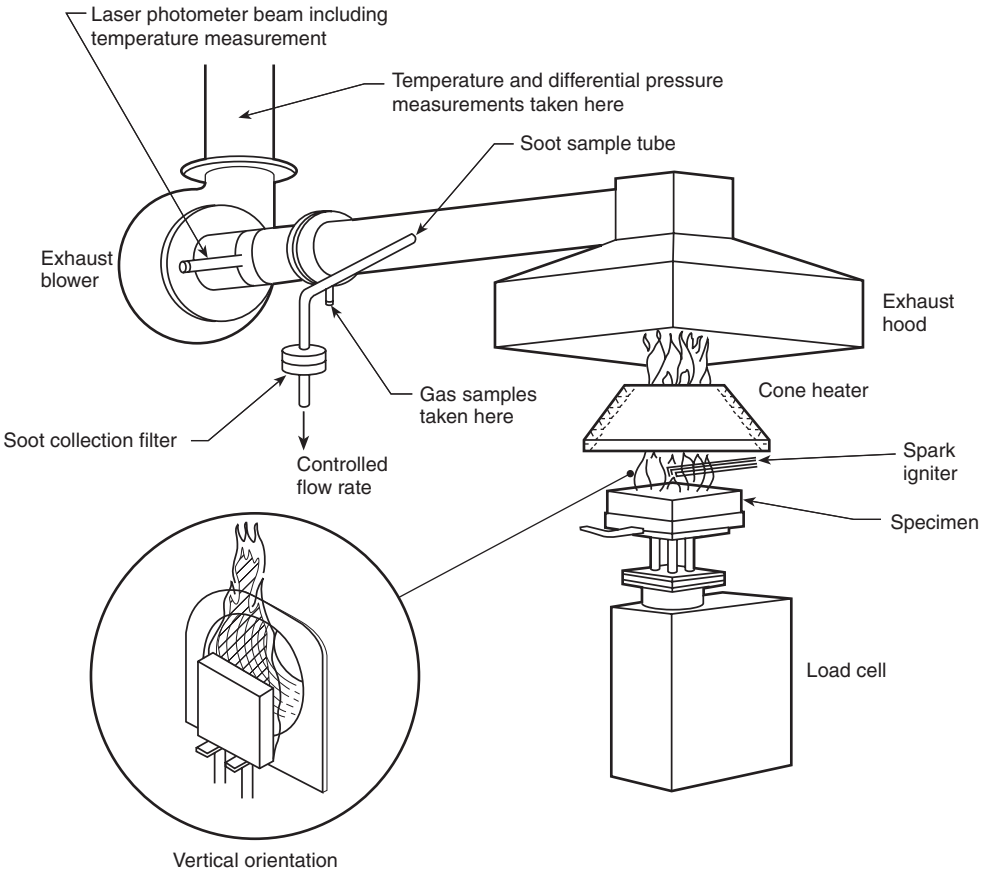

Figure 3-1.4. ***Bench-scale cone calorimeter.***

feature of most real fires. For other combustibles, neither data nor guidance is available.

A very similar problem is faced when the modeler has available full-scale HRR data, but the test was run in a room of different size or ventilation conditions than is the intended application. Only two studies on this topic have been published in the literature. Kokkala and colleagues[26] compared some room wall/ceiling linings in a large room to the values obtained in the ISO 9705 room. Also, during the CBUF project some furniture fires were done in rooms of two scales.[10] Neither of these studies looked at this issue comprehensively enough to yield numerical guidance.

Modeling with Bench-Scale HRR Data

If full-scale data on HRR are available, then these are simply used in the fire model. In many cases, however, such data are not available, often due to cost of testing or unavailability of large-size specimens. In such cases, it is desirable to be able to use bench-scale data, denoted as $\dot{q}''$ and measured in units of $kW \cdot m^{-2}$. With the bench-scale HRR, there are two main questions: (1) can it be predicted from some more fundamental measurements? and (2) how can the full-scale HRR be predicted from the bench-scale HRR?

Predicting Bench-Scale HRR from Fundamental Considerations

The former question has been of considerable interest to fire researchers for a number of years now, but practical engineering methods are not yet in hand. The task of predicting from more fundamental measurements is often described as creating a pyrolysis model because the degradation of a material when it is exposed to heat is known as pyrolysis. When a material heats up, degrades, ignites, and burns, complicated physical and chemical phenomena take place.

In addition to a change of phase, there is often flow of moisture, which must be accounted for simultaneously with heat flow. The material may undergo several different types of phase changes during the decomposition process, each accompanied by changes in density and porosity. Bubbles may be created within the bulk of the material and migrate to the surface. These may be accompanied by molten flow ejection at the surface. Oxygen may or may not directly interact with the surface to create a glowing combustion. Chemical reactions are commonly several in number and occur at different temperature regimes.

Finally, the material may undergo large-scale cracking, buckling, or sloughing. Each of these physical phenomena may significantly affect the rate of specimen

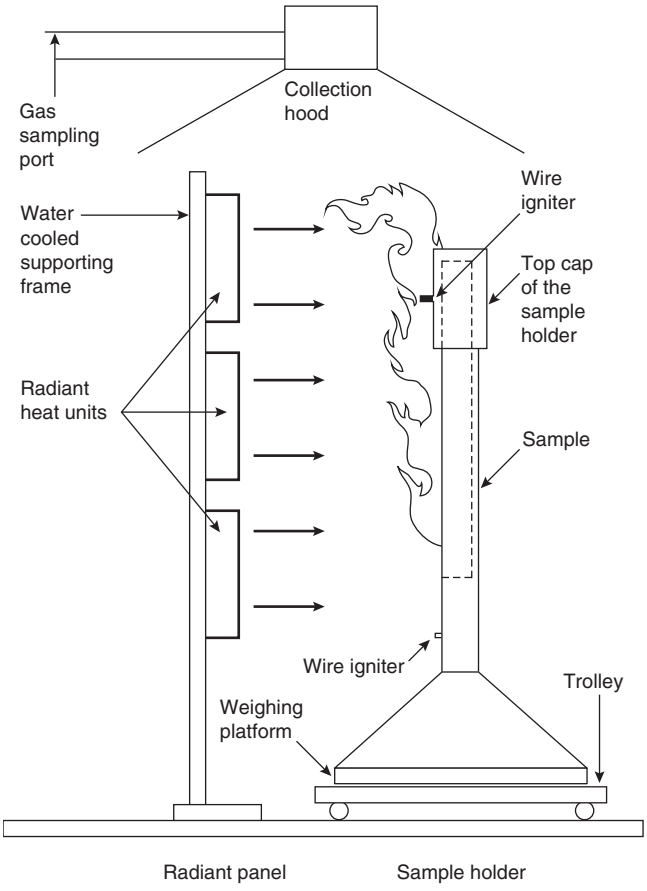

Figure 3-1.5. ***Intermediate scale ICAL calorimeter.***

decomposition. From even this very brief description, it is clear that computing the pyrolysis of a material may be an enormously difficult task. Thus, today, for any fire hazard analysis purposes, HRR is invariably measured, rather than being computed from more fundamental theory.

Readers wishing to look more closely at the type of modeling needed to represent the pyrolysis process can refer to the dissertation of Parker[27] as a good example of how charring materials need to be treated. Some half-dozen other dissertations have been written on the same topic. Melting-type materials have proved to be even more interesting as a subject of advanced research. Several hundred papers have been published on various aspects of modeling the pyrolysis behavior of just one common material, poly(methylmethacrylate). References 28–34 can provide an introduction to this research.

Predicting Full-Scale HRR from Bench-Scale Data: Overview

Prediction of full-scale HRR is probably the single most important engineering issue for successfully modeling fires. Schematically, we may write that

$$\dot{q} = \int \dot{q}'' dA \tag{2}$$

This representation does not fully reveal the difficulties involved. More explicitly,

$$\dot{q}(t) = \int \dot{q}''(t, x, y, z) dA(t) \tag{3}$$

This makes more clear that the instantaneous per-unit-area HRR is a function of time and also of the location of the burning element. The instantaneous burning area, $A(t)$, is also a function of time. In addition, while we have not written this explicitly, $\dot{q}''(t)$ depends on the heating boundary conditions to the element. This quantity is usually identified as the *heat flux* or *irradiance* incident upon the element. The latter term is commonly used since, in full-scale fires, heating is dominated by the radiant component.

By examining the nature of $dA(t)$, we can also identify the role of flame spread in characterizing the HRR of full-scale fires. A bench-scale HRR test specimen is usually ignited nearly instantaneously over its entire surface. Full-scale fires, by contrast, nearly always exhibit finite spread rates. The flame spread velocity in a full-scale fire can be identified with the movement of the boundaries of the flame-covered area $dA(t)$. Flame spread may be occurring in several directions over walls, ceilings, floors, and over individual surfaces of discrete commodities burning in a space. Consequently, it can be seen that tracking flame spread and $dA(t)$ is a major undertaking. This task, by its nature, is incompatible with zone-type fire models because it presumes that a mechanism is in place to track very small surface elements. Even the publicly available field models have not yet attempted this task, although some work with proprietary models has been started.[35]

Our approach will have to be restricted to identifying some of the attempts that have been made to simplify the problem in order to make it tractable for zone modeling. Simplifications are not yet possible for the general case. Instead, we must examine specific combustibles, for which appropriate flame spread representations have been worked out. This is illustrated in a number of discussions in the following sections. Before we do this, however, it is important to examine in more detail some of the variables that influence the HRR.

Predicting Full-Scale HRR from Bench-Scale Data: The Role of Irradiance

Engineering variables such as HRR, ignitability, flame spread, and so on are sometimes viewed as material fire properties. This is a useful view, but it must be kept in mind that such 'properties' are not solely defined by the physical/chemical nature of the substance. Instead, they are also determined by the boundary conditions of exposure. Boundary conditions can be divided into two types: (1) intended, and (2) unintended. Intended boundary conditions include irradiance (heat fluxes in room fires are dominated by the radiant component, so irradiance and imposed heat flux are used interchangeably) and thickness. Unintended boundary conditions, sometimes known as *apparatus dependencies*, include such factors as edge effects, perturbations due to nonuniform heating, drafts and uncontrolled air velocities, and so

forth. The latter are usually small if a well-designed test apparatus was used for measuring the response of the specimen.

The most significant intended boundary condition is the heat flux imposed on the specimen. This variable is crucial and no reduced-scale HRR results have meaning without knowing the irradiance. A test apparatus can impose a very wide range of specimen irradiances. For example, the cone calorimeter is capable of irradiances from zero to 100 kW·m^{-2}. For the user of the data, the crucial question becomes what irradiance to select when requesting a test. There are no simple answers to this, but we summarize here the main conclusions of Babrauskas.[36]

The major consideration in the selection of the test irradiance must come from a knowledge of heat fluxes associated with real fires. In theory, this could range from zero to an upper value which would be

$$\varepsilon\sigma(T_f^4 - T_o^4)$$

where

ε = emissivity

σ = Stefan-Boltzmann constant (5.67×10^{-11} kW·m^{-2}·K^{-4})

T_f = flame temperature (K)

T_o = ambient temperature (K)

But the emissivity approaches 1 for larger flames, and the ambient temperature contribution is insignificant, since $T_o \ll T_f$. The adiabatic flame temperature for most organic fuels is approximately 2300 K.[37] This would give a maximum irradiance limit of some 1500 kW·m^{-2}. This limiting value is, of course, nearly 10 times the actual maximum that is found in building fires of normal types. Thus, it is evident that the theoretical bounds to possible heat fluxes do not offer any guidance for testing. Instead, it is necessary to look at experimental data of heat fluxes found in actual building fires. We divide this into several types of building fires to be examined.

Heat fluxes in the vicinity of ignition sources: First, we must be clear by what is meant by *ignition source.* The innate definition of the term does not have limits—a burning building can be the ignition source to its neighboring building, as can a fire bomb. For discussion here, however, ignition sources can be limited to those that are small with respect to a fully developed room fire. Since the latter will be in the range of over 1 MW, the range of fires considered to be ignition sources might be taken as less than approximately 300 kW. A NIST study examined various ignition sources, ranging from 5 kW to over 300 kW.[38] The sources included both realistic igniting objects (cigarettes, matches, burning paper lunch bags, etc.) and schematic ones (small gas burners and wood cribs). It was found that, as the power output of the ignition source increased, the peak heat flux generally did not increase. Instead, only the area covered by the peak heat flux progressively increased. For flames ranging from a 0.3-kW Bunsen-type burner to a 50-kW wastebasket, the peak fluxes were remarkably constant at 30–40 kW·m^{-2}. Thus, for HRR from objects being ignited with a small ignition source, a test irradiance of 35 kW·m^{-2} can be selected. There are some unusual sources having a much higher flux, and these are discussed by Babrauskas.[36]

For larger burners, such as used in room fire tests, higher heat fluxes may have to be assumed. For porous square-faced gas burners, the wall heat flux was found to depend on the burner face size.[39] In some cases, fluxes up to 65–80 kW·m^{-2} were noted, although for most cases fluxes of 30–50 kW·m^{-2} are considered appropriate.[40]

At the extreme, ignition can occur due to a high velocity jet, such as from a failure on an oil-drilling rig. There, heat fluxes in the vicinity of 150–300 kW·m^{-2} have been observed.[41] Such situations, however, are very specialized. For ignitions from small wood cribs or other solid-fuel ignition sources, it can be estimated that the heat flux to adjacent objects is in the same 35-kW·m^{-2} range as for small flaming sources. The picture is more complicated, however, for the heat flux from these sources to the object underneath. These heat fluxes may be much higher,[36] but they are highly nonuniform and difficult to model.

Heat fluxes in preflashover room fires: After ignition, the combustibles in a room can be considered to be exposed to preflashover conditions. Heat fluxes occurring in preflashover room fires will vary widely. Away from the initial source of fire there will be essentially no heating at all. Near a small initial fire source, heat fluxes of the sort described in the preceding section will be seen. With increasing fire spread and involvement, a hot gas layer will build up below the ceiling. The heat fluxes will be significantly hotter within this layer than in lower spaces. Söderbom[42] found values typically $<$45 kW·m^{-2} at the center of the ceiling during preflashover fires. The value at the floor level is, of course, always $<$20 kW·m^{-2} prior to flashover, since attaining 20 kW·m^{-2} at floor level is one definition of flashover.[15] Since there is surprisingly little general guidance on this point, the user will have to make some assumptions or ad hoc calculations.

Heat fluxes on burning walls: Heat fluxes from burning items of larger types have, in general, not been studied in enough detail to be systematically known. The notable exception is for upward flame spread on vertical surfaces. For this configuration, a number of studies have explored the heat fluxes from the flame to the yet-unignited portion of the surface. Hasemi studied this problem in detail[43] and provided correlations. For his experiments, peak values of approximately 25 kW·m^{-2} were seen for the region downstream of the ignited area, but before the tip of the flames; beyond the flame tip, fluxes were no longer constant, but dropped off further downstream. Additional similar data have also been presented in a summary form.[44] Work by Kulkarni and coworkers has enlarged the diversity of material types that have been studied.[46] The value of 25 kW·m^{-2} is seen from these more extensive studies to be the lower bound of where data are clustered—most of the data are in the interval from 25 to 45 kW·m^{-2}. Thus, a value of 35 kW·m^{-2} might better capture the mean behavior.

A 35-kW·m^{-2} heat flux, then, can be used to characterize the peak level of heating to a vertical surface ele-

ment from its own upstream flame, just prior to its ignition. This value will need to be increased if the material is so situated as to be in a hot gas layer that is accumulating in the upper reaches of the room. Apart from the data of Söderbom, discussed above, this additional heating has not been studied in detail.

Heat fluxes in postflashover room fires: The maximum temperatures actually seen in postflashover room fires are approximately 1100°C. A perfect black-body radiator at that temperature would produce heat fluxes of approximately 200 kW·m^{-2}. Actual heat fluxes measured in postflashover room fires can come close to this value, but are usually somewhat lower. For instance, examining the extensive room burn data of Fang,[46] one finds the ranges of experimental results shown in Table 3-1.1.

One might reasonably conclude that a heat flux of approximately 150 kW·m^{-2} would be needed to properly represent the environment of the postflashover room fire. Today's bench-scale HRR apparatuses, however, can only go to about 100 kW·m^{-2} or less. Interestingly, the inability realistically to create the heat fluxes of the postflashover fire has not been seen to be a problem in fire testing. Often, the situation is avoided in its entirety by assuming that the maximum burning rate that will occur within the room is consistent with the available oxygen supply.[47] Nonetheless, if for more detailed fire modeling the HRR of individual items in the postflashover fire would be required, such high heat-flux values would be required.

The Dependence of the HRR on the Heat Flux

In the simplest case, the relationship of the HRR to the irradiance is very simple, as shown in Figure 3-1.6. Here, we see that the HRR depends in a linear manner on the irradiance. The curve does not pass through the origin due to the existence of flame flux. The total heat flux seen by the specimen can be viewed as comprised of two components: the external irradiance and the flux from its own flame. Only if the flame flux = 0 will the curve pass through the origin. Otherwise, the x-axis intercept is equal to (minus) the flame flux.

Flame flux is very difficult to measure experimentally, as decomposing materials tend to foul the instrumentation and invalidate the readings. A value of approximately 35 kW·m^{-2} has been reported for the flame flux of PMMA burned in the horizontal orientation in the cone calorimeter.[48] In another study, estimates of flame flux were made for several plastics burned in a similar manner.[49] These showed 30, 25, and 14 kW·m^{-2}, respectively, for nylon, polyethylene, and polypropylene. The furniture research program CBUF[10] determined that the flame fluxes in the cone calorimeter associated with fabric/foam composites are in the range 20–25 kW·m^{-2}.

Finally, some data are available[50] for liquids in containers of similar size as a cone calorimeter specimen holder. Flame fluxes of about 10–15 kW·m^{-2} are seen for alcohols and about 15–20 kW·m^{-2} for some hydrocarbons (heptane, methylmethacrylate, toluene, styrene). The value appears to depend only slightly on the chemical nature of the fuel. Gore et al.[50] specifically determined that this value does not increase with increasing fuel-sooting tendencies. All the above data refer specifically to the horizontal specimen orientation. There is very little data for the vertical orientation, although Janssens deduces that for wood products the vertical orientation flame flux is approximately 10–15 kW·m^{-2}, of which only about 1 kW·m^{-2} is due to radiation.[51]

With regard to linearity, the following very broad generalization can be made: for many products, over a substantial heat flux range, the HRR is linearly proportional to the heat flux. This generalization, however, will be seen to have only limited utility, since it is rarely known a priori whether it will be obeyed. Furthermore, there is a distinct tendency for most materials and products to deviate from linearity at very high and at very low heat fluxes. This behavior is best illustrated by an example. Some data obtained by Sorathia and coworkers[52] on advanced composites are shown in Figure 3-1.7. It is clear that the results are somewhat linear, but not precisely so. Some old, but still suggestive, data were obtained in the 1970s by Parker.[53] His results for a number of fire-retardant grades of polyurethane foam are shown in Figure 3-1.8. Of the five formulations shown, three show somewhat linear behavior, whereas two clearly do not. For most categories of specimens, however, substantially more linear behavior can be seen.

Predicting Full-Scale HRR from Bench-Scale Data: The Effect of Thickness

The same material may be used in different applications of varying thicknesses. Thickness does affect the HRR response. In general, a thin material will show a

Table 3-1.1 ***Heat Fluxes Measured in Postflashover Room Fires***

	Heat flux (kW·m^{-2})		
	Ceiling	Walls	Floor
Maximum	106–176	116–229	119–143
Average	68–147	91–194	—

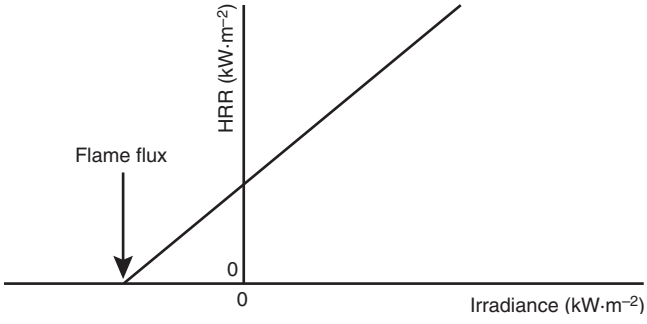

Figure 3-1.6. ***The simplest form of HRR dependence on irradiance.***

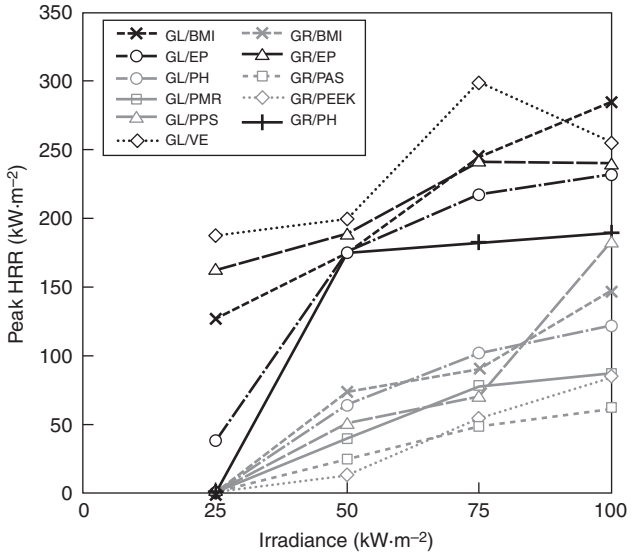

Figure 3-1.7. ***Response to irradiance of some advanced composite materials. Reinforcements: GL = glass, GR = graphite. Resins: BMI = bismaleimide, EP = epoxy, PAS = polyaryl sulfone, PEEK = poly(ether ether ketone), PH = phenolic, PMR = monomer-reactant polyimide, PPS = polyphenylene sulfide, VE = vinyl ester.***

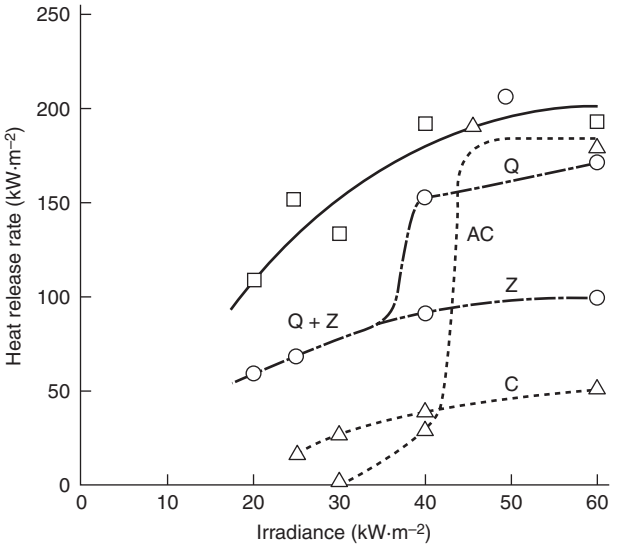

Figure 3-1.8. ***The results for FR polyurethane foams, as measured in the NBS I calorimeter by Parker.***

spike of HRR, whereas a thick product will commonly (but not always) show some quasi-steady period of burning. This variable has surprisingly been little explored and not much guidance is available. Perhaps the best illustrative example is due to Paul;[54] his data for PMMA are shown in Figure 3-1.9. This illustrates that near-steady burning behavior can be seen when the thickness approaches approximately 20 mm. This is true for many solid materials—thicknesses of this range are required in order to approach steady-burning conditions. A compilation of thickness data for polyethylene,[55] for example, shows that even 10-mm-thick specimens have not reached steady burning.

For foams, by contrast, no reasonable amount of thickness will normally show steady-state burning. Of special interest are polystyrene (PS) foams. These are normally very low-density foams of about 16 kg·m^{-3}. When exposed to heat, PS foams tend to collapse their cell struc-

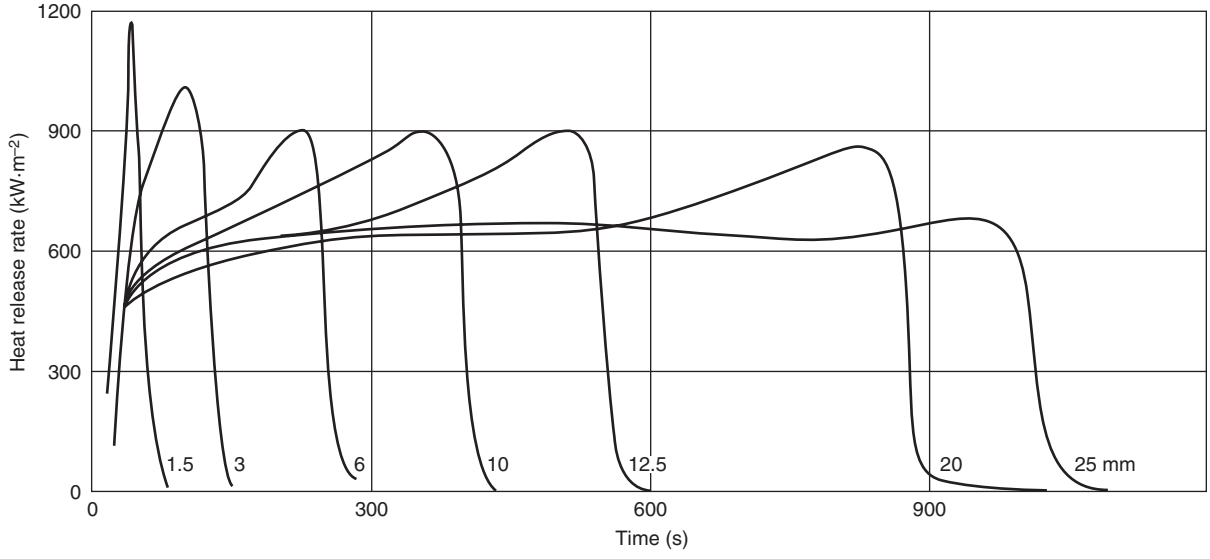

Figure 3-1.9. ***HRR for PMMA of various thicknesses.***

ture and become a thin liquid film. This occurs before ignition takes place. Thus, after ignition, what is burning is a thin coating on whatever was the substrate. This is the reason why the HRR of PS foams tends to be so apparatus dependent that it is hard to discern any intrinsic response of the material at all: its performance is totally dominated by the specimen holder and edge conditions.[56]

Predicting Full-Scale HRR from Bench-Scale Data: The Effect of Orientation

Routine testing in the cone calorimeter is specified by the ASTM standard to be done only in the horizontal orientation. This is because (1) many products show serious testing difficulties (e.g., melting) when tested in the vertical orientation and (2) conversely, the vertical orientation does not provide a better simulation of the burning of vertical objects. This is because there is no direct connection between flame fluxes in a bench-scale test and in a real-scale fire. The actual fluxes occurring in a real-scale fire are determined by many factors, including size of room, thickness of hot gas layer, flame spread occurring over other surfaces, and so forth. None of these are subject to the control of the bench-scale apparatus but, rather, must be specifically modeled.

Orientation effects will also make a difference during the bench-scale testing of specimens. Even though routine testing is done only in the horizontal orientation, a small body of work exists for which both orientations were explored. This is best illustrated by the results of two round robins that were conducted on the cone calorimeter, one under the auspices of ASTM and one under ISO. The data were taken at two irradiances, 25 and 50 $kW \cdot m^{-2}$, and the results are briefly summarized in the Appendix to ASTM E1354.[20] Such results are especially valuable since the values tabulated are the best estimate and are not subject to the specific errors of any one particular laboratory. A comparison for the peak HRR is shown in Figure 3-1.10, while the comparison for the 180-s average value of HRR is given in Figure 3-1.11. In both cases, the data points plotted represent all the data analyzed within the two round robins for which horizontal and vertical orientation results were obtained on a product.

For the peak HRR, a least-square regression gives that

$$\dot{q}_{pk}''(V) = 0.71\dot{q}_{pk}''(H) \tag{4}$$

while for the 180-s average HRR, the corresponding relation is

$$\dot{q}_{180}''(V) = 0.72\dot{q}_{180}''(H) \tag{5}$$

Both can be adequately approximated by the general relation that

$$\dot{q}''(V) = 0.7\dot{q}''(H) \tag{6}$$

This clearly verifies that the thin, boundary layer–type flames occurring in the vertical orientation provide a lower heat flux than the pool-like flames in the vertical orientation.

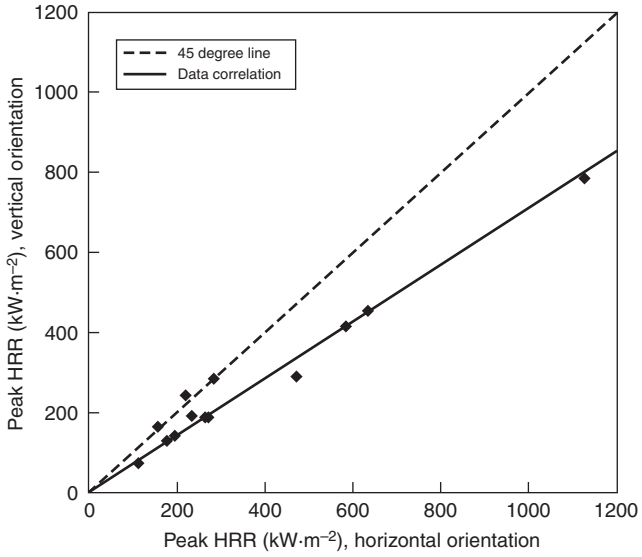

Figure 3-1.10. ***Orientation effect on the peak HRR, as determined from two cone calorimeter round robins.***

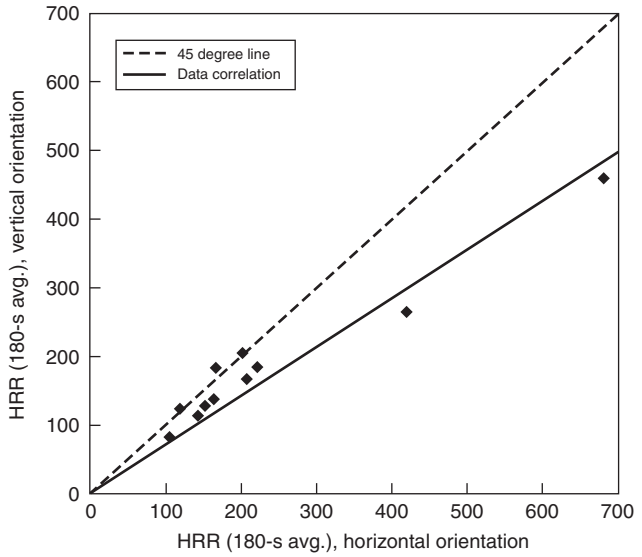

Figure 3-1.11. ***Orientation effect on the 180-s average HRR, as determined from two cone calorimeter round robins.***

Predicting Full-Scale HRR from Bench-Scale Data: Other Controlling Variables

Numerous other variables can, in principle, affect the HRR of specimens. This can include local velocities, scale and intensity of turbulence, and so on. For room fire modeling purposes, such effects can be assumed to be small. Two effects that are often of specific interest, however, are scale and vitiation effects. Scale effects are, in principle, normalized out when the per-unit-area variable is computed. These effects will not be zero, however. One factor

affecting them is the flame flux found in the bench-scale test apparatus. This will have some scale effect.

The studies in this area are not extensive. A study using a custom cone calorimeter with 200-mm × 200-mm specimen size tested horizontally found only a very small-scale effect, when compared to standard cone data.[57] A comparison between the ICAL and cone calorimeters for a series of wood products showed that systematic differences were surprisingly small, despite the 10× difference in linear dimension of the specimens.[58] Note, however, that in this case the specimens were tested in the vertical orientation. In such orientation, specimen flames are thin and there is little variation with scale. Of additional guidance is a study by Orloff[59] in which a vertical 3.56-m-high PMMA slab was burned. The mass loss rate, per unit area, was found to be

$$\dot{m}'' = 5.32 + 3.97x \quad (7)$$

where x is the vertical distance (m). Note that this result implies that there is but little variation for specimens with height <0.5 m, but significant increases for very large specimens.

In the case of objects burning in the horizontal orientation, large pool flames surmount the specimen. The flux from such flames will vary greatly with scale. Guidance provided for estimating burning rates of pools (see below) can be directly applied to this case.

HRR for Real Products

For many objects and commodities, published HRR are not available; thus, laboratory tests will have to be run if an answer is needed. For some commodities, however, exemplar data have been published and are available to the public. The tabulated test data can be very useful as generic representatives of items constructed of these materials, and with this general geometry. Where the analysis is intended to evaluate a specific product, that product should be tested in a suitable calorimeter and the data then used in the analysis. It must be strongly emphasized that in no case should generic database information be used when the purpose of the analysis is to seek regulatory approval for a product or to demonstrate the performance of a specific product in a court of law. In all such cases, actual laboratory testing on the item in question must be done.

In the case of a few product categories, methods are available for estimating large-scale HRR on the basis of bench-scale HRR data. The question then becomes, where can bench-scale HRR data be found? For a few product categories, some data are provided in the sections below. For the user interested in a more comprehensive look at bench-scale HRR data, the textbook *Heat Release in Fires*[22] and the cone calorimeter bibliography[60] are good sources. Also, Section 3, Chapter 4, "Generation of Heat and Chemical Compounds," provides some data on pure chemicals.

For convenience, the sections below are arranged alphabetically by type of product. However, many of the ideas are an offshoot of pioneering studies on pool fires. Thus, it is recommended that the user first read through the section on pools before progressing to other product categories.

Artificial Plants

Some data are shown in Figure 3-1.12.[61]

Bookcases, Casegoods, and Storage Units

In most cases, for storage furniture the fire hazard is created by the contents, not by the furniture item itself. An exception is modular storage units made of thermoplastic materials, which tend to burn very vigorously,[62] but quantitative HRR data have not been published. Storage furniture made of wood or wood covered with thin layers of thermosetting plastic tend to resist ignition unless filled with combustible contents. Some data are illustrated in Figure 3-1.13. The test arrangement for metal

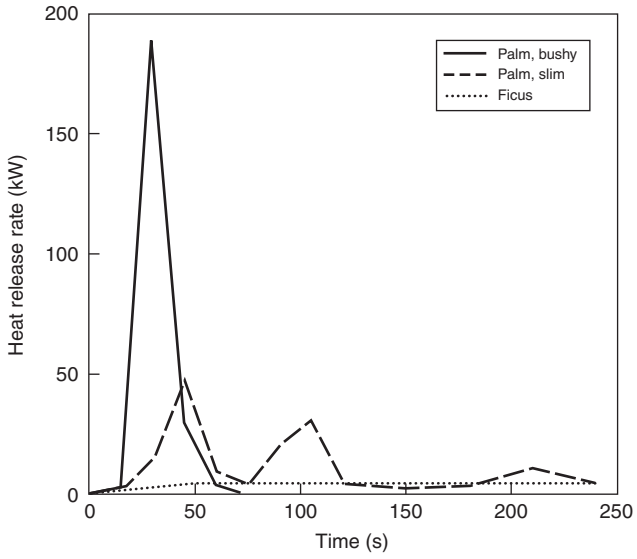

Figure 3-1.12. ***Artificial plants.***

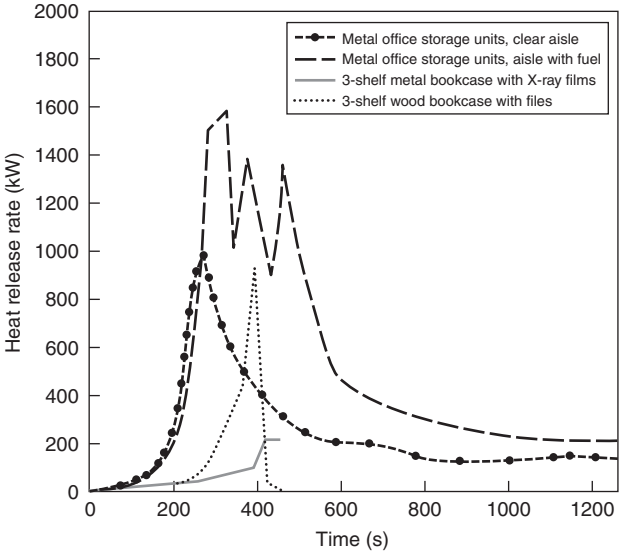

Figure 3-1.13. ***Storage units.***

office storage units[110] involved two tiers of shelving with a 0.76-m aisle in between. Each test contained 480 kg of paper fuel load in shelving units totaling 1.67 m^2 of floor area. For the configuration with fuel in the aisle, only 3 kg was placed in the aisle, but this extra fuel provided a major difference in fire severity. The data on X-ray film shelves and wooden bookcases are from Särdqvist.[61] For storage of paper files, it is known that the arrangement is more important than the quantity of fuel. Especially, storing files in cardboard boxes so that they can exfoliate exacerbates burning. Exfoliation occurs when paper folders are placed parallel, rather than perpendicular, to the front of the shelf. When fire attacks the front, folders progressively fall out and burn in the aisle. While well known, this effect has not been documented with HRR testing.

Cabinets (Electronic, Business Machine, etc.)

A limited amount of testing of business machine cabinets was reported by Babrauskas et al.,[63] as shown in Figure 3-1.14. Two series of tests on steel cabinets used for housing nuclear power-plant control electronics were conducted by VTT.[64,65] These showed HRR peaks of 100–200 kW. The authors also proposed computation formulas for predicting the HRR level that causes internal cabinet flashover and that causes burning to reach a ventilation limit.[66] Such computations are based on the assumption that air flow occurs only through fixed cabinet openings.

Carpets and Other Floor Coverings

Carpets that are in the room of fire origin are not likely to contribute significantly to fire growth. This has been demonstrated experimentally.[67] It is also consistent with modeling considerations: the floor area is convectively cooled and normally has the smallest view factor to the hot regions, which tend to be in the upper regions. The same material may be much more hazardous if installed on wall surfaces, although it must be pointed out that commercial textile wall coverings are normally similar, but not identical, to carpeting.

The hazard from floor coverings arises when an unsuitable product is used in a corridor, especially one that is an escape path. In such situations, very rapid flame spread and high HRR can result due to the fact that the corridor floor covering becomes involved due to a room fire feeding it. Not only carpeting, but solid materials such as linoleum and wood parquet flooring are also subject to becoming fully involved down the length of a corridor. A recent study has quantified this behavior and has also provided a predictive method.[68] It is shown that floor coverings with a peak HRR of less than 200 $kW \cdot m^{-2}$, measured in the cone calorimeter under an irradiance of 25 $kW \cdot m^{-2}$ tend not to show accelerating flame spread down a corridor.

Some carpeting materials can present a rapid fire spread hazard when installed on stairs. A residential carpet installed over a stairway has been measured to produce a peak HRR of 3 MW.[69] The test carpet was 80 percent acrylic and 20 percent nylon; no other types of carpeting were explored.

Chairs, Stackable

Stackable chairs are most commonly used in hotels and banqueting facilities. These chairs typically have metal legs and frame and only a small amount of combustible padding or structural material. Thus, a single chair can be expected to represent negligible hazard. However, when not in active use, they are stored in tall piles and many of these piles may be aggregated together. The hazard of even a single pile of modest height can be notable. Figure 3-1.15 illustrates some typical data on nonupholstered, molded chairs.[61] Figure 3-1.16 illustrates

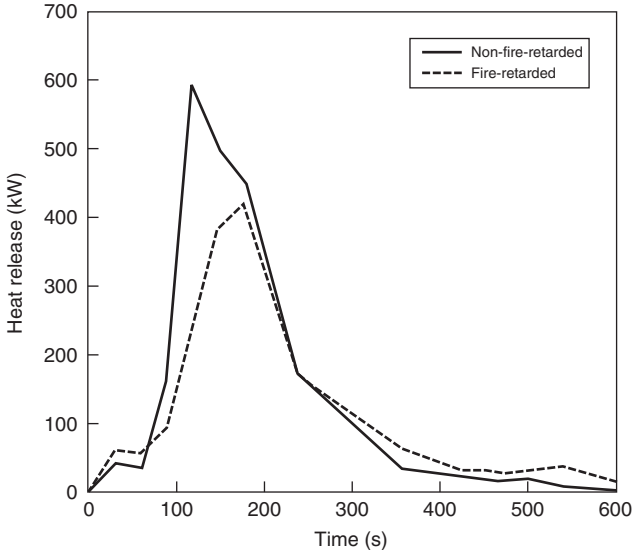

Figure 3-1.14. ***Business machine cabinets made from polyphenylene oxide plastic.***

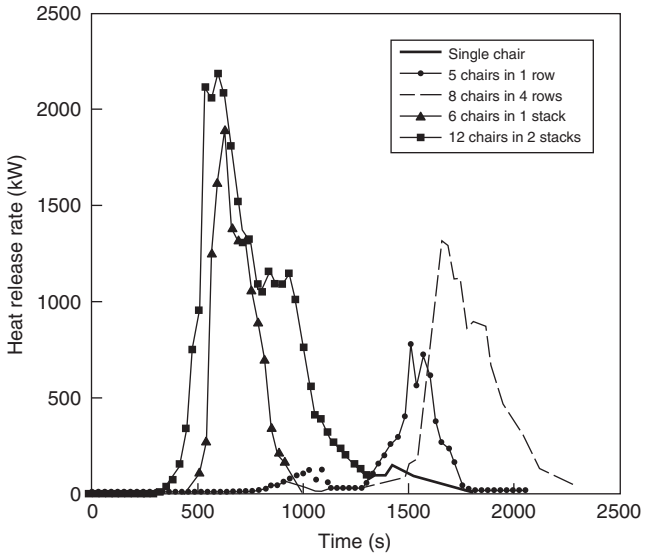

Figure 3-1.15. ***Stackable chairs, polypropylene with steel frame, no padding.***

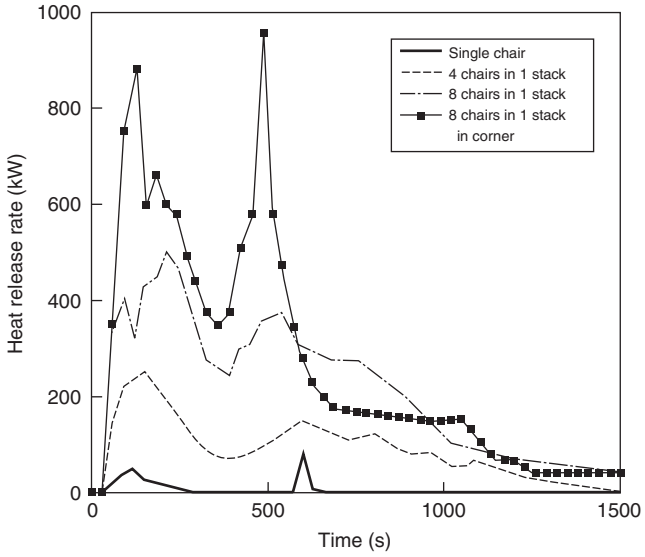

Figure 3-1.16. ***Metal-frame, upholstered stacking chairs.***

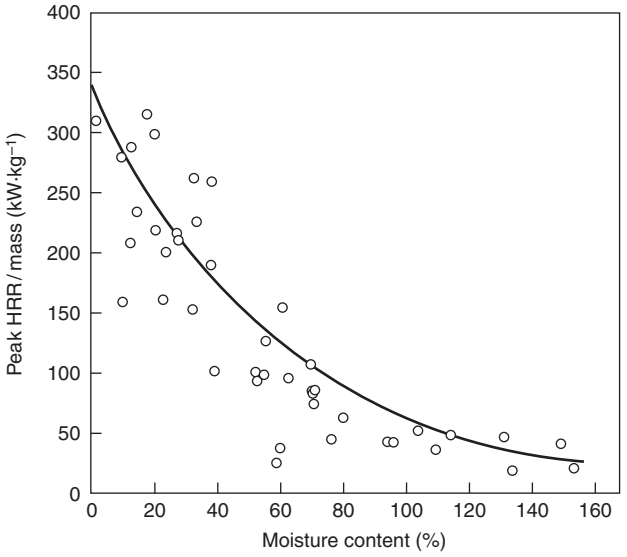

Figure 3-1.17. ***The peak HRR for Douglas fir Christmas trees, as a function of moisture and mass.***

some data on lightly upholstered chairs.[70] For the latter, the effect of radiant augmentation from burning in a corner is also illustrated.

Christmas Trees

Some tests on Christmas trees were reported by VTT[71] and by Damant and Nurbakhsh.[72] Newer studies, however, indicated that these tests, which examined only a few trees, did not capture the full range of HRR values associated with Christmas trees. The main variables that govern the HRR of Christmas trees are the following:

- Moisture content of the needles
- Mass of the tree
- Species
- Ignition source used

Moisture is the dominant variable and it had not been studied previously. The results of an extensive series of fire tests[73] on Douglas fir (*Pseudotsuga menziesii*) trees are shown in Figure 3-1.17, while the HRR of typical tests is illustrated in Figure 3-1.18. The tested trees were about 2.1 m tall, had an average mass of 11 kg, and had been watered according to various watering programs. The average tree was kept for 10 days prior to testing. The relation of the curve fit in Figure 3-1.17 is

$$\dot{q}/\text{mass} = e^{5.84-0.017M}$$

where M = moisture of needles (%) and the units of $\dot{q}/\text{mass}$ are $\text{kW}\cdot\text{kg}^{-1}$. Moisture is measured on a dry basis, so values can readily exceed 100 percent; also note that it is the needle moisture that governs the burning behavior—trunk moisture is not a relevant variable. To ignite Douglas fir trees with a small flame requires that the moisture content be below 50–60 percent. Otherwise, ignition is still possible if using larger combustible objects. In the work reported, the trees that could not be ignited by a small flame were all ignited by first igniting wrapped gift packages placed under the tree. For design purposes, it should be adequate to assume that the heat-release curve is a triangle. This requires knowing only the peak HRR and the total heat released. To estimate the latter, it was found in the tests that the Christmas trees showed an effective heat of combustion of 13.1 $\text{MJ}\cdot\text{kg}^{-1}$.

Thus, from knowing the mass of the tree and the effective heat of combustion, the total heat release may be

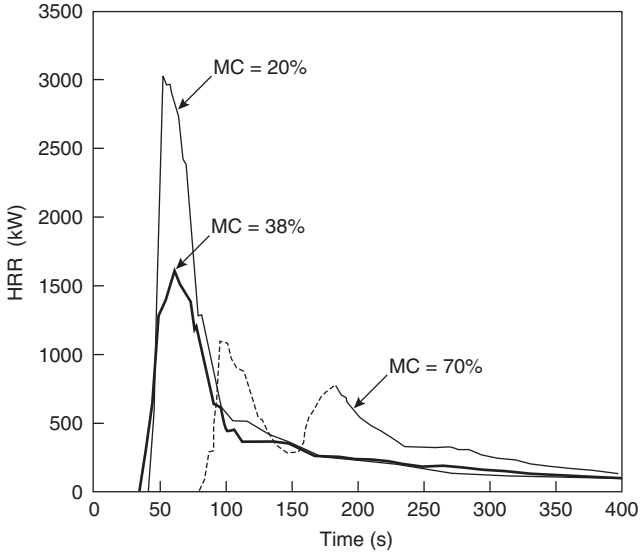

Figure 3-1.18. ***Typical HRR curves of Douglas fir Christmas trees.***

estimated. The needle moisture may not be known for design purposes. It is governed both by the watering program and by the innate biology, for example, the species, of the tree. No model is available at the present time that can predict moisture. However, research indicated that Douglas firs are a notably short-lasting species. The data points shown in Figure 3-1.17, with one exception, represent trees that had been on display for less than 16 days; some were watered carefully and regularly, while others were not. Other species of Christmas trees, such as Noble fir or Fraser fir are considered to be longer lasting, but are less commonly bought.

A smaller test series on Scotch pine trees was reported by Stroup et al.[74] They examined trees of 2.3–3.1-m height and mass between 9.5 and 20.0 kg; with one exception, the trees were of mass 12.7 kg or greater. Apart from one tree that is not considered here since it was not successfully ignited, the trees were left without water for three weeks in a room at 50 percent relative humidity and 23°C. Ignition was with an electric match to a lower branch of the tree. The Scotch pines were substantially taller and heavier than the Douglas firs, so it is not surprising that higher peak HRR values were attained. The peak HRR values ranged from 1620 to 5170 kW. Normalized per mass, the average was 183 $kW \cdot kg^{-1}$, with the range being 103–259 $kW \cdot kg^{-1}$. The moisture of the branches was not recorded, but presumably was <20 percent in all cases. Comparing to the above results, Douglas firs showed about 160–330 $kW \cdot kg^{-1}$. This would suggest that there is a species effect and that Scotch pines show an HRR/mass ratio ≈ 0.75 of that found for Douglas firs. This conclusion is very tentative, however, since the test programs did not use the same test protocol. Part of the difference might also be attributed to a height effect, since this cannot separately be taken into account.

Clothing Items

Two men's jackets (anoraks) were tested by SP[10] as potential ignition sources. One was a polyester jacket with an outer fabric comprising 65/35 percent cotton/polyester, an inner fabric of 100 percent polyamide, and a filling of 100 percent polyester wadding. Total weight was 739 g. The other was an acrylic jacket with a fabric of nylon/Taslan and a filling of 100 percent acrylic wadding. Total weight was 618 g. The HRR of these jackets are shown in Figure 3-1.19.

Coffee Makers

The HRR of several coffee makers is shown in Figure 3-1.20.[61] The units had total weights of 0.8 to 1.3 kg.

Computer Tapes

A test was conducted on a set of open steel shelves holding 90 computer tapes.[75] The tapes were 300 mm in diameter and the total mass of 99 kg was distributed on four shelves, two tiers deep. The results are indicated in Figure 3-1.21.

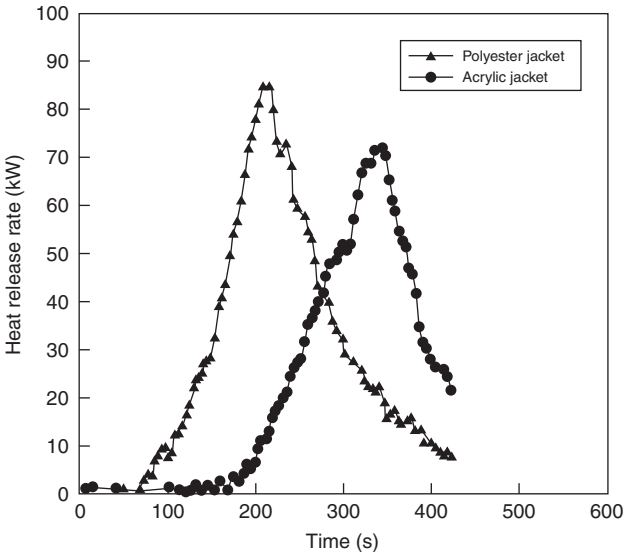

Figure 3-1.19. ***Two men's jackets.***

Cribs (Regular Arrays of Sticks)

Cribs here are taken to mean regular, three-dimensional arrays of sticks. Each stick is of a square cross section and of a length much greater than its thickness. The sticks are placed in alternating rows, with an air space separating horizontally adjacent sticks. (See Figure 3-1.22). Wood crib burning rates have been studied longer than any other product, with early data available from the 1930s.[76] Different analysis formulas have been presented over the years by numerous authors. Here we present a method of analysis[25] based largely on the voluminous experimental data of Nilsson[77] on wood cribs and the func-

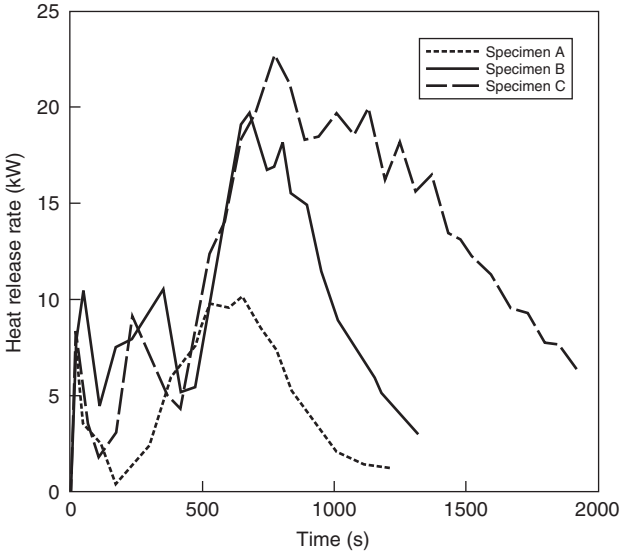

Figure 3-1.20. ***Coffee makers.***

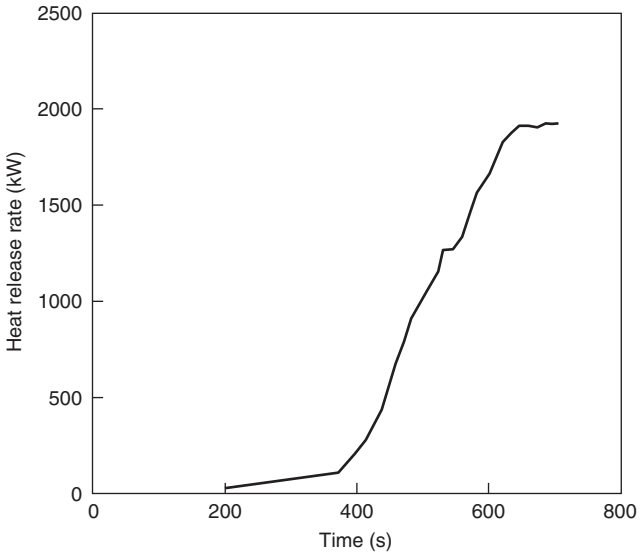

Figure 3-1.21. ***A rack of computer tapes.***

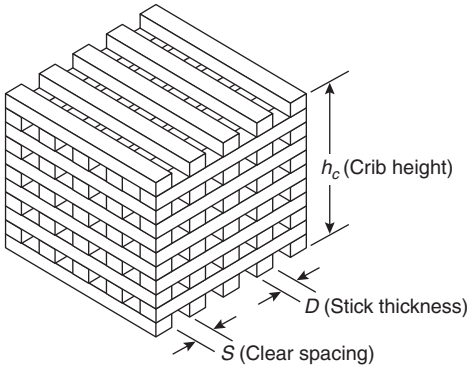

Figure 3-1.22. ***General arrangement of a wood crib.***

tional form suggestions of Yamashika and Kurimoto.[78] The scant available data on plastic cribs are from Harmathy[79] and Quintiere and McCaffrey.[80] The conditions of most interest are when cribs are ignited instantaneously, as with the use of a small amount of combustible liquid underneath. The first group of equations below represents this case. There is occasionally an interest in a crib fire where only one end of a crib is ignited, and a slow fire propagation is seen. An analysis for this situation has also been made.[81] A similar analysis is also available for the center-ignited, fire-spreading crib scenario.[82]

For cribs ignited uniformly overall, it is observed that the burning rate can be governed by one of three conditions: (1) the natural limit of stick surfaces burning freely; this limit applies to cribs with wide interstick spacings; (2) the maximum flow rate of air and combustion products through the air holes in the crib; this governs for tightly packed cribs; and (3) the maximum oxygen that can be supplied to the room; this effect is discussed separately, below. The numerical expressions corresponding to the three conditions are as follows:

(1) Fuel surface control:

$$\dot{m} = \frac{4}{D} m_o v_p \left(1 - \frac{2 v_p t}{D}\right) \tag{8a}$$

or

$$\dot{m} = \frac{4}{D} m_o v_p \left(\frac{m}{m_o}\right)^{1/2} \tag{8b}$$

with

$$m = m_o - \sum_i^t \dot{m}_i(t_i)\,\Delta t \tag{9}$$

(2) Crib porosity control:

$$\dot{m} = 4.4 \times 10^{-4} \left(\frac{S}{h_c}\right)\left(\frac{m_o}{D}\right) \tag{10}$$

(3) Room ventilation control:

$$\dot{m} = 0.12 A_v \sqrt{h_v} \tag{11}$$

The *least* of Equations 8a, 10, or 11 is to be taken as the governing rate (Equation 11 is discussed below). Equation 8b is necessary instead of the simpler Equation 8a when a switch of burning regime occurs during the course of the fire, for example, the burning changes from porosity control to fuel surface control at some point. This can happen since Equation 8a (or 8b) is a time-dependent expression. Thus, a crib may start burning under porosity or room ventilation–controlled conditions, then later switch to fuel surface control.

In the above equations, D is the stick thickness, m_o is the crib initial mass, t is the time since ignition, h_c is crib height, S is the clear spacing between sticks, and room ventilation variables are A_v, the ventilation opening area, and h_v, the ventilation opening height. The fuel surface regression velocity, v_p, is taken as dependent on the stick thickness and on the fuel type, as shown in Table 3-1.2. The experimental data for the plastic materials are extremely scant, however, so the values should be viewed as indicative rather than quantitative.

For the case of the center-ignited crib, the burning regimes are divided according to whether the flame spread has reached the edge of the crib at a particular time. This time is defined as t_0.

$$t_0 = 15.7n \tag{12}$$

Table 3-1.2 ***Fuel Type versus Regression Velocity v_p for Cribs***

Material	v_p
Wood	$2.2 \times 10^{-6} D^{-0.6}$
Polymethylmethacrylate	$1.4 \times 10^{-6} D^{-0.6}$
Thermosetting polyester	$3.1 \times 10^{-6} D^{-0.6}$
Rigid polyurethane foam	$3.8 \times 10^{-6} D^{-0.6}$

where n = the number of sticks per row. For time $t < t_0$, the following relation holds:[82]

$$\dot{m} = 0.0254 m_o \frac{v_p t^2}{n^2 D} \tag{13}$$

For $t > t_0$, Equations 8a through 11 are used. The heat release rate is determined from Equation 1. For plastics, the heat of combustion is commonly fairly constant and can be taken from tabulations or from cone calorimeter testing. For wood cribs, commonly the heat of combustion is taken to be 12×10^3 kJ·kg^{-1}. However, as illustrated in Figure 3-1.1, the heat of combustion of wood is a varying function of time. A better procedure would be either to predict the HRR of wood cribs directly, without going through Equation 1, or else to be able to have recourse to a realistic value of $\Delta h_c(t)$. Neither of these possibilities have currently been developed.

Room fire effects: Experimentally, it has long been observed[77] that, unlike a pool fire, which can burn in a room in a highly fuel-rich manner, a wood crib does not burn more than approximately 30 to 40 percent fuel rich. Conditions more fuel rich than that are not sustained, presumably, because of the highly vitiated air being supplied to the crib under those conditions. The stoichiometric fuel pyrolysis rate can be estimated as[11]

$$\dot{m}_p(st) = \frac{1}{r} \cdot 0.5 A_v \sqrt{h_v} \tag{14}$$

where the stoichiometric air/fuel mass ratio, r, for wood can be taken as $r = 5.7$. Comparing, then, the maximum pyrolysis rate given by Equation 11 with the stoichiometric rate given by Equation 14, it can be seen that a limit of approximately 37 percent fuel rich is reached when Equation 11 becomes the governing limit to the burning rate. Similar limits may possibly exist for other classes of combustibles, but experimental data are only available for wood cribs.

Curtains

The heat content and burning rate of curtains are generally moderate, but they are combustible and can contribute to the severity of fires by quickly propagating fire over large surfaces. Moore has done the most extensive study of curtains and draperies.[83] His test specimens were ignited with a match along the bottom. The results are summarized in Table 3-1.3 and Figure 3-1.23. His results show primarily the effect of fabric weight. Lightweight fabrics, of weight around 125 kg·m^{-2}, can show heat-release-rate peaks almost as high as heavy ones (around 300 kg·m^{-2}); however, their potential to ignite surrounding objects is much smaller, as demonstrated in Figure 3-1.23. These conclusions hold for both thermoplastic and cellulosic materials, but not for constructions using foam backings, for which insufficient data were available. Whether the curtain was in the closed or in the open position seemed to make little difference. The reason for the more severe fire performance of the heavyweight curtains was largely due to their increased burning time, which was typically about twice that for the lightweight curtains.

Table 3-1.3 ***Heat Release Rate Data for Curtains***

Type of Fiber	Weight (g/m^2)	Configuration	Peak HRR (kW)	Number of Wall and Ceiling Panels Ignited[a]
Cotton	124	Closed	188	1
Cotton	260	Closed	130	7
Cotton	124	Open	157	0
Cotton	260	Open	152	7
Cotton	313	Closed	600	3
Rayon/cotton	126	Closed	214	0
Rayon/cotton	288	Closed	133	6
Rayon/cotton	126	Open	176	0
Rayon/cotton	288	Open	191	2
Rayon/cotton	310	Closed	177	8
Rayon/acetate	296	Closed	105	4
Acetate	116	Closed	155	0
Cotton/polyester	117	Closed	267	1
Cotton/polyester	328	Closed	338	5
Cotton/polyester	117	Open	303	0
Rayon/polyester	367	Closed	658	2
Rayon/polyester	268	Closed	329	7
Rayon/polyester	53	Closed	219	0
Cotton/polyester	328	Open	236	7
Polyester	108	Closed	202	0
Acrylic	99	Closed	231	0
Acrylic	354	Closed	1177	8
Acrylic	99	Open	360	0
Acrylic	354	Open	NA	7
Cotton/polyester/ foam	305	Closed	385	1
Rayon/polyester/ foam	284	Closed	326	0
Rayon/fiberglass	371	Closed	129	5
Rayon/fiberglass	371	Closed	106	5

Nominal curtain size: two curtains each, 2.13 m high by 1.25 m wide. Wall area covered: 2.13 m high by 1.0 m wide (in closed position).

[a]Maximum possible number of panels to ignite = 10.

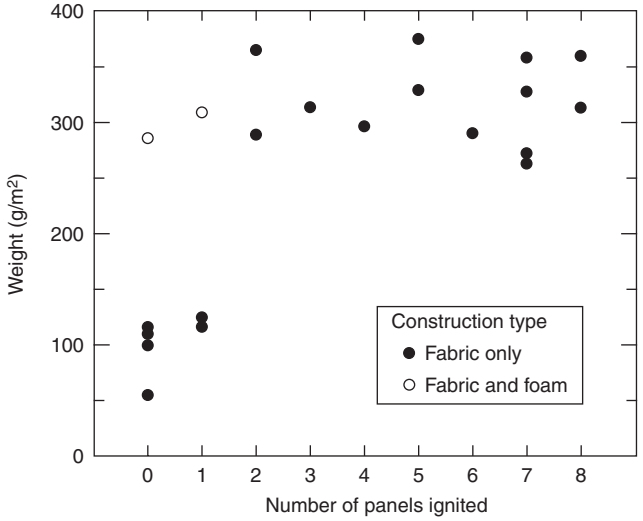

Figure 3-1.23. ***Effect of fabric weight on number of curtain panels ignited.***

Additional data on the HRR of curtains have been published by VTT[71] and by SP.[84]

Dressers

A test of a wooden dresser has been conducted by NIST.[85] See Figure 3-1.24.

Electric Cable Trays

Cable tray fires present almost an endless plethora of combinations of cable materials, tray construction, stacking, ignition sources, and so forth. Only a very few of these have been explored. The most systematic studies available are those from Tewarson et al.[86] and Sumitra.[87]A useful engineering analysis of their data has been prepared by Lee.[88] Lee provided a basic correlation of Tewarson's and Sumitra's data (see Figure 3-1.25), which shows that the peak full-scale heat-release rate $\dot{q}_{fs}$ (kW·m^{-2}) can be predicted according to bench-scale heat release rate measurements

$$\dot{q}_{fs} = 0.45\dot{q}''_{bs} \cdot A$$

where $\dot{q}''_{bs}$ is the peak bench-scale HRR (kW·m^{-2}), measured under 60-kW·m^{-2} irradiance, and A is the exposed tray area actively pyrolyzing (m^2). The active pyrolysis area, in turn, is estimated from Figure 3-1.26, which gives dA/dt as a function of $\dot{q}''_{bs}$. Thus, at any given time, t,

$$A(t) = A_o + \frac{dA}{dt} \cdot t$$

Finally, Table 3-1.4 gives a selection of measured values of $\dot{q}''_{bs}$ for various cable types.

Industrial Stored Commodities

Pallet loads of plastic-based commodities are commonly stored in factories, warehouses, and wholesale establishments.[89] Pellets of SBR (styrene-butadiene rubber) were packed in paper bags and loaded on a wooden pallet. The pallet was overwrapped with clear plastic film and spillage did not occur during testing. The full-pallet test was ignited with a propane torch at the bottom. The half-pallet test was ignited with a propane torch at the top. The full-pallet test (Figure 3-1.27) showed an HRR of close to

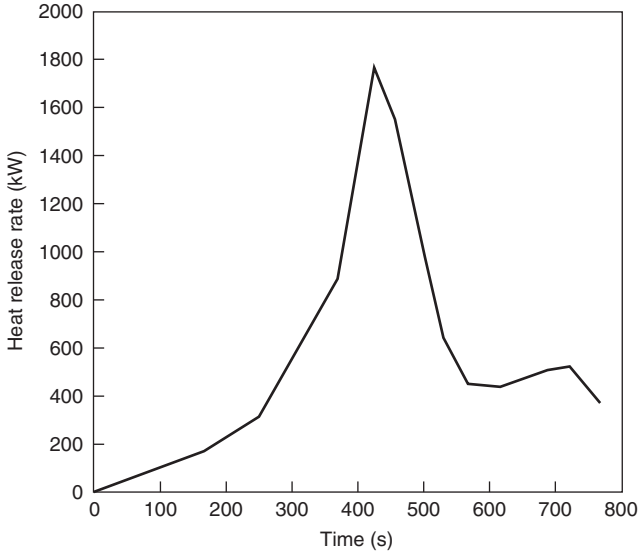

Figure 3-1.24. ***Wooden dresser.***

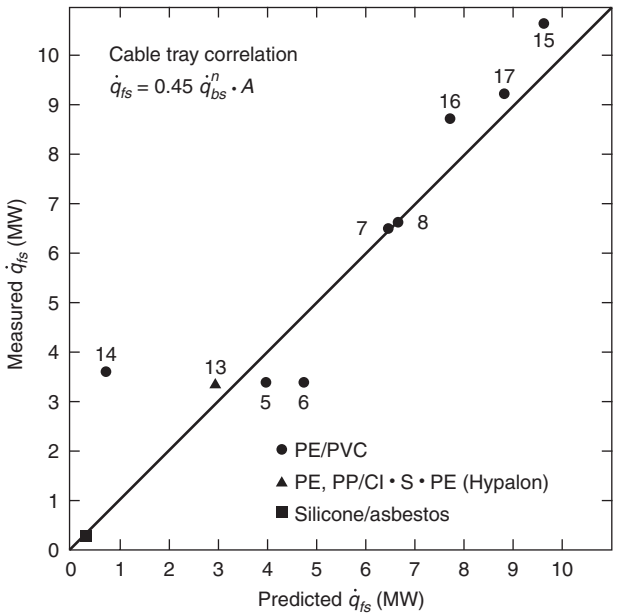

Figure 3-1.25. ***Heat release rate correlation for cable trays (numbers at data points identify full-scale tests).***

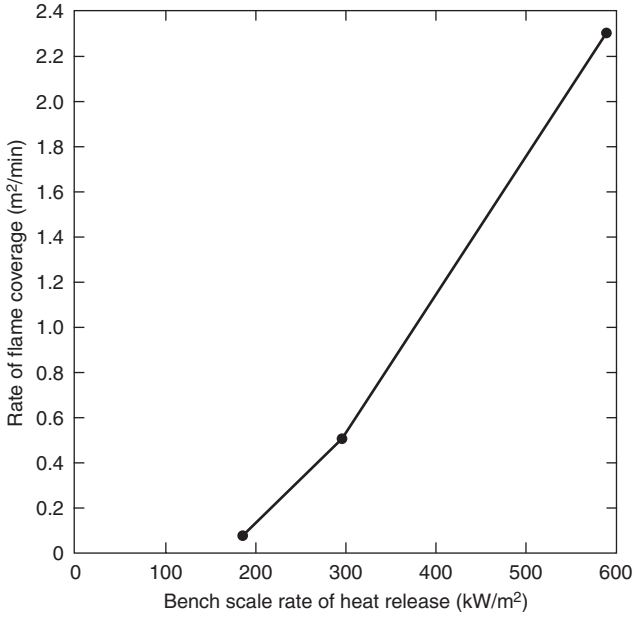

Figure 3-1.26. ***Effect of bench-scale cable heat release rate on full-scale rate of flame coverage.***

Table 3-1.4 ***Heat Release Rates of Typical Cables in Bench-Scale Tests***

Specimen Number	Cable Sample	IEEE 383 Test	$\dot{q}''_{bs}$ (kW/m^{-2})
20	Teflon	Pass	98
21	Silicone, glass braid	Pass	128
10	PE, PP/Cl·S·PE	Pass	177
14	XPE/XPE	Pass	178
22	Silicone, glass braid asbestos	Pass	182
16	XPE/Cl·S·PE	Pass	204
18	PE, nylon/PVC, nylon	[a]	218
19	PE, nylon/PVC, nylon	[a]	231
15	FRXPE/Cl·S·PE	Pass	258
11	PE, PP/Cl·S·PE	Pass	271
8	PE, PP/Cl·S·PE	Pass	299
17	XPE/Neoprene	Pass	302
3	PE/PVC	[a]	312
12	PE, PP/Cl·S·PE	Pass	345
2	XPE/Neoprene	[a]	354
6	PE/PVC	[a]	359
4	PE/PVC	Fail	395
13	XPE/FRXPE	Pass	475
5	PE/PVC	Fail	589
1	IDPE	[a]	1071

[a]Test not conducted.

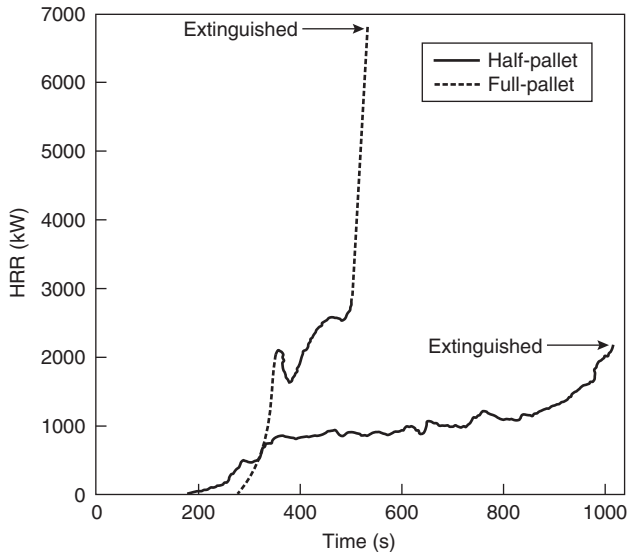

Figure 3-1.27. ***HRR of bags of SBR pellets on a wooden pallet.***

7 MW when conditions required that the commodity be extinguished; peak HRR conditions had not been reached.

Heskestad[90,91] analyzed a large series of palletized* storage tests conducted at FRMC in 1975 by Dean.[92] These experiments predated the availability of HRR calorimeters, so Heskestad obtained peak HRR values by using mass-loss-rate data and values of effective heat of combustion. The test arrangement was $2 \times 2 \times 3$ pallets high, with a flue space running in only one direction. Heskestad also analyzed a later series of rack storage tests by Yu and Kung.[93,94] The test arrangement was 2×2, with heights being 2, 3, or 4 pallets, and with flue spaces running in both directions. Heskestad's tabulated peak HRR values are given in Table 3-1.5. The peak HRR values were obtained by dividing the value in kilowatts by the floor area occupied by the commodity. The cardboard cartons with metal liner are FMRC Standard Class II Commodity, while the PS cups are FMRC Standard Plastic Commodity. Note that there does not exist a scaling rule that would enable HRR values to be computed for stack/rack heights other than those tested. Thus, the reported values could conservatively be applied to shorter heights, but cannot be extrapolated to greater heights. Older data[95] are given in Table 3-1.6; these have not been reanalyzed by Heskestad.

Additional FMRC data for different commodities loaded onto wooden pallets are shown in Figure 3-1.28. The PET (polyethylene terephthalate) bottle test[96] used 46 bottles of a 2-L size packed into single-wall corrugated cardboard boxes. Each box contained 2.55 kg of plastic and 1.29 kg of cardboard. Total test arrangement comprised 8 pallet loads arranged in a $2 \times 2 \times 2$ arrangement. Each pallet contained 8 cartons of the size $0.53 \times 0.53 \times 0.53$ m. The newspaper test[97] comprised 8.2 kg of shredded newsprint placed in a $0.53 \times 0.53 \times 0.51$ m single-wall corrugated cardboard box of 2.73 kg. Eight cartons comprised one pallet load. The pallets were arranged in a $2 \times 2 \times 2$ arrangement. The egg carton test[98] used foam polystyrene egg cartons of 12-egg capacity. Polyethylene bags were used to hold 200–216 of these egg cartons, open and nested into each other. Each pallet held about 20.4 kg of egg cartons. Each pallet contained about 22.7 kg of wood, and the load also contained about 0.4 kg of polyethylene. In this test, a low density of water extinguishment was applied, but this did not appear to reduce significantly the HRR of the commodity. Only the convective portion of the HRR was measured. Polystyrene shows a very high radiant heat-release fraction; thus, to account for the radiant fraction and for the diminution due to water spraying, the total HRR curve shown in Figure 3-1.28 was estimated by multiplying the measured convective portion by two times.

Packaged computers and computer accessories were tested by Hasegawa et al.[99,100] They tested pallet loads of packaged goods and also individual items, as packaged and boxed in individual cardboard boxes. The items were ignited using a line burner placed near the bottom edge of the package or stack. Ignition sources in the range of 50–200 kW were used. Table 3-1.7 identifies the specimens tested, while Figure 3-1.29 through Figure 3-1.32 show the results. The monitors were 16.8 kg each, while the desktop computers were 4.9 kg each. The pallet load in test P1 collapsed during testing and the full HRR was not registered; consequently, it was retested with supported sides.

A stack of expanded polystyrene boards was burned by Dahlberg at SP and results are reported by Särdqvist.[96] The total stack size was $1.2 \times 1.2 \times 1.2$ m, with a mass of

Palletized denotes a storage configuration where pallets are stored directly on top of each other, without use of shelving.

Table 3-1.5 ***HRR Values of Palletized and Rack Storage Commodities Tested at FMRC***

Test	Commodity	Storage Height (m)	Peak HRR ($kW \cdot m^{-2}$)	Time of Peak (s)
SP-4	PS jars in compartmented CB cartons	4.11	16,600	439
SP-13	PS foam meat trays, wrapped in PVC film, in CB cartons	4.88	10,900	103
SP-23	PS foam meat trays, wrapped in paper, in CB cartons	4.90	11,700	113
SP-30A	PS toy parts in CB cartons	4.48	5,210	120
SP-35	PS foam insulation	4.21	26,000	373
SP-44	PS tubs in CB cartons	4.17	6,440	447
SP-15	PE bottles in compartmented CB cartons	4.20	5,330	434
SP-22	PE trash barrels in CB cartons	4.51	28,900	578
SP-43	PE bottles in CB cartons	4.41	4,810	190
SP-6	PVC bottles in compartmented CB cartons	4.63	8,510	488
SP-19	PP tubs in compartmented CB cartons	4.26	5,870	314
SP-34	PU rigid foam insulation	4.57	1,320	26
SP-41	Compartmented CB cartons, empty	4.51	2,470	144
RS-1	CB cartons, double triwall, metal liner	2.95	1,680	260
RS-2	" "	2.95	1,490	89
RS-3	" "	2.95	1,680	180
RS-4	" "	4.47	2,520	120
RS-5	" "	4.47	2,250	240
RS-6	" "	5.99	3,260	210
RS-7	PS cups in compartmented CB cartons	2.90	4,420	95
RS-8	" "	2.90	4,420	100
RS-9	" "	2.90	4,420	120
RS-10	" "	4.42	6,580	100
RS-11	" "	5.94	8,030	148

CB, cardboard; PE, polyethylene; PP, polypropylene; PS, polystyrene; PU, polyurethane

Table 3-1.6 ***Miscellaneous Stored Commodities Tested by FMRC***

Commodity	Storage Height (m)	Peak HRR (kW/m^{-2})
Fiberglass (polyester) shower stalls, in cartons	4.6	1400
Mail bags, filled	1.52	400
PE letter trays, filled, stacked on cart	1.5	8500
PE and PP film in rolls	4.1	6200

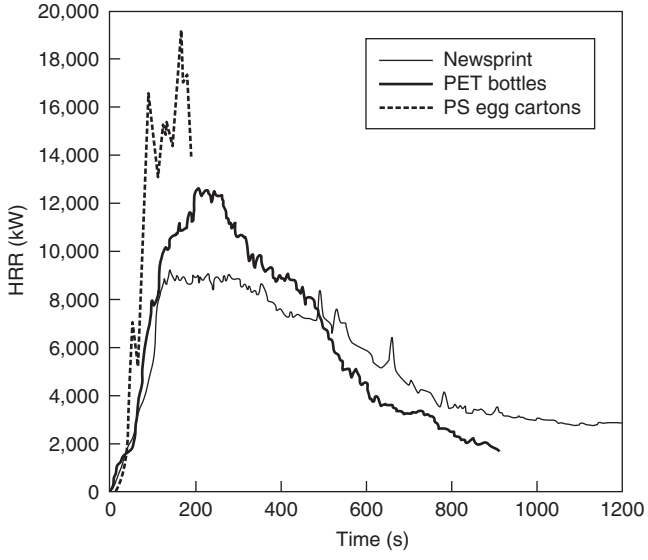

Figure 3-1.28. ***FMRC results for several additional commodities.***

1.4 kg. Ignition was with a 1-MW burner at the side of the stack. The HRR curve is shown in Figure 3-1.33. Numerous other example data are tabulated by Särdqvist.[96]

A study has been reported on burning pallet loads of organic peroxides.[101] Liquids were packaged in plastic containers within cardboard boxes, while solids were packaged in cardboard drums. The data are given only for a few packaging configurations with sufficient data not being available to generalize HRR predictions to other configurations.

For all rack storage tests, the times are very strongly affected by the ignition source location. Not enough data exist to make general correlations, but Figure 3-1.34 illustrates the basic effect. The storeroom test[102] comprised a mocked-up small storeroom in a retail shop, with miscellaneous goods boxed in cardboard boxes, placed on shelving 2.4 m high. A small amount of additional shelving was provided across an aisle 1.4 m wide. The FMRC

Table 3-1.7 ***Boxed Computer Items Tested by Hasegawa et al.***

Code	Items	Peak HRR (kW)
P1	Boxed monitors, 1 pallet of 12	4,700
P8	Boxed monitors, 1 pallet of 12, point-source ignition	5,030
P5	Boxed monitors, 1 pallet of 12 (stabilized from collapse)	6,400
P6	Boxed monitors, 2 pallets (side-by-side) of 12 each	17,300
P10	Boxed monitors, stack of 2 pallets high, 10 per pallet	14,100
P3	Boxed desktop computers, 1 pallet of 16	1,400
P7	Boxed desktop computers, pallet of 16 with boxed accessory boxes on top	8,190
P9	Polystyrene foam in boxes	6,730
P11	Monitor boxes, 1 pallet of 12	4,600

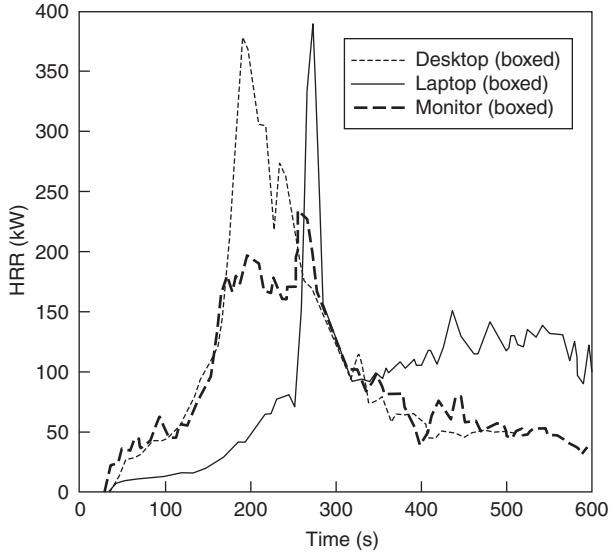

Figure 3-1.29. ***Single, packaged, and boxed computers and monitors.***

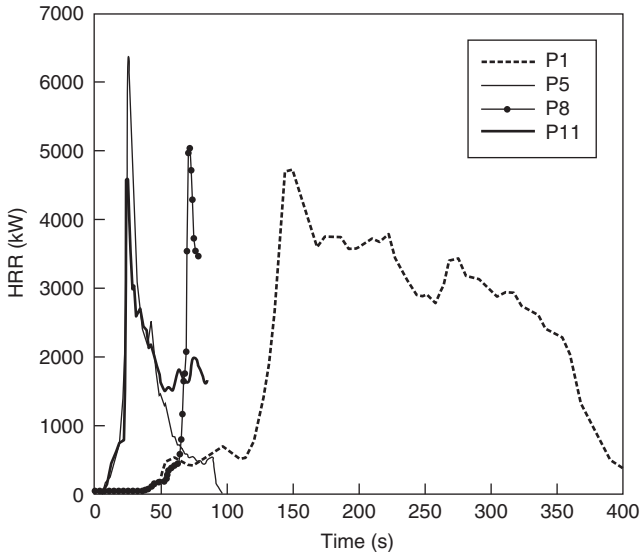

Figure 3-1.30. ***Pallets of packaged, boxed computer monitors.***

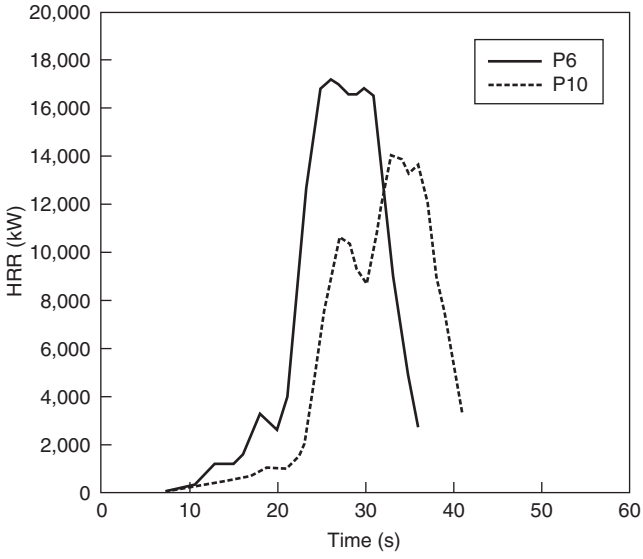

Figure 3-1.31. ***Pallets of packaged, boxed computer monitors.***

test involved pallets in a $2 \times 2 \times 2$ arrangement. In the storeroom test, ignition was at the base of the face of the main storage rack. The FMRC test[103] used the standard FMRC procedure whereby an ignitor is also placed at the base, but is located internally, at the two-way intersection of flue spaces between piles. The data for the storeroom test are plotted as real time, while the FMRC test data were shifted 470 s to make the steep HRR rise portions coincide. From a comparison of this kind, one can roughly estimate that igniting a rack at the front face causes events to occur 470 s later than would happen if ignition were at the center of the flue spaces.

Kiosks

NIST has reported[104] some HRR results on full-scale tests of kiosks. These are manned booths used in shopping malls, exhibitions, and other places wherein a small amount of merchandise display or sales occur. Some HRR curves are illustrated in Figure 3-1.35 for a kiosk, built largely of wood, that measured 1.2 m $\times$ 1.2 m $\times$ 2.1 m high. Tests 2–5 are all of the same-sized kiosk, but refer to various configurations of the openable panels. Test 5 appears to have been more severe since all the panels were

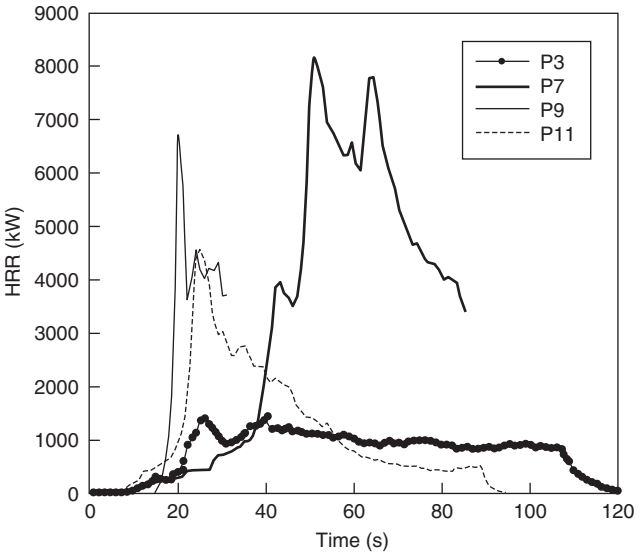

Figure 3-1.32. ***Pallets of miscellaneous computer items.***

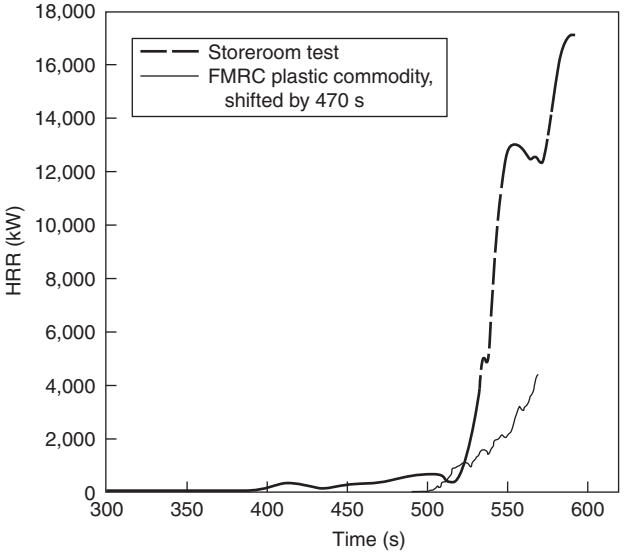

Figure 3-1.34. ***Effect of ignition source location on fire development.***

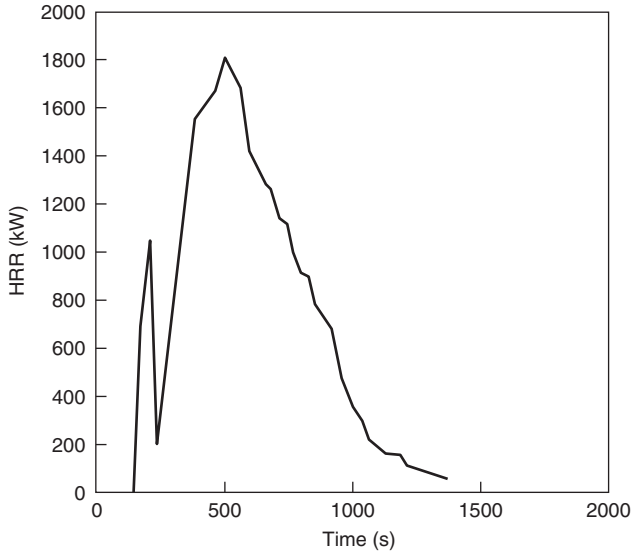

Figure 3-1.33. ***Stack of foam polystyrene boards.***

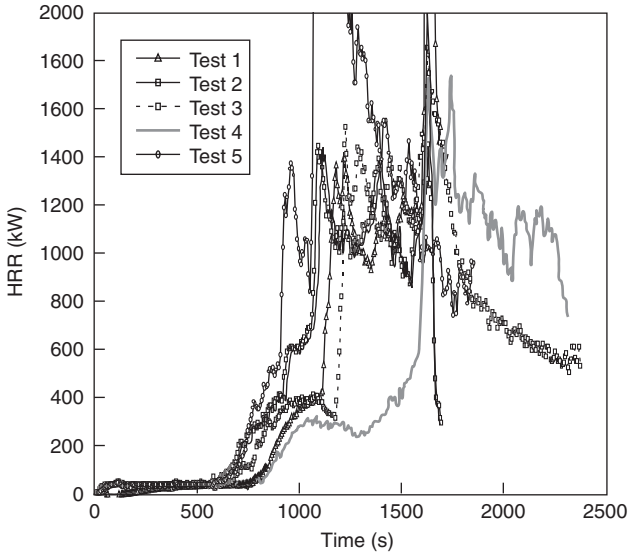

Figure 3-1.35. ***Display kiosks.***

closed. Test 1 involved the same kiosk placed in a room, rather than in the furniture calorimeter.

Mattresses

Despite the relatively simple shape of mattresses, the prediction of mattress HRR from bench-scale data is difficult. Even the use of full-scale HRR data is problematic, due to a peculiarity of mattress fires. Most other combustibles interact only modestly with their environment, until large HRR values are reached or until room flashover is being approached. Liquid pools on the other hand, as discussed below, interact very strongly with a room, if either the room size or the available ventilation are not very large in comparison to the pool's HRR. The identical phenomenon is observed with mattresses. Thus, there may not be a single value of the HRR of a mattress, because the HRR must be considered in relation to the room itself.

Some example data are compiled in Table 3-1.8 to illustrate the peak full-scale HRR values that are found for common material combinations.[38] The full-scale test protocol used a complete set of bedding; ignition was achieved with a wastebasket. Figure 3-1.36 illustrates the relation of bench-scale to full-scale data from the same data set, where full-scale testing was done under conditions not leading to significant room fire effect. Not enough specimens were tested to develop a usable correlation, so the results should be taken only as indicative.

Table 3-1.8 ***Some Mattress Heat Release Rate Data***

Padding Material	Ticking Material	Combustible Mass (kg)	Peak HRR, Full-Scale[a] (kW)	Bench-Scale HRR[b] (kW·m^{-2})
Latex foam	PVC	19	2720	479
Polyurethane foam	PVC	14	2630	399
Polyurethane foam	PVC	6	1620	138
Polyurethane foam	Rayon	6	1580	179
Polyurethane foam	Rayon	4	760	NA
Neoprene	FR cotton	18	70	89
Cotton/jute	FR cotton	13	40	43

[a]Full-scale data are for small or no room effect.

[b]Bench-scale data are peak values taken at 25 kW·m^{-2} irradiance.

Some full-scale data obtained under conditions where a strong room interaction effect was seen are shown in Table 3-1.9.[105,106] The full-scale test setup was different for this data set, in that no bedding was used and ignition was with a burner flame at the edge of the mattress. Thus, some mattresses were able to show essentially zero HRR since bedding was not available to sustain burning, and the ignition source could be evaded by receding specimens. A relation between full-scale and bench-scale results from this study is shown in Figure 3-1.37. The results of the behavior in that study follow:

- Mattresses with a bench-scale HRR (180-s average value) of < 165 kW·m^{-2} led to room fires of less than 100 kW.
- Mattresses with a bench-scale HRR (180-s average value) of > 165 kW·m^{-2} generally led to room fires on the order of 1 to 2 MW.
- The transition between those extremes was very abrupt.

The sharp transition between trivial fires and room flashover conditions can be attributed to the details of the test room, but also to the use of an ignition source that specimens of intermediate characteristics could evade.

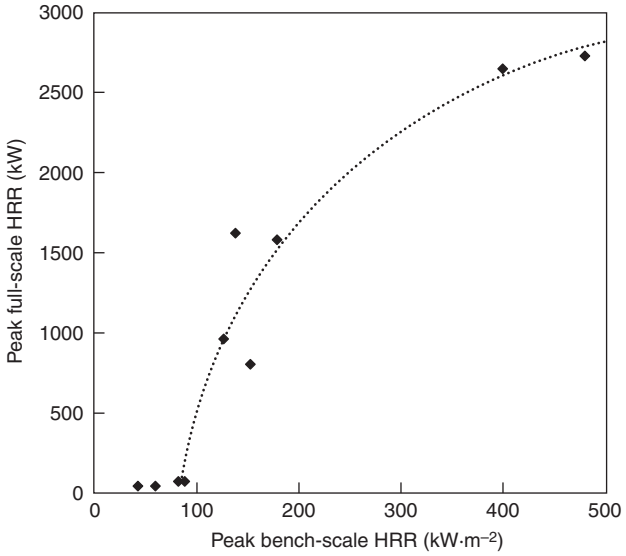

Figure 3-1.36. ***HRR of mattresses predicted from bench-scale results. Full-scale tests under conditions of negligible room effect; bench-scale HRR measured at 25-kW·m^{-2} irradiance.***

Additional data on mattress HRR have been published by SP[107] and by Lund University.[108] The latest study on mattress HRR has been the CBUF project.[10] The CBUF study included full-scale room fire tests, open-burning furniture calorimeter tests, and cone calorimeter tests. The mattress results are given in Table 3-1.10. In both of the full-scale test environments, no bedding was used, but a square-head burner was applied to the top surface of the specimen, precluding complications from any receding surface behavior. The bench-scale test data presented were obtained at a 35 kW·m^{-2} irradiance. The results indicate that, when tested in the standard ISO 9705 room, a very drastic room effect occurs for open-air HRR values over about 300 kW.

Table 3-1.9 ***Some Mattress Heat Release Rate Data***

Padding Material	Ticking Material	Combustible Mass (kg)	Peak HRR, Full Scale[a] (kW)	180-s Average HRR, Bench Scale (kW·m^{-2})
Polyurethane foam	Unidentified fabric	8.9	1716	220
Melamine-type PUR/cotton batting/polyester fiber pad	Polyester/polypropylene	NA	547	169
Polyurethane foam/cotton batting/polyester fiber pad	Unidentified fabric	NA	380	172
Polyurethane foam/polyester fiber pad	PVC	NA	335	195
Melamine-type PUR	FR fabric	15.1	39	228
FR cotton batting	PVC	NA	17	36
FR cotton batting	Polyester	15.7	22	45
Neoprene	PVC	14.9	19	31

[a]Full-scale data include room effect of small bedroom.

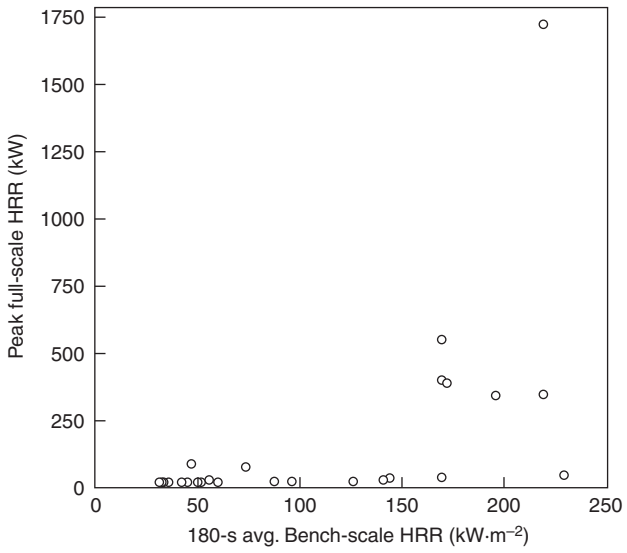

Figure 3-1.37. ***HRR of mattresses predicted from bench-scale results. Full-scale tests under conditions of significant room effect; bench-scale HRR measured at 35-kW· m^{-2} irradiance.***

The bench-scale data indicated that when widely varying mattress thicknesses exist, a simple relation of bench-scale to full-scale HRR cannot be sought, even if only predictions of open-burning (furniture calorimeter) results would be desired. As a first cut, it was concluded that mattresses can be grouped into two categories—those leading to propagating fires (the mattress being consumed in flaming combustion during a relatively short time), and those that do not. The former can be considered of the highest hazard, while the latter present only trivial hazard. Since, for practical reasons, all mattress composites must be tested in the cone calorimeter using a 50-mm thickness, to take into account effects due to thin mattresses, a thickness factor is defined:

$$\text{Th. fac.} = \min\left(\frac{\text{thickness (mm)}}{50}, 1.0\right)$$

For mattresses where the innersprings are used, the thickness is measured from the top of the mattress down to top of the metal springs; it is not the total thickness. To determine whether the mattress fire will be propagating or not, the following rules were developed:

$$\text{if} \quad \dot{q}''_{180} \cdot (\text{Th.Fac.}) < 100 \text{ kW·m}^{-2} \quad \textbf{and} \quad \dot{q}''_{60} < 250 \text{ kW·m}^{-2}$$

$$\text{then} \quad \dot{Q} < 80 \text{ kW} \quad \text{(nonpropagating fire)}$$

$$\text{else,} \quad \dot{Q} > 80 \text{ kW} \quad \text{(propagating fire)}$$

The HRR values over 80 kW in fact are flashover values of up to 2.5 MW, but the scheme does not assign a specific HRR number. Qualitatively, this scheme reflects the type of abrupt behavior change found in earlier studies (Figure 3-1.37), but here some more refined rules were developed that avoid nonpredictions that would occur from simple correlation. During the same CBUF project, a greatly more sophisticated mattress fire model has been developed by Baroudi et al.; this model is not easy to use, but details are given by Sundström[10] and Babrauskas et al.[109]

Office Workstations

Office worker cubicles (workstations) have been tested in several projects at NIST.[110–112] Figure 3-1.38 shows that very severe fire conditions can be generated by these arrangements. In some cases, fires of nearly 7 MW were recorded from the burning of a single person's workstation. The identification of the main conditions in these tests is given in Table 3-1.11. In one test series[111] replicates were tested in an open furniture calorimeter, then the configuration was tested again in a room test; this is illustrated in Figure 3-1.39.

Pallets

Conceptually, a wood pallet is a similar arrangement to a wood crib. The geometry, however, is different. Instead of being composed of identical rows of square-section sticks, pallets are made up of rectangular elements in a traditionally dimensioned configuration, Figure 3-1.40. The fire safety concern with pallets arises when they are idle and stacked many units high. Krasner[113] has reported on a number of tests in which the burning rate of pallets was measured. A typical experimental heat-release-rate curve is shown in Figure 3-1.41. This curve shows that,

Table 3-1.10 ***Results on Mattress from the CBUF Study***

Peak HRR Furniture Calorimeter (kW)	Peak HRR Room (kW)	Springs	Thickness (mm)	Thickness Factor	$\dot{q}''_{60}$	$\dot{q}''_{180}$	$\dot{q}''_{180} \times$ Thickness Factor	$\dot{q}''_{tot}$	Propagating Fire
26	42	sofabed	22	0.44	162	135	59	50	N
31	45	N	50	1.00	136	82	82	21	N
47	61	Y	10	0.20	225	227	45	43	N
47	NA	Y	20	0.40	111	118	47	45	N
275	NA	N	90	1.00	111	118	118	45	Y
348	471	Y	20	0.40	327	159	64	30	Y
313	1700	N	100	1.00	256	191	191	62	Y
917	2550	N	140	1.00	232	198	198	37	Y

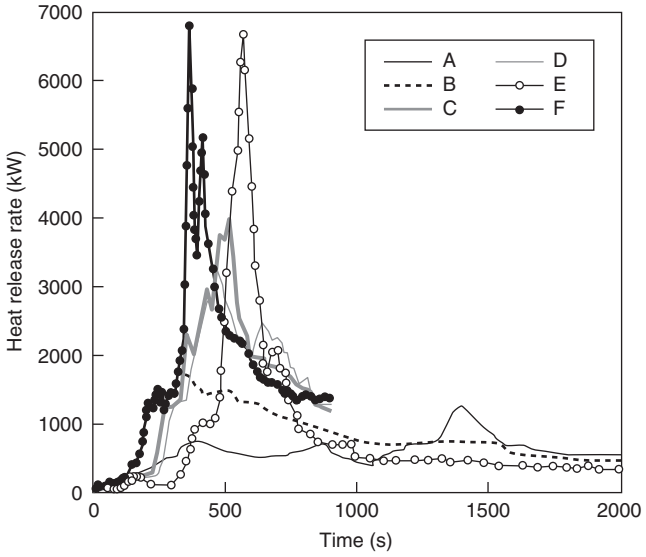

Figure 3-1.38. ***Office workstations.***

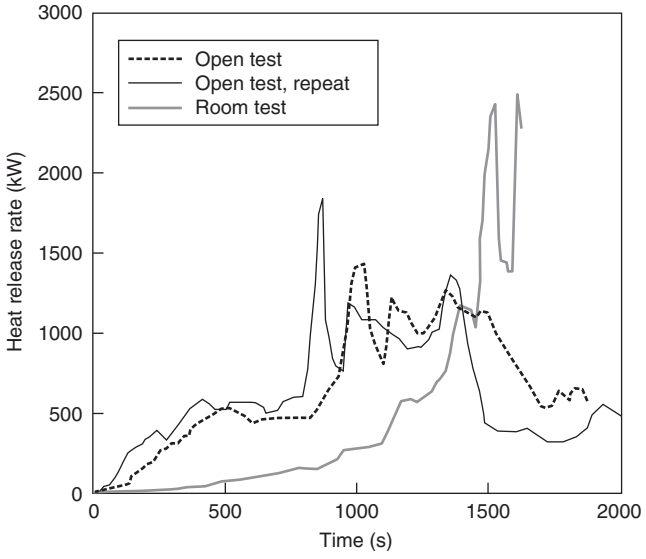

Figure 3-1.39. ***Identical workstations with old-style wood furniture tested under open burning and under room fire conditions.***

much like for a wood crib, a substantially constant plateau burning can be seen if the stack is reasonably high. The results for a standard pallet size of 1.22 × 1.22 m can be given as a general heat-release-rate expression:

$$\dot{q} = 1368(1 + 2.14h_p)(1 - 0.03M)$$

where h_p is stack height (m), M is moisture (%), and a net heat of combustion of 12×10^3 kJ·kg^{-1} has been assumed. For convenience in applying to nonstandard pallet sizes, this can be expressed on a per-unit-pallet-floor-area basis as

$$\dot{q}'' = 919(1 + 2.14h_p)(1 - 0.03M)$$

Table 3-1.11 ***Identification of Workstations in Figure 3.1.38***

Code	Combustible Mass (kg)	Description	Number of Sides with Acoustic Panels	Reference
A	291	Mostly old-style wood furniture	0	110
B	291	Semi-modern furniture	1	110
C	335	Modern furniture	2	112
D	—	Modern furniture	3	112
E	291	Modern furniture	4	110
F	—	Modern furniture	4	112

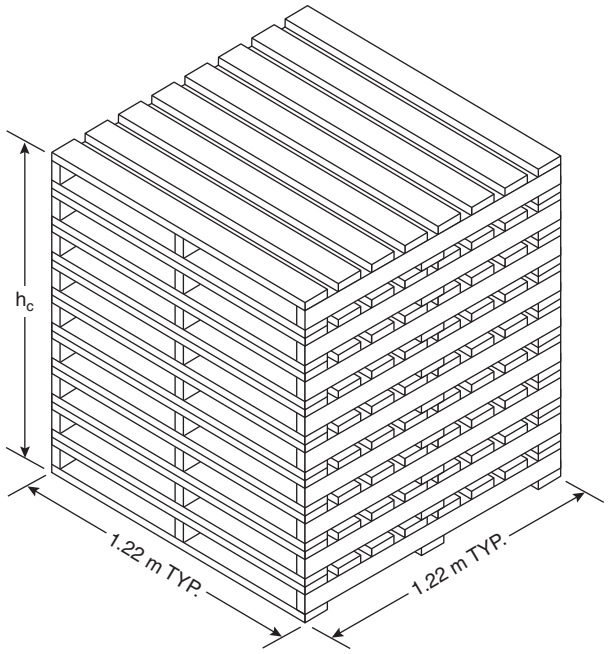

Figure 3-1.40. ***The geometric arrangement of a stack of wood pallets.***

The agreement between the above equations and experimental data is seen to be good over a wide range of pallet heights (Figure 3-1.42), but the expressions do somewhat overpredict the burning rates if applied to short stacks, with stack height $h_p < 0.5$ m.

Pillows

Pillow tests have been reported by NIST[114] and SP.[10] The results are given in Figure 3-1.43.

Pipe Insulation

The available data are from a configuration in which pipe insulation is used to cover the entire ceiling of a test

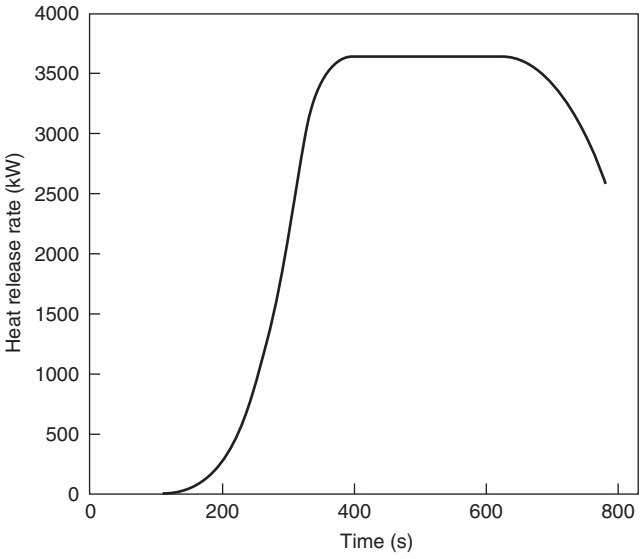

Figure 3-1.41. ***HRR of a typical wood pallet stack (1.22 × 1.22 × 1.22 m high).***

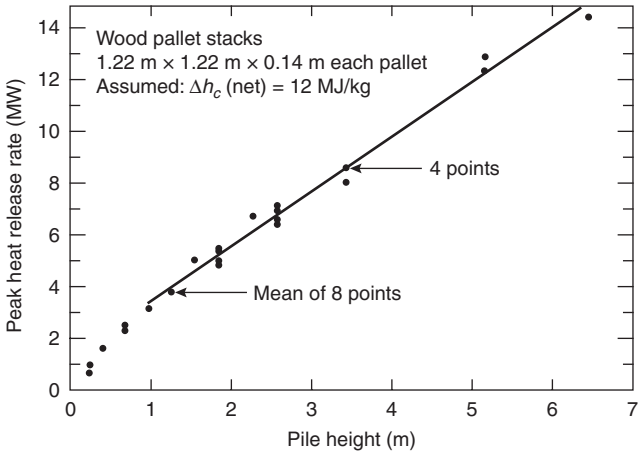

Figure 3-1.42. ***Dependence of pallet HRR on stack height.***

room. The test method used is a variant of ISO 9705, especially configured for pipe insulation testing.[115] Data on this configuration have been published by Wetterlund and Göransson[116] and by Babrauskas.[117]

Pools, Liquid or Plastic

Possibly the simplest geometric arrangement of fuel is a liquid (or thermoplastic) pool. Over the last four decades, an enormous number of studies have been conducted in which pool burning was considered theoretically or measured empirically. The most systematic early study was by two Russian researchers, Blinov and Khudiakov.[118] Their results were analyzed by Hottel,[119] who pointed out that conservation of energy can be applied to the pool:

$$\dot{q} = \dot{q}'' \times A = (\dot{q}''_r + \dot{q}''_c - \dot{q}''_{rr} - \dot{q}''_{\text{loss}})\left(\frac{\Delta h_c}{\Delta h_g}\right)A$$

where

$\dot{q}$ = the heat-release rate of the pool; double-prime denotes per unit area

A = the area of the pool (m²)

$\dot{q}''_r$ = the radiant heat flux absorbed by the pool

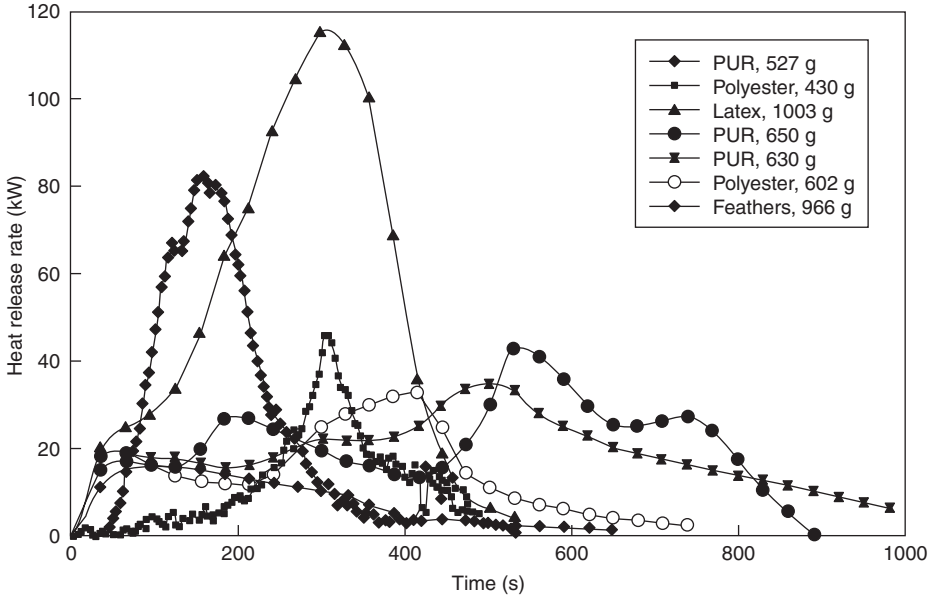

Figure 3-1.43. ***Pillows.***

$\dot{q}''_c$ = the convective heat flux to the pool
$\dot{q}''_{rr}$ = the heat flux reradiated from the surface of the pool
$\dot{q}''_{\text{loss}}$ = wall conduction losses and nonsteady terms (lumped together)

The heat of gasification is Δh_g (kJ/kg^{-1}), while the (lower, or net) heat of combustion is Δh_c. Note that some authors use the symbol L for the heat of gasification. The heat of gasification is defined as the enthalpy required to bring a unit of mass of liquid-phase substance at 25°C to the gaseous state at the temperature T_b, its boiling point. It should not be confused with the latent heat of evaporation Δh_v, which is the enthalpy required to change a unit mass of liquid to a gas at 25°C. The relation between these two quantities is

$$\Delta h_g = \Delta h_v + (T_b - 25) \times C_{pv}$$

where we have taken the simplification that C_{pv}, the heat capacity of the vapor (kJ/kg^{-1}·K^{-1}), is a constant. An extensive tabulation of these constants is provided by Babrauskas.[120]

Hottel's analysis of Blinov and Khudiakov's data showed two basic regimes are possible: radiatively dominated burning for large pool diameters, D, and convectively dominated burning for small D. Furthermore, in the convective regime, the flow can be either laminar or turbulent (being always turbulent for radiatively driven pools), while in the radiative regime, the flames can be optically thin or thick. These distinctions can, in the simplest analysis, be made solely on the basis of pool diameter. Such a simple classification is possible if the pool is strictly circular, radiant heating is only from the pool's flames and not augmented by external sources, and there are no interferences to the flow streamlines that could trip the onset of turbulence. In such a simplified case, the regimes can be identified as in Table 3-1.12.

In the convective limit (small pools), one may make the following approximation:

$$\dot{q} = \dot{q}''_c \cdot \frac{\Delta h_c}{\Delta h_g} \cdot A$$

However, the values of $\dot{q}''_c$ to be taken are not easily determined. Some additional details are given by Babrauskas.[121] For fire hazard analysis purposes, liquid pool fires will rarely be significantly dangerous if they are smaller than about 0.2 m in diameter. Thus, it will often only be necessary to treat pools burning in the radiative regime. In the radiative regime, it is found that data for most organic liquids can be well correlated by

$$\dot{q} = \Delta h_c \dot{m}''_\infty (1 - e^{-k\beta D}) \times A$$

Table 3-1.12 ***The Burning Regimes for Liquid Pools***

Diameter (m)	Burning Mode
< 0.05	Convective, laminar
0.05–0.2	Convective, turbulent
0.2–1.0	Radiative, optically thin
> 1.0	Radiative, optically thick

This requires determining two empirical constants: $\dot{m}''_\infty$ and the term kβ. These constants are given in Table 3-1.13 for a number of common fuels. The net heat of combustion, Δh_c, is also listed in the table. In principle, a slightly lower value, the *effective heat of combustion*, should be used instead of the net heat of combustion that is determined with oxygen bomb calorimetry. Some bench-scale values of a combustion efficiency factor to convert oxygen bomb values into experimentally measured values are given in Section 3, Chapter 4. For most liquids, however, the bench-scale values are not greatly below unity and realistic large-scale measurements are not available; thus the improvement in accuracy by extrapolating from bench-scale results may be nil.

Alcohol fuels show minimal radiative flux, in comparison to other fuel types. Thus, the best recommendation previously had been to use constant values of $\dot{m}''$, independent of diameter. Based on some newer test results,[122] it is clear that a diameter effect does exist, although it cannot be expressed in standard form. Thus, it is recommended that for methanol or ethanol the following values be used: $\dot{m}'' = 0.015$ ($D < 0.6$ m); $\dot{m}'' = 0.022$ ($0.6 < D < 3.0$ m); and $\dot{m}'' = 0.029$ ($D > 3.0$ m).

The above discussion implicitly assumed that the pool depth is at least several millimeters. If liquids are spilled on a horizontal surface that has no low spots and no diking, then a liquid layer will form that is less than 1 mm thick. *Thin-layer pools* of this nature (which can occur in arson cases) show a lower HRR than do pools of greater depths. Putorti et al.[123] studied gasoline spills on wood parquet, vinyl floor tiles, and carpeting. When a specified volume of liquid is spilled, the problem to be solved can be separated into two components: (1) determining the area of the spill, or, equivalently, the spill thickness; and (2) determining the HRR per unit area. For wood floors, Putorti found the $A = 1.5V$, where A = area (m^2) and V = volume (L). For vinyl tile, a similar relation was also found, but with the constant being 1.8. Converted into layer thicknesses, the thickness for wood was 0.67 mm and for vinyl tile it was 0.56 mm.

Earlier work has indicated that a relation of this kind should only be applied to smooth floor surfaces. For rough, absorptive surfaces a constant thickness is not obtained, and larger spill volumes produce, effectively, greater layer thicknesses.[124] Putorti's study with carpets both indicated large differences between carpet types and also showed that the data could not be represented as a constant layer thickness. The HRR per-unit-area values are shown in Figure 3-1.44. For solid-surface pours, spill areas were in the range 0.4–1.8 m^2. As presented above, pools of large depths in this size range would show HRR values of 1900–2400 kW·m^{-2}.

Thus, carpet-surface values are about 70–80 percent of values that would have been computed using the normal pool fire formulas. The smooth-surface values, however, are only about one-fifth of the values that would be found for pools of sizable depths. A similar study by Gottuk et al. (to be published) also describes HRR values for spills on hard surfaces that are, very roughly, about one fifth of those for normal pools. The relationships found by Putorti can only be expected to hold on dead-flat surfaces. If surfaces are crooked, then ponding at low spots will occur and uniform spill depths should never be anticipated.

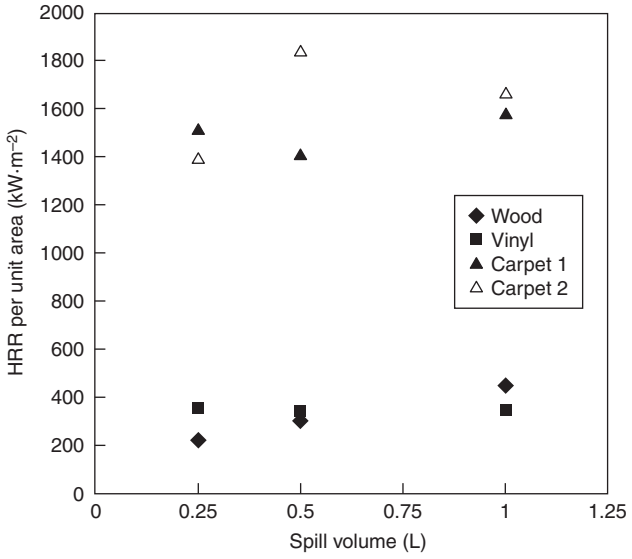

Figure 3-1.44. ***Thin pools of gasoline over various surfaces.***

The discussion above pertains only to *open-burning* fires. Thus, the literature-derived burning rates can be used only in the case of a very large, well-ventilated room (compared to the size of the fire). If calculations show that the free-burning pool would cause a temperature rise of more than, say, 100°C, then it is clear that radiative feedback will start being important and such an approximation cannot be made. No simple formulas exist for computing the enhanced burning rates when a pool receives significant room radiation. If computations under these conditions are necessary, the theoretical study of Babrauskas and Wickström[11] should be consulted. The computer program COMPF2[125] can also be used to treat this case.

The problem of pool burning is interesting from a combustion science point of view, and over the years there has been a very large number of studies that attempted to go beyond empirical predictions.[50,126–128] In addition, work is going on to provide more detailed experimental measurements for specific fuels.[129,130]

Television Sets

A limited amount of data are available on the HRR of television sets. Ahonen et al.[71] tested two old televisions with large wood cabinets. Babrauskas et al.[63] tested small

Table 3-1.13 ***Pool Burning: Thermochemical and Empirical Constants for a Number of Common Organic Fuels***

Material	Density (kg/m^{-3})	Δh_g (kJ/kg^{-1})	Δh_c (MJ/kg^{-1})	$\dot{m}''$ (kg/m^{-2}s^{-1})	k (m^{-1})
Cryogenics					
Liquid H_2	70	442	120.0	0.017 (±0.001)	6.1 (±0.4)
LNG (most CH_4)	415	619	50.0	0.078 (±0.018)	1.1 (±0.8)
LPG (mostly C_3H_8)	585	426	46.0	0.099 (±0.009)	1.4 (±0.5)
Alcohols					
Methanol (CH_3OH)	796	1195	20.0	See text	See text
Ethanol (C_2H_5OH)	794	891	26.8	See text	See text
Simple organic fuels					
Butane (C_4H_{10})	573	362	45.7	0.078 (±0.003)	2.7 (±0.3)
Benzene (C_6H_6)	874	484	40.1	0.085 (±0.002)	2.7 (±0.3)
Hexane (C_6H_{14})	650	433	44.7	0.074 (±0.005)	1.9 (±0.4)
Heptane (C_7H_{16})	675	448	44.6	0.101 (±0.009)	1.1 (±0.3)
Xylenes (C_8H_{10})	870	543	40.8	0.090 (±0.007)	1.4 (±0.3)
Acetone (C_3H_6O)	791	668	25.8	0.041 (±0.003)	1.9 (±0.3)
Dioxane ($C_4H_8O_2$)	1035	552	26.2	0.018	5.4
Diethyl ether ($C_4H_{10}O$)	714	382	34.2	0.085 (±0.018)	0.7 (±0.3)
Petroleum products					
Benzine	740	—	44.7	0.048 (±0.002)	3.6 (±0.4)
Gasoline	740	330	43.7	0.055 (±0.002)	2.1 (±0.3)
Kerosene	820	670	43.2	0.039 (±0.003)	3.5 (±0.8)
JP-4	760	—	43.5	0.051 (±0.002)	3.6 (±0.1)
JP-5	810	700	43.0	0.054 (±0.002)	1.6 (±0.3)
Transformer oil, hydrocarbon	760	—	46.4	0.039	0.7
Fuel oil, heavy	940–1,000	—	39.7	0.035 (±0.003)	1.7 (±0.6)
Crude oil	830–880	—	42.5–42.7	0.022–0.045	2.8 (±0.4)
Solids					
Polymethylmethacrylate	1184	1611	24.9	0.020 (±0.002)	3.3 (±0.8)
Polyoxymethylene $(CH_2O)_n$	1425	2430	15.7		
Polypropylene $(C_3H_6)_n$	905	2030	43.2		
Polystyrene $(C_8H_8)_n$	1050	1720	39.7		

polystyrene television cabinets of two types, fire-retardant and not. Since the circuit components contribute negligible HRR in comparison to the outer shell, only the cabinets were tested. Two very small (personal size) units were tested side-by-side in each test. This can represent either two appliances or simply the mass of one larger set. The results are given in Figure 3-1.45.

Transport Vehicles and Components

Passenger car HRR was measured at the Fire Research Station[131] and at VTT.[132] The FRS laboratory examined a 1982 Austin Maestro and a 1986 Citroën BX. VTT examined a Ford Taunus, a Datsun 160, and a Datsun 180. The dates of manufacture were stated only as late 1970s. In the FRS tests, the Austin measured a peak of 8.5 MW, while the Citroën a peak of 4.5 MW. For the VTT tests, the peak HRR values were all approximately 1.5–2.0 MW. These numbers are rather widely disparate and it is not fully clear why, except that this is not due to the fraction of polymer content onboard. The HRR curves are shown in Figure 3-1.46.

Tests on transport seating (Figure 3-1.47) were also done at SP.[133] They measured an array of four double bus seats and a similar arrangement of train seats. The foam was HR polyurethane, while the cover was a viscose/wool/polyester/polyamide blend for the bus seats and 100 percent wool fabric for the train seats.

Vehicle tires can ignite from an overheated axle and can release a substantial amount of heat if they burn. There is one study in the literature that documents such a fire. Hansen[134] burned a pair of 285/80 R22.5 truck tires mounted in a tandem wheel arrangement. The HRR curve is given in Figure 3-1.47. Vehicle tires are also prone to be ignited and to burn in tire dumps. The HRR will depend directly on the geometry and on the amount of tires involved. Some quantitative HRR experiments have been reported[135] on experiments done at the Fire Research Station. These experiments were for flaming tires, but most recent tire dump problems have been associated with a smoldering condition and no HRR quantification under these conditions has been reported.

Half a tram car was tested at SP.[61] The most recent HRR data on transport vehicles came from a European research program where nearly two dozen vehicles were tested, including cars, buses, trams, trucks, and rail vehicles. The peak HRR values for many of these tests ranged about 10–35 MW (Figure 3-1.48). However, one test involved a truck loaded with 2 metric tons of modern upholstered furniture. The peak HRR for this vehicle was found

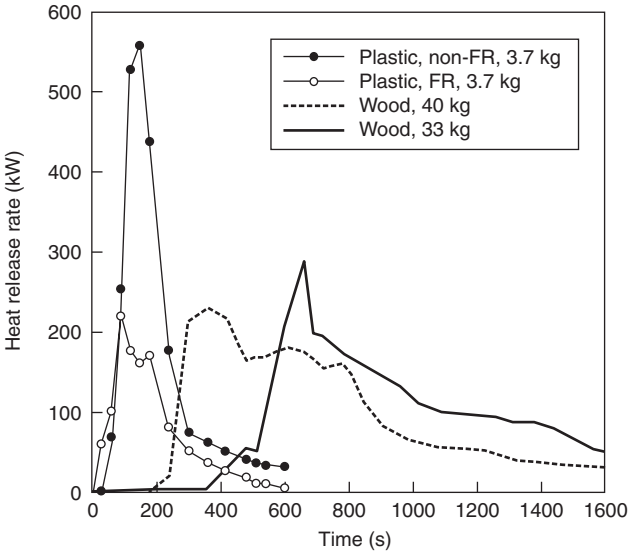

Figure 3-1.45. ***Television sets.***

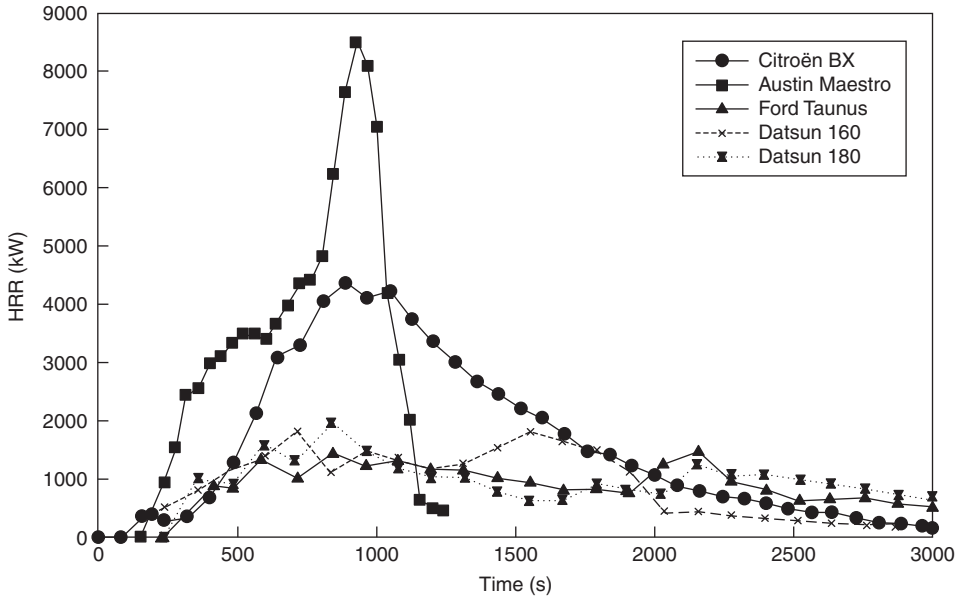

Figure 3-1.46. ***Passenger cars.***

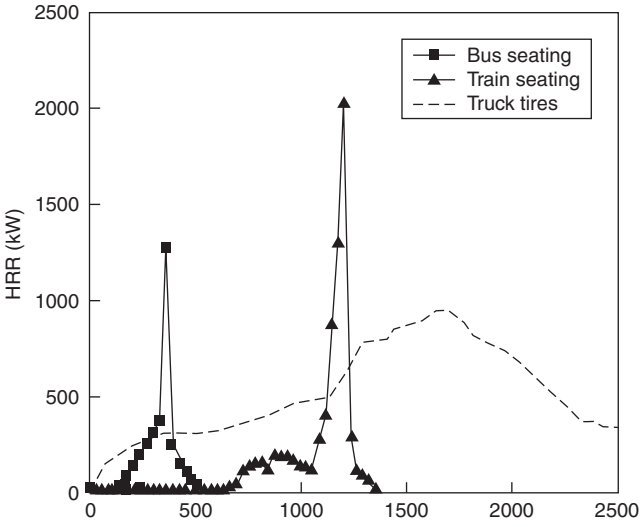

Figure 3-1.47. ***Vehicle seating and tires.***

to be approximately 120 MW. These series of tests have been documented in a book dedicated to the subject of tunnel safety.[136]

Trash Bags and Containers

Bench-scale measurements of trash are not readily feasible, due to the naturally irregular arrangement of these combustibles. There are full-scale test results available, however, that can suggest appropriate values to be used in different circumstances. A small bathroom-size (6.6-L) plastic wastebasket stuffed with 12 milk cartons shows an HRR of about 50 kW, sustained for about 200 s; this has been used extensively as an ignition source in early HRR testing.[38] Some typical trash-bag fires are shown in Figure 3-1.49.[88] Lee has correlated the peak heat release values according to the effective base diameter and packing density.[88] Figure 3-1.50 shows that the total burning rate (kW) increases with effective base diameter, but decreases with the tighter packing densities. Figure 3-1.51, conversely, illustrates that when the results are normalized per unit base area, a downward trend can be seen. The correlations according to packing density should only be considered rough observations, and not firm guidelines. Table 3-1.14 shows some additional data,[71] in which, over a certain range, increasing packing density increases the heat release rate. For design purposes, the range of 50 kW to 300 kW appears to cover the bulk of the expected fires from normal residential, office, airplane, or similar occupancy trash bags and trash baskets.

Upholstered Furniture

The HRR of upholstered furniture can be determined in three different ways: (1) by room fire testing; (2) by testing in the furniture calorimeter; (3) by conducting bench-scale tests in the cone calorimeter and then using a mathematical method to predict the full-scale HRR. Of all the occupant goods that can be found in a normal residence, upholstered furniture normally has the highest HRR, thus knowledge of its performance is essential for many applications. Until the 1970s, upholstered furniture used to be made from traditional materials. Thus, in the United States during the 1950s and 1960s, furniture commonly had a wood frame, steel springs, cotton batting padding, and an upholstery fabric of a natural fiber such as wool, silk, or cotton. A fraction of the furniture used latex foam padding instead of cotton batting. In earlier-yet times, furniture was commonly stuffed with rubberized

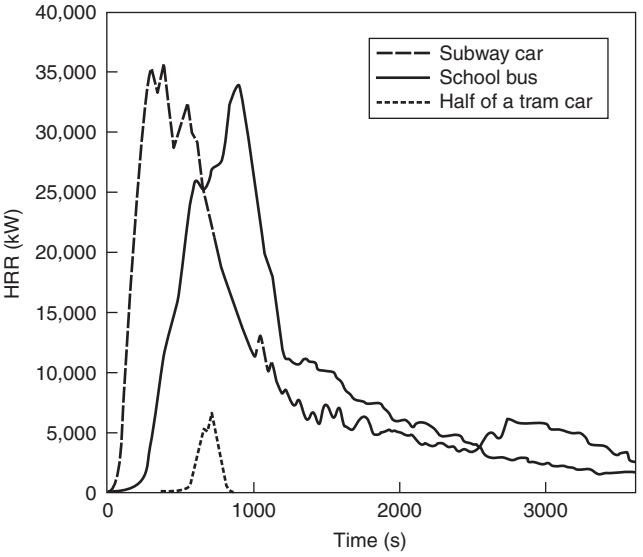

Figure 3-1.48. ***Transport vehicles.***

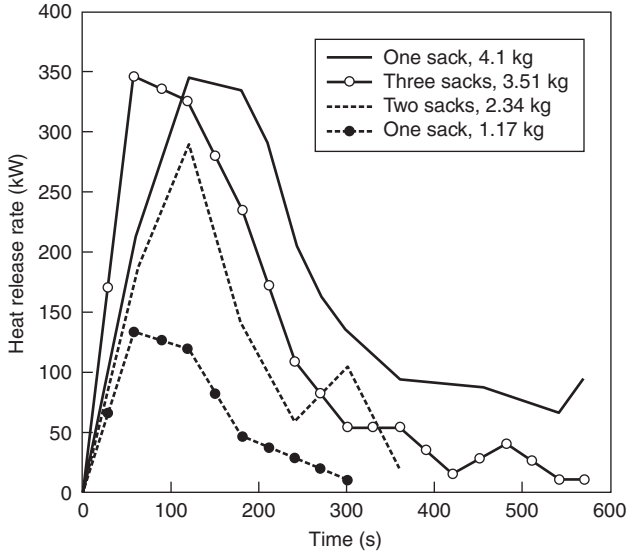

Figure 3-1.49. ***Trash bags.***

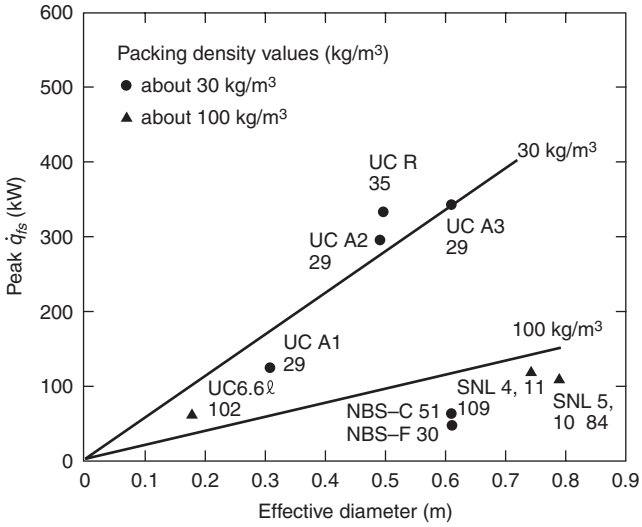

Figure 3-1.50. ***Trash heat release rates (total HRR).***

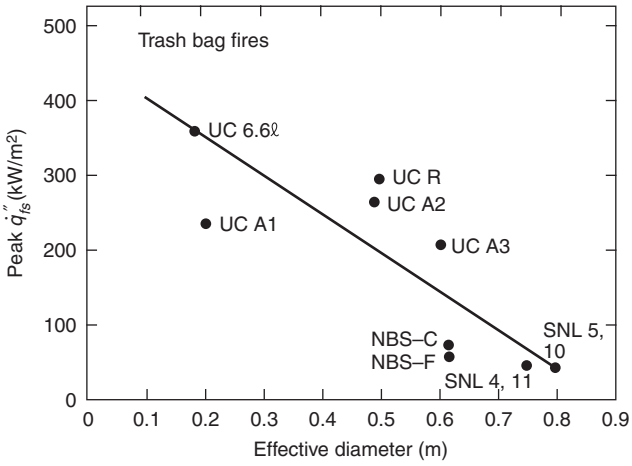

Figure 3-1.51. ***Trash heat release rates, normalized per unit base area.***

horse hair. By the 1970s, however, the predominant padding material became polyurethane foam, and fabric selection became very wide, including both thermoplastic synthetics and natural fibers. The HRRs of the modern furniture were found to be many times those of traditional types,[137] apart from the special case of latex foam. The latter shows HRR values distinctly higher than for polyurethane foam, but the material has a finite life and few specimens would survive to this day.

Figure 3-1.52 illustrates several furniture items tested at NIST.[2] Chair F21 used polyurethane foam complying with the California TB 117 standard[138] and polyolefin fabric. A specimen using ordinary polyurethane foam gave essentially identical results. This level of performance represents a very common but, unfortunately, worst-performance furniture item widely bought by consumers. Specimen F32 is a sofa made from the same materials. Chair F24 illustrates the large improvement in HRR when cotton fabric is substituted for polyolefin fabric. The peak HRR decreases by about one-third, from 2 MW to 700 kW. Further improvements, at present, are not readily available on the retail market. Contract furniture can be procured to advanced specifications, however, notably California TB 133.[138] The latter limits the peak HRR to values less than 80 kW, which will present negligible fire hazard in almost any circumstance.

A cone calorimeter–based prediction method was proposed by Babrauskas and Walton, based on data obtained in 1982.[139] This was the earliest effort, and was based on a data set comprising materials primarily from the 1970s. Since that time, however, the materials in use by the furniture makers have changed substantially, and, especially, some highly improved materials became available to the contract furniture market. In addition, predictive techniques readily available in the early 1980s were less sophisticated than those developed more recently. Thus, during the course of the European fire research program CBUF, two new predictive models were developed.[10,109] Model I is a relatively simple model and is described below briefly. A more advanced model was also developed and its details are provided in the above references.

To use the CBUF Model I, cone calorimeter data must first be obtained at an irradiance of 35 $kW \cdot m^{-2}$. A well-controlled specimen preparation method is needed, and this is provided in ASTM E1474.[140] Then, one determines if the furniture item is likely to sustain a propagating fire, or whether a moderate external flame source will simply result in limited burning and no propagation. This is determined from the 180-s average of cone calorimeter HRR results. If $\dot{q}''_{180} < 65\ kW/m^{-2}$, then no propagation is

Table 3-1.14 ***Some Data Obtained at VTT on 14-L Polyethylene Wastebaskets Showing Effect of Packing Density and Basket Construction***

Basket Sides	Basket Mass (kg)	Filling Type	Filling Mass (kg)	Filling Density (kg/m^{-3})	Peak HRR (kW)	Total Heat Released (MJ)
Solid	0.63	Shredded paper	0.20	14	4	0.7
Netted	0.63	Milk cartons	0.41	29	13	3.0
Solid	0.53	Shredded paper	0.20	14	18	7.3
Netted	0.53	Milk cartons	0.41	29	15	5.8

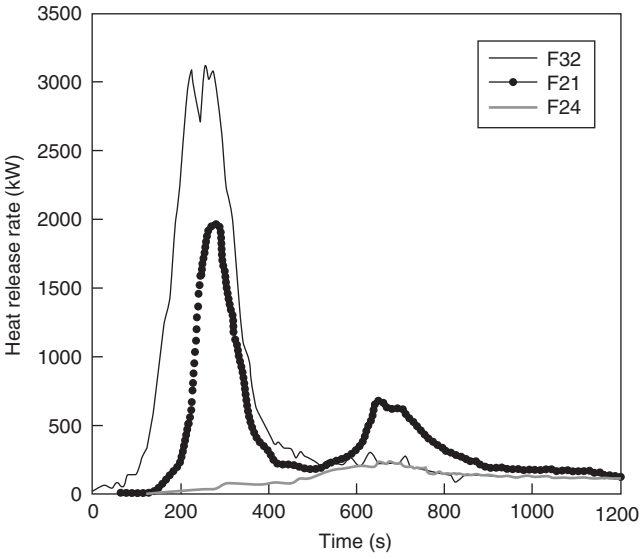

Figure 3-1.52. ***Several upholstered furniture items tested by NIST.***

assumed to occur; otherwise further calculations are made to estimate the peak HRR. The scheme is as follows:

$$\text{if} \quad (x_1 > 115) \quad \text{or} \quad (\dot{q}''_{35-\text{tot}} > 70 \quad \text{and} \quad x_1 > 40) \quad \text{or}$$
$$(\text{style} = \{3,4\} \quad \text{and} \quad x_1 > 70) \qquad \text{then} \quad \dot{q}_{fs} = x_2$$

Else,

$$\text{if} \quad x_1 < 56 \qquad \text{then} \quad \dot{q}_{fs} = 14.4x_1$$
$$\text{else,} \quad \dot{q}_{fs} = 600 + 3.77x_1$$

where $x_1 = (m_{\text{soft}})^{1.25}$ (style factor A) $(\dot{q}''_{35-pk} + \dot{q}''_{35-300})^{0.7}$ $(15 + t_{ig-35})^{-0.7}$ and the subscript 35 denotes that the cone calorimeter HRR tests run at a 35-kW·m^{-2} irradiance. The m_{soft} is the mass of the soft, that is, combustible, parts of the item (kg); it includes fabric, foam, interliner, dust cover, and so forth, but does not include the frame nor any rigid support pieces. In addition,

$$x_2 = 880 + 500(m_{\text{soft}})^{0.7} \text{ (style factor A)} \left(\frac{\Delta h_{c,\text{eff}}}{\dot{q}''_{35-\text{tot}}}\right)^{1.4}$$

Here, $\Delta h_{c,\text{eff}}$ is the test-average effective heat of combustion in the cone calorimeter (MJ·kg^{-1}), and $\dot{q}''_{35-\text{tot}}$ is the total heat released at a flux of 35 kW·m^{-2}. Another correlation predicts the total heat release:

$$q_{\text{tot}} = 0.9m_{\text{soft}} \times \Delta h_{c,\text{eff}} + 2.1(m_{\text{comb,tot}} - m_{\text{soft}})^{1.5}$$

where $m_{\text{comb,tot}}$ denotes the total combustible mass of the item (kg), that is, everything except metal parts.

Finally, the time to peak, t_{pk} (s) for the full-scale item is estimated as

$$t_{pk} = 30 + 4900(\text{style factor B}) \times (m_{\text{soft}})^{0.3}(\dot{q}''_{\text{pk\#2}})^{-0.5}(\dot{q}''_{\text{trough}})^{-0.5}(t_{\text{pk\#1}} + 200)^{0.2}$$

where the peak and trough subscripts refer to the fact that, in the general case, the cone calorimeter HRR of furniture composites shows two main peaks and one trough in between them. The style factors are obtained from Table 3-1.15. With these values computed, a triangular HRR curve can then be constructed. The peak HRR and the time to peak are given directly, while the base width of the triangle is determined from the calculated total heat release of the furniture item.

Wall/Ceiling Lining Materials

Combustible interior finish materials are substantially more difficult to treat than free-standing combustibles. They cannot be measured in a device such as the furniture calorimeter, and require any full-scale study to be a room fire. The materials cover a large area, but the area of active flame involvement is generally not predictable, except after flashover, when in many cases it can be assumed that all surfaces are involved. In the early 1980s, a series of wall materials was studied by Lee at NIST[15] in full-scale, and also in bench-scale, room fires with the cone calorimeter. This work comprised the first attempted correlation between bench scale and full scale for wall lining materials. For several materials in the test series, which included both cellulosics and plastics, it was found that, after flashover, the per-unit-area, full-scale heat-release rates, were approximately the same as the values obtained from the cone calorimeter. Lee's work did not yet lead to a predictive method, since no technique for estimating the flame-covered area, $A(t)$, was found.

At about the same time, Babrauskas found that full-scale fire development on wall/ceiling linings could be

Table 3-1.15 ***Style Factors Used in the CBUF Model for Predicting Upholstered Furniture Heat Release Rates***

Type of Furniture	Style Factor A	Style Factor B
Armchair, fully upholstered, average amount of padding	1.0	1.0
Sofa, 2-seat	1.0	0.8
Sofa, 3-seat	0.8	0.8
Armchair, fully upholstered, highly padded	0.9	0.9
Armchair, small amount of padding	1.2	0.8
Wingback chair	1.0	2.5
Sofa-bed (convertible)	0.6	0.75
Armchair, fully upholstered, metal frame	1.0	0.8
Armless chair, seat and back cushions only	1.0	0.75
Two-seater, armless, seat and back cushions only	1.0	1.0

approximated[141] by the expression $\dot{q}''_{bs-pk}/t_{ig}$, where the HRR value and the ignition time were obtained from the cone calorimeter. The $1/t_{ig}$ factor effectively represented the growth of $A(t)$, but such a scheme was only semi-quantitative.

The first successful quantitative method came with the work of Wickström and Göransson in 1987.[142] The model was based on the premise that the full-scale scenario involves the combustible materials located on the walls and ceiling of the ISO 9705 room. Note that the same material is expected to be placed on both walls and ceiling. The model uses the principle of area convolution and elaborates on Babrauskas' assumption that $1/t_{ig}$ controls the growth of the burning area. The model was later extended and extensively validated in the European research program EUREFIC, *EU*ropean *RE*action to *FI*re *C*lassification.[143] The primary assumptions in the model are

1. The burning area growth rate and the HRR are decoupled.
2. The burning area growth rate is proportional to the ease of ignition, that is, the inverse of the time to ignition in small scale.
3. The history of $\dot{q}''$ at each location in the full scale is to be the same as in the cone calorimeter test.

The model pays mind to the observation that burning patterns on wall/ceilings can be very different and, especially, that some products stop spreading fire under certain conditions, while others continue. The basic area growth regimes are illustrated in Figure 3-1.53, where the regimes are marked in Roman numerals. The fire spread may follow three different routes. At points A and B fire spread may or may not continue, based on whether a calculated fictitious surface temperature is higher than a critical value. The calculation is based on data from the cone calorimeter. Within the different flame spread regimes, the burning area growth rate depends on ignitability, that is, time to ignition in the cone calorimeter. Once the flame spread rate is determined, the HRR is calculated assuming that $\dot{q}''$ is the same in small and large scale. This is understood to be a simplification. The HRR depends on the actual heat flux level received by the product as a function of time. Experience showed, however, that the errors average out and can be included in empirical constants. The method is only moderately difficult to apply, but the description is somewhat lengthy. Details are contained in Babrauskas and Grayson.[22] This reference also contains graphs illustrating the kind of agreement that is obtained between predictions and experiments.

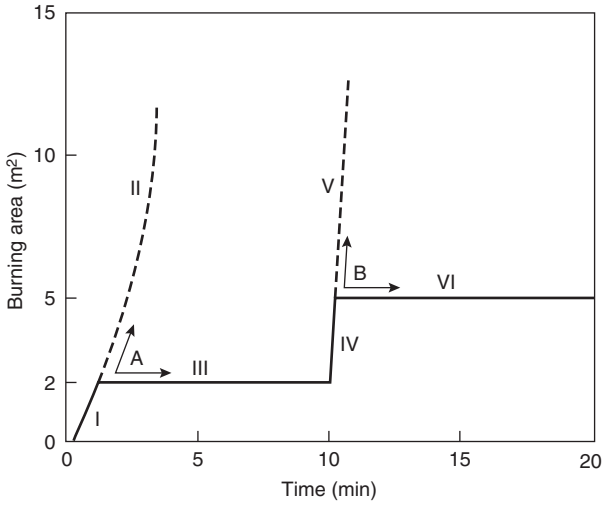

Figure 3-1.53. ***EUREFIC fire spread regimes.***

While highly successful for its intended purpose, the EUREFIC model does have notable limitations. This model:

- Can only treat the standard ISO 9705 room, with the standard doorway for ventilation
- Only predicts the ISO 9705 100 kW/300 kW burner
- Requires that the material be on both walls and ceiling
- Cannot deal with products that do not ignite in the cone calorimeter at a 25-kW·m^{-2} irradiance.

It must be remembered that the primary purpose for developing this model was to predict product performance categories to be obtained in the ISO 9705 test, while only using bench-scale cone calorimeter data. For its intended purpose, it has been an unquestionable success.

The above limitations indicate that the EUREFIC model, while a major breakthrough, was certainly not the final answer to modeling needs for wall/ceiling products. Two extensions have been proposed to generalize the applicability of this model. Göransson, one of the developers of the EUREFIC model, proposed an extension[144] to encompass a huge-scale room. Such a test room was constructed at VTT. Its dimensions were 6.75 m by 9.0 m, with a ceiling height of 4.9 m. The door opening, 0.8 by 2.0 m high, however, was the same as for the ISO 9705 room. The burner operation was at the 100-kW level for 10 min, then at 300 kW for another 10 min, finally at 900 kW for 10 more minutes. An extended model was created for this situation by introducing a new set of regimes to correspond to the 900-kW burner level. In addition, it was found that the constant had to be modified for the 100-kW and 300-kW time periods. The agreement between model and prediction was very good, but only five tests were available for validation at the huge scale.

A second extension was developed by Sumathipala and coworkers.[145,146] This model extends the applicability to the case of the room fire test studied by Lee.[15] The dimensions of that room are almost identical to the ISO room. The differences arise because (a) the two burner regimes are 40 kW and 160 kW, (b) the burner face size is different, and (c) the product is normally mounted on walls only, rather than walls and ceiling. The authors, however, in their development work included tests of both rooms in both mounting configurations. The success of these extensions confirms that the basic ideas behind the EUREFIC model are sound and can potentially have flexibility. On the other hand, it must be borne in mind that even the extensions are hard-wired configurations and do not yet approach a technique that could be applicable towards user-selected room sizes, burner levels, and product configurations.

Perhaps the most ambitious model so far for wall/ceiling products has been one developed by Karlsson and coworkers.[147,148,149] Karlsson's model incorporates much more of current concepts of plumes, flame length calculations, ceiling jets, and similar constructs than does the EUREFIC model. The model has the same hard-wired limitations that the EUREFIC model has in terms of ignition sources, product configuration, and room size being fixed. Another wall/ceiling model was developed by Quintiere and Cleary[40,150,151] and extended by Janssens and coworkers.[152]

Wardrobes

Information on the HRR of wardrobes is available from a NIST study.[153] The test wardrobes are illustrated in Figure 3-1.54; data are given in Table 3-1.16 and Figure 3-1.55. The wardrobes were outfitted with a small amount of clothing, or simulated clothing, and some paper. Tests were not run on the clothes items by themselves. However, since in the case of the steel wardrobe, the only other combustible present was the paint on the metal, it is reasonable to assign a value of about 270-kW peak for the 1.93-kg clothes load. The most important conclusion, however, was that, for combustible constructions, the peak HRR is inversely dependent on wardrobe panel thickness (and, by contrast, no simple connection to combustible specimen mass is seen). Thus, while the total heat content of the 19-mm particleboard specimen is high (see Table 3-1.16), its peak HRR is quite low, since flame spread and fire involvement proceed more slowly over a thick material.

Windows, Plastic

In applications where vandal resistance is needed, polycarbonate windows are sometimes used. This material is combustible, and limited testing was reported by Peacock et al.[154] The tests indicated that it is hard to derive an innate HRR value. The windows do not burn unless a sustained flame or heat source is applied. In that case, the HRR of the product increases with increasing severity of the ignition source. For a 50-kW exposure source, a test window showed an additional 50-kW HRR, with a burning time of approximately 80 s. For a 200-kW exposure source, the window peak HRR was about an additional 250 kW, but with a longer duration of about 200 s, at progressively diminishing HRR values.

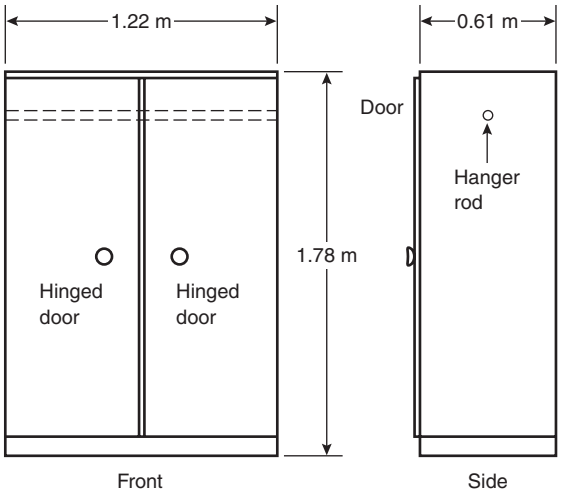

Figure 3-1.54. ***Configuration of the tested wardrobes.***

Estimating the HRR for General Combustibles

The previous edition of the Handbook suggested a hypothetical method for estimating the HRR for general combustibles. This was based on some very simplified assumptions, especially that flame spread could, in the first approximation, be ignored. Further experience gained with additional classes of combustibles, as discussed above, suggests that such a condition will only very rarely hold. Furthermore, the user has no way of knowing when it might hold. Thus, prudent design practice should now demand that first recourse be made to the specific sections above that may address the modeler's needs. If they do not, then testing is indicated. For the modeler wishing to start up a major research activity, the schemata outlined for upholstered furniture, mattresses, and wall/ceiling lining should serve as illustrations of appropriate starting points in theory and practice. It must be pointed out, however, that such research programs have proved to be complex and that quick or inexpensive results cannot be expected.

Uncertainty of HRR Measurements

As in any engineering measurement, uncertainty in HRR measurements can be subdivided into (1) bias and (2) random error, sometimes termed *precision uncertainty.* Bias is properly minimized by use of calibration standards; for HRR testing this often comprises a metered flow of a calibration gas of high purity. Another source of bias that can be minimized, when appropriate, is specific to oxygen consumption calorimetry bases measurements. For most testing, a standard oxygen consumption constant value of 13.1 $MJ \cdot kg^{-1}$ of oxygen consumed is used. A small number of substances of fire safety interest show oxygen consumption constants substantially different from this standard value. If the molecular composition of the substance is known, a correction can always be made to eliminate this source of bias.

Most of the instruments in which the HRR measurements are made have been subjected to round robins (interlaboratory trials) to quantify the magnitude of random error that can be expected. Comparative values have been compiled by Janssens,[155] as shown in Table 3-1.17. For a number of them, several round robins have been conducted, thus the data shown are identified by year. SBI denotes the European Single Burning Item test,[156] which is a regulatory HRR test for building products that uses two wall panels in a corner configuration, without a ceiling. Observe that the values tabulated refer to the 95 percent confidence intervals; standard deviations can be obtained by dividing the figures shown by 2.8.

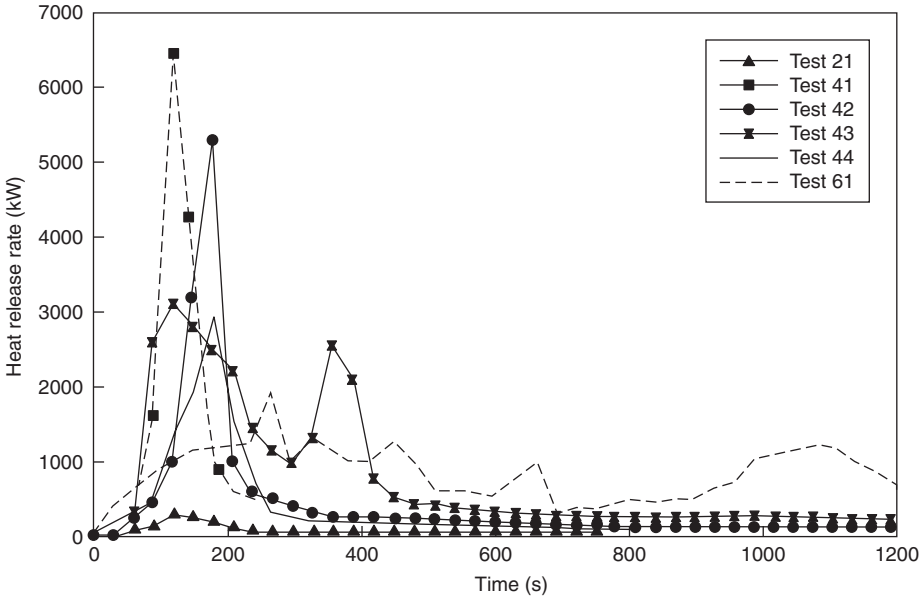

Figure 3-1.55. ***Various wardrobes.***

Table 3-1.16 ***The Heat Release Rate Properties of Wardrobes***

Test Number	Construction	Wardrobe Combustible Mass (kg)	Clothing and Paper (kg)	Peak HRR (kW)	Total Heat Released (MJ)	Average Heat of Combustion (MJ/kg^{-1})
21	Steel	0	1.93	270	52	18.8
43	Plywood, 12.7 mm thick	68.3	1.93	3100	1068	14.9
41	Plywood, 3.2 mm thick, unpainted	36.0	1.93	6400	590	16.9
42	Plywood, 3.2 mm thick, 1 coat FR paint	37.3	1.93	5300	486	15.9
44	Plywood, 3.2 mm thick, 2 coats FR paint	37.3	1.93	2900	408	14.2
61	Particleboard, 19 mm thick	120.3	0.81	1900	1349	17.5

Table 3-1.17 ***The 95 Percent Confidence Limits for Heat Release Rate Test Apparatuses as Determined from Recent Round Robins***

				Peak HRR		Total HRR	
Apparatus	Year	Labs	Levels	*r* (%)	*R* (%)	*r* (%)	*R* (%)
Cone calorimeter	2000	4	16	17	23	8	15
ICAL	1999	3	8	56	67	72	118
SBI	1997	16	30	38	54	47	71
Room calorimeter	1994	12	5	65	79	25	41

Note that *r* denotes the repeatability value whereas *R* denotes the reproducibility value.

References Cited

1. V. Babrauskas, and R.D. Peacock, "Heat Release Rate: The Single Most Important Variable in Fire Hazard," *Fire Safety J.* 18, pp. 255–272 (1992).
2. V. Babrauskas, J.R. Lawson, W.D. Walton, and W.H. Twilley, "Upholstered Furniture Heat Release Rates Measured with a Furniture Calorimeter," *NBSIR 82-2604,* National Bureau of Standards, Washington, DC (1982).
3. G. Heskestad, "A Fire Products Collector for Calorimetry into the MW Range" *FMRC J. I. OC2El.RA,* Factory Mutual Research Corp., Norwood, MA (1981).
4. "Standard Test Method for Fire Testing of Real Scale Upholstered Furniture Items," *ASTM E 1537,* American Society for Testing and Materials, Philadelphia (1993).
5. "Standard Test Method for Fire Testing of Real Scale Mattresses," *ASTM E 1590,* American Society for Testing and Materials, Philadelphia (1994).
6. "Pipe Insulation: Fire Spread and Smoke Production—Full-Scale Test," *NT FIRE 036,* NORDTEST, Espoo, Finland (1988).
7. "Upholstered Furniture: Burning Behaviour—Full-Scale Test," *NT FIRE 032,* 2nd ed., NORDTEST, Espoo, Finland (1991).
8. "Standard Fire Test of Limited-Smoke Cables, UL 1685," Underwriters Laboratories, Northbrook, IL (1991).
9. M.M. Hirschler, "Use of Heat Release Calorimetry in Standards," in *Fire Calorimetry, DOT/FAA/CT-95/46,* Federal Aviation Administration, Atlantic City International Airport, NJ, pp. 69–80 (1995).
10. B. Sundström (ed.), "Fire Safety of Upholstered Furniture—The Final Report on the CBUF Research Programme," *Report EUR 16477 EN,* Directorate-General Science, Research and Development (Measurements and Testing), European Commission, Distributed by Interscience Communications Ltd., London (1995).
11. V. Babrauskas, and U.G. Wickström, "Thermoplastic Pool Compartment Fires," *Combustion and Flame,* 34, pp. 195–201 (1979).
12. M. Dahlberg, "Error Analysis for Heat Release Rate Measurement with the SP Industry Calorimeter," *SP Report 1994:29,* Swedish National Testing and Research Institute, Borås (1994).
13. L.Y. Cooper, "Some Factors Affecting the Design of a Calorimeter Hood and Exhaust," *J. Fire Prot. Engineering,* 6, pp. 99–112 (1994).
14. F.L. Fisher and R.B. Williamson, "Intralaboratory Evaluation of a Room Fire Test Method," *NBS-GCR-83-421,* National Bureau of Standards, Washington, DC (1983).
15. B.T. Lee, "Standard Room Fire Test Development at the National Bureau of Standards," in *Fire Safety: Science and Engineering, ASTM STP 882* (T.Z. Harmathy, ed.), American Society for Testing and Materials, Philadelphia (1985).
16. B. Sundström, "Room Fire Test in Full Scale for Surface Products," *Rapport SP-RAPP 1984:16,* Statens Provningsanstalt, Borås, Sweden (1984).
17. "Surface Products: Room Fire Tests in Full Scale," *NT FIRE 025,* NORDTEST, Espoo, Finland (1986).
18. "International Standard—Fire Tests—Full Scale Room Test for Surface Products," *ISO 9705:1993(E),* International Organization for Standardization, Geneva (1993).
19. V. Babrauskas, "Development of the Cone Calorimeter—A Bench Scale Heat Release Rate Apparatus Based on Oxygen Consumption," *Fire and Materials,* 8, pp. 81–95 (1984).
20. "Standard Test Method for Heat and Visible Smoke Release Rates for Materials and Products Using an Oxygen Consumption Calorimeter," *ASTM E 1354,* American Society for Testing and Materials, Philadelphia (1997).
21. "International Standard—Fire Tests—Reaction to Fire—Part 1: Rate of Heat Release from Building Products (Cone Calorimeter Method)," *ISO 5660-1:1993(E),* International Organization for Standardization, Geneva (1993).
22. V. Babrauskas and S.J. Grayson (eds.), *Heat Release in Fires,* Elsevier Applied Science Publishers, London (1992).
23. J. Urbas and G.E. Luebbers, "The Intermediate Scale Calorimeter Development," *Fire and Materials,* 19, pp. 65–70 (1995).
24. "Standard Test Method for Determining of Fire and Thermal Parameters of Materials, Products, and Systems Using an Intermediate Scale Calorimeter (ICAL)," *ASTM E 1623,* American Society for Testing and Materials, Philadelphia.
25. V. Babrauskas, "A Closed-Form Approximation for Post-Flashover Compartment Fire Temperatures," *Fire Safety J.,* 4, pp. 63–73 (1981).
26. M. Kokkala, U. Göransson, and J. Söderbom, "Five Large-Scale Room Fire Experiments. Project 3," *EUREFIC Fire Research Program (VTT Publications 104),* VTT-Technical Research Center of Finland, Espoo (1992).
27. W.J. Parker, "Prediction of the Heat Release Rate of Wood," Ph.D. Dissertation, George Washington University, Washington, DC (1988).
28. T. Hirata, T. Kashiwagi, and J.E. Brown, "Thermal and Oxidative Degradation of Poly(methylmethacrylate): Weight Loss," *Macromolecules,* 18, pp. 1410–1418 (1984).
29. T. Kashiwagi, T. Hirata, and J.E. Brown, "Thermal and Oxidative Degradation of Poly(methylmethacrylate): Molecular Weight," *Macromolecules,* 18, pp. 131–138 (1985).
30. C. Vovelle, J.L. Delfau, M. Reuillon, J. Bransier, and N. Laraqui, "Experimental and Numerical Study of the Thermal Degradation of PMMA," in *Papers of ITSEMAP International Meeting of Fire Research and Test Centers,* Avila, Spain, pp. 43–66 (1986).
31. K.A. Holland and I.D. Rae, "Thermal Degradation of Polymers, Part 3. Thermal Degradation of a Compound Which Models the Head-to-Head Linkage in Poly(Methyl Methacrylate)," *Australian J. of Chemistry,* 40, pp. 687–692 (1987).
32. L.E. Manring, "Thermal Degradation of Saturated Poly(methylmethacrylate)," *Macromolecules,* 21, pp. 528–530 (1988).
33. A. Inaba, T. Kashiwagi, and J.E. Brown, "Effects of Initial Molecular Weight on Thermal Degradation of Poly(methyl methacrylate), Part 1," *Polymer Degradation and Stability,* 21, pp. 1–20 (1988).
34. K.D. Steckler, T. Kashiwagi, H.R. Baum, and K. Kanemaru, "Analytical Model for Transient Gasification of Noncharring Thermoplastic Materials," in *Fire Safety Science—Proceedings of the Third International Symposium,* Elsevier Applied Science, New York, pp. 895–904 (1991).
35. K. Opstad, "Modelling of Thermal Flame Spread on Solid Surfaces in Large-Scale Fires," Ph.D. Dissertation, Norges Tekniske Høgskole, Trondheim, Norway (1995).
36. V. Babrauskas, "Specimen Heat Fluxes for Bench-Scale Heat Release Rate Testing," *Fire and Materials,* 19, pp. 243–252 (1995).
37. "Basic Considerations in the Combustion of Hydrocarbon Fuels in Air," *NACA Report 1300,* National Advisory Committee for Aeronautics, Washington, DC (1957).
38. V. Babrauskas and J.F. Krasny, "Fire Behavior of Upholstered Furniture," *NBS Monograph 173,* National Bureau of Standards, Washington, DC (1985).
39. M. Kokkala and M. Heinilä, "Flame Height, Temperature, and Heat Flux Measurements on a Flame in an Open Corner of Walls," *Project 5 of the EUREFIC Fire Research Programme,* Valtion Teknillinen Tutkimuskeskus, Espoo, Finland (1991).

40. J.G. Quintiere, "A Simulation Model for Fire Growth on Materials Subject to a Room-Corner Test," *Fire Safety J.,* 20, pp. 313–339 (1993).
41. A.J. Parker, A.B. Wenzel, and T. Al-Hassan, "Evaluation of Passive Fire Protection by Jet Fire Test Procedure," Paper 4-d in Twenty-Ninth Loss Prevention Symposium, American Institute of Chemical Engineers, New York (1995).
42. J. Söderbom, "EUREFIC—Large Scale Tests According to ISO DIS 9705," *Project 4 of the EUREFIC Fire Research Programme, SP Report 1991:27,* Statens Provningsanstalt, Borås, Sweden (1991).
43. Y. Hasemi, "Experimental Wall Flame Heat Transfer Correlations for the Analysis of Upward Wall Flame Spread," *Fire Science and Technology,* 4, pp. 75–90 (1984).
44. J.G. Quintiere, "The Application of Flame Spread Theory to Predict Material Performance," *J. of Research of the National Bureau of Standards,* 93, pp. 61–70 (1988).
45. A.K. Kulkarni, C.I. Kim, and C.H. Kuo, "Turbulent Upward Flame Spread for Burning Vertical Walls Made of Finite Thickness," *NIST-GCR-91-597,* National Institute of Standards and Technology, Gaithersburg, MD (1991).
46. J.B. Fang and J.N. Breese, "Fire Development in Residential Basement Room," *NBSIR 80-2120,* National Bureau of Standards, Gaithersburg, MD (1980).
47. V. Babrauskas and R.B. Williamson, "The Historical Basis of Fire Resistance Testing, Parts I and II," *Fire Technology,* 14, pp. 184–194, 205, 304–316 (1978).
48. B.T. Rhodes, "Burning Rate and Flame Heat Flux for PMMA in the Cone Calorimeter" M.S. Thesis, University of Maryland, *NIST-GCR-95-664,* National Institute of Standards and Technology, Gaithersburg, MD (1994).
49. D. Hopkins, Jr. and J.G. Quintiere, "Material Fire Properties and Predictions for Thermoplastics," *Fire Safety J.,* 26, pp. 241–268 (1996).
50. J. Gore, M. Klassen, A. Hamins, and T. Kashiwagi, "Fuel Property Effects on Burning Rate and Radiative Transfer from Liquid Pool Flames," in *Fire Safety Science—Proceedings of the Third International Symposium,* Elsevier Applied Science, London, pp. 395–404 (1991).
51. M. Janssens, "Cone Calorimeter Measurements of the Heat of Gasification of Wood," in *INTERFLAM '93: Sixth International Fire Conference Proceedings,* Interscience Communications Ltd., London, pp. 549–558 (1993).
52. U. Sorathia, T. Dapp, J. Kerr, and J. Wehrle, "Flammability Characteristics of Composites," *DTRC SME 89/90,* U.S. Navy, David Taylor Research Center, Bethesda, MD (1989).
53. J.W. Rowen and J.W. Lyons, "The Importance of Externally Imposed Heat Flux on the Burning Behavior of Materials," *J. Cellular Plastics,* 14, pp. 25–32 (1978).
54. K. Paul, unpublished data, RAPRA Technology, Shawbury, England.
55. P. Elliot, R.H. Whiteley, and J.E. Staggs, "Steady State Analysis of Cone Calorimeter Data," in *Proceedings of the Fourth International Fire and Materials Conference,* Interscience Communications Ltd., London, pp. 35–42 (1995).
56. T.G. Cleary, and J.G. Quintiere, "Flammability Characterization of Foam Plastics," NISTIR 4664, National Institute of Standards and Technology, Gaithersburg, MD (1991).
57. R.M. Nussbaum and B.A.L. Östman, "Larger Specimens for Determining Rate of Heat Release in the Cone Calorimeter," *Fire and Materials,* 10, pp. 151–160 (1986); and 11, p. 205 (1987).
58. M. Janssens and J. Urbas, "Comparison of Small and Intermediate Scale Heat Release Data," in *INTERFLAM '96,* Interscience Communications Ltd., London, pp. 285–294 (1996).
59. L. Orloff, A.T. Modak, and R.L. Alpert, "Burning of Large-Scale Vertical Wall Surfaces," in *Sixteenth International Symposium on Combustion,* The Combustion Institute, Pittsburgh, pp. 1345–1354 (1976).
60. V. Babrauskas, "Cone Calorimeter Annotated Bibliography 1982–1991," *Tech. Note 1296,* National Institute of Standards and Technology, Gaithersburg, MD (1992).
61. S. Särdqvist, "Initial Fires: RHR, Smoke Production and CO Generation from Single Items and Room Fire Tests, *LUTVDG/TVBB-3070-SE,* Lund University, Dept. of Fire Safety Engineering, Lund, Sweden (1993).
62. P.S. Klitgaard and R.B. Williamson, "The Impact of Contents on Building Fires," *J. Fire and Flammability/Consumer Product Flammability Supplement,* 2, pp. 84–113 (1975).
63. V. Babrauskas et al., "Fire Hazard Comparison of Fire-Retarded and Non-Fire-Retarded Products," *NBS Special Publication SP 749,* National Bureau of Standards, Washington, DC (1988).
64. J. Mangs and O. Keski-Rahkonen, "Full Scale Experiments on Electronic Cabinets," *VTT Publications 186,* Valtion Teknillinen Tutkimuskeskus, Espoo, Finland (1994).
65. J. Mangs and O. Keski-Rahkonen, "Full Scale Experiments on Electronic Cabinets II," *VTT Publications 269,* Valtion Teknillinen Tutkimuskeskus, Espoo, Finland (1996).
66. O. Keski-Rahkonen and J. Mangs, "Maximum and Minimum Rate of Heat Release during Flashover in Electronic Cabinets of NPPS," Paper presented at *Fire Safety in Power Plants and Industrial Installations, SMiRT 13 Post Conference Seminar No. 6, Gramado, Brazil,* Valtion Teknillinen Tutkimuskeskus, Espoo, Finland (1995).
67. K.M. Tu and S. Davis, "Flame Spread of Carpet Systems Involved in Room Fires," *NBSIR 76-1013,* National Bureau of Standards, Washington, DC (1976).
68. P. Vandevelde and P. Van Hees, "Wind Aided Flame Spread of Floor Coverings, Development and Evaluation of Small and Large Scale Tests," in *INTERFLAM '96,* Interscience Communications Ltd., London, pp. 57–67 (1996).
69. S. Ames, R. Colwell, and K. Shaw, "The Fire Behaviour and Fire Testing of Carpet Used as a Stair Covering," in *INTERFLAM '96,* Interscience Communications Ltd., London, pp. 69–77 (1996).
70. R.B. Williamson and N.A. Dembsey, "Advances in Assessment Methods for Fire Safety," *Fire Safety J.,* 20, pp. 15–38 (1993).
71. A. Ahonen, M. Kokkala, and H. Weckman, "Burning Characteristics of Potential Ignition Sources of Room Fires," *Research Report 285,* Technical Research Centre, Espoo, Finland (1984).
72. G. Damant and S. Nurbakhsh, "Christmas Trees—What Happens When They Ignite?" *Fire and Materials,* 18, pp. 9–16 (1994).
73. V. Babrauskas and E. Stauss, to be published.
74. D.W. Stroup, L. DeLauter, J. Lee, and G. Roadarmel, "Scotch Pine Christmas Tree Fire Tests," *FR 4010,* National Institute of Standards and Technology, Gaithersburg, MD (1999).
75. J.S. Steel, unpublished data, National Institute of Standards and Technology, Gaithersburg, MD (1985).
76. F. Folke, "Experiments in Fire Extinguishment," *NFPA Quarterly,* 31, p. 115 (1937).
77. L. Nilsson, "The Effect of Porosity and Air Flow on the Rate of Combustion of Fire in an Enclosed Space," *Bulletin 18,* Lund Institute of Technology, Lund, Sweden (1971).
78. S. Yamashika and H. Kurimoto, "Burning Rate of Wood Crib," *Rept. of Fire Res. Inst. Japan,* 41, p. 8 (1976).
79. T.Z. Harmathy, "Experimental Study on the Effect of Ventilation on the Burning of Piles of Solid Fuels," *Comb. and Flame,* 31, p. 259 (1978).
80. J.G. Quintiere and B.J. McCaffrey, "The Burning of Wood and Plastic Cribs in an Enclosure, Vol. 1," *NBSIR 80-2054,* National Bureau of Standards, Washington, DC (1980).

81. W.L. Fons, H.B. Clements, and P.M. George, "Scale Effects on Propagation Rate of Laboratory Crib Fires," in *Ninth International Symposium on Combustion,* The Combustion Institute, Pittsburgh (1962).
82. M.A. Delichatsios, "Fire Growth Rates in Wood Cribs," *Comb. and Flame,* 27, p. 267 (1976).
83. L.D. Moore, "Full-Scale Burning Behavior of Curtains and Drapes," *NBSIR 78-1448,* National Bureau of Standards, Washington, DC (1978).
84. I. Wetterlund and U. Göransson, "A Full-Scale Fire Test Method for Free-Hanging Curtain and Drapery Textiles," *SP Report 1988:45,* Swedish National Testing Institute, Borås (1988).
85. National Insitute of Standards and Technology, unpublished data, Gaithersburg, MD.
86. A. Tewarson, J.L. Lee, and R.F. Pion, "Categorization of Cable Flammability, Part 1. Experimental Evaluation of Flammability Parameters of Cables Using Laboratory-Scale Apparatus," *EPRI Project RP 1165-1,* Factory Mutual Research Corp., Norwood, MA (1979).
87. P.S. Sumitra, "Categorization of Cable Flammability. Intermediate-Scale Fire Tests of Cable Tray Installations," *Interim Report NP-1881, Research Project 1165-1,* Factory Mutual Research Corp., Norwood, MA (1982).
88. B.T. Lee, "Heat Release Rate Characteristics of Some Combustible Fuel Sources in Nuclear Power Plants," *NBSIR 85-3195,* National Bureau of Standards, Washington, DC (1985).
89. V. Babrauskas, unpublished test results (1997).
90. G. Heskestad, "Flame Heights of Fuel Arrays with Combustion in Depth," in *Fire Safety Science—Proceedings of the Fifth International Symposium,* International Association for Fire Safety Science, Melbourne, Australia, pp. 427–438 (1997).
91. G. Heskestad, "Flame Heights of Fuel Arrays with Combustion in Depth," *FMRC J.I. 0Y0J3.RU(2),* Factory Mutual Research Corp., Norwood, MA (1995).
92. R.K. Dean, "Stored Plastics Test Program," *FMRC Serial No. 20269,* Factory Mutual Research Corp., Norwood, MA (1975).
93. H.-Z. Yu and H.-C. Kung, "Strong Buoyant Plumes of Growing Rack Storage Fires," in *Twentieth Symposium (International) on Combustion,* The Combustion Institute, Pittsburgh, pp. 1547–1554 (1984).
94. H.-Z. Yu and H.-C. Kung, "Strong Buoyant Plumes of Growing Rack Storage Fires," *FMRC J.I. 0G2E7.RA(1),* Factory Mutual Research Corp., Norwood, MA (1984).
95. "Guide for Smoke and Heat Venting," *NFPA 204,* National Fire Protection Association, Quincy, MA (1998).
96. J.L. Lee and R.K. Dean, "Fire Products Collector Tests of Polyethylene Terephthalate (PET) Plastic Bottles in Corrugated Carton," *FMRC J.I. 0N0J6.RA070(A),* Factory Mutual Research Corp., Norwood, MA (1986).
97. J.L. Lee, "Combustibility Evaluation of Shredded Newsprint Commodity and an Improved Polyurethane Foam Packaging Product Using the Fire Products Collector," *FMRC J.I. 0K0E6.RANS,* Factory Mutual Research Corp., Norwood, MA (1984).
98. H.-Z. Yu, "RDD and Sprinklered Fire Tests for Expanded Polystyrene Egg Crates," *FMRC J.I. 0R2E3.RA(1),* Factory Mutual Research Corp., Norwood, MA (1990).
99. H. Hasegawa, N.J. Alvares, and J.A. White, "Fire Tests of Packaged and Palletized Computer Products," *Fire Technology,* 35, pp. 294–307 (1999).
100. H. Hasegawa, personal communication (2000).
101. T.A. Roberts, R. Merrifield, and S. Tharmalingam, "Thermal Radiation Hazards from Organic Peroxides," *J. Loss Prev. Process Industries,* 3, pp. 244–252 (1990).
102. V. Babrauskas, unpublished test data (1997).
103. H.-Z. Yu and P. Stavrianidis, "The Transient Ceiling Flows of Growing Rack Storage Fires," *FMRC J.I. 0NIJ0.RA(3),* Factory Mutual Research Corp., Norwood, MA (1989).
104. H.E. Mitler, "Input Data for Fire Modeling," in *Thirteenth Meeting of the UJNR Panel on Fire Research and Safety, NISTIR 6030, vol. 1,* National Institute of Standards and Technology, Gaithersburg, MD, pp. 187–199 (1997).
105. V. Babrauskas, "Bench-Scale Predictions of Mattress and Upholstered Chair Fires," in *Fire and Flammability of Furnishings, ASTM STP 1233,* American Society for Testing and Materials, Philadelphia, pp. 50–62 (1994).
106. G.H. Damant and S. Nurbakhsh, *Heat Release Tests of Mattresses and Bedding Systems,* State of California, Bureau of Home Furnishings and Thermal Insulation, North Highlands, CA (1991).
107. G. Holmstedt and I. Kaiser, "Brand I Vårdbäddar," *SP-RAPP 1983:04* Statens Provningsanstalt, Borås, Sweden (1983).
108. B. Andersson, "Fire Behaviour of Beds and Upholstered Furniture—An Experimental Study," *LUTVDG/ISSN 0282-3756,* Lund University, Dept. of Fire Safety Engineering, Lund, Sweden (1985).
109. V. Babrauskas, D. Baroudi, J. Myllymäki, and M. Kokkala, "The Cone Calorimeter Used for Predictions of the Full-Scale Burning Behaviour of Upholstered Furniture," *Fire and Materials,* 21, pp. 95–105 (1997).
110. W.D. Walton and E.K. Budnick, "Quick Response Sprinklers in Office Configurations: Fire Test Results," *NBSIR 88-3695,* National Bureau of Standards, Gaithersburg, MD (1988).
111. D. Madrzykowski and R.L. Vettori, "Sprinkler Fire Suppression Algorithm for the GSA Engineering Fire Assessment System," *NISTIR 4833,* National Bureau of Standards, Gaithersburg, MD (1992).
112. D. Madrzykowski, "Office Work Station Heat Release Rate Study: Full Scale vs. Bench Scale," in *INTERFLAM '96,* Interscience Communications Ltd., London, pp. 47–55 (1996).
113. L.M. Krasner, "Burning Characteristics of Wooden Pallets as a Test Fuel," *Serial 16437,* Factory Mutual Research Corp., Norwood, MA (1968).
114. V. Babrauskas, "Pillow Burning Rates," *Fire Safety J.,* 8, pp. 199–200 (1984/85).
115. "Pipe Insulation: Fire Spread and Smoke Production—Full-Scale Test," *NT FIRE 036,* NORDTEST, Espoo, Finland (1988).
116. I. Wetterlund and U. Göransson, "A New Test Method for Fire Testing of Pipe Insulation in Full Scale," *SP Report 1986:33,* Swedish National Testing Institute, Borås (1986).
117. V. Babrauskas, "Toxic Fire Hazard Comparison of Pipe Insulations: The Realism of Full-Scale Testing Contrasted with Assessments from Bench-Scale Toxic Potency Data Alone," in *ASIAFLAM '95,* Interscience Communications Ltd., London, pp. 439–452 (1995).
118. V.I. Blinov and G.N. Khudiakov, "Diffusion Burning of Liquids," *NTIS No. AD296762,* U.S. Army Translation (1961).
119. H.C. Hottel, "Review Certain Laws Governing Diffusive Burning of Liquids," by V.I. Blinov and G.N. Khudiakov," *Fire Research Abstracts and Reviews,"* 1, pp. 41–44 (1958).
120. V. Babrauskas, tables and charts in *Fire Protection Handbook,* 18th ed., National Fire Protection Assn., Quincy, MA, pp. A-1 to A-17 (1997).

121. V. Babrauskas, "Estimating Large Pool Fire Burning Rates," *Fire Technology,* 19, pp. 251–261 (1983).
122. A. Gosse, personal communication, BG Technologies Ltd. (2000).
123. A.D. Putorti, Jr., J.A. McElroy, and D. Madrzykowski, "Flammable and Combustible Liquid Spill/Burn Patterns" *NIJ 604-00,* National Institute of Justice, U.S. Department of Justice, Washington, DC (2000).
124. A.T. Modak, "Ignitability of High-Fire-Point Liquid Spills," *EPRI NP-1731,* Electric Power Research Inst., Palo Alto, CA (1981).
125. V. Babrauskas, "COMPF2: A Program for Calculating Post-Flashover Fire Temperatures," *Tech. Note 991,* National Bureau of Standards, Washington, DC (1979).
126. A. Hamins, S.J. Fischer, T. Kashiwagi, M.E. Klassen, and J.P. Gore, "Heat Feedback to the Fuel Surface in Pool Fires," *Combustion Science and Technology,* 97, pp. 37–62 (1994).
127. K.C. Adiga, D.E. Ramaker, P.A. Tatem, and F.W. Williams, "Modeling Pool-Like Gas Flames of Propane," *Fire Safety J.,* 14, pp. 241–250 (1989).
128. K.C. Adiga, D.E. Ramaker, P.A. Tatem, and F. Williams, "Modeling Thermal Radiation in Open Liquid Pool Fires," in *Fire Safety Science—Proceedings of the Second International Symposium,* International Association for Fire Safety Science, Hemisphere Publishing Corp., New York, pp. 241–250 (1989).
129. H. Koseki and G.W. Mulholland, "Effect of Diameter on the Burning of Crude Oil Pool Fires," *Fire Technology,* 27, pp. 54–65 (1991).
130. H. Koseki, "Boilover and Crude Oil Fire," *J. Applied Fire Science,* 3, pp. 243–272 (1993/1994).
131. M. Shipp and M. Spearpoint, "Measurements of the Severity of Fires Involving Private Motor Vehicles," *Fire and Materials,* 19, pp. 143–151 (1995).
132. J. Mangs and O. Keski-Rahkonen, "Characterization of the Fire Behaviour of a Burning Passenger Car, Part I: Car Fire Experiments," *Fire Safety J.,* 23, pp. 17–35 (1994).
133. U. Göransson, and A. Lundqvist, "Fires in Buses and Trains: Fire Test Methods," *SP Report 1990:45,* Swedish National Testing and Research Institute," Borås (1990).
134. P.A. Hansen, "Fire in Tyres: Heat Release Rate and Response of Vehicles," *STF25 A95039, SINTEF NBL,* Norwegian Fire Research Laboratory, Trondheim, Norway (1995).
135. M.P. Shipp, "Fire Spread in Tyre Dumps," in *INTERFLAM '96.* Interscience Communications Ltd., London, pp. 79–88 (1996).
136. *Proceedings of the International Conference on Fires in Tunnels, SP—Swedish National Testing and Research Institute, Borås,* Interscience Communications Ltd, London (1994).
137. V. Babrauskas, "Upholstered Furniture Heat Release Rates: Measurements and Estimation," *J. Fire Sciences* 1, pp. 9–32 (1983).
138. Flammability Information Package (contains Technical Bulletins 116, 117, 121, 133, 106, and 26). Bureau of Home Furnishings, Dept. of Consumer Affairs, State of California, North Highlands (1987).
139. V. Babrauskas and W.D. Walton, "A Simplified Characterization for Upholstered Furniture Heat Release Rates," *Fire Safety J.,* 11, pp. 181–192 (1986)
140. "Standard Test Method for Determining the Heat Release Rate of Upholstered Furniture and Mattress Components or Composites Using a Bench-Scale Oxygen Consumption Calorimeter," *E 1474-96a,* American Society for Testing and Materials, Philadelphia (1996).
141. V. Babrauskas, "Bench-Scale Methods for Prediction of Full-Scale Fire Behavior of Furnishings and Wall Linings," *SFPE Technical Report 84-10,* Society of Fire Protection Engineers, Boston (1984).
142. U. Wickström and U. Göransson, "Prediction of Heat Release Rates of Surface Materials in Large-Scale Fire Tests Based on Cone Calorimeter Results," *J. Testing and Evaluation,* 15, pp. 364–370 (1987).
143. *Proceedings of the International EUREFIC Seminar 1991,* Interscience Communications Ltd, London (1991).
144. U. Göransson, "Model, Based on Cone Calorimeter Results, for Explaining the Heat Release Rate Growth of Tests in a Very Large Room," in *INTERFLAM '93: Sixth Intl. Fire Conf. Proc.,* Interscience Communications Ltd., London, pp. 39–47 (1993).
145. K. Sumathipala, A.K. Kim, and G.D. Lougheed, "A Comparison of ASTM and ISO Full-Scale Room Fire Test Methods," in *Proceedings of Fire and Materials, Second International Conference,* Interscience Communications Ltd., London, pp. 101–110 (1993).
146. K. Sumathipala, A.K. Kim, and G.D. Lougheed, "Configuration Sensitivity of Full-Scale Room Fire Tests," in *Proceedings of Fire and Materials, Third International Conference,* Interscience Communications Ltd., London, pp. 237–246 (1994).
147. B. Karlsson and S.E. Magnusson, "An Example Room Fire Model," in *Heat Release in Fires,* Elsevier Applied Science, London, pp. 159–171 (1992).
148. B. Karlsson, "Models for Calculating Flame Spread on Wall Lining Materials and the Resulting Heat Release Rate in a Room," *Fire Safety J.,* 23, pp. 365–386 (1994).
149. S.E. Magnusson and B. Sundström, "Combustible Linings and Room Fire Growth—A First Analysis," in *Fire Safety: Science and Engineering,* ASTM STP 882, American Society for Testing and Materials, Philadelphia, pp. 45–69 (1985).
150. T.G. Cleary and J.G. Quintiere, "A Framework for Utilizing Fire Property Tests," in *Fire Safety Science—Proceedings of the Third International Symposium,* Elsevier Applied Science, London, pp. 647–656 (1991).
151. J.G. Quintiere, G. Haynes, and B.T. Rhodes, "Applications of a Model to Predict Flame Spread over Interior Finish Materials in a Compartment," *J. Fire Prot. Engineering,* 7, p. 1013 (1995).
152. M. Janssens, O. Grexa, M. Dietenberger, and R. White, "Predictions of ISO 9705 Room/Corner Test Using a Simple Model," in *Proceedings of Fire and Materials Fourth International Conference,* Interscience Communications Ltd., London, pp. 73–83 (1995).
153. J.R. Lawson, W.D. Walton, and W.H. Twilley, "Fire Performance of Furnishings as Measured in the NBS Furniture Calorimeter, Part I," *NBSIR 83-2787,* National Bureau of Standards, Gaithersburg, MD (1983).
154. R.D. Peacock, P.A. Reneke, J.D. Averill, R.W. Bukowski, and J.H. Klote, "Fire Safety of Passenger Trains, Phase II: Application of Fire Hazard Analysis Techniques," National Institute of Standards and Technology, Gaithersburg, MD (2000).
155. M.L. Janssens, "Heat Release Rate," *FORUM Workshop on Measurement Needs for Fire Safety,* National Institute of Standards and Technology, Gaithersburg, MD (2000).
156. D.A. Smith and K. Shaw, "Single Burning Item (SBI) Test: The Euroclasses and Transitional Arrangements," in *INTERFLAM '99,* Interscience Communications Ltd., London, pp. 1–9 (1999).

CHAPTER 2

Calorimetry

Marc Janssens

Introduction

Heat release rate is the primary variable that determines the contribution to compartment fire hazard from materials. This was clearly demonstrated by Babrauskas and Peacock in a recent sensitivity study using the NIST fire hazard assessment software Hazard I.[1] However, the importance of heat release rate in fire hazard assessment was first recognized three decades ago by Smith at Ohio State University.[2] Smith and co-workers developed one of the first bench-scale heat release rate test methods.[3] They also proposed various procedures to assess compartment fire hazard on the basis of the bench-scale data, ranging from simple calculation methods[4] to a complex computer model.[5] This work was initiated at a time when the most accurate measuring techniques for heat release rate were not available, and when computer fire modeling was still in its infancy. Moreover, Smith advocated a practical approach based on engineering judgment and intuition rather than detailed science. Hence, his test and fire hazard assessment methods were far from perfect and received major criticism.[6,7] Nevertheless, Smith deserves recognition as one of the pioneers of heat release rate calorimetry.

There are several reasons why heat release rate is so important. First, it is directly related to mass loss rate. The toxic fire hazard of a material is a function of the release rate of toxic gases, which is the product of total mass loss rate and yield of these gases. Thus, the fire hazard of material A, which has a high yield of toxic gases, is less than that of material B with a lower yield, if the mass loss rate of A under identical exposure conditions is significantly lower. For example, many fire retardant treatments increase the yield of toxic gases, but dramatically reduce the mass loss rate, resulting in a lower fire hazard. This was illustrated in the study by Babrauskas and Peacock.[1] Second, the heat released by a material burning in a compartment results in a temperature rise of the hot layer gases and compartment walls and ceiling. Part of the radiation from hot surfaces and gases strikes the fuel surface, resulting in an increase in the mass loss rate over that if the material were to burn outside a compartment. Increased heat release enhances this thermal feedback effect.

With compartment fire hazard assessment as the primary application, there is a need for high quality heat release rate data, and, consequently, for devices and methods to measure it accurately. There are two basic approaches to evaluate the fire hazard of a material. The first option consists of an experimental evaluation in full scale. Typically, this approach requires multiple large scale fire tests covering all relevant fire and end-use conditions. The second option is the use of bench-scale data, primarily heat release rate, in conjunction with a calculation procedure to estimate full-scale fire performance. This second approach is significantly more versatile, and time and cost efficient. With the continuous improvement of the predictive capability and accuracy of fire models and calculation methods, it has become the preferred approach. With this in mind, the emphasis of this chapter is on bench-scale calorimetry.

Many reaction-to-fire test methods include an (often crude) measure of heat release rate.[8–12] However, with one exception (model box test in Japan[12]), these test methods were developed several decades ago and their measuring techniques are inaccurate and obsolete. Moreover, exposure conditions were not well defined and controlled, therefore it is difficult to relate the results of these early tests to real fire performance. The discussion in this chap-

Dr. Marc Janssens is associate professor in the Fire Safety Engineering Technology program at the Department of Engineering Technology of the University of North Carolina at Charlotte. His research has focused on computer fire modeling, fire hazard and risk assessment, fire test standards development, and the experimental and theoretical evaluation of material flammability with emphasis on heat release calorimetry.

ter does not include these reaction-to-fire tests, and is limited to calorimetric methods that were developed primarily for measuring heat release rate. These heat release test methods vary widely in concept and features. Four measuring techniques have been used and are described in detail below. This is followed by a discussion of the effect of various bench-scale calorimeter features and construction details. Then, a brief description is given of the many bench-scale calorimeters that were developed since the early 1970s. A comparison between these calorimeters is also included. The chapter is concluded with a discussion of some large-scale calorimeters, and a section on the uncertainty of heat release rate measurements. However, it is appropriate to start with a review of different methods for using heat release rate data in fire hazard assessment, illustrating the kind of data a bench-scale calorimeter needs to provide.

Use of Bench-Scale Heat Release Rate Data

Because of the volume of available data, a general discussion of this subject would be either incomplete or very lengthy. Therefore, the focus here is on one particular fire scenario; namely, wall linings in a room/corner test. Such a test consists of a small room with a single ventilation opening in the front narrow wall. Specimens of the material to be evaluated are attached to walls and/or ceiling. A gas burner ignition source is placed in contact with the walls in one of the rear corners. Products of combustion emerging through the ventilation opening are collected in a hood, and extracted through an exhaust duct. Instrumentation is located in the duct to measure the mole fraction of various gas species, total flow rate, smoke obscuration, and so on. Room/corner test methods have become a popular tool to evaluate the fire hazard of linings and have been standardized throughout the world.[13–16] These tests are discussed in more detail in the section on large-scale calorimeters.

Techniques for using bench-scale data to predict performance in the room/corner test differ widely in degree of complexity and sophistication. Requirements for the calorimeter that provides bench-scale data vary accordingly.

Interpretation of Bench-Scale Data in Terms of Material Properties

The most sophisticated technique to predict room/corner test performance uses heat release rate and other bench-scale measurements to obtain material properties. These properties (ideally) are apparatus-independent, and are used as input for a computer model that predicts full-scale fire performance. The two properties that are related to heat release rate are the effective heat of combustion, $\Delta h_{c,\mathrm{eff}}$ (kJ·g^{-1}), and the heat of gasification, Δh_g (kJ·g^{-1}). These properties are described below.

The effective heat of combustion is the ratio of heat release rate to mass loss rate

$$\Delta h_{c,\mathrm{eff}} = \frac{\dot{q}''}{\dot{m}''} \tag{1}$$

where

$\dot{q}''$ = heat release rate per unit exposed area (kW·m^{-2})

$\dot{m}''$ = mass loss rate per unit exposed area (g·m^{-2}·s^{-1})

The symbol $\Delta h_{c,\mathrm{eff}}$ is used to make a distinction between this property and the lower calorific value measured in an oxygen bomb calorimeter, $\Delta h_{c,\mathrm{net}}$. The latter is measured in a small container under high pressure and in pure oxygen, conditions that are not representative of real fires. The conditions in the new types of bench-scale calorimeters resemble those in real fires much more closely. For some fuels, in particular gases, $\Delta h_{c,\mathrm{eff}}$ is nearly identical to $\Delta h_{c,\mathrm{net}}$. However, for most solid materials $\Delta h_{c,\mathrm{eff}}$ is significantly lower and is the value to be used for fire hazard assessment. The issue is revisited in the next section.

The second material property is heat of gasification, Δh_g, defined as the net heat flow into the material required to convert one mass unit of solid material to volatiles. The net heat flux into the material can be obtained from an energy balance at the surface of the specimen (see Figure 3-2.1). Typically, a sample exposed in a bench-scale calorimeter is heated by external heaters and by its own flame. Heat is lost from the surface in the form of radiation. Due to the small sample size, the flame flux is primarily convective, and flame absorption of external heater and specimen surface radiation can be neglected. Hence, Δh_g can be defined as

$$\Delta h_g = \frac{\dot{q}''_{\mathrm{net}}}{\dot{m}''} = \frac{\dot{q}''_e + \dot{q}''_f - \dot{q}''_l}{\dot{m}''} \tag{2}$$

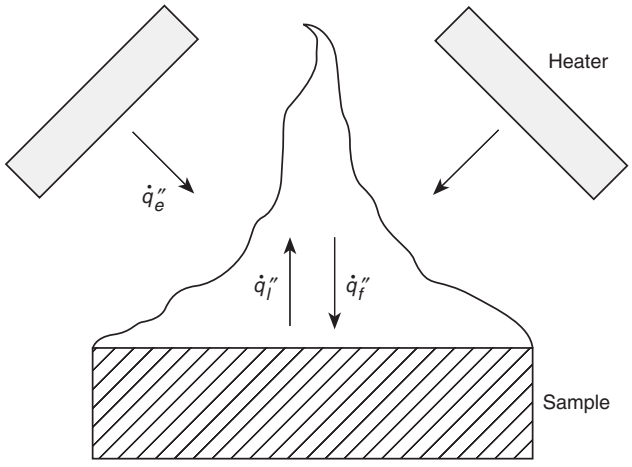

Figure 3-2.1. ***Surface heat balance.***

If the flame is approximated as a homogeneous gray gas volume, the fluxes in the numerator of equation (2) can be written as

$$\dot{q}''_f = \dot{q}''_{f,c} + \dot{q}''_{f,r} = h^*(T_f - T_s) + \sigma\varepsilon_f T_f^4 \approx h^*(T_f - T_s) \quad (3)$$

and

$$\dot{q}''_l = \sigma\varepsilon_s(T_s^4 - T_\infty^4) \quad (4)$$

where

h^* = convection coefficient, corrected for blowing (kW·m^{-2}·K^{-1})
$\dot{q}''_e$ = incident heat flux from external heaters (kW·m^{-2})
$\dot{q}''_f$ = flame flux (kW·m^{-2})
$\dot{q}''_{f,c}$ = convective fraction of the flame flux (kW·m^{-2})
$\dot{q}''_{f,r}$ = radiative fraction of the flame flux (kW·m^{-2})
$\dot{q}''_l$ = radiative losses from the surface (kW·m^{-2})
$\dot{q}''_{\text{net}}$ = net heat flux into the sample (kW·m^{-2})
T_f = flame temperature (K)
T_s = surface temperature (K)
T_∞ = ambient temperature (K)
ε_f = flame emissivity
ε_s = surface emissivity
σ = Boltzmann constant ($5.67 \cdot 10^{-11}$ kW·m^{-2}·K^{-4})

Some materials exhibit nearly steady mass loss rates when exposed to a fixed irradiance, $\dot{q}''_e$. For these materials, T_s reaches a steady value after a short initial transient period, and all terms in Equations 1–4 are approximately constant. Δh_g can then be obtained by measuring steady mass loss rates over a range of irradiance levels, and by plotting $\dot{m}''$ as a function of $\dot{q}''_e$. Δh_g is calculated as the reciprocal of the slope of a straight line fitted through the data points. $\dot{q}''_l - \dot{q}''_f$ is obtained as the intercept of this line with the abscissa. Tewarson et al.[17] and Petrella[18] have used this technique to obtain average Δh_g values for a large number of materials. Tewarson et al. also conducted tests in vitiated O_2/N_2 mixtures, and found $\dot{q}''_f$ to decrease linearly with decreasing oxygen concentration. Analysis of these additional experiments made it possible to separate $\dot{q}''_f$ and $\dot{q}''_l$.

Many materials, in particular those that form an insulating char layer as they burn, take a long time to reach steady burning conditions or may never reach steady conditions. Equations 1–4 are still valid for such materials, but the heat and mass fluxes and resulting $\Delta h_{c,\text{eff}}$ and Δh_g values vary with time. Tewarson and Petrella have used the same techniques to determine average Δh_g values for nonsteady burning materials using average mass loss rates. They found that average $\dot{m}''$ is still an approximately linear function of $\dot{q}''_e$. However, the average heat of gasification values obtained in this manner may not have any physical meaning. Physically meaningful nonsteady values for Δh_g can be obtained from Equation 2, with $\dot{q}''_f$ and $\dot{q}''_l$ calculated according to Equations 3 and 4 respectively. In order to do this, ε_s, T_s, ε_f, and T_f need to be measured, calculated or estimated in some way. Surface temperature is the most important and most difficult to determine. Flame temperature and emissivities are nearly constant over the duration of a test, and can be estimated more easily.[19–21] Urbas and Parker used thermocouples to measure T_s for wood specimens tested in the cone calorimeter.[22] The problem with this technique is maintaining good contact between the thermocouple and the exposed surface. Parker and Urbas designed a special tension system to hold the thermocouple hot junction against the char surface as this surface recedes during a test. The technique worked quite well, but the tension system made testing rather tedious. Urbas used an infrared pyrometer to measure T_s for wood specimens in an intermediate scale calorimeter.[23] This technique is much more practical, but not without problems. First, the pyrometer must operate in a specific wavelength range so that the flame becomes transparent. The sensor used by Urbas responds to infrared radiation between 8 and 12 μm. This is well above the radiation bands of CO_2 and H_2O, and in a region where, given the high flame temperature (compared to the surface temperature), soot radiation is negligible. Second, a pyrometer measures emitted and reflected radiation from a surface. Hence, assuming the surface acts as a gray body radiator, surface emissivity must be known to calculate T_s from this measurement. For wood char, Urbas found $\varepsilon_s \approx 1$ and confirmed this by comparing pyrometer and thermocouple measurements. For many other materials $\varepsilon_s < 1$, so that reflected radiation from the heater might be a problem. An alternative approach to determine T_s is by calculation. Janssens obtained T_s as a function of time for wood specimens exposed in the cone calorimeter by solving the equation for heat conduction through the char layer using an integral technique.[24] The resulting values for Δh_g compared well with those by Urbas. A drawback of this approach is that thermal properties of the material or its char are needed.

Another problem with unsteady values of $\Delta h_{c,\text{eff}}$ and Δh_g is the fact that time from ignition in a bench-scale test does not correspond directly to that in a full-scale room/corner fire. Considering a small element of the wall lining that is exposed in a room/corner test, incident heat flux varies with time as the compartment fire grows. In a bench-scale calorimeter, incident heat flux is nearly constant. Hence, the time axis of the unsteady $\Delta h_{c,\text{eff}}$ and $\Delta h_{c,\text{net}}$ curves must be transformed to a variable that also can be used for unsteady exposure conditions. Smith proposed using cumulative heat release rate to scale the time axis.[25] Mitler suggested cumulative mass loss.[26] Janssens plotted Δh_g curves for wood as a function of char depth.[24] Since char depth was defined as being proportional to cumulative mass loss, this approach is analogous to Mitler's.

With $\Delta h_{c,\text{eff}}$ and Δh_g for a material, performance in a room/corner test can be predicted. First, the exposed surface of the material is subdivided into smaller elements so that the incident heat flux to each element is approximately uniform. Then, a model is needed to determine the net heat flux into every element. This requires calculation of radiative and convective heat transfer between the different surfaces, gas volumes, and flames in the compartment coupled with the solution of compartment-wide mass, energy, and species conservation equations.

$\dot{m}''$ can be calculated for every segment as the ratio of $\dot{q}''_{net}$ to Δh_g. The heat release rate from every segment is then obtained by multiplying $\dot{m}''$ with $\Delta h_{c,eff}$, with adjustment for oxygen vitiation or starvation. Note that, although $\Delta h_{c,eff}$ and Δh_g are the most important properties, other properties are needed to estimate the time to ignition of every element and the resulting flame spread over the surface. As the fire grows and conditions in the compartment change, the sequence of calculations must be repeated for subsequent time steps. Due to the required spatial subdivision of the exposed surfaces which can be adapted to the gas phase mesh, field models are ideally suited for this kind of application. Nevertheless, only a few attempts to use such models for simulating room/corner tests have been reported.[27,28] This is probably because field models are very complex. Consequently, the number of field model users is small and most of them are not concerned with modeling the room/corner test. Fortunately, a simple model developed by Quintiere indicates such a level of detail is not needed to obtain reasonable predictions.[29] Quintiere assumed the total burning area is exposed to a uniform heat flux, and estimated this flux on the basis of experimental data for flame fluxes and hot layer temperatures as a function of heat release rate. Constant values were used for $\Delta h_{c,eff}$ and Δh_g, where the latter was determined from a reciprocal of the slope of a straight line fitted through data points of peak $\dot{m}''$ plotted against $\dot{q}''_e$ measured in the cone calorimeter.

If heat release measurements are first converted to material properties to use them for fire hazard assessment, the bench-scale calorimeter that is used must have certain features. If unsteady values for $\Delta h_{c,eff}$ and Δh_g are used, the calorimeter must be capable of measuring $\dot{m}''$ and the addition of instrumentation to measure T_s must be practical (unless T_s is calculated or estimated in some other way). If average or steady values for $\Delta h_{c,eff}$ and Δh_g are sufficient, only the total mass loss over the duration of a test is needed, and measuring $\dot{m}''$ is not required. If the model addresses the effect of oxygen vitiation or starvation on $\Delta h_{c,eff}$, it must be possible to operate the calorimeter in atmospheres different from ambient. If the model keeps track of the concentration of gas species and soot, the calorimeter must be capable of measuring soot and gas yields. The calorimeter must also be capable of running tests over a wide range of (steady) irradiance levels.

The discussion in this subsection is useful in clarifying a common misconception. Often it is believed that materials which are used in a particular orientation in practice should be tested in that orientation. This is not necessarily correct. Heat release rate as such is independent of specimen orientation. However, the heat release rate in a calorimeter under otherwise identical exposure conditions is higher in the horizontal than in the vertical orientation. This is because the heat feedback from the flame is much greater in the horizontal orientation. In that orientation, the flame is a relatively large volume of hot gas located above the specimen. The flame is only a thin sheet in front of a vertical sample, leading to a much lower heat feedback. Neither of these situations is comparable to that in a real fire, where burning areas are much larger and heat flux from the flame is much greater regardless of orientation of the fuel surface. Hence, the best approach is to interpret bench-scale measurements in terms of material properties that are independent of the test apparatus. These material properties can then be used to predict full-scale performance using a method which accounts for the effect of the enhanced heat flux from large flames. The above reasoning indicates that bench-scale testing in the vertical orientation is preferable, because the heat feedback to the flame is smaller and errors of flame flux estimates are relatively less important. However, for practical reasons, it is often preferable to run bench-scale tests in the horizontal orientation to avoid problems with, for example, melting and dripping of the specimen.

Direct Use of Heat Release Rate Curves at Multiple Irradiance Levels

If the differences between surface heat losses and flame fluxes in full-scale versus bench-scale are ignored or compensated for by an adjustment to the calculated external full-scale heat flux, heat release curves obtained over a range of irradiance levels can be used without conversion to material properties. This approach was suggested by Smith.[5] Heat release rate is measured as a function of time at three or four irradiance levels in the range of 20 to 65 $kW \cdot m^{-2}$. Then, the time axis is transformed, for reasons discussed in the previous subsection, by using cumulative heat release. Smith also developed a computer model to predict the incident heat flux to the burning area which is subdivided into smaller elements. Heat release from an element at a certain time is based on interpolation between the measured heat release curves, corresponding to the cumulative heat release from that element at that time and to the calculated incident heat flux. Smith and Green demonstrated that this interpolation method is reasonably accurate by running tests in their calorimeter while varying the incident heat flux.[30] The heat release rate curves measured under dynamic exposure conditions could be predicted quite accurately from interpolation between measurements of heat release rate under constant irradiance levels. A calorimeter that is to produce data suitable for this use must be capable of exposing specimens over a fairly wide range of constant irradiance levels.

Direct Use of Heat Release Rate Curves at a Single Irradiance Level

The approach outlined in the previous subsection can be simplified even further, if a heat release curve at a single irradiance level is used. This irradiance level is chosen so that it is a representative average (over space and time) of heat flux levels occurring in room/corner tests, typically between 25 and 50 $kW \cdot m^{-2}$. Thus, the dynamic effects of the room fire on the exposure level are ignored while the dynamics of the heat release curve are largely maintained. The single heat release curve is used in combination with a flame spread algorithm to predict heat release rate as a function of time in the room/corner test. The flame spread algorithm can be very simple, but needs at least some ignition data for the material. Transformation of the time axis for the heat release curve is not

necessary. As time proceeds, the burning area expands as new sections of the material are ignited. The flame spread algorithm calculates at every time step how large this newly ignited section is. Once ignited, the heat release rate from this section is obtained from the heat release curve for the same time relative to ignition. Thus, the total burning area and heat release at any time is obtained as a convolution integral. The most widely known room/corner test simulation of this nature was developed by Wickström and Göransson.[31] A calorimeter that is to provide data suitable for this use must be capable of providing heat release data at a single irradiance level, and some ignition data for the flame spread algorithm.

Regression Analysis

A regression analysis is the least sophisticated method. A room/corner test result that is indicative of the fire hazard of a material, for example, time to flashover, is correlated against a heat release parameter in combination with one or several other parameters measured in the calorimeter. This heat release parameter is typically the average heat release rate over a fixed period of time measured at one irradiance level. A (usually linear) statistical model is developed, and a regression analysis is performed to obtain model constants that give the best predictions for a given set of bench-scale and full-scale data. The resulting equation can then be used to predict full-scale performance on the basis of bench-scale data for materials that have not been tested in the room/corner test. Reasonable correlations of this type for the International Standards Organization (ISO) room/corner test were reported by Östman et al.[32] and Karlsson.[33] Clearly, with this approach the dynamics of the heat release curve are lost entirely. There is no difference in the prediction of full-scale performance for two materials with heat release curves of very different shape, provided the average heat release rate and other bench-scale measurements used in the correlation are identical. The predictions are valid for one scenario and geometry only. A positive aspect of this method is that the most rudimentary bench-scale calorimeter is sufficient to provide the necessary bench-scale data.

Summation of Bench-Scale Test Data Use

It is thus obvious that there is a wide variety of methods to use bench-scale heat release rate data for predicting real fire hazard of a material. In general, the versatility of the approach varies inversely with its complexity. A method using material properties can usually be applied over a range of conditions and configurations. Simple regression analyses are locked into one specific full-scale fire scenario. As an example, Quintiere's model can be used for different ignition sources (e.g. ASTM vs. ISO burner), specimen configurations (materials on walls only vs. walls and ceiling), and geometries. Östman's correlation only predicts time to flashover for one specific set of room/corner test conditions.

It must be stressed that, although heat release rate is the most important parameter, it is not the only parameter that needs to be included in a hazard analysis. Other factors related to piloted ignition, smoke release rate, opposed-flow flame spread, and so on, must be considered also. The Babrauskas/Peacock study illustrated that fire hazard is most sensitive to changes in the heat release rate of the burning fuel, but varies with other material characteristics as well.

Techniques for Measuring Heat Release Rate

Sensible Enthalpy Rise Method

Consider the energy balance of a gas-phase control volume enclosing the flame of a burning specimen (see Figure 3-2.2). Air enters the control volume at a flow rate $\dot{m}_a$ and temperature T_a. The enthalpy of this air can be written as

$$h_a = h_a^0 + c_p(T_a - T_0) \tag{5}$$

where

h_a = enthalpy of air at temperature T_a (kJ·kg^{-1})
h_a^0 = enthalpy of air at reference temperature T_0 (kJ·kg^{-1})
c_p = average specific heat of air between T_0 and T_a (kJ·kg^{-1}·K^{-1})
T_a = temperature of the air entering the combustion zone (K)
T_0 = reference temperature (K)

Part of the heat flux that strikes the exposed surface is conducted into the specimen. This heat flow raises the temperature of the solid, and decomposes some fraction into combustible fuel vapors. These vapors are generated at a rate $\dot{m}_v$, and enter the control volume at temperature T_v. Under the assumption that specific heat of all gases is

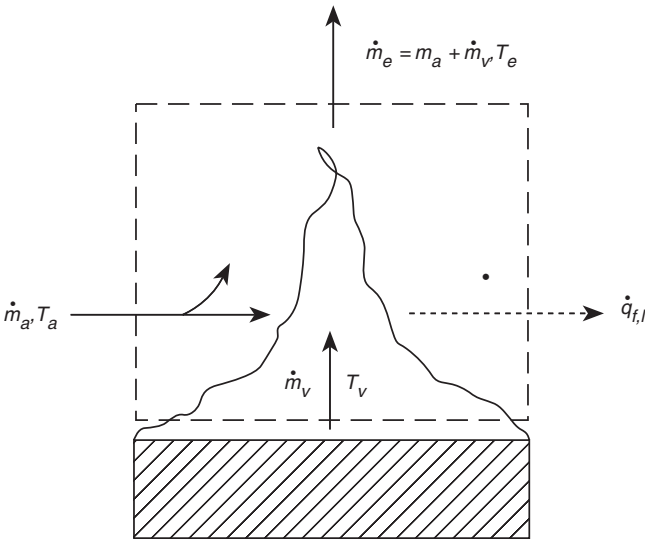

Figure 3-2.2. ***Gas-phase energy balance.***

approximately constant and temperature-independent (a reasonable approximation), the enthalpy of the fuel vapors can be written as

$$h_v = h_v^0 + c_p(T_v - T_0) \tag{6}$$

where

h_v = enthalpy of volatiles at temperature T_v (kJ·kg^{-1})

h_v^0 = enthalpy of volatiles at reference temperature T_0 (kJ·kg^{-1})

T_v = temperature of volatiles entering the combustion zone (K)

The fuel vapors mix with air, and are converted in the flame to products of combustion. The total flow rate, $\dot{m}_e$, of combustion products, which includes some excess air, has a temperature T_e and enthalpy given by

$$h_e = h_e^0 + c_p(T_e - T_0) \tag{7}$$

where

h_e = enthalpy of combustion products at temperature T_e (kJ·kg^{-1})

h_e^0 = enthalpy of combustion products at reference temperature T_0 (kJ·kg^{-1})

T_e = temperature of combustion products leaving the control volume (K)

T_e is higher than the mass-weighted average of T_a and T_v, because of the heat released by combustion in the flame, $\dot{q}$. However, only a fraction of this heat contributes to the temperature rise of the gases. This fraction is referred to as the convective fraction of the heat release rate. The remaining fraction of $\dot{q}$ is lost and is denoted as $\dot{q}_{f,l}$. For the most part, $\dot{q}_{f,l}$ is lost in the form of thermal radiation to the walls of the apparatus (closed configuration) or to the environment (open configuration). A small part of $\dot{q}_{f,l}$ consists of convective and radiative feedback to the fuel surface. Assuming gas phase transients can be neglected, application of the first law of thermodynamics for the control volume in Figure 3-2.2 results in

$$\dot{q}_{f,l} = \dot{m}_a h_a + \dot{m}_v h_v - \dot{m}_e h_e \tag{8}$$

As an example, suppose now that the same flow rates of air and volatiles, both at temperature T_0, are mixed in a hypothetical combustion chamber. Furthermore, assume the combustion reactions are identical to those in the calorimeter in Figure 3-2.2, and the products of combustion are cooled down to the reference temperature T_0 without condensing water. This hypothetical situation is shown in Figure 3-2.3. Application of the first law of thermodynamics for the combustion chamber control volume in Figure 3-2.3 leads to

$$\dot{q} = \dot{m}_a h_a^0 + \dot{m}_v h_v^0 - \dot{m}_e h_e^0 \tag{9}$$

Here, $\dot{q}$ is equal to the total rate of heat released by combustion in the flame. This heat release rate is identical in Figure 3-2.2 and Figure 3-2.3, but it is distributed in different ways. By expressing the heat released per unit mass of volatiles, an effective heat of combustion can be defined as

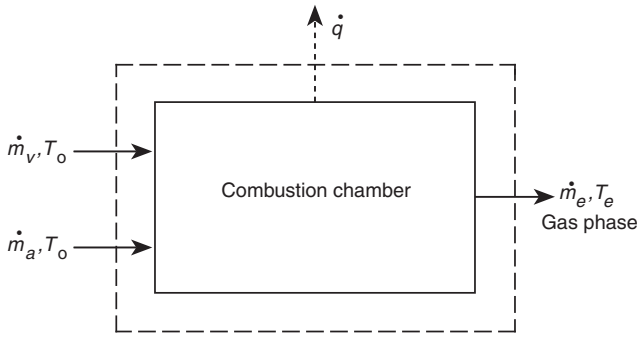

Figure 3-2.3. ***Hypothetical combustion chamber.***

$$\dot{m}_v \Delta h_{c,\text{eff}} \equiv \dot{q} \tag{10}$$

or per unit exposed area

$$\dot{m}''_v \Delta h_{c,\text{eff}} \equiv \dot{q}'' \tag{11}$$

$\Delta h_{c,\text{eff}}$ is for the combustion reactions as they take place in the calorimeter. As explained in the previous section, $\Delta h_{c,\text{eff}}$ must be distinguished from the net heat of combustion, $\Delta h_{c,\text{net}}$, measured in an oxygen bomb calorimeter. The difference between $\Delta h_{c,\text{eff}}$ and $\Delta h_{c,\text{net}}$ is very significant for charring materials such as wood. In an oxygen bomb calorimeter, nearly all the mass of wood is consumed, leaving a small fraction of noncombustible ash (usually less than 1 percent by mass). The net heat of combustion, $\Delta h_{c,\text{net}}$, of dry wood is in the range of 16–18 kJ·g^{-1}. When exposed under real fire conditions, only 70–80 percent of the mass is converted to volatiles that burn almost completely. The heat of combustion of the volatiles, $\Delta h_{c,\text{eff}}$, measured in a bench-scale calorimeter is only 12–13 kJ·g^{-1}. A solid char residue remains, primarily consisting of carbon, with a net heat of combustion of approximately 30 kJ·g^{-1}. In an oxygen bomb calorimeter, most of this char is also burnt, explaining why $\Delta h_{c,\text{net}}$ exceeds $\Delta h_{c,\text{eff}}$ by 25–50 percent. Even for materials that do not form a char, $\Delta h_{c,\text{eff}}$ can be significantly lower than $\Delta h_{c,\text{net}}$ if combustion of the volatiles in the bench-scale calorimeter is incomplete. In this case, the products of combustion contain measurable amounts of combustible components such as CO, soot, unburnt hydrocarbons, and so forth. The ratio of $\Delta h_{c,\text{eff}}$ to $\Delta h_{c,\text{net}}$ is defined as combustion efficiency, χ. For clean-burning gaseous fuels, such as methane, χ is close to unity. For fuels that produce sooty flames, including gases, χ can be significantly lower. For example, χ for acetylene is approximately 0.75. χ values for a number of gases, liquids and solids are listed in Chapter 4 of Section 3.

Substitution of equations 5, 6, 7, and 9 into 8 leads to

$$\begin{aligned}\dot{q} - \dot{q}_{f,l} = {} & c_p \dot{m}_e (T_e - T_0) - c_p \dot{m}_a (T_a - T_0) \\ & - c_p \dot{m}_v (T_v - T_0)\end{aligned} \tag{12}$$

For most combustible materials, the stoichiometric air to fuel ratio ranges between 3 and 16. Moreover, bench-scale calorimeters are usually operated with excess air. For example, the standard initial flow rate in the cone calorimeter is 30 $g \cdot s^{-1}$. Based on the oxygen consumption method discussed later in this chapter, the stoichiometric flow rate of air for a 10 kW fire (practical upper limit in the cone calorimeter) can be calculated as [10 kW]/[3 kJ per g of air] = 3.3 $g \cdot s^{-1}$. Thus, the air supply in the cone calorimeter is at least nine times stoichiometric, or at least $9 \times 3 = 27$ times the generation rate of volatiles. Usually, the ratio is much greater. Hence, $\dot{m}_v$ is negligible compared to $\dot{m}_a$ and Equation 12 can be approximated as

$$\dot{q} - \dot{q}_{f,l} \approx \dot{m}_a c_p (T_e - T_a) \tag{13}$$

This equation is the basis for the sensible enthalpy method. Heat release rate is calculated from the temperature rise $T_e - T_a$ of the gases flowing through a calorimeter. A schematic of a calorimeter based on this principle is shown in Figure 3-2.4.

There are a few problems with the practical implementation of this technique. The main concern is that only a fraction of the heat released in the flame is used to raise the sensible enthalpy or temperature of the gases. Therefore, another method is needed to recover or measure the loss term, $\dot{q}_{f,l}$. Some calorimeters have water-cooled walls that trap most of the losses. These losses can be estimated by measuring the enthalpy rise of the cooling water. However, due to the additional hardware and instrumentation, such calorimeters are rather complex and difficult to operate. A more popular method relies on a gas burner calibration to determine $\dot{q}_{f,l}$, under the assumption that the losses are fuel-independent. Defining the loss fraction, χ_R, by

$$\dot{q} - \dot{q}_{f,l} \equiv (1 - \chi_R)\dot{q} \tag{14}$$

The symbol χ_R is chosen for this fraction, since $\dot{q}_{f,l}$ consists primarily of radiation. If the calorimeter is operated with a constant air flow rate $\dot{m}_a$, Equation 13 can then be written as

$$\dot{q} \approx \frac{\dot{m}_e c_p}{1 - \chi_R} (T_e - T_a) \equiv k(T_e - T_a) \tag{15}$$

The calibration factor, k, is determined from a gas burner calibration with known $\dot{q}$. By repeating the calibration over a range of heat release rate levels, k can be determined as a function of $\dot{q}$ or T_e. If the specimen is enclosed with the heater, Equation 15 is still valid, provided a reference temperature T_r is used instead of T_a. The temperature difference $T_r - T_a$ results from the heat transfer between the heater and the air flow through the enclosure. T_r is therefore a function of heater setting, to be determined via calibration.

Smith's rate of heat release test developed at Ohio State University is the most well known and most widely used calorimeter based on the sensible enthalpy rise method.[3] The test is described in detail in a following section.

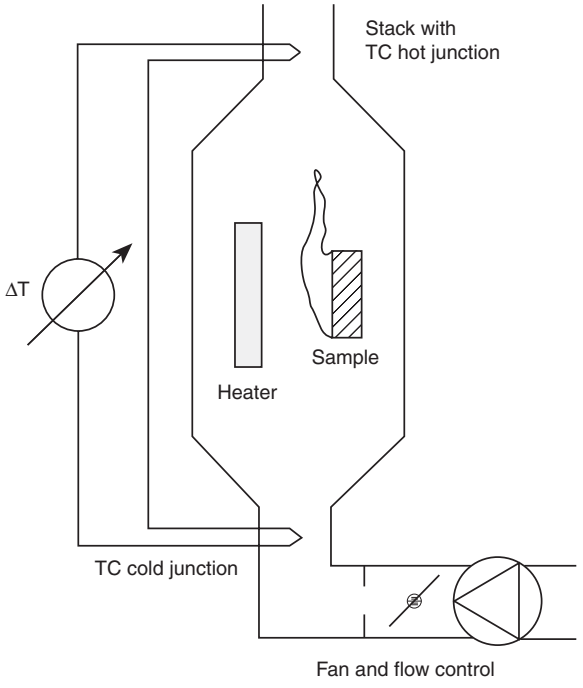

Figure 3-2.4. ***Sensible enthalpy rise calorimeter.***

Substitution Method

For practical reasons, calorimeters based on the sensible enthalpy rise method use a closed configuration. The specimen and heater(s) are located inside a metal box, which may be (partly) insulated. The dynamic response of the enclosure to changes in the thermal environment creates major problems in the practical implementation of the sensible enthalpy rise method. After ignition, part of the heat released by a burning sample is transferred by radiation to the enclosure walls. A fraction of this heat is stored in the walls, causing an increase of its temperature, in turn resulting in an enhanced heat transfer with the air flowing through the box. The result is that, for a material which quickly reaches steady burning conditions, there is a delay for T_e to reach the corresponding steady temperature. A similar phenomenon occurs when heat release rate from the specimen decreases, or after the specimen burns out and heat release rate goes back to zero. Under unsteady burning conditions, T_e constantly lags behind the temperature corresponding to the instantaneous heat release rate. Several methods have been suggested to mathematically address this problem, but none are completely satisfactory.[34–37]

The substitution method was developed to eliminate problems associated with thermal lag. The method requires two runs to determine heat release rate of a material under a given set of conditions. The first run uses a similar arrangement as shown in Figure 3-2.4. The temperature difference $T_e - T_a$ is measured as a function of time. The second run uses the same apparatus, air flow rate, and irradiance. However, the specimen is replaced by a noncombustible dummy specimen and a substitution

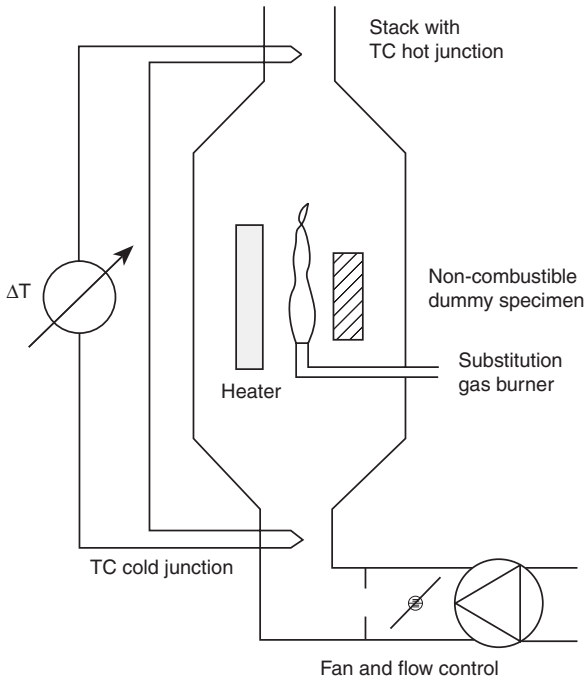

Figure 3-2.5. ***Second run with substitution calorimeter.***

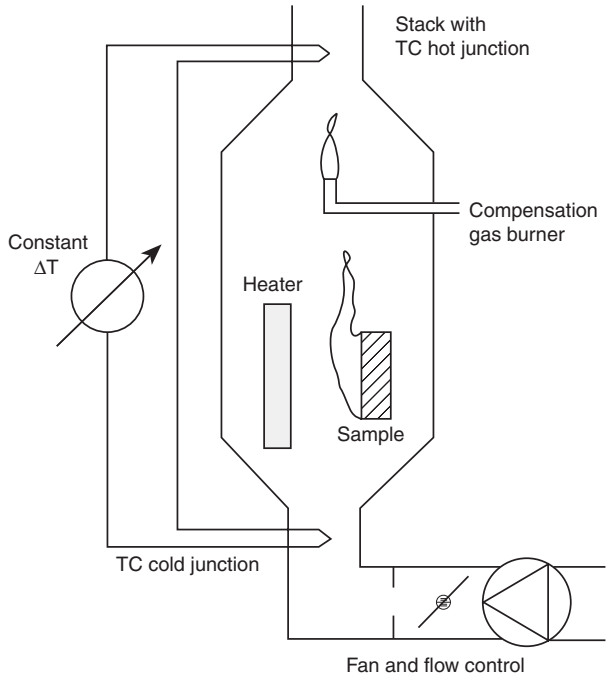

Figure 3-2.6. ***Compensation calorimeter.***

gas burner. The flow of gas to the burner is controlled in such a way that the temperature difference $T_e - T_a$ closely follows the curve measured during the first run. Figure 3-2.5 shows a schematic of the substitution run.

Presumably, the dynamics are identical in both runs. Hence, problems with thermal lag have been eliminated, and the heat release rate of the specimen can be determined from the fuel flow rate to the burner in the second run. Unfortunately, implementation of this method is not trivial, since a sophisticated control system is needed for the second run. Moreover, due to the addition of substitution runs, the number of tests needed to evaluate a material are doubled.

The substitution method was first implemented at Factory Mutual.[38] The apparatus was designed to measure the heat release rate from roof assemblies. The test method is briefly discussed in the section on large-scale calorimeters. A bench-scale substitution calorimeter developed at the Forest Products Laboratory[39] is described in more detail in the section on bench-scale calorimeters.

Compensation Method

A compensation calorimeter is similar to a substitution calorimeter, except that the burner is operated while a specimen is exposed. A schematic is shown in Figure 3-2.6. Initially, the burner flow rate is chosen so that the corresponding heat release rate exceeds that of any material to be tested. During a test, the gas flow rate to the burner is controlled so that $T_e - T_a$ remains constant. The heat release rate corresponding to the reduction in flow rate to the burner is equal to the heat release rate from the specimen.

The compensation method also eliminates problems with the dynamic response of the calorimeter enclosure. In theory, a compensation calorimeter is operated at a constant temperature. This would resolve another problem associated with the assumption that $\dot{q}_{f,l}$ is fuel independent, while in reality it is not ($\dot{q}_{f,l}$ is a strong function of the sootiness of the flame). In practice, however, the specimen and burner have to be separated to prevent radiation from the burner flame enhancing irradiance to the specimen. Hence, the calorimeter enclosure is not truly isothermal, and the problem remains unresolved. As with substitution calorimeters, the burner flow control system makes compensation calorimeters rather complex and difficult to operate. As a result, they are suitable only for research and not for routine testing.

Compensation calorimeters developed at the National Bureau of Standards[40,41] and Stanford Research Institute[42] are described in following sections.

Oxygen Consumption Method

In 1917, Thornton showed that for a large number of organic liquids and gases, a more or less constant net amount of heat is released per unit mass of oxygen consumed for complete combustion.[43] Huggett found this also to be true for organic solids and obtained an average value for this constant of 13.1 kJ·g^{-1} of oxygen.[44] His value may be used for practical applications and is accurate, with very few exceptions, to within ±5 percent. Thornton's rule implies that it is sufficient to measure the oxygen consumed in a combustion system in order to determine the net heat released. This idea is the basis for the oxygen consumption method for measuring heat release rate in fire tests.

Perhaps the first application of the oxygen consumption principle in fire research was performed by Parker on the ASTM E-84 tunnel test.[45] During the late 1970s and early 1980s, the oxygen consumption technique was refined at the National Bureau of Standards (NBS, currently the National Institute of Standards and Technology or NIST). The oxygen consumption method is now recognized as the most accurate and practical technique for measuring heat release rates from experimental fires. It is widely used throughout the world, both for bench-scale and large-scale applications.

The basic requirement to use the oxygen consumption technique is that all of the combustion products are collected and removed through an exhaust duct. At a distance downstream sufficient for adequate mixing, both flow rate and composition of the gases are measured. A schematic of an oxygen consumption calorimeter is shown in Figure 3-2.7. It is not necessary to measure the inflow of air, provided the flow rate is measured in the exhaust duct. Therefore, oxygen consumption calorimeters are typically open, to avoid that part of $\dot{q}_{f,l}$ is reflected by the calorimeter walls and reaches the specimen surface. This would result in an uncontrolled irradiance, in addition to that from the heater.

The practical implementation of the oxygen consumption method is not straightforward. Application of Thornton's rule to the combustion system shown in Figure 3-2.8 leads to the following equation for the heat release rate

$$\dot{q} = E\left(\dot{m}_a Y_{O_2}^a - \dot{m}_e Y_{O_2}^e\right) \tag{16}$$

where

E = heat release per mass unit of oxygen consumed ($\approx$13.1 kJ·g^{-1})

$Y_{O_2}^a$ = mass fraction of oxygen in the combustion air (0.232 g·g^{-1} in dry air)

$Y_{O_2}^e$ = mass fraction of oxygen in the combustion products (g·g^{-1})

The problems with the use of this equation are threefold. First, oxygen analyzers measure the mole fraction and not

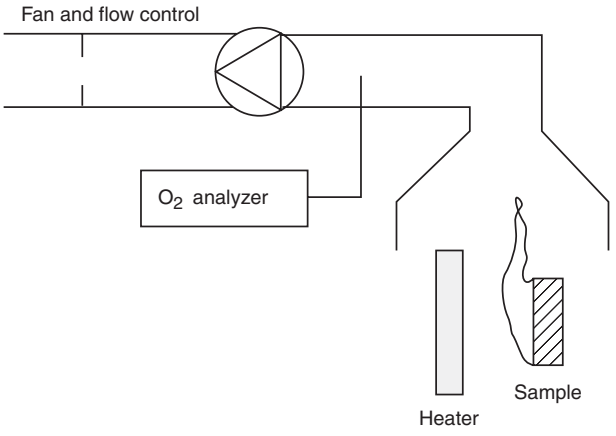

Figure 3-2.7. ***Oxygen compensation calorimeter.***

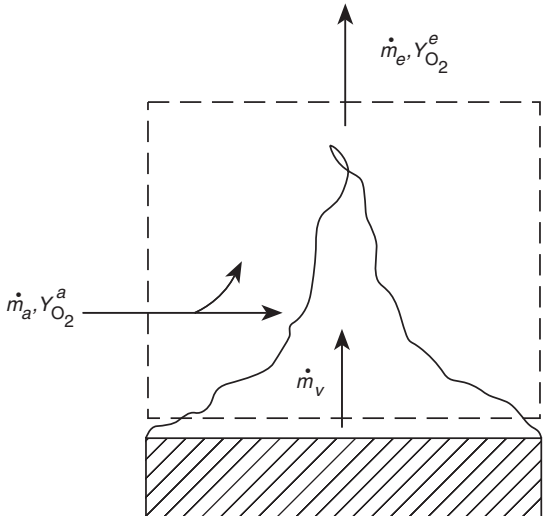

Figure 3-2.8. ***Gas-phase oxygen balance.***

the mass fraction of oxygen in a gas sample. Mole fractions can be converted to mass fractions by multiplying the mole fraction with the ratio between molecular mass of oxygen and molecular mass of the gas sample. The latter is usually close to the molecular mass of air ($\approx$29 g·mol^{-1}). Second, water vapor is removed from the sample before it passes through a paramagnetic analyzer, so that the resulting mole fraction is on a dry basis. This problem can be avoided by using a zirconium oxide analyzer, which measures oxygen mole fraction in a hot and wet sample. However, the performance of such analyzers is significantly inferior to that of paramagnetic instruments, making them unsuitable for accurate oxygen consumption calorimetry.[46] Third, flow meters measure volumetric rather than mass flow rates. The volumetric flow rate in the exhaust duct, normalized to the same pressure and temperature, is usually slightly different from the inflow rate of air because of expansion due to the combustion reactions.

Equations for calculating rate of heat release by oxygen consumption for various applications were developed by Parker[47] and Janssens.[48] The differences in treatment and equations to be used are mainly due to the extent to which gas analysis is made. As a minimum, the oxygen concentration must be measured. However, accuracy can be improved by adding instrumentation for measuring the concentration of CO_2, CO and H_2O. Equations for the most common configurations of the gas analysis system are given below. Detailed derivations are not repeated here, and can be found in the aforementioned references. Modified equations to address specific circumstances or problems, such as heat release rate measurements during suppression experiments or from fires with significant soot yields, can also be found in the literature.[49,50]

Only O_2 is measured: In this case all water vapor (by a cooling unit and a moisture sorbent) and CO_2 (by a chemical sorbent) must be removed from the exhaust gas sam-

ple stream before O_2 is measured. This leads to the assumption that the sample gas only consists of O_2 and N_2. The resulting equation for calculating heat release rate is

$$\dot{q} = E\frac{\phi}{1+\phi(\alpha-1)}\dot{m}_e\frac{M_{O_2}}{M_a}(1-X^a_{H_2O}-X^a_{CO_2})X^{Aa}_{O_2} \quad (17)$$

with

$$\phi = \frac{X^{Aa}_{O_2}-X^{Ae}_{O_2}}{(1-X^{Ae}_{O_2})X^{Aa}_{O_2}} \quad (18)$$

where

ϕ = oxygen depletion factor

α = volumetric expansion factor

M_{O_2} = molecular mass of oxygen (28 g·mol^{-1})

M_a = molecular mass of the combustion air (29 g·mol^{-1} for dry air)

$X^a_{H_2O}$ = actual mole fraction of water vapor in the combustion air

$X^a_{CO_2}$ = actual mole fraction of carbon dioxide in the combustion air

$X^{Aa}_{O_2}$ = measured mole fraction of oxygen in the combustion air

$X^{Ae}_{O_2}$ = measured mole fraction of oxygen in the exhaust flow

As the composition of the fuel is usually not known, some average value has to be used for α. Complete combustion of carbon in dry air results in $\alpha = 1$. If the fuel is pure hydrogen, α is equal to 1.21. A recommended average value for α is 1.105. $X^a_{H_2O}$ can be calculated from the relative humidity and temperature in the laboratory. Typically it is less than a few percent in a temperature-controlled laboratory. $X^a_{CO_2}$ in dry air is 330 ppm. Note that the symbols for oxygen mole fraction measured in the combustion air (prior to a test) and the exhaust flow include a superscripted *A*. This is to make a distinction between the actual and measured mole fractions of oxygen, with the latter on a dry gas sample basis.

Equation 17 is expected to be accurate to within ±10 percent, provided combustion is complete (i.e., all of the carbon is converted to CO_2). The error might be larger if CO or soot production is considerable, or if a significant amount of combustion products consist of species other than CO_2 or H_2O (e.g., HCl). The error is partly due to the uncertainty of E and α. If more exact values are available, accuracy can be improved by using those instead of the generic values of 13.1 kJ·g^{-1} and 1.105.

O_2 and CO_2 are measured: In this case, only water vapor is trapped before the exhaust gas sample reaches the analyzers. The rate of heat release is given by Equation 17, with the minor modification that $X^a_{CO_2}$ is not included in the expression inside parentheses. In addition, ϕ is slightly different and follows from

$$\phi = \frac{X^{Aa}_{O_2}(1-X^{Ae}_{CO_2})-X^{Ae}_{O_2}(1-X^{Aa}_{CO_2})}{(1-X^{Ae}_{O_2}-X^{Ae}_{CO_2})X^{Aa}_{O_2}} \quad (19)$$

where

$X^{Aa}_{CO_2}$ = measured mole fraction of carbon dioxide in the air (≈330 ppm)

$X^{Ae}_{CO_2}$ = measured mole fraction of carbon dioxide in the exhaust flow

Generally, adding CO_2 measurement does not greatly improve accuracy of $\dot{q}$.

O_2, CO_2, and CO are measured: If a significant fraction of carbon in the fuel is converted to CO instead of CO_2, the equations may have to be corrected to take incomplete combustion into account. Heat release rate is now calculated from

$$\dot{q} = \left[E\phi-(E_{CO}-E)\frac{1-\phi}{2}\frac{X^{Ae}_{CO}}{X^{Ae}_{O_2}}\right]\cdot\frac{\dot{m}_e}{1+\phi(\alpha-1)}\frac{M_{O_2}}{M_a}(1-X^a_{H_2O})X^{Aa}_{O_2} \quad (20)$$

with

$$\phi = \frac{X^{Aa}_{O_2}(1-X^{Ae}_{CO_2}-X^{Ae}_{CO})-X^{Ae}_{O_2}(1-X^{Ae}_{CO_2})}{(1-X^{Ae}_{O_2}-X^{Aa}_{CO_2}-X^{Ae}_{CO})X^{Aa}_{O_2}} \quad (21)$$

where

E_{CO} = heat release per mass unit of oxygen consumed for combustion of CO to CO_2 (≈17.6 kJ·g^{-1})

X^{Ae}_{CO} = measured mole fraction of carbon monoxide in the exhaust flow

One might wonder under what conditions the CO correction becomes significant. Figure 3-2.9 shows the ratio of heat release rate obtained by ignoring CO to the actual heat release rate, as a function of the ratio of measured CO to CO_2 mole fractions in the exhaust flow for

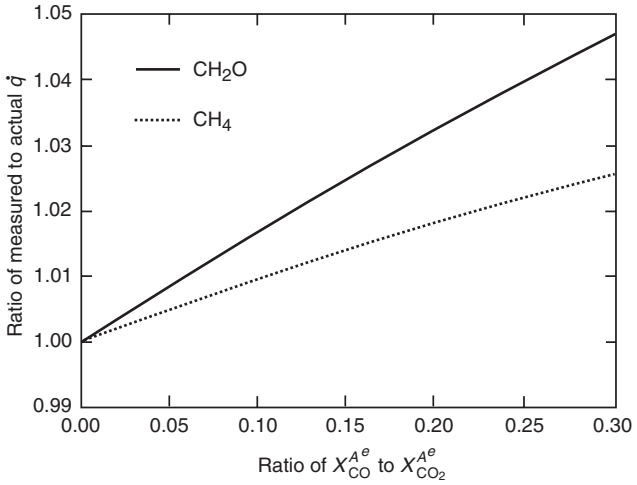

Figure 3-2.9. ***Effect of ignoring CO production on $\dot{q}$ error.***

methane and for a gaseous fuel of composition $(CH_2O)_n$. According to Roberts,[51] the molecular formula of the latter represents the thermal degradation products of beech wood. For the CO effect examined here, this fuel represents a worst case since it contains enough oxygen for combustion of all hydrogen. Methane gives a practical lower limit for the error, because it is the hydrocarbon with the highest hydrogen to carbon ratio. There is some experimental evidence that the yield of CO in underventilated fires reaches an upper limit approximately equal to 0.2 kg of CO per kg of fuel, when the equivalence ratio exceeds unity.[52] For the fuels considered here, the limit corresponds to a ratio of $X_{CO}^{A^e}$ to $X_{CO_2}^{A^e}$ of 0.27. Figure 3-2.9 indicates that, even under the worst conditions, the error by ignoring CO generation is less than 5 percent.

O_2, CO_2, CO, and H_2O are measured: Often the combustion products comprise only O_2, CO_2, CO, H_2O, and N_2 in significant amounts. In that case the expansion factor no longer has to be estimated, but can be calculated. Heat release rate is calculated from

$$\dot{q} = \left[E\phi - (E_{CO} - E)\frac{1-\phi}{2}\frac{X_{CO}^{A^e}}{X_{O_2}^{A^e}} \right] \dot{m}_a \frac{M_{O_2}}{M_a}(1 - X_{H_2O}^a)X_{O_2}^{A^a} \tag{22}$$

with

$$\frac{\dot{m}_a}{M_a} = \frac{(1 - X_{H_2O}^e)(1 - X_{O_2}^{A^e} - X_{CO_2}^{A^e} - X_{CO}^{A^e})}{(1 - X_{H_2O}^a)(1 - X_{O_2}^{A^a} - X_{CO_2}^{A^a})} \cdot \frac{\dot{m}_e}{18 + 4(1 - X_{H_2O}^e)(X_{O_2}^{A^e} + 4X_{CO_2}^{A^e} + 2.5)} \tag{23}$$

where

$X_{H_2O}^e$ = actual mole fraction of water vapor in the exhaust flow

The oxygen depletion factor, ϕ, is still determined according to Equation 21.

The oxygen consumption technique is the most accurate and convenient way to measure net release rate. Problems due to thermal lag are eliminated. Instrumentation delay and response times can be accounted for relatively easily.[53] Drawbacks of the technique are the high cost of instrumentation (only the best available oxygen analyzers are adequate), and the need for a rigorous calibration and maintenance schedule. Nevertheless, the benefits outweigh the disadvantages.

Solid or volatile heat release rate? An interesting question is whether the oxygen consumption technique measures heat release rate for the volatiles or the solid fuel. As explained in previous sections, thermal methods approximately measure heat release rate from the volatiles. However, Huggett's constant of 13.1 $kJ \cdot g^{-1}$, is based on the average net heat of combustion for a large set of materials. Hence, one would expect that oxygen consumption calorimetry gives the heat released by the fuel in its natural state at ambient temperature, since that is how the fuel is supplied in an oxygen bomb calorimeter. The question can be examined in more detail for some synthetic polymers, by comparing the net heat of combustion of the polymer to that of the corresponding monomer. If one were to burn a monomer in an oxygen consumption calorimeter, the products of complete combustion would be the same as for the corresponding polymer, provided test conditions are identical. Therefore, measured heat release rate would be the same in the two cases. However, the net heat of combustion is higher for the monomer. The difference with the net heat of combustion of the polymer is the net heat released in the polymerization process. Table 3-2.1 gives values for the net heat of combustion of 9 polymers and their monomers. The former are taken from Huggett,[44] the latter are obtained by adding the heat of polymerization as reported in the literature.[54] Table 3-2.1 confirms that the oxygen consumption technique measures net heat release rate of a solid fuel. The heat release rate from the volatiles is always higher, but not by as much as indicated in the last column of the table, because only a fraction of polymeric fuels decomposes back into the monomer (see Section 1, Chapter 7).

Table 3-2.1 ***Net Heat of Combustion of Some Polymers and Their Monomers***

Polymer	$\Delta h_{c,net}$ ($kJ \cdot g^{-1}$ fuel)	$\Delta h_{c,net}$ ($kJ \cdot g^{-1}$ O_2)	Monomer (state)	$\Delta h_{c,net}$ ($kJ \cdot g^{-1}$ fuel)	$\Delta h_{c,net}$ ($kJ \cdot g^{-1}$ O_2)	Diff (%)
Polyethylene	–43.3	–12.65	C_2H_4 (g)	–47.2	–13.78	8.9
Polypropylene	–43.3	–12.66	C_3H_6 (g)	–45.8	–13.39	5.8
Polybutadiene	–42.8	–13.14	C_4H_6 (l)	–44.1	–13.56	3.2
Polystyrene	–39.9	–12.97	C_8H_8 (l)	–40.5	–13.19	1.7
Polyvinylchloride	–16.4	–12.84	C_2H_3Cl (g)	–18.0	–14.10	9.8
Polyvinylidene chloride	–8.99	–13.61	$C_2H_2Cl_2$ (l)	–9.77	–14.79	8.7
Polyvinylidene fluoride	–13.3	–13.32	$C_2H_2F_2$ (g)	–15.6	–15.61	17.2
Polymethylmethacrylate	–24.9	–12.98	$C_5H_8O_2$	–25.4	–13.26	2.2
Polyacrylonitrile	–30.8	–13.61	C_3H_3N (l)	–32.2	–14.25	4.7
Average		–13.09			–13.99	6.9

Effects of Bench-Scale Calorimeter Construction Details

In this section, the effects of some calorimeter construction details on quality and accuracy of the measurements are examined. The discussion results in some guidelines for building the "ideal" calorimeter for a certain application.

Open or Closed Configuration

Calorimeters which utilize a measuring technique other than oxygen consumption consist of a closed box configuration. Combustion air is supplied to one side of the box, and combustion products are removed from the opposite side. Sample, heater, and ignition device typically are located inside the box. Advantages of a closed configuration are that air flow rate can be measured at the inlet under clean and soot-free conditions, the combustion air can be heated, and the oxygen concentration in the air can be increased (by adding O_2) or decreased (by adding N_2) over ambient. Disadvantages are the thermal lag due to heating or cooling of the enclosure walls, and uncontrolled radiation feedback from the enclosure walls to the specimen.

To resolve the first problem, various numerical procedures have been proposed for correcting the temperature signal measured with calorimeters based on the sensible enthalpy rise method.[34–37] These procedures are based on a mathematical model of the calorimeter consisting of two first order systems in series. The first system has a rather small time constant (between 8 and 30 seconds for various calorimeters), which is related to the heat capacity of the gases flowing through the calorimeter. The second system has a large time constant (200 to 930 seconds for various calorimeters), which is associated with the heat capacity of the calorimeter walls. The correction procedures adjust the output signal for thermal lag, using discrete forward and inverse Laplace transform techniques. In spite of the complex calculations, the resulting correction may not always be accurate due to the crude mathematical model for the calorimeter. A more convenient, and perhaps as accurate correction method relies on an electronic compensator.[55,56] The compensator electronically corrects the output signal of the exhaust thermocouples, based on the negative feedback of a wall temperature signal. The oxygen consumption method also has a time delay, but with properly adjusted sampling flows and oxygen analyzer, this delay consists almost entirely of the transport time for a gas sample from the combustion zone to the analyzer.[57] Since flow rates in the exhaust duct and sampling lines do not change significantly during a test, this delay time is approximately constant. It can be determined with gas burner calibrations, and can be easily accounted for by shifting the gas analysis data over the appropriate time interval. When an inferior oxygen analyzer is used, its internal response time might become significant. In such a case, the analyzer output signal can be corrected numerically for time delays in a similar way as temperature measurements. Oxygen analyzers behave as a first or second order system, and the appropriate time constants can be obtained from step response measurements. However, it is highly recommended that only the best and most accurate analyzers for oxygen consumption calorimetry be used, in which case internal delays are not a problem.

The second problem can only be eliminated by using blackened water-cooled calorimeter walls. If the walls are allowed to heat or cool freely, they emit radiation which varies with time. Part of this radiation reaches the specimen surface and enhances the irradiance from the heater in an uncontrolled fashion. Obviously, the need for water-cooled walls makes the apparatus much more complex and costly.

In conclusion, problems with thermal lag and radiation feedback to the specimen can be eliminated by using an open configuration. Solid objects must be water-cooled, or sufficiently remote from heater and specimen so that they do not interfere with the controlled irradiance to the specimen. A closed configuration can only be recommended for specialized applications (e.g., to study the effect of oxygen concentration or temperature of the combustion air on heat release rate and burning behavior).

Type of Heater

Heat release rates must be measured at constant heat flux levels over a range that is relevant for the fire of interest. The heat flux can be provided with a gas burner flame in contact with the specimen, or with a radiant panel remote from the specimen.

Incident heat flux from impinging gas burner flames can only be adjusted over a narrow range. To increase the heat flux from a gas burner, either flame size has to be increased, or a fuel with higher soot yield has to be used. Usually, these parameters can be adjusted only slightly, or not at all. It is very difficult to set and maintain a specific heat flux level since a major fraction of the heat transfer is convective. Moreover, the burner gas and combustion products mix with fuel volatiles, which affects burning behavior. In short, impinging flames are not desirable as the external heat source in heat release rate calorimeters.

It is much easier to create constant and uniform exposure conditions if the incident heat flux is primarily radiative. Porous gas panels as well as electrical heating elements are used for this purpose. The irradiance can be adjusted by changing the power of the heater, or by changing the distance between heater and specimen. If the second method is used, there are practical upper and lower limits to the range of irradiance levels that can be created. If the heater is too close to the specimen, convective heat transfer becomes significant. Therefore, the upper limit corresponds to the minimum distance that has to be maintained in order to ensure predominantly radiative heat transfer. The lower limit is determined by the uniformity of the incident irradiance, which drops with increasing distance between heater and specimen. The exact limits depend on the geometrical configuration, power of the heater, and the degree of nonuniformity of the incident heat flux profile that is deemed acceptable.

Another important aspect is the ability of the heater to maintain the irradiance at a constant level during a test.

If the heater is operated at a constant power level, incident irradiance changes during testing. At the start of a test, a cold sample is inserted. The sample acts as a heat sink, resulting in a decrease of the heater temperature, and consequently a decrease of the incident irradiance. After ignition, the heat released by the specimen results in an increase to the heater temperature and incident irradiance. Therefore, in order to maintain incident irradiance during a test, it is necessary to keep the temperature of the heater constant. This is very difficult with a gas panel, but relatively straightforward for electrical heating elements. With the oxygen consumption method, another drawback of using a gas panel is that its products of combustion result in an oxygen depletion that is usually much larger than the oxygen consumed for combustion of the specimen. Thus, small fluctuations in panel flow can result in significant error of the measured heat release rate. This baseline problem can be avoided by using a separate exhaust system for the heater.

It is clear from the previous discussion that an electrical heater is preferable to a gas panel. High and low temperature electrical heaters are used. The former are commonly Tungsten filament lamps that operate at temperatures close to 2300 K. According to Wien's displacement law, peak irradiance from such lamps is at a much shorter wavelength than for real fires, with temperatures in the range of 600 to 1400 K. Piloted ignition studies on plastics and wood have shown that these materials absorb much less radiation in the visible and near-infrared range, than at higher wavelengths.[58,59] On the basis of these findings, it can be concluded that high temperature electrical heating elements are not suitable for use in fire testing. It is therefore recommended that commercially available low temperature elements be used. Such elements typically operate between 800 and 1200 K, a range that is representative of real fire exposure conditions.

Type of Ignition Pilot

Heat release rate tests are most often conducted with an ignition pilot. The use of a pilot reduces the variation in time to sustained flaming between multiple tests conducted under identical test conditions. Because the duration of the preheat period prior to ignition affects burning rate after ignition, use of a pilot also improves repeatability of heat release rate measurements. Furthermore, piloted ignition is used because it is representative of most real fires, and conservative in other cases. The ignition pilot in bench-scale fire tests consists of a small gas burner flame, a glowing wire, or an electric spark. An impinging flame should not be used because it locally enhances the incident heat flux to the specimen. Another problem with pilot flames is that they are sometimes extinguished by fire retardants or halogens in the fuel volatiles. A glowing wire is not an efficient method for igniting fuel volatiles, sometimes leading to poor repeatability. An electric spark remains stable when fire retardants or halogens are present. However, it occupies a small volume, so that the positioning of the spark plug is more critical than with other types of ignition pilots. In conclusion, each type of pilot has its drawbacks. Nonetheless, a spark ignitor is probably the best type of ignition pilot for heat release rate tests.

Sample Size

The ideal situation would be if small-scale heat release rate data could be used directly to predict burning rate in real scale fires. Unfortunately, the minimum bench-scale sample size that is required to allow for such a straightforward prediction is not practical. As described in previous sections, the burning rate of a specimen is a direct function of the net heat flux transferred to the fuel. The net flux is equal to the total of external heat flux, flame convection and flame radiation, minus radiative heat losses from the fuel surface and heat losses (or gains) at the specimen edges. The Russian work on the effect of diameter on pool fire burning rate by Blinov and Khudiakov gives some insight into this problem. A detailed discussion of this work and its implications is given by Drysdale.[60] If the pool diameter is less than 0.03 m, flame convection is laminar and burning rate increases with decreasing diameter. If the pool diameter exceeds 1 m, flame convection is turbulent and burning rate is independent of diameter. There is a transition region between these two limits, with a minimum burning rate for a pool diameter of approximately 0.1 m. Therefore, the sample size in a heat release rate calorimeter must be at least 1 m for the results to be independent of scale, which is not feasible in practice. The Russian pool fire data also indicate that heat transfer at the edges becomes excessive at diameters below 0.1 m. Therefore, sample size in bench-scale calorimeters should be at least 0.1 m. To predict real scale burning rates, differences in flame heat transfer and heat transfer at the edges have to be accounted for. Nussbaum and Östman reported ignition and heat release data for 13 materials and two sample sizes.[61] Increase in sample size from 0.1×0.1 m to 0.2×0.2 m resulted in a slight reduction of piloted ignition time. Average heat release rate over the first minute after ignition on a per-unit-area basis increased by approximately 12 percent at exposure levels exceeding 25 $kW \cdot m^2$. Larger increases were observed at the 25 $kW \cdot m^{-2}$ exposure level, and for peak heat release rate. Janssens and Urbas presented a comparison of heat release rate data for nine wood products obtained in the cone and an intermediate-scale calorimeter.[62] A 100-fold increase in sample size only resulted in a 10 percent increase of the heat release rate. The modest effect can be explained by the fact that the heat feedback from the flame is relatively insensitive to sample area for testing in the vertical orientation, in particular for materials that do not produce very luminous flames, such as wood.

Depending on the specimen size in a bench-scale test, there is a limit on the degree of nonuniformity and irregularity of the product being tested, if the test conditions are to be representative of end-use conditions. Therefore, there might be some merit in choosing a specimen size that exceeds the minimum of 0.1 m. However, the main trade-off is that a larger specimen requires a larger and more powerful heater to ensure uniform incident irradiance to the specimen. It should be recognized that, no matter what the specimen size is, there are assemblies and

composites for which it is not possible to prepare representative bench-scale specimens. Intermediate-scale or full-scale tests are needed to evaluate the fire performance of such assemblies and composites.

An issue that is closely related to specimen size is that of edge effects. These effects have been studied extensively in the cone calorimeter. ASTM[63] and ISO[64] standards of the cone calorimeter prescribe that, except for calibrations with PMMA, the specimen is to be wrapped with aluminum foil on the sides and bottom. The main purpose of the foil is to eliminate mass transfer along all boundaries except the exposed face of the specimen. Furthermore, the ISO standard requires all tests be conducted in the horizontal orientation with the stainless steel edge frame. Further details on the cone calorimeter specimen preparation and test conditions can be found in Section 3, Chapter 3. Toal et al. tested several materials with and without foil wrapping, and with and without the edge frame.[65,66] They found that the edge frame reduces peak heat release rate and lengthens the burning time. Lengthened burning time is to be expected, because the edge frame is a relatively large mass of steel that acts as a heat sink, reducing the energy transferred to the specimen. Urbas and Sand were also concerned with the heat sink effect of the edge frame.[67] They designed an alternative edge frame, comprising an insulating collar made of medium-density or high-density refractory material. Their conclusion was that the best edge conditions are obtained using the insulating frame with insulation material that most closely resembles the specimen in thermal properties. Babrauskas et al. conducted a very extensive study of the effects of specimen edge conditions on heat release rate.[68] The objective of this study was to further examine the issues raised by Toal et al. and by Urbas and Sand, and to develop definitive recommendations. Specimens of 10 materials were tested in the horizontal orientation at 50 $kW \cdot m^{-2}$ using three configurations; without edge frame, with edge frame, and with an insulated edge frame akin to that developed by Urbas and Sand. All specimens were wrapped in aluminum foil. The study concluded that the use of an insulated frame gives heat release rate values that are slightly closer to the expected true values. However, the insulated frame makes the test procedure significantly more complicated, so that it is not recommended for routine testing. If the standard edge frame is used, Babrauskas et al. recommend heat release rate data be expressed on the basis of an effective exposure area of 0.0081 m^2. The standard edge frame reduces the actual exposed area from 0.1×0.1 m to 0.094×0094 m, or from 0.01 m^2 to 0.0088 m^2. The recommendation by Babrauskas et al. to further reduce the exposed area to an effective value of 0.0081 m^2 indicates that the heat sink effect of the edge frame reduces heat release rate values by approximately 8 percent. Tsantaridis and Östman tested 11 products in the cone calorimeter in the horizontal orientation at 50 $kW \cdot m^{-2}$, with and without the edge frame.[69] They also found that the use of the edge frame results in a reduction of heat release rate greater than what can be explained by the reduction of the exposed area. For the average heat release over the first three minutes following ignition, they found an average reduction of 8 percent, identical to Babrauskas et al. However, for maximum heat release rate they found reductions as high as 25 percent. It can be concluded from these studies that the sample holder configuration in a bench-scale heat release rate test may have a significant effect on the measurements, and that this should be accounted for if the test data are used to predict performance in real fires.

Specimen Orientation

As previously explained, products do not necessarily have to be tested in the same orientation as they are used. For practical reasons, the preferred orientation for bench-scale testing is horizontal facing upward. The vertical orientation might be preferable for collecting specialized data for research purposes.

Air Flow

Standard rate of heat release test methods are operated under overventilated conditions. Plenty of excess air is supplied, so that the measurements are not affected by lack of oxygen. However, specialized studies have been conducted to evaluate the effect of ventilation and vitiation.[70] Such studies require a closed configuration. The original ISO heat release rate apparatus had the capability of heating the combustion air, so that the effect of air temperature on heat release rate could be studied.[71]

Other Measurements

Heat release rate calorimeters often include additional instrumentation to measure parameters that are important in characterizing the fire performance of materials. Perhaps the most important additional measurement is that of mass loss rate. Most calorimeters can be provided with a load cell to measure specimen mass loss, but this can be very difficult in a closed configuration. Mass loss rate is obtained from numerical differentiation of the mass loss measurements. Smoke meters are added to measure smoke obscuration in the exhaust duct. Both white light and laser light systems are being used. Toxic gas species can be measured in the exhaust duct with additional gas analysis equipment. Such equipment ranges from standard infrared CO and CO_2 analyzers to complex online Fourier transform infrared (FTIR) instrumentation. Whether instrumentation can be added depends mainly on the design and construction details of the calorimeter.

Survey of Bench-Scale Calorimeters

Numerous bench-scale heat release rate calorimeters have been developed since the early 1970s. Many of these calorimeters are described in detail here.

The Ohio State University (OSU) Apparatus

Originally designed by Smith at Ohio State University,[3] the OSU apparatus is one of the most widely used and best known bench-scale calorimeters. The test method

was first published as a proposed ASTM standard in 1980. In 1983 it was adopted as ASTM Standard Test Method E906, and the method has not changed since then.[55] A schematic view of the apparatus is shown in Figure 3-2.10. The apparatus consists of an insulated metal box. The conical wall section between the combustion chamber and the stack is hollow. Air flows through this cavity and mixes with the combustion products downstream of the thermocouple hot junctions. However, recovery of a significant fraction of wall heat losses is not fully accomplished. Some features of the OSU apparatus are described below.

Measuring technique: Heat release rate is determined by the sensible enthalpy rise method. The temperature of inflowing air, and outflowing gases are measured with a thermopile of three type K thermocouples. The hot junctions are located symmetrically along a diagonal of the stack cross section, above the baffle plate. The cold junctions are located below the air distributor plate. An electrical compensator is used to correct the temperature signals for thermal lag. The factor k in Equation 15 is obtained from line burner calibration runs.

Configuration: Heater and specimen are located inside a box with approximate dimensions of $0.2 \times 0.41 \times 0.64$ m. The side walls of the box are insulated, and the hollow top wall section is cooled with air.

Heater: The vertical radiant heat source measures approximately 0.3×0.3 m, and consists of four silicon carbide heating elements. A steel masking plate is located in front of the elements to improve uniformity of the incident heat flux distribution over the specimen. The maximum incident heat flux to a vertical specimen is approximately 65 $kW \cdot m^{-2}$.

Ignitor: The optional ignition source is a pilot flame of 2 $ml \cdot s^{-1}$ methane, premixed with 14 $ml \cdot s^{-1}$ air. The pilot flame is either impinging on the specimen at the bottom (point ignition), or is located in the gas phase at the top of the specimen (pilot ignition), or is not used.

Specimen size and orientation: For testing in the vertical orientation, specimens with an exposed area of 0.15×0.15 m are positioned parallel to the heating elements. Specimens can be tested in the horizontal orientation with the aid of an aluminum reflector foil, which reflects the radiation from the heating elements to the specimen. In this case, maximum irradiance is reduced to 50 $kW \cdot m^{-2}$ and specimen size is 0.11×0.15 m. The use of the reflector plate is awkward and cumbersome, so that testing in the horizontal orientation with the OSU apparatus is not recommended.

Air flow: Total air flow rate is 40 $l \cdot s^{-1}$, of which only 10 $l \cdot s^{-1}$ passes through the combustion chamber and the remaining 30 $l \cdot s^{-1}$ flows through the upper hollow wall section. Nevertheless, the air flow rate through the combustion chamber contains enough oxygen to feed a 36 kW fire. Because, the heat release rate from test specimens rarely exceeds 20 kW, burning conditions in the OSU apparatus are always overventilated. The air flow rates are measured accurately with standard orifices.

Additional measurements: The ASTM E906 standard does not include a mass loss measurement but has a smoke measuring system with a white light source in the stack.

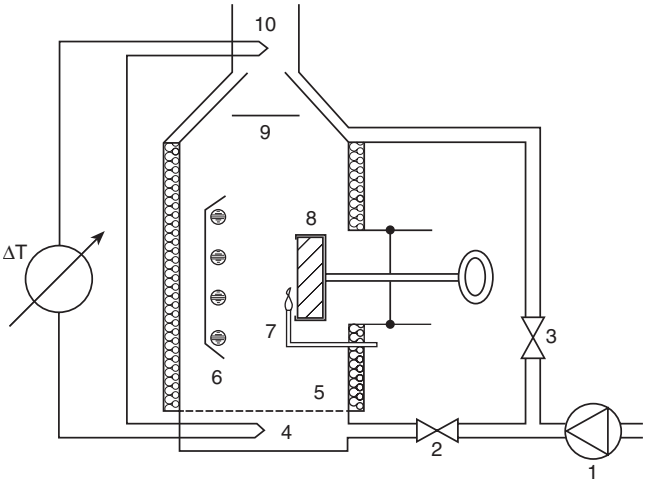

1 Air supply fan
2 Main flow control
3 By-pass flow control
4 TC cold junctions
5 Air distributor plate
6 Heating elements
7 Gas pilot
8 Sample and holder
9 Baffle plate
10 TC hot junctions

Figure 3-2.10. ***Schematic of the OSU apparatus.***

Federal Aviation Administration (FAA) version of the OSU apparatus: In 1978 the FAA established a committee to examine the factors affecting the ability of aircraft cabin occupants to survive in a post-crash environment. The committee recommended research to evaluate the fire performance of cabin materials, and development of a method using radiant heat for testing cabin materials. As a result, the FAA conducted an extensive series of full-scale fire tests and evaluated numerous bench-scale tests for their capability to provide results that correlate well with full-scale performance. The OSU apparatus, standardized as ASTM E906, was found to be the most suitable for material qualification. Improved flammability standards and requirements for airplane cabin interior materials based on ASTM E906 first went into effect in 1986.[72] The limits for acceptance were based on heat release rate measured at an irradiance level of 35 $kW \cdot m^{-2}$. Peak heat release rate could not exceed 100 $kW \cdot m^{-2}$, and average heat release rate over the first two minutes following ignition had to be 50 $kW \cdot m^{-2}$ or less. Originally, the test method used by the FAA was identical to ASTM E906. Since then, modifications have been made.[73] The FAA method now uses a thermopile of five thermocouples, a lighter sample holder, and a modified test procedure to minimize problems associated with thermal lag.[37] The FAA criteria for acceptance were revised in 1990 to 65 $kW \cdot m^{-2}$ for peak heat release rate during the five-minute test, and to 32.5 $kW \cdot m^{-2}$ for average heat release rate over the first two minutes following ignition.[72]

OSU Apparatus Modified for Oxygen Consumption

When oxygen consumption calorimetry became the preferred method for measuring rate of heat release, laboratories in the United States, Canada, and Sweden modified their OSU apparatus. These modifications typically

consisted of the elimination of the original thermopile, the addition of a gas sampling probe and gas analysis equipment, and some adjustments to the air flow rates. A brief summary of these investigations follows.

Modified OSU apparatus at NBS: As part of an investigation of combustion of mattresses exposed to flaming ignition sources, a number of mattress materials were tested at NBS in a modified OSU apparatus.[6,74] The following modifications were made to the standard OSU apparatus:

- The oxygen consumption technique was used instead of the sensible enthalpy rise method.
- The air flow through the hollow upper wall section was cut off to increase sensitivity of the oxygen measurement.
- The air flow rate through the combustion chamber was increased to 12 $l \cdot s^{-1}$.
- Specimen size was reduced to 0.1×0.1 m.
- The aluminum reflector foil was replaced by a more durable steel plate.

As a result of this study, good agreement was found between heat release rates measured in the modified OSU apparatus, and a classification of mattresses based on performance in full-scale experiments.

Modified OSU apparatus at the National Research Council of Canada (NRCC): The oxygen consumption method was compared with the three thermal methods, and was found to be preferable.[75] As a result, the OSU apparatus at NRCC was modified for oxygen consumption calorimetry and for measuring heat release rates at reduced air flow rates. Air regulators and flow meters were replaced so that the flow rates through the combustion chamber and through the upper hollow wall section could be set between 0.8 and 10 $l \cdot s^{-1}$, and between 0.8 and 30 $l \cdot s^{-1}$, respectively. At lower flow rates, longer flames were observed. The stack of the apparatus was extended to ensure all combustion took place inside the apparatus. For a wood specimen exposed to 25 $kW \cdot m^{-2}$, it was found that both air flow rates could be reduced to 2.5 $l \cdot s^{-1}$ without significant incomplete combustion or flaming outside the apparatus.

Modified OSU apparatus at Lund University: The OSU apparatus at Lund University in Sweden was also modified for oxygen consumption calorimetry.[76] The air flow through the upper hollow wall section was cut off, and the stack of the apparatus was extended.

Modified OSU apparatus at the Forest Products Laboratory: Two significant modifications were made to the FPL apparatus, in addition to the inclusion of instrumentation for oxygen consumption calorimetry.[77] An auxiliary heat flux meter was added beneath the specimen, to monitor incident irradiance during a test. Measurements obtained with this auxiliary meter indicated that the incident irradiance to a burning wood specimen increases significantly during a test. For example, the incident irradiance to a Douglas fir plywood specimen at the end of a 10-minute burning period increased by 20 percent over the 35 $kW \cdot m^{-2}$ baseline. The increase is due to the fact that the heater elements in the OSU calorimeter are supplied with constant power and are not temperature controlled, and that the calorimeter walls are allowed to heat up (or cool down) during testing. The fact that exposure conditions in the OSU calorimeter are not constant is a major weakness of the apparatus. It is nearly impossible to remedy this problem. The addition of an auxiliary heat flux meter is highly recommended. Thus, at least the time-varying exposure conditions are known. The second modification at FPL was the addition of a load cell to measure specimen mass loss during a test. This was a rather difficult task due to the geometry of the apparatus, and the mechanism for inserting specimens. The FPL load cell design seemed to be satisfactory, demonstrating the feasibility of measuring mass loss in the OSU apparatus.

The NBS I Calorimeter

This apparatus was developed by Parker and Long at NBS.[40] It consists of a combustion chamber at the bottom, a control chamber in the middle, and a mixing chamber at the top. Gases flow through the apparatus from bottom to top. The apparatus has the following features.

Measuring technique: Heat release rate is determined by the compensation method. The flow rate of propane to an auxiliary burner in the control chamber is adjusted to maintain the temperature in the mixing chamber at a constant level between 370 and 470°C. Additional air supplied to the control room greatly eliminates heat losses to the walls of this part of the apparatus.

Configuration: Three heaters and the specimen are located inside the combustion chamber with approximate dimensions of $0.33 \times 0.33 \times 0.36$ m.

Heaters: Three walls of the combustion chamber consist of gas panels, capable of producing a heat flux to the specimen of up to 100 $kW \cdot m^{-2}$. Incident irradiance to the specimen is checked with a copper disk heat flux meter.

Ignitor: Ignition of the specimen is nonpiloted.

Specimen size and orientation: The vertical specimen measures 0.114×0.15 m with a maximum thickness of 25 mm. The specimen holder fits into an opening in the remaining combustion chamber wall that faces the three radiant panel walls.

Air flow: Air is supplied to the combustion chamber at a rate of 63 $l \cdot s^{-1}$. The products of combustion are further diluted in the control chamber with air at a rate of 69 $l \cdot s^{-1}$. The dilution air is induced through the porous walls of the control chamber, and serves to reduce the temperature of the exhaust gases. This reduces measurement errors and thermal stresses in the mixing chamber wall material. The errors result primarily from the assumption that constant temperature of the exhaust gases is equivalent to constant heat content. This is only approximately correct because of differences in specific heat between various gas species in the exhaust stream and air.

Additional measurements: The apparatus does not include any additional instrumentation, and specimen mass loss and smoke obscuration are not measured.

Stanford Research Institute Calorimeter: A scaled-up version of the NBS I calorimeter was constructed at Stanford Research Institute.[42] The redesigned combustion

chamber measured approximately 0.86 × 0.68 × 0.98 m. Maximum specimen size was increased to 0.46 × 0.61 m, and the radiant heat flux range was reduced to 15–70 $kW \cdot m^{-2}$.

The FPL Calorimeter

This apparatus was developed by Brenden at the Forest Products Laboratory in Madison, Wisconsin.[39] The apparatus has the following features.

Measuring technique: Heat release rate is determined by the substitution method. The flow rate of propane to the substitution burner in the combustion chamber is adjusted during a second run so that the temperature-time curve of the exhaust gases traces that measured during the experiment with the test specimen. Combustion chamber walls and the unexposed side of the specimen holder are water-cooled. Heat losses through walls and specimen are accounted for by measuring the enthalpy rise of the cooling water.

Configuration: The apparatus consists of a water-cooled combustion chamber with approximate dimensions of 0.76 × 0.43 × 1.09 m.

Heater: The specimen is exposed to the heat flux from a premixed gas burner flame. Experiments were conducted[78] using approximately 0.5 $l \cdot s^{-1}$ natural gas mixed with 5 $l \cdot s^{-1}$ air, generating a total heat flux to the specimen between 30 and 40 $kW \cdot m^{-2}$.

Ignitor: The burner flame impinges on the specimen and also acts as ignition pilot.

Specimen size and orientation: The vertical specimen measures 0.45 × 0.45 m with a maximum thickness of 0.1 m.

Air flow: In addition to that supplied to the premixed burner, secondary air is supplied at the bottom of the combustion chamber. Various wood products were tested[78] with a secondary air flow rate of 14 $l \cdot s^{-1}$. The maximum total flow rate of air that can be supplied is 130 $l \cdot s^{-1}$.

Additional measurements: The apparatus does not include any additional instrumentation.

The FMRC Fire Propagation Apparatus

The Factory Mutual Research Corporation (FMRC) fire propagation apparatus was initially developed to measure convective heat release rate and generation rates of smoke and combustion products.[79] Originally, only convective heat release rate was measured on the basis of enthalpy rise of the exhaust gases. Test results reported since the late 1970s also include total heat release rates calculated from oxygen consumption or carbon dioxide generation. In the 1980s, the FMRC apparatus was constructed in industrial laboratories in France, Germany, and the United States. Tewarson used the apparatus to determine fire hazard indices[80] and material properties for fire modeling.[17] He also investigated the effect of environmental conditions (such as oxygen concentration in the combustion air) on heat release rate and burning behavior. The results of his extensive research are summarized in Section 3, Chapter 4. The FMRC fire propagation apparatus has the following features.

Measuring technique: Total heat release rate is determined by the oxygen consumption method. Tewarson also used carbon dioxide generation to calculate heat release rate. However, the amount of energy generated per mass unit of carbon monoxide generated is much more fuel dependent than the amount of energy produced per mass unit of oxygen consumed. Therefore, this technique is not as universally accepted as the oxygen consumption method.

Configuration: Tests are conducted in a semi-open environment. The specimen is located inside a quartz tube, 0.61 m in length and 0.17 m in diameter. A mixture of oxygen and nitrogen is supplied at the bottom of the tube. A stainless steel funnel and vertical exhaust duct are located at some distance above the tube. Dilution air is entrained in the area between the tube and the exhaust system. The total flow of gases through the exhaust duct is determined by measuring pressure drop across a precalibrated orifice.

Heater: Four heaters, which are located coaxially outside the quartz tube, are used to generate an incident heat flux to the specimen with a maximum of 70 $kW \cdot m^{-2}$. The electrical heaters operate at high temperatures, so that the spectral distribution of the emitted radiation is not representative of that present in most fires. This problem is discussed in detail in a previous section.

Ignitor: A small pilot flame is located approximately 10 mm above the center of the specimen.

Specimen size and orientation: The specimen is circular and has a diameter of 0.1 m. Maximum thickness is 50 mm. The specimen is tested in the horizontal orientation.

Air flow: Total gas flow rate supplied to the bottom of the quartz tube can be set between 0 and 8.3 $l \cdot s^{-1}$. Oxygen content of the combustion air can vary between 0 and 60 percent. Oxygen concentrations below ambient are used for simulating ventilation-controlled fires. Oxygen concentrations above ambient are used to increase flame radiation simulating larger fires.[81] Pure nitrogen is used to determine the heat of gasification.

Additional measurements: The apparatus includes instrumentation to measure specimen mass loss, smoke obscuration, smoke corrosivity, and soot and gas species concentrations in the exhaust flow.

The First ISO Rate of Heat Release Apparatus

The apparatus discussed here never made it beyond a prototype. In 1984, ISO/TC92/SC1 initiated development of an international standard test method for measuring heat release rate of building products on the basis of the cone calorimeter. The cone calorimeter is discussed in a subsequent section, and more in detail in a separate chapter. The development of an ISO heat release rate test method started more than ten years earlier, in the early 1970s. The original design was based on the British fire propagation test, BS 476 part 6. Much of the development work was conducted by three laboratories; two in England (Fire Research Station, and Timber Research and Development Association) and one in Denmark (Danish National Testing Institute). The prototype apparatus based on the sensible enthalpy rise method was finalized

in 1980. The apparatus was modified for oxygen consumption calorimetry a few years later, and some of the technical problems with the prototype were resolved. The resulting apparatus is described in detail in a report issued by the laboratory that conducted the work between 1980 and 1982.[71] The features of this apparatus are briefly discussed here.

Measuring technique: Heat release rate is determined by the oxygen consumption method.

Configuration: Specimen and heater are located inside an insulated box with approximate dimensions $0.1 \times 0.38 \times 0.38$ m.

Heater: The radiant panel measures 0.3×0.38 m, and consists of nine electrical elements. Maximum irradiance to the specimen is between 60 and 70 $kW \cdot m^{-2}$. The power to the heating elements is controlled to keep panel temperature constant during testing.

Ignitor: A small hydrogen pilot flame is located in front of the specimen.

Specimen size and orientation: The exposed area of the specimen is 0.205×0.205 m. Maximum thickness is 125 mm. The specimen can be tested in any orientation by rotating the entire apparatus.

Air flow: Experiments have been conducted at an air flow rate of 8.3 $l \cdot s^{-1}$. Air can be preheated to 100°C with heating elements located in the inlet duct. When testing specimens in the vertical orientation, direction of the air flow is from top to bottom. This results in a more uniform heat feedback from the flame to the specimen surface. When testing specimens in the horizontal orientation, air flows from one side to the other.

Additional measurements: The apparatus does not include instrumentation to measure specimen mass loss or other parameters.

The NBS II Calorimeter

This apparatus was derived from the NBS I calorimeter to accommodate larger specimens.[41] It has the following features.

Measuring technique: Heat release rate is determined by the compensation method. Gas flow to the burner is adjusted to maintain the temperature in the stack at a constant value of approximately 400°C. The same apparatus without compensation burner was used to explore its suitability for oxygen consumption calorimetry.

Configuration: Radiant panels, specimen, and compensation burner are located in the same chamber with approximate dimensions of $1.07 \times 1.37 \times 1.07$ m. When testing in the vertical orientation, two specimens are positioned back-to-back to approximate adiabatic rear boundary conditions.

Heaters: Two gas panels are located in front of two of the combustion chamber walls, forming an array of 0.3×0.6 m. Four panels are located in front of the remaining two walls, forming an array of 0.6×0.6 m. The specimen is positioned in the center between all panel arrays. Irradiance to the specimen can be set between 25 and 80 $kW \cdot m^{-2}$.

Ignitor: An electric spark is used as the ignition pilot at the top of vertical specimens, and over the edge of horizontal specimens. Various other pilot flame configurations can be used as an option.

Specimen size and orientation: Initially, specimens of 0.3×0.3 m were tested in the vertical orientation. Babrauskas used the apparatus to test mattress samples of 0.15×0.3 m in the horizontal orientation.[74] A heat flux meter adjacent to the specimen was used to monitor incident irradiance during tests.

Air flow: Air is supplied at the bottom of the combustion chamber and to the premixed gas panel burners. The products are extracted through the stack at the top of the combustion chamber.

Additional measurements: The specimen is mounted on a load cell. Instrumentation is provided in the stack for measuring smoke obscuration and concentration of oxygen, carbon dioxide, and carbon monoxide.

The Cone Calorimeter

The cone calorimeter was developed at NBS by Dr. Vytenis Babrauskas in the early 1980s.[57] It is presently the most commonly used bench-scale rate of heat release apparatus. The apparatus and test procedure are standardized in the United States[63] and internationally.[64] The cone calorimeter is described in detail in a separate chapter, and its main features are summarized here.

Measuring technique: Heat release rate is determined by the oxygen consumption method. The gas flow rate in the exhaust duct is calculated from the pressure drop across, and temperature at, an orifice plate in the duct.

Configuration: Cone heater, spark ignitor, sample holder, and load cell are located underneath a hood. The standard configuration is open, with free access of air to the combustion zone.

Heater: The heater consists of a 5 kW electrical heating element, wound inside an insulated stainless steel conical shell. Hence, the apparatus is named cone calorimeter. The heater can be oriented horizontally or vertically, to perform tests in either orientation. When tests are performed in the horizontal orientation, the specimen is positioned approximately 25 mm beneath the bottom plate of the cone heater. Flames and products of combustion rise and emerge through a circular opening at the top of the heater. Maximum irradiance to the specimen exceeds 100 $kW \cdot m^{-2}$.

Ignitor: An electric spark is used as the ignition pilot at the top of vertical specimens, and over the center of horizontal specimens.

Specimen size and orientation: Specimen size in both orientations is 0.1×0.1 m.

Air flow: Combustion products and dilution air are extracted through the hood and exhaust duct by a high-temperature fan. The initial flow rate can be adjusted between 10 and 32 $l \cdot s^{-1}$. Volumetric flow rate remains relatively constant during testing. Some cone calorimeters include additional instrumentation to optionally control and maintain the mass flow rate through the exhaust duct.

Additional measurements: The specimen is mounted on a load cell. Most cone calorimeters include instrumentation for measuring smoke obscuration (using a laser light source, described in ASTM E1354 and ISO 5660-2) and

concentration of soot, carbon dioxide, carbon monoxide, and other gases.

Larger cone heater at Trätek: A conical heater was designed at the Swedish Wood Research Institute (Trätek) double the size of that in cone calorimeter.[61] The larger heater was used to study the effect of specimen size on heat release rate.

The Trätek Calorimeter

The Swedish Wood Research Institute developed an open oxygen consumption calorimeter using the apparatus built by Sensenig at NBS as a model.[82,83] The apparatus, which now has been replaced by a cone calorimeter, has the following features.

Measuring technique: Heat release rate is determined by the oxygen consumption method. Oxygen concentration is measured with a zirconium oxide cell. This analyzer has the advantage that oxygen concentration is measured in a hot and wet gas sample, which greatly simplifies the calculations. However, the accuracy of zirconium oxide cells is inferior to that of paramagnetic oxygen analyzers. For this reason, the laboratory later changed to a paramagnetic analyzer after it acquired a cone calorimeter.[46] The gas flow rate in the exhaust duct is calculated from center-line velocity measured with a Pitot tube, and gas temperature.

Configuration: Heater, pilot flame, sample holder, and balance are located underneath a hood. The standard configuration is open, with free access of air to the combustion zone.

Heater: The heater measures approximately 0.3×0.3 m, and consists of tubular medium-wave infrared lamps. Maximum irradiance to the specimen is 50 $kW \cdot m^{-2}$. The irradiance level is adjusted by changing the distance between heater and specimen. Various heater operating conditions were examined, and conditions were chosen that result in the closest match with the spectral distribution of radiation from wood and oil flames.

Ignitor: A small pilot flame at the top of the specimen was found to result in the quickest involvement of the entire exposed specimen area.

Specimen size and orientation: Specimen size is 0.15×0.15 m. Specimens are positioned in the vertical orientation, parallel to the heating panel.

Air flow: Combustion products and dilution air are extracted through the hood and exhaust duct. The initial flow rate through the duct can be varied, but tests were conducted with a flow rate of approximately 20 $l \cdot s^{-1}$.

Additional measurements: The specimen is mounted on an electronic balance to measure mass loss. A white light source system is used for measuring smoke obscuration in the exhaust duct.

Comparison between Bench-Scale Calorimeters

How do results obtained with different calorimeters for the same material compare? A number of comparisons are reported in the literature. Sensenig tested particleboard, Type X gypsum board, medium-density fiberboard, and polyurethane foam in his oxygen consumption calorimeter, and according to ASTM E906.[83] Specimen holder, orientation, specimen size (0.15×0.15 m), mounting method, ignition pilot, and heat flux were identical to eliminate some of the possible sources of variation. The heat release curves from the two methods agreed quite well. In general, results from the OSU apparatus were slightly higher. Chamberlain compared heat release rates for 10 wood products measured in a slightly modified NBS I calorimeter to results from the NBS II calorimeter.[84] Poor correlations were found for peak heat release rate and average heat release rate over the first minute. Agreement was much better for 5-minute and 10-minute averages. This indicates that the dynamic response of the two methods is very different. Östman et al. reported on a comparison of heat release data for 13 building materials, obtained with the modified OSU apparatus at Lund, the cone calorimeter, and the Trätek apparatus.[85] Agreement was remarkably good with a correlation coefficient exceeding 90 percent for average heat release rate over the first minute following ignition. Babrauskas compared peak heat release rate from various calorimeters for five aircraft wall paneling materials.[86] He found good agreement between the FMRC apparatus and the cone calorimeter. However, he also found that the peak heat release rate from the OSU apparatus was approximately 50 percent of the peak from the cone calorimeter. Whether thermopile or oxygen consumption were employed seemed to have only a minor effect on the results from the OSU apparatus. Unfortunately, correlation of average heat release rate was not reported, so that a comparison with the Swedish work is not possible.

Tran compared heat release rate curves for Douglas fir plywood from the cone calorimeter, and the OSU apparatus at FPL modified for oxygen consumption.[77] First and second peaks agreed well, but the OSU data exceeded the cone calorimeter data by up to 20 percent between the peaks. The increased burning rate can be explained by the enhanced irradiance to the specimen due to temperature rise of the calorimeter walls and heater during a test. Tran tested the same material in the OSU apparatus with the vertical specimen holder from the cone calorimeter and found no effect.

Finally, two comparative studies were recently conducted involving electrical cables. Gandhi et al. measured shorter ignition times and lower heat release rates in the FMRC combustibility apparatus than in the cone calorimeter for communication cables.[87] Carman et al. compared oxygen consumption and thermopile measurements for six different types of cables.[88] Good agreement was obtained between the two measurement techniques under flaming conditions.

Heat release data from bench-scale calorimeters are always apparatus dependent. Differences in geometry, test conditions, and mounting methods explain discrepancies between the results from different calorimeters. Apparatus-specific factors must be considered and accounted for in a comparison between different calorimeters, or when the data are used to predict performance in real scale.

Large-Scale Heat Release Rate Calorimeters

There are two primary reasons for conducting a full-scale fire test: to validate computer fire models that are used for hazard assessment, or to evaluate the fire performance of products and assemblies for which bench-scale tests are not representative. Many types of full scale fire test rigs have been equipped with instrumentation to measure heat release rate. This became even more feasible with the development of the oxygen consumption method. These experimental arrangements can be categorized in the following groups: scaled-up heat release rate calorimeters, furniture calorimeters, room tests, industrial-size calorimeters, and other large scale fire tests equipped with instrumentation for measuring heat release rate.

Scaled-Up Heat Release Rate Calorimeters

These are larger scale versions of the bench-scale calorimeters discussed in previous sections. A sample of one to several square meters is exposed to a constant or preprogrammed thermal exposure.

Perhaps the oldest calorimeter of this type is the Factory Mutual Construction Materials Calorimeter.[38] A specimen of 1.22×1.22 m is exposed for 10–30 minutes to the standard ASTM E119 temperature-time curve, compressed into a much shorter time. Maximum heat flux is 150 $kW \cdot m^{-2}$. The specimen is horizontal facing downward and is exposed to a furnace operated with premixed heptane burners. Heat release rate is determined with the substitution method.

In recent years, a number of large scale panel tests have been developed. These tests consist of a large radiant gas panel and a flat specimen parallel to the panel. Panel and specimen are located beneath a hood and exhaust system. Heat release rate is measured by oxygen consumption. A calorimeter of this type was developed in Canada for facade systems.[89] The test is capable of exposing specimens of 1.22×2.08 m to a maximum irradiance of 30 $kW \cdot m^{-2}$. An intermediate-scale calorimeter of the same type was developed in the United States, primarily to evaluate the heat release rate from construction assemblies.[90] Sample size is 1×1 m, with a maximum irradiance of 60 $kW \cdot m^{-2}$. The method is now standardized by ASTM under designation E1623.[91]

Furniture Calorimeters

Furniture calorimeters have been developed in the United States,[92] the Nordic countries,[93] and England.[94] These calorimeters measure heat release rate from objects such as chairs, sofas, mattresses, and so on. The primary use of this kind of information is for input into compartment fire models and smoke transport models, which form part of fire hazard assessment. The specimen is placed on a load cell platform, beneath a hood and exhaust system. Instrumentation is provided in the exhaust duct to measure flow rate, oxygen and other gas species concentrations, and smoke obscuration. In the United States, standard methods have been developed by ASTM for the evaluation of single or stacked chairs and mattresses.[95–97]

Room Tests

Room fire experiments are routinely conducted throughout the world for various reasons. Since the development of oxygen consumption calorimetry, heat release has become one of the routine measurements. Until a few years ago there was little or no standardization in the way room tests were carried out. In the 1970s it was recognized that there was a need for a standard room fire test procedure, in particular for evaluating wall and ceiling lining materials. On the basis of observations made in earlier tests, it was concluded that a room/corner scenario was the best choice for such a standardized procedure. Two major developments greatly contributed to the standardization of a room/corner fire test. The first development was the use of gas burner ignition sources over wood cribs. Gas burners are repeatable and reproducible. They have the advantage that a wide range of steady or time-varying exposure levels can easily be obtained. The second development was that of oxygen consumption calorimetry.

Most of the work toward the development of a standard room/corner test was done in the late 1970s and early 1980s in the United States. The need for a standard room fire test and some aspects of its design were discussed by Benjamin in 1977.[98] Subsequent research in North America to arrive at a standard full scale test was conducted primarily by Williamson and co-workers at the University of California (UCB)[99] and by Lee at NBS.[100]

Considerable research has also been conducted in the Nordic countries. A detailed project to construct a full-scale room calorimeter was undertaken in Sweden.[101,102] No oxygen consumption measurements were made at the time. A heat balance was obtained by comparing the theoretical heat release from combustion of gaseous fuel to the sum of the heat losses. The heat losses consisted of convection through the doorway, conduction through the walls and ceiling, and radiation through the doorway. Heat convection through the doorway was estimated by measuring gas velocity and temperature at many points in the doorway. Heat conduction through the surrounding surfaces was calculated using total heat flux, radiation, and surface temperature data. Heat loss by radiation through the door was calculated from radiometer measurements. Initially, a series of quasi-steady calibration tests were conducted in an inert room. Three different circular propane gas burners were used with a diameter of 0.2, 0.3, and 0.4 m respectively. Heat balance calculations showed reasonable agreement, with convection losses being dominant. In subsequent tests with surface finishes, a heptane pool fire with a heat release rate of about 50 kW was used as the ignition source.

Ahonen et al. at the Technical Research Center of Finland studied the effects of different gas burner ignition sources on room/corner fire growth.[103] Three different burner sizes (0.17 m × 0.17 m, 0.305 m × 0.305 m, and 0.5 m × 0.5 m) and three square wave output levels (40 kW, 160 kW, and 300 kW) were used, leading to a total of nine combinations. Oxygen consumption calorimetry was

implemented for measuring heat release rate. The burner was placed in a rear corner of the room. In all tests, the walls and ceiling, except for the front wall, were lined with a 10 mm particle board of fairly high density (720 $kg \cdot m^{-3}$). The following six criteria were used to determine the time to flashover:

- Flames emerging through the door (flameover)
- A total heat release rate of 1 MW
- Total heat flux to the floor of 20 $kW \cdot m^{-2}$
- A minimum rate of smoke production
- 600°C at the geometric center of the room
- Total heat flux to the floor of 50 $kW \cdot m^{-2}$

With the time to flashover defined as the average of the six criteria, the following remarkable results were obtained:

- At the 40 kW level, the medium-sized burner resulted in flashover first, followed by the smaller burner and then the larger burner.
- At 160 kW, the largest burner resulted in flashover first, quickly followed by the other two configurations.
- At 300 kW, the trend was the same as at 160 kW with an even smaller spread between the three results.

The effect of burner size was most significant at the lowest power level, where the medium sized burner was the most severe. At higher exposure levels, the size of the burner was not important. Radiative and convective heat transfer from the burner flame was shown to depend on burner size and power level and had a significant effect on the performance of the material tested. On the basis of the results, the medium burner size and power level were recommended.

Based on the work at NBS and UCB, ASTM drafted a proposal for a standard room/corner test. The proposal was printed in the gray pages of the Annual Book of Standards in 1982 and 1983,[13] but was never formally published as an ASTM standard. The draft specifies dimensions and geometry of the test compartment, burner size and exposure level, and basic instrumentation and measurements required. The compartment has a floor area of 2.44 m by 3.66 m, interior room height is 2.44 m. A single door in the middle of a square wall is 0.76 m wide and 2.03 m high. A sand burner ignition source is located in a corner opposite from the door. All combustion products emerging through the door are collected in a hood. Measurements are made in the exhaust duct to calculate heat release rate via oxygen consumption. The National Fire Protection Association recently published room test standard NFPA 286, which is nearly identical to the ASTM proposed standard.[15] The ignition source specified in NFPA 286 is a sand burner with an area of 0.3×0.3 m at 0.3 m off the floor. The net heat output is 40 kW for 5 min followed by 160 kW for 10 min. A few years prior to publication of NFPA 286 the National Fire Protection Association developed NFPA 265, which is a slightly different room test procedure specifically for the evaluation of textile wallcoverings.[14] The two NFPA room test standards use the same burner, but NFPA 265 requires that it be placed at a 50 mm standoff distance from the back and side walls and be supplied with propane to result in a net heat output of 40 kW for 5 min followed by 150 kW for 10 min. The protocol described in NFPA 265 has been specified for more than 10 years in the U.S. model building codes to qualify textile wallcoverings and is based on extensive research conducted at UCB.[104]

Parallel to the development of the ASTM proposal for a room/corner test, ISO has developed an international room test standard. The ISO standard was published in 1992[16] and is based primarily on the Nordic research described above. The concept is identical to that of the draft ASTM method. The dimensions of the test room and ventilation opening are basically the same, but the ISO standard allows ignition sources and specimen configurations other than those described in the ASTM document. The primary ignition source in ISO 9705 is a sand burner with an area of 0.17×0.17 m at 0.17 m off the floor. The net heat output is 100 kW for 10 min followed by 300 kW for another 10 min.

Industrial-Size Calorimeters

The first industrial-size calorimeter for fires into the MW range was built at Factory Mutual around 1980.[105] This calorimeter, also referred to as the FM Fire Products Collector, was designed to measure heat and other fire products from test fires up to a size associated with sprinkler activation in commodity warehouse storage and other representative occupancies. Approximately 10 years later, a similar industrial-size calorimeter for heat release rate measurements up to 10 MW was constructed at the National Testing Laboratory (SP) in Sweden.[106] Since then several other laboratories, such as the National Research Council of Canada, the Fire Research Station in the UK, and Underwriters Laboratories and Southwest Research Institute in the United States, developed the capability of measuring heat release rate from large fires into the MW range. Cooper presented useful guidelines to address the special challenges associated with calorimetry of large fires.[107]

Other Large-Scale Fire Tests

The oxygen consumption method makes it possible to measure heat release rate on almost any fire test. Measurements are reported in the literature for very small fires (kW range) up to 100 MW. Standard fire endurance tests have been instrumented for oxygen consumption calorimetry.[108,109] Exhaust systems of entire laboratories have been equipped for the technique. There are virtually no limits.

Uncertainty of Heat Release Rate Measurements

The accuracy of a measured value indicates how well it agrees with the true value. The difference between a measured and the true value is referred to as the measurement error. Measurement errors consist of two components: bias error and precision error.

Bias error is fixed or systematic, that is, it does not vary when experiments are repeated (within a single lab-

oratory) or reproduced (in another laboratory). For example, the E value used to determine heat release rate on the basis of oxygen consumption (Equations 17, 20, and 22) may be a source of bias error. Use of a generic E value for a fuel of unknown composition results in an error that is always the same regardless of when, where, and how many times the experiment is conducted.

Precision errors are random in nature. For example, the turbulent flow in the exhaust duct of an oxygen consumption calorimeter results in fluctuations of the differential pressure across the bidirectional probe. Therefore, single-point velocity measurements are likely to slightly deviate from the mean.

The uncertainty of a measurement is the interval around the measured value within which the true value lies with a certain probability, usually 95 percent. In many cases the measured value is calculated from other independent measurements through a functional relationship. For example, heat release rate measured on the basis of oxygen consumption is calculated from differential pressure, temperature, and oxygen concentration measurements according to Equation 17. Standard mathematical techniques can be used to determine the uncertainty of heat release rate measurements on the basis of the uncertainties associated with all sources of error in the equation. Dahlberg performed such an uncertainty analysis for the industrial-size calorimeter at SP and reported values of ±7 percent and ±12 percent depending on the use of the CO correction (i.e., for Equations 20 and 17, respectively).[110] Enright and Fleischmann reported an uncertainty of ±5 percent for the cone calorimeter.[111] These uncertainties are significantly below the precision obtained from interlaboratory trials involving oxygen consumption calorimeters. For example, the most recent cone calorimeter round robin resulted in estimates for the peak heat release rate repeatability and reproducibility of 17 percent and 23 percent, respectively.[112] The discrepancies can be explained by the fact that the uncertainty analyses did not account for dynamic errors and sample, operator, and heat flux variations.

Nomenclature

c_p	specific heat at constant pressure (kJ·kg^{-1}·K^{-1})
E	heat release per mass unit of oxygen consumed (kJ·g^{-1})
E_{CO}	heat release per mass unit of oxygen consumed for combusion of CO to CO_2 (kJ·g^{-1})
h	convection coefficient (kW·m^{-2}·s^{-1}) or enthalpy (kJ·kg^{-1})
k	OSU calorimeter calibration factor (kW·K^{-1})
M	molecular mass (g·mol^{-1})
$\dot{m}$	mass loss rate or mass flow (g·s^{-1})
$\dot{q}$	heat flow (kW)
T	temperature (K)
X	mole fraction (mol·mol^{-1})
Y	mole fraction (g·g^{-1})

Greek

α	volumetric expansion factor
χ_R	radiative heat loss fraction
$\Delta h_{c,\text{eff}}$	effective heat of combusion (kJ·g^{-1})
Δh_g	heat of gasification (kJ·g^{-1})
ε	emissivity
ϕ	oxygen depletion factor
σ	Boltzman constant (5.67 · 10^{-11} kW·m^{-2}·K^{-4})

Subscripts

a	air
c	convective
CO	carbon monoxide
CO_2	carbon dioxide
e	external or exhaust
f	flame
H_2O	water vapor
l	loss
net	net
O_2	oxygen
r	radiative
s	surface
v	volatiles
∞	ambient

Superscripts

A	analyzer
a	air
e	exhaust
$''$	per unit area
*	corrected for blowing
0	reference

References Cited

1. V. Babrauskas and R. Peacock, "Heat Release Rate: The Single Most Important Variable in Fire Hazard," *Fire Safety J.*, 18, pp. 255–272 (1992).
2. E. Smith, "An Experimental Determination of Combustibility," *Fire Technology*, 7, pp. 109–119 (1971).
3. E. Smith, "Heat Release Rate of Building Materials," in *Ignition, Heat Release and Noncombustibility of Materials* (A. Robertson, ed.), American Society of Testing and Materials, West Conshohocken, PA, pp. 119–134 (1972).
4. E. Smith, "Application of Release Rate Data to Hazard Load Calculations," *Fire Technology*, 10, pp. 181–186 (1974).
5. E. Smith and S. Satija, "Release Rate Model for Developing Fires," *J. of Heat Transfer*, 105, pp. 282–287 (1983).
6. V. Babrauskas, "Performance of the OSU Rate of Heat Release Apparatus Using PMMA and Gaseous Fuels," *Fire Safety J.*, 5, pp. 9–20 (1982).
7. M. Janssens, "Critical Analysis of the OSU Room Fire Model for Simulating Corner Fires," in *Fire and Flammability of Furnishings and Contents* (A. Fowell, ed.), American Society for

Testing and Materials, West Conshohocken, PA, pp. 169–185 (1994).
8. BS476, *Fire Tests on Building Materials and Structures. Part 6: Method for Test for Fire Propagation for Products,* British Standards Institution, London, UK (1981).
9. DIN 4102, *Part 1: Fire Behavior of Building Materials and Building Components; Building Materials; Terminology, Calibration and Test Procedures,* DIN, Berlin, Germany (1984).
10. NF P 92-501, *Safety against Fire—Building Materials—Reaction to Fire Tests—Radiation Test Used for Rigid Materials or Materials on Rigid Substrate (Flooring and Finishes) of All Thicknesses, and for Flexible Materials Thicker than 5 mm,* AFNOR, Paris, France (1985).
11. NT Fire 0004, *Building Products: Heat Release and Smoke Generation,* NORDTEST, Helsinki, Finland (1985).
12. "Designation of Semi-Non-Combustible Materials and Fire Retardant Materials," *Notification No. 1231,* Ministry of Construction, Tokyo, Japan (1986).
13. "Proposed Method for Room Fire Test of Wall and Ceiling Materials and Assemblies," *ASTM Annual Book of Standards,* American Society for Testing and Materials, Philadelphia, pp. 958–978 (1983).
14. NFPA 265, *Standard Methods of Fire Tests for Evaluating Room Fire Growth Contribution of Textile Wall Covering,* National Fire Protection Association, Quincy, MA (1998).
15. NFPA 286, *Standard Methods of Fire Tests for Evaluating Contribution of Wall and Ceiling Interior Finish to Room Fire Growth,* National Fire Protection Association, Quincy, MA (2000).
16. ISO 9705, *Full-Scale Room Test,* International Standards Organization, Geneva, Switzerland (1992).
17. A. Tewarson and R. Pion, "Flammability of Plastics, I. Burning Intensity," *Combustion and Flame,* 26, pp. 85–103 (1976).
18. V. Petrella, "The Mass Burning Rate of Polymers, Wood and Liquids," *J. of Fire and Flammability,* 11, pp. 3–21 (1980).
19. N. Iqbal and J. Quintiere, "Flame Heat Fluxes in PMMA Pool Fires," *J. of Fire Protection Engineering,* 6, pp. 153–162 (1994).
20. B. Rhodes and J. Quintiere, "Burning Rate and Heat Flux for PMMA in the Cone Calorimeter," *Fire Safety J.,* 26, pp. 221–240 (1996).
21. D. Hopkins and J. Quintiere, "Material Fire Properties and Predictions for Thermoplastics," *Fire Safety J.,* 26, pp. 241–268 (1996).
22. W. Parker and J. Urbas, "Surface Temperature Measurements on Burning Wood Specimens in the Cone Calorimeter and the Effect of Grain Orientation," *J. of Fire and Materials,* 17, 5, pp. 205–208 (1993).
23. J. Urbas, "Non-Dimensional Heat of Gasification Measurements in the Intermediate Scale Heat Release Apparatus," *J. of Fire and Materials,* 17, pp. 119–123 (1993).
24. M. Janssens, "Cone Calorimeter Measurements of the Heat of Gasification of Wood," *Proceedings of the Interflam '93 Conference,* Interscience Communications, London, England, pp. 549–558 (1993).
25. E. Smith, "Math Model of a Fire in a Compartment Having Combustible Walls and Ceiling," in *AIChE Symposium Series 246,* 81, pp. 64–74 (1985).
26. H. Mitler, "Predicting the Spread Rates of Fires on Vertical Surfaces," in *23rd Symposium (International) on Combustion,* The Combustion Institute, pp. 1715–1721 (1990).
27. K. Opstad, "Fire Modeling Using Cone Calorimeter Results," in *Proceedings of the Eurefic Seminar,* Interscience Communications, London, England, pp. 65–71 (1991).
28. Y. Zhenghua and G. Holmstedt, "CFD and Experimental Studies of Room Fire Growth on Wall Lining Materials," *Fire Safety J.,* 27, pp. 201–238 (1996).
29. J. Quintiere, "A Simulation Model for Fire Growth on Materials Subject to a Room-Corner Test," *Fire Safety J.,* 20, pp. 313–339 (1993).
30. E. Smith and T. Green, "Release Rate Tests for a Mathematical Model," *Mathematical Modeling of Fires,* (J. Mehaffey, ed.), American Society for Testing and Materials, West Conshohocken, PA, pp. 7–20 (1987).
31. U. Wickström and U. Göransson, "Full-Scale/Bench-Scale Correlations of Wall and Ceiling Linings," *J. of Fire and Materials,* 16, pp. 15–22 (1992).
32. B. Östman and R. Nussbaum, "Correlation Between Small-Scale Rate of Heat Release and Full-Scale Room Flashover for Surface Linings," in *Fire Safety Science, Proceedings of the 2nd International Symposium,* Hemisphere Publ. Co., New York, pp. 823–832 (1989).
33. B. Karlsson, "Modeling Fire Growth on Combustible Lining Materials in Enclosures," Ph.D. Dissertation, University of Lund, Sweden (1992).
34. D. Evans and L. Breden, "Time Delay Correction for Heat Release Rate Data," *Fire Technology,* 14, pp. 85–96 (1978).
35. D. Bluhme and R. Getka, "Rate of Heat Release Test - Calibration, Sensitivity and Time Constants of ISO RHR Apparatus," *NORDTEST Project 115-77,* National Institute for Testing of Materials, Copenhagen, Denmark (1979).
36. P. Vandevelde, "An Evaluation of Heat Release Criteria in Reaction-to-Fire Tests," *J. of Fire and Materials,* 4, pp. 157–162 (1980).
37. A. Abramowitz and R. Lyon, "Effect of Instrument Response Time on Heat Release Rate Measurements," *J. of Fire and Materials,* 19, pp. 11–17 (1995).
38. N. Thompson and E. Cousins, "The FM Construction Materials Calorimeter," *NFPA Quarterly,* 52, pp. 186–192 (1959).
39. J. Brenden, "Apparatus for Measuring Rate of Heat Release from Building Materials," *J. of Fire and Flammability,* 6, pp. 50–64 (1975).
40. W. Parker and M. Long, "Development of a Heat Release Rate Calorimeter at NBS," in *Ignition, Heat Release and Noncombustibility of Materials,* (A. Robertson, ed.), American Society of Testing and Materials, pp. 135–151 (1972).
41. J. Tordella and W. Twilley, "Development of a Calorimeter for Simultaneously Measuring Heat Release and Mass Loss Rate," *NBSIR 83-2708,* National Bureau of Standards, Gaithersburg, MD (1983).
42. S. Martin, "Characterization of the Stanford Research Institute Large-Scale Heat-Release Rate Calorimeter," *NBS-GCR 76-54,* National Bureau of Standards, Gaithersburg, MD (1975).
43. W. Thornton, "The Relation of Oxygen to the Heat of Combustion of Organic Compounds," *Philosophical Magazine and Journal of Science,* 33 (1917).
44. C. Huggett, "Estimation of the Rate of Heat Release by Means of Oxygen Consumption," *J. of Fire and Materials,* 12, pp. 61–65 (1980).
45. W. Parker, "An Investigation of the Fire Environment in the ASTM E-84 Tunnel Test," *NBS Technical Note 945,* National Bureau of Standards, Gaithersburg, MD (1977).
46. R. Nussbaum, "Oxygen Consumption Measurements in the Cone Calorimeter—A Direct Comparison between a Paramagnetic Cell and a High-Temperature Cell," *J. of Fire and Materials,* 11, pp. 201–203 (1987).
47. W. Parker, "Calculations of the Heat Release Rate by Oxygen Consumption for Various Applications," *NBSIR 81-2427,* National Bureau of Standards, Gaithersburg, MD (1982).
48. M. Janssens, "Measuring Rate of Heat Release by Oxygen Consumption," *Fire Technology,* 27, pp. 234–249 (1991).

49. S. Brohez, C. Delvosalle, G. Marlair, and A. Tewarson, "Soot Generation in Fires: An Important Parameter for Accurate Calculation of Heat Release," in *Fire Safety Science, Proceedings, 6th International Symposium,* Poitiers, France, pp. 265–276 (2000).
50. B. Dlugogorski, J. Mawhinney, and V. Duc, "Measurement of Heat Release Rates by Oxygen Consumption Calorimetry in Fires Under Suppression," in *Fire Safety Science, Proceedings, 4th International Symposium,* Ottawa, Canada, pp. 877–888 (1994).
51. A. Roberts, "Ultimate Analysis of Partially Decomposed Wood Samples," *Combustion and Flame,* 8, pp. 345–346 (1964).
52. V. Babrauskas, "The Generation of CO in Bench-Scale Fire Tests and the Prediction for Real-Scale Fires," in *Proceedings of the 1st Fire and Materials Conference,* Interscience Communications, London, England, pp. 155–177 (1992).
53. B. Messerschmidt and P. van Hees, "Influence of Delay Times and Response Times on Heat Release Rate Measurements," *J. of Fire and Materials,* 24, pp. 121–130 (2000).
54. H. Sawada, *Thermodynamics of Polymerization,* Marcel Dekker, New York (1976).
55. ASTM E906, "Test Method for Heat and Visible Smoke Release Rates for Materials and Products," in *Annual Book of ASTM Standards,* American Society for Testing and Materials, West Conshohocken, PA, pp. 658–683 (1999).
56. ASTM E1317, "Standard Test Method for Flammability of Marine Surface Finishes," in *Annual Book of ASTM Standards,* American Society for Testing and Materials, West Conshohocken, PA, pp. 696–713 (1999).
57. V. Babrauskas, "Development of the Cone Calorimeter—A Bench-Scale Heat Release Rate Apparatus Based on Oxygen Consumption," *J. of Fire and Materials,* 8, pp. 81–95 (1984).
58. A. Koohyar, "Ignition of Wood by Flame Radiation," Ph.D. Dissertation, University of Oklahoma, Norman, OK (1967).
59. J. Hallman, "Ignition Characteristics of Plastics and Rubber," Ph.D. Dissertation, University of Oklahoma, Norman, OK (1971).
60. D. Drysdale, *An Introduction to Fire Dynamics,* John Wiley and Sons, Chichester, England, pp. 153–160 (1985).
61. R. Nussbaum and B. Östman, "Larger Specimens for Determining Rate of Heat Release in the Cone Calorimeter," *J. of Fire and Materials,* 10, pp. 151–160 (1986).
62. M. Janssens and J. Urbas, "Comparison of Small and Intermediate Scale Heat Release Rate Data," in *Proceedings of the Interflam '96 Conference,* Interscience Communications, London, England, pp. 285–294 (1996).
63. ASTM E1354, "Test Method for Heat and Visible Smoke Release Rates for Materials and Products Using an Oxygen Consumption Calorimeter," in *Annual Book of ASTM Standards,* American Society for Testing and Materials, West Conshohocken, PA, pp. 750–767 (1999).
64. ISO 5660–1, *Rate of Heat Release of Building Products (Cone Calorimeter),* International Standards Organization, Geneva, Switzerland (1992).
65. B. Toal, T. Shields, and W. Silcock, "Observations on the Cone Calorimeter," *J. of Fire and Materials,* 14, pp. 73–76 (1989).
66. B. Toal, T. Shields, and W. Silcock, "Suitability and Preparation of Samples for the Cone Calorimeter," *Fire Safety J.,* 16, pp. 85–88 (1990).
67. J. Urbas and H. Sand, "Some Investigations on Ignition and Heat Release of Building Materials Using the Cone Calorimeter," in *Proceedings of the Interflam '90 Conference,* Interscience Communications, London, England, pp. 183–192 (1990).
68. V. Babrauskas, W. Twilley, and W. Parker, "The Effect of Specimen Edge Conditions on Heat Release Rate," *J. of Fire and Materials,* 17, pp. 51–63 (1993).
69. L. Tsantaridis and B. Östman, "Communication: Retainer Frame Effects on Cone Calorimeter Results for Building Products," *J. of Fire and Materials,* 17, pp. 43–46 (1993).
70. V. Babrauskas, W. Twilley, M. Janssens, and S. Yusa, "A Cone Calorimeter for Controlled-Atmosphere Studies," *J. of Fire and Materials,* 16, pp. 37–43 (1992).
71. D. Bluhme, "ISO RHR Test Apparatus with Oxygen Consumption Technique," *NORDTEST Project 115-77, Dantest,* Copenhagen, Denmark (1982).
72. *Federal Register,* 51, pp. 26206–26221 (1986).
73. "Aircraft Material Fire Test Handbook," *DOT/FAA/CT-89/15,* US Department of Transportation, Federal Aviation Administration, Atlantic City, NJ (1990).
74. V. Babrauskas, "Combustion of Mattresses Exposed to Flaming Ignition Sources, Part II: Bench-Scale Tests and Recommended Standard Test," *NBSIR 80-2186,* National Bureau of Standards, Gaithersburg, MD (1981).
75. Y. Tsuchiya, "Methods of Determining Heat Release Rate: State-of-the-Art," *Fire Safety J.,* 5, pp. 49–57 (1982).
76. J. Blomqvist, "Rate of Heat Release of Building Materials, Experiments with an OSU Apparatus Using Oxygen Consumption," *Report LUTVDG/(TVBB-3017),* Lund University, Sweden (1983).
77. H. Tran, "Modifications to an Ohio State University Apparatus and Comparison with Cone Calorimeter Results," in *Heat and Mass Transfer in Fires, Proceedings of the AIAA/ASME Thermophysics and Heat Transfer Conference,* HTD 141, 1990, American Society of Mechanical Engineers, Seattle, WA, pp. 131–139 (1990).
78. J. Brenden, "Wood-Base Building Materials: Rate of Heat Release," *J. of Fire and Flammability,* 6, pp. 274–293 (1975).
79. A. Tewarson, "Heat Release Rates from Burning Plastic," *J. of Fire and Flammability,* 8, pp. 115–130 (1977).
80. A. Tewarson, "Reliable Small-Scale Fire Testing Apparatus," *Modern Plastics,* pp. 58–62 (1980).
81. A. Tewarson, J. Lee, and R. Pion, "The Influence of Oxygen Concentration on Fuel Parameters for Fire Modeling," *18th Symposium (International) on Combustion,* Combustion Institute, pp. 563–570 (1981).
82. G. Svensson and B. Östman, "Rate of Heat Release by Oxygen Consumption in an Open Test Arrangement," *J. of Fire and Materials,* 8, pp. 206–216 (1984).
83. D. Sensenig, "An Oxygen Consumption Technique for Determining the Contribution of Interior Wall Finishes to Room Fires," *NBS Technical Note 1128,* National Bureau of Standards, Gaithersburg, MD (1980).
84. D. Chamberlain, "Heat Release Rate Properties of Wood-Based Materials," *NBSIR 82-2597,* National Bureau of Standards, Gaithersburg, MD (1983).
85. B. Östman, G. Svensson, and J. Blomqvist, "Comparison of Three Test Methods for Measuring Rate of Heat Release," *J. of Fire and Materials,* 9, pp. 176–184 (1985).
86. V. Babrauskas, "Comparative Rates of Heat Release from Five Different Types of Test Apparatuses," *J. of Fire Sciences,* 4, pp. 148–159 (1986).
87. P. Gandhi, L. Caudill, and T. Chapin, "Comparison of Cone Calorimeter Data with FM3972 for Communication Cables," in *Proceedings of the Fifth Fire and Materials Conference,* Interscience Communications, London, England, pp. 217–227 (1998).
88. J. Caman, D. Price, G. Milnes, and D. Purser, "Comparison of Heat Release Rates as Measured by Oxygen Depletion and Thermopile Techniques," in *Proceedings of the Interflam '99 Conference,* Interscience Communications, London, England, pp. 1367–1371 (1999).

89. I. Oleszkiewicz and G. Crampton, "Heat Release from Combustion of Large-Scale Wall Assemblies," in *Abstracts of the 1st Heat Release and Fire Hazard Symposium,* Interscience Communications, London, England, 1991, pp. 18–22.
90. J. Urbas and J. Shaw, "Testing Wall Assemblies on an Intermediate Scale Calorimeter (ICAL)," *Fire Technology,* 29, pp. 332–349 (1993).
91. ASTM E1623, "Test Method for Determination of Fire and Thermal Parameters of Materials, Products, and Systems Using an Intermediate Scale Calorimeter (ICAL)," in *Annual Book of ASTM Standards,* American Society for Testing and Materials, West Conshohocken, PA, pp. 875–892 (1999).
92. V. Babrauskas, J. Lawson, W. Walton, and W. Twilley, "Upholstered Furniture Heat Release Rates Measured with a Furniture Calorimeter," *NBSIR 82–2604,* National Bureau of Standards, Gaithersburg, MD (1982).
93. NT Fire 032, *Upholstered Furniture: Burning Behavior—Full Scale Test,* NORDTEST, Helsinki, Finland (1987).
94. S. Ames and S. Rogers, "Large and Small Scale Fire Calorimetry Assessment of Upholstered Furniture," in *Proceedings of the Interflam '90 Conference,* Interscience Communications, London, England, pp. 221–232 (1990).
95. ASTM E1537, "Test Method for Fire Testing of Upholstered Furniture," in *Annual Book of ASTM Standards,* American Society for Testing and Materials, West Conshohocken, PA, pp. 807–826 (1999).
96. ASTM E1590, "Test Method for Fire Testing of Mattresses," in *Annual Book of ASTM Standards,* American Society for Testing and Materials, West Conshohocken, PA, pp. 841–861 (1999).
97. ASTM E1822, "Test Method for Fire Testing of Stacked Chairs," in *Annual Book of ASTM Standards,* American Society for Testing and Materials, West Conshohocken, PA, pp. 930–950 (1999).
98. I. Benjamin, "Development of a Room Fire Test," *Fire Standards and Safety,* American Society for Testing and Materials, Philadelphia, PA, pp. 300–311 (1977).
99. F. Fisher and R. Williamson, "Intralaboratory Evaluation of a Room Fire Test Method," *NBS GCR 83-421,* National Bureau of Standards, Gaithersburg, MD (1983).
100. B. Lee, "Standard Room Fire Test Development at the National Bureau of Standards," *Fire Safety Science and Engineering,* American Society for Testing and Materials, Philadelphia, PA, pp. 29–42 (1985).
101. B. Sundström and U. Wickström, "Fire: Full Scale Tests," *Technical Report SP-RAPP 1980:14,* National Testing Institute, Borås, Sweden (1980).
102. B. Sundström and U. Wickström, "Fire: Full Scale Tests, Calibration of Test Room—Part 1," *Technical Report SP-RAPP 1980:48,* National Testing Institute, Borås, Sweden (1981).
103. A. Ahonen, C. Holmlund, and M. Kokkala, "Effects of Ignition Source in Room Fire Tests," *Fire Science and Technology,* 7, pp. 1–13 (1987).
104. D. Belles, F. Fisher, and R. Williamson, "Evaluating the Flammability of Textile Wall Coverings," *Building Standards,* 56, pp. 8–14, 52 (1987).
105. G. Heskestad, "A Fire Products Collector for Calorimetry into the MW Range," *Technical Report FMRC J. I 0C2E1.RA,* Factory Mutual Research Corporation, Norwood, MA (1981).
106. M. Dahlberg, "The SP Industry Calorimeter—For Rate of Heat Release Rate Measurements up to 10 MW," *SP Report 1992:43,* Swedish National Testing and Research Institute, Borås, Sweden (1992).
107. L. Cooper, "Some Factors Affecting the Design of a Calorimeter Hood and Exhaust," *J. of Fire Protection Engineering,* 6, pp. 99–112 (1994).
108. J. Brenden and D. Chamberlain, "Heat Release Rates from Wall Assemblies," *Research Paper FPL-RP-476,* Forest Products Laboratory, Madison, WI (1986).
109. H. Tran and R. White, "Heat Release from Wood Wall Assemblies Using Oxygen Consumption Method," *Fire and Polymers: Hazards, Identification, and Prevention,* ACS Symposium Series 425, American Chemical Society, Washington, DC, pp. 411–428 (1990).
110. M. Dahlberg, "Error Analysis for Heat Release Rate Measurements with the SP Industry Calorimeter," *SP Report 1994:29,* Swedish National Testing and Research Institute, Borås, Sweden (1994).
111. P. Enright and C. Fleischmann, "Uncertainty of Heat Release Rate Calculation of the ISO 5660–1 Cone Calorimeter Standard Test Method," *Fire Technology,* 35, pp. 153–169 (1999).
112. J. Urbas, "BDMC Interlaboratory Cone Calorimeter Test Program," *J. of Fire and Materials,* in press.

CHAPTER 3

The Cone Calorimeter

Vytenis Babrauskas

Introduction

Section 3, Chapter 2 describes the history and development of techniques for measuring heat release rate (HRR). This chapter outlines features and details of today's preferred instrument for measuring bench-scale HRR—the cone calorimeter. Other cone calorimeter measuring functions are:

1. Effective heat of combustion
2. Mass loss rate
3. Ignitability
4. Smoke and soot
5. Toxic gases

The cone calorimeter is based on the concept of oxygen consumption calorimetry, which is also presented in Section 3, Chapter 2.

This chapter provides both an introduction to and description of cone calorimeter measurement technology. The cone calorimeter has recently assumed a dominant role in bench-scale fire testing of various products; therefore, an emphasis will be placed on the *why* of various design features. When conducting tests, the cone calorimeter operator needs to consult several other documents. Testing will presumably be in conformance with either ISO 5660[1] or ASTM E1354.[2] In addition, the "User's Guide for the Cone Calorimeter"[3] should be consulted. This chapter, thus, does not emphasize the operational aspects, which are documented in the above references, but provides the reader with an overall feel for the equipment. Space is not available in the Handbook to fully discuss the applications of cone calorimeter data, apart from the review of data given in Section 3, Chapter 1. Extensive guidance on using cone calorimeter data is given in a textbook on this subject.[4] It also provides example data compilations and information on using cone calorimeter data for predictions of fires.

Dr. Vytenis Babrauskas is the president of Fire Science and Technology Inc., a company specializing in fire safety research, fire testing issues, and fire science applications to fire investigations and litigations.

Summary of Features

A schematic view of the cone calorimeter is shown in Figure 3-3.1. Figure 3-3.2 shows a commercial instrument, while Figure 3-3.3 identifies some of the major components. The more salient operational features and limits of the apparatus are

• Specimen size	100 mm × 100 mm, thickness of 6 to 50 mm
• Specimen orientation	Horizontal, face up (standard testing) or vertical (reserved for exploratory studies)
• Specimen back-face conditions	Very low loss insulating ceramic fibrous material
• Load cell live load capacity	500 g
• Load cell tare capacity	3.5 kg
• Load cell resolution	0.005 g
• Ignition	Electric spark
• Heating flux range	0 to 110 $kW \cdot m^{-2}$
• Flux uniformity, horizontal	Typically 2 percent
• Flux uniformity, vertical	Typically 7 percent
• Sensing principle	Oxygen consumption, only
• Maximum instantaneous output	In excess of 20 kW
• Normally calibrated range	0 to 12 kW
• Linearity over 0 to 12 kW range	5 percent
• Noise intrinsic to oxygen meter	20 ppm O_2
• Noise in HRR measurement, over 0 to 12 kW range	2.5 percent
• Smoke meter operating range	0 to 20 m^{-1} (linear)
• Smoke meter resolution	0.01 m^{-1}
• Soot sampler mass fraction range	0 to 1 part in 200 (of exhaust gas flow)

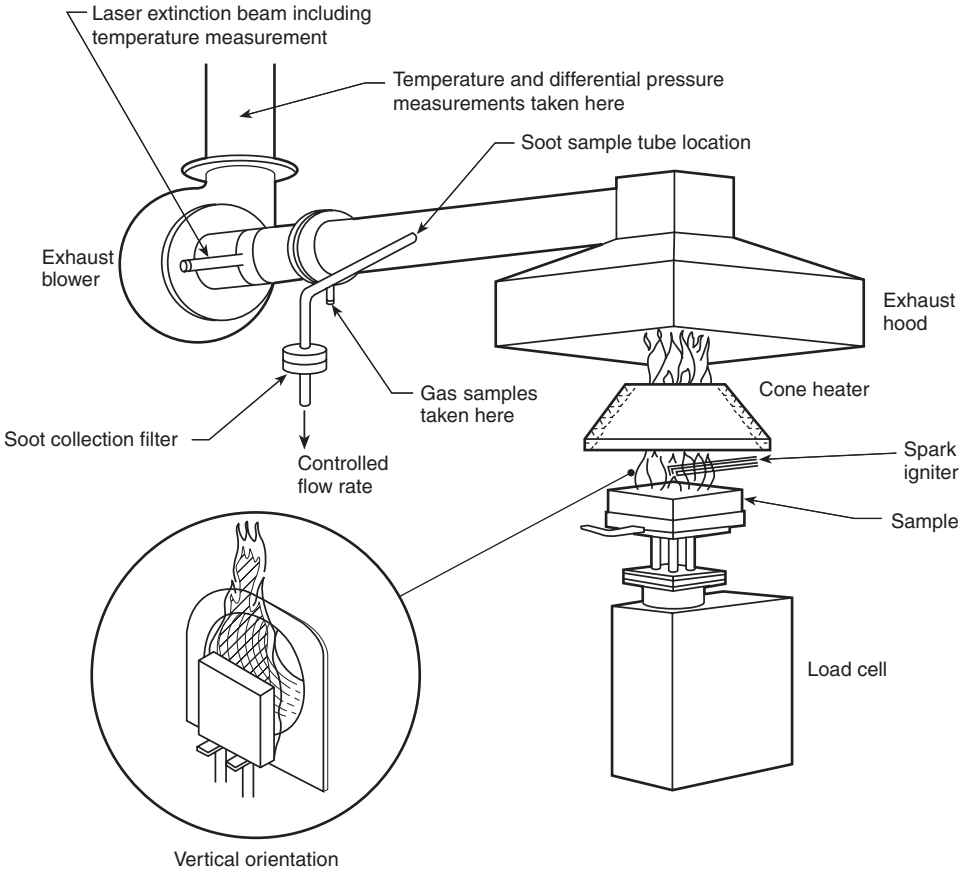

Figure 3-3.1. ***Schematic view of the cone calorimeter.***

Operating Principle

It is emphasized at this point that the cone calorimeter has been designed to use *only* oxygen consumption calorimetry as its measurement principle. Other calorimeters that on occasion use oxygen consumption principles, for example, the Factory Mutual Research Corporation (FMRC) flammability apparatus (see Section 3, Chapter 2), sometimes incorporate a sensible enthalpy flow measurement technique to arrive at the *convective component* of the heat release rate. In the design of the cone calorimeter, such an approach was deemed to be misleading. The implicit assumption behind this type of measurement is that the fraction of the total heat release being manifest as the sensible flow enthalpy is a property of the material being tested. Such is not, in fact, the case. The convective fraction is dependent on details of the apparatus design, and also on the scale of the specimen.[5]

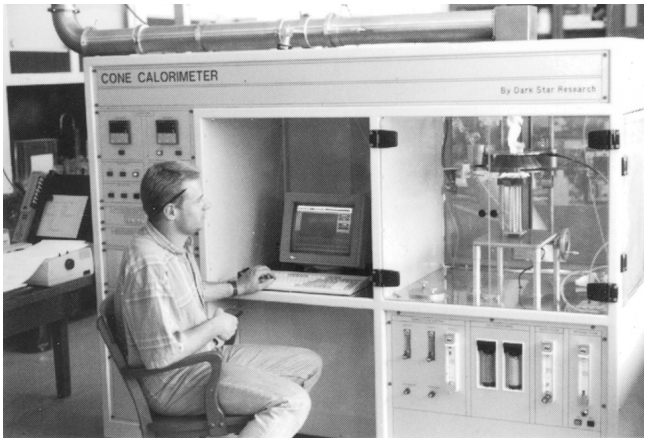

Figure 3-3.2. ***A commercial cone calorimeter. (Photo courtesy Dark Star Research.)***

Where high-quality results are required, such as in the cone calorimeter, current-day practice demands that a paramagnetic oxygen analyzer be used. The various manufacturers use measuring schemes that differ in detail, but all rely on the same paramagnetic principle whereby the sensing element is sensitive to the partial pressure of oxygen in the cell. The most significant interferents to this detection principle are NO and NO_2, both of which show a strong paramagnetic response, but not as strong as that of oxygen. Interferents are never a problem in fire testing, however, since O_2 levels measured are 10 to 21 percent, while concentrations of NO_x are rarely above 100 ppm.

Unlike in applications where oxygen levels are monitored as simply one of many indications of fire hazard, in HRR work it is essential that the instrumentation be designed for the highest possible resolution. Thus, both the

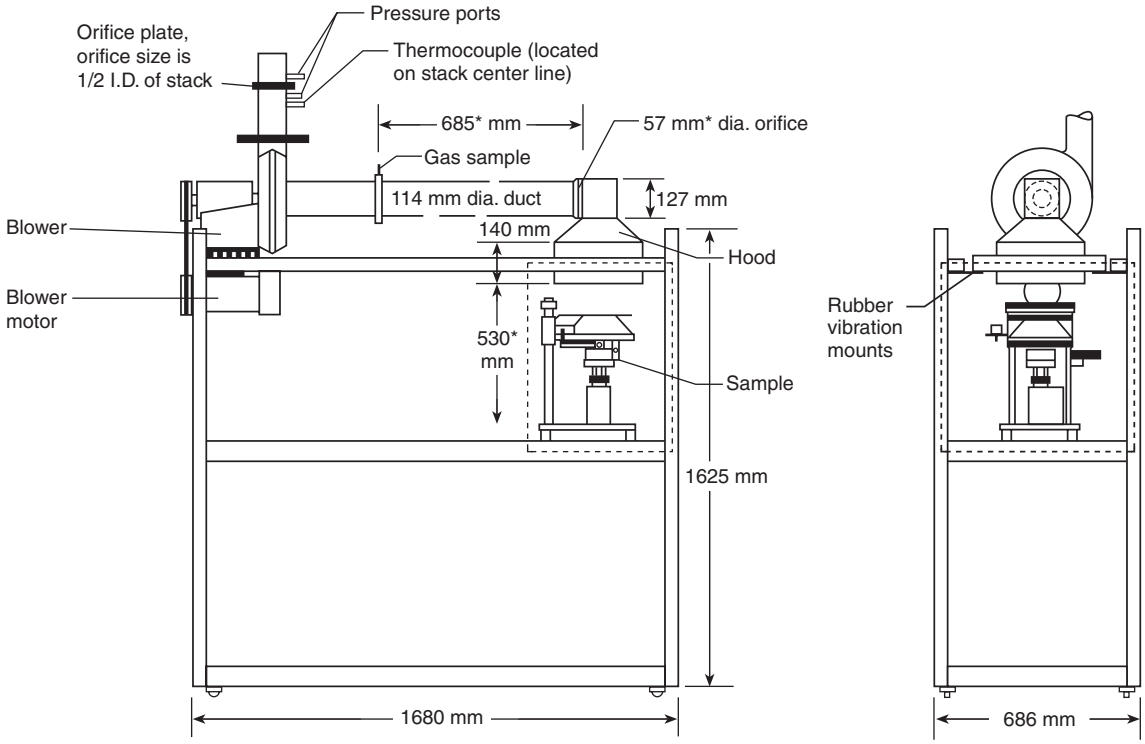

Figure 3-3.3. ***View of major components of the cone calorimeter.***

ASTM and the ISO standards specify that the short-term noise + drift of the oxygen analyzer must be ≤50 ppm O_2. The best-grade commercial instruments are able to meet a 20 ppm O_2 limit. In addition, the standards provide a significant amounts of detail on the layout of the gas sampling system, including desiccation, mass flow control, and bypass flows. All of these aspects have to be in conformance with the specifications for good repeatability and reproducibility performance (see Figure 3-3.3) to be achieved.

Because the detection principle responds to oxygen partial pressure, there needs to be a compensation for changes in atmospheric pressure. This can be done with a mechanical back-pressure regulator or by measuring the pressure and correcting electrically. If this compensation is not made, there can be significant error in the calculated heat release rate. Carbon dioxide, the other major component expected to be in the oxygen analyzer, causes less than 0.3 percent error in the oxygen reading. Extensive practice advice on selecting, setting up, and calibrating oxygen analysis systems is given in References 3 and 4.

The Radiant Heater

After establishing the operating principle, the next most important feature is the type of heater. In general, such a heater should be able to achieve adequately high irradiances, have a relatively small convective heating component, present a highly uniform irradiance over the entire exposed face of the specimen, and be designed so as not to change its irradiance when the main voltage varies, when heater element aging occurs, or when the apparatus retains some residual heat from the exposure given to a prior specimen.

Range of heat fluxes needed for testing: A room fire burning near its maximum rate can show gas temperatures over 1000°C, producing corresponding irradiances to walls and contents of 150 $kW \cdot m^{-2}$. Testing under such extreme conditions may not be required; nonetheless, if post-flashover fires are to be stimulated, irradiances of over 75 $kW \cdot m^{-2}$ should be available, and preferably closer to 100 $kW \cdot m^{-2}$. A significant convective component would negate the purpose of having a radiant ignition test. Rather low convective fluxes can be achieved for specimens oriented horizontally, face up, and with the prevailing airflow being upwards. For vertical specimens, orientation is considered, and it becomes evident that a boundary layer will normally be expected to develop that will add some convective component. The convective boundary layer component is not uniform over the height of a specimen; thus it is seen that better uniformity can also be expected under conditions where the convective component is minimized.

Choice of heater type: In a real fire, the ignition source is, in most cases, in the vicinity of a combustible. The radiation spectrum depends on the size of the fire. A very small fire can show a substantial fraction of its radiation at wavelengths characteristic of H_2O, CO_2, and other combustion products.[6] For larger fires—certainly for

room fires reaching a hazardous condition—the radiation from the soot tends to dominate. The result is an approximation to a grey-body radiation.[7] For such a grey-body radiation the temperature is typically in the vicinity of 1000°C.[8] Experimentally, heater choices for test apparatuses have included gas-fired panels, electric resistance heaters, flames, and high-temperature lamps. Electrical heaters tend to have a near-grey-body characteristic and, assuming a dull or oxidized surface condition, a high emissivity. Gas-fired panels derive a substantial portion of their radiation from the ceramic face; thus, while there are discrete molecular wavelength peaks, overall the radiation shows a grey-body continuum, typically in the range of 700 to 1000°C.[9] High-temperature lamps, which have been used by several investigators,[6,10] typically have radiating temperatures of 2200 to 3000°C. The spectral distribution of such a source—further limited by a translucent enclosure—is much different from one operating at 1000°C. Whether this change in spectral characteristics is important depends on the surface of the material to be ignited. For a material with a radiant absorbance independent of wavelength, this source variation would not matter. Hallman, however, has reported data for a large number of plastics and shows that while there are some specimens with negligible wavelength dependence to their absorbance, the majority show strong variations.[6] Hallman also measured ignition times of plastics with both a flame source and high-temperature lamps. The effect on ignition times ranges from negligible to more than an order of magnitude, depending on the specimen. For a general-purpose test, flames would probably be the least desirable source of heating. For a bench-scale test, flame size has to be kept small. This means that such flames are optically thin, their emissivity is low, and higher heat fluxes cannot be achieved unless a strong convective component is added.

Design details: Once an electrical radiant heater had been decided upon, design details were also influenced by work at NIST with earlier types of calorimeters. One of the primary requirements of the heater is that it not change the irradiance impressed on the specimen when the specimen ignites. This undesired event is, of course, exactly what happens with several of the older types of calorimeters. The specimen's flames directly heat up nearby ironwork, which, in turn, radiates to the specimen. The heater which had been viewing a cold specimen prior to ignition, also starts to view a hot flame afterwards. The result is that its efficiency increases drastically, giving a rise to its radiating temperature. Based on these observations, guidelines were formulated so that the specimen must, as much as possible, view only

1. A temperature-controlled heater
2. A water-cooled plate
3. The open-air, ambient-temperature environment

Reliance on item 2 increased costs significantly; thus, it was more desirable to use only items 1 and 3. Prior to the development of the cone calorimeter, fire test apparatuses typically controlled the power (or fuel rate) into the heater, but did not maintain it at a fixed temperature.

The conical shape: The cone calorimeter derives its name from the conical shape of the heater. (See Figure 3-3.4.) The decision had been made to use an electric resistance heater, running at a realistic maximum temperature of about 950°C, but its material and shape still had to be determined. Based on poor experiences with exposed-wire resistance heaters and with silicon carbide rod-type heaters, the tube heater was chosen. The tube heater consists of a resistive wire element inside a protective tube, swaged over a packing of inorganic insulation. The tube is made of Incoloy™ and can be bent to a desired shape.

To determine the best shape, the conical heater used in the ISO 5657 ignitability apparatus[11] was examined. This seemed to be a promising shape. The proper shape had to have a hole in the middle, since otherwise a hot spot would occur at the sample center, where the radiation view factor is the highest. The same heater had to serve in both horizontal and vertical orientations. In the horizontal orientation, it was essential that all the products of combustion flow out the hole in the middle, and not "splash" on the heater coil itself, nor escape from the underside. The original ISO 5657 design proved to be unsuitable in the former respect. It also had problems with durability and assembly. Thus a totally new design was created, one that looks, however, superficially similar to the ISO 5657 cone. With the actual cone calorimeter design, the flames from the specimen do not splash on the heater coil. Instead, a sheath of cold air is pulled up, surrounding the flame plume. Thus, there is not a concern that any surface reactions occur on the heater coil.

The space between the inner and outer cones is packed with refractory fiber. This arrangement helps keep the outside of the unit cool and also helps bring the heater up to operating temperature rapidly.

Emissivity of the heater: The emissivity was characterized by Janssens.[12] The heater coil, once installed and fired up a few times, becomes essentially radiatively black. The emissivity itself cannot be directly measured; however, it is possible to compute an approximate view factor, *F,* for the cone heater. The possibility of measure-

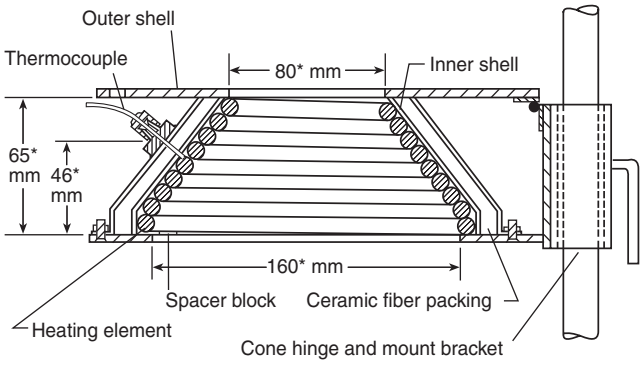

*Indicates a critical dimension

Figure 3-3.4. ***Cross-sectional view through the cone heater.***

ments is based on a simultaneous determination of the heater surface temperature and the heat flux falling on the heat flux meter, with the meter held in place at the same location where a specimen is situated. Over the range of fluxes of 10 to 90 $kW \cdot m^{-2}$, Janssens determined the $\varepsilon \times F$ product to be 0.73, with F being computed as 0.78. Then, solving for ε gives $\varepsilon = 0.91$. Since the temperatures of the heater closely resemble those in room fires, and the emissivity approaches 1.0, this means that the spectral distribution is likely to be very close to that expected from room fires (neglecting the molecular radiation contribution from CO_2 and H_2O).

Convective fraction of the heating flux: During the development of the cone calorimeter at NIST, a study was conducted to determine the fraction of the heating flux, which is accounted for by the convective contribution.[13] When measured with respect to a water-cooled heat flux meter, the results showed that, in the horizontal specimen orientation, the convective contribution was immeasurably small. In the vertical orientation, the fraction was typically 8 to 12 percent. Janssens later remeasured the vertical configuration[12] using a more accurately calibrated heat flux meter and found that, even for the vertical orientation, the convective transfer is immeasurably small. Thus, it can be stated that the objective of having a test method where the heating is primarily radiant was successfully met. For modeling of test results, however, one may be more interested in the possibility of convective heat transfer to a specimen that is heated, or even burning, not to a calibration meter constrained by its water-cooling jacket at near-room temperature. Janssens also made some determinations of such actual specimen heating. The direction of the heat transfer was such as to represent a heat loss from the specimen in all cases. A single convective heat transfer coefficient could not be derived, however, since the value was dependent on the irradiance level from the heater. Janssens' results could be represented by:

Irradiance from Heater ($kW \cdot m^{-2}$)	Convective Heat Transfer Coefficient h_c ($W \cdot m^{-2} \cdot K^{-1}$)
20	9.0
40	18.0
60	27.0

For practical work, Janssens recommended that an average value of $h_c = 13.5$ $W \cdot m^{-2} \cdot K^{-1}$ should be appropriate for work over the common irradiance range of 20 to 40 $kW \cdot m^{-2}$. The actual details of this small amount of convective heat transfer are pertinent only to certain specialized studies. For most work, it is entirely adequate to assume that the specimen heating is entirely radiative.

Uniformity of the heating flux: The uniformity of the heating flux over the face of the specimen in the cone calorimeter has been described.[13] Over the range of irradiances from 25 to 100 $kW \cdot m^{-2}$, the ratio of the flux at the specimen center to average flux varied only from 1.00 to 1.06. The peak deviations from average were typically 2 percent in the horizontal orientation and 7 percent in the vertical. Deviations are higher in the vertical orientation, since the effect of convective fluxes, due to the boundary layer flow, is more pronounced there. Additional measurements have been made in the specimen-depth plane. Control of the surface of the specimen was a special concern to the designers of the ISO apparatus, where a special compressive loading mechanism is provided that attempts to relevel the exposed surface, in case the specimen recedes due to melting. In the cone calorimeter, measurements have been made in the horizontal orientation using a small, 6-mm diameter Gardon-type heat flux gage. A flux mapping was obtained starting at the initial surface, and progressing down to the maximum depth of a specimen, which is 50 mm. A normal aluminum foil rectangular specimen wrap was used for these tests, but without any specimen. The results show that, at heating fluxes of both 25 and 50 $kW \cdot m^{-2}$, the deviations over the entire specimen depth are less than 10 percent, and can, therefore, be neglected. (See Figure 3-3.5.) At the lower depths, reflection from the aluminum foil probably assists in maintaining this uniformity.

Orientation of the heater and specimen: It is seen that the normal orientation of the specimen should be horizontal, face up, with the heater being parallel, face down. This allows thermoplastics, liquids, and other melting or dripping samples to be successfully tested. For certain application exploratory studies, it was considered desirable to allow testing in a vertical orientation. Thus, provision was made to swing the heater 90 degrees into a vertical orientation. Vertical orientation testing may be preferable when probing the flame regions, or measuring specimen surface temperatures is desired. Figures 3-3.6 and 3-3.7 show the comparative horizontal and vertical heater orientations, respectively. It is especially emphasized that no standard testing should be specified for the vertical orientation, *even for products that are normally used in a vertical orientation.* The ASTM standard[2] was amended in 1992 to clarify that the vertical orientation is only for special research studies and not for product testing.

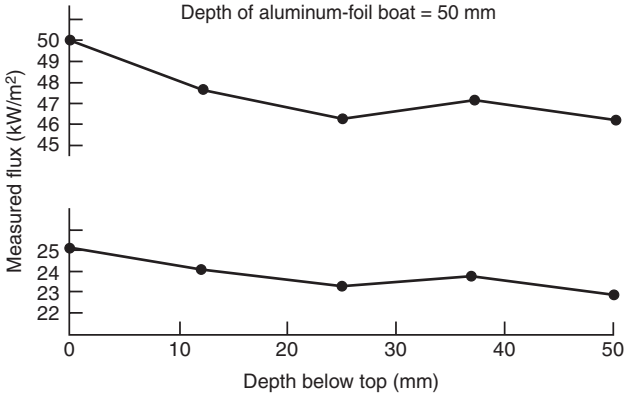

Figure 3-3.5. ***Measured flux at various positions below the top surface of a specimen.***

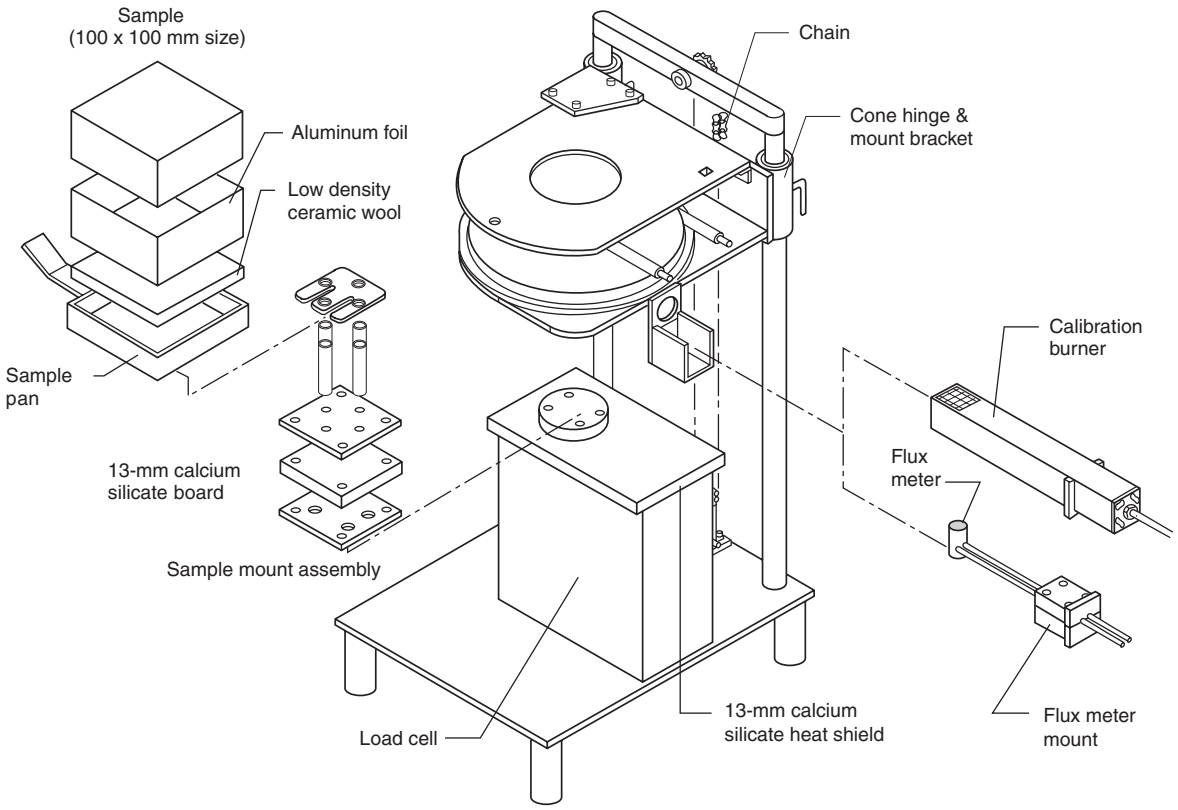

Figure 3-3.6. ***Heater in the horizontal (standard) orientation.***

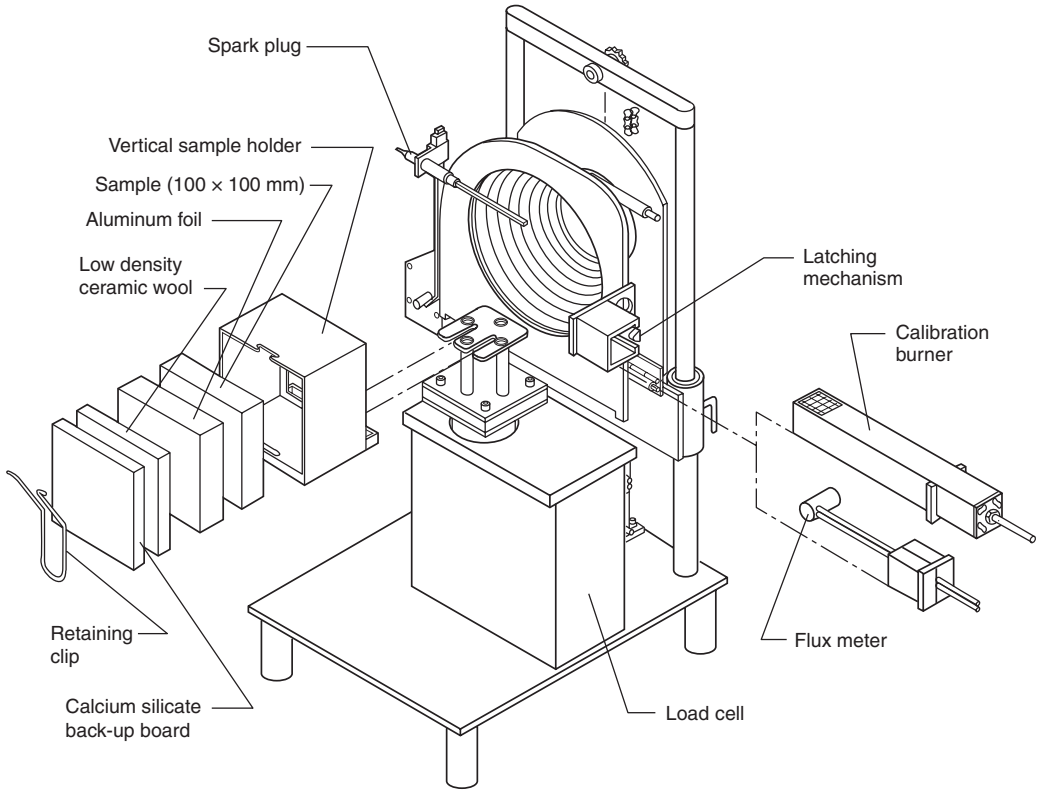

Figure 3-3.7. ***Heater in the vertical orientation.***

Airflow

The feasible airflow rate through the system is bound by certain limits. It must not be so fast that ignition results are improperly affected. It must also not be so slow that products of combustion spill out of the hood. If this were a closed system, one would also be concerned about airflow being so slow that the air/fuel ratio drops into the fuel-rich regime. The standard cone calorimeter, however, has been designed for ambient air testing, and this consideration does not apply.

Systematic guidance in this area was not available. However, as an example of the effect of airflow, measurements were made at NIST using the OSU apparatus. Specimens of black polymethylmethacrylate (PMMA) were exposed in the horizontal orientation to a heating flux of 35 $kW \cdot m^{-2}$. With an airflow rate of 12 $\ell \cdot s^{-1}$ through the combustion chamber, the ignition time was 209 s. When the airflow rate was doubled to 24 $\ell \cdot s^{-1}$, the specimen ignition time increased to 403 s. By contrast, Table 3-3.1 shows comparative results with the cone calorimeter; it can be seen a flow rate of 24 $\ell \cdot s^{-1}$ was found to be satisfactory. That flow rate was also about a factor of 2 greater than the minimum at which no spill out of the hood occurs.

The exhaust system uses a high-temperature cast-iron blower to exhaust the gases, and an orifice plate flowmeter. (See Figure 3-3.8.) The orifice plate flowmeter is instrumented with a differential pressure transducer and a thermocouple. For specialized studies, where the entire combustion system is glass enclosed,[14] it is possible to go to flow rates below 12 $\ell \cdot s^{-1}$. With such enclosed systems, accurate measurements can be made down to about 9 $\ell \cdot s^{-1}$ using the standard orifice plate. For lower flow rates, down to about 5 $\ell \cdot s^{-1}$, the standard orifice plate is replaced by one with a smaller opening.

Table 3-3.1 ***Effect of Exhaust Hood Airflow on Ignition Times in the Cone Calorimeter[a]***

Material	Thickness (mm)	Orientation	Fan Setting	Ignition Time[b] (s)
PMMA	13	Horizontal	no fan	71
PMMA	13	Horizontal	24 $\ell \cdot s^{-1}$	76
PMMA	13	Horizontal	41 $\ell \cdot s^{-1}$	67
PMMA	13	Vertical	no fan	86
PMMA	13	Vertical	24 $\ell \cdot s^{-1}$	84
PMMA	13	Vertical	41 $\ell \cdot s^{-1}$	77
Redwood	13	Horizontal	no fan	23
Redwood	13	Horizontal	24 $\ell \cdot s^{-1}$	24
Redwood	13	Horizontal	41 $\ell \cdot s^{-1}$	31
Redwood	13	Vertical	no fan	22
Redwood	13	Vertical	24 $\ell \cdot s^{-1}$	27
Redwood	13	Vertical	41 $\ell \cdot s^{-1}$	29

[a]At an irradiance of 35 $kW \cdot m^{-2}$

[b]Typical ignition time scatter was on the order of $\pm 10\%$ (1σ, $N = 3$)

Means of Ignition

In some cases no external ignition source is desired, and specimen testing is to be done solely on the basis of autoignition. In most cases, however, an external ignition source is desirable. This ignition source should, in general, not impose any additional localized heating flux on the specimen. Apparatus designs have been developed,

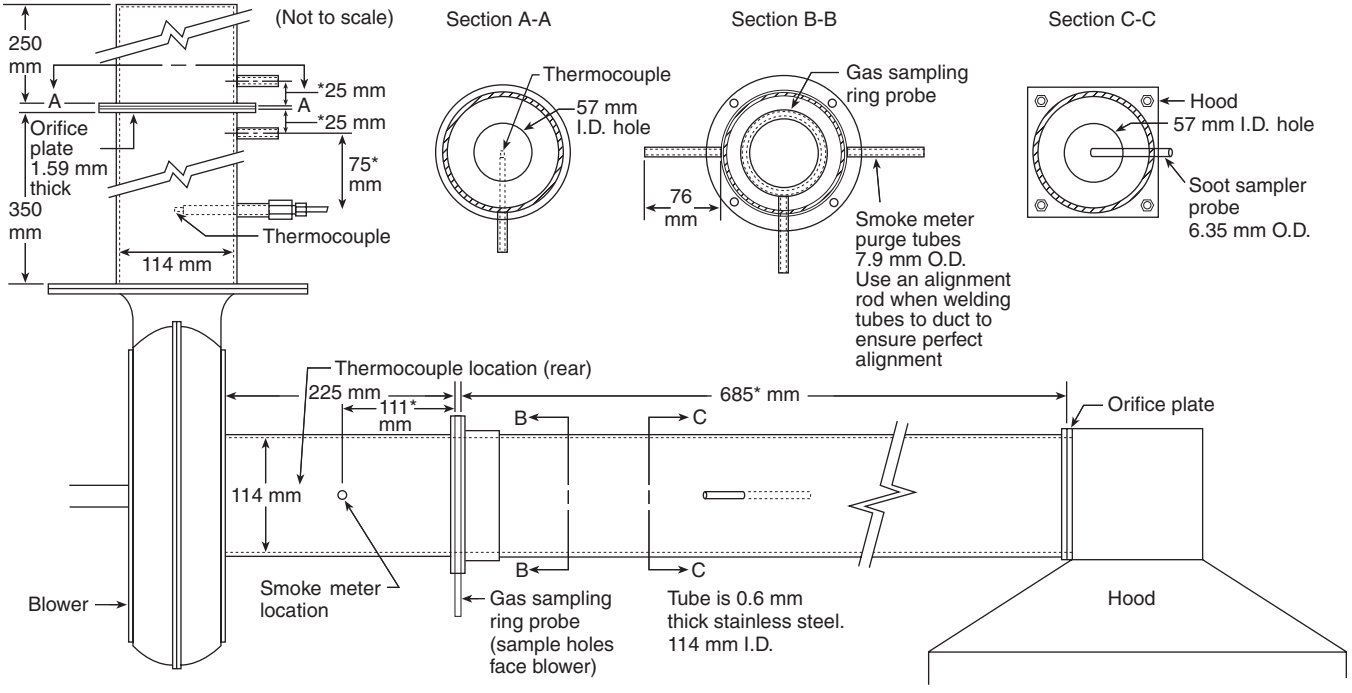

*Indicates a critical dimension

Figure 3-3.8. ***Exhaust duct.***

with impinging pilots that can, in some cases, produce such high localized heat fluxes as to burn a hole through the specimen at the point of impingement, yet not ignite it outside of that region. (See Reference 15.) Applications for such devices tend to be specialized, since the general objective of radiant ignition testing is to produce data that can be analyzed in the context of an assumed one-dimensional heat flow. A design using an impinging pilot has an additional difficulty. Since most of the specimen face is not yet heated to the ignition temperature when ignition first begins in the vicinity of the pilot, no unique ignition time can be determined. Instead, there is a significant time spread between when ignition first occurs at the initial location, to when the final portions of the face have been ignited.

The ignitor should reliably ignite a combustible gas mixture in its vicinity. Thus, the location of the ignitor must be chosen so that it is near the place where maximum evolution of pyrolysate gases is expected. Some materials are highly fire-retardant treated, and, when heated, emit vapors that tend to extinguish a pilot flame. The ignitor has to be designed so as not to be extinguished by fire-retardant compounds coming from the specimen, nor by airflows within the test apparatus.

The ISO 5657 apparatus was designed with a "dipping" gas pilot, which is periodically thrust for a short while down close to the specimen face, then retracted. This solution, however, introduces an uncertainty into ignition times and provides further complexity. A gas pilot, based on experience, also requires oxygen premix to be used if a flame that is both small and resistant to blowout is to be achieved.[16] With highly fire-retardant-bearing products, even such precautions are not likely to lead to a reliable pilot; thus, for instance, the ISO 5657 apparatus uses a second pilot to reignite the main pilot. Pilot stability also tends to be crucially dependent on the physical condition of the pilot tube tip, and significant maintenance can be necessary. Finally, if used in a heat release apparatus, a gas pilot can add noise to the baseline of the heat release measurement. Initial experimental results at NBS, using a more tractable alternative (i.e., electric spark ignition) were obtained with the NBS-II calorimeter, where a spark plug arrangement was provided for ignition. This development was successful, and so a similar electric pilot was designed for the cone calorimeter. The location of the ignitor should be at the place where the lower flammable limit is expected to first be reached when the specimen begins its pyrolysis. It should, however, not be so close to the specimen surface that minor swelling of the specimen would interfere with the ignition function. In the cone calorimeter, the ignitor locations were chosen so that, when testing in the horizontal orientation, the spark plug gap is located 13 mm above the *center* of the specimen; in the vertical orientation, the spark plug gap is located at the specimen plane and 5 mm above the *top* of the specimen holder.

The actual spark plug arrangement is shown in Figure 3-3.9. The spark plug is provided by a special-purpose 10-kV ignition transformer. The spark plug is moved in and out by remote control, operated by an air motor that rotates the shaft on which the spark plug rests. A reversible lock bar is used to adjust the spark-plug-to-heater distance when changing from the horizontal to the vertical orientation (the spark gap is 13 mm away from the heater baseplate in the horizontal orientation, but 25 mm away in the vertical).

Specimen Area and Thickness

Both specimen area and thickness may be expected to have some effect on the ignitability and the heat release rate. The main practical size and thickness limitations come from the fact that the specimens to be tested should exhibit primarily one-dimensional heat transfer. Thus, the configuration should be such that excessive edge effects are not seen. If the specimen thickness is such that it is thermally thick (the heat wave penetration depth being less than the physical depth), then further increases in thickness are not expected to change ignitability results. For thinner specimens, however, there can be expected to be a thickness effect, and the backing or substrate material's thermophysical properties can be of importance.

Specimen area: Janssens[12] studied in some detail the general problem of area effect on ignition. The effect is seen to be smaller when irradiances are high rather than low. The exact magnitude of the effect is also dependent on the specimen's thermophysical properties. For specimens of area 0.01 m^2 or larger, however, his results show an increase in ignition time of only about 10 percent over what would be seen with a specimen of infinite area. Later, Nussbaum and Östman[17] studied specimens in an experimental apparatus somewhat similar to the cone calorimeter, but accommodating 200 $\times$ 200 mm specimens. Their comparison of the ignition times of these larger specimens against the standard 100 $\times$ 100 mm ones shows that quadrupling the specimen area decreases the ignition time by about 20 percent.

For heat release rate, the specimen size affects the measurement, since flame volume is larger over larger specimens; consequently the flame radiation tends to approach a value of higher emissivity. Nussbaum and Östman also examined the heat release rates from the larger size specimens; the differences were generally of the same order of magnitude as the repeatability of the results. Babrauskas, in commenting on these data,[18] discussed tests on larger size, horizontal PMMA samples, where each doubling of the specimen's area increased the heat release rate, per unit area, by about 10 percent. The more general treatment of the horizontal specimen, of course, is as a liquid pool. Section 3, Chapter 1, Heat Release Rate, gives details on the size effect for burning pools. It can be seen that the diameter has to be greater than about 1 m before the specimen area effect becomes negligible.

The effect of specimen size for vertical samples was examined at Factory Mutual Research Corporation (FMRC) in a series of experiments on PMMA walls.[19,20] The FMRC studies showed little size effect for specimen heights up to 200 mm; beyond 200 mm there was approximately a linear dependence of $\dot{q}''$ on the height. This was true up to the maximum height tested, that is, 3.56 m. Unlike horizontal pools, the rate of heat release was not leveling off at even these sizes, and estimates suggested that

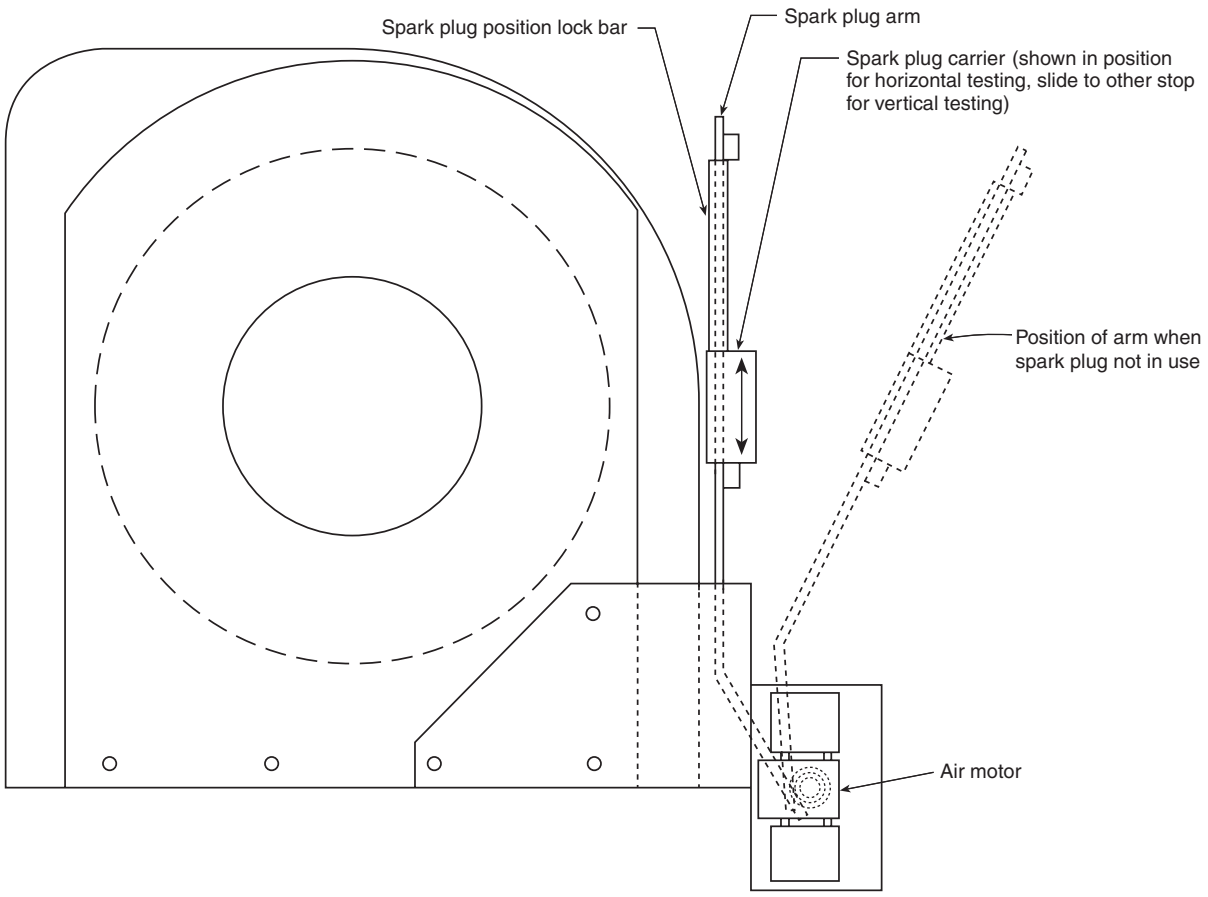

Figure 3-3.9. ***Spark plug, carrier, and air motor.***

the specimen size would have to be increased by another order of magnitude before a leveling off would be seen.

The conclusion from the above studies was that 100 mm × 100 mm was a suitable size for bench-scale testing, but that the bench-scale $\dot{q}''$ rates will always be somewhat lower than for full-scale fires.

Specimen thickness: The cone calorimeter is intended for testing actual commercial products. Thus the specimen thickness should be, as much as possible, the thickness of the finished product. There are limitations at both ends of the scale, however. The instrument is restricted to testing specimens not thicker than 50 mm. For products that in their finished state are greater than 50 mm thick, it can readily be seen that, for almost any realizable combination of thermophysical properties and incident radiant fluxes, a 50-mm specimen is thermally thick, and increasing thickness would not change the ignition times.[21,22] By making calculations for various densities and heat fluxes, it was found that for particleboard the minimum thickness required to ensure that the specimen is thermally thick can be represented by

$$\ell = 0.6\,\frac{\rho}{\dot{q}''} \qquad (1)$$

where

ℓ = thickness (mm)
ρ = density (kg·m^{-3})
$\dot{q}''$ = heat flux (kW·m^{-2})

This is probably a reasonable rule of thumb for other materials as well. The proportionality of the required thickness to $\rho/\dot{q}''$ is derived from classical heat conduction theory by equating the time for the front surface to reach the ignition temperature to the time for the rear surface temperature to begin to rise, assuming that the thermal conductivity is proportional to the density. Numerical calculations were necessary to determine a suitable constant because of the impact of the front surface heat losses.

For materials that are not thermally thick at the time of ignition, the nature of the backing material or substrate can influence the measured value of the ignition time. In the cone calorimeter, the substrate is a blanket of refractory ceramic fiber material, having a nominal density of 65 kg·m^{-3}. In use, the material assumes a more compacted density of roughly 100 kg·m^{-3}. Whenever possible, materials whose thicknesses are less than the minimum suggested in the above formula should be mounted on that substrate material over which they will actually be used. As a practical guide for testing unknown commercial

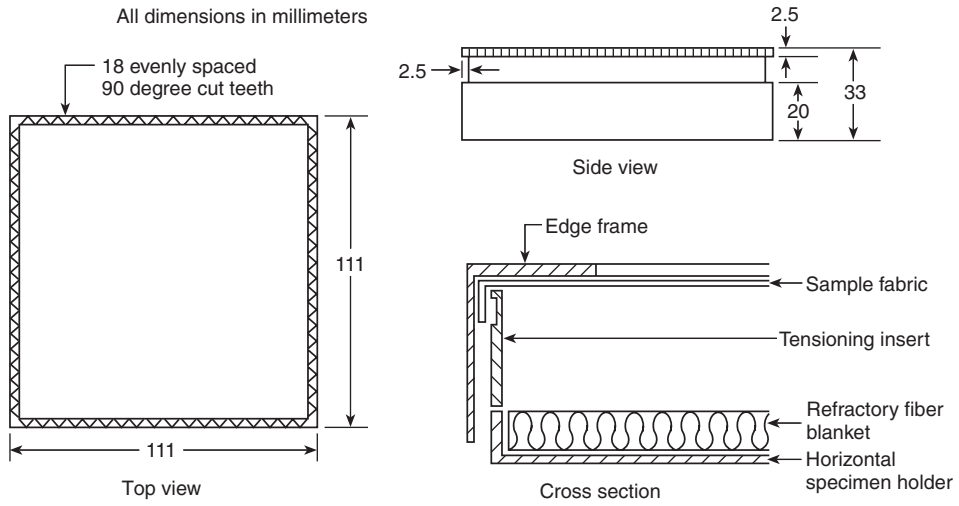

Figure 3-3.10. ***Special holder for testing fabrics and similar thin materials.***

samples, it is desirable to specify that any specimens less than 6 mm thick should always be considered as needing to be tested over their in-use substrate.

Fabrics are a special case. Thin fabrics are sometimes used for constructing air-supported structures; these should be tested with an air space in back, simulating the usage conditions. A special holder has been constructed that allows the fabrics to be pulled taut and held above a dead-air space. (See Figure 3-3.10.)

Sample Testing Specifications

Specimen Orientation and Specimen Holders

As discussed, both a horizontal and vertical specimen orientation are provided. It is considered that the horizontal orientation is standard, while the vertical orientation is reserved for special-purpose testing only. The specimen holders in Figures 3-3.11 and 3-3.12 show the two specimen holders, respectively. With proper precautions, the horizontal orientation can be used for testing liquids and melting materials. The vertical orientation has a small melt trough that can only catch a very small amount of molten material. Also, some specimens, when tested in the vertical orientation, show a tendency to lose physical strength and fall out of the holder. This does not happen in the horizontal orientation.

To present a standardized heat flow boundary condition to the rear face of the specimen, all specimens are backed by a 13-mm layer of low-density (nominal 65 $kg \cdot m^{-3}$) ceramic fiber blanket. Such a blanket is the most insulating product readily available for use. In the vertical orientation, there are several layers of rigid millboard behind the blanket, sufficient in thickness to fill out the depth of the specimen holder. The specimen is wrapped in a single sheet of aluminum foil, covering the sides and bottom. The aluminum foil serves to limit the flow of molten material and prevent it from seeping into the refractory blanket.

Load Cell

Many ancillary measurements made in the cone calorimeter (such as yields of various gas species) require the use of a load cell. Transducers had been tried in various earlier apparatuses, but most suffered because they were not designed for purely single-axis linear motion. That is, if the weight of the specimen was not well balanced, or differential heating stresses occurred, it was likely that a mechanical moment (or *torque*) would be applied to the device, with the transducer then being prone to jamming. For the cone calorimeter, a commercial-

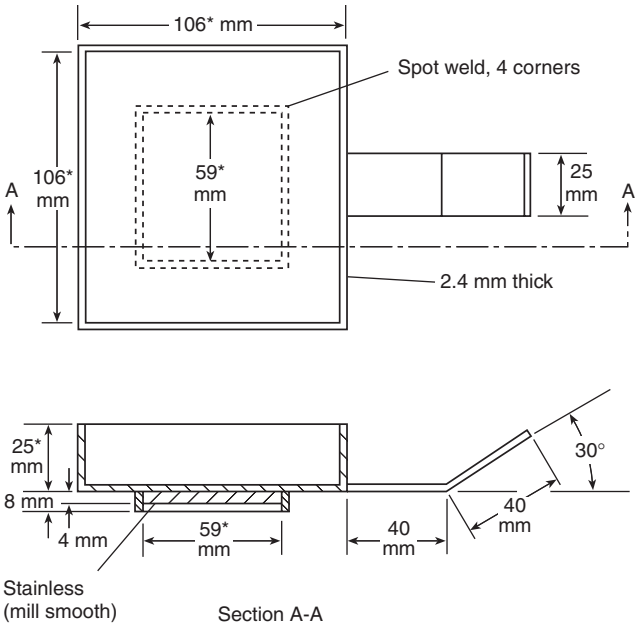

*Indicates a critical dimension

Figure 3-3.11. ***Horizontal orientation specimen holder.***

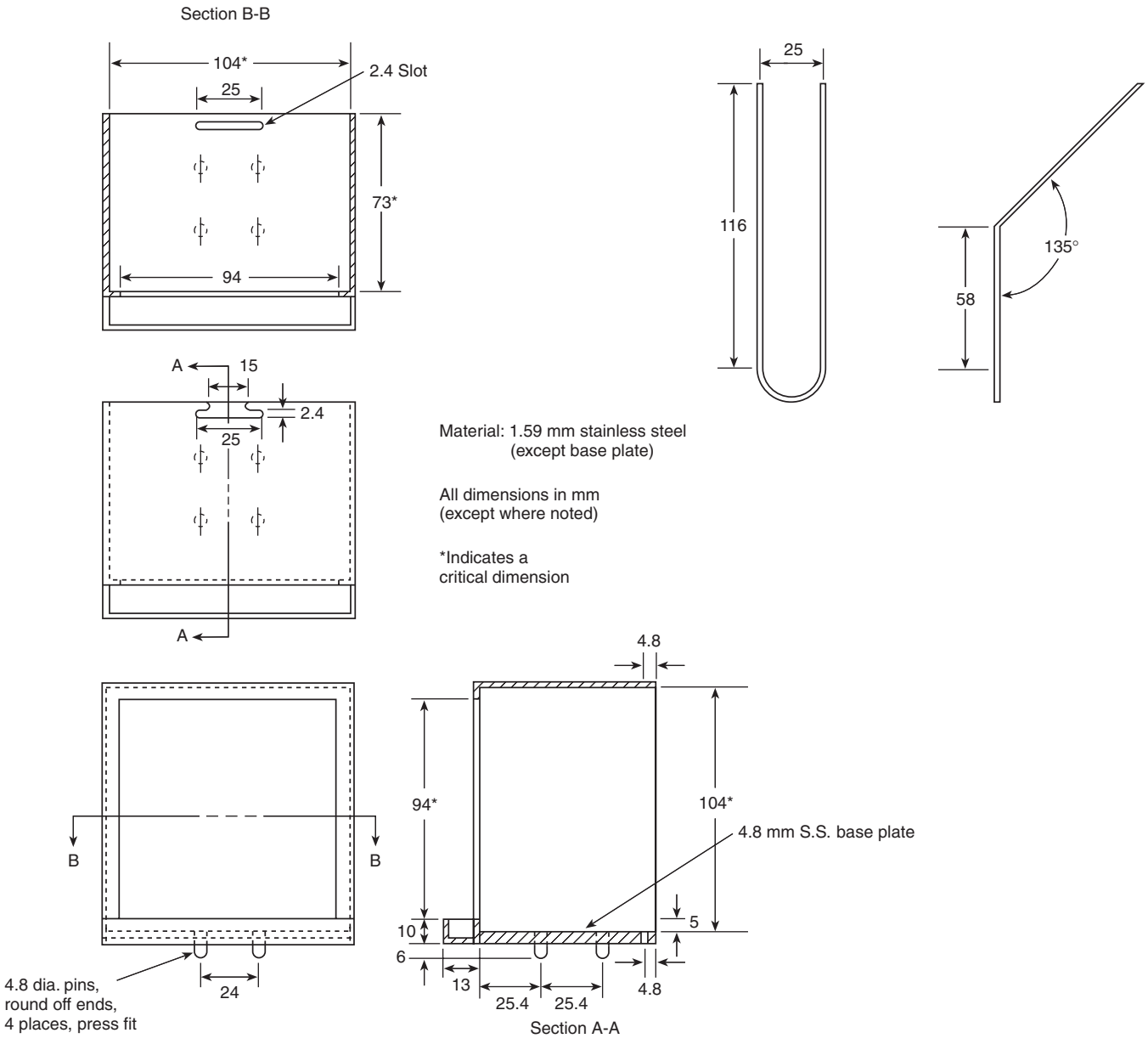

Figure 3-3.12. ***Vertical orientation specimen holder.***

design load cell was found that permits only up-and-down axial motion, while being insensitive to torques or forces from other directions.

The load cell has to accommodate two different orientation specimen holders, and may need to hold additional fixtures. All of these can have substantial—and different—weights, yet must allow accurate mass determination for low-density specimens. The solution adopted was a weighing system that has a large (3.5 kg) mechanical tare adjustment range, along with a sensitive weighing range (500 g). A resolution of 0.005 g is readily achievable.

Figures 3-3.6 and 3-3.7 show, respectively, how the horizontal and vertical orientation specimen holders are accommodated on the load cell. The horizontal holder has a square recess on the bottom and simply is placed straight down. The vertical holder is more conveniently inserted in a direction of moving toward the heater; thus the specimen is correctly located by four mounting pins on the bottom. In both cases there is a positive specimen location, and the operator does not have to be concerned with how far to insert the holder.

Edge Conditions

Edge effects: In an apparatus such as the cone calorimeter, it is desired that the small-scale test specimen would behave, as much as is possible, like a correspondingly sized element of the full-scale object. If one is dealing with

relatively large, flat, full-scale objects, then heat and mass transfer will occur only in the direction perpendicular to the exposed face. There will be no heat or mass flow along either of the face directions. The guidance to be derived from this conceptual model in designing the bench-scale test environment is clear: there should be a minimum of heat or mass transfer at the specimen edges. The aluminum foil used to wrap the specimen usually serves to minimize any mass transfer that may occur. The heat transfer situation, however, is more complicated.

In the vertical specimen orientation, the specimen has to be restrained against falling out; therefore, the vertical specimen holder incorporates a small lip extending 3 mm along the edges. In the horizontal orientation, no special measures need to be taken against falling out. Thus, for many types of specimens it is satisfactory to simply cover the edges and bottom with aluminum foil, leaving the top exposed in its entirety.

Some categories of specimens, however, present special problems. These are specimens that either have a propensity to ignite first along the outside edge, or ones that, when ignited, burn disproportionately vigorously near the edges. Such behavior is often found with wood specimens and with certain composites. This problem is alleviated by using a stainless steel edge frame for the horizontal orientation, which, in the same way as the vertical holder, provides a 3-mm lip around the edge of the specimen face. (See Figure 3-3.13.)

For specimens showing unrepresentative edge burning, the situation can be viewed as a spurious heat gain along the edges, when compared against a hypothetical ideal situation of exactly zero heat loss/gain at the edges. When an edge frame is applied, the opposite situation can tend to result, that is, a net heat loss from the specimen is observed.[23] The ideal situation, where a specimen is prevented from showing unrepresentative increased edge burning, but is equally not sustaining any losses to an edge frame, may be difficult to approach in practice. This is still a topic of active study at several institutions.

In some cases, an edge frame is needed for thermostructural reasons. Some specimens, especially certain composites, can show pronounced edge warping and curling when subjected to heat. The burning of such a specimen would be highly non-uniform if its edges were not held down with an edge frame. In many cases, an edge frame is all that is required. In some cases, however, additional measures, such as a wire grid (see below), are required.

For the testing of electric cables, there can be a pronounced tendency for pyrolysis gases to flow along the length of the cable interior, and to burn only at the edges, not uniformly over the surface. For such specimens, it has often been found useful to coat the cable ends with a sodium silicate cement, such as Insa-Lute Adhesive Cement Paste No. 1, produced by the Sauereisen Cements Co. When the ends are sealed in such a manner, a knife puncture must be made in the face of each piece of cable to avoid pressure buildup and rupture.

Intumescing samples: A common difficulty with fire test specimens is when they intumesce, either before ignition or during the burning. The simplest solution used in

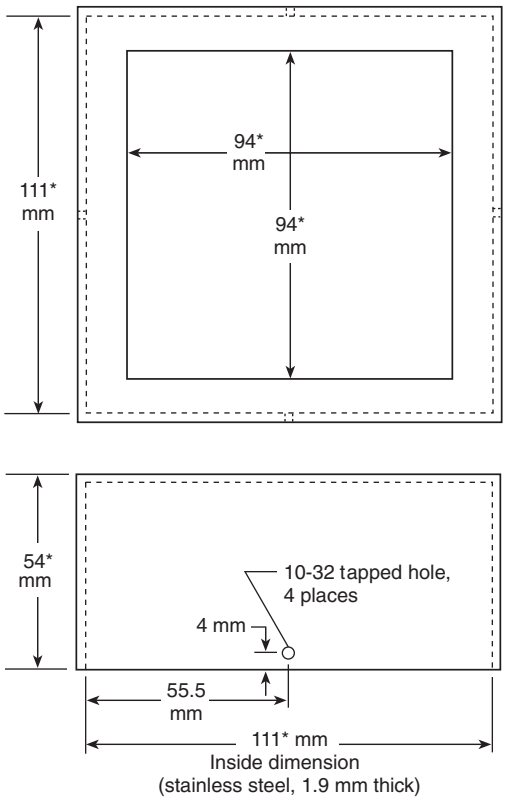

*Indicates a critical dimension

Figure 3-3.13. ***Edge frame for the horizontal specimen holder.***

the cone calorimeter, which suffices in many, but not all, cases, is the use of a *wire grid* placed on top of the specimen. Figure 3-3.14 shows a medium-weight grid. For minimizing the effect on the measurements, the grid weight should be the smallest possible consistent with providing adequate mechanical restraint to the particular specimen being tested. Mikkola[24] demonstrated that the effects on the measurements will be negligible if the average grid mass is $<0.6\ kg \cdot m^{-2}$ of specimen face area. This mass corresponds to quite a thin, small grid and will practically be usable only in occasional cases. Additional guidance is given in the NBS "User's Guide for the Cone Calorimeter,"[25] but testing laboratories will, on occasion, be required to devise their own special schemes for mounting and restraint.

Smoke Measurement

One of the most essential ancillary measurements performed with the cone calorimeter is smoke obscuration. This system was devised due to widespread dissatisfaction with older, closed-box types of smoke tests.[26,27] A large number of both practical and theoretical difficulties were found with closed-box systems, and these were successfully resolved by developing a flow-through smoke measuring system, using a helium-neon laser as the light source, and a sophisticated quasi-dual-beam

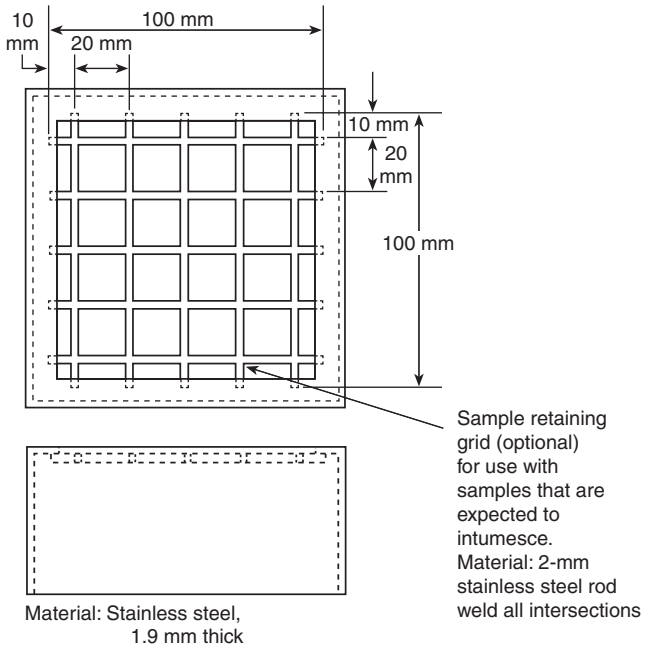

Figure 3-3.14. ***Wire grid.***

measuring arrangement. Figure 3-3.15 shows the overall arrangement of the laser photometer. It is mounted on the exhaust duct at the location shown in Figure 3-3.8. A thermocouple is also mounted nearby, since the calculations require a determination of the actual volume flow rate in the duct at the photometer location. The user should consult Reference 27 for details explaining the operation of the laser photometer. Briefly, the light from the laser goes, via two beam splitters, into two detectors. The light reaching the compensation detector is not attenuated by smoke; its signal serves as the reference to cancel out fluctuations in laser output power. The main beam detector measures a signal that is attenuated by the smoke. The optical path is purged by a minute flow of room air through a purge system. The flow is maintained by the pressure differential in the exhaust duct.

For certain research purposes, it is advantageous, in addition to obtaining optical smoke obscuration measurement, also to record the gravimetric soot yield. That is, the grams of soot evolved, per gram of specimen burned, can be measured. To do this, a soot mass sampler is connected to the port indicated in section C-C of Figure 3-3.8. A known mass fraction of the exhaust duct flow is passed through a measuring filter, and is weighed before and after the test.

Calibration Equipment

Two basic calibrations are needed: (1) the calibration of the temperature controller for the conical heater, and (2) the actual heat release rate calibration. The temperature controller is calibrated using a Schmidt-Boelter-type heat flux meter. The heat flux meter is equipped with a locating collar and is inserted in place of the specimen, with its face at the same place that the specimen face would be located. No specimen holder is used for this operation. Figures 3-3.6 and 3-3.7 show the insertion of the heat flux meter.

The heat release rate is calibrated by the use of a calibration burner, again inserted into the same bracket as is used for the heat flux meter. (See Figure 3-3.16.) The calibration burner, however, instead of always being inserted facing the heater, is inserted so that the discharge opening faces upward. Calibration is accomplished by controlling the flow of high-purity methane going to the burner and comparing it to a known value and using the net heat of combustion for pure CH_4 as 50 $MJ \cdot kg^{-1}$.

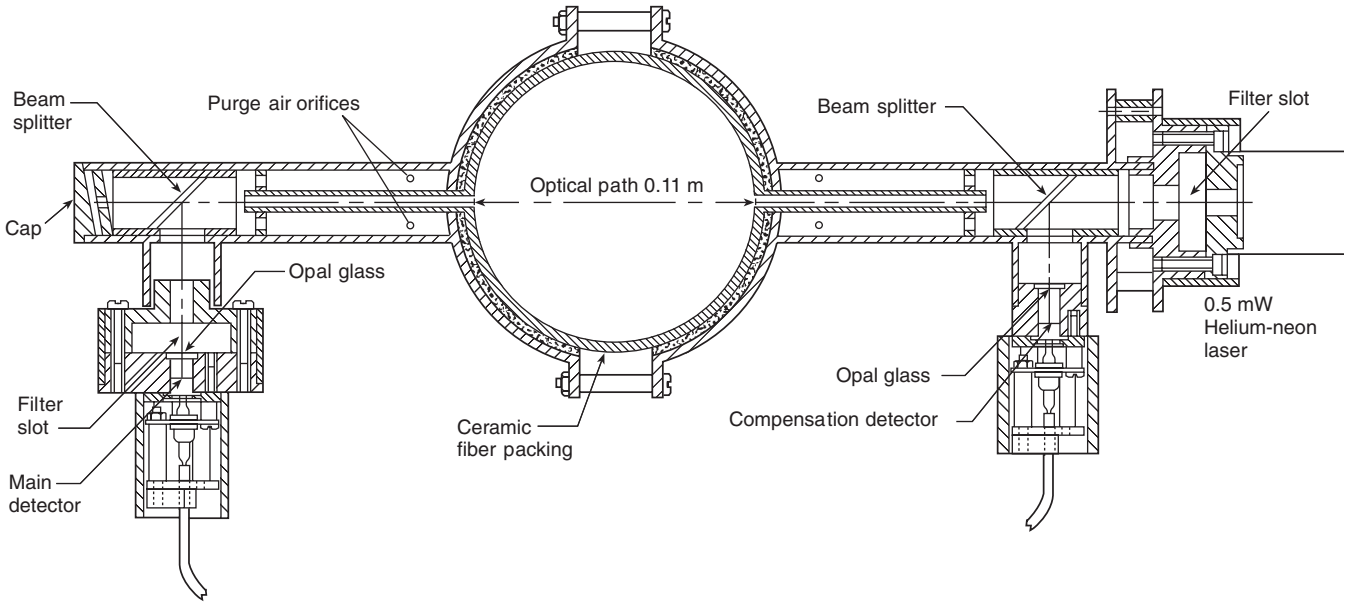

Figure 3-3.15. ***Laser photometer.***

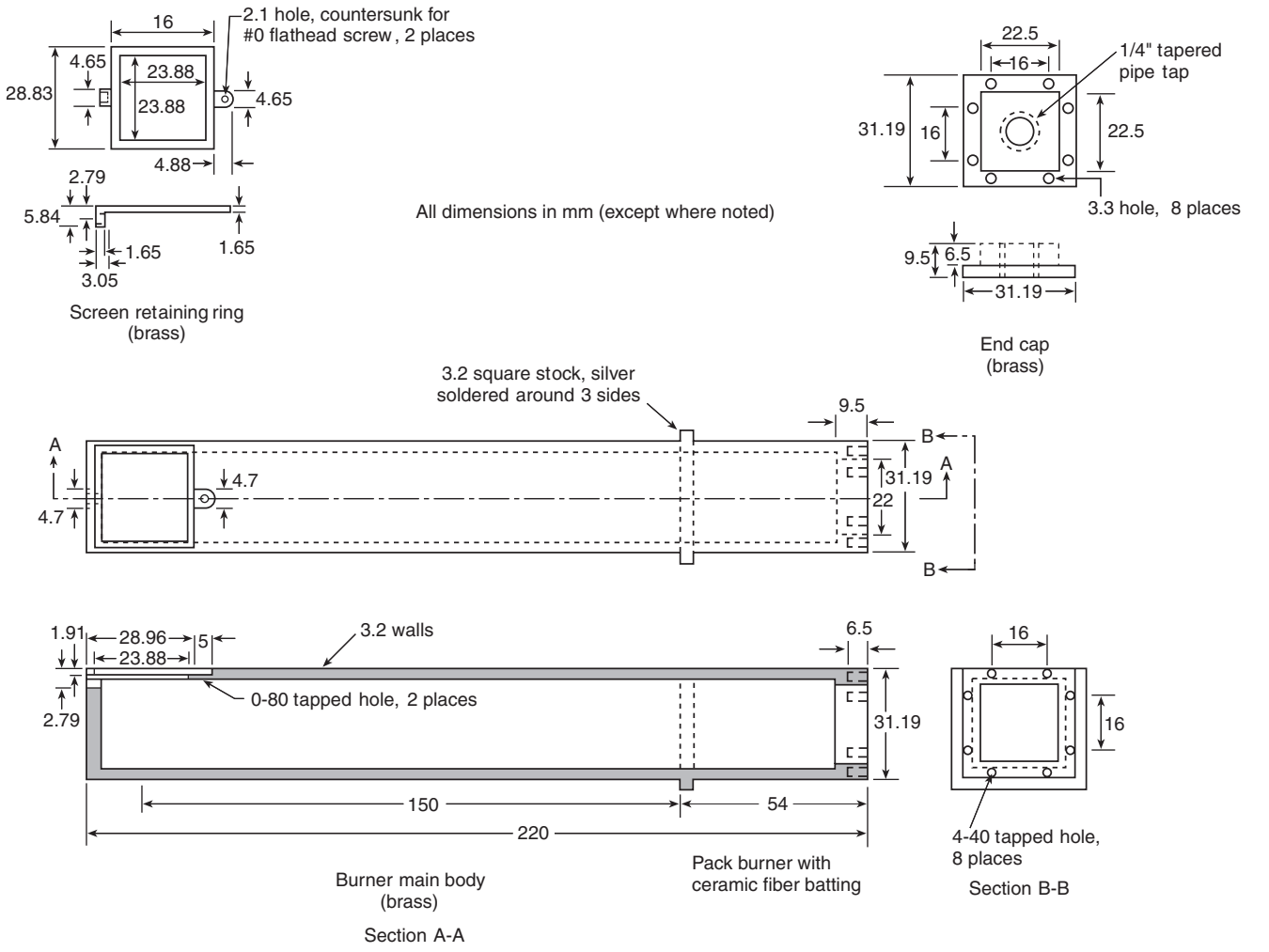

Figure 3-3.16. ***Calibration burner.***

The laser photometer is calibrated by neutral-density glass filters. These are inserted into a filter slot in front of the main beam detector. An auxiliary filter slot is provided in front of the laser. This serves to check the correct balancing of the dual-beam system's common mode rejection ratio.

The NBS "User's Guide to the Cone Calorimeter"[25] details how calibrations are performed.

Miscellaneous Details

Ring Sampler

The combustion products flowing through the exhaust system can be heavily laden in soot. Soot would cause rapid clogging of the oxygen measurement system if precautions were not taken. The most important precaution is the specially designed ring sampler. (See Figure 3-3.17.) The sampler is installed in the exhaust duct with the intake holes facing *away* from the direction of airflow. A number of small holes are used so as to provide a certain degree of smoothing with respect to duct flow turbulence.

Additional Gas Analyzers

Many users of cone calorimeters provide not just an oxygen analyzer, but also additional gas analyzers to help in determining the combustion chemistry and toxicity. CO and CO_2 analyzers are simply fitted into the same sampling line serving the oxygen analyzer. Other analyzers, for example, H_2O, HCI, and total unburned hydrocarbons, require a completely separate, heated sampling line system. Such a system also needs to have a heated soot filter at the front.

Measurements Taken with the Cone Calorimeter

The relevant ISO or ASTM standards mandate certain minimum variables to be recorded. In practice, it is normally desired to make the data from the test be as complete as possible. Cone calorimeter data are normally handled as data tables and files standardized according to the FDMS prescription.[28] A complete set of data from the

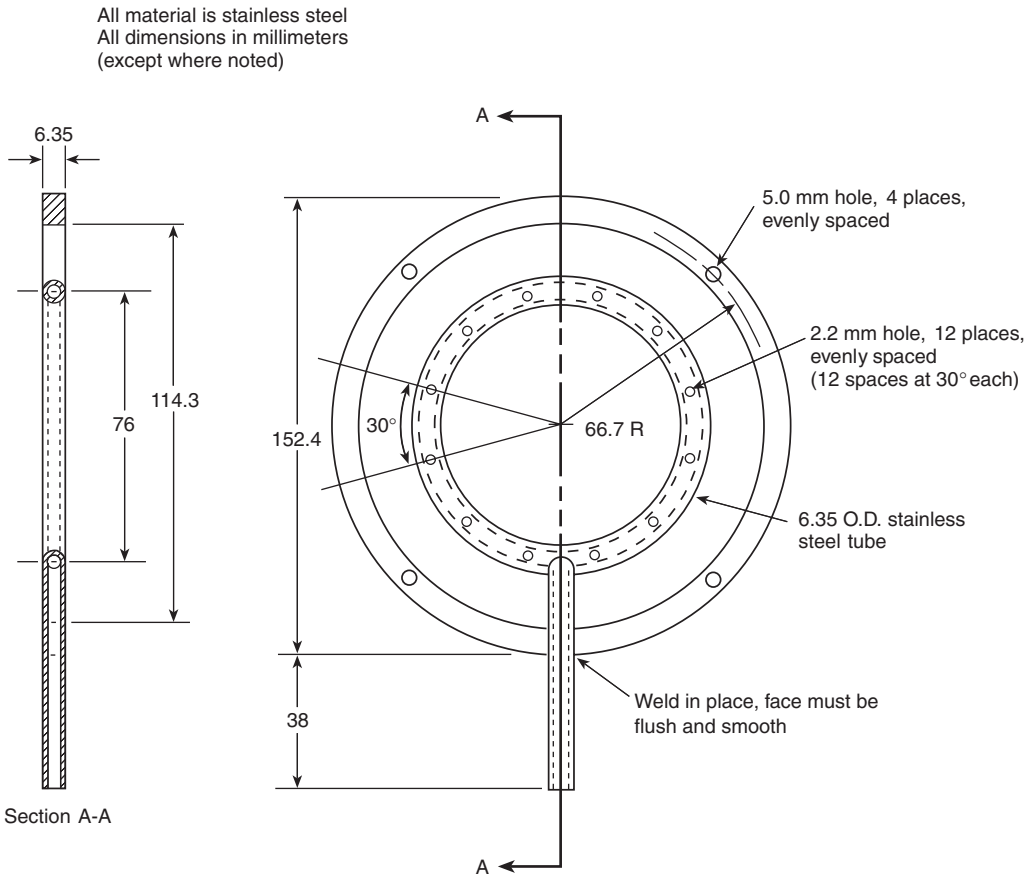

Figure 3-3.17. ***Ring sampler.***

cone calorimeter are illustrated there. Here, the more important ones of these are given, somewhat augmenting the ISO and ASTM set. Note that most of these items must be reported for each test run, but a complete test consists of three runs.

Identification	Various data items must be included here
Preparation	Any non-standard specimen preparation details must be reported
Test no.	Serial number of test; also information on testing laboratory, operator, and so forth.
Irradiance	The heating flux set for the test ($kW \cdot m^{-2}$)
Exhaust flow rate	Recorded for completeness, usually the standard value of 24 $\ell \cdot s^{-1}$
Orientation	Horizontal or vertical
Spark ignition	Yes or no
Edge frame	Yes or no
Wire grid	Yes or no
Area of specimen	(m^2), since may be nonstandard in special cases
Specimen initial mass	(g)
Specimen final mass	(g)
Time to ignition	This, according to the ISO and ASTM standards, is for "sustained flaming" (s)
Time to flameout	(s)
Peak $\dot{q}''$	($kW \cdot m^{-2}$)
Peak $\dot{m}''$	($g \cdot s^{-1} \cdot m^{-2}$)
Total $\dot{q}$	($MJ \cdot m^{-2}$)
O^2 consumption const.	($kJ \cdot kg^{-1}$); this is set to a specific value if known, otherwise to 13100
Eff. heat of combustion	($MJ \cdot kg^{-1}$), reported for period of entire test run
Specific extinction rate	($m^2 \cdot kg^{-1}$), reported for period of entire test run
Avg. mass loss rate	Computed over period starting when 10 percent of the ultimate specimen mass loss rate has occurred and ending at the time when 90 percent of the ultimate specimen mass loss has occurred ($g \cdot s^{-1} \cdot m^{-2}$)
Avg. $\dot{q}''$ (60 s)	Computed for the first 60 s after ignition ($kW \cdot m^{-2}$)
Avg. $\dot{q}''$ (180 s)	Computed for the first 180 s after ignition ($kW \cdot m^{-2}$)
Avg. $\dot{q}''$ (300 s)	Computed for the first 300 s after ignition ($kW \cdot m^{-2}$)

Note in the above 60, 180, and 300 s averages that, if the test is ended before having burned, say, 300 s, a proper average can still be correctly computed (i.e., at the end of the averaging period a number of zeroes are used for data points past the end of the test). Since users are often confused by this point, it must be emphasized: *It is not sensible to report an "average heat-release rate" without specifying the time interval.* The reason has to do with the question of what is the *end* of the test. The ISO and ASTM standards specify that the end of the test is considered to be:

1. After all flaming and other signs of combustion cease
2. While there may still be vestigial combustion evidence, but the mass loss rate has become very small (less than 150 $g \cdot m^{-2}$ being lost during any 1 min)
3. 60 min have elapsed

These rules are needed for establishing some uniformity among testing laboratories. They do not, however, mean that it is technically sound to compare the average $\dot{q}''$ of one material that may have burned for 10 min., with another that may have burned for 5 min. It is technically sound, however, to compare their burning over the first one, three, and so forth, minutes of test.

Further information on the form, units, and usage of fire properties measured in the cone calorimeter can be found in Reference 29; specific information on the smoke and soot properties measured in the cone calorimeter is given in Reference 26.

Repeatability and Reproducibility

The repeatability, *r,* and reproducibility, *R,* of the cone calorimeter were studied in two sets of interlaboratory trials, one sponsored by ISO and one by ASTM. According to the ISO instructions,[30] the definitions of repeatability and reproducibility were taken as

$$r = 2.8\ \sigma_r$$
$$R = 2.8\ \sigma_R$$

where σ_r is the repeatability standard deviation, σ_R is the reproducibility standard deviation, and the 2.8 factor comes from the fact the probability level of 95 percent is being specified.

From the results of the interlaboratory trials, values for *r* and *R* were calculated for six variables. These variables, chosen as being representative for the test results were: t_{ign}, $\dot{q}''_{max}$, $\dot{q}''_{180}$, q''_{tot}, $\Delta h_{c,eff}$, and σ_f. A linear regression model was used to describe *r* and *R* as a function of the mean overall replicates and overall laboratories for each of the six variables. The regression equations are given below. The range of mean values over which the fit was obtained is also indicated.

The results for time to sustained flaming, t_{ign}, in the range of 5 to 150 s were

$$r = 4.1 + 0.125\ t_{ign}$$
$$R = 7.4 + 0.220\ t_{ign}$$

The results for peak heat release rate, $\dot{q}''_{max}$, in the range of 70 to 1120 $kW \cdot m^{-2}$ were

$$r = 13.3 + 0.131\ \dot{q}''_{max}$$
$$R = 60.4 + 0.141\ \dot{q}''_{max}$$

The results for 180-s average heat release rate, $\dot{q}''_{180}$, in the range of 70 to 870 $kW \cdot m^{-2}$ were

$$r = 23.3 + 0.037\ \dot{q}''_{180}$$
$$R = 25.5 + 0.151\ \dot{q}''_{180}$$

The results for total heat released, q''_{tot}, in the range of 5 to 720 $MJ \cdot m^{-2}$ were

$$r = 7.4 + 0.068\ q''_{tot}$$
$$R = 11.8 + 0.088\ q''_{tot}$$

The results for effective heat of combustion, $\Delta h_{c,eff}$, in the range of 7 to 40 $kJ \cdot g^{-1}$ were

$$r = 1.23 + 0.050\ \Delta h_{c,eff}$$
$$R = 2.42 + 0.055\ \Delta h_{c,eff}$$

The results for average specific extinction area, σ_f, in the range of 30 to 2200 $m^2 \cdot kg^{-1}$ were

$$r = 59 + 0.076\ \sigma_f$$
$$R = 63 + 0.215\ \sigma_f$$

A comparison of the cone calorimeter repeatability and reproducibility to the values obtained for the ISO 5657 radiant ignition test showed the cone calorimeter results to be about a factor of 2 better.

Special Cone Calorimeters

The standard cone calorimeter has been designed for using room air for its combustion. All standard testing is done under such conditions. For special combustion studies, however, it can be of interest to explore the burning of materials at oxygen levels other than 21 percent. Such a unit has been constructed at NIST; Reference 14 gives details. This NIST controlled-atmosphere unit has already been used for studies of the burning of materials under conditions where the oxygen in the air supply is <21 percent, with N_2 or CO_2 being mixed into the air stream. (See Figure 3-3.18.) It has also been used for pyrolysis studies under pure nitrogen flow conditions. In principle, it could also be used for studies of enriched-oxygen atmospheres; however, the necessary safety procedures for handling high-concentration oxygen streams are different. A unit for handling O_2 > 21 percent mixtures has been constructed for NASA, but data are not yet available from it. A controlled-atmosphere unit is also appropriate for use when airflow rates of less than 12 $\ell \cdot s^{-1}$ are required.

Figure 3-3.18. ***The NIST controlled-atmosphere cone calorimeter.***

All of the present cone calorimeter designs, both standard and otherwise, have been designed for use only under *ambient* pressures. There is interest at this time from at least one research group to design and construct a unit for aerospace studies that would function under *nonambient* pressures.

References Cited

1. ISO 5660, International Standard, "Fire Tests—Reaction to Fire—Rate of Heat Release from Building Products," International Organization for Standardization, Geneva (1993).
2. ASTM E1354, *Standard Test Method for Heat and Visible Smoke Release Rates for Materials and Products Using an Oxygen Consumption Calorimeter,* American Society for Testing and Materials, Philadelphia.
3. W.H. Twilley and V. Babrauskas, "User's Guide for the Cone Calorimeter," NBS Special Publication SP 745, U.S. Natl. Bur. Stand., Gaithersburg, MD (1988).
4. V. Babrauskas and S.J. Grayson, eds., *Heat Release in Fires,* Elsevier, London (1992). Distributed in the U.S. by NFPA.
5. B.J. McCaffrey and G. Cox, "Entrainment and Heat Flux of Buoyant Diffusion Flames," NBSIR 82–2473, U.S. Natl. Bur. Stand. (1982).
6. J.R. Hallman, "Ignition Characteristics of Plastics and Rubber," Ph.D. dissertation, University of Oklahoma, Norman (1971).
7. B. Hägglund and L-E. Persson, "The Heat Radiation from Petroleum Fires," FOA Rapport C 20126-D6(A3), Försvarets Forskningsanstalt, Stockholm (1976).
8. V. Babrauskas, "Estimating Large Pool Fire Burning Rates," *Fire Technology, 19,* pp. 251–261 (Nov. 1983).
9. J.J. Comeford, "The Spectral Distribution of Radiant Energy of a Gas-Fired Radiant Panel and Some Diffusion Flames," *Comb. and Flame, 18,* pp. 125–132 (1972).
10. A. Tewarson, "Physico-Chemical and Combustion/Pyrolysis Properties of Polymeric Materials," NBS-GCR-80–295, U.S. Natl. Bur. Stand., Gaithersburg, MD (1980).
11. ISO 5657, "Fire Tests—Reaction to Fire—Ignitability of Building Products," International Organization for Standardization, Geneva (1986).
12. M.L. Janssens, "Fundamental Thermophysical Characteristics of Wood and Their Role in Enclosure Fire Growth," Ph.D. dissertation, University of Gent, Belgium (1991).
13. V. Babrauskas, "Development of the Cone Calorimeter—A Bench-Scale Heat Release Rate Apparatus Based on Oxygen Consumption," *Fire and Materials, 8,* pp. 81–95 (1984).
14. V. Babrauskas, W.H. Twilley, M. Janssens, and S. Yusa, "A Cone Calorimeter for Controlled-Atmospheres Studies," *Fire and Materials, 16,* pp. 37–43 (1992).
15. ASTM E906, "Standard Test Method for Heat and Visible Smoke Release Rates for Materials and Products," American Society for Testing and Materials, Philadelphia.
16. V. Babrauskas, "Combustion of Mattresses Exposed to Flaming Ignition Sources, Part II. Bench-Scale Tests and Recommended Standard Test," NBSIR 80-2186, U.S. Natl. Bur. Stand. (1981).
17. R.M. Nussbaum and B.A.-L. Östman, "Larger Specimens for Determining Rate of Heat Release in the Cone Calorimeter," *Fire and Materials, 10,* pp. 151–160 (1986).
18. V. Babrauskas, Letter to the editor, *Fire and Materials, 11,* p. 205 (1987).
19. L. Orloff, J. deRis, and G.H. Markstein, "Upward Turbulent Fire Spread and Burning of Fuel Surfaces," in *Fifteenth Symp. (Intl.) on Combustion,* The Combustion Institute, Pittsburgh pp. 183–192 (1974).
20. L. Orloff, A.T. Modak, and R.L. Alpert, "Burning of Large-Scale Vertical Wall Surfaces," in *Sixteenth Symp. (Intl.) on Combustion,* The Combustion Institute, Pittsburgh, pp. 1345–1354 (1976).
21. W.D. Weatherford, Jr. and D.M. Sheppard, "Basic Studies of the Mechanism of Ignition of Cellulosic Materials," *Tenth Symp. (Intl.) on Combustion,* The Combustion Institute, Pittsburgh, pp. 897–910 (1965).
22. H.R. Wesson, J.R. Welker, and C.M. Sliepcevich, "The Piloted Ignition of Wood by Thermal Radiation," *Comb. and Flame, 16,* pp. 303–310 (1971).
23. J. Urbas and H. Sand, "Some Investigations on Ignition and Heat Release of Building Materials Using the Cone Calorimeter," in *Interflam '90, Fifth Intl. Fire Conf. Proc.,* Interscience Communications, Ltd., London, pp. 183–192 (1990).
24. E. Mikkola, unpublished study, VTT, Espoo, Finland (1989).
25. W.H. Twilley and V. Babrauskas, "User's Guide for the Cone Calorimeter," *NBS Special Publication SP 745,* U.S. Natl. Bur. Stand., Gaithersburg, MD (1988).
26. V. Babrauskas and G. Mulholland, "Smoke and Soot Data Determinations in the Cone Calorimeter," in ASTM STP 983, *Mathematical Modeling of Fires,* American Society for Testing and Materials, Philadelphia, pp. 83–104 (1987).
27. P.J. Geake, "Smoke Characterisation by Laser Diffraction," Ph.D. Dissertation, Polytechnic of the South Bank, London (1988).
28. V. Babrauskas, R.D. Peacock, M. Janssens, and N.E. Batho, "Standardizing the Exchange of Fire Data—The FDMS," *Fire and Materials,* 15, pp. 85–92 (1991).
29. V. Babrauskas, "Effective Measurement Techniques for Heat, Smoke, and Toxic Fire Gases," in *Fire: Control the Heat . . . Reduce the Hazard,* QMC Fire & Materials Centre, London, pp. 4.1–4.10 (1988).
30. ISO 5725, "Precision of Test Methods—Determination of Repeatability and Reproducibility for a Standard Test Method by Inter-Laboratory Tests," International Organization for Standardization, Geneva (1986).

Additional Readings

Apparatus Development

J.E. Leonard, P.A. Bowditch, and V.P. Dowling, "The Development of a Controlled Atmosphere Cone Calorimeter," *DBCE Doc 98/038,* CSIRO, Highett, Vic., Australia (1998).

V. Babrauskas and I. Wetterlund, "Choice of Optical Calibration Filters for Laser Photometers," *Fire Safety J.,* 24, pp. 197–199 (1995).

V. Babrauskas, "The Development and Evolution of the Cone Calorimeter: A Review of 12 Years of Research and Standardization," *Fire Standards in the International Marketplace, ASTM STP 1163* (Arthur F. Grand, ed.), American Society for Testing and Materials, Philadelphia, pp. 3–22 (1995).

M.R. Christy, R.V. Petrella, and J.J. Penkala, "Controlled-atmosphere Cone Calorimeter," *Fire and Polymers II,* ACS Symp. Series 599, American Chemical Society, Washington, pp. 498–517 (1995).

Building Products

G. Cowles and P. Collier, "The Safety of Exterior Wall Claddings," *Build,* New Zealand No. 42, pp. 28–30 (1997).

C. Wade, "Fire Performance of External Wall Claddings under a Performance-based Building Code," *Fire and Materials,* 19, pp. 127–132 (1995).

Composites

F.-Y. Hshieh and H.D. Beeson, "Flammability Testing of Flame-retarded Epoxy Composites and Phenolic Composites," *Fire and Materials,* 21, pp. 41–49 (1997).

U. Sorathia, R. Lyon, R.G. Gann, and L. Gritzo, "Materials and Fire Threat," *Fire Technology,* 33, pp. 260–275 (1997).

A.G. Gibson and J. Hume, "Fire Performance of Composite Panels for Large Marine Structures," *Plastics, Rubber and Composites Processing and Applications,* 23, pp. 175–183 (1995).

Electric Wires and Cables

Y. Nakagawa, "A Comparative Study of Bench-Scale Flammability Properties of Electric Cables with Different Covering Materials," *J. Fire Sciences,* 16, pp. 179–205 (1998).

M.A. Barnes, P.J. Briggs, M.M. Hirschler, A.F. Matheson, and T.J. O'Neill, "A Comparative Study of the Fire Performance of Halogenated and Non-halogenated Materials for Cable Applications. Part I, Tests on Materials and Insulated Wires," *Fire and Materials,* 20, pp. 1–16 (1996). "Part II, Tests on Cables," *Fire and Materials,* 20, pp. 17–37 (1996).

P.J. Elliot and R.H. Whiteley, "A Cone Calorimeter Test for the Measurement of Flammability Properties of Insulated Wire," *Polymer Testing '96,* Rapra Technology Ltd., Shawbury, pp. 3-1–3-9 (1996).

Error Analysis

P.A. Enright and C.M. Fleischmann, "Uncertainty of Heat Release Rate Calibration of the ISO 5660-1 Cone Calorimeter Test Standard," *Fire Technology,* 35, pp. 153–169 (1999).

Extinguishment

B. Moghtaderi, B.Z. Dlugogorski, E.M. Kennedy, and D.F. Fletcher, "Effects of the Structural Properties of Solid Fuels on Their Re-ignition Characteristics," *Fire and Materials,* 22, pp. 165–166 (1998).

J.C. Yang, C.I. Boyer, and W.L. Grosshandler, "Minimum Mass Flux Requirements to Suppress Burning Surfaces with Water Sprays," *NISTIR 5795,* Natl. Inst. Stand. and Technol., Gaithersburg, MD (1996).

Fabrics

E. Yanai, T. Suzuki, and T. Yamada, "A Study of the Flammability of Non-flame-retardant and Flame-retardant Materials by Using Cone Calorimeter," *Intl. Symp. on Fire Science and Technology,* Korean Institute of Fire Science & Engineering, Seoul, pp. 85–92 (1997).

Floor Coverings

P. Van Hees and P. Vandevelde, "Mathematical Models for Wind-Aided Flame Spread of Floor Coverings," *Fire Safety Science—Proc. 5th Intl. Symp.,* Intl. Assn. for Fire Safety Science, Boston, pp. 321–332 (1997).

B.A.-L. Östman, "European Fire Tests for Flooring," *Interflam '96,* Interscience Communications Ltd, London, pp. 819–826 (1996).

Furniture

V. Babrauskas and I. Wetterlund, "Testing of Furniture Composites in the Cone Calorimeter: A New Specimen Preparation Method and Round Robin Results," *Fire Safety J.,* 30, pp. 179–194 (1998).

V. Babrauskas, D. Baroudi, J. Myllymäki, and M. Kokkala, "The Cone Calorimeter Used for Predictions of the Full-scale Burning Behaviour of Upholstered Furniture," *Fire and Materials,* 21, pp. 95–105 (1997).

Industrial and Agricultural Chemicals

J. Hietaniemi, R. Kallonen, and E. Mikkola, "Burning Characteristics of Selected Substances: Production of Heat, Smoke and Chemical Species," *Fire and Materials,* 23, pp. 171–185 (1999).

J. Hietaniemi, R. Kallonen, and E. Mikkola, "Fires at Chemical Warehouses: A Cone Calorimeter Study on the Burning Characteristics and Fire Effluent Composition of Selected Chemical Compounds," VTT Research Note 1810, Valtion Teknillinen Tutkimuskeskus, Espoo, Finland (1997).

K.-M. Tu, A. Aaronson, and R. Hombek, "A Study of the Combustion Characteristics of Fire Resistant Industrial Fluids Using the Cone Calorimeter," *Proc. 21st Intl. Conf. on Fire Safety,* Product Safety Corp., Sissonville, WV, pp. 42–55 (1996).

H. Breulet and S. Desmet, "Characterization of Industrial Liquids by Means of the Cone Calorimeter," *Industrial Fires II—Workshop Proceedings,* Report EUR 15967 EN, European Commission, Luxembourg, pp. 223–235 (1995).

Plastics

F. Gensous and S. Grayson, "Improved Procedure for Testing Intumescent Materials Using the Cone Calorimeter," *Interflam '96,* Interscience Communications Ltd, London, pp. 977–981 (1996).

A.F. Grand, "The Use of the Cone Calorimeter to Assess the Effectiveness of Fire Retardant Polymers under Simulated Real Fire Test Conditions," *Interflam '96,* Interscience Communications Ltd., London, pp. 143–152 (1996).

M. Hirschler, "Comparative Analysis of Effectiveness of Fire Retardants Using Heat Release Calorimetry," *Flame Retardants '96,* Interscience Communications Ltd., London, pp. 199–214 (1996).

D. Hopkins, Jr. and J.G. Quintiere, "Material Fire Properties and Predictions for Thermoplastics," *Fire Safety J.,* 26, pp. 241–268 (1996).

L. Costa, G. Camino, G. Bertelli, and G. Borsini, "Mechanistic Study of the Combustion Behaviour of Polymeric Materials in Bench-scale Tests. I. Comparison between Cone Calorimeter and Traditional Tests," *Fire and Materials,* 19, pp. 133–142 (1995).

J. Rychly and L. Costa, "Modelling of Polymer Ignition and Burning Adopted for Cone Calorimeter Measurements: The Correlation between the Rate of Heat Release and Oxygen Index," *Fire and Materials,* 19, pp. 215–220 (1995).

Room Fire Models

M. Dietenberger and O. Grexa, "Analytical Model of Flame Spread in Full-scale Room/Corner Tests," ISO 9706, *Fire and Materials '99, 6th Intl. Conf.,* Interscience Communications Ltd., London, pp. 211–222 (1999).

C.A. Wade, D. LeBlanc, J. Ierardi, and J.R. Barnett, "A Room-Corner Fire Growth and Zone Model for Lining Materials," *Proc. 2nd Intl. Conf. on Fire Research and Engineering,* Society of Fire Protection Engineers, Bethesda, MD, pp. 106–117 (1998).

C.L. Beyler, S.P. Hunt, N. Iqbal, and F.W. Williams, "A Computer Model of Upward Flame Spread on Vertical Surfaces," *Fire Safety Science—Proc. 5th Intl. Symp.,* Intl. Assn. for Fire Safety Science, Boston, pp. 297–308 (1997).

M. Kokkala, D. Baroudi, and W.J. Parker, "Upward Flame Spread on Wooden Surface Products: Experiments and Numerical Modelling," *Fire Safety Science—Proc. 5th Intl. Symp.,* Intl. Assn. for Fire Safety Science, Boston, pp. 309–320 (1997).

G. Grant and D. Drysdale, "Numerical Modelling of Early Flame Spread in Warehouse Fires," *Fire Safety J.,* 24, pp. 247–278 (1995).

M. Janssens, O. Grexa, M. Dietenberger, and R. White, "Predictions of ISO 9705 Room/Corner Test Using a Simple Model," *Proc. Fourth Intl. Fire and Materials Conf.,* Interscience Communications Ltd., London, pp. 73–83 (1995).

B. Karlsson, "Models for Calculating Flame Spread on Wall Lining Materials and the Resulting Heat Release Rate in a Room," *Fire Safety J.,* 23, pp. 365–386 (1994).

Smoke Production

A.W. Heskestad and P.J. Hovde, "Empirical Prediction of Smoke Production in the ISO Room Corner Fire Test by Use of ISO Cone Calorimeter Fire Test Data," *Fire and Materials,* 23, pp. 193–199 (1999).

Theoretical Pyrolysis Studies of Materials

J.E.J. Staggs, "Modelling Thermal Degradation of Polymers Using Single-step First-order Kinetics," *Fire Safety J.,* 32, pp. 17–34 (1999).

J.E.J. Staggs and R.H. Whiteley, "Modelling the Combustion of Solid-phase Fuels in Cone Calorimeter Experiments," *Fire and Materials,* 23, pp. 63–69 (1999).

M.I. Nelson, "A Dynamical Systems Model of Autoignition in the Cone Calorimeter," *Fire Safety Science—Proc. 5th Intl. Symp.,* Intl. Assn. for Fire Safety Science, Boston, pp. 547–558 (1997).

M.I. Nelson, J. Brindley, and A. McIntosh, "A Mathematical Model of Ignition in the Cone Calorimeter," *Combustion Science and Technology,* 104, pp. 33–54 (1995).

Toxicity Studies

H. Pottel, "The Toxic Potency of the Smoke of Burning Carpets: A Cone Calorimeter and FTIR Study," *UNITEX,* No. 6, pp. 56–65 (1996).

B. Andersson, G. Holmstedt, and S. Särdqvist, "Production of Toxic Gases—Scaling Effects," *Industrial Fires II—Workshop Proceedings, Report EUR 15967 EN,* European Commission, Luxembourg, pp. 155–166 (1995).

V. Babrauskas, "Generation of CO in Bench-scale Fire Tests and the Prediction for Real-scale Fires," *Fire and Materials,* 19, pp. 205–213 (1995).

R. Kakko, V. Christiansen, E. Mikkola, R. Kallonen, L. Smith-Hansen, and K.H. Jørgensen, "Toxic Combustion Products of Three Pesticides," *J. Loss Prevention in the Process Industries,* 8, pp. 127–132 (1995).

H. Pottel, "The Use of Partial Least Squares (PLS) in Quantitative FTIR: Determination of Gas Concentrations in Smoke Gases of Burning Textiles," *Fire and Materials,* 19, pp. 221–231 (1995).

Transportation

R.D. Peacock, R.W. Bukowski, and S.H. Markos, "Evaluation of Passenger Train Car Materials in the Cone Calorimeter," *Fire and Materials,* 23, pp. 53–62 (1999).

Wood Materials and Vegetation

J. Fangrat, Y. Hasemi, M. Yoshida, and T. Hirata, "Surface Temperature at Ignition of Wooden Based Slabs," *Fire Safety J.,* 27, pp. 249–259 (1997).

O. Grexa, E. Horváthová, and A. Osvald, "Cone Calorimeter Studies of Wood Species," *Intl. Symp. on Fire Science and Technology,* Korean Institute of Fire Science & Engineering, Seoul, pp. 77–84 (1997).

B. Moghtaderi, V. Novozhilov, D.F. Fletcher, and J.H. Kent, "A New Correlation for Bench-scale Piloted Ignition Data of Wood," *Fire Safety J.,* 29, pp. 41–59 (1997).

B. Moghtaderi, V. Novozhilov, D.F. Fletcher, and J.H. Kent, "Mathematical Modelling of the Piloted Ignition of Wet Wood Using the Heat-Balance Integral Method," *J. Applied Fire Science,* 6, pp. 91–107 (1996/97).

R.H. White, D. DeMars, and M. Bishop, "Flammability of Christmas Trees and Other Vegetation," *24th Intl. Conf. on Fire Safety,* Product Safety Corp., Sissonville WV, pp. 99–110 (1997).

R.H. White, D.R. Weise, and S. Frommer, "Preliminary Evaluation of the Flammability of Native and Ornamental Plants with the Cone Calorimeter," *Proc. 21st Intl. Conf. on Fire Safety,* Product Safety Corp., Sissonville, WV, pp. 256–265 (1996).

CHAPTER 4

Generation of Heat and Chemical Compounds in Fires

Archibald Tewarson

Introduction

Fire hazard is characterized by the generation of calorific energy and products, per unit of time, as a result of the chemical reactions between surfaces and vapors of materials and oxygen from air. If heat is the major contributor to hazard, it is defined as thermal hazard.[1] If fire products (smoke, toxic, corrosive, and odorous compounds) are the major contributors to hazard, it is defined as nonthermal hazard.[1] Various tests are used to determine the generation per unit of time of (1) the calorific energy, defined as the heat release rate, and (2) fire products. The heat release rate and generation rates of fire products normalized by the generation rate of material vapors, airflow, and so forth, defined as fire properties, are used in models to predict (1) heat release rate to assess the thermal hazard and fire protection needs; and (2) generation rates of fire products to assess the nonthermal hazard due to reduced visibility, and smoke damage, toxicity, corrosivity, and protection needs.

The region where vapors are generated is defined as the pyrolysis region and its leading edge as the pyrolysis front. The initiation of flaming fire is defined as ignition. Ignition is a process where vapors generated by heating the surface of a material mix with air, form a combustible mixture, ignite, and a fire is initiated. The region where the ignition process occurs is defined as the *ignition zone.* Minimum heat flux at or below which a material cannot generate the combustible mixture is defined as the *critical heat flux* (CHF).[1–4] The resistance of a material to generate a combustible mixture is defined as the *thermal response parameter* (TRP).[1–4] The higher the CHF and TRP values, the longer it takes for the material to heat up, ignite, and initiate a fire, and thus the lower the fire propagation rate.

Depending on the magnitude of the heat flux provided by external sources and the flame of the material burning in the ignition zone, the pyrolysis front and flame can move beyond the ignition zone. The movement of the pyrolysis front is defined as fire propagation. The rate of movement of the pyrolysis front on the surface is defined as the fire propagation rate.

Heat and chemical compounds are generated as a result of the chemical reactions between (1) pyrolyzing material vapors and oxygen in the gas phase, and (2) pyrolyzing material surface and oxygen in the solid phase. Heat generated in chemical reactions is defined as the *chemical heat*.[2–4] The rate of generation of chemical heat is defined as the *chemical heat release rate.* The chemical heat release rate distributes itself into a convective component, defined as the *convective heat release rate,* and into a radiative component, defined as the *radiative heat release rate*.[2–4] Convective heat release is associated with the flow of a hot products-air mixture, and radiative heat release is associated with the electromagnetic emission from the flame.

In a majority of cases, hazards to life and property are due to fires in enclosed spaces, such as in buildings. In general, fires in enclosed spaces are characterized by an upper and a lower layer. The main constituents of the upper layer are the hot fire products, and the main constituent of the lower layer is fresh air. In early stages, a building fire is well ventilated, and is easy to control and extinguish. However, if the fire is allowed to grow, especially with limited enclosure ventilation and large material surface area, the chemical reactions between oxygen from air and products of incomplete combustion (smoke, CO, hydrocarbons, and other intermediate products) remain incomplete, resulting in an increase in nonthermal hazard. Rapid increase in the generation rates of products of incomplete combustion and growth rate of the fire, due to sudden and dramatic involvement of most of the exposed material surfaces, is termed flashover. Flashover is the most dangerous condition in a fire.

Heat release rate and generation rates of fire products as well as their nature are governed by (1) fire initiation within the ignition zone; (2) fire propagation rate beyond

Dr. Archibald Tewarson is senior research specialist at Factory Mutual Research. His research has focused on chemical aspects of fires.

the ignition zone; (3) fire ventilation; (4) external heat sources; (5) presence or absence of the fire suppression/extinguishing agents; and (6) materials: (a) their shapes, sizes, and arrangements; (b) their chemical natures; (c) types of additives mixed in; and (d) presence of other materials. In this handbook most of these areas have been discussed from a fundamental as well as applied views. For example, the mechanisms of thermal decomposition of polymers, which govern the generation rates of material vapors, is discussed by Beyler in Section 1, Chapter 7; generation rate of heat (or heat release rate) from the viewpoint of thermochemistry is discussed by Drysdale in Section 1, Chapter 5. Flaming ignition of the mixture of material vapors and air is discussed by Kanury in Section 2, Chapter 11; and surface flame spread by Quintiere in Section 2, Chapter 12.

Several other chapters in this handbook relate to the subjects discussed here and should be consulted for complete information. The chapters are as follows: Section 3, Chapter 2 by Janssens on calorimetry; Section 3, Chapter 3 by Babrauskas on the cone calorimeter; Section 2, Chapter 5 by Gottuk and Roby on the effect of combustion conditions on species production; Section 2, Chapter 13 by Mulholland on smoke production and properties. Physical and combustion properties of selected fuels in air, heats of combustion and related properties of pure substances, plastics, and miscellaneous materials listed in Appendix C should be consulted for information that may not be included in this chapter. This chapter presents the applications of the principles discussed in several chapters in this handbook to determine the fire properties of materials. Simple calculations have been included in the chapter to show how the properties can be used for various applications.

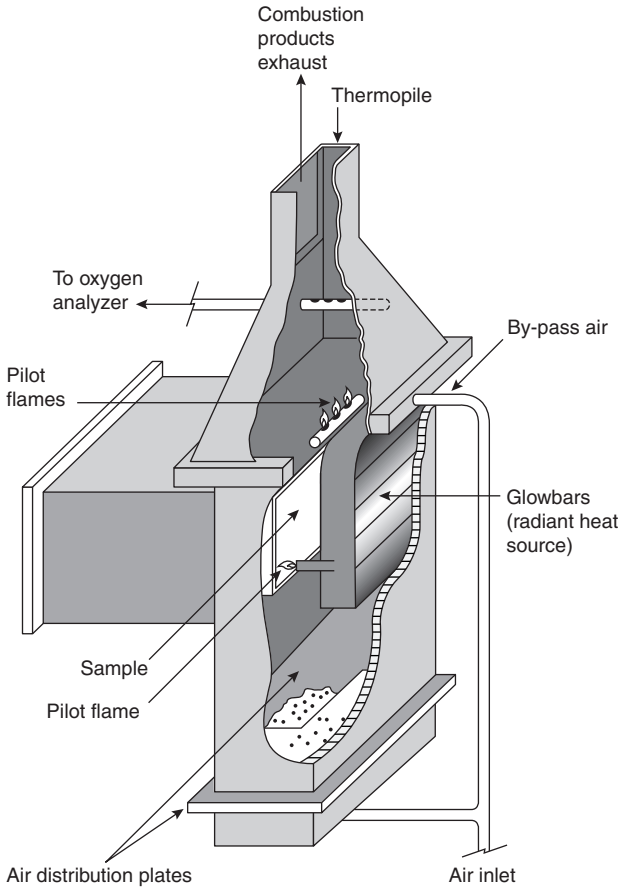

Figure 3-4.1. ***Ohio State University's (OSU, ASTM E906-83) heat release rate apparatus.[5–8]***

Concepts Governing Generation of Heat and Chemical Compounds in Fires

Fire Initiation (Ignition)

The fundamental ignition principles are described in detail by Kanury in Section 2, Chapter 11. The principles suggest that, for fire initiation, a material has to be heated above its CHF value (CHF value is related to the fire point). The CHF value can be determined in one of the several heat release rate apparatuses, for example, Ohio State University's (OSU) heat release rate apparatus,[5–8] shown in Figure 3-4.1; the ASTM E2058 fire propagation apparatus (FPA),[1–4,9–16] shown in Figures 3-4.2, parts (a) and (b); and the cone calorimeter,[17–19] shown in Figure 3-4.3. The design features, test conditions, and types of measurements for the three apparatuses are listed in Table 3-4.1.

Typically the CHF values are determined by exposing the horizontal sample (e.g., about 100-mm diameter or about 100 × 100-mm square and up to about 100-mm in thickness with blackened surface in the flammability apparatus) to various external heat flux values until a value is found at which there is no ignition for about 15 min.

As the surface is exposed to heat flux, initially most of the heat is transferred to the interior of the material. The ignition principles suggest that the rate with which heat is transferred depends on the ignition temperature (T_{ig}), ambient temperature (T_a), material thermal conductivity (k), material specific heat (c_P), and the material density (ρ). (See Section 2, Chapter 11.) The combined effects are expressed by a parameter defined as the thermal response parameter (TRP) of the material[1–4,9–15]

$$\mathrm{TRP} = \Delta T_{ig}\sqrt{k\rho c_P\left(\frac{\pi}{4}\right)} \tag{1}$$

where ΔT_{ig} ($= T_{ig} - Ta$) is the ignition temperature above ambient (K). The units are as follows: k is in kW/m·K, ρ is in g/m^3, c_P is in kJ/g·K, and TRP is in kW·s$^{1/2}$/m^2. TRP is a very useful parameter for the engineering calculations to assess resistance to ignition and fire propagation.

The ignition principles (see Section 2, Chapter 11) suggest that, for thermally thick materials, the inverse of the square root of time to ignition is expected to be a linear function of the external heat flux away from the CHF value:

$$\sqrt{\frac{1}{t_{ig}}} = \frac{(\dot{q}''_e - \mathrm{CHF})}{\mathrm{TRP}} \tag{2}$$

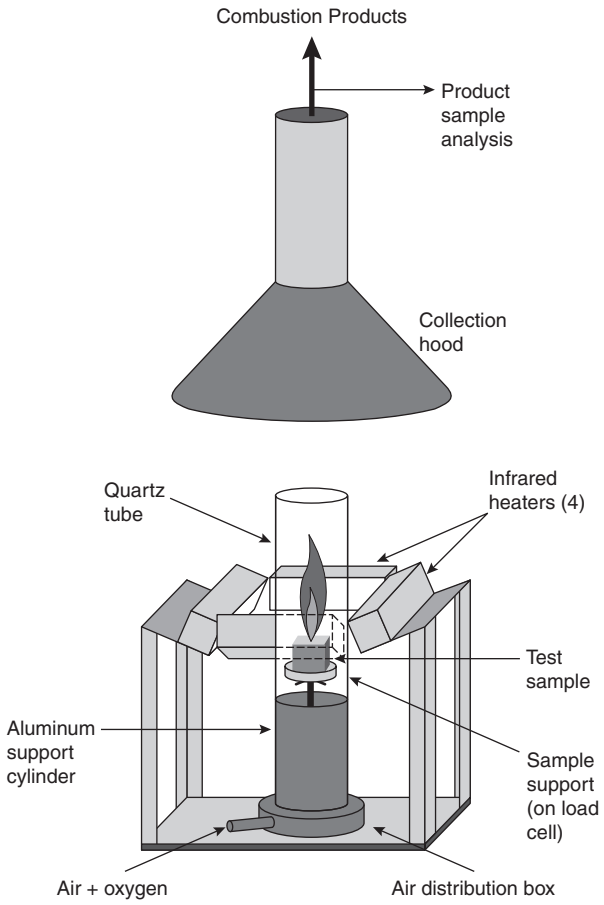

Figure 3-4.2(a). ***ASTM E2058 fire propagation apparatus designed by the Factory Mutual Research (FMR). Sample configuration for ignition, pyrolysis, and combustion tests.[1–4,9–16]***

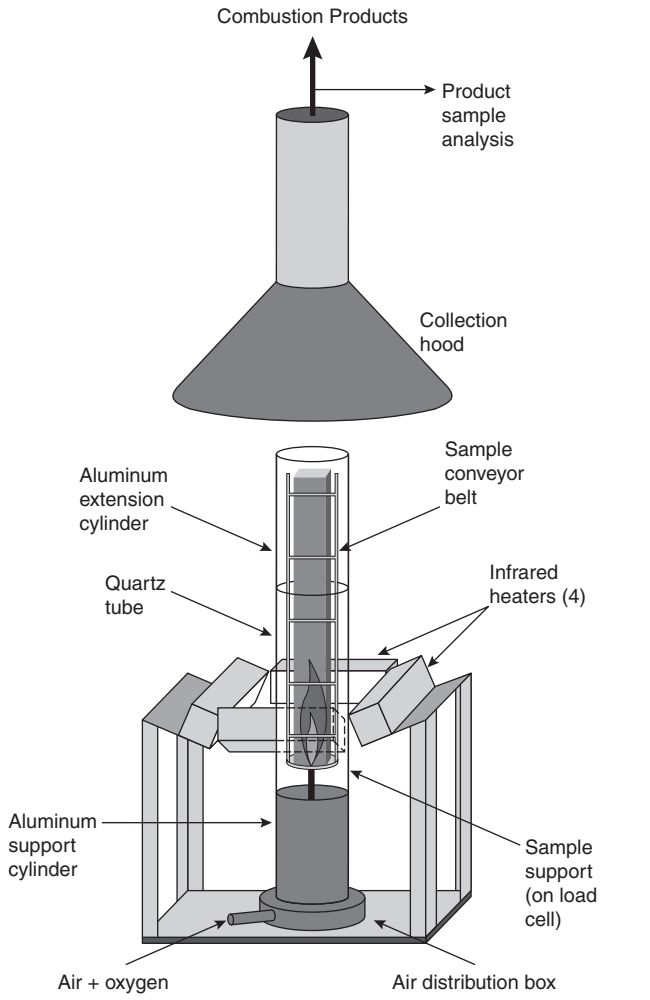

Figure 3-4.2(b). ***ASTM E2058 fire propagation apparatus designed by the Factory Mutual Research (FMR). Sample configuration for fire propagation tests.[1–4,9–16] A conveyor belt sample is shown.***

where t_{ig} is time to ignition (s) and $\dot{q}''_e$ is the external heat flux (kW/m^2). CHF is in kW/m^2. Most commonly used materials behave as thermally thick materials and satisfy Equation 2, such as shown by the data in Figure 3-4.4 for polymethylmethacrylate (PMMA); in Figure 3-4.5 for heavy corrugated paper sheets, measured in the ASTM E2058 fire propagation apparatus; and in Figure 3-4.6 for nonblackened samples, measured in the cone calorimeter. The cone calorimeter data are taken from Reference 20.

The value of TRP is determined, for example, in the ASTM E2058 fire propagation apparatus, by (1) measuring the time to ignition for 100 × 100-mm square or 100-mm diameter and up to 25-mm-thick samples at different external heat flux values for samples with surfaces blackened with a very thin layer of black paint or fine graphite powder to avoid errors due to differences in the radiation absorption characteristics of the materials, and (2) performing a linear regression analysis of the data away from critical heat flux, following Equation 2, and recording the inverse of the slope of the line.

The value of TRP for a surface that is not blackened is higher than the value for the blackened surface. For example, for nonblackened and blackened surfaces of polymethylmethacrylate (PMMA), TRP = 383 and 274 kW·s$^{1/2}$/m^2, respectively, from the ASTM E2058 fire propagation apparatus.[2] The value for TRP for a blackened surface of PMMA is close to the value calculated from the known T_{ig}, k, ρ, and c_P values for PMMA.[2]

TRP depends on the chemical as well as the physical properties of materials, such as the chemical structure, fire retardants, and thickness. For example, Figure 3-4.7 shows that TRP increases with sample thickness and increases in the amount of passive fire protection agent used, such as provided by a surface coating to a heavy corrugated paper sheet.

CHF and TRP values for materials derived from the ignition data measured in the ASTM E2058 fire propagation apparatus and the cone calorimeter (as reported in Reference 20) are listed in Table 3-4.2. In the cone calorimeter, the surface was not blackened, and thus the values of TRP may be somewhat higher than expected from the T_{ig}, k, ρ, and c_P values.

Examples of the values of T_{ig}, k, ρ, c_P, and measured and calculated TRP values are listed in Table 3-4.3.

Table 3-4.1 ***Design Features, Test Conditions, and Types of Measurements for OSU and ASTM E2058 Fire Propagation Apparatuses, and NIST Cone Calorimeter***

Design and Test Conditions	OSU[a]	ASTM E2058 Fire Propagation Apparatus[b]	Cone[c]
Inlet gas flow	Co-flow	Co-flow/natural	Natural
Oxygen concentration (%)	21	0 to 60	21
Co-flow gas velocity (m/s)	0.49	0 to 0.146	NA
External heaters	Silicon carbide	Tungsten-quartz	Electrical coils
External heat flux (kW/m^2)	0 to 100	0 to 65	0 to 100
Exhaust product flow (m^3/s)	0.04	0.035 to 0.364	0.012 to 0.035
Horizontal sample dimensions (mm)	110 × 150	100 × 100	100 × 100
Vertical sample dimensions (mm)	150 × 150	100 × 600	100 × 100
Ignition source	Pilot flame	Pilot flame	Spark plug
Heat release rate capacity (kW)	8	50	8
Measurements			
Time to ignition	Yes	Yes	Yes
Material gasification rate	No	Yes	Yes
Fire propagation rate	No	Yes	No
Generation rates of fire products	Yes	Yes	Yes
Light obscuration by smoke	Yes	Yes	Yes
Optical properties of smoke	No	Yes	No
Electrical properties of smoke	No	Yes	No
Gas-phase corrosion	No	Yes	No
Chemical heat release rate	Yes	Yes	Yes
Convective heat release rate	Yes	Yes	No
Radiative heat release rate	No	Yes	No
Flame extinction			
By water	No	Yes	No
By halon	No	Yes	No
By halon alternates	No	Yes	No

[a]As specified in ASTM E906-83[7] and by DOT/FAA[8]

[b]As specified in ASTM E2058 fire propagation apparatus

[c]As specified in ASTM E1354-90[19]

EXAMPLE 1:

In a fire, newspaper and polypropylene are exposed to a heat flux value of 50 kW/m^2. Estimate which material will ignite first, assuming physical conditions to be very similar for both the materials.

SOLUTION:

From Table 3-4.2, for newspaper and polypropylene, CHF = 10 and 15 kW/m^2, respectively, and TRP = 108 and 193 kW·s$^{1/2}$/m^2, respectively. Substituting these values in Equation 2 with $\dot{q}''_e$ = 50 kW/m^2, the times to ignition are calculated to be 6 and 24 sec for newspaper and polypropylene, respectively. Thus, newspaper will ignite first.

EXAMPLE 2:

Halogenated materials are obtained by replacing hydrogen atoms with halogen atoms in the chemical structures of the materials. For example, a unit in polyethylene (PE) consists of C_2H_4. If a hydrogen atom (H) is replaced by a chlorine atom (Cl) in a PE unit, it becomes a unit of rigid polyvinylchloride (PVC), that is, C_2H_3Cl. If two H atoms are replaced by two fluorine atoms (F) in a PE unit, it becomes a unit of Tefzel (ethylene tetrafluorethylene), that is, $C_2H_2F_2$. If all the hydrogen atoms are replaced by four F atoms in a PE unit, it becomes a unit of Teflon (polytetrafluoroethylene), that is, C_2F_4. Show how the replacement of hydrogen atoms by the halogen atoms affects the ignitability of the materials.

SOLUTION:

From Table 3-4.2, for PE (high density), PVC (rigid), Tefzel, and Teflon, the CHF values are 15, 15, 27, and 38 kW/m^2, respectively, and the TRP values are 321, 406, 356, and 682 kW·s$^{1/2}$/m^2, respectively. In the calculations, it is assumed that these materials are exposed to a uniform heat flux of 60 kW/m^2 in a fire under very similar physical conditions. From Equation 2, using $\dot{q}''_e$ = 60 kW/m^2, the times to ignition for PE (high density), PVC (rigid), Tefzel, and Teflon are calculated to be 40, 64, 91, and 755 sec, respectively. Thus, resistance to ignition increases as the hydrogen atom is replaced by the halogen atom in the chemical structure of PE. The higher the number of hydrogen atoms replaced by the halogen atoms in the structure, the higher the resistance to ignition. When all the hydrogen atoms are replaced by the fluorine atoms, the material becomes highly resistant to ignition.

Fire Propagation

The fundamental surface flame spread principles are described by Quintiere in Section 2, Chapter 12. According to these principles, the fire propagation process, as

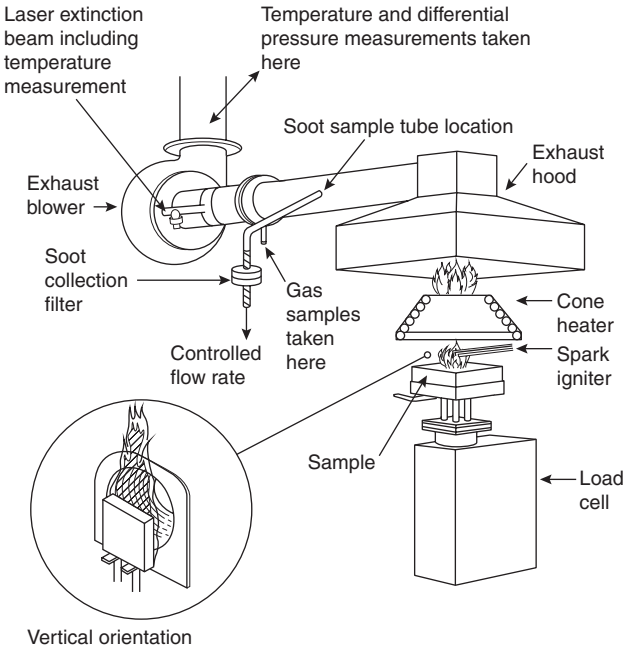

Figure 3-4.3. ***The cone calorimeter (ASTM E1354-90) designed at the National Institute of Standards and Technology (NIST).[17–19]***

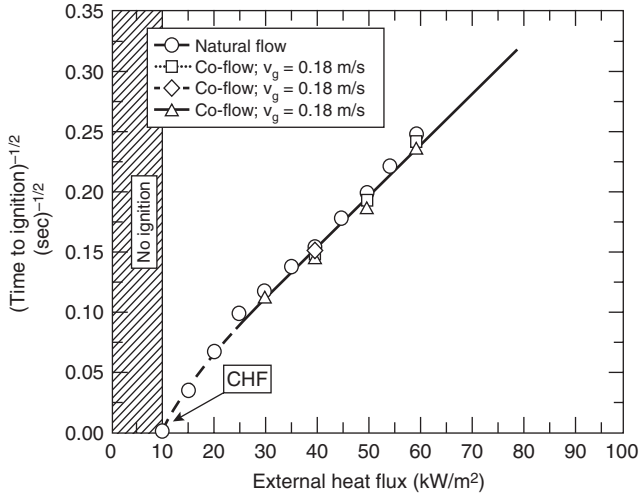

Figure 3-4.4. ***Square root of the inverse of time to ignition versus external heat flux for 100 × 100 × 25-mm-thick polymethylmethacrylate (PMMA) slab with blackened surface. Data measured in the ASTM E2058 fire propagation apparatus and reported in Reference 2 are shown.***

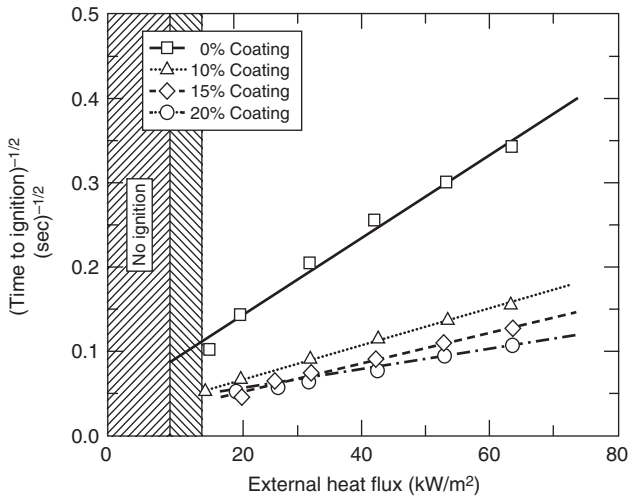

Figure 3-4.5. ***Square root of the inverse of time to ignition versus external heat flux for two 100 × 100 × 11-mm-thick sheets of heavy corrugated paper with blackened surface. Data measured in ASTM E2058 fire propagation apparatus.***

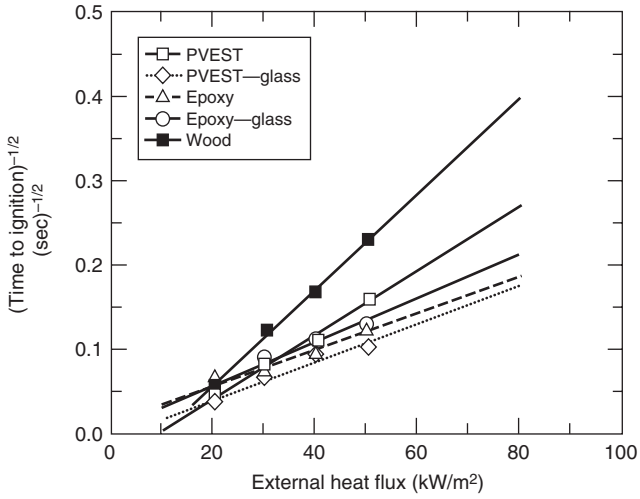

Figure 3-4.6. ***Square root of the inverse of time to ignition versus external heat flux for 100 × 100-mm nonblackened surfaces of 10 × 11-mm-thick polyvinyl ester (PVEST), 11-mm-thick epoxy, and 6-mm-thick wood (hemlock). Data measured in the cone calorimeter as reported in Reference 20 are shown.***

indicated by surface flame spread, can be explained as follows.

As a material is exposed to heat flux from internal and/or external heat sources, a combustible mixture is formed that ignites, and a flame anchors itself on the surface in the ignition zone. As the vapors of the material burn in the flame, they release heat with a certain rate, defined as the chemical heat release rate.* Part of the chemical heat release rate is transferred beyond the ignition zone as conductive heat flux through the solid and as convective and radiative heat fluxes from the flame. If the heat flux transferred beyond the ignition zone satisfies CHF, TRP, and gasification requirements of the material, the pyrolysis and

*In earlier papers, it was defined as the actual heat release rate, $\dot{Q}_A$.

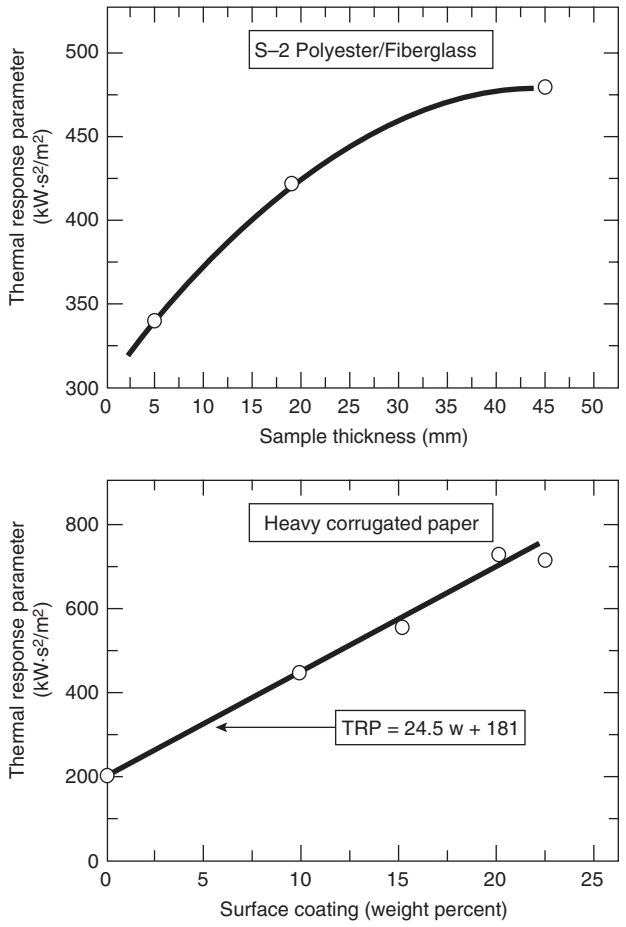

Figure 3-4.7. ***Thermal response parameter versus thickness for S-2 polyester/fiberglass sample and weight percent of surface coating for the heavy corrugated paper. Data measured in the ASTM E2058 fire propagation apparatus. w is weight %.***

flame fronts move beyond the ignition zone and the flame anchors itself over additional surface. Due to increase in the burning surface area, flame height, chemical heat release rate, and heat flux transferred ahead of the pyrolysis front all increase. The pyrolysis and flame fronts move again, and the process repeats itself and burning area increases. Fire propagation on the surface continues as long as the heat flux transferred ahead of the pyrolysis front (from the flame or external heat sources) satisfies CHF, TRP, and gasification requirements of the material.

The rate of movement of the pyrolysis front is generally used to define the fire propagation rate:

$$u = \frac{dX_p}{dt} \tag{3}$$

where u is the fire propagation rate (mm/s or m/s), and X_p is the pyrolysis front (mm or m).

The fire propagation rate can be determined in one of the several apparatuses: (1) the LIFT described by Quintiere in Section 2, Chapter 12; (2) the ASTM E2058 fire

Table 3-4.2 ***Critical Heat Flux and Thermal Response Parameter of Materials***

Materials	CHF (kW/m²) ASTM E2058 Fire Propagation Apparatus	TRP (kW·s$^{1/2}$/m²) ASTM E2058 Fire Propagation Apparatus	TRP (kW·s$^{1/2}$/m²) ASTM E1354-90[a]
Natural materials			
Flour	10	218	—
Sugar	10	255	—
Tissue paper	10	95	—
Newspaper	10	108	—
Wood (red oak)	10	134	—
Wood (Douglas fir)	10	138	—
Corrugated paper (light	10	152	—
Corrugated paper (heavy)			
No coating	10	189	—
Coating (10% by weight)	15	435	—
Coating (15% by weight)	15	526	—
Coating (20% by weight)	15	714	—
Wood (hemlock)	—	—	175
Wool 100%	—	—	252
Wood (Douglas fir/fire retardant, FR)	10	251	—
Synthetic materials			
Epoxy resin	—	—	457
Polystyrene (PS)	13	162	—
Acrylic fiber 100%	—	—	180
Polypropylene (PP)	15	193	291
PP/FR panel	15	315	—
Styrene-butadiene (SB)	10	198	—
Crosslinked polyethylenes (XLPE)	15	224–301	—
Polyvinyl ester	—	—	263
Polyoxymethylene	13	269	—
Nylon	15	270	—
Polyamide-6	—	—	379
Polymethylmethacrylate (PMMA)	11	274	—
Isophthalic polyester	—	—	296
Acrylonitrile-butadiene-styrene (ABS)	—	—	317
Polyethylene (high density) (PE)	15	321	364
PE/nonhalogenated fire retardants	15	652–705	—
Polyvinyl ester panels	13–15	440–700	—
Modified acrylic (FR)	—	—	526
Polycarbonate	15	331	—
Polycarbonate panel	16	420	—
Halogenated materials			
Isoprene	10	174	—
Polyvinylchloride (PVC)	10	194	—
Plasticized PVC, LOI = 0.20	—	—	285
Plasticized PVC, LOI = 0.25	—	—	401
Plasticized PVC, LOI = 0.30	—	—	397
Plasticized PVC, LOI = 0.35	—	—	345
Rigid PVC, LOI = 0.50	—	—	388
Rigid PVC1	15	406	—
Rigid PVC2	15	418	—
PVC panel	17	321	—

[a]Calculated from the ignition data reported in Reference 20.

(continued)

Table 3-4.2 ***Critical Heat Flux and Thermal Response Parameter of Materials (Continued)***

Materials	CHF (kW/m^2) ASTM E2058 Fire Propagation Apparatus	TRP ($kW \cdot s^{1/2}/m^2$) ASTM E2058 Fire Propagation Apparatus	TRP ($kW \cdot s^{1/2}/m^2$) ASTM E1354-90[a]
Halogenated materials (cont.)			
PVC fabric	26	217	—
PVC sheets	15	446–590	—
Ethylene tetrafluoroethylene (ETFE), Tefzel	27	356	—
Fluorinated ethylene-propylene (FEP), Teflon	38	682	—
Teflon fabric	50	299	—
Teflon coated on metal	20	488	—
Composite and fiberglass-reinforced materials			
Polyether ether keton—30% fiberglass	—	—	301
Isophthalic polyester—77% fiberglass	—	—	426
Polyethersulfone—30% fiberglass	—	—	256
Polyester 1—fiberglass	—	—	430
Polyester 2—fiberglass	10	275	—
Polyester 3—fiberglass	10	382	—
Polyester 4—fiberglass	15	406	—
Polyester 5—fiberglass	10	338	—
Epoxy Kevlar (thin sheet)	—	—	120
Epoxy fiberglass (thin sheet)	10	156	198
Epoxy graphite	15	395	—
Epoxy 1—fiberglass	10	420	—
Epoxy 2—fiberglass	15	540	—
Epoxy 3—fiberglass	15	500	—
Epoxy 4—fiberglass	10	388	
Epoxy resin—69% fiberglass	—	—	688
Epoxy-graphite 1	—	481	—
Epoxy-graphite 1/ceramic coating (CC)	—	2273	—
Epoxy-graphite 1/intumescent coating (IC)	—	962	—
Epoxy-graphite 1/IC-CC	—	1786	—
Polyvinyl ester 1—69% fiberglass	—	—	444
Polyvinyl ester 2—fiberglass	—	281	—
Polyvinyl ester 2—fiberglass//CC	—	676	—
Polyvinyl ester 2—fiberglass/IC	—	1471	—
Polyvinyl ester 2—fiberglass/IC-CC	—	1923	—
Graphite composite	40	400	—
Phenolic fiberglass (thin sheet)	33	105	172
Phenolic fiberglass (thick sheet)	20	610	—
Phenolic-graphite 1	20	333	—
Phenolic-graphite 2	—	—	400
Phenolic kevlar (thin sheet)	20	185	258
Phenolic kevlar (thick sheet)	15	403	—
Phenolic-graphite 1/CC	—	807	—
Phenolic-graphite 1/IC	—	1563	—

Materials	CHF (kW/m^2) ASTM E2058 Fire Propagation Apparatus	TRP ($kW \cdot s^{1/2}/m^2$) ASTM E2058 Fire Propagation Apparatus	TRP ($kW \cdot s^{1/2}/m^2$) ASTM E1354-90[a]
Foams (wall-ceiling insulation materials, etc.)			
Polyurethane foams	13–40	55–221	—
Polystyrene foams	10–15	111–317	—
Phenolic	20	610	—
Phenolic laminate—45% glass	—	—	683
Latex foams	16	113–172	—
Materials with fiberweb, net-like and multiplex structures			
Polypropylenes	8–15	108–417	—
Polyester-polypropylene	10	139	—
Wood pulp-polypropylene	8	90	—
Polyester	8–18	94–383	—
Rayon	14–17	161–227	—
Polyester-rayon	13–17	119–286	—
Wool-nylon	15	293	—
Nylon	15	264	—
Cellulose	13	159	—
Cellulose-polyester	13–16	149–217	—
Electrical cables—power			
PVC/PVC	13–25	156–341	—
PE/PVC	15	221–244	—
PVC/PE	15	263	—
Silicone/PVC	19	212	—
Silicone/cross linked polyolefin (XLPO)	25–30	435–457	—
EPR (ethylene-propylene rubber/EPR)	20–23	467–567	—
XLPE/XLPE	20–25	273–386	—
XLPE/EVA (ethyl-vinyl acetate)	12–22	442–503	—
XLPE/Neoprene	15	291	—
XLPO/XLPO	16–25	461–535	—
XLPO, PVF (polyvinylidine fluoride) XLPO	14–17	413–639	—
EPR/Chlorosulfonated PE	14–19	283–416	—
EPR, FR	14–28	289–448	—
Electrical cables—communications			
PVC/PVC	15	131	—
PE/PVC	20	183	—
XLPE/XLPO	20	461–535	—
Si/XLPO	20	457	—
EPR-FR	19	295	—
Chlorinated PE	12	217	—
ETFE/EVA	22	454	—
PVC/PVF	30	264	—
FEP/FEP	36	638–652	—
Conveyor belts			
Styrene-butadiene rubber (SBR)	10–15	336–429	—
Chloroprene rubber (CR)	20	760	—
CR/SBR	15	400	—
PVC	15–20	343–640	—

[a]Calculated from the ignition data reported in Reference 20.

Table 3-4.3 ***Thermal Properties and Thermal Response Parameter Values of Polymers***[a]

Polymers	T_{ig} (°C)	$\rho \times 10^{-3}$ (g/m³)	c_P (kJ/Kg·K)	$k \times 10^{-3}$ (kW/m·K)	TRP Exp	TRP Cal
Polyethylene	443	0.94	2.15	0.42	454	345
Polypropylene-1	443	0.93	2.20	0.20	288	240
Polypropylene-2	443	0.90	2.20	0.20	323	237
Polypropylene-3	443	1.06	2.08	0.20	277	208
Polypropylene-4	443	NM	NM	0.20	310	NM
Polypropylene-5	443	1.04	1.93	0.20	333	238
Polycarbonate-1	497	1.18	1.51	0.20	357	252
Polycarbonate-2	497	1.19	2.06	0.20	434	296
Polycarbonate-3	580	1.20	1.20	0.21	455	273
Polyvinylchloride-1	357	1.20	1.37	0.21	263	176
Polyvinylchloride-2	374	1.95	1.14	0.21	215	214
Nylon 6	497	0.12	2.19	0.24	154	106
Polyethyleneterephthalate	374	0.66	1.32	0.15	174	113
Polymethylmethacrylate	378	1.19	2.09	0.27	274	259
Teflon, PTFE	700	2.18	1.01	0.25	654	444
Teflon, FEP	700	2.15	1.20	0.25	680	484
Tefzel, ETFE	540	1.70	0.90	0.23	481	273
Kel-F, PCTFE	580	2.11	0.90	0.22	460	321
Halar, ECTFE	613	1.69	1.01	0.15	450	265
Polysulfone	580	1.24	1.30	0.28	469	333
Polyetheretherketone	580	1.32	1.82	0.25	550	382

[a]Data taken from Reference 21.

propagation apparatus (50- and 500-kW scales)—the 50-kW scale apparatus is shown in Figure 3-4.2(b); and (3) the fire products collector (10,000-kW scale ASTM E2058 fire propagation apparatus) shown in Figure 3-4.8. Examples of the type of data obtained from the ASTM E2058 fire propagation apparatus are shown in Figures 3-4.9 through 3-4.12. In Figure 3-4.12, heat release rates increase linearly with time during downward fire propagation, very similar to the pyrolysis front values for the downward fire propagation in Figure 3-4.9.

The slopes of the lines in Figures 3-4.9 through 3-4.12 represent fire propagation rates. The upward fire propagation rate is much faster than the downward fire propagation rate. For downward fire propagation, linear increases in the pyrolysis front and heat release rates indicate decelerating fire propagation behavior. For upward fire propagation, nonlinear increases in the pyrolysis front indicate accelerating fire propagation behavior.

Relationship between fire propagation rate, flame height, pyrolysis front, and heat release rate: Numerous researchers have found the following relationship between the flame height and pyrolysis front (as discussed by Quintiere in Section 2, Chapter 12 and reviewed in References 2 and 22)

$$X_f = aX_p^n \tag{4}$$

where

X_f = flame height (m)

$a = 5.35$

$n = 0.67$ to 0.80

for steady wall fires.[2] X_p is in m.

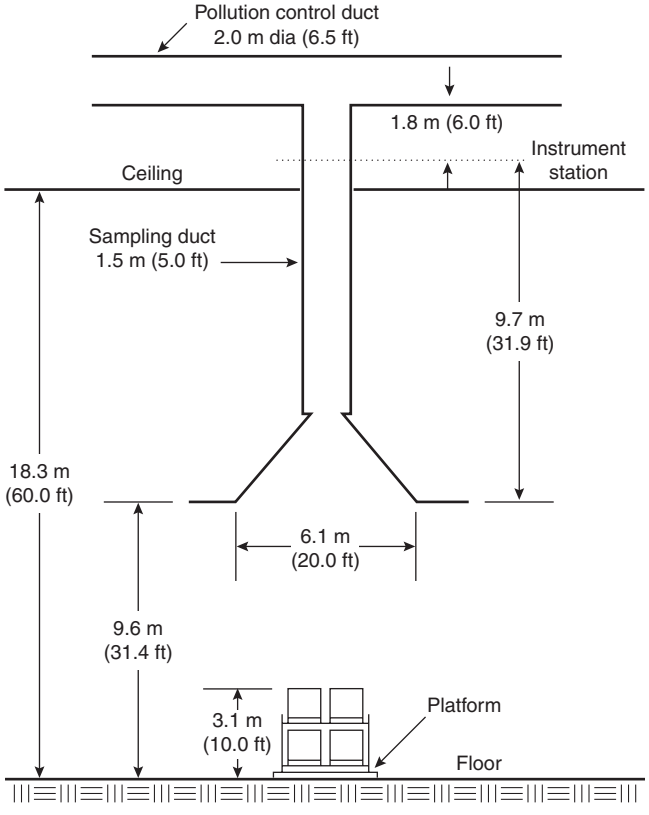

Figure 3-4.8. ***The fire products collector (10,000-kW-scale ASTM E2058 fire propagation apparatus) for large-scale combustion and fire propagation tests. Corrugated boxes with various products, arranged in two-pallet loads × two-pallet loads × two-pallet loads high are shown. The fire products collector is designed by the Factory Mutual Research Corporation.***

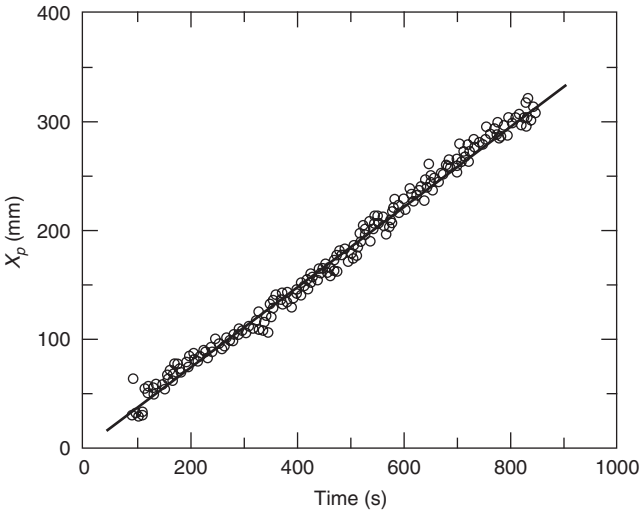

Figure 3-4.9. ***Pyrolysis front versus time for the downward fire propagation for 300-mm-long, 100-mm-wide, and 25-mm-thick PMMA vertical slab under opposed airflow condition in the ASTM E2058 fire propagation apparatus. Airflow velocity = 0.09 m/s. Oxygen mass fraction = 0.334. (Figure is taken from Reference 2.)***

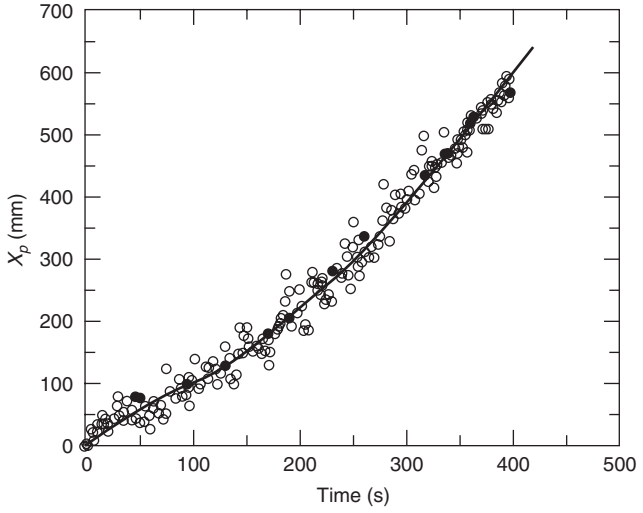

Figure 3-4.10. ***Pyrolysis front versus time for the upward fire propagation for 600-mm-long, 100-mm-wide, and 25-mm-thick PMMA vertical slab under co-airflow condition in the ASTM E2058 fire propagation apparatus. Airflow velocity = 0.09 m/s. Oxygen mass fraction = 0.233. (Figure is taken from Reference 2.)***

Fire propagation data for PMMA from the ASTM E2058 fire propagation apparatus[2] and for electrical cables from several standard tests for cables (ICEA, CSA FT-4, and UL-1581)[9] satisfy Equation 4, as shown in Figure 3-4.13, with $a = 5.32$ and $n = 0.78$. The visual measurement of the pyrolysis front as damage length is used for the acceptance criterion in many of the standard tests for electrical cables. For example, for upward fire propagation

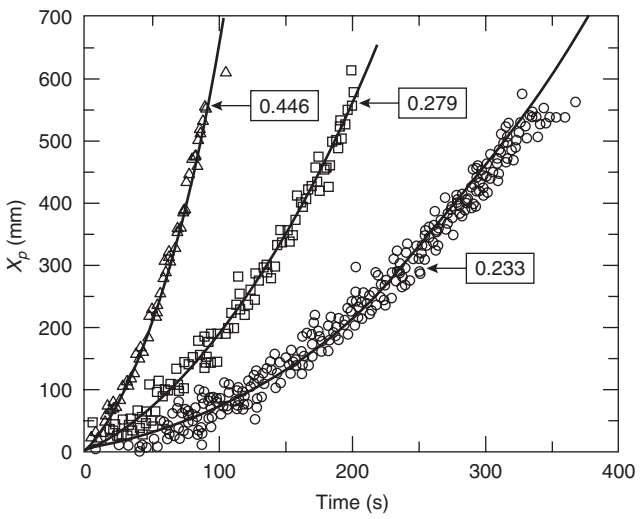

Figure 3-4.11. ***Pyrolysis front versus time for the upward fire propagation for 600-mm-long and 25-mm-thick diameter PMMA cylinder under co-airflow condition in the ASTM E2058 fire propagation apparatus. Airflow velocity = 0.09 m/s. Numbers inside the frames are the mass fractions of oxygen in air. (Figure is taken from Reference 2.)***

in the CSA FT-4, damage length less than 60 percent of the total length of the cable tray for 20-min exposure time is used as the acceptance criterion.[9] For horizontal fire propagation in the UL-1581 test, flame length of less than 40 percent of the total length of the cable tray is used as the acceptance criterion.[9]

The relationship between the flame height and the chemical heat release rate, expressed as the normalized chemical heat release rate (NCHRR) is defined as

$$\text{NCHRR} = \frac{\dot{Q}'_{ch}}{\rho c_p T_a g^{1/2} X_p^{3/2}} \tag{5}$$

where

$\dot{Q}'_{ch}$ = chemical heat release rate per unit width (kW/m)
ρ = density of air (g/m^3)
c_p = specific heat of air (kJ/g·K)
T_a = ambient temperature (K)
g = acceleration due to gravity (m^2/s)

X_p is in m.

Many researchers have shown that the ratio of the flame height to pyrolysis front is a function of the heat release rate, such as the following relationship (as discussed by Quintiere in Section 2, Chapter 12 and reviewed in References 2 and 22)

$$\frac{X_f}{X_p} = a[\text{NCHRR}]^n \tag{6}$$

where a and n are constants. This relationship reported in the literature (as reviewed in Reference 2) for methane, ethane, and propylene is shown in Figure 3-4.14. The data

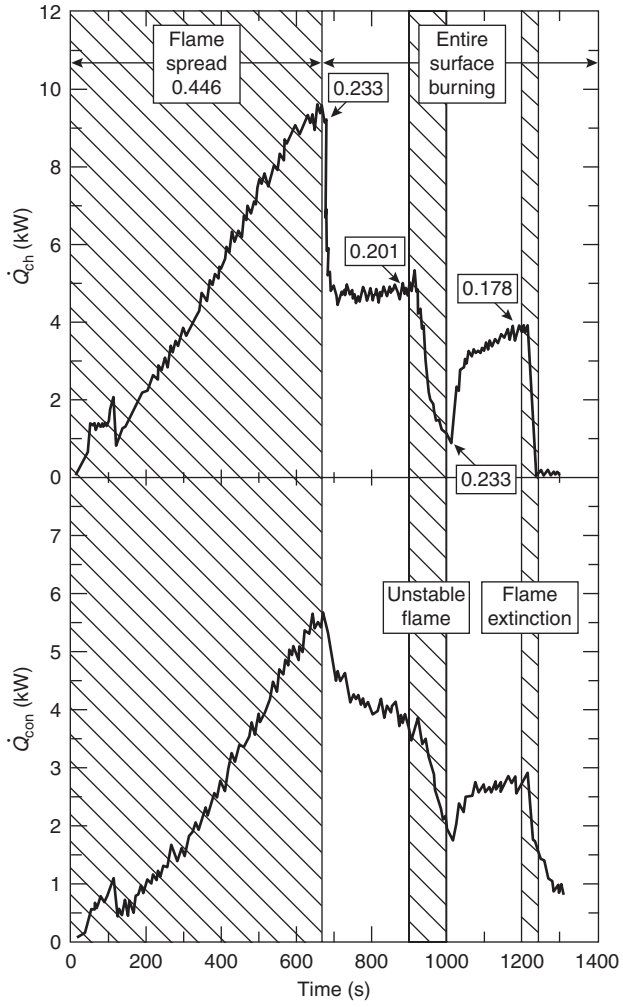

Figure 3-4.12. ***Chemical and convective heat release rate versus time for the downward fire propagation, combustion, and flame extinction for 300-mm-long, 100-mm-wide, and 25-mm-thick PMMA vertical slab under opposed airflow condition in the ASTM E2058 fire propagation apparatus. Airflow velocity = 0.09 m/s. Numbers inside the frames are the mass fractions of oxygen in air. (Figure is taken from Reference 2.)***

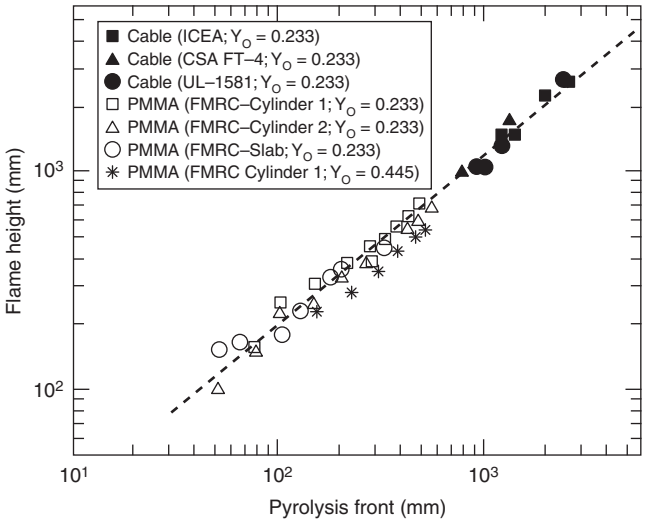

Figure 3-4.13. ***Flame height versus pyrolysis front for the upward fire propagation in normal air. Data are for the vertical fire propagation for electrical cables contained in 2.44-m-long, 310-mm-wide, and 76-mm-deep trays in standard tests for electrical cables (ICEA, CSA FT-4, and UL-1581) and for 600-mm long PMMA slabs (100-mm-wide and 25-mm-thick) and cylinder (25-mm diameter) in the ASTM E2058 fire propagation apparatus. Data for fire propagation in an oxygen mass fraction of 0.445 are also included. (Figure is taken from References 2 and 9.)***

for the upward fire propagation for PMMA from the ASTM E2058 fire propagation apparatus[2] and for the electrical cables from the several standard tests for cables (UL-1581, ICEA, and CSA FT-4) also satisfy this relationship as indicated in Figure 3-4.14.[9]

In Figure 3-4.14, data in the lower left-hand corner are for the low-intensity polyvinylchloride (PVC) electrical cable fire propagation in the standard tests for cables. These data show that for NCHRR < 0.2, $X_f/X_p < 1.5$ and $n = 1/10$. This is a characteristic property of materials for which there is either no fire propagation or a limited fire propagation beyond the ignition zone. These materials are defined as Group 1 materials.[4,9–15] Cables with Group 1 material characteristics pass the standard tests for cables (UL-910, CSA FT-4, UL-1581, and ICEA). The data for higher intensity fire propagation in Figure 3-4.14 show that (1) for $0.2 >$ NCHRR < 5, $n = 2/3$ and $1.5 > X_f/X_p < 20$ (PMMA fire propagation and methane combustion); and (2) for NCHRR > 5, $n = 1/2$ and $X_f/X_p > 20$ (ethane and propylene combustion). Thus, the ratio of the flame height to pyrolysis front is a good indicator of the fire propagation characteristics of the materials. Materials for which flame height is close to the pyrolysis front during fire propagation can be useful indicators of decelerating fire propagation behavior.

Researchers have also developed many correlations between the flame heat flux transferred ahead of the pyrolysis front and heat release rate for downward, upward, and horizontal fire propagation (as discussed by Quintiere in Section 2, Chapter 12 and reviewed in References 2 and 22). For example, small- and large-scale fire propagation test data from the ASTM E2058 fire propagation apparatus [Figure 3-4.2(b)] and fire products collector (Figure 3-4.8) suggest that, for thermally thick materials with highly radiating flames, the following semi-empirical relationship is satisfied:[3]

$$\dot{q}_f'' \propto \left(\frac{\chi_{rad}}{\chi_{ch}} \dot{Q}'_{ch} \right)^{1/3} \tag{7}$$

where $\dot{q}_f''$ is the flame heat flux transferred ahead of the pyrolysis front (kW/m^2) and χ_{rad} is the radiative fraction of the combustion efficiency, χ_{ch}. The fire propagation rate is expressed as[3]

$$\sqrt{u} \propto \frac{[(\chi_{rad}/\chi_{ch})(\dot{Q}'_{ch})]^{1/3}}{TRP} \tag{8}$$

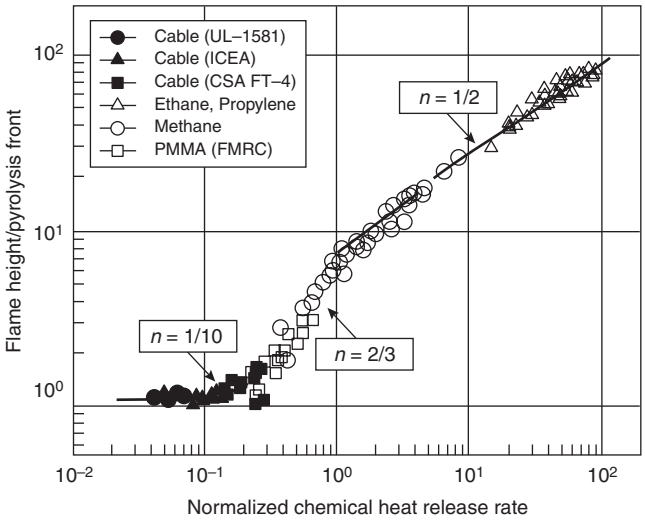

Figure 3-4.14. ***Ratio of flame height to pyrolysis front versus the normalized chemical heat release rate for the upward fire propagation in normal air. Data for the diffusion flames of methane, ethane, and propylene are from the literature. Data for the cables are from the standard tests for electrical cables (ICEA, CSA FT-4, and UL-1581).[9] Data for PMMA are from the ASTM E2058 fire propagation apparatus for 600-mm-long vertical PMMA slabs (100-mm-wide, 25-mm-thick) and cylinders (25-mm-diameter).[2] (Figure is taken from Reference 9.)***

In a simplified form of Equation 8, the right-hand side of Equation 8 multiplied by 1000 is defined as the *fire propagation index* (FPI):[4,9–15]

$$\text{FPI} = \frac{1000(0.42\dot{Q}'_{ch})^{1/3}}{\text{TRP}} = \frac{750(\dot{Q}'_{ch})^{1/3}}{\text{TRP}} \qquad (9)$$

FPI describes the fire propagation behavior of materials under highly flame-radiating conditions prevalent in large-scale fires. The small- and large-scale fire propagation test data and understanding of the fire propagation suggest that the FPI values can be used to classify the materials into four groups:[2–4,9–15]

1. *FPI < 7 (Nonpropagating) Group N-1 Materials*—Materials for which there is no fire propagation beyond the ignition zone. Flame is at critical extinction condition.
2. *7 < FPI < 10 (Decelerating Propagation): Group D-1 Materials*—Materials for which fire propagates beyond the ignition zone although in a decelerating fashion. Fire propagation beyond the ignition zone is limited.
3. *10 < FPI < 20 (Nonaccelerating Propagation): Group 2 Materials*—Materials for which fire propagates slowly beyond the ignition zone.
4. *FPI > 20 (Accelerating Propagation): Group 3 Materials*—Materials for which fire propagates rapidly beyond the ignition zone.

The FPI values for the upward fire propagation, under highly flame-radiating conditions, have been determined for numerous materials in the ASTM E2058 fire propagation apparatus. The highly radiating conditions are created by using a value of 0.40 for the mass fraction of oxygen. Two sets of tests are performed:

1. *Thermal response parameter test.* Ignition tests are performed in the ASTM E2058 fire propagation apparatus [Figure 3-4.2(a)], and TRP value is determined from the time to ignition versus external heat flux as described in the subsection on fire initiation (ignition).
2. *Upward fire propagation test.* Fire propagation tests for vertical slabs, sheets, or cables are performed in the ASTM E2058 fire propagation apparatus [50- and 500-kW scale, Figure 3-4.2(b)]. About 300- to 600-mm-long, up to about 100-mm-wide, and up to about 100-mm-thick samples are used. The bottom 120 to 200 mm of the sample is in the ignition zone, where it is exposed to 50 kW/m^2 of external heat flux in the presence of a pilot flame. Beyond the ignition zone, fire propagates by itself, under co-airflow condition with an oxygen mass fraction of 0.40. During upward fire propagation, measurement is made for the chemical heat release rate as a function of time in each test.

TRP value and the chemical heat release rate are used in Equation 9 to calculate the FPI as a function of time. The FPI profile is used to classify materials into Group 1, 2, or 3.

Application of the Fire Propagation Index (FPI) to classify materials:

Electrical cables. The FMRC standard for cable fire propagation Class No. 3972[14] is used to classify electrical cables, based on their upward fire propagation behavior, under highly flame-radiating conditions (oxygen mass fraction = 0.40), for protection needs in noncombustible occupancies. A noncombustible occupancy is defined as an occupancy where only specific types of combustibles are present, ignition sources are relatively small, and their contributions toward thermal and nonthermal hazards are negligible compared to the contributions of the combustibles. TRP and upward fire propagation tests are performed, and Equation 9 is used to calculate the FPI, as described above. Figure 3-4.15 shows an example of a typical profile for the FPI versus time for a polyethylene (PE)/polyvinylchloride (PVC) cable. This cable does not pass any of the standard electrical cable tray fire tests, and the FPI profile in Figure 3-4.15 shows that it is a Group 3 cable.

The following fire protection guidelines are recommended by FMRC for grouped cables:[11,13,14]

1. Group 1 cables do not need additional fire protection in noncombustible occupancies with noncombustible construction.
2. Group 2 cables can be used without additional fire protection in noncombustible occupancies with noncombustible construction under certain conditions.
3. Group 3 cables need fire protection.

Table 3-4.4 lists FPI values for selected electrical cables, composites, and conveyor belts.

EXAMPLE 3:

What type of fire behavior is represented by a 300-mm-wide, 8-m-high, and 25-mm-thick vertical sheet of a

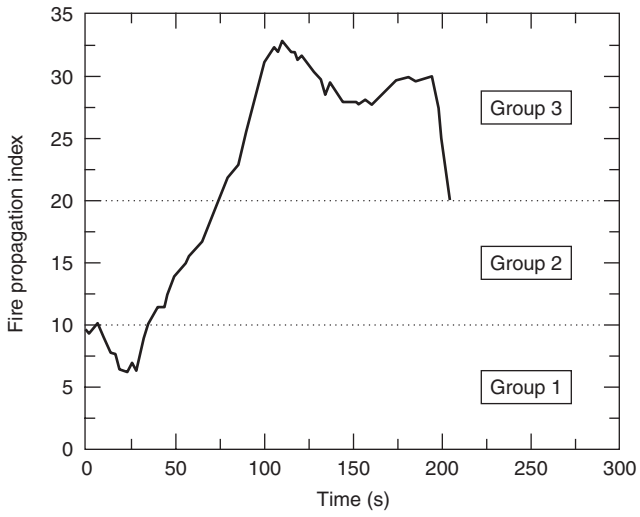

Figure 3-4.15. ***Fire Propagation Index versus time for a polyethylene (PE)/polyvinylchloride (PVC) Group 3 cable determined in the ASTM E2058 fire propagation apparatus. This cable does not pass any standard tests for electrical cables.***

material with a TRP value of 95 kW·s$^{1/2}$/m^2 if the peak chemical heat release during the upward fire propagation is 50 kW?

SOLUTION:

Fire propagation behavior is assessed by the FPI value. For the material, the chemical heat release rate per unit width, $\dot{Q}'_{ch} = 50/0.3 = 167$ kW/m. Substituting this value in Equation 9, with TRP = 95 kW·s$^{1/2}$/m^2, FPI = 43. The TRP value is greater than 20, and thus the material is a Group 3 material and represents an accelerating fire propagation behavior.

EXAMPLE 4:

A noncombustible cable spreading room has an old and a new area with a 3-hr-rated solid fire wall between the two. The old area is filled with several trays of polyethylene (PE)/polyvinylchloride (PVC) communications cables, and the new area is filled with several trays of crosslinked polyolefin (XLPO/XLPO) communications cables. In order to determine the fixed fire protection needs for these two areas, cable samples were submitted to a testing laboratory. The laboratory reported the following test data:

1. *Ignition data.*

Heat flux (kW/m^2)	30	40	50	60	100
Time to ignition (s)					
PE/PVC	76	27	14	8	2
XLPO/XLPO	—	716	318	179	45

2. *Peak chemical heat release rate.* During vertical fire propagation for 0.60-m-long cable sample in a highly radiating environment (oxygen mass fraction = 0.40), the following data were measured:

Cable	Peak chemical heat release rate per unit cable circumference (kW/m^2)
PE/PVC	100
XLPO/XLPO	20

The data were used to calculate the FPI values, which suggested that the area with PE/PVC cable trays needed fixed fire protection, whereas the area with XLPO/XLPO cable trays did not need fixed fire protection. Do you agree?

SOLUTION:

The TRP values from the linear regression analysis of the ignition data are 131 and 535 kW·s$^{1/2}$/m^2 for the PE/PVC and the XLPO/XLPO cable samples, respectively. The data for $\dot{Q}'_{ch}$ are given. Thus, from Equation 9, the FPI values for the PE/PVC and the XLPO/XLPO cable samples are 29 and 4, respectively. The FPI values suggest that the PE/PVC cable is a Group 3 cable and is expected to have an accelerating fire propagation behavior, and the

Table 3-4.4 ***Fire Propagation Index for Cables, Composites, and Conveyor Belts, Determined in the ASTM E2058 Fire Propagation Apparatus***

	Diameter/ Thickness (mm)	FPI	Group	Fire Propagation[a]
Power cables				
PVC/PVC	4–13	11–28	2–3	P
PE/PVC	11	16–23	3	P
PVC/PE	34	13	2	P
Silicone/PVC	16	17	2	P
Silicone/XLPO	55	6–8	1	N-D
EP/EP	10–25	6–8	1	N-D
XLPE/XLPE	10–12	9–17	1–2	D-P
XLPE/EVA	12–22	8–9	1	D
XLPE/Neoprene	15	9	1	D
XLPO/XLPO	16–25	8–9	1	D
XLPO, PVF/XLPO	14–17	6–8	1	N-D
EP/CLP	4–19	8–13	1–2	D-P
EP, FR/None	4–28	9	1	D
Communications cables				
PVC/PVC	4	36	3	P
PE/PVC	4	28	3	P
PXLPE/XLPO	22–23	6–9	1	N-D
Si/XLPO	28	8	1	D
EP-FR/none	28	12	2	P
PECl/none	15	18	2	P
ETFE/EVA	10	8	1	D
PVC/PVF	5	7	1	N
FEP/FEP	8	4	1	N
FEP/FEP	10	5	1	N
Conveyor belts[b]				
Styrene-butadiene rubber (SBR)		8–11	1–2	D-P
Chloroprene rubber (CR)		5	1	P
CR/SBR		8	1	D
PVC		4–10	1–2	N-P

[a]P: propagation; D: decelerating propagation; N: no propagation.

[b]3 to 25 mm thick.

XLPO/XLPO is a Group 1 cable and fire propagation is expected to be either limited to the ignition zone or decelerating. These calculations support that the cable spreading room area filled with the PE/PVC cable trays would need fixed fire protection, whereas it would not be needed for the area filled with the XLPO/XLPO cable trays.

Conveyor belts. A conveyor belt standard is being developed at the Factory Mutual Research Corporation (FMRC) following the FMRC standard for cable fire propagation Class No. 3972.[14] TRP and upward fire propagation tests are performed, and Equation 9 is used to calculate the FPI as described above.

Conveyor belts are classified as propagating or nonpropagating. For an approximately 600-mm-long and 100-mm-wide vertical conveyor belt, the data measured in the ASTM E2058 fire propagation apparatus under highly flame-radiating conditions show that the nonpropagating fire condition is satisfied for FPI $\leq$ 7.0 for the belts that show limited fire propagation in the large-scale fire propagation test gallery of the U.S. Bureau of Mines.[12,23]

Table 3-4.4 lists FPI values for selected conveyor belts taken from References 12 and 23.

EXAMPLE 5:

Conveyor belts are made of solid woven or piles of elastomers, such as styrene-butadiene rubber (SBR), polychloroprene rubber (CR), polyvinylchloride (PVC), reinforced with fibers made of polymers, such as nylon. In large-scale fire propagation tests in a tunnel, fire on the surface of a CR-based conveyor belt was found to be nonpropagating, whereas for a CR/SBR-based conveyor belt fire was found to be propagating. Small-scale tests showed that the CR- and CR/SBR-based conveyor belts had the following fire properties, respectively: (1) CHF = 20 and 15 kW/m^2, (2) TRP = 760 and 400 kW·s$^{1/2}$/m^2, and (3) peak $\dot{Q}'_{ch}$ = 114 and 73 kW/m under highly flame-radiating conditions (oxygen mass fraction = 0.40). Show that small-scale test results are consistent with the large-scale fire propagation behaviors of the two conveyor belts, using the criterion that, for nonpropagating fire behavior, the FPI is equal to or less than 7.

SOLUTION:

Substituting the TRP and $\dot{Q}'_{ch}$ values in Equation 9, the FPI values for the CR- and CR/SBR-based conveyor belts are 5 and 8, respectively. Thus, the CR-based conveyor belt is expected to have a nonpropagating fire behavior, whereas the CR/SBR-based conveyor belt is expected to have a propagating fire behavior. The small-scale test results, therefore, are consistent with the large-scale fire propagation behaviors of the two conveyor belts.

Polymeric materials for clean rooms. The microchip devices are manufactured, many at a time, on disks of semiconducting materials called wafers.[24] Wafers are manufactured in several stages: material preparation, crystal growth and wafer preparation, wafer fabrication, and packaging. The area where wafer fabrication takes place is called a *clean room.* The cleanliness of the room is highly controlled in order to limit the number of contaminants to which the wafer is exposed. The stringent requirements of the solid-state devices define levels of cleanliness that far exceeds those of almost any other industry. Contamination in a clean room is defined as anything that interferes with the production of wafers and/or their performance. The overall clean room design principle is to build a sealed room that is supplied with clean air, is built with polymeric materials that are noncontaminating, and includes systems to prevent accidental contamination from outside, from the interactions of the polymeric materials and the wafer cleaning liquids, from operators, and from accidental fires.

In 1997, Factory Mutual Research introduced a new methodology, identified as the 4910 Test Protocol,[25] for testing the fire propagation and smoke development behaviors of polymeric materials for use in clean rooms for the semiconductor industry. For the acceptance of polymeric materials, two criteria need to be satisfied: (1) Fire Propagation Index (FPI) $\leq$ 6 (m/s$^{1/2}$)/(kW/m)$^{2/3}$ and (2) Smoke Development Index (SDI) $\leq$ 0.4 (g/g) (m/s$^{1/2}$)/(kW/m)$^{2/3}$.

In the 4910 Test Protocol,[25] Fire Propagation Index (FPI) is formulated from (1) the thermal response parameter (TRP), which relates the time to ignition to the net heat flux, and (2) the chemical heat release rate measured during the upward fire propagation in air having a 40 percent oxygen concentration to simulate flame heat transfer at large scale. SDI is related to the smoke release rate and is obtained by multiplying the FPI value by the smoke yield as shown in Figure 3-4.16. The smoke yield is defined as the ratio of the total mass of smoke released per unit mass of the vapors from the polymeric material burned.

The FPI and SDI values for various polymeric materials determined from the tests in the ASTM E2058 fire propagation apparatus are listed in Table 3-4.5, where data are taken from References 4, 10, and 25 to 29.

It can be noted from Table 3-4.5 that specialty polymeric materials (highly halogenated thermoplastics and high temperature thermosets) have low FPI and SDI values and several of them satisfy the 4910 test protocol criteria [FPI $\leq$ 6 (m/s$^{1/2}$)/(kW/m)$^{2/3}$ and SDI $\leq$ 0.4

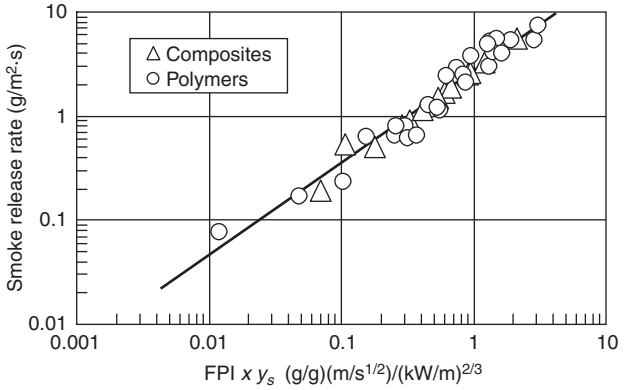

Figure 3-4.16. ***Peak smoke rates measured in the combustion tests in normal air with imposed external heat flux of 50 kW/m² versus peak FPI values from the propagation tests in air with 40 percent oxygen concentration multiplied by the smoke yields from the combustion tests. Tests were performed in the ASTM E2058 fire propagation apparatus.***

Table 3-4.5 ***Fire Propagation Index and Smoke Development Index for Polymeric Materials***[a]

Polymeric Material	FPI $(m/s^{1/2})/(kW/m)^{2/3}$	SDI $(g/g)(m/s^{1/2})/(kW/m)^{2/3}$
Fire-retarded or unmodified electrical cables		
Polyvinyl chloride(PVC)/polyvinyl chloride PVC)	36	4.1
Polyethylene (PE)/polyvinyl chloride (PVC)	28	3.8
Silicone/polyvinyl chloride (PVC)	17	2.0
Modified electrical cables		
Polyvinylchloride (PVC)	8	1.2
High-temperature polyvinylchloride (PVC)	7	0.69
Polyethylene (PE)/ethylvinylacetate (EVA)	5	0.40
Ordinary polymeric materials		
Fire-retarded polystyrene (FR-PS)	34	5.60
Fire-retarded polybutyleneterephthalate (FR-PBT)	32	2.20
Unmodified polymethylmethacrylate, (U-PMMA)	23	1.1
Unmodified polyoxymethylene, (U-POM)	15	0.03
Fire-retarded (FR) vinyl ester	10	2.5
Unmodified wood slab	14	0.20
Unmodified polyethylene (U-PE)	30	1.4
Polyethylene with 25% chlorine	15	1.7
Polyethylene with 36% chlorine	11	1.5
Polyethylene with 48% chlorine	8	1.9
Modified polyethylene (M-PE)-1	7	0.64
Modified polyethylene (M-PE)-2	6	0.65
Unmodified polypropylene (U-PP)	31	1.7
Fire-retarded polypropylene (FR-PP)	30	2.1
Modified polypropylene (M-PP)-1	11	3.0
Modified polypropylene (M-PP)-2	7	0.95
Modified polypropylene (M-PP)-3	7	0.35
Modified polypropylene (M-PP)-4	6	0.41
Modified polypropylene (M-PP)-5	5	0.40
Modified polypropylene (M-PP)-6	5	0.19
Modified polypropylene (M-PP)-7	5	0.21
Modified polypropylene (M-PP)-8	4	0.19
Fire-retarded flexible polyvinylchloride (FR-PVC)	16	1.6
Unmodified rigid polyvinylchloride (U-PVC)-1	8	0.86
Unmodified rigid polyvinylchloride (U-PVC)-2	7	1.2
Modified rigid polyvinylchloride (M-PVC)-1	6	0.31
Modified rigid polyvinylchloride (M-PVC)-2	5	0.64
Modified rigid polyvinylchloride (M-PVC)-3	4	0.15
Modified rigid polyvinylchloride (M-PVC)-4	3	0.16
Modified rigid polyvinylchloride (M-PVC)-5	3	0.29
Modified rigid polyvinylchloride (M-PVC)-6	2	0.11
Modified rigid polyvinylchloride (M-PVC)-7	2	0.04
Modified rigid polyvinylchloride (M-PVC)-8	2	0.06
Modified rigid polyvinylchloride (M-PVC)-9	1	0.03
Chlorinated rigid polyvinylchloride (CPVC, Corzan)	3	0.13
Highly halogenated specialty polymeric materials		
Unmodified polyvinylidenefluoride (U-PVDF Kynar)-1	5	0.14
Unmodified polyvinylidenefluoride (U-PVDF)-2	4	0.08
Unmodified ethylenechlorotrifluoroethylene (U-ECTFE, Halar)	4	0.15
Unmodified ethylenetetrafluoroethylene (U-ETFE, Tefzel)	7	0.17
Unmodified perfluoroalkoxy (U-PFA, Teflon)	2	0.01
Unmodified fluorinated ethylene-propylene (U-FEP, Teflon)	3	0.01
High-temperature specialty polymeric materials		
Phenol formaldehyde	5	0.06
Polyetheretherketone (PEEK)	4	0.03
Melamine	7	0.24
Unmodified polycarbonate (U-PC)	14	4.2
Modified polycarbonate (M-PC)-1	10	4.2
Modified polycarbonate (M-PC)-2	7	4.0
Unmodified polysulfone (U-POS)	18	1.49
Modified polysulfone (M-POS)-1	11	1.4
Modified polysulfone (M-POS)-2	11	0.32
Modified polysulfone (M-POS)-3	7	1.2
Modified polysulfone (M-POS)-4	7	0.25
Modified polyetherimide (M-PEI)-1	6	0.24
Modified polyetherimide (M-PEI)-2	6	0.04
Modified polyetherimide (M-PEI)-3	5	0.46
Unmodified polyphenyleneoxide (U-PPO)	9	1.6
Glass fiber–reinforced ordinary polyesters		
Glass fiber–reinforced fire-retarded polyester (FR-PES)-1	21	5.4
Glass fiber–reinforced fire-retarded polyester (FR-PES)-1	16	7.4
Glass fiber–reinforced fire-retarded polyester (FR-PES)-1	14	4.0
Glass fiber–reinforced modified polyester (M-PES)-1	11	5.5
Glass fiber–reinforced modified polyester (M-PES)-1	10	5.2
Glass fiber–reinforced modified polyester (M-PES)-1	9	3.1
Composites		
Fire-retarded polyester (30%)/glass fibers (70%)-1	13	0.91
Fire-retarded polyester (30%)/glass fibers (70%)-2	10	0.68
Unmodified phenolic (16%)/Kevlar fibers (84%)	8	0.33
Modified phenolic (20%)/glass fibers (80%)	3	0.07
Fire-retarded epoxy (35%)/glass fibers (65%)-1	11	2.1
Fire-retarded epoxy (35%)/glass fibers (65%)-2	10	0.94
Fire-retarded epoxy (35%)/glass fibers (65%)-3	9	1.2
Modified epoxy (24%)/glass fibers (76%)-1	5	0.61
Modified epoxy (29%)/graphite fibers (71%)	5	0.54
Modified epoxy and phenolic (18%)/glass fibers (82%)	2	0.18
Modified polyphenylenesulfide (16%)/glass fibers (84%)	3	0.29
Modified cyanate (27%)/graphite fibers (73%)	4	0.41

[a]Data taken from References 4, 10, and 25 to 29.

$(g/g)(m/s^{1/2})/(kW/m)^{2/3}$] for acceptance as clean room materials. These polymeric materials have high thermal stability with reduced release of carbon, hydrogen, and halogen atoms, as can be noted from their decomposition temperatures listed in Table 3-4.6, where data are taken from Reference 30.

Ordinary thermoplastics (such as PE, PP, and PVC) can also be modified such that they behave similarly to the specialty polymeric materials and have low FPI and SDI values to satisfy the 4910 Test Protocol criteria for acceptance as clean room materials.

Composites and fiberglass-reinforced materials. The use of composites and fiberglass-reinforced materials is increasing very rapidly because of low weight and high strength in applications such as aircraft, submarines, naval ships, military tanks, public transportation vehicles including automobiles, space vehicles, tote boxes, pallets, chutes, and so forth. Fire propagation, however, is one of the major concerns for the composites and fiberglass-reinforced materials; the FPI concept thus is used.[4,10] For the determination of the FPI for the composites and fiberglass-reinforced materials, the TRP and upward fire propagation tests are performed and Equation 9 is used, as discussed previously for electrical cables and conveyor belts.

The FPI concept used for the composites and fiberglass-reinforced materials is based on the knowledge gained during the development of the FMRC standard for cable fire propagation Class No. 3972[14] and FMRC studies on conveyor belts.[12,23] The nonpropagating fire condition is satisfied in the ASTM E2058 fire propagation apparatus for FPI ≤ 6.0, for about 600-mm-long and 100-mm-wide vertical composites and fiberglass-reinforced materials, under highly flame-radiating conditions (oxygen mass fraction = 0.40), very similar to the conveyor belts.

Table 3-4.5 lists FPI values for selected composites and fiberglass-reinforced materials taken from References 4 and 10.

Table 3-4.6 *Decomposition Temperature, Char Yield, and Limiting Oxygen Index for Polymeric Materials*[a]

Polymeric Material	Decomposition Temperature (°C)	Char Yield (%)	Limiting Oxygen Index (%)
Polybenzobisoxazole (PBO)	789	75	56
Polyparaphenylene	652	75	55
Polybenzimidazole (PBI)	630	70	42
Polyamideimide (PAI)	628	55	45
Polyaramide (kevlar)	628	43	28
Polyetherketoneketone (PEKK)	619	62	40
Polyetherketone (PEK)	614	56	40
Polytetrafluoroethylene (PTFE)	612	0	95
Polyetheretherketone (PEEK)	606	50	35
Polyphenylsulfone (PPSF)	606	44	38
Polypara(benzoyl)phenylene (PX)	602	66	41
Fluorinated cyanate ester	583	44	40
Polyphenylenesulfide (PPS)	578	45	44
Polyetherimide (PEI)	575	52	47
Polypromellitimide (PI)	567	70	37
Polycarbonate (PC)	546	25	26
Polysulfone (PSF)	537	30	30
Polyethylene (PE)	505	0	18
Polyamide 6 (PA6)-nylon	497	1	21
Polyethyleneterephthalate (PET)	474	13	21
Acrylonitrile-butadiene-styrene (ABS)	470	0	18
Polyurethane elastomer (PU)	422	3	17
Polymethylmethacrylate (PMMA)	398	2	17
Polychlorotrifluoroethylene	380	0	95
Polyvinylchloride (PVC)	370	11	50
Polystyrene (PS)	364	0	18
Polyoxymethylene (POM)	361	0	15
Polyvinylidenefluoride (PVDF)	355	0	44

[a]Data are taken from Reference 30.

Interior finish wall/ceiling materials. Since 1971, Factory Mutual Research Corporation has used the 25-ft corner test as a standard test. The 25-ft corner test is performed in a 7.6-m (25-ft)-high, 15.2-m (50-ft)-long and 11.6-m (38-ft)-wide building corner configuration to evaluate the burning characteristics of interior finish wall and ceiling materials.[31–34] The materials tested are typically panels with a metal skin over an insulation core material. The materials installed in the corner configuration are subjected to a growing exposure fire (peak heat release rate of about 3 MW) comprised of about 340 kg (750 lb) of 1.2-m (4-ft) × 1.2-m (4-ft) wood (oak) pallets stacked 1.5 m (5 ft) high at the base of the corner. The material is considered to have failed the test if within 15 min either (1) fire propagation on the wall or ceiling extends to the limits of the structure, or (2) flame extends outside the limits of the structure through the ceiling smoke layer.

The fire environment within the 25-ft corner test structure has been characterized through heat flux and temperature measurements.[31,33] It has been shown that the fire propagation boundary (pyrolysis front) measured by visual damage is very close to the critical heat flux (CHF) boundary for the material, as shown in Figure 3-4.17, taken from Reference 32. This relationship is in agreement with the general understanding of the fire propagation process. Through small- and large-scale fire propagation tests for low-density, highly char-forming wall and ceiling insulation materials, using the ASTM E2058 fire propagation apparatus [Figure 3-4.2(a)], fire products collector (Figure 3-4.8), and 25-ft corner test (Figure 3-4.17), a semi-empirical relationship has been developed for fire propagation rate for a 15-min test in the 25-ft corner test[31–33]

$$\frac{X_p}{X_t} = \frac{\dot{Q}''_{con}}{\text{TRP}} \tag{10}$$

where

X_p = average fire propagation length along the eaves (Figure 3-4.17) of the 25-ft corner test (pyrolysis front) measured visually (m)

X_t = total available length [11.6-m (38 ft)] in the 25-ft corner test

$\dot{Q}''_{con}$ = convective heat release rate (kW/m^2)

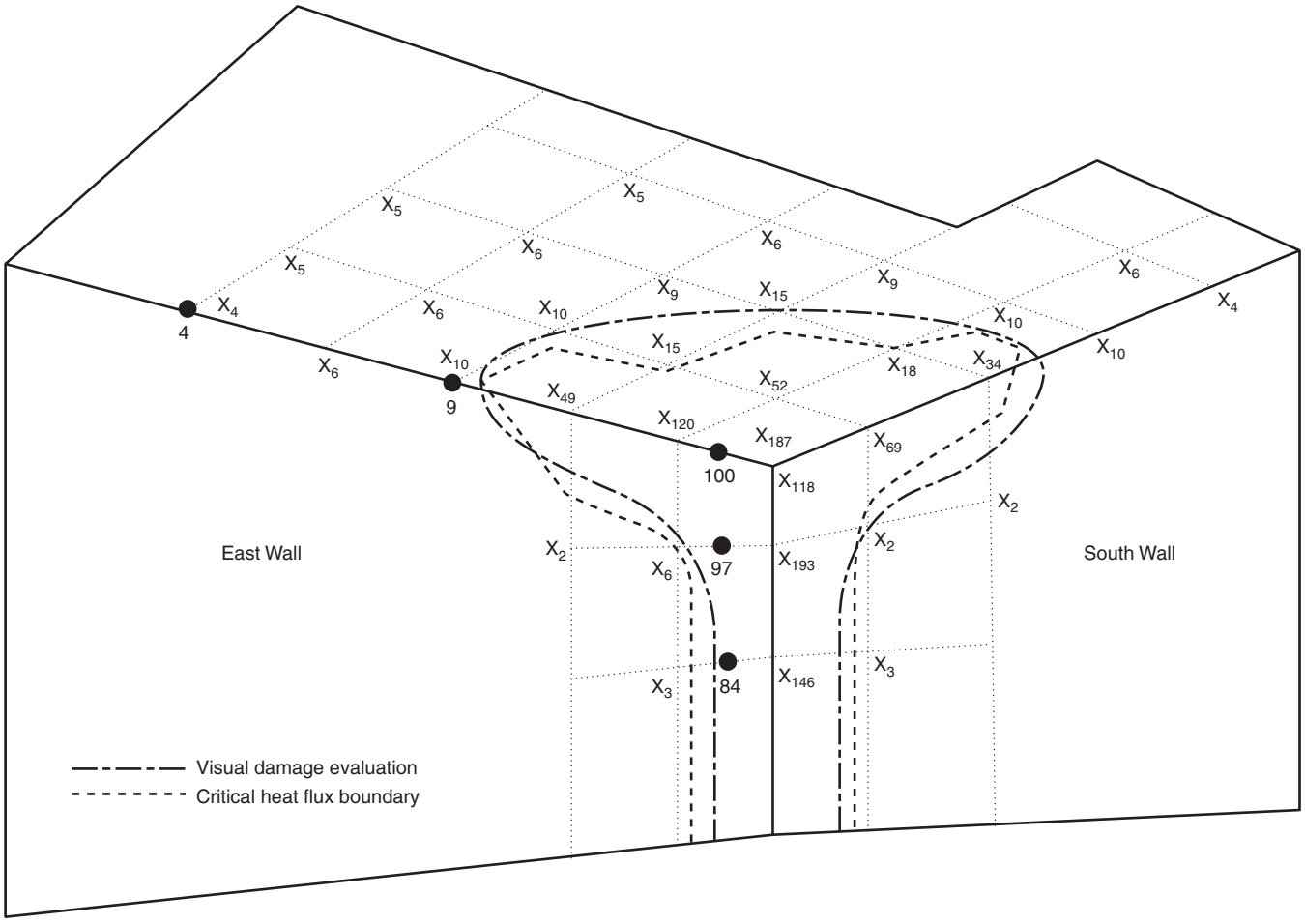

Figure 3-4.17. ***Critical heat flux boundary and visual observations for the extent of fire propagation in the FMRC 25-ft corner test for a product that passes the tests.[32]***

The right-hand side of Equation 10 with the convective heat release rate measured at 50 kW/m² of external heat flux is defined as the convective flame spread parameter (FSP_c).[32,33] Figure 3-4.18 shows a correlation between the convective flame spread parameter obtained from the ASTM E2058 fire propagation apparatus and the normalized fire propagation length in the FMRC 25-ft corner test. Pass/fail regions, as determined from the 25-ft corner test, are indicated in the figure. Materials for which $FSP_c \leq 0.39$ pass the 25-ft corner test, and materials for which $FSP_c \geq 0.47$ are judged to be unacceptable (i.e., fail).[32–34] The region where the FSP_c values are greater than 0.39 but less than 0.47 is uncertain.[32–34]

The correlation and pass/fail criterion shown in Figure 3-4.18 have been adopted in the FMRC Class No. 4880 for insulated wall or wall and ceiling panels.[34] In this standard, the 25-ft corner test has been replaced by the ASTM E2058 fire propagation apparatus [Figure 3-4.2(a)] tests. Two sets of tests are performed in the apparatus:[32–34]

1. *Thermal response parameter test.* Ignition tests are performed using approximately 100-mm × 100-mm and up to 100-mm-thick samples. Times to ignition at various external heat flux values are measured to determine the TRP as described earlier.
2. *Convective heat release rate test.* Combustion tests are performed using about 100-mm × 100-mm and up to 100-mm-thick samples. Samples are burned in normal air under an external heat flux exposure of 50 kW/m². During the test, measurement is made for the convective heat release as a function of time.

The data for the TRP and convective heat release rate at 50 kW/m² of external heat flux are used to calculate the flame spread parameter (FSP_c) that accepts or rejects the sample.

Flaming and Nonflaming Fires

During fire propagation, the surface of the material regresses in a transient fashion with a rate slower than the fire propagation rate.[2] The surface regression becomes steady after fire propagates throughout the available surfaces. The surface regression continues until all the combustible components of the material are exhausted. During fire propagation and surface regression, the material generates

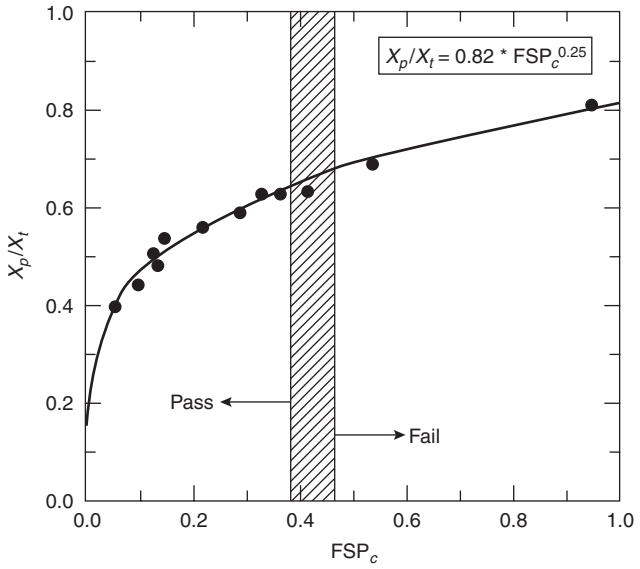

Figure 3-4.18. ***Normalized fire propagation length measured in the 25-ft corner test versus the convective flame spread parameter obtained from the ASTM E2058 fire propagation apparatus. (Figure is taken from References 32 and 33.)***

vapors at a transient or steady rate. The generation rate of the material vapors is measured by the mass loss rate. In the presence of a flame and/or external heat flux, the mass loss rate, under steady state, is expressed as[2,4,16]

$$\dot{m}'' = \frac{(\dot{q}''_e + \dot{q}''_{fr} + \dot{q}''_{fc} - \dot{q}''_{rr})}{\Delta H_g} \qquad (11)$$

where

$\dot{m}''$ = mass loss rate (g/m²·s)

$\dot{q}''_{fr}$ = flame radiative heat flux transferred to the surface (kW/m²)

$\dot{q}''_{fc}$ = flame convective heat flux transferred to the surface (kW/m²)

$\dot{q}''_{rr}$ = surface re-radiation loss (kW/m²)

ΔH_g = heat of gasification (kJ/g)

total flame heat flux to the surface $\dot{q}''_f = \dot{q}''_{fr} + \dot{q}''_{fc}$

According to Equation 11, the generation rate of material vapors is governed by the external and flame heat flux, surface re-radiation loss, and the heat of gasification.

Heat of gasification: The heat of gasification for a melting material is expressed as[35]

$$\Delta H_g = \int_{T_a}^{T_m} c_{p,s}\, dT + \Delta H_m + \int_{T_m}^{T_v} c_{p,l}\, dT + \Delta H_v \qquad (12)$$

where

ΔH_g = heat of gasification (kJ/g)

$c_{p,s}$ = specific heat of solid in kJ/g·K

$c_{p,l}$ = specific heat of molten solid in kJ/g·K

ΔH_m = heat of melting vaporization at melting temperature in kJ/g

ΔH_v = heat of vaporization at vaporization temperature in kJ/g

T_a = ambient temperature

T_m = melting temperature

T_v = vaporization temperature in K

For materials that do not melt, but sublime, decompose, or char, Equation 12 is modified accordingly. The heat of gasification can be determined from (1) the parameters on the right-hand side of Equation 12, which can be quantified by the thermal analysis techniques or calculated from the properties listed in the literature; and (2) nonflaming tests using apparatuses, such as the OSU heat release rate apparatus, the ASTM E2058 fire propagation apparatus, or the cone calorimeter. The following are some examples of the techniques:

1. *Heats of gasification of polymers from the differential scanning calorimetry.* The $c_{p,s}$, $c_{p,l}$, ΔH_m, and ΔH_v values for polymers have been quantified in the FMRC laboratory.[35] The techniques involve measurement of the specific heat as a function of temperature, such as shown in Figure 3-4.19 for polymethylmethacrylate, measured in the FMRC Flammability Laboratory. The specific heat increases with temperature; a value close to the vaporization temperature of PMMA is used in Equation 12. Further measurements are made of the heats of melting and vaporization. Some examples of the data measured in our laboratory are listed in Table 3-4.7.
2. *Heat of gasification from the literature data for the heats of gasification for various molecular weight hydrocarbons (alkanes).* The *CRC Handbook of Chemistry and Physics*[36] listing for the heats of gasification for liquid and solid

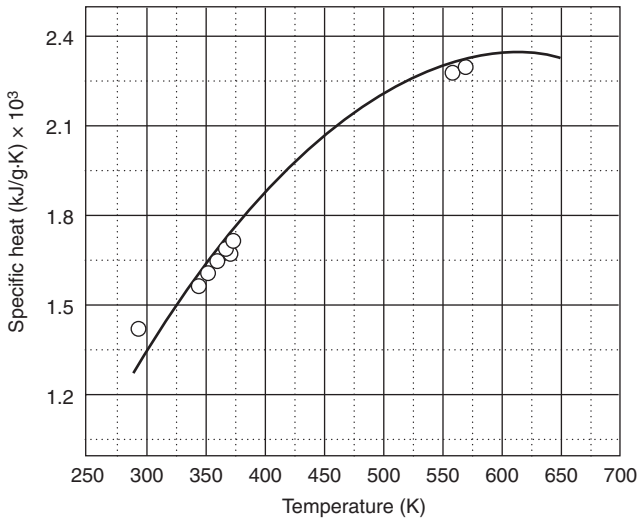

Figure 3-4.19. ***Specific heat of polymethylmethacrylate versus temperature measured by a differential scanning calorimeter at the flammability laboratory of the Factory Mutual Research Corporation.***

Table 3-4.7 *Surface Re-Radiation and Heats of Gasification of Various Materials*

Materials	Surface Re-radiation (kW/m^2)	Heat of Gasification (kJ/g)			
		Flam. App.[a]	Cone[b]	DSC[c]	Cal[d]
Distilled water	0.63	2.58	—	2.59	2.58
Hydrocarbons (alkanes)					
Hexane	0.50	—	—	—	0.50
Heptane	0.63	—	—	—	0.55
Octane	0.98	—	—	—	0.60
Nonane	1.4	—	—	—	0.64
Decane	1.8	—	—	—	0.69
Undecane	2.3	—	—	—	0.73
Dodecane	2.8	—	—	—	0.77
Tridecane	3.0	—	—	—	0.81
Tetradecane	3.0	—	—	—	0.85
Hexadexane	3.0	—	—	—	0.92
Natural materials					
Filter paper	10	3.6	—	—	—
Corrugated paper	10	2.2	—	—	—
Wood (Douglas fir)	10	1.8	—	—	—
Plywood/FR	10	1.0	—	—	—
Particleboard	—	—	3.9	—	—
Synthetic materials					
Epoxy resin	—	—	2.4	—	—
Polypropylene	15	2.0	1.4	2.0	—
Polyethylene (PE) (low density)	15	1.8	—	1.9	—
PE (high density)	15	2.3	1.9	2.2	—
PE foams	12	1.4–1.7	—	—	—
PE/25% chlorine (CI)	12	2.1	—	—	—
PE/36% CI	12	3.0	—	—	—
PE/48% CI	10	3.1	—	—	—
Rigid polyvinylchloride (PVC)	15	2.5	2.3	—	—
PVC/plasticizer	10	1.7	—	—	—
Plasticized PVC, LOI = 0.20	10	2.5	2.4	—	—
Plasticized PVC, LOI = 0.25	—	—	—	—	—
Plasticized PVC, LOI = 0.30	—	—	2.1	—	—
Plasticized PVC, LOI = 0.35	—	—	2.4	—	—
Rigid PVC, LOI = 0.50	—	—	2.3	—	—
Polyisoprene	10	2.0	—	—	—
PVC panel	17	3.1	—	—	—
Nylon 6/6	15	2.4	—	—	—
Polyoxymethylene (Delrin)	13	2.4	—	2.4	—
Polymethylmethacrylate (Plexiglas)	11	1.6	1.4	1.6	—
Polycarbonate	11	2.1	—	—	—
Polycarbonate panel	16	2.3	—	—	—
Isophthalic polyester	—	—	3.4	—	—
Polyvinyl ester	—	—	1.7	—	—
Acrylonitrile-butadiene-styrene (ABS)	10	3.2	2.6	—	—
Styrene-butadiene	10	2.7	—	—	—
Polystyrene (PS) foams	10–13	1.3–1.9	—	—	—
PS (granular)	13	1.7	2.2	1.8	—
Polyurethane (PU) foams					
Flexible polyurethane (PU) foams	16–19	1.2–2.7	2.4	1.4	—
Rigid polyurethane (PU) foams	14–22	1.2–5.3	5.6	—	—
Polyisocyanurate foams	14–37	1.2–6.4	—	—	—
Phenolic foam	20	1.6	—	—	—
Phenolic foam/FR	20	3.7	—	—	—
Ethylenetetrafluoroethylene (Tefzel)	27	0.9	—	—	—
Fluorinated ethylene propylene, FEP (Teflon)	38	2.4	—	—	—
Tetrafluoroethylene, TFE (Teflon)	48	0.8–1.8	—	—	—
Perfluoroalkoxy, PFA (Teflon)	37	1.0	—	—	—
Composite and fiberglass-reinforced materials					
Polyether ether ketone—30% fiberglass	—	—	7.9	—	—
Polyethersulfone—30% fiberglass	—	1.8	—	—	—
Polyester 1—fiberglass	—	—	2.5	—	—
Polyester 2—fiberglass	10	1.4	—	—	—
Polyester 3—fiberglass	10	6.4	—	—	—
Polyester 4—fiberglass	15	5.1	—	—	—
Polyester 5—fiberglass	10	2.9	—	—	—
Phenolic fiberglass (thick sheet)	20	7.3	—	—	—
Phenolic Kevlar (thick sheet)	15	7.8	—	—	—

[a]From the ASTM E2058 fire propagation apparatus under nonflaming fire conditions.

[b]Calculated from the cone calorimeter data reported in References 20 and 41 for the mass loss rate at various external heat flux values in flaming fires.

[c]From the flammability laboratory using the differential scanning calorimetry.

[d]Calculated from the data reported in the *CRC Handbook*.[36]

hydrocarbons (alkanes) satisfies the following relationship in the molecular weight range of 30 to 250 g/mol:

$$\Delta H_g = -3.72 \times 10^{-6} M^2 + 0.0042M + 0.164 \quad (13)$$

where M is the molecular weight of the hydrocarbon (g/mol).

The heats of gasification calculated from Equation 13 for various alkanes are listed in Table 3-4.7.

3. *Heat of gasification from the literature data for the specific heats and heats of vaporization.* Water will be used as an example. The specific heat of liquid water, $c_{p,l}$ is 0.0042 kJ/g-K,[37] and the heat of vaporization of water at 373 K is 2.26 kJ/g.[37] Assuming the ambient temperature to be 298 K and the vaporization temperature to be 373 K, the heat of gasification of water from Equation 12 is calculated as follows:

$$\int_{298}^{373} c_{p,l}\, dT = 0.0042(373 - 298) = 0.32 \text{ kJ/g}$$

$$\Delta H_{v,373} = 2.26 \text{ kJ/g}$$

$$\Delta H_g = 0.32 + 2.26 = 2.58 \text{ kJ/g}$$

From the differential scanning calorimetry, the heat of gasification of water determined in the FMRC Flammability Laboratory is 2.59 kJ/g, which is in excellent agreement with the calculated value. These two values for the heat of gasification of water are listed in Table 3-4.7.

4. *Heat of gasification from the nonflaming tests using the ASTM E2058 fire propagation apparatus.* The measurement for the heat of gasification from the nonflaming fire tests in the ASTM E2058 fire propagation apparatus was introduced in 1976.[35] In nonflaming fires, $\dot{q}''_f = 0$, and Equation 11 becomes

$$\dot{m}'' = \frac{\dot{q}''_e - \dot{q}''_{rr}}{\Delta H_g} \quad (14)$$

where mass loss rate is a linear function of the external heat flux, and the heat of gasification is the inverse of the slope of the straight line. This equation provides a convenient method to determine the heat of gasification in the nonflaming tests, where mass loss rate of the sample is measured at various external heat flux values. The heat of gasification is determined from the linear regression analysis of the average steady-state mass loss rate as a function of the external heat flux. In the ASTM E2058 fire propagation apparatus tests, approximately 100- × 100-mm square and up to 100-mm-thick samples are used with co-flowing nitrogen or air with an oxygen mass fraction of about 0.10.

Figure 3-4.20 shows a plot of the vaporization rate of water in a 0.0072 m² Pyrex glass dish against time at 50 kW/m² of external heat flux, measured in the ASTM E2058 fire propagation apparatus. The figure also includes the predicted mass loss rate using Equation 14, where

$$\dot{q}''_{rr} = \varepsilon\sigma(T_v^4 - T_a^4) \quad (15)$$

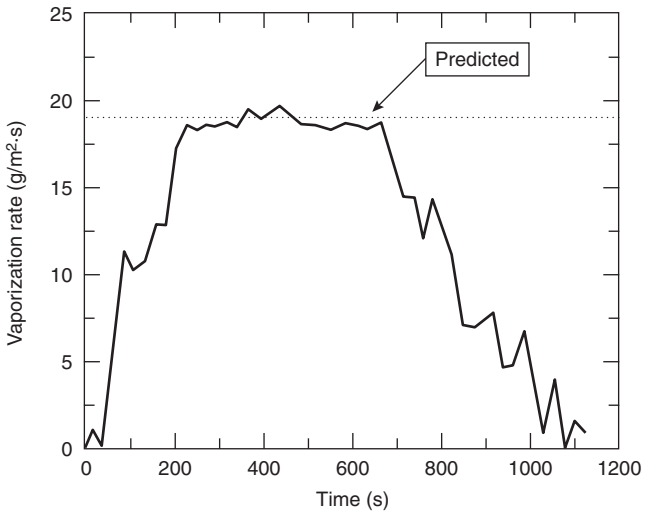

Figure 3-4.20. ***Vaporization rate of water versus time measured in the ASTM E2058 fire propagation apparatus using 99.69 g of water in a Pyrex dish with an area of 0.0072 m². Water was exposed to an external heat flux of 50 kW/m².***

where ε is the emissivity of water (0.95 to 0.963 in the temperature range 298 to 373 K),[38] and σ is the Stefan-Boltzmann constant (56.7 × 10⁻¹² kW/m²-deg⁴). For water, $T_v = 373$ K and $T_a = 298$ K, and thus $\dot{q}''_{rr} = 1$ kW/m². From Equation 14, using $\dot{q}''_e = 50$ kW/m², $\dot{q}''_{rr} = 1$ kW/m², and $\Delta H_g = 2.57$ kJ/g, $\dot{m}'' = 19.0$ g/m²·s. There is excellent agreement between the measured and predicted values at the steady state in Figure 3-4.20. Water vaporization tests and calculations are routinely used for the calibration of the ASTM E2058 fire propagation apparatus.

Heats of gasification determined from the mass loss rate as a function of external heat flux in nonflaming fire conditions in the ASTM E2058 fire propagation apparatus are listed in Table 3-4.7 for selected materials. Excellent agreement can be noted between the heats of gasification determined from the ASTM E2058 fire propagation apparatus and those obtained from the differential scanning calorimetry.

Heat of gasification can also be determined from the flaming fires if high external heat flux values are used such that $\dot{q}''_e \gg \dot{q}''_{fr} + \dot{q}''_{fc} - \dot{q}''_{rr}$ in Equation 11. This method has been used to calculate the heat of gasification from the cone calorimeter data for the mass loss rate in flaming fires reported in the literature.[20,39] The values calculated from the cone calorimeter data are also listed in Table 3-4.7 and show a general agreement with the values from the ASTM E2058 fire propagation apparatus.

EXAMPLE 6:

Estimate the ignition temperature of a material with a CHF of 11 kW/m². Assume its surface emissivity to be unity, ambient temperature to be 20°C, and vaporization temperature to be approximately equal to the ignition temperature.

SOLUTION:

From Equation 15,

$$11(\text{kW/m}^2) = 56.7 \times 10^{-12}(\text{kW/m}^2\cdot\text{deg}^4)(T_v^4)(\text{deg})^4 - 56.7 \times 10^{-12}(\text{kW/m}^2\cdot\text{deg}^4) \times (298)^4(\text{deg})^4$$

$$T_v \cong \left[\frac{11 \times 10^{12}}{56.7} + (298)^4\right]^{1/4} \cong (1940 \times 10^8 + 78.9 \times 10^8)^{1/4} \cong 670 \text{ K}$$

By assumption, vaporization temperature is equal to the ignition temperature, which is 670 K (397°C).

EXAMPLE 7:

A material with a surface re-radiation loss of 10 kW/m^2 and heat of gasification of 1.8 kJ/g was found to be involved in a fire with an exposed area of 2 m^2. The combined flame and external heat flux exposure to the material was estimated to be 70 kW/m^2. Estimate the peak mass loss rate at which the material may have been burning in the fire in terms of g/m^2·s and g/s.

SOLUTION:

From Equation 11,

$$\dot{m}'' = \frac{70 - 10}{1.8} = 33 \text{ g/m}^2\cdot\text{s}$$

The estimated peak mass loss rate that the material may have been burning in the fire is 33 g/m^2·s, or $33 \times 2 = 67$ g/s.

Flame heat flux: For flaming fires, in the absence of external heat flux, from Equation 11

$$\dot{m}'' = \frac{(\dot{q}''_{fr} + \dot{q}''_{fc} - \dot{q}''_{rr})}{\Delta H_g} \tag{16}$$

The results from numerous small- and large-scale fire tests show that, as the surface area of the material increases, the flame radiative heat flux increases and reaches an asymptotic limit, whereas the flame convective heat flux decreases and becomes much smaller than the flame radiative heat flux at the asymptotic limit in large-scale fires.[40] It is also known that, in small-scale fires of fixed size with buoyant turbulent diffusion flames, as the oxygen mass fraction is increased, the flame radiative heat flux increases and reaches an asymptotic limit comparable to the asymptotic limit in large-scale fires, whereas the flame convective heat flux decreases and becomes much smaller than the flame radiative heat flux.[41]

The effect of the mass fraction of oxygen on the flame radiative and convective heat fluxes in small-scale fires is shown in Figure 3-4.21 for 100- × 100-mm square × 25-mm-thick slabs of polypropylene. The data were measured in the ASTM E2058 fire propagation apparatus.[41] The increase in the flame radiative heat flux with increase in the mass fraction of oxygen is due to the increase in the flame temperature and soot formation and decrease in the residence time in the flame.[41] The oxygen mass fraction

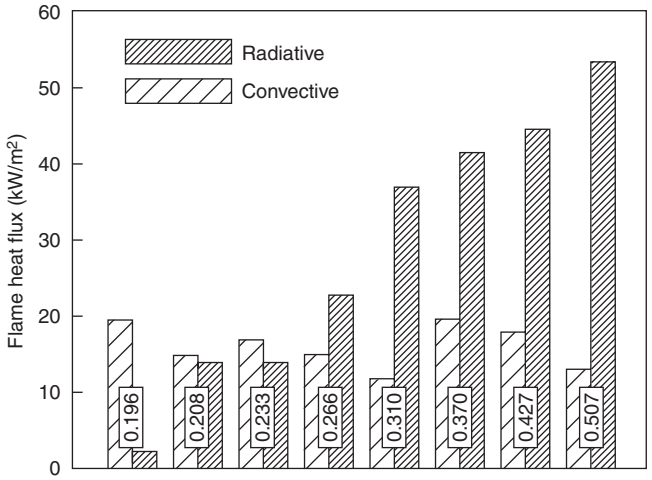

Figure 3-4.21. ***Flame radiative and convective heat fluxes at various oxygen mass fractions for the steady-state combustion of 100- × 100-mm square × 25-mm-thick slabs of polypropylene in the ASTM E2058 fire propagation apparatus under co-airflow velocity of 0.09 m/s. Data taken from Reference 41. Mass fractions of oxygen are indicated by the numbers inside the frames.***

variation technique to simulate large-scale flame-radiative heat flux conditions in small-scale fires is defined as the *flame radiation scaling technique.*[4]

In the flame radiation scaling technique, the flame radiative and convective heat fluxes are determined from (1) the measurements for the mass loss rate at various oxygen mass fractions in the range of 0.12 (close to flame extinction) to about 0.60, under co-airflow conditions; (2) the convective heat transfer coefficient for the ASTM E2058 fire propagation apparatus, derived from the combustion of methanol; (3) the mass transfer number; and (4) Equation 16. In the ASTM E2058 fire propagation apparatus, the asymptotic limit is reached for the oxygen mass fraction ≥ 0.30. At the asymptotic limit, Equation 16 can be expressed as

$$\dot{m}''_{\text{asy}} = \frac{\dot{q}''_{f,\text{asy}} - \dot{q}''_{rr}}{\Delta H_g} \tag{17}$$

where subscript asy represents the asymptotic limit. The asymptotic values for the mass loss rate and flame heat flux determined from the flame radiation scaling technique in the ASTM E2058 fire propagation apparatus are listed in Table 3-4.8. The measured asymptotic values of the mass loss rate reported in the literature and flame heat flux in large-scale fires are also listed in Table 3-4.8. Flame heat flux values for the large-scale fires are derived from the asymptotic values of the mass loss rate and known values of surface re-radiation losses and heats of gasification.

The data in Table 3-4.8 show that the asymptotic flame heat flux values, determined in the ASTM E2058 fire propagation apparatus, using the flame radiation scaling technique, are in good agreement with the values

Table 3-4.8 ***Asymptotic Values of Mass Loss Rate and Flame Heat Flux[a]***

	$\dot{m}''$ (g/m²·s)		$\dot{q}_f''$(kW/m²)	
Material	S*	L[b]	S*	L[b]
Aliphatic carbon-hydrogen atoms[c]				
Polyethylene	26	—	61	—
Polypropylene	24	—	67	—
Heavy fuel oil (2.6–23 m)	—	36	—	29
Kerosene (30–80 m)	—	65	—	29
Crude oil (6.5–31 m)	—	56	—	44
n-Dodecane (0.94 m)	—	36	—	30
Gasoline (1.5–223 m)	—	62	—	30
JP-4 (1.0–5.3 m)	—	67	—	40
JP-5 (0.60–17 m)	—	55	—	39
n-Heptane (1.2–10m)	~66	75	32	37
n-Hexane (0.75–10 m)	—	77	—	37
Transformer fluids (2.37 m)	27–30	25–29	23–25	22–25
Aromatic carbon-hydrogen atoms[c]				
Polystyrene (0.93 m)	36	34	75	71
Xylene (1.22 m)	—	67	—	37
Benzene (0.75–6.0 m)	—	81	—	44
Aliphatic carbon-hydrogen-oxygen atoms[c]				
Polyoxymethylene 16	—	50	—	
Polymethylmethacrylate (2.37 m)	28	30	57	60
Methanol (1.2–2.4 m)	20	25	22	27
Acetone (1.52 m)	—	38	—	24
Aliphatic carbon-hydrogen-oxygen-nitrogen atoms				
Flexible polyurethane foams	21–27	—	64–76	—
Rigid polyurethane foams	22–25	—	49–53	—
Aliphatic carbon-hydrogen-halogen atoms				
Polyvinylchloride	16	—	50	—
Tefzel (ETFE)	14	—	50	—
Teflon (FEP)	7	—	52	—

Mass loss rates are from the data reported in the literature.

[a]Small-scale fires, pool diameter fixed at 0.10 m, flame radiation scaling technique was used in the ASTM E2058 fire propagation apparatus, $Y_O \geq 0.30$.

[b]Large-scale fires in normal air.

[c]Numbers in m in parentheses are the pool diameters used in large-scale fires.

measured in the large-scale fires. The asymptotic flame heat flux values vary from 22 to 77 kW/m², dependent primarily on the mode of decomposition and gasification rather than on the chemical structures of the materials. For example, for the liquids, which vaporize primarily as monomers or as very low molecular weight oligomer, the asymptotic flame heat flux values are in the range of 22 to 44 kW/m², irrespective of their chemical structures. For polymers, which vaporize as high molecular weight oligomer, the asymptotic flame heat flux values increase substantially to the range of 49 to 71 kW/m², irrespective of their chemical structures. The independence of the asymptotic flame heat values from the chemical structures of materials is consistent with the dependence of flame radiation on optical thickness, soot concentration, and flame temperature in large-scale fires.

EXAMPLE 8:

Calculate the peak mass loss rate for polypropylene in large-scale fires, burning in the open, with no external heat sources in the surroundings.

SOLUTION:

In the calculation Equation 16 will be used. From Table 3-4.7, $\dot{q}''_{rr} = 15$ kW/m² and $\Delta H_g = 2.0$ kJ/g, and from Table 3-4.8, $\dot{q}''_{f,\text{asy}} = 67$ kW/m². Using these values in Equation 16,

$$\dot{m}'' = \frac{67 - 15}{2.0} = 26.0 \text{ g/m}^2\cdot\text{s}$$

EXAMPLE 9:

Calculate the peak mass loss rate for polypropylene in large-scale fires burning in the open in the presence of a burning object, which provides 20 kW/m² of heat flux to the polypropylene surface, in addition to its own flame heat flux of 67 kW/m².

SOLUTION:

In the calculation, Equation 11 will be used with $\dot{q}''_e = 20$ kW/m². From Table 3-4.7, $\dot{q}''_{rr} = 15$ kW/m² and $\Delta H_g = 2.0$ kJ/g and from Table 3-4.8, $\dot{q}''_{f,\text{asy}} = 67$ kW/m². Using these values in Equation 11,

$$\dot{m}'' = \frac{67 + 20 - 15}{2.0} = 36.0 \text{ g/m}^2\cdot\text{s}$$

Heat Release Rate

The determination of heat release rate in fires has been influenced by the principles and techniques used for the controlled combustion in the heating and power industries. Heat in the flowing combustion products (convective heat) and thermal radiation are used to generate steam, heat a furnace or space, produce mechanical power in internal combustion engines or gas turbines, and so forth. Heat is generated by injecting fuel (gas, liquid, or solid) into a hot environment, where it undergoes evaporation, gasification, and thermal decomposition or pyrolysis. Fuel vapors react chemically with oxygen and produce heat and products, such as carbon monoxide (CO), carbon dioxide (CO_2), hydrocarbons, water (H_2O), and soot. Theoretical air requirement for complete combustion is estimated from an empirical guide, which suggests that, for every 10.6 kJ of heat in the fuel burned, 3.4 g of air are required for complete combustion.[42] Equivalently, the heat of combustion per unit mass of oxygen consumed (ΔH_0^*) is 13.4 kJ/g. Using $\Delta H_0^* \approx 13.4$ kJ/g to determine the heat release rate in fires from the mass consumption rate of oxygen is discussed in References 16 and 43. This technique is defined as the *oxygen consumption* (OC) *calorimetry.*

A combustion process is characterized by its *combustion efficiency,* defined as the fraction of heat of complete combustion released in the chemical reactions, which is the ratio of the chemical heat release rate to the heat release rate for complete combustion or the ratio of the chemical heat of combustion to net heat of complete com-

bustion. The calorific energy generated in chemical reactions leading to complete combustion per unit mass of fuel, water produced being in the vapor state, is defined as the *net heat of complete combustion.* The calorific energy generated in chemical reactions leading to varying degrees of incomplete combustion per unit mass of the fuel consumed is defined as the *chemical heat of combustion.* In the heating and power industries, combustion efficiency is determined routinely from the waste products (flue gas) analysis, especially for CO, CO_2, and O_2, and from the measurements of temperature in the combustion products-air mixture and thermal radiation. For higher combustion efficiency, *mass fuel-to-air ratio* relative to the *stoichiometric mass fuel-to-air ratio* or the *equivalence ratio* is controlled by maintaining desired primary and secondary airflow.

The net heat of complete combustion is measured in the oxygen bomb calorimeter and is calculated from the standard heats of formation of the materials, CO_2 and H_2O (the standard heat of formation of O_2 in its standard state being zero). For example, for polymethylmethacrylate (PMMA) and polystyrene (PS), the net heats of complete combustion measured in the oxygen bomb calorimeter by the FMRC Flammability Laboratory are 25.3 and 39.2 kJ/g, respectively; and from the standard heats of formation, they are 24.9 and 39.8 kJ/g, respectively. For soot generated from the combustion of PMMA and PS, the net heats of complete combustion measured in the oxygen bomb calorimeter by the FMRC Flammability Laboratory are 33.9 and 32.1 kJ/g, respectively, and 32.8 kJ/g from the standard heats of formation of graphite and CO_2.

In fires, complete combustion is rarely achieved and products of incomplete combustion, such as CO and smoke, are quite common. An example of incomplete combustion is given in Table 3-4.9, where chemical heat of combustion and combustion efficiency decrease as CO, carbon, and ethylene are formed at the expense of CO_2 and H_2O with reduced O_2 consumption, a typical condition found in the ventilation-controlled fires.[44] The chemical heat of combustion is the ratio of the chemical heat release rate to the mass loss rate. The upper limit of the combustion efficiency is 1.00, corresponding to complete combustion, and the lower limit is 0.46, corresponding to unstable combustion leading to flame extinction for combustion efficiency ≤ 0.40.[44,45]

Table 3-4.9 ***Chemical Heat of Combustion and Combustion Efficiency of Polymethylmethacrylate***

Reaction Stoichiometry	ΔH_{ch} (kJ/g)[a]	χ_{ch}
$C_5H_8O_2$ (g) + 6.0 O_2 (g) = 5CO_2 (g) + 4H_2O (g)	24.9	1.00
$C_5H_8O_2$ (g) + 5.5 O_2 (g) = 4CO_2 (g) + 4H_2O (g) + CO (g)	22.1	0.89
$C_5H_8O_2$ (g) + 4.5 O_2 (g) = 3CO_2 (g) + 4H_2O (g) + CO (g) + C (s)	18.2	0.73
$C_5H_8O_2$ (g) + 3.0 O_2 (g) = 2CO_2 (g) + 3H_2O (g) + CO (g) + C (s) + 0.50 C_2H_4 (g)	11.5	0.46

[a]Standard heat of formation in kJ/mol: PMMA ($C_5H_8O_2$) (g) = –442.7; O_2 (g) = 0; CO_2(g) = 393.5; H_2O (g) = –241.8; CO (g) = –110.5; C (s) = 0; and C_2H_4 (g) = +26.2, where g is the gas and s is the solid.

Chemical heat release rate: The chemical heat release rate is determined from the *carbon dioxide generation* (CDG) and *oxygen consumption* (OC) *calorimetries.*

The CDG calorimetry:[2–4,16,28,29,41,44,46] The chemical heat release rate is determined from the following relationships:

$$\dot{Q}''_{ch} = \Delta H^*_{CO_2}\dot{G}''_{CO_2} + \Delta H^*_{CO}\dot{G}''_{CO} \tag{18}$$

$$\Delta H^*_{CO_2} = \frac{\Delta H_T}{\Psi_{CO_2}} \tag{19}$$

$$\Delta H^*_{CO} = \frac{\Delta H_T - \Delta H_{CO}\Psi_{CO}}{\Psi_{CO}} \tag{20}$$

where

$\dot{Q}''_{ch}$ = chemical heat release rate (kW/m²)
$\Delta H^*_{CO_2}$ = net heat of complete combustion per unit mass of CO_2 generated (kJ/g)
ΔH^*_{CO} = net heat of complete combustion per unit mass of CO generated (kJ/g)
ΔH_T = net heat of complete combustion per unit mass of fuel consumed (kJ/g)
Ψ_{CO_2} = stoichiometric yield for the maximum conversion of fuel to CO_2 (g/g)
Ψ_{CO} = stoichiometric yield for the maximum conversion of fuel to CO (g/g)
$\dot{G}''_{CO_2}$ = generation rate of CO_2 (g/m²·s)
$\dot{G}''_{CO}$ = generation rate of CO (g/m²·s)

The values for the net heats of complete combustion per unit mass of fuel consumed and CO_2 and CO generated are listed in Tables 3-4.10 through 3-4.13. The values depend on the chemical structures of the materials. With some exceptions, the values remain approximately constant within each generic group of fuels. The average values are also listed in the tables. From the average values, $\Delta H^*_{CO_2}$ = 13.3 kJ/g ± 11 percent and ΔH^*_{CO} = 11.1 kJ/g ± 18 percent. In the CDG calorimetry, the CO correction for well-ventilated fires is very small because of the small amounts of CO generated. The variations of 11 and 18 percent in the $\Delta H^*_{CO_2}$ and ΔH^*_{CO} values, respectively, would reduce significantly if values for low molecular weight hydrocarbons with small amounts of O, N, and halogen were used in averaging.

For the determination of the chemical heat release rate, generation rates of CO_2 and CO are measured and either the actual values or the average values of the net heat of complete combustion per unit mass of CO_2 and CO generated are used. The measurements for the generation rates of CO_2 and CO are described in the subsection entitled "Generation Rates of Chemical Compounds and Fire Ventilation."

The OC calorimetry:[2–4,17–19,28,29,41,43,44,46,47] The chemical heat release rate is determined from the following relationships:

$$\dot{Q}''_{ch} = \Delta H^*_O \dot{C}''_O \tag{21}$$

$$\Delta H^*_O = \frac{\Delta H_T}{\Psi_O} \tag{22}$$

where

ΔH^*_O = net heat of complete combustion per unit mass of oxygen consumed (kJ/g)
$\dot{C}''_O$ = mass consumption rate of oxygen (g/m²·s)
Ψ_O = stoichiometric mass-oxygen-to-fuel ratio (g/g)

The values for the net heats of complete combustion per unit mass of oxygen consumed are listed in Tables 3-4.10 through 3-4.13 along with the values for the net heats of complete combustion per unit mass of fuel consumed and CO_2 and CO generated. The average values of the net heat of complete combustion per unit mass of oxygen consumed are also listed in the tables. The values depend on the chemical structures of the materials. With some exceptions, the values remain approximately constant within each generic group of fuels. From the average values, ΔH^*_O = 12.8 kJ/g ± 7 percent. The ΔH^*_O value of 12.8 kJ/g is close to 13.4 kJ/g used in the heating and power industries[42] and 13.1 kJ/g ± 5 percent reported in Reference 43. The variation of 7 percent would reduce significantly if values for low molecular weight hydrocarbons with small amounts of O, N, and halogen were used in averaging.

For the determination of the chemical heat release rate, mass consumption rate of oxygen is measured, and either the actual values or the average values of the net heats of complete combustion per unit mass of oxygen consumed are used. The measurement for the consumption rate of oxygen is described in the subsection entitled "Generation Rates of Chemical Compounds and Fire Ventilation."

Convective heat release rate: The convective heat release rate is determined from the *gas temperature rise* (GTR) *calorimetry,* where the following relationship is used:[2–7,16,41,44]

$$\dot{Q}''_{con} = \frac{\dot{W} c_P (T_g - T_a)}{A} \tag{23}$$

where

$\dot{Q}''_{con}$ = convective heat release rate (kW/m²)
c_P = specific heat of the combustion product-air mixture at the gas temperature (kJ/g·K)
T_g = gas temperature (K)
T_a = ambient temperature (K)
$\dot{W}$ = total mass flow rate of the fire product-air mixture (g/s)
A = total exposed surface area of the material (m²)

Radiative heat release rate: Chemical heat release rate consists of a convective and a radiative component. Some fraction of the chemical heat release rate may be lost as conductive heat. In systems where heat losses are negligibly small, the radiative heat release rate can be obtained from the difference between the chemical and convective heat release rates:[2–4,16,41,44]

$$\dot{Q}''_{rad} = \dot{Q}''_{ch} - \dot{Q}''_{con} \tag{24}$$

where $\dot{Q}''_{rad}$ is the radiative heat release rate (kW/m²).

Use of GTR, CDG, and OC calorimetries: In 1972 the GTR calorimetry was used for the first time by the Ohio State University (OSU) to determine the heat release rate.[5,6] The apparatus used is now known as the OSU heat release rate apparatus; it is shown in Figure 3-4.1. The OSU apparatus is an ASTM[7] and an FAA standard test apparatus.[8] In the GTR calorimetry, it is assumed that almost all the thermal radiation from the flame is transferred to the flowing fire products-air mixture, as the flames are inside an enclosed space and heat loss by conductive heat transfer is negligibly small. The OC calorimetry has now been adapted to the OSU apparatus.[51]

The CDG, OC, and GTR calorimetries were used for the first time during the mid-1970s by the Factory Mutual Research Corporation (FMRC) to determine the chemical, convective, and radiative heat release rates.[35,52–54] The apparatus used is now known as the ASTM E2058 fire propagation apparatus (50-kW scale); it is shown in Figure 3-4.2(a). Heat release rate from the CDG and OC calorimetries in the ASTM E2058 fire propagation apparatus was defined as the actual heat release rate until 1986,[16,41,48,52–55] but after 1986 it was changed to the chemical heat release rate to account for the effects of (1) the chemical structures of the materials and additives; (2) fire ventilation; (3) the two dominant modes of heat release, that is, convective and radiative; and (4) the effects of the flame extinguishing and suppressing agents.

The ASTM E2058 fire propagation apparatus is a standard test apparatus for electrical cables[14] and for wall and ceiling insulation materials, replacing the 25-ft corner test;[34] and is expected to be adopted as a standard test apparatus for conveyor belts, composites, sample storage commodities, and other applications related to the commercial and industrial fire protection needs in the future.

In 1982 the National Institute of Standards and Technology (NIST) used the OC calorimetry,[17,18] following the methodology described in Reference 43. The apparatus developed to use this methodology, known as the cone calorimeter, is shown in Figure 3-4.3. The cone calorimeter became an ASTM standard test apparatus in 1990.[19]

Sampling ducts have been designed for the ASTM E2058 fire propagation apparatus and the cone calorimeter to measure the mass generation rates of CO_2 and CO and mass consumption rate of oxygen for use in the CDG and OC calorimetries. (See Equations 18 and 21.) The CDG and OC calorimetries are used in the ASTM E2058 fire propagation apparatus (50-, 500-, and 10,000-kW scale). In the OSU apparatus and the cone calorimeter, only the OC calorimetry is used.

The CDG and OC calorimetries are also used in numerous large-scale fire tests, such as the CDG calorimetry in the wind-aided turbulent horizontal flame spread in large-scale fire test galleries at the Londonderry Occupa-

Table 3-4.10 ***Net Heats of Complete Combustion per Unit Mass of Fuel and Oxygen Consumed and Carbon Dioxide and Carbon Monoxide Generated for Carbon- and Hydrogen-Containing Fuels***[a]

Fuel	Formula	ΔH_T (kJ/g)	ΔH_O^* (kJ/g)	ΔH_{CO_2} (kJ/g)	ΔH_{CO}^* (kJ/g)
Normal alkanes					
Methane	CH_4	50.1	12.5	(18.2)	(18.6)
Ethane	C_2H_6	47.1	12.7	16.2	15.4
Propane	C_3H_8	46.0	12.9	15.3	14.0
Butane	C_4H_{10}	45.4	12.7	15.1	13.7
Pentane	C_5H_{12}	45.0	12.6	14.7	13.2
Hexane	C_6H_{14}	44.8	12.7	14.6	12.9
Heptane	C_7H_{16}	44.6	12.7	14.5	12.8
Octane	C_8H_{18}	44.5	12.6	14.4	12.7
Nonane	C_9H_{20}	44.3	12.7	14.3	12.5
Decane	$C_{10}H_{22}$	44.4	12.7	14.3	12.4
Undecane	$C_{11}H_{24}$	44.3	12.7	14.3	12.4
Dodecane	$C_{12}H_{26}$	44.2	12.7	14.2	12.3
Tridecane	$C_{13}H_{28}$	44.2	12.7	14.2	12.3
Kerosene	$C_{14}H_{30}$	44.1	12.7	14.1	12.2
Hexadecane	$C_{16}H_{34}$	44.1	12.7	14.2	12.3
		Average	**12.7**	**14.6**	**12.9**
Substituted alkanes					
Methylbutane	C_5H_{12}	45.0	12.6	14.7	13.1
Dimethylbutane	C_6H_{14}	44.8	12.7	14.6	13.0
Methylpentane	C_6H_{14}	44.8	12.7	14.6	12.9
Dimethylpentane	C_7H_{16}	44.6	12.7	14.5	12.9
Methylhexane	C_7H_{16}	44.6	12.6	14.4	12.7
Isooctane	C_8H_{18}	44.5	12.6	14.4	12.7
Methylethylpentane	C_8H_{18}	44.5	12.6	14.4	12.7
Ethylhexane	C_8H_{18}	44.5	12.6	14.4	12.7
Dimethylhexane	C_8H_{18}	44.5	12.7	14.5	12.8
Methylheptane	C_8H_{18}	44.5	12.6	14.4	12.7
		Average	**12.6**	**14.6**	**12.8**
Cyclic alkanes					
Cyclopentane	C_5H_{10}	44.3	12.8	13.9	11.9
Methylcyclopentane	C_6H_{12}	43.8	12.7	13.9	11.9
Cyclohexane	C_6H_{12}	43.8	12.7	13.8	11.7
Methylcyclohexane	C_7H_{14}	43.4	12.7	13.8	11.7
Ethylcyclohexane	C_8H_{16}	43.2	12.7	13.8	11.7
Dimethylcyclohexane	C_8H_{16}	43.2	12.7	13.8	11.7
Cyclooctane	C_8H_{16}	43.2	12.7	13.9	11.9
Decalin	$C_{10}H_{18}$	42.8	12.7	13.4	11.0
Bicyclohexyl	$C_{12}H_{22}$	42.6	12.6	13.3	11.0
		Average	**12.7**	**13.8**	**11.6**
Normal alkenes					
Ethylene	C_2H_4	48.0	13.8	15.0	13.6
Propylene	C_3H_6	46.4	13.4	14.6	12.9
Butylene	C_4H_8	45.6	14.3	14.3	12.5
Pentene	C_5H_{10}	45.2	14.3	14.3	12.5
Hexene	C_6H_{12}	44.9	12.9	14.1	12.2
Normal alkenes *(continued)*					
Heptene	C_7H_{14}	44.6	12.9	14.1	12.2
Octene	C_8H_{16}	44.5	12.9	14.1	12.1
Nonene	C_9H_{18}	44.3	12.9	14.1	12.1
Decene	$C_{10}H_{20}$	44.2	12.9	14.1	12.2
Dodecene	$C_{12}H_{24}$	44.1	12.9	14.1	12.2
Tridecene	$C_{13}H_{26}$	44.0	12.9	14.1	12.2
Tetradecene	$C_{14}H_{28}$	44.0	12.9	14.1	12.2
Hexadecene	$C_{16}H_{32}$	43.9	12.9	14.1	12.1
Octadecene	$C_{18}H_{36}$	43.8	12.9	14.1	12.1
		Average	13.2	14.2	12.4
Cyclic alkenes					
Cyclohexene	C_6H_{10}	43.0	13.0	13.4	11.0
Methylcyclohexene	C_7H_{12}	43.1	12.9	13.4	11.1
		Average	13.0	13.4	11.1
Dienes					
1-3 Butadiene	C_4H_6	44.6	13.7	13.7	11.5
Cyclooctadiene	C_8H_{12}	43.2	13.3	13.3	10.9
		Average	**13.5**	**13.5**	**11.2**
Normal alkynes					
Acetylene	C_2H_2	47.8	(15.6)	14.3	12.4
Heptyne	C_7H_{12}	44.8	13.4	13.9	11.8
Octyne	C_8H_{14}	44.7	13.3	14.0	11.9
Decyne	$C_{10}H_{18}$	44.5	13.2	13.9	11.9
Dodecyne	$C_{12}H_{22}$	44.3	13.2	14.0	12.0
		Average	**13.3**	**14.0**	**12.0**
Arenes					
Benzene	C_6H_6	40.1	13.0	11.9	8.7
Toluene	C_7H_8	39.7	12.9	12.1	9.0
Styrene	C_8H_8	39.4	13.1	12.0	8.8
Ethylbenzene	C_8H_{10}	39.4	12.9	12.3	9.4
Xylene	C_8H_{10}	39.4	13.0	12.4	9.5
Propylbenzene	C_9H_{12}	39.4	12.9	12.5	9.6
Trimethylbenzene	C_9H_{12}	39.2	12.9	12.5	9.7
Cumene	C_9H_{12}	39.2	12.9	12.9	9.6
Naphthalene	$C_{10}H_8$	39.0	12.9	11.3	7.7
Tetralin	$C_{10}H_{12}$	39.0	12.9	12.2	9.2
Butylbenzene	$C_{10}H_{14}$	39.0	12.9	12.7	9.9
Diethylbenzene	$C_{10}H_{14}$	39.0	13.7	13.5	11.1
p-Cymene	$C_{10}H_{14}$	39.0	13.0	12.5	9.6
Methylnaphthalene	$C_{11}H_{10}$	38.9	12.9	11.5	8.1
Pentylbenzene	$C_{11}H_{16}$	38.8	13.0	12.8	10.2
Triethylbenzene	$C_{12}H_{18}$	38.7	12.7	12.7	10.0
		Average	**13.0**	**12.4**	**9.4**

[a]Data from References 48 and 49. Numbers in parentheses not used for averaging.

tional Safety Centre in Australia and Pittsburgh Research Center, U.S. Bureau of Mines.[56,57]

In the GTR calorimetry, a thermopile located in the flue gas chimney is used in the OSU apparatus, and a thermocouple located in the sampling duct is used in the ASTM E2058 fire propagation apparatus, where heat losses by conduction are negligibly small. The cone calorimeter has not been designed for the GTR calorimetry.

The radiative heat release rate is determined from the difference between the chemical and convective heat release rates only in the ASTM E2058 fire propagation apparatus.

Table 3-4.11 ***Net Heats of Complete Combustion per Unit Mass of Fuel and Oxygen Consumed and Carbon Dioxide and Carbon Monoxide Generated for Carbon-, Hydrogen-, and Oxygen-Containing Fuels***[a]

Fuel	Formula	ΔH_T (kJ/g)	ΔH_O^* (kJ/g)	ΔH_{CO_2} (kJ/g)	ΔH_{CO}^* (kJ/g)
Alcohols					
Methyl alcohol	CH_4O	20.0	13.4	14.5	12.9
Ethyl alcohol	C_2H_6O	27.7	13.2	14.5	12.7
n-Propyl alcohol	C_3H_8O	31.8	13.3	14.5	12.7
Isopropyl alcohol	C_3H_8O	31.8	13.3	14.5	12.7
Allyl alcohol	C_3H_6O	31.4	14.2	13.8	11.7
n-Butyl alcohol	$C_4H_{10}O$	34.4	13.3	14.5	12.8
Isobutyl alcohol	$C_4H_{10}O$	34.4	13.3	14.5	12.8
Sec-butyl alcohol	$C_4H_{10}O$	34.4	13.3	14.5	12.8
Ter-butyl alcohol	$C_4H_{10}O$	34.4	13.3	14.5	12.8
n-Amyl alcohol	$C_5H_{12}O$	36.2	13.3	14.5	12.8
Isobutyl carbinol	$C_5H_{12}O$	36.2	13.3	14.5	12.8
Sec-butyl carbinol	$C_5H_{12}O$	36.2	13.3	14.5	12.8
Methylpropylcarbinol	$C_5H_{12}O$	36.2	13.3	14.5	12.8
Dimethylethylcarbinol	$C_5H_{12}O$	36.2	13.3	14.5	12.8
n-Hexyl alcohol	$C_6H_{14}O$	37.4	13.3	14.5	12.7
Dimethylbutylalcohol	$C_6H_{14}O$	37.4	13.3	14.5	12.7
Ethylbutyl alcohol	$C_6H_{14}O$	37.4	13.3	14.5	12.7
Cyclohexanol	$C_6H_{12}O$	37.3	13.7	14.1	12.2
Benzyl alcohol	C_7H_8O	32.4	13.0	11.4	8.0
n-Heptyl alcohol	$C_7H_{16}O$	39.8	13.7	15.0	13.6
n-Octyl alcohol	$C_8H_{18}O$	40.6	13.7	15.0	13.6
n-Nonyl alcohol	$C_9H_{20}O$	40.3	13.4	14.7	13.0
		Average	**13.3**	**14.5**	**12.8**
Aldehydes					
Formaldehyde	CH_2O	18.7	(17.5)	12.7	10.1
Acetaldehyde	C_2H_4O	25.1	13.8	12.6	9.7
Butyraldehyde	C_4H_8O	33.8	13.9	13.9	11.7
Crotonaldehyde	C_4H_6O	34.8	15.2	13.8	11.8
Benzaldehyde	C_7H_6O	32.4	13.4	11.2	7.5
Ethyl hexaldehyde	$C_8H_{16}O$	39.4	13.7	12.7	9.9
		Average	**14.2**	**13.3**	**10.6**
Ketones					
Acetone	C_3H_6O	29.7	13.4	13.1	10.5
Methylethyl ketone	C_4H_8O	32.7	13.4	13.4	11.0
Diethyl ketone	$C_5H_{10}O$	33.7	12.9	13.2	10.7
Cyclohexanone	$C_6H_{10}O$	35.9	13.8	13.3	11.0
Methyl butyl ketone	$C_6H_{12}O$	35.2	12.9	13.3	11.0
Di-acetone alcohol	$C_6H_{12}O_2$	37.3	(16.9)	(16.4)	(15.7)
Dipropyl ketone	$C_7H_{14}O$	38.6	13.8	14.3	12.5
Phenylbutyl ketone	$C_{11}H_{14}O$	34.8	12.6	11.6	(8.4)
		Average	**13.2**	**13.2**	**11.1**
Acids					
Formic acid	CH_2O_2	5.7	16.4	5.96	0
Acetic acid	$C_2H_4O_2$	14.6	13.7	9.95	5.65
Benzoic acid	$C_7H_6O_2$	24.4	12.4	9.66	5.18
Cresylic acid	$C_8H_8O_2$	34.0	(16.0)	13.1	10.6
Esters					
Ethyl formate	$C_2H_6O_2$	20.2	13.3	11.3	7.8
n-Propyl formate	$C_4H_8O_2$	23.9	13.2	12.0	8.8
n-Butyl formate	$C_5H_{10}O_2$	26.6	13.0	12.3	9.4
Methyl acetate	$C_3H_6O_2$	20.2	13.3	11.3	7.8
Ethyl acetate	$C_4H_8O_2$	23.9	13.2	12.0	8.8
n-Propyl acetate	$C_5H_{10}O_2$	26.6	13.0	12.3	9.4
n-Butyl acetate	$C_6H_{12}O_2$	28.7	13.0	12.6	9.8
Isobutyl acetate	$C_6H_{12}O_2$	28.7	13.0	12.6	9.8
Amyl acetate	$C_7H_{14}O_2$	30.3	13.0	12.8	10.1
Cyclohexyl acetate	$C_8H_{14}O_2$	31.5	13.3	12.7	10.0
Octyl acetate	$C_{10}H_{20}O_2$	33.6	12.9	13.1	10.6
Ethylacetoacetate	$C_6H_{10}O_3$	30.3	(17.6)	(14.9)	(13.5)
Methyl propionate	$C_4H_8O_2$	23.9	13.2	12.0	7.4
Ethyl propionate	$C_5H_{10}O_2$	26.6	13.0	12.3	9.4
n-Butyl propionate	$C_7H_{14}O_2$	30.3	13.0	12.8	10.1
Isobutyl propionate	$C_7H_{14}O_2$	30.3	13.0	12.8	10.1
Amyl propionate	$C_8H_{18}O_2$	31.6	12.9	12.9	10.3
Methyl butyrate	$C_5H_{10}O_2$	26.6	13.0	12.3	9.4
Ethyl butyrate	$C_6H_{12}O_2$	28.7	13.0	12.6	9.8
Propyl butyrate	$C_7H_{14}O_2$	30.3	13.0	12.8	10.1
n-Butyl butyrate	$C_8H_{16}O_2$	31.6	12.9	12.9	10.3
Isobutyl butyrate	$C_8H_{16}O_2$	31.6	12.9	12.9	10.3
Ethyl laurate	$C_{14}H_{28}O_2$	37.2	13.3	13.8	11.6
Ethyl lactate	$C_5H_{10}O_3$	30.8	(18.9)	(16.5)	(16.0)
Butyl lactate	$C_7H_{14}O_3$	33.3	(16.8)	(15.8)	(14.8)
Amyl lactate	$C_8H_{16}O_3$	34.3	(16.4)	(15.6)	(14.5)
Ethyl benzoate	$C_9H_{10}O_2$	34.5	(15.4)	13.1	10.5
Ethyl carbonate	$C_5H_{10}O_3$	30.8	(18.9)	(16.5)	(16.0)
Ethyl oxalate	$C_4H_6O_4$	28.7	(20.2)	(16.6)	(20.2)
Ethyl malonate	$C_5H_8O_4$	32.2	(17.9)	(19.3)	(20.4)
		Average	**13.0**	**12.5**	**9.7**
Others					
Camphor	$C_{10}H_{16}O$	38.8	13.7	13.4	11.1
Cresol	C_7H_8O	34.6	13.7	12.1	9.1
Resorcinol	$C_6H_6O_2$	26.0	13.7	10.8	5.9
Acrolein	C_3H_4O	29.1	14.6	12.3	9.4

[a]Data from References 48 and 49. Numbers in parentheses not used for averaging.

Figure 3-4.22 shows a typical example of the heat release rate profile. The profile is for the chemical heat release rate of polypropylene, determined from the CDG and OC calorimetries in the ASTM E2058 fire propagation apparatus (500-kW scale). The polypropylene samplewas 100 mm in diameter and 25 mm in thickness. It was exposed to an external heat flux of 50 kW/m^2 under co-flowing normal air. In the figure, solid, molten, and boiling-liquid zones are indicated.

In the solid zone in Figure 3-4.22, combustion is at the steady state between about 400 and 900 sec. During the steady-state combustion, a very thin liquid film is present at the surface. In the molten zone, the thickness of the liquid film and chemical heat release rate increase rapidly during combustion. At the end of the zone, the entire sample is present as a liquid. In the boiling-liquid zone, the liquid boils vigorously, chemical heat release rate increases exponentially until the sample is consumed, the base diameter of the flame is considerably larger than the diameter of the sample dish (100 mm), and the flames are as high as 1.5 m (5 ft). This zone is the most dangerous zone.

Table 3-4.12 ***Net Heats of Complete Combustion per Unit Mass of Fuel and Oxygen Consumed and Carbon Dioxide and Carbon Monoxide Generated for Carbon-, Hydrogen-, Nitrogen-, and Sulfur-Containing Fuels[a]***

Fuel	Formula	ΔH_T (kJ/g)	ΔH_O^* (kJ/g)	$\Delta H_{CO_2}^*$ (kJ/g)	ΔH_{CO}^* (kJ/g)
C-H-N fuels					
Acrylonitrile	C_3H_3N	24.5	8.5	9.8	5.4
Diethylamine	$C_4H_{11}N$	38.0	11.2	15.8	14.8
n-Butylamine	$C_4H_{11}N$	38.0	11.2	15.8	14.8
sec-Butylamine	$C_4H_{11}N$	38.0	11.2	15.8	14.8
Pyridine	C_5H_9N	32.2	11.0	11.6	8.2
Aniline	C_6H_7N	33.8	11.2	11.9	8.7
Picoline	C_6H_7N	33.8	11.2	11.9	8.7
Triethylamine	$C_6H_{15}N$	39.6	11.6	15.2	13.8
Toluidine	C_7H_9N	34.9	11.3	12.1	9.1
Dimethylaniline	$C_8H_{11}N$	35.7	11.5	12.3	9.3
Di-*n*-butylamine	$C_8H_{19}N$	40.6	11.9	14.9	13.4
Quinoline	C_9H_7N	36.1	12.4	11.8	8.5
Quinaldine	$C_{10}H_9N$	36.7	12.4	11.9	8.7
Butylaniline	$C_{10}H_{15}N$	37.0	11.7	12.5	9.7
Tri-*n*-butylamine	$C_{12}H_{27}N$	41.6	12.1	14.6	12.9
		Average	**11.5**	**15.4**	**14.1**
C-H-S fuels					
Carbon disulfide	CS_2	13.6	10.8	(23.5)	(27.0)
Thiophene	C_4H_4S	31.9	14.0	15.2	14.0
Methylthiophene	C_5H_6S	33.2	13.6	14.8	13.2
Thiophenol	C_6H_6S	34.1	13.8	14.2	12.3
Hexyl mercaptan	$C_6H_{14}S$	33.0	11.6	14.8	13.2
Thiocresol	C_7H_8S	34.9	13.5	14.1	12.1
Heptyl mercaptan	$C_7H_{16}S$	33.7	11.6	14.4	12.7
Cresolmethylsulfide	$C_8H_{11}S$	36.2	13.4	15.9	15.0
Decylmercaptan	$C_{10}H_{22}S$	34.9	11.5	13.8	11.7
Dodecyl mercaptan	$C_{12}H_{26}S$	35.5	11.5	13.6	11.4
Hexyl sulfide	$C_{12}H_{26}S$	35.5	11.5	13.6	11.4
Heptyl sulfide	$C_{14}H_{30}S$	35.9	11.5	13.4	11.1
Octyl sulfide	$C_{16}H_{34}S$	36.3	11.5	13.3	10.9
Decyl sulfide	$C_{20}H_{42}S$	36.8	11.4	13.1	10.7
		Average	**11.3**	**13.1**	**11.5**

[a]Data from References 48 and 49. Numbers in parentheses not used for averaging.

The chemical heat release rate profiles from the CDG and OC calorimetries are very similar, as expected.

Energy released in a fire: The total amount of heat generated as a result of chemical reactions in the combustion of a material is defined as the chemical energy. The chemical energy has a convective and a radiative component:

$$E_{ch} = E_{con} + E_{rad} \tag{25}$$

where

E_{ch} = chemical energy (kJ)
E_{con} = convective energy (kJ)
E_{rad} = radiative energy (kJ)

The chemical energy and its convective and radiative components are calculated by the summation of the respective heat release rates:

$$E_i = A \sum_{n=t_{ig}}^{n=t_{ex}} \dot{Q}_i''(t_n)\Delta t_n \tag{26}$$

where

E_i = chemical, convective, or radiative energy (kJ)
A = total surface area of the material burning (m^2)
t_{ig} = the ignition time (s)
t_{ex} = flame extinction time (s)

The total mass of the material lost during combustion is measured directly from the initial and final mass and is calculated by the summation of the mass loss rate:

$$W_f = A \sum_{n=t_{ig}}^{n=t_{ex}} \dot{m}''(t_n)\Delta t_n \tag{27}$$

where W_f is the total mass of the material lost in the combustion (g).

Heat release rate can also be expressed as the product of the mass loss rate and the heat of combustion:

$$\dot{Q}_i'' = \Delta H_i \dot{m}'' \tag{28}$$

where ΔH_i is the chemical, convective, or radiative heat of combustion (kJ/g). The average chemical, convective, or radiative heats of combustion are calculated from the relationship based on Equations 26 and 27:

$$\Delta \overline{H}_i = \frac{E_i}{W_f} \tag{29}$$

where $\Delta \overline{H}_i$ is the average chemical, convective, or radiative heat of combustion (kJ/g). The average chemical heat of combustion determined in the cone calorimeter is defined as the effective heat of combustion.[17–19]

Heat release parameter (HRP): Heat release parameter (HRP) is defined as the amount of energy generated per unit amount of energy absorbed. From Equations 11 and 28,

$$\dot{Q}_i'' = \left(\frac{\Delta H_i}{\Delta H_g}\right)(\dot{q}_e'' + \dot{q}_f'' - \dot{q}_{rr}'') \tag{30}$$

where $\Delta H_i/\Delta H_g$ is defined as the chemical, convective, or radiative HRP, $(HRP)_{ch}$, $(HRP)_{con}$, or $(HRP)_{rad}$, respectively.[4] The HRP values are characteristic fire properties of materials, but depend on fire ventilation. The chemical HRP is independent of fire size.

In Figure 3-4.22, the theoretical prediction is from Equation 30, with chemical HRP = 19, external heat flux = 50 kW/m^2, and surface re-radiation = 18 kW/m^2 with negligibly small flame heat flux. The theoretical prediction is very close to the measured value in the solid zone.

Experimental data support Equation 30, as shown in Figures 3-4.23 through 3-4.25, where the average peak or steady-state chemical heat release rates are plotted against

Table 3-4.13 ***Net Heats of Complete Combustion per Unit Mass of Fuel and Oxygen Consumed and Carbon Dioxide and Carbon Monoxide Generated for Polymeric Materials[a]***

Fuel	Formula[b]	ΔH_T^c (kJ/g)	ΔH_O^* (kJ/g)	$\Delta H_{CO_2}^*$ (kJ/g)	ΔH_{CO}^* (kJ/g)
Carbon-hydrogen atoms in the structure					
Polyethylene	CH_2	43.6	12.8	13.9	11.8
Polypropylene	CH	43.4	12.7	13.8	11.7
Polyisobutylene	CH_2	43.7	12.7	13.9	11.9
Polybutadiene	$CH_{1.5}$	42.8	13.1	13.1	10.7
Polystyrene	CH	39.2	12.7	12.2	9.2
Expanded polystyrene					
GM47	$CH_{1.1}$	38.1	12.4	11.3	7.7
GM49	$CH_{1.1}$	38.1	12.4	11.3	7.7
GM51	CH	35.6	11.6	10.8	7.0
GM53	$CH_{1.1}$	37.6	12.4	11.3	7.7
		Average	**12.5**	**12.4**	**9.5**
Carbon-hydrogen-oxygen-nitrogen atoms in the structure					
Polyoxymethylene	CH_2O	15.4	14.4	10.5	6.6
Polymethylmethacrylate	$CH_{1.6}O_{0.4}$	25.2	13.1	11.5	8.0
Polyester	$CH_{1.4}O_{0.22}$	32.5	13.9	12.5	9.6
Epoxy	$CH_{1.3}O_{0.20}$	28.8	12.1	10.8	6.9
Polycarbonate	$CH_{0.88}O_{0.19}$	29.7	13.1	10.7	6.9
Cellulose triacetate	$CH_{1.3}O_{0.67}$	17.6	13.3	9.6	5.1
Polyethyleneterephthalate	$CH_{0.80}O_{0.40}$	22.0	13.2	9.6	5.1
Rigid phenolic foam	$CH_{1.1}O_{0.24}$	36.4	(16.8)	(14.0)	(12.0)
Polyacrylonitrile (PAN)	$CHN_{0.33}$	30.8	10.7	12.3	9.4
Red Oak	$CH_{1.7}O_{0.72}N_{0.001}$	17.1	13.2	10.2	6.0
Douglas Fir	$CH_{1.7}O_{0.74}N_{0.002}$	16.4	12.4	9.5	5.0
Nylon	$CH_{1.8}O_{0.17}N_{0.17}$	30.8	11.9	13.3	10.8
Flexible polyurethane foams					
GM21	$CH_{1.8}O_{0.30}N_{0.05}$	26.2	12.1	11.5	8.0
GM23	$CH_{1.8}O_{0.35}N_{0.06}$	27.2	13.7	12.5	9.7
GM25	$CH_{1.7}O_{0.32}N_{0.07}$	24.6	12.0	11.1	7.5
GM27	$CH_{1.7}O_{0.03}N_{0.08}$	23.2	11.2	10.4	6.2
Carbon-hydrogen-oxygen-nitrogen atoms in the structure *(continued)*					
Rigid polyurethane foams					
GM29	$CH_{1.1}0_{0.23}N_{0.10}$	26.0	12.6	10.7	6.8
GM31	$CH_{1.2}0_{0.22}N_{0.10}$	25.0	11.9	10.2	6.1
GM37	$CH_{1.2}0_{0.20}N_{0.08}$	28.0	12.7	11.2	7.5
Rigid polyisocyanurate foams					
GM41	$CH_{1.0}O_{0.19}N_{0.11}$	26.2	12.5	10.4	6.4
GM43	$CH_{0.93}O_{0.20}N_{0.11}$	22.2	10.8	8.9	(4.0)
		Average	**12.5**	**10.9**	**7.2**
Carbon-hydrogen-chlorine atoms in the structure					
Polyethylene with					
25% chlorine	$CH_{1.9}Cl_{0.13}$	31.6	12.7	13.4	10.8
36% chlorine	$CH_{1.8}Cl_{0.22}$	26.3	12.8	12.9	10.2
48% chlorine	$CH_{1.7}Cl_{0.36}$	20.6	12.8	12.3	9.4
Polychloroprene	$CH_{1.3}Cl_{0.30}$	25.3	13.3	12.7	9.5
Polyvinylchloride	$CH_{1.5}Cl_{0.50}$	16.4	11.7	11.7	8.2
Polyvinylidenechloride	CHCl	9.0	13.5	9.8	(5.5)
		Average	**12.8**	**12.1**	**9.6**
Carbon-hydrogen-fluorine atoms in the structure[d]					
Teflon TFE	CF_2	6.2	9.7	(7.1)	(1.1)
Teflon FEP	$CF_{1.8}$	4.8	(6.9)	(5.0)	(0)
Tefzel ETFE	CHF	12.6	12.6	9.2	(4.4)
Teflon PFA	$CF_{1.7}O_{0.01}$	5.0	(8.0)	(5.3)	(0)
Kel-F (CTFE)	$CF_{1.5}Cl_{0.50}$	6.5	11.8	8.6	(3.5)
Halar (E-CTFE)	$CHF_{0.75}Cl_{0.25}$	12.0	9.8	9.8	(5.4)
Kynar (PVF_2)	CHF	13.3	12.4	9.1	(4.2)
Tedlar (PVF)	$CH_{1.5}F_{0.50}$	13.5	(6.5)	(7.1)	(1.1)
Carbon-hydrogen-oxygen-silicone atoms in the structure					
Silicone-1	$CH_{1.3}O_{0.25}Si_{0.18}$	21.7	12.6	11.0	7.4
Silicone-2	$CH_{1.5}O_{0.30}Si_{0.26}$	21.3	13.9	12.4	9.4
Silicone-3	$CH_3O_{0.50}Si_{0.50}$	25.1	14.5	21.0	23.0

[a] From the data measured in the FMRC Flammability Laboratory.

[b] From the data for the elemental composition of the polymeric materails measured in the FMRC Flammability Laboratory.

[c] From the data measured by the FMRC Flammability Laboratory in the oxygen bomb calorimeter and corrected for water as a gas and for the residue.

[d] Trade names from Reference 50.

the net heat flux. Linear relationship between the chemical heat release rate and net heat flux is satisfied. For the condition $\dot{q}_e'' \gg \dot{q}_f'' - \dot{q}_{rr}''$, the average value of the HRP is calculated from the summation of the heat release rate and the external heat flux:

$$\overline{(\mathrm{HRP})_i} = \frac{E_i}{A \sum_{n-t_{ig}}^{n-t_{ex}} \dot{q}_e'' \Delta t_n} \tag{31}$$

Complete and incomplete combustion: In fires, combustion is never complete. Thus, the chemical heat release rate or the chemical heat of combustion is less than the heat release rate for complete combustion or the net heat of complete combustion. The ratio of the chemical heat release rate to the heat release rate for complete combustion or the ratio of the chemical heat of combustion to net heat of complete combustion is defined as combustion efficiency:[2–4,16,41,44]

$$\chi_{\mathrm{ch}} = \frac{\dot{Q}_{\mathrm{ch}}''}{\dot{Q}_T''} = \frac{\dot{m}'' \Delta H_{\mathrm{ch}}}{\dot{m}'' \Delta H_T} = \frac{\Delta H_{\mathrm{ch}}}{\Delta H_T} \tag{32}$$

where χ_{ch} is the combustion efficiency and $\dot{Q}_T''$ is the heat release rate for complete combustion (kW/m^2). The convective and radiative components of the combustion efficiency are defined in a similar fashion:[2–4,16,41,44]

$$\chi_{\mathrm{con}} = \frac{\dot{Q}_{\mathrm{con}}''}{\dot{Q}_T''} = \frac{\dot{m}'' \Delta H_{\mathrm{con}}}{\dot{m}'' \Delta H_T} = \frac{\Delta H_{\mathrm{con}}}{\Delta H_T} \tag{33}$$

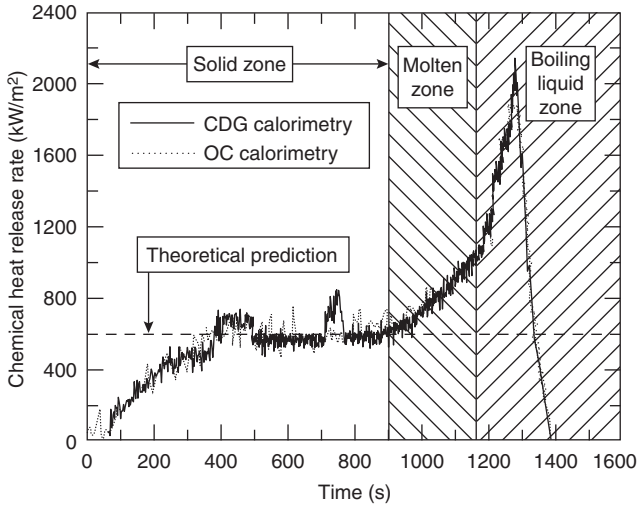

Figure 3-4.22. ***Chemical heat release rate for 100-mm diameter and 25-mm-thick slab of polypropylene exposed to an external heat flux of 50 kW/m² and 0.09 m/s co-flowing normal air in the ASTM E2058 fire propagation apparatus. The theoretical prediction is based on the heat release parameter for polypropylene listed in Table 3-4.15.***

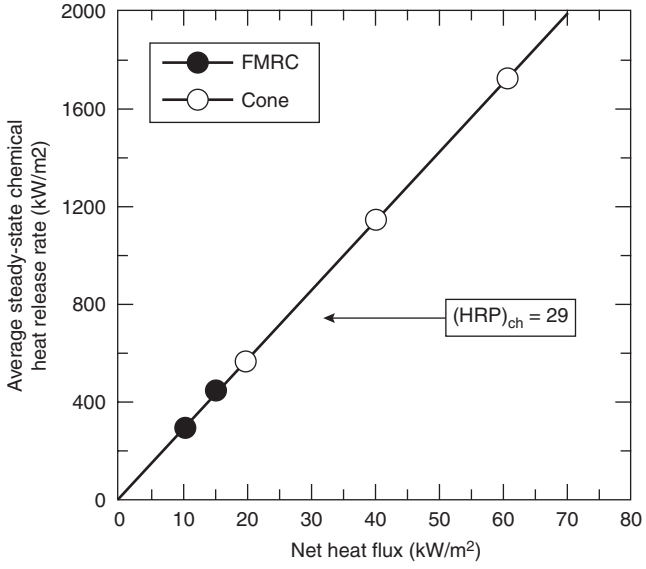

Figure 3-4.23. ***Average steady-state chemical heat release rate versus net heat flux for polystyrene slab. Net heat flux is the sum of the external and flame heat flux minus the surface re-radiation.***

$$\chi_{\text{rad}} = \frac{\dot{Q}''_{\text{rad}}}{\dot{Q}''_{T}} = \frac{\dot{m}''\Delta H_{\text{rad}}}{\dot{m}''\Delta H_{T}} = \frac{\Delta H_{\text{rad}}}{\Delta H_{T}} \tag{34}$$

where χ_{con} is the convective component of the combustion efficiency and χ_{rad} is the radiative component of the combustion efficiency. From the definitions,

$$\Delta H_{\text{ch}} = \Delta H_{\text{con}} + \Delta H_{\text{rad}} \tag{35}$$

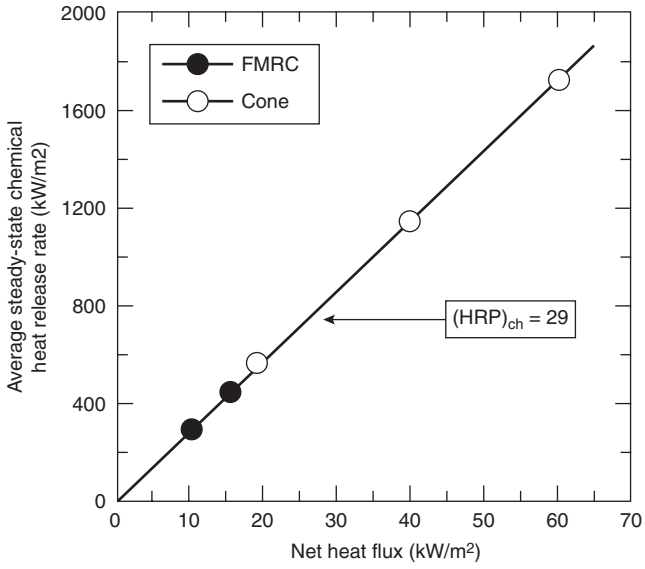

Figure 3-4.24. ***Average steady-state chemical heat release rate versus the net heat flux for high molecular weight hydrocarbon liquid burning in a 100-mm-diameter dish. The cone calorimeter data were measured at the research laboratory of the Dow-Corning Corporation, Midland, Michigan. Net heat flux is the sum of the external and flame heat flux minus the surface re-radiation.***

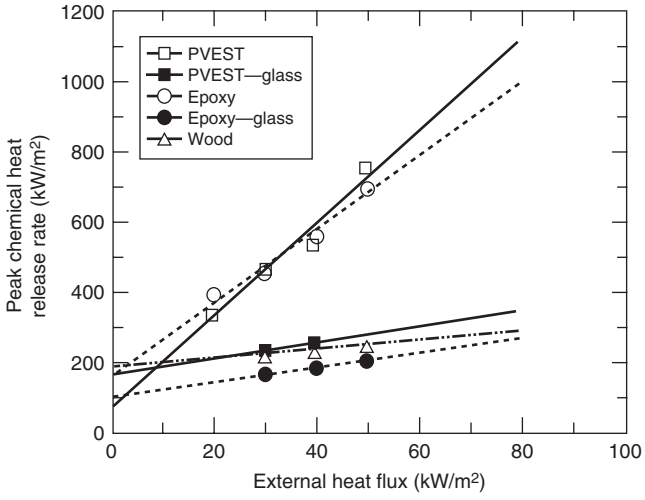

Figure 3-4.25. ***Peak chemical heat release rate versus the external heat flux for 100- × 100-mm × 3- to 11-mm-thick slab of polyvinyl ester (PVEST), PVEST/fiberglass, epoxy, epoxy/fiberglass, and wood (hemlock). Data measured in the cone calorimeter as reported in Reference 20 are shown.***

$$\chi_{\text{ch}} = \chi_{\text{con}} + \chi_{\text{rad}} \tag{36}$$

The chemical, convective, and radiative heat release rates, heats of combustion, and combustion efficiencies depend on the chemical structures of the materials and fire ventilation. The distribution of the chemical heat into convec-

tive and radiative components changes with fire size. The larger the fire size, the larger the fraction of the chemical heat distributed into the radiative component.

The chemical, convective, and radiative heats of combustion and the HRP values for the well-ventilated fires are listed in Tables 3-4.14 and 3-4.15, respectively. Comparisons between the limited data from the OSU apparatus, ASTM E2058 fire propagation apparatus, and cone calorimeter are satisfactory.

EXAMPLE 10:

Heptane was burned in a 2-m-diameter pan, and measurements were made for the mass loss rate, mass generation rates of CO and CO_2, and mass consumption rate of O_2. The average values in g/m²·s for the mass loss rate, mass generation rates of CO and CO_2, and mass consumption rate of O_2 were 66, 9, 181, and 216 respectively. For large-scale fires of heptane, the literature values are $\chi_{ch} = 0.93$, $\chi_{con} = 0.59$, and $\chi_{rad} = 0.34$. The net heat of complete combustion for heptane reported in the literature is 44.6 kJ/g. Calculate the chemical heat release rate and show that it is consistent with the rate based on the literature value of the combustion efficiency. Also calculate the convective and radiative heat release rates.

SOLUTION:

From Table 3-4.10, the net heat of complete combustion per unit mass of oxygen consumed is 12.7 kJ/g; the net heat of complete combustion per unit mass of CO_2 generated is 14.5 kJ/g; and the net heat of complete combustion per unit mass of CO generated is 12.8 kJ/g. From the CDG calorimetry (Equation 18),

$$\dot{Q}''_{ch} = 14.5 \times 181 + 12.8 \times 9$$
$$= 2625 + 115 = 2740 \text{ kW/m}^2$$

From OC calorimetry (Equation 21),

$$\dot{Q}''_{ch} = 12.7 \times 216 = 2743 \text{ kW/m}^2$$

The chemical heat release rate from the CDG and OC calorimetries are in excellent agreement, the average being 2742 kW/m².

The chemical heat of combustion is the product of net heat of complete combustion (44.6 kJ/g) and the combustion efficiency (0.93), which is 41.5 kJ/g.

The chemical heat release is the product of the mass loss rate (66 g/m²·s) and chemical heat of combustion (41.5 kJ/g), which is 2739 kW/m², compared to the averaged value 2742 kW/m² from the CDG and OC calorimetries. Thus, the chemical heat release determined from the measurements is consistent with the rate from the literature value of the combustion efficiency.

The convective heat release rate is equal to the convective heat of combustion and the mass loss rate. The convective heat of combustion is equal to the convective component of the combustion efficiency ($\chi_{con} = 0.59$) times the net of complete combustion (44.6 kJ/g). Thus, the convective heat release rate for heptane is $66 \times 0.59 \times 44.6 = 1737$ kW/m². In a similar fashion, the radiative heat release rate is $66 \times 0.34 \times 44.6 = 1001$ kW/m².

EXAMPLE 11:

From the flame radiation scaling technique, the asymptotic mass loss rate values in g/m²·s expected in large-scale fires, as listed in Table 3-4.8, for polyethylene, polystyrene, polyvinylchloride, and Teflon are 26, 36, 16, and 7, respectively. The chemical heats of combustion in kJ/g listed in Table 3-4.14 for these materials are 38.4, 27.0, 5.7, and 4.1, respectively. Estimate the chemical heat release rates expected in large-scale fires of polyethylene, polystyrene, polyvinylchloride, and Teflon. (In this chapter Teflon refers mainly to FEP, except in cases where it is identified otherwise.)

SOLUTION:

The chemical heat release rate is calculated from Equation 28. The chemical heat release rates estimated in the large-scale fires are (1) polyethylene: $26 \times 38.4 = 998$ kW/m²; (2) polystyrene: $36 \times 27.0 = 972$ kW/m²; (3) polyvinylchloride: $16 \times 5.7 = 91$ kW/m²; and (4) Teflon: $7 \times 4.1 = 28$ kW/m².

EXAMPLE 12:

Heat release rate is the product of the HRP and the net heat flux absorbed by the material, as indicated in Equation 30. This concept is used in various models to predict fire propagation and heat release rates, whereas values for the HRP are taken from a handbook such as this handbook, and net heat flux is estimated through correlations. The lower the value of the HRP for a fixed value of the net heat flux, the lower the heat release rate.

The values for the surface re-radiation, flame heat flux for large-scale fires, and chemical HRP are listed in Tables 3-4.7, 3-4.8, and 3-4.15, respectively. Calculate the chemical heat release rates expected in large-scale fires of heptane, kerosene, polyethylene, polypropylene, polystyrene, polymethylmethacrylate, polyvinylchloride, and Teflon.

SOLUTION:

The chemical heat release rates are calculated from the relationship $[(\text{HRP})_{ch} \times (\dot{q}''_f - \dot{q}''_{rr})]$, which is Equation 30:

1. heptane: $(75)(37 - 1) = 2700$ kW/m²
2. kerosene: $(47)(29 - 1) = 1316$ kW/m²
3. polyethylene: $(17)(61 - 15) = 782$ kW/m²
4. polypropylene: $(19)(67 - 15) = 988$ kW/m²
5. polystyrene: $(16)(75 - 13) = 992$ kW/m²
6. polymethylmethacrylate: $(15)(57 - 11) = 690$ kW/m²
7. polyvinylchloride: $(2)(50 - 15) = 70$ kW/m²
8. Teflon: $(2)(52 - 38) = 28$ kW/m²

The example shows the importance of the chemical HRP, flame heat flux, and surface re-radiation.

Heat release rate and fire ventilation: In the majority of fires, hazards are due to fires occurring in enclosed spaces. In early stages, a building fire is well-ventilated and is easy to control and extinguish. However, if the fire is allowed to grow, especially with limited enclosure ventilation and large material surface area, it becomes a ventilation-controlled fire and can lead to flashover, a very dangerous condition. In ventilation-controlled fires, the chemical reactions between oxygen from air and products of incomplete combustion from the decomposed and

Table 3-4.14 ***Yields of Fire Products and Chemical, Convective, and Radiative Heats of Combustion for Well-Ventilated Fires[a]***

Material	ΔH_T (kJ/g)	y_{CO_2} (g/g)	y_{CO} (g/g)	y_{ch} (g/g)	y_s (g/g)	ΔH_{ch} (kJ/g)	ΔH_{con} (kJ/g)	ΔH_{rad} (kJ/g)
Common gases								
Methane	50.1	2.72	—	—	—	49.6	42.6	7.0
Ethane	47.1	2.85	0.001	0.001	0.013	45.7	34.1	11.6
Propane	46.0	2.85	0.005	0.001	0.024	43.7	31.2	12.5
Butane	45.4	2.85	0.007	0.003	0.029	42.6	29.6	13.0
Ethylene	48.0	2.72	0.013	0.005	0.043	41.5	27.3	14.2
Propylene	46.4	2.74	0.017	0.006	0.095	40.5	25.6	14.9
1,3-Butadiene	44.6	2.46	0.048	0.014	0.125	33.6	15.4	18.2
Acetylene	47.8	2.60	0.042	0.013	0.096	36.7	18.7	18.0
Common liquids								
Methyl alcohol	20.0	1.31	0.001	—	—	19.1	16.1	3.0
Ethyl alcohol	27.7	1.77	0.001	0.001	0.008	25.6	19.0	6.5
Isopropyl alcohol	31.8	2.01	0.003	0.001	0.015	29.0	20.6	8.5
Acetone	29.7	2.14	0.003	0.001	0.014	27.9	20.3	7.6
Methylethyl ketone	32.7	2.29	0.004	0.001	0.018	30.6	22.1	8.6
Heptane	44.6	2.85	0.010	0.004	0.037	41.2	27.6	13.6
Octane	44.5	2.84	0.011	0.004	0.038	41.0	27.3	13.7
Kerosene	44.1	2.83	0.012	0.004	0.042	40.3	26.2	14.1
Benzene	40.1	2.33	0.067	0.018	0.181	27.6	11.0	16.5
Toluene	39.7	2.34	0.066	0.018	0.178	27.7	11.2	16.5
Styrene	39.4	2.35	0.065	0.019	0.177	27.8	11.2	16.6
Hydrocarbon	43.9	2.64	0.019	0.007	0.059	36.9	24.5	12.4
Mineral oil	41.5	2.37	0.041	0.012	0.097	31.7	—	—
Polydimethyl siloxane	25.1	0.93	0.004	0.032	0.232	19.6	—	—
Silicone	25.1	0.72	0.006	0.008	—	15.2	12.7	2.5
Chemicals and solvents								
Tetrahydrofuran (C_4H_8O)	32.2	2.29	0.021	—	—	30.3	—	—
Phenol (C_6H_6O)	31.0	2.63	0.057	—	0.099	27.6	13.3	14.3
Acetronitrile (C_2H_3N)	29.6	2.04	0.025	—	0.026	29.0	23.0	6.0
Ethylisonicotate ($C_8H_9O_2N$)	26.3	2.37	0.029	—	0.142	24.3	12.8	11.5
Adiponitrile ($C_6H_8N_2$)	33.1	2.35	0.045	—	0.045	31.1	22.1	9.0
Hexamethylenediamine ($C_6H_{16}N_2$)	35.3	2.28	0.029	—	0.045	32.6	15.7	16.9
Toluenediisocyanate ($C_9H_6O_2N_2$)	23.6	1.77	0.052	—	0.141	19.3	11.1	8.2
Diphenylmethanediisocyanate MDI ($C_{15}H_{10}O_2N_2$)	27.1	0.95	0.042	—	0.154	19.6	13.7	5.9
Polymeric MDI ($C_{23}H_{19}O_3N_3$)	29.6	1.22	0.032	—	0.165	23.3	15.0	8.3
Isoproturon ($C_{12}H_{18}ON_2$)	32.8	1.70	0.056	—	0.115	23.9	14.0	9.9
3 Chloropropene (C_3H_5Cl)	23.0	0.75	0.076	—	0.179	10.8	6.9	3.9
Monochlorobenzene (C_6H_5Cl)	26.4	0.86	0.083	—	0.232	11.2	—	—
Dichloromethane (CH_2Cl_2)	6.0	0.11	0.088	—	0.081	2.0	—	—
1,3 Dichloropropene ($C_3H_4Cl_2$)	14.2	0.35	0.090	—	0.169	5.6	—	—
Ethylmonochloroacetate ($C_4H_7O_2Cl$)	15.7	1.24	0.019	—	0.138	14.1	10.1	4.0
Chloronitrobenzoic acid ($C_7H_4O_4NCl$)	15.9	0.39	0.057	—	—	4.4	—	—
Aclonifen ($C_{12}H_9O_3N_2Cl$)	19.7	0.68	0.063	—	0.186	7.0	—	—
2,6 Dichlorobenzonitrile (dichlobenil) ($C_7H_3NCl_2$)	17.8	0.39	0.068	—	—	4.3	—	—
Diuron ($C_9H_{10}ON_2Cl_2$)	20.3	0.76	0.080	—	0.159	10.2	7.7	2.5
Trifluoromethylbenzene ($C_6H_5CF_3$)	18.7	1.19	0.069	—	0.185	10.8	5.1	5.7
Metatrifluoromethylphenylacetonitrile ($C_9H_6NF_3$)	16.0	0.89	0.058	—	0.168	7.3	4.0	3.3
Tetramethylthiurammonosulfide ($C_6H_{12}N_2S_3$)	22.6	1.06	0.041	—	—	19.6	—	—
Methylthiopropionylaldehyde (C_4H_8OS)	25.0	1.62	0.001	—	0.005	23.8	18.8	5.0
Pesticides								
2,4 D acid (Herbicide, $C_8H_6O_3Cl_2$)	11.5	0.50	0.074	—	0.163	4.5	3.0	1.5
Mancozeb ($C_4H_6N_2S_4Mn)_iZn_{0,4}$)	14.0	0.50	—	—	—	9.5	—	—
Folpel ($C_9H_4O_2NSCl_3$)	9.1	0.37	0.072	—	0.205	3.6	—	—
Chlorfenvinphos ($C_{12}H_{24}O_4Cl_3P$)	18.0	0.43	0.011	—	0.288	7.7	—	—
Chlormephos ($C_5H_{12}O_2S_2ClP$)	19.1	0.51	0.075	—	0.055	13.9	—	—

(continued)

Table 3-4.14 ***Yields of Fire Products and Chemical, Convective, and Radiative Heats of Combustion for Well-Ventilated Fires[a] (Continued)***

Material	ΔH_T (kJ/g)	y_{CO_2} (g/g)	y_{CO} (g/g)	y_{ch} (g/g)	y_s (g/g)	ΔH_{ch} (kJ/g)	ΔH_{con} (kJ/g)	ΔH_{rad} (kJ/g)
Natural materials								
Tissue paper	—	—	—	—	—	11.4	6.7	4.7
Newspaper	—	—	—	—	—	14.4	—	—
Wood (red oak)	17.1	1.27	0.004	0.001	0.015	12.4	7.8	4.6
Wood (Douglas fir)	16.4	1.31	0.004	0.001	—	13.0	8.1	4.9
Wood (pine)	17.9	1.33	0.005	0.001	—	12.4	8.7	3.7
Corrugated paper	—	—	—	—	—	13.2	—	—
Wood (hemlock)[b]	—	—	—	—	0.015	13.3	—	—
Wool 100%[b]	—	—	—	—	0.008	19.5	—	—
Synthetic materials—solids (abbreviations/names in the nomenclature)								
ABS[b]	—	—	—	—	0.105	30.0	—	—
POM	15.4	1.40	0.001	0.001	—	14.4	11.2	3.2
PMMA	25.2	2.12	0.010	0.001	0.022	24.2	16.6	7.6
PE	43.6	2.76	0.024	0.007	0.060	38.4	21.8	16.6
PP	43.4	2.79	0.024	0.006	0.059	38.6	22.6	0
PS	39.2	2.33	0.060	0.014	0.164	27.0	11.0	16.0
Silicone	21.7	0.96	0.021	0.006	0.065	10.6	7.3	3.3
Polyester-1	32.5	1.65	0.070	0.020	0.091	20.6	10.8	9.8
Polyester-2	32.5	1.56	0.080	0.029	0.089	19.5	—	—
Epoxy-1	28.8	1.59	0.080	0.030	—	17.1	8.5	8.6
Epoxy-2	28.8	1.16	0.086	0.026	0.098	12.3	—	—
Nylon	30.8	2.06	0.038	0.016	0.075	27.1	16.3	10.8
Polyamide-6[b]	—	—	—	—	0.011	28.8	—	—
IPST[b]	—	—	—	—	0.080	23.3	—	—
PVEST[b]	—	—	—	—	0.076	22.0	—	—
Silicone rubber	21.7	0.96	0.021	0.005	0.078	10.9	—	—
Polyetheretherketone (PEEK-$CH_{0.63}O_{0.16}$)	31.3	1.6	0.029	—	0.008	17.5	—	—
Polysulfone (PSO-$CH_{0.81}O_{0.15}S_{0.04}$)	29.0	1.8	0.034	—	0.020	24.3	—	—
Polyethersulfone (PES-$CH_{0.67}O_{0.21}S_{0.08}$)	25.2	1.5	0.040	—	0.021	20.4	—	—
Polyetherimide (PEI-$CH_{0.68}N_{0.05}O_{0.14}$)	30.1	2.0	0.026	—	0.014	27.2	—	—
Polycarbonate (PC-$CH_{0.88}O_{0.13}$)	31.6	1.5	0.054	—	0.112	18.4	—	—
Polyurethane (flexible) foams								
GM21	26.2	1.55	0.010	0.002	0.131	17.8	8.6	9.2
GM23	27.2	1.51	0.031	0.005	0.227	19.0	10.3	8.7
GM25	24.6	1.50	0.028	0.005	0.194	17.0	7.2	9.8
GM27	23.2	1.57	0.042	0.004	0.198	16.4	7.6	8.8
Polyurethane (rigid) foams								
GM29	26.0	1.52	0.031	0.003	0.130	16.4	6.8	9.6
GM31	25.0	1.53	0.038	0.002	0.125	15.8	7.1	8.8
GM35	28.0	1.58	0.025	0.001	0.104	17.6	7.8	9.8
GM37	28.0	1.63	0.024	0.001	0.113	17.9	8.7	9.2
GM41	26.2	1.18	0.046	0.004	—	15.7	5.7	10.0
GM43	22.2	1.11	0.051	0.004	—	14.8	6.4	8.4
Polystyrene foams								
GM47	38.1	2.30	0.060	0.014	0.180	25.9	11.4	14.5
GM49	38.2	2.30	0.065	0.016	0.210	25.6	9.9	15.7
GM51	35.6	2.34	0.058	0.013	0.185	24.6	10.4	14.2
GM53	37.6	2.34	0.060	0.015	0.200	25.9	11.2	14.7
Polyethylene foams								
1	41.2	2.62	0.020	0.004	0.056	34.4	20.2	14.2
2	40.8	2.78	0.026	0.008	0.102	36.1	20.6	15.5
3	40.8	2.60	0.020	0.004	0.076	33.8	18.2	15.6
4	40.8	2.51	0.015	0.005	0.071	32.6	19.1	13.5

Table 3-4.14 ***Yields of Fire Products and Chemical, Convective, and Radiative Heats of Combustion for Well-Ventilated Fires[a] (Continued)***

Material	ΔH_T (kJ/g)	y_{CO_2} (g/g)	y_{CO} (g/g)	y_{ch} (g/g)	y_s (g/g)	ΔH_{ch} (kJ/g)	ΔH_{con} (kJ/g)	ΔH_{rad} (kJ/g)
Phenolic foams								
1[b]	—	—	—	—	0.002	10.0	—	—
2[b]	—	—	—	—	—	10.0	—	—
Halogenated materials (abbreviations/names in the nomenclature)								
Polyethylene with								
25% chlorine	31.6	1.71	0.042	0.016	0.115	22.6	10.0	12.6
36% chlorine	26.3	0.83	0.051	0.017	0.139	10.6	6.4	4.2
48% chlorine	20.6	0.59	0.049	0.015	0.134	7.2	3.9	3.3
PVC	16.4	0.46	0.063	0.023	0.172	5.7	3.1	2.6
PVC-1[b] (LOI = 0.50)	—	—	—	—	0.098	7.7	—	—
PVC-2[b] (LOI = 0.50)	—	—	—	—	0.076	8.3	—	—
PVC[b] (LOI = 0.20)	—	—	—	—	9.099	11.3	—	—
PVC[b] (LOI = 0.25)	—	—	—	—	0.078	9.8	—	—
PVC[b] (LOI = 0.30)	—	—	—	—	0.098	10.3	—	—
PVC (LOI = 0.35)	—	—	—	—	0.088	10.8	—	—
PVC panel	—	—	—	—	—	7.3	—	—
CPVC ($CH_{1.3}Cl_{0.70}$)	12.8	0.48	0.052	—	0.043	4.4	—	—
PVDF (CHF)	13.3	0.53	0.055	—	0.037	3.8	—	—
ECTFE ($CHF_{0.75}Cl_{0.25}$)	12.0	0.41	0.095	—	0.038	4.6	—	—
ETFE (Tefzel, CHF)	12.6	0.78	0.035	—	0.028	7.3	—	—
PFA (Teflon, $CF_{1.6}O_{0.01}$)	5.0	0.42	0.099	—	0.002	2.2	—	—
FEP (Teflon, $CF_{1.8}$)	4.8	0.25	0.116	—	0.003	1.3	—	—
TFE (Teflon, $CF_{1.8}$)	6.2	0.38	0.092	—	0.003	2.0	—	—
Building products[c]								
Particleboard (PB)	—	1.2	0.004	—	—	14.0	—	—
Fiberboard (FB)	—	1.4	0.015	—	—	14.0	—	—
Medium-density FB	—	1.2	0.002	—	—	14.0	—	—
Wood panel	—	1.2	0.002	—	—	15.0	—	—
Melamine-faced PB	—	0.8	0.025	—	—	10.7	—	—
Gypsumboard (GB)	—	0.3	0.027	—	—	4.3	—	—
Paper on GB	—	0.4	0.028	—	—	5.6	—	—
Plastic on GB	—	0.4	0.028	—	—	14.3	—	—
Textile on GB	—	0.4	0.025	—	—	13.0	—	—
Textile on rock wool	—	1.8	0.091	—	—	25.0	—	—
Paper on PB	—	1.2	0.003	—	—	12.5	—	—
Rigid PU	—	1.1	0.200	—	—	13.0	—	—
EPS	—	1.9	0.054	—	—	28.0	—	—
Composite and fiberglass-reinforced materials (FGR) (abbreviations/names in the nomenclature)								
PEEK/FGR[b]	—	—	—	—	0.042	20.5	—	—
IPST/FGR[b]	—	—	—	—	0.032	27.0	—	—
PES/FGR[b]	—	—	—	—	0.049	27.5	—	—
PEST1/FGR[b]	—	—	—	—	—	16.0	—	—
PEST2/FGR[b]	—	—	—	—	—	12.9	—	—
PEST1/FGR	—	—	—	—	—	19.0	—	—
PEST2/FGR	—	—	—	—	—	13.9	—	—
PEST3/FGR	—	1.47	0.055	0.007	0.070	17.9	10.7	7.2
PEST4/FGR	—	1.24	0.039	0.004	0.054	16.0	9.9	6.1
PEST5/FGR	—	0.71	0.102	0.019	0.068	9.3	6.5	2.8
Epoxy/FG[b]	—	—	—	—	0.056	27.5	—	—
PVEST/FGR	—	—	—	—	0.079	26.0	—	—
Kevlar/Phenolic	—	1.27	0.025	0.002	0.041	14.8	11.1	3.7
Phenolic-1/FGR	—	0.98	0.066	0.003	0.023	11.9	8.9	3.0
Phenolic-2/FGR[b]	—	—	—	—	0.016	22.0	—	—

(continued)

Table 3-4.14 ***Yields of Fire Products and Chemical, Convective, and Radiative Heats of Combustion for Well-Ventilated Fires[a] (Continued)***

Material	ΔH_T (kJ/g)	y_{CO_2} (g/g)	y_{CO} (g/g)	y_{ch} (g/g)	y_s (g/g)	ΔH_{ch} (kJ/g)	ΔH_{con} (kJ/g)	ΔH_{rad} (kJ/g)
Aircraft panel materials								
Epoxy/FGR/paint	—	0.828	0.114	0.016	0.166	11.3	6.2	5.1
Epoxy/Kevlar/paint	—	0.873	0.091	0.016	0.126	11.4	6.3	5.1
Phenolic/FGR/paint	—	1.49	0.027	0.002	0.059	22.9	11.5	11.4
Phenolic/Kevlar/paint	—	1.23	0.088	0.011	0.094	18.6	8.9	9.7
Phenolic/graphite/paint	—	1.67	0.026	0.003	0.062	24.6	14.0	10.6
Polycarbonate	—	—	—	—	—	20.5	—	—
Electric cables (abbreviations/names in the nomenclature)								
Polyethylene/Polyvinylchloride								
1	—	2.08	0.100	0.021	0.076	31.3	11.6	19.7
2	—	1.75	0.050	0.013	0.115	25.1	11.1	14.0
3	—	1.67	0.048	0.012	—	24.0	13.0	11.0
4	—	1.39	0.166	0.038	—	22.0	14.0	8.1
5	—	1.29	0.147	0.042	0.136	20.9	10.7	10.2
EPR/Hypalon								
1	—	1.95	0.072	0.014	—	29.6	15.8	13.9
2	—	1.74	0.076	0.022	—	26.8	17.0	9.8
3	—	1.21	0.072	0.014	—	19.0	12.3	6.7
4	—	0.99	0.090	0.085	0.082	17.4	6.6	10.8
5	—	0.95	0.122	0.024	—	17.3	7.5	9.8
6	—	0.89	0.121	0.022	0.164	13.9	9.2	4.7
Silicone								
1	—	1.65	0.011	0.001	—	25.0	17.5	7.3
2	—	1.47	0.029	0.001	—	24.0	20.0	4.0
XLPE/XLPE								
1	—	1.78	0.114	0.029	0.120	28.3	12.3	16.0
2	—	0.83	0.110	0.024	0.120	12.5	7.5	5.0
XLPE/Neoprene								
1	—	0.68	0.122	0.031	—	12.6	5.9	6.7
2	—	0.63	0.082	0.014	0.175	10.3	4.9	5.5
Silicone/PVC								
1	16.4	0.76	0.110	0.015	0.111	10.0	—	—
2	16.4	1.19	0.065	0.005	0.119	15.6	—	—
PVC/Nylon/PVC-Nylon								
1	—	0.63	0.084	0.024	—	10.2	5.0	5.2
2	—	0.49	0.082	0.032	0.115	9.2	4.8	4.4
PTFE								
1	—	0.180	0.091	0.012	0.011	3.2	2.7	0.4
2	6.2	0.383	0.103	—	0.005	5.7	—	—
Materials with fiberweb, netlike, and multiplex structure (abbreviations/names in the nomenclature)								
Olefin	—	1.49	0.006	—	—	16.5	13.3	3.2
PP-1	—	1.25	0.0029	—	—	14.0	10.8	3.2
PP-2	—	1.56	0.0048	—	—	17.2	10.5	6.7
Polyester-1	—	2.21	0.015	—	—	24.6	8.9	15.7
Polyester-2	—	1.51	0.0079	—	—	16.8	9.1	7.7
Polyester-3	—	2.55	0.020	—	—	28.5	22.6	5.9
Polyester-4	—	1.92	0.014	—	—	21.4	12.4	9.0
Rayon-1	—	1.80	0.043	—	—	20.3	14.1	6.2
Rayon-2	—	1.91	0.043	0.002	—	21.5	13.3	8.2
Rayon-3	—	1.18	0.047	—	—	13.5	8.3	5.2
Polyester-Rayon	—	1.52	0.005	—	—	16.8	9.1	7.7
Polyester-polyamide	—	1.82	0.008	—	—	20.2	10.4	9.8
Rayon-PE	—	1.50	0.027	—	—	16.9	8.72	8.2

Table 3-4.14 ***Yields of Fire Products and Chemical, Convective, and Radiative Heats of Combustion for Well-Ventilated Fires[a] (Continued)***

Material	ΔH_T (kJ/g)	y_{CO_2} (g/g)	y_{CO} (g/g)	y_{ch} (g/g)	y_s (g/g)	ΔH_{ch} (kJ/g)	ΔH_{con} (kJ/g)	ΔH_{rad} (kJ/g)
Two to eight 100- × 100- × 100-mm corrugated paper boxes with and without the polymers with three-dimensional arrangement (abbreviations/names in the nomenclature)[d]								
Empty	—	1.53	0.023	0.001	—	14.2	10.7	3.5
With PVC (62%-thick)	—	1.01	0.073	0.007	0.119	10.7	9.5	1.2
With PC (59%-thick)	—	1.73	0.047	0.002	0.061	18.4	13.5	4.9
With PS (58%-thick)	—	1.40	0.138	0.026	0.285	16.2	12.5	3.7
With PS (60%-thin)	—	1.88	0.068	0.020	0.140	19.4	10.1	9.3
With PS (40%-thin)	—	1.74	0.042	0.005	0.167	18.0	11.7	6.7
With ABS (59%-thick)	—	1.53	0.089	0.006	0.143	16.1	12.7	3.4
With PET (41%-thin)	—	1.87	0.050	0.006	0.053	19.9	11.8	8.1
With PU (40%-foam)	—	1.56	0.024	—	—	14.4	8.6	5.8
High-pressure liquid spray combustion[e]								
Hydraulic fluids								
Organic polyol esters								
1	36.6	—	—	—	—	35.5	—	—
2	35.7	—	—	—	—	35.1	—	—
3	40.3	—	—	—	—	37.2	—	—
4	37.0	—	—	—	—	35.7	—	—
Phosphate esters								
1	31.8	—	—	—	—	29.3	—	—
2	32.0	—	—	—	—	29.6	—	—
Water-in-oil emulsions								
1	27.6	—	—	—	—	2.5	—	—
Polyglycol-in-water								
1	11.0	—	—	—	—	10.4	—	—
2	11.9	—	—	—	—	11.1	—	—
3	14.7	—	—	—	—	12.2	—	—
4	12.1	—	—	—	—	10.6	—	—
Liquid fuels								
Mineral oil	46.0	—	—	—	—	44.3	—	—
Methanol	20.0	—	—	—	—	19.8	—	—
Ethanol	27.7	—	—	—	—	26.2	—	—
Heptane	44.4	—	—	—	—	40.3	—	—

[a]Data measured in the ASTM E2058 fire propagation apparatus. Data measured in the cone calorimeter are identified by superscripts [b] and [c]. Some of the data are corrected to reflect well-ventilated fire conditions. All the data are reported for turbulent fires, that is, materials exposed to higher external heat flux values.

Dashes: either not measured or are less than 0.001.

[b]Calculated from the data measured in the cone calorimeter as reported in References 20 and 39.

[c]Calculated from the data measured in the cone calorimeter as reported in Reference 58.

[d]100- × 100- × 100-mm corrugated paper boxes with and without the 99- × 99- × 99-mm polymer boxes or pieces on corrugated paper compartments. The boxes are arranged in one and two layers, about 12 mm apart, with one to four boxes in each layer, separated by about 12 mm. All the boxes are placed on a very light metal frame made of rods with screen base. Measurements made in the ASTM E2058 fire propagation apparatus; numbers in parentheses are the weight percents.

[e]Data from Reference 59 measured in high-pressure liquid spray combustion in the fire products collector (10,000-kW scale apparatus in Figure 3-4.8).

gasified material (e.g., smoke, CO, hydrocarbons, and other intermediate products) remain incomplete and heat release rate decreases.[44]

In ventilation-controlled fires, heat release rate depends on the air supply rate and the mass loss rate, in addition to other factors. For ventilation-controlled fires, the effects of the mass flow rate of air and fuel mass loss rate are characterized, most commonly, by the local equivalence ratio:

$$\Phi = \frac{S\dot{m}''A}{\dot{m}_{air}} \tag{37}$$

where

Φ = equivalence ratio
S = stoichiometric mass air-to-fuel ratio (g/g)
$\dot{m}''$ = mass loss rate (g/m²·s)
A = exposed area of the material burning (m²)
$\dot{m}_{air}$ = mass flow rate of air (g/s)

Generalized-state relationships between mass fractions of major species (O_2, fuel, CO_2, H_2O, CO, and H_2) and temperature as functions of local equivalence ratios

Table 3-4.15 ***Chemical and Convective Heat Release Parameters***

Materials	$(HRP)_{ch}$ ASTM E2058 Fire Propagation Apparatus	$(HRP)_{ch}$ ASTM E1354[a]	$(HRP)_{ch}$ Cal[b]	$(HRP)_{con}$ ASTM E2058 Fire Propagation Apparatus	$(HRP)_{con}$ ASTM E906[c]	$(HRP)_{con}$ Cal[b]
Liquids and gases (hydrocarbons, alkanes)						
Hexane	—	—	83	—	—	56
Heptane	—	—	75	—	—	50
Octane	—	—	68	—	—	46
Nonane	—	—	64	—	—	42
Decane	—	—	59	—	—	39
Undecane	—	—	55	—	—	36
Dodecane	—	—	52	—	—	34
Tridecane	—	—	50	—	—	32
Kerosene	—	—	47	—	—	17
Hexadexane	—	—	44	—	—	28
Solids (abbreviations/names in the nomenclature)						
ABS	—	14	—	—	—	—
Acrylic sheet	—	6	—	—	—	—
Epoxy	—	11	—	—	—	—
IPST	—	6	—	—	—	—
Polyamide	21	—	—	—	—	—
Polypropylene	19	—	—	11	—	—
Polyethylene	17	21	—	12	—	—
Polystyrene	16	19	—	6	—	—
Polymethylmethacrylate	15	14	—	10	—	—
Nylon	12	—	—	7	—	—
Polyamide-6	—	21	—	—	—	—
Filled phenolic foam—50% inert	—	1	—	—	—	—
Polycarbonate	9	—	—	—	—	—
Polyoxymethylene	6	—	—	5	—	—
Polyethylene/25% Cl	11	—	—	5	—	—
Plasticized-PVC-3, LOI 0.25	—	5	—	—	—	—
Plasticized-PVC-4, LOI 0.30	—	5	—	—	—	—
Plasticized-PVC-5, LOI 0.35	—	5	—	—	—	—
Polyethylene/35% Cl	4	—	—	2	—	—
Rigid PVC-1, LOI 0.50	—	3	—	—	—	—
Rigid PVC-2	2	3	—	1	—	—
PVC panel	2	—	—	—	—	—
Polyethylene/48% Cl	2	—	—	—	—	—
PVEST	—	13	—	—	—	—
ETFE (Tefzel)	6	—	—	—	—	—
PFA (Teflon)	5	—	—	—	—	—
FEP (Teflon)	2	—	—	—	—	—
TFE (Teflon)	2	—	—	—	—	—
Wood (hemlock)	—	1	—	—	—	—
Wood (Douglas fir)	7	—	—	5	—	—
Wool	—	5	—	—	—	—
Composites and fiberglass-reinforced materials (FGR) (abbreviations/names in the nomenclature)						
Bismaleimide/graphite/ceramic (CC)	—	1	—	—	—	—
Epoxy/FGR	—	2	—	—	—	—
Epoxy/graphite	2	—	—	—	—	—
Epoxy/graphite/CC	2	—	—	—	—	—
Epoxy/graphite/intumescent (IC)	2	—	—	—	—	—
IPST/FGR	—	1	—	—	—	—
PEEK/FGR	—	3	—	—	—	—
PES/FGR	—	1	—	—	—	—
PEST-1/FGR	3	—	—	—	—	—
PEST-2/FGR	8	—	—	—	—	—
PEST-3/FGR	10	—	—	—	—	—
PEST-4/FGR	3	—	—	—	—	—
PEST-5/FGR	3	—	—	—	—	—
PEST-6-FGR	3	—	—	—	—	—

Table 3-4.15 ***Chemical and Convective Heat Release Parameters (Continued)***

Materials	$(HRP)_{ch}$			$(HRP)_{con}$		
	ASTM E2058 Fire Propagation Apparatus	ASTM E1354[a]	Cal[b]	ASTM E2058 Fire Propagation Apparatus	ASTM E906[c]	Cal[b]
Composites and fiberglass-reinforced materials (FGR) (continued)						
Phenol/FGR	—	1	—	—	—	—
Phenolic/Kevlar	2	—	—	—	—	—
Phenol/graphite	1	—	—	—	—	—
PVEST-1/FGR	3	—	—	—	—	—
PVEST-1/FGR/CC	3	—	—	—	—	—
PVEST-1/FGR/IC	1	—	—	—	—	—
PVEST-2/FGR	7	—	—	—	—	—
PVEST-3/FGR	2	—	—	—	—	—
Aircraft panel materials						
Epoxy fiberglass	4	4	—	2	1	—
Epoxy Kevlar	4	4	—	2	2	—
Phenolic Kevlar	5	4	—	2	—	—
Phenolic graphite	4	3	—	1	—	—
Phenolic fiberglass	4	3	—	2	1	—
Polycarbonate panel	9	—	—	—	—	—
Foams						
Polystyrene						
GM53	20	—	—	6	—	—
GM49	19	—	—	8	—	—
GM51	18	—	—	9	—	—
Flexible polyurethane						
GM 21	7	—	—	3	3	—
GM 23	9	—	—	5	6	—
GM 25	14	—	—	6	4	—
GM 27	9	—	—	4	2	—
Phenolic	—	1	—	—	—	—
Electrical cables (abbreviations/names in the nomenclature)						
PVC/PVC-1 (Group 3)	15	—	—	—	—	—
PE/PVC (Group 3)	19	—	—	—	—	—
PP,PEST/PVC (Group 3)	11	—	—	—	—	—
PVC/PVC-2 (Group 3)	14	—	—	—	—	—
Chlorinated PE (Group 2)	5	—	—	—	—	—
PVC/PVC-3 (Group 2)	4	—	—	—	—	—
EPR/PVC (Group 2)	6	—	—	—	—	—
PVC/EPR (Group 2)	4	—	—	—	—	—
XLPE/XLPE (Group 2)	6	—	—	—	—	—
EPR/hypalon-1 (Group 2)	6	—	—	—	—	—
EPR/hypalon-2 (Group 2)	4	—	—	—	—	—
EPR/hypalon-3 (Group 1)	3	—	—	—	—	—
EPR/hypalon-4 (Group 1)	3	—	—	—	—	—
EPR/EPR-1 (Group 1)	3	—	—	—	—	—
EPR/EPR-2 (Group 1)	3	—	—	—	—	—
EPR/EPR-3 (Group 1)	2	—	—	—	—	—
XLPE-EVA-1 (Group 1)	3	—	—	—	—	—
XLPE-EVA-2 (Group 1)	3	—	—	—	—	—
ETFA (Group 1)	3	—	—	—	—	—
PVC/PVF_2 (Group 1)	1	—	—	—	—	—
FEP/FEP-1 (Group 1)	2	—	—	—	—	—
FEP/FEP-2 (Group 2)	2	—	—	—	—	—

[a]Calculated from the data reported in References 20 and 39.

[b]Calculated from the data in References 48 and 49.

[c]From Reference 60.

for hydrocarbon-air diffusion flames are available.[61] The relationships suggest that the generation efficiencies of CO, fuel vapors, water, CO_2, and H and the consumption efficiency of O_2 are in approximate thermodynamic equilibrium for well-ventilated combustion, but deviate from equilibrium for ventilation-controlled combustion. This concept has been used for fires of polymeric materials.[44] In the tests, chemical and convective heat release rates, mass loss rate, and generation rates of fire products have been measured for various equivalence ratios in the ASTM E2058 fire propagation apparatus [Figure 3-4.2(a)] and in the Fire Research Institute's (FRI) 0.022-m^3 enclosure in Tokyo, Japan, described in Reference 44. The combustion efficiency and its convective component are found to decrease as fires become fuel rich, due to increase in the equivalence ratio. The ratio of the combustion efficiency and its convective component or chemical and convective heats of combustion for ventilation-controlled to well-ventilated combustion is expressed as[44]

$$\zeta_{ch} = \frac{(\chi_{ch})_{vc}}{(\chi_{ch})_{wv}} = \frac{(\Delta H_{ch}/\Delta H_T)_{vc}}{(\Delta H_{ch}/\Delta H_T)_{wv}} = \frac{(\Delta H_{ch})_{vc}}{(\Delta H_{ch})_{wv}} \quad (38)$$

$$\zeta_{con} = \frac{(\chi_{con})_{vc}}{(\chi_{con})_{wv}} = \frac{(\Delta H_{con}/\Delta H_T)_{vc}}{(\Delta H_{con}/\Delta H_T)_{wv}} = \frac{(\Delta H_{con})_{vc}}{(\Delta H_{con})_{wv}} \quad (39)$$

where ζ_{ch} and ζ_{con} are the ratio of the combustion efficiency to its convective component, or chemical and convective heats of combustion for ventilation-controlled to well-ventilated combustion. Subscript *vc* represents ventilation-controlled fire, and *wv* represents well-ventilated fire.

The experimental data for the ratios of the chemical and convective heats of combustion for ventilation-controlled to well-ventilated fires at various equivalence ratios are shown in Figures 3-4.26 and 3-4.27. The data are measured in the ASTM E2058 fire propagation apparatus and the FRI's 0.022-m^3 enclosure, details of which are described in Reference 44. The data for the polymers indicated in the figures satisfy the following general correlations, irrespective of their chemical structures:[44]

$$\frac{(\Delta H_{ch})_{vc}}{(\Delta H_{ch})_{wv}} = 1 - \frac{0.97}{\exp(\Phi/2.15)^{-1.2}} \quad (40)$$

$$\frac{(\Delta H_{con})_{vc}}{(\Delta H_{con})_{wv}} = 1 - \frac{1.0}{\exp(\Phi/1.38)^{-2.8}} \quad (41)$$

The effects of ventilation on the chemical and convective heats of combustion are reflected by the magnitudes of the expressions within the parentheses on the right-hand sides of Equations 40 and 41. For a well-ventilated fire, $\Phi \ll 1.0$, $(\Delta H_{ch})_{vc} = (\Delta H_{ch})_{wv}$, and $(\Delta H_{con})_{vc} = (\Delta H_{con})_{wv}$.

As a fire changes from well ventilated to ventilation controlled, equivalence ratio increases and the magnitudes of the expressions within the parentheses on the right-hand sides of Equations 40 and 41 increase. Thus with increase in the equivalence ratio, the chemical and convective heats of combustion decrease. The decrease in the convective heat of combustion is higher than it is for the chemical heat of combustion, because the coefficients for the equivalence ratios are different. The correlation suggests that a higher fraction of the chemical heat of combustion is expected to be converted to the radiative heat of combustion as fires change from well ventilated to ventilation controlled. This is in general agreement with the observations for the ventilation-controlled fires in buildings.

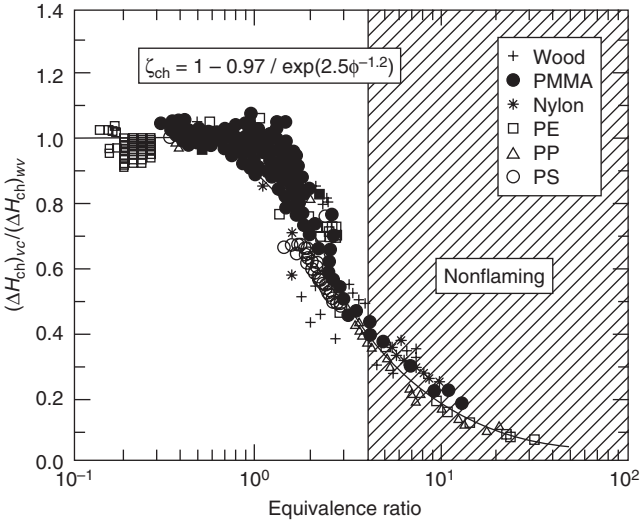

Figure 3-4.26. ***Ratio of the ventilation-controlled to well-ventilated chemical heat of combustion versus the equivalence ratio. Data are measured in the ASTM E2058 fire propagation apparatus and in the Fire Research Institute's enclosure.[44] Subscript vc represents ventilation-controlled fires, and subscript wv represents well-ventilated fires.***

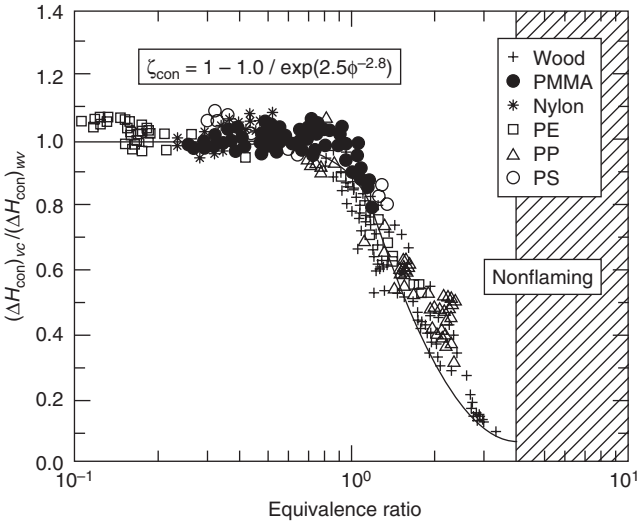

Figure 3-4.27. ***Ratio of the ventilation-controlled to well-ventilated convective heat of combustion versus the equivalence ratio. Data are measured in the ASTM E2058 fire propagation apparatus and in the Fire Research Institute's enclosure.[44] Subscript vc represents ventilation-controlled fires, and subscript wv represents well-ventilated fires.***

Equations 40 and 41 can be used in models for the assessment of the ventilation-controlled fire behavior of materials, using chemical and convective heats of combustion for well-ventilated fires such as from Table 3-4.14.

EXAMPLE 13:

Calculate the chemical heats of combustion at equivalence ratios of 1, 2, and 3 for red oak, polyethylene, polystyrene, and nylon using Equation 40 and data from Table 3-4.14 for well-ventilated fires.

SOLUTION:

	Chemical Heats of Combustion (kJ/g)			
Material	$\Phi \ll 1.0$	$\Phi = 1.0$	$\Phi = 2.0$	$\Phi = 3.0$
Red oak	12.4	11.4	8.3	6.2
Polyethylene	38.4	35.3	25.9	19.3
Polystyrene	27.0	24.9	18.2	13.6
Nylon	27.1	24.9	18.2	13.6

Generation of Chemical Compounds and Consumption of Oxygen

Chemical compounds (smoke, toxic, corrosive, and odorous compounds) are the main contributors to nonthermal hazard and thus the assessments of their chemical natures and generation rates, relative to the airflow rate, are of critical importance for the protection of life and property.

In fires, compounds are generated as a result of gasification and decomposition of the material and burning of the species in the gas phase with air in the form of a diffusion flame. In general, generation of the fire products and consumption of oxygen in diffusion flames occur in two zones.[44]

1. *Reduction zone.* In this zone, the material melts, decomposes, gasifies, and/or generates species that react to form smoke, CO, hydrocarbons, and other intermediate products. Very little oxygen is consumed in this region. The extent of conversion of the material to smoke, CO, hydrocarbons, and other products depends on the chemical nature of the material.
2. *Oxidation zone.* In this zone, the reduction zone products (smoke, CO, hydrocarbons, and other intermediates) react with varying degrees of efficiency with the oxygen from air and generate chemical heat and varying amounts of products of complete combustion, such as CO_2 and H_2O. The lower the reaction efficiency, the higher the amounts of reduction zone products emitted from a fire. The reaction efficiency of the reduction zone products with oxygen depends on the concentrations of the products relative to the oxygen concentration, temperature, and mixing of the products and air. For example, in laminar diffusion flames, smoke is emitted when the temperature of the oxidation zone falls below about 1300 K.

The hot ceiling layer in a building fire may be considered in terms of oxidation and reduction zone products. In building fires with plenty of ventilation, the concentrations of the reduction zone products are higher in the central region of the ceiling layer, whereas the concentrations of the oxidation zone products are higher closer to the room opening. As the air supply rate, or oxygen concentration available to the fire, decreases due to restrictions in the ventilation, the ceiling layer expands and starts occupying greater room volume with increase in the concentrations of the reduction zone products. Under these conditions, large amounts of the reduction zone products are released within the building increasing the nonthermal hazard.

The generation rate of a fire product is directly proportional to the mass loss rate, the proportionality constant being defined as the yield of the product:[1–4,9–16,41,44,45,48,49,52–55]

$$\dot{G}_j'' = y_j \dot{m}'' \tag{42}$$

where $\dot{G}_j''$ is the mass generation rate of product j (g/m²·s), and y_j is the yield of product j (g/g). The total mass of the product generated is obtained by the summation of the generation rate:

$$W_j = A \sum_{n=t_0}^{n=t_f} \dot{G}_j''(t_n) \Delta t_n \tag{43}$$

where

W_j = total mass of product j generated from the flaming and/or nonflaming fire of the material (g)

t_0 = time when the sample is exposed to heat (s)

t_f = time when there is no more vapor formation (s)

From Equations 27, 42, and 43, the average value of the yield of product j is

$$\overline{y_j} = \frac{W_j}{W_f} \tag{44}$$

The mass consumption rate of oxygen is also directly proportional to the mass loss rate:[1–4,9–16,33,36–39,42–45]

$$\dot{C}_{\mathrm{O}}'' = c_{\mathrm{O}} \dot{m}'' \tag{45}$$

where $\dot{C}_{\mathrm{O}}''$ is the mass consumption rate of oxygen (g/m²·s), and c_O is the mass of oxygen consumed per unit mass of fuel (g/g).

The mass generation rates of fire products and mass consumption rate of oxygen are determined by measuring the volume fractions of the products and oxygen and the total volumetric or mass flow rate of the fire products-air mixture:[2,3,44]

$$\dot{G}_j'' = \frac{f_j \dot{V} \rho_j}{A} = f_j \dot{W} \left(\frac{\rho_j}{\rho_g A} \right) \tag{46}$$

$$\dot{C}_{\mathrm{O}}'' = \frac{f_{\mathrm{O}} \dot{V} \rho_{\mathrm{O}}}{A} = f_{\mathrm{O}} \dot{W} \left(\frac{\rho_{\mathrm{O}}}{\rho_g A} \right) \tag{47}$$

where

f_j = volume fraction of product j

f_{O} = volume fraction of oxygen

$\dot{V}$ = total volumetric flow rate of the fire product-air mixture (m³/s)

$\dot{W}$ = total mass flow rate of the fire product-air mixture (g/s)

ρ_j = density of product j at the temperature of the fire product-air mixture (g/m³)

ρ_g = density of the hot fire product-air mixture (g/m³)

ρ_{O} = density of oxygen at the temperature of the fire product-air mixture (g/m³)

A = total area of the material burning (m²)

For volume fraction measurements, sampling ducts are used where fire products and air are well mixed, such as in the ASTM E2058 fire propagation apparatuses [Figure 3-4.2, parts (a) and (b) and 3-4.8] and in the cone calorimeter (Figure 3-4.3). Figure 3-4.28 shows the measurement locations in the sampling duct of the ASTM E2058 fire propagation apparatus. The volume fractions are measured by various types of instruments; for example, in the ASTM E2058 fire propagation apparatuses, they are measured continuously by (1) commercial infrared analyzers for CO and CO_2; (2) a high-sensitivity commercial paramagnetic analyzer for oxygen; (3) a commercial flame ionization analyzer for the mixture of low molecular weight gaseous hydrocarbons; and (4) by a turbidimeter, designed by the FMRC Flammability Laboratory,[62] for smoke. The turbidimeter measures the optical density defined as

$$D = \frac{\ln (I_0/I)}{\ell} \tag{48}$$

where

D = optical density (1/m)
I/I_0 = fraction of light transmitted through smoke
ℓ = optical path length (m)

The volume fraction of smoke is obtained from the following relationship:[62]

$$f_s = \frac{D\lambda \times 10^{-6}}{\Omega} \tag{49}$$

where

f_s = volume fraction of smoke
λ = wavelength of the light source (μm)
Ω = coefficient of particulate extinction taken as 7.0.[62]

In the ASTM E2058 fire propagation apparatuses, optical density is measured at wavelengths of 0.4579 μm (blue), 0.6328 μm (red), and 1.06 μm (IR). In the cone calorimeter, optical density is measured by using a helium-neon laser with a wavelength of 0.6328 μm (red).

From Equations 46 and 49,

$$\dot{G}_s'' = \frac{f_s \dot{V} \rho_s \times 10^{-6}}{A} = \left(\frac{D\lambda}{7}\right)\left(\frac{\rho_s \dot{V} \times 10^{-6}}{A}\right) = \left(\frac{D\lambda}{7}\right)\left(\frac{\rho_s}{\rho_a}\right)\left(\frac{\dot{W} \times 10^{-6}}{A}\right) \tag{50}$$

In the ASTM E2058 fire propagation apparatuses and the cone calorimeter, the fire products in the sampling duct are diluted about 20 times and thus the density of air, $\rho_a = 1.2 \times 10^3$ g/m^3, and the density of smoke, $\rho_s = 1.1 \times 10^6$ g/m^3, as suggested in Reference 62, are used:

$$\dot{G}_s'' = \left(\frac{1.1 \times 10^6 \times 10^{-6}}{7}\right)\left(\frac{\dot{V}}{A}\right)D\lambda = \left(\frac{1.1 \times 10^6 \times 10^{-6}}{7 \times 1.2 \times 10^3}\right)\left(\frac{\dot{W}}{A}\right)D\lambda \tag{51}$$

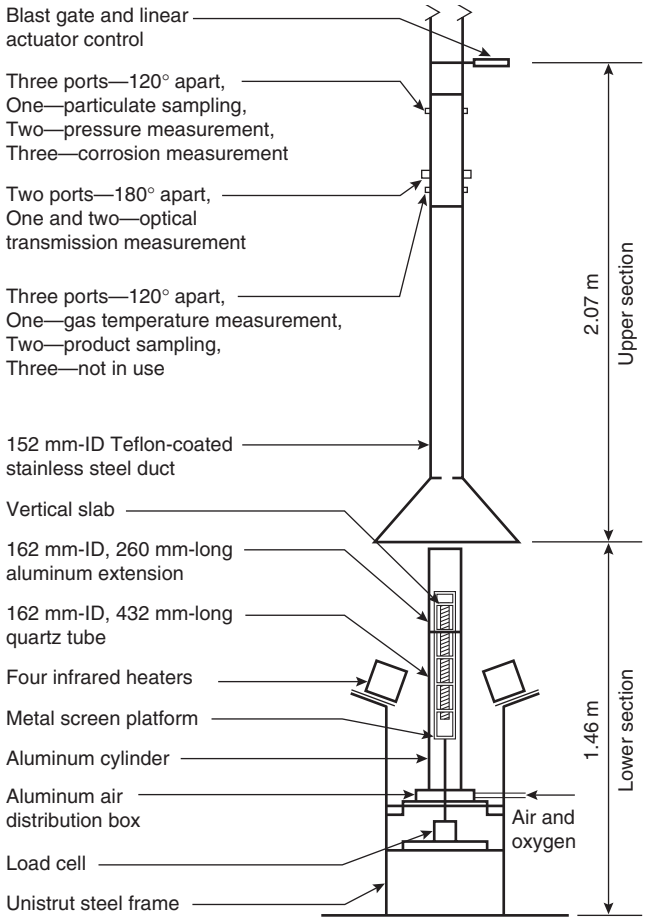

Figure 3-4.28. ***Sketch of the ASTM E2058 fire propagation apparatus showing locations where measurements are made for the product concentration, optical transmission, particulate concentration, and corrosion.***

For blue wavelength of light (λ = 0.4579 μm),

$$\dot{G}_s'' = 0.0720\left(\frac{D_{\text{blue}}\dot{V}}{A}\right) = 0.0600 \times 10^{-3}\left(\frac{D_{\text{blue}}\dot{W}}{A}\right) \tag{52}$$

For red wavelength of light (λ = 0.6328 μm),

$$\dot{G}_s'' = 0.0994\left(\frac{D_{\text{red}}\dot{V}}{A}\right) = 0.0829 \times 10^{-3}\left(\frac{D_{\text{red}}\dot{W}}{A}\right) \tag{53}$$

For infrared wavelength of light (λ = 1.06 μm),

$$\dot{G}_s'' = 0.1666\left(\frac{D_{\text{IR}}\dot{V}}{A}\right) = 0.1388 \times 10^{-3}\left(\frac{D_{\text{IR}}\dot{W}}{A}\right) \tag{54}$$

where D_{blue}, D_{red}, and D_{IR} are the optical densities measured at wavelengths of 0.4579, 0.6328, and 1.06 μm, respectively. These optical densities and total mass flow rate of the fire products-air mixture, $\dot{W}$, are measured continuously in the ASTM E2058 fire propagation apparatuses and the cone calorimeter, and A is known. The generation rates of smoke obtained from the optical densities at three wavelengths in the ASTM E2058 fire propagation appara-

tus are averaged. The smoke mass generated in the test is also measured continuously in the ASTM E2058 fire propagation apparatus by a commercial smoke mass monitoring instrument. The data are used to calculate the mass generation rate of smoke. The smoke generation rates obtained from the optical density and smoke mass monitor show very good agreement.

In the cone calorimeter, the smoke data are reported in terms of the average specific extinction area: (m^2/kg)[19]

$$\bar{\tau} = \frac{\sum_i \dot{V}_i D_i \Delta t_i}{W_f} \tag{55}$$

where $\bar{\tau}$ is the average specific extinction area determined in the cone calorimeter (m^2/g). Multiplying both sides of Equation 55 by $\rho_s \lambda \times 10^{-6}/7$ and rearranging

$$\bar{\tau}(\rho_s \lambda/7) \times 10^{-6} = \frac{\sum_i [(D_i \lambda \times 10^{-6}/7)\rho_s \dot{V}_i]\Delta t_i}{W_f} = \frac{W_s}{W_f} = \bar{y}_s \tag{56}$$

In the cone calorimeter, $\lambda = 0.6328$ μm for red wavelength and using $\rho_s = 1.1 \times 10^6$ g/m^3, as suggested in Reference 62, the average yield of smoke from the average specific extinction area determined in the cone calorimeter can be calculated from the following expression:

$$\bar{y}_s = 0.0994 \times 10^{-3} \bar{\tau} \tag{57}$$

where $\bar{y}_s$ is the average yield of smoke (g/g).

The smoking characteristics of a material are also reported in terms of *mass optical density* (MOD):[1,4,16,60]

$$\text{MOD} = \left[\frac{\log_{10}(I_0/I)}{\ell}\right]\left[\frac{\dot{V}}{A\dot{m}''}\right] = \left[\frac{D}{2.303}\right]\left[\frac{\dot{V}}{A\dot{m}''}\right] \tag{58}$$

From Equations 42 and 50, with $\rho_s = 1.1 \times 10^6$ g/m^3 and $\lambda = 0.6328$ μm,

$$y_s = \left(\frac{\lambda \rho_s}{7.0}\right)\left(\frac{D\dot{V} \times 10^{-6}}{A\dot{m}''}\right) = 0.0994\left(\frac{\text{MOD}}{2.303}\right) \tag{59}$$

MOD is generally reported with $\log_{10}$, however if it is changed to $\log_e$ and m^2/kg by multiplying it by 2.303 and dividing it by 1000, it becomes the specific extinction area, a terminology used in reporting the cone calorimeter data.

The average data for the yields of CO, CO_2, mixture of gaseous hydrocarbons, and smoke for well-ventilated fires are listed in Table 3-4.14.

EXAMPLE 14:

For a fiberglass-reinforced material, the following data were measured for combustion in normal air at an external heat flux value of 50 kW/m^2:

Total mass of the sample lost (g)	229
Total mass generated (g)	
CO	0.478
CO_2	290
Hydrocarbons	0.378
Smoke	6.31
Total energy generated (kJ)	3221

Calculate the average yields of CO, CO_2, hydrocarbons, and smoke and the average chemical heat of combustion.

SOLUTION:

The average yields are calculated from Equation 44, and the average chemical heats of combustion are calculated from Equation 29.

Average yields (g/g)	
CO	0.0021
CO_2	1.27
Hydrocarbons	0.002
Smoke	0.028
Average chemical heats of combustion (kJ/g)	14.1

EXAMPLE 15:

A circular sample of polystyrene, about 0.007 m^2 in area and 25 mm in thickness, was burned in normal air in the presence of external heat flux. In the test, measurements were made for the mass loss rate and light obscuration by smoke in the sampling duct with an optical path length of 0.149 m. The total volumetric flow rate of the mixture of fire products and air through the sampling duct was 0.311 m^3/s, and the wavelength of light source used was 0.6328 μm. At the steady-state combustion of polystyrene, the measured mass loss rate was 33 g/m^2·s with smoke obscuring 83.5 percent of the light. Calculate the yield of smoke from the data using a value of 1.1×10^6 g/m^3 for the density of smoke.

SOLUTION:

The optical density from Equation 48 is

$$D = \frac{\ln(I_0/I)}{\ell} = \frac{\ln(100/83.5)}{0.149} = 121\left(\frac{1}{\text{m}}\right)$$

The smoke generation rate from Equation 51 is

$$\dot{G}_s'' = \frac{1.1\dot{V}D\lambda}{7 \times A} = \frac{1.1 \times 0.311 \times 1.21 \times 0.6328}{7 \times 0.007} = 5.35 \text{ g/m}^2\cdot\text{s}$$

The smoke yield from Equation 42 is

$$y_s = \frac{5.35 \text{g/m}^2\cdot\text{s}}{33 \text{g/m}^2\cdot\text{s}} = 0.162 \text{ g/g}$$

Efficiencies of oxygen mass consumption and mass generation of products: A chemical reaction between oxygen and a fuel monomer of a material can be expressed as

$$F = \nu_O O_2 + \nu_N N_2 + \nu_{j_1} J_1 + \nu_{j_2} J_2 + \nu_N N_2 \tag{60}$$

where

F = fuel monomer of a material
ν_O = stoichiometric coefficient for oxygen
ν_N = stoichiometric coefficient and nitrogen
ν_{j_1}, ν_{j_2} = stoichiometric coefficients for the maximum possible conversion of the fuel monomer to products J_1 and J_2, respectively

The stoichiometric mass oxygen-to-fuel ratio for the maximum possible conversion of the fuel monomer is expressed as

$$\Psi_O = \frac{\nu_O M_O}{M_f} \tag{61}$$

where

Ψ_O = stoichiometric mass oxygen-to-fuel ratio for the maximum possible conversion of the fuel monomer to products

M_O = molecular weight of oxygen (32 g/mol)

M_f = molecular weight of the fuel monomer of the material (g/mol)

M_f is calculated from its elemental composition. For the elemental composition measurements, microanalytical techniques are used.

The stoichiometric yield for the maximum possible conversion of the fuel monomer of the material to a product is expressed as

$$\Psi_j = \frac{\nu_j M_j}{M_f} \tag{62}$$

where Ψ_j is the stoichiometric yield for the maximum possible conversion of the fuel monomer of the material to product j, and M_j is the molecular weight of product (g/mol).

The stoichiometric yields for some selected materials, calculated from the elemental composition data from the flammability laboratory, are listed in Table 3-4.16 for fuel monomer conversion to CO, CO_2, hydrocarbons, smoke, HCl, and HF. The stoichiometric yields depend on the number of atoms relative to the carbon atom. The yields provide an insight into the nature of products and the amounts of products expected to be generated in flaming and nonflaming fires, when expressed as the stoichiometric oxygen mass consumption rate and stoichiometric mass generation rates of products:

$$\dot{C}''_{\text{stoich,O}} = \Psi_O \dot{m}'' \tag{63}$$

$$\dot{G}''_{\text{stoich},j} = \Psi_j \dot{m}'' \tag{64}$$

where $\dot{C}''_{\text{stoich,O}}$ and $\dot{G}''_{\text{stoich},j}$ are the stoichiometric oxygen mass consumption rate and stoichiometric mass generation rate of product j for the maximum possible conversion of the fuel monomer to the product, respectively (g/m²·s).

In fires, the actual oxygen mass consumption rate and the mass generation rates of products are significantly less than the stoichiometric rates. The ratio of the actual oxygen mass consumption rate to stoichiometric rates is thus defined as the efficiency of oxygen mass consumption or product mass generation:[2–4,16,44]

$$\eta_O = \frac{\dot{C}''_{\text{actual,O}}}{\dot{C}''_{\text{stoich,O}}} = \frac{c_O \dot{m}''}{\Psi_O \dot{m}''} = \frac{c_O}{\Psi_O} \tag{65}$$

$$\eta_j = \frac{\dot{G}''_{\text{actual},j}}{\dot{G}''_{\text{stoich},j}} = \frac{y_j \dot{m}''}{\Psi_j \dot{m}''} = \frac{y_j}{\Psi_j} \tag{66}$$

where η_O is efficiency of oxygen mass consumption and η_j is the generation efficiency of product j. Subscript represents the actual oxygen mass consumption rate or the actual mass generation rate of a product.

EXAMPLE 16:

A material is made up of carbon, hydrogen, and oxygen. The weight of the material is distributed as follows: 54 percent as carbon, 6 percent as hydrogen, and 40 percent as oxygen. Calculate the chemical formula of the fuel monomer of the material.

SOLUTION:

From the atomic weights and the weight percent of the atoms, the number of atoms are as follows: carbon (C): 54/12 = 4.5; hydrogen (H): 6/1 = 6.0; and oxygen (O): 40/16 = 2.5. Thus the chemical formula of the fuel monomer of the material is $C_{4.5}H_{6.0}O_{2.5}$ or, dividing by 4.5, $CH_{1.33}O_{0.56}$.

EXAMPLE 17:

For the material in Example 16, calculate the stoichiometric mass oxygen-to-fuel ratio, stoichiometric mass air-to-fuel ratio, and stoichiometric yields for maximum possible conversion of the fuel monomer of the material to CO, CO_2, hydrocarbons, water, and smoke. Assume smoke to be pure carbon, and hydrocarbons as having the same carbon-atom-to-hydrogen-atom ratio as the original fuel monomer.

SOLUTION:

1. For stoichiometric yields of CO_2 and water and the stoichiometric mass oxygen and air-to-fuel ratio for the maximum possible conversion of the fuel monomer of the material to CO_2 and H_2O, the following expression represents the maximum possible conversion of the fuel monomer of the material to CO_2 and H_2O:

$$CH_{1.33}O_{0.56} + 1.06\ O_2 = CO_2 + 0.67\ H_2O$$

The molecular weight of the fuel monomer of the material is $1 \times 12 + 1.33 \times 1 + 0.56 \times 16 = 22.3$, the molecular weight of oxygen is 32, the molecular weight of CO_2 is 44, and the molecular weight of H_2O is 18. Thus,

$$\Psi_{CO_2} = \frac{44}{22.3} = 1.97$$

$$\Psi_{H_2O} = \frac{0.67 \times 18}{22.3} = 0.54$$

$$\Psi_O = \frac{1.06 \times 32}{22.3} = 1.52$$

The stoichiometric mass air-to-fuel ratio can be obtained by dividing Ψ_O by 0.233; that is, 1.52/0.233 = 6.52.

2. For stoichiometric yields of CO, hydrocarbons, and smoke for the maximum possible conversion of the fuel monomer of the material to these products, the following expressions represent the maximum possible conversion of the fuel monomer of the material to these products:

For CO,

$$CH_{1.33}O_{0.56} + zO_2 = CO + x(HO)$$

$$\Psi_{CO} = \frac{28}{22.3} = 1.26$$

Table 3-4.16 ***Stoichiometric Yields of Major Products***[a]

Material	Formula	Ψ_O	Ψ_{CO_2}	Ψ_{CO}	Ψ_s	Ψ_{hc}	Ψ_{HCl}	Ψ_{HF}
Carbon-Hydrogen Atoms in the Structure								
PE	CH_2	3.43	3.14	2.00	0.857	1.00	0	0
PP	CH_2	3.43	3.14	2.00	0.857	1.00	0	0
PS	CH	3.08	3.38	2.15	0.923	1.00	0	0
Expanded polystyrene								
GM47	$CH_{1.1}$	3.10	3.36	2.14	0.916	1.00	0	0
GM49	$CH_{1.1}$	3.10	3.36	2.14	0.916	1.00	0	0
GM51	CH	3.08	3.38	2.15	0.923	1.00	0	0
GM53	$CH_{1.1}$	3.10	3.36	2.14	0.916	1.00	0	0
Carbon-hydrogen-oxygen-nitrogen atoms in the structure								
POM	CH_2O	1.07	1.47	0.933	0.400	0.467	0	0
PMMA	$CH_{1.6}O_{0.40}$	1.92	2.20	1.40	0.600	0.680	0	0
Nylon	$CH_{1.8}O_{0.17}N_{0.17}$	2.61	2.32	1.48	0.634	0.731	0	0
Wood (pine)	$CH_{1.7}O_{0.83}$	1.21	1.67	1.06	0.444	0.506	0	0
Wood (oak)	$CH_{1.7}O_{0.72}N_{0.001}$	1.35	1.74	1.11	0.476	0.543	0	0
Wood (Douglas fir)	$CH_{1.7}O_{0.74}N_{0.002}$	1.32	1.72	1.10	0.469	0.536	0	0
Polyester	$CH_{1.4}O_{0.22}$	2.35	2.60	1.65	0.709	0.792	0	0
Epoxy	$CH_{1.3}O_{0.20}$	2.38	2.67	1.70	0.727	0.806	0	0
Polycarbonate	$CH_{0.88}O_{0.19}$	2.26	2.76	1.76	0.754	0.872	0	0
PET	$CH_{0.80}O_{0.40}$	1.67	2.29	1.46	0.625	0.667	0	0
Phenolic foam	$CH_{1.1}O_{0.24}$	2.18	2.60	1.65	0.708	0.773	0	0
PAN	$CHN_{0.33}$	2.87	2.50	1.59	0.681	0.681	0	0
Flexible polyurethane foams								
GM21	$CH_{1.8}O_{0.30}N_{0.05}$	2.24	2.28	1.45	0.622	0.715	0	0
GM23	$CH_{1.8}O_{0.35}N_{0.06}$	2.11	2.17	1.38	0.593	0.682	0	0
GM25	$CH_{1.7}O_{0.32}N_{0.07}$	2.16	2.22	1.41	0.606	0.692	0	0
GM27	$CH_{1.7}O_{0.30}N_{0.08}$	2.21	2.24	1.43	0.612	0.698	0	0
Rigid polyurethane foams								
GM29	$CH_{1.1}O_{0.23}N_{0.10}$	2.22	2.42	1.54	0.660	0.721	0	0
GM31	$CH_{1.2}O_{0.22}N_{0.10}$	2.28	2.43	1.55	0.662	0.729	0	0
GM37	$CH_{1.2}O_{0.20}N_{0.08}$	2.34	2.51	1.60	0.685	0.753	0	0
Rigid polyisocyanurate foams								
GM41	$CH_{1.0}O_{0.19}N_{0.11}$	2.30	2.50	1.59	0.683	0.740	0	0
GM43	$CH_{0.93}O_{0.20}N_{0.11}$	2.25	2.49	1.58	0.679	0.732	0	0
Carbon-hydrogen-oxygen-silicone atoms in the structure								
Silicone-1[b]	$CH_{1.3}O_{0.25}Si_{0.18}$	1.98	1.97	1.25	0.537	0.595	0	0
Silicone-2[c]	$CH_{1.5}O_{0.30}Si_{0.26}$	1.86	1.72	1.09	0.469	0.528	0	0
Silicone-3[d]	$CH_3O_{0.50}Si_{0.50}$	1.73	1.19	0.757	0.324	0.405	0	0
Carbon-hydrogen-oxygen-chlorine-fluorine atoms in the structure								
Fluoropolymers								
PVF (Tedlar)	$CH_{1.5}F_{0.50}$	1.74	1.91	1.22	0.522	0.587	0	0.435
PVF2 (Kynar)	CHF	1.00	1.38	0.875	0.375	0.406	0	0.594
ETFE (Tefzel)	$CH_{1.0}F_{0.99}$	1.01	1.38	0.880	0.377	0.409	0	0.622
E-CTFE (Halar)	$CHF_{0.75}Cl_{0.25}$	0.889	1.22	0.778	0.333	0.361	0.257	0.417
PFA (Teflon)	$CF_{1.7}O_{0.01}$	0.716	1.00	0.630	0.270	0	0	0.765
FEP (Teflon)	$CF_{1.8}$	0.693	0.952	0.606	0.260	0	0	0.779
TFE (Teflon)	CF_2	0.640	0.880	0.560	0.240	0	0	0.800
CTFE (Kel-F)	$CF_{1.5}Cl_{0.50}$	0.552	0.759	0.483	0.207	0	0.310	0.517
Chloropolymers								
PE-25% Cl	$CH_{1.9}Cl_{0.13}$	2.56	2.38	1.52	0.650	0.753	0.254	0
PE-36% Cl	$CH_{1.8}Cl_{0.22}$	2.16	2.05	1.30	0.558	0.642	0.368	0
Neoprene	$CH_{1.25}Cl_{0.25}$	1.91	2.00	1.27	0.546	0.602	0.409	0
PE-42% Cl	$CH_{1.8}Cl_{0.29}$	1.94	1.84	1.17	0.501	0.576	0.424	0
PE-48% Cl	$CH_{1.7}Cl_{0.36}$	1.73	1.67	1.06	0.456	0.521	0.493	0
PVC	$CH_{1.5}Cl_{0.50}$	1.42	1.42	0.903	0.387	0.436	0.581	0
$PVCl_2$	CHCl	0.833	0.917	0.583	0.250	0.271	0.750	0

[a]Calculated from the data for the elemental compositions of the materials in the FMRC Flammability Laboratory; subscript hc is total gaseous hydrocarbons; s is soot.
[b]$\eta_{SiO_2} = 0.483$.
[c]$\eta_{SiO_2} = 0.610$.
[d]$\eta_{SiO_2} = 0.811$.

For hydrocarbons,

$$CH_{1.33}O_{0.56} + zO_2 = CH_{1.33} + x(HO)$$

$$\Psi_{hc} = \frac{13.3}{22.3} = 0.60$$

For smoke,

$$CH_{1.33}O_{0.56} + zO_2 = C + x(HO)$$

$$\Psi_s = \frac{12}{22.3} = 0.54$$

EXAMPLE 18:

For the material in Examples 16 and 17, the generation efficiencies of CO_2, CO, hydrocarbons, and smoke are 0.90, 0.004, 0.002, and 0.036, respectively. The heat of gasification is 1.63 kJ/g, the surface re-radiation loss is 11 kW/m^2, and the predicted asymptotic flame heat flux value for large-scale fires is 60 kW/m^2. Calculate the yields and asymptotic values for the generation rates of CO_2, CO, hydrocarbons, and smoke expected in large-scale fires.

SOLUTION:

1. Yields from Equation 66 and data from Example 17:

$$y_{CO_2} = 0.90 \times 1.97 = 1.77 \text{ g/g}$$
$$y_{CO} = 0.004 \times 1.26 = 0.005 \text{ g/g}$$
$$y_{hc} = 0.002 \times 0.60 = 0.001 \text{ g/g}$$
$$y_s = 0.036 \times 0.54 = 0.019 \text{ g/g}$$

2. Asymptotic values for the mass loss rate from Equation 11:

$$\dot{m}'' = \frac{60 - 11}{1.63} = 30 \text{ g/m}^2\cdot\text{s}$$

3. Asymptotic values for the mass generation rates of products from Equation 42 and the above data:

$$\dot{G}''_{CO_2} = 1.77 \times 30 = 53 \text{ g/m}^2\cdot\text{s}$$
$$\dot{G}''_{CO} = 0.005 \times 30 = 0.159 \text{ g/m}^2\cdot\text{s}$$
$$\dot{G}''_{hc} = 0.001 \times 30 = 0.036 \text{ g/m}^2\cdot\text{s}$$
$$\dot{G}''_{s} = 0.019 \times 30 = 0.584 \text{ g/m}^2\cdot\text{s}$$

Generation rates of fire products and fire ventilation: As discussed previously, the effects of decrease in fire ventilation, as characterized by the increase in the local equivalence ratio, are reflected in the increase in the generation rates of the reduction zone products (smoke, CO, hydrocarbons, and others). For example, for flaming wood crib enclosure fires, as the equivalence ratio increases, the combustion efficiency decreases, flame becomes unstable, and the generation efficiency of CO reaches its peak for the equivalence ratio between about 2.5 and 4.0.[44]

The ventilation-controlled building fires are generally characterized by two layers: (1) a ceiling vitiated layer, identified as *upper layer,* and (2) an uncontaminated layer below, identified as *lower layer.* Incorporation of these two layers is the classical two-zone modeling of fires in enclosed spaces. Under many conditions, the depth of the upper layer occupies a significant fraction of the volume of the enclosed space. Eventually, the interface between the upper layer and the lower layer positions itself so that it is very close to the floor, very little oxygen is available for combustion, and most of the fuel is converted to the reduction zone products, that is, smoke, CO, hydrocarbons, and others.

Ventilation-controlled large- and small-enclosure and laboratory-scale fires and fires in the vitiated upper layer under the experimental hoods have been studied in detail, and are discussed or reviewed in References 44 and 63 through 66. The results from these types of fires are very similar. Detailed studies[44] performed for the generation rates of fire products for various fire ventilation conditions in the ASTM E2058 fire propagation apparatus [Figure 3-4.2(a)], and in the Fire Research Institute's (FRI) enclosure, show that with increase in the equivalence ratio (1) generation efficiencies of oxidation zone products, such as CO_2, and reactant consumption efficiency (i.e., oxygen) decrease, and (2) generation efficiencies of the reduction zone products, such as smoke, CO, and hydrocarbons increase.

Generalized correlations have been established between the generation efficiencies and the equivalence ratio for the oxidation and reduction zone products. The changes in the consumption or generation efficiencies of the products are expressed as ratios of the efficiencies for the ventilation-controlled (*vc*) to well-ventilated (*wv*) fires:

Reactants (oxygen)

$$\zeta_O = \frac{(\eta_O)_{vc}}{(\eta_O)_{wv}} = \frac{(c_O/\Psi_O)_{vc}}{(c_O/\Psi_O)_{wv}} = \frac{(c_O)_{vc}}{(c_O)_{wv}} \tag{67}$$

Oxidation zone products (carbon dioxide, water, etc.)

$$\zeta_{oxid} = \frac{(\eta_j)_{vc}}{(\eta_j)_{wv}} = \frac{(y_j/\Psi_j)_{vc}}{(y_j/\Psi_j)_{wv}} = \frac{(y_j)_{vc}}{(y_j)_{wv}} \tag{68}$$

where ζ_{oxid} is the oxidation zone product generation efficiency ratio.

Reduction zone products (smoke, carbon monoxide, hydrocarbons, etc.)

$$\zeta_{red} = \frac{(\eta_j)_{vc}}{(\eta_j)_{wv}} = \frac{(y_j/\Psi_j)_{vc}}{(y_j/\Psi_j)_{wv}} = \frac{(y_j)_{vc}}{(y_j)_{wv}} \tag{69}$$

where ζ_{red} is the reduction zone product generation efficiency ratio.

The relationships between the ratios of the mass of oxygen consumed per unit mass of fuel, the yields of the products for the ventilation-controlled to well-ventilated fires, and the equivalence ratio are shown in Figures 3-4.29 through 3-4.33. The ratios for oxygen and CO_2 (an oxidation zone product) do not depend on the chemical structures of the materials, whereas the ratios for the reduction zone products do depend on the chemical structures of the materials.

Oxygen and CO_2. The relationships for oxygen consumed and carbon dioxide generated are shown in Figures 3-4.29 and 3-4.30, respectively. The relationships are

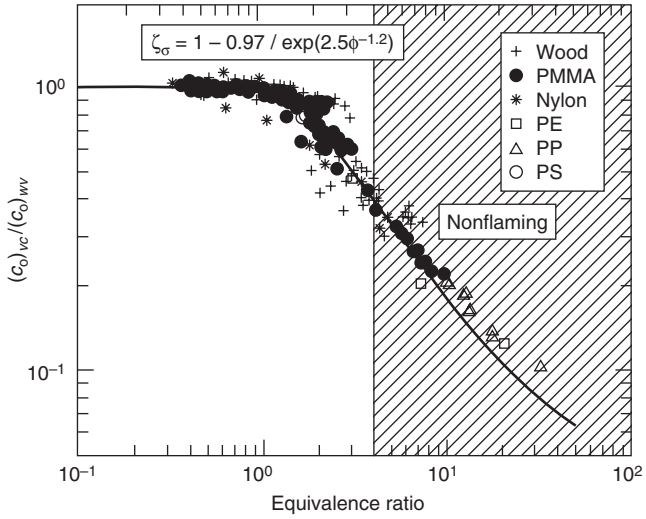

Figure 3-4.29. ***Ratio of the mass of oxygen consumed per unit mass of the fuel for ventilation-controlled to well-ventilated fires. Data are measured in the ASTM E2058 fire propagation apparatus and in the Fire Research Institute's enclosure.[44] Subscript vc represents ventilation-controlled fires, and subscript wv represents well-ventilated fires.***

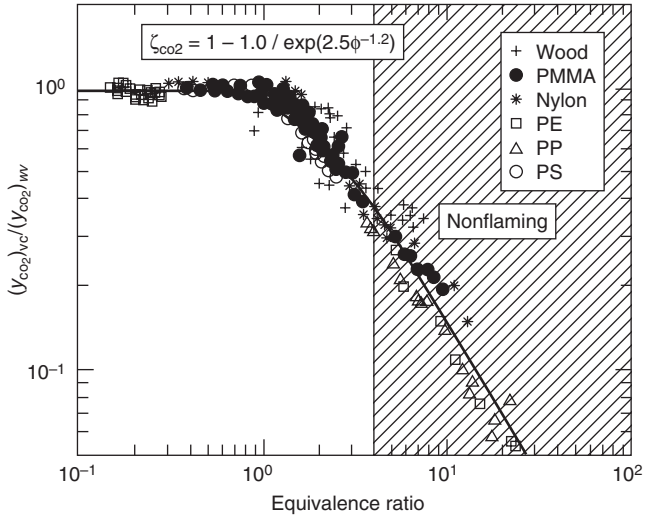

Figure 3-4.30. ***Ratio of the mass of carbon dioxide generated per unit mass of the fuel for ventilation-controlled to well-ventilated fires. Data are measured in the ASTM E2058 fire propagation apparatus and in the Fire Research Institute's enclosure.[44] Subscript vc represents ventilation-controlled fires, and subscript wv represents well-ventilated fires.***

very similar to the relationships for the chemical and convective heats of combustion ratios (Equations 40 and 41), as expected:

$$\frac{(c_O)_{vc}}{(c_O)_{wv}} = 1 - \frac{0.97}{\exp(\Phi/2.14)^{-1.2}} \tag{70}$$

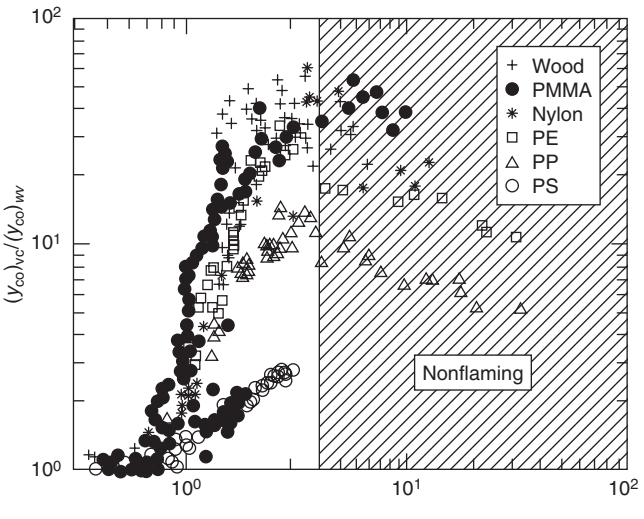

Figure 3-4.31. ***Ratio of the mass of carbon monoxide generated per unit mass of the fuel for ventilation-controlled to well-ventilated fires. Data are measured in the ASTM E2058 fire propagation apparatus and in the Fire Research Institute's enclosure.[44] Subscript vc represents ventilation-controlled fires, and subscript wv represents well-ventilated fires.***

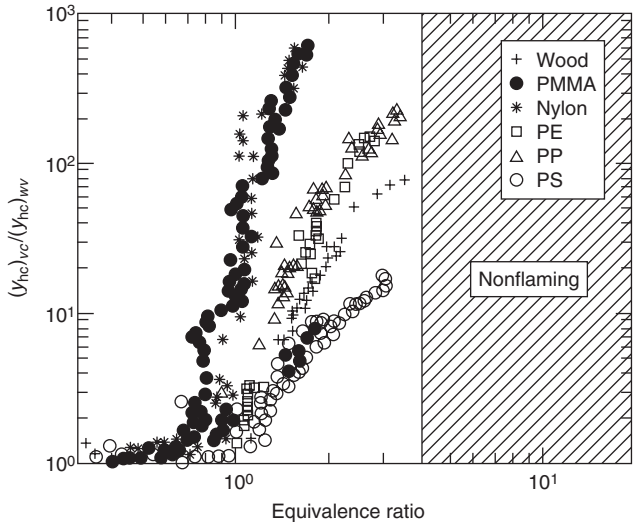

Figure 3-4.32. ***Ratio of the mass of hydrocarbons generated per unit mass of the fuel for ventilation-controlled to well-ventilated fires. Data are measured in the ASTM E2058 fire propagation apparatus and in the Fire Research Institute's enclosure.[44] Subscript vc represents ventilation-controlled fires, and subscript wv represents well-ventilated fires.***

$$\frac{(y_{CO_2})_{vc}}{(y_{CO_2})_{wv}} = 1 - \frac{1.00}{\exp(\Phi/2.15)^{-1.2}} \tag{71}$$

Carbon monoxide. The relationship between the ratio of the CO yields for ventilation-controlled to well-ventilated

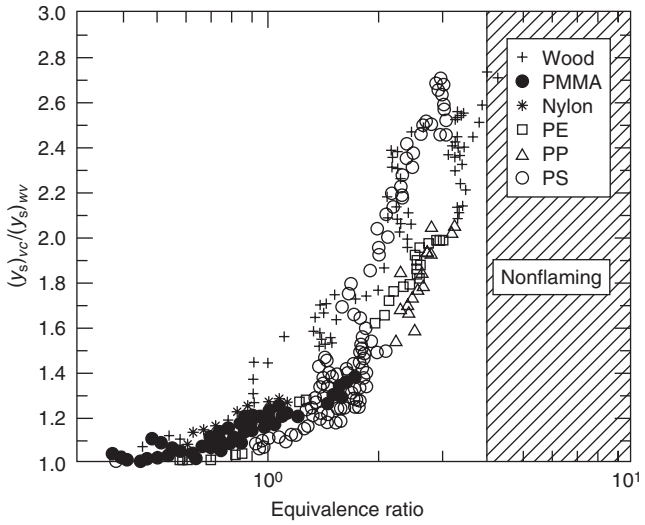

Figure 3-4.33. ***Ratio of the mass of smoke generated per unit mass of the fuel for ventilation-controlled to well-ventilated fires. Data are measured in the ASTM E2058 fire propagation apparatus and in the Fire Research Institute's enclosure.[44] Subscript vc represents ventilation-controlled fires, and subscript wv represents well-ventilated fires.***

fires and the equivalence ratio is shown in Figure 3-4.30. The data suggest the following relationship:[44]

$$\frac{(y_{CO})_{vc}}{(y_{CO})_{wv}} = 1 + \frac{\alpha}{\exp(2.5\Phi^{-\xi})} \tag{72}$$

where α and ξ are the correlation coefficients, which depend on the chemical structures of the materials. The values for the correlation coefficients for CO are listed in Table 3-4.17.

The increase in the ratio of the carbon monoxide yields for the ventilation-controlled to well-ventilated fires with the equivalence ratio is due to the preferential conversion of the fuel carbon atoms to CO. The experimental data show the following order for the preferential conversion: wood (C-H-O aliphatic structure) > PMMA (C-H-O aliphatic structure) > nylon (C-H-O-N aliphatic structure) > PE (C-H aliphatic linear unsaturated structure) > PP (C-H aliphatic branched unsaturated structure) > PS (C-H aromatic structure). A similar trend is found for the liquid and gaseous fuels, such as shown in Table 3-4.18.[44] The presence of O and N atoms in the fuels with aliphatic C-H structure appears to enhance preferential fuel carbon atom conversion to CO.

Table 3-4.17 ***Correlation Coefficients to Account for the Effects of Ventilation on the Generation Rates of CO, Hydrocarbons, and Smoke***

	CO		Hydrocarbons		Smoke	
Material	α	ξ	α	ξ	α	ξ
PS	2	2.5	25	1.8	2.8	1.3
PP	10	2.8	220	2.5	2.2	1.0
PE	10	2.8	220	2.5	2.2	1.0
Nylon	36	3.0	1200	3.2	1.7	0.8
PMMA	43	3.2	1800	3.5	1.6	0.6
Wood	44	3.5	200	1.9	2.5	1.2
PVC	7	8.0	25	1.8	0.38	8.0

Hydrocarbons. The relationship between the ratio of the hydrocarbon yields for ventilation-controlled to well-ventilated fires and the equivalence ratio is shown in Figure 3-4.32. The data suggest the following relationship:[44]

$$\frac{(y_{hc})_{vc}}{(y_{hc})_{wv}} = 1 + \frac{\alpha}{\exp(5.0\Phi^{-\xi})} \tag{73}$$

The correlation coefficient values for hydrocarbons are listed in Table 3-4.17. The numerator in the second term on the right-hand side of Equation 73 is 10 to 40 times that of CO, whereas the denominator is twice that for CO. This relationship suggests that there is a significantly higher preferential fuel conversion to hydrocarbons than to CO, with increase in the equivalence ratio. The order for the preferential fuel conversion to hydrocarbons is very similar to CO, except for wood; that is, PMMA > nylon > PE = PP > wood > PS. The exception for wood may be due to char-forming tendency of the fuel, which lowers the C-to-H ratio in the gas phase.

Smoke. The relationship between the ratio of the smoke yields for ventilation-controlled to well-ventilated fires and the equivalence ratio is shown in Figure 3-4.33. The data suggest the following relationship:[44]

$$\frac{(y_s)_{vc}}{(y_s)_{wv}} = 1 + \frac{\alpha}{\exp(2.5\Phi^{-\xi})} \tag{74}$$

The correlation coefficient values for smoke are listed in Table 3-4.17. The values of the correlation coefficients in

Table 3-4.18 ***Carbon Monoxide Generation Efficiency for Ventilation-Controlled and Well-Ventilated Combustion[a]***

	Well-Ventilated (wv)[b]	Ventilation-Controlled (vc) $\Phi \approx 4.0$		
Fuel	$\Phi < 0.05$	Ref. 64	Ref. 65	$\frac{(y_{CO})_{vc}}{(y_{CO})_{wv}}$
Methane	0.001	0.10	—	100
Propane	0.001	—	0.12	120
Propylene	0.004	0.10	—	25
Hexane	0.002	0.10	0.52[c]	50 (260[c])
Methanol	0.001	0.27	1.00[c]	270 (1000[c])
Ethanol	0.001	0.18	0.66[c]	180 (660[c])
Isopropanol	0.002	0.21	—	105
Acetone	0.002	0.21	0.63[c]	105 (315[c])

[a]Table taken from Reference 44.
[b]From ASTM E2058 fire propagation apparatus.
[c]Nonflaming.

the second term on the right-hand side of Equation 74 suggest that, with the increase in the equivalence ratio, the preferential fuel conversion to smoke is lower than it is to hydrocarbons and CO. Also, the order for the preferential conversion of the fuel carbon atom to smoke is opposite to the order for the conversion to CO and hydrocarbons, except for wood. The order is PS > wood > PE = PP > nylon > PMMA, suggesting that the order is probably due to decrease in the preference for the reactions between OH and CO compared to the reactions between OH and soot.

Other reduction zone products. Since the sum of the generation efficiencies of all the products for a material cannot exceed unity, the generation efficiency of products other than CO, CO_2, hydrocarbons, and smoke is

$$\eta_{other} = 1 - (\eta_{CO} + \eta_{CO_2} + \eta_{hc} + \eta_s) \qquad (75)$$

where η_{other} is the generation efficiency of products other than CO, CO_2, hydrocarbons, and smoke. The generation efficiency of other products can be calculated from Equations 71 through 75 using correlation coefficients from Table 3-4.17. The generation efficiency values for other products calculated in this fashion for various equivalence ratios are shown in Figure 3-4.34. The figure shows that, for equivalence ratios greater than 4, where fires are nonflaming, about 10 to 60 percent of fuel carbon is converted to products other than CO, CO_2, soot, and hydrocarbons.

The order for the preferential conversion of fuel carbon to other products in the nonflaming zone is PS (C-H aromatic structure) < PE & PP (C-H aliphatic structure) < wood (C-H-O aliphatic structure) < nylon (C-H-O-N aliphatic structure) < PMMA (C-H-O aliphatic structure). It thus appears that, in nonflaming fire, fuels with C-H structures are converted mainly to CO, smoke, and hydrocarbons, rather than to other products, whereas fuels with C-H-O and C-H-O-N structures are converted mainly to products other than CO, CO_2, smoke, and hydrocarbons. Some of the products include formaldehyde (HCHO) and hydrogen cyanide (HCN).[44]

Generation efficiencies of formaldehyde, hydrogen cyanide, and nitrogen dioxide. The experimental data for the generation efficiencies of formaldehyde, hydrogen cyanide, and nitrogen dioxide versus the equivalence ratio are shown in Figures 3-4.35 and 3-4.36.

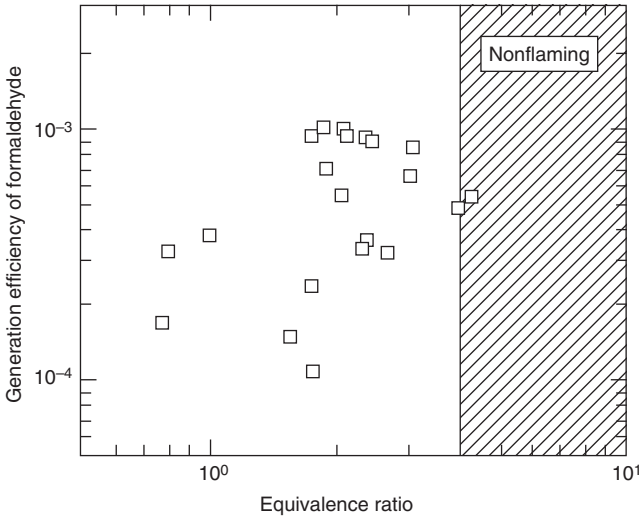

Figure 3-4.35. ***Generation efficiency of formaldehyde generated from wood versus the equivalence ratio.***

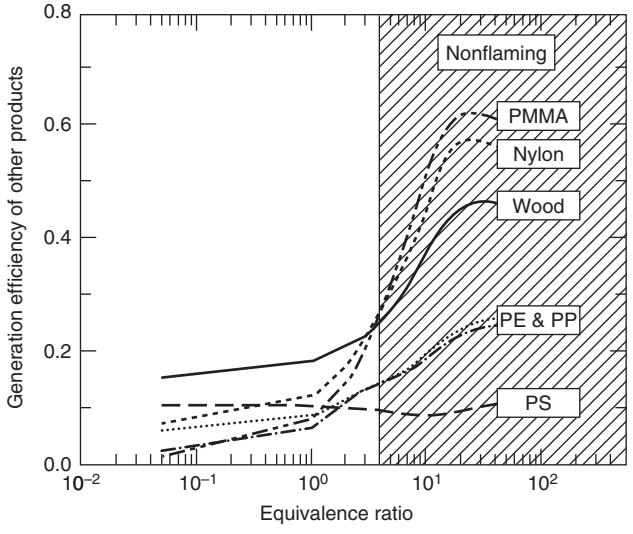

Figure 3-4.34. ***Generation efficiency of products other than CO, CO_2, hydrocarbons, and smoke versus the equivalence ratio.***

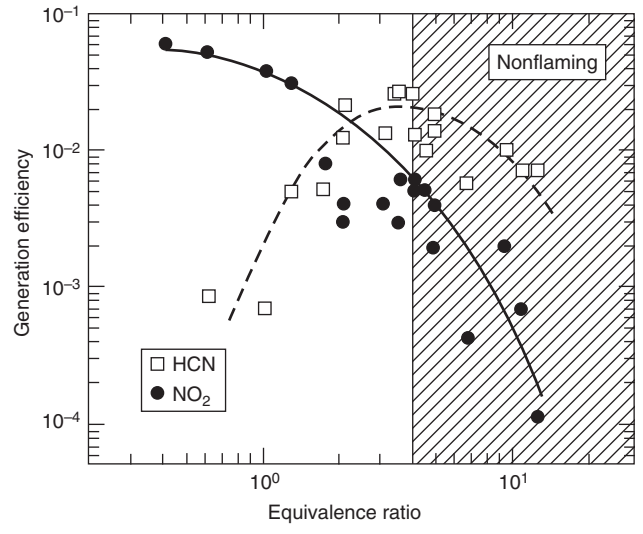

Figure 3-4.36. ***Generation efficiencies of hydrogen cyanide and nitrogen dioxide generated from nylon versus the equivalence ratio.***

Formaldehyde is generated in the pyrolysis of wood (C-H-O structure). It is attacked rapidly by oxygen (O) and hydroxyl (OH) radicals in the flame, if unlimited supply of oxygen is available. Thus, only traces of formaldehyde are found in well-ventilated fires. The generation efficiency of formaldehyde, however, increases with the equivalence ratio, indicating reduced concentrations of O and OH radicals and gas temperature due to lack of oxygen available for combustion.

In fires, hydrogen cyanide is formed in the reduction zone from materials with hydrogen and nitrogen atoms in the structure, such as nylon (C-H-O-N structure). Nitrogen dioxide (NO_2), on the other hand, is formed in the oxidation zone, as a result of the oxidation of hydrogen cyanide. The data in Figure 3-4.36 show that the generation efficiency of hydrogen cyanide increases and the generation efficiency of NO_2 decreases with the equivalence ratio. This observation supports that O and OH radical concentrations decrease with increase in the equivalence ratio. The decrease in the generation efficiency of hydrogen cyanide in the nonflaming fire suggests decrease in the fuel mass transfer rate.

Relationship between the generation efficiencies of CO_2 and CO. The relationship between the generation efficiencies of CO_2 and CO is shown in Figure 3-4.37, where the data are taken from Reference 44. CO is generated in the reduction zone of the flame as a result of the oxidative pyrolysis of the fuel, and is oxidized to CO_2 in the oxidation zone of the flame. The generation efficiency of CO_2 is independent of the chemical structure of the fuel (Figure 3-4.30), whereas the generation efficiency of CO depends on the chemical structure of the fuel (Figure 3-4.31). In Figure 3-4.37, the curves represent approximate predictions based on the correlation coefficients from Table 3-4.17 and Equations 71 and 72.

The relationship between the generation efficiencies of CO_2 and CO is quite complex. The boundary of the shaded region marked *air* in Figure 3-4.37 is drawn using the data for the well-ventilated combustion for equivalence ratios less than 0.05. The boundary of the *air* region may be considered as equivalent to the lower flammability limit. No flaming combustion is expected to occur in this region, as the fuel-air mixture is below the lower flammability limit; however, nonflaming combustion, generally identified as smoldering, may continue. The boundary of the shaded region marked *fuel* is drawn using the data for the ventilation-controlled combustion for equivalence ratio of 4.0, and may be considered as equivalent to the upper flammability limit. In the *fuel* region, no flaming combustion is expected to occur, as the fuel-air mixture is above the upper flammability limit; however, nonflaming processes may continue. The shaded region marked *chemical structure* and drawn to the right of the methanol curve is an imaginary region as it is not expected to exist, because there are no stable carbon-containing fuel structures below the formaldehyde with a structure of HCHO. For the stable fuels with C-H-O structures, formaldehyde (HCHO) and methanol (CH_3OH) have the lowest molecular weights (30 and 32, respectively). Thus, data for HCHO and CH_3OH probably would be comparable.

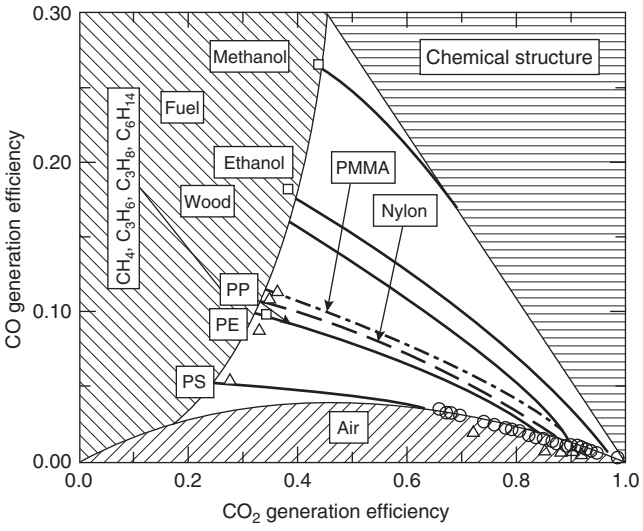

Figure 3-4.37. ***Relationship between the generation efficiencies of CO_2 and CO. Data taken from Reference 44.***

The curves in Figure 3-4.37 show that, in flaming combustion, with increase in the equivalence ratio, the preference for fuel carbon atom conversion to CO, relative to the conversion to CO_2, follows this order: methanol (C-H-O structure) > ethanol (C-H-O structure) > wood (C-H-O structure) > PMMA (C-H-O structure) > nylon (C-H-O-N structure) > PP (C-H aliphatic unsaturated branched structure) ≥ (CH_4, C_3H_6, C_3H_8, C_6H_{14}) ≥ PE (C-H aliphatic unsaturated linear structure) > PS (C-H aromatic unsaturated structure). Thus for fires in enclosed spaces, generation of higher amounts of CO relative to CO_2 at high local equivalence ratios is expected for fuels with C-H-O structures compared to the fuels with C-H structures. The reason for higher amounts of CO relative to CO_2 for fuels with C-H-O structures is that CO is easily generated in fuel pyrolysis, but is oxidized only partially to CO_2 due to limited amounts of oxidant available.

Relationship between the generation efficiencies of CO and smoke: The relationship between the generation efficiencies of CO and smoke is shown in Figure 3-4.38, where data are taken from Reference 44. CO and smoke are both generated in the reduction zone of the flame as a result of the oxidative pyrolysis of the fuel, and their generation efficiencies depend on the chemical structure of the fuel (Figures 3-4.31 and 3-4.33). In Figure 3-4.38, the curves represent approximate predictions based on the correlation coefficients from Table 3-4.17 and Equations 72 and 74.

The relationship in Figure 3-4.38 is quite complicated. The boundary of the shaded region marked *air* is drawn using the data for the well-ventilated combustion for equivalence ratios less than 0.05. The boundary of the shaded region marked *fuel* is drawn using the data for the ventilation-controlled combustion for equivalence ratio of 4.0. The boundary for the region marked *air* may be considered as equivalent to the lower flammability limit, and the boundary for the region marked *fuel* may be considered as equivalent to the upper flammability limit.

In Figure 3-4.38, the order for the preference for fuel carbon atom conversion to smoke relative to conversion

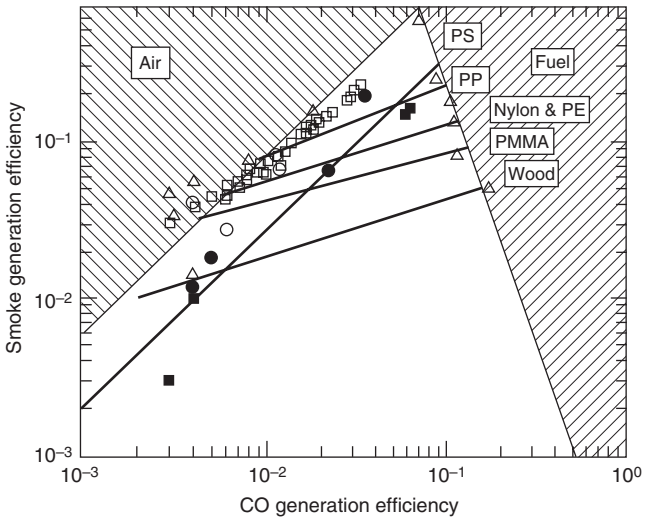

Figure 3-4.38. ***Relationship between the generation efficiencies of CO and smoke. Data taken from Reference 44.***

to CO is wood (C-H-O structure) < PMMA (C-H-O structure) < nylon (C-H-O-N structure) < PP (C-H aliphatic unsaturated branched structure) ≈ PE (C-H aliphatic unsaturated linear structure) < PS (C-H aromatic structure). The generation efficiency of smoke for PS, which is a polymer with aromatic C-H structure, is the highest. The generation efficiency of smoke for wood, which is a polymer with aliphatic C-H-O structure, is the lowest.

Generalized Relationships to Calculate Chemical, Convective, and Radiative Heats of Combustion and Yields of Products at Various Equivalence Ratios

The following relationship is the generalized form of Equations 40, 41, and 70 through 74:

$$fp = fp_{\infty}\left[1 + \frac{\alpha}{\exp(\Phi)/\beta)^{-\xi}}\right] \tag{76}$$

where

fp = fire property
α, β, and ξ = correlation coefficients characteristic of the chemical structures of the polymers
subscript ∞ = infinite amount of air
fp = constant for each polymer when determined under turbulent flame conditions

The fire properties are heat of combustion (or combustion efficiency) and yields (or generation efficiencies) of products. Three conditions can be identified: (1) for $\Phi \gg \beta$, $fp = fp_{\infty}(1 + \alpha)$; (2) for $\Phi \ll \beta$, $fp = fp_{\infty}$; and (3) $\Phi \approx \beta$, $fp \approx fp_{\infty}(1 + \alpha/2.7)$. Thus, the parameter α is associated primarily with the magnitude of the fire properties in nonflaming fires (high Φ values). The parameter β is associated with the fire properties in the transition region between the fires with an infinite amount of air and the fires with a very restricted amount of air. The parameter ξ is associated with the range of Φ values for the transition region. A high value of α is indicative of a strong effect of ventilation on the fire and its properties and vice versa. High values of β and ξ are indicative of rapid change of fire from flaming to nonflaming by a small change in the equivalence ratio, such as for the highly fire-retarded or halogenated materials for which flaming combustion in normal air itself is unstable.

Chemical heat of combustion versus equivalence ratio for the nonhalogenated polymers: From Equation 76,

$$\Delta H_{ch} = \Delta H_{ch,\infty}\left[1 - \frac{0.97}{\exp(\Phi/2.15)^{-1.2}}\right] \tag{77}$$

The values of $\Delta H_{ch,\infty}$ for several polymers are listed in Table 3-4.14.

Chemical heat of combustion versus equivalence ratio for the halogenated polymers (polyvinylchloride):

$$\Delta H_{ch} = \Delta H_{ch,\infty}\left[1 - \frac{0.30}{\exp(\Phi/0.53)^{-11}}\right] \tag{78}$$

As can be noted from the terms inside the brackets in Equations 77 and 78, the effect of ventilation on the chemical heat of combustion is much stronger for PVC than it is for the nonhalogenated polymers. The effect for PVC occurs at $\Phi \geq 0.4$, which is significantly lower than $\Phi \geq 2.0$ found for the nonhalogenated polymers.[44,68] For PVC homopolymer, the flaming combustion changes to nonflaming combustion for $\Phi \geq 0.70$, which is also significantly lower than $\Phi \geq 4.0$ found for the nonhalogenated polymers. This attribute is consistent with the highly halogenated nature of PVC and its mode of decomposition. The decomposition of PVC is characterized by the release of HCl, which is initiated at temperatures as low as about 100°C. At temperatures of up to 200 to 220°C, HCl is the major effluent. Presence of oxygen in the air enhances HCl release. The generation of HCl from PVC leads to the formation of double bonds and release of various aromatic/unsaturated hydrocarbons (benzene, ethylene, propylene, butylene, etc.).

Convective heats of combustion versus equivalence ratio for the nonhalogenated polymers: From Equation 76,

$$\Delta H_{con} = \Delta H_{con,\infty}\left[1 - \frac{1.0}{\exp(\Phi/1.38)^{-2.8}}\right] \tag{79}$$

The values of $\Delta H_{con,\infty}$ for several polymers are listed in Table 3-4.14.

Radiative heats of combustion versus equivalence ratio for the nonhalogenated polymers: Radiative heats of combustion are obtained from the difference between the chemical and the convective heats of combustion:

$$\Delta H_{rad} = \Delta H_{ch} - \Delta H_{con} \tag{80}$$

Consumption of oxygen for the nonhalogenated polymers: From Equation 76,

$$c_O = c_{O,\infty}\left[1 - \frac{0.97}{\exp(\Phi/2.14)^{-1.2}}\right] \quad (81)$$

Yield of carbon dioxide for the nonhalogenated polymers: From Equation 76,

$$y_{CO_2} = y_{CO_2,\infty}\left[1 - \frac{1.0}{\exp(\Phi/2.15)^{-1.2}}\right] \quad (82)$$

$y_{CO_2,\infty}$ values are listed in Table 3-4.14.

Yield of carbon dioxide for the halogenated polymers (PVC): From Equation 76,

$$y_{CO_2} = y_{CO_2,\infty}\left[1 - \frac{0.30}{\exp(\Phi/0.53)^{-11}}\right] \quad (83)$$

From the terms inside the brackets in Equations 82 and 83, a stronger effect of ventilation on the yield of CO_2 for PVC than for the nonhalogenated polymers can be noted. $y_{CO_2,\infty}$ values are listed in Table 3-4.14.

Yields of carbon monoxide, hydrocarbons, and smoke for the nonhalogenated polymers: From Equation 76,

Polystyrene

$$y_{CO} = y_{CO,\infty}\left[1 + \frac{2.0}{\exp(\Phi/1.44)^{-2.5}}\right] \quad (84)$$

$$y_{hc} = y_{hc,\infty}\left[1 + \frac{25}{\exp(\Phi/2.45)^{-1.8}}\right] \quad (85)$$

$$y_s = y_{s,\infty}\left[1 + \frac{2.8}{\exp(\Phi/2.02)^{-1.3}}\right] \quad (86)$$

The $y_{CO,\infty}$, $y_{hc,\infty}$, and $y_{s,\infty}$ values are listed in Table 3-4.14.

Polyethylene and Polypropylene

$$y_{CO} = y_{CO,\infty}\left[1 + \frac{10}{\exp(\Phi/1.39)^{-2.8}}\right] \quad (87)$$

$$y_{hc} = y_{hc,\infty}\left[1 + \frac{220}{\exp(\Phi/1.90)^{-2.5}}\right] \quad (88)$$

$$y_s = y_{s,\infty}\left[1 + \frac{2.2}{\exp(\Phi/2.50)^{-1.0}}\right] \quad (89)$$

The $y_{CO,\infty}$, $y_{hc,\infty}$, and $y_{s,\infty}$ values are listed in Table 3-4.14.

Polymethylmethacrylate

$$y_{CO} = y_{CO,\infty}\left[1 + \frac{43}{\exp(\Phi/1.33)^{-3.2}}\right] \quad (90)$$

$$y_{hc} = y_{hc,\infty}\left[1 + \frac{1800}{\exp(\Phi/1.58)^{-3.5}}\right] \quad (91)$$

$$y_s = y_{s,\infty}\left[1 + \frac{1.6}{\exp(\Phi/4.61)^{-0.60}}\right] \quad (92)$$

The $y_{CO,\infty}$, $y_{hc,\infty}$, and $y_{s,\infty}$ values are listed in Table 3-4.14.

Wood

$$y_{CO} = y_{CO,\infty}\left[1 + \frac{44}{\exp(\Phi/1.30)^{-3.5}}\right] \quad (93)$$

$$y_{hc} = y_{hc,\infty}\left[1 + \frac{200}{\exp(\Phi/2.33)^{-1.9}}\right] \quad (94)$$

$$y_s = y_{s,\infty}\left[1 + \frac{2.5}{\exp(\Phi/2.15)^{-1.2}}\right] \quad (95)$$

The $y_{CO,\infty}$, $y_{hc,\infty}$, and $y_{s,\infty}$ values are listed in Table 3-4.14.

Nylon

$$y_{CO} = y_{CO,\infty}\left[1 + \frac{36}{\exp(\Phi/1.36)^{-3.0}}\right] \quad (96)$$

$$y_{hc} = y_{hc,\infty}\left[1 + \frac{1200}{\exp(\Phi/1.65)^{-3.2}}\right] \quad (97)$$

$$y_s = y_{s,\infty}\left[1 + \frac{1.7}{\exp(\Phi/3.14)^{-0.8}}\right] \quad (98)$$

The $y_{CO,\infty}$, $y_{hc,\infty}$, and $y_{s,\infty}$ values are listed in Table 3-4.14.

Yields of Carbon Monoxide, Hydrocarbons, and Smoke for the Halogenated Polymers (Polyvinylchloride)

From Equation 76,

$$y_{CO} = y_{CO,\infty}\left[1 + \frac{7}{\exp(\Phi/0.42)^{-8.0}}\right] \quad (99)$$

$$y_{hc} = y_{hc,\infty}\left[1 + \frac{25}{\exp(\Phi/0.42)^{-1.8}}\right] \quad (100)$$

$$y_s = y_{s,\infty}\left[1 + \frac{0.38}{\exp(\Phi/2.02)^{-8.0}}\right] \quad (101)$$

From the above relationships for PVC, for $0.40 \geq \Phi \geq 1.0$, the maximum CO and smoke yields reach about 60 percent of the stoichiometric yields, listed in Table 3-4.16. For nonhalogenated polymers, the maximum CO and smoke yields reach ≤ 30 percent of the stoichiometric yields for $\Phi \geq 2.0$. Polystyrene is the only polymer, within the above group of polymers, for which the smoke yield exceeds that of PVC. These trends suggest that CO and smoke are generated much easier from PVC than from the nonhalo-

genated polymers, possibly due to the formation of double bonds, as HCl is eliminated at temperatures as low as 100°C from the PVC structure, and formation of various compounds occurs with aromatic/unsaturated bonds.

For nonhalogenated polymers considered with $\Phi \geq 4.0$, the CO yield is lowest and the smoke yield is highest for polystyrene, an aromatic ring-containing polymer; whereas, for polymethylmethacrylate, an aliphatic carbon-hydrogen-oxygen-atom-containing polymer, the CO yield is highest and smoke yield is lowest. This result suggests that aromatic ring structure promotes smoke formation, whereas the strong C-O bond in the structure remains intact as ventilation is reduced.

EXAMPLE 19:

Following Example 13, calculate the yields of CO and smoke at equivalence ratios of 1, 2, and 3 for polystyrene, polyethylene, wood, and nylon using Equations 84 and 86, 87 and 89, 93 and 95, and 96 and 98, respectively.

SOLUTION:

	Yield (g/g)							
	$\Phi \ll 1.0$		$\Phi = 1.0$		$\Phi = 2.0$		$\Phi = 3.0$	
Material	CO	Smoke	CO	Smoke	CO	Smoke	CO	Smoke
Polystyrene	0.060	0.164	0.070	0.202	0.137	0.331	0.162	0.417
Polyethylene	0.024	0.060	0.043	0.071	0.191	0.098	0.238	0.117
Wood	0.004	0.015	0.018	0.018	0.145	0.028	0.171	0.034
Nylon	0.038	0.075	0.149	0.086	1.04	0.105	1.28	0.120

Prediction of Fire Properties Using Smoke Point

Smoke emission characteristics of fuels have been expressed for decades by smoke point, defined as a minimum laminar axisymmetric diffusion flame height (or fuel volumetric or mass flow rate) at which smoke just escapes from the flame tip.[48,49,69–84] Smoke-point values have been measured for numerous gases, liquids, and solids.[48,49,69–74]

Almost all the knowledge on smoke formation, oxidation, and emission from diffusion flames is based on the combustion of fuels containing carbon and hydrogen atoms (hydrocarbons).[71,76–79] On the basis of the chemical structure, hydrocarbons are divided into two main classes: (1) aliphatic and (2) aromatic. Fuels containing both aliphatic and aromatic units are known as arenes. Aliphatic fuels have open-chain structure, and aromatic fuel structures consist of benzene rings. Aliphatic hydrocarbons are divided into three families: (1) alkanes (C_nH_{2n+2}), where n is an integer—the suffix *ane* indicates a single bond; (2) alkenes (C_nH_{2n})—the suffix *ene* indicates a double bond, and *diene*, two double bonds between carbon-carbon atoms; and (3) alkynes ($C_{2n}H_{2n-2}$)—the suffix *yne* indicates a triple bond. The integer n can vary from one in a gas, such as methane, to several thousands in solid polymers, such as polyethylene. In cyclic aliphatic fuels, carbon atoms are also arranged as rings. Dienes are classified as (1) conjugated—double bonds alternate with single bonds, (2) isolated—double bonds separated by more than one single bond, and (3) allens—double bonds with no separation. Conjugated dienes are more stable than other dienes.

Solid carbon particles present in smoke are defined as soot.[71,76] Soot is generally formed in the fuel-rich regions of the flame and grows in size through gas-solid reactions, followed by oxidation (burnout) to produce gaseous products, such as CO and CO_2. Time that is available for soot formation in the flame is a few milliseconds. Soot particle inception occurs from the fuel molecule via oxidation and/or pyrolysis products, which typically includes unsaturated hydrocarbons, especially acetylene, polyacetylenes, and polyaromatic hydrocarbons (PAH). Acetylene, polyacetylenes, and PAH are relatively stable with respect to decomposition. Acetylene and PAH are often considered the most likely precursors for soot formation in flames. PAH have the same role in diffusion flames for both aliphatic and aromatic fuels. In all flames, irrespective of the fuel, initial detection of soot particles takes place on the centerline when a temperature of 1350 K is encountered. Thus, even though the extent of conversion of a fuel into soot may significantly change from fuel to fuel, a common mechanism of soot formation is suggested.

Soot production in the flame depends on the chemical structure, concentration, and temperature of the fuel and flame temperature, pressure, and oxygen concentration.[71,76–79] The diffusion-controlled flame ends when fuel and oxidant are in stoichiometric ratio on the flame axis. The flame is followed by a soot after-burning zone, which is partially chemically controlled. The soot oxidation zone increases from about 10 to 50 percent of the visible flame length as the soot concentration increases. Flame luminosity and smoke emission in the plume depend on overall soot production and oxidation. Flames emit soot when soot temperature in the oxidation zone falls below 1300 K. The soot temperature decreases downstream because of radiation losses and diffusion of fresh cold air, both of which quench soot oxidation. At high soot concentrations, flame emissivity approaches unity, and flame luminosity becomes independent of the amount of soot.

Smoke point, carbon-to-hydrogen ratio, aromaticity, and flame temperature have been suggested as useful parameters to assess relative smoke emission characteristics of fuels in laminar diffusion flames.[48,49,69–74] The soot-forming tendency of fuels is inversely proportional to smoke point. General trends observed for smoke points for hydrocarbon fuels in laminar diffusion flames are aromatics < alkynes < alkenes < alkanes. Smoke-point values have been correlated with flame radiation, combustion efficiency and its convective and radiative components, and generation efficiencies of products.[48,49,69–74] Figures 3-4.39 through 3-4.41 show the relationships between the smoke point and the combustion efficiency and its convective and radiative components, and generation efficiencies of CO and smoke. The data were measured in the ASTM E2058 fire propagation apparatus [Figure 3-4.2(a)], and reported in References 48 and 49. The following relationships have been found from the data:[48,49]

$$\chi_{ch} = 1.15 L_{sp}^{0.10} \tag{102}$$

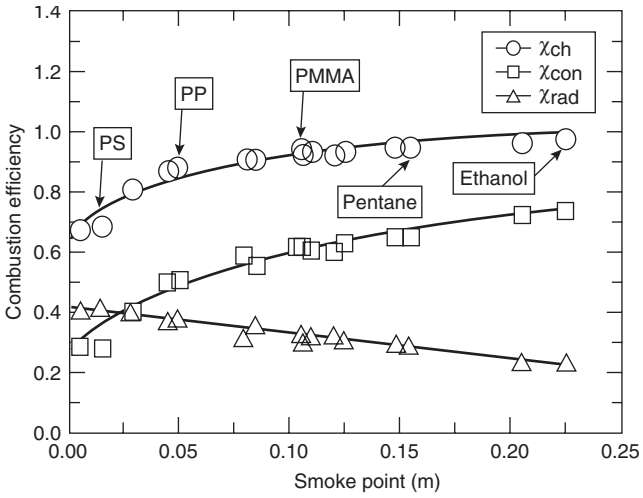

Figure 3-4.39. ***Relationships between the combustion efficiency and its convective and radiative components, and the smoke point. Data were measured in the ASTM E2058 fire propagation apparatus, and reported in References 48 and 49.***

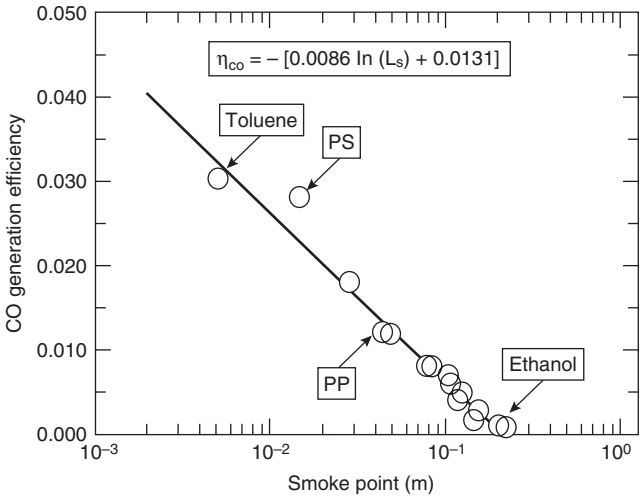

Figure 3-4.40. ***Relationships between the CO generation efficiency and the smoke point. Data were measured in the ASTM E2058 fire propagation apparatus, and reported in References 48 and 49.***

where χ_{ch} is the combustion efficiency (–), and L_{sp} is the smoke point (m) as measured in the ASTM E2058 fire propagation apparatus.

$$\chi_{rad} = 0.41 - 0.85 L_{sp} \tag{103}$$

where χ_{rad} is the radiative component of the combustion efficiency (–). This correlation is very similar to the one reported in the literature.[72]

$$\chi_{con} = \chi_{ch} - \chi_{rad} \tag{104}$$

where χ_{con} is the convective component of the combustion efficiency (–).

$$\eta_{CO} = -[0.0086 \ln (L_{sp}) + 0.0131] \tag{105}$$

where η_{CO} is the generation efficiency of CO (–).

$$\eta_s = -[0.0515 \ln (L_{sp}) + 0.0700] \tag{106}$$

where η_s is the generation efficiency of smoke (–).

The highest value of L_{sp} that has been measured is 0.240 m for ethane. Although methane and methanol would be expected to have smoke points higher than 0.240 m, they have not been measured experimentally. Since the combustion efficiency cannot exceed unity and the generation efficiencies of CO and smoke cannot be negative, the relationships in Equations 102 through 106 are valid for $0 > L_{sp} \leq 0.240$ m.

Smoke point decreases with increase in the molecular weight. The smoke-point values for monomers and polymers, however, show different types of dependencies: (1) the smoke-point values for ethylene and polyethylene

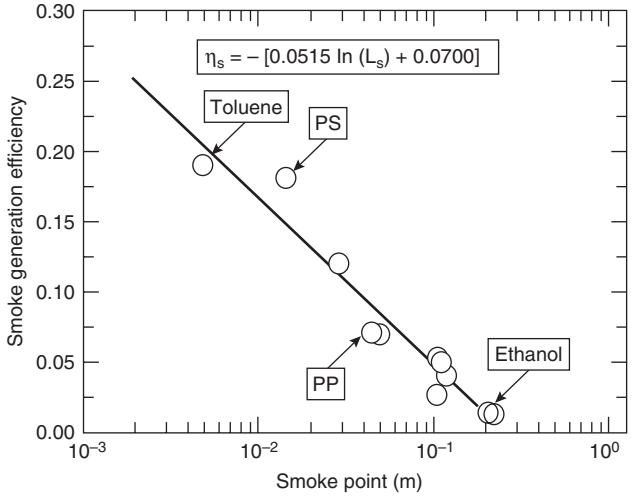

Figure 3-4.41. ***Relationships between the smoke generation efficiency and the smoke point. Data were measured in the ASTM E2058 fire propagation apparatus, and reported in References 48 and 49.***

are 0.097 and 0.045 m, respectively; (2) the smoke-point values for propylene and polypropylene are 0.030 and 0.050 m, respectively; and (3) the smoke-point values for styrene and polystyrene are 0.006 and 0.015 m, respectively. The smoke-point data for polymers support the accepted vaporization mechanisms of polymers;[85] that is, polyethylene, polypropylene, and polystyrene vaporize as higher molecular weight oligomers rather than as monomers, and thus, their smoke-point values are different than the values for the monomers. The smoke-point

values suggest that polyethylene is expected to have higher smoke emission than ethylene, whereas polypropylene and polystyrene are expected to have lower smoke emissions than propylene and styrene.

The correlations show that emissions of CO and smoke are very sensitive to changes in the smoke-point values compared to combustion efficiency and its convective and radiative components. This condition is expected from the understanding of the relationship between the smoke point and chemical structures of fuels. For example, a decrease of 33 percent in the smoke-point value of 0.15 m to 0.10 m produces a decrease of 4 and 12 percent in the combustion efficiency and its convective component, respectively, and an increase of 14 percent in the radiative component of the combustion efficiency; however, the generation efficiencies of CO and smoke increase by 89 and 67 percent, respectively.

Equations 102 through 106 can be used to estimate the fire properties of gases, liquids, and solids from their smoke-point values. The smoke-point values, however, depend strongly on the apparatus and cannot be used as reported. One of the approaches is to establish correlations between the smoke-point values measured in different apparatuses and a single apparatus for which relationships such as given in Equations 102 through 106 are available. This type of approach has been described in References 38 and 39 for the ASTM E2058 fire propagation apparatus, where smoke-point values for 165 fuels, reported in the literature, were translated to the values for the ASTM E2058 fire propagation apparatus. The fire properties (chemical, convective, and radiative heats of combustion and yields of CO and smoke) estimated in this fashion, from Equations 102 through 106, are listed in Tables 3-4.19 through 3-4.21. In the tables, molecular formula and weight, stoichiometric mass air-to-fuel ratio, and net heat of complete combustion have also been tabulated. The estimated data in the tables have been validated by direct measurements in the small- and large-scale fires using several fuels.[48,49]

The data in Tables 3-4.19 through 3-4.21 show linear dependencies on the molecular weight of the fuel monomer within each group:[48,49]

$$\Delta H_i = h_i + \frac{m_i}{M} \tag{107}$$

$$y_j = a_j \pm \frac{b_j}{M} \tag{108}$$

where

ΔH_i = net heat of complete combustion or chemical, convective, or radiative heat of combustion (kJ/g)

y_j = yield of product j (g/g)

M = molecular weight of fuel monomer (g/mol)

h_i = mass coefficient for the heat of combustion (kJ/g)

m_i = molar coefficient for the heat of combustion (kJ/mol)

a_j = mass coefficient for the product yield (g/g)

b_j = molar coefficient for the product yield (g/mol)

The coefficients depend on the chemical structures of the fuel; m_i and b_j become negative with the introduction of oxygen, nitrogen, and sulfur atoms into the chemical structure. Relationships in Equations 107 and 108 support the suggestion[79] that generally smaller molecules offer greater resistance to smoke formation and emission. The relationships suggest that for gases, liquids, and solids gasifying as high molecular weight fuels, $\Delta H_i \approx h_i$ and $y_j \approx a_j$.

The variations of chemical, convective, and radiative heats of combustion and yields of CO and smoke with the chemical structures of the fuels are similar to the smoke-point variations.

EXAMPLE 20:

The following smoke-point values have been reported in the literature:

Polymer	PE	PP	PMMA	PS
Smoke point (m)	0.045	0.050	0.105	0.015

For well-ventilated conditions, estimate (1) the chemical, convective, and radiative heats of combustion using Equations 102 through 104 and data for the net heat of complete combustion from Table 3-4.14; and (2) yields of CO and smoke using Equations 105 and 106 and stoichiometric yields from Table 3-4.16.

SOLUTION:

1. From Equations 102 through 104 and Table 3-4.14,

Polymer	PE	PP	PMMA	PS
ΔH_T (kJ/g)	43.6	43.4	25.2	39.2
ΔH_{ch} (kJ/g)	36.8	37.0	23.1	29.6
ΔH_{con} (kJ/g)	20.6	21.1	15.0	14.0
ΔH_{rad} (kJ/g)	16.2	15.9	8.1	15.6

2. From Equations 105 and 107 and Table 3-4.16,

Polymer	PE	PP	PMMA	PS
Ψ_{CO}	2.00	2.00	1.40	2.15
Ψ_s	0.857	0.857	0.600	0.923
y_{CO} (g/g)	0.027	0.025	0.009	0.050
y_s (g/g)	0.077	0.072	0.028	0.135

Nonthermal Damage Due to Fire Products

Damage due to heat is defined as thermal damage, and damage due to smoke, toxic, and corrosive products is defined as nonthermal damage. Nonthermal damage depends on the chemical nature and deposition of products on the walls, ceilings, building furnishings, equipment, components, and so forth, and the environmental conditions. The severity of the nonthermal damage increases with time. Examples of nonthermal damage to property are corrosion, electrical malfunctions, discoloration, and odors.

Most commercial and industrial occupancies are susceptible to nonthermal fire damage. Examples of typical commercial and industrial occupancies are telephone

Table 3-4.19 ***Combustion Properties of Fuels with Carbon and Hydrogen Atoms in the Chemical Structure***

Hydrocarbon	Formula	*M* (g/mol)	S	Heat of Combustion (kJ/g) ΔH_T	ΔH_{ch}	ΔH_{con}	ΔH_{rad}	Yield (g/g) CO	Smoke
Normal alkanes									
Ethane	C_2H_6	30	16.0	47.1	45.7	34.1	11.6	0.001	0.013
n-Propane	C_3H_8	44	15.6	46.0	43.7	31.2	12.5	0.005	0.024
n-Butane	C_4H_{10}	58	15.4	45.4	42.6	29.6	13.0	0.007	0.029
n-Pentane	C_5H_{12}	72	15.3	45.0	42.0	28.7	13.3	0.008	0.033
n-Hexane	C_6H_{14}	86	15.2	44.8	41.5	28.1	13.5	0.009	0.035
n-Heptane	C_7H_{16}	100	15.1	44.6	41.2	27.6	13.6	0.010	0.037
n-Octane	C_8H_{18}	114	15.1	44.5	41.0	27.3	13.7	0.010	0.038
n-Nonane	C_9H_{20}	128	15.0	44.4	40.8	27.0	13.8	0.011	0.039
n-Decane	$C_{10}H_{22}$	142	15.0	44.3	40.7	26.8	13.9	0.011	0.040
n-Undecane	$C_{11}H_{24}$	156	15.0	44.3	40.5	26.6	13.9	0.011	0.040
n-Dodecane	$C_{12}H_{26}$	170	14.9	44.2	40.4	26.4	14.0	0.011	0.041
n-Tridecane	$C_{13}H_{28}$	184	14.9	44.2	40.3	26.3	14.0	0.012	0.041
n-Tetradecane	$C_{14}H_{30}$	198	14.9	44.1	40.3	26.2	14.1	0.012	0.042
Hexadecane	$C_{16}H_{34}$	226	14.9	44.1	40.1	26.0	14.1	0.012	0.042
Branched alkanes									
Methylbutane	C_5H_{12}	72	15.3	45.0	40.9	27.2	13.8	0.012	0.042
Dimethylbutane	C_6H_{14}	86	15.2	44.8	40.3	26.3	14.0	0.014	0.046
Methylpentane	C_6H_{14}	86	15.2	44.8	40.3	26.3	14.0	0.014	0.046
Dimethylpentane	C_7H_{16}	100	15.1	44.6	39.9	25.7	14.1	0.015	0.049
Methylhexane	C_7H_{16}	100	15.1	44.6	39.9	25.7	14.1	0.015	0.049
Trimethylpentane	C_8H_{18}	114	15.1	44.5	39.6	25.3	14.3	0.016	0.052
Methylethylpentane	C_8H_{18}	114	15.1	44.5	39.6	25.3	14.3	0.016	0.052
Ethylhexane	C_8H_{18}	114	15.1	44.5	39.6	25.3	14.3	0.016	0.052
Dimethylhexane	C_8H_{18}	114	15.1	44.5	39.6	25.3	14.3	0.016	0.052
Methylheptane	C_8H_{18}	114	15.1	44.5	39.6	25.3	14.3	0.016	0.052
Cyclic alkanes									
Cyclo-Pentane	C_5H_{10}	70	14.7	44.3	39.2	24.1	15.1	0.018	0.055
Methylcyclopentane	C_6H_{12}	84	14.7	43.8	38.2	23.0	15.2	0.019	0.061
Cyclohexane	C_6H_{12}	84	14.7	43.8	38.2	23.0	15.2	0.019	0.061
Methylcyclohexane	C_7H_{14}	98	14.7	43.4	37.5	22.3	15.2	0.021	0.066
Ethylcyclohexane	C_8H_{16}	112	14.7	43.2	36.9	21.7	15.3	0.021	0.069
Dimethylcyclohexane	C_8H_{16}	112	14.7	43.2	36.9	21.7	15.3	0.021	0.069
Cyclooctane	C_8H_{16}	112	14.7	43.2	36.9	21.7	15.3	0.021	0.069
Decalin	$C_{10}H_{18}$	138	14.4	42.8	36.2	20.9	15.3	0.023	0.073
Bicyclohexyl	$C_{12}H_{22}$	166	14.5	42.6	35.7	20.4	15.3	0.023	0.076
Alkenes									
Ethylene	C_2H_4	28	14.7	48.0	41.5	27.3	14.2	0.013	0.043
Propylene	C_3H_6	42	14.7	46.4	40.5	25.6	14.9	0.017	0.095
Butylene	C_4H_8	56	14.7	45.6	40.0	24.8	15.2	0.019	0.067
Pentene	C_5H_{10}	70	14.7	45.2	39.7	24.2	15.4	0.020	0.065
Hexene	C_6H_{12}	84	14.7	44.9	39.4	23.9	15.5	0.021	0.064
Heptene	C_7H_{14}	98	14.7	44.6	39.3	23.7	15.6	0.021	0.063
Octene	C_8H_{16}	112	14.7	44.5	39.2	23.5	15.7	0.022	0.062
Nonene	C_9H_{18}	126	14.7	44.3	39.1	23.3	15.8	0.022	0.062
Decene	$C_{10}H_{20}$	140	14.7	44.2	39.0	23.2	15.8	0.022	0.061
Dodecene	$C_{12}H_{24}$	168	14.7	44.1	38.9	23.1	15.9	0.023	0.061
Tridecene	$C_{13}H_{26}$	182	14.7	44.0	38.9	23.0	15.9	0.023	0.061
Tetradecene	$C_{14}H_{28}$	196	14.7	44.0	38.8	22.9	15.9	0.023	0.060
Hexadecene	$C_{16}H_{32}$	224	14.7	43.9	38.8	22.8	16.0	0.023	0.060
Octadecene	$C_{18}H_{36}$	252	14.7	43.8	38.7	22.8	16.0	0.023	0.060
Polyethylene	$(C_2H_4)_n$	601	14.7	43.6	36.8	20.6	16.2	0.027	0.077
Polypropylene	$(C_3H_6)_n$	720	14.7	43.4	37.0	21.1	15.9	0.025	0.072
Cyclic alkenes									
Cyclohexene	C_6H_{10}	82	14.2	43.0	35.7	20.2	15.5	0.029	0.085
Methylcyclohexene	C_7H_{12}	96	14.3	43.1	35.8	19.8	16.0	0.029	0.085
Pinene	$C_{10}H_{16}$	136	14.1	36.0	33.5	18.9	14.6	0.039	0.114

Table 3-4.19 ***Combustion Properties of Fuels with Carbon and Hydrogen Atoms in the Chemical Structure (Continued)***

Hydrocarbon	Formula	*M* (g/mol)	*S*	Heat of Combustion (kJ/g) ΔH_T	ΔH_{ch}	ΔH_{con}	ΔH_{rad}	Yield (g/g) CO	Smoke
Alkynes and Butadiene									
Acetylene	C_2H_2	26	13.2	47.8	36.7	18.7	18.0	0.042	0.096
Heptyne	C_7H_{12}	96	14.3	44.8	36.0	18.8	17.1	0.036	0.094
Octyne	C_8H_{14}	110	14.4	44.7	35.9	18.9	17.1	0.036	0.094
Decyne	$C_{10}H_{18}$	138	14.4	44.5	35.9	18.9	17.0	0.035	0.094
Dodecyne	$C_{12}H_{22}$	166	14.5	44.3	35.9	18.9	17.0	0.035	0.094
1, 3-Butadiene	C_4H_6	54	14.0	44.6	33.6	15.4	18.2	0.048	0.125
Arenes									
Benzene	C_6H_6	78	13.2	40.1	27.6	11.0	16.5	0.067	0.181
Toluene	C_7H_8	92	13.4	39.7	27.7	11.2	16.5	0.066	0.178
Styrene	C_8H_8	104	13.2	39.4	27.8	11.2	16.6	0.065	0.177
Ethylbenzene	C_8H_{10}	106	13.6	39.4	27.8	11.2	16.6	0.065	0.177
Xylene	C_8H_{10}	106	13.6	39.4	27.8	11.2	16.6	0.065	0.177
Indene	C_9H_8	116	13.0	39.2	27.9	11.3	16.6	0.065	0.176
Propylbenzene	C_9H_{12}	120	13.7	39.2	27.9	11.3	16.6	0.065	0.175
Trimethylbenzene	C_9H_{12}	120	13.7	39.2	27.9	11.3	16.6	0.065	0.175
Cumene	C_9H_{12}	120	13.7	39.2	27.9	11.3	16.6	0.065	0.175
Naphthalene	$C_{10}H_8$	128	12.9	39.0	27.9	11.3	16.6	0.065	0.175
Tetralin	$C_{10}H_{12}$	132	13.5	39.0	27.9	11.4	16.6	0.064	0.174
Butylbenzene	$C_{10}H_{14}$	134	13.8	39.0	27.9	11.4	16.6	0.064	0.174
Diethylbenzene	$C_{10}H_{14}$	134	13.8	39.0	27.9	11.4	16.6	0.064	0.174
p-Cymene	$C_{10}H_{14}$	134	13.8	39.0	27.9	11.4	16.6	0.064	0.174
Methylnaphthalene	$C_{11}H_{10}$	142	13.0	38.9	28.0	11.4	16.6	0.064	0.174
Pentylbenzene	$C_{11}H_{16}$	148	13.9	38.8	28.0	11.4	16.6	0.064	0.173
Dimethylnaphthalene	$C_{12}H_{12}$	156	13.2	38.8	28.0	11.4	16.6	0.064	0.173
Cyclohexylbenzene	$C_{12}H_{16}$	160	13.7	38.7	28.0	11.4	16.6	0.064	0.173
Diisopropylbenzene	$C_{12}H_{18}$	162	14.0	38.7	28.0	11.4	16.6	0.064	0.173
Triethylbenzene	$C_{12}H_{18}$	162	14.0	38.7	28.0	11.4	16.6	0.064	0.173
Triamylbenzene	$C_{21}H_{36}$	288	14.3	38.1	28.2	11.6	16.6	0.063	0.169
Polystyrene	$(C_8H_8)_n$	200	13.2	39.2	29.6	14.0	15.6	0.050	0.135

Table 3-4.20 ***Combustion Properties of Fuels with Carbon, Hydrogen, and Oxygen Atoms in the Chemical Structure***

Hydrocarbon	Formula	*M* (g/mol)	S	Heat of Combustion (kJ/g) ΔH_T	ΔH_{ch}	ΔH_{con}	ΔH_{rad}	Yield (g/g) CO	Smoke
Aliphatic esters									
Ethyl formate	$C_3H_6O_2$	74	6.5	20.2	19.9	13.5	6.3	0.003	0.011
n-Propyl formate	$C_4H_8O_2$	88	7.8	23.9	23.4	15.4	8.0	0.005	0.019
n-Butyl formate	$C_5H_{10}O_2$	102	8.8	26.6	26.0	16.7	9.3	0.007	0.025
Methyl acetate	$C_3H_6O_2$	74	6.5	20.2	19.9	13.5	6.3	0.003	0.011
Ethyl acetate	$C_4H_8O_2$	88	7.8	23.9	23.4	15.4	8.0	0.005	0.019
n-Propyl acetate	$C_5H_{10}O_2$	102	8.8	26.6	26.0	16.7	9.3	0.007	0.025
n-Butyl acetate	$C_6H_{12}O_2$	116	9.5	28.7	28.0	17.8	10.2	0.008	0.029
Isobutyl acetate	$C_6H_{12}O_2$	116	9.5	28.7	28.0	17.8	10.2	0.008	0.029
Amyl acetate	$C_7H_{14}O_2$	130	10.0	30.3	29.5	18.6	11.0	0.009	0.033
Cyclohexyl acetate	$C_8H_{14}O_2$	142	10.2	31.5	30.6	19.1	11.5	0.010	0.035
Octyl acetate	$C_{10}H_{20}O$	172	11.2	33.6	32.6	20.2	12.5	0.012	0.039
Ethyl acetoacetate	$C_6H_{10}O_3$	130	7.4	30.3	29.5	18.6	11.0	0.009	0.033
Methyl propionate	$C_4H_8O_2$	88	7.8	23.9	23.4	15.4	8.0	0.005	0.019
Ethyl propionate	$C_5H_{10}O_2$	102	8.8	26.6	26.0	16.7	9.3	0.007	0.025
n-Butyl propionate	$C_7H_{14}O_2$	130	10.0	30.3	29.5	18.6	11.0	0.009	0.033
Isobutyl propionate	$C_7H_{14}O_2$	130	10.0	30.3	29.5	18.6	11.0	0.009	0.033
Amyl propionate	$C_8H_{16}O_2$	144	10.5	31.6	30.8	19.2	11.6	0.010	0.035
Methyl butyrate	$C_5H_{10}O_2$	102	8.8	26.6	26.0	16.7	9.3	0.007	0.025
Ethyl butyrate	$C_6H_{12}O_2$	116	9.5	28.7	28.0	17.8	10.2	0.008	0.029
Propyl butyrate	$C_7H_{14}O_2$	130	10.0	30.3	29.5	18.6	11.0	0.009	0.033

(continued)

Table 3-4.20 ***Combustion Properties of Fuels with Carbon, Hydrogen, and Oxygen Atoms in the Chemical Structure (Continued)***

Hydrocarbon	Formula	*M* (g/mol)	S	Heat of Combustion (kJ/g) ΔH_T	ΔH_{ch}	ΔH_{con}	ΔH_{rad}	Yield (g/g) CO	Smoke
Aliphatic esters									
n-Butyl butyrate	$C_8H_{16}O_2$	144	10.5	31.6	30.8	19.2	11.6	0.010	0.035
Isobutyl butyrate	$C_8H_{16}O_2$	144	10.5	31.6	30.8	19.2	11.6	0.010	0.035
Ethyl laurate	$C_{14}H_{28}O$	228	12.0	37.2	35.6	26.5	9.1	0.008	0.031
Ethyl oxalate	$C_4H_6O_4$	102	6.1	28.7	27.7	21.3	6.4	0.001	0.003
Ethyl malonate	$C_5H_8O_4$	132	7.7	32.2	31.0	23.4	7.5	0.003	0.015
Ethyl lactate	$C_5H_{10}O_3$	118	7.0	30.8	29.6	22.5	7.1	0.001	0.010
Butyl lactate	$C_7H_{14}O_3$	146	8.5	33.3	32.0	24.1	7.9	0.004	0.018
Amyl lactate	$C_8H_{16}O_3$	160	9.0	34.3	32.9	24.7	8.2	0.005	0.021
Ethyl carbonate	$C_5H_{10}O_3$	118	7.0	30.8	29.6	22.5	7.1	0.001	0.010
Aliphatic alcohols									
Methyl alcohol	CH_4O	32	6.4	20.0	19.1	16.1	3.0	0.001	0.001
Ethyl alcohol	C_2H_6O	46	9.0	27.7	25.6	19.0	6.5	0.001	0.008
n-Propyl alcohol	C_3H_8O	60	10.3	31.8	29.0	20.6	8.5	0.003	0.015
Isopropyl alcohol	C_3H_8O	60	10.3	31.8	29.0	20.6	8.5	0.003	0.015
n-Butyl alcohol	$C_4H_{10}O$	74	11.1	34.4	31.2	21.6	9.6	0.004	0.019
Isobutyl alcohol	$C_4H_{10}O$	74	11.1	34.4	31.2	21.6	9.6	0.004	0.019
Sec butyl alcohol	$C_4H_{10}O$	74	11.1	34.4	31.2	21.6	9.6	0.004	0.019
Ter butyl alcohol	$C_4H_{10}O$	74	11.1	34.4	31.2	21.6	9.6	0.004	0.019
n-Amyl alcohol	$C_5H_{12}O$	88	11.7	36.2	32.7	22.2	10.4	0.005	0.022
Isobutyl carbinol	$C_5H_{12}O$	88	11.7	36.2	32.7	22.2	10.4	0.005	0.022
Sec butyl carbinol	$C_5H_{12}O$	88	11.7	36.2	32.7	22.2	10.4	0.005	0.022
Methylpropyl carbinol	$C_5H_{12}O$	88	11.7	36.2	32.7	22.2	10.4	0.005	0.022
Dimethylethyl carbinol	$C_5H_{12}O$	88	11.7	36.2	32.7	22.2	10.4	0.005	0.022
n-Hexyl alcohol	$C_6H_{14}O$	102	12.1	37.4	33.7	22.7	11.0	0.006	0.024
Dimethylbutyl alcohol	$C_6H_{14}O$	102	12.1	37.4	33.7	22.7	11.0	0.006	0.024
Ethylbutyl alcohol	$C_6H_{14}O$	102	12.1	37.4	33.7	22.7	11.0	0.006	0.024
Allyl alcohol	C_3H_6O	58	9.5	31.4	28.6	20.4	8.2	0.003	0.014
Cyclohexanol	$C_6H_{12}O$	100	11.7	37.3	33.6	22.6	11.0	0.005	0.024
Aliphatic ketones									
Acetone	C_3H_6O	58	9.5	29.7	27.9	20.3	7.6	0.003	0.014
Methyl ethyl ketone	C_4H_8O	72	10.5	32.7	30.6	22.1	8.6	0.004	0.018
Cyclohexanone	$C_6H_{10}O$	98	11.2	35.9	33.7	24.1	9.6	0.005	0.023
Di-acetone alcohol	$C_6H_{12}O_2$	116	9.5	37.3	35.0	24.9	10.1	0.006	0.026
Other aliphatic fuels									
Monoethyl ether	$C_6H_{10}O_2$	90	8.4	26.7	25.8	20.0	5.8	0.001	0.007
Monoethylether acetate	$C_7H_{12}O_3$	132	7.8	32.2	31.0	23.2	7.7	0.001	0.011
Monoethylether diacetate	$C_6H_{10}O_4$	146	6.1	33.3	32.0	24.2	7.9	0.001	0.009
Glycerol triacetate	$C_9H_{14}O_6$	218	6.0	36.9	35.4	26.3	9.1	0.002	0.011
Other aromatic fuels									
Benzaldehyde	C_7H_6O	106	10.4	32.4	21.2	8.1	13.2	0.062	0.166
Benzyl alcohol	C_7H_8O	108	10.8	32.6	22.9	9.8	13.1	0.050	0.137
Cresylic acid	C_8H_8O	136	9.1	34.0	25.1	11.6	13.5	0.039	0.107
Ethyl benzoate	$C_9H_{10}O_2$	150	9.6	34.5	27.4	14.1	13.3	0.030	0.084
Phenylbutyl ketone	$C_{11}H_{14}O$	162	11.9	34.8	26.3	12.6	13.7	0.041	0.115

central offices, computer rooms, power-plant control rooms, space satellites in operation, under construction or in storage, department and grocery stores, hotels, restaurants, various manufacturing facilities, and transportation vehicles such as aircraft, ships, trains, and buses.

For this chapter, the subject of corrosion for commercial and industrial occupancies has been reviewed based on the knowledge derived from the telephone central office (TCO) experience for the deposition of atmospheric pollutants and fire products on equipment, severity of corrosion damage, and ease of cleaning the equipment.[86–89] Galvanized zinc or zinc-chromated finishes represent a major portion of the structural components of the TCO equipment and the HVAC ductwork.[87–89] Unfortunately all zinc surfaces are sensitive to corrosion attack by corrosive products. For example, on exposure to HCl gas, zinc forms zinc chloride, which is very hygroscopic and picks up moisture from air with relative humidity as

Table 3-4.21 ***Combustion Properties of Fuels with Carbon, Hydrogen, Nitrogen, and Sulfur Atoms in the Chemical Structure***

Hydrocarbon	Formula	*M* (g/mol)	*S*	Heat of Combustion (kJ/g) ΔH_T	ΔH_{ch}	ΔH_{con}	ΔH_{rad}	Yield (g/g) CO	Smoke
Aliphatic fuels with carbon, hydrogen, and nitrogen									
Diethylamine	$C_4H_{11}N$	73	14.6	38.0	34.0	21.3	12.6	0.012	0.039
n-Butylamine	$C_4H_{11}N$	73	14.6	38.0	34.0	21.3	12.6	0.012	0.039
Sec-Butylamine	$C_4H_{11}N$	73	14.6	38.0	34.0	21.3	12.6	0.012	0.039
Triethylamine	$C_6H_{15}N$	101	14.6	39.6	35.3	22.0	13.3	0.014	0.044
Di-*n*-butylamine	$C_8H_{19}N$	129	14.6	40.6	36.1	22.4	13.7	0.014	0.047
Tri-*n*-butylamine	$C_{12}H_{27}N$	185	14.7	41.6	37.0	22.9	14.1	0.015	0.049
Aromatic fuels with carbon, hydrogen, and nitrogen									
Pyridine	C_5H_5N	79	12.6	32.2	24.0	11.5	12.5	0.037	0.104
Aniline	C_6H_7N	93	12.9	33.8	25.0	11.7	13.3	0.043	0.119
Picoline	C_6H_7N	93	12.9	33.8	25.0	11.7	13.3	0.043	0.119
Toluidine	C_7H_9N	107	13.2	34.9	25.8	11.9	13.9	0.048	0.130
Dimethylaniline	$C_8H_{11}N$	121	13.3	35.7	26.4	12.1	14.3	0.051	0.139
Quinoline	C_9H_7N	129	12.5	36.1	26.7	12.1	14.5	0.052	0.143
Quinaldine	$C_{10}H_9N$	143	12.7	36.7	27.1	12.2	14.8	0.055	0.149
Butylaniline	$C_{10}H_{15}N$	149	13.6	37.0	27.2	12.2	15.0	0.056	0.151
Aliphatic fuels with carbon, hydrogen, and sulfur									
Hexyl mercaptan	$C_6H_{14}S$	118	12.2	33.0	30.1	17.9	12.2	0.012	0.040
Heptyl mercaptan	$C_7H_{16}S$	132	12.5	33.7	30.4	18.1	12.3	0.013	0.044
Decyl mercaptan	$C_{10}H_{22}S$	174	13.0	34.9	31.1	18.4	12.7	0.016	0.051
Dodecyl mercaptan	$C_{12}H_{26}S$	202	13.3	35.5	31.4	18.6	12.8	0.017	0.054
Hexyl sulfide	$C_{12}H_{26}S$	202	13.3	35.5	31.4	18.6	12.8	0.017	0.054
Heptyl sulfide	$C_{14}H_{30}S$	230	13.4	35.9	31.6	18.7	13.0	0.018	0.057
Octyl sulfide	$C_{16}H_{34}S$	258	13.6	36.3	31.8	18.8	13.1	0.019	0.059
Decyl sulfide	$C_{20}H_{42}S$	314	13.8	36.8	32.1	18.9	13.2	0.020	0.061
Aromatic fuels with carbon, hydrogen, and sulfur									
Thiophene	C_4H_4S	84	9.8	31.9	23.4	10.8	12.6	0.031	0.086
Methylthiophene	C_5H_6S	98	10.5	33.2	24.1	10.9	13.2	0.039	0.107
Thiophenol	C_6H_6S	110	10.6	34.1	24.6	11.0	13.6	0.045	0.122
Thiocresol	C_7H_8S	124	11.1	34.9	25.0	11.0	14.0	0.050	0.135
Cresolmethyl sulfide	$C_8H_{11}S$	155	11.6	36.2	25.7	11.1	14.5	0.058	0.155

low as 10 percent to form electrically conductive liquid zinc chloride solution. The solution flows on the surfaces, drips down or runs onto equipment, resulting in very serious electrical shorting problems. In two major TCO losses, zinc chloride played a key role in both the rate of restoration as well as the ability to salvage equipment.

In TCO fires involving PVC-based cables, contamination levels in the range of about 5 to 900 microgram/cm^2 have been observed.[87–89] In general, an electronic switch would be expected to accumulate zinc chloride levels in the range of about 5 to 9 microgram/cm^2 from the interaction with the environment over its expected lifetime of over 20 years. Clean equipment is expected to have less than 2 microgram/cm^2 of chloride contamination, whereas contaminated equipment can have as high as 900 microgram/cm^2. Thus, equipment contamination levels and ease of restoration have been classified into four levels,[87–89] as listed in Table 3-4.22.

Corrosion

Corrosion is defined as an unwanted chemical reaction and/or destruction or deterioration of a material because of reaction with its environment. Factors that are considered to be important for the extent of corrosion damage are (1) oxygen, (2) nature and concentrations of the fire products, (3) relative humidity, (4) temperature, (5) nature of the target and its orientation relative to the flow of the fire products-air mixture, (6) flow velocity of the fire products-air mixture, (7) presence of extinguishing agents, (8) techniques used for cleaning the exposed surface and their implementation time after the fire, and others.

Most of the knowledge on corrosion damage has been based on air pollution, for example, due to acid rain. Acid deposition is generally described as *acid rain.*[90] Rain usually includes all forms of precipitation (rain, snow, sleet, hail, etc.). Acid deposition is a broader term and includes the uptake of gases by surfaces, impact of fog, and settling of dust and small particles.[90] Precipitation is one of the principal removal mechanisms by which the atmosphere cleanses itself. Acids in rain precipitation result mainly from sulfuric, nitric, and hydrochloric acids, either absorbed directly into precipitation or formed in the aqueous phase from precursor compounds.

In general, all forms of pollution deposition not involving precipitation are referred to as dry, including dew

Table 3-4.22 ***Contamination Levels for the Surface Deposition of Chloride Ions for Electronic Equipment***[a]

Chloride Ion (microgram/cm^2)	Level	Damage/Cleaning/Restoration
2	One	No damage expected. No cleaning and restoration required.
<30	Two	Equipment can be easily restored to service by cleaning, with little impact on long-term reliability.
30 to 90	Three	Equipment can also be restored to service by cleaning, as long as no unusual corrosion problem arise, and the environment is strictly controlled soon after the fire.
>90	Four	The effectiveness of cleaning the equipment dwindles, and the cost of cleaning quickly approaches the replacement cost. Equipment contaminated with high chloride levels may require severe environmental controls even after cleaning, in order to provide potentially long-term reliable operation.

[a]Data taken from Reference 87.

and fog processes.[90] With the exception of nitric acid vapors, most gases do not readily deposit on dry, inert surfaces. However, if the gas is soluble in water, the presence of a liquid film (e.g., resulting from condensation) will generally accelerate dry deposition. In these cases, the amount deposited on the surfaces will depend not only on the concentration of the pollutant, but also on the relative frequency of encountering a wet surface.

Data in Figure 3-4.42, taken from Reference 91, show that the deposition of HCl on wet filter paper is almost four times as high as the deposition on dry paper, in agreement with Reference 90. HCl was generated by exposing PVC to an external heat flux of 20 kW/m^2 in an inert environment in the ASTM E2058 fire propagation apparatus. The chloride ion deposition is high in the initial stages and decreases with time, which is consistent with the decomposition mechanism of PVC. The decomposition of PVC is characterized by the release of HCl, which is initiated at a temperature as low as about 100°C. At a temperature of up to about 200 to 220°C, HCl is the major effluent. Presence of oxygen in the air enhances HCl release. The generation of HCl from PVC leads to the formation of double bonds and release of CO and various aromatic/unsaturated hydrocarbons (benzene, toluene, ethylene, propylene, butylene, etc). The yields of some of these products from the combustion and pyrolysis of PVC are listed in Table 3-4.23, taken from Reference 92.

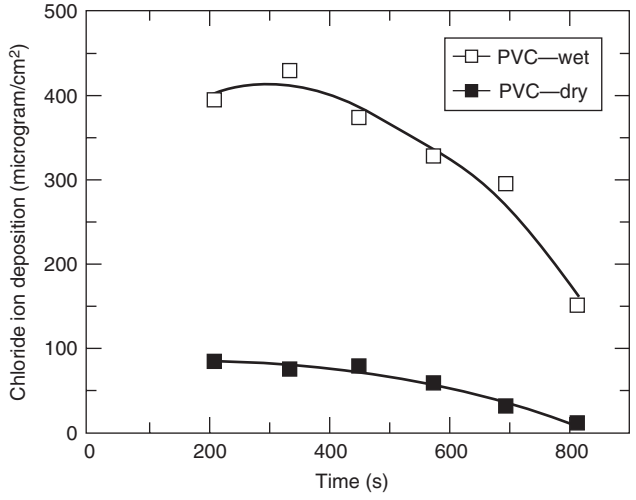

Figure 3-4.42. ***Deposition of HCl on wet and dry cellulosic filter paper during the pyrolysis of PVC at an external heat flux of 20 kW/m² under co-airflow with 10 percent of oxygen concentration in the ASTM E2058 fire propagation apparatus. Flow velocity 0.09 m/s with filter paper at right angle to the flow. Data used in figure are taken from Reference 91.***

Deposition of HCl on walls of enclosures has also been quantified in larger-scale fire tests. For example, in the fire tests with PVC floor covering performed in a 2.8- × 2.8- × 2.4-m-high unventilated room, about 50 percent of the original chloride ions in PVC were deposited on the walls.[93] With the exception of vinyl film (wallpaper) and super-gloss enamel paint on polyethylene, the chloride ion deposition on all other surfaces was in the range of 30 to 90 microgram/cm^2. The differences in the chloride ion deposition on various materials on the wall appear to be related to the hydrophilic (water-attracting) and hydrophobic (water-repelling) nature of the surfaces, that is, filter paper is hydrophilic and vinyl film is hydrophobic, in agreement with Reference 90. This deposition corresponds to the third level of contamination for TCOs. (See Table 3-4.22.)

The corrosion damage in fires follows the basic corrosion relationship,

$$D_{corr} = \mu c^m t^n \tag{109}$$

where

D_{corr} = metal corrosion (penetration depth or metal loss in microns, angstroms, mils)
t = exposure time (min, day)
c = concentration of the corrosive product (g/m^3)
μ, m, n = empirical constants

The constant μ may be defined as a corrosion parameter characteristic of the corrosive nature of the product. The constant n is a function of the corrosion resistance characteristics of the film at the surface. When the film on the surface protects the surface and inhibits further corrosion by diffusion, $n = 1/2$.[90] When the film is permeable to corrosive gases and offers no protection, $n = 1$.[90]

For short-term exposure of metal surfaces to aqueous solutions of corrosive fire products, $n = 1$, and from Equation 109,

$$\dot{R}_{corr} = \mu c^m \tag{110}$$

where $\dot{R}_{corr}$ is corrosion rate (Å/min).

For long-term exposure of metal surfaces to aqueous solutions of corrosive fire products, as a protective layer

Table 3-4.23 ***Yield of CO, HCl, Benzene, and Toluene from the Combustion/Pyrolysis of Polyvinylchloride***[a]

Combustible[b]	Air/Inert	Yield (g/g)			
		CO	HCl	Benzene	Toluene
PVC homopolymer					
Rigid PVC sheet (49.3% Cl)	inert	—	0.480	0.022	0.002
	air	—	0.479	0.022	0.001
Rigid PVC-1	inert	—	0.555	0.058	0.008
	air	—	0.472	0.044	0.004
Rigid PVC-2	air	0.356	0.513	—	—
PVC resin	air	—	0.486	0.048	0.001
PVC homopolymer-1	air	0.422	0.583	0.031	0.001
PVC homopolymer-2	air	0.413	0.584	0.036	0.001
PVC homopolymer-3	air	0.299	0.500	0.029	0.001
PVC homopolymer-4	air	0.429	0.580	0.043	0.004
PVC + plasticizer					
PVC (33% Cl) + dioctylphthalate (67%)	air	0.275	0.269	—	—
PVC (31% Cl) + tricresylphosphate	air	0.248	0.269	—	—
PVC + plasticizer + acid neutralizer					
PVC (%) + dioctylphthalate (%) + K_2CO_3 (%)					
42.4 + 42.4 + 15.2	N_2	—	0.171	—	—
38.2 + 38.2 + 23.6	N_2	—	0.111	—	—
32.5 + 32.5 + 35.0	N_2	—	0.029	—	—
PVC (%) + dioctylphthalate (%) + $CaCO_3$ (%)					
45.5 + 45.5 + 9.0	N_2	—	0.221	—	—
41.7 + 41.7 + 16.0	N_2	—	0.171	—	—
35.7 + 35.7 + 28.6	N_2	—	0.117	—	—
Electrical cables					
PVC jacket	air	—	0.277–0.408	—	—
FR PVC insulation	air	—	0.204–0.285	—	—
Insulation (51% PVC + 49% Plasticizer + additives)	air	0.067	0.273	0.010	0.001
Insulation (57% PVC + 43% Plasticizer + additives)	air	0.090	0.333	0.011	0.001
PVC cable	air	—	0.263	0.033	0.001
General products					
Floor tile (33% PVC + 70% $CaCO_3$ + inert)	air	0.031	0.073	0.001	—
PVC-nylon brattice cloth	air	—	0.174	0.048	0.001
PVC-nylon fabric	air	—	0.254	0.051	0.001
FR PVC-nylon product	air	—	0.206	0.025	0.001
FR PVC	air	—	0.300	0.020	0.001

[a]From Reference 92.

[b]FR—fire retarded, K_2CO_3—potassium carbonate; $CaCO_3$—calcium carbonate.

of corrosion byproducts is formed at the surface, $n = 1/2$, and from Equation 109,

$$\dot{R}_{corr} = \frac{\mu c^m}{t^{1/2}} \tag{111}$$

showing that corrosion rate decreases with time.

Figure 3-4.43 shows a plot of the corrosion rate of a mild steel probe exposed to aqueous solutions of hydrochloric and nitric acid of varying concentrations for 24 hrs. The data used in the figure are taken from Reference 81. No protective layer is formed for 24 hrs, and thus Equation 110 is followed. From linear regression analysis, $\mu = 2.08$ (Å/min)$(g/m^3)^{-1/2}$ and $m = 1/2$. This relationship suggests that the corrosion rate does not increase rapidly with the concentration of the corrosive products. For example, if the concentration of the corrosive product is increased ten times, the corrosion rate would increase only by a factor of three.

For corrosion in the gas phase, the presence of water is essential or the volume fraction of water ≠ 0. The experimental data for corrosion in the gas phase suggest that $m = 1$ in Equation 110, which can be expressed in the following modified form:

$$\dot{R}_{corr} = \frac{\mu y_{corr} \dot{m}'' A}{f_{water} \dot{V}} \tag{112}$$

where

y_{corr} = yield of the corrosive product (g/g)

$\dot{m}''$ = mass loss rate of the material ($g/m^2 \cdot s$)

A = total exposed surface area of the material (m^2)

f_{water} = volume fraction of water generated in the combustion of the material and present in the humid air

$\dot{V}$ = total volumetric flow rate of fire product-air mixture (m^3/s)

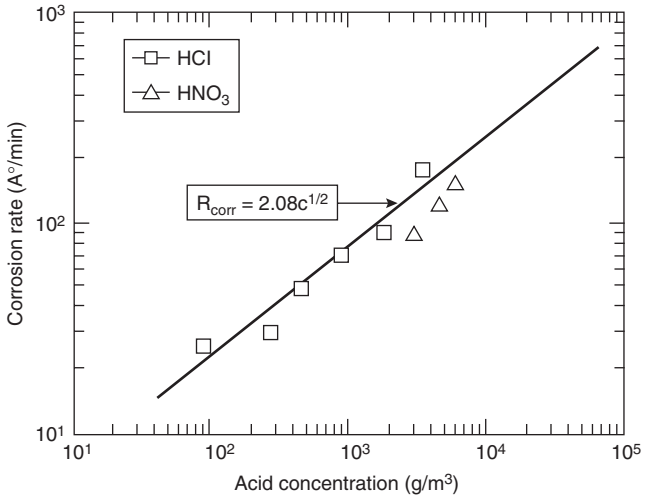

Figure 3-4.43. ***Corrosion rate of a mild steel probe versus hydrochloric and nitric acid concentrations. Data used in figure are taken from Reference 91.***

All the terms in Equation 112 can be measured, and thus the corrosion parameter, μ, can be calculated for the generalized application of the corrosion data.

Corrosion measurements: For corrosion measurements, fire products are generated in small-scale tests and the corrosion is measured by exposing metal probes to the products in the gas phase at various relative humidities or in the aqueous solutions of the products. The common test methods are as follows:

1. The ASTM E2058 fire propagation apparatus test method [Figures 3-4.2(a), 3-4.2(b), and 3-4.27][1,68,91,94–96]
2. The cone calorimeter test method (Figure 3-4.3)[97,98]
3. The radiant combustion/exposure test method[97,98]
4. The CNET (Centre National d'Etudes des Telecommunications) corrosion test method[97,100,101]
5. The DIN 57472 test method[97,102]
6. The DIN 53436 with metal sheets and CNET corrosion probe test method[103]

Corrosion measurements in the gas phase. The measurements are made in the ASTM E2058 fire propagation apparatus, the cone calorimeter, the CNET, and the radiant combustion/exposure test methods. For the measurements, either high-sensitivity Rohrback Cosasco (RC) atmospheric metal corrosion probes or CNET metal corrosion probes are used.

The RC corrosion probes are manufactured by a vacuum deposition technique to obtain an open matrix with little resistance to in-depth diffusion of products, resulting in rapid corrosion. It is designed to monitor short-term corrosion (16 to 24 hr) for environments with small concentrations of corrosive products. The RC probe consists of two metal strips (5,000 to 90,000 Å) embedded in an epoxy-fiberglass plate. One metal strip is coated and acts as a reference, and the other noncoated metal strip acts as a sensor. As the sensor strip corrodes and loses its thickness, its resistance changes. The change in resistance, which represents the extent of corrosion of the metal, is measured as a function of time, by the difference in the resistance between the two strips. The probe readings remain reliable up to about half the thickness of the metal strip (probes are identified as 2500 to 45,000 Å probes).

The CNET probe consists of an epoxy-fiberglass plate embedded with about 170,000 Å thick copper conductors. The change in the resistance of the probe is recorded at the beginning and at the end of the test to determine the extent of corrosion.

The corrosion in the gas phase is measured during the tests every min and every hr after the test for 16 to 24 hr. The corrosion rate is calculated as a function of time, using the following type of relationship:

$$\dot{R}_c = \frac{D_{c_1} - D_{c_2}}{t_2 - t_1} \tag{113}$$

where

$\dot{R}_c$ = corrosion rate in Å/min
D_{c1} = metal thickness in angstroms at time t_1 (s)
D_{c_2} = metal thickness in angstroms at time t_2 (s)

Data have been reported in the literature for the gas-phase corrosion, mass loss rate, and total volumetric rate of fire products-air mixture with relative humidity maintained approximately constant. From Equation 112,

$$\frac{\dot{R}_{\text{corr}}}{(\dot{m}'' A/\dot{V})} = \frac{\mu y_{\text{corr}}}{f_{\text{water}}} \tag{114}$$

where f_{water} is approximately constant, and thus the values of $\dot{R}_{\text{corr}}/(\dot{m}'' A/\dot{V})$ can be used to assess the relative corrosion nature of the fire products generated from various materials. Tables 3-4.24 and 3-4.25 list the values of the corrosion rate per unit fuel vapor concentration, $\dot{R}_{\text{corr}}/(\dot{m}'' A/\dot{V})$. The data show the following:

1. For significant gas-phase corrosion, it is necessary to have hydrogen atoms in the structure of the halogenated materials as suggested by the stoichiometric yields listed in Table 3-4.16. For example, the corrosion rates per unit fuel vapor concentration for PVC (hydrogen atoms in the structure) and Teflon (no hydrogen atoms in the structure) differ by a factor of 7. The difference is probably due to (a) the inefficiency of the hydrolysis process during the conversion of fluorocarbon products generated from Teflon to HF, and (b) the high water solubility of HCl generated from PVC.
2. The corrosion rates per unit fuel vapor concentration for halogenated materials with hydrogen atoms in the structure are high [greater than 0.14 (Å/min)/(g/m^3)], whereas they are negligibly small for fires of nonhalogenated materials [less than 0.007 (Å/min)/(g/m^3)], as expected.
3. Fire retardation of nonhalogenated materials by halogenated materials increases the corrosion rate per unit fuel vapor concentration for the nonhalogenated materials from less than 0.007 to 0.011 to 0.046 (Å/min)/(g/m^3). These values, however, are still about 1/10 the values for the halogenated materials.

Table 3-4.24 ***Corrosion Rate per Unit Fuel Vapor Concentration in the Gas Phase for Flaming and Nonflaming Fires with Variable Oxygen Concentration in the ASTM E2058 Fire Propagation Apparatus and the Radiant Combustion/Exposure Chamber***

Polymer[a]	O_2 (%)	F/NF[b]	Water Present[c]	Corrosion Rate[d] FLAM[e]	Corrosion Rate[d] RC/E[f]
EVA	21	F	no	nd	0.001
EVA-FR1	21	F	no	nd	0.021
PE	21	F	no	nd	0.002
PE-FR1	21	F	no	nd	0.024
PE-FR1	21	F	yes	nd	0.036
PE-FR2	21	F	no	nd	0.022
PE-FR2	21	F	yes	nd	0.024
PE-FR2	21	F	no	nd	0.014
PE-FR2	21	F	yes	nd	0.016
PE/25% Cl	10	N	yes	0.14	nd
PE/36% Cl	10	NF	yes	0.15	nd
PE/48% Cl	10	NF	yes	0.19	nd
PVC	10	NF	yes	0.15	nd
	21	NF	no	nd	0.027
	21	NF	yes	0.12	0.087
	21	F	yes	1.0	nd
TFE	0	NF	yes	0.0036	nd
	10	NF	yes	0.011	nd
	40	NF	yes	0.035	nd
	21	F	yes	0.42	nd

FR-1, red phosphorus fire retardant; FR-2, bromine fire retardant; EVA, ethylene-vinyl acetate copolymer; PE, polyethylene; Cl, chlorine; TFE, tetrafluoroethylene (Teflon); and nd, not determined.

[a]See nomenclature.

[b]F: flaming, NF: nonflaming.

[c]Increased humidity in the gas phase with water.

[d]Per unit fuel vapor concentration (Å/min)(g/m^3)

[e]The ASTM E2058 fire propagation apparatus test method.[1,68,91,94–97]

[f]The radiant combustion/exposure test method,[98,100] 1500-min average.

Table 3-4.25 ***Corrosion Rate per Unit Fuel Vapor Concentration in the Gas Phase for Flaming Fires in Air in the Radiant Combustion/Exposure Chamber[97]***

Sample Description	Corrosion Rate[a]
Crosslinked polyolefin (XLPO) + metal hydrate	0.007
HD polyethylene (PE) + chlorinated PE blend	>0.098
Chlorinated PE + fillers	>0.098
Ethylvinylacetate (EVA) PO + ATH filler	0.012
Polyphenylene oxide/polystyrene (PS) blend	0.005
Polyetherimide	0.002
Polyetherimide/siloxane copolymer	0.005
Intumescent polypropylene (PP)	0.025
Polyolefin copolymer + mineral filler	0.046
XLPO + mineral filler	0.011
XLPO + ATH	0.003
XLPO + ATH	0.007
EVA-PO + mineral filler	0.013
PO + mineral filler	0.016
CLPE + chlorinated additive	>0.098
Polyvinylidene fluoride	>0.098
Polytetrafluoroethylene	>0.098
Polyvinylchloride (PVC)	>0.098
PVC wire	>0.098
PE homopolymer	0.006
Douglas fir	0.006
EVA-PO copolymer	0.003
Nylon 6,6	0.008
XLPE copolymer + brominated additives	0.091

[a]Per unit fuel vapor concentration (Å/min)/(g/m^3); average gas-phase concentration ≈ 17.0 g/m^3.

4. Increase in the corrosion rate per unit fuel vapor concentration due to the presence of water is not significant for halogenated materials with hydrogen atoms in the structure, as expected, as water is generated in the combustion process.
5. Increase in the oxygen concentration in the environment increases the corrosion rate per unit fuel vapor concentration.

Corrosion measurements in the aqueous solution. The measurements are made in the ASTM E2058 fire propagation apparatus and the DIN 57472 test methods. For the measurements, Rohrback Cosasco (RC) loop-type metal corrosion probes are used. The probes are exposed to the aqueous solutions of the fire products. The probe consists of a metal loop attached to an epoxy-fiberglass rod, with a built-in reference. The metal loop acts as a sensor. As the sensor loop corrodes and loses its thickness, its resistance changes. The extent of corrosion is measured by the difference in the resistance between the loop and the reference. The corrosion rate is determined from Equation 113.

The fire products are either bubbled directly into known volumes of water or are collected in the gas phase on cellulose-based filter papers of known area. After the test, the color, odor, and mass of the products deposited on the filter papers are determined. The fire products are extracted with a known volume of deionized water.

The corrosion in the aqueous solution is measured every hour for 16 to 24 hr. In some cases, concentrations of corrosive ions, such as chloride, bromide, and fluoride, are also determined using selective ion electrodes in the ASTM E2058 fire propagation apparatus test method. In the DIN 57472 test standard, pH and conductivity of the solution are measured.

The solution-phase corrosion parameters measured by the ASTM E2058 fire propagation apparatus test method show that they are comparable for all the halogenated materials and are significantly higher than the values for the gas phase.

Smoke Damage

Smoke is a mixture of black carbon and aerosol.[104,105] Smoke is generated by many sources and is released to the environment, causing pollution, reduction in visibility, and nonthermal damage (discoloration, odor, electrical shorting and conduction, corrosion, etc.). The estimated influx of black carbon to the environment from burning is

0.5 to 2×10^{15} g/yr.[104] Black carbon is often called charcoal, soot, elemental carbon, and so forth.[104] The particulate organic matter (POM) in aerosols consists of[104] (1) hydrocarbons—these are the alkanes, alkenes, and some aromatics, with aliphatics constituting the greatest fraction, and range from C_{17} to C_{37}; (2) polycyclic aromatic hydrocarbons; (3) oxidized hydrocarbons—these classes include acids, aldehydes, ketones, quinones, phenols, and esters, as well as the less stable epoxides and peroxides, and may be produced directly in combustion processes or through oxidations in the atmosphere; (4) organonitrogen compounds—the aza-arenes are the only types of this class that have been so far analyzed, and they are one or two orders of magnitude less than the polycyclic aromatic hydrocarbons; and (5) organosulfur compounds—heterocyclic sulfur compounds, such as benzothiazole, have been reported in urban aerosols.

The environmental behavior of black carbon introduced by combustion processes depends on the characteristics of the source, aerosol properties, chemical composition of black carbon, and meteorology.[104] The yield of black carbon depends on the material and combustion conditions, as discussed in previous sections. Table 3-4.26 lists data, taken from Reference 104, for the yield of black carbon from some industrial combustion processes.

Multimodal distributions of black carbon issuing from flames, diesel engines, and freeway traffic show that the *nuclei mode* has a geometric mean radius between 0.0025 and 0.020 microns and probably results from the condensation of gaseous carbon moieties.[104] The *accumulation mode* encompasses particles in the size range 0.075 to 0.25 microns and apparently results from the coagulation and condensation of the nuclei mode particles.[104] Finally in the case of vehicular emissions there is a *coarse mode* at several microns that is attributed to the precipitation of fine particles on the walls of exhaust systems and a subsequent entrainment in the issuing gases.[104] The coal-fired utility boilers produce soot with peaks at particle radius of about 0.05 microns.[104] Long-range transport of particles shows that about 60 percent of the soot is less than 0.05 microns radius size class.[104] The larger particles are probably removed preferentially from the air during its travel.

In fires, large variations in smoke particle size, due to coagulation and condensation, have been found. As the smoke moves away from the fire origin, large particles settle down to the floor, leaving small particles in the gas phase,[106] similar to the long-range transport in the atmosphere discussed in Reference 104. The data from various fires show that initially the smoke particles are in the coarse mode. The particle size decreases slowly with time, suggesting that large particles settle down from the hot layer at the ceiling.

Relationships between transport of heat and smoke generated in large enclosure fires and for smoke characterization have been developed and data have been reported for the most frequently occurring smoke particle radius.[107] These data are listed in Table 3-4.27, which shows that radii of the smoke particles vary between 0.062 to 0.09 microns, belonging to the lower end of the accumulation mode.

It thus appears that, in fires, smoke damage in the room of fire origin is expected to be due to particles of several microns in radius in the coarse mode, whereas smoke damage downstream of the fire is expected to be due to particles with radius less than 0.1 micron in the lower end of the accumulation mode.

Although concentration, size, physical, and optical properties, and chemical composition of smoke particles have been studied in detail, very little is known about the charges on the particles.[108] It has been suggested that soot nucleation and growth occur near the highly ionized regions of the flames in combustion processes, possibly suggesting that some of the charges are transferred to smoke particles. In hydrocarbon-oxygen flames, the following reaction is considered to be the dominant reaction for the charge separation:[108]

$$CH + O = CHO^+ + e^- \qquad (115)$$

Charges on smoke particles generated in flaming and nonflaming fires of wood, cotton wick, polyurethane, heptane with 3 percent toluene, and an alcohol have been examined.[108] The results show that, in nonflaming fires,

Table 3-4.26 ***Yield of Black Carbon from Some Industrial Combustion Processes[104]***

Fuel	Source	Yield (g/kg)
Natural gas	Steam generator	3×10^{-4}
	Domestic water heater	0.1
	Heating boiler	0.01–0.07
Gasoline	Automobile engine	0.1
Diesel	Automobile engine	2–4
	Truck/bus engine	0.6–1
Jet A	Aircraft turbine	0.5–3
Fuel oil (#2)	Utility turbine	0.08

Table 3-4.27 ***Most Frequently Occurring Smoke Particle Radii in Fires of Some Materials[107]***

Material	Smoke Particle Radius (microns)
Coal	0.078
Polystyrene	0.078
Kerosene	0.079
Polypropylene	0.079
Polyethylene	0.077
Propylene	0.076
Ethylene	0.072
Heptane	0.077
Propane	0.068
Nylon	0.075
PMMA	0.068
Douglas fir	0.062
Polyethylene with chlorine	0.090
Polychloroprene	0.090
PVC	0.083
Styrene-butadiene rubber with chlorine	0.073

initially a very small fraction of particles is charged. During aging, the charge increases slowly. For flaming polyurethane fires, where large amounts of black carbon are generated, smoke carries a high initial charge; 70 percent of the particles in the size interval from 0.018 to 0.032 microns are charged. Similar results are found for heptane. Flaming wood fires, however, show particle charges between that of nonflaming fires of wood and cotton wick and that of flaming fires of polyurethane. In the flaming fire of alcohol, there is no smoke.

Char and black carbon are efficient absorbers of HCl. In the combustion of plasticized PVC wire, about 25 percent of the original chloride ions are retained in the char, and the ions are predominantly inorganic in nature.[109] In the combustion of PE-PVC cables in rooms, smoke particles that settle down in the room contain about 33 percent by weight of inorganic chloride ions, and less than 2 percent of the theoretically expected mass of the chloride ions leaves the enclosure.[106] In the combustion of 79.5 percent PVC-20.5 percent PE, 19 mg of HCl/g of smoke is loosely bound and 27 mg of HCl/g of smoke is tightly bound to carbon.[110]

It thus appears that, for nonthermal fire damage, the important factors are (1) concentrations of fire products and their deposition on surfaces, (2) chemical and physical nature of the products, (3) nature of the surfaces, (4) presence of moisture, and other factors. These factors depend on (1) fire initiation and spread, (2) generation rates of fire products and their chemical and physical natures, (3) relative humidity and temperature, (4) in-flow rate of air and its mixing with the products and the flow velocity of the mixture, (5) nature and orientation of the target relative to the flow of the products, (6) exposure duration, (7) presence or absence of fire extinguishing agents, and so forth.

Fire Control, Suppression, and Extinguishment

For the prevention of loss of life and property in fires, both active and passive fire protection techniques are used.[111] Passive fire protection is provided by (1) modifying the chemical structures of the materials for high resistance to ignition and fire propagation, (2) incorporating fire retardants within the materials, (3) coating and wrapping the surfaces, (4) separating materials by inert fire barriers, (5) modifying configuration and arrangement of materials, and so forth. Active fire protection is provided by the application of agents to control, suppress, and/or extinguish fires. The most commonly used liquid and gaseous agents at the present time are water, CO_2, N_2, and halons* 1211 ($CBrClF_2$), 1301 ($CBrF_3$), and 2402 ($CBrF_2CBrF_2$). Because of the contribution of halons to depletion of the stratospheric ozone layer, they will not be used in the future. There is thus an intense effort underway to develop alternative fire suppressants to replace ozone-layer-depleting halons.

The mechanisms of passive and active fire protection are generally known.[45,111–118] Flame extinction by liquid and gaseous agents is mainly due to physical processes (such as removal of heat from the flame and burning surface and creation of nonflammable mixtures) and/or chemical processes (such as termination of chemical reactions). The effectiveness of water is mainly due to removal of heat from the burning surface as a result of vaporization. The effectiveness of halons is mainly due to termination of chemical reactions. N_2 and CO_2 are effective mainly due to creation of nonflammable mixtures by reducing mass fraction of oxygen.

Passive Fire Protection

Passive fire protection is provided by various chemical and physical means, as follows.

Increasing the resistance to ignition and fire propagation by increasing the critical heat flux (CHF) and thermal response parameter (TRP) values: The critical heat flux is expressed as

$$\text{CHF} \approx \sigma(T_{ig}^4 - T_a^4) \tag{116}$$

where

σ = Stefan-Boltzmann constant (56.7×10^{-12} kW/m^2·K^4)
T_{ig} = ignition temperature (K)
T_a = ambient temperature (K)

TRP is defined in Equations 1 and 2, and its relationship to fire propagation in Equations 8 and 9.

The relationships between time to ignition, fire propagation rate, fire propagation index, and TRP (Equations 2, 8, and 9) show that the time to ignition is directly proportional to the TRP value to the power 2; and the fire propagation rate and the fire propagation index are inversely proportional to the TRP value to the power 2 and 1, respectively. Thus the higher the TRP value, the longer the time to ignition, the slower the fire propagation rate, and the lower the FPI value. For high TRP values with FPI < 7, there is no fire propagation beyond the ignition zone, defined as the nonfire-propagating behavior. Also, for materials with high CHF values, higher heat flux exposure is required to initiate a fire.

The CHF and TRP values can be increased by modifying the pertinent parameters, such as increase in the chemical bond dissociation energy and decrease in thermal diffusion (combination of the density, specific heat, and thermal conductivity). Figures 3-4.44 and 3-4.45 show the CHF and TRP values for a tri-wall corrugated paper sheet containing various amounts of a passive fire protection agent (identified as agent A here); the data were obtained from the ignition experiments in the ASTM E2058 fire propagation apparatus. Figure 3-4.46 shows the TRP value for a single-wall corrugated paper sheet containing various amounts of the passive fire protection agent A; the data were obtained from the ignition experiments in

*The numbers represent: first, number of carbon atoms; second, number of fluorine atoms; third, number of chlorine atoms; fourth, number of bromine atoms.

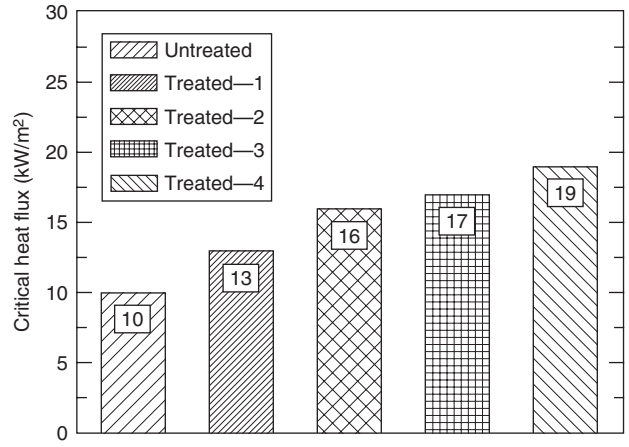

Figure 3-4.44. ***Critical heat flux for untreated and treated tri-wall corrugated paper sheet. The amount of passive fire protection agent is increasing from Treated 1 to 4. Data obtained from the ignition experiments in the ASTM E2058 fire propagation apparatus. Numbers indicated on top of each bar are the critical heat flux values.***

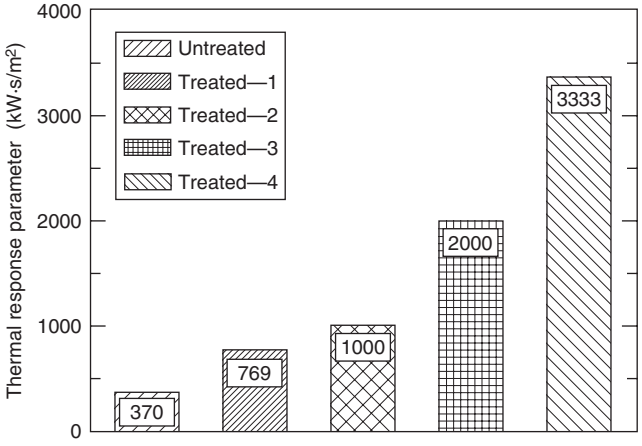

Figure 3-4.45. ***Thermal response parameter for untreated and treated tri-wall corrugated paper sheet. The amount of passive fire protection agent is increasing from Treated 1 to 4. Data obtained from the ignition experiments in the ASTM E2058 fire propagation apparatus. Numbers indicated on top of each bar are the TRP values.***

the ASTM E2058 fire propagation apparatus. The CHF and TRP values increase with increase in the amount of agent; thus, the passive fire protection agent would complement the active fire protection agents. Corrugated paper boxes treated with higher amounts of the passive fire protection agent are expected to require reduced amounts of the active fire protection agents for fire control, suppression, or extinguishment compared to the amounts of the active fire protection agents required for the untreated boxes.

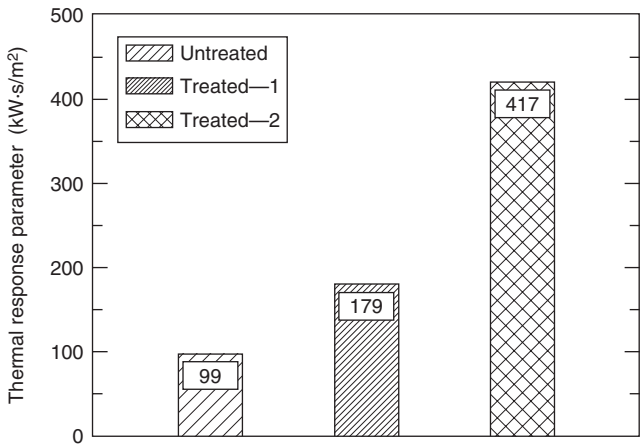

Figure 3-4.46. ***Thermal response parameter for untreated and treated single-wall corrugated paper sheet. The amount of passive fire protection agent is increasing from Treated 1 to 2. Data obtained from the ignition experiments in the ASTM E2058 fire propagation apparatus. Numbers indicated on top of each bar are the TRP values.***

The passive fire protection requirements for various materials can be assessed from the data for CHF and TRP listed in Table 3-4.2.

Decreasing the values of the heat release parameter (HRP) and the flame heat flux: Heat release rate is equal to the heat release parameter (HRP) times the net heat flux (Equation 30). HRP is the ratio of the heat of combustion to heat of gasification, and thus the HRP value can be decreased by decreasing the heat of combustion and/or increasing the heat of gasification by various chemical and physical means. An examination of data in Table 3-4.14 for heats of combustion shows that introduction of oxygen, nitrogen, sulfur, halogen, and other atoms into the chemical structures of the materials reduces the heat of combustion. For example, the heat of combustion decreases when the hydrogen atoms attached to carbon atoms in polyethylene are replaced by the halogen atoms, such as by fluorine in Teflon. The chemical heat of combustion decreases from 38.4 kJ/g to 4.2 kJ/g (Table 3-4.14), and the chemical HRP value decreases from 17 to 2 (Table 3-4.15).

The HRP values can also be reduced by increasing the heat of gasification and decreasing the heat of combustion by retaining the major fraction of the carbon atoms in the solid phase, a process defined as charring. Several passive fire protection agents are available commercially to enhance the charring characteristics of materials.

Figure 3-4.47 shows the reduction in the chemical heat release rate as a result of increase in charring of a tri-wall corrugated paper sheet by the passive fire protection agent A; the data were obtained from the combustion experiments in the ASTM E2058 fire propagation apparatus. The amount of the agent A is increasing from Treated 1 to 3. There is a very significant decrease in the chemical heat

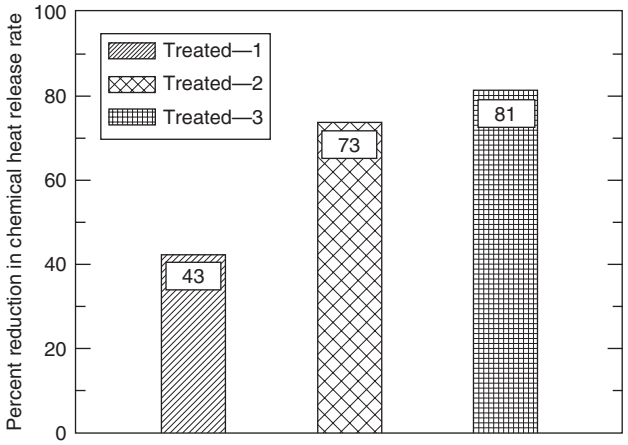

Figure 3-4.47. ***Percent reduction in the chemical heat release rate of untreated tri-wall corrugated paper sheet by a passive fire protection agent. The amount of the passive fire protection agent is increasing from Treated 1 to 3. Data from the combustion experiments in the ASTM E2058 fire propagation apparatus. Numbers indicated on top of each bar are the percent reductions in the chemical heat release rate.***

release rate of the tri-wall corrugated paper sheet by the passive fire protection agent A, which will complement the active fire protection agents. Corrugated paper boxes treated with higher amounts of the passive fire protection agent are expected to require reduced amounts of the active fire protection agents for fire control, suppression, or extinguishment compared to the one required for the untreated boxes.

The effect on flame heat flux by passive fire protection is determined by using the radiation scaling technique, where combustion experiments are performed in oxygen concentration higher than the ambient values. Very little is known about this subject. Table 3-4.8 lists some of the flame heat flux values derived from the radiation scaling technique, but no systematic study has been performed for the effectiveness of passive fire protection. For liquids that vaporize primarily as monomers or as very low molecular weight oligomers, the flame heat flux values are in the range of 22 to 44 kW/m^2, irrespective of their chemical structures. For solid materials, which vaporize as high molecular weight oligomers, the flame heat flux values increase substantially to the range of 49 to 71 kW/m^2, irrespective of their chemical structures. The independence of the asymptotic flame heat values from the chemical structures of materials is consistent with the dependence of flame radiation on optical thickness, soot concentration, and flame temperature in large-scale fires. Passive fire protection agents, which can reduce the molecular weight of the vaporized materials, would be effective in reducing the flame heat flux and complement the active fire protection agents.

Changing the molten behavior of materials: Figure 3-4.22 shows the chemical heat release rate versus time for the well-ventilated combustion of a 90-mm-diameter and 25-mm-thick slab of polypropylene exposed to an external heat flux of 50 kW/m^2. The data were measured in the ASTM E2058 fire propagation apparatus. For about 900 sec, the polypropylene slab burns as a solid with a thin liquid layer at the surface. The measured and calculated values of the heat release rate under this condition agree very well. The heat release rate was calculated from Equation 30 with $\dot{q}''_e \geqslant \dot{q}''_f - \dot{q}''_{rr}$.

Between about 900 and 1150 sec, the polypropylene slab melts rapidly. At about 1150 sec, the entire sample changes to a liquid and burns as a boiling-liquid pool fire. The chemical heat release rate triples at this stage. This stage is the most dangerous in a fire and presents a serious challenge to the active fire protection agents, such as water applied as a spray from sprinklers. Inert passive fire protection agents that eliminate the boiling-liquid pool fire stage will be effective in complementing the active fire protection agents, such as water.

Changing the nature of the fire products: Nonhalogenated passive fire protection agents or agents that reduce or eliminate the release of halogenated and highly aromatic products and enhance release of aliphatic products, rich in hydrogen and oxygen atoms but poor in carbon atoms, are effective in reducing the nonthermal damage due to smoke and corrosion. Some of the passive fire protection agents, available commercially, interact with the materials in the solid as well as in the gas phase during pyrolysis and combustion.

The critical parameter that needs to be examined in the presence and absence of the passive fire protection agents is the ratio of the generation rate of products [such as for smoke, CO, corrosive products (HCl), and others] to heat release rate. The effectiveness of the passive fire protection agent is reflected in the small values of the ratios at fire control, suppression, and/or extinguishment stages.

Active Fire Protection

Active fire protection is provided by applying agents to the flame and/or to the surface of the burning material. The fire control, suppression, and extinguishment have been described by the fire point equation.[114,116] According to the fire point theory, the convective heat flux from the flame to surface as flame extinction condition is reached is expressed as[114,116]

$$\dot{q}''_{fc} = \phi \Delta H_T \dot{m}''_{\text{cr}} \tag{117}$$

where

$\dot{q}''_{fc}$ = convective flame heat flux from the flame to the surface as the extinction condition is reached (kW/m^2)

ϕ = maximum fraction of combustion energy that the flame reactions may lose to the sample surface by convection without flame extinction and is defined as the kinetic parameter for flame extinction

ΔH_T = net heat of complete combustion (kJ/g)

$\dot{m}''_{\text{cr}}$ = critical mass loss rate for flame extinction (g/m^2·s)

The kinetic parameter is defined as[114,116]

$$\phi = \frac{\Delta H_{g,\text{con}}}{\Delta H_T} \tag{118}$$

where $\Delta H_{g,\text{con}}$ is the flame convective energy transfer to the fuel per unit mass of fuel gasified (kJ/g). The kinetic parameter is expected to be higher for fast-burning material vapors and lower for slower burning material vapors, such as materials containing halogens, sulfur, and nitrogen. It is suggested that, at flame extinction, combustion is controlled primarily by the convective heat transfer, and thus the critical mass loss rate would follow Spalding's mass transfer number theory:[113]

$$\dot{m}''_{\text{cr}} = \frac{h}{c_P} \ln (B_{\text{cr}} + 1) \tag{119}$$

where

h = convective heat transfer coefficient (kW/m²·K)
c_P = specific heat of air (kJ/g·K)
B_{cr} = critical mass transfer number

The critical mass transfer number is defined as

$$B_{\text{cr}} = \frac{Y_{\text{O}}\Delta H^*_{\text{O}} - c_P(T_s - T_a)}{\Delta H_{g,\text{con}}} \tag{120}$$

where

Y_{O} = oxygen mass fraction
ΔH^*_{O} = net heat of complete combustion per unit mass of oxygen consumed (kJ/g), which is approximately constant (Tables 3-4.10 through 3-4.13)
T_s = surface temperature (*K*)
T_a = ambient temperature (*K*)

For ambient conditions, $Y_{\text{O}}\Delta H_T \gg c_P(T_s - T_a)$. From equations 118 through 120,

$$\phi = \frac{Y_{\text{O}}\Delta H^*_{\text{O}}}{\Delta H_T \exp(\dot{m}''_{\text{cr}} c_P/h) - 1} \tag{121}$$

The fire point theory[114,116] and experimental data show that the critical mass loss rate for flame extinction is similar to the critical mass loss rate for ignition;[16,63,115,117,119] the critical mass loss rate for ignition, however, has to be measured at the time period where the sustained flame is just being established. The data for the critical mass loss rate for ignition and flame extinction and the kinetic parameter for flame extinction are listed in Table 3-4.28. The values for the critical mass loss rate for ignition from the ASTM E2058 fire propagation apparatus (Reference 16) are measured at the time period where the sustained flame is just being established, and thus are higher than the values from the University of Edinburgh (Reference 119). The University of Edinburgh data are probably measured just before the sustained flame is established. For polymethylmethacrylate, the critical mass loss rate for ignition from the ASTM E2058 fire propagation apparatus (Reference 16) agrees with the critical mass loss rate for flame extinction from Reference 117.

Table 3-4.28 ***Critical Mass Loss Rate for Ignition and Kinetic Parameter for Flame Extinction***

	Critical Mass Loss Rate (g/m²·s)		Kinetic Parameter	
Material	Ref. 16[a]	Ref. 119[b]	Ref. 16[a]	Ref. 119[b]
Polyoxymethylene	4.5	1.7	0.43	1.05
Polymethylmethacrylate	3.2	1.9	0.28	0.53
Polyethylene	2.5	1.3	0.27	—
Polypropylene	2.7	1.1	0.24	0.50
Polyethylene foams				
1	2.6	—	0.24	—
2	2.6	—	0.25	—
3	2.5	—	0.25	—
4	2.6	—	0.25	—
Chlorinated polyethylenes				
25% chlorine	6.6	—	0.15	—
36% chlorine	7.5	—	0.09	—
48% chlorine	7.6	—	0.08	—
Polystyrene	4.0	0.80	0.21	0.78
Polystyrene foams				
GM47	6.3	—	0.11	—
GM49	4.9	—	0.14	—
GM51	6.3	—	0.10	—
GM53	5.7	—	0.11	—
Polyurethane foams (flexible)				
GM21	5.6	—	0.16	—
GM23	5.3	—	0.17	—
GM25	5.7	—	0.15	—
GM27	6.5	—	0.12	—
1/$CaCO_3$	7.2	—	0.19	—
Polyurethane foams (rigid)				
GM29	7.9	—	0.10	—
GM31	8.4	—	0.09	—
GM35	6.9	—	0.11	—
Polyisocyanurate foams (rigid)				
GM41	6.8	—	0.12	—
GM43	5.5	—	0.15	—
Phenolic foam	5.5	—	0.17	—

[a]Ignition data measured in the ASTM E2058 fire propagation apparatus.
[b]Ignition data measured at the University of Edinburgh, U.K.

The data in Table 3-4.28 show that the values of the kinetic parameter are higher for the aliphatic materials than the values for the aromatic and chlorinated materials, which is opposite to the trend for the heat of combustion. The data suggest that the materials can be arranged in the following decreasing order of the kinetic parameter values (using FMRC values): polyoxymethylene ($\phi = 0.43$) > polymethylmethacrylate $\phi = 0.28$) > polyethylene, polypropylene, and polyethylene foams ($\phi = 0.27$ to 0.25) > polystyrene ($\phi = 0.21$) > polyurethane, polystyrene, and polyisocyanurate foams and chlorinated polyethylenes

($\phi = 0.09$ to 0.19). As expected from the fire point theory,[114,116] the reactivity of the vapors in the gas phase follows the kinetic parameter.

The combustion efficiency and product generation efficiencies follow the reactivity of the vapors in the gas phase, such as shown in Figure 3-4.48 for the combustion efficiency. The lower the value of the kinetic parameter (Equation 121), the lower the reactivity of the material vapors, which is reflected in the (1) reduced values of the combustion efficiency (Equations 32 through 34), (2) reduced values of the generation efficiencies (Equation 66) of the oxidation zone products (such as CO_2), and (3) increased values of the generation efficiencies of the reduction zone products (such as smoke, CO, and hydrocarbons).

The flame extinction can also be expressed in terms of the critical heat release rate:

$$\dot{Q}''_{\text{cr},i} = \Delta H_i \dot{m}''_{\text{cr}} \tag{122}$$

where $\dot{Q}''_{\text{cr},i}$ is the critical heat release rate (chemical, convective, or radiative in kW/m^2), and ΔH_i is the heat of combustion (chemical, convective, and radiative in kJ/g). Table 3-4.29 lists the critical chemical, convective, and radiative heat release rates for flame extinction, where critical mass loss rate values are taken from Table 3-4.28 and heats of combustion from Table 3-4.14.

The data in Table 3-4.29 suggest that the critical heat release rate for flame extinction is weakly dependent on the chemical nature of the material, contrary to the critical mass loss rate. The critical heat release rates thus can be averaged, which are 100 ± 7, 53 ± 9, and 47 ± 10 kW/m^2 for the chemical, convective, and radiative heat release rates, respectively. For materials with highly reactive vapors, such as polyethylene, large amounts of extinguishing agent are needed to reduce the heat release rate to the critical value. For materials with highly nonreactive vapors, such as Teflon, it is difficult to reach the critical heat release rate values unless high external heat flux is applied.

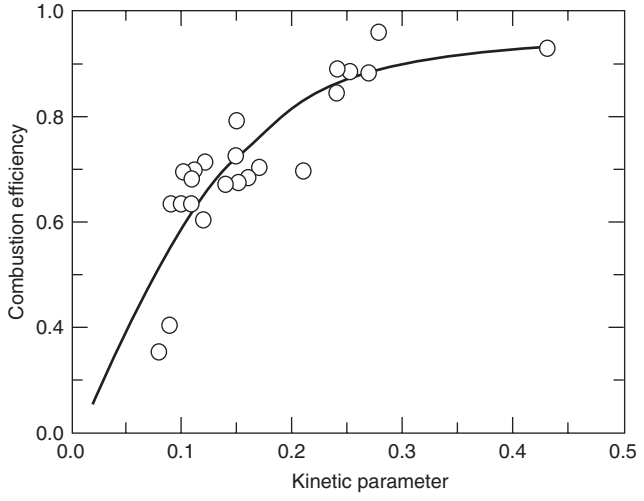

Figure 3-4.48. ***Kinetic parameter for flame extinction versus the combustion efficiency and production generation efficiencies. Data are measured in the ASTM E2058 fire propagation apparatus.***

Table 3-4.29 ***Critical Chemical, Convective, and Radiative Heat Release Rates for Flame Extinction[a]***

	Critical Heat Release Rate (kW/m^2)		
Material	Chemical	Convective	Radiative
Polyoxymethylene	(65)	50	(14)
Polymethylmethacrylate	77	53	24
Polyethylene	96	55	42
Polypropylene	104	61	43
Polyethylene foams	88	51	38
Chlorinated polyethylenes	95	48	47
Polystyrenes	108	44	64
Polyurethane foams (flexible)	101	48	53
Polyurethane foams (rigid)	102	44	58
Average	96 ± 10	51 ± 6	46 ± 12

[a]Critical mass loss rates from the ASTM E2058 fire propagation apparatus, and heats of combustion from Table 3-4.14.

The energy balance at the surface as the flame extinction condition is reached is[113]

$$\dot{m}'' = \frac{\phi \Delta H_T \dot{m}''_{\text{cr}} + \dot{q}''_e - \dot{q}''_{rr} - \dot{q}''_{\text{agent}}}{\Delta H_g} \tag{123}$$

$$\dot{Q}''_i = \frac{\Delta H_i}{\Delta H_g} (\phi \Delta H_T \dot{m}''_{\text{cr}} + \dot{q}''_e - \dot{q}''_{rr} - \dot{q}''_{\text{agent}} \tag{124}$$

where

$\dot{q}''_e$ = external heat flux (kW/m^2)

$\dot{q}''_{rr}$ = surface re-radiation loss (kW/m^2)

$\dot{q}''_{\text{agent}}$ = heat flux removed from the surface or from the flame by the agent as the flame extinction condition is reached (kW/m^2)

ΔH_i = chemical, convective, or radiative heat of combustion (kJ/g)

ΔH_g = heat of gasification (kJ/g)

$\Delta H_i / \Delta H_g$ is defined as the heat release parameter (HRP).

Flame suppression/extinguishment by water: The heat flux removed from the surface of a burning material by water, as a result of vaporization, is expressed as[113]

$$\dot{q}''_w = \varepsilon_w \dot{m}_w \Delta H_w \tag{125}$$

where

ε_w = water application efficiency

$\dot{m}''_w$ = water application rate per unit surface area of the material (g/m^2·s)

ΔH_w = heat of gasification of water (2.58 kJ/g)

If only part of the water applied to a hot surface evaporates and the other part forms a puddle, such as on a horizontal surface, blockage of flame heat flux to the surface and escape of the fuel from the material surface are expected. Equation 125 thus is modified as

$$\dot{q}''_w = \dot{m}''_w(\varepsilon_w \Delta H_w + \delta_w) \quad (126)$$

where δ_w is the energy associated with the blockage of flame heat flux to the surface and escape of the fuel vapors per unit mass of the fuel gasified (kJ/g).

From Equations 123 and 126,

$$\dot{m}''_w = \frac{\dot{q}''_e}{\varepsilon_w \Delta H_w + \delta_w} + \frac{\phi \Delta H_T \dot{m}''_{cr} - \dot{q}''_{rr} - \dot{m}'' \Delta H_g}{\varepsilon_w \Delta H_w + \delta_w} \quad (127)$$

At flame extinction, $\dot{m}'' = \dot{m}''_{cr}$ and from Equation 127

$$\dot{m}''_{w,ex} = \frac{\dot{q}''_e}{\varepsilon_w \Delta H_w + \delta_w} + \frac{\dot{m}''_{cr}(\phi \Delta H_T - \Delta H_g) - \dot{q}''_{rr}}{\varepsilon_w \Delta H_w + \delta_w} \quad (128)$$

where $\dot{m}''_{w,ex}$ is the water application rate per unit surface area of the material for flame extinction (g/m²·s). As discussed in Reference 113, in the absence of the external heat flux with no water puddle formation at the surface, the critical water application rate for flame extinction is

$$\dot{m}''_{w,cr} = \frac{\dot{m}''_{cr}(\phi \Delta H_T - \Delta H_g) - \dot{q}''_{rr}}{\varepsilon_w \Delta H_w} \quad (129)$$

where $\dot{m}''_{w,cr}$ is the critical water application rate (g/m²·s), which is related to the fundamental fire property of the material. The calculated values of the critical water application rate for materials are listed in Table 3-4.30, where efficiency of water application was taken as unity. The values were calculated from Equation 128, using data from Table 3-4.14 for the net heats of complete combustion, from Table 3-4.28 for the critical mass loss rate and the kinetic parameter, from Table 3-4.7 for the heats of gasification and surface re-radiation loss, and using a value of 2.59 kJ/g for the heat of gasification of water.

All the materials listed in Table 3-4.30 burn in normal air without the external heat flux, except polyethylene with 36 and 48 percent chlorine by weight. The critical water application rate for flame extinction for materials that do not burn in normal air without the external heat flux is zero. The materials in Table 3-4.30 that burn without the external heat flux can be arranged in the following order of increased water application rate required for flame extinction: polyoxymethylene, polymethylmethacrylate, and polyethylene with 25 percent chlorine (2.1 to 2.5 g/m²·s) < polyethylene and polypropylene (3.5 to 4.1 g/m²·s) < polystyrene (5.1 g/m²·s).

The data in Table 3-4.30 suggest that the critical water application rate required for flame extinction, with no water puddle at the surface, can be calculated to support the experimental data. The input data for the calculation can be obtained from the measurements for the fire properties in the small-scale apparatuses, such as the oxygen bomb calorimetry, the ASTM E2058 fire propagation apparatus, the OSU apparatus, and the cone calorimeter. The properties and respective tests are (1) surface re-radiation loss (from the CHF and critical mass loss rate, using ignition tests), (2) heat of gasification using the non-flaming tests, (3) net heat of complete combustion from the oxygen bomb calorimeter, and (4) kinetic parameter (Equation 121) where the ratio of the convective heat transfer coefficient to specific heat is needed. The ratio can be obtained from the methanol combustion at variable oxygen mass fractions and external heat flux for known inlet airflow rates, a procedure that has been used in the ASTM E2058 fire propagation apparatus for such applications.[41]

The first term on the right-hand side of Equation 128 can be considered as the term to account for the effects of fire size as well as the shapes and arrangements of the materials. As the fire intensity increases due to changes in the shape, size, and arrangements of the material, heat flux to the surface of the material increases, and water application

Table 3-4.30 ***Critical Water Application Rates for Flame Extinction***

Material	$\dot{q}''_{rr}$ (kW/m²)	ΔH_T (kJ/g)	ΔH_g (kJ/g)	$\dot{m}''_{cr}$ (g/m²·s)	ϕ (g/m²·s)	Critical Water Appl. Rate (g/m²·s)
Polyoxymethylene	13	15.4	2.4	4.5	0.43	2.3
Polymethylmethacrylate	11	25.2	1.6	3.2	0.28	2.5
Polyethylene	15	43.6	1.8	2.5	0.27	3.8
Polypropylene	15	43.4	2.0	2.7	0.24	3.0
Polyethylene foams						
1	12	41.2	1.7	2.6	0.24	3.6
2	13	40.8	1.4	2.6	0.25	3.8
3	12	40.8	1.8	2.5	0.25	3.5
4	12	40.8	1.5	2.6	0.25	4.1
Chlorinated polyethylenes						
25% chlorine	12	31.6	2.1	6.6	0.15	2.1
36% chlorine	12	26.3	3.0	7.5	0.12	0
48% chlorine	10	20.6	3.1	7.6	0.13	0
Polystyrene	13	39.2	1.7	4.0	0.21	5.1

rates above and beyond the critical water application rate for flame extinction thus would be required. For example, water application rate for extinguishment of fires burning at the asymptotic limits can be calculated from (1) the values of the flame heat flux to the surface listed in Table 3-4.8, in place of the external heat flux in Equation 128; and (2) the data for the critical water application rate for flame extinction listed in Table 3-4.30. The calculated water application rates for extinguishment of fires burning at the asymptotic limits are listed in Table 3-4.31. The data show that the first term of Equation 128 becomes very dominant at the asymptotic limit compared to the second term, which is the critical water application rate. In Table 3-4.31, the water application rates at the asymptotic limits are thus calculated on the basis of flame heat flux alone.

Numerous small- and large-scale tests have been performed to assess the extinguishment of fires by water sprays.[113–118,120–123] For example, small-scale fire suppression/extinguishment tests are performed in the ASTM E2058 fire propagation apparatus [Figures 3-4.2(a) and (b)], and large-scale fire suppression/extinguishment tests are performed in the fire products collector (Figure 3-4.8) and at the FMRC Test Center, mostly at the 30-ft site (Figure 3-4.49).[35,45,111,112,115,120–124]

Table 3-4.31 *Water Application Rate for the Extinguishment of Fires at the Asymptotic Limits*[a]

Material	$\dot{m}''_{w,cr}$ (g/m²·s)	$\dot{q}''_f$ (kW/m²)	Water Appl. Rate (g/m²·s)
Aliphatic carbon-hydrogen atoms			
Polyethylene	3.8	61	27
Polypropylene	3.0	67	29
Heavy fuel oil (2.6–23 m)	?	29	11[b]
Kerosene (30–80 m)	?	29	11[b]
Crude oil (6.5–31 m)	?	44	17[b]
n-Dodecane (0.94 m)	?	30	12[b]
Gasoline (1.5–223 m)	?	30	12[b]
JP-4 (1.0–5.3 m)	?	40	16[b]
JP-5 (0.60–17 m)	?	39	15[b]
n-Heptane (1.2–10 m)	?	37	14[b]
n-Hexane) 0.75–10 m)		37	14[b]
Transformer fluids (2.37 m)			
Aromatic carbon-hydrogen atoms			
Polystyrene (0.93 m)	5.1	75	34
Xylene (1.22 m)	?	37	14[b]
Benzene (0.75–6.0 m)	?	44	17[b]
Aliphatic carbon-hydrogen-oxygen atoms			
Polyoxymethylene	2.3	50	22
Polymethylmethacrylate (2.37 m)	2.5	60	26
Methanol (1.2–2.4 m)	?	27	10[b]
Acetone (1.52 m)	?	24	9[b]
Aliphatic carbon-hydrogen-halogen atoms			
Polyvinylchloride	0	50	19
Tefzel (ETFE)	0	50	19
Teflon (FEP)	0	52	20

[a]For water application efficiency of unity with no water puddle at the surface.

[b]Calculated from the flame heat flux alone. Because water does not stay at the surface, the flame extinction of liquid pool fires with water is not an efficient process. The efficiency of unity used in the calculations thus may not be correct and actual water application rates would probably be higher than calculated.

Small-scale fire suppression/extinguishment tests using water and materials with two- and three-dimensional configurations burning in co- and natural-airflow conditions: Several studies have been performed for these types of configurations and airflow conditions.[111–118] For example, small-scale fire suppression/extinguishment tests using water are performed in the ASTM E2058 fire propagation apparatus, under co- and natural airflow conditions. In the tests, measurements are made, in the presence and absence of water, for the critical heat flux (CHF); thermal response parameter (TRP); mass loss rate; chemical, convective, and radiative heat release rates; generation rates of CO and CO_2; hydrocarbons; smoke; optical transmission through smoke; corrosion in the gas phase; and other products (depending on the need).

The test samples used, with and without the external heat flux, consist of (1) two-dimensional samples: 100 × 100 mm square and 100-mm-diameter circular samples up to 50 mm in thickness; and (2) three-dimensional samples identified as *sample commodities:* (a) cross piles of sticks, defined as the *crib*—single crib is used in the test; and (b) 50-, 75-, and 100-mm cubic boxes—one to eight boxes are arranged in one to four layers with a separation of about 12 mm between the boxes and the layers. The designation used for the arrangement of the boxes is as follows: number of boxes along the length × number of boxes along the width × number of layers, that is,

1. One box with a single layer: 1 × 1 × 1 sample commodity,
2. Two boxes with a single layer: 2 × 1 ×1 sample commodity,
3. Two boxes with two layers: 1 × 1 × 2 sample commodity,
4. Three boxes with three layers: 1 × 1 × 3 sample commodity,
5. Four boxes with four layers: 1 × 1 × 4 sample commodity,
6. Four boxes with a single layer: 2 × 2 × 1 sample commodity,
7. Eight boxes with two layers: 2 × 2 × 2 sample commodity.

There are provisions to use more than eight boxes and four layers. The arrangements have strong effect on the fire intensity as shown in Figure 3-4.50, where chemical heat release rate is plotted against time for 100-mm cubic box with one box to a layer for a total of four layers. Visual flame heights from the bottom of the first box are indicated for two arrangements. The data were measured in the ASTM E2058 fire propagation apparatus. The data show that the increase in the chemical heat release rate is more than expected from the increase in the surface area. For example, the surface area increases by a factor of 4 from one to four boxes, whereas the peak chemical heat release rate increases by a factor of 5, even though all the surface areas are not burning. This relationship is indica-

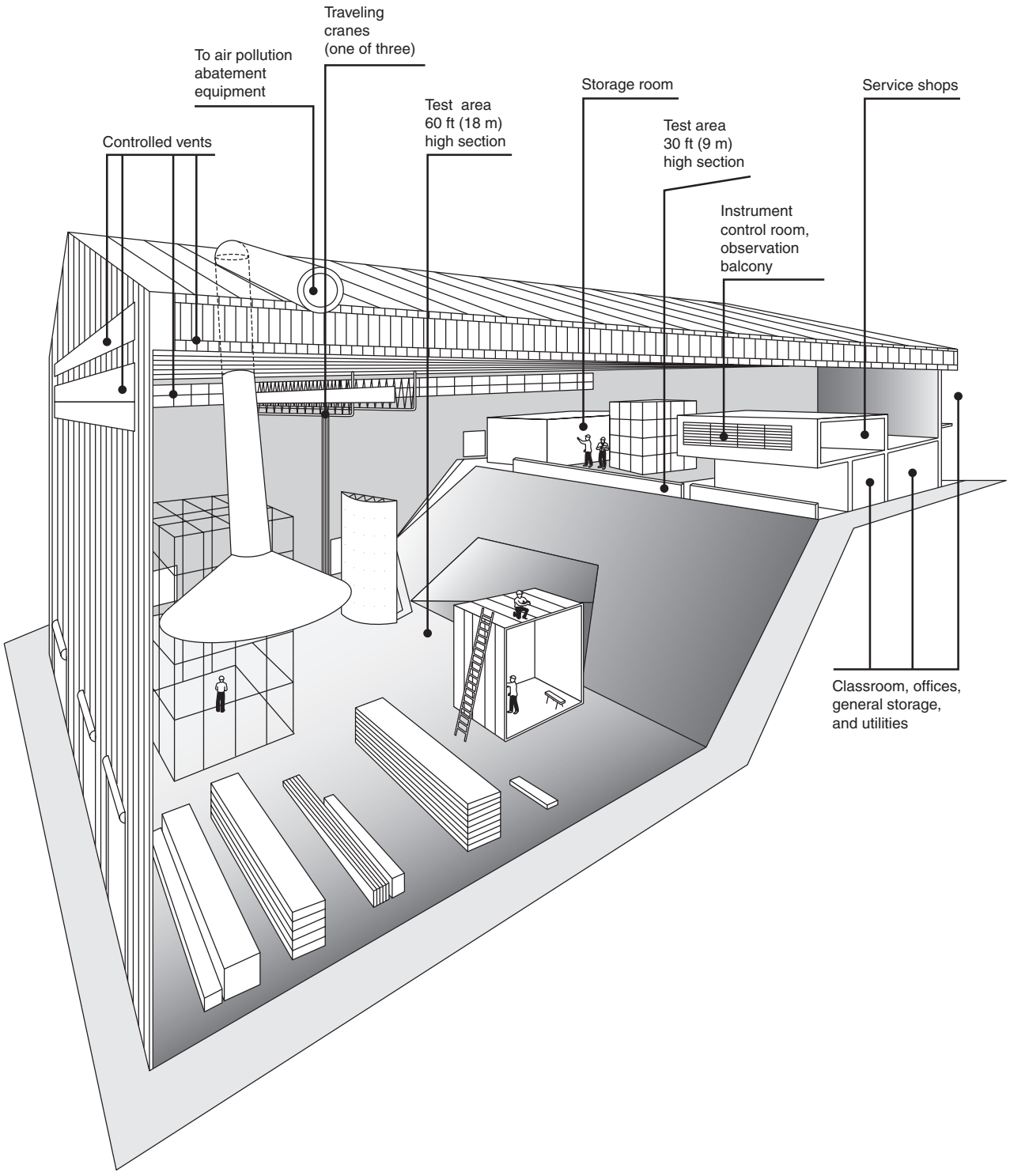

Figure 3-4.49. ***The Factory Mutual Research Corporation's Test Center at West Gloucester, Rhode Island, where large-scale fire tests are performed.***

tive of the enhancement of the flame heat flux in a three-dimensional arrangement.

In the three-dimensional arrangement of the sample commodities, the water application rate for fire suppression/extinguishment is expected to be governed by the first term rather than by the second term in Equation 128 (see Table 3-4.31), due to the enhancement of the flame heat flux. With water application efficiency of unity and

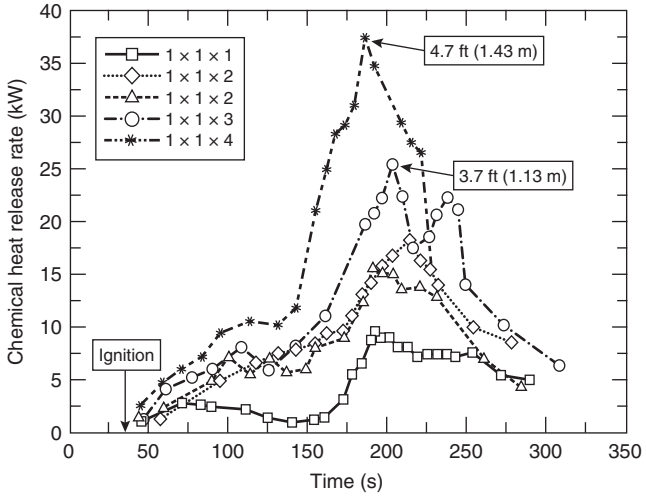

Figure 3-4.50. ***Free-burning chemical heat release rate versus time for 100-mm cubic empty corrugated paper boxes arranged as one box per layer for a total of four layers. Each layer is about 12 mm apart. Visual flame heights are indicated for two arrangements. Data were measured in the ASTM E2058 fire propagation apparatus.***

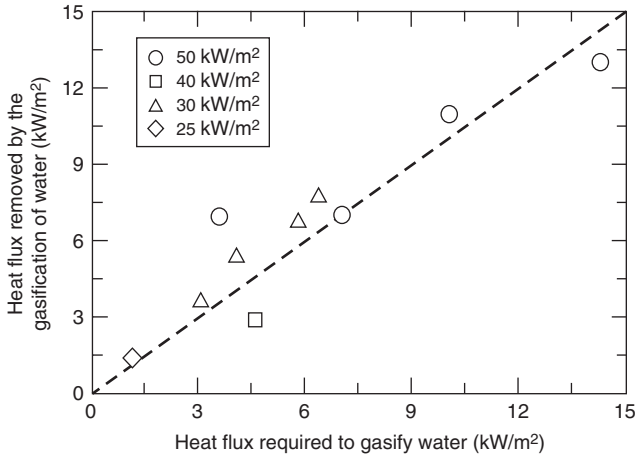

Figure 3-4.51. ***Average heat flux removed from the surface by the gasification of water versus the average heat flux required for the gasification of water. The data are for 100-mm-diameter and 13-mm-thick horizontal wetted slabs of the Whatman No. 3 cellulosic filter paper. The slabs were exposed to external heat fluxes in the range of 25 to 50 kW/m² in the ASTM E2058 fire propagation apparatus under co-flow conditions in normal air. The slabs were wetted with different amounts of water until saturation. Data are taken from Reference 124.***

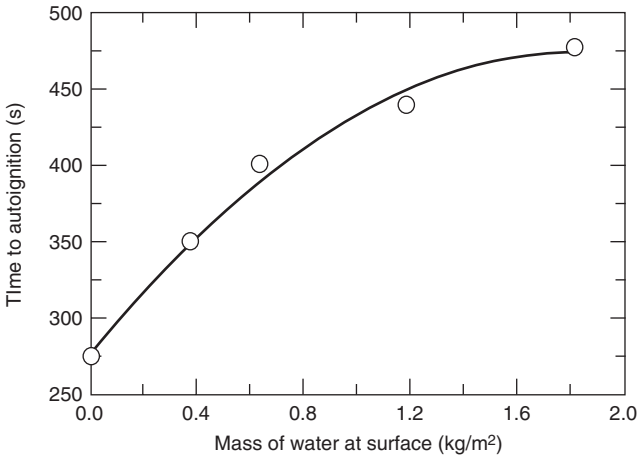

Figure 3-4.52. ***Time to autoignition versus the total amount of water used to wet the 100-mm-diameter and 13-mm-thick horizontal wetted slabs of the Whatman No. 3 cellulosic filter paper. The slabs were exposed to external heat fluxes in the range of 25 to 50 kW/m² in the ASTM E2058 fire propagation apparatus under co-flow conditions in normal air. The slabs were wetted with different amounts of water until saturation. Data are taken from Reference 124.***

no water puddle at the surface, the water application rate required for flame suppression/extinguishment for the three-dimensional arrangement of sample commodities, from Table 3-4.31 for solids, is expected to be in the range of 19 to 34 g/m²·s. These rates are about ten times the critical water application rates for flame extinction (Table 3-4.30).

Figures 3-4.51 through 3-4.53 show examples of the fire extinguishment test data from the ASTM E2058 fire propagation apparatus for 100-mm-diameter and 13-mm-thick circular Whatman No. 3 cellulosic filter paper slabs.[124] Figure 3-4.51 is a plot of the average heat flux removed from the surface of wet filter paper by the gasification of water versus the average heat flux required to gasify the water. The average heat flux removed from the surface, during the test time period, is calculated from Equation 123 using the measured values of the mass loss rate with and without the water on the surface, and the values from Table 3-4.7 for the heats of gasification and surface re-radiation loss of filter paper. The average heat flux required to gasify the water, during the test time period, is calculated from Equation 125 using the measured values of the mass of water applied to the surface, where efficiency of application is unity. As expected from the published literature on this subject,[111–118,128] there is excellent agreement between the heat flux removed from the surface by water and heat flux required to gasify it.

The data in Figure 3-4.52 show that the time to sustained autoignition for the filter paper increases with increase in the amount of water at the surface, as expected due to removal of energy by (1) the gasification of water and (2) blockage of flame heat flux to the surface and escape of the fuel vapors. It is well known that the wetting action of water delivered from sprinklers is effective in resisting the fire jump across the aisles of stored commodities in warehouses. The wetting action of water is considered to be one of the major advantages of the sprinkler fire protection.

Figure 3-4.53 shows the percent reduction in the chemical heat release rate versus the water application

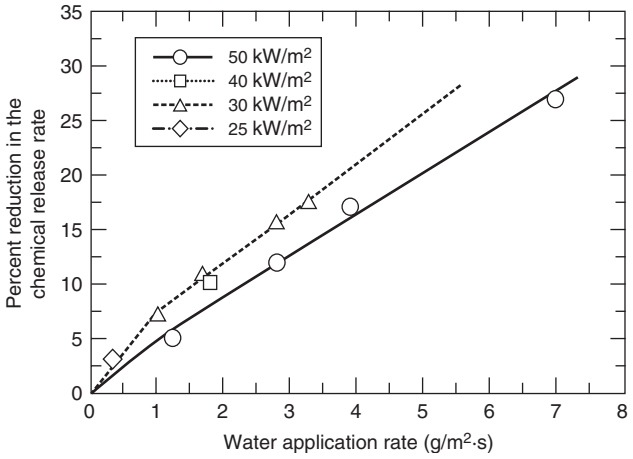

Figure 3-4.53. ***Percent reduction in the chemical heat release rate versus the water application rate for the combustion of 100-mm-diameter and 13-mm-thick horizontal wetted slabs of the Whatman No. 3 cellulosic filter paper. The slabs were exposed to external heat fluxes in the range of 25 to 50 kW/m² in the ASTM E2058 fire propagation apparatus under co-flow conditions in normal air. Data are taken from Reference 124.***

rate for the cellulosic filter paper sample exposed to various heat fluxes. From Equation 124, the reduction in the chemical heat release rate for a fixed external heat flux value can be expressed as follows:

$$\dot{Q}''_{ch} - \dot{Q}''_{ch,w} = \frac{\Delta H_{ch}}{\Delta H_g}\dot{q}''_w \qquad (130)$$

where $\dot{Q}''_{ch,w}$ is the chemical heat release rate in the presence of water (kW/m²). $\Delta H_{ch}/\Delta H_g$ is the HRP. From Equations 126 and 130,

$$\dot{Q}''_{ch} - \dot{Q}''_{ch,w} = \text{HRP}(\varepsilon_w \Delta H_w + \delta_w)\dot{m}''_w \qquad (131)$$

In the tests, the water was applied directly to the surface and there was no puddle formation on the surface, thus $\varepsilon_w = 1$ and $\delta_w = 0$. For cellulosic filter paper, HRP = 3.6 and the heat of gasification of water is 2.6 kJ/g. Using these values in Equation 131,

$$\frac{\dot{Q}''_{ch} - \dot{Q}''_{ch,w}}{\dot{Q}''_{ch}} \times 100 = \left[\frac{100 \times 3.6 \times 2.6}{\dot{Q}''_{ch}}\right]\dot{m}''_w \qquad (132)$$

or, the percent reduction in the chemical heat release rate is

$$\frac{\dot{Q}''_{ch} - \dot{Q}''_{ch,w}}{\dot{Q}''_{ch}} \times 100 = \frac{936}{\dot{Q}''_{ch}}\dot{m}''_w \qquad (133)$$

Equation 133 suggests that a plot of the percentage reduction in the chemical heat release rate versus the water application rate should be a straight line with a slope of $936/\dot{Q}''_{ch}$. For the external heat flux values of 25, 30, 40, and 50 kW/m², the free-burning chemical heat release rates are 120, 190, 210, and 235 kW/m², respectively. Thus, the slopes at these fluxes are 7.8, 4.9, 4.5, and 4.0 $(g/m^2 \cdot s)^{-1}$, respectively. The slopes of the lines from the experimental data for 30 and 50 kW/m² in Figure 3-4.53 are 4.7 and 3.9 $(g/m^2 \cdot s)^{-1}$, respectively, in excellent agreement with the expected slopes from Equation 133. Thus, the experimental data support the heat balance mechanism for flame extinction by the gasification of water, as long as there is no water puddle at the surface.

Small-scale fire suppression/extinguishment tests using water with horizontal and vertical slabs burning under natural airflow condition. Several studies have been performed in this type of configuration.[113–118] For example, fire extinguishment tests have been performed with water applied to the burning vertical and horizontal slabs of polymethylmethacrylate (PMMA), polyoxymethylene (POM), polyethylene (PE), and polystyrene (PS).[117] The horizontal slabs were 0.18-m squares and the vertical slabs were 0.18 m wide and 0.37 m high.[117] The slabs were exposed to external heat flux values in the range 0 to 17 kW/m² in normal air in the presence of water applied at a rate of 0 to 7.8 g/m²·s.[117] The water application efficiency was close to unity.

Figure 3-4.54 shows the time to flame extinction and mass loss rate for various external heat fluxes applied to the surface of the vertical PMMA slab burning in normal air with a water application rate of 5.2 g/m²·s; the data in the figure are taken from the study reported in Reference 117. With increase in the external heat flux, the time to flame extinction increases until, close to the critical heat flux (CHF) value of 11 kW/m² (Table 3-4.2), it goes to infinity (no flame extinction). The mass loss rate data in Figure 3-4.54 show that, close to the CHF value, the mass loss rate approaches the critical rate of 3.2 g/m²·s, determined from the ignition experiments (Table 3-4.29). These data support the fire point theory.[114,116]

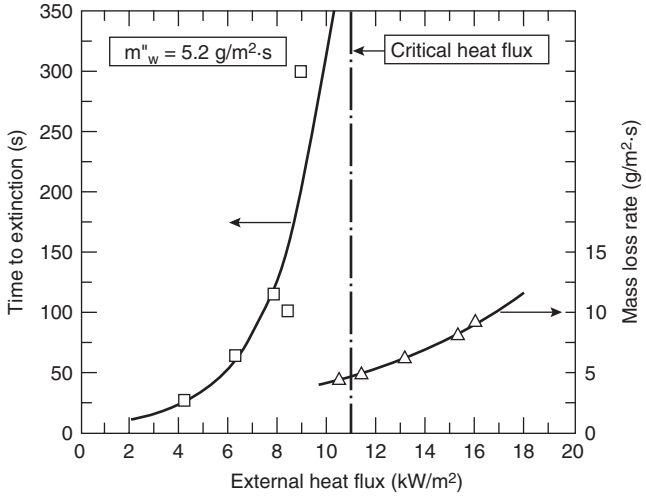

Figure 3-4.54. ***Time to flame extinction and mass loss rate at various external heat fluxes for the combustion of a 0.18-m-wide, 0.37-m-high, and 50-mm-thick vertical slab of polymethylmethacrylate in the presence of water with an application rate of 5.2 g/m²·s. Data are taken from the study reported in Reference 117.***

Figure 3-4.55 shows water application rates required for flame extinction for vertical slabs of polymethylmethacrylate (PMMA), polyoxymethylene (POM), polystyrene (PS), and polyethylene (PE) burning in normal air with various external heat flux exposure. The data satisfy Equation 127:

Polymethylmethacrylate

Vertical

$$\dot{m}''_w = 0.37\dot{q}''_e + 1.67 \ (R^2 = 0.99) \quad (134)$$

Horizontal

$$\dot{m}''_w = 0.22\dot{q}''_e + 1.56 \ (R^2 = 0.99) \quad (135)$$

Polyoxymethylene

Vertical

$$\dot{m}''_w = 0.42\dot{q}''_e + 1.97 \ (R^2 = 0.98) \quad (136)$$

Horizontal

$$\dot{m}''_w = 0.24\dot{q}''_e + 2.08 \ (R^2 = 0.99) \quad (137)$$

Polystyrene

Horizontal

$$\dot{m}''_w = 0.22\dot{q}''_e + 3.1 \ (R^2 = 0.98) \quad (138)$$

Equations 134 and 136 show that, for vertical slabs, the inverse of the slope is equal to 2.7 and 2.3 kJ/g for PMMA and POM, respectively, which are close to the heat of gasification of water (2.6 kJ/g). Thus, the effect of a water puddle at the surface is negligible as expected for the vertical surfaces. Equations 135, 137, and 138 show that, for horizontal surfaces, the inverse of the slopes for PMMA, POM, and PS are 4.6, 4.1, and 4.6 kJ/g, respectively, which are almost twice the value for the heat of gasification of water. The data for the horizontal slabs thus suggest that the blockage of flame heat flux and escape of the fuel from the surface are as important as the gasification of water. The energy associated with the blockage is about the same magnitude as the energy associated with the gasification of water.

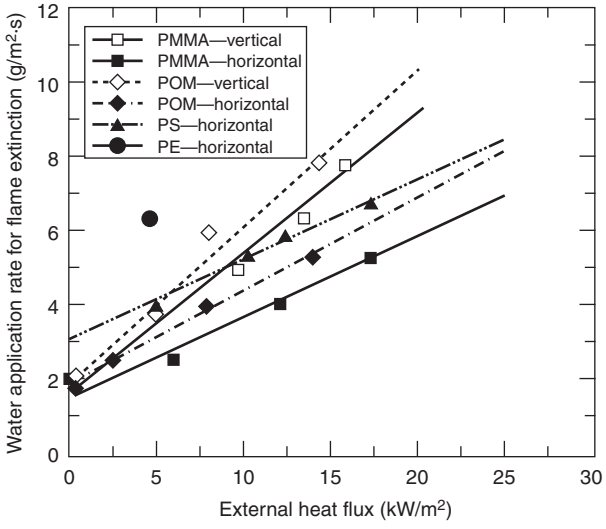

Figure 3-4.55. ***Water application rate required for flame extinction of horizontal and vertical slabs of polymethylmethacrylate (PMMA), polyoxymethylene (POM), polystyrene (PS), and polyethylene (PE) burning in normal air at various external heat fluxes. Data are taken from the study reported in Reference 117.***

Large-scale fire suppression/extinguishment tests using water. Numerous large-scale fire suppression/extinguishment tests have been performed.[111–118,121–124] In almost all cases, the materials are heterogeneous and the configurations are three dimensional, identified as *commodities.* Tests are performed under natural airflow conditions with water applied from a series of sprinklers. The sprinklers are either at the ceiling or close to the top surface of the commodities. At FMRC, large-scale fire suppression/extinguishment tests are performed in the fire products collector (Figure 3-4.8) and at the FMRC Test Center, mostly at the 30-ft site (Figure 3-4.50).[35,45,111,112,115,120–124]

FMRC classifies a stored commodity by its potential fire protection challenge, which is essentially dependent on the commodity's ability to release heat in a fire in the presence of water.[120] Most stored commodities are classified into one of the six classes, such as the following examples.[120]

Noncombustible: Do not burn and do not, by themselves, require sprinkler protection.

Combustibles: Class I: Example—noncombustible products on wood pallets or noncombustible products packaged in ordinary corrugated paper boxes or wrapped in ordinary paper on wood pallets. Class I commodity is simulated by glass jars in compartmented corrugated paper boxes.

Class II: Example—Class I products in more combustible packaging, such as wood crates or multiple-thickness corrugated boxes. Class II commodity is simulated by metal-lined double tri-wall corrugated paper boxes.

Class III: Example—packaged or unpackaged wood, paper, or natural-fiber cloth, or products made from them, on wood pallets. Class III commodity is simulated by using paper cups in compartmented corrugated paper boxes.

Class IV: Class I, II, and III commodities containing no more than 25 percent (by volume) or 15 percent by weight of high-heat-release-rate synthetic materials. Class IV commodity is simulated by polystyrene (15 percent by weight) and paper cups in compartmented corrugated paper boxes.

Group A plastics: Simulated by polystyrene cups in compartmented corrugated paper boxes.

For the tests in the fire products collector, the commodities are used in a $2 \times 2 \times 2$ arrangement (two pallet

loads along the length × two pallet loads along the width × two layers).[111,112,120,123] Each pallet load consists of a wood pallet with eight 0.53-cubic corrugated paper boxes, containing products under test, in a 2 × 2 × 2 arrangement (two boxes along the length × two boxes along the width in two layers, with boxes touching each other). Each pallet load is a 1-m (42-in.) cube of product and separated by about 150 mm. This arrangement leads to the test commodity consisting of eight pallet loads with 64 corrugated paper boxes containing products with overall dimensions of 2.3 m (7.5 ft) × 2.3 m (7.5 ft) × 2.9 m (9.7 ft) high.

In the fire products collector (10,000-kW-scale ASTM E2058 fire propagation apparatus) fire suppression/extinguishment tests, water is applied at the top of the commodity, in a uniform fashion, with application rates in the range of 0 to 407 g/m²·s (0 to 0.6 gpm per sq ft). The range of the water application rates is about ten times the predicted range for the three-dimensional arrangements (Table 3-4.31 with water application efficiency of unity and no water puddles at the surfaces). It thus appears that blockage of flame heat flux to the surface and escape of fuel vapors are as important as gasification of water for the fire suppression/extinguishment of the commodities, similar to the flame extinction for horizontal slabs (Equations 135, 137, and 138) in small-scale tests, discussed previously.

Figure 3-4.56 shows the calculated values of the free-burning average peak heat release rate for the simulated Class I through Group A plastic commodities. In the calculations data measured in the fire products collector (10,000-kW-scale ASTM E2058 fire propagation apparatus) were used.[124] The Class I through Class III commodities were made of cellulosic materials and had lower heat release rates. This behavior is expected on the basis of the values of (1) surface re-radiation loss and heat of gasification (Table 3-4.7), (2) flame heat flux (close to polyoxymethylene, Table 3-4.8), (3) heat of combustion (Table 3-4.14), and (4) heat release parameter (Table 3-4.15) for wood and paper. The heat release rates for Class I through Class III commodities increase gradually from Class I through Class III.

Introduction of polystyrene from about 15 percent (Class IV) to 100 percent (plastics Group A) inside the corrugated paper boxes results in an exponential increase in the chemical and radiative heat release rates as indicated in Figure 3-4.56. This behavior is expected on the basis of the higher values of (1) heat of gasification (Table 3-4.7), (2) flame heat flux (Table 3-4.8), (3) heat of combustion (Table 3-4.14), and (4) heat release parameter (Table 3-4.15) for polystyrene compared to the values for the cellulosic materials in Class I through III commodities. The higher intensity fire due to the introduction of polystyrene is also indicated by the higher water applications rates required for fire suppression/extinguishment in Figure 3-4.57. The higher water requirement for fire suppression/extinguishment for Class IV and plastics Group A commodities is expected from Equation 128, due to higher value of the flame heat flux which dominates the water application rate requirements.

Flame Extinction by the Processes in the Gas Phase

The process of flame extinction by gaseous, powdered, and foaming agents and by increase in the local equivalence ratio is predominantly a gas-phase process and thus is different from the process of flame extinction by water,

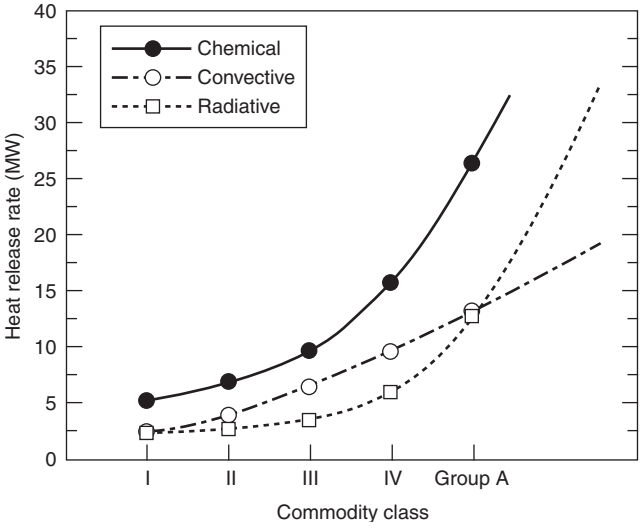

Figure 3-4.56. ***Calculated average peak heat release rates for free-burning fires of simulated commodities from the data measured in the fire products collector (10,000-kW-scale ASTM E2058 fire propagation apparatus). Data are taken from References 111, 112, 120, 123, and 124.***

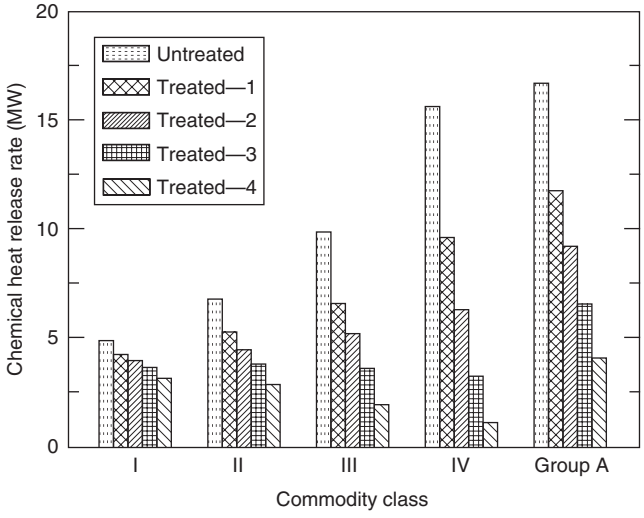

Figure 3-4.57. ***Calculated average peak chemical heat release rates at various water application rates for fires of simulated commodities from the data measured in the fire products collector (10,000-kW-scale ASTM E2058 fire propagation apparatus). Data are taken from References 111, 112, 120, 123, and 124. One gpm/ft² = 769 g/m²·s.***

which occurs predominantly in the solid phase at the surface of the material. The kinetic parameter for flame extinction defined in Equation 118, however, is still applicable:[113]

$$\phi = \frac{\phi_0 - \kappa Y_{j,\text{ex}}\left[\dfrac{1 + \Delta c_P(T_{\text{ad}} - T_a) + \Delta H_D}{\Delta H_{\text{O}}^* Y_{\text{O}}}\right]}{1 - Y_{j,\text{ex}}} \qquad (139)$$

where

ϕ = kinetic parameter in the presence of the extinguishing agent
ϕ_0 = kinetic parameter in the absence of the extinguishing agent
κ = ratio between the kinetic parameters at the flame temperature and at the adiabatic flame temperature
$Y_{j,\text{ex}}$ = mass fraction of the extinguishing agent
Δc_p = difference between the heat capacities of the extinguishing agent and the fire products (kJ/g·K)
T_{ad} = adiabatic flame temperature at the stoichiometric limit (K)
T_0 = initial temperature of the reactants (K)
ΔH_D = heat of dissociation (kJ/g)

Equation 139 shows that the addition of an extinguishing agent reduces the kinetic parameter from its normal value and includes the effects of four flame extinction mechanisms:[113] (1) dilution, effects are included in the $\kappa Y_{j,\text{ex}}$ term; (2) added thermal capacity, effects are included in Δc_p; (3) chemical inhibition, effects are included through increases in T_{ad} value; for most fuels the adiabatic flame temperature at the stoichiometric limit is about 1700 K;[113] more reactive fuels, such as hydrogen, have lower adiabatic flame temperature at the stoichiometric limit, and less reactive or retarded materials have higher values of the adiabatic flame temperature at the stoichiometric limit; and (4) kinetic chain breaking and endothermic dissociation through Δc_P and ΔH_D terms.

From Equation 123, in the presence of an extinguishing agent that works in the gas phase,

$$\dot{m}'' = \frac{\phi \Delta H_T \dot{m}''_{\text{cr}} + \dot{q}''_e - \dot{q}''_{rr}}{\Delta H_g} \qquad (140)$$

For a fixed value of the external heat flux, the addition of an extinguishing agent reduces the normal value of the kinetic parameter by one or more of the four mechanisms expressed by Equation 139; the mass loss rate decreases and approaches the critical value at which the flame is extinguished. Increase in the external heat flux would increase the mass loss rate, and further addition of the extinguishing agent would be needed to reduce the mass loss to its critical value and to reestablish the flame extinction condition. Continued increase in the extinguishing agent with external heat flux will result in the first term in the denominator on the right-hand side of Equation 140 to become zero, and the equation will represent a nonflaming fire.

For a fixed airflow rate, as is generally the case in enclosure fires where the extinguishing agent working in the gas phase is used, increase in the mass loss rate due to external heat flux results in an increase in the equivalence ratio, defined in Equation 36. As the equivalence ratio increases and approaches values of 4.0 and higher, the combustion efficiency approaches values less than or equal to 0.40, flames are extinguished, and nonflaming conditions become important.[44,45] Thus, the upper limit for the application of the extinguishing agent working in the gas phase is dictated by the equivalence ratio $\geq$ 4.0 and/or the combustion efficiency $\leq$ 0.40. Under nonflaming conditions, increase in the external heat flux increases the generation rate of the fuel vapors and the reduction-zone products.

Flame Extinction by Reduced Mass Fraction of Oxygen

Flame extinction by reduced mass fraction of oxygen can be the result of (1) dilution and heat capacity effects due to the addition of inert gases, such as N_2 and CO_2; and (2) chemical effects due to the retardation of chemical reactions and reduction in the flame heat flux to the surface, especially the radiative component.

Theoretical and experimental analyses have been performed for flame extinction by reduced oxygen mass fractions. For example, for polymethylmethacrylate (PMMA), an oxygen mass fraction value of 0.180 is predicted for flame extinction[125] compared to the experimental values of 0.181 for a 70-mm-wide, 190-mm-high, and 19-mm-thick vertical PMMA slab[126] and 0.178 for a 100-mm-wide, 25-mm-thick, and 300- and 610-mm-high vertical slabs of PMMA, and 25-mm-diameter and 610-mm-high vertical cylinder of PMMA.[2] The critical values of the chemical, convective, and radiative heat release for PMMA are 106, 73, and 33 kW/m^2, respectively,[2] showing a trend similar to one reported in Table 3-4.29. At oxygen mass fractions equal to or less than 0.201, flames are unstable and faint blue in color.[2]

The effect of increased external heat flux on flame extinction due to reduced oxygen mass fraction has been examined for the buoyant turbulent diffusion flames. For example, for rectangular and circular horizontal PMMA slabs, 0.06 to 0.10 m^2 in area and 0.03 to 0.05 m in thickness, exposed to external heat flux values of 0, 40, 60, and 65 kW/m^2, flame extinction is found at oxygen mass fractions of 0.178, 0.145, 0.134, and 0.128, respectively.[35] The data support Equation 140 and show that, for buoyant turbulent diffusion flames, flaming can occur up to relatively low oxygen mass fraction values. The only condition is that, in the gas phase, the reactant-oxidizer mixture is within the flammability limit.

The effect of reduced oxygen mass fraction on flame extinction of materials in the three-dimensional arrangement, where flame heat flux is enhanced, has been examined. Figure 3-4.59 shows an example where chemical heat release rates at oxygen mass fractions of 0.233, 0.190, and 0.167 versus time are shown for the combustion of 50-mm cubes of empty corrugated paper boxes in a 2 × 2 × 2 arrangement. The weight of each box is about 13 g (839 g/m^2). The measurements are from the ASTM E2058 fire propagation apparatus.

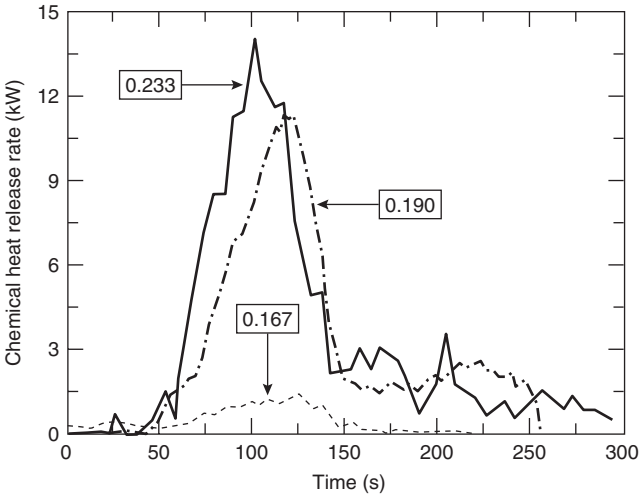

Figure 3-4.58. ***Chemical heat release rate versus time for 50-mm empty corrugated paper boxes in a 2 × 2 × 2 arrangement (two boxes along the length × two boxes along the width × two layers, for a total of eight boxes separated by about 12 mm). Measurements were made in the ASTM E2058 fire propagation apparatus with no external heat flux under the co-flow condition at various oxygen mass fractions, which are indicated in the figure.***

In Figure 3-4.58, at oxygen mass fraction of 0.167, the flame is close to the extinction condition, only 10.5 percent of the initial weight of the boxes is consumed, which is equivalent to consumption of a single box with a surface area of about 0.0155 m². The peak chemical heat release rate close to flame extinction, in Figure 3-4.59, is about 1.5 kW or 97 kW/m², using a surface area of 0.0155 m². This value is in excellent agreement with the average value in Table 3-4.29, derived from the critical mass loss rates for ignition. The data in Figure 3-4.59 for the three-dimensional arrangement of the corrugated boxes thus support the fire point theory,[114,116] independence of the critical heat release rate for flame extinction from the geometrical arrangement and surface areas of the materials, and Equations 139 and 140 as originally formulated in Reference 113.

Nomenclature

A	total exposed surface area of the material (m²)
a_j	mass coefficient for the product yield (g/g)
b_j	molar coefficient for the product yield (g/mol)
B_{cr}	critical mass transfer number ($Y_O\Delta H^*_O/\Delta H_{g,con}$)
CHF	critical heat flux (kW/m²)
$\dot{C}''_O$	mass consumption rate of oxygen (g/m²·s)
$\dot{C}''_{stoich,O}$	stoichiometric mass consumption rate of oxygen (g/m²·s)
c_O	mass of oxygen consumed per unit mass of fuel (g/g)
c_P	specific heat (kJ/g·K)
Δc_P	difference between the heat capacities of the extinguishing agent and the fire products (kJ/g·K)
CDG	carbon dioxide generation calorimetry
D	optical density $\{[\ln (I_0/I)]/\ell\}$ (1/m)
D_{corr}	metal corrosion (penetration depth or metal loss in microns, angstroms, mils)
E_i	total amount of heat generated in the combustion of a material (kJ)
f_j	volume fraction of a product
fp	fire property
FPI	Fire Propagation Index 1000 $(0.42\dot{Q}''_{ch})^{1/3}$/TRP
FSP_c	convective flame spread parameter
$\dot{G}''_j$	mass generation rate of product j (g/m²·s)
$\dot{G}''_{stoich,j}$	stoichiometric mass generation rate of product j (g/m²·s)
GTR	gas temperature rise calorimetry
ΔH_i	heat of combustion per unit mass of fuel vaporized (kJ/g)
ΔH_{CO}	heat of complete combustion of CO (10 kJ/g)
ΔH_D	heat of dissociation (kJ/g)
ΔH_g	heat of gasification at ambient temperature (kJ/g)
$\Delta H_{g,con}$	flame convective energy transfer to the fuel per unit mass of fuel gasified (kJ/g)
ΔH_m	heat of melting at the melting temperature (kJ/g)
ΔH_T	net heat of complete combustion per unit of fuel vaporized (kJ/g)
ΔH_v	heat of vaporization at the vaporization temperature (kJ/g)
ΔH_w	heat of gasification of water (2.58 kJ/g)
ΔH^*_{CO}	net heat of complete combustion per unit mass of CO generated (kJ/g)
$\Delta H^*_{CO_2}$	net heat of complete combustion per unit mass of CO_2 generated (kJ/g)
ΔH^*_O	net heat of complete combustion per unit mass of oxygen consumed (kJ/g)
HRP	heat release parameter ($\Delta H_i/\Delta H_g$)
h_i	mass coefficient for the heat of combustion (kJ/g)
I/I_0	fraction of light transmitted through smoke
j	fire product
k	thermal conductivity (kW/m·K)
L_{s_p}	smoke point (m)
ℓ	optical path length (m)
$\dot{m}''$	mass loss rate (g/m²·s)
$\dot{m}''_w$	water application rate per unit surface area of the material (g/m²·s)
M	molecular weight (g/mol)
m_i	molar coefficient for the heat of combustion (kJ/mol)
MOD	mass optical density ($D\dot{V}/A\dot{m}''$) (m²/g)
$\dot{m}_{air}$	mass flow rate of air (g/s)
OC	oxygen consumption calorimetry
$\dot{q}''_e$	external heat flux (kW/m²)
$\dot{q}''_f$	flame heat flux (kW/m²)

$\dot{Q}_i''$ heat release rate per unit sample surface area ($\dot{m}''\Delta H_{ch}$) (kW/m^2)
$\dot{Q}_i'$ heat release rate per unit sample width (kW/m)
$\dot{R}_{corr}$ corrosion rate (Å/min)
S stoichiometric mass air-to-fuel ratio (g/g)
t time (s)
t_f time at which there is no more vapor formation (s)
t_0 time at which the sample is exposed to heat (s)
T temperature (K)
ΔT_{ig} ignition temperature above ambient (K)
TRP thermal response parameter [$\Delta T_{ig}(k\rho c_p)^{1/2}$] (kW·s$^{1/2}$/m^2)
u fire propagation rate (dX_p/dt) (mm/s or m/s)
v_g co-flow air velocity (m/s)
$\dot{V}$ total volumetric flow rate of fire product-air mixture (m^3/s)
$\dot{W}$ total mass flow rate of the fire product-air mixture (g/s)
W_f total mass of the material lost in the flaming and nonflaming fire (g)
W_j total mass of product j generated in the flaming and nonflaming fire (g)
X_f flame height (m or mm)
X_p pyrolysis front (m or mm)
X_t total length available for fire propagation (m or mm)
y_j yield of product j ($\dot{G}_j''/\dot{m}''$)
$Y_{j,ex}$ mass fraction of the extinguishing agent
Y_O mass fraction of oxygen

Greek

α correlation coefficient (nonflaming fire)
β correlation coefficient (transition region)
δ_w energy associated with the blockage of flame heat flux to the surface and escape of fuel vapors per unit mass of the fuel gasified (kJ/g)
ε_w water application efficiency
ϕ kinetic parameter for flame extinction
ξ correlation coefficient (transition region)
Φ equivalence ratio ($S\dot{m}''/\dot{m}_{air}$)
χ_{ch} combustion efficiency $\dot{Q}''_{ch}/\dot{m}''\Delta H_T$)
χ_{con} convective component of the combustion efficiency $\dot{Q}''_{con}/\dot{m}''\Delta H_T$)
χ_{rad} radiative component of the combustion efficiency $\dot{Q}''_{rad}/\dot{m}''\Delta H_T$)
η_j generation efficiency ($\dot{G}_j''/\dot{m}''\Psi_j$)
κ ratio between the kinetic parameters for the flame temperature and adiabatic flame temperature
λ wavelength of light (μm)
σ Stefan-Boltzmann constant (56.7×10^{-12} kW/m^2·K^4)
τ average specific extinction area (m^2/g)
μ corrosion parameter (Å·min·ml)
ρ density (g/m^3)
ν_j stoichiometric coefficient of product j
ν_O stoichiometric coefficient of oxygen
Ψ_j stoichiometric yield for the maximum conversion of fuel to product j
Ψ_O stoichiometric mass oxygen-to-fuel ratio (g/g)
ζ ratio of fire properties for ventilation-controlled to well-ventilated combustion
ζ_{oxid} oxidation zone product generation efficiency ratio
ζ_{red} reduction zone product generation efficiency ratio

Subscripts

a air or ambient
ad adiabatic
asy asymptotic
ch chemical
con convective
corr corrosion
cr critical
e external
ex extinguishment
f flame or fuel
fc flame convective
fr flame radiative
g gas
g, con flame convective energy for fuel gasification
i chemical, convective, radiative
ig ignition
j fire product
n net
0 initial
oxid oxidation zone of a flame
rad radiation
red reduction zone of a flame
stoich stoichiometric for the maximum possible conversion of fuel monomer to a product
rr surface re-radiation
s surface
vc ventilation-controlled fire
w water
wv well-ventilated fire
∞ infinite amount of air

Superscripts

· per unit time (s^{-1})
′ per unit width (m^{-1})
″ per unit area (m^{-2})

Definitions

Chemical heat of combustion — calorific energy generated in chemical reactions leading to varying degrees of incomplete combustion per unit fuel mass consumed

Convective heat of combustion	calorific energy carried away from the flame by the fire products-air mixture per unit fuel mass consumed
Heat of gasification	energy absorbed to vaporize a unit mass of fuel originally at ambient temperature
Heat release parameter	calorific energy generated per unit amount of calorific energy by the fuel
Kinetic parameter for flame extinction	maximum fraction of combustion energy that the flame reactions may lose to the sample surface by convection without flame extinction
Net heat of complete combustion	calorific energy generated in chemical reactions leading to complete combustion, with water as a gas, per unit fuel mass consumed
Radiative heat of combustion	calorific energy emitted as thermal radiation from the flame per unit fuel mass consumed

Abbreviations

ABS	acrylonitrile-butadiene-styrene
CPVC	chlorinated polyvinylchloride
CR	neoprene or chloroprene rubber
CSP (or CSM)	chlorosulfonated polyethylene rubber (Hypalon)
CTFE	chlorotrifluoroethylene (Kel-F)
E-CTFE	ethylene-chlorotrifluoroethylene (Halar)
EPR	ethylene propylene rubber
ETFE	ethylenetetrafluoroethylene (Tefzel)
EVA	ethylvinyl acetate
FEP	fluorinated polyethylene-polypropylene (Teflon)
IPST	isophthalic polyester
PAH	polyaromatic hydrocarbons
PAN	polyacrylonitrile
PC	polycarbonate
PE	polyethylene
PEEK	polyether ether ketone
PES	polyethersulphone
PEST	polyester
PET	polyethyleneterephthalate (Melinex, Mylar)
PFA	perfluoroalkoxy (Teflon)
PMMA	polymethylmethacrylate
PO	polyolefin
POM	polyoxymethylene
PP	polypropylene
PS	polystyrene
PTFE	polytetrafluoroethylene (Teflon)
PU	polyurethane
$PVCl_2$	polyvinylidene chloride (Saran)
PVDF	Polyvinylidenefluoride (Kynar)
PVEST	polyvinylester
PVF	polyvinyl fluoride (Tedlar)
PVF_2	polyvinylidene fluoride (Kynar, Dyflor)
PVC	polyvinylchloride
SBR	styrene-butadiene rubber
TFE	tetrafluoroethylene (Teflon)
XLPE	crosslinked polyethylene

References Cited

1. ASTM E2058, *Standard Methods of Test for Measurement of Synthetic Polymer Material Flammability Using a Fire Propagation Apparatus (FPA),* American Society for Testing and Materials, Philadelphia (in press).
2. A. Tewarson and S.D. Ogden, "Fire Behavior of Polymethylmethacrylate," *Combustion and Flame,* 89, pp. 237–259 (1992).
3. A. Tewarson and M.M. Khan, "Flame Propagation for Polymers in Cylindrical Configuration and Vertical Orientation," in *Twenty-Second Symposium (International) on Combustion,* Combustion Institute, Pittsburgh, PA, pp. 1231–1240 (1988).
4. A. Tewarson, "Flammability Parameters of Materials: Ignition, Combustion, and Fire Propagation," *J. Fire Science,* 10, pp. 188–241 (1994).
5. E.E. Smith, "Measuring Rate of Heat, Smoke, and Toxic Gas Release," *Fire Technology,* 8, pp. 237–245 (1972).
6. E.E. Smith, "Heat Release Rate of Building Materials," *Ignition, Heat Release, and Non-combustibility of Materials,* ASTM STP 502, American Society for Testing and Materials, Philadelphia, pp. 119–134 (1972).
7. ASTM E906-83, "Standard Test Method for Heat and Visible Smoke Release Rates for Materials and Products," The American Society for Testing and Materials, Philadelphia (1984).
8. C.P. Sarkos, R.A. Filipczak, and A. Abramowitz, "Preliminary Evaluation of an Improved Flammability Test Method for Aircraft Materials," *Technical Report DOT/FAA/CT-84/22,* Federal Aviation Administration, Atlantic City, NJ.
9. A. Tewarson, "Flame Spread in Standard Tests for Electrical Cables," *Technical Report J.I.OMO2E1.RC-2,* Factory Mutual Research, Norwood, MA (1993).
10. A. Tewarson and D. Macaione, "Polymers and Composites—An Examination of Fire Spread and Generation of Heat and Fire Products," *J. Fire Sciences,* 11, pp. 421–441 (1993).
11. A. Tewarson and M.M. Khan, "A New Standard Test Method for the Quantification of Fire Propagation Behavior of Electrical Cables Using Factory Mutual Research Corporation's Small-Scale Flammability Apparatus," *Fire Technology,* 28, pp. 215–227 (1992).
12. M.M. Khan, "Classification of Conveyor Belts Using Fire Propagation Index," *Technical Report J.I.OT1E2.RC,* Factory Mutual Research, Norwood, MA (1991).
13. A. Tewarson and M.M. Khan, "Electrical Cables—Evaluation of Fire Propagation Behavior and Development of Small-Scale Test Protocol," *Technical Report J.I.OM2E1.RC,* Factory Mutual Research, Norwood, MA (1989).
14. *Specification Standard for Cable Fire Propagation, Class No. 3972,* Factory Mutual Research, Norwood, MA (1989).
15. A. Tewarson, "A Study of Fire Propagation and Generation of Fire Products for Selected Cables Used by the United States Navy," *Technical Report J.I.OP3N3.RC/OP1N3.RC,* Factory Mutual Research, Norwood, MA (1988).
16. A. Tewarson, "Experimental Evaluation of Flammability Parameters of Polymeric Materials," *Flame Retardant Polymeric Materials (*M. Lewin., S.M. Atlas, and E.M. Pearce, eds.), pp. 97–153, Plenum Press, New York (1982).
17. V. Babrauskas, "Development of the Cone Calorimeter—A Bench-Scale Heat Release Rate Apparatus Based on Oxygen Consumption," *Technical Report NBSIR 82-2611,* National Institute of Standards and Technology, Gaithersburg, MD (1982).
18. *Heat Release and Fires* (V. Babrauskas and S.J. Grayson, eds.), Elsevier Publishing Company, London (1992).
19. ASTM E1354-90, *Standard Test Method for Heat and Visible Smoke Release Rates for Materials and Products Using Oxygen*

Consumption Calorimeter, American Society for Testing and Materials, Philadelphia, PA (1990).

20. M.J. Scudamore, P.J. Briggs, and F.H. Prager, "Cone Calorimetry—A Review of Tests Carried Out on Plastics for the Association of Plastics Manufacturers in Europe," *Fire and Materials,* 15, pp. 65–84 (1991).
21. A. Tewarson, I.A. Abu-Isa, D.R. Cummings, and D.E. LaDue, "Characterization of the Ignition Behavior of Polymers Commonly Used in the Automotive Industry," *Fire Safety Science—Proceedings of the Sixth International Symposium,* University of Poitiers, France (in press).
22. A.C. Fernandez-Pello and T. Hirano, "Controlling Mechanisms of Flame Spread," *Combustion Science and Technology,* 32, pp. 1–31 (1983).
23. V. Apte, R. Bilget, and A. Tewarson, "Replacing a Regulatory Large-Scale Flammability Test for Conveyor Belts with a Small-Scale Test," Interflam 2001, 9th International Conference, Edinburgh, UK (2001).
24. P.V. Zant, *Microchip Fabrication: A Practical Guide to Semiconductor Processing,* McGraw-Hill Inc., New York, 2nd ed. (1990).
25. *Test Standard, Factory Mutual Research Corporation, FMRC Clean Room Materials Flammability Test Protocol, Class Number FMRC 4910,* Factory Mutual Research, Norwood, MA (1997).
26. A. Tewarson, M.M. Khan, P.K. Wu, and R.G. Bill, "Flammability of Clean Room Polymeric Materials for the Semiconductor Industry," *Fire and Materials,* 25, pp. 31–42 (2001).
27. A. Tewarson, R.G. Bill, R.L. Alpert, A. Braga, V. DeGiorgio, and G. Smith, "Flammability of Clean Room Materials," *J.I. OYOE6.RC,* Factory Mutual Research, Norwood, MA (1999).
28. A. Tewarson and D. Macaione, "Polymers and Composites—An Examination of Fire Spread and Generation of Heat and Fire Products," *J. Fire Sciences,* 11, pp. 421–441 (1993).
29. A. Tewarson, "Fire Hardening Assessment (FHA) Technology for Composite Systems," *Technical Report ARL-CR-178,* Army Research Laboratory, Aberdeen Proving Ground, MD (1994).
30. R.E. Lyon, "Solid-State Thermochemistry of Flaming Combustion," *Final Report DOT/FAA/AR-99/56,* Federal Aviation Administration, Atlantic City, NJ (1999).
31. J.S. Newman and A. Tewarson, "Flame Spread Behavior of Char-Forming Wall/Ceiling Insulations," *Fire Safety Science—Proceedings of the Third International Symposium,* Elsevier Applied Science, New York, pp. 679–688 (1991).
32. J.S. Newman, "Integrated Approach to Flammability Evaluation of Polyurethane Wall/Ceiling Materials," Polyurethanes World Congress Oct. 10–13, Society of the Plastics Industry, Washington, DC (1993).
33. J.S. Newman, "Cost-Effective Method for Flammability Characterization of Alternate Polyols and Blowing Agents," in *Proceedings of the SPI 32nd Annual Technical/Marketing Conference,* Society of the Plastics Industry, Washington, DC (1989).
34. *Approval Standard for Class I A) Insulated Wall or Wall and Roof/Ceiling Panels, B) Plastic Interior Finish Materials, C) Plastic Exterior Building Panels, D) Wall/Ceiling Coating Systems, E) Interior or Exterior Finish Systems, Class No. 4880,* Factory Mutual Research, Norwood, MA (1993).
35. A. Tewarson and R.F. Pion, "Flammability of Plastics. I. Burning Intensity," *Combustion and Flame,* 26, pp. 85–103 (1976).
36. *CRC Handbook of Chemistry and Physics,* 61st ed. (R.C. Weast and M.J. Astle, eds.), CRC Press, Inc., Boca Raton, FL (1980).
37. M.A. Paul, *Physical Chemistry,* D.C. Heath and Company, Boston, MA, p. 46 (1962).
38. D.Q. Kern, *Process Heat Transfer,* McGraw-Hill Book Company, New York, p. 72 (1950).
39. M.M. Hirschler, "Fire Hazard and Toxic Potency of the Smoke from Burning Materials," *J. Fire Sciences,* 5, pp. 289–307 (1987).
40. H.C. Hottel, "Review: Certain Laws Governing the Diffusive Burning of Liquids by Blinov and Khudiakov (1957) Dokl Akad Nauk SSSR, Vol. 113, 1094, 1957," *Fire Research Abstract and Reviews,* 1, pp. 41–45 (1959).
41. A. Tewarson, J.L. Lee, and R.F. Pion, "The Influence of Oxygen Concentration on Fuel Parameters for Fire Modeling," *Eighteenth Symposium (International) on Combustion,* Combustion Institute, Pittsburgh, PA, pp. 563–570 (1981).
42. J.C. Macrae, *An Introduction to the Study of Fuel,* Elsevier Publishing Company, London (1966).
43. C. Hugget, "Estimation of Rate of Heat Release by Means of Oxygen Consumption Measurements," *Fire & Materials,* 4, pp. 61–65 (1980).
44. A. Tewarson, F.H. Jiang, and T. Morikawa, "Ventilation-Controlled Combustion of Polymers," *Combustion and Flame,* 95, pp. 151–169 (1993).
45. A. Tewarson and M.M. Khan, "Extinguishment of Diffusion Flames of Polymeric Materials by Halon 1301," *J. Fire Sciences,* 11, pp. 407–420 (1993).
46. C. Costa, G. Treand, F. Moineault, and J.L. Gustin, "Assessment of the Thermal and Toxic Effects if Chemical and Pesticide Pool Fires Based on Experimental Data Obtained Using the Tewarson Apparatus," *Transactions IchemE.,* Institution of Chemical Engineers, 77, B, pp. 154–164 (1999).
47. A. Tewarson, "Flammability Properties of Engine Compartment Fluids, Part 1: Combustion Properties of Fluids Containing Carbon, Hydrogen and Oxygen," *Technical Report OBIR7.RC,* Factory Mutual Research, Norwood, MA (1998).
48. A. Tewarson, "Prediction of Fire Properties of Materials Part 1: Aliphatic and Aromatic Hydrocarbons and Related Polymers," *Technical Report NBS-GCR-86-521,* National Institute of Standards and Technology, Gaithersburg, MD (1986).
49. A. Tewarson, "Smoke Point Height and Fire Properties of Materials," *Technical Report NBS-GCR-88-555,* National Institute of Standards and Technology, Gaithersburg, MD (1988).
50. *Handbook of Plastics and Elastomers* (C.A. Harper, ed.), McGraw-Hill Book Company, New York (1975).
51. Y. Tsuchiya and J.F. Mathieu, "Measuring Degrees of Combustibility Using an OSU Apparatus and Oxygen Depletion Principle," *Fire Safety Journal,* 17, pp. 291–299 (1991).
52. A. Tewarson, "Heat Release Rates from Samples of Polymethylmethacrylate and Polystyrene Burning in Normal Air," *Fire & Materials,* 1, pp. 90–96 (1976).
53. A. Tewarson and F. Tamanini, "Research and Development for a Laboratory-Scale Flammability Test Method for Cellular Plastics," *Technical Report No. 22524, RC76-T-64,* National Institute of Standards and Technology, Gaithersburg, MD (1976).
54. A. Tewarson, "Heat Release Rate in Fires," *J. Fire & Materials,* 8, pp. 115–121 (1977).
55. A. Tewarson, "Physico-Chemical and Combustion/Pyrolysis Properties of Polymeric Materials," *Technical Report NBS-GCR-80-295,* National Institute of Standards and Technology, Gaithersburg, MD (1980).
56. A.R. Apte, R.W. Bilger, A.R. Green, and J.G. Quintiere, "Wind-Aided Turbulent Flame Spread and Burning over Large-Scale Horizontal PMMA Surfaces," *Combustion and Flame,* 85, pp. 169–184 (1991).
57. F.J. Perzak and C.P. Lazzara, "Flame Spread over Horizontal Surfaces of Polymethylmethacrylate," in *Twenty-Fourth Symposium (International) on Combustion*, Combustion Institute, Pittsburgh, PA, pp. 1661–1667 (1992).
58. L. Tsantarides and B. Ostman, "Smoke, Gas, and Heat Release Data for Building Products in the Cone Calorimeter,"

Technical Report I 8903013, Swedish Institute for Wood Technology Research, Stockholm, Sweden (1989).

59. M.M. Khan, "Characterization of Liquid Fuel Spray Fires," *Heat and Mass Transfer in Fire and Combustion Systems,* 223, American Society of Mechanical Engineers, New York (1992).
60. A. Tewarson and R.G. Zalosh, "Flammability Testing of Aircraft Cabin Materials," in *73rd Symposium AGARD Conference Proceedings, No. 467, Aircraft Fire Safety,* National Technical Information Service, Springfield, VA, pp. 33–1 to 33–12 (1989).
61. Y.R. Sivathanu and G.M. Faeth, "Generalized State Relationships for Scalar Properties in Nonpremixed Hydrocarbon/Air Flames," *Combustion and Flame,* 82, pp. 211–230 (1990).
62. J.S. Newman and J. Steciak, "Characterization of Particulates from Diffusion Flames," *Combustion and Flame,* 67, pp. 55–64 (1987).
63. D. Drysdale, *An Introduction to Fire Dynamics,* Wiley, New York, pp. 278–400 (1985).
64. C.L. Beyler, "Major Species Production by Diffusion Flames in a Two-Layer Compartment Fire Environment," *Fire Safety J.,* 10, pp. 47–56 (1986).
65. C.L. Beyler, in *Fire Safety Science—Proceedings of the Third International Symposium,* Elsevier Applied Science, New York, pp. 431–440 (1986).
66. E.E. Zukowski, in *Fire Safety Science—Proceedings of the Third International Symposium,* Elsevier Applied Science, New York, pp. 1–30 (1986).
67. T. Morikawa, "Effects of Supply Rate and Concentration of Oxygen and Fuel Location on CO Evolution in Combustion," *J. Fire Science,* 1, pp. 364–378 (1983).
68. A. Tewarson, F. Chu, and F.H. Jiang, "Combustion of Halogenated Polymers," in *Fire Safety Science Fourth International Symposium,* Elsevier Applied Science, New York, pp. 563–574 (1994).
69. ASTM D 1322-80, *Standard Test Method for Smoke Points of Aviation Turbine Fuels,* American Society for Testing and Materials, Philadelphia (1980).
70. J. deRis and X. Cheng, "The Role of Smoke-Point in Material Flammability Testing," in *Fire Safety Science—Proceedings of the Fourth International Symposium,* Elsevier Applied Science, New York, pp. 301–312 (1994).
71. I. Glassman, "Soot Formation in Combustion Processes," in *Twenty-Second Symposium (International) on Combustion,* Combustion Institute, Pittsburgh, pp. 295–311 (1986).
72. G.H. Markstein, "Correlations for Smoke Points and Radiant Emission of Laminar Hydrocarbon Diffusion Flames," in *Twenty-Second Symposium (International) on Combustion,* Combustion Institute, Pittsburgh, pp. 363–370 (1986).
73. L. Orloff, J. deRis, and M.A. Delichatsios, "Radiation from Buoyant Turbulent Diffusion Flames," *Combustion and Flame,* 69, pp. 177–186 (1992).
74. J.H. Kent, "Turbulent Diffusion Flame Sooting—Relationship to Smoke-Point Tests," *Combustion and Flame,* 67, pp. 223–233 (1987).
75. J.H. Kent, "A Quantitative Relationship Between Soot Yield and Smoke Point Measurements," *Combustion and Flame,* 63, pp. 349–358 (1986).
76. J.H. Kent and Gg. Wagner, "Why Do Diffusion Flames Emit Soot," *Combustion Science and Technology,* 41, pp. 245–269 (1984).
77. O.L. Gulder, "Influence of Hydrocarbon Fuel Structure Constitution and Flame Temperature on Soot Formation in Laminar Diffusion Flames," *Combustion and Flame,* 78, pp. 179–194 (1989).
78. O.L. Gulder, "Soot Formation in Laminar Diffusion Flames at Elevated Temperatures," *Combustion and Flame,* 88, pp. 74–82 (1992).
79. B.S. Haynes and H.Gg. Wagner, "Soot Formation," *Progress in Energy and Combustion Sciences,* 7, pp. 229–273 (1981).
80. U.O. Koylu and G.M. Faeth, "Structure of Overfire Soot in Buoyant Turbulent Diffusion Flames at Long Residence Times," *Combustion and Flame,* 89, pp. 140–156 (1992).
81. U.O. Koylu, Y.R. Sivathanu, and G.M. Faeth, "Carbon Monoxide and Soot Emissions from Buoyant Turbulent Diffusion Flames," in *Fire Safety Science—Proceedings of the Third International Symposium,* Hemisphere Publishing Co., New York, pp. 625–634 (1991).
82. U.O. Koylu and G.M. Faeth, "Carbon Monoxide and Soot Emissions from Liquid-Fueled Buoyant Turbulent Diffusion Flames," *Combustion and Flame,* 87, pp. 61–76 (1991).
83. Y.R. Shivathanu and G.M. Faeth, "Soot Volume Fractions in the Overfire Region of Turbulent Diffusion Flames," *Combustion and Flame,* 81, pp. 133–149 (1990).
84. D.B. Olson, J.C. Pickens, and Gill, "The Effects of Molecular Structure on Soot Formation, II. Diffusion Flames," *Combust. and Flame,* 62, pp. 43–60 (1985).
85. S.L. Madorsky, *Thermal Degradation of Organic Polymers,* Interscience Publishers, John Wiley & Sons, Inc., New York, p. 192 (1964).
86. "Network Reliability: A Report to the Nation, Compendium of Technical Papers," Federal Communications Commission's Network Reliability Council, National Engineering Consortium, Chicago (1993).
87. B.T. Reagor, "Smoke Corrosivity: Generation, Impact, Detection, and Protection," *J. Fire Sciences,* 10, pp. 169–179 (1992).
88. B.T. Reagor and C.A. Russell, "A Survey of Problems in Telecommunications Equipment Resulting from Chemical Contamination," *IEEE Transactions,* CHMT-9, 2, p. 209 (1986).
89. B.T. Reagor and C.A. Russell, "A Survey of Manufacturing Problems in Telecommunications Equipment," *Proceedings of the International Conference on Electrical Contacts, Electromechanical Components, and Their Applications,* Nagoya, Japan (1986).
90. F.W. Lipfert, "Effects of Acidic Deposition on the Atmospheric Deterioration of Materials," in *Material Performance,* pp. 12–19 (1987).
91. F.L. Chu, "Development and Application of Nonthermal Damage Assessment Techniques," *Technical Report J.I. OV1J1.RC,* Factory Mutual Research, Norwood, MA (1992).
92. A. Tewarson, "The Effects of Fire-Exposed Electrical Wiring Systems on Escape Potential from Buildings, Part I: A Literature Review of Pyrolysis/Combustion Products and Toxicities—Poly(Vinyl Chloride)," *Technical Report No. 22491, RC75-T-47,* Factory Mutual Research, Norwood, MA (1975).
93. K.G. Martin and D.A. Powell, "Toxic Gas and Smoke Assessment Studies on Vinyl Floor Coverings with the Fire Propagation Tests," *Fire and Materials,* 3, pp. 132–139 (1979).
94. A. Tewarson, "Non-Thermal Damage," *J. Fire Sciences,* 10, pp. 188–241 (1992).
95. A. Tewarson and M.M. Khan, "Generation of Smoke from Electrical Cables," *Proceedings of the ASTM Symposium on Characterization and Toxicity of Smoke* (H.K. Hasegawa, ed.), ASTM STP 1082, American Society for Testing and Materials, Philadelphia, pp. 100–117 (1988).
96. A. Tewarson, M.M. Khan, and J.S. Steciak, "Combustibility of Electrical Wire and Cable for Rail Rapid Transit Systems, Vol. 1. Flammability," *Technical Report DOT-TSC-UMTA-83-*

4.1, National Technical Information Service, Springfield, VA (1982).

97. S.L. Kessel, C.E. Rogers, and J.G. Bennett, "Corrosive Test Methods for Polymeric Materials, Part 5—A Comparison of Four Test Methods," *J. Fire Sciences,* 12, pp. 196–233 (1994).
98. P.A. Dickinson, "Evolving Fire Retardant Materials Issues: A Cable Manufacturer's Perspective," *Fire Technology,* 4, pp. 345–368 (1992).
99. A.F. Grand, "Evaluation of the Corrosivity of Smoke Using a Laboratory Radiant Combustion Exposure Apparatus," *J. Fire Sciences,* 10, pp. 72–93 (1992).
100. P. Rio, "Presentation de l'essai Corrosivite mis au point au CNET-Lab-SER/ENV," *Centre National d'Etudes des Telecommunications* (1983).
101. M.F. Bottin, "The ISO Static Test Method for Measuring Smoke Corrosivity," *J. Fire Science,* 10, pp. 160–168 (1992).
102. "Testing of Cables, Wires, and Flexible Cords, Corrosivity of Combustion Gases," *DIN 57472, Part 813 Standard,* Verband Deutscher Elektrotechniker (VDE) Specification 0472 (1983).
103. E. Barth, B. Muller, F.H. Prager, and F. Wittbecker, "Corrosive Effects of Smoke: Decomposition with the DIN Tube According to DIN 53436," *J. Fire Sciences,* 10, pp. 432–454 (1992).
104. E.D. Goldberg, *Black Carbon in the Environment: Properties and Distribution,* John Wiley & Sons, New York (1985).
105. *Particulate Carbon Formation During Combustion (*D.C. Siegla and G.W. Smith, eds.), Plenum Press, New York (1981).
106. S.P. Nolan, "A Review of Research at Sandia National Laboratories Associated with the Problem of Smoke Corrosivity," *Fire Safety Journal,* 15, pp. 403–413 (1989).
107. J.S. Newman, "Smoke Characterization in Enclosure Environments," in *Proceedings of the ASTM Symposium on Characterization and Toxicity of Smoke* (H.K. Hasegawa, ed.), ASTM STP 1082, American Society for Testing and Materials, Philadelphia, pp. 123–134 (1988).
108. H. Burtscher, A. Reiss, and A. Schmidt-Ott, "Particle Charge in Combustion Aerosols," *J. Aerosol Science,* 17, p. 47 (1986).
109. J.J. Beitel, C.A. Bertelo, W.F. Carroll, R.O. Gardner, A.F. Grand, M.M. Hirschler, and G.F. Smith, "HCl Transport and Decay in a Large Apparatus, II. Variables Affecting Hydrogen Chloride Decay," *J. Fire Sciences,* 5, pp. 105–145 (1987).
110. J.P. Stone, R.N. Hazlett, J.E. Johnson, and H.W. Carhart, "The Transmission of HCl by Soot from Burning PVC," *J. Fire and Flammability,* 4, pp. 42–57 (1973).
111. A. Tewarson, and M.M. Khan, "The Role of Active and Passive Fire Protection Techniques in Fire Control, Suppression, and Extinguishment," in *Fire Safety Science—Proceedings of the Third International Symposium,* Hemisphere Publishing Co., New York, pp. 1007–1017 (1991).
112. "Small-Scale Testing: The Role of Passive Fire Protection in Commodity Classification," *FMRC Update,* 4, 3, Factory Mutual Research, Norwood, MA (1990).
113. C. Beyler, "A Unified Model of Fire Suppression," *Journal of Fire Protection Engineering,* 4, pp. 5–16 (1992).
114. D.J. Rashbash, "The Extinction of Fire with Plain Water: A Review," in *Fire Safety Science—Proceedings of the First International Symposium,* Hemisphere Publishing Co., New York, pp. 1145–1163 (1986).
115. G. Heskestad, "The Role of Water in Suppression of Fire: A Review," *J. Fire and Flammability,* 11, pp. 254–262 (1980).
116. D.J. Rashbash, "A Flame Extinction Criterion for Fire Spread," *Combustion and Flame,* 26, pp. 411–412 (1976).
117. R.S. Magee and R.D. Reitz, "Extinguishment of Radiation-Augmented Plastics Fires by Water Sprays," in *Fifteenth Symposium (International) on Combustion,* Combustion Institute, Pittsburgh, pp. 337–347 (1975).
118. D.J. Rashbash, "The Extinction of Fires by Water Sprays," *Fire Research Abstracts and Reviews,* 4, pp. 28–52 (1962).
119. H.E. Thomson, and D.D. Drysdale, "Critical Mass Flow Rate at the Firepoint of Plastics," in *Fire Safety Science—Proceedings of the Second International Symposium,* Hemisphere Publishing Co., New York, pp. 67–76 (1989).
120. "Advances in Commodity Classification, A Progress Report," *FMRC Update,* 4, 1, Factory Mutual Research, Norwood, MA (1990).
121. C. Yao, "The Development of the ESFR Sprinkler System," *Fire Safety Journal,* 14, pp. 65–73 (1988).
122. H.C. Kung, H. You, W.R. Brown, and B.G. Vincent, "Four-Tier Array Rack Storage Fire Tests with Fast-Response Prototype Sprinklers," in *Fire Safety Science—Proceedings of the Second International Symposium,* Hemisphere Publishing Co., New York, pp. 633–642 (1989).
123. J.L. Lee, "Extinguishment of Rack Storage Fires of Corrugated Cartons Using Water," in *Fire Safety Science—Proceedings of the First International Symposium,* Hemisphere Publishing Co., New York, pp. 1177–1186 (1986).
124. M.M. Khan and A. Tewarson, "Passive Fire Protection for Materials and Storage Commodities," in *Flame Retardancy, Educational Symposium No. 28, Rubber Division, American Chemical Society, Fall 1992,* Paper J, The University of Akron, Akron, OH, pp. 1–30 (1992).
125. H. Kodama, K. Miyasaka, and A.C. Fernandez-Pello, "Extinction and Stabilization of a Diffusion Flame on a Flat Combustible Surface with Emphasis on Thermal Controlling Mechanisms," *Combustion Science and Technology,* 54, pp. 37–50 (1987).
126. A.K. Kulkarni and M. Sibulkin, "Burning Rate Measurements on Vertical Fuel Surfaces," *Combustion and Flame,* 44, pp. 185–186 (1982).

CHAPTER 5

Compartment Fire Modeling

James G. Quintiere

Introduction

An approach for predicting various aspects of fire phenomena in compartments has been called *zone* modeling. It is based on a conceptual representation for the compartment fire process, and is an approximation to reality. Any radical departure by the fire system from the basic concept of the zone model can seriously affect the accuracy and validity of the approach. The zone model simply represents the system as two distinct compartment gas zones: an upper volume and a lower volume resulting from thermal stratification due to buoyancy. Conservation equations are applied to each zone and serve to embrace the various transport and combustion processes that apply. The fire is represented as a source of energy and mass, and manifests itself as a plume, which acts as a pump for the mass from the lower zone to the upper zone through a process called *entrainment.*

The zone modeling approach emerged in the mid-1970s when the effort to study the developing fire in a compartment intensified. Careful measurements and observations revealed characteristics of the compartment fire system. The upper and lower layers (zones) were deemed relatively uniform in temperature and composition. Distinct phenomena were discerned that could be studied in isolation, enabling better predictions of their roles in the compartment fire system.

Fowkes,[1] in his work with Emmons on the Home Fire Project, was the first to publish a basis for the zone model approach in his description of the "Bedroom Fire" series conducted at Factory Mutual Research Corporation. Almost simultaneously, computer models based on the zone model approach were produced by Quintiere,[2] Pape and Waterman,[3] and Mitler[4] working with Emmons. Since then the development of such computer models has been prolific. They have extended the early efforts from a single room to computer codes that can address a number of interconnected rooms, using a number of new fire phenomena and computer features. These advances in fire science, together with the development of the personal computer, have given the engineer a convenient tool for investigating the hazard of fire in buildings. A notable illustration of this tool is the software "Hazard I," developed by the National Institute of Standards and Technology (NIST).[5] At this time, numerous computer codes and software packages exist based on the zone model approach. In a recent survey, Friedman[6] cited 21 zone models in use around the world.

This chapter outlines the basic conservation equations for the gas zones, and describes the various transport and combustion processes that make up the system. These processes are referred to as the submodels of the system. As such, they can contribute subroutines to computer codes, which implement the mathematical solution. Discussion of submodels will be limited, but the reader will be referred to appropriate references. In most cases, other chapters of *The SFPE Handbook of Fire Protection Engineering* will be cited. No discussion of a computer code or its numerical solution algorithm will be addressed, since these are issues more of style and mathematics. The presentation will elucidate the mathematical basis of the zone model, its assumptions, its features, and its scope of application. Each user of this approach must sufficiently understand its basis to assess its accuracy and validity. When used correctly, zone models predict the average macroscopic features of compartment fires. There are many examples of comparisons to data that illustrate their level of accuracy, and these will not be repeated here. The user must be skilled in assessing the quality of the data and submodels that directly influence the variables of the problem of interest. It is hoped that the discussion that follows will make the user more knowledgeable or sensitive in making these quality assessments.

Conservation Equations

The building block of the zone model is the conservation equations for the upper and lower gas zones. These

Dr. J. G. Quintiere is the John L. Bryan Professor of Fire Protection Engineering at the University of Maryland. His research has focused on fire growth and flame spread.

equations are developed either (1) by using fundamental equations of energy, mass, and momentum transport in control volume form as applied to the zones, or (2) by using differential equations that represent the conservation laws and integrating them over the zones. However, the momentum equation will not be explicitly applied, since information needed to compute velocities and pressures is based on assumptions and specific applications of momentum principles at vent boundaries of the compartment. An extensive review of control volume equations for mass, species, and energy conservation in a combustion system has been presented by Quintiere[7] and serves as reference for the equations that follow.

Figure 3-5.1 illustrates a typical zone model for a compartment fire process. It shows a fire plume and a door vent. The hot combustion gases that collect in the upper space of the room and spill out of the vent constitute the upper-layer zone. A control volume, CV_1, is defined to enclose the gas in this upper layer and the fire plume. The lower interface of the upper layer moves with the control volume such that no mass is transferred across this thermally stratified region. The velocity of the control volume along this interface, $\overline{w}$, is equal to the fluid velocity, $\overline{v}$. The temperature of the upper layer is greater than that in the lower layer (zone) which includes all the remaining gas in the room, and is delineated by a second control volume, CV_2. It has been assumed in zone modeling that the volume of the fire plume is small relative to the gas layer or zone volumes, and therefore its effect has been ignored. In general, multiple fire plumes can occur at any height in the room, and multiple vents or mass transport can take place between the zones (CV_1 and CV_2) and the surroundings. In each case mass transport must be appropriately described in terms of the system variables; however, this may not always be easy or known. The properties of the upper and lower zones are assumed to be spatially uniform, but can vary with time. Thus, temperature, T, and species mass concentration, Y_i, are properties associated with ideal upper and lower homogeneous gas layers. Other assumptions in the application of the conservation laws to the zones are listed below:

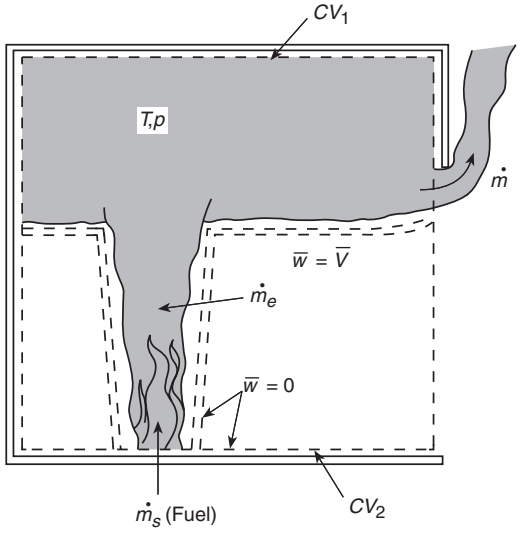

Figure 3-5.1. ***Control volumes selected in zone modeling.***

1. The gas is treated as an ideal gas with a constant molecular weight and constant specific heats: c_p and c_v.
2. Exchange of mass at free boundaries is due to pressure differences or shear mixing effects. Generally these are caused by natural or forced convection, or by entrainment processes.
3. Combustion is treated as a source of mass and energy. No mechanism from first principles is included to resolve the extent of the combustion zone.
4. The plume instantly arrives at the ceiling. No attempt is made to account for the time required to transport mass vertically or horizontally in the compartment. Hence, transport times are not explicitly accounted for in zone modeling.
5. The mass or heat capacity of room contents is ignored compared to the enclosure wall, ceiling, and floor elements; that is, heat is considered lost to the structure, but not to the contents. Where room contents shield boundary structural surfaces, some compensations can occur in the analysis, but for cluttered rooms this assumption may be poor.
6. The horizontal cross section of the enclosure is a constant area, A. In most cases of zone modeling, rectilinear compartments have been considered. However, this is not a necessary assumption, and enclosures in which A varies with height can easily be handled.
7. The pressure in the enclosure is considered uniform in the energy equation, but hydrostatic variations account for pressure differences at free boundaries of the enclosure; that is, $p \gg \rho g H$. In general, the enclosure pressure, p, is much greater than the variations due to hydrostatics. For example, for $p = 1$ atm $= 14.7$ psi $= 10^2$ kPa (kN/m^2) $= 10^5$ Pa, the hydrostatic variation for a height, $H = 1$ m, gives a pressure difference of $\rho g H = 1.2$ kg/m^3 $\times$ 9.8 m/s^2 $\times$ 1 m $= 10$ kg/m·s^2 $= 10$ Pa (N/m^2).
8. Mass flow into the fire plume is due to turbulent entrainment. Entrainment is the process by which the surrounding gas flows into the fire plume as a result of buoyancy. Empirically, the inflow velocity linearly depends on the vertical velocity in the plume.
9. Fluid frictional effects at solid boundaries are ignored in the current models.

Conservation of Mass

The conservation of mass for a control volume states that the rate of change of mass in the volume plus the sum of the net mass flow rates out is zero for J flow streams

$$A\frac{d}{dt}(\rho z_l) + \sum_{\substack{j=1 \\ \text{(net out)}}}^{J} \dot{m}_j = 0 \qquad (1)$$

where

ρ = density of the gas in the control volume (or zone)

z_l = the height of the zone

For the illustration in Figure 3-5.1, applying Equation 1 to the upper layer (CV_1) would give

$$\sum_{j=1}^{3} \dot{m}_j = \dot{m} - \dot{m}_e - \dot{m}_s \qquad (2)$$

where

$\dot{m}$ = mass flow rate out of the door

$\dot{m}_e$ = mass rate of entrainment into the fire plume

$\dot{m}_s$ = mass rate of gaseous fuel supplied

Mass flows at the boundaries can occur due to many phenomena. Therefore, the user or designer of a zone model must include the appropriate mass flow phenomena. For example, in addition to the mass rates in Equation 2, mass flows can occur due to forced convection from wind or ventilation effects, from shear entrainment as flows affect layer interfaces, or from cold plumes that could plunge through hot layers.

Conservation of Species

The mass conservation of species i is given by Y_i. By using Equation 1 and applying the conservation of mass for species i to a control volume, it follows that

$$\rho z_l A \frac{dY_i}{dt} + \sum_{j=1}^{J} \dot{m}_j (Y_{ij} - Y_i) = \dot{\omega}_i \qquad (3)$$

where

Y_{ij} = mass concentration of species i leaving the control volume through the j flow stream

$\dot{\omega}_i$ = mass production rate of species due to combustion

The production term, $\dot{\omega}_i$, in principle, can be described through a knowledge of the chemical equation of the reaction or its particular stoichiometry. Thus, stoichiometric coefficients can be used to represent the production of species and the consumption of oxygen in terms of the mass rate of fuel *reacted.* Stoichiometry is not easily determined, and the fuel gases as they emerge from the pyrolysis of solids can take many chemical forms that differ from the solid fuel's original molecular composition. A partial way to overcome these complications has been to represent the mass production of species for fire in terms of the rate of mass *loss* for the pyrolyzing fuel. Hence, one must be careful to distinguish between the mass of fuel lost and that reacted, and to relate available species yield data to the particular fire conditions of the application. Yield is defined as the mass ratio of species to fuel lost. The yields or production rates may change with fire conditions, and therefore, in general, will not be consistent with data from small-scale tests. For example, the production rate of CO changes markedly with air-to-fuel ratio.

Conservation of Energy

The conservation of energy for the control volume is applied along with Equation 1 and the equation of state, $p = \rho RT$, to give

$$\rho c_p z_l A \frac{dT}{dt} - z_l A \frac{dp}{dt} + cp \sum_{\substack{j=1 \\ \text{(net out)}}}^{J} \dot{m}_j (T_j - T) \qquad (4)$$

$$= \dot{\omega}_F \Delta H - \dot{Q}_{\text{net loss}}$$

where

T = temperature of the gases within the control volume

T_j = temperature of the gases in the j flow stream crossing the control volume boundary

$\dot{Q}_{\text{net loss}}$ = net rate of heat transfer lost at the boundary

ΔH = the heat of combustion (taken as a positive quantity)

$\dot{\omega}_F$ = the rate at which the fuel supplied is *reacted*

Usually in zone models it is assumed that all of the fuel supplied can react, provided there is sufficient oxygen available. One assumption on the sufficiency of oxygen is to consider that all the fuel supplied is reacted as long as the oxygen concentration in that control volume is greater or equal to zero, that is,

$$\dot{\omega}_F = \dot{m}_s \quad \text{if} \quad Y_o \geq 0 \qquad (5)$$

Thereafter, an excess rate of fuel can exist that can be transported into adjoining zones or control volumes where a decision must be made about whether it can continue to react. At this condition, all of the net oxygen supplied to the control volume is reacted, so that, as long as $Y_o = 0$

$$\dot{\omega}_F = r \times (\text{net mass rate of oxygen supplied}) \qquad (6)$$

where r is the stoichiometric fuel-to-oxygen mass ratio. This condition when $Y_o = 0$ in compartment fires is termed the ventilation-limited condition. At this moment, significant changes take place in the nature of the chemical reaction. Notably, incomplete combustion is more likely, and for hydrocarbon fuels this leads to a significant increase in the yield of carbon monoxide and soot. Thus, care must be used in interpreting the results of zone models once ventilation-limited conditions arise, particularly with respect to the prediction of species concentrations and the extent of burning. Material data used for well-ventilated conditions will no longer apply. The issue of what constitutes a flammable mixture in a compartment gas layer and combustion in a vitiated layer has not yet been resolved satisfactorily. Thus, combustion under ventilation-limited conditions has not been adequately addressed for a zone model, and needs more study.

The first term on the left side of Equation 4 arises due to the change of internal energy with the control volume. If the temperature is not changing rapidly with time, this term can be small and its elimination gives rise to a quasi-steady approximation for growing fires that allows a more simple analysis. The second term arises from the rate of work done by pressure as the gas layer expands or contracts due to the motion of the thermal stratification interface. Having been rearranged, this term now is expressed as rate of pressure, p, increase for the compartment and is essentially caused by net heat or mass additions to the compartment gases. Except for the rapid accumulation of

mass or energy, for compartments with small openings to the surroundings, this pressure rise is small, and the pressure nominally remains at nearly the ambient pressure. For example, an addition of 100 kW to a 40 m^3 gas volume in a room with a 0.1 m^2 vent area gives rise to roughly an increase of 10 Pa in less than 10^{-2} s over normal ambient pressure of 10^5 Pa.[7] Any increase in pressure within the compartment could give rise to a flow of mass through a vent, and this term in Equation 4 may be associated with a *volumetric expansion* effect, as referred to by some. Conversely, a reduction in energy release rate will cause the pressure to drop relative to the ambient. This phenomenon, when cycling between heating and cooling, explains the *breathing effect* for fires in closed buildings.

The third term of Equation 4 accounts for the enthalpy flow rates and only applies to j flow streams that enter the control volume, since $T_j = T$ for all flow streams leaving, as long as the uniform temperature assumption still applies.

Summary

The zone model for the compartment fire system consists of two zones: the upper and lower gas layers. The solution process for the layer properties can be visualized by considering the conservation Equations 1, 3, and 4 applied to each zone. The species equation can yield the Y_i for each layer. The mass and energy equations comprise four equations that permit the determination of the two layer temperatures, one layer height (since the height of the other layer is directly found by difference from the total height of the compartment), and the compartment pressure (which is assumed uniform by Equation 7). The densities are found from the ideal gas equation of state in which approximately ρT is a constant. To complete this solution process, each source or transport term in the equations must be given in terms of the above layer properties, or auxiliary relationships must be included for each new variable introduced. The source terms are associated with the $\dot{\omega}_i$ terms, and the transport terms include the j mass flow rates and the boundary heat transfer rates. The extent to which source and transport relationships are included reflects the sophistication and scope of the zone model. Some source and transport terms are essential to a basic zone model, others can be specified as approximations to reality, and others can be ignored when physically irrelevant. These source and transport relationships can be termed *submodels* and can comprise subroutines of a zone model computer code. The nature of these submodels is discussed below.

Source Term Submodels

The principal source term is the rate of fuel supplied. In an experimental fire this can be known if the fire source is simulated by a gas burner. In the other extreme, the mass of fuel supply can be a result of a spreading fire over an array of different solid fuels. In general,

$$\dot{m}_s = f(\text{fuel properties, heat transfer}) \tag{7}$$

in which the heat transfer to the fuel results from the flame configuration and the heated compartment. The fuel properties are still not completely defined or conventionally accepted for fire applications, since no general theory exists for pyrolysis, and theories of flame spread and ignition are couched in terms of effective fire properties, which are modeling parameters. Nevertheless, data exist for fuel fire properties and can enable approximate models for $\dot{m}_s$ of reasonable accuracy. For example, Tewarson describes how the mass supply and energy release can be determined from fuel properties, and tabulates properties for a number of solid fuels. (See Section 3, Chapter 4.) For realistic items under well-ventilated conditions, Babrauskas has compiled results that could serve as initial estimates for $\dot{m}_s$ in compartment fires. (See Section 3, Chapter 1.)

The rate of energy release, $\dot{\omega}_F \Delta H$, required by Equation 4 has already been discussed through Equations 5 and 6. The point should be made that the heat of combustion, ΔH, employed must be with respect to the mass of fuel gases pyrolyzed, given by such data as Tewarson's, and is not the theoretical oxygen bomb value for the solid fuel. (See Section 3, Chapter 4.) Due to incomplete combustion, ΔH will be less than the theoretical value, in general.

The production of species can be described in terms of species yield, γ_i, such that

$$\dot{\omega}_i = \gamma_i \dot{m}_s \tag{8}$$

For well-ventilated fires, γ_i may be reasonably constant for a given fuel, as tabulated by Tewarson. (See Section 3, Chapter 4.) In general, it can vary with time and can significantly vary as ventilation-limited conditions are approached and achieved. For example, Tewarson shows that γ_i for CO can vary with equivalence ratio, Φ, where

$$\Phi = \frac{\text{mass of fuel available}/\text{mass of oxygen available}}{r} \tag{9}$$

where r is the stoichiometric value for complete combustion. Zukoski et al.[8] have shown how this relationship may be applied to compartment fires. The equivalence ratio, Φ, may be computed in a zone (or upper layer) where combustion has occurred by computing the mass concentrations of the "available" fuel and oxygen in the zone. This is done by Equation 3 in which $\dot{\omega}_i$ is set equal to zero for both the fuel and oxygen, since this yields the available Y_F and Y_o values, not their actual concentrations in the layer following combustion. The generality of considering $\gamma_i = \gamma_i(\Phi)$ for zone models is still under study, and its use must be considered as exploratory. Nevertheless, it currently offers the only practical approach for estimating species, such as CO, under ventilation-limited conditions in compartment fires.

Mass and Heat Transport Submodels

Entrainment

An essential feature of a zone model is the mass rate of entrainment, $\dot{m}_e$, relationship for the fire plume. This relationship allows the principal mechanism for flow

between the lower and upper stratified gas layers. Considerable work has been performed to develop entrainment relationships for pool fires or axisymmetric gas burner fires. Unfortunately both the ideal theoretical plume models and correlations based on data vary widely, and no consensus exists among zone models in practice for the optimum pool fire entrainment model. Rockett[9] illustrates the variations in results he found using different fire entrainment models in the Harvard/NIST Mark VI compartment fire zone model. He found that the layer height, entrainment rate, and layer gas temperature varied by roughly a factor of two among the various models. More useful data rather than ideal mathematical models are clearly needed to resolve this issue of accuracy for a simple pool fire. Yet even a perfect entrainment relationship for an axisymmetric pool fire would not necessarily be perfect in a zone model, because a plume in a compartment can be subject to nonsymmetric airflows that can bend the plume and thus affect its entrainment rate. Usually wind effects will increase the entrainment rate.

Rockett[9] has shown that the effect of the entrainment model is crucial to predictions for the developing fire. This research suggests that the entrainment model must be representative of the actual object burning. However, no entrainment models exist for a wall, corner, or item of furniture; this dramatizes the lack of much-needed research in this area. Yet, this does not mean that the zone model has a fatal flaw; it simply means much more systematic data are necessary to expand the versatility of the zone model and its accuracy. Moreover, if a zone model with its selected entrainment relationship tracks well with data from an experimental fire scenario, it can be assumed accurate for simulating the process and can be used with some assurance for that scenario. A catalogue of empirical entrainment relationships for various object fires developed from specialized entrainment apparatus would help resolve the entrainment issue. This apparatus could be developed from the large calorimeter intended to measure energy release rate in which the fire plume is collected in a hood-duct system and the total flow rate is recorded.

Vent Flows through Openings in Vertical Partitions

Classic models of fire in a room or building represent the structure with an opening, such as a door or window, to the ambient surroundings. Fire-induced flows through such openings have been well studied, and a widely accepted model exists to compute these flows based on the temperature distribution of the gases on either side of the opening. The theoretical basis of the computation is orifice flow utilizing Bernoulli's equation along a streamline, as illustrated in Figure 3-5.2. The velocity at station two is given by

$$v_2 = \sqrt{\frac{2(\rho_1 - \rho_2)}{\rho_1}} \tag{10}$$

where v_1 is assumed to be zero. The mass flow rate is computed by integration over the flow area, A, adjusted by a flow coefficient, C:

$$\dot{m} = C \int \rho_1 v_2 \, dA \tag{11}$$

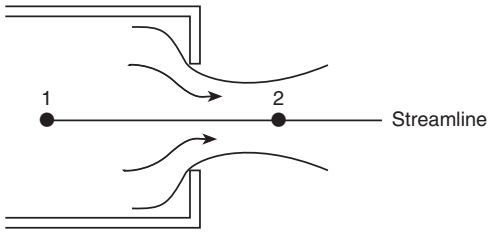

Figure 3-5.2. ***Orifice flow.***

Emmons suggests that a value of 0.68 for C has an accuracy of ±10 percent, except at very low flow rates at the beginning of a fire. (See Section 2, Chapter 3.) In general, C will depend on the Reynolds number. Figure 3-5.3 depicts examples of typical vent flows through an opening in a vertical partition. In both cases Equations 10 and 11 apply, but the pressure distribution must be described appropriately. For example, in the pure natural convection case shown in Figure 3-5.3 (a), the pressure is determined by the static pressure with respect to the floor pressure, $p(0)$. Actually it is the floor pressure that applies in Equation 4 and in the perfect gas equation of state.

The assumption is that the flow velocities are small compared to the vent flow velocities, justifying the static pressure computation. Thus, the vertical pressure distribution on either side of the opening is computed as

$$p(z) = p(0) - \int_0^z \rho g \, dz \tag{12}$$

McCaffrey and Rockett[10] illustrate the accuracy of the hydrostatic assumption in Figure 3-5.4. The sign of the pressure difference across the opening determines the flow direction. Emmons presents the general equations that enable this computation to be included in a zone model. (See Section 2, Chapter 3.) It is by far the most accurate of the submodels, and provides the basis for linking rooms together in a zone model, which allows smoke and fire growth computations for a large building.

The flow through an opening in a horizontal partition can be compared to that for the vertical partition, provided the pressure difference is large enough. If there is only a single vent from the fire compartment through a horizontal partition, such as a ceiling, the flow must be oscillatory or bi-directional. The latter case implies a zero pressure

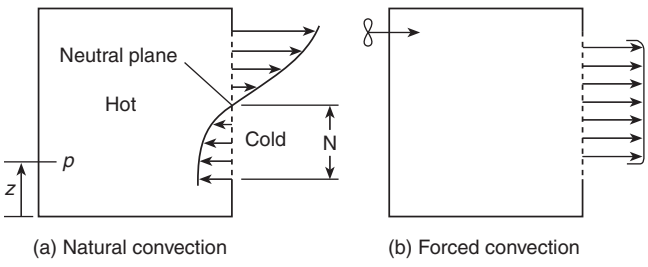

Figure 3-5.3. ***Typical vent flows.***

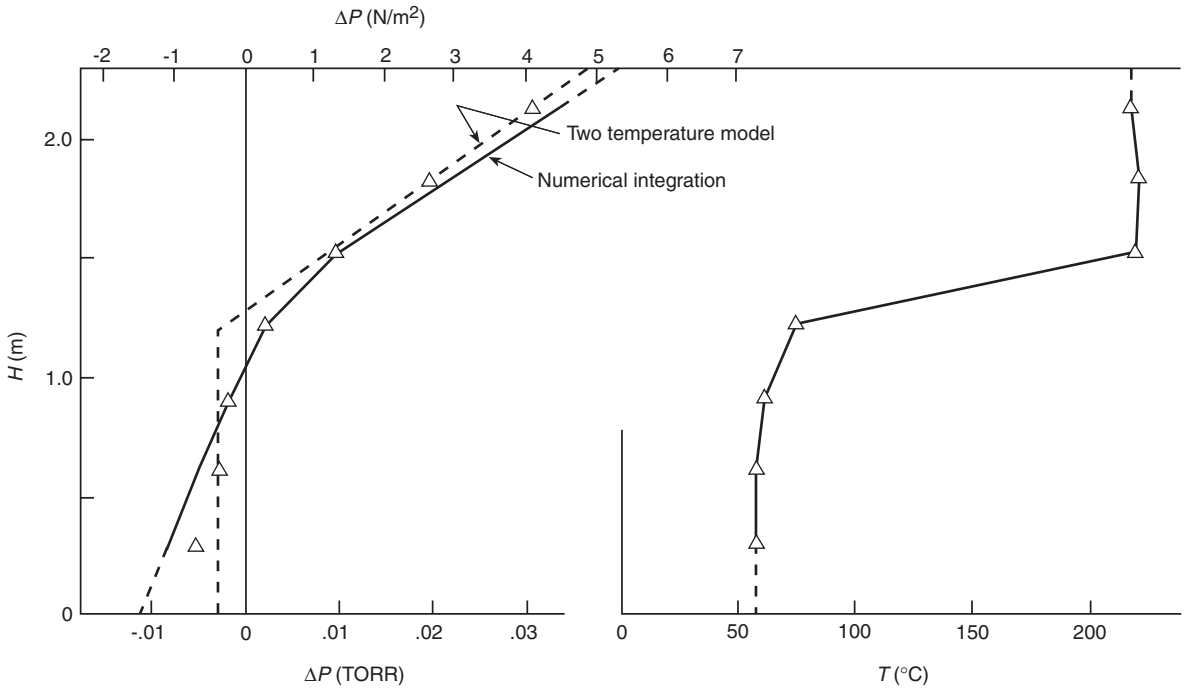

Figure 3-5.4. ***Vertical pressure difference across a room vertical partition compared to a computation based on room fire temperature distribution and a two-temperature zone model approximation using the hydrostatic pressure assumption.[10]***

difference, with gravity solely determining the flow. A theory for this case has been developed by Epstein[11] and has been implemented by Cooper.[12] For orifice-like vents with zero pressure difference, the volumetric exchange flow rate, $\dot{V}$, given by Epstein,[11] is approximately

$$\dot{V} = 0.055\left[D^5 g(\rho_1 - \rho_2)\left(\frac{\rho_1 + \rho_2}{2}\right)\right]^{1/2} \qquad (13)$$

where D is the diameter of the vent and ρ_1 and ρ_2 are the corresponding fluid densities on either side of the vent. For vents of significant depth, L, the coefficient in Equation 13 depends on L/D.

Convective Heat Transfer to Surfaces

The $\dot{Q}_{\text{net loss}}$ term in Equation 4 is composed of the convective and radiative heat loss to the boundary surfaces of the layer control volumes. This involves both heat transfer from the gas layers at their bulk temperatures and the heat transfer from the flame. Consistent treatment of the flame and layer gas heat transfer must be carried out for the zone model. If the flame becomes large and fills the upper layer, one cannot count the flame and gas heat transfer without being redundant.

Convective heat transfer to a ceiling by a fire plume has been widely studied at modest scales, such that flame radiation may have been insignificant. Alpert[13] specifically examined only convective heating in contrast to studies by You and Faeth[14] and Kokkala[15] who included flame effects.

In general, convective effects will vary along the ceiling, walls, and floor, and depend on the nature and position of the fire. In some cases an *adiabatic wall temperature* has been appropriately introduced since the driving force for convective heat transfer locally is not the bulk gas layer temperature, but the local boundary layer temperature, which is not explicitly computed. Convective heat transfer data for the walls and floor of a fire compartment or for rooms beyond the fire compartment have not been developed. Hence, most zone models use estimates from natural convection correlations.

Radiative Heat Transfer

The theory of radiative heat transfer is adequate to develop the needed components for the zone model. However, the theory is not sufficiently developed to predict flame radiation from first principles without very sophisticated modeling of the soot and temperature distributions. Hence, flame radiation is relegated to empirical practices. Radiation from a smoke layer is easier to deal with within the context of a uniform property gas layer for the zone model. One difficulty still is the availability of property data to determine the contribution of smoke particulates to the layer radiation properties. The discussion presented by Tien et al. can be used to begin a development of the radiative equations needed by the zone model. (See Section 1, Chapter 4.) Also, the presentation by Mudan and Croce gives empirical approaches to dealing with flame radiation. (See Section 3, Chapter 11.) The report by Forney[16] lays out the theory and equations

describing radiation exchange between the gas layers and boundary surfaces.

Conduction Heat Transfer

The radiative and convective heat transfer from the gas must be balanced by conduction heat transfer through the boundary surfaces. This balancing requires a numerical solution to a partial differential equation in conjunction with the ordinary differential equations in time describing the conservation of energy and mass for the gas layers. Usually zone models have considered only one-dimensional conduction, which should be adequate for most applications. Most multiple-compartment models do not consider communication by conduction into the next compartment, treating the structural elements as thermally thick instead. In principle, there is no difficulty with developing an accurate algorithm for conduction through the boundary elements for any conditions. For more information, the reader is referred to the discussion by Rockett and Milke. (See Section 1, Chapter 2.)

Mixing between the Layers

The primary exchange of fluid between the lower and upper gas layers is due to the buoyant effect of the fire plume. Secondary, but significant, mixing processes can occur due to the other effects. These are shown in Figure 3-5.5 and include three phenomena:

1. Exchange due to a cold flow injected into the hot layer
2. Exchange due to shear mixing associated with vent flows
3. Exchange due to wall flows

Phenomenon 1 is the inverse of the hot fire plume penetrating the upper layer. In both cases the fluid at the edge of the plume may not be buoyant enough to penetrate the respective layer. A comparable situation is a cold forced jet introduced vertically into the lower layer. Depending on the relative temperatures, it may not escape the lower layer and, therefore, may not penetrate into the upper layer. These are issues that can be resolved to some extent by research available in the literature on buoyant plumes and jets.

Phenomenon 2 has not been sufficiently studied. Data suggest that the flow rate of the mixed stream can be significant relative to the vent flow rate, especially for small vents.[17] A correlation for the mixing rate has been developed from saltwater simulation experiments.[18]

Phenomenon 3 has been discussed by Jaluria.[19] He presents relationships that allow the estimation of the rate of transfer of cold fluid adjacent to the wall in the hot upper gas layer into the cold lower gas layer or vice versa.

All of these flows tend to blur the sharp distinction between the upper and lower gas layers, reducing their degree of stratification. Obviously, if sufficient mixing occurs, the layer may appear to become well-mixed or destratified. Destratification should occur naturally in the context of the zone model, and one should not have to switch to a well-mixed compartment model under these conditions.

Relationships for all of these secondary flows have not been developed with confidence nor with full acceptance. Although they are important for improving the accuracy of a zone fire model, little work has gone forward to establish their validity.

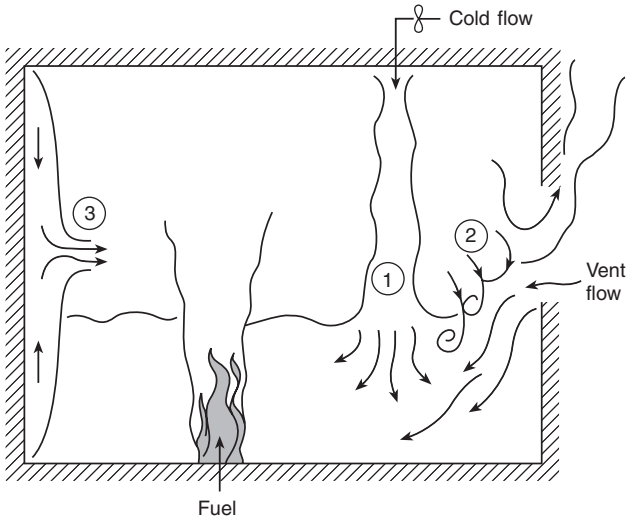

Figure 3-5.5. ***Secondary flows—mixing phenomena. 1. A cold plume descending from the upper layer into the lower layer; 2. Shear mixing of an entering vent flow stream; 3. Wall flows due to local buoyancy effects.***

Forced Flow Effects

The effect of forced airflow on the fire conditions and smoke spread due to mechanical or natural wind forces has always been an issue in large building fires. Wind effects and the resultant pressure distribution around a tall building has become a standard element of design data for structural design, but this has not been utilized for fire safety design. The movement of smoke through a building due to the mechanical ventilation system has been simulated by network models that treat the compartment volume as uniform in properties, and include the pressure losses due to vents and duct friction. A two-layer zone model has not been linked to the mechanical ventilation system in a building. To create a link, one must include the full-pressure-flow characteristics of fans in both directions to allow for the possibility of the backflow of smoke against the direction of airflow in the ducts. An attempt at this linkage has been presented by Klote and Cooper,[20] who hypothesize a fan characteristic relationship. Ultimately an experimental study will be needed to lay a foundation for this analysis.

Fire Growth Rate

In most all zone models, the fire source is considered an input quantity, based on some experimental or empirical data. This limits the simulation capability of a zone model, since fire growth and spread is not modeled. Also the effects of compartment feedback due to thermal and vitiation (oxygen depletion) effects are not taken into account. The versatility and utility of a zone model can only

be improved by developing techniques for accommodating the fire growth of realistic building contents and architectural elements. This process will have an impact on the use and development of flammability tests for hazard analysis and product acceptability.

Embedded Submodels

The detailed physics that one can include in a zone model are only limited by current research and imagination. The zone model can be versatile in accommodating new phenomena, even if they appear inconsistent with the uniform property layer assumption. By analogy to the relationship between inviscid flow and boundary layer flow in the analysis of aerodynamic bodies, the layer properties can be regarded as first-order approximation for higher order analysis. Flame and boundary layer phenomena within the compartment can be computed by regarding the layer properties as infinite reservoirs. These phenomena can be computed after the primary layer properties are computed. Examples of embedded phenomena are shown in Figure 3-5.6. Although the combustion region is assumed to be of negligible volume at the zone model for mutation, the flame height can be computed along with the velocity and temperature distributions in an axisymmetric fire plume.[21] Other embedded phenomenon are: (1) the ceiling jet, (2) the computation of temperature distributions over the ceiling, (3) the deposition of soot and other products of combustion on surfaces, and (4) the heating and degradation of structural elements.

Unresolved Phenomena

Some significant phenomena are not addressed by the zone-modeling approach for fire, such as vent flames, transient flow in corridors, and shaft flows. (See Figure 3-5.7.) These phenomena require more research and new strategies to enable them to be included into a zone model. Vent flames are significant for fire growth into the next compartment and usually follow flashover. Information about their rate of heat transfer and extent needs to be computed. Transient corridor flows are important in the analysis of smoke transport through long corridors. The current zone model methodology yields an instantaneous layer, which would descend, but the actual process produces a transient ceiling jet. Flows in vertical shafts involve the interaction of plumes with walls, pressure-driven effects, and turbulent mixing.

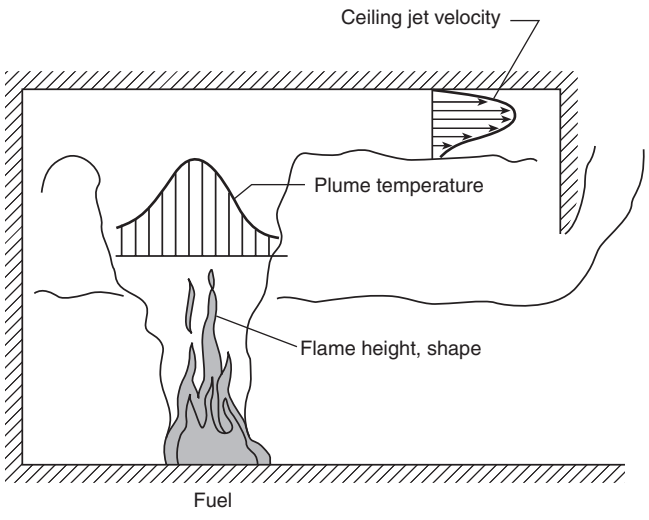

Figure 3-5.6. ***Examples of embedded phenomena.***

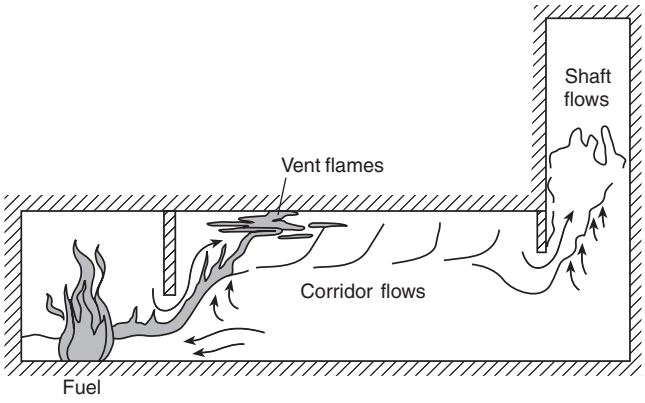

Figure 3-5.7. ***Examples of significant phenomena absent from zone models.***

Selected Reading and Comments

Zone models provide the integrating framework for the phenomena of fire and its fire protection engineering components. Many zone models have been constructed for fire predictions in compartments. They involve the basic conservation equations, submodels describing the particular phenomena included, and the mathematical algorithm for solution. Some have developed user-friendly interfaces. Most provide documentation on the model and its use. The interested reader is referred to some published models for more detailed information.[22–24] Many zone-model computer models exist, similar both in substance and the ability to analyze fire effects in buildings. They can stimulate needed research. However, more effort appears to have gone into the computer code developments rather than the experimental research needed for improvement in the model.

Nomenclature

A	area compartment floor
C	flow coefficient
c_p	specific heat at constant pressure
c_v	specific heat at constant volume
g	acceleration due to gravity
H	compartment height
J	number of flow streams in control volume
m	mass

p pressure
Q heat transfer
r stoichiometric fuel-to-oxygen mass ratio
R ideal gas constant
t time
T temperature
v fluid velocity
V volume
w control volume velocity
Y mass fraction
z_l height of control volume or zone
ΔH heat of combustion
γ_i yield of species i
ρ density
Φ equivalence ratio
$\dot{\omega}_F$ consumption rate of fuel
$\dot{\omega}_i$ production rate of species

Subscripts

e entrained
F fuel
i species
j flow stream
s supplied

Superscripts

$\dot{(\,)}$ per unit time

References Cited

1. N.D. Fowkes, "A Mechanistic Model of the 1973 and 1974 Bedroom Test Fires," in *A Study of Room Fire Development: The Second Full-Scale Bedroom Fire Test of the Home Fire Project* (P.A. Croce, ed.), (July 24, 1974), Vol. II, FMRC Tech. Rept. No. 21011.4, pp. 8–50 (1975).
2. J. Quintiere, "Growth of Fire in Building Compartments," in *Fire Standards and Safety* (A.F Robertson, ed.), ASTM STP614, American Soc. for Testing and Materials, pp. 131–167 (1977).
3. R. Pape and T. Waterman, "Modification to the FIRES Pre-Flashover Room Fire Computer Model," *IITRI Project J6400,* IIT Res. Inst., Chicago, IL (1977).
4. H.E. Mitler, "The Physical Basis for the Harvard Computer Fire Code," *Home Fire Proj. Tech. Rept. No. 34,* Harvard Univ., Cambridge, MA (1978).
5. R.W. Bukowski, R.D. Peacock, W.W. Jones, and C.L. Forney, "HAZARD I: Technical Reference Guide," *NIST Handbook 146,* Vol. II (1989).
6. R. Friedman, *Survey of Computer Models for Fire and Smoke,* 2nd ed., Factory Mutual Research Corp., Norwood, MA (1991).
7. J.G. Quintiere, "Fundamentals of Enclosure Fire Zone Models," *J. of Fire Protection Engr.,* 1, 3 (1989).
8. E.E. Zukoski, S.J. Toner, J.H. Morehant, and T. Kubota, "Combustion Processes in Two-Layered Configurations," *Fire Safety Science—Proc. 2nd Int. Symp.,* Hemisphere Publishing Corp., New York, pp. 255–304 (1989)
9. J.A. Rockett, "Using the Harvard/NIST Mark VI Fire Simulation," *NISTIR 4464,* Nat. Inst. of Standards and Technology (1990).
10. B.J. McCaffrey and J.A. Rockett, "Static Pressure Measurements of Enclosure Fires," *J. of Fire Research,* Nat. Bur. Stand. (1977).
11. M. Epstein, "Buoyant-Driven Exchange Flow Through Small Openings in Horizontal Partitions," *Jour. of Heat Transfer,* American Soc. for Testing and Materials, 110 (1988).
12. L.Y. Cooper, "An Algorithm and Associated Computer Subordinate for Calculating Flow Through a Horizontal Ceiling Flow Vent in a Zone-Type Compartment Fire Model," *NISTIR 4402,* Nat. Inst. of Stand. and Technology (1990).
13. R.L. Alpert, "Convective Heat Transfer in the Impingement Region of a Buoyant Plume," *Jour. of Heat Transfer,* American Soc. for Testing and Materials, 109 (1987).
14. H.Z. You and G.M. Faeth, "Ceiling Heat Transfer During Fire Plume and Fire Impingement," *Fire and Materials,* 3, 3 (1979).
15. M.A. Kokkala, "Experimental Study of Heat Transfer to Ceiling from an Impinging Diffusion Flame," *Fire Safety Science—Proc. of 3rd Inter. Symp.,* G. Cox and B. Langford, ed., Elsevier Applied Science, London (1991).
16. G.P. Forney, "Computing Radiative Heat Transfer Occurring in a Zone Model," *NISTIR 4709,* Nat. Inst. of Stand. and Technology (1991).
17. B.J. McCaffrey and J.G. Quintiere, "Buoyancy-Driven Countercurrent Flows Generated by a Fire Source," *Heat Transfer and Turbulent Buoyant Convection,* Vol. II (D.B. Spalding and N. Afgan, ed.), Hemisphere Pub. Co., pp. 457–472 (1977).
18. C.S. Lim, E.E. Zukoski, and T. Kubota, "Mixing in Doorway Flows and Entrainment in Fire Flames," Cal. Inst. of Technology, NBS Grant No. NB82NADA3033 (1984).
19. Y. Jaluria, "National Convection Wall Flows," in *SFPE Handbook of Fire Protection Engineering* (P.J. DiNenno, et al., eds.), National Fire Protection Association, Quincy, MA, pp. 2-50–2-63 (1995).
20. J.H. Klote and L.Y. Cooper, "Model of a Simple Fan-Resistance Ventilation System and Its Application to Fire Modeling," *NISTIR 89-4141,* Nat. Inst. of Stand. and Technology (1989).
21. B. McCaffrey, "Flame Height," in *SFPE Handbook of Fire Protection Engineering* (P.J. DiNenno, et al., eds.), National Fire Protection Association, Quincy, MA, pp. 2-1–2-8 (1995).
22. H.W. Emmons, H.E. Mitler, and L.N. Trefethen, "Computer Fire Code III," *Home Fire Proj. Tech Rept. No. 25,* Harvard Univ. Cambridge, MA (1978).
23. T. Tanaka, "A Model of Multicompartment Fire Spread," *NBSIR 83-2718,* Nat. Bur. Stand. (1983).
24. R.D. Peacock, W.W. Jones, R.W. Bukowski, and C.L. Forney, "Technical Reference Guide for the HAZARD I Fire Hazard Assessment Method," Ver. 1.1, *NIST Hdbk 146,* Nat. Inst. of Stand. and Tech. (1991).

CHAPTER 6

Estimating Temperatures in Compartment Fires

William D. Walton and Philip H. Thomas

Introduction

The ability to predict temperatures developed in compartment fires is of great significance to the fire protection professional. There are many uses for a knowledge of compartment fire temperatures, including the prediction of (1) the onset of hazardous conditions, (2) property and structural damage, (3) changes in burning rate, (4) ignition of objects, and (5) the onset of flashover.

The fundamental principles underlying compartment fires are presented in Section 3, Chapter 5. This chapter gives a number of simplified solution techniques.

Fire Stages

In this chapter, compartment fires are defined as fires in enclosed spaces, which are commonly thought of as rooms in buildings, but may include other spaces such as those found in transportation vehicles such as ships, planes, trains, and the like.

Compartment fires are often discussed in terms of growth stages.[1] Figure 3-6.1 shows an idealized variation of temperature with time along with the growth stages. The growth stages are

1. Ignition
2. Growth
3. Flashover
4. Fully developed fire
5. Decay

While many fires will not follow this idealization, it provides a useful framework for the discussion of compartment fires. All fires include an ignition stage but, beyond that, may fail to grow, or they may be affected by manual or automatic suppression activities before going through all of the stages listed above.

Mr. William D. Walton is a research fire protection engineer with the Building and Fire Research Laboratory, National Institute of Standards and Technology.

Dr. Philip H. Thomas is retired from the Fire Research Station, Borehamwood, England.

Growth Stage Definitions

Ignition stage: The period during which the fire begins.

Growth stage: Following ignition, the fire initially grows primarily as a function of the fuel itself, with little or no influence from the compartment. The fire can be described in terms of its rate of energy and combustion product generation. A discussion of energy generation or burning rate can be found in Section 3, Chapter 1. If sufficient fuel and oxygen are available, the fire will continue to grow, causing the temperature in the compartment to rise. Fires with sufficient oxygen for combustion are said to be fuel controlled.

Flashover: Flashover is generally defined as the transition from a growing fire to a fully developed fire in which all combustible items in the compartment are involved in fire. During this transition there are rapid changes in the compartment environment. Flashover is not a precise term, and several variations in definition can be found in the literature. Most have criteria based on the temperature at which the radiation from the hot gases in the compartment will ignite all of the combustible contents. Gas temperatures of 300 to 650°C have been associated with the onset of flashover, although temperatures of 500 to 600°C are more widely used.[2] The ignition of unburnt fuel in the hot fire gases, the appearance of flames from openings in a compartment, or the ignition of all of the combustible contents may actually be different phenomena.

Fully developed fire: During this stage, the heat release rate of the fire is the greatest. Frequently during this stage

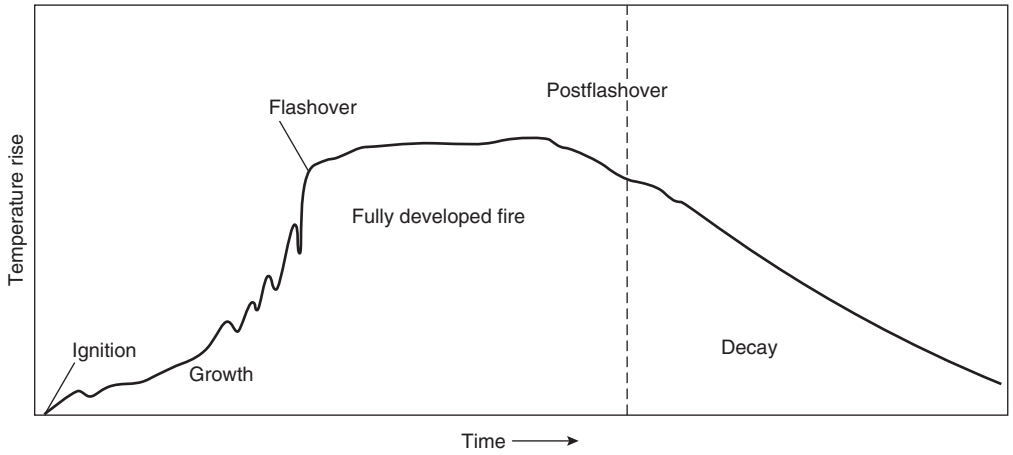

Figure 3-6.1. ***General description of room fire in absence of fire control.***

more fuel is pyrolized than can be burned with the oxygen available in the compartment. In this case, the fire is said to be ventilation controlled. If there are openings in the compartment, the unburned fuel will leave the compartment in the gas flow and may burn outside of the compartment. During the fully developed stage, the environment within the compartment has a significant effect on the pyrolysis rate of the burning objects.

Decay stage: Decay occurs as the fuel becomes consumed, and the heat release rate declines. The fire may change from ventilation to fuel controlled during this period.

Compartment Fire Phenomena

Compartment Fire Model

In order to calculate or predict the temperatures generated in a compartment fire, a description or model of the fire phenomena must be created. This model will be described in terms of physical equations which can be solved to predict the temperature in the compartment. Such a model is, therefore, an idealization of the compartment fire phenomena. Consider a fire which starts at some point below the ceiling and releases energy and products of combustion. The rate at which energy and products of combustion are released may change with time. The hot products of combustion form a plume, which, due to buoyancy, rises toward the ceiling. As the plume rises, it draws in cool air from within the compartment, decreasing the plume's temperature and increasing its volume flow rate. When the plume reaches the ceiling, it spreads out and forms a hot gas layer which descends with time as the plume's gases continue to flow into it. There is a relatively sharp interface between the hot upper layer and the air in the lower part of the compartment. The only interchange between the air in the lower part of the room and the hot upper layer assumed is through the plume. As the hot layer descends and reaches openings in the compartment walls (e.g., doors and windows), hot gas will flow out the openings and outside air will flow into the openings. This description of compartment fire phenomena is referred to as a two-layer or zone model. The basic compartment fire phenomena are shown schematically in Figure 3-6.2.

The two-layer-model concept assumes that the compositions of the layers are uniform, that is, that the temperature and other properties are the same throughout each layer. Although the temperature of the lower layer will rise during the course of the fire, the temperature of the upper layer will remain greater and is the most important factor in compartment fires. The assumptions may be less valid for very large spaces or for long, narrow spaces such as corridors and shafts.

Calculation of Compartment Fire Temperatures

The basic principle used to calculate the temperature in a compartment fire is the conservation of energy. As applied to the hot upper layer, the conservation of energy can be simply stated as follows: the energy added to the hot upper layer by the fire equals the energy lost from the hot layer plus the time rate of change of energy within the hot upper layer. From the time rate of change of en-

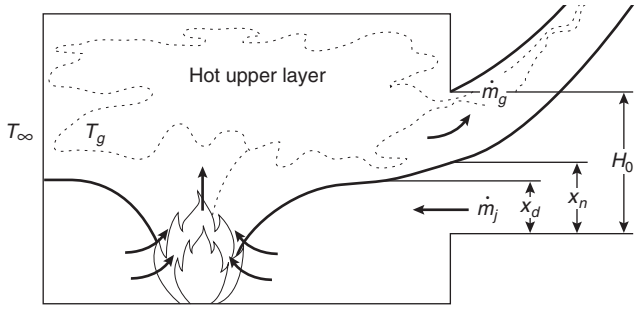

Figure 3-6.2. ***Two-layer model with no exchange between layers except the plume.***

ergy within the hot layer, the temperature of the layer can be computed. Conservation of energy can also be applied to the lower layer. Since the volume of the upper layer changes with time, and mass flows in and out of the upper layer, conservation of mass must be used along with the conservation of energy. Because the energy generated by the fire and the temperatures in the compartment vary as a function of time, the application of conservation of energy will result in a series of differential equations. For the purposes of examining the components of the conservation of energy, the steady-state expressions for the conservation of energy for the hot upper layer will be used.

The transport of energy in a compartment fire is a very complex process. In order to formulate expressions for the conservation of energy in a practical way, a number of assumptions must be made. It is possible to formulate the equations for the conservation of energy in a number of ways, based on the level of detail desired. The expressions and assumptions used in this chapter are based on those commonly found in the fire research literature and represent a somewhat simplified description of the phenomena. Additional details may be found in the references cited.

The steady-state conservation of energy for the hot upper gas layer in a compartment can be simply stated as follows: the energy generated by the fire and added to the hot layer equals the energy lost from the hot layer through radiation and convection plus the energy convected out the compartment openings.

Energy Generated by the Fire

The energy generated by the fire is the primary influence on the temperature in a compartment fire, and much research has been conducted in predicting the energy release rate of many fuels under a variety of conditions. This discussion will focus on flaming combustion, as it is most important in generating a significant temperature rise in a compartment. A discussion of smoldering combustion is found in Section 2, Chapter 9. As a fuel is heated and releases pyrolysis products, these products react with oxygen, generating heat and producing flames. The rate of energy release is equal to the mass loss rate of the fuel times the heat of combustion of the fuel:

$$\dot{Q} = \dot{m}_f \Delta h_c \tag{1}$$

where

$\dot{Q}$ = energy release rate of the fire (kW)

$\dot{m}_f$ = mass burning rate of the fuel (kg/s)

Δh_c = effective heat of combustion of the fuel (kJ/kg)

The effective heat of combustion is the heat of combustion which would be expected in a fire where incomplete combustion takes place. This amount is less than the theoretical heat of combustion as measured in the oxygen bomb calorimeter. The effective heat of combustion is often described as a fraction of the theoretical heat of combustion. The effect of fluctuations is largely neglected.

In fuel-controlled fires, there is sufficient air to react with all the fuel within the compartment. In ventilation-controlled fires, there is insufficient air within the compartment, and some of the pyrolysis products will leave the compartment, possibly to react outside the compartment. For calculating the temperatures produced in compartment fires, the primary interest is the energy released within the compartment.

The pyrolysis rate of the fuel depends on the fuel type, its geometry, and the fire-induced environment. The energy generated in the compartment by the burning pyrolysis products then depends on the conditions (temperature, oxygen concentration, etc.) within the compartment. While the processes involved are complex, and some are not well understood, there are two cases where some simplifying assumptions can lead to useful methods for approximation of the energy released by the fire.

Free-burning fires are defined as those in which the pyrolysis rate and the energy release rate are affected only by the burning of the fuel itself and not by the room environment. This definition is analogous to a fire burning out of doors on a calm day. Babrauskas has provided a collection of data on free-burning fires in Section 3, Chapter 1. This data is most useful for estimating burning rates of primarily horizontal fuels in preflashover fires, where the primary heating of the fuel is from the flames of the burning item itself. Vertical fuels, such as wall linings and fuels located in the upper hot gas layer, will likely be influenced by the preflashover room environment.

Ventilation-controlled fires are defined as those in which the energy release rate in the room is limited by the amount of available oxygen. The mass flow rate of air or oxygen into the room through a door or window can be calculated from the expressions described below and in Section 2, Chapter 3. For most fuels, the heat released per mass of air consumed is a constant approximately equal to 3000 KJ/kg.[3] Therefore, the rate of energy release of the fire can be approximated from the air inflow rate.

The amount of energy released by the fire which enters the hot upper layer is a function of the fire, layer conditions, and geometry. For most fires, approximately 35 percent of the energy released by the fire leaves the fire plume as radiation.[4] (A discussion of flame radiation can be found in Section 2, Chapter 12.) In a compartment fire, a fraction of the radiated energy reaches the upper layer. The majority of the remaining energy released by the fire is convected into the upper layer by the plume. As the plume rises, it entrains air from the lower layer, thus reducing its temperature and increasing the mass flow rate. For a first approximation, it can be assumed that all of the energy generated by the fire is transported to the upper layer. For a complete discussion of fire plumes see Section 2, Chapter 1.

Conservation of Mass

The mass flow into the compartment and the flow out are related by

$$\dot{m}_g = \dot{m}_a + \dot{m}_f \tag{2}$$

where $\dot{m}_f$ is the mass burning rate of the fuel (kg/s).

The mass flow rate of hot gas out of a window or door is given by Rockett:[5]

$$\dot{m}_g = \frac{2}{3} C_d W_0 \rho_\infty \left[2g \frac{T_\infty}{T_g} \left(1 - \frac{T_\infty}{T_g} \right) \right]^{1/2} (H_0 - X_N)^{3/2} \quad (3)$$

where

$\dot{m}_g$ = mass flow rate of hot gas out an opening (kg/s)
C_d = orifice constriction coefficient (typically ≈ 0.7)
W_0 = opening width (m)
H_0 = opening height (m)
ρ_∞ = ambient air density (kg/m²)
g = acceleration due to gravity, 9.8 m/s²
X_N = height of neutral plane (m)
T_g = temperature of the hot upper gas layer (K)
T_∞ = ambient temperature (K)

The mass flow rate of air into a door or window is given by

$$\dot{m}_a = \frac{2}{3} C_d W_0 \rho_\infty \left[2g \left(1 - \frac{T_\infty}{T_g} \right) \right]^{1/2} (X_N - X_d)^{1/2} (X_N + X_d/2) \quad (4)$$

where X_d = height of the interface (m).

The expressions for mass flow in and mass flow out cannot be solved directly for T_g since the height to the neutral plane and interface are unknown. The complete solution of these equations requires expressions for plume entrainment and additional energy equations and is normally carried out only in computer fire models. If the mass burning rate of the fuel is small compared with the mass flow rate of air into the compartment, the mass flow out of the opening may be approximated as equal to the mass inflow rate. Flows out of vents in the ceiling are discussed in Section 3, Chapter 11.

For preflashover fires in compartments with typical doors or windows, the neutral plane and interface can be approximated at the midlevel of the opening. This approximation can only be made after the initial smoke filling of the compartment is complete, and flow in and out of the opening is established.

For fires nearing flashover and post-flashover fires, the interface between the upper and lower layers is located near the floor, and the flow reaches a maximum for a given upper gas temperature. Rockett has shown the temperature dependence on the flow becomes small above 150°C, and the flow into the compartment can be approximated as a constant multiplied by[5] $A_0\sqrt{H_0}$.

Rockett calculated values for this constant of 0.40 to 0.61 kg/s·m$^{5/2}$, depending on the discharge coefficient of the opening. Thomas and Heselden estimate the value of this constant at 0.5 kg/s·m$^{5/2}$, which is the value most commonly found in the literature.[6] The resulting approximation is then

$$\dot{m}_a = 0.5 A_0 \sqrt{H_0} \quad (5)$$

where

A_0 = area of opening (m²)
H_0 = height of opening (m)

The term $A_0\sqrt{H_0}$ is commonly known as the ventilation factor. The first use of this type of opening flow analysis for evaluating postflashover-fire test data is attributed to Kawagoe.[7] From early work analyzing such data, the empirical observation was made that wood fires in rooms with small windows appeared to burn at a rate approximately stoichiometric. Although flames emerging from the windows implied that some fuel was burning outside, calculations often suggested that enough air was entering the fire for stoichiometric burning. Empirical observations on wood fires[7] led to

$$\dot{m}_f = 0.09 A_0 \sqrt{H_0} \quad (6)$$

There is now a body of data[8] that modifies this simple proportionality between $\dot{m}_f$ and $A_0\sqrt{H_0}$.

The Conseil International du Bâtiment (CIB) experiments upon which Law[9] has based her method shows a dependance on A_T. It seems possible that the wide use of Equation 6 is a result of a concentration of experimental fires in rooms of a limited range of

$$\frac{A_T}{A_0\sqrt{H_0}}$$

where

A_T = total area of the compartment enclosing surfaces (m²)

Traditionally, energy balances were often stated in terms of the energy produced by the burning fuel and, thereby, led to an effective heat of combustion of the fuel. However, this practice in principle leads to the same result—the energy produced is related to the air flow for ventilation-controlled fires. Kawagoe[7] and Magnusson and Thelandersson[10] used 10.75 MJ/kg for the effective heat of combustion of wood in the flaming phase for fully developed compartment fires. With 16.4 MJ/kg for the heat of combustion of wood volatiles, this setup corresponds to a combustion efficiency of 10.75/16.4, which is virtually identical to the 0.65 used in several computer models.

By far the majority of data is based on experiments in which the fuel was cellulosic, and much of the experimental data are based on wood in the form of cribs. For the postflashover burning of a different fuel with a different chemistry, the burning rate expressions may still be used, as long as the fuel is a hydrocarbon producing approximately 3000 kJ for each kg of air consumed in the combustion process. Because different fuels react differently to the thermal environment and will pyrolyze at different rates according to the energy requirements to produce volatiles, one can only estimate temperatures by evaluating the differences, or obtain maximum temperatures by using stoichiometry. Fuels more volatile than wood will probably produce lower temperatures inside a compartment, even if the excess fuel produces a greater hazard outside the compartment. The assumptions that the energy is related to the air flow and that the fuel is in stoichiometric proportion will give an upper estimate of temperatures for ventilation-controlled fires. Since Equation 6 is close to stoichiometric, it could, coupled with the

Table 3-6.1 ***Heat Balance Measured in Experimental Fires in a Compartment of 29 m² Floor Area with a Fire Load of Wood Cribs***

Fire Load (kg)	Window Area (m^2)	Heat Release (kcal/s)	Heat Loss from Hot Gases (%)			
			Effluent Gas	Structural Surfaces	Feedback to Fuel	Window Radiation
877	11.2	1900	65	15	11	9
	5.6	1900	52	26	11	11
1744	11.2	3200	61	15	11	13
	5.6	2300	53	26	12	9
	2.6	1600	47	30	16	7

effective heat of combustion of wood, give results close to an upper temperature limit for other fuels.

Conservation of Energy

The heat generated by burning materials within a compartment is absorbed by the enclosing surfaces of the compartment and any other structural surfaces, by the surfaces of the fuel, and by the incoming air and any excess fuel. Heat is lost to the exterior in the flames and hot gases that exit from the openings in the compartment enclosing surfaces and by radiation through the openings. An example of an experimental heat balance measured in a small compartment is given in Table 3-6.1. For this compartment, unglazed windows provided ventilation from the start of the fire.

Table 3-6.1 illustrates the significant amount of heat loss in the effluent gases and shows that, with decreasing window area, a larger proportion of the heat released will be absorbed by the enclosing surfaces. The total heat released, assuming a complete burnout, is directly proportional to the amount of the fire load, but the rate of heat release may also be controlled by the ventilation. In this example, with the lower fire load, both window areas give sufficient ventilation for the fuel to burn at its maximum (free-burning) rate but, with the doubled fire load, the burning rate is not doubled, because the window area restricts the ventilation needed.

Methods for Predicting Preflashover Compartment Fire Temperatures

The solution of a relatively complete set of equations for the conservation of energy requires the solution of a large number of equations which vary with time. Although individual energy transport equations may be solved, in general there is not an explicit solution for a set of these equations. As a result, one of two approaches can be taken. The first is an approximate solution which can be accomplished by hand using a limiting set of assumptions. The second is a more complete solution utilizing a computer program. In either case, a number of methods have been developed. The methods presented are those which appear most widely accepted in the fire protection community. Each method employs assumptions and limitations which should be understood before employing the method. The methods presented in this chapter predict average temperatures and are not applicable to cases where prediction of local temperatures are desired. For example, these methods should not be used to predict detector or sprinkler actuation or the temperatures of materials as a result of direct flame impingement.

Method of McCaffrey, Quintiere, and Harkleroad

McCaffrey, Quintiere, and Harkleroad have used a simple conservation of energy expression and a correlation with data to develop an approximation of the upper layer temperature in a compartment.[11] Applying the conservation of energy to the upper layer yields

$$\dot{Q} = \dot{m}_g c_p (T_g - T_\infty) + q_{\text{loss}} \tag{7}$$

where

$\dot{Q}$ = energy (heat) release rate of the fire (kW)
$\dot{m}_g$ = gas flow rate out the opening (kg/s)
c_p = specific heat of gas (kJ/kg·K)
T_g = temperature of the upper gas layer (K)
T_∞ = ambient temperature (K)
q_{loss} = net radiative and convective heat transfer from the upper gas layer (kW)

The left-hand side of Equation 7 is the energy generated by the fire. On the right-hand side, the first term is the heat transported from the upper layer in the gas flow out an opening. The second term is the net rate of radiative and convective heat transfer from the upper layer, which is approximately equal to rate of heat conduction into the compartment surfaces. The rate of heat transfer to the surfaces is approximated by

$$q_{\text{loss}} = h_k A_T (T_g - T_\infty) \tag{8}$$

where

h_k = effective heat transfer coefficient (kW/m·K)
A_T = total area of the compartment enclosing surfaces (m^2)

Substituting Equation 8 into Equation 7 yields the nondimensional temperature rise in terms of two dimensionless groups:

$$\frac{\Delta T_g}{T_\infty} = \frac{\dot{Q}/(c_p T_\infty \dot{m}_g)}{1 + h_k A_T/(c_p \dot{m}_g)} \tag{9}$$

where ΔT_g is the upper gas temperature rise above ambient ($T_g - T_\infty$) (K).

The mass flow rate of hot gas out of a window or door can be rewritten from Equation 3:

$$\dot{m}_g = \frac{2}{3} C_d W_0 H_0^{3/2} \rho_\infty \left[2g \frac{T_\infty}{T_g} \left(1 - \frac{T_\infty}{T_g} \right) \right]^{1/2} \left(1 - \frac{X_N}{H_0} \right)^{3/2} \tag{10}$$

where

C_d = orifice constriction coefficient
W_0 = opening width (m)
H_0 = opening height (m)
ρ_∞ = ambient air density (kg/m^2)
g = acceleration due to gravity, 9.8 m/s^2
X_N = height of neutral plane (m)

Since X_N primarily depends on T_g, $\dot{Q}$, and geometric factors (H_0 and W_0), $\dot{m}_g$ may be replaced by $\sqrt{g}\rho_\infty A_0 \sqrt{H_0}$ in the two dimensionless variables in Equation 10, without any loss in generality. The effects of T_g and $\dot{Q}$ are incorporated into the correlation via other terms. Based on an analysis of test data, Equation 9 was written as a power-law relationship:

$$\Delta T_g = 480 \left(\frac{\dot{Q}}{\sqrt{g} c_p \rho_\infty T_\infty A_0 \sqrt{H_0}} \right)^{2/3} \left(\frac{h_k A_T}{\sqrt{g} c_p \rho_\infty A_0 \sqrt{H_0}} \right)^{-1/3} \tag{11}$$

where

A_0 = area of opening (m^2)
H_0 = height of opening (m)

The numbers 480, 2/3, and −1/3 were determined by correlating the expression with the data from over 100 experimental fires. These data included both steady-state and transient fires in cellulosic and synthetic polymeric materials and gaseous hydrocarbon fuels. Compartment height ranged from 0.3 m to 2.7 m and floor areas from 0.14 m^2 to 12.0 m^2. The compartments contained a variety of window and door sizes. The term raised to the 2/3 power in Equation 11 represents the ratio of the energy released to the energy convected, and the term raised to the −1/3 power represents the energy lost divided by the energy convected.

Substituting the values for ambient conditions of

g = 9.8 m/s^2
c_p = 1.05 kJ/kg·K
ρ_∞ = 1.2 kg/m^3
T_∞ = 295 K

into Equation 11 yields[12,13]

$$\Delta T_g = 6.85 \left(\frac{\dot{Q}^2}{A_0 \sqrt{H_0} h_k A_T} \right)^{1/3} \tag{12}$$

The heat transfer coefficient can be determined using a steady-state approximation when the time of exposure, t, is greater than the thermal penetration time, t_p, by

$$h_k = k/\delta \quad \text{for} \quad t > t_p \tag{13}$$

The thermal penetration time is defined as

$$t_p = \left(\frac{\rho c}{k} \right) \left(\frac{\delta}{2} \right)^2 \tag{14}$$

where

ρ = density of the compartment surface (kg/m^3)
c = specific heat of the compartment surface material (kJ/kg·K)
k = thermal conductivity of compartment surface (kW/m·K)
δ = thickness of compartment surface (m)
t = exposure time (s)
t_p = thermal penetration time (s)

When the time of exposure is less than the penetration time, an approximation based on conduction in a semi-infinite solid is

$$h_k = \left(\frac{k \rho c}{t} \right)^{1/2} \quad \text{for} \quad t \le t_p \tag{15}$$

If there are several wall and/or ceiling materials in the compartment, an area-weighted average for h_k should be used.

The limitations as stated by McCaffrey et al. on the use of this method for estimating temperatures are as follows:

1. The correlation holds for compartment upper layer gas temperatures up to approximately 600°C.
2. It applies to steady-state as well as time-dependent fires, provided the primary transient response is the wall conduction phenomenon.
3. It is not applicable to rapidly developing fires in large enclosures in which significant fire growth has occurred before the combustion products have exited the compartment.
4. The energy release rate of the fire must be determined from data or other correlations.
5. The characteristic fire growth time and thermal penetration time of the room-lining materials must be determined in order to evaluate the effective heat transfer coefficient.
6. The correlation is based on data from a limited number of experiments and does not contain extensive data on ventilation-controlled fires nor data on combustible walls or ceilings. Most of the fuel in the test fires was near the center of the room.

Example of McCaffrey et al. method: Calculate the upper layer temperature of a room 3 × 3 m in floor area and

2.4 m high with a door opening 1.8 m high and 0.6 m wide. The fire source is a steady 750 kW fire. The wall-lining material is 0.016 m (5/8 in.) gypsum plaster on metal lath. Perform the calculation at times of 10, 60, and 600 s after ignition. Using Equation 11,

$$\Delta T_g = 480\left(\frac{\dot{Q}}{\sqrt{g}c_p\rho_\infty T_\infty A_0\sqrt{H_0}}\right)^{2/3}\left(\frac{h_k A_T}{\sqrt{g}c_p\rho_\infty A_0\sqrt{H_0}}\right)^{-1/3}$$

where

$c_p = 1$ kJ/kg·K
$T_\infty = 27°C$ (300 K)
$\rho_\infty = 1.18$ kg/m^3
$A_0 = 1.8$ m $\times$ 0.6 m $= 1.08$ m^2
$g = 9.8$ m/s^2
$H_0 = 1.8$ m
$\dot{Q} = 750$ kW
$A_T = A_{walls} + A_{floor} + A_{ceiling} - A_{openings}$
$= 4 \times (3 \times 2.4) + (3 \times 3) + (3 \times 3) - 1.08$
$= 28.8$ m^2 + 9 m^2 + 9 m^2 − 1.08
$= 45.72$ m^2

The wall heat loss coefficient, h_k, is a function of time.

a. Calculate the thermal penetration time, t_p.

$$t_p = \left(\frac{\rho c}{k}\right)\left(\frac{\delta}{2}\right)^2$$

where

ρ = wall material density (1440 kg/m^3)
$k = 0.48 \times 10^{-3}$ kW/m·c
$c = 0.84$ kJ/kg°C
$\delta = 0.016$ m
$t_p = 161.3$ s

b. Calculate h_k at 10, 60, and 600 s.

For $t < t_p$ (10, 60 s),

$$h_k = \left(\frac{k\rho c}{t}\right)^{1/2} \qquad k\rho c = 0.581$$

1. At $t = 10$ s,

$$h_k = \left(\frac{0.581}{10}\right)^{1/2} = 0.24\text{kW/m·K}$$

2. At $t = 60$ s,

$$h_k = \left(\frac{0.581}{60}\right)^{1/2} = 0.098\text{kW/m·K}$$

3. For $t > t_p$ (600 s) at $t = 600$ s,

$$h_k = \frac{k}{\delta} = \frac{0.48 \times 10^{-3}}{0.016} = 0.03\text{kW/m·K}$$

c. Calculate the compartment temperature at the three times using Equation 11.

1. At $t = 10$ s,

$$\Delta T_g = 480\left[\frac{750}{(\sqrt{9.8})(1)(1.18)(300)(1.08)(\sqrt{1.8})}\right]^{2/3} \cdot \left[\frac{(0.24)(45.72)}{(\sqrt{9.8}(1)(1.18)(1.08)(\sqrt{1.8})}\right]^{-1/3}$$
$$= 480(0.47)^{2/3}(2.05)^{-1/3}$$
$$= 227 \text{ K}$$

2. At $t = 60$ s,

$$\Delta T_g = 480(0.47)^{2/3}(0.837)^{-1/3}$$
$$= 307 \text{ K}$$

3. At $t = 600$ s,

$$\Delta T_g = 480(0.47)^{2/3}(0.26)^{-1/3}$$
$$= 453 \text{ K}$$

Method of Foote, Pagni, and Alvares

The Foote, Pagni, and Alvares method follows the basic correlations of McCaffrey, Quintiere, and Harkleroad and adds data for forced-ventilation fires. Using Equation 9 and not introducing an expression for doorway flow results in the expression[14]

$$\frac{\Delta T_g}{T_\infty} = 0.63\left(\frac{\dot{Q}}{\dot{m}_g c_p T_\infty}\right)^{0.72}\left(\frac{h_k A_T}{\dot{m}_g c_p}\right)^{-0.36} \tag{16}$$

where

ΔT_g = upper gas temperature rise above ambient (K)
T_∞ = ambient air temperature (K)
$\dot{Q}$ = energy (heat) release rate of the fire (kW)
$\dot{m}_g$ = compartment mass ventilation rate (kg/s)
c_p = specific heat of gas (kJ/kg·K)
h_k = effective heat transfer coefficient (kW/m·K)
A_T = total area of the compartment-enclosing surfaces (m^2)

The coefficient and exponents are based on data from well-ventilated tests in a compartment with a 6 × 4 m floor area and a height of 4.5 m with ventilation rates of 110 to 325 g/s. The compartment exhaust was through a 0.65 × 0.65 m duct located 3.6 m above the floor. Four air inlet openings were 0.5 × 0.12 m high, with centerlines 0.1 m above the floor. A methane gas burner fire in the center of the floor with heat release rates of 150 to 490 kW resulted in upper gas temperatures of approximately 100 to 300°C.

Foote et al. have shown that the correlation for forced-ventilation fires agrees well with the data presented by McCaffrey et al. for free ventilation fires with

$$\dot{m} \approx 0.1(\rho_\infty\sqrt{g}A_0\sqrt{H_0})$$

Example of Foote et al. method: Estimate the temperature in a 5 × 5 m in floor area × 4 m high compartment having 0.025-m-(1-in.)-thick concrete walls. The forced-ventilation rate is 2.4 m^3/s of air (5000 cfm). Perform the calculation for $t > t_p$. The fire size is given as 1000 kW; ambient air conditions at 300 K. Using Equation 16,

$$\frac{\Delta T_g}{T_\infty} = 0.63\left(\frac{\dot{Q}}{\dot{m}c_p T_\infty}\right)^{0.72}\left(\frac{h_k A_T}{\dot{m}c_p}\right)^{-0.36}$$

where

$\dot{Q} = 1000$ kW
$T_\infty = 300$ K
$c_p = 1.0$ kJ/kg·K
$A_T = 4 \times (5 \times 4) + 2\,(5 \times 5) = 105$ m^2
$\dot{m}_g = (2.4\ m^3/s)\,(1.18\ kg/m^3) = 2.8$ kg/s

Calculate h_k for $t > t_p$. For 0.025-m-thick concrete,

$\delta = 0.025$ m
$\rho = 2000$ kg/m^3
$k = 1.4 \times 10^{-3}$ kW/m·K
$c_p = 0.88$ kJ/kg · K

$$t_p = \left(\frac{\rho c}{k}\right)\left(\frac{\delta}{2}\right)^2 = \left[\frac{(2000)\cdot(0.88)}{1.4\times10^{-3}}\right]\left(\frac{0.025}{2}\right)^2 = 196\text{s} \quad \text{for} \quad t > t_p$$

$$h_k = \frac{k}{\delta} = \frac{1.4\times10^{-3}}{0.025} = 0.056\text{kW/m}^2\cdot\text{K}$$

$$\frac{\Delta T_g}{T_\infty} = (0.63)\left[\frac{1000}{(2.8)(1)(300)}\right]^{0.72}\left[\frac{(0.056)(105)}{(2.8)(1)}\right]^{-0.36}$$

$$\Delta T_g = (0.14)(T_\infty) = 164\text{ K}$$
$$T_g = 164 + 300\text{ K} = 464\text{ K}$$

Method of Beyler and Deal

Beyler and Deal compared a number of methods for naturally ventilated compartments to test data and recommend the method of McCaffrey, Quintiere, and Harkleroad for naturally ventilated compartments. Beyler offers an improved correlation for compartments where the forced-ventilation flow rate is known.[15,16] This method begins by applying the conservation of energy in the upper layer of a compartment. Combining Equations 7 and 8 yields

$$\dot{Q} = \dot{m}_g c_p (T_g - T_\infty) + h_k A_T (T_g - T_\infty) \qquad (17)$$

where:

$\dot{Q}$ = energy (heat) release rate of the fire (kw)
$\dot{m}_g$ = gas flow rate out the opening (kg/s)
c_p = specific heat of gas (kJ/kg·K)
T_g = temperature of the upper gas layer (K)
T_∞ = ambient temperature (K)
h_k = effective heat transfer coefficient (kW/m·K)
A_T = total area of the compartment enclosing surfaces (m^2)

Rearranging Equation 17a yields

$$\Delta T_g = \frac{\dot{Q}}{\dot{m}_g c_p + h_k A_T} \qquad (17a)$$

or

$$\frac{\Delta T_g \dot{m}_g c_p}{\dot{Q}} = \frac{1}{1 + (h_k A_T)/\dot{m}_g c_p} \qquad (17b)$$

where $\Delta T_g = T_g - T_\infty$.

A nondimensional temperature rise is defined as

$$\Delta T^* \equiv \frac{\Delta T_g \dot{m}_g c_p}{\dot{Q}} \qquad (18)$$

and the ratio of the bounding surface loss to the ventilation losses is defined as

$$Y^* \equiv 1 + \frac{h_k A_T}{\dot{m}_g c_p} \qquad (19)$$

By plotting ΔT^* as a function of ΔY^* for data with experiments with known ventilation rates Beyler and Deal developed a correlation for the effective heat transfer coefficient of

$$h_k = 0.4 \max\left(\sqrt{\frac{k\rho c}{t}}, \frac{k}{\delta}\right) \qquad (20)$$

where

k = thermal conductivity of the compartment surface (kW/m·K)
ρ = density of the compartment surface (kg/m^3)
c = specific heat of the compartment surface material (kJ/kg·K)
δ = thickness of the compartment surface (m)
t = exposure time (s)

The expression switches from transient to steady state at a thermal penetration time of $t_p = (\rho c/k)\delta^2$ rather than $t_p = (\rho c/k)(\delta/2)^2$ used by McCaffery et al. and Foote et al. For the data set Beyler and Deal evaluated, the standard error for their method was 29 K as compared to 51 K for the method of Foote et al., even though the equation uses only one fitting constant.

Beyler and Deal demonstrated that this method works for ventilation to the lower part of the compartment (with or without a plenum) as well as for ventilation to the upper part of the compartment. The Beyler and

Deal method was based on data up to 2000 s into fire tests. At longer times, the heat loss model breaks down.

Example of Beyler and Deal method: Estimate the temperature in a 5 m × 5 m floor area and 4 m high compartment with 0.025 m (1 in.)-thick concrete walls. The forced-ventilation rate is 2.4 m^3/s of air (5000 cfm). Perform the calculation for $t > t_p$.The fire size is given as 1000 kW; ambient air conditions at 300 K. Using Equation 17a,

$$T_g - T_\infty = \frac{\dot{Q}}{\dot{m}_g c_p + h_k A_T}$$

where

$\dot{Q} = 1000$ kw
$\dot{m}_g = (2.4\ m^3/s)\ (1.18\ kg/m^3) = 2.8$ kg/s
$c_p = 1.0$ kJ/kg·K
$T_\infty = 300$ K
$A_T = 4(5 \times 4) + 2(5 \times 5) = 105\ m^2$

a. Calculate h_k for $t > t_p$. For 0.25-m-thick concrete,

$\delta = 0.25$ m
$\rho = 2000\ kg/m^3$
$k = 1.4 \times 10^{-3}$ kW/m·K
$c = 0.88$ kJ/kg·K

$$h_k = 0.4\left(\frac{k}{\delta}\right) = 0.4\left(\frac{1.4 \times 10^{-3}}{0.25}\right) = 0.0224\ kW/m^2{\cdot}K$$

b. Calculate the compartment temperature using Equation 17a.

$$T_g - 300 = \frac{1000}{(2.8)(1.0) + (0.0224)(105)}$$

$$T_g = 494\ K$$

Method of Peatross and Beyler

The correlations used in the McCaffrey, Quintiere, and Harkleroad method and the Beyler and Deal method are based on the assumption of normal insulating-wall materials. For highly conductive walls such as steel, Peatross and Beyler suggest the use of an alternative heat transfer coefficient.[17] Using a lumped mass analysis for heat transfer through the wall which is appropriate for a highly conductive wall yields

$$m''_w c \frac{dT_w}{dt} = h_g(T_g - T_w) - h_\infty T_w \qquad (21)$$

where

m''_w = mass per unit area of the wall (kg/m^2)
c = specific heat of the wall (kJ/kg·K)
T_w = wall temperature (K)
t = time (s)
h_g = heat transfer coefficient on the hot side of the wall (kW/m·K)
T_g = upper layer temperature (K)
h_∞ = heat transfer coefficient on the ambient side of the wall (kW/m·K)

Solving for the wall temperature with the initial condition of the wall at ambient temperature yields

$$T_w = \frac{h_g T_g}{h_g + h_\infty}\left[1 - \exp\left(-\frac{h_g - h_\infty}{m''_w c}\,t\right)\right] \qquad (22)$$

The heat transfer through the wall, $\dot{q}''$, may be expressed in terms of the heat transfer to the hot side of the wall or in terms of an overall effective heat transfer coefficient, h_k.

$$\dot{q}'' = h_g(T_g - T_w) = h_k(T_g - T_\infty) \qquad (23)$$

Solving for h_k yields

$$h_k = h_g - \frac{h_g^2}{h_g + h_\infty}\left[1 - \exp\left(-\frac{h_g - h_\infty}{\rho\delta c}\,t\right)\right] \qquad (24)$$

where

ρ = density of the wall (kg/m^3)
δ = thickness of the wall (m)

From the above equations it can be seen that

$$h_k = \frac{h_g h_\infty}{h_g + h_\infty} \quad \text{at} \quad t = \infty$$

$$h_k = h_g \quad \text{at} \quad t = 0$$

From a number of experiments, Peatross and Beyler found the heat transfer coefficients of 30 W/m^2·K for h_g and 20 W/m^2·K for h_∞. Substituting these values yields

$$h_k = 30 - 18\left[1 - \exp\left(-\frac{50}{\rho\delta c}\,t\right)\right] \qquad (25)$$

The h_k calculated with this method can be used directly in the Beyler and Deal method. It must be multiplied by 2.5 for use in the McCaffery, Quintiere, and Harkleroad method to account for the 0.4 fitting constant in the h_k in the Beyler and Deal method.

Example of Peatross and Beyler method for forced ventilation: Estimate the temperature in a 5 m × 5 m floor area and 4 m-high compartment having 0.00635 m- (0.25 in.)-thick, 0.5 percent carbon steel walls. The forced-ventilation rate is 2.4 m^3/s of air (5000 cfm). Perform the calculation for $t = 200$ s. The fire size is given as 1000 kW; ambient air conditions at 300 K. Using equation 17a,

$$T_g - T_\infty = \frac{\dot{Q}}{\dot{m}_g c_p + h_k A_T}$$

where

$\dot{Q} = 1000$ kw
$\dot{m}_g = (2.4\ m^3/s)\ (1.18\ kg/m^3) = 2.8$ kg/s
$c_p = 1.0$ kJ/kg·K
$T_\infty = 300$ K
$A_T = 4(5 \times 4) + 2(5 \times 5) = 105\ m^2$

a. Using equation 25, calculate h_k for $t = 200$ s. For 0.25-m-thick, 0.5 percent carbon steel,

$\delta = 0.00635$ m
$\rho = 7833$ kg/m^3
$c = 0.465$ kJ/kg·K

$$h_k = 30 - 18\left[1 - \exp\left(-\frac{50}{\rho\delta c}t\right)\right]$$
$$= 30 - 18\left\{1 - \exp\left[-\frac{50}{(7833)(0.00635)(0.465)}200\right]\right\}$$
$$= 12 \text{ kW/m}^2\text{·K}$$

b. Calculate the compartment temperature using Equation 17a.

$$T_g - 300 = \frac{1000}{(2.8)(1.0) + (12)(105)}$$
$$T_g = 301 \text{ K}$$

Method of Beyler

For compartments with no ventilation the quasi-steady approximation used in many of the methods is not appropriate since the conditions in the compartment will not reach steady state. Beyler applied a nonsteady energy balance to the closed compartment expressed by the differential equation[15]

$$mc_p\frac{dT}{dt} = \dot{Q} = h_k A_T \Delta T_g \tag{26}$$

where

$\dot{Q}$ = energy (heat) release rate of the fire (kw)
m = mass of the gas in the compartment (kg/s)
c_p = specific heat of gas (kJ/kg·K)
$\Delta T_g = T_g - T_\infty$
T_g = temperature of the upper gas layer (k)
T_∞ = ambient temperature (K)
h_k = effective heat transfer coefficient (kW/m·K)
A_T = total area of the compartment enclosing surfaces (m^2)
ρ = density of the compartment surface (kg/m^3)
δ = thickness of the compartment surface (m)
t = exposure time (s)

In this case a "closed" compartment has sufficient leaks to prevent pressure buildup, but the leakage is ignored. The mass of the fuel is ignored, and the initial temperature is assumed to be ambient temperature. For constant heat release rate, the solution to Equation 26 is

$$\Delta T_g = \frac{2K_2}{K_1^2}\left(K_1\sqrt{t} - 1 + e^{-K_1\sqrt{t}}\right) \tag{27}$$

where

$$K_1 = \frac{2(0.4\sqrt{k\rho c})}{mc_p} \tag{28}$$

$$K_2 = \frac{\dot{Q}}{mc_p} \tag{29}$$

where

k = thermal conductivity of the compartment surface (kW/m·K)
c = specific heat of the compartment surface material (kJ/kg·K)

which include the fitting coefficient. Beyler used data with a maximum temperature rise of 150°C to develop this correlation.

Example of Beyler method: Estimate the temperature in a 5 m × 5 m in floor area and 4-m-high "closed" compartment having 0.025 m- (1 in.)-thick concrete walls. Perform the calculation for $t = 120$ s. The fire size is given as 100 kW; ambient air conditions at 300 K. Using Equation 27,

$$\Delta T = \frac{2K_2}{K_1^2}\left(K_1\sqrt{t} - 1 + e^{-K_1\sqrt{t}}\right)$$

where

$T_\infty = 300$ K
$t = 120$ s

a. Calculate K_1 using Equation 28.

$$K_1 = \frac{2(0.4\sqrt{k\rho c})}{mc_p}$$
$$= \frac{2\left(0.4\sqrt{(1.4\times10^{-3})(2000)(0.88)}\right)}{(118)(1.0)}$$
$$= 0.01064$$

where

$m = (100 \text{ m}^3)(1.18 \text{ kg/m}^3) = 118$ kg
$c_p = 1.0$ kJ/kg·K
$\rho = 2000$ kg/m^3
$k = 1.4 \times 10^{-3}$ kW/m·K
$c = 0.88$ kJ/kg·K

b. Calculate K_2 using Equation 29.

$$K_2 = \frac{\dot{Q}}{mc_p}$$
$$= \frac{100}{(118)(1.0)}$$
$$= 0.84746$$

where

$m = (100 \text{ m}^3)(1.18 \text{ kg/m}^3) = 118$ kg
$c_p = 1.0$ kJ/kg·K

c. Calculate the compartment temperature using Equation 27.

$$T_g - 300$$
$$= \frac{(2)(0.84746)}{(0.01064)^2}\left((0.01064)\sqrt{120} - 1 + e^{-(0.01064)\sqrt{120}}\right)$$
$$T_g = 397.8 \text{ K}$$

Methods for Predicting Postflashover Compartment Fire Temperatures

Method of Babrauskas

The following method is based on the work of Babrauskas.[18,19] The upper gas temperature, T_g, is expressed according to a series of factors, each one accounting for a different physical phenomenon:

$$T_g = T_\infty + (T^* - T_\infty) \cdot \theta_1 \cdot \theta_2 \cdot \theta_3 \cdot \theta_4 \cdot \theta_5 \tag{30}$$

where $T*$ is an empirical constant = 1725 K, and the factors θ are in Equations 36, 41, 43, 44, 46, and 47.

Burning rate stoichiometry, θ_1: The dimensionless stoichiometric coefficient ϕ is defined as

$$\phi = \frac{\dot{m}_f}{\dot{m}_{f,st}} \tag{31}$$

where $\dot{m}$ is the fuel mass pyrolysis rate (kg/s), and $\dot{m}_{f,st}$ is the stoichiometric mass burning rate (i.e., no excess fuel and no excess oxygen).

$$\dot{m}_{f,st} = \frac{0.5A_0\sqrt{H_0}}{r} \tag{32}$$

where the ratio r is such that 1 kg fuel + r kg air → (1 + r) kg products. The value of r is readily computable for fuels containing carbon, hydrogen, and/or oxygen from the chemical formula of the fuel, taking the products to be CO_2, H_2O, and N_2.

$$\begin{aligned} &C_xH_yO_z + wO_2 + w\left(\frac{79}{21}\right)N_2 \rightarrow \\ &xCO_2 + \frac{y}{2}H_2O + w\left(\frac{79}{21}\right)N_2 \end{aligned} \tag{33}$$

where

$$w = \frac{2x + y/2 - z}{2} \tag{34}$$

and

$$r = \frac{[w + w(3.76)]28.97}{12.01x + 1.00y + 16.00z} \tag{35}$$

At stoichiometry ϕ = 1, and it is greater than 1 for fuel-rich burning and less than 1 for fuel-lean conditions.

The effect of ϕ on gas temperatures was evaluated by numerical computations using the COMPF2 computer program.[20] The efficiency factor, θ_1, accounts for deviation from stoichiometry and is shown in Figure 3-6.3. It is seen that the fuel-lean and the fuel-rich regimes exhibit a very different dependence. For the fuel-lean regime, the results can be approximated by

$$\theta_1 = 1.0 + 0.51 \ln \phi \quad \text{for} \quad \phi < 1 \tag{36}$$

Similarly, in the fuel-rich regime a suitable approximation is

$$\theta_1 = 1.0 - 0.05(\ln \phi)^{5/3} \quad \text{for} \quad \phi > 1 \tag{37}$$

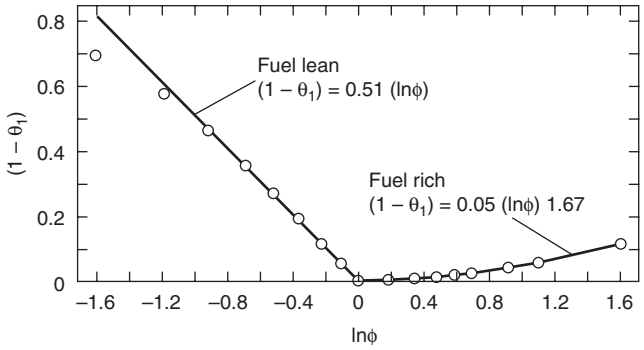

Figure 3-6.3. ***Effect of equivalence ratio.***

If heat release rate, $\dot{Q}$, rather than mass loss rate, $\dot{m}$, is used, then

$$\phi = \frac{\dot{Q}}{\dot{Q}_{\text{stoich}}} \tag{38}$$

And, since the stoichiometric heat release rate is

$$\dot{Q} = 1500A_0\sqrt{H_0} \tag{39}$$

then

$$\phi = \frac{\dot{Q}}{1500A_0\sqrt{H_0}} \tag{40}$$

The value of $\dot{Q}$ can be determined from Section 3, Chapter 1.

A separate procedure is necessary for pool fires, due to the strong radiative coupling. Here

$$\theta_1 = 1.0 - 0.092(-\ln\eta)^{1.25} \tag{41}$$

where

$$\eta = \left(\frac{A_0\sqrt{H_0}}{A_f}\right)\frac{0.5\Delta h_p}{r\sigma(T_g^4 - T_b^4)} \tag{42}$$

where

Δh_p = heat of vaporization of liquid (kJ/kg)
A_f = pool area (m^2)
σ = Stefan-Boltzmann constant (5.67×10^{-11} $kW/m^2 \cdot K^4$)
T_b = liquid boiling point temperature (K)

This expression unfortunately requires an estimate for T_g to be made, so for the pool fire case, a certain amount of iteration is necessary. The relationship above is plotted in Figure 3-6.4.

Wall steady-state losses, θ_2: The next efficiency factor, θ_2, accounts for variable groups of importance involving the wall surface (which is defined to include the ceiling) properties: area A_T(m^2), thickness L (m), density ρ (kg/m^3), thermal conductivity k (kW/m·K), and heat capacity c_p(kJ/kg·K). This factor is given as

$$\theta_2 = 1.0 - 0.94\exp\left[-54\left(\frac{A_0\sqrt{H_0}}{A_T}\right)^{2/3}\left(\frac{L}{k}\right)^{1/3}\right] \tag{43}$$

and is shown in Figure 3-6.5.

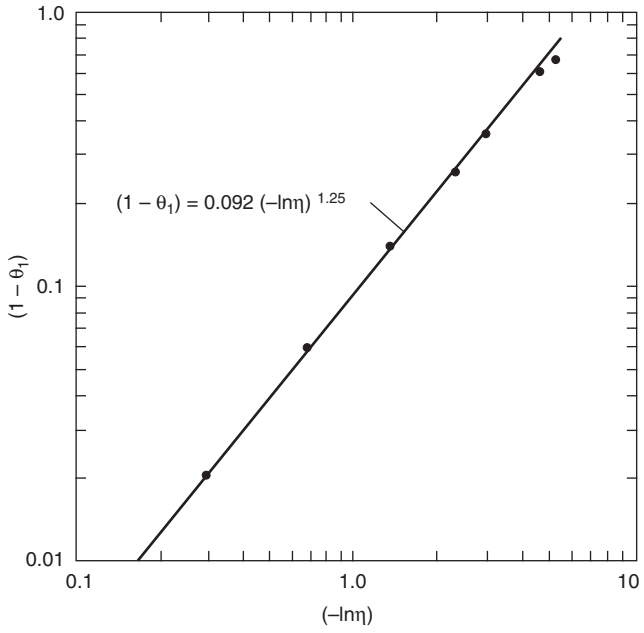

Figure 3-6.4. ***Effect of pool diameter.***

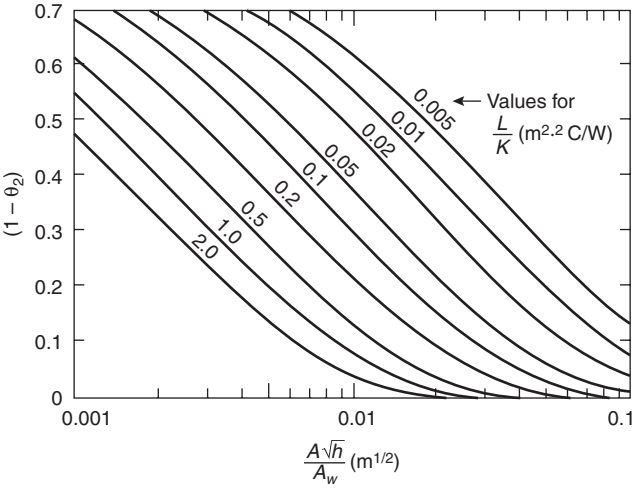

Figure 3-6.5. ***Effect of wall steady-state losses.***

Wall transient losses, θ_3: For the transient case, the above relationship predicts the asymptotic temperature value. An additional time-dependent factor, however, is needed. See Figure 3-6.6.

$$\theta_3 = 1.0 - 0.92 \exp\left[-150\left(\frac{A_0\sqrt{H_0}}{A_T}\right)^{0.6}\left(\frac{t}{k\rho c_p}\right)^{0.4}\right] \qquad (44)$$

If only steady-state temperatures need to be evaluated, then $\theta_3 = 1.0$.

Wall effects for t just slightly greater than zero are not well modeled with the above relationships for $\theta_2 \times \theta_3$; however, this condition is not a serious limitation, since the method is only designed for postflashover fires.

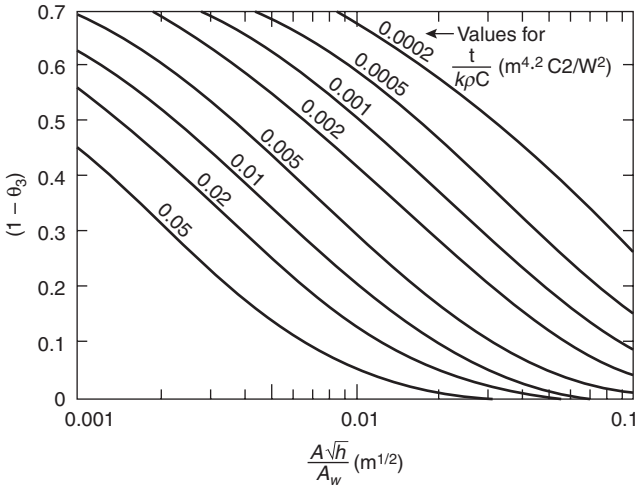

Figure 3-6.6. ***Effect of wall transient losses.***

For transient fires, the possibility of two separate effects must be considered. First, the wall loss effect, represented by Equation 44, in all fires, exhibits a nonsteady character. Second, the fuel release rate may not be constant. Since in the calculational procedure the previous results are not stored, it is appropriate to restrict consideration to fires where $\dot{m}_f$ does not change drastically over the time scale established by θ_3. This "natural" time scale can be determined as the time when the response has risen to 63 percent of its ultimate value, that is, at $\theta_3 = 0.63$, and is

$$t = 2.92 \times 10^{-6}(k\rho c_p)\left(\frac{A_T}{A_0\sqrt{H_0}}\right)^{1.5} \qquad (45)$$

Opening height effect, θ_4: The normalization of burning rate and wall loss quantities with the ventilation factor $A_0\sqrt{H_0}$ does not completely determine the total heat balance. An opening of a given $A_0\sqrt{H_0}$ can be tall and narrow or short and squat. For the shorter opening, the area will have to be larger. Radiation losses are proportional to the opening area and will, therefore, be higher for the shorter opening. By slight simplification, a representation for θ_4 can be made as

$$\theta_4 = 1.0 - 0.205H_0^{-0.3} \qquad (46)$$

as shown in Figure 3-6.7.

Combustion efficiency, θ_5: The fire compartment is viewed as a well, but not perfectly, stirred reactor. Thus a certain "unmixedness" is present. A maximum combustion efficiency, b_p, can be used to characterize this state. Since the model assumes infinitely fast kinetics, any limitations can also be included here. Data have not been available to characterize b_p in real fires, but agreement with measured fires can generally be obtained with b_p values in the range 0.5 to 0.9. The effect of b_p variation can be described by

$$\theta_5 = 1.0 + 0.5 \ln b_p \qquad (47)$$

as shown in Figure 3-6.8.

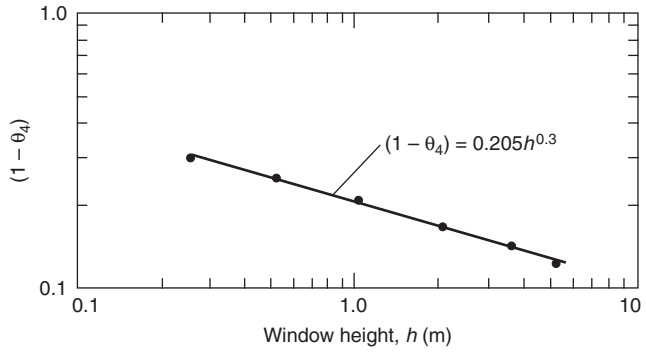

Figure 3-6.7. ***Effect of window height.***

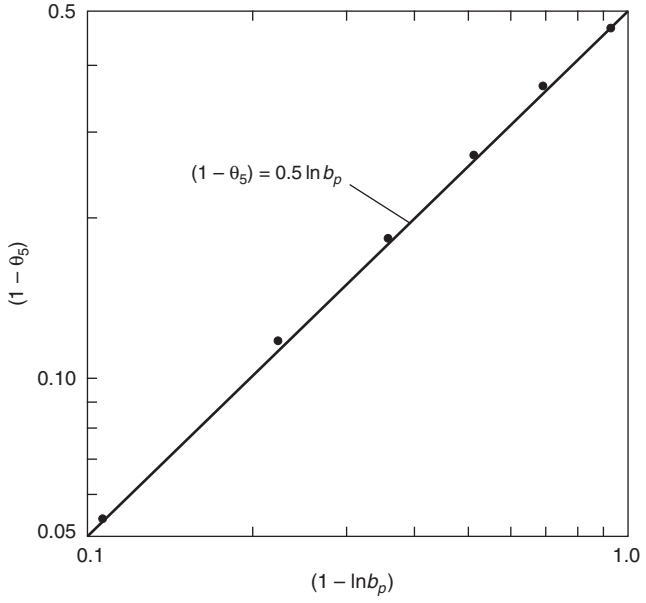

Figure 3-6.8. ***Effect of b_p, the maximum combustion efficiency.***

Method of Law

The area of structural surface to which heat is lost is expressed by $(A_T - A_0)$. For a given fire load, compartments with different values of A_T, A_0, and height H_0 will have a different heat balance, and thus the temperatures in the compartments will differ. This is illustrated in Figure 3-6.9 which shows how temperature varies with

$$\Omega = \frac{(A_T - A_0)}{A_0\sqrt{H_0}}$$

For low values of Ω (i.e., high ventilation), the rate of heat release is at a maximum, but the heat loss from the window is also large and the resultant temperature is low. For high values of Ω (i.e., low-ventilation areas), there is little heat loss to the outside, but the rate of heat release is also small and the resultant temperature is, again, low.

The curve in Figure 3-6.10 has been derived from many experimental fires conducted internationally by CIB.[8] For design purposes, Law has defined it as follows:

$$T_{g(\max)} = 6000\,\frac{(1 - e^{-0.1\Omega})}{\sqrt{\Omega}} \tag{48}$$

where

$$\Omega = \frac{(A_T - A_0)}{A_0\sqrt{H_0}}$$

and

A_T = total area of the compartment enclosing surfaces (m^2)
A_0 = area of opening (m^2)
H_0 = height of opening (m)

This equation represents an upper limit of fire temperature rise for a given Ω. However, if the fire load is low, this value may not be obtained. The importance of the effect of fire load also depends on A_0 and A_T, and can be expressed as

$$T_g = T_{g(\max)}(1 - e^{-0.05\psi}) \tag{49}$$

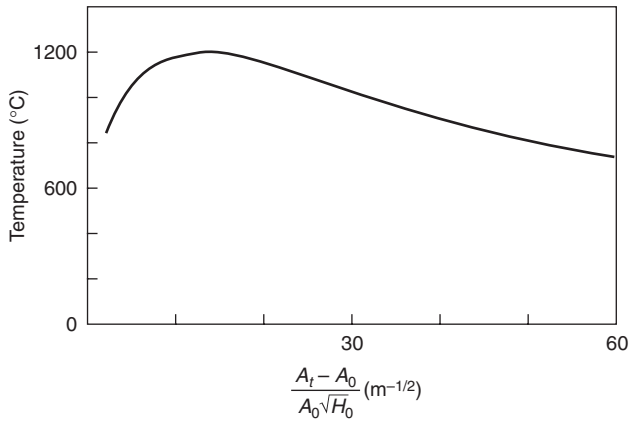

Figure 3-6.9. ***Average temperature during fully developed period measured in experimental fires in compartments.***

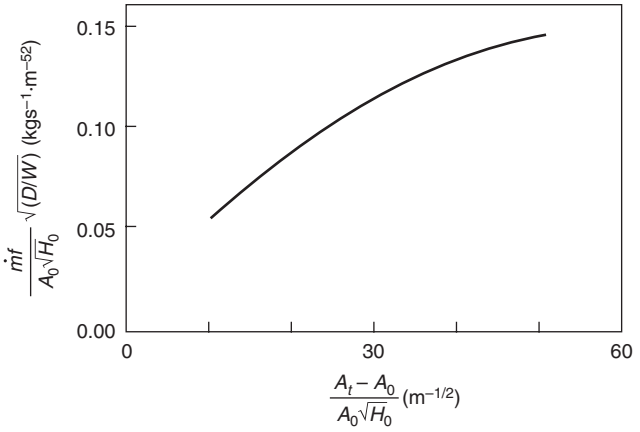

Figure 3-6.10. ***Variation of a rate of burning during fully developed period measured in experimental fires in compartments.***

where

$$\psi = \frac{L}{[A_0(A_T - A_0)]^{0.5}}$$

where L is the fire load (wood) in kg.

The effect of the fire on the structure depends not only on the value of T_g but also on the duration of heating. The effective fire duration, τ, in seconds, is given by

$$\tau = \frac{L}{\dot{m}_f} \tag{50}$$

where $\dot{m}_f$ is the rate of burning measured in kg/s.

Equation 6 implies that the smaller the value of $A_0\sqrt{H_0}$ the lower the rate of burning and the longer the duration. Assuming a complete burnout, therefore, the effect on the structure tends to be more severe for large values of Ω given for small $A_0\sqrt{H_0}$.

For design purposes the following equation has been developed to express the correlation of experimental results:[9]

$$\dot{m}_f = 0.18A_0\sqrt{H_0(W/D)}1 - e^{-0.036\Omega})\xi < 60 \tag{51}$$

where

W = compartment width (m)

D = compartment depth (m)

$$\xi = \frac{\dot{m}_f}{A_0\sqrt{H_0}}\left(\frac{D}{W}\right)^{1/2}$$

Equation 51 is shown in Figure 3-6.10 over the range where the data lie. Both equations are for ventilation-controlled fires. When there is ample ventilation, so that the fuel is free burning, the value of $\dot{m}_f$ depends on L and the type of fuel. For example, domestic furniture has a free-burning fire duration of about 20 min, giving τ = 1200 s and $\dot{m}_f = L/1200$.

The temperatures discussed above are averages measured during the fully developed period of the fire. It is assumed that all fires are ventilation controlled, with the simple relationship for rate of burning given by Equation 51, which is near stoichiometric burning, and it is assumed that combustion of 1 kg of wood releases 18.8 MJ in total.

Swedish Method

The Swedish method, developed by Magnusson and Thelandersson,[10] is based on the conventional mass and energy balance equations. The fire itself is not modeled; heat release rate curves are provided as input and, in all instances, the energy release must be less than stoichiometric. The method does not take into account that the actual mass loss rate may be greater than stoichiometric, with the excess fuel burning outside the compartment. A computer program SFIRE (versions 1 through 3) is available to perform this method. The results from the computer program have been compared with a large number of full-scale fire experiments, both in the fuel- and ventilation controlled regimes, with good agreement between theory and experiment. It should be added, however, that most of the experiments involved wood crib fires, which inherently burn slower and produce less excess fuel load than furnishings and other combustibles found in practical fire loads. In the Swedish method, the fire load is expressed in relation to A_T as $\dot{Q}$ 18.8 L/A_T MJ/m^2.

The design curves approved by the Swedish authorities were computed on the basis of systemized ventilation-controlled heat-release curves taken from Reference 10. Figure 3-6.11 shows some typical curves. The curves are calculated for wall, floor, and ceiling materials with "normal" thermal properties from an energy balance which assumes a uniform temperature in the compartment.

Predicting Flashover

One of the uses of predicted compartment fire temperatures is the estimation of the likelihood of flashover. The methods used are similar to those used in the prediction of temperature. In one case, that of McCaffrey et al., the method is simply an extension of the temperature calculation.

Method of Babrauskas

Babrauskas uses the energy balance for the upper layer given in Equation 7, where the gas flow rate out of the opening is approximated by[21]

$$\dot{m}_g \approx 0.5A_0\sqrt{H_0} \tag{52}$$

The primary energy loss is assumed to be radiation to 40 percent of the wall area which is at approximately ambient temperature:

$$q_{\text{loss}} = \varepsilon\sigma(T_g^4 - T_\infty^4)(0.40A_T) \tag{53}$$

where

ε = emissivity of the hot gas

σ = Stefan-Boltzmann constant 5.67×10^{11} kW/m^2·K^4

Combining Equations 7, 52, and 53, using a gas temperature for flashover of 873 K, a specific heat of air of 1.0 kJ/kg·K, an emissivity of 0.5, and assuming the correlation between compartment wall and opening area of

$$\frac{A_T}{A_0\sqrt{H_0}} \approx 50$$

yields a minimum $\dot{Q}$ required for flashover,

$$\dot{Q} = 600A_0\sqrt{H_0} \tag{54}$$

The air flow into the compartment has been approximated as

$$0.5A_0\sqrt{H_0}$$

The maximum amount of fuel which can be burned completely with this air is known as the stoichiometric amount. For most fuels, the heat released per mass of air consumed is a constant approximately equal to 3000 kJ/kg. Therefore, the stoichiometric heat release rate $\dot{Q}_{\text{stoich}}$ can be calculated

$$\begin{aligned}\dot{Q}_{\text{stoich}} &= 3000\dot{m}_g = 3000(0.5_0\sqrt{H_0}) \\ &= 1500A_0\sqrt{H_0}\end{aligned} \tag{55}$$

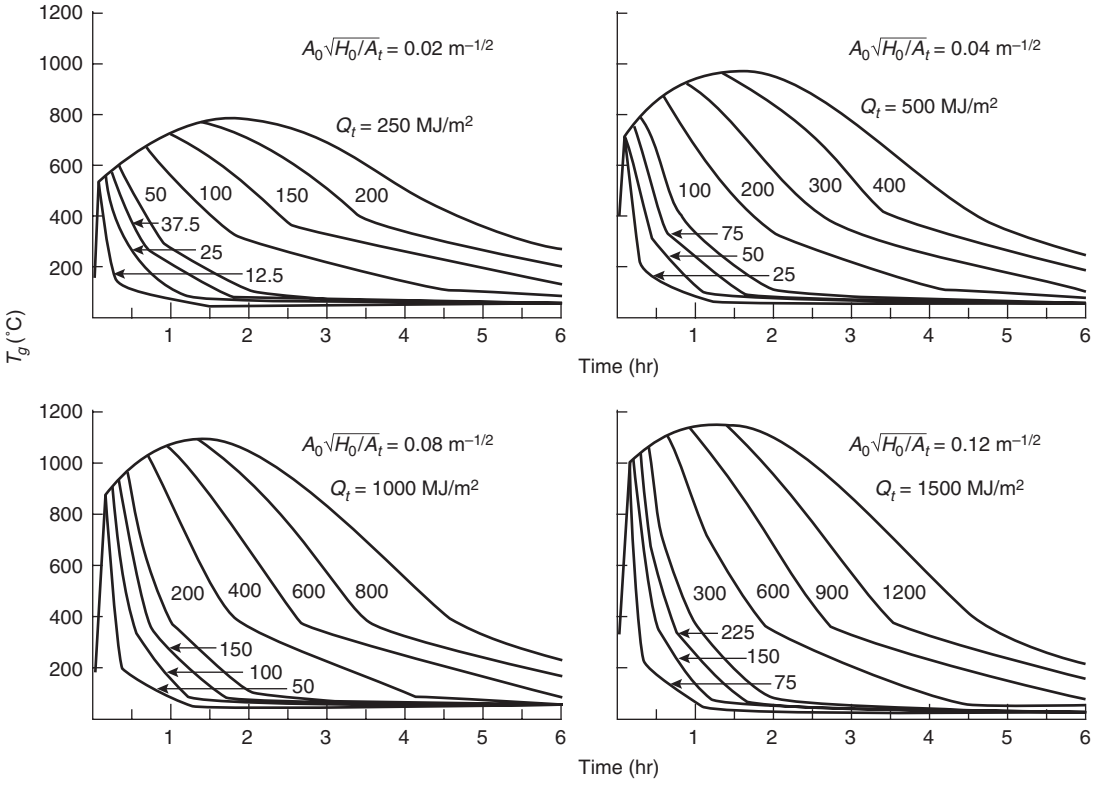

Figure 3-6.11. ***Examples of gas temperature-time curves of postflashover compartment fires for different values of the fire load density $\dot{Q}_t$ MJ per unit of total internal surface Area, A_t, and the opening factor $A_0\sqrt{H_0/A_t}$. Fire compartment, type A—from authorized Swedish standard specifications.[10]***

From this derivation, it is shown that the minimum $\dot{Q}$ required for flashover equals 0.4 $\dot{Q}_{stoich}$. Comparing these results with fire tests, Babrauskas found that the data falls within a range of $\dot{Q} = 0.3\dot{Q}_{stoich}$ to $\dot{Q} = 0.7\dot{Q}_{stoich}$. A best fit of the data suggests

$$\dot{Q} = 0.5\dot{Q}_{stoich}$$

which, substituting into Equation 55 yields

$$\dot{Q} = 750A_0\sqrt{H_0} \tag{56}$$

The 33 test fires used had energy release rates from 11 to 3840 kW, with fuels primarily of wood and polyurethane. Ventilation factors $A_0\sqrt{H_0}$ ranged from 0.03 to 7.51 m$^{5/2}$, and surface area to ventilation factor ratios

$$\frac{A_T}{A_0\sqrt{H_0}}$$

ranged from 9 to 65 m$^{-1/2}$.

Example of Babrauskas' method: Calculate the heat release rate necessary to cause flashover, using the method of Babrauskas. Assume the same room as in the McCaffrey et al. method example for predicting compartment fire temperatures. From Equation 56

$$\dot{Q} = 750A_0\sqrt{H_0}$$

where

A_0 = 1.08 m^2
H_0 = 1.8 m
$\dot{Q}$ = (750)(1.08)(1.8)$^{1/2}$ = 1087 kW

Method of McCaffrey, Quintiere, and Harkleroad

The method of McCaffrey, Quintiere, and Harkleroad for predicting compartment fire temperatures may be extended to predict the energy release rate of the fire required to result in flashover in the compartment.

Equation 11 can be rewritten as

$$\dot{Q} = \left[\sqrt{g}c_p\rho_\infty T_\infty^2\left(\frac{\Delta T_g}{480}\right)^3\right]^{1/2}(h_k A_T A_0\sqrt{H_0}) \tag{57}$$

Selecting an upper gas temperature of 522°C and ambient temperature of 295 K or ΔT_g = 500°C for flashover, and substituting values for the gravitational constant (g = 9.8 m/s^2), the specific heat of air (c_p = 1.0 kJ/kg·K), and the density of air (ρ_∞ = 1.18 kg/m^3), and rounding 607.8 to 610 yields

$$\dot{Q} = 610(h_k A_T A_0\sqrt{H_0})^{1/2} \tag{58}$$

where

h_k = effective heat transfer coefficient [(kW/m)/K]
A_T = total area of the compartment surfaces (m^2)
A_0 = area of opening (m^2)
H_0 = height of opening (m)

Using Equation 12 yields a slightly different value, 623.6 rounded to 620, of the leading coefficient because of the difference in the value used for the specific heat of air

$$\dot{Q} = 620(h_k A_T A_0 \sqrt{H_0})^{1/2} \quad (59)$$

The use of either 610 or 620 is acceptable within the accuracy of the expression.

Example of McCaffrey et al. method: Estimate the energy release rate required for flashover of a compartment. Assume the same room as in the McCaffrey et al. method example for predicting compartment fire temperatures. Assuming $\Delta T_g = 500°C$ as a condition for flashover, and air properties at 295 K, use Equation 45

$$\dot{Q} = 610(h_k A_T A_0 \sqrt{H_0})^{1/2}$$

where

$$h_k = \frac{k}{\delta} = \frac{0.48 \times 10^{-3}}{0.016} = 0.03 \text{ kW/m·K}$$

$A_T = 45.72 \text{ m}^2$
$A_0 = 1.08 \text{ m}^2$
$H_0 = 1.8 \text{ m}$

Therefore,

$$\dot{Q} = 610[(0.03)(45.72)(1.08)(\sqrt{1.8})]^{1/2}$$
$$= 860 \text{ kW}$$

Method of Thomas

Thomas uses the energy balance for the upper layer shown in Equation 7, where the gas flow rate out of the opening is approximated by[2]

$$\dot{m}_g \approx 0.5 A_0 \sqrt{H_0} \quad (60)$$

Thomas develops an expression for $\dot{q}_{\text{loss}}$ which assumes the area for the source of radiation for roughly cubical compartments is $A_T/6$:

$$\dot{q}_{\text{loss}} \approx h_c(T_g - T_w)\frac{A_T}{2} + \varepsilon\sigma(2T_g^4 - T_w^4 - T_{\text{flr}}^4)\frac{A_T}{6} \quad (61)$$

where

A_T = total area of the compartment-enclosing surfaces (m^2)
h_c = convective heat transfer coefficient ($kW/m^2 \cdot K$)
T_w = temperature of the upper walls (K)
T_{floor} = temperature of the floor (K)

From experimental data, Thomas developed an average for $\dot{q}_{\text{loss}}$ of 7.8 A_T. Using an upper layer temperature of 577°C or a ΔT_g of 600°C for flashover criterion and c_p = 1.26 kJ/kg·K yields an expression for the minimum rate of energy release for flashover:

$$\dot{Q} = 7.8A_T + 378A_0\sqrt{H_0} \quad (62)$$

Comparison of Methods for Predicting Flashover

Babrauskas has compared the effect of room wall area on the energy release required for flashover, using the above methods.[22] The results of his comparisons, along with some experimental data for rooms with gypsum board walls, are shown in Figure 3-6.12. The graph shows the energy required for flashover as a function of compartment wall area, both normalized by the ventilation factor $A_0\sqrt{H_0}$. Babrauskas observes that over the range of compartment sizes of most interest, all of the methods produce similar results. The method of McCaffrey et al. diverts from the others for small room sizes. Babrauskas notes that all of the methods are a conservative representation of the data.

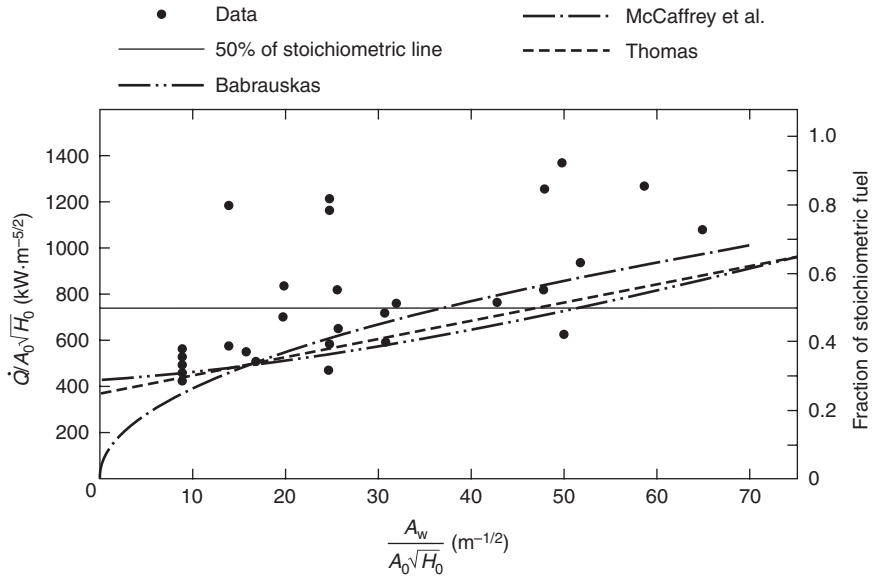

Figure 3-6.12. ***The effect of room wall area (gypsum walls) on the heat required for flashover.***

Nomenclature

A_T	total area of the compartment enclosing surfaces (m^2)
$A_{ceiling}$	area of compartment ceiling (m^2)
A_f	pool fire area (m^2)
A_{floor}	area of compartment floor (m^2)
$A_{openings}$	area of compartment openings (m^2)
A_{walls}	area of compartment walls (m^2)
c	specific heat of the wall (kJ/kg·K)
C_d	orifice constriction coefficient
c_p	specific heat of gas (kJ/kg·K)
D	compartment depth (m)
g	acceleration due to gravity, 9.8 m/s^2
h_c	convective heat transfer coefficient
Δh_c	effective heat of combustion of the fuel (kJ/kg)
h_g	heat transfer coefficient on the hot side of the wall (kW/m·K)
h_k	effective heat transfer coefficient (kW/m·K)
h_∞	heat transfer coefficient on the ambient side of the wall (kW/m·K)
H_o	opening height (m)
k	thermal conductivity of the wall (kW/m·K)
L	fire load, wood (kg)
m	mass of the gas in the compartment (kg/s)
$\dot{m}_a$	mass flow rate of air into an opening (kg/s)
$\dot{m}_g$	gas flow rate out the opening (kg/s)
$\dot{m}_f$	mass burning rate of fuel (kg/s)
$\dot{m}_{f,st}$	stoichiometric mass burning rate of fuel (kg/s)
$\dot{m}''_w$	mass per unit area of the wall (kg/m^2)
q_{loss}	net radiative and convective heat transfer from the upper gas layer (kW)
$\dot{Q}$	energy (heat) release rate of the fire (kW)
$\dot{Q}_{stoich}$	stoichiometric heat release rate (kW)
t	time (s)
t_p	thermal penetration time (s)
T_b	liquid boiling point (K)
T_{flr}	temperature of the floor (K)
T_g	temperature of the upper gas layer (K)
T_w	wall temperature (K)
T_∞	ambient temperature (K)
W	compartment width (m)
W_o	opening width (m)
X_d	height of the interface (m)
X_N	height of neutral plane (m)

Greek characters

δ	thickness of the wall (m)
ε	emissivity of the hot gas
ρ	density of the wall (kg/m^3)
ρ_∞	ambient air density (kg/m^3)
σ	Stefan-Boltzmann constant, 5.67×10^{-11} $kW/m^2 \cdot K^4$

Subscripts

a	air
b	boiling
ceiling	ceiling
d	thermal discontinuity
f	fuel
g	gas
floor	floor
loss	loss
N	neutral plane
o	opening
openings	openings
p	penetration
stoich	stoichiometric
T	total
w	wall
walls	walls
∞	ambient

Superscripts

$\cdot$	per unit time (s^{-1})
$''$	per unit area (m^{-1})

References Cited

1. D. Drysdale, "The Pre-Flashover Compartment Fire," *An Introduction to Fire Dynamics,* John Wiley and Sons, Chichester, England, pp. 278–303 (1985).
2. P.H. Thomas, "Testing Products and Materials for Their Contribution to Flashover in Rooms," *F. and Matls.,* 5, 3, pp. 103–111 (1981).
3. C. Huggett, "Estimation of Rate of Heat Release by Means of Oxygen Consumption Measurements," *F. and Matls.,* 4, 2, pp. 61–65 (1980).
4. J. de Ris, *Fire Radiation—A Review,* Tech. Report FMRC, RC78-BT-27, Factory Mutual Research Corporation, Norwood, pp. 1–41 (1978).
5. J.A. Rockett, "Fire Induced Gas Flow in an Enclosure," *Comb. Sci. and Tech.,* 12, pp. 165–175 (1976).
6. P.H. Thomas and A.J.M. Heselden, "Fully Developed Fires in Single Compartments," *Fire Research Note No. 923,* Fire Research Station, Borehamwood, England (1972).
7. K. Kawagoe, "Fire Behaviour in Rooms," Report of the Building Research Institute, Ibaraki-ken, Japan, No. 27 (1958).
8. P.H. Thomas and A.J.M. Heselden, "Fully Developed Fires in Single Compartments," *CIB Report No. 20,* A Co-operating Research Programme of the Conseil International du Batiment, Joint Fire Research Organization Fire Research Note 923/197.
9. M. Law, *Structural Engr.,* 61A, 1, p. 25 (1983).
10. S.E. Magnusson and S. Thelandersson, "Temperature-Time Curves of Complete Process of Fire Development. Theoretical Study of Wood Fuel Fires in Enclosed Spaces," *Civil Engineering and Building Construction Series No. 65,* Acta Polytechnica Scandinavia, Stockholm, Sweden (1970).
11. B.J. McCaffrey, J.G. Quintiere, and M.F. Harkleroad, "Estimating Room Fire Temperatures and the Likelihood of Flashover Using Fire Test Data Correlations," *Fire Tech.,* 17, 2, pp. 98–119 (1981).

12. J.G. Quintiere, "A Simple Correlation for Predicting Temperature in a Room Fire," *NBSIR 83–2712,* National Bureau of Standards, Washington, D.C. (June 1983).
13. J.R. Lawson and J.G. Quintiere, "Slide-Rule Estimates of Fire Growth," *NBSIR 85-3196,* National Bureau of Standards, Washington, D.C. (June 1985).
14. K.L. Foote, P.J. Pagni, and N.J. Alvares, "Temperature Correlations for Forced-Ventilated Compartment Fires," in *Proceedings of the First International Symposium,* International Association for Fire Safety Science, Hemisphere Publishing, pp. 139–148 (1986).
15. C. Beyler, " Analysis of Compartment Fires with Forced Ventilation," *Fire Safety Science—Proceedings of the Third International Symposium,* Elsevier Science, New York, pp. 291–300 (1991).
16. S. Deal and C. Beyler, "Correlating Preflashover Room Fire Temperatures," *J. of Fire Prot. Engr.*, 2, 2, pp. 33–88 (1990).
17. M. J. Peatross and C.L. Beyler, "Thermal Environmental Prediction in Steel-bounded Preflashover Compartment Fires," in *Fire Safety Science—Proceedings of the Fourth International Symposium,* International Association for Fire Safety Science, Boston, pp. 205–216 (1994).
18. V. Babrauskas, "A Closed-form Approximation for Post-Flashover Compartment Fire Temperatures," *F. Safety J.,* 4, pp. 63–73 (1981).
19. V. Babrauskas and R. B. Williamson, "Post-Flashover Compartment Fires: Basis of a Theoretical Model," *Fire and Matls.,* 2, 2, pp. 39–53 (1978).
20. V. Babrauskas, "COMPF2—A Program for Calculating Post-Flashover Fire Temperatures," *NBS TN 991,* National Bureau of Standards, Washington, D.C. (1979).
21. V. Babrauskas, "Estimating Room Flashover Potential," *Fire Tech.,* 16, 2, pp. 94–104 (1980).
22. V. Babrauskas, "Upholstered Furniture Room Fires—Measurements, Comparison with Furniture Calorimeter Data, and Flashover Predictions," *J. of F. Sci.,* 2, pp. 5–19 (1984).

CHAPTER 7

Zone Computer Fire Models for Enclosures

William D. Walton

Introduction

Computer programs are used in many areas of fire protection design, including suppression system design, smoke control system design, and egress analysis. The emphasis in this chapter is on zone computer fire models for enclosures. Zone fire models are computer programs designed to predict the conditions resulting from a fire in an enclosure. These models solve the equations based on the zone assumptions describing the fire-induced conditions within an enclosure.

Computer fire models can provide a faster and more accurate estimate of the impact of a fire and the measures used to prevent or control the fire than many of the methods previously used. While manual calculation methods provide good estimates of specific fire effects (e.g., prediction of time to flashover), they are not well suited for comprehensive analyses involving the time-dependent interactions of multiple physical and chemical processes present in developing fires.

The state of the art in computer fire modeling is changing rapidly. Understanding of the processes involved in fire growth is improving, and, thus, the technical basis for the models is improving. The capabilities, documentation, and support for a given model can change dramatically over a short period of time. In addition, computer technology itself (both hardware and software) is advancing rapidly. A few years ago, a large mainframe computer was required to use most of the computer fire models. Today, all of the zone fire models can be run on personal computers. Therefore, rather than provide an exhaustive review of rapidly changing state-of-the-art available computer models, the following discussion will focus on a representative selection. The reader is guided to References 1 and 2 for a comprehensive review of computer fire models.

Mr. William D. Walton is a research fire protection engineer with the Building and Fire Research Laboratory, National Institute of Standards and Technology.

Enclosure Fire Models

There are two major classes of computer models for analyzing enclosure fire development. *Stochastic* or *probabilistic models* generally treat fire growth as a series of sequential events or states. These models are sometimes referred to as *states transition models.* Mathematical rules are established to govern the transition from one event to another (e.g., from ignition to established burning). Probabilities are assigned to each transfer point based on analysis of relevant experimental data, historical fire incident data, and computer model results. For a complete discussion of stochastic models, see Section 3, Chapter 16.

In contrast, *deterministic models* represent the processes encountered in a compartment fire by interrelated mathematical expressions based on physics and chemistry. These models may also be referred to as *room fire* models, *computer fire* models, or *mathematical fire* models. Ideally, such models represent the ultimate capability: discrete changes in any physical parameter could be evaluated in terms of the effect on fire hazard. While the state of the art in understanding fire processes will not yet support the *ultimate* model, a number of computer models are available that provide reasonable estimates of selected fire effects.

The newest type of deterministic fire model is the *field* model. This type of model solves the fundamental equations of mass, momentum, and energy for each element in an enclosure space that has been divided into a grid of smaller units. A complete discussion of field modeling can be found in Section 3, Chapter 8. Although field model technology and use have advanced rapidly in recent years, it should be noted that field models require substantial computer resources and are relatively complex to use.

The most common type of physically based fire model is the *zone* or *control volume* model, which solves the conservation equations for distinct and relatively large regions (control volumes). A complete discussion of the fundamental principles behind the zone fire model formulation can be found in Section 3, Chapter 5. A number of

zone models exist, varying to some degree in the detailed treatment of the fire phenomena. The dominant characteristic of this type of model is that it divides the room(s) into a hot, upper layer and a cooler, lower layer. (See Figure 3-7.1.) The model calculations provide estimates of key conditions for each of the layers as a function of time. Zone modeling has proved to be a practical method for providing estimates of fire processes in enclosures.

The beginnings of pre-flashover zone fire modeling can be traced to the mid-1970s with the publication of a description of the fundamental equations by Quintiere.[3] Based on these equations, the first zone fire model published was RFIRES by Pape and Waterman,[4] followed shortly by the HARVARD model by Emmons and Mitler.[5] The development of zone fire models was facilitated both by the advancement in the understanding of the basic physics of fire growth in a compartment and advances in, and the availability of, mainframe computers. Following the publication of these two models a number of zone fire models for mainframe computers were introduced. In 1985 the first zone model, ASET-B, written specifically for the newly available IBM-compatible personal computers, was introduced by Walton.[6] Since that time additional models have been introduced, and most of the models written for mainframe computers have been converted for use in personal computers.

No zone fire model is *best* for all applications. The selection of a zone fire model for a particular application depends on a number of factors. While most of the zone fire models are based on the same fundamental principles, there is significant variation in features among the different models. The decision to use a model should be based on an understanding of the assumptions and limitations for the particular model. In general the more detailed the model outputs, the more extensive the model inputs, and the greater the computer execution time required. When using any computer fire model, it is always a good idea to test the sensitivity of the model outputs to changes in model inputs. If small changes in model inputs result in large changes in model outputs, the user must exercise great care in selecting the input values.

A key issue in selecting a model is model validation. Comparison of model results with experimental data is valuable for determining the applicability of a model to a particular situation. Comparisons of model results with experimental data are limited, and the number of comparisons varies widely among the models. The model user should carefully examine model validation comparisons before selecting a model. Frequently, experienced model users will use more than one model to evaluate a particular situation. If several models provide similar results this can increase the confidence in the results. Similar results do not, however, guarantee that the results accurately represent the physical conditions being modeled, since most of the zone fire models are based on the same basic assumptions.

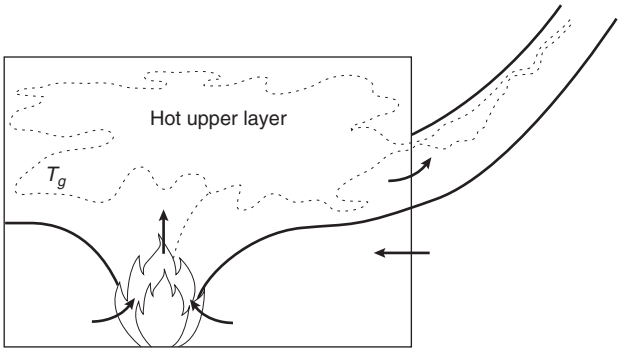

Figure 3-7.1. ***Two-layer model with no exchange between layers except the plume.***

Overview of Representative Zone Fire Models

ASET Computer Program

ASET (available safe egress time) is a program for calculating the temperature and position of the hot upper smoke layer in a single room with closed doors and windows. ASET can be used to determine the time to the onset of hazardous conditions for both people and property. The required program inputs are the heat-loss fractions, the height of the fuel above the floor, criteria for hazard and detection, the room ceiling height, the room floor area, a heat release rate, and (optional) species generation rate of the fire. The program outputs are the temperature, thickness, and (optional) species concentration of the hot upper smoke layer as a function of time, and the time to hazard and detection. ASET can examine multiple cases in a single run. ASET was written in FORTRAN by Cooper and Stroup.[6]

ASET-B Computer Program

ASET-B is a program for calculating the temperature and position of the hot upper smoke layer in a single room with closed doors and windows. ASET-B is a compact version of ASET, designed to run on personal computers. The required program inputs are a heat-loss fraction, the height of the fire, the room ceiling height, the room floor area, the maximum time for the simulation, and the rate of heat release of the fire. The program outputs are the temperature and thickness of the hot upper smoke layer as a function of time. Species concentrations and time to hazard and detection, calculated by ASET, are not calculated in the compact ASET-B version. ASET-B was written in BASIC by Walton.[6]

COMPBRN III Computer Program

COMPBRN III is primarily used in conjunction with probabilistic analysis for the assessment of risk in the nuclear power industry. The model is based on the assumption of a relatively small fire in a large space, or a fire involving large fuel loads early during the pre-flashover fire growth period. The model's strengths are (1) emphasis on the thermal response of elements within the enclosure to a fire within the enclosure, and (2) model simplicity. The temperature profile within each element is computed,

and an element is considered ignited or damaged when its surface temperature exceeds the user-specified ignition or damage temperature. The model outputs include the total heat release rate of the fire, the temperature and depth of the hot gas layer, the mass burning rate for individual fuel elements, the surface temperatures, and the heat flux at user-specified locations. COMPBRN III was written by Siu et al.[7]

COMPF2 Computer Program

COMPF2 is a computer program for calculating the characteristics of a post-flashover fire in a single building compartment, based on fire-induced ventilation through a single door or window. It is intended both for performing design calculations and for the analysis of experimental burn data. Wood, thermoplastics, and liquid fuels can be evaluated. A comprehensive output format is provided that gives gas temperatures, heat-flow terms, and flow variables. The documentation includes input instructions, sample problems, and a listing of the program. The program was written in FORTRAN by Babrauskas.[8]

CSTBZ1 Computer Program

CSTBZ1 is a computer program for post-flashover fires, based on similar basic assumptions as those of COMPF2. The equations of mass and energy conservation are written without neglecting the fuel source term, and several vertical openings in a room can be considered. The equation of heat diffusion into the walls is solved either by a classical explicit finite difference method, or by a new modal approach that offers the capability of storing in a file a few numbers characterizing a given wall, leading to a rapid calculation of the superficial wall temperatures. A sophisticated numerical algorithm was used to solve the equations through uncoupling. The program was written by Curtat and Bodart.[9]

CFAST Computer Program

The CFAST (consolidated model of fire growth and smoke transport) is an upgrade of the FAST program[10] and incorporates numerical solution techniques originally implemented in CCFM program.[11] FAST is now the graphical user interface program for CFAST. CFAST is a multi-room model that predicts within a structure resulting from a user-specified fire. CFAST version 4.0.1 can accommodate up to 30 compartments with multiple openings between compartments and to the outside. The required program inputs are the geometrical data describing the compartments and connections; the thermophysical properties of the ceiling, walls, and floors; the fire as a rate of mass loss; and the generation rates of the products of combustion. The programs outputs are the temperature and thickness of, and species concentrations in, the hot, upper layer and the cooler, lower layer in each compartment. Also given are the surface temperatures and heat transfer and mass flow rates. CFAST also includes mechanical ventilation, a ceiling jet algorithm, capability of multiple fires (up to 30), heat transfer to targets, detection and suppression systems, and a flame spread model. CFAST was written in FORTRAN by Jones, et al.[12,13]

BRANZFIRE Computer Program

BRANZFIRE is a zone fire model for predicting the fire environment in an enclosure, resulting from a room-corner fire involving walls and ceilings. The zone fire model uses conservation equations based on those found in CFAST.[12] BRANZFIRE predicts ignition, flame spread, and the resultant heat released by the wall and ceiling lining material subjected to a burner fire. The model considers upward flame spread on the walls and beneath the ceiling, lateral flame spread on the walls, and downward flame spread from the ceiling jet. Wall and ceiling flame spread properties are computed from cone calorimeter data. Program outputs include layer height, species concentrations, gas temperatures, visibility, wall temperatures, and heat release rate. BRANZFIRE was written in Visual Basic by C. Wade.[14,15,16]

JET Computer Program

JET is a two-zone single compartment model where the compartment is enclosed by a combination of draft curtains and walls. The ceiling may contain fusible links and vents where the vents operate in response to the fusing of the links. The ceiling vents remove hot, upper layer gas from the compartment. The fire is characterized by a time-dependent heat release rate, a time-dependent radiative fraction, and either a constant or variable fire diameter, which is determined using a heat release rate per unit area for the burning material. Inputs also include the thermal properties of the ceiling. Program outputs include the ceiling jet temperature and velocity, link temperature, and activation times. JET was written in FORTRAN by W. D. Davis.[17]

FIRST Computer Program

FIRST is the direct descendant of the HARVARD V[5] program developed by Emmons and Mitler. The program predicts the development of a fire and the resulting conditions within a room given a user-specified fire or user-specified ignition. It predicts the heating and possible ignition of up to three targets. The required program inputs are the geometrical data describing the rooms and openings, and the thermophysical properties of the ceiling, walls, burning fuel, and targets. The generation rate of soot must be specified, and the generation rates of other species may be specified. The fire may be entered either as a mass loss rate or in terms of fundamental properties of the fuel. Among the program outputs are the temperature and thickness of, and species concentrations in, the hot, upper layer and the cooler, lower layer in each compartment. Also given are surface temperatures and heat transfer and mass flow rates. The FIRST program was written in FORTRAN by Mitler and Rockett.[18]

FPETOOL Computer Program

FPETOOL is the descendent of the FIREFORM program.[19] It contains a computerized selection of relatively simple engineering equations and models useful in estimating the potential fire hazard in buildings. The calculations in FPETOOL are based on established engineering

relationships. The FPETOOL package addresses problems related to fire development in buildings and the resulting conditions and response of fire protection systems. The subjects covered include smoke filling in a room, sprinkler/detector activation, smoke flow through (small) openings, temperatures and pressures developed by fires, flashover and fire severity predictions, fire propagation (in special cases), and simple egress estimation. The largest element in FPETOOL is a zone fire model called FIRE SIMULATOR. FIRE SIMULATOR is designed to estimate conditions in both pre- and post-flashover enclosure fires. The inputs include the geometry and material of the enclosure, a description of the initiating fire, and the parameters for sprinklers and detectors being tracked. The outputs include the temperature and volume of the hot smoke layer; the flow of smoke from openings; the response of heat-actuated detection devices, sprinklers, and smoke detectors; oxygen, carbon monoxide, and carbon dioxide concentrations in the smoke; and the effects of available oxygen on combustion. FPETOOL was written in BASIC by Nelson.[20]

LAVENT Computer Program

LAVENT is a program developed to simulate the environment and the response of sprinkler elements in compartment fires with draft curtains and fusible-link-actuated ceiling vents. The zone model used to calculate the heating of the fusible links includes the effects of the ceiling jet and the upper layer of hot gases beneath the ceiling. The required program inputs are the geometrical data describing the compartment, the thermophysical properties of the ceiling, the fire elevation, the time-dependent heat release rate of the fire, the fire diameter or the heat release rate per unit area of the fire, the ceiling vent area, the fusible-link response time index (RTI) and activation temperature, the fusible-link positions along the ceiling, the link assignment to each vent, and the ambient temperature. A maximum of 5 ceiling vents and 10 fusible links are permitted in the compartment. The program outputs are the temperature and height of the hot layer, the temperature of each link, the ceiling jet temperature and velocity at each link, the radial temperature distribution along the interior surface of the ceiling, the activation tie of each link, and the area opened. LAVENT was written in FORTRAN.[21]

WPI/FIRE Computer Program

WPI/FIRE is a direct descendant of the HARVARD V[5] and FIRST[18] programs. It includes all of the features of the HARVARD program version 5.3 and many of the features of the FIRST program. WPI/FIRE also includes the following additional features: improved input routine, momentum-driven flows through ceiling vents, two different ceiling jet models for use in detector activation, forced ventilation for ceiling and floor vents, and an interface to a finite difference computer model for the calculation of boundary surface isotherms and hot spots. The WPI/FIRE program was written in FORTRAN by Satterfield and Barnett,[22] and additions to the program continue to be developed by graduate students at the Center for Fire Safety Studies, Worcester Polytechnic Institute.

References Cited

1. R. Friedman, *An International Survey of Computer Models for Fire and Smoke,* 2nd ed. (Dec. 1991). Available from Library, Factory Mutual Research Corporation, 1151 Boston-Providence Turnpike, Norwood, MA 02062.
2. R. Friedman, "An International Survey of Computer Models for Fire and Smoke," *Jour. of Fire Prot. Engr.,* 4, 3, pp. 83–92 (1992).
3. J. Quintiere, "Growth of Fires in Building Compartments," ASTM STP 614, American Society for Testing and Materials, Philadelphia, PA (1977).
4. R. Pape, T.E. Waterman, and T.V. Eichler, "Development of a Fire in a Room from Ignition to Full Room Involvement—RFIRES," *NBS-GCR-81-301,* National Bureau of Standards, Washington (1981).
5. H.E. Mitler, "The Harvard Fire Model," *F. Safety J.,* 9, pp. 7–16 (1985).
6. W.D. Walton, "ASET-B A Room Fire Program for Personal Computers," *NBSIR 85-3144,* National Bureau of Standards, Washington, DC (1985).
7. V. Ho, N. Siu, and Apostolakis, "COMPBRN III—A Fire Hazard Model for Risk Analysis," *Fire Safety J.,* 13, 2–3, pp. 137–154 (1988).
8. V. Babrauskas, "COMPF2—A Program for Calculating Post-Flashover Fire Temperatures," NBS TN 991, National Bureau of Standards, Washington, DC (1979).
9. M.R. Curtat and X.E. Bodart, *1st Symposium International Association for Fire Safety Science,* Hemisphere Publications, Gaithersburg, MD, p. 637 (1986).
10. W.W. Jones, "A Multicompartment Model for the Spread of Fire, Smoke and Toxic Gases," *F. Safety J.,* 9, pp. 55–79 (1985).
11. G.P. Forney and L.Y. Cooper, "The Consolidated Compartment Fire Model (CCFM) Computer Application. VENTS, Parts I, II, III, IV," *NISTIR,* National Institute of Standards and Technology, Gaithersburg, MD (1990).
12. W.W. Jones, G.P. Forney, R.D. Peacock, and P.A. Reneke, "A Technical Reference for CFAST: An Engineering for Estimating Fire and Smoke Transport," TN-1431, National Institute of Standards and Technology, Gaithersburg, MD (2000).
13. R.D. Peacock, P.A. Reneke, W.W. Jones, R.W. Bukowski, and G.P. Forney, "A User's Guide for FAST: Engineering Tools for Estimating Fire Growth and Smoke Transport," SP-921, 2000 Edition, National Institute of Standards and Technology, Gaithersburg, MD (2000).
14. C.A. Wade, D. LeBlanc, J. Ierardi, and J.R. Barnett, "A Room-Corner Fire Growth & Zone Model for Lining Materials," Second International Conference on Fire Research and Engineering (ICFRE2), National Institute of Standards and Technology and Society of Fire Protection Engineers, Gaithersburg, MD, pp. 106–117 (1998).
15. C. Wade and J. Barnett, "A Room-Corner Fire Model Including Fire Growth on Linings and Enclosure Smoke-Filling," *J. of Fire Prot. Engr.,* 8(4), pp. 183–193 (1997).
16. C. Wade, "Branzfire-Engineering Software for Evaluating Hazard of Room Lining Materials," in *Conference Proceedings on the Eight International Interflam Conference,* Interscience Communications Limited, London, pp. 1147–1152 (1999).
17. W.D. Davis, "The Zone Fire Model Jet: A Model for the Prediction of Detector Activation and Gas Temperature in the

Presence of a Smoke Layer," *NISTIR 6324,* National Institute of Standards and Technology, Gaithersburg, MD (1999).

18. H.E. Mitler and J.A. Rockett, "User's Guide to FIRST, A Comprehensive Single-Room Fire Model," *CIB W14/88/22,* National Bureau of Standards, Gaithersburg, MD (1987).
19. H.E. Nelson, "FIREFORM—A Computerized Collection of Convenient Fire Safety Computations," *NBSIR 86-3308,* National Bureau of Standards, Gaithersburg, MD (1986).
20. H.E. Nelson, "FPETOOL: Fire Protection Engineering Tools for Hazard Estimation," *NISTIR 4380,* National Institute of Standards and Technology, Gaithersburg, MD (1990).
21. Y.L. Cooper, "Estimating the Environment and the Response of Sprinkler Links in Compartment Fires with Draft Curtains and Fusible-Link-Actuated Ceiling Vents Theory," *F. Safety J.,* 16, pp. 137–163 (1990).
22. D.B. Satterfield and J.R. Barnett, "User's Guide to WPI-FIRE Version 2 (WPI-2)—A Compartment Fire Model," Worcester Polytechnic Institute, Center for Fire Safety Studies, Worcester, MA (Aug. 1990).

Additional Readings

L.Y. Cooper and D.W. Stroup, "ASET—A Computer Program for Calculating Available Safe Egress Time," *F. Safety J.,* 9, pp. 29–45 (1985).

B. Hagglund, "A Room Fire Simulation Model," *FOA C 20501-D6,* National Defense Research Institute, Sweden (June 1983).

B. Hagglund, "Simulating the Smoke Filling in Single Enclosures," *FOA C 20513-D6,* National Defense Research Institute, Sweden (October 1983).

J.A. Swartz et al., *Final Technical Report on Building Fire Simulation Model,* Vols. I and II, National Fire Protection Association, Quincy (1983).

T. Tanaka, "A Model of Multiroom Fire Spread," *NBSIR 83-2718,* National Bureau of Standards, Washington (1983).

E.E. Zukoski and T. Kubota, "Two-Layer Modeling of Smoke Movement in Building Fires," *F. and Matls.,* 4, 1, p. 17 (1980).

CHAPTER 8

Modeling Enclosure Fires Using CFD

Geoff Cox and Suresh Kumar

Introduction

It was in the early 1920s, that Lewis Richardson first demonstrated the feasibility of solving, using numerical methods, the governing equations of fluid flow.[1] His purpose was weather prediction, but it was not for another 50 years that the technology we now know as *computational fluid dynamics* (or *CFD*) began to emerge as a general tool for the analysis of the full breadth of fluid flow problems, including those associated with fire.

Solution of the Reynolds-averaged Navier-Stokes equations using numerical simulation tools has now become commonplace in the design and analysis of many practical engineering problems. This advance has been driven by the availability of commercial CFD software together with massive increases in computer speed accompanied by ever-reducing hardware costs.

This technology evolved outside the fire community and has been imported into it, in contrast to zonal models (Section 3, Chapter 7), which were developed within this discipline. This has far-reaching implications since the same basic CFD technology is also being exploited, developed, tested, and verified for an extremely wide range of applications. Problems and successes demonstrated elsewhere can often be exploited in the fire context, although as we will see, many issues are unique to fire and can only be the responsibility of the fire community. But the same tools that are used to study, for example, heat transfer in an internal combustion engine can also be used to explore, for example, indoor air movement, early detection of smoke, and the dispersion of combustion products within the atmospheric boundary layer.

The study of fire spread inside buildings and indeed other enclosures such as ships and aircraft is another such application. CFD provides the potential to study these extremely complicated problems that are only partially amenable to reduced-scale physical modeling because of the very large number of nondimensional groups that need to be preserved to simulate full-scale behavior.

The starting point for CFD models is the "exact" system of coupled partial differential equations that describe the balance between the competing influences on the transport of mass, momentum, chemical species, and energy within the fire and throughout the enclosure containing it. However, rigorous solution of the "exact" equations, resolving fully the length and time scales that occur in the flows associated with the turbulent combustion characteristic of fire, is still beyond the capabilities of even the largest computers currently available. To capture the details of the chemical reaction zone in a fire would require a characteristic mesh size below 1 mm. As a consequence it is necessary to simplify the system of exact equations by some form of modeling.

Most practical approaches (see Reference 2, for example) solve the so-called Reynolds-averaged Navier-Stokes (RANS) equations.* These are obtained from the exact equations by first time-averaging them and then solving the resulting continuous equations in discretized form over the domain of interest. The full rigor of the initial balance equations is now lost because of problems associated with the terms that result from averaging the turbu-

Geoff Cox is technical director of the U.K. Fire Research Station where he has been conducting research since 1973. He is visiting professor at Cranfield University and chairman of the International Standards Technical Committee on Fire Safety.

Dr. Suresh Kumar joined the U.K. Fire Research Station in 1980, and heads the CFD fire-modeling team. His major research interests are in fire science, fire modeling, and fire safety engineering. He has pioneered the development of the CFD models JASMINE and TUNFIRE for fire safety design and hazard assessment.

*A density-weighted variant of Reynolds averaging (Favre averaging) is often necessary for the treatment of regions where density fluctuations have a significant effect. This is not usually a serious issue in smoke movement studies but can be close to the fire source. This treatment is not presented here but will be found, for example, in Cox.[1]

lent transport processes. These terms, which describe the contributions of turbulent mixing and its influences on chemical kinetics and radiant heat transfer, need to be modeled. In most practical computer models this is achieved by use of the two-equation $k \sim \varepsilon$ turbulence model (k is the kinetic energy of the turbulence and ε is its rate of dissipation), and it is here where full rigor is lost.

An alternative approach is to exploit large-eddy simulation techniques,[3,4] where the larger turbulent vortices are simulated rigorously but the finer-scale turbulent motions are either modeled in a similar fashion to RANS modeling[4] or perhaps ignored entirely.[3] It is important to realize that neither of these approaches capture the length and times scales associated with the details of the combustion processes involved. These can only be described by the submodels employed.

A full, direct numerical simulation that solves the exact equations rigorously currently remains beyond the scope of problems of practical interest although research with this approach is growing apace,[5] certainly improving our understanding of fine-scale behavior.

In addition to the uncertainties associated with the modeling of turbulent flow, others are also introduced as a result of the numerical methods used to solve the continuous equations no matter which strategy is adopted. Recognition of the limitations in each of these departures from rigor is essential for the successful practical exploitation of CFD to solve fire problems.

It should be recognized that this topic, like most involving computation, is rapidly evolving and that this chapter can represent only a snapshot in time of current capability. Where 1000 mesh points represented the upper limit of capability for discretization in the early 1980s, one or two thousand times that number would, as we write, be quite routine! However the principles will be largely unchanged although their outreach will grow with time. While treatment of smoke movement problems is more mature, there is considerable research in progress at the time of writing on some of the more detailed issues relating to the combustion science involved (e.g., flame spread, oxygen vitiation) where the challenges are prodigious indeed.

This chapter does not dwell on the theoretical underpinning to CFD. This is too large a topic to be dealt with in this brief and hopefully practical chapter. Such detail will be found in very many textbooks and reviews on the topic. Cox,[2,6] for example, specifically addresses these issues in the fire context, while many (Patankar,[7] and Versteeg and Malalasekera,[8] for example) discuss them in a more general sense. Kumar[9] provides a full review of turbulence modeling and its application to fire problems. The chapter here places more emphasis on the use of CFD in a practical environment and on fire-specific issues that are essential for proper exploitation of the CFD methodology.

Currently CFD is being used by the practicing fire protection engineer primarily for the assessment of smoke control problems. Most of what is presented here is directed toward assisting in the proper use of the methodology for that purpose. However, some information is also provided on more advanced applications so that the potential of the methodology can be appreciated.

The Principles

The simplifications and assumptions that are essential in the synthesis of zone fire modeling as exemplified in Section 3, Chapter 7 are unnecessary when using the very different philosophy of field (or CFD) modeling. Instead, the full, partial differential equation set, expressing the principles of local conservation of mass, momentum, energy, and species, the *field equations*, are solved using numerical methods subject only to the boundary conditions of the problem.

Solutions are obtained on a numerical grid of typically hundreds of thousands or millions, if they can be afforded, of elementary control volumes filling the domain of interest.

The numerical mesh is chosen to provide acceptably accurate approximations to the field equations. Unlike the few large, physically contrived control volumes of the zonal models, field models ensure local conservation of the governing equations in the many thousands or millions of relatively small control volumes situated for the convenience of numerical approximation.

Whether a fire plume is deflected from the vertical by a door jet through an enclosure opening and as a consequence entrains extra air or, perhaps, rises only part way to the ceiling before losing its buoyancy should be determined by the solution of the equations and not by prior assumption.

This chapter concentrates on the Reynolds-averaged approach to CFD modeling. This engineering approach, pioneered in the wider context by Spalding and his coworkers,[10] has made particular use of the two-equation $k \sim \varepsilon$ turbulence model to provide a predictive capability for the treatment of practical problems. This is the approach adopted by all commercial packages to date, although some offer alternatives; the $k \sim \varepsilon$ model still remains the industry workhorse. Here the physical and chemical processes occurring at length scales less than that of the numerical grid are replaced by approximate models that attempt to describe their subgrid behavior.

The Modeling of Turbulent Flow

Before we go on to describe CFD modeling any further, it is important to understand the choices available for the treatment of turbulence in these problems. Turbulence is generated at large scale, typically of the order of a few meters and representative of physical lengths associated with the generation of shear layers in the flow—maybe a room or doorway dimension or a fire width. Without any further stimulus, this turbulent energy decays, and with it turbulent eddy sizes become smaller and smaller until they are small enough for the energy to be dissipated by viscous forces. It is at these finest length scales that fuel/air mixing takes place and at which chemical reaction occurs.

A schematic spectral plot (Figure 3-8.1) of turbulent energy with inverse eddy dimension illustrates these different scales. A notional fine-wire thermocouple trace from within the fire, as shown in Figure 3-8.2, presents this same information in a different form.

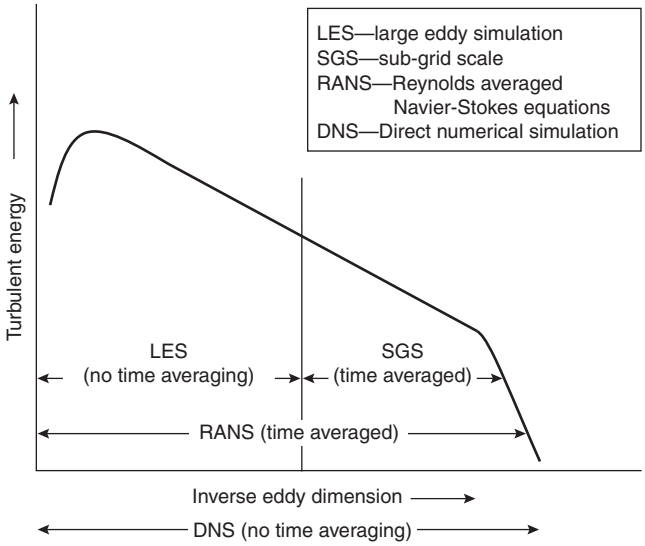

Figure 3-8.1. ***Schematic representation of turbulent energy spectrum showing different modeling treatments.***

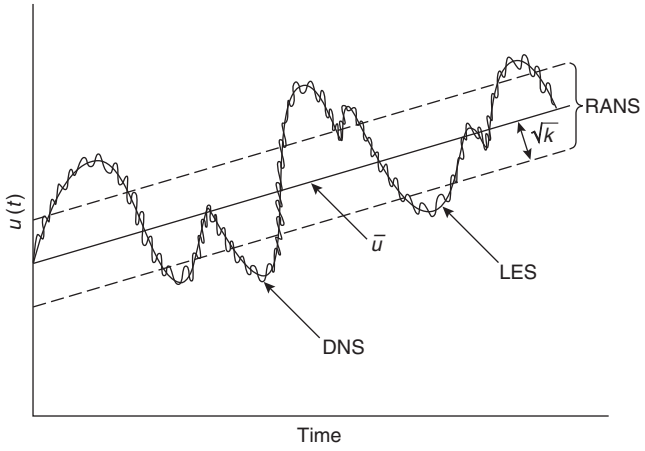

Figure 3-8.2. ***Schematic representation of different treatments for turbulence.***

We can use these illustrations to explain different treatments that the CFD methodology can employ for fire simulation purposes. The RANS model solves only for time-averaged properties. The very important influences of turbulent fluctuations are dealt with by turbulence models, which encompass influences over the whole length-scale range by replacing the very complex correlations between fluctuating variables, using modeled equations. Although turbulent fluctuations are time averaged, the time evolution of the averages is followed in much the same way as a thermocouple of a relatively long time constant measures an experimental average.

The large-eddy simulation (LES) avoids time averaging of fluctuations at scales larger than the mesh size. Thus the larger eddy influences are rigorously represented. However, below the mesh size, certainly at length scales associated with the chemical reaction, fluctuations are either totally ignored[3] or perhaps time averaged in a similar way to that used in the RANS approach.[4] The thermocouple analogue here is of a much shorter time constant than previously, able to follow some larger fluctuations but not the small-scale detail.

Finally and not yet possible at practical scale, because of computing limitations, is for the simulation to follow fluctuations at all length scales right down to those associated with viscous dissipation and without any time averaging. The thermocouple analogue here is of a thermocouple of zero time constant. This technique, generally referred to as direct numerical simulation (DNS), will remain the preoccupation of the research community for many years to come.

The Governing Equations for the RANS Approach

The governing equations for the RANS models start with the set of time-mean, turbulence-modeled conservation equations for mass, momentum, energy, and species together with transport equations for the turbulence variables k and ε. These equations (eight and more) can be conveniently written in terms of a general time-mean variable, ϕ:

$$\frac{\partial}{\partial t}(\rho\phi) + \frac{\partial}{\partial x_j}(\rho u_j \phi) = \frac{\partial}{\partial x_j}\left(\Gamma_\phi \frac{\partial \phi}{\partial x_j}\right) + S_\phi \qquad (1)$$

This equation "simply" describes the principles of conservation for each of the many elementary control volumes filling the domain of interest. The first term represents the time rate of change of the property within the volume; the second, the influences of convection on the volume; the third, the influences of diffusion; and the last term, any generation or destruction involved. This last term might, for example, in the case of enthalpy conservation, describe radiant heat exchanges with adjacent volumes and surfaces. It is also this term that describes the buoyancy forces in the momentum equations and the effects of buoyancy on turbulent mixing in the k and ε equations.

Equation 1 describes momentum conservation when ϕ stands for u_i, energy conservation when ϕ stands for h, and mass continuity when $\phi = 1$. It also describes the transport of turbulence kinetic energy, when $\phi = k$, and its dissipation rate, when $\phi = \varepsilon$, in addition to the conservation of the mixture fraction when $\phi = f$, and the conservation of the species i when $\phi = Y_i$. The Γ_ϕ term is an effective exchange coefficient appropriate to ϕ, which includes the effects of both molecular and turbulent diffusion. S_ϕ is a source term.

With the conservation equations written in this form, the meaning of Γ_ϕ and S_ϕ for each property is given in Table 3-8.1. Each variable is a time average of the true fluctuating variable.

The values of the empirical constants C_1, C_2, C_μ, σ_k, and σ_t are those recommended by Jones and Whitelaw[11] and obtained from detailed studies of nonbuoyant shear flows. It has been common practice to use these in application to enclosure fire problems. Some discussion of these constants in the fire context will be found in Cox.[2]

Table 3-8.1 ***Effective Exchange Coefficients and Source Terms in Generic Transport Equation for ϕ (Equation 1).***

Transport of	ϕ	Γ_ϕ	S_ϕ
Mass	1	0	0
Momentum	u_i	μ_{eff}	$-\frac{\partial p}{\partial x_i} + \frac{\partial}{\partial x_j}\left[\mu_{\text{eff}}\frac{\partial u_j}{\partial x_i}\right] + g_i$
Enthalpy	h	$\frac{\mu_{\text{eff}}}{\sigma_h}$	$\frac{\partial p}{\partial t} + S_{h,\text{rad}}$
Kinetic energy of turbulence	k	$\frac{\mu_{\text{eff}}}{\sigma_k}$	$G_k + G_B - \rho\varepsilon$
Rate of dissipation of turbulent energy	ε	$\frac{\mu_{\text{eff}}}{\sigma_\varepsilon}$	$\frac{\varepsilon}{k}[(G_k + G_B)C_1 - C_2\rho_\varepsilon]$
Mixture fraction	f	$\frac{\mu_{\text{eff}}}{\sigma_f}$	0
Mass fraction of fuel	Y_f	$\frac{\mu_{\text{eff}}}{\sigma_Y}$	S_f

where $G_k = \mu_t\left(\frac{\partial u_i}{\partial x_j} + \frac{\partial u_j}{\partial x_i}\right)\frac{\partial u_i}{\partial x_j}$

$G_B = -\beta g\frac{u_t}{\sigma_t}\frac{\partial T}{\partial x_j}$

$\mu_{\text{eff}} = \mu_l + \mu_t$

$\mu_t = C_\mu\rho\frac{k^2}{\varepsilon}$

and

$C_1 = 1.44$, $C_2 = 1.92$, $C_\mu = 0.09$, $\sigma_k = 1.0$, $\sigma_\varepsilon = 1.3$, $\sigma_t = \sigma_h = \sigma_f = \sigma_Y = 0.7$.

We will return later to the issues associated with the influence of buoyancy on turbulent mixing.

Many fire engineers will exploit one of the general-purpose commercial CFD packages currently available in which all the above detail has been coded for them and they may feel that they have no need for this detail. However, extremely important for the fire application is the G_B term. It is this that describes the influences of fire-generated density gradients on turbulent mixing.

In the bulk flow, buoyancy forces disturb the simple picture of isotropic turbulence assumed by the traditional $k \sim \varepsilon$ model. Turbulent mixing in a rising plume is enhanced by buoyancy while in a stably stratified ceiling layer it will be inhibited. In this respect the modeling of turbulent mixing in compartment fires requires particular attention. The production term in the k equation associated with the buoyancy forces,

$$G_B = -\beta g\frac{\mu_t}{\sigma_t}\frac{\partial T}{\partial x_j} \tag{2}$$

takes on opposite signs in regions of stable and unstable stratification. This term, which describes the exchange of turbulent kinetic energy with potential energy, represents a source in the unstable situation of the fire plume, where heated gases emerge beneath cool gases, but it becomes a sink in the hot gas ceiling layer, where the opposite occurs.

It is important that the fire-engineering practitioner ensures that this term is either activated or is coded for when using commercial codes. An illustration of the consequence of omitting this term is graphically illustrated by Figure 3-8.3, taken from Markatos et al.[12]

This treatment for turbulent buoyant mixing has proved its worth in many comparisons of predictions with experimental data and its success can be measured particularly by, for example, the "blind" simulations of Miles et al.[13] These will be discussed in the section on validation below.

Special Treatment for Flow Close to Walls

The CFD model solves discretized forms of the continuous Equation set 1 throughout the domain of study subject to the boundary conditions for the problem. To cope with regions very close to solid surfaces such as walls or obstructions where the flow changes from turbulent to laminar, the RANS models use universal wall laws to describe this transition. This is necessary because very close gridding in these regions would be required to capture this behavior numerically thus substantially increasing computational cost and effort.

Generally, the turbulent boundary layer can be split into a laminar, viscous sublayer closest to the wall ($y^+ < 5$), an inertial log-law sublayer ($30 < y^+ < 400$) where the flow is fully turbulent but where the shear stress can be considered uniform, and between them ($5 < y^+ < 30$) a region of transition between laminar and turbulent flow.

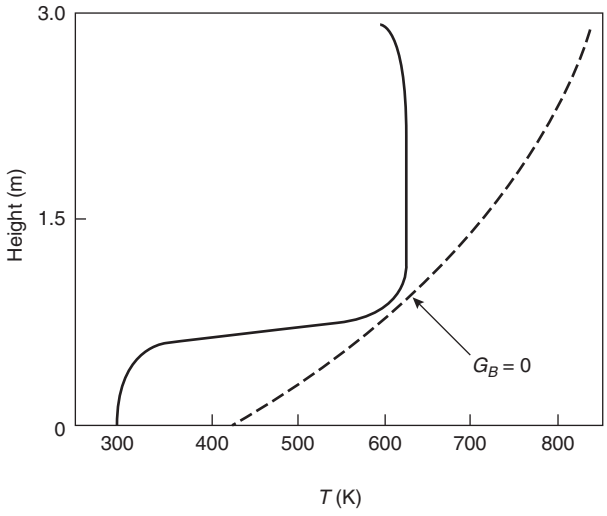

Figure 3-8.3. ***Predicted gas temperature profile with and without including buoyancy in $k \sim \varepsilon$ turbulence model.***

It is general practice to locate the near-wall node point close enough to the wall to be in the inertial sublayer. Then the velocity and enthalpy profiles between the near-wall node and the wall are

$$u^+ = \frac{1}{\kappa}\ln(Ey^+) \tag{3}$$

$$h^+ = \sigma_t(u^+ + P_j) \tag{4}$$

where

$$y^+ = \frac{\rho k_P^{1/2} C_\mu^{1/4} y_P}{\mu} \tag{5}$$

and

$$h^+ = \frac{\rho^{1/2}\tau_w^{1/2}(h_w - h_P)}{\dot{q}''_w} \tag{6}$$

κ is the von Karman constant relating mixing length to distance from the wall. E is a parameter that lumps together the effects of the viscous sublayer. Its value depends upon the surface roughness of the wall as does P_j, which represents the resistance of the laminar sublayer to the transport of enthalpy. For smooth surfaces E is often taken as 9.0 and P_j is given by the function

$$P_j = 9.24\left[\left(\frac{\sigma}{\sigma_t}\right)^{3/4} - 1\right]\left[1 + 0.28\exp - 0.007\left(\frac{\sigma}{\sigma_t}\right)\right] \tag{7}$$

which is -2.77 for $\sigma/\sigma_t = 0.7$, or is zero for $\sigma/\sigma_t = 1.0$. For general finish brick, E could be as low as 0.064 and P_j should then be 6.56.

Where there is a requirement to provide a very fine mesh close to the wall—perhaps for faithful representation of a ceiling jet, then the near-wall node will most likely need to be in the laminar or transitional regions. For $y^+ < 11$, a linear velocity profile,

$$u^+ = y^+ \tag{8}$$

should be used instead of Equation 3. Strictly speaking, Equation 3 is valid for $y^+ < 5$ (laminar sublayer), but it can be used up to $y^+ = 11$, which corresponds to the intersection point of the linear (Equation 8) and the logarithmic (Equation 3) velocity profiles.

For $11 < y^+ < 30$ (bridging the laminar and inertial sublayers), the log-law Equation 3 can still be used. However, for $y^+ < 30$, Equations 3 and 8 should ideally be coupled with a low Reynolds number k-ε turbulence model.[14] Otherwise, the boundary values of k and ε obtained from the standard high Reynolds number k-ε turbulence model will not be accurate.

Combustion Models

With the material described so far, supplemented by a prescription of the appropriate boundary conditions, we are in a position to examine buoyant flows that emerge from fires—a significant aspect of the smoke movement problem. It is often tempting simply to represent the fire source in such simulations as a volumetric heat source $\dot{q}'''$.

Such a simplified treatment of the fire source cannot properly capture the effects of distributed combustion that can play such an important part in fire problems. For more realistic simulations, models need to be incorporated to describe the influences of combustion and radiative heat exchange.

The purpose of incorporating a combustion model in smoke movement simulations is two-fold. First, it allows the process of fuel-air mixing, and therefore of distributed heat release, an essential feature of fire, to be determined by both flow conditions and by the shortage of one or other reactant. Prejudgment of heat-releasing control volumes is avoided, thus admitting natural treatments for wind-blown flames and of flame extension due to underventilation. Second, predictions of chemical species yield and transport become possible both to provide estimates of, for example, local toxic species concentrations and of thermal radiation absorption/emission properties of fire gases.

Most models assume for engineering purposes that the combustion process can be represented as a single, one-step reaction:

$$F + sO \rightarrow (1 + s)P \tag{9}$$

where F, O, and P simply represent the masses of fuel, oxidant, and product. At this stage it is not necessary to consider their detailed chemical compositions—this is only manifest by the stoichiometric air requirement of the fuel. In principle the task now involves solution of the species conservation equation (Equation 1, when $\phi = Y_i$) for each of the components in the reaction. However, the influences of turbulence on the source terms in these equations causes considerable further complexity.

By recasting the species conservation equations in terms of a conserved scalar, the mixture fraction

$$f = \frac{\beta - \beta_O}{\beta_F - \beta_O} \tag{10}$$

where $\beta = Y_f - (Y_o/s)$ is a conserved variable and the F and O refer to fuel and oxidant streams, respectively, and making the assumption that component diffusivities are equal, it is then possible to eliminate the source term in determining the degree of mixing between fuel and oxidant.

Spalding's eddy break-up model[15] allows for the influences of turbulence on chemical reaction. This assumes that the rates of chemical reaction are infinitely fast and that the mean rate of consumption of fuel at the molecular level is controlled by the rate of molecular mixing of reactants, in turn proportional to the rate of dissipation of turbulent eddies.

Magnussen and Hjertager[16] modified Spalding's original model such that this rate was controlled by the "deficient" reactant, air or fuel. Thus in the case of fire in the open, it is the local fuel concentration that controls the reaction, except of course immediately above the fuel bed. In

ventilation-controlled enclosure fires, the air is deficient and it is then the oxygen concentration that controls the reaction. A third controlling term based on mean property kinetics is sometimes added to limit the rate of reaction of cold mixtures:

$$S_f = -C\rho\frac{\varepsilon}{k}\min\left\{Y_f, \frac{Y_{ox}}{s}, Y_f Y_{ox} B \exp\left(\frac{-E}{RT}\right)\right\} \qquad (11)$$

Magnussen et al.[17] with an assumption of isotropic turbulence suggests for C a functional form,

$$C = 23.6\left(\frac{\nu\varepsilon}{k^2}\right)^{1/4} \qquad (12)$$

but it is common practice to assume C to be a dimensionless constant of the order of 4.[16]

This assumption for source term closure permits the transport equation for fuel mass fraction to be solved in addition to that for the mixture fraction to provide predictions of mass fraction of each component of the simplified chemical reaction. Application of this type of treatment to fire problems has been reasonably successful,[13,18,19] as it has been in other areas of combustion engineering.

The model has the merit of simplicity and permits the enthalpy to be released over a distributed volume determined by the enclosure geometry and availability of air. The phenomenon of flame lengthening as a consequence of ventilation control is incorporated by this modeling approach.

Concentrations of the stable species, CO_2 and H_2O, can then be deduced by assuming that they occupy the products of combustion in their stoichiometric proportions. An assumption of local thermodynamic equilibrium will allow detailed chemical species concentrations to be determined using procedures such as those embodied within the NASA-Lewis series of computer programs.[20]

The effects of finite-rate chemical kinetics and nonequilibrium kinetics are, however, not treated by such a scheme. For the realistic prediction of partially oxidized species, such as CO, and soot, more sophistication is needed. These will not be discussed here but the reader can consult Cox[2] and Moss[21] for more complex strategies. These are still primarily in the research domain and are unlikely, at the time of writing, to be used by the fire engineer. An estimate of CO concentration can be established by exploiting the equilibrium assumption. Although this can produce considerable overprediction of CO compared to the measured data,[22] such information can, as long as the limitations are recognized, be useful in obtaining engineering estimates of upper bounds of toxic hazard.

Radiant Heat Transfer

Two quite distinct difficulties need to be addressed for the realistic modeling of radiant heat transfer in enclosure fires. The first concerns the geometric problem associated with the exchange of radiant energy between remote emitters and receivers, solid surfaces, and the soot particulate/gas phase mixtures of flames and smoke aerosols. The second difficulty concerns the calculation of local emissive powers and absorptivities. The relative contributions from soot and gaseous emissions vary substantially between flame and smoke products. A successful model must be able to cope with not only these differences, but also those between relatively dense smoke layers and the almost transparent layers of the incoming air. In addition, as with fluid flow and combustion chemistry, the effect of turbulent fluctuations in temperature and composition must be considered particularly at the fire source itself. In most practical treatments of far-field conditions in enclosure fires, these effects are ignored. Recent work on this issue is presented in References 2, 21, and 23.

The influences of radiant heat transfer on the governing equations are exerted through the source term in the enthalpy conservation equation.

Exact solutions are not possible for most practical applications; instead, several approximate methods have been developed and have been applied to compartment fire problems.

Flux Methods

A substantial simplification becomes possible if the spatial and angular distributions of radiation intensity can be separated. This is the approach of the flux methods. If the spectral intensity is assumed uniform on given intervals of solid angle, then the radiative transfer equation reduces to a series of coupled, linear, ordinary differential equations in terms of spatially averaged radiation intensities or fluxes.

The solid angles are assumed to coincide with the faces of a control volume in Cartesian space and the radiant flux across each face is assumed uniform (Figure 3-8.4). Then, when F_i^+ is the flux passing through the

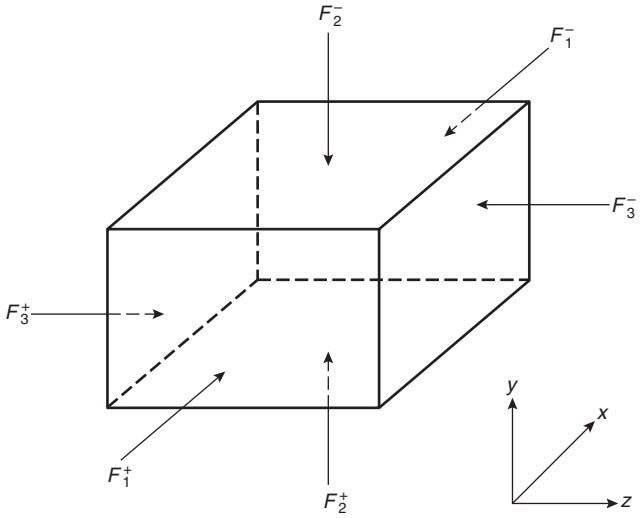

Figure 3-8.4. ***Six-flux distribution of a radiating control volume.***

control volume in the positive i direction and F_i^- is the flux in the negative i direction,

$$\frac{dF_i^+}{dx_i} = -(a+s)F_i^+ + aE_b + \frac{s}{6}\sum_{i=1}^{3}(F_i^+ + F_i^-) \quad (13)$$

$$\frac{dF_i^-}{dx_i} = (a+s)F_i^- - aE_b - \frac{s}{6}\sum_{i=1}^{3}(F_i^+ + F_i^-) \quad (14)$$

where a and s are local absorption and scattering coefficients and E_b is the blackbody emissive power of the control volume.

By combining these and differentiating with respect to x_i, we obtain

$$\begin{aligned}\frac{d}{dx_i}\left[\Gamma_R \frac{d}{dx_i}(F_i^+ + F_i^-)\right] &= -S_i \\ &= (a+s)(F_i^+ + F_i^-) - 2aE_b - \frac{s}{3}\sum_{i=1}^{3}(F_i^+ + F_i^-)\end{aligned} \quad (15)$$

where

$$\Gamma_R = \frac{1}{a+s} \quad (16)$$

This equation has the same form as the generic conservation Equation 1 and can be solved using the same numerical algorithm. The radiative contribution to the source term in the enthalpy equation for each control volume is then

$$S_{h,\text{rad}} = -\sum_{i=1}^{3} S_i = a\sum_{i=1}^{3}(F_i^+ + F_i^-) - 6aE_b \quad (17)$$

This model is attractive for CFD using the Cartesian grid since it computes the fluxes in Cartesian coordinate directions and exploits the same numerical techniques as employed to solve the hydrodynamic equations. It is often sufficient for the treatment of smoke movement problems. However, it does have a number of serious limitations, the most important of which, for application to fire, is its inability to model radiant transfer accurately at angles oblique to the Cartesian grid.

Discrete Transfer Method

The discrete transfer (DT) method developed by Lockwood and Shah[24] overcomes many of these difficulties, combining computational economy with greater realism. It utilizes features of the zone, flux, and Monte Carlo methods by tracing rays of electromagnetic radiation through the computational domain between boundaries. However, rather than their directions being generated at random, they are instead chosen in advance in a similar way to choosing the location of the hydrodynamic mesh. The technique involves solving the radiative transfer equation along the paths of these rays chosen to emanate usually from the centers of the bounding, hydrodynamic control volume faces (Figure 3-8.5).

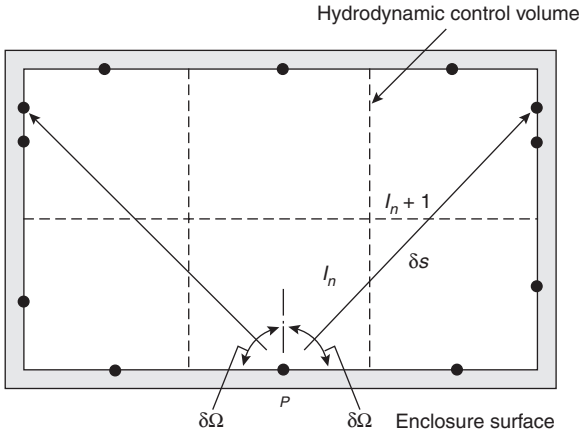

Figure 3-8.5. ***Schematic of discrete transfer method showing two representative rays.***

The number and direction of rays from each such point are chosen, a priori, to provide the desired level of accuracy in the same way as the finite-difference grid is selected for undertaking the hydrodynamic calculation. The hemisphere around each point is divided into segments of equal circumferential area over which the intensity is assumed uniform.

A simple recurrence relationship is solved for each ray as it traverses from one bounding surface to another:

$$I_{n+1} = I_n \exp[-(a+s)\delta s] + \frac{E^*}{\pi}\{1 - \exp[-(a+s)\delta s]\} \quad (18)$$

where

I_{n+1} = the intensity leaving the nth hydrodynamic control volume

I_n = the intensity entering the nth control volume

δs = the pathlength through the control volume

and

$$E^* = \frac{a}{a+s}\cdot E_b + \frac{s}{4(a+s)}\int_{\Omega'=0}^{4\pi} I\, d\Omega' \quad (19)$$

It has been assumed that temperatures, absorption, and scattering coefficients are uniform within the hydrodynamic control volume.

The net gain or loss of radiant energy in each control volume is then deduced from the numbers of rays crossing it and this can be introduced into the enthalpy conservation equation as before, for the nth control volume:

$$S_{h,\text{rad}} = \sum_{\substack{\text{all rays}\\ \text{through } n}} (I_{n+1} - I_n)\Omega\,\delta\Omega\,\delta A \quad (20)$$

where δA is the area of the cell surface.

Accuracy clearly improves with increased numbers of rays, but Bressloff[25] demonstrates that between 16 and 32 rays emitted from each boundary control surface should be adequate for the prediction of heat transfer in

the gas phase for smoke movement problems. The method can, though, create erroneous "fingers" of high heat flux and "hot spots" on boundaries in the directions of high ray density. These errors are reduced, the greater the number of rays used and, of course, the finer the hydrodynamic grid. More information on the accuracy of the DT treatment in application to fire problems will be found in References 26–28.

Radiative Properties of the Combustion Products

For each of these methods, computations for local absorptance and emittance are required. In an enclosure fire, conditions vary considerably from the comparatively transparent entrained air close to the floor to the highly emissive, luminous flames of the fire source and the optically dense ceiling smoke layer.

The simplest treatment for the smoke layer assumes it to be a gray gas of prescribed absorption coefficient.[29] More realistic treatments allow absorptance and emittance to be determined from the local predictions within each hydrodynamic control volume of concentration of CO_2, H_2O, and soot. There exist a hierarchy of models for the computation of these local properties.

Lockwood and Malalasekera[30] used the mixed gray gas model developed by Truelove[31] in conjunction with the discrete transfer model to model room fire growth. This is particularly attractive because it links the physical realism of Beer's law with the simplicity of the gray gas approximation. By assuming that the combustion product mixture is composed of a number of gray gases (CO_2, H_2O) and soot, the model defines total emissivity/absorptivity of the gas/soot mixture as

$$\varepsilon_m = \sum_{j,j'} b_{m,j,j'}(T)[\![1 - \exp\{[-a_{g,j}(p_w + p_c) - a_{s,j'}c]\delta_s\}]\!] \quad (21)$$

where the temperature-dependent weighting coefficient, $b_{m,j,j'}(T)$, represents the fraction of blackbody energy in the wavelength region where the absorption coefficient is $a_{g,j}$ for the gas mixture and $a_{s,j'}$ for the soot mixture, and should satisfy the sum rules:

$$\begin{aligned} \sum_{j'} b_{m,j,j'}(T) &= b_{g,j}(T) \\ \sum_{j} b_{m,j,j'}(T) &= b_{s,j'}(T) \end{aligned} \quad (22)$$

The weighting coefficients $b_{m,j,j'}(T)$ are obtained by a least-squares fit of Equation 21 to the mixture of the total emittance data evaluated from the measured gas and soot spectral properties.

Recently, Bressloff et al.[26] have demonstrated the benefits of the computational efficiency of this relatively simple model compared to more accurate but relatively expensive wide- and narrow-band models.[32–35]

Modak[33] developed a relatively simple wide-band model based on a curve-fitting method for the spectral data for homogeneous, isothermal mixtures of soot, CO_2, and H_2O that does not involve spectral calculations. He determined mixture absorptivity from

$$\alpha = \alpha_s + \alpha_g - \alpha_s\alpha_g \quad (23)$$

where α_s is the soot absorptivity, given by

$$\alpha_s \cong 1 - \exp(1 - 12bofv\,\delta s T_s) \quad (24)$$

and α_g is the absorptivity of the molecular species CO_2 and H_2O, given by

$$\alpha_g = \varepsilon_g\left(\frac{T}{T_s}\right)^{0.65-0.2\xi} \qquad \xi = \frac{p_w}{(p_w + p_c)} \quad (25)$$

where

T = the temperature of the local gas mixture
T_s = the blackbody temperature of the soot
f_v = the soot volume fraction
p_w and p_c = the partial pressures of water and carbon dioxide
ε_g = the emissivity of the CO_2-H_2O mixture that is determined by curve fitting to detailed spectral calculations using the method of Felske and Tien[35]

An application of this treatment can be found in Reference 29.

Yan and Holmstedt[36] have recently developed a very efficient narrow-band model for fire applications that they claim is twenty times faster than existing narrow-band models.

In flaming regions where fluctuations in species concentration and temperature are large, the time-mean treatments described here are likely to underpredict radiative transfer.[37,38] To capture these effects, more sophistication is required than is presented here. References 21 and 38 discuss these treatments in some detail.

Boundary Conditions

The boundary conditions to be used will clearly be dependent on the problem of concern. Those for the momentum equations at solid boundaries have been outlined above. Naturally ventilated fires, though, entrain air from the surrounding environment driven by pressure differences caused by the fire's buoyant acceleration. It is thus necessary to represent an infinite physical region in the finite computational domain. This is generally achieved by taking the computational boundary a long way from the region of the primary flow. The pressure is fixed at this plane while velocity derivatives normal to the boundary are set to zero. At this free boundary, at points of outflow, the derivatives of the scalar fields are set to zero while at points of inflow, ambient conditions are specified.

Heat will be lost from the fire into the structure at a rate determined by both the thermal properties of the bounding walls and time. Early in the fire the walls will be cold and heat-transfer rates, all other things being equal, will be at their highest. Later as the walls get heated, the rate will reduce. Convective and radiative

energy exchanges with control volume faces at the bounding walls must balance conductive loss into the bulk of the solid.

This can be achieved by coupling the solution to a time-dependent, heat conduction equation for the walls. There are a number of ways of treating this. The simplest is to assume that the process can be described by a series of quasi-steady, one-dimensional approximations to the heat conduction equation,

$$\dot{q}''_{\text{tot}} = -k_S \frac{\partial T}{\partial x} \tag{26}$$

By assuming that the thermal wave penetrates a distance $\delta(t)$ into the solid boundary of thickness d (see Figure 3-8.6), the quasi-steady approximation gives[39]

$$\delta(t) = \frac{2}{\sqrt{\pi}} \left(\frac{k_S t}{\rho_S c_S} \right)^{1/2} \tag{27}$$

where t is the elapsed time from ignition, and k_s, ρ_s, and c_s are respectively the thermal conductivity, density, and specific heat of the solid.

This simple approximation appears to be reasonably acceptable for use in smoke movement applications where the transience of the gas phase is much shorter than that of the solid walls. Since it underestimates heat flux in the bounding walls, it is not sufficiently accurate for application to surface heat-transfer problems (see the Validation section below). Here the quasi-steady approximation will be inadequate and a more accurate solution of Equation 26 is required.

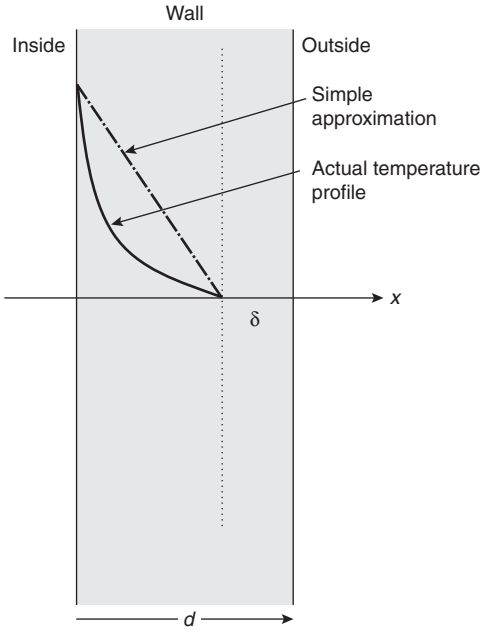

Figure 3-8.6. ***Simple illustration of one-dimensional conduction.***

Numerical Solution Method

Equation 1 describes the local conservation principles for the continuous behavior of ϕ within the domain of interest. The objective of the numerical method is to descretize these nonlinear partial differential equations in space and time and then to solve the resulting set of simultaneous algebraic equations. The discretized form of the generic Equation 1 can be written as

$$A_P^{\phi} \phi_P = \sum_{nb} A_i^{\phi} \phi_i + b^{\phi} \tag{28}$$

where *nb* stands for all neighboring nodes surrounding the node *P*. A_i^{ϕ} and A_P^{ϕ} are the influence coefficients that comprise convection and diffusion of the property ϕ.

Details of the procedures involved are very complex and cannot be discussed in detail here. They will be found elsewhere (e.g., References 2, 7, and 40).

Ideally, fire-engineering practitioners would prefer not to concern themselves with solution details but with CFD. It is essential to understand the various pitfalls and possible sources of error that may occur. Of course, in numerical approximation, a measure of success of the solution is whether it has converged, meaning, literally, is the numerical solution approaching that of the continuous equations? Converged solutions will be approached by a series of fit-and-try techniques. Successive guesses for the variables are substituted into the equations until each side balances to within acceptable errors. This is repeated over and over many times in a process known as iteration. On any given grid, when the difference between right and left sides—the residuals of the discretized equations—are low for every variable and when examined over the whole field, then the solution might be considered to be converged. However, as we see below, it is essential to demonstrate that the solution is also grid independent before we can be content that we have a reasonably accurate solution to the coupled, continuous equation set.

Some insight can be obtained by considering a discretized form of a continuous spatial derivative at the node point *P*,

$$\left(\frac{\partial \phi}{\partial x} \right)_P = \frac{\phi_w - \phi_P}{\Delta x} - \left[\frac{1}{2} \Delta x \left(\frac{\partial^2 \phi}{\partial x^2} \right)_P + \text{H.O.T.} \right] \tag{29}$$

where H.O.T. stands for higher-order terms.

This form of the equation uses an upwind differencing approximation based on only two node points on the numerical mesh—the central node, *P*, and upwind, west node, *W*, in this case. This is quite common practice in practical CFD modeling where unconditionally stable solutions are required.

As Δx becomes vanishingly small, it is clear that the terms in the brackets become insignificant. Of course, in reality Δx is finite, and sometimes larger than would be ideal, and thus omission of these terms represents a truncation error in the numerical derivative. Since the largest of these terms, the first in the squared brackets, has the same physical form as does the diffusion equation for ϕ, this is often referred to as *numerical diffusion.* More accurate, higher-order schemes based on additional node points are also

available in most CFD software but tend to give rise to numerical stability problems. However, this simple illustration explains why it is important to use as fine a grid as can be afforded and not to be content with a solution until reasonable grid independence can be demonstrated.

Since an iterative method is used for obtaining the final converged solution, it is desirable to restrict variations in the field values of the solution variable ϕ from one iteration to the next as this reduces the chance of divergence. This process, known as relaxation can be applied in two different ways. A direct way of applying this, the so-called underrelaxation of field variables, is where the "new" solution resulting from the next step of the iterative process does not completely replace its predecessor but only has a weighted influence on it, for example,

$$\phi_P^{\text{new}} = K_\phi \phi_P^{\text{new}} + (1 - K_\phi)\phi_P^{\text{old}}; \qquad 0 < K_\phi < 1 \tag{30}$$

where the superscripts "old" and "new" represent the values of ϕ before and after iteration and K_ϕ is a relaxation factor for the variable ϕ. This relaxation factor can differ for the particular equation being solved. The smaller K_ϕ is, the smaller the change in the field variables and heavier the underrelaxation.

The choice of K_ϕ is crucial for achieving a stable and rapid solution. For larger K_ϕ, the solution may experience oscillations that can lead to solution divergence. For smaller K_ϕ, although the solution follows a stable route to convergence, the speed of convergence may be so slow that it becomes effectively "frozen" (when K_ϕ approaches zero).

It is normal practice to use heavy underrelaxation in CFD (for stability of the solution), but it is important to realize that the solution may only change very slowly as a consequence. It is therefore not safe to assume that simply because the residuals or differences, between the left and right side of an equation do not change, convergence has been achieved. This may occur because the equation has been too heavily underrelaxed.

Another way of achieving relaxation is based on inertial relaxation or the method of "false" time steps.[7] Here, instead of applying relaxation to the field variable, the discretized control volume equations are modified by incorporating an inertial relaxation term, K_{in}:

$$(A_P^\phi + K_{\text{in}})\phi_P = \sum_{nb} A_i^\phi \phi_i + b^\phi + K_{\text{in}}\phi_P^{\text{old}}; \qquad K_{\text{in}} \geq 0 \tag{31}$$

where

$$K_{\text{in}} = \frac{\rho_P \text{Vol}_P}{\delta_{\text{ft}}} \tag{32}$$

Here ρ_P is the fluid density at P, Vol_P is the volume of grid cell P and δ_{ft} is a relaxation factor called the false time step (applicable to both steady-state and transient solutions). The larger K_{in}, or the smaller δ_{ft}, the greater the underrelaxation. Similar caution as for the above must be exercised in assessing the convergence of the solution.

When examining a numerical solution, it is also necessary to demonstrate that global mass and enthalpy balances have been achieved. Global mass inflow rates at enclosure openings together with fuel mass release rates must balance mass outflow rates to within acceptable accuracy. Heat lost by conduction into the enclosing structure together with convected and radiated loss through openings must balance the heat released by the fire source.

Validation

The foregoing text has outlined the basic principles involved in the use of CFD. Here some consideration is given to issues associated with the validation and verification of these models in the fire context. Every commercial CFD code includes a series of test cases to demonstrate the capabilities of the software in application to some classic fluid flow problems. It is important to recognize that while these do validate the technology in general terms, the responsibility for ensuring validity for the application resides with the fire community.

Why is this necessary? The turbulence models used in RANS software have tended to be developed for turbulent shear flow rather than for buoyant convective flow. Thus the assumptions that are made of isotropic turbulence in the standard $k \sim \varepsilon$ model are not strictly valid. The treatments available to describe the influences of buoyancy on turbulent mixing (Equation 2) need to be explored for their validity, as do, of course, many of the other submodels (e.g., for combustion, radiation, etc.) used to describe the whole process.

The general issue of the validity of CFD model simulations is something that the American Association for Aeronautics and Astronautics have addressed in a recent guide.[41] They use the following definitions of validation and verification:

Validation. The process of determining the degree to which a model is an accurate representation of the real world from the perspective of the intended users of the model

Verification. The process of determining that a model implementation accurately represents the developer's conceptual description of the model and the solution of the model

In the fire context, for example, the turbulence, combustion, and radiation models need to be validated to test their representation of reality. Whether the model equations are then solved to adequate accuracy is then the issue of verification.

The fire literature contains many comparisons of CFD predictions with experimental data (e.g., 42–51). These studies contain elements of both validation and verification. Most, however, have been conducted with a prior knowledge of the experimental results. One of the most important model validation studies has involved a recent series of blind simulation tests conducted under the auspices of Conseil International du Batiment's Fire Commission CIB W14.[52] Both zonal and CFD models were applied by various users to round robin test problems for which experimental data were available but not released to users until after their simulations had been submitted.

The experiment used for the model evaluation illustrated here was one of a series performed in the 1980s in the VTT testing hall in Finland, but the results were not published. Two wooden cribs were located inside an enclosure containing a single high-level slot opening (Figure 3-8.7). One of these cribs was ignited and fire was allowed to spread from the first to the second crib. This is a particularly severe test of the modeling methodology since the fire reaches flashover after 20 min or so and continues to burn for approximately 2 hours. This is a severe challenge to both the combustion model and also to the computer hardware requirements needing to compute transient predictions for such a long period.

Other than the geometry and the thermal properties of the wall materials, the only information supplied for the blind simulations was the measured, individual mass loss rates for each crib together with an effective heat of combustion. Mass loss rates were determined from the raw weight loss data through which a smooth curve had been fitted and time derivatives determined. Figure 3-8.8 shows the resultant mass loss rates for the two cribs. A measurement of the effective heat of combustion from oxygen depletion calorimetry throughout the duration of the fire was also supplied (Figure 3-8.9).

A selection of the results from the JASMINE CFD model is illustrated here (Figures 3-8.10–3-8.13).[13] It will be seen that gas temperatures and major gas species concentrations have been reasonably well reproduced. Although not perfect, agreement can be seen to be generally acceptable for many practical purposes. The discrepancy evident in the minimum oxygen concentrations is almost certainly due to instrumentation sensitivity limitations at low concentrations.

The poorest performance of the model was in its predicted total heat flux to the bounding surfaces (Figure 3-8.13). Although reasonably acceptable in terms of its impact on local gas temperatures (see Figure 3-8.12), this is not sufficiently accurate for use in the study of heat transfer to structural elements or to new fuel about to ignite as a consequence of the initial fire.

It is likely that this performance results from the crude one-dimensional heat conduction approximation, Equation 26 assumed here, where the linear approximation to the surface temperature gradient underestimates actual heat fluxes at the surface. This is yet to be proved,

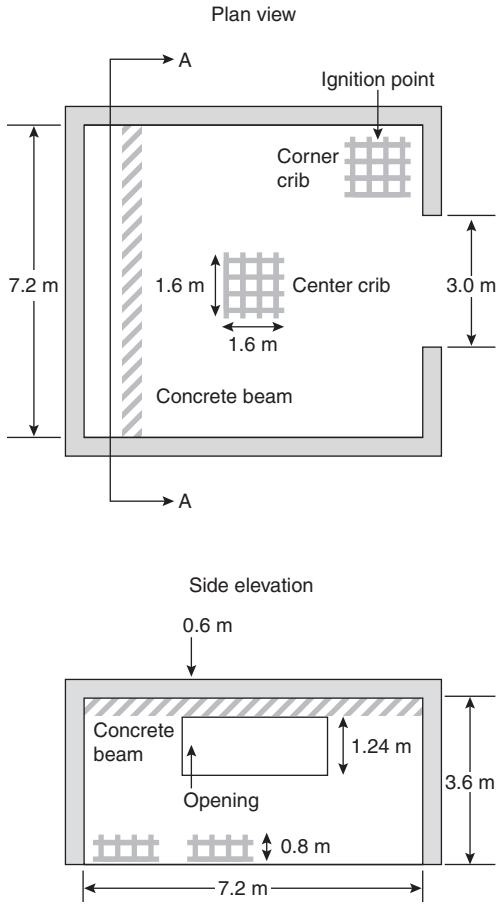

Figure 3-8.7. ***Geometry of the experiment.***

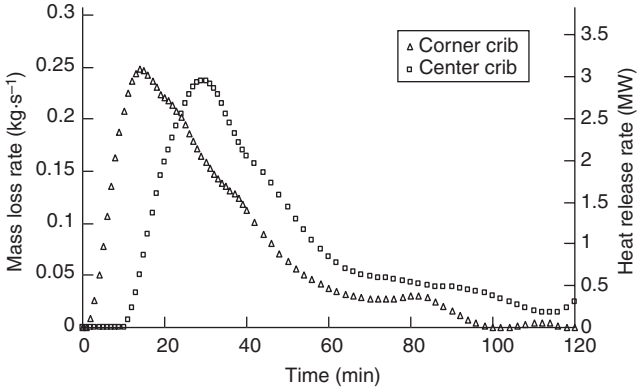

Figure 3-8.8. ***Mass loss and heat release rates of the two wooden cribs.***

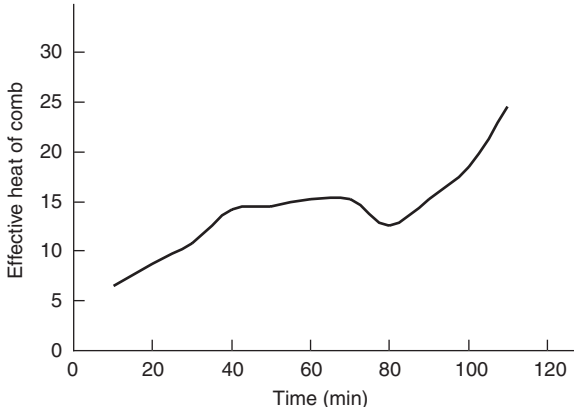

Figure 3-8.9. ***Measured heat of combustion as a function of time.***

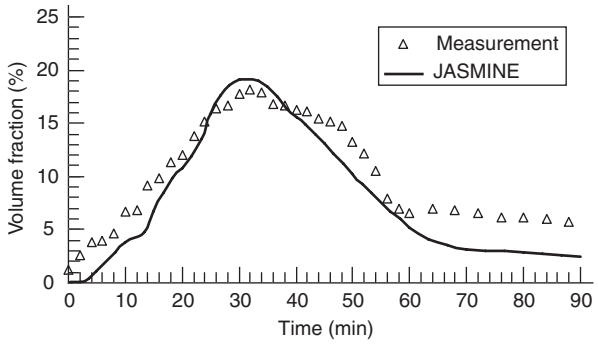

Figure 3-8.10. ***Comparison of predicted and measured CO_2 volume fraction near the center of the ceiling.***

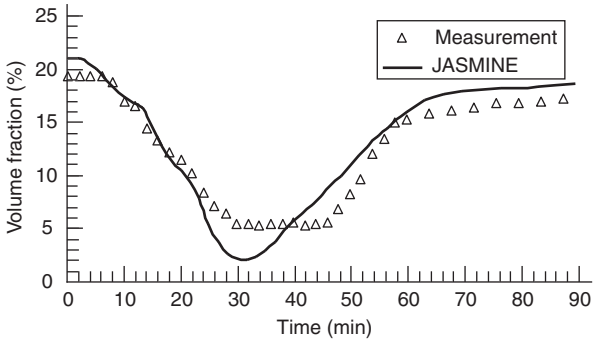

Figure 3-8.11. ***Comparison of predicted and measured O_2 volume fraction near the center of the ceiling.***

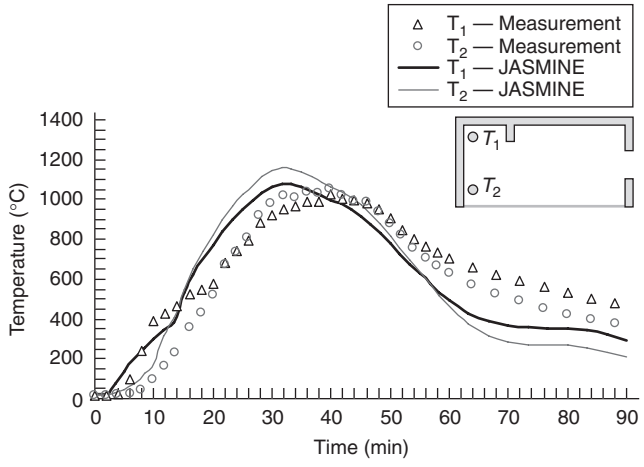

Figure 3-8.12. ***Predicted and measured gas temperatures close to the back wall.***

but these results suggest that the combinations of assumptions adopted together with the CFD methodology are fit for purpose for the exploration of gas phase calculations but that the simple conduction treatment adopted in this study is not appropriate for examination of solid phase questions.

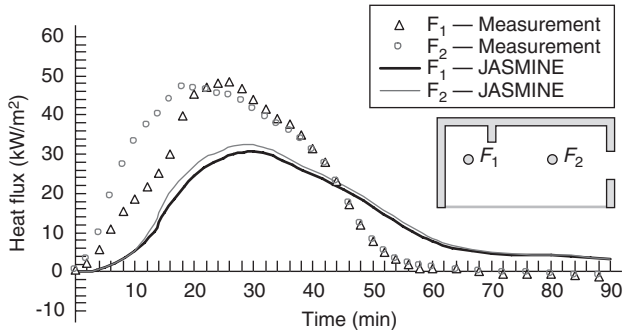

Figure 3-8.13. ***Predicted and measured surface fluxes from gas to normal density concrete bores.***

Ensuring Proper Use

So far we have discussed in outline the principles and content of CFD models. We now need to turn to the issues surrounding their proper use. The performance of the model depends on the proper description of physical and chemical processes for the particular problem, combined with appropriate initial and boundary conditions.

There are two essential components to this process—the first concerning the treatment of fire science and the second concerning establishment of a good numerical solution.

An example of the possible misuse of the modeling methodology as a result of incorrect prescription of the fire itself might be to characterize the fire source by a known or prescribed heat-release rate but then to associate that heat-release rate with an inappropriate fuel area. Close attention needs to be paid, for example, to the relative influences of momentum and buoyancy at the fire source. They are represented by the nondimensional heat-release rate (or source Froude number), Q^*:

$$Q^* = \frac{Q}{\rho_a c_p T_a D^2 \sqrt{gD}} \tag{33}$$

where

Q = heat release rate of the fire

D = characteristic fuel dimension (say, diameter of the fuel base)

g = acceleration due to gravity

The value of Q^* above anything around 2.5 is not representative of buoyant fires but is more appropriate for higher-momentum jet fires. If the problem concerns the normal unwanted fire, then it is likely that too small a fuel area has been associated with the heat release rate. Of course, if the hazard being modeled is a high-pressure gas-pipe leakage, then a higher Q^* is perfectly reasonable.

Another problem can occur when no combustion model is employed and instead a volumetric heat source is used to describe the fire. Too small a volume will yield gas temperatures in the source that are much too high. The authors have seen examples of peak gas temperature predictions of over 5000°C in such sources when the adiabatic flame temperature—an absolute limit on gas temperature—is unlikely to exceed, say 2000°C. Clearly this kind of erroneous source description grossly misrepresents buoyant acceleration and indeed buoyant turbulent mixing at the source. Such errors are easy to avoid with proper attention to the characteristics of buoyant fires.

Measured time-averaged gas temperatures in a fire seldom exceed around 1300°C. Since the CFD code spatially averages these temperatures over the mesh spacing, it is unlikely that model will predict temperatures as high as this. Anything above this temperature should be treated with caution and anything above the adiabatic flame temperature must be incorrect.

Other key features that need to be scrutinized closely when studying a numerical solution are, in addition to the fire source itself, the thermal plume above the flame tip, the resulting ceiling jet and upper hot gas layer, together with wall and vent flows. Simple calculations can be undertaken to check these components of the overall solution.

Concerning the numerical description of the problem an extremely important requirement is that the free boundary conditions outside a compartment opening, for example, or surrounding an unbounded fire, are far enough away as not to influence the solution in the region of interest. Providing a constant-pressure boundary condition across a doorway opening will not, for example, allow the proper inflow and outflow characteristics to be established.

It is comparatively easy to produce impressive-looking visual images of the fluid flow with modern software, but it is essential to demonstrate that the solution is reasonably well converged, by checking for sensitivity to further numerical iteration and further mesh refinement.

A checklist of some of the more important considerations that need to taken concerning the problem set-up and examination of the solution is listed here.

Considerations of Numerical Aspects

1. Resist the temptation to undertake two-dimensional simulations. These can provide physically misleading solutions. Think where the air entrained into the fire would come from if the problem were really two-dimensional.
2. Choose the mesh to capture the main physical features of the flow ensuring that the near-wall nodes satisfy the criterion $y^+ < 400$ (see Equation 5). Ensure an adequately fine mesh resolution for the fire source and at enclosure openings.
3. Ensure that the aspect ratio of cells is not too large—typically not larger than 50.
4. Analyze the accuracy of the solution by a grid refinement study preferably using at least three different grid resolutions—ideally by doubling the grid cells in all directions. For these buoyant flows, special attention should be given to the vertical mesh spacing.
5. It is likely that a first-order numerical differencing scheme will be used at least initially since it is stable, but, if possible, as convergence is approached use a second- or higher-order scheme.
6. It is not advisable to change too many relaxation parameters at once, as it then becomes difficult to analyze which of the changes has influenced the solution.
7. In transient simulations, be sure that the time step is adapted to the choice of the grid and check the influence of the time step on the results. For a rapidly developing fire, more iterations per time step are generally needed.
8. Normalized mass and momentum continuity errors, and residual errors for all the solved variables, should be less than about 0.01, preferably less than 0.001. In an ideal simulation, the residuals will decrease steadily. However, in practice some equations may oscillate for a while but should eventually decrease (in a damped oscillatory manner).
9. Examine convergence by following monitor data, especially pressure, at critical locations (e.g., in the plume, in the hot gas layer, and in ventilation openings). Monitor values should gradually settle down to their converged levels.
10. Global mass and heat balances should be better than 95 percent in one or more analysis regions. One of these regions should encompass the entire enclosure or building. Generally, global mass balance is achieved quite easily—regardless of the quality of the solution. Global heat balance is often more difficult and a good indicator of how well a solution is converged.
11. Be careful when exploiting an assumed axis of symmetry. When a simulation is run on half a domain for economy, undertake a simulation on the full domain using the half-domain results as the initial condition.
12. Explore difficulties in achieving a steady-state solution by utilizing transient simulations. There may be no steady solution if physical oscillation is present.

Considerations of Fire Science

1. Use a combustion model to allow a proper coupling between local air flow and distributed heat release.
2. Check that Q^* is representative of the fire of concern, for buoyant fires $Q^* < 2.5$.
3. It is important to incorporate radiative loss from the flaming region. The fire plume can lose up to 50 percent of its heat by radiation.
4. Ensure that boundary heat losses are accounted for. These can cause ceiling layers to loose their buoyancy and cool wall currents to fall through a buoyant layer.
5. Check ventilation conditions:

- What is the role of compartment leakages?—See Reference 53 for a discussion of this issue.
- Has the HVAC been modeled if it is important?
- Are underventilated conditions likely, and, if so, have they been accounted for in the combustion modeling?

6. Check whether modeling of fire protection measure (e.g., detector, sprinkler, etc.) is required. Realistic reproduction of the ceiling jet characteristics, and therefore a reasonably fine underceiling mesh resolution, will be needed to predict the likelihood of detector or sprinkler activation. Impingement point details, if important, will not be accurately captured by the standard $k \sim \varepsilon$ model.
7. For smoke movement problems, a six-flux radiation model is normally adequate. However, for boundary heat transfer predictions, a more sophisticated method such as the discrete transfer method should be considered.
8. Ensure that free boundaries are chosen carefully. A free-pressure boundary should be far enough from any ventilation openings not to affect flows through them (for example, with the ISO room, this should at least be equal to the length of the room). Avoid steep pressure gradients near the free-pressure boundary and ensure that simulations are reasonably insensitive to the boundary position.
9. Do the predictions of the fire source make sense? For example, flame temperature should not exceed 1300°C. Anything higher than 2000°C must be incorrect due to an erroneous source specification; anything higher than 1300°C should be examined closely.
10. Compare flame temperature, flame height, plume entrainment, upper-layer temperature, ceiling jet properties, and so on with empirical correlations.

There will be occasions when the model may suggest unexpected behavior. In a physical model, although presenting a surprise for the engineer, such behavior would nonetheless be believable. However, with a numerical simulation, such an outcome is disturbing because it can have one of two explanations. Either it is genuine as in the physical simulation, or it is the result of some misleading numerical artifact. The possibility of the latter cannot be completely discounted with such complex simulations. It is therefore essential that simple calculations be used to "shadow" the numerical simulations.

During the official enquiry[54] into the King's Cross underground fire in London, such an unexpected outcome was predicted by the CFD analysis.[55,56] The flames on a wooden passenger escalator were predicted not to rise in a vertical plume as might at first sight be expected but to lay down in the trench of the escalator. It was only with a study of sensitivity of the results to fire source conditions as well as subsequent physical testing that these numerical predictions were demonstrated to be correct. And indeed, *with hindsight,* not unexpected!

The flames were shown to lay down only when the air required for entrainment into the fire could be provided from above and below the fire, but not from the sides, that is, after the fire had spread across the width of the escalator (Figure 3-8.14).[56] The fluid mechanics here were locally, essentially two-dimensional. With the fire confined to one side of the escalator, and with local flow three-dimensional, the flames did indeed rise vertically (Figure 3-8.15). This phenomenon with hindsight was already well known from experiences of forest fires accelerating up slopes due to flame leaning.

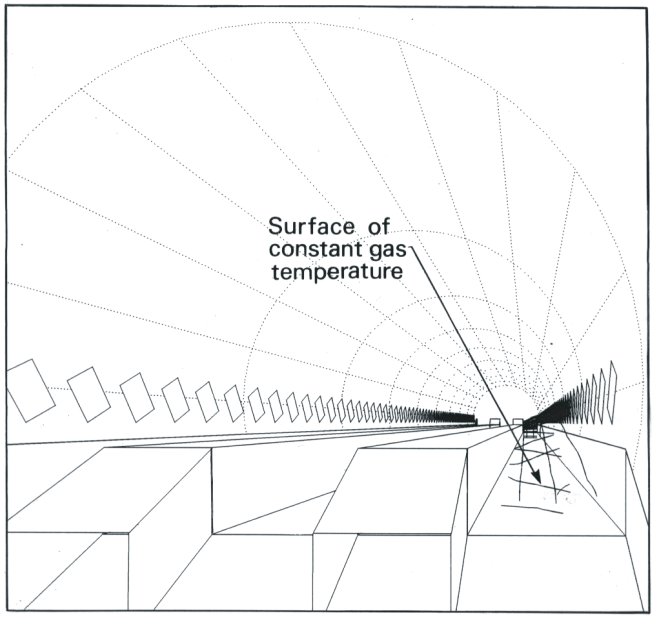

Figure 3-8.14(a). ***A 1.6-MW fire across the whole width of the channel.***

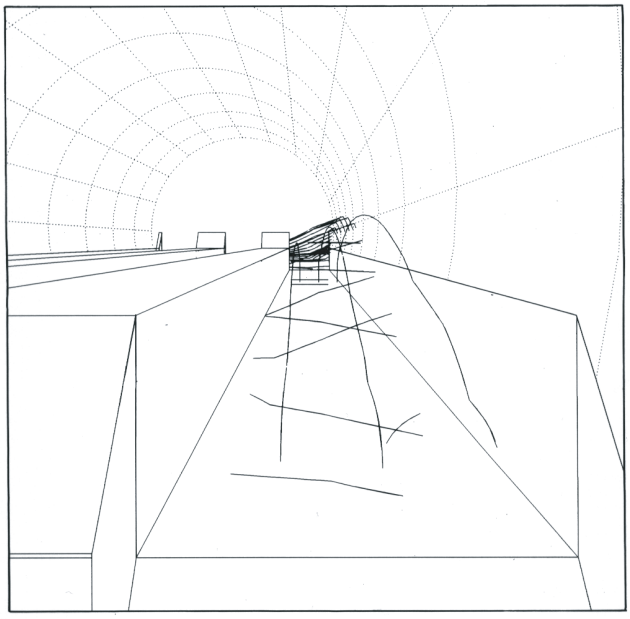

Figure 3-8.14(b). ***Enlargement of (a) with advertisements removed.***

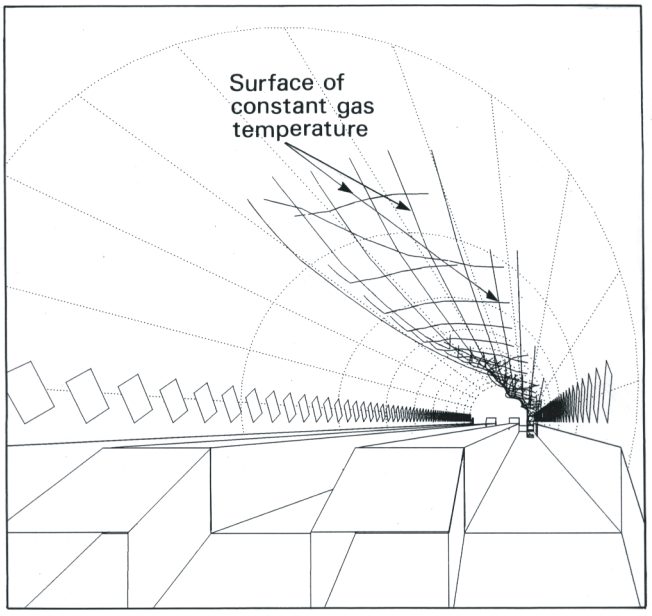

Figure 3-8.15. ***A 0.5-MW fire across one-third of the channel width.***

Some Practical Applications

Most commercial applications of CFD have been restricted to the assessment of smoke control design strategies particularly in large buildings. It is in these kinds of structures where the traditional building regulations are often not readily applicable and an engineered solution is, of necessity, required. Covered shopping malls, atrium hotels, leisure complexes, airport and railway terminals are just some examples of where the technology is finding its utility for the practicing engineer. Often these structures are unique in nature (e.g., the Millenium Dome in London), but increasingly the codes are being used for more routine problems. An example of the use of CFD for a very large atrium leisure complex is outlined in the Appendix at the end of this chapter. An illustration of the use of CFD to model smoke movement in conjunction with a passenger egress model is provided in Figure 3-8.16. The illustration shows the progress of the combustion products 3 min from ignition of a luggage fire in the terminal building of Brussels International Airport. In this example, the heat release history of the luggage fire source has been taken from experimental data and used as input to the CFD model. The occupants are making their escape based on assumed detection of this fire at one minute.

Figure 3-8.17 illustrates another application of the CFD methodology to an exploration of heat transfer within a fire-resistant furnace.[57] The figure shows predicted gas and furnace surface temperature contours in addition to gas flow streamlines and some gas temperature contours for a commercial fire-resistance wall furnace powered by natural gas and following the standard ISO 834 time-temperature curve. The DT model was used for the treatment of radiant heat transfer but assumed a constant absorption coefficient throughout the furnace. Thermocouple temperatures by which the furnace was controlled were simulated by use of *virtual thermocouples*

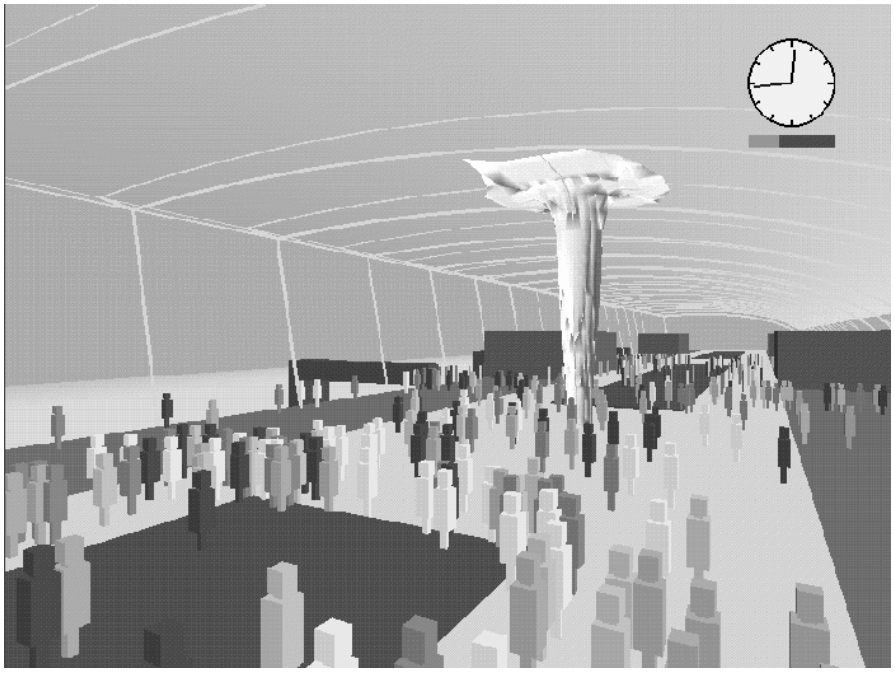

Figure 3-8.16. ***Simulation of smoke spread and human egress in the design for the Brussels airport passenger terminal.***

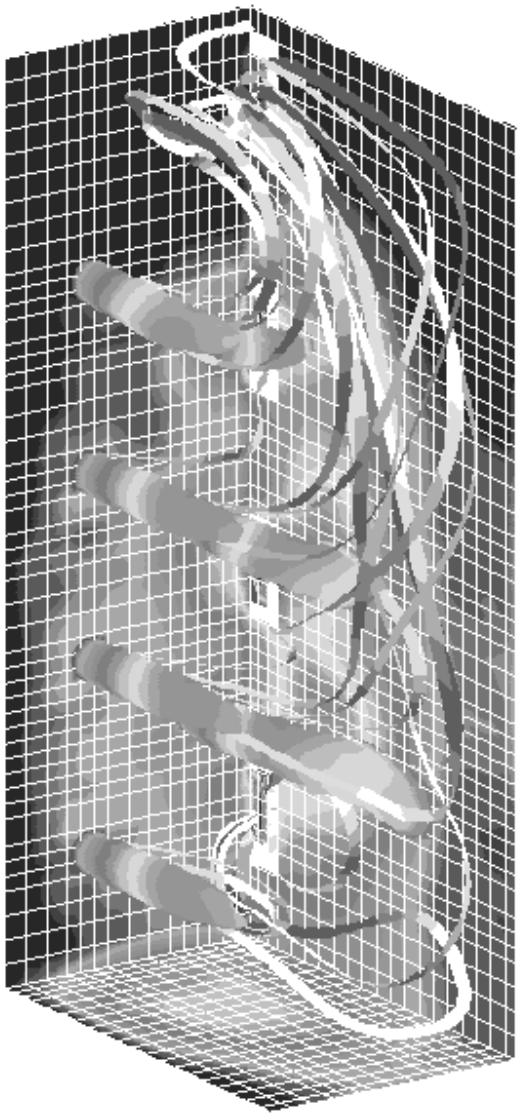

Figure 3-8.17. ***Predicted gas and furnace surface temperature contours and flow streamlines.***

to account for thermocouple heat transfer and thermal inertia.

More Advanced Application

The CFD methodology has the potential to be used for more complex problems than those associated with smoke movement. The interaction of water sprinklers with the smoke layer is one such example. Another is the issue of flame spread. Both these problems are, though, extremely complex. A brief outline is provided of the approaches that are being applied by the research community that may be of practical utility in the future.

Solid Phase Combustion

The behavior of solid combustibles can be described by applying the conservation principles within the bulk of the solid subject to the boundary conditions set by the gas phase. For a porous solid, the mass continuity and energy conservation equations will often be sufficient if the solid can be assumed to offer no resistance to the flow of the gaseous pyrolysates from within its bulk. Then the mass continuity equation is

$$\frac{\partial \rho_s}{\partial t} + \frac{\partial}{\partial x_j}(\rho u_j) = 0 \tag{34}$$

where ρ_s is the instantaneous local density of the solid, and the energy conservation equation is

$$\frac{\partial}{\partial t}(\rho_s c_s T_s) + \frac{\partial}{\partial x_j}(\rho u_j c_p T_s) = \frac{\partial}{\partial x_j}\left(k_s \frac{\partial T_s}{\partial x_j} - \dot{q}_R\right) - H_p \frac{\partial \rho_s}{\partial t} \tag{35}$$

where H_p is the heat of pyrolysis. The terms on the left side of Equation 35 represent the unsteady accumulation of energy in the solid together with the energy carried by the gas pyrolysates through the elementary control volume. The right side comprises terms describing thermal conduction, the influence of in-depth absorption of thermal radiation, and the energy lost in the phase change. An Arrhenius pyrolysis rate equation closes the system of equations:

$$\frac{\partial \rho_s}{\partial t} = -B\rho_s \exp\left(-\frac{E_s}{RT_s}\right) \tag{36}$$

These equations can now be solved subject to the boundary condition at the solid surface that

$$\dot{q}''_{\text{net}} = -k_s \frac{\partial T}{\partial x_j} \tag{37}$$

where $\dot{q}''_{\text{net}}$ represents the net heat transfer to the solid from the gas phase. As has been discussed earlier, the accurate prediction of surface heat transfer is an extremely complex issue and further research is required before robust predictions can be made.

Extensive studies of this kind have been conducted by di Blasi et al.[58] for the study of flame spread over well-behaved materials such as polymethylmethacrylate and to a lesser degree wood. Others have adopted a similar methodology for the study of both flame spread and pyrolysis from these materials.[59,60]

Figure 3-8.18 illustrates the application of such an approach to the modeling of flame spread over samples of polymethylmethacrylate within an experimental wind tunnel. These predictions are compared with the measurements of Chao and Fernandez-Pello[61] who varied wind speed, oxygen concentration, and turbulence intensity in the approach flow. The figure shows conditions at a time 25 s after ignition from the front edge of the PMMA slabs over both floor and ceiling samples for an oxygen mass fraction of 0.5, a wind speed of 2 m/s and a turbulence intensity of 10 percent. The predictions clearly show the greater progress of the flame in the floor-mounted case. This, perhaps surprising, result is also shown in the experiment and appears to be the result of the lower flame thickness under the ceiling, resulting from the influences of buoyancy.

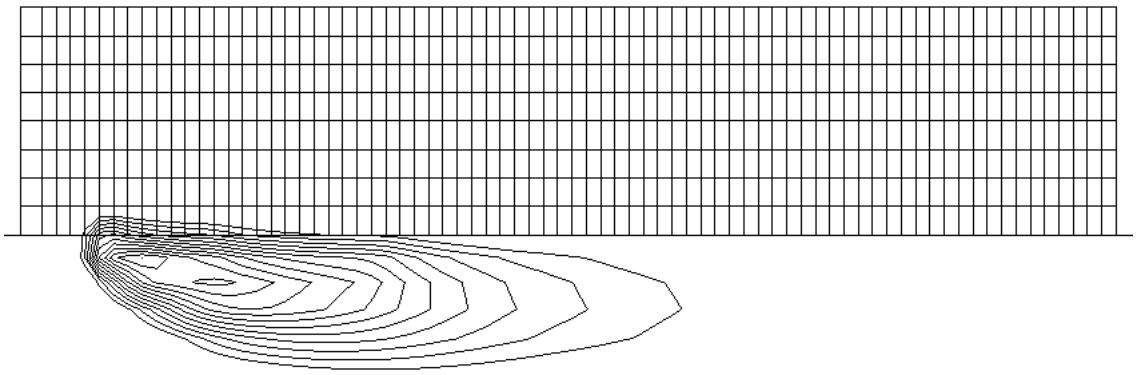

Figure 3-8.18(a). ***Flame spread over a ceiling-mounted sample of PMMA in a wind tunnel as illustrated by isotherm contours 25 s from ignition (wind speed 2 m/s, oxygen concentration 0.5, and turbulence intensity 10%).***

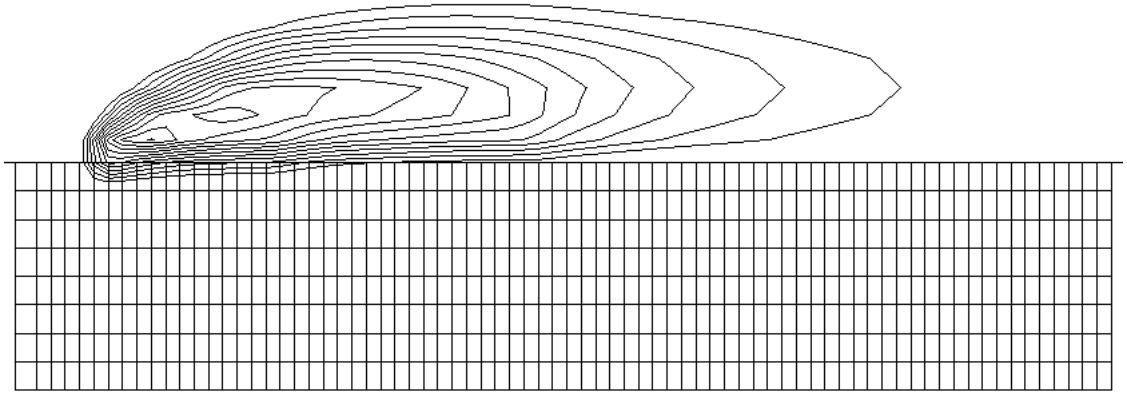

Figure 3-8.18(b). ***Flame spread over a floor-mounted sample of PMMA in a wind tunnel as illustrated by isotherm contours for the same conditions as in Figure 3-8.18(a).***

However, for the full range of products to be found in building structures, a rigorous analysis such as this is not a practical proposition. Physical effects such as delamination, cracking, and bubbling are not readily amenable to such a treatment, and a more pragmatic approach needs to be adopted.

Here a coupling between gas and solid phases exploiting standardized fire test data is likely to be the most successful. Some modeling, exploiting this more pragmatic approach, has been described, for example, by Opstad[62] and Yan and Holmstedt.[59]

The Influence of Water Sprays on Combustion Products

Naturally, if the solid phase combustion processes are difficult to model, the further complexity of added water at the fire source makes the task even more complex. However, some studies have been undertaken of the interactions of water sprays on fire gases remote from the source to explore the likelihood of smoke being drawn down to floor level by sprinkler sprays.

To model these processes, extra contributions to the gas phase source terms are added in the enthalpy and momentum equations to describe heat and momentum exchange between phases. Furthermore, a mass source term is also needed to account for mass addition from the spray to the gas by evaporation.

These can be obtained by using Lagrangian particle-tracking techniques to trace the trajectories of the droplets through the flow field.[63] For a water droplet of diameter D, subject to gravitational acceleration and viscous drag forces, its equation of motion can be written (e.g., see Reference 64) as

$$\frac{dv_i}{dt} = -\left(\frac{18\mu}{\rho_d D^2}\right)\left(\frac{C_D\,\mathrm{Re}}{24}\right)(v_i - u_i) + g \qquad (38)$$

where

v_i = droplet velocity in the i direction
u_i = gas velocity in the i direction
ρ_d = liquid density
C_D = drag coefficient
R = Reynolds number based on the droplet diameter

$$\mathrm{Re} = \frac{\rho D}{\mu} | v_i - u_i | \tag{39}$$

The diameter of the evaporating droplet can be determined from the expression

$$\frac{dD}{dt} = \frac{C_b}{2D}(1 + 0.23\,\mathrm{Re}^{1/2}) \tag{40}$$

and a vaporization rate constant can be expressed as

$$C_b = \frac{8k}{\rho c_p} \ln\left[1 + \frac{c_p}{L}(T_g - T_d)\right] \tag{41}$$

where k, ρ, and c_p are for the surrounding gas and L is the latent heat of vaporization of the droplet. The droplet temperature as it traverses the flow field can be determined from

$$\frac{dT}{dt} = 6k(2 + 0.6\,\mathrm{Re}^{1/2}\sigma^{1/3})\frac{(T_g - T_d)}{\rho_d D^2 c_{p,d}} \tag{42}$$

where $c_{p,d}$ is the specific heat of the liquid.

These ordinary differential equations permit the location, velocity, size, and temperature of each droplet or each size range of droplets to be determined as functions of time.

The contributions that the droplets make to the source terms in the gas phase equations are evaluated by summing the contributions to each gas phase control volume of each size range as it enters and leaves the volume element.

The boundary conditions for the gas phase calculation will be as has already been discussed, but for the droplet calculation will depend upon initial values of velocity, size, and temperature of the droplets. Such information is not readily available although there has been some recent effort to obtain such data for typical sprinkler heads (e.g., see Reference 65).

Figure 3-8.19 illustrates a simple calculation of spray-fire interactions in a forced ventilated enclosure fire. Immediately above a 400-kW pool fire is an imaginary sprinkler injecting, at a velocity of 10 $m \cdot s^{-1}$ a line of droplets of 0.5-mm diameter. Their progress through the fire plume is shown with the stars representing the point at which complete evaporation has occurred. Only very few of the droplets reach the floor of the compartment, most being lifted by the buoyant plume to evaporate at a high level. Work of this kind is in its infancy, but calculations such as these demonstrate the potential.

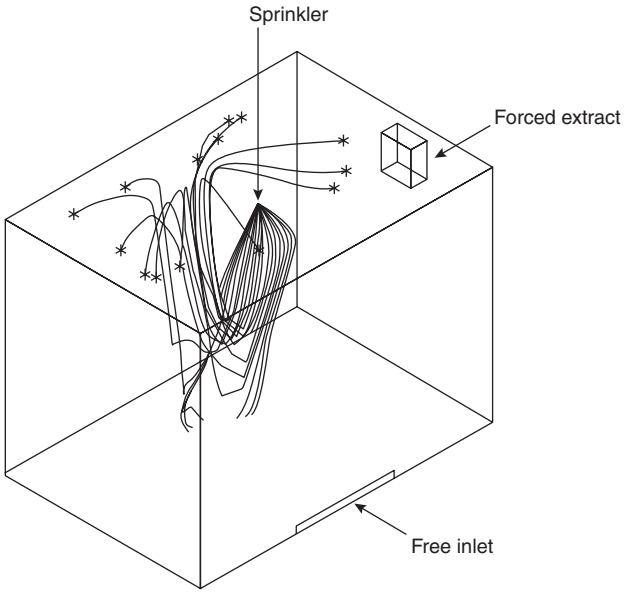

Figure 3-8.19. ***Predicted trajectories of water droplets.***

Software and Hardware Issues

Software tends to be divided between the fire-specific computer programs that have been developed by fire research laboratories and general-purpose programs available from commercial software vendors. The latter contain much of the same fundamental treatments for turbulence and thermal radiation but often not the fire-specific components. In essence, all are alike although they do differ in detail. Each has its strengths and weaknesses. Usually the commercial programs are more highly developed in terms of their numerical efficiency and incorporation of a broader range of treatments for some of the more general physical aspects but do not have the same pedigree of validation as the fire-specific codes.

The RANS fire-specific programs include JASMINE,[18] SOFIE,[46] SMARTFIRE,[50] and KAMELEON.[19] In the general-purpose category are PHOENICS,[66] CFX,[67] FLUENT,[68] and STAR-CD.[69] The NIST LES model[3] is unique in the sense that it is the only LES fire model that has so far been used for practical three-dimensional fire applications.

Workstations and top-end PCs are quite suitable for calculation of smoke movement problems. Hardware costs continue to drop, and while, as always, the fastest machine available will always be preferable, a $5,000 machine should be enough to allow three-dimensional smoke movement simulations to be conducted on a 100,000 node mesh. Steady-state simulations should be completed overnight with transient simulations up to around 10-min real time over a couple of days.

Annual licenses on commercial software range from around $10,000 to $20,000. For fire-specific software, license costs are lower. The higher prices of the commercial software tend to reflect the greater degree of software support, documentation, and maintenance available, although this tends, of course, to be of a general nature, with naturally less support available from commercial vendors for fire problems.

Conclusion

The use of CFD fire modeling in fire safety design is growing rapidly. Such models are no longer restricted to just the academic developers and research institutions. Many building design offices now have access to CFD codes offering the ability to design smoke control systems with the same tools as can be used to assess building

ventilation. The possibility of simulating ambient air movements both before and after the outbreak of fire also offers a powerful new capability for examination of early fire detection strategies. With the increasing trend toward performance-based regulation, such simulation tools will inevitably become increasingly attractive, particularly now that they can be used on personal computers. The relatively low license and hardware costs now ensure much greater accessibility than ever before.

However, education and training costs to ensure proper use cannot be ignored. It is relatively easy to run modern CFD software to produce impressive color images that may look plausible, but without proper consideration of the issues we have raised in this chapter, there are serious risks that the models will be misused. Hopefully this contribution will go some way to guide fire safety engineers on the proper use of this extremely powerful technology.

Appendix: An Exemplification of the Use of CFD for Smoke Control in a Large Atrium Building

This study was undertaken on behalf of local building control authorities to assess the effectiveness of a smoke control design based on traditional calculation methods. CFD was used because of the unique size of the building (regulations and traditional design approaches outside their normal expected range of validity).

The Building

The particular building of concern here was a large, six-story atrium complex designed for use as an indoor leisure park. An outline of the atrium design is shown in Figure 3-8.A1. The atrium building was a single envelope of overall dimensions 150 m long, 62 m wide, and 52 m high. Inside, the proposed design consisted of a central atrium approximately 104 m long, 27 m wide, and 40 m high, with five floors of galleries, each approximately 17.5 m in width and 6 m high, open to the central atrium. The side elevation of the gallery on the first floor is shown in Figure 3-8.A2.

Main doorways, 6 m wide by 5 m high, were situated at either end of the main atrium, providing both means of escape for occupants on the atrium floor and for the provision of replacement air for the high-level powered extraction systems.

Ventilation

Fans capable of handling six air changes per hour—165 m^3/s (the recommendation of the local building control authority) were proposed to be installed at the top of the atrium void. These were to be activated on fire detection by beam detector at first floor level. On each gallery the fresh air supply at ceiling level of 1.7 m^3/s in each partitioned smoke zone switched to an extraction of 29 m^3/s on fire detection. The fan capacities had been calculated based on traditional methods and for a steady 5-MW fire.

Fire Safety Objectives

The purpose of the study was to assess the validity of the smoke control strategy based on traditional calculation methods. The occupants of a gallery were assumed to be able to escape to a place of safety within 10 min of fire detection—no egress calculations were performed.

Fire Scenarios

Three main fire scenarios were considered for the galleries. The first scenario corresponded to a growing fire situated centrally at the front part of the first gallery floor. The second examined that same fire now at the back of

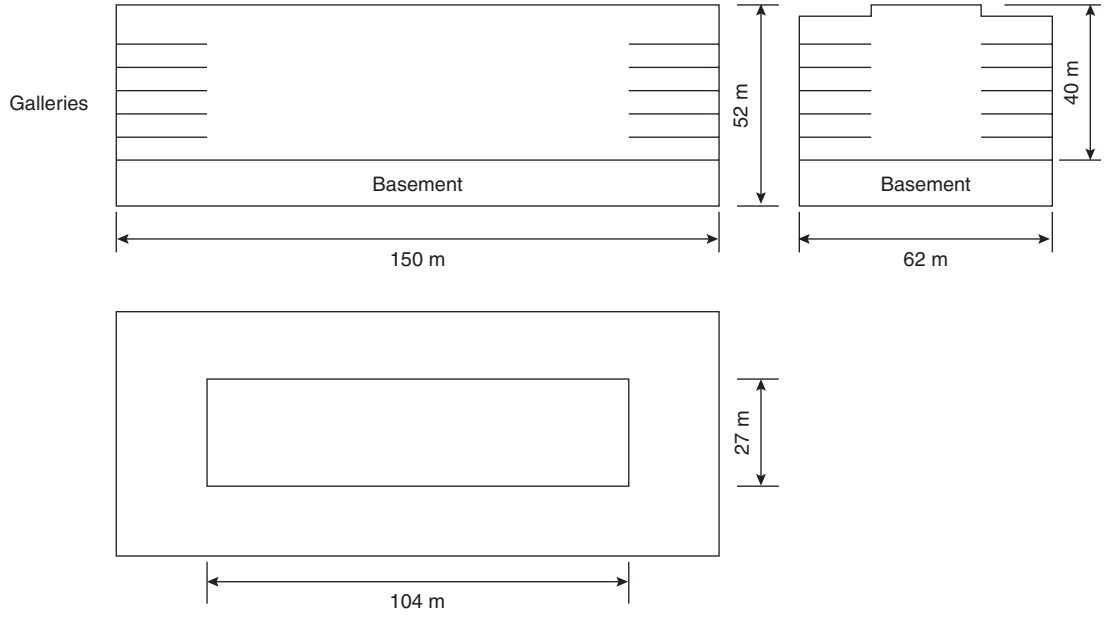

Figure 3-8.A1. ***Outline of large atrium surrounded by open galleries.***

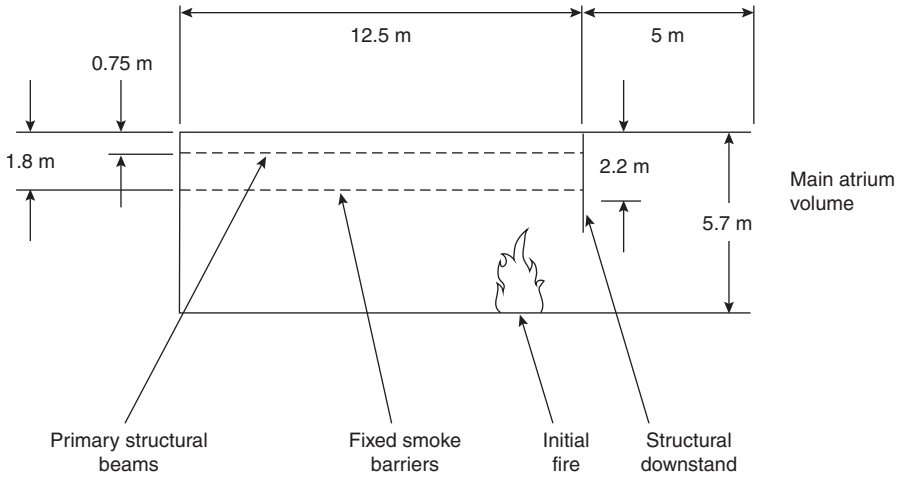

Figure 3-8.A2. ***Gallery—side elevation.***

the gallery. The concern here was to explore the likely effects of a fire close to a reservoir screen. The third scenario corresponded to a fire on the floor of the atrium, situated along the centerline and 25 m from one end.

Design Fire Sizes

Design fires were chosen after discussions with representatives of designers and local building control and fire service representatives. Exponentially growing fires, with an initial rate of heat release of 100 kW, were assumed for each fire scenario. For the gallery cases, the fire was assumed to grow exponentially, with a doubling time of 1 min until the calculated operation of the first sprinkler head. The rate of heat release was then assumed to drop suddenly to one-half of its value at that time and then to continue to grow exponentially, but more slowly, with a doubling time of 3 min. The area of the fire source was also allowed to increase such that the local rate of heat release per unit area did not exceed 0.5 MW/m^2.

For the atrium fire, the rate of heat release was allowed to grow exponentially, doubling every minute until it reached 3.2 MW (at 5 min), at which level it was assumed constant.

Detection and Fire Suppression Activation Criteria

Fire detection was assumed to occur when the product mass fraction exceeded 1.4×10^{-3} at the detector head locations. This empirical value was taken to be equivalent to 20-m visibility through the smoke from polyurethane mattress fires. Sprinkler activation was determined from the rate of rise of gas temperature in the control volumes occupied by sprinkler heads and by assuming a response time index for each sprinkler head to be 210 m$^{1/2}$·s$^{1/2}$.

Prefire Conditions

For the gallery fire, an ambient air temperature of 20°C has been assumed throughout the computational domain. For the atrium fire, the air temperature has been assumed to increase linearly from 20°C at floor level to 45°C just under the ceiling.

Results and Discussion

Gallery fire: Figure 3-8.A3(a) shows the times for the operation of detectors D1 and D2 in the fire zone, detector

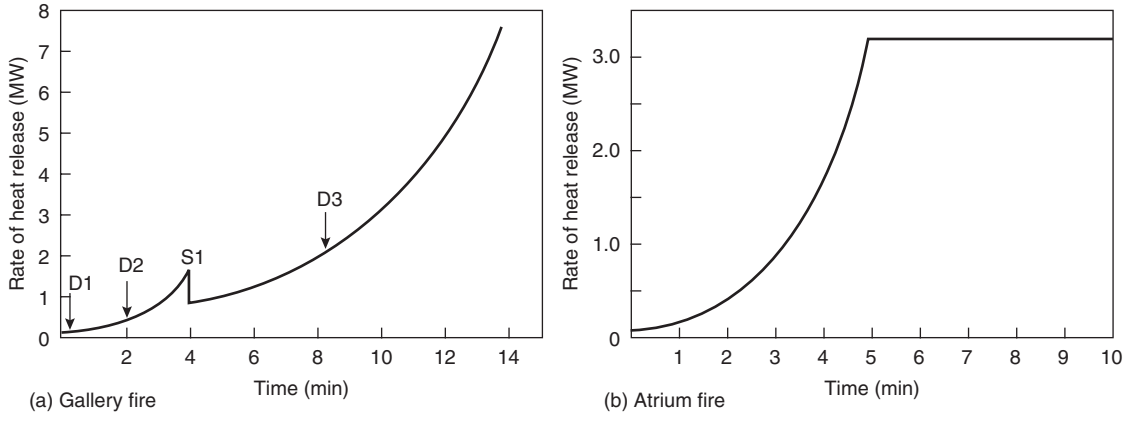

Figure 3-8.A3. ***Design fires for atrium complex.***

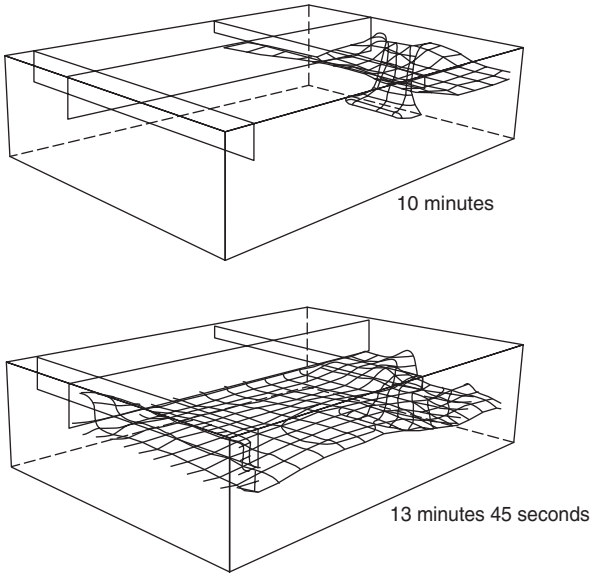

Figure 3-8.A4. ***Evolution of hazardous gas temperature of 80°C from above, looking toward main atrium volume.***

D3 in the adjacent zone, and the operation time for the first sprinkler nearest to the fire. It can be seen that the detector adjacent to the fire operated almost immediately. Figure 3-8.A4 shows the evolution of the contour of a hazardous, breathable gas temperature (80°C).

It can be seen that this hazardous contour takes about 10 min to reach the structural beam and crosses the smoke barrier (toward the adjacent smoke zone) in 11 min (not shown) and then starts spilling into the atrium as well as to the adjacent zone. This suggests that for the growing fire considered, the proposed extraction system would be able to cope with the smoke produced until 11 min have elapsed from the start of the fire.

The sprinkler operation pattern is shown in Figure 3-8.A5. By the time the rate of heat release had reached 5 MW (at 12 min), 14 sprinkler heads were predicted to have operated. This is well within the maximum operating area of the ordinary hazard group III sprinkler system specified under LPC rules for automatic sprinkler installations.[70]

Should the fire continue to grow in the way assumed, however, then by the time 7.5 MW was reached, 40 heads would have operated, well in excess of the LPC rules for assumed maximum area. The system would, therefore, "overrun" in these circumstances.

Atrium fire: The progress of a number of predicted visibility contours on a vertical slice through the center of the atrium is illustrated in Figure 3-8.A6. The model predicts that a beam detector, at the first gallery floor level, detects the fire at 65 s when its heat output has reached 200 kW. On detection, the mechanical extract system operates and the escape doors at both ends of the atrium open to admit replacement air. The sudden opening of the doors causes the rising smoke plume to be deflected sideways, so much so that the dense smoke extends across the floor of the atrium, threatening occupants over a distance of 20 m to 30 m. As the fire continues to grow, producing greater buoyancy, the plume slowly recovers. However, smoke at floor level does remain a problem until around 8 min. Smoke also enters the galleries at a high level, but since its temperature, optical density, and toxic gas concentration are below significant levels, this does not cause serious concern.

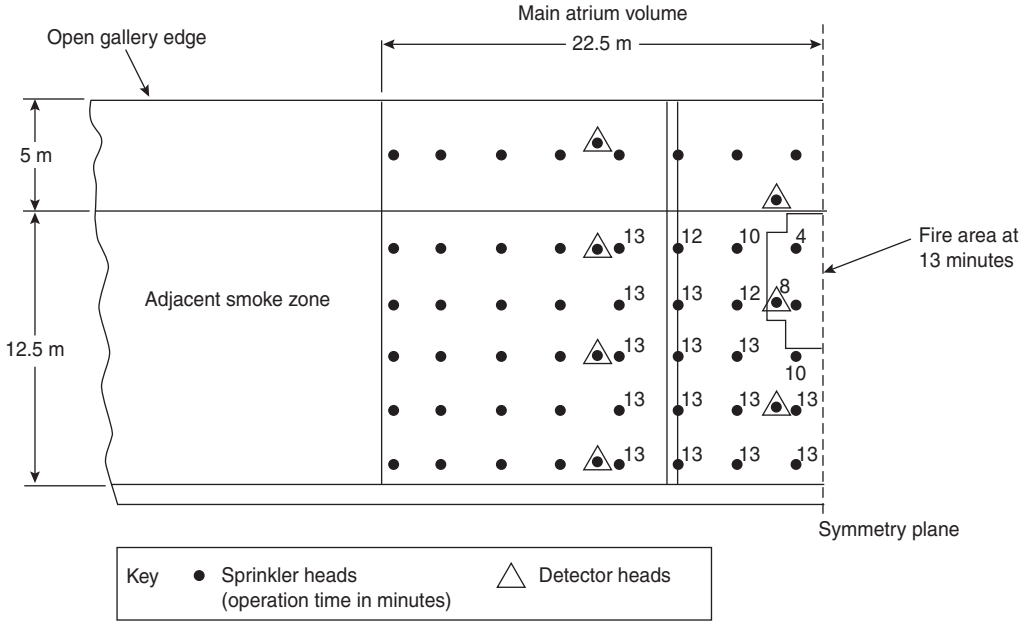

Figure 3-8.A5. ***Sprinkler operation pattern in gallery smoke zone.***

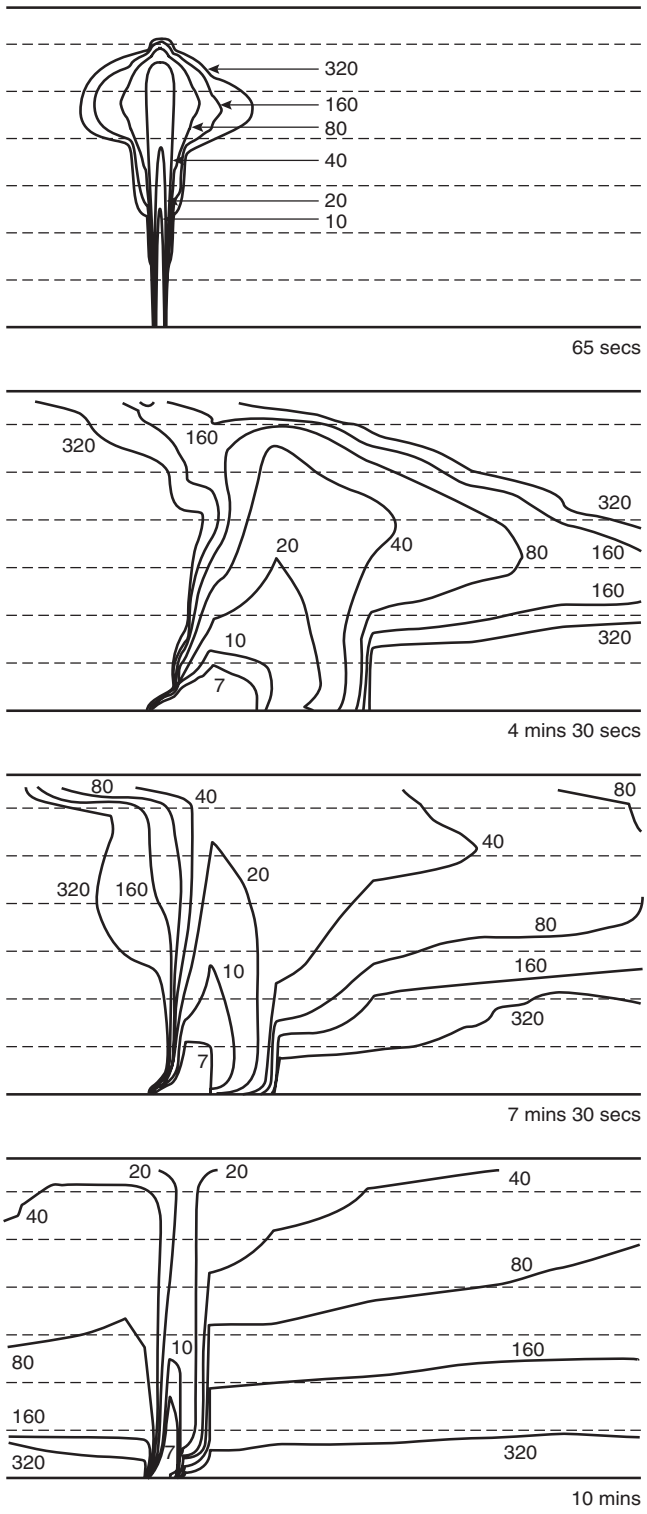

Figure 3-8.A6. ***Evolution of predicted visibility contours (m) on a vertical slice through the center of the atrium.***

Conclusion

The model predictions suggest that management of the smoke extraction system required attention in the main atrium. A progressive increase of the extraction rate would be one solution to the deflection of the smoke along the atrium, as would a redesign of the air inlets to prevent jetting.

Nomenclature

a	radiation absorption coefficient (Equations 13–21)
A_i^{ϕ}	influence coefficients (Equations 28, 31)
b^{ϕ}	source and time-dependent terms (Equations 28, 31)
b	weighting coefficient (Equations 21, 22)
B	pre-exponential factor (Equations 11, 36)
c	soot concentration (Equation 21)
c_p	specific heat
C_1, C_2 C_{μ}	constants in $k \sim \varepsilon$ model (Table 3-8.1)
C_D	drag coefficient (Equation 38)
C_b	evaporation constant (Equations 40, 41)
d	wall thickness (Figure 3-8.6)
D	fuel base diameter (Equation 33); droplet diameter (Equations 38–40, 42)
E	constant in log-law of wall (Equation 3), activation energy (Equation 11)
E_b	blackbody emissive power (Equations 13–21)
f	mixture fraction (Table 3-8.1, Equation 10)
f_v	soot volume fraction (Equation 24)
F	Fuel (Equation 9)
F_i	radiative flux in ith direction (Equations 13–17)
G	turbulent generation term (Table 3-8.1)
g	acceleration due to gravity
H.O.T.	higher-order terms (Equation 29)
h	enthalpy
I	radiation intensity (Equation 18)
k	thermal conductivity (Equations 26, 35), turbulent kinetic energy (Table 3-8.1, Equations 11, 12)
K_{ϕ}, K_{in}	underrelaxation and inertial relaxation factors (Equations 30–32)
l	pathlength (Equation 21)
L	latent heat of vaporization
O	oxidant (Equation 9)
p	pressure
p_w, p_c	partial pressures for water vapor and CO_2 (Equations 21, 25)
P_j	constant in Equation 4 representing resistance of laminar sublayer
P	product (Equation 9)
$\dot{q}''$	flux
$\dot{Q}$	heat release rate
Q^*	nondimensional heat release rate (or source Froude number)
R	gas constant (Equation 11)
Re	Reynolds number
s	stoichiometric requirement of fuel (Equations 9, 11), scattering coefficient
S	source term (Table 3-8.1)

t	time
T	temperature
u	gas velocity
v	droplet velocity
Vol	cell volume
x	spatial coordinate
y	distance from wall (Equation 5)
Y	mass fraction (Table 3-8.1; Equation 11)

Greek

α	radiation absorptivity (Equations 23–25)
β	conserved scalar (Equation 10)
γ	coefficient of thermal expansion (Equation 2)
Γ	exchange coefficient (Table 3-8.1)
ε	rate of dissipation of turbulent kinetic energy (Table 3-8.1, Equation 11)
κ	von Karman constant (Equation 3)
λ	radiation wavelength (Equation 24)
μ	absolute viscosity (Table 3-8.1; Equation 5)
ν	kinematic viscosity
ρ	density
σ	Prantdl/Schmidt numbers (Table 3-8.1)
ϕ	general fluid property variable (Table 3-8.1)
Ω	solid angle (Equations 19, 20)
ξ	normalized partial pressure (Equation 25)

Superscripts

$+$	dimensionless property in wall functions
$-$	time average
$'$	fluctuating property, correction
$''$	per unit area
$'''$	per unit volume
$*$	guessed value; derived expression; nondimensional parameter
t	near wall value

Subscripts

i,j,k	three Cartesian coordinate directions
a	ambient
b	blackbody
B	buoyancy
c	convective
d	liquid drop
f	fuel
k	shear
l	laminar
nb	neighboring node
o	oxidant
ox	oxygen
P	nodal point
R	radiation
s	solid, soot
st	stoichiometric value
t	turbulent
tot	total
w	wall

References Cited

1. L.F. Richardson, "Volume 1: Meteorogy and Numerical Analysis," Collected Papers, Cambridge University Press (1993).
2. G. Cox, *Combustion Fundamentals of Fire,* Academic Press, London (1995).
3. K.B. McGrattan, H.R. Baum, and R.G. Rehm, "Large Eddy Simulations of Smoke Movement," *F. Safety J.,* 30, p. 161 (1998).
4. X. Zhou, K.H. Luo, and J.J.R. Williams, "Dynamic Behaviour in Reacting Plumes," in *Proceedings of the Twenty-Eighth Symposium (International) on Combustion,* Combustion Institute, Pittsburgh (2000).
5. L. Vervisch and T. Poinsot, "Direct Numerical Simulation of Non-Premixed Turbulent Flames," *Ann. Rev. Fluid Mech.,* 30, p. 655 (1998).
6. G. Cox, *Turbulent Closure and the Modelling of Fire Using CFD,* Phil. Trans. Roy. Soc., London, A 356, p. 2835 (1998).
7. S.V. Patankar, *Numerical Heat Transfer and Fluid Flow,* Hemisphere, Washington, DC (1980).
8. H.K. Versteeg and W.M.G. Malalasekera, *An Introduction to Computational Fluid Dynamics,* Longman, London (1995).
9. S. Kumar, "Mathematical Modelling of Natural Convection in Fire—A State of the Art Review of the Field Modelling of Variable Density Turbulent Flow," *Fire Materials,* 7, pp. 1–24 (1983).
10. S.V. Patankar and D.B. Spalding, "A Computer Model for Three-Dimensional Flow in Furnaces," in *Fourteenth Symposium (International) on Combustion,* Combustion Institute, Pittsburgh, pp. 605–614 (1973).
11. W.P. Jones and J.H. Whitelaw, "Calculation Methods for Reacting Turbulent Flows: A Review," *Combustion & Flame,* 48, p. 1 (1982).
12. N.C. Markatos, M.R. Malin, and G. Cox, "Mathematical Modelling of Buoyancy Induced Smoke Flow in Enclosures," *Int. J. Heat Mass Transfer,* 25, pp. 63–75 (1982).
13. S.D. Miles, S. Kumar, and G. Cox, "Comparison of 'Blind Predictions' of a CFD Model with Experimental Data," in *Proceedings of the Sixth International Symposium on Fire Safety Science,* IAFSS, Boston, pp. 543–554 (2000).
14. B.E. Launder and B.I. Sharma, "Application of the Energy Dissipation Model of Turbulence to the Calculation of Flow Near a Spinning Disc," *Lett. Heat and Mass Transf.,* 1, pp. 131–138 (1974).
15. D.B. Spalding, "Mixing and Chemical Reaction in Steady State Confined Turbulent Flames," in *Thirteenth Symposium (International) on Combustion,* Combustion Institute, Pittsburgh, pp. 649–657 (1971).
16. B.F. Magnussen and B.H. Hjertager, "On Mathematical Modelling of Turbulent Combustion with Special Emphasis on Soot Formation and Combustion," in *Sixteenth Symposium (International) on Combustion,* Combustion Institute, Pittsburgh, pp. 719–729 (1976).
17. B.F. Magnussen, B.H. Hjertager, J.G. Olsen, and D. Bhaduri, "Effects of Turbulent Structure and Local Concentrations on Soot Formation and Combustion in Acetylene Diffusion Flames," in *Seventeenth Symposium (International) on Combustion,* Combustion Institute, Pittsburgh, pp. 1383–1393 (1978).

18. G. Cox and S. Kumar, "Field Modelling of Fire in Forced Ventilated Enclosures," *Combust. Sci. Technol,* 52, pp. 7–23 (1987).
19. J. Holen, M. Brostrom, and B.F. Magnussen, "Finite Difference Calculation of Pool Fires," *Twenty-Third Symposium (International) on Combustion,* Combustion Institute, Pittsburgh, pp. 1677–1683 (1990).
20. S. Gordon and B.J. McBride, "Computer Program for Calculation of Complex Chemical Equilibrium Compositions, Rocket Performance, Incident and Reflected Shocks and Chapman-Jouguet Detonations," *NASA SP-273* (1971).
21. J.B. Moss, "Turbulent Diffusion Flames," *Combustion Fundamentals of Fire,* Academic Press, London (1995).
22. S.K. Liew, K.N.C. Bray, and J.B. Moss, "A Flamelet Model of Turbulent Non-Premixed Combustion," *Combus. Sci. Technol.* 27, pp. 69–73 (1981).
23. G.M. Faeth, S.M. Jeng, and J. Gore, "Radiation from Fires," in *Heat Transfer in Fire and Combustion Systems,* 45, p. 137 (1985).
24. F.C. Lockwood and N.G. Shah, "A New Radiation Solution Method for Incorporation in General Combustion Prediction Procedures," in *Proceedings of the Eighteenth Symposium (International) on Combustion,* Combustion Institute, Pittsburgh, pp. 1405–1414 (1981).
25. N.W. Bressloff, "CFD Prediction of Coupled Radiation Heat Transfer and Soot Production in Turbulent Flames," Ph.D. Thesis, Cranfield University, UK (1996–1997).
26. N.W. Bressloff, J.B. Moss, and P.A. Rubini, "Application of a New Weighting Set for the Discrete Transfer Radiation Model," in *Proceedings of the Third European Conference on Industrial Furnaces and Boilers,* Lisbon, Portugal (1995).
27. P.S. Cumber, "Ray Effect Mitigation in Jet Fire Radiation Modelling," *Int. J. Heat Mass Transf.,* 43, pp. 935–943 (2000).
28. M. Aksit, P. Mackie, and P.A. Rubini, "Coupled Radiative Heat Transfer and Flame Spread Simulation in a Compartment," in *Proceedings of the Third International Seminar on Fire and Explosion Hazards,* Lake Windermere, UK, pp. 343–354 (2000).
29. S. Kumar, A.K. Gupta, and G. Cox, "Effects of Thermal Radiation on the Fluid Dynamics of Compartment Fires," in *Proceedings of the Third International Symposium on Fire Safety Science,* Elsevier, London, p. 345 (1991).
30. F.C. Lockwood and W.M.G. Malalasekera, "Fire Computation: the Flashover Phenomenon," in *Proceedings of the Twenty-Second Symposium (International) on Combustion*, Combustion Institute, Pittsburgh, pp. 1319–1328 (1988).
31. J.S. Truelove, "Mixed Grey Gas Model for Flame Radiation," Harwell, UK Atomic Energy Authority Report AERE HL 76/3448, (1976).
32. W.L. Grosshandler, "Radiative Heat Transfer in Non-Homogeneous Gases: A Simplified Approach," *Intl. J. Heat Mass Transfer,* 23, p. 1447 (1980).
33. A.T. Modak, "Radiation from the Products of Combustion," *Fire Res.,* 1, pp. 339–361 (1978–79).
34. B. Leckner, "Spectral and Total Emissivity of Water Vapour and Carbon Dioxide," *Combust. Flame,* 19, pp. 33–48 (1972).
35. J.D. Felske and C.L. Tien, "Calculation of the Emissivity of Luminous Flames," *Combust. Sci. Technol.,* 7, pp. 25–31 (1973).
36. Z. Yan and G. Holmstedt, "Fast, Narrow-Band Computer Model for Radiation Calculations," *Numerical Heat Transfer,* 31B, p. 61 (1997).
37. G. Cox, "On Radiant Heat Transfer from Turbulent Flames," *Combust. Sci. Technol.,* 17, pp. 75–78 (1977).
38. J.P. Gore and G.M. Faeth, "Structure and Spectral Radiation Properties of Turbulent Ethylene/Air Diffusion Flames," in *Twenty-First Symposium (International) on Combustion,* Combustion Institute, Pittsburgh, pp. 1521–1531 (1987).
39. H.S. Carslaw and J.C. Jaeger, *Conduction of Heat in Solids,* Oxford University Press, England (1959).
40. C.T. Shaw, *Using Computational Fluid Dynamics,* Prentice Hall, London (1992).
41. Guide for the Verification & Validation of CFD Simulations, American Institute of Aeronautics & Astronautics, Guide G-077-1998, AIAA, Reston, VA (1998).
42. S. Kumar and G. Cox, "The Application of a Numerical Field Model of Smoke Movement to the Physical Scaling Compartment Fires," in *Numerical Methods in Thermal Problems,* pp. 837–848 (1983).
43. S. Kumar and G. Cox, "Mathematical Modelling of Fire in Road Tunnels," in *Proceedings of the Fifth International Symposium on Aerodynamics and Ventilation of Vehicle Tunnels,* BHRA, Cranfield, UK, p. 61 (1985).
44. W.H. Ayres, "Fundamental Studies of the Extinguishment of Pool Fires in a Cross Wind," Ph.D. Thesis, University of Sheffield, UK (1988).
45. F.C. Lockwood and W.M.G. Malalasekera, "Fire Computation: the Flashover Phenomenon," in *Twenty-Second Symposium (International) Combustion,* Combustion Institute, Pittsburgh, pp. 1319–1328 (1988).
46. M.J. Lewis, J.B. Moss, and P.A. Rubini, "CFD Modelling of Combustion and Heat Transfer in Compartment Fires," in *Proceedings of the Fifth International Symposium on Fire Safety Science,* International Association for Fire Safety Science, Melbourne, Australia, pp. 463–474 (1997).
47. N.L. Crauford, S.K. Liew, and J.B. Moss, "Experimental and Numerical Simulation of a Buoyant Fire," in *Comb. Flame,* 61, p. 63 (1985).
48. G. Cox, S. Kumar, and N.C. Markatos, "Some Field Model Validation Studies," in *Proceedings of the First International Symposium on Fire Safety Science,* Hemisphere, Washington, DC, pp. 159–171 (1986).
49. Y.L. Sinai, "Validation of CFD Modelling of Unconfined Pool Fires with Cross Wind: Flame Geometry," *Fire Safety J.,* 24, p. 1 (1995).
50. L. Kerrison, N. Mawhinney, E.R. Galeas, N. Hoffmann, and M.K. Patel, "A Comparison of Two Fire Field Models with Experimental Room Fire Data," in *Proceedings of the Fourth International Symposium on Fire Safety Science,* IAFSS, Ottawa, Canada, pp. 161–172 (1994).
51. S. Nam, "Numerical Simulation of Smoke Movement in Clean Room Environments," *Fire Safety J.,* 34, p. 169 (2000).
52. S. Hostikka and O. Keski-Rahkonen, "Design and Simulation Reports of CIB W14 Round Robin for Code Assessment, Scenario B," *VTT Building Technology Internal report RTE119-IR-2,* Espoo, Finland (1998).
53. Y. Sinai, "Comments on the Role of Leakages in Field Modelling of Under-Ventilated Compartment Fires," *Fire Safety J.,* 33, p. 11 (1999).
54. D. Fennel, "Investigation into the King's Cross Underground Fire," Her Majesty's Stationery Office, London (1988).
55. S. Simcox, N.S. Wilkes, and I.P. Jones, "Computer Simulation of the Flows of Hot Gases from the Fire at the King's Cross Underground Station," *Fire Safety J.,* 18, p. 49 (1992).
56. G. Cox, R. Chitty, and S. Kumar, "Fire Modelling and the King's Cross Fire Investigation," *Fire Safety J.,* 15, p. 7 (1989).
57. S. Welch and P. Rubini, "Three Dimensional Simulation of a Fire Resistance Furnace," in *Proceedings of the Fifth International Symposium on Fire Safety Science,* IAFSS, Melbourne, Australia, pp. 1009–1020 (1997).
58. C. di Blasi, S. Crescitelli, G. Russo, and A.C. Fernandez-Pello, "Model of the Flow Assisted Spread of Flames over a Thin Charring Combustible," in *Proceedings of the Twenty-Second*

Symposium (International) on Combustion, Combustion Institute, Pittsburgh, pp. 1205–1212 (1988).

59. Z. Yan and G. Holmstedt, "CFD and Experimental Studies of Room Fire Growth on Wall Lining Materials," *Fire Safety J.,* 27, p. 201 (1996).
60. V. Novozhilov, B. Moghtaderi, D.F. Fletcher, and J.H. Kent, "Computational Fluid Dynamics Modelling of Wood Combustion," *Fire Safety J.,* 27, p. 69 (1996).
61. Y.H.C. Chao and A.C. Fernandez-Pello, "Concurrent Horizontal Flame Spread: The Combined Effect of Oxidiser Flow Velocity, Turbulence and Oxygen Concentration," *Comb. Sci. Tech.,* 19, pp. 110–111 (1995).
62. K. Opstad, "Modelling of Thermal Flame Spread on Solid Surfaces in Large Scale Fires," Doctoral Thesis, University of Trondheim, Norway (1995).
63. C.T. Crowe, M.P. Sharma, and D.E. Stock, "The Particle-Source-in-Cell Model for Gas Droplet Flows," *ASME Journal of Fluids Engineering,* 99, p. 325 (1977).
64. F. Boysan, W.H. Ayres, J. Swithenbank, and Z. Pan, "Three Dimensional Model of Spray Combustion in Gas Turbine Combustors," *J. Energy,* 6, p. 368 (1982).
65. S. Kumar, G.M. Heywood, and S.K. Liew, "Superdrop Modelling of a Sprinkler Spray in a Two-Phase CFD-Particle Tracking Model," in *Proceedings of the Fifth International Symposium on Fire Safety Science,* Melbourne, Australia, p. 889 (1997).
66. http://www.cham.co.uk
67. http://www.aeat.com/cfx
68. http://www.fluent.com
69. http://www.cd.co.uk
70. *Rules for Automatic Sprinkler Installations,* Loss Prevention Council, UK (1996).

CHAPTER 9

Smoke and Heat Venting

Leonard Y. Cooper

Introduction

Objectives of Venting by Design

Smoke and heat venting is the removal of hot smoky gases from the upper parts of one or more rooms of a fire-containing facility and the introduction of relatively cool and uncontaminated air into the lower parts of the rooms from adjacent spaces or from the outside environment. Smoke removal by venting may be driven by (1) natural convection (i.e., buoyancy-driven forces), occurring either fortuitously (e.g., natural venting of smoke through broken windows near the top of a room of fire origin) or by design (e.g., a well-designed system of fusible-link-actuated ceiling vents); by (2) mechanical ventilation (i.e., fan-driven smoke removal); or by (3) a combination of these.

The main objectives of venting by design are (1) to facilitate escape of people from fire environments by restricting spread of smoke and hot gases into escape routes; (2) to facilitate fire fighting by enabling fire fighters to enter the building and to see the seat of the fire; and (3) to reduce property damage from fires due to exposure to smoke and hot gases.

The Focus of This Chapter

The focus of this chapter is on fire safety problems involving smoke venting of single spaces of fire origin and/or freely connected (i.e., via relatively large connecting openings) adjacent spaces by designed use of ceiling- or near-ceiling-mounted vents. Typical, relevant compartment geometries are (1) large, open, ceiling vent–deployed warehouse-type spaces (see Figure 3-9.1), possibly divided by ceiling-mounted screens or draft curtains into separate, freely-connected, curtained spaces; and (2) multiple-space, atrium-like facilities (see Figure 3-9.2) involving fire near the floor of a ceiling-vented atrium (Space 1) or fire in a ground- or mezzanine-level shop (Space 2A or Space 2B) adjacent and freely connected to a ceiling-vented atrium.

This chapter is concerned with basic engineering concepts underlying the design of complete venting systems

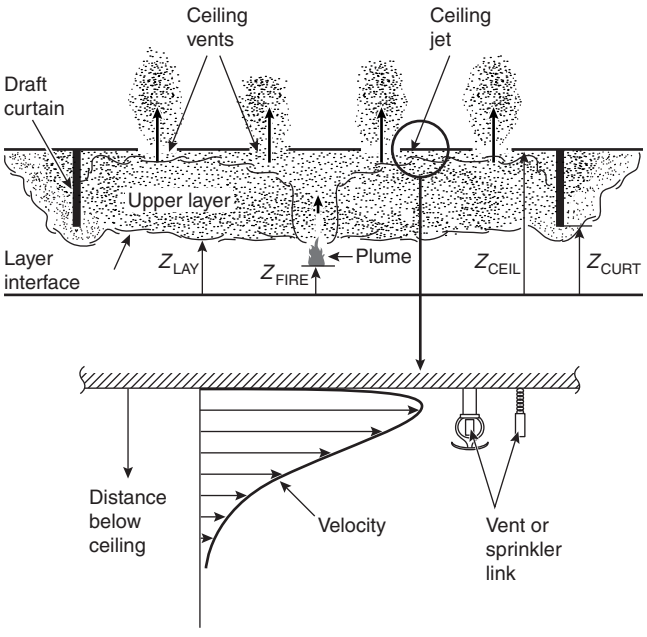

Figure 3-9.1. ***Fire in a building space with draft curtains and ceiling vents.***

Dr. Leonard Y. Cooper was a research engineer in the Building and Fire Research Laboratory of the National Institute of Standards and Technology from 1978 to 1998. Since 1998 he has been senior scientist/engineer at Hughes Associates Inc., a fire protection engineering research and development firm. Since 1978 he has focused on applying a broad range of the physical and mechanical engineering sciences to develop and transfer research results into technically sound engineering practices in the field of applied fire safety. His research has included the development of mathematical models of fire phenomena and on the assembly of these into compartment fire models and associated computer programs for practical and research-oriented compartment fire simulations.

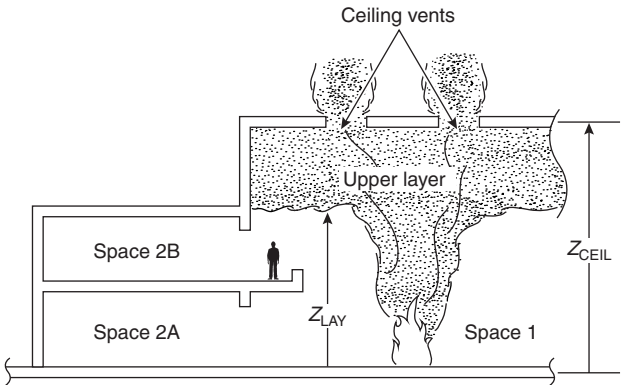

Figure 3-9.2. ***Fire near the floor of a ceiling-vented atrium with ground- and mezzanine-level shops.***

for the above types of facility. These include the provision of vents and inlets, fans, and allied features, such as ceiling-mounted screens or draft curtains, where the latter would be deployed to divide a space into separate curtained compartments to limit the smoke from spreading outside an arbitrary, curtained compartment of fire origin.

Venting phenomena become significantly more complex when venting is used in conjunction with active sprinkler systems. The first part of the chapter deals with the traditional aspects of venting in the absence of operating sprinklers. The extent of current knowledge on the interaction of vents and sprinklers and the design of combined vent/sprinkler systems is discussed at the end of the chapter.

It is beyond the scope of this chapter to be exhaustive on all aspects of the subject of smoke and heat venting. In this regard, the reader is particularly encouraged to complement the material presented here with that provided in References 1–4, each of which provides design-type guidance on aspects of smoke and heat venting, and in Section 4, Chapter 13, "Smoke Management in Covered Malls and Atria."

A major feature of this chapter is the presentation of the actual equations required for the design of successful smoke- and heat-venting systems. Many of these equations can be found in References Cited. When introducing these equations, it is an important objective of the presentation here to include their physical bases and their logical context. This is done to enhance the reader's understanding of basic concepts and, to the extent possible, to avoid their inappropriate use.

Simulating Fire-Generated Environments and the Action of Venting

Criteria for Successful Vent Design

A ceiling-vent design is successful to the extent that it controls the fire-generated environment of fire origin according to any of a variety of possible specified criteria. For example, if the likely growth rate of a fire in a particular burning commodity is known, a vent system with large enough vent area, designed to provide for timely opening of the vents, should be expected to lead to rates of smoke removal consistent with a fire-safe environment. Regarding life safety objectives, the design should allow occupants of the space enough time to exit safely. Regarding property protection, fire fighters arriving at the fire at a specified time subsequent to fire detection should be able to approach and attack the fire successfully and protect commodities in adjacent spaces from being damaged.

Evaluating the Success of a Particular Vent Design

To evaluate the success of a particular vent design and/or design strategy it is necessary to predict the development of the fire environment in the fire compartment as a function of any of a number of physical characteristics that define, and may have a significant effect on, the fire environment. Examples of such characteristics are floor-to-ceiling height and area of the compartment spaces and thermal properties of its ceilings, walls, and floors; type of barriers that separate the space of fire origin and adjacent spaces (e.g., full walls with vertical door-like vents or ceiling-mounted draft curtains); material type and arrangement of burning commodities (in the case of warehouse configurations, e.g., wood pallets in 3 m $\times$ 3 m arrays and stacked 2 m high); type, location, and method of deployment of devices that detect the fire and actuate the opening of deployed ceiling vents, or initiate the operation of sprinklers [e.g., fusible links of specified Response Time Index (RTI) that are distributed at a specified spacing and mounted at a specified distance below the ceiling]; and size of the open area of deployed ceiling vents themselves.

Fire environments can involve substantially steady-state phenomena, but it is more typical for time-dependent phenomena to play a prominent role in real fire safety problems of interest. In most cases, the best way to predict the fire environment and to evaluate the likely effectiveness of a vent design is to use a reliable mathematical model that simulates the various, relevant physical phenomena that come into play during the fire scenario. Such a tool of analysis would be designed to solve well-formulated mathematical problems, based on relevant principles of physics and fundamentally sound, well-established empirical relationships. In this regard, venting phenomena are part of the general phenomena of fire and smoke spread through single- or multiroom compartments. Indeed, any compartment fire model that can simulate the development of fire-generated conditions in enclosed facilities can typically also be used as an engineering tool for the design and analysis of venting.

Even for a particular class of problem, like the engineering problem associated with successful vent design, there is a good deal of variation among applicable mathematical models that are available or among those that could be developed to carry out the task. Such models would differ from one another by the number and detail of individual physical phenomena taken into account. Thus, the above list of physical characteristics that define and may have a significant effect on the fire scenario does not include outside wind conditions, which could have an important influence on the fire-generated environment. A

model may or may not include the effect of wind. One that included this effect would be more difficult to develop and validate and more complicated to use, but, if well developed, it would be significantly more reliable than a model that assumes a quiescent outside environment.

In the next section a group of phenomena is described that, taken together, represents a physical basis for estimating the fire-generated environment and the response of fusible vent or sprinkler links in well-ventilated compartment fires with draft curtains and fusible-link-actuated ceiling vents. The phenomena include growth of the smoke layer in the curtained compartment; flow dynamics of the buoyant fire plume; flow of smoke through open ceiling vents; flow of smoke below draft curtains; continuation of the fire plume in the upper layer; heat transfer to the ceiling surface and thermal response of the ceiling; velocity and temperature distribution of the plume-driven, near-ceiling flow (called the *ceiling jet*) and response of near-ceiling-deployed fusible links. An understanding of and capability of accounting quantitatively for these phenomena is a basic requirement for understanding and simulating their simultaneous action.

The Physical Basis for Simulating Fire-Venting Phenomena

The Basic Fire Scenario

Unless noted otherwise, the discussion of basic phenomena is couched in terms of a generic Figure 3-9.1–type of fire scenario and facility. As will be mentioned, these considerations are also directly applicable to Figure 3-9.2–type scenarios.

The reader is referred to the first part of Section 3, Chapter 10, "Compartment Fire-Generated Environment and Smoke Filling," for a complementary and somewhat more general qualitative discussion of phenomena for generic two-room compartment fire scenarios. The discussion there is applicable to all configurations of Figures 3-9.1 and 3-9.2.

Refer to Figure 3-9.1. Consider the space of fire origin defined by ceiling-mounted draft curtains and with near-ceiling, fusible-link-actuated ceiling vents and sprinklers. The curtained area can be considered one of several such spaces in a large building compartment. Also, by specifying that the curtains be deep enough, they can be thought of as simulating the walls of a single uncurtained compartment. The first part of this chapter identifies and discusses critical physical phenomena that determine the overall environment in the curtained space up to the time of actuation of sprinklers, if they are deployed. The objective is to identify and describe the phenomena in a manner that captures the essential features of this generic class of fire scenario, and allows for a complete and general, but appropriately concise and simple, simulation.

The overall building compartment is assumed to have near-floor inlet vents that are large enough to maintain the inside environment, below any near-ceiling smoke layers which may form, at outside-ambient conditions. It is assumed that a two-layer zone-type model describes adequately the phenomena under investigation. The characteristics of the lower layer, from the floor, at $z = 0 = z_{FLOOR}$, to the bottom of the upper smoke layer, at $z = z_{LAY}$, are assumed to be well described by those of the outside ambient. In general, the upper smoke-layer thickness changes with time, but at any instant it is assumed to be uniform in space, with absolute temperature, T_{LAY}, and density, ρ_{LAY}.

Mass and energy are transferred continuously to and from the upper and lower layers by a variety of mechanisms to be discussed. Conservation of energy and mass along with the perfect gas law is applied to the layers. This leads to equations that require estimates of components of heat transfer, enthalpy flow, and mass flow to the layers. Qualitative and some key quantitative features of these phenomena are described and presented below.

Hydrostatic Pressure Variation as a Function of Elevation within the Fire Space and in the Outside Environment

The hydrostatic pressure of a standard ambient atmosphere at sea level is $P_{AMB} = 101325$ Pa. Also, air at nearly standard atmospheric conditions can be well approximated as a perfect gas with equation of state

$$P = \rho RT \tag{1}$$

where P, T, and ρ are absolute pressure, temperature, and density, respectively, and $R = 286.8$ J/(kg·K) is the gas constant for air. For an ambient temperature, assumed here to be $T_{AMB} = 293$ K, it follows from Equation 1 that, for a quiescent standard atmosphere, $\rho_{AMB} = 1.2$ kg/m^3.

It is generally accepted that for the accuracy required in fire model simulations, the equation of state of fire-heated and -contaminated air, that is, smoke, can be taken to be that of air. Therefore, Equation 1 represents the equation of state for ambient air and for smoke at arbitrary temperatures that are realizable in fires.

The momentum equation, that is, hydrostatics, leads to

$$P(z) = P(z_0) - \int_{z_0}^{z} \rho(\eta) g d\eta \equiv P(z_0) + \Delta P(z) \tag{2}$$

where z_0 is a datum elevation and $g = 9.8$ m/s^2 is the acceleration of gravity.

Using Equation 1 in Equation 2, it can be shown[5] that relative variations in $P(z)$ are negligible throughout typical buildings, even when a building includes a fire environment, and throughout the "nearby" outside environment. In particular, throughout buildings and local outside environments

$$P(z) = P(z_0)[1 + O(\delta)] \approx P(z_0) \tag{3}$$

where

$$\delta = \frac{\rho g (z - z_0)}{P(z_0)} \ll 1 \tag{4}$$

The fact that δ is generally small can be shown for the outside environment, for example, by considering changes in

elevation from a z_0 datum of the order of 100 m and by adopting the estimate, $\rho = \rho_{OUT}(z) \approx \rho_{AMB}$. Then, assuming that $P_{OUT}(z_0) \approx P_{AMB}$, it follows from Equation 4 that

$$\begin{aligned}\delta_{OUT} &= \frac{\rho_{OUT} g(z - z_0)}{P_{OUT}(z_0)} \\ &\approx \frac{(1.2\ \text{kg/m}^3)(9.8\ \text{m/s}^2)(100\ \text{m})}{[10^5\ \text{kg/(ms}^2)]} \\ &= 0.012\end{aligned}$$

and, from Equation 3, that changes in $P_{OUT}(z)$ throughout the 100-m elevation range will generally (only) be of the order of 1 percent.

It is concluded from Equations 3 and 4 that throughout all practical fire environment–related spaces, including the nearby outside ambient,

$$\rho T \approx \rho_{AMB} T_{AMB} = \frac{P_{AMB}}{R} = \text{constant} \qquad (5)$$

Although Equation 5 is a generally valid approximation, and $\Delta P(z)$ of Equation 2 is typically relatively small throughout fire environment–related spaces, these latter variations in pressure as a function of elevation will be seen to play an important role in determining the rate of buoyancy-driven flows through vents. Using again the approximation $\rho = \rho_{OUT}(z) \approx \rho_{AMB} =$ constant in Equation 2 leads to the following estimate for the elevation-dependent variation of the outside environment

$$\begin{aligned}\Delta P_{OUT}(z) \equiv P_{OUT}(z) - P_{OUT}(z_0) &= -\int_{z_0}^{z} \rho_{OUT}(\eta) g d\eta \\ &\approx -\rho_{AMB} g(z - z_0) \qquad (6)\end{aligned}$$

Flow through Vents

General theory: The reader is referred to Section 2, Chapter 3, "Vent Flows," for a general discussion on the topic of flow through vents.

Consider a vent (i.e., an opening) in a wall-, ceiling-, or floorlike partition, and, for purpose of discussion, designate the two sides/spaces that are connected by the vent as sides/spaces 1 and 2. In most cases of practical interest here, flow is driven through such a vent mainly by cross-vent hydrostatic pressure differences from the high- to the low-pressure side of the vent, where the traditional means of calculating vent-flow rates is by using an orifice-type flow calculation.

At a particular elevation, somewhat removed from the vent opening, that is, on either side of the partition where velocities of the vent flow are relatively small, assume that the environment is relatively quiescent in the sense that the pressure there is well represented by the hydrostatic pressure. Relative to a common datum elevation, the hydrostatic pressure distributions, $P_1(z)$ and $P_2(z)$, associated with side/space 1 and 2, respectively, on both sides of the vent are calculated from Equation 2. Then, $\Delta P_{1\text{-}2}$, the cross-vent difference of these distributions is constructed from

$$\Delta P_{1\text{-}2}(z) \equiv P_1(z) - P_2(z) \qquad (7)$$

At any particular elevation, the average velocity of the vent flow at a vent opening, V_{VENT}, assumed to be in the direction normal to the plane of the vent opening and from the high- to the low-pressure side of the vent, can typically be well estimated from Bernoulli's equation as applied to flow through orifices

$$|V_{VENT}(z)| = C\left[\frac{2|\Delta P_{1\text{-}2}(z)|}{\rho_{VENT}(z)}\right]^{1/2} \qquad (8)$$

where $\rho_{VENT}(z)$ is the density of the vent flow (i.e., the density at elevation z in the space, 1 or 2, from which the vent flow originates) and C is the flow coefficient, or coefficient of contraction of the flow subsequent to its passage through the vent opening.

Where the Equation 8 formulation is valid, then for relatively narrow vents (e.g., the characteristic horizontal or vertical span of the vent is relatively small compared to the horizontal or vertical span, respectively, of the partition in which it is contained), C is typically taken to be

$$C \approx 0.61 \qquad (9)$$

This is the value associated with relatively high Reynolds-number flows through sharp-edged, circular orifices.

For relatively wide vents (e.g., the width and height of the vent are of the order of the width and height, respectively, of the space from which the vent flow originates), there is no significant contraction of the vent flow subsequent to its passage through the vent, and

$$C \approx 1.0 \qquad (10)$$

Equations 8 and 10 will be used below in estimating the rate of smoke flow below draft curtains.

Once $V_{VENT}(z)$ is obtained from Equation 8, the mass flow rate through the vent is finally calculated by integrating the mass-flow-rate flux across the entire area of the vent. For example, in the case of vents located in vertical wall partitions, the intergral would be from the bottom to the top elevations of the vent opening, z_{BOT} and z_{TOP}, respectively. (Note that an important feature of flows through vents in vertical wall partitions, e.g., flows through open doors or windows or under draft curtains, is that the direction of the flow, i.e., the velocity of the flow, can change direction as a function of elevation because of changes in sign with elevation of $\Delta P_{1\text{-}2}$.)

The orientation of a vent; horizontal and vertical vents: Define α as the angle that the normal to the plane of a vent opening makes with the vertical. Throughout this chapter, vents with $\alpha = 0$ will be designated as *horizontal* vents in the sense that the planes of the openings of such vents define horizontal planes. Similarly, vents with $\alpha = 90°$ will be designated as *vertical* vents.

Flow through nonhorizontal vents or through horizontal strips of nonhorizontal vents where $\Delta P_{1\text{-}2}$ does not change sign: For flow configurations where $\Delta P_{1\text{-}2}$ does not change signs across the area of a nonhorizontal vent, or across the area of a horizontal strip of a nonhorizontal vent

(a *horizontal strip* of a vent is defined as a portion of the vent between two horizontal planes), the above-indicated mass-flow-rate-flux integral leads to the following final representation for the total flow rate, $\dot{m}_{VENT}$, through the vent or through the vent strip:

$$\dot{m}_{VENT} = \left(\frac{1}{\sin\alpha}\right)\int_{z_{BOT}}^{z_{TOP}} W_{VENT}(\eta)\rho_{VENT}(\eta)\left|V_{VENT}(\eta)\right| d\eta, \quad \alpha > 0 \tag{11}$$

where $W_{VENT}(z)$ is the width of the vent at elevation z; z_{TOP} and z_{BOT} are the elevations at the top and bottom of the vent or of the strip, respectively; and $|V_{VENT}(z)|$ and $\rho_{VENT}(z)$ are determined from Equation 8 and from the direction of the flow.

Flow through horizontal vents: For horizontal vents, ΔP_{1-2} is uniform in sign and magnitude, V_{VENT} is uniform in direction and magnitude across the entire vent area, and

$$\dot{m}_{VENT} = A_{VENT}\rho_{VENT}\left|V_{VENT}(z_{VENT})\right| \tag{12}$$

where A_{VENT} is the area of the vent, z_{VENT} is the uniform elevation of the vent, and $\left|V_{VENT}(z_{VENT})\right|$ is obtained from Equations 7 and 8.

Flow through Ceiling Vents in a Figure 3-9.1–Type Fire Scenario

Cross-vent pressure, velocity, and mass-flow rate: Consider Figure 3-9.1–type fire scenarios. For well-designed smoke vent systems, it will be seen from considerations of Equation 2 that the buoyancy of the high-temperature smoke in the fire-containing curtained space will lead to an inside pressure at the ceiling that is larger than the outside pressure. Open ceiling vents there will lead to the desired outflow of smoke through the open vents according to Equations 8 and 12.

For a well-designed smoke vent system, it is assumed that there are always low-elevation (below any inside smoke layer that would have developed), open, inlet-/makeup-air vents connecting the inside space to the outside environment. The flow of outside air into the lower levels of the enclosed space is assumed to maintain the inside environment, outside any smoke layer, at a pressure, temperature, and density that is well approximated by that of the outside environment.

For the above assumptions to be valid, it is necessary that at any particular time during a fire scenario, the total area of the open inlet vents, A_{INLET}, is relatively large compared to A_{VENT}, large enough so that the pressure drop across the inlet vents is negligible compared to the pressure drop across any open ceiling vents. As will be seen, the latter assumption will typically be valid if the total area of the inlet vents is at least 1.5–2 times the total area of open ceiling vents.

Using Equation 6, the assumptions of negligible, below-smoke-layer, inside-to-outside pressure, temperature, and density differences *inside the facility but outside or below the smoke layer* lead to the result:

$$P_{IN}(z) = P_{OUT}(z) = P_{OUT}(z_0) - \rho_{AMB}g(z - z_0), \quad z \le z_{LAY} \tag{13}$$

where P_{IN} is the hydrostatic pressure inside the facility. A continuation of $P_{IN}(z)$ upward and *into the smoke layer in the curtained space of fire origin* is determined from Equations 2 and 13 as

$$P_{IN}(z) = P_{IN}(z_{LAY}) - \rho_{LAY}g(z - z_{LAY}), \quad z_{LAY} < z \le z_{CEIL} \tag{14}$$

and $\Delta P_{IN\text{-}OUT}$, the inside-to-outside pressure difference *inside the curtained space of fire origin* according to Equation 7, is found from Equations 6, 13, and 14 as

$$\Delta P_{IN\text{-}OUT}(z) = \begin{cases} 0, & z \le z_{LAY} \\ (\rho_{AMB} - \rho_{LAY})g(z - z_{LAY}) > 0, & z_{LAY} < z \le z_{CEIL} \end{cases} \tag{15}$$

From Equation 15, the *inside-to-outside pressure difference across horizontal ceiling vents is*

$$\begin{aligned} &\Delta P_{IN\text{-}OUT}(z_{CEIL}) \\ &\quad = (\rho_{AMB} - \rho_{LAY})g(z_{CEIL} - z_{LAY}) \\ &\quad = \rho_{AMB}g(z_{CEIL} - z_{LAY})\frac{(T_{LAY} - T_{AMB})}{T_{LAY}} > 0 \end{aligned} \tag{16}$$

Within the smoke layer, in general, and at $z = z_{CEIL}$ in particular, it is seen from Equations 15 and 16 that the inside pressure is always greater than the outside pressure. Thus, as expected, the flow through ceiling vents is from the smoke layer in the inside space to the outside space. Therefore, $\rho_{VENT} = \rho_{LAY}$. Using this last result with Equations 5, 8, 9, and 12 leads to the following estimate for $V_{VENT}(z)$, and $\dot{m}_{VENT}$ *for horizontal ceiling vents:*

$$\begin{aligned} V_{VENT} &= 0.61\left[2\frac{\Delta P_{IN\text{-}OUT}(z_{CEIL})}{\rho_{LAY}}\right]^{1/2} \\ &= 0.61\left[2\frac{\Delta P_{IN\text{-}OUT}(z_{CEIL})T_{LAY}}{(\rho_{AMB}T_{AMB})}\right]^{1/2} \end{aligned} \tag{17}$$

$$\begin{aligned} &\dot{m}_{VENT} \\ &\quad = A_{VENT}\rho_{LAY}V_{VENT} \\ &\quad = 0.61A_{VENT}\left[2\rho_{AMB}T_{AMB}\frac{\Delta P_{IN\text{-}OUT}(z_{CEIL})}{T_{LAY}}\right]^{1/2} \end{aligned} \tag{18}$$

Using Equations 16 and 18, the following final and particularly interesting representation for $\dot{m}_{VENT}$ *for horizontal ceiling vents* is obtained:

$$\begin{aligned} &\frac{(\dot{m}_{VENT}/A_{VENT})}{\{0.61\rho_{AMB}[g(z_{CEIL} - z_{LAY})/2]^{1/2}\}} \\ &\quad = \left[4\left(1 - \frac{T_{AMB}}{T_{LAY}}\right)\frac{T_{AMB}}{T_{LAY}}\right]^{1/2} \end{aligned} \tag{19}$$

From the above it is seen that the left side of Equation 19 is a function only of T_{LAY}/T_{AMB}. Also, it is easily shown that this dimensionless vent flow–rate variable has a maximum value of 1 when $T_{LAY} = 2T_{AMB}$. For example, for the currently adopted value of $T_{AMB} = 293$ K, the maximum possible flow rate from a ceiling vent above an arbitrary depth of smoke layer will occur when the temperature of the layer is $T_{LAY} = 2(293\text{ K}) = 586$ K. If T_{LAY} is larger or smaller than T_{AMB} then there will be a reduction in the vent flow rate from the maximum possible value. (Although larger layer temperatures would lead to greater buoyancy of the layer and larger cross-vent pressure drops, these increased pressure drops, which are proportional to V^2_{VENT}, would not be great enough to sustain the earlier mass flow rate. This is the case because, with the now-reduced layer density, a larger flow velocity would be required to maintain the previous mass flow rate.)

All the above are well illustrated in Figure 3-9.3 where the left side of Equation 19 is plotted as a function of T_{LAY}/T_{AMB}. From this plot it is seen that if $T_{LAY}/T_{AMB} > 1.3$, that is, $T_{LAY} - T_{AMB} > 90$ K for $T_{AMB} = 293$ K, the effect of T_{LAY} on $\dot{m}_{VENT}$ is minimal and $\dot{m}_{VENT}$ will always be within 80 percent of its maximum possible value. The plot also indicates that T_{LAY} values much smaller than $1.3T_{AMB}$ will lead to significant reductions in $\dot{m}_{VENT}$.

Generic plots of $P_{IN}(z)$, $P_{OUT}(z)$, and $\Delta P_{IN\text{-}OUT}(z)$ and an illustration of the flow through a ceiling vent are presented in Figure 3-9.4.

EXAMPLE 1:

Flow through a horizontal ceiling vent: As an example of the above, consider horizontal ceiling vents above a 3-m-thick smoke layer that is 100 K greater than $T_{AMB} = 293$ K. From Equations 16 and 17 the cross-vent pressure difference and the velocity will be

$$\Delta P_{IN\text{-}OUT}(z_{LAY}) = 1.2(\text{kg/m}^3)(9.8)(\text{m/s}^2)(3\text{ m})\frac{(100)}{(393)}$$
$$= 9.0\text{ kg/(m·s}^2) = 9.0\text{ Pa}$$

$$V_{VENT} = 0.61\left[2(9.0\text{ kg/m·s})\frac{(393/293)}{(1.2\text{ kg/m}^2)}\right]^{1/2}$$
$$= 2.7\text{ m/s}$$

and, from Equations 5 and 18 and the latter result for V_{VENT}, the mass flow rate of smoke flow per unit area of vent will be

$$\dot{m}_{VENT}/A_{VENT} = 1.2\ (\text{kg/m}^3)\left(\frac{293}{393}\right)(2.7)\text{ m/s}$$
$$= 2.4\ (\text{kg/s})/\text{m}^2$$

Flow through Shallow Vents on a Sloping Roof

Consider flow through a vent on a sloping roof as depicted in Figure 3-9.5. Here, the cross-vent pressure difference, $\Delta P_{IN\text{-}OUT}(z)$, would again be obtained from Equation 15. Designate z_{MID} as the elevation of the middle of the vent and, as depicted in the figure, consider scenarios where the entire vent is above the bottom of the smoke layer, that is, $z_{BOT} - z_{LAY} > 0$ and $\rho_{VENT}(z) = \rho_{LAY}$. Then, for the entire surface defined by the vent opening, $\Delta P_{IN\text{-}OUT}(z)$ will be uniformly well approximated by $\Delta P_{IN\text{-}OUT}(z_{MID})$ if the vent is shallow in the sense that half the height of the vent, $(z_{TOP} - z_{BOT})/2$, is small compared to the depth of the portion of the smoke layer below z_{MID}, that is,

$$\Delta P_{IN\text{-}OUT}(z)$$
$$= \Delta P_{IN\text{-}OUT}(z_{MID})\left[1 - \frac{(z_{MID} - z)}{(z_{MID} - z_{LAY})}\right] \qquad (20)$$
$$\approx \Delta P_{IN\text{-}OUT}(z_{MID})$$

if (criterion for a "shallow" vent):

$$0 < \frac{(z_{TOP} - z_{BOT})/2}{(z_{MID} - z_{LAY})} \ll 1 \qquad (21)$$

When Equation 21 is satisfied, Equation 20 and the constant value, ρ_{LAY}, for $\rho_{VENT}(z)$ can be used in Equation 8.

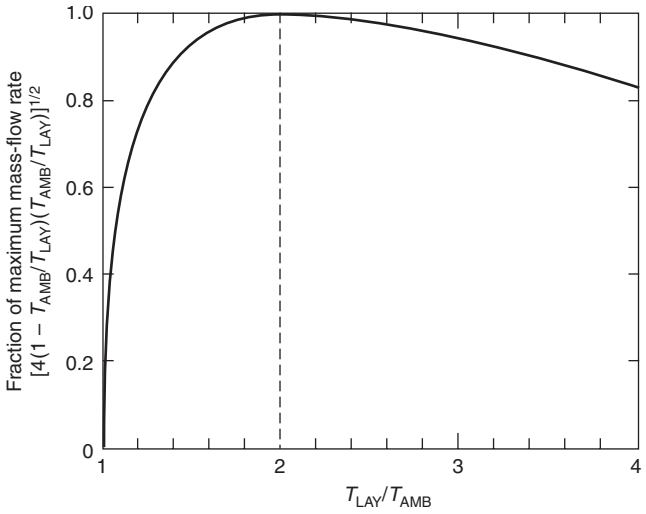

Figure 3-9.3. ***Plot of $(\dot{m}_{VENT}/A_{VENT})/\{0.61\rho_{AMB}[g(z_{CEIL} - z_{LAY})/2]^{1/2}\}$ as a function of T_{LAY}/T_{AMB} according to Equation 19.***

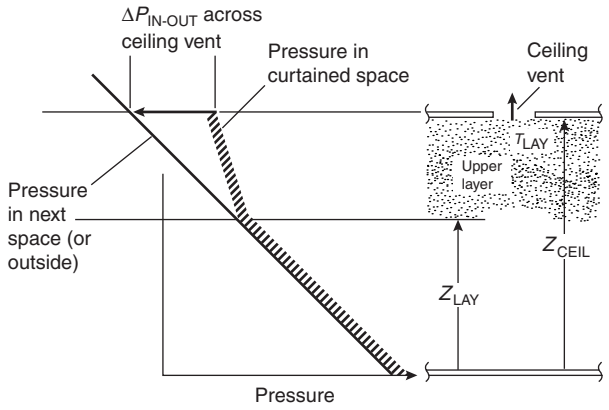

Figure 3-9.4. ***Flow through a ceiling vent.***

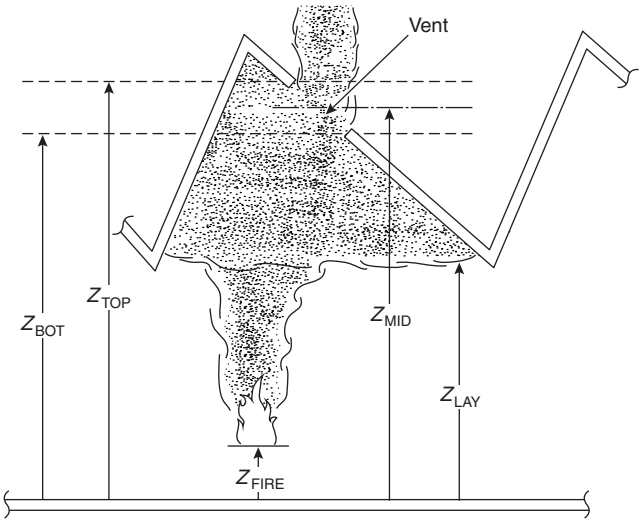

Figure 3-9.5. ***Flow through a vent in a sloping roof.***

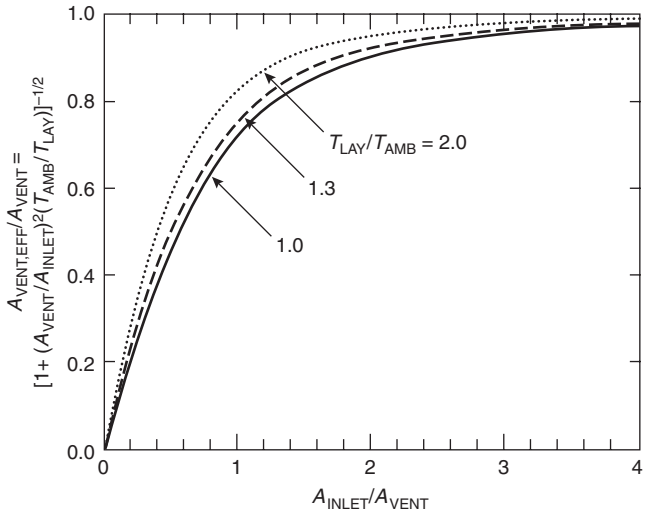

Figure 3-9.6. ***Plot of $A_{VENT,EFF}/A_{VENT}$ as a function of A_{INLET}/A_{VENT} for fixed values T_{LAY}/T_{AMB} = 1, 1.3, and 2 according to Equation 22.***

Then Equation 11 is well approximated by Equation 12 with z_{VENT} replaced by z_{MID}, and the results of Equations 17–19 for flow through horizontal vents is valid for flow through shallow sloped vents if z_{CEIL} is replaced by z_{MID}.

The Effect of Limited Inlet-Vent Area on the Flow through Ceiling Vents in Figure 3-9.1–Type Fire Scenarios

The above results depend on the assumption that A_{INLET}, the total area of the inlet vents, is large enough compared to the total area of open ceiling vents (in the curtained space of fire origin) that the inside-to-outside cross-inlet-vent pressure drop is small compared to the cross-ceiling-vent pressure drop of Equation 16. If the inlet-vent area is *not* large enough, then, based on the $\Delta P_{IN\text{-}OUT}(z_{LAY})$ and V_{VENT} estimates of Equations 16 and 17, respectively, Equations 18 and 19 can still be used to estimate $\dot{m}_{VENT}$ provided the *actual* A_{VENT} in these latter equations is replaced by an *effective* vent area, $A_{VENT,EFF}$, according to[6]

$$\frac{A_{VENT,EFF}}{A_{VENT}} = \left[1 + \left(\frac{A_{VENT}}{A_{INLET}}\right)^2 \left(\frac{T_{AMB}}{T_{LAY}}\right)\right]^{-1/2} \qquad (22)$$

$A_{VENT,EFF}/A_{VENT}$ as a function of A_{INLET}/A_{VENT} is plotted in Figure 3-9.6 for fixed values $T_{LAY}/T_{AMB} = 1$, 1.3, and 2. As can be seen from Equation 22 and from the plot, the larger the value of T_{LAY}/T_{AMB}, the smaller the impact of reduced A_{INLET}/A_{VENT} on reductions below 1 of $A_{VENT,EFF}/A_{VENT}$. It can also be seen in the plot that for $T_{LAY}/T_{AMB} > 1.3$, where the 1.3 value corresponds to the above-identified lowest T_{LAY} for effective venting, $A_{VENT,EFF}/A_{VENT}$ will exceed 0.9, that is, the ceiling vents will be more than 90 percent effective, if $A_{INLET}/A_{VENT} > 1.8$.

The Effect of Outside Wind Conditions on the Flow through Ceiling Vents in Figure 3-9.1–Type Fire Scenarios

General considerations: Assume that there is a prevailing wind condition in the outside environment. Depending on the wind speed, V_{WIND}, and the wind direction relative to the outside building geometry and relative to the geometry of possible nearby buildings, and assuming that all vents on the outside surface of the building are closed, the aerodynamic flow around the building will lead to the establishment of a location-dependent pressure distribution along the outside building surface

$$P_{SURF}(\text{position}) = P_{OUT}(z) + \frac{C_{PRES}(\text{position})\rho_{ATM}V_{WIND}^2}{2} \qquad (23)$$

where C_{PRES} is the local pressure coefficient. Example values of C_{PRES} for flow around an isolated, low, square building are shown in Figure 3-9.7.

If the building vents are open and if vent areas are relatively small compared to the building surface areas, then pressures near the vent openings, but away from any local

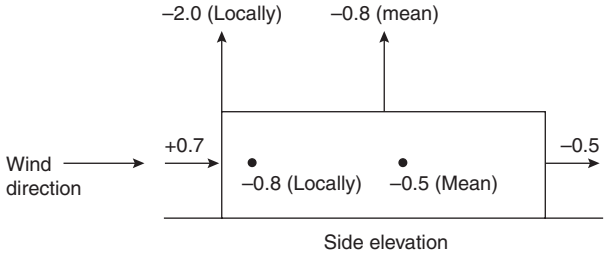

Figure 3-9.7. ***Pressure coefficients for an isolated, low, square building.***

through-vent flows that may develop, will be substantially unchanged from the above-mentioned, closed-vent pressure distribution. Also, while the near-vent pressure distributions generally vary from vent to vent, they will be relatively uniform for any particular vent. Under these conditions, a determination of flow rates into and/or out of vents and through the interior of the building would be based on an interior building flow analysis, with pressure-specified boundary conditions at the open vents.

A single, open inlet vent or multiple openings at the same P_{SURF}: If there is only one open inlet vent, say in the upwind side of the building leading to a relatively high pressure differential there *above* the local hydrostatic pressure [the upwind $C_{PRES} = 0.7$ value of Figure 3-9.7 indicates, e.g., that for $V_{WIND} = 10$ m/s, P_{SURF} at the vent would be $0.7\rho_{ATM}V_{VENT}^2/2 \approx 0.7(1.2)(10)^2/2$ kg/(ms^2) = 42 Pa greater than P_{OUT}], or if there are several open vents, all at locations on the outside surface of the building where pressures are substantially identical, then, *independent* of the magnitude of V_{WIND}, the wind will have no effect on the inflow or outflow through the vents. Thus, if the air inside the building is uniformly at the outside air temperature (assumed to be uniform) and if there is no mechanical ventilation, then the effect of the wind will be simply to bring the interior hydrostatic pressure at the location of the vent(s) to the aerodynamic-flow-specified value, P_{SURF}; the interior of the building will be "pressurized" as a result of the open vent(s), but there will be no wind-induced interior flows. If there is a fire in the room with the open vent (e.g., the vent is a broken window), then, in the usual way, there will be fresh air inflow into the room toward the bottom of the vent and buoyant smoke outflow toward the top of the vent, all this taking place at an aerodynamic-flow-specified, elevated hydrostatic pressure within the room.

If the open vent is in a side of the building facing downwind, that is, exposed to the wake of the flow, then, as in Figure 3-9.7, C_{PRES} typically will be negative. The pressure at the vent will be relatively low, at the outside, local hydrostatic pressure *reduced* by an amount on the order of $\rho_{ATM}V_{VENT}^2/2$. There will again be no wind-induced flow at the vent.

Two inlet vents, one on the upwind side and one on the downwind side of the building: If there are two inlet vents in the walls of the building, one upwind and one downwind (again, no heating and no mechanical ventilation), then there *will* be wind-induced flow through the vents and within the building. There will be inlet air at the high-pressure upwind vent and outlet air at the low-pressure downwind vent, with levels of through-vent flows and of interior hydrostatic pressures determined by an appropriate analysis that accounts for conservation of momentum (i.e., Bernoulli's equation) and mass at the exterior vents and at room-to-room vents within the interior of the building. The changes in hydrostatic pressures within the rooms of the building, over and above the hydrostatic pressures that would be in evidence in a quiescent environment, would be somewhere between the wind-induced pressures at the locations of the high-pressure vent and the low-pressure vent.

Wind-modified pressures at roof surfaces and wind-modified action of ceiling vents: As in the Figure 3-9.7 example (also see Figure 1-1.34 of Section 1, Chapter 1, "Introduction to the Mechanics of Fluids"), independent of wind direction, roof surfaces of flat-roofed buildings tend to have negative, wind-induced pressure coefficients. (This is not the case for sloping roofs, for which pressure coefficients can be positive or negative, depending on wind direction.) Therefore, if the interior, wind-induced hydrostatic pressures are higher than those associated with a quiescent environment, say, the result of open vents in the upwind side of the building, then the flow of smoke through ceiling vents can be enhanced significantly by virtue of increased, favorable, cross-vent pressures. However, for reduced interior pressures, say, the result of open vents on the downwind side of the building, the effect of wind conditions can disrupt completely the desired smoke-removing action of ceiling vents, even reducing the *direction* of the cross-vent pressures and, as a result, the direction of the flow through the vents, that is, from outside to inside.

For a square, low, flat-roofed building configuration like that of Figure 3-9.7, it seems that the latter problem would not exist if, say, identical open inlets are provided on all four sides. Thus, the figure indicates that the smallest of the pressure coefficients at such side vents would be greater than -0.8 and the pressure coefficients on the roof surface would typically be less than -0.8. As a result, wind-modified, cross-ceiling-vent pressure differentials would always exceed a design value that was based on a windless outside environment. All this would lead to enhanced wind-induced performance of roof vents. (Note: The reader is referred to the end of Section 1, Chapter 1, "Introduction to the Mechanics of Fluids," for additional discussion on the effect of wind on the action of ceiling vents.)

The Effect of Combined Buoyancy- and Pressure-Driven Flow through Horizontal Ceiling Vents

Flow through horizontal vents when $\Delta P_{IN\text{-}OUT} = 0$: At the beginning of the section Flow through Vents, it was stated that "flow is driven through vents . . . *mainly* by cross-vent hydrostatic pressure differences" (italics added). In the case of horizontal vents, there is another phenomenon that can affect significantly the validity and the accuracy of the present flow estimates, which were based solely on hydrostatic pressure differences and on use of the traditional Bernoulli equation flow model, referred to below as the *standard flow model.* The phenomenon involves a buoyancy-driven instability, the basic feature of which is explained here by considering an example two-layer scenario with horizontal ceiling vents where $\Delta P_{IN\text{-}OUT}(z_{CEIL}) = 0$.

Analysis of the Figure 3-9.1 scenario, which assumed a quiescent outside environment, led to the Equation 16 estimate of $\Delta P_{IN\text{-}OUT}(z_{CEIL})$. As indicated, for a non-zero-thickness smoke layer, the latter is always positive. However, as discussed in the previous section, wind conditions and poorly positioned inlet vents can lead to scenarios where, even in the case of a relatively high-temperature,

low-density, upper smoke layer, $\Delta P_{\text{IN-OUT}}(z_{\text{CEIL}})$ can be brought to zero (and even to negative values). For $P_{\text{IN-OUT}}(z_{\text{CEIL}}) = 0$, the standard flow model equation of Equations 8 or 17 and then Equation 18 leads to the estimate, $V_{\text{VENT}} = \dot{m}_{\text{VENT}} = 0$. However, under these circumstances it is clear that the standard flow model does not describe either quantitatively or qualitatively the real state of the vent flow.

The fundamental problem[7–9] here involves a "heavy" fluid (the relatively low-temperature and high-density outside air) positioned above an open vent, below which is a "light" fluid (the relatively buoyant, high-temperature, and low-density smoke). This is an unstable configuration (i.e., a zero-flow configuration cannot be sustained), and it will lead to an unsteady and purely buoyancy-driven, exchange-type flow through the vent; the relatively buoyant smoke inside the facility will flow up through the vent to the outside, and the more dense, cool, outside air will flow down through the vent into the inside space. (The flow phenomenon is analogous to the exchange flow that is observed during the emptying of an open upside-down bottle, initially filled with liquid, where the bottle opening is analogous to the vent, and where the liquid above and the air below are analogous to the "heavy" outside air and the "light" smoke, respectively.)

Flow through horizontal vents for positive, moderate $\Delta P_{\text{IN-OUT}}$: Assume now that $\Delta P_{\text{IN-OUT}}(z_{\text{CEIL}})$ is increased from zero through positive values (with or without a quiescent outside environment). The above exchange flow will persist, but there will be a *reduction* in the above-described outside-to-inside flow component and an *increase* in the inside-to-outside flow component. As $\Delta P_{\text{IN-OUT}}(z_{\text{CEIL}})$ is increased further, flow through the vent will eventually become unidirectional, from inside to outside, that is, the flow will be qualitatively similar to that predicted by the standard flow model. When unidirectional flow is first achieved, the flow condition is referred to as the *flooding-flow condition*[7]; the corresponding value of $\Delta P_{\text{IN-OUT}}(z_{\text{CEIL}})$ is designated as ΔP_{FLOOD}, the flooding-flow cross-vent pressure; and the corresponding vent flow velocity is designated V_{FLOOD}, the *flooding-flow velocity.*

For vent areas with moderate aspect ratios, for example, circular or square vents or moderate-aspect-ratio rectangular vents, with length of sides, L_1 and L_2, satisfying $0.5 \le L_1/L_2 \le 2.0$, ΔP_{FLOOD} and V_{FLOOD} can be estimated from[7]

$$\Delta P_{\text{FLOOD}} = 0.97\left(1 + \frac{\varepsilon}{2}\right)\exp(1.1\varepsilon) g \rho_{\text{AMB}} \left(1 - \frac{T_{\text{AMB}}}{T_{\text{LAY}}}\right) D_{\text{VENT}}$$

$$V_{\text{FLOOD}} = 0.195(g D_{\text{VENT}}^5 \varepsilon)^{1/2} \exp(0.55\varepsilon) \qquad (24)$$

$$\varepsilon \equiv \frac{(1 - T_{\text{AMB}}/T_{\text{LAY}})}{(1 + T_{\text{AMB}}/T_{\text{LAY}})};$$

$$D_{\text{VENT}} = (4A_{\text{VENT}}/\pi)^{1/2}$$

where D_{VENT} is the equivalent diameter of a single vent of interest (i.e., A_{VENT} of Equation 24 is the area of a *single* vent, as distinguished from the previous usage, where it denoted the total area of *all* open vents).

A plot of $V_{\text{VENT}}/V_{\text{FLOOD}}$ vs. $\Delta P_{\text{IN-OUT}}(z_{\text{CEIL}})/\Delta P_{\text{FLOOD}} > 1$, that takes into account the effect of combined buoyancy- and pressure-driven flow, is presented in Figure 3-9.8. Included in the figure is a plot of relevant data[10] acquired in a reduced-scale experimental facility involving fan-specified cross-vent pressure differentials with a cold-air over hot-air configuration. The figure also includes a second plot of the same variables, but where V_{VENT} is the vent flow velocity predicted with the standard flow model, for example, using Equation 19 in the present application under conditions of a quiescent outside environment.

As seen in the Figure 3-9.8 plots,[7] the value of V_{VENT} at the flooding-flow condition is estimated to be less than one-third of the value obtained from the standard flow model. In particular, at the flooding-flow condition the effective value for the flow coefficient, $C_{\text{EFF,FLOOD}}$, is estimated to be[7]

$$C_{\text{EFF,FLOOD}} = 0.178 \quad \text{instead of } C = 0.61 \qquad (25)$$

As $\Delta P_{\text{IN-OUT}}(z_{\text{CEIL}})$ is increased beyond ΔP_{FLOOD}, it eventually would become large enough for the Equation 19 standard-flow-model result to provide good estimates for V_{VENT}. In this regard, it is seen in the plots of Figure 3-9.8 that, for example, the standard flow model will overpredict V_{VENT} by no more than 20 percent of actual values once $\Delta P_{\text{IN-OUT}}(z_{\text{CEIL}})/\Delta P_{\text{FLOOD}}$ exceeds 3.

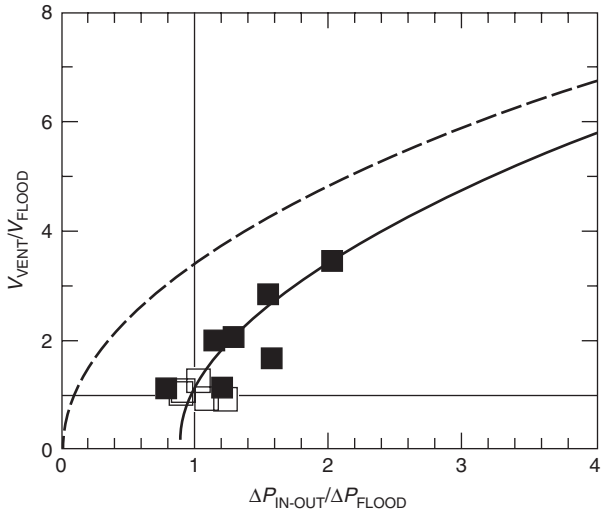

Figure 3-9.8. ***Plot of $V_{\text{VENT}}/V_{\text{FLOOD}}$ vs. $\Delta P_{\text{IN-OUT}}(z_{\text{CEIL}})/\Delta P_{\text{FLOOD}}$; a result[7] that accounts for the combined effects of buoyancy- and pressure-driven flows through a ceiling vent (———); experimental data:[9] flooding-flow conditions (□) and nonflooding-flow conditions (■); and Bernoulli's equation, which ignores the effect of buoyancy-driven instability (- - - -).***

EXAMPLE 2:

Flow through a ceiling vent: As in Example 1, consider horizontal ceiling vents above a 3-m-thick smoke layer that is 100 K greater than T_{AMB} = 293 K. As determined there, for large inlet vents and a zero-wind condition $P_{IN\text{-}OUT}(z_{CEIL})$ = 9.0 Pa. From Equation 24 it is now determined that $\varepsilon \equiv (1 - 293/393)/(1 + 293/393) = 0.14$ and $\Delta P_{FLOOD} = 0.97(1 + 0.14/2)\exp[1.1(0.14)/2](9.8)(1.2)(1 - 293/393)(4/\pi)^{1/2}(A_{VENT}/m^2)^{1/2}$ Pa $= 3.7(A_{VENT}/m^2)^{1/2}$ Pa. Based on the above, it is therefore estimated that the Example 1 result (from standard-flow-model considerations) of $\dot{m}_{VENT}/A_{VENT}$ = 2.4 (kg/s)/m² will overpredict the correct vent-flow rate, but by no more than 20 percent of the expected value if $\Delta P_{IN\text{-}OUT}(z_{CEIL})/P_{FLOOD} = 9.0/[3.7(A_{VENT}/m^2)^{1/2}] > 3$, that is, provided $A_{VENT} < 0.65$ m². In practical terms it is noted that 0.65 m² is a small area for a single vent unit. (U.S. vent-system designs typically use single-vent units with dimensions ranging from 1.2 m × 1.2 m = 1.5 m² to 1.8 m × 2.6 m = 4.7 m².) In practical full-scale venting systems, a 0.65-m² maximum-allowable limit on the area of single-vent units would represent a problematic design constraint with a relatively large number of vent units required for a specified total vent area and corresponding to relatively high costs of implementation. It is also noteworthy that the results of Equation 24 and of Figure 3-9.8 have only been validated for a limited number of reduced-scale tests, involving vents with areas less than 0.65 m². There do not appear to be any available, reliable flow-rate vs. pressure data for flow-through vent units with areas in the range 1.5 m² to 4.7 m² or greater.

Plug-Holing

The phenomenon of plug-holing: Refer to Figure 3-9.9. This depicts the phenomenon of flow being extracted from an upper layer through a ceiling vent, where extraction at a specified volumetric flow rate leads to the average flow velocity, V_{VENT}. For this configuration, define the Froude number, F, and the layer thickness, h, as

$$F \equiv \frac{V_{VENT}A_{VENT}}{\{[g(\rho_{AMB} - \rho_{LAY})/\rho_{AMB}]^{1/2}h^{5/2}\}}; \qquad h = z_{CEIL} - z_{LAY} \tag{26}$$

For large enough F, the interface of the layer, as indicated in the figure, will be depressed a distance h_{DEP} that is comparable to h. Results presented in the literature[11,12] lead to the following conclusions for circular vents:

1. If $F > F_{CRITICAL} = 1.6$, then $h_{DEP}/h = 1$ and flow through the vent will include some fluid from the lower-layer environment, that is, $\dot{m}_{VENT} > \rho_{LAY}V_{VENT}A_{VENT}$.
2. The condition $F/F_{CRITICAL} = 1$ represents a scenario where $h_{DEP}/h = 1$, but where, for this critical value of F and for all smaller values, flow through the vent is entirely from the upper-layer environment, that is, $\dot{m}_{VENT} = \rho_{LAY}V_{VENT}A_{VENT}$.
3. If $F/F_{CRITICAL} = 1 - \delta_1$ where $0 < \delta_1 \ll 1$, then $h_{DEP}/h = 1 - \varepsilon_1(\delta_1)$ where $\lim_{\delta_1 \downarrow 0} \varepsilon_1(\delta_1) \downarrow 0$.

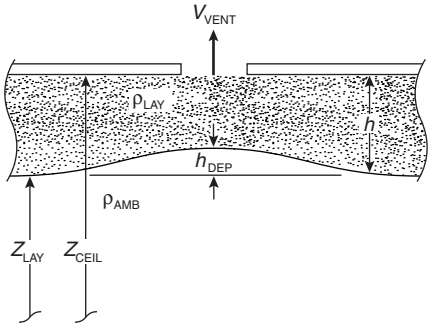

Figure 3-9.9. ***The phenomenon of plug-holing.***

4. If $0 < F/F_{CRITICAL} = \delta_2 \ll 1$, then $h_{DEP}/h = \varepsilon_2(\delta_2)$ where $\lim_{\delta_2 \downarrow 0} \varepsilon_2(\delta_2) \downarrow 0$. (27)

(In the list above, the meaning of the limits in items 3 and 4 is if δ_1 or δ_2 approach zero through positive values, then ε_1 or ε_2 will approach zero through positive values.)

Note that there are no results available in the literature that provide a quantitative estimate of the relationship between h_{DEP}/h and $0 < F/F_{CRITICAL} < 1$. Nevertheless, it is reasonable to expect that

$$\lim_{F/F_{CRITICAL} \to 0} \frac{h_{DEP}}{h} = \beta \frac{F}{F_{CRITICAL}} \qquad \textit{where } 0 < \beta = \text{constant} = 0(1) \tag{28}$$

It is also reasonable to expect that the above conclusions can be extended to moderate-aspect-ratio vents other than circular vents, for example, square vents or moderate-aspect-ratio rectangular vents.

The phenomenon of Figure 3-9.9, where the layer interface is depressed to the elevation of the ceiling as a result of $F/F_{CRITICAL} > 1$, that is, where flow through the vent is extracted partially from the ambient lower layer, is known as plug-holing. (Note: The reader is referred to References 4, 13, and 14 for additional discussion on the topic of plug-holing.)

Plug-holing and natural venting: It is possible to apply the above result to the natural vent flow problems of current interest. Thus, if $F/F_{CRITICAL}$ is small, say,

$$\text{if } F/F_{CRITICAL} < 0.2, \quad \text{then, } h_{DEP}/h \text{ will be small, on the order of } F/F_{CRITICAL} \tag{29}$$

according to Equation 28; that is, if $F/F_{CRITICAL}$ is small, then the layer-interface depression of Figure 3-9.9 will be small. Now, if the vent flow leading to the F value is the result of natural ventilation and not forced mechanical ventilation, then the traditional results of Equations 16–19 associated with natural venting will be relevant. From these latter equations and from the definition of Equation 26, it follows that in natural venting, when there is no plug-holing and $h_{DEP}/h \approx 1$,

$$\frac{F}{F_{CRITICAL}} = 0.54\left(\frac{\rho_{AMB}}{\rho_{LAY}}\right)^{1/2}\frac{A_{VENT}}{h^2} \tag{30}$$

The requirement of internal consistency between the conditions of Equation 28 and those of 29 and 30 leads to the following final result: in natural venting through moderate-aspect-ratio vents, if

$$\left(\frac{\rho_{AMB}}{\rho_{LAY}}\right)^{1/2}\frac{A_{VENT}}{(z_{CEIL}-z_{LAY})^2} < 0.4 \tag{31}$$

then the plug-holing phenomenon will be insignificant; if Equation 31 is not satisfied, then plug-holing can be significant.

Therefore, if Equation 31 is satisfied, then all earlier results for flow through ceiling vents will be relevant. If Equation 31 is not satisfied, then, because of possible plug-holing, the earlier results can be unreliable.

EXAMPLE 3:

Maximum vent area for avoiding plug-holing in the Example 1 venting scenario: As in Example 1, consider horizontal ceiling vents above a 3-m-thick smoke layer that is 100 K greater than T_{AMB} = 293 K. Applying the criterion of Equation 31, it is determined that plug-holing will be avoided in the Example 1 venting scenario if moderate-aspect-ratio vents are used and if the area of individual vents satisfy

$$\begin{aligned} A_{VENT} &< 0.4\,\frac{(z_{CEIL}-z_{LAY})^2}{(\rho_{AMB}/\rho_{LAY})^{1/2}} \\ &= 0.4\,\frac{(3\text{ m})^2}{(293/393)^{1/2}} \\ &= 4.2\text{ m}^2 \end{aligned}$$

Smoke Flow under Draft Curtains

Velocity of flow under draft curtains: Refer to Figure 3-9.10. If and when the layer interface in the curtained space of fire origin drops below the bottom of the draft curtains, smoke will start to flow out of this space and into adjacent spaces. Here, the "vent" consists of the open area in the plane of and below the draft curtain, at $z < z_{CURT}$. As with ceiling vents, the flow rate here is determined by the cross-vent hydrostatic pressure difference, which now varies with z. Here the flow is from within the curtained space to the adjacent curtained space, where it is assumed that the outside environment conditions still persist in the adjacent spaces, from z_{FLOOR} up to z_{CEIL}, that is, it is assumed that any smoke that may have already "spilled into" the adjacent space has not yet modified significantly the initial outside-ambient environment. Thus, the pressure in the adjacent space, P_{ADJ}, is estimated from Equation 6 as

$$P_{ADJ}(z) \approx P_{OUT}(z) = P_{OUT}(z_0) - \rho_{AMB}g(z-z_0), \quad z_{FLOOR} < z \le z_{CEIL} \tag{32}$$

$P_{IN}(z)$ is again given by Equations 13 and 14, and the cross-vent pressure difference, $\Delta P_{IN\text{-}ADJ}(z)$, which is again (essentially) always positive, is estimated from

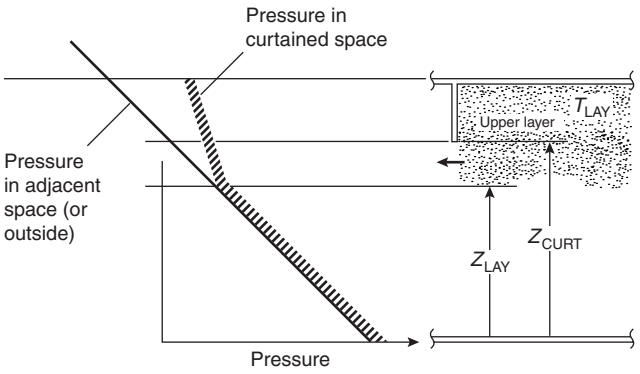

Figure 3-9.10. ***Flow below a draft curtain.***

$$\Delta P_{IN\text{-}ADJ}(z) \equiv P_{IN}(z) - P_{ADJ}(z) \approx \Delta P_{IN\text{-}OUT}(z) > 0 \tag{33}$$

according to Equation 15. Also, since the pressure is again higher in the curtained space of fire origin than the adjacent space, once again, $\rho_{VENT} = \rho_{LAY}$.

In the present configuration, the velocity at the below-curtain vent will vary with z, where this variation is determined from Equations 8, 15, and 33:

$$\begin{aligned} V_{VENT}(z) &= \left[\frac{2\Delta P_{IN\text{-}ADJ}(z)}{\rho_{LAY}}\right]^{1/2} \\ &= \left[\frac{2\Delta P_{IN\text{-}ADJ}(z)T_{LAY}}{(\rho_{AMB}T_{AMB})}\right]^{1/2} \end{aligned} \tag{34}$$

where, for the present vent configuration, Equation 10 was used to provide the appropriate choice for C.

Mass-flow rate under draft curtains: Let L_{CURT} be the total length of the draft curtains that separate the curtained space of fire origin from all adjacent spaces, that is,

$$W_{VENT}(z) = L_{CURT} = \text{constant} \tag{35}$$

Then, Equations 15, and 33–35 in Equation 11, with $\alpha = 90°$, lead to the following estimate for $\dot{m}_{CURT,}$ the total mass flow rate under the draft curtains from the curtained space of fire origin to all adjacent spaces,

$$\dot{m}_{CURT} = \begin{cases} 0 & \text{if } z_{LAY} \ge z_{CURT} \\ \left(\dfrac{L_{CURT}}{3}\right)[8(z_{CURT}-z_{LAY})^3\rho_{LAY}(\rho_{AMB}-\rho_{LAY})g]^{1/2} & \\ = \left(\dfrac{L_{CURT}}{3}\right)\rho_{AMB}\left(\dfrac{T_{AMB}}{T_{LAY}}\right) & \\ \quad \times\left[\dfrac{8(z_{CURT}-z_{LAY})^3 g(T_{LAY}-T_{AMB})}{T_{AMB}}\right]^{1/2} & \\ \quad \text{if } z_{LAY} < z_{CURT} \end{cases} \tag{36}$$

EXAMPLE 4:

Smoke flow under draft curtains: As an example of the above, consider a 3.5-m-thick smoke layer where, as in Examples 1, 2, and 3, T_{LAY} is 100 K greater than T_{AMB} = 293 K. Here, let z_{LAY} be 0.5 m below z_{CURT} (i.e., the depth of the draft curtains are 3.0 m), and let the curtained space of fire origin be away from any walls, with a square plan area of 30 m × 30 m, that is, with L_{CURT} = 4(30 m) = 120 m. Then, from Equation 36 it is determined that

$$\dot{m}_{CURT} = (120\text{ m}/3)(1.2\text{ kg/m}^3)\left(\frac{293}{393}\right)\left[8(0.5\text{ m})^3(9.8\text{ m/s}^2)\left(\frac{100}{293}\right)\right]^{1/2}$$
$$= 66\text{ kg/s}$$

Based on Example 1, it is seen from Figure 3-9.1 that if the fire in the curtained area is nearly steady and if the mass flow rate of smoke in the fire plume, at an elevation 3 m below the ceiling, is approximately 66 kg/s, then smoke spilling below the curtains will be avoided if there are approximately (66 kg/s)/[2.4 (kg/s)/m^2] = 28 m^2 of open ceiling vents in the ceiling of the curtained space of fire origin. If no open ceiling vents are provided, then there will be spilling below the curtains to an approximate depth of 0.5 m. In the latter case, smoke spilling into, and smoke filling of, the adjacent spaces will continue until all adjacent spaces are filled with smoke from the ceiling to a depth of approximately 3.5 m, after which the depth of the smoke layer will continue to develop uniformly throughout the entire building space, always increasing in thickness.

Convected Mass and Enthalpy to the Smoke Layer from the Fire Plume

Different plume models: The major contributor of convected mass and enthalpy to the smoke layer is from the fire plume. This is depicted in Figure 3-9.11. If the plume is unobstructed at least to the top of its combustion zone, it is assumed that the rate of energy release of the fire's combustion zone, $\dot{Q}_{TOTAL}$, does not vary significantly from free-burn values. It is also assumed that a fixed fraction, λ_{RAD}, of this energy is radiated from the combustion zone and that above the combustion zone the rest of $\dot{Q}_{TOTAL}$,

$$\dot{Q}_{CONV} \equiv (1 - \lambda_{RAD})\dot{Q}_{TOTAL} \tag{37}$$

is convected upward in the plume. Generally applicable estimates of λ_{RAD} and $\dot{Q}_{CONV}$ for full-scale hazardous fires (see Section 3, Chapter 10, "Compartment Fire-Generated Environment and Smoke Filling") are

$$\lambda_{RAD} = 0.35; \qquad \dot{Q}_{CONV} = 0.65\dot{Q}_{TOTAL} \tag{38}$$

Regarding the radiation transfer, for relatively early times in the fire development, for example, prior to the activation of sprinklers when they are deployed, it is reasonable to assume that the smoke layer is relatively transparent, that is, that all radiation heat transfer from the fire, at the rate $\lambda_{RAD}\dot{Q}_{TOTAL} \approx 0.35\dot{Q}_{TOTAL}$, is incident on the bounding surfaces of the compartment.

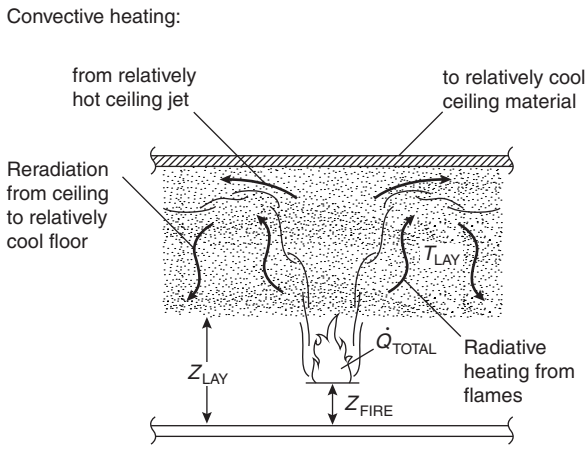

Figure 3-9.11. ***The fire, the fire plume, and heat transfer to the ceiling.***

A plume model is selected from the several available in the literature,[15] and it is used to determine the rate of mass and enthalpy flow in the plume at the elevation of the layer interface, $z = z_{LAY}$. It is assumed that all this flow penetrates the layer interface and enters the upper layer.

In general, the mass-flow rate in the plume, $\dot{m}_{PLUME}$, increases with elevation above the base of the fire, $z - z_{FIRE}$, as a result of lateral entrainment into the rising hot and buoyant plume gases. Estimates of $\dot{m}_{PLUME}$ for four different plume models are presented here: *pool fire, large fire, free line fire,* and *near-wall line fire.* The first two of these are for a plume above a fire with effective circular base of diameter, D_{FIRE}, where A_{FIRE} is the effective plan area of the fire and

$$D_{FIRE} = \left(\frac{4A_{FIRE}}{\pi}\right)^{1/2} \tag{39}$$

The other two models are for plumes above a linelike fire of effective length, L_{FIRE}. For such fires, $\dot{Q}_{CONV}$ and $\dot{m}_{PLUME}$ can be specified in terms of the convected energy-release rate per unit length, $\dot{Q}'_{CONV}$, and mass-flow rate per unit length, $\dot{m}'_{LINE}$, respectively,

$$\dot{Q}'_{CONV} \equiv \frac{\dot{Q}_{CONV}}{L_{FIRE}} \tag{40}$$

$$\dot{m}'_{LINE} \equiv \frac{\dot{m}_{PLUME}}{L_{FIRE}} \tag{41}$$

Pool fire; $\dot{m}_{PLUME}$ at arbitrary elevations: The following is one of the several available estimates for $\dot{m}'_{PLUME}$ above a pool fire.[16] It is valid at arbitrary elevation above the base of the fire. For a pool fire at arbitrary elevation, with $\dot{m}_{PLUME}$ measured in kg/s; $\dot{Q}$ and $\dot{Q}_{CONV}$ in kW; and z, z_{FIRE}, L_{FLAME}, and D_{FIRE} in m:

$$\dot{m}_{\mathrm{PLUME}}(z) = \begin{cases} 0.0054\dot{Q}_{\mathrm{CONV}}(z - z_{\mathrm{FIRE}})/L_{\mathrm{FLAME}} \\ \qquad \text{if } 0 < (z - z_{\mathrm{FIRE}})/L_{\mathrm{FLAME}} < 1; \\ 0.071\dot{Q}_{\mathrm{CONV}}^{1/3}(z - z_{\mathrm{FIRE}} - L_{\mathrm{FLAME}} + 0.166\dot{Q}_{\mathrm{CONV}}^{2/5})^{5/3} \\ \times [1 + \varepsilon\dot{Q}_{\mathrm{CONV}}^{2/3}(z - z_{\mathrm{FIRE}} - L_{\mathrm{FLAME}} + 0.166\dot{Q}_{\mathrm{CONV}}^{2/5})^{-5/3}] \\ \qquad \text{if } (z - z_{\mathrm{FIRE}})/L_{\mathrm{FLAME}} \geq 1 \end{cases} \quad (42)$$

where L_{FLAME}, the length of the reacting flaming region of the fire, and ε are

$$\varepsilon = 0.0054/0.071 - (0.166)^{5/3} = 0.0259168209\ldots \simeq 0.026 \quad (43)$$

$$L_{\mathrm{FLAME}}/D_{\mathrm{FIRE}} = \begin{cases} 0 \text{ if } \Lambda < 0; \\ \Lambda \text{ if } \Lambda \geq 0 \end{cases} \quad (44)$$

and where $\Lambda = [0.083/(1 - \lambda_{\mathrm{RAD}})^{2/5} + 0.166]\dot{Q}_{\mathrm{CONV}}^{2/5}/D_{\mathrm{FIRE}} - 1.02$

Large fire: The following is an estimate[6] for $\dot{m}_{\mathrm{PLUME}}$ above large fires of perimeter P. Use of the model is restricted to elevations above the base of the fire that are so small compared to D_{FIRE}, for example, $z_{\mathrm{LAY}} - z_{\mathrm{FIRE}} < 2D_{\mathrm{FIRE}}$, that the entire temperature of the plume volume to that height can be reasonably estimated as T_{AMB} + 900 K. The model is applicable to large fires in the sense that the maximum elevation considered, that is, the maximum elevation of the smoke-layer interface, is expected to be close enough to the base of the fire that the lateral bounds of the plume there still mostly coincide with the lateral bounds of the lower, continuously flaming region of the fire, where temperatures are relatively uniform at the maximum value of approximately 900 K above the inlet air at T_{AMB} (see Figure 2-1.3 of Section 2, Chapter 1, "Fire Plumes"), that is, approximately 1200 K. For a large fire, where $z - z_{\mathrm{FIRE}} < 2D_{\mathrm{FIRE}}$:

$$\dot{m}_{\mathrm{PLUME}}(z)/(\mathrm{kg/s}) = 0.18(\mathrm{P/m})[(z - z_{\mathrm{FIRE}})/\mathrm{m}]^{3/2} \quad (45)$$

or, alternatively,

$$\dot{m}_{\mathrm{PLUME}}(z) = 0.18P(z - z_{\mathrm{FIRE}})^{3/2};$$

with $\dot{m}_{\mathrm{PLUME}}(z)$ in kg/s and P, z, and z_{FIRE} in m. (When other equations "like" Equation 45 are presented below, they will *not* be presented with their "alternative" forms. The reader that prefers the alternative-type form is advised to construct it by analogy to the Equation 45 example.)

Note that an unusual feature of the Equation 45 estimate for $\dot{m}_{\mathrm{PLUME}}$ is that it is independent of $\dot{Q}_{\mathrm{TOTAL}}$.

Free line fire: The following is an estimate for $\dot{m}'_{\mathrm{PLUME}}$ above a free line fire:[17]

$$\dot{m}'_{\mathrm{LINE}}(z)/[\mathrm{kg/(m{\cdot}s)}] = 0.18[(z - z_{\mathrm{FIRE}})/m][\dot{Q}'_{\mathrm{CONV}}/(\mathrm{kW/m})]^{1/3} \quad (46)$$

where the above result is for a wedgelike plume that rises above a line fire (or a linelike source of high-temperature smoke) that is removed enough from walls so that the plume can entrain "freely" from both its sides, and where the estimate of Equation 46 is expected to be useful for $z - z_{\mathrm{FIRE}} < O(L_{\mathrm{FIRE}})$, that is, for elevations above the fire base of the order of the length of the line fire. Note that the line fire plume cannot be expected to maintain its two-dimensional, wedgelike character much beyond $z = z_{\mathrm{FIRE}} + L_{\mathrm{FIRE}}$. For higher elevations, the plume flow rate would perhaps be best estimated with the pool-fire estimate of Equations 42–44, using an appropriate, effective base diameter, D_{FIRE}.

Near-wall line fire: If the line fire is immediately adjacent to a wall, so that is can only entrain on one side of the wedgelike plume (or, if the buoyant source of the plume is smoke from a fire in an adjacent room that enters the space of interest through a wide vent opening, where the smoke is unobstructed in its ascent along the wall immediately above the vent opening), then it will be referred to here as a *near-wall line fire.* Using a plume reflection–type principle, an estimate of $\dot{m}'_{\mathrm{LINE}}$ for this case can be obtained with the use of Equation 46 by "doubling $\dot{Q}'_{\mathrm{CONV}}$ and halving the resulting $\dot{m}'_{\mathrm{LINE}}$" that is, for a near-wall line fire:

$$\dot{m}'_{\mathrm{LINE}}(z)/[\mathrm{kg/(m{\cdot}s)}] = (0.18/2)(z - z_{\mathrm{FIRE}})/\mathrm{m})[2\dot{Q}'_{\mathrm{CONV}}/(\mathrm{kW/m})]^{1/3} \quad (47)$$

where, as was the case for Equation 46, it is again reasonable to expect that Equation 47 cannot be used with confidence much beyond $z = z_{\mathrm{FIRE}} + L_{\mathrm{FIRE}}$. The estimate of Equation 47 is consistent with the assumption that below a z-elevation of interest the integrated heat transfer losses from the plume to the adjacent wall are small compared to the convected enthalpy in the plume at that elevation.

EXAMPLE 5:

$\dot{m}'_{\mathrm{LINE}}$ in a balcony spill plume: The plume flow estimate of Equation 46 for a free line fire would be applicable in determining $\dot{m}'_{\mathrm{LINE}}$ in so-called balcony spill plumes[2] (see Figure 3-9.12). Consider the following example problem.

PROBLEM:

Referring to Figure 3-9.12, consider a $\dot{Q}_{\mathrm{TOTAL}}$ = 5 MW pool-like fire of A_{FIRE} = 4 m^2 (i.e., from Equation 39, $D_{\mathrm{FIRE}}/\mathrm{m} = [4(4)/\pi]^{1/2} = 2.3$) below a balcony of width W = 3 m. Let H = 3 m be the elevation of the balcony above the base of the fire, that is, $H = z_{\mathrm{BALCONY}} - z_{\mathrm{FIRE}}$ = 3 m. Assume that $\dot{Q}_{\mathrm{CONV}} = 0.65\ \dot{Q}_{\mathrm{TOTAL}}$ = 3.25 MW. After impinging on the lower surface of the balcony, assume that the smoke from the pool-fire plume flows below and (eventually and mostly) toward the edge of the balcony, without significant additional entrainment and without significant heat transfer losses. The smoke then spills upward from below the balcony, continuing upward as a free line fire–generated spill plume. Whatever the actual position of the pool fire relative to the edge of the balcony,

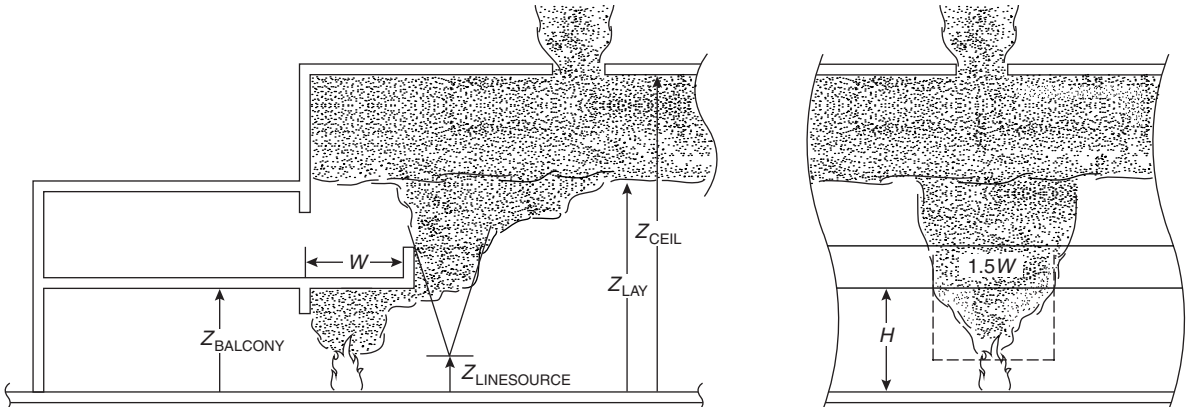

Figure 3-9.12. ***Scenario of Example 5 involving a balcony spill plume.***

it is expected that the effective lengths of the spill plume and of its free line-fire source, L_{PLUME} and $L_{FIRE} = L_{PLUME}$, respectively, will be of the order of W, say, between W and $2W$. Therefore, estimate $L_{FIRE} = L_{PLUME} \approx 1.5W = 4.5$ m.

Designate the elevation of the unknown, equivalent, free line-fire source for the spill plume as $z_{LINESOURCE}$ and the mass-flow rate of the pool-fire plume at the elevation of balcony impingement as $\dot{m}_{PLUME}(z_{BALCONY})$. Then, at the edge of the balcony, the criterion of equivalency between mass-flow rate in the spill plume, $\dot{m}'_{LINE}(z_{BALCONY})$, and in the pool-fire plume is

$$\dot{m}'_{LINE}(z_{BALCONY}) = \dot{m}_{PLUME}(z_{BALCONY})/L_{FIRE}$$

Consider the problem of determining the total mass-flow rate in the spill plume at an elevation of 3 m above the balcony, that is, 6 m above the base of the fire, where, for life safety considerations, it is desired to ensure that z_{LAY} of the smoke layer that would fill the upper parts of the space would never fall below this elevation, that is, $z_{LAY} - z_{FIRE} = 6$ m.

SOLUTION:

From the above-specified information it can be estimated from Equations 42–44 that $L_{FLAME} = 4.4$ m and

$$\dot{m}_{PLUME}(z_{BALCONY}) = 12.0 \text{ kg/s}$$

Also, from Equation 40, $\dot{Q}'_{CONV}$ for the equivalent free line-fire source is

$$\dot{Q}'_{CONV} = \frac{\dot{Q}_{CONV}}{L_{FIRE}} = \left(\frac{3250}{4.5}\right) \text{kW/m} = 722 \text{ kW/m}$$

Using the latter two results, Equation 46, and the above criterion of equivalency leads to

$$\begin{aligned}\dot{m}'_{LINE}(z_{BALCONY})/[\text{kg/(m·s)}] &= 0.18[(z_{BALCONY} - z_{LINESOURCE})/\text{m}](722)^{1/3} \\ &= (12.0)/(4.5) = 2.7\end{aligned}$$

from which it is determined that

$$(z_{BALCONY} - z_{LINESOURCE})/\text{m} = 2.7/[0.18(722)^{1/3}] = 1.7$$

that is, the equivalent free line-fire source is 1.7 m below the elevation of the balcony and (3 + 1.7) m = 4.7 m below the elevation of interest. Using Equation 46 again, it is finally determined that

$$\begin{aligned}\dot{m}'_{LINE}(z - z_{LINESOURCE} = 4.7 \text{ m}) &= 0.18(4.7)(722)^{1/3} \text{ kg/(m·s)} \\ &= 7.6 \text{ kg/(m·s)}\end{aligned}$$

For the continuation free line-fire plume at $z = z_{FIRE} + 6$ m $= z_{BALCONY} + 3$ m,

$$\dot{m}_{PLUME} = \dot{m}'_{LINE} L_{FIRE} = (7.6)(4.5) \text{ kg/s} = 34.2 \text{ kg/s}$$

For comparison with the latter result, it has also been estimated from Equations 42–44 that for the pool fire "in the open," away from under the balcony at $z = z_{FIRE} + 6$ m $= z_{BALCONY} + 3$ m:

$$\dot{m}_{PLUME} = 26.0 \text{ kg/s}$$

Therefore, with the fire located under the balcony rather than "in the open," it is estimated that there will be a 31 percent increase of the mass-flow rate of smoke that flows into the upper layer, an increase from 26 kg/s to 34 kg/s.

ALTERNATIVE SOLUTION:

Reference 2 provides the following estimate for $\dot{m}_{SPILLPLUME}(z_B \equiv z - z_{BALCONY} > 0)$, the mass flux in spill plumes like the one of the present problem. For balcony spill plumes[2] at elevation z,

$$\dot{m}_{SPILLPLUME}(z_B \equiv z - z_{BALCONY} > 0)/(\text{kg/s}) = 0.39[(\dot{Q}_{TOTAL}/\text{kW})(L_{PLUME}/\text{m})^2]^{1/3}(z_B + 0.25H)/\text{m} \quad (48a)$$

or

$$\dot{m}_{SPILLPLUME}(z_B \equiv z - z_{BALCONY} > 0)/(\text{lb/s}) = 0.12\{[\dot{Q}_{TOTAL}/(\text{BTU/s})][L_{PLUME}/\text{ft}]^2\}^{1/3}(z_B + 0.25H)/\text{ft} \quad (48b)$$

where $z_B \equiv z - z_{BALCONY}$ is the elevation above the balcony, $\dot{Q}_{TOTAL}$ is the total heat release rate of the fire below the balcony, and H and L_{PLUME}, as before, are the elevation of the balcony above the base of the fire and the effective length of the spill plume at the edge of the balcony, respectively.

In the present problem, $\dot{Q}_{TOTAL} = 5$ MW, L_{PLUME} is *estimated* to be $L_{PLUME} \approx 1.5$; $W = 4.5$ m, where $W = 3$ m is the width of the balcony; $z_B = 3$ m; and $H = 3$ m. Using these values in Equation 48a leads to

$$\dot{m}_{SPILLPLUME} = 0.39[5(10^3)(4.5)^2]^{1/3}[3 + 0.25(3)]\text{kg/s}$$
$$= 68 \text{ kg/s}$$

The latter result for mass flow rate in the spill plume is seen to be approximately 2.0 times the flow rate estimate of the earlier free line-fire plume analysis (68 kg/s here vs. 34 kg/s there) and approximately 2.6 times the earlier estimate for flow rate above the pool fire if it were "in the open" (68 kg/s here vs. 26 kg/s there).

Continuation of the Plume's Rise in the Smoke Layer

Refer again to Figure 3-9.11. As the plume flow enters the upper layer, the forces of buoyancy, which act to drive the plume toward the ceiling, are reduced immediately because of the temperature increase of the upper-layer environment over that of the lower ambient. As a result, the continued ascent of the plume gases will be less vigorous, that is, at reduced velocity, than it would have been in the absence of the layer. Also, as they continue their ascent within the layer, the temperature of the plume gases will now be higher than they would have been in the absence of the layer. Such higher temperatures are a result of the modified plume entrainment, which is now from the relatively high-temperature upper layer rather than the ambient-temperature lower layer. Methods of predicting the characteristics of the modified upper-layer plume flow are available.[18,19]

The Ceiling Jet and Convective Heat Transfer to the Ceiling

Having penetrated the interface, the plume continues to rise toward the ceiling of the curtained compartment. As it impinges on the ceiling surface, the plume flow turns and forms a relatively high-temperature, high-velocity, turbulent ceiling jet that flows radially outward along the ceiling and transfers heat to the relatively cool ceiling surface.[18–22] The ceiling jet is cooled by convection and the ceiling material is heated in-depth by conduction. Eventually, the now-cooled ceiling jet reaches the extremities of the curtained space, where it turns and is deposited into and mixed with the upper layer.[23,24] The convective heat-transfer rate and the ceiling surface temperature on which it depends are both strong functions of the radial distance from the point of plume/ceiling impingement, decreasing rapidly with increasing radius.

Thermal Response of the Ceiling

The thermal response of the ceiling is driven by transient heat conduction. For times of interest here, radial gradients in ceiling surface conditions are small enough so that the conduction heat transfer is quasi-one-dimensional in space. Thus, the thermal response of the ceiling can be obtained from the solution to a set of one-dimensional conduction problems at a few discrete radial positions. These would be solved subject to net convection and radiation heat-flux boundary conditions. Interpolation in the radial direction between the solutions would lead to a sufficiently smooth representation of the distributions of ceiling surface temperature and convective heat transfer rate. The latter of these would be integrated over the ceiling surface to obtain the net instantaneous rate of convective heat transfer losses from the ceiling jet.[22]

The Ceiling Jet and the Response of Fusible Links and Other Thermal Sensor Devices

Convective heating and thermal response of near-ceiling-deployed fusible links or other near-ceiling thermal sensor devices (e.g., liquid-filled glass bulbs that burst at their design temperatures and actuate a sprinkler or thermoplastic vent covers designed to soften and "drop out" at specified actuation design temperatures, thereby opening "initially covered" vents) are determined from the local time-dependent distributions of ceiling jet velocity and temperature. These distributions will depend on vertical distance below the ceiling and radial distance from the fire-plume axis. If and when the link-fuse temperature or temperature that otherwise actuates a particular devise is reached, the device or devices operated by the link, for example, a single vent, a group of vents ganged together, or a sprinkler, will be actuated.

For radial distances of interest, relatively near to the plume, the ceiling jet is an inertially dominated flow, that is, only initial velocity, and not initial temperature or buoyancy, plays a significant role in the development of ceiling jet velocity distribution. This velocity distribution, depicted in Figure 3-9.13, can be estimated from the characteristics of the plume, upstream of ceiling impingement. The ceiling jet temperature distribution, depicted in Figure 3-9.14 for either a relatively "hot" or relatively "cool" ceiling surface, is then estimated from the now-known velocity, upper-layer temperature, ceiling surface temperature, and ceiling surface heat flux distributions.

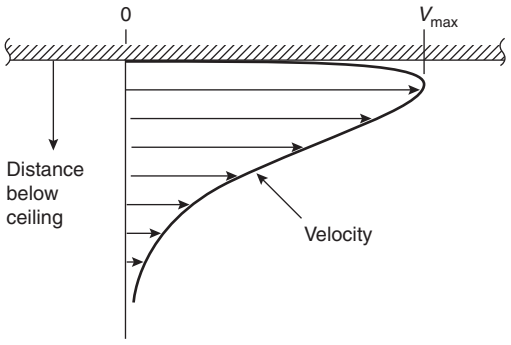

Figure 3-9.13. ***Ceiling jet velocity.***

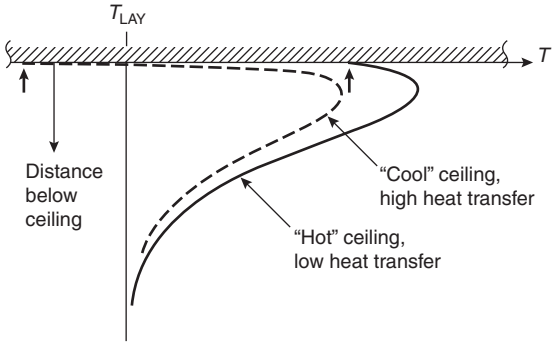

Figure 3-9.14. ***Ceiling jet temperature.***

The LAVENT Model and Computer Code

The mathematical fire model and associated computer program LAVENT (fusible-*L*ink-*A*ctuated *VENT*s)[25–27] was developed and is available to simulate most of the phenomena described above. (LAVENT uses the plume model of Equations 43–44. In its current form, it does not take into account wind effects, the reduced effectiveness of vents as a result of limited-area inlet vents, that is, Equation 22, or the buoyancy-driven vent-flow modification discussed in the context of Equations 24 and 25.) All phenomena simulated in LAVENT, some of which were described above with supporting equations and others were presented here only qualitatively, have been presented with detailed model equations.[25] The LAVENT model can be used to simulate on a time-dependent basis and to study parametrically a wide range of Figure 3-9.1–type fires.

Full documentation for LAVENT, including its theoretical basis,[25] a user guide for the computer code,[26] and sample problems using the code, is also included in Appendices A, B, and C, respectively, of NFPA 204.[1]

The Minimum Depth of Draft Curtains

The ceiling jet in the curtained space of fire origin will have a depth[25] of the order of $0.1(z_{CEIL} - z_{FIRE})$. Consistent with the modeling concepts used throughout this chapter, the effects of the upper layer can only be expected to be generally reliable once the upper layer submerges (i.e., is thicker than) the ceiling jet. In this regard, when draft curtains are used, it is recommended[1] that they have a minimum depth of $0.2(z_{CEIL} - z_{FIRE})$, that is,

$$\text{depth of curtains} \equiv z_{CEIL} - z_{CURT} \geq 0.2(z_{CEIL} - z_{FIRE}) \quad (49)$$

Required Vent Areas

Time-Dependent and Steady-State Design Problems

As mentioned above, it is typical for time-dependent phenomena to play a prominent role in fire safety problems of real interest. This is certainly the case with problems involving fire venting, where the characteristics of hazardous fires and their corresponding plume dynamics, the thicknesses of smoke layers and their temperature, the number (i.e., the area) of active (i.e., open) vents (e.g., in a system involving individual fusible-link-actuated vents), and so on all change with time during the course of fire development. An analysis that accounts for such interacting phenomena on a time-dependent basis must inevitably involve use of a computer fire model (i.e., rather than "hand" calculations), like LAVENT. Nevertheless, for design purposes it often possible, and it has been traditional to formulate such problems as involving substantially steady-state phenomena.

A steady-state vent-design problem formulation would typically involve (1) a specified steady-state design fire threat, including, for example, the elevation and area of the fire (possibly the fuel type and the configuration of the fuel array) and its characteristic energy-release rate, (2) a minimum acceptable value for z_{LAY}, and (3) relevant building design features, for example, the elevation of deployed ceiling vents, $z = z_{CEIL}$. The actual design problem would be to determine total area of open vents required to maintain the smoke-layer interface at $z = z_{LAY}$.

Solving the Steady-State Design Problem

Smoke-flow rate from the plume to the layer: The steady-state problem solution first requires a determination of $\dot{m}_{PLUME}(z_{LAY})$. This would be obtained from the description of the specified fire and with the use of a relevant plume model equation. To achieve the design objective, that is, to ensure that the elevation of the layer will be maintained at $z = z_{LAY}$, the flow rate out of the vents will have to match $\dot{m}_{PLUME}(z_{LAY})$.

The average temperature of the smoke layer: As the plume gases rise from the base of the fire toward z_{LAY}, they entrain and mix with the lower-layer environment at temperature T_{AMB}. For free plumes that are not bound by or in contact with solid surfaces, the convected energy in the plume gases is conserved at $\dot{Q}_{CONV}$. (There will be convective heat transfer losses from a plume along portions of its length where it is in contact with wall surfaces, e.g., along the length of a plume above a near-wall-type line fire.) Therefore an estimate for $T_{PLUME}(z_{LAY})$, the average temperature of plume gases as they enter the smoke layer, is

$$T_{PLUME}(z_{LAY}) - T_{AMB} = \frac{\dot{Q}_{CONV}}{[\dot{m}_{PLUME}(z_{LAY})C_P]} \quad (50)$$

where C_P is the specific heat at constant pressure of air.

A fraction, K, of $\dot{Q}_{CONV}$ will be transferred from the smoke layer to bounding surfaces of the enclosure.[1] As a result of this, the temperature of the smoke-layer gases, T_{LAY}, will be less than $T_{PLUME}(z_{LAY})$

$$T_{LAY} - T_{AMB} = \frac{K\dot{Q}_{CONV}}{[\dot{m}_{PLUME}(z_{LAY})C_P]} \quad (51)$$

A reasonably accurate determination of K would involve a generally difficult analysis of the net rate of heat transfer from the upper-layer gases to upper-layer-exposed and -bounding surfaces of the facility. For example, to es-

timate convection heat transfer rates, the analysis would require appropriate predictions of the characteristics of fire plume–driven boundary flows adjacent to the ceiling and wall surfaces that bound the smoke layers.

It has been recommended that $K = 0.5$ can be generally used as a representative value in Equation 51.[1] However, no value for K should be used that leads to a $T_{LAY} - T_{AMB}$ estimate that exceeds 900 K, where the latter value represents the maximum temperature within flames/plumes above free-burning pool fires, that is, the maximum temperature near the base of the fire, within the continuous flaming region (see Section 2, Chapter 1, "Fire Plumes").

In view of the typical significant uncertainty in the value of K, there will be a corresponding significant uncertainty in the value determined for T_{LAY} in Equation 51. Therefore, from the earlier result presented below Equation 19 and in Figure 3-9.3, it is a fortunate circumstance that, for T_{LAY} values that are at least 90 K greater than T_{AMB}, vent mass flow rates are relatively insensitive to T_{LAY}.

Determining the required total vent area: For the design problem at hand, the above results provide estimates for $\dot{m}_{PLUME}(z_{LAY})$ (Equation 42–44 for pool fires, Equation 45 for large fires, Equation 46 for free line fires, and Equation 47 for near-wall line fires) and T_{LAY} (Equation 51). From these and from the specified values for the design smoke-layer depth, $z_{CEIL} - z_{LAY}$, the required total area for all vents would be determined by requiring $\dot{m}_{VENT} = \dot{m}_{PLUME}(z_{LAY})$ and by using the $\dot{m}_{VENT}/A_{VENT}$ estimate of Equation 19. This leads to the following general result for required total vent area:

$$A_{VENT} = \frac{1.16[\dot{m}_{PLUME}(z_{LAY})/\rho_{AMB}]}{[(z_{CEIL} - z_{LAY})(1 - T_{AMB}/T_{LAY})T_{AMB}/T_{LAY}]^{1/2}} \quad (52)$$

EXAMPLE 6:

Required total vent area for large fires; a general result and an example application: Consider relatively steady burning of a 5-m × 5-m square array of combustibles on the floor of a warehouse facility with ceiling elevation of 9 m. The warehouse is subdivided with ceiling-mounted draft curtains where the bottom of the draft curtains are at an elevation of 6 m. It is desired to provide enough ceiling vent area in each curtained space so that, for an arbitrary curtained space of fire origin, the smoke layer that is established will not fall below the bottom of the curtains and will not flow into and threaten commodities stored in adjacent compartments.

For this example problem, $z_{FIRE} = 0$, $z_{LAY} = 6$ m, and $z_{CEIL} = 9$ m and, from Equation 39, $D_{FIRE} = [4(5)(5)/\pi]^{1/2}$ m = 5.64. Therefore, the fire and problem constraints satisfy the condition of Equation 45, that is, $z_{LAY} - z_{FIRE} = 6$ m $< 2D_{FIRE} = 11.3$ m, and the fire can be considered to be a large fire with P = 4(5 m) = 20 m. As noted earlier, a large fire is one where the gas temperature throughout the entire volume of the plume at and below the relevant, relatively low elevations are uniformly at a characteristic temperature of 1200 K. For plume temperatures of such magnitude and for upper-layer heat-transfer losses associated with any reasonable value of K, it is clear from Equation 18 and from Figure 3-9.3 that for large fires,

$$\left[4\left(1 - \frac{T_{AMB}}{T_{LAY}}\right)\frac{T_{AMB}}{T_{LAY}}\right]^{1/2} \approx 1$$

Using this last observation and Equation 45 in Equation 52 leads to the following *general* result for the total required vent area for large fires where $z - z_{FIRE} < 2D_{FIRE}$:

$$A_{VENT}/m^2 = 0.11(P/m)[(z_{LAY} - z_{FIRE})/m]^{3/2}/[(z_{CEIL} - z_{LAY})/m]^{1/2} \quad (53)$$

where the latter result is equivalent to the result in Reference 6 for the required vent area for large fires. (Note that in contrast to $\dot{m}_{PLUME}(z)$ of Equation 45 and the required vent area of Equation 53 for large fires, neither of which depend on $\dot{Q}_{CONV}$, the plume models and the required vent area for all other types of design fires *will* depend on $\dot{Q}_{CONV}$.)

Applying the Equation 53 result to the Example 6 problem at hand leads to the result

$$A_{VENT}/m^2 = 0.11(20)(6)^{3/2}/(3)^{1/2} = 18.6$$

The Design Fire

The required vent area for a facility is the minimum vent area that leads to the fire-safe design of the facility (successful removal of smoke according to some adopted design-venting objective) when it is threatened by a particular design fire. The design fire would be an appropriate characterization of a fire associated with the burning of a likely assembly of combustibles expected to be found in the particular facility of interest.

As an example of guidance on constructing an analytic estimate of an appropriate design fire for a particular facility, the reader is referred to Tables 5-5.2(b) and 6-1.4.6.3 of Reference 1. Each of these tables is a catalogue of burning characteristics for a wide range of practical arrays of combustibles, where table entries are based on measurements from full-scale experimental fires. Table 5-5.2(b), "Unit Heat Release Rate for Commodities," lists parameters (energy release rate per unit plan area of the combustible array) that allow a description of steady burning of different kinds of combustibles. Table 6-1.4.6.3, "Continuous Growth Fires," lists parameters (t_g, time for the fire to grow from the effective initiation of flaming ignition to 1000 kW) that allow a description of fire growth in different combustibles that is approximated as being proportional to time-squared, that is, t^2 fire growth:

$$\dot{Q}_{TOTAL} \approx 1000\left(\frac{t}{t_g}\right)^2 \quad (54)$$

Mechanical Ventilation

There are a variety of situations where smoke vent designs should appropriately rely partially or totally on mechanical ventilation. Examples include situations

where (1) there is a concern that wind-modified cross-vent pressures may reduce seriously the efficiency of a natural vent system; (2) the temperature of the smoke is likely to be so low that, according to the considerations of Equation 19 and Figure 3-9.3, natural venting would not be economical, for example, the total, required natural vent area is excessive; and (3) natural venting would be impractical, for example, a smoke-venting capability is desired at intermediate floors of a multifloor facility or there are other building design constraints that preclude the use of ceiling vents.

The design concept for a system that involves mechanical ventilation is the same as one that relies entirely on natural vents. The design fire plume inflow to the smoke layer at its desired minimum elevation is established, and suitable ventilation fans are chosen that will provide the necessary extraction of smoke at some elevation within the smoke layer.

The operating characteristics of the fans used in a design must take into account the temperature of the smoke that is being extracted.

It is possible to use mechanical ventilation with natural vents to remove the generic requirement of large, open inlet vents. Thus, if most doors and windows at elevations below z_{LAY} are closed and leakage there to the outside is limited, then mechanical ventilation can be used to force fresh air into the facility below z_{LAY}. The idea would be to use fans to pressurize the interior of the facility, and to push the smoke out through open vents located above z_{LAY}, for example, through fusible-link-actuated ceiling vents within a curtained space of fire origin. In this way the difficult problem of designing fans to operate under unfavorable and typically unknown, high-temperature conditions is avoided.

The issue of plug-holing can be a particular concern when using mechanical ventilation for smoke removal.

The reader is referred to Chapter 4 of Reference 2 for a discussion on issues related to equipment and controls of mechanical ventilation systems used for smoke venting.

Designing Systems That Successfully Combine Smoke Vents with Sprinklers

The Difficulty and Controversy of Combining Vent and Sprinkler Systems

The fire safety benefits of vents and sprinklers are different. In appropriate applications, it is evident that fire safety would be enhanced if both sets of benefits could be achieved simultaneously. However, it is not at all clear that a simple combining of the two technologies will lead to a combining of their respective benefits. (Here, *simple combining* of the technologies means deploying the technologies according to design rules that apply for each, in the absence of the other.) Indeed, the varied physical phenomena, that are the basis for the success of the two technologies when deployed independently, to a greater or lesser extent can be expected to be interactive when deployed together. Thus, design features of the smoke and heat vents can modify sprinkler performance and the design features of the sprinklers can be expected to modify smoke and heat vent performance. As an example of the latter, consider the following.

The water spray associated with sprinkler systems will inherently lead to some cooling of the smoke that rises from the fire's combustion zone and begins to fill the protected space. This is cooling that would not have occurred in the absence of the sprinklers and that would not have been taken into account in a deployed smoke and heat vent design that was based solely on the considerations presented earlier in this chapter. Because the sprinkler spray cools the smoke, the designed effectiveness of the vents to remove the smoke will have been reduced; the mass rate of smoke flowing out of the vents will be less than the design value.

If the extent of the interactions of sprinklers and smoke vents can be shown to be small, or always leading to enhanced benefits, than the idea of a simple combining of the two technologies will succeed. However, if the interaction is significant in the sense that a benefit is modified greatly, and negatively so, then appropriate design modifications to the combined system would have to be identified and implemented. (Thus, in the above example, if sprinkler cooling of the smoke is shown to lead to significant reduction in vent flow rate, then the vent design would have to be appropriately modified, i.e., a larger vent area would be required for a successful design.)

The task of obtaining a clear understanding of the above-mentioned interaction phenomena and the task of developing methods for identifying appropriate design modifications, when required, have been shown to involve difficult and controversial issues. At the time this chapter was prepared no generally accepted technical guidelines existed on the effective design of combined venting/sprinkle systems.

Resolving Claims and Counterclaims on the Benefits of Combined Vent/Sprinkler Systems

Past studies of combined vent/sprinkler systems: Published and unpublished reports of the results of combined sprinkler/vent studies typically conclude that certain enhanced and/or reduced benefits accrue from combining the two technologies, that is, positive and/or negative claims. Also, over the years, many analyses of the results of these studies by people not directly involved in the work have also been published. These analyses invariably conclude with positive or negative claims of the benefits of combining venting and sprinkler technologies, opinions that are partly, and at times entirely, different from the opinions espoused in the corresponding original report of the work in question. Finally, published opinions on the effects of combining vents with sprinklers are often based on simple logical arguments. In some cases even these latter opinions can appear to be contradictory.

There is one study[28] that identified and reviewed 34 position papers on the subject and that evaluated the validity of generic claims and counterclaims on the benefits of combined vent/sprinkler systems. A listing of the

claims and counterclaims so identified and a summary of conclusions on their validity follow.

Claims and counterclaims:[28] In the literature, claims that have been made *in favor* of vent/sprinkler systems can be reduced to the following three:

1. Smoke and heat vents limit the distribution of products of combustion in the facility whether deployed sprinklers are operative or inoperative.
2. Smoke and heat vents decrease the number of activated sprinklers.
3. Smoke and heat vents assist the fire department in identifying the location of the fire within the facility and in reducing the need for manual roof venting.

In the literature, claims that have been made *against* vent/sprinkler systems can be reduced to the following four:

1. Smoke and heat vents will cause enhanced burning rates.
2. Smoke and heat vents will delay sprinkler activation.
3. Smoke and heat vents increase the number of activated sprinklers.
4. Smoke and heat vent flow rates are insufficient to realize any benefit.

Validity of claims for and against combined vent/sprinkler systems: After evaluating reports of studies of combined vent/sprinkler systems, it has been concluded based on the evidence that[28]

- Venting does not have a negative effect on sprinkler performance.
- Successful performance of sprinklers does not rely upon reduced oxygen concentrations.
- Venting has no effect on the activation times of early sprinklers and does not affect the total number of sprinklers activated.
- If a fire is directly beneath a vent, activations of the first sprinklers may be delayed slightly, but there is no evidence that this will have a significant impact on sprinkler performance.
- Venting does limit the spread of products of combustion by releasing them from the building (within the curtained compartment of fire origin) near the source of the fire; this improves visibility for building occupants, whose concern is for rapid egress, and for fire fighters, whose concern is to find the seat of the fire to complete fire extinguishment.
- By limiting the spread of smoke and heat, venting also reduces smoke and heat damage to the building.
- In the event that sprinklers do not operate, venting remains a valuable aid in controlling the fire manually.
- Early vent activation has no detrimental effects on sprinkler performance.
- In many fires, current vent design practices, for example, those of NFPA 204,[1] are likely to limit the number of vents operated to one, and, in successful sprinkler operations, vents may not operate at all.
- Design practices should use methods which ensure early operation of vents; vent operation should be ganged so that the benefit of roof vents is fully realized.
- When deployed with vents and draft curtains, a sprinkler design needs to take full account of draft curtains as obstructions.
- Draft curtains should be placed in aisles rather than over storage.

Toward a Methodology for the Design of Combined Vent/Sprinkler Systems

General criteria for successful vent design: Taking the above conclusions into account and drawing on current knowledge of basic physical phenomena involved in vent/sprinkler interactions, it would appear that a consensus on the design of combined sprinkler/vent systems would result by meeting the following general criteria for successful vent design:

1. *A successful vent design, whether deployed with or without sprinklers, is one that leads to the benefits of improved visibility and safety during a fire to the extent that venting removes from a protected facility the highest temperature and most hazardous smoke and slows to an acceptable rate or stops, say, above eye elevation, the growth of the upper smoke layer.*
2. *When draft-curtain compartmentation is included in the vent design, a significant, additional possible benefit comes about to the extent that the smoke is contained successfully within the curtained compartment of fire origin by action of the venting there. Then the losses to building contents will be correspondingly confined to the contents found in the curtained compartment of fire origin.*

The design question is, Without reducing the designed effectiveness of sprinklers to control a fire, how can these criteria on vent design be met when taking proper account of the cooling and mixing actions of discharging sprinklers? To answer this question is to achieve a full-consensus design for combined vent/sprinkler systems.

Interaction of sprinkler spray and smoke layer: The action of sprinkler sprays on the smoke layer includes a combination of evaporative cooling and dilution of the smoke, where the latter is by virtue of spray-driven mixing, via entrainment dynamics, of the relatively cool and uncontaminated lower-layer gases and the upper layer.[29–41] Provided sprinkler spray–reduced smoke temperature and associated loss of buoyancy it is not too great, it would appear that the effect of evaporative cooling of the smoke, even if accompanied by moderate sprinkler spray–driven mixing, can be offset by additional vent capacity. However, it seems that even without significant evaporative cooling, sprinkler spray–driven mixing action can be so effective that it leads to a precipitous increase in the volume of smoke (i.e., in the depth of the smoke layer) and to a corresponding precipitous decrease from an originally high-temperature concentrated smoke to a much lower-temperature and now-voluminous and -diluted smoke. If and when the latter vigorous mixing occurs, then even impractically large increases in vent capacity would not likely lead to any significant measure of the benefits of

venting. The latter phenomenon is commonly referred to as *smoke-logging.* A vent design that is developed to meet the above general criteria must be based on a credible analysis that accounts for and avoids the phenomena of smoke logging.

There is experimental evidence that smoke logging can be controlled by venting,[42] and a preliminary analysis to explain the phenomenon has been provided.[29,30] Thus, it has been reported that "preliminary tests in [a] . . . large-scale mall . . . showed that, under some conditions, [a] . . . smoke layer could be brought down by a manually operated sprinkler spray, [and that] smoke logging then occurred rapidly, with a high smoke density at low level. However, under some conditions, the smoke layer was not disturbed by a sprinkler spray."[30]

To summarize the above, the major benefits of venting can be achieved, even when used in combination with sprinklers, by identifying and adopting a technically sound design that can be shown to meet the above general criteria for successful vent design. Such criteria can be met only up to the time that smoke logging occurs, or provided that smoke logging does not occur. To determine that the benefits *are* achievable, and that they are in fact achieved in any particular design, requires an analysis and resolution of underlying issues of sprinkler/smoke-layer interaction.

Sprinkler spray–driven cooling, mixing, and smoke logging can be resolved with computer fire-model simulations: From the simplest modeling concepts and through evidence of measurements, it is clear that the action of sprinklers reduce the temperature of the fire environment. However, in terms of past experimental studies, there has been no attempt to deal with the very difficult task of isolating and understanding these effects of temperature reduction in the context of the complex phenomena of sprinkler spray cooling (by heat-transfer and mass-transfer exchanges between spray droplets and the gases that fill the space) and sprinkler spray–driven smoke transport and mixing (transport of room gases by spray-generated pressure distributions and gas/spray-droplet momentum exchanges). What *is* known through visual measurements, but only anecdotally so, is that spray-driven mixing and transport of an initially stable and growing upper smoke layer can and often does lead to onset of smoke logging, whereby the mixing actions of sprinkler sprays are so vigorous as to effectively and continuously mix the continuous supply of newly generated smoke from the fire plume with all the rest of the (smokey) gas that fills the space. As indicated above, it is not reasonable to expect to achieve the desired benefits of venting subsequent to the initiation of smoke logging.

Given a *design fire* and a reliable means of predicting the corresponding sequencing of sprinkler actuation, resolution of the issue of sprinkler spray–driven cooling, mixing, and smoke logging would be based on a fire-model simulation that takes appropriate account of interactions of the sprinkler sprays and the fire environment and that predicts that vent design objectives have been achieved.

There is some indication that analytic fire-modeling methods can be used to resolve the above issues.[41] Reference here is to a mathematical model of the generic interaction of a downward-directed sprinkler spray and a two-layer fire environment. The model simulates the action of the sprinkler spray, including the effects of evaporative cooling and the spray-driven mixing of the elevated-temperature, upper smoke layer and the relatively cool and uncontaminated lower layer. The analysis led to the identification of six possible generic configurations of sprinkler/layer interaction.[40,41] Of the possible configurations, the one that will prevail at a given time during the development of a particular fire was found to depend mainly on the thickness and temperature of the upper smoke layer and on the momentum, spread angle, and characteristic droplet size of the sprinkler spray. In any particular fire scenario, the action of open vents and/or draft-curtain compartmentation could provide some control of the thickness and temperature of the layer, and, therefore, of sprinkler/layer interactions that would prevail.

Of the six above-referenced configurations of sprinkler/vent interaction, four were found to be particularly favorable in the present context, in the sense that they would *maximize* the success of a combined sprinkler/vent design. The idea is that with proper vent design the favorable configurations could lead to the desired control of the smoke-layer depth while minimizing smoke mixing to the lower layer to the point that any smoke there is only in a highly dilute state. Thus, for a given set of sprinkler spray characteristics, if the smoke layer is kept relatively thin and/or not too buoyant (i.e., its temperature is not too high), then the rates of both mass and enthalpy flow entrained into the upper-layer part of the sprinkler's "spray cone of influence" would be relatively insignificant (compared to the corresponding rates associated with the fire-plume flow to the upper layer). As a result, the combined action of cooling and momentum-exchange in the spray cone would be strong enough to transport all of the limited amounts of upper-entrained smoke through the layer interface, and well into the depth of the lower layer, there to be mixed eventually, with negligible consequences, into the rest of the lower-layer gases.

For the above configurations, the overall impact on undesirable mixing of the smoke in the protected space would be minimal. In particular, if it were possible and practical to design a vent system that would keep the smoke layer thin enough to maintain any of the above-referenced configurations of sprinkler/vent interaction for a significant length of time (i.e., by deploying a vent system that would remove from the upper layer most of the continuously in-flowing smoke from the fire plume), then, in the context of the above criteria, the resulting, combined sprinkler/vent system would achieve desired system objectives.

In contrast to the above, of the six possible configurations of sprinkler/vent interaction there were two that are particularly *unfavorable* in the sense that they would *minimize* the likely success of a combined sprinkler/vent design. These configurations could lead to relatively vigorous mixing between the smoke layer and the lower layer, leading to a rapid growth of the upper smoke layer and, possibly, to smoke logging.

Note that at least for the early part of a typical fire scenario, immediately subsequent to one or more rapid-

response sprinkler discharges, the condition of a relatively thin and not-too-high-temperature upper smoke layer will *always* prevail. These are exactly the basic conditions of the first and favorable of the above-mentioned flow configurations. Consistent with experience, smoke logging at such times is never observed.

Resolving the problem of sprinkler skipping and vent skipping: In terms of achieving vent/sprinkler design objectives, it is important to introduce, discuss, and identify a possible means of resolving problems associated with the phenomena known as *sprinkler skipping* and *vent skipping.*

The first sprinkler discharge introduces sprinkler-spray flows to the developing fire environment. This initial spray and the ones to follow are made up of ensembles of droplets of various sizes and velocities that flow from the respective sprinkler nozzles. Although the spray characteristic of a given sprinkler head design will have certain measurable overall characteristics, it is well beyond the scope of current technology to describe all aspects of the spray, which will, in any event, vary from one nominally identical manufactured sprinkler head to another. Furthermore, even a perfect knowledge of the initial conditions of the droplet trajectories would be of little use in the practical estimate of the precise subsequent droplet trajectories. One reason for this is that the droplet trajectories, especially those of the early discharging sprinklers, will be influenced significantly, by interaction with the relatively unpredictable (because of uncertainties of fire location, growth, etc.) and vigorous upward-moving plume flow. For example, some of the droplets, the ones that leave the vicinity of the sprinkler head with relatively small initial speed, will be accelerated rapidly, by droplet/plume-gas momentum exchanges, to the point where they closely track the trajectories of, and are convected along with, the plume flow. Furthermore, for the larger of these droplets, this close plume tracking will occur well before they evaporate and reach thermodynamic equilibrium with the surrounding plume flow. In the usual way, the plume flow, which now transports random and unpredictable numbers of water droplets, forms the ceiling jet which flows past the downstream sprinkler heads. This is the ceiling jet, which is supposed to heat, fuse the links (or break the bulbs) of, and initiate discharge of these downstream sprinkler heads, the water sprays from which are critical for controlling the fire.

In the above scenario, if ceiling jet–convected water droplets strike a sprinkler link or bulb, then, because of effects of evaporative cooling, there will be a significant reduction of its rate of heating. This can lead to a significant delay in sprinkler discharge. It is the resulting, unpredictable, and deleterious delay in sprinkler discharge that is referred to as *sprinkler skipping.*

The basic principles of traditional automatic vent actuation (i.e., by the melting action of fusible links heated by the high-temperature, high-velocity, ceiling-jet flow) are identical to the principles of fusible-link-actuated, automatic sprinkler discharge. Therefore, the above discussion on the phenomenon of sprinkler skipping is totally relevant and identical to a corresponding phenomenon involving vents, designated as *vent skipping.* Thus, as in the case of sprinklers, the otherwise predictable automatic opening of fusible-link-actuated vents is subject to random and unpredictable water droplet–cooling delays in vent opening.

Accounting for sprinkler skipping and vent skipping in design: In traditional sprinkler design (i.e., assuming the absence of vents), the effects of sprinkler skipping on the ability of a sprinkler design to control a fire are taken into account empirically via the empirical experimental design process. In this regard, the relatively large numbers of sprinkler heads involved in a typical sprinkler installation and the relatively small number of expected skipped sprinklers, apparently leads to a natural robustness of sprinkler systems relative to the deleterious effects of sprinkler skipping.

In contrast to traditional sprinkler design, when vents and sprinklers are used *together,* the random and unpredictable effects of vent skipping are *not* now taken into account in the design of automatic vent systems. Also, the numbers of installed vent units per unit area of protected space, the *installed vent density,* is typically much smaller than the corresponding *installed sprinkler-head density.* Therefore, when using traditional automatic vent design methods, an appropriate correction for vent skipping would appear to be warranted, for example, by increasing the total design vent area in a compartment by some appropriate safety factor.

In terms of combined vent/draft-curtain designs, and as an alternative to traditional automatic, fusible-link-actuated vents, which involve inevitably the problem of vent skipping, it would appear that more controllable and more reliable means of ensuring timely and effective vent action are available. One generic possibility would involve *ganging,* that is, opening together at an appropriate controlled time all or most vent units in the compartment of fire origin, for example, by signals from smoke detectors or by appropriate indicators of sprinkler discharge.[43] A ganging strategy that could be well integrated into a reliable, consensus sprinkler/vent design is one where all vents of the fire compartment are ganged to open together immediately following first sprinkler discharge. Alternatively, by using achievable, "smart" vent-opening control, it should be possible to develop more sophisticated vent actuation strategies, for example, immediately following first sprinkler discharge, open all vents beyond the first or second ring of sprinklers (as identified, say, by the sprinkler of first discharge), and open all other vents after sprinkler control is indicated. The latter strategy would be augmented by an appropriate increase in vent area, over that of the design value, to account for the associated reduced number of early-opened vents.

A Consensus Approach to the Design of Combined Sprinkler/Vent Systems

Using mathematical fire models to achieve design objectives: The above discussion indicates that effective sprinkler/vent systems are feasible, and that mathematical fire models with a proven capability for simulating sprinkler/smoke interactions can be used as the basis for a consensus

approach to identify and establish effective sprinkler/vent system designs.

The capabilities of mathematical models to simulate sprinkler/smoke interactions have been reviewed.[44,45] The models considered were those that are complete in the sense that they can be used to simulate successfully both isolated sprinkler/smoke interactions and full fire scenarios, where the latter would be used to establish the success of sprinkler/vent designs. Both zone-type and field model–type simulation approaches were found to offer excellent possibilities for addressing the problem. In the usual way, the two approaches are complementary in the sense that the zone model approach would be most applicable and appropriate for parametric studies and as a practical design tool, while the field model approach would be most applicable for simulating and studying the details of specific scenarios that are of particular interest and concern, for example, the discharge sequence of sprinklers and the effectiveness of a vent design in specific fire scenarios where draft curtains are almost directly above the fire.

A sprinkler/vent design approach that uses zone-type fire model simulations might involve application of an advanced version of LAVENT that would include the sprinkler/smoke-interaction simulation model[41] discussed earlier. A successful preliminary implementation of this approach, with a revised prototype model called LAVENTS (fusible *L*ink-*A*ctuated *VENT*s and *S*prinklers), has already been presented.[46] Relevant successes using the field model approach have also been reported. Examples of these include applications of the LES (*L*arge *E*ddy *S*imulation) model,[47–50] the JASMINE model,[51,52] and others.[53,54]

A set of example guidelines for design of a consensus sprinkler/vent system: To fix ideas that are consistent with the above discussion, the following example guidelines for design of a consensus sprinkler/vent system are provided.

1. Establish sprinkler design in the traditional way, that is, develop design parameters using full-scale testing involving effective, rapid, sprinkler-activation strategies in the absence of vents (rapid in the sense that the test/design problem solved is one involving an effectively unconfined ceiling where smoke-layer buildup is negligible in that it does not effect the timing or sequence of early sprinkler discharge).
2. Establish a vent design objective. In cases where sprinkler action is expected to control the fire (i.e., the fire will not exceed a specified, maximum energy-release rate), the design objective for Figure 3-9.1–type scenarios might be for the vents to maintain indefinitely the smoke from spreading beyond the curtained compartment of fire origin (i.e., the smoke-layer interface does not descend below the bottom of the draft curtains). If the latter design objective is shown to be too ambitious, or, in cases where sprinkler action is expected only to slow, but not to stop the growth of the fire, the design objective would be for the vents to maintain the smoke from spreading beyond the curtained compartment of fire origin for a specified time interval, for example, the time expected for the fire department to respond and initiate an attack on the fire.
3. Adopt a practical/achievable strategy of early opening of all vents in the compartment of fire origin, for example, ganged operation of all vents in the curtained compartment of fire origin based on and subsequent to first sprinkler activation.
4. Using an appropriate consensus compartment fire model, one with a proven capability of simulating the time-dependent interaction of sprinklers, vents, and draft curtains, develop a vent design that meets the established design objectives.

Nomenclature

A_{FIRE}	effective plan area of fire
A_{INLET}	total area of open inlet vents
A_{VENT}	total area of ceiling vents or area of a single unit vent
$A_{VENT,EFF}$	effective area of vent
C	flow coefficient, (Equation 8)
$C_{EFF,FLOOD}$	effective value of C for flooding-flow condition
C_P	specific heat at constant pressure of air
C_{PRES}	local pressure coefficient
D_{VENT}	equivalent diameter of a single vent, (Equation 24)
D_{FIRE}	effective diameter of base of fire, (Equation 39)
F	Froude number, (Equation 26)
$F_{CRITICAL}$	critical value of F
g	acceleration of gravity, 9.8 m^2/s
h	$z_{CEIL} - z_{LAY}$
h_{DEP}	depressed distance of layer interface
K	fraction of $\dot{Q}_{CONV}$ (Equation 51)
L_{CURT}	length of draft curtains
L_{FIRE}	effective length of line fire
L_{FLAME}	mean flame height (Equation 43)
L_1, L_2	length of sides of rectangular vent
$\dot{m}_{CURT}$	mass flow rate under a draft curtain
$\dot{m}'_{LINE}$	mass flow rate per unit length for plume from line fire (Equation 41)
$\dot{m}_{PLUME}$	mass flow rate in the plume
$\dot{m}_{SPILLPLUME}$	mass flow rate in a spill plume (Equation 48)
$\dot{m}_{VENT}$	mass flow rate through vent
P	absolute pressure
P_{ADJ}	P in space adjacent to curtained space
P_{AMB}	P of standard ambient environment, 101325 Pa
P_{IN}	P inside the facility
P_{OUT}	P of outside environment
P_{SURF}	P along outside building surface
P_1, P_2	P in space 1, 2

$\dot{Q}_{CONV}$	portion of $\dot{Q}_{TOTAL}$ convected in plume (Equation 37)
$\dot{Q}'_{CONV}$	convected energy release rate per unit length for line fire (Equation 40)
$\dot{Q}_{TOTAL}$	total rate of fire energy release
R	gas constant for air, 286.8 (J/kg·K)
T	absolute temperature
T_{AMB}	characteristic T of ambient environment, 293 K
T_{LAY}	T of smoke layer
T_{OUT}	T of outside environment
t_g	time for t-squared fire to grow to 1000 kW
V_{FLOOD}	V_{VENT} for flooding-flow condition
V_{VENT}	average velocity of vent flow at the vent opening
V_{WIND}	wind speed
W_{VENT}	width of vent
z	elevation
$z_{BALCONY}$	z at bottom of balcony
z_{BOT}	z at bottom of vent
z_{CEIL}	z at ceiling
z_{CURT}	z at bottom of curtain
z_{FIRE}	z at base of fire
z_{FLOOR}	z at floor
z_{LAY}	z at bottom of upper smoke layer
$z_{LINESOURCE}$	z of line-fire source
z_{MID}	z at middle of nonhorizontal vent
z_{TOP}	z at top of vent
z_{VENT}	z of horizontal vent
z_0	z at datum

Greek

α	angle between normal to vent area and the vertical
β	a constant (Equation 28)
ε	defined in Equation 24
ε	defined in Equation 44
$\Delta P(z)$	$P(z) - P(z_0)$
$\Delta P_{IN\text{-}ADJ}(z)$	$P_{IN}(z) - P_{ADJ}(z)$
ΔP_{FLOOD}	$\Delta P_{IN\text{-}OUT}(z_{CEIL})$ for flooding-flow condition
$\Delta P_{IN\text{-}OUT}(z)$	$P_{IN}(z) - P_{OUT}(z)$
$\Delta P_{1\text{-}2}(z)$	$P_1(z) - P_2(z)$
δ	a measure of normalized P (Equation 4)
η	dummy variable of integration
Λ	dimensionless flame length (Equation 44)
λ_{RAD}	fraction of $\dot{Q}_{TOTAL}$ radiated to far field
ρ	density
ρ_{AMB}	characteristic ρ of ambient environment, 1.2 kg/m^3
ρ_{LAY}	ρ of smoke layer
ρ_{OUT}	ρ of outside environment
ρ_{VENT}	ρ of vent flow

References Cited

1. NFPA 204, *Guide for Smoke and Heat Venting,* NFPA, Quincy, MA (1998 edition).
2. NFPA 92B, *Guide for Smoke Management Systems in Malls, Atria, and Large Areas,* NFPA, Quincy, MA (2000).
3. H.P. Morgan, et al. "Design Methodologies for Smoke and Heat Exhaust Ventilation," *Fire Research Station,* Watford, United Kingdom (1999).
4. T. Butcher, ed., *CIBSE Relationships for Smoke Control Calculations, Technical Memoranda TM:1995,* Chartered Institution of Building Services Engineers, London (1995).
5. L.Y. Cooper and G.P. Forney, "The Consolidated Compartment Fire Model (CCFM) Computer Code Application CCFM. VENTS—Part I: Physical Basis," *NISTIR 90-4342,* National Institute of Standards and Technology, Gaithersburg, MD (1990).
6. P.H. Thomas, et al. "Investigations into the Flow of Hot Gases in Roof Venting," *Fire Research Technical Paper No. 7,* HMSO, London (1963).
7. L.Y. Cooper, "Combined Buoyancy- and Pressure-Driven Flow through a Horizontal, Circular Vent," *Journal of Heat Transfer,* 117, pp. 659–667 (1995).
8. L.Y. Cooper, "Calculating Combined Buoyancy- and Pressure-Driven Flow through a Horizontal, Circular Vent; Application to a Problem of Steady Burning in a Ceiling-Vented Enclosure," *Fire Safety Journal,* 27, pp. 23–35 (1996).
9. L.Y. Cooper, "VENTCF2: An Algorithm and Associated Computer Subroutine for Calculating Flow through a Horizontal Ceiling/Floor Vent in a Zone-Type Compartment Fire Model," *Fire Safety Journal,* 28, pp. 253–287 (1997).
10. G. Heskestad and R.D. Spalding, "Inflow of Air Required at Wall and Ceiling Appertures to Prevent Escape of Fire Smoke," FMRCJ.I.OQ4E4.RU, Factory Mutual Research Corporation, Norwood, MA (1991).
11. J.S. Turner, *Buoyancy Effects in Fluids,* Cambridge Press (1973).
12. I.R. Wood, "Selective Withdrawal from a Stably Stratified Fluid," *Journal of Fluid Mechanics,* 32, pp. 209–223 (1968).
13. D. Spratt and A. Heselden, "Efficient Extraction of Smoke from a Thin Layer under a Ceiling," *Fire Research Note No. 1001,* Fire Research Station, Department of the Environment and Fire Offices' Committee, Joint Fire Research Organization, Watford, UK (1974).
14. J.H. Shanley and C.L. Beyler, "Horizontal Vent Flow Modeling with Helium and Air," *Fire Safety Science—Proceedings of the Second International Symposium,* (T. Wakamatsu, et al. eds.), Hemisphere, New York, pp. 305–313 (1989).
15. C.L. Beyler, "Fire Plumes and Ceiling Jets," *Fire Safety Journal,* 11, pp. 53–75 (1986).
16. G. Heskestad, "Engineering Relations for Fire Plumes," *Fire Safety Journal,* 7, pp. 25–32 (1984).
17. E.E. Zukoski, "Development of a Stratified Ceiling Layer in the Early Stages of a Closed-Room Fire," *Fire and Materials,* 2, 2, pp. 54–62 (1978).
18. L.Y. Cooper, "A Buoyant Source in the Lower of Two Homogeneous, Stably Stratified Layers," *20th International Symposium on Combustion,* Combustion Institute, Pittsburgh, pp. 1567–1573 (1984).
19. L.Y. Cooper, "Convective Heat Transfer to Ceilings above Enclosure Fires," *19th Symposium (International) on Combustion,* Combustion Institute, Pittsburgh, pp. 933–939 (1982).
20. L.Y. Cooper, "Heat Transfer from a Buoyant Plume to an Unconfined Ceiling," *Journal of Heat Transfer,* 104, pp. 446–451 (1982).

21. L.Y. Cooper and A. Woodhouse, "The Buoyant Plume-Driven Adiabatic Ceiling Temperature Revisited," *Journal of Heat Transfer,* 108, pp. 822–826 (1986).
22. L.Y. Cooper and D.W. Stroup, "Thermal Response of Unconfined Ceilings above Growing Fires and the Importance of Convective Heat Transfer," *Journal of Heat Transfer,* 109, pp. 172–178 (1987).
23. L.Y. Cooper, "Ceiling Jet–Driven Wall Flows in Compartment Fires," *Combustion Science and Technology,* 62, pp. 285–296 (1988).
24. L.Y. Cooper, "Fire-Plume Generated Ceiling Jet Characteristics and Convective Heat Transfer to Ceiling and Wall Surfaces in a Two-Layer Zone-Type Fire Environment: Uniform Temperature Ceiling and Walls," *Fire Science and Technology,* 13, 1 and 2, pp. 1–17 (1993).
25. L.Y. Cooper, "Estimating the Environment and the Response of Sprinkler Links in Compartment Fires with Draft Curtains and Fusible Link-Actuated Ceiling Vents," *Fire Safety Journal,* 16, pp. 137–163 (1990).
26. W.D. Davis and L.Y. Cooper, "Estimating the Environment and the Response of Sprinkler Links in Compartment Fires with Draft Curtains and Fusible Link-Actuated Ceiling Vents—Part II: User Guide for the Computer Code LAVENT," *NISTIR 89-4122,* National Institute of Standards and Technology, Gaithersburg, MD (1989).
27. National Institute of Standards and Technology, LAVENT software, Gaithersburg, MD.
28. C.L. Beyler and L.Y. Cooper, "Interaction of Sprinklers With Smoke Vents," in press *Fire Technology.*
29. M.L. Bullen, "The Effect of a Sprinkler on the Stability of a Smoke Layer beneath a Ceiling," *Fire Research Note No. 1016,* Department of the Environment and Fire Officers' Committee, Joint Fire Research Organization, Watford, England (1974).
30. M.L. Bullen, "The Effect of a Sprinkler on the Stability of a Smoke Layer beneath a Ceiling," *Fire Technology,* 13, 1, pp. 21–34 (1977).
31. R.L. Alpert, "Calculated Interaction of Sprays with Large-Scale Buoyant Flows," *Journal of Heat Transfer,* 106, pp. 310–317 (1984).
32. A.J. Gardiner, *First Report on the Interaction between Sprinkler Sprays and the Thermally Buoyant Layers of Gases from Fires,* South Bank Polytechnic, London (1985).
33. A.J. Gardiner, *Second Report on the Interaction between Sprinkler Sprays and the Thermally Buoyant Layers of Gases from Fires,* South Bank Polytechnic, London (1986).
34. A.J. Gardiner, *Third Report on the Interaction between Sprinkler Sprays and the Thermally Buoyant Layers of Gases from Fires,* South Bank Polytechnic, London (1988).
35. A.J. Gardiner, *Fourth Report on the Interaction between Sprinkler Sprays and the Thermally Buoyant Layers of Gases from Fires,* South Bank Polytechnic, London (1988).
36. L.A. Jackman, *Second Report on the Interaction between Sprinkler Sprays and the Thermally Buoyant Layers of Gases from Fires,* South Bank Polytechnic, London (1990).
37. L.A. Jackman, *Third Report on the Interaction between Sprinkler Sprays and the Thermally Buoyant Layers of Gases from Fires,* South Bank Polytechnic, London (1991).
38. L.A. Jackman, P.F. Nolan, A.J. Gardiner, and H.P. Morgan, *Mathematical Model of the Interaction of Sprinkler Spray Drops with Fire Gases,* South Bank University, London, Swedish Fire Research Board, and National Institute of Standards and Technology (NIST), Fire Suppression Research, First International Conference on Fire Suppression Research, May 5–8, 1992, Stockholm, Sweden, (V. Sjolin, D.D. Evans, and N.H. Jason, eds.), pp. 209–227 (1992).
39. G. Heskestad, "Sprinkler/Hot Layer Interaction," *NIST-GCR-91-590,* National Institute of Standards and Technology (NIST), Gaithersburg, MD (1991).
40. L.Y. Cooper, "The Interaction of an Isolated Sprinkler Spray and a Two-Layer Compartment Fire Environment. Phenomena and Model Simulations," *Fire Safety Journal,* 25, 2, pp. 89–107 (1995).
41. L.Y. Cooper, "The Interaction of an Isolated Sprinkler Spray and a Two-Layer Compartment Fire Environment," *International Journal Heat and Mass Transfer,* 38, 4, pp. 679–690 (1995).
42. P.L. Hinkley, "Work by the Fire Research Station on the Control of Smoke in Covered Shopping Centers," *BRE Paper CP 83/75,* Building Research Establishment (BRE), Fire Research Station (FRS), London (1975).
43. A.J.M. Heselden, "The Interaction of Sprinklers and Fire Venting," *Fire Surveyor,* 11, 5, pp. 13–28 (1982).
44. G. Holmstedt, "Sprinkler and Fire Venting Interaction," *Literature Survey on Modeling Approaches and Experiments Available and Recommendations for Further Studies, 92178 AR GH/AB,* Swedish Fire Research Board, Stockholm, Sweden (1992).
45. B. Persson and H. Ingason, "Modeling of Interaction between Sprinklers and Fire Vents," *SP Report 1996:32,* Swedish National Testing and Research Institute, Sweden (1996).
46. L.Y. Cooper, "LAVENTS—A Computer Program to Model the Interaction between Sprinklers, Smoke Layers, and Smoke Vents," presented at the *International Conference on Smoke Ventilation and Sprinklers—Aspects of Combined Use,* Fire Research Station, Borehamwood, England (1992).
47. K.B. McGrattan, A. Hamins, D.W. Stroup, "Sprinkler, Smoke and Heat Vent, Draft Curtain Interaction—Large-Scale Experiments and Model Development," *NISTIR 6196,* National Institute of Standards and Technology (NIST), Gaithersburg, MD (1998).
48. K.B. McGrattan, H.R. Baum, and R.G. Rehm, "Large Eddy Simulations of Smoke Movement," *Fire Safety Journal,* 30, pp. 161–178 (1998).
49. K.B. McGrattan and D.W. Stroup, "Sprinkler, Vent and Draft Curtain Interaction: Experiment and Computer Simulation," *National Institute of Standards and Technology (NIST),* Gaithersburg, MD (1997).
50. K.B. McGrattan and D.W. Stroup, "Large Eddy Simulations of Sprinkler, Vent and Draft Curtain Performance," *Fire Suppression and Detection Research Application, Symposium, Research and Practice: Bridging the Gap, Proceedings,* National Fire Protection Research Foundation, February 12–14, 1997, Orlando, FL, pp. 59–68 (1997).
51. H. Touvinen, "Validation of Ceiling Jet Flows in a Large Corridor with Vents Using the CFD Code JASMINE," *Fire Technology,* 32, 1, pp. 25–49 (1996).
52. H. Touvinen and L.Y. Cooper, "Validation of Ceiling Jet Flows in a Large Corridor with Vents Using the CFD Code JASMINE: Errata and Additional Remarks," *Fire Technology,* 33, 2, pp. 183–186 (1997).
53. R.N. Mawhinney, E.R. Galea, and M.K. Patel, "Euler-Lagrange Modeling of Fire/Sprinkler Interactions," *Fire Safety Science—Proceedings of the Fifth International Symposium,* International Association of Fire Safety Science (IAFSS), Australia, p. 1336 (1997).
54. W.K. Chow and A.C. Tang, "Experimental Studies on Sprinkler Water Spray Smoke Layer Interaction," *Journal of Applied Fire Science,* 4, 3, pp. 171–184 (1994–95).

CHAPTER 10

Compartment Fire-Generated Environment and Smoke Filling

Leonard Y. Cooper

Fire Safety of Building Designs

Introduction

The following generic problem must be solved if one is to be able to establish the fire safety of building designs:

Given: Initiation of a fire in a compartment or enclosed space.

Predict: The environment that develops at likely locations of occupancy, at likely locations of fire/smoke sensor hardware (e.g., detectors and sprinkler links), and in locations of safe refuge and along likely egress paths.

Compute: The time of fire/smoke sensor hardware response and the time of onset of conditions untenable to life and/or property. This computation would be carried out from the above predictions, using known response characteristics of people, hardware, and materials.

The above is only a simple sketch of the overall problem that is likely to be associated with the interesting details of many real fire scenarios. A long-term challenge of fire science and technology is to solve the above type of problem, even when it is formulated in elaborate detail. Compartment fire modeling is the branch of fire science and technology which develops the necessary tools to address this generic problem.

This chapter will describe some of the key phenomena that occur in compartment fires, and it will focus on smoke filling which is one of the simplest quantitative global descriptions of these phenomena. A specific smoke-filling model will be presented, and solutions to its model equations will be discussed along with example applications.

Compartment Fire-Generated Environment

Figures 3-10.1 through 3-10.8 depict the various phenomena that make up the compartment fire-generated environment to be predicted when compartment fire modeling is adopted. These figures are intended to illustrate the representative conditions at different instants of time in two generic compartment spaces: (1) an almost-fully enclosed single-room compartment of fire origin and (2) an almost-fully enclosed, freely connected, two-room compartment made up of the room of fire origin and an adjacent space. A description of the phenomena depicted in these figures follows. The physical bases of assumption that can be used to simplify descriptions of some of these phenomena are included in the discussion. Some of these will be important in placing the simple smoke-filling model into the perspective of the overall complex dynamic fire environment.

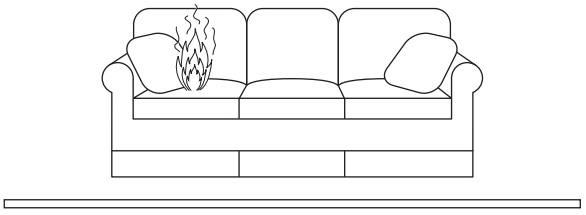

Figure 3-10.1. ***Events immediately after ignition.***

Dr. Leonard Y. Cooper was a research engineer in the Building and Fire Research Laboratory of the National Institute of Standards and Technology from 1978–1998. Since 1998 he has been a senior scientist/engineer at Hughes Associates Inc., a fire protection engineering research and development firm. Since 1978 he has focused on applying a broad range of the physical and mechanical engineering sciences to develop and transfer research results into technically sound engineering practices in the field of applied fire safety. His research included the development of mathematical models of fire phenomena and on the assembly of these into compartment fire models and associated computer programs for practical and research-oriented compartment fire simulations.

Room of Fire Involvement

Fire growth in the combustible of fire origin: An unwanted ignition leading rapidly to flaming is assumed to occur within an enclosed space. This ignition is depicted in Figure 3-10.1 as occurring on the cushion of a couch in, say, a residential type of occupancy. It is, however, important to realize that all of the discussion to follow, and Figure 3-10.1 itself, is also relevant to fire scenarios which may develop in other kinds of occupancies, for example, as a result of ignitions in stacked commodity warehouse enclosures, places of assembly, and so forth.

Within a few seconds of ignition, early flame spread quickly leads to a flaming fire with a power output of the order of a few tens of kW (a power level characteristic of a small wastepaper basket fire). The fire continues to grow. Besides releasing energy, the combustion process also yields a variety of other products, including toxic and nontoxic gases and solids. Together, all of these products are referred to as the "smoke" produced by the fire.

With an adequate description of the ignition source and the involved combustible (e.g., ignited paper match on the corner of a couch whose frame, cushioning and finishing materials, and construction were well defined), one would hope that fire science and technology would provide methods to predict the fire spread and growth process from onset of ignition. Toward this end, ongoing research on flame spread and combustion is under way in a variety of fire research institutions throughout the world. (Examples of such research include boundary layer analyses and experiments with flame spread on idealized materials and geometries; and flame spread tests and rate of heat release tests on small samples of real material composites.) However, for the present and the foreseeable future, it is beyond the state-of-the-art of fire technology to make the required fire growth prediction with any generality. This situation leads to a dilemma for the modeler of compartment fire environments, because the physical and chemical mechanisms which govern the dynamics of the combustion zone actually drive the basic intra-compartment smoke migration phenomena whose simulations are being sought.

A practical engineering solution to the above dilemma, proposed and supported by Cooper,[1,2] lies in the following compromise in simulation accuracy:

> Prior to the time of potential flashover, it is reasonable to neglect the effect of the enclosure on flame spread and to assume that, from the time of ignition to the time shortly before potential flashover, the combustion zone in a particular grouping of combustibles develops as it would in a free-burn situation.

[Free burn here is defined as a burn of the combustibles in a large (compared to the combustion zone), ventilated space with relatively quiescent atmosphere.] To implement these ideas, one simply uses empirical, free-burn test data (which may or may not be presently available) to describe the combustion physics of a fire whose hazard is being evaluated. This compromise would, in the course of time, be supplanted by analytic models of flame spread and fire growth to the extent the future results of research lead to satisfactory methods for predicting such phenomena.

The implementation of the above compromise is, in principle, relatively simple. But for general use, it must be supported by an extensive data base acquired from a series of actual full-scale free-burn tests. This kind of data is being acquired with some regularity at fire test laboratories such as those of the National Institute of Standards and Technology and the Factory Mutual Research Corporation.[3–5]

Development of the plume: As depicted in Figure 3-10.2, a large fraction, λ_r, of the rate of energy released in the high-temperature combustion zone is transferred away by radiation. The transferred energy, $\lambda_r \dot{Q}(t)$, irradiates nearby surfaces of the combustible and faraway wall, ceiling, etc., surfaces which are in the line-of-sight of the combustion zone. The actual value of λ_r associated with the free-burn of a specific array of combustibles is often deduced from data acquired during the aforementioned type of free-burn tests. For typical hazardous flaming fires, λ_r is usually of the order of 0.35.

Because of the elevated temperature of the products of combustion, buoyancy forces drive them out of the growing combustion zone and up toward the ceiling. In this way, a plume of upward-moving elevated-temperature gases and particulates is formed above the fire. For the full height of the plume and at its periphery, relatively quiescent and cool gases are entrained laterally and mixed with the plume as it continues its ascent to the ceiling. As a result of this entrainment, the total mass flow in the plume continuously increases, and the average temperature and average concentration of products of combustion in the plume continuously decrease with increasing height. With reasonable accuracy, the plume dynamics at any instant of time can be quantitatively described as a function of the rate of energy, $(1 - \lambda_r)\dot{Q}(t)$, convected up from the combustion zone. A description of the concentration of combustion products in the plume would require, in addition, the combustion zone's rate of product generation. With regard to predictions of the dynamics of the plume, results can be provided at a variety of different levels of detail.[6–8] For example, Zukoski et al.

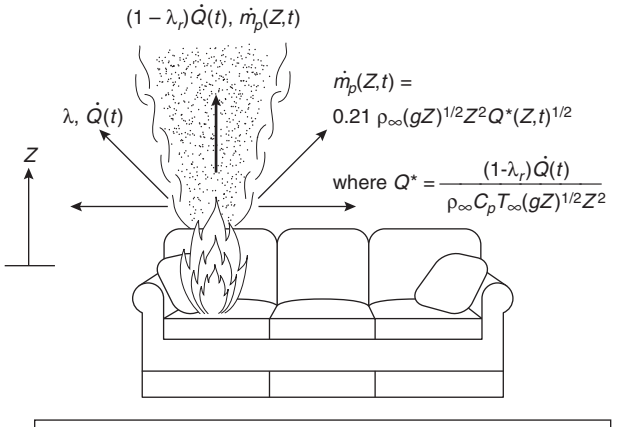

Figure 3-10.2. ***Development of the plume.***

provide the formula in Figure 3-10.2 as an estimate of the mass flux in the plume, $\dot{m}_p$, at a distance Z above the combustion zone.[7]

Plume-ceiling interaction: As depicted in Figure 3-10.3, when the hot plume gases impinge on the ceiling, they spread across it forming a relatively thin radial jet. This jet of hot gases contains all of the smoke generated from the combustion zone, and all the ambient air which was entrained along the length of the plume.

As the hot jet moves outward under the ceiling surface, it entrains ambient air from below. It transfers energy by conduction to the relatively cool adjacent ceiling surface, and by convection to the entrained air. It is retarded by frictional forces from the ceiling surface above, and by turbulent momentum transfer to the entrained air from below. As a result of all this flow and heat transfer activity, the ceiling jet continuously decreases in temperature, smoke concentration, and velocity, and increases in thickness with increasing radius.

Research reported in the literature has led to results for predicting the quantitative aspects of ceiling-jet dynamics that can be used for selecting and locating smoke detectors and fusible link sprinkler head actuators, and for the mathematical modeling of overall compartment fire environments.[9–18]

With regard to detectors and fusible links, knowledge of the properties of the ceiling jet is the key to the prediction of the response of properly deployed devices in real fire scenarios. With regard to the overall modeling of compartment fire environments, the basic information that must be extracted from the ceiling-jet properties is the rate of heat transfer to the ceiling surface. Experiments have shown that this heat transfer can be significant, of the order of several tens of percent of the total energy released by the combustion zone, and, as a result, it is key to predicting the temperature of the smoke which ultimately spreads throughout the enclosure. Also, a reasonable estimate of this rate of heat transfer is required for estimating temperatures of the ceiling surface material itself.

Ceiling jet-wall interaction: The ceiling jet continues to move radially outward under the ceiling surface, and it eventually reaches the bounding walls of the enclosure. As depicted in Figure 3-10.4, the ceiling jet (now somewhat reduced in temperature from its highest levels near the plume) impinges and turns downward at the ceiling-wall juncture, thereby initiating a downward-directed wall jet.

The downward wall jet is of higher temperature and lower density than the ambient air into which it is being driven. The jet is, therefore, retarded by buoyancy in its downward descent, and at some distance below the ceiling the downward motion of the smoky jet is eventually halted. The wall jet is also retarded (probably to a lesser degree) by frictional forces at the wall surface, and it is cooled by conductive/convective heat transfer to relatively cool wall surfaces. Momentum and heat transfer from the jet occur away from the wall as the jet's outer flow is sheared off and driven back upward on account of buoyancy. In its turn, the now upward-moving flow entrains ambient air in a manner which is reminiscent of entrainment into the original fire plume. Eventually a relatively quiescent upper gas layer is formed below the continuing ceiling-jet flow activity.

The strength of the wall-jet flow activity will be determined by the characteristics of the ceiling jet at the position of its impingement with the wall. For fire scenarios where the proximity of the walls to the fire is no greater than a room height or so, it is reasonable to speculate that, based on test results,[19,20] rates of conductive/convective heat transfer to wall surfaces can be significant, of the order of tens of percent of the fire's energy release, and that entrainment to the upward moving, reverse portion of the wall flow can lead to significant variations of the early rate of thickening of the upper gas layer. On the other hand, if walls are several room heights from the fire, then it is possible that the ceiling jet will be relatively weak by the time it reaches the walls, in the sense that ceiling jet-wall interactions may not play an important role in the dynamics of the overall fire environment.

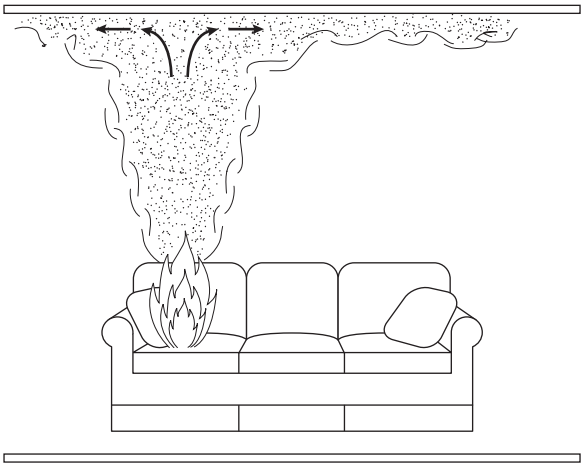

Figure 3-10.3. ***The plume-ceiling interaction.***

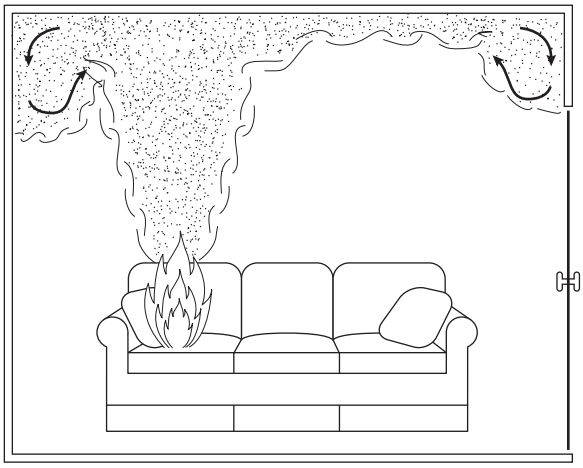

Figure 3-10.4. ***Ceiling jet-wall interaction.***

Besides being important in the prediction of the overall fire environment, knowledge of the flow and temperature environments local to vigorous ceiling jet-wall interaction zones would be the key to predicting the response of wall-mounted smoke detectors, fusible links, and so forth.

Development and growth of the upper layer—"smoke filling": The gases in the ceiling and wall jets redistribute themselves across the upper volume of the room. Eventually, a relatively quiescent, elevated temperature upper smoke layer of uniform thickness is formed below the continuing ceiling-jet flow activity. As the thickness of this layer grows, it eventually submerges the flows generated by the ceiling jet-wall interactions. The bottom of the layer is defined by a distinctive material interface which separates the lower ambient air from the upper, heated, smoke-laden gases. With increasing time the level of the smoke layer interface continues to drop, and the temperature and smoke concentration of the upper layer continue to rise.

In general, one would hope that fire detection, successful occupant alarm, and, if appropriate, successful intervention hardware response would occur during the state of fire growth described above. As suggested earlier, rationally engineered design in this regard would be possible with predictions of the dynamic fire environments local to deployed devices, and with predictions of the resulting response of such devices.

For reasons already mentioned, some detail in the description of plume, ceiling-jet, and ceiling jet-wall flow dynamics is required. However, for the purpose of understanding the impact of the overall fire environment on life and property safety, simplified descriptions compatible with the aforementioned detail would suffice and, for a variety of practical reasons, would actually be preferable. For this reason, available predictive models of compartment fire environments commonly describe the bulk of upper layer environment in terms of its spatially averaged properties. Thus, at any instant of time, it is typically assumed that the portion of the room which contains the fire-generated products of combustion, that is, the smoke, is confined to an upper layer of the room. This upper layer is described as having changing thickness and changing, but spatially uniform, temperature and concentration of combustion products. Actual full-scale testing of compartment fire environments has indicated that such a simple means of describing the distribution of products of combustion represents a reasonable compromise between accuracy in simulation and practicability in implementation.

Figure 3-10.5 is a generic depiction of the compartment fire environment at the stage of fire development under discussion. At this stage, whether or not the space of fire involvement is fully enclosed (i.e., all doors and windows are closed and only limited leakage occurs at bounding partitions) or is freely communicating with adjacent space(s) (e.g., open or broken windows, open doors to the outside environment or to an adjacent enclosed space of limited or virtually unlimited extent) becomes very important in the subsequent development of the fire environment. In the sense that the upper layer thickness and temperature would grow most rapidly, the fully enclosed space with most leakage near the floor would lead to the most rapid development of potentially life and property threatening conditions.

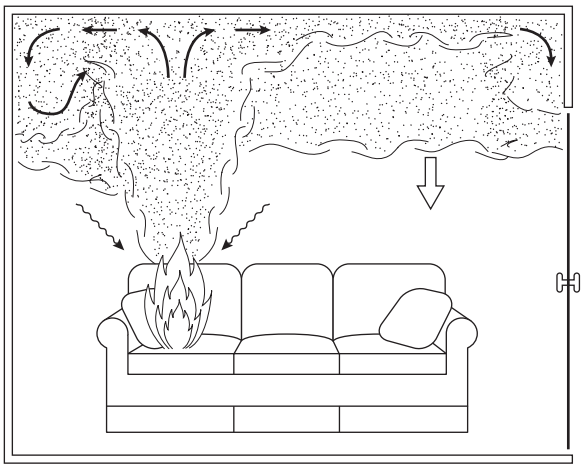

Figure 3-10.5. ***Fully enclosed space with developed growing upper layer.***

Referring again to the depiction in Figure 3-10.5, the fire plume below the smoke layer interface continues to entrain air as it rises to the ceiling. However, as the hot plume gases penetrate the layer interface and continue their ascent, additional entrainment is from an elevated temperature, smoke-laden environment. Also, once the plume gases enter the smoke layer, they are less buoyant relative to this layer than they were relative to the cool lower layer of ambient air. Thus, the continued ascent of plume gases is less vigorous than it would otherwise be in the absence of the upper layer.

The new and more complex two-layer state of the enclosure environment requires that some modification of the earlier referenced quantitative descriptions of the plume, ceiling-jet, and ceiling jet-wall flow dynamics be introduced. Modifications along these lines are proposed by Cooper.[21,22]

As depicted in Figure 3-10.6, potentially significant wall flow can develop during the descent of the layer interface. This flow is expected to occur away from regions of vigorous ceiling jet-wall interactions. It is distinct from the previously described upper wall jet and develops because of relatively cool upper wall surfaces which bound the elevated-temperature upper smoke layer. The smoke which is adjacent to these wall surfaces is relatively cool and, therefore, more dense than its surroundings. As a result of this density difference, a continuous, downward-directed wall flow develops which is injected at the smoke interface into the lower, relatively smoke-free layer. Once in the lower layer, the smoke-laden wall flow, now of higher temperature than its surroundings, will be buoyed back upward to either mix with and contaminate the lower layer or to entrain additional (i.e., in addition to the fire plume) lower layer air into the upper layer.

It is noteworthy that the wall effect just described has been observed in full- and reduced-scale fire tests, and that it appears to be particularly significant in enclosures

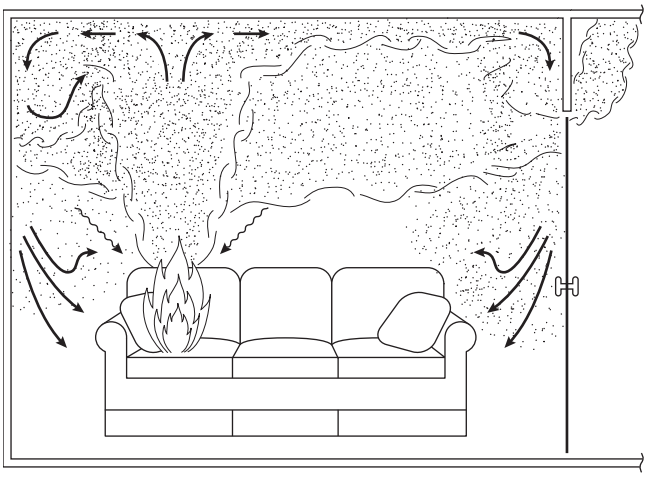

Figure 3-10.6. ***Further "smoke filling."***

with relatively large ratios of perimeter-to-ceiling height (e.g., in corridors).[23]

As a result of its elevated temperature, the smoky upper layer transfers energy by radiation to the ceiling and upper wall surfaces which contain it. As depicted in Figures 3-10.4 and 3-10.5 by the downward-directed arrows, the layer also radiates to the lower surfaces of the enclosure and its contents. Initially, the only significant role of this downward radiation is its effect on human tissue. Indeed, only for downward-directed radiation fluxes significantly in excess of life-threatening levels (characterized by smoke layer temperature levels of the order of 200°C, or by flux levels of the order of 2.5 kW/m^2) would the radiant energy feedback to enclosure surfaces and combustibles have a significant impact on fire growth and spread, and on the overall fire environment.[1,24]

Once radiation feedback becomes of general significance, for example, when the average upper layer temperature reaches 300 to 400°C, it is likely that the potential for flashover will develop within a relatively short time interval (compared to the time interval between ignition and the onset of a life-threatening environment). The events which develop during this time interval will be referred to here as the "transition stage" of fire development.

The onset of life-threatening conditions, which could be caused by any one of a number of reasons, would occur prior to the transition stage of fire development. Before this event can be predicted, quantitative criteria defining a "life-threatening environment" must be established. These criteria must be defined in terms of those physical parameters for which predictive models of compartment fire environments can provide reasonable estimates. Consistent with the earlier discussion, such parameters include the smoke layer thickness (or vertical position of its interface) and temperature. The concentration of potentially hazardous components of the smoke in the upper layer would also be of basic importance. Criteria for the onset of a life-threatening environment could, for example, be based on the following consideration (which would neglect the effect of lower layer contamination due to wall flows):

When the smoke layer interface is above some specified, characteristic face-elevation, an untenable environment would occur if and when a hazardous radiation exposure from the upper layer is attained. Such an exposure could be defined by a specified upper layer critical temperature. If the interface is below face-elevation, then untenability would occur if and when a second critical smoke layer temperature is attained. However, the latter temperature would be lower than the former one, and untenable conditions would result from burns or the inhalation of hot gases. Once the interface dropped below face elevation, untenability would also occur if and when a specified critical concentration (or a specified exposure dosage) of some hazardous product of combustion was attained.[2]

Transition stage of fire development: Any detailed analysis and prediction of the fire environment during the transition stage of fire development must, of necessity, take account of the effects of upper layer and upper surface reradiation, in general, and of the complex effects of radiation-enhanced fire growth, in particular. Such an analysis would require a mathematical model of compartment fire phenomena which would be significantly more sophisticated than that which would be required to predict the fire environment prior to, and possibly even following, the transition stage.

Regarding the potential difficulty, uncertainty, inconvenience, and/or cost of carrying out transition stage analysis, it is noteworthy that conservative designs for life and property safety may be possible by implementing a strategy of fire environment analysis which avoided the details of the transition stage entirely. This is done by conservatively assuming that the relatively brief time interval associated with the transition stage shrinks to a flashover jump condition at a relatively early time in the fire scenario.[1]

Smoke Spread from the Room of Fire Involvement to Adjacent Spaces

Smoke and fresh air exchange between a room of fire involvement and an adjacent space: Under this and the following subheading, smoke spread phenomena associated with a fire-involved room and a communicating adjacent space will be discussed. Reference here will be made to a fully enclosed, two-room space with relatively large common penetrations (e.g., open doors or windows) through which smoke and ambient air exchange will be so significant as to render inadequate an analysis which treats the room of fire involvement as an isolated enclosure. Regarding the two-room spacial configuration, Figures 3-10.1 through 3-10.5 are still relevant to the early development of conditions within the fire room. As the smoke layer interface drops to the level of the soffit of the communicating doorway(s) or window(s), significant amounts of smoke start to move into the adjacent space from above, while significant amounts of ambient air are driven out of the adjacent space (and into the fire room) from below. From that time on, as depicted in Figure 3-10.7, an interdependent smoke-filling process in each of

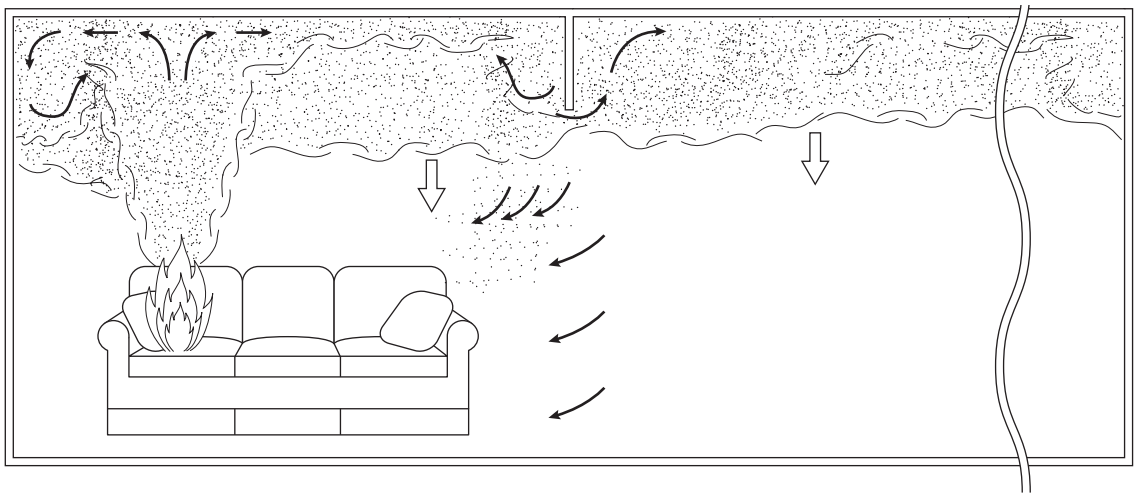

Figure 3-10.7. ***Smoke and fresh air exchange between a room of fire involvement and an adjacent space.***

the two spaces is initiated, and the adjacent space starts to develop a two-layer type of environment.

Throughout the course of typical real-fire scenarios, changes in the absolute pressures of facility spaces are, at the most, of the order of one percent. Yet, dynamic elevation-dependent pressure differences that exist between the rooms of fire involvement and adjacent spaces are large enough to drive a significant cross-door exchange of smoke and ambient air.

Toward the left side of Figure 3-10.8 is a sketch of the vertical static pressure distribution, $P_{fire}(Z)$, of the room of fire involvement. This is the pressure distribution that is measured in the bulk of the relatively quiescent-environment room, away from vigorous door and plume flows. Notice that the rate of change of pressure with elevation is uniform and relatively large between the floor and the smoke interface, and is uniform and relatively small within the smoke layer. The reason for this is that the temperature-dependent density throughout each of the two layers is assumed to be uniform, and the lower layer is more dense (i.e., of lower temperature) than the upper one. The pressure at the floor is designed as $P_{fire}(Z = 0) = P_{fire,0}$.

Toward the right side of Figure 3-10.8 is a sketch of the vertical static pressure, $P_{adj}(Z)$, in the adjacent space. There, the change of slope occurs at the elevation of the adjacent space's smoke interface, which is above the smoke interface in the fire room. Also, the slope of the pressure distribution above the interface is consistent with a smoke layer somewhat more dense or cooler than the smoke

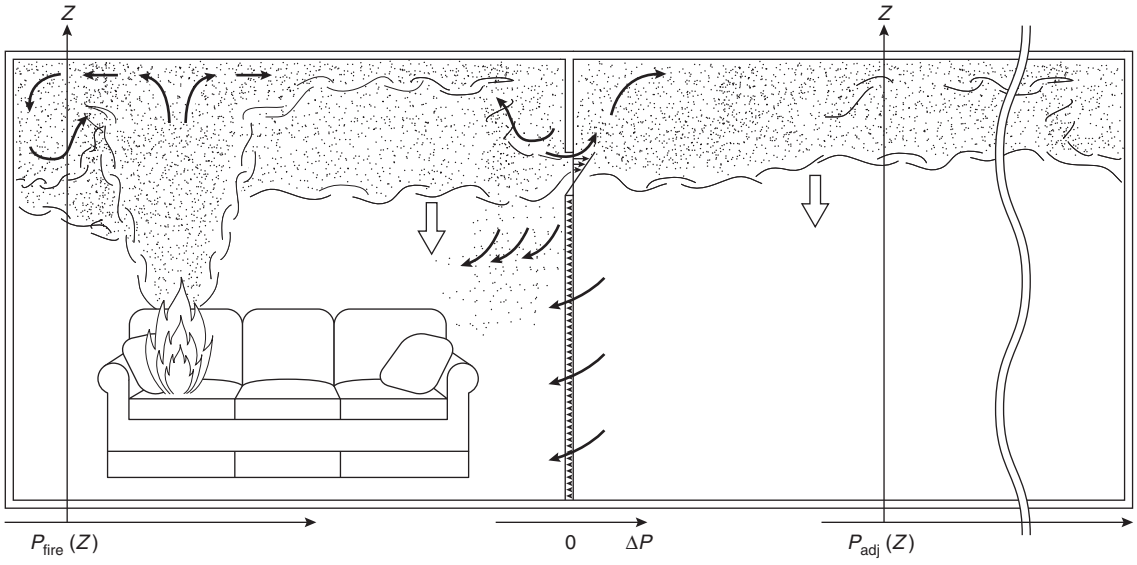

Figure 3-10.8. ***Figure 3-10.7 with sketches of pressure distributions.***

layer in the fire room. Finally, the pressure at the floor is designated as $P_{adj}(Z) = P_{adj,0}$. The two pressure distributions can be compared by the plot of the pressure difference, $\Delta P(Z) = P_{fire}(Z) - P_{adj}(Z)$,which is sketched in the doorway of Figure 3-10.8. At Z elevations below the soffit where ΔP is positive, gases are driven from the fire room into the adjacent space. At elevations where ΔP is negative, gases are driven from the adjacent space into the fire room. At the unique elevation, called the neutral plane, where ΔP is zero, the gases tend to remain stagnant in both spaces. This is the elevation in the doorway which divides outgoing fire room smoke above from inflowing adjacent space air below.

At any given elevation, it is typical in the modeling of fire-generated doorway/window flows to use Bernoulli's equation to estimate the velocity, $V(Z)$, of the flow coming out of or into the fire room. The flow is assumed to be accelerated from rest to a dynamic pressure, $\rho V^2(Z)/2 = \Delta P(Z)$, where ρ is the density of the gas from which the streamlines originate. Also, at any elevation, the flow is assumed to be constricted at the *vena contracta* of the inlet/outlet jet, as with an orifice, to a fraction, C, of the width $W(Z)$ of the doorway. Then the total rate of mass flow across the doorway per unit height at any elevation would be

$$\rho C V(Z) W(Z) = C W(Z) \sqrt{2\rho \Delta P(Z)}$$

Imposing conservation principles at any instant of time when the layer thicknesses and densities (temperatures) in the two rooms are known, leads to the instantaneous values of $\Delta P(Z = 0)$ and neutral plane elevation.

An in-depth presentation of results for calculating total inlet and outlet mass flows and for general application of the above considerations is presented by Zukoski and Kubota.[25] Results on most appropriate values to use for C have been obtained from full-scale fire experiments.[26]

Door plume, ceiling jet, and smoke filling of the adjacent space: Having been driven into the adjacent space by the cross-door pressure differential, the doorway smoke jet is buoyed upward toward the ceiling due to its relatively low density (high temperature). The upward buoyant flow, depicted in Figure 3-10.7, is analogous to the previously discussed fire plume and, with minor modifications, can be quantitatively described by the same kinds of equations. In using these equations, the enthalpy flow rate of the inflowing smoke jet replaces the strength, $\dot{Q}(t)$, of the fire plume, and the smoke jet buoyancy source elevation, taken to be at or near the neutral plane elevation, replaces the elevation of the fire's combustion zone. Further quantitative details on one possible set of door-plume flow calculations are available.[25]

Just as the doorway smoke jet rises up in the adjacent space, is diluted by entrained fresh ambient air, and is mixed with the upper layer in the manner of a fire plume, so the relatively cool and dense ambient doorway jet enters the fire room, drops down past the upper layer, is contaminated by entrained smoke, and is mixed with the lower layer. This mechanism of lower layer smoke contamination in the room of fire involvement is in addition to the previously described wall flow mechanism which was depicted in Figure 3-10.6.

Figure 3-10.7 depicts the fire environment after the adjacent space upper layer is already well established. At earlier times, adjacent space smoke movement phenomena are closely related to those effects described above (i.e., Figures 3-10.3 and 3-10.4 and associated text) for the room of fire involvement. Thus, the doorway smoke jet plume impinges on the adjacent space ceiling, leads to the development of a ceiling jet which interacts with wall surfaces, and eventually redistributes itself to form a growing, upper layer of uniform thickness.

As was the case for the room of fire involvement, knowledge of adjacent space ceiling and upper wall properties is of fundamental importance in predicting the response of adjacent-space-deployed fire detection/intervention hardware, and the temperature of the adjacent space environment. Also, contamination of the lower layer by smoke injection from downward-directed wall flows can play a relatively more important role in adjacent spaces than in the fire room itself.[23]

All the above adjacent room effects must be predicted quantitatively with reasonable accuracy, since the fire-generated environments in the fire room and in adjacent spaces are strongly coupled by cross-door mass and energy exchanges. Also, of key importance is the ability to predict the onset of adjacent space environmental conditions which are untenable for life or property.

Multiroom and multilevel fire/smoke compartments: The discussion in the last two subparagraphs was related to the two-room illustration of Figure 3-10.7. However, the general principles of smoke migration are no different in fire/smoke compartments of more than two connected spaces.

In multiroom or even multilevel compartments, smoke migration occurs as smoke in successive rooms fills to the door/window soffits, and then starts to "spill out" into the adjacent spaces. At the same time, in each room where filling has been initiated, the phenomena related to plumes, ceiling jets, different wall flows, and upper layer/lower layer mixing are also taking place. In each of the spaces, these various phenomena are generally coupled together through the connecting door/window flows. For this reason, all effects must be analyzed simultaneously. For example, in a multiroom fire/smoke compartment one needs to satisfy the principle of conservation of mass when it is applied not just to a single doorway but to all envelopes which completely bound each compartment. To do so, one needs to solve for the pressure difference distributions and the resulting inflows and outflows across all intercompartment penetrations.

Some Special Classes of Multiroom Fire Scenarios

Single room vented to the outside: One practical, special class of the multiroom fire scenario is the single room of fire involvement which is vented to the outside ambient environment. One can carry out an analysis of the fire environment in such vented spaces by bringing to bear all considerations relevant to the Figure 3-10.7 discussion

and by assuming the adjacent space to be arbitrarily large, that is, large enough so that it would never be filled with smoke to the point where such smoke would interact with the fire room itself. The pressure distribution of the adjacent space from the floor to the top of the door/window would be specified to be the same as that of an outside ambient environment. Dynamics of the plume, which is driven by the smoke flow entering the adjacent space from the fire room, would not be affected by the adjacent space ceiling or far wall surfaces. All inflow to the fire room would be uncontaminated ambient air.

Treating the adjacent space in the above manner leads to considerable simplification in modeling mathematically the room fire environment. It is noteworthy in this regard that the only mathematical models developed specifically to predict post-flashover fire environments are related to this configuration of a single room of fire involvement vented to the outside ambient environment.

Single room vented to large space: Another important class of fire scenario, which is directly related to the last one, is the single room of fire involvement which is actually vented to a very large space. Such is the configuration, for example, when a room of fire involvement is vented to a large atrium.

Under these circumstances one could analyze the fire environment which develops in the large containing space (the atrium) as one would analyze the environment in a space with a single isolated fire (e.g., see Figures 3-10.4 through 3-10.6). Here, the energy and products of combustion release rates of the fire would be taken to be the enthalpy and combustion products' flow rates of the effluent from the doorway/window jet of the fire room. As before (i.e., independent of changes in the large, but finite, adjacent space), and at least for some significant time into the fire, the development of the environment in the fire room itself and the resulting door/window smoke flow could hopefully be predicted analytically. Short of analytic predictions, however, actual measurements of the door/window effluent acquired in full-scale free-burn tests of the fire room, up to and even beyond flashover, could be used as data input in the analysis of the large adjacent space problem.

The combined experimental/analytic approach has been used to predict the environment which develops in large prison cell blocks during fires in single cells of different design.[27]

Single room and freely connected multiroom fire compartments: For those times of fire development when the compartment of fire involvement consists of a single enclosed space, analysis of the fire environment is considerably simplified. This is because an accounting of inflow and outflow at windows and doors (which are presumably closed) is not required.

When the fire compartment is partitioned into separate but freely connected spaces, the relatively simple, single-enclosed-space analysis, where the area of the single space is taken to be the total area of the fire compartment, can continue to be relevant. Here, "freely connected" refers to fire scenarios and spacial configurations where common openings between rooms are large enough, and/or the energy release rate of the fire is small enough, so that smoke layers remain reasonably uniform in thickness, temperature, and product concentration through the bulk of the compartment area.

Quantitative criteria for establishing whether a specific fire compartment is freely connected relative to a specified fire threat are not yet available. However, the concept of the freely connected, multiroom fire/smoke compartment has been shown to be valid during full-scale multiroom fire experiments[2,28]

Smoke Spread Outside the Smoke Compartment of Fire Involvement

The above paragraphs addressed the development of the fire-generated environment by describing fire/smoke compartments of fire involvement. Yet, the original outline of the generic fire safety problem is also relevant to the general problem of predicting smoke environments throughout an entire facility.

Figure 3-10.9 illustrates a practical concept for modeling the development of smoke environments both inside and outside the smoke compartment of fire involvement. Facility spaces that would be included in the smoke compartment (on the left of the figure) are distinguished from those included in the rest of the building or facility (on the right) by the detail which is required to describe or model mathematically the fire-generated environments within them. In the smoke compartment of fire involvement, smoke would spread within a room, and would be driven from room to room by strong buoyancy forces which lead to layered smoke environments. These environments must be analyzed in the context of (at least) a two-layer model with associated phenomena of plume flow, surface flows, and so forth. In the rest of the building, it is reasonable to describe the smoke in each space as being uniformly dispersed. Here, dynamic changes in the smoke distribution in the environment come about from room-

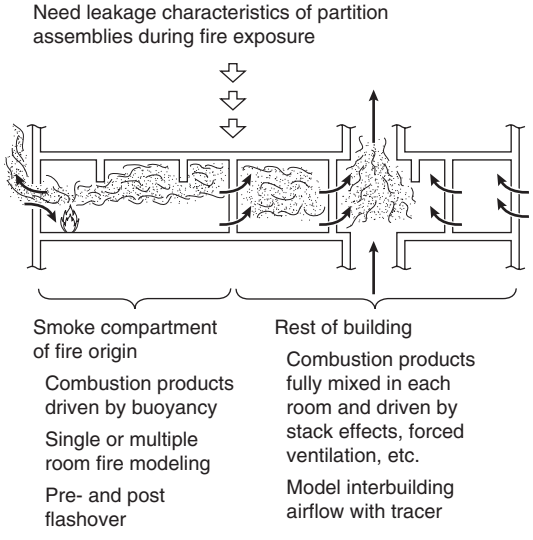

Figure 3-10.9. ***A concept for modeling smoke spread throughout complex facilities.***

to-room pressure differences which are generated by stack effects, wind effects, and forced ventilation, leading to smoke movement, mixing, and dilution.

The fire compartment is the source of smoke to the rest of the building. The rate of introduction of this smoke depends on the pressure differences across common partition assemblies, and on their leakage characteristics.[29] Once the rate of smoke leakage across common portions can be expressed quantitatively, the rest of the building problem can be analyzed with a model of smoke movement similar to those presented by Wakamtsu[30] and Evers and Waterhouse.[31]

Mathematical Models and Computer Codes for Predicting the Compartment Fire Environment

In recent years, many mathematical models and associated computer codes for predicting dynamic compartment fire environments have been developed. These can be divided into two types: field models and zone models.

Incorporating global partial differential equations which describe the relevant combustion, flow, and heat transfer processes, field models formulate and solve initial/boundary value problems for the unknown variables in compartment fire scenarios. Zone models, however, describe the compartment fire phenomena in terms of coupled submodel algorithms or sets of equations. Each equation set describes a single fire-generated process associated with an actual physical zone of the compartment space. The processes and corresponding zones typically correspond to the ones identified in Figures 3-10.1 through 3-10.8, and as discussed above.

There is a good deal of variation between all types of compartment fire models. Significant differences tend to be in (1) the number and detail of the individual physical phenomena that are taken into account (2) the number and complexity of interconnected fire compartment spaces that can be analyzed and (3) in the most common situation, when a computer is required to solve the model equations, the capability of the computer hardware that is required to carry out the calculations, the user-friendliness of the computer program, and its available documentation.

The intended use for which a given model was developed is probably the most important feature leading to its uniqueness. Such uses can differ widely: for example, at one extreme; to understand and predict coupled, compartment fire-generated processes with the greatest possible accuracy and generality; and at the other, to provide a common-use, firesafety-practitioner's tool for analysis and design. As will be seen, a set of equations which describes the dynamic smoke filling phenomenon in and of itself would constitute a compartment fire model of the simplest variety whose use could fall squarely at the latter extreme of the spectrum.

ASET—A Model for Predicting the Smoke Filling Process in a Room of Fire Origin

The smoke filling process is an essential feature of any zone-type compartment fire model. It basically involves three zones: the fire's combustion zone, the plume, and the upper smoke layer. The last section presented a relatively detailed qualitative description of many of the processes which make up the overall dynamic compartment fire environment. This section will formulate a mathematical model of the smoke filling process.

The model to be presented was originally developed within the context of life safety in fires.[1,2,24] In particular it was developed to provide estimates of the Available Safe Egress Time (ASET) in compartments of fire origin, where the available safe egress time is defined as the length of the time interval between fire detection/successful alarm and the onset of life safety hazard. Accordingly, the model has been given the name ASET.

Since life safety considerations are primary, the model focuses attention on phenomena which develop between the times of fire ignition and the onset of hazardous conditions. This allows significant simplifications in the modeling which would not be otherwise justified, vis-à-vis the use of the simplest possible smoke filling process to describe the fire-generated environments of interest.

The basic phenomena of the smoke filling process are outlined as follows:

The fire starts at some position below the ceiling of the enclosure and releases energy and products of combustion in some time-dependent manner. As the fire develops from ignition, buoyancy forces drive the high-temperature products of combustion upward toward the ceiling. In this way, a plume of upward-moving elevated temperature gases is formed above the fire. All along the axis of the plume relatively quiescent and cool ambient air is laterally entrained and mixed with the plume gases as they continue their ascent to the ceiling. As a result of this entrainment, the total mass flow rate in the plume continuously increases, and the average temperature and average concentration of products of combustion in the plume continuously decrease with increasing height. When the plume gases impinge on the ceiling they spread across it, forming a relatively thin, stably stratified upper layer. As the plume gas upward-filling process continues, the upper gas layer grows in depth, and the relatively sharp interface between it and the cool ambient air layer below continuously drops.

In this section, a simple mathematical model of these phenomena, which captures the essential features of the dynamic fire environment, is constructed. The major elements of the model include the turbulent buoyant plume theory[32] together with experimental plume results,[33] the theory of the dynamics of such plumes in confined spaces,[34] and the application of the plume dynamics theory to the fire problem as presented.[35] Figure 3-10.10 presents a simple illustration of the model's smoke filling flow dynamics. The variables introduced there will be defined in this section.

Initial Value Problem for the Temperature of the Upper Layer and the Position of the Interface

To take a conservative approach, the partitions of the room of fire origin are assumed to have all major penetrations (e.g., doors, windows, and vents) closed. Any leakage from the room resulting from fire-driven gas expansion is assumed to occur near the floor level. The

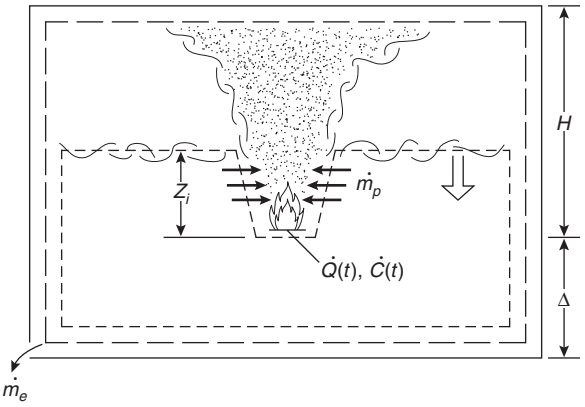

Figure 3-10.10. ***Simple illustration of fire-in-enclosure flow dynamics.***

sketch of Figure 3-10.7 is compatible with these assumptions, both of which lead to some conservatism in the eventual prediction of the time for onset of untenability.

The fire's combustion zone is modeled as a point source of energy release which is effectively located at or above the floor level. The mass flow rate of fuel introduced from this zone into the plume is neglected compared with the mass flow rate of entrained air. Except for the buoyancy forces that they produce, density variations in the flow field are neglected (i.e., the Boussinesq approximation is invoked). Using the fact that the absolute pressure throughout the space varies only insignificantly from a constant uniform value, the density, ρ, can be related to the absolute temperature, T, at any time and spatial position through the perfect gas law according to

$$\rho T = \text{constant} = \rho_a T_a \tag{1}$$

where ρ_a and T_a are the density and absolute temperature, respectively, of the ambient air.

The time-varying total energy release rate of the combustion zone is defined by $\dot{Q}(t)$. It is assumed that $\dot{Q}(t)$ can be approximated by the free-burn energy release rate of the characteristic fuel assembly whose hazard-producing characteristics are under investigation and for which $\dot{Q}(t)$ is known. This assumption is consistent with the fact that onset of hazardous conditions within the enclosure will occur at temperature and depleted-oxygen levels which are low compared with those levels at which variations from free-burn will begin to be significant.

The fraction of $\dot{Q}$ which effectively acts to heat the plume gases and to ultimately drive the plume's upward momentum is $(1 - \lambda_r)$, where λ_r is approximately the fraction of $\dot{Q}$ lost by radiation from the combustion zone and plume.

The total mass flow in the plume, $\dot{m}_p$, and the mass mixing cup temperature of the plume, $\overline{T}_p$, at a distance Z above the fire (but below the layer interface) can be estimated by[7,35]

$$\frac{\overline{T}_p}{T_a} - 1 = \frac{(\dot{Q}^*)^{2/3}}{0.210}, \quad 0 < Z \le Z_i(t) \tag{2}$$

$$\dot{m}_p = 0.210 \rho_a (gZ)^{1/2} Z^2 (\dot{Q}^*)^{1/3}, \quad 0 < Z \le Z_i(t) \tag{3}$$

where $\dot{Q}^*$ is defined as

$$\dot{Q}^* = \frac{(1 - \lambda_r)\dot{Q}}{\rho_a C_p T_a (gZ)^{1/2} Z^2}$$

and where g is the acceleration of gravity, C_p is the specific heat at constant pressure, assumed to be constant and uniform throughout the space, and $Z_i(t)$ is the time-varying distance above the fire of the interface which separates a growing upper layer of elevated-temperature (product of combustion-laden gas) and a lower shrinking layer of ambient air. The mass flow rate of gas, $\dot{m}_e$, leaking out of the room's floor-level leakage paths can be estimated from[35]

$$\dot{m}_e = \begin{cases} \dfrac{(1 - \lambda_c)\dot{Q}}{C_p T_a}, & -\Delta < Z_i(t) \\ \dfrac{(1 - \lambda_c)\dot{Q}}{C_p \overline{T}_h}, & -\Delta = Z_i(t) \end{cases} \tag{4}$$

where Δ is the height of the fire above the floor, and λ_c is the instantaneous fraction of $\dot{Q}$ lost to the bounding surfaces of the room and its contents (i.e., $\lambda_c = \dot{Q}_{\text{loss}}/\dot{Q}$). Also, assuming that the upper layer is well mixed, $\overline{T}_h$ is taken to be its absolute temperature. By using Equation 2, $\overline{T}_h$ can be related to the average upper layer density, $\overline{\rho}_h$, which is defined by

$$\overline{\rho}_h = \frac{1}{(H - Z_i)} \int_{Z_i}^{H} \rho dZ \tag{5}$$

The total rate of energy loss characterized by λ_c occurs as a result of a variety of convective and radiative heat transfer exchanges between the room's gases and the above-mentioned surfaces. Equation 6 brings attention to the fact that, by the time the layer interface drops to the floor, that is, when $Z_i = -\Delta$, all ambient air has been pushed out of the room. At all subsequent times, the entire room is filled with, and defines the bounds of, the upper layer, and the room's leakage gases are at upper layer rather than ambient conditions.

A mass balance for the lower, shrinking volume of ambient air results in

$$\rho_a A \frac{dZ_i}{dt} = \begin{cases} -\dot{m}_e - \dot{m}_p(Z = Z), & 0 < Z_i(t) \le H \\ -\dot{m}_e, & -\Delta < Z_i(y) \le 0 \\ 0, & -\Delta = Z_i(t) \end{cases} \tag{6}$$

where A is the area and H is the height of room of fire origin, and where estimates for $\dot{m}_e$ and $\dot{m}_p$ are provided in Equations 3 and 4.

Using Equations 2 and 7 in an energy balance for the upper layer results in

$$1 - \frac{\overline{\rho}_h}{\rho_a} = 1 - \frac{T_a}{\overline{T}_h} = \frac{\int_0^t (1 - \lambda_c)\dot{Q} d\xi}{\rho_a C_p T_a A (H - Z_i)}, \quad -\Delta < Z_i < H \tag{7}$$

$$(1 - \lambda_c)\dot{Q} = (\Delta + H)\rho_a C_p T_a A \left(\frac{1}{\overline{T}_h}\right) \frac{d\overline{T}_h}{dt}, \quad Z_i = -\Delta \tag{8}$$

Equations 4 and 6 are now used in Equation 6, and Equation 7 is recast into differential form. After some manipulation, the following pair of governing equations for Z_i and $\overline{T}_h$ result

$$\frac{dZ_i}{dt} = \begin{cases} -C_1\dot{Q} - C_2\dot{Q}^{1/3}Z_i^{5/3}, & 0 < Z_i \le H \\ -C_1\dot{Q}, & -\Delta < Z_i \le 0 \\ 0, & Z_i = -\Delta \end{cases} \tag{9}$$

$$\frac{d\overline{T}_h}{dt} = \begin{cases} \dfrac{\overline{T}_h[C_1\dot{Q} - (\overline{T}_h/T_a - 1)C_2\dot{Q}^{1/3}Z_i^{5/3}]}{H - Z_i}, & \\ & 0 < Z_i \le H \\ \dfrac{\overline{T}_h C_1\dot{Q}}{H - Z_i}, & -\Delta \le Z_i \le 0 \end{cases} \tag{10}$$

$$\left.\begin{aligned} C_1 &= \frac{1 - \lambda_c}{\rho_a C_p T_a A} \\ C_2 &= \left(\frac{0.21}{A}\right)\left[\frac{(1 - \lambda_r)g}{(\rho_a C_p T_a)}\right]^{1/3} \end{aligned}\right\} \tag{11}$$

The problem now becomes one of simultaneously solving Equations 9 and 10 subject to the appropriate initial conditions. For the present purpose, these initial conditions can be taken as those relating to one of two different cases.

Case 1: $\dot{Q}(t = 0) \equiv \dot{Q}_0 \neq 0$.

Here assume

$$\lim_{t\to 0}\dot{Q} \approx \dot{Q}_0 + \dot{Q}_0' t \tag{12}$$

where

$$\dot{Q}_0' = \frac{d\dot{Q}}{dt} \quad \text{at } t = 0$$

Then, solve Equations 9 and 10 subject to the initial conditions

$$\begin{aligned} Z_i(t = 0) &= H \\ \overline{T}_h(t = 0) &= T_a\left(1 + \frac{C_1\dot{Q}_0^{2/3}}{C_2 H^{5/3}}\right) \\ &= T_a + \left(\frac{1 - \lambda_c}{1 - \lambda_r}\right)[\overline{T}_p(t = 0) - T_a] \end{aligned} \tag{13}$$

where the value for $\overline{T}_h(t = 0)$ was obtained with the use of Equation 7. Using Equation 7 further, an analysis of the apparent singularity of Equation 10 at $t = 0$ leads to the result

$$\lim_{t\to 0}\frac{d\overline{T}_h}{dt} = T_a\left(\frac{C_1}{C_2}\right)\left(\frac{\dot{Q}_0^{2/3}}{6H^{8/3}}\right)\cdot\left(\frac{2\dot{Q}_0' H}{\dot{Q}_0} + 5(C_1\dot{Q}_0 + C_2 H^{2/3}\dot{Q}_0^{1/3})\right) \tag{14}$$

Case 2: $\dot{Q}(t = 0) = 0$

Here assume

$$\lim_{t\to 0}\dot{Q} \approx \dot{Q}_0' t \tag{15}$$

Then solve Equations 9 and 10 subject to the initial conditions

$$Z_i(t = 0) = H,\ \overline{T}_h(t = 0) = T_a \tag{16}$$

In this case, analysis of the problem leads to the following small time estimates:

$$\lim_{t\to 0} Z_i \approx H - \left(\frac{3}{4}\right)C_2\dot{Q}_0'^{1/3}H^{5/3}t^{4/3} \tag{17}$$

$$\lim_{t\to 0}\overline{T}_h \approx T_a + \left(\frac{2}{3}\right)T_a\left(\frac{\dot{Q}_0'^{2/3}}{H^{5/3}}\right)\left(\frac{C_1}{C_2}\right)t^{2/3} \tag{18}$$

Safe Available Egress Time from the Solution to the Initial Value Problem for Upper Layer Thickness and Temperature

The above initial value problem for Z_i and $\overline{T}_h$ would be solved by a numerical integration procedure. For the purpose of using the equations to determine onset of hazardous conditions, the solution would be terminated in a given problem at the time, t_{HAZ}, when

$$\overline{T}_h \ge \overline{T}_{h(\text{HAZ})} \tag{19}$$

(layer temperature reaches a hazardous value associated with an untenable flux of thermal radiation)

or

$$Z_i \le Z_{i(\text{HAZ})} \tag{20}$$

(interface reaches a characteristic face elevation, $Z_{i(\text{HAZ})}$, and the upper layer gases are assumed to be hazardous for human ingestion or significantly impairing to human vision).

From the computed history of Z_i and $\overline{T}_h$, and compatible with the detection criterion which is invoked, the time of detection could also be obtained. This would be defined as that time, t_{DET}, when, for example

$$\overline{T}_h \ge \overline{T}_{h(\text{DET})} \tag{21}$$

(layer temperature detection criterion)

and/or

$$\frac{d\overline{T}_h}{dt} \ge \left(\frac{d\overline{T}_h}{dt}\right)_{\text{DET}} \tag{22}$$

(layer rate of temperature rise detection criterion)

The time of detection corresponding to other detection criteria which were similarly related to Z_i and $\overline{T}_h$, and so forth, could also be obtained. Finally, the time of detection could be explicitly specified, for example, "immediate" detection, $t_{DET} = 0$, as a result of the guaranteed presence of alert occupants.

From all the above, the desired value for ASET is computed from

$$\text{ASET} = t_{HAZ} - t_{DET}$$

The computer program ASET has been developed to carry out the solution to the above problem for arbitrarily specified $\dot{Q}(t)$. The program is written in American National Standards Institute (ANSI) FORTRAN and it is supported by a user's manual.[24]

A simplified version of the program, ASET-B, written in BASIC and containing all necessary equation-solving software, has also been developed, and it is supported by its own user's manual.[36]

Initial Value Problem for the Concentration of Products of Combustion

In this subsection, equations for estimating the concentration of products of combustion in the upper layer are developed.

The time-varying rate at which a combustion product of interest is generated within the combustion zone is designated by $\dot{C}(t)$. The dimensions of $\dot{C}(t)$ are u_c per unit time, where u_c is a dimensional unit appropriate for the particular product. For example, u_c could have the dimensions of mass, number of particles, number of particles with mass between m and $(m + dm)$, and so forth.

Just as $\dot{Q}(t)$ is approximated by free-burn energy release rate data, so it is assumed that $\dot{C}(t)$ can be approximated by the free-burn product generation rate of the fuel assembly under investigation. As is the case with $\dot{Q}$, $\dot{C}$ is assumed to be known, say, from experimental free-burn measurements.

The average concentration of product in the upper layer is defined as the average amount of product (dimension u_c) per unit mass of upper layer mixture. The concentration is designated by $M(t)$. It is assumed that the mass fraction of the product in the upper layer is always small compared to 1.

Conservation of the product results in

$$\frac{d}{dt}\left[\overline{\rho}_h MA(H - Z_i)\right] = \dot{C}, \quad -\Delta < Z_i \le H \tag{23}$$

$$\frac{d}{dt}\left[\overline{\rho}_h MA(H + \Delta)\right] = \dot{C} - \dot{m}_e M, \quad Z_i = -\Delta \tag{24}$$

Manipulation of Equations 23 and 24 with the use of Equations 9 and 10 leads to the following equation for M:

$$\frac{dM}{dt} = \begin{cases} \left(\dfrac{\overline{T}_h}{T_a \rho_a A}\right)\dfrac{\dot{C} - \rho_a A C_2 \dot{Q}^{1/3} Z^{5/3} M}{H - Z_i}, & 0 < Z_i < H \\ \dfrac{[\overline{T}_h/(T_a \rho_a A)]\dot{C}}{H - Z_i}, & -\Delta \le Z_i \le 0 \end{cases} \tag{25}$$

With solutions for Z_i and $\overline{T}_h$ from earlier considerations, Equation 25 can be solved for M once appropriate initial conditions are established. For this purpose, the two cases must be considered again.

Case 1(a): $\dot{Q}(t = 0) \equiv \dot{Q}_0 \neq 0$; $\dot{C}(t = 0) \equiv \dot{C}_0 \neq 0$.

Here assume

$$\lim_{t \to 0} \dot{C} \approx \dot{C}_0 + \dot{C}_0' t \tag{26}$$

where

$$\dot{C}_0' = \frac{d\dot{C}}{dt} \quad \text{at } t = 0$$

Then, solve Equation 25 subject to

$$M(t = 0) = \frac{\dot{C}_0}{C_2 A H^{5/3} \rho_a \dot{Q}_0^{1/3}} = \frac{\dot{C}_0}{\dot{m}_p(t = 0)} \tag{27}$$

Here, an analysis of the apparent zero time singularity of Equation 25 leads to the result that

$$\lim_{t \to 0} \frac{dM}{dt} = \left(\frac{5}{6}\right)\left(\frac{C_1}{C_2}\right)\left(\frac{\dot{Q}_0^{2/3}\dot{C}_0}{\rho_a A H^{8/3}}\right) \cdot \frac{1 + H(3\dot{C}_0'/\dot{C} - \dot{Q}_0'/\dot{Q}_0)}{5\dot{Q}_0\dot{C}_1} + (C_2/C_1)(H^{5/3}/\dot{Q}_0^{2/3})] \tag{28}$$

Case 1(b): $\dot{Q}(t = 0) \equiv \dot{Q}_0 \neq 0$; $C(t = 0) \equiv C_0 \neq 0$.

Here assume

$$\lim_{t \to 0} \dot{C} \approx \dot{C}_0' t \tag{29}$$

Then, solve Equation 25 subject to

$$M(t = 0) = 0 \tag{30}$$

In this case, analysis of Equation 25 leads to the following small time estimate

$$\lim_{t \to 0} M = \frac{\dot{C}_0' t}{2\rho_a A^{5/3} Q^{1/3} C_2} = \frac{\dot{C}_0' t}{2\dot{m}_p(t = 0)} \tag{31}$$

Case 2(b): $\dot{Q}(t = 0) = 0$; $\dot{C}(t = 0) = 0$.

(Note that the condition $\dot{Q}(t = 0) = 0$, $C(t = 0) \neq 0$, i.e., nonzero product generation rate with a zero heat release rate, is not allowed.) Here assume Equation 29. Then solve Equation 25 subject to Equation 30. In this case, analysis of Equation 25 leads to

$$\lim_{t \to 0} M = \frac{2\dot{C}_0' t^{2/3}}{3\rho_a A C_2 H^{5/2} \dot{Q}_0'^{1/3}} \tag{32}$$

Using Combustion Product Concentrations to Establish the Time of Detection and the Onset of Untenability

When a fire's rate of generation of products of combustion is known, the upper layer concentrations can be

estimated from the considerations of the previous section. Under such circumstances, it would be possible to apply detection and hazard criteria which are more detailed than those discussed earlier.

In the case of detection, the response of a detection device which is sensitive to the presence of the predictable combustion product can be simulated. For example, the time of detection, t_{DET}, would be predicted to be the time when the upper layer concentration of the product attained a detectable level, M_{DET}.

In the case of hazard, a criterion for the onset of untenability could depend on a variety of possible conditions involving all of the environmental parameters, Z_i, $\overline{T}_h$, and M. For example, assume that estimates of the fire's generation rate of water and CO are available. Then, the time-varying values for Z_i, $\overline{T}_h$, M_{water}, and M_{CO} could be computed, and the time of onset of untenability could be estimated to be the earliest time when (1) the interface was still above a characteristic elevation, Z_F, and $\overline{T}_h$ exceeded a specified hazardous overhead value (associated with an untenable flux of thermal radiation), or (2) the interface was below Z_F, and the upper layer CO concentration or temperature and humidity conditions were such as to be hazardous for human ingestion.

All of the above considerations are taken into account in the ASET computer program. Predictions of product of combustion concentration are not yet included in ASET-B.

Available Safe Egress Time from Rooms of Fire Origin—Some Example Calculations

Assumptions on the Disposition of Energy Release and Their Implications

In order to use the proposed fire model for a specified free-burn fire, values of λ_r and λ_c are required. While appropriately chosen constant-λ values should prove to be adequate for most engineering applications, the model described can, through specified dynamic variations in these λs, readily accept more detailed characterizations of the gas-to-room surface heat transfer phenomena.

Depending on the fuel and its configuration, the total radiant power output in fire combustion zones is in the range of 15 to 40 percent of the total rate of heat release.[38,39] Based on this and, for example, on data presented by Cooper,[40] it appears that $\lambda_r = 0.35$ is a reasonable choice for the type of growing hazardous fires under consideration. Except where noted otherwise, this value will be used in all calculations described in this chapter.

Using the 0.35 value for λ_r, and taking account of convective heat transfer considerations, an appropriate value for λ_c was developed.[41] It was found to lie in the approximate range 0.6 to 0.9. The lower value, 0.6, would relate to high aspect ratio spaces (ratio of ceiling span to room height) with smooth ceilings and with fires positioned far away from walls. The intermediate values and the high, 0.9, value for λ_c would relate to low aspect ratio spaces, fire scenarios where the fire position is within a room height or so from walls and/or spaces with highly irregular ceiling surfaces. In the latter types of situations, which are representative of most realistic fire scenarios, it is not presently possible to provide general rules to accurately estimate λ_c within this 0.6 to 0.9 range. This fact has strong implications on the capability for establishing accurate estimates for the average upper layer temperature. This can be seen from Equation 10, where, early in the fire and at times of relatively cool upper layer temperatures ($\overline{T}_h/T_a$ close to 1), $d\overline{T}_h/dt$ and, ultimately, $\overline{T}_h - T_a = \Delta\overline{T}_h$ are seen to be proportional (through the factor C_1) to $(1 - \lambda_c)$. In contrast to the upper layer temperature estimate and at times of relatively small values of $\Delta\overline{T}_h/T_a = \overline{T}_h/(T_a - 1)$, the upper layer-lower layer interface position history is not nearly as sensitive to inaccuracies in λ_c. At such times, the second term on the right-hand side of the first line of Equation 9, which is independent of λ_c, will dominate the first term, the two terms being in the ratio of $\dot{m}_p$ to $\dot{m}_e$ (compare to the first line of Equation 6).

The above discussion leads to the following guidelines for selection and use of a value for λ_c, when a reliable estimate of its actual value is not otherwise available:

1. For the purpose of computing a conservative estimate of the time when a hazardous temperature or a hazardous interface elevation will be attained (i.e., the predicted t_{HAZ} will be less than the observed t_{HAZ}), one should select $\lambda_c = 0.6$.
2. For the purpose of a conservative estimate of detection time when detection is by temperature or rate of temperature rise of the upper layer (i.e., the predicted t_{DET} will be greater than the actual t_{DET}), one should select $\lambda_c = 0.9$.
3. When fire detection is by temperature or rate of temperature rise, a reasonably accurate (as compared with a conservative) estimate of detection time is achievable only (1) in large aspect ratio, smooth ceiling spaces where detection is based on a $\lambda_c = 0.6$ computation of average upper layer temperature, and (2) in other configurations where detectors are deployed near the ceiling in some regular grid array, and where the time of detection is based on estimates of actual maximum ceiling-jet temperature (i.e., predictions of average upper layer temperature are not the basis for determining likely time of detection). For such estimates, the reader is referred to Section 4, Chapter 1 of this handbook.

Available Safe Egress Time in a Semi-Universal Fire

For the smoke filling model to have utility to practitioners of fire safety, it is necessary that the significant elements of potentially threatening fire scenarios be identified. It is also necessary for the results of fire hazard analyses to be presented in a concise and practical manner. This subsection provides an example of how the whole concept might proceed in practice.

First, one must identify quantitative characteristics of a particular, potentially threatening, free-burn fire of concern. Cooper deals with some practical considerations that would be useful in deducing such characteristics.[1] For the present, a composite, semi-universal-type fire has been constructed from the data of Friedman.[41] The fire's energy release history is plotted in Figure 3-10.11. The fire is

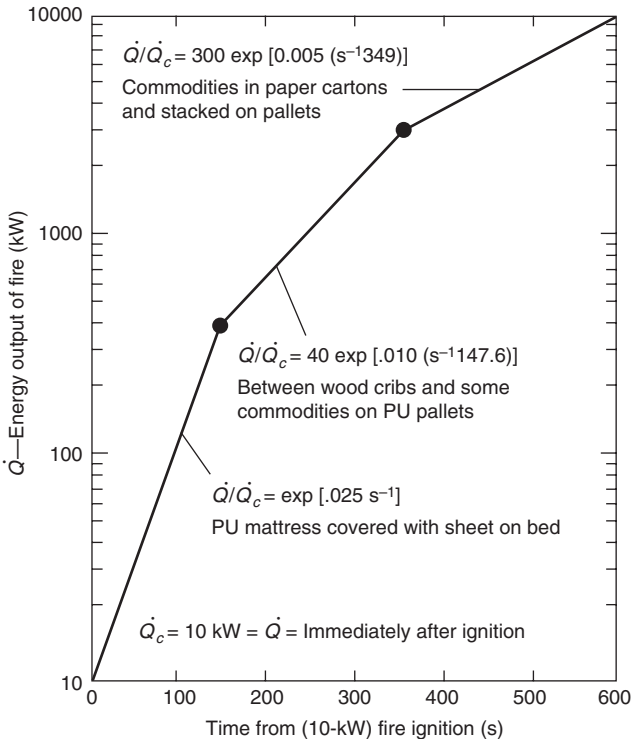

Figure 3-10.11. ***Free-burn energy release rate from a semi-universal fire. A fictitious construction from the data of O'Neill and Hayes.[44]***

assumed to be initiated from a 10 kW ignition source. Initially, it grows exponentially at a rate which is characteristic of a fire initiated in a polyurethane mattress with bedding. This early growth rate would be characteristic of the early growth of fires in a variety of occupancies which typically contain upholstered polyurethane cushioning, for example, hospital patient and lobby rooms, residential spaces, and auditoriums. It is also consistent with the (unreported) early growth state of fires in large assemblies of commodities stacked on pallets. Beyond 400 kW, the fire of Figure 3-10.11 is assumed to grow at a rate which is similar to and/or which bounds the anticipated growth of fires initiated in a variety of different types of commodities stacked on pallets. The portion of the semi-universal fire beyond 400 kW is no doubt also representative of other threatening fires in large mercantile and/or business occupancies.

The fire of Figure 3-10.11 was assumed to be initiated in a variety of different-size spaces. The geometries of these spaces are characterized by areas ranging from 28 to 929 m^2 and by heights ranging from 2.4 to 6.1 m.

Two possible criteria for fire detection are considered in the analysis of available safe egress time. These include using ASET to calculate instantaneous detection (by whatever means) and detection when the upper gas layer reaches an average temperature of 57°C. The utility of the latter detection criterion is at present strictly speculative. It is included here only to illustrate the type of results which one might hope to generate by solution of the model equations and use of the ASET computer program. (The results could also be obtained with ASET-B.)

The criterion adopted for the onset of hazardous conditions is an upper layer interface position 0.91 m above the floor, or an average upper layer temperature of 183°C (corresponding to a heat flux of 0.25 W cm^{-2} at the floor), whichever comes first.

It is assumed that 35 percent of the fire's instantaneous energy release rate is radiated from the combustion zone (λ_r = 0.35) and that a total of 60 percent of this energy release rate is transferred to the interior surfaces of the room and its contents, that is, 40 percent of this energy is retained in the upper layer products of combustion (λ_c = 0.60). Recall that the latter choice of λ_c would be appropriate for large aspect ratio spaces with smooth ceiling, but, in any event, the choice of λ_c would have a minor impact on estimated egress times in cases where criteria of detection or hazard are not dependent on upper layer gas temperature.

With the above range of parameters, the quantitative details of the last section were used to estimate available safe egress times with the ASET program. The results of these computations are presented in Figure 3-10.12. In this figure, ASET = $t_{HAZ} - t_{DET}$ is plotted as a function of room area for different parametric values of room height and for different detection criteria.

As an example of the utility of Figure 3-10.12, consider a scenario where a fire is initiated in an occupied, 500 m^2, nominal, 6.1 m-high ceiling auditorium outfitted with polyurethane cushion seats (which are assumed to be the most significant fuel load). Then, from Figure 3-10.12 one would estimate an available safe egress time of approximately 450 s. This assumes immediate detection as a result of occupant recognition and verbal alarm to fellow occupants at the time of fire initiation. If the auditorium is to be considered safe relative to successful egress, then a further study would have to reveal that the time required for a capacity crowd to evacuate the auditorium is less than 450 s.

The following general features of the results of Figure 3-10.12 are worth noting:

1. As is well known, for life safety as it relates to safe egress, temperature detectors are not particularly effective.

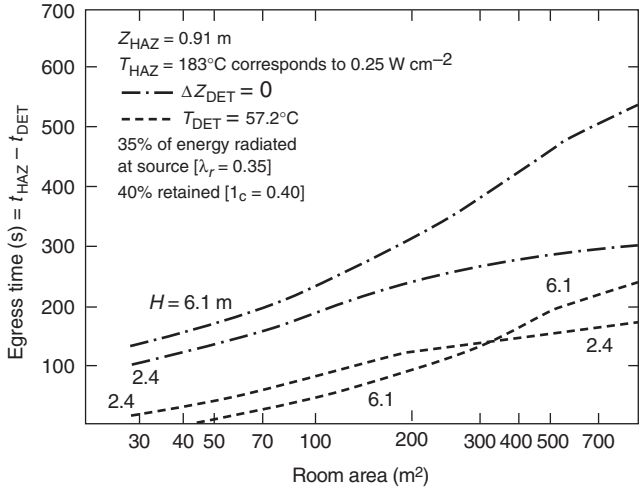

Figure 3-10.12. ***Estimates of available egress times from the semi-universal fire of Figure 3-10.11.***

2. For a given curve, increasing room area eventually leads to an abrupt reduction in the curve's slope. This is the result of a shift in the triggering mechanism for onset of hazardous conditions. On the left side of the change in slope (smaller areas), untenability occurs as a result of the layer interface dropping to the 0.91 m level. On the right side (larger areas), untenability occurs as a result of thermal radiation from a hot upper layer.

Based on the previously developed model equations, the calculation procedure described in this section has been generalized and incorporated with other example calculations into the ASET computer program user's manual.[24] For a fire scenario of interest, this computer program carries out ASET calculations corresponding to user-supplied inputs which describe the fire threat, room size, and appropriate user-specified detection and hazard criteria.

A Possible Extension in the Model's Utility

An Experimental, Full-Scale, Multi-Room Fire Scenario

This section compares the results of a full-scale, multi-room fire experiment with calculations based on ASET. The experiment was one of a series of tests in a mockup hospital patient room/corridor building space.[44]

A plan view of the building space is presented in Figure 3-10.13. The space is made up of a room of area 14.4 m^2 connected by an open doorway to a corridor-lobby configuration of area 74.3 m^2.

A fire is initiated in a wastepaper basket next to the corner of a polyurethane mattress covered with bedding. The burn characteristics of this assembly were studied prior to the room burns of this series.[5] The wastepaper basket/mattress fuel energy release rate, as derived from weight loss measurements, is plotted in Figure 3-10.14. For the purpose of the present analysis, it is assumed that this energy release rate was reproduced in the actual test run under review.

The model, which has been quantitatively described so far, is a single-room or room-of-fire-origin model. Thus,

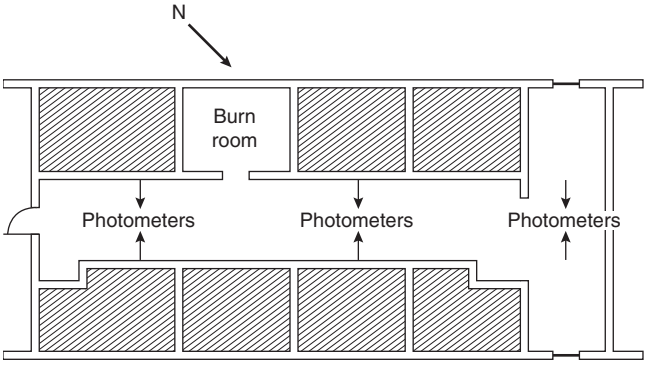

Figure 3-10.13. ***Plan view of hospital room/corridor mockup space.***

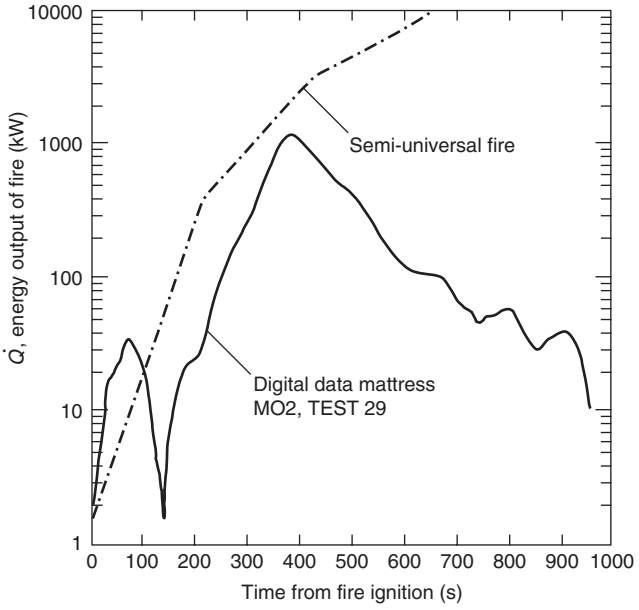

Figure 3-10.14. ***Energy release rate of wastepaper basket/mattress fuel assembly.***

it may not be immediately obvious at what point, if any, it will have relevance to the present fire scenario. It would appear that a two-room or multi-room flow dynamics model would generally be required to study the room-corridor-lobby scenario under consideration. (For example, a two-room example flow calculation for a set of fire and room size parameters which somewhat corresponds to the present scenario has been considered[25]). Nevertheless, it is possible that a simple, single-room modeling approach to fire scenarios involving relatively free-flowing multi-space configurations can be adequate for the purpose of obtaining engineering estimates of available egress times in the range of conditions that occurred in the referenced hospital patient room/corridor test.

Model Predictions Compared with Experimental Results

Room of fire origin: For early times into the fire, prior to the time when the upper layer interface drops to the level of the connecting doorway soffit, the single-room model is completely relevant. Up to that moment, the open doorway acts as the lower leakage path referred to earlier. Using the energy release data of Figure 3-10.14, and taking the fire source to be effectively at the floor, the model was used to compute the product of combustion-filling history of a 14.4 m^2 room up to the time that the upper layer thickness exceeded the existing ceiling-to-soffit dimension of 0.41 m. λ_c was estimated at 0.72.[40] The time for the interface to reach the soffit was computed to be 21 s following ignition.

Adjacent space: Once the smoke flows under the soffit and starts to fill the large corridor-lobby space, a two-room model is required to describe the gas migration and

exchange between the two spaces. This would continue to be true for at least some intermediate time interval. Following this, the single-room model can again be relevant.

If the fire is small enough or the doorway is large enough so that flows through the doorway remain relatively weak, the adjacent space will eventually attain and maintain a smoke layer thickness essentially identical to that of the room of fire origin. After some time interval, the histories of the elevations of the layer interfaces in both the corridor/lobby and room of fire origin spaces will be similar and can be computed from a single-room model, where the single room has an area equal to the combined area of both spaces. Time intervals when the upper layer thickness of the two rooms is not similar would encompass (1) the initial time when the room of fire origin fills up with smoke to the level of the doorway soffit and (2) the subsequent time interval when the upper layer thickness of the adjacent space grows from zero to a value close to that of the room of fire origin.

For fire scenarios where the above is applicable, significant simplifications occur in that the relatively simple single room of fire origin model can be used to study the effects of fire growth when far more complicated multiroom models would, at first hand, appear to be required.

To test the above ideas, the single-room model was used to predict the history of a single interface elevation and the average upper layer temperature within the combined patient room/corridor space. Using the energy release rate of Figure 3-10.14 and a total room area of 88.7 m^2, the history of the interface elevation and of the average upper layer temperature was computed. An effective λ_c for this combined space scenario is expected to be greater than the above $\lambda_c = 0.72$ value used for the single room of fire origin because of the additional heat transfer to the corridor surfaces. A value of $\lambda_c = 0.85$ was selected for the calculation. This was done with the anticipation that comparisons between computed and experimental average upper layer temperatures would reveal an appropriate correction to this λ_c value. (Recall that the upper layer temperature difference, $\Delta\overline{T}_h$, is approximately proportional to $1 - \lambda_c$.) The results of the computation for interface position and upper layer temperature are presented in Figures 3-10.15 and 3-10.16, respectively.

For the purpose of comparing results for the analytic and experimental interface position, an operational definition of the experimental interface position was required. This definition was based on the outputs of a total of six photometers placed at three different elevations and at one to three different positions (see Figure 3-10.13) in the corridor and lobby. The measured optical density (OD) outputs of these photometers are indicated in Figure 3-10.17. From these outputs, and for the purpose of defining a time when the smoke layer interface position passes the elevations of these photometers, there is still ambiguity as to what value of OD should constitute the presence of a smoke layer. Four different OD values, 0.01, 0.02, 0.03, and 0.04, were used as possible definitions for a minimum upper layer OD. Using the photometer outputs, the result of these four possible interface definitions leads to four possible sets of experimental data points for the interface elevation versus time. These are plotted in Figure 3-10.15 together with the theoretical results of the interface motion.

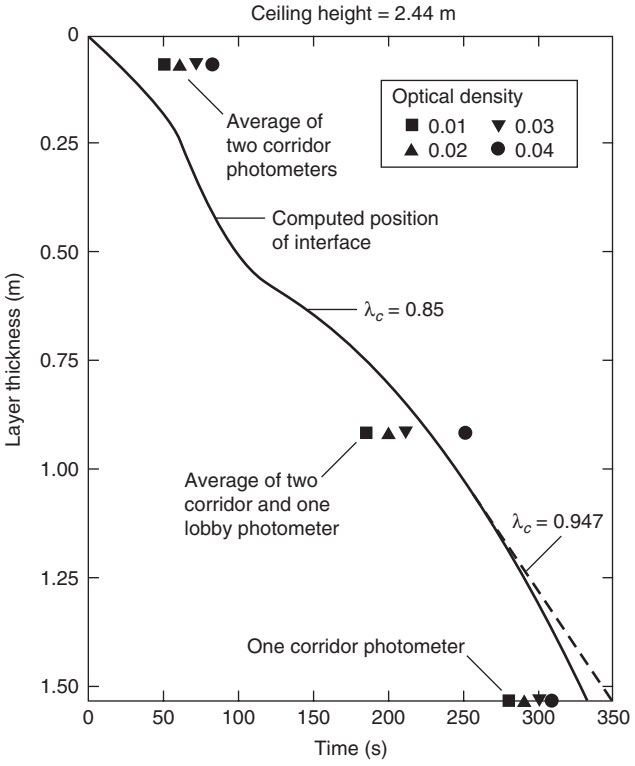

Figure 3-10.15. ***History of interface position.***

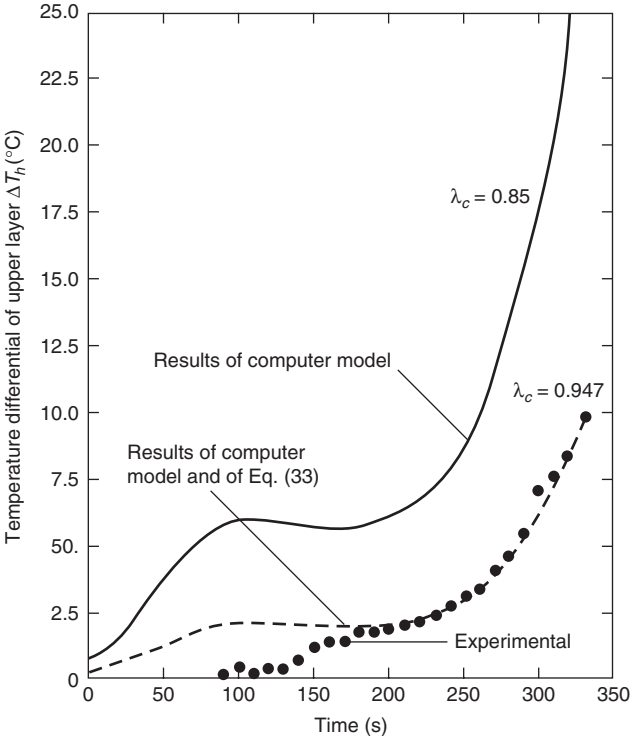

Figure 3-10.16. ***History of average upper layer temperature.***

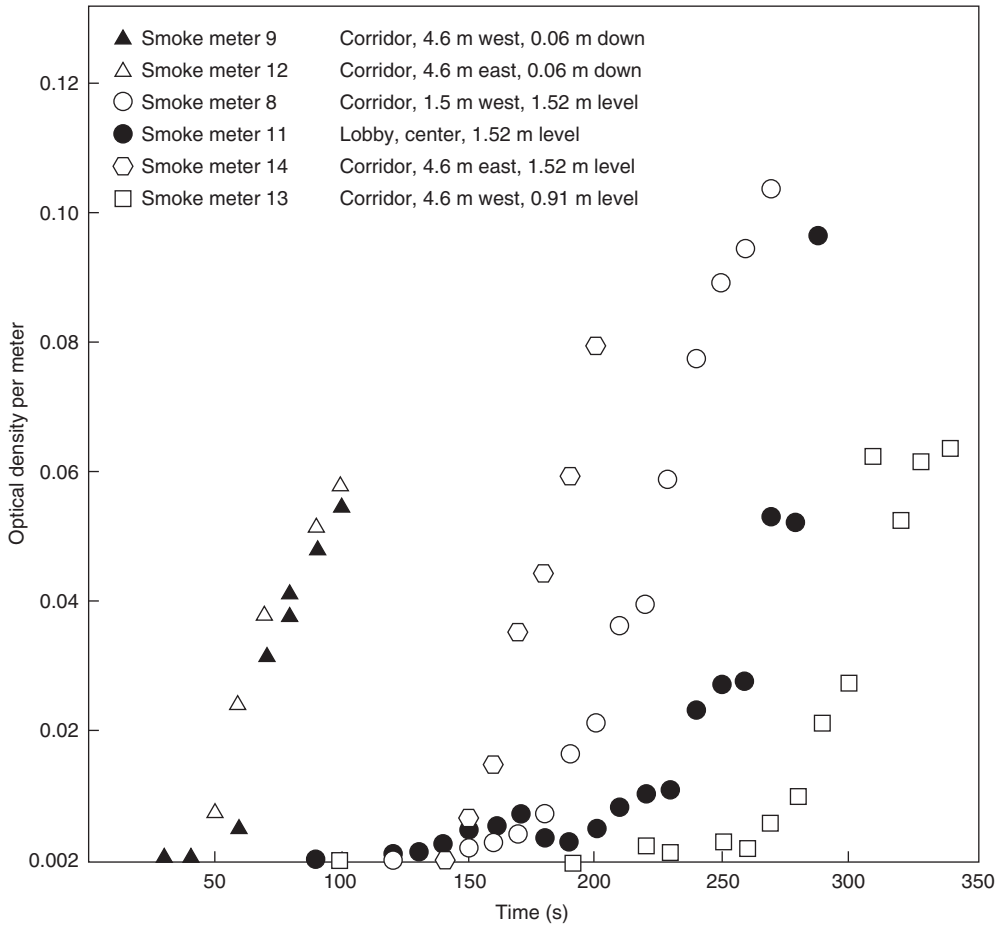

Figure 3-10.17. ***Optical densities measured by the photometers.***

The favorable agreement between the results of theoretical and experimental interface position at the lower two of the three photometer locations illustrates the capability of the single-room model, in the present multi-room fire scenario, to predict the growth of the potentially hazardous upper smoke layer thickness. A favorable comparison at the uppermost photometer elevation located 0.06 m from the ceiling was not to be expected. This is because of the fact that, in the present multi-space configuration, the single-room model implemented in the manner described is clearly not adequate to predict the early growth in the corridor-lobby portion of the test space. Subsequent testing in the Figure 3-10.13 test space has corroborated the potential utility of the model in providing practical simulations of multi-room fire environments.[28]

Gas temperatures were measured by two thermocouple trees located in the center of the corridor 4.6 m on either side of the room of fire origin doorway. No temperature data were acquired in the lobby space. At any given time, the equi-elevation thermocouples of these two trees measured temperature differences, $(T - T_a)$, which agreed to within 20 percent of one another. For the purpose of comparing analytic and experimental average upper layer temperature histories, an appropriate instantaneous weighting of the measured temperatures of the limited number of these corridor thermocouples was required. At a given instant of time, this weighing has to be consistent with the estimate/measurement of the interface position as well as with the relative position of the thermocouples in question. A plot of the measured average upper layer temperature history deduced from such a data reduction scheme is presented along with the plot of the computed temperature history in Figure 3-10.16. As noted earlier, if a different λ_c has been used in the computation then, to a first approximation (i.e., using the principle of proportionality between $\Delta\overline{T}_h$ and $1 - \lambda_c$), one would anticipate a shift from the originally computed $\Delta\overline{T}_h(t)$ (with $\lambda_c = 0.85$) to a new temperature history $\Delta\overline{T}_h^{(\text{new})}(t)$ [with $\lambda_c = \lambda_c^{(\text{new})}$], where

$$\Delta\overline{T}_h^{(\text{new})}(t) = [(1 - \lambda_c^{(\text{new})})/(1 - 0.85)]\Delta\overline{T}_h(t) \qquad (33)$$

In view of the above, it is possible to bring the predicted analytic $\overline{T}_h$ plot into coincidence with the experimental $\overline{T}_h$ plot for at least one instant of time by a new choice, $\lambda_c^{(\text{new})}$, for λ_c. Such coincidence is attained at $t =$ 330 s (when the computed layer interface is at the potentially hazardous position 0.91 m from the corridor floor) by the specific choice of $\lambda_c^{(\text{new})} = 0.947$. Using this latter value of $\lambda_c^{(\text{new})}$ in Equation 33, an adjusted average upper

layer temperature history was computed and plotted. (See Figure 3-10.16.)

The single-room model was also used to recompute the interface position and temperature histories corresponding to $\lambda_c = 0.947$. These are plotted in Figures 3-10.15 and 3-10.16, respectively. For the parameters of the present scenario, the proximity of the $\lambda_c = 0.85$ and $\lambda_c = 0.947$ plots of Figure 3-10.15 illustrates the relative insensitivity of the interface position history to changes in λ_c. The variations between the two $\lambda_c = 0.947$ temperature history estimates are so small that they cannot be discerned in most of the Figure 3-10.15 plot. For this scenario, this illustrates the insensitivity of interface position on λ_c.

As can be noted in Figure 3-10.16, the experimental and newly calculated estimates for the upper layer temperature history are in good agreement in the time interval 175–330 s but in poor agreement at earlier times. Besides the fact that earlier times are likely to require analysis by a multi-room model, it is worth noting that the relatively complicated nature of the energy transfers which are being simulated may preclude sharper estimates of $\overline{T}_h$ with a single, constant value of λ_c. In this regard, results indicate that for fires in the present test space, λ_c can vary in time over a wide range of values.[28]

Solutions to the Model Equations for a Special Class of Growing Fires

As was indicated in the last two sections, the ASET smoke filling model equations are easily solved with the use of the ASET or ASET-B computer programs for any particular fire specified by $\dot{Q}(t)$, $C(t)$, and parameters H, A, Δ, λ_r, and λ_c. However, the approach of solving the equations for one set of conditions at a time does not lead readily to insight into solutions of generic problems of interest. For example, to obtain the results of Figure 3-10.12, solutions to the equations were required over a range of input values of A for each of the two input values of H. If more H values were of interest, and if, for example, one wished to study the effect of varying λ_c and/or Δ, then the volume of computer output would quickly become massive and unwieldy. In general, insight into the environment generated by a class of fire scenario (e.g., the semi-universal fire of Figure 3-10.11 in a room of arbitrary H, A, Δ, λ_r, and λ_c) is most clear when solutions can be obtained and displayed by means of limited numbers of graphs, charts, or tables. In this section, features of such a solution for an important, practical class of fire scenario will be displayed graphically, and explanation on how to extract practical results from this will be presented by way of examples. Some very useful and surprising time-of-smoke-filling estimates are obtained from this solution, and these will also be presented.

$Q \propto t^n$ Fire and Its Governing Equations

This subsection will present and solve Equations 9 through 11 and 25 for the broad class of fires whose $\dot{Q}(t)$ can be reasonably approximated by growth rates proportional to t^n for arbitrary $n \geq 0$ and whose product of combustion generation rates, $C(t)$, are approximately proportional to $\dot{Q}(t)$. This class of fire includes the constant fire, $n = 0$, and the t^2 growing fires, $n = 2$, both of which have been used in a variety of different references to describe the burning of many practical assemblies of combustibles. To be definite, it is assumed that $\dot{Q}$ and C can be approximated by

$$\dot{Q}(t) = \dot{Q}_0 \left(\frac{tH^{3/2}g^{1/2}}{A} \right)^n ; \quad C(t) = \beta Q(t) \tag{34}$$

where $\dot{Q}_0$ represents a characteristic energy release rate, n is any non-negative integer, and β is a constant of proportionality of appropriate dimension.

Notice that for the constant fire problem, $n = 0$ in Equation 34 and $\dot{Q}_0$ is simply the specified constant energy release rate of the fire. Also, the energy release rate in many practical fires is simulated by $n = 2$-type fires and is approximated by[4]

$$\dot{Q}(t) = \left(\frac{1000}{t_g^2} \right) t^2 \text{ kW} \tag{35}$$

where t_g, the growth time of the fire, is defined as the time for the fire to grow in a t^2-type manner from a small flaming fire to a fire of approximately 1000 kW. Equation 34 for $n = 2$ and Equation 35 lead to the result that for these "t-squared" fires, $\dot{Q}_0$ should be chosen as[4]

$$\dot{Q}_0 = \frac{1000A^2}{(t_g^2 g H^3)} \quad \text{kW for } \dot{Q} \sim t^2 \text{ fires} \tag{36}$$

It is convenient to introduce the following dimensionless variables and parameters:

$$\left.\begin{aligned}
&\zeta = \frac{Z_i}{H} && \text{(interface elevation)}\\
&\phi = \frac{T}{T_a} && \text{(upper layer temperature)}\\
&\mu = \frac{(1-\lambda_c)M}{\beta C_p T_a} && \text{(upper layer product concentration)}\\
&\tau = \frac{3[(1-\lambda_r)Q_0^*]^{1/3}(tH^{3/2}g^{1/2}/A)^{(n+3)/3}}{n+3} && \text{(time)}\\
&\varepsilon = \frac{(1-\lambda_c)[(n+3)/3]^{2n^*(n+3)}Q_0^{*2/(n+3)}}{(1-\lambda_r)^{(n+1)/(n+3)}} && \text{(fire strength)}\\
&\dot{Q}_0^* = \frac{\dot{Q}_0}{\rho_a C_p T_a g^{1/2} H^{5/2}} && \text{(characteristic energy release rate)}\\
&\delta = \frac{\Delta}{H} && \text{(fire elevation)}
\end{aligned}\right\} \tag{37}$$

Using the above definitions in the model Equations 7, 9, 10, 13, and 16 through 18, eventually leads to the following equations for τ, ϕ, and μ:

$$\frac{d\zeta}{d\tau} = \begin{cases} -\varepsilon\tau^{2n^*(n+3)} - 0.210\zeta^{5/3}; & 0 < \zeta \leq 1 \\ -\varepsilon\tau^{2n^*(n+3)}; & -\delta < \zeta \leq 0 \\ 0; & \zeta = -\delta \end{cases} \tag{38}$$

$$\phi = \left\{1 - \frac{(n+3)\varepsilon\tau^{3(n+1)/(n+3)}}{3(n+1)(1-\zeta)}\right\}^{-1}; \qquad -\delta < \zeta \le 1$$
$$\frac{d\phi}{d\tau} = \frac{\varepsilon\phi\tau^{2n/(n+3)}}{(1+\delta)}; \qquad \zeta = -\delta \tag{39}$$

$$\mu = \phi - 1; \qquad -\delta \le \zeta \le 1 \tag{40}$$

where Equation 38 must be solved subject to

$$\zeta(\tau = 0) = 1 \tag{41}$$

and where early time estimates for ζ, ϕ, and μ are

for $n = 0$:

$$\left.\begin{aligned} &\lim_{\tau\to 0}\frac{\zeta - 1}{1 + \varepsilon/0.210} = -0.210\tau + \text{higher order terms in } \tau \\ &\lim_{\tau\to 0}\frac{\phi}{(1+\varepsilon/0.210)} = \lim_{\tau\to 0}\frac{\mu+1}{1+\varepsilon/0.210} = 1 + \frac{5\varepsilon\tau}{6} \\ &\qquad + \text{higher order terms in } \tau \end{aligned}\right\} \tag{42}$$

for $n > 0$:

$$\left.\begin{aligned} &\lim_{\tau\to 0}(\zeta - 1) = -0.210\tau + \text{higher order terms in } \tau \\ &\lim_{\tau\to 0}(\phi - 1) = \lim_{\tau\to 0}\mu \\ &\quad = \frac{(n+3)\varepsilon\tau^{2n/(n+3)}}{3(n+1)(0.210)} + \text{higher order terms in } \tau \end{aligned}\right\} \tag{43}$$

Equation 38 describes the rate of descent of the interface as it passes through the regions above the fire ($0 < \zeta < 1$), below the fire ($-\delta < \zeta < 0$), and at the floor ($\zeta = -\delta$). Equations 39 and 40 describe the corresponding upper layer temperature and product concentration. Equations 42 and 43 are useful in starting a numerical solution to Equations 38 and 39.

Discussion of the Equations

The last subsection presented the equations which govern the dynamics of the interface, ζ, the upper layer temperature, ϕ, and the upper layer product concentration, μ. From Equation 40, the solution for μ would follow directly from the solution for ϕ. From the time of ignition to the time that the interface drops to the floor of the enclosure, a solution for ϕ could be obtained from Equations 39, 42, and 43, provided a solution for ζ was available. Beyond that time, the solution for ϕ could be determined by a direct integration of the second line of Equation 39.

With the above observations, attention is drawn to the solution for ζ. From ignition at $\tau = 0$ until $\tau = \tau_0 \equiv \tau(\zeta = 0)$, corresponding to the time when the interface drops to $\zeta = 0$, ζ is governed by Equation 41 and the first line of Equation 38. No general closed form solution is possible, and a numerical solution for $\zeta(\tau; \varepsilon, n)$ is in order. Once this has been obtained, the solution can be extended beyond τ_0 by direct integration of the second and third lines of Equation 38.

Solutions from Ignition to τ_0

In general, there is no particular problem in using a computer to integrate Equation 38 numerically and obtain ζ. However, in terms of generating a display of working graphical solutions which include times when ζ is small and positive, a problem does arise in the limit as ε approaches 0 (e.g., for small, dimensionless fire strength, $\dot{Q}^*$). Applying such a limit to the first line of Equation 38 leads, in a first approximation, to the total neglect of the earlier referenced (left-hand) expansion term in comparison to the (right-hand) entrainment term. This corresponds, physically, to the situation of an interface that approaches the elevation of the fire, $\zeta = 0$, asymptotically in time. In the present nomenclature, and for a source whose strength grows as t^n, the solution for $\varepsilon = 0$ is found to be

$$\zeta(\tau;\ \varepsilon = 0, n) = \zeta^{(0)}(\tau) = \left[1 + 0.210\left(\frac{2}{3}\right)\tau\right]^{-3/2} \tag{44}$$

This result is plotted in Figure 3-10.18 along with numerically obtained, non-zero ε solutions for ζ.

From Equation 44 it is clear that for $\varepsilon = 0$, $\zeta \to 0$ as $\tau \to \infty$. But, for a fixed n and an arbitrarily small but non-zero ε, a $\zeta = 0$ position of the interface will, in fact, be attained at some finite, large $\tau = \tau_0$.

This small ε behavior of ζ and its proximity to the $\varepsilon = 0$ solution can be observed in Figure 3-10.18. As can be seen, the smaller the value of ε and the closer the value of n to 0, the longer in time the actual solution is accurately approximated by the $\varepsilon = 0$ solution.

The small ε limit is very important in problems of physical interest. As an example, consider a constant ($n = 0$) smolder source of 0.5 kW, located a distance of 2 m below a ceiling with $\lambda_r = 0.1$ and $\lambda_c = 0.75$. This leads to $\varepsilon = 5.3\ (10^{-4})$. As an example of a relatively strong fire, consider a constant flaming fire of 5,000 kW (e.g., a burning gasoline spill approximately 1 m in radius) located 5 m below a ceiling, with $\lambda_r = 0.35$ and $\lambda_c = 0.75$. This leads to $\varepsilon = 6.0\ (10^{-2})$. In terms of a "small ε" criterion, the latter fire is still relatively weak.

Time, Temperature, and Concentration When the Smoke Drops to the Fire Elevation

Numerically computed τ_0, ε pairs were obtained and plotted by Cooper[43] for a variety of different n values. The corresponding values for $\phi_0 = \phi(\tau_0; \varepsilon, n)$ were also obtained and plotted. All these results are reproduced here in Figure 3-10.19. From these plots and for arbitrary ε and n, it is possible to find the time, t_0, which corresponds to τ_0, for the smoke layer to drop to the fire elevation at $Z = 0$. The plots also provide an estimate for $\phi_0 = \phi(t_0)$, from which it is possible to obtain the $t = t_0$ upper layer temperature, T_0, and (if applicable) the product of combustion concentration, M_0. The most interesting general feature of Figure 3-10.19 is that, for a given n, the value of the ordinate

$$\varepsilon^{2(n+3)/[3(n+5)]}\tau_0(\varepsilon;\ n) = f(\varepsilon;\ n) \tag{45}$$

is relatively uniform over a broad ε range of interest. For example, for $n = 0$, 1, and 2

$$\begin{aligned} \varepsilon^{2/5}\tau_0(\varepsilon;\ n = 0) &= f(\varepsilon;\ n = 0) = 4.3(1 \pm 0.15) \\ \varepsilon^{1/3}\tau_0(\varepsilon;\ n = 1) &= f(\varepsilon;\ n = 1) = 3.4(1 \pm 0.16) \\ \varepsilon^{10/33}\tau_0(\varepsilon;\ n = 2) &= f(\varepsilon;\ n = 2) = 3.0(1 \pm 0.17) \end{aligned} \tag{46}$$

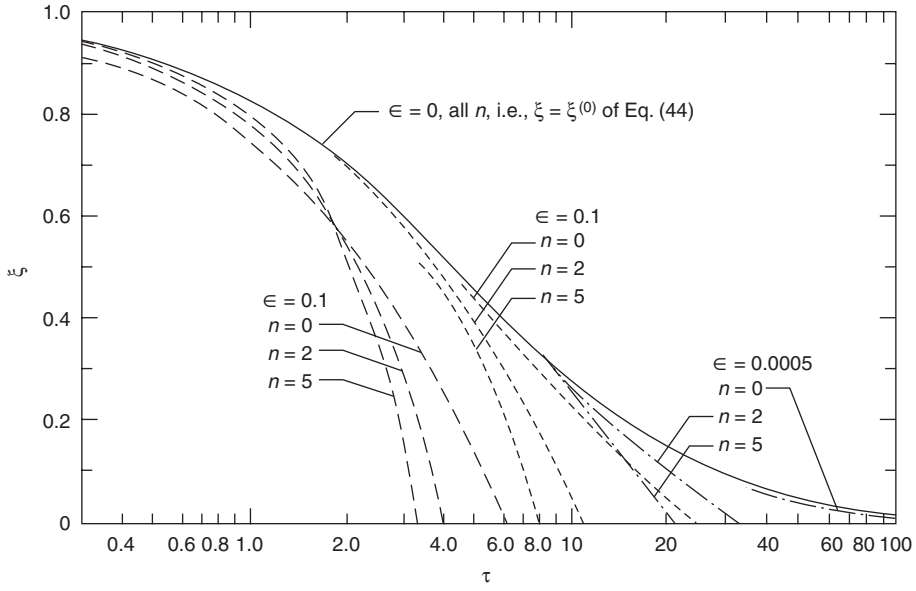

Figure 3-10.18. ***Plots of $\zeta(\tau)$ for different values of n and ε, $0 < \tau \leq \tau_0$.***

for ε in the range

$$0.2(10^{-4}) < \varepsilon < 0.2(10^{-1}) \tag{47}$$

[With somewhat larger errors, Figure 3-10.19 indicates that estimates of τ_0 coming from Equation 46 would remain valid even for ε significantly smaller than $0.2(10^{-4})$.] This result can be expressed in practical terms as a general solution for t_0

$$t_0 = [f(\varepsilon; n)]^{3/(n+3)} \left\{ \frac{[A(n+3)/3]^5 [\rho_a C_p T_a t_0^n / Q(t_0)]^3}{(1-\lambda_c)^2 (1-\lambda_r) g} \right\}^{1/(3n+5)} \tag{48}$$

where the $f(\varepsilon;n)$ are provided in Equation 46, or can be found from Figure 3-10.19. Also,

$$\varepsilon = (1-\lambda_c) \left\{ \frac{[A(n+3)/3]^{2n} [Q(t_0)/t_0^n]^2}{(1-\lambda_r)^{(n+1)} (\rho_a C_p T_a)^2 g^{(n+1)} H^{(3n+5)}} \right\}^{1/(n+3)} \tag{49}$$

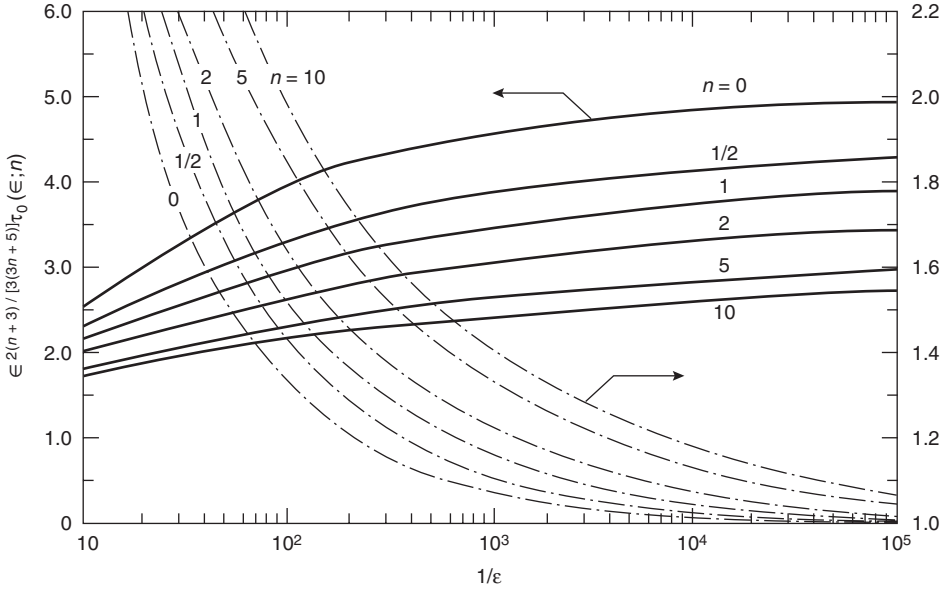

Figure 3-10.19. ***Plots of $\varepsilon^{2(n+3)/[3(n+5)]}\tau_0$ and φ_0 as functions of $1/\varepsilon$ for different values of n.***

Thus, the analysis has led to a remarkable practical result, namely, for fires which grow at rates which are approximately proportional to t^n and for a wide range of fire elevations and room heights of practical interest, the time for a smoke layer to drop from the ceiling to the elevation of the fire is relatively independent of H.

Taking ρ_a, T_a, C_p, and g to be

$$\rho_a = 1.18 \text{ kg/m}^3, \quad T_a = 294 \text{ K}, \quad g = 9.8 \text{ m/s}^2$$
$$C_p = 240 \text{ cal/(kgK)} = 1.005 \text{ Ws/m}^3 \tag{50}$$

Equations 48 and 49 for $n = 0$, 1, and 2 become

$n = 0$:

$$t_0 = 91.4(1 \pm 0.15)\frac{A/Q^{3/5}}{[(1-\lambda_c)^2(1-\lambda_r)]^{1/5}}$$

$$\varepsilon = 9.43(10^{-3})\left(\frac{Q^2}{H^5}\right)^{1/3}\left(\frac{1-\lambda_c}{1-\lambda_r}\right)^{1/3} \tag{51}$$

(A in m^2, Q in kW, t_0 in sec, H in m)

$n = 1$:

$$t_0 = 20.2(1 \pm 0.12)\left[A^5\frac{[t_0/Q(t_0)]^3}{[(1-\lambda_c)^2(1-\lambda_r)]}\right]^{1/8}$$

$$\varepsilon = 1.98(10^{-2})\left(A\frac{Q(t_0)/t_0}{1-\lambda_r}\right)^{1/2}\frac{1-\lambda_c}{H^2} \tag{52}$$

(A in m^2, Q in kW, t_0 in sec, H in m)

$n = 2$:

$$t_0 = 10.5(1 \pm 0.10)\left[A^5\frac{[t_0^2/Q(t_0)]^3}{(1-\lambda_c)^2(1-\lambda_r)}\right]^{1/11}$$

$$\varepsilon = 3.68(10^{-2})(1-\lambda_c)\left[A^4\frac{[Q(t_0)/t_0^2]^2}{H^{11}(1-\lambda_v)^3}\right]^{1/5} \tag{53}$$

(A in m^2, Q in kW, t_0 in sec, H in m)

or, in terms of t_g of Equation 35[4]

$n = 2$:

$$t_0 = 1.60(1 \pm 0.10)\left[\frac{A^5t_g^6}{(1-\lambda_c)^2(1-\lambda_r)}\right]^{1/11}$$

$$\varepsilon = 0.583(1-\lambda_c)\left[\frac{(A/t_g)^4}{H^{11}(1-\lambda_r)^3}\right]^{1/5} \tag{54}$$

(A in m^2, Q in kW, t_0 and t_g in sec, H in m)

where all the above t_0 estimates are subject to the ε range of Equation 47.

Some Solution Results for $Z_i(t)$, $T(t)$, and $\mu(t)$

Plots of general solutions for $Z_i(t)$, $T(t)$, and $\mu(t)$ are presented in Figure 3-10.20 for $n = 0$, 1, and 2. These plots are useful up to the times when the interface either drops to the floor of the compartment or to an elevation 0.2 H below the fire, whichever event occurs first.

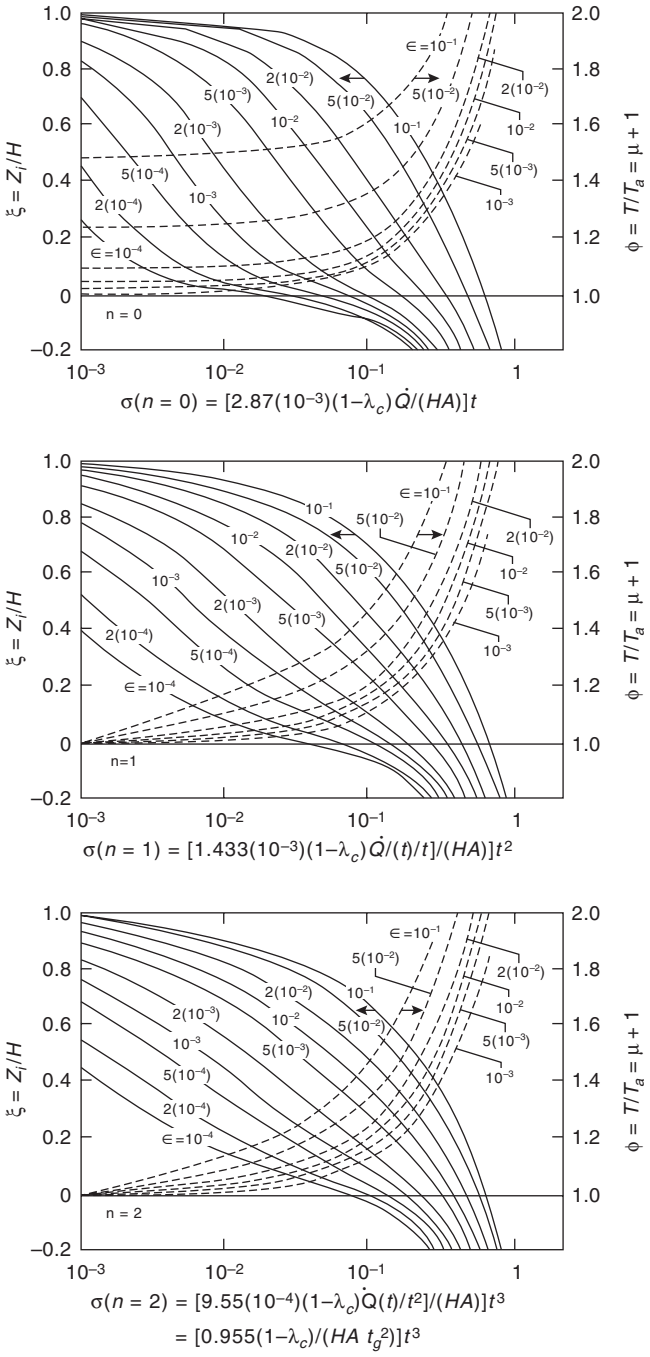

Figure 3-10.20. ***Plots of $Z_i(t)$, $T(t)$, and $\mu(t)$ up to the time when $Z_i = -0.2\,H$ or $Z_i = Z_{floor}$, whichever comes first, for different values of ε and for n = 0, 1, and 2. ($\dot{Q}$ in kW; t and t_g in s; H in m; and A in m^2.)***

As can be noted, the abscissa of the Figure 3-10.20 plots, which have been taken from Cooper,[43] are in the form

$$\sigma = \{\text{constant}\} t^{n+1}$$

The σ of Figure 3-10.20 corresponds to

$$\sigma = \left[\frac{n+3}{3(n+1)}\right] \varepsilon \tau^{3(n+1)/(n+3)} \tag{55}$$

under the ambient property assumptions of Equation 50. Cooper found σ to be a convenient variable for describing the upper layer environment after the interface had dropped below the fire elevation, $Z_i = 0$, and even subsequent to the time that the interface drops to the compartment floor, that is, when $Z_i = -\Delta$.[43] A description of solutions to our problem at these latter times is beyond the scope of this chapter, and the reader is referred to Cooper's work for a full discussion of the relevant results.[43]

Using the $\dot{Q} \sim t^n$ Solution Plots of Figures 3-10.19 and 3-10.20 to Predict Characteristics of Compartment Fire-Generated Environments

To illustrate the use of the solution plots of Figures 3-10.19 and 3-10.20, they will now be applied to two example problems. The first example will involve a problem of smoldering combustion. The second example illustrates the use of the theory in predicting the environment produced in an enclosure which contains a specific large-scale flaming fire hazard.

EXAMPLE 1:

Smoldering combustion: Smoldering experiments reported by Quintiere et al. were carried out in a single-room compartment of height 2.44 m and floor area 8.83 m^2.[45] The opening to the enclosure was formed by a closed undercut door, where the undercut formed a 0.76 m × 0.025 m open horizontal slit at floor level. A smoldering ignition source was placed in the enclosure with the top surface of the source at an elevation of 0.33 m. Gas analysis was carried out at four equidistant elevations, the inlets of sampling tubes extending horizontally approximately 0.5 m from the walls.

The tests evaluated two different smolder sources: a loosely packed bed of cotton, and blocks of flexible polyurethane foam. Mass loss rates, $\dot{m}$, were found to be approximately linear in time throughout the first hour of the two tests, that is,

$$\dot{m} = \alpha t \qquad 0 < t < 60 \text{ min} \tag{56}$$

where

$$\alpha = \begin{cases} 0.21 \text{ g/min}^2 & \text{for polyurethane} \\ 0.33 \text{ g/min}^2 & \text{for cotton} \end{cases}$$

The heats of combustion, H_c, of the materials as well as the ratios, γ, of mass-of-CO produced to mass of material lost were obtained in a separate small-scale apparatus. These were found to be

$$H_c = \begin{cases} (11 \pm \text{) kJ}/g_{\text{cotton}} \\ (15 \pm 8) \text{ kJ}/g_{\text{polyurethane}} \end{cases} \tag{57}$$

$$\gamma = \begin{cases} 0.11 g_{CO}/g_{\text{cotton}} \\ \left(0.10 \begin{matrix} +0.01 \\ -0.04 \end{matrix}\right) g_{CO}/g_{\text{polyurethane}} \end{cases} \tag{58}$$

The results of the previous section will be used to predict the environment which developed in the enclosure during the course of the two different material evaluations.

Comparting Equations 56 through 58 to Equation 34 leads to

$$\begin{aligned} \dot{Q} = \alpha H_c t = \dot{Q}_0 \left[\frac{t H^{3/2} g^{1/2}}{A}\right]^n \\ \dot{C}_{CO} = \alpha \gamma t = \beta \dot{Q} \end{aligned} \tag{59}$$

where $\dot{C}_{CO}$ is measured in g_{CO} per unit time. From the above, it is concluded that

$$n = 1; \qquad \frac{Q(t)}{t} = \alpha H_c; \qquad \beta = \frac{\gamma}{H_c} \tag{60}$$

Also

$$H = 2.11 \text{ m}, \qquad \Delta = 0.33 \text{ m}, \qquad A = 8.83 \text{ m}^2 \tag{61}$$

Radiant losses from the combustion zone are neglected, that is, $\lambda_r = 0$. Considerations by Cooper,[40] together with the experimental results of Mulholland et al. and Veldman et al.,[46,13] indicate that for a $\lambda_r = 0$ combustion zone in an enclosure with proportions similar to the present one, $\lambda_c \approx 0.6$. This λ_c will be used here.

Using the λ_c value 0.6 and Equations 50, 57, 58, and 60 in the μ definition of Equation 37 and the result of Equation 40 leads to

$$\phi = 1 + 135 M_{\text{cotton}} = 1 + 204 M_{\text{polyurethane}} \tag{62}$$

where, for example, M_{cotton} is the upper layer concentration of CO ($g_{\text{CO}}/g_{\text{upper layer}}$) during smoldering of the cotton source.

From Equations 56 and 57

$$\frac{Q(t)}{t} = \alpha H_c \approx \begin{cases} 0.21(15) \text{ kJ/min}^2 = 9(10^{-4}) \\ \quad \text{kW/s for polyurethane} \\ 0.33(11) \text{ kJ/min}^2 = 9(10^{-4}) \\ \quad \text{kW/s for cotton} \end{cases} \tag{63}$$

All parameters of the problem required to estimate t_0 and ε from Equation 52 are now available. These are found to be

$$t_0 = 1400 \text{ sec}; \qquad \varepsilon = 1.6(10^{-4}) \tag{64}$$

The value of ε satisfies the ε range of Equation 47 thereby establishing the validity of the t_0 estimate.

From the value of ε, it is now possible to use Figure 3-10.19 to obtain ϕ_0. Thus, for $1/\varepsilon = 0.61(10^4)$ and for $n = 1$ it is found from the Equation 36 definition of ϕ that

$$\phi_0 = 1.07 \rightarrow T(t_0) = 1.07T_a = 315\ \text{K} = 42°\text{C} \tag{65}$$

Also, from Equation 62, this result for ϕ_0 yields

$$\left.\begin{aligned} M_{\text{cotton}}(t_0) &= \frac{1.07-1}{135} \\ &= 5(10^{-4})\frac{g_{\text{CO}}}{g_{\text{upper layer}}} \\ &= 5(10^2)\ \text{ppm CO} \end{aligned}\right\} \tag{66}$$

$$\left.\begin{aligned} M_{\text{polyurethane}}(t_0) &= \frac{1.07-1}{204} \\ &= 3(10^{-4})\frac{g_{\text{CO}}}{g_{\text{upper layer}}} \\ &= 3(10^2)\ \text{ppm CO} \end{aligned}\right\}$$

The smoke interface reaches the floor at the time, t_f, corresponding to

$$\zeta_f = \frac{Z_i(t_f)}{H} = -\frac{\Delta}{H} = \delta = -0.16 \tag{67}$$

From the $n = 1$ plots of Figure 3-10.20, it is found that this occurs at t_f corresponding to

$$\begin{aligned} \sigma = 0.3 &= \sigma_f(\zeta = \zeta_f;\ n = 1) \\ &= \left\{1.4(10^{-3})(1-\lambda_c)\left[\frac{\dot{Q}(t)/t}{HA}\right]\right\}t_f^2 \\ &\qquad (\dot{Q}\ \text{in kW};\ t\ \text{in s};\ H\ \text{in m};\ A\ \text{in m}^2 \\ &= \left\{1.4(10^{-3})(1-0.6)\left[\frac{9(10^{-4})}{(2.1)(8.8)}\right]\right\}t_f^2 \\ &= 0.3(10^{-7})t_f^2 \end{aligned} \tag{68}$$

(for both the cotton and polyurethane) at which time

$$\phi(t_f) = \phi_f \approx 1.25 \tag{69}$$

The following results are obtained from Equations 68 and 69 and with the use of Equation 62:

$$\begin{aligned} t_f &= 3(10^3)\ \text{sec} \\ M_{\text{cotton}}(t_f) &= \frac{1.25-1}{135} = 1.9(10^3)\ \text{ppm CO} \\ M_{\text{polyurethane}}(t_f) &= \frac{1.25-1}{204} = 1.2(10^3)\ \text{ppm CO} \end{aligned} \tag{70}$$

Thus, the above estimate indicates that the interface reached the floor elevation somewhat prior to the 60-min duration of the tests. The reader is referred to Cooper's studies for further discussion of comparisons between calculated and experimental results.[43]

EXAMPLE 2:

Hazard development in enclosures containing some larger scale fires: NFPA 204M, *Guide for Smoke and Heat Venting*, provides a catalogue of experimentally determined energy release rates for the growth stages of flaming fires in practical fuel assemblies.[4] The $\dot{Q}$ of all items in this listing is proportional to t_2. For example, the $\dot{Q}$ of many items can be estimated by

$$t_g = 100\ \text{sec} \tag{71}$$

Using Equation 35, this corresponds to

$$\dot{Q} = 0.10t^2\ \text{kW/s}^2 \tag{72}$$

The latter items include wood pallets stacked 3.0 to 4.6 m high, many different types of polyethylene, polypropylene, polystyrene and PVC commodities in cartons stacked 4.6 m high, and a horizontal polyurethane mattress.

The results of Figures 3-10.19 and 3-10.20 will be used to characterize the hazard development in enclosures which contain Equation 71-type fires.

From Equations 54 and 71 and the abscissa for $n = 2$ of Figure 3-10.20

$$\begin{aligned} t_0 &\approx 20\left[\frac{A^5}{(1-\lambda_c)^2(1-\lambda_r)}\right]^{1/11} \\ \varepsilon &= 1.5(10^{-2})\left[\frac{(1-\lambda_c)A^{4/5}}{1-\lambda_r)^{3/5}H^{11/5}}\right] \\ \sigma(n=2) &= 0.96(10^{-4})\left(\frac{1-\lambda_c}{HA}\right)t^3 \\ &\qquad (t\ \text{in sec};\ H\ \text{in m};\ A\ \text{in m}^2) \end{aligned} \tag{73}$$

With Equation 73, Figures 3-10.19 and 3-10.20 can now be used to answer a wide variety of hazard-related questions. For illustrative purposes, two such questions will be addressed here.

QUESTION 1:

Flaming ignition is initiated in stacked commodities of the "t_g = 100 s variety" which are contained in a warehouse of height 6 m and floor area 1500 m^2. At what time does the upper layer attain the potentially untenable temperature (due to downward radiation) of 183°C, and what is the elevation of the layer interface at this time?[1] At what time does the upper layer completely fill the warehouse?

ANSWER:

Consistent with recommendations by Cooper,[2] assume $\lambda_r = 0.35$, and, for the purpose of a hazard analysis of this type, conservatively assume that $\lambda_c = 0.6$. Take H to be the floor-to-ceiling dimension, 6 m, and Δ to be zero. Then, for $A = 1500$ m^2, Equation 73 leads to

$$\begin{aligned} t_0 &= 680\ \text{sec} \\ \varepsilon &= 5.2(10^{-2}) \\ \sigma(n=2) &= 4.7(10^{-9})t^3 \end{aligned} \tag{74}$$

Notice that the above value for $\varepsilon = 5.2\ (10^{-2}) > 0.2\ (10^{-1})$ is somewhat outside the Equation 47 range. As a result, the above $t_0 = 680$ s estimate is not reliable. A better value for t_0, estimated from Equation 48 and Figure 3-10.19, is found to be $t_0 \approx 600$ s.

The $\varepsilon = 5.2\ (10^{-2})$ value corresponds to $1/\varepsilon = 19$ which, for $n = 2$ in Figure 3-10.19, is found to correspond (somewhat off-scale) to

$$\phi_0 \approx 2.4 \rightarrow T(t_0) = 2.4T_a = 710\ \text{K} = 433°\text{C} \qquad (75)$$

At the time, t_u, of potential untenability, $T_u = T(t_u)$ is assumed to be 183°C (456 K). Thus

$$\phi_u = \phi(t_u) = \frac{T_u}{T_a} = \frac{456}{294} = 1.55 \qquad (76)$$

For $\varepsilon = 5.2\ (10^{-2})$, the $n = 2$ plots of Figure 3-10.20 can be interpolated at $\phi = \phi_u = 1.55$ to yield

$$\sigma_u = \sigma(t_u) \approx 0.2 = 4.7(10^{-9})t_u^3 \rightarrow t_u = 350\ \text{sec} \qquad (77)$$

which, in turn, is seen to correspond to

$$\zeta_u = \zeta(t_u) = \frac{Z_i(t_u)}{H} = 0.45 \qquad (78)$$

Using this last value for ζ_u along with $H = 6$ m leads to

$$Z_i(t_u) = 0.45(6)\ \text{m} = 2.7\ \text{m} \qquad (79)$$

The above results are summarized as follows: the upper smoke layer will fill the compartment at $t_0 = 600$ s, at which time its average temperature will be approximately 430°C. The potentially untenable condition of $T = 183$°C will occur at $t_u = 350$ s, at which time the layer interface is 2.7 m above the floor.

QUESTION 2:

Flaming ignition is initiated in a polyurethane mattress 0.6 m above the floor of a hospital ward with floor-to-ceiling dimension of 3 m and floor area 100 m^2. At what time, t_u, does the upper layer interface reach the potentially untenable elevation, $Z_u = 1.5$ m, and what is the upper layer temperature, T_u, at this time?

ANSWER:

Take $\lambda_c = 0.8$, and $\lambda_r = 0.35$. Also, $H = 2.4$ m, $\Delta = 0.6$ m, $Z_u = 0.9$ m, and $A = 100$ m^2. Then, Equation 73 leads to

$$\begin{aligned} t_0 &= 230\ \text{sec} \\ \varepsilon &= 2.3(10^{-2}) \\ \sigma(n=2) &= 8.0(10^{-8})t^3 \end{aligned} \qquad (80)$$

Also, at the time of untenability

$$Z_i(t_u)H = \frac{Z_u}{H} = \frac{0.9}{2.4} = 0.38 \qquad (81)$$

For $\varepsilon = 2.3(10^{-2})$, the $n = 2$ plots of Figure 3-10.20 can be interpolated to obtain the desired values of $\sigma(t_u)$, and then $\phi(t_u)$ corresponding to $Z_i/H = 0.38$. Thus

$$\begin{aligned} &\sigma(t_u) = 0.18 = 80(10^{-9})t_u^3 \rightarrow t_u = 130\ \text{sec} \\ &\phi(t_u) = 1.33 \rightarrow T(t_u) = 1.33T_a = 391\ \text{K} = 118°\text{C} \end{aligned} \qquad (82)$$

In Equation 80, t_0 is the time for the smoke interface to drop to the level of the mattress which is 0.6 m above the floor. As an additional point of information, for $\varepsilon = 2.3(10^{-2})$, corresponding to $1/\varepsilon = 44$, and for $n = 2$, Figure 3-10.19 provides the result

$$\phi_0 = 1.94 \rightarrow T(t_0) = 1.94T_a = 570\ \text{K} = 297°\text{C} \qquad (83)$$

Notice that this result can also be obtained approximately from Figure 3-10.20. To do so, select the value of $\sigma = \sigma(t_0)$ when $\zeta = Z_i/H = 0$, and find the corresponding value for $\phi = \phi(t_0)$, all on the $\varepsilon = 2(10^{-2})$ curves. This leads to $\phi(t_0) = 1.88 \approx 1.94$.

The above results are summarized as follows: the smoke layer interface will drop to the 1.5-m elevation at $t = 130$ s, at which time its average temperature will be approximately 118°C. Also, the interface will reach the mattress elevation at $t = 230$ s and have an average temperature of 297°C.

References Cited

1. L.Y. Cooper, "A Concept for Estimating Available Safe Egress Time in Fire," *F. Safety J.*, 5, pp. 135–144 (1983).
2. L.Y. Cooper, "A Mathematical Model for Estimating Available Safe Egress Time in Fires," *F. and Matls.*, 6, pp. 135–144 (1982).
3. E.G. Butcher and A.C. Parnell, *Smoke Control and Fire Safety Design*, Spon, London (1979).
4. G. Heskestad, "Appendix A," in *NFPA 204M, Guide for Smoke and Heat Venting,* National Fire Protection Association, Quincy, MA (1991).
5. V. Babrauskas, "Combustion of Mattresses Exposed to Flaming Ignition Sources, Part I, Full-Scale Tests and Hazard Analysis," in *NBSIR 77-1290,* National Bureau of Standards, Gaithersburg, MD (1977).
6. G. Heskestad, "Engineering Relations for Fire Plumes," *F. Safety J.*, 7, pp. 25–32 (1984).
7. E.E. Zukoski, T. Kubota, and B. Cetegen, "Entrainment in Fire Plumes," *F. Safety J.*, 3, pp. 107–121 (1980/81).
8 B.J. McCaffrey, "Purely Buoyant Diffusion Flames: Some Experimental Results," in *NBSIR 79-1910,* National Bureau of Standards, Gaithersburg, MD (1979).
9. R.L. Alpert, "Turbulent Ceiling-Jet Induced by Large-Scale Fires," *Comb. Science Tech.*, 11, pp. 197–213 (1975).
10. G. Heskestad, "Similarity Relations for the Initial Convective Flow Generated by Fire," *Paper 72-WA/HT-17,* Winter Annual Meeting, ASME (1972).
11. G. Heskestad and M.A. Delichatsios, "Environments of Fire Detectors—I: Effect of Fire Size, Ceiling Heights, and Material," 1: "Measurements," *FMRC Report NBS-GCR-77-86,* 2: "Analysis," *FMRC Report NBS-GCR-77-95,* National Bureau of Standards, Gaithersburg, MD (1977).
12. G. Heskestad and M.A. Delichatsios, "Environments of Fire Detectors—II: Effect of Ceiling Configuration," 1: "Measure-

ments," *FMRC Report NBS-GCR-78-128,* 2: "Analysis," *FMRC Report NBS-GCR-78–129,* National Bureau of Standards, Gaithersburg, MD (1978).
13. C.C. Veldman, T. Kubota, and E.E. Zukoski, "An Experimental Investigation of Heat Transfer from a Buoyant Plume to a Horizontal Ceiling—Part I: Unobstructed Ceiling," *C.I.T. Report NBS-GCR-77-97,* National Bureau of Standards, Gaithersburg, MD (1975).
14. L.Y. Cooper, "Heat Transfer from a Buoyant Plume to an Unconfined Ceiling," *J. of Heat Transfer,* 104, pp. 446–451 (1982).
15. L.Y. Cooper and A. Woodhouse, "The Buoyant Plume-Driven Adiabatic Ceiling Temperature Revisited," *J. of Heat Transfer,* 108, pp. 822–826 (1986).
16. L.Y. Cooper and D.W. Stroup, "The Thermal Response of Unconfined Ceilings above Growing Fires and the Importance of Convective Heat Transfer," *J. of Heat Transfer,* 109, pp. 172–178 (1987).
17. R.L. Alpert, "Calculation of Response Time of Ceiling Mounted Fire Detectors," *Fire Tech.,* 3, pp. 181–195 (1972).
18. I. Benjamin, G. Heskestad, R. Bright, and T. Mayes, *An Analysis of the Report on Environments of Fire Detectors,* Fire Detection Institute (1979).
19. D. Goldman and Y. Jaluria, "Effect of Opposing Buoyancy on the Flow in Free and Wall Jets," *J. of Fluid Mech.*, 166, pp. 41–56 (1986).
20. L.Y. Cooper, "Ceiling Jet Properties and Wall Heat Transfer Near Regions of Ceiling Jet-Wall Impingement," in *NBSIR 86-3307,* National Bureau of Standards, Gaithersburg, MD (1986).
21. L.Y. Cooper, "Convective Heat Transfer to Ceilings above Enclosure Fires," in *Proceedings of 19th Symposium (International) on Combustion,* Combustion Institute, Haifa, Israel (1982).
22. L.Y. Cooper, "A Buoyant Source in the Lower of Two, Homogeneous, Stably Stratified Layers—A Problem of Fire in an Enclosure," in *Proceedings of 20th Symposium (International) on Combustion,* Combustion Institute, Pittsburgh, pp. 1567–1573 (1984).
23. L.Y. Cooper, "On the Significance of a Wall Effect in Enclosures with Growing Fires," *Comb. Science Tech.*, 40, pp. 19–39 (1984).
24. L.Y. Cooper and D.W. Stroup, "Calculating Available Safe Egress Time (ASET)—A Computer Program and User's Guide," *NBSIR 82-2578,* National Bureau of Standards, (1982). Also, a condensed version: "ASET—A Computer Program for Calculating Available Safe Egress Time," *F. Safety Jour.*, 9, pp. 29–45 (1985).
25. E.E. Zukoski and T. Kubota, "Two-Layer Modeling of Smoke Movement in Building Fires," *F. and Matls.*, 4, 1, pp. 17–27 (1980).
26. K. Steckler, J. Quintiere, and W. Rinkinen, "Flow Induced by Fire in a Compartment," in *Proceedings of 19th Symposium (International) on Combustion,* Combustion Institute, Pittsburgh (1982).
27. NFPA 101, *Life Safety Code,* (A-15-3.1.3), National Fire Protection Association, Quincy, MA (1994).
28. L.Y. Cooper, M. Harkelroad, J. Quintiere, and W. Rinkinen, "An Experimental Study of Upper Hot Layer Stratification in Full-Scale Multiroom Fire Scenarios," *J. of Heat Transfer,* 104, pp. 741–749 (1982).
29. L.Y. Cooper, "The Need and Availability of Test Methods for Measuring the Smoke Leakage Characteristics of Door Assemblies," in *Fire Safety: Science and Engineering,* ASTM STP 882, ASTM, Philadelphia, pp. 310–329 (1985).
30. T. Wakamatsu, "Calculation of Smoke Movement in Buildings," in *Res. Paper 34,* Building Research Institute, Tokyo (1968).
31. E. Evers and A. Waterhouse, "A Computer Model for Analyzing Smoke Movement in Buildings," in *SCS Ltd. Report CP 68/78* for Fire Research Station, Borehamwood, UK (1978).
32. B.R. Morton, G.I. Taylor, and J.S. Turner, "Turbulent Gravitational Convection from Maintained and Instantaneous Sources," in *Proceedings of Royal Society (London),* Ser. A, 234, pp. 1–23 (1956).
33. S. Yokoi, "On the Heights of Flames from Burning Cribs," *BRI Report 12,* Ministry of Construction, Japanese Government (1963).
34. W.D. Baines and J.S. Turner, "Turbulent Buoyant Convection from a Source in a Confined Region," *J. of Fluid Mech.*, 37, Part 1, pp. 51–80 (1969).
35. E.E. Zukoski, "Development of a Stratified Ceiling Layer in the Early Stages of a Closed-Room Fire," *F. and Matls.,* 2, pp. 54–62 (1978).
36. W.D. Walton, "ASET-B: A Room Fire Program for Personal Computers," in *NBSIR 85-3144-1,* National Bureau of Standards, Gaithersburg, MD (1985).
37. D. Burgess and M. Hertzberg, "Radiation from Pool Fires" in *Heat Transfer in Flames,* ed. By N.H. Afgan and J.M. Beer, Chap. 27, Wiley and Sons, New York (1974).
38. J. DeRis, "Fire Radiation—A Review," *Tech. Report FMRC RC 78-BT-27,* Factory Mutual Research Corp., Norwood, MA (1978).
39. A.T. Modok and P.A. Croce, "Plastic Pool Fires," *Comb. Flame*, 30 (1977).
40. L.Y. Cooper, "Estimating Safe Available Egress Time from Fires," *NBSIR 80-2172,* National Bureau of Standards, Gaithersburg, MD (1981).
41. R. Friedman, "Quantification of Threat from a Rapidly Growing Fire in Terms of Relative Material Properties," *F. and Matls.*, 2, pp. 27–33 (1978).
42. T. Tanaka, "A Model on Fire Spread in Small-Scale Building," in *Third Joint Meeting US-Japan Panel on Fire Research and Safety,* UJNR, Washington, DC (1978).
43. L.Y. Cooper, "The Development of Hazardous Conditions in Enclosures with Growing Fires," *Comb. Science and Tech.*, 22, pp. 279–297 (1983).
44. J.G. O'Neill and W.D. Hayes, "Full-Scale Fire Tests with Automatic Sprinklers in a Patient Room" *NBSIR 79-1749,* National Bureau of Standards, Gaithersburg, MD (1979).
45. J. Quintiere, M. Birky, and G. Smith, "An Analysis of Smoldering Fires in Closed Compartments and Their Hazard Due to Carbon Monoxide," *F. and Matls.*, 6, p. 99 (1982).
46. G. Mulholland, T. Handa, O. Sugawa, and H. Yamamoto, "Smoke Filling in an Enclosure," *20th National Heat Transfer Conference,* Milwaukee (1981).

CHAPTER 11

Fire Hazard Calculations for Large, Open Hydrocarbon Fires

Craig L. Beyler

Introduction

A major challenge in industrial fire protection is controlling the impact from large, open hydrocarbon fires. The primary mechanism for injury of damage from such fires is thermal radiation. Depending upon the circumstances and conditions leading to such an event, a different type of open fire may result. For example, ignited releases can produce pool fires, jet flames, vapor cloud fires, or fireballs, all of which behave differently and exhibit markedly different radiation characteristics. This chapter presents detailed techniques for calculating impacts from large, open hydrocarbon fires. Examples are included throughout this chapter to illustrate the application of these expressions.

The first section of this chapter discusses hydrocarbon pool fires, an area in which considerable work has been done, including various important geometric parameters (e.g., flame height), thermal radiation models, and atmospheric absorption of radiation. The second section deals with turbulent jet flames and flares, first presenting significant geometric effects and thermal radiation models, then discussing aerodynamic effects on radiant energy and flame stability.

While the above cases involve primarily steady-state thermal radiation, the third section considers two very important cases that involve unsteady radiant effects—burning vapor clouds and fireballs. Although developmental work in both of these areas is still ongoing, limited data are available to lend some confidence to the use of these models.

The following part of this introduction presents an event tree for the release of a flammable material to guide the user's selection of appropriate potential impacts and model application. It cannot be overstressed that prudent judgment should be exercised in the application of any of these calculation schemes to yield a safe and fair evaluation of scenarios of interest.

Event Tree for Flammable Material Release

Figure 3-11.1 depicts a typical event tree for the release of a flammable material, showing the pathways that lead to the various types of open fires. For this purpose, assume the release occurs from a pressurized container since all types of open fires may be realized from a pressurized release. In this example, the pressurized container may be either a large vessel (for storage, reaction, batching, etc.) or a pipeline (for transfer, fittings, instruments, etc.). The pressure may be the result of either normal operations or abnormal external events. For example, a tank may be pressurized because it contains a compressed liquid or because it has been exposed to an external fire; a pipeline may be pressurized because of a pumping operation or because of steam tracing on a blocked-in segment. Finally, the release may be due to a major failure (e.g., spontaneous tank failure) or a minor accident (e.g., breakage of a fitting).

While tracing the pathways in the event tree, note that a release may or may not be accompanied by immediate ignition. With immediate ignition, that is, following the left branch of the tree, a jet flame will result if the release is from a relatively small opening. Such a release could be either vapor or liquid and, if liquid, could also involve flashing of liquid into vapor and/or accumulation of liquid. If the release is the result of a major spill and there is immediate ignition, the result is usually a fireball, the size of which is strongly affected by the amount of flash vaporization and liquid entrainment that occurs upon release.

If ignition does not occur immediately upon release, the right branch of the event tree is followed. Releases through relief valves, either accidental or intentional, may

Dr. Craig L. Beyler is the technical director of Hughes Associates, Fire Science and Engineering. He was the founding editor of the *Journal of Fire Protection Engineering* and serves on a wide range of committees in the fire safety community. This chapter is based on the chapter written by Krishna Mudan and Paul Croce for the first and second editions of the SFPE Handbook of Fire Protection Engineering.

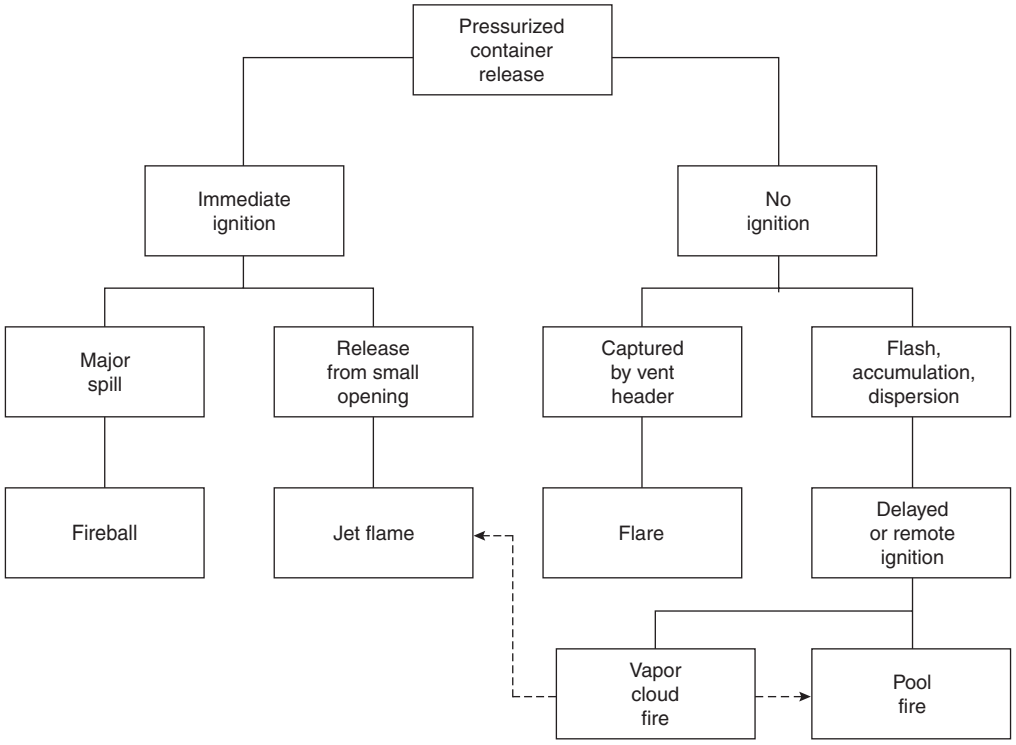

Figure 3-11.1. ***Example event tree for release of flammable material.***

be captured by a vent header system and directed to a flare. Flares must accordingly be designed for expected accident or operational flow capacities, and the design should include consideration of resulting hazard zones.

If the unignited release is to the atmosphere, the spill will be accompanied by flash vaporization, liquid entrainment, accumulation, and/or vapor dispersion. A delayed local ignition following accumulation results in a pool fire whose characteristics are strongly influenced by the geometry of containment (or lack thereof).

Absence of a local ignition source, either immediate or delayed, allows a vapor cloud to form as the vapors disperse downwind. A portion of this vapor cloud will be flammable, and depending upon the size of the release, the flammable region could extend significantly downwind. A remote ignition source can ignite the cloud, resulting in a vapor cloud fire that burns from the point of ignition back toward the source of the cloud, that is, the release point. Note also that the event tree shows dashed pathways from the vapor cloud fire to a pool fire or a jet flame. This is intended to show that the transient burning of the vapor cloud fire back to the release point can initiate a subsequent steady burning jet flame or pool fire, and consideration must be given to potential impacts from both types of fire.

Finally, this event tree represents an example of potential pathways leading to hazardous open fires. Scenarios will be encountered that will be similar to the event tree depicted in Figure 3-11.1 or to parts thereof, but it is important to recognize that in all cases, the event tree must be structured to reflect the actual scenario under consideration.

Hydrocarbon Pool Fires

The thermal radiation hazards from hydrocarbon pool fires depend on a number of parameters, including the composition of the hydrocarbon, the size and shape of the pool, the duration of the fire, its proximity to the object at risk, and the thermal characteristics of the object exposed to the fire. The objectives of this section of the chapter are to review available techniques for determining the thermal radiation hazards from liquid hydrocarbon pool fires under various credible spill conditions.

The state of the art of predicting the thermal environment of hydrocarbon pool fires consists essentially of semiempirical methods, some of which are based on experimental data. Needless to say, such semiempirical methods are always subject to uncertainties.

Estimating the thermal radiation field surrounding a fire involves the following three major steps:

1. Geometric characterization of the pool fire; that is, the determination of burning rate and the physical dimensions of the fire. In calculating thermal radiation, the size of the fire implies the time-averaged size of the visible envelope.
2. Characterization of the radiative properties of the fire; that is, the determination of the average emissive power of the flames. The intensity of thermal radiation

emitted by pool fires depends upon a number of parameters, including fuel type, fire size, flame temperature, and composition. The major sources of emission in large hydrocarbon fires are the water vapor, carbon dioxide, and soot.

3. Calculation of radiant flux at a given location. This can be accomplished once the geometry of the fire, its radiation characteristics, and the location, geometry, and orientation of the receiver are known. For large distances (hundreds of meters), the absorption of thermal radiation in the intervening atmosphere becomes appreciable. This is dependent on the pathlength, flame temperature, and the relative humidity in the atmosphere.

References 1–7 provide general information concerning radiation heat transfer relevant to pool fires, and References 8–39 are specific studies of pool fire radiation heat transfer underpinning the methods of analysis.

Pool Fire Geometry

The flame geometry for the solid flame model is generally determined by assuming that the flame is a solid, gray emitter having a regular well-defined shape such as a circular or a tilted cylinder. The dimension of the flame area characterized by the flame base diameter, visible flame height, and the flame tilt. The flame diameter is dependent on the pool size (spill volume and/or spill rate). The flame height appears to depend on the flame diameter and the burning rate. These factors, which influence the flame geometry, are discussed in this chapter.

The pool fire geometry is determined by the manner and location of the fuel release. Section 2, Chapter 7 provides detailed means for predictions of the extent of the spill or pool, the spread of flame over the fuel surface, and the resulting burning rate. This information will be required for determination of the flame height and the radiation analyses that follow.

The height or length of a flame is a significant indicator of hazard since it directly relates to flame heat transfer and the propensity to impact surrounding objects. A plume of hot gases rises above a flame, the temperature, velocity and width of this plume change as it rises due to the mixing of the plume with the surrounding. The height and temperature of the flame are important in estimating the ignition of adjacent combustibles. Above the fuel source, the flaming region is characterized by high temperature and is generally luminous. Flame from the pool fires fluctuate periodically so that the tip of the flame will be significantly different from the length of the continuous combustion (or luminous) region. Consequently, flame height has been defined by various criteria in order to correlate data. Investigators have used the degree of luminous flame intermittency, flame temperature, or visible estimations. Hence, correlations for flame height could have inherent variation with the instantaneous flame length due to factors involving flame fluctuation and flame definition. For additional information, see Section 2, Chapter 1, "Fire Plumes."

Flame length: Many investigators have developed correlations for turbulent flame lengths in a quiescent air environment. Most are based on the dimensional analysis of experimental data; some are based on approximate theoretical models involving some empirical factors.

Thomas[40] has developed a correlation for the mean visible height of turbulent diffusion flames (in the absence of wind), based on the experimental data of laboratory-scale wood crib fires and dimensional analysis considerations. The correlation for a circular fire is

$$\frac{H}{D} = 42\left(\frac{\dot{m}''}{\rho_a\sqrt{gD}}\right)^{0.61} \tag{1}$$

where $\dot{m}''$ = mass burning rate per unit pool area (in kg/m^2·s) and ρ_a = ambient air density (kg/m^3). For rectangular fires of small aspect ratios, an area equivalent to a circular fire diameter may be used.

The presence of wind may also alter the visible length of flames. The correlation developed by Thomas,[40] based on wood crib fires, is

$$\frac{H}{D} = 55\left(\frac{\dot{m}''}{\rho_a\sqrt{gD}}\right)^{0.67} u^{*-0.21} \tag{2}$$

where u^* is the nondimensional wind velocity given by

$$u^* = \frac{u_w}{(g\dot{m}''D/\rho_v)^{1/3}} \tag{3}$$

Moorhouse[34] conducted several large-scale tests of liquified natural gas (LNG) pool fires. The crosswind and downwind motion picture data were analyzed to determine the flame length. The correlation given by Moorhouse is

$$\frac{H}{D} = 62\left(\frac{\dot{m}''}{\rho_a\sqrt{gD}}\right)^{0.254} u_{10}^{*-0.044} \tag{4}$$

where u_{10}^* is the nondimensional wind speed determined using Equation 3 with measured wind speed at a height of 10 m. In both Equations 14 and 16, u_{10}^* is assigned a value of unity if it is less than 1.

Heskestad[41,42] has correlated data from a wide variety of sources including pool fires and buoyant jets using the following equation:

$$\frac{H}{D} = 0.235\frac{\dot{Q}^{2/5}}{D} - 1.02 \tag{5}$$

where $\dot{Q}$ is measured in kW. It can be shown that $\dot{Q}^{2/5}/D$ is proportional to the nondimensional burning rate, $\dot{m}''/(\rho_a\sqrt{gD})$, raised to the 2/5 power.

Figure 3-11.2 shows the flame height to diameter ratio, H/D, as a function of the nondimensional burning rate, $\dot{m}''/(\rho_a\sqrt{gD})$, for a range of pool fire data assembled by Mudan.[14] In addition, the Thomas, Moorhouse, and Heskestad flame heights are shown.

Flame tilt angle: Flame length under wind conditions have been studied by several investigators. Figure 3-11.3 illustrates a general schematic for the windblown flame. The pool fire flame follows a curved trajectory, and the angle, θ, approximates the trajectory. The vertical and hor-

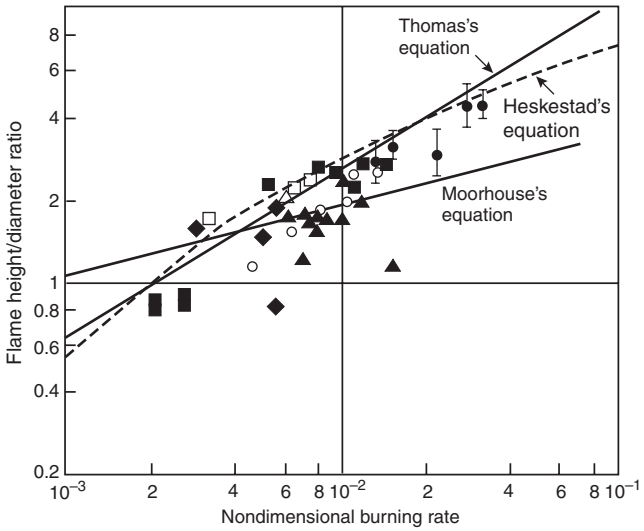

Figure 3-11.2. ***Flame heights for various hydrocarbon pool fires on land and water.[14]***

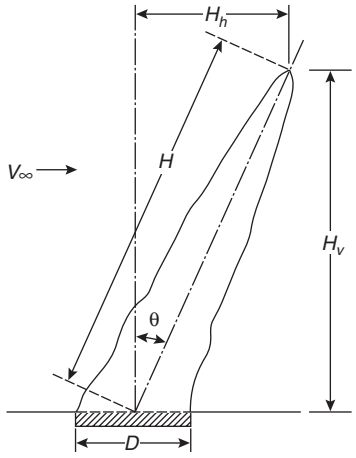

Figure 3-11.3. ***Flame inclinations due to wind.***

izontal components of the flame length measured along the angle are also shown in the figure.

Walker and Sliepcevick[43] and Emori and Saito[44] derived correlations from small-scale experiments. They correlated the angle of inclination as a function of cross-wind velocity, v_∞, but the results do not compare well with larger-scale data.

Thomas[40] developed the following correlation for flame tilt angle, θ, based on the data from two-dimensional wood cribs:

$$\cos\theta = 0.7\left[\frac{u_w}{(g\dot{m}''D/\rho_a)^{1/3}}\right]^{-0.49} \tag{6}$$

Based on the measured values, the American Gas Association (AGA)[39] proposed the following correlation to determine the flame tilt angle, θ:

$$\cos\theta = \begin{cases} 1 & \text{for } u^* \le 1 \\ 1/\sqrt{u^*} & \text{for } u^* \ge 1 \end{cases} \tag{7}$$

where u^* is the nondimensional wind velocity given by Equation 3 with a wind velocity measured at a height of 1.6 m. In Figure 3-11.4, a comparison of observed flame tilt angle is shown for various hydrocarbons pool fires with correlations given by Equations 6 and 7. Although there is considerable scatter in the measured flame tilt, the correlation given by Equation 7 represents the flame tilt most accurately. Defaveri et al.[45] have studied the effects of wind on high-momentum flames.

Geometry of trench fires: Trench fires have received little attention to date. Small laboratory-scale *n*-hexane and heptane fires have been conducted under wind-free conditions. Moorhouse[16] conducted limited large-scale LNG trench fires with aspect ratios ranging from 1.5 to 2.5. More recently, Mudan and Croce[17] reported on large-scale tests with LNG trenches having aspect ratios of up to 30.0. All the data seem to indicate that flame geometry of trench fires is more sensitive to wind conditions than is flame geometry of conventional pool fires. Flame height was found to be a strong function of trench width rather than length. Indeed, for large aspect ratios, the trench fire seemed to break up into small flamelets having a typical base dimension of the trench width, *W*.

Based on an extensive analysis of the motion picture data of LNG trench fires, Mudan and Croce[17] suggested that the trench fire geometry can be represented by a modified Froude number. The definition of the modified Froude number is

$$\mathrm{Fr}' = \frac{u_w}{2\sqrt{gW}} \tag{8}$$

where

u_w = wind speed, m/s
W = trench width, m
g = acceleration due to gravity, m/s²

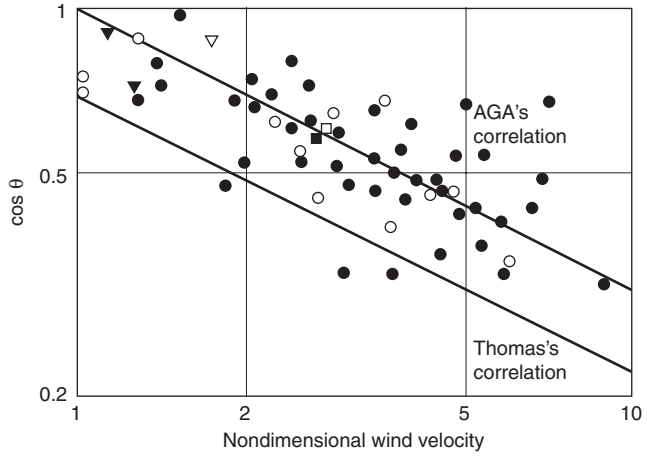

Figure 3-11.4. ***Relationship between nondimensional wind velocity and flame tilt angle.[14]***

The measured flame length as a function of the modified Froude number is shown in Figure 3-11.5. The flame length correlation is

$$\frac{H}{W} = \begin{cases} 2.2 & \mathrm{Fr}' \geq 0.25 \\ 0.88(\mathrm{Fr}')^{-0.65} & 0.25 < \mathrm{Fr}' \leq 0.1 \\ 4.0 & \mathrm{Fr}' \leq 0.1 \end{cases} \quad (9)$$

The flame drag and flame tilt are given by the following expressions.

Flame drag:

$$\frac{W'}{W} = \begin{cases} 3.5 & \mathrm{Fr}' \geq 0.25 \\ 23.3(\mathrm{Fr}')^{1.37} & 0.25 < \mathrm{Fr}' \leq 0.1 \\ 1 & \mathrm{Fr}' < 0.1 \end{cases} \quad (10)$$

Flame tilt:

$$\cos\theta = \begin{cases} 0.56 & \mathrm{Fr}' \geq 0.25 \\ 0.36(\mathrm{Fr}')^{-0.32} & 0.25 \leq \mathrm{Fr}' \leq 0.042 \\ 1 & \mathrm{Fr}' \leq 0.042 \end{cases} \quad (11)$$

The essential features of the suggested correlations defined by Equations 9, 10, and 11 are

1. The flame geometry (length, drag, and tilt) is independent of the ambient conditions for Froude numbers greater than about 0.25. For example, the critical wind speed for a 4-m-wide trench will be about 3 m/s. For wind speeds greater than 3 m/s, the trench fire geometry does not change significantly.
2. For very low Froude numbers (extremely low-wind to no-wind cases), the flame geometry parameters are dependent on the trench width.
3. For in-between Froude numbers, the flame length decreases with increasing wind speed and the flame drag and tilt increase.

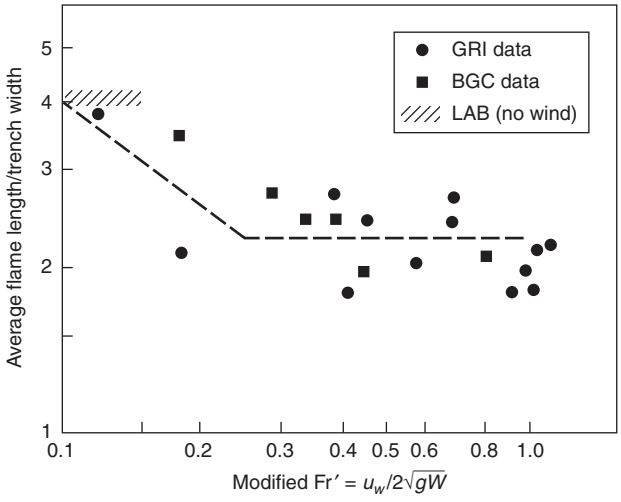

Figure 3-11.5. ***Nondimensional flame height as a function of the Froude number.[17]***

Caution must be exercised in using the correlations given by Equations 9, 10, and 11 since they are based only on LNG fire data.

Thermal Radiation Hazards from Liquid Hydrocarbon Pool Fires

Calculation Procedure—Flame Radiation to External Target

This section provides methods for assessing the impact of radiation from pool fires to potential targets. The goal is to provide methods for calculating safe separation distances between fire sources and potential targets that would be damaged or adversely affected by radiation from the fire. The methods in this section include a range of levels of detail and rigor. Some methods are most appropriate for very crude initial hazard assessments, while the more detailed methods are capable of better predictions though requiring more engineering effort. Where separations exist and a simple method demonstrates that the separation is far more than required for safety, it may not be necessary to perform a more rigorous analysis. In other more critical applications, the highest accuracy methods available are required.

The methods presented in this section have been evaluated and included by the Society of Fire Protection Engineers (SFPE) in *Engineering Guide on Pool Fire Radiation.*[46] In that reference, the methods are described fully, the assumptions inherent in the methods are identified, limits of applicability are assessed, and available input data and data sources are identified. The accuracy of the methods are examined through comparisons of the methods with available experimental data.

Calculation Methods

Estimating the thermal radiation incident upon an object involves the following three major steps:

(1) Determine the geometric characteristics of the pool fire, that is, determine the burning rate and physical dimensions of the fire.
(2) Determine thermal radiation characteristics of the fire.
(3) Calculate the incident radiant flux at the target location.

It is extremely important that a single methodology be used for all three steps of this process. The available methods include empirical elements that, if indiscriminately used, can lead to unpredictable results. Because of this fact, each method is described fully and independently from other methods, even when some elements of the analysis appear similar.

Four methods for estimating radiation from pool fires were identified and evaluated.[46] Two methods are generally classifiable as simple screening methods and two are more detailed procedures. The screening methods include a very simple correlation developed by Shokri and Beyler,[47] and the classical point source model. The more detailed procedures are those developed by Shokri and Beyler[47] and by Mudan.[14]

Screening Methods

Shokri and Beyler correlation: Based on experimental data from large-scale pool fire experiments, Shokri and Beyler[47] developed a simple correlation of radiant heat flux at ground level as a function of the radial position of a vertical target. The incident heat-flux correlation (in kW/m^2) is given by

$$\dot{q}'' = 15.4\left(\frac{L}{D}\right)^{-1.59} \tag{12}$$

where D is the diameter of the pool fire and L is the distance from the center of the pool fire to the target edge. Note that the edge of the circular pool has a value of L/D of 0.5. While this correlation was determined from circular pool fires, an equivalent-area circular source can be used for noncircular pools with an aspect ratio of approximately one. The equivalent diameter is given by

$$D = \sqrt{\frac{4A}{\pi}} \tag{13}$$

where A is the surface area of the noncircular pool.

This method assumes that the pool is circular or nearly circular. It assumes that the target is vertical and located at ground level. It is known that the radiant heat flux is maximized near the midheight of the radiating source and that a target facing the center of radiation will give the maximum heat flux at a given location. As such, at heights above ground level the radiant flux is expected to exceed that given by Equation 12.

Figure 3-11.6 shows a semilogarithmic plot of the data from Hugglund and Persson,[18] Yamaguchi and Wakasa,[19] Seeger,[20] Yumoto,[21] Dayan and Tien,[22] and May and McQueen[23] with the correlation given by Equation 12. Figure 3-11.7 shows a comparison of the measured and predicted heat fluxes for the original data included in Figure 3-11.6 as well as additional data from the literature that were not used to develop the correlation.

A safety factor of 2 is recommended for use with Equation 12.[46] Figure 3-11.8 shows a comparison of all the available data to the predictions using Equation 12 with a safety factor of 2. Figure 3-11.8 clearly shows that essentially all the data is overpredicted by Equation 12 with a safety factor of 2 applied. The safety factor of 2 is a recommendation for use in design applications. Where a realistic result is required, no safety factor should be applied.

Point source model: To predict the thermal radiation field of flames, it is customary to model the flame by a point source located at the center of real flame. The point source model is the simplest configurational model of a radiant source. Whereas more realistic radiator shapes give rise to very complex configuration factor equations, the point source model provides a simple relationship that varies with the inverse square of the distance, R. For an actual point source of radiation or a spherical source of radiation, the distance R is just the distance from the point or from the center of the sphere to the target. See Figure 3-11.9 for a graphic representation of relevant nomenclature.

The point source model is widely used (see Drysdale[48] for example), though it has really never been developed as a rigorous methodology. The method as presented and evaluated here follows the development as given by Drysdale.[48]

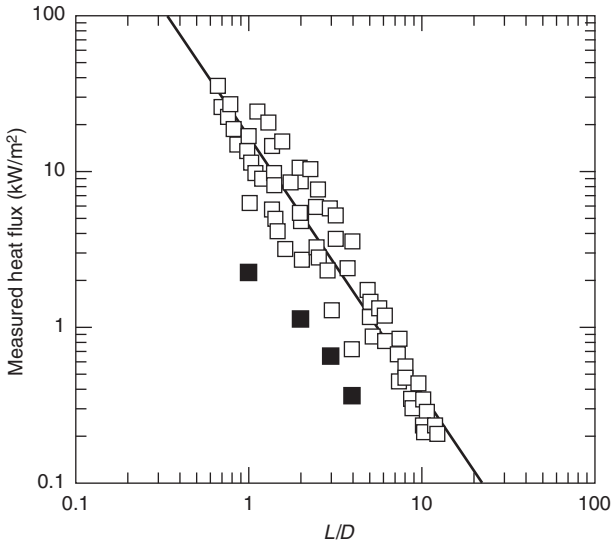

Figure 3-11.6. ***Measured incident radiant heat flux at ground level to a vertical target as a function of the distance from the pool center to the target normalized by the pool diameter. Solid symbols are 50-m-diameter kerosene data. The solid line is Equation 12.[47]***

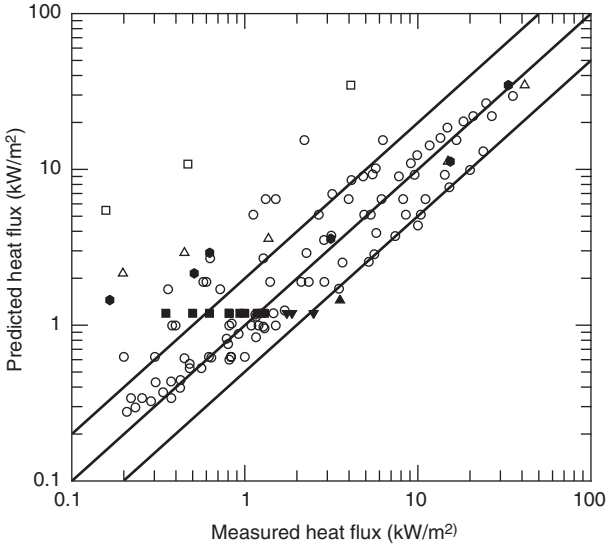

Figure 3-11.7. ***Comparison of measured and calculated radiative heat flux from large pool fires using the Shokri and Beyler correlation (Equation 12). Solid lines indicate equality of measured and predicted heat fluxes based on the correlation developed by Shokri and Beyler.[47]***

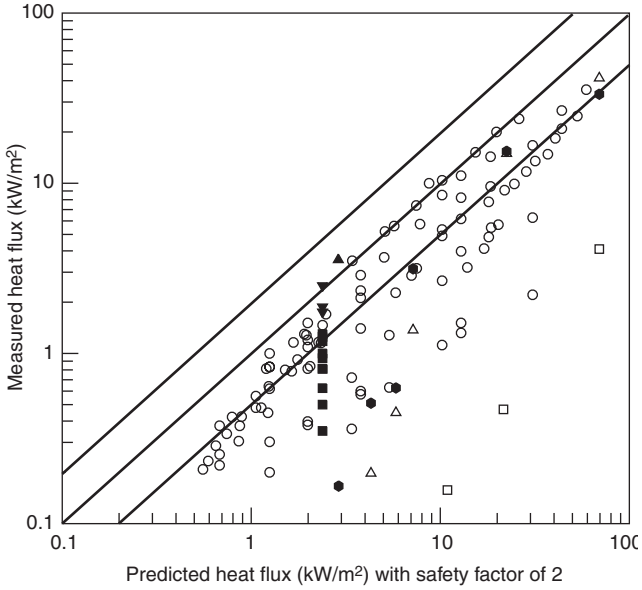

Figure 3-11.8. ***Comparison of measured and calculated radiative heat flux from large pool fires using the Shokri and Beyler correlation (Equation 12) and a safety factor of 2. Solid lines indicate equality of measure and predicted heat fluxes based on the correlation developed by Shokri and Beyler[47] with a safety factor of 2.***

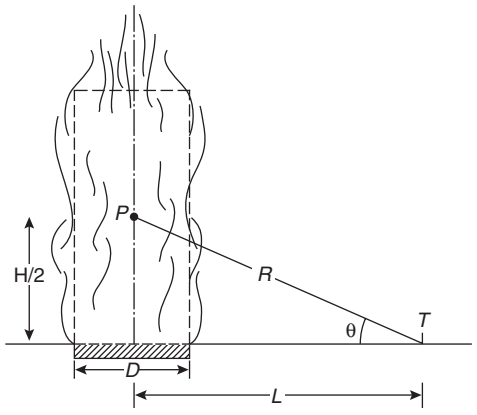

Figure 3-11.9. ***Nomenclature for use with the point source model.***

The incident radiative heat flux is given by

$$\dot{q}'' = \frac{\dot{Q}_r \cos\theta}{4\pi R^2} \tag{14}$$

where

$\dot{Q}_r$ = the total radiative energy output of the fire

θ = the angle between the normal to the target and the line of sight from the target to the point source location

R = the distance from the point source to the target

The location of the equivalent point source, *P,* is at the center of the pool fire and at the midheight of the flame. The flame height in meters is given by the Heskestad[41] correlation, Equation 5:

$$H = 0.235\dot{Q}^{2/5} - 1.02D \tag{5}$$

where $\dot{Q}$ is the heat release of the pool fire in kW and D is the diameter of the pool fire in meters.

If the pool has a length-to-width ratio near one, an equivalent diameter can be used for noncircular pools in the determination of the flame height. The equivalent diameter is given by Equation 13:

$$D = \sqrt{\frac{4A}{\pi}} \tag{13}$$

where A is the surface area of the noncircular pool.

The distance from the point source location to the target location is given by the Pythagorean theorem:

$$R = \sqrt{L^2 + H_T^2} \tag{15}$$

where H_T is the height of the target relative to the height of the equivalent point source at $H/2$, and L is the horizontal distance from center of the pool to the target.

For a target on the ground, $H_T = H/2$. For a target at the midheight of the flame, $H_T = 0$.

The radiative energy output is given by the radiative fraction, χ_r, multiplied by the total heat release rate:

$$\dot{Q}_r = \chi_r \dot{Q} = (0.21 - 0.0034D)\dot{Q} \tag{16}$$

where the radiative fraction is a function of both the fuel and the pool area and D is the pool diameter in meters.

The radiative fraction deduced from the experiments[46] is plotted in Figure 3-11.10 as a function of pool diameter, *D.* The radiative fractions were determined using the point source method for the most remote data point for each experiment. The curve fit used in Equation 16 above is also shown in Figure 3-11.10. At pool diameters above 50 m, the radiative fraction for 50 m should be used.

Estimating the thermal radiation from a pool fire to a target involves the following steps based on the point source model:

1. Determine the heat release rate, $\dot{Q}$.
2. Determine the diameter of the pool fire, or use Equation 13 for noncircular pools.
3. Determine the location of the equivalent point source, *P.* The equivalent point source is on the centerline of the pool at a height equal to one-half the flame height given by Equation 5.
4. Calculate the distance, *R,* from the equivalent point source location to the target location using Equation 15.
5. Determine the radiative output of the flame from Equation 16.
6. Calculate the radiative heat flux to the target using Equation 14.

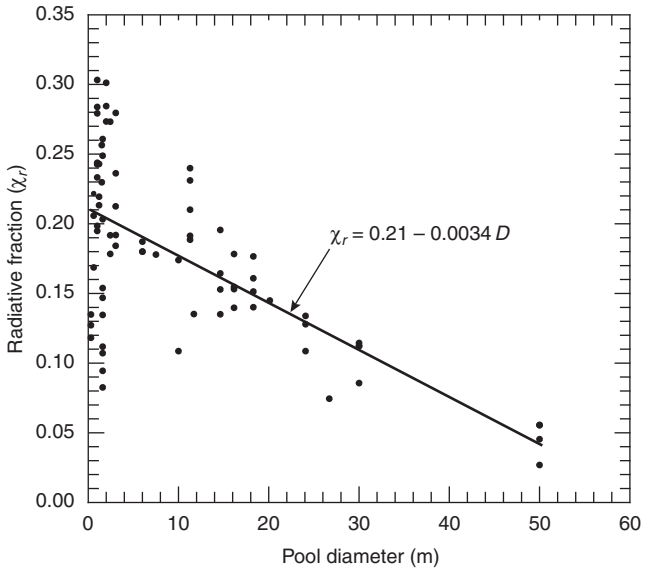

Figure 3-11.10. ***Radiative fraction (χ_r) as a function of pool diameter. The solid line is a curve fit to the data.[46]***

Figure 3-11.11 shows a comparison of all the available data with the prediction of the point source model.[46] The lines shown on the plot reflect predictions that are one-half and twice those of the measured data. At heat fluxes above about 5 kW/m^2, there are systematic, nonconservative results.

The point source configuration factor is known to be a very simplistic representation of a pool fire. It is a correct assumption at large distances from the fire. A theoretical analysis of radiation from a small pool fire by Modak[49] indicated that the point source model is within 5 percent of the correct incident heat flux when $L/D > 2.5$. This result is, however, dependent upon the specific flame modeled and was not derived from experimental data. The method is known to underpredict incident heat fluxes at closer locations (e.g., see Drysdale[48]). The poor performance at heat fluxes above 5 kW/m^2 indicate that the point source model is not a good choice under conditions where ignition of combustibles is to be considered.

A safety factor of 2 is recommended for use with the point source model at heat fluxes less than 5 kW/m^2. Figure 3-11.12 is a comparison of predicted and measured heat fluxes with the inclusion of the recommended factor of safety. The vertical line is located at the maximum heat flux for which the point source model is recommended for use. Figure 3-11.12 clearly shows that essentially all the data is overpredicted by the point source model with a safety factor of 2 applied for heat fluxes less than 5 kW/m^2. The safety factor of 2 is a recommendation for use in design applications. Where a realistic result is required, no safety factor should be applied.

Detailed Methods

Shokri and Beyler: Shokri and Beyler[47] have described a method for prediction of radiation from pool fires based on the pool fire radiation data available in the open literature. They correlated experimental data of flame radia-

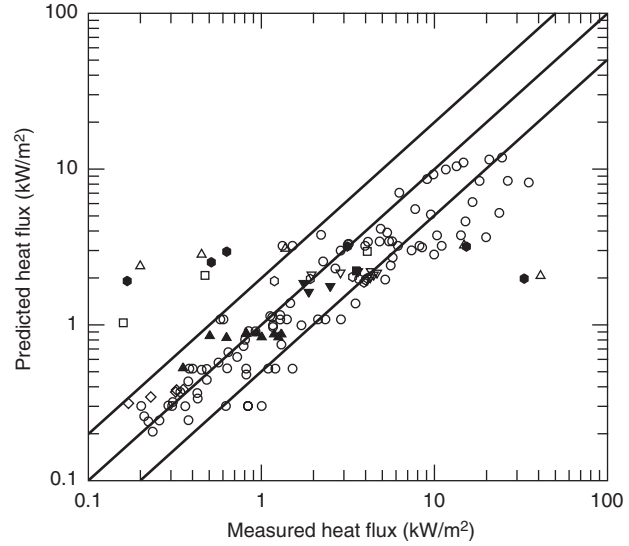

Figure 3-11.11. ***Comparison of measured and calculated radiative heat flux from large pool fires using the point source model. Solid lines indicate equality of measured and predicted heat fluxes based on the point source model.***

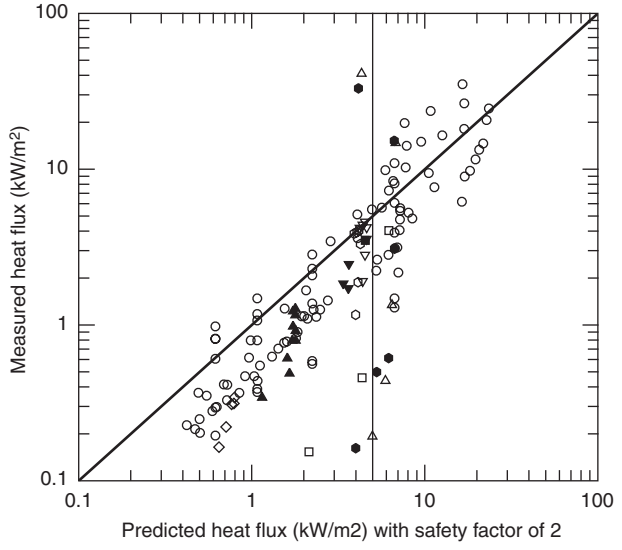

Figure 3-11.12. ***Comparison of measured and calculated radiative heat flux from large pool fires using the point source model and a safety factor of 2. Solid lines indicate equality of measured and predicted heat fluxes based on the point source model.***

tion to external targets in terms of an average effective emissive power of the flame. The flame is assumed to be a cylindrical, blackbody, homogeneous radiator with an average emissive power.

Shokri and Beyler[47] have treated radiant heat transfer from a source to a target based on the concept of the angle factor, also variously known as the shape, geometrical, configuration, or view factors, including those given by many authors.[1,3,50–57] and the incident radiative flux (in kW/m²) to a target outside the flame, $\dot{q}''$, is given by

$$\dot{q}'' = EF_{12} \tag{17}$$

where E is the emissive power of the pool fire flame, kW/m², and F_{12} is the view or configuration factor between the target and the flame.

The configuration factor is a function of the target location, the flame height and diameter, and lies between zero and one. When a target is very close to a flame, the configuration factor approaches one since everything viewed by the target is the flame. The flame is idealized as a cylinder with a diameter equal to the pool diameter, D, and a height equal to the flame height, H_f. If the pool has a length-to-width ratio near one, an equivalent-area circular source can be used for noncircular pools in the determination of flame height. For noncircular pools, the effective diameter will be defined as the diameter of a circular pool with an area equal to the actual pool area given by Equation 13:

$$D = \sqrt{\frac{4A}{\pi}} \tag{13}$$

where A is the surface area of the noncircular pool.

Flame height of the pool fire flame is determined using the Heskestad[41] correlation given by Equation 17:

$$H = 0.235\dot{Q}^{2/5} - 1.02D \tag{5}$$

where

H = flame height,

$\dot{Q}$ = heat release of the pool fire, kW

D = diameter of the pool fire, m

Given the diameter and height of the flame, the view factor, F_{12}, is determined using Equation 18 applicable to cylindrical radiation sources. For horizontal and vertical target orientations, expressions for estimating the configuration factor are found in Equations 18a and 18b, respectively.

$$F_{12,H} = \frac{(B - 1/S)}{\pi\sqrt{B^2 - 1}} \tan^{-1}\sqrt{\frac{(B+1)(S-1)}{(B-1)(S+1)}} - \frac{(A - 1/S)}{\pi\sqrt{A^2 - 1}} \tan^{-1}\sqrt{\frac{(A+1)(S-1)}{(A-1)(S+1)}} \tag{18a}$$

$$F_{12,V} = \frac{1}{\pi S}\tan^{-1}\left(\frac{h}{\sqrt{S^2-1}}\right) - \frac{h}{\pi S}\tan^{-1}\sqrt{\frac{(S-1)}{(S+1)}} + \frac{Ah}{\pi S\sqrt{A^2-1}}\tan^{-1}\sqrt{\frac{(A+1)(S-1)}{(A-1)(S+1)}} \tag{18b}$$

where

$$A = \frac{h^2 + S^2 + 1}{2S}, \qquad B = \frac{1 + S^2}{2S}$$

$$S = \frac{2L}{D}, \qquad h = \frac{2H}{D}$$

and

L = distance between the center of the cylinder to the target

H = height of the cylinder

D = cylinder diameter

See Figure 3-11.13, parts (a) and (b) for an illustration of the nomenclature.

The maximum configuration or shape factor at a point is given by the vectorial sum of the horizontal and vertical view factors:

$$F_{12,\max} = \sqrt{F_{12,H}^2 + F_{12,V}^2} \tag{19}$$

Precalculated maximum view factors are shown in Figures 3-11.14(a) to 3-11.14(e). Each figure gives the maximum view factor for a flame of a particular flame height to pool radius ratio (H/R_p): 2, 3, 4, 5, and 6, respectively.

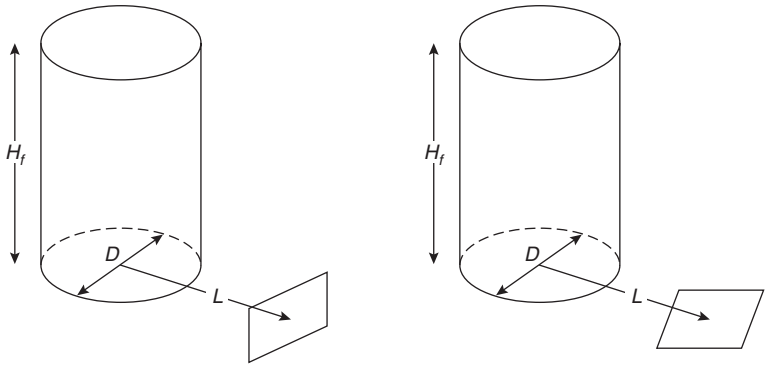

Figure 3-11.13(a). ***Cylindrical flame-shape configuration factor geometry for vertical and horizontal targets at ground level.***

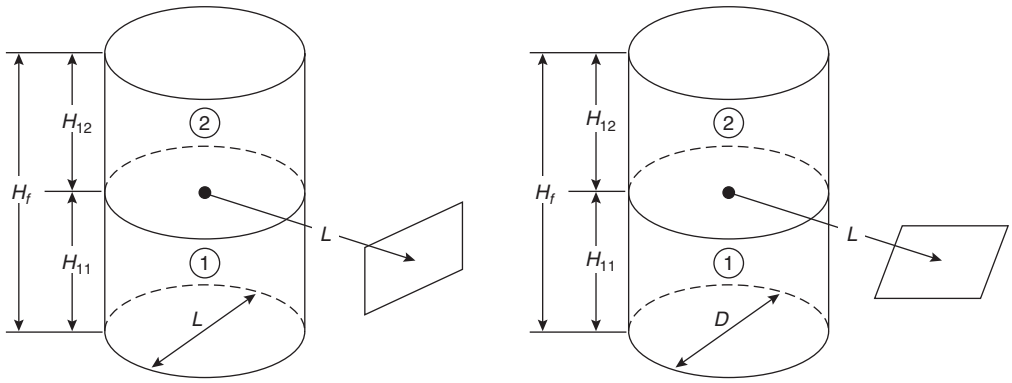

Figure 3-11.13(b). ***Two-cylinder representations of the configuration factor for target above ground level.***

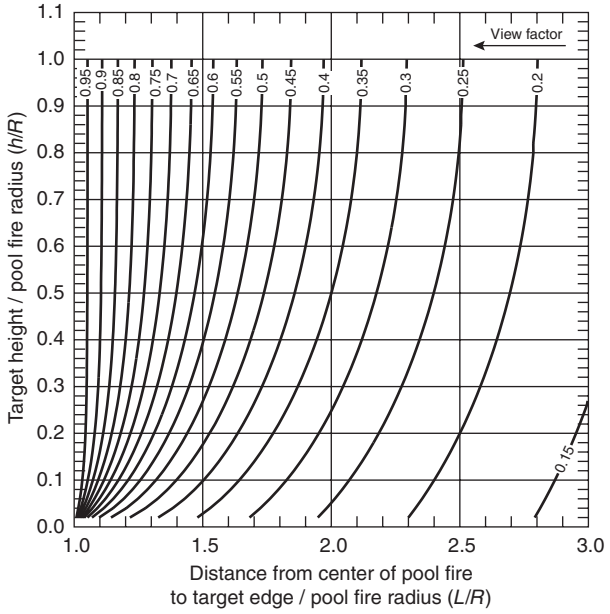

Figure 3-11.14(a). ***Maximum configuration factor for a flame height to pool fire radius ratio $H/R_p = 2$.***

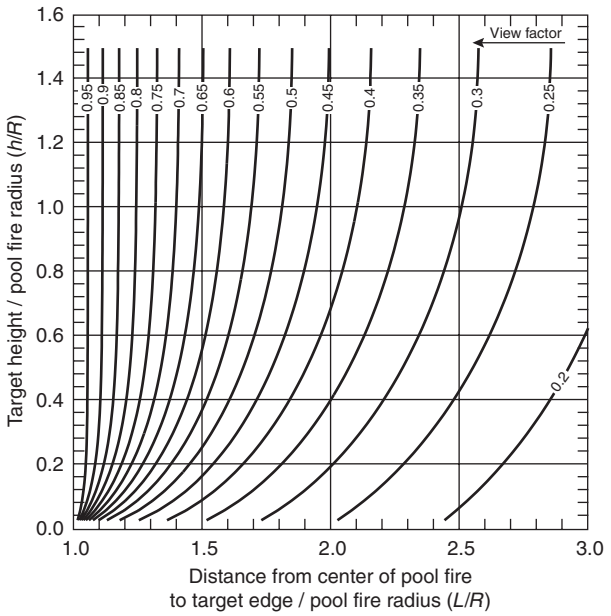

Figure 3-11.14(b). ***Maximum configuration factor for flame height to pool fire radius of ratio $H/R_p = 3$.***

The target location is defined in each figure by the ratio of the target height to the pool radius, and the ratio of the distance of the target from the pool center to the pool radius. The view factors are represented as contours. The figures only include target locations up to one-half the flame height. The curves for target heights above one-half the flame height are symmetric about the half-height and as such need not be included. For example, the view factor for a target at one-fourth of the flame height and three-fourths of the flame height are identical.

Shokri and Beyler[47] determined the effective emissive power of the flame by fitting experimental measurements of radiant heat flux from pool fires to external targets. The effective emissive power of the pool fire in terms of effective pool diameter is given by the following correlation:

$$E = 58(10^{-0.00823D}) \qquad (20)$$

This represents the average emissive power over the whole of the flame and is significantly less than the emissive powers that can be attained locally. The emissive power is reduced with increasing pool diameter due to the increasing prominence of black smoke outside the flame that obscures the radiation from the luminous flame. Figure 3-11.15 is a comparison of Equation 20 with the data used by Shokri and Beyler[47] to develop Equation 20.

Figure 3-11.16 shows a comparison of the predicted and measured heat fluxes, using the best fit emissive power for each experiment (the value plotted in Figure 3-11.15). Figure 3-11.16 shows that the cylindrical model is an excellent representation of the view factor over a wide range of conditions. Figures 3-11.15 and 3-11.16 together illustrate that the major uncertainty is in the definition of the emissive power and not in the view factor model. Figure 3-11.17 shows the overall performance of the model.

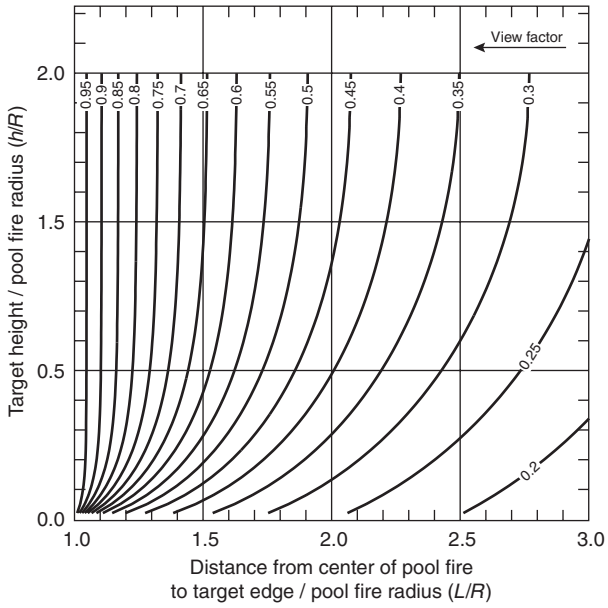

Figure 3-11.14(c). ***Maximum view factor for a flame height to pool fire radius ratio $H_f/R = 4$.***

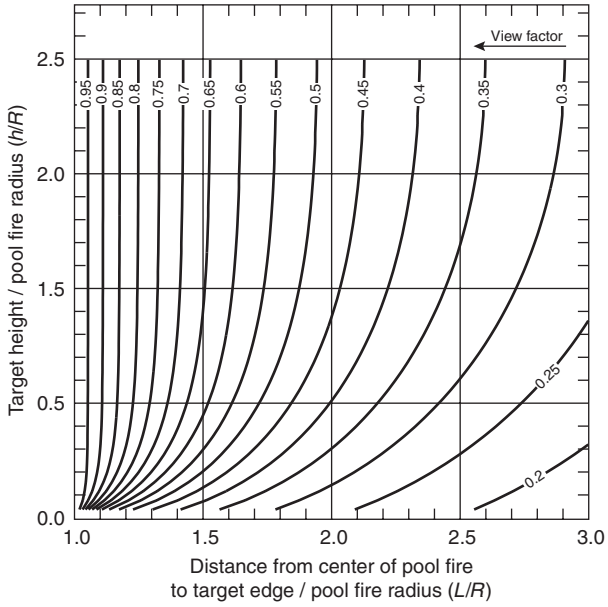

Figure 3-11.14(d). ***Maximum configuration factor for a flame height to pool fire radius ratio $H/R_p = 5$.***

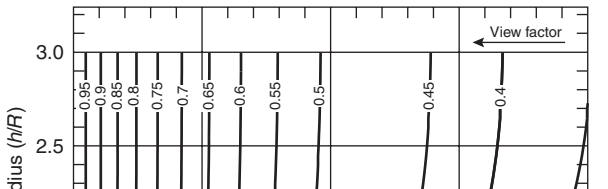

Figure 3-11.14(e). ***Maximum configuration factor for a flame height to pool fire radius ratio $H/R_p = 6$.***

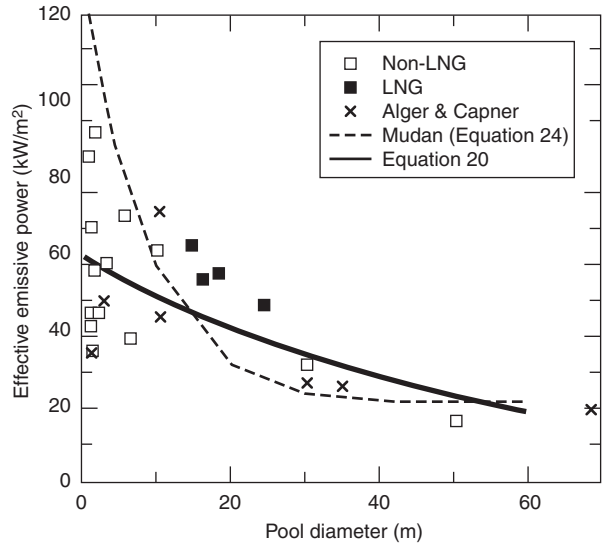

Figure 3-11.15. ***Effective emissive power as a function of the pool diameter determined by Shokri and Beyler.[47] The solid line is Equation 20 and the dashed line is Equation 24.***

Summary of the procedure for the Shokri and Beyler pool fire radiation method: Estimating the thermal radiation field surrounding a fire involves the following steps based on the method developed by Shokri and Beyler:[47]

1. Determine the heat release rate, $\dot{Q}$.
2. Determine the height of the pool fire flame from Equation 15.
3. Calculate the view factor from Equation 18 (and Equation 19 if needed). If the target is above ground level, then a two-cylinder representation is required. Alternatively, the precalculated view factors in Figure 3-11.14 may be used.
4. Determine the effective emissive power of the flame from Equation 20.
5. Calculate the radiative heat flux to the target using Equation 17.

Factor of safety: A safety factor of 2 is recommended for use with the Shokri and Beyler method.[46] Since this method is most applicable at heat fluxes greater than 5 kW/m^2, the recommended factor of safety is only applicable for heat fluxes above this level. Figure 3-11.18 is a

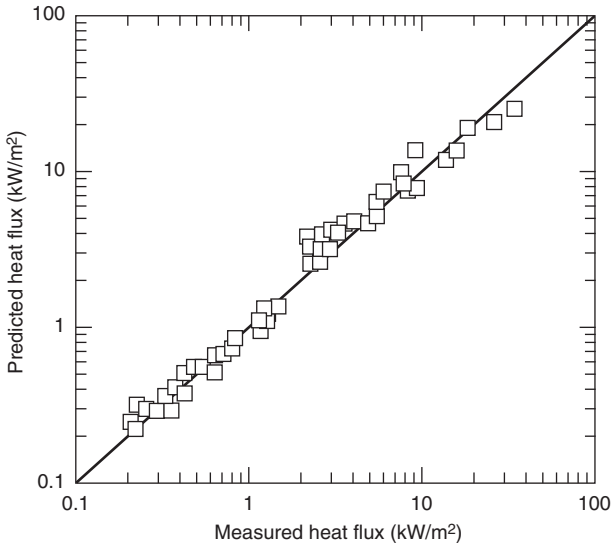

Figure 3-11.16. ***Comparison of measured and calculated incident radiant heat flux using effective emissive powers. The solid line indicates equality of the measured and predicted heat fluxes based on the method developed by Shokri and Beyler.[47]***

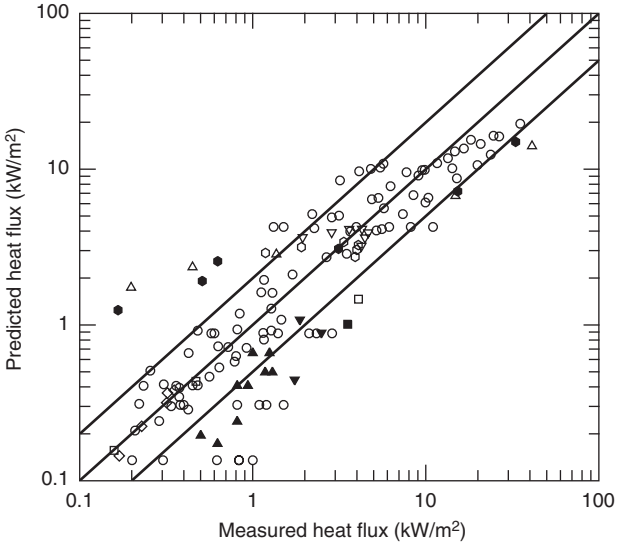

Figure 3-11.17. ***Comparison of measured and calculated radiative heat flux from large pool fires using the detailed method developed by Shokri and Beyler.[47] Solid lines indicate equality of measured and predicted heat fluxes based on the detailed method developed by Shokri and Beyler.[47]***

comparison of predicted and measured heat fluxes with the inclusion of the recommended factor of safety. The vertical line is located at the minimum heat flux for which the Shokri and Beyler model is recommended for use. Figure 3-11.18 clearly shows that essentially all of the data are overpredicted by the Shokri and Beyler model with a safety factor of 2 applied for heat fluxes greater than 5 kW/m². The safety factor of 2 is a recommendation for use in design applications. Where a realistic result is required, no safety factor should be applied.

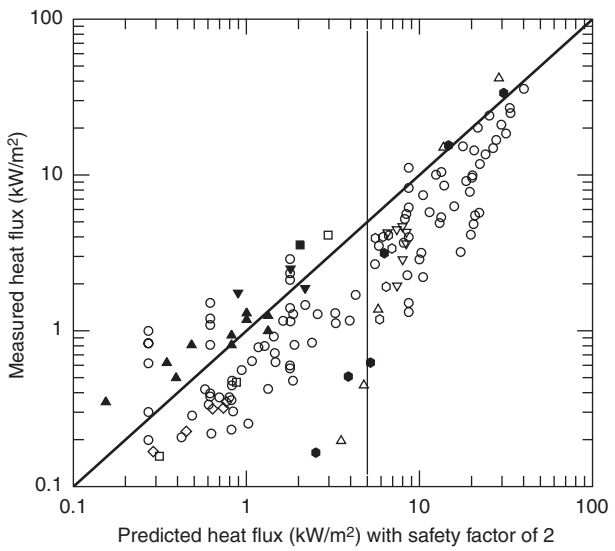

Figure 3-11.18. ***Comparison of measured and calculated radiative heat flux from large pool fires using the detailed method developed by Shokri and Beyler and a safety factor of 2. Solid lines indicate equality of measured and predicted heat fluxes based on the detailed method developed by Shokri and Beyler[47] with a safety factor of 2.***

Mudan method: Mudan[14] has presented a method for estimating thermal radiation from pool fires for no-wind conditions and for windblown flames. The thermal radiation intensity to an element outside the flame envelope is given by the following equation:

$$\dot{q}'' = EF_{12}\tau \tag{21}$$

where

E = average emissive power at flame surface, kW/m²
F_{12} = view factor
τ = atmospheric transmissivity

Equation 21 is used with the assumption that the flame is a vertical or tilted cylinder. This requires the flame diameter and height to be determined. The flame diameter is taken to be the pool diameter, D. See Figure 3-11.19 for general nomenclature.

The flame height correlation used in this method is based on the correlation of mean visible height, H_f, of turbulent diffusion flames (in absence of wind) developed by Thomas.[40] The correlation for a circular fire is given by Equation 1:

$$\frac{H}{D} = 42\left(\frac{\dot{m}''_\infty}{\rho_a\sqrt{gD}}\right)^{0.61} \tag{1}$$

where

D = pool diameter
$\dot{m}''_\infty$ = mass burning rate per unit pool area, kg/m²·s
ρ_a = ambient air density, kg/m³
g = gravitational acceleration, 9.8 m/s²

If the pool has a length-to-width ratio near one, an equivalent-area circular source can be used for noncircular

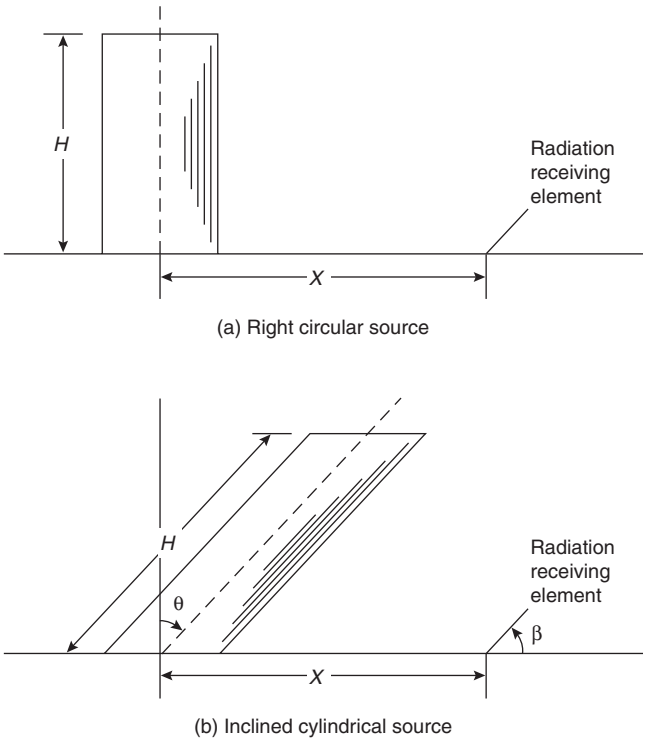

Figure 3-11.19. ***Configuration factor calculation geometries for right and inclined cylinders.***

pools in the determination of the flame height. For noncircular pools, the effective diameter will be defined as the diameter of a circular pool with an area equal to the actual pool area, given by Equation 13 as

$$D = \sqrt{\frac{4A}{\pi}} \tag{13}$$

In the presence of wind, the flame length is given by the following correlation developed by Thomas[40] (Equation 2):

$$\frac{H}{D} = 55\left(\frac{\dot{m}''_\infty}{\rho_a\sqrt{gD}}\right)^{0.67} (u^*)^{-0.21} \tag{2}$$

where u^* is the nondimensional wind velocity given by Equation 2:

$$u^* = \frac{u_w}{(g\dot{m}''_\infty D/\rho_v)^{1/3}} \tag{3}$$

where u_w is the wind speed, m/s, and ρ_v is the fuel vapor density, kg/m^3.

In the presence of a significant wind, the flame may not remain vertical, and a flame tilt angle due to the wind is relevant to the assessment of radiation. The American Gas Association (AGA)[39] proposed the following correlation to determine the flame tilt (Equation 7):

$$\cos\theta = \begin{cases} 1 & \text{for } u^* \le 1 \\ 1/\sqrt{u^*} & \text{for } u^* \ge 1 \end{cases} \tag{7}$$

where u^* is the nondimensional wind velocity given by Equation 20 with the wind velocity measured at a height of 1.6 m above the ground.

The turbulent flame is approximated by a cylinder. Under wind-free conditions, the cylinder is vertical (Figure 3-11.19(a)). Under the influence of wind, the cylinder is assumed to be tilted (Figure 3-11.19(b)). View factors for horizontal and vertical targets of a vertical cylinder for no-wind conditions are as follows:

$$F_{12,V} = \frac{1}{\pi S}\tan^{-1}\left(\frac{h}{\sqrt{S^2-1}}\right) - \frac{h}{\pi S}\tan^{-1}\sqrt{\frac{(S-1)}{(S+1)}} + \frac{Ah}{\pi S\sqrt{A^2-1}}\tan^{-1}\sqrt{\frac{(A+1)(S-1)}{(A-1)(S+1)}} \tag{22a}$$

$$F_{12,H} = \frac{(B-1/S)}{\pi\sqrt{B^2-1}}\tan^{-1}\sqrt{\frac{(B+1)(S-1)}{(B-1)(S+1)}} - \frac{(A-1/S)}{\pi\sqrt{A^2-1}}\tan^{-1}\sqrt{\frac{(A+1)(S-1)}{(A-1)(S+1)}} \tag{22b}$$

where

$$S = \frac{2L}{D} \qquad h = \frac{2H}{D}$$

$$A = \frac{h^2+S^2+1}{2S} \qquad B = \frac{1+S^2}{2S}$$

and

L = distance between the center of the pool fire and the target
H = height of the pool fire
D = pool fire diameter

If the target is either at ground level or at the flame height, then a single cylinder can represent the flame. If the target is above the ground, then two cylinders must be used to represent the flame. One cylinder represents the flame below the height of the target, and the other represents the flame above the height of the target. See Figure 3-11.13b for an illustration of the nomenclature. The overall view factor is the sum of the two component view factors.

The maximum configuration factor at a point is given by the vectorial sum of the horizontal and vertical target configuration factors given by Equation 19:

$$F_{12,\max} = \sqrt{F_{12,H}^2 + F_{12,V}^2} \tag{19}$$

The configuration exchange factor for windblown flame has been given by Mudan,[54] who employed a contour integral approach developed by Sparrow[55] to determine closed-form equations for view factors from a tilted cylinder.

The view factor for a tilted cylindrical flame with a circular base is as follows:

$$\pi F_V = \frac{a\cos\theta}{b - a\sin\theta}\,\frac{a^2+(b+1)^2-2b(1+\sin\theta)}{\sqrt{AB}}\tan^{-1}\sqrt{\frac{A}{B}}\left(\frac{b-1}{b+1}\right)^{1/2} + \frac{\cos\theta}{\sqrt{C}}\times\left[\tan^{-1}\frac{ab-(b^2-1)\sin\theta}{\sqrt{b^2-1}\sqrt{C}} + \tan^{-1}\frac{(b^2-1)\sin\theta}{\sqrt{b^2-1}\sqrt{C}}\right] - \frac{a\cos\theta}{(b-a\sin\theta)}\tan^{-1}\sqrt{\frac{b-1}{b+1}} \tag{23a}$$

$$\pi F_H = \tan^{-1}\sqrt{\frac{b+1}{b-1}} - \frac{a^2+(b+1)^2-2(b+1+ab\sin\theta)}{\sqrt{AB}} \times \tan^{-1}\sqrt{\frac{A}{B}\left(\frac{b-1}{b+1}\right)}^{1/2} + \frac{\sin\theta}{\sqrt{C}} \times \left[\tan^{-1}\frac{ab-(b^2-1)\sin\theta}{\sqrt{b^2-1}\sqrt{C}} + \tan^{-1}\frac{(b^2-1)^{1/2}\sin\theta}{\sqrt{C}}\right] \quad (23b)$$

where

$a = H/R$

$b = L/R$

$A = a^2 + (b+1)^2 - 2a(b+1)\sin\theta$

$B = a^2 + (b-1)^2 - 2a(b-1)\sin\theta$

$C = 1 + (b^2-1)\cos^2\theta$

When the angle of tilt is zero, Equations 23a and 23b reduce to Equations 22a and 22b, respectively. The maximum configuration factors at the target location are determined using Equation 19. Figures 3-11.20 and 3-11.21 show the calculated configuration factor for no-wind conditions and underwind conditions for a target at ground level. For the no-wind condition, Figure 3-11.14 can also be used to determine the view factor for a more general set of target locations.

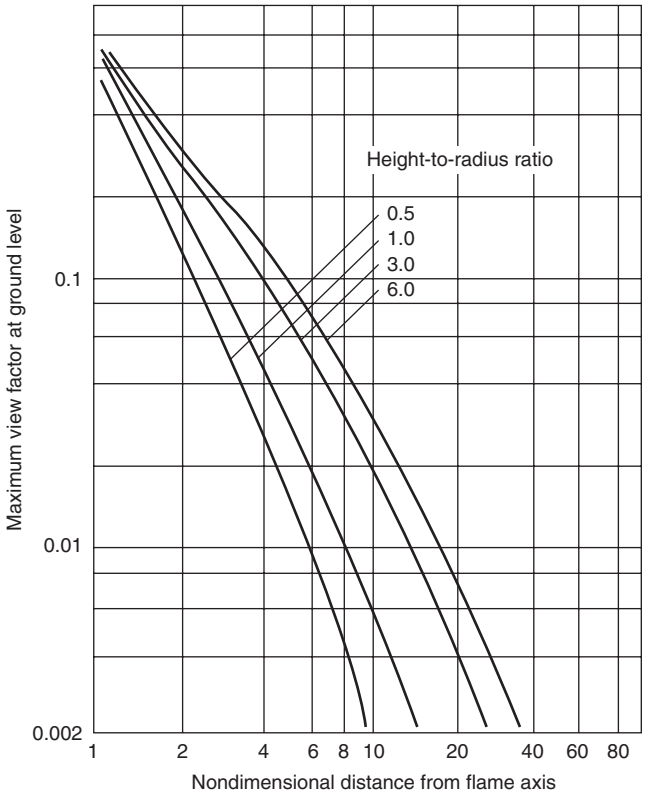

Figure 3-11.20. ***Maximum configuration factors for a ground-level object from a right circular cylinder. The nondimensional distance from the flame is L/R.***

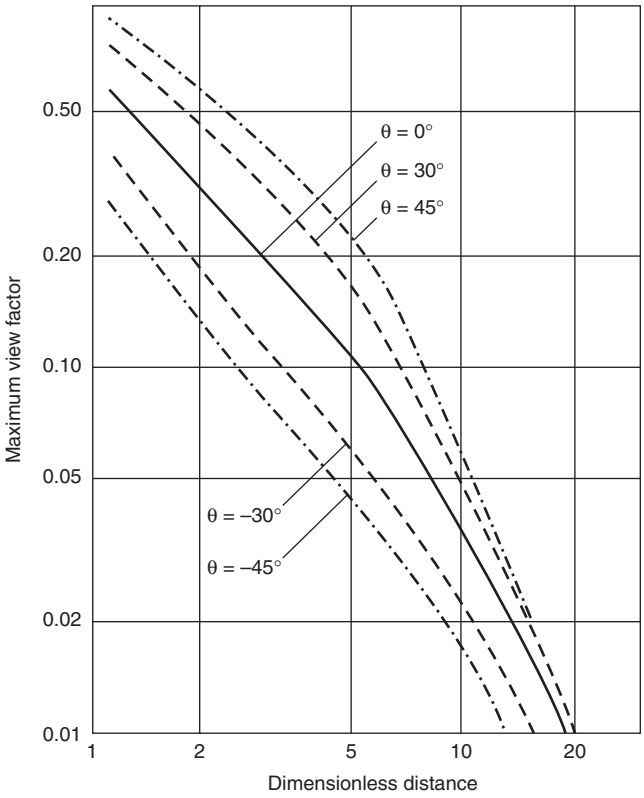

Figure 3-11.21. ***Maximum configuration factors for tilted circular cylinders with targets at ground level. The dimensionless distance is L/R.***

The emissive power, E, of the flame is given by the following correlation:

$$E = E_{\max}e^{-sD} + E_s[1 - e^{-sD}] \quad (24)$$

where

E = equivalent blackbody emissive power, 140 kW/m^2

s = extinction coefficient, 0.12 m^{-1}

D = equivalent pool diameter, m

E_s = emissive power of smoke, 20 kW/m^2

Atmospheric Absorption

The radiation from the fire to surrounding objects will be partially attenuated by absorption and scattering along the intervening path. The principal constituents of the atmosphere that absorb thermal radiation are water vapor (H_2O) and carbon dioxide (CO_2). Table 3-11.1 indicates the composition of various gases in the atmosphere. The CO_2 content in the atmosphere is generally constant at about 330 ppm by volume. The water vapor content varies strongly with temperature and humidity. Figure 3-11.22 indicates the relationship between atmospheric temperature, relative humidity, and the amount of precipitable water vapor in a given pathlength.

The principal absorption bands for water vapor are at 1.8, 2.7, and 6.27 μm. Minor absorption bands also exist at 0.94, 1.1, 1.38, and 3.2 μm. Strong absorption by CO_2 existing in the 2.7-μm region, the 4.3-μm region, and the

Table 3-11.1 ***Composition of Constituent Gases in the Atmosphere and Their Concentrations***

Constituent Gas	Concentration in Atmosphere (% by volume)
Nitrogen	78.088
Oxygen	20.949
Argon	0.93
Carbon dioxide	0.033
Neon	1.8×10^{-3}
Helium	5.24×10^{-4}
Methane	1.4×10^{-4}
Krypton	1.14×10^{-4}
Nitrous oxide	5.0×10^{-5}
Carbon monoxide	2.0×10^{-5}
Xenon	8.6×10^{-6}
Hydrogen	5.0×10^{-6}
Ozone	Variable
Water vapor	Variable (depends on temperature and relative humidity)

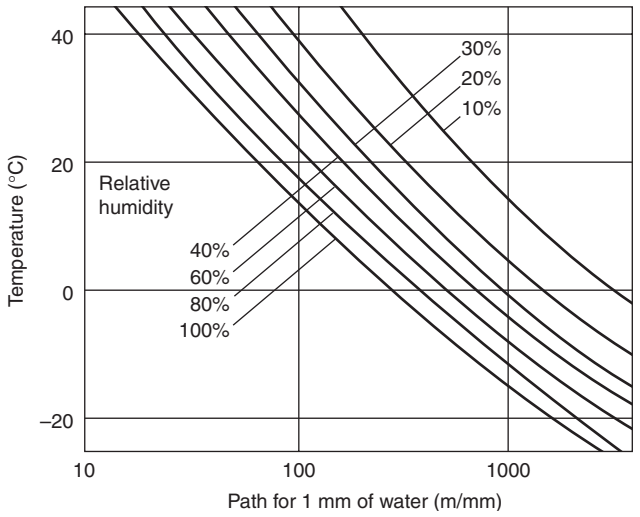

Figure 3-11.22. ***Variation of precipitable water content of the atmosphere with temperature, humidity, and pathlength.***

region between 11.4 and 20 μm. Weaker absorption bands are present at 1.4, 1.6, 2.0, 4.8, 5.2, 9.4, and 10.4 μm. As the temperature of the emitting or absorbing species increases, the bands tend to broaden.

A useful concept for the quick estimation of atmospheric absorption of continuum radiation is the "equivalent bandwidth of complete absorption." One calculates the integral of absorption over an absorption band and interprets the result as the width of a "rectangular," *complete* absorption band equivalent to the real band profile. For a continuum source, the effect of such opaque bands is then easy to estimate. Three absorption bands in the range of interest (1.5 through 5.5 μm) can be described in this way. These are the water vapor bands at 1.87 and 2.7 μm and the 4.3-μm, CO_2 band. The water absorption beyond about 4.7 μm is not as readily dealt with, since the band structure is not narrow compared to the range of interest. However, the fraction of total energy from a 1300-K blackbody that lies beyond 4.7 μm is about 25 percent and that beyond 5.5 μm is only 19 percent. The results of total absorption bandwidth calculations for the above three bands of interest are given in Tables 3-11.2 and 3-11.3. These calculations are based on the data available in the *Infrared Handbook*.[56] Also given in the tables are the fractions of a 1300-K blackbody energy that will be absorbed in each of these bands.

The absorption by the water vapor and carbon dioxide in a certain length of the atmosphere of blackbody radiation from a source can also be calculated using the emissivity charts published by Hottel and Sarofim.[57] The procedure to calculate the absorption in the water vapor band is as follows:

1. Determine the partial pressure of water vapor, in atmospheres, based on

$$p'_w = \frac{RH}{100} \exp\left(14.4114 - \frac{5328}{T_a}\right) \tag{25}$$

   where RH is the relative humidity and T_a is the ambient temperature in Kelvin.
2. Define a pathlength, L (in m), from the flame surface to observer. Determine the partial pressure-pathlength parameter:

$$p_w L = p'_w L(T_s/T_a) \tag{26}$$

   where
   T_s = source surface temperature (K)
   T_a = ambient temperature (K)
3. For the source temperature, and $p_w L$, determine the water vapor emissivity, ε_w, using emissivity plots given in Figure 3-11.23.

Table 3-11.2 ***Total Absorption Bandwidth for 1.87-μm and 2.7-μm Bands at 300 K***

	1.87-μm Band		2.7-μm Band	
Precipitable Water (mm)	Total Absorption Bandwidth, $\Delta\lambda$ (μm)	Fraction of 1300-K Blackbody Energy Absorbed	Total Absorption Bandwidth, $\Delta\lambda$ (μm)	Fraction of 1300-K Blackbody Energy Absorbed
5	0.16	0.04	0.58	0.16
2	0.12	0.03	0.51	0.14
1	0.1	0.03	0.45	0.12
0.1	0.033	0.01	0.22	0.06
0.01	0.01	0.003	0.07	0.02

Table 3-11.3 ***Total Absorption Bandwidth for 4.3-μm CO_2 Band at 300 K***

Pathlength through the Atmosphere (m)	Total Absorption Bandwidth $\Delta\lambda$ (μm)	Fraction of 1300-K Blackbody Energy Absorbed
1000	0.28	0.04
100	0.22	0.03
10	0.17	0.02
1	0.065	0.01
0.3	0.033	0.004

4. Calculate the water vapor absorption coefficient.

$$\alpha_w = \varepsilon_w (T_a/T_s)^{0.45} \tag{27}$$

The procedure to determine the absorption by carbon dioxide is very similar. The partial pressure of CO_2 remains relatively constant at about 3×10^{-4} atm. The absorption coefficient is given by

$$\alpha_c = \varepsilon_c (T_a/T_s)^{0.65} \tag{28}$$

The emissivity of the carbon dioxide band is shown in Figure 3-11.24. There is also a correction factor due to spectral overlap for the calculation of emissivity of a CO_2–H_2O mixture. This effect, however, accounts for a change in emissivity of about 5 percent at 1200 K and even less at higher temperatures.[57]

The transmissivity is given by

$$\tau = 1 - \alpha_w - \alpha_c \tag{29}$$

and is used in determining the thermal radiation hazard. The procedure outlined in this section may be simplified further if it is assumed that the flame temperature and the ambient temperature remain constant. For most hydrogen fuels, the flame temperature is approximately

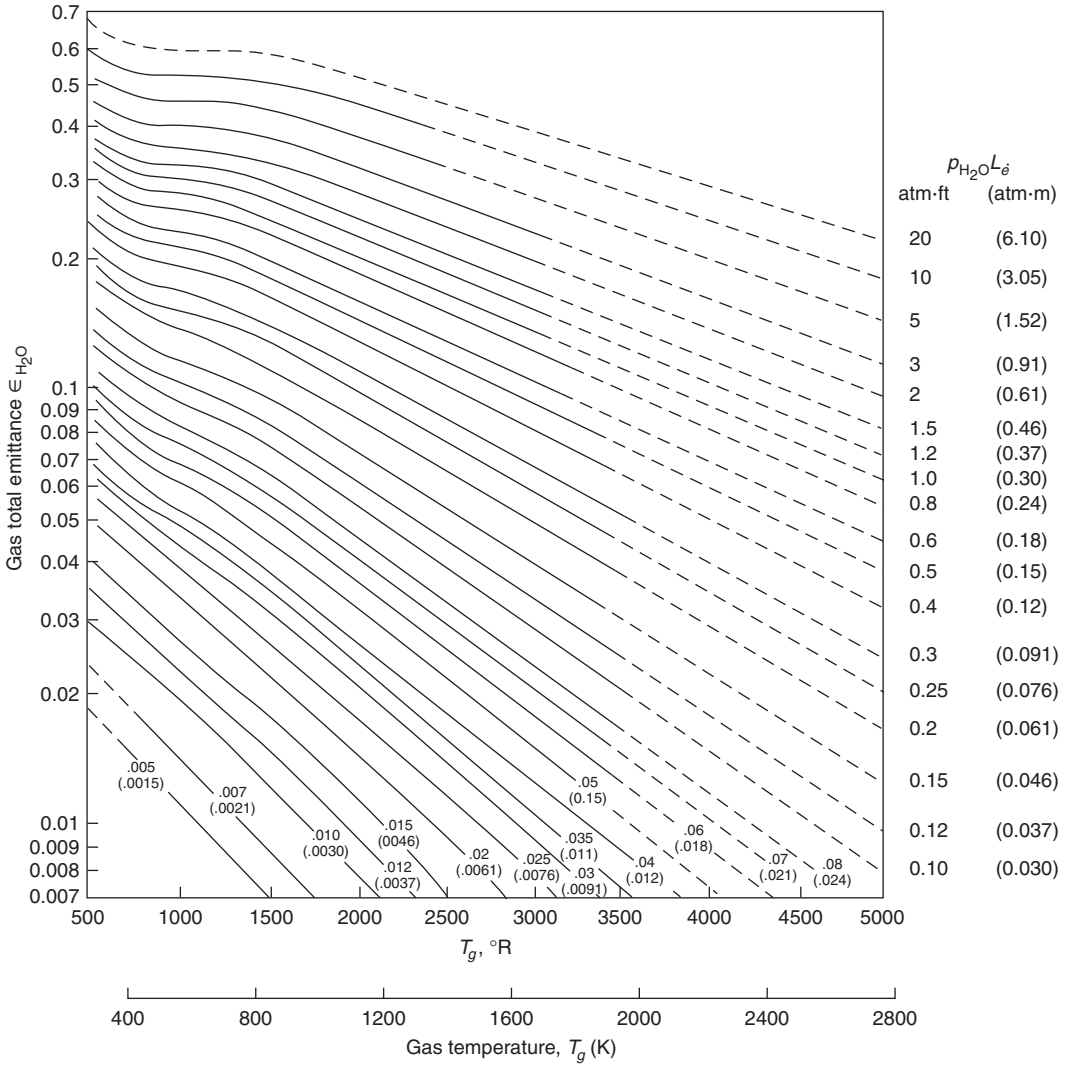

Figure 3-11.23. ***Total emissivity of water-vapor in a mixture of total pressure of 1 atm.[57]***

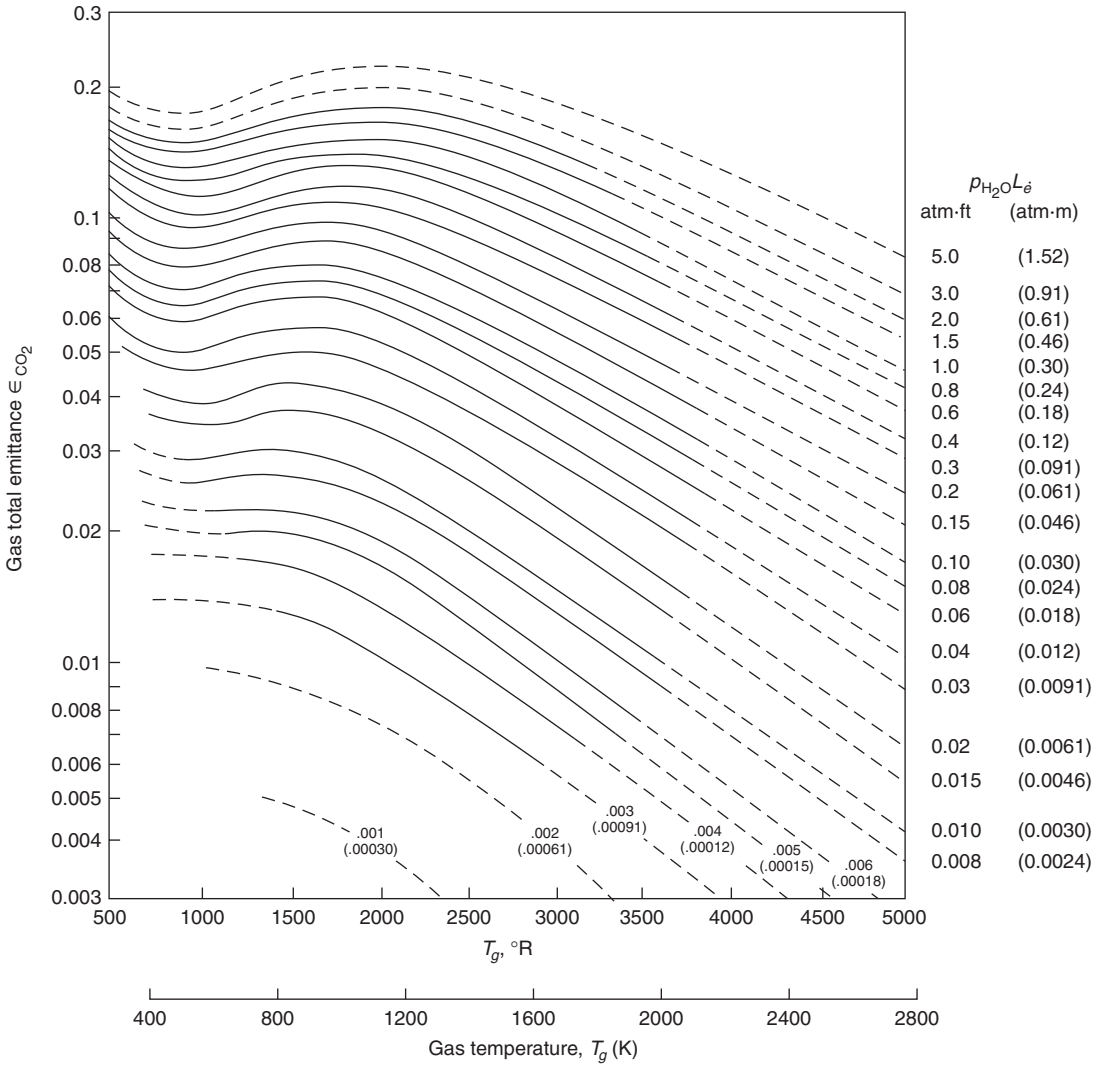

Figure 3-11.24. ***Total emissivity of carbon dioxide in a mixture of total pressure of 1 atm[57] where p_{CO_2} is the partial pressure of carbon dioxide and L_e is the equivalent pathlength.***

1400 K. If it is assumed that the typical ambient temperature is 293 K (20°C), the transmissivity may be plotted as a function of pathlength. In Figure 3-11.25 the transmissivity is shown as a function of pathlength for various relative humidities. Figure 3-11.25 provides a quick estimate of atmospheric absorption of thermal radiation.

Summary of the procedure for the Mudan pool fire radiation method: Estimating the thermal radiation field surrounding a fire involves the following steps based on the method developed by Mudan:[14]

1. Determine the height of the pool fire flame and tilt angle from Equations 1, 2, 3, and 7.
2. Calculate the configuration factor from Equations 19, 22, and 20. Figures 3-11.14, 3-11.20, or 3-11.21 may be used where appropriate.
3. Determine the effective emissive power of the flame from Equation 24.
4. Calculate the radiative heat flux to target using Equation 21.

Figure 3-11.26 shows a comparison of data with the predictions of this method.[46] The predictions tend to be conservative, and the differences between measured and predicted values are relatively uniform over the full range of heat fluxes. No validation data are available for wind-tilted conditions.

A safety factor of 2 is recommended for use with the Mudan method.[46] Figure 3-11.27 is a comparison of predicted and measured heat fluxes with the inclusion of the recommended factor of safety. Figure 3-11.22 clearly shows that essentially all the data are overpredicted by the Mudan model with a safety factor of 2. The safety factor of 2 is a recommendation for use in design applications. Where a realistic result is required, no safety factor should be applied.

Summary and General Recommendations

Table 3-11.4 summarizes the methods included in this section and their ranges of applicability. All the methods

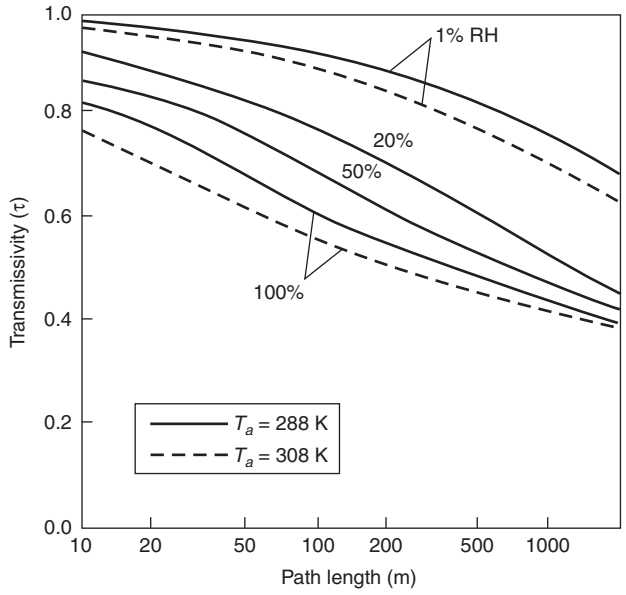

Figure 3-11.25. ***Transmissivity as a function of path-lengths; source temperature 1400 K.***

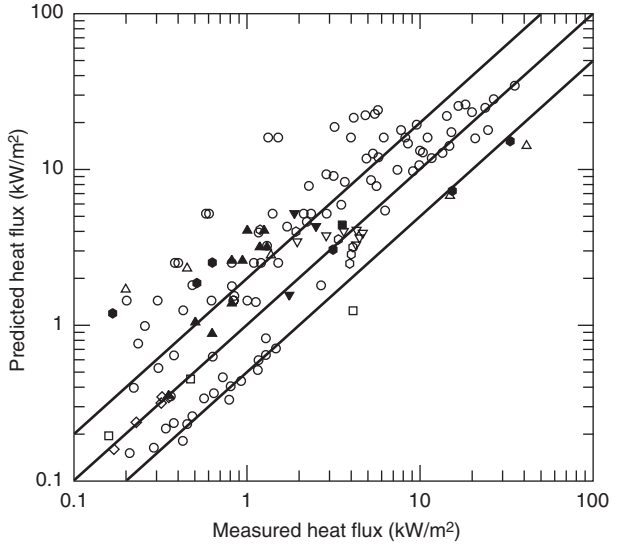

Figure 3-11.26. ***Comparison of measured and calculated radiative heat flux from large pool fires using the detailed method developed by Mudan.[14] Solid lines indicate equality of measured and predicted heat fluxes based on the detailed method developed by Mudan.[14]***

used with the indicated safety factors provide conservative results. However, the variations in the predicted versus measured heat fluxes (i.e., the goodness of fit) vary considerably between methods. Methods that minimize these variations are inherently more reliable in that the method better explains the experimental data. The methods that minimize the variation are the point source model and the Shokri and Beyler method, when used in their applicable ranges. Table 3-11.5 shows the correlation coefficient of each method over the indicated ranges of application. The methods with the greatest correlation coefficient better explain the variations observed in the database. While at less than 5 kW/m² there is little difference between the performance of the point source model and the Mudan[14] model, the simplicity of the point source model argues for its use.

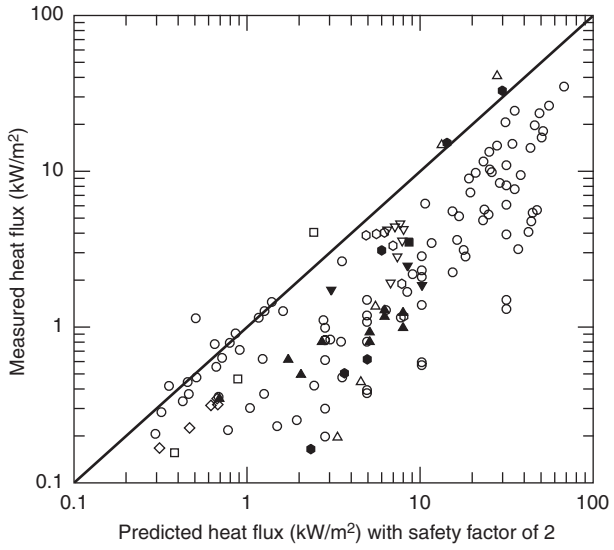

Figure 3-11.27. ***Comparison of measured and calculated radiative heat flux from large pool fires using the detailed method developed by Mudan with a safety factor of 2. Solid lines indicate equality of measured and predicted heat fluxes based on the detailed method developed by Mudan with a safety factor of 2.[14]***

Table 3-11.4 ***Summary of the Methods***

Method	Range of Use (kW/m²)	Recommended Safety Factor	Preferred Methods
Shokri and Beyler correlation	All heat fluxes, ground level only	2	—
Point source model	0–5 kW/m²	2	< 5 kW/m²
Shokri and Beyler model	> 5 kW/m²	2	> 5 kW/m²
Mudan model	All heat fluxes	2	—

Table 3-11.5 ***Correlation Coefficients for the Methods***

Heat-Flux Calculation Method	Correlation Coefficient	Correlation Coefficient with Safety Factor
Point source model (below 5 kW/m²)	0.51	0.38
Mudan model (below 5 kW/m²)	0.53	0.34
Shokri and Beyler model (above 5 kW/m²)	0.52	0.66
Mudan model (above 5 kW/m²)	0.35	0.57

The point source model and the Shokri and Beyler model are the preferred models based on both the conservative nature of these methods and the minimization of the variations between the data and the experiments.

Because heat fluxes below 5 kW/m² cannot lead to ignition of combustibles, any analysis involving a combustible target should be performed using the Shokri and Beyler model. Since pain and second-degree burns can occur at 5 kW/m², many analyses involving human exposure can be performed using the simple point source model. If exposure is less than 1 min, it may be necessary to use the more complex Shokri and Beyler model for human exposure.

Illustration of the calculation procedure: In this section two sample calculations are presented to illustrate the calculation procedure for the thermal radiation from pool fires.

EXAMPLE 1:

Toluene from a tank is assumed to spill to form a pool in a diked area of 12-m diameter. The distance from the center of the pool fire to the target edge is assumed to be 30 m.

Calculate flame radiative heat flux to the target at ground level with no wind (Figure 3-11.28) using:

(a) Shokri and Beyler correlation
(b) Point source model
(c) Shokri and Beyler detailed method using shape factor algebra
(d) Mudan detailed method using shape factor algebra

CALCULATION PROCEDURE:

Properties of toluene (Babrauskas, Section 3, Chapter 1)

Heat of combustion, $\Delta H_c = 40550$ kJ/kg

Mass burning rate, $\dot{m}''_\infty = 0.1126$ kg/m²·s

Properties of air at 20°C, $\rho_a = 1.2$ kg/m³

(a) Heat flux from the Shokri and Beyler correlation, Equation 12:

$$\dot{q}'' = 15.4\left(\frac{L}{D}\right)^{-1.59}$$

where $L = 30$ m and $D = 12$ m. Therefore, heat flux to the target is

$$\dot{q}'' = 15.4\left(\frac{30}{12}\right)^{-1.59} = 3.6 \text{ kW/m}^2$$

(b) Heat flux from point source model, Equation 14:

$$\dot{q}'' = \frac{\dot{Q}_r \cos\theta}{4\pi R^2}$$

The radiative energy output, $\dot{Q}_r$, is given by the radiative fraction, χ_r, multiplied by the total heat-release rate, $\dot{Q}$, from Equation 16:

$$\dot{Q}_r = \chi_r \dot{Q}$$

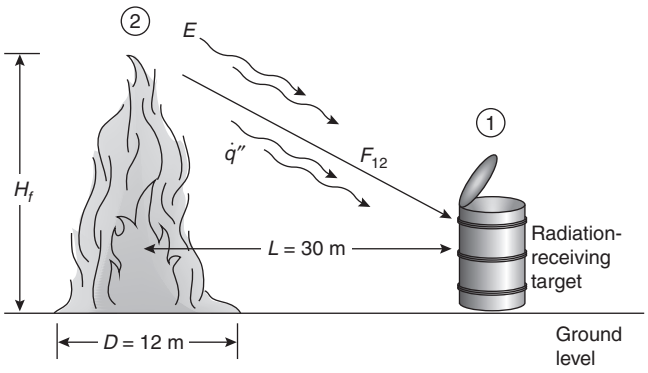

Figure 3-11.28. ***Toluene pool fire with target at ground level.***

Figure 3-11.12 can be used to determine χ_r from curve fit to the experimental data as

$$\chi_r = 0.21 - 0.0034D$$

and $\dot{Q}$, total heat release rate, is given by

$$\dot{Q} = \dot{m}''_\infty \Delta H_c A$$

and A, area of the pool, can be expressed from Equation 13:

$$A = \frac{\pi}{4} D^2$$

Combining the above equations yields

$$\dot{Q}_r = (0.21 - 0.0034D)\left(\dot{m}''_\infty \Delta H_c \frac{\pi}{4} D^2\right) = 87{,}371 \text{ kW}$$

The distance, R, from the point source location to the target location is given by the Pythagorean theorem, Equation 15:

$$R = \sqrt{L^2 + H_T^2}$$

where $L = 30$ m and H_T is given by

$$H_T = \frac{H}{2}$$

H is the height of the flame from Equation 5:

$$H = 0.23\dot{Q}^{2/5} - 1.02D = 32.11 \text{ m}$$

$$H_T = \frac{0.23(\dot{m}''_\infty \Delta H_c (\pi/4) D^2)^{2/5} - 1.02D}{2} = 16 \text{ m}$$

$$R = \sqrt{30^2 + 16^2} = 34 \text{ m}$$

The angle, θ, between the normal to the target and the line of sight from the point source location can be estimated as

$$\theta = \tan^{-1}\left(\frac{1}{2}\frac{H}{L}\right) = 0.49 \text{ rad}$$

The heat flux from the point source model is

$$\dot{q}'' = \frac{\dot{Q}_r \cos\theta}{4\pi R^2} = \frac{87371 \times \cos(0.49)}{4 \times \pi \times 34^2} = 5.3 \text{ kW/m}^2$$

(c) Heat flux from the Shokri and Beyler detailed method using shape factor algebra with target at ground level and no wind, Equation 17:

$$\dot{q}'' = EF_{12}$$

The emissive power of the flame, E, is given by Equation 20:

$$E = 58(10^{-0.00823D})$$

$$E = 58(10^{-0.00823\times 12}) = 46.2 \text{ kW/m}^2$$

Equation 18a can be used to determine the shape factor in the horizontal direction:

$$F_{12,H} = \frac{[B - (1/S)]}{\pi\sqrt{B^2 - 1}} \tan^{-1}\sqrt{\frac{(B+1)(S-1)}{(B-1)(S+1)}} - \frac{[A - (1/S)]}{\pi\sqrt{A^2 - 1}} \tan^{-1}\sqrt{\frac{(A+1)(S-1)}{(A-1)(S+1)}}$$

Equation 18b can be used to determine the shape factor in vertical direction:

$$F_{12,V} = \frac{1}{\pi S}\tan^{-1}\left(\frac{h}{\sqrt{S^2-1}}\right) - \frac{h}{\pi S}\tan^{-1}\sqrt{\frac{(S-1)}{(S+1)}} + \frac{Ah}{\pi S\sqrt{A^2-1}}\tan^{-1}\sqrt{\frac{(A+1)(S-1)}{(A-1)(S+1)}}$$

where

$$S = \frac{2L}{D} = \frac{2 \times 30}{12} = 5$$

$$H_f = 0.23\dot{Q}^{2/5} - 1.02D = 32.11 \text{ m}$$

$$h = \frac{2H_f}{D} = \frac{2 \times 32.11}{12} = 5.35$$

$$A = \frac{h^2 + S^2 + 1}{2S} = \frac{5.35^2 + 5^2 + 1}{2 \times 5} = 5.46$$

$$B = \frac{(1 + S^2)}{2S} = 2.6$$

Substituting values of A, B, S, and h in the shape factor equation to determine $F_{12,H}$ and $F_{12,V}$, the $F_{12,H}$ is equal to 0.039, and $F_{12,V}$ is equal to 0.088.

The maximum shape factor at a point is given by the vectorial sum of the horizontal and vertical shape factors:

$$F_{12,\max} = \sqrt{F_{12,H}^2 + F_{12,V}^2}$$

Therefore, the maximum shape factor at a point is equal to 0.097. Therefore, heat flux to the target is

$$\dot{q}'' = EF_{12,\max} = 48 \times 0.097 = 4.5 \text{ kW/m}^2$$

(d) Heat flux from the Mudan detailed method using shape factor algebra with target at ground level and no wind, Equation 21:

$$\dot{q}'' = EF_{12}\tau$$

The emissive power of the flame, E is given by Equation 24:

$$E = E_{\max}e^{-sD} + E_s(1 - e^{-sD})$$

$$E = 140e^{-0.12\times 12} + 20(1 - e^{-0.21\times 12}) = 48.43 \text{ kW/m}^2$$

Equation 22a can be used to determine the shape factor in the horizontal direction:

$$F_{12,H} = \frac{[B - (1/S)]}{\pi\sqrt{B^2 - 1}} \tan^{-1}\sqrt{\frac{(B+1)(S-1)}{(B-1)(S+1)}} - \frac{[A - (1/S)]}{\pi\sqrt{A^2 - 1}} \tan^{-1}\sqrt{\frac{(A+1)(S-1)}{(A-1)(S+1)}}$$

and Equation 22b can be used to determine the shape factor in vertical direction:

$$F_{12,V} = \frac{1}{\pi S}\tan^{-1}\left(\frac{h}{\sqrt{S^2-1}}\right) - \frac{h}{\pi S}\tan^{-1}\sqrt{\frac{(S-1)}{(S+1)}} + \frac{Ah}{\pi S\sqrt{A^2-1}}\tan^{-1}\sqrt{\frac{(A+1)(S-1)}{(A-1)(S+1)}}$$

$$H_f = 42D\left(\frac{\dot{m}''_\infty}{\rho_a\sqrt{gD}}\right)^{0.61} = 27.79 \text{ m}$$

$$h = \frac{2H_f}{D} = \frac{2 \times 27.79}{12} = 4.63$$

$$S = \frac{2L}{D} = \frac{2 \times 30}{12} = 5$$

$$A = \frac{h^2 + S^2 + 1}{2S} = \frac{4.63^2 + 5^2 + 1}{2 \times 5} = 4.74$$

$$B = \frac{(1 + S^2)}{2S} = 2.6$$

Substituting values of A, B, S, and h in the shape factor equation to determine $F_{12,H}$ and $F_{12,V}$, $F_{12,H}$ is equal to 0.035, and $F_{12,V}$ is equal to 0.084.

The maximum shape factor at a point is given by the vectorial sum of the horizontal and vertical shape factors:

$$F_{12,\max} = \sqrt{F_{12,H}^2 + F_{12,V}^2}$$

Therefore, the maximum shape factor at a point is equal to 0.091.

Therefore, heat flux to the target is

$$\dot{q}'' = EF_{12,V}\tau = 48.43 \times 0.091 \times 1 = 4.45 \text{ kW/m}^2$$

Table 3-11.6 summarizes the results for each of the methods.

EXAMPLE 2:

Calculate flame radiative heat flux from a 10-m-diameter toluene pool fire to a vertical target 2 m above the ground at 12 m from the center of the pool (Figure 3-11.29) with no wind, using:

(a) Shokri and Beyler method using shape factor algebra
(b) Mudan method using shape factor algebra

CALCULATION PROCEDURE:

(a) Heat flux from the Shokri and Beyler detailed method using shape factor algebra with target height 2 m above ground level and no wind

Table 3-11.6 ***Summary of the Heat Flux from 12-m-Diameter Toluene Pool Fire to 30-m Target at Ground Level with No Wind***

Heat Flux Calculation Method	Heat Flux (kW/m^2)
(a) Shokri and Beyler correlation	3.6
(b) Point source model	5.3
(c) Shokri and Beyler method using shape factor algebra	4.5
(d) Mudan method using shape factor algebra	4.45

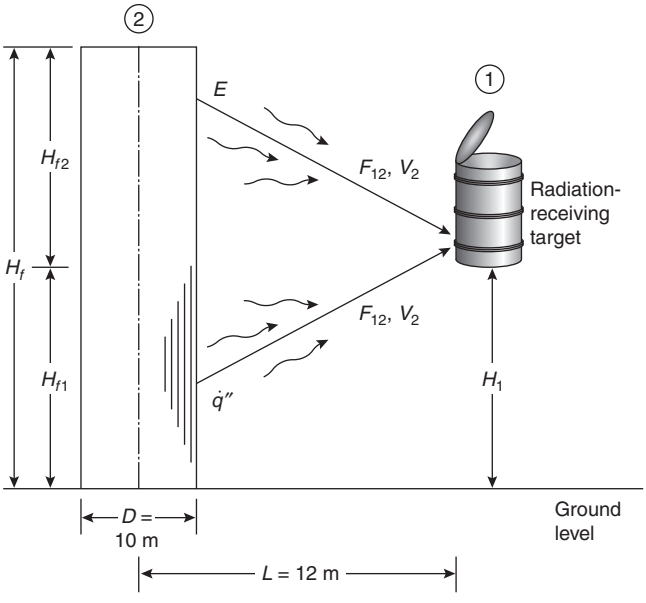

Figure 3-11.29. ***Toluene pool fire with target above ground level.***

Properties of toluene (Babrauskas, Section 3, Chapter 1)

Heat of combustion, $\Delta H_c = 40550$ kJ/kg
Mass burning rate, $\dot{m}''_\infty = 0.1126$ kg/m^2·s
Properties of air at 20°C $\rho_a = 1.2$ kg/m^3

Heat flux is given by Equation 17:

$$\dot{q}'' = EF_{12}$$

The emissive power of the flame, E, is given by Equation 20:

$$E = 58(10^{-0.00823D})$$

$$E = 58(10^{-0.00823\times 10}) = 48 \text{ kW/m}^2$$

The flame height, H, is given by Equation 17:

$$H = 0.23\dot{Q}^{2/5} - 1.02D$$

where

$\dot{Q} = \dot{m}''_\infty \Delta H_c A$ kW
$\dot{Q} = 360{,}000$ kW
$H = 28$ m

Since the target is above the ground, but it is not at the flame height, two cylinders must be used to represent the flame. Since the target is strictly vertical, it is not necessary to calculate the horizontal shape factor.

The shape factor for the target located above ground level can be calculated from Figures 3-11.14(a) to 3-11.14(e) or by the following method. For the vertical target, Equation 18b can be used to determine the shape factor at location H_{f1}:

$$F_{12,V1} = \frac{1}{\pi S}\tan^{-1}\left(\frac{h_1}{\sqrt{S^2-1}}\right) - \frac{h_1}{\pi S}\tan^{-1}\sqrt{\frac{(S-1)}{(S+1)}} + \frac{A_1 h_1}{\pi S\sqrt{A_1^2-1}}\tan^{-1}\sqrt{\frac{(A_1+1)(S-1)}{(A_1-1)(S+1)}}$$

$$S = \frac{2L}{D} = \frac{2\times 12}{10} = 2.4$$

$$H_{f1} = \frac{2H_{f1}}{D} = \frac{2\times 2}{10} = 0.4$$

$$A_1 = \frac{H_{f1}^2 + S^2 + 1}{2S} = \frac{0.4^2 + 2.4^2 + 1}{2\times 2.4} = 1.44$$

Substituting values of A_1, S, and H_{f1} in the shape factor equation to determine $F_{12,V1}$, the $F_{12,V1}$ is equal to 0.066. Shape factor at location H_{f2} is given by

$$F_{12,V2} = \frac{1}{\pi S}\tan^{-1}\left(\frac{H_{f2}}{\sqrt{S^2-1}}\right) - \frac{H_{f2}}{\pi S}\tan^{-1}\sqrt{\frac{(S-1)}{(S+1)}} + \frac{A_2 H_{f2}}{\pi S\sqrt{A_2^2-1}}\tan^{-1}\sqrt{\frac{(A_2+1)(S-1)}{(A_2-1)(S+1)}}$$

$$S = \frac{2L}{D} = \frac{2 \times 12}{10} = 2.4$$

$$H_{f2} = \frac{2H_{f2}}{D} = \frac{2(H_f - H_{f1})}{D} = \frac{2(28-2)}{10} = 5.2$$

$$A_2 = \frac{H_{f2}^2 + S^2 + 1}{2S} = \frac{5.2^2 + 2.4^2 + 1}{2 \times 2.4} = 7.04$$

Substituting values of A_2, S, and H_{f2} in the shape factor equation to determine $F_{12,V2}$, $F_{12,V2}$ is equal to 0.206. Therefore, total shape factor is given by

$$F_{12,V} = F_{12,V1} + F_{12,V2} = 0.066 + 0.206 = 0.27$$

Therefore, heat flux to the target at 2 m above ground is

$$\dot{q}'' = EF_{12,V} = 48 \times 0.27 = 13.0 \text{ kW/m}^2$$

(b) Heat flux from Mudan[14] method using shape factor algebra with target height 2 m above ground level and no wind

Heat flux is given by Equation 21:

$$\dot{q}'' = EF_{12}\tau$$

The emissive power of the flame, E, is given by Equation 21:

$$E = E_{\max} e^{-sD} + E_s(1 - e^{-sD})$$

$$E = 140e^{-0.12\times10} + 20(1 - e^{-0.21\times10}) = 56.14 \text{ kW/m}^2$$

The flame height, H, is given by Equation 1:

$$H_f = 42D\left(\frac{\dot{m}''_\infty}{\rho_a\sqrt{gD}}\right)^{0.61} = 25.4 \text{ m}$$

Since the target is above the ground, but it is not at the flame height, two cylinders must be used to represent the flame. Since the target is strictly vertical, it is not necessary to calculate the horizontal shape factor.

The shape factor for the target located above ground level can be calculated from the Figures 3-11.16(a) to 3-11.16(e) or by the following method. For the vertical target, Equation 22b can be used to determine the shape factor at location H_1:

$$F_{12,V1} = \frac{1}{\pi S}\tan^{-1}\left(\frac{H_1}{\sqrt{S^2-1}}\right) - \frac{H_1}{\pi S}\tan^{-1}\sqrt{\frac{(S-1)}{(S+1)}} + \frac{A_1H_1}{\pi S\sqrt{A_1^2-1}}\tan^{-1}\sqrt{\frac{(A_1+1)(S-1)}{(A_1-1)(S+1)}}$$

$$S = \frac{2L}{D} = \frac{2 \times 12}{10} = 2.4$$

$$H_1 = \frac{2H_{f1}}{D} = \frac{2 \times 2}{10} = 0.4$$

$$A_1 = \frac{H_1^2 + S^2 + 1}{2S} = \frac{0.4^2 + 2.4^2 + 1}{2 \times 2.4} = 1.44$$

Substituting values of A_1, S, and h_1 in the shape factor equation to determine $F_{12,V1}$, $F_{12,V1}$ is equal to 0.066.

Shape factor at location H_2 is given by

$$F_{12,v2} = \frac{1}{\pi S}\tan^{-1}\left(\frac{H_2}{\sqrt{S^2-1}}\right) - \frac{H_2}{\pi S}\tan^{-1}\sqrt{\frac{(S-1)}{(S+1)}} + \frac{A_2H_2}{\pi S\sqrt{A_2^2-1}}\tan^{-1}\sqrt{\frac{(A_2+1)(S-1)}{(A_2-1)(S+1)}}$$

$$S = \frac{2L}{D} = \frac{2 \times 12}{10} = 2.4$$

$$h_2 = \frac{2H_{f2}}{D} = \frac{2(H_f - H_{f1})}{D} = \frac{2(24.5-2)}{10} = 4.5$$

$$A_2 = \frac{H_2^2 + S^2 + 1}{2S} = \frac{4.5^2 + 2.4^2 + 1}{2 \times 2.4} = 5.62$$

Substituting values of A_2, S, and h_2 in the shape factor equation to determine $F_{12,V2}$, $F_{12,V2}$ is equal to 0.206. Therefore, total shape factor is given by

$$F_{12,V} = F_{12,V1} + F_{12,V2} = 0.066 + 0.188 = 0.27$$

Therefore, heat flux to the target at 2 m above ground is

$$\dot{q}'' = EF_{12,V} = 56.14 \times 0.25 = 15.2 \text{ kW/m}^2$$

Heat Transfer to Targets within Pool Fires

Temperatures within pool fires have been widely measured and reported.[58] Over a very wide range of pool sizes (0.1–50-m diameter), the maximum time-averaged flame temperatures are generally observed to be approximately 900–1100°C. Table 3-11.8 shows measured maximum average temperatures reported in the literature. This maximum has been found to be remarkably independent of the fuel. The maximum time-averaged temperature is observed on the pool centerline over approximately the lower 40 percent of the flame height.

Effective radiation temperatures can be measured with optical pyrometers, narrow angle radiometers, or scanning spectrometers. These measurements tend to

Table 3-11.7 ***Summary of the Heat Flux from 10-m-Diameter Toluene Pool Fire to 12-m Target at 2 m High above Ground Level with No Wind***

Heat Flux Calculation Method	Heat Flux (kW/m²)
(a) Shokri and Beyler method using shape factor algebra	13.0
(b) Mudan method using shape factor algebra	15.2

Table 3-11.8 ***Maximum Time-Averaged Temperatures of Pool Fires***

	°C
Cox and Chitty[59]	1000
McCaffrey[60]	820
Terai and Nitta[61]	770
Kung and Stavrianidis[62]	920
Hägglund and Persson[18]	1000
Russell and Canfield[63]	1100
Gregory, Keltner, and Mata[64]	1000
Johnson, Linley, and Mansfield[32]	1200
Anderson et al.[65]	1000

yield maximum, average, effective radiation temperatures somewhat larger than the actual maximum temperatures, up to 1200°C (see Wayne and Kinsella,[66] Hägglund and Persson[18]), which is a reflection of the fourth-power dependence of radiation on temperature. The radiation is affected by the maximum temperature excursions rather than simply the average. Effective radiation temperatures measured outside the flame can be significantly lower than this due to obscuration by smoke outside the flame.

Average fluxes to objects immersed in flames have been widely measured. Most of the work that has been reported was performed to assess the energy input to liquid tanks for the purpose of determining venting requirements while the remainder of the work has been performed to assess the heating of weapons and nuclear fuel containers. Most of this work has focused on objects located in the lower portions of the flame where the maximum temperatures and fluxes are expected. Table 3-11.9 summarizes the results of a number of investigations and assessments of existing data. Based on the available data, a maximum time-averaged heat flux of 120 kW/m^2 is a reasonable, conservative representation of the available data. These investigations include data in which the size of the object was small relative to the size of the flame, but the objects were sized to represent tanks and/or weapons. The object was fully immersed in optically thick flames on all sides.

Measurements made with objects comparable inside to the pool fire are far less common (Taylor et al.,[67] McLain[68]). Heat fluxes in this situation are less than those observed when the object is much smaller than the pool fire. This results from the reduced flame pathlengths observed. The flames are not uniformly optically thick as seen by the object. Measurements of heating rates to objects on the order of 1–3 m in size heated by comparably sized pool fires result in average heat fluxes in the range 75–85 kW/m^2 (see Table 3-11.9). These heat fluxes were deduced from measured rates of the temperature of tank contents.

The extinction coefficient, k, of pool fires has been measured by several investigators. Typically, pool fires are found to have average extinction coefficients of about 2 1/m. An extinction coefficient of 2 1/m is consistent with the observation that pool fires reach their asymptotic, radiatively dominated burning rate at pool diameters of 1 m.

Table 3-11.9 ***Large-Scale Pool Fire Maximum Average Heat-Flux Measurements***

Large Calorimeters	kW/m^2
Gregory, Keltner, and Mata[69]	120
Wachtell and Langhaar[70]	85
Anderson et al.[65]	100
National Academy of Science[71] (average of data in the literature pre-1970)	110
Moodie[72]	100
Tunc and Venart[73]	105
McLain[68]	85[a]
Taylor et al.[67]	75[a]
Small Calorimeters	**kW/m^2**
Russell and Cansfield[63]	170
Gregory, Keltner, and Mata[69]	160

[a]Object site comparable to pool fire.

The effect of the object size on flame heat fluxes has not been systematically studied. However, it has been observed that larger objects, even if significantly smaller than the flame, do yield smaller heat fluxes than smaller objects. Gregory, Keltner, and Mata[69] have observed this effect in 9-m × 18-m pool fires with objects up to 1.4 m in diameter. They found fluxes to 1.4-m-diameter calorimeters were 30–40 percent less than for 0.1–0.2-m-diameter calorimeters. Similarly, measurements using conventional heat-flux transducers (Gardon or Schmidt/Boelter) tend to yield higher fluxes than observed with calorimeters, which are sized to represent normal tanks or weapons. Table 3-11.9 summarizes available heat flux data as measured with small calorimeters. It is thought that these effects result from two phenomena. First, the larger calorimeters effectively average the fluxes over the size of the calorimeter. This spacial averaging process tends to reduce the measured fluxes. Second, the larger calorimeters can significantly perturb the flame in the region surrounding the calorimeter, yielding reduced temperatures surrounding the calorimeter. The size of the region affected scales with the diameter of the calorimeter. With small calorimeters, this length is small compared to 1/k so that the radiant fluxes are not much affected. For large calorimeters, the reduction in local flame temperature may be significant over radiative length scales, and radiant fluxes are reduced.

Most measurements that have been performed have been made in the center of the flame where the highest fluxes are expected. Relatively few measurements have been made within the flame near the flame edge. Temperature profiles have been measured by Russell and Canfield[63] and Johnson, Linley, and Mansfield.[32] Their temperature results indicate that temperatures are reduced to about half the centerline value at one-half the pool radius. Russell and Canfield[63] made small-scale calorimeter measurements about 0.3 m from the visible flame edge. Measurements made facing the flame edge were less than 20 kW/m^2 while measurements made facing the body of the flame were about 135 kW/m^2. This

value should be compared to fluxes measured on the centerline of the fire of 160 kW/m^2 made with Gardon gages. This indicates that fluxes within the flame are relatively constant until and unless the radiative pathlengths are small enough to reduce the flame emissivity as discussed previously.

Thermal Radiation from Jet Flames

Large turbulent diffusion flames are encountered in a processing environment as a result of an accidental release of hydrocarbon vapors or the intentional disposal of unwanted gases in a flare. Flaring is the combustion process that has been the traditional method for safe disposal of large quantities of unwanted flammable gases and vapors in the petroleum industry. With the advent of air quality standards, flaring has also taken on an added importance as a method of industrial environmental control, since most gases that could previously be vented to the atmosphere must now be burned in a flare. The flaring of gases in the petroleum industry occurs in three ways:

1. *Production flaring.* In a production oil field where no provision exists for collecting and processing of gas, there is a requirement for safe disposal of flammable gases. There was a time when almost all gas released was flared, but the great value now placed on natural gas has made gas recovery economical for some fields. Nevertheless, if gas occurs in small quantities that are uneconomical to process or if the gas is so sour that processing is expensive, it can still be flared.
2. *Process flaring.* Flaring also takes place in petrochemical plants, oil refineries, and gas processing plants where the flare system is one of the off-site facilities. In process flaring, the gas that leaks past safety valves protecting various process units is brought to the flare and burned. This gas feeds the small flames that burn almost continuously on refinery stacks. Process flaring can occur at much greater rates when process units are evacuated during a shutdown or when off-specification products are produced during start-up.
3. *Emergency flaring.* This occurs when large volumes of volatile liquids or flammable gases have to be disposed of safely in an emergency such as fire, power failure, or overpressure in a process vessel.

The flaring process involves the release of a tremendous amount of energy. Since a portion of this energy release is in the form of thermal radiation, it represents a substantial hazard to personnel, equipment, and the environment. The sizing of flare system, both in diameter and height, is of major importance to ensure personnel safety during flaring operations. The ability to predict the thermal radiation field from flares is essential in the design of a reasonably sized, safe operating flare. Experimental data on thermal radiation from full-scale flares are rare, and when available at all, the flow rate and composition of the flared gases are usually unknown. However, several scale-model studies have been conducted to examine the geometric and radiative characteristics of flares.

The geometric characteristics of hydrocarbon flares are similar to turbulent jet flames. In fact, many of the geometric descriptions of flares are based on small-scale turbulent jet flame experiments. The base diameter of a flare stack, height of the stack, and composition of the burning substance are often known to the user. In modeling accidental releases of hydrocarbon gases, these relevant data may have to be estimated.

The analytical models describing the geometric characteristics of turbulent jet diffusion flames are described in the following section. The models describe parameters such as the flame height, flame width, and flame tilt. Thermal radiation models, the aerodynamic effects on radiation heat transfer, and blowout stability of jet flames, as well as calculation procedures are also described in this section.

Geometry of Turbulent Jet Flames

Combustion in a flare or jet fire occurring in the form of a strong turbulent flame may be buoyancy or momentum dominated. Such a flame presents a number of challenging phenomena for study, including the effect of crosswind on flame shape and size; radiation and formation; and dispersion of smoke and other gaseous pollutants. While applying these models to industrial flares, it is also important to recognize the effects of steam in suppressing smoke formation and thermal radiation. The fundamentals of combustion in flares have been studied by Brzustowski,[74–76] Brzustowski and Sommer,[77] and Brzustowski et al.[78,79]

Turbulent Jet Flame Height in Stagnant Surroundings

A reasonable measure of progress of burning of a diffusion flame is its height or length. At low velocities the flame is generally attached to the point of release, but at higher velocities it becomes detached, may become unstable, and extinguish. If, however, the flame impinges on an obstruction, this may serve to stabilize it. Predicting the height or length of the diffusion flame of gas jet burning in still air has long been considered one of the classical solved problems in combustion science. State of the art papers on this subject were published by Hottel and Hawthorne,[80] and Hawthorne et al.[81] Hottel and Hawthorne[80] considered the case of a primary fuel jet of higher velocity issuing into an infinite atmosphere of air with allowance for primary air in the fuel jet. They observed the progressive change in the flame shape and size as the nozzle velocity is increased. This is illustrated in Figure 3-11.30, which is based on the work of Hottel and Hawthorne[80] and further interpretation by Gugan.[82] In the laminar regime the flame length is approximately proportional to the velocity, while in the turbulent regime it is independent of velocity. Turbulence spreads from the flame tip downwards. As velocity increases there are successively a region where the flame may be on the port or lifted, a region where only a lifted flame occurs, and a point beyond which there is blow-off.

Hawthorne et al.,[81] in the earliest attempts, have developed a set of experimental data and a theoretical model for flame length for turbulent flame jets. They envisage the flame as an inverted cone with the apex on the

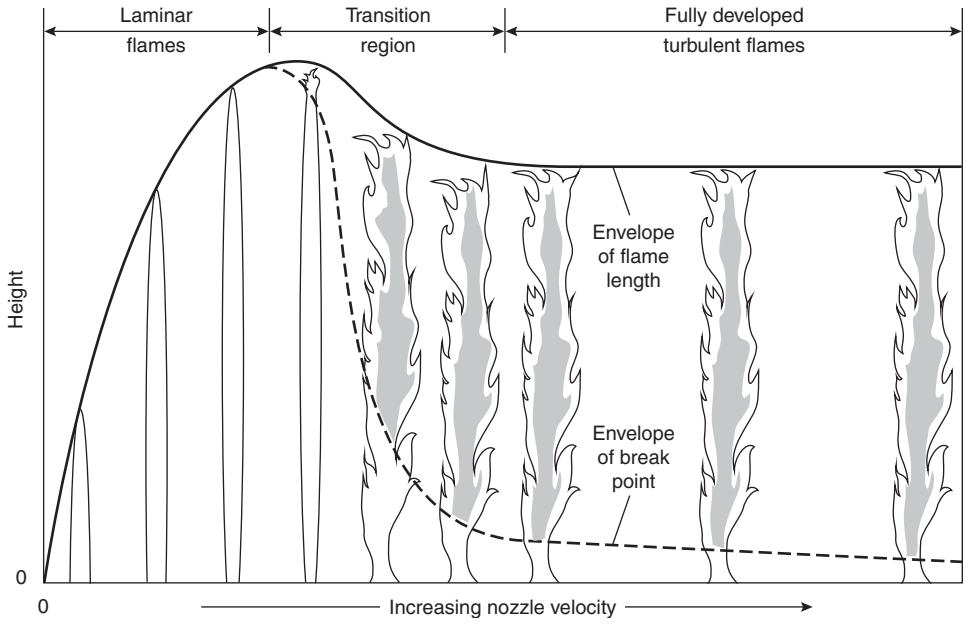

Figure 3-11.30. ***Progressive change in flame type with increasing jet velocity.***

orifice. The equation for the length of the flame was shown to be expressible, largely from momentum consideration, in the form

$$L = \frac{5.3 d_j}{C_T}\left\{\frac{T_F}{\alpha_T T_j}\left[C_T + (1 - C_T)\frac{M_a}{M_f}\right]\right\}^{1/2} \qquad (30)$$

where

L = length of visible turbulent flame measured from the break point, m
d_j = jet diameter, m
C_T = fuel concentration in stoichiometric fuel-air mixture
α_T = Mole of reactant per mole of product for stoichiometric fuel-air mixture
M_a, M_f = molecular weight of air and fuel
T_F, T_j = adiabatic flame temperature and temperature of jet fluid (absolute)

The factor 5.3 appearing in Equation 30 is the ratio of visible length to the width of the flame at the point where stoichiometric air has been entrained. This factor was determined from experimental data.

Equation 30, for determining the flame length, reduces to a much simpler expression for most hydrocarbon gases. The value of parameters C_T, α_T, and T_F/T_j for various hydrocarbons are given in Table 3-11.10.

Table 3-11.10 ***Constant for Equation 41***

Hydrocarbon Fuel	C_T	α_T	T_F/T_j
Methane	0.091	1.0	7.4
Ethane	0.074	1.04	9.0
Propane	0.038	0.96	7.6

Since C_T is typically much less than unity, α_T is approximately unity and T_F/T_j varies between 7 and 9. Equation 30 may be approximated by the following equation:

$$L = \frac{15 d_j}{C_T}\left(\frac{M_a}{M_f}\right)^{1/2} \qquad (31)$$

Momentum-controlled flame lengths as discussed above are generally 200 to 300 times the jet nozzle diameter. While these are the tallest possible jet flames, over a wide range of conditions, jet flames are buoyancy controlled.

A number of investigators have measured jet flame lengths.[74,77,83–86] All their flame height results are in the form of a power law of the Froude number, u^2/gD, where u is the nozzle velocity and d is the nozzle diameter. Flame heights, L, are correlated as

$$\frac{L}{D} \approx (\mathrm{Fr})^{1/5} \sim \left(\frac{u^2}{gD}\right)^{1/5} \sim \frac{Q^{2/5}}{D}$$

where Q is the heat release rate. All the available results can satisfactorily be described by

$$L = 0.2 Q^{2/5}$$

Figure 3-11.31 from McCaffrey[86] shows L/D as a function of $u/\sqrt{gD}$, $\sqrt{\mathrm{Fr}}$. The correlation is seen to hold over a range of about five decades in $\sqrt{\mathrm{Fr}}$. The low end of the correlation corresponds to pool fires and the high end corresponds to momentum-dominated flames.

Kalghatgi[87] and McCaffrey and Evans[88] have studied the stability and lift-off characteristics of momentum jet flames. These phenomena have a profound effect on flame radiation as indicated in Figure 3-11.31.

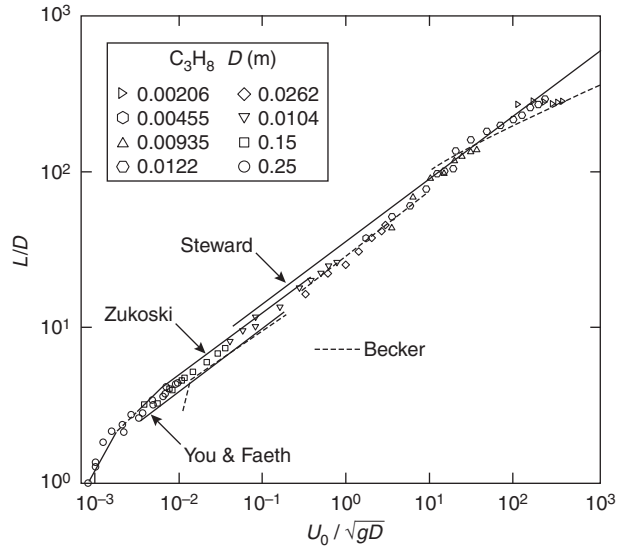

Figure 3-11.31. ***Flame height per nozzle diameter as a function of $u\sqrt{gD}$.***

Brzustowski[74] and Brzustowski and Sommer[77] proposed that the end of a turbulent diffusion flame at very high Reynolds number occurs at that point on the axis of maximum fuel concentrations where the fuel concentration equals the lean limit. In theory, this criterion can be applied to any flow configuration for which cold-flow concentration data at sufficiently high Reynolds number are available. Brzustowski[74] has also used some full-scale flare test data to support the lean limit criterion. With this criterion, the flame length for momentum-dominated jets is given by the following equation:

$$\frac{L}{d_j} = \frac{Y_{fj}}{0.32}\left(\frac{\rho_j}{\rho_a}\right)^{1/2}\left[1 + \frac{M_a}{M_f}\left(\frac{1}{0.297C_L} - 1\right)\right] \quad (33)$$

For a flame where buoyancy is the dominating force, the flame length is given by

$$\frac{L}{d_j} = 2.96\left(\frac{\rho_j}{\rho_a}\right)^{1/2} \mathrm{Fr}^{1/5} Y_{fj}^{3/5} \times \left[1 + \frac{M_a}{M_f}\left(\frac{1}{0.297C_L} - 1\right)\right]^{3/5} \quad (34)$$

where, C_L = fuel concentration at the lean flammability limit, by volume. Fr is the Froude number. Since C_L is about 5 percent or less for most hydrocarbons and M_a/M_f is approximately unity, Equations 33 and 34 may be simplified to the following two equations for momentum- and buoyancy-dominated flames, respectively.

$$\frac{L}{d_j} = \frac{10.5}{C_L}\left(\frac{M_a}{M_f}\right)^{1/2} \quad (35)$$

$$\frac{L}{d_j} = 6.1\left(\frac{u_j^2}{d_j g}\right)^{1/5}\left(\frac{1}{C_L}\right)^{3/5}\left(\frac{\widetilde{C}_a T_a}{\Delta\widetilde{H}}\right)^{1/5} \quad (36)$$

where $\widetilde{C}_a$ = molar heat capacity of air and $\Delta\widetilde{H}$ = molar heat of combustion.

Equations 35 and 36 are functionally very similar to the expressions obtained by Hawthorne et al.[81] and Putnam and Speich.[84] These expressions indicate the similarity in three independent experiments.

Turbulent Jet Flame Length in Crosswind Conditions

A series of controlled experiments have been conducted by Brzustowski et al.[89] and Gollahalli et al.[90] in wind tunnels involving hydrogen and propane flames in the presence of wind. The work indicates that in such fires the initial effect of cross flow was to shorten the flame, after which increases in a cross-flow velocity caused increases in the flame length. Shortly before blowoff conditions were reached, flame length was observed to decrease with an increase in crosswind.

The results obtained by Brzustowski et al.[89] and Gollahalli et al.[90] with zero-wind condition are consistent with the model equations given in the previous section. Based on wind tunnel data and limited comparison with full-scale data, Brzustowski[76] has proposed the following procedure to determine the flame shape in the presence of crosswind for a jet flame.

1. Calculate the dimensionless lean limit concentration:

$$\overline{C}_L = C_L\left(\frac{u_j}{u_w}\right)\left(\frac{M_f}{M_a}\right) \quad (37)$$

2. If $\overline{C}_L \le 0.5$, then $\overline{S}_L = 2.04\,(\overline{C}_L)^{-1.03}$
   If $\overline{C}_L > 0.5$, then $\overline{S}_L = 2.71\,(\overline{C}_L)^{-0.625}$
3. If $\overline{S}_L > 2.35$, then $\overline{X}_L = \overline{S}_L - 1.65$.
   If $\overline{S}_L \le 2.35$, then determine $\overline{X}_L$ by following the equation

$$\overline{S}_L = 1.04\overline{X}_L^2 + 2.05\overline{X}_L^{0.28} \quad (38)$$

4. Determine the dimensionless rise, $\overline{Z}_L$, of the flame tip above flame tip:

$$\overline{Z}_L = 2.04\overline{X}_L^{0.28} \quad (39)$$

5. Calculate dimensional coordinates of the flame tip using the following equation:

$$X = \overline{X}_L d_j\left(\frac{\rho_j}{\rho_a}\right)^{1/2}\left(\frac{u_j}{u_w}\right)$$
$$Z = \overline{Z}_L d_j\left(\frac{\rho_j}{\rho_a}\right)^{1/2}\left(\frac{u_j}{u_w}\right) \quad (40)$$

Kalghatki[91] conducted a series of 103 small-scale wind tunnel experiments to determine the size and shape of turbulent hydrocarbon jet diffusion flames in the presence of crosswind. The tests were conducted with methane, propane, ethylene, and commercial butane. The

burner diameter ranged from 6 to 22 mm, and the range of velocities were between 13 and 200 m/s. The crosswind velocities were varied from 2.6 to 8.1 m/s. Based on these tests, Kalghatki[91] concluded that the turbulent jet flame can be described by a frustum of a cone and the geometry of a jet flame under influence of wind can be represented by five geometric parameters:

1. Angle α_B, subtended by the burner tip and the tip of the flame with respect to vertical
2. Angle α, subtended by the flame with respect to vertical
3. Vertical length, L_{BV}, of the flame tip from the plane of the burner
4. The flame base width, W_1
5. The flame tip width, W_2

These parameters are expressed in terms of a dimensional variable called *effective source diameter* and a nondimensional velocity, R. The definitions of these two parameters are

$$D_s = D\left(\frac{\rho_j}{\rho_a}\right) \tag{41}$$

where

D = source diameter, m

ρ_j = density of jet fuel, kg/m^3

ρ_a = density of ambient air, kg/m^3

$$R = \frac{U}{U_j} \tag{42}$$

where

U = crosswind speed, m/s

U_j = jet velocity, m/s

In Figure 3-11.32 the variation of the vertical flame length parameter is shown as a function of the nondimensional velocity, R. Also shown in Figure 3-11.32 are the correlations suggested by Brzustowski for propane, methane, and ethylene. In order to predict the actual flame length, the flame tilt with respect to the burner axis must be known. Figure 3-11.33 shows the data on flame tilt and the comparison with Brzustowski's calculation procedure. It is seen that the calculation procedure underestimates the flame tilt. Therefore, the measured flame

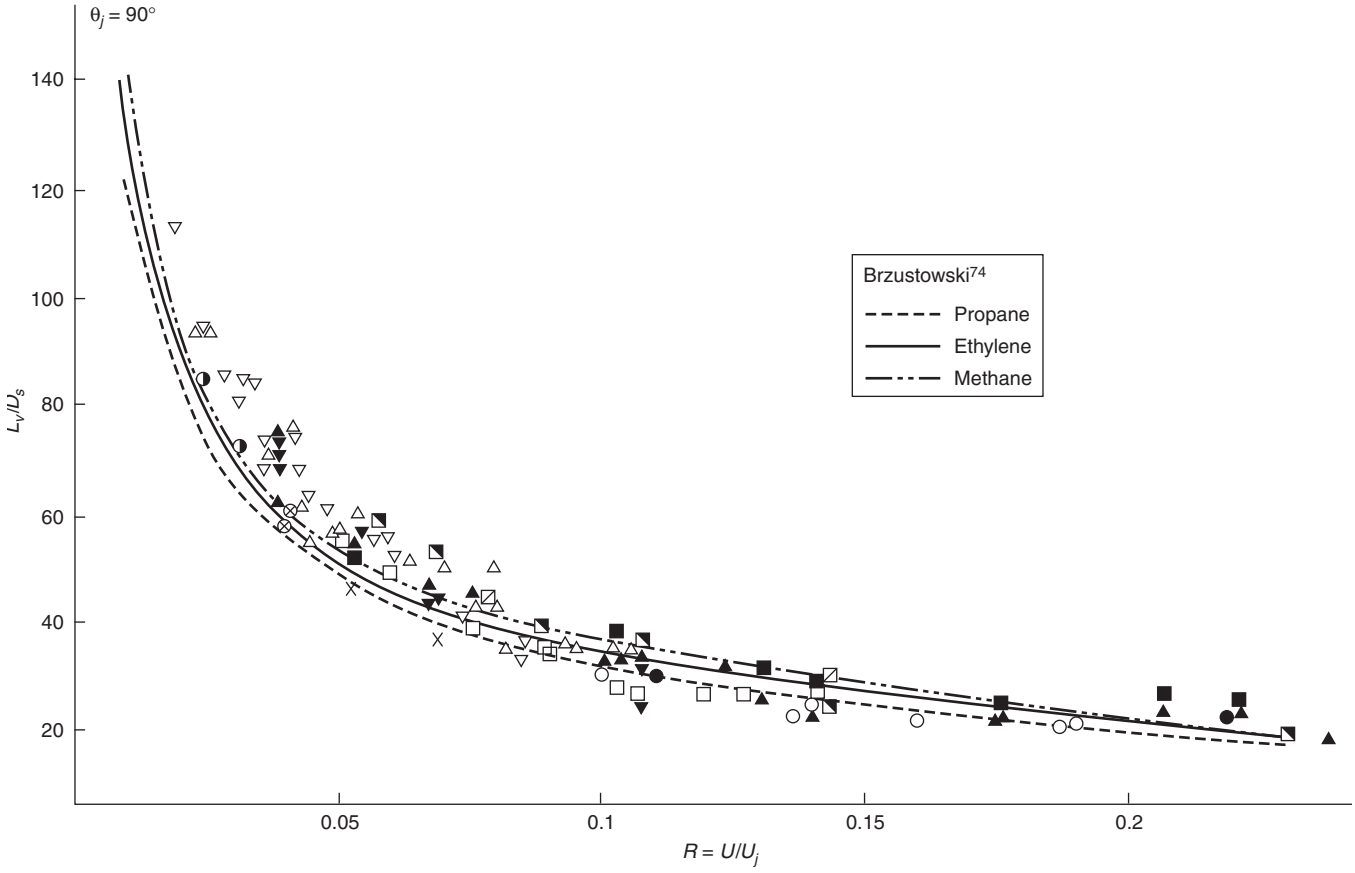

Figure 3-11.32. ***Variation of the flame length above burner tip with velocity ratio, R.[91]***

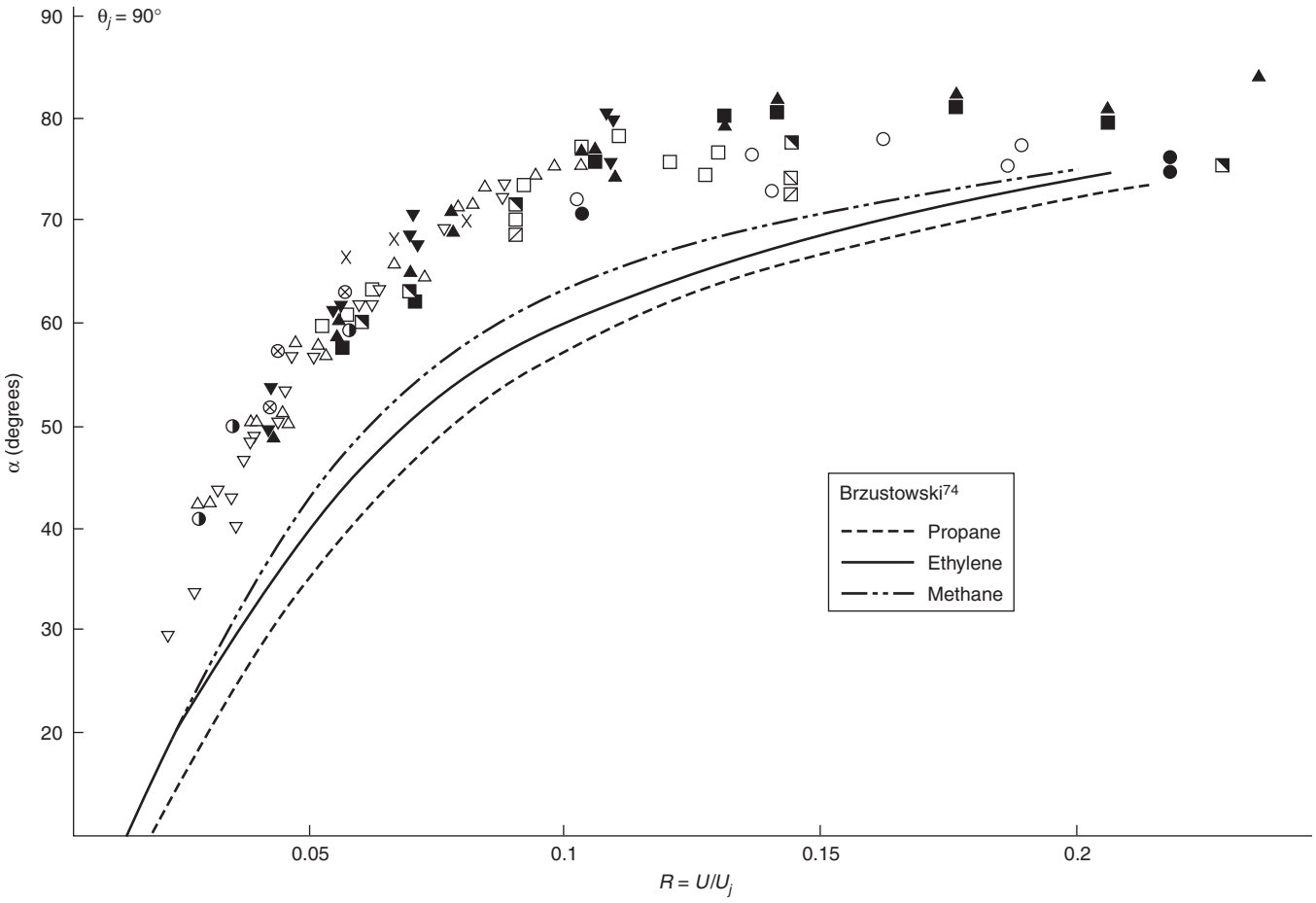

Figure 3-11.33. ***Variation of angle of tilt with velocity ratio, R.[91]***

lengths are slightly larger than the ones predicted using Brzustowski's model. Based on these results, Kalghatki[91] suggests the following correlations to determine the flame length and flame tilt parameters.

$$\alpha_B = 94 - \frac{1.6}{R} - 35R \tag{43}$$

$$\alpha = 94 - \frac{1.1}{R} - 30R \tag{44}$$

$$\frac{L_{BV}}{D_s} = 6 + \frac{2.35}{R} + 20R \tag{45}$$

Here the angles α are in degrees. The range of validity of these correlations are for the values of R greater than 0.02 and less than 0.25. The upper limit for R is not a serious limitation to the applicability of the model. For values of R less than 0.02, the wind-free data may be used to determine the flame lengths and the tilt may be assumed to be zero. It should be noted that the flame length given by Equation 45 determines only the vertical component. Actual inclined flame height is given by dividing Equation 45 by the cosine of the angle of tilt given by Equation 43. It is worth noting that the actual inclined flame length ratio is independent of the velocity ratio and is relatively constant at a value of about 120. This indicates that the majority of the tests conducted in this program were momentum-dominated turbulent jets. Recently, Sonju and Hustad[92] conducted an experimental study on turbulent diffusion flames. The flare diameters ranged from 2.3 to 80 mm and the velocities ranged from 5 to 250 m/s. Their data indicate that the flame length is proportional to the one-fifth power of the Froude number. For Froude numbers greater than 100,000, the flame lengths appear to be independent of the Froude number. These results are consistent with the data of Putnam and Speich.[84]

Turbulent Jet Flame Diameter in Crosswind Conditions

The work of Hawthorne et al.[81] described above also includes jet flame diameter calculation. They observed that the jet diameter increases as a function of distance. The measured spreading angles were in the range of 3 to 8 degrees (one-half angle). The equivalent diameter for

thermal radiation calculations can be calculated from the following equation:

$$\frac{D_c}{d_j} = \sec\theta + \frac{L}{d_j}\sin\theta\sec^2\theta \quad (46)$$

The data of Kalghatki[91] for the base and tip widths of the flames indicate the spreading angle is a function of the nondimensional velocity ratio, R. For a jet flame in windblown surroundings, Kalghatki[91] gives the following correlation of jet diameter:

$$\frac{W_2}{D_s} = 80 - \frac{0.57}{R} - 570R + 1470R^2 \quad (47)$$

$$\frac{W_1}{D_s} = 49 - \frac{0.22}{R} - 380R + 950R^2 \quad (48)$$

From these calculations, it can also be deduced that the cone half-angle for the frustum decreases from a value of about 5 degrees at $R = 0.025$ to a value of about 2.8 degrees at $R = 0.2$. Therefore, at large, relative wind speeds, a diffusion flame takes an almost cylindrical shape. The data of Sonju and Hustad,[92] indicates that the flame diameter increases as one-fifth power of the flame Froude number. The suggested constants, proportionally, for methane and propane flames are 2.5 and 4.0, respectively.

Kalghatki[91] also conducted some limited tests with nonorthogonal jet flames and concluded that the flame lengths are dependent on wind direction. These tests were conducted with relative wind angles varying from 45° to 135° (with 90° representing orthogonal cross flow). The value of the nondimensional velocity was greater than 0.025. The data indicate that for a given angle of tilt, the flame length remains relatively constant; however, the flame length decreases with increasing angle of tilt. The data of flame length and wind direction over the entire velocity ratios are shown in Figure 3-11.34. As can be seen from Figure 3-11.34, there appears to be a linear relationship between flame length and wind direction. The correlation suggested by Kalghatki[91] is

$$\frac{L_B}{D_s} = 163 - 0.64\theta_j \quad (64)$$

where θ_j is the angle between wind and jet (degrees).

Aerodynamic effects on flame stability: A jet diffusion flame in still air will lift off the tip of the burner and form a stable lifted flame when the flow velocity through the burner is increased beyond a limiting value known as the lift-off stability limit. If the flow velocity is increased further, the flame is extinguished at some limiting rate known as the *blowout stability* limit.

At the base of a lifted diffusion flame, the local turbulent burning velocity will be equal to the local flow velocity. If the flow rate through the burner is increased, the flow velocity will also increase and the base of the flame will be blown downstream to a new position where the turbulent burning velocity equals local flow velocity. The flame will blow out when the change in the burning velocity cannot keep up with the flow velocity anywhere in the jet as one moves downstream from the base of the jet flame.

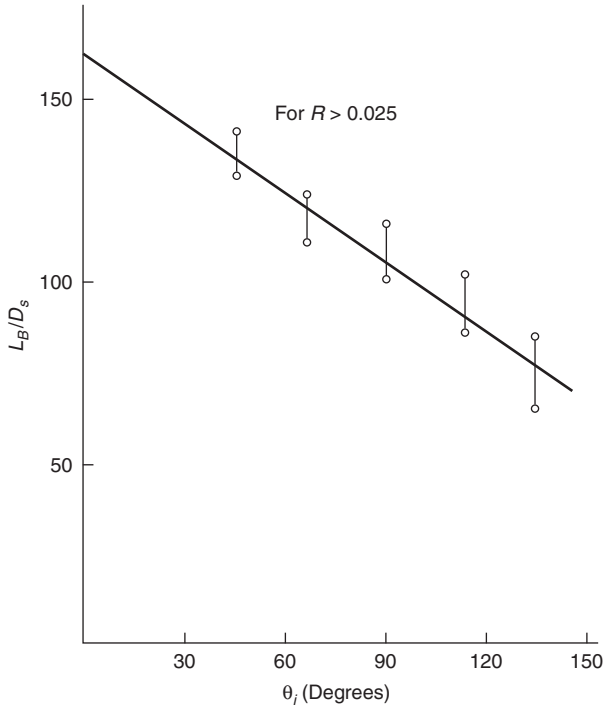

Figure 3-11.34. ***Variation of flame length with jet axis orientation.[91]***

The distance along the burner axis where the mean concentration equals the stoichiometric level is independent of the flow velocity and is given by the following equation:

$$\frac{H}{d_e} = 4\frac{\tilde{\theta}_e}{\tilde{\theta}_s}\left(\frac{\rho_e}{\rho_a}\right)^{1/2} + 5.8 \quad (49)$$

where

H = height along the jet axis, m
d_e = effective jet diameter, m
$\tilde{\theta}_e$ = fuel mass fraction at jet exit
$\tilde{\theta}_s$ = stoichiometric fuel mass fraction
ρ_e = jet mixture density, kg/m^3
ρ_a = ambient air density, kg/m^3

The effective jet diameter is defined as follows.
For subsonic jets:

$$d_e = d_j \qquad \text{for } M < 1$$

For choked flow:

$$d_e = d_j\left[\frac{2 + (\gamma - 1)M^2}{\gamma + 1}\right]^{(\gamma+1)/(\gamma-1)}\frac{1}{\sqrt{M}} \quad (50)$$

where

d_j = jet diameter, m
M = Mach number after expansion to ambient pressure
γ = ratio of specific heats

All things being equal, the larger of the value of H, the more scope there will be for the base of the flame to seek a new stable position as the flow velocity is increased, and therefore it will be more difficult to blow out the flame. Similarly, larger values of burning velocity will lead to larger flow velocities to blow out the flame. The critical velocity at the burner exit for blowout will depend upon the burning velocity, density ratio, and the Reynolds number based on H.

$$\frac{U_e}{S_u} = f\left(R_H, \frac{\rho_e}{\rho_a}\right) \tag{51}$$

where

U_e = critical velocity at jet exit, m/s
S_u = maximum burning velocity, m/s
R_H = Reynolds number given by

$$R_H = HS_u\frac{\mu_e}{\mu_e} \tag{52}$$

where μ_e = dynamic viscosity.

The typical values of the relevant parameters for typical fuels are given in Table 3-11.11.

Kalghatki[87] conducted a systematic study of the blowout stability of jet diffusion flames in still air. The fuel gases used were methane, propane, ethylene, acetylene, and commercial butane. The burner diameters ranged from 0.2 to 12 mm. The universal stability limit is given by the following equation:

$$\overline{U}_e = 0.017R_H(1 - 3.5 \times 10^{-6}R_H) \tag{53}$$

where

$$\overline{U}_e = \frac{U_e}{S_u}\left(\frac{\rho_e}{\rho_a}\right)^{1.5} \tag{54}$$

The validity of Equation 53 is shown in Figure 3-11.35. It should be noted that Equation 53 is valid only up to a Reynolds number of 100,000.

Table 3-11.11 ***Relevant Properties of Hydrocarbon Gases to Determine Blowout Stability***

Gas	Molecular Weight	Dynamic Viscosity at 0°C (micropoises)	Maximum Burning Rate S_u (m/s)	Ratio of Specific Heats	Stoichiometric Air-Fuel Ratio
Methane	16	102.7	0.39	1.31	17.2
Propane	44	74	0.45	1.13	15.7
Ethylene	28	91	0.75	1.255	14.9
Acetylene	26	93.5	1.63	1.25	13.3
Butane	54	80	0.44	1.1	15.7
Hydrogen	2	84	3.06	1.33	34.7

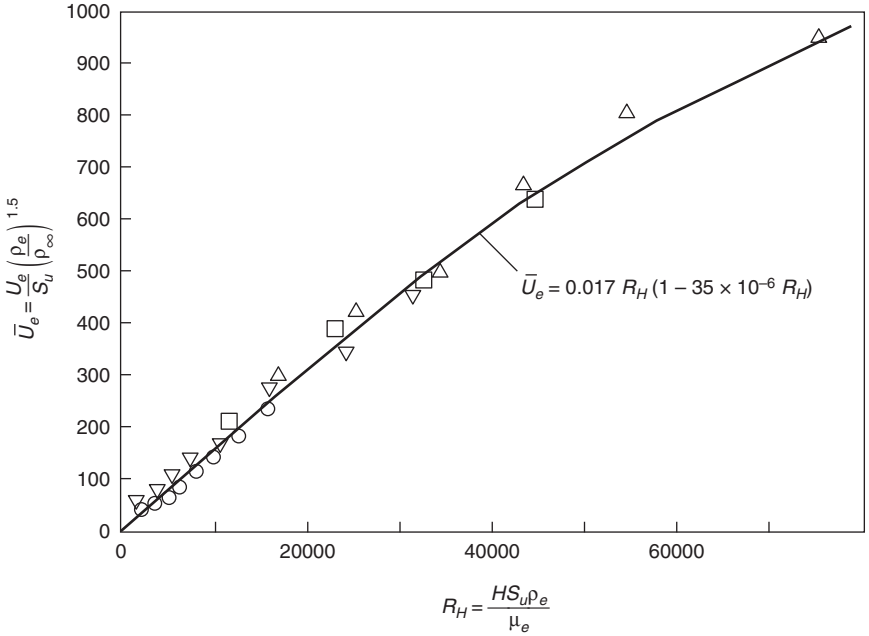

Figure 3-11.35. ***Universal blowout stability curve for diffusion flames.[87]***

Thermal Radiation Hazards from Hydrocarbon Jet Flames

Point Source Model for Jet Flame Radiation

For incident heat flux from a jet flame to a target outside the flame, it is customary to model the flame by a point located at the center of the real flame, as mentioned earlier in the pool fire section. The radiant heat flux per unit area and per unit time received by a target at a distance R from the point source is given by

$$\dot{q}'' = \frac{\dot{Q}_r \cos\theta}{4\pi R^2} \tag{55}$$

where Q_r is the radiative output given by the radiation fraction, χ_r, multiplied by the total heat release rate:

$$\dot{Q}_r = \chi_r Q$$

The geometrical aspects of the representation of thermal radiation field given by the point source model are surprisingly accurate for flare stacks, even in the case of long windblown flames. Many of the early experimental investigations relevant to jet flames were concerned with flares. The work covers a variety of jet flames, including flames of natural gas and of liquified petroleum gas (LPG). Representative accounts of work using natural gas are those by Chamberlain,[93] Johnson, Brightwell, and Carsely[94] at Shell, and by Cook, Fairweather, Hammonds, and Hughes[95] at British Gas. Accounts of work on jet flames of LPG at Shell and British Gas have been given by Hirst[96] and Tam and Cowley.[97] The work on flames formed part of a study of emission and gas dispersion of jets as well as of combustion.

Hirst[78] describes experiments using liquefied propane. Tests were carried out using orifices ranging from 9 to 52 mm in diameter and pressures from about 6 to 20 bar. Both horizontal and vertical releases were studied. A series of tests were done with vertical releases. The liquid rose in a strongly divergent cone bending with the wind. The cone angle was typically 30° for the plume but up to 90° in the flash region. The releases usually reached a steady state before ignition. The visible clouds at ignition were large, extending up to 45 m vertically and 70 m downwind. In most cases fireballs formed and in several tests rose to 100 m; the most fully developed fireballs occurred at low wind speeds. The overpressure generated by the flames were also measured. The maximum observed fell from some 3 bar at 20 m from the release point to about 0.8 bar at 100 m.

Other tests were done with horizontal releases. One of the features measured in these trials was the distance reached by the flame. Figure 3-11.36 gives the relation between the mass flow and the impingement distance of the flame for a 50-mm-diameter pipe. In one of the trials in which a 35-m-long jet flame from a full bore release of 7.9 kg/s from a 50-mm pipe at pressure of 13 bar. The combustion energy was 365 MW. The maximum surface emissive power was 250 kW/m^2 and occurred 25 m from the release point and just before the flame underwent transition from the momentum-dominated to the buoyancy-dominated condition. However, for such full-scale bore

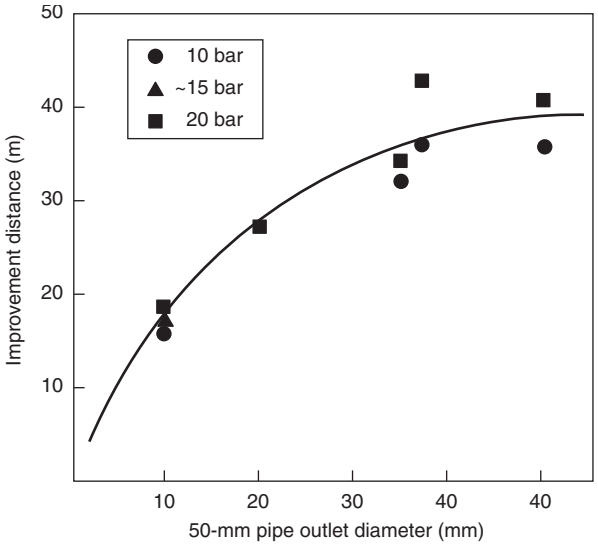

Figure 3-11.36. ***Jet flames: flame impingement distance versus mass flow for propane.[57]***

discharges the heat radiation within the flame was complex, and steady heat fluxes were mainly in the range 50–220 kW/m^2 and depended on the discharge conditions and the target distance. The maximum temperature occurred at a distance of 4 m and had a value of 1570 K.

Brzustowski[98] considered a flare (in the presence of high crosswind) as a uniformly radiating cylinder. He observed that the thermal radiation flux given by point source model is similar to those predicted using a cylindrical source model except at distances very close to the source. Brzustowski[98] also computed radiation heat flux for vertical elements parallel and perpendicular to the wind direction and has concluded that the corrected point source model and the uniform cylinder radiation model essentially yield very similar results.

Brzustowski, Gollahalli, and Sullivan[89] carried out small- and pilot-scale experiments to study the radiative characteristics of turbulent flares using commercial-grade methane and propane. Small-scale test data were taken at jet velocities from 6.8 to 70 m/s with jet Reynolds numbers from 7500 to 94,000, and ratios of crosswind velocity to jet velocity from 0 to 0.113. Pilot-scale experiments were conducted on an outdoor site with the flare modeled by a vertical 25-mm inner-diameter pipe 1.5 m high. In these tests, provisions were made for injecting steam into the gas below the tip of the flare. The incident heat flux at various distances was measured with and without steam.

Oenbring and Sifferman[99] compared the point source model predictions with full-scale measurements. The full-scale data consisted of radiation measurements in the Oenbring and Sifferman[99] studies that were conducted at the oil refinery facility in Conoco's Ponca City, Oklahoma, and in the Gillis gas plant facility in Los Angeles, California. The Gillis flare stack was 40 cm (16 in.) in diameter and 23 m high. The gas velocity ranged from a Mach number of 0.2 to 0.49. All test data indicate that the inverse square law predicts the thermal radiation accurately.

Radiative Fraction for Jet Flames

In order to predict the incident heat flux accurately, it is necessary to determine the fraction of total combustion energy resulting in thermal radiation. In general, the fraction of heat radiated depends on the efficiency of combustion and soot formation and on the heat lost by convection to the entrained air.

Most thermal radiation prediction models tends to ignore the details of the combustion process and concentrate on the overall combustion efficiency, or fraction of the energy that is radiated to the environment. Markstein[7] conducted a series of radiation measurements on propane turbulent diffusion flames. The total radiative powers of the flames were determined using wide-angle radiometer. The flow rates varied from 44 to 412 cm^3/s. A collimated beam radiometer was used to measure the radiation characteristics of different parts of the flames. Based on these measurements, Markstein[7] concluded that the thermal radiation from diffusion flames is at a maximum at approximately the center of the flame and tapers off on either side, forming a Gaussian distribution. The total radiative power of the flame was observed to be directly proportional to the total heat-release rate. Figure 3-11.37 shows that the fraction of combustion energy released in the form of radiation is approximately 20 percent for the propane diffusion flames. Burgess and Hertzberg[37] measured the fraction of combustion energy radiated to the surroundings for several gaseous fuels. Tan[100] and Kent[101] have also suggested values for the radiated energy for a variety of fuels.

Table 3-11.12 compares the values of radiative fraction, χ_r suggested by various investigators. The parameter f_s in Table 3-11.12 represents the fuel mass fraction at which carbon particles begin to form. For any hydrocarbon fuel, C_nH_m burning in air, the fraction f_s is given by

$$f_s = \frac{12n + m}{12n + m + [n/2(137.3)]} \tag{56}$$

For the same entrainment/mixing history, a gas with a higher value of f_s has less tendency to form solid carbon particles than a gas with a lower value of f_s. Higher values of f_s, therefore, correspond to lower radiation levels.

Examination of Table 3-11.12 shows good qualitative agreement. Propane and butane have similar values of f_s, and their χ_r values are comparable. Methane and hydrogen have lower values of χ_r and higher f_s values. But ethylene has a lower value of f_s and, except in one study by Burgess and Hertzberg,[37] the χ_r values are also lower. This

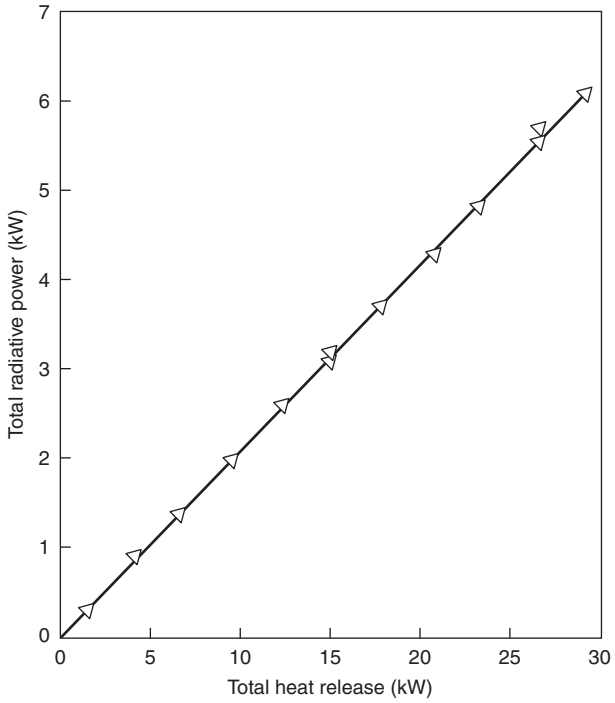

Figure 3-11.37. ***Radiative power for propane diffusion flames.[7]***

may be partially due to straight molecular weight corrections applied by Tan[100] and Kent.[101]

The intensity of flame radiation may be affected by the medium through which it passes. An appreciable attenuation may occur when radiation is transmitted from a source to a target through the atmosphere. The values of radiative fraction χ_r in Table 3-11.12 are properties of the fuel only. They do not take into account the variation of the operating parameters such as stack exit velocity, crosswind velocity, and the presence of air steam. However, these parameters have a profound influence on the temperature profiles and affect the fraction of combustion energy radiated, χ_r.

Figure 3-11.38 shows the radiative fraction measured by McCaffrey over six decades: $u/\sqrt{gD}$. Comparing this figure with Figure 3-11.31 shows that the radiative fraction is constant in the buoyancy-controlled regime, but for momentum-controlled jet flames, the radiative fraction decreases until blowoff occurs.

Table 3-11.12 ***Comparison of Radiative Fraction, χ_r of Various Fuels***

Fuel	f_s	χ_r Brzustowski[98]	χ_r Burgess and Hertzberg[37]	χ_r Tan[100]	χ_r Kent[101]	χ_r McCaffrey[86]
Hydrogen	1.0	0.2	0.17	—	—	—
Methane (C_1)	0.189	0.2	0.23	0.20	0.19	0.22
Ethylene (C_2)	0.170	0.25	0.36	0.26	0.25	0.38
Propane (C_3)	0.176	0.30	—	0.32	0.32	0.302
Butane (C_4)	0.175	0.30	0.30	0.37	0.37	—
C_5 and higher	—	0.40	—	—	—	—

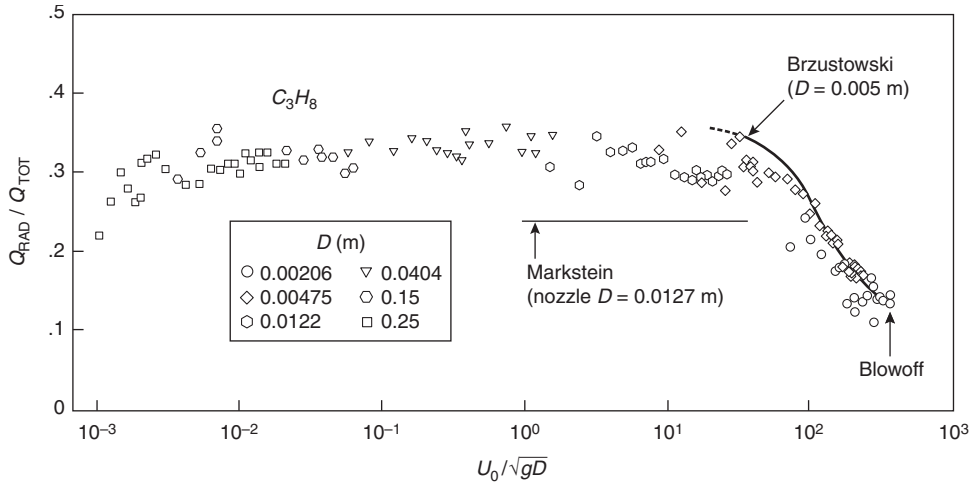

Figure 3-11.38. ***Radiative fraction measured by McCaffrey.[86]***

Evans and Pfenning[102] and McCaffrey[103,104] have studied jet flame extinction via water spray. They also document significant reductions in flame radiation at subsuppression water spray addition rates of up to 50 percent.

Brzustowski, Gollahalli, Gupta, Kaptein, and Sullivan[79] conducted a series of laboratory-scale tests on the effects of jet velocity and free stream velocity on the fraction of energy radiated, χ_r, from the turbulent flames. Figure 3-11.39 shows the effect of jet velocity on radiation in the absence of crosswind for methane and propane flames. Also drawn in Figure 3-11.39 are the suggested values of radiative fraction χ_r from Tan[100] and Kent.[101] As can be seen from Figure 3-11.39 the fraction of energy radiated, χ_r, is strongly dependent on jet velocity and decreases with increasing jet velocity. Figure 3-11.40 shows the effects of crosswind velocity on the radiant energy. In general, increasing crosswind velocity appears to increase the fraction of energy radiated, χ_r.

The significant departures of measured values of χ_r from the values previously published (which do not take into account the aerodynamic effects) can be understood in relation to variation of the detailed temperature profiles in the flames. The underlying explanation deals with the competing processes by which the products of hydrocarbon pyrolysis near the flare stack oxidize directly or form soot that burns in the downstream portion of the flames. Quite obviously, predictions based on the traditional values of χ_r would have overestimated the thermal radiation in all these laboratory-scale experiments. Brzustowski, Gollahalli, Gupta, Kaptein, and Sullivan[79] also measured thermal radiation from a full-scale flare. The 0.406-m-diameter flare was operating at about 25 percent of the design flaring rate. The best estimates of jet velocity and wind velocity were 28 and 4 m/s, respectively. The flame length was measured to be 25 m and flame tip was about 10 m above the flare tip level. The value of χ_r calculated from the radiation measurements at two ground sections 0.223 was about 30 percent lower than the values predicted using the Tan[100] and Kent[101] approaches.

Figure 3-11.41 shows the fraction of net heat release radiated as a function of the flare Reynolds number for a 5-cm (2-in.) natural gas flare from Straiz, O'Leary, Brennan, and Kardan.[105] The Reynolds numbers in these tests are comparable to full-scale Reynolds numbers (of the order of 10^5 to 10^6). The fraction of energy radiated, χ_r, shows a significant departure at higher Reynolds numbers from its traditionally assumed value of 0.2.

It is quite evident that the aerodynamics of the flow have a significant effect on the radiation from a large

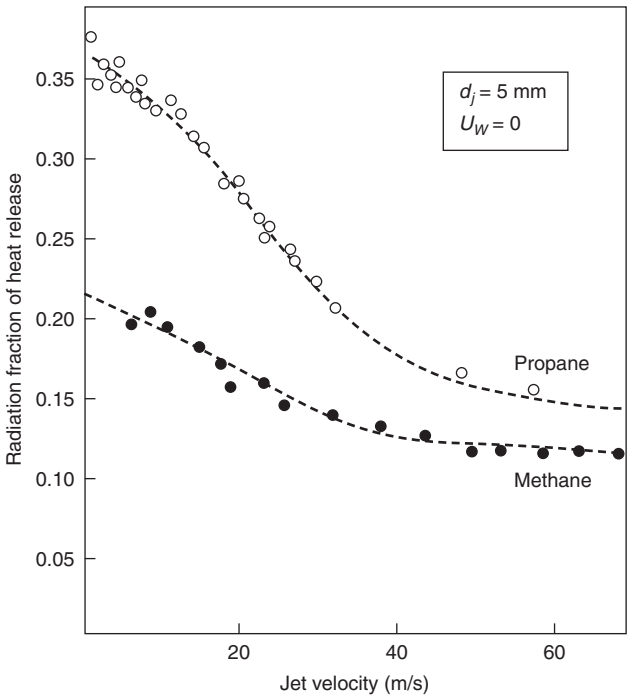

Figure 3-11.39. ***Effect of jet velocity on radiated fraction of combustion energy.***

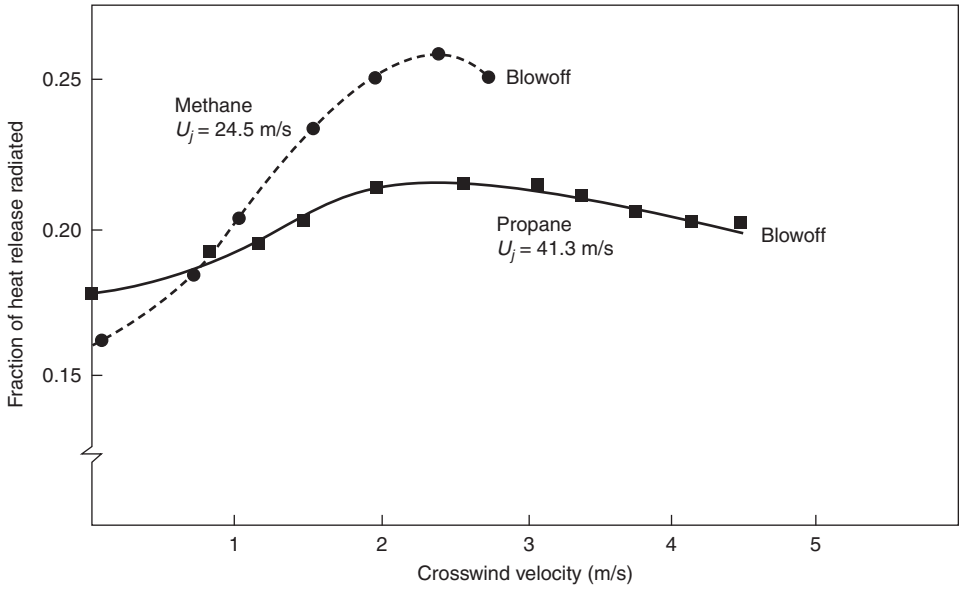

Figure 3-11.40. ***Effect of crosswind velocity on radiated fraction of combustion energy.***

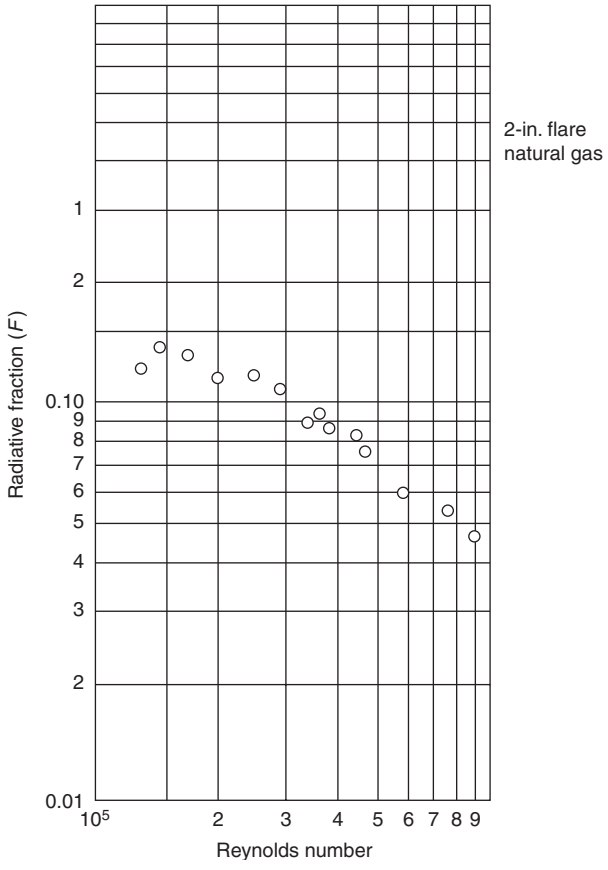

Figure 3-11.41. ***Radiative fraction for natural gas flames full-scale tests.***[105]

turbulent diffusion flame. However, the radiation data described above were obtained on the laboratory-scale experiments, and their validity for large flames encountered in an offshore environment cannot be taken for granted.

Line and Cylinder Models for Jet Flame Radiation

As mentioned in the previous section, a point source model is a simple representation of a jet flame and applies only at large distance from the fire. The point source model can be inaccurate for target positions close to the fire. This is particularly important when one is evaluating safe separation distances for storage of hydrocarbon fuels.

The tilted cylinder model discussed in the pool fire section can be used to overcome the inaccuracy of the point source model to determine the thermal radiation from large diffusion flames. This model assumes that the fire can be represented by a solid body of a simple geometrical shape, and all thermal radiation is emitted from its surface.

The incident radiation per unit area per unit time is given by

$$\dot{q}'' = FE\tau \tag{57}$$

where

E = surface emissive power of flame, kW/m^2

F = configuration factor

τ = atmospheric attenuation factor (transmissivity)

The configuration factor is the fraction of the radiation falling directly on the receiving target. The shape or configuration factor depends on the shapes of the fire and receiving target, and on the distance between them.

The surface emissive power is the total radiative power leaving the surface of the fire approximated by the following equation:[106]

$$E = E_{bb}(1 - e^{-\kappa L}) \tag{58}$$

where

E_{bb} = equivalent blackbody emissive power, kW/m^2
κ = extinction coefficient, m^{-1}
L = effective pathlength, m

The blackbody emissive power E_{bb} can be calculated by

$$E_{bb} = \sigma T_f^4 \tag{59}$$

where σ is the Stefan-Boltzmann constant (5.67×10^{-11} kW/m^2·K^4) and T_f is the flame temperature (K).

Fumarola, de Faveri, Pastorino, and Ferraiolo[107] suggested a line source model to compute radiation from jet flames. An elemental length of the flame is assumed to radiate similar to a point source model. The total incident heat flux at any observer location is computed by integrating the heat flux due to an elemental source over the flame length. They compare their results with Brzustowski[98] and the Oenbring and Sifferman model and observed that their model predicted lower-incident heat fluxes at ground level.

Galant, Grouset, Martinez, Micheau, and Allemand[109] proposed a three-dimensional numerical model to estimate the flame geometry and thermal radiation from large diffusion flames. The model considers the variation in flow conditions based on a pseudo-stream-function formulation and includes effects of turbulence, combustion, and soot concentration. The model has been validated with field experiments of up to 254-mm (10-in.) diameter methane jets and agreement between predicted and measured heat flux is within 15 percent.

Jet Fire Impingement Exposure

The severity of the thermal exposure from impinging jet flames far exceeds that observed for pool fire exposures. Heat fluxes of up to 250 and 300 kW/m^2 for two-phase LPG and sonic natural gas jets, respectively, have been measured in large-scale jet flame tests (e.g., Cowley and Prichard[110]). In these tests where the flame fully engulfed a cylindrical target, heat fluxes averaged over the impingement area were 200 kW/m^2 for sonic natural gas jets and were 150 kW/m^2 for two-phase LPG jets.

The severity of jet flame impingement exposures results from highly radiative, optically thick flames with high convective heat fluxes. The radiative and convective components of the total heat flux tend to be roughly equal in the high heat flux regions of the target (Parker[111]). Wighus and Dransgsholt[112] report temperatures as high as 1200°C and impingement velocities of up to 80 m/s in gaseous propane jet flames. They also found that the temperatures observed at the location of peak velocity were lower for higher gas velocities. For instance, they measured 1150°C at 30 m/s and 650°C at 80 m/s. They measured heat fluxes as high as 340 kW/m^2 in some tests, and the radiative fraction of the total heat flux tended to be about 2/3. Their results would indicate that differences found by Cowley and Prichard[110] for natural gas and two-phase LPG flames were primarily the result of the two-phase nature of the LPG release rather than differences between natural gas and propane gaseous flame properties.

Unsteady Thermal Radiation Analysis

Liquefied fuel gases having boiling points below normal ambient temperatures have come to be stored and transported in large quantities. Liquefied natural gas (LNG) is stored for peak demand use. It is also transported by sea in bulk carriers designed for cryogenic cargos. Liquefied petroleum gas (LPG) is stored under pressure and is transported by trucks, railroad tank cars, and by sea in bulk carriers. While liquefied hydrogen has been used in limited quantities as a rocket fuel, serious consideration is being given to its use as a fuel for aircraft and possibly highway vehicles. Because volatile fuels are being transported in rapidly increasing volumes, speculation is being devoted to the kinds of accidents that could result from the release of these fuels.

The failure of a container carrying a pressurized cargo will result in the flash evaporation of a portion of the released liquid and the sudden formation of a vapor cloud from the evolved vapors. Upon contact with an ignition source, one of two situations may occur: the generation of a propagating plume flame, or the formation of a fireball. If the vapor puff is ignited immediately after its formation, it may burn as a rising sphere, usually referred to as a *fireball.* The rapid combustion of vapor clouds in the form of fireballs has been observed in several accidents involving vehicles carrying liquid propane. Here some of the accidents where a fireball has been reported to be observed are reviewed.

In the General Accounting Office report to the U.S. Congress regarding liquefied energy gases safety, an accident is cited involving a tractor-semitrailer carrying 34 m^3 (9000 gal) of LPG. About 2 min after the accident, a fireball of about 123 m (135 yd) in diameter was observed. The radiant heat from the fireball burned several people, a house, several other buildings, and some 12 acres of woods.

The National Fire Protection Association has maintained descriptions of several accidents involving LGP where a rising fireball was observed. One such accident happened in Oneonta, New York, where a freight train derailed involving 27 cars, 7 of which contained 120 m^3 (33,000 gal) of liquid propane. Seconds after the derailment, a huge fireball erupted from the area where the tank cars were piled up. It is believed that this fireball was the result of ignition of LPG when one of the tank cars split open. The fireball heated other tanks carrying LPG, which resulted in several BLEVEs (boiling liquid expanding vapor explosions).

One of the most cited fireballs occurred in Crescent City, Illinois, when a freight train carrying 15 cars derailed, 10 of them containing 130 m^3 (34,000 gal) of LPG each. One of the derailed tank cars rode up and over the pile and tore a hole in another tank car containing propane, causing the release of gas that produced the first

fireball. There were several subsequent explosions that lasted for hours and destroyed 24 individual living quarters and 18 businesses.

The fireballs resulting from such accidents are large—usually of the order of about 100 m in diameter. The duration of the fireball is on the order of a few seconds because of rapid mixing with the surrounding air. During this brief period, a fraction of the combustion energy present in the initial mass of vapor is radiated as thermal energy to the surroundings. The adverse effect of this thermal radiation to population and property depends on the intensity and the duration of the radiation.

If, however, the vapor cloud is allowed to travel with the wind and is ignited at a location away from the source, the resulting vapor fire assumes the form of a propagating plume flame. In both cases, an unsteady diffusion flame is produced. However, the flame geometry is defined by the particular mode of burning. Accordingly, the levels of resulting thermal radiation differ significantly for each mechanism. The unique behavior of these vapor cloud fires is discussed in this chapter. The following sections present an analysis of burning vapor clouds that define a plume fire; a discussion of the formation and burning of a hydrocarbon fireball; and a sample calculation procedure for burning of a vapor cloud in the form of a fireball.

Thermal Radiation from Burning Vapor Clouds

Estimating the thermal radiation field surrounding a burning vapor cloud involves geometric characterization of the cloud, that is, the time-averaged size of the visible envelope. It also requires estimation of the radiative properties of the fire, that is, the average emissive power, and so forth. Finally, the radiant intensity at a given location must be determined. Since the burning behavior of a moving vapor cloud can be best described as unsteady, the standard equations for pool fires do not apply. In the discussion that follows, the flame geometry and effective thermal radiation parameters that characterize a burning vapor cloud are identified.

Given a spill of a volatile, flammable chemical, initially a pool is formed. As the pool vaporizes due to heat transfer from the medium surface (land or water), a vapor cloud is formed above the pool. These vapors are entrained by the ambient wind, and are dispersed in the downwind direction. Two conditions must be met for a burning cloud to be produced; first, there must be an ignition source located away from the spill point; second, the concentration within the vapor cloud must be within the flammability limit range for that material. Assuming these conditions exist, the fire that results is in the form of a propagating plume flame.

Based on experiments with spills of LNG on water, Mudan[113] and Raj et al.[38] identified three stages of vapor fire development. First, a transient turbulent flame spreads through the cloud. The flame propagates in both upwind and downwind directions. The second stage in the development of a vapor fire is the steady-state propagation toward the liquid pool. At this location, there appears to be a stationary diffusion flame. The third and final stage of burning results in a small pool fire at the source location. Based on limited experimental data on vapor cloud fires, the burning behavior and resultant flame geometry can be analyzed.

Flame propagation velocity: Within a few seconds after ignition, flames tend to spread quickly both upwind and downwind of the ignition source. Flame travel in both directions is consistent if the ignition occurs after the flammable vapor cloud travels over it. The flames are initially contained within the cloud, but subsequently extend in the form of a flame plume above the cloud. This is consistent with premixed burning of the regions in the cloud that are within flammable limits prior to flame arrival, followed by diffusive burning of the richer regions in the cloud. After consuming the flammable vapors downwind of the ignition source, the downwind edge of the flame starts moving toward the spill point. Generally, the flame zone is normal to the wind direction.

During this transient flame growth, an *average* flame propagation velocity with respect to the ground can be determined by noting the location of the upwind edge of the flame at various time intervals. The flame speed with respect to gases may be obtained by adding the wind speed to the flame speed with respect to the ground. The initial, rapid propagation of the flame in the premixed vapor cloud can also be measured by the same technique.

Wind speed plays a significant role in the vapor cloud propagation. The flame velocity tends to increase with wind speed. Also, an increase in wind velocity increases the dispersion process. The ignition delay is also affected by the wind speed. Clearly, for a fuel-rich vapor cloud, an increase in mixedness will increase the flame propagation velocity. However, if the fuel concentration is well below stoichiometry, a further increase in ignition delay may, in fact, cause a decrease in flame propagation speed.

Mizner and Eyre[36] conducted vapor fire tests with propane spilled on water. The spill rates of propane varied from 2.1 to 5.6 m^3/min and the ignition source was located approximately 130 m from the spill point. The wind speeds varied between 6 and 7 m/s. The flame propagation velocities measured by locating the upwind edge of the flame as a function of time. Their analysis indicates that the flame propagation velocity (with respect to the ground) varies between 3.75 and 4.8 m/s.

In Figure 3-11.42 the measured flame propagation velocities (with respect to unburnt gases) are shown for various wind speeds. The data indicate that there is no significant variation in the flame propagation velocities for methane (LNG) and propane (LPG). The maximum laminar burning velocity for methane is 0.45 m/s; laminar flame speed is 3.5 m/s; and the typical expansion ratio is 7.4. The corresponding properties for propane are 0.52, 4.0, and 7.6 m/s, respectively. Since these properties are somwhat similar for methane and propane, it is reasonable to expect the turbulent flame propagation velocities to be similar.

Flame geometry model: Fay and Lewis[114] proposed a model for unsteady burning of unconfined fuel vapor clouds. Based on small-scale experiments with methane, ethane, and propane, and a simple entrainment model, they gave expressions to compute the maximum diameter, height, and duration for complete combustion. The model

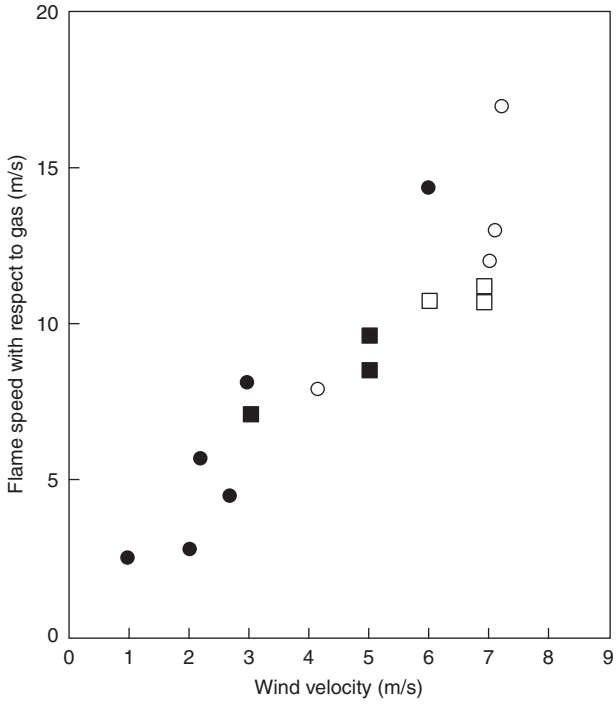

Figure 3-11.42. ***Flame propagation velocities for LPG and LNG vapor fires.[113]***

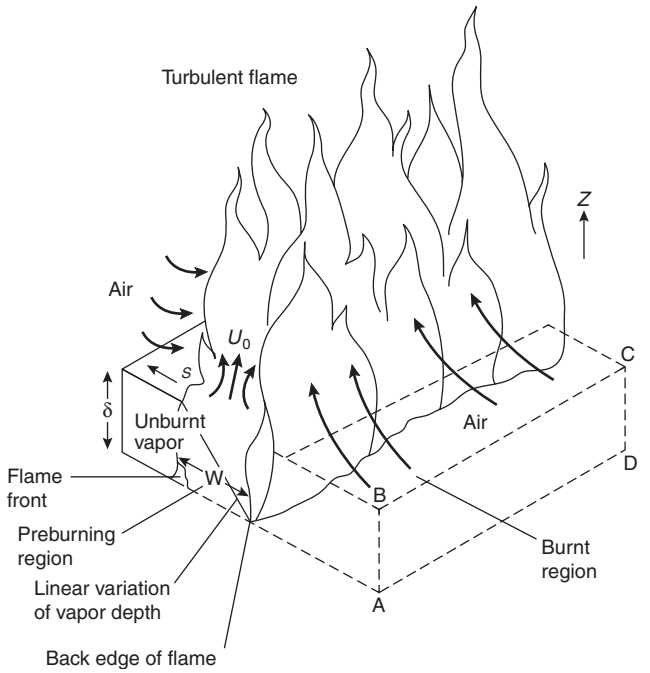

Figure 3-11.43. ***Schematic diagram showing the unconfined burning of a pure flammable vapor cloud.***

suggested by Fay and Lewis[114] assumes that the unsteady, turbulent diffusion flame is in the form of a fireball. The correlations given by the authors are validated over a range of small-scale experimental data (up to 200 cm^3) with methane, ethane, and propane gases at room temperature. However, experiments conducted with cold propane vapors ignited in an open environment do not show evidence of a fireball. In fact, the experiments performed by Shell[36] with LNG and LPG, and earlier tests involving LNG vapor fires, fail to confirm Fay and Lewis's[114] proposition that diffusive burning in unconfined vapor clouds takes place only in the form of a fireball.

Raj and Emmons[115] presented a theoretical analysis to estimate the ground level width of a large combustible vapor cloud. The model is based on the principle that the plume above a heat source is characterized by the strength of the heat source. In the case of a burning vapor plume, the rate of burning controls the plume characteristics, and the rate of burning itself is a function of the gas velocity within the plume.

The essential features of the Raj and Emmons[115] model are illustrated in Figure 3-11.43. The assumptions made in the model development are as follows:

1. The geometry of the burning vapor cloud is two dimensional.
2. The burning is controlled by natural convection (buoyancy).
3. The flame propagation velocity with respect to unburnt gases is relatively constant.
4. The depth of the vapor cloud is uniform and is not affected by the flame.
5. The variation of the depth of vapor in the preburning zone is linear.
6. The steady-state turbulent flame correlation for the ratio of visible flame height to base width is valid.

Using experimentally derived values for flame height-to-width ratio and flame propagation velocity, Raj and Emmons[115] gave the following equation to determine the flame width as a function of time:

$$\tau = \left(\frac{\mathrm{Fr}_f}{\mathrm{Fr}}\right)^{1/3}\left\{\frac{\pi}{3\sqrt{3}} + \frac{2}{3}\ln\left[\frac{\sqrt{\chi^2+\chi+1}}{(1-\chi)}\right] - \frac{2}{\sqrt{3}}\tan^{-1}\left[\frac{2}{\sqrt{3}}\left(\chi+\frac{1}{2}\right)\right]\right\} \quad (60)$$

and

$$\chi = \left[\left(\frac{\mathrm{Fr}}{\mathrm{Fr}_f}\right)^{1/3}\xi\right]^{1/2}$$

where

$\xi = W/\delta$

$\tau = 2\,St/\delta$

$\mathrm{Fr}_f = S^2/g\delta$ = flame Froude number

Fr = Froude number = U_0^2/gW

S = flame propagation velocity, m/s

g = acceleration due to gravity, m/s^2

δ = unburnt vapor cloud thickness, m

U_0 = upward velocity at flame base, m/s

W = flame width, m

Raj and Emmons[115] estimated the Froude number based on Steward's[39] data on flame heights for hydrocarbon diffusion flames. The analysis indicates the following relationship for the flame height in a linear heat source.

$$\left(\frac{H}{W}\right)_{\text{stoichiometric}} = 4.98N_{\text{co}}^{1/3} \tag{61}$$

where N_{co} is the combustion number defined as follows:

$$N_{\text{co}} = \text{Fr}\frac{\rho_0'^2\omega[r + \omega/\rho_0']^2}{(1-\omega)^3} \tag{62}$$

where

ρ_0' = density ratio = density of vapor at flame base/density of air.

r = stoichiometic air/fuel mass ratio

ω = inverse volumetric expansion ratio and is defined as follows:

$$\omega = \frac{1}{(1 + Q_c/rC_pT_a)} \tag{63}$$

where

Q_c = heat of combustion, J/kg

C_p = specific heat, J/kg·K

T_a = ambient temperature, K

The maximum width of the vapor fire is given by the following equation:

$$\xi_\infty = \frac{W_\infty}{\delta} = \left(\frac{\text{Fr}}{\text{Fr}_f}\right)^{-1/3} \tag{64}$$

Steward's[85] data indicates that nearly 400 percent excess air is entrained in the fire plume. The typical height-to-width ratios measured in Steward's[85] data range between 5 and 50. Raj and Emmons assumed a height-to-width ratio of 2 for LNG vapor fires and demonstrated that Equation 64 predicts the observed behavior of flame width.

Experimental data on methane and propane vapor fires indicate that the flame width varies as the cloud propagates back to the spill point. Typically, it has been observed that the flame width increases as a function of time until all the flammable vapor is consumed. The width of the fire reduces to the dimension of the pool. That rate of increase in flame width appears to be slightly less than the flame propagation velocity (with respect to the ground).

The flame length variation can also be estimated as a function of flame width. It is interesting to note that flame length also increases slightly with time, but the ratio of the flame length to flame width is relatively constant. A plot of flame length-to-width ratios for propane vapor flames is shown in Figure 3-11.44.[113] In general, flame length is about 40 percent of the flame width. The data of Mizner and Eyre[36] show that the typical flame length-to-width ratio varies between 20 and 40 percent. It is worth noting that vapor fire flame length-to-width ratios are significantly less than flame height-to-diameter ratios for pool fires.

The time-dependent flame width may be calculated using Equation 64. Figure 3-11.45 compares the computed flame width to measured flame widths as a function of time. Although there is considerable scatter in the data, the overall agreement between predicted and observed growth rates is good.

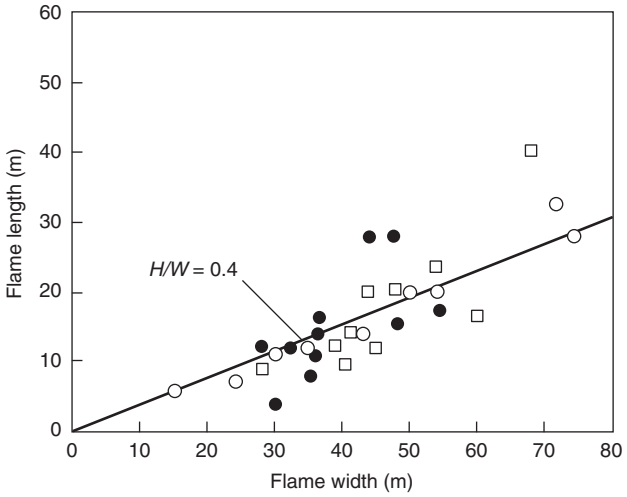

Figure 3-11.44. ***Flame length as a function of flame width.[113]***

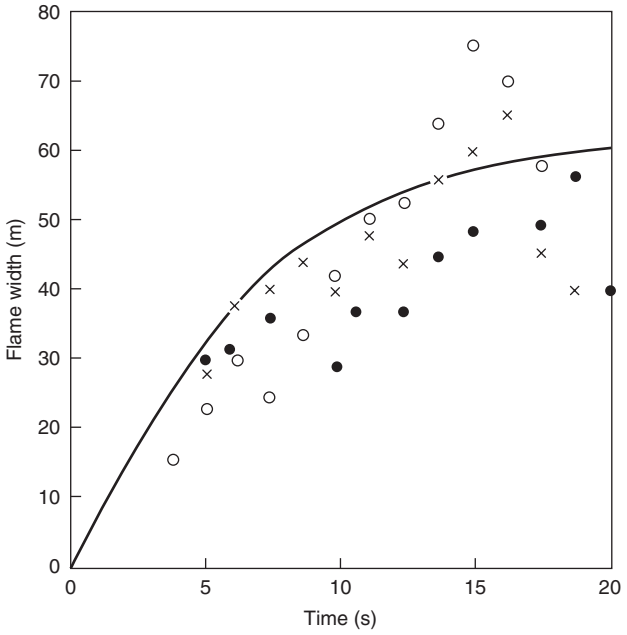

Figure 3-11.45. ***Comparison of predicted and measured flame widths for LPG vapor fires.[113]***

Thermal radiation: The incident flux received by a stationary observer from a propagating vapor is a complex function of several factors. First, the emissive power, which defines the radiative properties of the fire, should be determined. Since the duration of a vapor fire is short, and the steady burning period is even shorter, it is difficult to assign an averaging time for determining emissive powers and average incident fluxes. There is, however, a

short period over which the thermal radiation appears to have less fluctuation. This duration can be used in determining average incident fluxes and corresponding emissive powers.

Another important geometrical parameter influencing the thermal radiation from vapor fires is the area of the visible flame. If the flame is optically thick, the thermal radiation increases with an increase in the flame surface area. The area increases rapidly immediately following ignition because both the flame width and flame height increase with time. Therefore, the flame area increases approximately like the square of time. Once the flammable vapors are consumed, the flame area decreases rapidly. The incident flux also increases rapidly due to increasing flame area and drops off as the burnout process begins. The distance to the flame surface is also a key parameter. Since the flame is in motion, the distance varies continuously until the cloud approaches the spill points where a pool fire is formed. Coupled with the variation in distance is the changing effect of absorption by the water vapor and carbon dioxide in the atmosphere. And finally, the geometry of the flame relative to the observer influences the view factor, that is, that portion of flame "seen" by the observer. Therefore, it is evident that the transient nature of the burning process, effected by the changing geometry, severely limits a detailed characterization of thermal radiation from a vapor cloud fire.

For a simple rectangular flame geometry, the centerline horizontal and vertical view factors can be determined using the following equations:[2]

$$F_h = \frac{1}{2\pi}\left(\tan^{-1}\gamma + \frac{X}{\sqrt{1+X^2}}\tan^{-1}\frac{Y}{\sqrt{1+X^2}}\right) \tag{65}$$

$$F_v = \frac{1}{2\pi}\left(\frac{X}{\sqrt{1+X^2}}\tan^{-1}\frac{Y}{\sqrt{1+X^2}} + \frac{Y}{\sqrt{1+Y^2}}\tan^{-1}\frac{X}{\sqrt{1+Y^2}}\right) \tag{66}$$

where X = flame length divided by observer distance, and Y= flame width divided by observer distance.

For asymmetric configurations, trigonometic variations of Equations 65 and 66 can be used to determine the appropriate view factors. The leading edge of the flame (with respect to the observer) may be calculated using the ignition location and the flame propagation velocity. The time dependent flame width may be calculated using Equation 64. Since flame height is related to flame width, the crosswind radiation may be calculated using appropriate view factors. The incident thermal flux is given by the following equation:

$$\dot{q}''_{\text{crosswind}} = EF_{V,H}\tau \tag{67}$$

where τ represents the atmospheric transmissivity.

A similar procedure may be adopted to calculate incident thermal radiation in the downwind direction. Here the flame is moving away from the observer at flame propagation speed. Therefore, the downwind incident flux will be at its maximum at the time of ignition (assuming ignition occurs at the downwind edge of the cloud) and will decrease rapidly.

Because of the complex phenomena of a vapor fire, a simple calculation procedure cannot be developed to determine the incident thermal flux. A numerical program based on equations described in this section may be used to determine the time-dependent thermal flux.

Thermal Radiation from Hydrocarbon Fireballs

Fireball combustion occurs when volatile hydrocarbons are released and rapidly ignited. In order to characterize the radiation from fireballs, it is necessary to define the size and dynamics of the fireball and then to assess the radiation based on these results.

Fireball Size and Dynamics

The maximum size of a fireball is governed primarily by the mass of the fuel released and vaporized. While the fireballs are rarely spherical, an equivalent spherical volume is widely used to characterize the size of a fireball. The maximum diameter of the equivalent spherical fireball is given by

$$D = 5.8\ \text{m}^{1/3} \tag{68}$$

where D is the maximum diameter in meters and m is the mass of fuel in kilograms. This expression was synthesized by Roberts[116] from prior work and has been adopted by others since that time (see CPSS[117]). The maximum fireball diameter is independent of the initial pressure of the fuel so long as the pressure and temperature are sufficient to vaporize the fuel. Hasegawa and Sato[118,119] suggest that for propane at or above normal ambient temperature (20°C) complete vaporization will occur.

While the maximum size of the fireball is independent of the release pressure, the dynamics of the fireball are dependent upon the momentum of the release, which results from the flash evaporation of the fuel. For momentum-dominated fireballs, the burning duration is given by

$$t_d = 0.45m^{1/3} \tag{69}$$

(see CPSS[117]), where t_d is in seconds and m is in kilograms. For buoyancy-dominated fireballs, such as would be expected for atmospheric pressure releases, the burning duration is given by

$$t_d = 2.6m^{1/6} \tag{70}$$

(see CPSS[117]) where t_d is in seconds and m is in kilograms. Not only do burning durations differ for momentum-dominated and buoyancy-dominated fireballs, but the growth histories of the fireballs over their lifetime also differ. For momentum-dominated fireballs, the maximum fireball diameter is reached quickly with the fireball diameter growing initially as the one-fourth power of time

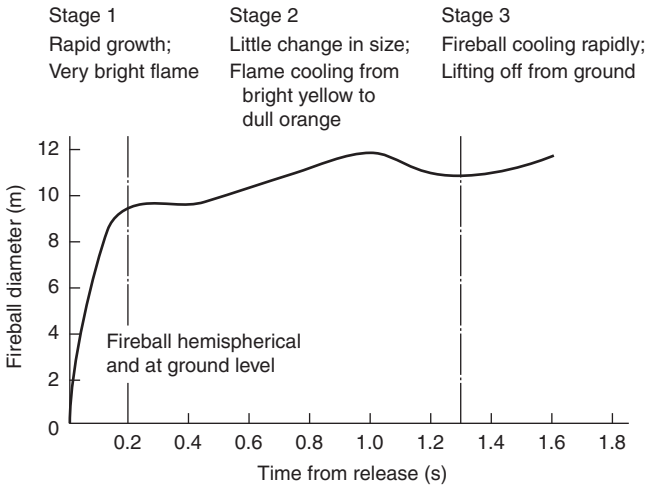

Figure 3-11.46. ***Fireball development as a function of time; 7.5 kg LPG released from cylinder bursting.[116]***

(see Figure 3-11.46). The fireball diameter remains approximately constant over its lifetime. Conversely, the size of a buoyancy-dominated fireball initially grows as the square of time, controlled by buoyant entrainment processes (Fay and Lewis[114]).

Comparing the above fireball duration equations, it becomes clear that for large fuel masses, the momentum-dominated duration exceeds the buoyancy-dominated duration. Since buoyancy is ever present, the duration should never exceed the buoyancy-dominated duration. As such, even pressurized releases will be dominated by buoyancy for very large masses (greater than about 30,000 kg), and the buoyancy-dominated expression should be used.

For buoyancy-dominated fireballs, not only is the entrainment rate lower, but the fireball rises during its lifetime. As such, during its lifetime the fireball lifts off from the ground. Roberts[116] adopts the correlation of Hardee and Lee[120] for the time to fireball liftoff:

$$t_e = 1.1m^{1/6} \tag{71}$$

where t_e is in seconds and m is in kilograms. As one would expect, the liftoff time scales in the same manner as the buoyant fireball duration, with the liftoff time being about 40 percent of the burning duration. Based on the work of Fay and Lewis,[114] the maximum rise height of a buoyancy-dominated fireball is approximately five-thirds of the maximum fireball diameter. As such, the maximum rise heights range from one to five-thirds of the maximum fireball diameter for both momentum- and buoyancy-dominated fireballs.

Fireball Radiation

Radiation models for fireballs use either the point source or spherical source model. The expressions are essentially equivalent under the simplest conditions but vary with geometric conditions where the target cannot view the entire fireball.

Point Source Fireball Model

For the point source model, the incident radiant flux, q, is given by

$$q = \tau\chi_R \cdot \frac{\dot{Q}}{4\pi L^2}\cos\theta \tag{72}$$

where

τ = atmospheric transmissivity
χ_R = radiative fraction
$\dot{Q}$ = heat release rate
L = distance from the target to the point source location
θ = angle of the target relative to the line of sight connecting the source and target

The heat release rate is normally estimated by assuming that the total heat content of the fireball, Q, is released uniformly over the fireball duration.

$$\dot{Q} = \frac{Q}{t_d} \tag{73}$$

The radiative fraction is generally in the range 0.1 to 0.4. Roberts[116] correlated the data of Hawegawa and Sato[118,119] to obtain the following correlation for the radiative fraction as a function of the fuel vapor pressure:

$$\chi_R = 0.27P^{0.32} \tag{74}$$

where P is the storage pressure (in MPa), and the original data included vapor pressures from 0.2 to 1.4 MPa.

The distance from the point source to the target is given by simple geometry as

$$L = \sqrt{R_T^2 + (Z_p - H_T)^2} \tag{75}$$

where

R_T = horizontal distance from the release to the target
H_T = target height
Z_p = height of the point source

The appropriate selection of Z_p is the average height of the center of the fireball. This can range from $D/2$ for high-momentum releases with no buoyancy effects to $5/6$ D for buoyancy-dominated releases.

Spherical Fireball Model

The spherical fireball model assumes that the fireball can be characterized as having an average fireball surface emissive power, E, and a diameter, D. The incident radiant flux to a target outside the fireball is given by

$$q = \tau EF \tag{76}$$

where τ is the transmissivity of the atmosphere between the fireball and the target and F is the configuration factor.

The configuration factor is strictly a geometric factor. Figure 3-11.47 shows the relevant geometric details required for the determination of the configuration factor where ϕ is the half-angle subtended by the fireball; θ is the angle of the normal to the target relative to the axis to the fireball; L is the separation of the target from the fireball center; and r is the fireball radius ($r = D/2$).[117] When $\theta < \pi/2 - \phi$, the configuration factor is simply

$$F = \left(\frac{r^2}{L^2}\right)(\cos\theta) \qquad \text{for } \theta < \frac{\pi}{2} - \phi \tag{77}$$

When $\theta > \pi/2 - \phi$, portions of the fireball are not visible to the target and the configuration factor is more complex.

$$\begin{aligned} F = {} & \frac{1}{2} - \frac{1}{\pi}\sin^{-1}\left[\frac{(L^2 - r^2)^{1/2}}{L\sin\Theta}\right] \\ & + \frac{r^2}{\pi L^2}\cos\Theta\cos^{-1}\left[-\frac{(L^2 - r^2)^{1/2}}{r}\cos\Theta\right] \\ & - \frac{1}{\pi L^2}(L^2 - r^2)^{1/2}(r^2 - L^2\cos^2\Theta)^{1/2} \\ & \text{for } \Theta > \frac{\pi}{2} - \Phi \end{aligned} \tag{78}$$

where

r = radius of fireball ($r = D/2$), m
D = diameter of fireball, m
L = distance to center of sphere, m
Θ = angle between normal to surface and connection of point to center of sphere, rad
2Φ = view angle, rad

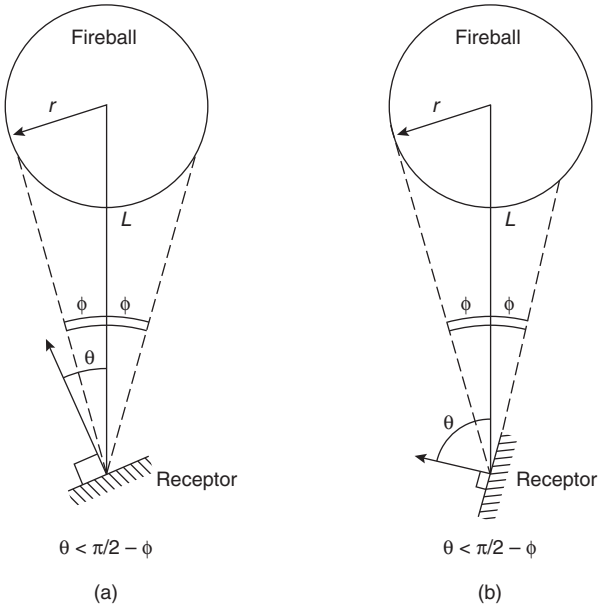

Figure 3-11.47. ***Geometry of a radiative sphere (fireball). (a) Receptor "sees" the whole fireball. (b) Receptor "sees" part of the fireball.***

The appropriate selection of Z_p is the average height of the center of the fireball. This can range from $D/2$ for high-momentum releases with no buoyancy effects to $5/6D$ for buoyancy-dominated releases.

The emissive power of the fireball surfaces have been measured by several investigators and have been found to be in the range of 100–450 kW/m^2. Pape et al.[121] have correlated the data of Hasegawa and Sato in a form similar to the radiative fraction correlation by Roberts.[116]

$$E = 235P^{0.39} \tag{79}$$

where E is the emissive power in kW/m^2 and P is the vapor pressure in MPa. Measurements by Johnson et al.[122] for 1000 and 2000 kg butane and propane releases at 0.75 and 1.6 MPa yielded surface emissive powers in the range of 320–370 kW/m^2. An emissive power for large-scale releases of 350 kW/m^2 is widely used.

Thermal Radiation Hazards

Thermal radiation from hydrocarbon fires may pose significant hazards to both personnel and property. Hazards to personnel result from exposure to intense thermal radiation, causing severe burn injury. In the following subsection the criteria for thermal radiation hazard assessment for determining safe separation distances for personnel are discussed. Discussions of the effects on combustibles and structures can be found elsewhere in the handbook.

Criteria for Thermal Radiation Hazard Assessment

The thermal radiation from a fire may cause burns on bare skin if the intensity of radiation is sufficiently large and if the exposure is of sufficient duration. A more comprehensive treatment of skin burn injury calculations is provided by the SFPE engineering guide.[123] Skin burns occur over a continuous range of severity, starting from a burn so minor that the skin is barely damaged and extending through complete destruction of all skin layers to the underlying tissues or bone. Several classifications of skin burn severity have been proposed, each depending on the degree of skin damage. The most familiar classification is to divide skin burns into three degrees. Even with these three degrees, there are several recognized sublevels. For present purposes, the following levels of burn severity can be used, with the attached simple descriptions:

1. *First degree.* The mildest level of skin burn, characterized by erythema (reddening), but no formation of blisters. The mildest of first-degree burns are not particularly painful and commonly present no medical problem. They may, in fact, not even cause symptoms other than a mild impression of warmth. More severe first-degree burns will produce some pain, but no permanent damage. Flaking or scaling of the skin will occur several days after exposure because of damage to the outer skin layer.
2. *Second degree.* An intermediate level of skin burn, characterized by formation of blisters. Blister depth may be shallow, with only the surface layers of the skin

damaged, resulting in a moderate second-degree burn, or with nearly the full depth of the skin destroyed, that is, a severe second-degree burn.

3. *Third degree.* Deep burns, characterized by destruction of all skin layers. The underlying tissue may also be destroyed.

The medical problems of burns covering large areas of the body include the severe loss of fluid and the extreme potential for infection following the loss of a large portion of the protective layers of the skin. Survival of healthy adults and teenagers can normally be expected if less than 20 percent of the body surface has second- and third-degree burns (percent body areas: head 7 percent, arms 14 percent, and hands 5 percent). Survivability decreases rapidly for persons who have more than 50 percent of body surface covered by full-thickness burns, and even with intensive medical care, it is unlikely to find survivors.

Pain and tissue damage are both related to heating of the skin. The skin consists of two main layers: the epidermis, which is a thin (0.05 to 0.1 mm) outer layer, and the derma, which is an inner layer (1 to 2 mm thick). Since the skin is a complex system, there is no perfect mathematical model available for describing its response to heating under all conditions. However, simplified models can be used as an aid in predicting skin response to heating. The simplest analysis begins with the assumption that the skin and underlying tissue behave as a one-dimensional medium with constant thermal properties. Heat transfer is due to conduction only, and the temperature field anywhere in the medium is given by the following equation:[124]

$$\frac{\delta T}{\delta t} = \alpha^2 \frac{\delta^2 T}{\delta X^2} \tag{80}$$

where

T = temperature at time t and distance x below the skin surface

$\alpha^2 = k/\rho c$ = thermal diffusivity, m^2/s

k = thermal conductivity, w/m·K

ρ = density, kg/m^3

c = specific heat, J/kg·K

The solution to Equation 80 depends on the initial and boundary conditions. If it is assumed that the skin and the underlying tissue are at a uniform temperature, T_0, and that at time zero a constant heat flux of $\dot{q}''$ is applied, the initial and boundary conditions are as follows:

$$\left.\begin{array}{lll} t \le 0 & x \ge 0 & T = T_0 \\ t > 0 & x = 0 & \dfrac{\delta T}{\delta x} = -\dfrac{\dot{q}''}{k} \end{array}\right\} \tag{81}$$

Equation 81 indicates that the heat flux, $\dot{q}''$, produces a temperature gradient in the epidermis that is inversely proportional to the value of thermal conductivity. The solution to Equation 80 with the initial and boundary conditions indicated in Equation 81 is as follows:

$$T = \frac{\dot{q}''}{k}\left[\frac{2a\sqrt{t}}{\sqrt{\pi}} \exp\left(-\frac{x^2}{4a^2 t}\right) - x\, erfc\left(\frac{x}{2a\sqrt{t}}\right)\right] \tag{82}$$

The *erfc* is the complementary error function. The increase in skin surface temperature ($x = 0$) is given by the following equation:

$$T_s - T_0 = \frac{2\dot{q}''\sqrt{t}}{\sqrt{\pi k \rho c}} \tag{83}$$

The data of Buettner[124] obtained by having volunteers expose their forearms to varying degrees of thermal radiation indicate that the threshold pain is felt by human beings when the average temperature of 0.1-mm depth of skin is increased to about 45°C. The data indicate that the time required for pain can be correlated with the intensity of radiation by the following equation:

$$t_p = \left[\frac{35}{\dot{q}''}\right]^{1.33} \tag{84}$$

where

t_p = time required for pain, s

$\dot{q}''$ = incident thermal radiation, kW/m^2

The deviation of Equation 84 from Equation 83 is attributed to slightly higher surface temperature for higher thermal flux for pain threshold.

In Figure 3-11.48 the time required to cause pain is shown as a function of the incident thermal flux. The sources of data used in Figure 3-11.48 include "pricking" and "threshold" pain.[124–127] All the sources of data show general agreement on the time required for pain at low fluxes. No pain was shown, regardless of the exposure duration, for thermal fluxes below 1.7 kW/m^2 (the solar constant is about 1 kW/m^2 on a clear summer day). At higher fluxes, the time required for pain diverges for the several studies. However, Equation 84 appears to predict the time required for pain with reasonable accuracy.

When the skin surface temperature reaches about 55°C, blistering of the skin occurs. Mehta et al.[128] determined that the severity of the burn depends on the energy absorbed after the skin temperature has reached a temperature of 55°C. If the amount of energy absorbed is 41.8 kJ/m^2, pain or mild second-degree burns will be experienced. For an additional exposure of 83.6 kJ/m^2, a blister or severe second-degree burn will become evident. Finally, for an exposure of greater than 162.2 kJ/m^2, severe third-degree burns will result and the skin tissue will be permanently damaged. Figure 3-11.49 shows the time required for blister formation for human skin as measured by Stoll and Greene[127] and Mehta et al.[128] The times required are quite similar for threshold blisters and full blisters, showing that there is little practical difference between the two. Mixter[129,130] has compared the degree of burns to human skin with that of pigs and found a good correlation. Mixter's[129] data for second-degree burns to white pigs are also shown in Figure 3-11.49. The difference in Mixter's data and other sources of data is attributed primarily to the source of thermal radiation. Stoll and Greene used a 1000-W projection lamp and Mixter used a carbon arc source.

The data shown in Figures 3-11.48 and 3-11.49 are useful for estimating the time for threshold pain and how rapidly human skin burns will result at various levels of

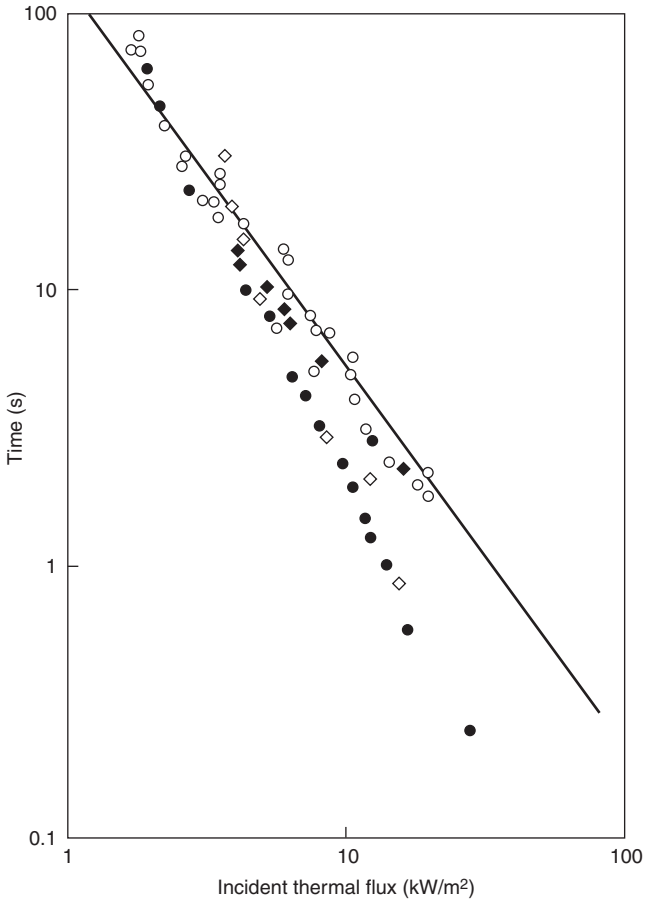

Figure 3-11.48. ***Time required for pain due to exposure to thermal radiation.[114]***

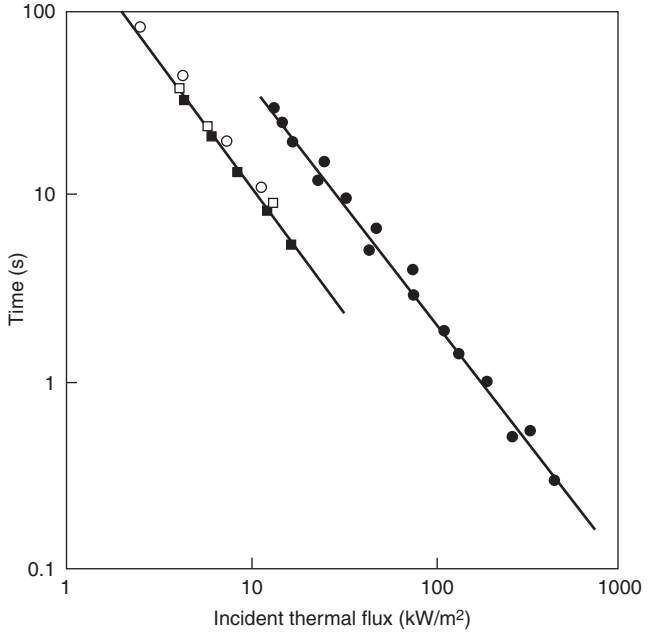

Figure 3-11.49. ***Time required for skin burns by thermal radiation; data sources.[114]***

radiant exposure. These data, however, do not aid in determining the radiant flux levels at which fatalities may be expected. The only source of data on large-scale deaths from thermal radiation are analyses of fatalities from nuclear weapons. Since the exposure times are typically very short, interpretation of these data is somewhat subjective.

Eisenberg et al.[131] analyzed the data on the relation between thermal radiation intensity and burn injury for nuclear explosions at different yields. The results of their analysis are shown in Figure 3-11.50 for significant injury threshold, 1 percent lethality, near 50 percent lethality, and near 100 percent lethality for various incident radiation intensities. Also shown in Figure 3-11.50 are the second-degree burn data collected by Mixter.[129] These data correspond very closely to the significant injury threshold.

The *United States Federal Safety Standards for Liquefied Natural Gas Facilities* (49 *CFR,* Part 193, 1980) suggest an acceptable level of 5 kW/m² for direct exposure of human beings. At this incident flux, exposure time on bare skin before unbearable pain is about 13 s and second-degree burns may occur in about 40 s. This level can, therefore, be used as a criterion for injury. The level at which fatality is likely to occur is more difficult to define. If we assume the duration of exposure to be the same, at about 40 s, Figure 3-11.50 can be used to determine a fatality threshold of about 10 kW/m². This level may, therefore, be used in determining the hazard zone for fatality.

Summary

In the previous sections, we have given detailed techniques for computing impacts of large, open hydrocarbon fires. In particular, we have addressed steady-state thermal radiation from pool fires and flame jets and unsteady-state thermal radiation from vapor fires and fireballs.

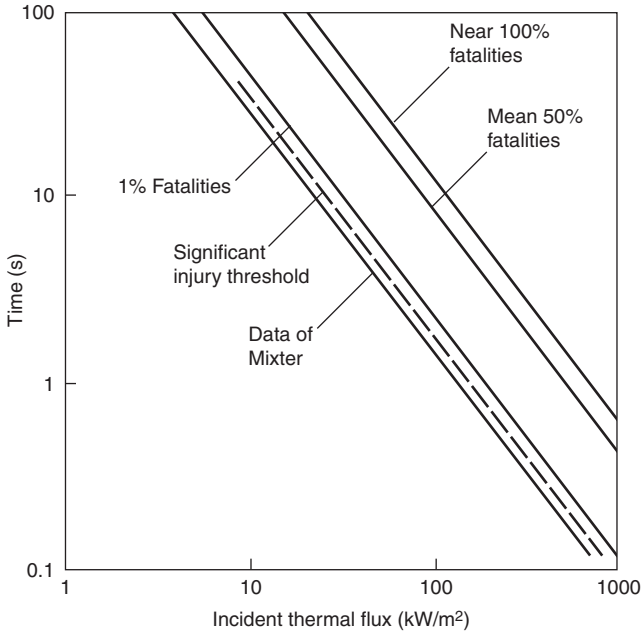

Figure 3-11.50. ***Fatality levels for thermal radiation.[131]***

Particular emphasis has been placed on supporting the assessment methodology with available experimental data. These models can be used to appropriate impact criteria to evaluate the fire and flammability hazards associated with hydrocarbon releases.

References Cited

1. E.M. Sparrow and R.D. Cess, *Radiation Heat Transfer,* Brooks Publication Company, Belmont, CA (1966).
2. E.M. Sparrow and R.D. Cess, *Radiation Heat Transfer,* Revised Edition, McGraw-Hill, New York (1978).
3. R. Siegel and J.R. Howell, *Thermal Radiation Heat Transfer,* Third Edition, Hemisphere Publishing Corporation, Washington, DC (1992).
4. M.F. Modest, *Radiation Heat Transfer,* McGraw-Hill, New York (1993).
5. W.H. McAdams, *Heat Transmission,* Third Edition, McGraw-Hill, New York (1954).
6. D.Q. Kern, *Process Heat Transfer,* McGraw-Hill, New York (1950).
7. G.H. Markestein, "Radiative Energy Transfer from Turbulent Diffusion Flames," *Combustion and Flame,* 27, pp. 51–53 (1976).
8. V.I. Blinov and G.N. Khudiakov, "Certain Laws Governing Diffusive Burning of Liquids," *SSSR Doklady,* Academiia Nauk, pp. 1094–1098 (1957).
9. H.C. Hottel, "Certain Laws Governing Diffusive Burning of Liquids," *Fire Research Abstract and Revision,* 1, p. 41 (1959).
10. J. DeRis and L. Orloff, "A Dimensionless Correlation of Pool Burning Data," *Combustion and Flame,* 10, pp. 381–388 (1972).
11. D.S. Burgess, A. Strasser, and J. Grumer, "Diffusive Burning of Liquid Fuels in Open Trays," *Fire Research Abstract and Revision,* 3, p. 177 (1961).
12. J. Grumer, A. Strasser, T.A. Kubala, and D.S. Burgess, "Uncontrolled Diffusive Burning of Some New Liquid Propellants," *Fire Research Abstract and Revision,* 3, p. 159 (1961).
13. M.G. Zabetakis and D.S. Burgess, "Research in Hazards Associated with the Production and Handling of Liquid Hydrogen," *U.S. Bureau of Mines Report, RI 5707,* Pittsburgh, PA (1961).
14. K.S. Mudan, "Thermal Radiation Hazards from Hydrocarbon Pool Fires," *Progress Energy Combustion Science,* 10, pp. 59–80 (1984).
15. S.R. Gollahalli and H.F. Sullivan, "Liquid Pool Fires—A Review," *Research Report #23,* University of Waterloo, Canada (1973).
16. J. Moorhouse, "Scaling Criteria for Pool Fires Derived from Large-Scale Experiments," *I. Chem. Sym.,* 71, pp. 165–179 (1982).
17. K.S. Mudan and P.A. Croce, "Thermal Radiation Model for LNG Trench Fires," *ASME Winter Annual Meeting,* New Orleans (1984).
18. B. Hagglund and L. Persson, "The Heat Radiation from Petroleum Fires," *FOA Report C 20126-D6 (A3),* Stockholm, Sweden (1976).
19. T. Yamaguchi and K. Wakasa, "Oil Pool Fire Experiments," *Fire Safety Science—Proceedings of the First International Symposium* (Grant and Pagni, eds.), Hemisphere Publishing Corporation, Washington, DC, pp. 911–918 (1986).
20. P.G. Seeger, "On the Combustion and Heat Transfer in Fires of Liquid Fuels in Tanks," in *Heat Transfer in Fires* (P.L. Blackshear, ed.), Scripta Book Company, Washington, DC, pp. 95–126 (1974).
21. T. Yumoto, "Fire Spread between Two Oil Tanks," *Journal of Fire and Flammability,* 8, p. 494 (1977).
22. T. Dayan and V.L. Tien, "Radiant Heating from a Cylindrical Column," *Combustion Science and Technology,* 9, pp. 51–56 (1974).
23. W.G. May and W. McQueen, "Radiation from Large Liquefied Natural Gas Fires," *Combustion Science and Technology,* 7, pp. 51–56 (1973).
24. M. Klassen and J.P. Gore, "Structure and Radiation Properties of Pool Fires," *NIST-GCR-94-651,* U.S. Department of Commerce, Building and Fire Research Laboratory, National Institute of Standards and Technology, Gaithersburg, MD (1994).
25. H. Koseki and G.W. Mulholland, "The Effect of Diameter on the Burning of Crude Oil Pool Fire," *Fire Technology,* 27, 1, pp. 54–65 (1991).
26. H. Koseki and T. Yumoto, "Air Entrainment and Thermal Radiation from Heptane Pool Fires," *Fire Technology,* 24, 1, pp. 33–47 (1988).
27. H. Koseki and T. Yumoto, "Burning Characteristics of Heptane in 2.7-m Square Dike Fires," *Fire Safety Science—Proceedings of the Second International Symposium* (Wakamatsu et al., eds.), Hemisphere Publishing Corporation, Washington, DC, pp. 231–240 (1989).
28. T. Yumoto, "An Experimental Study on Heat Radiation from Oil Tank Fire," *Fire Research Institute, Report No. 33—Report of Oil Tank Fire,* Fire Research Institute , Tokyo, p. 23 (1971).
29. "Report of Oil Tank Fire Experiment," Japan Society of Safety Engineering (1979).
30. "Report of Oil Tank Fire Extinguishment," Technical Report No. 8, Fire Research Institute (FRI), Tokyo (1976).
31. T.T. Fu, "Heat Radiation from Fires of Aviation Fuels," *Fire Technology,* 10, 1, pp. 54–67 (1973).
32. H.T. Johnson, L.J. Linley, and J.A. Mansfield, "Measurement of the Spatial Dependence of Temperature and Gas and Soot Concentrations within Large Open Hydrocarbon Fuel Fires," *NASA Technical Memorandum 58230,* Lyndon B. Johnson Space Center, Houston (1982).
33. P.K. Raj, K.S. Mudan, and A.N. Moussa, "Experiments Involving Pool and Vapour Fires from Spills of LNG on Water," *Report No. CG-D-55-79, NTIS AD7707,* U.S. Coast Guard, Washington, DC (1979).
34. J. Moorhouse, "Scaling Criteria for Pool Fires Derived from Large-Scale Experiments," *I. Chemical Symposium,* pp. 165–179 (1982).
35. R.S. Alger, R.C. Corlett, A.S. Gordon, and F.A. Williams, "Some Aspects of Turbulent Pool Fires," *Fire Technology,* 15, 2, pp. 142–156 (1979).
36. G.A. Mizner and J.A. Eyre, "Radiation from Liquefied Gas Fire on Water," *Combustion Science and Technology,* 35, pp. 33–57 (1983).
37. D.S. Burgess and M. Hertzberg, "Radiation from Pool Fires," in *Heat Transfer in Fire* (N.H. Afgan and J.R. Beer, eds.), Scripta Book Company, Washington, DC, pp. 413–430 (1974).
38. P.K. Raj, K.S. Mudan, and A.N. Moussa, "Experiments Involving Pool and Vapour Fires from Spills of LNG on Water," *Report No. CG-D-55-79, NTIS AD77073,* U.S. Coast Guard, Washington, DC (1979).
39. "LNG Safety Research Program," *Report IS 3-1,* American Gas Association (1974).
40. P.H. Thomas, "The Size of Flames from Natural Fires," *Ninth Symposium (International) on Combustion,* Combustion Institute, Pittsburgh, pp. 844–859 (1962).
41. G. Heskestad, "Luminous Height of Turbulent Diffusion Flames," *Fire Safety Journal,* 5, 2, pp. 103–108 (1983).
42. G. Heskestad, "Peak Gas Velocities and Flame Heights of Buoyancy-Controlled Turbulent Diffusion Flames," *Eighteenth*

Symposium (International) on Combustion, Combustion Institute, Pittsburgh, pp. 951–960 (1981).

43. J.R. Welker and C.M. Sliepcevich, "Bending of Wind-Blown Flames from Liquid Pools," *Fire Technology,* 2, 2, pp. 127–135 (1966).
44. I. Emori and K. Saito, "Scaling Correlation and Smoke Observations of Oil Tank Fires Under Wind-blown Conditions," *Chemical and Physical Process in Combustion, Fall Technical Meeting, Combustion Institute/Eastern States Section,* Providence, RI, Vol. 67, pp. 1–4 November (1983).
45. D.M. Defaveri, A. Vidili, R. Pastorino, and G. Ferraiolo, "Wind Effects on Diffusion Flames of Fires of High Source Momentum," *Journal of Hazardous Materials,* 22, pp. 86–100 (1989).
46. "Assessing Flame Radiation to External Targets from Pool Fires," *SFPE Engineering Guide,* Society of Fire Protection Engineers (SFPE), Bethesda, MD (1999).
47. M. Shokri and C.L. Beyler, "Radiation from Larger Pool Fires," *SFPE Journal of Fire Protection Engineering,* 4, 1, pp. 141–150 (1989).
48. D. Drysdale, *An Introduction to Fire Dynamics,* Second Edition, John Wiley and Sons, New York, p. 148 (1999).
49. A. Modak, "Thermal Radiation from Pool Fires," *Combustion and Flame,* 29, pp. 177–192 (1977).
50. J.R. Howell, *A Catalog of Radiation Configuration Factors,* McGraw-Hill, New York (1982).
51. H.C. Hottel, "Radiant Heat Transmission," in W.H. McAdams, McGraw-Hill, New York (1954).
52. J.H. McGurie, "Heat Transfer by Radiation," *Fire Research Special Report 2,* HM Stationary Office, London (1953).
53. D.C. Hamilton and W.R. Morgan, "Radiant-Interchange Configuration Factors," *National Advisory Committee for Aeronautic (NACA), Technical Note 2836,* Washington, DC (1952).
54. K.S. Mudan, "Geometric View Factors for Thermal Radiation Hazard Assessment," *Fire Safety Journal,* 12, 2, pp. 89–96 (1987).
55. E.M. Sparrow, "A New Simpler Formulation for Radiative Angler Factors," *Journal of Heat Transfer,* ASME, 85, pp. 81–88 (1963).
56. *Handbook of Military Infrared Technology* (W.L. Wolfe, ed.), Office of National Research, Washington, DC (1965).
57. H.C. Hottel and A.F. Sarofim, *Radiative Transfer,* McGraw-Hill, New York (1967).
58. C.L. Beyler, "Fire Plumes and Ceiling Jets," *Fire Safety Journal,* 11, pp. 53–75 (1986).
59. G. Cox and R. Chitty, *Combust. Flame,* 60, p. 219 (1985).
60. B. McCaffrey, *NBSIR 79-1910,* National Bureau of Standards, Washington, DC (1979).
61. T. Terai and K. Nitta, *Symposium of Architectural Institute of Japan,* Nagoya (1976).
62. H.C. Kung and P. Stavrianidis, *Nineteenth International Symposium on Combustion,* Combustion Institute, Pittsburgh, p. 905 (1982).
63. L.H. Russell and J.A. Canfield, "Experimental Measurement of Heat Transfer to a Cylinder Immersed in a Large Aviation Fuel Fire," *Journal of Heat Transfer* (1973).
64. J.J. Gregory, N.R. Keltner, and R. Mata, Jr., "Thermal Measurements in Large Pool Fires," *Journal of Heat Transfer,* 111, (1989).
65. C. Anderson et al., "Effects of a Fire Environment on a Rail Tank Car Filled with LPG," *Report No. FRA-OR&D 75-31,* U.S. Department of Transportation, Federal Railroad Administration, Washington, DC (1974).
66. F.D. Wayne and K. Kinsella, "Spectral Emission Characteristics of Large Hydrocarbon Pool Fires," *84-WA/HT-74,* The American Society of Mechanical Engineers, New York (1984).
67. A.J. Taylor et al., "Engulfment Fire Tests on Road Tanker Sections," *Rarde Technical Report 7/75,* Controller HMSO, London (1975).
68. W.H. McLain, "Investigation of the Fire Safety Characteristics of Portable Tanks Polyethylene Tanks Containing Flammable Liquids," *Report No. CG-M-1-88,* U.S. Coast Guard, Washington, DC (1988).
69. J.J. Gregory, N.R. Keltner, and R. Mata, Jr., "Thermal Measurements in Large Pool Fires," *SAND-87-0094C,* Sandia National Laboratories, Albuquerque (1987).
70. G.P. Wachtell and J.W. Langhaar, "Fire Test and Thermal Behavior of 150-Ton Lead-Shielded Cask," *DP 1070, Engineering and Equipment, TID-4500,* E.I. DuPont De Nemours and Co., Wilmington, DE (1966).
71. National Academy of Science Committee on Hazardous Materials, Division of Chemistry and Chemical Technology (National Research Council, ed.), *Pressure-Relieving Systems for Marine Cargo Bulk Liquid Containers,* National Academy of Sciences, Washington, DC (1973).
72. K. Moodie et al., "Total Pool Fire Engulfment Trials on a 5-Tonne LPG Tank," *HSE Internal Report No. IR/L/FR/87/27,* London (1987).
73. M. Tunc and J.E.S. Venart, "Incident Radiation from an Engulfing Pool Fire to a Horizontal Cylinder, Part I & II" *Fire Safety Journal,* 8, pp. 81–95 (1984/1985).
74. T.A. Brzustowski, "A New Criterion for the Length of a Gaseous Turbulent Diffusion Flame," *Combustion Science and Technology,* 6, pp. 313–319 (1973).
75. T.A. Brzustowski, "Flaring in the Energy Industry," *Progress Energy Combustion Science,* 2, pp. 129–141 (1976).
76. T.A. Brzustowski, "Flaring: State of the Art," *Loss Prevention,* 11, p. 15 (1977).
77. T.A. Brzustowski and E.C. Sommer, "Predicting Radiant Heating from Flares," *Proceedings of the API Division of Refining,* 53, p. 865 (1973).
78. T.A. Brzustowski, S.R. Gollahalli, M.P. Gupta, M. Kaptein, and H.F. Sullivan, "The Turbulent Hydrogen Diffusion Flame in a Cross Wind," *Combustion Science and Technology,* 11, pp. 29–33 (1975).
79. T.A. Brzustowski, S.R. Gollahalli, M.P. Gupta, M. Kaptein, and H.F. Sullivan, "Radiant Heating from Flares," *ASME Paper 75-HT-4,* American Society of Mechanical Engineers (ASME), New York (1975).
80. H.C. Hottel and W.R. Hawthorne, "Diffusion in Laminar Flame Jets," *Third Symposium (International) on Combustion,* Combustion Institute, Pittsburgh, pp. 254–266 (1949).
81. W.R. Hawthorne, D.S. Weddell, and H.C. Hottell, "Mixing and Combustion on Turbulent Gas Jet," *Third Symposium (International) on Combustion,* Combustion Institute, Pittsburgh, pp. 266–288 (1949).
82. K. Gugan, "Flixborough—A Combustion Specialist's Viewpoint," *Chemical Engineering,* 309, London (1976).
83. F.P. Ricou and D.B. Spalding, "Measurements of Entrainment by Axisymmetrical Turbulent Jets," *Journal of Fluid Mechanics,* II, p. 21 (1961).
84. A.A. Putnam and C.F. Speich, "A Model Study of the Interaction of Multiple Turbulent Diffusion Flames," *Ninth Symposium (International) on Combustion,* Combustion Institute, Pittsburgh, pp. 867–877 (1963).
85. F.R. Steward, "Prediction of the Height of Turbulent Diffusion Buoyant Flames," *Combustion Science and Technology,* 2, pp. 203–212 (1970).

86. B. McCaffrey, "Some Measurements of the Radiative Power Output of Diffusion Flames," *WSS/CI 81-15, Western States Section,* Combustion Institute, Pittsburgh (1981).
87. B. Kalghatgi, "Blow-Out Stability of Gaseous Jet Diffusion Flames, Parts I and II," *Comb. Sci. Tech.,* 26, p. 233–250 (1981).
88. B. McCaffrey and D. Evans, "Very Large Methane Jet Diffusion Flames," *Twenty-First Symposium (International) on Combustion,* Combustion Institute, Pittsburgh, pp. 25–31 (1986).
89. T.A. Brzustowski, S.R. Gollahalli, and H.F. Sullivan, "The Turbulent Hydrogen Diffusion Flames in a Cross-Wind," *Combustion Science and Technology,* II, pp. 29–33 (1975).
90. S.R. Gollahalli, T.A. Brzustowski, and H.F. Sullivan, "Characteristics of a Turbulent Propane Diffusion Flame in a Cross-Wind," *Transactions of CSMC,* 3, pp. 205–214 (1975).
91. G.T. Kalghatki, "The Visible Shape and Size of a Turbulent Jet Diffusion Flame in a Crosswind," *Combustion and Flame,* 52, pp. 91–106 (1983).
92. O.K. Sonju and J. Hustad, "An Experimental Study of Turbulent Jet Diffusion Flame in a Crosswind," *Norwegian Maritime Research,* pp. 2–11 (1984).
93. G.A. Chamberlain, "Developments in Design Methods for Predicting Thermal Radiation from Flares," *Chemical Engineering Research Des.,* 65, p. 299 (1987).
94. A.D. Johnson, H.M. Brightwell, and A.J. Carsley, "A Model for Predicting the Thermal Radiation Hazards from Large-Scale Horizontally Released Nature Gas Jet Fires," *Hazards,* XII, p. 123 (1994).
95. D.K. Cook, M. Fairweather, J. Hammonds, and D.J. Hughes, "Size and Radiative Characteristics of Natural Gas Flares," *Chemical Engineering Research Des.,* 65, pp. 310, 318 (1987).
96. W.J.S. Hirst, "Combustion of Large Scale Jet-Releases of Pressurised Liquid Propane," *Comm.* 1241 (London: Institution of Gas Engineers) (1984).
97. V.H.Y. Tam and L.T. Cowley, "Consequence of Pressurised LPG Release—A Full-Scale Experiment," *Gastect 88, Paper 4.3* (1989).
98. T.A. Brzustowski, "Predicting Radiant Heating from Flares," *Esso Engineering Research and Development Report, EE 15ER.71* (1971).
99. P.R. Oenbring and T.R. Sifferman, "Flare Design—Are Current Methods Too Conservative?" *Hydrocarbon Processing,* pp. 124–129 (1980).
100. S.H. Tan, "Flare System Design Simplified," *Hydrocarbon Processing,* 46, pp. 172–176 (1967).
101. G.R. Kent, "Practical Design of Flare Stacks," *Hydrocarbon Processing,* 43, pp. 121–125 (1964).
102. D. Evans and D. Pfenning, "Water Sprays Suppress Gas-Well Blowout Fires," *Oil and Gas Journal,* 83, pp. 80–86 (1985).
103. B. McCaffrey, "Jet Diffusion Flame Suppression Using Water Sprays, An Interim Report," *Comb. Sci. Tech.,* 40, pp. 107–136 (1984).
104. B. McCaffrey, "Momentum Diffusion Flame Characteristics and the Effects of Water Spray," *Comb. Sci. Tech.,* 63, pp. 315–335 (1989).
105. J.F. Straitz III, J.A. O'Leary, J.E. Brennan, and C.J. Kardan, "Flare Testing and Safety," *Loss Prevention,* II, pp. 23–30 (1977).
106. W.W. Yuen and C.L. Tien, "Simple Calculation Scheme for the Luminous Flame Emissivity," *Sixteenth Symposium (International) on Combustion,* Combustion Institute, Pittsburgh, pp. 1481–1487 (1976).
107. G. Fumarola, D.M. de Faveri, R. Pastorino, and G. Ferraiolo, "Determining Safety Zones for Exposure to Flare Radiation," *Institute of Chemical Engineering Symposium, Series 82, Loss Prevention and Safety Promotion,* pp. G23–G30 (1983).
108. P.R. Oenbring and T.R. Sifferman, "Flare Design Based on Full-Scale Plant Data," *Forty-Fifth Midyear Meeting, API Refining Department Proceedings,* 59, Houston (1980).
109. S. Galant, D. Grouset, G. Martinez, P. Micheau, and J.B. Allemand, "Three-Dimensional Steady Parabolic Calculations of Large Scale Methane Turbulent Diffusion Flames to Predict Flare Radiation Under Cross-Wind Conditions," *Twentieth Symposium (International) on Combustion,* Combustion Institute, Pittsburgh, pp. 531–540 (1984).
110. L. Cowley and M. Prichard, "Large-Scale Natural Gas and LPG Jet Fires and Thermal Impact on Structures," *GASTECH 90 Conference,* Amsterdam (1990).
111. A. Parker, "Evaluating High-Temperature Intumescent Insulation Materials Under Fire and Blast Conditions," *Insulation Materials: Testing and Applications: Third Volume, ASTM STP 1320* (Graves and Zarr, eds.), American Society for Testing and Materials, Philadelphia (1997).
112. Wighus and Dransgsholt, "Impinging Jet Fire Experiments—Propane 14 MW Laboratory Tests," *Report STF25 A92026, SINTEF NB,* Norwegian Fire Research Laboratory (1993).
113. K.S. Mudan, "Hydrocarbon Pool and Vapor Fire Data Analysis," *U.S. DOT Report DE-AC01-83EP16008,* U.S. Department of Transportation, Washington, DC (1984).
114. J.A. Fay and D.H. Lewis, "Unsteady Burning of Unconfined Fuel Vapor Clouds," *Sixteenth Symposium (International) on Combustion,* Combustion Institute, Pittsburgh pp. 1397–1405 (1976).
115. P.K. Raj and H.W. Emmons, "On the Burning of a Large Flammable Vapor Cloud," *Combustion Institute/Central and Western States Sections (Joint Meeting): Flammability and Burning Characteristics of Materials and Fuels,* San Antonio, Combustion Institute, Pittsburgh, pp. 1–23 (1975).
116. A.F. Roberts, "Thermal Radiation Hazards from Releases of LPG from Pressurized Storage," *Fire Safety Journal,* 4, pp. 197–212 (1982).
117. Center for Chemical Process Safety, *Guidelines for Evaluating the Characteristics of Vapor Cloud Explosions, Flash Fires, and BLEVE's,* American Institute for Chemical Engineers, New York, pp. 157–180 (1994).
118. K. Hasegawa and K. Sata, "Study of Fireball Following Steam Explosion of *n*-Pentane," *Loss Prevention and Safety Promotion,* 2, p. 297 (1977).
119. K. Hasegawa and K. Sata, "Experimental Investigation of the Unconfined Vapor Cloud Explosions of Hydrocarbons," *Technical Memorandum 12,* Fire Research Institute, Tokyo (1978).
120. H.C. Hardee and D.O. Lee, "Thermal Hazard from Propane Fireballs," *Trans. Plan. Tech.,* 2, pp. 121–128 (1973).
121. R.P. Pape et al., "Calculation of the Intensity of Thermal Radiation from Large Fires," *Loss Prevention Bulletin,* 82, pp. 1–11 (1988).
122. D.M. Johnson, M.J. Pritchard, and M.J. Wickens, "Large Scale Catastrophic Releases of Flammable Liquids," *Commission of the European Communities Report, Contract No. EV4T.0014.UK(H),* Brussels (1990).
123. SFPE, *Predicting 1st and 2nd Degree Skin Burns from Thermal Radiation,* Society of Fire Protection Engineers, Bethesda, MD (2000).
124. K. Buettner, "Effects of Extreme Heat and Cold on Human Skin, II. Surface Temperature, Pain and Heat Conductivity in Experiments with Radiant Heat," *J. Ap. Phys.,* 3, p. 703 (1951).
125. J.D. Hardy, I. Jacobs, and M.D. Meizner, "Thresholds of Pain and Reflex Contraction as Related to Noxious Stimulation," *J. Ap. Phys.,* 5, pp. 725–739 (year?).

126. N. Bigelow, I. Harrison, H. Goodell, and H.G. Wolf, "Studies on Pain: Quantitative Measurements of Two Pain Sensations of the Skin, with Reference to the Nature of Hyperalgesia of Peripheral Neuritis," *J. of Clinical Invest.,* 24, pp. 503–512 (1945).

127. A.M. Stoll and L.C. Greene, "Relationship between Pain and Tissue Damage Due to Thermal Radiation," *J. Ap. Phys.,* 14, pp. 373–382 (1959).

128. A.K. Mehta, F. Wong, and G.C. Williams, "Measurement of Flammability and Burn Potential of Fabrics," *Summary Report to NSF—Grant #GI-31881,* Fuels Research Laboratory, Massachusetts Institute of Technology, Cambridge (1973).

129. G. Mixter, "The Empirical Relation between Time and Intensity of Applied Thermal Energy in Production of 2+ Burns in Pigs," *University of Rochester Report No. UR-316, Contract W-7044 eng49,* New York (1954).

130. G. Mixter, "Thermal Radiation Burns beneath Fabric Systems," *Annals of the New York Academy of Sciences,* 82, pp. 701–713 (1959).

131. N.A. Eisenberg, et al., "Vulnerability Model. A Simulation System for Assessing Damage Resulting from Marine Spills," *NTIS AD-AD015-245,* Springfield, VA (1975).

CHAPTER 12

Behavioral Response to Fire and Smoke

John L. Bryan

Introduction

The determination of the behavioral response of individuals in fire incidents has been examined for approximately 40 years by research studies. Individuals were administered a questionnaire by fire department personnel at the time of a fire incident,[1,2] were mailed questionnaires, or were interviewed following the fire incident. An individual's behavioral response in a fire incident appears to be affected by

1. The variables of the building in which the fire incident occurs
2. The perceived physical cues of the fire severity at the time the individual becomes aware of the fire

The behavioral response of the building occupants may vary if they perceive physical cues (an odor of smoke), in contrast to observed cues (smoke obscuring the means of egress). There is some evidence that the recognition of fire protection systems, provided within the building, may be a factor in an individual's perception of the severity of the fire incident threat. It would appear that the most important individual decisions and behavioral responses usually involve perceived life-threatening situations that occur in the initial stages of the fire incident, prior to fire department arrival. In their studies of health care facilities, Lerup et al.[3] have indicated the importance of the participants initial behavior in the following manner:

> In the process of investigating these case studies we have come to believe that the period between detection of the fire and the arrival of the fire department is the most crucial life saving period in terms of the first compartment. (The area in direct contact with the room of origin and the fire.)[3]

Dr. John L. Bryan is Professor Emeritus, Department of Fire Protection Engineering at the University of Maryland. Currently a consultant located in Frederick, Maryland, his major interest is in the field of human behavior in fires.

The behavioral response of the individuals intimately involved with the initiation of the fire, or those who were aware of the initial fire cue, often appeared to be a determinant to the outcome of the fire incident. It should be realized that altruistic behavior observed in most fire incidents, with the behavioral response of the occupants in a deliberate, purposeful manner, appears to be the most frequent mode of behavioral response. The nonadaptive flight or panic type behavioral response appears to be an infrequent, unusual, or unique participant behavioral response in most fire incidents.

Awareness of Cues

The manner in which an individual is alerted to the occurrence of a fire may predispose the perception of the threat involved. The alerting means, communication mode, and message content were discussed by Keating and Loftus,[4] in their study on vocal alerting systems in buildings. It would appear that variations in voice quality, pitch, or volume, as well as the content of the message, may provide reinforcing threat cues to occupants.

Proulx and Sime,[5] in their study involving evacuation drills in an underground rapid transit station, found the use of directive public announcements with an alerting alarm bell was the most conducive to creating an immediate effective evacuation. Ramachandran,[6] in his review of the research on human behavior in fires in the United Kingdom since 1969, has summarized the effectiveness of alarm bells as awareness cues in the following manner:

> The response to fire alarm bells and sounders tends to be less than optimum. There is usually skepticism as to whether the noise indicated a fire alarm and, if so, is the alarm merely a system test or drill?[6]

Ramachandran[7] indicated that the development of "informative fire warning systems," which utilize a graphic display with a computer-generated message and a high-pitched alerting tone, has reduced the observed

delay times in the initiation of practice evacuations. Cable,[8] in his study of the response times of staff personnel to the fire alarm signal in Veterans Administration hospitals, found the greatest delay in response time with the coded alarm-bell-type systems. Kimura and Sime[9] found, in the evacuation of two lecture halls with college students, the verbal instructions of the lecturer were the determining factor in the choice of the use of the fire exit over the normal entrance and exit. The research literature developed from practice evacuations tends to indicate that the use of verbal directive informative messages may be the most effective in reducing the delay in evacuation initiation.

However, it should be noted that if the verbal directive messages are in conflict with other awareness cues, (e.g., the odor or sight of smoke) the credibility of the message may be questioned and the information disregarded by the occupants. One of the few documented cases of this type of situation occurred in the South Tower of the World Trade Center on April 17, 1975. As reported by Lathrop,[10] the fire occurred at approximately 9:04 a.m. in a trash cart in a storage area on the 5th floor, adjacent to an open stairway door. This allowed the smoke to infiltrate the 9th through 22nd floors. The occupants of these floors moved into the core area of the building. At 9:10 a.m., a verbal message from the building communications center monitoring these core lobby areas advised the occupants to remain calm and return to their office areas. In spite of this announcement, the occupants remained in the core lobby areas and became more concerned about the smoke conditions. Thus, with the occupants on the affected floors becoming more anxious, an evacuation message was announced at 9:16 a.m.

Burns[11] reported on the explosion and fire on February 26, 1993, which severely affected both towers of the World Trade Center, and the Vista Hotel, wherein simultaneous occupant evacuations occurred. The explosion disrupted the structure's communications center, and the occupants, having experienced the explosion, loss of power, and floor areas infiltrated with smoke within minutes, evacuated without the established verbal directional announcements utilized in practice evacuations.

Fahy and Proulx, in their questionnaire study of 406 trained fire wardens located in both towers of the World Trade Center at the time of this explosion and fire, found these individuals reported being alerted in the follow manner:[12]

> Respondents mentioned hearing or feeling the explosion, losing lights or telephones, noticing smoke or dust, hearing sirens and alarms, getting information from others, and seeing other people evacuating the area.

Bryan[1] found that most of the participants in a study of residential fire incidents became aware of the fire incident by the odor of the smoke. However, if the categories "notified by others" and "notified by family" are combined in this residential fire incident study, the process of personal notification becomes the most frequent means of the initial awareness of the fire incident. (See Table 3-12.1.) The noise category included sounds generated from persons moving downstairs, persons moving through corridors, and other related fire incident sounds, including the breaking of glass and the movement of fire department apparatus.

Table 3-12.2 compares the means of awareness of the British population from Wood's study[2] and the U.S. population from Bryan's study.[1] The number of categories were reduced (from the 11 categories indicated in Table 3-12.1) because the British study had fewer categories. U.S. population responses were adapted to the British categories. There was only one significant difference in the means of awareness between the two populations, with 15 percent of the British population having become aware of the fire incident upon observing flame, as contrasted with 8.1 percent of the U.S. population.

Concerning the awareness of the occupants to smoke detectors, Berry[13] indicated in his study of the National Fire Protection Association–recommended smoke detector noise level of 85 dBA[14] that individuals with hearing impairments, or those taking sleeping pills or medication, may require a detector noise level exceeding 100 dBA. Cohen[15] has indicated that flashing or activated visual light signals are effective indicators of fire alarm system activation in occupancies populated by hearing impaired persons. NFPA *101,® Life Safety Code,®* in 1981, initially permitted the flashing of the exit signs with the activation

Table 3-12.1 ***Means of Awareness of the Fire Incident by the Study Population[1]***

Means of Awareness	Participants	Percent
Smelled smoke	148	26.0
Notified by others	121	21.3
Noise	106	18.6
Notified by family	76	13.4
Saw smoke	52	9.1
Saw fire	46	8.1
Explosion	6	1.1
Felt heat	4	0.7
Saw/Heard fire department	4	0.7
Electricity went off	4	0.7
Pet	2	0.3
$N = 11$	569	100.0

Table 3-12.2 ***Means of Awareness of the Fire Incident for the British and the U.S. Study Population[1,2]***

Means of Awareness	British Percent	U.S. Percent	$P_1 - P_2$	$SE_{P_1 - P_2}$	CR
Flame	15.0	8.1	6.9	1.64	4.21[a]
Smoke	34.0	35.1	1.1	2.27	0.48
Noises	9.0	11.2	2.2	1.41	1.56
Shouts and told	33.0	34.7	2.7	2.25	1.20
Alarm	7.0	7.4	0.4	1.23	0.33
Other	2.0	2.8	0.8	0.70	1.14
$N = 6$	2193	569			

[a]Critical ratio significant at or above the 1 percent level of confidence.

of an audible fire alarm system. This provision has been continued in the 2000 edition.[16]

Kahn[17] conducted a study with 24 male subjects relative to their being awakened by an audible smoke detector alarm signal and their identification of supplemental fire cues. Kahn found these subjects slept through the alarm signals with a signal-to-noise ratio of 10 dBA at their ears, and consistently failed to identify the awakening smoke detector cue as well as radiant heat and smoke odor cues as fire warnings. Noble et al.[18] have indicated the alarm signal-to-noise ratio is attenuated by physical surroundings. An audible smoke detector or alarm signal may be reduced by 40 dBA in passing through a ceiling or wall, and by 15 dBA in passing through a door. In addition, it was found that the signal could be masked to an ineffective level by a typical residential air conditioner with a noise level of 55 dBA.

The recognition of ambiguous fire incident cues as indicators of a possible emergency condition, appears to be inhibited by the presence of other persons in some occupancies. Latane and Darley,[19] in their experimental studies of the inhibition of adaptive behavioral responses to emergencies, created an experimental situation involving college students. While the students were completing a written questionnaire, the experimenters would introduce smoke into the room through a small vent in the wall. If the subject left the room and reported the smoke, the experiment was terminated. If the subject had not reported the presence of the smoke within a six-minute interval from the time the smoke was first noticed, the experiment was considered completed. Subjects alone in the room reported the smoke in 75 percent of the cases. When two passive subjects were introduced in the room with each subject, only 10 percent of the groups reported the smoke. When the total experimental group consisted of three unknowing subjects, one of the individuals reported the smoke in only 38 percent of the groups. Of the twenty-four persons involved in the eight unknowing subject groups, only one person reported the smoke within the first four minutes of the experiment. In the situations involving subjects alone in a room, 55 percent of the subjects had reported the smoke within two minutes and 75 percent reported smoke in four minutes.

Latane and Darley reported that noticing the smoke was apparently delayed by the presence of other persons, with the median delay of 5 seconds for single subjects and 20 seconds for both of the group conditions. These results would appear to indicate the inhibiting influences that may be imposed on individuals in public places. Latane and Darley reported the behavioral response of nine of the unknowing subjects in the ten passive research situations as follows:

> The other nine stayed in the waiting room as it filled up with smoke, doggedly working on their questionnaire, and waving the fumes away from their faces. They coughed, rubbed their eyes, and opened the window but did not report the smoke.[19]

Latane and Darley suggest that, while trying to interpret ambiguous threat cues as to whether a situation requires a unique response, the individual is influenced by the behavioral response of others who are exposed to the identical cues. If these other individuals remain passive and appear to interpret the situation as a nonemergency, this inhibiting social influence may reinforce this nonemergency interpretation for an individual. This behavioral experiment may help explain the reported tendency of persons (1) to disregard initial ambiguous fire incident cues, or (2) to interpret the cues as a nonemergency condition, when the fire incident occurs with a social audience of other persons, as in a restaurant, motion picture theater, or department store. This experimental study may also be helpful in understanding the incidents reported to fire departments that have been delayed by occupants for periods of minutes or even hours. In the report of the Arundel Park fire,[20] several of the participants indicated that when they reentered the hall after observing the fire from outside the building, they warned other participants and suggested they leave, but they were laughed at and the warning was disregarded.

Latane and Darley indicated that social inhibition, diffusion of responsibility, and mimicking appear to be primarily responsible for the inhibition of adaptive and assistance behavior responses by participants in emergency situations. It would appear that the inhibition of behavioral responses in the early stages of a fire incident (when the fire incident cues are relatively ambiguous) may predispose participants to a nonadaptive type of flight behavior, since the available evacuation time has been expended. In some fire incidents it appears to be difficult to get occupants of a building to evacuate because of the variables of social inhibition and diffused responsibility. The tendency to mimic the interpretation of cues and the behavior responses of others (as established by Latane and Darley) appears to be a frequent occurrence in fire incidents in restaurants, hotels, and other places of public assembly.

Perception of the Fire Incident

Withey[21] has examined seven psychological and physical processes that an individual may utilize in an attempt to perceive, identify, structure, and evaluate the situational fire incident cues. It would appear that six of these individual perceptual processes, as presented in Figure 3-12.1, may be critical factors in the perception of a fire.[22]

Recognition: The process of recognition occurs when the individual identifies the ambiguous fire cues as an indication of a fire incident, and thus becomes aware of the fire. The initial perceptual cues may be very ambiguous, and may not positively indicate a fire incident. The cues are produced by a continuous dynamic physical process, with an increasing intensity due to the fluid mechanics properties of flame, heat, and smoke production. Withey also indicated that the usual mental state and predisposition of an individual is to recognize threat cues in terms of the most probable occurrence, typically as related to a prior personal experience, and in the form of an optimistic favorable outcome. The optimistic outcome aspect of an individual's perception of fire incident cues may be a result of the influence of the individual's concept of a personal invulnerability to risk.

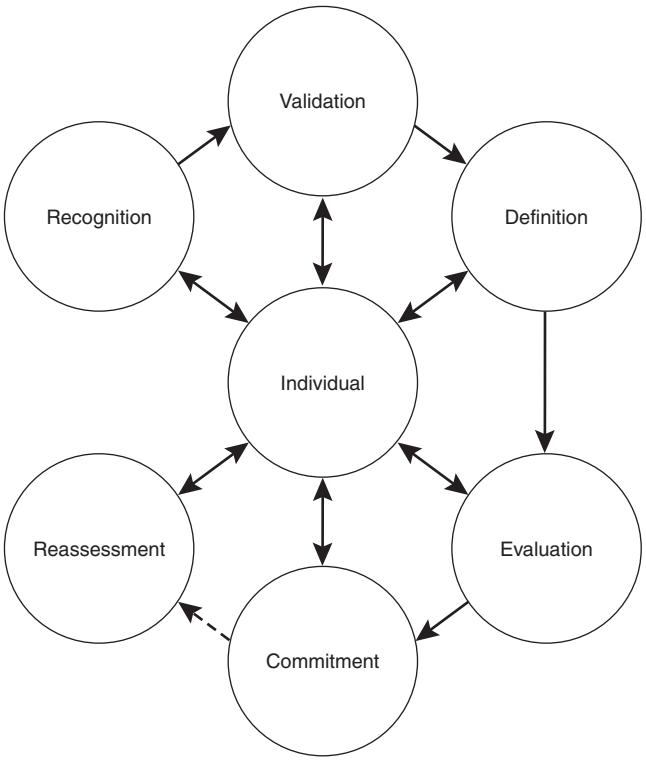

Figure 3-12.1. ***The decision processes of the individual in a fire.***

The concept of threat recognition appears to be a very important problem in fire protection. The decision that initiates the activation of the fire alarm, the evacuation of the building occupants, or suppression of the fire may be delayed or postponed if the individuals involved do not perceive the cues as indicative of an emergency fire situation. Apparently, the ambiguous nature of the fire cues, and the unstructured nature of many public and social groups, require the appearance of significant amounts of smoke, or sudden and threatening flames before most individuals without specialized fire prevention instruction or prior fire incident experiences perceive a threatening fire to be present.

Validation: The process of validation apparently consists of the individual attempting to validate an initial perception of the fire cues, primarily by seeking verbal reassurance of the minor and insignificant character of the fire incident. When the perceived cues are ambiguous, however, the individual often attempts to obtain additional information. Thus, the person is aware that something is happening in the immediate environment, but is not sure exactly how the cues define the event. The process of validation is often conducted by persons exposed to the identical cues. In a study concerned with the individual's perception of cues from the explosion of a fireworks plant, Killian[23] found from the study population of 139 persons that 85 individuals (61 percent) obtained definitive information as to the source and nature of the explosion or smoke, from someone in person or someone who telephoned.

Latane and Darley[19] established that the physical presence of others during the recognition and validation processes inhibit and structure the behavioral responses of an individual.

Definition: The definition process is considered to be the procedure whereby the individual attempts to relate the information concerning the fire to the perceived and contextual variables, including the qualitative nature of the fire relative to their location, the magnitude of deprivation implied by the fire, and the time context and sequence of the implied deprivation. The generation of stress and anxiety in the individual appears to be most rapid and severe before the individual defines the initial ambiguous cues with structure for the situation. It is often apparent to the individual that the situation requires structure and interpretation before the cues can be defined and assimilated. The role concept of the individual, as well as the physical environment created by the fire incident, appear to be critical factors in the situation, relative to the personalization of the fire threat. The most important physical aspects in the definition process are the generation, intensity, and propagation of smoke, flames, and thermal exposure.

Evaluation: The individual's process of evaluating the fire incident may be described as the cognitive and psychological activities necessary for the individual to respond to the threat. The individual's ability to develop alternate strategies to cope with the fire incident—through psychological and physiological mechanisms that are designed to reduce the stress and anxiety levels of the individual—provide a basis for an initial decision to be formulated for an overt behavioral response. Because of the brief time span involved in the generation and propagation of the fire, it should be remembered that these cognitive processes (including the process of evaluation) may have to be accomplished within several seconds.

Sime[24] has emphasized the importance of the individual's perception of the time available for evacuation or to obtain a refuge, as being an estimation by the individual of the fire threat. Thus, he indicates the perceived time available is dependent upon the information and communication provided to the occupants concerning the location and development of the fire.

The individual's evaluation process may include the formulation of adaptation, escape, or defense procedures. Therefore, the variables of the physical environment in which the fire occurs may be critical in the evaluation process. These determinants and critical variables may be (1) the physical location of the individual in relation to the means of egress, (2) the location and proximity of other members of the population at risk, (3) the physically perceived untenable effects of the fire, and (4) the overt behavioral response of other individuals in the population. During the cognitive process of evaluation, the individual may decide to evacuate the building (flight) or to obtain a fire extinguisher or activate a manual fire alarm station (fight). During the evaluation process, the individual is

very perceptive to the overt actions and communications of the other members of the at-risk population. Thus, the behavioral responses of observed individuals may be mimicked, resulting in mass adaptive or nonadaptive behavior instead of selective individualized behavior.

In his classic studies of nonadaptive group behavior, Mintz[25] developed the concept of this mode of behavior being directly dependent upon the individual's perception of the reward structure of the situation. A heterogeneous population within a building, having perceived and defined a fire threat, would probably initially perceive a reward structure conducive to group and individual cooperative and adaptive behavior responses. Theoretically, all occupants should be able to proceed to and reach the provided means of egress. However, because of the locations of the exits and the relative positions of the individuals within the area, the perceived reward structure for the individuals located farther from the means of egress could provide for the initiation of competitive behavior between occupants. With cooperative behavior, some individuals could perceive that it would be impossible for them to reach an exit in time to escape the deprivation effects of the fire. Once the pattern of competitive behavior becomes observable by one or more individuals, this pattern may become the norm for the group and result in selective, individual competitions to reach the means of egress. Such competitive behavior may be normalized in the group by each individual's perception of the reward structure, or their probability of obtaining the reward. In this fire the reward is to obtain the means of egress.

In the individual's evaluation process, cultural, sociological or economic influences, or the assumption of a particular individual psychological role may be critical to the formulation of behavioral response strategies. The individual in a familiar role, suitable for the fire incident (i.e., those with fire fighting training or experience) and in familiar surroundings, may experience less anxiety and will probably select more adaptive behavior responses than individuals in an unfamiliar role who are confronted with the occurrence of an unfamiliar threat, in unfamiliar surroundings.

Jones and Hewitt[26] conducted detailed interviews with 40 occupants of a 27-story office building who had evacuated the building during a fire incident. (It should be noted that the fire occurred at 9:00 p.m., when the fire management plan was not in effect due to the reduced occupancy of the building.) In this situation it appeared that the leadership and the evacuation group formation were related to the fire training and the normal roles of the occupants. These investigators found the relationship between the occupancy roles and the normal or emergent leadership of the occupants to be the critical factor in a successful evacuation, with the following variables:

> the social and organizational characteristics of the occupancy, including what a person knows (or believes) of the situation, whether the person is alone or part of a group, the normal roles that people hold within the occupancy, and the organizational structure or framework. One factor that appears to be related to the chosen evacuation strategy of an occupant is the presence of leadership and the form which that leadership takes.[26]

Horiuchi, Murozaki, and Hokugo[27] reported on a questionnaire study of 458 occupants of an eight-story office building involved in a fire incident. These researchers found significant differences between the normal occupants of the building (familiar with the building) and those occupants attending training sessions in the building (not familiar with the building), relative to their actions, selection of evacuation routes, and effectiveness in achieving an exit. The regular occupants of the building engaged in fire-fighting actions and alerted or assisted other occupants, while the occupants not familiar with the building primarily engaged in evacuation behavior.

Commitment: The process of commitment consists of the mechanisms utilized by the individual to initiate the behavioral responses necessary to achieve the behavioral response strategies that were formulated in the evaluation process. This overt behavioral response to the perceived threat of the fire incident results in completion, partial completion, or noncompletion of the response strategy. Thus, if the response strategy is not completed, the individual immediately becomes involved in the cognitive process of reassessment and commitment. If the behavioral response results in success, however, the anxiety and stress created by the situation are relieved for the individual, even though the fire incident may have increased in severity.

Reassessment: The process of reassessment and overcommitment may be the most stressful of the individual's cognitive processes, because of the failure of previous attempts to achieve the formulated response strategies to the fire incident. More intense psychological and physiological energy is allocated to the behavioral responses, and the individual tends to become less selective in the risks involved in the behavioral response. If successive failures are encountered, the individual becomes more frustrated, anxiety levels increase, and the probability of success decreases. At the Arundel Park fire incident, the number of persons who selected windows as a means of escape from the building increased when the individuals were involved in a secondary evacuation response.[20]

This analysis has been an attempt to understand the cognitive processes of the individual through an examination of the variables related to the processes of recognition, validation, definition, evaluation, commitment, and reassessment. It should be noted that these cognitive processes are dynamic and are constantly being modified in relation to the magnitude, velocity, and intensity of their covert and overt responses. The behavioral responses of the individuals (relative to their psychological and physiological dynamic activity) will probably be below normal during the recognitive process, when the individual is concentrating on the ambiguous perceptual cues. During the process of validation and the definition of the threat, there is usually overt communication and verbalization with adjacent members of the risk population. The period of above normal activity appears to occur

initially during the process of commitment, and often transfers to a hyperactive level during the process of reassessment and recommitment. It should be remembered that the stress and anxiety generated will tend to increase for the individual as these cognitive and physical behavioral responses result in failure to achieve risk reduction through evacuation or fire control.

The physical variables of the fire incident consist of the flame appearance, the flame, smoke or heat proximity, and the velocity of flame or smoke propagation. These fire incident variables will tend to predispose the individual to a higher level of behavioral response activity, considering the individual's perception of these variables as increasing the personal risk. However, it should be noted that during the process of reassessment and commitment, the individual's physical activity may reach the hyperactive level, or at the other extreme, be expressed as a state of complete physical immobility with a subnormal activity level and a complete loss of the ability to communicate in a coherent manner. These individuals may appear to perceive the fire incident as too severe for their capabilities of adaptability. They appear to be overwhelmed by the stress generation and abandon their attempts to formulate a response strategy. Thus, in ceasing to attempt any cognitive or physical adaptive behavioral response, they instead adopt a complete cognitive withdrawal from the fire incident environment through psychological withdrawal from reality. A schematic presentation of the dynamics of the behavioral response activity levels of the individual are illustrated in Figure 3-12.2.

Breaux et al.[28] have developed a conceptual model of the cognitive decision processes of the individual in the fire incident. Instead of the six processes adopted from Withey,[21] Breaux et al. have utilized only three processes: recognition/interpretation, behavior (with either action or inaction), and the outcome of the action (that involves the evaluation and long term effects of the behavior.) The evaluation of the behavior is similar to the process of reassessment in Withey's conceptual model. Both the recognition/interpretation process and the behavior process have cognitive inputs that are critical to the decision-making processes. These cognitive inputs involve past experience, the factors immediately arising, and the current state factors, which all impact the recognition/interpretation process. Breaux et al. have emphasized that the individuals in the fire incident may not know precisely at an early stage that they are involved in a fire, and may not know where the fire has developed in relation to their location

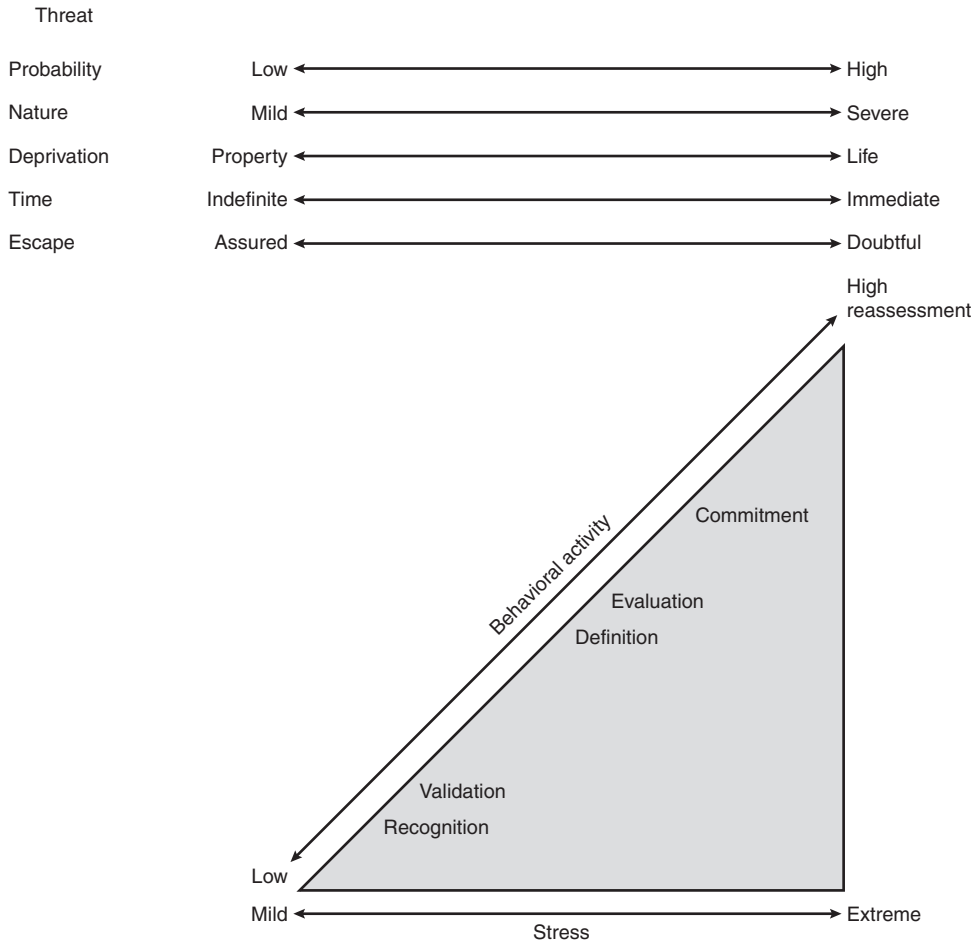

Figure 3-12.2. ***The behavioral activity dynamics of the individual in a fire incident.***

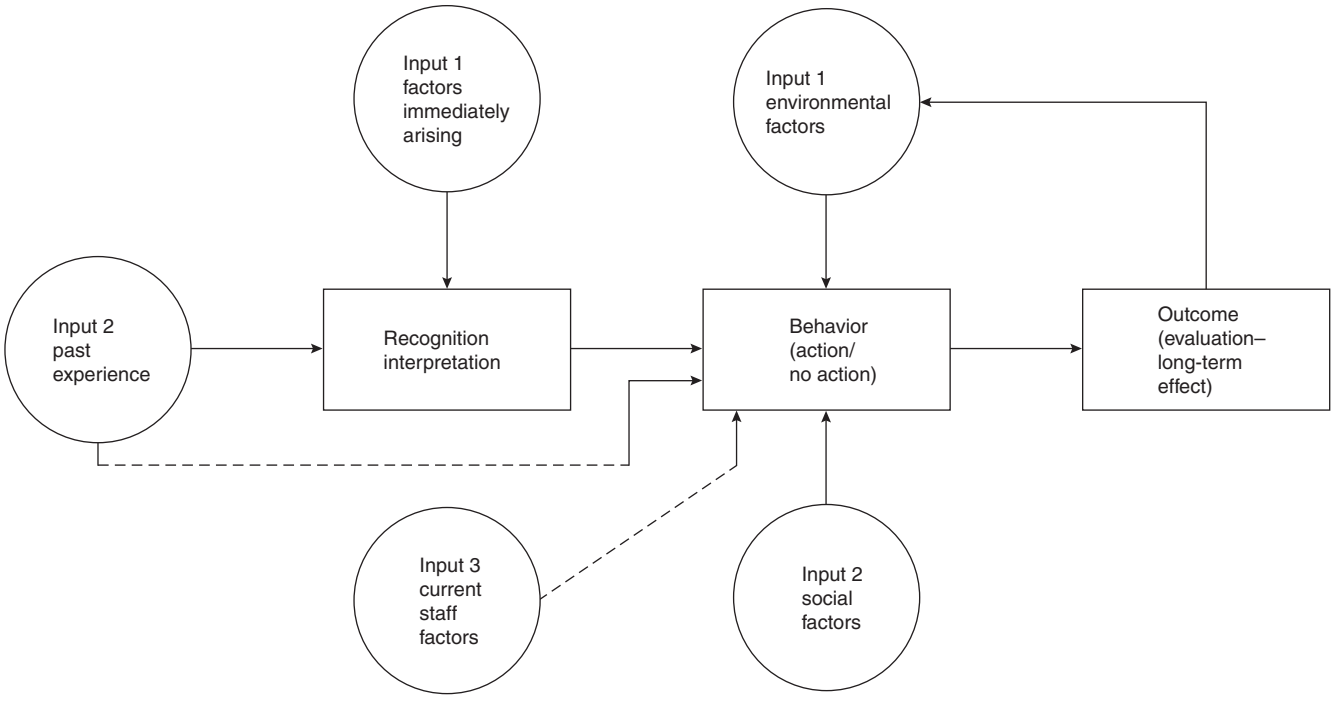

Figure 3-12.3. ***Suggested heuristic systems model of human behavior in fire incidents.***

in the building, or their specific location relative to the means of egress. The conceptual model developed by Breaux et al. is shown in Figure 3-12.3.

Bickman et al.[29] have modified the conceptual model of Breaux et al. into one that involves fire as a physical event, with the individual processes of the detection of cues, the definition of the situation, and the coping behavior. Bickman et al. have developed assumptions relative to the behavior responses that increase the probability of detection and the probability of fire suppression, and thus affect the various activities in the coping behavior aspects of their conceptual model.

Proulx[30] has developed a stress model to demonstrate the generation and various levels of stress within the individual involved in the decision process during a fire incident. This stress model is illustrated in Figure 3-12.4, and should be compared with the behavioral activity dynamics of the individual in a fire incident presented in Figure 3-12.2. The left side of Figure 3-12.4 indicates the information to be processed by the individual, and the right side indicates the resulting emotional state. The five loops in the model are described by Proulx in the following manner:

> The first loop of the stress model starts with the perception of ambiguous information. This information is decoded in the processing system (PS in the figure) for interpretation. Given that the available information may not allow for a straightforward assessment of the situation, people will at first minimize or deny the situation. These defensive strategies of avoidance lead to an absence of reaction.

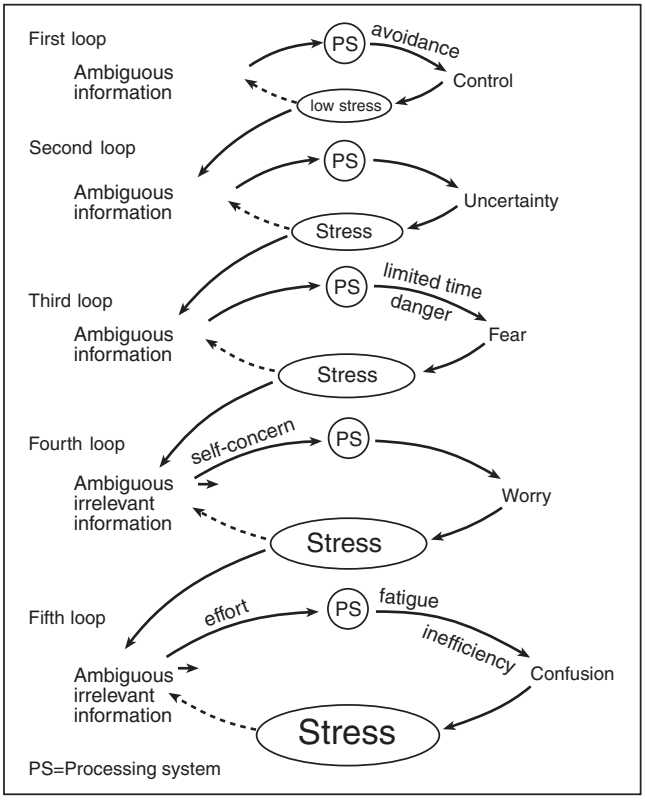

Figure 3-12.4. ***Stress model of people in a fire.[30]***

Although individuals may vary considerably in their appraisal of the same event, the repeated perception of ambiguous information will eventually generate a state of uncertainty which will then induce a feeling of stress. Some time can be spent going repeatedly through this second loop of the stress model.

The third loop of the stress model is related to the interpretation of the situation as an emergency. The thicker line around the processing system expresses the pressure of the overload of information with which the person tries to deal at once. The fear felt by the person is a manifestation of a specific appraisal of the environment.

The fourth loop of the model relates to the person's processing of irrelevant information and is represented by the very thick line around the processing system. This irrelevant information creates worry and more stress. The irrelevant information, created by the person, is caused by concern for his or her own performance in coping with the situation. Perceived feelings of arousal and fear, uncertainties regarding how to proceed with the problem, difficulties in interpreting what exactly is going on, and self-estimation of the efficiency of already-applied actions will become additional information to process.

The fifth and last loop of the model supposes an investment of more mental effort to master the problem, momentarily reducing the pressure on the processing system but resulting in fatigue and inefficiency manifested in a state of confusion.[30]

Proulx indicates that definitive, valid, and directive information provided to occupants of a building in a fire incident are the most effective stress reducers and thus tend to minimize the response delays created in the first and second loops of the stress model.

Chubb[31] identified a model of incident command procedure decision processes used by fire department officers, with the possibility that it be used for improvement and training in the decision process for building occupants in a fire situation. The decision model was developed from the theory of naturalistic decision-making, which has evolved from studies of decision-makers in complex, time-critical situations. The critical variables of the naturalistic decision-making theory appear to have many of the environmental and psychological features of the fire situation involving building occupants. Chubb has identified these critical variables as

- Ill-defined goals and ill-structured tasks
- Uncertainty, ambiguity, and missing data
- Shifting and competing goals
- Dynamic and continually changing conditions
- Real-time reactions to changed conditions
- Time stress
- High stakes
- Organizational goals and norms
- Experienced decision-makers[31]

Figure 3-12.5 is an illustration of the recognition-primed decision (RPD) model developed by Klein[32] from the studies of fire department officers. Chubb has correctly indicated that the limitation of this model, when applied to building occupants, is the lack of the fire officers' training and experience in building fires. That is, the static abilities relative to the mental and physical capabilities of building occupants are expected to be more varied and limited than those of fire officers. Chubb indicates that successful recognition-primed decision-making is dependent on the occupant training and practice of the fire safety plans, with the decision support system in the building consisting of egress signs, emergency lighting, and verbal communication systems.

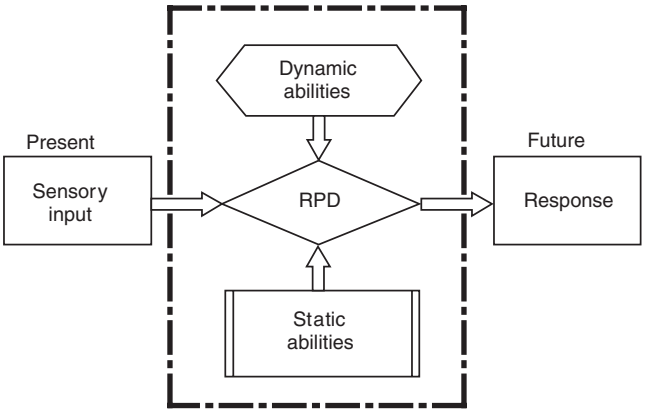

Figure 3-12.5. ***Recognition-primed decision model.[31]***

Behavioral Responses of Occupants

A study by Wood[2] involved 952 fire incidents and 2,193 individuals interviewed by fire department personnel at the fire incident scene in Great Britain. Wood found the most frequent behavioral responses to fire could be categorized as evacuation of the building, fighting or containing the fire, and the notification of other individuals or the fire brigade. Bryan[1] found similar types of broad categorization of behavioral response in a United States study primarily concerned with residential occupancies. This residential fire incident study involved interviews of 584 participants in 335 fire incidents, by fire department personnel who used a structured questionnaire at the scene of the fire incident.

Table 3-12.3 presents the initial first actions in the studies of both the British and United States populations. The behavior of the individuals in both studies varied relative to their gender, with the female and male behavior being primarily divided along culturally determined primary group roles. The males were predominantly more active in fighting the fire, while the females were predominantly concerned with alerting others and assisting others in evacuating the building.

There were ten statistically significant differences between the British and United States populations. The United States population was predominant at the five or one percent level of confidence for the first actions of "notified others," "got dressed," "got family," "left area," and "entered the building." A greater percentage of the British population engaged in the first actions of "fought fire," "went to fire area," "closed door to fire area," "pulled fire alarm," and "turned off appliances."

Table 3-12.3 ***First Actions of the British and U.S. Study Populations[1,2]***

Actions	British Percent	U.S. Percent	$P_1 - P_2$	$SE_{P_1 - P_2}$	CR
Notified others	8.1	15.0	6.9	1.38	5.00[a]
Searched for fire	12.2	10.1	2.1	1.51	1.39
Called fire department	10.1	9.0	1.1	1.40	0.79
Got dressed	2.2	8.1	5.9	0.85	6.94[a]
Left building	8.0	7.6	0.4	1.27	0.31
Got family	5.4	7.6	2.2	1.11	1.98[b]
Fought fire	14.9	10.4	4.5	1.63	2.76[a]
Left area	1.8	4.3	2.5	0.70	3.57[a]
Nothing	2.1	2.7	0.6	0.69	0.87
Had others call Fire Department	2.8	2.2	0.6	0.76	0.79
Got personal property	1.2	2.1	0.9	0.55	1.64
Went to fire area	5.6	2.1	3.5	1.01	3.47[a]
Removed fuel	1.2	1.7	0.5	0.53	0.94
Enter building	0.1	1.6	1.5	0.30	5.00[a]
Tried to exit	1.6	1.6	0	0	0
Closed door to fire area	3.1	1.0	2.1	0.76	2.76[a]
Pulled fire alarm	2.7	0.9	1.8	0.70	2.57[b]
Turned off appliances	4.1	0.9	3.2	0.85	3.20[a]
$N = 18$	2193	580			

[a]Critical ratios significant at or above the 1 percent level of confidence.

[b]Critical ratio significant at or above the 5 percent level of confidence.

The general classification of the first, second, and third actions for both the British and United States populations were categorized as "evacuation," "reentry," "fire fighting," "moved through smoke," and "turned back" behavior. The behavioral comparison of the two populations is presented in Table 3-12.4.There was a statistically significant difference between the populations in every behavioral response category except the "moved through smoke" behavior.

An interesting aspect of the actions of the participants involved in the United States study are the modifications in the first, second, and third behavior response actions of the participants. Table 3-12.5 presents these three actions for the total population of 584 individuals in the U.S. study. It should be noted how the action of "notified others" accounted for 15 percent of the first actions and by the time of the third actions, accounted for only 5.8 percent of the behavioral actions. A similar reduction in the frequency of the behavioral response actions can be observed with the action of "searched for the

Table 3-12.4 ***Human Behavior of the British and U.S. Study Population[1,2]***

Behavior	British Percent	U.S. Percent	$P_1 - P_2$	$SE_{P_1 - P_2}$	CR
Evacuation	54.5	80.0	25.5	2.30	11.09[a]
Reentry	43.0	27.9	15.1	2.30	6.57[a]
Fire fighting	14.7	22.9	8.2	1.74	4.71[a]
Moved through smoke	60.0	62.7	2.7	2.29	1.18
Turned back	26.0	18.3	7.7	2.01	3.83[a]
$N = 5$	2193	584			

[a]Critical ratios significant at or above the 1 percent level of confidence.

Table 3-12.5 ***Compilation of the First, Second, and Third Action of the U.S. Study Populations[1]***

Actions	1st Action Percent	2nd Action Percent	3rd Action Percent
Notified others	15.0	9.6	5.8
Searched for fire	10.1	2.4	0.8
Called fire department	9.0	14.6	12.7
Got dressed	8.1	1.8	0.3
Left building	7.6	20.9	35.9
Got family	7.6	5.9	1.4
Fought fire	4.6	5.7	11.5
Got extinguisher	4.6	5.3	1.6
Left area	4.3	2.8	1.1
Woke up	3.1	0	0
Nothing	2.7	0	0
Had others call fire department	2.2	4.0	4.1
Got personal property	2.1	3.8	0.8
Went to fire area	2.1	1.0	0
Removed fuel	1.7	1.0	1.1
Enter building	1.6	0.8	1.1
Tried to exit	1.6	2.4	0.5
Went to fire alarm	1.6	1.8	1.1
Telephoned others—relatives	1.2	0.6	1.1
Tried to extinguish	1.2	1.8	1.9
Closed door to fire area	1.0	0.2	0.3
Pulled fire alarm	0.9	0.6	0.5
Turned off appliances	0.9	0.6	0.3
Check on pets	0.9	1.4	0.5
Await fire department arrival	0	1.0	3.6
Went to balcony	0.2	0.8	2.7
Removed by fire department	0	0	1.6
Open doors—windows	0.2	0.4	1.1
Other	3.9	8.8	6.6
$N = 29$	100.0	100.0	100.0

fire" which is involved with a reduction in the activity from 10.1 percent as the first action to 0.8 percent for the third action. The behavioral actions of "got dressed" and "got family" presented this same tendency toward a reduction in the frequency of the action with the progression during the fire incident. In contrast, an increase in the frequency of the action from the first to the third actions may be noted with the actions of "called fire department," "left building," and "fought fire."

Canter, Breaux, and Sime[33] developed a decomposition diagram of the acts of 41 persons in 14 domestic fires. This study was conducted in the United Kingdom, and the domestic occupancies were similar to those studied by Wood[2] and Bryan.[1] The decomposition diagram is shown in Figure 3-12.6, and should be compared with Tables 3-12.3 through 3-12.5. The sequence of the first, second, and third actions of the U.S. study population is generally similar to the action sequence in Figure 3-12.6.

Behavior According to Gender

The differences between the first behavioral response actions of the occupants according to gender has been examined by Bryan.[1] Table 3-12.6 presents the initial actions of the United States study population relative to the gender of the participants.

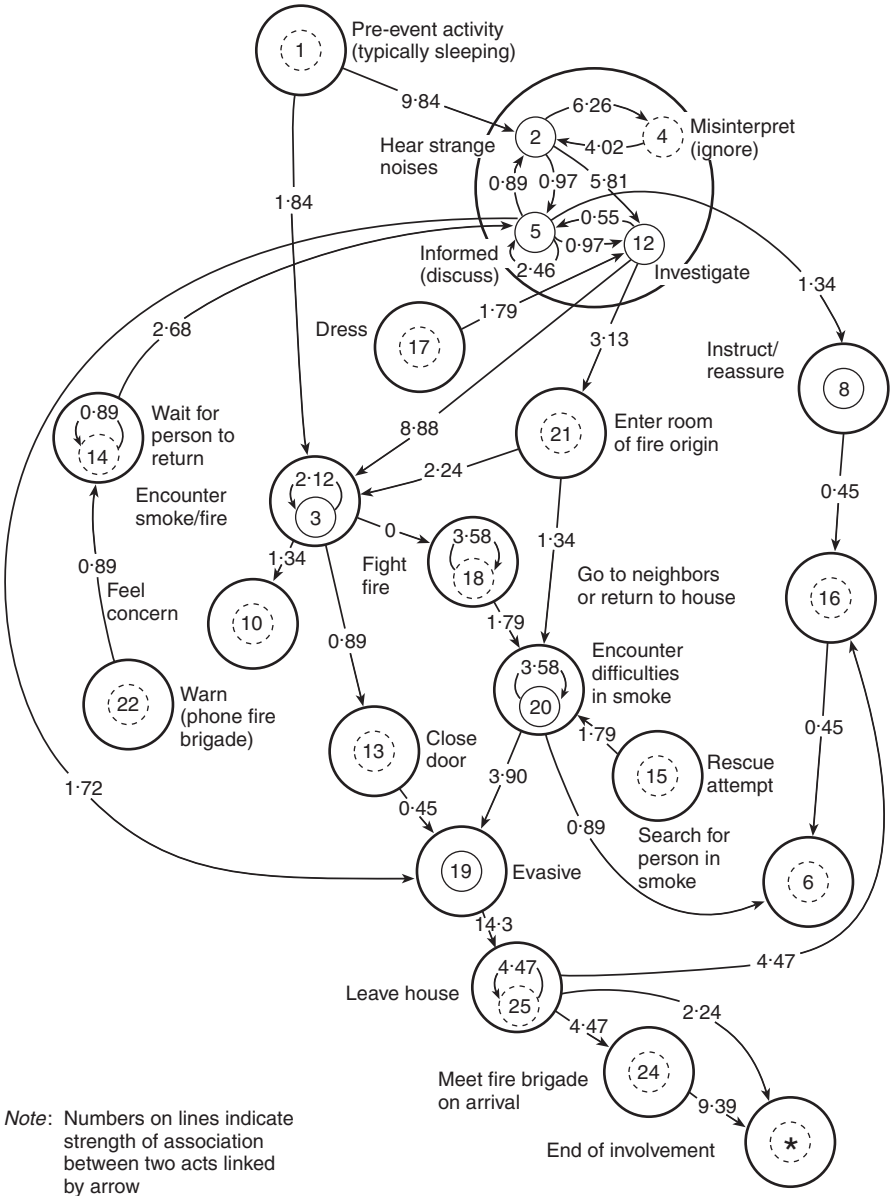

Figure 3-12.6. ***Decomposition diagram—domestic fires.[33]***

Table 3-12.6 ***First Actions of the U.S. Study Population Classified as to the Gender of the Participant[1]***

First Action	Male Percent	Female Percent	$P_1 - P_2$	$SE_{P_1 - P_1}$	CR
Notified others	16.3	13.8	2.5	2.98	0.83
Searched for fire	14.9	6.3	8.6	2.51	3.43[a]
Called fire department	6.1	11.4	5.3	2.41	2.19[b]
Got dressed	5.8	10.1	4.3	2.30	1.87
Left building	4.2	10.4	6.2	2.22	2.79[a]
Got family	3.4	11.0	7.6	2.22	3.42[a]
Fought fire	5.8	3.8	2.0	1.77	1.13
Got extinguishers	6.9	2.8	4.1	1.77	2.31[b]
Left area	4.6	4.1	0.5	1.70	0.29
Woke up	3.8	2.5	1.3	1.45	0.90
Nothing	2.7	2.8	0.1	1.38	0.72
Had others call fire department	3.4	1.3	2.1	1.23	1.71
Got personal property	1.5	2.5	1.0	1.17	0.85
Went to fire area	1.9	2.2	0.3	1.20	0.25
Removed fuel	1.1	2.2	1.1	1.08	1.02
Enter building	2.3	0.9	1.4	1.02	1.37
Tried to exit	1.5	1.6	0.1	1.05	0.09
Went to fire alarm	1.1	1.9	0.8	1.02	0.78
Telephone others—relatives	0.8	1.6	0.8	0.91	0.87
Tried to extinguish	1.9	0.6	1.3	0.91	1.43
Closed door to fire area	0.8	1.3	0.5	0.87	0.57
Pulled fire alarm	1.1	0.6	0.5	0.75	0.66
Turned off appliances	0.8	0.9	0.1	0.79	0.12
Check on pets	0.8	0.9	0.1	0.79	0.12
Other	6.5	2.5	4.0	1.70	2.35[b]
$N = 25$	262	318			

[a]Critical ratios significant at or above the 1 percent level of confidence.

[b]Critical ratios significant at or above the 5 percent level of confidence.

There were significant statistical differences between males and females in the categories of "searched for fire," "called fire department," "got family," and "got extinguishers." Male participants were predominant in fire fighting activities. Thus, 14.9 percent of the males participated in the behavioral response of "searched for fire" as opposed to 6.3 percent of the females, and 6.9 percent of the males were involved in the action of "got extinguishers" as opposed to 2.8 percent of the females. In the United States population, females differed significantly from the males in the warning and evacuation activities—11.4 percent of the females "called fire department" as their initial behavioral response action as opposed to 6.1 percent of the males. In relation to the evacuation behavior, 10.4 percent of the females "left building" as the first behavioral response action, contrasted with 4.2 percent of the males. The cultural role influence on female participants is probably explicitly indicated in the concern for other family members, with the indication that 11 percent of the females "got the family" as the first behavioral response, while only 3.4 percent of the males engaged in this behavioral response. It should be noted that the male actions of "searched for fire" or "fought fire" were matched by the female actions of "called fire department" and "got family." This identical pattern of behavioral responses has also been observed in fire incidents in health care and educational occupancies.

Behavior in Hotel Fire Incidents

The fire protection engineering concepts related to the protection of the occupants of high-rise buildings have been examined and analyzed following the fire in the MGM Grand Hotel in Clark County, Nevada, on November 21, 1980.[34] This hotel fire involved both injuries and fatalities among the guests.

The management of the MGM Grand Hotel, and the Clark County Fire Department under Chief Roy L. Parrish, in cooperation with the National Fire Protection Association (NFPA),[35] conducted an intensive study of the guests registered in the hotel for the evening of November 20 to 21, 1980, to determine how the occupants became aware of the fire incident and their behavioral responses.

The MGM Grand Hotel fire was discovered by an employee of the hotel who entered the deli-restaurant located on the casino level of the hotel at approximately 7:10 a.m. on November 21, 1980. This restaurant area was unoccupied at the time, and the hotel operator was immediately notified to call the fire department. The Clark

County Fire Department received the notification by the direct telephone line call from the hotel at 7:17 a.m., and the first fire company arrived on the scene from a fire station directly across the street on Flamingo Road at approximately 7:18 a.m. The hotel telephone operators were forced from their switchboard positions by the smoke immediately after they had initiated an announcement on the public address system, at approximately 7:20 a.m., for the evacuation of the casino area. The fire reached a flashover condition in the deli area, immediately spread from east to west through the main casino area, and extended out the west portico doors on the casino level immediately following the arrival of the initial fire department personnel.

An addition to the hotel was being constructed adjacent to the west end of the building, and construction workers there participated in warning guests and assisted in the fire fighting and evacuation of guests. The heat and smoke extended from the casino area through seismic joints, elevator shafts, and stairways throughout the 21 residence floors of the hotel. The heat was intense enough on the 26th (top) floor to activate automatic sprinkler heads located in the lobby area adjacent to the elevator shafts.

Due to the rapid early evacuation of the telephone staff, guests in their rooms were not alerted by the hotel public address system or the local fire alarm system. Guests who became alerted early in the fire incident, or guests already awake and dressed, were able to escape prior to the smoke conditions becoming untenable on the residential floors. Guests alerted later in the progression of the fire incident remained in their rooms or moved to other rooms, often with other occupants. The flame propagation did not extend above the casino level, with the exception of very minor extension into two guests' rooms on the 5th floor. The fire resulted in 85 fatalities to guests and hotel employees in the following areas of the hotel:[34] 14 persons were found on the casino level, 29 persons were found in guest rooms, 21 persons were found in corridors and lobbies, 9 persons were found in the stairways, and 5 persons were found in elevators. The victims were located on the casino level, and the 16th through 25th floors, with the majority of fatalities found between the 20th and the 25th floors.

Figure 3-12.7 is a diagram of the guest floor arrangement and layout of the MGM Grand Hotel which was used in the occupant questionnaire study conducted by the National Fire Protection Association.[35] Of the nine individuals found in the stairways it should be noted that two persons were found in Stairway number 1 at the extreme south end of the south wing on the 17th floor, six persons were found between the 20th and 23rd floors in Stairway number 2 at the central end of the south wing, and one individual was found at the ground-floor level of

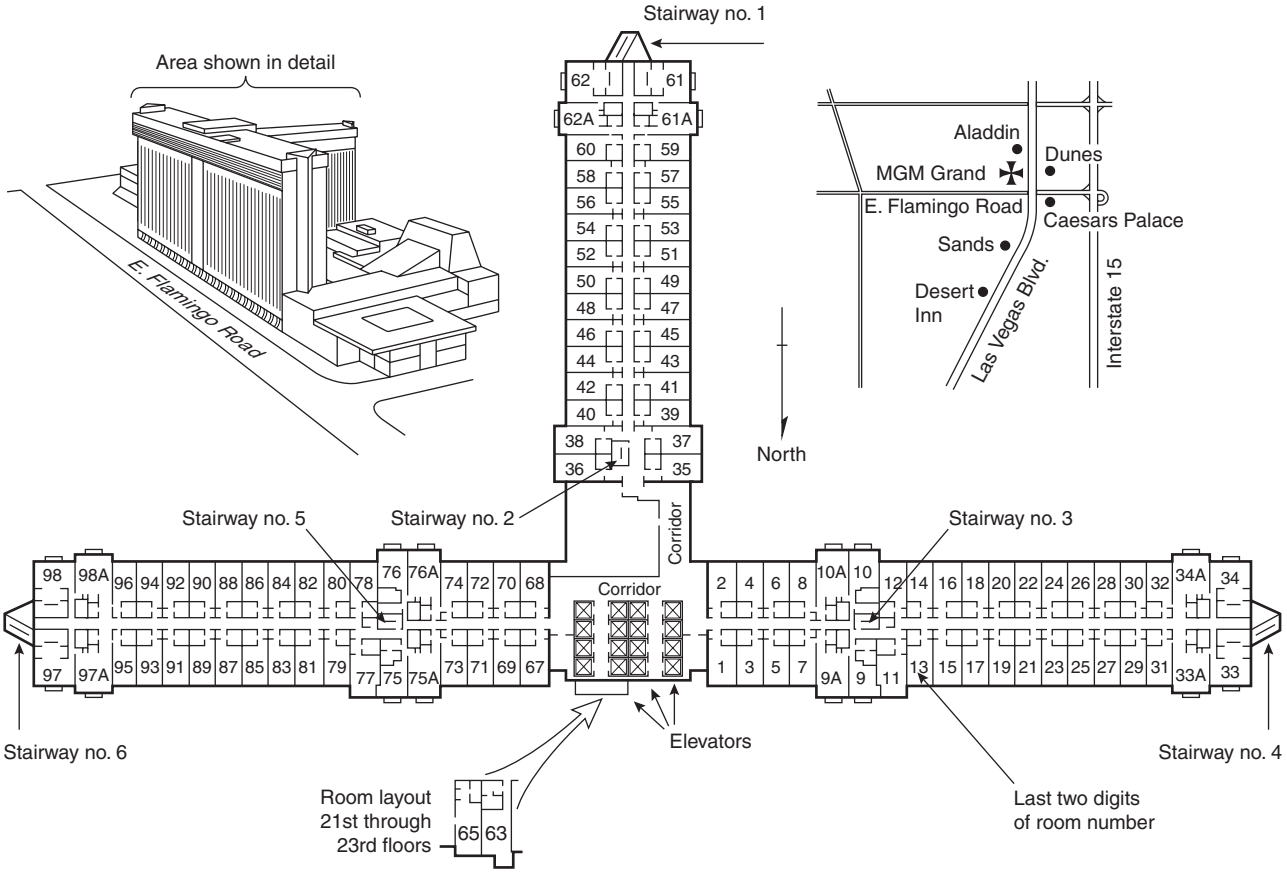

Figure 3-12.7. ***Residential floor diagram of the MGM Grand Hotel.***

Stairway number 4 at the extreme west end of the west wing.

Various estimates have been provided of the number of guests and fire department personnel that suffered injuries at the MGM Grand Hotel fire. Morris[36] indicated that 619 persons were transported to hospitals from the fire scene, and another 150 guests were treated at the Las Vegas Convention Center, where the survivors had been transported. It should be realized that the MGM Grand Hotel fire was a unique fire incident in several aspects. First, it was the second most serious hotel fire in the United States, being surpassed in terms of the loss of life only by the Winecoff Hotel fire in Atlanta, Georgia, on December 7, 1946. Second, it was the first high-rise fire in the United States in which helicopter evacuation was involved for about 300 guests, while the fire department rescued approximately 900 guests.

The Clark County Fire Department obtained from the management of the MGM Grand Hotel a list of the guests registered in the hotel for the evening of November 20 to 21, 1980. This list was transmitted to the NFPA, which prepared a three-page, 28-item questionnaire, with the floor plan of the guest rooms attached as the fourth page. A total of 1960 questionnaires were mailed on December 19, 1980, and 554 questionnaires were returned. Included with the questionnaire was an interview request form by which the respondents indicated their willingness to be interviewed in person about their experience. Of the 554 questionnaires returned, a response rate of approximately 28 percent, 455 individuals (or 82 percent of the response study population) indicated they would be willing to be interviewed.

The ages of the questionnaire respondents ranged from 20 to 84 years, with an average age of 45 years. The questionnaire population consisted of 331 males and 222 females, with one respondent not indicating a gender classification. The population included 103 individuals who indicated they were alone at the time they became aware of the occurrence of the fire within the hotel. The presence of other persons, especially if members of the individual's primary group, has previously seemed to determine the response of some individuals in residential fire incidents.[1]

Table 3-12.7 ***Compilation of the Initial Five Actions of Guests in the MGM Grand Hotel Fire Incident[35]***

	Percent of Population				
Actions	First	Second	Third	Fourth	Fifth
Dressed	16.8	11.6	6.5	—	—
Opened door	15.9	11.7	6.7	3.4	—
Notified roommates	11.6	3.0	—	—	—
Dressed partially	10.1	7.5	4.5	—	—
Looked out window	9.7	5.7	—	—	—
Got out of bed	4.5	—	—	—	—
Left room	4.3	5.4	8.1	2.4	2.0
Attempted to phone	3.4	3.6	—	2.8	—
Went to exit	2.5	10.3	9.5	16.1	6.7
Put towels around door	1.6	2.5	3.0	6.8	7.7
Felt door for heat	1.3	2.3	—	—	—
Wet towels for face	1.3	3.7	6.3	4.6	7.9
Got out of bath	1.1	—	—	—	—
Attempted to exit	1.1	3.0	5.8	4.3	—
Secured valuables	—	6.8	4.3	—	—
Notified other room	—	3.4	2.2	—	—
Returned to room	—	—	3.9	8.4	4.1
Went down stairs	—	—	3.9	5.4	21.3
Left hotel	—	—	3.4	2.6	2.0
Notified occupants	—	—	3.0	—	—
Went to another exit	—	—	—	3.6	4.8
Went to other room	—	—	—	3.6	3.6
Went to other room/others	—	—	—	3.4	8.7
Looked for exit	—	—	—	2.4	—
Broke window	—	—	—	—	4.3
Offered refuge in room	—	—	—	—	1.8
Went upstairs to roof	—	—	—	—	2.9
Went to balcony	—	—	—	—	1.8
Other	14.8	19.5	28.9	30.2	20.4
Total (percent)	100.0	99.1	96.9	90.4	79.6
Number of guests	554	549	537	501	441

The initial five behavioral responses of the 554 guests as elicited from the NFPA questionnaire study are presented in Table 3-12.7. The five most frequent first behavioral responses were "dressed," "opened door," "notified roommates," "dressed partially," and "looked out window." The guests involved in the first responses were predominantly engaged in attempting to define and structure the fire cues relative to the severity of the threat to themselves. Approximately 8 percent of the study population initiated or attempted to initiate their evacuation behavior with the first response, as indicated by the actions of "attempted to exit," "went to exit," and "left room." Sixteen individuals, 2.9 percent of the population, initiated actions to improve the room as an area of refuge with the actions "wet towels for face" and "put towels around door." The behavioral responses of the guests in this questionnaire study could be classified as evacuation responses or refuge preparation responses. The responses relating to the evacuation behavior appeared to be initiated early if the means of egress were clear of smoke, or the smoke was determined to be nonthreatening by the guests. However, if the smoke was heavy, the guests appeared to initiate the behavioral response of staying in their rooms or moving to more suitable rooms with responses designed to prevent smoke migration into the rooms and to protect themselves from the smoke.

Examination of Table 3-12.7 indicates the five most frequent behavioral responses reported by guests as second actions were "opened door," "dressed," "went to exit," "dressed partially," and "secured valuables." Approximately 19 percent of the study population reported they were still involved in the dressing actions prior to initiating evacuation or seeking refuge.

Examination of the third behavioral responses of the 537 guests in the study population indicated the responses of the guests generally progressed to evacuation, attempted evacuation, and notification responses. Thus,

approximately 25 percent of the MGM Grand Hotel fire incident study population was involved in evacuation-related behavioral responses, and approximately 10 percent of the guests were involved in attempted evacuations as identified by their third responses of "attempted to exit" and "returned to room." The alerting and notification actions of the guests were involved with the third behavioral responses of "notified occupants" and "notified other room."

The fourth behavioral responses of the guests in the study population indicated a progression of the guests to evacuation, attempted evacuation, and self-protection or room refuge procedural responses. The most frequent action of the guests in their fourth responses was the behavior of "went to exit" (approximately 16 percent of this population). However, combining the guests involved with this action with the guests utilizing the actions of "went down stairs," "went to another exit," "left hotel," and "left room," there were 151 guests (approximately 30 percent of the fourth action guest population) involved in evacuation actions. The process of the guests forming convergence clusters was noted in this hotel fire. This action involved individuals clustering together in rooms as areas of refuge, with the clustered individuals characterized as individuals usually not known to each other prior to the occurrence of the fire incident. The fourth responses of "went to other room" and "went to other room/others," are explicit indicators of the initiation and formation of convergence clusters.

The fifth behavioral responses of the guests were primarily for self-protection, including the improvement of the room as an area of refuge, and evacuation behavior. The primary evacuation behavioral responses would consist of the fifth responses of "went downstairs," "went to exit," and "went to another exit." Thus, the guests involved with evacuation actions consisted of 175 individuals (approximately 40 percent of this study population). The guests who decided not to evacuate and were thus concerned with finding refuge utilized the fifth actions of "went to other room/others," "wet towels for face," "put towels around door," "broke window," "returned to room," "went to other room," "offered refuge in room," and "went to balcony." Approximately 40 percent of the fifth response study population was involved in the finding refuge, and self-protection actions.

Convergence Clusters

The phenomenon of occupant convergence cluster formation in a fire incident was initially noticed in a study of the occupant behavior in a 1979 high-rise apartment building fire.[37] Convergence clusters appear to involve the convergence of the occupants of the building in specific rooms selected as being areas of refuge. In the MGM Grand Hotel fire, the guests tended to select rooms on the north side of the east and west wings, and rooms on the east side of the south wing, due to the prevailing atmospheric conditions and the external smoke migration. In addition, guests reported that people had converged in rooms that had balconies and doors leading to the balconies because of the ease of ventilation, the reduced-smoke exposure, improved visibility, and the communication advantages the balconies offered. The guests who reported their participation in the convergence behavior in rooms with other persons provided either numerical estimates of the persons occupying the room or suite, or indicated only that "others" or "other persons" were present.

Table 3-12.8 lists the rooms that were identified by guests as being areas of refuge for a total of three or more persons with individuals other than the original occupants of the room. This table also presents the estimates of the length of time the convergence cluster was maintained in the rooms. The duration of the cluster was usually maintained until assistance was obtained for evacuation, or until the occupants were notified by fire or rescue personnel to evacuate. The number of persons shown in the table indicates the total number of persons in the clusters for the total number of rooms identified on the floor. The smallest number of people identified as a single cluster involved three persons, and the largest was 35 persons.

The greatest number of rooms used for convergence clusters, and of course the largest population participating in convergence clusters, was located on the 17th floor of the hotel. No convergence clusters were identified by guests as occurring on the 6th, 21st, or 26th floors. It would appear that convergence clusters may serve as an anxiety and tension-reducing mechanism for individuals

Table 3-12.8 ***Compilation of the Time Duration, Room Numbers, and Number of Guests Involved in Convergence Clusters in the MGM Grand Hotel Fire Incident[35]***

Floor	Room Number	Time (Hours)	Persons	
			Number	Percent
7	731	0.6	3	0.7
8	827, 840	1.5–1.75	14[a]	3.3
9	927	2.5	5	1.2
10	1009A, 1025, 1034, 1060	1.2	53	12.7
11	1129, 1115	1.5–2	30[a]	7.2
12	1261, 1225, 1233A	2–3	53	12.7
14	1433A, 1461A, 1451, 1416A	1.5–2	8[a]	1.9
15	1501, 1533A, 1510	2–3	38[a]	9.1
16	1643, 1625, 1633, 1629, 1627, 1615	2–3.5	35[a]	8.4
17	1725, 1775, 1731, 1719 1762, 1756, 1733A	2–2.5	84	20.1
18	1819, 1802, 1850	2–3	20	4.8
19	1929, 1919, 1962A, 1961, 1925	2–3.5	13[a]	3.1
20	2027, 2013, 2030	2–3	13	3.1
22	2213, 2221, 2229	2.5–3.5	25	6.0
23	2329, 2314, 2342, 2331, 2308, 2340	2.5–3.25	20[a]	4.8
24	2446	3.5	4	0.9
25	2512, 2509A	3.5	[a]	0
Total	17 57		418	100.0
Range	7–25 1–7	0.6–3.5	3–84	0–20.1

[a]Persons indicated only as "Others."

confronted with a fire incident perceived as life threatening. The action of "offered refuge in room," which was previously identified in the discussion of the fifth behavioral responses, is a definitive indication of the formation of a convergence cluster.

In addition to the detailed human behavior study of the MGM Grand Hotel fire,[38] the NFPA conducted a similar questionnaire study of the guest's behavior in the Westchase Hilton Hotel fire.[39]

Figure 3-12.8 presents the decomposition diagram for eight multiple-occupancy fires with the acts of 96 persons.[33] These multiple-occupancy fires in the United Kingdom involved hotel occupancies. Figure 3-12.8 and Table 3-12.7 should be compared to illustrate the similarity of the occupants' behavior in both of these studies.

Nonadaptive Behavior

The classic types of nonadaptive behavior in a fire incident involve the disregard of adaptive actions, behavior that might facilitate the evacuation of others, or inhibit the propagation of the smoke, heat, or flame from a fire incident. Nonadaptive behavior may consist of a single behavioral response, such as leaving the room of fire origin without closing the door to the room, thus allowing the

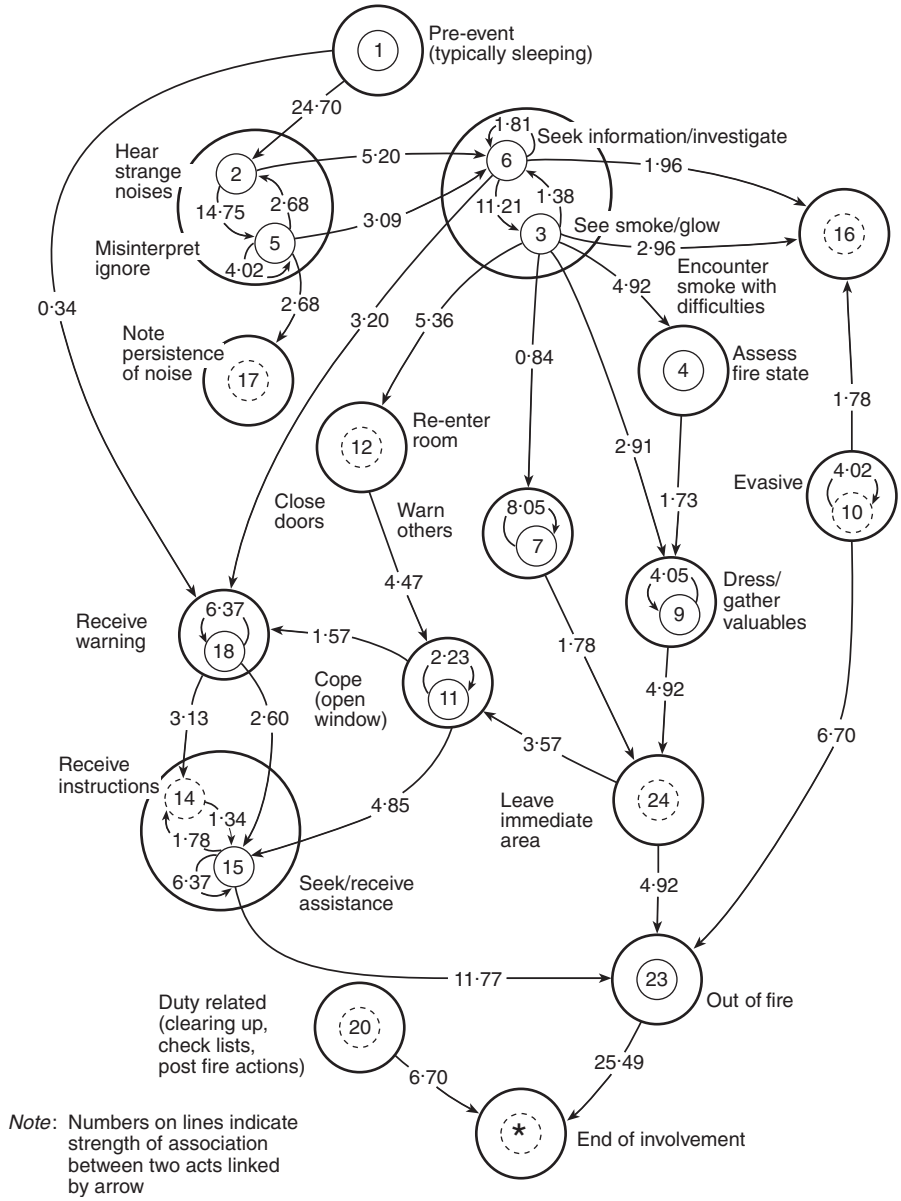

Figure 3-12.8. ***Decomposition diagram—multiple-occupancy fires.[33]***

fire to propagate throughout the structure and endanger the lives of other individuals. However, the more generalized concept of nonadaptive behavior consists of a population fleeing the fire incident, without regard for others, and inflicting physical injuries on themselves and others.

Nonadaptive behavior responses may be an omission, such as forgetting to close a door, or may involve a response that, although well meaning and positive in intent, results in negative consequences. When the action of a behavioral response results in the extinguishment of the fire and the reduction of the threat, the behavior may be said to be adaptive. However, when such a behavioral response is ineffective because the fire was more developed than perceived, a more adaptive response might have been to warn others and notify the fire department. Thus, it would appear that some behavior which appears to be nonadaptive, in reality, is behavior that would have appeared to be adaptive if it had only been successful. Injuries suffered by persons in fire incidents may be cues to nonadaptive or risky behavior by the individual.

Panic Behavior

The concept of panic behavior is the nonadaptive behavioral response that is always discussed following fire incidents, such as the Beverly Hills Supper Club fire,[40] where multiple fatalities occurred.

According to most definitions, panic is a flight or fleeing type of behavioral response that also involves extravagant and injudicious effort. Panic is not likely to be limited to a single individual but may be mimicked and adopted by a body of persons. Schultz[41] has defined a panic type of behavior reaction from his simulation experiments:

> A fear-induced flight behavior which is nonrational, nonadaptive, and nonsocial, which serves to reduce the escape possibilities of the group as a whole.[41]

The concept of panic is often used to explain the occurrence of multiple fatalities in fires even when there is no physical, social, or psychological evidence indicating that competitive, injudicious flight behavior actually occurred. Representatives of the media and public officials often label various types of fire incident behavioral responses as panic. The evidence accumulated from interviews with participants and the questionnaires completed by occupants provided no evidence of the classical group type of panic behavior, with competitive flight for the exits in the Beverly Hills Supper Club fire.[42]

Sime[43] has indicated that panic as a concept is primarily a description of the behavior, not an explanation of the behavior. He pointed out that the concept is used to support the introduction of requirements in building laws or ordinances to provide for the fire safety of the building occupants. Sime has also very aptly shown the difference between the use of the concept to describe other persons' behavior in a fire incident, and the use of the concept to describe an individual's behavior which is accompanied by a high state of concern and anxiety. As Sime has indicated, simply because an individual identifies behavior as being associated with a panic reaction does not necessarily identify the behavior as being the classic panic type behavioral response. Sime also indicates the outcome of the behavior affects its labeling, and that the actual behavior of people in a fire is most likely to be misinterpreted when the outcome of the fire incident has been unfortunate.

As Sime indicated, the use of the concept of panic must be separated from the use of the terms anxiety or fear. The concept of self-destructive or animalistic panic type behavioral responses to fire incident stimuli, such as the presence of flames or smoke, has not been supported by the research on human behavior in fire incidents. As indicated by Sime,[43] Quarantelli,[44] and others,[1,2,4,45] panic behavior in which the flight response is characterized by actual physical competition between the participants, and personal injuries, is rare.

In his interview study of 100 participants of single-dwelling residential fires, Keating[45] reported no instances of panic behavior and instead found primarily altruistic, helpful behavioral responses.

Ramachandran,[6] in his review of studies on human behavior in fires in the United Kingdom, has developed the following conclusion relative to nonadaptive behavior:

> In the stress of a fire, people often act inappropriately but rarely panic or behave irrationally. Such behavior, to a large extent, is due to the fact that information initially available to people regarding the possible existence of a fire and its size and location is often ambiguous or inadequate.[6]

Reentry Behavior

The study of the 1956 Arundel Park fire documented the initial examination of the phenomenon of reentry behavior.[20] Some codes and regulations affecting the design of the means of egress appeared to assume that pedestrian traffic will only move away from the fire area or floor of the building involved. The Arundel Park study[20] indicated that approximately one-third of the individuals interviewed had reentered the building.

It is apparent that the means of egress components—primarily doors, stairways, and corridors—may be subjected to two-way movement from building occupants or other personnel. The behavioral response of the occupant who after safely leaving the building turns around and reenters has been observed most frequently in the residential fire incident. The occupant is often completely aware of the occurrence of the fire in the building and of the specific portions of the building involved in the area of fire origin and smoke propagation. Table 3-12.9 presents the number of individuals who reentered in the Arundel Park fire from the interviewed population of 61 persons. The reasons for the reentry behavior, and the fact that the reentry participants were predominantly male in this fire incident, should be noted.

The Arundel Park fire incident occurred in an assembly occupancy being utilized for a church-sponsored oyster roast, which is a family event. Thus, the primary group cultural role of father or husband may have been a critical variable in the reentry behavior in the population interviewed and may have resulted in the fact that the reentry participants were mostly male. Reentry behavior should not be considered as nonadaptive behavior since this type of behavior response is often engaged in to assist or rescue

Table 3-12.9 ***Reasons for Reentry Behavior by Occupants in the Arundel Park Fire, Classified by Gender of the Occupants[20]***

Gender	Reentered and Left Same Exit	Reentered and Left Different Exit	Stated Reason for Reentrance
M	1		Turn off kitchen stoves
M	1	1	Tell people to leave
M	3	1	To help
M	1		Assist people
M	2	3	Find wife
M	2	2	Assist fire fighting
M & 1 F		5	No stated reason
21 M & 1 F	10	12	

persons remaining or believed to be remaining in the fire incident building. The reentry behavior is often engaged in by parents when children are missing during a fire incident. This reentry behavior is often undertaken in a rational, deliberate, and purposeful manner, without the emotional anxiety or self-anxiety characteristics often associated with nonadaptive behavior. However, reentry behavior has usually been considered nonadaptive since it negatively affects the efficient and effective egress of other persons in the building (i.e., those initially leaving the building are impeded at any egress selected for reentry).

The reasons elicited from participants in reentry behavior in residential occupancies[1] in the United States are presented in Table 3-12.10. It would appear from the total study population of 584 persons that 162 people or approximately 27.9 percent engaged in reentry behavior. The most frequent reason for reentry behavior in this study was "to fight the fire," followed by "to obtain personal property," "to check on the fire," "to notify others," "to assist the fire department," and "to retrieve pets." These six reentry behavioral response reasons accounted for approximately 73 percent of reentry behavior.

Table 3-12.11 compares the reentry behavior of the British[2] and the United States[1] study populations. It should be noted that all of the behavioral response reasons were significantly different statistically, with the exception of the reason "save personal effects." The United States population was predominant with the reentry reasons of "save personal effects," "call the fire department," "rescue pets," "notify others," "assist fire department," and "assist the evacuation." The British population was predominant with the reentry reasons of "fight the fire," "observe the fire," "shut doors," "await fire department," and "fire not severe."

Table 3-12.10 ***Reasons for Reentry of the Population in the Project People Study[1]***

Reasons	Participants	Percent
Fight fire	36	22.2
Obtain personal property	28	17.2
Check on fire	18	11.0
Notify others	13	8.0
Assist fire department	12	7.4
Retrieve pets	12	7.4
Call fire department	9	5.5
Assist evacuation	4	2.5
Taken to hospital	3	1.8
Turn power back on	2	1.2
Rescue from balcony	1	0.6
Help injured family member	1	0.6
Turn off gas	1	0.6
Open windows	1	0.6
Close door	1	0.6
No apparent danger	1	0.6
Entered non-danger area	1	0.6
Responsibility	1	0.6
Due to fire	1	0.6
Told to by others	1	0.6
Not reported	16	9.8
$N = 21$	163	100.0
Range = 1–36	Percent of Participant Population = 27.9	

Occupant Fire Fighting Behavior

Occupants who engaged in fire fighting behavior during fire incidents have been predominantly male. This behavior is now believed to be primarily a culturally determined and assumed aspect of the male role in certain social and occupational situations.

However, in the study of 335 primarily residential fire incidents,[1] it was found that 37.3 percent of those who chose to fight the fire were females, with the youngest participant being a seven-year-old girl. The fire fighting population in this study of 134 persons consisted of 50 females and 84 males. The age range of those who engaged

Table 3-12.11 ***Comparison of Reasons for Reentry Behavior of British and U.S. Study Populations[1,2]***

Reasons	British Percent	U.S. Percent	$P_1 - P_2$	$SE_{P_1 - P_2}$	CR
Fight fire	36.0	22.2	13.8	4.02	3.34[a]
Observe fire	19.0	11.0	8.0	3.25	2.46[b]
Save personal effects	13.0	17.2	4.2	2.91	1.44
Shut doors	10.0	0.6	9.4	2.38	3.95[a]
Await fire department	9.0	0	9.0	2.26	3.98[a]
Call fire department	2.0	5.5	3.5	1.32	2.65[a]
Rescue pets	2.0	7.4	5.4	1.40	3.86[a]
Fire not severe	5.0	1.2	3.8	1.74	2.18[b]
Notify others	0	8.0	8.0	0.92	8.69[a]
Assist fire department	0	7.4	7.4	0.88	8.41[a]
Assist evacuation	0	2.5	2.5	0.54	4.63[a]
$N = 11$	943	163			

[a]Critical ratios significant at or above the 1 percent level.

[b]Critical ratios significant at or above the 5 percent level of confidence.

in the fire fighting behavior varied from the seven-year-old girl to an 80-year-old man. The distribution of the participants relative to sex and age is presented in Table 3-12.12. Approximately 23 percent of the total study population were involved in occupant fire fighting behavior.

The majority of those involved in the fire fighting behavior were between 28 and 37 years old, consisting of approximately 30 percent of the fire fighting behavior population. Statistically significant differences in the behavioral responses of the males and females were shown in the responses of "got extinguisher" and "fought fire." Approximately 15 percent of the male population reacted by obtaining extinguishers. Approximately 26 percent of the male population reported they fought the fire when they first became aware of the fire incident, as opposed to approximately 10 percent of the female occupants. The female members of the population predominantly notified the fire department before initiating the fire fighting type of behavioral response. Approximately 33 percent of the females versus 25 percent of the males reacted to the fire incident by initially notifying the fire department as indicated in Table 3-12.13.

The occupant fire fighting behavioral responses appear most prevalent in occupancies in which the individuals are emotionally or economically involved (primarily their homes) or where such behavior is a result of training or an assigned occupational role. A total of 285 individuals at some time during a fire incident engaged in one of the six actions defined as a fire fighting behavioral response, and a total of 252 individuals participated in one of the four actions relative to notification of the fire department.

In the study by Crossman et al.[46] of residential fire incidents in Berkeley, California, a total of 180 persons were involved in fire fighting behavioral responses. The total of 208 fire incidents for this study included approximately 167 fire incidents, or approximately 80 percent, that had not been reported to the fire department. The majority of the 167 unreported fire incidents had been extinguished by the occupants of the building involved in the fire incident or the occupants assisted by neighbors. Table 3-12.14 presents the study's percentage distribution of the individuals responsible for extinguishing the fire. Six percent of these fire incidents self-extinguished, and 52 percent of the fires were extinguished by the individual engaged in the activity that created the fire incident. As a means of comparison, the fire incidents in the Project People Study[1] may have consisted of incidents that were judged uncontrollable by the occupants and resulted in the notification of the fire department. It should be remembered that approximately 90 percent of the fire occurrences in the National Fire Prevention and Control Administration National Household Fire Incident Survey[47] had also not been reported to the fire department.

The types of occupancies in which equipment provided within the occupancy was used to fight the fire are shown in Table 3-12.15. The apparently high frequency of residential occupancies, with 64 percent of the occupancies being either single-family dwellings or apartments, may be a variable created by the fire incident population of this study. This residential occupancy distribution may also be representative of many urban areas where the fire problems are essentially concentrated in residential occupancies.

In the Project People Study,[1] 107 of the 584 participants did not voluntarily leave the building after becoming aware of the fire incident. The reasons given for their remaining in the building are presented in Table 3-12.16. Fifty-two occupants, or approximately 49 percent of the population staying in the building, reported that they remained because they intended to engage in fire control or

Table 3-12.12 ***Gender and Age of U.S. Participants Engaging in Fire Fighting Behavior[1]***

Gender	Participants	Percent
Male	84	62.7
Female	50	37.3
Total	134	100.0
Age		
7–17	8	5.9
18–27	31	23.1
28–37	41	30.6
38–47	27	20.1
48–57	16	11.9
58–67	2	1.5
68–80	3	2.2
Unknown	6	4.7
Total	134	100.00
Percent of Participant Population = 22.9		

Table 3-12.13 ***Comparison of the Gender of the Participants Engaging in Fire Fighting and Notification of the Fire Department[1]***

Action	Male Percent	Female Percent	$P_1 - P_2$	$SE_{P_1 - P_2}$	CR
Searched for fire	17.2	9.1	8.1	4.23	1.91
Got extinguisher	15.6	6.0	9.6	3.95	2.43[b]
Fought fire	25.6	9.7	15.9	4.83	3.29[a]
Removed fuel	3.4	3.1	0.3	2.17	0.14
Tried to extinguish	5.3	2.8	2.5	2.49	1.00
Went to fire area	3.1	2.8	0.3	2.07	0.14
Total	70.2	33.5	36.7	6.01	6.11[b]
N =	184	101			
Called fire department	25.6	33.0	7.4	5.83	1.27
Had others call fire department	9.2	7.5	1.7	3.27	0.52
Went to fire alarm	3.8	3.8	0	0	0
Pulled fire alarm	1.9	1.6	0.3	1.65	0.18
Total	40.5	45.9	5.4	6.31	0.85
N =	106	146			

[a]Critical ratio significant at or above the 1 percent level of confidence.
[b]Critical ratio significant at or above the 5 percent level of confidence.

Table 3-12.14 ***Percentage of Occupants Extinguishing Residential Fires in Berkeley, CA[46]***

Fire Suppressed by	Percent
Person engaged in heat-using activity	52.8
Other member(s) of household	28.3
Friends and neighbors	8.9
Fire department	18.9
Burnout	6.1
Total	115.0
Single individual	80.7
Group effort	19.3
Total	100.0

Table 3-12.15 ***Occupancies in Which Fire Fighting Equipment Was Utilized by Participants in Fire Fighting Behavior[1]***

Occupancy	Incidents	Percent
Dwelling (1 Family)	23	35.9
Apartment (<29 Units)	18	28.1
Restaurant	3	4.8
Apartment (>20 Units)	3	4.8
Manufacturing	2	4.8
Hotel and motel	2	3.2
School	3	3.2
Billiard center	1	1.5
City club	1	1.5
Hospital	1	1.5
Dwelling (2 Family)	1	1.5
College dormitory	1	1.5
Service station	1	1.5
Office	1	1.5
Photographic laboratory	1	1.5
Other	2	3.2
N = 16	64	100.00

Table 3-12.16 ***Elicited Reasons of Participants for Not Voluntarily Leaving the Fire Incident Building[1]***

Reason	Participants	Percent
Fight fire	52	48.7
Notify others	7	6.5
Blocked by smoke	7	6.5
Blocked by fire	5	4.7
Overcome by smoke	5	4.7
Search for fire	3	2.8
Needed help	2	1.9
Secure property	2	1.9
Afraid of fire spread	2	0.9
No fire in area	1	0.9
Help others	1	0.9
Does not know	1	0.9
No response to fire department	1	0.9
Home	1	0.9
Return to area	1	0.9
Not reported	16	15.0
N = 15	107	100.0
Range = 1–52	Percent of Participant Population = 15.6	

fire fighting activities. The other most frequent reasons for remaining in the fire incident building were to notify others of the fire occurrence or because the means of egress were obscured by smoke. Approximately 15 percent of the study population voluntarily remained within the fire building.

Occupant Movement through Smoke

The movement of the occupants through smoke is sometimes related to the fire fighting behavior and the alerting of others, and is often a component of the evacuation behavior in many fire incidents.[1,2] The principal variables influencing an occupant's decision to move through smoke appear to be recollection of the location of the exit, and ability to estimate the travel distance required. Secondary variables are the perception of the severity of the smoke (determined by observation of the appearance of the smoke), the smoke density, and the presence or absence of heat with smoke.[38,39] It should be recognized that to achieve evacuation, occupants have moved through smoke for extended distances (over 20 m) under conditions of extremely limited visibility (less than 4 m) at personal risk. Occupants sometimes have also been forced to turn back and not complete the evacuation.

Jin and Yamada[48] reported on a study involving 31 subjects (14 males and 17 females), traveling a maximum distance of 10.5 m in a corridor exposed to smoke from smoldering cedar crib chips. The smoke extinction coefficient varied from 0.1 to 1.2 l/min. The subjects were also exposed to an increasing heat exposure from radiant heaters at the end of the corridor, with a mean temperature at the end of the corridor of 82°C. At five points in the corridor the subjects were stopped and asked arithmetic questions to be solved mentally. Both walking speed in the corridor and the mental arithmetic capability decreased with the increase in smoke density and the increased radiant heat exposure.

Fahy and Proulx[12] in their questionnaire study of 406 trained fire wardens in the World Trade Center explosion and fire found that 94 percent of the respondents in Tower 1 and 70 percent of the respondents in Tower 2 moved through smoke. In addition, the study reported that approximately 75 percent of these individuals turned back during their evacuation because of smoke, crowding, locked doors, breathing difficulty, fear and poor visibility. It was also reported that some occupants continued to move through smoke, even when they perceived the smoke to be worsening and they believed they may have been moving toward the fire.

Table 3-12.17 compares the distance moved through smoke for the 1316 persons in the British study[2] and the 322 persons in the United States study[1] who reported that they moved through smoke. It may be of interest to note that 60 percent of the population in the British study and 62.7 percent of the population in the United States study reported that they moved through smoke. Apparently building occupants will move through smoke in an evacuation process. An important variable may be both the smoke density and the visibility distance available to the occupants during the evacuation process, as well as their familiarity with the means of egress.

Table 3-12.17 ***Compilation of the Distance Moved through Smoke for Participants in Both the British and U.S. Study Populations[1,2]***

Distance Moved (feet)	British Percent	U.S. Percent	$P_1 - P_2$	$SE_{P_1 - P_2}$	CR
0–2	3.0	2.3	0.7	1.02	0.69
3–6	18.0	8.4	9.6	2.23	4.30[a]
7–12	30.0	17.1	12.9	2.71	4.76[a]
13–30	19.0	45.5	26.5	2.62	10.11[a]
31–36	5.0	2.0	3.0	1.25	2.40[b]
37–45	4.0	4.1	0.1	1.19	0.08
46–60	5.0	11.0	6.0	1.47	4.08[a]
>60	15.0	9.6	5.4	2.10	2.57[b]
N =	1316	322			

[a]Critical ratios significant at or above the 1 percent level of confidence.
[b]Critical ratios significant at or above the 5 percent level of confidence.

Table 3-12.18 ***Compilation of the Visibility Distance for the British and the U.S. Populations When They Moved through Smoke[1,2]***

Visibility Distance (feet)	British Percent	U.S. Percent	$P_1 - P_2$	$SE_{P_1 - P_2}$	CR
0–2	12.0	10.2	1.8	1.99	0.90
3–6	25.0	17.2	7.8	2.65	2.94[a]
7–12	27.0	20.2	6.8	2.73	2.49[b]
13–30	11.0	31.7	21.7	2.24	9.69[a]
31–36	3.0	2.2	0.8	1.03	0.78
37–45	3.0	3.7	0.7	1.08	0.65
46–60	3.0	7.4	4.4	1.21	3.64[a]
>60	17.0	7.4	9.6	2.24	4.29[a]
N =	1316	322			

[a]Critical ratios significant at or above the 1 percent level of confidence.
[b]Critical ratios significant at or above the 5 percent level of distance.

Table 3-12.18 presents the visibility distance of the British and the United States occupants as they moved through the smoke in evacuating the fire incident buildings. Occupants reported their movement through smoke in relatively high smoke-density conditions, with visibility below 4 m for 64 percent of the British population and for 47.6 percent of the United States population.

Table 3-12.19 relates the distance moved through smoke for the United States population to the visibility distance.[1]

The visibility distance for both the British and the United States populations at the time the participants were forced to turn back is presented in Table 3-12.20. It is interesting to compare Table 3-12.20 with Table 3-12.18 because very few of the participants turned back when the visibility distance exceeded 10 m, with the greater percentage of occupants having turned back at the reduced visibility levels. Comparing the visibility distance below 4 m in Table 3-12.19, it is obvious that 91 percent of the British population who turned back and 76.4 percent of the United States population initiated their behavior at visibility distances of less than 4 m.

Table 3-12.19 ***Comparison of the Movement through Smoke with the Visibility Distance Significance of These Differences in the Participant Population[1]***

Distance Moved	Participants	Percent
Greater than visibility	170	46.4
Equal to visibility	128	35.0
Less than visibility	68	18.6
N = 3	366	100.0

Greater than Visibility Percent	Equal to Visibility Percent	Less than Visibility Percent	$P_1 - P_2$	$SE_{P_1 - P_2}$	CR
46.4	35.0		11.4	5.77	1.97[b]
46.4		18.6	27.8	6.98	3.98[a]
	35.0	18.6	16.4	6.83	2.40[b]
170	128	68			

[a]Critical ratios significant at or above the 1 percent level of distance.
[b]Critical ratios significant at or above the 5 percent level of confidence.

Table 3-12.20 ***Compilation of the Visibility Distance for the British and the U.S. Populations at the Time They Initiated the Turned Back Behavior[1,2]***

Visibility Distance (feet)	British Percent	U.S. Percent	$P_1 - P_2$	$SE_{P_1 - P_2}$	CR
0–2	29.0	31.8	2.8	5.31	0.53
3–6	37.0	22.3	14.7	5.57	2.64[a]
7–12	25.0	22.3	2.7	5.02	0.54
13–30	6.0	17.6	11.6	3.07	3.78[a]
31–36	0.5	1.3	0.7	0.90	0.77
37–45	1.0	0	1.0	1.10	0.91
46–60	0.5	4.7	4.2	1.16	3.62[a]
>60	1.0	0	1.0	1.10	0.91
N =	570	85			

[a]Critical ratios significant at or above the 1 percent level of confidence.

Proulx[49] in the study of the occupant's response to a fire in a 25 story high-rise apartment building received 137 questionnaires returned, with 68 percent of the occupants over 60 years of age. One hundred fourteen of the occupants, or 83 percent, attempted to evacuate during the fire, and 96, or 84 percent, of those attempting to evacuate moved through smoke. Forty-five percent of those moving through smoke indicated they could see "nothing at all" or "little," and 30 percent said they could see 12 to 15 m in the corridor. Of the 114 occupants who attempted to evacuate 61, or 54 percent, were successful, and 53, or 46 percent, were unsuccessful due to the smoke

conditions in the corridors or stairs. Relative to the 53 unsuccessful occupants 29, or 55 percent, returned to their own apartments and 24 occupants, or 45 percent, sought refuge in other apartments.

Heskestad and Pederson[50] have reported on five large "escape through smoke" experiments involving more than 300 persons with various way guidance systems. In all of these experiments the visibility was less the 3 m due to the induced smoke conditions. Two of the experiments involved the test situation modeled on a ship staircase and a ship or hotel corridor. One of these experiments involved an emergency training mock-up, one experiment used a corridor in a health care facility, and one experiment used portions of a passenger ferry. Variables measured during the experiments were the occupants time to travel through the experimental facility and the number of incorrect decisions made during the travel. These experiments found that tactile and audible way guidance systems appear to be as suitable as the visible systems in assisting the individuals movements through smoke.

Jin[51] has reported on his numerous studies involving the effectiveness of guidance sign systems with human subjects in smoke environments. The improvements resulting from these experiments include a pictorial exit sign, flashing exit signs, and a flashing row of lights at floor level indicating the direction of egress travel. The flashing row of lights was effective in a heavy smoke level of 1.0 l/m with the spacing of the lights at 0.5 m and the flashing velocity is 4 m/s.

Handicapped or Impaired Occupants

The problems involving fires in occupancies designed for permanently or temporarily disabled persons, such as nursing homes and hospitals, appear to have been properly alleviated in recent years due to building design, adequate staff training, and preparation to protect the occupants until evacuation is possible.[52] An extensive study of human behavior in health care facilities[53,54] indicated the nursing staff performed their professional roles even in situations with a high degree of personal risk.

The few fire incidents that have been studied, in which handicapped persons have been involved in other occupancies, have primarily been in residential occupancies. In both of these cases the handicapped individuals were assisted in a successful evacuation by other occupants. The one instance involved a wheelchair occupant[38] and the other situation involved a blind occupant.[44]

Pauls[55] has indicated from a number of practice evacuations in high-rise office buildings in Canada that approximately 3 percent of the occupants will be unable to use the stairs due to conditions that permanently or temporarily limit mobility. Paul's population included occupants with heart conditions and individuals recovering from surgery, illnesses, and accidents.

Isner and Klem[56,57] in their reports of the explosion and fire in the World Trade Center indicated that normal power was lost with the occurrence of the explosion at approximately 12:18 p.m., and the emergency generators failed about 20 min. later, with all the remaining power to the World Trade Center complex being disconnected at approximately 1:32 p.m. Thus, the simultaneous evacuation of both able and disabled occupants from Towers 1 and 2 were conducted in darkness with varying smoke conditions in the stairways. These simultaneous evacuations may have involved the largest number of occupants and the longest evacuation times of any fire-induced evacuations of buildings in the United States.

Juillet,[58] in one of the first documented studies of this type, reported on the interview study of 27 occupants with disabilities who were evacuated from one of the two towers in the World Trade Center during the explosion and fire. Of those interviewed, fourteen had mobility impairments, three had sight or hearing impairments, three were pregnant, two had cardiac conditions, and seven had respiratory conditions. Juillet[59] indicated it was believed the total disabled population in both Towers 1 and 2 at the time of the incident was between 100 and 200 persons, with approximately 100 occupants having been identified previously. The average evacuation time of the 27 study participants was 3.34 hrs, with a reported range of evacuation times from 40 min. to over 9 hrs. The predominate means of evacuation was through the stairs, with assistance from other evacuees or emergency personnel. The altruistic behavior, characteristic in many fire incidents with large populations,[37,38] appeared to have been exhibited in this fire incident with the disabled occupants, as reported by Juillet:

> in the absence of communications by authorities, they gladly accepted assistance—from colleagues and even from complete strangers—in evacuating. These caring groups of people who assisted the disabled protected their "charges" until they were safely evacuated and moved away from the building.[58]

The Fire SERT Centre at The University of Ulster recently completed the most extensive and detailed analytical and experimental studies of the evacuation capabilities of disabled individuals. Boyce, Shields, and Silcock conducted a series of studies in Northern Ireland to determine the number and characteristics of disabled persons who may be expected to frequent public buildings, and to determine the capabilities of these persons to complete an evacuation. The initial study determined the number and types of disabled persons expected to occupy public assembly occupancies.[60] This study found that 12 percent of the mobile population of Northern Ireland out in public are disabled persons and 2 percent of these disabled persons require assistance. Table 3-12.21 presents the number of disabled adults and children by their degree of mobility expressed as a percentage of the total mobile population. Table 3-12.22 illustrates the disabled persons in public who have experienced evacuation difficulties as percentages of the total mobile population. Table 3-12.23 indicates the involvement of disabled persons in social and recreational occupancies relative to their degree of mobility.

Additional valuable data presented in this study involved the frequency with which disabled persons go out in public. In addition, data was presented relative to the severity of disability among disabled adults who live in

Table 3-12.21 ***Numbers of Disabled Adults and Children Who Go Out by Degree of Mobility, Expressed as Percentages of the Total Mobile Population (i.e., Able-Bodied People and Mobile Disabled People) in N. Ireland.[60]***

	Adults			Children			Total (adults and children)		
Disability	Unassisted	Assisted	Total	Unassisted	Assisted	Total	Unassisted	Assisted	Total
Locomotion	6.0	1.6	7.6	0.2	0.1	0.3	6.2	1.7	7.9
Wheelchair Users	0.05	0.09	0.14	—	—	—	0.05	0.09	0.14
Zimmer/rollator user	0.13			—	—	—	0.13		
Walking stick/crutch	1.27	1.52	6.91	—	—	—	1.27	1.52	6.91
No aid	3.99			—	—	—	3.99		
Reaching and Stretching	1.8	0.8	2.6	0.0	0.0	0.1	1.8	0.8	2.6
Dexterity	2.2	0.9	3.0	0.1	0.0	0.1	2.2	0.9	3.1
Seeing	2.0	0.9	2.9	0.04	0.04	0.2	2.1	0.9	3.0
Blind	0.02	0.05	0.06	0.0	0.0	0.01	0.02	0.05	0.07
Hearing	4.2	0.8	5.0	0.1	0.1	0.2	4.3	0.9	5.2
Deaf	0.1	0.1	0.1	0.0	—	0.0	0.1	0.1	0.1
Mental/behavioral	2.0	0.7	2.7	0.3	0.2	0.4	2.3	0.9	3.2

Percentages for each disability do not sum to totals given in Table 2 because many individuals have more than one disability.

Percentages for wheelchair users and walking aid users do not sum to total since some data is missing.

Source: K. E. Boyce, T. J. Shields and G. W. H. Silcock, "Toward the Characterization of Building Occupancies for Fire Safety Engineering: Prevalence, Type, and Mobility of Disabled People," *Fire Technology,* 35, 1, p. 41 (1999).

Table 3-12.22 ***Number of Disabled Adults Who Go Out and Experience Difficulty, Expressed as Percentages of Total Mobile Population of N. Ireland[60]***

	Go out Unassisted Degree of Difficulty			Assisted Degree of Difficulty			Total Degree of Difficulty		
Action	Some	Great	Impossible	Some	Great	Impossible	Some	Great	Impossible
Go up and down stairs	2.4	1.1	0.2	0.2	0.6	0.2	2.59	1.69	0.43
Climb outside steps	1.5	0.8	0.2	0.3	0.4	0.2	1.81	1.14	0.40
Cross door saddles	0.1	0.1	0.03	0.2	0.1	0.01	0.32	0.13	0.04
Go through doors	0.1	0.03	0.01	0.1	—	0.01	0.15	0.03	0.02
Turn door knobs	0.3	0.1	0.03	0.2	0.07	0.05	0.43	0.13	0.08

Since these percentages are based on adults, only the actual percentages of the mobile population in N. Ireland who experience difficulty may be higher.

Source: K. E. Boyce, T. J. Shields, and G. W. H. Silcock, "Toward the Characterization of Building Occupancies for Fire Safety Engineering: Prevalence, Type, and Mobility of Disabled People," *Fire Technology,* 35, 1, p. 42 (1999).

communal facilities and go out for meals and drinks, and for adults who are employed. The perceived value of this information and data relative to the application of performance codes was stated as follows:[61]

> The information provided in this analysis has important implications for characterizing building occupancies. It establishes that public buildings are frequented by a significant number of disabled people and that the nature of their disabilities and how well they can be expected to evacuate without assistance during an emergency will be a function of the use of the building or part of the building. Characterizing buildings and characterizing occupants as required by performance-based codes, are not mutually exclusive activities, a fact that has not yet percolated through the design professions.

The second study by Boyce, Shields, and Silcock[62] involved the experimental observations and measurement of the movement of disabled persons on a horizontal corridor, on inclined ramps, and on stairs. The observations included the velocity of movement, rest periods required, assistance required and the physical aids utilized relative to their degree of ambulatory disability. One hundred seven persons completed the horizontal corridor without assistance, 54 males and 53 females, ages 20 to 85. The velocity of this population relative to their ambulatory disability is presented in Table 3-12.24. Sixteen of the 28 manual wheelchair users needed assistance to traverse the 50 m long corridor with the 90 degree turn 8 m from the starting point. Only 34 participants were capable of participating in the stair movement studies involving ascending and descending travel, 30 of these without assistance and 4 with assistance, including three blind persons.

In general the movement velocity was slightly faster in descending travel on ramps while on the stairs the ascending movement was faster, as indicated in a comparison of Tables 3-12.25 and 3-12.26. The authors indicated the following from these experiments:[63]

Table 3-12.23 ***Extent of Involvement of Disabled Adults and Children in Various Social and Recreational Activities by Degree of Mobility[60]***

	Adults			Children			Totals		
Activity	Unassisted	Assisted	Total	Unassisted	Assisted	Total	Unassisted	Assisted	All
Participates in theatre, ie, opera, musicals, ballet, cinema	9,756 (6.5)	2,514 (9.6)	12,270 (7.0)	1,028 (14.0)	387 (7.3)	1,415 (11.3)	10,784 (6.9)	2,901 (9.5)	13,685 (7.3)
Goes shopping[a]	1,532 (58.5)	2,233 (40.0)	3,765 (40.1)	153 (81.0)	53 (28.0)	206 (75.7)	2,235 (79.6)	1,330 (23.5)	3,565 (42.1)
Participates indoor sport/spectates sport	13,161 (8.9)	1,006 (4.0)	14,167 (8.1)	3,205 (44.0)	1,084 (20.5)	4,289 (3.4)	16,366 (10.5)	2,090 (6.8)	18,456 (9.9)
Attends ordinary social club	8,052 (5.4)	898 (3.6)	8,950 (5.1)	— —	— —	— —	8,052 (5.4)	898 (3.6)	8,950 (5.1)
Stayed in hotel/other holiday accommodation	40,220 (27.0)	4,437 (17.6)	44,657 (25.6)	— —	— —	— —	40,220 (25.7)	4,437 (14.5)	44,657 (23.9)
Goes out for meals/drinks[a]	1,318 (50.3)	2,032 (36.4)	3,350 (40.9)	— —	— —	— —	1,277 (45.5)	2,032 (35.8)	3,350 (39.6)
Is employed	18,896 (12.7)	229 (0.9)	19,125 (11.0)	— —	— —	— —	18,896 (12.1)	229 (0.7)	19,125 (10.2)
Attends ordinary school	350 (0.2)	0 (0.0)	350 (0.2)	0 (0.0)	0 (0.0)	0 (0.0)	350 (0.2)	0 (0.0)	350 (0.2)
Attends college of further education	316 (0.2)	0 (0.0)	316 (0.2)	0 (0.0)	0 (0.0)	0 (0.0)	316 (0.2)	0 (0.0)	316 (0.2)

[a]Asked of disabled persons living in communal establishments only

Source: K. E. Boyce, T. J. Shields, and G. W. H. Silcock, "Toward the Characterization of Building Occupancies for Fire Safety Engineering: Prevalence, Type, and Mobility of Disabled People," *Fire Technology,* 35, 1, p. 44 (1999).

Table 3-12.24 ***Speed on Horizontal by Presence/Absence of Locomotion Disability and Walking Aid—Unassisted Ambulant[62]***

Subject Group	Mean (m/s)	Standard Deviation (m/s)	Range (m/s)	Interquartile Range (m/s)
All disabled ($n = 107$)	1.00	0.42	0.10–1.77	0.71–1.28
With locomotion disability ($n = 101$)	0.80	0.37	0.10–1.68	0.57–1.02
no aid ($n = 52$)	0.95	0.32	0.24–1.68	0.70–1.02
crutches ($n = 6$)	0.94	0.30	0.63–1.35	0.67–1.24
walking stick ($n = 33$)	0.81	0.38	0.26–1.60	0.49–1.08
walking frame or rollator ($n = 10$)	0.57	0.29	0.10–1.02	0.34–0.83
Without locomotion disability ($n = 6$)	1.25	0.32	0.82–1.77	1.05–1.34

Source: K. E. Boyce, T. J. Shields, and G. W. H. Silcock, "Toward the Characterization of Building Occupancies for Fire Safety Engineering: Capabilities of Disabled People Moving Horizontally and on an Incline," *Fire Technology,* 35, 1, p. 54 (1999).

Table 3-12.25 ***Speed on Stairs (ascent) by Presence/Absence of Locomotion Disability—Unassisted Ambulant[62]***

Subject Group	Mean (m/s)	Standard Deviation (m/s)	Range (m/s)	Interquartile Range (m/s)
With locomotion disability ($n = 30$)	0.38	0.14	0.13–0.62	0.26–0.52
no aid ($n = 19$)	0.43	0.13	0.14–0.62	0.35–0.55
crutches ($n = 1$)	0.22	—	0.13–0.31	0.26–0.45
walking stick ($n = 9$)	0.35	0.11	0.18–0.49	
rollator ($n = 1$)	0.14	—	—	—
Without disability ($n = 8$)	0.70	0.24	0.55–0.82	0.55–0.78

Source: K. E. Boyce, T. J. Shields, and G. W. H. Silcock, "Toward the Characterization of Building Occupancies for Fire Safety Engineering: Capabilities of Disabled People Moving Horizontally and on an Incline," *Fire Technology,* 35, 1, p. 64 (1999).

The abilities of disabled people cover a wide spectrum with respect to movement on horizontal and inclined planes. Given the significant differences in the capabilities of those using different mobility aids and the inherent differences in their spatial requirements, it is suggested that, for evacuation modeling purposes, they be considered separately.

Escape times are usually determined from characteristic travel speeds coupled with premovement times. From this study it is apparent that, for some disabled people, it may also be necessary to include periods of rest and time to negotiate changes in direction. This paper's findings should help designers derive characteristic

Table 3-12.26 ***Speed on Stairs (descent) by Presence/Absence of Locomotion Disability—Unassisted Ambulant[62]***

Subject Group	Mean (m/s)	Standard Deviation (m/s)	Range (m/s)	Interquartile Range (m/s)
With locomotion disability				
(n = 30)	0.33	0.16	0.11–0.70	0.22–0.45
no aid (n = 19)	0.36	0.14	0.13–0.70	0.20–0.47
crutches (n = 1)	0.22	—	—	—
walking stick (n = 9)	0.32	0.12	0.11–0.49	0.24–0.46
rollator (n = 1)	0.16	—	—	—
Without disability (n = 8)	0.70	0.26	0.45–1.10	0.53–0.90

Source: K. E. Boyce, T. J. Shields, and G. W. H. Silcock, "Toward the Characterization of Building Occupancies for Fire Safety Engineering: Capabilities of Disabled People Moving Horizontally and on an Incline," *Fire Technology,* 35, 1, p. 65 (1999).

times for disabled people traversing any typical escape route.

The detailed observations made during the movement studies suggest that, in designing accessible escape routes, more attention needs to be focused on the real, rather than the perceived needs of disabled people. Consideration should be given to the nature and position of support systems such as handrails, and the positioning of doors in escape routes, since these will influence the progress and the flight behaviors of some disabled occupants.

The third study by Boyce, Shields, and Silcock[64] was an experimental study of door operation and egress. One hundred four ambulatory disabled persons, 54 male and 50 female, ages 25 to 85 participated in this study. The disabilities of the participants involved 5 using crutches, 28 using a walking stick and 8 using a walker. The time to negotiate a standard single leaf door with a clear width opening of 750 mm is presented in Table 3-12.27, with the type of door operation and the closer force on the door leaf. In addition to the ambulatory disabilities other critical disabilities for this action involved 45 persons with a minor reaching and stretching disability and 58 with a dexterity disability. Table 3-12.28 presents the failure rates and the time to negotiate the door for the seven manual wheelchair users. The manual wheelchair users, in general, took more time to push the door open than to pull the door open. It also took these wheelchair users three to four times longer than the ambulatory disabled persons to negotiate the door.

The fourth study by Boyce, Shields, and Silcock[65] was an experimental study to determine the ability of disabled persons to locate and read three types of exit signs: nonilluminated, internally illuminated and light emitting diode (LED) signs. The signs were placed in a clear atmosphere in a room, 2.3 m from the floor with a maximum viewing distance of 85 m. The distances at which the participants were able to read the exit signs were measured. A total of 118 disabled persons participated in this study, including 25 persons with a vision disability. Table 3-12.29 presents the distances at which the participants could read the signs. The LED signs appeared to be the most visible and legible by the disabled persons with and without vision disabilities.

Klote, Alvord, Levin, and Groner[66] examined the design considerations needed to enable the elevators in tall buildings to be utilized for the evacuation of disabled oc-

Table 3-12.27 ***Time to Negotiate Door for Each Door Setting by Mobility Aid—Ambulant Disabled[64]***

	No Aid (n = 63)			Crutch Users (n = 5)		Walking Stick Users (n = 28)			Walking Frame/ Rollator Users (n =8)	
Closing Force (N)	Mean (s)	Standard Deviation (s)	Range	Mean (s)	Range	Mean (s)	Standard Deviation (s)	Range (s)	Mean (s)	Range
Push										
21	3.0	0.8	1.7–4.5	3.7	3.6–3.8	3.7	1.5	2.3–7.4	7.9	2.0–12.8
30	3.5	2.2	1.9–15.0	3.0	2.5–3.2	3.8	1.5	2.5–7.3	6.3	2.2–10.5
42	3.7	1.5	1.6–10.2	3.8	2.9–5.2	4.0	1.6	2.3–7.5	5.2	2.1–10.3
51	4.1	2.4	1.0–14.3	3.6	3.1–3.9	4.3	2.4	1.5–10.7	7.9	2.0–14.3
60	4.0	1.9	1.3–13.0	3.8	3.6–4.1	3.7	1.5	1.7–7.9	5.2	2.0–10.3
70	4.3	2.0	1.7–11.2	3.9	3.3–4.6	4.6	2.1	2.5–11.1	6.2	1.7–11.2
Pull										
21	3.3	1.5	1.5–7.6	2.8	2.2–4.0	3.6	1.4	1.8–7.6	5.7	2.0–8.2
30	3.2	1.0	1.5–5.2	—	—	3.2	0.9	1.8–4.9	5.2	4.3–6.0
42	3.7	1.8	1.4–12.6	4.0	2.9–6.3	3.9	1.4	1.9–6.8	4.7	2.6–6.9
51	3.8	1.6	1.5–10.2	3.6	2.5–4.6	4.6	2.2	1.5–9.5	6.3	2.5–11.2
60	4.1	1.9	1.5–11.4	3.6	2.7–4.7	4.1	1.7	1.4–7.4	8.9	1.9–17.0
70	4.6	2.2	1.5–12.6	4.6	2.6–4.7	4.9	2.3	2.1–9.7	3.2	1.9–6.7

Source: K. E. Boyce, T. J. Shields, and G. W. H. Silcock, "Toward the Characterization of Building Occupancies for Fire Safety Engineering: Capability of Disabled People to Negotiate Doors," *Fire Technology,* 35, 1, p. 73 (1999).

Table 3-12.28 ***Percentage Failure and Time to Negotiate Door for Each Door Setting—Manual Wheelchair Users[64]***

Closing Force Leading Edge (*N*)	No. of Failures (%)	No. (%) Successful	Mean (s)	Median (s)	Range (s)
Push ($n = 7$)					
30	1 (14.3)	6 (85.7)	13.1	7.4	3.6–39.0
42	1 (14.3)	6 (85.7)	13.3	10.7	3.6–36.0
51	2 (28.6)	5 (71.4)	10.0	7.4	3.6–20.5
60	2 (28.6)	5 (71.4)	10.5	10.5	3.5–17.4
70	2 (28.6)	5 (71.4)	11.6	6.7	3.6–26.3
Pull ($n = 7$)					
30	2 (28.6)	5 (71.4)	13.5	11.3	3.7–34.0
42	3 (42.9)	4 (57.1)	12.8	6.8	3.8–34.0
51	3 (42.9)	4 (57.1)	10.5	7.0	3.8–24.0
60	5 (71.4)	2 (28.6)	4.2	4.2	2.8–4.6
70	5 (71.4)	2 (28.6)	4.3	4.3	3.7–5.0

Source: K. E. Boyce, T. J. Shields, and G. W. H. Silcock, "Toward the Characterization of Building Occupancies for Fire Safety Engineering: Capability of Disabled People to Negotiate Doors," *Fire Technology,* 35, 1, p. 74 (1999).

cupants. In the explosion and fire in the World Trade Center with the loss of power in both Towers 1 and 2, including the emergency power, occupants were trapped in elevators in both buildings. Burns[11] indicated Tower 1 had 99 elevator cars, with many of them occupied. One 6- by 8-ft car, when opened, revealed 9 unconscious occupants, after an estimated exposure to the smoke in the shaft for approximately 2 hrs at the 9th floor level. Sherwood[67] reported that one 9- by 12-ft elevator car was stuck for 6 hrs at the 41st floor level of Tower 2 with 72 occupants: 62 elementary-school children and 10 adults.

NFPA *101,® Life Safety Code®*[16] in the 1991 edition permitted the use of elevators with fire fighter service from areas of refuge, which were also specified in this edition. In 1997 the *Life Safety Code®* permitted the use of a fire fighter service elevator with special features to be used as a second means of egress from towers with specifications on the occupant load, the provision of automatic sprinklers, the egress arrangement, and capacity.

Summary

Canter et al.[68] have stated the crux of the behavioral response in fire incidents in the following manner: "Behavior in fires can be understood as a logical attempt to deal with a complex, rapidly changing situation in which minimal information for action is available." It is suggested by Swartz[69] that the goals of codes should be "reoriented to increase the likelihood of informed decisions being made by people in fires." The examinations of the behavior in the Beverly Hills Supper Club fire led to the recommendation by Pauls and Jones[70] that "fire safety education should consider and be based on people's erroneous conceptions about distance being related to safety, and the time needed to escape from a fire emergency." Thus, more than a decade of detailed systematic research on human behavior in fires has resulted in the following consensus of the behavior of most persons, by Sime:[43]

> Despite the highly stressful environment, people generally respond to emergencies in a 'rational' often altruistic manner, insofar as is possible within the constraints imposed on their knowledge, perceptions and actions by the effects of the fire. In short, "instinctive," "panic"type reactions are not the norm.

There is a complex relationship between the physical and social environment in which the behavior occurs, which is complicated by the individual's perception of the ambiguous fire cues and primarily influenced by the person's relevant training and previous fire experience. It must be recognized that the fire cues are a product of a rapidly changing dynamic process which is constantly altering the decisions of the occupant within the building.

Table 3-12.29 ***Distance at Which Subjects Can Read Exit Signs by Presence/Absence of Seeing Disability[65]***

Type of Sign and Subject Group	Mean (m)	Median (m)	Standard Deviation (m)	Range (m)	Interquartile Range (m)
Non-illuminated exit sign					
All disabled ($n = 105$)	13.3	15.0	3.1	1.0–15.0	12.0–15.0
With seeing disability ($n = 25$)	11.4	12.0	4.0	1.0–15.0	9.7–15.0
Without seeing disability ($n = 80$)	13.7	15.0	2.7	6.0–15.0	15.0–15.0
Illuminated exit sign					
All disabled ($n = 118$)	14.2	15.0	2.7	1.0–15.0	15.0–15.0
With seeing disability ($n = 25$)	12.9	15.0	4.6	1.0–15.0	15.0–15.0
Without seeing disability ($n = 93$)	14.5	15.0	1.8	6.0–15.0	15.0–15.0
LED sign					
All disabled ($n = 83$)	14.6	15.0	1.6	5.0–15.0	15.0–15.0
With seeing disability ($n = 23$)	14.0	15.0	2.6	5.0–15.0	15.0–15.0
Without seeing disability ($n = 60$)	14.7	15.0	1.2	7.0–15.0	15.0–15.0

Source: K. E. Boyce, T. J. Shields, and G. W. H. Silcock, "Toward the Characterization of Building Occupancies for Fire Safety Engineering: Capability of People with Disabilities to Read and Locate Exit Signs," *Fire Technology,* 35, 1, p. 83 (1999).

Pauls and Jones[70] have summarized this decision dilemma as follows: "What is an appropriate action at one stage may be quite inappropriate a minute later."

Paulsen[52] has emphasized the limited time constraints imposed on the occupant in a fire incident building as follows:

> With very limited time available in which to decide on a course of action, people involved in fires often face difficult decisions. Decisions may be intellectually difficult in the context of limited knowledge of the engineered safety or the basic configuration of the occupied structure or limited knowledge of the development of the fire itself. Decisions may be difficult because of the sometimes counterinstinctive nature of the correct response, because some additional risk to one's self is incurred by a decision to alert or assist others.

References Cited

1. J.L. Bryan, *Smoke as a Determinant of Human Behavior in Fire Situations,* University of Maryland, College Park (1977).
2. P.G. Wood, *Fire Research Note 953,* Building Research Establishment, Borehamwood, UK (1972).
3. L. Lerup, D. Conrath, and J. Koh Liu, *NBS-GCR-77-93,* National Bureau of Standards, Gaithersburg, MD (1978).
4. J.P. Keating and E.F. Loftus, *Psych. Today,* 14 (1981).
5. G. Proulx and J.D. Sime, "To Prevent Panic in an Underground Emergency: Why Not Tell People the Truth?" *Fire Safety Science—Proceedings of the Third International Symposium,* Elsevier Applied Science, New York, pp. 843–852 (1991).
6. G. Ramachandran, "Human Behavior in Fires—A Review of Research in the United Kingdom," *Fire Technology,* 26, 2, pp. 149–155 (1990).
7. G. Ramachandran, "Informative Fire Warning Systems," *Fire Technology,* 27, 1, pp. 66–81 (1991).
8. E.A. Cable, "Cry Wolf Syndrome: Radical Changes Solve the False Alarm Problem," Department of Veterans Affairs, Albany, NY (1994).
9. M. Kimura and J.D. Sime, "Exit Choice Behavior During the Evacuation of Two Lecture Theatres," *Fire Safety Science—Proceedings of the Second International Symposium,* Hemisphere Publishing Corp., Washington, DC, pp. 541–550 (1989).
10. J.K. Lathrop, "Two Fires Demonstrate Evacuation Problems in High-Rise Buildings," *Fire Journal,* 70, 1, pp. 65–70 (1976).
11. D.J. Burns, "The Reality of Reflex Time," *WNYF,* 54, 3, pp. 26–29 (1993).
12. R.F. Fahy and G. Proulx, "Collective Common Sense: A Study of Human Behavior During The World Trade Center Evacuation," *NFPA Journal,* 87, 2, pp. 61, 64 (1995).
13. C.H. Berry, *Fire J.,* 72, p. 105 (1978).
14. NFPA 74, *Household Fire Warning Equipment,* National Fire Protection Association, Quincy, MA (1975).
15. H. C. Cohen, *Fire J.,* 76, p. 70 (1982).
16. NFPA *101, Life Safety Code,* National Fire Protection Association, Quincy, MA (2000).
17. M.J. Kahn, *Fire Tech.,* 20, p. 20 (1984).
18. E.H. Nober, H. Pierce, A. Well, C.C. Johnson, and C. Clifton, *Fire J.,* 75, p. 86 (1981).
19. B. Latane and J.M. Darley, *J. of Person. and Soc. Psych.,* 10, p. 215 (1968).
20. J.L. Bryan, *A Study of the Survivors' Report on the Panic in the Fire at Arundel Park Hall, Brooklyn, Maryland, on January 29, 1956,* University of Maryland, College Park (1957).
21. S.B. Withey, in *Man and Society in Disaster,* Basic, New York (1962).
22. J.L. Bryan, *Human Behavior Factors and the Fire Occurrence,* University of Maryland, College Park (1971).
23. R.M. Killian, R. Quick, and F. Stockwell, *A Study of Response to the Houston, Texas, Fireworks Explosion,* National Academy of Science, Washington, DC (1956).
24. J.D. Sime, "Perceived Time Available: The Margin of Safety in Fires," *Fire Safety Science—Proceedings of the First International Symposium,* Hemisphere Publishing Corp., Washington, DC, pp. 561–570 (1986).
25. A. Mintz, *J. of Abn. and Soc. Psych.,* 66, p. 150 (1950).
26. B.K. Jones and J.A. Hewitt, "Leadership and Group Formation in High-Rise Building Evacuations," *Fire Safety Science—Proceedings of the First International Symposium,* Hemisphere Publishing Corp., Washington, DC, pp. 513–522 (1986).
27. S. Horiuchi, Y. Murozaki, and A. Hokugo, "A Case Study of Fire and Evacuation in a Multi-Purpose Office Building, Osaka, Japan," *Fire Safety Science—Proceedings of the First International Symposium,* Hemisphere Publishing Corp., Washington, DC, pp. 523–532 (1986).
28. J. Breaux, D. Canter, and J. Sime, *Psychological Aspects of Behavior of People in Fire Situations,* University of Surrey, Guilford, UK (1976).
29. L. Bickman, P. Edelman, and M. McDaniels, *NBS-GCR-78-120,* National Bureau of Standards, Gaithersburg, MD (1977).
30. G. Proulx, "A Stress Model for People Facing a Fire," *Journal of Environmental Psychology,* 13, pp. 137–147 (1993).
31. M. Chubb, "Human Factors Lessons for Public Fire Educators: Lessons from Major Fires," Education Section, National Fire Protection Association, Phoenix (1993).
32. G.A. Klein and D. Klinger, "Naturalistic Decision Making," CSERIAC Gateway, Wright-Patterson AFB, Crew System Ergonomics Information Analysis Center, pp. 1–4 (1991).
33. D. Canter, J. Breaux, and J. Sime, "Domestic, Multiple-Occupancy, and Hospital Fires," in *Fires and Human Behaviour (*David Canter, ed.), John Wiley & Sons, New York, pp. 117–136 (1980).
34. R.L. Best and D.P. Demers, *Fire J.,* 76, p. 19 (1982).
35. J.L. Bryan, *Fire J.,* 76, p. 37 (1982).
36. G.P. Morris, *F. Command,* 68, p. 20 (1981).
37. J.L. Bryan and P.J. DiNenno, *NBS-GCR-79-187,* National Bureau of Standards, Gaithersburg, MD (1979).
38. J.L. Bryan, *An Examination and Analysis of the Dynamics of the Human Behavior in the MGM Grand Hotel Fire,* National Fire Protection Association, Quincy, MA (1983).
39. J.L. Bryan, *An Examination and Analysis of the Dynamics of the Human Behavior in the Westchase Hilton Hotel Fire,* National Fire Protection Association, Quincy, MA (1983).
40. R.L. Best, *Fire J.,* 72, p. 18 (1978).
41. D.P. Schultz, *Contract Report NR 170-274,* University of North Carolina, Charlotte (1968).
42. Kentucky State Police, *Investigative Report to the Governor, Beverly Hills Supper Club Fire,* Kentucky State Police, Frankfort (1977).
43. J.D. Sime, in *Fire and Human Behavior,* John Wiley and Sons, New York (1980).

44. E.L. Quanrantelli, *Panic Behavior in Fire Situations: Findings and a Model from the English Language Research Literature,* Ohio State University, Columbus (1979).
45. J.P. Keating, *Fire J.,* 76, p. 57 (1982).
46. E.R.F. Crossman, W.B. Zachary, and W. Pigman, *UCBFRG/WP 75-5,* University of California, Berkeley (1975).
47. National Fire Prevention and Control Administration, *Highlights of the National Household Fire Survey,* U.S. Fire Administration, Washington, DC (1976).
48. T. Jin and T. Yamada, "Experimental Study of Human Behavior in Smoke-Filled Corridors," *Fire Safety Science—Proceedings of the Second International Symposium,* Hemisphere Publishing Corp., Washington, DC, pp. 511–519 (1989).
49. G. Proulx, "The Impact of Voice Communication Messages During A Residential Highrise Fire," *Human Behavior in Fire Proceedings of the First International Symposium,* Fire SERT Centre, University of Ulster, pp. 265–274 (1998).
50. A.W. Heskestad and K.S. Pederson, "Escape Through Smoke: Assessment of Human Behavior and Performance of Wayguidance Systems," *Human Behavior in Fire Proceedings of the First International Symposium,* Fire SERT Center, University of Ulster, pp. 631–638 (1998).
51. T. Jin, "Studies on Human Behavior and Tenability in Fire Smoke," *Fire Safety Science—Proceedings of the Fifth International Symposium,* International Association for Fire Safety Science, pp. 3–21 (1997).
52. R.L. Paulsen, *Fire Tech.,* 20, p. 15 (1984).
53. J.L. Bryan, P.J. DiNenno, and J.A. Milke, *NBS-GCR-80-297,* National Bureau of Standards, Gaithersburg, MD (1979).
54. J.L. Bryan, J.A. Milke, and P.J. DiNenno, *NBS-GCR-80200,* National Bureau of Standards, Gaithersburg, MD (1979).
55. J.L. Pauls, in *Human Response to Tall Buildings,* Dowden, Hutchinson and Ross, Stroudsburg, Germany (1977).
56. M.S. Isner and T.J. Klem, "Fire Investigation Report, World Trade Center Explosion and Fire, New York, New York, February 26, 1993," National Fire Protection Association, Quincy, MA (1993).
57. M.S. Isner and T.J. Klem, "Explosion and Fire Disrupt World Trade Center," *NFPA Journal,* 87, 6, pp. 91–104 (1993).
58. E. Juillet, "Evacuating People with Disabilities," *Fire Engineering,* 126, 12, pp. 100–103 (1993).
59. E. Juillet, Personal Communication, (Jan. 18, 1994).
60. K.E. Boyce, T.J. Shields, and G.W.H. Silcock, "Toward the Characterization of Building Occupancies for Fire Safety Engineering: Prevalence, Type, and Mobility of Disabled People," *Fire Technology,* 35, 1, pp. 35–50 (1999).
61. K.E. Boyce, T.J. Shields, and G.W.H. Silcock, "Toward the Characterization of Building Occupancies for Fire Safety Engineering: Prevalence, Type, and Mobility of Disabled People," *Fire Technology,* 35, 1, p. 48 (1999).
62. K.E. Boyce, T.J. Shields, and G.W.H. Silcock, "Toward the Characterization of Building Occupancies for Fire Safety Engineering: Capabilities of Disabled People Moving Horizontally and on an Incline," *Fire Technology,* 35, 1, pp. 51–67 (1999).
63. K.E. Boyce, T.J. Shields, and G.W.H. Silcock, "Toward the Characterization of Building Occupancies for Fire Safety Engineering: Capabilities of Disabled People Moving Horizontally and on an Incline," *Fire Technology,* 35, 1, pp. 66–67 (1999).
64. K.E. Boyce, T.J. Shields, and G.W.H. Silcock, "Toward the Characterization of Building Occupancies for Fire Safety Engineering: Capability of Disabled People to Negotiate Doors," *Fire Technology,* 35, 1, pp. 68–78 (1999).
65. K.E. Boyce, T.J. Shields, and G.W.H. Silcock, "Toward the Characterization of Building Occupancies for Fire Safety Engineering: Capability of People with Disabilities to Read and Locate Exit Signs," *Fire Technology,* 35, 1, pp. 79–86 (1999).
66. J.H. Klote, D.M. Alvord, B.M. Levin, and N.E. Groner, "Feasibility and Design Considerations of Emergency Evacuation by Elevators," NISTIR 4870, NIST, Building and Fire Research Laboratory, Gaithersburg, MD (1992).
67. J. Sherwood, "Darkness and Smoke," *WNYF,* 54, 3, pp. 56–60.
68. D. Canter, J. Breaux, and J. Sime, *Human Behavior in Fires,* University of Surrey, Guilford, England (1978).
69. J.A. Swartz, *Fire J.,* 73, p. 73 (1979).
70. J.L. Pauls and B.K. Jones, *Fire J.,* 74, p. 35 (1980).

CHAPTER 13

Movement of People: The Evacuation Timing

Guylène Proulx

Introduction

This chapter is an updated version of the chapter "Movement of People" written originally by Jake Pauls. Most of the initial material is still in the chapter, for example, basic crowd movement characteristics (density, speed, and flow) with some new examples. Extensive descriptions are given of building evacuation models developed by Pauls, based on empirical studies in Canada. The effective-width model for evacuation flow is highlighted, especially in relation to prediction formulas for the total evacuation time of large buildings. Some original material has been included regarding the time delay to start an evacuation, the movement of people with disabilities, and occupant movement in smoke. Although all the answers on these new themes are not yet available, it was felt important to include these issues in this chapter. A limited number of studies have been conducted on these questions; however, with the ever-increasing use of performance-based design, it has become essential for the fire safety engineer to consider their impact on fire safety.

Note of Caution

A caution must be given regarding limitations in the quantitative methods currently available for people's movement in buildings. Some traditional assumptions about people's behavior in fires have been shown to be erroneous by research, especially that conducted during the last three decades. (See Section 3, Chapter 12.) Some models of evacuation behavior, such as the so-called hydraulic model, although applicable to certain situations, should not be applied indiscriminately to any situation. Valuable here are the views of John Archea, abstracted from his remarks (summarized by Pauls[1]) at the International Life Safety and Egress Seminar in 1981.

> Most egress rules were developed in their present form some twenty years before research was done.
>
> Research on people's movement falls into two schools: the carrying capacity school which examines exit flow capacity, and the human response school which says that exit capacity may be a necessary condition for safe egress, but it is not a sufficient condition. In the former, the "safe end" of the egress route is emphasized as the key point where egress is to be evaluated. The human response school looks at what happens at the other end of the route—the threatened end of the egress route. The former assumes that people will, upon hearing an alarm, drop what they are doing and immediately evacuate in an orderly fashion, without interacting with each other. Actually, people tend to ignore or downplay the initial fire cues, eventually they investigate conditions, compare with their experience, and then decide on actions that may have little to do with what is assumed in code rules for egress. Such activities take time. Another finding is that familiar entry routes are more likely to be used for evacuation than egress routes that have never been experienced before. Consequently, routes that are being counted on to "drain" the building of its occupants may be disregarded in an actual evacuation.
>
> Traditional exit technology also relies on what is called the "hydraulic model." There are three assumptions in the hydraulic model: occupants are alert, able-bodied, and ambulatory; fire safety depends on the safe end of the evacuation

Guylène Proulx is a research officer at the Fire Risk Management Program of the National Research Council of Canada, since 1992. She holds a Ph.D. in architectural planning from the University of Montreal specializing in environmental psychology. She focuses her research on investigating human response to alarms, evacuation movement, typical actions taken, timing of escape, time to start evacuation, and social interaction during a fire. She is a member of the National Fire Protection Association (NFPA), the Society of Fire Protection Engineers (SFPE), the Human Factors and Ergonomics Society (HFES), and the International Association for Fire Safety Science (IAFSS).

system; and there is a high-density building population that will tax the capacity of the exit system. There are two phases to evacuation: the time to start and the movement phase. The hydraulic model deals only with the latter. Liquid flow or ball-bearing models do not account for the fact that people will take time to investigate the situation, help one another or that they have different degrees of familiarity with particular routes.

Archea's remarks raise basic questions about long-standing approaches to the design of means of egress. A related chapter, "Behavioral Response to Fire and Smoke" (Section 3, Chapter 12), should be consulted for some of the background research that is helping to describe people's actual behavior when encountering fire. Additional research on the topic of fire-related human behavior, especially the behavior associated with egress, is found in the following literature review.

Literature Review

The following should be regarded as an indicative survey rather than a complete review of technical contributions to the subject of evacuation. Some additional background is provided in reviews by Stahl and Archea,[2] Stahl, Crosson, and Margulis,[3] Paulsen,[4] and Pauls.[5]

Early Committee Documents

The 1935 report *Design and Construction of Building Exits*[6] described committee deliberations; however, it is sometimes incorrectly spoken of as a research document. Because it contains a mix of traditional practice with some empirical studies, the report is often misinterpreted regarding qualitative and quantitative aspects of exit use by crowds; for example, the unit exit width and unrealistically high flow figures, such as 45 persons per min per unit of exit width downstairs, are concepts that predated the 1935 work. These errors influence time-based egress design calculations even today.

Sharing many of the characteristics of the 1935 report, and building upon some of its contents, is its British counterpart, *Post-War Building Studies, No. 29*.[7] This report helped to establish the nominal 2.5-min clearing time for a space (based on a reported successful evacuation time of 2.5 min in the Empire Palace Theatre fire in Edinburgh in 1911), and it suggested the use of very high flows to perform the population capacity calculation (i.e., 40 persons per min per 530 mm or 21 in. of exit width).

General Research on Crowd Movement

The post-war era also marked the beginning of modern studies of crowd movement, notably in Japan by Kikuji Togawa, whose many technical insights and empirical data were reported in 1955.[8] Among his mathematical presentations we find an equation for "time required for escape." It takes into account the flow time for an egress element plus the time needed to traverse some distance in the egress system. This general form of equation appears often in the egress literature.

Post-war publications by Russian experts included highly abstract treatment of evacuation, but did not provide the kind of empirical detail presented by Togawa. Most often referenced is the book titled (in its 1978 English translation) *Planning for Foot Traffic Flow in Buildings,* by Predtechenskii and Milinskii.[9] Their work is little known (and used even less) in North America; however, some of their abstract treatment and graphical techniques have been applied by Kendik,[10,11] using data from evacuation observations in Germany in 1977.

Often mentioned in some egress literature is a small-scale study by an operations research team that worked for the London Transport Board. The team's observations and tests were described in an unpublished research report,[12] and highlights were published by Hankin and Wright.[13] The former unpublished report has been widely circulated, referenced, and misapplied by people who compounded some original defects in the report, such as the failure to distinguish between maximum and mean flows. Again, as with earlier widely referenced but not critically read documents, this has led to overly optimistic predictions of egress time in some calculations. There are other problems inherent as well in applying data from a special-population transit context to the context of evacuation via (unfamiliar) routes, such as exit stairs. Caution on this should also be heeded when applying some of the work by Togawa[8] and Fruin.[14]

John Fruin is a prominent researcher in North America whose well-known book *Pedestrian Planning and Design*[14] is now available in a revised edition. It is a comprehensive reference book on crowd movement. Fruin's work is often referred to in time-based analyses; however, these analyses sometimes tend either to misuse the data for levels of service E and F (which Fruin recommends to be used rarely, if at all, in analysis or design situations) or to combine high-flow density assumptions with relatively high-speed assumptions (an unrealistic combination). Used conservatively (including width deductions for the edge effect also reported by Fruin), there is much similarity between movement characteristics recommended by Fruin and those coming from Pauls' studies.

Between 1972 and 1982, many field observations—mostly unanalyzed and unpublished—were conducted by the National Research Council of Canada. These observations concentrated on people's movement in large assembly-occupancy buildings and large-scale events, such as the 1976 Commonwealth Games in Edmonton. This work provided further empirical underpinning to the effective-width model for crowd flow on egress routes.

The work on evacuation and human behavior in fire has known a renewed of enthusiasm with the arrival of many new researchers in the 1990s. The number of papers on this subject at conferences such as the International Association for Fire Safety Science (IAFSS), Interflam, and First International Symposium on Human Behavior in Fire, and at NFPA's meetings demonstrates the vitality of the field in the last decade.

Research on Tall Buildings

Near the end of the 1960s the matter of high-rise fire safety became a rapidly growing concern to safety officials

and committees working on standards and codes. Among the papers prepared at that time on the matter of evacuation time of tall buildings and the design of exit stairs were ones by Galbreath,[15] Melinek and Booth,[16] and Melinek and Baldwin.[17] These papers contained a reworking of some of the "classical" reports from the 1930s and 1950s to provide formulas relating exit stair width and minimum total evacuation time. Few new data were presented, and the formulas in general seriously underestimated total evacuation times of such buildings.

Beginning in 1969, Pauls began comparatively systematic and detailed observations of many evacuation drills in tall buildings, especially in Ottawa, Canada. Ignoring relatively inaccessible early references, the work is represented in general conference publications and periodical articles[18–20] and in published analyses and applications, especially on the "effective-width model."[21–27] Although dealing largely with evacuation situations where a "hydraulic model" is valid (e.g., there is queuing by people waiting to use egress routes, and much of the activity is relatively simple crowd movement dedicated to egress), this work bridged between movement studies and concurrent studies examining people's behavior in fires (especially in Great Britain and the U.S.). The behavioral studies identified the role played by nonevacuation behavior before, during, and even in place of simple evacuation movement—all of which tend to significantly increase the actual evacuation times of buildings.

Mention should be made of more recent studies of evacuation of tall buildings, mostly in drills but some in connection with serious fires. Many of these studies have been published in conference proceedings. The most highlighted book on this subject is the *Proceedings of the First International Symposium on Human Behaviour in Fire,* 1998, available through FireSERT at the University of Ulster, Belfast, United Kingdom.

By way of a very general and incomplete summary, some conclusions can be drawn regarding movement of people in fire:

1. Panic is very rare even in fires. Normal patterns of behavior, movement route choices, and relationships with others tend to persist during emergency situations.
2. People's behavior tends to be altruistic and reasonable, especially in light of the limited and often ambiguous information available to people at the time of the event.
3. After perceiving a fire cue, such as the fire alarm signal or smelling smoke, people often ignore these initial cues or spend time investigating, seeking information about the nature and seriousness of the situation, which creates a delay time before starting evacuation movement.
4. Faced with ambiguous information and short time for decision making, people are likely to apply a well-run decision plan when choosing an evacuation route, consequently moving toward their most familiar way out of the building.
5. Evacuation, and response to fire generally, is often a social response; people tend to act as a group and to attempt to evacuate with people with whom they have emotional ties.
6. Problems that are encountered during normal building use will tend to persist and exacerbate situations in emergencies. Included are faulty communication, circulation hazards, wayfinding problems.

A key assumption, based on such findings, is that the movement of people observed in normal building use and in evacuation drills is a good basis for predicting their movement in a fire emergency. Specifically, people should not be expected to react faster or move more efficiently in a fire emergency than they do normally. Therefore, much of the evacuation technology, derived from careful documentation of realistic evacuation drills (e.g., without prior warning), is a good basis for developing guidelines for the design and use of emergency egress systems. This is a key to the validity of much of the technology presented in this chapter as well as to the validity of evaluation procedures for egress systems.

Crowd Behavior and Management

Crowd incidents, in which people are seriously injured or killed due to crushing or trampling, are not restricted to emergencies (such as fire), to conditions of crowd violence, or even simply to exuberance of some members of a crowd. Such events can occur, and have occurred, at sports events, religious gatherings, and rock music concerts. Serious injury and even death can occur during entry, occupancy, and evacuation of a building. It can happen under conditions that might, in every other respect, appear to be nearly normal, even to people in close proximity to those hurt in the incident.

An introduction to some problems and solutions for crowd safety has been provided by Pauls[28] and Fruin.[29,30] Pauls notes crowd incidents in Britain, Canada, and the United States and refers to reports such as the one by SCION,[31] prepared after 66 football fans died in a crowd crush on a stairway in 1971 in Ibrox Park, Glasgow (which influenced a U.K. standard for sports grounds);[32] the report of a special committee set up after 11 people were crushed in a crowd waiting to get into a rock concert in Cincinnati in 1980;[33] and a record of a meeting of experts called together by the U.S. National Bureau of Standards (NBS)[34] in response to the Cincinnati committee. Recent contributions to the literature include the reports of British Inquiries into the Hillsborough stadium crush that killed 95 soccer fans in 1989, the Bradford stadium fire, plus crowd incidents in Brussels and Sheffield.[35–38] Crowd safety engineering is also the subject of a book.[39]

Among the NBS report[34] design recommendations, mostly in relation to ingress, some recommendations have wide applicability:

1. Strive for simplicity in all access and movement routes; this lessens the need for directional graphics and ushers.
2. Capacity-handling channels should be continuous walking surfaces, such as ramps. Stairs are satisfactory to shorten channels not subject to heavy pedestrian loads.
3. To the greatest extent possible, ingress systems should be "reversible" and usable whenever emergency egress is necessary.

Among technical papers appended to the NBS report 94 was one by Fruin, entitled "Crowd Disasters—A Sys-

tems Evaluation of Causes and Countermeasures" (which was subsequently republished).[29,40] This paper discusses four fundamental elements—time, space, information and energy—in relation to the following aspects of serious crowd incidents:

1. Rapid accumulation of queuing persons as demand for a facility outstrips its capacity.
2. Pedestrian densities that approach the critical density of about 8 persons/m^2 (less than 1.5 ft^2/person) leave no space between people. Shock waves, causing individuals to move involuntarily as much as 3 m (10 ft) laterally, can be seen moving through crowds in this situation.
3. Competitive rushing by a crowd away from something is termed "panic" by Fruin, and competitive rushing toward some objective (such as in the Cincinnati incident) is termed a "craze."

In relation to the second item on this list and to the unusual physical forces in crowd incidents, Fruin notes[29]

> The combined pressures of massed pedestrians and shock-wave effects through crowds at the critical density level produce forces which are impossible for individuals or even small groups of individuals to resist. Reports of persons being literally lifted out of their shoes and of clothes being torn off are a common result of the forces involved in crowd incidents. Survivors of crowd disasters report difficulty in breathing due to crowd pressures, and asphyxia is a more typical cause of death than trampling by the crowd. In the Glasgow, Scotland, soccer stadium incident in which 66 persons died, the failure of a steel railing under crowd pressures contributed to the piling up of pedestrians. The bending of a steel-pipe railing under crowd pressures was reported at the Cincinnati Coliseum incident. The force required to bend a 50-mm (2-in.) diameter steel railing, applied 0.75 m (30 in.) above the base, is estimated at 500 kg (1100 lb.).

Fruin lists countermeasures for critical density levels, such as provision of adequate pedestrian processing capacity and control of demand (e.g., arrival process). Also recommended are dispersion of routes as well as separation of waiting pedestrians into smaller groups. The U.K. *Guide to Safety at Sports Grounds*[32] calls for systems of rails placed across the tops of wide stairs to break up large mass flows onto stairs into smaller flows that will not tax the stair's capacity so severely, thus reducing crowd forces to safe levels, a method sometimes termed "metering." Under this U.K. guide—made mandatory retroactively through reference in British regulations—such crowd control rails, as well as all guardrails, must be designed to resist loads that are much greater than called for in North American code requirements for guardrails.

Crowd incidents often exhibit what can be termed a failure of front-to-back communication, which was well represented in the rock concert incident at the Toronto's Exhibition Stadium in July 1980.[41] People at the back of a crowd or bulk queue may contribute unknowingly to the forces that can build up in the crowd, forces that can reach crushing levels in the middle of the crowd or at the front, especially where forward movement is stopped by a barrier. The people being crushed are unable to communicate their plight to those at the back. For example, this was exhibited very well during the Hillsborough stadium crush in 1989.[35,42] Thirty minutes away from kickoff, the terrace section (standing spectators) of the Leppings Lane stand was near capacity, although some room was still available in the outer pens. Outside, several thousand fans, some without tickets, were trying to push and force their way forward. With the congestion building up outside to dangerous levels, the police made the decision to open a gate into the stadium. Suddenly the intense pressure from outside was dramatically transferred inside to the narrow confines of a tunnel that was the quickest way to the terrace. The extreme pressure at the back of the crowd pinned the people at the front against the steel-wire fence. Some of the victims trapped were women and children who thought being in front was the safest place to watch the game. Five minutes after it started, the match was interrupted, with visual indication from television coverage that injuries might have occurred on the terrace. In total, 95 people died, suffocated, or were trampled to death, and another 400 were injured.

There is a distinction between "crowd management" and "crowd control." Designers and managers of places where crowds assemble should be aware of this distinction, which is carefully drawn, at least by leading North American crowd behavior experts. To manage a crowd is to make use of design and operating features based on the subtle and beneficial exploitation of people's natural behavior. This requires a good understanding of a crowd's reason for being, and the collective motivation of its members. Crowd control, on the other hand, is a more extreme, disruptive line of defense when crowd management is not successful; it might include dramatic police actions to subdue mob violence with force against force. Unfortunately, little literature exists that can be referenced here for guidance; designers or consultants working on projects subject to use by crowds should seek the advice of experienced facility and event managers as well as use their own powers of observation. Examples of crowd control—which have little to offer designers and managers—may be viewed on television news accounts of riots. Examples of generally very good crowd management can be seen at the Disney complexes.

Basic Movement Characteristics and Relationships

Crowd movement is quantitatively specified using three fundamental characteristics, all of which are expressed as rates. These are density, speed, and flow. Density is the number of persons in a unit area of walkway (e.g., 2.0 persons/m^2). Often this characteristic is referred to by using the inverse of density, that is, the area per person or pedestrian module, for example, 0.5 m^2 (5.4 square ft^2) per person. Speed is simply the distance covered by a moving person in a unit of time [e.g., 1.0 m/s (3.3 ft/s)]. The term "flow" is often used in a casual, nontechnical way when the general term "movement" is implied, or

when speed is actually being specified. Flow is specifically the number of people that pass some reference point in a unit of time (e.g., 2.0 persons/s). These three characteristics are related, along with path width, in the fundamental traffic equation (which, incidentally, applies to motor vehicles as well as pedestrians)

$$\text{flow} = \text{speed} \times \text{density} \times \text{width} \qquad (1)$$

For example, the density, speed, and flow values shown above are consistent with what would be obtained with this equation, assuming the walkway's width is 1.0 m (3.3 ft). Note that, to be correct, a consistent set of units must be used, and speed must be measured along the slope of the walkway.

Also important is that speed is dependent on density. People can move quickly with a normal gait if there is a great deal of space between them. The closer they are to each other, the more constrained is their movement until, when very close together, they can only shuffle along slowly. Aside from these speed implications, high-density situations are also uncomfortable to varying degrees, depending on culture, social setting, and the relationship to those nearby. Expressed quantitatively, when the pedestrian density is less than about 0.5 persons/m^2 (21 ft^2/person), people are able to move along walkways at about 1.25 m/s (4.1 ft/s), an average unrestricted walking speed. With greater density, speed decreases, and it decreases very markedly with very high densities, reaching a standstill when density reaches 4 or 5 persons/m^2 (2.1 to 2.6 ft^2/person), equivalent to a fairly crowded elevator situation. This is also similar to the situation in a closely packed bulk queue of people anxiously waiting or competing to get through an entrance. Speeds of movement are more variable at low densities. When density is low, it is not necessarily accurate to calculate high speeds of movement. In fact, at low density, the main factors that will determine speed are more likely to be occupants' characteristics such as age, limitations, and grouping. For example, a family group is likely to move at the speed of its slowest member, being a child or a senior person.

On stairs, the speeds of movement are slightly lower and, at low densities, relatively fit people can average about 1.1 m/s (3.6 ft/s) descending along the stair slope [a horizontal speed component of about 0.8 m/s (2.6 ft/s)]. The speed-density relation data from a study by Pauls[23] in uncontrolled total evacuations of tall office buildings are shown in Figure 3-13.1. A curve representing similar speed-density findings reported by Fruin[14] is included in Figure 3-13.1 along with a regression equation for Pauls's data. (Note that Fruin's data were not derived from observations of evacuation in buildings.)

Given these dynamics as illustrated in Figures 3-13.1 and 3-13.2, there is a relatively complex relationship between flow and density. As shown in Figure 3-13.2, flow is small at both low and very high densities, but it attains a peak or optimum value at some intermediate density ranging around 2.0 persons/m^2, depending on whether people are on a level walkway or on a stairway. Equation 2 describes the flow-density relation obtained empirically for stairs used in total evacuations of tall office buildings.[23]

$$\text{flow} = [1.26(\text{density})] - [0.33(\text{density})^2] \qquad (2)$$

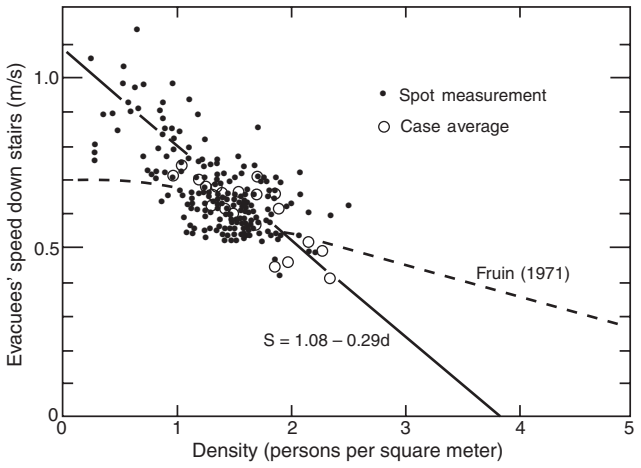

Figure 3-13.1. ***Relation between speed and density on stairs in uncontrolled total evacuations.***

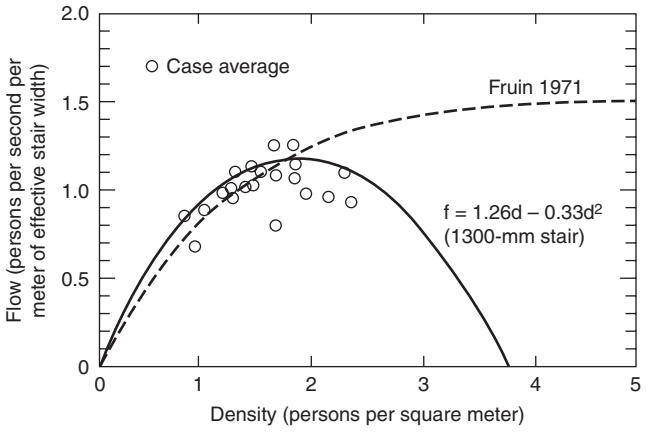

Figure 3-13.2. ***Relation between flow and density on stairs in uncontrolled total evacuations.[61]***

These basic characteristics and relationships are often described in publications on pedestrian movement.[14] Little should be made of the differences in the curves at the high-density end in Figure 3-13.2. As seen from the data points in Figure 3-13.1, these conditions are rarely or never observed, and the differences are mainly of academic interest.

Put into simple terms, the optimum flow conditions observed in uncontrolled total evacuation drills on a typical 1120-mm (44-in.) wide exit stair in a well-populated office building evacuation are as follows:

1. Each person would occupy slightly less than two treads.
2. There would be a descent of one storey every 15 seconds.
3. One person per second would pass a fixed point.

Going further, for evacuees on such an optimally-loaded stairway, there would be one evacuee on every other stair, staggered left and right. These conditions are similar to those expected with level of service E, the busiest level of service recommended for stairs by Fruin.[14]

Expressed abstractly, the optimum flow conditions for evacuation downstairs include

1. Density of 2.0 persons/m^2
2. Speed of 0.5 m/s along the stair slope
3. Flow of 1.18 persons/(m·s) of effective stair width

Note that a stair's effective width is 300 mm (12 in.) less than its nominal width (credited in building codes); for example, a nominal width of 1120 mm (44 in.) equates to an effective width of 812 mm (32 in.).[23,24,26] This is described more completely in the following subsection.

Fruin's Levels of Service

Chapter 4 of Fruin's *Pedestrian Planning and Design*[14] is much used as a basis for deciding on appropriate pedestrian values to be used in dynamic exit calculations. The book's central concepts and data are also available in several other publications.[43,44]

Fruin describes six levels of service (A through F) for walkways, stairways, and queuing. Level A provides the highest standard with the least chance of congestion; level F provides the lowest—Fruin notes, an unacceptably low—standard with much congestion. Chapter 4 describes the levels of service in terms of flow as a function of area per persons, or "pedestrian module"—the inverse of crowd density—while Chapter 3 describes how speed varies with the module. For emergency movement and limited space situations, usually of concern to a fire protection engineer, levels of service C, D, and E should be used. Expressed in Fruin's original imperial-units form, pedestrian modules range, respectively, from about 25 to 5 ft^2/person (2.3 to .5 m^2/person) on walkways and 10 to 4 ft^2/person (0.9 to .4 m^2/person) on stairways. Corresponding flows range from 10 to 25 PFM [persons per foot (of effective width) per minute] [.5 to 1.4 persons/(m·s) of effective width] on walkways and 7 to 17 PFM [.4 to .9 person/(m·s)] on stairways (plus or minus 1 PFM [(0.5 person/(m·s)], respectively, depending on whether descent or ascent is required). Speeds of movement, which are more variable at low densities, range in average value from 250 to 100 ft/min (1.27 m/s to .51 m/s) on walkways and from 115 to 70 ft/min (.58 m/s to .36 m/s) (along the slope) on stairs. It is estimated that ramps with slopes up to about 5 percent do not decrease movement speed; a 10 percent upward slope decreases speed by about 10 percent; an unusually steep 20 percent upward slope leads to a 25 percent reduction in speed.

Fruin also reports reductions in walkway effective width due to edge effects; however, he did not carry his work as far as Pauls did in relation to stairs, nor did he carry out detailed documentation of the effective width of corridors as did Habicht and Braaksma,[45] who reported edge effects of about 150 mm (6 in.) at each corridor wall, edge effects similar to what Pauls found at stair walls.

Evacuation Timing

The level-of-service characteristics, described previously, are stated in terms of rates. Most important, however, is the total time needed for evacuation to be completed. The total time taken for people to move past or through one part of a circulation system, which is the flow time, must be distinguished from the movement time, which is time taken to go from a point of origin to some destination, such as a remote place of safety. The flow time is simply a function of the crowd flow capacity of the usable width of a particular circulation element and the population or number of people to be moved through it. Population, capacity, and flow time are related as follows:

$$\text{population} = \text{flow capacity} \times \text{flow time} \qquad (3)$$

Evacuation time is relatively complex, and it is more difficult to control and predict than is flow time. The total evacuation time contains two major components: (1) the delay time to start evacuation movement and (2) the time needed to travel to a place of safety.

The time available for a safe evacuation of the occupants in the event of a fire is limited to the time when untenability conditions occur in the evacuation route. In a way to visualize the timing of escape, Figure 3-13.3 illustrates the different components of the time available (this

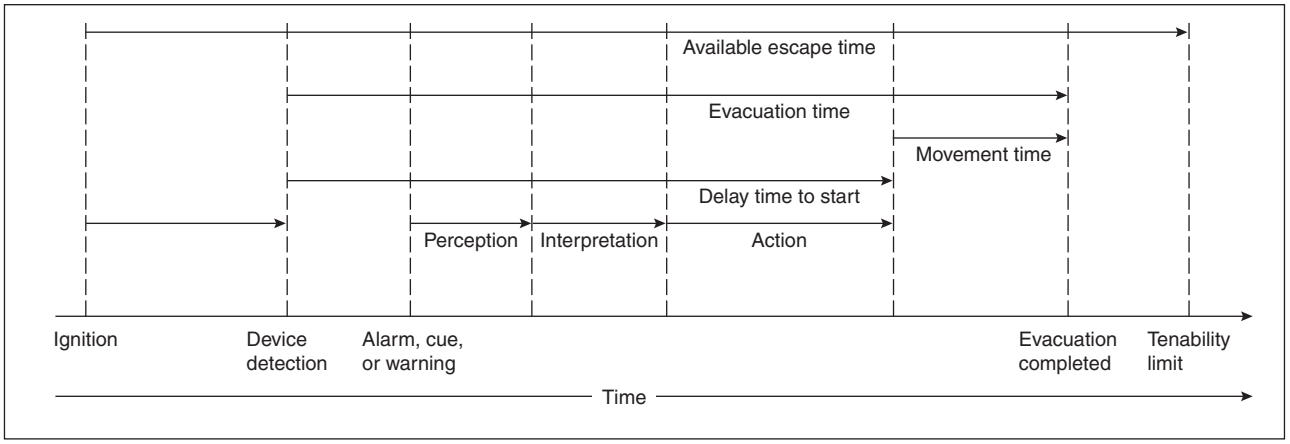

Figure 3-13.3. ***Sequence of occupant response to fire.***

figure is largely inspired by British Standard (BS) Draft for Development document DD240, 1997,[46] and the FIRECAM occupant response model, 1992[47]).

The time of ignition is the starting time of the fire event. Then a time should be calculated for the detection to take place. Detection could take a few seconds to a few hours, depending on the type of fire and the detection devices in place. An elapsed time should be calculated between detection and alarm activation. In some cases, these two events are almost simultaneous, but there could be a delay, for example, if occupants have to manually activate the fire alarm signal at a pull-station. When the fire alarm signal, or cue, has been perceived, then a time to start should be calculated. The fire alarm may not be activated or may not work, so occupants will eventually perceive some cues from the fire or will receive a warning by others. The delay time to start comprises 3 subcomponents: perception, interpretation, and action. Perception is the time occupants will take to perceive the fire alarm signal; it could also be a fire cue or warning by others. Interpretation of this information will take some time, and different actions will be taken to investigate or search for more information before a decision to evacuate is made. Once the decision to evacuate is made, occupants will engage in other actions before leaving, such as getting dressed, gathering children, or finding valuables. After the perception-interpretation-action process has taken place, then the occupants will start to move. Movement time should be calculated from the flow time through various elements of the egress system and the travel time to move along an egress route. The evacuation time is calculated from the time of alarm signal activation until the last occupant to evacuate has reached a location of safety. This time should be less than the time when untenability occurs (some say half the time).

Delay Time to Start

The time occupants will take to initiate their evacuation movement once they have perceived some cues of the fire can be a difficult figure to estimate. In the past, no such delay was considered, which made calculation easier but provided totally inaccurate evacuation times. Traditionally, it was assumed that as soon as the occupants would perceive fire cues or the fire alarm signal, they would start to evacuate the building. Victims reporting their behavior during fires have always challenged this assumption of immediate response. In the calculation of an expected total time to evacuate a building, it is now a common practice to add some time to account for a delay to start evacuation.

The literature on time delay to start is still scarce, but data from case studies are appearing constantly. It is important to mention that what is called here delay time to start or time to start is considered under "premovement," particularly in the British literature. This denomination of premovement is a bit peculiar, since occupants' behavior during this premovement time is usually to move around trying to figure out the situation. Therefore, there could be a lot of movement during this premovement time; this explains why the expression *delay time to start* is preferred here.

It was suggested in former editions of this chapter that a safe bet to account for the delay time to start would be to double the calculated time to move to obtain the overall time to evacuate. Many fire safety engineers, however, have found this approach too demanding on their design and prefer to add 15 to 30 s to account for the delay time to start. Is 30 s reasonable, or is 3 min more realistic? Instead of picking up numbers in the air, it is important to closely study the available research findings.

The delay time to start has been studied in two ways: during evacuation drills and from fire victim interviews. Some tend to denigrate the fire drill studies, although they are perfectly representative of a fire situation, especially if the drill is nonannounced. Fire drills represent exactly the situation that would face occupants if the fire were located in a remote area or on an upper floor of the building and the only sign of fire would be the sudden sound of the fire alarm signal.

In Canada, Proulx's obtained the time to start of over 500 occupants of 7 mid-rise and high-rise residential buildings during evacuation drills.[48] For ethical reasons, occupants of these residential buildings received a note a few weeks before the exercise informing them that a fire drill would be conducted in their building without informing them of the date and time. Video cameras located in the building corridors recorded the exact time occupants took to leave their apartments. A questionnaire filled out after the drill provided essential information on occupants' perception of the fire alarm, their interpretation of the signal, their actions before leaving their apartment, and their evacuation movement. Around 25 percent of the occupants in each building thought it was a real fire when they heard the fire alarm.

Significant variations were observed for the time to start in the 7 residential buildings studied. A clear distinction was made between buildings with a good or a poorly audible fire alarm signal. From the questionnaires, when over 80 percent of the respondents mentioned that the fire alarm was loud enough in their apartment, it was judged that the building had a good audible fire alarm signal. In 3 of the buildings studied, where the alarm had good audibility, the mean delay time to start evacuation was 2 min 49 s. In these buildings, three-quarters of the evacuation time was used for the delay time to start and one-quarter in movement time. So for an evacuation that lasted in total 4 min, 3 min were spend in time to start and 1 min to move to the outside.

A fourth building where the alarm was judged good by the occupants had 5 min 19 s as a mean time to start evacuation. The latter was a winter evacuation, which required putting on coat, boots, mitts, and hat, which explains the longer time to start. In a fifth building with good alarm, most occupants decided to evacuate onto their balconies instead of the procedure that required occupants to leave to ground level. The mean time for occupants to appear onto their balconies was 2 min 25 s.

Two of the residential buildings studied by Proulx had over 20 percent of the occupants who judged that the alarm was not loud enough inside their suites. These occupants took an extra long time to start, since many started 2 to 3 min after hearing the arriving fire trucks or after firefighters knocked at their door. For these two

buildings, although some started in the initial 2 min, others took as long as 25 min to start, for an overall mean time to start of 9 min.

Some may wonder what were the occupants doing during these 2 to 3 min after hearing the fire alarm (or the fire trucks) before starting to evacuate. From the questionnaires, occupants mentioned that they got dressed, were gathering children, pets, purse, wallet, and keys. Some put away supper, had a look on their balcony, or gave a call to the superintendent before leaving their apartments. Six of these evacuation drills were conducted in the summer on a week day at around 7:30 p.m., and the winter evacuation was on a Saturday at 11:00 a.m. It is not known what would be the delay time to start evacuation at night, but it is likely to be longer than the times observed during the day. It is also interesting to know that in all these evacuation drills, many occupants (maybe as much as half the occupants present) never came out, and many refused to answer the firefighters who knocked at their doors. This behavior might be more prevalent at night.

Evacuation drills were studied by Proulx in three office buildings.[49,50] Occupants received no warning of this exercise, since these Canadian government buildings conduct evacuation drills annually. Data on time to start was gathered using video cameras. The individual time to start of over 1000 occupants was recorded. The mean time to start for the three buildings was 50 s. Although all these office workers had received training and were fully aware of the evacuation procedure, they nevertheless spent time finishing phone calls, saving data on computers, securing files, and gathering belongings before leaving their desks. Many had to be prompted to move by their local fire warden.

In their fascinating evacuation study of a large retail store, Shields, Boyce, and Silcock[51] found that staff response had the most determinant effect on the occupant time to start their evacuation. They conducted an unannounced evacuation drill of a Marks & Spencer's store using video cameras to record behavior and movement, and a questionnaire administered to evacuees after the drill. The fire alarm was activated in the entire store. Although floor staff were not aware of the drill, their fast response was essential in prompting customers movement. The average time to start moving for customers after the sound of the alarm was 25 s with a maximum of 55 s. Cash counters were closed within 30 s of the alarm sounding. Customers in the changing rooms were all evacuated by staff within 60 s. Clearly, the fast staff response during this drill had a major impact on the fast evacuation of the store.

Time to start evacuation was studied in an underground transport system by Proulx and Sime[52]. This study demonstrated the importance of the cue received to prompt evacuation movement. In the underground levels of the station, passengers never started to evacuate after the activation of the fire alarm signal: they kept waiting for their trains, reading, standing, and never made a move to evacuate. When staff appeared to prompt movement, passengers complied immediately. The same response was observed with the use of precise live messages from the voice communication system. The messages informed the passengers of the type of incident and its location, and instructed them on what to do. Only 15 s after the voice communication message, passengers started to move.

The delay time to start has also been studied through reports of fire victims. Although it is recognized that victims may have difficulty reporting accurately the delay time they took before starting to evacuate, there are interview techniques that can help to obtain acceptable estimates.[53,54] In Australia, Brennan used such interview techniques to obtain detailed accounts of fire victims.[55] She studied a severe high-rise office fire that started in a stack of polyurethane-padded chairs stored on the third level of a 14-story building. The fire grew rapidly, emitting a large quantity of smoke. The central fire alarm system never sounded. Victims reported becoming aware of the incident by seeing and smelling smoke or being warned by others. From the interviews, it was estimated that the mean time to start evacuation was approximately 2 min 30 s.

Brennan also studied the occupants' behavior during a high-rise residential fire that occurred at night.[56] From interviews with victims, it was estimated that occupants took around 10 min to start evacuation after hearing the fire alarm and seeing light smoke in the corridor. It should be noted that it is estimated that only half the occupants of that building actually evacuated during that fire.

Studies of two high-rise residential fires in Canada that resulted in six fatalities in stairwells in one case and one fatality in the suite of origin in the other case were studied by Proulx.[57,58] The high-rise fire with six fatalities occurred at night in the winter time. According to the occupant accounts, the fire alarm was not audible in many of the apartments; these occupants learned about the fire from the warning of others. Victims estimated their time to start evacuation at 10 to 30 min for occupants who attempted to evacuate. In the second case study, all occupants heard the fire alarm since there was a sounder in every suite. Occupants waited for instructions from the voice communication system. Evacuees estimated that they took 5 min before starting to evacuate after receiving the evacuation order.

These different studies on the delay time to start show the marked difference in response time according to the type of warning obtained. The time to start will vary according to the information available. The fire alarm signal is probably the less reliable cue of a fire since there are a large number of false alarms, test alarms, or prank alarms in some buildings that have reduced the credibility of this signal as an indication of a real fire.[59] Fire cues, such as smelling something burning or seeing smoke come forth has very ambiguous, initializing investigation response from occupants more than evacuation movement. Obtaining a warning by others appears to be a better indication of an actual problem. Messages delivered through a voice communication system or directly by staff seem to be the signals that are taken most seriously by occupants as indicating a requirement to promptly leave the area.

Building Characteristics and Occupant Characteristics

From the case studies reported above, a marked difference in delay time to start evacuation is found according to the type of occupancy studied. In office buildings,

occupants appear as more readily prepared to move than in residential occupancies. In fact, it is not so much the type of occupancy that makes a difference, but the characteristics of the building and of the occupants. For example, a characteristic of the building that would make a difference in the delay time to start is the visual access to other occupants and what goes on in the building. In a residential building, occupants are by themselves in their suites; they don't have access to the overall behavior of others, and they don't have an overview of the space, such as in an open-plan office or a cinema. This lack of visual access is likely to increase the delay time to start, since occupants will have to take time to obtain more information before making the decision to evacuate. An occupant characteristic that could make a difference is the alertness of the occupant; for example, in an office building, occupants are dressed, awake, and alert. These conditions could be completely different for a family group in a hotel room at night. The time to prepare to start evacuation for a family with children in the middle of the night could be extensive compared to somebody who is at work.

A number of such characteristics that could have an impact on the time delay to start evacuation have been identified and discussed in BS DD240.[46] Here are some of the characteristics with some findings of the most recent work on human behavior in fire. The most salient building characteristics are as follows:

Type of warning system: The fire alarm signal is usually the basic warning system. It is, however, the signal that occupants will take the longest to respond to if they have received no training or if the alarm is often activated for no-fire reasons. The use of a voice communication system with informative live messages is probably the best way to initiate a fast response. Prerecorded messages, in comparison, are rarely as effective in making occupants start to move and less informative in content as live messages. The audibility and the intelligibility of these systems should be assessed to ensure occupants will perceive the information provided. The voice communication system, coupled with closed-circuit TV, could allow an officer to provide precise information to the occupants regarding the unfolding event and instructions tailored to the location of different groups.

Building layout and wayfinding: The way each floor and the whole building are organized has an impact on the possibility for the occupant to have developed a mental map of the space. When looking for information or devising a plan of action, occupants are likely to spend more time obtaining information in a building where wayfinding is difficult.

Visual access: The way the building is designed may or may not provide occupants with visual access to the behavior of others, which could be an important source of information for people. Visual access could also improve the perception of fire cues or strobe lights as well as the location of the closest exit.

Focal point: In buildings where occupants focus their attention on the stage, the screen, or the ambient atmosphere (e.g., at a discotheque or rave party), the animation of this focal point will have to stop and full lighting should resume for occupants to pay attention to the fire situation. Information regarding the expected response of occupants should be provided from a figure of authority at the focal point.

Training: An essential part of a fast occupant response. Training is more a characteristic of the building than of people, since training should be specifically tailored to each building evacuation procedure. Although a person who has received training may transfer this knowledge to another location, it is common to observe that well-trained people did not take any action when the fire alarm rang in another building. Overall, training of the occupants is usually performed only in institutions such as schools and some work environments. In public buildings, occupants are unlikely to be trained for that specific building. Consequently, staff have to be very well trained to efficiently prompt occupant movement. Staff also have to be in sufficient numbers to cover the full space.

Frequency of false alarm: The number of false alarms in a building is an important determinant of the efficiency of this system to warn occupants. A large number of false alarms could be estimated at three or more alarms over a period of 6 months. A fire alarm signal, by itself, rarely triggers evacuation movement, unless training and other information is provided. However, the fire alarm is a very good way to alert occupants and prepare them to receive complementary information or to look for information. If the number of false alarms is important, it could be expected that the delay time to start will be endlessly extended since occupants are unlikely to look for information and will be less receptive to other cues.

Some occupant characteristics are as follows:

Familiarity: Occupants who are familiar with a building, who have participated in evacuation drills, and are aware of the evacuation procedure are more likely to start evacuation rapidly.

Responsibility: In single-family houses, occupants respond rapidly when the smoke alarm goes off because they know they are responsible for it; no one else will take care of that problem. In a public building, such as a museum or a shopping center, visitors don't feel responsible if the fire alarm goes off. They assume that they will be told if something is really happening. The delay to start will depend on the fast and precise voice communication information provided and the staff behavior and instruction.

Social affiliation: Occupants are likely to attempt to gather with people with whom they have emotional ties before starting evacuation, such as a family group. This activity of gathering members may take time, especially if members are not together at the start of the incident.

Commitment: People who are committed to an activity will take a long time to turn their attention toward an unexpected situation. For example, people waiting in line to board a plane, eating in a restaurant, or gambling at the

casino are all committed to these activities and will be reluctant to turn their attention to an alarm bell or some strange smell of smoke. However, at the cinema, if the movie is stopped and lights are turned on, attention of the occupants will be captured right away and information to prompt their time to start can be provided.

Alertness and limitation: A fire in the middle of the night in a hotel or residential building will require a longer time to respond since most occupants will be asleep. Another dimension to this characteristic is the possibility that occupants may have some limitation that will extend their response time. These limitations could be perceptual, physical, or intellectual, or might be due to the consumption of medication, drugs, or alcohol. It is important to estimate the proportion of occupants who will have a longer delay time to start due to alertness conditions or a limitation.

Staff or warden: The speed with which occupants will respond to the fire alarm or other fire cues is largely dependent on their status in the building and the behavior and instruction of staff and wardens. Consequently, the training of staff and wardens is paramount. To be readily recognized, they need to wear distinctive uniforms and show their authority through their behavior. The delay time to start could be dramatically shortened by the behavior and instruction of well-trained staff and wardens.

The preceding building and occupant characteristics should be taken into account when estimating a time delay to start evacuation. In the past, the delay time to start has always been neglected, which usually explains the discrepancy between the calculated evacuation time and the observed evacuation time during fire drills. Some have suggested that the delay time in a real fire should be shorter than in a drill, since signs of the fire should trigger fast occupant response. Interviews with victims show another story. In fact, the initial signs of a fire are usually judged extremely ambiguous, which tend to further increase the delay time to start of occupants.

Delay Time Calculation

For calculation purpose of a total evacuation time, a delay time to start has to be calculated. All researchers in the field of human behavior in fire are hesitant at suggesting numbers because of the limited research findings in this area. Nevertheless, due to the fast development of the performance-based approach to look at new innovative fire safety design systems for buildings, some data to account for the delay time to start evacuation by occupants is essential. In 1997, the British Standards Institute published the Draft for Development DD240.[46] Although initially meant as a British Standard on Fire Safety Engineering, public comments received on the draft code of practice suggested to the relevant committee to publish this document as a Draft for Development, so information contained in DD240 is essentially provisional until a review is conducted. DD240 provides a flexible but formalized framework to fire safety design.

Table 21 of DD240, reproduced here as Table 3-13.1 (with some modification to the terminology), suggests some delay time to start evacuation for different occupancies according to the warning systems available in the building.[46] The time to start depends mainly upon the type of warning system provided in the building, the type of occupancy, and the characteristics of the occupants. (The type of warning considered here offers a slight variation from the same concept presented by DD240.)

Table 3-13.1 ***Estimated Delay Time to Start Evacuation in Minutes***

Occupancy Type	W1 (min)	W2 (min)	W3 (min)
Offices, commercial and Industrial buildings, schools, colleges and universities (Occupants awake and familiar with the building, the alarm system, and evacuation procedure.)	< 1	3	> 4
Shops, museums, leisure-sport centers, and other assembly buildings (Occupants awake but may be unfamiliar with building, alarm system, and evacuation procedure.)	< 2	3	> 6
Dormitories, residential mid-rise and high-rise (Occupants may be asleep but are predominantly familiar with the building, alarm system, and evacuation procedure.)	< 2	4	> 5
Hotels and boarding houses (Occupants may be asleep and unfamiliar with the building, alarm system, and evacuation procedure.)	< 2	4	> 6
Hospitals, nursing homes, and other institutional establishment (A significant number of occupants may require assistance.)	< 3	5	> 8

W1: live directives using a voice communication system from a control room with closed-circuit television facility, or live directives in conjunction with well-trained, uniformed staff that can be seen and heard by all occupants in the space
W2: nondirective voice messages (prerecorded) and/or informative warning visual display with trained staff
W3: warning system using fire alarm signal and staff with no relevant training

Source: Adapted from *Fire Safety Engineering in Buildings, Part 1: Guide to the Application of Fire Safety Engineering Principles,* Table 21, British Standard Institutue, DD240, London, 1997.

Occupants are likely to respond more rapidly to a warning system that will provide more information for decision making. To take into account fire scenario, DD240 suggests that the times given in Table 3-13.1 be

> adjusted in relation to the assumed rate of fire growth,
>
> (a) for occupants in a small room/space of fire origin who can clearly see smoke and flames at a distance, adopt the relevant time given for W1,
> (b) for occupants in a large room/space of fire origin who can clearly see smoke and flames at a distance, adopt the relevant time given for W2, unless W1 is in operation,
> (c) for occupants outside the room/space of fire origin who cannot clearly see smoke and flames, adopt the time given for the warning system in operation.[46]

Further, it should be emphasized that in some types of occupancies such as factories, some time for shutdown of equipment may have to be added to the time given in Table 3-13.1.

Equations for Total Evacuation Time

Several equations for total evacuation time, such as the ones from Togawa[8] or Melinek and Booth[16] appear formidably complex; the calculation benefits they promise are hidden behind scientific notation systems. In using such formidable equations, there is a danger of getting sidetracked by their apparent sophistication. Like computer models, they may tend to keep us from understanding the world as it actually exists; the equations and models can take on a reality of their own. Therefore, the emphasis in this section is on minimizing the complexity of the mathematics and maximizing the awareness, using simple language and graphs, of real processes that many existing models depict incompletely.

Empirical Method by Pauls

While early Canadian research on evacuation did not get into the mathematical abstraction found in some other researchers' work, it did utilize many simple graphic representations of people's movement, merging, and queuing in evacuations of tall buildings.

In contrast to previous contributors to evacuation technology, Pauls began by observing as many evacuation drills as possible in tall office buildings, being careful to record many aspects of each exercise in great detail, and then developing relations that best described what was actually observed.[23,60] This method revealed defects in earlier literature on matters of crowd configuration on stairs, maximum and mean flows, and actual evacuation populations—all of which were sources of error in other predictions.

Altogether, 29 drills were observed in buildings ranging from 8 to 21 stories high, in which traditional, uncontrolled total evacuation procedures were used. Generally, all stairways in each building were monitored at ground-floor discharge points and at selected heights, often through the use of instrumented, moving observers. An average of two stairways were documented for each drill, thus giving 58 cases for analysis. (A smaller number of drills were documented where the procedure involved a selective or sequenced controlled evacuation procedure, with either partial or total evacuation. These controlled evacuations are not covered by any of the equations provided here and are separately discussed under the section titled "Evacuation Procedures in Tall Office Buildings.")

By way of background to the prediction equations developed from Pauls's study, the effective-width model for crowd movement must be defined. This empirically based model describes flow as a linear function of a stair's effective width—the width remaining once edge effects are deducted [150 mm (6 in.) in from each wall boundary and 90 mm (3.5 in.) in from each handrail centerline]. (See Figure 3-13.4.) The effective-width model takes into account the propensity of people to sway laterally—especially when walking slowly in a crowd—and, therefore, to arrange themselves in a staggered configuration, not in regular lanes, as assumed in the traditional unit-width model based on presumed static dimensions of people's shoulders.[23] For example, a stair designed to provide two of the traditional units of exit width has a nominal width of 1120 mm (44 in.) and an effective width of 820 mm (32 in.), causing crowds to take up a staggered formation.

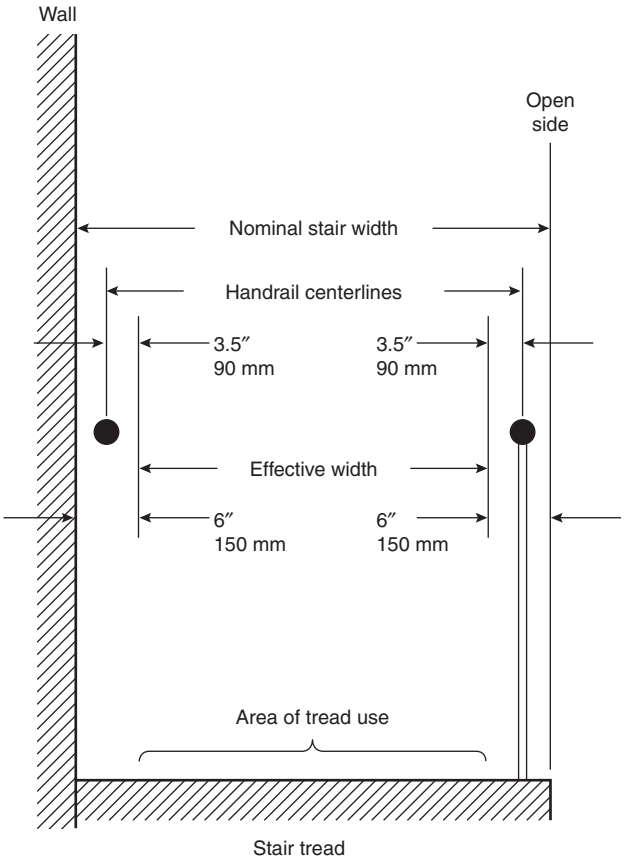

Figure 3-13.4. ***Measurement of effective stair width in relation to walls and handrails.***

Another finding underlying the effective-width approach is that mean evacuation flow (per meter of effective stair width) varies in a nonlinear fashion with evacuation population (per meter of effective stair width), as shown in Figure 3-13.5. The regression equation is designated here as Equation 4.

$$f = 0.206\rho^{0.27} \tag{4}$$

where f and ρ have the metric units shown in Figure 3-13.5.

Other factors besides effective stair width, influencing the mean flow in evacuations are people's use of extra clothing (for protection against precipitation or cold conditions outside a building), plus various building design and use factors, including normal stair use.[23] Regarding building design, the assumed influence of stair-step geometry on crowd flow is considered below.

Equation 5 (with dimensions in mm) and Equation 6 (with dimensions in inches) relate effective stair width, w,

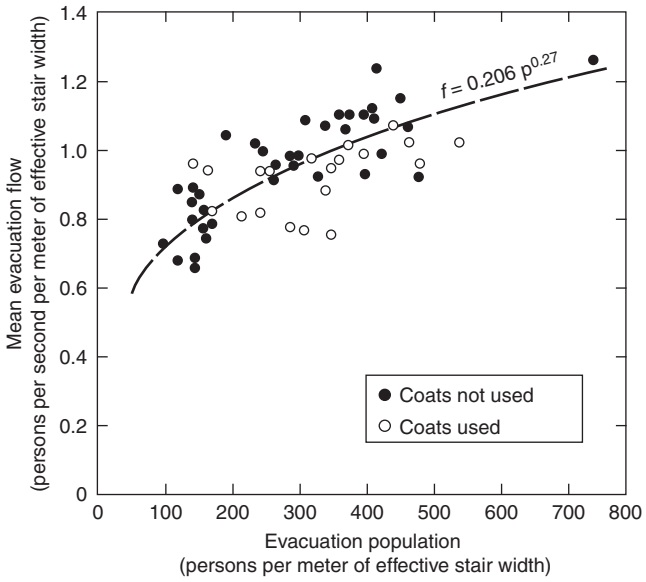

Figure 3-13.5. ***Effect of population on flow down stairs in uncontrolled total evacuations.[61]***

actual total population, P, and the expected flow time, t, in seconds. These equations can be translated into a somewhat more useful form and graphed as shown in Figure 3-13.6, which relates effective stair width per person and the resulting flow time for a crowd moving down stairs. Three curves are provided to show the assumed effect of various step geometries on crowd movement efficiency. It should be noted that some of Pauls's early publications of equations similar to Equations 5 and 6 differ slightly, because they were based on stairs with step geometries approximately described by the highest of the three curves. Equations 5 and 6 relate to the middle curve.

$$w = \frac{8040}{t^{1.37}} P \tag{5}$$

$$w = \frac{317}{t^{1.37}} P \tag{6}$$

In relation to evacuation time prediction, the preceding equations and graphs have dealt only with flow time. For uncontrolled total evacuations of tall office buildings, there is a simple way of predicting the time to start needed for flow to build up to half its mean level. This empirically derived time to start is shown in Figure 3-13.7. When added to flow time, based on empirically determined mean flows, the 41 s (0.68 min.) accounts for travel time plus all or part of the other subcomponents of minimum evacuation time discussed previously. The extent to which the 41 s is adequate depends on the experience of the building occupants and the manner in which the evacuation is initiated and run. Evacuations in cases of actual fire or other emergencies are assumed to take longer, as discussed earlier.

From Equation 4, and from the 41 s time to start shown in Figure 3-13.7, the first of two prediction equations shown in Figure 3-13.8 is derived. The prediction

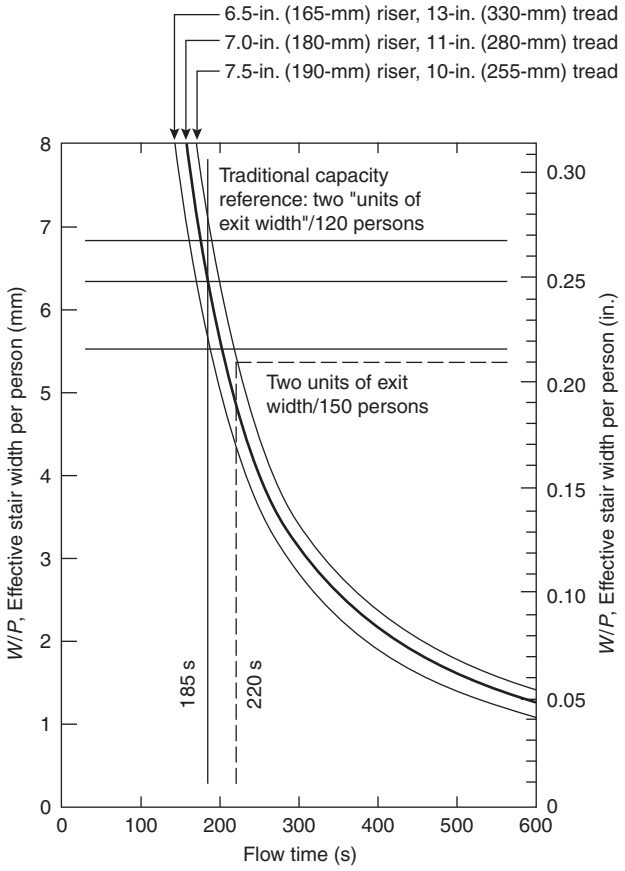

Figure 3-13.6. ***Relationship between effective stair width per person and flow time for several step geometries.***

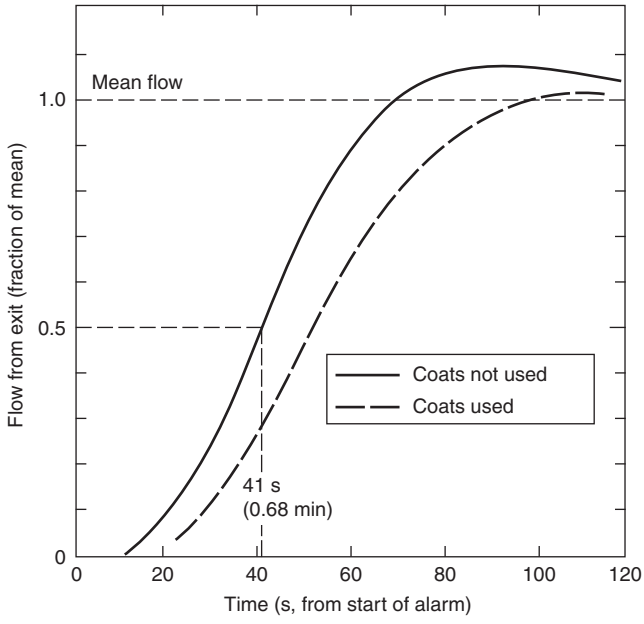

Figure 3-13.7. ***Buildup of flow from exits in uncontrolled total evacuations of tall office buildings.***

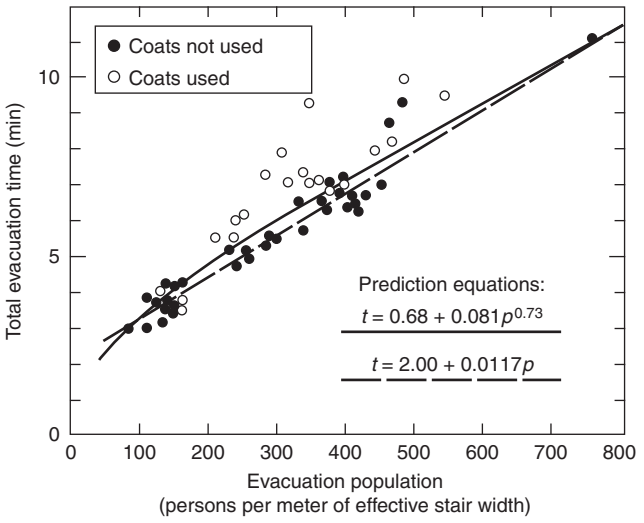

Figure 3-13.8. ***Predicted and observed total evacuation times for tall office buildings.***

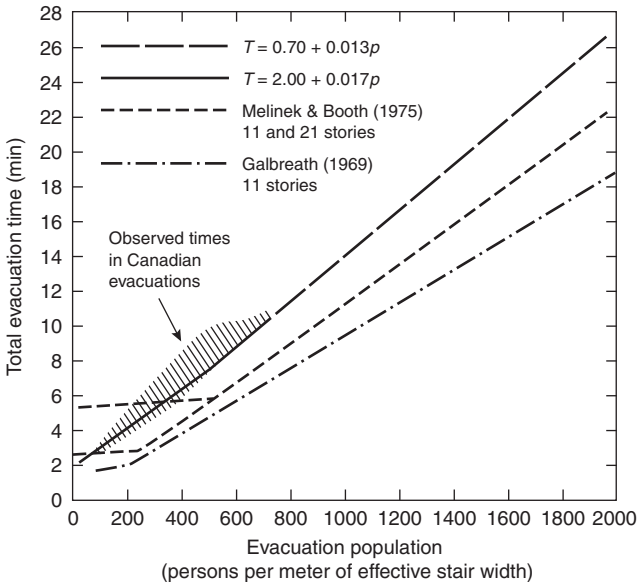

Figure 3-13.9. ***Predicted and observed total evacuation times for tall office buildings incorporating results from other investigators.***

equations apply to cases where there are no more than 800 persons/m of effective stair width. (The upper equation in Figure 3-13.8 is Equation 7, and the lower one is Equation 8.) Note that there is a good match between the prediction curve (Equation 7) and the observed total evacuation times for the uncontrolled evacuations, especially in those cases where extra outdoor clothing was not used. Using Equation 7, the net error in predicting total evacuation times for 50 cases in buildings 8 to 15 stories high was 0.2 percent. The simplified linear equation, Equation 8, also fits these data very well.

$$T = 0.68 + 0.081p^{0.73} \quad (7)$$

$$T = 2.00 + 0.0117p \quad (8)$$

where T is the minimum time, in minutes, to complete an uncontrolled total evacuation by stairs, and p is the actual evacuation population per meter of effective stair width, measured just above the discharge level of the exit. (Note the upper limit of 800 persons per meter of effective stair width.) This also applies to Equation 4.

Buildings that will be less accurately predicted with Equations 7 and 8 are the taller ones with very low populations on each floor. With such buildings, the total evacuation time is influenced by the travel distance and people's ability to descend stairs quickly, that is, at about 10 s/story, rather than the 15 to 20 s observed in evacuations with higher populations. The observed times departing most from the prediction lines in Figure 3-13.8 were for buildings with 18 to 20 stories.

For buildings with more than 800 persons per meter of effective stair width, Equation 9 provides a good basis for predicting times for uncontrolled total evacuations in tall office buildings.

$$T = 0.70 + 0.0133p \quad (9)$$

Figure 3-13.9 shows Equations 8 and 9, along with prediction lines based on equations proposed by Melinek and Booth[16] and Galbreath,[15] plus a cross-hatched area showing where observed times lie.

Another indication of the accuracy of these prediction equations for uncontrolled total evacuations of office buildings is provided in Figure 3-13.10. This compares predicted and observed evacuation times for approximately 1700 people evacuating an 8-story, 6-exit Canadian office building in March 1983 (in cold-weather conditions), as documented by Public Works Canada.

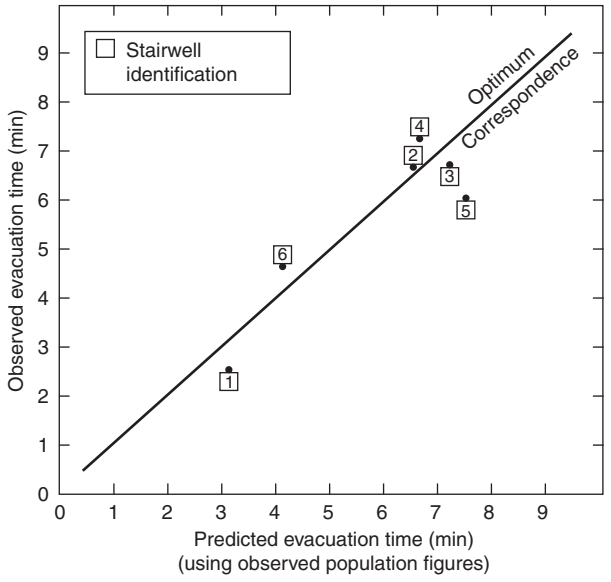

Figure 3-13.10. ***Comparison of predicted and observed evacuation times for an office building.***

Actual Populations in Office Buildings

A cautionary note must be given here regarding the prediction of actual populations in buildings. In many buildings with assembly occupancies, the prediction of maximum population will be relatively straightforward, based on seat counts and floor area of waiting spaces [where an area of 0.3 to 0.6 m^2/person (3 to 6 ft^2/person) is a reasonable assumption]. However, studies in Canadian office buildings strongly support a case for assuming that each actual office building occupant has an average of about 25 m^2 (268 ft^2) of gross rentable area.[23,61] This contrasts sharply with the traditional occupant-load assumption in codes and standards which assume 9.3 m^2 (100 ft^2) of gross rentable area per occupant. Codes and standards give estimates of actual occupants that may be incorrect by a factor of more than 2. Typical workspace counts also overestimate office populations (sometimes by 15 percent).

Evacuation Procedures in Tall Office Buildings

Evacuations of multistory office buildings can be thought of as being one of two types: uncontrolled total evacuation, and controlled selective evacuation. The former is dependent largely on the nature of evacuation sequencing or deference behavior required, and the latter on the type of control imposed and the availability of a voice communication system to manage the evacuation.

Figures 3-13.11 and 3-13.12 illustrate patterns of evacuee movement, over time and space, for a hypothetical traditional (uncontrolled) total evacuation and a controlled selective evacuation. Traces represent the movement of the last persons to leave each floor. The slopes of the traces represent the speed of movement down an exit stairway; horizontal lines represent queuing. For a more complete discussion of modeling evacuation using such diagrams, including combined use of elevators and stairs, see References 18 and 19.

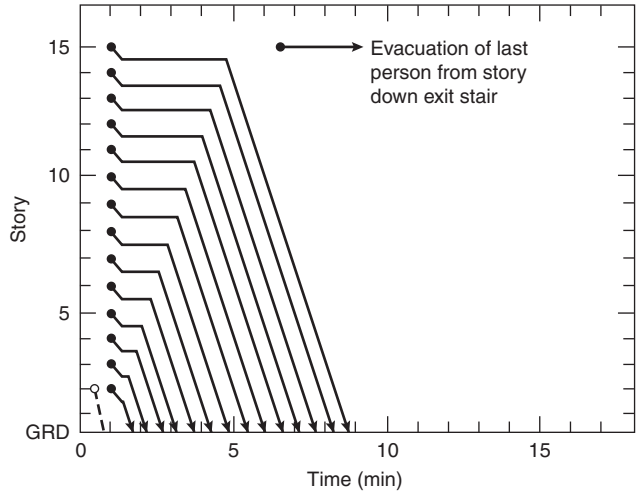

Figure 3-13.11. ***Hypothetical uncontrolled total evacuation of a 15-story office building.***

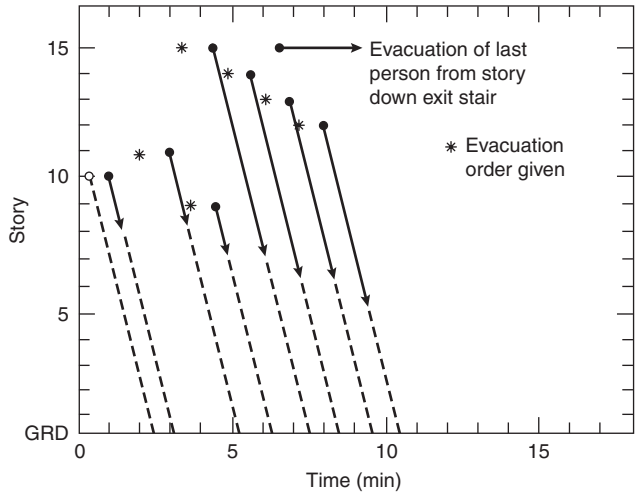

Figure 3-13.12. Hypothetical controlled selective evacuation of 15-story office building.

Based on Canadian observations of 29 evacuation drills in office buildings, ranging from 8 to 21 stories in height, Figure 3-13.11 shows what can be reasonably expected in an uncontrolled total evacuation of a 15-story building occupied by 70 able-bodied persons per floor—a fairly high-population condition that would be expected with about 1400 m^2 (15,000 ft^2) on each floor. It is assumed that there is an equal division of evacuation demand for two standard 1120 mm (44 in.) exit stairs and a mean egress flow of approximately one person per second discharging from each exit. Descent speed is 3.6 floors per minute (about 0.5 m/s along the stair slope), and each evacuee has slightly less than two treads of stair area (0.5 m^2/person).

Based on Canadian observations of ten evacuation drills, Figure 3-13.12 depicts a controlled selective evacuation, in this case, a partial evacuation of only the tenth-floor fire area, the floors above, and the ninth floor. Compared to the evacuation depicted in Figure 3-13.11, the movement traces are steeper, indicating faster descent speeds; however, there is also greater space between traces, indicating that densities are lower than depicted in Figure 3-13.11. Resulting flows in each exit are considerably lower.

In both cases, about 9 min are required to move all occupants to areas below a presumed fire area—the tenth floor in the case of Figure 3-13.12. Because of the time required to initiate and control the selective sequential evacuation, it takes approximately the same time to move 490 persons to safety (below the ninth floor) as it does to move all 980 occupants to the ground in the uncontrolled total evacuation depicted in Figure 3-13.11. Rather than jump to the conclusion that uncontrolled total evacuation is better or more efficient, it must be considered that, if there really was a fire on the tenth floor, and if all occupants attempted simultaneous egress, and if the usual rules of deference shown in Figure 3-13.11 applied, occupants of the most immediately threatened floors would

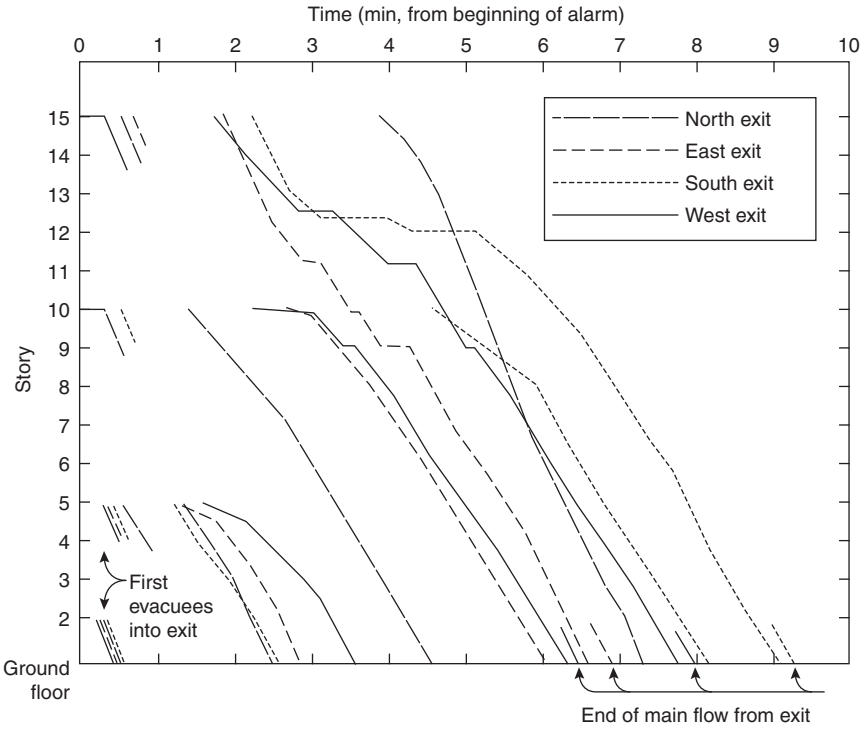

Figure 3-13.13. ***Movement of observers with evacuees during an uncontrolled total evacuation.***

have to queue in the vicinity of those floors for several minutes. With the stairwell doors being open on the fire floor, all the upper floors would become contaminated by smoke, and descending occupants from floors above the fire floor would have to move in smoke.

An increasingly common conclusion is that, although uncontrolled total evacuation is not demanding of building management systems, it is too upsetting for occupants who are indiscriminately evacuated (if indeed they can be encouraged, with ambiguous alarm systems, to evacuate at all). On the other hand, the uncontrolled total evacuation process is simple, and there is no need for relatively sophisticated systems and training, which are expensive and may involve a long delay time before occupants who should evacuate become notified to start their evacuation.

Uncontrolled Total Evacuation

One drill case study entailed the 1972 evacuation of 1453 persons, using uncontrolled total evacuation procedures, from a 15-story office building via four 1140-mm exit stairs. The total evacuation time ranged between 6.6 and 9.3 min. The time variation was largely due to unbalanced demand on the four exits—the result of unequally sized catchment areas and an overcompensating attempt to redistribute some of the demand to predesignated exits on several floors. The average total evacuation time was 7.8 min, a figure close to the predicted 7.0 minute time. (See calculations below.) The difference is largely explained by the fact that evacuees experienced slight delays and less efficient movement down stairs because outdoor clothing was used. The attempt to have people on several floors move to more remote, predesignated, but less familiar exits also added minor delays.

Figure 3-13.13 shows the traces of movement of instrumented observers, using the exit stairs with evacuees, during this uncontrolled total evacuation. In this evacuation, some people were on the fifteenth floor up to 4 min, and their queuing on exit stairs, near this level, lasted up to 4 min from the initiation of the general fire alarm system. It was usually less than 2 min at lower levels. Conditions were much like those noted in relation to Figure 3-13.9; each evacuee occupied an average area equivalent to two stair treads, and descent speed was typically 3.5 stories/min below the seventh floor—conditions that would be unduly arduous or impossible for only a few percent of typical office workers. In the case of this drill, such persons and some assistants (73 persons altogether) descended a central, fifth stairway reserved, in this evacuation, for their use.

The building was recently rebuilt with the same floor areas, but with only the central exit stairway and another one in the largest wing left intact. However, its occupants still are expected to utilize the uncontrolled total evacuation procedure. Given the difficulties of obtaining a balanced use of the remaining exits, it is not unreasonable to predict that the total evacuation time will now be approximately twice what was achieved in the 1972 drill.

Sample computations of uncontrolled total evacuation time: Here it is useful to consider the evacuation time prediction for this building in somewhat greater detail.[24]

This building has a cruciform plan with a total of 33,000 m^2 (350,000 ft^2) of gross rentable area on 14 office floors. One of the four wings is larger in area than the other three; thus, there is unlikely to be an equal population using each exit stairway during an evacuation. For the first computations, the unmodified stairway arrangement will be assumed, with one exit stair at the center of the building and one exit stair at the end of each of the four wings. Subsequent computations will consider the modified case with only two stairways.

For the original, unmodified situation we will assume that the exit stairs have extensive normal use, partly because the building is occupied largely by a single government department. The center stairway has a relatively high level of normal use because of its location near the elevators and its entry door in the ground-floor lobby. The fire emergency procedures call for this stairway to be used only by handicapped persons and others assisting them in emergencies. The stairs have a nominal width of 1140 mm (45 in.) and a dogleg configuration, with two 180-degree turns per story. The step geometry provides a riser height of 180 mm (7 in.) and a tread depth of 250 mm (10 in.). Stair wall finishes have a semirough texture. Assume that the building is slightly more densely occupied than the average noted earlier (specifically, assume one actual occupant for every 22 m^2 instead of the 25 m^2 noted in the subsection "Actual Populations in Office Buildings"). Given this kind of information about the office building, as well as the knowledge that the occupants are accustomed to periodic evacuation drills, a prediction of the flow and evacuation time performance when the traditional uncontrolled total evacuation procedure is used can be attempted.

First, an estimate is made of the total number of occupants to be evacuated. At 22 m^2 per actual occupant and a total gross-rentable office area of 33,000 m^2, the anticipated evacuation population is 1500 people. It can be assumed that 2 percent of these (i.e., 30 people) cannot or should not evacuate down the stairs in a high-flow situation with relatively able-bodied evacuees and should elect to use the central stairway. Typically, only a few of these people would have such severe mobility impairments that they would need to be assisted by more than one other person to get down the stairs. If an average of one person to assist each of these 30 handicapped patrons is included, the central stairway will then be used by approximately 60 persons; this leaves 1440 persons using the four remaining exit stairs at the building perimeter. As a first approximation, it can be assumed that these stairs will be used equally, even though one of the four wings is larger than the others. Each of the four 1140 mm (45 in.) stairs would thus carry 360 evacuees.

Next, by deducting 300 mm (12 in.) from the nominal stairway width, it can be calculated that each of the stairs has an effective width of 840 mm (33 in.). The anticipated mean evacuation flow can be indirectly calculated using any of a number of methods, such as the methods set out in Equations 4, 5, or 6 and in Figure 3-13.6. The easiest method is to use Figure 3-13.6, interpolating between the two upper curves to account for the step geometry. Each stair provides 2.33 mm (0.09 in.) of effective width per person; thus, we can read off an expected flow time of 390 s, estimated to the closest 10 s (and having two significant figures). The mean flow is obtained simply by dividing the population per stairway (360 persons) by the time (390 s), giving a mean flow of 0.92 person/s.

This uncontrolled evacuation prediction can be adjusted to take into account some modifying factors in addition to the step geometry adjustment[26] already built into Figure 3-13.6 (and further discussed in Pauls).[62] For example, the stair walls are slightly rough; therefore, it is reasonable to expect some reduction in flow.[23] A 4 percent reduction in flow would be a reasonable assumption. The fact that this evacuation was held during somewhat cool weather, and therefore some of the evacuees wear or carry outdoor clothing, should be taken into account. Assume this leads to a 6 percent reduction in the flow. On the positive side, an adjustment for the fact that the building occupants are familiar with evacuation drills and that there is fairly extensive normal use of the stairs (although this is likely to be more the case for the center stairway than for the perimeter stairs) should be considered. There might, in fact, be some confusion as relatively able-bodied people go first to the normally used center stairway only to be redirected to one of the perimeter stairs. There may also be some confusion and delay as the exit stairway in the largest wing develops more extensive queuing at exit doors and, as a result, people either decide on their own to try another stairway or are directed by fire wardens to use another stairway. Thus, on the positive side, it is prudent to assume an adjustment of only 2 percent for normal stair use and familiarity with evacuation drills.

It is sufficiently accurate (given the underdeveloped state of the art) simply to add up the negative and positive factors to give a net adjustment of minus 8 percent for the expected flow. This results in an adjusted flow prediction of 0.83 person/s (50 persons/min) on each of the four perimeter stairs. A well-documented, cool-weather evacuation drill in the same setting had the following mean flows, in person per second: 0.85, 0.83, and 0.80—remarkably similar to the prediction. The differences are largely explainable by the fact that the four stairs were not equally used in the evacuation drill, despite efforts by the building's fire emergency staff to balance usage. Too many evacuees were, in fact, diverted to one of the stairways, which thereby served 448 people. They had been diverted from the largest wing, where the stairs were used by 385 people. The other two stairs served 329 and 291 people, respectively, for a total of 1453, compared with the initial assumption of 1440.

Repeating the above computations, using Figure 3-13.6 and the actual stair populations (448, 385, 329, 291), with the adjustments described above, mean flows of 0.88, 0.84, 0.81, and 0.78 person/s, respectively—all within 4 percent of the observed flows—can be predicted. Thus, it is possible to make some very accurate predictions for the relatively straightforward, traditional, uncontrolled total evacuations of tall office buildings, if we understand some basic factors of building design and use.

As to the matter of minimum total uncontrolled evacuation time, a simple prediction can be made with the 390 s (6.5 min) flow time (read from Figure 3-13.6), which assumes equal usage by 360 people of each of the four perimeter stairs. Adjusting this time by the 8 percent

figure gives an adjusted flow time of 7.0 min. Adding the suggested 0.68 min startup time (the time for flow to build up to half its mean value, read from Figure 3-13.7), a predicted total evacuation time is 7.7 min. Alternatively, without including any adjustments, Figure 3-13.8 or Equations 7 or 8 could be used to calculate an approximate, slightly underestimated total evacuation time in the range of 7.4 to 7.0 min.

The observed total evacuation times were 9.3, 8.2, 7.0, and 6.6 min, respectively, for the stairs, listed in descending order of population. This range of observed times is mainly a result of the nonuniform distribution of evacuees among the four perimeter exits. The average observed time was 7.8 min, compared with the (adjusted) prediction of 7.7 min. In fact, the adjusted predicted times, using the actual populations, are found (using Figure 3-13.6) to be 9.2, 7.9, 7.2, and 6.6 min, respectively, in order of decreasing population, all within 4 percent of observed times.

Finally, the predicted minimum total uncontrolled evacuation time should be computed for the building in its modified form, with only two exit stairs and with a similar total population. Having 1400 people (assuming 100 per floor) equally distributed between the two stairs, each with an effective width of 840 mm (33 in.), would lead to a flow time in excess of the 10-min (600-s) limit of Figure 3-13.6. Because the population per meter of effective stair width, 833, slightly exceeds the 800 limit for most of the formulas suggested, Equation 9 should be used here. Doing so gives an unadjusted minimum total evacuation time of 11.8 min. However, there will be great difficulty achieving balanced usage between the two remaining exit stairs. The central one could easily have a usage 40 percent higher than the other stairway.[23] In this case, (assuming a 817- and 583-person split between the exit stairs) the minimum, unadjusted total evacuation time would be approximately 13.7 min, or about twice what was the case when the building had 5 exits.

These examples demonstrate that traditional total uncontrolled evacuations can be relatively easily understood and predicted in the case of tall office buildings. Such calculation of total evacuation time provides the overall time for occupants to evacuate a building when no particular incident is happening. It should be kept in mind that for a situation where an actual fire is occurring, the time delay to start evacuation would be longer if signs of the fire are present; means of egress could be blocked by smoke, and occupants above the fire floor would be unable to leave. These fire conditions could entirely change the total evacuation time of a high-rise office building.

Controlled Selective Evacuation

The other actual evacuation to be described here occurred in a 21-story office building in 1971 and was one of the first large-scale attempts at a controlled, selective evacuation in Ottawa. (Figure 3-13.14 shows heavier traces depicting actual movement of observers; lighter traces depict the movement pattern predicted several days before the drill, based on estimated populations on individual floors. Given that this was done very early on in the Ottawa study, it shows a remarkably accurate prediction capability.) Although the evacuation drill consisted of the total clearing of the building—some 2100 persons evacuating over a 30-min period—it did utilize the selective, sequential procedure which could have been terminated after 6 min, with the clearing of only the presumed fire floor and two adjacent floors. The drill simulated a worst-case scenario with a fire on the third floor. For this case, a concern for smoke movement to upper floors suggested a procedure that first clears the fire-floor area, then all floors above this, starting with the twenty-first floor and progressing downward.

This evacuation drill, also described in detail by Pauls and Jones,[27] included a dramatic example of what can go wrong when fire safety management personnel misuse the communication systems needed to manage such sequential evacuations. There had been no earlier large-scale attempt to test all aspects of such an evacuation procedure. Due to an incorrectly set switch on a control console, there was a delay in getting the first announcement over the public-address system, following approximately 1.5 min of a standard fire alarm. The first announcement successfully carried over the public address, nearly 3 min into the drill, was made by an obviously flustered, inadequately prepared person who said, "Ladies and gentlemen. We have to evacuate this building. The alarm has been set on the third floor. Please evacuate. Other floors stand by."

This ambiguous announcement was followed by a slightly different one in French—bilingualism being de rigueur in government-occupied buildings in Ottawa. Confusion followed. As many as 350 persons left their floors before they were supposed to, most going down one of the two 1040-mm (41-in.) wide exit stairs. This premature evacuation confused and delayed the intended earlier evacuation of floors 3, 4, and 2. According to a questionnaire returned shortly after the drill by a sample of 176 evacuees (an 88 percent mailback return rate), some people thought they heard the announcer say that a fire had been reported on the third floor. Of the 176 respondents, 43 percent reported interpreting the situation as an actual fire after hearing the first public-address announcement. Regarding their interpretation of the situation before this announcement, with only the ringing of the building's fire alarm system, only 17 percent of the questionnaire respondents thought it was a fire, nearly 60 percent thought it was due to a circuit malfunction, and 16 percent thought it was a drill.

Turning to the conditions faced by evacuees in the two exit stairs, with the confused evacuation procedure, there was extensive queuing and slow progress by some evacuees who prematurely left the twenty-first floor via the south exit. In this exit, some 4 min were required for them to move between the nineteenth and seventeenth floors, and they took 10 min to descend the full distance to the ground. In the other exit, where there was minimal premature evacuation, descent speed was fairly consistent at about 3.8 stories/min, resulting in a 5.3-min descent time from the twenty-first floor.

It is useful to contrast these conditions with what would likely occur in a traditional, uncontrolled total evacuation of the building's 2100 able-bodied occupants via the two 1040-mm stairs. According to Equation 9, an uncontrolled evacuation would take a minimum of nearly 20 min. If all 2100 people were simultaneously standing at their respective floor's exits, there would be only 0.17 m^2 of stair area, or about one-half tread, per person. For evac-

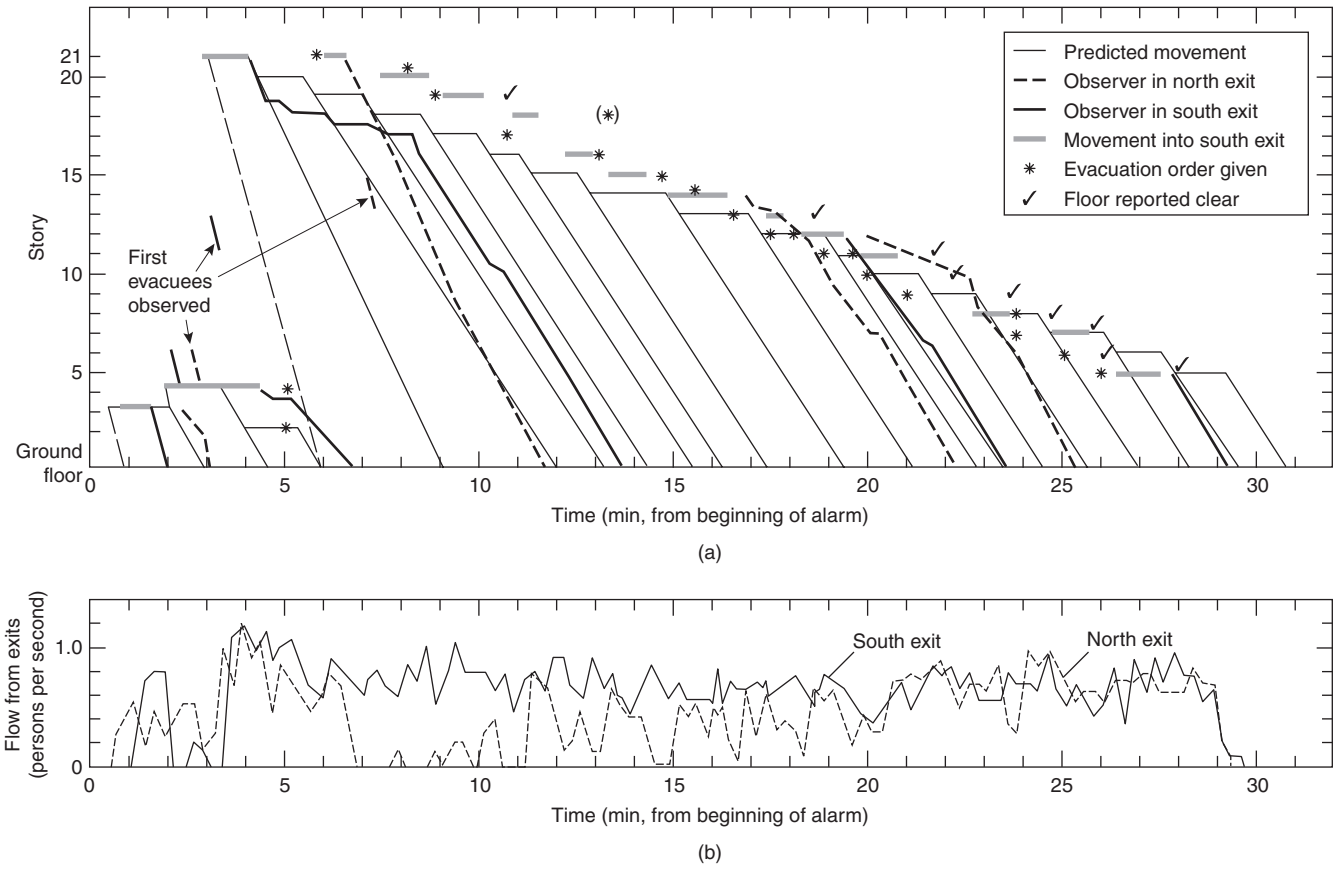

Figure 3-13.14. ***Predicted and observed movement, plus flow, in a sequential evacuation exercise.***

uees from the highest floors, such queuing might last for 14 of the 20 min.

Whether queuing and evacuation delays create an upsetting situation for the people involved is a good question, and it raises the broader question about how aware typical occupants of high-rise buildings are of the kinds of queuing and movement conditions they might face in a major evacuation. Should they be made aware of such aspects of building safety? By what means? Who has the responsibility for doing it? An important attempt to address this issue was included in the *Report of the Ontario Public Inquiry into Fire Safety in High-rise Buildings*.[63] The report is highly recommended to anyone concerned with fire safety in tall buildings.

Occupants with Disabilities

During the last three decades, there has been a growing effort at providing access for all people in most buildings. It is now well-rooted in the regulation of developed countries to require accessibility to all new or refurbished public buildings. Since most people with disabilities or limitations, as well as the elderly, are determined to stay autonomous and to go out and about, buildings are increasingly occupied by mixed-ability occupants. This phenomenon has to be taken into account in fire safety design.

The prevalence of the population with disabilities appears quite similar among developed countries. The 1991 national census in Canada showed that 15.5 percent reported some level of disability (1 percent were under 15 years old, 7.4 percent were between 15 and 64 years old and 7.1 percent were over 64 years old).[64] Among Canadians with disabilities, 93.7 percent were living in private households, and only 5 percent of them were unable to leave their homes. It is not known how many disabled go out of their home regularly, but among the disabled children under 15 years old, 92 percent were attending school (88 percent were in regular schools), and out of the disabled people between the age of 15 and 64 years of age, 56 percent were holding a job (compared to 81 percent of the able population). The type of limitation identified by disabled adults were limitation in mobility (53 percent), agility (50 percent), intellectual (32 percent), hearing (24 percent), seeing (10 percent), and speaking (9 percent). Many respondents reported more than one disability.

In the United States it was estimated, through the 1994 Survey of Income and Program Participation, that 20.6 percent of the American population had some level of disability.[65] This survey excluded people living in institutions. This high percentage of people with disabilities reflects the passage of the 1990 Americans with Disabilities Act, which brought an increased interest in obtaining accurate statistics and increased awareness of disabled people to identify themselves. From this survey it is estimated that among

the overall population over 6 years old, 3.3 percent used a wheelchair and 9.6 percent used a cane, crutches, or a walker for 6 months or longer. The employment rate for people 21 to 64 years of age was 82.1 percent in the able-bodied population and 52.4 percent among those with a disability.

In the United Kingdom the population census of 1984 showed that 14 percent of the population could be classified as disabled. A detailed survey conducted in Northern Ireland in 1989 estimated that 17 percent of the population could be classified as disabled. Out of this group, 11 percent were confined to their homes while the very large majority were able to go out with assistance or, for most of them, without assistance. An in-depth study of this data showed that disabled people constitute 12 percent of the total mobile population of Northern Ireland who are out and about in the community, and just over 10 percent of that mobile population are disabled people who may be unassisted.[66] Among the disabled people who go out, 55 percent go out every day, and 93 percent go out at least once a week. So it is reasonable to assume that disabled people are regularly visiting public buildings.

In the fire field, so far, efforts have been concentrated in identifying means to provide life safety to people with disabilities. Special procedures have been identified following reports of the experience of occupants with disabilities who survived a fire or went through an evacuation.[67,68] The "egressibility" of occupants with disabilities has become an essential subject to take into account during fire safety design. Egressibility supposes the possibility of everyone leaving a building or reaching an area of safety in case of an emergency. The egressibility concept does not mean that every occupant should egress the same way or through the same route; rather, it intends to promote equivalent opportunity of life safety for everyone.[69]

Different options are being implemented to provide adequate life safety for everyone.[70] The area of refuge concept is one such option. It received limited success during testing,[71] but the area of refuge concept remains an interesting option if supplemented with complementary fire safety provisions. Providing safe elevators in buildings is another option.[72–76] The buddy system, which supposes that one or a few persons are assigned the responsibility to look after or to report the presence of a person with limitation in the case of an emergency, has not proven to be always satisfactory in practice but is used in many work environments. Techniques for carrying mobility impaired persons have been detailed in booklets.[70,77] More evacuation devices are being purchased. These devices can be used with minimum effort to transport people; however, they have to be kept in a convenient place, and some training is needed to use them efficiently. Visual alarms are implemented for the hearing impaired. Another strategy is to keep a list of the people who might have problems evacuating available for the responding firefighters. According to many firefighters, however, most lists are incomplete, since people are free to register on the list. Furthermore, these lists are often out-of-date, as people may have moved in or out of the building without the list being updated. In assessing the effectiveness of the various strategies, it can be seen that no single life safety option or technique will solve all of the problems. It is more likely that a combination of different options will increase life safety.

All these strategies have pros and cons and should be tailored to specific occupancies. One consideration that has been originally left out is the fact that some occupants with disabilities are likely to attempt to evacuate, no matter the strategy in place. Many disabled people might be mobility-impaired, but usually they are still mobile to some degree—either by themselves, with the aid of a technical device, or with the assistance of others. Consequently, it is essential to obtain some knowledge on the egress capacity of the population with disabilities. The Fire SERT research group at the University of Ulster, Northern Ireland, has developed a substantial body of data on the egress capabilities of disabled people who go out and about in the community. Their results, published in *Fire Technology* (1999), are an essential source of reference to anyone who has to take into account the escape capacities of people with disabilities.[66,78–80] Only partial data of the Fire SERT studies are reported here.

To obtain this data, the Fire SERT group met with 155 disabled participants who regularly visited 5 day centers. Among the disabled people studied, 121 could move without help, and 34 requested assistance throughout the experiment. The movement speeds achieved on a straight horizontal surface are presented in Table 3-13.2.

Table 3-13.2 ***Speed on a Horizontal Surface***

Subject Group (number)	Mean (m/s)	Standard Deviation (m/s)	Range (m/s)	Interquartile Range (m/s)
All disabled (n = 107)	1.00	0.42	0.10–1.77	0.71–1.28
With locomotion disability (n = 101)	0.80	0.37	0.10–1.68	0.57–1.02
no aid (n = 52)	0.95	0.32	0.24–1.68	0.70–1.02
crutches (n = 6)	0.94	0.30	0.63–1.35	0.67–1.24
walking stick (n = 33)	0.81	0.38	0.26–1.60	0.49–1.08
walking frame or rollator (n = 10)	0.57	0.29	0.10–1.02	0.34–0.83
Without locomotion disability (n = 6)	1.25	0.32	0.82–1.77	1.05–1.34
Electric wheelchair (n = 2)	0.89	—	0.85–0.93	—
Manual wheelchair (n = 12)	0.69	0.35	0.13–1.35	0.38–0.94
Assisted manual wheelchair (n = 16)	1.30	0.34	0.84–1.98	1.02–1.59
Assisted ambulant (n = 18)	0.78	0.34	0.21–1.40	0.58–0.92

Table 3-13.3 ***Speed on Stairs***

Subject Group (number)	Mean (m/s)	Standard Deviation (m/s)	Range (m/s)	Interquartile Range (m/s)
Ascent				
With locomotion disability (n = 30)	0.38	0.14	0.13–0.62	0.26–0.52
no aid (n = 19)	0.43	0.13	0.14–0.62	0.35–0.55
crutches (n = 1)	0.22	—	0.13–0.31	0.26–0.45
walking stick (n = 9)	0.35	0.11	0.18–0.49	—
rollator (n = 1)	0.14	—	—	—
Without disability (n = 8)	0.70	0.24	0.55–0.82	0.55–0.78
Descent				
With locomotion disability (n = 30)	0.33	0.16	0.11–0.70	0.22–0.45
No aid (n = 19)	0.36	0.14	0.13–0.70	0.20–0.47
Crutches (n = 1)	0.22	—	—	—
Walking stick (n = 9)	0.32	0.12	0.11–0.49	0.24–0.46
Rollator (n = 1)	0.16	—	—	—
Without disability (n = 8)	0.70	0.26	0.45–1.10	0.53–0.90

The speed on stairs was measured for participants who passed a screening test; this reduced the sample to 30 people who could negotiate stairs, although they all had a locomotion disability. Eight people who had no disability were included for comparison, as presented in Table 3-13.3. The researchers observed that participants had to rest repeatedly along the route. Also, more than 35 percent of the participants went up the stairs taking one step at a time; 44 percent went down the stairs the same way. In general, the participants were more confident going up the stairs than they were coming down. Finally, 91 percent of unassisted subjects chose to use the handrail when going up and 94 percent when coming down.

The capacity of disabled people to negotiate doors was also studied by the Fire SERT group. They examined the necessary time for disabled people to go through a door by pulling and pushing the door, which was closing with different forces. Partial results are shown in Table 3-13.4. The researchers observed that the analysis of these data suggests that the ability of disabled people to negotiate doors, subjected to a range of closing forces, may depend on different factors. These include the use of a technical aid such as a walker, since it implies a relatively slow movement speed and particular technique in maneuvering the technical aid though the door; how old the participant was, since this is inherently related to strength; and the presence and severity of a dexterity, or reaching and stretching, disability.

The Fire SERT group also studied the capability of people with disabilities to read and locate exit signs. They compared a nonilluminated exit sign, an internally-illuminated sign, and a light emitting diode (LED). They concluded that for people with seeing impairments, LED signs were the easiest to see and read.[80]

It has been demonstrated that people with intellectual disability can learn to evacuate a building. However, for this skill to be maintained, substantial repeated training is

Table 3-13.4 ***Time in Seconds to Negotiate Doors***

Closing Force (N)	No Aid (n = 63)			Crutch Users (n = 5)		Walking Stick (n = 28)			Walking Frame/ Rollator (n =8)	
	Mean (s)	Standard Deviation	Range (s)	Mean (s)	Range (s)	Mean (s)	Standard Deviation	Range (s)	Mean (s)	Range (s)
Push										
21	3.0	0.8	1.7–4.5	3.7	3.6–3.8	3.7	1.5	2.3–7.4	7.9	2.0–12.8
30	3.5	2.2	1.9–15.0	3.0	2.5–3.2	3.8	1.5	2.5–7.3	6.3	2.2–10.5
42	3.7	1.5	1.6–10.2	3.8	2.9–5.2	4.0	1.6	2.3–7.5	5.2	2.1–10.3
51	4.1	2.4	1.0–14.3	3.6	3.1–3.9	4.3	2.4	1.5–10.7	7.9	2.0–14.3
60	4.0	1.9	1.3–13.0	3.8	3.6–4.1	3.7	1.5	1.7–7.9	5.2	2.0–10.3
70	4.3	2.0	1.7–11.2	3.9	3.3–4.6	4.6	2.1	2.5–11.1	6.2	1.7–11.2
Pull										
21	3.3	1.5	1.5–7.6	2.8	2.2–4.0	3.6	1.4	1.8–7.6	5.7	2.0–8.2
30	3.2	1.0	1.5–5.2	—	—	3.2	0.9	1.8–4.9	5.2	4.3–6.0
42	3.7	1.8	1.4–12.6	4.0	2.9–6.3	3.9	1.4	1.9–6.8	4.7	2.6–6.9
51	3.8	1.6	1.5–10.2	3.6	2.5–4.6	4.6	2.2	1.5–9.5	6.3	2.5–11.2
60	4.1	1.9	1.5–11.4	3.6	2.7–4.7	4.1	1.7	1.4–7.4	8.9	1.9–17.0
70	4.6	2.2	1.5–12.6	4.6	2.6–4.7	4.9	2.3	2.1–9.7	3.2	1.9–6.7

necessary, with incentives and in a variety of realistic scenarios.[81] The speeds of movement of people with an intellectual disability could be comparable to the speeds of able occupants, although their time delay to start could be very long, especially during night evacuation.

Movement in Smoke

For a long time it was assumed that during an evacuation when occupants encountered smoke, they would stop, turn back, and find another means of egress. It is acknowledged now that many people are prepared to move in smoke. It is estimated that over 60 percent of evacuees in small residential buildings move through smoke to evacuate. A study of the behavior of occupants who evacuated after the bomb blast at the World Trade Center in 1993 showed that 94 percent of the occupants of Tower 1 moved through smoke.[82] Detailed study of the evacuation of two high-rise residential buildings showed that around 96 percent of the occupants located above the fire floor moved through smoke. The only occupants who managed to escape without meeting any smoke were occupants located under the fire floor or occupants who started their evacuation very early during the fire. In fact, movement through smoke is a recurring event in actual fires.[57,58] The fact that movement in smoke is so prevalent during high-rise fire evacuation can be explained by the simultaneous evacuation movement of a large number of occupants. Occupants of the fire floor who evacuate their floor will allow the stairwell to become contaminated when opening the door to that stairwell. Even if the stairwell is pressurized, the repeated movement of occupants from the fire floor to the stairwells and occupants opening doors to the same stairwells on all upper floors will allow this means of egress to become contaminated. In a way, the stairwells of a high-rise building might be the most dangerous place to be during a fire, after the room of fire origin and the fire floor.

Although it seems well known by the public that it is the smoke that kills people in fires,[83] occupants are still prepared to move through smoke to reach safety. The public knowledge that smoke kills does not mean that they are a good judge of the potential lethal effect of smoke. Victims are reporting that they made it through smoke because they moved very fast, or were breathing through a cloth or holding their breath to protect themselves. In fact, these people were extremely lucky because smoke kills, and it kills fast—a couple of breaths could be enough to lose consciousness.

As was discussed in Section 3, Chapter 12, the principal motivation to move through smoke was the knowledge of an exit location and the ability to estimate the travel distance to that exit. Another motivation that can be found in high-rise buildings is the strong desire of occupants to reach ground level. Also, when occupants start their evacuation, it is possible that no smoke was visible, but eventually during their descent, this situation changed (usually within seconds). In these circumstances, some occupants may persist and continue down, others will turn back, while some others may seek refuge.

The presence of smoke has a major impact on occupants' speed of movement. T. Jin in Japan is a pioneer in this field.[84] He tested individual subjects in a 20-m-long corridor filled with two types of smoke analogous to the early stage of a fire, a highly irritant white smoke produced by burning wood cribs and a less irritant black smoke produced by burning kerosene. The visibility in irritant smoke decreased sharply at smoke density extinction coefficient exceeding 0.5 l/m. The occupant speed of movement, which was over 1 m/s at the introduction of smoke, went down to a stop after a few meters in the irritant smoke. Participants could not keep their teary eyes open in irritant smoke. In the nonirritant smoke, participants moved initially at over 1 m/s and slowed down to 0.5 m/s when the extinction coefficient reached 1.0 l/m.

Jensen in Norway tested over 80 subjects in a test facility looking at the performance of different wayguidance systems in smoke.[85] Under smoke optical density of 1.09 and 1.58 l/m, speeds of movement were around 0.2 to 0.4 m/s, which seems to be the ultimate speed of movement in heavy smoke conditions, independent of any egress information system used. Those who have survived catastrophic fires moved on average only 10 m in heavy smoke. At a speed of 0.2 m/s, this equals a time exposure of 50 s.

Tenability studies show that people's movement in smoke before incapacitation varies widely according to a number of factors such as the weight, fitness, and activity of the person or the mix and concentration of the gases developed by the fire. Generally speaking, occupants have only a few minutes available for movement in smoke before incapacitation occurs. Education, training, and evacuation procedures all recommend to avoid moving in smoke, but occupants are still moving in smoke in many fires.

Another problem of movement through smoke is the fast obscuration of the ceiling-mounted luminaires, which gives an impression of total black out. Interviews of fire victims who traveled through smoke are consistent; the occupants insist that the power was out during their evacuation even though no electric fault can be found after the fire. Consequently, it was the smoke density that was obscuring the light fixtures. To alleviate the problem of moving in black-out conditions, the installation of a wayguidance photoluminescent system is gaining popularity. The characteristics of this material to efficiently guide occupants in the dark are particularly interesting. This material could provide support to evacuees where standard lighting and emergency lighting have failed. In the Jensen study,[85] photoluminescent material positioned as a continuous line at floor level and at 1 m from the floor were better than luminaires and lit signs to guide occupants in smoke conditions. In a field study by Proulx,[50] it was found that speeds of movement in a stairwell with a photoluminescent wayguidance system, in black-out conditions, were comparable to speeds of movement in fully-lit stairwells.

Time-Based Egress Analysis

The need to have realistic, verifiable estimates of egress-time criteria and accompanying movement assumptions should be recognized by fire protection engineers and other consultants conducting time-based egress

analyses (sometimes termed "timed exit analyses" or "dynamic exit analyses"). Such analyses are prepared to help get official approval for a building design that otherwise might not meet specific egress requirements in a code. In some cases, the assumptions and calculation methods used in such analyses should be seriously questioned. Currently, authorities having such analyses thrust on them may have difficulty judging their value; they can only fall back on the reputation of the consulting firm and/or the bulk of a report and the apparent (perhaps illusory) sophistication of its calculations.

One should be especially critical of discussions in which egress-time criteria are equated in simple fashion to hazard development times. As noted above in relation to the "life safety evaluation," there should be a factor of safety, especially in view of the incomplete technical grasp of both egress and fire issues at the present time. For example, in a conservative approach, the time available should be at least twice as long as the time required.

This chapter has emphasized egress capacity or flow issues more than travel distance or speed issues. The former are generally more important in building spaces occupied by more than a few persons. Time-based egress analyses usually address both sets of issues and state the total evacuation time for a space as the sum of a flow time and a travel time. In some situations, the travel time component is simply the time taken by the person closest to the exit to move from his or her point of origin to the point considered a place of safety or refuge. Careful judgment is required to predict this speed and the actual flow of those following the first person. A simple, conservative approach would assume a modest speed for the first person, and a speed similar to the congested speed for those following behind. In this case, it is reasonable to predict the minimum total evacuation time (not including communication and decision-making times) as the sum of this first person's travel time and the flow time of those following, based on an assumed mean-flow calculation. (Note that the term *minimum total evacuation time* is used here; some consultants have erroneously reported that their time-based exit analyses predict maximum total evacuation times.)

For example, if the first person is 18.3 mm (60 ft) from a 914-mm- (36-in.-) wide (nominal width) exit door and is followed by 100 people, the two time components are travel time—0.3 min [18 m (60 ft) divided by 61 m (200 ft) per min]—and flow time through the doorway—2.0 min (100 persons divided by 50 persons/min)—for a total of 2.3 min for the minimum total evacuation time. Note that in reality, the first person might walk at a free walking speed; however, it is very unlikely that other people would be close behind. Therefore, it is unreasonable to assume that those immediately behind the fast-walking first person would achieve a mean flow of 50 persons/min, a conservative figure for sustained mean flow through a nominal 914-mm (36-in.) doorway. Further information on reasonable movement rates is provided in Table 3-13.1.

One of the errors in some time-based exit analyses occurs as inconsistent, unrealistic assumptions are made about simultaneous high speed and high density of crowd movement, a combination that appears, according to Equation 1, to give a high flow. (Equation 1, the fundamental equation for traffic movement, describes flow as the product of speed, density, and path width.)

Due to interference among closely spaced people, high densities do not permit high speeds of movement, a fact illustrated by Figure 3-13.1 in relation to crowd movement down stairs. Moreover, optimum flows occur only at speeds that are about 60 percent of the speeds at which individuals can move freely. (See Figure 3-13.2 in relation to stairs and, generally, the subsection "General Research on Crowd Movement.")

The moderate conditions, shown in Table 3-13.5, are reasonable approximations for predicting speeds, densities, and flows in calculations of minimum egress time for many situations (especially in view of the fact that other behavior not involving simple movement directed to the exit will often be a larger factor in determining evacuation time). The figures given for corridors apply to all walkways with level or moderate slope (less than 1:12). The figures for stairs assume relatively good step geometry and handrail provision. The figures are based on work by Fruin[14] and by Pauls (as discussed earlier in this chapter); however, they are simplified and optimistic because there are no reductions for edge effects. Nominal per-foot measurements are used here. The resultant errors will be acceptable so long as egress times calculated using these assumptions are considered minimum times for egress movement only. (Figure 3-13.6 is an example of a more sophisticated approach to stair flow capacity.)

Sample Calculation Using Table 3-13.5

Given a crowd of 170 people using a corridor 1520 mm (5.0 ft) wide leading to a doorway 914 mm (3.0 ft) in nominal width and then a stairway 1220 mm (4.0 ft) in nominal width, what mean flow should be assumed for evacuation purposes? Which of the egress facilities governs this flow? What is expected minimum flow time? And what crowd conditions can be expected in these three facilities?

Using moderate conditions, it is predicted that the corridor will serve 100 persons/min, the doorway will serve 51 persons/min, and the stair will serve 48 persons/min. Therefore, the stair capacity governs the flow. The flow time is expected to be 170 divided by 48, or 3.5 min, a time similar to the implied standard in current egress standards. At a flow of 48 persons/min through each facility

Table 3-13.5 ***Crowd Movement Parameters for Various Facilities and Conditions***

Facility	Crowd Condition	Density (ft^2)	Speed (ft/min)	Flow (min/ft)
Stair	Minimum	<0.05	150	<5
Stair	Moderate	0.10	120	14
Stair	Optimum	0.19	95	18
Stair	Crush	0.30	<40	<12
Corridor	Minimum	<0.05	250	<12
Corridor	Moderate	0.10	200	20
Corridor	Optimum	0.20	120	24
Corridor	Crush	0.30	<60	<18
Doorway	Moderate	0.10	170	
Doorway	Optimum	0.22	120	
Doorway	Crush	0.30	<50	

For SI units: 1 ft = 0.3048 m; 1 ft^2 = 0.093 m^2.

and without any queuing, the corridor will be minimally crowded with an average crowd density of about 0.5 person/m^2 (0.05 person/ft^2), and the doorway and stair will be used at comfortable, moderate levels.

From Figures 3-13.5 and 3-13.6, it can be understood that, with greater population per width of egress facility (and with queuing for the facility), there may be a higher, more efficient flow. In these cases, it may be appropriate to use the optimum values presented in Table 3-13.1; however, caution must be exercised with the localized crowding conditions that may result, especially on stairs and at doors. For example, if there were 800 people using the facilities described in this subsection, the stair would continue to govern the flow time, but with a higher mean flow, the flow time could be 11.1 min. Movement would be restricted to a shuffling pace, with extensive queuing, and a few percent of the people might have difficulty dealing with the sustained high-density conditions.

Movement Assumptions for Simple, First-Approximation Calculations

Although very incomplete, the following will be useful in doing rough, preliminary calculations. Differing crowd compositions and abilities may alter these values up or down by about one-third. Adverse design conditions will reduce effectiveness by as much as one-third. (These values are comparable with those described as "Levels of Service D and E.")[14]

Stairs: A high-quality stairway that allows convenient counterflow and two-abreast movement, with a width of 1220 mm (4 ft) between handrail centerlines—giving an effective width of just over 1 m—will carry a flow of about one person/s under moderate flow conditions. Speed along the slope will be approximately 0.5 m/s (2 ft/s), or one typical office building story every 15 s. Each person will occupy an average of two stair treads.

Level passageways and moderate-slope ramps: A clear width of 1.22 m (4 ft) will permit a flow of 1.33 persons/s under moderate flow conditions. Speed will be approximately 1.0 m/s (3.33 ft/s). Density will be approximately 1 person per 1 m^2 (10 ft^2).

Doorways: A common 910 mm (3 ft) nominal width doorway will permit a flow of 1 person/s under moderate to optimum flow conditions.

The ratio of clear widths for similar flow, comparing stairs and the other facilities, is 4:3; that is, a 1.22-m (4-ft) clear stair width is well matched to a 1-m (3-ft) clear doorway width. Hence the ratios of 4:3 and 3:2 used in common code rules for egress widths are approximately correct and, in the case of the latter 3:2 ratio, err on the side of safety because the code rules are based on stairs' nominal width (not counting handrail incursions or other edge effects).

Other circulation facilities: For completeness, a few other circulation facilities can be noted even though they are not necessarily given egress capacity credit by codes and standards because of a variety of use and maintenance difficulties. A 1.22-m (4-ft) nominal width escalator will carry 1.5 persons/s. A typical revolving door will permit a flow of 0.5 person/s. A turnstile will permit a flow of 0.5 to 1.0 person/s depending on ticket or coin collection procedures.

Summary

A quantitative approach to the movement of people must be balanced by a qualitative understanding of the context within which the movement takes place. In cases of fire or other emergencies, egress movement is part of a complex behavior pattern. Calculations addressing time to start and movement directed to egress from a space or building must be considered as providing only minimum evacuation times. Nonetheless, such calculations are useful for making comparisons among design options and for using equivalency approaches to satisfy legal requirements for means of egress.

Calculation methods on movement developed by Pauls and delay time to start developed by Proulx have been emphasized as a result of field studies of evacuation and other movement of people in buildings. Much additional work is required to develop such methods and to revise requirements in codes and standards so that an integrated systematic approach to fire protection, egress provision, and everyday movement safety is the norm.

References Cited

1. J.L. Pauls, "International Life Safety and Egress Seminar, Maryland, November 1981: Summary of Presentations and Discussion," *F. Safety J.*, 5, p. 213 (1983).
2. F.I. Stahl and J.C. Archea, "Assessment of the Technical Literature on Emergency Egress from Buildings." *NBSIR 77-1313,* National Bureau of Standards, Gaithersburg, MD (1977).
3. F.I. Stahl, J.J. Crosson, and S.T. Margulis, "Time-Based Capabilities of Occupants to Escape Fires in Public Buildings: A Review of Code Provisions and Technical Literature." *NBSIR 82-2480,* National Bureau of Standards, Gaithersburg, MD (1982).
4. R.L. Paulsen, Human Behavior and Fire Emergencies: An Annotated Bibliography. *NBSIR 81-2438,* National Bureau of Standards, Gaithersburg, MD (1981).
5. J.L. Pauls, "Development of Knowledge about Means of Egress." *Fire Tech.*, 20, 2, p. 28 (1984).
6. *Design and Construction of Building Exits,* National Bureau of Standards, Washington, DC (1935).
7. *Fire Grading of Buildings, Part III, Personal Safety, Post-War Building Studies,* Her Majesty's Stationery Office, London (1952).
8. K. Togawa, *Report No. 14,* Building Research Institute, Tokyo (1955).
9. V.M. Predtechenskii and A.I. Milinskii, *Planning for Foot Traffic Flow in Buildings,* Amerind Publishing, New Delhi (1978).
10. E. Kendik, "Assessment of Escape Routes in Buildings and a Design Method for Calculating Pedestrian Movement." *Technology Report 85-4,* Society of Fire Protection Engineers, Boston (1985).
11. E. Kendik, *Proceedings of the First International Symposium on Fire Safety Science,* Hemisphere, New York (1984).

12. London Transport Board, *Second Report of the Operational Research Team on the Capacity of Footways,* London Transport Board, London (1958).
13. B.D. Hankin and R.A. Wright, *Oper. Res. Quart.*, pp. 9–81 (1959).
14. J.J. Fruin, *Pedestrian Planning and Design,* revised ed., Elevator World Educational Services Division, Mobile, AL (1987).
15. M. Galbreath, *Fire Research Note 8,* National Research Council of Canada, Ottawa (1969).
16. S.J. Melinek and S. Booth, *Current Paper CP 96/75,* Building Research Establishment, Borehamwood, UK (1975).
17. S.J. Melinek and R. Baldwin, *Current Paper CP 95/75,* Building Research Establishment, Borehamwood, UK (1975).
18. J.L. Pauls, "Movement of People in Building Evacuations," in D.J. Conway (ed.), *Human Response to Tall Buildings,* Chap. 21. Dowden, Hutchinson and Ross, Stroudsburg, PA, pp. 281–292 (1977).
19. J.L. Pauls, "Management of Movement of Building Occupants in Emergencies," in *Proceedings of Second Conference on Designing to Survive Severe Hazards,* Illinois Institute of Technology Research Institute, Chicago, pp. 103–130 (1977).
20. J.L. Pauls, "Evacuation of High Rise Office Buildings." *Buildings,* 84 (May 1978).
21. Board for the Coordination of the Model Codes, *Report on Means of Egress,* Council of American Building Officials, Falls Church, VA (1985).
22. NFPA *101, Code for Safety to Life from Fire in Buildings and Structures,* NFPA, Quincy, MA (1994).
23. J.L. Pauls, "Building Evacuation: Research Findings and Recommendations." in *Fires and Human Behaviour,* John Wiley and Sons, New York, pp. 251–275 (1980).
24. J.L. Pauls, "Effective-Width Model for Evacuation Flow in Buildings," in *Proceedings of Workshop on Engineering Applications of Fire Technology,* National Bureau of Standards, Washington, DC, pp. 215–232 (1980).
25. J.L. Pauls, "Effective-Width Model for Crowd Evacuation Flow on Stairs," *Proceedings of 6th International Fire Protection Engineering Seminar,* Karlsruhe, Germany, pp. 295–306 (1982).
26. J.L. Pauls, "The Movement of People in Buildings and Design Solutions for Means of Egress." *Fire Technology,* 20, 1, pp. 27–47 (1984).
27. J.L. Pauls and B.K. Jones, "Building Evacuation: Research Methods and Case Studies," in *Fires and Human Behaviour,* John Wiley and Sons, New York, pp. 227–249 (1980).
28. J.L. Pauls, *Building Practice Note 35,* National Research Council of Canada, Ottawa (1982).
29. J.J. Fruin, *Audit. News,* 22, p. 4 (1984).
30. J.J. Fruin, *Crowd Dynamics and the Design and Management of Public Places,* Conference, Los Angeles (1985).
31. SCICON, *Safety in Football Stadia: A Method of Assessment, Scientific Control Systems,* London (1972).
32. Home Office/Scottish Home and Health Dept., *Guide to Safety at Sports Grounds (Football),* Her Majesty's Stationery Office, London (1976).
33. *Report of the Task Force on Crowd Control and Safety,* City of Cincinnati (1980).
34. T.F. Ventre, F.I. Stahl, and G.E. Turner, *NBSIR 81-2361,* National Bureau of Standards, Gaithersburg, MD (1981).
35. The Rt. Hon. Lord Justice Taylor, *The Hillsborough Stadium Disaster,* Interim and Final Reports, Her Majesty's Stationery Office, London (1990).
36. T.J. Klem, *Fire J.*, 80, p. 128 (1986).
37. Popplewell, *Committee Report 9585,* Her Majesty's Stationery Office, London (1985).
38. Popplewell, *Committee Report 9710,* Her Majesty's Stationery Office, London (1986).
39. R.A. Smith and J.F. Dickie (eds.), *Engineering for Crowd Safety,* Elsevier, Amsterdam (1993).
40. D.M. Alvord, *NS-GCR 85-496,* National Bureau of Standards, Gaithersburg, MD (1985).
41. J.L. Pauls, "Observations of Crowd Conditions at Rock Concert in Exhibition Stadium, Toronto, 16 July 1980." *Building Research Note No. 185,* National Research Council of Canada, Ottawa (1982).
42. J.M. Lewis and M.L. Kelsey, "The Crowd Crush at Hillsborough: The Collective Behavior of an Entertainment Crush," *Disasters, Collective Behavior, and Social Organisation,* Kent State Univ., OH (1994).
43. J.J. Fruin, *Elev. World,* 33, p. 52 (1985).
44. ITE Technical Council Committee 5-R, *Traffic Eng.*, May 34, (1976).
45. T.A. Habicht and J.P. Braaksmal, *J. Trans. Eng.*, 110, p. 80 (1984).
46. British Standards Institute, *Fire Safety Engineering in Buildings, Part 1: Guide to the Application of Fire Safety Engineering Principles,* DD240, London (1997).
47. G. Proulx and G. Hadjisophocleous, "Occupant Response Model: A Sub-Model for the NRCC Risk-Cost Assessment Model," *Proceedings of the Fourth International Symposium on Fire Safety Science,* Ottawa, Canada (1994).
48. G. Proulx and R.F. Fahy, "The Time Delay to Start Evacuation: Review of Fire Case Studies," *Proceedings of the Fifth International Symposium on Fire Safety Science,* Melbourne, Australia (1997).
49. G. Proulx and J. Pineau, "Differences in the Evacuation Behaviour of Office and Apartment Building Occupants," *Proceedings of the Human Factors and Ergonomics Society 40th Annual Meeting,* Philadelphia (1996).
50. G. Proulx, B. Kyle, and J. Creak, "Effectiveness of a Photoluminescent Wayguidance System," *Fire Tech.* In press (2001).
51. T.J. Shields, K.E. Boyce, and G.W.H. Silcock, "Towards the Characterization of Large Retail Stores," *Proceedings of the First International Symposium on Human Behaviour in Fire,* Belfast, UK (1998).
52. G. Proulx and J.D. Sime, "To Prevent 'Panic' in an Underground Emergency: Why Not Tell People the Truth?," *Proceedings of the Third International Symposium on Fire Safety Science,* Elsevier, London (1991).
53. P. J. Keating and F. E. Loftus, "Post Fire Interviews: Development and Field Validation of the Behavioral Sequence Interview Technique," *NBS-GCR 84-477,* National Bureau of Standards, Washington, DC (1984).
54. A.J. Chapman and D.J. Perry, "Applying the Cognitive Interview Procedure to Child and Adult Eyewitnesses of Road Accidents," *Applied Psychology: An International Review,* 44, 4 (1995).
55. P. Brennan, "Timing Human Response in Real Fires," *Proceedings of the Fifth International Symposium on Fire Safety Science,* Melbourne, Australia (1997).
56. P. Brennan, "Victims and Survivors in Fatal Residential Building Fires," *Proceedings of the First International Symposium on Human Behaviour in Fire,* Belfast, UK (1998).
57. G. Proulx, "Critical Factors in High-Rise Evacuations," *Fire Prevention,* 291, pp. 24–27 (1996).
58. G. Proulx, "The Impact of Voice Communication Messages during a Residential Highrise Fire," *Proceedings of the First International Symposium on Human Behaviour in Fire,* Belfast, UK (1998).
59. G. Proulx, "Occupant Response to Fire Alarm Signals," *NFPA Fire Alarm Code Handbook, Supplement 4,* Quincy, MA (1999).

60. J.L. Pauls, "The 7-11 Stair: Should It Be Required for Residential Construction? (Rebuttal to National Association of Home Builders.)" The Building Official and Code Administrator, May–June 1985, pp. 16–35. *The Building Official and Code Administrator*, 26 (May–June 1985).
61. B.M. Johnson and J.L. Pauls, "Study of Personnel Movement in Office Buildings," *Health Impacts of the Use, Evaluation and Design of Stairways in Office Buildings,* Health and Welfare Canada, Ottawa (1977).
62. J.L. Pauls, "The Stair Event: Some Lessons for Design," *Proceedings of Conference, People and the Man-Made Environment,* Sydney, pp. 99–109 (1980).
63. J.B. Webber, *Report of the Ontario Public Inquiry into Fire Safety in High-Rise Buildings,* Queen's Printer of Ontario, Ontario (1983).
64. Statistics Canada, *1991 Census Handbook, Reference, Catalogue 92-305E,* Statistics Canada, Ottawa (1992).
65. U.S. Census Bureau, "Americans with Disabilities: 1994–95," *Current Population Reports P70-61,* http://www.census.gov:80/hhes/www/disable/census.html.
66. K.E. Boyce, T.J. Shields, and G.W.H. Silcock, "Toward the Characterization of Building Occupancies for Fire Safety Engineering: Prevalence, Type, and Mobility of Disabled People," *Fire Tech.,* 35, 1, pp. 35–50 (1999).
67. K.E. Dunlop and T.J. Shields, "Real Fire Emergency Evacuation of Disabled People," *CIB W14,* Belfast, UK (1994).
68. E. Juillet, "Evacuating People with Disabilities," *Fire Eng.,* 126, 12, pp. 100–103 (1993).
69. J. Pauls and E. Juillet, "Life Safety of People with Disabilities: How Far Have We Progressed?" in *Proceedings of CIB W14 Symposium and Workshops: Fire Safety Engineering in the Process of Design, Part 1: Symposium: Engineering Fire Safety for People with Mixed Abilities,* Ulster, Northern Ireland, pp. 17–40 (1993).
70. U.S. Fire Administration, *Emergency Procedures for Employees with Disabilities in Office Occupancies,* Emmitsburg, MA (1995).
71. J.H. Klote, H.E. Nelson, S. Deal, and B.M. Levin, "Staging Areas for Persons with Mobility Limitations," *NISTIR 4770,* U.S. Department of Commerce Technology Administration, Gaithersburg, MD (1992).
72. B.J. Semple, "Vertical Exiting: Are Elevators Another Way Out?" *NFPA Journal,* 87, 3, (1993).
73. J.H. Klote and G.T. Tamura, "Design of Elevator Smoke Control Systems for Fire Evacuation," *ASHRAE Transactions,* 97, 2, pp. 634–642 (1991).
74. *Proceedings of the Symposium on Elevators and Fire,* Baltimore, MD, The American Society of Mechanical Engineers, New York, February (1991).
75. N.E. Groner and B.M. Levin, "Human Factors Considerations in the Potential for Using Elevators in Building Emergency Evacuation Plans," *NIST-GCR-92-615,* National Institute of Standards and Technology, Gaithersburg, MD (1992).
76. G.M.E. Cooke, "Assisted Means of Escape of Disabled People from Fires in Tall Buildings," *BRE Information Paper, IP 16/91,* Fire Research Establishment, Garston, UK (1991).
77. B. Johnson, "Evacuation Techniques for Disabled Persons," *National Research Council of Canada,* Springfield Environmental Research Ltd. (1983).
78. K.E. Boyce, T.J. Shields, and G.W.H. Silcock, "Toward the Characterization of Building Occupancies for Fire Safety Engineering: Capabilities of Disabled People Moving Horizontally and on an Incline," *Fire Tech.,* 35, 1, pp. 51–67 (1999).
79. K.E. Boyce, T.J. Shields, and G.W.H. Silcock, "Toward the Characterization of Building Occupancies for Fire Safety Engineering: Capabilities of Disabled People to Negotiate Doors," *Fire Tech.,* 35, 1, pp. 66–78 (1999).
80. K.E. Boyce, T.J. Shields, and G.W.H. Silcock, "Toward the Characterization of Building Occupancies for Fire Safety Engineering: Capabilities of People with Disabilities to Read and Locate Exit Signs," *Fire Tech.,* 35, 1, pp. 79–86 (1999).
81. M. Rowe and J.H. Kedesdy, "Fire Evacuation Skills Training for Institutionalized Mentally Retarded Adults," *Behavioral Residential Treatment,* 3, 2 (1988).
82. F.R. Fahy and G. Proulx, "Collective Common Sense: A Study of Human Behavior during the World Trade Center Evacuation," *NFPA Journal,* 9, 2, pp. 59–67 (1995).
83. G. Proulx, R.F. Fahy, J. Comeletti, M. Appy, and E. Kirtley, "Home Fire Safety Class for Working Adults," *IR 803,* National Research Council of Canada (1999).
84. T. Jin, "Studies on Human Behavior and Tenability in Fire Smoke," *Proceedings of the Fifth International Symposium on Fire Safety Science,* Melbourne, Australia (1997).
85. G. Jensen, "Evacuating in Smoke," *IGS AS,* Trondheim, Norway (1993).

CHAPTER 14

Emergency Movement

Harold E. "Bud" Nelson and Frederick W. Mowrer

Introduction

Prediction of the movement of occupants during egress is an essential aspect of performance-based building fire safety analysis methods. In general, life safety from fire is achieved if the required safe egress time (RSET) is shorter than the available safe egress time (ASET), where the ASET is defined as the time when fire-induced conditions within an occupied space or building become untenable. Methods to evaluate the development of fire-induced conditions and tenability criteria to determine the ASET are addressed in other chapters of this handbook. The RSET can be subdivided into a number of discrete time intervals, the sum of which constitute the total RSET:

$$RSET = t_d + t_a + t_o + t_i + t_e \quad (1)$$

where

t_d = time from fire ignition to detection

t_a = time from detection to notification of occupants of a fire emergency

t_o = time from notification until occupants decide to take action

t_i = time from decision to take action until evacuation commences

t_e = time from the start of evacuation until it is completed

The RSET elements t_d and t_a may involve hardware, such as fire detection devices and fire alarm equipment, and human response, such as discovery of fire, or other indication of fire, and giving the alarm. The elements t_o and t_i relate the individual and collective responses of the occupants until they commence evacuation. The theory and design of detection and alarm systems are covered elsewhere in this handbook. The theory of human response is addressed in Section 3, Chapter 12 "Behavioral Response to Fire and Smoke."

This chapter primarily addresses different methods that can be used to estimate the last of the RSET elements, t_e, the evacuation time. Included in the coverage of this chapter are those human behavioral responses that affect the flow and efficiency of the emergency movement.

This chapter also identifies models that have been developed to evaluate emergency movement in buildings and provides guidance on the criteria for model selection.

Elements of Emergency Movement

Research-based methods for predicting the flow of groups of persons in emergencies have emerged in recent years. The major contributors include Predtechenskii and Milinskii,[1] Fruin,[2] and Pauls.[3,4] The methods developed are, in most cases, compatible and supportive of each other. All are based on the relationship between the speed of movement and population density of the evacuating stream of persons. In general, these methods assume that

1. All persons will start to evacuate at the same instant.
2. Occupant flow will not involve any interruptions caused by decisions of the individuals involved.
3. All or most of the persons involved are free of disabilities that would significantly impede their ability to keep up with the movement of a group.

The approach is often referred to as a hydraulic model of emergency egress.

Separate works by investigators, such as Wood,[5] Bryan,[6] and Keating and Loftus[7] have concentrated on the decisions and resulting actions taken by individuals in actual fires. Sime[8] and MacLennan[9] have examined the

Harold E. "Bud" Nelson, a senior research engineer at Hughes Associates, Inc., in Columbia, Maryland, is a past president of the SFPE. He has focused on hazard analysis and application of scientific principles to the solution of real-world fire safety problems.

Frederick W. Mowrer is an associate professor in the Department of Fire Protection Engineering at the University of Maryland. He currently serves on the board of directors of the SFPE and is the chair of the SFPE Technical Steering Committee. His research interests include material flammability evaluation, enclosure fire dynamics, and fire risk assessment.

impact of occupant decisions and choices of actions on evacuation time.

In this chapter, the product of hydraulic model calculations is termed modeled evacuation time. Actual egress time is the time required for the occupants to actually leave a building. Generally, the actual egress time will exceed the modeled time. Since the modeled evacuation time is an approximation based on data from evacuation drills and fire experience, it is therefore possible that the modeled evacuation time can exceed the actual evacuation time. The difference between modeled evacuation time and actual evacuation time can be expressed in terms of an apparent evacuation efficiency using the relationship

$$t_e = t_{me} e \quad (2)$$

where

t_{me} = modeled evacuation time (s)
e = apparent evacuation efficiency

Apparent evacuation efficiency, e, is a function of elements that interfere with the assumed hydraulic evacuation flow. Typical examples of efficiency elements are

1. Delays caused by egress management activities of wardens or others directing the evacuation
2. Time delays involved in stopping and restarting of flows at merging points
3. Delays, self-instituted by individuals, that retard their start or slow their progress
4. Inefficient balance in the use of exit facilities, where some emergency routes are overtaxed while others are underutilized

All of these factors can reduce evacuation efficiency. However, all of the elements will seldom come to bear on a single evacuation.

The first step in appraising emergency movement usually is to calculate the modeled egress time. The use of model calculations provides a reproducible base of reference in appraising the impact of overall systems, individual components, or changes in systems. If, however, the results of the modeled evacuation time are to be compared to a realistically expected evacuation time or to expected fire growth, it is important that the user understand that the modeled evacuation time is seldom achieved in reality. Accurate estimation of expected evacuation time requires the calculation of the modeled evacuation time and an appraisal of evacuation efficiency. (See Equation 2.) The actual time from fire initiation to evacuation includes the expected movement time (t_e) and the other elements in Equation 1 that describe RSET. This chapter separately addresses the use of hydraulic flow calculations to estimate modeled evacuation time and delays in initiation and evacuation efficiency factors.

Hydraulic Flow Calculations

The estimation of modeled evacuation time utilizes a series of expressions that relate data acquired from tests and observations to a hydraulic approximation of human flow. While the expressions indicate absolute relationships, there is considerable variability in the data. Figure 3-14.1, abstracted from Section 3, Chapter 13, shows a typical relationship between the source data and the derived equation. The equations and relationships presented in the following paragraphs can be used independently or collected to solve a complex egress problem. Such a coordinated collection of equations is demonstrated in the sample problem.

Effective Width, W_e

Persons moving through the exit routes of a building maintain a boundary layer clearance from walls and other stationary obstacles they pass. This clearance is needed to accommodate lateral body sway and assure balance.

Discussion of this crowd movement phenomena is found in the works of Pauls,[3] Fruin,[2] and Habicht and Braaksma.[10] The useful (effective) width of an exit path is the clear width of the path less the width of the boundary layers. Figures 3-14.2 and 3-14.3 depict effective width and boundary layer. Table 3-14.1 is a listing of boundary layer widths. The effective width of any portion of an exit route is the clear width of that portion of an exit route less the sum of the boundary layers.

Clear width is measured

1. From wall to wall in corridors or hallways
2. As the width of the treads in stairways
3. As the actual passage width of a door in its open position
4. As the space between the seats along the aisles of assembly arrangement
5. As the space between the most intruding portions of the seats (when unoccupied) in a row of seats in an assembly arrangement

The intrusion of handrails is considered by comparing the effective width without the handrails and the effective width using a clear width from the edge of the handrail. The smaller of the two effective widths then

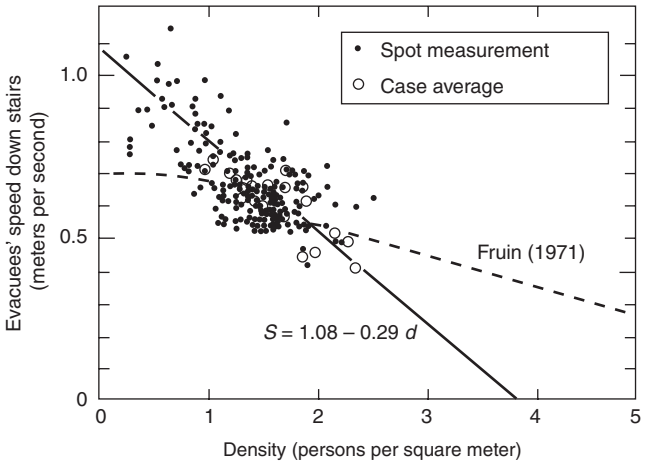

Figure 3-14.1. ***Relation between speed and density on stairs in uncontrolled total evacuations. Dashed line from Fruin.[2]***

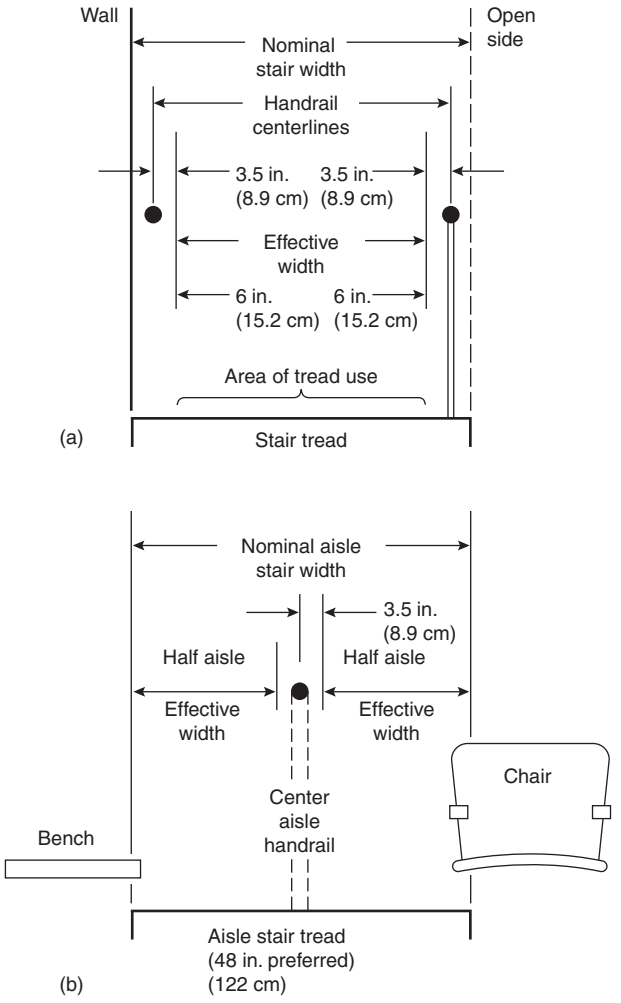

Figure 3-14.2. ***Measurements of effective width of stairs in relation to walls, handrails, and seating.***

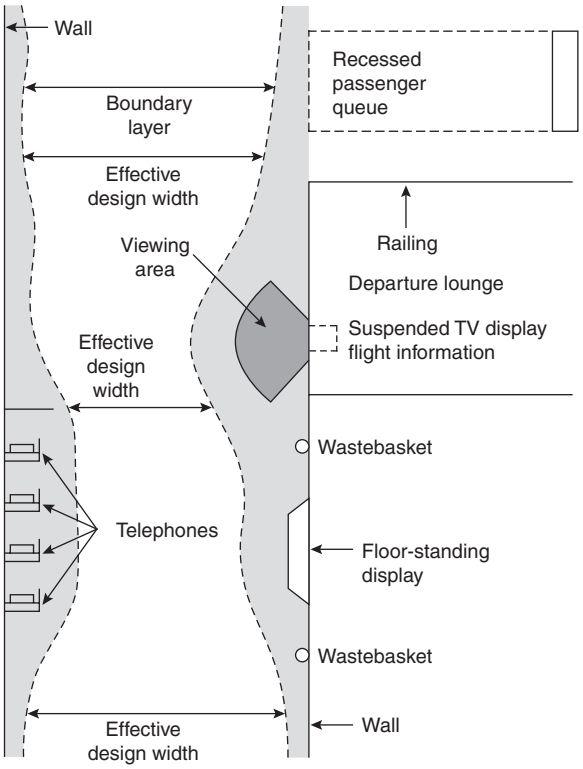

Figure 3-14.3. ***Public corridor effective width.***

Table 3-14.1 ***Boundary Layer Widths***

	Boundary Layer	
Exit Route Element	(in.)	(cm)
Stairways—wall or side of tread	6	15
Railings, handrails[a]	3.5	9
Theater chairs, stadium benches	0	0
Corridor, ramp walls	8	20
Obstacles	4	10
Wide concourses, passageways	<18	46
Door, archways	6	15

[a]Where handrails are present, use the value if it results in a lesser effective width.

applies. Using the values in Table 3-14.1, only handrails that protrude more than 2.5 in. need be considered. Minor midbody height or lower intrusions such as panic hardware are treated in the same manner as handrails. Where an exit route becomes either wider or narrower, only that portion of the route has the appropriate greater or lesser clear width.

Density, *D*

Density is the measurement of the degree of crowdedness in an evacuation route and is expressed in persons per unit area. The calculations in this chapter are based on density expressed in persons per square foot (or persons per square meter).

Unless information on the dispersion of occupants indicates otherwise, the density of the first exit element (aisle, corridor, ramp, etc.) is based on all of the served occupants. This information will demonstrate the capacity limits of the route element and produce a value representing the maximum capacity of the element.

Conversely, if the egressing population is widely dispersed, in terms of reaching the exit route element, the calculation is based on an appropriate time step. At each time increment, the density of the exit route is based on those that have entered the route minus those that have passed from it.

The density factors in subsequent portions of the egress system are determined by calculation. The calculation methods involved are contained in the section of this chapter titled "Transitions."

Speed—Movement Velocity of Exiting Individuals, *S*

Observations and experiments have shown that evacuation flow speed of a group is a function of the population

density. The relationships presented in this section have been derived from Fruin,[2] Pauls,[3] and Predtechenskii and Milinskii.[1]

If the population density is less than about 0.05 persons/ft² (0.54 persons/m²) of exit route (20 ft²/person; 1.85 m²/person), individuals will move at their own pace, independent of the speed of others. If the population density exceeds about 0.35 persons/ft² (3.8 persons/m²), no movement will take place until enough of the crowd has passed from the crowded area to reduce the density.

Between the density limits of 0.05 and 0.35 persons/ft² (0.54 and 3.8 persons/m²) the relationship between speed and density can be considered as a linear function. The equation of this function is

$$S = k - akD \quad (3)$$

where

S = speed along the line of travel

D = density in persons per unit area

k = constant, as shown in Table 3-14.2

= k_1; and $a = 2.86$ for speed in ft/min and density in persons/ft²

= k_2; and $a = 0.266$ for speed in m/s and density in persons/m²

Table 3-14.2 shows evacuation speed constant.

Figure 3-14.4 is a graphic representation of the relationship between speed and density. The speeds determined from Equation 2 are along the line of movement; for stairs the speeds are along the line of the treads. Table 3-14.3 provides convenient multipliers for converting vertical rise of a stairway to a distance along the line of movement. The travel on landings must be added to the values derived from Table 3-14.3.

The maximum speed is that occurring when the density is less than 0.05 persons/ft² (0.54 persons/m²). These maximum speeds are listed in Table 3-14.4.

Within the range listed in Tables 3-14.2, 3-14.3, and 3-14.4, the evacuation speed on stairs varies approximately as the square root of the ratio of tread width to tread height. There is not sufficient data to appraise the likelihood that this relationship holds outside this range.

Table 3-14.2 ***Constants for Equation 2, Evacuation Speed***

Exit Route Element		k_1	k_2
Corridor, Aisle, Ramp, Doorway		275	1.40
Stairs			
Riser (in.)	Tread (in.)		
7.5	10	196	1.00
7.0	11	212	1.08
6.5	12	229	1.16
6.5	13	242	1.23

1 in. = 25.4 mm.

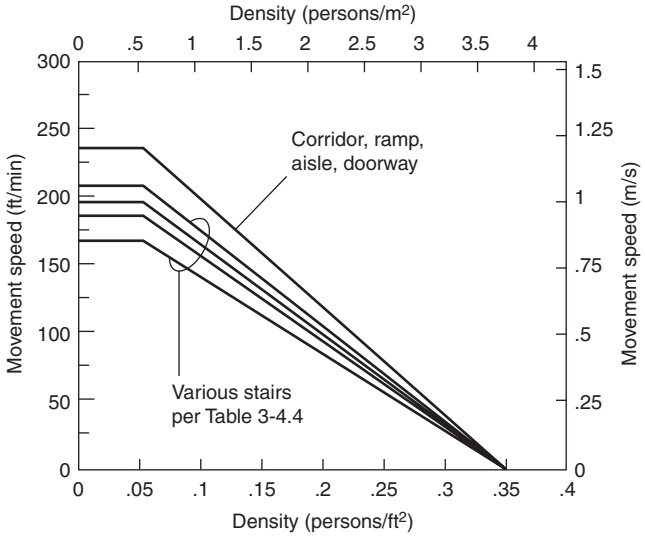

Figure 3-14.4. ***Evacuation speed as a function of density. S = k – akD, where D = density in persons/ft² and k is given in Table 3-14.2. Note that speed is along line of travel.***

Table 3-14.3 ***Conversion Factors for Relating Line of Travel Distance to Vertical Travel for Various Stair Configurations***

Stairs Riser (in.)	Tread (in.)	Conversion Factor
7.5	10.0	1.66
7.0	11.0	1.85
6.5	12.0	2.08
6.5	13.0	2.22

Table 3-14.4 ***Maximum (Unimpeded) Exit Flow Speeds***

		Speed (along line of travel)	
Exit Route Element		(ft/min)	(m/s)
Corridor, Aisle, Ramp, Doorway		235	1.19
Stairs			
Riser (in.)	Tread (in.)		
7.5	10	167	0.85
7.0	11	187	0.95
6.5	12	196	1.00
6.5	13	207	1.05

Specific Flow, F_s

Specific flow, F_s, is the flow of evacuating persons past a point in the exit route per unit of time per unit of effective width, W_e, of the route involved. Specific flow is expressed in persons/min/ft of effective width (if the value of $k = k_1$ from Table 3-14.2), or persons/s/m of ef-

fective width (if the value of $k = k_2$ from Table 3-14.2). The equation for specific flow is

$$F_s = SD \tag{4}$$

where

F_s = specific flow
D = density
S = speed of movement

F_s is in persons/min/ft² when density is in persons/ft² and speed in ft/min; F_s is in persons/s/m² when density is in persons/m² and speed in m/s.

Combining Equations 2 and 3 produces

$$F_s = (1 - aD)kD \tag{5}$$

where k is as listed in Table 3-14.2.

The relationship of specific flow to density is shown in Figure 3-14.5. In each case the maximum specific flow occurs when the density is 0.175 persons/ft² (1.9 persons/m²) of exit route space. There is a maximum specific flow associated with each type of exit route element; these are listed in Table 3-14.5.

Calculated Flow, F_c

The calculated flow, F_c, is the predicted flow rate of persons passing a particular point in an exit route.

The equation for actual flow is

$$F_c = F_s W_e \tag{6}$$

where

F_c = calculated flow
F_s = specific flow
W_e = effective width

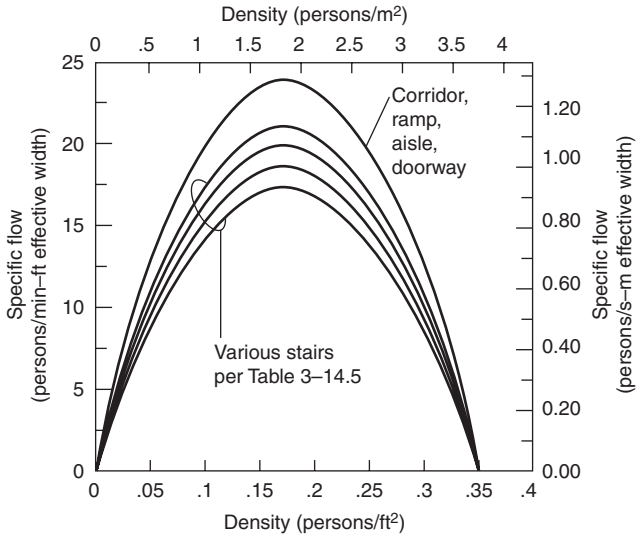

Figure 3-14.5. ***Specific flow as a function of density.***

Table 3-14.5 ***Maximum Specific Flow, F_{sm}***

Exit Route Element		Maximum Specific Flow: Persons/min/ft of Effective Width	Maximum Specific Flow: Persons/s/m of Effective Width
Corridor, Aisle, Ramp, Doorway		24.0	1.3
Stairs			
Riser (in.)	Tread (in.)		
7.5	10	17.1	0.94
7.0	11	18.5	1.01
6.5	12	20.0	1.09
6.5	13	21.2	1.16

Combining Equations 4 and 5 produces

$$F_c = (1 - aD)kDW_e \tag{7}$$

F_c is in persons/min when $k = k_1$ (from Table 3-14.2), D is persons/ft², and W_e is ft.

F_c is in persons/s when $k = k_2$ (from Table 3-14.2), D is persons/m², and W_e is m.

Time for Passage, t_p

Time for passage, t_p, that is, time for a group of persons to pass a point in an exit route, can be expressed as

$$t_p = \frac{P}{F_c} \tag{8}$$

where t_p is time for passage (t_p is in min where F_c is persons/min; t_p is in s where F_c is persons/s). P is population in persons.

Combining Equations 6 and 7 yields

$$t_p = \frac{P}{(1 - aD)kDW_e} \tag{9}$$

Transitions

Transitions are any points in the exit system where the character or dimension of a route changes or where routes merge. Typical examples of points of transition include the following:

1. Any point where an exit route becomes wider or narrower. For example, a corridor may be narrowed for a short distance by an intruding service counter or similar element. The calculated density, D, and specific flow, F_s, differ before reaching, while passing, and after passing the intrusion.
2. The point where a corridor enters a stairway. There are actually two transitions: one occurs as the egress flow passes through the doorway, the other as the flow leaves the doorway and proceeds onto the stairs.
3. The point where two or more exit flows merge, for example, the meeting of the flow from a cross aisle into a main aisle that serves other sources of exiting

population. It is also the point of entrance into a stairway serving other floors.

The following rules apply to determining the densities and flow rates following the passage of a transition point:

1. The flow after a transition point is a function, within limits, of the flow(s) entering the transition point.
2. The calculated flow, F_c, following a transition point cannot exceed the maximum specific flow, F_{sm}, for the route element involved multiplied by the effective width, W_e, of that element.
3. Within the limits of Rule 2, the specific flow, F_s, of the route departing from a transition point is determined by the following equations:

(a) For cases involving one flow into and one flow out of a transition point,

$$F_{s(\text{out})} = \frac{F_{s(\text{in})} W_{e(\text{in})}}{W_{e(\text{out})}} \tag{10a}$$

where

$F_{s(\text{out})}$ = specific flow departing from transition point
$F_{s(\text{in})}$ = specific flow arriving at transition point
$W_{e(\text{in})}$ = effective width prior to transition point
$W_{e(\text{out})}$ = effective width after passing transition point

(b) For cases involving two incoming flows and one outflow from a transition point, such as that which occurs with the merger of a flow down a stair and the entering flow at a floor,

$$F_{s(\text{out})} = \frac{F_{s(\text{in}-1)} W_{e(\text{in}-1)} + F_{s(\text{in}-2)} W_{e(\text{in}-2)}}{W_{e(\text{out})}} \tag{10b}$$

where the subscripts (in – 1) and (in – 2) indicate the values for the two incoming flows.

(c) For cases involving other merger geometries, the following general relationship applies:

$$[F_{s(\text{in}-1)} W_{e(\text{in}-1)}] + \cdots + [F_{s(\text{in}-n)} W_{e(\text{in}-n)}] = [F_{s(\text{out}-1)} W_{e(\text{out}-1)}] + \cdots + [F_{s(\text{out}-n)} W_{e(\text{out}-n)}] \tag{10c}$$

where the letter n in the subscripts (in – n) and (out – n) is a number equal to the total number of routes entering (in – n) or leaving (out – n) the transition point.

4. Where the calculated specific flow, F_s, for the route(s) leaving a transition point, as derived from the equations in rule 3, exceeds the maximum specific flow, F_{sm}, a queue will form at the incoming side of the transition point. The number of persons in the queue will grow at a rate equal to the calculated flow, F_c, in the arriving route minus the calculated flow leaving the route through the transition point.
5. Where the calculated outgoing specific flow, $F_{s(\text{out})}$, is less than the maximum specific flow, F_{sm}, for that route(s), there is no way to predetermine how the incoming routes will merge. The routes may share access through the transition point equally, or there may be total dominance of one route over the other. For conservative calculations, assume that the route of interest is dominated by the other route(s). If all routes are of concern, it is necessary to conduct a series of calculations to establish the bounds on each route under each condition of dominance.

Impact of Smoke Conditions on Ability to Evacuate

Evacuation Speed in a Smoke-Laden Environment

The emergency movement speeds reported in most sources were derived from experiments and observations conducted in smoke-free environments. While most emergency egress of populations do occur in environments that are smoke free or nearly so, some emergency evacuations involve movement through smoke conditions. Both the density and optic-irritating properties of the smoke can impact movement speed. Jin[11] reports the results and analysis of several series of investigations he conducted, involving human subjects moving through a smoke-laden environment. Jin used two types of smoke, a highly irritating smoke produced by burning wood cribs with narrow spacing between the sticks and a less irritating smoke produced by burning kerosene. The graph in Figure 3-14.6 is typical of the results observed. With the less irritating smoke movement speed decreased gradually as the extinction coefficient increased. With the highly irritating smoke, the evacuation movement speed dropped precipitously once the extinction coefficient reached 0.4/m. Where evacuation through smoke is involved, the movement speed of evacuation should be no greater than that appropriate for the expected density and irritation properties of the smoke. Pending further research the adjustment should be made using the values plotted in Figure 3-14.6.

Probability of Movement through Smoke-Obscured Environment

Table 3-14.6 summarizes data compiled in the United Kingdom[12] and in the United States[13] relating to the visibility distance of smoke and the percentage of building occupants who moved through smoke having the corresponding density. Roughly 40 to 50 percent of occupants

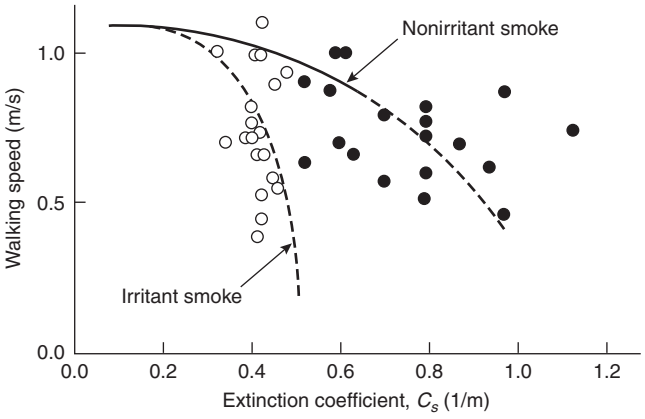

Figure 3-14.6. ***Walking speed in fire smoke.***

Table 3-14.6 ***Compilation of Visibility Distance for Populations Moving through Smoke***

Visibility Distance		U.K. Sample Population (%)	U.S. Sample Population (%)
(ft)	(m)		
0–2	0–0.6	12.0	10.2
3–6	0.9–1.8	25.0	17.2
7–12	2.1–3.6	27.0	20.2
13–30	4.0–9.1	11.0	31.7
31–36	9.4–11.0	3.0	2.2
37–45	11.3–13.7	3.0	3.7
46–60	14.0–18.3	3.0	7.4
>60	>18.3	17.0	7.4

moved through smoke at visibility distances of less than 12 ft (3.7 m), while 7 to 17 percent of occupants required visibility distances of greater than 60 ft (18.3 m). This range seems to be the demarcation between those occupants willing to move through smoke to an exit (the majority) and those who are reluctant to travel through smoke (the minority). It should be noted that the data in Table 3-14.6 are subjective and are indicative of visibility to both normal objects and backlit exit signs, as the building occupants interviewed were viewing both types of objects while trying to egress.

Users of the data in Table 3-14.6 need to realize that the data in both of the referenced studies was derived, for the most part, from fires in residential properties housing occupants familiar with the means of egress. Also, in the majority of the cases, travel distance through the smoke was 30 ft or less. Additionally, due to the age of the studies (1972 and 1979) these data should be verified with any available more current data.

EXAMPLE:

Consider an office building (Figure 3-14.7) with the following features:

1. There are nine floors, 300 by 80 ft (91 by 24 m).
2. Floor to floor height is 12 ft (3.7 m).
3. Two stairways are located at the ends of the building (no dead ends).
4. Each stair is 44 in. (1.12 m) wide (tread width) with handrails protruding 2.5 in. (63 mm).
5. Stair risers are 7 in. (178 mm) wide and treads are 11 in. (279 mm) high.
6. There are two 4-ft by 8-ft (1.2-m by 2.4-m) landings per floor of stairway travel.
7. There is one, 36-in. (0.91 m) clear width, door at each stairway entrance and exit.
8. The first floor does not exit through stairways.
9. Each floor has a single 8-ft- (2.4-m-) wide corridor extending the full length of each floor. Corridors terminate at stairway entrance doors.
10. There is a population of 300 persons/floor.

SOLUTION A—First Order Approximation:

1. Assumptions.

The prime controlling factor will be either the stairways or the door discharging from them. Queuing will occur; therefore the specific flow, F_s, will be the maximum specific flow, F_{sm}. All occupants start egress at the same time. The population will use all facilities in the optimum balance.

2. Estimate flow capability of a stairway.

From Table 3-14.1, the effective width, W_e, of each stairway is $44 - 12 = 32$ in. (2.66 ft) [813 mm (0.81 m)]. Also, the effective width, W_e, of each door is $36 - 12 = 24$ in. (2 ft) [609 mm (0.61 m)]. The maximum specific flow, F_{sm}, for the stairway (from Table 3-14.5) is 18.5 persons/min/ft (60 persons/min/m) effective width. Specific flow, F_s, equals maximum specific flow, F_{sm}. Therefore, using Equation 6, the flow from each stairway is limited to $18.5 \times 2.66 = 49.2$ persons/min.

3. Estimate flow capacity through a door.

Again from Table 3-14.5, the maximum specific flow through any 36-in. (0.9-m) door is 24 persons/min/ft (78.7 persons/min/m) effective width. Therefore, using Equation 6, the flow through any door is limited to $24 \times 2 = 48$ persons/min. Since the flow capacity of the doors is less than the flow capacity of the stairway served, the flow is controlled by the stairway exit doors (48 persons/stairway exit door/min).

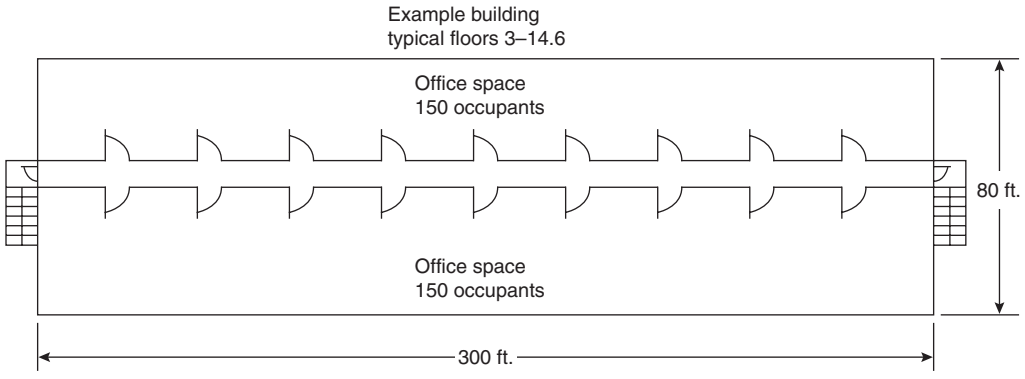

Figure 3-14.7. ***Floor plan for example.***

4. Estimate the speed of movement for estimated stairway flow.

From Equation 3 the speed of movement down the stairs is $212 - (2.86 \times 212 \times 0.175) = 105$ ft/min (32 m/min). The travel distance between floors (using the conversion factor from Table 3-14.3) is $12 \times 1.85 = 22.2$ ft (6.8 m) on the stair slope plus 8 ft (2.4 m) travel on each of the two landings, for a total floor-to-floor travel distance of $22.2 + (2 \times 8) = 38.2$ ft (11.6 m). The travel time for a person moving with the flow is $38.2/105 = 0.36$ min/floor.

5. Estimate building evacuation time.

If all of the occupants in the building start evacuation at the same time, each stairway can discharge 48 persons/min. The population of 2400 persons above the first floor will require approximately 25 min to pass through the exit. An additional 0.36 min travel time is required for the movement from the second floor to the exit. The total minimum evacuation time for the 2400 persons located on floors 2 through 9 is estimated at 25.4 min.

SOLUTION B—More Detailed Analysis:

1. Assumptions.

The population will use all exit facilities in the optimum balance; all occupants start egress at the same time.

2. Estimate flow density (D), speed (S), specific flow (F_s), effective width (W_e), and initial calculated flow (F_c) typical for each floor.

Divide each floor in half to produce two exit calculation zones, each 150 ft (45.7 m) long. Determine the density, D, and speed, S, if all occupants try to move through the corridor at the same time, that is, 150 persons moving through 150 ft of an 8-ft- (2.4-m-) wide corridor:

D = 150 persons/1200 ft² corridor area = 0.125 persons/ft².

From Equation 3, $S = k - akD$.

From Table 3-14.2, $k = 275$.

$S = 275 - (2.86 \times 275 \times 0.125) = 177$ ft/min (54 m/min).

From Equation 5, $F_s = (1 - aD)kD$.

$F_s = [1 - (2.86 \times 0.125)] \times 275 \times 0.125 = 22$ persons/ft (72 persons/m) effective width/min.

From Table 3-14.5, F_s, is less than the maximum specific flow, F_{sm}; therefore, F_s is used for the calculation of calculated flow.

From Table 3-14.1, the effective width of the corridor is $8 - (2 \times 0.5) = 7$ ft (2.13 m)

From Equation 7, calculated flow, $F_c = (1 - aD)kDW_e$.

$F_c = [1 - (2.86 \times 0.125)] \times 275 \times 0.125 \times 7 = 154$ persons/min.

Note: At this stage in the calculation, calculated flow, F_c, is termed initial calculated flow for the exit route element (i.e., corridors) being evaluated. This term is used because the calculated flow rate can be sustained only if the discharge (transition point) from the route can also accommodate the indicated flow rate.

3. Estimate impact of stairway entry doors on exit flow.

Each door has a 36-in. (0.91 m) clear width. From Table 3-14.1, effective width, W_e, is $36 - 12 = 24$ in. (2 ft) (0.605 m).

From Table 3-14.5, the maximum specific flow, F_{sm}, is 24 persons/min/ft effective width.

From Equation 10,

$$F_{s(\text{door})} = [F_{s(\text{corridor})}W_{e(\text{corridor})}]/W_{e(\text{door})}F_{s(\text{door})}$$
$$= (22 \times 7)/2 = 77 \text{ persons/min/ft}$$
$$(25.3 \text{ persons/min/m}) \text{ effective width}$$

Since F_{sm} is less than the calculated F_s, the value of F_{sm} is used. Therefore, the effective value for specific flow is 24.

From Equation 6 the initial calculated flow, $F_c = F_sW_e = 24 \times 2 = 48$ persons/min through a 36-in. (0.91-m) door. Since F_c for the corridor is 154 while F_c for the single exit door is 48, queuing is expected. The calculated rate of queue buildup will be $154 - 48 = 106$ persons/min.

4. Estimate impact of stairway on exit flow.

From Table 3-14.1, effective width, W_e, of the stairway is $44 - 12 = 32$ in. (2.66 ft) (0.81 m).

From Table 3-14.5, the maximum specific flow, F_{sm}, is 18.5 persons/ft (60 persons/m) effective width.

From Equation 10, the specific flow for the stairway, $F_{s(\text{stairway})}$, is $24 \times 2/2.66 = 18.0$ persons/ft (59 persons/m) effective width. In this case, F_s is less than F_{sm} and F_s is used.

The value of 18.0 for F_s applies until the flow down the stairway merges with the flow entering from another floor.

Using Figure 3-14.4 or Equation 5 and Table 3-14.2, the density of the initial stairway flow is approximately 0.146 persons/ft² (1.6 person/m²) of stairway exit route.

From Equation 3 the speed of movement during the initial stairway travel is $212 \times (2.86 \times 212 \times 0.146) = 123$ ft/min (37.5 m/min).

From Solution A, the floor-to-floor travel distance is 38.2 ft (11.6 m). The time required for the flow to travel one floor level is $38.2/123 = 0.31$ min (19 s).

Using Equation 6, the calculated flow, F_c, is $18.0 \times 2.66 = 48$ persons/min.

After 0.31 min, 15 (48×0.31) persons will be in the stairway from each floor feeding to it. If floors 2 through 9 exit all at once, there will be $15 \times 8 = 120$ persons in the stairway. After this time the merging of flows between the flow in the stairway and the incoming flows at stairway entrances will control the rate of movement.

5. Estimate impact of merger of stairway flow and stairway entry flow on exit flow.

From Equation 10,

$$F_{s(\text{out-stairway})} = \{[F_{s(\text{door})} \times W_{e(\text{door})}] + [F_{s(\text{in-stairway})} \times W_{e(\text{in-stairway})}]\}/W_{e(\text{out-stairway})}$$
$$= [(24 \times 2) + (18 \times 2.66)]/2.66$$
$$= 36 \text{ persons/ft effective width}$$

From Table 3-14.5, F_{sm} for the stairway is 18.5 persons/min/ft effective width. Since F_{sm} is less than the calculated F_s, the value of F_{sm} is used.

6. Track egress flow.

Assume all persons start to evacuate at time zero. Initial flow speed is 177 ft/min. Assume that congested flow

will reach the stairway in 30 s. At 30 s, flow starts through stairway doors. F_c through doors is 48 persons/min for the next 19 s. At 49 s, 120 persons are in each stairway and 135 are waiting in a queue at each stairway entrance door.

Note: Progress from this point on depends on which floors take dominance in entering the stairways. Any sequence of entry may occur. To set a boundary, this example estimates the result of a situation where dominance proceeds from the highest to the lowest floor.

The remaining 135 persons waiting at each stairway entrance on the ninth floor enter through the door at the rate of 48 persons/min. The rate of flow through the stairway is regulated by the 48 persons/min rate of flow of the discharge exit doors. The descent rate of the flow is 19 s/floor.

Thus:

at 218 s (3.6 min)	all persons have evacuated the 9th floor
at 237 s (4.0 min)	the end of the flow reaches the 8th floor
at 401 s (6.7 min)	all persons have evacuated the 8th floor
at 420 s (7.0 min)	the end of the flow reaches the 7th floor
at 584 s (9.7 min)	all persons have evacuated the 7th floor
at 603 s (10.1 min)	the end of the flow reaches the 6th floor
at 767 s (12.8 min)	all persons have evacuated the 6th floor
at 786 s (13.1 min)	the end of the flow reaches the 5th floor
at 950 s (15.8 min)	all persons have evacuated the 5th floor
at 969 s (16.2 min)	the end of the flow reaches the 4th floor
at 1133 s (18.9 min)	all persons have evacuated the 4th floor
at 1152 s (19.2 min)	the end of the flow reaches the 3rd floor
at 1316 s (21.9 min)	all persons have evacuated the 3rd floor
at 1335 s (22.3 min)	the end of the flow reaches the 2nd floor
at 1499 s (25.0 min)	all persons have evacuated the 2nd floor
at 1518 s (25.3 min)	all persons have evacuated the building

Evacuation Efficiency Factors

Decisions

Humans require time to make decisions. In general, people are hesitant to undertake overt actions unless they clearly accept the need for such action.

In group situations, group interaction is extremely important to decision making. Latane and Darley[14] pointed out the tendency of many individuals to defer emergency decision making until action is clearly required. More recently MacLennan[9] in his experiments in Australia has classified and is now quantifying this as a factor he and Sime call "associative." MacLennan has noted that persons in groups often delay response to a warning alarm until it is clear that the group accepts the need to take emergency action. Prior training, organization, and real-time fire information can reduce the delay in the time to take emergency action.

Levin,[15] in analyzing data from many sources related to emergency action in residences, has proposed the division of speed of response into four categories. These categories, which Levin terms ambiguity classes, are based on the initial interpretation of the cues by the individual involved. Levin's classes are

A. Respondent believes that there may be a fire (but is not certain).
B. Respondent believes that it is likely there is a fire.
C. Respondent is sure there is a fire and has seen sufficient smoke to believe that it is a dangerous fire.
D. Respondent has seen flames.

With one major exception, the universal response to ambiguity Class A is to seek information. In the sample studied by Levin, the exception to the general rule occurred with those responsible for persons incapable of taking care of themselves (small children, invalids). These individuals immediately took action to evacuate or otherwise safeguard their charges.

Conversely, in an ambiguity Class D situation emergency action was always taken.

In ambiguity Classes B and C some persons continued to seek information while others undertook other types of emergency action. These actions included attacking the fire, calling the fire department, giving the alarm, and evacuating the building. For the limited number of cases that Levin classified in ambiguity Classes B and C (20 in Class B, and 19 in Class C), the portion of the persons who sought information rather than take emergency action was approximately 50 percent in ambiguity Class B and 35 percent in Class C.

Investigation Time

As noted in the preceding paragraphs, individuals often seek information to clarify the ambiguities inherent in fire situations. This reaction is particularly the case for persons alone or in small groups. Sime[8] has tracked individuals involved in hotel fires, and his data demonstrate significant amounts of apparently nonproductive movement. This movement is assumed to be prompted by individuals seeking information they feel is necessary to make a proper decision. From an engineering standpoint, this response emphasizes the potential of increasing evacuation efficiency by providing clear information to the occupants of a building about the occurrence and location of the fire, and the condition of the exit routes.

Other Actions

When an individual has decided to take action in response to perceived fire danger, that action may or may not contribute to a speedy evacuation. Figure 3-14.8 diagrammatically shows a variety of the types of actions that are likely to occur. In actual fire situations many individuals undertake actions they believe will mitigate the

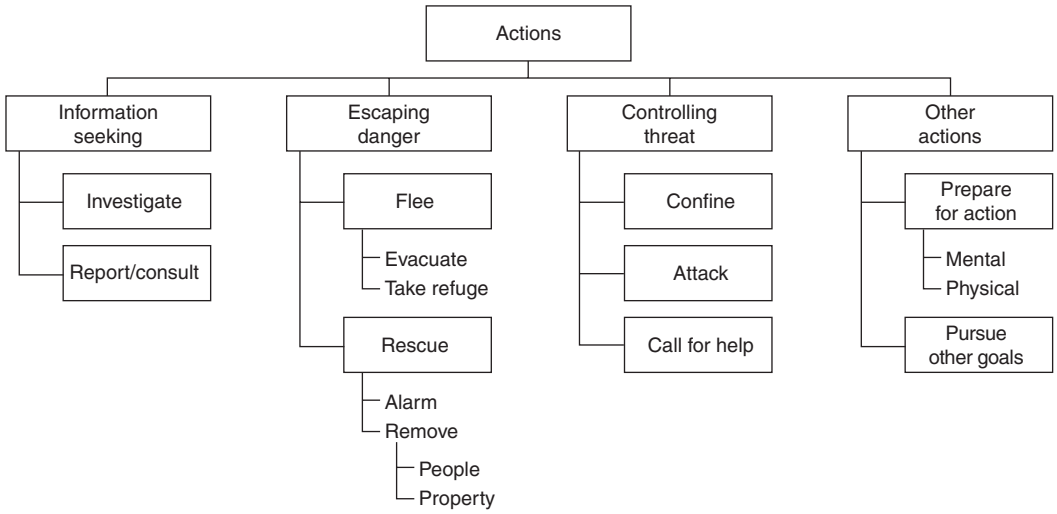

Figure 3-14.8. ***Types of actions.***

fire, help others, or aid in making decisions. Often these actions do not contribute to their evacuation; these alternative actions may be contributing to safety, detrimental to safety, laudable, or mistaken. All actions, however, impact on evacuation efficiency.

Providing real-time information to building occupants and ensuing rapid response of emergency forces can mitigate delays with a minimum of impact on the desirable effects of nonevacuation actions.

Way Finding

Way finding is most important in situations involving a relatively small number of individuals evacuating a location where they are not familiar with the emergency exit system. This situation typically occurs in hotels, multitenant office buildings, and similar structures where persons seldom use the stairways.

The classic solution to the problem of way finding is the provision of exit signs and exit directional signs. Ozel[16] has summarized the current view of researchers in way-finding problems and related these findings to fire evacuation conditions. A person's ability to find his or her way in an emergency relates to how well that person perceives his or her position and surroundings. The term frequently used is *cognitive mapping*. Most people maintain their cognitive mapping images in simple, regularized forms, such as straight lines and rectangles. In this concept, exit signs are only part of the overall ability of a person to perceive a suitable cognitive map.

Other factors that are rated of high importance to way finding include (1) the complexity of the space as related to common layouts or similar types of buildings (e.g., double-loaded corridors terminating at exits are simple while arrangements involving complex curves or unusual angles are complex); and (2) the presence of distinguishing marks or other indications of points of special attention. Of particular importance are both exit routes and dead ends or other spaces that should not be entered in exiting the building.

Way finding affects evacuation efficiency in facilities where the population density is low and the occupants are unfamiliar with the evacuation routes. In such facilities the efficiency is greatest when (1) the routes are simple, and (2) the exit points are evident in both their location and assurance (to the evacuee) that they truly lead to safety.

Way-finding efficiency decreases as the layout complexity increases. Some factors increasing complexity are unusual arrangements of corridors, obtuse angles, concentric corridors, undifferentiated enclosures (where one cannot orient oneself with respect to the exterior), and exit access doors that appear the same as every other door.

Conversely, all aspects that tend to simplify and identify the exit route decrease the time involved in way finding.

Merging Conflicts

Modeled evacuation time calculations assume that the flow of people is similar to that of a hydraulic fluid. As such, the merger of two flows (persons entering at a floor into a stairwell that is already flowing with evacuees from higher floors) is assumed to regulate itself according to the capabilities of the stairwell and the amount of flow from each of the sources.

In emergency evacuation drills MacLennan[9] has observed significant interruption of the continuity of flow when one flow is stopped and another is started at a merger point. The greatest merging flow efficiency occurs when, once a flow uses an exit route to its full capacity, it blocks all other entry until it has cleared past the point of merger. In actual evacuations, however, there is normally a sharing of access at merger points. This situation results in breaks in the egress flow that can have a significant affect on the capacity. MacLennan has seen effects as high as

30 to 50 percent reduction in the stairwell flow from this cause alone.

Wardens

MacLennan's work indicates that the most efficient flow occurs in a situation where all occupants are fully trained and promptly evacuated upon signal without the assistance of wardens.

Where occupants are not so trained it is often necessary to have a trained warden system. While this system is essential, MacLennan's observations indicate that wardens impose a reduction in egress efficiency. The amount of reduction will depend upon the type of organization and the evacuation procedures. The impact on evacuation efficiency is the greatest when wardens hold occupants in a ready position until the wardens are directed from another point to initiate evacuation.

Self-Regulation

In high-density situations (e.g., heavily populated offices, auditoriums, etc.) individuals often withhold themselves from the evacuation procedure until the crowd lessens (i.e., density is reduced). When these persons arrive at critical exit points so that the main crowded path, normally the stairway, is continuously fed by a short queue, their action will have no impact. However, when the self-induced delay reduces the feed of the critical point, a reduction in egress efficiency will occur.

Uneven Use of Exit Facilities

If some exit facilities are used proportionally more than others, the efficiency of the egress system will decrease. Some exit paths will be utilized while others will be overtaxed.

The impact of uneven exit use can be estimated as a function of (1) the distribution of exits relative to the distribution of population, (2) the degree that the exits will be used for either building entry or for common use within the structure, and (3) all of the cognitive mapping factors discussed under "Way Finding."

Evacuation Efficiency Factors—Summary

In his analysis, MacLennan found that large multifloor office buildings (some high-rise) demonstrated evacuation times in the range of twice the modeled time where a highly organized evacuation system was present; and up to three times the modeled evacuation time when there had been no training and no organization.

It is expected that MacLennan's findings represent reasonable norms but are subject to many variations (e.g., education level, cultural background, age, and gender) that need to be considered in any individual evaluation.

Emergency Movement Models

A number of models have been developed to calculate building emergency movement times. Gwynne and Galea[17] identified 22 different such models in a review based on available published literature. This includes 16 models that were available at the time of the review and 6 models known to be under development. The 16 available models are as follows:

BGRAF[18]
CRISPII[19]
DONEGAN'S ENTROPY MODEL[20]
EGRESS[21]
E-SCAPE[22]
EVACNET+[23]
EVACSIM[24]
EXIT89[25]
EXITT[26]
EXODUS[27,28]
MAGNETMODEL[29]
PAXPORT[30]
SIMULEX[31,32]
TAKAHASHI'S MODEL[33]
VEGAS[34,35]
WAYOUT[36]

Gwynne and Galea[17] critically appraised these evacuation models on the basis of four characteristics.

Nature of the Model Application

Three fundamentally different approaches are used in different evacuation models. These include optimization, simulation, and risk assessment. The optimization models generally assume that occupants evacuate a building in the most efficient manner. The evacuation paths and the flow characteristics of people and exits are considered optimal. The population is considered to be a homogeneous ensemble without individual behavior.

The simulation models attempt to represent the behaviors and movements observed in evacuations to realistically represent the actual paths and decisions taken during an evacuation. The behavioral sophistication employed by these models varies greatly, and consequently so does the accuracy of the results.

Risk assessment models attempt to identify fire hazards associated with evacuation. Repeated runs of the model are made to assess statistically significant variations associated with different design changes, including different fire protection measures.

The Enclosure Representation

The enclosure from which the evacuation takes place must be represented in all evacuation models. Two methods are usually used to represent the enclosure: fine networks and course networks. In each case, the enclosure is subdivided. The resolution of the subdivision distinguishes the fine network from the course network. In the course network models, the geometry is defined in terms of partitions based on the actual structure. Typically, each node represents a room or a corridor. Nodes are connected by arcs representing actual connections within the structure.

In the fine network approaches, the entire floor space of the enclosure is covered by a fairly uniform network of tiles or nodes. Nodes are connected with neighboring nodes, with the number of connections depending on the model. In a fine network, a large space may have thousands of nodes; in this way, the geometry of a space, including internal obstructions, can be accurately represented along with the location of each individual during an evacuation.

The Population Perspective

The population in an enclosure can be represented in one of two perspectives: a global or an individual perspective. Models that use the global perspective treat the population as an homogeneous ensemble without individual characteristics. These models represent evacuation on the basis of the number of occupants who escaped, not on the basis of individuals. With the global perspective, only a distributed or average attribute can be assigned to the population.

Models that use the individual perspective allow for personal attributes to be assigned to individual occupants, either by the user of the model or through a random process, in order to represent a diverse population. These personal attributes are then used in the decision-making and movement process of each individual. This process is typically independent of other individuals, although it does not, preclude group interaction and behavior.

The Behavioral Perspective

To consider the decision-making processes of occupants during an evacuation, a model must have a method of determining behavior. This method will be influenced by the representations used for the population and the enclosure and the broad range of potential behaviors of individuals. Some models do not apply any behavioral rules. These models rely completely on the physical movement of the population and the physical representation of the building according to deterministic equations. For models that do consider behavior, the perspective used can be classified into four categories: implicit, rule-based, functional analogy-based, and artificial intelligence-based. Implicit models do not declare behavioral rules, but rather assume the rules to be implicitly represented through methods and data incorporating psychological and sociological influences.

Rule-based models explicitly recognize the behavioral traits of individual occupants and apply a system that allows occupants to make decisions according to a defined set of rules. In the simpler rule-based methods, the same decisions are triggered by the same stimuli in a deterministic way. Other rule-based methods use either a stochastic approach to apply the rules or a combination of deterministic and stochastic approaches.

Functional analogy-based models apply an equation, or a system of equations, to the entire population, based on a field of study believed to be analogous to some aspect of human behavior. In artificial intelligence-based models, artificial intelligence has been applied to mimic human behavior based on various stimuli.

The behavior of people under fire conditions is influenced by their interactions with other people, with the enclosure and with the fire-induced environment. The decision making of people under fire conditions is influenced and complicated by a number of psychological, sociological, and physiological factors. Because of the behavioral and decision-making factors, some of which are not yet well understood, human behavior is the most complex and difficult aspect of evacuation to simulate.

In addition to the models reviewed by Gwynne and Galea[17] is the model EGRESS TIME, contained in the collection of models and procedures FPETOOL.[37] In terms of the characteristics used by Gwynne and Galea,[17] this model would be judged as an optimization model, having a course network, and limited attention to individual population perspectives.

Model Selection Factors

It is beyond the scope of this chapter to review the features, capabilities, uses, limitations, validation, availability, and costs of the evacuation models identified above. Instead, some of the factors that should be considered in the selection of a model for a particular application are presented, based on the foregoing discussion. These factors are presented in the form of a series of questions on a number of topics that a potential user should ask about an evacuation model before deciding to use it for a particular application. These questions are listed by topic.

Evacuation Model Type

Is the model based on optimization, simulation, or risk assessment?
Is the type of model suitable for the application?
What are the limitations of the model with respect to the application?

Enclosure Representation

Is the model based on a fine network or a course network?
How are different spaces and areas within spaces represented?
How are connections between spaces represented?
How are obstructions within a space represented?
How do these representations influence the model results?
How many nodes, connections, and obstructions can the model handle?
How are the data entered to represent spaces, connections, and obstructions?

Population Perspective

Does the model use a global or an individual perspective?
If the perspective is global, what general characteristics of the population are represented?
If the perspective is individual, what individual characteristics of the population are represented?
How are the individual or global characteristics of the population entered in the model?

Behavioral Perspective

What type of behavioral perspective does the model employ—none, implicit, rule-based, functional analogy-based, or artificial intelligence-based?
How does the model treat people-people interactions and their effects on behavior?
How does the model treat people-enclosure interactions and their effects on behavior?
How does the model treat people-environment interactions and their effects on behavior?
How does the model address physiological factors that influence decision making?
How does the model address psychological factors that influence decision making?
How does the model address sociological factors that influence decision making?

Model Validation

Has the model been validated? If so, how and to what extent?
How has the model validation been reported?

Model Implementation

Has the model been implemented on a computer?
What computer platforms does the model support?

Model Support

Is the model currently supported by the author(s)?
Is the model supported by another agency?
Is the model still being developed? If so, how are users notified of upgrades?

Model Costs

What is the initial cost of the model?
What are the ongoing costs for upgrades, support, and maintenances

Appropriateness to Task

What inputs does the model require of the user? Are these available?
Does the model consider elements needed for the task at hand, for example,
speed of movement, impact of density on speed?
queuing or other congestion?
merging of flows?
premovement decisions?
decisions/actions during movement?
Does the model produce an output meeting the needs of the task at hand?

Nomenclature

D	density in persons per unit area
e	apparent evacuation efficiency
F	flow
k	constant from Table 3-14.2
P	population
S	speed along the line of travel
t	time
W	width

Subscripts

1	speed in ft/min and density in persons/ft^2
2	speed in m/s and density in persons/m^2
ae	actual evacuation
c	calculated
(corridor)	corridor
(door)	door
d	delay
e	effective
(in $-$ *n*)	prior to point *n*
me	modeled evacuation
(out $-$ *n*)	after point *n*
p	passage
s	specific
sm	maximum specific
(stairway)	stairway

References Cited

1. V.M. Predtechenskii and A.I. Milinskii, *Planning for Foot Traffic in Buildings* (translated from the Russian), Stroizdat Publishers, Moscow (1969). English translation published for the National Bureau of Standards and the National Science Foundation, Amerind Publishing Co., New Delhi, India (1978).
2. J.J. Fruin, *Pedestrian Planning Design,* Metropolitan Association of Urban Designers and Environmental Planners, Inc., New York (1971).
3. J.L. Pauls, "Effective-Width Model for Evacuation Flow in Buildings," in *Proceedings, Engineering Applications Workshop,* Society of Fire Protection Engineers, Boston (1980).
4. J.L. Pauls, "Calculating Evacuation Time for Tall Buildings," in *SFPE Symposium: Quantitative Methods for Life Safety Analysis,* Society of Fire Protection Engineers, Boston (1986).
5. P.G. Wood, "The Behavior of People in Fires," *Fire Research Note 953,* Building Research Establishment, Fire Research Station, Borehamwood, United Kingdom (1972).
6. J.L. Bryan, *Smoke as a Determinant of Human Behavior in Fire Situations,* University of Maryland, College Park (1977).
7. J.P. Keating and E.F. Loftus, "Post Fire Interviews: Development and Field Validation of the Behavioral Sequence Interview Technique," *Report GCR-84-477,* National Bureau of Standards, Gaithersburg, MD (1984).
8. J.D. Sime, "Escape from Building Fires: Panic or Affiliation?," Ph.D. Dissertation, University of Surrey, UK (1984).
9. H.A. MacLennan, "Towards an Integrated Egress/Evacuation Model Using an Open System Approach, Fire Safety Science," in *Proceedings of the First International Symposium,* Hemisphere Publishing Corporation, Washington, DC (1986).
10. A.T. Habicht and J.P. Braaksma, "Effective Width of Pedestrian Corridors," *Journal of Transportation Engineering,* 110, 1 (1984).

11. T. Jin, "Studies on Human Behavior and Tenability in Fire Smoke," *Proceedings, 5th International Symposium on Fire Safety Science,* pp. 3–22 (1997).
12. P.G. Wood, *Fire Research Note 953,* Building Research Establishment, Borehamwood, United Kingdom (1972).
13. J.L. Bryan, *Smoke as a Determinant of Human Behavior in Fire Situation,* University of Maryland, College Park (1977).
14. B. Latane and J.M. Darley, "Group Inhibition of Bystander Intervention in Emergencies," *Journal of Personality Psychology,* 10, 3, pp. 215–221 (1968).
15. B.M. Levin, "Design as a Function of Response to Fire Cues," in *Proceedings of American Institute of Architects "Research and Design 85: Architectural Applications of Design and Technology Research,"* Los Angeles (1985).
16. F. Ozel, *Way Finding and Route Selection in Fires,* New Jersey Institute of Technology, Newark, NJ (1986).
17. S. Gwynne and E.R. Galea, "A Review of the Methodologies and Critical Appraisal of Computer Models Used in the Simulation of Evacuation from the Built Environment," Research Report, Society of Fire Protection Engineers, (undated).
18. F. Ozel, "Simulation Modeling of Human Behaviour in Buildings," *Simulation,* pp. 377–384 (1992).
19. J.N. Fraser-Mitchell, "An Object-Oriented Simulation (CRISPII) for Fire Risk Assessment," in *Proceedings of the Fourth International Symposium of Fire Safety Science* (T. Kashiwagi, ed.), pp. 793–804 (1994).
20. H.A. Donegan, A.J. Pollock, and I.R. Taylor, "Egress Complexity of a Building," in *Proceedings of Fourth International Symposium on Fire Safety Science* (T. Kashiwagi, ed.), pp. 601–612 (1994).
21. N. Ketchell, S.S. Cole, and D.M. Webber, "The EGRESS Code for Human Movement and Behaviour in Emergency Evacuation," *Engineering for Crowd Safety* (R.A. Smith and J.F. Dickie, eds.), Elsevier, London, pp. 361–370 (1994).
22. E. Reisser-Weston, "Simulating Human Behaviour in Emergency Situations," *RINA International Conference of Escape, Fire, and Rescue* (1996).
23. T.M. Kisko and R.L. Francis, "EVACNET+: A Computer Program to Determine Optimal Evacuation Plans," *Fire Safety Journal,* 9, pp. 211–220, (1985).
24. L.S. Poon and V.R. Beck, "EVACSIM: Simulation Model of Occupants with Behavioural Attributes in Emergency Evacuation of High Rise Buildings," in *Proceedings of Fourth International Symposium on Fire Safety Science* (T. Kashiwagi, ed.), pp. 681–692 (1994).
25. R.F. Fahy, "An Evacuation Model for High Rise Buildings" in *Proceedings of the Third International Symposium on Fire Safety Science* (G. Cox and B. Langford, eds.), Elsevier, London, pp. 815–823 (1991).
26. B. Levin, "EXITT: A Simulation Model of Occupant Decisions and Actions in Residential Fires," in *Proceedings of the Second International Symposium on Fire Safety Science* (T. Wakamatsu, Y. Hasemi, A. Seizawa, P. Seeger, P. Pagni, and C. Grant, eds.), pp. 561–570 (1989).
27. M. Owen, E.R. Galea, and P.J. Lawrence, "The Exodus Evacuation Model Applied to Building Evacuation Scenarios," *J. of Fire Protection Engr.* 8, 2, pp. 65–86 (1996).
28. E.R. Galea and J.M.P. Galparsoro, "EXODUS: An Evacuation Model for Mass Transport Vehicles," *Fire Safety Journal,* 22, pp. 341–366 (1994).
29. S. Okasaki and S. Matsushita, "A Study of Simulation Model for Pedestrian Movement with Evacuation and Queuing," *Engineering for Crowd Safety* (R.A. Smith and J.F. Dickie, eds.), Elsevier, London, pp. 271–280 (1993).
30. J. Barton and J. Leather, "Paxport: Passenger and Crowd Simulation," *Passenger Terminal* 95, pp. 71–77 (1995).
31. P. Thompson and E. Marchant, "A Computer Model for the Evacuation of Large Building Populations," Fire Safety Journal, 24, pp. 131–148 (1995).
32. P.A. Thompson and E.W. Marchant, "Simulex; Developing New Computing Modelling Techniques For Evaluation," Proceedings of the Fourth International Symposium on Fire Safety Science, (T. Kashiwagi, ed.), International Association for Fire Safety Science, pp. 613–624 (1994).
33. K. Takahashi, T. Tanaka, and S. Kose, "An Evacuation Model for Use in Fire Safety Design of Buildings," in *Proceedings of the Second International Symposium on Fire Safety Science,* (T. Wakamatsu, Y. Hasemi, A. Seizawa, P. Seeger, P. Pagni, and C. Grant, eds.), Hemisphere, pp. 551–560 (1989).
34. G.K. Still, "New Computer System Can Predict Human Response to Building Fires," *Fire,* 84, pp. 40–41 (1993).
35. G.K. Still, "Simulating Egress Using Virtual Reality: A Perspective View of Simulation and Design," *IMAS 94, Fire Safety on Ships* (1994).
36. V.O. Shestopal and S.J. Grubits, "Evacuation Model for Merging Traffic Flows in Multi-Room and Multi-Storey Buildings," in P*roceedings of the Fourth International Symposium on Fire Safety Science,* (T. Kashiwagi, ed.), pp. 625–632, (1994).
37. H.E. Nelson, *FPETOOL: Fire Protection Tools for Hazard Estimation,* NISTIR 4380, National Institute of Standards and Technology, Gaithersburg, MD (1990).

CHAPTER 15

Stochastic Models of Fire Growth

G. Ramachandran

Introduction

Apart from changes in environmental conditions, such as wind velocity and direction, humidity, and temperature, the spread of fire in a building is governed by physical and chemical processes evolved from a variety of burning materials arranged in different ways. Multiple interactions among these processes at different times during fire growth cause uncertainties in the pattern of fire development. Although different patterns of fire development can be simulated by varying the input values to the parameters of a deterministic model, there is a need to determine the uncertainty (probability) with which each pattern is likely to occur in a real fire in any type of building considered. The likely pattern of fire spread can only be predicted within limits of confidence expressed in probabilistic terms.

Nondeterministic models[1] (or indeterministic models as defined by Kanury[2]), rather than deterministic techniques, offer rational methods of evaluating the uncertainties in the pattern of fire growth and are of two types: (1) probabilistic and (2) stochastic. The first type generally deals with a final outcome, such as area damaged, financial loss, or fire severity, and is considered as a continuous random variable reaching various levels in a fire according to a probability distribution.[3] Large values of the variable follow an extreme value distribution. (See Section 5, Chapter 8.) A semi-probabilistic approach is provided by a fault tree[4] in which the probability of occurrence of a top event (e.g., fire spreading beyond the room of origin) is estimated by assigning discrete (not continuous) probabilities to sub-events leading to the top event. Models of the first type (i.e., probability distributions and fault trees) do not consider in detail the underlying physical processes and their variation over the duration (time) of fire growth. Such "static" models can provide sufficient tools for fire protection and insurance problems concerned with "collective risk" in a group of buildings.

Stochastic models constitute the subject matter of this chapter, and may be regarded as "dynamic," since they are capable of predicting the course of fire development in a particular building. In these models, the various states, realms, or phases occurring sequentially in space and time during fire growth are specified together with the associated probability distributions. Depending on the nature of these distributions, a fire stays in each state for a random length of time and moves randomly from state to state. The sojourn and transition probabilities may be regarded as "noise" terms superimposed over a deterministic pattern of fire growth.

After describing the basic features of stochastic modeling of fire spread, two types of stochastic models are discussed in detail: (1) Markov chains and (2) networks. Attention is also drawn to the application of other stochastic models, such as random walk, diffusion processes, percolation theory, epidemic models, and branching processes. The next-to-last section in this chapter discusses briefly a new type of stochastic model based on the "stochastic differential equation" which is currently being developed in Australia.

The models discussed in this chapter mainly relate to the growth of fire and not to the spread of smoke or other combustion products.

Dr. G. Ramachandran retired in November 1988 as head of the Operations Research Section at the Fire Research Station, United Kingdom. Since then he has been practicing as a consultant in risk evaluation and insurance. He is a visiting professor at the Universities of Manchester, and Leeds. His research has focused on statistical and economic problems in fire protection and actuarial techniques in fire insurance. In October 1998 he published a book on the economics of fire protection.

Basic Features

Probability Distributions

Consider the burning of a particular object in a room as a random (stochastic) process, with $Q(t)$ denoting the

probability that the object is still burning at time t. In a simple model the process may be assumed to be Poisson,[5] so that $Q(t)$ has the exponential form

$$Q(t) = \exp(-\mu t) \tag{1}$$

In this model the probability of extinction of fire during the short period $(t, t + \partial t)$ denoted by $\mu(t)$ has been assumed to have the constant value μ independent of t. The function $Q(t)$ can also be interpreted as the probability that the duration of burning of the object considered is greater than t. Then, the (cumulative) probability distribution function

$$F(t) = 1 - Q(t) \tag{2}$$

is the probability that the duration of burning is less than or equal to t. The parameter μ is the "instantaneous probability" of extinction of fire, whereas $\lambda(= 1 - \mu)$ is the "instantaneous probability" of fire surviving.

The value of μ will vary depending on whether it is a free-burning fire or a fire extinguished by fire fighting (e.g., by fire brigade or sprinklers). The value of μ for any object burning under specified conditions can be estimated by carrying out replicated extinction experiments with the object. If $\bar{t}$ is the mean (average) duration of burning of the object

$$\mu = 1/\bar{t} \tag{3}$$

according to the properties of an exponential probability distribution. This distribution was implied in Kida's probabilistic analysis of extinction experiments.[6]

Spread to Another Object

In a simple model, as discussed earlier, it can be assumed that a fire involving one object spreads to another object if it survives (i.e., not extinguished) with the probability λ.

$$\lambda + \mu = 1 \tag{4}$$

The model can be expanded to include an (instantaneous) probability w to denote the event of fire not spreading, even though it is not extinguished, that is, the fire continues to burn without spreading. In this case[5]

$$\lambda + \mu + w = 1 \tag{5}$$

and, following the derivation of Equation 1,

$$\begin{aligned} Q_1(t) &= \exp[-(\lambda + \mu)t] \\ &= \exp(-t + wt) \end{aligned} \tag{6}$$

where $Q_1(t)$ is the probability that the fire is burning at time t without spreading. The duration of burning in this case follows an exponential probability distribution with mean duration given by the reciprocal of $(\lambda + \mu)$ or of $(1 - w)$.

The length of time a fire involving an object burns affects future fire spread to another object: heat output (fire severity) increases with time. Equation 5 can, therefore, be modified such that, during a short time interval immediately after time t,

$$\lambda(t) + \mu(t) + w(t) = 1 \tag{7}$$

The instantaneous probabilities $\lambda(t)$, $\mu(t)$, and $w(t)$ are functions of the continuous random variable t. However, in practical problems, one can consider t in minutes and one minute as a short time interval such that the probabilities are denoted by $\lambda(i)$, $\mu(i)$, and $w(i)$ with $i = 1, 2, 3, \ldots$. The probability $w(i)$ applies to a single minute and, hence, it is likely to be small. One can, therefore, write

$$Q_1^1(t + 1) = w(1) \cdot w(2) \cdot \cdots \cdot w(t) \tag{8}$$

to denote the probability of fire burning during the time period $(t + 1)$ without spreading. Equation 8 follows from Equation 6. If $w(i)$ is a constant w as in Equation 6, it may be seen that

$$Q_1^1(t) = w^t \tag{9}$$

General Model

The probability distribution for duration of burning can have other forms, such as uniform and log-normal, although an exponential distribution has been postulated for the sake of simplicity. Following Ramachandran[5] and Aoki,[7] the following probabilities can be defined in the general case for the fire involving the object ignited first:

$q_1(t + 1)$ = probability of burning at the beginning of the $(t + 1)^{\text{th}}$ period or end of the t^{th} period without spreading before that period

$P_1(t + 1)$ = cumulative probability of becoming extinguished before the end of the $(t + 1)^{\text{th}}$ period

$S_1(t + 1)$ = cumulative probability of spreading before the end of the $(t + 1)^{\text{th}}$ period

With subscript 1 denoting the object ignited first, the following equations are easily derived:

$$q_1(t + 1) = q_1(t) \cdot w_1(t) = \prod_{r=1}^{t} w_1(r)$$

as in Equation 8, since $q_1(1) = 1$.

$$P_1(t + 1) = \sum_{r=1}^{t+1} q_1(r) \cdot \mu_1(r)$$

$$S_1(t + 1) = \sum_{r=1}^{t+1} q_1(r) \cdot \lambda_1(r)$$

The parameters $\lambda_1(r)$, $\mu_1(r)$, and $w_1(r)$ are probabilities of spreading, becoming extinguished, and burning without spreading during the r^{th} period.

The following equations with similar definitions can be derived for the second object to which fire can spread from the object first ignited. (The subscript 2 has been used for the second object.)

$$q_2(t+1) = q_2(t) \cdot w_2(t) + q_1(t) \cdot \lambda_1(t),\ q_2(1) = 0$$

$$P_2(t+1) = \sum_{r=2}^{t+1} q_2(r) \cdot \mu_2(r)$$

$$S_2(t+1) = \sum_{r=2}^{t+1} q_2(r) \cdot \lambda_2(r)$$

The probabilities $q_2(t+1)$, $P_2(t+1)$, $S_2(t+1)$ and their associated parameters $w_2(t)$, $\lambda_2(t)$, and $\mu_2(t)$ pertain to the second object and are "conditional," given that the fire has spread to the second object.

In the first of the equations mentioned above it has been assumed that the second object starts burning in the second minute after the ignition of the first object in the first minute. The probability of this event is likely to be low such that $q_2(2)$ has a small value. The time of occurrence of sustained or established burning of the second object depends upon the incubation or latent period beyond which the fire involving the first object becomes capable of spreading to the second object.[8] This time and the spread probability $\lambda_1(r)$ also depend upon the distance between the two objects.[8] Radiation of heat to an object generally decreases in inverse proportion to the square of the distance of the object from the burning object. Fire spread may not occur if the unignited object is located beyond a "critical distance" from the burning object.[9]

As r varies, $q_1(r)$ gives rise to a discrete or continuous probability distribution for the object first ignited. This distribution can be ascertained by carrying out experiments with the two objects considered by varying the distance between them. In the continuous case, if the instantaneous probabilities are assumed as constants, the average duration of burning of the first object before spreading to the second object is an estimate of $(1/1 - w_1)$, assuming an exponential distribution. Applying this result to the discrete case with constant probabilities, for any specified distance between the two objects,

$$q_1(t+1) = w_1^t$$

as in Equation 9. An exponential distribution with constant probabilities need not be assumed if the mathematical form of $w_1(t)$ and its variation with the distance between the two objects can be established from an analysis of the experimental data. These data would also provide an estimate of $\lambda_1(t)$ for any distance between the object ignited first and the second object. The value of $\mu_1(t)$ can then be obtained from the equation

$$\mu_1(t) = 1 - \lambda_1(t) - w_1(t)$$

It can be verified that, since $q_1(1) = 1$,

$$\begin{aligned} P_1(t+1) + S_1(t+1) &= \sum_{r=1}^{t+1} q_1(r)[\mu_1(r) + \lambda_1(r)] \\ &= \sum_{r=1}^{t+1} q_1(r)[1 - w_1(r)] \\ &= \sum_{r=1}^{t+1} [q_1(r) - q_1(r+1)] \\ &= 1 - q_1(t+2) \end{aligned}$$

As t increases, $q_1(t)$ will decrease toward zero such that the sum of the two cumulative probabilities will tend to unity. Hence, as one would have expected, the probability of burning without spreading will tend to zero with the passage of time, and the fire involving the first object would have either been extinguished or spread to the second object.

In the language of stochastic modeling, the spread probability, $\lambda_1(r)$, is the transition probability at time r, and may be redefined as $\lambda_{12}(r)$ to denote the spread from the object first ignited to the second object. Other objects in a room may be considered as the first or second object such that, in the general case, $\lambda_{ij}(r)$ is the probability of spreading from the i^{th} object to the j^{th} object at time r. Based upon the distances between them, the objects can be arranged in order in a diagram to analyze the sequential spread of fire from object to object at any time r. (See Figure 3-15.1.) This simple analysis may be sufficient for all practical purposes, although a fire from one object can spread to another object directly or indirectly through the ignition of another object.

As t increases, $q_i(t)$ will tend to zero and the cumulative probability of extinguishment, $P_i(t+1)$, to a limiting value E_i. This value, E_i, denotes the probability of fire being extinguished ultimately, with the spread limited to the i^{th} object. Correspondingly, the cumulative probability of spreading, $S_i(t+1)$, will tend to $(1 - E_i)$. The following equations may be specified in the limiting case:

$$\begin{aligned} E_1 &= \mu_1 & \lambda_1 &= 1 - \mu_1 \\ E_2 &= \lambda_1 \cdot \mu_2 & \lambda_2 &= 1 - \mu_2 \\ E_3 &= \lambda_1 \cdot \lambda_2 \cdot \mu_3 & \lambda_3 &= 1 - \mu_3 \end{aligned}$$

and so on, such that, in general terms

$$E_i = \lambda_1 \cdot \lambda_2 \ldots \lambda_{i-1} \cdot \mu_i; \quad \lambda_i = 1 - \mu_i \tag{10}$$

$$P_i = \sum_{j=1}^{i} E_j \tag{11}$$

The equations aforementioned provide values for μ_i for $i = 1, 2, 3 \ldots$ which may be regarded as the limiting probability of extinguishment for the i^{th} object, given (conditional) that the fire has spread to this object. The parameter λ_i is the limiting and conditional probability of spread beyond the i^{th} object.

The model mentioned above for objects in the room of fire origin can be extended to include structural barriers

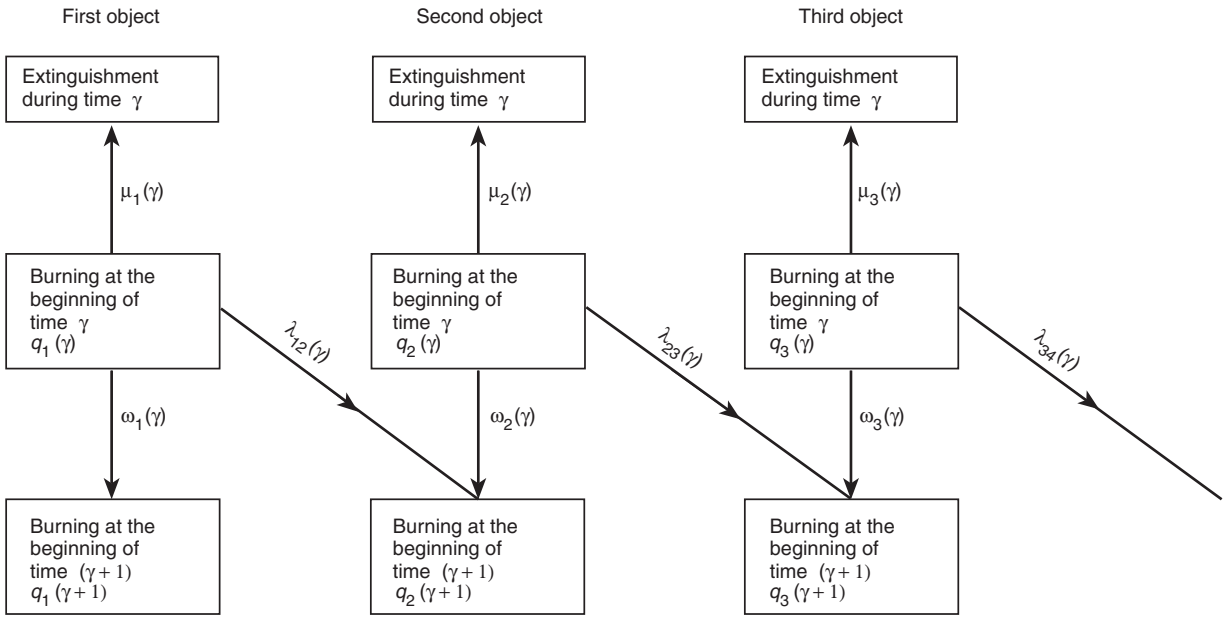

Figure 3-15.1. ***Probability diagram for spread of fire from object to object at time γ.***

and objects in corridors and other rooms on the same floor or different floors of a building. This procedure involves complex calculations, since a fire in a room can spread to an adjoining room in the same or upper floor; a fire can also spread through several paths. The problem of fire spread throughout a building can be simplified to some extent by applying network models, which are discussed later.

Markov Model

Mathematical Representation

A considerable amount of statistical and experimental data are needed for applying the model for fire spread from object to object. For practical purposes it may be sufficient to consider fire spreading through a number of spatial modules,[10] phases,[11] or realms.[12] These stages of fire growth can generally be defined as *states* such that fire spreads, moves, or makes a transition from state to state.

The movement of fire from state to state is governed by a *transition probability*, which is a function of time since the start of the fire. The fire also spends a certain length of time in each state before making the transition; this duration follows a temporal probability distribution. The state occupied by fire at any moment in time is governed by transition probabilities and temporal probability distributions. Represented mathematically, if the fire is in state a_i at the n^{th} minute, it can be in state a_j at the $(n + 1)^{\text{th}}$ minute, according to the transition probability $\lambda_{ij}(n)$. The transition probabilities are most conveniently handled in matrix form. One may write, dropping (n) for convenience, with m states,

$$P = \begin{bmatrix} \lambda_{11} & \lambda_{12} & \cdot & \cdot & \lambda_{1m} \\ \lambda_{21} & \lambda_{22} & \cdot & \cdot & \lambda_{2m} \\ \cdot & \cdot & \cdot & \cdot & \cdot \\ \cdot & \cdot & \cdot & \cdot & \cdot \\ \lambda_{m1} & \lambda_{m2} & \cdot & \cdot & \lambda_{mm} \end{bmatrix}$$

where

$$\sum_{j=1}^{m} \lambda_{ij} = 1 \qquad i = 1, 2, \ldots, m$$

The probability distribution of the system at time n can be expressed as the vector

$$\mathbf{P} = (q_1\, q_2\, q_3 \ldots q_m)$$

where q_i is the probability of the fire burning in the i^{th} state at time n. Since a fire can be in one of the m states at a given time

$$\sum_{i=1}^{m} q_i = 1$$

The m^{th} state may denote the state of fire having been extinguished if such a state is included in the model considered. The vector given by the product $p \cdot \mathbf{P}$ expresses the probabilities of burning in different states one transition (minute) later.

As an example, consider a model of fire growth in a room in which the i^{th} state represents i objects burning. Suppose, with $m = 4$ and no extinguishment, the process

stops with the occurrence of flashover when all four objects are ignited. There is no recession in growth and, hence, there is no transition to a lower state from a higher state. With these assumptions, let the transition matrix be

$$P = \begin{bmatrix} 0.4 & 0.3 & 0.2 & 0.1 \\ 0 & 0.5 & 0.3 & 0.2 \\ 0 & 0 & 0.6 & 0.4 \\ 0 & 0 & 0 & 1 \end{bmatrix}$$

If, at time n, the probabilities of fire burning in different states is given by

$$p_n = (0.1 \quad 0.2 \quad 0.3 \quad 0.4)$$

it can be seen by performing the matrix multiplication, that the probability of fire burning in different states at time $(n + 1)$ is given by

$$p_{n+1} = (0.04 \quad 0.13 \quad 0.26 \quad 0.57)$$

Hence, at time $(n + 1)$, the probability of the fire being in the third state, for example, is 0.26, and the probability of flashover (4^{th} state) is 0.57.

Markov Chains

Markov chains are used for repetitive situations in which there is a set of probabilities that define the likelihood of transition from one state to another. A chain comprises a sequence of such transitions. In a Markov chain, the transition probabilities satisfy the following properties:[4]

1. Each state belongs to a finite set of all possible states.
2. The characteristics of any state do not depend upon any other previous state.
3. For each pair of states (i, j) there is a probability λ_{ij} that state j occurs immediately after state i occurs.

The transition probabilities can be specified in a matrix form P as discussed previously, with the aid of a hypothetical example. Berlin[4] and Watts[10] have illustrated the use of this matrix by modeling a "random walk" among five adjacent spaces.

Markov chains may possess a number of special characteristics, one of which is called an *absorbing state.* The system remains in an absorbing state once it enters this state. A fire burning out (self-termination) and a fire getting extinguished by an extinguishing agent are examples of absorbing states. State i is an absorbing state if row i of the transition matrix has a value of $\lambda_{ij} = 1$ and all other values in the row are zero.

Markov Process

The next step is to consider a slightly more complex model called the *Markov process*, a stochastic or random process where the probability of occurrence of some future state of the system, given its present state, is not altered by information concerning past states. That is, the history of the process has no influence on its future. This lack of a historical influence is often referred to as a *memoryless* or *Markovian* property of a process.

In a Markov process with stationary transition probabilities, the value of $\lambda_{ij}(n)$ is a constant independent of the time variable n. Following this process Berlin[12] estimated stationary transition probabilities for six realms (states) for residential occupancies: (I) nonfire state, (II) sustained burning, (III) vigorous burning, (IV) interactive burning, (V) remote burning, and (VI) full room involvement. These realms were defined by critical events, such as heat release rate, flame height, and upper room gas temperature. Development of fire over time was considered as a "random walk" through these realms.

Based on data from over a hundred full-scale fire tests, Berlin[12] calculated transition probabilities as in Table 3-15.1. The information in this table indicates that, when a fire is in Realm III, there is a 75 percent chance of growth to Realm IV, and a 25 percent chance of recession to Realm II. Figure 3-15.2 is the transition diagram

Table 3-15.1 ***Transition Descriptors for a Typical Room in a Residential Occupancy***

Fire Type: Smoldering fire in a couch with cotton cushions.

Realm Transition			Temporal Distribution		
From	To	Transition Probability	Type	Mean	Standard Deviation
II	I	0.33	Uniform	2.0	5.0
II	III	0.67	Log-normal	8.45	0.78
III	II	0.25	Uniform	1.0	2.0
III	IV	0.75	Normal	5.55	3.22
IV	III	0.25	Uniform	1.5	9.0
IV	V	0.75	Uniform	0.5	3.5
V	IV	0.08	Uniform	0.6	6.0
V	VI	0.92	Log-normal	5.18	4.18

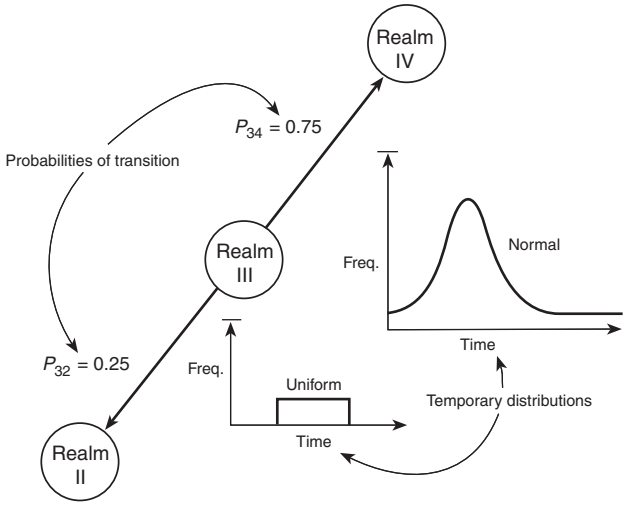

Figure 3-15.2. ***Realm transition descriptors.***

defined by the transition probabilities in Table 3-15.1. Realm I, no fire, is an absorbing state, since all fires eventually terminate in this state. The process also ends when Realm VI (full room involvement) is reached; for this reason, this state also is an absorbing state. Berlin[12] used uniform, normal, and log-normal distributions to describe temporal probability distributions for the different states.

Among many questions asked about fire development using the Markov model is what maximum extent of fire growth represents the most extreme condition. The portion of fires that does not grow beyond Realm II is the probability (0.33) of transition from Realm II to I. If M_3 is the long-run (limiting) probability of fire reaching Realm III, but not growing beyond, then[12]

$$M_3 = \frac{\lambda_{21} + \lambda_{23} \cdot \lambda_{31}}{1 - \lambda_{23} \cdot \lambda_{32}} - \lambda_{21} \tag{12}$$

Using the figures in Table 3-15.1 and noting that $\lambda_{31} = 0$, it may be seen that $M_3 = 0.07$. Beyond Realm III is more difficult, as described by Berlin.[12] Probabilities of maximum extent of flame development as estimated by Berlin are given in Table 3-15.2. Berlin has also discussed other fire effects, such as probability of self-termination and distribution of fire intensity.

One of the major weaknesses of the Markov model regards the "stationary" nature of the transition probabilities. It is assumed that these probabilities remain unchanged regardless of the number of transitions representing the passage of time. The length of time a fire burns in a given state affects future fire spread. For example, the probability of a wall burn-through increases with fire severity which is a function of time. The time spent by fire in a particular state may also depend on how that state was reached (i.e., whether the fire was growing or receding). Some fires may grow quickly and some grow slowly, depending on high or low heat release. In a Markov model with stationary transition probabilities no distinction is made between a growing fire and a dying fire.

Berlin[12] has estimated that 99 percent of all fires will terminate within twelve transitions. This result is based on the assumption of stationary transition probabilities that may be nearly true for a few fluctuations between the same realms where different materials would be contributing to the burning process. However, the fire will eventually consume all fuels, in which case the probabilities of termination from all realms will be equal to one. Therefore, Berlin's approach represents a worst-case analysis.

Table 3-15.2 ***Maximum Extent of Flame Development***

Maximum Flame Extent	Probability of Flame Extent
Realm II	0.33
Realm III	0.07
Realm IV	0.02
Realm V	0.58

State Transition Model

According to Berlin's Markov model, a fire in a particular realm can either grow to a higher realm or recede to a lower realm. There is no transition to the nonfire (absorbing) state (Realm I) from any realm higher than Realm II, except Realm VI (full room involvement) which is also an absorbing state. Receding to a lower state may be true to some extent when describing fire growth in terms of flame spread, but such an assumption is not possible in the case of spatial spread of fire in which, as discussed previously, fire spreads sequentially from one object to another. According to this model, if fire spreads to an object it cannot spread backwards to the object from which it spread. The fire involving an object either spreads forward to other objects, gets extinguished, or stays with the object without spreading.

Complex computational procedures would be involved in a stochastic model for fire spread from object to object in a room or to different rooms. Hence, consistent with the fire statistics available, particularly in the United Kingdom and United States, a simplified model based on the following three main states can be considered for fire development in a room:

S_1 Fire confined to the object first ignited

S_2 Fire spreading beyond the object first ignited but confined to the contents of the room

S_3 Fire spreading beyond room of origin but confined to the building

A fourth state may be added to denote extinguishment or burning out (self-termination) of fire; this is an absorbing state, since a fire process cannot leave this state after entering it. The third state, S_3, is also an absorbing state, since a spreading fire will eventually terminate within the building of origin; spreading beyond the building is not considered.

The three states ($i = 1, 2, 3$) mentioned above generate a state transition model, distinct from Berlin's Markov model. This model was used by Ramachandran[5] for evaluating the transition (spread) probabilities $\lambda_i(t)$ and the probabilities $\mu_i(t)$ for extinguishment or transition to the fourth state. The value of $\lambda_3(t)$ was taken as zero, since fire spread beyond the building was not considered. The probability of burning in a state without spreading was also considered with the aid of the parameter $w_i(t)$ $[= 1 - \lambda_i(t) - \mu_i(t)]$. The duration of burning was divided into subperiods, each of a fixed length of five minutes.

Statistics furnished by fire brigades in the United Kingdom related to fires that were extinguished during each time period since ignition. Hence, Ramachandran[5] used the extreme value technique, with some assumptions, to estimate the number of fires that were burning in a particular stage at the beginning of each subperiod. With the aid of these estimates and the actual numbers of fires that were extinguished, approximate values were obtained for the extinguishment and spread probabilities (as functions of time) and probability distributions of duration of burning in each state. The equations given previously for the general model were utilized for this purpose. Four materials ignited first in the bedroom of a

dwelling were considered for illustrating the application. Tables 3-15.3 and 3-15.4 and Figures 3-15.3 and 3-15.4 are examples extracted from this study. Aoki[7] described fire growth with similar states based on the spatial extent of spread; his analysis was similar to that of Ramachandran[5]

Table 3-15.3 ***Bedroom Bedding (Probabilities)***

Period (t) (min)	First State		Second State		Third State
	$\mu(t)$	$\lambda(t)$	$\mu(t)$	$\lambda(t)$	$\mu(t)$
1–5	0.0055	0.0745	—	—	—
6–10	0.0385	0.1170	0.7026	0.1747	—
11–15	0.0631	0.0602	0.8507	0	0.4894
16–20	0.0407	0.0780	0.8319	0	0.3750
21–25	0.0406	0.1887	0.7576	0.1688	0.8667
26–30	0.1071	0.1730	0.8474	0.0329	0.4878
31–35	0.0723	0.1131	0.8206	0.0676	0.7143
36–40	0.0449	0.1071	0.8218	0.0172	0.5455
41–45	0.0205	0.0758	0.7293	0.2632	0.8333
46–50	0.0160	0.1451	0.8750	0	0.4737
51–55	0.0476	0.2508	0.7350	0.1282	0.5500
56–60	0.0860	0.2308	0.7816	0.0862	0.5417
61–65	0.0861	0.2417	0.7840	0.0800	0.5769
66–70	0.0739	0.1478	0.7444	0.1556	0.6190
71–75	0.0316	0.1519	0.8205	0.1795	0.5455
76–80	0.0233	0.1860	0.6250	0.0833	0.6316
81–85	0.0294	0	0.6774	0	0.4286
86–90	0.0101	0.4950	0.2500	0.3182	0.7500

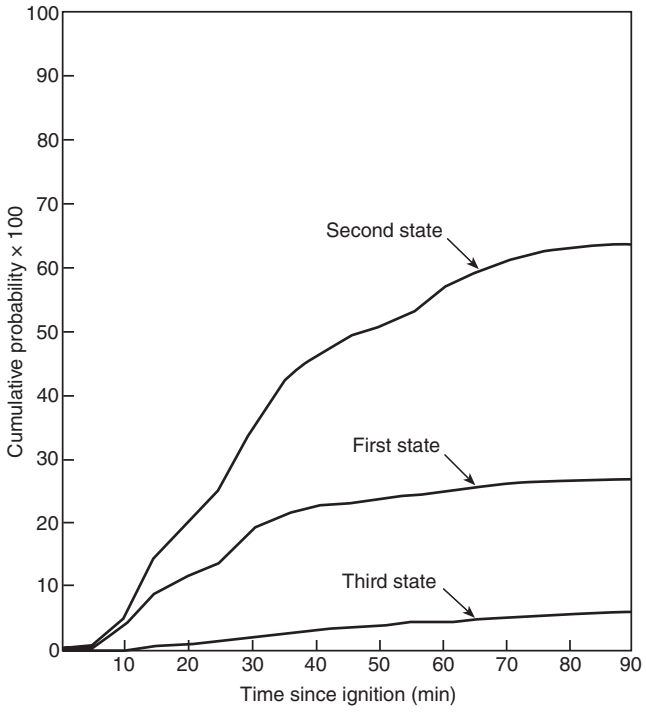

Figure 3-15.3. ***Bedding—cumulative probability of extinguishment.***

Table 3-15.4 ***Bedroom Bedding (Average Times)***

	First State	Second State	Third State
Duration of burning in the state (min)	24.5	5.9	8.5
Extinguishment time in the state (min)	26.2	32.2	44.1
Time for spreading beyond the state (min)	27.9	38.9	[a]

[a]Spread beyond the third state (building) is not considered.

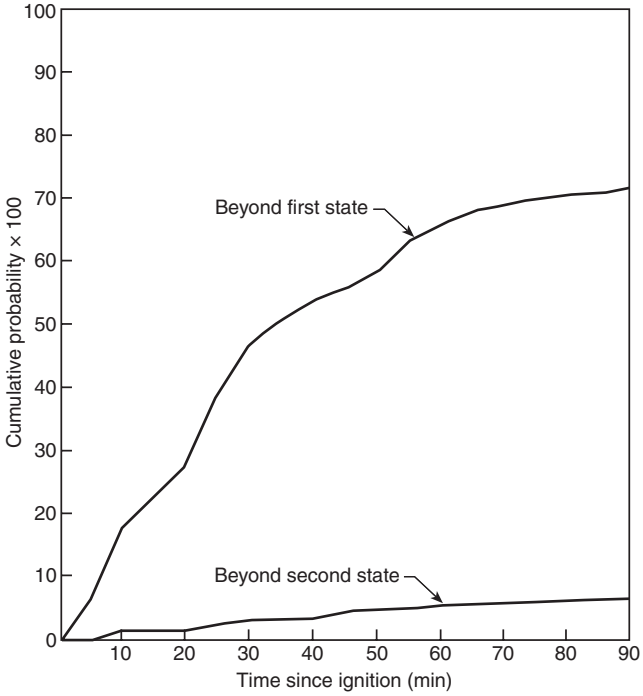

Figure 3-15.4. ***Bedding—cumulative probability of spreading.***

and Morishita[11] and considered eight phases of spatial spread of fire, including spread to the ceiling.

In a later study, Ramachandran[3] added another state between S_2 and S_3 to denote the event of fire involving the structural barriers of a room, assumed to occur after fire has spread beyond S_1 and S_2 but still confined to the room. This intermediate state was considered as generally consecutive to S_2, although a fire can spread directly from S_1 and involve the structural boundaries. Fire statistics available in the United Kingdom permit the incorporation of this additional state into a state transition model. As shown in Figure 3-15.5, only the limiting probabilities λ_i and μ_i specified in Equation 10 were estimated.

Fire statistics provided estimates for $E_i (i = 1 \text{ to } 4)$, the proportion of fires extinguished in the i^{th} state. The condition that

$$\sum_{j=1}^{4} E_j = 1$$

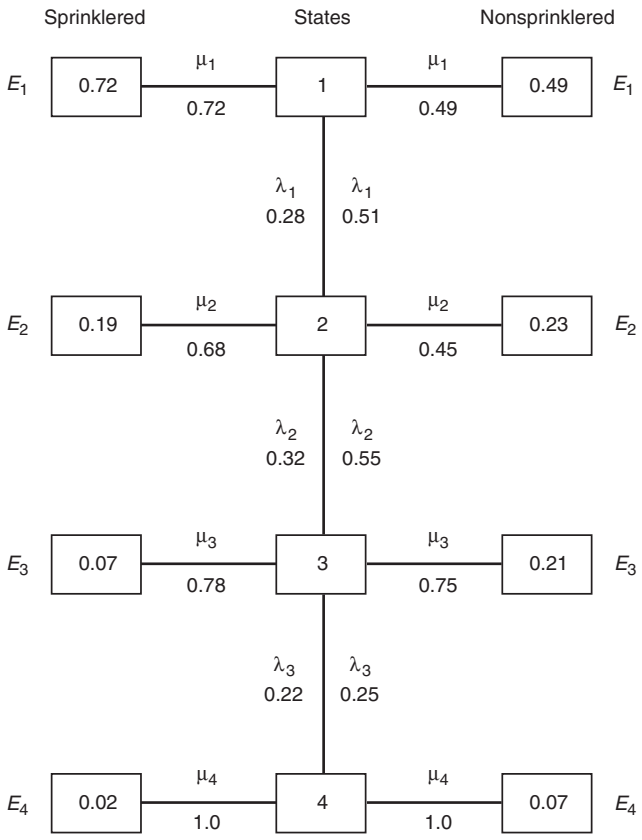

E_1 = Probability of confinement to items first ignited = μ_1

E_2 = Probability of spreading beyond item first ignited but confinement to contents of room of fire origin = $\lambda_1 \cdot \mu_2$

E_3 = Probability of spreading beyond item first ignited and other contents but confinement to room of fire origin and involvement of structure = $\lambda_1 \cdot \lambda_2 \cdot \mu_3$

E_4 = Probability of spreading beyond room of fire origin but confinement in the building = $\lambda_1 \cdot \lambda_2 \cdot \lambda_3 \cdot \mu_4$ ($\mu_4 = 1$)

Figure 3-15.5. ***Probability tree—textile industry.***

follows from the assumption that $\mu_4 = 1$ and, hence, $\lambda_4 = 0$; fire spread beyond the building of origin was not considered.

The parameter μ_1 is the same as λ_{21} in Berlin's model in which the first state (Realm I) is the nonfire state and the second state and above are fire states (Realms II through VI). Also λ_1 is the same as Berlin's λ_{23}, and μ_2 corresponds to λ_{31}. With these changes and the assumption that there is no recession of fire growth ($\lambda_{32} = 0$), the value of M_3 in Equation 12 is equal to

$$E_2 = \lambda_1 \cdot \mu_2$$

as derived from Equation 10.

In Figure 3-15.5, the product $\lambda_1 \cdot \lambda_2 (= E_3 + E_4)$ may be regarded as the probability of flashover, and λ_3 as the probability of failure of the structural boundaries of the room.[13] For the following reasons fire statistics do not provide a valid estimate of λ_3. Figures for the number of fires that spread beyond the room of origin include: (1) fires that spread by destruction of barrier elements (wall, floor, ceiling) as well as (2) those that spread by convection through a door or window left open or through some other opening. In the latter case, the barrier elements would still be structurally sound. A "room," as recorded in fire brigade reports, is not necessarily a "fire compartment." Using a probabilistic model[13] or other methods, the value of λ_3 for any compartment of given fire resistance can be estimated and multiplied by the probability of flashover to provide an estimate of probability of spread beyond the compartment of origin.

The probabilities provided by a stochastic model can be regarded as "noise" terms superimposed over a deterministic trend in fire growth over space and time. The trend can be predicted by a deterministic model, such as an exponential model.[3] Table 3-15.5 is an example based on such a model and fire incidence statistics.[13] The estimates of time in this table have been measured from the time of occurrence of established burning at the end of the first state, denoting confinement of fire to object first ignited. The percentage figures in Table 3-15.5 have provided the probabilities for constructing the probability tree in Figure 3-15.5.

To represent the interaction between human behavior and fire dynamics, Beck[14] developed a series of stochastic

Table 3-15.5 ***Textile Industry, U.K., Extent of Fire Spread and Average Area Damaged***

	Sprinklered[a]			Nonsprinklered		
Extent of Spread	Average Area Damaged (m^2)	Percentage of Fires	Time (min)	Average Area Damaged (m^2)	Percentage of Fires	Time (min)
Confined to item first ignited	4.43	72	0	4.43	49	0
Spread beyond item but confined to room of fire origin						
Contents only	11.82	19	8.4	15.04	23	6.2
Structure involved	75.07	7	24.2	197.41	21	19.4
Spread beyond room	1000.00	2		2000.00	7	
Average	30.69	100		187.08	100	

[a]System operated

state transition models and interrelated deterministic models. His sequential fire growth model was based on the six realms defined by Berlin,[12] with the remote burning state denoting flashover. His results, reproduced in Table 3-15.6, are applicable to office buildings. P_I in this table is the same as E_i in Equation 10. Adopting a different notation and starting with $P_1 = \mu_1$, the conditional probabilities of extinguishment, μ_i, and conditional probabilities of spread, λ_i ($= 1 - \mu_i$), were calculated according to Equation 10. The probability of a fully developed fire, given a fire defined by P_{FDF}/F, is given by the product $\lambda_1 \cdot \lambda_2 \cdot \lambda_3 \cdot \lambda_4$. The probability of spread beyond the compartment of fire origin, P_{VI}, is given by the product of P_{FDF}/F and λ_5 or by $\lambda_1 \cdot \lambda_2 \cdot \lambda_3 \cdot \lambda_4 \cdot \lambda_5$.

Beard[15] proposed a state transition model by considering a number of "critical events" with directional characteristics that a fire may pass through and the times between critical events. For example, critical heat event CHE2U referred to "fire passing through 2 kW on the way up," whereas CHE2D referred to "fire passing through 2 kW on the way down." The time between two critical events was assumed to have a temporal probability distribution independent of the time between earlier critical events. A particular succession of critical events formed a chain; specific times between critical events were referred to as a *sequence* within the chain. Based on assumed forms for transition probabilities and temporal probability distributions, Monte Carlo simulation was employed to generate randomly particular chains and sequences. A generated sequence to smoke and toxic gases was related to the corresponding sequence for the burning rate. Based on the concentration of carbon monoxide, Beard employed the concept of "fraction of fatality," with fatality resulting at a unit value for this fraction. He applied the model to a particular case involving flaming ignition on a bed in a hospital ward. He concluded that there would be a very large (greater than 80 percent) likelihood of having multiple fatalities if a fire exceeds 50 kW. One of the several assumptions used by him was that the fire did not spread beyond the ward.

Williamson[16] introduced a state transition model for analyzing and reporting the results of fire growth experiments performed under conditions resembling actual fire conditions. Three preflashover states were defined as follows:

J The period of time from the beginning of the experiment to ignition of the specimen

K The period of time from ignition of the specimen until flames touch the ceiling

L The period of time from when the flames first touch the ceiling until full involvement (flashover) occurs

Histograms and cumulative distribution functions of the state durations provided a graphical representation of fire performance. Examples were chosen to illustrate the method. Traditional cellulosic and cementitious walls and ceilings were compared to plastic materials in the same configuration.

Networks

State Transition Model

There is a probability p_f for flashover occurring in a room or compartment which depends on the objects in the room and their spatial arrangement apart from ventilation and other factors. Given flashover, the fire can breach the structural boundaries of the room with a probability p_b and spread beyond the room with a probability $p_s (= p_f \cdot p_b)$. The value of p_b depends on the level of fire severity attained after flashover and the fire resistance of the structural elements, such as walls, ceilings, and floors. The probability of failure of a room or compartment of given fire resistance, p_b, can be estimated from the joint probability distribution of fire severity and fire resistance expressed in units of time.[13] Fire resistance of a compartment will be reduced and the failure probability p_b increased by weakness caused by penetrations, such as piping or cables through walls, doors, windows, or other openings in the structural barriers.

Each room or corridor in a building has, therefore, an independent probability p_s of fire spreading beyond its boundaries. Using these probabilities for different rooms and corridors, fire spread in a building can be considered as a discrete propagation process of burning among points that abstractly express the rooms, spaces, or elements of a building. In a simple analysis, states classified by the burning situation of individual points can be incorporated in a state transition model.[17]

Consider, for example, three adjoining rooms, R_1, R_2, and R_3, that provide the following four states with the fire commencing with the ignition of objects in R_1.

1. Only R_1 is burning.
2. R_1 and R_2 are burning (and not R_3).
3. R_1 and R_3 are burning (and not R_2).
4. All three rooms are burning.

There is no transition from the

1. First to the fourth state
2. Second to the third state
3. Third to the second state
4. Second or third or fourth to the first state (recession of fire growth).

Table 3-15.6 ***Probabilities of Extinguishment: Fire-Growth and Suppression Model***

System Configuration	P_I	P_{II}	P_{III}	P_{IV}	P_V	P_{VI}	P_{FDF}/F
No sprinkler	0.5673	0.0038	0.0017	0.3282	0.0666	0.0324	0.0990
Sprinkler	0.5673	0.3827	0.0201	0.0232	0.0045	0.0022	0.0067

A transition from the second to the fourth state involves the spread of fire to R_3 from R_1 or R_2. The probability for this transition is, therefore, the sum of probabilities for spread from R_1 to R_3 and R_2 to R_3. Likewise, the probability of transition from the third to the fourth state is the sum of probabilities for spread from R_1 to R_2 and R_3 to R_2. A fire can burn in the same state without transition to another state. The process terminates when the fourth state is reached.

With the assumptions mentioned above, the following transition matrix can be formed with p_{ij} denoting the probability, p_s, of fire spread from room i to room j per unit time.[17] The unit may be longer than one minute, say, five minutes since one is considering spread from room to room after the occurrence of flashover. The values of p_{ij} may be considered as constants in a state transition model with stationary transition probabilities.

$$\mathbf{P}=\begin{bmatrix} 1-p_{12}-p_{13} & p_{12} & p_{13} & 0 \\ 0 & 1-p_{13}-p_{23} & 0 & p_{13}+p_{23} \\ 0 & 0 & 1-p_{12}-p_{32} & p_{12}+p_{32} \\ 0 & 0 & 0 & 1 \end{bmatrix}$$

During the initial period, since only R_1 is burning, the probability of burning in different states is given by the probability distribution of the system

$$\mathbf{p_0} = (1 \quad 0 \quad 0 \quad 0)$$

The probability distribution of the system after one unit of time is given by

$$\mathbf{p_1} = \mathbf{p_0} \cdot \mathbf{P} = (1-p_{12}-p_{13} \quad p_{12} \quad p_{13} \quad 0)$$

and after two units of time by the following row vector which, for convenience, has been written as a column vector

$$\mathbf{p_2} = p_1 \cdot P = \begin{bmatrix} (1-p_{12}-p_{13})^2 \\ 2p_{12}(1-p_{13}) - p_{12}^2 - p_{12} \cdot p_{23} \\ 2p_{13}(1-p_{12}) - p_{13}^2 - p_{13} \cdot p_{32} \\ p_{12} \cdot p_{23} + 2p_{12} \cdot p_{13} + p_{13} \cdot p_{32} \end{bmatrix}$$

The probability distributions of the system for later periods can be obtained by repeating the matrix multiplication as described above. This process will generate for each state a probability distribution for burning in that state as a function of time. For the first state (only R_1 burning), for example, the probability after n units of time is $(1-p_{12}-p_{13})^n$. The probability distributions for the other three states can be obtained by performing the calculations on a computer. The distribution for any state will provide an estimate of average transition time to that state. For estimating the average transition time to the fourth state, denoting the burning of all three rooms, Morishita[17] has proposed a method based on partitioning the matrix **P**. He has also discussed the stochastic process for a system in which extinguishment is attempted. For purposes of illustration he has applied the model to a hypothetical small house.

By carrying out further calculations and adding the corresponding probabilities, cumulative probabilities over time can be estimated for burning in the four states. The cumulative probabilities would generally tend to some limits as the value of n denoting time increases. The limiting value of the cumulative probability for the fourth state (all three rooms burning) and the corresponding time would be of special interest. This probability can be reduced and the associated time increased by (1) increasing the structural fire resistance of the rooms to reduce the probability of barrier failure, p_b, and (2) installing sprinklers to reduce the probability of flashover, p_f. With these safety measures probability of fire spread from room to room, p_s, will be reduced. Consequently the cumulative probability of fire being confined to the room of origin, R_1, will increase; this probability for a duration of t minutes is given by

$$\sum_{n=1}^{t} (1-p_{12}-p_{13})^n$$

where p_{12} and p_{13} are the probabilities of spreading from R_1 to R_2 and R_3 per unit time.

Network Models

The model described above can be extended to provide cumulative probabilities, at time n or limiting, for the burning of more than three rooms, but this will involve tedious and complex calculations. It would be simpler to consider fire spread between two given rooms through intermediate rooms and corridors in terms of discrete values attached to the probability p_s of spread beyond a room. This probability may be the limiting value for the cumulative probability given by, say, $E_4(= \lambda_1 \cdot \lambda_2 \cdot \lambda_3)$ in Figure 3-15.5. Alternatively, the time taken by fire to breach the boundaries of a room may be ascertained from deterministic (scientific) models and a probability assigned to this time, t_s, used for p_s in the stochastic model. The duration t_s is the sum of t_f representing the time to the occurrence of flashover after the start of established burning and t_b representing the time for which the barriers of the room can withstand fire severity after flashover. The latter time may be the endurance of barrier elements as measured by a standard fire resistance test, such as ASTM E119, *Standard Test Methods for Fire Tests of Building Construction and Materials.* As mentioned earlier $p_s = p_f \cdot p_b$.

Consider, as an example, the simple layout of Figure 3-15.6(a), relating to four rooms, and the corresponding graph shown in part (b), which also shows the probability (p_{ij}) of fire spread between each pair of rooms (i, j). The probability p_{ij} refers to p_s as defined herein, whereas Dusing et al.[18] and Elms and Buchanan[19] have considered only the barrier failure probabilities denoted by p_b, ignoring the probability of flashover denoted by p_f. The specific problem considered by these authors was to compute the probability of fire spread from room 1 to 4, which might follow any of the four paths, that is, (1) → (2) → (4); (1) → (3) → (4); (1) → (2) → (3) → (4); and (1) → (3) → (2) → (4).

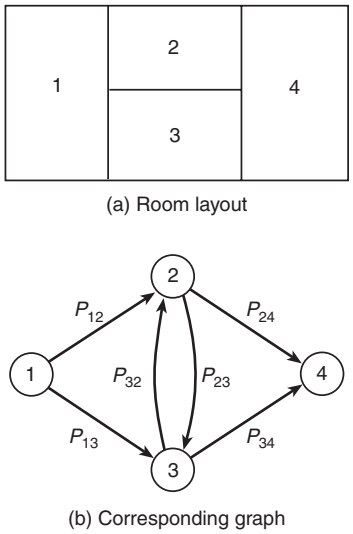

Figure 3-15.6. ***Simple diagram for fire spread.***

Using the event space method, Elms and Buchanan[19] considered first all possible "events" or combinations of fire spreading or not spreading along various links. If a_{ij} represents spread of fire along link ij, and $\overline{a}_{ij}$ represents fire not spreading along the link, then one event might be

$$[a_{12}, \overline{a}_{13}, a_{23}, \overline{a}_{32}, \overline{a}_{24}, a_{34}]$$

There will be $2^6 = 64$ events that will be all-exclusive, as any pair of events will contain at least one link for which fire spreads in one event and does not spread in the other. The probability of each event occurring is the product of the probabilities of its elements, assuming that the elements are independent. Thus, for the example given above, the event probability will be

$$p_{12}(1 - p_{13})p_{23}(1 - p_{32})(1 - p_{24})p_{34}$$

and the overall probability is the sum of all 64 event probabilities.

The complete event space can be represented as a tree with 64 branches. The probability of fire spread for each event (branch) is obtained by multiplying all the link probabilities in a branch. However, not all branches have to be computed in full. The computation can be curtailed, while still allowing for all cases. For this purpose, Elms and Buchanan[19] have described a method of constructing the tree and its ordering to identify or search possible paths of links leading to node (room) 4 from node 1. This procedure is known as a "depth-first search" of a graph. In this algorithm, a path is a series of nodes or rooms in a building; the construction of a branch, which is part of a particular event, is based on an underlying path. Each branch allowing fire spread must contain at least one path. Figure 3-15.7 shows the actual tree as it would be computed by the algorithm. The total probability of spread from node 1 to node 4 is given by the sum of all the branch probabilities. The calculation is carried out for each pair of rooms,

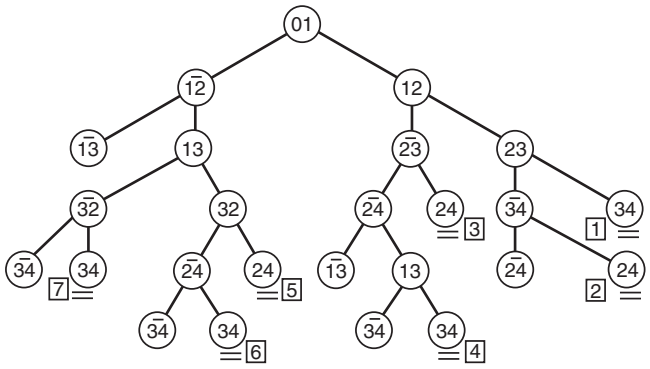

Figure 3-15.7. ***Modified event space tree.***

and the results assembled in a "fire spread matrix." The diagonal elements of the matrix are unity.

Various means have been employed to curtail the algorithm to prevent the computer developing excessively lengthy branches that would, as the branch probability decreases with branch length, have little effect on the result. The first means is to restrict the length of a fire spread path to a maximum number of compartments. The second approach is to terminate development of a branch if the cumulative branch probability drops below a certain fraction of the running total of the branch-spread probabilities calculated up to that point. The third means is to terminate development of a branch if the underlying path length becomes greater than a specified amount more than the length of the shortest possible path between the two rooms being considered.

In the computer-based technique of Elms and Buchanan[19] as described above, a building is represented as a network by defining compartments as nodes and the links between these nodes as possible paths for fire spread from compartment to compartment in a multicompartment building. The core of this model is a probabilistic network analysis to compute the probability of fire spreading to any compartment within the building. A series of further refinements were added when the model was applied to analyze the effects of fire resistance ratings on the likely fire damage to buildings.[20]

Time Dimension

Elms and Buchanan[19] did not consider the dimension of time explicitly, although it was implicit in many of their functions. The probability of fire spreading from one compartment to another was considered irrespective of how long it might take. As a result, the analysis did not take into account any intervention (e.g., the fire service). In this respect the model represented a worst-case scenario and assumed that the fire would eventually burn itself out.

The model of Elms and Buchanan[19] was not concerned with the process of fire growth and assumed that the spread was solely a function of the probable effects of a fully developed fire. The probability of flashover was not considered in this model. Platt[21] has proposed a new network model in which fire resistance and severity are

related to real time instead of equating these two parameters to the time based on the ISO standard fire which is not necessarily representative of the real time. The model computes the probability that fire will have spread to any part of a building after an elapsed time t. The essential features of Platt's model[21] are described in the following paragraphs.

The spread of fire to an adjacent compartment may be via the following paths:

1. Through an open doorway
2. Vertical spread via windows
3. Through a barrier, such as a wall, closed door, or ceiling

Two models are considered for estimating fire growth as a function of time. The first model is based on the exponential relationship between fire area and growth time as suggested by Ramachandran.[22] The second model uses the parabolic relationship between rate of heat release and growth time as proposed by Heskestad.[23] This model is used in conjunction with the relationship between compartment temperature and rate of heat flow to provide an estimate of flashover time, which is taken as the time when ceiling temperature reaches 600°C. The temperature is a function of the ventilation characteristics of the compartment, the type of fuel material, its configuration, and the thermal properties of the structural boundaries.

A figure of 49 percent is used to represent the probability that the initial fire will not result in flashover. Subsequent ignitions caused by fire spread are given a 100 percent probability of reaching flashover. This assumption may overestimate the spread of fire, since a barrier may fail in the very latter stages of a fully developed fire, which may not then have the momentum to initiate further ignition.

The real time of the fire duration, t, representing fire severity, s, is estimated by the ratio of fuel load to rate of combustion which is a function of ventilation and dimensional characteristics of the compartment. A formula suggested by CIB[24] is used to estimate the equivalent time, t_e involving the real parameters of the compartment. The approved fire resistance rating (FRR) of a barrier element, modified for weakness and another factor, is multiplied by the ratio (t/t_e) to yield an equivalent FRR denoted by R. R and fire severity, s, are not independent but quite rightly they have been assumed to be independent random variables with log-normal probability distributions. Under this assumption, the probability of fire spread through a barrier is estimated through the safety factor (R/s) which is also a log-normal variate. The probability of fire spread via an open door is assumed to be 100 percent. The probability of fire spreading vertically up the facade of a building via windows is equated to the probability that the height of the external flames is greater than or equal to the height of the spandrel.

A comparison is then made between these values and the design values of the barrier and door fire resistance and the spandrel heights. The output from these comparisons is a series of probabilities that fire will spread via each of the three possible paths described earlier. Combining these individual probabilities gives an overall probability of fire spreading to an adjacent compartment. Repeated for each compartment within the building, these values collectively form the adjacency fire spread matrix whose values represent the probability that fire will spread from compartment i to an adjacent compartment j. The expected time for fire to spread to an adjacent compartment, given that fire does spread, provides values for the adjacency fire spread time matrix.

By combining the two matrices providing probabilities and expected times for fire spread between adjacent compartments, the analysis computes the probability of fire spreading from an initial compartment i to any compartment j. The fire may spread along any path, but is conditional on having arrived at compartment j in a given time. The resulting matrix (i.e., global fire spread matrix) may be considered as a three-dimensional matrix with each layer being evaluated at a different time. Once the fire spread matrix has been formed, Platt's model[21] is very similar to that of Elms and Buchanan[20] except that, in the former model, the probability of spread is dependent on time, whereas, in the latter model the probability of fire spreading is irrespective of the time taken.

Ling and Williamson[25] have proposed a model in which a floor plan is first transformed into a network similar to the process described by Dusing et al.[18] and Elms and Buchanan.[19] Each link in their network represents a possible route of fire spread, and those links between nodes corresponding to spaces separated by walls with doors are possible exit paths similar to those developed by Berlin et al.[26] The space network is then transformed into a probabilistic fire spread network as in the example in Figure 3-15.8 with four rooms, Rm 1 to Rm 4, and two corridor segments C_1 and C_2. In this figure, Rm 1 has been assumed as the room of fire origin, but it would be a simple modification to reformulate the problem for another room of origin. With Rm 1 and Rm 1′, with a "prime" denoting the preflashover and post-flashover stages, the first link is represented by

$$\underset{(p_f,\, t_f)}{\text{Rm 1} \rightarrow \text{Rm 1}'}$$

where p_f represents the probability of flashover and t_f represents the time to flashover. The nodes denoted by a prime represent a fully developed (i.e., post-flashover) fire in the compartment.

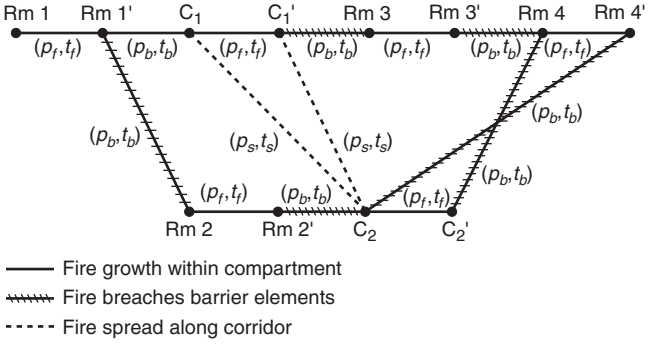

Figure 3-15.8. ***Probabilistic network of fire spread of Rm 1 to C_2.***

In Figure 3-15.8, three different types of links are identified. The first corresponds to the fire growth in a compartment, the second to the fire breaching a barrier element, and the third to fire spread along the corridors. To each link i, a pair of numbers (p_i, t_i) is assigned, with p_i representing the distributed probability that a fire will go through link i, and t_i representing the time distribution that it will take for such a fire to go through link i. The section of the corridor, C_1, opposite Rm 1, is treated as a separate fire compartment and is assigned a (p_f, t_f) for the link from C_1 to C_1'. The number pair (p_s, t_s) represents the probability and time for the preflashover spread of fire along the corridor from C_1 to C_2. As a first approximation, p_s may be considered to be governed by the flame spread classification of the corridor's finish materials on the walls and ceiling, as measured by a test method such as the tunnel test in ASTM E84, *Standard Test Method for Surface Burning Characteristics of Building Materials*.

Once full involvement occurs in the section C_1 of the corridor outside Rm 1 (i.e., node C_1' is reached) the fire spread in the corridor is influenced more by the ventilation in the corridor and by the contribution of Rm 1 than by the material properties of the corridor itself. Thus there is a separate link, C_1' to C_2, that has its own (p_s, t_s). The number pair (p_b, t_b) represents the probability of failure of the barrier element, with t_b representing the endurance of the barrier element.

Once one has constructed the probabilistic network, the next step is to solve it by obtaining a listing of possible paths of fire spread with quantitative probabilities and times associated with each path. For this purpose, Ling and Williamson[25] have adopted a method based on "emergency equivalent network," developed by Mirchandani[27] to compute the expected shortest distance through a network. (The word *shortest* has been used instead of *fastest* to be consistent with the literature.) This new equivalent network would yield the same probability of connectivity and the same expected shortest time as the original probabilistic network. In this method, each link has a Bernoulli probability of success and the link delay time is deterministic.

It must be noted that there are multiple links between nodes in the equivalent fire spread network. For example, the door between Rm 1 and the corridor could be either open or closed at the time the fire flashed over in Rm 1. Ling and Williamson[25] assumed, as an example, that there is a 50 percent chance of the door being open and that an open door has zero fire resistance. Furthermore, they assumed that the door, if closed, would have a 5-min fire rating. With further assumptions they constructed the equivalent fire spread network (Figure 3-15.9) with twelve possible paths for the example in Figure 3-15.8 to find the expected shortest time for the fire in Rm 1 to spread to the portion of corridor C_2. This network changes to Figure 3-15.10 with ten possible paths if self-closing 20-min fire-rated doors had been installed in the corridor, assuming that the reliability of the self-closures is perfect and that doorstops had not been allowed. Note that the links have been renumbered for Figure 3-15.10.

For the two equivalent networks shown in Figures 3-15.9 and 3-15.10, all of the possible paths are listed in Tables 3-15.7 and 3-15.8 with increasing time and with all the component links identified. Each of these paths can be described by a fire scenario; for instance, path 1 in Table 3-15.7 consisting of links ℓ_1, ℓ_2, and ℓ_4, would be

> "The fire flashes over, escapes from Rm 1 through an open door into the corridor C_1 and spreads along the corridor to C_2."

The probability of that scenario (0.13) is strongly dependent on the probability (0.5) for the occurrence of flashover in Rm 1 and of the probability (0.5) that the door will be open. The time of 17.5 min is composed of the times of 10 min for flashover and 7.5 minutes for fire to spread in the corridor from C_1 to C_2.

Ling and Williamson[25] have derived a formula for calculating from the figures in Tables 3-15.7 and 3-15.8, the probability of connectivity R, which is 0.5 for both the networks (Figures 3-15.9 and 3-15.10). This probability is a direct result of the assumed probability of 0.5 for flashover in the room of fire origin and the occurrence of unity probabilities in the remaining links that make up certain paths through the network. According to another formula, the expected shortest time is 29.6 min for Figure 3-15.9, and increases to 47.1 min for Figure 3-15.10 due to the presence of the 20-min fire-rated door. The equivalent

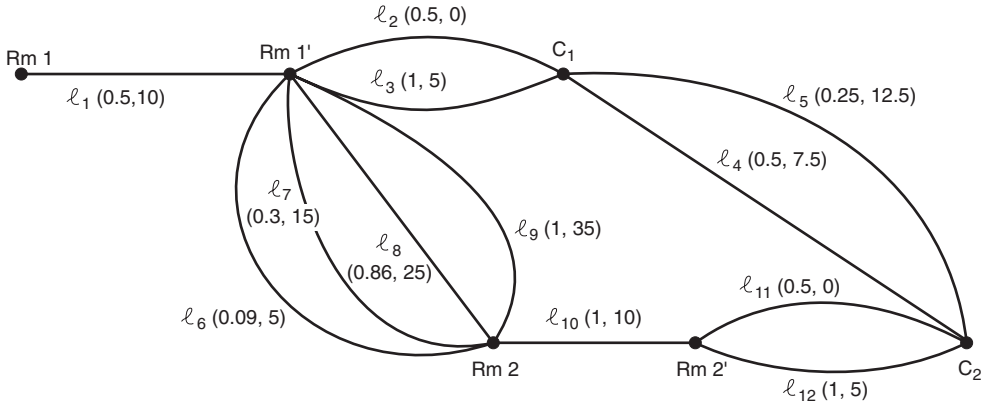

Figure 3-15.9. ***Equivalent fire spread network with 5-min unrated doors.***

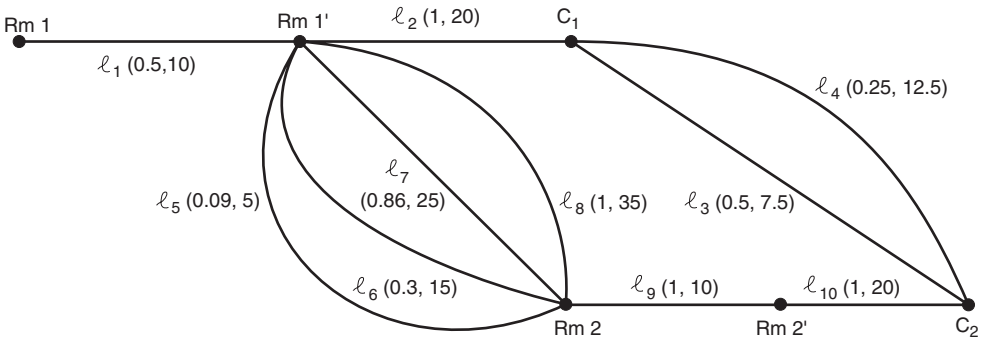

Figure 3-15.10. ***Equivalent fire spread network with self-closing 20-min fire-rated doors.***

Table 3-15.7 ***Pathways through the Example Fire Spread Equivalent Network Assuming 5-Min Unrated Corridor Doors, as Shown in Figure 3-15.9***

Paths	Component Links	Probability p_i	Time t_i (min)
1	1-2-4	1/8 = 0.13	17.5
2	1-2-5	1/16 = 0.06	22.5
3	1-3-4	1/4 = 0.25	22.5
4	1-6-10-11	1/44 = 0.02	25.0
5	1-3-5	1/8 = 0.13	27.5
7	1-6-10-12	1/22 = 0.05	30.0
8	1-7-10-12	3/40 = 0.08	35.0
9	1-8-10-11	3/14 = 0.21	40.0
10	1-8-10-12	3/7 = 0.43	50.0
11	1-9-10-11	1/4 = 0.25	55.0
12	1-9-10-12	1/2 = 0.50	60.0

Table 3-15.8 ***Pathways through the Example Fire Spread Equivalent Network Assuming Self-Closing 20-Min Fire-Rated Corridor Doors, as Shown in Figure 3-15.10***

Paths	Component Links	Probability p_i	Time t_i (min)
1	1-2-3	1/4 = 0.25	37.5
2	1-2-4	1/8 = 0.13	42.5
3	1-5-9-10	1/22 = 0.5	45
4	1-6-9-10	3/20 = 0.15	55
5	1-7-9-10	3/7 = 0.43	65
6	1-8-9-10	1/2 = 0.50	75

fire spread network thus facilitates an evaluation of design changes and affords ready comparison of different strategies to effect such changes.

Random Walk

In a simple stochastic representation, the fire process involving any single material or number of materials can be regarded as a random walk. The fire takes a random step every short period either to spread with a probability λ or to get extinguished (or burnout) with a probability μ(= 1 − λ). The parameter λ denotes the success probability of the fire, whereas μ denotes the success probability of an extinguishing agent. The problem is similar to two gamblers, A (fire) and B (extinguishing agent), playing a sequence of games, the probability of A winning any particular game being λ. If A wins a game he or she acquires a unit stake by destroying, say, a unit of the floor area; if he or she loses the game, no stake is gained. In the latter case, A does not lose his or her own stake to B; an already burned out area is a loss that cannot be regained. Extinguishment can also be considered as an absorbing boundary to the random walk, just as it is an absorbing state in a state transition model.

A random walk will lead to an exponential model described in Equations 1 through 3. In these equations, if one writes $c = \mu - \lambda$ such that $\mu = (1 + c)/2$, since $\mu + \lambda = 1$

$$Q(t) = \exp\left[\frac{-(1+c)t}{2}\right] \tag{13}$$

The fire-fighting effort is adequate if c is positive with μ greater than λ and, hence, greater than ½; it is inadequate if c is negative with μ less than λ and, hence, less than ½. If $c = 0$, such that $\mu = \lambda = ½$, there is an equal balance between fire-fighting efforts and the propensity of fire to spread.

Associated with the random variable t denoting time, there is another random variable x denoting damage which may be expressed in terms of, say, area destroyed. Damage in fire has an exponential relationship with duration of burning,[22] such that the logarithm of x is directly proportional to t as a first approximation. This assumption would lead to Pareto distribution

$$\phi(x) = x^{-w}, \quad x > 1 \tag{14}$$

denoting the probability of damage exceeding the value x. This distribution is used in economic problems concerned with, for example, income distribution to describe the fact that there are a large number of people with low incomes and a small number of people with high incomes. The damage is small in most of the fires, with high levels of damage occurring only in a small number of fires.

The use of Pareto distribution for fire damage originally proposed by Benckert and Sternberg[28] was later supported by Mandelbrot[29] who derived this distribution following a random walk process. For all classes of Swedish houses outside Stockholm, the value of the exponent w was found to vary between 0.45 and 0.55. A value of $w = 0.5$ in Equation 14 would imply, as discussed with reference to Equation 13, an equal balance between firefighting efforts and the propensity of fire to spread and cause damage.

The parameter μ in Equations 1 and 2 is known as the *hazard* or *failure rate* given by the ratio

$$\frac{f(t)}{Q(t)}$$

where $f(t)$ is the probability density function obtained as the derivative of $F(t)$ in Equation 2. A constant value for μ would denote a random failure. For a Pareto distribution in Equation 14, the failure rate is w/x, such that, with a constant value for w, the failure rate would decrease as x increases, indicating that, in terms of damage, a fire can burn forever without getting extinguished. A constant value for μ or w is somewhat unrealistic, particularly for a fire that is fought and extinguished at some stage. A fire will also burn out when all the available fuel is consumed or when it stops spreading due to the arrangement of objects in a room or building. For the reasons mentioned above, although the failure rate can decrease in the early stages of fire development denoting a success for fire spread, it would eventually increase ("wear out failure"), since fire extinguishing efforts would succeed ultimately.[30] There may be a long intermediate stage of steady growth of fire with μ remaining as a constant. The failure rate as a function of time would, hence, resemble a "bathtub" whose cross-section is composed of two curves sloping downwards representing the early and final stages of fire growth, connected at the bottom by a long straight line representing the intermediate stage.

Erving et al.[31] presented an approach to the theory of burning velocity in which a flame front moves forward at a rate determined by the random walk of chemical energy. The flame velocity is estimated by the value of a parameter which is a "collision rate" divided by a "reaction rate," both determined at the point of maximum reaction velocity. Empirical activation energies were given by the authors for certain hydrocarbon flames.

In the context of fire spread, random walk is a one-dimensional process describing the damage by random functions of time rather than by a random function of time and space. The random walk indicates the position of the fire (i.e., damage at any time). At every unit of time, there is a change in position indicated by an increment to the damage or no change due to absorption (extinguishment or burning out). Generally the walk is considered in discrete time. If the walk is continuous in time such that the increments are Gaussian, this leads to a diffusion process.[32] (A diffusion process is an approximation to Brownian motion, a phenomenon well known in many branches of science and technology.) The normal, or diffusion, term is one of two possible components of a general additive stochastic process, the other component being a discontinuous or transition term arising from occurrences of events at random times. The Markov chains discussed earlier belong to the second type of component. A linear superposition of the two components provides a solution to an equation governing a general additive process.

Percolation Process

In random walk and diffusion models, randomness is a property of the moving object, whereas in a percolation process, randomness is a property of the space in which the object moves.[33] Thus the transition the object suffers when at a particular point is random but, if the object ever returns to this point, it would suffer the same transition as before. The process is described by a stochastic field on the space (i.e., a vector field of transition numbers). Percolation process deals with deterministic flow in a random medium, in contrast with random walk and diffusion models which are concerned with random flow in a deterministic medium.

Broadbent and Hammersley[34] considered the walk as taking place on a graph consisting of a number of sites, connected by directed bonds, passage being possible only along such a "bond." If such a graph obeys certain connectivity requirements, it is termed a *crystal.* In a randomized version, each bond of the crystal has an independent probability of being blocked, and it is desired to know what effect this has on the probability of communication from one site A to another site B; this is not the same as from B to A, since communication has a direction.

If fire is considered as the moving object, the movement takes place in a space or medium that has a certain random property although the object (fire) itself has some randomness associated with it. Buildings in an area, for example, are somewhat randomly distributed. Buildings are also connected by directed bonds, with spread (flow) of fire being possible only along the bonds. Each bond has an independent probability of blocking or preventing fire spread; this depends on the nature of a building and its contents, wind conditions, and the distances between buildings. A percolation problem also arises when one considers a network some of whose links, chosen at random, may be blocked, and one wishes to know the effect of this random blockage on flow through the network. Such a problem would be encountered in predicting fire spread in a forest or from building to building in an urban area.

Apparently for the reasons mentioned above, Hori[35] considered percolation process for the modeling of fire spread from building to building. Sasaki and Jin[36] were concerned with the actual application of this model and estimation of probabilities of fire spread. By using the data contained in the fire incidence reports for Tokyo, urban fires were simulated and the average number of burnt buildings per fire estimated. Apart from distances between buildings and wind velocity, the following factors were also regarded as having some effect on the probability of fire spread: building construction, building size and shape, window area, number of windows, indoor construction materials, furniture, walls, fences, gardens, and trees.

For the model, the first factor was classified into three groups: (1) wood construction, (2) mortar (slow burning) construction, and (3) concrete (fireproof) construction. The wind velocity was classified into two groups: (1) 0 to 2.5 m/s and (2) 2.5 to 5.0 m/s. In the former case, fire spread was assumed to be undirectional (isotropic) whereas, in the latter case, the data were subdivided into smaller groups according to the directions of fire spread: the windward direction, the leeward direction, or direction perpendicular to that of the wind (the sideward direction). Fire incidents in which wind velocity was larger than 5.1 m/s were excluded due to their small number. If the number of burnt buildings was i and that of unburnt ones was j, the probability of fire spread was expressed as $i/(i + j)$.

The data were divided by every meter of the distance between buildings, or every 2 m or more in case the data were few. The exponential function $\exp(-cd)$ was used for estimating the probability of spread between two buildings as a function of distance d between them. Using the least square method, the values of c were obtained for different building construction and wind velocity categories. The analysis revealed that building construction was the main factor responsible for fire spread. The simulations did not evaluate the changes in the pattern of spread according to time.

In a recent study, Nahmias et al.[37] have examined the feasibility of applying percolation theory to the spread of fires in forests. For studying the effect of randomness on the propagation of fire the authors have built a square network model containing combustible and noncombustible blocks randomly distributed, with a variable concentration, the parameter q denoting the fraction of noncombustible elements. In the absence of wind, the propagation was found to be consistent with a model of invasion percolation on a square site lattice with nearest neighbor interaction leading to a threshold not far from the theoretical value $q = 0.39$. The threshold was larger with wind blowing on the model. The largest threshold value obtained was $q = 0.65$. The final state of the model after combustion was represented for different values of wind velocity and fraction values q. The observation of this state can bring out the directed, nonlocal, and correlated characters of the contagion.

Epidemic Theory

For predicting fire spread in a large urban area, Albini and Rand[38] have proposed a model that has some similarity with chain-binomial models of Reed and Frost[39] for the spread of an epidemic. The authors envisaged fires in "locales," which may be single buildings or blocks of buildings. A number of these are presumed to be alight initially and randomly distributed and to stay alight for a time T in the absence of fire fighting. At time T, this generation of fires can spread fire and then die out, leaving a second generation to burn for a second period T, and so on.

Fire spread is assumed to take place only at the end of each fire interval. For the $(n + 1)^{th}$ interval, the *a priori* probability that any locale is burning is P_n and that it has not yet been burnt is A_n. It follows that

$$A_n = (1 - P_0)(1 - P_1) \ldots (1 - P_n)$$
$$P_{(n+1)} = A_n \cdot B_n$$

where B_n is the probability that during the $(n + 1)^{th}$ interval, fire spreads into a "locale" previously unburnt. To obtain B_n, Albini and Rand[38] introduced parameters defining the following three probabilities:

1. Probability that during the $(n + 1)^{th}$ interval there are just m locales burning out of N possible locales adjacent to a given locale
2. Probability that at least one of the m burning locales spreads fire
3. *A priori* probability that fire will spread during any interval of duration T from a burning locale to an unburnt neighbor

Based on the aforementioned parameters the authors obtained an upper and lower approximation for B_n and narrow limits for $(1 - A_n)$, the probability of a locale being burnt.

The Albini and Rand[38] model allowing for fire fighting was based on a number of idealizations. First, fire-fighting effort was assumed to be constant. The authors introduced a parameter M for the fraction of burning locales wherein all fire fighters in a city could extinguish that fraction during the given time interval out of all possible burning locales. Fire fighting was assumed to be continuous throughout the time interval. A fire not extinguished may or may not spread; if extinguished it cannot spread. Under the assumptions mentioned above, the authors have derived an expression for the probability $P_{(n+1)}$ defined earlier. Albini and Rand considered directional spread of fire assuming that from an isolated locale the probability of spread forward and backward was the same and the directional element in the spread arose only from the initial condition. Spatial variation was included in the model by connecting the probability of spread to the probability that any building was itself burning and separated from any of its neighbors not yet burning by less than the appropriate "safe" distance for radiation or brand transfer.

Thomas[40] drew attention to the possible relevance of epidemic theory to fire spread in a building, and compared the model of Albini and Rand[38] with a deterministic epidemic model based on a continuous propensity of fire to spread. He found the results of both models to be in reasonable agreement as to their basic features, but concluded that neither would be appropriate for addressing spread in a single building where the number of "locales" is not large. For such a situation a stochastic treatment is necessary to allow for the finite chance that the initiating fires can burn out before spreading, a chance that is negligible when the number of initial fires is large.

Stochastic Differential Equation

Introduction

Most of the models developed to date use statistical data provided by real fires for quantifying, in terms of

probabilities, uncertainties caused by factors which cannot be controlled. These models do not explicitly consider the underlying physical processes. On the other hand, models such as zone, field, and others involving computational fluid dynamics (CFD) are based on physiochemical and thermodynamic theories supported by experimental data. These models are essentially deterministic since they do not explicitly consider the uncertainties or randomness affecting the spread of a real fire. In order to avoid complex calculations which cannot be performed even with the aid of advanced computer programs, deterministic models use simplified equations which treat as fixed values parameters which are clearly variables. Exclusion of parameters that can affect fire spread is another source of uncertainty generally ignored by a deterministic model. For these reasons, the development of a real fire is unlikely to follow exactly the pattern predicted by a deterministic model even for the early stage involving the material or object first ignited. More uncertainties are involved when a fire spreads from object to object in a room.

For the reasons mentioned above, there is a need to develop models which couple deterministic and stochastic processes governing the spread of a real fire in a room or building. Ramachandran[41] suggested one such model in which heat output and area damage in a real fire are considered as correlated variables for predicting the rate of fire growth (and "doubling time") according to an exponential model.[22] This method, in conjunction with the probability distribution of area damage, can provide estimates for the time of flashover in a compartment and for the probability of flashover. Another method is to introduce additional parameters in a deterministic model to take account of uncertainties and derive the stochastic version of the deterministic model. One such method, based on the stochastic differential equation,[42] is currently being developed in Australia and has the following basic features.

The Deterministic Model

The deterministic version of the stochastic model derived by Hasofer and Beck[42] for compartment fires is a one-zone model consisting of three variables: the gas temperature T (°C), the rate of fuel burning R (g/min), and the oxygen mass fraction in the compartment x. Eventually x is converted into the percentage oxygen deficiency $D = 23 - 100x$. The initial temperature is $T_0 = 20$°C and the time t is measured in min. The basic laws used to derive the equations are discussed by Dysdale,[43] section 10.3.2.

The following parameters have been used in the model:

Variable parameters

V (volume of compartment) = 21.6 m^3
S (inside surface area of compartment) = 46.88 m^2
A (area of opening) = 1.6 m^2
B_{max} (total fuel mass) = 172.8 kg
R_0 (initial burning rate) = 8.38 g/min
h (height of opening) = 2 m

Fixed Parameters

ρ (gas specific gravity) = 490 g/m^3 at 500°C
= 1300 g/m^3 at 20°C
C_p (specific heat of gas) = 0.001 kJ/gK
σ (Stefan Boltzmann constant) = 3.4×10^{-9} kJ/min·m^{2}K^4
ε (gas emissivity) = 0.015
ν (mass of oxygen used up by 1 g of fuel) = 1.36 g

The values of the variable parameters refer to a flashover fire.

With Q_L denoting the net rate of heat loss from the enclosure, the heat balance equation is

$$C_p \rho V \frac{dT}{dt} = H_B R - Q_L \tag{15}$$

where H_B is the net combustion heat per gram of fuel, R is the fuel-burning rate, and ρ is taken to be some average gas specific gravity. Rewriting Equation 15

$$\frac{dT}{dt} = \beta R - q(T) \tag{16}$$

where $\beta = H_B/C_p\rho V$ and $q(T) = Q_L/C_p\rho V$. By expressing the total heat loss rate Q_L as the sum of radiation loss rate and convection loss rate, the following equation has been derived under some assumptions:

$$q(T) = \sum [(T + 273)^4 - (T_0 + 273)^4] + \Phi(T - T_0) \tag{17}$$

for some values of the calibration parameters Σ and Φ.

Let the oxygen fraction in the incoming air be y (= 0.23). Then, assuming homogenous mixing, the following differential equation is derived for oxygen mass balance:

$$\frac{dD}{dt} = \delta(k_1 - D)R - \mu D \tag{18}$$

where

$D = 100y - 100x = 23 - 100x$
$\delta = 1/\rho V$
$k_1 = 100(y + \nu)$
$\mu = m_a/\rho V$

The new symbol m_a denotes the ventilation rate in g/min. Equation 18 applies only as long as the oxygen concentration is above 7 percent. When that value is reached, it remains steady at that value until the burning rate starts diminishing.

For the burning rate R, the differential equation

$$\frac{dR}{dt} = \alpha(k - D)z \tag{19}$$

has been derived under the assumptions that R is an increasing function of the gas temperature T, and R stops increasing when the oxygen fraction falls below 0.126. R rises only slowly for low temperatures. For z, which is

slowly increasing for small T, the following calibration formula has been used:

$$z = 22T\left(1 - \frac{1}{1 + (0.001T)^2}\right) \tag{20}$$

Equation 19 is applicable as long as there is still some fuel not burning. When most of the combustible material has been consumed, the burning rate quickly decreases exponentially. Equations 16, 18, and 19 require the specification of the initial burning rate, R_0.

The three-variable model described above was calibrated to the output of the National Research Council of Canada (NRCC) model[44] with the particular set of values of the variable and fixed parameters listed earlier, by choosing appropriate values for the calibration parameters. These values were chosen as follows. A discrete version of the NRCC model, at intervals of 0.02 min. was obtained. Denoting the values of the gas temperature, the burning rate, and the oxygen deficiency by T_N, R_N, and D_N, respectively, discrete versions of the model were run with varying values of the parameters. An optimization algorithm was used to obtain the values of the parameters that minimized the distance function

$$\Delta = \sum C_1^2(T_N - T)^2 + C_2^2(R_N - R)^2 + C_3^2(D_N - D)^2 \tag{21}$$

where $C_1 = 0.001$, $C_2 = 0.008$, and $C_3 = 23$. These values of the Cs were chosen so as to obtain comparable fits for the three variables at their maximum values.

The values of the calibration parameters obtained were as follows:

$$\alpha = 2.5;\ \beta = 0.1125 \qquad \Phi = 0.399 \qquad \Sigma = 1.875 \times 10^{-10}$$
$$\delta = 1.5 \times 10^{-5} \qquad \mu = 0.58 \qquad k = 10.4 \qquad k_1 = 158$$
$$R_0 = 280\ \text{g/min} \qquad B_{\max} = 82.5\ \text{kg} \tag{22}$$

The Stochastic Model

The set of three deterministic equations derived in Equations 16, 18, and 19 have been turned into a set of stochastic differential equations by adding on the right hand side forcing functions, which are white noise multiplied by some function of the variables. The purpose of these forcing functions is to model the intrinsic variability of the fire phenomenon due, for example, to the turbulent behavior of the hot gases. The forcing function adopted is a standard Brownian motion differential $d\mathbf{W}$ with independent components (each with mean zero and variance dt) multiplied by an appropriate function of the variables. The standard form for describing the behaviour of a set of n coupled variables is

$$d\mathbf{X} + \boldsymbol{\alpha}(\mathbf{X}, t)\,dt = \boldsymbol{\beta}(\mathbf{X}, t)\,d\mathbf{W} \tag{23}$$

where $\mathbf{X}$, $\boldsymbol{\alpha}$, and $d\mathbf{W}$ are vectors of length n and $\boldsymbol{\beta}$ is an $n \times n$ matrix. Since the future behavior of the vector $\mathbf{x}$ is independent of its past values, given its present value, it is a Markov vector.

The model does not make $\boldsymbol{\alpha}$ and $\boldsymbol{\beta}$ depend explicitly on the time; they are functions of $\mathbf{x}$ only. It is further assumed that the forcing functions for each of T, D, and R are independent, such that the matrix β is diagonal. Another assumption is that the randomness of the fire will increase with increasing temperature. Bearing in mind that the variance of a scalar forcing function differential βdw is $\beta^2 dt$, the following set of stochastic differential equations have been obtained:

$$\begin{aligned} &dT - \beta R\,dt + q(T)\,dt = f_1(T)\,d\mathbf{W}_1 \\ &dD - \delta(k_1 - D)R\,dt + \mu D\,dt = f_2(T)\,d\mathbf{W}_2 \\ &dR - \boldsymbol{\alpha}(k - D)z\,dt = f_3(T)\,d\mathbf{W}_3 \end{aligned} \tag{24}$$

where $q(T)$ is given by Equation 17 and $z(T)$ by Equation 20. The functions $f_1(T)$, $f_2(T)$, and $f_3(T)$ are appropriately chosen increasing functions of T.

Due to a great paucity of information about the intrinsic variability of enclosure fires, it is presently difficult to determine precise formulas for the functions f_1, f_2, and f_3. Experiments specifically designed to provide data for identifying these functions have been planned to be carried out at the Centre for Environmental Safety and Engineering Risk, Victoria University of Technology, Australia. Statistical variability is another problem whose source is lack of knowledge of the parameters governing the fire. The most important unknown parameter is the initial burning rate which is a nonnegative quantity and, hence, can be assumed to have a lognormal probability distribution. Other parameters affecting the fire are the geometry of the compartment, the size of the openings and whether they are open or shut, and the nature, amount, and position of the fuel load. If these parameters are also unknown, further parameters of the model must be allocated a probability distribution to cater for the added uncertainty. With additional reasonable assumptions regarding the variability of the phenomenon, the probability of extreme values of the fire load can be estimated by a Monte Carlo simulation and used as an input to the probabilistic fire risk analysis of the building under consideration.

Simulation–Illustration

To illustrate the capacity of the model to simulate the intrinsic variability of a fire, a Monte Carlo simulation was performed, using Equation 24 and the parameter values in Equation 22. The functions f_i were chosen as follows:

$$f_1(T) = \frac{\Phi T}{1000} \tag{25}$$

$$f_2(T) = \frac{15\Phi T}{1000} \tag{26}$$

$$f_3(T) = \frac{12\Phi T}{10^6} \tag{27}$$

By varying the parameter Φ, varying degrees of stochasticity may be achieved. Figure 3-15.11 ($\Phi = 50$) and Figure 3-15.12 ($\Phi = 100$) illustrate the type of fire curve obtained.

Since (T, D, R) is a Markov vector and initially all three components increased monotonically, any decrease in the initial burning rate R_0 will just shift the fire curves in Figures 3-15.11 and 3-15.12 to the right. This is illustrated in Figure 3-15.13 for $R_0 = 150$. Thus, choosing a random value for R_0 and a nonzero value for Φ will produce curves similar to Figures 3-15.11 and 3-15.12, but shifted either to the right or to the left.

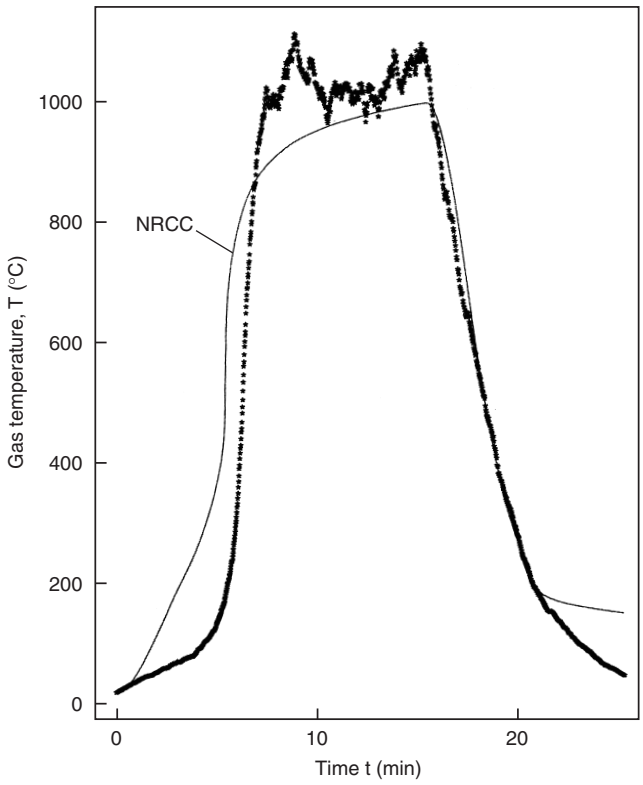

Figure 3-15.11. ***Stochastic model. Gas temperature. ϕ = 50.***

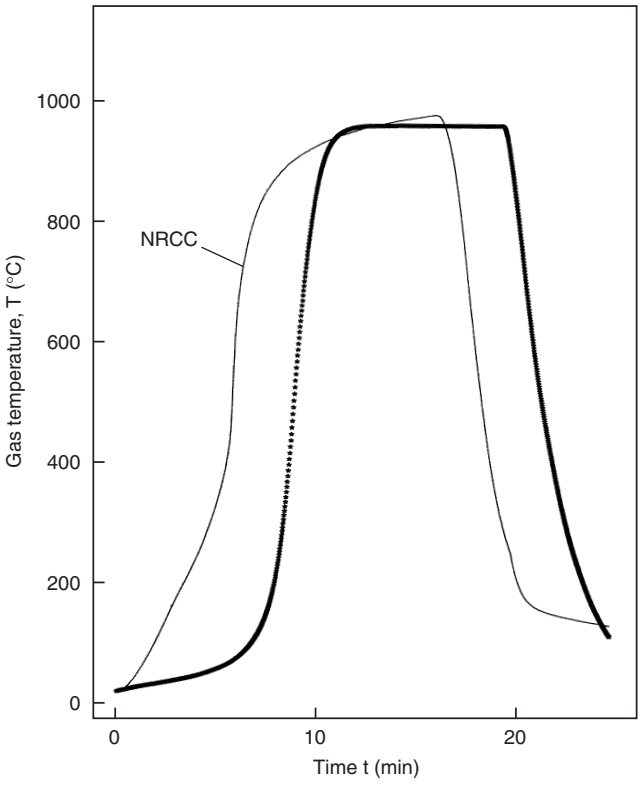

Figure 3-15.13. ***Deterministic model. Effect of reducing R_0 to 150.***

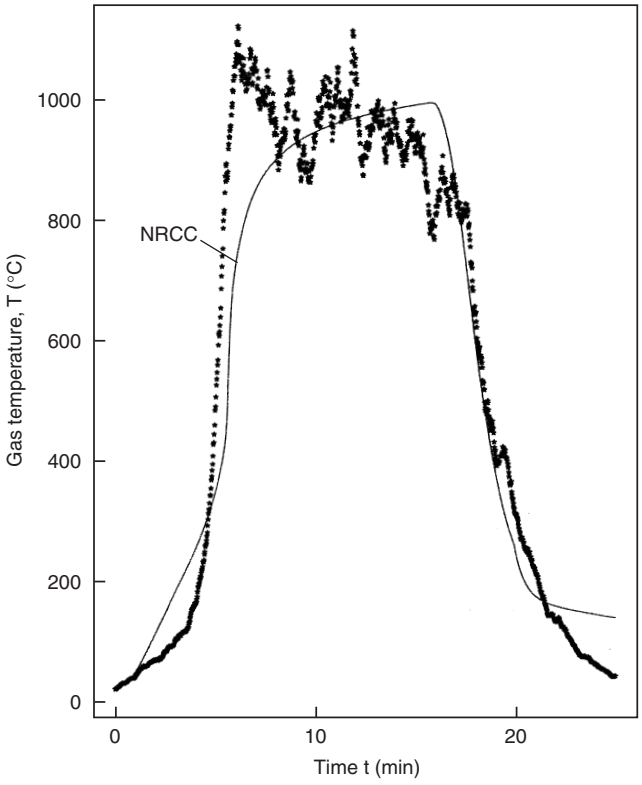

Figure 3-15.12. ***Stochastic model. Gas temperature. ϕ = 100.***

The main projected use of the stochastic fire curves such as Figures 3-15.11 and 3-15.12 is as an input to modules which will calculate the effect of the fire on fire barriers and subsequently trace the possible spread of fire to adjacent compartments. As an illustration of the kind of results obtainable, Hasofer and Beck[42] studied one particular measure of fire severity, normalized heat load, H, proposed by Harmathy and Mehaffy.[45] They obtained histograms of the values of H based on 1500 simulations of the fire curves with $\Phi = 100$ for two cases. In the first case, both the initial burning rate, R_0, and the total fuel mass, B_{max}, were considered as fixed quantities. In this case, in degrees Celsius, the mean of H was 8063.5 and the standard deviation was 849.8. In the second case, R_0 and B_{max} were considered as independent random variables with lognormal distributions. The parameters mean and coefficient of variation had the values of 280 and 0.3 for R_0 and 82.5 and 0.3 for B_{max}. The mean of H increased only slightly to 8222.2, but the standard deviation almost tripled to 2471.6.

A histogram was drawn for the maximum temperature reached, based on 1500 simulations with $\Phi = 100$ and R_0 and B_{max} as independent random variables. This exercise revealed values of 1181.1 and 176.6 for the mean and standard deviation, respectively, of the maximum temperature.

The stochastic model discussed above only takes account of uncertainties governing certain parameters in a deterministic model of fire spread relating to a single material or object. The model does not take account of uncertainties governing the spread of fire from object to object.

However, it may be possible to use the outputs of this model for different objects to construct the matrix of transition probabilities required for a Markov model, discussed earlier, for fire spread from object to object in a room or compartment. Further research in bridging the gap between deterministic fire growth models and stochastic fire growth models is currently being carried out at Victoria University of Technology in Australia.

Other Models

Branching processes[46] can be relevant for fire spread in a building in which a material first ignited (first generation) ignites one or more other materials (second generation), which ignite other materials (third generation), and so on, leading to the spread of fire throughout the building. The number of offsprings (burning materials) vary randomly from one generation to another, depending on the distances between ignited and unignited materials, ventilation, and other factors affecting fire spread. Hence, there is a need to develop a branching process model applicable to random environment.[47]

For predicting the damage to buildings and other properties resulting from incendiary or nuclear attacks, Phung and Willoughby[48] considered two types of stochastic models. In the first model, the entire fire front was regarded as a random walker moving along a linear row of cells or small square areas. In each short time interval the front may be in one of three states: (1) die or stop permanently, (2) spread or move one cell forward, or (3) pause or stay where it is. Simple probability considerations provide an estimate of the probability P_n that, at time t, the fire will be n cell units long after an initial condition of being lit at time zero

$$P_n = \exp[-(\lambda + \mu)t]\lambda^n t^n$$

The parameters λ and μ are, respectively, the probabilities for forward spread and burnout during a short time interval. The fire will stay where it is, with probability $[1 - (\mu + \lambda)]$.

The second stochastic model of Phung and Willoughby was called *fuel-state* model, because it dealt explicitly with the state of the fuel in each cell. In the burning process, the fuel changes from the unignited to the burnout state passing through the flaming state. A cell will be in one of these three states at any time with probabilities U, F, and B for unignited, flaming, and burnout states, respectively. In a two-dimensional array of cells, the cell dimension can be so chosen that a burning cell can ignite the immediate neighbor cells but not those that are farther away. Under this assumption, an unignited cell can be ignited by one or more of its eight (8) immediate burning neighbors with probability

$$P = 1 - (1 - P_1)(1 - P_2) \ldots (1 - P_8)$$

where P_1, P_2 … P_8 denotes the chances of ignition by the neighbors. These eight spread probabilities are not necessarily symmetrical, due to factors such as wind and topography. Using the formulation described, differential equations are derived for U, F, and B for each cell with the condition $(U + F + B) = 1$, solutions of which can be obtained by numerical calculations using computers, if necessary.

References Cited

1. G. Ramachandran, "Non-Deterministic Modeling of Fire Spread," *Journal of Fire Protection Engineering,* 3(2), pp. 37–48 (1991).
2. A.M. Kanury, "On the Craft of Modeling in Engineering and Science," *Fire Safety Journal,* 12, pp. 65–74 (1987).
3. G. Ramachandran, "Probabilistic Approach to Fire Risk Evaluation," *Fire Technology,* 24, 3, pp. 204–226 (1988).
4. G.N. Berlin, "Probability Models in Fire Protection Engineering," *SFPE Handbook of Fire Protection Engineering* (P.J. DiNenno, et al., eds.), National Fire Protection Association, Quincy, MA (1988).
5. G. Ramachandran, "Stochastic Modeling of Fire Growth," *Fire Safety: Science and Engineering,* ASTM STP 882 (T.A. Harmathy, ed.), American Society for Testing and Materials, Philadelphia, PA, pp. 122–144 (1985).
6. H. Kida, "On the Fluctuations of the Time Required to Extinguish Small Liquid Diffusion Flames with Sprays of Several Salt Solutions," Report of Fire Research Institute of Japan, No. 29, Mitaka, Japan, 25–33 (1969).
7. Y. Aoki, "Studies on Probabilistic Spread of Fire," Research Paper No. 80, Building Research Institute, Tokyo, Japan (1978).
8. G. Ramachandran, "Stochastic Modeling of Fire Growth," CIB Workshop on Mathematical Modeling of Fire Growth, Paris, France (1981).
9. C.R. Theobald, "The Critical Distance for Ignition from Some Items of Furniture," Fire Research Note No. 736, Fire Research Station, Boreham Wood, Herts, U.K. (1968).
10. J.M. Watts, Jr., "Dealing with Uncertainty: Some Applications in Fire Protection Engineering," *Fire Safety Journal,* II, pp. 127–134 (1986).
11. Y. Morishita, "Establishment of Evaluating Method for Fire Safety Performance," *Research Project on Total Evaluating System on Housing Performances,* Building Research Institute, Tokyo, Japan (1977).
12. G.N. Berlin, "Managing the Variability of Fire Behavior," *Fire Technology,* 16, pp. 287–302 (1980).
13. G. Ramachandran, "Probability-Based Fire Safety Code," *Journal of Fire Protection Engineering,* 2(3), pp. 75–91 (1990).
14. V.R. Beck, "A Cost-Effective Decision-Making Model for Building Fire Safety and Protection," *Fire Safety Journal,* 12, pp. 121–138 (1987).
15. A.N. Beard, "A Stochastic Model for the Number of Deaths in a Fire," *Fire Safety Journal,* 4, pp. 169–184 (1981/82).
16. R.B. Williamson, "Fire Performance Under Full-Scale Test Conditions—A State Transition Model," *Sixteenth Symposium (International) on Combustion,* The Combustion Institute, Pittsburgh, PA, pp. 1357–1371 (1976).
17. Y. Morishita, "A Stochastic Model of Fire Spread," *Fire Science and Technology,* 5, 1, pp. 1–10 (1985).
18. J.W.A. Dusing, A.H. Buchanan, and D.G. Elms, "Fire Spread Analysis of Multi-Compartment Buildings," Research Report 79/12, Department of Civil Engineering, University of Canterbury, New Zealand (1979).
19. D.G. Elms and A.H. Buchanan, "Fire Spread Analysis of Buildings," Research Report R35, Building Research Association of New Zealand, Judgeford (1981).

20. D.G. Elms and A.H. Buchanan, "The Effects of Fire Resistance Ratings on Likely Fire Damage in Buildings," Research Report 88/4, Department of Civil Engineering, University of Canterbury, New Zealand (1988).
21. D.G. Platt, "Modeling Fire Spread: A Time-Based Probability Approach," Research Report 89/7, Department of Civil Engineering, University of Canterbury, New Zealand (1989).
22. G. Ramachandran, "Exponential Model of Fire Growth," *Fire Safety Science—Proceedings of the First International Symposium* (C.E. Grant and P.J. Pagni, eds.), Hemisphere Publishing Corporation, New York, pp. 657–666 (1986).
23. G. Heskestad, "Engineering Relations for Fire Plumes," Technology Report 82-8, Society of Fire Protection Engineers, Boston, MA (1982).
24. "Design Guide: Structural Fire Safety, CIB W14 Workshop," *Fire Safety Journal,* 10, 2, pp. 81–138 (1986).
25. W.T.C. Ling and R.B. Williamson, "The Modeling of Fire Spread Through Probabilistic Networks," *Fire Safety Journal,* 9 (1986).
26. G.N. Berlin, A. Dutt, and S.M. Gupta, "Modeling Emergency Evacuation from Group Homes," Annual Conference on Fire Research, National Bureau of Standards, Gaithersburg, MD (1980).
27. P.B. Mirchandani, *Computations and Operations Research,* 3, Pergamon Press, Elmsford, NY, pp. 347–355 (1976).
28. L.G. Benckert and I. Sternberg, "An Attempt to Find an Expression for the Distribution of Fire Damage Amount," *Transactions of the Fifteenth International Congress of Actuaries,* 11, pp. 288–294 (1957).
29. B. Mandelbrot, "Random Walks, Fire Damage Amount and Other Paretian Risk Phenomena," *Operations Research,* 12, pp. 582–585 (1964).
30. G. Ramachandran, "The Poisson Process and Fire Loss Distribution," *Bulletin of the International Statistical Institute,* 43, 2, pp. 234–236 (1969).
31. H. Evring, J.C. Giddings, and L.G. Tensmeyer, "Flame Propagation: The Random Walk of Chemical Energy," *The Journal of Chemical Physics,* 24(4), pp. 857–861 (1956).
32. S. Karlin, *A First Course in Stochastic Processes,* Academic Press, New York (1966).
33. J.M. Hammersley and D.C. Handscomb, "Percolation Processes," *Monte Carlo Methods,* Methuen & Co. Ltd., London, Chapter II (1964).
34. S.R. Broadbent and J.M. Hammersley, "Percolation Processes, 1, Crystals and Mazes," *Proceedings of the Cambridge Philosophical Society,* 53, pp. 629–641 (1957).
35. M. Hori, "Theory of Percolation and Its Applications," *Nippon Tokeigakkai-shi,* 3, p. 19 (1972).
36. H. Sasaki and T. Jin, "Probability of Fire Spread in Urban Fires and Their Simulations," Report No. 47, Fire Research Institute, Tokyo, Japan (1979).
37. J. Nahmias, H. Tephany, and E. Guyon, "Propagation de la Combustion sur un Reseau Heterogene Bidimensionnel," *Revue Phys. Appl.,* 24, pp. 773–777 (1989).
38. F.A. Albini and S. Rand, "Statistical Considerations on the Spread of Fire," IDA Research and Engineering Support Division, Washington, DC (1964).
39. N.J.T. Bailey, "Reed and Frost Model," *The Elements of Stochastic Processes,* John Wiley and Sons, New York, Chapter 12, Section 5 (1964).
40. P.H. Thomas, "Some Possible Applications of the Theory of Stochastic Processes to the Spread of Fire," Internal Note No. 223, Fire Research Station, Boreham Wood, Herts, U.K. (1965).
41. G. Ramachandran, "Heat Output and Fire Area," *Proceedings of the International Conference on Fire Research and Engineering,* Society of Fire Protection Engineers, Orlando, FL, pp. 481–486 (1995).
42. A.M. Hasofer and V.R. Beck, "A Stochastic Model for Compartment Fires." *Fire Safety Journal,* 28, pp. 207–225 (1997).
43. D.D. Drysdale, *An Introduction to Fire Dynamics,* John Wiley and Sons, Chichester, UK (1985).
44. H. Takeda and D. Yung, "Simplified Fire Growth Models for Risk-Cost Assessment in Apartment Buildings," *Journal of Fire Protection Engineering,* 4, 2, pp. 53–66 (1992).
45. T.Z. Harmathy and J.R. Mehaffy, "Normalized Heat Load: A Key Parameter in Fire Safety Design," *Fire and Materials,* 61, pp. 27–31 (1982).
46. T.E. Harris, *The Theory of Branching Processes,* Springer-Verlag, Berlin (1963).
47. W.E. Wilkinson, "Branching Processes in Stochastic Environments," Ph.D. Thesis, University of North Carolina, Chapel Hill (1968).
48. P.D. Phung and A.B. Willoughby, "Prediction Models for Fire Spread Following Nuclear Attacks," Report No. URS641-6, URS Corporation, Burlingame, CA (1965).

CHAPTER 16

Explosion Protection

Robert Zalosh

Introduction

Combustible gases, vapors, and dusts/powders represent explosion hazards when and if they are mixed with air (or some other oxidant) in proportions between the lower and upper flammable limits. The explosion hazard is associated with the premixing of fuel and oxidant in a confined environment prior to the introduction of an ignition source. Upon ignition, flame propagates through the fuel-oxidant mixture, and the confinement prevents the unrestrained expansion of the combustion products. The result is the rapid development of a potentially damaging pressure increase.

Explosion hazard evaluations usually entail (1) recognizing the potential formation of a flammable fuel-air mixture, (2) identifying potential ignition sources present after fuel-air mixture formation, and (3) determining the resulting explosion pressures and their implications with regard to structural damage potential. Explosion protection measures interrupt this sequence of explosion events either by (1) preventing fuel-air mixture formation (e.g., by ventilation or inerting), (2) eliminating potential ignition sources (e.g., by grounding equipment to prevent electrostatic discharges), or (3) limiting pressure buildup (e.g., by explosion venting or explosion suppression). This chapter provides an engineering framework for performing this type of explosion hazard and protection measure evaluation.

Flammability, Explosibility, and Inerting

Gases and Vapors

Flammable limit concentrations for gases and vapors are traditionally determined in a glass test vessel that allows observation of any flame propagation. In some cases, the test vessel is a 5- to 10-cm-diameter, 1.5-m-long, glass tube,[1] while in other cases a 5-liter-capacity (22-cm-diameter) flask is used.[2] A spark situated either at the open lower end of the tube, or near the center of the flask is triggered to determine the flammability of a gas-air mixture of known concentration. If ignition results in flame propagation to the top of the tube, or upward and outward from the center of the flask,[2] the mixture is deemed flammable. The lower flammable limit is the average value of (1) the lowest gas/vapor concentration capable of supporting flame propagation and (2) the largest concentration that does not result in flame propagation. Similarly, the upper flammable limit is average value of (1) the highest gas/vapor concentration for which flame propagation is observed and (2) the lowest concentration at which there is no propagation. The chapter in this handbook entitled "Flammability Limits of Premixed and Diffusion Flames" (Section 2, Chapter 7) has tabulated values of the lower and upper flammable limits reported previously by Zabetakis.[1]

Flammability limit testing is also sometimes performed in pressure vessels that allow pressure increases to indicate flame propagation. Since this type of test is a more direct measure of explosion hazards, the data are usually called explosion limits. In some cases (e.g., methane lower limit and hydrogen upper limit) the flammability limits and explosibility limits are virtually the same, but in other cases (e.g., methane upper limit and hydrogen lower limit) there can be substantial differences. In practice, flammability limits are used when the criterion is the prevention of flame propagation, and explosibility limits are used either when the criterion is the avoidance of a significant overpressure, or when flammability limits are needed at elevated temperatures or pressures.[3] Upper flammable limits are more sensitive to pressure variations than lower limits, except at very low pressures (typically less than one-tenth of an atmosphere) where the two limits suddenly narrow and the gas or vapor becomes nonflammable.[4]

The maximum safe oxygen concentration for explosion prevention via inerting is called the limiting oxidant

Dr. Robert Zalosh is a professor of fire protection engineering at Worcester Polytechnic Institute. He previously worked for Factory Mutual Research Corporation where he initiated the explosion research group and was manager of the applied research department. Professor Zalosh has been a member of the NFPA Committee on Explosion Protection Systems for more than 20 years.

concentration (LOC) in NFPA 69, *Standard on Explosion Prevention Systems,* 1997 edition.[5] Representative values for the limiting oxygen concentration for nitrogen inerting and carbon dioxide inerting are listed in Table 3-16.1. The LOC for carbon dioxide inerting of all of the flammable vapors/gases in Table 3-16.1 except hydrogen is in the range 11.5 to 14.5 volume percent, whereas the corresponding range for nitrogen inerting is 9.5 to 12 volume percent.

The volume percent of inert gas needed to reduce the oxygen concentration to the LOC values shown in Table 3-16.1 is

$$\% \text{ Inert} = 100 - 4.76(\text{LOC})[1 + (F/A)] \qquad (1)$$

where *F/A* is the fuel/air volumetric ratio for the most challenging gas-air mixture for inerting. Values of *F/A* can be determined if the complete fuel-air-inert flammability diagram is available. Flammability diagrams for methane and for *n*-hexane are given in the chapter "Flammability Limits of Premixed and Diffusion Flames." The *F/A* corresponding to the nose of the methane flammability diagram is the stoichiometric ratio of 0.105. The *F/A* corresponding to the nose of the *n*-hexane flammability diagram is approximately 0.03, which is somewhat greater than the stoichiometric ratio for hexane-air. Since the worst-case *F/A* value is $\ll 1$ for most flammable gases and vapors, a reasonably conservative approximation for use in the absence of the complete flammability diagram would be to set $F/A = 0$ in evaluating the volume of inert gas needed via Equation 1.

It is important to recognize that practical applications of flammability/explosibility data for explosion hazard evaluations should account for nonuniform or stratified vapor-air mixtures. The accuracy, response-time, and reliability of the oxygen monitoring instrumentation is another important consideration. Based on these considerations, the guidelines for inerting systems given in NFPA 69 state that the maximum allowable oxygen concentration should be at least 2 volume percent below the LOC when the concentration is continuously monitored. If the oxygen concentration is not continuously monitored, a greater margin of safety is needed.

Table 3-16.1 ***Limiting Oxygen Concentrations for Fuel-Air Mixtures with Added N_2 or CO_2[5]***

Fuel	Limiting Oxygen Concentration for Nitrogen Inerting	Limiting Oxygen Concentration for Carbon Dioxide Inerting
	Gases and vapors	
Acetone	11.5	14
n-Butane	12	14.5
Ethanol	10.5	13
Ethylene	10	11.5
n-Heptane	11.5	14.5
Hydrogen	5.0	5.2
Methane	12	14.5
Methyl Ether	10.5	13
Propane	11.5	14.5
Toluene	9.5	—
	Combustible dusts	
Aluminum	5	2
Cellulose Acetate	9	11
Coal, Bituminous	14	17
Coal, Subbituminous	—	15
Corn Starch (17 μm)	9	—
Epoxy Resin	—	12
Nylon	—	13
Polycarbonate	—	15
Silicon	11	12
Stearic Acid and Metal Stearates	10.6	13
Sulfur	—	12
Zinc	9	10
Zirconium	0	0

Combustible Dusts and Powders

Combustible dusts and powders pose a potential explosion hazard when their characteristic particle size is smaller than 100 to 400 micrometers (depending on material combustibility) and they are suspended in air at a concentration between the lower and upper explosive limits. Typical lower explosive limits for dusts with characteristic particle sizes less than about 100 micrometers are in the 30- to 60-g/m^3 range, which is roughly equal to the range for many flammable gases and vapors when expressed in these units. The upper explosive limit for dusts is typically[4] between 2000 and 6000 g/m^3, but it is a difficult measurement to make and an even more difficult measurement to apply as a practical explosion prevention measure.

Contemporary laboratory testing to determine dust explosibility is conducted with a near-spherical vessel of 20- to 30-liter volume. Figure 3-16.1 is a schematic drawing of a typical 20-l spherical apparatus. The weighed dust sample is placed into an auxiliary dust chamber and is air-injected into the sphere via a perforated dispersion

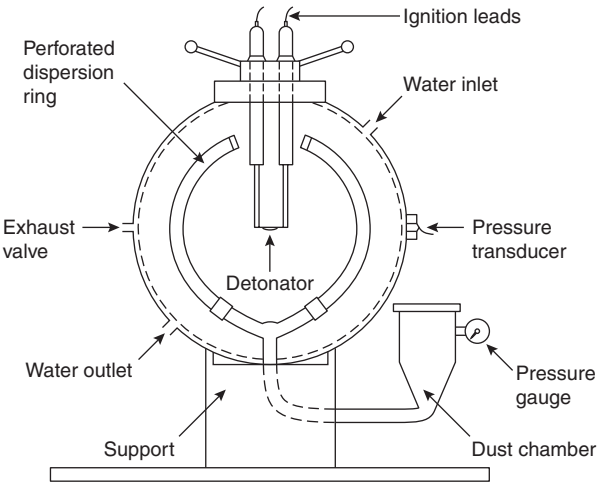

Figure 3-16.1. ***Twenty-liter spherical dust explosion apparatus.***

ring. An electrical spark or pyrotechnic igniter located in the center of the sphere ignites the dust cloud after a suitable time delay for dispersion. ASTM E1515,[6] the American standard for determining the minimum explosible concentration (MEC), specifies using either a 2500 J or 5000 J pyrotechnic igniter in a 20-l test vessel. Results are sensitive to the ignition source used and the level of turbulence in the test vessel at the time of ignition. In some cases, MEC results are so sensitive to the igniter energy that tests are needed in a 1-m^3 vessel to minimize ignition energy effects.

Minimum explosible dust concentrations, as determined in a 1-m^3 vessel, are shown in Table 3-16.2 for representative industrial and agricultural dusts. More comprehensive tabulations are available.[7,8] The MEC for a given material generally decreases with decreasing particle size, until a limiting size is reached, below which there is no further reduction of the MEC. Apparently, the combustion reaction is limited by the rate of devolatilization (which is dependent on particle surface area) at particle diameters above this limiting size, whereas the flame propagation rate is limited by vapor phase thermochemistry below this limiting size. This explanation is consistent with the equivalence of flammable gas and small-particle combustible dust lower limit concentrations for generically similar materials. For a given material and particle size, the MEC decreases linearly with increasing temperature.[9]

One inherent difficulty in using minimum explosible concentration data is the unknown or deceivingly minimal dust concentrations in many industrial facilities. An example might be a situation in which there is concern about possible explosive dust concentrations in a plastic powder silo. Even if suspended dust concentrations were measured during normal loading and unloading operations, considerably higher concentrations can be generated during upset conditions such as the use of vibrations or air blasts to dislodge powder flow obstructions.

One dust explosion prevention measure for equipment in which dust concentrations cannot be maintained below the MEC, is to use an inert gas to reduce the oxygen concentration. Limiting oxygen concentration data for several dusts are shown in Table 3-16.1. The data for carbon dioxide inerting of organic dusts are in the range 11 volume percent to 15 volume percent, but the LOC values for some of the metals are significantly lower. In fact, the zero LOC for zirconium is indicative of its pyrophoric behavior as a powder. As with the MEC, the LOC for a given dust decreases linearly with increasing temperature, according to the correlations presented by Siwek.[9]

The minimum ignition temperature (MIT) for a dust cloud is usually determined in an apparatus known as the Godbert-Greenwald furnace. A dust sample is air-injected into the top of the preheated vertical tube, and thermocouple measurements indicate whether the dust is ignited before it exits the bottom of the tube. Most of the dusts listed in Table 3-16.2, and in the more extensive tabulation by Eckhoff,[7] have cloud MIT values in the range 440°C to 750°C.

Dust layer ignition temperatures are usually measured using a 5-mm-thick layer of dust deposited on a hot plate with a temperature control. The temperature is in-

Table 3-16.2 ***Explosibility Data for Representative Powders and Dusts[7]***

Material	Median Particle Size (μm)	Minimum Explosive Concentration (g/m^3)	Minimum Cloud Ignition Temp (°C)	Minimum Layer Ignition Temp (°C)	Minimum Ignition Energy (mJ)	P_{max} (bar·g)	K_{ST} (bar·m/s)
Activated carbon	18	60	790	>450	—	8.8	44
Aluminum	<10	60	560	430	—	11.2	515
Ascorbic acid	39	60	460	Melts	—	9.0	111
Calcium stearate	<10	30	580	>450	16	9.2	99
Coal, bituminous (high volatility)	4	60	510	260	—	9.1	59
Corn starch	<10	—	520	>450	300	10.2	128
Epoxy resin	26	30	510	Melts	—	7.9	129
Fructose	200	60	440	440	180	7.0	28
Methyl cellulose	37	30	410	450	29	10.1	209
Milk powder	165	60	460	330	75	8.1	90
Napthalene	95	15	660	>450	<1	8.5	178
Paper tissue dust	54	30	540	300	—	8.6	52
Phenolic resin	<10	15	610	>450	—	9.3	129
Polyethylene, l.d.	<10	30[a]	420	Melts	—	8.0	156
Polyethylene, l.d.	150	125	480	Melts	—	7.4	54
Polyvinylchloride	25	125	750	>450	>2000	8.2	42
Rubber	80	30	500	230	13	8.5	138
Silicon	<10	125	>850	>450	54	10.2	126
Sugar	10	60	440	Melts	14	8.3	75
Zinc	<10	250	570	440	—	6.7	125

[a]This MEC for polyethylene was determined in a 1.2 liter cylinder.

creased slowly until the dust layer begins to glow. As is evident from the data in Table 3-16.2, the dust layer ignition temperature is often significantly lower than the dust cloud minimum ignition temperature. This is a ramification of the increased heat dissipation rates in a dust cloud compared to the interior of a dust layer.

An important consideration in applying the dust cloud and dust layer ignition temperature data is the frequent occurrence of nonuniform hot wall temperatures. An example is the situation in which a small hot spot is created by mechanical friction, perhaps in a blender or a pulverizer. Data presented by Siwek and Cesana[10] suggest that the small spot (with a temperature of at least 900°C) in a mill or similar process equipment can ignite a dust cloud if the MIT < 600°C as determined in furnace tests.

The minimum ignition energy (MIE) for an electrical spark discharge within a combustible dust cloud is measured via a standardized test conducted in a 1.2-l cylindrical tube, sometimes called a modified Hartmann tube. The International Electrotechnical Commission (IEC) test method described by Siwek and Cesana[10] allows for spark energies in the range from 1 mJ to several hundred mJ. MIE data for the dust samples in Table 3-16.2 range from less than 1 mJ to more than 2000 mJ. For a given material, the MIE is known to be influenced by the following parameters:

- The MIE decreases as the spark duration increases, due to the presence of either inductance or resistance in the capacitive discharge circuit. For example, adding a series inductance in the range 0.1 to 1.0 H, or a series resistance in the range 10^4 to 10^5 Ω, decreases the MIE by an order of magnitude. The practical significance of this is that it takes more spark energy for an electrostatic (capacitive) discharge to ignite a dust cloud than for a spark in electrical equipment due perhaps to actuation of an electromechanical switch. The MIE data in Table 3-16.2 were obtained with long duration inductive discharges.
- The MIE decreases as the dust median particle size increases; Siwek and Cesana[10] show that the variation is to the –2.5 power of particle diameter.
- The MIE varies with dust concentration, but the most sensitive concentration depends on the particular material. The data in Table 3-16.2 are for the most sensitive concentration.
- The MIE decreases with increasing air-dust temperature.
- The MIE and the MIT increase with increasing velocity of the dust-air mixture.

The theoretical spark energy can be calculated for simple electrical discharges. For example, the energy (J) in a purely capacitive discharge is $1/2CV^2$, where C is the capacitance (F), and V is the stored voltage prior to discharge. In the case of a purely inductive circuit, the theoretical spark energy is $1/2Li^2$, where L is the circuit inductance, and i is the current (A). The inductance spark energy can be compared directly to the MIE for a particular dust to assess the likelihood of ignition; the capacitive spark energy comparison should account for the higher ignition energies associated with short duration capacitive discharges. The energy associated with mechanical friction and impact sparks is much more difficult to determine. Siwek and Cesana[10] state that such sparks will only ignite dusts with MIE values <10 mJ and MIT values <500°C.

EXAMPLE 1:

Coal feed rates and airflow rates at two coal pulverizers are as follows. At Pulverizer A the bituminous coal feed rate is 1.9 kg/s and the airflow rate is 7.1 m^3/s. At Pulverizer B the coal feed rate is 13.9 kg/s and the airflow rate is 7.1 m^3/s.

Are the pulverizer outlet coal dust concentrations within the explosive range? If both coals have a Godbert-Greenwald furnace ignition temperature of 510°C, would you expect a dust explosion to occur if there is a frictional hot spot or a frictional spark in the pulverizer?

SOLUTION:

The pulverizer outlet coal dust concentration during steady-state operation is equal to the coal feed rate divided by the airflow rate. The concentrations for these two pulverizers are 0.27 kg/m^3 for Pulverizer A and 1.96 kg/m^3 for Pulverizer B. The Pulverizer A concentration is well within the explosive limits for typical bituminous coals. The Pulverizer B concentration is close to the reported upper explosive limit for coal (2 to 4 kg/m^3). Since the MIT of both coals is in the range 500 to 600°C, we would expect them to be ignitable by sustained mechanical friction that produces wall temperatures in the range 600 to 900°C depending on the size of the heated area; we would not expect ignition by short-duration mechanical impact sparks because the cloud MIT is greater than 500°C. This suggests that a temperature monitor in the pulverizer could be used to shut down the pulverizer well before the wall temperature approaches 600°C, either from mechanical friction or smoldering coal.

EXAMPLE 2:

An elevated silo with an electrical capacitance of 500 picofarads is used to store a pharmaceutical powder with a minimum ignition energy of 10 mJ for inductive sparks and 50 mJ for capacitive sparks. If the silo is not adequately grounded, what would its minimum voltage have to be in order for an electrostatic spark to ignite the cloud of powder in the silo, or being discharged from the silo?

SOLUTION:

The voltage needed to generate an electrostatic spark of capacitive energy E is equal to $\sqrt{2E/C}$, which in this case is equal to

$$\sqrt{\frac{2(50 \times 10^{-3}\ \text{J})}{500 \times 10^{-12}\ \text{F}}} = 1.4 \times 10^4\ \text{V} = 14\ \text{kV}$$

A very high voltage of this magnitude may indeed be generated from the continuous impact/friction of the powder during filling and unloading. Although grounding of the silo would prevent high voltage from accumulating on the silo itself, there is also a hazard associated with electrostatic charge accumulation on ungrounded

objects and equipment in the silo, and possibly on the powder itself if it has a high electrical resistivity.

Closed Vessel Deflagrations

Ignition of either a gas-air mixture or a dust cloud in an unvented enclosure will usually result in a deflagration (i.e., flame propagation at subsonic speed away from the ignition site). The pressure developed in the enclosure is dependent on the extent of flame propagation, and the temperature and composition of the burned gas. If the flame has propagated throughout the enclosure, the ratio of the deflagration pressure to the initial pressure in the enclosure can be obtained from the ideal gas equation as it applies to the postdeflagration and predeflagration gas-air mixtures, both of which occupy the same enclosure volume. Thus

$$\frac{P_m}{P_0} = \frac{n_b T_b}{n_0 T_0} \tag{2}$$

where

P_m = pressure developed at the completion of a closed vessel deflagration

P_0 = initial pressure in the enclosure

n_b = number of moles of burned gas at the completion of the deflagration

n_0 = number of moles of gas-air mixture initially in the enclosure

T_b = temperature of the burned gas at the completion of the deflagration

T_0 = initial temperature of the gas-air mixture

Equation 2 is applicable to both gas deflagrations and dust deflagrations. However, in the case of dust deflagrations, the effect of the dust does not appear explicitly in the equation because only the gas temperature and composition determine the deflagration pressure. Conservative estimates of burned gas temperature and composition can be obtained using the assumption that combustion occurs adiabatically at constant volume. Thus, the calculation of deflagration pressures becomes an exercise in thermochemical equilibrium in which the initial fuel-oxidant mixture is specified to react adiabatically at constant volume. Various computer codes can be used to do these calculations.

Calculated results obtained with the STANJAN code (written and distributed by Professor William Reynolds of Stanford University) are shown in Figure 3-16.2(a) for the adiabatic, constant-volume flame temperature, for methane-air, propane-air, and hydrogen-air mixtures of varying concentration. The fuel concentration used in Figure 3-16.2 is the equivalence ratio, defined as the fuel-to-air ratio divided by the stoichiometric fuel-to-air ratio. In terms of fuel volume fraction, x, the equivalence ration is equal to $[x(1 - x_{st})]/[x_{st}(1 - x)]$, where x_{st} is the stoichiometric volume fraction of fuel. The stoichiometric fuel volume fraction for methane–air is 0.095, for propane–air is 0.040, and for hydrogen–air is 0.296. The calculated adiabatic constant-volume flame temperatures shown in Figure 3-16.2(a) are generally 200°C to 400°C higher than the corresponding adiabatic, isobaric flame temperatures for the same fuel–air concentrations.

Calculated adiabatic constant-volume deflagration pressures for the same fuel-air mixtures are shown in Figure 3-16.2(b). The maximum pressures for each flammable gas occur at fuel equivalence ratios in the range 1.1 to 1.2 (i.e., at slightly richer than stoichiometric concentrations). These worst-case deflagration pressures are in the range 8 to 9.6 atm abs. Theoretical values of P_m at an equivalence ratio of 0.5, which corresponds to the lower flammable limit for methane and propane, are in the range 6 to 6.5 atm abs. Experimental measurements of closed vessel deflagration pressures agree well with the theoretical values of P_m at near-stoichiometric concentrations, but are significantly less than the theoretical values at concentrations near the lower and upper flammable limits. The reasons

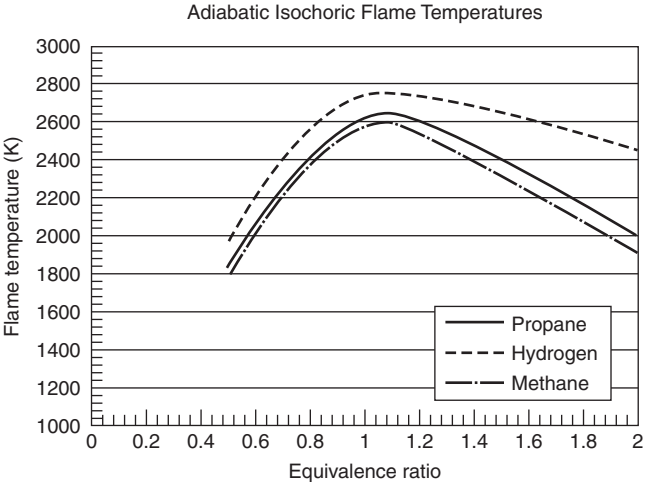

Figure 3-16.2(a). ***Calculated adiabatic, constant-volume flame temperatures as a function of equivalence ratio.***

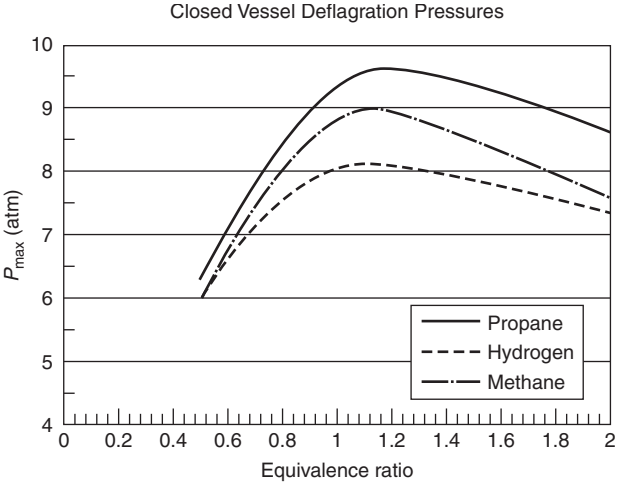

Figure 3-16.2(b). ***Flammable gas-air deflagration pressures as a function of fuel equivalence ratio.***

for the deviation at near-limit concentrations are 1) incomplete combustion due to flame propagation through only a portion of the enclosure and 2) slow flame propagation allowing time for heat losses from the burned gas mixture to the enclosure walls. As an example of the incomplete combustion, extensive deflagration testing of lean hydrogen–air mixtures has shown that the fraction of hydrogen burned ranges from zero to one as the hydrogen concentration increases from its lower limit of 4 volume percent to 8 volume percent, and remains equal to approximately one (complete combustion) as the hydrogen concentration ranges from 8 volume percent to about 40 volume percent (equivalence ratio of 1.6).

Measured values of P_{max} (worst-case P_m) are shown in Table 3-16.3 for twelve flammable gases and vapors. All but two values are in the range 6.8 bar to 8.1 bar g. The two exceptions are acetylene (P_{max} = 10.6 bar g) and ammonia (P_{max} = 5.4 bar g).

Theoretical values of P_m can also be calculated for combustible dusts using a thermochemical equilibrium computer code, such as the NASA code CET89, that contains extensive properties for condensed phase materials. Experimental values of P_m depend on particle size as well as dust concentration. The effect of particle size is illustrated by the data in Figure 3-16.3. The value of P_{max} for three of the four dusts is invariant with particle size providing the median particle diameter is no greater than 100 μm. However, for polyvinylchloride (which is significantly less combustible than the other three materials), P_{max} decreases with increasing median particle size for all particles greater than 20 μm, and cannot be ignited at all at particle sizes of 150 μm and larger. The effect of dust concentration on P_{max} is such that the worst-case concentration often occurs at a concentration of about 500 g/m³, which for many organic materials is roughly twice the stoichiometric concentration, and five to ten times the minimum explosible concentration. Values of P_{max} for the twenty dust samples listed in Table 3-16.2 are in the range 6.7 bar g to 11.2 bar g (i.e., about the same range as the values of P_{max} for flammable gases and vapors).

Table 3-16.3 ***Deflagration Parameters for Flammable Gases and Vapors in Air[8]***

Gas or Vapor	P_{max} (bar g)	Laminar Burning Velocity (cm/s)	K_G (bar·m/s)
Acetylene	10.6	166	1415
Ammonia	5.4	—	10
n-Butane	8.0	45	92
Diethyl ether	8.1	47	115
Ethane	7.8	47	106
Hydrogen	6.8	312	550
Isopropyl alcohol	7.8	41	83
Methane	7.1	40	55
Methyl alcohol	7.5	56	75
n-Pentane	7.8	46	104
Propane	7.9	46	100
Toluene	7.8	41	94

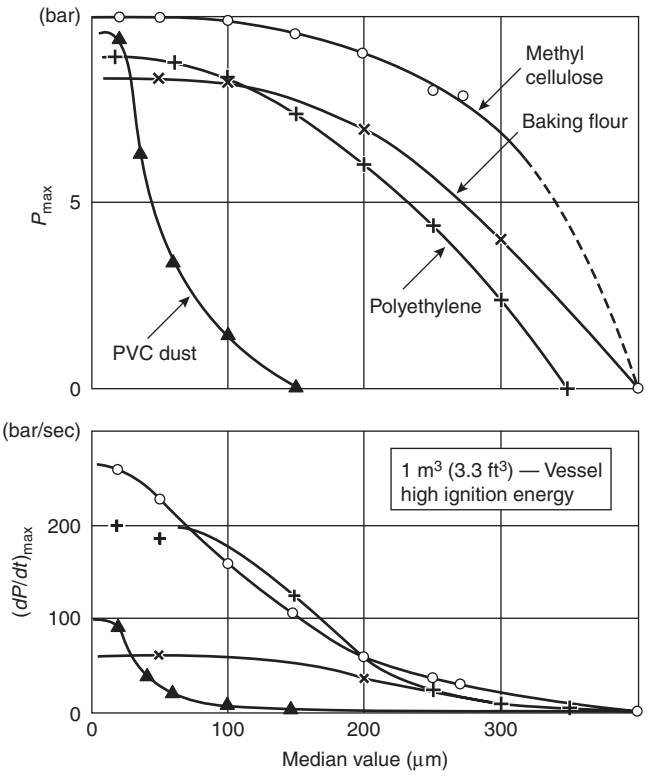

Figure 3-16.3. ***Effect of particle size on deflagration pressure and rate-of-pressure rise.[8]***

The rate of pressure rise during a deflagration is primarily dependent on the rate of flame propagation and the vessel size, as well as the flame temperature. Theoretical calculations are usually based on the following assumptions. First, it is assumed that the flame speed is small in comparison to sound speed so that the pressures in the enclosure are spatially uniform at any given time during the deflagration. The rate of flame propagation relative to the unburned gas ahead of the flame front is called the burning velocity, S_u. The mass burning rate is

$$\frac{dm_b}{dt} = -\frac{dm_u}{dt} = \rho_u \chi S_u A_f \qquad (3)$$

where

m_b = mass of burned gas in enclosure at time t
m_u = mass of unburned gas in enclosure at time t
ρ_u = density of unburned gas at time t
A_f = surface area of flame front at time t
χ = ratio of turbulent burning velocity to laminar burning velocity

Flame propagation into a near-stoichiometric gas-air mixture will occur as an expanding spherical flame until the flame approaches the walls of the enclosure. Laminar burning velocities have been measured for worst-case concentrations of many gases and vapors. Values are listed for the twelve gases/vapors in Table 3-16.3. Representative

values for the alkanes and many other hydrocarbons are 40 to 47 cm/s. Expansion of the burned gas, and the corresponding motion of the unburned gas away from the ignition site as the flame propagates, causes the actual flame velocity relative to a fixed observer (i.e., the flame speed) to be significantly larger than the burning velocity. Before any compression occurs, the flame speed is $(T_b/T_0)S_u$, which is equal to 350 to 440 cm/s for many hydrocarbons at near-stoichiometric concentrations. Turbulent motion of the unburned gas can further increase the burning velocity and flame speed, as represented either by the augmentation factor χ, or by generating wrinkled or distorted flames with corresponding larger flame surface areas, A_f.

A second key assumption invoked in most theoretical models of closed vessel deflagrations is that the fractional pressure rise at any time during the deflagration is equal to the fraction of the total mass burned, that is,

$$\frac{P - P_0}{P_m - P_0} = \frac{m_b}{m_0} \tag{4}$$

where

P = deflagration pressure at time t

m_0 = total mass in the enclosure

The justification for Equation 4 is that it has been verified by more complicated models, such as the Complete Computer Solution described by Bradley and Mitcheson,[11] as well as by experimental data reported in that paper and in Lewis and von Elbe.[12] Equation 4 can also be used to calculate the maximum pressure developed in enclosures that are partially with fuel-air mixtures (i.e., partial volume deflagrations).

The third assumption needed for a closed vessel deflagration model is the type of thermodynamic process undergone by the unburned gas as it is compressed. The most common assumption is that the unburned gas is compressed isentropically [i.e., $P/P_0 = (\rho/\rho_u)^\gamma$], where γ is the ratio of specific heats of the unburned gas (1.4 for most flammable hydrocarbon-air mixtures). Although it is not necessary, it is also common to assume the flame continues to propagate spherically such that its radius at any time t is r_b in a vessel of radius a. The resulting equations for $P(t)$ and $r_b(t)$ are

$$\frac{dP}{dt} = \frac{3\chi S_u}{a}\left(\frac{P}{P_0}\right)^{1/\gamma}(P_m - P_0)\left(\frac{r_b}{a}\right)^2 \tag{5}$$

$$\left(\frac{r_b}{a}\right)^2 = \left[1 - \left(\frac{P_0}{P}\right)^{1/\gamma}\left(\frac{P_m - P}{P_m - P_0}\right)\right]^{2/3} \tag{6}$$

Equations 5 and 6 can be solved simultaneously starting from the initial condition that $r_b/a = \varepsilon$ at $t = 0$, where ε is some small number $\ll 1$ representing the kernel of flame at ignition. An example solution for $P(t)$ and $r_b/a(t)$ for the case S_u = 45.5 cm/s, $\chi = 1$, P_m = 640 kPa g, a = 7.15 m is shown in Figures 3-16.4(a) and 3-16.4(b). The curve in Figure 3-16.4(a) labeled *numerical solution* refers to the numerical integration of Equation 5. The curve labeled *analytical approximation* refers to the following simplified solution for $P(t)$ early in the deflagration when $(P - P_0)/P_0 \ll 1$.

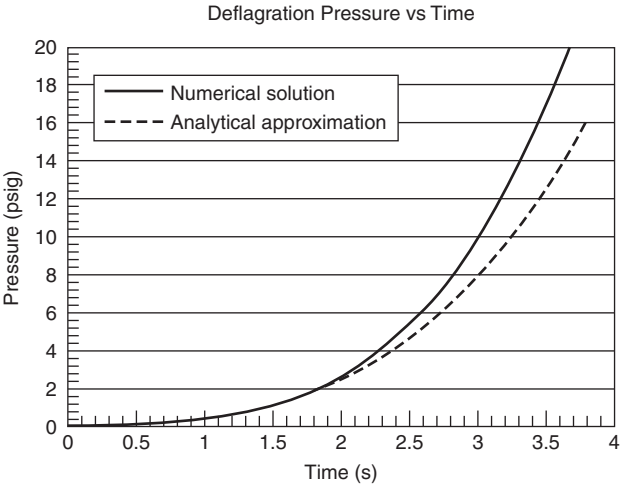

Figure 3-16.4(a). ***Pressure versus time for a closed vessel deflagration with S_u = 45.5 cm/s, a = 7.15 m, and P_m = 640 kPa g.***

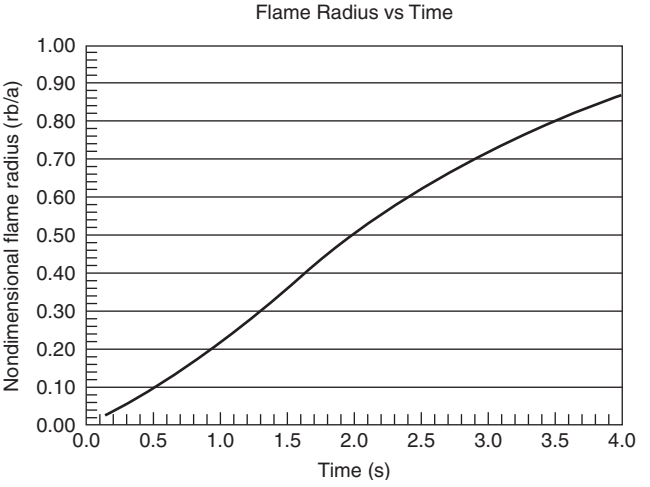

Figure 3-16.4(b). ***Calculated nondimensional flame radius during deflagration.***

$$\frac{P - P_0}{P_0} = \left(\frac{1}{\gamma} + \frac{P_0}{P_m - P_0}\right)^2\left(\frac{P_m - P_0}{P_0}\right)^3\left(\frac{\chi S_u t}{a}\right)^3 \ll 1 \tag{7}$$

The analytical approximation in Figure 3-16.4(a) is virtually identical to the numerical solution when $P < 2$ psig, and only differs by about 20 percent up to P = 8 psig. The flame radius at the time P = 2 psig is equal to half the enclosure vessel radius, and it is equal to 80 percent of the vessel radius when P = 16 psig. Since the pressure ultimately increases to 93 psig in this particular deflagration, it is clear that most of the pressure increase occurs when

the flame has propagated very close to the enclosure wall, such that the entire enclosure is almost filled with flame.

The continued integration of Equation 5 up to $P = P_m$ would require an empirical correlation to account for the variation of S_u with increased pressure and temperature of the unburned gas as it is compressed. Bradley and Mitcheson[11] have carried out nondimensionalized solutions using such correlations. Their results indicate that the time, t_m, at which P reaches P_m can be approximated as

$$t_m = \frac{a}{0.3S_u}$$

where the burning velocity is the mean value of the burning velocities at the beginning and end of the deflagration (i.e., when $P = P_0$ and $P = P_m$). In other words, the mean flame speed, a/t_m, during the deflagration is equal to 3.3 times the mean burning velocity.

Experimental measurements of the rate-of-pressure-rise in a closed vessel explosion are often characterized in terms of the parameter, K_G, defined as

$$K_G = \left(\frac{dP}{dt}\right)_{\max} V^{1/3} \tag{8}$$

where V is the vessel volume, and the maximum rate of pressure rise is measured at the inflection point in the P-versus-time curve. Theoretically, there is no inflection point (because there is no heat loss or other mechanism to decelerate the flame), and $(dP/dt)_{\max}$ occurs when $P = P_m$. Based on Equation 5, the theoretical relationship between K_G and S_u is

$$K_G = 4.84\chi S_u \left(\frac{P_m}{P_0}\right)^{1/\gamma} (P_m - P_0) \tag{9}$$

Experimentally determined values of K_G listed in Table 3-16.3 for the various gases and vapors indicate that they generally increase as S_u increases, but that they are not necessarily linearly proportional to S_u. This is a manifestation of the fact that the turbulence factor, χ, varies among the individual gases and vapors in a manner that cannot be predicted a priori.

The effect of turbulence on the rate-of-pressure-rise is even more important in the case of dust explosions. There is inherently some level of turbulence in every dust explosion because some type of disturbance or initial motion is needed to generate the dust cloud. One convenient, albeit indirect, measure of the turbulence level is the time delay between the beginning of dust injection and ignition actuation. The turbulent motion in the vessel is a maximum when the dust is first injected, and decays significantly by the time the entire dust cloud has entered the vessel. Figure 3-16.5 shows how the ignition delay time influences the values of $P_{\max}$ and $(dP/dt)_{\max}$ measured in a 1-m^3 vessel with coal dust and with aluminum dust. In view of the importance of this effect, a standardized test method has been developed[13] in the interest of obtaining reproducible results in different test vessels and laboratories. Values of $K_{ST} = [(dP/dt)_{\max}]V^{1/3}$ obtained for various dusts using this standardized injection and ignition delay methodology are listed in Table 3-16.2. Except for aluminum, all of the dusts listed have K_{ST} values no greater than 208 bar·m/s. A more direct measure of turbulence level is the root-mean-square fluctuating air velocity in the vessel. Measurements of this rms velocity as a function of time following the initiation of dust injection have been carried out by several researchers and their results are summarized in Eckhoff's textbook.[7] Eckhoff also provides a summary of some theoretical models for closed vessel dust deflagrations that are analogous to the one described for gas explosions, but account for the finite particle burn time and corresponding finite flame thickness in dust explosions.

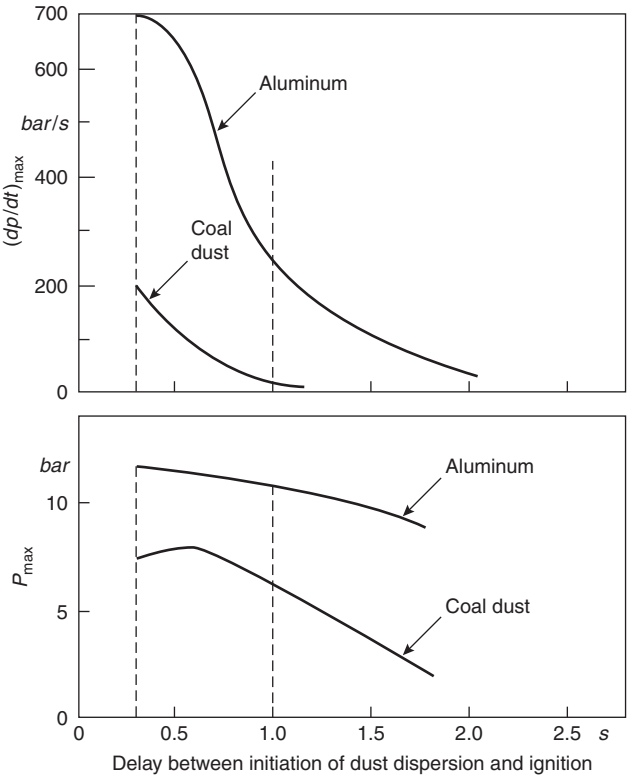

Figure 3-16.5. ***Effect of ignition delay time on deflagration pressure and rate-of-pressure-rise.[7]***

One special consideration in dust explosions is the propensity for damaging secondary explosions. These secondary dust explosions arise when a gas or dust deflagration in some process equipment causes the equipment to fail (because it cannot withstand the closed vessel deflagration pressure, $P_{\max}$), and produce a strong disturbance in the form of a blast wave and associated air motion. This disturbance often causes the dust that has settled on walls and floors to be put into suspension and form a combustible dust cloud. Even if the subsequent cloud occupies only a small fraction of the building, it is often ignited by the flame that has also emerged from the breached process equipment. If the secondary explosion occurs in an occupied building, it can produce numerous

casualties as well as building structural damage. The quantities of dust needed to generate a particular pressure rise can be estimated using Equation 4.

EXAMPLE 3:

Approximately 200 g of *n*-butane are released into an aerosol can–filling room due to a valve misalignment on one large deodorant can. Suppose the butane mixes in stoichiometric proportions with a portion of the air in the $4 \times 4 \times 3$ m room and is subsequently ignited. What will the peak pressure be in the absence of any explosion venting?

SOLUTION:

Equation 4 can be used to solve this problem if we first calculate the mass of butane needed to fill the entire room with a stoichiometric butane-air mixture. We can do this calculation in terms of the mixture density, ρ_0, and the butane mass fraction as follows:

$$m_0 = \left(\frac{x_{\text{but}} M_{\text{but}}}{M_{\text{mix}}}\right)\rho_0 V$$

where the mixture molecular weight, M_{mix}, is calculated based on the stoichiometric concentration of butane (3.1 volume percent).

$$\begin{aligned} M_{\text{mix}} &= x_{\text{but}} M_{\text{but}} + (1 - x_{\text{but}}) M_{\text{air}} \\ &= (0.031)(58) + (1 - 0.031)(28.8) = 29.7 \end{aligned}$$

The mixture density (which is not much different than air density) is calculated from the ideal gas equation:

$$\begin{aligned} \rho_0 &= \frac{M_{\text{mix}} P_0}{R T_0} = \frac{(29.7 \text{ kg/kmol})(101 \times 10^3 \text{ Pa})}{(8314 \text{ J/kmol} - \text{K})(298 \text{ K})} \\ &= 1.21 \text{ kg/m}^3 \end{aligned}$$

$$\begin{aligned} \text{Therefore, } m_0 &= \left[\frac{(0.031)(58)}{29.7}\right](1.21 \text{ kg/m}^3)(48 \text{ m}^3) \\ &= 3.52 \text{ kg.} \end{aligned}$$

and $m_b/m_0 = (0.20 \text{ kg})/(3.52 \text{ kg}) = 0.057$.

Using the value for $P_m - P_0$ for *n*-butane in Table 3-16.3,

$$P - P_0 = (8.0 \text{ bar g})(0.057) = 0.456 \text{ bar g} = 6.6 \text{ psig.}$$

We note that since this pressure is greater than the strength of rooms in industrial facilities, some form of explosion venting and explosion suppression would be needed. We also note that this scenario is entirely possible even though the 200 g of *n*-butane released would be too small to form a flammable mixture if it was dispersed uniformly throughout the 48 m^3 enclosure.

EXAMPLE 4:

Determine the value of χ, the ratio of turbulent-to-laminar burning velocity, corresponding to the K_G value listed in Table 3-16.3 for *n*-butane.

SOLUTION:

The value of χ can be calculated using Equation 9 as follows:

$$\begin{aligned} \chi &= \frac{K_G}{4.84 S_u \left(\dfrac{P_m}{P_0}\right)^{1/\gamma} (P_m - P_0)} \\ &= \frac{92 \text{ bar} - \text{m/s}}{4.84(0.45 \text{ m/s})(9.0)^{1/1.4}(8 \text{ bar})} = 1.10 \end{aligned}$$

This suggests that the flame speed in the test used to determine K_G was not significantly faster than the speed corresponding to the laminar burning velocity for a worst-case butane-air mixture.

EXAMPLE 5:

A coal-fired power plant has bituminous coal dust layers with a mass-per-floor-area of 1000 g/m^2 in an enclosure with a 4-m ceiling height. Assume the coal dust layer is dispersed by a primary explosion such that it forms a worst-case dust cloud with a concentration of 500 g/m^3 in the lower portion of the enclosure. What would the pressure increase due to a secondary explosion in the enclosure without any explosion venting be?

SOLUTION:

Equation 4 can be used to solve this problem if we use both m_b and m_0 on a per-unit-floor-area basis. Thus, $m_0/A = (500 \text{ g/m}^3)(4 \text{ m}) = 2000 \text{ g/m}^2$, and we are given $m_b/A = 1000 \text{ g/m}^2$. Using the value of $P_m - P_0$ for bituminous coal in Table 3-16.2,

$$P - P_0 = (9.1 \text{ bar g})(1/2) = 4.55 \text{ bar g} = 66 \text{ psig}$$

If the volumetric bulk density of the coal dust layer is equal to a typical value of 500 kg/m^3, the corresponding coal dust layer thickness would be

$$\frac{1.00 \text{ kg/m}^2}{500 \text{ kg/m}^3} = 2 \times 10^{-3} \text{ m} = 2 \text{ mm}$$

Detonations

A detonation is an explosion in which the combustion wave (i.e., flame) propagates at supersonic speeds through the unburned fuel. Detonations are fundamentally different than the closed vessel deflagrations described in the previous section of this chapter. Since flames in a deflagration propagate at speeds well below the speed of sound (which is about 340 m/s in room temperature air), the pressure increase during a deflagration occurs virtually uniformly throughout the enclosure as the explosion evolves. In contrast, the pressure rise during a detonation is highly nonuniform and occurs virtually instantaneously as the shock wave propagates through the gas–air mixture. If the flame speed is slightly less than the speed of sound, such that the pressure rise is nonuniform but shock waves do not occur, the explosion is called a quasi-detonation.

The practical significance of this fundamental difference between detonations and deflagrations is that they require different approaches to explosion protection. The sudden, spatially nonuniform pressure rise during a detonation or quasi-detonation precludes the use of explosion venting or explosion suppression systems. Furthermore, the high-peak, short-duration detonative pressure loads warrant special considerations in the evaluation of structural resistance.

The peak pressure during a detonation can be calculated from the classical Chapman-Jouguet theory, which is a combination of thermochemical equilibrium and gas dynamic conservation equations across the detonation front.[12,14] Figure 3-16.6 shows calculated detonation pressures as a function of fuel concentration for seven different flammable gases. Chapman-Jouguet calculations for these and other mixtures can be conducted with both the STANJAN and CET89 computer codes mentioned previously for deflagration calculations. Burgess et al.[14] and others have suggested that a good approximation to the Chapman-Jouguet detonation pressure, P_{CJ}, is $P_{CJ} = 2P_m$ (i.e., twice the closed vessel deflagration pressure). This approximation represents a much simpler alternative to the Chapman-Jouguet theory of calculating detonation pressures. As indicated in Figure 3-16.6, P_{CJ} for a near-stoichiometric gas-air mixture initially at atmospheric pressure is in the range 16 to 20 atmospheres.

The pressure distribution behind the C-J detonation front is shown in Figure 3-16.7 for the case of a detonation wave propagating in both directions away from the initiation site in a tube. Behind the propagating detonation front the pressure decreases to a plateau value equal to about 0.35 P_{CJ}. The speed of propagation is equal to the C-J Mach number times the speed of sound in the unburned gas-air mixture. If the tube has one or more closed ends, the detonation wave will be reflected and propagate in the reverse direction with increased amplitude. If the end wall is rigid, the reflected shock wave for many gas-air mixtures is equal to 2.76 P_{CJ}. If the end wall is open, the detonation wave will be reflected as a rarefaction wave propagating back toward the detonation initiation site.

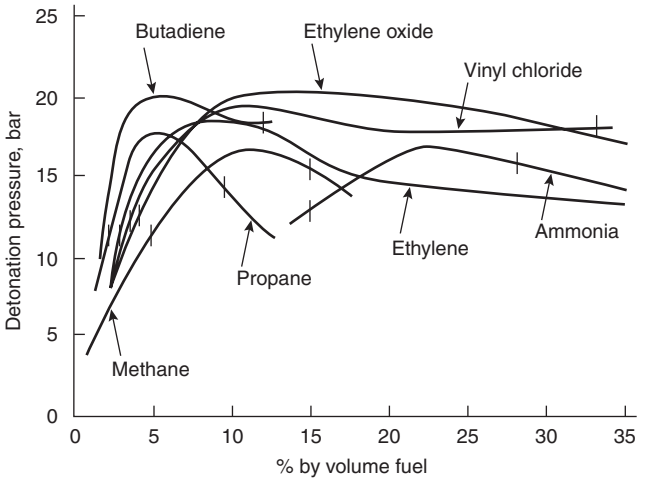

Figure 3-16.6. ***Calculated Chapman-Jouguet detonation pressures.***

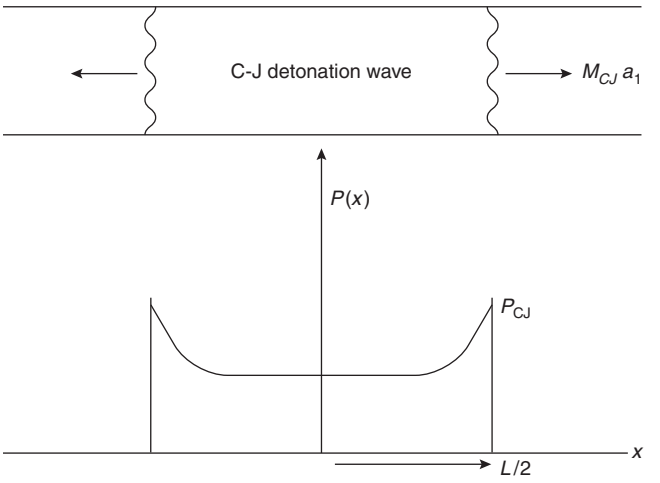

Figure 3-16.7. ***Pressure distribution in C-J detonation wave propagating through a tube.***

The structural load associated with a detonation wave depends on the impulse, I_D, per unit area, where

$$I_D(x,t) = \int_{t_a}^{t} [p(x,t) - p_a]\, dt \tag{10}$$

The detonation front arrival time, t_a, is equal to $x/(M_D a_1)$, where x is the distance from the detonation initiation site, M_D is the detonation Mach number, and a_1 is the speed of sound in the unburned gas-air mixture.

Neglecting any reflected waves, Sichel[15] has shown that a good approximation for I_D is

$$I_D = \frac{0.35 \rho_1 a_1 M_D x}{(\gamma_2 + 1)} \tag{11}$$

where γ_2 is the ratio of specific heats in the burned gas; in many cases γ_2 is equal to 1.2. The C-J detonation Mach numbers for several stoichiometric gas–air mixtures are listed in Table 3-16.4. They are in the relatively narrow range 4.9 to 5.5. The unburned gas sound speed for most stoichiometric hydrocarbon-air gas mixtures is in the narrow range 330 m/s to 350 m/s, while for hydrogen it is 403 m/s.

An interesting aspect of Equation 11 is that the specific impulse is linearly proportional to the distance from detonation initiation site. Burgess et al.[16] note that pipeline detonations often cause periodic ruptures along the pipeline length, with each break serving as a pressure relief expansion, requiring the pressure duration/impulse to rebuild to the structural failure threshold again by propagating over another length of pipe. Methods to assess the structural damage potential from these impulsive loads generated during detonations are described by Baker et al.[17] One after-the-fact indication of

Table 3-16.4 ***Detonation Mach Numbers and Cell Sizes for Stoichiometric Gas-Air Mixtures***

Gas	C-J Mach Number	Cell Width (cm)[19]
Acetylene	5.46	0.98
n-Butane	—	5.0–6.2
Ethane	—	5.4–6.2
Ethylene	—	2.8
Hydrogen	4.89	1.5
Hydrogen sulfide	—	10
Methane	5.17	28
Propane	5.38	6.9
Propylene	—	5.4

C-J Mach numbers were calculated with the STANJAN computer code.

structural failure due to detonative loads is the occurrence of fragmented structural debris associated with brittle failure, as opposed to the bulging and more ductile failure of structural steel subjected to deflagration pressures beyond the yield point.

In view of the drastically different explosion protection considerations for detonations, it is important to assess the potential for a detonation to occur as opposed to a deflagration. Some guidance, as described below, can be offered for this assessment, but there are no exact criteria to provide an unequivocal answer.

The detonability length scale is the detonation cell width, S_c, shown in Figure 3-16.8. As indicated in Figure 3-16.8, the detonation front consists of a complicated network of curved shock segments that propagate transversely to the detonation propagation direction. The transverse wave structure includes curvilinear triangles with a width S_c. If a smoke foil is inserted on the inner wall of a detonation tube, the detonation cells create a diamond- or fish-scale-shaped pattern on the smoke foil. Detonation cell widths are measured from the traces deposited on these smoke foils as described, for example, by Gelfand et al.[18] The same is true for chemical induction length as a qualitative measure of detonability.

Detonation cell widths can also be correlated with the detonation reaction zone length in a one-dimensional representation of the shock wave initiated chemically reacting flow behind the leading edge of a detonation. This model, which is called a ZND model (the initials stand for three original model developers), requires some chemical kinetics data as well as an assumption about heat losses and drag associated with the tube wall. The calculations and their relationship to cell size are described by Gelfand et al.,[18] by Shepherd,[20] and by Stamps et al.[21]

Detonation cell widths measured or calculated for nine different stoichiometric gas-air mixtures are listed in Table 3-16.4. Values range from about 1 cm for acetylene to about 28 cm for methane. These values were obtained at atmospheric pressure and room temperature. Higher initial pressures and temperatures would result in smaller cell widths. Furthermore, some of the gases listed in Table 3-16.4 have smaller cell widths at some fuel-rich concentrations, with minimum values for a given fuel being as much as 40 percent smaller than the values shown in the table.

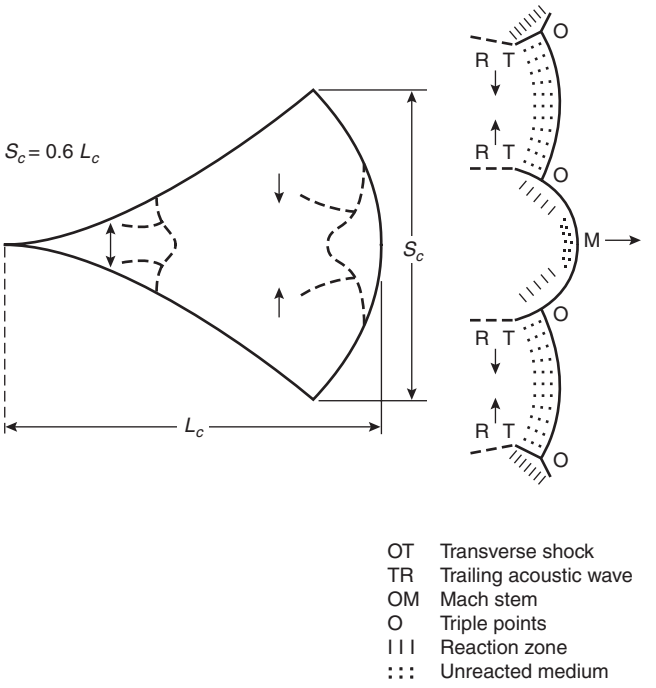

Figure 3-16.8. ***Detonation cell structure.[18]***

A sustained detonation can only occur if the characteristic length scale of the gas-air mixture is greater than some multiple of the detonation cell width. The value of the multiplication factor depends on the geometry. In the case of a pipe, the detonation will not propagate down the pipe if the pipe diameter is less than about $S_c/3$. The detonation will not propagate from open end of the pipe into the surrounding gas mixture if the pipe diameter is less than 13 S_c.

What is the likelihood of a detonation occurring in an enclosure or cloud larger than the critical size indicated by the detonation cell size? The answer depends on the strength of the ignition source and the presence of either a highly elongated geometry or an exceptionally high level of turbulence for promoting flame acceleration. The minimum ignition source energy required for the direct initiation of a detonation ranges from a low of about 5 kJ for acetylene and hydrogen in air to a high estimated to be 93,000 kJ for methane. Since these initiation energies are many orders of magnitude larger than the energies associated with accidental ignition sources, direct initiation can be precluded from almost all accident initiation scenarios.

In the case of a weak (typically accidental) ignition source in a pipe or some other elongated enclosure, the deflagration-to-detonation transition (DDT) distance depends upon the following parameters.

Mixture reactivity. The more reactive the mixture, the more rapid is the flame acceleration to DDT.

Enclosure or pipe wall roughness and the presence of obstruction. The rougher the pipe interior surface or the more obstructions present, the shorter is the transition length to DDT.

Enclosure or pipe diameter. The larger the pipe or enclosure diameter, the shorter is the transition to DDT.

Initial pressure and temperature. The higher the initial temperature and pressure, the shorter is the transition length to DDT.

Initial turbulence level. The more turbulence or initial gas velocity in the enclosure, the shorter is the DDT transition length.

Figure 3-16.9 illustrates how mixture reactivity influences the DDT length/diameter ratio for the case of a smooth walled 2-inch (5-cm) diameter pipe.[22] The ratio of DDT transition length to pipe diameter is plotted as a function of the ratio of nitrogen/oxygen concentration for methane, for ethane, and for propane at near-worst-case fuel/oxygen ratios that produce stoichiometric combustion with CO formation instead of CO_2. The L_{DDT}/diameter ratio increases rapidly as the nitrogen/oxygen ratio increases for all three alkanes, with the transition length being shortest for propane and longest for methane. In these experiments, the largest N_2/O_2 ratio at which transition occurred (last data point on each curve), was less than the 3.76 ratio corresponding to air. In other words, the L_{DDT}/diameter ratio for these alkanes in air (at a 2-inch pipe diameter) is larger than the largest ratio (120) measurable in these experiments. The three arrows in the graph represent the absence of transition at the indicated N_2/O_2 ratio. These data are consistent with the experimental observations of Flessner and Bjorkland,[23] who did *not* see DDT with gasoline-air mixtures in a 15-cm-diameter, 16-m-long smooth wall pipe, but saw DDT at a distance of 74 pipe diameters when they inserted an expanded metal liner in the pipe entrance to simulate a rough wall section.

Sherman and Berman[24] have developed a semiquantitative methodology to categorize the probability of detonations occurring in specific industrial accident scenarios by subjectively extrapolating the experimental data on the various effects mentioned above. They categorize gas mixture reactivities on the basis of detonation cell size, and they categorize enclosure geometries on the basis of size, confinement, level of obstructions, amount of venting, and so on. They have applied their methodology to the case of a possible hydrogen detonation during hypothesized severe accident scenarios in one particular nuclear plant containment building.

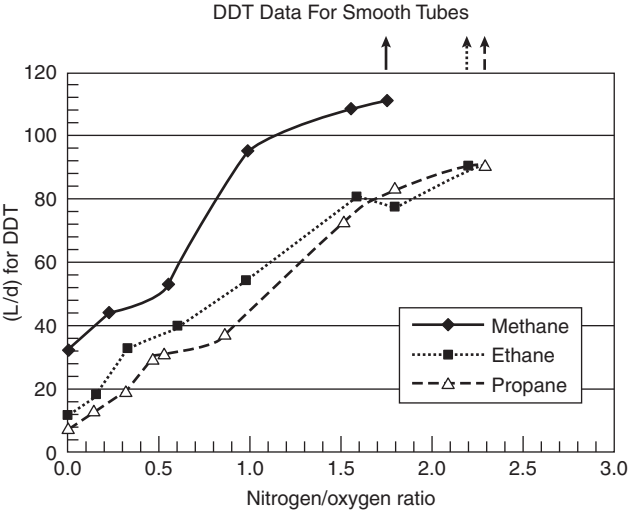

Figure 3-16.9. ***Deflagration-to-detonation transition length data.[23]***

Although most accidental explosions are deflagrations, there are some occasional well-documented accounts of detonation incidents. One excellent example is the Jacobs et al.[25] description of a particularly destructive detonation in a section of a petroleum refinery in which a gas mixture of 3 percent naptha, 19 percent oxygen, and 78 percent inert gas at 105 psig was accidentally allowed to enter several large pieces of process equipment connected by over 1000 ft of piping. Their account of the incident includes a description of the flame propagation path and associated pressures (3000–4000 psi in some locations) developed.

EXAMPLE 6:

A large process oven is heated with a burner utilizing a 1-cm-diameter, 5-m-long fuel line containing a stoichiometric propane-air mixture. What is the likelihood of a detonation occurring in the oven and the fuel line as a result of a delayed ignition after the oven has been inadvertently filled with a fuel-air mixture? How would the situation change if a stoichiometric hydrogen-air mixture replaced the propane-air mixture in the fuel line?

SOLUTION:

From Table 3-16.4, S_c = 6.9 cm for a stoichiometric propane-air mixture. Thus, the minimum pipe diameter for detonation propagation in this case is $S_c/3$ = 2.3 cm. Therefore, a sustained propane-air detonation will not propagate through the 1-cm fuel line. If the propane is replaced by hydrogen, $S_c/3$ = 0.50 cm, and a fuel line detonation would be possible, particularly in view of the 500:1 length to diameter ratio.

In order for the detonation to be transmitted into the oven, the fuel line would have to be larger than 13 S_c = 20 cm for hydrogen. Thus, the oven should not experience a detonation. Explosion venting could be a viable form of explosion protection for the oven.

EXAMPLE 7:

If a detonation did propagate through a stoichiometric hydrogen-air mixture in the fuel line, what would the specific impulse be on the pipe wall? Neglect any reflected shock wave effects, and use a sound speed of 400 m/s for the unburned stoichiometric hydrogen-air mixture.

SOLUTION:

Before using Equation 11 to evaluate the specific impulse, we need to calculate the molecular weight and density of the stoichiometric hydrogen-air mixture.

$$\rho_{mix} = \frac{M_{mix}}{M_{air}}\rho_{air}$$

$$= \frac{(0.295)(2) + (1 - 0.295)(28.8)}{28.8}(1.2\ \text{kg/m}^3)$$

$$= 0.87\ \text{kg/m}^3$$

Using the C-J detonation Mach number for stoichiometric hydrogen-air listed in Table 3-16.4,

$$I = \frac{0.35(0.87\ \text{kg/m}^3)(400\ \text{m/s})(4.89)(5\ \text{m})}{(1.2 + 1)}$$
$$= 1354\ \text{Pa·s}$$

If we assume the pressure is effectively relieved when the detonation reaches the open end of the tube, the detonation duration in the 5 m long pipe is

$$\frac{5\ \text{m}}{4.89(400\ \text{m/s})} = 2.56\ \text{m·s}$$

The average pressure exerted on the pipe wall is I/t_{dur} = 530 kPa = 77 psig. This value is about one-third of the C-J detonation pressure. Structural analysts familiar with dynamic loadings can use these values and the pipe wall properties to determine whether the fuel line should survive the detonation.

Explosion Venting

Explosion venting is the discharge of combustion gases during a deflagration to maintain pressures below the enclosure damage threshold. The enclosure can be a room, a building, or a piece of process equipment. The fuel may be a combustible gas, dust, mist, or hybrid dust-gas mixture. The discharge vent opening is usually covered initially by one or more blowoff panels, rupture discs, or other engineered vent devices. Since explosion vents usually open after the explosion is initiated to limit the pressure rise, they cannot be used for detonations because the maximum pressure occurs instantaneously when the shock front reaches a given location.

The most effective explosion venting systems are those that deploy early in the deflagration, have as large a vent area as possible, and allow unrestricted venting of combustion gases. Early vent deployment requires that the vent release at the lowest possible pressure without interfering with normal operations and pressure fluctuations in the enclosure. In the case of vents on exterior walls and roofs of buildings, the minimum feasible vent release pressure is usually slightly larger than the highest expected differential pressure associated with wind loads (typically 0.14 to 0.21 psig; i.e., 0.96 to 1.44 kPa).

The amount of vent area needed for effective explosion venting depends on the size of the enclosure and the rate of pressure rise within it. According to Equation 5, the rate of pressure rise in an unvented enclosure is proportional to the product of the mixture effective burning velocity and flame surface area, and varies inversely with the enclosure volume. The rate of pressure reduction due to venting is proportional to the product of vent area and gas velocity through the vent. The vent velocity is dependent on the instantaneous pressure in the enclosure and the composition of the vented gas (i.e., the relative proportions of burned and unburned gas). These considerations have been implemented in the formulation of theoretical models, scaling correlations for test data, and guidelines for determining the required vent area.

Theoretical Models

Most of the theoretical models are for vented gas explosions because their effective burning velocities and flame surface areas are more amenable to modeling than those of dust explosions. The two categories of gas explosion models are (1) two-fluid models and (2) computational fluid dynamics (CFD) models. The two-fluid models are conceptually similar to the closed vessel model described previously, but include provisions for modeling the vented flow and various types of flame accelerations and turbulent combustion with possible highly wrinkled flame surface areas. Zalosh[26] has reviewed the status of these models through 1995.

Computational fluid dynamics models are much more sophisticated and complicated than the relatively simple two-fluid models. They solve for the spatial distribution of gas velocities, gas composition, and thermodynamic variables throughout a computational grid that can be either fixed or adaptive to the instantaneous flow and combustion field. Two distinguishing features of each of these models are their formulations for turbulence generation and for turbulent combustion rates. Although they are too complicated and computationally burdensome for routine deflagration vent design, several of these models are being used now for special applications such as offshore platform modules with highly congested equipment. Popat et al.[27] have provided a comparative review of four popular CFD models used in Europe, including their success in pre-test predictions.

Although dust explosions are more difficult to model than gas explosions, there have been several noteworthy efforts summarized by Eckhoff.[7] Some of these explicitly utilize the gas explosion parameters (burning velocity and flame surface area) and provide prescriptions to evaluate them from experimental data. Others use the closed vessel K_{ST} parameter as a representation of the effective burning rate. One recent burning velocity type model developed by Tamanini[28] at FMRC has been utilized to correlate dust-explosion-venting test data.

Test Data and Correlations

Crucial aspects of both vented gas explosion and vented-dust-explosion testing and data correlations are (1) mixture reactivity, (2) turbulence sources (both initial turbulence and obstacle-flame interaction turbulence), (3) vessel volume (scale) effects, and (4) vessel geometry (primarily length/diameter ratio), as well as the vent parameters: vent area, vent release pressure, and vent panel inertia. Vented-gas-explosion testing has the additional complication of various flame instabilities, some of which are dependent on ignition location, enclosure wall lining, and the presence of equipment within the enclosure. Dust-explosion testing has the additional complications of ignition source strength and dust cloud uniformity, as well as the time delay between dust dispersion and ignition.

Rather than attempt to review the numerous vented-explosion test programs, we will briefly focus on the testing that seems to have had the greatest influence on the development of data correlations and our current understanding of vented-explosion phenomenology. In this regard, perhaps the most influential and most extensive testing has been the large-scale testing conducted by Bartknecht and his protégés at the Ciba-Geigy Test Center in Basel, Switzerland. Their test vessels ranged in size from 2.4 m^3 to 250 m^3, and had a pressure rating of 10 bar so they could be used for both vented and unvented tests.[29] Most of their testing has been with dusts using energetic igniters and worst-case dust concentrations. Their data have been correlated in the various versions of the VDI Guideline for Dust Explosion Venting.[30]

Recent efforts in explosion venting data correlations have utilized nondimensional parameters that lend themselves to data interpolation and extrapolation. The nondimensional pressure parameter is

$$\pi = \frac{\Delta P_{\text{red}}}{\Delta P_{\text{max}}}$$

and the nondimensional vent parameter is

$$\Gamma = \frac{a_{CD} \cdot A_v \cdot P_0}{V^{2/3} \cdot K_{ST}}$$

where

A_v = vent area (m^2)
V = enclosure volume (m^3)
K_{ST} = ASTM E1226 (20-l vessel) dust reactivity (bar·m/s)
P_{red} = reduced pressure in vented explosion (bar·ga)
P_{max} = unvented explosion pressure (bar·ga)
P_{stat} = vent deployment pressure (bar·ga)
P_0 = initial pressure (= 1 bar·abs)
a_{CD} = vent discharge coefficient × sound speed = $C_D a_1$ = 230 m/s

The current FMRC correlation[31] uses the π parameter and a modified form of the Γ parameter in which a volume-adjusted K_{ST} parameter is used, and P_{max} replaces P_0 in the numerator. The particular correlation of π (Γ) was developed to provide a best fit to the Bartknecht data.

Gas explosion venting correlations relate the pressure parameter, π, to one of two alternate forms of the nondimensional vent parameter.

1. The Swift-Epstein[32] form of the vent parameter is

$$\Gamma_{S\text{-}E} = \frac{\chi S_u A_s}{C_D A_v} \sqrt{\frac{\rho_1}{P_{\text{red}}}}$$

where A_s is the interior surface area of the enclosure, that is, the maximum flame surface area at the time the enclosure is completely filled with flame.

2. The Bradley-Mitcheson[33] form of the vent parameter is

$$\Gamma_{B\text{-}M} = \frac{A_v a_1}{V^{2/3} S_u \left(\frac{M_1 T_f}{M_b T_1} \right)}$$

where T_f is the adiabatic isobaric flame temperature and M_b is the burned gas molecular weight. Molkov[34] has subsequently modified the Bradley-Mitcheson vent parameter to include the ratio χ/C_D, and has developed correlations for this ratio that account for turbulent flame stretch.

The turbulence parameter, χ, is particularly difficult to estimate and correlate for the vented gas explosions that produce flame instabilities. These flame instabilities produce complicated pressure-versus-time traces with multiple pressure peaks and oscillations such as shown in Figure 3-16.10. Depending on conditions (as described by Cooper et al.[35]), the maximum pressure during a vented explosion can correspond to any one of the four types of pressure peaks shown in Figure 3-16.10.

Explosion Venting Guidelines

The following vent area guidelines are based on data obtained from numerous tests in relatively large-scale enclosures with near worst-case gas-air or dust-air mixture compositions. The specific test programs are referenced in NFPA 68.[8] In some cases, the data was correlated using the parameters described previously. In other cases (particularly for gas explosions), the data were enveloped rather than correlated. Separate guidelines are offered for low-strength and high-strength enclosures, with the nominal demarcation between the two corresponding to a damage threshold pressure of 1.5 psig (0.1 bar ga). The reason for this demarcation is that the high-strength guidelines were primarily developed from European test programs, which did not include low-pressure tests, while many of the U.S. test programs featured large, low-strength structures.

Low-strength enclosures: The low-strength enclosure guidelines are currently based on the Swift-Epstein correlation parameter described previously. Thus the required vent area required to maintain pressures below the damage threshold, P_{red}, is proportional to the internal surface

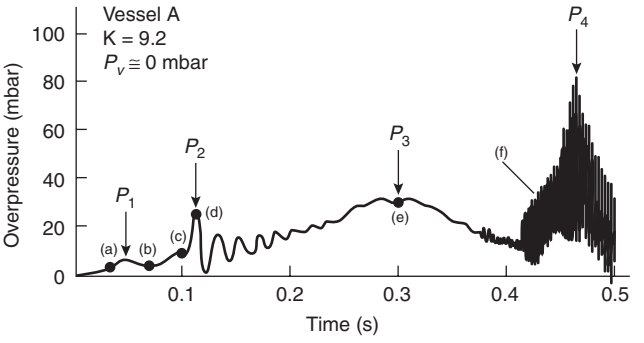

Figure 3-16.10. ***Pressure-time profile typical of an explosion in a near-cubic vessel with a low failure pressure explosion relief.[35]***

area of the enclosure. The general form of this venting equation is

$$A_v = \frac{CA_s}{\sqrt{P_{red}}} \quad (12)$$

where

A_v = vent area (ft² or m²)
C = fuel characteristic constant (psig$^{1/2}$ or kPa$^{1/2}$) specified in Table 3-16.5
A_s = internal surface area of enclosure (ft² or m²)
P_{red} = overpressure damage threshold (psig or kPa)

The intended range of applicability of Equation 12 is

- 0.35 psig $< P_{red} <$ 1.5 psig
- $P_{red} - P_{stat} > 0.35$ psi, where P_{stat} = vent opening pressure
- enclosure length/diameter (hydraulic) < 3

The recommended values of C in Table 3-16.5 represent the highest values inferred on the basis of test data presented in 18 references cited in NFPA 68.[8] Test conditions encompassed both quiescent and initially turbulent fuel-air mixtures in enclosures with volumes ranging from 0.18 to 82.3 m³.

For a given fuel, most of the data correspond to C values well below those given in Table 3-16.5. For example, the most likely value of C for propane is about one-third of the recommended value of 0.17. On the other hand, it is entirely possible for the recommended C value as used in Equation 12 to underestimate the pressure developed in a vented explosion with an extremely high level of turbulence, such as might occur in a hammermill, for example.

Values of C for other gases should be based on test data. In lieu of such data, a reasonable guess that is consistent with the Swift-Epstein correlation could be made by multiplying the 0.17 psig$^{1/2}$ value for propane (for which the most data are available) by the ratio of the burning velocity of the other gas to that for propane.

High-strength enclosures: The vent area recommended in NFPA 68 for compact ($L/D \leq 2$) high-strength enclosures subject to gas explosions is

$$A_v = \left[(0.127 \log_{10} K_G - 0.0567)P_{red}^{-0.582} + 0.175P_{red}^{-0.572}(P_{stat} - 0.1)\right]V^{2/3} \quad (13)$$

where $P_{stat} \leq 0.5$ bar and $P_{red} \leq 2$ bar.

Table 3-16.5 *C Values in Swift-Epstein Equation*[8]

Fuel	English Unit C (psig)$^{1/2}$	Metric Unit C (bar)$^{1/2}$
Anhydrous ammonia	0.05	0.013
Methane	0.14	0.037
Gases with S_u values < 60 cm/s	0.17	0.045
Dusts with $K_{ST} < 200$ bar·m/s	0.10	0.026
Dusts with $K_{ST} > 200$ and < 300 bar·m/s	0.12	0.030
Dusts with $K_{ST} > 300$ bar·m/s	0.20	0.051

For enclosures with $L/D > 2$, there is an equation for an incremental vent area to cope with the higher rates of pressure rise in elongated enclosures subject to flame acceleration.

The current (1998) version of NFPA 68 has the same equation for dust explosions in high-strength enclosures as is in VDI 3673. However, the committee has proposed the following new equation for dust explosions in compact enclosures for the 2002 Edition of NFPA 68.

$$A_v = (8.535 \times 10^{-5})(1 + 1.75P_{stat})K_{ST}V^{0.75}\sqrt{\frac{(1-\Pi)}{\Pi}} \quad (14)$$

where $\Pi = P_{red}/P_{max}$ as in the general correlations, V is in m³ and A_v is in m².

An equation for an incremental vent area for enclosures with $L/D > 2$ is also being proposed as of this writing. If approved by NFPA in the fall of 2001, Equation 14 and the auxiliary L/D equation will appear in the next version of NFPA 68, and will be recommended for low-strength as well as high-strength enclosures.

One limitation of all the explosion-vent guidelines as they are currently formulated, is that they do not account for application-specific turbulence levels and equipment obstruction levels. In other words, the implication in using the guidelines is that either the turbulence and equipment levels in the application are comparable to those used in the test data from which the guidelines were based, or else the vent designer is inherently accepting a certain ill-defined level of conservatism by assuming that the application turbulence and equipment obstruction levels are significantly lower than those used in the testing. By the same token, most of the guidelines do not account for the extent of the enclosure filled with combustible mixture. Current research, such as that described by Tamanini[36,37] is providing a basis for overcoming these limitations.

EXAMPLE 8:

Suppose the $4 \times 4 \times 3$ in room of Example 3 has a damage threshold pressure of 1.0 psig. What would be the minimum vent area to maintain pressures under this value for a worst-case butane–air mixture explosion? Assume the gas mixture is initially at rest and the vent release pressure is 0.2 psig.

SOLUTION:

For this room,

$$A_s = 2[4(4) + 4(3) + 4(3)] = 80 \text{ m}^2$$

Since butane has a burning velocity similar to that for propane, from Table 3-16.5, $C = 0.17$. Therefore, using Equation 9,

$$A_v = 80(0.17)/1.0 = 13.6 \text{ m}^2 \ (146 \text{ ft}^2)$$

EXAMPLE 9:

A 400-m³ electrostatic precipitator used in a power plant firing bituminous coal is to be equipped with lightweight explosion vents. If the damage threshold pressure for the precipitator is 1.2 bar (17.4 psig), its L/D ratio is 1.5, and the vent static release pressure is 0.4 bar (5.8 psig), what is the minimum vent area needed? Assume the bitu-

minous coal has the explosibility parameters listed in Table 3-16.2.

SOLUTION:

From the Table 3-16.2 listing for bituminous coal, K_{ST} = 59 bar·m/s and P_{max} = 9.1 bar g. Therefore, $\pi = 1.2/9.1 = 0.132$. Substituting into Equation 14,

$$A_v = (8.535 \times 10^{-5})[1 + 1.75(0.40)](59)(400)^{0.75}\sqrt{\frac{1 - 0.132}{0.132}}$$

$$= 1.96 \text{ m}^2$$

We note that since the vent area is linearly proportional to K_{ST}, which can vary substantially among various coals (and other generic materials for that matter), it is important to base the calculated vent area on data for site-specific samples. Note also that the calculated vent area does not account for the weight (inertia) of the vent panel. A procedure to determine the additional vent area required for heavy vent panels will appear in the next edition of NFPA 68.

Explosion Suppression Systems

An explosion suppression system is designed to detect and suppress an incipient explosion before the pressure rises to the enclosure damage threshold. Suppression is achieved by the rapid discharge of an extinguishing agent from pressurized containers mounted on the protected enclosure. The sequence of events is pictured in Figure 3-16.11. A pressure or flame radiation detector senses the incipient explosion while only a small fraction of the flammable gas or dust has burned. The sensor signal triggers the discharge of suppression agent into the enclosure. When the agent reaches the expanding flame front, it quenches the flame and thereby suppresses the explosion.

One important advantage of explosion suppression systems versus explosion venting is that there is no discharge of flame or fuel. Thus suppression systems can often be used more readily on indoor equipment and on equipment containing toxic materials. One major disadvantage of the system is the high cost associated with both the installation of a complex system and the refilling and resetting of the system after a discharge.

The basic components of an explosion suppression system include detectors, an electrical power supply and control system, and a set of rapid action extinguishing units. Pressure sensing detectors are usually used in applications involving dust explosion hazards, while gas explosion applications can employ either pressure sensors or ultraviolet radiation detectors, depending on the required response line (UV detectors provide the fastest response time) and concerns for spurious activation and/or optical shielding of the detectors. Electrical power supplies and control systems include appropriate interlocks for self-monitoring and for shutting down processes and triggering alarms at system activation. Extinguishing agents traditionally used in explosion suppression systems have been either halogenated hydrocarbons (halons) or chemical powders. Dry chemicals, such as monoammonium phosphate and sodium bicarbonate, are still being used to protect many unoccupied facilities and equipment. However, the recent phaseout of halon production, because of ozone depletion concern, has triggered an ongoing search for new liquid and gaseous

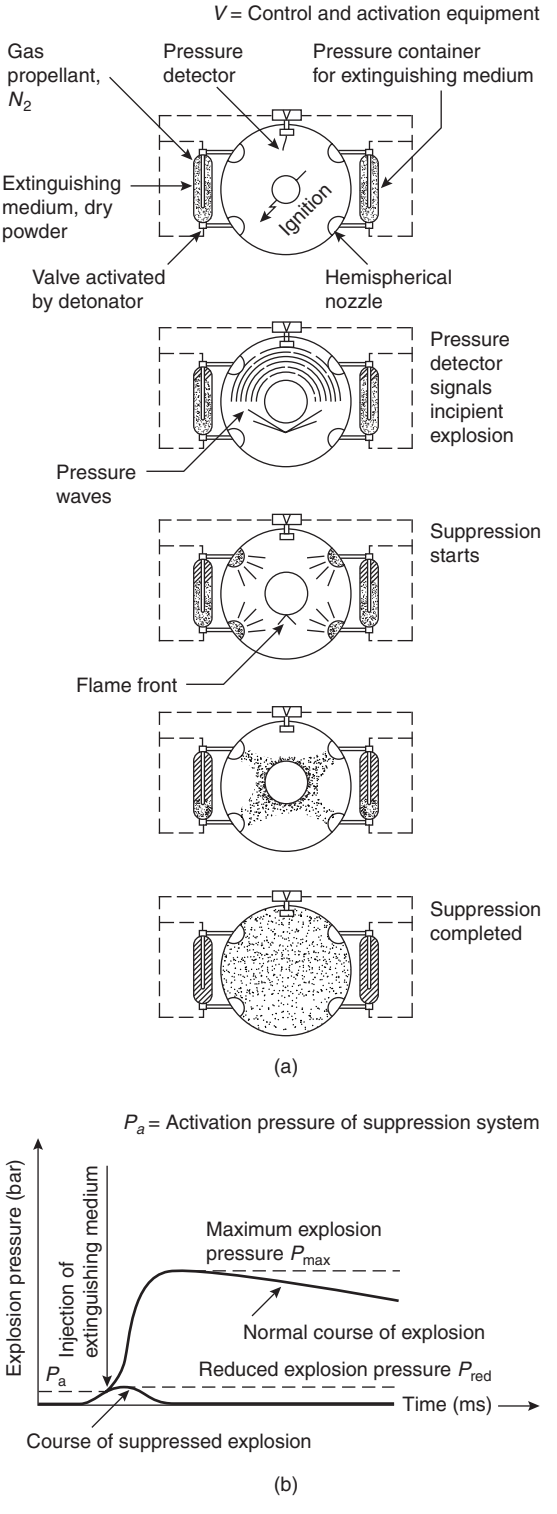

Figure 3-16.11. ***(a) Explosion suppression system. (b) Pressure versus time diagram of a normal and a suppressed explosion.[4]***

agents (primarily perfluorocarbons and hydrofluorocarbons), and has generated renewed interest in water and aqueous salt solutions for explosion suppression of potentially occupied facilities, such as aerosol propellant filling rooms and gas compressor stations.

Several test programs have provided data on the quantity of agent, activation times and pressures, and method of agent dispersal needed for effective suppression. These programs have encompassed a variety of flammable gases and dusts, have ranged in scale from laboratory vessels[38] to a 500-m^3 tanker pump room,[39] and include many tests in the 250-m^3 Ciba-Geigy test vessel mentioned previously.[40] The ISO and Factory Mutual standards[41,42] specify that testing should be conducted in a vessel of at least 1-m^3 volume, and should include tests with and without suppression agents.

Bartknecht[43] has systematically investigated the effect of enclosure size on the quantity of dry chemical agent needed for effective suppression. His data indicate that the required quantity of agent is proportional to the enclosure volume (i.e., there is a certain critical agent concentration) for volumes under about 5 m^3, but that the required amount of agent is proportional to the two-thirds power of the enclosure volume beyond 9 m^3. This change in scaling suggests that the dry chemical suppression mechanism changes from advance inerting of unburned fuel ahead of the flame front in small vessels, to actual quenching of the flame front in large vessels. Chatrathi and Going[44] have recently reported on testing using dry chemical suppression agents in both modes: inerted (injected into the vessel with combustible dust) and post-ignition suppression. His inerted test results were used to determine minimum inerting concentrations for mono-ammonium phosphate and sodium bicarbonate.

Recent fundamental research with various suppression agents has elucidated the suppression mechanisms associated with various agents and fuel combinations. Many agents provide the thermal heat sink effect that is the most clearly understood mechanism. Some agents also provide a chemical inhibition effect (via free-radical scavenging), but the magnitude of this effect is dependent upon the flame speed as well as the chemical compositions of the fuel and agent.[45,46]

The importance of the flame speed in assessing suppression agent and system effectiveness can best be appreciated in terms of the components contributing to what Chatrathi and Going[44] call the *total suppressed pressure* (TSP). These components can be expressed in the following equation:

$$\mathrm{TSP} = P_A + \Delta P_{\mathrm{inj}} + \Delta P_{\mathrm{comb}} \qquad (15)$$

where

P_A = deflagration pressure at the time of agent discharge actuation

ΔP_{inj} = incremental pressure associated with the discharge of propellant gas and any gaseous agent into the enclosure

ΔP_{comb} = incremental pressure associated with the combustion that occurs as the agent travels to the flame front and actually suppresses the deflagration

The first term in Equation 15 can be minimized through the selection of fast-acting detectors and the use of very fast opening suppression agent containers. The second term is usually only an important consideration in small enclosures (Chatrathi and Going report that ΔP_{inj} = 1.4 psig when one 2.5 l container, pressurized to 900 psig with nitrogen is injected into a 1-m^3 closed vessel). The third term is the most difficult to characterize because it includes consideration of agent dispersal as well as the chemically reacting interaction of the agent with the expanding flame front. In terms of minimizing agent travel time to the flame front, it is clear that the use of a large number of well distributed small agent containers would be preferable to use of fewer large containers. Moore's testing[47] has verified this conjecture. If the agent travel time can be calculated, and the agent is assumed to be instantly effective once it reaches the flame front, the value of ΔP_{comb} can be estimated using Equations 6 and 7.

The ΔP_{comb} term in Equation 15 will inevitably increase with increasing fuel K_{ST} or K_G, as well as with the increasing turbulence level associated with the application explosion scenario. The highest challenge K_{ST} material subjected to explosion suppression tests has been aluminum dust. Early results described by Bartknecht[43] showed the limitations of the first generation suppression systems and agents in suppressing aluminum dust explosions. The recent results of Chatrathi and Going suggest that the TSP of aluminum dust can now be reduced to 10–20 percent of $P_{\max}$. This is significantly larger than the TSP achieved with organic fuels, which is usually less than 5 percent of $P_{\max}$.

The choice of a suitable suppression agent and number/location of agent containers involves some very practical considerations as well as consideration of the maximum pressure developed in the suppressed explosion. Some of these considerations include agent compatibility with process materials, agent toxicity, environmental impact, and agent retention time for applications in which there is a threat of repeated ignitions.

Blast Waves

If explosion prevention and explosion suppression measures are not successful, a blast wave will emanate from the breached enclosure. The blast wave will propagate into the surrounding atmosphere and will decay with distance from the enclosure. One of the most common questions with regard to explosion protection is whether or not the blast wave at a particular location will be sufficiently strong to cause damage or injury. Simplified methodology to address this question is presented here along with reference citations for more thorough and extensive analyses.

If we confine our attention to distances that are large in comparison to the characteristic diameter of the breached enclosure, we can deal with relatively simple far-field blast wave scaling correlations. The characteristic shape of the far-field blast wave is shown in Figure 3-16.12. It consists of a shock wave with a pressure rise, P_s, followed immediately by a rarefaction wave in which the pressure decays to some value below atmo-

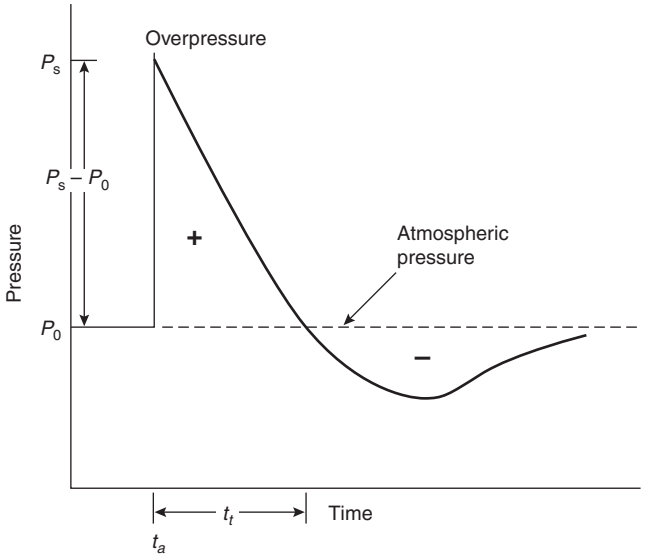

Figure 3-16.12. ***Far-field blast wave.***[49]

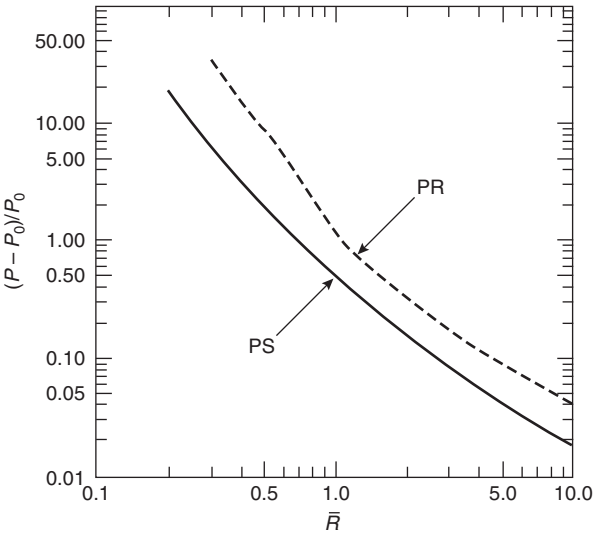

Figure 3-16.13. ***Blast wave pressure versus scaled distance.***

spheric pressure, and then a gradual recovery to atmospheric pressure, P_0. Sometimes the final pressure recovery occurs in the form of a second shock, and the shape takes the form of a slightly deformed letter *N*, thus leading to the term *N wave.*

Blast wave correlations are often in the form of a nondimensional pressure $(P_s - P_0)/P_0$ and a nondimensional distance from the blast source. The nondimensional distance, $\overline{R}$, is defined as

$$\overline{R} = R\left(\frac{P_0}{E}\right)^{1/3} \tag{16}$$

where R is the actual distance from the blast source (m), E is the blast wave energy (J), and P_0 is in *Pa*.

The correlation for nondimensional pressure versus $\overline{R}$ is shown in Figure 3-16.13. The curve labeled PS in Figure 3-16.13 refers to the incident overpressure, while the curve labeled PR refers to the reflected blast wave pressure resulting from a blast wave being reflected head-on from a rigid wall. Neither curve in Figure 3-16.13 accounts for the reflection of the shockwave off the ground surface. The usual procedure for including ground surface reflection is to use twice the calculated blastwave energy when using the correlations in Figure 3-16.13.

The implication in this type of blast wave scaling correlation is that the blast wave is characterized by only one parameter, the blast energy, E. In theoretical models of blast wave pressure, the energy is assumed to be released instantaneously, at a single point. This approach is called ideal blast wave theory. The correlations for ideal blast waves are based on a combination of theory and test data from condensed phase, compact explosives. Baker[17,48] describes the development of these correlations, which include nondimensional blast wave impulses, positive-phase durations, and many other parameters. The impulse is particularly important for doing dynamic structural response analyses, such as those described by Kinney and Graham.[49]

Can the blast waves from various accidental explosions be predicted from these ideal blast wave correlations? In some cases the answer is unequivocally yes. A good example is the blast wave from a ruptured pressure vessel containing a gas that is not ignited upon release. The energy associated from this type of physical explosion is the energy of expansion of the gas as it goes from an initial pressure, P_1, to atmospheric pressure. A perfect gas isentropic expansion representation of this energy is

$$E = \frac{(P_1 - P_0)V}{\gamma - 1} \tag{17}$$

where V is the vessel volume and γ is the gas ratio of specific heats. Other approaches to this problem, including the assessment of vessel fragment shrapnel effects, are described in the AIChE Consequence Analysis Guidelines.[50]

If the breached vessel fails as a result of an internal combustion explosion, or if the vessel is vented per explosion venting guidelines, the blast wave analysis is considerably more complicated because there is a combustion energy contribution to the total blast wave energy. Correlations to predict blast waves from vented explosions are contained in NFPA 68, and more recent developments, including two-dimensional considerations, are described by Forcier and Zalosh.[51]

Another special consideration in breached vessel blast waves is the blast wave and fragment shrapnel released when a liquefied gas undergoes a boiling liquid expanding vapor explosion (BLEVE) as a result of severe fire exposure. Correlations for BLEVEs are described in *Guidelines for Evaluating the Characteristics of Vapor Cloud Explosions, Flash Fires, and BLEVEs,*[52] and some of the research leading to these correlations are described in Baurer et al.,[53] Hasegawa and Sato,[54,55] and Fay and Lewis.[56] These publications include correlations for the size and radiation emitted from the rising fireball that occurs in most BLEVEs.

One final special consideration is the blast wave associated with vapor cloud explosions. These explosions occur when a very large cloud of flammable gas or vapor is ignited in a highly obstructed environment such as a chemical or petrochemical plant with a high density of process equipment and storage vessels. The strength of the blast wave that occurs in a vapor cloud explosion is dependent on the flame speed that develops and the degree of confinement in and around the vapor cloud.

Early assessments of vapor cloud explosion blast waves were conducted using the idealized blast wave type correlations described here, along with some rough guess at the energy yield (i.e., the fraction of the available combustion energy actually contributing to the blast wave). However, these early efforts were not very successful because 1) most of the interest is in the near-field rather than the far-field, and 2) even the far field assessments were not accurate because the blast wave strength and impulse decays far less rapidly than that of an ideal blasé wave. Two other types of blast wave models are utilized now for vapor cloud explosions. The simpler current approach involves an empirical estimate for the flame speed in different applications, along with results of one-dimensional flame propagation (or piston propagation) nonideal blast wave calculations. This approach, which is still evolving, is described in *Guidelines for Evaluating the Characteristics of Vapor Cloud Explosions, Flash Fires, and BLEVEs,*[52] Strehlow,[57] and van den Berg.[58] The second current approach is to utilize CFD models of the actual two-dimensional or three-dimensional flame propagation, in which the flame speed and acceleration are calculated as part of the solution. The models used for this approach are essentially the same models referenced earlier for CFD calculations of vented gas explosions.[27] Which of these two approaches will see more widespread use in the future depends, in large part, on the availability of faster and more powerful computers, along with the education of potential users of these sophisticated models. In a sense, this issue is only a microcosm of the more general question of what level of modeling will be utilized for performance based explosion hazard assessments.

References Cited

1. M.G. Zabetakis, "Flammability Characteristics of Combustible Gases and Vapors," *U.S. Bureau of Mines Bulletin 627,* Washington (1965).
2. ASTM E 661, "Standard Test Method for Concentration of Limits of Flammability of Chemicals," American Society for Testing and Materials, Philadelphia, PA (1995).
3. ASTM E 918-83, "Standard Practice for Determining Limits of Flammability at Elevated Temperature and Pressure," American Society for Testing and Materials, Philadelphia, PA (1993).
4. M. Hertzberg, "The Flammability Limits of Gases, Vapors, and Dusts: Theory and Experiment," *Fuel-Air Explosions,* p. 3, Univ. of Waterloo Press (1982).
5. NFPA 69, *Standard on Explosion Prevention Systems,* National Fire Protection Association, Quincy, MA (1997).
6. ASTM E 1515-98, "Standard Test Method for Minimum Explosible Concentration of Combustible Dusts," American Society for Testing and Materials (1998).
7. R. Eckhoff, *Dust Explosions in the Process Industries,* 2nd Edition, Butterworth Heinemann (1996).
8. NFPA 68, *Guide for Venting of Deflagrations,* National Fire Protection Association, Quincy, MA (1998).
9. R. Siwek, "Determination of Technical Safety Indices and Factors Influencing Hazard Evaluation of Dusts," *J. Loss Prevention in the Process Industries,* 9, pp. 21–31 (1996).
10. R. Siwek and C. Cesana, "Ignition Behavior of Dusts: Meaning and Interprertation," *Process Safety Progress,* 4, pp. 107–119 (1995).
11. D. Bradley and A. Mitcheson, "Mathematical Solutions for Explosions in Spherical Vessels," *Combustion and Flame,* 26, pp. 201–217 (1976).
12. B. Lewis and G. von Elbe, *Combustion, Flames, and Explosions of Gases,* Academic Press, New York (1961).
13. ASTM E-1226, "Standard Test Method for Pressure and Rate of Pressure Rise for Combustible Dusts," American Society for Testing and Materials, Philadelphia, PA (1988).
14. R. Strehlow, *Combustion Fundamentals,* McGraw-Hill, New York (1984).
15. M. Sichel, "Simplified Calculation of Detonation Induced Impulse," (1980).
16. D.S. Burgess, J.N. Murphy, N.E. Hanna, and R.W. Van Dolah, *Large-Scale Studies of Gas Detonations,* U.S. Bureau of Mines RI 7196, Washington (1971).
17. W.E. Baker, P.A. Cox, P.S. Westine, J.J. Kulesz, and R.A. Strehlow, *Explosion Hazards and Evaluation,* Elsevier, New York (1983).
18. B.E. Gelfand, S.M. Frolov, and M.A. Nettleton, "Gaseous Detonations," *Progress in Energy and Combustion Science,* 17, pp. 327–371 (1991).
19. A. Sulmistras, I.O. Moen, and A.J. Saber, "Detonations in Hydrogen Sulphide-Air Clouds," Defense Research Establishment Suffield, Ralston, Alberta *Report No. 11* 40 (1985).
20. J.E. Shepherd, "Chemical Kinetics of Hydrogen-Air-Diluent Detonations," *Dynamics of Explosions: Progress in Astronautics and Aeronautics,* 106, pp. 263–293 (1986).
21. D.W. Stamps, W.B. Benedick, and S.R. Tieszen, "Hydrogen-Air Diluent Detonation Study for Nuclear Reactor Safety Analysis," *Sandia Report NUREG/CR-5525* (1991).
22. R.P. Lindstedt and H.J. Michels, "Deflagration to Detonation Transition in Mixtures of Alkane LNG/LPG Constituents with O_2/N_2," *Combustion and Flame,* 72, pp. 63–72 (1988).
23. Flessner and Bjorklund, *Coast Guard Report* (1980).
24. M.P. Sherman and M. Berman, "The Possibility of Local Detonations during Degraded-Core Accidents in the Bellefonte Nuclear Power Plant," *Nuclear Technology,* 81, pp. 63–77 (1988).
25. R.B. Jacobs, W.L. Bulkley, J.C. Rhodes, and T.L. Speer, "Gaseous Detonation," *Chemical Engineering Progress,* 53, pp. 565–573 (1957).
26. R. Zalosh, "Review of Gas Deflagration Venting Models," *Proceedings of the First International Seminar on Fire and Explosion Hazard of Substances and Venting of Deflagrations,* All-Russian Research Institute for Fire Protection, pp. 166–181 (1995).
27. N. Popat, C. Catlin, B. Arntzen, R. Lindstedt, B. Hjertager, T. Solberg, O. Saeter, and A. van den Berg, "Investigations to Improve and Assess the Accuracy of Computational Fluid Dynamic Based Explosion Models," *Journal of Hazardous Materials,* 45, pp. 1–25 (1996).
28. F. Tamanini, "Characterization of Mixture Reactivity in Vented Explosions," *14th International Colloquium on the Dynamics of Explosions and Reactive Systems* (1993).

29. W. Bartknecht, "Pressure Venting of Dust Explosions in Large Vessels," *Proceedings of the 20th Annual Loss Prevention Symposium* (1986).
30. VDI 3673, "Pressure Venting of Dust Explosions," *Verein Deutscher Ingenieure,* VDI Verlag GmbH, Dusseldorf, Germany (1995).
31. F. Tamanini and J. Valiulis, "Improved Guidelines for the Sizing of Vents in Dust Explosions," *J. Loss Prevention in the Process Industries,* 9, pp. 105–118 (1996).
32. I. Swift and M. Epstein, "The Performance of Low Pressure Explosion Vents," *20th AIChE Loss Prevention Symposium* (1986).
33. D. Bradley and A. Mitcheson, "The Venting of Gaseous Explosions in Spherical Vessels," *Combustion and Flame,* 32, pp. 221–236 (1978).
34. V. Molkov, A. Korolchenko, A. Ya, and S. Alexandrov, "Venting of Deflagrations in Buildings and Equipment: Universal Correlation," *Proceedings of Fifth International Symposium on Fire Safety Science,* IAFSS, pp. 1249–1260 (1997).
35. M.G. Cooper, M. Fairweather, and J.P. Tite, "On the Mechanisms of Pressure Generation in Vented Explosions," *Combustion and Flame,* 65, pp. 1–14 (1986).
36. F. Tamanini, "Vent Sizing in Partial-Volume Deflagrations and Its Application to the Case of Spray Dryers," *J. Loss Prevention in the Process Industries,* 9, pp. 339–350 (1996).
37. F. Tamanini and J. Chafee, "Mixture Reactivity in Explosions of Stratified Fuel Layers," *Proceedings of the 34th AIChE Loss Prevention Symposium* (2000).
38. M. Hertzberg, K. CashdoUar, L. ZJochower, and D. Ng, "Inhibition and Extinction of Explosions in Heterogeneous Mixtures," *Twentieth International Symposium on Combustion,* pp. 1691–1700 (1984).
39. R. Richards, "Development of Explosion Suppression System Requirements for Shipboard Pump Rooms," *U.S. Coast Guard Report CG-D-79-76, N77S Document #ADA031308,* (1976).
40. P. Moore, "Towards Large Volume Explosion Suppression Systems," *EuropEx Newsletter,* 4, pp. 2–4 (1987).
41. ISO 6184/4, "Explosion Protection Systems—Part 4: Determination of Efficacy of Explosion Suppression Systems," *International Standard ISO 6184/4* (1985).
42. Factory Mutual Approval Standard 5700, "Explosion Suppression Systems," FMRC (1999).
43. W. Bartknecht, *Explosions: Course, Prevention, Protection,* Springer-Verlag, New York (1981).
44. K. Chatrathi and J. Going, "Dust Deflagration Extinction," *Proceedings of the 34th Annual Loss Prevention Symposium* (2000).
45. I. Moen, S. Ward, P. Thibault, J. Lee, R. Kaystautas, T. Dean, and C. Westbrook, "The Influence of Diluents and Inhibitors on Detonations," *Twentieth International Symposium on Combustion,* pp. 1717–1725 (1984).
46. G.W. Gmurczyk and W.L. Grosshandler, "Suppression Effectiveness Studies of Halon-Alternative Agents in a Detonation/Deflagration Tube," *Proceedings of the 1994 Halon Options Technical Working Conference,* New Mexico Engineering Research Institute (1994).
47. P. Moore, "Explosion Suppression Trials," *EuropEx Newsletter,* 1, pp. 3–7 (1986).
48. W.E. Baker, *Explosions in Air,* University of Texas Press, Austin (1973).
49. G. Kinney and K. Graham, *Explosive Shocks in Air,* 2nd Edition, Springer-Verlag (1985).
50. *Guidelines for Consequence Analysis of Chemical Releases,* AIChE Center for Chemical Process Safety (1999).
51. T. Forcier and R. Zalosh, "External Pressures Generated by Vented Gas and Dust Explosions," *J. of Loss Prevention in the Process Industries,* 13, pp. 411–417 (2000).
52. *Guidelines for Evaluating the Characteristics of Vapor Cloud Explosions, Flash Fires, and BLEVEs,* AIChE Center for Chemical Process Safety (1994).
53. B. Baurer, K. Hess, H. Giesbrecht, and W. Louckel, "Modelling of Vapour C1oud Dispersion and Deflagration after Bursting of Tanks Filled with Liquefied Gas," *Proceedings of the 2nd Intemational Symposium on Loss Prevention and Safety Promotion in the Process Industries,* pp. 305–321 (1977).
54. K. Hasegawa and K. Sato, "Study on the Fireball Following Steam Explosion of n-Pentane," *Proceedings of the 2nd International Symposium on Loss Prevention and Safety Promotion in the Process Industries,* pp. 297–304 (1977).
55. K. Hasegawa and K. Sato, "Experimental Investigation of the Unconfined Vapour-Cloud Explosions of Hydrocarbons," *Technical Memorandum No. 12,* Japanese Fire Research Institute (1978).
56. J.A. Fay and D.H. Lewis, Jr., "Unsteady Burning of Unconfined Vapor Clouds," *16th International Symposium on Combustion,* pp. 1397–1405 (1977).
57. R.A. Strehlow, "The Blast Wave from Deflagrative Explosions—An Acoustic Approach," *AlChE Loss Prevention Symposium,* 14, pp. 145–152 (1981).
58. A.C. van den Berg, "The Multi-Energy Method: A Framework for Vapour Cloud Explosion Blast Prediction," *J. of Haz. Matls.,* 12, pp. 1–10 (1985).

Section Four
Design Calculations

Section 4 Design Calculations

CHAPTER 1

Design of Detection Systems

Robert P. Schifiliti, Brian J. Meacham, and Richard L. P. Custer

Introduction

Fire detection and alarm systems are recognized as key features of a building's fire prevention and protection strategy. This chapter presents a systematic technique to be used by fire protection engineers in the design and analysis of detection and alarm systems. The majority of discussion is directed toward systems used in buildings. However, many of the techniques and procedures also apply to systems used to protect planes, ships, outside storage yards, and other nonbuilding environments.

Scientific research on fire growth and the movement of smoke and heat within buildings provides fire protection engineers with information and tools that are useful in the design of fire detection systems. Also, studies of sound production and transmission allow communication systems to be engineered, thus eliminating the uncertainty in locating fire alarm sounders. All of this information allows engineers and designers to design systems that meet specific, identifiable goals.

Sections 1, 2, and 3 of this handbook introduced and discussed a series of concepts and tools for use by fire protection engineers. This chapter shows how some of these tools can be used collectively to design and evaluate detection and alarm systems.

Robert P. Schifiliti, P.E., is a fire protection consultant based in Reading, Massachusetts, and an adjunct associate professor of fire protection engineering at Worcester Polytechnic Institute. He specializes in fire detection and fire alarm system design and analysis.

Brian J. Meacham, Ph.D., P.E., is Principal Risk Consultant and Principal Fire Protection Consult for Arup Fire, located in Massachusetts. Dr. Meacham is a fellow of the Society of Fire Protection Engineers.

Richard Custer, M.Sc., is Technical Director and Principal Fire Analyst for Arup Fire. Mr. Custer is a fellow of the Society of Fire Protection Engineers.

A Note about Precision

When solving multiple equations with numerous variables from many sources, it is often easy to overlook the importance of precision and confidence in the final answer. This acknowledgment is particularly true since engineers have progressed from slide rulers to calculators to computers in a relatively short span of time. Most calculations in this chapter have been done using a computer—most often with a simple spreadsheet. The generally accepted practice for these types of tools is to round off only the final answer to the correct number of significant digits.

The standard and most widely taught rule for rounding is to round off using the same number of significant digits as the least precisely known number used in the calculation. An alternate rule suggests using one more significant figure than suggested by the standard rule. It has been shown that the alternate rule is more accurate and does not lead to loss of data as does the standard rule.[1,2] The alternate rule for rounding has been used in this chapter. For more information or to refresh your knowledge of precision, rounding, and significant figures, consult the references or a standard text on engineering and scientific measurements.

Overview of Design and Analysis

To design a fire detection and alarm system, it is first necessary to establish the system's goals. These goals are established by model codes, the property owner, risk manager, insurance carriers, and/or the authority having jurisdiction. Ultimately, the goals of the system can be put in four basic categories:

1. Life safety
2. Property protection
3. Business protection
4. Environmental concerns

Some designers include heritage conservation in the list of goals. However, the protection of historic property is really another form of property and mission protection, although the methodology and extent for protection may vary.

When designing for life safety, it is necessary to provide early warning of a fire condition. The fire detection and alarm system must provide a warning early enough to allow complete evacuation of the danger zone before conditions become untenable. The fire detectors or fire alarm system may be used to activate other fire protection systems, such as special extinguishing systems and smoke control systems, that are used to help maintain a safe environment during a fire.

In some situations, the life safety mission of a detection system is enhanced by providing information to occupants. This situation is often the case in *stay-in-place* or *defend-in-place* strategies or partial evacuation/relocation strategies. The detection system is used to provide information about the location and extent of the fire. Instructions are then given to the target audience.

Property protection goals are principally economic. The objective is to limit damage to the building structure and contents. Maximum acceptable losses are established by the property owner or risk manager. The goal of the system is to detect a fire soon enough to allow manual or automatic extinguishment before the fire exceeds acceptable damage levels.

Goals for the protection of a mission or business are determined in a manner similar to that used in property protection. Here, fire damages are limited to prevent undesirable effects on the business or mission. Some items that need to be considered are the effects of loss of raw or finished goods, loss of key operations and processes, and loss of business to competitors during downtime. Other concerns include the availability and lead time for obtaining replacement parts. If the equipment to be protected is no longer available or requires several months for replacement, the ability to stay in business during and after an extended period of downtime may be jeopardized.

Protection of the environment is also a fire protection concern. Two examples are (1) toxicity of products of combustion and (2) contamination by fire protection runoff water. Should large quantities of contaminants be expected from a large fire, the goal of the system may well be to detect a fire and initiate appropriate response prior to reaching a predetermined mass loss from burning materials or quantity of fire suppression agent discharged.

Once the overall goals have been set, specific performance and design objectives for a performance-based design can be established.[3–5] Performance-based fire protection design requires that specific performance objectives, rather than generic prescriptive requirements, be met. A typical prescriptive requirement would be to provide a smoke detector for every 84 m² (900 ft²) or 9-m (30-ft) spacing. In prescriptive design, speed of detection and the fire size at detection for such an installation are not known or considered explicitly. In addition, if some action must be taken in response to the alarm in order to control the fire, the expected damage is also unknown.

Implementation of a fire safety performance objective requires that the objective be stated first by the client in terms of acceptable loss. The client loss objectives must then be (1) expressed in engineering terms that can be quantified using fire dynamics, and (2) related to design fires, design fire environments, and the performance characteristics of fire suppression equipment. For example, the client loss objective may be to prevent damage to essential electronic equipment in the compartment of origin. To meet this objective, one must first define what *damage* is. This damage could be expressed in terms of the thickness of the smoke layer. Other criteria, such as temperature or concentration of corrosive combustion products, or a combination of criteria, could also be used.

Based on a study of the likelihood of ignition and fire growth scenarios, a design fire needs to be established. The design fire is characterized by its heat release rate, $\dot{Q}$, at any moment in time; its growth rate, dq/dt; a combustion product rate dcp/dt, such as smoke particulate, toxic or corrosive species, and so forth; and production rate, dp/dt. The design fire may be determined by (1) a combination of small- and large-scale testing specific to the application or (2) analysis of data taken from studies reported in the literature.

For a given fire safety design objective, there will be a point, $\dot{Q}_{do}$, on the design fire curve where the energy and product release rates will produce conditions representative of the design objective. Given that there will be delays in detecting the fire, notifying the occupants, accomplishing evacuation, or initiating suppression actions, the fire will need to be detected at some time in advance of $\dot{Q}_{do}$. In order to account for these delays, a critical fire size, $\dot{Q}_{cr}$, can be defined as the point on the design fire curve at which the fire must be detected in order to meet the design objectives for a given spacing or radial distance from the fire.

There are two types of delays that influence the size of the fire at detection: (1) those that are variable and (2) those that are fixed. Variable delays represent transport lag and are related to radial distance of the detector from the fire, ceiling height, and the convective heat release rate of the fire. Fixed delays are associated with system characteristics, such as alarm verification time. Adding the fixed delays to $\dot{Q}_{cr}$ defines another point on the design fire curve: $\dot{Q}_i$ or the *ideal* fire; that is, the fire that would be detected with no transport delay.

The design fire, $\dot{Q}_{do}$, has been defined as the fire size (in terms of peak heat release and given growth rate history) that corresponds to the maximum acceptable loss fire, and the critical fire, $\dot{Q}_{cr}$, as the maximum fire size at time of detection that allows actions to be taken to limit the continually growing fire to the design fire limit. The time needed to take the limiting actions is the response lag. The total system response time, then, is the amount of time required between the critical fire and the design fire for all the actions to take place before $\dot{Q}_{do}$ is reached, and is the sum of the fixed and variable delays and the response lag. The various design and evaluation points on a design fire curve are shown in Figure 4-1.1.

For example, if the design fire is determined to be 1500 kW and manual suppression will be employed, the critical fire can be selected at a moment in time that permits detection, notification, and response before the 1500 kW fire size is reached. If the total system response

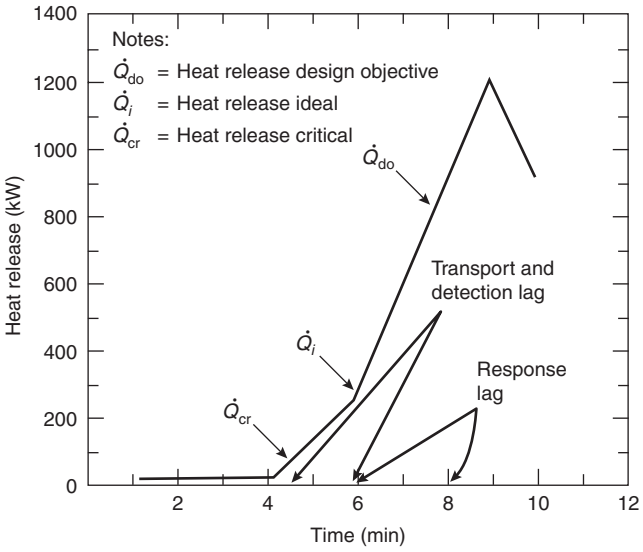

Figure 4-1.1. ***Design fire curve.***

time is estimated to be 3 min, the critical fire would be at the size determined at 3 min prior to reaching 1500 kW using the estimated fire growth rate.

Expressing fire size or fire load as an energy release and growth rate may be thought of in the same way that structural engineers use earthquake zone maps to design for potential earthquakes. Electrical engineers might compare fire loads to fault currents used in designing overcurrent protection devices. At the present time, design fire, critical fire, and total system response time requirements are not established by any building codes. It is the job of the design engineer to work with the building owner and local code officials to establish the performance requirements for a given system application.

Once the goals of a system have been established, several probable fire scenarios should be outlined. The occupancy of the building and the expected fuels should be analyzed to establish an expected fire growth rate and an expected maximum heat release rate. Fire loss reports and fire test data can be used to help estimate heat release rates and the production of smoke and fire gases. It is important that different fire scenarios be evaluated to establish how the system design or response might change as a result of varying fire conditions. Several possible fire scenarios should be outlined using the techniques presented elsewhere in this handbook.

When designing a system, select the most likely fire scenario as the basis of the design. Once the design requirements for spacing and detector type are established, the system's response can be analyzed using the other possible fire scenarios. If the alternate fire scenarios cause the design not to meet the established goals, design changes can be made and retested, if warranted.

The several fire scenarios used when analyzing a system will produce upper and lower bounds or a range of system performance characteristics. The fire scenarios selected should include best and worst case fires as well as several likely scenarios for the particular building characteristics and occupancy.

For the purposes of design or analysis, detection and alarm systems have three basic elements: detection, processing, and signaling. The first, detection, is that part of the system that senses fire. The second element involves the processing of signals from the detection portion of the system. Finally, the processing section of the system activates the signaling portion in order to alert occupants and perform other auxiliary signaling operations. Auxiliary functions may include smoke control, elevator capture, fire department signaling, and door closing.

This chapter focuses on the detection and signaling elements of a fire alarm system. Engineering methods for the design and analysis of heat detector response are presented along with several examples. A method to calculate the audibility of fire alarm sounders is also presented. The selection of a system's control panel and the design of auxiliary functions is beyond the scope of this chapter.

Detection

To design the detection portion of a fire alarm system, it is necessary to determine where fire detectors should be placed in order to respond within the goals established for the system. Several different detector types might respond to the expected fire, so it may be necessary to develop several candidate system designs, using various combinations of detector types in order to optimize the system's performance and cost.

A fire signature[6] is some measurable or sensible phenomenon present during combustion. Table 4-1.1 is a cross-reference of fire signatures and commercially available detector types. The table shows the predominant fire signature to which the detector responds.

Heat Detection

This section discusses an engineering method for determining the placement of heat detectors on a large flat ceiling.

The present practice in designing fire detection systems using heat detectors is to space the detectors at intervals equal to spacings established by tests at Underwriters Laboratories Inc. Listed spacings are determined in full-scale fire tests.[7]

In the Underwriters Laboratories Inc. (UL) test, a burning pan of 190-proof denatured alcohol is located in the center of a test room. Sprinkler heads having a 160°F (71°C) rated operating temperature are located on the ceiling in a square array having 10-ft (3-m) sides. The fire is in the center of the square. The distance between the fire and the ceiling is varied so that the 160°F (71°C) sprinkler head being used operates in approximately 2 min.

As shown in Figure 4-1.2, detectors of the type being tested are located at the corners of squares having 20-, 30-, 40-, and 50-ft (6.1-, 9.1-, 12.2-, and 15.2-m) sides. The spacing of the last detector to operate prior to a sprinkler head operating becomes the detector's listed spacing. A similar testprocedure is employed by Factory Mutual Research Corporation (FMRC) to arrive at an approved detector spacing.

Table 4-1.1 ***Fire Signatures and Commercially Available Detectors***

Fire Signature/ Detector Type	Electromagnetic Radiation Wave Length 1700 to 2900 Angstroms	Electromagnetic Radiation (thermal) 6500 to 8500	Invisible Products of Combustion Less Than 0.1 Micron	Visible Smoke and Products of Combustion More Than 0.1 Micron	Rapid Change in Temperature	High Temperature
Ultraviolet detector	X					
Infrared detector		X				
Sub-micron particle detector						
Wilson cloud chamber			X			
Infrared particle detector						
Smoke detector						
photoelectric				X		
ionization			X			
photo beam				X		
Rate-of-rise heat detector					X	
Rate anticipation heat detector						X
Fixed temperature heat detector						X

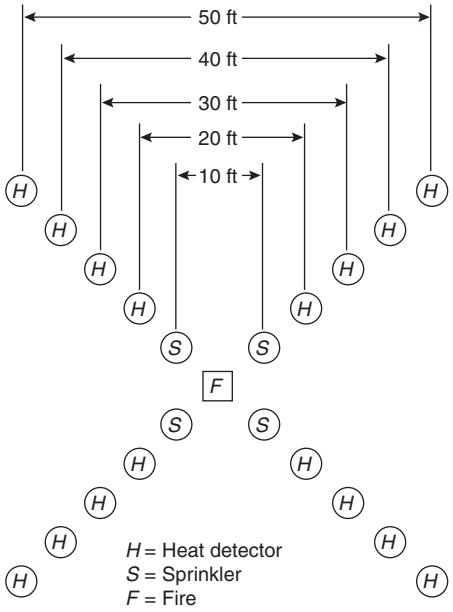

Figure 4-1.2. ***Detector test layout.***

Most codes require that detectors be spaced at intervals equal to the UL or FMRC spacing. NFPA 72, National Fire Alarm Code®,[8] 1999 edition, requires that the installed spacing be less than the listed spacing to compensate for high ceilings, beams, and air movement. High ceilings mean that the fire plume will entrain more ambient air as it rises. This condition has the effect of cooling the gases and reducing the concentration of fire products. Beams, joists, walls, or sloped ceilings alter the flow of combustion products. This situation can serve to restrict or enhance the operation of a fire detector. For instance, consider the case where a fire detector is located on a ceiling between two parallel beams and a fire occurs at floor level between the beams. If the distance between the beams is small compared to the horizontal distance from the fire to the detector, the beams will act as a channel directing the flow of hot gas to the detector, thus speeding operation. NFPA 72 allows detector spacing to be increased beyond the listed spacing in areas, such as corridors, with narrow walls to confine the smoke and heat produced by the fire. Systems can be designed using this type of code approach; however, this approach will not permit quantitative assessment of detector response or measure the ability of a given system design to meet specific design goals relating to fire size, allowable damage, or hazard.

The best possible location for a heat detector is directly over the fire. If there are specific hazards to be protected, the design should include detectors directly overhead or inside of the hazard. In areas without specific hazards, detectors should be spaced evenly across the ceiling. When detectors are evenly spaced, as shown in Figure 4-1.3, the point that is farthest from any detector will be in the middle of four detectors. The spacing between detectors is

$$S = 2^{1/2} r \tag{1}$$

For a given detector, the problem is to determine the maximum distance the detector can be located from the fire and still respond within the design goals of the system. This requires a method for predicting detector response, based on fire size and growth rate, ceiling height, and detector characteristics.

Fire plume and ceiling-jet models can be used to estimate the temperature and velocity of fire gases flowing past a detector. The heat transfer can be calculated, and the response of the detector can be modeled.

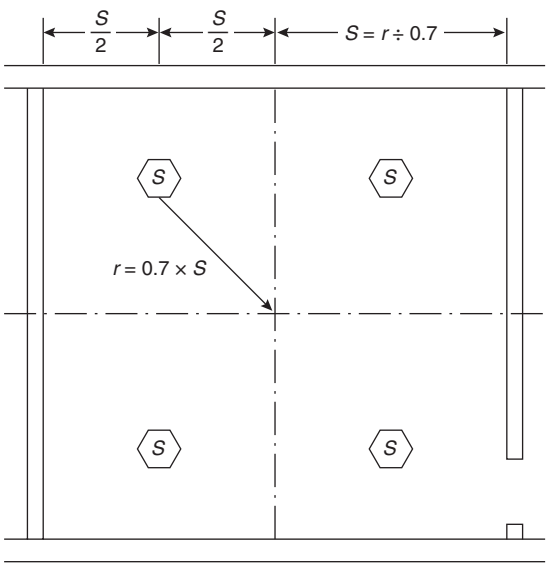

Figure 4-1.3. ***Detector spacing.***

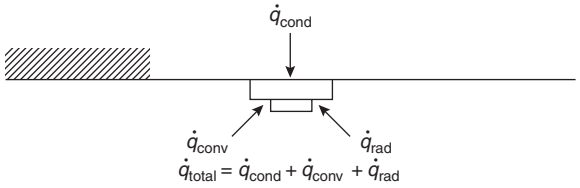

Figure 4-1.4. ***Heat transfer to a ceiling-mounted detector.***

Figure 4-1.4 describes the heat transfer taking place between a heat detector and its environment. The total heat transfer rate to the unit, $\dot{q}_{total}$, can be expressed by the relationship

$$\dot{q}_{total} = \dot{q}_{cond} + \dot{q}_{conv} + \dot{q}_{rad} \quad \text{(kW or Btu/s)} \tag{2}$$

where

$\dot{q}_{cond}$ = conduction
$\dot{q}_{conv}$ = convection
$\dot{q}_{rad}$ = radiation heat transfer rates

During the initial stage of fire growth, radiation heat transfer can be neglected. Also, the elements of most commercially available heat detectors are thermally isolated from the remainder of the unit. In these cases, it can be assumed that the heat lost from the heat-sensitive element by conduction to other parts of the detector, and to the ceiling by conduction, is negligible in comparison to the convection heat transfer taking place. This exclusion leaves a net rate of heat transfer to the detector equal to $\dot{q}_{conv}$. The convective heat transfer rate to the detector is described by

$$\dot{q} = \dot{q}_{conv} = hA(T_g - T_d) \quad \text{(kW or Btu/s)} \tag{3}$$

where

h = convective heat transfer coefficient in kW/(m²·°C) or Btu/(s·ft²·°F)
A = area being heated
T_d = detector temperature
T_g = temperature of the gas heating the detector

Treating the detector element as a lumped mass, m (kg or lbm), the change in its temperature is found by

$$\frac{dT_d}{dt} = \frac{\dot{q}}{mc} \quad \text{deg/s} \tag{4}$$

where c is the specific heat of the element being heated and has units of kJ/(kg·°C) or Btu/(lbm·°F) and $\dot{q}$ is the heat transfer rate. This equation leads to the following relationship for the change in temperature of the detector with respect to time:

$$\frac{dT_d}{dt} = \frac{hA(T_g - T_d)}{mc} \tag{5}$$

Heskestad and Smith[9] have proposed use of a time constant, τ, to describe the convective heat transfer to a particular detector element:

$$\tau = \frac{mc}{hA} \quad \text{s} \tag{6}$$

$$\frac{dT_d}{dt} = \frac{T_g - T_d}{\tau} \tag{7}$$

Note that τ is a function of the mass, area, and specific heat of the particular detector element being studied. For a given fire-gas temperature and velocity and a particular detector design, an increase in mass increases τ. A larger τ results in slower heating of the element.

The convective heat transfer coefficient, h, is a function of the velocity of the gases flowing past the detector element and the shape of the detector element. For a given detector, if the gas velocity is constant, h is constant. It has been shown[10] that the convective heat transfer coefficient for spheres, cylinders, and other objects similar to a sprinkler or heat detector element is approximately proportional to the square root of the Reynolds number, Re:

$$\text{Re} = \frac{ud}{v} \tag{8}$$

where

u = gas velocity
d = diameter of a cylinder or sphere exposed to convective heating
v = kinematic viscosity of the gas

For a given detector, this equation means that h and, hence, τ, is approximately proportional to the square root of the velocity of the gases passing the detector. This relationship can be expressed as a characteristic response time index, RTI, for a given detector:

$$\tau u^{1/2} \simeq \tau_0 u_0^{1/2} = \text{RTI} \tag{9}$$

Thus, if τ_0 is measured in the laboratory at some reference velocity u_0, this expression is used to determine the τ at any other gas velocity, u, for that detector. The product, $\tau u^{1/2}$, is the response time index, RTI.

The use of RTI as a heat transfer function is a simplification. The determination of RTI assumes that τ (and therefore h) is proportional to the square root of the gas velocity, regardless of the magnitude of the velocity. The flow of gases past irregularly shaped objects such as detectors and sprinklers is very complex. Even the flow past cylinders is too complex to use a simple relationship for the heat transfer coefficient (i.e., constant RTI). Hollman showed that the heat transfer coefficient (and therefore τ) is actually proportional to the Reynolds number raised to a fractional power, n, that varies from 0.330 to 0.805 depending on the value of the Reynolds number.[10] For values of Re between 40 and 4000, which is probably the range for most fire detection scenarios, the value of n is given as 0.466. This value is close to 0.5 (square root), but may explain some of the variation found in the experimental determination of τ and RTI.

Plunge tests performed on a variety of heat detectors by Bissell[11] show variations in τ and RTI, while other tests produced reasonable results for a variety of test parameters. It is possible that further analysis may show that an RTI based on $n = 0.5$ is reasonable and that the potential errors are insignificant in the context of fire and detector modeling. On the contrary, it may be found that some other value for n produces better results.

The exponent n may vary over ranges of Reynolds numbers less than those reported by Hollman. Some detector geometries are aerodynamically designed to channel fire gases to the detector element. The ability to affect the gas flow is a function of both the flow velocity and whether the flow is turbulent or laminar. These effects introduce additional variables that complicate the determination of a heat transfer function.

An added source of error in heat transfer modeling is that the temperature-sensing element of a heat detector is never completely isolated from the detector body. This setup results in conductive heat loss that may not be accounted for when using only one time constant. Kokkala has shown that for some detectors as much as 10 percent of the heat gained by convection is lost by conduction to the detector body.[12] A two-time-constant approach, similar to the *C* parameter used in modeling the response of sprinkler heads, is suggested by Kokkala. In a plunge test, the velocity may be high enough so that the conduction heat loss is negligible when compared to the heat gain by convection. In actual fire conditions, this conduction heat loss may contribute to the variation in RTI as it is currently used.

The magnitude of the potential error resulting from the assumption that RTI is constant has not been investigated. Future research and analysis should also consider the possibility that it might be best to test and report several discrete values for τ (hence h).[13] An example is using a plunge test to find τ at three different velocities. The slow, medium, and fast velocities should be representative of the range of possible fire-gas velocities.

A continuous curve of τ versus u for every model detector would be ideal. However, the economic feasibility of testing must be considered. At the present time, heat detectors are tested in ovens to determine their operating temperatures, and are tested in full-scale fire tests to determine their listed spacing (relative sensitivity). A single oven could be used to test for operating temperature and τ at several different velocities as discussed above. This type of testing would be more repeatable (precise), have a lower environmental impact, and give results that can be directly used by engineers in performance-based analysis and design. The test data could be used to calculate a listed spacing comparable to that determined in the present full-scale test so that current code-based design methods could continue to be used.

The remainder of the calculations in this chapter will be made using RTI as a heat transfer function. The user will readily see how other functions, when available, can be incorporated into the equations to effect other solutions.

Heskestad and Smith[9] developed a test apparatus at Factory Mutual Research Corporation to determine the RTI of sprinkler heads. In the test, called a *plunge test*, the sprinkler head is suddenly lowered into the flow of a hot gas. The temperature and velocity of the gas are known and are constant during the test. The equation for the change in the detector temperature is then

$$\frac{dT_d}{dt} = \left(\frac{1}{\tau}\right)(T_g - T_d) \tag{10}$$

Since the gas temperature is constant during the test, the solution to this equation is

$$T_d - T_a = (T_g - T_a)\left[1 - \exp\left(\frac{-t}{\tau}\right)\right] \tag{11}$$

where T_a is the ambient, or initial, temperature of the sprinkler or detector at time $t = 0$. T_d is the temperature of the detector at time t. Rearranging the equation gives

$$\tau = \frac{t}{\ln\left[(T_g - T_a)/(T_g - T_d)\right]} \tag{12}$$

By measuring the response time, t_r, of the unit in the plunge test, this equation can be used to calculate τ_0 at the test velocity u_0. This calculation is done by substituting the response temperature and time for T_d and t. The sensitivity of the detector or sprinkler can then be expressed as

$$\tau_0(\text{at } u_0) = \frac{t_r}{\ln\left[(T_g - T_a)/(T_g - T_r)\right]} \text{ (s)} \tag{13}$$

In terms of the response time index, this equation becomes

$$\text{RTI} = \frac{t_r u_0^{1/2}}{\ln\left[(T_g - T_a)/(T_g - T_r)\right]} \tag{14}$$

The RTI has units of $m^{1/2}s^{1/2}$ or $ft^{1/2}s^{1/2}$.

A plunge test can be used to determine the RTI for a heat detector or a sprinkler. Knowing the RTI, the change in temperature of similar units can be calculated for any history of fire gases flowing past it. The form of the heat transfer equation is

$$\frac{dT_d}{dt} = \frac{u^{1/2}(T_g - T_d)}{\text{RTI}} \tag{15}$$

This equation is used to calculate the temperature of a fixed-temperature heat detector or sprinkler exposed to

fire gases. The equation can be used to determine the time at which the unit reaches its operating temperature.

The use of a lumped mass model may not hold for rate-of-rise heat detectors and rate-compensated heat detectors. The heat transferred to a fixed-temperature heat detector either heats a sensing element until it melts, or it heats two dissimilar metals of a snap disk. In each case, the element itself is exposed to the hot gases. This result is not true for rate-of-rise heat detectors or rate-compensated heat detectors.

Most commercial rate-of-rise heat detectors operate when the expansion of air in a chamber exceeds the rate at which the air can escape through a small vent hole. For this type of detector, it is also necessary to model heat transfer from the detector body to the air in its chamber. Then, the expansion of the air and its escape through a vent hole must be accounted for. The response time index determined in a plunge test may not be constant as fire-gas velocities or temperatures vary. Hence, RTI is only an approximation of how the detector responds. Also, it has been hypothesized, but not tested, that rate-of-rise detectors may be modeled by simply comparing the rate of change of gas temperature to their rated response threshold.[13] This hypothesis may be true since their rated response in degrees per minute or degrees per second is actually the measured rate of gas temperature change in the test apparatus. Thus, it would be expected that if the velocity of the fire gases was on the same order of magnitude as in the test, the rate of change of gas temperature would be the measure for detector response.

A rate-compensated detector consists of a metallic shell surrounding two bowed metal struts. There are electrical contacts on the struts. The struts and shell expand at different rates as the detector is heated. When heated fast, the outer shell expands and causes the bowed struts to straighten and close the contacts, signaling an alarm. This condition usually occurs at temperatures below the rated operating temperature. However, if the unit is heated more slowly, the difference between the expansion rates of the inner and outer parts is such that the contacts close at or near the unit's rated temperature. For rates of temperature rise up to approximately 22°C/min (40°F/min), rate-compensated detectors tend to respond when the surrounding gas temperature reaches the unit's rated operating temperature.[14]

Obviously, the rate-compensated type of heat detector cannot be treated as a lumped mass when calculating its response to a fire. However, at rates of temperature rise less than approximately 22°C/min (40°F/min), they can be modeled by simply assuming that they respond when the surrounding gas temperature reaches their operating temperature.

From the discussion above, it is evident that the response of fixed-temperature heat detectors can be modeled. It is necessary to know the temperature at which the detector is rated to operate. For rate-of-rise heat detectors, it is necessary to know the rate of change in the detector's temperature at which it will alarm. The RTI or τ_0 and u_0 for the detector are also needed.

In order to calculate the response of a heat detector, it is necessary to know the temperature and velocity of the gases flowing past it. Some fire plume models or ceiling-jet models may give functional relationships for temperature and velocity that can be substituted into the heat transfer equation and integrated. Other models may not be suitable for an analytical solution. In this case, the fire model should be used to produce data on time-versus-temperature and time-versus-gas velocities. These data can then be used to numerically solve the detector heat transfer equation.

Most fire and ceiling-jet models do not model the temperature and velocity profile as a function of distance from the ceiling. This lapse introduces error and uncertainty in the results. Marrion[15] showed that maximum temperature and velocity occurs between 1 and 3 in. (25 and 76 mm) below the ceiling for small (5- to 7-in. [127 to 178 mm] diameter) gasoline pan fires with a ceiling clearance of about 14 ft (4.3 m). Others have reported maximums at a distance down from the ceiling of approximately one-tenth the distance from the fuel to the ceiling. Alpert[16] reports ceiling jet thickness to be approximately 5 to 12 percent of the ceiling to fuel distance. Users are cautioned when modeling detector mechanisms that are not within this range.

When the responses of multiple detectors or sprinklers are modeled, no provisions are made to account for sprinkler spray cooling of the room, and therefore, the activation of additional elements (beyond the first) may be inaccurately predicted. For more information on this topic the reader is referred to the references for works by Cooper, Delichatsios and Alpert, and Heskestad.[17–19]

Heat Detection—Steady-State Fires

Alpert[16] presented the following series of equations to calculate temperature and velocity of fire gases in a ceiling jet as a function of heat release rate and position for steady-state fires:

$$T_g - T_a = \frac{[5.38(\dot{Q}/r)^{2/3}]}{H}\,°\text{C} = \frac{[4.74(\dot{Q}/r)^{2/3}]}{H}\,°\text{F}$$

where $r/H > 0.18$, and

$$T_g - T_a = \frac{(16.9\dot{Q}^{2/3})}{H^{5/3}}\,°\text{C} = \frac{(14.9\dot{Q}^{2/3})}{H^{5/3}}\,°\text{F}$$

where $r/H \leq 0.18$, and

$$u = \frac{(0.20\dot{Q}^{1/3}H^{1/2})}{r^{5/6}}\,\text{m/s} = \frac{(0.25\dot{Q}^{1/3}H^{1/2})}{r^{5/6}}\,\text{ft/s}$$

where $r/H > 0.15$, and

$$u = 0.95\left(\frac{\dot{Q}}{H}\right)^{1/3}\,\text{m/s} = 1.2\left(\frac{\dot{Q}}{H}\right)^{1/3}\,\text{ft/s}$$

where $r/H \leq 0.15$.

In the above series of equations,

T_g = maximum, near ceiling, fire-gas temperature in °C or °F
T_a = ambient temperature in °C or °F
$\dot{Q}$ = total heat release rate of the fire in kW or BTU/min
r = radial distance from the axis of the fire plume in m or ft
H = height above the origin of the fire in m or ft
u = maximum, near ceiling, fire-gas velocity in m/s or ft/s

This model assumes that the temperature and velocity of the fire gases at a point away from the source are related to the instantaneous heat release rate of the fire. This assumption neglects the time required for transport of the fire gases from the source to the detector. Also, because the correlations are based on the total heat release rate rather than only the convective heat release rate, errors will be introduced when the convective fraction differs from that in the tests used to develop the correlations.

For a constant gas temperature and constant gas velocity, the basic heat transfer equation can be solved:

$$\frac{dT_d}{dt} = \frac{T_g - T_d}{\tau} \tag{7}$$

$$dT_d = \int_0^t \frac{1}{\tau}(T_g - T_d)\,dt$$

$$\Delta T_d = T_d - T_a = (T_g - T_a)\left[1 - \exp\left(\frac{-t}{\tau}\right)\right]°\text{C}$$

or, substituting the equation for RTI

$$\Delta T_d = T_d - T_a = (T_g - T_a)\left[1 - \exp\left(\frac{-tu^{1/2}}{\text{RTI}}\right)\right]°\text{C}$$

The response of heat detectors to fires with ceiling jets having a near constant gas temperature and velocity can be modeled using the above equations.

EXAMPLE 1:

A 4-m^2 pool of kerosene is burning under a flat ceiling that is 6 m high. The ambient temperature is 20°C. What would be the temperature of a ceiling-mounted heat detector having an RTI of 55 m$^{1/2}$s$^{1/2}$ after a 30-s exposure if it were located 6 m from the center of the plume?

SOLUTION:

From Table 3-4.11 in this handbook the chemical heat of combustion of kerosene is 40.3 kJ/g. The convective heat of combustion is listed as 26.2 kJ/g, which is a convective fraction of about 65 percent. For Alpert's correlations we must use the total heat release rate, hence the total or chemical heat of combustion. This calculation assumes that the convective fraction will be approximately the same as the convective fraction in the experimental data Alpert used to develop the correlations for temperature and velocity. From Table 3-4.5 the mass burning rate is given as approximately 67 g/m^2·s. The total heat release rate is

$$\dot{Q} = H_c \dot{m}'' A \text{ kW}$$

$$\dot{Q} = 40.3(67)4 \text{ kW}$$

$$\dot{Q} = 10{,}800 \text{ kW}$$

An r/H ratio greater than 0.18 indicates that the detector is located in the ceiling jet temperature profile. In this example,

$$\frac{r}{H} = \frac{6}{6} = 1 > 0.18$$

Therefore,

$$T_g - T_a = \frac{[5.38(\dot{Q}/r)^{2/3}]}{H}\,°\text{C}$$

$$T_g - 20 = \frac{[5.38(10{,}800/6)^{2/3}]}{6}\,°\text{C}$$

$$T_g - 20 = 132.7°\text{C}$$

$$T_g = 153°\text{C}$$

The velocity of the fire gases in the ceiling jet is given by

$$u = \frac{(0.20\dot{Q}^{1/3}H^{1/2}}{r^{5/6}} \text{ m/s}$$

$$u = \frac{[0.20(10.800)^{1/3}(6)^{1/2}]}{6^{5/6}} \text{ m/s}$$

$$u = 2.4 \text{ m/s}$$

The resulting detector temperature after 120 s is now calculated:

$$\Delta T_d = T_d - T_a = (T_g - T_a)\left[1 - \exp\left(\frac{-tu^{1/2}}{\text{RTI}}\right)\right]°\text{C}$$

$$\Delta T_d = (153 - 20)\left[1 - \exp\left(\frac{-30(2.4)^{1/2}}{55}\right)\right]°\text{C}$$

$$\Delta T_d = 76°\text{C}$$

$$T_d = 76 + T_a = 76 + 20 = 96°\text{C}$$

EXAMPLE 2:

What would be the response time of the detector in the above example if its temperature rating was 57°C?

SOLUTION:

$$\Delta T_d = T_d - T_a = (T_g - T_a)\left[1 - \exp\left(\frac{-tu^{1/2}}{\text{RTI}}\right)\right]°\text{C}$$

Rearranging and substituting the rated response temperature T_r for T_d, and response time t_r for t,

$$t_r = \frac{\text{RTI}}{u^{1/2}} \ln\left(\frac{T_g - T_a}{T_g - T_r}\right)°\text{C}$$

$$t_r = \frac{55}{2.4^{1/2}} \ln\left(\frac{153 - 20}{153 - 57}\right)°\text{C}$$

$$t_r = 12 \text{ s}$$

Heat Detection, Growing Fires, and Quasi-Steady-State Modeling

A growing fire can be modeled by assuming the fire to be composed of a series of increasing steady heat release rates. This model is referred to as quasi-steady-state modeling. The first step is to break the heat release rate curve into a series of small time intervals. For each interval, use the average heat release rate for that interval to calculate the fire-gas temperature and velocity. Then, starting at ambient temperature, calculate the change and resulting temperature of the detector at the end of the first interval. Using that new detector temperature at the start of the next interval, use the next gas temperature and ve-

locity to calculate the detector temperature at the end of the interval. Continue until you have reached the time of interest or until the detector temperature exceeds its operating temperature.

EXAMPLE 3:

A stack of wood pallets is burning under a flat ceiling that is 6 m high. Table 4-1.2, showing heat release rates, is given below. The ambient temperature is 20°C. What would be the temperature of a ceiling-mounted heat detector having an RTI of 55 $m^{1/2} \cdot s^{1/2}$ after a 180-s exposure if it were located 6 m from the center of the plume?

SOLUTION:

As in the previous examples, the detector is located in the developed ceiling jet. The first step is to calculate the change in temperature and the velocity for each heat release rate in the table. For the period 0 to 10 s, the heat release rate is given as 5 kW. The change in temperature and the velocity of the ceiling jet at the detector are

$$T_g - T_a = \frac{\left[5.38\left(\frac{\dot{Q}}{r}\right)^{2/3}\right]}{H}\,°C$$

$$T_{g,1} - T_a = \frac{\left[5.38\left(\frac{5}{6}\right)^{2/3}\right]}{6} = 0.794°C$$

$$T_{g,1} = 20.794°C$$

$$u = \frac{(0.20\dot{Q}^{1/3}H^{1/2})}{r^{5/6}}\ \text{m/s}$$

$$u_1 = \frac{[0.20(5)^{1/3}(6)^{1/2}]}{6^{5/6}} = 0.188\ \text{m/s}$$

Next calculate the change in detector temperature ΔT_d as a result of that exposure by assuming the temperature and velocity to be steady over short intervals.

$$\frac{dT_d}{dt} = \frac{T_g - T_d}{\tau} = \frac{u^{1/2}(T_g - T_d)}{RTI}$$

Table 4-1.2 ***Example 3—Heat Release Rates***

Δt	$\dot{Q}$	Δt	$\dot{Q}$
0	0	100	469
10	5	110	567
20	19	120	675
30	42	130	792
40	75	140	919
50	117	150	1055
60	169	160	1200
70	230	170	1355
80	300	180	1519
90	380		

$$\Delta T_d = T_{d,n} - T_{d,n-1} = \frac{u_n^{1/2}(T_{g,n} - T_{d,n-1})}{RTI}\Delta t°C$$

$$T_{d,n} = \left[\frac{u^{1/2}(T_{g,n} - T_{d,n-1})}{RTI}\Delta t\right] + T_{d,n-1}°C$$

Initially, the detector is not exposed to hot gases and is at ambient temperature. For the first step or interval, the detector is exposed and the resulting detector temperature at the end of the interval ($T_{d,1}$) is calculated.

$$T_{d,1} = \left[\frac{u^{1/2}(T_{g,1} - T_{d,0})}{RTI}\Delta t\right] + T_{d,0}°C$$

$$T_{d,1} = \left[\frac{(0.188)^{1/2}(20.794 - 20)}{55}10\right] + 20 = 20.063°C$$

To simplify the process, set up a table or a spreadsheet, as shown in Table 4-1.3, to complete the calculations. Rounding to two significant digits is done last. After 120 seconds of exposure the detector temperature is approximately 32°C. If the dectector were rated at 57°C, it would not have responded.

Heat Detection—Potential Errors: Steady-State and Quasi-Steady-State Modeling

There are many sources of potential error in these calculations. These include the following: uncertainty in the operating temperature, uncertainty in the ambient temperature, and inaccuracies in the fire-gas temperature and velocity correlations. Because the magnitude of these potential errors is unknown or unreported, a tolerance or confidence interval for the answer cannot be estimated.

In addition, it has been assumed that use of the ceiling-jet model is valid for the examples above. The model assumes an infinite ceiling for the ceiling jet to flow outward without encountering walls and developing a layer. In the first example, the gas velocity was 2.4 m/s, and the calculation was done for a period of 120 s. The leading edge of the ceiling jet would then be approximately 48 m (2.4 m/s × 120 s) from the fire location. This dimension can be used

Table 4-1.3 ***Example 3—Spreadsheet Calculations***

t	$\dot{Q}$	ΔT_g	T_g	u	ΔT_d	T_d
0	0	0		0	0	20
10	5	0.794	20.794	0.188	0.063	20.063
20	19	1.934	21.934	0.294	0.184	20.247
30	42	3.281	23.281	0.383	0.341	20.588
40	75	4.830	24.830	0.464	0.525	21.114
50	117	6.496	26.496	0.538	0.718	21.832
60	169	8.301	28.301	0.609	0.918	22.749
70	230	10.194	30.194	0.674	1.112	23.861
80	300	12.170	32.170	0.737	1.297	25.158
90	380	14.247	34.247	0.797	1.476	26.633
100	469	16.393	36.393	0.855	1.641	28.274
110	567	18.603	38.603	0.911	1.792	30.066
120	675	20.896	40.896	0.965	1.935	32.001

as a test to determine if additional error is possible because limitations of the model have been exceeded.

Evans and Stroup[20] published a computer program called DETACT-QS, which uses Alpert's equations to calculate the response of heat detectors. That program requires the following input: ceiling height, H; ambient temperature, T_a; distance from fire axis to detector, r; detector response or activation temperature, T_r; and detector response time index (RTI). The user must also input history of time versus heat release rate for the fire. The program uses the quasi-steady-state method demonstrated above to calculate the detector response.

Heat Detection—Power-Law Fires

Heskestad and Delichatsios[8] presented functional relationships for modeling the temperature and velocity of fires whose heat release rates grow according to the power-law relationship:

$$\dot{Q} = \alpha t^p \text{ kW}$$

where

α = constant for a particular fuel describing the growth of the fire (kW/s^2)
t = time (s)
p = positive exponent
$\dot{Q}$ = heat release rate (kW)

NFPA 72, Appendix B, uses a constant called the *fire growth time*, t_g, in lieu of α to describe the fire intensity. The fire growth time is defined as the time at which a power-law fire would reach a heat release rate of 1055 kW (1000 Btu/s). In terms of t_g, the power-law equation becomes

$$\dot{Q} = \left(\frac{1055}{t_g^2}\right) t^p \text{ kW}$$

The nondimensional functional relationships given by Heskestad and Delichatsios[21] for temperature and velocity of fire gases in a ceiling jet are

$$u_p^* = \frac{u}{(A^{1/(3+p)}\alpha^{1/(3+p)}H^{(p-1)/(3+p)})}$$
$$u_p^* = f\left(t_p^*, \frac{r}{H}\right) \tag{16}$$

$$\Delta T_p^* = \frac{\Delta T}{A^{2/(3+p)}(T_a/g)\alpha^{2/(3+p)}H^{-(5-p)/(3+p)}}$$
$$\Delta T_p^* = g\left(t_p^*, \frac{r}{H}\right) \tag{17}$$

where

$$A = \frac{g}{C_p T_a \rho_0} \tag{18}$$

$$t_p^* = \frac{t}{A^{-1/(3+p)}\alpha^{-1(3+p)}H^{4/(3+p)}} \tag{19}$$

All variables are described in this chapter's nomenclature section.

For $p = 2$ power-law fires, the above nondimensional equations reduce to the following:

$$u_2^* = \frac{u}{(A^{1/5}\alpha^{1/5}H^{1/5})}$$

$$\Delta T_2^* = \frac{\Delta T}{A^{2/5}(T_a/g)\alpha^{2/5}H^{-3/5}}$$

$$t_2^* = \frac{t}{A^{-1/5}\alpha^{-1/5}H^{4/5}}$$

Heskestad and Delichatsios[21] presented correlations to the functional relationships for fires whose release rates vary according to the power-law equation, with $p = 2$. These fires are referred to as t^2 fires. It has been shown[22,23] that the $p = 2$ power-law fire growth model can be used to model the heat release rate of a wide range of fuels. The original correlations were used in several publications and popular calculation programs for ceiling-jet and heat-detector modeling, including the first two editions of this handbook.[8,9,20,23–26]

Subsequently Heskestad and Delichatsios found that an incorrect value for the heat of combustion of wood resulted in the correlations being in error. All examples in this chapter that use these correlations have been updated or replaced. The corrected data correlations are as follows:[27]

$$t_{2f}^* = 0.861\left(1 + \frac{r}{H}\right)$$

t_{2f}^* is the nondimensional time at which the heat front reaches the detector. When $t_2^* < t_{2f}^*$, the heat front has not reached the detector position. Therefore, $\Delta T_2^* = 0$.

For $t_2^* \geq t_{2f}^*$,

$$\Delta T_2^* = \left[\frac{(t_2^* - t_{2f}^*)}{(0.146 + 0.242r/H)}\right]^{4/3}$$

This relationship may also be expressed as

$$\Delta T_2^* = \left[\frac{(t_2^* - t_{2f}^*)}{D}\right]^{4/3}$$

where

$$D = 0.146 + 0.242\frac{r}{H}$$

$$\frac{u_2^*}{(\Delta T_2^*)^{1/2}} = 0.59\left(\frac{r}{H}\right)^{-0.63}$$

The above correlations assume that the convective heat release rate is approximately 75 percent of the total heat release rate. The following equations are more useful forms and are used with the nondimensional equations for ΔT_2^* and u_2^* by first multiplying α by the convective fraction X:

$$\alpha_c = X\alpha \text{ kW/s}^2$$

$$t_{2f}^* = 0.813\left(1 + \frac{r}{H}\right) \tag{20}$$

$$\Delta T_2^* = 0$$

when $t_2^* < t_{2f}^*$.

For $t_2^* < t_{2f}^*$,

$$\Delta T_2^* = \left[\frac{(t_2^* - t_{2f}^*)}{(0.126 + 0.210r/H)} \right]^{4/3} \tag{21}$$

This may also be expressed as

$$\Delta T_2^* = \left[\frac{(t_2^* - t_{2f}^*)}{D} \right]^{4/3}$$

where

$$D = 0.126 + 0.210 \frac{r}{H} \tag{22}$$

$$\frac{u_2^*}{(\Delta T_2^*)^{1/2}} = 0.59 \left(\frac{r}{H} \right)^{-0.63} \tag{23}$$

Beyler found that these correlations for temperature and velocity could be substituted into the heat transfer equation and integrated.[28] Beyler's analytical solution was published in *Fire Technology*[29] and is repeated here.

The analytical solution for the instantaneous rate of change of detector temperature is

$$\frac{dT_d(t)}{dt} = \frac{4}{3} \frac{\Delta T}{\Delta T_2^*} \Delta T_2^{*1/4} \frac{(1 - e^{-Y})}{(t/t_2^*)D} \tag{24}$$

The analytical solution for change in detector temperature is

$$\Delta T_d = T_d(t) - T_d(0) = \frac{\Delta T}{\Delta T_2^*} \Delta T_2^* \left[1 - \frac{(1 - e^{-Y})}{Y} \right] \tag{25}$$

where

$$Y = \frac{3}{4} \sqrt{\frac{u}{u_2^*}} \sqrt{\frac{u_2^*}{(\Delta T_2^*)^{1/2}}} \left(\frac{\Delta T_2^*}{\mathrm{RTI}} \right) \left(\frac{t}{t_2^*} \right) D \tag{26}$$

and as previously defined,

$$D = 0.126 + 0.210 \frac{r}{H} \tag{22}$$

In a design situation, the objective is to determine the spacing of detectors required to respond to a specific fire scenario. The detector must respond when the fire reaches a certain threshold heat release rate or in a specified amount of time. Time and heat release rate are interchanged using the fire growth model. The steps in solving this type of problem using the $p = 2$ power-law model are outlined below and are discussed in more detail in the examples following this section. The referenced equation numbers assume that the correlations used are the ones for a variable convective fraction. The procedure would be the same if using the correlations for the fixed, 75 percent convective fractions except that α is not multiplied by the convective fraction when used in the equations. For design problems,

1. Determine the environmental conditions of the area being considered.
   a. ambient temperature, T_a (convert to absolute temperature)
   b. ceiling height or height above fuel, H
2. Estimate the fire growth characteristic α or t_g for the fuel expected to be burning. If t_g is used, calculate the corresponding α. Multiply α by the convective fraction to get α_c before using in the equations.
3. Establish the goals of the system: required response time t_r or maximum permitted threshold heat release rate $\dot{Q}_T$.
4. Select the detector type to be used. For fixed-temperature units, this choice establishes the detector response temperature T_r and its RTI, or τ_0 and u_0.
5. Make a first estimate of the distance, r, from the fire to the detector necessary to meet the system goals.
6. Assume that the fire starts obeying the power-law model at time $t = 0$.
7. Set the initial temperature of the detector and its surroundings at ambient temperature.
8. Using Equation 20, calculate the nondimensional time, t_{2f}^*, at which the initial heat front reaches the detector.
9. Calculate the factor A defined in Equation 18.
10. If the equations for a variable convective fraction are used, multiply α by the convective fraction X to get α_c and use result that with the required response time in Equation 19 to calculate the corresponding value of t_2^*.
11. If t_2^* is greater than t_{2f}^*, continue with Step 12. If not, try a new detector position, r, closer to the fire and return to Step 8.
12. Calculate the ratio u/u_2^* using Equation 16.
13. Calculate the ratio $\Delta T/\Delta T_2^*$ using Equation 17.
14. Use Equation 21 to calculate ΔT_2^*.
15. Equation 23 is used to calculate the ratio $u_2^*/(\Delta T_2^*)^{1/2}$.
16. Use Equations 22 and 26 to calculate D and Y.
17. Equation 25 can now be used to calculate the resulting temperature of the detector.
18. If the temperature of the detector is below its operating temperature, this procedure must be repeated using a smaller r. If the temperature of the detector exceeds its operating temperature, a larger r can be used.
19. Repeat this procedure until the detector temperature is about equal to its operating temperature. The required spacing of detectors is then $S = 1.41r$.

This same procedure is used to estimate the response of rate-of-rise heat detectors. The difference is that in Step 17, Equation 24 is used to calculate rate of change of the detector temperature. This result is then compared to the rate at which the detector is designed to respond.

The discussion and procedure so far has centered around the solution of a design problem. The question asked was, How far apart must detectors of a specific design be spaced to respond within specific goals to a certain set of environmental conditions and a specific fire scenario?

The second type of problem that must be addressed is the analysis of an existing system or the analysis of a proposed design. Here the spacing of detectors or sprinklers is known. The engineer must still estimate the burning characteristics of the fuel and the environmental conditions of the space being analyzed. The equations can then be solved in a reverse fashion to determine the rate of heat release or the time to detector response. The technique is as follows:

1. Determine the environmental conditions of the area being considered.
   a. ambient temperature, T_a (convert to absolute temperature)

b. ceiling height or height above fuel, H
2. Estimate the fire growth characteristic α or t_g for the fuel expected to be burning. If t_g is used, calculate the corresponding α. Multiply α by the convective fraction to get α_c before using in the equations.
3. Determine the spacing of the existing detectors or sprinklers. The protection radius is then $r = S/\sqrt{2}$.
4. Determine the detector's rated response temperature and its RTI, or τ_0 and u_0.
5. Make a first estimate of the response time of the detector or estimate the heat release rate at detector response and calculate the corresponding response time using the power-law equation.
6. Assume that the fire starts obeying the power-law model at time $t = 0$.
7. Set the initial temperature of the detector and its surroundings at ambient temperature.
8. Using Equation 20, calculate the nondimensional time, t^*_{2f}, at which the initial heat front reaches the detector.
9. Calculate the factor A defined in Equation 18.
10. Use the estimated response time along with Equation 19 to calculate the corresponding value of t^*_2.
11. If t^*_2 is greater than t^*_{2f}, continue with Step 12. If not, try a longer estimated response time or a larger estimated heat release rate and return to Step 8.
12. Calculate the ratio u/u^*_2 using Equation 16.
13. Calculate the ratio $\Delta T/\Delta T^*_2$ using Equation 17.
14. Use Equation 21 to calculate ΔT^*_2.
15. Equation 23 is used to calculate the ratio $u^*_2/(\Delta T^*_2)^{1/2}$.
16. Use Equations 22 and 26 to calculate D and Y.
17. Equation 25 can now be used to calculate the resulting temperature of the detector.
18. If the temperature of the detector is below its operating temperature, this procedure must be repeated using a longer estimated response time. If the temperature of the detector exceeds its operating temperature, a smaller t_r can be used.
19. Repeat this procedure until the detector temperature is about equal to its operating temperature. The resulting response time, t_r, can be used to calculate either the total heat release rate or the convective heat release rate at response using the power-law equation.

As in the design problem, this technique can be used to estimate the response of existing systems of rate-of-rise heat detectors. The difference is that in Step 4 the set point or rate of temperature rise at which the detector will respond must be determined from the manufacturer's data. In Step 17, Equation 24 is used to determine the rate at which the temperature of the detector is changing.

Heat Detection—Potential Errors: Power-Law Fire Modeling

When the exact conditions of velocity and temperature of fire gases flowing past a detector are not known, errors are introduced in the design and analysis of fire detector response. Graphs in Heskestad and Delichatsios' report show the errors in calculated fire-gas temperatures and velocities.[22] An exact treatment of these errors is beyond the scope of this chapter, though some discussion is warranted.

Plots of actual data and calculated data show that errors in ΔT^*_2 can be as much as 50 percent, though generally there appears to be much better agreement.[22,23] The maximum errors occur at r/H values of about 0.37. All other plots of actual and calculated data, for various r/H, show much smaller errors. In terms of the actual change in temperature over ambient, the maximum errors are on the order of 5 to 10°C. The larger errors occur with faster fires and lower ceilings.

At $r/H = 0.37$, the errors are conservative when the equations are used in a design problem. That is, the equations predicted lower temperatures. Plots of data for other values of r/H indicate that the equations predict slightly higher temperatures.

Errors in fire-gas velocities are related to the errors in temperatures. The equations show that the velocity of the fire gases is proportional to the square root of the change in temperature of the fire gases.[22] In terms of heat transfer to a detector, the detector's change in temperature is proportional to the change in gas temperature and the square root of the fire-gas velocity. Hence, the expected errors bear the same relationships.

Based on the discussion above, errors in predicted temperatures and velocities of fire gases will be greatest for fast fires and low ceilings. Sample calculations simulating these conditions show errors in calculated detector spacings on the order of plus or minus 1 m, or less.[23]

Similar to Alpert's steady-state model, the power-law ceiling-jet model assumes a flat infinite ceiling. If the leading edge of the ceiling jet has passed the detector position and not reached a wall or other obstruction, then the model is within its stated parameters. The nondimensional time that the heat front reaches some position, r/H, is given by the equation for t^*_{2f}. The corresponding nondimensional time at response is given by the equation for t^*_2. Setting these equal to each other and solving for r at $t = t_r$ gives the radial distance from the fire to the leading edge of the heat front. Using the equations for a user-entered convective fraction,

$$t^*_{2f} = 0.813\left(1 + \frac{r}{H}\right)$$

and

$$t^*_2 = \frac{t_r}{A^{-1/5}\alpha_c^{-1/5}H^{4/5}}$$

$$t^*_{2f} = t^*_2$$

$$0.813\left(1 + \frac{r}{H}\right) = \frac{t_r}{A^{-1/5}\alpha_c^{-1/5}H^{4/5}}$$

$$r = \frac{(t_r/A^{-1/5}\alpha_c^{-1/5}H^{4/5})/0.813 - 1}{H} = \frac{t^*_2/0.813 - 1}{H}$$

Selection of Data for Design and Analysis

In order to calculate the required spacing of heat detectors or sprinklers to respond to a given fire, the following information is required:

1. *System goals:* desired fire size (heat release rate) at response or time to detector response from the start of open flaming

2. Fire growth constant α or t_g
3. Ambient temperature
4. Height above the fuel or ceiling height

In addition to the above, the heat capacity of air at constant pressure, C_p, the density of air, ρ_0, and the gravitational constant, g, are used in the calculations. It is also necessary to know the characteristics of the detector for which the spacing calculations are being made. Specifically, the response temperature and the RTI of the detector must be known.

Establishing system goals is not within the scope of this chapter. However, it should be pointed out that, no matter what the goals are, they must be expressed in terms of heat release rate or time to detector response. The system's goals may actually be to limit damages to some dollar value, provide adequate escape time, or limit the production of toxic gases. In order to calculate required detector spacing using this system, these goals would have to be translated. For instance, as the fire grows, at what time or heat release rate must the detector respond so that the fire department can be summoned and extinguish the fire before damage levels are exceeded or conditions become untenable due to toxic gases?

Table 4-1.4 is a list of furniture calorimeter tests done at the National Bureau of Standards.[16,24] The tests provide

Table 4-1.4 ***Summary of NBS Calorimeter Tests***

Test No.	Description	Fire Growth Time (s) (t_g)	α (kW/s²)	Virtual Time (s)	Maximum Heat Release Rate (kW)
Test 15	Metal wardrobe 41.4 kg (total)	50	0.4220	10	750
Test 18	Chair F33 (trial loveseat) 39.2 kg	400	0.0066	140	950
Test 19	Chair F21 28.15 kg (initial stage of fire growth)	175	0.0344	110	350
Test 19	Chair F21 28.15 kg (later stage of fire growth)	50	0.4220	190	2000
Test 21	Metal wardrobe 40.8 kg (total) (average growth)	250	0.0169	10	250
Test 21	Metal wardrobe 40.8 kg (total) (later growth)	120	0.0733	60	250
Test 21	Metal wardrobe 40.8 kg (total) (initial growth)	100	0.1055	30	140
Test 22	Chair F24 28.3 kg	350	0.0086	400	700
Test 23	Chair F23 31.2 kg	400	0.0066	100	700
Test 24	Chair F22 31.9 kg	2000	0.0003	150	300
Test 25	Chair F26 19.2 kg	200	0.0264	90	800
Test 26	Chair F27 29.0 kg	200	0.0264	360	900
Test 27	Chair F29 14.0 kg	100	0.1055	70	1850
Test 28	Chair F28 29.2 kg	425	0.0058	90	700
Test 29	Chair F25 27.8 kg (later stage of fire growth)	60	0.2931	175	700
Test 29	Chair F25 27.8 kg (initial stage of fire growth)	100	0.1055	100	2000
Test 30	Chair F30 25.2 kg	60	0.2931	70	950
Test 31	Chair F31 (loveseat) 39.6 kg	60	0.2931	145	2600
Test 37	Chair F31 (loveseat) 40.40 kg	80	0.1648	100	2750
Test 38	Chair F32 (sofa) 51.5 kg	100	0.1055	50	3000
Test 39	½-in. Plywood wardrobe w/ fabrics 68.8 kg	35	0.8612	20	3250
Test 40	½-in. Plywood wardrobe w/ fabrics 68.32 kg	35	0.8612	40	3500
Test 41	⅛-in. Plywood wardrobe w/ fabrics 36.0 kg	40	0.6594	40	6000
Test 42	⅛-in. Ply. wardrobe w/ fire-ret. (int. fin. initial)	70	0.2153	50	2000
Test 42	⅛-in. Ply. wardrobe w/ fire-ret. (int. fin. later)	30	1.1722	100	5000
Test 43	Repeat of ½-in. Plywood wardrobe 67.62 kg	30	1.1722	50	3000
Test 44	⅛-in. Ply. wardrobe w/ F-R., latex paint 37.26 kg	90	0.1302	30	2900
Test 45	Chair F21 28.34 kg (large hood)	100	0.1055	120	2100
Test 46	Chair F21 28.34 kg	45	0.5210	130	2600
Test 47	Chair adj. back metal frame, foam cush. 20.8 kg	170	0.0365	30	250
Test 48	Easychair CO7 11.52 kg	175	0.0344	90	950
Test 49	Easychair 15.68 kg (F-34)	200	0.0264	50	200
Test 50	Chair metal frame minimum cushion 16.52 kg	200	0.0264	120	3000
Test 51	Chair molded fiberglass no cushion 5.28 kg	120	0.0733	20	35
Test 52	Molded plastic patient chair 11.26 kg	275	0.0140	2090	700
Test 53	Chair metal frame w/ padded seat and back 15.5 kg	350	0.0086	50	280
Test 54	Loveseat metal frame w/ foam cushions 27.26 kg	500	0.0042	210	300
Test 55	Group chair metal frame w/ foam cushion 6.08 kg	Never exceeded 50 kW heat release rate			
Test 56	Chair wood frame w/ latex foam cushions 11.2 kg	500	0.0042	50	85
Test 57	Loveseat wood frame w/ foam cushions 54.60 kg	350	0.0086	500	1000
Test 61	Wardrobe ¾-in. particleboard 120.33 kg	150	0.0469	0	1200
Test 62	Bookcase plywood w/ aluminum frame 30.39 kg	65	0.2497	40	25
Test 64	Easychair molded flexible urethane frame 15.98 kg	1000	0.0011	750	450
Test 66	Easychair 23.02 kg	75	0.1876	3700	600
Test 67	Mattress and boxspring 62.36 kg (later fire growth)	350	0.0086	400	500
Test 67	Mattress and boxspring 62.36 kg (initial fire growth)	1100	0.0009	90	400

a database of heat release rate, particulate production, and radiation from a variety of common furnishings. The table provides the corresponding α or t_g for the calorimeter tests.[23] The virtual time data in the table is the approximate time at which the heat release rate in the test began to follow the $p = 2$ power-law model ($\dot{Q} = \alpha t^2$ kW). Prior to this time, the behavior of the fire cannot be predicted with this model. Figure 4-1.5 shows some test data along with a power-law curve superimposed.

The data in Table 4-1.4 can be used to select α or t_g for use in spacing calculations. However, in many cases the data in this table will not match the scenario being studied. If the heat-release-rate-versus-time history can be obtained or approximated for the expected fuel, the α or t_g can be calculated using curve fitting techniques.[23]

In most cases, since the exact fuel that will be involved in a fire cannot be known, the rigorous calculation of α is not warranted. Engineering judgment can be used to select an α or t_g that approximates the severity of the fire. The data in Table 4-1.4 suggest a range of 50 to 500 s for t_g. Only a few rapidly developing fires had a t_g below 50 s. Three slow fires had values above 500 s for t_g.

Table 4-1.4 also lists the maximum heat release rate reached during the power-law growth. The heat release rate model $\dot{Q} = \alpha t^2$ does not predict when a fuel package stops following the model or when the fuel is depleted. This task is an important point often missed by many designers. A simple test is to calculate the mass of fuel consumed from $t = 0$ to the time of interest. For $p = 2$ power-law fire growth rate, the total energy consumed is

$$E = \int_{t=0}^{t} \dot{Q} = \int_{t=0}^{t} \alpha t^2 \text{ kJ}$$

$$E = \frac{\alpha t^3}{3} \text{ kJ}$$

Knowing the heat of combustion, H_c, for the fuel permits calculation of the mass of fuel necessary to release a given amount of energy in the time period:

$$E = mH_c \text{ kJ}$$

$$m = \frac{E}{H_c} \text{ g or kg (depending on the units for } H_c)$$

When doing a design or analysis, try several different fire growth rates to determine the effect of their variance on the calculations. In some cases, the effect will be minimal. In other cases, this type of sensitivity analysis will show that a more thorough analysis of the possible fuels and fire scenarios is warranted.

The selection of an ambient temperature can have a measurable effect on the calculations. The calculations assume that the detector or sprinkler starts out at the same temperature as the ambient air when the fire starts. Hence, if a temperature of 20°C is assumed for the spacing calculations and the actual temperature at the time of the fire is 10°C, the system's goals will not be met. For design calculations to be conservative, the lowest expected ambient temperature should be used.

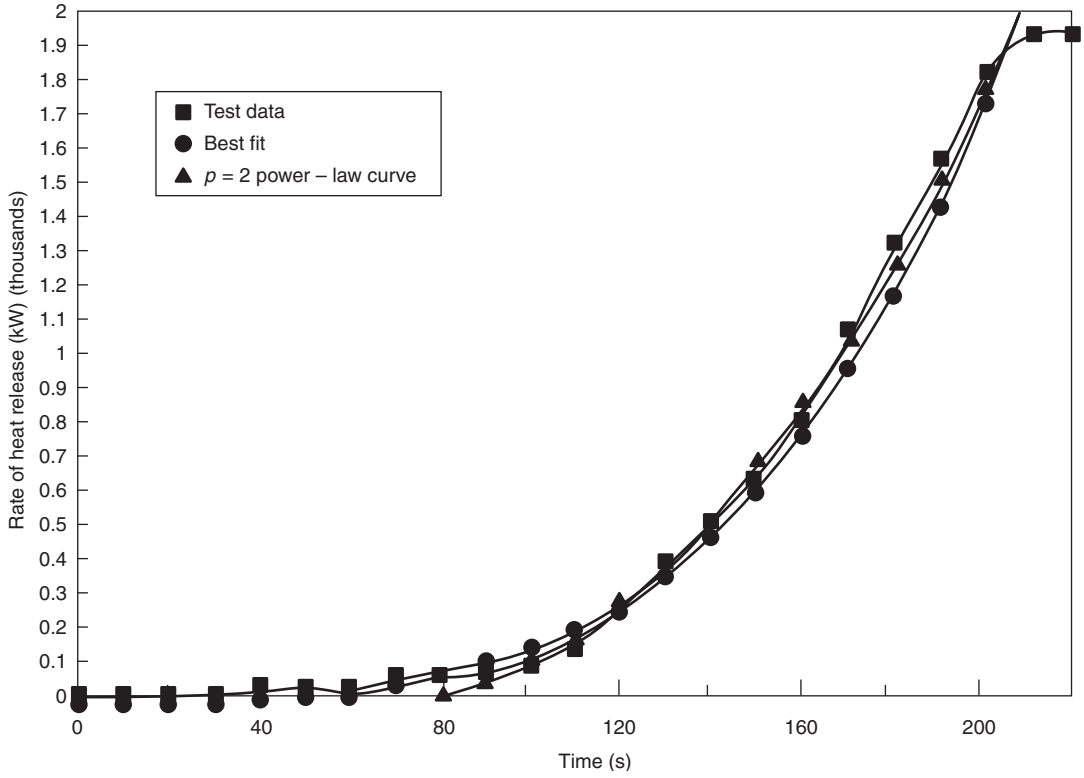

Figure 4-1.5. ***Test 27 chair.***

The relationships presented by Heskestad and Delichatsios[21] are correlated to fire test data using the ceiling height above the fuel surface for H. If this height varies, the larger value of H will produce more conservative results in the calculations for detector spacing or response. The most conservative results are obtained when the floor-to-ceiling height is used, since this height is the maximum vertical distance from fuel to detector.

The values for C_p, ρ_0, and g should be 1.040 kJ/(kg·K), 1.1 kg/m^3, and 9.81 m/s^2, respectively. Slight variations in these constants have negligible effects on the calculations.

As previously mentioned, the design or analysis calculations are done for a particular detector or sprinkler. Therefore, it is necessary to know the unit's operating temperature. The response time index or τ_0 and u_0 are also needed. Operating temperature is obtained from manufacturer's data. The detector's sensitivity is best determined by conducting a plunge test.[9]

In the absence of plunge test data, a detector's UL-listed spacing can be used as a measure of detector sensitivity. Heskestad and Delichatsios analyzed UL test data and calculated time constants, τ_0, for various combinations of UL-listed spacing and detector operating temperature.[22] The Appendix Subcommittee of NFPA 72 expanded the table to include a larger selection of detectors.[8] That table is reproduced here as Table 4-1.5.

Heat Detection Design and Analysis Examples Using the Power-Law Fire Model

Analysis and design problems will be used to show how fire protection engineers can use the techniques presented in this chapter. The examples show the sensitivity of these techniques to changes in variables and input parameters. A design problem is first worked by hand to solve the equations presented earlier in the section on heat detection. The remaining examples were worked using a spreadsheet written to solve the equations.

Table 4-1.5 ***Time Constants for Any Listed Detector τ_0 (s)***[a]

Listed Spacing (ft)	UL (°F)						FMRC All Temp.
	128°	135°	145°	160°	170°	196°	
10	400	330	262	195	160	97	195
15	250	190	156	110	89	45	110
20	165	135	105	70	52	17	79
25	124	100	78	48	32		48
30	95	80	61	36	22		36
40	71	57	41	18			
50	59	44	30				
70	36	24	9				

These time constants are based on an analysis of the Underwriters Laboratories Inc. and Factory Mutual Research Corporation listing test procedures. Plunge test results performed on the detector to be used will give a more accurate time constant.

[a]At a reference velocity of 5 ft/s

(Reproduced from NFPA 72–1993, Appendix B.[8])

EXAMPLE 4:

A fire detection system is being designed for an unsprinklered manufacturing building. The area being considered has a large, flat ceiling 5.0 m high. Ambient temperature is normally 20°C, but on weekends it is cut back to 10°C. It will be assumed that the fire scenario involves the ignition of a stack of wood pallets. The pallets are stacked 1.5 m (5 ft) high. Fire tests[8] show that this type of fire follows the $p = 2$ power-law equation with a t_g of approximately 150 s. The corresponding α can be calculated:

$$\dot{Q} = \alpha t^2 \text{ kW}$$

$$\alpha = \frac{1055}{t_g^2} = \frac{1055}{150^2} = 0.047 \text{ kW/s}^2$$

The goal is to detect the fire before it reaches a total heat release rate of 2500 kW. Fixed-temperature heat detectors will be used. The detectors have a 57°C (135°F) operating temperature and a UL-listed spacing of 30 ft. From Table 4-1.5 the time constant is found to be 80 s. This time constant is referenced to a gas velocity of 1.5 m/s and can be used with Equation 9 to calculate the detector's RTI.

First, use the power-law equation to calculate the time that the fire would reach a total heat release rate of 2500 kW:

$$\dot{Q} = \alpha t^2 \text{ kW}$$

$$t = \sqrt{\frac{\dot{Q}}{\alpha}} = \sqrt{\frac{2500}{0.047}} = 231 \text{ s}$$

The RTI is calculated using Equation 9 and a reference velocity, u_0, of 1.5 m/s (5 ft/s):

$$\text{RTI} = \tau_0 u_0^{1/2} = 80\sqrt{1.5} = 98 \text{ m}^{1/2}\text{s}^{1/2}$$

As described previously in Step 5 for design of a proposed system, it is necessary to make a first guess at the required detector spacing. In this case, try using $r = 6.0$ m. Use Equation 20 to calculate the nondimensional time, t_{2f}^*, at which the initial heat front reaches the detector. Use the distance from the top of the fuel package to the ceiling for H.

$$t_{2f}^* = 0.813\left(1 + \frac{r}{H}\right)$$

$$t_{2f}^* = 0.813\left(1 + \frac{6.0}{3.5}\right) = 2.207$$

Next, Equation 18 is used to calculate A. Note that in this equation the ambient temperature, T_a, must be expressed as an absolute temperature. In this case add 273 to °C to get K (Kelvin).

$$A = \frac{g}{C_p T_a \rho_0}$$

$$A = \frac{9.81}{1.040(10 + 273)1.1} = 0.030$$

The nondimensional time corresponding to the required response time is now calculated. However, first we must calculate α_c:

$$\alpha_c = X\alpha = 0.70(0.047) = 0.033 \text{ kW/s}^2$$

$$t_2^* = \frac{t}{A^{-1/5}\alpha_c^{-1/5}H^{4/5}}$$

$$t_2^* = \frac{231}{(0.030)^{-1/5}(0.033)^{-1/5}(3.5)^{4/5}} = 21.256$$

Since $t_2^* > t_{2f}^*$, we know that the heat front has passed the detector location. Next, the ratio of the velocity to the nondimensional velocity is calculated:

$$u_2^* = \frac{u}{(A^{1/5}\alpha_c^{1/5}H^{1/5})}$$

$$\frac{u}{u_2^*} = A^{1/5}\alpha_c^{1/5}H^{1/5}$$

$$\frac{u}{u_2^*} = (0.030)^{1/5}(0.033)^{1/5}(3.5)^{1/5} = 0.322$$

The ratio of the change in gas temperature to the nondimensional gas temperature is calculated:

$$\Delta T_2^* = \frac{\Delta T}{A^{2/5}(T_a/g)\alpha_c^{2/5}H^{-3/5}}$$

$$\frac{\Delta T}{\Delta T_2^*} = A^{2/5}\left(\frac{T_a}{g}\right)\alpha_c^{2/5}H^{-3/5}$$

$$\frac{\Delta T}{\Delta T_2^*} = (0.030)^{2/5}\left(\frac{283}{9.81}\right)(0.033)^{2/5}(3.5)^{-3/5} = 0.855$$

The nondimensional change in gas temperature is now calculated:

$$D = 0.126 + 0.210\left(\frac{6.0}{3.5}\right) = 0.486$$

$$\Delta T_2^* = \left[\frac{(t_2^* - t_{2f}^*)}{D}\right]^{4/3}$$

$$\Delta T_2^* = \left[\frac{(21.256 - 2.207)}{0.486}\right]^{4/3} = 133.142$$

Next, the ratio $u_2^*/(\Delta T_2^*)^{1/2}$ is calculated:

$$\frac{u_2^*}{(\Delta T_2^*)^{1/2}} = 0.59\left(\frac{r}{H}\right)^{-0.63}$$

$$\frac{u_2^*}{(\Delta T_2^*)^{1/2}} = 0.59\left(\frac{6.0}{3.5}\right)^{-0.63} = 0.420$$

Y is now calculated:

$$Y = \frac{3}{4}\sqrt{\frac{u}{u_2^*}}\sqrt{\frac{u_2^*}{(\Delta T_2)^{1/2}}}\left(\frac{\Delta T_2^*}{\text{RTI}}\right)\left(\frac{t}{t_2^*}\right)D$$

$$Y = \frac{3}{4}\sqrt{0.322}\sqrt{0.420}\left(\frac{133.142}{98}\right)\left(\frac{231}{21.256}\right)(0.486) = 1.979$$

The resulting temperature of the detector at $t = 231$ s, $T_d(t)$, can now be calculated. Assume that the temperature of the detector at the start of the fire, $T_d(0)$, is the same as ambient temperature, T_a.

$$\Delta T_d = T_d(t) - T_d(0) = \frac{\Delta T}{\Delta T_2^*}\Delta T_2^*\left[1 - \left(\frac{1 - e^Y}{Y}\right)\right]$$

$$\Delta T_d = T_d(t) - T_d(0)$$

$$= 0.855(133.142)\left[1 - \left(\frac{1 - e^{-1.979}}{1.979}\right)\right]$$

$$\Delta T_d = T_d(t) - T_d(0) = 64.264$$

$$T_d(t) = \Delta T_d + T_d(0) = 64.264 + 10 = 74.264 = 74°\text{C}$$

After 231 s, when the heat release rate has reached 2500 kW, the detector located 6 m from the fire axis has reached an approximate temperature of 74°C. Note that the answer has been rounded to two significant digits, one more than the least precision of any of the variables. This rule is the alternate rule for rounding as discussed in the introduction of this chapter.

The detector actuation temperature is 57°C. This result indicates that the detector has responded before the fire has reached 2500 kW. Since the calculated temperature is higher than the actuation temperature, a larger r can be tried. The calculations should be repeated until the calculated detector temperature is approximately equal to the actuation temperature.

For this example the answer converges on a radial distance of approximately 7.4 m. The spacing between detectors is

$$S = r\sqrt{2} = 7.4\sqrt{2} = 10.5 \text{ m}$$

EXAMPLE 5:

This example will show how an existing heat detection system or a proposed design can be analyzed to determine its response time or fire size at response. The scenario used in Example 4 will be repeated, except that the manufacturing building has an existing system of heat detectors, which are spaced evenly on the ceiling at 15.0-m intervals. The detector characteristics are the same as above. The actuation temperature is 57°C and the RTI is 98 $\text{m}^{1/2}\cdot\text{s}^{1/2}$. The ceiling height is 5 m, and the height of the pallets is 1.5 m. Ambient temperature is 10°C. α is 0.047 kW/s^2 ($t_g = 150$ s) and α_c is 0.033 kW/s^2.

The maximum radial distance from the fire axis to a detector is calculated first, using Equation 5.

$$S = r\sqrt{2} \text{ m}$$

$$r = \frac{S}{\sqrt{2}} = \frac{15.0}{\sqrt{2}} = 10.6 \text{ m}$$

The next step in the analysis is to estimate the response time of the detector or the fire size at response. In the design above, the fire grew to about 2500 kW in 231 s when the detector at a distance of 7 m responded. The radial distance in this example is larger and should result in

a slower response and larger fire size at response. A first guess at response time might be 6 min or 360 s. The fire size (total heat release rate) at 360 s is

$$\dot{Q} = \alpha t^2 \text{ kW}$$

$$\dot{Q} = 0.047(360)^2 = 6091 \text{ kW}$$

The remaining calculations for the resulting detector temperature are similar to those in Example 4. Rather than show the detail, a spreadsheet was used to complete the calculations. The resulting detector temperature at 360 s was calculated to be approximately 84°C.

This result indicates that the detector response time is less than the estimated 6 min. Therefore, a smaller response must be tried. If the calculated temperature were lower than the actuation temperature, a larger t would be tried. The calculations are repeated until the calculated detector temperature is approximately equal to the actuation temperature. In this case, the response time converges at 295 s. This result corresponds to a fire size at response of 4070 kW. It is at this time and heat release rate that the detector temperature reaches its actuation temperature of 57°C.

This example assumes that the fire continues to follow the power-law relationship through the burning period. If there is not enough fuel available, it is possible for the heat release rate curve to flatten out before reaching 4070 kW. These calculations do not predict when this development will happen. These calculations also do not predict how the detector temperature changes after the fire stops following the power-law relationship. It may be that sufficient heat continues to be released and the detector eventually responds. It is also possible for the fire gases to cool sufficiently to preclude detector actuation unless additional fuel becomes involved in the fire.

Comparing Example 4 with Example 5 shows how detector spacing affects response time. A difference in spacing of 4.4 m (15 − 10.6 m) results in a difference of approximately 64 s in the detector response time. Because the fire is accelerating according to the $p = 2$ power-law relationship, the resulting difference in fire size at response is 1570 kW.

EXAMPLE 6:

A warehouse is used to store sofas and other furniture. The sofas are similar to one tested by the National Bureau of Standards in their furniture calorimeter.[30] Burning characteristics are assumed to be similar to the sofa used in Test 38:[23,30] $\alpha = 0.1055$ kW/s^2, $t_g = 100$ s; peak heat release rate = 3000 kW. The sofas are stored one or two high. Assume a convective fraction of 65 percent.

The building has a flat roof and ceiling. The distance from the floor to the ceiling is 4.6 m. When the sofas are stacked two high, the distance from the top of the fuel package to the ceiling is 2.4 m. Ambient temperature in the warehouse is kept above 10°C. (See Figure 4-1.6.)

Based on maximum allowable property loss goals established by the owner, it is desirable to detect a fire and notify the fire department prior to a second fuel package becoming involved. The original NBS report[30] contains data on radiation measured during Test 38. This information can be used along with other techniques presented in this handbook to determine when a second item might ignite. For instance, it might be determined that furniture across a 2-m aisle might ignite when the fire reaches a total heat release rate of 3000 kW. The objective would then be to detect the fire soon enough so that the fire can be extinguished or controlled before the fire reaches total 3000 kW. In this example, it is assumed that the fire must be detected when it reaches a total heat release rate of about 2000 kW.

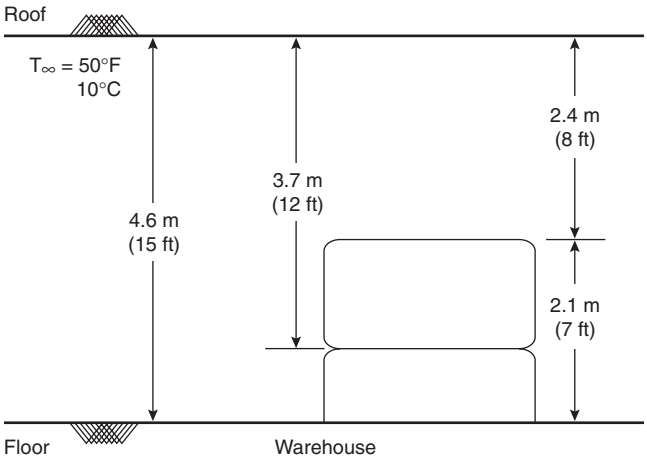

Figure 4-1.6. ***Example 6—Warehouse.***

The fire detection system will consist of fixed-temperature heat detectors connected to a control panel that is, in turn, connected to the local fire department. The detector to be used has a fixed temperature rating of 57°C and an RTI of 42 $m^{1/2} \cdot s^{1/2}$.

The problem is determining the spacing of detectors required to detect this fire. When the computer program runs, the user is prompted for all of the above information. In this example, the data are fixed except for the distance from the ceiling to the flame origin. If the distance between the top of the fuel and the ceiling (2.4 m) is used, the calculations indicate that the detectors must be spaced 7.3 m apart to respond when the fire reaches a heat output of 2000 kW.

For a worst-case analysis, the distance from the floor to the ceiling (4.6 m) is used. This distance results in a required detector spacing of 5.9 m.

A more realistic worst-case scenario would be when the sofas are not stacked two high. With one sofa on the floor, the distance from the fuel to the ceiling would be about 3.7 m. The required detector spacing would then be 6.5 m.

These results are summarized in Table 4-1.6. This table clearly shows the relationship between ceiling height and detector response. The greater the distance from the fire to the ceiling, the closer the detectors must be spaced to respond within the goals of the system. Designs based on the floor-to-ceiling distance are conservative and representative of a worst-case condition. More realistic designs are based on the most probable or the greatest expected vertical clearance between fuel and detector.

Table 4-1.6 ***Example 6—Ceiling Height or Height above Fuel versus Detector Spacing***

Ceiling Height, H (m)	Required Spacing, S (m)
2.4	10.3
3.7	9.2
4.6	8.4

Table 4-1.7 ***Example 7—Ceiling Height or Height above Fuel versus Response Time***

Ceiling Height, H (m)	Response Time, t_r (s)
2.4	140
3.7	150
4.6	160

EXAMPLE 7:

For the same conditions in Example 6, if the detector spacing is fixed at 10.3 m ($r = 7.3$ m), how does the ceiling height affect the response time of the system?

Using the spreadsheet, the results, after rounding, are summarized in Table 4-1.7.

EXAMPLE 8:

This example will show how to select a detector type to economically meet the system's goals. The fire scenario and goals used in Examples 6 and 7 will be used: $H = 2.4$ m; $T_a = 10$°C; RTI = 42 $m^{1/2} \cdot s^{1/2}$; X = 65 percent, $t_g = 100$ s.

In Example 6, it was found that heat detectors with a fixed temperature rating of 57°C and an RTI of 42 $m^{1/2} \cdot s^{1/2}$ must be spaced 10.3 m apart to meet the system's goals—a response at 2000 kW. Here, the spacing of rate-of-rise heat detectors will be estimated.

The detector to be used is rated to respond when its temperature increases at a rate of 11°C/min or more. The detector's RTI will be assumed to be the same as the detector in Example 6. The calculation procedure is the same as for fixed temperature detectors except that, in the last step, the equation for the rate of temperature change is used:

$$\frac{dT_d(t)}{dt} = \frac{4}{3}\frac{\Delta T}{\Delta T_2^*}\Delta T_2^{*\,1/4}\frac{(1 - e^{-Y})}{(t/t_2^*)D}$$

Solving the equations, it is found that the rate-of-rise heat detectors can be spaced up to 25 m apart and respond at approximately 2000 kW total heat release rate.

If the total area of the warehouse is 5000 m^2, approximately 48 fixed-temperature heat detectors would be required to meet the established goals. The same goals can be met with approximately 8 rate-of-rise heat detectors. Additional detectors might be required due to of obstructing beams or walls. It should also be pointed out that the use of m^2 for calculating the required number of units is only an estimate. The detector does not cover an area that is 625 m^2 (25 m × 25 m). It is covering a circular area having a radius no more than about 17.7 m. That is, all points on the ceiling must be within the protection radius of a detector for the calculations to be valid. If one used a "rated area" for a detector rather than a radial measurement, it could be concluded that a single detector in this example could cover a space that was 125 m long if it were only 5 m wide.

By trying different detector types or detectors with higher sensitivities, project goals might be met with a fewer number of detectors. The scenario in this example shows that, to detect the same fire, a much greater number of fixed-temperature heat detectors than rate-of-rise heat detectors is required. This conclusion is not always the case. Many fires will develop slowly and cause high ceiling temperatures without ever exceeding the rate of temperature rise necessary to actuate a rate-of-rise heat detector. As a backup, most commercially available rate-of-rise heat detectors have a fixed-temperature element also. The rate-of-rise element and the fixed-temperature element should be considered separately when designing or analyzing a system.

EXAMPLE 9:

In this example, a combination fixed-temperature and rate-of-rise heat detector will be analyzed and the response of the two elements will be compared. For an installed spacing of 10.0 m ($r = 0.707$ m), the effect of fire growth rate on response time will be shown. The following conditions from examples 6, 7, and 8 will be repeated: $H = 2.4$ m; $T_a = 10$°C; RTI = 42 $m^{1/2} \cdot s^{1/2}$; X = 65 percent. The fixed-temperature element response threshold is $T_r = 57$°C, and the rate-of-rise threshold is $dTr/dt = 11$°C/min.

The results are shown in Table 4-1.8 and Figure 4-1.7. For fire growth times up to $t_g = 509$ s, the rate-of-rise element responds faster. For fires that grow slower (increasing t_g), the fixed-temperature element will respond faster.

For larger installed spacings, such as the 25-m spacing calculated in the previous example for the spacing of the rate-of-rise detector, the crossover point occurs sooner. The results for a 25-m spacing are shown in Table 4-1.9 and Figure 4-1.8. For fire growth times up to $t_g = 228$ s, the rate-of-rise element responds faster. For fires that grow slower (increasing t_g), the fixed-temperature element will respond faster.

Table 4-1.8 ***Response Time as a Function of Fire Growth Time, t_g***

	Response Time, t_r (s)	
t_g	Fixed-Temperature	Rate-of-Rise
50	85	31
100	135	53
200	219	98
300	297	155
400	373	241
500	447	426
509	454	454
600	521	835

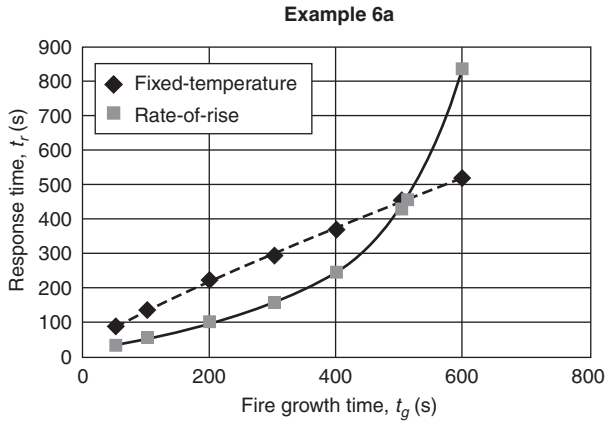

Figure 4-1.7. ***Response time as a function of fire growth time, t_g.***

Table 4-1.9 ***Response Time as a Function of Fire Growth Time, t_g***

	Response Time, t_r (s)	
t_g	Fixed-Temperature	Rate-of-Rise
50	168	77
100	269	140
200	448	355
228	497	497
300	619	1330

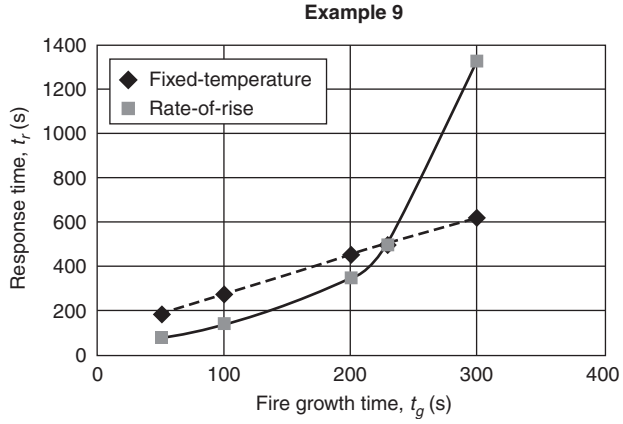

Figure 4-1.8. ***Response time as a function of fire growth time, t_g.***

EXAMPLE 10:

In this example, the effects of fire growth rate on detector spacing will be examined. The scenario used in Examples 6 through 9 will be used again. The following conditions from these examples will be repeated: $H = 2.4$ m; $T_a = 10$°C; RTI = 42 $m^{1/2} \cdot s^{1/2}$; X = 65 percent. The fixed temperature element response threshold is $T_r = 57$°C and the rate-of-rise threshold is $dT_r/dt = 11$°C/min.

In Examples 6, 7, and 8, the rate of fire growth followed the power-law equation with an α of 0.1055 kW/s^2 or $t_g = 100$ s. Calculations were done for several values of t_g. The results are summarized in Table 4-1.10 and Figure 4-1.9.

For fixed-temperature detectors, if the fire grows at a faster rate (smaller t_g), a smaller spacing is required to meet the system's goals. If the fire grows at a slower rate, a larger detector spacing is allowed. This relationship clearly shows the effects of thermal lag on detector response. At slow rates of growth, the detector is immersed in the hot fire gases and, despite thermal lag, has time to absorb the heat before the fire reaches the maximum permissible heat release rate. The effects of thermal lag are less important at slow rates of fire growth.

The rate-of-rise detector also experiences thermal lag. However, the curve peaks at approximately $t_g = 110$ $m^{1/2} \cdot s^{1/2}$ and $S = 25$ m. For the rate-of-rise detector, as

Table 4-1.10 ***Required Detector Spacing as a Function of Fire Growth Time, t_g***

	Required Spacing (m)	
t_g	Fixed-Temperature	Rate-of-Rise
50	7.2	23
75	9	24
100	10	25
110	11	25
120	11	24
150	12	24
200	14	22
300	15	18
400	16	14
500	17	12
600	18	10

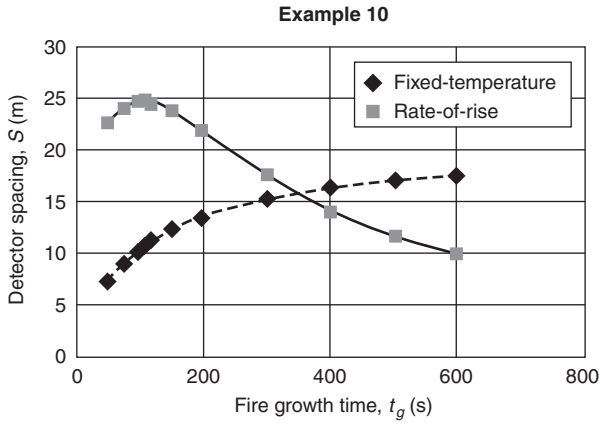

Figure 4-1.9. ***Required detector spacing as a function of fire growth time, t_g.***

the fire growth rate slows (larger t_g), thermal lag decreases as it did for the fixed temperature detector. However, as the rate of fire growth slows, so does the rate of change of the detector's temperature. For this particular detector and fire scenario, at fire growth times greater than about 110 s, the detector spacing must be reduced so that the threshold rate of change of the detector temperature is reached before the maximum permissible heat release rate is reached.

EXAMPLE 11:

In this example a detector is exposed to the ceiling jet for a fire with $t_g = 150$ s and a 75 percent convective fraction. Ambient temperature is 10°C. The ceiling is 4 m high, and the detector is located at a radial distance of 5 m from the fire. The RTI of the detector is 50. Plot the detector temperature and the fire-gas temperature at the detector location for t up to 240 s.

The detector remains at ambient temperature until the ceiling jet first reaches the detector position. At what time does the ceiling jet first reach the detector? This result is found by setting $t_{2f}^* = t_2^*$ and solving for t. First, α_c is calculated:

$$\alpha = \frac{t_g^2}{1055} = \frac{1055}{150^2} = 0.047 \text{ kW/s}^2$$

$$\alpha_c = X\alpha = 0.75(0.047) = 0.035 \text{ kW/s}^2$$

$$t_{2f}^* = t_2^*$$

$$0.813\left(1 + \frac{r}{H}\right) = \frac{t}{A^{-1/5}\alpha_c^{-1/5}H^{4/5}}$$

$$t = 0.813\left(1 + \frac{r}{H}\right) = A^{-1/5}\alpha_c^{-1/5}H^{4/5} \text{ s}$$

$$t = 0.813\left(1 + \frac{5}{4}\right) = (0.030^{-1/5})(0.035^{-1/5})(4^{4/5})$$
$$= 21.86 = 22 \text{ s}$$

The heat front reaches the detector at about 22 s, and heating begins. Prior to this point, the detector and gas temperature surrounding the detector are at ambient temperature.

The method to calculate the detector temperature is the same as in previous examples. To calculate the change in ceiling-jet gas temperature, combine the following equations and solve to ΔT:

$$\Delta T_2^* = \frac{\Delta T}{A^{2/5}(T_a/g)\alpha_c^{2/5}H^{-3/5}}$$

and

$$\Delta T_2^* = \left[\frac{(t_2^* - t_{2f}^*)}{(0.126 + 0.210r/H)}\right]^{4/3}$$

$$\Delta T = A^{2/5}\left(\frac{T_a}{g}\right)\alpha_c^{2/5}H^{-3/5}\left[\frac{(t_2^* - t_{2f}^*)}{(0.126 + 0.210r/H)}\right]^{4/3}$$

A spreadsheet solution is shown in Table 4-1.11 and graphed in Figure 4-1.10.

EXAMPLE 12:

A sprinkler system is being installed in a large exhibition hall. The building has a flat roof deck supported by open space frame trusses. The distance from the underside of the roof deck to the floor is 12 m. Ambient temperatures do not usually fall below 5°C.

Table 4-1.11 ***Example 11—Ceiling Jet and Detector Temperature as a Function of Time***

t (s)	T_g (s)	T_d (s)
22	10	10
30	12	10
40	15	10
50	19	11
60	24	13
70	29	15
80	34	18
90	39	21
100	45	25
110	51	30
120	58	35
130	64	40
140	71	46
150	78	52
160	85	59
170	93	66
180	100	73
190	108	81
200	116	88
210	124	96
220	132	104
230	140	112
240	148	120

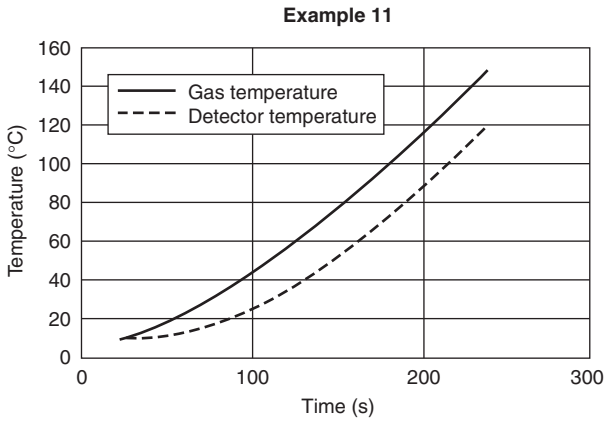

Figure 4-1.10. ***Example 11—Ceiling jet and detector temperature as a function of time.***

Three different designs for the sprinkler system have been proposed. All three are designed to provide the same water density over a specified area. Each proposal uses a sprinkler with a temperature rating of 74°C and an RTI of 110 $m^{1/2} \cdot s^{1/2}$. The only difference among the three systems is the spacing of the sprinklers and the branch lines that feed them. The first proposal uses a square array with a spacing of 3.0 m. The second and third proposals are based on square array spacings of 3.7 m and 4.6 m, respectively.

What effect will the three different spacings have on the size of the fire when the system responds? Assume two different fire scenarios. In the first, the fire grows at a moderate rate with $t_g = 200$ s. The second fire scenario has a slower fire growth rate with $t_g = 500$ s. For both, assume a convective fraction of 75 percent. Results of the calculations are shown in Table 4-1.12 after rounding.

The calculations show an increase of about 25 percent in the fire size at response when the spacing is increased 50 percent from 3.0 to 4.6 m. The increased spacing may result in a lower system cost. However, closer spacings mean that the sprinkler system will probably respond sooner. The fire protection engineer can use this type of analysis to assist in choosing a system that best meets the project's overall goals.

EXAMPLE 13:

A fire impacting elevator machinery can result in passengers or fire fighters being carried to a fire floor or being trapped between floors. Elevator safety codes generally do not require any sprinkler protection or detection at the top of shafts since the fuel load is typically insufficient to actuate a sprinkler or affect persons in the cars.

Smoke detection is used in elevator lobbies and machine rooms to recall elevators to a safe level when smoke threatens the elevator shaft. The presence of sprinklers in the elevator machine room presents another risk: the possibility of water discharge on energized controllers and motors and on the elevator brakes. To reduce this risk, in addition to smoke detection, heat detectors may be used to ensure that equipment is de-energized upon or prior to the discharge of water. To accomplish this task, some codes may require a heat detector with a lower temperature rating and a lower RTI within 0.61 m of every sprinkler in an elevator machine room. Are these requirements sufficient to assure response before the sprinkler to a range of possible fire scenarios?

Table 4-1.12 ***Example 12—Effects of Sprinkler Spacing on Fire Size at Response and Time to Response***

	$t_g = 200$ s		$t_g = 200$ s	
S (m)	t_r (s)	$\dot{Q}_T$ (kW)	t_r (s)	$\dot{Q}$ (kW)
3.0	350	3300	800	2700
3.7	370	3600	840	3000
4.6	400	4100	890	3400

SOLUTION:

For this example, use an ambient temperature of 15°C and a ceiling height or clearance of 4 m. Assume the actuation temperature of the sprinklers is 74°C and the actuation temperature of the heat detectors is 57°C. The RTI of the sprinklers is 110 $m^{1/2} \cdot s^{1/2}$, and the RTI of the detectors is 42 $m^{1/2} \cdot s^{1/2}$. Spacing of the sprinklers is 3.0 m. Calculate the response of the sprinkler and the heat detector to a fast fire, $t_g = 50$ s, and a slow fire, $t_g = 600$ s. Assume a 75 percent convective fraction.

A sprinkler spacing of 3.0 m results in a worst case radial distance of 2.12 m. The heat detector could be an additional 0.61 m beyond at $r = 2.73$ m. The results of the calculations are summarized in Table 4-1.13.

These calculations show that the heat detector will respond before the sprinkler. Depending on the actual conditions, additional calculations should be tried for different fire scenarios and for changes in other variables such as RTI, ambient temperature, ceiling clearance, and so forth.

Smoke Detection

In order to determine whether or not a smoke detector will respond to a given $\dot{Q}_{cr}$, a large number of factors must be evaluated. These include the following: smoke aerosol characteristics, aerosol transport, detector aerodynamics, and sensor response.

Smoke aerosol characteristics at the point of generation are a function of the fuel composition, the combustion state (smoldering or flaming), and the degree of vitiation of the combustion air. The characteristics considered include particle size and distribution, particle number or concentration at various sizes, composition, color, and refractive index. Given the dynamic nature of fire growth and spread and fuels involved, ventilation conditions will change over time, thus affecting the smoke produced.

Transport considerations include (1) changes to the aerosol characteristics that occur with time and distance from the source and (2) transport time. Changes in the aerosol largely relate to the particle size and concentration, and result from the processes of sedimentation, agglomeration, and coagulation. Transport time is a function of the characteristics of the travel path from the source to the detector, which include ceiling height and configuration (sloped, beamed, etc.), intervening barriers such as doors, and buoyancy effects such as layering and thermal inversions.

Table 4-1.13 ***Example 13—Sprinkler and Heat Detector Response to Different Fire Growth Rates***

	Response Time (s)	
	$t_g = 50$ s	$t_g = 600$ s
Sprinkler	65	370
Heat Detector	50	300

Once smoke reaches the detector, other factors become important, namely the aerodynamic characteristics of the detector and the type of sensor. The aerodynamics of the detector relate to the ease with which smoke can pass through the detector housing and enter the sensor. In addition, the location of the entry portion of the housing relative to the velocity profile of the detector normal to the plane of the ceiling is also a factor. Finally, different sensing modes (e.g., ionization or photoelectric) will respond differently, depending on the characteristics of the transported aerosol. Within the family of photoelectric devices, there will be variations depending upon the wavelengths of light and the scattering angles employed. Also, algorithms used to sample and weight the sensor's response are introduced by the manufacturer and affect the detector's response.

Standard practice for the design of smoke detection systems is much the same as that for heat detection systems. Recommended spacing criteria are established based on detector response to a specific parameter, such as the optical density within an enclosure. A variety of smoke tests are used to verify that the detector responds between defined upper and lower activation thresholds and within required response times to a range of different types of smoke. This information translates into recommended spacing criteria that is intended to ensure that the detector responds within defined parameters. In some cases, the recommended spacing can be increased, or must be decreased, depending on factors such as compartment configuration and air flow velocity.[8]

In applications where estimating the response of a detector is not critical, the recommended spacing criteria provide sufficient information for the design of a basic smoke detection system. If the design requires detector response within a certain time frame, optical density, specified heat release rate, or temperature rise, then additional analysis may be required. In this case, information concerning the expected fuel, fire growth, sensor, and compartment characteristics is required. The following examples show various performance-based approaches to evaluating smoke detector response.

Modeling Smoke Detector Response—General

The response of smoke detectors to fire conditions is not easily modeled. The response characteristics of smoke detectors vary widely compared with thermal detectors. In addition, less is known about the production and transport of smoke in the early stages of a fire. Natural and forced air currents have a larger effect on the movement of smoke at the time of interest (very early in the fire) than they do on the stronger thermal currents required to alarm heat detectors.

A comparison of how smoke detectors operate with the smoke measurement methods most often employed and reported by researchers shows that smoke measurements do not generally include the factors that we need to model smoke detector response.[13] Thus, there is a gap between the data generated by fire researchers and the data needed to model smoke detector response.

For example, fire researchers most often measure and report data on heat release rate, temperature and velocity of fire gases, and the optical density or obscuration per unit distance of the smoke at various locations. Of these, only optical density and obscuration relate to smoke. Although called *obscuration,* it is more accurately called *attenuation* since the light beam may be absorbed, reflected, or refracted by the smoke. These are calculated as follows:

Percent obscuration, *O:*

$$O = 100\left(I - \frac{I}{I_0}\right)$$

Percent obscuration per unit distance, O_u

$$O_u = 100\left[1 - \left(\frac{I}{I_0}\right)^{1/l}\right]$$

Optical density, *D*

$$D = \log_{10}\left(\frac{I_0}{I}\right) = -\log_{10}\left(\frac{I}{I_0}\right)$$

Optical density per unit distance, D_u (m^{-1})

$$D_u = \frac{D}{l} = \frac{1}{l}\log_{10}\left(\frac{I_0}{I}\right) = -\frac{1}{l}\log_{10}\left(\frac{I}{I_0}\right)\ \mathrm{m}^{-1}$$

where I_0 is the initial intensity of a light beam reaching a photocell, I is the intensity of the light beam in the presence of smoke, and l is the distance between the source and the photocell.

Optical density and obscuration are useful data for evaluating visibility. However, the only commercially available smoke detector that operates by sensing the attenuation of a light beam is the projected-beam-type smoke detector. Further, these measurements are sensitive to the wavelength of light used. Thus, to be valuable for estimating the response of a projected-beam smoke detector, the data must be measured and reported using the same wavelength as the light source used by the detector.

The two most common types of smoke detectors are ionization type and photoelectric type. Neither type operates using light attenuation. Without a correlation between the optical density data and the response characteristics of a particular detector, accurate modeling is not possible.

In addition, detectors often use complex response algorithms rather than simple threshold or rate-of-change response levels. The algorithms are used to reduce false and nuisance alarms and to enhance fire signature matching. These algorithms vary from detector to detector and are generally not published by the manufacturers. Thus, even if correlations between optical density and the response of scattering- and ionization-type smoke detectors were available, the actual response of each model is affected by the signal sampling algorithm.

Nevertheless, there are methods that can be used to grossly estimate smoke detector response. These estima-

tion methods may not provide accurate prediction of time to detector response because the potential errors in the estimation methods are not generally known and the response algorithms for a particular detector are not known. Without knowledge of the accuracy of the models and the potential errors, these estimation methods should not be used to compare detector response to other model calculations such as egress time calculations or time to untenability. Estimation methods are best used to compare changes in the response of a particular detector as a result of changes in spacing or location, while holding all other variables constant.

In addition to these estimation methods, actual fire tests with detectors present may provide information to compare smoke detector response to other factors such as egress time, structural response, heat release rate, and so forth. Product performance tests may be sources of data. Although, the actual response may not be reported in manufacturer's literature, the minimum and maximum permissible performance imposed by the test standard provides ranges of possible response.

Modeling Smoke Detector Response—Light Obscuration Smoke Detectors

For projected-beam-type detectors, fire or smoke models that calculate the optical density per unit length, D_u, in a space or the total optical density in the path of the detector, D, may be used to determine when the detector would respond. Manufacturer specifications will typically indicate at what levels of total obscuration or total optical density the detectors respond. Projected-beam smoke detectors generally have adjustable response thresholds.

Many fire models estimate the unit optical density, D_u, in a uniform upper layer or volume. This method is referred to as zone modeling. The optical density over the entire length of the beam is then determined by multiplying D_u by the path length, l. The path length is the distance between the source and receiver or the projected-beam smoke detector. This method assumes homogenous distribution of smoke throughout the path, an assumption which may not be valid.

Another method to model the response of projected-beam obscuration-type detectors is to calculate the unit optical density, D_u, at several discrete points or in several discrete segments between the source and the receiver of the projected-beam smoke detector. This approach is a form of field modeling. The optical density per unit length is then multiplied by the length of that particular segment. The total optical density of the path is then the sum of all of the densities for the individual segments.

Modeling Smoke Detector Response—Light Scattering (Photoelectric) Smoke Detectors

The amount of light scattered by smoke is very complex and is related to factors such as the particle number density and size distribution, refractive index, the wavelength of the light source, and the angle between the source and the receiver. Some of these variables can be described by the manufacturer for a particular detector. Some require information about the smoke produced by the fuel and its transport to the detector location.

Information about smoke properties related to light scattering is presently limited to a few types of fuels and is not readily available to practicing fire protection engineers. In addition, the data may not be in a useable format. For instance, the data must match the wavelength of the light source used in the detector being modeled. Scattering data at other wavelengths introduces errors and uncertainties.

Meacham has shown that it is possible to model the response of light-scattering detectors using information about smoke properties obtained by small-scale testing of various fuels.[31,32] However, the recommended test methods have not been further developed, tested, or incorporated into fire test programs.

At the present time, there are no practical methods available to directly model the response of light-scattering-type detectors. However, obscuration or optical density modeling, as discussed above for obscuration-type detectors, can be used in a limited way to estimate scattering-type smoke detector response.

A scattering-type detector responds at different optical densities for different types of smoke. For example, a scattering-type smoke detector that responds at an optical density of .029 m^{-1} (2.0%/ft obscuration) to smoke produced by a smoldering gray cotton lamp wick may not respond until an optical density of 0.15 m^{-1} (10%/ft) is reached for smoke from a kerosene fire. At the response threshold, both types of smoke are scattering the same amount of light to the receiver of the scattering photoelectric smoke detector. There are many factors involved in this effect. One is that the darker smoke from the kerosene fire does not reflect as much light as the lighter colored smoke from the lamp wick.

Another way to understand the differing response of a scattering-type detector to two types of smoke is to consider the amount of light being scattered when both smoke samples have the same optical density. Both samples of smoke equally block our vision of the light reflected by an object. One type of smoke may be composed of large, highly reflective smoke particles that cause the incident light to scatter in many directions. Thus, it reduces the amount of light in the forward direction. The other type of smoke may consist of a smaller number of larger particles that absorb light more readily than they reflect it. Though they have equal optical densities, one is more likely to scatter light and set off a scattering-type detector.

In order to model the response of a scattering-type detector using obscuration or optical density, it is necessary to know the optical density required for a particular type of smoke to alarm a particular model detector. For example, many manufacturers label their smoke detectors with a unit optical density, D_u, or unit obscuration, O_u, based on a calibration test that is part of UL standard number 268.[33] That number indicates the unit optical density required for that detector to respond to smoke having very specific characteristics. The optical density required to alarm a particular detector as quoted by the manufacturer is just

one value for a given particle size distribution, concentration, color, and so on used in the laboratory calibration test of that model detector. If the smoke and conditions are similar to that used in the test of the detector, the specified alarm threshold can be used in calculations.

It is not sufficient to have data for a particular fuel and detector combination. It is known that smoke changes as it moves away from a fire.[34] There may be changes in the number, size, shape, and velocity of the particles. The optical density at response to any smoke signature other than the laboratory calibration test will be different and will vary with different fuels and burning modes.

Threshold response data to various fuels for a particular detector are not readily available. Some manufacturers may provide data if available and when requested. Product performance and safety tests as well as fire tests with detectors present are useful sources of limiting performance data. Product standards typically test detectors in rooms with specified fuels and smoke buildup rates and velocities. The detectors must respond at certain levels or within certain time limits. While the exact performance data may not be made available, the test limits are useful for estimating the range of possible detector response.

Modeling Smoke Detector Response—Ionization Smoke Detectors

The signal produced by the chamber of an ionization detector has been shown to be proportional to the product of the number of particles and their diameter.[35–38] The exact signal produced by an ionization smoke detector is given by a more complex equation in the literature and requires an additional number called the chamber constant. The chamber constant varies with each different model of detector.

Given the quantity and size distribution of smoke particles and the chamber constant (from the manufacturer), it is possible to model the ionization smoke detector. Unfortunately, there are no fire models that provide the required detector model input. In addition, manufacturer specifications do not presently include chamber constants.

Newman modified the chamber theory to account for ionization detector sensitivity to the small electrical charge carried by some fire aerosols.[39] Newman also developed a method to model ionization smoke detector sensitivity as a function of the soot yielded by a particular fuel. Using his method, the change in a detector's signal, ΔI, can be related to the optical density of smoke measured at a particular wavelength, $D_{u\lambda}$.

To use the method proposed by Newman it is necessary to know what change in detector chamber signal, ΔI, will cause a detector or system to alarm. Although manufacturers do not presently provide this data, they may be persuaded to do so in the future.

Newman's work was done using a small-scale apparatus and three ionization smoke detectors. A wider range of tests, including some full-scale testing, is needed to verify this method. Presently, the only way to model ionization detector response is to use the optical density estimations as discussed for scattering-type photoelectric smoke detectors.

Modeling Smoke Detector Response—Entry Resistance

In addition to smoke characteristics and the detector's operating mechanism, the ability to get the smoke into the chamber affects the response of the unit. For spot-type photoelectric- and ionization-type smoke detectors, entry resistance is caused by bug screens, chamber design, and the detector's aerodynamic characteristics.

In a scenario where the optical density at the detector location is increasing with time, the optical density inside the detector chamber will always be less than that outside the detector chamber. Similarly, if a detector is placed in a smoke stream having a constant optical density, there will be a time delay before the optical density inside the chamber approaches that outside the detector. As with heat transfer to heat detectors, smoke entry resistance can be characterized by a detector time constant, τ:

$$\frac{dD_{\mathrm{ui}}}{dt} = \frac{1}{\tau}\left(D_u - D_{\mathrm{ui}}\right) \mathrm{s^{-1}\cdot m^{-1}}$$

where

D_{ui} ($\mathrm{m^{-1}}$) = optical density per unit length inside the detector chamber

D_u ($\mathrm{m^{-1}}$) = optical density per unit length outside the detector

τ = detector time constant (s)

If the time constant and the rate of change of optical density outside the detector are constant, then this equation can be solved. Further, substituting D_{ur} for the optical density outside the detector at response and D_{uo} for the optical density required inside the detector to produce response yields the following:[40,41]

$$D_{\mathrm{ur}} = D_{\mathrm{uo}} + \tau\left(\frac{dD_u}{dt}\right)\left\{1 - \exp\left[-D_{\mathrm{ur}}\frac{1}{\tau}\left(\frac{dD_u}{dt}\right)\right]\right\} \mathrm{m^{-1}}$$

Heskestad proposed that the time constant could be represented by the following:

$$\tau = \frac{L}{u} \mathrm{s}$$

where L is the detector's characteristic length and u is the velocity of the ceiling jet flowing past the detector.

The characteristic length is thought to be a property of the detector that is independent of the smoke and ceiling-jet properties. It is interpreted as the distance the smoke would travel at the velocity u before the optical density inside the detector reaches the value outside of the detector. Combining the equations,

$$D_{\mathrm{ur}} = D_{\mathrm{uo}} + \frac{L}{u}\left(\frac{dD_u}{dt}\right)\left\{1 - \exp\left[-D_{\mathrm{ur}}\frac{u}{L}\left(\frac{dD_u}{dt}\right)\right]\right\} \mathrm{m^{-1}}$$

The exponential term is small compared to the rest of the equation, allowing the equation to be simplified.[40] Simplification of the equation is not necessary when calculations are made using a computer. However, the simplified form clearly shows the effect of entry resistance:

$$D_{ur} = D_{uo} + \tau\left(\frac{dD_u}{dt}\right) \text{ m}^{-1}$$

or

$$D_{ur} = D_{uo} + \frac{L}{u}\left(\frac{dD_u}{dt}\right) \text{ m}^{-1}$$

This form of the entry resistance equation clearly shows that when the optical density outside a detector is increasing with time, the optical density inside the detector will lag behind if there is any entry resistance.

Heskestad and, later, Bjorkman et al.[42] have plotted test data to determine the L number for a variety of smoke detectors. Additional work has been done by Marrion and by Oldweiler to study the effects of detector position and gas velocity on the L number.[15,43]

Bjorkman et al., Marrion, and Oldweiler all observed variations in L that may be attributed to a dependence on velocity. Marrion's and Oldweiler's data also imply that there may also be a dependence on the characteristics of the smoke. Table 4-1.14 below summarizes the results from the works cited above.

Examination of the data and analysis work cited above shows that more work needs to be done to study the effects of low velocities and smoke characteristics on detector entry characteristics. The sharp increase in L at lower velocities appears to indicate that entry resistance may be related to smoke particle size. It is also possible that L is a function of the smoke momentum at low velocities. Thus, the time lag would be inversely proportional to the velocity squared.

Table 4-1.14 ***Range of Characteristic Length (L) Numbers***

Researcher	Ionization Detector L (m)	Scattering Detector L (m)
Heskestad[40]	1.8	15[a]
Bjorkman et al.[42]	3.2 ± 0.2[b]	5.3 ± 2.7[c]
Marrion[15]	Not tested	7.2,[d] 11.0–13.0,[e] 18.4[f]
Oldweiler[43]	4.0–9.5,[g] 4.3–14.2[h]	Not tested

[a] older style detector with more elaborate labyrinth

[b] L determined by best fit for three test velocities

[c] L based on a single test velocity and a limited number of tests (complete equation used)

[d] low L number at low test velocity

[e] range of L for several fuels and detector positions

[f] L increased by adding "fence" to further restrict smoke entry

[g] range of L for a variety of velocities using simplified equation for entry resistance

[h] range of L for a variety of velocities using simplified equation for entry resistance

Engineers can use L as a measure of entry resistance and the resulting time lag. However, in scenarios where the ceiling-jet velocity is low, there will be greater uncertainty in the results.

Without validation of L as a measure of lag time, manufacturers and test laboratories are not measuring or reporting L in their literature. Nevertheless, the range of L numbers reported in Table 4-1.14 can be used to estimate possible errors in detector response time.

Smoke Detection Calculation Examples

EXAMPLE 14:

The smoke level measured outside of a detector at the time of response in a laboratory calibration test is listed on manufacturers' specifications as the optical density or obscuration required to alarm the unit. Because of entry resistance, the smoke level inside the detector will be less. The specified response is for a particular type of smoke and is measured in a laboratory test apparatus. An example of one calibration test is the gray smoke test listed in the UL 268 smoke detector test standard.[33]

In the test, the smoke detector response threshold must not exceed 0.0581 m^{-1} (4.0%/ft). Velocity in the test chamber is 9.8 m/min. The test starts with clear air. A smoldering cotton lamp wick is used to increase the optical density in the test chamber. The rate of increase of optical density in the chamber must fall within the following limits:

$$3.7 \times 10^{-3} \leq \frac{dD_u}{dt} \leq 5.3 \times 10^{-3} \text{ m}^{-1}\cdot\text{min}^{-1}$$

What is the range of optical density inside of the detector at the time of response (D_{uo}) if the detector has an L of 3 m? What would it be if the detector had an L of 14 m?

SOLUTION:

For L = 3 m and $dDu/dt = 3.7 \times 10^{-3}$ $\text{m}^{-1}\cdot\text{min}^{-1}$,

$$D_{ur} = D_{uo} + \frac{L}{u}\left(\frac{dD_u}{dt}\right) \text{ m}^{-1}$$

$$D_{uo} = D_{ur} - \frac{L}{u}\left(\frac{dD_u}{dt}\right) \text{ m}^{-1}$$

$$D_{uo} = 0.0581 - \frac{3}{9.8}(3.7 \times 10^{-3}) = 0.057 \text{ m}^{-1}$$

For $L = 3$ m and $dD_u/dt = 5.3 \times 10^{-3}$ $\text{m}^{-1}\cdot\text{min}^{-1}$,

$$D_{uo} = 0.0581 - \frac{3}{9.8}(5.3 \times 10^{-3}) = 0.056 \text{ m}^{-1}$$

For $L = 14$ m and $dD_u/dt = 3.7 \times 10^{-3}$ $\text{m}^{-1}\cdot\text{min}^{-1}$,

$$D_{uo} = 0.0581 - \frac{14}{9.8}(3.7 \times 10^{-3}) = 0.053 \text{ m}^{-1}$$

For $L = 14$ m and $dD_u/dt = 5.3 \times 10^{-3}$ $\text{m}^{-1}\cdot\text{min}^{-1}$,

$$D_{uo} = 0.0581 - \frac{14}{9.8}(5.3 \times 10^{-3}) = 0.051 \text{ m}^{-1}$$

These calculations indicate that the actual quantity of this particular type of smoke required to alarm the detector varies from 0.051 to 0.057 m^{-1} or from 3.5 to 3.9 percent/ft.

Smoke production and characteristics. The fuel characteristics of primary concern for smoke detection are (1) material and (2) mode of combustion. These two parameters are important for determining pertinent features of expected products of combustion, such as particle size, distribution, concentration, and refractive index. The importance of these features with regard to smoke detection are well documented[6,31,32] and are discussed by Mulholland in Section 2, Chapter 13.[34] Assuming a well-mixed smoke-filled volume, data on smoke characteristics for given fuels can provide an estimation of detector response.

EXAMPLE 15:

The design objective is to detect the smoke from a flaming 200-g (0.5-lb) polyurethane pillow in less than 2 min. The pillow is located in a 36 m^2 room with a ceiling height of 2.5 m (8 ft). Assume that the pillow is burning at a steady rate of 50 g/min. Can the design objective be met? What assumptions are required?

SOLUTION:

The total mass loss at 2 min is 100 g. Given this information, the optical density in the room can be calculated from the relationship (see Section 2, Chapter 13):

$$D_u = \frac{D_m M}{V_c} \tag{29}$$

where D_m [mass optical density (m^2/g)] can be taken from Table 2-13.5 in Section 2, Chapter 13 as 0.22 m^2/g.

$$D_u = \frac{(0.22\ m^2/g)(100\ g)}{(36\ m^2)(2.5\ m)} = 0.244\ m^{-1}$$

Assuming the detector will respond at the UL upper sensitivity limit of 0.14 m^{-1} (black smoke),[33] it can be assumed that the detector will respond within 2 min. This approach is simplified, however, and assumes that the smoke is confined to the room, is well mixed, can reach the ceiling level, and can enter the detector.

EXAMPLE 16:

Polyurethane mattresses are stored in a room that is 50 m × 75 m × 10 m high. A goal has been set to detect a flaming fire before approximately 350 g of fuel has been consumed. Using a projected beam smoke detector with sensitivity settings that can vary from 20 percent to 70 percent total obscuration in 10 percent increments, what is the minimum sensitivity setting for response to this fire? Assume the smoke is mixed evenly throughout the space.

SOLUTION:

The mass optical density, D_m, for a flaming polyurethane mattress is given in this handbook on p. 2-264 as 0.22 m^2/g. The volume of the room is 37,500 m^3.

From the equation for mass optical density, calculate the resulting unit optical density in the room when 350 g of fuel is consumed:

$$D_m = \frac{D_u V}{\Delta m}\ m^2/g$$

$$D_u = \frac{\Delta m D_m}{V}\ m^{-1}$$

$$D_u = \frac{350(0.22)}{37{,}500} = 0.002\ m^{-1}$$

Knowing D_u and assuming the path length of the beam to be 75 m, the ratio of light reaching the receiver of the unit can be calculated:

$$\frac{I}{I_0} = 10^{-D_u I}$$

$$\frac{I}{I_0} = 10^{-0.002(75)} = 0.708$$

Next, the percent obscuration caused by the smoke is calculated:

$$O = 100\left(1 - \frac{I}{I_0}\right)$$

$$O = 100(1 - 0.708) = 29.2$$

Thus, a projected beam smoke detector would have to be set to respond at about 30 percent total obscuration or less to meet the design objective.

Discussion related to the use of D_m. The previous two examples used the mass optical density, D_m, to calculate the expected optical density, D_u, in a space when a certain mass of fuel was consumed. D_m data are typically measured in small-scale tests due to the need for accurate measurements of mass loss and optical density. The use of D_m from small-scale tests to calculate the resulting D_u in a large-scale scenario introduces error. Some comparisons show qualitative correlation. However, it has been reported that the correlation breaks down with complex fires.[34]

Stratification. In the context of this chapter, smoke dilution refers to a reduction in the quantity of smoke available for detection at the location of the detector. This dilution can occur either through natural convection (entrainment in the plume or the ceiling jet) or by effects of a heating or ventilation system. In many cases, forced ventilation systems with high exchange rates cause the most concern. In the early stages of fire development, when smoke production rate is small and the plume is weak, smoke can easily be drawn out of the room and away from area smoke detectors. In addition, high velocity air flows out of supply and into return vents creating defined patterns of air movement within a room. Such flows can either keep smoke away from detectors that are located outside of these paths, or, in some cases, inhibit smoke from entering a detector located directly in the air flow path.

Although there currently are no quantitative methods for estimating either smoke dilution or air flow effects on smoke detector siting, these factors must be considered qualitatively. It should be clear, however, that the air flow effects become larger as the required fire size at detection, $\dot{Q}_{cr}$, gets smaller. If the application warrants, it

may be useful to obtain velocity profiles of the air movement within a room or to perform small-scale smoke tests under various conditions to aid in the smoke detector placement analysis.

The potential for smoke stratification is another concern in the detection of low-energy fires and fires in rooms or volumes with very high ceilings. Stratification occurs when the temperature within the plume equals that of the surrounding air, and there is insufficient thermal energy from the fire to force the smoke higher. Once this point of equilibrium is reached, the smoke layer will maintain its height above the fire, regardless of the ceiling height, until additional energy is provided.

Unlike the effects of air flow on smoke dilution, stratification effects can be calculated using the relationship[44]

$$\dot{q}_{conv} > 0.352 H^{5/2} T_s^{3/2} \quad (27)$$

where

$\dot{q}_{conv}$ = convective heat release rate in W
H = distance from the top of the fuel package (base of the fire) to the ceiling level in m
T_s = difference in ambient gas temperature in °C between the fuel location and ceiling level

This same relationship can also be found in NFPA 92B, *Guide for Smoke Management Systems in Malls, Atria, and Large Areas,* 1991 edition.[45]

EXAMPLE 17:

The design objective is to detect the pyrolysis of overheated PVC cable insulation in a 7-m (23-ft) high, 100-m^2 (1076-ft^2) room. The room is air conditioned, with a temperature differential of 10°C (18°F) between the base of the switch equipment and the ceiling. The proposed design has smoke detectors mounted at the ceiling level. Assuming the critical fire size is 1000 W, will there be sufficient thermal energy to force the smoke to the ceiling level?

SOLUTION:

In this case, one can rearrange Equation 27 and solve for *H:*

$$H < \left(\frac{\dot{q}_{conv}}{0.352 T_s^{3/2}} \right)^{2/5}$$

where $\dot{Q}_{cr}$= 1000 W, and T_s = 10°C (18°F). This result indicates that the highest level of smoke rise is estimated to be 6 m (20 ft). As a result, the design objective may not be achieved by the proposed design. This approach is also valid for evaluating the effects of stratification in a high-ceiling room where a larger fire might be expected. However, the effects of heating and air conditioning systems and warm or cold walls are not considered.

EXAMPLE 18:

The design objective is to detect the flaming combustion of a chair located in the lobby of an office building in order to initiate smoke management functions. The lobby is located at the lowest level of a 20-m (64-ft) high atrium. The atrium has offices on three sides and a glass facade to the outside on the other. The atrium is air conditioned, with a temperature differential of 20°C (36°F) between the lobby and the ceiling level. The proposed design is for smoke detectors to be mounted at the ceiling level. Is there sufficient thermal energy to force the smoke to the ceiling level?

SOLUTION:

First, a value for $\dot{Q}_{cr}$ must be selected for the burning chair. From an analysis of the chair and a review of published heat release data, it is determined that the chair most closely resembles the metal frame chair with padded seat used in Test 53 of the NIST furniture heat release rate tests.[8] This chair had a maximum heat release rate of 280 kW, which can be used as $\dot{q}_{conv}$ (or in this case $\dot{Q}_{cr}$, the critical fire) in Equation 27. Equation 27 can then be rearranged to solve for *H:*

$$H < \dot{Q}_{cr} / (0.352 T_s^{3/2})^{2/5}$$

where $\dot{Q}_{cr}$ = 280,000 W and T_s = 20°C (36°F). In this case, the highest point of smoke rise is estimated to be 38 m (125 ft). Thus, the smoke would be expected to reach the ceiling-mounted detector.

It should be noted that air flow concerns were not considered in Examples 12, 13, and 14. In some cases, a system supplying air at a low level and exhausting at an upper level may actually help transport the smoke to the upper levels of a room, where in other cases it may serve to inhibit smoke movement. It should also be noted that, simply because the smoke reaches the level of the detector, there is no guarantee that it can enter the sensor chamber.

Velocity analog. Spot-type smoke detectors, whether commercial or residential, or ionization- or light-scattering type, all require smoke to enter the detection chamber in order to be sensed. This requirement is another factor that must be considered when attempting to estimate smoke detector response. Smoke entry into the detector can be affected in several ways, for example, due to insect screens, chamber configuration, and proximity of the detector to the ceiling.

As previously discussed in this chapter, Heskestad[46] introduced the concept of smoke detector lag to explain the difference between the optical density outside (D_{ur}) and inside (D_{uo}) of a detector at the time of activation. Although studies of this relationship have provided useful information concerning smoke detector lag,[15,41] the difficulty in quantifying L for different detectors and relating it to siting requirements has limited its usefulness. In its stead, the concept of critical velocity (u_c) has been introduced.[4,47]

Critical velocity, in this context, refers to the lowest gas velocity required for smoke entry into the sensor chamber at a level to sound an alarm at a given threshold. Experimental work has shown this requirement to be in the range of 0.15 m/s for the detectors tested in one study.[47] When velocities fell below this value, the smoke level outside the detector at the time a specified analog output level was reached rose dramatically compared to levels when the velocity was above the critical value. This figure can be useful for design and evaluation purposes, as it is close to the low-velocity value (0.16 m/s) at which a detector must respond in the UL smoke detector sensi-

tivity chamber in order to be listed.[33] Thus, the location of a velocity of 0.16 m/s in the ceiling jet for a given fire and ceiling height can be considered as a first approximation design radius for detector siting purposes. It should be noted that the ceiling-jet velocity correlations assume a horizontal, smooth ceiling. A detailed discussion of ceiling-jet flows by Evans is presented in Section 2, Chapter 2. The critical velocity approach can be illustrated with a simplified example.

EXAMPLE 19:

The new owners of a hotel have established a fire detection design objective that the smoke detection system in the grand ballroom must be able to detect a 50-kW fire. The ballroom is 50 m (160 ft) long by 30 m (96 ft) wide with a 7.1-m (23-ft) high smooth ceiling. The existing smoke detectors are installed at a listed spacing of 10 m on center and have a critical velocity of 0.15 m/s. Assuming the fire starts at a point equally spaced between the existing smoke detectors, will the velocity of the ceiling jet from a 50-kW fire be sufficient to force smoke into the detection chamber? Assume there will be no ventilation system effects.

SOLUTION:

The stated design objective is to detect a 50-kW fire. Because it is not stated whether the fire is steady state or growing, this solution will assume a steady-state fire of 50 kW. This assumption allows the use of Alpert's[16] velocity correlations for a steady-state fire. Alpert provides two equations that can be used: one for $r/H = 0.15$, and the other for $r/H > 0.15$. This correlation is generally considered to be valid when r/H is between 0.15 and 2.1. Therefore, the ratio r/H must be determined first. In addition, the fire source should be at a distance of at least 1.8 times the ceiling height from the nearest enclosure wall.

The installed spacing is 10 m (32 ft) on center. Using the relationship $S = 2^{1/2}r$, the radial distance is found to be approximately 7.1 m (23 ft). Given that H is also 7.1 m (23 ft), the ratio r/H is found to be 1.0. This value is greater than 0.15; thus the following equation can be used:

$$U = \frac{0.195\dot{Q}^{1/3}H^{1/2}}{r^{5/6}}$$

By entering the values of $\dot{Q} = 50$ kW, $H = 7.1$ m (23 ft), and $r = 7.1$ m (23 ft), a velocity of 0.37 m/s is calculated. This indicates that, for a steady-state 50-kW fire, there will be sufficient velocity to force smoke into the detectors at their existing locations.

However, if the 50 kW fire as stated is the design fire, $\dot{Q}_{do}$, and it was determined that the critical fire, $\dot{Q}_{cr}$, was only 5 kW, the resulting velocity using the steady-state correlation at 5 kW would be 0.17 m/s—very close to the critical velocity of 0.16 m/s. Furthermore, with a relatively small fire and a relatively high ceiling, stratification is likely to be a factor and should be considered. Assuming the room is air conditioned, with a temperature differential of 10°C from the top of the fuel package to the ceiling level, the smoke from a 5-kW fire would stratify at a level of about 7.3 m (23.4 ft)—very close to the ceiling height of 7.1 m (23 ft). Given probable dilution of smoke and errors in approximations, it could be considered unlikely that a 5-kW fire would be detected under the defined conditions.

In addition to illustrating how the concept of critical velocity can be used for the design of smoke detection systems, it clearly points out the need to adequately define performance and design objectives, and to select correlations that fit those objectives. First, the objectives should be stated in terms of both the design fire and the critical fire. A 50-kW design fire is significantly different from a 50-kW critical fire, and the design for one may not meet the requirements for the other. Second, care should be taken in selecting a ceiling-jet velocity correlation that most closely fits the design objectives. Unless the hazard analysis indicates that the maximum fire size of $\dot{Q}_{do}$ will be 50 kW, it may be better to apply a ceiling-jet velocity correlation, based on a growing fire. In this case, the fire growth rate must also be estimated as part of the evaluation. The following example shows the importance of these factors by using the same ballroom as described in Example 19, and provides more specific performance and design parameters.

EXAMPLE 20:

After additional consultation, the owners of the hotel described in Example 19 have modified their objectives as follows: assuming that a fire will begin in a chair, the smoke detection system for the grand ballroom must be able to detect the fire and initiate an internal response before it spreads beyond the chair of origin. The typical fuel load within the room consists of metal-framed chairs with padded seats and backs, and plywood tables with cotton tablecloths.

The response time from when the alarm signal is indicated at the annunciator until the first staff member arrives is estimated to be 60 s. The delay time from detector activation until alarm initiation, as measured at the sensor, is 10 s. Because of the potential for nuisance alarms, the detection system employs an alarm verification feature that has a minimum delay time of 15 s and a maximum delay time of 60 s.

The existing smoke detectors are installed at a UL-listed spacing of 10 m on center and have a critical velocity of 0.15 m/s. Assuming the fire starts at a point equally spaced between the existing smoke detectors, and there are no ventilation system effects, can the existing smoke detection system be expected to meet the design objectives?

SOLUTION:

The complete solution to a problem like this one may require several steps; for example, determination of the design fire, determination of the critical fire, estimation of ceiling jet velocity at $\dot{Q}_{cr}$, estimation of smoke production or optical density, and analysis of possible stratification effects. In all cases, however, determination of the design fire and the critical fire is essential.

Given that the goal is to detect the fire while in the chair of origin, a first step might be to estimate the fire size within the chair that could ignite the cotton tablecloth. From analysis of the chair and a review of published heat release data, it is determined that the chair most closely resembles the metal frame chair with padded seat and back used in Test 53 of the NIST furniture heat release rate

tests.[8] This chair had a maximum heat release rate of 280 kW; a fire growth rate of ≈ 0.0086 kW/s^2; a growth time, t_g, of 350 s; and a virtual start time, t_v, of 50 s.

Assuming that the fire would likely grow up the seatback of the chair and that the seatback is located approximately 0.5 m from the tablecloth, an estimate of the energy output required for ignition of the tablecloth can be made. In this case, using the radiant ignition routine in FIREFORM[48] and assuming the fuel being easy to ignite (ignition flux of 10 kW/m^2) with a separation distance of 0.5 m, it is estimated that the tablecloth will ignite when the total energy output from the burning chair reaches 139 kW. These parameters define the design fire.

The next step is to calculate the time for the design fire to reach the threshold limit of 139 kW. Using the relationship $\dot{Q} = \alpha t^2$, a time of 118 s (about 2 min) is calculated. This calculation is growth time of the fire after it begins to follow an exponential growth rate until the design fire size is reached. Given that the fire would probably start as smoldering combustion, the actual growth time could be considerably larger (1 to 2 hr possible).

The critical fire size can then be estimated by subtracting the various response times and estimating the heat release rate at that moment in time. In this regard, reasonable time delays should be used based on the information provided. The focus should be on obtaining the "most reasonable" worst-case delay for the situation. From the problem statement, this delay is estimated based on the response times given, using the following equation:

$$t_{\text{response}} = t_{\text{transport}} + t_{\text{verify}} + t_{\text{system}} + t_{\text{staff}}$$

where the following assumptions are made:

transport = smoke transport time (unknown)
verify = verification time (60 s maximum)
system = system response time (10 s)
staff = staff response time (60 s)

Momentarily ignoring the smoke transport time and assuming prompt staff response, the result is a maximum detection system response time of 130 s. However, in an actual fire situation, the smoke detector verification time should be at its minimum of 15 s, and not at its maximum of 60 s. Making this assumption, the total response time (still ignoring smoke transport time) is 85 s. This result is less than the 127 s time to ignition of the tablecloth and is used to help define the critical fire size ($\dot{Q}_{\text{cr}}$).

Here, the 85 s is subtracted from the 127 s (that defines the design fire), and the relationship $\dot{Q} = \alpha t^2$ is used to calculate the heat release rate at that moment in time. The result is a heat release rate of 15 kW. Assuming no smoke transport time, this result would be the critical fire size at which detection must occur in order to detect the fire and cause the required response before the design fire size is reached.

The next step is to factor in a lag due to the smoke transport time. In order to account for smoke transport lag, Brozovsky[47] suggests a safety factor that is equivalent to a heat release rate that is 80 percent of the maximum fire size at the time of detection. This factor would result in a critical fire size of 12 kW and a corresponding response time of 37 s. These values can then be used to determine if the ceiling-jet velocity will exceed 0.16 m/s.

Although several simplifications have been made, this example outlines a methodology for estimating the potential for detector response, given the concepts of design fire and critical fire. In addition, the cross-checking utilized points out the importance of understanding the limitations and boundary conditions of correlations and empirical relationships; i.e., simply because one condition can be met, it does not automatically mean that all others will be met as well, and the complete scenario should be considered. Engineering of smoke detection, especially for low-energy fires, can be a difficult task, and the application of any method for this purpose should include clear statements of all assumptions made.

Temperature approximation method for modeling smoke detection. The temperature approximation theory is another method used to estimate the optical density produced by flaming fires. The theory hypothesizes that the mass concentration of smoke particles at a point is proportional to the change in temperature due to the fire (at that point).[49] The following assumptions are necessary:

1. Particle size distribution is constant in space and time.
2. Mass generation rate is proportional to mass burning rate.
3. There is no heat transfer between particles or between the particles and the confining surfaces.
4. The smoke does not continue to react as it travels.

Heskestad then hypothesized that the ratio of optical density to temperature rise would be a constant for a particular fuel and burning mode (flaming, smoldering, vertical combustion, horizontal combustion, etc.). There are actually three parts to this hypothesis.

The first is that each fuel and burning mode results in a unique optical density required to alarm a particular model and type of detector. This aspect was discussed previously regarding photoelectric, ionization, and projected-beam smoke detectors. This phenomenon is regularly observed, explained by theory, and accepted by the scientific and engineering community.

The second part of the hypothesis is that for each fuel and burning mode the optical density at a point is proportional to the mass concentration of particles:

$$D_u \propto C$$

The final part of the hypothesis is that, for each fuel and burning mode, the mass concentration of particles is proportional to the change in temperature at a point:

$$C \propto \Delta T$$

Combining these proportionalities, optical density is proportional to the change in gas temperature for a given fuel and combustion mode:

$$D_u \propto \Delta T$$

Therefore, the ratio of optical density to temperature rise is constant for a given fuel:

$$\frac{D_u}{\Delta T_g} = \text{CONSTANT}$$

This hypothesis assumes that the only way to move the smoke particles from the source to the detector at the ceiling is by buoyant forces.

Heskestad and Delichatsios examined experimental data for obscuration and temperature rise at various locations on a ceiling for different fuels. They concluded that while the data showed some variation in time at different radial positions relative to the fire source, the ratio could be approximated as a constant. Table 4-1.15 lists the ratios recommended by Heskestad and Delichatsios for various fuels.

Examining the original data, the last column has been added to show the range of values for each fuel. Averages have also been calculated and listed in the last row of the table for reference.

Others experiments have resulted in data that differ from that of Heskestad and Delichatsios. Bjorkman et al. reported values for polyurethane that are approximately one half that reported by Heskestad and Delichatsios.[42] The data produced by Heskestad and Delichatsios show the ratio of optical density to temperature rise was not constant. The authors concluded that the variation was the result of slowly changing characteristics of the smoke particles as they left the flaming source and traveled in the plume and ceiling jet. Nevertheless, they concluded that a constant value could be used as a rough approximation to allow engineers to model optical density produced by a fire. Although it has not yet been done, it is possible to examine their original data and place error bars on the values recommended in Table 4-1.15.

A fire model can be used to calculate the temperature rise at a smoke detector location or in a layer. Then, using the ratios reported by researchers, the optical density at that location as a function of time can be approximated.

Discussion related to the use of fire models for heat and smoke detector modeling. Some computer fire models or sets of computational tools include routines for calculating heat or smoke detector response. It is important for users to understand the underlying detector models being used so that limitations and potential errors can be understood. For heat detection, most computational tools use a lumped mass model as described in this chapter. However, for smoke detection some use a temperature rise model, and some use a mass optical density or specific extinction area model. The specific extinction area σ_f is similar to the mass optical density except that it is based on calculations using the natural log, e, rather than $\log_{10}$. Most do not include entry resistance modeling. Some permit the use of fuel-specific parameters for smoke yield and mass optical density. Others use preset values.

Table 4-1.15 ***Ratios Recommended by Heskestad and Delichatsios for Various Fuels***

Material	$10^2 D_u/\Delta T$ (1/ft °F)	Range of Values
Wood	0.02	0.015–0.055
Cotton	0.01/0.02	0.005–0.03
Paper	0.03	Data not available
Polyurethane	0.4	0.2–0.55
Polyester	0.3	Data not available
PVC	0.5/1.0	0.1–1.0
Foam rubber PU	1.3	Data not available
Average	0.4	0.005–1.3

Radiant Energy Detection

During the combustion process, electromagnetic radiation is emitted over a broad range of the spectrum. Currently, however, fire detection devices operate only in one of three bands: ultraviolet (UV), visible, or infrared (IR), where the wavelengths are defined within the following ranges:[8]

Ultraviolet	0.1	to	0.35 microns
Visible	0.35	to	0.75 microns
Infrared	0.75	to	220 microns

Selection of a specific sensor type for fire detection is based on a number of factors, including fuel characteristics, fire growth rate, ambient conditions, resulting control or extinguishing functions, and environmental conditions in the detection area. More specifically, it includes evaluation of the radiant energy absorption of the atmosphere, presence of nonfire-related radiation sources, the electromagnetic energy of the spark, ember or fire to be detected, the distance from the fire source to the sensor, and characteristics of the sensor.

These factors are important for several reasons. First, a radiation sensor is primarily a *line-of-sight* device, and must "see" the fire source. If there are other radiation sources in the area, or if atmospheric conditions are such that a large fraction of the radiation may be absorbed in the atmosphere, the type, location, and spacing of the sensors may be affected. In addition, the sensors react to specific wavelengths, and the fuel must emit radiation in the sensors' bandwidth. For example, an infrared detection device with a single sensor tuned to 4.3 microns (the CO_2 emission peak) cannot be expected to detect a noncarbon-based fire. Furthermore, the sensor must be able to respond reliably within the required time, especially when activating an explosion suppression system or similar fast-response extinguishing or control system.

Once the background information has been determined, the detection system can be designed. Standard practice for the design of radiant energy detection devices is based on application of generalized fire size versus distance curves that are derived using the inverse square law:[8]

$$S = \frac{kP \exp^{\zeta d}}{d^2}$$

where

S = radiant power reaching the detector (W)
k = proportionality constant for the detector
P = radiant power emitted by the fire
ζ = the extinction coefficient of air
d = the distance between the fire and the detector

This relationship is used to produce sensor response information for specific fuels. By then plotting the normalized fire size versus the normalized distance, the resulting curve defines the maximum distance at which the tested sensor can be expected to consistently detect a fire of a defined size (usually provided in m²). By testing a sensor using various fuels, a family of curves can be developed to assist in system design. These curves (sometimes given in tabular form) are usually provided by the sensor manufacturer.

Before applying the distance obtained from such a curve, one must also consider the sensors' field of view. Because the radiation sensor is a line-of-sight device, the sensitivity of the device to a defined fire size decreases as the fire location is moved off the optical axis of the device. This result means that a fire of X m², which is detectable at a distance Y m on axis from the sensor, may not be detectable at the same distance Y m if it is located 30 degrees off axis. Limitations of viewing angles are also provided by manufacturers.

Ambient conditions should also be considered as part of the evaluation and design process. Factors, such as humidity and dust, can affect the absorption of radiation in the atmosphere, thus limiting the amount of radiation reaching the sensor for a given fire size. Similarly, temperature can affect the relative sensitivity of a sensor. As the ambient temperature increases, the relative sensitivity can decrease. Even if the decrease is small, it can affect the response of the sensor to the expected fire.

Radiation Detection Example

EXAMPLE 21:

The design objective is to detect a 1.0 m² (11 ft²) pool fire of JP4 aircraft fuel in a large hangar in order to activate a fixed suppression system. The hangar dimensions are 50 m (160 ft) by 80 m (257 ft) with a 20-m (64-ft) ceiling height. The ambient temperature at the ceiling level varies between 15°C (59°F) and 60°C (140°F), depending on time of day and season. The humidity also varies by season, with relative humidity of 90 percent possible. What steps should be taken during system design?

SOLUTION:

The first step should be selection of a detection device. Because the hazard is carbon based, IR detection at 4.3 microns is suitable. Also, because IR detectors generally provide a larger surveillance area per device than UV detectors, they could be more cost effective than UV detection in this case.

One should then determine possible sources of interfering radiation and select a device that is resistant to these extraneous sources. Such resistance to false response can be obtained by filtering, use of multiple sensors (e.g., two- or three-channel detector), or a combination.

The next step is to review the manufacturer's data to determine mounting criteria based on the size of the critical fire [1.0 m² (11 ft²)]. Generally, this step begins with the fire size versus distance curve or table. If only a curve is provided, one must then determine the mounting height and lateral distance limits of the detector. Lateral distances are important as related to the sensors' field of view.

Given this information, a device layout design can be made. This design should consider all possible obstructions, and result in all parts of the hangar being monitored. One such design is illustrated in Figure 4-1.11.

As part of the layout, one should consider the possible effects of reduced device sensitivity due to angular displacement, temperature, and humidity. Because manufacturers' criteria vary on these parameters, typical values are used in this solution to illustrate their effects.

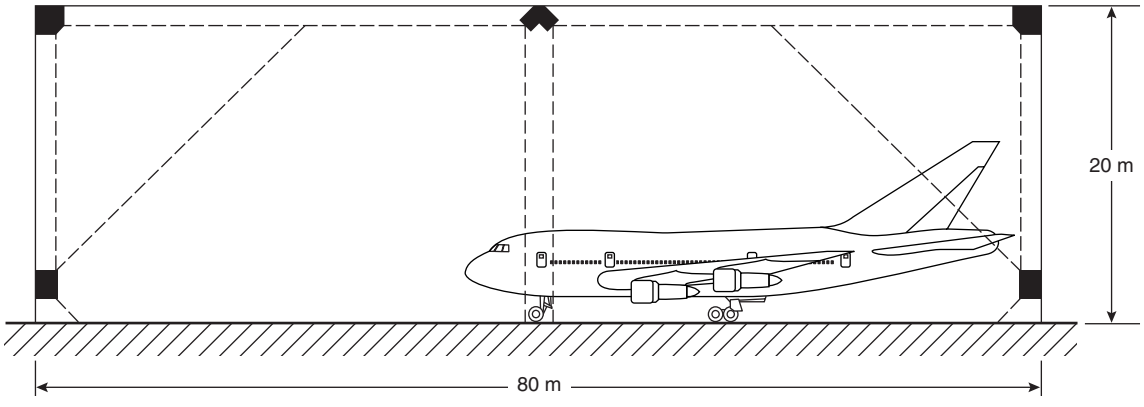

Figure 4-1.11. ***IR detector layout for an aircraft hangar.***

For example, the proposed layout has devices utilizing a field of view of 45 degrees. Assuming the nominal sensitivity is such that a 1.0 m^2 (11 ft^2) fire can be detected at 40 m (128 ft), and there is a reduction in sensitivity of 30 percent due to angular displacement, the distance at which a 1.0 m^2 (11 ft^2) fire can be detected at 45 degrees is reduced to 28 m (90 ft). If the manufacturers' data indicate a further reduction in sensitivity for temperature, for example 3 percent at 50°C (122°F), the distance is reduced to about 26.8 m (86 ft). If there are further reductions due to humidity, for example a 3 percent reduction at 90 percent relative humidity, the resulting detection distance at 45 degrees is about 25.6 m (82 ft).

In this example, the viewing distance at 45 degrees is a maximum of 20 m (64 ft), and the design can be considered valid. Had the sensitivity decreased such that the distance dropped below 20 m (64 ft), an alternative layout or different devices must be used. In all cases, the manufacturers' literature should be consulted to determine all pertinent increases or reductions in detector sensitivity due to fuel, distance, angular displacement, and environmental conditions.

Designing Fire Alarm Audibility

In most cases, the purpose of a fire detection and alarm system is to alert the occupants of a building that an emergency exists and to initiate evacuation. In situations such as high-rise or industrial buildings, it may be desirable to provide the occupants with more information, such as the nature and location of the fire. In either case, the purpose of the system is defeated if the signal is not heard and understood by the occupants.

This section demonstrates a method for fire protection engineers to estimate the relative effectiveness and cost of various fire alarm alerting systems during the design process. In the past, the selection and location of fire alarm devices has been based on experience and engineering judgment. The use of this simplified methodology can save thousands of dollars in retrofit costs required to correct deficiencies in an alarm system.

The transmission of sound from a source to a target is a function of many factors, such as humidity; air viscosity and temperature; the frequency of the signal; the location of the source relative to the target; the construction of walls, floors, and ceilings; and the furnishings in the area. *Architectural Acoustics*[50] contains a good discussion of these and many other factors affecting sound transmission and loss.

Sound power and sound pressure levels are expressed in decibels (dB) relative to a reference. It is assumed that the reader is familiar with this system of measurement. Throughout this chapter sound power level (SWL or L_W) in decibels is referenced to 10^{-12} W. Sound pressure level (SPL or L_p) in decibels is referenced to 2×10^{-5} Pa. This discussion also assumes that the reader is familiar with the concept of A-weighting. The purpose of A-weighting is to adjust sound pressure level measurements to correspond as closely as possible to the way humans perceive the loudness of the many different frequencies we hear. For instance, a 1000-Hz signal at an SPL of 20 dB would be clearly audible. A 100-Hz signal at the same SPL would not be heard. A-weighting allows a single number to describe the SPL produced by a signal containing frequencies between 20 and 20,000 Hz. The weighting of the various frequencies is established by an internationally accepted A-weighting curve.[51]

Typical fire alerting systems consist of a combination of audible and visual signals activated by fire detection systems. The audible devices are usually horns, bells, chimes, or speakers. The visual indicators are usually strobe lights, incandescent lamps, or, occasionally, revolving beacons.

In residential occupancies, fire alerting systems should be capable of awakening a sleeping person and informing him or her that a fire emergency exists. Several studies have been done to establish the sound pressure level required to achieve this goal.[52,53] These studies suggest an SPL between 55 and 70 dBA will awaken a college-age person with normal hearing. The minimum required SPL is also a function of the background noise or signal-to-noise ratio. These levels establish the SPL required to alert or be audible. They do not address the problem of how the person will perceive the sound or react to it.

Until recently, fire codes did not set forth the SPL that a fire alarm system must produce within a building. NFPA 72[8] requires signals to be 15 dBA above ambient in areas where people may be sleeping. British standards require fire alarm signals to produce a sound pressure level of 65 dBA or 5 dBA above ambient noise in areas where occupants are not sleeping.[54] A sound pressure level of 75 dBA at the head of the bed is required in occupancies where people may be sleeping.

The audible design requirements listed above and the remaining discussion and examples in this section all use dBA as a measure of audibility. However, it should be pointed out that for a sound to be perceived as audible, it need only penetrate or be greater than the background noise level at one particular frequency bandwidth. For example, certain facilities such as manufacturing plants may have a background noise level in excess of 85 dBA. An installed fire alarm may produce only 75 dBA at a certain location. Nevertheless, occupants will hear and respond to the fire alarm system. Why? The reason is because the background noise that contributes to the 85 dBA is mostly low frequency sound and the fire alarm is mostly high and midrange frequencies. Figure 4-1.12 illustrates this concept. Like two picket fences, one behind the other, only one picket or octave band must be taller for us to perceive the presence of the second fence or signal. While the balance of this section uses dBA, the procedure and methods apply equally well to work done in a single frequency band.

Visual signals are located to assist people in deciphering potentially confusing alarm signals. The visual signals also help alert occupants in high background noise environments.

Butler, Bowyer, and Kew[51] have described a method to estimate sound pressure levels at some location remote from the sound source. Formulas presented in their

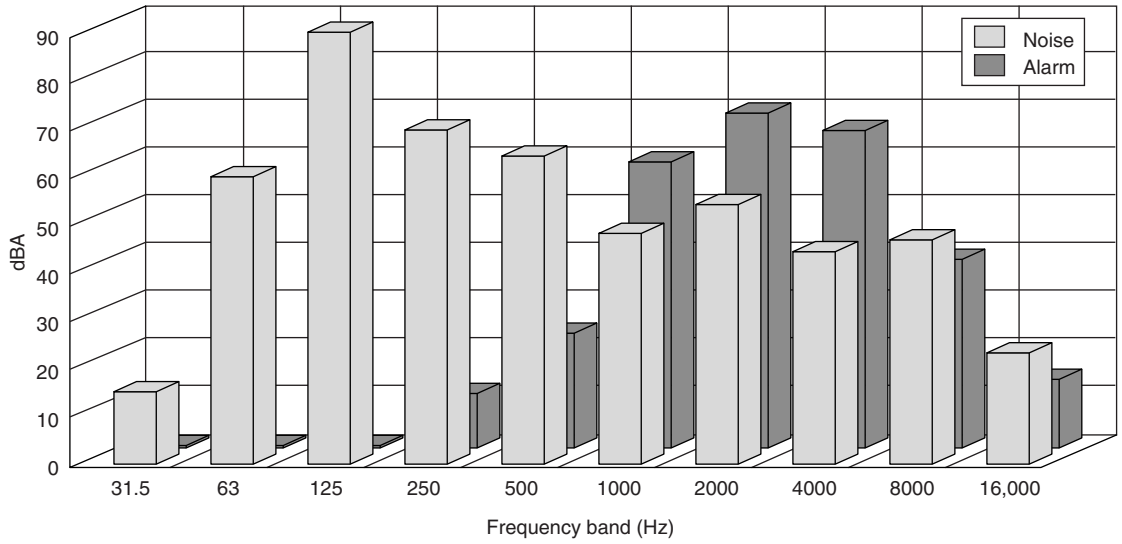

Figure 4-1.12. ***Penetration of noise by alarm.***

study are analogous to standard sound attenuation formulas found in other references.[50,55] They have been simplified by replacing complex terms with constants for which they have provided tables of data (see Tables 4-1.16 through 4-1.29). The equations and data presented in their study provide a straightforward method for analyzing proposed designs. The same equations and data can be used to determine the power requirement and maximum allowable spacing of signaling devices required to achieve a specified sound pressure level. The technique presented in their study is suitable for acoustically simple buildings only. Complex building arrangements and materials may require a more rigorous analysis using other methodologies which are beyond the scope of this chapter.

To demonstrate how signaling systems can be designed and analyzed, two scenarios will be considered. Both scenarios are based on a typical dormitory or office layout. The building has long corridors with rooms of equal size on each side. Each room is approximately 5 m wide by 6 m deep. The walls consist of two layers of Sheetrock (total of 25.4 mm thick) separated by wood studs. The wall cavities contain 75-mm-thick mineral fiber insulation. The floors are concrete with carpeting. The ceiling is 3 m high and consists of acoustical tiles. The room doors are solid core with good edge seals. The alerting systems will be designed to achieve a 75 dBA sound pressure level at the farthest point in the rooms.

In the first scenario, wall-mounted fire alarm speaker/light combinations are spaced equally in the corridor. Calculations determine the maximum allowable spacing of the speakers in order to achieve the design goal of 75 dBA in the rooms.

In the second scenario, speakers are placed in each room as well as in the corridor. Calculations determine the size of the speaker and the power needed to drive that speaker to achieve the design goal of 75 dB. Calculations are also presented to determine the required spacing of speakers in the corridor to achieve a sound level of 65 dB.

Table 4-1.16 ***Adjustment for Mounting Position of Sounder (C_1)***

Sounder Position	C_1
Wall/ceiling mounted (more than 1 m from any other major surface)	+5
Wall/ceiling mounted (closer than 1 m to one other major surface)	+7

Table 4-1.17 ***Adjustment for Distance (C_2) with Distance from Source (m)***

Distance from Source (m)	C_2
1	−11
2	−17
3	−21
6	−27
12	−33
15	−35
20	−37
25	−39
30	−41
40	−43
50	−45
60	−47
80	−49
100	−51

Unless otherwise noted, the following formulas and data are from Butler, Bowyer, and Kew.[51]

Scenario A:

In this scenario, the fire alerting system, or sounder, will consist of wall-mounted speaker/light combinations in the corridors only.

L_W is the sound power level of a horn, bell, speaker, or any sounder (dBA referenced to 10^{-12} W).

$$L_W = L + 20 \log_{10} r + 11 \text{ dB}$$

where L is the manufacturer's stated output in dBA at a distance r meters. A typical compression driver-type fire alarm speaker powered at 2 W has an L equal to 94 dBA at 3.05 m.[56] Therefore,

$$L_W = 94 + 20 \log_{10} (3.05) + 11$$
$$L_W = 115 \text{ dB}$$

L_{P1} is the sound pressure level (dBA referenced to 2×10^{-5} Pa) produced outside of a room wall from one speaker.

$$L_{P1} = L_W + C_3 + C_4 + C_5$$

where

C_3 = correction for the number of directions that the sounder propagates

C_4 = correction for the characteristics of the corridor walls, ceiling, and floor

C_5 = function of the distance from the sounder to the center of the bedroom wall

From Table 4-1.18[51] C_3 is -3 dB, because the speaker propagates in two directions along the corridor; from Table 4-1.19 C_4 is -9 dB, because the floor and ceiling are acoustically soft; and C_5 is unknown since the required spacing of the corridor speakers has not yet been determined. Table 4-1.20 provides C_5 values for determined distances.

A worst-case condition exists for a room located farthest from a speaker. In this situation the room is located equally between two speakers. Since each unit propagates sound to the room, the sound pressure level outside of the room is higher than if there were only one speaker. The sound pressure level is not double that for a single speaker. For equally spaced sounders, Table 4-1.21 indicates to add 3 dB to the level expected from a single unit. Therefore,

$$L_{P1} = 115 - 3 - 9 + C_5 + 3$$
$$L_{P1} = 106 + C_5$$

L_{P2} is the sound pressure level at the farthest point in a room. To achieve the established goals, L_{P2} must be 75 dBA. In this situation, with the speaker located outside of the occupied space,

$$L_{P2} = L_{P1} - R + C_2 + C_6 + C_7 + 11 \text{ dBA}$$

Table 4-1.18 ***Adjustment for Number of Directions of Sound Propagation (C_3)***

Number of Directions	C_3
Single direction (e.g., positioned at one end of a corridor)	0
Two-directional (e.g., positioned in the length of a corridor)	–3
Three-directional (e.g., positioned at a T junction of corridors)	–5

Table 4-1.19 ***Adjustment Based on the Finishes in the Corridor (C_4)***

Surface Finishes	C_4
Hard (e.g., walls and ceiling with solid surfaces and tarazzo floor)	0
Medium (e.g., acoustic ceiling, plastered solid walls with 5% coverage of soft surfaces and floor of composite tiles)	–8
Soft (e.g., acoustic ceiling, plastered solid walls with 5% coverage of soft surfaces and carpets on felt on concrete floor)	–9

Table 4-1.20 ***Adjustment for Distance from Source to Mid-Point of the Partition (C_5)***

Distance from Source (m)	C_5
1	0
3	–4
6	–8
10	–10
12	–11
15	–12
20	–14
30	–15
50	–17

Table 4-1.21 ***Addition of Two Sound Pressure Levels***

Difference between the Two Levels (dB to Be Added)	Add to the Higher Level (dB)
0	3
1	2
2	2
3	2
4	2
5	1
6	1
7	1
8 or more	0

Table 4-1.22 ***Factor for Area of Partition between Sounder and Receiver (C_6)***

Partition area (m^2)	C_6
2	+3
4	+6
8	+9
10	+10
15	+11.5
20	+13
30	+15
50	+17
80	+19
100	+20
200	+23

where

R = average sound reduction index for the wall

C_2 = function of the distance from the wall to the point of interest

C_6 = function of the area of the room wall (see Table 4-1.22)

C_7 = function of the frequency of the sound reaching the wall (see Table 4-1.23)

Table 4-1.23 ***Adjustment for Frequency of Maximum Output of Sounders (C_7)***

Frequency of Sounder	C_7
500 Hz	0
1000 Hz	–3
2000 Hz	–5
4000 Hz	–9

In this case, from data presented by Butler, Bowyer, and Kew,[51] the sound reduction index R for the wall is about 40 dB. (See Table 4-1.24.) This value is based on incident sound in the range of 100 to 3150 Hz. Sound attenuation through the door is about 26 dB. (See Table 4-1.24.) The average sound reduction index, R, for the combined door and wall is 34 dB, if the door is 10 percent of the area. (See Table 4-1.25.) C_2 is found to be −27 dB, because there are 6.5 m from the center of the wall to the corner of the room. (See Table 4-1.25.) Since the wall is 15 m^2, C_6 is +11.5 dB. (See Table 4-1.22.) If it is assumed that the sound reaching the wall is a maximum at a frequency of 2000 Hz, $C_7 = 15$ dB. (See Table 4-1.23.) Therefore,

$$L_{P2} = (106 + C_5) - 34 - 27 + 11.5 - 5 + 11 \text{ dBA}$$

$$L_{P2} = 62.5 + C_5 \text{ dBA}$$

Table 4-1.24 ***Second Reduction Indices (dB) for a Selection of Typical Structures (100–3150-Hz Frequency Range)***

Building Element	Weight of partition (kg/m^2)	Average Attenuation (dB)
Walls and Partitions		
1. 100-mm-dense concrete with or without plaster	250	45
2. 150-mm "no fines" concrete with 12-mm plaster on both faces	250	45
3. 115-mm brickwork with 12-mm plaster on both faces	250	45
4. 115-mm brickwork unplastered	195	42
5. 300-mm lightweight concrete precast blocks with well-grouted joints	190	42
6. 75-mm clinker blockwork with 12-mm plaster on both faces	115	40
7. 50-mm-dense concrete	120	40
8. 25.4-mm plasterboard (2 layers) separated by timber studding (75 mm) and mineral fiber blanket	—	40
9. 200-mm lightweight concrete precast blocks with well-grouted joints	122	40
10. 150-mm lightweight concrete precast blocks with well-grouted joints	93	37
11. 50-mm clinker blocks with 12-mm plaster on both faces	—	35
12. 63-mm hollow clay blocks with 12-mm plaster on both faces	—	35
13. 9.5-mm plasterboard (2 layers) separated by timber studding (75-mm with 12-mm) on plaster on both faces	—	35
14. 6-mm plywood/hardboard (2 layers) separated by timber studding (50- and 50-mm) mineral fiber blanket	—	30
15. 19-mm chipboard on a supporting frame	—	25
16. 0.8-mm sheet steel	—	25
17. 21-mm tongued and grooved softwood boards tightly clamped on a support frame	—	20
18. 3.2-mm hardboard (2 layers) separated by 44-mm polystyrene core	—	20
Doors		
19. Flush panel, hollow core, hung with one large air gap	9	14
20. Flush panel, hollow core, hung with edge sealing	9	20
21. Solid hardwood, hung with edge sealing	28	26
Windows		
22. Single glass in heavy frame	15	24
23. Double-glazed 9-mm panes in separate frames 50-mm cavity	62	34
24. Double-glazed 6-mm panes in separate frames 100-mm cavity	112	38
25. Double-glazed 6-mm and 9-mm panes in separate frames 200-mm cavity, absorbent blanket in reveals	215	58

Table 4-1.25 ***Average Sound Reduction Indices (dB) of Partitions Incorporating a Door of 26-dB Attenuation (i.e., heavy door with edge sealing) (100–3150-Hz Frequency Range)***

Door Representing Percentage of Total Area of Partition	Sound reduction index of partition without glazing					
	25 dB	30 dB	35 dB	40 dB	45 dB	50 dB
100%	26	26	26	26	26	26
50%	25	27	28	28	28	28
25%	25	28	30	31	31	31
10%	25	28	32	34	35	35
5%	25	28	33	36	38	38

Table 4-1.26 ***Average Sound Reduction Indices (dB) of Partitions Incorporating a Door of 14-dB Attenuation (i.e., one with large air gaps) (100–3150-Hz frequency range)***

Door Representing Percentage of Total Area of Partition	Sound reduction index of partition without glazing					
	25 dB	30 dB	35 dB	40 dB	45 dB	50 dB
100%	14	14	14	14	14	14
50%	16	16	16	16	17	17
25%	19	19	19	19	20	20
10%	21	23	23	23	23	23
5%	23	25	26	26	26	26

Table 4-1.27 ***Average Sound Reduction Indices (dB) of Partitions Incorporating a Door of 20-dB Attenuation (i.e., light door with edge sealing) (100–3150-Hz frequency range)***

Door Representing Percentage of Total Area of Partition	Sound reduction index of partition without glazing					
	25 dB	30 dB	35 dB	40 dB	45 dB	50 dB
100%	20	20	20	20	20	20
50%	21	22	22	22	22	23
25%	23	24	25	25	25	26
10%	24	27	28	29	29	29
5%	24	28	30	32	32	32

Table 4-1.28 ***Combined Sound Reduction Indices for Combination of Standard Doors and Glazing (100–3150-Hz frequency range)***

Area of (24 dB) Glazing (m^2)	Sound Reduction Index for Standard Size Door (1.54 m^2)		
	14 dB	20 dB	26 dB
	Insulation Values for Combined Door and Glazing		
1	16	21	25
2	17	22	25
4	18	22	24
6	19	23	24
8	20	23	24
10	20	23	24
12	21	23	24
16	21	23	24
20	22	23	24

If there were no loss of sound pressure level between the speaker and the room wall due to distance, C_5 would be zero and L_{P2} would be 62.5 dBA. This result shows that even if the two speakers were right outside the room, the goal of 75 dBA in the room would not be met. In fact, the resultant noise level in the room would be slightly less than the 65 dBA required by British standards[54] to alert nonsleeping persons. The sound level of 62.5 dBA would exceed the 55 dBA reported by Nober et al.[32] to alert sleeping college-age persons in a quiet ambient setting.

To meet the goal of 75 dBA in the room, either the sound system or the environment would have to be changed. Fire alarm speakers are normally available with multiple power taps such as 4, 2, 1, 1/2, and 1/4 W. A single unit may allow choice of two or three different power levels, which allows balancing of the system after installation.

If a 4-W power input were used, this would be a doubling of the 2 W originally tried in the previous calculation. Because decibels are logarithmic, a doubling of power results in a change of 3 dB in L_W ($10 \times \log_{10} 2 = 3$). This action alone would not be sufficient to meet the 75-dBA goal. In addition, the higher sound pressure level in the immediate vicinity of the speaker might be discomforting. If the fire alarm system were also used for voice communication, a speaker tapped at 4 W in a small corridor might sound very distorted and be unintelligible.

It is also possible to change the sound pressure level in dBA by changing the frequency of the source. In general, the higher the frequency, the higher the attenuation as the sound waves pass through a wall. Hence, a lower frequency would increase the sound pressure level in the room. In the calculations above, it was assumed that the predominant frequency of the source was 2000 Hz. This frequency resulted in a C_7 of -5 dBA. According to Table 4-1.23, if this frequency were 500 Hz, C_7 would be 0 dBA. This adjustment would increase the SPL in the room by 5 dBA.

Changes could be made to the building design that would make it possible to meet the design goal. For instance, the use of a lighter-weight door or one without good edge sealing could increase sound transmission to the room by as much as 12 dBA. (See Tables 4-1.26 through 4-1.29.) However, changes such as this one would tend to defeat other goals such as fire resistance and resistance to smoke spread. If the floor and ceiling were hard surfaces without carpeting or tiles, C_4 could be increased from -9 to 0 dBA. (See Table 4-1.30.) Changes

Table 4-1.29 ***Average Sound Reduction Indices for a Partition Whose Surface Is a Combination of Glass, Door, and Wall Partition (100–3150-Hz frequency range)***

	Sound Reduction Value of Partition without Glazing or Door											
	30 dB			35 dB			40 dB			45 dB		
Door + Glazing as Percentage of Total Partition Area	Insulation Value of Combined Door and Glazing (dB) (from Table 4-1.27)											
	15	20	25	15	20	25	15	20	25	15	20	25
5	26	28	30	28	31	33	28	32	36	28	33	37
10	24	27	29	24	29	32	25	30	34	25	30	35
20	22	25	28	21	26	31	22	27	32	22	27	32
30	20	24	28	20	25	29	20	25	30	20	25	30
50	18	23	27	18	23	28	18	23	28	18	23	28
75	16	21	26	16	21	26	16	21	26	16	21	26
100	15	20	25	15	20	15	15	20	25	15	20	25

Table 4-1.30 ***Average Sound Reduction Indices (dB) of Partitions Incorporating Single Glazing (100–3150-Hz frequency range)***

Percentage of Glazing (24 dB)	25 dB	30 dB	35 dB	40 dB	45 dB	50 dB
100%	24	24	24	24	24	24
75%	24	25	25	25	25	25
50%	24	26	27	27	27	27
33%	25	27	28	29	29	29
25%	25	27	29	30	30	30
10%	25	29	31	33	34	35
5%	25	29	33	35	36	37
2½%	25	30	34	37	39	40
—	25	30	35	40	45	50

such as this would probably be resisted for reasons other than fire safety.

The only remaining alternative is to provide speakers in each of the rooms.

Scenario B:

In this case, a speaker in each room powered at only 1/4 W will be tried in addition to the speaker in the corridor. The problem, then, is to select a speaker with a sound power output that can meet the goal of 75 dB at the pillow.

L = ? at r = 3.05 m (3.05 m is a commonly used reference point.)

$$L_W = L + 20 \log_{10} r + 11 \text{ dB}$$
$$L_W = L + 20 \log_{10} (3.05) + 11 \text{ dB}$$
$$L_W = L + 21 \text{ dB}$$

L_{P2} is the sound level at the bed. In this case, with the speaker in the occupied space,

$$L_{P2} = L_W + C_1 + C_2 \text{ dBA}$$

where C_1 is a correction for how close the sounder is to an adjacent surface, and C_2 is a correction for the distance from the speaker to the bed. In this case, the speaker is on the wall and close to the ceiling. Therefore,[51] C_1 is +7 dB, and C_2 is −27 dB (approximately 6.5 m from the speaker to the bed). (See Tables 4-1.16 and 4-1.17.) Therefore,

$$L_{P2} = (L + 21) + 7 - 27 \text{ dBA}$$
$$L_{P2} = L + 1 \text{ dBA}$$

To get L_{P2} = 75 dBA, L must be at least 74 dBA. The smallest and least expensive fire alarm speaker available is a 4-in. paper cone speaker. A typical speaker of this size and type, powered at 1/4 W, has an L equal to 75 dB at 3.05 m.[58] This speaker would meet the design goal in the room, without even considering any sound contribution from corridor-mounted speakers.

For the corridor speakers in Scenario B, L_{P1} is the sound pressure level at a point farthest from a speaker.

$$L_{P1} = L_W + C_3 + C_4 + C_5 \text{ dBA}$$

where C_3 and C_4 are the same as in Scenario A (−3 and −9 dB, respectively). C_5 is a function of the spacing, which is to be determined. If a single corridor speaker tapped at only 1/4 W is used, with an L of 85 dB at 3.05 m,[56]

$$L_W = L + 20 \log_{10} r + 11 \text{ dB}$$
$$L_W = 85 + 20 \log_{10} (3.05) + 11 \text{ dB}$$
$$L_W = 106 \text{ dB}$$
$$L_{P1} = 106 - 3 - 9 + C_5 \text{ dBA}$$
$$L_{P1} = 94 + C_5$$

The goal is to maintain a 65-dBA sound pressure level in the corridors (L_{P1}).

Therefore, C_5 must be −29 dBA or more for L_{P1} to be 65 dBA or higher. From Table 4-1.20,[51] it is found that distance of 50 m between source and target in the corridor could be exceeded and still meet the 65-dBA goal.

Cost Analysis

Scenario A:

For comparison purposes, assume that sufficient changes could be made to the building and alarm system to allow speakers to be mounted in the corridor only at a spacing of 3 m. A typical dormitory with about 30 bedrooms per floor requires approximately 24 speakers per floor in the corridors. In a building with seven floors, this requirement amounts to 168 speakers. At 2 W per speaker, the result would be 336 W. This setup requires three 125-W power amplifiers at an installed cost of about $1400.00 each. This amount does not include other fixed costs, such as control equipment and detectors, that are the same for each of the scenarios.

Assume each corridor unit to be a speaker/light combination. The average installed cost, including backbox, wiring back to a control panel on the first level, and conduit, would total to about $135.00 per unit. The total cost is then

$$\text{TOTAL} = (3 \times \$1400.00) + (168 \times \$140.00)$$
$$\text{TOTAL} = \$27{,}720$$

Scenario B:

In this case, there are thirty 4-in paper cone speakers per floor at an average cost of $100.00, installed. Assume a total of four speaker/light units per floor in the corridors. The calculations show that the system goals are met with only one or two units in the corridors. However, the halls may be split by smoke doors or they may be irregular in shape. Also, system reliability is increased by using more than one unit.

Each bedroom speaker and corridor speaker is powered at 1/4 W. For seven floors, this setup gives a total power requirement of 59.5 W. Therefore, one 60-W amplifier, at a unit cost of $1125.00, is needed. The total cost is then

$$\text{TOTAL} = \$1125.00 + (7 \times 30 \times \$100.00) + (7 \times 4 \times \$135.00)$$
$$\text{TOTAL} = \$25{,}905.00$$

Summary

The estimates show the relative costs of the different scenarios, not the actual costs. The real costs of the systems are affected by factors such as whether the building is new or existing. If existing, the price is affected by the extent of other renovations. Also, the estimates do not reflect the cost of other parts of the system. The balance of the system includes such items as smoke and heat detectors, equipment for elevator capture, and air handler controls.

The relative costs of the two systems in Scenarios A and B under "Cost Analysis" differ by only 7 percent. In a building of this size and type, such a small margin cannot be considered significant enough to conclude that one system is more economical than the other.

The small difference in the costs of the two systems is due to the additional cost of amplifiers needed to power the system that has only corridor units. The total number of units (corridor + room) in Scenario B is 70 more than in Scenario A. The reduced power requirement offsets the added cost of their installation.

Scenario A has a higher equipment cost but a lower installation cost than Scenario B. This result means that the relative costs of the two systems will be slightly sensitive to the type of equipment used and the cost of installation labor. By changing the figures used in the cost estimates, it can be shown that the variance is only a few percent and probably not significant.

If the building were four stories or less in height, the difference in relative cost reduces to about two percent. Again, this amount is not considered to be a significant difference.

By increasing the size of the building to twelve stories, Scenario B becomes significantly less expensive than Scenario A. Above this height, the combined use of room and corridor units becomes increasingly economically attractive.

Changing the size of each floor has about the same effect as changing the height of the building. Therefore, increasing the floor area makes Scenario B more viable. A reduction in floor area and building height does not make the corridor-only system attractive, unless the building is only a few stories in height. Then, a voice system is probably not needed. From an economics standpoint, a corridor-only horn/light system is probably best, since the cost of these units is generally less than that of speakers. Again, this conclusion assumes that sufficient changes could be made to the building design to increase the level of sound penetrating the corridor walls.

Obviously, if the sound loss from the corridor to the individual rooms is less, Scenario A starts to look better. This situation has the effect of raising the height above which Scenario B becomes significantly less expensive. However, changing construction features to reduce sound loss may reduce the passive fire resistance of the structure below an acceptable level as well as decrease the privacy level.

There are other factors to consider when choosing between different systems. In Scenario A, the quantity of speakers in the corridors and the high power levels driving each speaker (2 W each) can cause sound distortion. Voice messages may not be intelligible in the bedrooms even though there is enough sound to wake a sleeping occupant. Also, the high sound levels (106 dBA plus) in the corridors approach uncomfortable levels.

It is clear from the discussions above that a system with room speakers in conjunction with corridor units is the most desirable case. That system has the added advantage of eliminating most of the uncertainties in the design of the system. It is easier and more accurate to calculate sound levels at a point in the same room as the sound source than it is to estimate sound losses through composite walls.

This cost-benefit analysis shows that a fire alarm alerting system with units in each office or bedroom can be installed at about the same cost or less than a corridor-

only system. In addition, there is a higher confidence level that the system with the sounders in each room will perform its intended function: to awaken and alert sleeping occupants.

Designing Fire Alarm Visibility

Visual alarm notification is an important part of a fire alarm system. This visual aspect is especially important in cases where the ambient noise level is high, building occupants may be sleeping, or building occupants or their visitors may have hearing impairments. In these cases, it should be expected that the visual alarm will be required to alert occupants and initiate evacuation or relocation. As such, one first needs to determine a suitable intensity required to obtain this function.

In many cases, a suitable intensity can be obtained from regulatory documents, such as building codes, fire codes, or the Americans with Disabilities Act. These references typically give a required appliance intensity and a maximum size space that can be covered by an appliance with that intensity. If additional guidance is needed, reference can be made to appropriate documentation on alerting of persons by visual means.[57] It is also possible that a reference may cite a required level of illumination to alert someone. This requirement should not be confused with the intensity of the lamp providing the signal. The two are related by the inverse square law where E is the illumination (lumens per unit area), I is the intensity of the light source (candela), and d is the on-axis distance between the light source and the point where the illumination is measured. See Figure 4-1.13.

$$E = \frac{I}{d^2}$$

In cases where flashing signals are required, the source strength or output is cited as *effective intensity.* Effective intensity is used to equate the perceived brightness of a flashing light to that of a steady light. It can be calculated using the relationship,[58]

$$I_e = \frac{\left(\int_{t_1}^{t_2} I\,dt\right)}{(a + t_2 - t_1)} \tag{28}$$

where

I_e = effective intensity
I = instantaneous intensity
t_1 = the time (s) of the beginning of that part of the flash where I exceeds I_e
t_2 = the time (s) of the ending of that part of the flash where I exceeds I_e

In the United States, the value of 0.2 is usually used for the constant a. This relationship is shown graphically in Figure 4-1.14.

If the duration of the flash is less than one millisecond, Equation 28 can be further simplified to[58]

$$I_e = 5 \int I\,dt$$

where the integration is performed over the complete flash cycle.

As part of a test program to determine signaling applications for the hearing impaired, UL determined that an illumination of 0.398 lumens/m^2 (0.037 lumens/ft^2) as viewed on axis from a single flashing light source located in the center of one wall of a 6.1 m by 6.1 m (20 ft by 20 ft) room was the minimum required by their objective. It was also determined that, by increasing the "square" dimensions in increments of 3 m (10 ft) in both directions (length

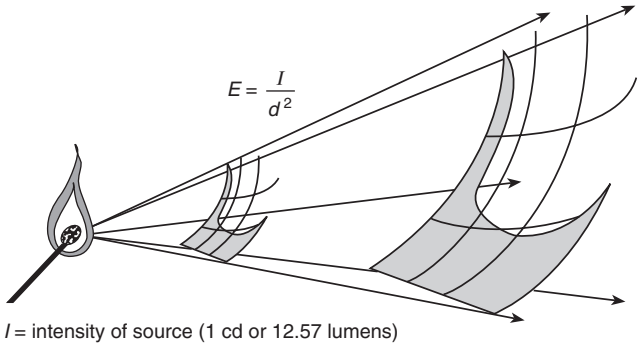

I = intensity of source (1 cd or 12.57 lumens)

E = illumination [1 lumen/ft^2 or 1 footcandle (1 lumen/m^2 or 1 lux or 0.0926 footcandle)]

d = distance from source to object (ft or m)

Figure 4-1.13. ***Relationship between intensity of lamp and level of illumination required to alert someone.***

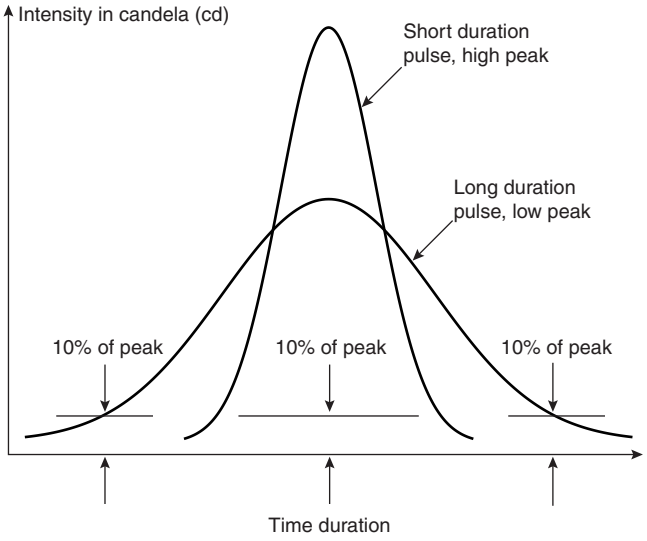

Figure 4-1.14. ***Peak versus effective intensity. (Source: R.P. Schifiliti Associates, Inc., Reading, MA)***

and width), the minimum illumination value of 0.398 lumens/m^2 could be used to extrapolate the required signal intensity as the room size increased.

For example, if the room size were increased to 12.2 m by 12.2 m (40 ft by 40 ft), the effective intensity, cd eff, of the flashing strobe signal could be determined using the inverse square law and solving for *I:*

$$E = \frac{I}{d^2}\text{; therefore}$$

$$I = Ed^2 = (0.398 \text{ lumens/m}^2)(12.2 \text{ m}^2) = 59.2 \text{ candela}$$

Thus, one signal rated at 60 cd eff would be sufficient for the space. Using the same approach, but smaller squares, one would also find that two signals rated at 30 cd eff, or four signals rated at 15 cd eff each, would also be applicable.

Designers should check with the authority having jurisdiction or the current edition of NFPA 72 regarding the use of multiple flashing lights.

EXAMPLE 22:

The design objective is to evaluate the visual alarm notification system installed in a large open space for suitability in providing signals for the hearing impaired. The space is 21 m (70 ft) by 37 m (120 ft), with a 6.5-m (20-ft) ceiling height. The notification appliances are located 2 m (6.5 ft) above floor level and are spaced as shown in Figure 4-1.15. The signals are rated at 45 cd eff each. Is the required illumination of 0.398 lumens/m^2 currently provided?

SOLUTION:

The first step is to section off the space into blocks that are anticipated to be covered for each signal. In this case, the result is six blocks, each 12.2 m (40 ft) long by 10.5 m (34 ft) wide. This step is illustrated in Figure 4-1.16.

Given these dimensions, one could calculate the illumination at point A, where

$$E = \frac{45 \text{ cd}}{(10.5 \text{ m})^2} = 0.41 \text{ lumens/m}^2$$

This is greater than the minimum required illumination of 0.398 lumens/m^2. However, application of this method requires the blocks of coverage by a signal to be square, with the lateral distance (90 degrees) being equal to one-half the coverage distance on-axis. In this case, the lateral distance is 12.2 m (40 ft), and this is the figure that should be used to calculate the illumination throughout the entire block. In doing this, one finds that the illumination provided is

$$E = \frac{45 \text{ cd eff}}{(12.2 \text{ m})^2} = 0.29 \text{ lumens/m}^2$$

which is below the minimum required 0.398 lumens/m^2. This outcome results in areas of the space not having the required illumination. This outcome is illustrated in Figure 4-1.17.

To determine what intensity is required for the signals in order to provide the required 0.398 lumens/m^2, the inverse square law can be applied using the value $d = 12.3$ m. This application results in a required incident intensity of 60 cd eff for each existing signal location.

By applying this method of dividing spaces into squares and applying the inverse square law, the intensity of signals and their required spacing can be calculated for spaces of any shape and size. Tradeoffs can be made between the number of signals and the intensity of signals to best fit the application (e.g., one signal of 60 cd eff versus four properly spaced signals of 15 cd eff each).

In cases where a minimum required illumination at all points in a space is specified (as opposed to the minimum effective intensity on-axis within a square), the illumination can be calculated using the inverse square law, the cosine law, and the cosine cubed law. In this case, the inverse square law provides the illumination on-axis, application of the cosine law provides the illumination at a perpendicular surface within the same plane as the signal, and application of the cosine cubed law provides the illumination at parallel surfaces within the same plane as the signal.

With this information, it should be possible to calculate visual fire alarm signals for most situations. In all cases, a value for the required effective intensity at some point within the room is required. If not provided at the beginning of the design process, one should determine an effective intensity based on the specific application and the condition of the occupants being alerted.

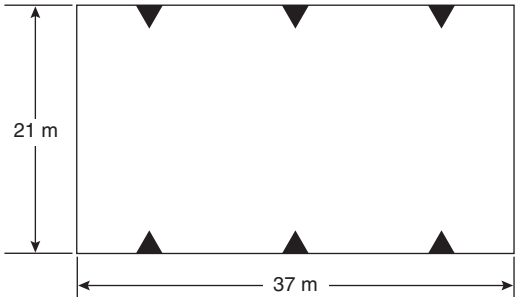

Figure 4-1.15. ***Notification appliance* (▲) *locations.***

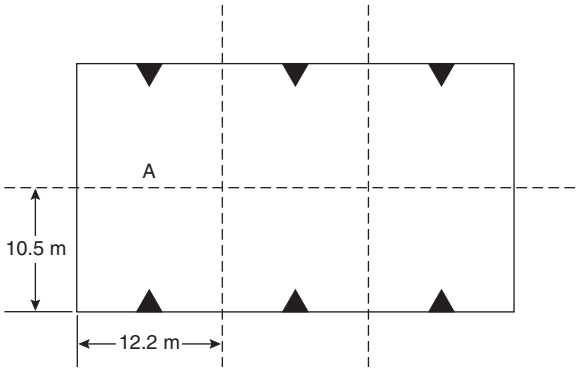

Figure 4-1.16. ***Sections for anticipated signal* (▲) *coverage.***

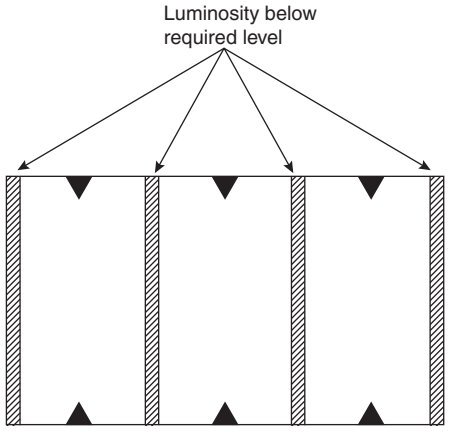

Figure 4-1.17. ***Diagram of subadequate luminosity intensity.***

Nomenclature

α	fire intensity coefficient (Btu/s^3 or kW/s^2)
A	area (m^2 or ft^2)
A	$g/(C_pT_a\rho_0)$ [m^4/(s^2·kJ) or ft^4/(s^2·Btu)]
c	specific heat of detector element [Btu/(lbm·R) or kJ/(kg·K)]
C_p	specific heat of air [Btu/(lbm·R) or kJ/(kg·K)]
d	diameter of sphere or cylinder (m or ft)
D	$0.188 + 0.313\ r/H$
Δt	change in time (s)
ΔT	increase above ambient in temperature of gas surrounding a detector (°C or °F)
ΔT_d	increase above ambient in temperature of a detector (°C or °F)
ΔT_p^*	change in reduced gas temperature
f	functional relationship
g	functional relationship
g	gravitational constant (m/s^2 or ft/s^2)
h_c	convective heat transfer coefficient [kW/(m^2·°C) or Btu/(ft^2·s·°F)
H	ceiling height or height above fire (m or ft)
ΔH_c	heat of combustion (kJ/mol)
H_f	heat of formation (kJ/mol)
L_P	sound pressure level
L_W	sound power level
m	mass (lbm or kg)
p	positive exponent
$\dot{q}$	heat release rate (Btu/s or kW)
$\dot{q}_{cond}$	heat transferred by conduction (Btu/s or kW)
$\dot{q}_{conv}$	heat transferred by convection (Btu/s or kW)
$\dot{q}_{rad}$	heat transferred by radiation (Btu/s or kW)
$\dot{q}_{total}$	total heat transfer (Btu/s or kW)
$\dot{Q}$	heat release rate (Btu/s or kW)
$\dot{Q}_{cr}$	critical heat release rate
$\dot{Q}_{do}$	design heat release rate
$\dot{Q}_i$	ideal heat release rate
$\dot{Q}_p$	predicted heat release rate (Btu/s or kW)
$\dot{Q}_T$	threshold heat release rate at response (Btu/s or kW)
r	radial distance from fire plume axis (m or ft)
ρ_0	density of ambient air (kg/m^3 or lb/ft^3)
Re	Reynolds number
RTI	response time index (m$^{1/2}$·s$^{1/2}$ or ft$^{1/2}$·s$^{1/2}$)
S	spacing of detectors or sprinkler heads (m or ft)
t	time (s)
t_c	critical time—time at which fire would reach a heat release rate of 1000 Btu/s (1055 kW) (s)
t_r	response time (s)
t_v	virtual time of origin (s)
t_{2f}	arrival time of heat front (for $p = 2$ power-law fire) at a point r/H (s)
t_{2f}^*	reduced arrival time of heat front (for $p = 2$ power-law fire) at a point r/H (s)
t_p^*	reduced time
T	temperature (°C or °F)
T_a	ambient temperature (°C or °F)
T_d	detector temperature (°C or °F)
T_g	temperature of fire gases (°C or °F)
T_s	rated operating temperature of a detector or sprinkler (°C or °F)
U	velocity (m/s)
u	instantaneous velocity of fire gases (m/s or ft/s)
u_0	velocity at which τ_0 was measured (m/s or ft/s)
u_p^*	reduced gas velocity
v	kinematic viscosity (m^2/s or ft^2/s)
x	vectorial observation point (m or ft)
Y	defined in Equation 27
τ	detector time constant—$mc/(hA)$ (s)
τ_0	measured at reference velocity u_0 (s)

References Cited

1. C. Mulliss and W. Lee, "On the Standard Rounding Rule for Multiplication and Division," *Chinese Journal of Physics,* 36, 3, pp. 479–487 (1998).
2. W. Lee, C. Mulliss, and H.-C. Chiu, "On the Standard Rounding Rule for Addition and Subtraction," *Chinese Journal of Physics,* 38, 1, pp. 36–41 (2000).
3. R. Custer, "Selection and Specification of the 'Design Fire' for Performance-Based Fire Protection Design," in *Proceedings, SFPE Engineering Seminar,* Phoenix, AZ, Society of Fire Protection Engineers, Boston (1993).
4. R. Custer, B. Meacham, and C. Wood, "Performance-Based Design Techniques for Detection and Special Suppression Applications," in *Proceedings of the SFPE Engineering Seminars on Advances in Detection and Suppression Technology,* San Francisco, Society of Fire Protection Engineers, Boston (1994).
5. SFPE Engineering Guide to Performance-Based Fire Protection. Society of Fire Protection Engineers. Published by National Fire Protection Association, Quincy, MA (2000).
6. R. Custer and R. Bright, "Fire Detection: The State-of-the-Art," *NBS Tech. Note 839,* National Bureau of Standards, Washington, DC (1974).

7. UL 521, *Standard for Safety Heat Detectors for Fire Protective Signaling Systems,* Underwriters Laboratories Inc., Northbrook, IL (1993).
8. NFPA 72, *National Fire Alarm Code,* NFPA, Quincy, MA (1999).
9. G. Heskestad and H. Smith, *FMRC Serial Number 22485,* Factory Mutual Research Corp., Norwood, MA (1976).
10. J.P. Hollman, *Heat Transfer,* McGraw-Hill, New York (1976).
11. W. Bissell, "An Investigation into the Use of the Factory Mutual Plunge Tunnel and the Resulting RTI for Fixed Temperature Fire Detectors," Master's Thesis, Worcester Polytechnic Institute, Worcester, MA (1988).
12. M. Kokkala, "Thermal Properties of Heat Detectors and Sprinklers," *Nordtest Brand Symposium,* Boras, Sweden (1986).
13. R.P. Schifiliti and W.E. Pucci, "Fire Detection Modeling: State of the Art," The Fire Detection Institute, Bloomfield, CT (1996).
14. "Discussion of a New Principle in Fire Detection, Rate Compensation," Fenwal, Inc., Ashland, MA (1951).
15. C. E. Marrion, "Lag Time Modeling and Effects of Ceiling Jet Velocity on the Placement of Optical Smoke Detectors," Master's Thesis, Worcester Polytechnic Institute, Center for Firesafety Studies, Worcester, MA (1989).
16. R. Alpert, *Fire Tech.,* 8, p. 3 (1972).
17. L.Y. Cooper, "Interaction of an Isolated Sprinkler and a Two Layer Compartment Fire Environment," National Institute of Standards and Technology, Gaithersburg, MD (1991).
18. M. Delichatsios and R. L. Alpert, "Calculated Interaction of Water Droplet Sprays with Fire Plumes in Compartments," *NBS-GCR 86-520,* Center for Fire Research, National Bureau of Standards, Washington, DC (1986).
19. G. Heskestad, "Sprinkler/Hot Layer Interaction," *NIST-GCR 91-590,* National Institute of Standards and Technology, Gaithersburg, MD (1991).
20. D.D. Evans and D.W. Stroup, "Methods to Calculate the Response Time of Heat and Smoke Detectors Installed Below Large Unobstructed Ceilings," *NBSIR 85-3167,* National Bureau of Standards, Gaithersburg, MD (1985).
21. G. Heskestad and M.A. Delichatsios, "The Initial Convective Flow in Fire," *17th Symposium on Combustion,* Combustion Institute, Pittsburgh, PA (1978).
22. G. Heskestad and M.A. Delichatsios, "Environments of Fire Detectors—Phase I: Effect of Fire Size, Ceiling Height, and Material," Volume I: "Measurements" (NBS-GCR-77-86), (1977), Volume II: "Analysis" (NBS-GCR-77-95), National Technical Information Service (NTIS), Springfield, VA (1977).
23. R.P. Schifiliti, "Use of Fire Plume Theory in the Design and Analysis of Fire Detector and Sprinkler Response," Master's Thesis, Worcester Polytechnic Institute, Center for Firesafety Studies, Worcester, MA (1986).
24. D.W. Stroup, D.D. Evans, and P. Martin, *NBS Special Publication 712,* National Bureau of Standards, Gaithersburg, MD (1986).
25. *SFPE Handbook of Fire Protection Engineering,* NFPA, Quincy, MA (1988 and 1995).
26. NFPA 72, *National Fire Alarm Code,* NFPA, Quincy, MA, 1984 through 1996 editions.
27. G. Heskestad and M. Delichatsios, "Update: The Initial Convective Flow in Fire," *Fire Safety Journal,* 15, pp. 471–475 (1989).
28. C. Beyler, personal communication (1985).
29. C. Beyler, "A Design Method for Flaming Fire Detection," *Fire Technology,* 20, 4, pp. 9–16 (1984).
30. J.R. Lawson, W.D. Walton, and W.H. Twilley, *NBSIR 83-2787,* National Bureau of Standards, Washington, DC (1983).
31. B.J. Meacham, "Characterization of Smoke from Burning Materials for the Evaluation of Light Scattering-Type Smoke Detector Response," Master's Thesis, Worcester Polytechnic Institute, Center for Firesafety Studies, Worcester, MA (1991).
32. B.J. Meacham and V. Motevalli, "Characterization of Smoke from Smoldering Combustion for the Evaluation of Light Scattering-Type Smoke Detector Response," *J. of Fire Protection Engineering, SFPE,* 4, 1, p. 17 (1992).
33. UL 268, *Standard for Safety Smoke Detectors for Fire Protective Signaling Systems,* Underwriters Laboratories, Inc., Northbrook, IL (1989).
34. G. Mulholland, "Smoke Production and Properties," *SFPE Handbook of Fire Protection Engineering,* 2nd ed., Quincy, MA (1995).
35. J. Hoseman, "Uber Verfahren zur Bestimmung der Korngrossenverteilung Hokkonzentrierter Polydispersionen von MiePartikeln," Ph.D. Thesis, Aachen, Germany (1970).
36. C.D. Litton, "A Mathematical Model for Ionization Type Smoke Detectors and the Reduced Source Approximation," *Fire Technology,* 13, 4, pp. 266–281 (1977).
37. R.W. Bukowski and G.W. Mulholland, "Smoke Detector Design and Smoke Properties," TN 973, U.S. Department of Commerce, National Bureau of Standards, Washington, DC (1978).
38. C. Helsper, H. Fissan, J. Muggli, and A. Scheidweiler, "Verification of Ionization Chamber Theory," *Fire Technology,* 19, 1, p. 14 (1983).
39. J. Newman, "Modified Theory for the Characterization of Ionization Smoke Detectors," in *Fire Safety Science—Proceedings of the Fourth International Symposium,* International Association for Fire Safety Science, Ottawa, Ontario (1994).
40. G. Heskestad, "Generalized Characteristics of Smoke Entry and Response for Products-of-Combustion Detectors," in *Proceedings, 7th International Conference on Problems of Automatic Fire Detection,* Rheinish-Westfalischen Technischen Hochschule, Aachen, Germany (1975).
41. M. Kokkala et al., "Measurements of the Characteristic Lengths of Smoke Detectors," *Fire Technology,* 28, 2, p. 99 (1992).
42. J. Bjorkman, O. Huttunen, and M. Kokkala, "Paloilmaisimien toimintaa kuvaavat laskentamallit (Calculation Models for Fire Detector Response)," *Research Notes 1036,* Technical Research Center of Finland (1989).
43. A. Oldweiler, "Investigation of the Smoke Detector L Number in the UL Smoke Box," Master's Thesis, Worcester Polytechnic Institute, Worcester, MA (1995).
44. M.A. Delichatsios, "Categorization of Cable Flammability, Detection of Smoldering, and Flaming Cable Fires," Interim Report, Factory Mutual Research Corporation, Norwood, MA (1980).
45. NFPA 92B, *Guide for Smoke Management Systems in Malls, Atria, and Large Areas,* NFPA, Quincy, MA (1991).
46. G. Heskestad, *FMRC Serial Number 21017,* Factory Mutual Research Corp., Norwood, MA (1974).
47. E.L. Brozovsky, "A Preliminary Approach to Siting Smoke Detectors Based on Design Fire Size and Detector Aerosol Entry Lag Time," Master's Thesis, Worcester Polytechnic Institute, Center for Firesafety Studies, Worcester, MA (1991).
48. S. Deal, "Technical Reference Guide for FPEtool Version 3.2," *NISTIR 5486,* National Institute for Standards and Technology, Gaithersburg, MD (1994).

49. G. Heskestad and M.A. Delichatsios, "Environments of Fire Detectors, Phase I: Effects of Fire Size, Ceiling Heights, and Material," Volume II, *Analysis Technical Report Serial Number 11427,* RC-T-11, Factory Mutual Research Corp., Norwood, MA (1977).
50. K.B. Ginn, *Architectural Acoustics,* Bruel and Kjaer (1978).
51. H. Butler, A. Bowyer, and J. Kew, "Locating Fire Alarm Sounders for Audibility," Building Services Research and Information Association, Bracknell, UK (1981).
52. E.H. Nober, H. Pierce, A. Well, and C.C. Johnson, *NBS-GCR-83-284,* National Bureau of Standards, Washington, DC (1980).
53. M.J. Kahn, "Detection Times to Fire-Related Stimuli by Sleeping Subjects," *NBS-GCR-83-435,* National Bureau of Standards, Washington, DC (1983).
54. *British Standard Code of Practice CP3,* British Standards Institution, London (1972).
55. C. Davis and D. Davis, *Sound System Engineering,* Howard H. Sams and Co., Inc., Indianapolis, IN (1975).
56. *Product Catalog,* Fire Control Instruments, Newton, MA (1986).
57. UL 1971, *Standard for Safety Signaling Devices for the Hearing Impaired,* Underwriters Laboratories, Inc., Northbrook, IL (1992).
58. "Nomenclature and Definitions for Illuminating Engineering," *IES RP-16-1987,* Illuminating Society of North America, New York (1987).

Additional Reading

V. Babrauskas, J.R. Lawson, W.D. Walton, and W.H. Twilley, *NBSIR 82-2604,* National Bureau of Standards, Washington, DC (1982).

CHAPTER 2

Hydraulics

John J. Titus

Introduction

Hydraulics may be regarded as the application of knowledge about how fluids behave to the solution of practical problems in fluid flow. It is generally held to describe the behavior and effects of water in motion in both closed conduits and open channels. In the field of fire protection we are concerned primarily with the closed conduit flow regime. In this chapter we will restrict our discussion to the behavior and properties of water flowing in pipes as the phenomenon of paramount interest.

Fluid Statics

Physical Properties of Fluids

Solution of any flow problem requires a basic knowledge of the physical properties of the fluid being considered. A brief description of the most basic properties follows.

1. Density: $\rho = \frac{m}{V}$

The density of a fluid is the mass of the fluid per unit volume, expressed in SI units as kg/m^3 and in English, or U.S. customary, units as slugs/ft^3 (or lbf·s^2/ft^4). The density of water at 4°C (~40°F) is 1000 kg/m^3 (1.94 lbf·s/ft^4).

2. Specific weight: $\gamma = \rho g$

As the representation of the force exerted by gravity on a unit volume of fluid, specific weight takes on units of weight per unit volume. At 4°C, the specific weight of water is 9.81 kN/m^3 (62.4 lb/ft^3).[1]

John J. Titus, P.E., is a former research associate at the Center for Fire-safety Studies at Worcester Polytechnic Institute, Worcester, Massachusetts. He has been active in engineering design and contracting of fire suppression and detection systems since 1971. Mr. Titus is a partner in MBS Fire Technology, Inc., a fire protection engineering consulting firm based in central Massachusetts.

3. Specific gravity (relative density): Specific gravity is the ratio of a liquid's density or specific weight to that of water at 4°C.

4. Viscosity: The term *viscosity* refers to a proportionality constant in the equation relating cross-sectional velocity variations (or rate of fluid deformation) to shear stresses developed in the fluid flow. (See the section of this chapter titled "Fluid Energy Losses in Pipe Flows.") Viscosity can be considered a measure of a fluid's resistance to deformation or shear or, alternatively, its readiness to flow when acted upon by an external force. In engineering analyses it is useful to think of viscosity as a momentum diffusivity term.

Viscosity is commonly expressed in one of two forms: absolute (or dynamic) viscosity, μ, which is the proportionality constant referred to above, or kinematic viscosity, ν, which is related to the absolute viscosity by the equality

$$\nu = \frac{\mu}{\rho}$$

A wide variety of units is used to express viscosity, depending not only on U.S. customary or SI formulations but also on older English and metric conventions as well as on the type of instrument used to measure this fluid property. A unit based on the c.g.s. (centimeter, gram, second) convention of the old metric system has gained wide favor in the representation of absolute viscosity. This unit, called the *poise*, has dimensions of dyne·seconds per square centimeter or grams per centimeter·second. The centipoise, which equals 0.01 poise, is the form of preference since the viscosity of water at 20°C (68°F) equals one centipoise to a very close approximation. In the English system the unit of viscosity is pound-seconds per square foot. One lb·s/ft^2 equals 478.8 poise.

5. Fluid pressure: Pressure is a force per unit area that arises when a fluid is subjected to a compressive stress. Units may be Newtons/m^2, lb/ft^2, lb/in.^{2}, or the equiva-

lent. Pascal's law states that the pressure in a fluid at rest is the same in all directions, a condition different from that for a stressed solid where the stress on a plane depends upon the orientation of that plane. For an infinitesimal fluid element in a larger static body of fluid, a free body diagram of the vertical forces may be drawn as in Figure 4-2.1. The pressure difference $[(p + dp) - p]$ is due only to the weight of the fluid element. Since the weight of the element is given by $mg = \rho g\, dz\, dA$, a summing of forces in the vertical direction gives

$$dp\, dA = -\rho g\, dz\, dA \tag{1a}$$

$$dp = -\rho g\, dz \tag{1b}$$

In integral form, Equation 1b becomes

$$\int_1^2 \frac{dp}{\rho g} = -\int_1^2 dz = -(z_2 - z_1) \tag{2}$$

where the path endpoints 1 and 2 refer to different elevation levels.

To integrate Equation 2, it is necessary to establish a functional relation between pressure p and the term ρg. Where density varies with pressure, the fluid is considered compressible, and the functional relation may be complex. For fluids that may be considered incompressible, such as water, ρ is a constant at any specified temperature. Equation 2 then becomes

$$p_2 - p_1 = -\rho g(z_2 - z_1) \tag{3}$$

The term $(z_2 - z_1)$ may be called a static *pressure head,* which can be expressed in feet, inches, or meters of water, or some height unit of any liquid. A simplified form of Equation 3 is often written

$$\rho = \gamma h \tag{4}$$

where h = elevation of the column of liquid above a reference surface (i.e., $z_2 - z_1$). For water at 60°F (15.6°C), γ is taken equal to 62.4 lb/ft^3 (16.02 kg/m^3). The pressure corresponding to a head of h feet, then, is $0.433h$ lb/in.^{2} (psi), or approximately 3 kPa per meter elevation. The head corresponding to a pressure of one psi (0.07 bar) is, inversely, 2.3 ft (0.7 m). Note that Equation 4 is valid only for a homogeneous, noncompressible fluid at rest, and that regardless of the shape of the container, points in the same horizontal plane experience the same pressure.

The vertical distance h is termed the *head* of a fluid. A pressure due only to the weight of a column of fluid is called a static pressure and can be measured by a standard Bourdon-type gage (see Figure 4-2.4). Such a measure is generally referred to as gage pressure. The term *absolute pressure* takes into account the pressure exerted by the atmosphere as well, which at sea level is approximately 14.7 psi (1 bar), equivalent to a 33.9-ft- (10.3-m-) high column of water. A pressure less than atmospheric is called a vacuum pressure, a perfect vacuum being zero absolute pressure. Since most fluid properties of interest are not significantly affected by small changes in atmospheric pressure, most fluids calculations are in terms of gage pressure, although this fact is not often indicated in standard calculation nomenclature. When they are explicitly identified, gage pressure is denoted by the term psig and absolute pressure by psia. If not stated otherwise, psi may be taken to designate gage pressure.

Pressure Measuring Devices

1. Manometer tube: Pressure measurement in a manometer tube is obtained by measuring the vertical displacement of a relatively heavy fluid (usually mercury), which will rise a smaller vertical distance than water in proportion to the ratio of its specific weight to that of water. Depending on the actual arrangement of the manometer tubing, a gage equation can be written to solve for the pressure head. For the manometer shown in Figure 4-2.2, the gage equation is written by proceeding from the open

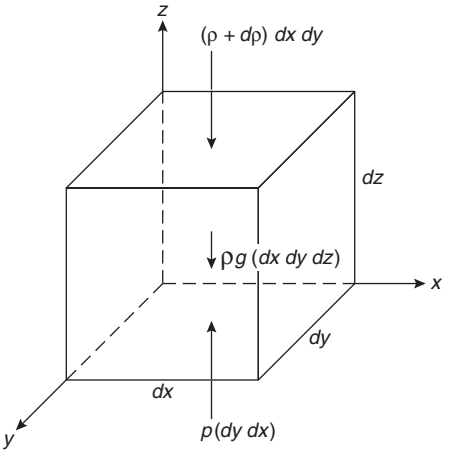

Figure 4-2.1. ***Notation for basic equation of fluid statics.***

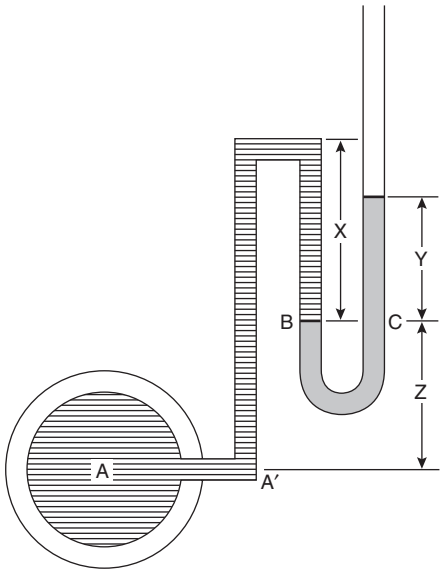

Figure 4-2.2. ***Manometer.***

end through the tube to point A', adding terms when descending a column and subtracting when ascending. Using mercury as the manometer fluid, we can write

$$(y + z)\gamma_{Hg} - z\gamma_{Hg} - x\gamma + (x + z)\gamma = p_A \qquad (5)$$

Combining terms, generalizing the result, and expressing in terms of feet of water (head),

$$\frac{P_A}{\gamma} = ys + z \qquad (6)$$

where s is the specific gravity of the manometer fluid.

2. Piezometer tube (Figure 4-2.3): Literally a *pressure measuring tube,* a piezometer consists essentially of a narrow tube rising from a container enclosing a fluid under pressure. Through the relation among pressure, height, and specific weight, the height to which the fluid rises in the tube represents the pressure of the contained fluid. While useful for some laboratory work, piezometer tubes are not generally feasible in practical applications.

3. Bourdon gauge (Figure 4-2.4): The standard pressure measuring device used in a wide variety of fluid pressure measurement applications is the Bourdon gauge. The gauge contains a curved tube of elliptical cross section that undergoes a change in curvature with change in pressure. A dial hand, connected to the inner tube through a linkage system, indicates gauge pressure on a numerical dial face. Bourdon gauges are factory calibrated and reasonably accurate instruments if not damaged by pressure surge or impact force. A field reading, unless known to be correct, cannot be assumed to be accurate and should be checked by independent means.

Forces on Submerged Plane Areas Due to Fluid Pressure

It is sometimes of interest to determine the magnitude of the resultant force on a submerged area and the location of the center of pressure where the resultant force

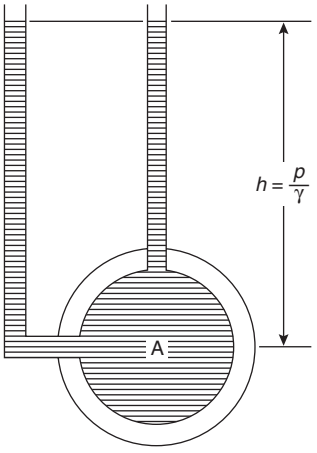

Figure 4-2.3. ***Piezometer.***

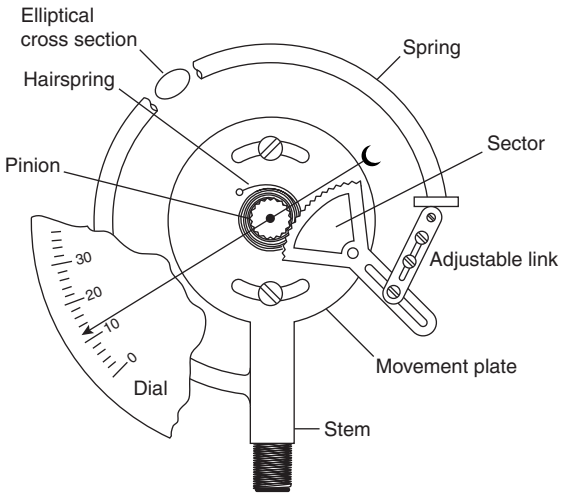

Figure 4-2.4. ***Standard Bourdon gauge.***

can be assumed to act. Consider the following example of a tank that has a rectangular window in an inclined wall (Figure 4-2.5). The magnitude of the resultant force can be determined from

$$F_R = \gamma h_c A \qquad (7)$$

The center of pressure of the area is the point at which the resultant force can be considered to act. Its location is determined from the relation

$$l_p = l_c + \frac{I}{l_c A} \qquad (8)$$

where I = the moment of inertia of the area about its centroidal axis.

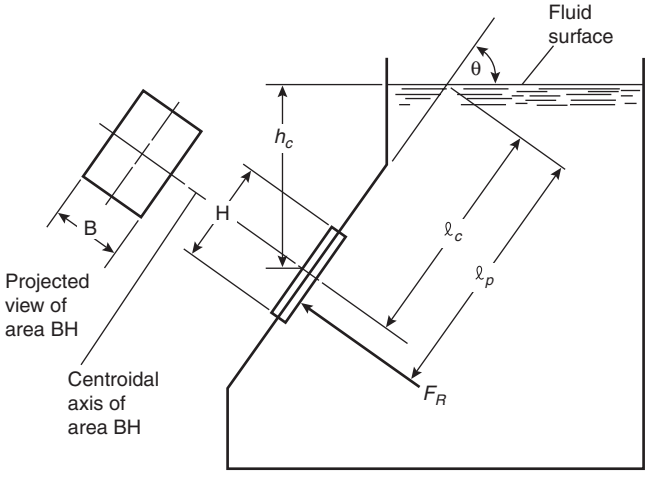

Figure 4-2.5. ***Tank with a rectanglar window in an inclined wall.***

For a vertical wall, the center of pressure is located at a distance $d/3$ from the bottom (where d is the total depth below the free surface), and at a distance $l/3$ from the bottom of an inclined wall or area (where l is the length of the face of the wall).

Conservation Laws in Fluid Flows

Fluid flow may be characterized as uniform or nonuniform, steady or unsteady, compressible or incompressible, laminar or turbulent, rotational or irrotational, and one-, two-, or three-dimensional or some combination thereof. Real flows may be modeled as approximations of ideal flows when real properties do not depart significantly from the ideal characteristics defined by these terms.

For example, uniform flow occurs when the average velocity of a fluid does not change in either magnitude or direction anywhere along the flow path. Thus, liquid flow in a constant head pipeline of unchanging diameter is considered uniform flow. Steady flow, on the other hand, is determined with reference to a stationary point in the flow path. For steady flow to occur, the velocity of flow at that point must remain constant with time. This condition implies that the fluid density, the pressure head, and the volume rate of flow also are invariant with time. Thus, liquid flow in a constant head pipeline of varying diameter may be considered steady, nonuniform flow. It is important to note that a flow may be considered uniform (no change in magnitude or direction of the velocity) in a curved pipeline as long as the reference direction of the velocity vector is taken in the direction of the flow. We can then say that the velocity of the fluid does not change direction with respect to its enclosing boundaries.

We can also consider this flow one-dimensional whenever it is permissible to say that velocities or accelerations normal to the general direction of the flow are negligible. Clearly, real flow in a real-world structure has three dimensions, but a one-dimensional analysis is highly desirable as it represents a considerable mathematical simplification. Fortunately, a very large number of practical engineering flow problems involving water can be modeled as one-dimensional, steady flow problems, particularly many pipeline flows. In such cases it is possible to apply basic physical principles of conservation of mass and conservation of energy in the direction of flow to obtain the energy balance at any point in the flow. In fire flow hydraulics, it is common practice to introduce additional simplifying assumptions, such as the requirements that the fluid be incompressible and that flow properties be invariant with temperature and pressure. It then follows directly that with no flow additions or subtractions, the volumetric flow rate at any point in a fluid stream must be a constant. This statement of mass conservation, known as the equation of continuity, can be expressed mathematically as

$$\rho_1 A_1 v_1 = \rho_2 A_2 v_2 = \text{constant} \tag{9}$$

If the fluid is considered incompressible, as is the case with water, Equation 9 becomes

$$A_1 v_1 = A_2 v_2 = \text{constant} = Q \tag{9a}$$

By applying the principal of conservation of energy to a flowing fluid, an expression can be derived that gives the theoretical net energy balance of the fluid at any point along its flow path. This is known as the Bernoulli equation, which can be written as

$$\frac{p_1}{\gamma} + \frac{v_1^2}{2g} + z_1 = \frac{p_2}{\gamma} + \frac{v_2^2}{2g} + z_2 \tag{10}$$

In this form, units are ft lb/lb of fluid or, simply, ft of fluid. Each term thus represents a fluid head. Multiplying each term by the specific weight, γ, converts the equation to units of pressure. Changes in internal energy of the fluid are ignored and are assumed to be negligible. The form of Equation 10 suggests that the flow of liquid (or transport of fluid energy) results from three principal causes: pressure difference, gravity, and inertia. Equation 10 expresses an ideal condition fulfilled by the three components of head corresponding to these three causes. The assumption of incompressibility (i.e., constant density) requires that the product of the velocity of flow and the cross-sectional area of the flow of any conserved portion of the stream be constant; the ideal flow streamlines, therefore, converge as the velocity increases and diverge as the velocity decreases. If it could be assumed that the total Bernoulli head were, indeed, constant or, equivalently, if it were possible to obtain total head simply as a function of the coordinates of the moving fluid element, then many hydrokinetic problems could be solved theoretically by mathematically manipulating and extrapolating the Bernoulli equation. Unfortunately, this is not the case. Other energy transfers are possible, and these require use of a more general form of the equation. In addition to the pressure, velocity, and position (elevation) energies possessed by the fluid at sections 1 and 2, energy may be added to the fluid (work done on the fluid by a pump), lost by the fluid (through friction), or extracted from the fluid (work done by the fluid). Therefore, we write the Bernoulli energy conservation expression in the more general form

$$\underbrace{\left(\frac{p_1}{\gamma} + \frac{v_1^2}{2g} + z_1\right)}_{\text{Energy at Section 1}} + \underbrace{h_A}_{\text{Energy Added}} - \underbrace{h_L}_{\text{Energy Lost}} - \underbrace{h_E}_{\text{Energy Extracted}} = \underbrace{\left(\frac{p_2}{\gamma} + \frac{v_2^2}{2g} + z_2\right)}_{\text{Energy at Section 2}} \tag{10a}$$

EXAMPLE 1:

Water flows from a reservoir through a pipeline as shown in the following diagram. The flow is considered frictionless and discharges freely at point *C*.

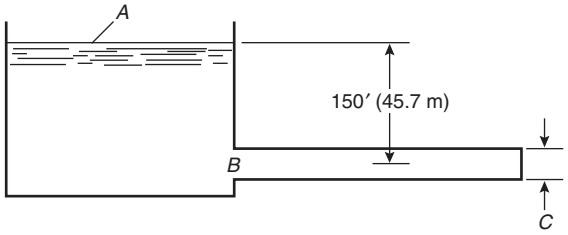

(a) What is the total head (total specific energy) at point *B?*

(b) What is the discharge velocity at point *C?*

SOLUTION:

(a) At *A*, both the velocity and gage pressures are considered to be zero. By Bernoulli, then, the total head would be written as

$$h_A = 0 + 0 + 150 \text{ ft} = 150 \text{ ft}$$

or, in SI unit equivalents,

$$h_A = 0 + 0 + 45.7 \text{ m} = 45.7 \text{ m}$$

At *B*, the fluid has a nonzero velocity head and is under hydrostatic pressure. As long as we consider the flow frictionless, the total head is constant. Therefore,

$$h_B = h_A = 150 \text{ ft (45.7 m)}$$

(b) At *C*, the pressure head is again zero, since the discharge is at atmospheric pressure. Once more by Bernoulli,

$$h_C = 0 + \frac{v^2}{2g} + 0$$

$$v^2 = 2(32.2)(150)$$

$$v = 98.3 \text{ ft/s}$$

or, in SI unit equivalents,

$$v^2 = 2(9.81)(45.7)$$

$$v = 29.9 \text{ m/s}$$

Note that we could calculate the actual values of the pressure and velocity heads at point *B* if we had more information about the system. For example, we could determine $\dot{Q}$, the discharge at point *C*, knowing the area and type of discharge opening (see the section of this chapter titled "Free Discharge at an Opening"). This determination is simply an application of the continuity equation. Knowing the pipeline diameter at point *B* allows us to apply continuity constraints once again to calculate v_B from which the velocity head may be determined. The pressure head at *B* is simply a function of the weight of the vertical column of water.

The components of the Bernoulli equation may be expressed graphically in terms of energy levels existing at any points in the flow regime. In Figure 4-2.6 a simple system representing a realistic flow is shown. Water flows from a reservoir (with presumed constant surface elevation) to atmosphere. The flow is accompanied by losses of energy represented by h_L. The losses may occur in many places such as at valves, bends, and sudden changes in pipe diameter. Generally, the most important loss is that due to friction between the moving fluid and the pipe wall. Since there are always energy losses in real flows, the total energy of the system decreases in the direction of flow. The line connecting all points representing the total energy is called the *energy gradient* (EG). It must always decrease in the direction of flow unless energy is added to the system, such as by a pump. The *hydraulic gradient* (HG) connects the points representing the sum of static pressure and elevation energies (i.e., the heights to which water in piezometer tubes would rise). Note that the hydraulic gradient may increase in the direction of flow if velocity head is converted to pressure head at any point (such as at an increase in pipe diameter). Thus, the relationship between the energy and hydraulic gradients can be written as

$$\text{EG} = \text{HG} + \frac{v^2}{2g} \tag{11}$$

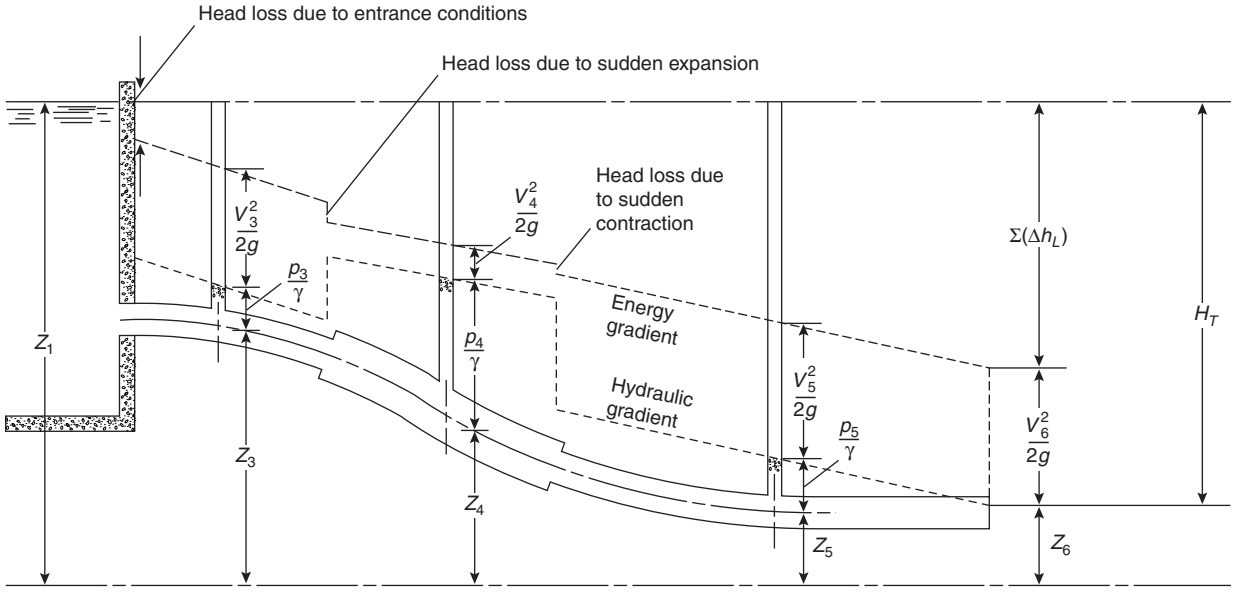

Figure 4-2.6. ***Realistic flow characteristics.***

Fluid Energy Losses in Pipe Flows

General Considerations

That part of hydraulics which treats fluid energy losses due to friction in piping is well known and well utilized in fire protection engineering. Losses to friction are due to shear stresses set up within a moving fluid in a conduit by an imposed pressure gradient. Flow driven by the pressure force is restrained by drag forces acting at the conduit wall. To better visualize this phenomenon, it is useful to introduce the concept of the boundary layer. For many fluids, such as air or water, motion through a stationary conduit or pipe is characterized in most practical situations by a nearly constant velocity cross section everywhere except in a very thin layer near the wall of the pipe. This layer thickness may be as little as 0.1 mm but may vary significantly with the nature of the fluid, the velocity of flow, and the surface roughness of the conduit. We may visualize boundary layer flow (see Figure 4-2.7) in terms of a velocity profile. Theory* holds that a very thin (molecular) layer of fluid sticks to the conduit wall. The tendency of the next fluid layer to move due to an imposed force creates a shearing stress, τ, between the layers. If the boundary is thought of as many fluid lamina sliding on each other, then we can expect the velocities of these lamina to increase with distance y from the wall until, at the edge of the boundary layer, the local velocity reaches the free-stream velocity of the fluid. The factor relating the velocity profile to the developed stress in the fluid is termed the fluid viscosity. The relationship was expressed mathematically by Newton as

$$\tau = \mu \frac{du}{dy} \tag{12}$$

The smaller the value of fluid viscosity, the thinner the boundary layer will be. The first layer of fluid sticks or adheres to the surface of the conduit while lamina above it successively slide on each other, exerting drag forces that, for most fluids, are proportional to the viscosity (so-called Newtonian fluids). The rate of change of the velocity between successive lamina is a measure of the unit shearing force between them. A curve joining the tips of velocity vectors plotted for the different lamina in the boundary layer is called a velocity profile. Laminar (smooth, streamline) flow [see Figure 4-2.8(a)] is characterized by a parabolic velocity profile with maximum velocity attained at the theoretical centerline of the flow. Turbulent flow, by contrast, is rough (nonstreamline) flow [see Figure 4-2.8(b)], characterized by an essentially uniform average velocity across the flow section, with only a very thin boundary layer close to the wall where viscous forces predominate. The velocities associated with laminar flows are generally so low as to be impracticable from a design standpoint. Most flows of interest, therefore, are turbulent, and the use of an assumed uniform or average velocity to calculate kinetic energy and velocity pressures

*Early theoretical development of the boundary layer concept is due primarily to Prandtl.[2,3]

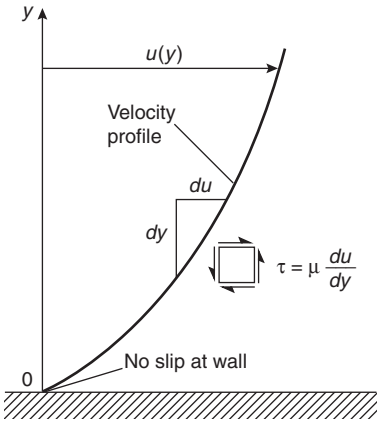

Figure 4-2.7. ***Velocity profile.***

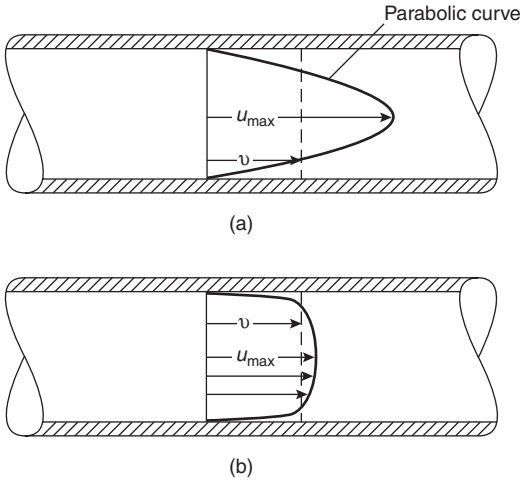

Figure 4-2.8. ***Laminar (a) and turbulent (b) pipe flow velocity profiles for the same volume.***

does not introduce significant error. In those atypical situations where relatively large velocity heads are involved (such as where a pump adds a large amount of energy), a correction factor may be used to relate the actual average kinetic energy to the kinetic energy calculated using average velocity. From continuity considerations,

$$\text{KE} = \int_A \rho u^3 \, dA = \alpha \rho \int_A v^3 \, dA \tag{13}$$

where

KE = true kinetic energy of the flow
v = average velocity of flow
α = kinetic energy correction factor

For incompressible fluids

$$\alpha = \frac{1}{A} \int_A \left(\frac{u}{v} \right)^3 dA \tag{14}$$

and has the value of approximately 1.1 for most turbulent flow problems. Since the velocity head in water distribution piping is small, this correction factor is usually ignored.

While the development of boundary layer theory and the theory of viscous forces has led to an improved theoretical understanding of the mechanics of pipe flows, most flows of interest in fire protection cannot be fully analyzed from theoretical considerations alone. Fire protection flows are almost always turbulent flows. Despite a great expenditure of effort to develop a general predictive theory of turbulent flow phenomena, a fully descriptive theory does not yet exist. While it is postulated that head losses arise because of friction between the fluid and the pipe wall, there is an additional head loss contribution due to turbulence within the fluid. In turbulent flows the rate of head loss, unfortunately, is not simply a function of velocity but depends also on pipe wall roughness. It is further complicated by the changing interaction between these variables at different velocities and roughness element sizes. Within the last century, however, a large body of empirical flow data has been collected, analyzed, and reduced by several investigators. The major features and limits of applicability of the more important results are presented in the following paragraphs.

Fluid Flow Energy Loss Equations

Theoretical development of the physical relationships describing pipe flows dates from about the middle of the nineteenth century, when Chezy postulated a fundamental proportionality between volumetric flow and pipe size based on the continuity equation. His formula is commonly given as

$$Q = \frac{\pi D^2}{4} v = \frac{\pi D^2}{4} \frac{C}{2} \sqrt{DS} \tag{15}$$

and may also be written as

$$S = \left(\frac{8Q}{\pi C}\right)^2 D^{-5} \tag{16}$$

where D and S are pipe diameter and slope of the energy grade line, respectively. The factor C is a proportionality factor incorporating a significant degree of physical uncertainty. Since, by definition

$$S = \frac{h_L}{L}$$

we may write

$$h_L = \left(\frac{8}{\pi C}\right)^2 \frac{L}{D^5} Q^2 \tag{17}$$

as an expression for pipe flow head loss as a function of pipe diameter and discharge. Use of this equation was limited by uncertainties relating to evaluations of the C-factor, which is not, in fact, a constant for a given size conduit or wall condition as was originally thought.

A theoretically more satisfying approach was taken by Darcy, Weisbach, and others. Their formula, which bears the names of the two primary investigators, is generally written as

$$h_L = f \frac{L}{D} \frac{v^2}{2g} \tag{18}$$

It postulates a basic proportionality between head loss and the kinetic energy of the flow, as well as to pipe length and diameter. The proportionality factor f, known as the friction factor, became the subject of extensive theoretical and experimental investigation. The value of f for laminar flow can be shown theoretically to be a simple linear function of the Reynolds number, Re, where $\mathrm{Re} = D_e v \rho/\mu$. The term D_e is the equivalent flow diameter, which is the actual inside diameter of a circular pipe flowing full. The equivalent diameter, D_e, can be found from the hydraulic radius, r_h, which is defined as the area in flow divided by the wetted perimeter. The wetted perimeter does not include the free fluid surface.

$$D_e = 4r_h$$

For Re less than about 2000 (corresponding to low velocity flows or fluids of high viscosity) the relation is

$$f = \frac{64}{\mathrm{Re}} \tag{19}$$

In turbulent flows the roughness of the pipe walls becomes a much more significant factor, and a simple expression to determine f is unavailable.

A systematic investigation of the actual characterisitics of piping inner wall surfaces was first performed by Nikuradse in 1933. To simulate varying degrees of roughness in commercial pipes due to corrosion or surface finish, Nikuradse glued sand grains of known sizes to the inside walls of test pipes. The resulting logarithmic plot of friction factor versus Re is shown in Figure 4-2.9. Although the tests are from Nikuradse, the plot is called Stanton's diagram in recognition of his earlier (1914) elucidation of the relation between friction factor and Reynolds number. Note that at sufficiently high Re, the friction factor depends almost entirely on pipe roughness and is essentially independent of Re. In these plots the roughness parameter is expressed as the ratio of the root mean square grain diameter to the pipe diameter. The resulting ratio is termed the relative roughness and is represented mathematically as ε/D. Typical roughnesses of new commercial pipe is shown in Table 4-2.1. Several later investigators developed mathematical formulas for expressing Nikuradse's results. Chief among them were Colebrook, Moody, and VonKarman.

Moody plotted various equations on a graph similar to the earlier work of Stanton. The resulting Moody diagram (Figure 4-2.10) is widely used today in conjunction with the Darcy-Weisbach equation to compute friction losses for water flowing in pipe. Figure 4-2.11 (page 4-53) presents relative roughness values for use with the Moody diagram over a wide range of conditions. Other diagrams have been developed for use with the Darcy-Weisbach equation[4,5] when parameters other than h_L are sought. Essentially, the alternative graphical formulations employ a rearrangement of variables to facilitate solving for some other unknown such as Q or D.

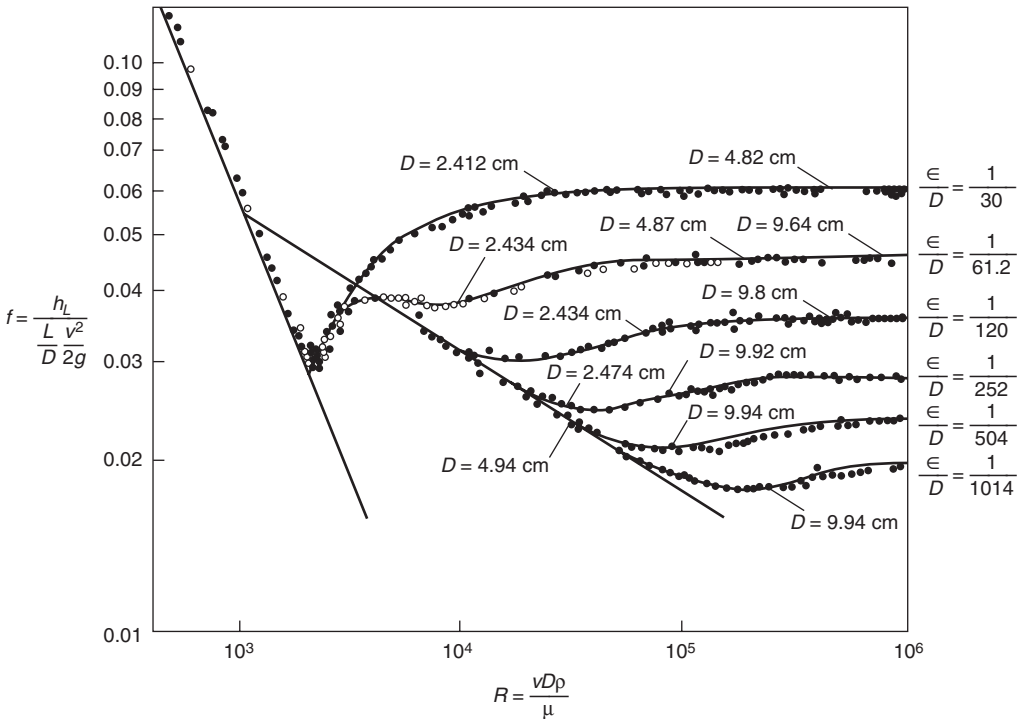

Figure 4-2.9. ***Nikuradse's sand-roughened-pipe tests.***

Table 4-2.1 ***Values of Absolute Roughness of New Clean Commercial Pipes***

Type of Pipe or Tubing	ε ft (0.3048 m) × 10^6		Probable Maximum Variation of *f* from Design (%)
	Range	Design	
Asphalted cast iron	400	400	–5 to +5
Brass and copper	5	5	–5 to +5
Concrete	1,000–10,000	4,000	–35 to +50
Cast iron	850	850	–10 to +15
Galvanized iron	500	500	0 to +10
Wrought iron	150	150	–5 to +10
Steel	150	150	–5 to +10
Riveted steel	3,000–30,000	6,000	–25 to +75
Wood stave	600–3,000	2,000	–35 to +20

Source: *Pipe Friction Manual, 3d ed.* Hydraulic Institute, *(1961).*

Both experimental and theoretical investigations have yielded uncertain results in the region known as the *critical zone,* wherein the flow changes from laminar to turbulent. Uncertainty may be expected since the transition point is difficult to define precisely and, in fact, varies over a considerable range of Re depending upon the direction of the transition (i.e., flow going from laminar to turbulent or from turbulent to laminar) and the local conditions affecting flow stability. As a practical consideration, however, this uncertainty is of little importance, since most real flows of interest fall well into the turbulent range.

Colebrook developed an empirical transition function for the region between smooth flow and complete turbulence. Flow in this region is sometimes referred to as hydraulically smooth or turbulent smooth. The equation has been presented in various forms, the following expression being commonly used:

$$\frac{1}{\sqrt{f}} = -0.86 \ln\left(\frac{\varepsilon/D}{3.7} + \frac{2.51}{\mathrm{Re}\sqrt{f}}\right) \tag{20}$$

An alternate and equivalent expression is

$$f = \left[1.14 - 2\log\left(\frac{\varepsilon}{D} + \frac{9.35}{\mathrm{Re}\sqrt{f}}\right)\right]^{-2} \tag{20a}$$

This relation forms the primary basis for the Moody diagram.

VonKarman used boundary layer theory to derive an expression characterizing the friction factor for fully turbulent flow within rough-walled pipes. The final numerical form of the equation,

$$\frac{1}{\sqrt{f}} = 1.4 + 2\log\frac{D}{\varepsilon} \tag{21}$$

was adjusted to agree more closely with Nikuradse's experimental results. As pipe roughness decreases, this expression approaches Colebrook's equation.

Perhaps the most widely used flow-energy loss relation is the empirically based Hazen-Williams formula, developed near the turn of the century from observations of

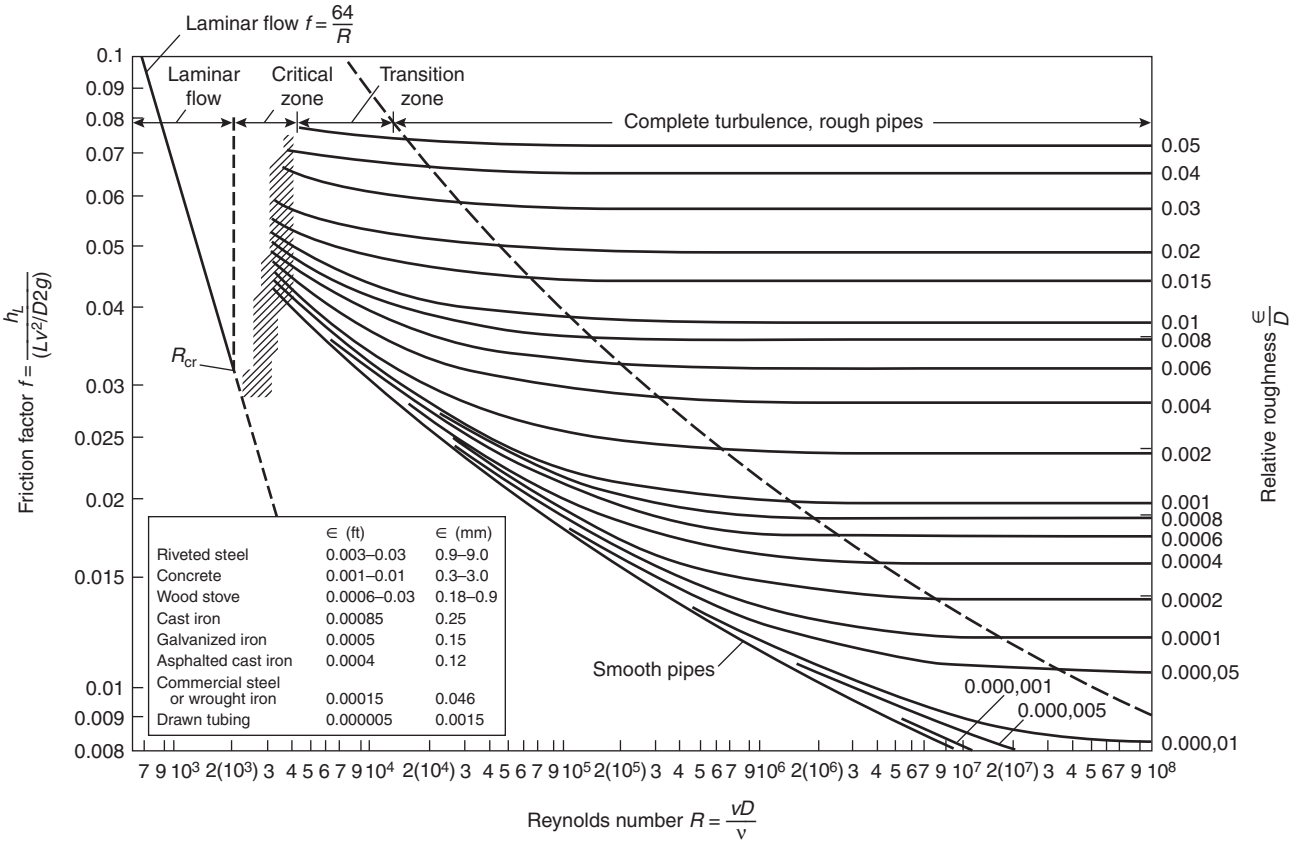

Figure 4-2.10. ***Moody diagram.***

a very large number of pipeline flows. The Hazen-Williams equation was originally written in the form

$$V = 0.113CD^{0.63}S^{0.54} \tag{22}$$

where V is the average velocity in feet per second, S is the slope of the energy grade line—that is, the loss of energy per unit length of the pipe—and D is the actual internal pipe diameter in inches. The coefficient C is a *friction* factor introduced as a constant to represent the roughness of the pipe walls. Table 4-2.2 presents a representative list of C coefficients for various piping materials. Note that the value of C can vary significantly with the piping material, the age of the pipe, and the corrosive qualities of the water.

The Hazen-Williams formula is also encountered in the form

$$Q = 0.285CD^{2.63}S^{0.54} \tag{22a}$$

where Q is volumetric flow rate in gpm and D is in inches. Yet another form, also in the same units for Q and D, is widely used in automatic sprinkler system design. It is arranged to solve for the pressure drop in psi per linear foot of pipe

$$p = \frac{4.52Q^{1.85}}{C^{1.85}D^{4.87}} \tag{22b}$$

In SI units

$$p = \frac{6.05Q^{1.85}}{C^{1.85}D^{4.87}} \times 10^5 \tag{22c}$$

where the units of Q are L/min, D is in mm, and p is in bars per meter of pipe.

Many manufacturers of fire protection equipment, many fire underwriters, and others have published Hazen-Williams-based pipe friction loss data (usually in tabular format) over applicable ranges of pipe sizes, flow rates, and C-factors. A useful calculation aid in a more compact format is the Hazen-Williams nomograph (Figure 4-2.12), which is reproduced here in its generalized form.

The Hazen-Williams formula may be used only for water at or around 60°F (15.6°C), as it does not contain any terms relating to the physical properties of the fluid. The formula does not actually have a sound theoretical basis, but still gives acceptable results in practice with a judicious choice of the C coefficient. Fundamentally, the C-factor is a proportionality constant and, as such, its *true* value depends as much upon the values chosen for the exponents as it does upon actual pipe roughness. The suggested values are the result of curve-fitting exercises and cannot be expected to accurately and evenly represent flow parameter relationships across the full range of

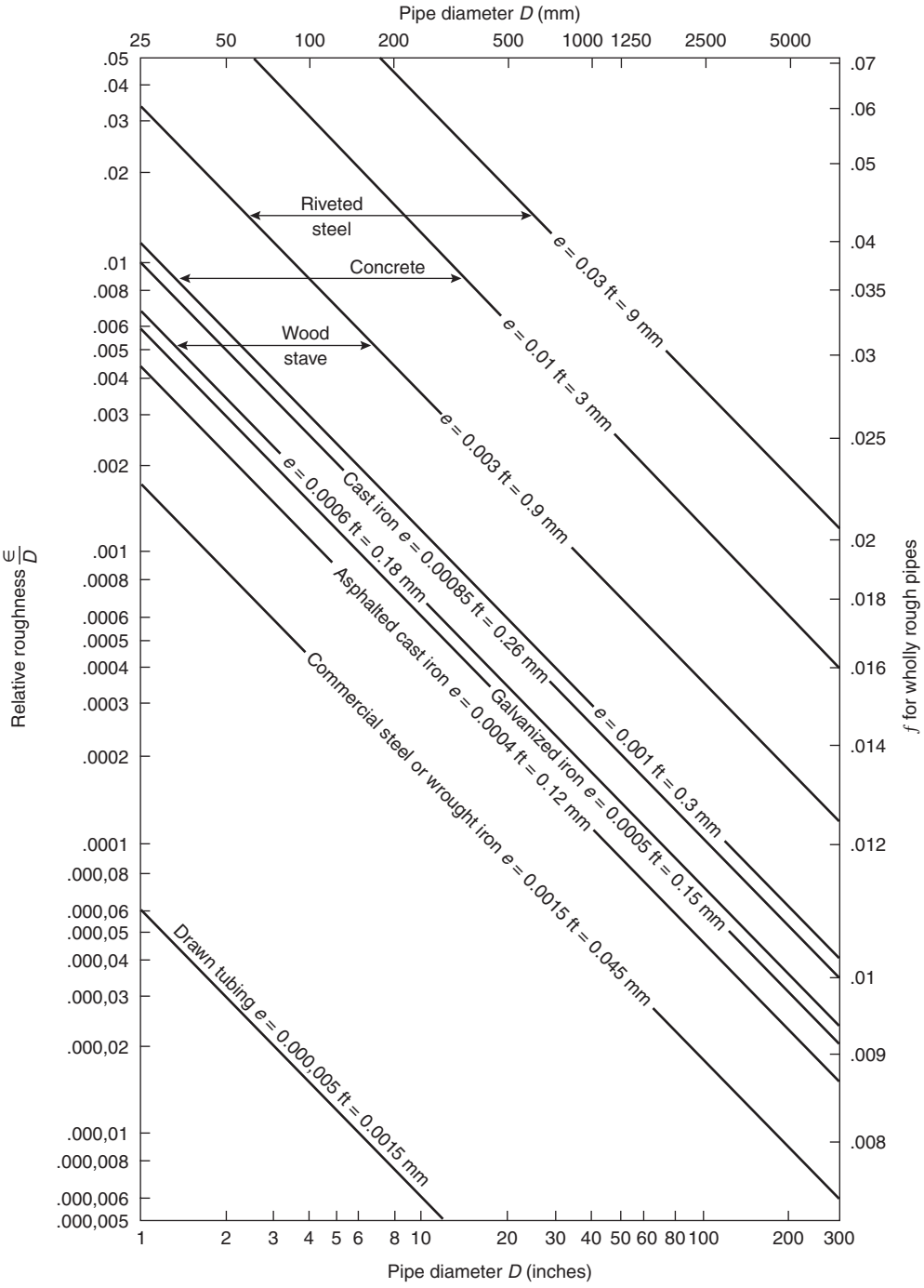

Figure 4-2.11. ***Relative roughness chart.***

observed flow velocities. Allowing the desirability of retaining constant exponents for D and S (i.e., a presumed theoretically stable correlation among all flow parameters in the equation), the value of C for any given flow scenario becomes a narrowly bounded variable that reflects the pipe roughness. Although as in the Chezy formula C is not actually a constant, for practical use it is assigned a constant value for a given presumed roughness. Unfortunately, as Table 4-2.2 shows, the Hazen-Williams equation is a much better model of smooth pipe flow than of rough pipe flow. As long as the flow velocity is close to that at which C was measured and as long as the pipe roughness is not excessive, the Hazen-Williams relation can be expected to give reliable results. It has

Table 4-2.2 ***Values of C in Hazen-Williams Formula***[a]

Type of Pipe	*C* values for certain pipe diameters					
	2.5 cm (1 in.)	7.6 cm (3 in.)	15.2 cm (6 in.)	30.5 cm (12 in.)	61 cm (24 in.)	122 cm (48 in.)
Uncoated cast iron—smooth and new		121	125	130	132	134
Coated cast iron—smooth and new		129	133	138	140	141
30 years old						
Trend 1—slight attack		100	106	112	117	120
Trend 2—moderate attack		83	90	97	102	107
Trend 3—appreciable attack		59	70	78	83	89
Trend 4—severe attack		41	50	58	66	73
60 years old						
Trend 1—slight attack		90	97	102	107	112
Trend 2—moderate attack		69	79	85	92	96
Trend 3—appreciable attack		49	58	66	72	78
Trend 4—severe attack		30	39	48	56	62
100 years old						
Trend 1—slight attack		81	89	95	100	104
Trend 2—moderate attack		61	70	78	83	89
Trend 3—appreciable attack		40	49	57	64	71
Trend 4—severe attack		21	30	39	46	51
Miscellaneous						
Newly scraped mains		109	116	121	125	127
Newly brushed mains		97	104	108	112	115
Coated spun iron—smooth and new		137	142	145	148	148
Old—take as coated cast iron of same age						
Galvanized iron—smooth and new	120	129	133			
Wrought iron—smooth and new	129	137	142			
Coated steel—smooth and new	129	137	142	145	148	148
Uncoated steel—smooth and new	134	142	145	147	150	150
Coated asbestos-cement—clean		142	149	150	152	
Uncoated asbestos-cement—clean		142	145	147	150	
Spun cement-lined and spun bitumen-lined—clean		147	149	150	152	153
Smooth pipe (including lead, brass, copper, polythene, and smooth PVC)—clean	140	147	149	150	152	153
PVC wavy—clean	134	142	145	147	150	150
Concrete—Scobey						
Class 1—C_s = 0.27; clean		69	79	84	90	95
Class 2—C_s = 0.31; clean		95	102	106	110	113
Class 3—C_s = 0.345; clean		109	116	121	125	127
Class 4—C_s = 0.37; clean		121	125	130	132	134
Best—C_s = 040; clean		129	133	138	140	141
Tate relined pipes—clean		109	116	121	125	127
Prestressed concrete pipes—clean				147	150	150

[a]The above table has been compiled from an examination of 372 records. It is emphasized that the Hazen-Williams formula is not suitable for the coefficient *C* values appreciably below 100, but the values in the above table are approximately correct at a velocity of 0.9 m/s (3 ft/s).

For other velocities the following approximate corrections should be applied to the values of *C* in the table above.

Values of *C* at 0.9 m/s	Velocities below 0.9 m/s for Each Halving, Rehalving of Velocity Relative to 0.9 m/s	Velocities above 0.9 m/s for Each Doubling, Redoubling of Velocity Relative to 0.9 m/s
C below 100	Add 5 percent to *C*	Subtract 5 percent from *C*
C from 100 to 130	Add 3 percent to *C*	Subtract 3 percent from *C*
C from 130 to 140	Add 1 percent to *C*	Subtract 1 percent from *C*
C above 140	Subtract 1 percent from *C*	Add 1 percent to *C*

been noted, however, that in rough pipes head loss varies with flow (and velocity) to the power of 2 rather than the power of 1.85 characteristic of smooth pipes.[6] This observation introduces a significant element of uncertainty into the hydraulic analysis of rough pipe with higher velocity flows.

EXAMPLE 2:

Water at 50°F (10°C) flows through 4 in. (102 mm) Schedule 40 welded steel pipe at a rate of 500 gpm (1892.7 l/m). Compare the friction head losses calculated by the Darcy-Weisbach and Hazen-Williams equations for flow through 100 ft of pipe.

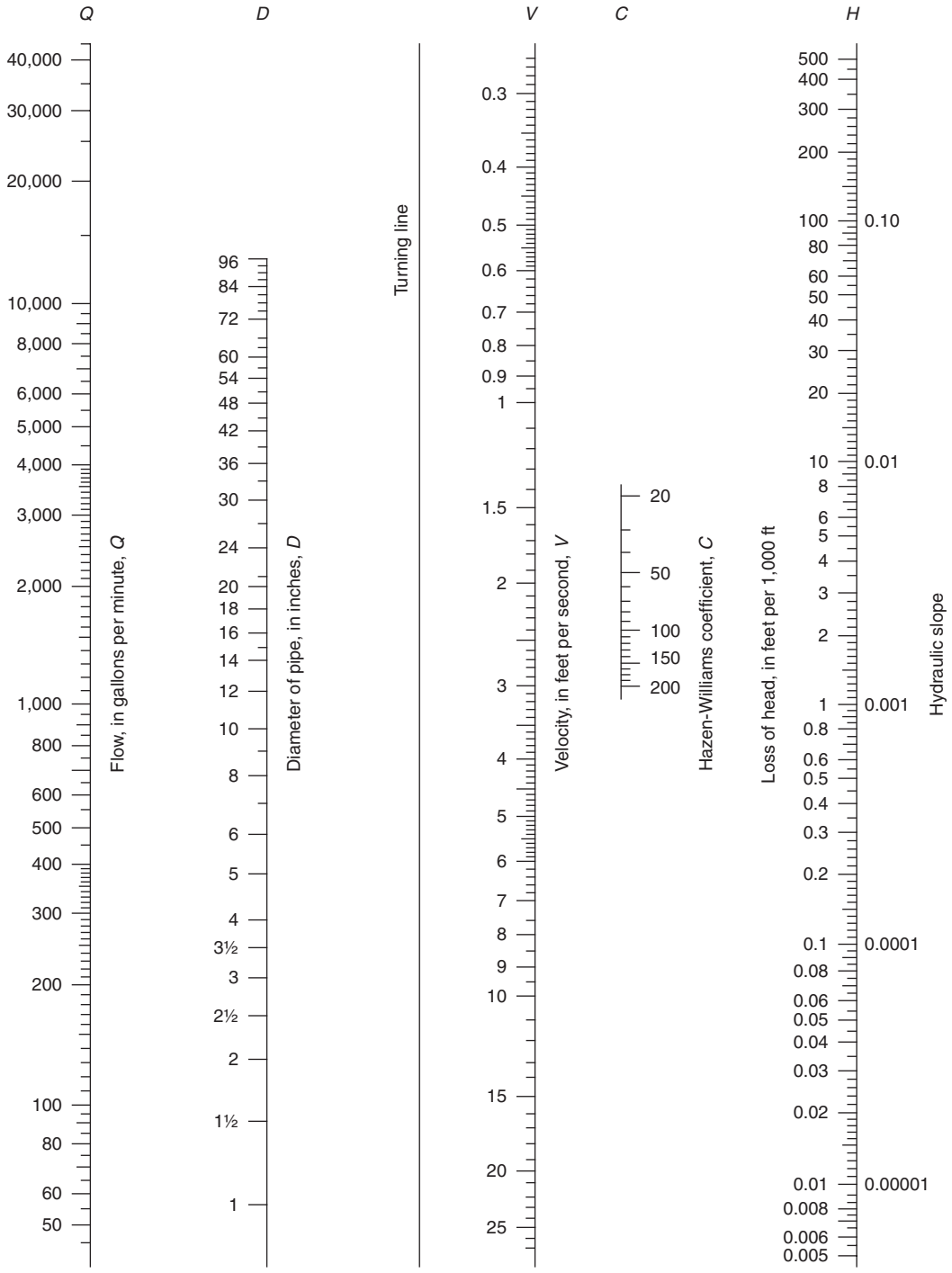

Figure 4-2.12. ***Nomograph for solution of the Hazen-Williams formula.***

SOLUTION:

Basic Data:
For 50°F water, $\nu = 1.41 \times 10^{-5}$ ft²/s
pipe flow area = 0.0884 ft²
$\varepsilon = 0.0002$
pipe inside diameter = 0.3355 ft = 4.026 in.

Using the Darcy approach, we first determine Re, ε/D, and then enter the Moody diagram (Figure 4-2.10).

Flow quantity = Q = 500 gpm ≡ 1.1140 cfs (31.54 l/s)

$$\text{Velocity } = v = \frac{Q}{A} = \frac{1.1140}{0.0884} = 12.60 \text{ fps } (3.8 \text{ m/s})$$

$$\text{Re} = \frac{Dv}{\nu} = \frac{0.3355(12.60)}{1.41 \times 10^{-5}} = 3.0 \times 10^5$$

$$\frac{\varepsilon}{D} = \frac{0.0002}{0.3355} = 0.0006$$

From the Moody friction chart, $f = 0.0188$.

From Equation 18

$$h_L = \frac{0.0188(100)(12.60)^2}{2(0.3355)(32.2)} = 13.8 \text{ ft} = 5.98 \text{ psi (0.41 bar)}$$

The Hazen-Williams approach—Equation 22b—does not take into account any variability in the physical properties of water. It is more straightforward to apply but will likely be less accurate. If we assume a *C*-factor of 100 and solve directly for pressure drop in psi per 100 ft we obtain

$$\Delta p = \frac{4.52(100)(500)^{1.85}}{(100)^{1.85}(4.026)^{4.87}} = 10.06 \text{ psi (0.69 bar)}$$

If we assume $C = 140$,

$$\Delta p = 5.40 \text{ psi (0.37 bar)}$$

a drop of nearly 50 percent and much closer to the Darcy result.

Accuracy in using Hazen-Williams clearly depends on a careful choice of *C*-factor. The Darcy result is not nearly so sensitive to choice of specific roughness ε.

Minor Losses

Flows through pipe fittings, valves, or other pipeline fixtures generate additional turbulence and, therefore, additional energy losses. These losses, although termed minor, can be very significant fractions of the total energy loss due to friction in a piping system. In particular, losses due to pipeline obstructions such as swing-type check valves and certain types of flow meters are equivalent to many feet (or meters) of straight pipe losses. Thus, in some instances minor losses may have to be considered major, particularly in systems where there are many fittings, valves, or other appurtenances. Empirical methods are used to determine these losses for a range of flow or obstruction geometries. One common method is to define a *minor loss coefficient* to express head loss as a function of velocity head. Thus,

$$h_L = k\frac{v^2}{2g} \tag{23}$$

where *k* is a dimensionless loss coefficient. It is sometimes convenient to express such losses in terms of *equivalent length of straight pipe,* or as pipe diameters that produce the same head loss. Thus, by Darcy-Weisbach,

$$\frac{L}{D} = \frac{k}{f} \tag{24}$$

Table 4-2.3 shows local loss coefficients for a number of fittings and flow patterns. Wherever possible manufacturers' data should be used, particularly for valves because of the wide variety of designs even for valves of the same generic type. Such data are often published in the form of flow coefficient or C_v values, which may be used in the equation

$$Q = C_v\sqrt{h_L} \tag{25}$$

C_v is determined from the relation

$$C_v = \pi D^2\sqrt{\frac{g}{8k}} \tag{26}$$

which results directly from a combination of the continuity equation with the equations above.

EXAMPLE 3:

Table 4-2.4 lists a number of equivalent lengths of standard Schedule 40 pipe for screwed steel fittings and valves. Using the table determine the equivalent length of the 2-in.-diameter pipe network shown below.

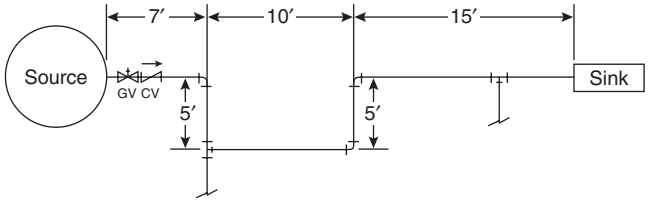

SOLUTION:

The line comprises

1 check valve	19.0 ft (5.7 m)
3 90° standard elbows	3 × 8.5 = 25.5 ft (7.7 m)
1 tee (flow through run)	7.7 ft (2.4 m)
1 tee (flow through branch or stem)	12.0 ft (3.7 m)
1 gate valve	1.5 ft (0.5 m)
straight pipe	42.0 ft (12.8 m)
	L_e = 107.7 ft (32.8 m)

The Darcy equation for determining friction losses through the network would then have the form

$$h_L = \frac{fL_e v^2}{2Dg}$$

Alternately, the loss coefficient approach may be used, where

$$h_L = k\frac{v^2}{2g}$$

This method must be used to find entrance and exit losses. For this example, however, we either refer to manufacturer's data for valve and fitting C_v values or calculate *k* from the relation

$$k = \frac{fL_e}{D}$$

Energy Losses in Pipe Networks

Flow networks may consist of pipes arranged in series, parallel, or some more complicated configuration. In

Table 4-2.3 *Local Loss Coefficients*

Use the equation $h_L = kv^2/2g$ unless otherwise indicated. Energy loss E_L equals h_v head loss in feet.

1

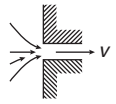

Perpendicular square entrance:
$k = 0.50$ if edge is sharp

2

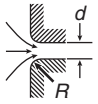

Perpendicular rounded entrance:

$R/d =$	0.50	0.1	0.2	0.3	0.4
$k =$	0.25	0.17	0.08	0.05	0.04

3

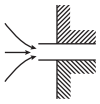

Perpendicular re-entrant entrance:
$k = 0.8$

4

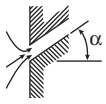

Additional loss due to skewed entrance:
$k = 0.505 + 0.303 \sin \alpha + 0.226 \sin^2 \alpha$

5

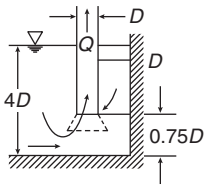

Suction pipe in sump with conical mouthpiece:

$$E_L = D + \frac{5.6Q}{\sqrt{2gD^{1.5}}} - \frac{v^2}{2g}$$

Without mouthpiece:

$$E_L = 0.53\ D + \frac{4Q}{\sqrt{2gD^{1.5}}} - \frac{v^2}{2g}$$

Width of sump shown: $3.5D$

(After I. Vágás)

6

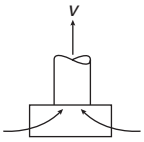

Strainer bucket:
$k = 10$ with foot value
$k = 5.5$ without foot value

(By Agroskin)

7

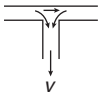

Standard tee, entrance to minor line:
$k = 1.8$

8

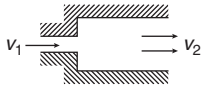

Sudden expansion:

$$E_L = \left(1 - \frac{v^2}{v^1}\right)^2 \frac{v_1^2}{2g} \quad \text{or} \quad E_L = \left(\frac{v^1}{v^2} - 1\right)^2 \frac{v_2^2}{2g}$$

9

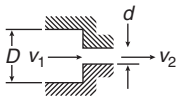

Sudden contraction:

$(d/D)^2 =$	0.01	0.1	0.2	0.4	0.6	0.8
$k =$	0.5	0.5	0.42	0.33	0.25	0.15

10

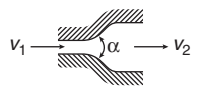

Diffusor:

$E_L = k(v_1^2 - v_2^2)/2g$

$\alpha° =$	20	40	60	80
$k =$	0.20	0.28	0.32	0.35

(Continued)

Table 4-2.3 ***Local Loss Coefficients (Continued)***

11

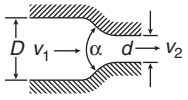

Confusor:

$E_L = k(v_1^2 - v_2^2)/2g$

$\alpha^\circ =$	6	10	20	40	60	80	100	120	140
k for $D = 3d$	0.12	0.16	0.39	0.80	1.0	1.06	1.04	1.04	1.04
$D = 1.5d$	0.12	0.16	0.39	0.96	1.22	1.16	1.10	1.06	1.04

12

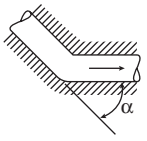

Sharp elbow:

$k = 67.6 \times 10^{-6}(\alpha^\circ)^{2.17}$

(By Gibson)

13

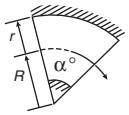

Bends:

$k = [0.13 + 1.85(r/R)^{3.5}]\sqrt{\alpha^\circ/180^\circ}$

(By Hinds)

14

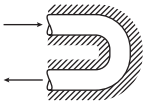

Close return bend:

$k = 2.2$

15

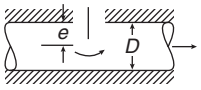

Gate valve:

$e/D =$	0	1/4	3/8	1/2	5/8	3/4	7/8
$k =$	0.15	0.26	0.81	2.06	5.52	17.0	97.8

16

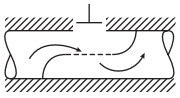

Global value:

$k = 10$ when fully open

17

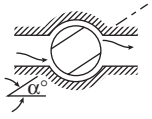

Rotary valve:

$\alpha^\circ =$	5	10	20	30	40	50	60	70	80
$k =$	0.05	0.29	1.56	5.47	17.3	52.6	206	485	∞

(By Agroskin)

18

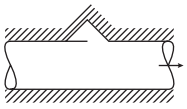

Check valves:

Swing type $k = 2.5$ when fully open

Ball type $k = 70.0$

Lift type $k = 12.0$

19

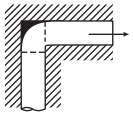

Angle valve:

$k = 5.0$ if fully open

20

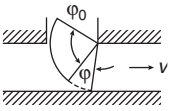

Segment gate in rectangular conduit:

$$k = 0.3 + 1.3\left[\left(\frac{1}{n}\right)\right]^2$$

where $n = \varphi/\varphi_0$ = the rate of opening with respect to the central angle

(By Abelyev)

21

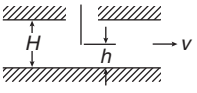

Sluice gate in rectangular conduit:

$$k = 0.3 + 1.9\left[\left(\frac{1}{n}\right) - n\right]^2$$

where $n = h/H$

(By Burkov)

Table 4-2.4 ***Typical Equivalent Lengths of Schedule 40 Straight Pipe for Screwed Steel Fittings and Valves (for any fluid in turbulent flow)***

	Equivalent Length (ft) Pipe Size		
Fitting Type	1" (25.7 mm)	2" (50.8 mm)	4" (101.6 mm)
Regular 90° elbow	5.2	8.5	13.0
Long radius 90° elbow	2.7	3.6	4.6
Regular 45° elbow	1.3	2.7	5.5
Tee, flow through line (run)	3.2	7.7	17.0
Tee, flow through stem	6.6	12.0	21.0
180° return bend	5.2	8.5	13.0
Globe valve	29.0	54.0	110.0
Gate valve	0.84	1.5	2.5
Angle valve	17.0	18.0	18.0
Swing check valve	11.0	19.0	38.0
Coupling or union	0.29	0.45	0.65

any case, an evaluation of friction losses for the flows is based on energy conservation principles applied to the flow junction points. Methods of solution depend on the particular piping configuration. In general, however, they involve establishing a sufficient number of simultaneous equations or employing a friction loss formula where the friction coefficient depends only on the roughness of the pipe (e.g., Darcy or Hazen-Williams).

Pipes in series: When two pipes of different sizes or roughnesses are connected in series [Figure 4-2.13(a)], head loss for a given discharge, or discharge for a given head loss, may be calculated by applying the energy equation between the bounding points, taking into account all losses in the interval. Thus, head losses are cumulative.

Series pipes may be treated as a single pipe of constant diameter to simplify the calculation of friction losses. The approach involves determining an equivalent length of a constant diameter pipe which has the same friction loss and discharge characteristics as the actual series pipe system. Minor losses due to valves and fittings are also included. Using the previous example once again, we note that application of the continuity equation to the solution allows the head loss to be expressed in terms of only one pipe size.

The lost head in equivalent feet of 6-in. pipe is then given in Darcy-Weisbach form by

$$h_L = f\left(\frac{L_e}{D}\right)\left(\frac{v^2}{2g}\right)$$

L_e can be obtained if f is known. Exact hydraulic equivalence in the velocity head terms depends upon f being a constant over the range of velocities applicable to the problem. In fact, f is not a constant over wide ranges of velocity. Since it varies only slightly with Reynolds number, however, solutions are sufficiently accurate.

Pipes in parallel: Two or more pipes connected as in Figure 4-2.13(b), so that flow is first divided among the pipes and is then rejoined, comprise a parallel pipe system. Flows in pipes arranged in parallel are also determined by application of energy conservation principles—specifically, energy losses through all pipes connecting common junction points must be equal. Each leg of the parallel network is treated as a series piping system and converted to a single equivalent length pipe. The friction losses through the equivalent length parallel pipes are then considered equal and the respective flows determined by proportional distribution. For a given Q, an outline of the procedure is as follows:

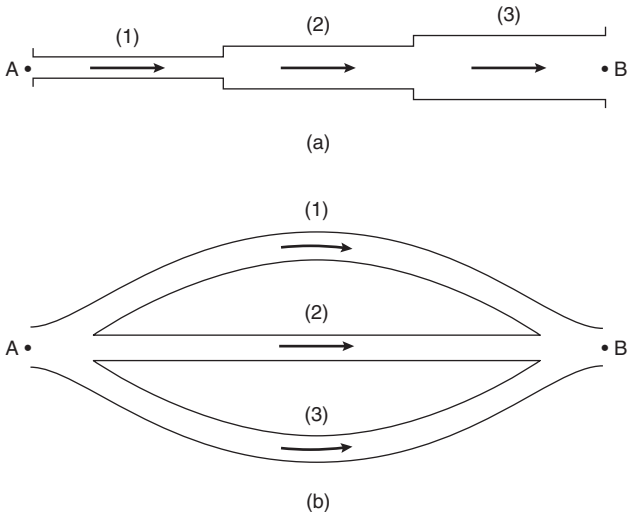

Figure 4-2.13. ***Energy losses in pipe network: (a) pipes in series, (b) pipes in parallel.***

1. Express each branch of the parallel system as an equivalent length of a single pipe size, including all minor losses between the bounding junction points.
2. Assume a discharge Q_1' through pipe branch 1.
3. Solve for h_L, using Q_1'.
4. Using h_L, find Q_2' and Q_3' for the remaining branches.
5. Knowing the proportional distribution of flow among the legs, Q_1', Q_2', and Q_3' are adjusted so that their sum equals the known Q; thus,

$$Q_1 = \frac{Q_1'}{\sum Q'}Q \quad Q_2 = \frac{Q_2'}{\sum Q'}Q \quad Q_3 = \frac{Q_3'}{\sum Q'}Q \qquad (27)$$

6. h_{L_1}, h_{L_2}, and h_{L_3} are computed for the values of Q_1, Q_2, and Q_3 as a check for correctness.

For judicious choice of assumed discharges, solutions are obtained rapidly that agree within a few percent, well within the range of accuracy of the assumed friction factors.

In the case where the head loss is known between points A and B, Q for each branch is found simply by solution of the equation for pipe discharge. The discharges are added to obtain the total flow through the system.

Compound piping networks: Energy loss calculations in compound piping configurations or networks employ

the same basic physical principles as for single pipes. That is, conservation of energy and conservation of mass (continuity) must be satisfied throughout the network. In particular, at each pipe junction

$$\sum Q = Q_1 + Q_2 + \cdots + Q_n = 0 \tag{28}$$

and around each closed loop or circuit

$$\sum h_L = h_{L_1} + h_{L_2} + \cdots + h_{L_n} = 0 \tag{29}$$

The general solution procedure involves setting up a sufficient number of independent equations of these two types and solving simultaneously for the unknowns. For complicated networks straightforward algebraic solution is clearly impractical. A very widely used relaxation method for systematic solution of large networks was developed by Hardy Cross in 1928. The method is well suited for solution by hand and is readily adaptable for machine computation.

We have seen that loss of head in a pipe may be represented generally by an equation of the form $h_L = KQ^n$ (where, for the Hazen-Williams formula, $n = 1.85$). For any single pipe in a network, we may write

$$Q = Q_0 + \Delta \tag{30}$$

where

Q = corrected flow
Q_0 = assumed flow
Δ = flow correction

The problem, so stated, reduces to finding Q to a desired degree of accuracy by successive evaluations of Δ based on updated estimates of Q_0. We solve for Δ as follows:

$$\begin{aligned} h_L = KQ^n &= K(Q_0 + \Delta)^n \\ &= K(Q_0^n + nQ_0^{n-1}\Delta + \cdots) \end{aligned} \tag{31}$$

If Δ is small relative to Q_0, the higher-order terms in the expansion may be neglected. Since, for any circuit, $\Sigma h_L = 0$, we may write

$$\sum KQ^n = 0 = \sum [KQ_0^n + KnQ_0^{n-1}\Delta] \tag{32}$$

to a good approximation. Solving for Δ we have

$$\Delta = \frac{-\sum KQ_0^n}{n\sum KQ_0^{n-1}} = \frac{\sum h_{L_0}}{n\sum (h_{L_0}/Q_0)} \tag{33}$$

The overall formulation is made algebraically consistent by designating clockwise flows positive and counterclockwise flows negative. The calculation procedure is controlled by the requirement that the algebraic sum of all assumed flows must equal zero at each pipe junction. The originally assumed flows are repeatedly and cyclically corrected until the Δ values are negligible, indicating that a hydraulic balance has been reached. Note that pipes common to two circuits are corrected twice in each cycle, once for each circuit. For a system where total head loss is known, flows can be balanced by correcting assumed head losses instead of flows.

Several other methods exist for determining flows and head losses in compound pipe networks. Many can be performed manually, although computer analysis is desirable and necessary for the more complex methods, particularly those involving unsteady flow. For a review of alternative methods, the reader is referred to Stephenson[7] and Walski.[6]

Flow Measurement and Discharge

Flow Measuring Devices

This section deals primarily with the basic principles of operation of some flow measuring devices in common use and, in particular, with the pitot tube and the pipeline differential flow meters that have been standardized by the ASME (American Society of Mechanical Engineers): namely, the Venturi, the flow nozzle, and the square-edge thin-plate concentric orifice.

In general, an incompressible fluid of density ρ, viscosity μ, flows with average velocity v through a metering element of diameter d. The metering element is located in a horizontal metering tube of roughness ε and diameter D. The flow through the element produces a pressure differential Δp sensed by pressure taps located a distance L apart. It can be shown by dimensional analysis that the fundamental parameters involved in fluid metering, namely L, ε, v, ρ, μ, d, D, and Δp, yield relational solutions conventionally formulated as follows:

$$\frac{d\rho v}{\mu} = \mathrm{Re}_d \qquad \text{metering element Reynolds number}$$

$$\frac{L}{D} \qquad \text{tap location ratio}$$

$$\frac{d}{D} = \beta \qquad \text{beta ratio}$$

$$\frac{\varepsilon}{D} \qquad \text{relative roughness}$$

$$\frac{v}{\sqrt{2g\Delta p/\rho}} = \overline{K} \qquad \text{flow coefficient (pressure coefficient)}$$

Since $v = \overline{K}\sqrt{2g\Delta p/\rho}$, the continuity equation allows the volumetric flow rate measured by the meter to be expressed as

$$Q = \overline{K}A_d\sqrt{2g\Delta p/\gamma} \tag{34}$$

where A_d is the flow area of the metering element.

Typically, flow meter calculations are based on the idealized flow of a one-dimensional, frictionless, incompressible fluid in a horizontal metering tube. Real conditions require corrections to the ideal formulation. Conventional corrections for the effects of variations from ideal geometry and flow velocity profile are achieved through the use of modification factors. Thus, in Equation 34 above, $\overline{K}$ in-

cludes pressure and flow modifications which are conventionally defined as

$$\overline{K} = CE \tag{35}$$

where C = coefficient of discharge defined as the ratio of actual flow rate to ideal rate and

$$E = \frac{1}{\sqrt{1 - \beta^4}}$$

and is known as the velocity of approach factor, since it accounts for the one-dimensional kinetic energy at the inlet tap.

The general volumetric flow metering equation is, then,

$$Q = \overline{K} A_d \sqrt{\frac{2g\Delta p}{\gamma}} = CEA_d \sqrt{\frac{2g\Delta p}{\gamma}} \tag{36}$$

Venturi flow meter: Figure 4-2.14 shows a schematically typical Venturi-type flow tube. The divergent cone section reduces the overall pressure loss of the meter. Pressure is sensed through a series of holes in the inlet cone and throat. These holes lead to an annular chamber, and the two chambers are connected to a pressure differential sensor such as a U-tube manometer. ASME standardized discharge coefficients are given in Table 4-2.5. Venturi tubes must be individually calibrated to obtain these coefficients outside the tabulated limits.

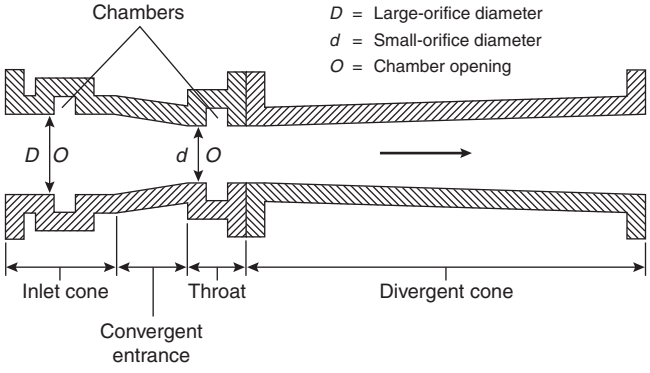

Figure 4-2.14. ***Venturi tube.***

Table 4-2.5 ***ASME Coefficients for Venturi Tubes***

Type of Inlet Cone	Re_2 Minimum	Re_2 Maximum	Value of C	Tolerance (%)
Machined		1,000,000	0.995	±1.00
Rough welded sheet metal	500,000	2,000,000	0.985	±1.50
Rough cast			0.984	±0.70

Determination of volumetric flow rate is a simple calculation employing the general flow metering formula—Equation 36—where C is the applicable tabulated value based on Re_d, and E is calculated directly from the beta ratio.

ASME flow nozzle: This nozzle is depicted in Figure 4-2.15. The pressure differential is sensed by either throat taps or pipe wall taps appropriately located. Coefficients of discharge for ASME flow nozzles may be accurately computed from the following equation:

$$C = 0.9975 - 0.00653\left(\frac{10^6}{\mathrm{Re}_d}\right)^a \tag{37}$$

where

$$a = \frac{1}{2} \text{ for } \mathrm{Re}_d < 10^6$$

$$a = \frac{1}{5} \text{ for } \mathrm{Re}_d < 10^6$$

Volumetric flow rates are calculated in the same manner as for the Venturi tube.

ASME orifice meters: Fluid flowing through a thin, square-edged orifice plate experiences a contraction of the flow stream some distance downstream from the orifice. The minimum area of flow is called the *vena contracta* and its location is a function of the beta ratio. Figure 4-2.16 shows the relative pressure difference due to the presence of the orifice plate and the location of the *vena contracta* with respect to beta. By inspection of Figure 4-2.16 it is clear that the actual location of the pressure taps is critical. Three distinct arrangements for tap locations are specified by the ASME for accurately measuring the pressure differential. These types of tap arrangements are called the flange, *vena contracta*, and the 1*D* and ½*D*. Each has certain advantages and disadvantages and affects the value of the discharge coefficient.

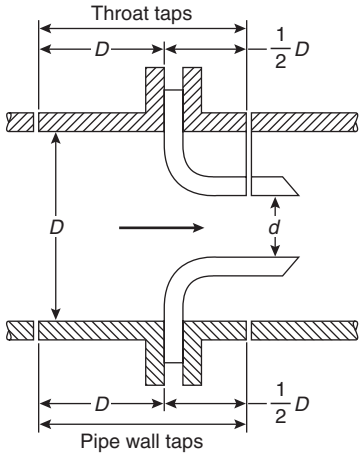

Figure 4-2.15. ***ASME flow nozzle.***

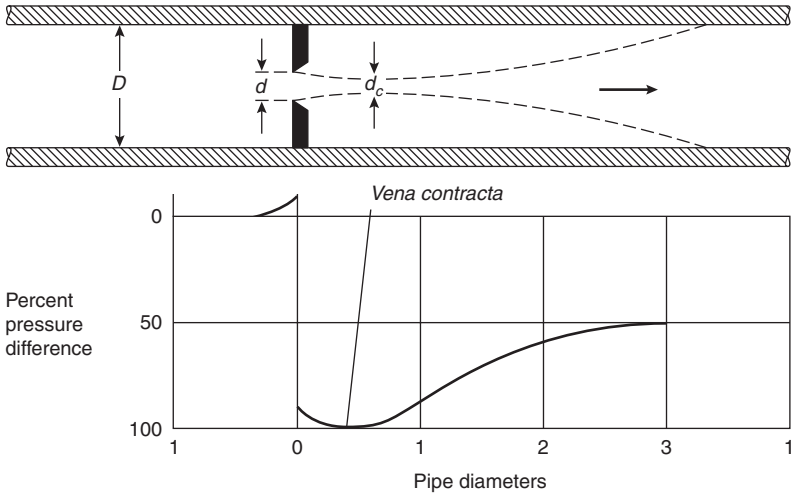

Figure 4-2.16. ***Relative pressure changes due to flow through an orifice.***

Discharge coefficients for orifice metering plates may be calculated from the equation

$$C = C_o + \frac{\Delta C}{\mathrm{Re}_d^{\alpha}} \tag{38}$$

where C_o and α are obtained from Table 4-2.6. Since the jet contraction downstream of the orifice can amount to nearly half of the orifice area, orifice discharge coefficients are in the order of 0.6 compared to the near-unity coefficients obtained with Venturi tubes and flow nozzles.

Pitot tube: A pitot tube is a device designed to sense stagnation or total pressure for the determination of velocity and volumetric flow rate. A number of commercial devices are available, some of which include a static pressure tap, that are designed for insertion into a water main under pressure through a standard pipe tap or corporation cock. The installed pitot tube measures velocity at a point in the fluid. Conventional practice assumes that the conversion of kinetic energy to flow work in the tube is frictionless. Thus, applying the energy equation to the generalized pitot tube diagram (Figure 4-2.17) we obtain

$$\frac{u_s^2 - u_i^2}{2g} + \frac{p_s - p_0}{\rho_0 g} = 0 \tag{39}$$

where

u_s = stagnation point velocity
u_i = ideal streamtube velocity
p_s = stagnation pressure
p_0 = static pressure

Since, by definition $u_s = 0$, solving for u_i we obtain

$$u_i = \sqrt{\frac{2g(p_s - p_0)}{\gamma_0}} = \sqrt{\frac{2g\Delta p}{\gamma_0}} \tag{40}$$

Typically, a pipe coefficient, C_p, which is independent of the geometry of the velocity profile, is defined as

$$C_p = \frac{\text{average velocity}}{\text{centerline velocity}}$$

For typical velocity profiles, C_p varies from about 0.75 to 0.97 but usually lies within a narrower range of about 0.80 to 0.90. Knowing the centerline velocity, the flow can be obtained simply by

$$Q = C_p A v_{\mathrm{CL}} \tag{41}$$

In situations where pipe velocity profiles are unknown, and therefore average velocities are not available, it may be necessary to obtain velocity measurements at many individual points. Given n velocities, the flow is then

$$Q = \sum_{i=1}^{n} v_i A_i \tag{42}$$

where

v_i = velocity at the ith point
A_i = area of annular ring of flow cross section for which velocity v_i is accurate

Detailed procedures for obtaining accurate pitot traverses are available in the literature along with suggestions for assessing the reliability of water audits, *C*-factor tests, and so forth, based on pitot gage measurements.[4,6] See the next section for a discussion of discharge measurements using pitot tubes.

Free Discharge at an Opening

Flow discharging to the atmosphere from a tank, hydrant, nozzle, or open conduit is affected by the area and shape of the opening. The total energy of the fluid is converted into kinetic energy at the orifice according to an

Table 4-2.6 ***Values of C_o, ΔC, and α for Use in Equation 38***

	D = 2 in. = 50 mm		D = 4 in. = 100 mm		D = 8 in. = 200 mm		D = 16. in. = 400 mm	
β	C_o	ΔC	C_o	ΔC	C_o	ΔC	C_o	ΔC
				Flange taps $\alpha = 1$				
0.20	0.5972	127	0.5946	200	0.5951	327	0.5955	551
0.30	0.5978	144	0.5977	209	0.5978	307	0.5980	457
0.40	0.6014	181	0.6005	256	0.6002	362	0.6001	514
0.50	0.6050	260	0.6034	386	0.6026	584	0.6022	903
0.60	0.6078	392	0.6055	622	0.6040	1015	0.6032	1710
0.70	0.6068	573	0.6030	953	0.6006	1637	0.5991	2898
				Vena contracta taps $\alpha = ½$				
0.20	0.5938	1.61	0.5928	1.61	0.5925	1.61	0.5924	1.61
0.30	0.5939	1.78	0.5934	1.78	0.5933	1.78	0.5932	1.78
0.40	0.5970	2.01	0.5954	2.01	0.5953	2.01	0.5953	2.01
0.50	0.5994	2.29	0.5992	2.29	0.5992	2.29	0.5991	2.29
0.60	0.6042	2.68	0.6041	2.68	0.6041	2.69	0.6041	2.70
0.70	0.6069	3.34	0.6068	3.37	0.6067	3.44	0.6068	3.57
				1D and ½D taps $\alpha = ½$				
0.20	0.5909	2.03	0.5922	1.41	0.5936	1.10	0.5948	0.94
0.30	0.5915	2.02	0.5930	1.50	0.5944	1.24	0.5956	1.12
0.40	0.5936	2.17	0.5951	1.72	0.5963	1.49	0.5974	1.38
0.50	0.5979	2.40	0.5978	1.99	0.5999	1.79	0.6007	1.69
0.60	0.6036	2.67	0.6040	2.31	0.6044	2.12	0.6048	2.11
0.70	0.6078	3.19	0.6072	2.98	0.6068	3.07	0.6064	3.51

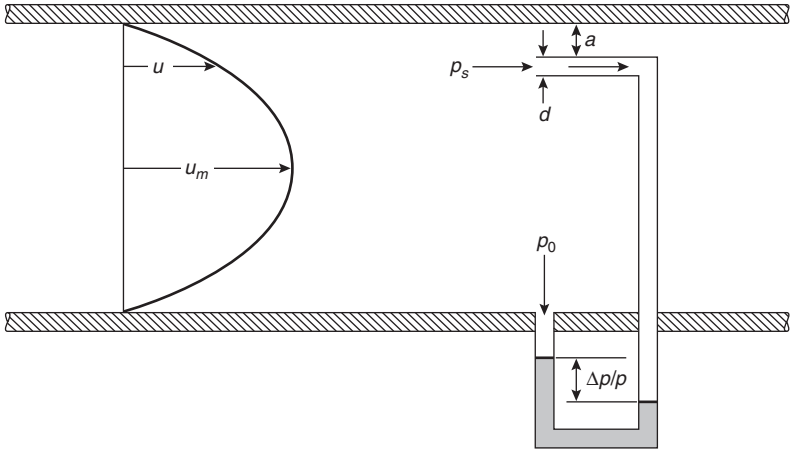

Figure 4-2.17. ***Pitot tube study.***

appropriate form of the Bernoulli equation. In the most general case of a closed pressurized tank,

$$\frac{v_0^2}{2g} = z_1 + \frac{p_1}{\rho} \tag{43}$$

$$v_0 = \left[2g\left(z_1 + \frac{p_1}{\rho}\right)\right]^{1/2} \tag{44}$$

Accounting for losses at the point of discharge,

$$v_0 = C_v\sqrt{2gh} \tag{45}$$

where C_v, the coefficient of velocity, is determined from the coefficients of discharge and contraction

$$C_v = \frac{C_d}{C_c}$$

Table 4-2.7 ***Orifice Coefficients for Water***

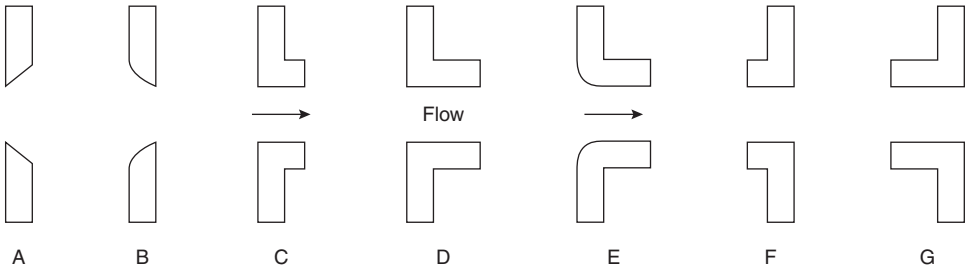

Illustration	Description	C_d	C_c	C_v
A	Sharp-edged	0.62	0.63	0.98
B	Round-edged	0.98	1.00	0.98
C	Short tube (fluid separates from walls)	0.61	1.00	0.61
D	Short tube (no separation)	0.82	1.00	0.82
E	Short tube with rounded entrance	0.97	0.99	0.98
F	Reentrant tube, length less than one-half of pipe diameter	0.54	0.55	0.99
G	Reentrant tube, length 2 to 3 pipe diameters	0.72	1.00	0.72
Not shown	Smooth, well-tapered nozzle	0.98	0.99	0.99

Commonly used values of orifice coefficients for water are given in Table 4-2.7. The orifice discharge can then be expressed as

$$Q_o = C_d A_o \sqrt{2gh} \tag{46}$$

and the head loss due to turbulence at the orifice as

$$h_L = \left(\frac{1}{C_v^2} - 1\right)\frac{v_0^2}{2g} \tag{47}$$

where

$\left(\frac{1}{C_v^2} - 1\right)$ = minor loss k-factor

For the general case of a tank of varying cross-sectional area being replenished with inflow, $\dot{Q}_{\text{IN}}$, the time to empty from height z_1 to z_2 is given by

$$t = \int_{z_1}^{z_2} \frac{A_t\, dz}{c_d A_o \sqrt{2gh} - \dot{Q}_{\text{IN}}} \tag{48}$$

where A_t is expressed as a function of z.

For a tank of constant cross section this simplifies to

$$t = \frac{2A_t\left(\sqrt{z_1} - \sqrt{z_2}\right)}{C_d A_o \sqrt{2g}} \tag{49}$$

EXAMPLE 4:

A 15-ft-diameter tank discharges water at 50°F through a 2-in.-diameter sharp-edged orifice. If the initial water depth in the tank is 10 ft and the tank is continuously pressurized to 50 psig, how long will it take to empty the tank?

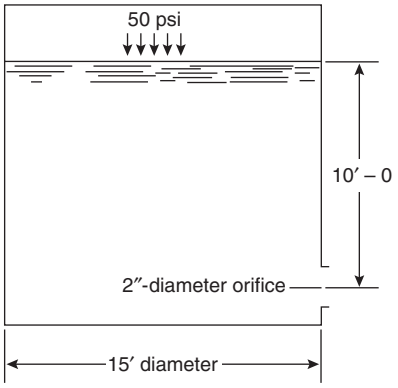

SOLUTION:

At 50°F (10°C),

$$\gamma = 62.4 \text{ lbm/ft}^3 \ (16.02 \text{ kgm/m}^3)$$

For the orifice:

$$A_o = \frac{\pi D^2}{4} = 3.14 \text{ ft}^2 \ (0.29 \text{ m}^2)$$

$$C_d = 0.62 \text{ (sharp-edged orifice)}$$

For the tank:

$$A_t = \frac{\pi D^2}{4} = 176.7 \text{ ft}^2 \ (16.4 \text{ m}^2)$$

$$h_0 = 10 + \frac{50(144)}{62.4} = 125.38 \text{ ft } (38.2 \text{ m})$$

$$h_1 = 0 + \frac{50(144)}{62.4} = 115.38 \text{ ft } (35.2 \text{ m})$$

The total pressure head on the discharging fluid results from both an elevation and a static pressure head. Therefore,

$$t = \frac{2A_t[(z_0 = p_0/\gamma)^{1/2} - (z_1 + p_1/\gamma)^{1/2}]}{C_d A_o \sqrt{2g}}$$

$$t = 10.4 \text{ s}$$

Discharge stream coordinates are given by

$$x = v_0 t = v_0 \sqrt{\frac{2y}{g}} = 2C_v \sqrt{zy} \quad (50a)$$

$$y = \frac{gt^2}{2} \quad (50b)$$

For the simpler case of a hydrant discharging to atmosphere, the flow can be determined by an appropriate form of Equation 36,

$$Q = 29.8D^2 C_d \sqrt{p} \quad (51)$$

where

Q = discharge (gpm)

D = outlet diameter (in.)

p = pressure detected by pitot gage (psi)

C_d = coefficient based on hydrant outlet geometry (usually taken to be 0.90 for full flow across a standard 2½-in. outlet)

In the absence of a pitot gage, hydrant flows may be estimated by observing the trajectory of the discharge stream. The horizontal component of the velocity does not change appreciably over time, thus allowing calculation of the velocity based on the height of the outlet and the distance traveled by the stream. Figure 4-2.18 presents the basic parameters. The velocity determined in this manner is at the *vena contracta* and is given by

$$v = \frac{x}{\sqrt{2y/g}} \quad (52)$$

The discharge is simply the product of this velocity and the area of the *vena contracta.* The method is relatively inaccurate due to the obvious difficulty of measuring the required area and the distance x. It is a useful bounding guide, however, in the absence of precision measuring devices.

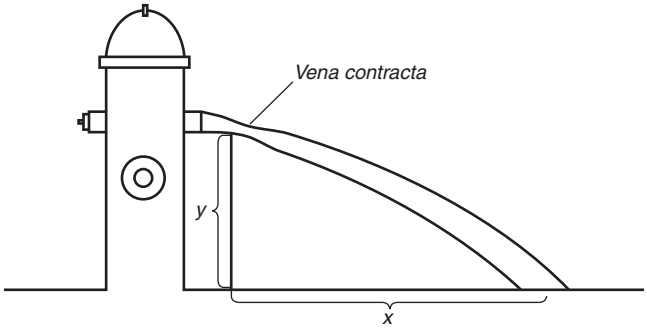

Figure 4-2.18. ***Determining discharge by the trajectory method.***

WATER HAMMER*

Water hammer in a pipeline is caused by a sudden stoppage of flow and is characterized by loud noise and vibration. The kinetic energy from the interrupted flow is transferred to the walls of the enclosing pipe or equipment, which expand under the increased pressure. Such pressures, or shock waves, can be severe enough to destroy the equipment and the pipeline itself.

Density changes due to pressure are assumed zero for nearly all hydraulic calculations, as water is considered incompressible for practical purposes even though it is about 100 times more compressible than steel. When shock waves arise in confined water, however, the compressibility of water becomes very significant, and water's elastic properties must be taken into account. The primary property of interest is the bulk modulus of elasticity, E, which is defined as the ratio of pressure change to the corresponding change of volume as determined by compression tests on volumes. (The bulk modulus is analogous to Young's modulus in solid mechanics, which is the ratio of linear stresses to linear strains as determined by tension tests.) The formula expressing the relationship between pressure and volume is

$$\Delta p = -E \frac{\Delta V}{V_0} \quad (53)$$

where the minus sign indicates that a positive change in pressure produces a decrease in volume. A modulus of compressibility, K, is also defined as the inverse of E.

Under normal conditions, water confined and flowing under pressure in a pipeline exerts pressure on the pipe walls according to the pressure-energy term of the energy equation. Any change in discharge within the system (due to valve closure, pump stoppage, etc.) results in a change of flow momentum. By virtue of the impulse-momentum relation, the momentum change will cause an impulse force to be created. This force in a pipeline is commonly referred to as water hammer.

The theory of water hammer, as developed by Zhukovsky, can be briefly illustrated as follows: a valve in a pipeline is closed instantaneously; the fluid impacts the closed gate and is decelerated to zero velocity, thereby creating a pressure shock. By Newton, pressure shocks in fluids of infinite extent travel at a velocity given by

$$c^* = \sqrt{\frac{KE}{\rho}} \quad (54)$$

where c^* is called the celerity (velocity) of the shock wave, KE is the kinetic energy of the fluid, and ρ is the fluid density. The pipe, however, is also elastic. Therefore, if the fluid in the pipe is compressed, the pipe will expand. The

*This discussion is patterned after the theory of water hammer as developed by N. J. Zhukovsky and as presented in Andrew L. Simon's *Practical Hydraulics,* 2nd ed.[4]

modulus of elasticity, E_c, of a system composed of fluid and pipe may be determined from the equation

$$\frac{1}{E_c} = \frac{1}{E} + \frac{D}{E_p w} \tag{55}$$

where

D = pipe diameter
w = thickness of the pipe wall
E_p = modulus of elasticity of the pipe material

Table 4-2.8 gives the modulus of elasticity for common pipe materials. The celerity of a shock wave in a pipe system of finite extent can then be computed from

$$\frac{c}{c^*} = \frac{1}{\sqrt{1 + ED/(E_p w)}} \tag{56}$$

which is plotted in Figure 4-2.19. The graph indicates the considerable influence of pipe rigidity on the velocity of the shock.

The shock waves that travel upstream and downstream from the valve closure eventually reach points in the system that correspond to large stationary energy stores (e.g., reservoirs) or other sudden closure points, which may vary in their ability to absorb or reflect the shock wave. If the shock is absorbed into a larger energy field it will disappear, and it will do so in time

$$t = \frac{L}{c} \tag{57}$$

where L is the distance from the energy reservoir to the shock wave point of origin. At the instant of shock absorption the compressed fluid, no longer balanced, begins to flow backward, creating a relief pressure shock that travels back to the valve. The time period T that the initial shock or impulse pressure acts on the valve is, therefore, the time required for the pressure wave to travel away from and back to the valve:

$$T = 2t = \frac{2L}{c} \tag{58}$$

Table 4-2.8 ***Modulus of Elasticity E_p of Various Pipe Materials***

	E_p		
Pipe Material	(psi)	(lb/ft²)	(kg/m²)
Lead	0.045×10^6	6.48×10^6	31.64×10^6
Lucite (at 73°F)	0.4×10^6	57.6×10^6	281.23×10^6
Rubber (vulcanized)	2×10^6	288×10^6	1406×10^6
Aluminum	10×10^6	1440×10^6	7030×10^6
Glass (silica)	10×10^6	1440×10^6	7030×10^6
Brass, bronze	13×10^6	1872×10^6	8489×10^6
Copper	14×10^6	2016×10^6	9842×10^6
Cast iron, gray	16×10^6	2304×10^6	$11{,}249 \times 10^6$
Cast iron, malleable	23×10^6	3312×10^6	$16{,}170 \times 10^6$
Steel	28×10^6	4023×10^6	$19{,}685 \times 10^6$

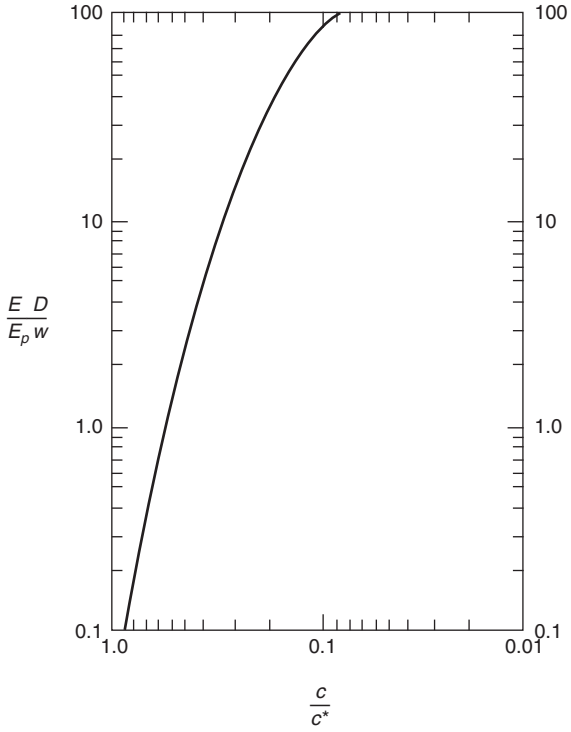

Figure 4-2.19. ***Celerity of pressure waves in pipes, c equals celerity in elastic pipe; c* equals celerity in fluid of infinite extent.***

At time T, all the fluid is moving backward at some velocity v. Since the valve is closed, there is no supply for this flow. A negative pressure shock is created at the valve. The shock travels to and back from the reservoir, as the flow is reversed. Such oscillations of pressure and periodic flow reversals persist until the kinetic energy is dissipated by friction. The process described will occur both upstream and downstream from the point of origin, though the initial shock will be positive upstream and negative downstream and the periodicities would not likely be equal.

The theoretical magnitude of the pressure shock at instantaneous valve closure can be determined directly from

$$p^* = \rho c \Delta v \tag{59}$$

and the pressure will oscillate in the pipe within the range

$$p = p_0 \pm p^* \tag{60}$$

In actuality, the time of closure of a valve is not zero but some finite time period which we may call T_c. The water hammer pressure increases gradually with the rate of closure of the valve. Depending on whether T_c is smaller or larger than T, we distinguish between quick and slow closure. For $T_c < T$, the shock pressure will attain its maximum value p^*. (In this sense, quick closure is equivalent to instantaneous closure.) For $T_c > T$, maximum pressure

will be somewhat less than p^* and may be calculated by the Allievi formula

$$p = p_0\left(\frac{N}{2} + \sqrt{\frac{N^2}{4} + N}\right) \tag{61}$$

in which

$$N = \left(\frac{Lv\rho}{p_0 T_c}\right)^2 \tag{61a}$$

In general the calculation of water hammer pressure rises, regardless of method, will tend to underestimate the actual values. Real systems will tend to experience superimposition of positive or negative pressure waves due to complex piping configurations. Discontinuities introduced by a variety of auxiliary valving and metering equipment complicate the analysis considerably. Other methods are available for analyzing water hammer effects on systems that may not be reasonably handled by the above idealized method.[8] Since water hammer can be extremely detrimental, often resulting in complete loss of the system, it is desirable to perform an analysis wherever such effects are of concern. Control over the development of damaging shock waves is achieved through use of slow-closing valves, pressure relief valves, or shock-absorbing devices.

Pumps

Pump Operating Characteristics

Pumps are mechanical devices that convert electrical or mechanical energy into hydraulic energy. There are many classes of pumps—for example, reciprocating, rotary, jet, ram, centrifugal—each class referring to different ways pumps move liquids. A common class of pump is the centrifugal and it is usually the only type we are concerned with in fire protection applications. Based on the way in which the impeller (the rotating component) imparts energy to the water, centrifugal pumps may be divided into several categories. Turbine or radial flow centrifugal pumps force water outward at right angles to the rotating axis. Mixed flow pumps force water in both radial and axial directions. Propeller pumps move water in the axial direction only. Any of these types may be single or multistage, where stage refers to the number of impellers on the pump's rotating shaft. The orientation of the shaft may be vertical or horizontal. The following discussion, while broadly applicable, is directed mainly to centrifugal pumps.

Figure 4-2.20 illustrates several of the terms commonly used to describe pump performance conditions. In general, pumping of liquids requires that the pressure at any point in the intake line be greater than the vapor

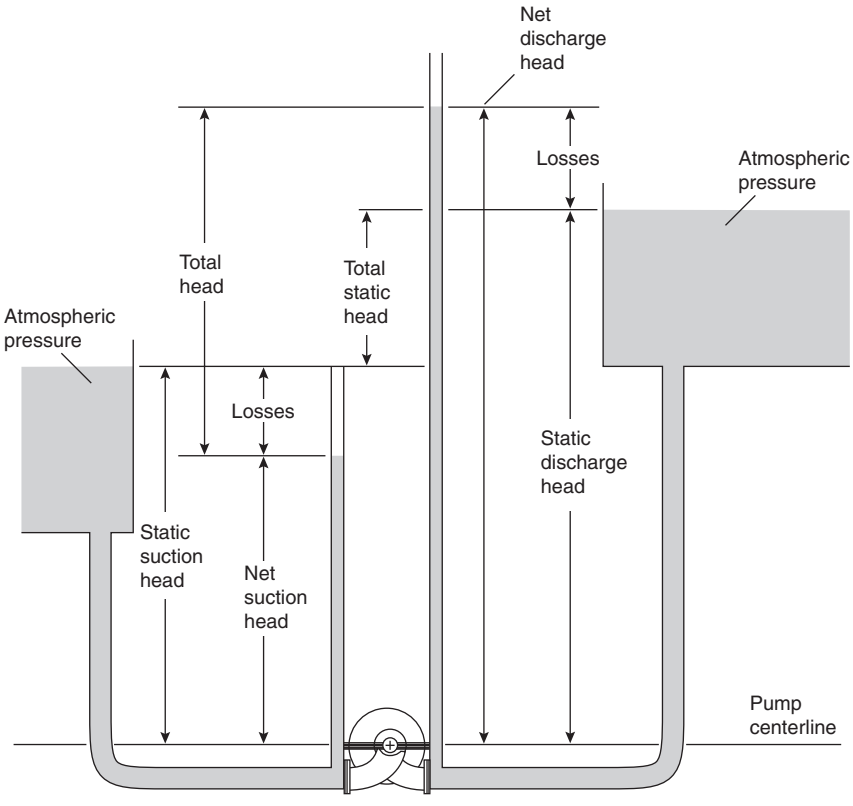

Figure 4-2.20. ***Pump head definitions.***

pressure of the liquid to avoid loss of prime and the highly destructive phenomenon known as cavitation. The pressure gradient that causes a liquid to move through the intake line to the pump impeller is termed the net positive suction head (NPSH). In pump selection, it is essential to determine that the *available* NPSH of the system exceeds the *required* NPSH for the pump under consideration. Required NPSH depends upon many factors relating to pump geometry and construction and intake system operating conditions, but it is defined simply as the difference between net suction head and vapor pressure at a given flow, or the energy needed to fill the pump on the intake side and overcome intake system head losses. If the net suction head is less than the vapor pressure of the water, the water will vaporize in the pump, producing cavitation. Small vapor bubbles formed in the low-pressure region will collapse violently upon entering regions of high pressure, causing localized stress concentrations and vibrations, ultimately leading to mechanical failure.

The required net positive suction head ($NPSH_{req}$) for any pump can be obtained from the manufacturer. The available net positive suction head ($NPSH_{av}$) must be calculated for each system. Because the total energy of a system is constant, the available NPSH may be determined at any point in the system. The general expression at the pump centerline follows from Bernoulli as

$$NPSH_{av} = \frac{(p_{gauge} + p_{atm})}{\rho g} + z - h_L - \frac{p_{vp}}{\rho g} \qquad (62)$$

where

h_L = friction head loss in intake system piping (in feet of water)

p_{vp} = vapor pressure (0.256 psia for water at 20°C)

Knowing the pressure and pipe friction loss terms, the pump can be set at a height, z, which will ensure that $NPSH_{av} > NPSH_{req}$.

Where a free surface exists on the intake side (such as at the surface of an intake reservoir) and the velocity at a point on the surface is negligible, the above expression simplifies to

$$NPSH_{av} = z - h_L + \frac{(p_{atm} - p_{vp})}{\rho g} \qquad (63)$$

For pumps of relatively low heads and large discharge capacities (common in fire protection applications) the available NPSH may be less than zero (h_L is large). These pumps should be installed well below the reservoir water level to eliminate the possibility of cavitation. For this reason and also to avoid accidental loss of prime, authorities having jurisdiction generally require *positive suction* installation. In such instances the pump should be of the vertical shaft type so that the motor can be installed at an elevation above any possible flood level.

The useful work done by a pump is the product of the weight of the liquid pumped and the head developed by the pump. The work per unit time in this context is the hydraulic horsepower, commonly called the water horsepower (WHP). For discharge, Q, in gpm, total dynamic head, h, in feet, and specific weight, γ, for water at 20°C (68°F),

$$WHP = \frac{Qh}{3960} \qquad (64)$$

The power required to actually drive the pump is the brake horsepower (BHP). The difference between water horsepower and brake horsepower is the power lost within the pump due to mechanical and hydraulic friction. The ratio of WHP to BHP is the pump efficiency, η_p. Similarly, the ratio of BHP to electrical or engine horsepower (EHP) is the motor efficiency, η_m. The overall efficiency is, then, the pump efficiency multiplied by the motor efficiency:

$$\eta = (\eta_p)(\eta_m) = \frac{WHP}{BHP} \cdot \frac{BHP}{EHP} \qquad (65)$$

Although WHP should be calculated using the specific weight of the fluid at known conditions of temperature and pressure, the variation for water is very small; it should be noted that pump motor sizes are chosen from standard available sizes in any case.

The interrelations of head, capacity, power, and efficiency for a given pump are known as the characteristics of the pump. They can be expressed graphically in the form of pump characteristic curves. Figure 4-2.21 shows a standard plot of the several variables at constant impeller speed (N). Note that the point of maximum operating efficiency on the head-capacity curve corresponds to the maximum value of the efficiency curve. The actual operating point of the pump, however, depends on the system demand (or system head) curve. The system head loss for any flow rate is the sum of the system friction head loss at that rate plus the total static head to be overcome in the system. Figure 4-2.22 illustrates the relationship. Recall from Figure 4-2.20 that the total static head is the difference in elevation between the discharge level and the suc-

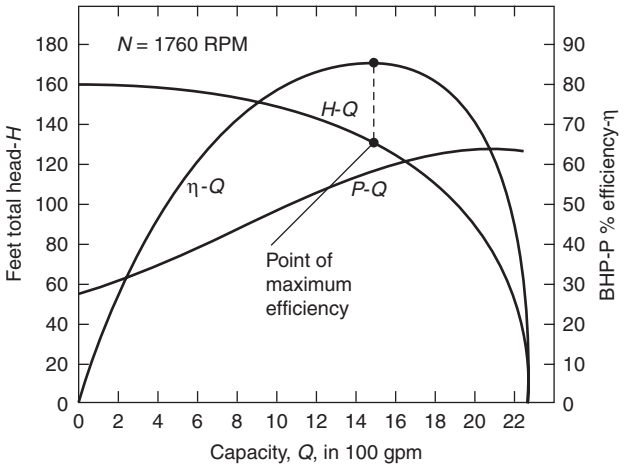

Figure 4-2.21. ***Centrifugal pump characteristics.***

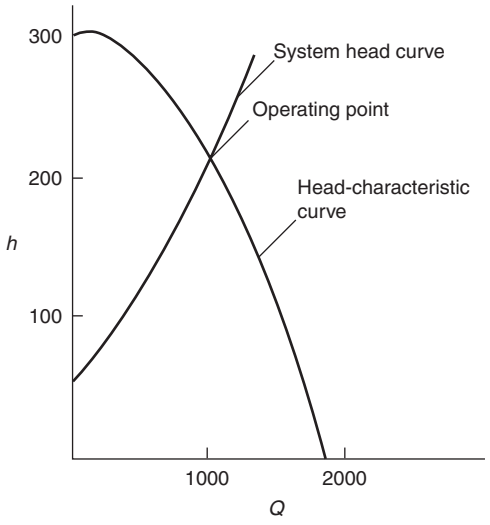

Figure 4-2.22. ***Graphical determination of operating point.***

tion level. System friction losses may be determined by calculations methods given in previous sections.

Pump Selection

Economical pump selection for fire protection applications requires consideration of the following factors:

1. The maximum discharge rate required under the most demanding design conditions
2. The total head-capacity relation (characteristic curve)
3. The suction head—in particular, the net positive suction head available
4. Pump speed and power source requirements
5. Pump spatial and environmental requirements
6. The maximum allowable system head downstream of the pump discharge

The usual design condition is that a system will be given or will be chosen from a very limited range of possibilities, and the proper pump must be selected. As shown in Figure 4-2.22, when the system demand curve and the pump head-capacity curve are superimposed, their intersection will determine the operating point of the pump. This point also locates the efficiency and, therefore, the power requirements. It is often economically desirable to select a pump such that its operating point is at or near its peak efficiency. In many fire protection applications, however, a pump may be called upon to operate very infrequently. Power consumption may, therefore, not be a significant factor relative to initial cost. Common practice in fire protection applications is to select a pump to operate at 150 percent of rated capacity at 65 percent of rated head (see NFPA 20[8])—that is, an operating point farther out along the characteristic curve. A pump is chosen such that its operating point so defined meets or exceeds the system demand curve at that point.

If the pump is to be used as a *booster* to increase supply main pressure, care must be exercised to select a pump having a maximum discharge head at zero flow (also known as *churn* head), which, when added to the maximum main's supply head, does not exceed the maximum allowable working pressure on the system. The maximum allowable working pressure prescribed by NFPA 13, for example, is 175 psig.[9]

Centrifugal Pump Affinity Relations

The abstract concept of *pump specific speed* has been developed to simplify the description of pump performance characteristics. It consolidates the discharge, head, and speed (rpm) at optimum performance into a single number. For a single stage, single suction pump, specific speed may be calculated from

$$N_s = \frac{NQ^{1/2}}{H^{3/4}} \tag{66}$$

where Q (in gpm) is taken at pump rpm, N, and total dynamic head, H. The specific speed of a pump is not actually a speed for that pump in any physical sense; it is defined as the speed in revolutions per minute at which a homologous (geometrically similar) pump would run if constructed to deliver 1 gpm against 1 ft total head at its peak efficiency. For pump impeller designs of identical proportions but different sizes, the specific speed is a constant performance index. That is, the performance of any impeller can be predicted from knowledge of the performance of any other geometrically similar impeller.

Changing the impeller diameter results in changes in discharge, total head, and delivered power. These changes occur according to the follow relations:

$$\frac{Q_1}{Q_2} = \left(\frac{D_1}{D_2}\right)^3 \frac{n_1}{n_2} \tag{67a}$$

$$\frac{H_1}{H_2} = \left(\frac{D_1}{D_2}\right)^2 \left(\frac{n_1}{n_2}\right)^2 \tag{67b}$$

$$\frac{Q_1}{Q_2} = \left(\frac{H_1}{H_2}\right)^{1/2} \left(\frac{D_1}{D_2}\right)^2 \tag{67c}$$

$$\frac{\mathrm{BHP}_1}{\mathrm{BHP}_2} = \left(\frac{D_1}{D_2}\right)^5 \frac{\rho_1}{\rho_2} \frac{n_1^3}{n_2^3} \tag{67d}$$

Since

$$\frac{N_1}{N_2} = \frac{D_1}{D_2} \tag{68}$$

a change in motor speed only will yield similar results. That is, a change in impeller size has the same effect on pump performance as a change in speed provided, of course, that there is no marked change in operating efficiency.

EXAMPLE 5:

A 6-in. (152.4-mm) pump operating at 1770 rpm discharges 1500 gpm (5678 l/m) of water at 40°F against a 120-ft (36.6-m) head.

(a) What discharge capacity and total head can be expected from a homologous 8-in. (203-mm) pump operating at 1170 rpm?
(b) If the pumps operate at an overall 80 percent efficiency, what is the 8-in. (203-mm) pump power requirement?

SOLUTION:

(a) From Equation 67b,

$$H_2 = \left[\frac{8^2(1170)^2}{(6)^2(1770)^2}\right](120) = 93.2 \text{ ft } (28.4 \text{ m})$$

From Equation 67a,

$$Q_2 = \left[\frac{(8)^3(1170)}{(6)^3(1770)}\right](1500) = 2350 \text{ gpm } (8895.5 \text{ l/m})$$

(b) From Equation 64,

$$\text{WHP} = \frac{2350(93.2)}{3960} = 55.3 \text{ HP}$$

Therefore,

$$\text{BHP} = \frac{55.3}{0.8} = 69.1 \text{ HP}$$

The motor chosen would be the next highest standard horsepower rating.

If more discharge or more head is required than a single pump can provide, two or more pumps may be combined to provide the necessary output. For example, when discharge is too little, pumps may be installed in parallel, sharing the same suction and inlet conditions. Figure 4-2.23 illustrates the principle. If a pump provides sufficient discharge but too little head, a second pump may be installed in series, the output of the first pump being fed directly into the suction of the second pump. Figure 4-2.24 depicts the series arrangement. A variety of compound arrangements are possible, depending on details of actual supply and demand, with economics being the prime arbiter.

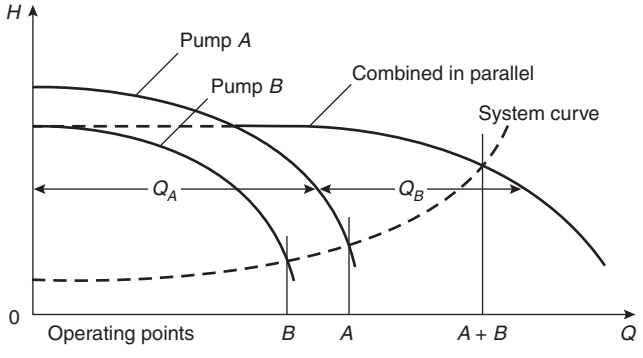

Figure 4-2.23. ***Two pumps combined in parallel.***

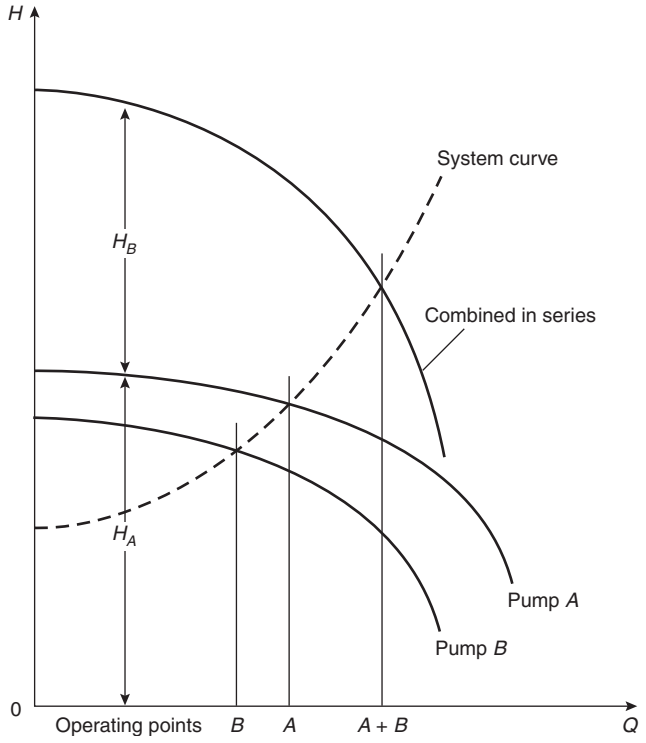

Figure 4-2.24. ***Two pumps combined in series.***

Nomenclature

A	area
C	proportionality constant or flow coefficient, Hazen-Williams C-factor
c	celerity of a shock wave
D	pipe diameter
d	element diameter
E	velocity of approach factor, bulk modulus of elasticity
f	Darcy-Weisbach friction loss factor
g	gravitational acceleration constant, 9.8 m/s^2
H	head of water
h	head
h_c	height of centroid
h_L	head loss
I	moment of inertia
K	proportionality constant or flow coefficient
k	proportionality constant or flow coefficient
L	length of conduit (in friction loss equations)
l	length or distance
m	mass

N pump rpm
p pressure
Q volumetric discharge rate
Re Reynolds number
S slope of energy gradient
s specific gravity
u stream velocity at a given point in flow cross section
V volume
v average stream velocity
z height above a reference datum (potential head)
α kinetic energy correction factor
β beta ratio
γ specific weight
Δ increment
ε pipe wall absolute roughness
η efficiency
μ absolute (dynamic) viscosity
ν kinematic viscosity
ρ density
τ fluid shear stress

References Cited

1. H.E. Hickey, *Hydraulics for Fire Protection,* National Fire Protection Association, Quincy, MA (1980).
2. R.P. Benedict, *Fundamentals of Pipe Flow,* Wiley-Interscience, New York (1980).
3. V.L. Streeter and E.G. Wylie, *Fluid Mechanics,* McGraw-Hill, New York (1979).
4. A.L. Simon, *Practical Hydraulics,* John Wiley & Sons, New York (1981).
5. F.M. White, *Fluid Mechanics,* McGraw-Hill, New York (1986).
6. T.M. Walski, *Analysis of Water Distribution Systems,* Van Nostrand Reinhold, New York (1984).
7. D. Stephenson, *Pipeflow Analysis,* Elsevier, Amsterdam (1984).
8. NFPA 20, *Installation of Centrifugal Fire Pumps,* National Fire Protection Association, Quincy, MA (1993).
9. NFPA 13, *Installation of Sprinkler Systems,* National Fire Protection Association, Quincy, MA (1994).

Additional Readings

R.A. Granger, *Fluid Mechanics,* Holt, Rinehart and Winston (CBS College Pub.), New York (1985).

N.H.C. Hwang, *Fundamentals of Hydraulic Engineering Systems,* Prentice-Hall, Englewood Cliffs, NJ (1981).

I.J. Karassik, ed., *Pump Handbook,* McGraw-Hill, New York (1986).

J.W. Murdock, *Fluid Mechanics and Its Applications,* Houghton Mifflin, Boston (1976).

CHAPTER 3

Automatic Sprinkler System Calculations

Russell P. Fleming

Introduction

Applications Where Water Is Appropriate

Water is the most commonly used fire extinguishing agent, mainly due to the fact that it is widely available and inexpensive. It also has very desirable fire extinguishing characteristics such as a high specific heat and high latent heat of vaporization. A single gallon of water can absorb 9280 Btus (2586.5 kJ) of heat as it increases from a 70°F (21°C) room temperature to become steam at 212°F (100°C).

Water is not the perfect extinguishing agent, however, and is considered inappropriate for the protection of certain water reactive materials. In some cases, the use of water can produce heat, flammable or toxic gases, or explosions. The quantities of such products must be considered, however, because application of sufficient water can overcome the reaction of minor amounts of these materials.

Another drawback of water is that it is more dense than most hydrocarbon fuels, and immiscible as well. Therefore, water will not provide an effective cover for burning hydrocarbons, or mix with them and dilute them to the point of not sustaining combustion. Instead, the hydrocarbons will float on top of the water, continuing to burn and possibly spread. To combat such fires, foam solutions can be introduced into the water to provide an effective cover and smother the fire. Applying water in a fine mist has also been successful.

However, even when water from sprinklers will not suppress the fire, its cooling ability can protect structural elements of a building by containing the fire until it can be extinguished by other means.

Russell P. Fleming, P.E., is vice president of engineering, National Fire Sprinkler Association, Patterson, New York. Mr. Fleming has served as a member of more than a dozen NFPA technical committees, including the Committee on Automatic Sprinklers. He currently serves on the Board of Directors of NFPA.

Types of Sprinkler Systems

Automatic sprinkler systems are considered to be the most effective and economical way to apply water to suppress a fire. There are four basic types of sprinkler systems:

1. A *wet pipe* system is by far the most common type of sprinkler system. It consists of a network of piping containing water under pressure. Automatic sprinklers are connected to the piping such that each sprinkler protects an assigned building area. The application of heat to any sprinkler will cause that single sprinkler to operate, permitting water to discharge over its area of protection.
2. A *dry pipe* system is similar to a wet system, except that water is held back from the piping network by a special dry pipe valve. The valve is kept closed by air or nitrogen pressure maintained in the piping. The operation of one or more sprinklers will allow the air pressure to escape, causing operation of the dry valve, which then permits water to flow into the piping to suppress the fire. Dry systems are used where the water in the piping would be subject to freezing.
3. A *deluge* system is one that does not use automatic sprinklers, but rather open sprinklers. A special deluge valve holds back the water from the piping, and is activated by a separate fire detection system. When activated, the deluge valve admits water to the piping network, and water flows simultaneously from all of the open sprinklers. Deluge systems are used for protection against rapidly spreading, high hazard fires.
4. A *preaction* system is similar to a deluge system except that automatic sprinklers are used, and a small air pressure is usually maintained in the piping network to ensure that the system is air tight. As with a deluge system, a separate detection system is used to activate a deluge valve, admitting water to the piping. However, because automatic sprinklers are used, the water is usually stopped from flowing unless heat from the fire has also activated one or more sprinklers. Some

special arrangements of preaction systems permit variations on detection system interaction with sprinkler operation. Preaction systems are generally used where there is special concern for accidental discharge of water, as in valuable computer areas.

These four basic types of systems differ in terms of the most fundamental aspect of how the water is put into the area of the fire. There are many other types of sprinkler systems, classified according to the hazard they protect (such as residential, in-rack, or exposure protection); additives to the system (such as antifreeze or foam); or special connections to the system (such as multipurpose piping). However, all sprinkler systems can still be categorized as one of the basic four types.

Applicable Standards

NFPA 13, *Standard for the Installation of Sprinkler Systems* (hereafter referred to as NFPA 13), is a design and installation standard for automatic sprinkler systems, referenced by most building codes in the United States and Canada.[1] This standard, in turn, references other NFPA standards for details as to water supply components, including NFPA 14, *Standard for the Installation of Standpipe and Hose Systems;* NFPA 20, *Standard for the Installation of Centrifugal Fire Pumps* (hereafter referred to as NFPA 20); NFPA 22, *Standard for Water Tanks for Private Fire Protection* (hereafter referred to as NFPA 22); and NFPA 24, *Standard for the Installation of Private Fire Service Mains and Their Appurtenances.*

For protection of warehouse storage, NFPA 13 traditionally referenced special storage standards that contained sprinkler system design criteria, including NFPA 231, *Standard for General Storage Materials* (hereafter referred to as NFPA 231); NFPA 231C, *Standard for Rack Storage of Materials* (hereafter referred to as NFPA 231C); NFPA 231D, *Standard for Rubber Tire Storage;* and NFPA 231F, *Standard for Roll Paper Storage.* However, beginning with the 1999 edition of NFPA 13 these standards were all merged into NFPA 13 to produce a consolidated sprinkler system design and installation standard.

Other NFPA standards contain design criteria for special types of occupancies or systems, including NFPA 13D, *Standard for the Installation of Sprinkler Systems in One- and Two-Family Dwellings and Manufactured Homes* (hereafter referred to as NFPA 13D); NFPA 15, *Standard for Water Spray Fixed Systems for Fire Protection;* NFPA 16, *Standard for the Installation of Foam-Water Sprinkler and Foam-Water Spray Systems;* NFPA 30, *Flammable and Combustible Liquids Code;* NFPA 30B, *Code for the Manufacture and Storage of Aerosol Products;* and NFPA 409, *Standard on Aircraft Hangars.*

Limits of Calculation in an Empirical Design Process

Engineering calculations are best performed in areas where an understanding exists as to relationships between parameters. This is not the case with the technology of automatic sprinkler systems. Calculation methods are widely used with regard to only one aspect of sprinkler systems: water flow through piping. There are only very rudimentary calculation methods available with regard to the most fundamental aspect of sprinkler systems, i.e., the ability of water spray to suppress fires.

The reason that calculation methods are not used is simply the complexity of the mechanisms by which water suppresses fires. Water-based fire suppression has to this point not been thoroughly characterized to permit application of mathematical modeling techniques. As a result, the fire suppression aspects of sprinkler system design are empirical at best.

Some, but not all, of the current sprinkler system design criteria are based on full-scale testing, including the criteria originally developed for NFPA 231C and 13D, and parts of NFPA 13, such as the material on the use of large drop and ESFR (early suppression fast response) sprinklers. Most of the NFPA 13 protection criteria, however, are the result of evolution and application of experienced judgment. In the 1970s, the capabilities of pipe schedule systems, which had demonstrated a hundred years of satisfactory performance, were codified into a system of area/density curves. This permitted the introduction of hydraulic calculations to what had become a cookbook-type method of designing sprinkler systems. It allowed system designers to take advantage of strong water supplies to produce more economical systems. It also permitted the determination of specific flows and pressures available at various points of the system, opening the door to the use of "special sprinklers." Special sprinklers are approved for use on the basis of their ability to accomplish specific protection goals, but are not interchangeable since there is no standardization of minimum flows and pressures.

Because of this history, the calculation methods available to the fire protection engineer in standard sprinkler system design are only ancillary to the true function of a sprinkler system. The sections that follow in this chapter address hydraulic calculations of flow through piping, simple calculations commonly performed in determining water supply requirements, and optional calculations that may be performed with regard to hanging and bracing of system piping. The final section of this chapter deals with the performance of a system relative to a fire, and the material contained therein is totally outside the realm of standard practice. This material is not sufficiently complete to permit a full design approach, but only isolated bits of total system performance.

Hydraulic Calculations

Density-Based Sprinkler Demand

Occupancy hazard classification is the most critical aspect of the sprinkler system design process. If the hazard is underestimated, it is possible for fire to overpower the sprinklers, conceivably resulting in a large loss of property or life. Hazard classification is not an area in which calculation methods are presently in use, however. The proper classification of hazard requires experienced judgment and familiarity with relevant NFPA standards.

Once the hazard or commodity classification is determined and a sprinkler spacing and piping layout has

been proposed in conformance with the requirements of the standard, the system designer can begin a series of calculations to demonstrate that the delivery of a prescribed rate of water application will be accomplished for the maximum number of sprinklers that might be reasonably expected to operate. This number of sprinklers, which must be supplied regardless of the location of the fire within the building, is the basis of the concept of the remote design area. The designer needs to demonstrate that the shape and location of the sprinkler arrangement in the design area will be adequately supplied with water in the event of a fire.

Prior to locating the design area, there is the question of how many sprinklers are to be included. This question is primarily addressed by the occupancy hazard classification, but the designer also has some freedom to decide this matter.

Figure 7-2.3.1.2 of the 1999 edition of NFPA 13 and corresponding figures in NFPA 231 and 231C contain area/density curves from which the designer can select a design area and density appropriate for the occupancy hazard classification. Any point on or to the right of the curve in the figure(s) is acceptable. The designer may select a high density over a small area, or a low density over a large area. In either event, the fire is expected to be controlled by the sprinklers within that design area, without opening any additional sprinklers.

EXAMPLE 1:

Using the sample area/density curve shown in Figure 4-3.1, many different design criteria could be selected, ranging from a density of 0.1 gpm/ft² (3.7 mm/min) over 5000 ft² (500 m²) to 0.17 gpm/ft² (6.9 mm/min) over 1500 ft² (139 m²). Either of these two points, or any point to the right of the curve [such as 0.16 gpm/ft² (6.5 mm/min) over 3000 ft² (276 m²)] would be considered acceptable. A selection of 0.15 gpm/ft² (6.1 mm/min) over 2400 ft² (221 m²) is indicated.

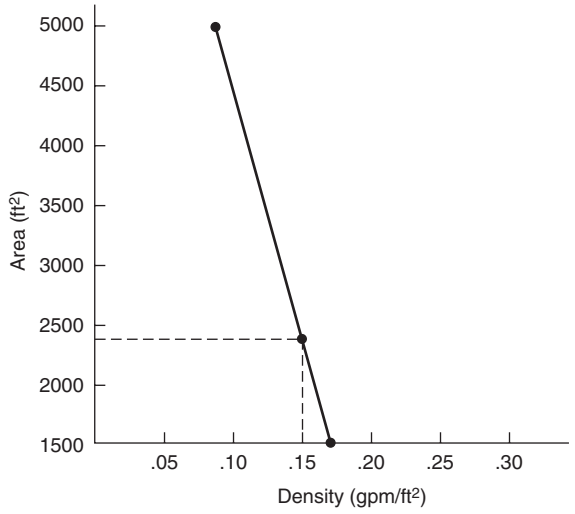

Figure 4-3.1. ***Sample area/density curve.***

Water is provided only for the number of sprinklers in the design area, since no water is needed for the sprinklers that are not expected to open. The actual number of sprinklers in the design area depends, of course, on the spacing of the sprinklers. NFPA 13 requires that the design area be divided by the maximum sprinkler spacing used, and that any fractional result be rounded up to the next whole sprinkler.

EXAMPLE 2:

Based on the point selected from the sample area/density curve above and the proposed maximum spacing of sprinklers, the number of sprinklers to be included in the design area can be determined. If sprinklers are spaced at 12 × 15 ft (3.66 × 4.57 m) so as to each protect an area of 180 ft² (16.72 m²), the design area of 2400 ft² (221 m²) would include

$$\frac{2400}{180} = 13.33 = 14 \text{ sprinklers}$$

The remote design area is required to have a rectangular shape, with the long side along the run of the branch lines. The length of the design area (needed to determine how many sprinklers along a branch line are contained within it) is found by multiplying the square root of the design area by a factor of 1.2. Again, any fractional result is rounded to the next whole sprinkler.

EXAMPLE 3:

If the 14 sprinklers from Example 2 were spaced 12 ft (3.66 m) along branch lines 15 ft (4.57 m) apart, the length of the rectangular area along the branch lines would be

$$\frac{1.2(2400)^{1/2}}{12} = \frac{1.2(49)}{12} = 4.9 = 5 \text{ sprinklers}$$

If the sprinklers were spaced 15 ft (4.57 m) along branch lines 12 ft (3.66 m) apart, the same length of the design area would include only 4 sprinklers.

NFPA 13 (1999) contains some exceptions to this method of locating a remote design area and determining the number of sprinklers to be supplied. Chapter 7 of the standard has special modifications to the design area based on factors such as the use of a dry system, the use of quick response sprinklers under flat smooth ceilings of limited height, and the existence of nonsprinklered combustible concealed spaces within the building. The chapter also contains a room design method, which can reduce the number of sprinklers expected to operate in a highly compartmented occupancy. Also, beginning in 1985, the standard adopted a four sprinkler design area for dwelling units and their adjacent corridors when residential sprinklers are installed in accordance with their listing requirements.

Figures in the appendix to Chapter 8 of NFPA 13 (1999 edition) show the normal documentation and the step-by-step calculation procedure for a sample sprinkler system. The starting point is the most remote sprinkler in the design area. For tree systems, in which each sprinkler is supplied from only one direction, the most remote sprinkler is generally the end sprinkler on the farthest branch line from the system riser. This sprinkler, and all

others as a result, must be provided with a sufficient flow of water to meet the density appropriate for the point selected on the area/density curve.

Where a sprinkler protects an irregular area, NFPA 13 prescribes that the area of coverage for the sprinkler must be based on the largest sides of its coverage. In other words, the area which a sprinkler protects for calculation purposes is equal to

$$\text{area of coverage} = S \times L$$

where S is twice the larger of the distances to the next sprinkler (or wall for an end sprinkler) in both the upstream and downstream directions, and L is twice the larger of the distances to adjacent branch lines (or wall in the case of the last branch line) on either side. This reflects the need to flow more water with increasing distance from the sprinkler, since increased flow tends to expand the effective spray umbrella of the sprinkler.

The minimum flow from a sprinkler must be the product of the area of coverage multiplied by the minimum required density

$$Q = \text{area of coverage} \times \text{density}$$

Most of the special listed sprinklers and residential sprinklers have a minimum flow requirement associated with their listings, which is often based on the spacing at which they are used. These minimum flow considerations override the minimum flow based on the area/density method.

EXAMPLE 4:

If a standard spray sprinkler protects an area extending to 7 ft (2.1 m) on the north side (half the distance to the next branch line), 5 ft (1.5 m) on the south side (to a wall), 6 ft (1.8 m) on the west side (half the distance to the next sprinkler on the branch line), and 4 ft (1.2 m) on the east side (to a wall), the minimum flow required for the sprinkler to achieve the density requirement selected in Example 1 can be found by completing two steps. The first step involves determining the area of coverage. In this case

$$S \times L = 2(6\text{ ft}) \times 2(7\text{ ft}) = 12\text{ ft} \times 14\text{ ft}$$
$$= 168\text{ ft}^2\ (15.6\text{ m}^2)$$

The second step involves multiplying this coverage area by the required density

$$Q = A \times \rho = 168\text{ ft}^2 \times 0.15\text{ gpm/ft}^2$$
$$= 25.2\text{ gpm}\ (95.4\text{ lpm})$$

Pressure Requirements of the Most Remote Sprinkler

When flow through a sprinkler orifice takes place, the energy of the water changes from the potential energy of pressure to the kinetic energy of flow. A formula can be derived from the basic energy equations to determine how much water will flow through an orifice based on the water pressure inside the piping at the orifice:

$$Q = 29.83 c_d d^2 P^{1/2}$$

However, this formula contains a factor, c_d, which is a discharge coefficient characteristic of the orifice and which must be determined experimentally. For sprinklers, the product testing laboratories determine the orifice discharge coefficient at the time of listing of a particular model of sprinkler. To simplify things, all factors other than pressure are lumped into what is experimentally determined as the K-factor of a sprinkler, such that

$$Q = K \times P^{1/2}$$

where K has units of gpm/(psi)$^{1/2}$ [lpm/(bar)$^{1/2}$].

If the required minimum flow at the most remote sprinkler is known, determined by either the area/density method or the special sprinkler listing, the minimum pressure needed at the most remote sprinkler can easily be found.

Since $Q = K(P)^{1/2}$, then $P = (Q/K)^2$

NFPA 13 sets a minimum pressure of 7 psi (0.48 bar) at the end sprinkler in any event, so that a proper spray umbrella is ensured.

EXAMPLE 5:

The pressure required at the sprinkler in Example 4 can be determined using the above formula if the K-factor is known. The K-factor to be used for a standard orifice (nominal ½-in.) sprinkler is 5.6.

$$P = \left(\frac{Q}{K}\right)^2 = \left(\frac{25.2}{5.6}\right)^2 = 20.2\text{ psi (1.4 bar)}$$

Once the minimum pressure at the most remote sprinkler is determined, the hydraulic calculation method proceeds backward toward the source of supply. If the sprinkler spacing is regular, it can be assumed that all other sprinklers within the design area will be flowing at least as much water, and the minimum density is assured. If spacing is irregular or sprinklers with different K-factors are used, care must be taken that each sprinkler is provided with sufficient flow.

As the calculations proceed toward the system riser, the minimum pressure requirements increase, because additional pressures are needed at these points if elevation and friction losses are to be overcome while still maintaining the minimum needed pressure at the most remote sprinkler. These losses are determined as discussed below, and their values added to the total pressure requirements. Total flow requirements also increase backward toward the source of supply, until calculations get beyond the design area. Then there is no flow added other than hose stream allowances.

It should be noted that each sprinkler closer to the source of supply will show a successively greater flow rate, since a higher total pressure is available at that point in the system piping. This effect on the total water demand is

termed hydraulic increase, and is the reason why the total water demand of a system is not simply equal to the product of the minimum density and the design area. When calculations are complete, the system demand will be known, stated in the form of a specific flow at a specific pressure.

Pressure Losses through Piping, Fittings, and Valves

Friction losses resulting from water flow through piping can be estimated by several engineering approaches, but NFPA 13 specifies the use of the Hazen-Williams method. This approach is based on the formula developed empirically by Hazen and Williams:

$$p = \frac{4.52Q^{185}}{C^{1.85}d^{4.87}}$$

where

p = friction loss per ft of pipe in psi

Q = flow rate in gpm

d = internal pipe diameter in inches

C = Hazen-Williams coefficient

The choice of C is critical to the accuracy of the friction loss determination, and is therefore stipulated by NFPA 13. The values assigned for use are intended to simulate the expected interior roughness of aged pipe. (See Table 4-3.1.)

Rather than make the Hazen-Williams calculation for each section of piping, it has become standard practice, when doing hand calculations, to use a friction loss table, which contains all values of p for various values of Q and various pipe sizes. In many cases the tables are based on the use of Schedule 40 steel pipe for wet systems. The use of other pipe schedules, pipe materials, or system types may require the use of multiplying factors.

Once the value of friction loss per foot is determined using either the previous equation or friction loss tables, the total friction loss through a section of pipe is found by multiplying p by the length of pipe, L. Since NFPA 13 uses p to designate loss per foot, total friction loss in a length of pipe can be designated by p_f, where

$$p_f = p \times L$$

In the analysis of complex piping arrangements, it is sometimes convenient to lump the values of all factors in the Hazen-Williams equation (except flow) for a given piece of pipe into a constant, K, identified as a friction loss coefficient. To avoid confusion with the nozzle coefficient K, this coefficient can be identified as FLC, friction loss coefficient.

$$\text{FLC} = \frac{(L \times 4.52)}{(C^{1.85}d^{4.87})}$$

The value of p_f is therefore equal to

$$p_f = \text{FLC} \times Q^{1.85}$$

Table 4-3.1 *C Values for Pipes*

Type of Pipe	Assigned C Factor
Steel pipe—dry and preaction systems	100
Steel pipe—wet and deluge systems	120
Galvanized steel pipe—all systems	120
Cement lined cast or ductile iron	140
Copper tube	150
Plastic (listed)	150

EXAMPLE 6:

If the most remote sprinkler on a branch line requires a minimum flow of 25.2 gpm (92.1 lpm) (for a minimum pressure of 20.2 psi [1.4 bar]) as shown in Examples 4 and 5, and the second sprinkler on the line is connected by a 12-ft (3.6-m) length of 1 in. (25.4 mm) Schedule 40 steel pipe, with both sprinklers mounted directly in fittings on the pipe (no drops or sprigs), the minimum pressure required at the second sprinkler can be found by determining the friction loss caused by a flow of 25.2 gpm (92.1 lpm) through the piping to the end sprinkler. No fitting losses need to be considered if it is a straight run of pipe, since NFPA 13 permits the fitting directly attached to each sprinkler to be ignored.

Using the Hazen-Williams equation with values of 25.2 for Q, 120 for C, and 1.049 for d (the inside diameter of Schedule 40 steel 1-in. pipe) results in a value of p = 0.20 psi (0.012 bar) per foot of pipe. Multiplying by the 12-ft (3.6-m) length results in a total friction loss of p_f = 2.4 psi (0.17 bar). The total pressure required at the second sprinkler on the line is therefore 20.2 psi + 2.4 psi = 22.6 psi (1.6 bar). This will result in a flow from the second sprinkler of $Q = K(P)^{1/2}$ = 26.6 gpm (100.7 lpm).

Minor losses through fittings and valves are not friction losses but energy losses, caused by turbulence in the water flow which increase as the velocity of flow increases. Nevertheless, it has become standard practice to simplify calculation of such losses through the use of "equivalent lengths," which are added to the actual pipe length in determining the pipe friction loss. NFPA 13 contains a table of equivalent pipe lengths for this purpose. (See Table 4-3.2.) As an example, if a 2-in. (50.8-mm) 90-degree long turn elbow is assigned an equivalent length of 3 ft (0.914 m), this means that the energy loss associated with turbulence through the elbow is expected to approximate the energy loss to friction through 0.914 m of 50.8 mm pipe. As with the friction loss tables, the equivalent pipe length chart is based on the use of steel pipe with a C-factor of 120, and the use of other piping materials requires multiplying factors. The equivalent pipe length for pipes having C values other then 120 should be adjusted using the following multiplication factors: 0.713 for a C value of 100; 1.16 for a C value of 130; 1.33 for a C value of 140; 1.51 for a C value of 150.

EXAMPLE 7:

If the 12-ft (3.6-m) length of 1-in. (25.4-mm) pipe in Example 6 had contained 4 elbows so as to avoid a building column, the pressure loss from those elbows could be approximated by adding an equivalent length of pipe to the friction loss calculation. Table 4-3.2 gives a value of 2 ft (0.610 m) as the appropriate equivalent length for standard elbows in 1 in. (25.4 mm) Schedule 40 steel pipe. For

Table 4-3.2 ***Equivalent Pipe Length Chart (for C = 120)***

Fittings and Valves	Fittings and Valves Expressed in Equivalent Feet of Pipe													
	¾ in.	1 in.	1¼ in.	1½ in.	2 in.	2½ in.	3 in.	3½ in.	4 in.	5 in.	6 in.	8 in.	10 in.	12 in.
45° Elbow	1	1	1	2	2	3	3	3	4	5	7	9	11	13
90° Standard Elbow	2	2	3	4	5	6	7	8	10	12	14	18	22	27
90° Long Turn Elbow	1	2	2	2	3	4	5	5	6	8	9	13	16	18
Tee or Cross (Flow Turned 90°)	3	5	6	8	10	12	15	17	20	25	30	35	50	60
Butterfly Valve	—	—	—	—	6	7	10	—	12	9	10	12	19	21
Gate Valve	—	—	—	—	1	1	1	1	2	2	3	4	5	6
Swing Check[a]	—	5	7	9	11	14	16	19	22	27	32	45	55	65

For SI Units: 1 ft = 0.3048 m.

[a]Due to the variations in design of swing check valves, the pipe equivalents indicated in the above chart are to be considered average.

4 elbows, the equivalent fitting length would be 8 ft (2.4 m). Added to the actual pipe length of 12 ft (3.6 m), the total equivalent length would be 20 ft (6 m). This results in a new value of p_f = 20-ft · 0.20 psi/ft = 4.0 psi (0.28 bar). The total pressure at the second sprinkler would then be equal to 20.2 psi + 4.0 psi = 24.2 psi (1.67 bar). The total flow from the second sprinkler in this case would be $Q = K(P)^{1/2}$ = 27.5 gpm (100.4 lpm).

Some types of standard valves, such as swing check valves, are included in the equivalent pipe length chart, Table 4-3.2. Equivalent lengths for pressure losses through system alarm, dry, and deluge valves are determined by the approval laboratories at the time of product listing.

Use of Velocity Pressures

The value of pressure, *P,* in the sprinkler orifice flow formula can be considered either the total pressure, P_t, or the normal pressure, P_n, since NFPA 13 permits the use of velocity pressures at the discretion of the designer. Total pressure, normal pressure, and velocity pressure, P_v, have the following relationship:

$$P_n = P_t - P_v$$

Total pressure is the counterpart of total energy or total head, and can be considered the pressure that would act against an orifice if all of the energy of the water in the pipe at that point were focused toward flow out of the orifice. This is the case where there is no flow past the orifice in the piping. Where flow does take place in the piping past an orifice, however, normal pressure is that portion of the total pressure which is actually acting normal to the direction of flow in the piping, and therefore acting in the direction of flow through the orifice. The amount by which normal pressure is less than total pressure is velocity pressure, which is acting in the direction of flow in the piping. Velocity pressure corresponds to velocity energy, which is the energy of motion. There is no factor in the above expression for elevation head, because the flow from an orifice can be considered to take place in a datum plane.

When velocity pressures are used in calculations, it is recognized that some of the energy of the water is in the form of velocity head, which is not acting normal to the pipe walls (where it would help push water out the orifice), but rather in the downstream direction. Thus, for every sprinkler (except the end sprinkler on a line), slightly less flow takes place than what would be calculated from the use of the formula $Q = K(P_t)^{1/2}$. (See Figure 4-3.2.)

NFPA 13 permits the velocity pressure effects to be ignored, however, since they are usually rather minor, and since ignoring the effects of velocity pressure tends to produce a more conservative design.

If velocity pressures are considered, normal pressure rather than total pressure is used when determining flow through any sprinkler except the end sprinkler on a branch line, and through any branch line except the end branch line on a cross main. The velocity pressure, P_v, which is subtracted from the total pressure in order to determine the normal pressure, is determined as

$$P_v = \frac{v^2}{2g} \times 0.433 \text{ psi/ft } (0.098 \text{ bar/m})$$

or

$$P_v = 0.001123Q^2/d^4$$

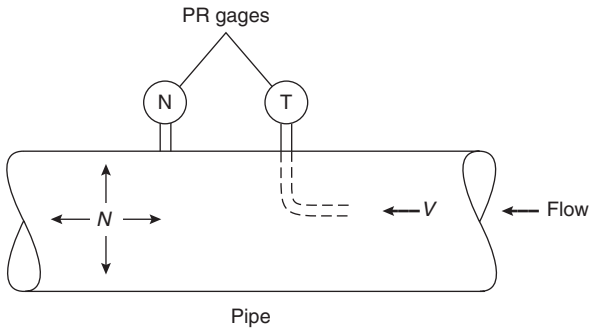

Figure 4-3.2. ***Velocity and normal pressures in piping.***

where Q is the upstream flow through the piping to an orifice (or branch line) in gpm and d is the actual internal diameter of the upstream pipe in inches.

Because NFPA 13 mandates the use of the upstream flow, an iterative approach to determining the velocity pressure is necessary. The upstream flow cannot be known unless the flow from the sprinkler (or branch line) in question is known, and the flow from the sprinkler (or branch line) is affected by the velocity pressure resulting from the upstream flow.

EXAMPLE 8:

If the pipe on the upsteam side of the second sprinkler in Example 6 were 3 in. Schedule 40 steel pipe with an inside diameter of 1.38 in. (35 mm), the flow from the second sprinkler would be considered to be 26.6 gpm (100.2 lpm) as determined at the end of Example 6, if velocity pressures were not included.

If velocity pressures were to be considered, an upstream flow would first be assumed. Since the end sprinkler had a minimum flow of 25.2 gpm (95.2 lpm) and the upstream flow would consist of the combined flow rates of the two sprinklers, an estimate of 52 gpm (196.8 lpm) might appear reasonable. Substituting this flow and the pipe diameter into the equation for velocity pressure gives

$$P_v = \frac{0.001123Q^2}{d^4}$$
$$= \frac{0.001123(52)^2}{(1.38)^4}$$
$$= 0.8 \text{ psi } (0.06 \text{ bar})$$

This means that the actual pressure acting on the orifice of the second sprinkler is equal to

$$P_n = P_t - P_v$$
$$= 22.6 \text{ psi} - 0.8 \text{ psi}$$
$$= 21.8 \text{ psi } (1.50 \text{ bar})$$

This would result in a flow from the second sprinkler of

$$Q = K(P)^{1/2}$$
$$= 26.1 \text{ gpm } (98.7 \text{ lpm})$$

Combining this flow with the known flow from the end sprinkler results in a total upstream flow of 51.3 gpm (194.2 lpm). To determine if the initial guess was close enough, determine the velocity pressure that would result from an upstream flow of 51.3 gpm (194.2 lpm). This calculation also results in a velocity pressure of 0.8 psi (0.06 bar), and the process is therefore complete. It can be seen that the second sprinkler apparently flows 0.5 gpm (1.9 lpm) less through the consideration of velocity pressures.

Elevation Losses

Variation of pressure within a fluid at rest is related to the density or unit (specific) weight of the fluid. The unit weight of a fluid is equal to its density multiplied by the acceleration of gravity. The unit weight of water is 62.4 lbs/ft^3 (1000 kg/m^3).

This means that one cubic foot of water at rest weighs 62.4 pounds (1000 kg). The cubic foot of water, or any other water column one foot high, thus results in a static pressure at its base of 62.4 pounds per square foot (304.66 kg/m^2). Divided by 144 sq in. per sq ft (1.020×10^4 kg/m^3 bar), this is a pressure of 0.433 pounds per sq in. per ft (0.099 bar/m) of water column.

A column of water 10 ft (3.048 m) high similarly exerts a pressure of 10 ft $\times$ 62.4 lbs/ft^2 $\times$ 1 ft/144 in.^{2} = 4.33 psi (3.048 m $\times$ 999.5 kg/m^2 $\div$ 1.020×10^4 kg/m^2 bar = 0.299 bar). The static pressure at the top of both columns of water is equal to zero (gauge pressure), or atmospheric pressure.

On this basis, additional pressure must be available within a sprinkler system water supply to overcome the pressure loss associated with elevation. This pressure is equal to 0.433 psi per foot (0.099 bar/m) of elevation of the sprinklers above the level where the water supply information is known.

Sometimes the additional pressure needed to overcome elevation is added at the point where the elevation change takes place within the system. If significant elevation changes take place within a portion of the system that is likely to be considered as a representative flowing orifice (such as a single branch line along a cross main that is equivalent to other lines in the remote design area), then it is considered more accurate to wait until calculations have been completed, and simply add an elevation pressure increase to account for the total height of the highest sprinklers above the supply point.

EXAMPLE 9:

The pressure that must be added to a system supply to compensate for the fact that the sprinklers are located 120 ft (36.6 m) above the supply can be found by multiplying the total elevation difference by 0.433 psi/ft (0.099 bar/m).

$$120 \text{ ft} \times 0.433 \text{ psi/ft} = 52 \text{ psi } (3.62 \text{ bar})$$

Loops and Grids

Hydraulic calculations become more complicated when piping is configured in loops or grids, such that water feeding any given sprinkler or branch line can be supplied through more than one route. A number of computer programs that handle the repetitive calculations have therefore been developed specifically for fire protection systems, and are being marketed commercially.

Determining the flow split that takes place in the various parts of any loop or grid is accomplished by applying the basic principles of conservation of mass and conservation of energy. For a single loop, it should be recognized that the energy loss across each of the two legs from one end of the system to the other must be equal. Otherwise, a circulation would take place within the loop itself. Also, mass is conserved by the fact that the sum of the two individual flows through the paths is equal to the total flow into (and out of) the loop. (See Figure 4-3.3.)

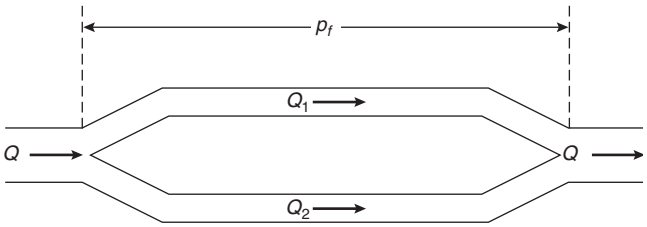

Figure 4-3.3. ***Example of a simple loop configuration.***

Applying the Hazen-Williams formula to each leg of the loop

$$p_f = L_1 \frac{4.52Q_1^{1.85}}{C_1^{1.85}d_1^{4.87}} = L_2 \frac{4.52Q_2^{1.85}}{C_2^{1.85}d_2^{1.85}}$$

Substituting the term FLC for all terms except Q,

$$p_f = \text{FLC}_1 Q_1^{1.85} = \text{FLC}_2 Q_2^{1.85}$$

This simplifies to become

$$\left(\frac{Q_1}{Q_2}\right)^{1.85} = \frac{\text{FLC}_2}{\text{FLC}_1}$$

Since Q_1 and Q_2 combine to create a total flow of Q, the flow through one leg can be determined as

$$Q_1 = \frac{Q}{[(\text{FLC}_1/\text{FLC}_2)^{0.54} + 1]}$$

For the simplest of looped systems, a single loop, hand calculations are not complex. Sometimes, seemingly complex piping systems can be simplified by substituting an "equivalent pipe" for two or more pipes in series or in parallel.

For pipes in series

$$\text{FLC}_e = \text{FLC}_1 + \text{FLC}_2 + \text{FLC}_3 + \cdots$$

For pipes in parallel

$$\left(\frac{1}{\text{FLC}_e}\right)^{0.54} = \left(\frac{1}{\text{FLC}_1}\right)^{0.54} + \left(\frac{1}{\text{FLC}_2}\right)^{0.54} + \cdots$$

For gridded systems, which involve flow through multiple loops, computers are generally used since it becomes necessary to solve a system of nonlinear equations. When hand calculations are performed, the Hardy Cross[2] method of balancing heads is generally employed. This method involves assuming a flow distribution within the piping network, then applying successive corrective flows until differences in pressure losses through the various routes are nearly equal.

The Hardy Cross solution procedure applied to sprinkler system piping is as follows:

1. Identify all loop circuits and the significant parameters associated with each line of the loop, such as pipe length, diameter, and Hazen-Williams coefficient. Reduce the number of individual pipes where possible by finding the equivalent pipe for pipes in series or parallel.
2. Evaluate each parameter in the proper units. Minor losses through fittings should be converted to equivalent pipe lengths. A value of all parameters except flow for each pipe section should be calculated (FLC).
3. Assume a reasonable distribution of flows that satisifies continuity, proceeding loop by loop.
4. Compute the pressure (or head) loss due to friction, p_f, in each pipe using the FLC in the Hazen-Williams formula.
5. Sum the friction losses around each loop with due regard to sign. (Assume clockwise positive, for example.) Flows are correct when the sum of the losses, dp_f, is equal to zero.
6. If the sum of the losses is not zero for each loop, divide each pipe's friction loss by the presumed flow for the pipe, p_f/Q.
7. Calculate a correction flow for each loop as

$$dQ = \frac{-dp_f}{[1.85\Sigma(p_f/Q)]}$$

8. Add the correction flow values to each pipe in the loop as required, thereby increasing or decreasing the earlier assumed flows. For cases where a single pipe is in two loops, the algebraic difference between the two values of dQ must be applied as the correction to the assumed flow.
9. With a new set of assumed flows, repeat steps 4 through 7 until the values of dQ are sufficiently small.
10. As a final check, calculate the pressure loss by any route from the initial to the final junction. A second calculation along another route should give the same value within the range of accuracy expected.

NFPA 13 requires that pressures be shown to balance within 0.5 psi (0.03 bar) at hydraulic junction points. In other words, the designer (or computer program) must continue to make successive guesses as to how much flow takes place in each piece of pipe until the pressure loss from the design area back to the source of supply is approximately the same (within 0.5 psi [0.03 bar]) regardless of the path chosen.

EXAMPLE 10:

For the small two-loop grid shown in Figure 4-3.4, the total flow in and out is 100 gpm (378.5 lpm). It is necessary to determine the flow taking place through each pipe section. The system has already been simplified by finding the equivalent pipe for all pipes in series and in parallel. The following values of FLC have been calculated:

Pipe 1 FLC = 0.001
Pipe 2 FLC = 0.002
Pipe 3 FLC = 0.003
Pipe 4 FLC = 0.001
Pipe 5 FLC = 0.004

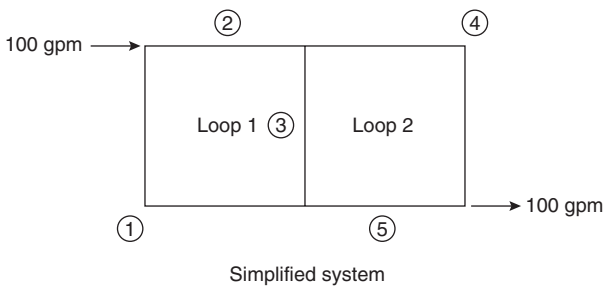

Figure 4-3.4. ***Simplified system, pipe in series.***

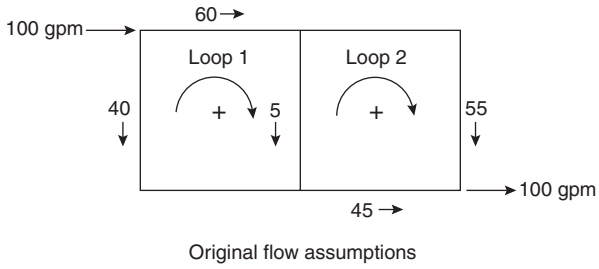

Figure 4-3.5. ***Original flow assumptions.***

Under step 3 of the Hardy Cross procedure, flows that would satisfy conservation of mass are assumed. (See Figure 4-3.5.) Steps 4 through 9 are then carried out in a tabular approach. (See Table 4-3.3.)

Making these adjustments to again balance flows, a second set of iterations can be made. (See Table 4-3.4.) For pipe segment 3, the new flow is the algebraic sum of the original flow plus the flow corrections from both loops. (See Figures 4-3.6 and 4-3.7.)

In starting the third iteration, it can be seen that the pressure losses around both loops are balanced within 0.5 psi. (See Table 4-3.5.) Therefore, the flow split assumed after two iterations can be accepted. As a final check, step 10 of the above procedure calls for a calculation of the total pressure loss through two different routes, requiring that they balance within 0.5 psi (0.03 bar):

Route through pipes 1 and 5:

$$\begin{aligned}\mathrm{FLC}_1,\ (Q_1)^{1.85} + \mathrm{FLC}_2(Q_2)^{1.85} &= 0.001(54.0)^{1.85} + 0.004(35.9)^{1.85} \\ &= 1.6 + 3.0 = 4.6 \text{ psi (0.32 bar)}\end{aligned}$$

Route through Pipes 2 and 4:

$$\begin{aligned}0.002(46.0)^{1.85} + 0.001(64.1)^{1.85} &= 2.4 + 2.2 \\ &= 4.6 \text{ psi (0.32 bar)}\end{aligned}$$

This is acceptable. Note that it required only two iterations to achieve a successful solution despite the fact that the initial flow assumption called for reverse flow in pipe 3. The initial assumption was for a clockwise flow of 5 gpm (18.9 lpm) in pipe 3, but the final solution shows a counterclockwise flow of 18.1 gpm (68.5 lpm).

Table 4-3.3 ***First Iteration***

Loop	Pipe	Q	FLC	p_f	dp_f	(p_f/Q)	$dQ = -dp_f/1.85[\sum(p_f/Q)]$	$Q + dQ$
1	1	–40	0.001	–0.92		0.023	dQ = –16.4	–56.4
	2	60	0.002	3.90		0.065		+43.6
	3	5	0.003	0.06		0.012		–11.4
					= 3.04	0.100		
2	3	–5	0.003	–0.06		0.012	dQ = 11.2	+6.2
	4	55	0.001	1.66		0.030		+66.2
	5	–45	0.004	–4.58		0.102		+33.8
					= –2.98	0.144		

Table 4-3.4 ***Second Iteration***

Loop	Pipe	Q	FLC	p_f	dp_f	(p_f/Q)	$dQ = -dp_f/1.85[\sum(p_f/Q)]$	$Q + dQ$
1	1	–56.4	0.001	–1.74		0.031		–54.0
	2	43.6	0.002	2.16		0.050		+46.0
	3	–22.6	0.003	–0.96		0.042	dQ = 2.4	–20.2
					= –0.54	0.123		
2	3	22.6	0.003	0.96		0.042		+20.5
	4	66.2	0.001	2.34		0.035		+64.1
	5	–33.8	0.004	–2.69		0.080	dQ = –2.1	+35.9
					= 0.61	0.157		

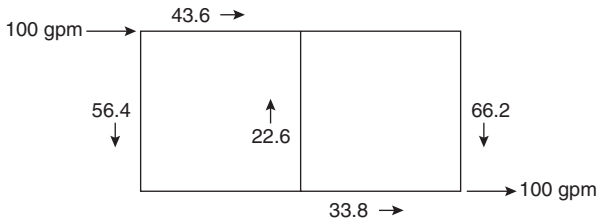

Figure 4-3.6. ***Corrected flows after first iteration.***

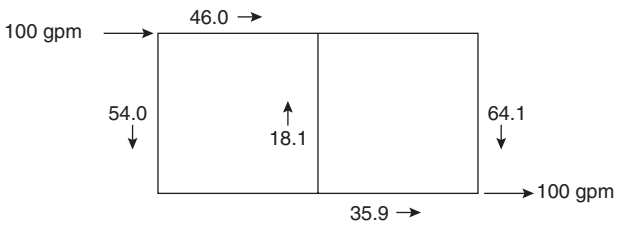

Figure 4-3.7. ***Corrected flows after second iteration.***

Table 4-3.5 ***Third Iteration***

Loop	Pipe	Q	FLC	p_f	dp_f	(p_f/Q)	$dQ = -dp_f/1.85[\sum(p_f/Q)]$	$Q + dQ$
1	1	–54.0	0.001	–1.60				
	2	46.0	0.002	2.38				
	3	–18.1	0.003	–0.64				
					= 0.14			
2	3	18.1	0.003	0.64				
	4	64.1	0.001	2.20				
	5	–35.9	0.004	–3.01				
					= –0.17			

Water Supply Calculations

Determination of Available Supply Curve

Testing a public or private water supply permits an evaluation of the strength of the supply in terms of both quantity of flow and available pressures. The strength of a water supply is the key to whether it will adequately serve a sprinkler system.

Each test of a water supply must provide at least two pieces of information—a static pressure and a residual pressure at a known flow. The static pressure is the "no flow" condition, although it must be recognized that rarely is any public water supply in a true no flow condition. But this condition does represent a situation where the fire protection system is not creating an additional flow demand beyond that which is ordinarily placed on the system. The residual pressure reading is taken with an additional flow being taken from the system, preferably a flow that approximates the likely maximum system demand.

Between the two (or more) points, a representation of the water supply (termed a water supply curve) can be made. For the most part, this water supply curve is a fingerprint of the system supply and piping arrangements, since the static pressure tends to represent the effect of elevated tanks and operating pumps in the system, and the drop to the residual pressure represents the friction and minor losses through the piping network that result from the increased flow during the test.

The static pressure is read directly from a gauge attached to a hydrant. The residual pressure is read from the same gauge while a flow is taken from another hydrant, preferably downstream. A pitot tube is usually used in combination with observed characteristics of the nozzle though which flow is taken in order to determine the amount of flow. Chapter 7 of NFPA 13 provides more thorough information on this type of testing.

Figure A-8-3.2(d) of NFPA 13 (1999 edition) is an example of a plot of water supply information. The static pressure is plotted along the *y*-axis, reflecting a given pressure under zero flow conditions. The residual pressure at the known flow is also plotted, and a straight line is drawn between these two points. Note that the *x*-axis is not linear, but rather shows flow as a function of the 1.85 power. This corresponds to the exponent for flow in the Hazen-Williams equation. Using this semi-exponential graph paper demonstrates that the residual pressure effect is the result of friction loss through the system, and permits the water supply curve to be plotted as a straight line. Since the drop in residual pressure is proportional to flow to the 1.85 power, the available pressure at any flow can be read directly from the water supply curve.

For adequate design, the system demand point, including hose stream allowance, should lie below the water supply curve.

EXAMPLE 11:

If a water supply is determined by test to have a static pressure of 100 psi (6.9 bar) and a residual pressure of 80 psi (5.5 bar) at a flow of 1000 gpm (3785 lpm), the pressure available at a flow of 450 gpm (1703 lpm) can be approximated by plotting the two known data points on the hydraulic graph paper as shown in Figure 4-3.8. At a flow of 450 gpm (1703 lpm), a pressure of 90 psi (6.2 bar) is indicated.

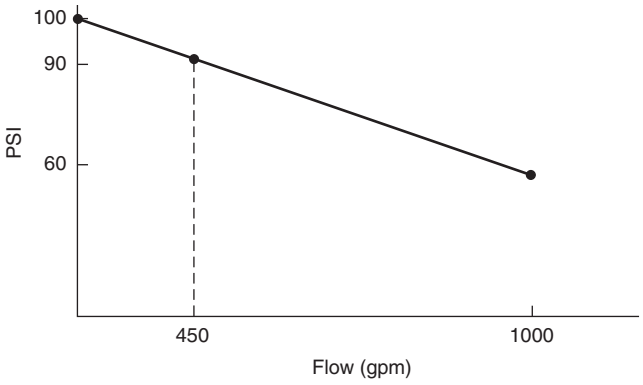

Figure 4-3.8. ***Pressure available from 450 gpm flow water supply.***

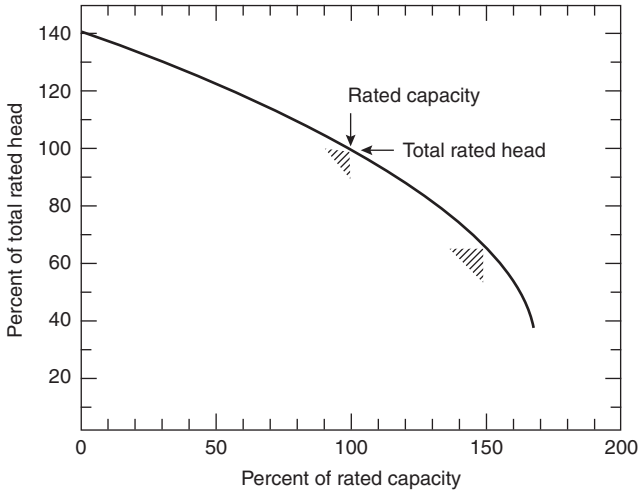

Figure 4-3.9. ***Pump performance curve.***

Pump Selection and Testing

Specific requirements for pumps used in sprinkler systems are contained in NFPA 20, which is cross-referenced by NFPA 13.

Fire pumps provide a means of making up for pressure deficiencies where an adequate volume of water is available at a suitable net positive suction pressure. Plumbing codes sometimes set a minimum allowable net positive suction pressure of 10 to 20 psi (0.69 to 1.38 bar). If insufficient water is available at such pressures, then it becomes necessary to use a stored water supply.

Listed fire pumps are available with either diesel or electric drivers, and with capacities ranging from 25 to 5000 gpm (95 to 18,927 lpm), although fire pumps are most commonly found with capacities ranging from 250 to 2500 gpm (946 to 9463 lpm) in increments of 250 up to 1500 gpm (946 up to 5678 lpm) and 500 gpm (1893 lpm) beyond that point. Each pump is specified with a rated flow and rated pressure. Rated pressures vary extensively, since manufacturers can control this feature with small changes to impeller design.

Pump affinity laws govern the relationship between impeller diameter, D, pump speed, N, flow, Q, pressure head, H, and brake horsepower, bhp. The first set of affinity laws assumes a constant impeller diameter.

$$\frac{Q_1}{Q_2} = \frac{N_1}{N_2} \qquad \frac{H_1}{H_2} = \frac{N_1}{N_2} \qquad \frac{\text{bhp}_1}{\text{bhp}_2} = \frac{N_1}{N_2}$$

These affinity laws are commonly used when correcting the output of a pump to its rated speed.

The second set of the affinity laws assumes constant speed with change in impeller diameter, D.

$$\frac{Q_1}{Q_2} = \frac{D_1}{D_2} \qquad \frac{H_1}{H_2} = \frac{D_1}{D_2} \qquad \frac{\text{bhp}_1}{\text{bhp}_2} = \frac{D_1}{D_2}$$

Pumps are selected to fit the system demands on the basis of three key points relative to their rated flow and rated pressure. (See Figure 4-3.9.) NFPA 20 specifies that each horizontal fire pump must meet these characteristics, and the approval laboratories ensure these points are met:

1. A minimum of 100 percent of rated pressure at 100 percent of rated flow.
2. A minimum of 65 percent of rated pressure at 150 percent of rated flow.
3. A maximum of 140 percent of rated pressure at 0 percent of rated flow (churn).

Even before a specific fire pump has been tested, therefore, the pump specifier knows that a given pump can be expected to provide certain performance levels. It is usually possible to have more than one option when choosing pumps, since the designer is not limited to using a specific point on the pump performance curve.

There are limits to flexibility in pump selection, however. For example, it is not permitted to install a pump in a situation where it would be expected to operate with a flow exceeding 150 percent of rated capacity, since the performance is not a known factor, and indeed available pressure is usually quick to drop off beyond this point.

NFPA 20 gives the following guidance on what part of the pump curve to use:[1]

> A centrifugal fire pump should be selected in the range of operation from 90 percent to 150 percent of its rated capacity. The performance of the pump when applied at capacities over 140 percent of rated capacity may be adversely affected by the suction conditions. Application of the pump at capacities less than 90 percent of the rated capacity is not recommended.
>
> The selection and application of the fire pump should not be confused with pump operating conditions. With proper suction conditions, the pump can operate at any point on its characteristic curve from shutoff to 150 percent of its rated capacity.

For design capacities below the rated capacity, the rated pressure should be used. For design capacities between 100 and 150 percent of rated capacity, the pressure

used should be found by the relationship made apparent by similar triangles.

$$\frac{0.35P}{0.5Q} = \frac{P' - 0.65P}{1.5Q - Q'}$$

where P and Q are the rated pressure and capacity, and P' is the minimum available pressure at capacity, Q', where $Q < Q' < 1.5Q$.

EXAMPLE 12:

A pump is to be selected to meet a demand of 600 gpm (2271 lpm) at 85 psi (5.86 bar). To determine whether a pump rated for 500 gpm (1893 lpm) at 100 psi (6.90 bar) would be able to meet this point without having an actual pump performance curve to work from, the above formula can be applied, with $P = 100$, $Q = 500$, and $Q' = 600$.

Inserting these values gives

$$\frac{(0.35)(100)}{(0.5)(500)} = \frac{[P' - (0.65)(100)]}{[(1.5)(500) - 600]}$$

$$\frac{35}{250} = \frac{(P' - 65)}{(750 - 600)}$$

$$P' = 65 + 21 = 86 \text{ psi (5.93 bar)}$$

Since the value of P' so calculated is greater than the 85 psi (5.86 bar) required, the pump will be able to meet the demand point.

Tank Sizing

Tank selection and sizing are relatively easy compared to pump selection. The most basic question is whether to use an elevated storage (gravity) tank, a pressure tank, or a suction tank in combination with a pump. Following that is a choice of materials. NFPA 22 is the governing standard for water tanks for fire protection, and includes a description of the types of tanks as well as detailed design and connection requirements.

From a calculation standpoint, tanks must be sized to provide the minimum durations specified by NFPA 13 or other applicable standards for the system design. Required pressures must still be available when the tanks are at the worst possible water level condition (i.e., nearly empty).

If the tank is intended to provide the needed supply without the use of a pump, the energy for the system must be available from the height of a gravity tank or the air pressure of a pressure tank.

An important factor in gravity tank calculations is the requirement that the pressure available from elevation [calculated using 0.433 psi per foot (0.099 bar/m)] must be determined using the lowest expected level of water in the tank. This is normally the point at which the tank would be considered empty.

In sizing pressure tanks, the percentage of air in the tanks must be controlled so as to ensure that the last water leaving the tank will be at an adequate pressure. While a common rule of thumb has been that the tank should be one-third air at a minimum pressure of 75 psi (5.17 bar), this rule does not hold true for systems with high pressure demands or where the tank is located a considerable distance below the level of the highest sprinkler.

For pipe schedule systems, two formulas have traditionally been used, based on whether the tank is located above the level of the highest sprinkler or some distance below.

For the tank above the highest sprinkler

$$P = \frac{30}{A} - 15$$

For the tank below the highest sprinkler

$$P = \left(\frac{30}{A} - 15\right) + \left(\frac{0.434H}{A}\right)$$

where

A = proportion of air in the tank

P = air pressure carried in the tank in psi

H = height of the highest sprinkler above the tank bottom in feet

It can be seen that these formulas are based simply on the need to provide a minimum pressure of 15 psi (1.03 bar) to the system at the level of the highest sprinkler, and an assumption of 15 psi (1.03 bar) atmospheric pressure.

Using the same approximation for atmospheric pressure, a more generalized formula has come into use for hydraulically designed systems:

$$P_i = \frac{P_f + 15}{A} - 15$$

where

P_i = tank air pressure to be used

P_f = system pressure required per hydraulic calculations

A = proportion of air in the tank

EXAMPLE 13:

A pressure tank is to be used to provide a 30-min-water supply to a system with a hydraulically calculated demand of 140 gpm (530 lpm) at a pressure of 118 psi (8.14 bar). Since there are sprinklers located adjacent to the tank, it is important that air pressure in the tank not exceed 175 psi (12.0 bar). To determine the minimum size tank that can be used, it is important not only to consider the total amount of water needed, but also the amount of air necessary to keep the pressures within the stated limits.

The above equation for hydraulically designed systems can be used to solve for A.

If $$P_i = \left[\frac{(P_f + 15)}{A}\right] - 15$$

then $$A = \frac{(P_f + 15)}{(P_i + 15)}$$

$$A = \frac{(118 + 15)}{(175 + 15)} = \frac{133}{190} = 0.70$$

This means that the tank will need to be 70 percent air if the air pressure in the tank is to be kept to 175 psi (12.0 bar).

The minimum water supply required is 30 min × 140 gpm = 4200 gallons (15,898 l).

Thus, the minimum tank volume will be such that 4200 gallons (15,898 l) can be held in the remaining 30 percent of volume.

$$0.3V = 4200 \text{ gal} \qquad V = \frac{4200}{0.3} = 14{,}000 \text{ gal tank (53,000 l)}$$

Hanging and Bracing Methods

Hangers and Hanger Supports

NFPA 13 contains a great deal of specific guidance relative to hanger spacing and sizing based on pipe sizes. It should also be recognized that the standard allows a performance-based approach. Different criteria exist for the hanger itself and the support from the building structure.

Any hanger and installation method is acceptable if certified by a registered professional engineer for the following:

1. Hangers are capable of supporting five times the weight of the water-filled pipe plus 250 pounds (114 kg) at each point of piping support.
2. Points of support are sufficient to support the sprinkler system.
3. Ferrous materials are used for hanger components.

The building structure itself must be capable of supporting the weight of the water-filled pipe plus 250 pounds (114 kg) applied at the point of hanging.

The 250 pound (114 kg) weight is intended to represent the extra loading that would occur if a relatively heavy individual were to hang on the piping.

Trapeze Hangers

Trapeze hangers are used where structural members are not located, so as to provide direct support of sprinkler lines or mains. This can occur when sprinkler lines or mains run parallel to structural members such as joists or trusses.

A special section of NFPA 13 addresses the sizing of trapeze hangers. Because they are considered part of the support structure, the criteria within NFPA 13 are based on the ability of the hangers to support the weight of 15 ft (5 m) of water-filled pipe plus 250 pounds (114 kg) applied at the point of hanging. An allowable stress of 15,000 psi (111 bar) is used for steel members. Two tables are provided in the standard, one of which presents required section moduli based on the span of the trapeze and the size and type of pipe to be supported, and the other of which presents the available section moduli of standard pipes and angles typically used as trapeze hangers.

In using the tables, the standard allows the effective span of the trapeze hanger to be reduced if the load is not at the midpoint of the span. The equivalent length of trapeze is determined from the formula

$$L = \frac{4ab}{(a + b)}$$

where L is the equivalent length, a is the distance from one support to the load, and b is the distance from the other support to the load.

EXAMPLE 14:

A trapeze hanger is required for a main running parallel to two beams spaced 10 ft (3.048 m) apart. If the main is located 1 ft 6 in. (0.457 m) from one of the beams, the equivalent span of trapeze hanger required can be determined by using the formula

$$L = \frac{4(1.5 \text{ ft})(8.5 \text{ ft})}{(1.5 \text{ ft} + 8.5 \text{ ft})} = 5.1 \text{ ft (1.554 m)}$$

Earthquake Braces

Protection for sprinkler systems in earthquake areas is provided in several ways. Flexibility and clearances are added to the system where necessary to avoid the development of stresses that could rupture the piping. Too much flexibility could also be dangerous, however, since the momentum of the unrestrained piping during shaking could result in breakage of the piping under its own weight or upon collision with other building components. Therefore, bracing is required for large piping (including all mains) and for the ends of branch lines.

Calculating loads for earthquake braces is based on the assumption that the normal hangers provided to the system are capable of handling vertical forces, and that horizontal forces can be conservatively approximated by a constant acceleration equal to one-half that of gravity.

$$a_h = 0.5g$$

NFPA 13 contains a table of factors that can be applied if building codes require the use of other horizontal acceleration values.

Since the braces can be called upon to act in both tension and compression, it is necessary not only to size the brace member to handle the expected force applied by the weight of the pipe in its zone of influence, but also to avoid a member that could fail as a long column under buckling.

The ability of the brace to resist buckling is determined through an application of Euler's formula with a maximum slenderness ratio of 300. This corresponds to the maximum slenderness ratio generally used under steel construction codes for secondary framing members. This is expressed as

$$\frac{\ell}{r} \leq 300$$

where ℓ = length of the brace and r = least radius of gyration for the brace.

The least radius of gyration for some common shapes is as follows:

pipe $\qquad r = \dfrac{(r_0^2 + r_i^2)^{1/2}}{2}$

rod $\qquad r = \dfrac{r}{2}$

flat $\qquad r = 0.29h$

Special care must be taken in the design of earthquake braces so that the load applied to any brace does not exceed the capability of the fasteners of that brace to the piping system or the building structure, and that the braces are attached only to structural members capable capable of supporting the expected loads.

Performance Calculations

Sprinkler Response as a Detector

Automatic sprinklers serve a dual function as both heat detectors and water distribution nozzles. As such, the response of sprinklers can be estimated using the same methods as for response of heat detectors. (See Section 4, Chapter 1.) Care should be taken, however, since the use of such calculations for estimating sprinkler actuation times has not been fully established. Factors, such as sprinkler orientation, air flow deflection, radiation effects, heat of fusion of solder links, and convection within glass bulbs, are all considered to introduce minor errors into the calculation process. Heat conduction to the sprinkler frame and distance of the sensing mechanism below the ceiling have been demonstrated to be significant factors affecting response, but are ignored in some computer models.

Nevertheless, modeling of sprinkler response can be useful, particularly when used on a comparative basis. Beginning with the 1991 edition, an exception within Section 4-1.1 of NFPA 13 permitted variations from the rules on clearance between sprinklers and ceilings " . . . provided the use of tests or calculations demonstrate comparable sensitivity and performance."

EXAMPLE 15:

Nonmetallic piping extending 15 in. (0.38 m) below the concrete ceiling of a 10-ft- (3.048 m-) high basement 100 ft by 100 ft (30.48 × 30.48 m) in size makes it difficult to place standard upright sprinklers within the 12 in. (0.30 m) required by NFPA 13 for unobstructed construction. Using the LAVENT[9] computer model, and assuming RTI values of 400 $ft^{1/2}{\cdot}s^{1/2}$ (221 $m^{1/2}{\cdot}s^{1/2}$) for standard sprinklers and 100 $ft^{1/2}{\cdot}s^{1/2}$ (55 $m^{1/2}{\cdot}s^{1/2}$) for quick-response sprinklers, it can be demonstrated that the comparable level of sensitivity can be maintained at a distance of 18 in. (0.457 m) below the ceiling. Temperature rating is assumed to be 165°F, and maximum lateral distance to a sprinkler is 8.2 ft (2.50 m) (10 ft × 13 ft [3.048 m × 3.962 m] spacing). Assuming the default fire (empty wood pallets stored 5 ft [1.52 m] high), for example, the time of actuation for the standard sprinkler is calculated to be 200 s, as compared to 172 s for the quick-response sprinkler. Since the noncombustible construction minimizes concern relative to the fire control performance for the structure, the sprinklers can be located below the piping obstructions.

Dry System Water Delivery Time

Total water delivery time consists of two parts. The first part is the trip time taken for the system air pressure to bleed down to the point where the system dry valve opens to admit water to the piping. The second part is the transit time for the water to flow through the piping from the dry valve to the open sprinkler. In other words

$$\text{water delivery time} = \text{trip time} + \text{transit time}$$

where water delivery time commences with the opening of the first sprinkler.

NFPA 13 does not contain a maximum water delivery time requirement if system volume is held to no more than 750 gal (2839 l). Larger systems are permitted only if water delivery time is within 60 s. As such, the rule of thumb for dry system operation is that no more than a 60 s water delivery time should be tolerated, and that systems should be divided into smaller systems if necessary to achieve this 1-min response. Dry system response is simulated in field testing by the opening of an inspector's test connection. The test connection is required to be at the most remote point of the system from the dry valve, and is required to have an orifice opening of a size simulating a single sprinkler.

The water delivery time of the system is recorded as part of the dry pipe valve trip test that is conducted using the inspector's test connection. However, it is not a realistic indication of actual water delivery time for two reasons:

1. The first sprinkler to open on the system is likely to be closer to the system dry valve, reducing water transit time.
2. If additional sprinklers open, the trip time will be reduced since additional orifices are able to expel air. Water transit time may also be reduced since it is easier to expel the air ahead of the incoming water.

Factory Mutual Research Corporation (FMRC) researchers have shown[3] that it is possible to calculate system trip time using the relation

$$t = 0.0352 \frac{V_T}{A_n T_0^{1/2}} \ln\left(\frac{p_{a0}}{p_a}\right)$$

where

t = time in seconds
V_T = dry volume of sprinkler system in cubic feet
T_0 = air temperature in Rankine degrees
A_n = flow area of open sprinklers in square feet
p_{a0} = initial air pressure (absolute)
p_a = trip pressure (absolute)

Calculating water transit time is more difficult, but may be accomplished using a mathematical model developed by FMRC researchers. The model requires the system to be divided into sections, and may therefore produce slightly different results, depending on user input.

Droplet Size and Motion

For geometrically similar sprinklers, the median droplet diameter in the sprinkler spray has been found to be inversely proportional to the $1/3$ power of water pressure and

directly proportional to the $^2/_3$ power of sprinkler orifice diameter such that

$$d_m \propto \frac{D^{2/3}}{P^{1/3}} \propto \frac{D^2}{Q^{2/3}}$$

where

d_m = mean droplet diameter
D = orifice diameter
P = pressure
Q = rate of water flow

Total droplet surface area has been found to be proportional to the total water discharge rate divided by the median droplet diameter

$$A_S \propto \frac{Q}{d_m}$$

where A_S is the total droplet surface area.

Combining these relationships, it can be seen that

$$A_S \propto (Q^3 p D^{-2})^{1/3}$$

When a droplet with an initial velocity vector of **U** is driven into a rising fire plume, the one-dimensional representation of its motion has been represented as[4]

$$\frac{m_1 d\mathbf{U}}{dt} = m_1 g - \frac{C_D \rho_g (\mathbf{U} + V)^2}{2S}$$

where

U = velocity of the water droplet
V = velocity of the fire plume
m = mass of the droplet
ρ_g = density of the gas
g = acceleration of gravity
C_D = coefficient of drag
S_f = frontal surface area of the droplet

The first term on the right side of the equation represents the force of gravity, while the second term represents the force of drag caused by gas resistance. The drag coefficient for particle motion has been found empirically to be a function of the Reynolds number (Re) as[5]

$$C_D = 18.5\ \mathrm{Re}^{-0.6} \qquad \text{for Re} < 600$$
$$C_D = 0.44 \qquad \text{for Re} > 600$$

Spray Density and Cooling

The heat absorption rate of a sprinkler spray is expected to depend on the total surface area of the water droplets, A_S, and the temperature of the ceiling gas layer in excess of the droplet temperature, T. With water temperature close to ambient temperature, T can be considered excess gas temperature above ambient.

Chow[6] has developed a model for estimating the evaporation heat loss due to a sprinkler water spray in a smoke layer. Sample calculations indicate that evaporation heat loss is only significant for droplet diameters less than 0.5 mm. For the droplet velocities and smoke layer depths analyzed, it was found that the heat loss to evaporation would be small (10 to 25 percent), compared to the heat loss from convective cooling of the droplets.

Factory Mutual Research Corporation researchers[7] have developed empirical correlations for the heat absorption rate of sprinkler spray in room fires, as well as convective heat loss through the room opening, such that

$$\dot{Q} = \dot{Q}_{\mathrm{cool}} + \dot{Q}_c + \dot{Q}_l$$

where

$\dot{Q}$ = total heat release rate of the fire
$\dot{Q}_{\mathrm{cool}}$ = heat absorption rate of the sprinkler spray
$\dot{Q}_c$ = convective heat loss rate through the room opening
$\dot{Q}_l$ = sum of the heat loss rate to the walls and ceiling, $\dot{Q}_s$, the heat loss rate to the floor, $\dot{Q}_f$, and the radiative heat loss rate through the opening, $\dot{Q}_r$

Test data indicated that

$$\dot{Q}_{\mathrm{cool}}/\dot{Q} = 0.000039\Lambda^3 - 0.003\Lambda^2 + 0.082\Lambda$$

for $0 < \Lambda \leq 33\ l/(\mathrm{min} \times \mathrm{kW}^{1/2} \times \mathrm{m}^{5/4})$

where Λ is a correlation factor incorporating heat losses to the room boundaries and through openings as well as to account for water droplet surface area.

$$\Lambda = (AH^{1/2}\dot{Q}_l)^{-1/2}(W^3 P D^{-2})^{1/3}$$

for $P = \dfrac{p}{(17.2\ \mathrm{kPa})}$ and $D = \dfrac{d}{0.0111\ \mathrm{m}}$

where

A = area of the room opening in meters
H = height of the room opening in meters
P = water pressure at the sprinkler in bar
d = sprinkler nozzle diameter in meters
W = water discharge in liters per minute

The above correlations apply to room geometry with length-to-width ratio of 1.2 to 2 and opening size of 1.70 to 2.97 m^2.

Suppression by Sprinkler Sprays

Researchers at the National Institute of Standards and Technology (NIST) have developed a "zeroth order" model of the effectiveness of sprinklers in reducing the heat release rate of furnishing fires.[8] Based on measurements of wood crib fire suppression with pendant spray sprinklers, the model is claimed to be conservative. The model assumes that all fuels have the same degree of resistance to suppression as a wood crib, despite the fact that tests have shown furnishings with large burning surface areas can be extinguished easily compared to the deep-seated fires encountered with wood cribs.

The recommended equation, which relates to fire suppression for a 610-mm-high crib, has also been checked for validity with 305-mm crib results. The equation is

$$\dot{Q}(t - t_{act}) = \dot{Q}(t_{act})\exp\left[\frac{-(t - t_{act})}{3.0(\dot{w}'')^{-1.85}}\right]$$

where

$\dot{Q}$ = the heat release rate (kW)

t = any time following t_{act} of the sprinklers (s)

$\dot{w}''$ = the spray density (mm/s)

The NIST researchers claim the equation is appropriate for use where the fuel is not shielded from the water spray, and the application density is at least 0.07 mm/s [4.2 mm/min. (0.1 gpm/ft²)]. The method does not account for variations in spray densities or suppression capabilities of individual sprinklers.

The model must be used with caution, since it was developed on the basis of fully involved cribs. It does not consider the possibility that the fire could continue to grow in intensity following initial sprinkler discharge, and, for that reason, should be restricted to use in light hazard applications.

Sprinklers are assumed to operate within a room of a light hazard occupancy when the total heat release rate of the fire is 500 kW. The significance of an initial application rate of 0.3 gpm/ft² (0.205 mm/s) as compared to the minimum design density of 0.1 gpm/ft² (0.07 mm/s) can be evaluated by the expected fire size after 30 s. With the minimum density of 0.07 mm/s (0.1 gpm/ft²), the fire size is conservatively estimated as 465 kW after 30 s. With the higher density of 0.205 mm/s (0.3 gpm/ft²), the fire size is expected to be reduced to 293 kW after 30 s. Corresponding values after 60 s are 432 kW and 172 kW, respectively.

Nomenclature

C	coefficient of friction
FLC	friction loss coefficient
Q	flow (gpm)
$\dot{w}''$	spray density (mm/s)

References Cited

1. *NFPA Codes and Standards,* National Fire Protection Association, Quincy, MA.
2. H. Cross, *Analysis of Flow in Networks of Conduits or Conductors,* Univ. of Illinois Engineering Experiment Station, Urbana, IL (1936).
3. G. Heskested and H. Kung, *FMRC Serial No. 15918,* Factory Mutual Research Corp., Norwood, MA (1973).
4. C. Yao and A.S. Kalelkar, *Fire Tech.,* 6, 4 (1970).
5. C.L. Beyler, "The Interaction of Fire and Sprinklers," *NBS GCR 77-105,* National Bureau of Standards, Washington, DC (1977).
6. W.K. Chow, "On the Evaporation Effect of a Sprinkler Water Spray," *Fire Tech.,* pp. 364–373 (1989).
7. H.Z. You, H.C. Kung, and Z. Han, "Spray Cooling in Room Fires," *NBS GCR 86-515,* National Bureau of Standards, Washington, DC (1986).
8. D.D. Evans, "Sprinkler Fire Suppression Algorithm for HAZARD," *NISTIR 5254,* National Institute of Standards and Technology, Gaithersburg, MD (1993).
9. W.D. Davis and L.Y. Cooper, "Estimating the Environment and Response of Sprinkler Links in Compartment Fires with Draft Curtains and Fusible-Link Actuated Ceiling Vents, Part 2: User Guide for the Computer Code LAVENT," *NISTIR/89-4122,* National Institute of Standards and Technology, Gaithersburg, MD (1989).

CHAPTER 4

Foam Agents and AFFF System Design Considerations

Joseph L. Scheffey

Introduction

Foams have been developed almost entirely from experimental work. While the technologies are rather mature, no fundamental explanations of foam extinguishment performance have been developed based on first principles. As a result, foams are characterized by (1) fire tests for which there is no general international agreement and (2) physical and chemical properties which may or may not correlate with empirical results. This chapter reviews the important parameters associated with foam agents, test methods used to evaluate foams, and relevant data in the literature that can be used to evaluate designs for special hazards. Because of their superior performance in extinguishing hydrocarbon fuel fires, the emphasis is on film-forming foams and thin pool fires (e.g., from spills). Situations involving fuels "in depth" are not evaluated in detail here.

Fire-fighting foam consists of air-filled bubbles formed from aqueous solutions. The solutions are created by mixing a foam concentrate with water in the appropriate proportions (typically 1, 3, or 6 percent concentrate to water). The solution is then aerated to form the bubble structure. Some foams, notably those that are protein-based, form thick, viscous foam blankets on hydrocarbon fuel surfaces. Other foams, such as film-formers, are much less viscous and spread rapidly on the fuel surface. The film-formers are capable of producing a vapor-sealing film of surface-active water solution on most of the hydrocarbon fuels of interest.

Since the foam is lighter than the aqueous solution that drains from the bubble structure, and lighter than flammable or combustible liquids, it floats on the fuel surface. The floating foam produces an air-excluding layer of aqueous agent, which suppresses and prevents combustion by halting fuel vaporization at the fuel surface. If the entire surface is covered with foam, the fuel vapor will be completely suppressed, and the fire will be extinguished. Low-expansion foams (i.e., foam volume: solution volume of $\leq 10:1$) are quite effective on two-dimensional (pool) flammable and combustible liquid fires, but not particularly effective on three-dimensional fuel fires. This is particularly true of three-dimensional fires involving a low flashpoint fuel. Typically, an auxiliary agent, such as dry chemical, is used with foam where a three-dimensional fire (running fuel or pressurized spray) is anticipated.

Joseph L. Scheffey, P.E., is director of Fire Protection RDT&E for Hughes Associates, Inc., Baltimore, Maryland.

Description of Foam Agents

There are no universally agreed-on definitions of foam agents or terms associated with fire-fighting foam. For example, where foam is referenced in NFPA standards, definitions vary from document to document. Because foams vary in performance, in terms of application rates and quantities required for extinguishment, agent definitions can be cast to accentuate positive attributes, such as "rapid knockdown" or "superior burnback resistance." Geyer et al. have described the composition of various foam agents, paraphrased as follows.[1]

1. *Protein foam.* Protein foam is a "mechanical" foam produced by combining (proportioning) foam concentrate and water and discharging the resulting solution through a mixing chamber. The mixing chamber introduces (aspirates) air, which expands the solution to create foam bubbles. The liquid concentrate consists primarily of hydrolyzed proteins in combination with iron salts. Hoof and horn meal and hydrolyzed feather meal are examples of proteinaceous materials used in protein-foam concentrates. No aqueous film is formed on the fuel surface with this type of agent.

2. *Fluoroprotein.* These agents are basically protein foams with fluorocarbon surface-active agents added. The varying degrees of performance are achieved by using different proportions of the base protein hydrolyzates and the fluorinated surfactants. While fluoroprotein foams generally have good fuel shedding capabilities and dry chemical compatibility, the solution that drains out from the expanded foam does not form a film on hydrocarbon fuels. However, the addition of the fluorinated surfactants may act to reduce the surface tension of the solution. This reduction may, in turn, decrease the viscosity of the expanded solution, thus promoting more rapid fire control when compared to protein foams.
3. *Aqueous film-forming foam (AFFF).* These agents are synthetically formed by combining fluorine-free hydrocarbon foaming compounds with highly fluorinated surfactants. When mixed with water, the resulting solution achieves the optimum surface and interfacial tension characteristics needed to produce a film that will spread across a hydrocarbon fuel. The foam produced from this agent will extinguish in the same vapor-excluding fashion as other foams. Further, the solution that results from normal drainage or foam breakdown produces an aqueous "film" that spreads rapidly and is highly stable on the liquid hydrocarbon fuel surface. It is this film formation characteristic that is the significant distinguishing feature of AFFF.

These definitions are by no means all-inclusive. For example, film-forming fluoroprotein (FFFP) foam is an agent that is produced by increasing the quantity and quality of the surfactants added to a protein hydrolyzate. By doing this, the surface tension of the resulting solution, which drains from the expanded foam, is reduced to the point where it may spread across the surface of a liquid hydrocarbon fuel. An alcohol-resistant concentrate is formulated to produce a floating polymeric skin for foam buildup on water-miscible fuels. This polymeric skin protects the foam from breakdown by polar solvents, for example, acetone, methanol, and ethanol.

The descriptions show that there are distinct chemical differences between protein-based foams and AFFF. In general, the surfactants used in aqueous foams are long-chained compounds that have a hydrophobic or hydrophilic (i.e., water repelling or water attracting, respectively) group at one end.[2] The molecular structure of a typical AFFF fluorinated surfactant is shown in Figure 4-4.1.[3] In this molecule, the perfluoroctyl group on the left is the hydrophobic group, while the propyltrimethylammonium group is the hydrophilic group. When these compounds are dissolved into solution with water, they will tend to group near the surface of the solution, aligned so that their hydrophobic ends are facing toward the air/solution interface. The advantage of this is that the perfluoroctyl group found in these compounds is also oliophobic (i.e., oil repelling) as well as hydrophobic.[4]

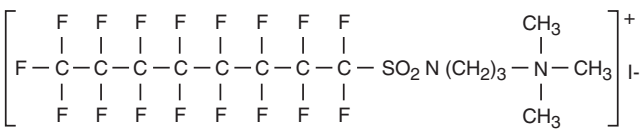

Figure 4-4.1. ***Typical AFFF fluorosurfactant molecule.[3]***

AFFF concentrates also contain hydrocarbon surfactants. These compounds are less hydrophobic than those containing the perfluoroctyl group. However, they do provide greater stability once the solution is expanded into a foam. As a result, the surface tension of the solution is reduced below that of water; the expanded foam produced from the solution is resistive to breakdown from heat, fuels, or dry chemical extinguishing agents; and the solution that drains out from the expanded foam is able to form a film on hydrocarbon fuels.

The importance of both the film formation and foam bubble characteristics of AFFF, resulting from the combination of fluorocarbon and hydrocarbon surfactants, was evaluated in early work by Tuve et al.[5] When a highly expanded, stiff formulation of AFFF was used, these researchers found it difficult to obtain good fire extinguishment and vapor sealing characteristics. The foam resisted flow, and drainage of the aqueous solution (film) was slow. The drainage was corrected by expanding the foam to a lesser degree. This pioneering AFFF formulation, with an expansion ratio of 8:1 and 25 percent drainage time of 6 min, appeared to offer the best compromise in characteristics. It provided a readily flowable foam that sealed up against obstructions, promoted the rapid formation of a surface-active film barrier on the fuel, and provided a sufficiently stable foam to resist burnback.

Fire Extinguishment and Spreading Theory

As noted by Friedman in his review of suppression theory, the mechanisms of foam fire extinguishment on two-dimensional pool fires have not been developed.[6] Usually, the fire extinguishment is described simply as a factor of the cessation of fuel vaporization at the fuel surface. As the fuel vapor decreases, the size of the combustion zone decreases. When the area is totally covered, extinguishment occurs. Cooling must occur to bring the vapor pressure of the fuel below that of its boiling point. Once the fuel is cooled, a layer of foam must then be applied either manually, or by spreading, to prevent combustion. Hanauska et al. have proposed fundamental extinguishment parameters, summarized in the following text.[7] A similar foam extinguishment model has been proposed by Persson and Dahlberg.[8]

Foam Loss Mechanisms

Fire extinguishment by foams can be summarized as shown in Figure 4-4.2. Foam having a temperature, T_i,

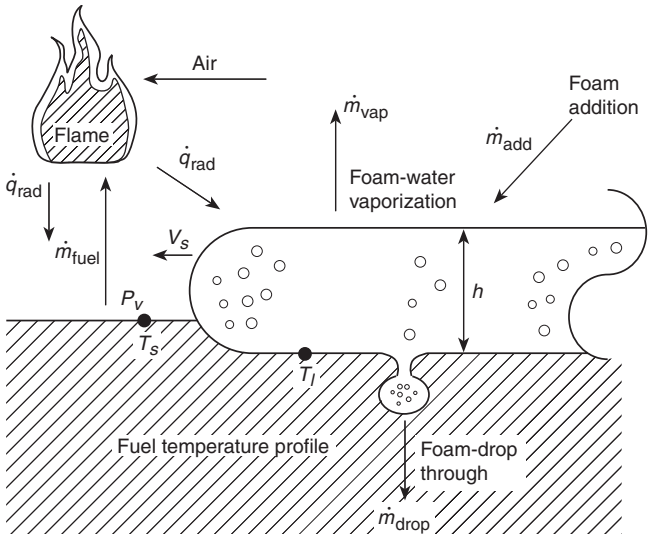

Figure 4-4.2. ***Illustration of the significant parameters affecting a foam's hydrocarbon fuel fire extinguishment capability.***

and depth, h, spreads at a rate of V_s along a fuel of temperature, T_s, and vapor pressure, P_v. Fuel is volatized by the fire at a rate of $\dot{m}_{fuel}$, which is a function of the radiative feedback, $\dot{q}_{rad}$. The foam is added by the discharge application, $\dot{m}_{add}$, and lost through evaporation, $\dot{m}_{vap}$, and drop-through, $\dot{m}_{drop}$.

The total mass loss of the foam is a function of the loss due to drop-through and the mass loss due to vaporization. The mass loss due to drop-through is at least partially dependent on the drainage of liquid from the foam. Evaporation of the liquid results primarily from radiant energy from the fire. Assuming that most of the radiation results in direct evaporation of the foam, the evaporation of foam can be characterized by

$$\dot{m}''_{vap} = \frac{\dot{q}''_{rad}}{\Delta H_v} \quad (1)$$

where ΔH_v is the combined latent and sensible heats of vaporization. Using a rough estimate of $\dot{q}''$ from large pool fires of 45–185 kW/m² yields an evaporation rate of 18 and 72 g·m²/s, assuming a heat of vaporization of 2563 kJ/kg. (See Section 2, Chapter 2.) To account for reflective and absorbed losses, Persson[9] has proposed a calculation method

$$\dot{m}''_{vap} = \dot{q}''_{rad} k_e \quad (2)$$

where k_e is an experimentally derived constant using different fluxes from a radiant exposure. For $\dot{q}''_{rad}$ values of 45 and 185 kW/m², Equation 2 yields values for $\dot{m}''_{vap}$ of 11 and 46 g·m²/s, respectively. Since the estimated $\dot{m}''_{vap}$ values based on Equation 1 at the same heat fluxes were 18 and 72 g·m²/s, the experimental mass loss rate results are about 62 percent lower than the theoretical loss. The difference between values is attributable to neglecting the reflected and absorbed losses in Equation 1. This indicates that about 48 percent of the radiant flux to the foam surface is either reflected from or absorbed into the foam blanket. The division between these two heat-transfer mechanisms is not clear and is an area for further study.

Foam loss can likewise be described theoretically, based on the downward force of gravity and the opposing forces due to surface tension and buoyancy. Alternately, a model mass loss due to drainage can be expressed as a time-averaged constant

$$\dot{m}_{drain} = k_d \quad (3)$$

where k_d is an experimentally determined drainage coefficient. From the data of Persson, the drainage coefficient can be estimated to be 17 to 25 g·m²/s.[9] The drainage rate was found to be relatively independent of the radiant heat flux to the foam, but highly dependent on the expansion ratio. Foams with lower expansion ratios will drain faster. For example, decreasing the expansion ratio by about half (11.3 to 5.3) increased the drainage rate by a factor of about 2 (55 to 105 g/min). Decreasing the expansion ratio changes fundamental parameters of the foam, which allows it to drain faster.

Experimental work on the foam model, particularly with regard to the effects of incident heat flux on the foam blanket, are continuing in the United States and Europe. Lattimer et al.[10] designed a test apparatus that was used to measure the behavior of foam when exposed to irradiance levels of 0–50 kW/m². The apparatus provided data on evaporation rate, drainage rate, foam destruction rate, foam temperature, heat penetration, and time to fuel ignition. The performance of a single AFFF formulation was characterized.

Evaporation rates were measured primarily to be a function of irradiance, making it possible to predict evaporation using the irradiance from the fire and an effective heat of vaporization. The AFFF foam evaluated in this study was determined to have an effective heat of vaporization of 4.87 ±0.75 MJ/kg. This result is slightly higher than that found by Ikasson and Persson,[11] 4.0 MJ/kg. Different AFFF formulations may explain this difference.

Foam drainage rate was measured to be insensitive to the irradiance level or the presence of a fuel layer below the foam. This was consistent with the findings of the Swedish researchers. For foams with expansion ratios ranging from 6.0–9.7, drain rate was determined to be a function of foam mass per unit area. A single curve was developed to characterize the drain rate for all foams with a thickness equal to or less than 75 mm. The drainage rate was measured to be constant down to a foam mass per unit area of 3.0 kg/m² and decreased linearly to zero by 1.5 kg/m². The steady-state drain-rate level decreased from 40 g·m²/s to 28 g·m²/s by increasing the expansion ratios from 6.0 to 9.7, respectively.

The drainage rate of low-expansion ratio foams (3.3) was as much as 4–10 times higher than levels measured at higher expansion ratios. The high level was attributed to the fluidity of the foam, which is affected by solution density in foam, breaking and coalescing of bubbles, and so-

lution viscosity. Measurements of foam fluidity for different AFFF foam expansion ratios and temperatures are necessary to further understand these trends in the data at low expansion ratios.

Foam depletion rate was measured primarily to be a function of the irradiance level incident on the foam. As irradiance increased, the foam depletion rate increased. Foam depletion rate was independent of the initial foam height and expansion ratio.

Heat penetration through the foam was measured to be a function of foam height and foam mass. For all of the different tests where heat penetration was measured, the data indicate that heat begins penetrating through the foam when the foam becomes approximately 50 ± 7 mm thick and has a foam mass of 4.2 ± 1.2 kg/m^2.

Ignition time in tests with JP-5 fuel layers was measured to be a function of both irradiance and initial foam height. Increases in irradiance and decreases in initial foam height were determined to decrease the time to ignition. This result was found to be independent of expansion ratio and initial fuel temperature. At ignition, nearly all of the AFFF (less than 0.8 kg/m^2) had been lost from the fuel surface.

Additional small-scale testing needs to be performed to quantify the foam losses and foam spread characteristics of other foam concentrates. Foam loss and spread data are expected to be concentrate dependent, and these data are necessary to further validate the performance of the foam extinguishment model.

Foam drainage is a complicated phenomenon that is highly time dependent. Besides the forces associated with the bubble structure, drainage is dependent on the continual changing geometries of the cells and other variable conditions, such as collapsing cells. Even though all aspects of this problem cannot be fully detailed, simplified models have been created that predict the drainage rate for foams. Kraynik has developed one such model that considers the drainage from a column of persistent foam.[12] The model contains no empirical parameters and assumes the foam is dry with very thin walls such that the liquid contained in the cell walls is negligible. In relaxing the assumptions, this basic model might ultimately be used to assess the effect of various fundamental parameters on foam drainage.

Foam Spread over Liquid Fuels

In order to predict the extinguishment of a liquid pool fire by fire-fighting foam, it is necessary to describe the process of spreading the foam over the liquid fuel surface. This process of foam spread on a liquid fuel is similar to the spread of a less dense liquid (such as oil) on a more dense liquid (such as water). This phenomenological approach to the spread of foam on a liquid pool fire is appropriate to the extent that foam can be treated as a liquid. Kraynik characterizes foams macroscopically as being Bingham fluids with a finite shear stress and nonnewtonian viscosity.[13] That is, foam displays an infinite viscosity up to some initial shear rate above which it displays a shear-rate dependent viscosity.

Since fuels typically have low viscosities (especially compared to foam viscosities at relatively low shear rates), it may be appropriate to model foam spread across a fuel surface using models developed for oil spread on water. These models assume that the oil spreads as a fluid with a viscosity much higher than the water on which it is spreading. The process of oil spread on water has been described in detail by Fay,[14] and Fay and Hoult.[15] Their phenomenologically based model describes three regimes of spread characterized by combinations of spreading forces and retarding forces. The first regime is the gravity-inertia regime, where the outward spread of the oil is driven by a gravity force and retarded by the inertia required to accelerate the oil. The second regime is the gravity-viscous regime, where the gravity-induced spreading is retarded by viscous dissipation in the water. Since the oil is much more viscous than the water, they assume that there is slug flow in the oil and that the viscous drag force is dominated by the velocity gradient in the water. The third regime is characterized by a surface-tension spreading force opposed by the viscous retarding force. By setting the spreading and retarding forces equal in each of the regimes, they developed equations to estimate the length of the spread as a function of time.

By treating the spread of foam on fuel as similar to the spread of oil on water, the equations developed by Fay and Hoult might be used to describe the spread of a foam blanket over a fuel pool as a function of time.[14] Since foam generally has a much higher viscosity than the fuel on which it is spreading, the assumption of slug flow made for the oil by Fay and Hoult should be reasonably valid for foam spread on fuel as well.[14] The equations are

$$\text{gravity-inertia regime:} \quad l = \left(\Delta g V t^2\right)^{1/4}$$

$$\text{gravity-viscous regime:} \quad l = \left(\frac{\Delta g V^2 t^{3/2}}{\nu^{1/2}}\right)^{1/6} \tag{4}$$

$$\text{surface-tension-viscous regime:} \quad l = \left(\frac{\sigma^2 t^3}{\rho^2 \nu}\right)^{1/4}$$

where

l = length of spread (cm)
$\Delta = (\rho_{fuel} - \rho_{foam})/\rho_{fuel}$
g = acceleration of gravity (981 cm/s^2)
V = foam volume (cm^3)
t = time (s)
ν = kinematic viscosity of fuel (cm^2/s)
σ = spreading coefficient (dynes/cm)
ρ = density of fuel or foam (g/cm^3)

Equation 4 represents an untested theoretical model of foam spread. The equation includes the parameters that are known or suspected to affect foam spread. They are presented here as an initial effort to understand foam flow based on first principles. They are not yet developed

for engineering use. The following discussion expands on this theory.

The transition from gravity-dominated spread to surface-tension-dominated spread can be shown to occur at a critical thickness of the foam layer, h_c, given by

$$h_c = \left(\frac{\sigma}{g\Delta\rho_{foam}}\right)^{1/2} \quad (5)$$

The transition from inertia to viscous-dominated retarding force occurs when the foam thickness, h, is equal to the viscous boundary layer thickness, δ, of the fuel, with

$$h = \frac{V}{l^2}$$
$$\delta = (\nu t)^{1/2} \quad (6)$$

The equations for length of spread can be used to generate preliminary estimates of the spread distance and area coverage for the placement of a volume of foam on a fuel surface. The equations are only estimates because they consider a force balance between just the dominant forces for each regime. All forces are actually present in each regime. Also, the densities of both fluids are considered to be very nearly equal for the development of the equation for the gravity-viscous regime. This is the case for oil spread on water, but may not be the case for foam on fuel.

Using approximations for fuel and foam characteristics, it can be shown that a positive spreading coefficient does not begin to affect the spread of foam until the foam layer has become very thin. For the placement of a volume of foam on a fuel, this may not occur until after significant time has passed, relative to the time scale for knockdown desired in many fire protection situations.

The equations for foam spread on fuel include many of the parameters known to be important to foam spread. However, the equations are independent of the foam viscosity. Observations indicate that low-viscosity nonrigid foams, such as AFFF, spread faster than high-viscosity rigid protein foams. The inclusion in the model of a term to account for this is desirable.

The equations for spread length so far have assumed that the foam spreads over the fuel as plug flow, with no relative movement within the foam itself. It is easy to conceive that the foam has the capability to flow over itself. The relative movement within the foam is equivalent to the foam flowing over a solid surface. The total foam flow might ultimately be modeled as the combination of the foam plug over the fuel and the flow within the foam layer itself.

According to Cann et al., several regimes exist for spread of a liquid on a solid that are similar to those described for spread of a liquid on a liquid.[16] Most of this spread occurs in a gravity-viscous force regime, where the spread is given by

$$l = \frac{kt}{\mu} \quad (7)$$

where k is an empirically determined constant, and μ is the foam viscosity.

Thus, the spread of foam over fuel can be characterized by two scenarios: (1) high-viscosity liquid spreading over a low-viscosity liquid and (2) a liquid spreading over a "solid." The spread of foam can be described by modifying Equation 4, as follows:

$$\text{gravity-inertia regime:} \quad l = (\Delta g V t^2)^{1/4} + \frac{kt}{\mu}$$
$$\text{gravity-viscous regime:} \quad l = \left(\frac{\Delta g V^2 t^{3/2}}{\nu^{1/2}}\right)^{1/6} + \frac{kt}{\mu} \quad (8)$$
$$\text{surface-tension regime:} \quad l = \left(\frac{\sigma^2 t^3}{\rho^2 \nu}\right)^{1/4} + \frac{kt}{\mu}$$

Kraynik describes foams as being characterized by a yield stress and shear thinning viscosity.[13] Thus, the foam viscosity in the equations above is not a constant but is a function of the shear rate. The stress in the foam is a result of the gravity-induced pressure gradient. As the foam flows out and becomes thin, the stress will be reduced. When the stress falls below the yield stress, the viscosity will become infinite and the second term, kt/μ, in the spread length equations will go to zero. The foam will flow simply as plug flow. Above the yield stress, the foam will have a finite viscosity, but this viscosity will be dependent on the yield stress.

An AFFF agent that is very free flowing will have a relatively small yield stress and will retain the second term in the spread length equations until it has flowed out to a very thin layer. A protein foam that is relatively stiff will have a large yield stress, and the second term will go to zero before the foam has spread very far. Above the yield stress, the viscosity of the AFFF will be lower than that of a protein foam, and the second term will provide a greater contribution to foam spread. The rheological properties described appear to have a significant impact on foam spread; however, the properties are not a part of any current specification and are rarely measured.

Foam Extinguishment Modeling

At present, modeling of foam extinguishment cannot be performed because of the large number of remaining uncertainties. A model would have to take into account the addition of foam to the fuel surface, the spread of foam on the fuel surface, and the foam loss mechanisms of evaporation and drop-through. The foam spread length equations can be used to estimate the area of foam coverage at a specific time and for a specific quantity of foam. Modeling at this time is limited because of the lack of established values for k_e (Equation 2) and k_d (Equation 3). Also, the yield stress and viscosity relationships for firefighting foams have not been quantified. Experimental work is needed to complete this modeling effort. Also, the actual method of application (e.g., from a handline nozzle or fixed device such as a sprinkler) must ultimately be

taken into account. Even so, preliminary calculations using this methodology are encouraging and support continued development.[7]

Surface Tension and Spreading Coefficient

Film-forming foams are defined by the ability of the aqueous solution draining from the foam to spread spontaneously across the surface of a hydrocarbon fuel. The fundamental relationship used to describe the spreading coefficient is

$$S_{a/b} = \gamma_b - \gamma_a - \gamma_l \quad (9)$$

where

$S_{a/b}$ = spreading coefficient (dynes/cm)
γ_b = surface tension of the lower liquid phase of a hydrocarbon fuel (dynes/cm)
γ_a = surface tension of the upper layer of liquid using AFFF solution (dynes/cm)
γ_l = interfacial tension between liquids *a* and *b* (dynes/cm)

Surface tension and interfacial tension can be measured using methods such as those described in ASTMD-1331, *Standard Test Methods for Surface and Interfacial Tension of Solutions of Surface-Active Agents.* Reagent-grade cyclohexane is typically used as a reference fuel. A du Nouy tensiometer, having a torsion balance with a 4- or 6-cm-circumference platinum-iridium ring, is lowered into the liquid and slowly pulled out until the liquid detaches from the ring's surface. The force recorded at the point where this separation occurs is the surface tension (dynes/cm) of the pure liquid. Similarly, the interfacial tension is the measurement of tension when the ring is pulled through the boundary layer between two liquids.

The Naval Research Laboratory developed some of the earliest quantitative data on the spreading coefficient of AFFF on hydrocarbons, as shown in Tables 4-4.1 and 4-4.2.[17] As fuel temperature increases, the surface tensions of both the fuel and solution decrease. The spreading coefficient may go to zero or go negative.[17,18]

While it has been shown that film-forming foams are superior fire extinguishing agents compared to other foams, there are no one-to-one correlations between bench-scale surface-tension/spreading coefficient data and fire control, extinguishment, and burnback resistance times. Both Scheffey et al.[19] and Geyer[20] have demonstrated that there is no direct correlation between fire extinguishment and spreading coefficient. As such, spreading coefficient data alone cannot be used as a relative predictor of fire performance.

Since the surface tensions of most AFFFs are approximately equal, there must be a balance between the surface tension of the fuel and the interfacial tension of the two liquids to create a positive spreading coefficient. It can be seen then that, while both the surface tension of the solution and the interfacial tension between the liquids have an impact on the spreading coefficient, the interfacial tension is usually the determining factor. For fuels, such as avgas or *n*-heptane, which have surface tensions in the range of 19 to 20 dynes/cm, either the foam surface tension or the interfacial tension, or both, must be reduced. Normally, the changes resulting from a modification of the formulation will be more significant for the interfacial-tension value than they will be for the foam surface-tension value. Still, a relationship between the two values does exist.[4] Therefore, in reducing the sum of the values to obtain a positive spreading coefficient, a delicate balance must be maintained.

Maintaining this balance and achieving a positive spreading coefficient is accomplished by controlling the amount and type of fluorinated surfactants used to formulate the agent. This at first seems beneficial, since a positive number on a low surface-tension fuel will ensure an even larger value with higher surface-tension fuels (e.g., JP-5 or motor gasoline). But, in reducing the interfacial tension, the agent may lose some of its fuel-shedding capabilities. The effects of adding too much fluorosurfactant to an aqueous solution and the result on foam bubble stability are described by Rosen[4] and Aubert et al.[2] This could be a problem that manifests itself only during actual fire testing. The type and amount of fluorosurfactants also affect the spreading coefficient.[19]

Despite the lack of one-to-one correlations between surface-tension spreading coefficient data and fire control, extinguishment, and burnback results, these criteria are useful in categorizing film-forming agents. The spreading coefficient test is used throughout the world as a standard indicator of aqueous film-forming foams. Although undocumented, it is believed that film formation results in improved viscosity (or associated mechanisms that improve spreading), ultimately resulting in superior extinguishing performance.

Table 4-4.1 ***Surface Tension of Hydrocarbon Liquids and Fuels[17]***

Hydrocarbon Liquid	Grade	Surface Tension at 25°C (dynes/cm)
Cyclohexane	Certified A.C.S.	24.2
n-Heptane	Certified spectroanalyzed	19.8
n-Heptane	Commercial	20.9
Isooctane	Certified A.C.S.	18.3
Avgas	115/145	19.4[a] 19.5[b]
JP-4	Navy specification	22.4[a] 22.8[b]
JP-5	Navy specification	25.6[a] 25.8[b]
Motor fuel	Regular	20.5[a] 21.5[b]
Naphtha	Stove and lighting	20.6

[a]Sample 1
[b]Sample 2

Table 4-4.2 ***Interfacial Tensions, Spreading Coefficients, and Film Formation Observations for Various Surfactant Solution-Hydrocarbon Liquid Combinations[17]***

Surfactant Solution	Hydrocarbon Liquid	Interfacial Tension (dynes/cm)	Spreading Coefficient (dynes/cm)	Film Formed
FC-194 (lot 107) (solution surface tension of 15.5 dynes/cm at 25°C)	Cyclohexane	4.3	4.4	Yes
	n-Heptane, certified	5.5	–1.2	No
	n-Heptane, commercial	4.3	1.1	Yes (very slow spread)
	Avgas[a]	4.6	–0.7	No
	JP-4[a]	3.6	3.3	Yes
	JP-5[a]	4.9	5.2	Yes
	Motor Fuel[a]	3.7	1.3	Yes
FC-195 (lot 9) (solution surface tension of 15.6 dynes/cm at 25°C)	Cyclohexane	3.2	5.4	Yes
	n-Heptane, certified	4.2	0.0	Yes (slow spread)
	Isooctane	2.5	0.2	Yes (slow spread)
	Avgas[a]	0.5	3.3	Yes
	JP-4[b]	3.6	3.6	Yes
	JP-5[b]	4.9	5.3	Yes
	Motor fuel[a]	2.6	2.3	Yes
	Naphtha	2.8	2.2	Yes
FC-195 (lot 10) (solution surface tension of 16.4 dynes/cm at 25°C)	Cyclohexane	1.5	6.3	Yes
	n-Heptane, certified	3.2	0.6	Yes
	Isooctane	2.8	–1.3	No
	Avgas[a]	2.1	1.0	Yes
	JP-4[a]	2.7	3.3	Yes
	JP-5[a]	4.2	5.0	Yes
	Motor fuel[a]	1.2	2.9	Yes
	Naphtha	0.8	3.4	Yes (slow spread)

[a]Sample 1
[b]Sample 2

Assessment of Fire Extinguishing and Burnback Performance

Standard Test Methods

Since a theory of foam spreading has not been developed, performance of foams is measured using fire tests. The use of bench-scale burning fuel trays (e.g., less than 1 m diameter) results in varying fuel burning rates. This was observed by Chiesa and Alger when they attempted to use a 15-cm by 45-cm pan for foam performance evaluation.[21] Data from their experiments are shown in Figure 4-4.3, which correlates control times observed when foam samples were tested using bench-scale apparatus (laboratory) and 4.6-m^2 (50-ft^2) fire tests (field method). Equal control times correspond to a 45-degree line. Since the majority of the points fall below this line, the laboratory test is more severe (about 35 percent) than the field test.

Fire test methods used by regulatory authorities for certification are usually on the order of 2.6 to 9.3 m^2 (28 to 100 ft^2). Foams must also meet additional test parameters related to storage, proportioning, and equipment factors.

Underwriters Laboratories Standard 162: Underwriters Laboratories (UL) 162, *Standard for Foam Equipment and Liquid Concentrates,* is the principle test standard for the listing of foam concentrates and equipment in the United States. Test procedures outlined in this standard have been developed to evaluate specific agent/proportioner/discharge device combinations. When a foam concentrate is submitted for testing, it must be accompanied by the discharge device and proportioning equipment with which it is to be listed. Listed products, including the agent, discharge device, and proportioner, are then described in the UL *Fire Protection Equipment Directory.*

Listed with a system, foam liquid concentrates are associated with discharge devices classified as Type I, II, or III. Type I devices deliver foam gently onto the flammable liquid fuel surface, for example, a foam trough along the inside of a tank wall. These devices are no longer evaluated in UL 162. Type II discharge devices deliver foam onto the liquid surface in a manner that results in submergence of the foam below the fuel surface, and restricted agitation at the fuel surface. Examples include subsurface injection systems, tank wall–mounted foam chambers, and applications where foam is bounced off the wall of a tank. Type III discharge devices deliver foam

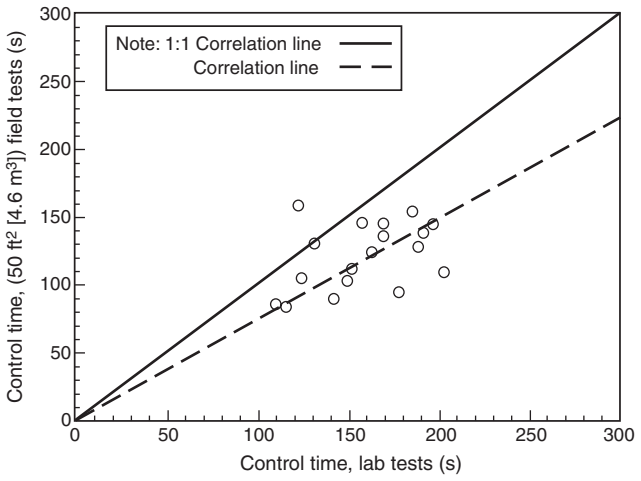

Figure 4-4.3. ***Correlation of control times observed in laboratory and field tests of foam.[21]***

directly onto the liquid surface and cause general agitation at the fuel surface, for example, by using hand-held nozzles. The flammable liquid fire tests in UL 162 include methods for sprinklers, subsurface injection, and topside discharge devices, including nozzles.

Class B fire test requirements for Types II and III discharge devices and sprinklers are shown in Table 4-4.3. Commercial grade *n*-heptane is placed in a square test pan. The area of the pan is a minimum of 4.6 m^2 (50 ft^2). The application rates ("densities" in UL 162, *Standard for Foam Equipment and Liquid Concentrates)* for various concentrates are outlined in Table 4-4.3.

In the test fire, the fuel is ignited and allowed to burn for 60 s. Foam is then discharged for the duration specified in Table 4-4.3. The foam blanket resulting from the foam discharge must spread over and completely cover the fuel surface, and the fire must be completely extinguished before the end of the foam discharge period.

After all the foam is discharged, the foam blanket formed on top of the fuel is left undisturbed for the period specified in Table 4-4.3. During the time the foam blanket is left undisturbed, a lighted torch is passed approximately 25.4 mm (1 in.) above the entire foam blanket in an attempt to reignite the fuel. The fuel must not reignite, candle, flame, or flash over while the torch is being passed over the fuel. However, candling, flaming, or flashover that self-extinguishes is acceptable, provided that the phenomenon does not remain in one area for more than 30 s.

After the attempts to reignite the fuel with the lighted torch are completed, a 305-mm- (12-in.-) diameter section of stovepipe is lowered into the foam blanket. The portion of the foam blanket that is enclosed by the stovepipe is removed with as little disturbance as possible to the blanket outside the stovepipe. The cleared fuel area inside the stovepipe is ignited and allowed to burn for 1 min. The stovepipe is then slowly removed from the pan while the fuel continues to burn. After the stovepipe is removed, the foam blanket must either restrict the spread of fire for 5 min to an area not larger than 0.9 m^2 (10 ft^2), or flow over and reclose the burning area.

When the UL 162 test is passed, the agent, proportioning device, and discharge device become listed. The

Table 4-4.3 ***Foam Application Rates and Duration to Burnback Ignition in UL 162 for Hydrocarbon Fuels***

Application	Foam Concentrate	Fuel Group	Test Application Density [lpm/m^2 (gpm/ft^2)]	Time of Foam Applicaton (min)	Maximum Extinguishment Density [l/m^2 (gal/ft^2)]	Duration until Burnback Ignition (min)	Minimum Application Rate [lpm/m^2 (gpm/ft^2)]
Type III discharge outlets	P, FP, S, FFFP[a]	Hydrocarbon	2.5 (0.06)	5	12.2 (0.03)	15	6.6 (0.16)
	AFFF, FFFP[a]	Hydrocarbon	1.6 (0.04)	3	4.9 (0.12)	9	4.1 (0.10)
Type II discharge outlets	P, FP, S, FFFP[a]	Hydrocarbon	2.5 (0.06)	5	12.2 (0.3)	15	4.1 (0.10)
	AFFF, FFFP[a]	Hydrocarbon	1.6 (0.04)	3	4.9 (0.12)	9	41. (0.10)
	All	Polar	[b]	5	—	15	[c]
Foam-Water sprinklers	P, FP, S	Hydrocarbon	6.6 (0.16)	5	30 (0.8)	15	6.6 (0.16)
Standard orifice sprinkler and spray systems	AFFF, FFFP	Hydrocarbon	4.1 (0.10)	5	20.4 (0.5)	15	6.6 (0.16)
		Polar	[b]	5	—	15	[d]

P = Protein FFFP = Film-forming fluoroprotein FP = Fluroprotein AFFF = Aqueous film-forming fluoroprotein S = Synthetic

[a]Film-forming fluoroprotein is to be tested at application densities of 2.5 and 1.6 Lpm/m^2 (0.06 and 0.04 gpm/ft^2).

[b]Application rate may vary among polar groups, as specified by the manufacturer.

[c]0.01 or 1.67 times test application rate, whichever is greater.

[d]0.16 or 1.6 times test application rate, whichever is greater.

Source: UL 162, *Standard for Foam Equipment and Liquid Concentrates,* March 1994.

fact that foam concentrate has a UL label does not mean it has been tested under all potential end-use conditions. The UL *Fire Protection Equipment Directory* must be referenced to determine with what equipment the concentrate has been tested and approved.

UL 162, *Standard for Foam Equipment and Liquid Concentrates,* is not an agent specification; therefore, there are no requirements for physical properties, such as film formation and sealability and corrosion resistance. Neither are there any provisions to test, on a large scale, the degree of dry chemical compatibility of an agent, or the effects of aging or mixing with agents of another manufacturer. Requirements for a positive spreading coefficient (greater than zero using cyclohexane) for film-forming foams recently have been implemented.[22]

U.S. military specification: The U.S. Military Specification, MIL-F-24385, is the AFFF procurement specification for the U.S. military and federal government. The U.S. military, in all likelihood, is the largest user of foam in the world. It is important to recognize that MIL-F-24385 is a procurement specification as well as a performance specification. Hence, there are requirements for packaging, initial qualification inspection, and quality conformance inspection, in addition to fire performance criteria. Equipment designs unique to the military, in particular U.S. Navy ships, also impact on the specification requirements (e.g., use of seawater solutions and misproportioning-related fire tests). These requirements have been developed based on research and testing at the Naval Research Laboratory and actual operational experience with protein and film-forming foams.

Table 4-4.4 summarizes the important fire extinguishment, burnback resistance, film formation, and foam quality requirements established by MIL-F-24385. The fire tests are conducted using 2.6 m^2 (28 ft^2) and 4.6 m^2 (50 ft^2) circular fire test pans. There are specific requirements to conduct a fire test of the agent after it has been subjected to an accelerated aging process (simulating prolonged storage) and after intentionally misproportioning the concentrate with water. In particular, the requirement to conduct a fire test of the agent at one-half of its design concentration is one of the most difficult tests. The 2.6-m^2 (28 ft^2) half-strength fire test must be extinguished in 45 s, only 15 s greater than allowed when the full-strength solution is used.

The physical and chemical properties evaluated for MIL-F-24385 agents are outlined in Table 4-4.5, along with the rationale for each test. These procedures have been developed based on experience and specific military requirements. For example, MIL-F-24385 requires that the agent be compatible with dry chemical agents. Dry chemical agents may be used as "secondary" agents in aviation and shipboard machinery space fires, for example, to combat three-dimensional fuel fires, where AFFF alone may have limited effectiveness. MIL-F-24385 requires that an agent's compatibility with potassium bicarbonate dry chemical agent (PKP) be demonstrated. The burnback time of the foam in the presence of the dry chemical is measured. Also, the concentrate of one manufacturer must be compatible with concentrates of the same type furnished by other manufacturers, as determined by fire tests and accelerated aging tests.

Table 4-4.4 ***Summary of the U.S. Military AFFF Specification (MIL-F-24385, Revision F) Key Performance Requirements***

Test Parameter	Revision F
Fire extinguishment	
2.6-m^2 (28-ft^2) fire test	
Application rate	2.9 lpm/m^2 (0.71 gpm/ft^2)
Maximum extinguishment time	30 s
Maximum extinguishment density	1.45 l/m^2 (0.036 gal/ft^2)
4.6-m^2 (50-ft^2) fire test[a]	
Application rate	1.6 lpm/m^2 (0.04 gpm/ft^2)
Minimum 40-s summation	320 s
Maximum extinguishment time	50 s
Maximum extinguishment density	1.34 l/m^2 (0.033 gal/ft^2)
Fire extinguishment—over- and under-proportioning [2.6-m^2 (28-ft^2) Test]	
One-half strength	
Maximum extinguishment time	45 s
Maximum extinguishment density	2.2 l/m^2 (0.054 gal/ft^2)
Quintuple (5 ×) strength	
Maximum extinguishment time	55 s
Maximum extinguishment density	2.7 l/m^2 (0.066 gal/ft^2)
Burnback resistance	
2.6-m^2 (28-ft^2) fire test	25% maximum at 360 s[b]
4.6-m^2 (50-ft^2) fire test	25% maximum at 360 s
Foam quality	
Expansion ratio	6.0 : 1 minimum
25% drainage	150 s minimum
Film formation	
Spreading coefficient	
Fuel	Cyclohexane
Minimum value	3 dynes/cm
Ignition resistance test	
Fuel	Cyclohexane
Pass/fail criteria	No ignition

[a]Saltwater only

[b]300 s for one-half-strength solutions; 200 s for quintuple-strength solutions

Standards outside the United States: The number of standards developed for foams outside the United States is quite substantial. A brief review of the literature yielded over 17 different standards and test methods.[23] Developments in the European community are reviewed here to provide examples of differences in test standards.

The International Civil Aviation Organization (ICAO) develops crash fire-fighting and rescue documents for its member bodies. The ICAO *Airport Services Guide,* Part 1, "Rescue and Firefighting," describes airport levels of protection to be provided and extinguishing

Table 4-4.5 ***Physical/Chemical Properties and Procurement Requirements of the AFFF Mil Spec***

Requirement	Rationale
Refractive index	Enable use of refractometer to measure solution concentrations in field; this is most common method recommended in NF PA 412[a]
Viscosity	Ensures accurate proportioning when proportioning pumps are used; for example, balance pressure proportioner or positive displacement injection pumps
pH	Ensures concentrate will be neither excessively basic or acidic; intention is to prevent corrosion in plumbing systems
Corrosivity	Limits corrosion of, and deposit buildup on, metallic components (various metals for 28 days)
Total halides/ chlorides	Limits corrosion of, and deposit buildup on, metallic components
Environmental impact	Biodegradability, fish kill, BOD/COD[b]
Accelerated aging	Film formation capabilities, fire performance, foam quality; ensures a long shelf life
Seawater compatibility	Ensures satisfactory fire performance when mixed with brackish or saltwater
Interagent compatibility	Allows premixed or storage tanks to be topped off with different manufacturers' agents, without affecting fire performance
Reduced- and over-concentration Fire test	Ensures satisfactory fire performance when agents are proportioned inaccurately
Compatibility with dry chemical (PKP) agents	Ensures satisfactory fire performance when used in conjunction with supplementary agents
Torque to remove cap	Able to remove without wrench
Packaging requirements	Strength, color, size, stackable, minimum pour, and vent-opening tamperproof seal; ensures uniformity of containers and ease of handling
Initial qualification inspection	Establish initial conformance with requirements
Quality conformance inspection (each lot)	Ensures continued conformance with requirements

[a]NFPA 412, *Standard for Evaluating Aircraft Rescue and Fire-Fighting Foam Equipment*, 1998 edition.

[b]BOD/COD: Biological oxygen demand/chemical oxygen demand

agent characteristics. Minimum usable amounts of extinguishing agents are based on two levels of performance: Level A and Level B. The amounts of water specified for foam production are predicted on an application rate of 8.2 lpm/m^2 (0.20 gpm/ft^2) for Level A, and 5.5 lpm/m^2 (0.13 gpm/ft^2) for Level B. Agents that meet performance Level B require less agent for fire extinguishment. ICAO foam test criteria are described in Table 4-4.6. Foams meeting performance Level B have an extinguishment application density of 2.5 l/m^2 (0.061 gal/ft^2). There are no surface-tension, interfacial-tension, and spreading coefficient requirements.

The International Organization for Standardization (ISO) has issued a draft specification for low-expansion foams, EN 1568-3.[24] The specification includes definitions for protein, fluoroprotein, synthetic, alcohol resistant, AFFF, and FFFP concentrates. A positive spreading coefficient is required for film-forming foams when cyclohexane is used as the test fuel. There are toxicity, corrosion, sedimentation, viscosity, expansion, and drainage criteria. The fire test uses a 2.4-m- (8-ft-) diameter circular pan with heptane as the fuel. The UNI 86 foam nozzle is used for either a "forceful" or "gentle" application method at a flow rate of 11.4 lpm (3 gpm). The application rate is 2.4 lpm/m^2 (0.06 gpm/ft^2). For the greatest performance level, a 3-min extinguishment time is required. This extinguishment time results in an extinguishment application density of 7.6 l/m^2 (0.19 gal/ft^2).

The proposed ISO/EN requirements for extinguishing and burnback are summarized in Table 4-4.7. There are three levels of extinguishment performance and four levels of burnback performance. For extinguishing performance, Class I is the highest class and Class III the lowest class. For burnback resistance, Level A is the highest level and Level D the lowest level.

Typical performance classes and levels for different concentrates are provided. Typical anticipated performance for AFFF is noted as Level IC, and Level IB for alcohol-type AFFF. For a fluoroprotein foam, performance is expected to be Level IIA for both alcohol-type and hydrocarbon-only concentrates.

Table 4-4.6 ***ICAO Foam Test Requirements***

Fire Tests	Performance Level A	Performance Level B
1. Nozzle (air aspirated)		
(a) Branch pipe	UNI 86 foam nozzle	UNI 86 foam nozzle
(b) Nozzle pressure	700 kPa (100 psi)	700 kPa (100 psi)
(c) Application rate	4.1 lpm/m^2 (0.10 gpm/ft^2)	2.5 lpm/m^2 (0.06 gpm/ft^2)
(d) Discharge rate	11.4 lpm (3.0 gpm)	11.4 lpm (3.0 gpm)
2. Fire size	≅ 2.8 m^2 (≅ 30 ft^2) (circular)	≅ 4.5 m^2 (≅ 48 ft^2) (circular)
3. Fuel (on water surface)	Kerosene	Kerosene
4. Preburn time	60 s	60 s
5. Fire performance		
(a) Extinguishing time	≤60 s	≤60 s
(b) Total application time	120 s	120 s
(c) 25% reignition time	≥5 min	≥5 min

Table 4-4.7 ***Maximum Extinction Times and Minimum Burnback Times from Proposed ISO/EN Specification***

		Gentle Application Test		Forceful Application Test	
Extinguishing Performance Class	Burnback Resistance Level	Extinction Time (min) Not More Than	Burnback Time (min) Not Less Than	Extinction Time (min) Not More Than	Burnback Time (min) Not Less Than
I	A	—	—	3	10
	B	5	15	3	Not tested
	C	5	10	3	Not tested
	D	5	5	3	Not tested
II	A	—	—	4	10
	B	5	15	4	Not tested
	C	5	10	4	Not tested
	D	5	5	4	Not tested
III	B	5	15	Not tested	Not tested
	C	5	10	Not tested	Not tested
	D	5	5	Not tested	Not tested

Comparison of small-scale tests: Table 4-4.8 outlines the large number of variables associated with foam performance and testing. These include factors such as foam bubble stability and fluidity, actual fire test parameters (e.g., fuel, foam application method and rate), and environmental effects. Even the fundamental methods of measuring foam performance (i.e., knockdown, control, and extinguishment) vary. For example, Johnson reported that FFFP fails the proposed ISO/EN gentle application tests because small flames persist along a small area of the tray rim.[25] As a result, the foam committees have proposed redefining extinction to include flames.

Given the variations and lack of fundamental foam spreading theory, it follows that tests and specifications for various foams and international standards have different requirements. The differences are reflected in Table 4-4.9, which compares four key parameters of MIL-F-24385, UL 162, ICAO, and ISO/EN standards for manual application (e.g., handline or turret nozzles). There is no uniform agreement among test fuel, application rate, the allowance to move the nozzle, and the extinguishment application density for AFFF. There is a factor of six difference between the lowest permitted extinguishment application density (MIL-F-24385) and the highest (ISO/EN). This significant difference is attributed, at least in part, to the fixed nozzle requirement in the ISO/EN specification.

No study has been performed to correlate test methods; given the significant differences in performance characteristics and requirements, it is unlikely that correlation between these test methods could be established, even when considering AFFF only. An AFFF that meets the ICAO standard could not be said to meet MIL-F-24385 without actual test data. The problem of correlating differences in small-scale tests was demonstrated by UL in a comparison of UL, MIL-F-24385, O-F-555B (U.S. government protein foam specification), and United Kingdom test methods.[26] In those tests, differences between different classes of agents (protein vs. AFFF) and between agents within a class (e.g., AFFF) were demonstrated. No correlations between test standards could be established.

The problem of correlation is compounded when a single test method is used in an attempt to assess different classes of foam (e.g., protein and AFFF). Attempts to use a single test method are problematic because of the inherent difference between these foams. That is, protein foams require air aspiration so that the foam floats on the fuel surface. This stiff, "drier" foam is viscous and does not inherently spread well without outside forces (e.g., nozzle stream force). AFFF, because of its film-formation characteristics, does not require the degree of aspiration that protein foams require. This heavier, "wetter" foam is inherently less viscous, which contributes to improved spreading and fluidity on fuel surfaces. This is related, at least in part, to the degree of aspiration of the foam. A more exact description of foam aspiration is appropriate. Thomas has described two levels of foam aspiration: (1) primary aspirated and (2) secondary aspirated.[27] Primary aspirated foam occurs when a foam solution is applied by means of a special nozzle designed to mix air with the solution within the nozzle. The consequence is foam bubbles of general uniformity. *Air-aspirated* foam refers to this primary aspirated foam. Secondary aspirated foam results when a foam solution is applied using a nozzle that does not mix air with the solution within the nozzle. Air is, however, drawn into the solution in-flight or at impact at the fire. Secondary aspirated foam is more commonly referred to as *non-air-aspirated* foam.

The correlation between foam solution viscosity and extinguishment time has been shown by Fiala, but the entire foam spreading and extinguishment theory has yet to be demonstrated based on first principles.[28] Thus, the test standards reference bench-scale methods that measure a factor of foam fluidity (e.g., spreading coefficient), but fail to recognize the total foam spreading system, including viscous effects. Fundamental understanding of foam mechanisms would promote the development of bench- and small-scale test apparatuses that potentially have greater direct correlation for predicting large-scale results.

There has been some criticism of the human element involved in many of the test methods. The human factor occurs when an operator is allowed to apply foam from a

Table 4-4.8 ***Variables Associated with Foam Performance and Testing***

I. Physical/chemical properties of foam solution
  A. Bubble stability
    1. Measures
      a. Expansion ratio
      b. Drainage rate
    2. Variables
      a. Water temperature
      b. Water hardness/salinity
      c. Water contamination
  B. Fluidity of foam
    1. Measures
      a. Viscosity
      b. Spreading rate
      c. Film formation
    2. Variables
      a. Fuel type and temperature
      b. Foam bubble stability
  C. Compatibility with auxillary agents
    1. Measures—fire and burnback test
    2. Variables
      a. Other foam agents|
      b. Dry chemical agents
  D. Effects of aging
    1. Measures—fire and burnback test
    2. Variable—shelf life of agent

II. Test methods to characterize foam performance
  A. Fuel
    1. Measures
      a. Vapor pressure
      b. Flash point
      c. Surface tension
      d. Temperature
    2. Variables
      a. Volatility
      b. Depth and size
      c. Initial temperature of air and fuel temperature
      d. Time fuel has been burning (e.g., short versus long, and depth of hot layer)
  B. Foam application method
    1. Measures
      a. Stream reach
      b. Aspiration of foam
      c. Foam stability, e.g., contamination by fuel
      d. Water content of foam
      e. Proportioning rate
    2. Variables
      a. Aspiration
        (1) Effect on stream reach
        (2) Degree to which foam is aspirated and the need to aspirate based on foam type

II B. 2. Variables (continued)
      b. Fixed versus mobile device
      c. Application technique
        (1) Indirect, for example, against backboard or sidewall
        (2) Direct
          (a) Gentle
          (b) Forceful
          (c) Subsurface injection
      d. Application location
        (1) High—need to penetrate plume
        (2) Low
      e. Application rate of foam
      f. Wind (as it affects stream reach)
        (1) Crosswind
        (2) With and against
      g. Effect of reduced or increased concentration due to improper proportioning
  C. Fire configuration
    1. Measures
      a. Fuel burning rate, radiation feedback to fire
      b. Propensity for reignition
      c. Surface tension
    2. Variables
      a. Pan/containment geometry
      b. Two-dimensional (pool) versus three-dimensional (running fuel/atomized pray)
      c. Presence and temperature of freeboard
      d. Wind (as it affects flame tilt and reradiation)
      e. Surface on which there is fuel
        (1) Rough
        (2) Smooth
        (3) Water substrate—“peeling” effect of fuel
  D. Measurement of results
    1. Measures
      a. Time to knockdown, control, extinguish, and burnback
        (1) Actual or estimated time by visual observations
        (2) ummation values, that is, summation of control at 10, 20, 30, and 40 sec
      b. Heat flux during extinguishment and burnback
    2. Variables—qualitative and quantitative methods to determine fire knockdown, extinguishment, and burnback
      a. 90 percent control—measure of ability of foam to quickly control the fire
      b. 99 percent (virtual extinguishment)—all but the last flame or edge extinguished
      c. Extinguishment—100 percent
      d. Burnback—25 percent, 50 percent

hand-held nozzle onto the burning test fire. Personnel are also called upon in some tests to qualitatively assess the percentage of fire involvement in the test pan during the burnback procedure. Using a fixed nozzle during a specification test eliminates the human element during extinguishment. For sprinkler applications, using a fixed nozzle is entirely appropriate and should yield results comparable to actual installations. For applications where movement is actually involved (e.g., fire-fighting handlines, crash-rescue truck turrets, and movable monitors on ships and at petrochemical facilities), the extinguishment densities in the fixed test application will generally exceed the densities found in actual applications in the field. (See Table 4-4.9 for differences in extinguishing densities for manual versus fixed applications.) Removal of the human element is certainly advisable from a test repeatability standpoint. However, removing the human element from approval fire tests has proved difficult. Both

Table 4-4.9 ***Examples of Extinguishment Application Densities of Various Test Standards***

Test Standard	Fuel	Application Rate [lpm/m² (gpm/ft²)]	Nozzle Movement Permitted	Extinguishment Application Density [l/m² (gal/ft²)]
MIL SPEC	Motor gasoline	1.6 (0.04)	Yes	1.34 (0.033)
UL 162	Heptane	1.6 (0.04)	Yes	4.9 (0.12)
ICAO	Kerosene	2.5 (0.06)	Yes (horizontal plane)	2.6 (0.061)
ISO/EN—Forceful	Heptane	2.5 (0.06)	No	7.6 (0.19)

U.S. and Canadian military authorities have investigated the use of fixed nozzles. Both organizations concluded that tests with human operators resulted in better correlation with large fires and overall repeatability.

Quantitative methods for evaluating burnback performance have been described by Scheffey et al.[19] and been adopted in ISO/EN and Scandinavian (NORDTEST) test methods. These methods involve the use of radiometers to establish a heat flux during full test-pan involvement. After extinguishment, the radiometers measure the increasing flux as the burnback fire grows. This increasing flux due to burnback is compared against the original flux. A cutoff is established so that the maximum burnback time is the time for the burnback flux to reach some percentage (e.g., 25 percent) of the original full-burning flux.

Critical Application Rates and Correlations between Small- and Large-Scale Tests

The previous section described the application rate differences in standard test methods between AFFF, fluoroprotein, and protein foams. These application rate differences were established based on full-scale testing. For sprinklers, much of the fundamental application rate differences were established during testing conducted by Factory Mutual Research Corporation (FMRC). (See section on foam-water sprinkler systems.) For manual applications, tests in the aviation fire protection field provide the basis for the fundamental application rates. The application rates specified in test standards are usually rates lower than those used in actual practice. (See Table 4-4.3.) There are two reasons for this: (1) a factor of safety is used when specifying rates in actual practice and (2) differences between individual foam agents are more readily apparent at critical application rates. To demonstrate how application rates are developed and how specification tests correlate with large-scale results, an example from aviation fire tests will be used. This example is based on a review of foam fire test standards performed by Scheffey et al. for the Federal Aviation Administration (FAA).[23]

Tests were conducted by the FAA to determine application rates for a single-agent attack to achieve fire control (e.g., 90 percent extinguishment of a fire area) within 1 min under a wide variety of simulated accident conditions. Two factors are important in addition to the application rate required for 1-min fire control: (1) the critical application rate, below which fires will not be extinguished independent of the amount of time an agent is applied; and (2) application density, which is the amount of foam per unit area to control or extinguish a fire.

Minimum application rates were originally developed by Geyer in tests of protein and AFFF agents.[29] These tests involved "modeling" tests with JP-4 pool fires of 21-, 30-, and 43-m (70-, 100-, and 140-ft) diameter. Large-scale verification tests with a B-47 aircraft and simulated shielded fires (requiring the use of secondary agents) were conducted with 34- and 43-m (110- and 140-ft) JP-4 pool fires. All tests were conducted with air-aspirating nozzles. The protein foam conformed to the U.S. government specification, O-F-555b, while the AFFFs used were in nominal conformance with MIL-F-24385 for AFFF. These tests were being performed at the time when the seawater-compatible version of MIL-F-24385 had just been adopted based on large-scale tests.

Figure 4-4.4 illustrates the results of the modeling experiments. The results show that, for a fire control time of 60 s, the application rate for AFFF was on the order of 1.6 to 2.4 lpm/m² (0.04 to 0.06 gpm/ft²), while the application rate for protein foam was 3.3 to 4.1 lpm/m² (0.08 to 0.10 gpm/ft²). The data indicated that the application rate curves become asymptotic at rates of 4.1 lpm/m² (0.1 gpm/ft²) and 8.2 lpm/m² (0.2 gpm/ft²) for AFFF and protein foam, respectively. Above these rates, fire control times are not appreciably improved. Likewise, critical application rates for fire control are indicated when control times increase dramatically. The single test with a fluoroprotein agent indicated that this agent, as expected, fell between AFFF and protein foam.

Large-scale auxiliary agent tests were conducted to identify increases in foam required when obstructed fires

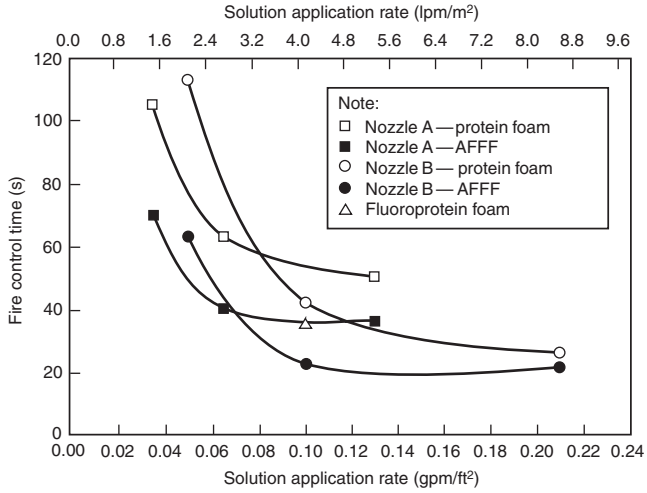

Figure 4-4.4. ***Fire control time as a function of solution application rate using protein foam and AFFF on JP-4 pool fires.[29]***

with an actual fuselage were added to the scenario. The results indicated that fire control times increased by a factor of 1 to 1.9 for AFFF and 1.5 to 2.9 for protein foams. It was estimated that the most effective foam solution application rates were 4.9 to 5.7 lpm/m² (0.12 to 0.14 gpm/ft²) for AFFF and 7.5 to 9 lpm/m² (0.18 to 0.22 gpm/ft²) for protein foam. This is the original basis of the recommendations adopted by ICAO of 5.5 lpm/m² (0.13 gpm/ft²) for AFFF and 8.2 lpm/m² (0.20 gpm/ft²) for protein foam. A rate of 7.5 lpm/m² (0.18 gpm/ft²) was subsequently established for fluoroprotein foam. These application rate values are still used by FAA, NFPA, and ICAO to establish minimum agent supplies at airports.

Tests of AFFF alone were conducted by Geyer.[30] These agents, selected from the U.S. Qualified Products List (MIL-F-24385 requirements), were tested on JP-4, JP-5, and aviation gasoline (avgas) fires. Air-aspirating nozzles were used with different AFFF agents. Example results are shown in Figure 4-4.5. Similar data were collected by holding the JP-4 fuel fire size constant at 743 m² (8000 ft²) and varying the flow rates to develop application rate comparisons. These data are shown in Figure 4-4.6.

Additional tests were conducted by Geyer et al. to verify the continuation of the reduction of water when AFFF agents were substituted for protein foam in aviation situations.[1] In 25-, 31-, and 44-m- (82.4-, 101-, and 143-ft-) diameter Jet A pool fires, AFFF, fluoroprotein, and protein foams were discharged with air-aspirating and non-air-aspirating nozzles. The data, summarized in Figure 4-4.7, validated the continued allowance of a 30 percent reduction in water requirement at certified U.S. airports when AFFF is substituted for protein foam.

Although some test criteria in standardized methods do not necessarily correlate directly with actual fire and

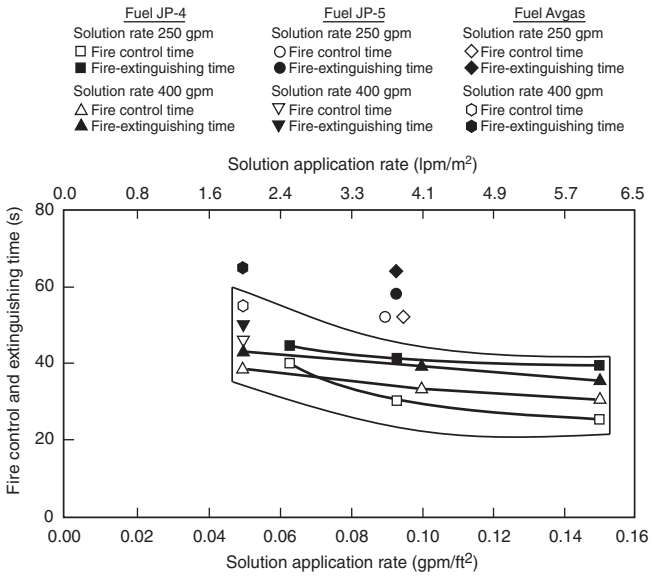

Figure 4-4.5. ***Fire control and extinguishing times as functions of the foam solution application rate using AFFF at 250 gpm (946 lpm), 400 gpm (1514 lpm), and 800 gpm (3028 lpm) on JP-4, JP-5, and avgas fires.[30]***

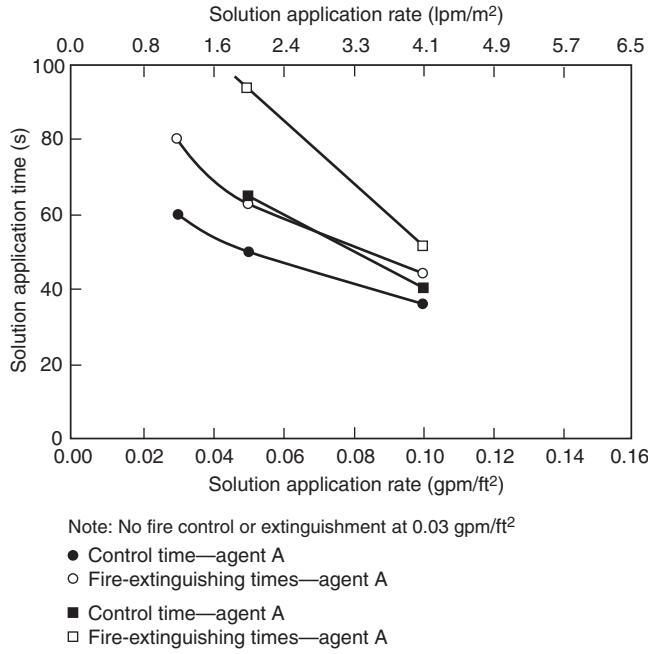

Figure 4-4.6. ***Fire control and extinguishing times as a function of solution application rate using AFFF at 250, 400, and 800 gpm on 743-m² (8000-ft²) JP-4 fuel fires.[30]***

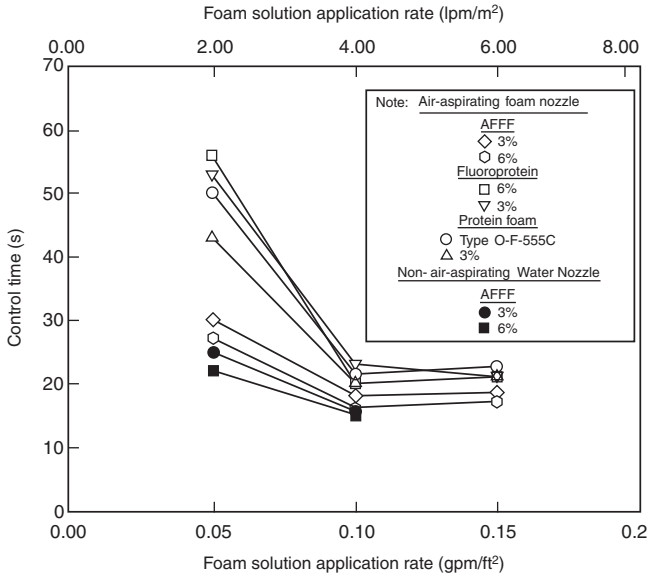

Figure 4-4.7. ***Fire control time as a function of solution application rate for AFFF, fluoroprotein, and protein foams for Jet A pool fires.[1]***

burnback performance, small-scale test data for AFFF formulated to the U.S. military specification (MIL-F-24385) has been shown to correlate with large-scale fire test results. This is based on a comprehensive review of small- and large-scale test data.[23] In these data, a key variable

was controlled; that is, all AFFF agents were formulated to meet MIL-F-24385. Ninety percent fire control times were used as the most accurate measure of fire knockdown performance, which were reported in all tests. The use of 90 percent control times eliminates the variability of total extinguishment, which might be dependent on test-bed-edge effects or running fuel fire scenarios. Data for tests using air-aspirated or non-air-aspirated nozzles were combined. Low-flashpoint [less than 0°C (32°F)] fuels were evaluated. The evaluation included only tests where manual application was used, eliminating the variable of fixed versus manual application.

The effects of application rate on control and extinguishment times, as demonstrated in Figures 4-4.4 through 4-4.7, were reconfirmed as shown in Figure 4-4.8. Control time increases exponentially as application rate decreases, particularly below 4.1 lpm/m² (0.10 gpm/ft²). Variability of the data is shown by the first standard deviation.

The scaling of small fires with large fires is shown in Figures 4-4.9 and 4-4.10, which relate the time needed to control the burning fuel surface as a function of fire size. The time needed to control a unit of burning area [s/ft² (s/m²)], designated as the specific control time, is plotted as a function of fire size. For low [1.2 to 2.5 lpm/m² (0.03 to 0.06 gpm/ft²)] and intermediate [2.8 to 4.1 lpm/m² (0.07 to 0.10 gpm/ft²)] application rates, the specific control times decrease linearly as a function of fire area. These data are in agreement with data from Fiala, which also indicate decreasing specific extinguishment control times as a function of burning area for increasing application rates of AFFF.[28] Also, Fiala showed that, for a constant application rate, AFFFs have lower specific extinguishment times as a function of burning area than those of protein and fluoroprotein foams. Obviously, this linear relationship must change at very large areas; otherwise, the specific control/extinguishment time would go to zero. This is evidenced in Figure 4-4.9, where the curve flattens at the high-area end of the plot.

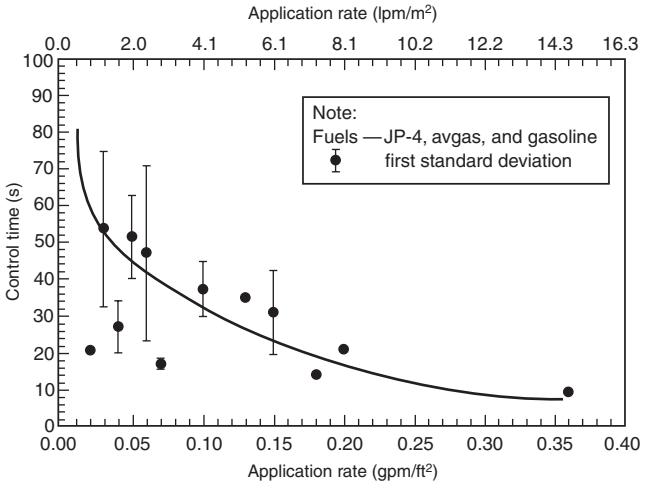

Figure 4-4.8. ***AFFF control time as a function of application rate.[23]***

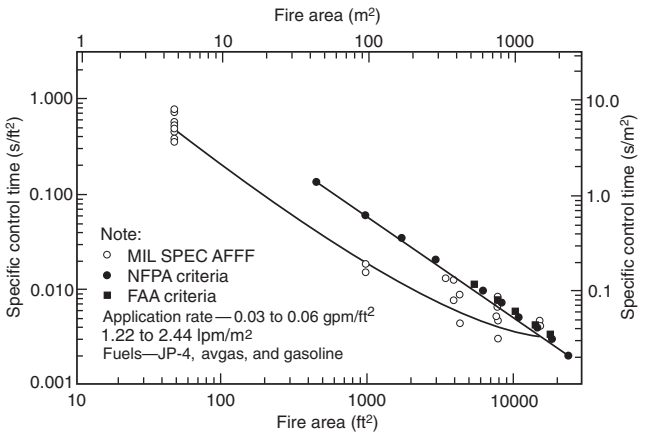

Figure 4-4.9. ***Specific control times for AFFF at low application rates.[23]***

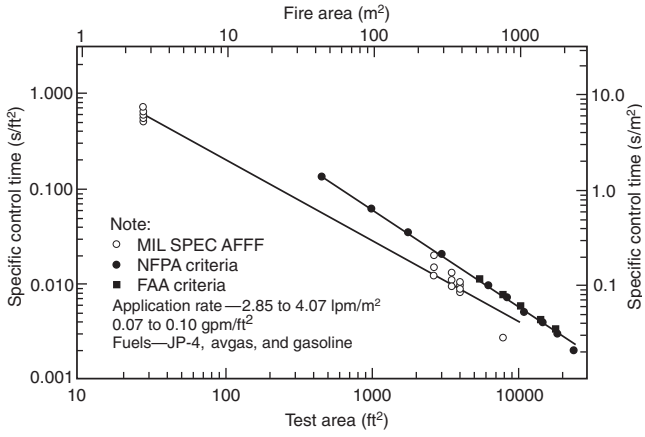

Figure 4-4.10. ***Specific control times for AFFF at intermediate application rates.[23]***

Figures 4-4.9 and 4-4.10 show that higher specific control times are required for MIL-F-24385 test fires [2.6 and 4.7 m² (50 and 20 ft²) compared to large fires. This is readily apparent as actual/control extinguishment times for the small fires are on the same order as results from large fires. FAA and NFPA criteria for minimum quantities of agent are also shown in Figures 4-4.9 and 4-4.10. These criteria are expressed in terms of specific control time as a function of area by using the required control time of 60 s and the practical critical fire areas for airports serving different sizes of aircraft. The data indicate that specific control times with MIL-F-24385 agents are roughly equivalent or less than the specific control times established by NFPA and FAA requirements for large fire areas. This relationship is true even with the AFFF discharged at rates 25 to 75 percent below the minimum NFPA/FAA discharge rate of 5.5 lpm/m² (0.13 gpm/ft²). From these data, it can be concluded that a scaling relationship exists between MIL-F-24385 small-scale tests and

actual large-scale crash rescue and fire-fighting applications. The MIL-F-24385 tests are more challenging than the larger tests in terms of specific control time, but this challenging test produces an agent that can meet NFPA and FAA requirements at less than the design application rate. This factor of safety accounts for variables in actual aviation crash situations, for example, running fuel fires, debris that may shield fires, and cross winds that may limit foam stream reach.

Aviation Fire Protection Considerations

Historical Basis for Foam Requirements

The underlying principle in aviation fire protection is to temporarily maintain the integrity of an aircraft fuselage after a mishap to allow passenger escape or rescue. When an aircraft is involved in a fuel spill fire, the aluminum skin will burn through in about 1 min. If the fuselage is intact, the sidewall insulation will maintain a survivable temperature inside the cabin until the windows melt out in approximately 3 min. At that time, the cabin temperature rapidly increases beyond survivable levels.

Aircraft rescue and fire-fighting (ARFF) vehicles are designed to reach an incident scene on the airport property in 2 to 3 min, depending on the standard enforced by the authority having jurisdiction (AHJ). Having reached the scene in this time frame, agent must be applied to control a fire in 1 min or less. The 1-min critical time for fire control is recognized by FAA, NFPA, and ICAO.

Minimum agent requirements on ARFF vehicles are established using the 1-min critical control time plus the anticipated spill area for the largest aircraft using the airport. A "theoretical critical fire area" has been developed, based on tests, and is defined as the area adjacent to the fuselage, extending in all directions to the point beyond which a large fuel fire would not melt an aluminum fuselage regardless of the duration of the exposure. A function of the size of an aircraft, the theoretical critical fire area was amended to a "practical critical fire area" after evaluation of actual aircraft fire incidents. The practical critical area, two-thirds the size of the theoretical critical area, is widely recognized by the aviation fire safety community, including FAA, NFPA, and ICAO. Vehicles must be equipped with sufficient agent and discharge devices to control a fire in the practical critical area within 1 min. Vehicles must also be equipped with secondary agent (dry chemical or Halon 1211) for use in combating three-dimensional fuel fires.

Agent Quantities and Standards

The previous text on critical application rates described the rationale used to develop design application rates used in aviation fire protection. These rates are 5.5 lpm/m^2 (0.13 gpm/ft^2) for AFFF, 7.5 lpm/m^2 (0.18 gpm/ft^2) for fluoroprotein foam, and 8.2 lpm/m^2 (0.28 gpm/ft^2) for protein foam. Using these rates, the practical critical fire area and the 60-s control time criteria, minimum agent quantities are established for airports serving different size aircraft. These criteria are contained in NFPA 403, *Standard for Aircraft Rescue and Fire-Fighting Services at Airports,* and the FAA Advisory Circular 150/5210-6C, "Aircraft Fire and Rescue Facilities and Extinguishing Agents." ICAO uses similar criteria. NFPA 403 recently adopted the 4.6 m^2 (50 ft^2) fire extinguishment and burnback criteria from MIL-F-24385 for AFFF agents. UL test criteria are acceptable for protein and fluoroprotein foams. Most airports in the United States use AFFF as the primary fire-fighting agent. Recognizing the limitations of its test methods for aviation applications, UL has deleted references to crash rescue fire fighting from the scope of UL 162, *Standard for Foam Equipment and Liquid Concentrates.* NFPA 403 recognizes that the standards for foam that it references are widely recognized throughout North America, but may not be recognized in other areas of the world. In particular, the ICAO test method has significantly different test parameters, including test fuel, application rate, and extinguishment density. The NFPA notes that it is incumbent on the national authority having jurisdiction to determine that alternative test methods meet the level of performance established by NFPA 403 test criteria.

NFPA 412, *Standard for Evaluating Aircraft Rescue and Fire-Fighting Foam Equipment,* provides field test methods to determine the adequacy of foam equipment on crash rescue vehicles. It includes criteria for foam expansion and drainage, and methods to determine foam solution concentration.

Expansion and drainage: Foam expansion and drainage requirements of the current version of NFPA 412, *Standard for Evaluating Aircraft Rescue and Fire-Fighting Foam Equipment,* are shown in Table 4-4.10.

NFPA 412 references a 1600-ml foam sample collector, which was originally adopted by ICAO and ISO/EN. This single method is used to obtain expansion and drainage measurements for all types of foams in hope that similar success could be obtained in using a single fire test method for all foams. The multiple categories of foam test classification in Table 4-4.7 for the ISO/EN method show how difficult this has been to achieve. Given the different methods of foam flow over a fuel surface, it may not be practical to use a common fire test method predicated on the current means of testing. Further development of fundamental foam-extinguishing principles is recommended.

Table 4-4.10 ***Foam Quality Requirements from NFPA 412***

Agent	Minimum Expansion Ratio	Minimum Solution 25% Drainage Time (min)
AFFF or FFFP		
Air aspirated	5:1	2.25
Non-air-aspirated	3:1	0.75
Protein	8:1	10
Fluoroprotein	6:1	10

The 1600-ml expansion and drainage test method replaced two other methods where a 1000-ml cylinder or 1400-ml pan was used as the collection device. MIL-F-24385 still uses the 1000-ml collection method. This situation, plus other different test methods, makes direct comparison of expansion and drainage data difficult. Tests performed by Underwriters Laboratories (UL) identified differences among the three test methods based on expansion and drainage results.[31] UL found that expansion ratios remained the same but that drainage was quicker using the 1600-ml method compared to the 1000-ml method for film-forming foams. Drainage time increased (i.e., doubled) for the protein foams when the 1600-ml method was used compared to the 1400-ml pan method.

No direct correlations have been established between expansion, drainage, and fire-extinguishing performance. There is a relationship between foam drainage and burnback. Longer drainage times generally result in longer burnback times.

The expansion and drainage data in Table 4-4.10 indicate the inherent differences between air-aspirated and non-air-aspirated film-forming foams. The data in Figure 4-4.7 showed that non-air-aspirated AFFF was more effective at critical application rates than air-aspirated AFFF. This conclusion was verified by Jablonski in tests with U.S. Air Force crash trucks as shown in Figure 4-4.11.[32] Even so, there continues to be debate over aspirated and non-air-aspirated foam for manual applications involving aviation fuel spills.

Under certain conditions, non-air-aspirated AFFF is not as effective as air-aspirated AFFF. The results of the foam tests in the United Kingdom[33,34] and the results from DiMaio et al.[35] described situations where air-aspirated AFFF resulted in better fire extinguishment performance than non-air-aspirated foam.

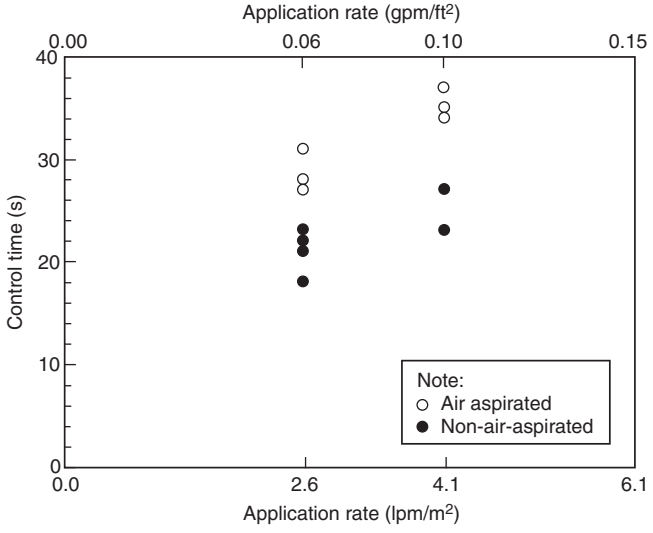

Figure 4-4.11. ***Effects of AFFF aspiration on JP-4 pool fire control times.[32]***

Given that one-to-one correlation between expansion, drainage, and fire-extinguishing performance is difficult to identify, there appears to be a lower limit where non-air-aspirated AFFF becomes ineffective. This has not been quantified, but it is speculated that poor performance occurs when AFFF expansion ratio is less than 2.5 to 3.0, and drainage is difficult to measure, that is, nearly instantaneous. This is based in part on unpublished data from the Naval Research Laboratory on shipboard bilge AFFF sprinklers[36] and the results of the U.K. tests.[33,34] The importance of this lower limit of foam aspiration is recognized in NFPA 412 criteria.

Foam concentration determination: The most common method of determining foam concentration in the field is by use of a hand-held refractometer. The refractive index, n, is defined as

$$n = \frac{\sin i}{\sin r} \tag{10}$$

where

$\sin i$ = angle of incidence

$\sin r$ = angle of refraction

This is depicted graphically in Figure 4-4.12.

Manufacturers report that the glycols in AFFF formulations create the necessary refractive characteristics to determine concentration. However, they also report that glycol has a potential detrimental impact on overall agent performance. Elimination of this compound might improve (slightly) the performance of AFFF, but the glycol is also needed as a fundamental component of agent mixing.

The refractive index of water at 20°C (68°F) is 1.333 (air has a refractive index of 1.0002926). Since the refractive index of a solution is proportional to the inverse of the solution density, and density is proportional to temperature, then

$$n \propto \frac{1}{T} \tag{11}$$

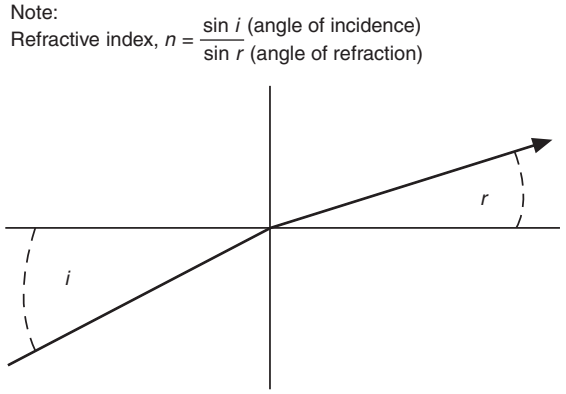

Figure 4-4.12. ***Refractive index of solutions.***

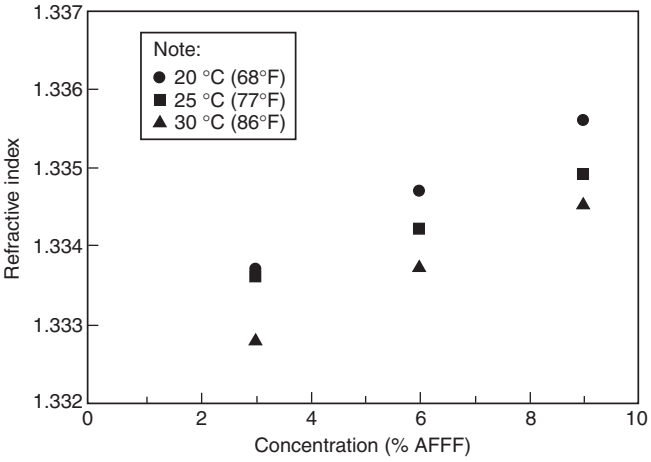

Figure 4-4.13. ***Effects of temperature on refractive index.***[37]

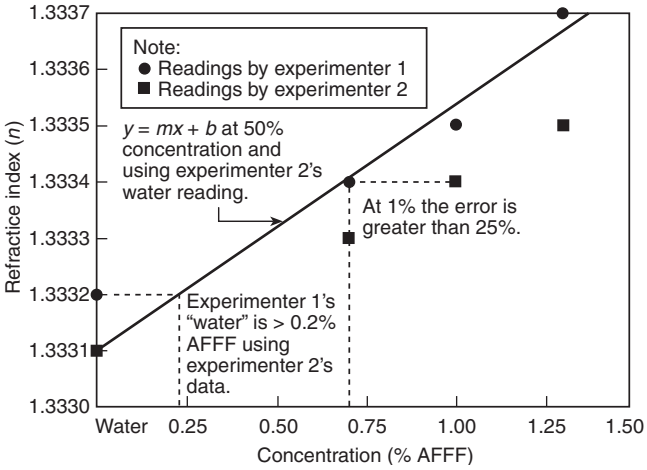

Figure 4-4.14. ***Refractive indices of 1 percent AFFF solutions in tap water.***

where T is the temperature. This relationship is illustrated in Figure 4-4.13. Any refractive index measurements must be made considering temperature. Some hand-held measurement devices are temperature compensated. It is good procedure to conduct concentration measurements at a constant temperature.

Other scales may be used. For example, the Brix scale is used as a measure of sucrose weight percent concentration. Units with this scale, commonly found in the food product industry, can be used to measure foam concentration. A typical range of a bench or hand-held refractometer is 1.3000 to 1.7000.

NFPA 412, *Standard for Evaluating Aircraft Rescue and Fire-Fighting Foam Equipment,* describes a method to determine foam concentration using the refractive method. In NFPA 412, the preparation of three standard solutions is recommended: one at the nominal concentration, one at one-third more than the nominal concentration, and one at one-third less than the nominal concentration. A plot of the refractive scale reading against the known foam concentration is made on graph paper. This plot establishes a "calibration" curve against which foam samples from a vehicle or system can be judged. Since refractive index is linear, a calibration curve can be created by

$$\text{AFFF \%}_{\text{sample}} = \frac{n_{\text{foam}} - n_{\text{water}}}{n_{\text{concentrate}} - n_{\text{water}}} \times 100 \qquad (12)$$

This method is used by the U.S. Navy for checking proportioning system accuracy onboard ships.

The limitations of the refractive index technique are described by Timms and Haggar.[37] The accuracy of the refractometer can become poor due to the focusing and setting of the refracted light junction on the cross hairs of the viewing window, and the reading of the graduated scale to four decimal places (where the scale is graduated only to three places). This effect is illustrated in Figure 4-4.14, where a calibration curve for a 1 percent AFFF concentrate was established using a straight line through the 50 percent concentration point and the "water" reading by one of the experimenters. Note that the error between readings by the two experimenters at 1 percent concentration exceeds 25 percent. In this example, differences in the baseline water reading will create substantial error in the calibration curve. These differences are exaggerated with 1 percent concentrates. At 3 percent or 6 percent, the experimental error in reading the refractometer, for field testing, is generally accepted as adequate.

Alternative methods for measuring AFFF concentration include total fluorine content, optical absorption methods, and electrical conductivity. Since neither the total fluorine content method nor optical absorption method is suited to field use, the conductivity method has been proposed. Since foams contain electrolytes, their conductance, G, can be measured and described as

$$G = \frac{1}{R}\,(\text{mhos}) \qquad (13)$$

where R = resistance (ohms). Conductivity, σ, is conductance per unit length:

σ = G/unit length
= mhos/cm
= siemens/cm

Since conductivity is directly proportional to temperature, conductivity increases with temperature. (See Figure 4-4.15.) Temperature compensation is appropriate when using this method.

Timms and Haggar showed the influence of the substrate water on both refractive index and conductivity.[37] (See Figures 4-4.16 and 4-14.17.) It is important to note the difference of the characteristic curve for a salt solution. AFFF actually reduces the conductivity of this highly conductive water. Note also that, while conductance may exhibit straight-line characteristics in the area of interest (0 to 10 percent), the overall curves from 0 to 100 percent are nonlinear.

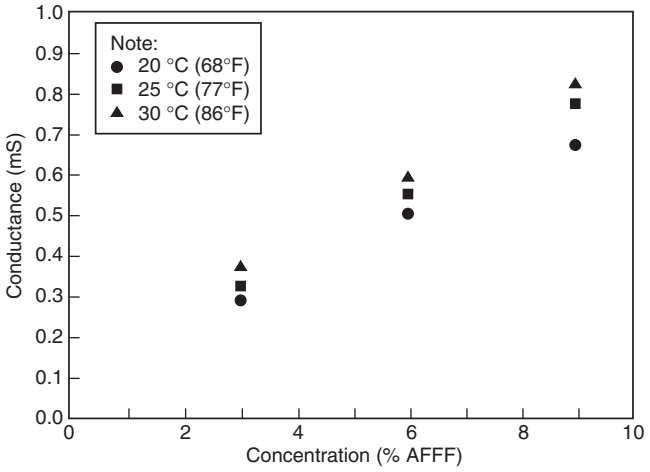

Figure 4-4.15. ***Effects of temperature on the conductance of AFFF solutions.[37]***

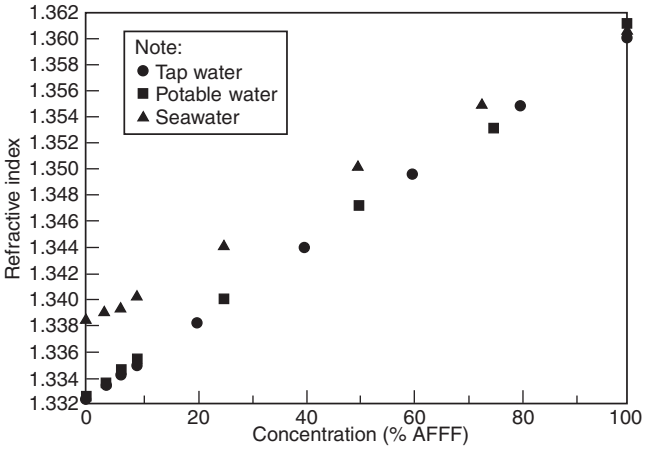

Figure 4-4.16. ***Effect of substrate water on refractive index of AFFF solutions.[37]***

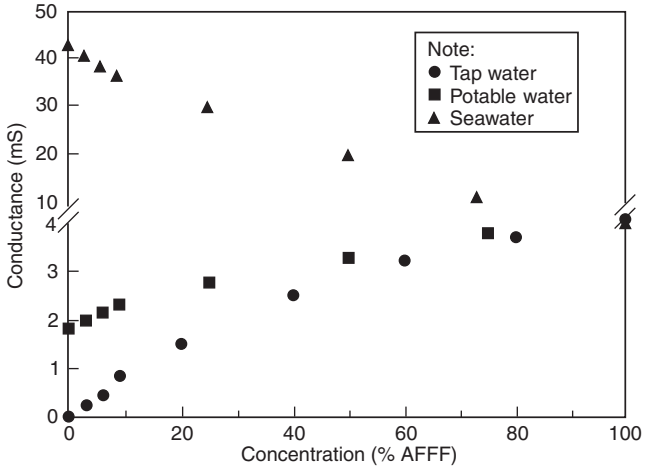

Figure 4-4.17. ***Effect of substrate water on conductivity of AFFF solutions.[37]***

Table 4-4.11 ***Sensitivity of Refractive Index and Conductivity Methods for Determining Foam Concentration[37]***

	Refractive Index	Conductance (mS)
3%	1.3337	0.318
6%	1.3343	0.558
Difference	0.0006	0.240
"Sensitivity"	0.0005 (0.5 in 1000)	0.43 (430 in 1000)

Table 4-4.12 ***Accuracy of Foam Test Measurements[37]***

Solution	Refractive Index	Electrical Conductance	Actual
A	4.5% ± 0.8%	3.5% ± 0.1%	3.50 ± 0.01%
B	5.1% ± 0.8%	5.5% ± 0.1%	5.50 ± 0.01%
C	8.7% ± 0.8%	8.5% ± 0.1%	8.50 ± 0.01%

The "sensitivity" of the two methods (i.e., refractive index and conductivity) was shown by these researchers by comparing the difference between readings for solutions of 3 percent and 6 percent divided by the reading at 6 percent. The sensitivities for tap water show that the conductivity method is more sensitive than the refractive index measure. (See Table 4-4.11.) In repeated readings of refractive index and conductivity, the foam concentration accuracy using conductivity was ± 0.1 percent, where the accuracy of the refractive index method was ± 0.8 percent. (See Table 4-4.12.)

The electrical conductivity method is now recognized in NFPA standards. NFPA 412 cautions against the use of this method for seawater applications. The electrical conductivity method, used for process control in the chemical industry, has recently been adapted for use as a proportioning controller for AFFF systems.

Aircraft Hangar Protection

The two objectives of aircraft hangar protection are (1) protect aircraft and (2) prevent collapse of the hangar roof structure, which is usually unprotected steel. The protection of the aircraft is the principle concern, since its value is generally many times that of the structure. This concern is particularly true for advanced military aircraft. Historically, these protection systems have been deluge-type sprinkler systems with open-head nozzles. They are activated by rapid-response detection systems.

Before the development of foam, water-deluge systems were used. The original foam-water sprinkler systems used protein foam. With the development of AFFF, research was performed to determine appropriate application rates and types of discharge devices. The research work, performed primarily by Factory Mutual Research Corporation (FMRC), provides the basis not only for current aircraft hangar protection criteria, but also for other sprinkler suppression system criteria.

Overhead sprinkler protection: Before the advent of foam, hangars were protected by conventional spray sprinklers using water. Water-deluge systems having discharge rates on the order of 10.4 lpm/m² (0.25 gpm/ft²) were used in conjunction with sloped floors and drains to protect aircraft. Even with these systems, activated by detection systems, burnthrough protection of aircraft fuselages (e.g., 1 min) could not be ensured. Ceiling temperatures in an 18.3-m- (60-ft-) high space on the order of 427 to 816°C (800 to 1500°F) have been recorded for fuel spill fires where this protection was provided. For a 121-m² (1300-ft²) JP-4 fuel fire, 927°C (1700°F) ceiling temperatures have been recorded within 30 s of ignition prior to deluge system discharge.

Protein foam systems, discharging at a rate of 8.2 lpm/m² (0.20 gpm/ft²), were an improvement on the water systems. Air-aspirating sprinklers were required to make effective protein foam. Because of the high centerline velocities of a pool fire plume, the foam flow from the perimeter toward the center of the fire was thought to be the dominant suppression mechanism.[38]

With the development of AFFF, FMRC conducted a series of tests for the U.S. military to establish appropriate design parameters. In a series of baseline comparison tests, FMRC compared AFFF with protein foam. The tests consisted of 83.6-m² (900-ft²) JP-4 pool fires in an 18.3-m-(60-ft-) high space. Air-aspirating, standard upright, and old-style upright sprinklers were evaluated at application rates of 4.1 to 8.2 lpm/m² (0.10 to 0.20 gpm/ft²). In one test, a low-level turret nozzle discharging AFFF was used in conjunction with sprinklers discharging water. Table 4-4.13 summarizes the results of the AFFF tests. A comparison of Tests 4 and 5 with Test 3 indicates improved results from the use of standard sprinklers compared to foam-water sprinklers. At application rates of 6.6 lpm/m² (0.16 gpm/ft²), the standard sprinklers were 1.3 to 1.6 times as effective in achieving extinguishment compared to air-aspirating foam-water sprinklers. At an application rate of 8.2 lpm/m² (0.20 gpm/ft²), the extinguishment times with AFFF from foam-water sprinklers were comparable to results from protein foam tests. Rapid suppression with the turret nozzle [at 8.3 lpm/m² (0.22 gpm/ft²)] combined with an overhead water system was demonstrated in Test 7. No adverse effects were evident from the water discharged from the overhead sprinklers after the foam ran out.

The superior performance of the standard sprinklers was attributed to more effective plume penetration by higher density foam particles. The maximum centerline velocities measured were 23.2 m/s (76 ft/s), with 15.2 m/s (50 ft/s) at the centerline of the fire. The fire plumes tended to bend due to air currents within the test building. Since the terminal velocity of the foam agents was estimated to be on the order of 9.1 m/s (30 ft/s) maximum, the droplets near the centerline never reached the fire. This result supports the theory that extinguishment occurs from the outside perimeter inward. Since foam droplets from standard sprinklers are about twice as dense as air-aspirated particles, the terminal velocities are greater. Greater velocities allow greater penetration of the fire plume. The same mechanisms explain why air-aspirated AFFF provides similar performance to protein foam. When the AFFF is air aspirated, there is no longer any advantage of increased droplet terminal velocity.

Table 4-4.13 ***Hangar Deluge System Tests by Factory Mutual Research Corporation[38]***

Test Conditions	Test No. 2	Test No. 3	Test No. 4	Test No. 5	Test No. 6	Test No. 7 (turret nozzle)
Type of Head	Foam-water	Foam-water	Standard	Standard	Standard	Old-style sprinkler
Spacing [m² head⁻¹ (ft² head⁻¹)]	7.4 (80)	9.3 (100)	12.1 (130)	12.1 130	9.3 (100)	9.3 (100)
Application rate [lpm/m² (gpm/ft²)]	8.2 (0.20)	6.6 (0.16)	6.6 (0.16)	6.6 (0.16)	5.2 to 4.4 (0.125 to 0.105)	6.6 (0.16) (water system)
End head pressure [kPa (psi)]	193 (28)	193 (28)	97 (14)	97 (14)	35 (5)	55 (8) (water system)
25% Drainage time (min)	2.5	2.1	0.5–0.8	1.0–1.3	0.5–0.7	No data recorded
50% Drainage time (min)	5.0	4.4	1.3–1.8	1.8–2.3	1.2–1.6	No data recorded
Expansion ratio	4.3 : 1	3.4 : 1	2.2 : 1	1 : 25	2.2 : 1	12 : 1
Extinguishment time (min : s)	2 : 22	2 : 15	1 : 45	2.3 : 1	3 : 05	≈0 : 33

Table 4-4.14 ***Estimated Particle Diameter vs. Terminal Velocity[40]***

Particle Diameter [mm (in.)]	Terminal Velocity [m/s (ft/s)]			
		Foam		
	Water	Expansion Ratio 2 : 1	Expansion Ratio 5 : 1	Expansion Ratio 10 : 1
12.7 (0.5)	See note[a]	10.1 (33)	6.7 (22)	4.6 (15)
6.3 (0.25)	10.4 (34)	7.3 (24)	4.6 (15)	3.4 (11)
2.5 (0.1)	6.7 (22)	4.6 (15)	2.7 (9)	—

[a]The breakup of water drops greater than about 6.3-mm (0.25-in.) diameter is highly probable due to instability.

Additional work by FMRC established estimates for the terminal velocity of foam, as shown in Table 4-4.14.[39,40] Plume theory was used to estimate roughly that velocity on the order of 18.3 m/s (60 ft/s) could be expected in an 18.3-m- (60-ft-) high space with an 83.6-m^2 (900-ft^2) JP-4 fire. This estimate was in good agreement with the experimental results. Based on an average foam particle diameter of 6.3 mm (0.25 in.), a maximum terminal velocity of 7.3 m/s (24 ft/s) could be expected. For a JP-4 pool fire, this translates into a 0.7-m^2- (8-ft^2-) maximum fire size before plume penetration is not possible.

The practical significance of AFFF discharged through non-air-aspirating sprinklers was demonstrated by Breen et al.[40] Air-aspirating sprinklers require 207-kPa (30-psi) nozzle pressure to be effective. Standard sprinklers can discharge effective AFFF solution at pressures as low as 69 kPa (10 psi). This had important retrofit considerations where foam proportioning system losses could be made up through reduced sprinkler pressures.

Additional tests were conducted with closed-head sprinklers in an 18.3-m- (60-ft-) high hangar.[41] Potential cost benefits would have resulted from reduced hardware costs and unwanted discharges from deluge systems. These tests demonstrated that this concept was not feasible for the hangar scenario because of the large number of sprinklers that opened during the 83.6-m^2 (900-ft^2) fire tests.

The superior performance of standard sprinklers compared to air-aspirating sprinklers is reflected in the criteria of NFPA 409, *Standard on Aircraft Hangars.* If standard sprinklers are used with AFFF, the design application rate for overhead deluge systems may be reduced to 6.6 lpm/m^2 (0.16 gpm/ft^2) from 8.2 lpm/m^2 (0.20 gpm/ft^2) required for air-aspirated sprinklers. This decrease represents a 20 percent reduction in foam required when standard sprinklers are used.

Low-level application of AFFF: With the increase in wingspan areas of large aircraft, it was recognized that significant damage could occur before extinguishment of the pool fire underneath the wing. Using overhead sprinklers only, FMRC demonstrated the times required for the foam to spread and extinguish fires. (See Table 4-4.13.) The concept of low-level application of foam, using monitors or turret nozzles, was developed to reduce extinguishment time where shielded fires may occur. This concept was later extended to include side-mounted nozzles and discharge outlets, and flush-mounted nozzles installed in a floor or deck.

These systems are effective because AFFF solution droplets do not have to penetrate the fire plume. They also typically deliver, at spot locations, high densities of foam. A high density allows the foam to gain a "bite" or toehold on the fire. Low-level AFFF systems have been used successfully for over two decades on U.S. Navy aircapable ships, protecting flight decks and special hazard areas.

Table 4-4.15 summarizes fire test data for low-level application of AFFF. As seen, control and extinguishment times are quite rapid. NFPA 409, *Standard on Aircraft*

Table 4-4.15 ***Fire Test Data for Low-Level Application of AFFF***

Reference	Test No.	Test Area [m^2 (ft^2)]	Fuel	Nozzle	Nozzle *k* Factor (gal/psi$^{0.5}$)	Maximum Spray Height[a] [m (ft)]	Spray Diameter[a] [m (ft)]	Nominal Application Rate [lpm/m^2 (gpm/ft^2)]	Control and Extinguishment Times
FMRC 1975[39]	3	83.6 (900)	JP-4	Turret nozzle (monitor)	50.3	50-degree arc, 8-s cycle time, 15-degree angle of elevation, 25.9 m (85 ft) from the center of the test pool		4.1 (0.10)	90% in 10 to 15 s 100% in 35 to 40 s
	4	83.6 (900)	JP-4	Turret nozzle (monitor)	50.3	50-degree arc, 8-s cycle time, 15-degree angle of elevation, 25.9 m (85 ft) from the center of the test pool		4.1 (0.10)	90% in 1 min 30 s[b] 100% in ≈ 2 min
	6	83.6 (900)	JP-4	Turret nozzle (monitor)	50.3	50-degree arc, 8-s cycle time, 15-degree angle of elevation, 25.9 m (85 ft) from the center of the test pool		4.1 (0.10)	90% in 20 s 100% in 25 s

Table 4-4.15 ***Fire Test Data for Low-Level Application of AFFF (Continued)***

Reference	Test No.	Test Area [m^2 (ft^2)]	Fuel	Nozzle	Nozzle k Factor (gal/$psi^{0.5}$)	Maximum Spray Height[a] [m (ft)]	Spray Diameter[a] [m (ft)]	Nominal Application Rate [lpm/m^2 (gpm/ft^2)]	Control and Extinguishment Times
FMRC 1973[38]	7	83.6 (900)	JP-4	Overhead OSS[c] + Turret nozzle	5.0	N/A	N/A	6.6 (0.16)[d] + 9.0 (0.22) 9.5 (0.38)	Control in 17 s[d] 100% in 33 s
Australia[42]	1	78.5 (846)	Aviation kerosene	P10 Pop-up	4.1	0.8 (2.6)	4.3 (14.1)	5.5 (0.13)	95% in 30 s
	2	78.5 (846)	Aviation kerosene	W-1 Pop-up	3.6	1.5 (4.9)	3.3 (10.8)	4.9 (0.12)	≈90% in 25 s[e]
	3	78.5 (846)	Aviation kerosene	P-10	4.1	0.8 (2.6)	3.3 (10.8)	5.5 (0.13)	98% in 30 s
Naval Weapons Center Phase III 1972[43]	5	697 (7500)	JP-5	Type S flush deck	5.5	1.8 (6)	12.2 (40)	1.6 (0.04)	50% in 30 s 90% in 60 s
	11	697 (7500)	JP-5	Type S flush deck	5.5	1.8 (6)	12.2 (40)	2.4 (0.06)	70% in 30 s 95% in 60 s
	9	697 (7500)	Avgas	Type S flush deck + deck edge	5.5 [114 lpm (30 gpm)	1.8 (6)	12.2 (40)	2.4 (0.06) + 1.6 (0.04) 4.1 (0.10)	15% in 30 s 50% in 60 s
	15	697 (7500)	Avgas	Type S flush deck + deck edge	5.5 [114 lpm (30 gpm)]	1.8 (6)	12.2 (40)	2.4 (0.06) + 1.6 (0.04) 4.1 (0.10)	40% in 30 s 70% in 60 s
Naval Weapons Center Pop-Up 1984[44]	10 and 10R	372 (4000)	JP-5	Type SB flush deck	5.1	1.8 (6)	9.1 to 12.2 (30 to 40)	2.4 (0.06)	60 to 90 s for 90% control; 99% in 2 min
	5, 5R, and 5R1	372 (4000)	JP-5	Bete pop-up	5.5	1.8 (6)	9.8 (32)	2.4 (0.06)	60 to 90 s for 90% control; 99% in ≈ 2 min
Naval Weapons Center Weapons Staging Area 1998[45]	I8	48.3 (520)	JP-5	Overhead side-mounted spray nozzles	1.9	NA	NA	8.6 (0.21)	90% in 15 s 99% in 52 s 100% in 57 s
	I11	48.3 (520)	JP-5	Overhead side-mounted spray nozzles	1.9	NA	NA	21.6 (0.53)	90% in 8 s 99% in 15 s 100% in 27 s
	II6[f]	66.9 (720)	JP-5	Low-Level fan	4.7	NA	NA	11.8 (0.29)	90% in 24 s 99% in 52 s 100% in 79 s
	II12[f]	66.9 (720)	JP-5	Low-Level fan	4.7	NA	NA	20.4 (0.50)	90% in 9 s 99% in 16 s

[a]Spray height and diameter at the pressure/flow used in the test

[b]An unplanned 69-kPa (10-psi) pressure drop in FMRC Test 4 caused a 4.6-m (15 ft) reduction in nozzle range, resulting in 90 percent control and extinguishment times 3 to 4 times those observed in Tests 3 and 6.

[c]No wing obstruction over fire test area

[d]The overhead deluge system discharging ordinary water was accidentally activated 12 sec later than the turret nozzle (5 sec before control was attained). The contribution, if any, of the overhead deluge system toward complete extinguishment was judged to be quite small compared to the turret nozzle.

[e]Wind-affected results

[f]Deck pool fire area was obstructed with simulated weapons carts.

Hangars, criterion of 4.1 lpm/m^2 (0.10 gpm/ft^2) for low-level applications is based on a fire control time of 30 s and extinguishment in 60 s. Data indicate that a JP-5 pool fire can be 90 percent controlled in 60 to 90 s and 99 percent extinguished in 2 min when an application rate of 2.4 lpm/m^2 (0.06 gpm/ft^2) is used. The system can be effective at rates as low as 1.6 lpm/m^2 (0.04 gpm/ft^2). For low-flash-point fuels (e.g., avgas), control time increases. Control and extinguishment times can be reduced by increasing the application rates on JP-5 fuel fires. Based on these results, the U.S. Navy adopted an AFFF application rate of 2.4 lpm/m^2 (0.06 gpm/ft^2) for protecting aircraft carrier flight decks.[46]

While they may help control a three-dimensional (spill) fire, low-level application systems cannot be assumed to suppress totally a running fuel fire. Running fuel fires at a spill rate of 189 lpm (50 gpm) are typically used in U.S. Navy flight-deck suppression tests using the flush-deck system. The running fuel fire, shielded by simulated aircraft debris, requires aggressive handline attack for extinguishment.[47]

Obstructions, such as parked vehicles, may block low-level nozzles. Testing for a flight-deck weapons staging area showed that a side-mounted low-level system could be effective even when nozzles are obstructed.[45] In these tests, 5 of the 12 deck-edge nozzles were obstructed to simulate vehicle tires blocking edge-mounted nozzles. Even with 40 percent reduction, the fire was controlled and extinguished in less than 1 min (compared to 15 to 30 s when unobstructed).

Cost of installation, maintainability, and reliability are factors when considering a low-level application system. Reliability issues with turrets/monitors have been identified by both FMRC and the U.S. Navy. The flush-deck system adopted by the U.S. Navy took considerable effort before a high degree of reliability and maintainability could be achieved. This open deluge nozzle, originally installed as a water washdown nozzle, incorporates a ball-check feature in the nozzle orifice to prevent debris from clogging the nozzle. Clean-out traps are installed in system piping for maintenance. Pop-up nozzles have been proposed as an alternative to flush-deck nozzles. These nozzles have their own reliability and maintainability issues. Unless there are very high costs associated with the loss of an aircraft, in-floor or flush-deck nozzles are generally cost-prohibitive for commercial aviation facilities. For high risk/cost applications, in-floor nozzles may be justified. This may be the case for advanced military aircraft; for example, research has been performed on an inverted deluge system that not only can suppress a pool fire, but also can cool exterior combustible components of the airframe. Initial installations have suffered from design and installation problems.[48] Lack of experience with these types of systems was the significant single cause of problems with these systems. Acceptance testing and maintenance were found to be lacking.

Side-mounted nozzles are the most reliable systems, consisting of open-pipe or -spray nozzles. The spreading rate of foam from an aspirated open-pipe system increases control and suppression time. Open-spray nozzles can be very effective, but their reach is limited.

New hangar fire protection design concepts: Issues related to asset protection, reliability of fixed systems, and environmental impact led the U.S. Navy to reevaluate their approach to hangar fire protection systems. A goal was established to install reliable and easily maintained fire protection systems that prevent damage to the hangar structure and to aircraft not directly involved in an initial spill fire ignition. This goal resulted in a multidiscipline study to address all associated technical issues.

All military service branches in North America have been plagued with false activation involving foam-water-deluge sprinkler systems over aircraft with open cockpits. These false activations have been caused by numerous sources including lightning strikes that introduced transient voltage spikes into the fire alarm system; water hammers in aging underground water distribution systems; accidental releases by maintenance personnel; deliberate acts of vandalism; accidental activation of manual pull stations; failure of pressure relief valves at pumping stations; roof-water leakage into overhead heat detection systems; and false activation of fire detection systems. This prompted the pursuit of alternative fire protection designs that would provide the desired level of protection.

Alternative designs included the use of closed-head AFFF overhead sprinkler systems and greater reliance on low-level monitor nozzle AFFF systems as the primary extinguishing component as described in the previous section. Low-level systems were originally designed to provide supplementary protection for the area shadowed from the overhead system by large wing areas. In pursuing these alternative designs, technical and operational issues and limitations of both existing and proposed new systems were identified:

- Thermally activated systems may result in unacceptably high damage to assets prior to fire control/extinguishment, particularly in very high bay hangar ceilings (see Reference 49).
- While it is readily accepted that conventional hangar fire protection systems were not designed to extinguish a three-dimensional fire, some fire protection engineers believed that AFFF extinguishing systems could be designed to control a spill fire and limit the area of the fire to only those aircraft intimate with the initial ignition source.
- Different aviation fuels are now commonly being used, e.g., JP-5 and JP-8 are now the predominant fuels, compared to the lower flashpoint JP-4 previously used.
- Low-level AFFF monitor nozzle systems are
  - —Relatively inefficient in terms of pattern distribution
  - —Unreliable
  - —Susceptible to blockage by equipment
  - —Commonly found out of service in the field
- Any new AFFF low-level nozzle should be designed for minimal overspray and should not be significantly impacted by water discharge from any water-only protection system.
- Optical fire detectors are
  - —Prone to false alarms
  - —Currently tested, listed, and approved using fuels that are not typical in aviation

—Subjected to few if any sourcess of false alarms in currently recognized approval standards

A concept was developed by the U.S. Navy to meet the desired performance goals. This concept included the following:

- Use of low-level AFFF deluge nozzles, having minimal overspray, to control/extinguish liquid fuel pool spill fires
- Operation of the low-level AFFF system using improved optical detectors designed to
  —Be highly immune to false alarms
  —Rapidly detect JP-5 fuel spill fires
- Installation of a quick-responding, closed-head, wet-pipe sprinkler system in the hangar ceiling
- Implementation of lessons learned from all military hangar design experiences in a comprehensive new, improved design

Most of the research and development associated with the process has been completed and is described in References 49 to 54. Two aspects of U.S. Navy research and development are germane to the performance of AFFF. The first involves the performance of AFFF when subjected to water spray from sprinklers. The second is a developmental effort initiated to design a reliable, low-profile AFFF nozzle that could be installed in the floors of hangars.

Twenty-three full-scale fire tests were conducted to evaluate the effects of overhead water sprinklers on AFFF foam blankets.[51] One AFFF application rate [4.0 lpm/m^2 (0.1 gpm/ft^2)] and two sprinkler application rates [6.5 and 10.2 lpm/m^2 (0.16 and 0.25 gpm/ft^2)] were included in this evaluation. The tests were conducted on a range of spill fires. The spill fires were produced using either JP-5 or JP-8 aviation fuels and were evaluated on a concrete pad with similar drainage characteristics typical of navy hangars. The spill fires continued to burn (i.e., were shielded) during water/foam application. The heating effect on the burnback resistance of foam, with and without sprinkler water application, was evaluated.

The results show that the use of water sprinklers in conjunction with a low level AFFF fire suppression system [with an application rate of 4.0 lpm/m^2 (0.1 gpm/ft^2)] had minimal effects on the ability of the system to suppress the fire and resist burnback. In all tests, the low-level AFFF system was capable of quickly extinguishing the test fire (control ~30 s and extinguishment ~1 min) independent of the sprinkler application rate. The time required for the fire to burnback across the fuel surface was apparently a function of the drainage characteristics of the hangar and was only slightly affected by the application of water through the overhead sprinklers. The tests also show that the flashpoint of the fuel has an effect on the control, extinguishment, and burnback resistance capabilities of the system. Although the burnback times for the lower flashpoint fuels were faster than the higher flashpoint fuels, the duration of protection was not significantly altered. These tests show that overhead water sprinklers have minimal effect on AFFF foam blankets, independent of the test fuel, particular fire, and sprinkler application rate. A combined low-level AFFF extinguishing system operating in conjunction with an overhead water sprinkler system provided adequate burnback protection during AFFF discharge, but this protection may be lost shortly (a few minutes) after the end of AFFF discharge.

The new low-level fire-extinguishing system was designed to discharge AFFF adequately across a hangar floor, to be less likely to be affected by obstructions, and to reduce the likelihood of damage to exposed aircraft electronic equipment.[53] To achieve these objectives, the nozzle was designed to

- Produce a nominal AFFF application rate of 4.0 lpm/m^2 (0.1 gpm/ft^2)
- Operate at a nominal pressure of 2.8 bar (40 psi)
- Provide coverage to a distance of 7.6 m (25 ft) from a hangar floor drainage trench (centerline of two parallel trenches spaced 15.2 m (50 ft) apart)
- Spray AFFF so that the pattern height does exceed 0.3 m (1 ft) above the deck

The nominal AFFF application rate of 4.0 lpm/m^2 (gpm/ft^2) was selected based on current design practices as described in the previous two sections of the chapter. The nozzle operating pressure was selected based on standard, commercially available pump performance curves and preliminary estimates of friction loss for the system.

Over 50 nozzles were evaluated for this application.[53] Testing of these nozzles indicated that, while a limited number of commercially available nozzles could meet the design requirements, manufacturing, installation, and operation of these nozzles under normal hangar conditions was not feasible. Existing pop-up nozzles were not designed for the high flow rates or spray characteristics required of this application. As a result of these deficiencies, a prototype nozzle was developed. The prototype concept was subsequently developed into a commercially available nozzle. Foam pattern, distribution, and flow tests were conducted by Underwriters Laboratories Inc. on a nozzle with a flow coefficient of 22.6 k (gpm/psi$^{1/2}$).

There is no universal agreement on the proper approach to military hangar fire protection in North America. For example, the U.S. Air Force recognizes the use of high-expansion foam. A number of these systems have recently been installed. The Canadian Ministry of Defense (MoD) is investigating the possible use of compressed-air foam. Additionally, the U.S. Army has evaluated the use of early–suppression fast-response (ESFR) closed-head water sprinkler protection for helicopter hangars.[55] FMRC concluded that both 93°C- (200°F-) temperature-rated ESFR sprinklers discharging at 345 kPa (50 psig) [41 lpm/m^2 (1.0 gpm/ft^2)] and 517 kPa (75 psig) [49 lpm/m^2 (1.2 gpm/ft^2)] and 141°C- (286°F-) temperature-rated, k = 5.6 (gpm/psi$^{1/2}$) quick-response sprinklers at 345 kPa (50 psig) [16 lpm/m^2 (0.40 gpm/ft^2)] can provide adequate fire protection for the hangar against a 61-m^2 (200-ft^2), 473-l (125-gal) JP-4 aviation fuel-pan fire. For some tests, fuel depletion was necessary for the fire to be controlled.

Foam-Water Sprinkler Systems

This chapter has dealt with foam characteristics, foam concentrate, test standards, and manual application techniques. In particular, applications in the aviation industry were described. The text on aircraft hangar protection introduced the concept of fixed foam protection systems. In particular, much of the foam-water sprinkler system test data was originally developed for aircraft hangars. Herein, additional foam-water sprinkler system design criteria are described. Again, emphasis is placed on AFFF systems since they are more effective for extinguishment than protein or fluoroprotein systems.

Codes, Standards, and Regulations

Overhead foam-water sprinkler systems, as specified in the NFPA standards, are generally designed to serve dual purposes: (1) to control and/or suppress a fuel spill fire and (2) when the foam runs out, to cool materials with water. Since the systems are designed to provide protection for flammable/combustible liquid hazards and ordinary combustibles, the specified application rates reflect this dual-protection approach. Table 4-4.3 shows the fundamental application rates used by Underwriters Laboratories on hydrocarbon fuel fires to evaluate sprinklers. The fire must be extinguished within 5 min for AFFF discharged at 4.1 lpm/m^2 (0.10 gpm/ft^2) for standard sprinklers and 6.6 lpm/m^2 (0.16 gpm/ft^2) for agents discharged from foam-water sprinklers (air aspirating). However, since most deluge and closed-head sprinkler systems are installed in industrial occupancies, they must meet highly protected risk (HPR) insurance requirements. As a result, the NFPA standard for deluge and closed-head AFFF systems (NFPA 16, *Standard on the Installation of Deluge Foam-Water Sprinkler and Foam-Water Spray Systems)* requires 6.6-lpm/m^2 (0.16-gpm/ft^2) minimum water application. This water application rate also provides a safety factor over the 4.1 lpm/m^2 (0.10 gpm/ft^2) rate at which AFFF discharged from sprinklers is effective on pool fires. The safety factor is reflected in Table 4-4.3 under the column heading Minimum Application Rate.

Table 4-4.16 summarizes current requirements from NFPA standards and guidelines. NFPA 11, *Standard for Low-Expansion Foam,* is geared toward petroleum and chemical industry protection. Previous requirements from NFPA 11 allowed 4.1 lpm/m^2 (0.10 gpm/ft^2) for loading racks, for example, tank truck loading facilities. The latest requirements for NFPA 11 eliminate this design criterion and reference NFPA 16 requirements, which require 6.6 lpm/m^2 (0.16 gpm/ft^2). In special situations, 4.1 lpm/m^2 (0.10 gpm/ft^2) is permitted by NFPA 11, but only where there is low-level or manual application for a hydrocarbon fuel spill. NFPA 16 is consistent in requiring 6.6 lpm/m^2 (0.16 gpm/ft^2); it references other NFPA standards for special exceptions, for example, NFPA 409, *Standard on Aircraft Hangars,* and NFPA 30, *Flammable and Combustible Liquids Code.* NFPA 409 requirements were previously discussed. Section 4, Chapter 5 provides an example for calculating foam quantities based on design application rates and areas to be protected.

With the publication of the 1998 edition of NFPA 11, marine foam application is now addressed. Foam application rates are required to be not less than the greatest of that required for deck spills, the largest tank, or the largest monitor solution flow rate as shown in Table 4-4.17 for hydrocarbon fuels and Table 4-4.18 for polar solvents. For polar solvents, standardized fire tests are used to determine the minimum foam design application

Table 4-4.16 ***NFPA Standards Related to AFFF Sprinkler Systems***

Standard[a]	Minimum AFFF Application Rate [lpm/m^2 (gpm/ft^2)]	Duration (min)
NFPA 11, (1998) *Low-Expansion Foam*	Indoor storage tank greater than 37 m^2 (400 ft^2) 6.6 (0.16)	30
	Loading rack monitors 4.1 (0.10)	15
	Diked areas Fixed low level (Class II hydrocarbon) 4.1 (0.10)	20
	Monitor 6.6 (0.16)	20
	Undiked areas for AFFF handlines 4.1 (0.10)	15
NFPA 16, *Standard for the Installation of Foam-Water Sprinkler and Foam-Water Spray Systems* (1999)	6.6 (0.16)	10 min; 7 min if above minimum design
NFPA 409, *Standard on Aircraft Hangars* (1995)	Overhead deluge 8.2 (0.20) for aspirated AFFF	10 min; 7 min if above minimum design
	6.6 (0.16) for non-air-aspirated AFFF	
	Supplemental low level (for shielded wing areas) 4.1 (0.10)	10 min

[a]See Additional Readings for complete titles and dates.

Table 4-4.17 ***Foam Application Rate for Marine Hydrocarbon Hazards (NFPA 11)***

Type of Hazard	Calculation of Rate
Deck spill	6.50 lpm/m^2 (0.16 gpm/ft^2) or 10% of the cargo block area
Largest tank	9.78 lpm/m^2 (0.24 gpm/ft^2) of the single largest tank area
Largest monitor	3.0 lpm/m^2 (0.074 gpm/ft^2) of the area protected by the largest monitor (not less than 1250 lpm)

Table 4-4.18 ***Foam Application Rate for Marine Polar Solvent Hazards (NFPA 11)***

Type of Hazard	Calculation of Rate
Deck spill	Rate for most hazardous polar solvent × 10% of the cargo block area
Most demanding tank	150% of the highest required foam application rate for the single largest tank
Largest monitor	45% of the highest required foam application rate applied over the area protected by the monitor (not less than 1250 lpm)

rate for the most difficult extinguishment case. Foam concentrates for hydrocarbon fuels must be approved using a 9.29-m^2 (100-ft^2) fire test similar to UL 162. The fixed-nozzle gasoline fire test has an extinguishment application density of 12.2 l/m^2 (0.30 gal/ft^2).

Model building and fire codes in the United States are in the process of adopting AFFF protection criteria for the storage of flammable and combustible liquids. Criteria of insuring authorities [e.g., Industrial Risk Insurers (IRI) and Factory Mutual (FM)] are similar to the NFPA requirements. Insurance authority guidelines should be referenced for specific projects, since there are differences in protection criteria.

Protection of Stored Flammable and Combustible Liquids

Flammable and combustible liquids are stored in containers ranging in size from less than one quart to several hundred gallons. These liquids may be stored for display in a retail outlet or "super store," or stored for distribution in a general-purpose warehouse housing many different combustibles, or stored in "liquid" warehouses containing large quantities of the liquid. NFPA 30, *Flammable and Combustible Liquids Code,* is the applicable NFPA protection document. This code includes requirements for tank storage, piping systems, containers, and operations. Criteria for suppression system protection is addressed in the sections dealing with container storage.

The protection of flammable and combustible liquids is a function of many factors, including the liquid properties, the ignition (which can be a factor of the storage occupancy), the packaging system (e.g., stored in cardboard cartons), the container design and material (e.g., steel, plastic, glass, fiberboard), and the arrangement of storage (e.g., rack versus pallet, storage height, aisle width, and mixture of other combustibles in the array). Based on these factors, a suppression system is provided to control or suppress the anticipated fire and protect the structure. The system may be designed to (1) control a fire so that the fire department can ultimately extinguish or suppress the burning material or (2) suppress the fire. Variables in suppression system design include sprinkler application rate, agent, orifice size, spacing, response time index (RTI), temperature rating, and provision of in-rack protection.

The basis of protection criteria in NFPA 30 is now well documented. Fire test references and associated citations in technical literature are now included with all protection tables.[56] The basis of the protection criteria can now be directly linked to test data or engineering extrapolations of the data. Material in Appendix E of NFPA 30 provides guidance and an example test protocol for evaluating protection of liquids stored in the containers. This includes consideration of the source of the fire, which may be a "point" ignition (i.e., small ignition) or a large spill/three-dimensional fire. Depending on other variables, such as container type and packaging material, one of these scenarios may be more difficult to protect. Appendix E of NFPA 30 provides detailed guidance on this subject.

Stored liquids may be protected using water sprinklers, foam, or other approved methods. Figure 4-4.18 shows a conceptual grouping of water and AFFF protection methods as a function of container type and storage method for water protection of liquids. The reader should consult Reference 56. The basis of AFFF protection is described in the following sections.

Protection of drum and tank storage: Some of the earliest work using AFFF sprinklers involved the protection of 208-l (55-gal) drums. In work conducted at Factory Mutual Research Corporation, sponsored by Allendale Insurance, Factory Insurance Association (FIA), and the 3M Company, the effectiveness of standard sprinklers supplied with AFFF for controlling drum fires was determined.[57] Five fire tests were conducted in simulated flammable liquid-drum storage using two types of storage arrangements. Three tests were conducted with two-, three-, and four-high palletized drum storage, respectively. Two tests were conducted with five-tier high-rack storage of palletized drums.

In all tests, a heptane fuel supply simulated leakage from the upper level of storage. Except for one rack-storage

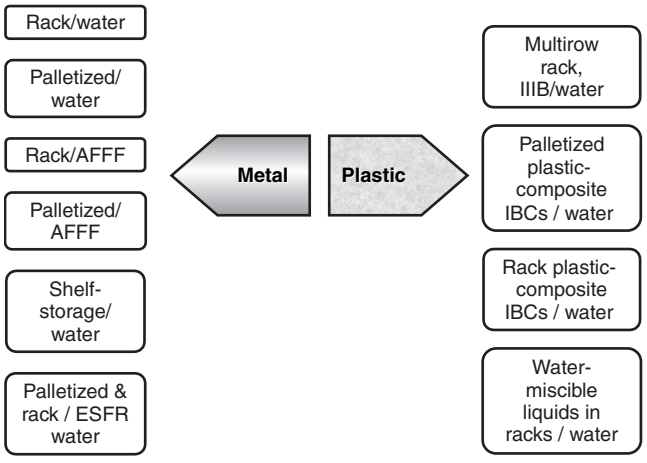

Figure 4-4.18. ***Grouping of NFPA 30 protection criteria for liquids.***

test that used a 57-lpm (15-gpm) spill rate, fuel spillage was 7.6 lpm (2 gpm). Ceiling protection employed high-temperature sprinklers at discharge rates of either 12.3 or 24.6 lpm/m^2 (0.30 or 0.60 gpm/ft^2). In-rack supplemental protection for the rack-storage tests was provided at three levels, with ordinary temperature sprinklers each discharging 113 lpm (30 gpm). The success of each test was based on storage stability, that is, no pile collapse, and limitation of drum pressure to 104 kPa (15 psig).

AFFF was effective in controlling spill fires on the floor. The exception was in areas not reached by the discharge from operating sprinklers, where the flow of foam was blocked by pallets. Protection was not effective on the three-dimensional spill fires. Fire exposure and resultant pressure development within drums was more severe with increased clearances between storage and sprinklers due to greater delays in sprinkler operation.

Generally, results were considered good in the rack-storage tests, where in-rack sprinklers were provided in each tier. For palletized storage, the AFFF protection controlled the floor fire although pallets hindered the spread of foam. Ceiling sprinklers alone did not adequately protect palletized storage where an elevated spill resulted in a three-dimensional fire within the pile.

The results of these tests were used, along with engineering judgment, to develop AFFF protection criteria in NFPA 30, *Flammable and Combustible Liquids Code.* AFFF protection of 12.3 lpm/m^2 (0.30 gpm/ft^2) at the ceiling for rack protection of metal drum/tank storage up to 7.6 m (25 ft) high. In-rack protection (e.g., sprinklers in alternating tiers or every tier) is a function of the liquid (flashpoint), container style (relieving vs. nonrelieving), and capacity of the container.

The results of the original Factory Mutual (FM) drum tests were extended in a series of tests conducted by Southwest Research Institute.[58] The objective was to test the effectiveness of relieving-style steel drums and varying degrees of overhead sprinkler protection to mitigate fire hazards associated with the storage of flammable liquids. Nylon plugs inserted in the 5.1-cm (2.0-in.) pour hole and 1.3-cm (0.5-in.) vent hole were designed to melt under fire conditions, allowing the drum to vent any built-up pressure. Heptane, a Class IB flammable liquid, was used as the stored commodity.

Tests were designed to model credible, worst-case loss scenarios involving the 208-l (55-gal) storage of the commodity. The fire modeled the accidental puncture of a full drum, and either an immediate or a delayed ignition source. Sprinkler suppression of the fire was monitored for the duration of the spill, and until flames were either under control or completely extinguished. Commodity was stacked in a 3 × 3 palletized array, to varying heights (2, 3, or 4 high), and protected with varying sprinkler types and densities.

The relieving-style closures were successful at mitigating the hazards associated with overpressurizing drums during a fire. The installed suppression systems were capable of either extinguishing or controlling the fire for the duration of the spill. A summary of the successful protection configurations for the commodity tested is provided in Table 4-4.19.

Table 4-4.19 ***Summary of Heptane-Palletized Drum Storage Tests[58]***

Test	Commodity	Protection (nominal application rates)
2 and 3	3 × 3, 2 high	3% AFFF at 12.3 lpm/m^2 (0.30 gpm/ft^2)
5	3 × 3, 2 high	ELO water-based at 24.6 lpm/m^2 (0.60 gpm/ft^2)
7	3 × 3, 3 high	ELO, 3% AFFF at 18.5 lpm/m^2 (0.45 gpm/ft^2)
8	3 × 3, 4 high	ELO, 3% AFFF at 24.6 lpm/m^2 (0.60 gpm/ft^2)

The fuel spill rate (7.6 vs. 56.8 lpm) was found to have a substantial impact on the fire exposure of the drums. When taken in conjunction with the effect of the ignition scenario, the fuel spill rate had a strong influence on the number of initial heads operating and on the duration of the fire exposure. The ignition of the fuel source also played a role in the number of heads actuated during a test. The immediate ignition of fuel (simulating a spill onto an existing ignition source) resulted in a slower growing fire, actuating fewer sprinkler heads. Alternately, an ignition scenario where a 7.6-l spill was allowed to develop prior to ignition resulted in the actuation of four heads within the first minute of fire exposure. A comparable test with the immediate ignition scenario resulted in only two heads operating in a time in excess of 2 min and 30 s. The involvement of fewer sprinkler heads and the prolonged fire exposure implied that the immediate ignition provided a more challenging scenario.

The AFFF system used in the test program was successful in generating a good blanket of foam within 1 to 2 min of actuation (depending on the number of initial heads actuated). The foam quality was such that it was free to flow over drum heads, providing cooling to the tops and sides of drums, and forming a blanket at the floor to suppress pool fires. The foam system (in Tests 6 through 8) was also effective at limiting the fire at the fuel introduction point, periodically extinguishing the source. In general, by the time fuel flow to the array was complete, the foam system had suppressed all pool fires, leaving only small pallet fires for manual suppression.

An initial survey of closure obstruction versus venting phenomenon indicated that there was little or no effect on the obstruction of a plug and its ability to vent. This is indicated by the low number of drums that exhibited bulging during tests. The bulging of a drum indicates an unusual buildup of pressure. This phenomenon was not consistent, even in drums where both closures were obstructed. It was also noted that even partial venting of either opening was sufficient in reducing the pressure within the drum.

Drum deformation was recorded on a subjective basis. Typical deformation involved bulging of the head of the drum by 1.2 to 2.5 cm (0.5 to 1.0 in.). In some cases, deformations were seen on the order of 7.6 to 10.2 cm (3 to 4 in.) with some unfurling of the head chime.

It is difficult to attribute the level of deformation with a corresponding internal pressure. Several drums were deformed to a degree consistent with hydrostatic pressures of 207 to 241 kPa (30 to 35 psi); however, no pressures of this magnitude were recorded. A possible reason for higher levels of deformation at lower pressures may lie in the exposed temperatures of the drums. Several drums were subjected to uneven heating. The uneven heating phenomenon is present where a drum is located directly above a pallet containing venting drums. This scenario sets the subject drum over an isolated flame source, heating it from below.

The results of these tests have been included in the NFPA 30 protection criteria tables for palletized steel drum storage up to four high when protected using AFFF. The use of listed relieving devices is recommended; the exact details of this listing procedure are being developed.

Liquid spill and container storage: Table 4-4.20 summarizes early closed-head AFFF sprinkler testing on a flammable liquid spill.[59] In a 9.1-m- (30-ft-) high ceiling room, *n*-heptane was discharged in a simulated spill to create a three-dimensional spill and a two-dimensional pool fire. Fuel spill rate was varied up to 113 lpm (30 gpm). AFFF application rates were 4.5 to 12.3 lpm/m^2 (0.11 to 0.30 gpm/ft^2). The primary variables were the temperature rating of the sprinkler and the application rate. Non-air-aspirating sprinklers were used. The data show that high-temperature-rated sprinklers activated at about the same time as ordinary temperature sprinklers, controlled the fire in comparable times (roughly 2 min control time), and resulted in significantly fewer sprinklers operating (7 versus 32). An increase in application rate when the high-temperature sprinklers were used resulted in fewer heads operating, but did not decrease overall control and extinguishment time. Fires were controlled, but not totally extinguished as a result of the three-dimensional spill fire. These tests showed the advantage of using high-temperature-rated sprinklers in AFFF closed-head suppression systems.

Table 4-4.20 ***Closed-Head Sprinkler Tests***[59]

Sprinkler Temperature Rating [°C (°F)]	Nominal Application Rate [lpm/m^2 (gpm/ft^2)]	Total Heads Opened	Sprinkler Operation and Control Times (min : s)
71 (160	4.5 (0.11)	34	First sprinkler—0:27 Final sprinkler—1:01 3:50 Control time
71 (160)	7.4 (0.18)	32	First sprinkler—0:22 Final sprinkler—1:08 1:00 to 1:20 for knockdown 2:20 Control time
138 (280)	7.4 (0.18)	7	First sprinkler—0:33 Final sprinkler—0:531 1:50 Control time
138 (280)	7.4 (0.18)	15	First sprinkler—0:28 Final sprinkler—1:44 2:20 Control time
138 (280)	7.4 (0.18)	17 to 19	First sprinkler—0:22 to 0:24 Final sprinkler—1:03 to 1:13 2:00 Control time
141 (286)	12.3 (0.30)	10	First sprinkler—0:24 Final sprinkler—1:10 2:25 Control time

In response to the concerns related to flammable liquid warehouse protection, the National Fire Protection Research Foundation (NFPRF) initiated the International Foam-Water Sprinkler Research Project. The objectives were to document the performance of foam-water sprinkler systems designed for real-world storage and ignition scenarios and provide a design basis and minimum design parameters for foam-water sprinkler systems. Five tasks were performed, including a literature search, range-finding tests, and large-scale tests involving palletized and rack storage of liquids.

The literature search identified over 1100 sources of information related to flammable liquid fires and foam protection, but a dearth of data related to water and foam-water sprinkler suppression of liquid storage fires.[60] The range-finding tests indicated that the Class IB flammable liquids (heptane) provided a greater challenge than water-miscible fuels (e.g., isopropanol).[61] Breach of steel containers exposed to a flammable liquid pool fire without sprinkler protection occurred over a range of times between 2 and 7.5 min, depending on the particular type of container. Plastic containers were quickly breached and discharged their contents to the exposing pool fire.

Large-scale tests were conducted under an 8.2-m- (27-ft-) high ceiling at the Underwriters Laboratories fire test facility in Northbrook, Illinois.[62] A series of 14 fire tests involving the protection of 3.8- and 18.9-l- (1- and 5-gal-) metal and 18.9-l (5-gal) plastic containers filled with heptane (Class IB flammable liquid) were conducted. The use of closed-head foam-water sprinkler systems for the protection of these fuel packages was investigated. Quantities of fuel used in the fire tests varied from 605 to 7260 l (160 to 1920 gal); fuel storage densities ranged from 160 to 1907 l/m^2 (3.9 to 46.5 gal/ft^2); and storage heights ranged from 4.3 to 42.7 m (1.3 to 13 ft). Each fire test was initiated using a 37.8-l (10-gal) flammable liquid (heptane) spill, recognizing the larger spill ignition scenarios observed in large-loss fires.

Fire tests involving palletized storage of 3.8-l (1-gal) metal F-style containers of heptane, packaged four containers in a corrugated cardboard carton, were conducted. The results indicated that the 37.8-l (10-gal) flammable liquid spill fire could be suppressed by a closed-head foam-water sprinkler system at a 16.4 lpm/m^2 (0.40 gpm/ft^2) design application rate for storage heights up to 3.3 m (10.7 ft) under the 8.2-m (27-ft) ceiling prior to any container breach or fuel loss. Fires involving 18.9-l (5-gal) metal containers of heptane could be suppressed by a closed-head foam-water sprinkler system application rate of 12.3 lpm/m^2 (0.30 gpm/ft^2) for a palletized storage height

of up to 3.6 m (12 ft). Plastic pour spouts in the 18.9-l (5-gal) tight-head metal containers safety vented and prevented container breaching.

Fires involving 18.9-l (5-gal) plastic containers of heptane could not be suppressed by a preprimed, closed-head foam-water sprinkler system with an application rate of 12.3 lpm/m^2 (0.30 gpm/ft^2), where containers were stacked one high [483 mm (19 in.)], due to container breaching and flammable liquid spillage prior to foam-water discharge.

Rack-storage tests also conducted in the NFPRF International Foam-Water Sprinkler Research Project did not lead to conclusive results.[63]

Based on the results of the NFPRF foam-water sprinkler testing, the FMRC original AFFF drum testing, and engineering judgment/extrapolation, the NFPA 30 Technical Committee adopted protection criteria for palletized and rack storage of liquids in metal containers when protected by AFFF. Variables that affect the specific level of protection include container size, class of liquid stored, inclusion of exterior packaging material, and storage height. Ceiling application rates are on the order of 12.3 to 16.4 lpm/m^2 (0.30 to 0.40 gpm/ft^2). Protection criteria shown in Table 4-4.21 are recommended for palletized storage of small containers that are nonrelieving style (i.e., do not readily vent when exposed to fire). Additional criteria are included in NFPA 30 for foam protection of palletized relieving-style containers based on extrapolation of the NFPRF data and engineering judgment. Where the hazard involves a water-miscible fuel, an alcohol-type foam should be used. The application rate should be at least as great as the rate established by foam listing requirements. AFFF solution should be discharged when four sprinklers are operating.

AFFF protection of flammable and combustible liquids should be used where large spills of low flashpoint fuels are a realistic scenario. Other protection options are available and have recently been adopted or are currently being considered by NFPA 30 and the model building/fire prevention codes. Designers of warehouse protection should have a thorough knowledge of these criteria and the available test data (including water-only protection) when considering design options for the protection of stored combustible and flammable liquids. Reference 56 and NFPA 30 provide detailed data and guidance for water-only protection. Additional guidance for warehouse protection is available from the Center for Chemical Process Safety.[64]

Table 4-4.21 ***AFFF Sprinkler Protection Requirements in NFPA 30 for Solid-Pile and Palletized Storage of Flammable and Combustible Liquids in Non-Relieving-Style Metal Containers of 18.9-l (5-gal) Capacity or Less***

Package Type	Cartoned	Uncartoned
Class liquid	IB, IC, II	IB, IC, II
Application rate [lpm/m^2 (gpm/ft^2)]	16.4 (0.40)	12.3 (0.30)
Area [m^2 (ft^2)]	186 (2000)	186 (2000)
Temperature rating [°C (°F)]	141 (286)	141 (286)
Maximum spacing [m^2/head (ft^2/head)]	9.3 (100)	9.3 (100)
Orifice size [mm (in.)]	13.3 (0.53)	12.5 or 13.3 (0.5 or 0.53)
Maximum height [m (ft)]	3.4 (11)	3.7. (12)
Hose [lpm (gpm)]	1891 (500)	1891 (500)
Water supply duration (min)	120	120
Foam supply duration (min)	15	15

Foam Environmental Considerations

There has been increasing concern about the consequences of the discharge of foam in the environment. This concern affects the users of foam, the manufacturers of foam agents, the fire safety authority having jurisdiction, and environmental authorities. Quantitative data and methods to evaluate environmental impact are not widely published or well developed. The issue is not a new or unique development but has received increased notice as a result of increased attention to environmental impact of fire-fighting agents.

Factors related to the impact of fire-fighting foam on the environment include

1. Discharge of foam solutions and fuel-contaminated foam solutions to waterways and the potential toxicity to aquatic life
2. Effects on water treatment facilities
3. Persistence and biodegradability of chemicals in foam concentrates and solutions
4. Combustion products of fuel/foam solutions

Perspective on the Use of Foam Agents

In order to assess the impact of foam on the environment, the likely scenarios under which AFFF may be discharged should be considered. Based on these scenarios, the overall impact can be assessed and, where appropriate, potential mitigation strategies can then be developed. Likely scenarios include uncontrolled fires, potential hazardous situations, fire-fighting training evolutions, and fixed or mobile vehicle suppression system discharge testing.

Uncontrolled fires: There are many fires for which foam may be used, including flammable liquid storage, process industry protection, aviation protection, and marine applications. For most fires, the elimination of foam as a suppression agent results in the potential for dramatically increased environmental impact. This impact results from the potential increase in hydrocarbon fuel effluent to the environment (due to smoke from uncontrolled burning and fuel/fire-fighting water effluent). Consider the example shown in Figure 4-4.19. A 929-m^2 (10,000-ft^2) section of a warehouse containing combustible and flammable liquids may be protected using traditional water sprinklers discharging at a rate of 12.3 lpm/m^2 (0.30 gpm/ft^2). If these sprinklers fail to control a large spill fire, the fire may develop and spread past the design area of the sprinklers. The example assumes the fire is contained within the fire wall; this may not always be the case for high-challenge fires. If the fire department aggressively combats the fire, a

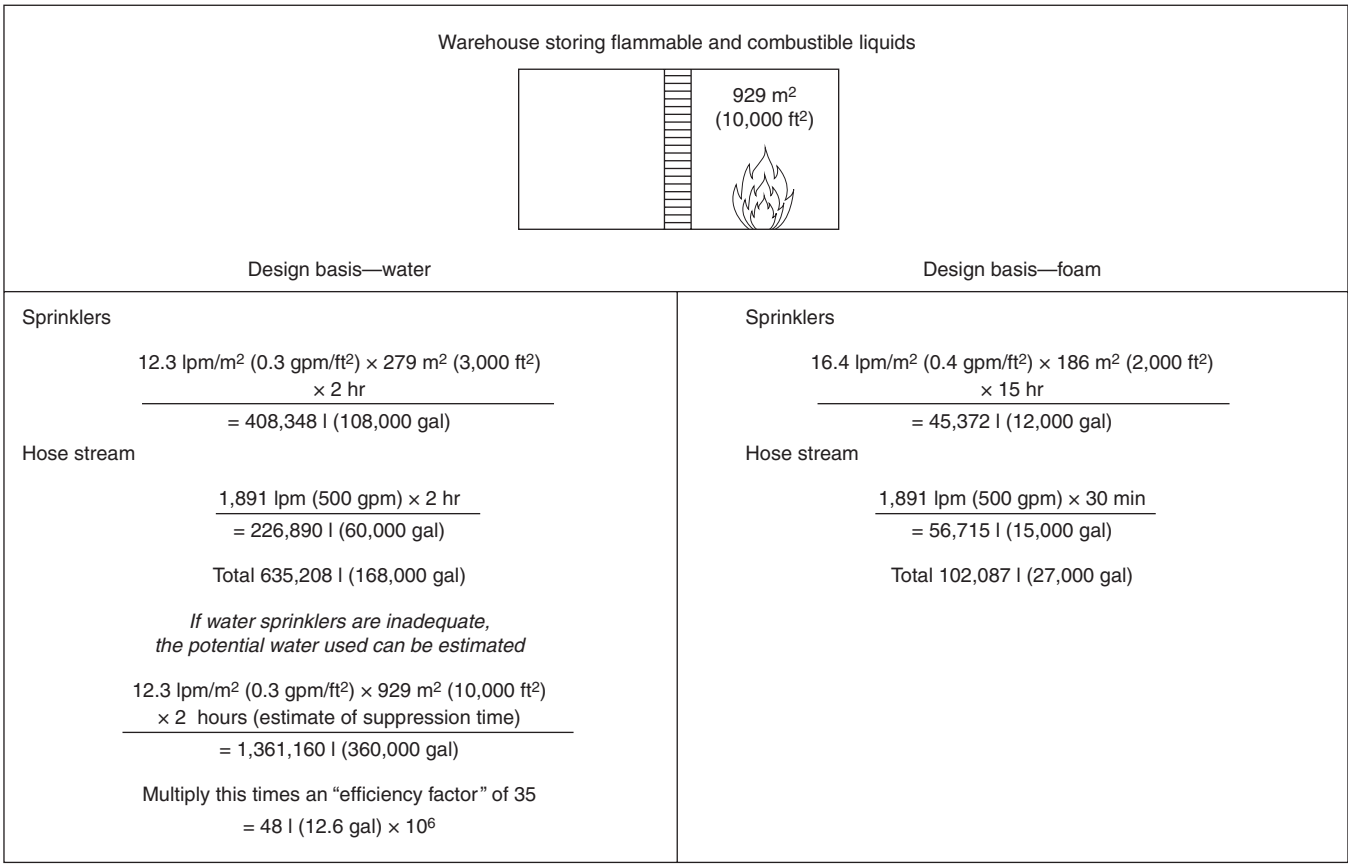

Figure 4-4.19. Example of potential effluent from flammable liquid warehouse fire.

rough estimate of fire-fighting water that may be used is 15 to 50 times the minimum anticipated agent required for suppression.[6,65,66] A rough estimate of the potential fuel-contaminated effluent (neglecting the actual quantities of hydrocarbon liquid) is shown in Figure 4-4.19. In the alternative situation, a properly specified foam-water sprinkler system designed for a high degree of reliability can control or suppress the fire. Using application rates and discharge times based on recent tests and building code requirements, the anticipated fuel/foam/water effluent for this scenario can be estimated. (See Figure 4-4.19.) The use of the foam-water system reduces the potential effluent by a factor of nearly 500 compared to the "unsuccessful" water sprinkler scenario where handlines are used. This reduction neglects the impact of smoke discharged to the atmosphere during the uncontrolled burning in the water-only scenario.

In some cases, it may be possible to collect the effluent from an uncontrolled fire. In other situations, it may not be possible. Any foam solution that has been used in fire suppression is likely to be contaminated with fuel and diluted with water.

Potential hazardous situations: Potential hazardous situations may result from a fuel spill where there is a likely ignition source. In this situation, foam may be applied for ignition prevention. The potential impact of ignition and resulting uncontrolled fire must be assessed against the potential additional environmental impact by discharging foam for ignition prevention. The potential environmental effects from an uncontrolled fire should be considered as described in the previous text. Another consideration is the assessment of any additional impact of foam when applied to a fuel spill. For example, would the resulting fuel with foam have any greater impact on the environment than the fuel alone? If so, how is this impact quantitatively determined?

Training evolutions: Fire-fighting training is usually conducted under conditions conducive to collection of fuel, water, and foam. A separation process might be used to recover fuel. Water/foam solution may then be treated or reused. Alternatively, simulated hydrocarbon fuel spill scenarios might be used, with a simulated foam agent. Propane-fired burners are typically used. The disadvantage of these systems is the potential loss of realism of the simulated fire/agent interaction. These techniques may potentially reduce training effectiveness. Quantitative comparisons have not been performed to assess these differences.

System discharge testing: Facilities protected by foam systems may have containment systems that can hold effluent. Requirements for these containment systems are becoming more widespread in model building and fire codes. An alternative to discharge testing with foam is the use of a simulant that can be measured using concentration determination methods. For example, salt solutions can be used as the "concentrate" to test AFFF systems, with the simulant concentration measured using the conductivity method. Simulators may be more difficult to use for protein-based systems, where viscosity factors influence proportioning system accuracy.

Methods of Assessment

Biodegradability: The primary component of AFFF solution is water. Examples of other components are nonfluorinated surfactants, glycol ethers, and fluorinated surfactants. Freeze-resistant concentrate may contain ethylene or propylene glycol. Alcohol-type foams contain xanthan or similar gums. The fluorinated surfactants are particularly resistant to biodegradation. Further, the less-effective protein-based foams were largely assumed to be nonpolluting because of their "natural" organic base. An early review of the available literature by Factory Mutual Research Corporation indicated that both types of agents, that is, AFFF and protein-based, present inherent environmental issues and that effluents containing either should be processed in some form of sewage treatment facility or diluted prior to discharge into a stream.[39]

A conventional method used to determine the biodegradability of a material is comparison of the chemical oxygen demand (COD) of the material with its biological oxygen demand (BOD). This method is particularly important for waste treatment facilities where the stability of the treatment process may be upset. The method typically used is specified in "Standard Methods for the Examination of Water and Wastewater."[67] BOD measures the amount of oxygen consumed by microorganisms in breaking down a hydrocarbon. COD measures the maximum amount of oxygen that could theoretically be consumed by microorganisms. Therefore, a BOD/COD ratio is representative of the ability of microorganisms to biodegrade the components in a foam. The higher the BOD/COD ratio, the more biodegradable the foam. Results reported for BOD/COD of AFFF range from 0.60 to 0.99. MIL-F-24385 requires a maximum COD of 500,000 mg/l and a minimum 20-day BOD/COD ratio of 0.65 for 6 percent concentrate. AFFF agents have been reported to have higher BOD and COD values than protein foams.[39] AFFF solutions are high-BOD materials compared to the normal influent to treatment plants. Large quantities can "shock load" wastewater treatment facilities.

The fluorochemical-based surfactants in AFFF have a carbon–fluorine chain that apparently does not break down in either the BOD or the COD test. The AFFF might then appear to be completely "biodegradable," even though the carbon–fluorine chain remains.

If nonbiodegradability concerns are based on the persistence of the fluorochemical surfactants, then the environmental impact tests currently used to assess foams do not address this concern. There is speculation that the undegradable material is biologically inert, but no published data confirms this. Since the fluorinated surfactants are required to create surface-tension reduction of the solution, replacement with less persistent chemicals is problematic. There is a need for a more thorough understanding and testing related to the environmental impact of fluorosurfactants and possible alternatives.

The persistence of fluorosurfactants in soil has recently been quantified in a study of fire-training facilities.[68] In a study of training sites having long-term use, perfluorocarboxylates were detected using gas chromatography/mass spectrometry. These chemicals were detected at sites that were inactive for a period of 7 to 10 years. The results are consistent with the view that biodegradation of the long chain perfluorocarbon is unlikely. The influence of the perfluorinated compounds on the biotransformation and transport of other cocontaminants (e.g., training fuel) and other site characterization parameters (e.g., dissolved organic carbon and inorganics) is unknown.

Methods for detecting AFFF in aqueous solutions have been investigated.[69] A Fourier Transform Infrared Spectroscopy (FTIR) method and drain-time test were found to be effective in evaluating the level of AFFF contamination in wastewater and soil. The drain-time method was proposed as a simple, easy-to-use field test. Using these methods, procedures were developed to estimate AFFF contamination levels in wastewater and soil. Analysis of wastewater and soil for AFFF contamination was broken into two groups: nonbiodegraded samples and biodegraded samples. Nonbiodegraded samples were screened for AFFF, then analyzed further if deemed necessary. Samples were initially screened using the drain-time test. Samples with no drain time contain less than a 1 : 240 dilution of AFFF (5 ppm of fluorosurfactant). If the sample had a drain time, it was recommended that the FTIR analysis be performed on the sample. In solutions with fluorosurfactants, FTIR analysis can provide a quantitative level of AFFF in the sample if the fluorosurfactant source solution is available to develop a calibration curve. Otherwise, FTIR provides a qualitative estimate of the AFFF level in the solution.

Biodegraded wastewater samples were difficult to analyze because the hydrocarbon surfactants and a portion of the fluorosurfactant molecule are degraded. With these foam-making constituents degraded, the drain-time test results were found to be unreliable. However, the fluorine-carbon tail of the fluorosurfactant is not biodegraded, making FTIR analysis on biodegraded samples possible. With biodegraded samples, FTIR analysis can provide a qualitative measure of AFFF levels.

Toxicity: In sufficient concentrations, foams may affect aquatic life. A number of fish toxicity studies have been performed. In tests using fathead minnows, the U.S. Air Force found that these fish could live in a simulated effluent stream containing 250-ppm AFFF without fatality for up to 8 days. LC_{50} values (i.e., the concentration causing deaths of 50 percent of the fish exposed) at 96 and 24 hr were 398 and 650 ppm, respectively.[70] MIL-F-24385

requires AFFF toxicity testing in accordance with ASTM E-729, using dynamic procedures with killifish. LC_{50} of 1000 mg/l for 6 percent concentrate is permitted.

Alone, these values may be considered as having a low degree of fish toxicity using environmental regulation rating scales. Localized concentrations in ponds or streams may exceed the values cited, if there is limited water movement.

Published data do not exist for the phytotoxicity of foam solutions; however, there have been no published reports of plant kills resulting from foam solution discharges.

Manufacturers report that thermal decomposition products from AFFF do not present a health hazard during fire fighting. Again, there are no data published in the literature. Manufacturers' product environmental data for AFFF include references to a test where a layer of AFFF was burned in a pan of gasoline inside an enclosure. Two measurements of hydrogen fluoride recorded above the sample were 0.23 and 0.16 ppm.[71]

Foaming and emulsification of fuels: The surfactants in AFFF solutions can cause foaming in treatment aeration ponds. This foaming process may suspend high BOD solids in the foam. If these are carried over to the outfall of the treatment facility, nutrient loading in the outfall waterway may result. Foam aeration may also cause foam bubble backup in sewer lines.

In uncontrolled fires, spills, and live fire-training scenarios, foams may contain suspended fuels. The fuel may become emulsified in the foam-water solution.

A bench-scale study has been conducted to evaluate the potential inhibitory effects of untreated AFFF wastewater on the biological nutrient removal process.[72] In this study, bench-scale reactors simulating the nitrification process were loaded at various AFFF concentrations, and the influence on process performance was evaluated. The results indicated that AFFF in concentrations between 10 ppm and 60 ppm did not show any inhibition to biological nitrification, and effluent did not exhibit any pass-through toxicity. These range-finding tests did indicate that nitrification inhibition did occur above 60 ppm AFFF. Some reductions in percent COD removal were observed as AFFF concentrations were increased.

Mitigation Strategies

Foam discharges are more easily handled where there is an in-place collection capability. This situation may be available at warehouses, tank farms, and fire-fighting training facilities. Where these facilities are not available, temporary diking is an alternative where time and resources permit.

Investigations have been conducted to develop foam/water separators using aeration and agitation techniques. To date, these techniques have not been optimized.

Discharge to water treatment facilities is recommended by many foam vendors when the solution is uncontaminated by fuel. Metering or dilution may be required to prevent levels of foam that will upset treatment facility reactions or cause excessive foaming. The use of defoamers to reduce aeration has been suggested.

Where fuels contaminate foam solutions, fuel/water separators might be used to skim off the hydrocarbon fuel. AFFF solutions have a tendency to form emulsions with fuels, potentially reducing the effectiveness of fuel/water separators. An alternative is to hold the solution in a pond or tank until the emulsion breaks and the separation process can be used. Agitation should be avoided to prevent the emulsion from reforming. In some situations (e.g., training), the fuel and treated water have been reused. Many fire-training facilities collect foam solution for ultimate discharge to water treatment facilities.

To ensure that unbalanced conditions do not occur in water treatment facilities, foam discharge should be carefully monitored. Different ranges of discharge rates have been suggested. This is an area requiring further investigation. Manufacturers of the foam solution should be consulted in conjunction with the wastewater treatment operator.

The entire area of environmental aspects of foam discharge requires additional evaluation and development of generally recognized guidance. Until generally recognized guidance is promulgated, users must rely on manufacturers' data and guidance. In all situations, discussions with the operator of the wastewater treatment facility and the environmental regulatory authorities are appropriate. Work is continuing in an effort to identify appropriate policy and criteria covering foam discharge for facilities having foam suppression systems. These efforts are focusing on identifying applicable codes and standards, analyzing environmental impact, and evaluating containment options.

Nomenclature

$AFFF\%_{sample}$	percentage of AFFF present in the sample
BOD	biological oxygen demand (mg/l)
γ_a	surface tension of liquid *a* (dynes/cm)
γ_b	surface tension of liquid *b* (dynes/cm)
γ_l	interfacial tension between liquids *a* and *b* (dynes/cm)
COD	chemical oxygen demand (mg/l)
ΔH_v	combined latent and sensible heads of vaporization (kJ/kg)
δ	viscous boundary layer thickness (cm)
G	conductance (mhos)
g	acceleration of gravity (cm/s^2)
h	foam thickness
h_c	critical thickness of the foam layer
i	angle of incidence
k	foam spreading coefficient, dimensionless or nozzle coefficient ($lpm/kPa^{1/2}$)
k_d	foam drainage coefficient, dimensionless
k_e	foam evaporation coefficient, dimenionless
l	length of foam spread
n	refractive index, dimensionless
μ	viscosity (cm^2/s)

$\dot{m}_{add}$	foam addition rate
$\dot{m}_{fuel}$	fuel mass loss rate
$\dot{m}_{drain}$	foam mass loss due to drainage
$\dot{m}_{drop}$	foam loss rate due to drop-out
$\dot{m}_{vap}$	foam mass loss rate due to vaporization
ν	kinetic viscosity (cm^2/s)
n_{water}	refractive index of water, dimensionless
n_{foam}	refractive index of foam solution, dimensionless
$n_{concentrate}$	refractive index of foam concentrate, dimensionless
P_v	vapor pressure of fuel
ρ_{fuel}	fuel density (g/cm^3)
ρ_{foam}	foam density (g/cm^3)
$\dot{q}''$	rate of heat transfer
$\dot{q}_{rad}$	rate of heat transfer due to radiation
q''_{rad}	radiative heat release rate from pool fire
R	resistance (ohms)
r	angle of refraction
σ	spreading coefficient (dynes/cm) or conductivity (mhos)
$S_{a/b}$	spreading coefficient between liquids *a* and *b* (dynes/cm)
T	temperature (°C)
t	time (s)
T_i	foam temperature (°C)
T_s	fuel temperature (°C)
V	volume (cm^3 or l^3)
v_s	spreading velocity of foam (cm/s)

Subscripts

add	addition of foam
drain	drainage of foam
drop	drop-out of foam
rad	radiation
vap	vaporization

Superscripts

·	rate of change, as in $\dot{m}$
″	per unit area

References Cited

1. G.B. Geyer, L.M. Neri, and C.H. Urban, "Comparative Evaluation of Fire Fighting Foam Agents," *Report FAA-RD-79-61,* Federal Aviation Administration, Washington, DC (1979).
2. J.H. Aubert, A.M. Kraynik, and P.B. Rand, "Aqueous Foams," *Scientific American,* 19, 1, pp. 74–82 (1988).
3. V.L. Francen, "Fire Extinguishing Composition Comprising a Fluoroaliphatic and a Fluorine-Free Surfactant," U.S. Patent 3,562,156 (1971).
4. M.J. Rosen, *Surfactants and Interfacial Phenomena,* John Wiley & Sons, New York, Chapters 1, 5, 7 (1989).
5. R.L. Tuve, H.B. Peterson, E.J. Jablonski, and R.R. Neill, , "A New Vapor-Securing Agent for Flammable Liquid Fire Extinguishment," *NRL Report 6057,* Washington, DC (1964).
6. R. Friedman, "Theory of Fire Extinguishment," *Fire Protection Handbook,* 17th ed. National Fire Protection Association, Quincy, MA, pp. 1–74 (1991).
7. C.P. Hanauska, J.L. Scheffey, R.J. Roby, and D.T. Gottuk, "Improved Formulations of Firefighting Agents for Hydrocarbon Fuel Fires," *SBIR Phase I Final Report* Hughes Associates, Inc., Baltimore, MD (1994).
8. B. Persson and M. Dahlberg, "A Simple Model of Foam Spreading on Liquid Surfaces," *SP Report 1994:27,* Swedish National Testing and Research Institute, Boras, Sweden (1994).
9. H. Persson, "Fire Extinguishing Foams—Resistance against Heat Radiation," *SR Report 1992:54,* Swedish National Testing and Research Institute, Sweden (1992).
10. B.Y. Lattimer, C.P. Hanauska, J.L. Scheffey, F.W. Williams, and W. Leach, "Behavior of Aqueous Film Forming Foams (AFFF) Exposed to Radiant Heating," *NRL Ltr Rpt Ser 6180/0013,* Naval Research Laboratory, Washington, DC (2000).
11. S. Ikasson and H. Persson, "Fire Extinguishing Foam—Test Method for Heat Exposure Characterisation," *SP Report 1997:09,* Swedish National Testing and Research Institute, Boras, Sweden (1997).
12. A.M. Kraynik, "Foam Drainage," *Sandia Report SAND-83-0844,* Sandia National Laboratories, Albuquerque, NM (1983).
13. A.M. Kraynik, "Foam Flows," *Annual Review of Fluid Mechanisms,* 20, pp. 325–357 (1988).
14. J.A. Fay, "The Spread of Oil Slicks on a Calm Sea," *Oil on the Sea* (D. P. Hoult, ed.), Plenum, New York, pp. 53–64 (1964).
15. J.A. Fay, and D.P. Hoult., "Physical Processes in the Spread of Oil on a Water Surface," *Coast Guard Final Report,* Massachusetts Institute of Technology, Cambridge, MA (1971).
16. P. Cann, H.A. Spikes, and G. Caporico, "Spreading of Perfluorinated Fluids on Metal Surfaces," *4th International Colloquium on Synthetic Lubricants and Operation Fluids,* Oatfildern, Germany, pp. 631–638 (1984).
17. H.E. Moran, J.C. Burnett, and J.T. Leonard, "Suppression of Fuel Evaporation by Aqueous Films of Fluorochemical Surfactant Solutions," *Naval Research Laboratory Report 7247,* Washington, DC (1971).
18. T. Briggs, and B. Abdo, "Emphasis on Spreading Quality of AFFF Could Be Misleading," *FIRE,* 80, 94, (1988).
19. J.L. Scheffey, R.L. Darwin, J.T. Leonard, C.R. Fulper, R.J. Ouellette, and C.W. Siegmann, "A Comparative Analysis of Film-Forming Fluoroprotein Foam (FFFP) and Aqueous Film-Forming Foam (AFFF) for Aircraft Rescue and Fire Fighting Services," *Hughes Associates, Inc. Report 2108-A01-90,* Hughes Associates Inc., Baltimore, MD (1990).
20. G.B. Geyer, "Status Report on Current Foam Fire Fighting Agents," *International Conference on Aviation Fire Protection,* Interlaken, Switzerland (1987).
21. P.J. Chiesa, and R.S. Alger, "Severe Laboratory Fire Test for Fire Fighting Foams," *Fire Technology,* 16, 1, pp. 12–21 (1980).
22. Underwriters Laboratories Inc., *Standard for Foam Equipment and Liquid Concentrates,* 6th ed., Northbrook, IL (1994).
23. J.L. Scheffey, J. Wright, and C. Sarkos, "Analysis of Test Criteria for Specifying Foam Firefighting Agents for Aircraft Rescue and Firefighting," *FAA Technical Report, DOT/FAA/CT-94/04,* Atlantic City, NJ (1994).
24. International Organization for Standardization, "Fire Extinguishing Media—Foam Concentrates—Part 3: Specification

for Low-Expansion Foam Concentrates for Surface Application to Water-Immiscible Liquids," *Draft European Standard EN 1568-3,* (2000).

25. B.P. Johnson, "A Comparison of Various Foams When Used against Large-Scale Petroleum Fires," Home Office Fire Research and Development Office, (1993).
26. W.M. Carey, and M.R. Suchomel, "Testing of Fire Fighting Foam," *Underwriters Laboratories Report No. CG-M-1-81,* Underwriters Laboratories Inc., Northbrook, IL (1980).
27. M.D. Thomas, "UK Home Office Research into Domestic Fire Fighting," *First International Conference on Fire Suppression Research Proceedings,* Stockholm, Sweden, pp. 283–289 (1993).
28. R. Fiala, "Aircraft Post-Crash Firefighting/Rescue," from *AGARD Aircraft Fire Safety Lecture Series No. 123* (1982).
29. G.B. Geyer, "Evaluation of Aircraft Ground Firefighting Agents and Techniques," *Technical Report AGFSRS 71-1,* Tri-Service System Program Office for Aircraft Ground Fire Suppression and Rescue, Wright-Patterson AFB, OH (1971).
30. G.B. Geyer, "Firefighting Effectiveness of Aqueous Film-Forming Foam (AFFF) Agents," *FAA Technical Report FAA-NA-72-48,* DOD Aircraft Ground Fire Suppression and Rescue Unit (ASD-TR-73-13), Washington, DC (1973).
31. W.M. Carey, "Improved Apparatus for Measuring Foam Quality," Underwriters Laboratories Inc., Northbrook, IL (1983).
32. E.J. Jablonski, "Comparative Nozzle Study for Applying Aqueous Film-Forming Foam on Large-Scale Fires," *U.S. Air Force Report, CEEDO-TR-78-22,* Tyndall AFB, Florida (1978).
33. J.A. Foster, "Additions for Hosereel Systems: Trials of Foam on 40 m^2 Petrol Fires," *Scientific Research and Development Branch Report 40/87,* Home Office, London (1987).
34. P.L. Parsons, "Trials of Foam on Petrol Fires at the Fire Service Technical College," *Scientific Advisory Branch Report No. 14/75,* Home Office, London (1976).
35. L.R. DiMaio, R.F Lange., and F.J. Cone, "Aspirating vs. Non-Aspirating Nozzles for Making Fire Fighting Foams—Evaluation of a Non-Aspirating Nozzle," *Fire Technology,* 20, 1, pp. 5–10 (1984).
36. J.L. Scheffey, "Submarine Bilge AFFF Sprinklers," *Naval Research Laboratory Project, 64561N-S1946-2024000,* unpublished data (1988).
37. G. Timms, and P. Haggar, "Foam Concentration Measurement Techniques," *Fire Technology,* 26, 1, pp. 41–50 (1990).
38. D.E. Breen, "Hangar Fire Protection with Automatic AFFF Systems," *Fire Technology,* 9, 2, pp. 119–131 (1973).
39. L.M. Krasner, D.E. Breen, and P.M. Fitzgerald, "Fire Protection of Large Air Force Hangars," *AFWL-TR-75-119,* Factory Mutual Research Corporation, Norwood, MA (1975).
40. D.E. Breen, L.M. Krasner, B.G. Vincent, and P.J. Chicarello, "Evaluation of Aqueous Film Forming Foam for Fire Protection in Aircraft Hangars," *FMRC Technical Report Ser. No. 21032,* Factory Mutual Research Corporation, Norwood, MA (1974).
41. L.M. Krasner, "Closed-Head AFFF Sprinkler Systems for Aircraft Hangars," *FMRC S. I. 0C6N3.RG, RC 79-T-58,* Factory Mutual Research Corporation, Norwood, MA (1979).
42. "Pop-Up-Type Floor-Mounted Foam Sprinklers for Aircraft Hangars," *Technical Record TR44/153/14(L),* Department of Housing and Construction, Australia.
43. *China Lake CVA Fire Fighting Tests, Phase III,* unpublished data (1972).
44. J.L. Scheffey, "Flow, Pattern, and Fire Performance Characteristics of a Prototype Pop-Up Nozzle for Use on Aircraft Carrier Flight Decks," *Report 2429-17,* Hughes Associates, Inc., Columbia, MD (1985).
45. J.L. Scheffey, and J.T. Leonard, "AFFF Protection for Weapons Staging Areas," *Fire Safety Journal,* 14, 14, pp. 47–63 (1988).
46. Department of the Navy, "General Specifications for Ships of the United States Navy, 1991 Edition," *NAVSEA S9AA0-AA-SPN-010/GEN-SPEC, Section 555,* Department of the Navy, Washington, DC.
47. H.W. Carhart, J.T. Leonard, R.L. Darwin, R.E. Burns, J.T. Hughes, and E.J. Jablonski, "Aircraft Carrier Flight Deck Fire Fighting Tactics and Equipment Evaluation Tests," *NRL Memorandum Report 5952,* Washington, DC (1987).
48. Rolf Jensen and Associates, "Comprehensive Aqueous Film Forming Foam Central Fire Suppression System Analysis/Report, B1-B Aircraft Hangars," *Technical Report A6406,* U.S. Air Force (1989).
49. J.E. Gott, D.L. Lowe, K.A. Notarianni, and W. Davis, "Analysis of High Bay Hangar Facilities for Fire Detector Sensitivity and Placement," *NIST TN 1423,* National Institute of Standards and Technology, Gaithersburg, MD (1997).
50. D.B. Szepezi, G.G. Back, J.L. Scheffey, F.W. Williams, and J.E. Gott, "Aircraft Hangar Fire Suppression System Evaluation—Intermediate Scale Studies," *NRL/MR/6180-99-8422,* Naval Research Laboratory, Washington, DC (1999).
51. G.G. Back, F.W. Williams, J.E. Gott, A.J. Parker, and J.L. Scheffey, "Aircraft Hangar Fire Protection System Evaluation Full Scale Study," *NRL Ltr Rpt Ser 6180/0620,* Naval Research Laboratory, Washington, DC (1998).
52. D.T. Gottuk, J.L. Scheffey, F.W. Williams, J.E. Gott, and R.J. Tabet, "Optical Fire Detection (OFD) for Military Aircraft Hangars: Final Report on OFD Performance to Fuel Spill Fires and Optical Stress," *NRL/MR/6180-00-8457,* Naval Research Laboratory, Washington, DC (2000).
53. A.J. Parker, G.G. Back, J.L. Scheffey, J.J. Schoenrock, J.P. Ouellette, F.W. Williams, J.E. Gott, and R.J. Tabet, "The Development of a Prototype Low-Level AFFF Nozzle System for U.S. Navy Aircraft Hangars," *NRL Ltr Rpt Ser 6180/0004* (2000).
54. J.L. Scheffey, A.J. Wakelin, J.E. Gott, R.J. Tabet, and F.W. Williams, "Aircraft Hangar Fire Suppression System Design Study," *NRL/MR* (in preparation), Naval Research Laboratory, Washington, DC (2000).
55. B.G. Vincent, H.C. Kung, and P. Stavrianidis, "Fire Protection for U.S. Army Helicopter Hangars," *FMRC J.I.OXON1.RA,* Factory Mutual Research Corporation, Norwood, MA (1993).
56. D.P. Nugent, *Directory of Fire Tests Involving Flammable and Combustible Liquids in Small Containers,* 2nd ed., Schirmer Engineering (2000).
57. R.M. Newman, P.M. Fitzgerald, and J.R. Young, "Fire Protection of Drum Storage Using 'Light Water' Brand AFFF in a Closed-Head Sprinkler System," *FMRC Technical Report Ser. No. 22464, RC 75-T-16,* Factory Mutual Research Corporation, Norwood, MA (1975).
58. Southwest Research Institute, "Performance Testing of Automatic Sprinkler Systems in the Protection of Palletized, 55-Gal Storage of Heptane in Self-Relieving Style, Steel Drums," *SwRI Project No. 01-2016-001,* San Antonio, TX (1999).
59. J.R. Young, and P.M. Fitzgerald, "The Feasibility of Using 'Light Water' Brand AFFF in a Closed-Head Sprinkler System for Protection against Flammable Liquid Spill Fires," *FMRC Technical Report RC 75-T-4, Ser. No. 22352,* Factory Mutual Research Corporation, Norwood, MA (1975).
60. Schirmer Engineering Corporation, "International Foam-Water Sprinkler Research Project: Task 1—Literature Search," *Technical Report No. 10-90001-04-00,* National Fire Protection Research Foundation, Quincy, MA (1992).
61. J.P. Hill, "International Foam-Water Sprinkler Research Project: Task 3—Range Finding Tests," *Technical Report OTOR6.RR,*

National Fire Protection Research Foundation, Quincy, MA (1991).

62. Underwriters Laboratories Inc., "International Foam-Water Sprinkler Research Project: Task 4—Palletized Storage Fire Tests 1 through 13," *Technical Report 91NK14873/NC987,* National Fire Protection Association, Quincy, MA (1992).
63. W.M. Carey, "International Foam-Water Sprinkler Research Project: Task 5—Rack Storage Fire Tests," *Technical Report,* National Fire Protection Research Foundation, Quincy, MA (1992).
64. Center for Chemical Process Safety, *Guidelines for Safe Warehousing of Chemicals*, American Institute of Chemical Engineers, New York, (1998).
65. D.J. Rasbash, "The Extinction of Fire with Plain Water: A Review," *Proceedings from the First International Symposium on Fire Safety Science,* (C.E. Grant and P.J. Pagni, eds.), National Institute of Standards and Technology, Gaithersburg, MD, pp. 1145–1163 (1986).
66. J.L. Scheffey and F.W. Williams, "The Extinguishment of Fires Using Low-Flow Water Hose Streams—Part II," *Fire Technology,* 27, 4, pp. 291–320 (1991).
67. American Public Health Association, "Standard Methods for the Examination of Water and Wastewater," 18th ed., Washington, DC (1992).
68. C.A. Moody and J.A. Field, "Determination of Perfluorocarboxylates in Groundwater Impacted by Fire-Fighting Activity," *Environmental Science & Technology*, 33, 16, pp. 2800-2806 (1999).
69. Hughes Associates, Inc., "Development of Detection Method for Aqueous Film Forming Foam (AFFF)," Armstrong Laboratories Environics Directorate, Dayton, OH (1997).
70. National Environmental Health Laboratory, "Biological Treatment of Fire Fighting Foam Waste," *Report No. REHL(K) 67–14,* Kelly AFB, Texas (1967).
71. "Light Water Brand AFFF Waste Disposal Recommendations and Hazard Evaluation," *3M Product Environmental Data Sheet,* 3M Company, St. Paul, MN (1991).
72. M. Enten-Unal, S. Paranjape, G.C. Schafran, and F.W. Williams, "Evaluation of the Effects of AFFF Inputs to the VIP Biological Nutrient Removal Process and Pass-Through Toxicity," *NRL/MR/6180-98-8141,* Naval Research Laboratory, Washington, DC (1998).

Additional Readings

ASTM D1331, *Standard Test Methods for Surface and Interfacial Tension of Solutions of Surface-Active Agents,* American Society for Testing and Materials, Philadelphia, PA (1995).

ASTM E729, "Standard Practice for Conducting Acute Toxicity Tests with Fish, Macroinvertebrates, and Amphibians," American Society for Testing and Materials, Philadelphia, PA (1996).

FAA, "Aircraft Fire and Rescue Facilities and Extinguishing Agents," *FAA Advisory Circular 150/5210-6C,* Federal Aviation Administration, Washington, DC (1985).

ICAO, "Rescue and Firefighting," *Airport Services Guide,* 3rd ed., International Civil Aviation Organization, Montréal, Québec (1990).

NFPA 11, *Standard for Low-Expansion Foam,* National Fire Protection Association, Quincy, MA (1998).

NFPA 13, *Standard for the Installation of Sprinkler Systems,* National Fire Protection Association, Quincy, MA (1999).

NFPA 16, *Standard for the Installation of Foam-Water Sprinkler and Foam-Water Spray Systems,* National Fire Protection Association, Quincy, MA (1999).

NFPA 30, *Flammable and Combustible Liquids Code,* National Fire Protection Association, Quincy, MA (2000).

NFPA 403, *Standard for Aircraft Rescue and Fire-Fighting Services at Airports,* National Fire Protection Association, Quincy, MA (1998).

NFPA 409, *Standard on Aircraft Hangars,* National Fire Protection Association, Quincy, MA (2001).

NFPA 412, *Standard for Evaluating Aircraft Rescue and Fire-Fighting Foam Equipment,* National Fire Protection Association, Quincy, MA (1998).

UL 162, *Standard for Foam Equipment and Liquid Concentrates,* Underwriters Laboratories Inc., Northbrook, IL (1994).

UL Fire Protection Equipment Directory, Underwriters Laboratories Inc., Northbrook, IL (2001).

U.S. Military Specification, MIL-F-24385, Department of the Navy, Washington, DC (2000).

U.S. Government, "Federal Specification, Foam Liquid, Fire Extinguishing, Mechanical," O-F-55B, (U. S. Government Protein Foam Specification), Washington, DC (1964).

CHAPTER 5

Foam System Calculations

Joseph L. Scheffey and Harry E. Hickey

Introduction

Foam agent fire protection is especially suited for the control and extinguishment of flammable and combustible liquid-type fire protection problems.

An impressive array of fire protection problems can be properly addressed using foam classification agents. The NFPA *Fire Codes*® discuss foam fire protection systems as suitable for the protection of numerous fire protection problems.[1] It is important to note that other classifications of fire extinguishing systems, including dry chemicals, wet chemicals, carbon dioxide, halon, and some special agents, may be suitable for similar hazards.

Table 4-5.1 identifies special hazards that may be suitable for adequate fire protection by different types of foam systems. Each special hazard is cross-referenced to one or more classifications of foam fire protection systems that are identified in NFPA standards as being suitable for the stated hazard. This table is useful for examining the scope and limitations of different types of foam application systems for special hazard fire protection. The referenced standards should be consulted concerning specification and design considerations for each specific problem condition.

Foam agent fire protection systems are suitable for Class A fires in ordinary combustible materials in addition to Class B fires (flammable and combustible liquids). Historically, portable foam fire extinguishers provided important fire protection for both Class A and Class B problems. The dual consideration of evaluating foam fire protection systems for both Class A and Class B fire protection problems is important. This consideration is especially important for mixed occupancy storage, which may be suitably protected by foam spray systems, foam water sprinkler or spray systems, or closed head sprinkler systems using aqueous film forming foam (AFFF) type foam agents.

Joseph L. Scheffey, P.E., is director of RDT&E at Hughes Associates, Inc., Baltimore, Maryland.

Dr. Harry E. Hickey is retired from the University of Maryland where he served as associate professor, Department of Fire Protection Engineering.

Objective Classification of Fire Problems for Foam Agent Fire Protection

The following objectives identify five performance areas for evaluating foam agent fire protection. Performance objectives may be combined for specific problem situations. These objectives form important considerations for the hydraulic design of foam agent systems.

Objective 1: Secure the surface of a flammable or combustible liquid that is not burning.

Flammable and combustible liquids emit vapors that may create a hazard condition. Flammable vapors may be suppressed by providing an adequate foam blanket over the surface area. Flammable liquid spills present a fire hazard. This hazard may be mitigated and/or controlled by the use of appropriate foam agent application.

Objective 2: Control and extinguish fires in flammable and combustible liquid hazardous locations in local areas within buildings.

Flammable and combustible liquids are often stored inside buildings in 55-gal (208-l) drums and other types of containers. These liquids are also used in association with manufacturing processes, industrial machinery, heating equipment, experimental activities, and so forth. The use of flammable and combustible liquids inside buildings may result in liquid spill and fuel ignition. Foam agents are appropriate for protecting localized flammable and combustible liquid problems inside buildings.

Objective 3: Extinguish fires in atmospheric storage tanks.

For nearly 100 years, foam agent fire protection has successfully extinguished fires in outdoor vertical atmospheric storage tanks. This type of protection still represents

Table 4-5.1 *Special Hazard Identification*[1]

	Protection Reference					
	NFPA 11			NFPA 11A	NFPA 16	
	Monitors	Foam Spray	Other Systems	High Expansion Foam	Foam-Water Sprinkler	Closed-Head Sprinkler
Aircraft protection						
1. Aircraft hangars (see NFPA 409)	X	X	X	X	X	X
2. Rooftop heliport construction and protection (see NFPA 418)		X	X		X	
3. Aircraft engine test facilities (see NFPA 423)		X		X	X	
Enclosed stockpiles						
1. Flammable liquids—flash point below 100°C (see NFPA 30)				X[a]		
2. Combustible liquids—flash point of 100°C and above (see NFPA 30)				X[a]		
3. Low-density combustibles (foam rubber, foam plastics, rolled tissue or crepe paper)				X[a]		
4. High-density combustibles—rolled paper (see NFPA 13)				X[a]		
5. Combustibles in containers (cartons, bags, fiber drums)				X[a]		
Nuclear power plants						
1. Fire protection for light water nuclear power plants (see NFPA 803)		X		X	X	
2. Nuclear research reactors (see NFPA 802)		X		X	X	
Protection of commodity storage						
1. Indoor general storage (see NFPA 13)				X		
2. Rack storage of materials (see NFPA 13)				X		
3. Storage of rubber tires (see NFPA 13)				X		
4. Storage of rolled paper (see NFPA 13)				X		
5. Archives and record center storage (see NFPA 232AM)				X		
6. Rack container storage of liquids (see NFPA 30)						X
Marine applications						
1. Machinery spaces		X			X	
2. Deck systems for petroleum and chemical tankers	X					
Special problems						
1. Production, storage, and handling of liquefied natural gas (LNG) (see NFPA 59A)		X		X	X	
2. Fire and dust explosions in chemical, dye, pharmaceutical, and plastics industry (see NFPA 654)		X		X	X	
3. Fires and explosions in wood processing and wood working facilities (see NFPA 664)		X		X		
4. Ovens and furnaces: design, location, and equipment (see NFPA 86)		X				
5. Mobile surface mining equipment (see NFPA 121)		X		X		
6. Tank vehicle and tank car loading and unloading (see NFPA 30)	X	X	X		X	X
7. Automotive service station filling areas (see NFPA 30A)		X				
8. Dipping and coating processes using flammable or combustible liquids (see NFPA 34)		X				
9. Manufacturer of organic coatings (protection of equipment mixers, solvent tanks, and open containers— see NFPA 35)		X		X[a]		
10. Laboratories using chemicals (see NFPA 45)		X			X	X
11. Storage and handling of liquefied petroleum gases at utility gas plants (see NFPA 59)		X		X	X	
Special problems identified in manufacturers' literature and/or identified foam standards and recommended practices						
1. Process structures and equipment		X				
2. Horizontal atmospheric tanks		X				
3. Pump rooms		X				
4. Dip tanks		X				
5. Engine test cells		X				
6. Transformer rooms				X		
7. Dike areas	X		X			

[a]Consider in conjunction with automatic sprinklers

one of the most successful uses of foam agents; in fact, foam agent fire protection is the primary means for the proper protection of atmospheric storage tanks. Foam agents have been successfully used to extinguish flammable and combustible liquid fires in atmospheric storage tanks with diameters up to 200 ft (61 m).

Objective 4: Extinguish fires in outdoor and indoor processing areas.

A large variety of industrial processes utilize flammable and combustible liquids. In most processing plants, these liquids pass through pipelines and are captured in holding tanks. Foam agents, properly selected for the specific hazard, are suitable for controlling and extinguishing fires in process equipment. However, foam agents are not suitable for coping with vertical running fires or fires where the flammable material is flowing from an orifice under pressure.

Objective 5: Protect, prevent, control, and extinguish fire problems in selected special hazards.

In addition to the other specified objectives, foam fire extinguishing agents provide appropriate fire protection for numerous special hazard problems. Some important special hazard conditions that are suitable for foam fire protection are included in the following list: (See also Table 4-5.1.)

Dike areas
Engine test cells
Transformers
Engine rooms
Laboratories using chemicals
Aircraft hangars
Nuclear research reactors
High density storage of combustibles
Rubber tires
Rack container storage of aerosols
Loading racks
Automotive service station filling areas
Ovens and furnaces

Basic Types of Foam System Protection

Foam fire protection systems are divided into four basic classifications by the National Fire Protection Association. Each of these classifications is briefly identified below. Conditions exist where it may be proper to use more than one classification of protection on a given fire problem. Examples of fixed foam systems are covered under supplemental topics later in this chapter on the hydraulic design of low expansion and high expansion foam systems.

Fixed Foam Systems

These systems are complete installations piped from a central foam station, discharging through fixed delivery outlets to the hazard to be protected. Any required pumping equipment is permanently installed. For example, a fixed system for a vertical atmospheric cone roof storage tank would include the following permanently installed equipment: water supply lines, foam proportioning equipment, a foam liquid storage tank, foam solution lines to the storage tank, all necessary control valves, a tank solution riser pipe, and one or more topside foam chambers. Other equipment may be added based on the complexity of the problem and associated hydraulic conditions.

Semifixed Foam Systems

Two separate classifications of semifixed foam systems are identified below. The first classification is more predominantly used in the United States, although one major oil company does use applications of the second classification. Common to both classifications is the concept that part of the total system is permanently installed and part of the system is provided by portable elements.

The first classification of semifixed systems indicates a type in which the fire hazard is equipped with fixed discharge outlets connected to piping that terminates at a safe distance. The fixed piping installation may or may not include a foam maker. Necessary foam producing materials are transported to the scene after the fire starts and are connected to the piping.

The second classification of semifixed systems indicates a type in which foam solutions are piped through the area from a central foam station, the solution being delivered through hose lines to portable foam makers such as monitors, foam towers, hose lines, and so forth.

Mobile Systems

Mobile systems basically consist of a unit on wheels that transports all of the required equipment and foam liquid necessary for making finished foam. This concept includes any foam producing unit which is mounted on wheels, and which may be self-propelled or towed by a vehicle. These units may be connected to an available water supply or may use a premixed foam solution. The original concept of a mobile foam system was called a "foam house on wheels," a mobile piece of fire apparatus with a UL-rated fire pump, an integral part of the pumping network, a foam liquid tank, and fire hose. Essentially this unit can double as a structural fire suppression unit. NFPA 11C, *Standard for Mobile Foam Apparatus,* covers the specifications and performance criteria for mobile systems.[1]

Portable Systems

Portable systems represent a rather economical approach to providing basic foam fire protection for small hazards. This classification considers that the foam producing equipment and materials, including the foam liquid, the proportion device(s), the discharge nozzle, the hose, and other required appliances, are transported by hand from a storage location to the incident scene. While portable systems are simple to operate, they are limited by their foam discharge rate capability; they may also be labor intensive to maintain a continuous foam supply over the required duration of discharge. Foam equipment manufacturers can provide technical information on a range of portable equipment.

Protection of Incipient Spills and Related Hazards

Portable fire extinguishers provide one method of protection for small flammable liquid storage hazards, fuel transfer hazards, and incipient spill fires.

Underwriters Laboratories (UL) has classified and listed chemical foam extinguishers. These extinguishers are now generally considered obsolete since their manufacture in the United States was discontinued in 1969. The National Fire Protection Association recommends that these units be replaced with currently available models.

Aqueous film forming foam agent portable fire extinguishers are used to replace the chemical-type foam extinguisher and provide protection for hazard conditions where this type of extinguishing agent is recommended. Extinguishers of this type are usually available in hand portable models of 2½-gal (9 l) capacity and in wheeled models having a liquid capacity of 33 gal (125 l). These extinguishers have ratings of 3A:20B and 20A:160B, respectively. The AFFF portable model closely resembles the stored pressure water extinguisher except for the special type of nozzle. NFPA 10, *Standard for Portable Fire Extinguishers,* should be consulted concerning the selection and placement of portable extinguishers.[1]

Protection for Fixed Roof Atmospheric Storage Tanks

Fixed or cone roof atmospheric storage tanks for the storage of flammable liquids can be protected by fire fighting foam. Several techniques are available for correctly applying foam to a cone roof tank fire. Each technique should be carefully considered with reference to the size of the storage tank, the flammable or combustible liquid being stored in a given tank, and the foam agent classification that is suitable for the hazard. Some fundamental concepts associated with the proper protection for fixed roof atmospheric storage tanks are discussed below. Each individual topic is further developed through design problems on cone roof atmospheric storage tanks.

Foam Monitors

One or more foam monitors may be positioned around the periphery of a cone roof tank to project foam over the tank shell and onto the surface of a burning liquid. This technique has been successfully used on numerous fires. However, NFPA 11, *Standard for Low-Expansion Foam,* clearly indicates that foam monitors may be considered the primary means of protection for fixed roof tanks when the tank is less than 60 feet in diameter. This indication represents a severe limitation on the recommended use of foam monitors for the protection of cone roof tanks.

Foam Handlines

Similar to the concept of providing foam protection with foam monitors, foam handlines may be positioned around the periphery of a cone roof tank to project foam over the tank shell and onto the surface of a burning liquid. Foam handlines have a flow range from 50 gpm (190 lpm) to less than 300 gpm (1136 lpm) and are only suitable for possible protection of fixed roof tanks with a diameter of less than 30 ft (9 m) and a height not greater than 20 ft (6 m). The selection of foam handline nozzles must be carefully considered to provide the correct total discharge for the flammable liquid problem to be protected.

Foam handlines are very important for supplemental fire protection requirements. Handlines delivering a minimum of 50 gpm (190 lpm) are very useful for extinguishing small spill fires and dike fires in the vicinity of a storage tank. The number of such supplemental foam hose streams is dependent on the diameter of the largest storage tank in the compound to be protected. (NFPA 11 should be consulted.)

Surface Application of Foam

One common and acceptable method of applying foam to the flammable liquid surface of a single roof storage tank is through fixed discharge outlets installed on the tank shell. Two distinct types of foam discharge outlets are available based on the hazard problem and the foam agent. Each type of device may be distinguished as follows:

Type I outlets: These approved discharge outlets will conduct and deliver foam gently onto the liquid surface without submergence of the foam below the flammable liquid surface and agitation of the surface. This type of device was originally intended to apply special alcohol resistant foams to polar solvent fuels. Today, Type I discharge outlets may be used with hydrocarbon fuels. (NFPA 11 should be consulted.)

Two classifications of Type I outlets are commercially available where this device is suitable. A porous tube is a Type I foam discharge outlet. The tube is coarsely woven and rolled up into a foam chamber so that there is an attached end at the foam maker and a free end. When foam is admitted to the tube at the foam chamber, the tube unrolls, dropping into the tank. The buoyancy of the foam causes the tube to rise to the surface, and foam flows out through the pores of the fabric directly onto the liquid surface.

A foam trough represents a second variety of a Type I discharge outlet. The trough consists of sections of steel sheet formed into a chute which is securely attached to the inside of the tank wall so that it forms a descending spiral from the top of the tank to within 4 ft (2 m) of the bottom.

Based upon advances in foam fire protection, porous tubes and foam chutes are rarely installed on new installations for the proper protection of cone roof atmospheric storage tanks.

Type II outlets: These approved discharge outlets do not deliver foam gently onto the liquid surface without submergence of the foam or agitation of the surface. An air foam chamber with a Type II outlet may be attached to the tank shell at the weak seam line. The Type II discharge outlet is positioned on the inside of the tank to permit discharge of the foam down the inside of the tank wall surface onto the flammable liquid surface. The number and discharge capacity of Type II foam chambers for a given

size (diameter) cone roof storage tank are presented in NFPA 11.

Portable foam towers: These devices represent specialized portable equipment that may be fitted with either a Type I or a Type II foam discharge outlet. A tower is a device that is brought to the scene of the fire, erected, and placed in operation for delivering foam to the burning surface of a tank after the fire starts. The Type II discharge outlets are shaped to apply foam inward toward the tank shell. The erection of foam towers adjacent to a burning tank and the operation of the foam towers may present a safety hazard to the personnel working with this equipment. The number of persons required to place foam towers in service is also a problem associated with these devices.

Subsurface Application of Foam

An alternative method of applying foam to a cone roof atmospheric storage tank is through subsurface injection, usually near the base of the tank but above the water bottom in the tank. This application technique involves injecting expanded foam into the flammable liquid near the bottom of the liquid level under controlled velocity conditions. The buoyancy of the foam allows the foam to slowly rise to the flammable liquid surface and spread across the surface to effect fire control and then total extinguishment.

There are three important conditions to consider in subsurface application of foam in fixed and semifixed systems.

1. Subsurface foam application is not considered suitable for the protection of Class IA hydrocarbon liquids.
2. Subsurface foam application is not currently suitable for polar solvent.
3. Subsurface and semisubsurface injection systems are not recommended for *open top* or *covered floating* roof tanks.

Semisubsurface Injection Method

A modified form of subsurface foam injection for cone roof tanks is used in a number of European countries. The modified technique is designated the semisubsurface injection method, based on the equipment used to insert the expanded foam into the tank shell. The semisubsurface injection method has not found any particular application in the United States.

Protection of Floating Roof Storage Tanks

In contrast to single roof tanks, floating roof tanks have a cover or roof over the flammable liquid that floats on the surface of the liquid and moves vertically with the liquid level in the tank. The floating roof may be open to the atmosphere. This physical arrangement of the tank is classified as an "open top floating roof tank." A permanently installed cover may be placed over the entire tank; this second designation is classified as a "covered floating roof tank."

The floating roof has a perimeter seal between the roof cover perimeter and the tank shell. The seal is necessary to prevent flammable vapors from escaping into the atmosphere and collecting over the floating roof. Three types of seal devices may be found on floating roof-type storage tanks: (1) a mechanical shoe seal or a pantograph-type seal, (2) a metal weather shield, and (3) a metal secondary seal.

NFPA 11 should be consulted for a description of each seal device and the physical arrangement of these devices. Some devices also require the use of a foam dam when protected by fixed foam fire protection systems. The requirements for foam dams are also given in the referenced standard.

The fire experience with floating roof tanks appears to be very good. Consequently, fixed foam outlets are not generally required on either open top floating roof tanks or covered floating roof tanks. When an oil company elects to protect these types of tanks or the local fire protection authority requests protection for these types of tanks, three different application techniques may be used for proper protection of open top floating roof tanks. A brief description of each technique follows.

Portable Nozzle Method

The basic fire problem associated with floating roof tanks is a fire burning in the seal area between the cover and the tank shell. Typically, the surface area of this fire is quite small. One technique to extinguish this type of fire is to advance a portable hose line to the top of the tank, supply foam to this hose line, and manually apply foam to the seal area. Personnel operating this hose line should be highly trained in this type of operation and follow established safety practices.

Catenary System Method

The catenary system consists of a series of foam makers at evenly spaced points in the roof near the seal. These foam makers are connected to a common section of piping which in turn is attached to a flexible hose that rides up and down with the access stairway to the roof cover. The stairway is fixed to the top of the tank shell, and the bottom portion of the stairway rides on a set of tracks attached to the floating cover. This arrangement allows the stairway to move both horizontally and vertically as the cover moves with the flammable liquid level.

At the time of a fire, foam solution is pumped under pressure through a vertical pipe and flexible hose to the foam makers. This system can be designed to discharge foam under the seal directly onto the flammable liquid, or foam can be discharged above the seal. Foam equipment manufacturers producing this type of equipment should be consulted for engineering data on design requirements, installation techniques, and hydraulic calculations.

Fixed Foam Maker Method

The fixed foam maker method consists of installing piping around the outside wall of the tank and connecting to it a series of foam makers installed on special mounting shields above the storage tank rim. The circumference of

the tank will determine the number of points needed for foam application. This method requires a foam dam to retain the foam over the seal or weather shield. This dam is normally 12 to 24 in. (305 to 610 mm) in height. Complete construction details of the foam dam may be found in the appendix of NFPA 11.

Covered floating roof tanks generally do not require fixed foam fire protection systems. There may be some cases of substandard installations or locations where local codes require proper protection for this classification of storage tank. The standards for fixed roof tanks should apply where it is required to protect covered floating roof-type tanks.

Protection of Storage or High-Volume Hazards with High-Expansion Foam

High-expansion foam is an agent for the control and extinguishment of both Class A and Class B fires. The classification of foam makes it particularly suitable as a flooding agent for use in confined spaces.

The development and application of high expansion foams for fire fighting purposes started with the work of the Safety in Mines Research Establishment in England concerning the difficult problem of fires in coal mines. It was found that by expanding an aqueous surface active agent solution to a semistable foam of about 1000 times the volume of the original solution, it was possible to force the foam down relatively long corridors, thus providing a means for transporting water to a fire inaccessible to ordinary hose streams. This work was expanded upon by the United States Bureau of Mines immediately after World War II.

Developmental work in the United States on high expansion foam has led to the refinement of specialized high expansion foam generating equipment for fighting fire in confined spaces, for specific applications to fire control problems in both municipal and industrial fire fighting, and for the protection of special hazard occupancies. Medium-expansion foam was developed to cover the need for a more wind-resistant foam than high-expansion foam for outdoor applications.

Concepts and Suitability for Medium- and High-Expansion Foams

Medium- and high-expansion foams are aggregations of bubbles that are mechanically generated by the passage of air or other bases through a net, screen, or other porous medium which is wetted by an aqueous solution of surface active foaming agents. Under proper conditions, fire fighting foams of expansions from 20:1 to 1000:1 can be generated. Such foams provide a unique agent for transporting water to inaccessible places, for total flooding of confined spaces such as basements, and for volumetric displacement of vapor, heat, and smoke. Extensive tests have demonstrated that under certain circumstances high expansion foam, when used in conjunction with water sprinklers, will produce more positive fire control and extinguishment than either extinguishment system by itself; this appears to be especially true with high rack storage of mixed commodities (e.g., high piled storage of paper stock and mixed storage of Class A and Class B materials). Optimum efficiency of high-expansion foam in any one type of hazard is dependent to some extent on the rate of application and also the foam expansion and stability.

Personal Safety

Persons should not enter a space filled with high-expansion foam without wearing full protective gear, self-contained breathing apparatus, an attached lifeline, and operating in a "buddy" system. A person who is immersed in high-expansion foam can experience disorientation and other psychological and personal discomforts. Foam entering any of the body cavities may cause severe irritation and membrane swelling.

Special Considerations

The proper design and application of high-expansion foam systems are directly related to a number of special system considerations. Special design factors include maximum submergence time and location of foam generating equipment.

A maximum time needs to be specified for filling the enclosed space to the proper depth with expanded foam. The time, expressed in minutes, is a function of the type of combustible material and the arrangement of the combustible material. An important consideration in maximum submergence time is whether stock material should be considered at a constant storage level in the space to be protected. Also of importance is whether the stock is protected by automatic sprinklers in addition to the high expansion foam. The basic objective is to control a developing fire before the fire has an opportunity to spread vertically over the face of a storage pile.

Fixed installations using high-expansion foam fire protection will probably involve the use of customized foam generating equipment to produce the cubic feet per minute requirement of foam discharge. The following points should be observed in the selection and placement of high-expansion foam generating equipment:

1. Two generators positioned remotely from each other are more effective and efficient than a single generator.
2. Generating equipment should be top mounted to avoid back pressures on the foam making equipment. Generators are normally mounted on external towers or special roof supports.
3. Generating equipment should be so positioned as to avoid product-of-combustion air intake. Induced smoke into the generating equipment can significantly reduce the quality and quantity of the foam produced.
4. To effectively dampen convection currents from a developing fire in an area to be protected, the capacity of each required foam generator should be the same.

All of the above information on types and classifications of foam systems serves as the background for actually designing a specific foam fire protection system. Some important limitations concerning both low- and high-expansion foam systems are presented in the following section before some problem examples.

Limitations of Foam Fire Protection Systems

This section discusses both low- and high-expansion foam systems. The limitations of foam fire protection must be addressed relative to each of these two system classifications. The following points should be reviewed during the proper selection and design of foam-type fire protection.

Limiting Factors for Low-Expansion Foam Systems

1. Low-expansion foam application is limited to the extinguishment of horizontal or two-dimensional fire problems. This type of foam application is not suitable for three-dimensional fires.
2. Low-expansion foam systems are limited by foam agent suitability for the defined flammable or combustible liquid. Basically, foam agents are suitable for either hydrocarbon fuels or polar solvents. Alcohol resistant-type foams may be approved for both hydrocarbons and polar solvents.
3. Different types and brands of foam concentrates may be incompatible and should not be mixed in storage.
4. Foam solution consists of 90 percent or more water. Foam system limitations should be evaluated with respect to the proper use of aqueous based agents on flammable materials and the electrical conductivity of the application method.
5. Foam systems are limited by the equipment appliances and devices used to proportion the foam and to deliver the finished foam onto a given hazard or fire problem. Equipment limitations pertaining to flow rate, operating pressure ranges, and proportioning ranges should be carefully considered in the selection and application of foam systems.

Limiting Factors for High-Expansion Foam Systems

1. Medium- and high-expansion foams are finding applications for a broad range of fire protection problems. However, unlike low-expansion foam systems, medium- and high-expansion foam fire protection systems should be specifically evaluated for each type of hazard condition. The fact that each system requires a feasibility study and individual design may be considered a form of limitation when contrasted to the design concepts for low-expansion foam systems.
2. NFPA 11A, *Standard for Medium- and High-Expansion Foam Systems*,[1] states that "under certain circumstances it may be possible to utilize medium and high expansion foam systems for control of fires involving flammable liquids or gases under pressure, but no general recommendations can be made in this standard due to the infinite variety of particular situations which can be encountered in actual practice." This statement is considered to be a design limitation.
3. Medium- and high-expansion foam systems should not be used on fires in the following hazards unless competent evaluation, including tests, indicates acceptability:
   (a) Chemicals, such as cellulose nitrate, which release sufficient oxygen or other oxidizing agents to sustain combustion
   (b) Energized unenclosed electrical equipment
   (c) Water reactive metals, such as sodium and potassium (Na, K)
   (d) Hazardous water reactive materials, such as triethylaluminum and phosphorous pentoxide
   (e) Liquefied flammable gas

Hydraulic Calculation for Atmospheric Storage Tanks Protected by Low-Expansion Foam Systems

This section of the chapter is concerned with the proper design and associated hydraulic calculations for foam fire protection systems protecting atmospheric storage tanks with low-expansion foam systems. The material presented is limited to fixed protection systems using either top mounted foam chambers or subsurface injection, as discussed in the first section of this chapter. A single flammable liquid storage tank problem is presented for developing the appropriate methods and techniques for computing the foam agent requirements, system hardware requirements, and the necessary hydraulic calculations to properly deliver the required rate of foam to the subject hazard. The single example will be calculated using topside application of foam and subsurface injection of foam. This approach permits comparison and contrast of the system design and hydraulic requirements between the two foam application methods.

EXAMPLE 1:

Problem statement. The single outside storage tank depicted in Figure 4-5.1 is to be protected by a completely fixed foam system. The topside foam chamber arrangement is used in this problem. Note that the foam system is connected to a domestic water supply. The water supply curve is illustrated in Figure 4-5.2. For this problem, consider that the water available for the foam system is limited to the street main flow characteristics. A foam system job work sheet and a complete set of hydraulic calculations are to be prepared for this problem.

SOLUTION:

Procedure statements. A systematic outline follows for the proper design and hydraulic assessment associated with the stated problem; reference is made to criteria established in NFPA 11. This standard should serve as a companion guide to the systematic evaluation of each problem scenario. Individual item information is transferred to the referenced problem job sheet (Figure 4-5.3) and the associated hydraulic calculation sheet (Figure 4-5.4).

Problem assessment. In addition to the physical layout of the design problem, information is required on the hazard to be protected. The nature of the hazard drives the problem design. The following steps identify the hazard and standard requirements associated with the hazard:

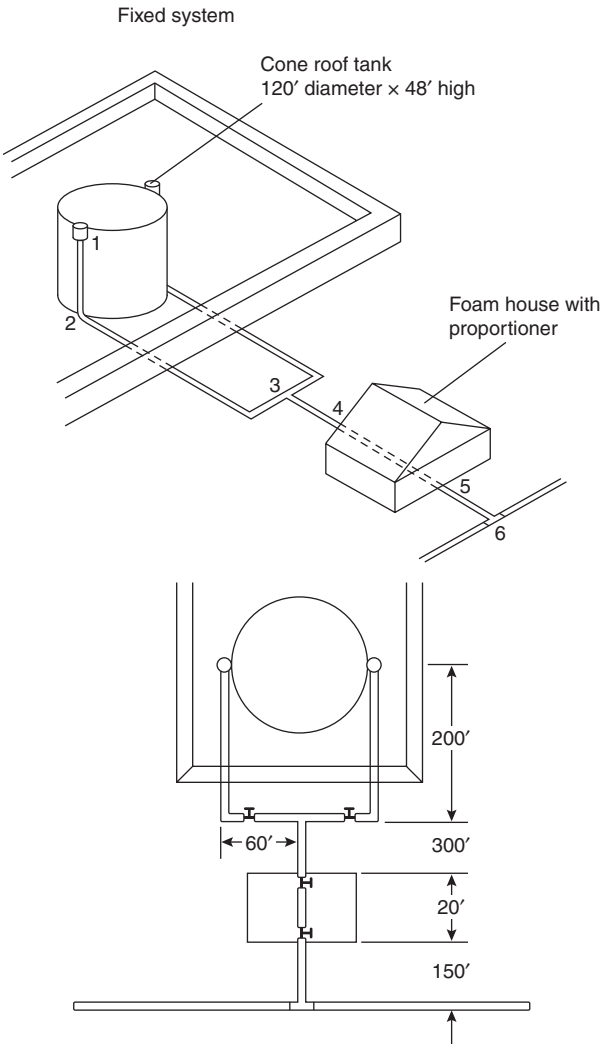

Figure 4-5.1. ***Single storage tank with fixed foam system protection. The numbers 1 through 6 in the top portion of the drawing represent the reference points for hydraulic calculations for Example 1.***

Step 1: Installation identification.

Refer to Figure 4-5.1. One vertical atmospheric storage tank is positioned in a dike area. The tank is protected by a fixed foam fire protection system and connected to the domestic water supply.

Step 2: Hazard classification.

Flammable liquid atmospheric storage tank

Step 3: Type of protection.

Fixed protection systems

Step 4: Hazard description.

120-ft diameter outdoor cone roof flammable liquid storage tank

Step 5: Flammable or combustible liquid area to be protected.

Calculate the flammable liquid surface area: Area $= 0.7854d^2$:

$$A = 0.7854(120)^2 = 11{,}310 \text{ ft}^2$$

Step 6: Flammable liquid or combustible liquid identification.

Gasoline—Sg. 0.72

Step 7: Foam application method.

Top mounted fixed foam chambers—Type II

Step 8: Description, number, and placement of foam application devices.

Several factors need to be simultaneously considered in responding to this step. The description should reference a given manufacturer's foam chamber because the flow and pressure characteristics of the foam chamber *may be* a factor or present options for the system design. Manufacturer's literature and the UL listing of foam equipment should be consulted on this matter.

For proprietary reasons, the selected foam chamber for this problem will be identified as an FMA chamber with an operating pressure range of 40 to 80 psi and a flow range from 300 to 700 gpm of foam solution.

The foam standard (NFPA 11) requires a minimum of two foam chambers for a 120-ft diameter tank. More foam makers may be used based on hydraulic considerations, or economies of scale based on equipment costs. Individual manufacturers of foam equipment must be consulted on these options.

Placement of foam makers should consider equal spacing around the upper tank perimeter and placement of the foam solution feed lines. If possible, maintain constant flow and pressure requirements of each device.

Step 9: Foam agent selected.

A 3 percent fluoroprotein foam is selected for the defined hazard. Note that the type of foam agent selected for a particular design problem may affect other variables or consideration in the foam system design. This caution is reflected in Step 10.

Step 10: Foam solution application rate.

Foam solution application rates for storage tanks containing liquid hydrocarbons should be at least 0.1 gpm/ft^2 of liquid surface area of the tank to be protected. It should be noted that other types of foam protection (e.g., portable nozzles) may require different application rates. Also, flammable and combustible liquids not classified as hydrocarbons may require different foam solution application rates. Reference should be made to NFPA 11 concerning design application rates.

The foam solution application rate for the stated problem is calculated as follows:

$$\text{rate (gpm)} = 0.1 \text{ gpm/ft}^2 \times 11{,}310 \text{ ft}^2 = 1131 \text{ gpm}$$

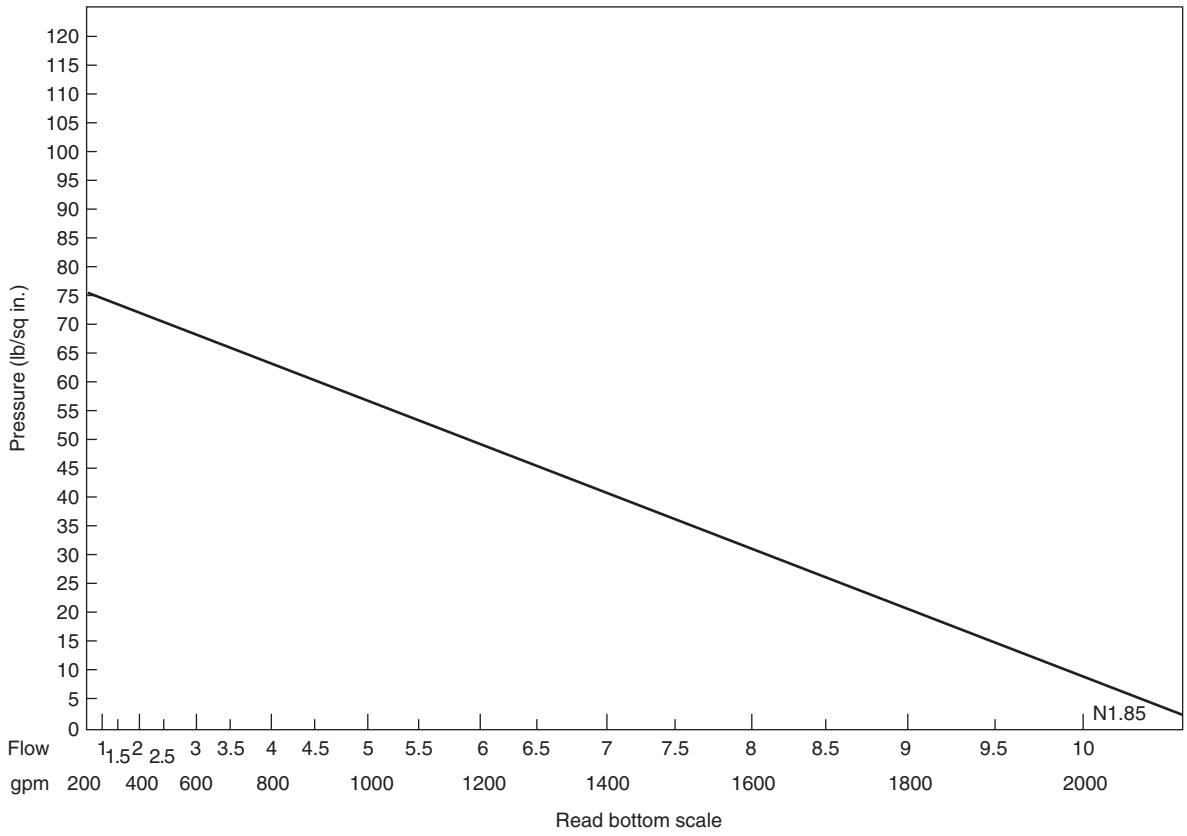

Figure 4-5.2. ***Water supply curve for fixed foam system for Examples 1 and 2.***

However, the total rate is divided equally between two foam makers so it is appropriate to specify a rate of 1132 gpm, or 566 gpm per foam maker.

Step 11: Foam concentrate rate.

The foam concentrate rate is based on the foam agent proportioning rate. A 3 percent fluoroprotein foam is selected for this problem (see Step 9). In other words, 3 percent of the calculated solution rate is the foam concentrate rate. This rate may be determined as follows:

$$\text{foam concentrate rate} = 0.03(\%) \times 1132 \text{ gpm}$$
$$= 34 \text{ gpm}$$

Note that a continuous supply of foam agent (concentrate) must be available at a rate of 34 gpm for the required duration of discharge (see Step 13).

Step 12: Water application rate.

Quite simply, the water application rate is the foam solution rate minus the foam concentrate rate. The water application rate proceeds as follows:

$$\text{water application rate} = 1132 \text{ gpm} - 34 \text{ gpm}$$
$$= 1098 \text{ gpm}$$

The water application rate can also be determined as 97 percent of the "solution" rate when using a 3 percent foam concentrate.

Step 13: Duration of discharge.

A minimum foam solution discharge time is specified in NFPA 11 to control and extinguish a fire in a cone roof atmospheric storage tank. Duration of discharge is dependent on the classification of flammable or combustible liquid and the *type* of discharge outlet. Information for the given problem is contained in NFPA 11. The requirement for protecting gasoline with Type II foam chambers is 55 min. of continuous foam solution discharge.

Step 14: Gallons of foam required.

The required foam supply for any given problem should properly consider a primary supply and a reserve supply. The primary supply is computed by multiplying the determined rate of foam agent required by the duration of discharge as follows:

$$\text{foam agent required} = 34 \text{ gpm} \times 55 \text{ min} = 1870 \text{ gal}$$

The authority having jurisdiction may require that equal quantity of foam be placed in reserve for a second fire.

FOAM SYSTEM JOB WORK SHEET

Sheet: 1 of: 1

Designer: Staff Date: 1986

Installation identification: Ourville Oil Company

Hazard classification: Flammable liquid atmospheric storage tank

Type of protection: Fixed protection system

Hazard description: 120 ft diameter outdoor cone roof flammable liquid storage tank

Flammable or combustible liquid area to be protected: 11,310 ft^2

Flammable or combustible liquid identification: Gasoline Sq. 0.72

Foam application method: Type II—fixed chambers

Description, number, and placement of foam application devices: 2—Chambers equally spaced

Foam agent selected: Fluoroprotein—3%

Foam solution application rate: 0.1 gpm per sq ft or 1131 gpm

Foam concentration rate: 34 gpm

Water application rate: 1098 gpm

Duration of discharge: 55 min

Gallons of foam required: 1870 gallons

Gallons of water required: 60,390 gallons

Water supply information: See Figure 4–5.2

Special foam design considerations:

Figure 4-5.3. ***Foam system job work sheet.***

Step 15: Gallons of water required.

The basic procedure follows the concept presented in Step 14. The water requirement is the product of the water rate times the time.

$$\text{water required} = 1098 \text{ gpm} \times 55 \text{ min} = 60{,}390 \text{ gal}$$

While the above calculation is straightforward, the answer may come as a surprise. Fixed foam protection systems for atmospheric storage tanks require a large quantity of water. The total quantity of water must be available at the site to assure foam delivery over the required time.

Step 16: Special foam system design considerations.

The first 15 steps in this problem analysis focus on fundamental considerations required to determine foam agent and water supply requirements. It is now appropriate to examine a series of special considerations that directly relate to the hydraulic design factors associated with this problem. Other design factors may be appropriate for different problems. However, the basic considerations outlined below should serve to guide similar calculations for other design problems.

1. Pipe size selection.
   Water supply pipe and foam solution pipe may be sized to minimize head loss between identified supply and demand points; pipe may also be designed on the basis of a mean velocity flow in a given section of pipe. A flow velocity of 10 ft per second may be used in the absence of other specific criteria for the determination of both water supply pipe and foam solution pipe. Pipe will be sized in this manner for the stated problem.
2. Valves in the pipe system.
   (a) The laterals of each foam chamber or fixed roof tank should be separately valved outside of the dike installation.

HYDRAULIC CALCULATIONS

Subject: Example problem 1 Job no.: _____

_____ Sheet no.: _____ Of: _____

_____ By: _____ Date: _____

_____ Chkd by: _____ Date: _____

Application rate: 0.1 gpm per sq ft Area: 11,130 sq ft

Minimum solution rate: 1131 gpm Actual solution rate: 1132 gpm

Foam maker pressure and rate: 50 psi–566 gpm Foam system: Chamber type 2

Water data: _____ Ref. drawing: Figure 4-5.1

Foam maker type and location	Added gpm	Total gpm	Pipe size (in.)*	Pipe & equivalent fitting lgth. (ft)**	Friction psi/ft C=100	Friction Total psi	Static psi	Proportioner psi	Req'd pres gpm
Starting point: 1	Elevation: 48 ft			Pressure at foam maker: 50 psi					
1	566	566							50
1–2		566	5.047	48'+(1E)8.6'=56.6'	0.0420	2.4	20.8		73.2
2–3		566	5.047	260'+(1GV)2'=(1T)25'					—
(2–3)				Σ = 287'	0.0420	12.1	—		85.3
3–4	566	1132	8.071	300'+(1GV)2'=302'	0.154	4.7	—		90.0
4–5		1132	8.071	18'+(1GV)2'=20'	0.154	0.3		4.0	94.3
5–6		#1098	8.071	150'=(1T)35'=185'	0.145	2.7			97.0
Σ at 6		1098							97.0

\# Water only

* "X" indicates extra hvy.—std. wt. otherwise

** See sheet for tabulation of pipe and fittings

Figure 4-5.4. ***Hydraulic calculation work sheet.***

(b) The water line to each proportioner inlet should be separately valved.
Note: Valves are properly shown in Figure 4-5.1.

3. Foam proportioner selection.
Several different foam proportioners are available from equipment manufacturers. It is very important to select foam proportioning equipment that meets the following requirements:
(a) Proper proportioning over the range of desired flows.
(b) Minimum or acceptable head loss across the proportioning device.
(c) Suitability for the foam agent selected.
(d) Capability of overcoming any back pressure limitations.

4. Water pumps.
The water supply in a given case may require a pressure boost to meet the foam chamber discharge requirements. Where a water pump is required, consideration must be given to the pump capacity, the

pressure profile, the pump horsepower requirement, and the pump intake-discharge positions with respect to the total installation of pipe.

Hydraulic analysis for Example 1: The supporting documentation above provides a foundation for conducting a hydraulic design for the problem depicted in Figure 4-5.1. The design parameters and associated calculations are presented in sequential steps below. All reference points conform to Figure 4-5.1. Computations are also charted on a hydraulic calculation sheet as shown in Figure 4-5.4.

Step 1: Starting point.

The design objective is to provide each of the two foam chambers with the required pressure to discharge the calculated quantity of foam solution. The stated problem requires a foam maker discharge of 566 gpm at 50 psi. An orifice plate is supplied by the foam equipment manufacturer to provide the correct discharge at the design pressure (50 psi). The design pressure is a function of the range of pressures that can be used with a specific manufacturer's foam chamber.

Step 2: Design tank riser.

The vertical pipe supplying the foam chamber (reference points 1–2) is sized on the basis of a maximum flow velocity of 10 feet per second. The pipe size is determined as follows:

Formula:

$$\text{Velocity} = \frac{0.40852 \times \text{gpm}}{d^2}$$

a. Solve for d
b. $10 \text{ fps} = \dfrac{0.4085 \times 566 \text{ gpm}}{d^2}$
c. $d^2 = 23.12$ in.
d. $d = 4.8$ in.
e. 5-in. pipe is selected. (Note: The authority having jurisdiction may require a 6-in. pipe.)

Step 3: Enter hydraulic calculation from reference points 1-2.

1. Friction loss, FL, is determined by the Hazen-Williams formula

$$\text{FL} = \frac{4.52 \times Q^{1.85}}{C^{1.85} \times d^{4.87}}$$

where

$Q = 566$ gpm

$C = 100$

$d = 5.047$ (internal diameter of pipe)

FL = 0.0420 psi/ft

2. Note: All friction losses and head losses are summed in the required pressure column.
3. The head loss, H_L, for 48 ft of elevation difference between reference points is computed as follows:

$$H_L = 0.433 \text{ psi/ft} \times 48 \text{ ft} = 20.8 \text{ psi}$$

4. The pipe section includes one standard elbow at reference point 2. For hydraulic calculations, fittings are treated as equivalent feet of pipe in accordance with NFPA 13, *Standard for the Installation of Sprinkler Systems*.[1]

Step 4: Enter hydraulic calculations from reference point 2 (bottom of tank) to reference point 3.

1. The flow is constant (566 gpm) so the pipe size remains the same at 5 in.
2. Pipe fittings include a globe valve outside the dike area and a standard tee at reference point 3.

Step 5: Enter hydraulic calculations from reference point 3 to the foam house (reference point 4).

1. The total foam solution flow (1132 gpm) is supplied by line 2-3.
2. Determine the pipe size based on a maximum flow velocity of 10 ft/s.
3. $\text{velocity} = \dfrac{0.4085 \times \text{gpm}}{d^2}$

$$10 \text{ fps} = \frac{0.4085 \times 1132 \text{ gpm}}{d^2}$$

$$d = 6.8 \text{ in.}$$

4. An 8-in. pipe is recommended between the foam house and reference point 3.
5. The friction loss in the stated line includes the linear distance plus the gate valve.
6. It should be observed that the required pressure at the discharge side of the foam house is 90.0 psi.

Step 6: Enter the hydraulic calculations in the foam house.

1. To the left of the top view, bottom half, Figure 4-5.1, is an illustration of the foam proportioning ratio controller inserted into the water line. The proportioning device selected for this problem has a friction loss of 4 psi at a solution flow rate of 1132 gpm. Foam equipment manufacturers should be consulted on head loss characteristics for specific devices. The ratio controller takes up a lineal distance of 2 ft leaving 18 ft of straight run pipe in the foam house.
2. The calculations provided do not include provisions for a water pump.

Step 7: Enter the hydraulic calculations from the foam house to the street main.

1. The flow rate in line 5-6 is 1098 gpm. Note the change in friction loss.
2. An 8-in. main is used to connect the street main to the foam house.

Step 8: Summary.

1. The water demand requirement at reference point 6 is 1098 gpm at 97.0 psi.
2. The hydraulic demand has been calculated to provide a foam solution flow of 566 gpm at 50 psi for *each* designated foam chamber.
3. The water supply curve referenced as Figure 4-5.2 shows 1098 gpm available at 53 psi. Therefore, a water

pump is required in the pump house to boost the pressure from 50 psi (loss of pressure from reference points 6 to 5 is approximately 3 psi) to 97 psi or approximately 50 psi. A pump can be engineered for this specific application.

EXAMPLE 2:

Overview statement. The flammable liquid storage tank presented as Example 1 is also presented as Example 2; only the method of fire protection changes. Example 2 considers the depicted 120-ft diameter storage tank to be protected with subsurface application of foam to the described hazard. The subsurface application technique requires new design considerations with respect to foam equipment and hydraulic calculations. The following principles should be observed in the design of subsurface application foam systems:

1. Foam solution is expanded outside of the dike area by a "high back pressure" foam maker. A typical foam expansion of 4:1 is achieved at the foam maker.
2. The expanded foam flows through a carefully designed pipeline from the foam maker to an opening in the tank shell just above the water bottom in the tank. In accordance with NFPA 11, *Standard for Low-Expansion Foam,* the foam velocity at the point of discharge into the tank contents shall not exceed 10 ft/s for Class IB liquids and 20 ft/s for other type liquids. An excessive input velocity to the tank can cause the foam to be saturated with fuel pickup.
3. Foam entering the product rises to the fuel surface by natural buoyancy.

Problem statement. A single outside storage tank illustrated in Figure 4-5.5 is to be protected by a completely fixed foam system. The subsurface foam application method is used for this problem. The Figure 4-5.2 water supply curve is to be applied with this problem. Consider that the water available for the foam system is limited to the street main flow characteristics. A foam system job work sheet and a complete set of hydraulic calculations are to be prepared for this problem.

Procedure statements. A systematic outline follows for the proper design and assessment associated with Example 2. Reference is made to criteria established in NFPA 11 by paragraph reference. NFPA 11 should serve as a companion guide to the systematic evaluation of each problem scenario. Individual item information is transferred to the referenced problem sheet (Figure 4-5.6) and the associated hydraulic calculation sheet (Figure 4-5.7).

Problem assessment. In addition to the physical layout of the design problem, information is required on the hazard to be protected. The nature of the hazard is identical to Example 1; only the method of protection changes. Some of the following steps are repeated for maintaining a sequence to the problem solution. New material will be explained in detail. Calculations for similar material are referenced to Example 1.

Step 1: Installation identification.

Refer to Figure 4-5.5. One vertical atmospheric storage tank is positioned in the dike area. The tank is protected by a fixed subsurface injection foam fire protection system and connected to the domestic water supply.

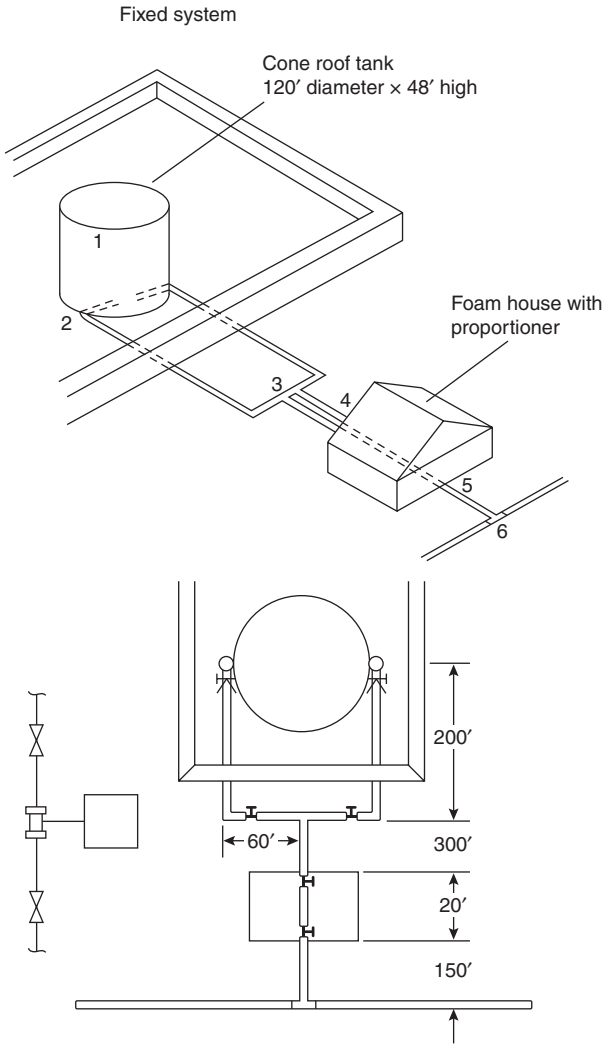

Figure 4-5.5. ***Subsurface application foam system with reference points used in Example 2.***

Step 2: Hazard classification.

Flammable liquid atmospheric storage tank

Step 3: Type of protection.

Subsurface application to fixed roof storage tanks (Re: NFPA 11, Section 3-2.4)

Step 4: Hazard description.

120-ft-diameter outdoor cone roof flammable liquid storage tank

Step 5: Flammable or combustible liquid area to the protected.

11,310 ft^2 (See Step 5—Example 1)

Step 6: Flammable liquid or combustible liquid identification.

Gasoline—Sq. 0.72

FOAM SYSTEM JOB WORK SHEET

Sheet: 1 of: 1

Designer: Staff Date: 1986

Installation identification: Ourville Oil Company

Hazard classification: Flammable liquid storage tank

Type of protection: Subsurface application to fixed roof storage tank

Hazard description: 120 ft diameter outdoor cone roof flammable liquid storage tank

Flammable or combustible liquid area to be protected: 11,310 ft^2

Flammable or combustible liquid identification: Gasoline — sq. 0.72 sq. 0.72

Foam application method: Subsurface application to a liquid hydrocarbon

Description, number, and placement of foam application devices: Two subsurface injection points positioned equal and opposite on the tank shell. A PHB foam maker is used.

Foam agent selected: 3%

Foam solution application rate: 1132 gpm

Foam concentration rate: 34 gpm

Water application rate: 1098 gpm

Duration of discharge: 55 min

Gallons of foam required: 1870

Gallons of water required: 60,390

Water supply information: See Figure 4-5.2

Special foam design considerations: Foam injection piping to be sized for a maximum fluid velocity of 10 fps

Figure 4-5.6. ***Foam system job work sheet.***

Step 7: Foam application method.

Subsurface application to a liquid hydrocarbon (Re: NFPA 11, Section 3-2.4)

Step 8: Description, number, and placement of foam application devices.

Several equipment design variables must be considered simultaneously in this step. Again, reference must be made to a specific foam manufacturer's equipment offerings or the conduct of a comparative analysis between two or more manufacturers of suitable equipment. The manufacturer's literature and the UL listing of foam equipment should be consulted on this matter.

The following substeps outline the key features of the design to be evaluated and computed at this overall step in the design development. Each substep may impact on other substeps and therefore all substeps must be evaluated before selecting a set of equipment and associated calculations.

Step 8(a): Velocity of approach into the storage tank.

Gasoline is a Class IB liquid, and therefore the injection velocity of the expanded foam into the product tank should not exceed 10 ft/s. This does not mean that the velocity of foam between the foam maker and the injection point has to be controlled to a maximum of 10 ft/s. Rather, the foam velocity at the physical point of entry to the product is the key consideration.

Remember that the foam is expanded at the entry point to the product. Special flow curves must be examined to determine velocity characteristics with expanded foam. These curves are not available in the current edition

HYDRAULIC CALCULATIONS

Subject: Example problem 2 Job no.: _____

Sheet no.: _____ Of: _____

By: _____ Date: _____

Chkd by: _____ Date: _____

Application rate: 0.1 gpm per sq ft Area: 11,130 sq ft

Minimum solution rate: 1132 gpm Actual solution rate: 1132

Foam maker pressure and rate: PHB–159 psi–566 gpm Foam system: Subsurface

Water data: Figure 4-5.2 Ref. drawing: _____

Foam maker type and location	Added gpm	Total gpm	Pipe size (in.)*	Pipe & equivalent fitting lgth. (ft)**	Friction psi/ft C=100	Friction Total psi	Static psi	Proportioner psi	Req'd pres psi
Starting point: 1		Elevation: 48 ft			Pressure at foam maker: 50 psi				
1		2264	10"				15		15
1–2		2264	10"	20	0.20	0.4			15
2–3				560+1CV(55)1GV(5)	0.40	24.8			40
				620					
∑3									40

Note: The demand pressure at 3 is less than the allowable pressure of 64.0 psi

* "X" indicates extra hvy.—std. wt. otherwise

** See sheet for tabulation of pipe and fittings

Figure 4-5.7. ***Hydraulic calculations.***

of NFPA 11; one must turn to manufacturer's literature on this topic.

A set of flow curves for expanded foam in various pipe diameters are included in the Appendix of the chapter with approval of National Foam System, Inc. Figure 4-5A.3 is consulted for this problem element.[2]

Table 3-2.4.2 of NFPA 11 indicates that two discharge outlets must be provided for a 120-ft-diameter tank. The foam solution rate for each outlet is given in Step 10 of this example and is equal to the calculations for Example 1: 566 gpm per outlet. However, the foam is expanded at the high back pressure foam maker using a ratio of 4:1. The expanded foam flow rate at each outlet is 2264 gpm. This is the value used when checking foam velocity.

A 10-in. pipe is required to maintain a foam velocity less than 10 ft/s when the rate of expanded foam is 2264 gpm (see Figure 4-5.A3). The pipe length upstream from the discharge point must be at least 20 times the

diameter of the pipe to establish uniform velocity. Therefore, a straight run of 10-in. pipe at least 17 ft in length is necessary.

The foam outlet is not required to be at the tank shell. Note that the 10-in. pipe is actually inserted into the tank. This design approach permits economizing the pipe sizes between the tank and the high back pressure foam maker. The high back pressure foam maker is to be positioned outside of the dike area. A gate valve and a check valve are installed adjacent to the tank shell.

Step 9: Foam agent selected.

A 3 percent fluoroprotein foam is selected for the defined hazard. The foams should be listed for subsurface injection.

Step 10: Foam solution application rate.

For tanks containing liquid hydrocarbons, the foam solution rate must be at least 0.10 gpm/sq ft of liquid surface area of the tank to be protected. The maximum rate must be 0.20 gpm/sq ft. (Re: NFPA 11, Table 3-2.4.3.)

The foam solution application rate for Example 2 is the same foam solution rate calculated for Example 1; the application rate is 1132 gpm.

Step 11: Foam concentrate rate.

The foam concentrate rate is determined in the same manner as set forth for Example 1. Using a 3 percent fluoroprotein foam, the requirement is 34 gpm for a total solution rate of 1132 gpm. This requirement impacts on Step 14 of this example.

Step 12: Water application rate.

The water application rate is also determined in the same manner as set forth in Example 1. The water application rate is the foam solution rate minus the foam concentrate rate: the water rate is 1098 gpm.

Step 13: Duration of discharge.

The minimum discharge time for subsurface application of foam is identical to the requirement for Type II application. (Re: NFPA 11, Section 3-2.4.3.) Gasoline product requires a total discharge time of 55 minutes.

Step 14: Gallons of foam required.

The gallons of foam required is computed in the same manner as set forth in Example 1. The primary foam supply is computed by multiplying the determined rate of foam agent by the duration of flow, which indicates a requirement of 1870 gal.

Step 15: Gallons of water required.

The water requirement is the product of the water rate times the discharge time, or 60,390 gal.

Step 16: Special foam system design considerations

One special design consideration is presented in Step 8(a) and involves the pipe requirements for injecting foam into the base of a storage tank under controlled velocity conditions. Other special conditions that apply specifically to subsurface injection of foam to storage tanks are given below.

1. *High-back-pressure foam maker.* A high-back-pressure foam maker is designed for capability to make foam and discharge the foam against considerable back pressure. The high-back-pressure foam maker selected for the example problem is designed to operate satisfactorily at inlet pressures of 100 to 300 psi and produce foam of 2:4 expansion against back pressures not exceeding 40 percent of the inlet pressure. With an inlet pressure of 150 psi, for example, 60 psi is available at the discharge for forcing the foam through a hose and/or piping into the storage tank and to overcome the fuel head in the tank. Manufacturers of high-back-pressure foam equipment should be consulted for obtaining flow and pressure characteristics and back pressure limitations. Two high-back-pressure foam makers are used with Example 2. The two foam makers are located in the foam house and are arranged for parallel operations. (See Figure 4-5.5.)
2. *Pipe size selection.* Expanded foam flowing in conduit (pipe) does not follow the head loss characteristics expressed in the Hazen-Williams formula. A set of flow curves have been developed for determining friction loss for expanded foam discharge by a high-back-pressure foam maker.[2] A set of these curves is provided in the Appendix to this chapter with the permission of National Foam System, Inc. (See Figures 4-5A.1 and 4-5A.2.)

   A flow velocity of 10 ft/s is used for the determination of pipe sizes flowing foam solution and water. If necessary, water supply pipe and foam solution pipe may be sized to minimize head loss between identified supply and demand points.
3. *Valves in the pipe system.* (Re: NFPA 11, Section 3-2.6.3.) For subsurface application, each foam delivery line must be provided with a valve and check valve, unless the latter is an integral part of the high-back-pressure foam maker or pressure generator to be connected at the time of use. When product lines are used for foam, product valving must be arranged to ensure foam enters only the tank to be protected.
4. *Foam proportioner selections.* The practices and procedures outlined in Example 1 apply to Example 2. However, to accommodate the pressure requirements associated with a high-back-pressure foam maker, a balanced proportioner would appear to provide the best level of constant proportioning over designated pressures.
5. *Water pumps.* The required pressure at the intake to the high-back-pressure device is approximately 150 psi. The static pressure on the water system is only 75 psi. Therefore, a water pump is required to boost the water-solution pressure in the foam hose. The most efficient approach to designing a required water pump installation is to select or design a pump-driver combination that will boost the available residual pressure to the required residual pressure at the demand flow. In

other words, with the right capacity pump, the driver horsepower is calculated to raise the pressure over the differential range. Other criteria must be used if a standard fire pump is required by the authority having jurisdiction.

Hydraulic analysis for Example 2: The information above provides a foundation for conducting a hydraulic design for the problem depicted in Figure 4-5.5. The design parameters and associated calculations are presented in sequential steps below. All reference points conform to Figure 4-5.2. Computations are also charted on a hydraulic calculation sheet, designated as Figure 4-5.7.

Step 1: Precalculation for high-back-pressure foam maker.

The hydraulic characteristics of the high-back-pressure foam maker must be considered before the computations start. A high-back-pressure foam maker delivering 550 gpm at 150 psi is selected for each finished foam line to the tank.

a. Determine a K value for the specified unit:

$$Q = K\sqrt{150}$$
$$K = 44.9$$

b. Required discharge per foam maker is 566 gpm.

c. Determine the required input pressure for a flow of 566 gpm:

$$566 \text{ gpm} = 44.9\sqrt{P}$$
$$P = 159 \text{ psi}$$

d. The available back pressure becomes 40 percent of 159, or 64.0 psi.

Remember: Head loss converted to psi between the foam maker discharge and the foam discharge outlet to the tank, plus the product head, must not exceed 64 psi.

Step 2: Size foam injection pipe to tank.

Step 8(a) under problem assessment for Example 2 establishes that a 10-in. pipe is required to maintain a flow velocity under 10 ft/s.

Step 3: Determine head loss from production storage.

Finished foam rising through the product must overcome the product head. Gasoline is the product for this series of problems with a Sq. = 0.72.

$$\text{psi loss} = 48 \text{ ft} \times 0.433 \text{ psi/ft} \times 0.72 \text{ Sq.}$$
$$\text{psi loss} = 15$$

Step 4: Size the foam supply line from the tank shell to the foam house.

The stated pipe is selected on the basis of the allowable friction loss of 64 psi minus the product head loss which equals 15 psi. Therefore, 49 psi (64 psi − 15 psi) can be dissipated from the tank to the foam maker through 500 ft of pipe and be used as an initial estimator; the flow rate is 2264 gpm. Figure 4-5.8 indicates a 6-in. pipe is required. A 6-in. check valve and a 6-in. gate valve will be installed on the foam supply line adjacent to the tank in

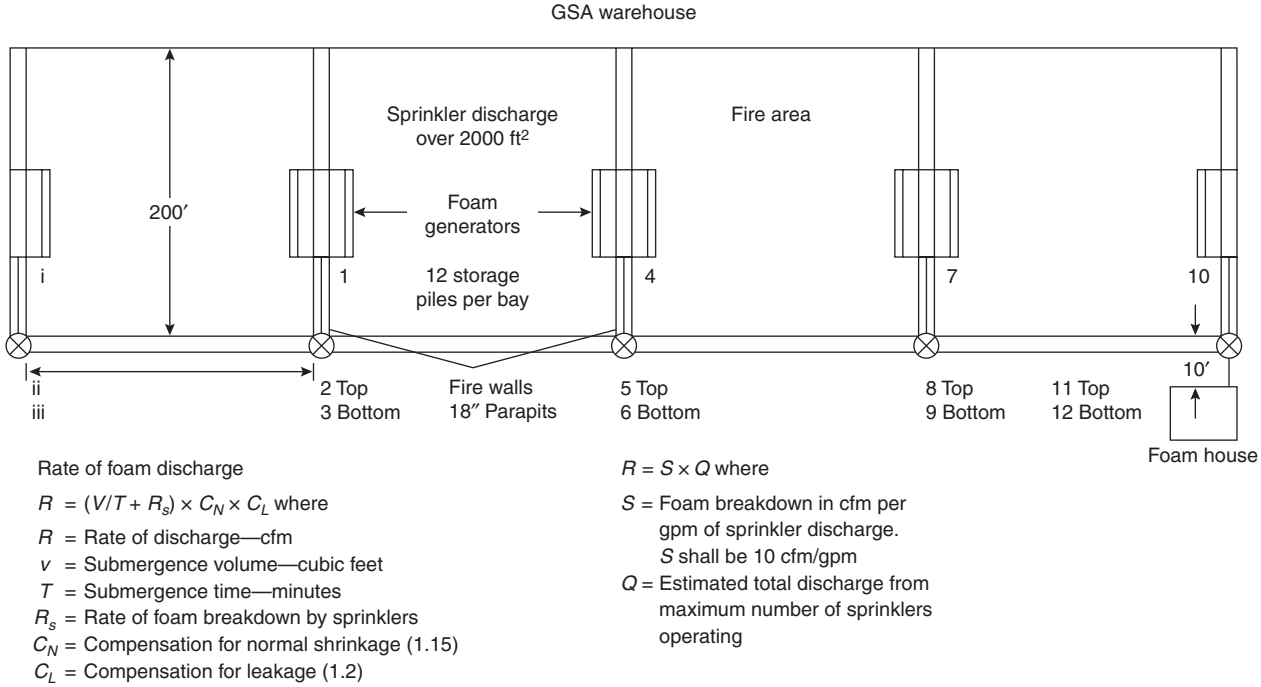

Figure 4-5.8. ***Typical four-bay warehouse complex.***

the dike area. The required friction loss calculations are presented in Figure 4-5.7.

Calculation note: Subsurface foam system hydraulics actually divide into two separate calculation sets, as follows: (1) the hydraulics between the high-back-pressure foam maker and the storage tank and (2) the hydraulics between the street main supply and the high-back-pressure foam maker.

Step 5: Street main to fire pump calculation.

The lateral supply line will be designated at a velocity of 10 ft/s. Recall that only water is moving through this line.

$$\text{Velocity} = \frac{0.4085 \times \text{gpm}}{d^2}$$

a. Solve for d

b. $10 \text{ ft/s} = \dfrac{0.4085 \times 1098 \text{ gpm}}{d^2}$

c. $d^2 = 44.85$ in.
d. $d = 6.69$ in.
e. Use an 8-in. pipe

Step 6: Piping in foam hose.

8-in.-diameter pipe will be used in the foam house to connect between the water pump, the foam proportioner, and the high-back-pressure foam maker.

High-Expansion Foam Systems

Many of the fundamental hydraulic concepts presented with low-expansion foam system design problems also apply to high-expansion foam systems. Some similarities and differences between the hydraulic design for high-expansion foam systems and low-expansion foam systems are presented in Table 4-5.2. In this analysis, a low-expansion foam system using top-mounted foam chambers is compared to an elevated high-expansion foam generator installation.

Example 3 considers the use of a high-expansion foam system in conjunction with automatic sprinkler protection for fire control and suppression in a specified government warehouse. Be careful to note the generator flow rates, foam concentrate rates, and water supply rates. One of the advantages for considering high-expansion foam for the protection of confined space hazards is the low rate of foam application and associative water rate when compared to other aqueous types of systems.

EXAMPLE 3:

Problem statement. An owner has elected to protect a number of warehouse complexes with a combination of automatic sprinklers and high-expansion foam. A typical four-bay warehouse complex is illustrated in Figure 4-5.8. The storage item is crude rubber piled 12 ft 6 in. high in 2000 ft² pile areas. The installed sprinkler design is 0.2 gpm/ft². The location of the high-expansion foam generators is illustrated on the 12-in. wide brick fire walls. Each foam generator is equipped with a set of remote-controlled baffels that permits directional flow of foam into adjacent fire areas. Custom generators are used that have a foam solution rate requirement of 1.83 gpm per 1000 ft³ of foam production. Three percent foam proportion with a UL-listed high-expansion foam is used for this system.

Procedure statements. The key consideration in high-expansion foam system design is the proper sizing of the foam-generating equipment to be used for a specific application. A special job work sheet is provided to systematically calculate the foam generation requirements. (See Figure 4-5.9.) Individual item information is transferred from the referenced job sheet to the associated hydraulic calculation sheet. (See Figure 4-5.10.) Reference is made to criteria established in NFPA 11A, *Standard for Medium- and High-Expansion Foam Systems.* This standard should serve as a companion guide to the systematic evaluation of the warehouse protection problem.

Problem assessment. The fundamental considerations of the hazard to be protected establish the elements of the

Table 4-5.2 ***Comparison of Design Criteria for Low-Expansion and High-Expansion Foam Systems***

Design/Hydraulic Step Function	Low-Expansion Foam System—Top Chamber	High-Expansion Foam System—Top Generator
Starting point	Foam chamber(s)	Foam generator(s)
Second determination	Foam solution requirement per chamber (gpm)	Expanded foam requirement per chamber (cfm)
Third determination	Foam solution delivery rate between foam maker and foam house	Same determination
Fourth determination	Size pipe from foam maker(s) to foam house	Size pipe from foam generator(s) to foam house
Fifth determination	Determine type and size of foam proportioner	Same determination
Sixth determination	Determine hydraulic requirements in foam house	Same determination
Seventh determination	Evaluate water supply/demand requirement at foam house	Same determination
Eighth determination	Assess requirement for water pump in foam house; recalculate hydraulic requirements in foam house	Same requirement

HIGH-EXPANSION FOAM SYSTEM JOB WORK SHEET

Sheet: 1 of: 1

Designer: Staff Date: 1986

Installation identification: GSA Defense Materials Warehouse

Hazard classification: High density combustibles

Type of protection: Dry pipe automatic sprinkler—fixed HI-X foam

Hazard description: Crude rubber in piles

Rate of discharge determination:

1. Submergence volume (cubic feet)
   v = floor area 40,000 sq ft × foam depth 14.5 ft = 580,000 cu ft
2. Submergence time (minutes) T = 5
3. Rate of foam breakdown by automatic sprinklers: $R_s = S \times Q$ where
   S shall be 10 cfm/gpm and Q shall be total discharge from operating sprinklers
   R_s = 10 cfm × 400 gpm = 4000 cfm
4. Compensation for normal foam shrinkage—C_N: C_N = 1.15
5. Compensation for leakage—C_L; C_L range is from 1 to 1.2: C_L = 1.1
6. Rate of discharger (cfm) = $(v/T + R_s) \times C_N \times C_L$ = 151,800

Description, number, and placement of foam generators: 2—80,000 cfm foam generators per storage bay. Placement on fire walls as shown

Foam solution rate: 146 gpm/generator × 2 = 292 gpm

Foam concentration rate: 3% proportion × 292 gpm = 9 gpm

Duration of discharge: 15 minutes of full operation

Gallons of foam required: Main and reserve = 270 gals

Gallons of water required: 4,245

Water supply information: Adequate for demand curve

Special foam system design considerations: System is activated by automatic sprinkler system dry pipe trip.

Figure 4-5.9. ***High-expansion foam system job work sheet.***

problem design. In the case of high-expansion foam, some subjective criteria needs to be established due to the lack of specific information in NFPA 11A. Subjective criteria will be fully noted in the problem development. The following steps identify the hazard and the standard calculations associated with the hazard.

Step 1: Installation identification.

Refer to Figure 4-5.8, a defense materials warehouse.

Step 2: Hazard classification.

High density combustibles. Note: The actual storage material is crude rubber provided in irregular flat sheets. This commodity is not specifically specified in Table 2-3.4 of NFPA 11A. Therefore, some judgment must be made when selecting foam submergence time as required for the calculations below.

Step 3: Type of protection.

The warehouse is protected by a drypipe automatic sprinkler system with a maximum discharge capability of 0.2 gpm/ft^2 over 2000 ft^2. This discharge density is not considered adequate protection for crude rubber in 2000 ft^2 piles. The automatic sprinkler protection is supplemented by a fixed high-expansion foam system. The foam generators are mounted on the coping section

HYDRAULIC CALCULATIONS

Subject: GSA Warehouse
Job no.: Sample problem 3
Sheet no.: 1 Of: 1
By: Staff Date: 1986
Chkd by: Date:
Application rate: NH gpm per sq ft
Area: 40,000 ft
Minimum solution rate: 1.83 gpm/1000 ft³
Actual solution rate: 185 gpm/1000 ft³
Foam maker pressure and rate: 50 psi @ 146 gpm
Foam system: Fixed
Water data:
Ref. drawing:

Foam maker type and location	Added gpm	Total gpm	Pipe size (in.)*	Pipe & equivalent fitting lgth. (ft)**	Friction psi/ft C=100	Friction Total psi	Static psi	Proportioner psi	Req'd pres psi
Starting point: 1	Elevation: 22 ft				Pressure at foam maker: 50 psi				
1	146	146							50
1–2–3		146	3.068	212′+E(7′)=1 T(15)	.0387	9.1	9.5		68.6
				234′					
2 @ 3									68.6
3–6		146	4.026	200′	.0103	2.06			70.7
6–9–12	148	294	4.026	400′	.0375	15.0			85.7
Foam house		294						4.0	89.7
System demand		294							90.0

* "X" Indicates extra hvy.—std. wt. otherwise

** See sheet for tabulation of pipe and fittings

Figure 4-5.10. ***Hydraulic calculations.***

to the fire walls that divide the warehouse into fire areas. Generators positioned on the internal fire walls are arranged to discharge foam into whichever compartment, as required.

Step 4: Hazard description.

The fundamental considerations associated with the hazard are given under Step 1. It should be further noted that 12 storage piles of 2000 ft² each are located in the designated fire areas. Each individual pile is approximately 12 ft 6 in. high. Due to the piling arrangement of the rubber and the burning characteristics of rubber, no deduction is made for "stock" in the rate discharge determination.

Step 5: Rate of discharge determination.

The basic design objective is to determine the rate of expanded foam discharge in cubic feet per minute to sub-

merge the hazard in a defined period of time. This determination can be accomplished by applying a rate formula developed by the NFPA Foam Committee. The formula is given in Figure 4-5.9, under sub-item 6. The formula can be applied by first calculating and then assigning values to the formula variables.

1. *Submergence volume* (Re: NFPA 11A, Section 2-3.3).
   Floor area: 200 ft × 200 ft = 40,000 ft²
   Foam Depth:
   (a) 1.1 × height = 1.1 × 12.5 = 13.75 ft
   (b) Height + 2 ft − 12.5 ft + 2 ft = 14.5 ft
   Use the larger of the two values or 14.5 ft for calculations.
   Volume = area × depth
   Volume = 40,000 ft² × 14.5 ft = 580,000 ft³
   (See Step 4—no deduction is made for stock)
2. *Submergence time* (Re: NFPA 11A, Section 2–3.4).
   5 minutes for high density materials with sprinkler protection
3. *Rate of foam breakdown for sprinklers* (Re: NFPA 11A, Section 2-3.5.2).
   (a) Discharge from sprinklers:

$$Q = 0.2 \text{ gpm/ft}^2 \times 2000 \text{ ft}^2 = 400 \text{ gpm}$$

   (b) Apply formula:

$$R_s = 10 \text{ cfm} \times 400 \text{ gpm} = 4000 \text{ cfm}$$

4. *Compensation for shrinkage.* Set at 1.15 as a constant (Re: NFPA 11A, Section 2-3.5.2).
5. *Compensation for leakage.* Use 1.1 to allow for some leakage around doors (Re: NFPA 11A, Section 2-3.5.2).
6. Apply formula:

$$\text{cfm} = (v/T + R_s) \times C_N \times C_L$$

$$\text{cfm} = (580{,}000 \text{ ft}^3/5 \text{ min} + 4000 \text{ cfm}) \times 1.15 \times 1.1$$

$$= 151{,}800 \text{ cfm}$$

Note: The foam breakdown from sprinklers is a relatively small value compared to the total cfm rate.

Step 6: Description, number, and placement of generators.

Custom-built foam generators will be required for this problem. Each generator will have a capacity of 80,000 cfm with a foam solution rate of 146 gpm. (See given information with problem statement.) Five generators will be required to protect the entire warehouse. Generators mounted on interior fire walls will be equipped with baffels arranged to discharge foam into either adjacent compartment; electrical controls will be operated from the foam house. Generators are actually mounted 22 ft above the finished floor.

Step 7: Foam solution rate.

The foam solution rate per generator is given in Step 6. The solution rate requirement is 1.83 gpm per 1000 ft³ of foam production.

Solution rate = 80,000 ft³/1000 ft³ × 1.83 gpm = 146 gpm

Two generators require 292 gpm.

Step 8: Foam concentrate rate.

The foam selected for this problem proportions at 3 percent. Therefore, the concentrate rate is 3 percent × 292 gpm = 9 gpm.

Step 9: Duration of discharge.

Duration of discharge for the foam systems should be checked with the authority having jurisdiction. A basic minimum discharge time is 15 minutes of continuous operation.

Step 10: Gallons of foam required.

It is assumed that enough foam will be placed in storage to meet both a main and a reserve requirement: 9 gpm × 15 min × 2 = 270 gal.

Step 11: Gallons of water required.

The primary water supply must provide a rate of 283 gpm for 15 minutes or 4245 gal. A like amount must be supplied for the secondary demand.

Step 12: The problem considers that the water supply to the foam house is adequate to meet the calculated demand for the system.

Step 13: The foam system is arranged to be activated by the automatic sprinkler system when the drypipe valve trips due to a sprinkler head operating. The system can also be activated manually.

Hydraulic analysis for Example 3

Step 1: The inlet pressure requirement for the foam generator is 50 psi.

Step 2: The foam solution line supplying each foam generator and the riser pipe to the top of the fire wall are sized on the basis of a maximum flow velocity of 10 ft/s.

$$\text{Velocity} = \frac{0.4085 \times \text{gpm}}{d^2}$$

a. $10 \text{ fps} = \dfrac{0.4085 \times 146 \text{ gpm}}{d^2}$
b. $10d^2 = 59.64$
c. $d^2 = 5.96$
d. $d = 2.44$
e. Use a 3-in. pipe

Since the same size pipe is used from the foam generator to ground level, the hydraulic analysis can go from reference point 1 to reference point 3. The elevation head to be considered is 22 ft.

Step 3: The flow and pressure demand at the base of each riser supplying a foam generator is the same, since the generator sizes are equal. It is necessary to calculate a flow constant at this location so the pressure points upstream can be correctly adjusted for higher pressure values developed by friction loss between supply points. The demand constant is calculated as follows:

(reference point 3)

$Q = K\sqrt{P}$

146 gpm = K 68.6

Step 4: The ground-level cross-main connecting the foam generator risers is sized on the basis of a maximum flow velocity of 10 ft/s. The flow from two generators is used for the flow computations.

$$\text{Velocity} = \frac{0.4085 \times \text{gpm}}{d^2}$$

a. $V = \dfrac{0.4085 \times 292 \text{ gpm}}{d^2}$

b. $10d^2 = 119.282$

c. $d^2 = 11.928$

d. $d = 3.45$

e. Use a 4-in. pipe

Step 5: Determine the actual flow characteristics for the high-expansion foam generator at reference point 4.

Use the *K* value (constant) determined in Step 3 to calculate the actual supply to the second foam generator at reference point 4. The new pressure at the riser base is (reference point 6) 70.7 psi from the hydraulic calculation sheet. The higher pressure is used with the *K* value to determine the actual flow for the second high-expansion foam unit.

$$Q = K\sqrt{P}$$

$$Q = 17.6\sqrt{70.7}$$

$$Q = 148$$

The actual flow increases by 2 gpm for the second generator.

Step 6: Determine the flow and pressure requirements at the foam house. Determine the friction loss for the total flow back to the foam hose and add in 4 psi for the foam proportioner.

Step 7: System demand.

The final system demand is 294 gpm at 90.0 psi at the foam proportioner inlet to supply the two high-expansion foam generators. The water supply to the foam house must meet this demand.

The Advent of Class A Foams

Class A foams have been used extensively in wildland fire suppression. The success of Class A foam for the confinement, control, and extinguishment of natural cover fuel fires suggests that this type of foam may be effective for structural fire protection as foam solution in fire streams. Initial research has been conducted to quantify the fire fighting efficiency of Class A foams to improve the operating efficiency of these foams when compared to plain water fire streams. The National Fire Protection Research Foundation has published research findings on Class A foam effectiveness: one in December 1993[3] and one in November 1994.[4] A synopsis of the findings are presented below.

The National Fire Protection Research Foundation (NFPRF) sponsored a research program with Underwriters Laboratories, Inc. (UL), to investigate the effectiveness of Class A foams by means of three discharge devices: (1) a standard spray nozzle, (2) an air-aspirated spray nozzle, and (3) by injecting compressed air into the Class A foam solution. This research investigation has two objectives: (1) to develop test data related to the fire fighting effectiveness of Class A foam solutions as compared to water only and (2) to conduct laboratory analysis of the Class A foam concentrate used in the performance tests.

Briefly, the initial fire test plan included a Class 20A wood crib fire with foam solution concentrates selected at 0.1, 0.3, and 0.5 percent. Adjunct variables included nominal expansion ratios of 5 for a standard nozzle at 15 gpm, 7.5 for an air-aspirated nozzle at 15 gpm, and 7.5 for injecting compressed air into the Class A foam solution.

The wood crib fire tests were conducted at UL's test facility located in Northbrook, Illinois, and are reported in the December 1993 publication.

In summary, the initial set of fire tests provide support of the following conclusions by the Technical Advisory Committee (TAC):

- Handheld hoselines supplied with Class A foam solutions provide enhanced fire fighting performance when compared to handheld hose lines supplied with water only.
- The best foam quality, as measured by retention and exposure protection tests, was achieved with compressed air foam.
- Results of the wood crib fire tests indicated superior characteristics in terms of fire control time for Class A foams when compared to water application only.
- Fire tests conducted with the air-aspirated test nozzle had the longest reignition times, while tests conducted with the Compressed Air Foam had the lowest crib weight losses.
- Exposure protection test results demonstrated the ability of the Class A foam to lengthen the ignition time of a combustible surface when compared to cribs protected by the same rate and duration of water.
- Retention-of-weight tests demonstrated that wood cribs exposed to Class A foam retain more weight than cribs treated with water.

The testing program outline above was very controlled in a laboratory setting. Foam applications were not subjected to many real world variables that could include wind, weather conditions, fuel geometry, pre-burn times, and human factors in the foam application. Despite such conditions, the reported testing program clearly supports a number of advantages for using Class A foam on structural type fires.

The Phase II research project report of 1994 reviews the conduct of structural fire suppression tests. These tests were also conducted at UL's test facilities in Northbrook, Illinois. A test cell measuring 30 by 36 by 30 ft was used for the Class A foam comparative analysis tests. Two fuel package scenarios were used as follows:

- The Series I UL 1626 residential fuel package consisted of a wood crib and simulated furniture positioned in one corner of the enclosure.
- The Series II fuel package consisted of a corner upholstered sofa scenario.

Fire test monitoring of the enclosure included measurements of the Class A foam solution or water flow rate; room temperature gradients at distances of 2, 9, 18, 24, 33, 48, and 72 in. below the ceiling; rate of heat release; oxygen content; smoke density; and heat flux. In each test series, observations were made of fire knockdown and damage to the walls of the enclosure and the fuel package.

Upon ignition, the fuel package was allowed to burn until flashover was achieved in the enclosure. Five seconds after flashover, a water application or a Class A foam solution was applied to suppress the fire using either a direct or indirect application method. The direct application method consisted of discharging the agent directly onto the walls of the enclosure and the fuel package. In contrast, the indirect application method consisted of discharging the agent first onto the ceiling and walls and then onto the fuel package.

The 1994 Class A Foam Study Report divides the summary information according to the Series I and II testing programs. The Series I abbreviated findings are summarized as follows:

- Class A foam using a direct application method took less time and quantity of agent to lower heat release to 500 KW than plain water.
- Class A Compressed Air Foam (CAF) using the indirect application method was more effective in reducing heat release values down to 500 KW.

The Series II abbreviated findings are limited to the following selective observations:

- The test results using Class A foam solutions generally provided for a reduced amount of total heat release from the fire and less damage to the sofa.
- Class A Compressed Air Foam applied at 7 gpm using the direct application method demonstrated the shortest time period and the lowest quantity of agent required to reduce the rate of heat released to 500 KW.
- The direct application method provides for a reduced amount of total heat release and less damage to the sofa when compared to the same tests conducted using the indirect application method.

Both reports recommend additional research on the application of Class A Foams with special attention given to hardware devices that include handheld fixed nozzles, proportioning equipment, and foam-generating equipment.

Additional research has been conducted by the National Institute of Standards and Technology.[5] The effectiveness of Class A foams on Class A and Class B fire threats were characterized. Four representative Class A foams were chosen for evaluation. A series of Class B fire suppression tests were conducted in conformance with UL 162 *Standard for Foam Equipment and Liquid Concentrates*. These tests utilized a 4.6-m^2 (50-ft^2) heptane pool fire and consisted of the suppression of the fire and then testing for reignition and burnback resistance. Agent was applied at 2.44 and 4.88 lpm/m^2 (0.06 and 0.12 gpm/ft^2), which is one and one-half and three times the rate required by the standard for AFFF application. The higher flow rates were used because the agents could not extinguish the fire at the standard AFFF application rate. The four agents had fire knockdown (control) times similar to AFFF, but two of the agents did not completely extinguish the fire in all the tests. AFFF had a higher resistance to burnback and longer time to re-ignition than the other four agents.

Full-scale fire experiments were conducted with 92.9-m^2 (1000-ft^2) gasoline pool fires. Agent application was made with a 454 lpm (120 gpm) hose stream (i.e., 4.88 lpm/m^2 [0.12 gpm/ft^2]). Two application techniques were used with each of the four agents in the large-scale tests. One application was made with a self-aspirating tube nozzle, and one application was made with a non-aspirating adjustable fog nozzle. AFFF and water were used as benchmark agents for these tests. Plain water could not extinguish this fire. AFFF exhibited better fire control and extinguishment characteristics, and substantially better burnback resistance, than those of the Class A foams.

In tests conducted for the U.S. Air Force, the Naval Research Laboratory assessed a compressed air foam system for possible use for aircraft hangar scenarios involving JP-8 fuel.[6] The breadboard unit used AFFF as the fire extinguishing agent. It was found that a commercial off-the-shelf non-air-aspirating nozzle was as effective as the air-aspirating nozzle provided with the unit. Air injection for aeration of the AFFF stream before discharge from the nozzle was found to be unnecessary.

Nomenclature

C	Hazen-Williams coefficient (constant)
C_L	foam leakage correction factor
C_N	normal foam shrinkage factor
d	internal pipe diameter (in.)
FL	friction loss (psi/ft)
K	nozzle discharge coefficient (gpm/$psi^{1/2}$)
Q	flow (gpm)
R	total foam generator capacity (cfm)
R_s	total rate of foam breakdown [$S \times Q$] (cfm/gpm)
S	rate of foam breakdown by sprinklers per gpm of sprinkler discharge (cfm/gpm)
T	submergance time (min)
V	velocity (ft/s)
v	submergence volume (ft^3)

References Cited

1. *National Fire Codes,* National Fire Protection Association, Quincy, MA.
2. "Flammable Liquid Storage Tank Protection," *National Foam Engineering Manual,* Section 6, National Foam, Lionville, PA (n. d.).
3. W.M. Carey, *National Class A Foam Research Project Technical Report,* National Fire Protection Research Foundation, Quincy, MA (December 1993).
4. W.M. Carey, *National Class A Foam Research Project Technical Report, Phase II,* National Fire Protection Research Foundation, Quincy, MA (December 1994).
5. D. Madrzykowski and D.W. Stroup, "Demonstration of Biodegradable, Environmentally Safe, Non-Toxic Fire Suppression Liquids," *NISTIR 6191,* National Institute of Standards and Technology Report, Gaithersburg, MD (1998).
6. S.A. Hill, J.L. Scheffey, F. Walker, and F.W. Williams, "Tests of Alternative Fire Protection Methods for USAF Hangars," *NRL/MR/6180-99-8337,* Naval Research Laboratory Report, Washington, DC (1999).

Appendix

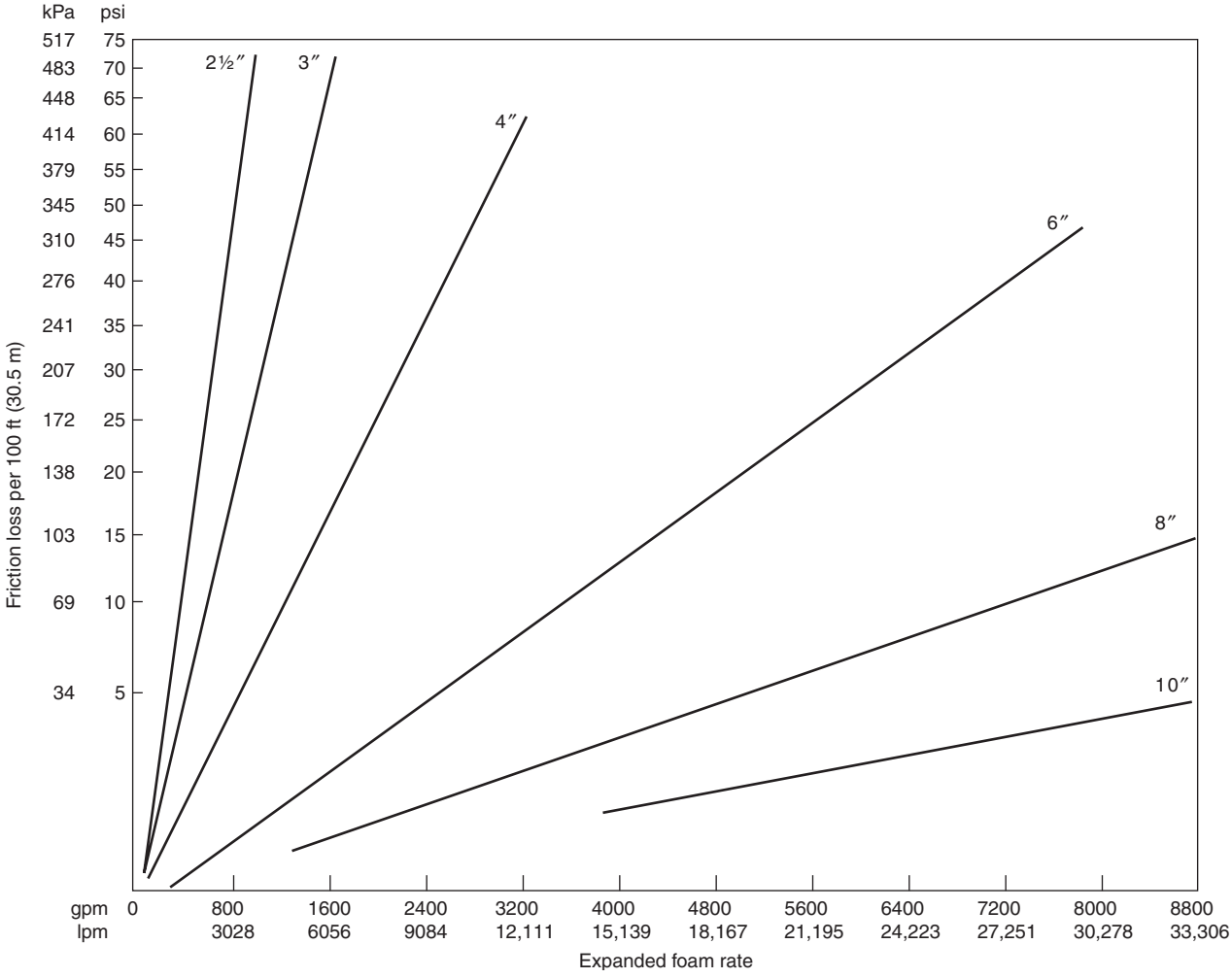

Figure 4-5A.1. ***Foam friction losses—4:1 expansion (2½", 3", 4", 6", 8", and 10" pipe).***

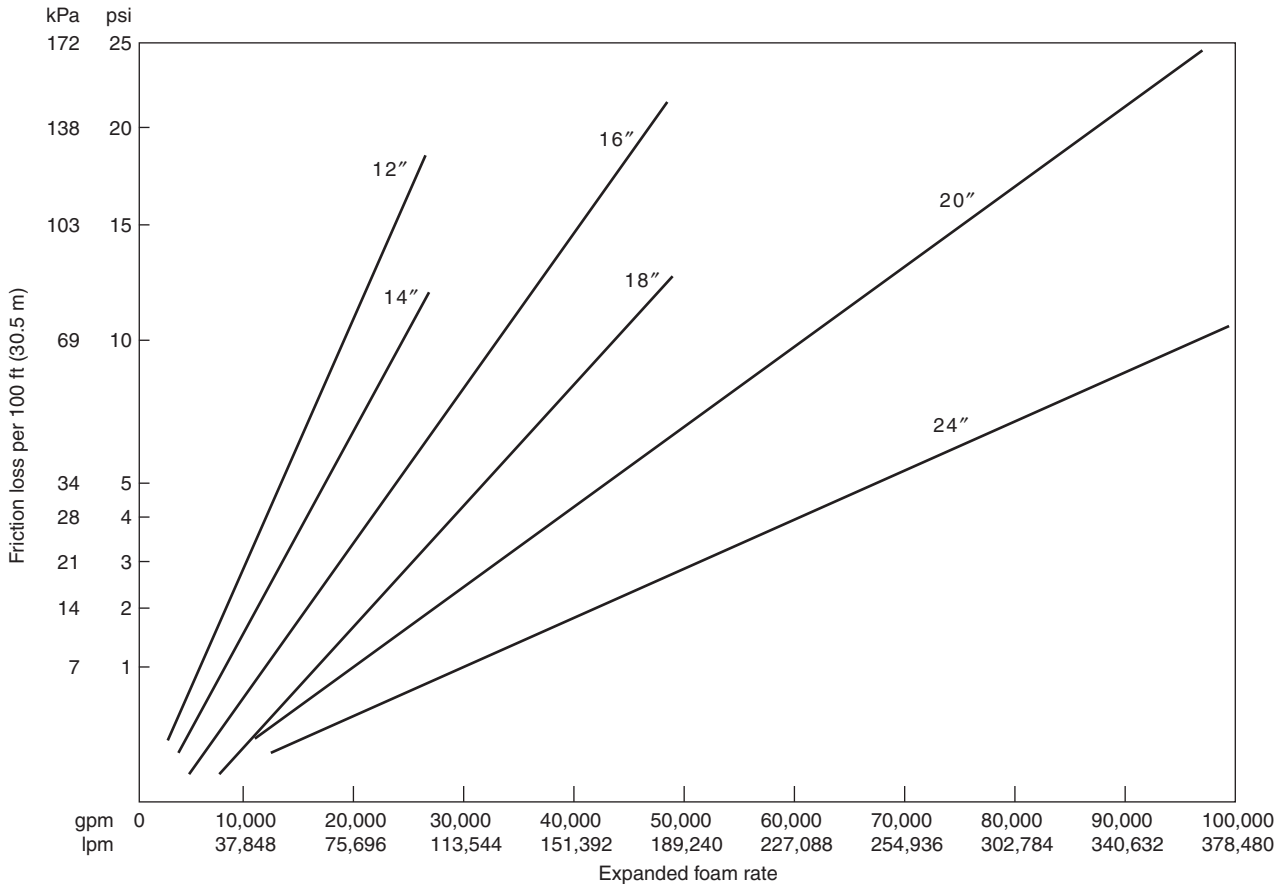

Figure 4-5A.2. ***Foam friction losses—4:1 expansion (12", 14", 16", 18", 20", and 24" pipe).***

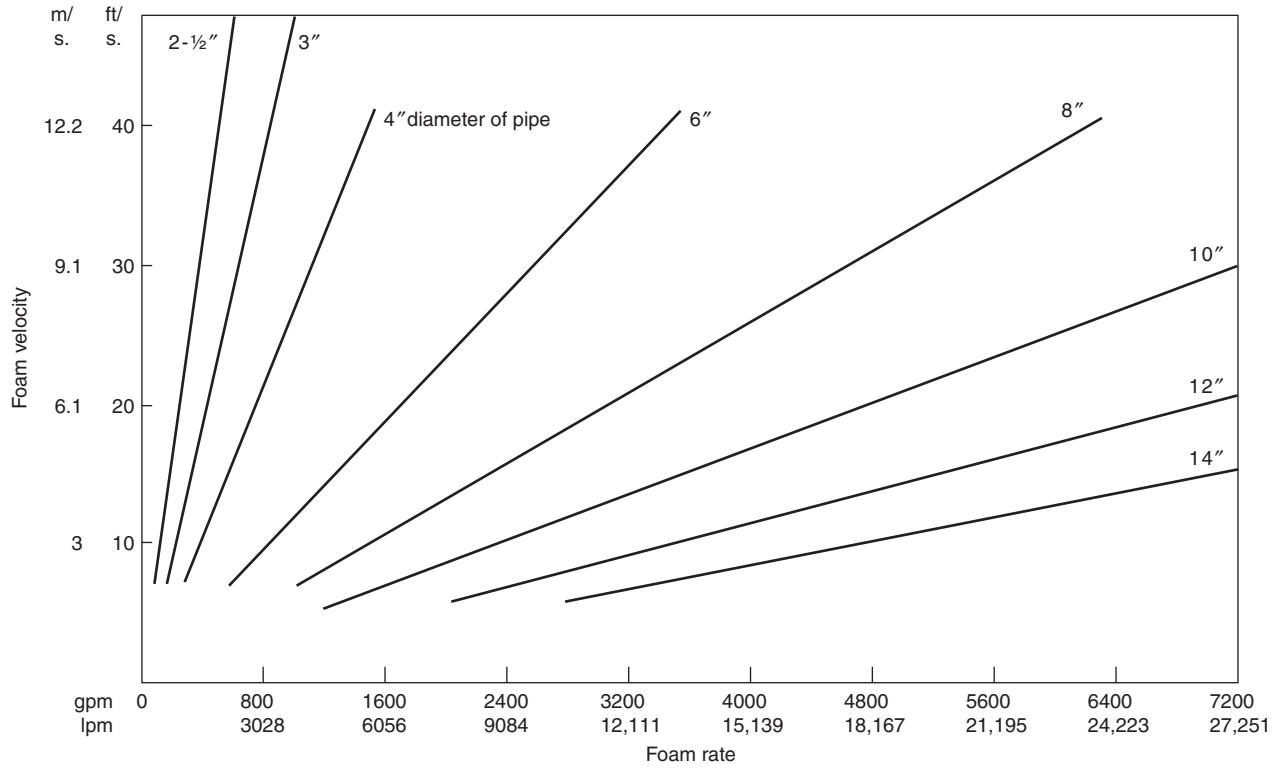

Figure 4-5A.3. ***Foam velocity versus pipe size (2½", 3", 4", 6", 8", 10", 12", and 14" pipe).***

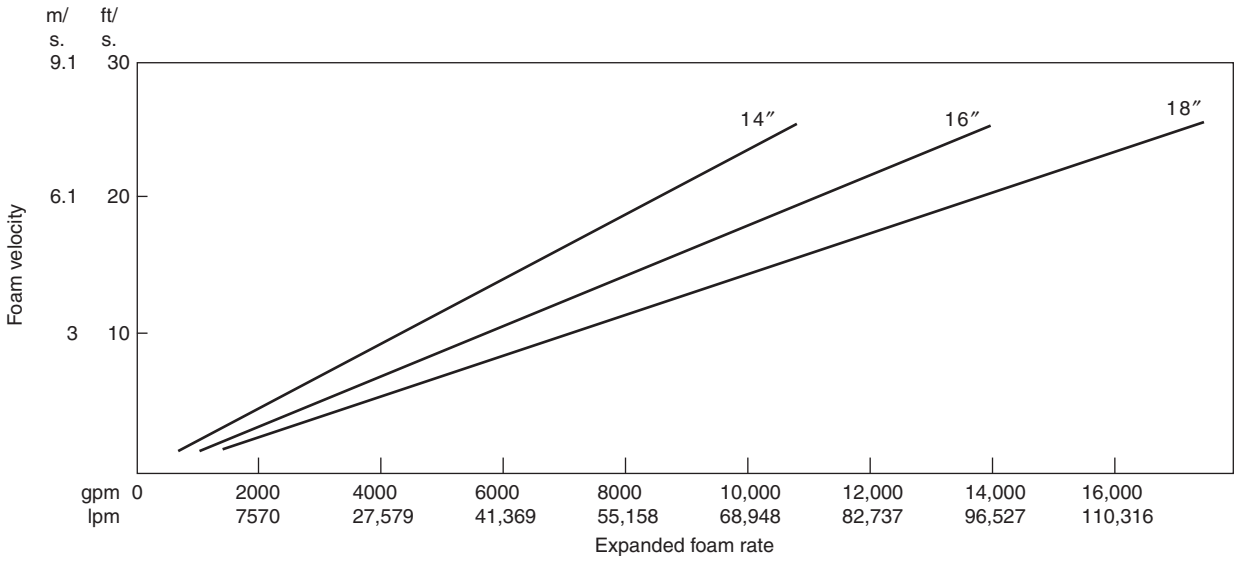

Figure 4-5A.4. ***Foam velocity versus pipe size—Schedule 40 pipe (14", 16", and 18" pipe).***

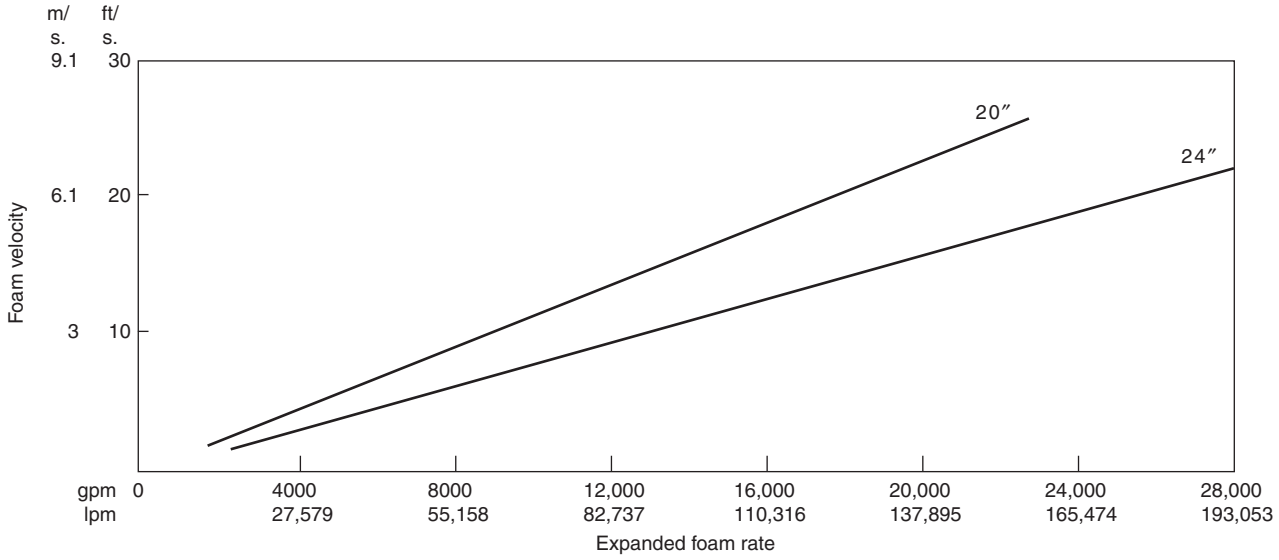

Figure 4-5A.5. ***Foam velocity versus pipe size—Schedule 40 pipe (20" and 24" pipe).***

CHAPTER 6

Halon Design Calculations

Casey C. Grant

Introduction

Halogenated agent extinguishing systems are a relatively recent innovation in fire protection, but, despite this, they already face extinction. As of January 1, 1994, the global production of fire protection halons in many countries ceased.

The obvious question is, "Why maintain this chapter on halon design calculations?" Although global production of fire protection halons essentially ceased on January 1, 1994, it is expected that this technology will continue for an extended period of time to address the modification and maintenance of existing systems, and new essential systems that will use recycled surplus stock.

The stratospheric ozone layer depletion issue is a problem confronting the global community unlike any other. Late in 1987, the United States and 24 other countries (including the European Economic Community) signed the Montreal Protocol to protect stratospheric ozone.[1] Originally, the protocol restricted the consumption of ozone-depleting chlorofluorocarbons (CFCs) to 50 percent of the 1986 use levels by 1998, and halon production was to be frozen in 1993 at 1986 production levels. But the November, 1992, Copenhagen revision to the Montréal Protocol accelerated this, such that all production of the chemicals ceased worldwide as of January 1, 1994.

The Montreal Protocol is based on unprecedented trade restrictions and is the first time nations of the world have joined forces to address an environmental threat in advance of fully established effects. The trade restrictions concern nations not participating in the agreement (the nonsignatories). Within one year of the agreement taking effect, each party shall ban the import of the bulk chemicals from the nonsignatory nations. About four years after the effective date of the agreement, imports of products containing the identified chemicals from nonsignatory nations would be banned. Within five years, products made with the chemicals (but not containing them) would be banned or restricted. This is truly significant since many products, including many electronic components, are currently manufactured using CFCs.

Today, high technology demands new and different fire protection techniques for which halon systems have proved ideal.

Casey C. Grant, P.E., is Secretary, NFPA Standards Council. He is a former member of the NFPA Technical Committee on Halogenated Fire Extinguishing Agent Systems and was previously supervisor of systems design engineering at Fenwal Incorporated.

Characteristics of Halon

Background, Definition, and Classifications of Halon Compounds

Although there are a variety of methods available for applying halogenated agents, the most common is the total flooding system. The most popular halogenated agent is Halon 1301, with its superior fire extinguishing characteristics and low toxicity. Halogenated agent extinguishing systems are a promising tool for the fire protection engineer and have great potential for solving many of our fire protection problems now and in the future.

Halogenated extinguishing agents are hydrocarbons in which one or more hydrogen atoms have been replaced by atoms from the halogen series: fluorine, chlorine, bromine, or iodine. This substitution confers flame extinguishing properties to many of the resulting compounds that make them ideal for certain fire protection applications.

The halogenated extinguishing agents are currently known simply as halons, and are described by a nomenclature that indicates the chemical composition of the materials without the use of chemical names. This simplified system was proposed by James Malcolm at the U.S. Army Corps of Engineers Laboratory in 1950 and avoids the use of possibly confusing names.[2] The United Kingdom and parts of Europe still use the initial capital "alphabet" system, that is, bromotrifluoromethane (Halon 1301) is BTM

and bromochlorodifluoromethane (Halon 1211) is BCF. The number definition for the chemical composition of Halon 1301, perhaps the most widely recognized halogenated extinguishing agent, is 1 (carbon), 3 (fluorine), 0 (chlorine), 1 (bromine), and 0 (iodine).

By definition, the first digit of the number represents the number of carbon atoms in the compound molecule; the second digit, the number of fluorine atoms; the third digit, the number of chlorine atoms; the fourth digit, the number of bromine atoms; and the fifth digit, if any, the number of iodine atoms. Trailing zeros in this system are not expressed. Figure 4-6.1 graphically demonstrates this concept by illustrating Halon 1301 in comparison to methane.

There are three halogen elements commonly found in halon extinguishing agents used for fire protection: fluorine (F), chlorine (Cl), and bromine (Br). Compounds containing combinations of fluorine, chlorine, and bromine can possess varying degrees of extinguishing effectiveness, chemical and thermal stability, toxicity, and volatility. In general, the relevant properties of these three halogen elements are characterized as shown in Table 4-6.1.

Due to the many chemical combinations available, the characteristics of halogenated fire extinguishing agents differ widely. It is generally agreed that the agents most widely used for fire protection applications are Halon 1301, Halon 1211, Halon 1011, and Halon 2402. Also somewhat common is Halon 122, which has been used as a test gas because of its economic advantages. However, because of its widespread use as a test agent, many individuals have wrongly assumed that Halon 122 is an effective fire extinguishing agent. Table 4-6.2 illustrates the halogenated hydrocarbons most likely to be used today.

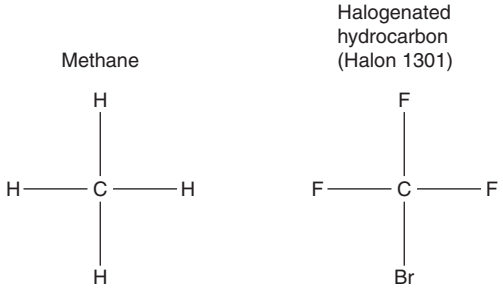

Figure 4-6.1. ***Molecular composition of methane and Halon 1301.***

Table 4-6.1 ***Contributing Characteristics of Fluorine, Chlorine, and Bromine***

	Fluorine	Chlorine	Bromine
Stability to compound	Enhances	—	—
Toxicity	Reduces	Enhances	Enhances
Boiling point	Reduces	Enhances	Enhances
Thermal stability	Enhances	Reduces	Reduces
Fire extinguishing effectiveness	—	Enhances	Enhances

Table 4-6.2 ***Halons Commonly Used for Fire Protection***

Chemical Name	Formula	Halon Number
Methyl bromide	CH_3Br	1001
Methyl iodide	CH_3I	10001
Bromochloromethane	CH_2BrCl	1011
Dibromodifluoromethane	CF_2Br_2	1202
Bromochlorodifluoromethane	CF_2BrCl	1211
Dichlorodifluoromethane[a]	CF_2Cl_2	122
Bromotrifluoromethane	CF_3Br	1301
Carbon tetrachloride	CCl_4	104
Dibromotetrafluoroethane	$C_2F_4Br_2$	2402

[a]A popular test gas without substantial fire extinguishing properties.

History

The earliest halogenated fire extinguishing agent known to be used for industrialized fire protection was carbon tetrachloride (Halon 104).[3] First becoming available as early as 1907, it was most widely used in hand-pump portable extinguishers and was popular due to its low electrical conductivity and lack of residue following application. Also referred to as "pyrene" extinguisher fluid, Halon 104 caused a number of accidental deaths and serious injuries due to its toxicity, and eventually its use was halted during the 1950s.

Methyl bromide (Halon 1001) gained popularity after it was discovered in the late 1920s to be a more effective extinguishing agent than carbon tetrachloride. Due to its high toxicity, it was never used in portable extinguishers even though it was used extensively in British and German aircraft and ships during World War II. Interestingly, methyl bromide possesses a narrow "flammability" range between 13.5 and 14.5 percent in air, though above and below this range it is an efficient fire extinguishant. Germany developed bromochloromethane (Halon 1011) in the late 1930s to replace methyl bromide, but it failed to enjoy widespread use until after World War II.[4]

Thus, prior to World War II, three halogenated fire extinguishing agents were available: Halon 104, Halon 1001, and Halon 1011. Yet because of their inherently high toxic nature, these agents slowly disappeared from typical system applications. By the mid-1960s Halon 104 and Halon 1001 were no longer being used, and Halon 1011 was only in limited use for specialized explosion suppression applications. Figure 4-6.2 represents a chronology chart that indicates the usage of these early halons as well as the halons more commonly used today.

Joint research was undertaken in 1947 by the U.S. Army Chemical Center and the Purdue Research Foundation to evaluate the fire suppression effectiveness and toxicity of the large number of available agents.[2] After testing more than 60 new agents, 4 were selected for further study: dibromodifluoromethane (Halon 1202), bromochlorodifluoromethane (Halon 1211), bromotrifluoromethane (Halon 1301), and dibromotetrafluoromethane

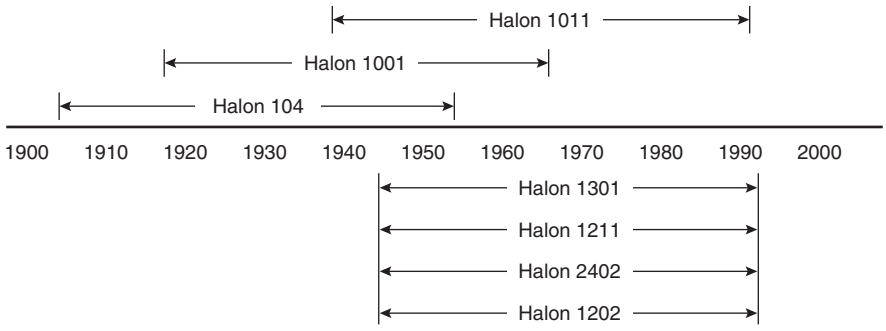

Figure 4-6.2. ***Time span usage of selected halons.***

(Halon 2402). Further testing revealed that Halon 1202 was the most effective yet also most toxic, while Halon 1301 was the second most effective and least toxic. As a result of this testing, the use of halon to provide fire protection for modern technology took on new dimensions. Halon 1202 was used by the U.S. Air Force for military aircraft engine protection while the Federal Aviation Administration (FAA) selected Halon 1301 for a similar application in commercial aircraft engine nacelles.[5] Portable extinguishers using Halon 1301 were implemented by the U.S. Army. The use of total flooding systems originated in 1963, and in the following five years several total flooding systems were installed based on carbon dioxide system technology.

In 1966, attention began to focus on the use of Halon 1301 for the protection of electronic data processing equipment. That year, the NFPA organized a Technical Committee (NFPA 12A) to standardize the design, installation, maintenance, and use of halon systems. Their resulting work was officially adopted by the NFPA membership as a standard in 1968.[6] Subsequent recognition that there were differences among the halon agents made it apparent that separate standards would be necessary. The initial halon standard, NFPA 12A, *Standard for Halon 1301 Fire Extinguishing Systems* (hereinafter referred to as NFPA 12A), focused on the use of Halon 1301 due to its high desirability and growing popularity.[7] Work on an additional standard, NFPA 12B, *Standard on Halon 1211 Fire Extinguishing Systems,* concerning the use of Halon 1211, was started in 1969 and was officially adopted by the NFPA as a standard in 1972.[8] A tentative standard on the use of Halon 2402 (NFPA 12CT) was established, but has not been officially adopted.[9]

Another NFPA committee directly concerned with the use of halon is the NFPA Committee on Electronic Computer/Data Processing Equipment (NFPA 75, *Standard for the Protection of Electronic Computer/Data Processing Equipment).*[10] Even though this standard was adopted in 1961, the use of halon was not considered until after 1972, when extensive testing by several major companies demonstrated that the use of Halon 1301 was suitable for protecting electronic computer and data processing equipment.[11] Halon 1301 eventually became the most widely used extinguishing agent for this purpose in the United States and throughout much of the world. However, certain areas of Europe have preferred Halon 1211 and 2402.

In anticipation of the worldwide production phaseout of fire protection halons, which eventually settled at January 1, 1994, for developed countries, a new committee was established during 1992 within the NFPA standards-making system designated as the Technical Committee on Alternative Protection Options to Halon. The committee's first document is NFPA 2001, *Standard on Clean Agent Fire Extinguishing Systems,* which addresses the design, installation, maintenance, and operation of total-flooding fire extinguishing systems that use halon replacement agents.[12]

Halon 1301

Attributes and limitations: Of all the halogenated extinguishing agents used in fire protection today, Halon 1301 is by a wide margin the most commonly used. The primary use of this agent is for the protection of electrical and electronic equipment, flammable liquids and gases, and surface-burning flammable solids such as thermoplastics. Areas normally or frequently occupied, air and ground vehicle engines, and other areas where rapid extinguishment is important or where damage to equipment or materials or cleanup after use must be minimized are also ideally protected by this agent. However, Halon 1301 is not a panacea, and it is appropriate to recognize its limitations as well as its attributes. The benefits of Halon 1301 are: fast chemical suppression, penetrating vapor, clean (no residue), noncorrosive, compact storage volumes, nonconductive, and colorless (no obscuration). There are also limitations to using Halon 1301: it has minimal extinguishing effectiveness on reactive metals and rapid oxidizers, it may have unfavorable side effects on deep-seated Class A fires, the agent is expensive, and it is potentially harmful to the environment. Obviously, the most significant limitation is the detrimental effect that the halons have on the earth's stratospheric ozone layer.

Because Halon 1301 inhibits the chain reaction of the combustion process, it chemically suppresses the fire very quickly, unlike other extinguishing agents that work by removing the fire's heat or oxygen. Stored as a liquid under pressure and released at normal room temperature as a vapor, Halon 1301 gets into blocked and baffled spaces readily and leaves no corrosive or abrasive residue after use. A high liquid density permits compact storage containers, which on a comparative weight basis, makes Halon 1301

approximately 2.5 times more effective as an extinguishing agent than carbon dioxide. Since it is virtually free of electrical conductivity, Halon 1301 is highly suitable for electrical fires. Halon 1301 is a colorless vapor when discharged into a hazard volume, though it sometimes temporarily clouds the volume due to the chilling of any moisture in the air. But of all its attributes, the most promising is that of people compatibility, for unlike other extinguishing agents, Halon 1301 is essentially nontoxic in the concentrations usually required for fire suppression.

There are several types of flammable materials on which Halon 1301 is ineffective and not recommended. Reactive metals such as potassium, Nak eutectic alloy, magnesium, sodium, titanium, and zirconium burn so intensely that they overpower the agent's extinguishing abilities.[5] Included with these are the metal hydrides such as lithium hydride, and petroleum solvents such as butyllithium. Autothermal decomposers and fuels that contain their own oxidizing agent will also burn freely in the presence of halon agents. These latter substances, such as gunpowder, rocket propellants, and cellulose nitrate, have an oxidizer physically too close to the fuel, and the agent cannot penetrate the fire zone fast enough. Halon is also not effective in preventing the combustion or reaction of chemicals capable of autothermal decomposition such as hydrazine or organic peroxides. Even though Halon 1301 is effective with certain surface-burning flammable solids such as thermoplastics, deep-seated Class A fires typically require relatively high agent concentrations for long soaking periods. When exposed to deep-seated fires for long periods of time, Halon 1301 may decompose into toxic and corrosive products of decomposition. Therefore, it is important that the agent be dispersed while the fire is small. The expense necessary to purchase, install, and maintain a properly functioning Halon 1301 system for more specific Class A hazards is often not economically justified. Halon 1301 fire suppression systems are usually not associated with everyday commodities, but instead are found in applications pertaining to highly valued risks.

Properties

Physical properties: On the average, Halon 1301 requires 10 percent less agent on a gas-volume basis than does Halon 1211 to extinguish any given fuel.[2] However, both agents are approximately 2.5 times more effective on a weight-of-agent basis than carbon dioxide. Halon 1301 is a gas at 70°F (21°C) with a vapor pressure of 199 psig. Although this pressure would adequately expel the material, it decreases rapidly to 56 psig (4 bar) at 0°F (–18°C) and to 17.2 psig (1.2 bar) at −40°F (−40°C). Therefore, it is necessary to increase the container pressure with dry nitrogen either to 360 or 600 psig (25 or 41 bar) at 70°F (21°C), ensuring adequate performance at all temperatures. Figure 4-6.3 demonstrates the temperature-pressure profile for Halon 1301 and Halon 1301 superpressurized with dry nitrogen.

Halon 1301 is normally stored in a pressure vessel as a liquid before it is released to occupy the hazard volume as a vapor. With a boiling point of −72°F (−58°C), it is approximately 1.5 times more dense than water in its liquid phase and approximately 5 times heavier than air in its vapor phase. Thus, Halon 1301 vapor will typically escape through openings in the low portions of a totally flooded volume. Other physical properties are shown in Table 4-6.3.

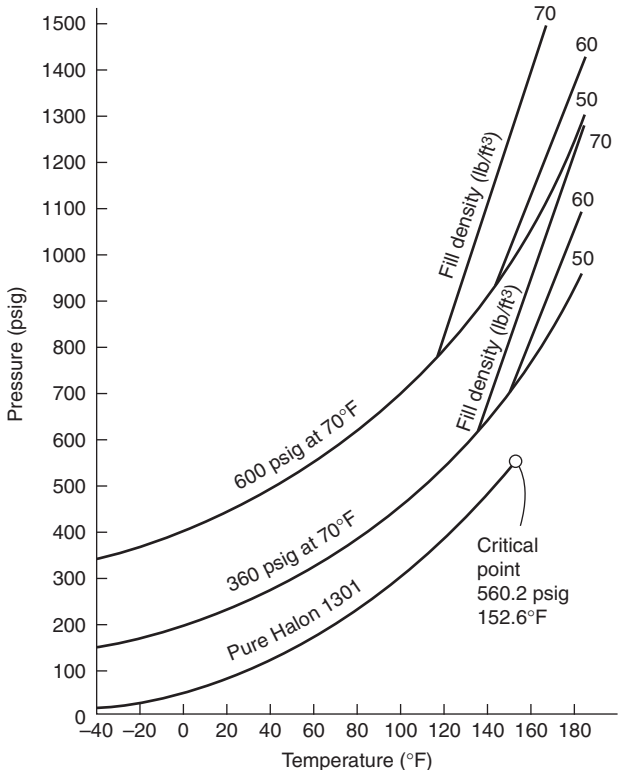

Figure 4-6.3. ***Temperature-pressure relationship for pure Halon.***

Traditionally, there were three distinct elements assumed for combustion: heat, fuel, and oxygen. Known as the fire triangle, this theory had to be modified as halons became more widely used and better understood. Typical fire extinguishment involves either removing the fuel from the fire, limiting oxygen to the fire (smothering), or removing the heat (quenching). The halons do not extinguish fire in any of these ways, but instead break up the uninhibited chain reaction of the combustion process. The tetrahedron of the fire, as it is now called, is shown in Figure 4-6.4.

Table 4-6.3 ***Selected Physical Properties of Halon 1301***

Boiling point	–72.0°F
Freezing point	–270.4°F
Specific gravity of liquid (@70°F)	1.57
Specific gravity of vapor (@70°F)	5.14
Liquid density @70°F	98.0 lb/ft³
Vapor density @70°F	7.49 lb/ft³ (standard)
Critical temperature	152.6°F
Critical pressure	575 PSIA

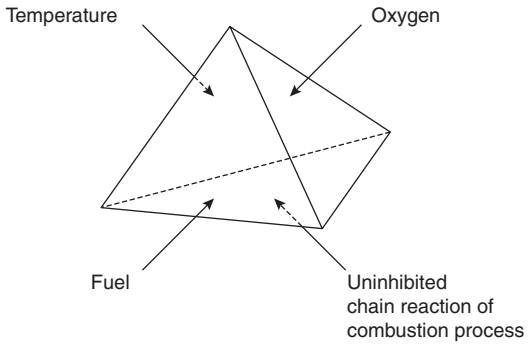

Figure 4-6.4. ***The tetrahedron of fire.***

The extinguishing mechanism of the halogenated agents is not completely understood, yet there is definitely a chemical reaction that interferes with the combustion process. The halogen atoms act by removing the active chemical species involved in the flame chain reaction. While all the halogens are active in this way, bromine is much more effective than chlorine or fluorine. With Halon 1301 (54 percent by weight bromine), it is the bromine radical that acts as the inhibitor in extinguishing the fire. Yet the fluorine in the molecule also serves a specific task since it is the fluorine that gives the agent thermal stability and keeps Halon 1301 from decomposing until approximately 900°F (480°C).[13]

Extinguishing effectiveness: As shown in Figure 4-6.5, the four types of fire are ordinary combustibles (Class A), flammable liquids and gases (Class B), electrical (Class C), and reactive metals (Class D).[5]

It was previously mentioned that Halon 1301 is ineffective on Class D fires and is not as desirable as other agents in extinguishing deep-seated Class A fires. The effectiveness of Halon 1301 on Class A fires is not as predictable as with other classes of fire. It depends to a large extent upon the burning material, its configuration, and how early in the combustion cycle the agent is applied. Most plastics behave as flammable liquids and can be extinguished rapidly and completely with 4 to 6 percent concentrations of Halon 1301.[7]

Other materials, particularly cellulosic products, can in certain forms develop deep-seated fires in addition to flaming combustion. The flaming portion of such fires can be extinguished with low 4 to 6 percent Halon 1301 concentrations, but the glowing deep-seated portion of the fire may continue under some circumstances. Even so, the deep-seated fire can be controlled since its rate of burning and consequent heat release will be reduced. Considerably higher concentrations (18 to 30 percent) of Halon 1301 are required to achieve complete extinguishment, but these levels are seldom economical to apply and their application may result in unwanted products of decomposition. However, the concept of controlling deep-seated fires with halogenated agents has been accepted in the respective NFPA standards.[7]

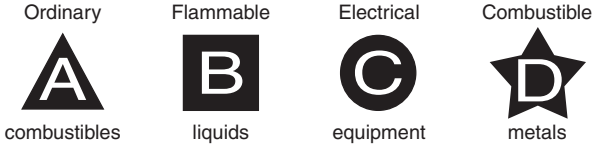

Figure 4-6.5. ***The four classes of fire.***

It is Class B and Class C fires for which halon is particularly well suited. The most common applications involve Class C electrical hazards, with the increase in popularity of Halon 1301 keeping well in stride with the development of high technology. Typically, electrical and electronic equipment are protected with a concentration of 5 percent Halon 1301 by volume, though a significantly lower concentration will suitably extinguish a potential fire.[14] The concentrations necessary to extinguish Class B fires have been the subject of much testing with results that vary widely. The effectiveness of halogenated agents on flammable liquid and vapor fires is quite dramatic, especially in total flooding systems. Rapid and complete extinguishment is obtainable with low concentrations of the agent.[7] To be effective, the fire must be contained (such as inside a building) so that the agent can react with it; Halon 1301 applied to large exterior running pool fires dissipates into the atmosphere without penetrating the flame zone.

Corrosive effects of undecomposed halons: Unlike Halon 1301 and Halon 1211, the early nonfluorinated halogenated agents had significant corrosive problems. Laboratory tests by DuPont in a 44-month exposure period with aluminum, magnesium, steel, stainless steel, titanium, and brass exposed to undecomposed Halon 1301 support the fact that this agent will not corrode these metals, which may all commonly be used in fixed fire extinguishing systems.[13] This is not surprising from a chemical standpoint because the presence of the fluorine atom in a molecule generally reduces its chemical reactivity and corrosive properties and increases its stability.

The presence of free water in systems containing Halon 1301 should be avoided. Free water is defined as the presence of a separate water phase in the liquid halon. When present in a small quantity, free water can provide a site for concentrating acid impurities into a corrosive liquid.[15] Free water should not be confused with dissolved water, which is not a problem in a Halon 1301 system.

Halon 1301 is inert toward most elastometers and plastics. In general, rigid plastics that are normally unaffected include polytetrafluorethylene, nylon, and acetal copolymers. Most of the commonly used plastics undergo little, if any, swelling in the presence of Halon 1301, with the exception of ethyl cellulose and possibly cellulose acetate/butyrate. Elastomers are particularly suitable when exposed to Halon 1301 for extended periods of time with the notable exception of silicone rubber.[13] Halons decomposed at high temperatures during suppression produce halogen acids and free halons that can be corrosive.

Toxicity

General toxic properties: The relative safety of Halon 1301 has been established through more than 30 years of medical research involving both humans and test animals. No significant adverse health effects have been reported from the proper use of Halon 1301 as a fire extinguishant since its original introduction into the marketplace.[7]

Early studies by the U.S. Army Chemical Center on Halon 1301 determined the approximate lethal concentration for a 15-minute exposure to be 83 percent by volume.[2] Animals exposed to concentrations below lethal levels exhibit two distinct types of toxic effects. Concentrations greater than 10 percent by volume produce cardiovascular effects such as decreased heart rate, hypotension, and occasional cardiac arrythmias.[16] Concentrations of Halon 1301 greater than 30 percent by volume result in central nervous system changes including convulsions, tremors, lethargy, and unconsciousness. Effects are considered transitory and disappear after exposure.[17]

Human exposure to concentrations of Halon 1301 greater than 10 percent by volume have shown indications of pronounced dizziness and a reduction in physical and mental dexterity.[18] With concentrations between 7 and 10 percent by volume, subjects experienced tingling of the extremities and dizziness, indicating mild anesthesia. Exposure to Halon 1301 concentrations less than 7 percent by volume have little effect, with the exception of a deepening in the tone of voice caused by a higher density in the medium between the vocal chords. The effects at all levels of concentration disappear quickly after removal from the exposure. Testing of Halon 1301 for potential teratogenic (i.e., altering the normal process of fetal development) and mutagenic (a carcinogen in humans) effects have indicated that no serious problems exist.[5]

Most fire protection applications today have a design concentration of 5 percent by volume, thus the question of toxicity is not usually a serious concern. Exposure limitations for Halon 1301 (indicated by NFPA 12A) are summarized in Table 4-6.4.[7]

In addition to possible toxic effects, liquid Halon 1301 (including the spray in the immediate proximity of a discharge) may freeze the skin on contact and cause frostbite. However, direct contact is necessary for this to occur and is unlikely, since with engineered Halon 1301 fire extinguishing systems the discharge nozzles are typically distant from all occupants.

Table 4-6.4 ***Permitted Exposure Time for Halon 1301***

Concentration (percent by volume)	Permitted Time of Exposure
Normally occupied areas	
0–7%	15 min
7–10%	1 min
Above 10%	Not permitted
Normally unoccupied areas	
0–7%	15 min
7–10%	1 min
10–15%	30 s
Above 15%	Prevent exposure

Products of decomposition: Consideration of the life safety of Halon 1301 must also include the effects of breakdown products which have a relatively higher toxicity than the agent itself. Upon exposure to flames or hot surfaces above approximately 900°F (480°C), Halon 1301 decomposes to form primarily hydrogen bromide (HBr) and hydrogen fluoride (HF).[19] Trace quantities of bromine (Br_2), carbonyl fluoride (COF_2), and carbonyl bromide ($COBr_2$) have been observed, but the quantities are generally too small to be of concern. Although small amounts of carbonyl halides (COF_2 and $COBr_2$) were reported in early tests, more recent studies have failed to confirm the presence of these compounds. Table 4-6.5 summarizes the predominant products of decomposition for Halon 1301.[20]

The primary toxic effect of the decomposition products is irritation. Even in concentrations of only a few parts per million, the decomposition products have characteristically sharp, acrid odors. This characteristic provides a built-in warning system since the irritation becomes severe well in advance of truly hazardous levels. In addition, the odor also serves as a warning that carbon monoxide and other potentially toxic products of combustion may be present. Prompt detection and rapid extinguishment of a fire will produce the safest post-extinguishment atmosphere.

Other Halons

Physical properties: The predominant halogenated agent in existence today for total flooding fire extinguishing systems is Halon 1301, though some areas of Europe have utilized Halon 1211 for this purpose. One reason for this use of Halon 1301 (besides toxicity) is the ability of the agent to vaporize and penetrate all portions of the hazard volume. Table 4-6.6 shows that Halon 1301 has the lowest boiling point and Halon 1211 has the second lowest.

With the discharge of a halon system at ambient temperature, Halon 1301 flashes to a vapor almost instantaneously, while Halon 1211 tends to pool momentarily. Agents with boiling points exceeding the temperature of the hazard volume will stay liquid until heated by the fire itself. These high boiling point halogenated agents have two distinct attributes: they can be projected in a liquid stream and they have a quenching effect in addition to

Table 4-6.5 ***Predominant Halon 1301 Decomposition Products***

Compound	Formula	ALC[a] for 15-min Exposure ppm by Volume in Air
Hydrogen fluoride	HF	2500
Hydrogen bromide	HBr	4750
Bromine	Br_2	550
Carbonyl fluoride	COF_2	1500
Carbonyl bromine	$COBr_2$	—

[a]Approximate lethal concentration

Table 4-6.6 ***Selected Physical Properties of Typical Halogenated Fire Extinguishing Agents***

Halon Number	Type of Agent	Approximate Boiling Point (°F)	Approximate Freezing Point (°F)	Specific Gravity of Liquid (@70°F)
104	Liquid	170	–8	1.59
1001	Liquid	40	–135	1.73
1011	Liquid	151	–124	1.93
1202	Liquid	76	–223	2.28
1211	Liquefied gas	25	–257	1.83
1301	Liquefied gas	–72	–270	1.57
2402	Liquid	117	–167	2.17

breaking the uninhibited chain reaction. Thus, portable extinguishers generally use Halon 1301 as a propellant for other halon agents.

Toxicity

One of the primary reasons that Halon 1301 is the most preferred of the halogenated agents is its relatively low toxicity, as discussed earlier. Table 4-6.7 compares the approximate lethal concentration of both the natural and decomposed vapors for a variety of fire extinguishing agents. Included with this list of halon agents is carbon dioxide for sake of comparison. As a natural vapor, Halon 1301 is the least toxic halogenated agent. Carbon dioxide may appear to compare favorably with Halon 1301, yet high concentrations of carbon dioxide are necessary for fire extinguishment, which also makes the hazard volume lethal to human occupants.

Halon in the Fire Protection Spectrum

Halogenated agent extinguishing systems are only one segment of the total fire protection spectrum. Good engineering judgment is necessary when trying to determine the applicability of halon and whether it should be used instead of, or in addition to, other fire protection measures. It must be clearly understood that halogenated agent extinguishing systems are not the panacea for all fire hazards, yet they do offer a safe method to extinguish certain fires in their very early stages. Thus, these systems are commonly applied to situations where even the smallest fire is absolutely unthinkable.

Table 4-6.7 ***Approximate Lethal Concentrations (ppm) for 15-min Exposure to Vapors of Various Fire Extinguishing Agents***

Formula	Halon Number	Natural Vapor	Decomposed Vapor
CCl_4	104	28,000	300
CH_3Br	1001	5,900	9,600
CH_2ClBr	1011	65,000	4,000
CF_2Br_2	1202	54,000	1,850
CF_2ClBr	1211	324,000	7,650
CF_3Br	1301	832,000	14,000
$C_2F_4Br_2$	2402	126,000	1,600
CO_2	—	658,000	658,000

Table 4-6.8 ***Necessary Control Measures for Computer Room Fire Stage Sequence***

Fire Stage	Control	Serious Danger Concern
1. Pre-ignition	Good housekeeping practices, control combustible furnishings and interior finish	
2. Initial pyrolysis	Smoke detection system	Occupants and business interruption
3. Incipient	Portable fire extinguishers, Halon 1301 automatic suppression system	Occupants and contents
4. Pre-flashover	Automatic sprinklers	Occupants and structure
5. Post-flashover	Fire walls, compartmentalization	Surrounding structures

As an example, total computer room fire protection might involve several different control measures addressing different possible fire conditions. Table 4-6.8 illustrates this concept, based on the different stages of a growing fire. The table is not a rigid description of the fire protection requirements of every computer room, but instead an example of how total fire protection is the overall objective when approaching a design situation.

An important factor of developing halogenated agent extinguishing systems is the interaction of all concerned individuals. To design, install, maintain, and operate a halon system requires a cooperative effort from a number of different groups. As shown in Figure 4-6.6, these individuals include the end users, consultants, manufacturers, installers, insurance representatives, and other selected authorities. Representatives from all these groups work together to develop and enhance model codes, which provide guidance and understanding for proper halon system usage.

System Configurations

Detection

The three primary parts of every halogenated agent extinguishing system are detection, control panel, and agent delivery. Since there is no single type of detector that offers the ultimate for every application, consideration must be given to the types of combustibles and combustion that are likely to occur in the protected area.

Photoelectric and ionization smoke detectors have different response characteristics to fires and can be susceptible to false or unwanted alarms. Thermal detectors, although more reliable, react more slowly to fire conditions. In certain applications, speed is critical and optical detectors would be required.

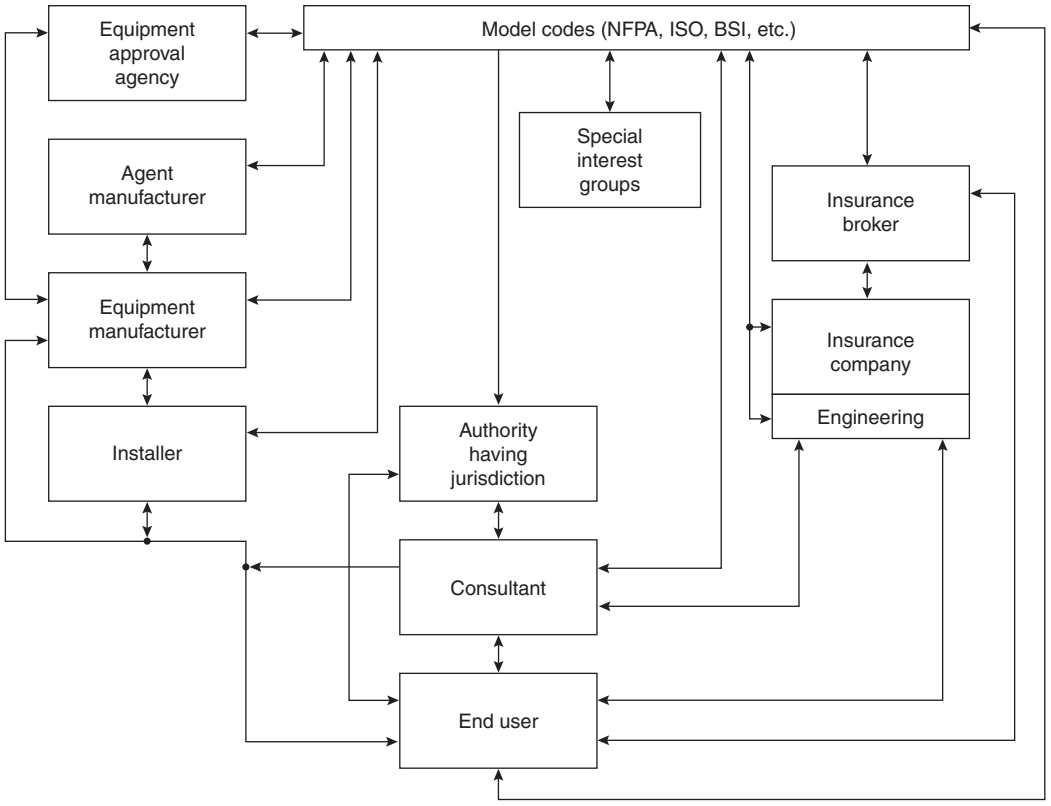

Figure 4-6.6. ***Typical inter-relationship of halon fire protection interests.***

To optimize the speed and reliability of detection systems, it is important to use two different types of detectors on two separate detection loops within the hazard area. This method is referred to as cross-zone detection. Each detection loop functions independently to provide both added reliability with a comforting degree of redundancy.[21]

Control Panels

Features: As its name implies, the control panel is the device that controls system operation and allows the system to function as designed. When a control panel protects more than one area, each individual area is referred to as a zone of protection. Each zone of every halon control panel has three different types of circuits: initiating, signaling, and release. A fire alarm zone and halon zone are compared in Table 4-6.9 to illustrate the differences between these circuit types. It is unusual for a single halon control panel to protect more than five zones at once due to the high number of circuits required. Fire alarm control panels, on the other hand, may have dozens of individual zones.

Initiating circuits provide the input into the panel and support automatic detectors, manual pull stations, and other initiating devices. Automatic detectors are normally cross-zoned, which implies two separate detection circuits. One circuit is required for prealarm and both circuits are necessary for halon release. The signaling circuits, sometimes referred to as bell or auxiliary circuits, are used for audible/visual alarms and other auxiliary functions. The release circuits allow the halon to release from the containers and are sometimes referred to as firing, solenoid, initiator, dump, or halon circuits.

Modes of operation: At any time, a halon control panel and the halon system could be in one of four modes of operation; as shown in Table 4-6.10 these include unpowered, normal, alarm, and trouble condition. The alarm condition is further definable with prealarm, prerelease, release, and postrelease condition. Typical systems utilizing cross-zoning detection activate, when required, into prealarm and/or release condition, but this often becomes more complicated with time delays, abort switches, and other auxiliary functions. Unless otherwise specified, manual pull stations activate all alarm conditions, override abort switches, if present, and immediately release the halon. These different alarm conditions provide a convenient mechanism for sequential operation

Table 4-6.9 ***Typical Control Unit Features***

	Halon Zone	Fire Alarm Zone
Initiating circuit	Two cross zone detection circuits	One circuit for detection
Signaling circuit	Multiple signaling sequence	Multiple signaling sequence
Release circuit	One circuit	None

Table 4-6.10 ***Modes of Control Panel Operation***

Unpowered condition	Off
Normal condition	On
Alarm condition:	
Prealarm	One detector activates.
Prerelease	Two cross-zoned detectors activate. Time delay starts.
Release	Time delay ends or manual pull station activates. Halon is released.
Postrelease	Halon has been released.
Trouble condition	Failure or disruption of field wiring. Insufficient power input.

of audible/visual signaling, equipment shutdown, fire service notification, and other auxiliary functions.

Control panel economics: As halogenated agent extinguishing systems become more numerous, the frequency of large-scale projects with multiple halon zones in a single facility is increasing. Today, entire data processing centers and telecommunications buildings are protected with Halon 1301 systems. To protect a large building with many halon zones, it may appear that the most effective way of configuring the system is by using a single large control panel with the capacity for all required halon zones. This is not true, since there is a limitation to the number of halon zones that any one halon panel can effectively manage. Figure 4-6.7 illustrates an alternative method, where the individual halon zones of a large building each have their own halon panel wired to give an alarm or trouble signal to a central fire alarm panel.

A typical halon zone requires an average of 12 wires to support all the necessary system functions. Thus, the cost of running multiple wires and large conduit instead of only two wires (for interpanel communication) often offsets the cost of smaller, more numerous panels located near the halon zones. This configuration offers flexibility for future consolidations or additions, which are common for high technology facilities. Aesthetics are enhanced at the master control location, and system operation is simplified. Installation checkout and servicing is easier when the halon control panel is within the hazard area. Finally, the overall system is more reliable due to less wiring, lack of design complexity, simplified maintenance, and multisource dependence.

Agent Delivery

In addition to the control panel and detection, the other primary part of every halogenated agent extinguishing system is agent delivery. The agent delivery includes the discharge nozzles, agent storage container(s), release mechanism, and associated piping. As shown in Table 4-6.11, three methods of agent delivery exist: (1) central storage, (2) modular, and (3) shared supply. Central storage has the container(s) centrally located, with the agent piped accordingly. This method is popular due to its similarity with carbon dioxide system technology (which helped develop early systems), along with usually having the lowest initial cost. Modular systems use smaller containers strategically located throughout the hazard area, with minimal piping. The high reliability of modular systems is based on lack of dependancy on piping integrity, negligible piping calculations, total system supervision, multisource dependence, and the inherent ability to be heat actuated regardless of catastrophic system failure. Modular systems are simple to design, are relatively easy to install, and have a high degree of future flexibility. Systems utilizing shared supply are essentially central storage systems with container(s) shared by more than one hazard volume. Even though fewer containers are used, directional valves and extensive piping do not often allow shared supply systems to be cost effective.

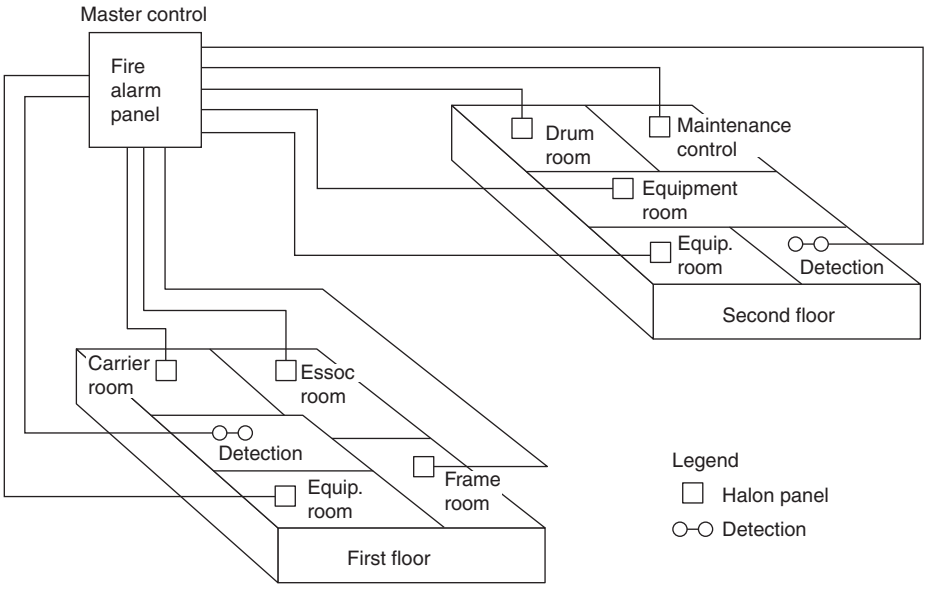

Figure 4-6.7. ***The network concept of control panel interface for a typical halon application.***

Table 4-6.11 ***Comparison of Different Methods of Agent Delivery***

	Central Storage	Modular	Shared Supply
Hardware cost	Moderate	High	Moderate
Installation cost	Moderate	Low	Moderate
Design simplicity	Difficult	Simple	Difficult
Installation simplicity	Difficult	Medium	Difficult
Operation and maintenance simplicity	Medium	Medium	Medium
Reliability	Moderate	High	Low
Future flexibility	Low	High	Low

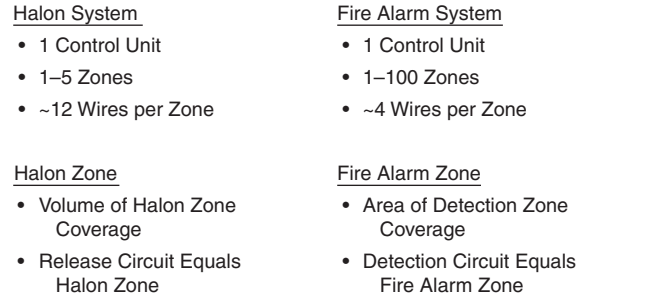

Figure 4-6.8. ***Halon/fire alarm differences.***

Adding to its unpopularity are its design and installation complexity, low reliability, and impaired future flexibility. When a shared supply halon system activates for one hazard, the remaining hazards become unprotected until the system is completely recharged.

Design Concepts and Methodology

Definitions and Terminology

Halogenated agent extinguishing systems are typically classified as either total flooding or local application systems. A total flooding system is designed to develop and maintain a concentration of halon that will extinguish fires in combustible materials located in an enclosed space. Local application systems are designed to apply the agent directly to a fire that may occur in an area or space that is not immediately enclosed. In addition to these, there are specialized applications, which may include combination total flooding/local application or partial flooding. The vast majority of installed halon systems today are the total flooding type using Halon 1301.

The definitions of halon system and halon zone are often confusing. This is especially true to individuals closely associated with the fire alarm industry, since fire alarm terminology is similar. Figure 4-6.8 defines the basic features of a halon system and halon zone and offers a comparison with each respective fire alarm counterpart.

A halon zone usually equates to an area of halon coverage functioning on a single release circuit, while the zones in a fire alarm system typically are each detection circuit. As an example, one halon zone could be a single computer room, whereas a fire alarm zone could be the entire floor of a building. A halon system also has much fewer (though more comprehensive) zones than a fire alarm system.

Halon Design Guidelines

The design process necessary for total flooding systems is easily quantified. The procedure can be separated into five definable steps: (1) hazard identification, (2) determination of agent quantity, (3) specification of operating requirements, (4) determination of hardware requirements, and (5) generation of postdesign information.

The initial step is to provide a definition of the hazard. This includes determining the fuels involved, the dimensions and configuration of the enclosure, the maximum and minimum net volumes, the status of occupancy, the expected hazard area temperature range, and possible unclosable openings. Based on this information, the minimum design concentration can be established. Next, the agent quantity is determined based upon the design concentration, the volume, minimum expected temperature, leakage due to ventilation or unclosable openings, and altitude above sea level. Usually, the gross volume is used to calculate the agent quantity to allow for extra agent to replace that lost through normal building leakage. However, agent concentrations must conform with the applicable toxicity criteria with respect to the minimum net volume and maximum temperature. The operating specifications are then required if they have not already been established. These will indicate how the system is to operate, the modes of operation, the type of agent delivery, and so forth. When these are known, the necessary hardware requirements must be obtained and the design of the system completed. The final step is to generate the postdesign information necessary for others to install, test, operate, and maintain the system. Postdesign information should contain all design calculations (including hydraulic calculations), complete blueprint drawings, and detailed information describing the testing, operation, and maintenance of the system.

Local Application and Special Systems

Local application systems are often installed to extinguish fires involving flammable liquids, gases, and surface burning solids. Such systems are designed to apply the agent directly to a fire that may occur in an area or space not immediately enclosed. They must be designed to deliver halon agent to the hazard being protected in such a manner that the agent will cover all burning surfaces during discharge of the system. Because of its lower volatility, Halon 1211 may be better suited than other forms of halon for local application systems. The lower volatility, plus a high liquid density, permits the agent to be sprayed as a liquid and thus propelled into the fire zone to a greater extent than is possible with other vaporized agents. Examples of areas protected by local application are spray booths, dip and quench tanks, oil-filled electric transformers, printing presses, heavy construction equipment, and vapor vents. An example of a local application system is shown in Figure 4-6.9.

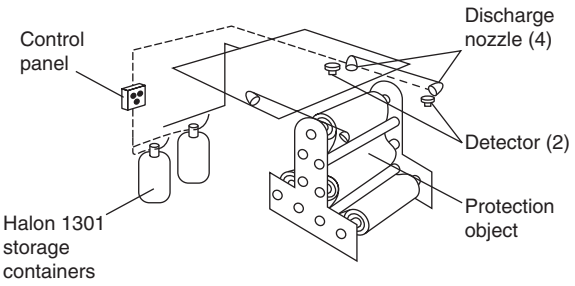

Figure 4-6.9. ***Local application system.***

Currently, NFPA standards do not set a minimum limit on the discharge time for a local application design. The rate of discharge and the amount of agent required for a given application must be determined by experimentation and evaluation. The most critical components of these systems are the discharge nozzles; the discharge velocity and rate must be sufficient to penetrate the flames and produce extinguishment but not be so great as to cause splashing or spreading of fuel and thus increase the fire hazard. The minimum design discharge quantity should not be less than 1.5 times the minimum quantity required for extinguishment at any selected design rate.[20] Also of critical importance are type and location of detectors.

As with other types of gaseous suppression systems, local application systems can be designed according to the rate-by-volume method or the rate-by-area method. The rate-by-area method determines nozzle discharge rates based on the exposed surface area of the hazard being protected. This method is less popular than the rate-by-volume method, which requires discharge rates sufficient to fill (within the discharge time) a volume whose imaginary boundaries extend a limited distance from the protected hazard. This method is favored since it performs similarly to total flooding systems. Important factors to be considered in the design of a local application system are the rate of agent flow, the distance and area limitations of the nozzles, the quantity of agent required, the agent distribution system, and the placement of detectors.

Unlike total flooding systems, only the liquid portion of the discharge is effective for local application systems. The computed quantity of agent needed for local application must be increased to compensate for the residual vapor in the storage container at the end of liquid flow. An additional 25 percent storage capacity is required in the absence of an enclosure that would prevent gas dissipation. Systems should also compensate for any agent vaporized in the pipe lines due to heat absorption from the piping. The heat transfer is important when the piping is at a higher temperature than the agent. The following equation determines the amount of agent increase necessary to compensate for this effect:[7]

$$W_x = \frac{2\pi kL(T_p - T_a)(t)}{3600h(\ln r_o/r_i)} \quad (1)$$

where

W_x = amount of agent increase, kg (lb)

k = themal conductivity of the piping, W/m·K (Btu·t/hr·ft²·°F)

L = linear length of the piping, m (ft)

T_p = pipe temperature, °C (°F)

T_a = agent temperature, °C (°F)

t = system discharge time

h = heat of vaporization of the agent at T_a, kJ/kg (Btu/lb)

r_o = outside pipe radius, mm (in.)

r_i = inside pipe radius, mm (in.)

Specialized systems using a variety of agents are in wide use throughout the world to protect hazards such as aircraft engine nacelles, military vehicles, emergency generator motors, earth moving equipment, and racing cars. The characteristic common to all these systems is that they can only be applied to the specific hazard for which they were designed and tested. One unusual concept used to protect aircraft flight simulator areas is known as partial flooding, where only the volume containing the simulator equipment receives the total flooding concentration, and not the expansive open areas above it. A design concentration of 7 percent is recommended to achieve a 5 percent concentration in the hazard area and should provide for a minimum agent height level relative to the agent concentration of approximately 1.5 m (5 ft) above the highest part of the hazard. The placement of the nozzle is critical and should be designed to direct agent discharge approximately 30 degrees below the horizontal plane. As shown in Figure 4-6.10, the savings associated

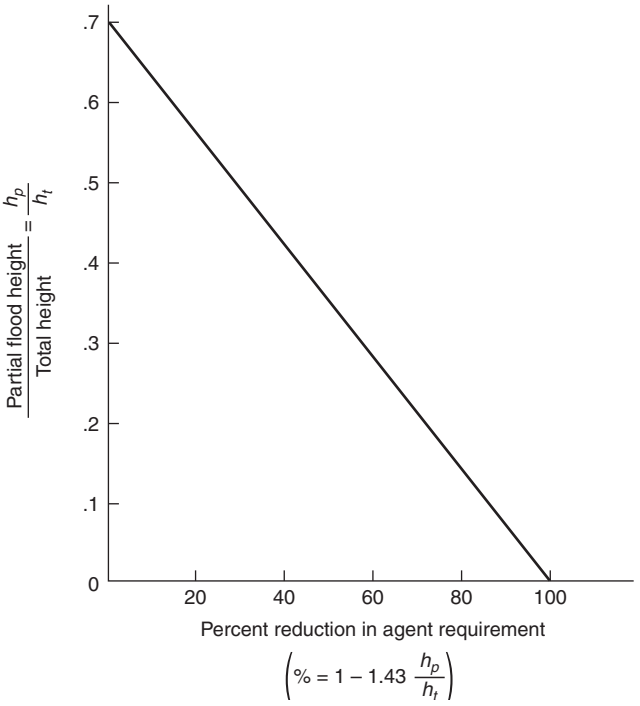

Figure 4-6.10. ***Agent reduction associated with partial flooding systems.***

with partial flooding systems can be substantial, especially in areas with very high ceilings.[19]

Agent Requirements: Total Flooding

Design Concentrations: Solid Fuels

Flammable solids may be classified as those that do not develop deep-seated fires and those that do. Class A combustible solids that develop deep-seated fires do so after exposure to flaming combustion for a certain length of time, which varies with the material. Some materials may begin as deep seated through internal heating such as spontaneous ignition. With respect to Halon 1301 total flooding systems, a fire is considered deep seated if a 5 percent concentration will not extinguish the fire within 10 min after agent discharge.[7] Materials that do not become deep seated undergo surface combustion only and may be treated much the same as those in a flammable liquid fire.

The presence of Halon 1301 in the vicinity of a deep-seated fire will extinguish the flame and reduce the rate of burning, yet the quantity of agent required for complete extinguishment of all embers is difficult to assess. Often it is impractical to maintain an adequate concentration of Halon 1301 for a sufficient time to ensure the complete extinguishment of a deep-seated fire. Factors affecting this concentration include

1. Nature of fuel
2. Time during which it has been burning
3. Availability of oxygen within the enclosure
4. Ratio of burning surface area to the volume of the enclosure
5. Geometric characteristics of the fuel
6. Fuel distribution within the enclosure

Table 4-6.12 illustrates the extinguishing concentrations of selected flammable solid fires as indicated by six different halon industry groups.[22]

Even where the fire has inadvertently become deep seated, application of a low Halon 1301 concentration has two benefits. First, all flaming combustion is halted, preventing rapid spread of the fire to adjacent fuels. Second, the rate of combustion is drastically reduced. These two characteristics justify the ability of Halon 1301 to control, if not extinguish, deep-seated fires. However, Halon 1301 systems that are specifically designed to extinguish deep-seated fires are seldom economical to apply and may not be as effective in these fires as other types of extinguishing systems.

Design Concentrations: Liquid and Gas Fires

There are two general types of flammable liquid or gas fires. First, a flammable or explosive mixture of vapors exists that must be prevented from burning, and second, fuel is burning that must be extinguished. Associated with each of these conditions is a minimum level of Halon 1301 extinguishing concentration, respectively known as inerting and flame extinguishment. When determining the halon design concentration, proper consideration must be given to the quantity and type of fuel

Table 4-6.12 ***Extinguishing Concentrations of Selected Flammable Solid Fires***

	Halon 1301 Concentration (percent by volume)					
	Factory Mutual	Fenwal	Ansul	DuPont	Safety First	Underwriter Labs
Surface Fires						
Polyvinyl chloride		2.0		2.6	3.8	
Polystyrene		3				
Polyethylene		3				
Stacked computer printout			5.1			
Polyester computer tape		5			3.8	
Wood crib 30 pcs. $^3/_4$" × $^7/_8$"	3					
Wood crib 24 pcs. 2" × 2" × 18"					3.8	
Wood crib 1A 50 pcs. 2" × 2" × 18"					3.8	3.88
Excelsior loose on floor					3.8	6.0
Shredded paper loose on floor					3.8	
Polyurethane foam				3	3.8	
Cotton lint					3.8	
Crumpled paper	3	6			3.8	
Wood pallets—stack of 10	3					
Deep-Seated Fires						
Shredded paper in wire basket					20	18.0
Polyester computer tape loose in open wire basket		10				
Charcoal	13					
Parallel wood blocks	20					
Glazed fox fur					6.5	

involved, the conditions under which it normally exists in the hazard, and any special conditions of the hazard itself. If certain hazards have explosion potential either before or following a fire due to the presence of volatile, gaseous, or atomized fuel, then special consideration should be given to vapor detection and explosion suppression measures.

As its name implies, the flame extinguishment concentration assumes that the given fuel is burning and that Halon 1301 injected into the air surrounding the fuel at the stated concentration will extinguish the fire.[7] Design concentrations for flame extinguishment are given in Table 4-6.13. These concentrations are not considered effective with premixed flames or explosive mixtures of fuel vapor in air, but instead apply to diffusion flames, where the flames emanate from pure fuel vapor, and oxygen suffuses into the flame zone from the outside. If the possibility of a subsequent reflash or explosion exists, then the flame extinguishing concentration is not sufficient. NFPA 12A[7] defines these conditions as "when both:

1. The quantity of fuel permitted in the enclosure is sufficient to develop a concentration equal to or greater than one-half of the lower flammable limit throughout the enclosure, and
2. The volatility of the fuel before the fire is sufficient to reach the lower flammable limit in air (maximum ambient temperature or fuel temperature exceeds the closed cup flash point temperature) or the system response is not rapid enough to detect and extinguish the fire before the volatility of the fuel is increased to a dangerous level as a result of the fire."

Most fuels exhibit about a 30 to 40 percent higher concentration for inerting than for flame extinguishment. The minimum inerting concentration suppresses the propagation of the flame front at the "flammability peak" or stoichiometric fuel/air composition and inerts the enclosure so that any fuel/air mixture will not burn. The higher inerting concentration is often considered safer to use even if the flame extinguishment concentration is feasible, yet the sacrifices include higher system cost and higher concentrations to which personnel may be exposed. (See Table 4-6.14.)

Table 4-6.13 ***Design Concentration for Flame Extinguishment***

Fuel	Minimum Design Concentration (percent by volume)
Acetone	5.0
Benzene	5.0
Ethanol	5.0
Ethylene	8.2
Methane	5.0
n-Heptane	5.0
Propane	5.2

Table 4-6.14 ***Halon 1301 Design Concentrations for Inerting***

Fuel	Minimum Concentration (percent by volume)
Acetone	7.6
Benzene	5.0
Ethanol	11.1
Ethylene	13.2
Hydrogen	31.4
Methane	7.7
n-Heptane	6.9
Propane	6.7

Includes a safety factor of 10 percent added to experimental values

It is possible to calculate whether the flame extinguishing concentration is acceptable by determining if the fuel present in the hazard will permit attainment of the one-half lower flammable limit of the fuel. The equation to determine the maximum allowable fuel loading (*MFL*) for flame extinguishment concentrations is

$$MFL = \frac{(K_c)(LFL)(MW)}{T} \tag{2}$$

where

MFL = maximum allowable fuel loading, kg/m^3 (lb/ft^3)
K_c = conversion factor, 0.06093 (0.00685)
LFL = lower flammable limit of fuel in air, percent volume
MW = molecular weight of fuel
T = temperature, K (R)

This can be compared with the actual fuel loading (*FL*), which is calculated by

$$FL = \frac{(VF)(W_{lt_2O})(SG)}{V} \tag{3}$$

where

FL = fuel loading, kg/m^3 (lb/ft^3)
VF = volumetric quantity of fuel, m^3 (ft^3)
W_{lt_2O} = specific weight of water, 997.9 kg/m^3 (62.3 lb/ft^3)
SG = specific gravity of fuel
V = volume of enclosure, m^3 (ft^3)

If the fuel loading, *FL*, exceeds the maximum allowable fuel loading, *MFL*, then the inerting concentration for the particular fuel should be used. Most applications involve a variety of fuels within a single enclosure. If the sum of the actual fuel loadings, *FL*, is greater than any single maximum allowable fuel loading, *MFL*, then the most stringent inerting concentration is recommended. If it is determined that a flame extinguishment concentration is sufficient, the value for the fuel requiring the greatest concentration is most applicable.

Calculation of Agent Quantity

The calculations necessary for determining the Halon 1301 total flooding quantity are dependent on temperature, volume of the enclosure, agent concentration, altitude with respect to sea level, and losses due to ventilation and leakage. Most applications are based on a static volume enclosure with all openings sealed and all ventilation systems shut down prior to discharge. This simplifies the calculation significantly. Often the ventilation system does not shut down but instead is dampered to allow recirculating air (without makeup air) to continue cooling sensitive electronic equipment and promote the mixing of halon and air. Total flooding quantities are still based on a static volume for these applications. However, in this instance, it may be necessary to include the volume of the ventilation ductwork in addition to the volume of the enclosure. The equation to determine the Halon 1301 total flooding quantity is

$$W = \frac{(V)(C)(A_c)}{S(100 - C)} \tag{4}$$

where

W = 3 weight of Halon 1301 required, kg (lb)

C = Halon 1301 concentration, percent by volume

A_c = altitude correction factor—(Refer to Table 4-6.15)

S = specific vapor volume based on temperature, m^3/kg (ft^3lb)

$S = 0.14781 + 0.000567T$; T = Temperature °C

$S = 2.2062 + 0.005046T$; T = Temperature °F

Application Rate

Discharge time and soaking period: When designing a Halon 1301 total flooding system, it is important to determine the system discharge time and soaking period.

As indicated in NFPA 12A, "the agent shall be completed in a nominal 10 seconds or as otherwise required by the authority having jurisdiction."[7] The reasons for a rapid discharge time include keeping unwanted products of decomposition to a minimum and achieving complete dispersal of agent throughout the enclosure. Sometimes a much faster application rate is required due to the possibility of a fast spreading fire; yet, discharge times longer than 10 s are sometimes necessary for areas such as museums requiring that turbulence be kept to a minimum, or areas with unavoidably difficult piping configurations.

Table 4-6.15 ***Correction Factors for Altitudes***

Altitude		Correction Factor
Feet	Meters	
3000	914	0.90
4000	1219	0.86
5000	1524	0.83
6000	1829	0.80
7000	2134	0.77
8000	2438	0.74
9000	2743	0.71
10000	3048	0.69
11000	3353	0.66
12000	3658	0.64
13000	3962	0.61
14000	4267	0.59
15000	4572	0.56

The soaking time is another important requirement for a Halon 1301 total flooding system. This is especially true for deep-seated fire or fires that may reflash. The most common application today for total flooding systems is the protection of valuable electronic equipment. Fires in these applications are almost always extinguished within a few seconds by the Halon 1301 agent, yet a 10-min soaking period is usually required. This estimated time period allows responsible individuals to arrive at the scene to take follow-up action. It is important to remember that halogenated agent extinguishing systems in most cases have only a single chance to control an unwanted fire.

Effects of ventilation: When Halon 1301 is discharged into a total flooding enclosure that is ventilated, some agent will be lost with the ventilating air. Assuming that ventilation must continue during and after discharge, a greater amount of agent is required to develop a given concentration. Also, to maintain the concentration at a given level requires continuous agent discharge for the duration of the soaking period. If an enclosure initially contains pure air, the Halon 1301 discharge rate required to develop a given concentration for agent at any given time after the start of discharge is[7]

$$R = \frac{(C)(E)}{(S)(100 - C)\left[1 - e^{(-Et_1/V)}\right]} \tag{5}$$

where

R = Halon 1301 discharge rate, kg/s (lb/s)

E = ventilation rate, m^3/s (ft^3/s)

t_1 = discharge time, s

e = natural logarithm base, 2.71828

The Halon 1301 discharge rate necessary to maintain a given concentration of agent is[7]

$$R = \frac{(C)(E)}{(S)(100 - C)} \tag{6}$$

After the agent discharge is stopped, the decay of the agent concentration with respect to time is[7]

$$C = C_0 e^{(-Et_2/V)} \tag{7}$$

where

C_0 = agent concentration at end of discharge, percent volume

t_2 = time after stopping discharge, s

Compensation for leakage: Occasionally a Halon 1301 total flooding system is designed for an enclosure that has openings that cannot be closed. An example may be a conveyor belt penetrating an enclosure wall, yet even these openings can sometimes be closed using inflatable seals. Halon 1301 discharged into an enclosure for total flooding will result in an air/agent mixture that has a higher specific gravity than the air surrounding the enclosure. Therefore, any openings in the lower portions of the enclosure will allow the heavier air/agent mixture to flow out and the lighter outside air to flow in. Fresh air entering the enclosure will collect toward the top, forming an interface between the air/agent mixture and fresh air. As the leakage proceeds, the interface will descend toward the bottom of the enclosure. The space above the interface will be completely unprotected, whereas the lower space will essentially contain the original extinguishing concentration. There are two methods of compensating for unclosable openings: initial overdose and extended discharge.

The initial overdose method provides for an adequate overdose of Halon 1301 to ensure a preestablished minimum of agent at the end of the desired soaking period. Mechanical mixing is required within the enclosure to prevent stratification of agent concentration and a descending interface. Also caution must be used to prevent personnel exposure to the high initial concentrations. The necessary initial concentration depends upon the extended protection time required, the opening height, the opening width, and the volume of the enclosure. Referring to Figure 4-6.11, the equation used to determine the initial concentration for a final concentration of 5 percent is[7]

$$G = \frac{(K)(W_o)(2g_cH^3)^{1/2}}{3V} \quad (8)$$

where

G = geometric constant
K = orifice discharge coefficient, 0.66
W_o = opening width, m (ft)
g_c = acceleration due to gravity, 9.81 m/s² (32.2 ft/s²)
H = opening height, m (ft)

The other method used to compensate for unclosable openings is extended discharge. This involves at least two separate piping systems: one to achieve the initial agent concentration, and the other to provide a continuous addition of Halon 1301 at a rate which will compensate for leakage out of the enclosure during the soaking period. The agent must be discharged in such a way that uniform mixing of agent and air is obtained. This mixing is often difficult due to the extremely low flow rates being discharged over the entire soaking period, occasionally resulting in small nozzles freezing due to air moisture. Based on the design concentration and opening height, Figure 4-6.12 can be used to determine the Halon 1301 makeup rate per unit opening width.

Assuming the design concentration of Halon 1301 is established in the enclosure initially, the time required for the interface to reach half-way down the enclosure height can be calculated. Referring to Figure 4-6.13, the geometric constant previously calculated for intial overdose is used to find the soaking time based on the initial design concentration.

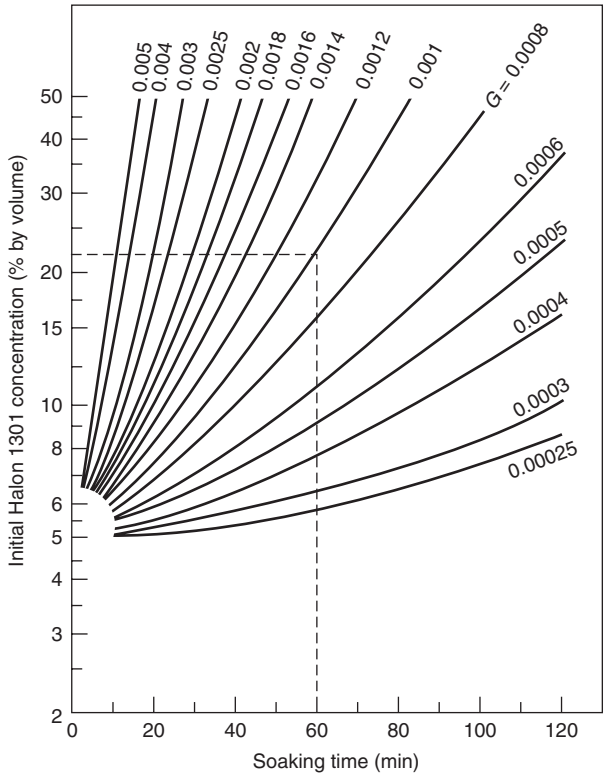

Figure 4-6.11. ***Initial amount of Halon 1301 to produce a 5 percent residual concentration in enclosures equipped for mechanical mixing.***

Flow Calculations

Piping Theory

The overall objective of designing a Halon 1301 piping system is to properly disperse the required concentration of Halon 1301 throughout the hazard volume within the specified time period. Systems must be engineered to operate quickly and effectively. The discharge time (usually a nominal 10 s as indicated by NFPA 12A) is a critical system constraint and is measured as the interval between the first appearance of liquid at the nozzle and the time when the discharge becomes predominantly gaseous.[7] The hydraulic calculations are considered to be the most difficult part of the entire design process, and are almost always calculated with the aid of computer programs due to the tedious nature of manual calculations.

As illustrated in Figure 4-6.14, the primary components of a Halon 1301 piping system are the agent storage

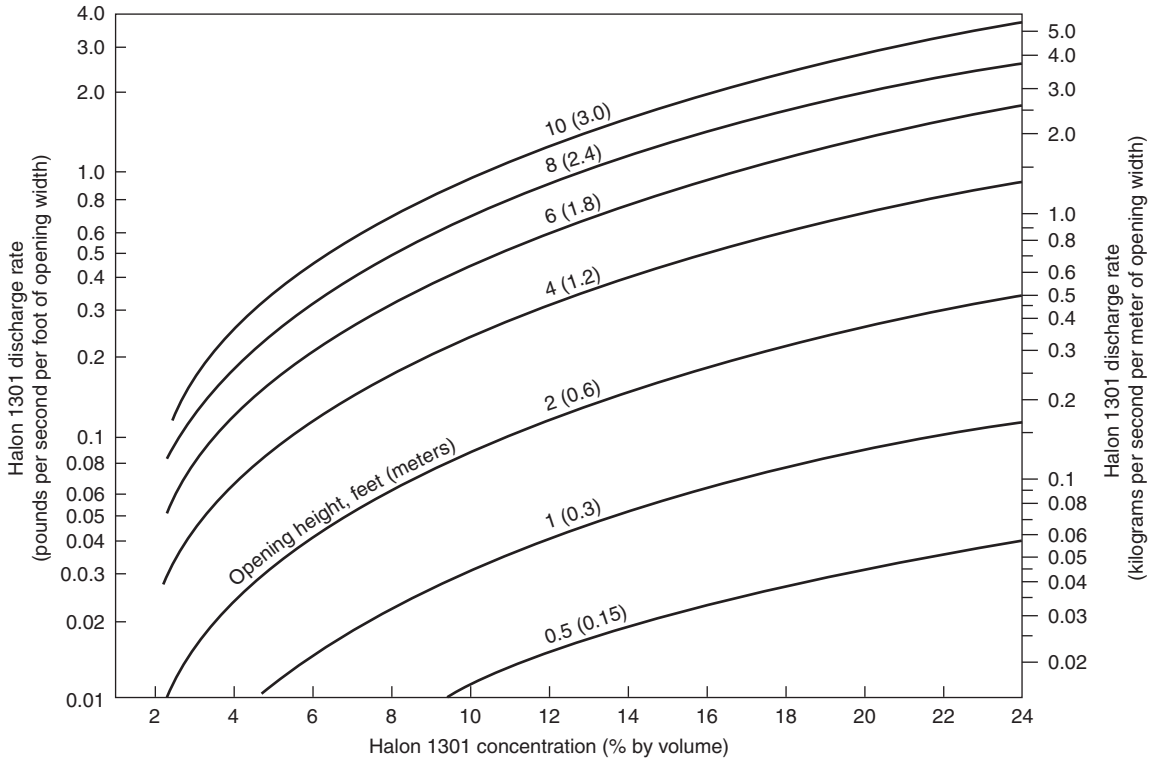

Figure 4-6.12. ***Extended discharge rate of Halon 1301 to maintain constant concentrations in enclosures with openings.***

container, the discharge nozzle, and the pipe. Often, more than one nozzle is required, complicating the calculations significantly. An attempt should always be made to keep the piping system simple and if possible, balanced. A balanced system has the actual and equivalent pipe lengths from container to each nozzle within ± 10 percent of each other and has equal design flow rates at each nozzle.[7]

As with sprinkler systems or other systems involving fluid flow, the methodology for solving Halon 1301 piping calculations involves seeking terminal characteristics based on property changes encountered due to the movement of the fluid. The system hydraulics are controlled by the selection of the orifice area at the discharge nozzle. This orifice area is calculated from the nozzle pressure, which is based on the starting pressure in the container and pressure losses in the pipe. Because the flow of Halon 1301 is nonsteady and has a change in phase from liquid to vapor, the calculations become highly complex. To simplify calculations, the average discharge conditions are determined so that they might reasonably represent the entire discharge time span. This time-independent model is based on the moment in time when half the liquid phase of the agent has left the nozzle. All the calculations for a 10 s discharge condition shown in Figure 4-6.15 would be solved at the mid-discharge condition (5 s). Hence, the critical characteristics that vary with discharge, such as the storage container pressure and the pressure-density relationship in the pipeline, are replaced with average time-independent values.[23]

By the time half of the liquid agent is out of the nozzle, the original pressure in the storage container has dropped considerably. To calculate the mid-discharge storage container pressure, the percent of agent still within the pipe must be determined. Also, the initial drop in pressure immediately after the start of discharge is nonlinear. As seen in Figure 4-6.16, the pressure recovery is due to the nitrogen vigorously boiling out of the halon/nitrogen mixture within the storage container.

Unlike water-based fluid flow, the pressure drop occurring when Halon 1301 flows through a pipe is nonlinear and is dependent on the pipeline agent density, not the distance traveled. The pipeline flow is two phase, with a mixture of liquid and vapor agent. As the agent travels in the pipe, the pressure and density decrease, which increases the velocity and the amount of halon vapor. Interestingly, the evolution of the nitrogen from the halon/nitrogen mixture in the storage container causes the halon to drop in temperature and become more dense. This phenomenon fortunately is not a factor in the calculations since a time-independent model is being used. The increase in density at any one location over the entire time span should not be confused with the decrease in density that occurs when the agent flows from one location to another.

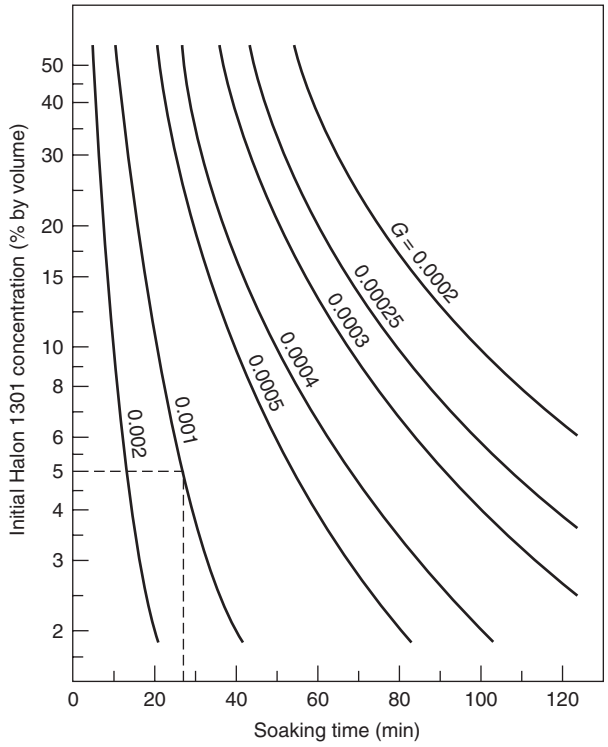

Figure 4-6.13. ***Time required for interface between efluxing Halon 1301/air mixtures and influxing air to descend to center of enclosures not equipped for mixing.***

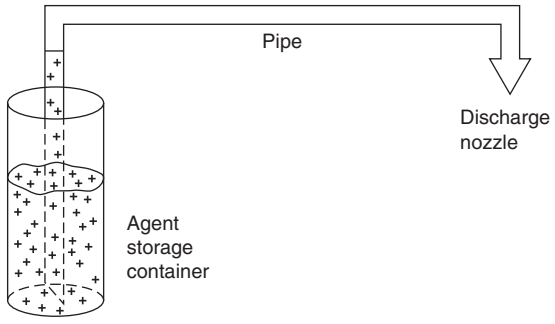

Figure 4-6.14. ***Primary components of a Halon 1301 piping system.***

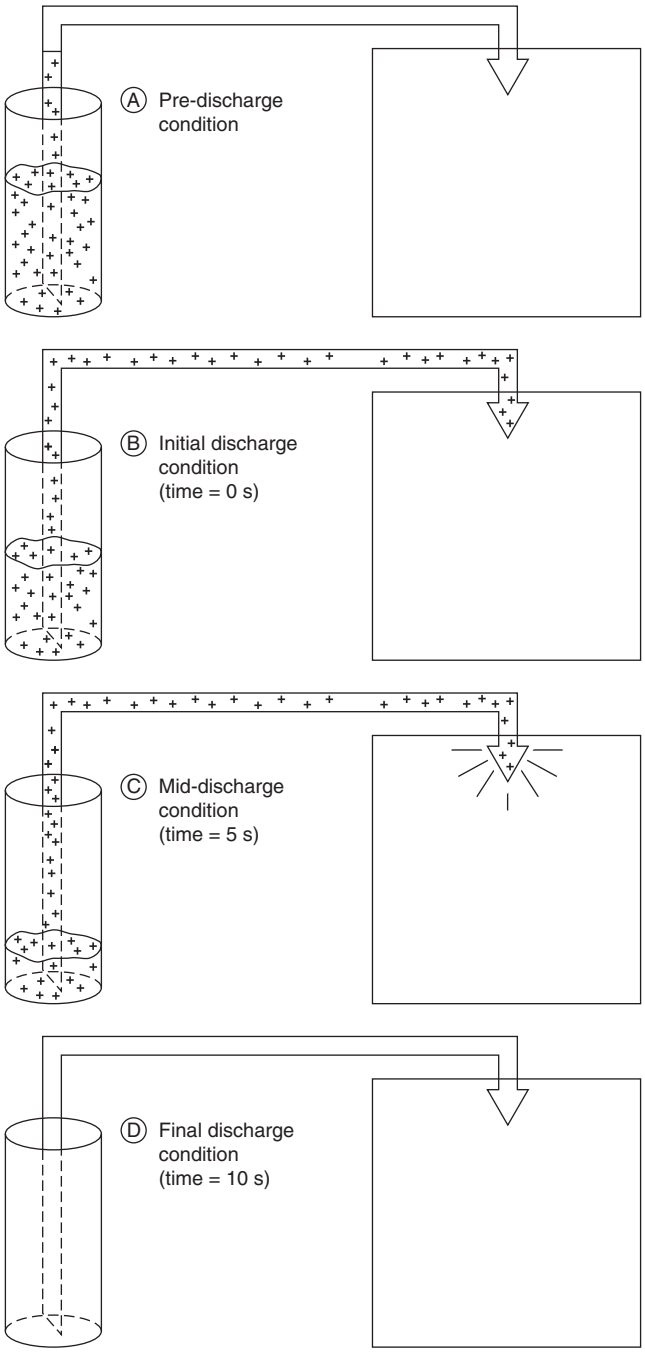

Figure 4-6.15. ***Summary of Halon 1301 discharge conditions based on a 10-s discharge.***

Guidelines and Limitations

Unrealistic distribution networks often fail to perform to specifications and are difficult if not impossible to predict from a calculation standpoint. As the piping system becomes more unrealistic, the calculations become more unreliable. To aid in the development of accurate calculations, certain fundamental limitations are necessary to ensure proper system design. These limitations are especially important with respect to computer programs since these programs have a tendency to be operated abusively with high expectations. Summarized below are the design constraints for Halon 1301 hydraulic calculations.[24]

1. Good design practice
2. Discharge time $\leq$ 10 s
3. Favorable system temperature

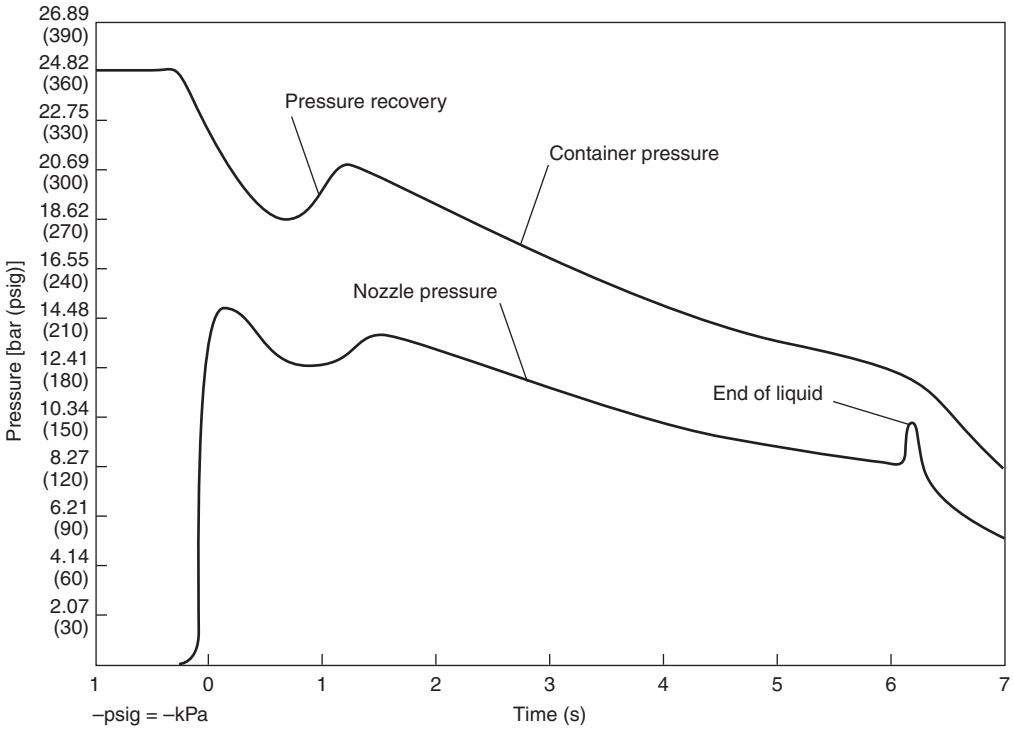

Figure 4-6.16. ***Pressure profile during system discharge.***

4. Initial container pressure = 2482.2 kPa (360 psig) or 4137.0 kPa (600 psig)
5. Initial container fill density ≤ 1121.4 kg/m^3 (70 lb/ft^3)
6. Percent in pipe ≤ maximum value
7. Turbulent flow ≥ minimum value
8. Nozzle pressure ≥ minimum value
9. Actual nozzle area ≤ percentage of feed pipe area
10. Actual nozzle area = calculated nozzle ±5 percent

Good design practice includes such items as favoring balanced systems, keeping the degree of flow/split imbalance below a maximum value, avoiding vertically installed tees, and avoiding nozzles on different floor levels which may separate the halon gas/vapor mixture. The values for some of the constraints are determined by the individuals developing computer programs that are verified by approval agencies through testing.

Calculation Procedure

The piping calculations comprise four steps:

1. Determining the necessary input data
2. Calculating the average storage container pressure
3. Calculating the nozzle pressure at each nozzle, and
4. Calculating the nozzle orifice areas

Pipeline calculations are performed for each segment of pipe having both a constant flow rate and a uniform pipe diameter; thus the piping network is divided into sections called junctions. Each discharge nozzle is also identified. The forms necessary for the input data, pressure calculations, and nozzle calculations are contained in Figures 4-6.17 and 4-6.18. Assuming the appropriate input data are known, the average storage container pressure is determined from Figure 4-6.19 based on the percent agent in pipe, which itself is determined by[7]

$$\% \text{ in pipe} = \frac{K_1}{\left(W_i/V_p\right) + K_2} \tag{9}$$

where

W_i = initial charge weight of Halon 1301, lb
V_p = internal pipe volume, ft^3 (See Table 4-6.16)
K_1 and K_2 = constants (See Table 4-6.17)

Once the average storage container pressure is known, Figures 4-6.18 and 4-6.20 and Equations 10 through 22 can be used to determine the nozzle orifice areas for a 360 psig system. Usually the calculations are based on a 10-s discharge time, though this is sometimes changed slightly to produce flow rates in accordance with Table 4-6.18. Turbulent pipeline flow can also be achieved by using smaller pipe sizes. Pipe diameters that are too small result in unacceptably high pressure losses; therefore, care must be used in pipe size selection. It is important to recognize that approximations have been made for Y and Z factors and nozzle coefficients. The calculation procedure presented here is only intended to demonstrate the current methodology and not to provide a rigorous solution. The necessary equations are[7,25]

System Halon weight _____ lb
Container fill density _____ lb/ft³
Discharge time _____ s

Form I: System summary

N1: _____ lb N3: _____ lb N5: _____ lb
N2: _____ lb N4: _____ lb N6: _____ lb

A	B	C	D	E	F	G	H	I	W	X	Y
Inputs									Outputs		
Junction number	Nozzle number	Flow rate *Q*	Pipe type	Pipe diameter *D*	Actual pipe length *L*	Fittings, equivalent length *L*	Total length *L*	Elevation change *h*	Junction pressure *P* (starting of from Form II)	Density at orifice *r* (Fig. 4–6.20)	Orifice area *F* (Eq. 22)

Figure 4-6.17. ***Halon 1301 piping calculation summary form.***

$$P_e = \frac{rL_e}{144} \quad (10)$$

where
Pe = elevation pressure, psig
r = agent density, lb/ft³
L_e = pipe elevation length, ft

$$A = 1.013D^{5.25} \quad (11)$$

where
A = pipe size factor
D = actual pipe diameter, in.

$$B = \frac{7.97}{D^4} \quad (12)$$

where
B = pipe size factor

$$Y_1 = -\left(\frac{a}{3}p_0^3 + \frac{b}{2}p_0^2 + cP_0 + d\right) \quad (13)$$

where
Y_1 = first Y factor
P_0 = junction starting pressure, psig
a, b, c, and d = constants (See Table 4-6.19)

Form II: Pressure calculations

J	K	L	M	N	O	P	Q	R	S	T	U	V
Initial pressure				Final pressure								
	Elevation			Pipe size factors								
Junction pressure	Density r (Fig. 4–6.20)	Pressure P_e (Eq. 10)	Corrected starting pressure P_0	A (Eq. 11)	B (Eq. 12)	1st Y factor Y_1 (Table 4–6.19, Eq.13)	1st Z factor Z_1 (Eqs. 14–17)	Temporary Y factor Y_t (Eq. 18)	Temporary pressure P_t (Table 4–6.19, Eq.19)	2nd Z factor Z_2 (Eqs.14–17)	2nd Y factor Y_2 (Eq. 20)	Final junction pressure P (Table 4–6.19, Eq. 21)

Figure 4-6.18. ***Halon 1301 pressure calculation summary form.***

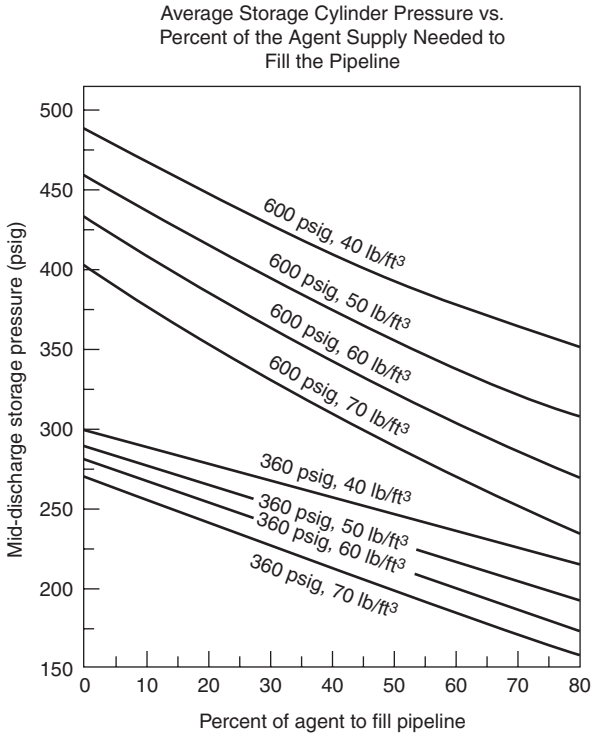

Figure 4-6.19. ***Mid-discharge storage container pressure.***

$$Z = 1.01790 - 0.01179(P - 160) \quad \text{for 70 lb/ft}^3 \text{ fill density} \tag{14}$$

$$Z = 0.96913 - 0.01098(P - 170) \quad \text{for 60 lb/ft}^3 \text{ fill density} \tag{15}$$

$$Z = 0.96412 - 0.01051(P - 175) \quad \text{for 50 lb/ft}^3 \text{ fill density} \tag{16}$$

$$Z = 0.95900 - 0.01008(P - 180) \quad \text{for 40 lb/ft}^3 \text{ fill density} \tag{17}$$

where
Z = Z factor
P = pressure, psig

$$Y_T = Y_1 + L\left(\frac{Q^2}{A}\right) \tag{18}$$

where
Y_T = temporary Y factor
Q = flow rate, lb/s

$$P_T^3 + \left(\frac{3b}{2a}\right)P_T^2 + \left(\frac{3c}{a}\right)P_T = -\left(\frac{3}{a}\right)Y_T - \left(\frac{3d}{a}\right) \tag{19}$$

where
P_T = temporary pressure, psig

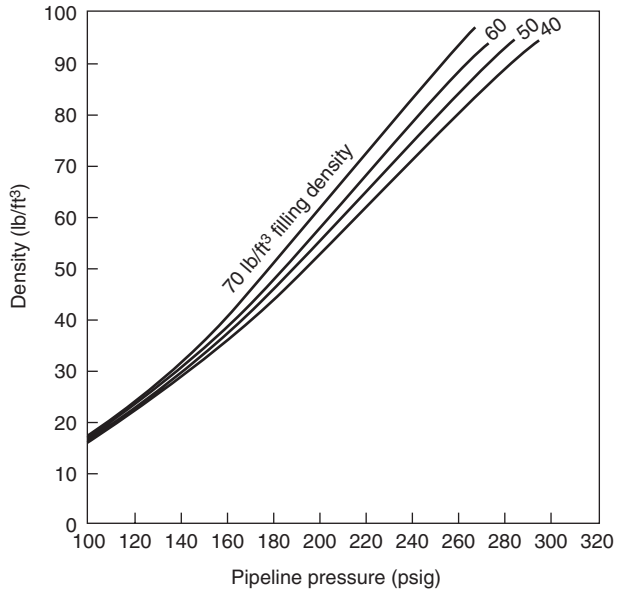

Figure 4-6.20. ***Pipeline density/pressure relationship for a 360 psig system.***

Table 4-6.16 ***Internal Volume of Steel Pipe***

Nominal Pipe Diameter (in.)	Schedule 40 Inside Diameter (in.)	ft³/ft	Schedule 80 Inside Diameter (in.)	ft³/ft
1/4	0.364	0.0007	0.302	0.0005
3/8	0.493	0.0013	0.423	0.0010
1/2	0.622	0.0021	0.546	0.0016
3/4	0.824	0.0037	0.742	0.0030
1	1.049	0.0060	0.957	0.0050
1 1/4	1.380	0.0104	1.278	0.0089
1 1/2	1.610	0.0141	1.500	0.0123
2	2.067	0.0233	1.939	0.0205
2 1/2	2.469	0.0332	2.323	0.0294
3	3.068	0.0513	2.900	0.0459
3 1/2	3.548	0.0687	3.364	0.0617
4	4.026	0.0884	3.826	0.0798

$$Y_2 = Y_T + B\left(Z_2 - Z_1\right)Q^2 \tag{20}$$

where

Y_2 = second Y factor

$$P^3 + \left(\frac{3b}{2a}\right)P^2 + \left(\frac{3c}{a}\right)P = -\left(\frac{3}{a}\right)Y_2 - \left(\frac{3d}{a}\right) \tag{21}$$

$$F = 1.5Q\left[1/f(rp)^{1/2}\right] \tag{22}$$

where

F = nozzle orifice area, in.²

f = nozzle coefficient (approximation = 0.7)

Table 4-6.17 ***Constants to Determine Percent of Agent in Piping***

Storage (psig)	Filling Density	K_1	K_2
600	70	7180	46
600	60	7250	40
600	50	7320	34
600	40	7390	28
360	70	6730	52
360	60	6770	46
360	50	6810	40
360	40	6850	34

Table 4-6.18 ***Minimum Design Flow Rates to Achieve Turbulent Pipeline Flow***

Nominal Pipe Diameter (in.)	Schedule 40 Minimum Flow Rate (lb/s)	Schedule 80 Minimum Flow Rate (lb/s)
1/8	0.20	0.11
1/4	0.34	0.24
3/8	0.68	0.48
1/2	1.0	0.79
3/4	2.0	1.9
1	3.4	2.8
1 1/4	5.8	4.8
1 1/2	8.4	7.5
2	13	13
2 1/2	19.5	17
3	33	26
4	58	48
5	95	81
6	127	109

For SI units: 1 lb/s = 0.454 kg/s

Table 4-6.19 ***Constant for Y Factor/Pressure Equations***

P Storage (psig)	Fill Density (lb/ft³)	a	b	c	d
360	70	3.571×10^{-4}	0.6971	–63.50	–5921
360	60	4.018×10^{-4}	0.6913	–64.01	–6333
360	50	3.125×10^{-4}	0.6238	–56.90	–7386
360	40	3.720×10^{-4}	0.6187	–55.55	–8120

Postdesign Considerations

Postdesign considerations are divided into two categories: system documentation and inspection/acceptance practices. Good halon system design is not complete until full documentation is provided for installation, acceptance, and eventual end user operation. Proper documentation is especially important to prevent the inadvertent discharge of a halon system for other than a fire, since replacement of the halon agent could be very difficult with future availability being dependent on recycled stock.

System Documentation

System documentation should include the items listed below. This material is necessary for others to install, test, operate, and maintain the system. Information can be recorded entirely on system drawings or in both a written manual and system drawings.

System manual

1. Design Data
   (a) Functional and operational description
   (b) Halon 1301 weight calculations
   (c) Hydraulic piping calculations
   (d) Special considerations
2. Installation, Maintenance, and Inspection Instructions

As-built system drawings

1. Floor Plan Layout
   (a) Suitable dimensions
   (b) Equipment locations
   (c) Special installation details
2. Electrical Schematic
3. Equipment Identification
4. Special Notes

Inspection and Acceptance

After installation, each system should be inspected and tested by technicians trained by the equipment manufacturer covering the items listed below:

1. Test system wiring for proper connection, continuity, and resistance to ground
2. Check system control unit in accordance with factory recommended procedures
3. Calibrate and test each detector in accordance with factory recommended procedures
4. Test each releasing circuit for proper resistance by means of a current-limiting meter
5. Test the operation of all ancillary devices such as alarms, dampers, magnetic closers, and so on.
6. Obtain a certificate of inspection signed and dated by the installing contractor and the authority having jurisdiction

An installation checklist is often used, which expands on the above items in complete detail.[26] These checklists are available from agent and equipment manufacturers, installers, insurance groups, and consultants.

When accepting a newly installed halon system, it is important to determine compliance with design specifications. In previous years, a full discharge test was required to provide unquestionable evidence of performance, yet this could be a costly and sometimes unnecessary burden carried by the end user. End users with multiple systems would often prove system acceptance based on the performance characteristics of their other systems.

The primary reason for discharge test failure, when it was performed, was because the hazard enclosure would not hold the design concentration over the entire soaking period.[27] Checking the enclosure for possible halon leakage points has always been difficult and is the only questionable part of the acceptance/inspection procedure. A method referred to as the enclosure integrity test has proved to be very effective for this problem, and validates the integrity of the protected enclosure.[7] This technique shows much promise and has potential for substantially enhancing the reliability of proper system operation.

The most immediate and effective use of fan pressurization techniques is for leakage path indication.[28] This involves pressurizing or depressurizing the enclosure with the fan pressurization apparatus and using an indicating device, such as a smoke pencil or acoustic sensor, to determine leakage paths. The installers' visual inspection of the enclosure now becomes very effective since even the smallest cracks can be located. Due to low cost and simplicity, a smoke source is usually the most desirable method for locating leaks, but an excellent alternative is the use of a directional acoustic sensor that can be selectively aimed at different sound sources.[29] Highly sensitive acoustic sensors are available that can detect air as it flows through an opening and are sensitive enough to clearly hear a human eye blink.[30] Openings can also be effectively detected by placing an acoustic source on the other side of the barrier and searching for acoustic transmission. Another method is to use an infrared scanning device if temperature differences across the boundary are sufficient.[31] These techniques are not quantitative, but they are effective, inexpensive, and easily performed.

Environmental Considerations

Scientific evidence indicates that fire protection Halon 1301 is one of several man-made substances adversely effecting the earth's ozone layer.[32] Ozone exists naturally as a thin layer of gas in the stratosphere that blocks the sun's harmful ultraviolet rays and thus is vital to life on earth. Several adverse environmental and direct health effects are linked to ozone layer depletion, and its preservation is of paramount concern to mankind. It's believed that Halon 1301 (and other chlorofluorocarbons) chemically destroy ozone when emitted into the atmosphere.

Earlier, the phase-out of full system discharge tests that were used to verify enclosure integrity received special attention since they accounted for a proportionately large percentage of fire protection halon emissions. Fortunately, the amount of fire protection Halon 1301 released for actual fires is relatively small. Testing a system by performing a full discharge test allows the release of Halon 1301, which on a cumulative basis may be potentially harmful to the environment and depletes relatively precious stocks of halon agent that should be dedicated to suppressing fires. The release of Halon 1301 should be minimized.

With regard to ozone layer depletion, halons used for fire protection are different than halons used for other industrial applications.[33] Fire protection halons are unique because of their essential mission to prevent the loss of life, minimize the loss of irreplaceable property, assure the continuity of vital operations, and reduce the amount of fire byproducts polluting the atmosphere. Efforts have

been made to minimize the release of fire protection halons for noncritical tasks like training, testing, and research. It is assumed that halon systems will remain in existence for many more years, despite the present worldwide restriction on their production.

Nomenclature

a constant (see Table 4-6.19)
A pipe size factor
A_c altitude correction factor—(refer to Table 4-6.15)
b constant (see Table 4-6.19)
B pipe size factor
c constant (see Table 4-6.19)
C Halon 1301 concentration, percent by volume
C_0 agent concentration at end of discharge, percent by volume
d constant (see Table 4-6.19)
D actual pipe diameter, in.
e natural logarithm base, 2.71828
E ventilation rate, m^3/s (ft/s)
f nozzle coefficient (approximation = 0.7)
F nozzle orifice area, $in.^2$
FL fuel loading, kg/m^3($1b/ft^3$)
g_c acceleration due to gravity, 9.81 m/s^2 (32.2 ft/s^2)
G geometric constant
h heat of vaporization of the agent at T_a, kJ/kg (Btu/lb)
H opening height, m (ft)
k thermal conductivity of the piping, W/m·K (Btu·t/hr·ft^2·f)
K orifice discharge coefficient, 0.66
K_c conversion factor, 0.06093 (0.00685)
L linear length of piping, m (ft)
L_e pipe elevation length, ft
LFL lower flammable limit of fuel in air, percent volume
MFL maximum allowable fuel loading, kg/m^3 (lb/ft^3)
MW molecular weight of fuel
P pressure, psig
P_0 junction starting pressure, psig
P_e elevation pressure, psig
P_T temporary pressure, psig
Q flow rate, lb/s
r agent density, lb/ft^3
R Halon 1301 discharge rate, kg/s (lb/s)
r_i inside pipe radius, mm (in.)
r_o outside pipe radius, mm (in.)
S specific vapor volume of Halon 1301 based on temperature, m^3/kg (ft^3/lb)
SG specific gravity of fuel
t system discharge time
T temperature, K (R)
t_1 discharge time, s
t_2 time after stopping discharge, s
T_a agent temperature, C (F)
T_p pipe temperature, C (F)
V enclosure volume, m^3 (ft^3)
VF volumetric quantity of fuel, m^3 (ft^3)
V_p internal pipe volume, ft^3 (See Table 4-6.16)
W_x amount of agent increase, kg (lb)
W_{h_2O} specific weight of water, 997.9 kg/m^3 (62.3 lb/ft^3)
W weight of Halon 1301 required, kg (lb)
W_o opening width, m (ft)
W_i initial charge weight of Halon 1301, lb
Y_1 first Y factor
Y_2 second Y factor
Y_T temporary Y factor
Z Z factor

References Cited

1. C.C. Grant, "Fire Protection Halons and the Environment: An Update Symposium," *Fire Technology,* 24, p. 1 (1988).
2. "The Halogenated Extinguishing Agents," *NFPA Quarterly,* 48, 8, Part 3 (1954).
3. D. Wharry and R. Hirst, *Fire Technology: Chemistry and Combustion,* Inst. of F. Engrs., Leicester, England (1974).
4. R. Strasiak, "The Development of Bromochloromethane (CB)," *WADC Technical Report 53–279,* Wright Air Development Center, Dayton, OH (1954).
5. *Fire Protection Handbook, Seventeenth Edition,* National Fire Protection Association, Quincy, MA (1991).
6. NFPA 12A-T, *Standard on Halogenated Fire Extinguishing Agent Systems,* National Fire Protection Association, Quincy, MA (1968).
7. NFPA 12A, *Standard on Halon 1301 Fire Extinguishing Systems,* National Fire Protection Agency, Quincy, MA (1992).
8. NFPA 12B, *Standard on Halon 1211 Fire Extinguishing Systems,* National Fire Protection Association, Quincy, MA (1990).
9. NFPA 12C-T, *Tentative Standard on Halon 2402 Fire Extinguishing Systems,* National Fire Protection Association, Quincy, MA (1983).
10. NFPA 75, *Standard for the Protection of Electronic Computer/Data Processing Equipment,* National Fire Protection Association, Quincy, MA (1992).
11. C. Ford, *Halon 1301 Computer Fire Test Program—Interim Report,* DuPont Co., Wilmington, DE (1972).
12. NFPA 2001, *Standard on Clean Agent Fire Extinguishing Systems,* National Fire Protection Agency, Quincy, MA (1994).
13. "DuPont Halon 1301 Fire Extinguishant," *Technical Bulletin B-29E,* DuPont Co., Wilmington, DE.
14. *Evaluation of Telephone Frame Fire Protection,* GTE/Fenwal, Holliston, MA (1970).
15. "Handling and Transferring 'Freon' FE 1301 Fire Extinguishing Agent," *Technical Bulletin FE-2,* DuPont Co., Wilmington, DE (1969).
16. D.G. Clark, *The Toxicity of Bromotrifluoromethane (FE 1301) in Animals and Man,* Ind. Hyg. Res. Lab., Imperial Chemical Industries, Alderley Park, Cheshire, England (1970).
17. R.D. Stewart, P.E. Newton, A. Wu, C. Hake, and N.D. Krivanek, *Human Exposure to Halon 1301,* Medical College of Wisconsin, Milwaukee, unpublished (1978).

18. The Hine Laboratories, Inc., *Clinical Toxicologic Studies on Freon Fe-1301, Report No. 1*, San Francisco, CA, unpublished report (1968).
19. J.L. Bryan, *Fire Suppression and Detection Systems,* Macmillan, New York (1982).
20. N. Sax, *Dangerous Properties of Industrial Materials,* Section 12, 2nd ed., Reinhold, New York (1963).
21. G.J. Grabowski, *Fire Detection and Actuation Devices for Halon Extinguishing System, An Appraisal of Halogenated Fire Extinguishing Agents,* National Academy of Sciences, Washington, D.C. (1972).
22. C. Ford, "Extinguishment of Surface and Deep-Seated Fires with Halon 1301," *Symposium of an Appraisal of Halogenated Fire Extinguishing Agents,* National Academy of Sciences, Washington, D.C. (1972).
23. H.V. Williamson, *Halon 1301 Flow Calculations—An Analysis of a Series of Tests Conducted by FEMA at the Fenwal Test Site,* Chemetron Corp., Hanover (1975).
24. C.C. Grant, "Computer Aided Halon 1301 Piping Calculations," *Fire Safety Journal,* (1985).
25. *Flow in Pipes—Pyroforane Halon 1301,* Produits Chimiques Ugine Kuhlmann, Corbevoie, France.
26. J.J. Brenneman and M. Charney, "Testing a Total Flooding Halon 1301 System in a Computer Installation," *Fire Journal,* 68, p. 6 (1974).
27. S.A. Chines, "Halon System Discharge Testing—An Authority Having Jurisdiction Point of View," *Seminar Paper for Fire Protection Halons and the Environment, NFPA Annual Meeting,* Cincinnati (1987).
28. C.C. Grant, "Controlling Fire Protection Halon Emissions," *Fire Technology,* 24, p. 1 (1988).
29. D.N. Keast, and H.S. Pei, "The Use of Sound to Locate Infiltration Openings in Buildings," *Proceedings of the ASHRAE-DOE Conference on the Thermal Performance of the Exterior Envelope of Buildings,* Orlando, FL, p. 85 (1979).
30. *Ultraprobe 2000 Data Sheet (acoustic sensor),* UE Systems, Elmsford, NY (2000).
31. A.K. Blomsterberg, and D.T. Harrje, "Approaches to Evaluation of Air Infiltration Energy Losses in Buildings," in *ASHRAE Transactions, Vol. 85, Pt. 2*, p. 797 (1979).
32. S.O. Andersen, "Halons and the Stratospheric Ozone Issue," *Fire Journal,* p. 56 (May/June 1987).
33. G. Taylor, "Achieving the Best Use of Halons," *Fire Journal,* 81, 3, p. 69 (1987).

CHAPTER 7

Halon Replacement Clean Agent Total Flooding Systems

Philip J. DiNenno

Introduction

The regulation of Halon 1301 under the Montreal Protocol and its amendments culminated in the phaseout of production of halons in the developed countries on December 31, 1993. This regulation engendered tremendous research and development efforts across the world in a search for replacements and alternatives. Over the past several years, several total flooding, clean agent alternatives to Halon 1301 have been commercialized, and development continues on others. In addition to clean total flooding gaseous alternatives, new technologies, such as water mist and fine solid particulate, are being introduced. This chapter focuses on total flooding clean agent halon replacements.

Table 4-7.1 is a summary of the most important halocarbon and inert gas extinguishing agents developed to date. The table gives the chemical name; trade name; American Society of Heating, Refrigerating, and Air-Conditioning Engineers, Inc. (ASHRAE) designation (for halocarbons); and chemical formula.

Characteristics of Halon Replacements

Clean fire suppression agents are defined as fire extinguishants that vaporize readily and leave no residue.[1] Clean agent halon replacements fall into two broad categories: (1) halocarbon compounds and (2) inert gases and mixtures. Halocarbon replacements include compounds containing carbon, hydrogen, bromine, chlorine, fluorine, and iodine. They are grouped into five categories: (1) hydrobromofluorocarbons (HBFC), (2) hydrofluorocarbons (HFC), (3) hydrochlorofluorocarbons (HCFC), (4) perfluorocarbons (FC or PFC), and (5) fluoroiodocarbons (FIC).

Philip J. DiNenno, P.E. is president of Hughes Associates Inc., a fire protection engineering research and development firm. He has been actively involved in the testing and development of halon replacement chemicals and alternative fire suppression technologies.

Table 4-7.1 ***Commercialized Halon Replacement Nomenclature***

Chemical Name	Trade Name	ASHRAE Designation	Chemical Formula
Perfluorobutane	CEA-410	FC-3-1-10	C_4F_{10}
Heptafluoropropane	FM-200	HFC-227ea	CF_3CHFCF_3
Trifluoromethane	FE-13	HFC-23	CHF_3
Chlorotetrafluoroethane	FE-24	HCFC-124	$CHClFCF_3$
Pentafluoroethane	FE-25	HFC-125	CHF_2CF_3
Dichlorotrifluoroethane (4.75%)	NAF-SIII	HCFC Blend A	$CHCl_2CF_3$
Chlorodifluoromethane (82%)			$CHClF_2$
Chlorotetrafluoroethane (9.5%)			$CHClFCF_3$
Isopropenyl-1-methylcyclohexene (3.75%)			
$N_2/Ar/CO_2$	Inergen	IG-541	N_2 (52%) Ar (40%) CO_2 (8%)
N_2/Ar	Argonite	IG-55	N_2 (50%) Ar (50%)
Argon	Argon	IG-01	Ar (100%)

While the characteristics of halocarbon clean agents vary widely, they share several common attributes:

1. All are *electrically nonconductive.*
2. All are *clean agents;* that is, they vaporize readily and leave no residue.
3. All are *liquefied gases* or display analogous behavior (e.g., compressible liquid).
4. All can be stored and discharged from typical Halon 1301 hardware (with the possible exception of HFC-23, which more closely resembles 600 psig [40 bar] superpressurized halon systems).
5. All (except HFC-23) use nitrogen superpressurization in most applications for discharge purposes.

6. All are less efficient fire extinguishants than Halon 1301 in terms of storage volume and agent weight. The use of most of these agents requires increased storage capacity.
7. All are total flooding gases after discharge. Many require additional care relative to nozzle design and mixing.
8. All produce more decomposition products (primary HF) than Halon 1301, given similar fire type, fire size, and discharge time.
9. All are more expensive at present than Halon 1301 on a weight (mass) basis.

Inert gas alternatives include nitrogen and argon, and blends of these. One inert gas replacement has a small fraction of carbon dioxide. Carbon dioxide is not an inert gas, because it is physiologically active and toxic at low concentrations (approximately 9 percent). Inert gas clean agents are stored as pressurized gases. They are electrically nonconductive, form stable mixtures in air, and leave no residue.

Extinguishing Mechanisms

Halocarbon clean agents extinguish fires by a combination of chemical and physical mechanisms, depending upon the compound. Chemical suppression mechanisms of HBFC and HFIC compounds are similar to Halon 1301; that is, the Br and I species scavenge flame radicals, thereby interrupting the chemical chain reaction. Other replacement compounds suppress fires primarily by extracting heat from the flame reaction zone, thereby reducing the flame temperature below that which is necessary to maintain sufficiently high reaction rates by a combination of heat of vaporization, heat capacity, and the energy absorbed by the decomposition of the agent.

Oxygen depletion also plays an important role in reducing flame temperature. The energy absorbed in decomposing the agent by breaking fluorine and chlorine bonds is quite important, particularly with respect to decomposition production formation. There is undoubtedly some degree of "chemical" suppression action in flame radical combustion with halogens, but it is considered to be of minor importance since it is not catalytic (e.g., one F radical combines with one H flame radical).

The lack of significant chemical reaction inhibition in the flame zone by HCFC, HFC, and FC compounds results in higher extinguishing concentrations relative to Halon 1301. The relative importance of the energy sink represented by breaking halogen species bonds results in higher levels of agent decomposition relative to Halon 1301.

Inert gas acts by reducing the flame temperature below thresholds necessary to maintain combustion reactions. This condition is created by reducing the oxygen concentration and by raising the heat capacity of the atmosphere supporting the flame. The addition of a sufficient quantity of inert gas to reduce the oxygen concentration below 12 percent (in air) will extinguish flaming fires. The agent concentration required is also a function of the heat capacity of the inert gas added. Hence, there are differences in minimum extinguishing concentration between inert gases.

Flame Suppression Effectiveness

Flame suppression effectiveness of total flooding halon replacement agents has been evaluated in a number of ways. The predominant small-scale test method for establishing flame extinguishing concentrations for liquid and gaseous fuels is the ICI cup burner or variations thereof.

Figure 4-7.1 is a schematic of the ICI cup burner. A small laminar flame is established above a "cup" of fuel surrounded by a cylindrical chimney. An air/agent mixture flows up the chimney surrounding the flame. The minimum concentration of agent (in air) at which the flame is extinguished is the minimum extinguishing concentration (MEC). There are many variations of the basic device as used by different laboratories. These variations include cup and chimney diameter, different mixing and measuring methods, chimney height, and agent/air mixture velocity past the flame.[2] Table 4-7.2 gives some indication of the variation in cup burner extinguishing concentration for a range of extinguishment concentrations for a range of agents with *n*-heptane as the fuel.

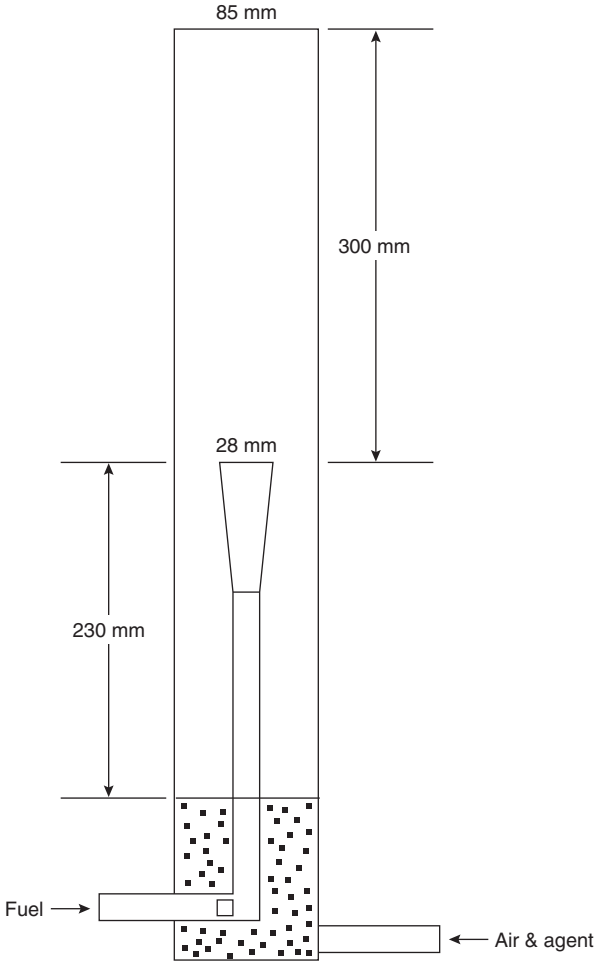

Figure 4-7.1. ***Schematic of ICI cup burner apparatus.[2]***

Table 4-7.2 ***n-Heptane Cup Burner Extinguishing Values from Various Investigators (from NFPA 2001,[1] except as noted)***

Reference	Nitrogen	FC-3-1-10	HFC-227ea	HFC-23	Halon 1301
Sheinson	30[3]	5.2	6.6	12	3.1
3M		5.9	—	—	3.9
NMERI[a]		5.0	6.3	12.6	2.9
Senecal, Fenwal		5.5	5.8	12 (13)	3 (3.5)
Robin			5.9	12.7	3.5
NIST[b]	32	5.3	6.2	12	3.2

[a]New Mexico Engineering Research Institute

[b]National Institute of Standards and Technology

Given the wide variation in test methods, the minimum extinguishing concentrations measured from these different devices are reasonably close.

The cup burner can also be used to establish the MEC for inert gases; Ansul obtained a value of 2.91 percent for IG-541. This result is in contrast to concentrations of 32, 41, and 23 percent by volume measured by the National Institute of Standards and Technology (NIST) for nitrogen, argon, and carbon dioxide, the components of Inergen.

NIST has conducted investigations on a wide range of halon replacement chemicals for aviation use. In order to give a wider perspective on the type and range of chemicals being evaluated for fire suppression use, Table 4-7.3 is included. The table gives cup burner *n*-heptane flame extinction data for a wide range of potential halon replacements.

Table 4-7.4 presents cup burner MEC for a range of fuels and agents taken from various sources. Where multiple values of the MEC were found, they are given. The nitrogen data are presented as representative inert gas values. Argon/N2 blend MEC values would be higher. These data should not be used for design purposes without ensuring that the concentrations are consistent with system manufacturer requirements and third-party approvals.

Table 4-7.5 presents cup burner and full-scale data from VdS. Table 4-7.6 is a compilation of "best values" of cup burner data from a range of sources compiled by Tapscott.

In addition to the cup burner apparatus, researchers at NIST have utilized an opposed-flow diffusion flame (OFDF) apparatus to rank halon replacements for fire extinguishing effectiveness. The OFDF burner is commonly used for combustion research. It has many advantages as a research tool for fundamental combustion studies. Its primary advantage is in its ability to relate the results to fundamental predictions of flame structure and conditions at flame extinction. The oxidizer (and suppressant) stream is forced down onto the fuel surface, exhaust gases are drawn down through an annulus or jacket around the fuel cup, and a flat flame is established. Water cooling is provided for the fuel cup and exhaust gas.

The OFDF burner can vary the turbulence intensity or strain rate of the flame. For most applications of clean agent fire suppression, the strain rate is not a major concern, but in specialized applications, such as engine nacelles with high fuel and oxidizer flow rates or in high-pressure spray or jet fires, the strain rate will substantially impact the minimum condition for extinguishment. Figure 4-7.2 is a sample plot showing the variation of the mole fraction of extinguishing agent versus the strain rate at extinction for n-heptane fuels for a range of suppressants. For typical natural fires, the strain rate is approximately 25 s^{-1}. At high strain rates, the flame is extinguished at lower agent concentrations.

Figure 4-7.3 shows the relationship between MEC for the cup burner and OFDF apparatus. As expected, the cup burner concentration is quite similar to the OFDF concentration at a low strain rate (25 s^{-1}), typical of natural fires. In all cases, the MEC of agent is much lower for high strain rate flames. This further reinforces the value of

Table 4-7.3 ***Agent Fraction in the Oxidizer Stream at Extinction of n-Heptane Cup Burner Flames[3]***

Agent Type	Agent	Mass Percent	Volume Percent
Inert	N_2	31	32
	CO_2	32	23
	He	6.0	31
	Ar	38	41
Nitrogen containing	NF_3	*a*	*a*
Silicon containing	SiF_4	36	13
Sodium containing	$NaHCO_3$ (10–20 μm)	3.0	*b*
Hydrofluorocarbons	CF_3H	25	12
	CF_2H_2	*c*	*c*
	CF_2H_2/C_2HF_5	30	15
	CH_2FCF_3	29	10
	CHF_2CF_3	29	8.7
	$CF_3CH_2CF_3$	27	6.5
	C_3HF_7	28	6.2
Fluorocarbons	CF_4	37	16
	C_2F_6	30	8.1
	C_3F_6	29	7.3
	C_3F_8	30	6.3
	$c\text{-}C_4F_8$	32	6.3
	C_4F_{10}	32	5.3
Chlorine containing	CHF_2Cl	28	12
	$CHCl_2F$	32	11
	CH_3CF_2Cl	*c*	*c*
	$CF_2 = CHCl$	*c*	*c*
	$CF_2 = CFCl$	31	10
	$CHFClCF_3$	26	7.0
Bromine containing	CF_3Br	14	3.1
	CF_2Br_2	16	2.6
	CH_2BrCF_3	17	3.5
	$CH_2 = CHBr$	*c*	*c*
	$CF_2 = CFBr$	27	6.3
	$CF_2 = CHBr$	24	6.0
Iodine containing	CF_3I	18	3.2

[a]Acted as an oxidizer, promoted flame stability

[b]Solid powder not expressed in volume percent.

[c]Agent observed to be flammable.

Table 4-7.4 ***Cup Burner Minimum Extinguishing Concentrations***

	Cup Burner Extinguishment Concentration (Vol %)				
Fuel	HFC-227ea[b]	FC-3-1-10	HFC-23	HCFC Blend A	N_2
Acetone	6.8	5.5[e]			
Acetonitrile	3.7				
AV gas	6.7				
n-Butanol	7.1				
n-Butyl acetate	6.6				
Cyclopentanone	6.7				
Diesel no. 2	6.7				
Ethanol	8.1	6.8[e]			
Ethyl acetate	5.6				
Ethylene glycol	7.8				
Gasoline (unleaded)	6.5				
n-Heptane	6.0[a]	5.2[c]	12.0[c]	12.6[d]	32[a]
	5.8–6.6[c]	5.0[d]	12.6[d]		
Hydraulic fluid	5.8	4.3–4.5[a]			22–26[a]
JP-4	6.6				
JP-5	6.0[a]	4.8[a]			27[a]
	6.6[c]				
Methane	6.2				
Methanol	10.0	9.4[e]			
Methyl ethyl ketone	6.7				
Methyl isobutyl ketone	6.6				
Morpholine	7.3				
Propane	6.3	6.0[a]			32.5[a]
i-Propanol	7.3				
Pyrrolidine	7.0				
Tetrahydrofuran	7.2				
Toluene	5.8				
Turbo hydraulic oil 2380	5.1				
Xylene	5.3				

[a]From Reference 3
[b]From Reference 4
[c]From Reference 5
[d]From Reference 6
[e]From Reference 7

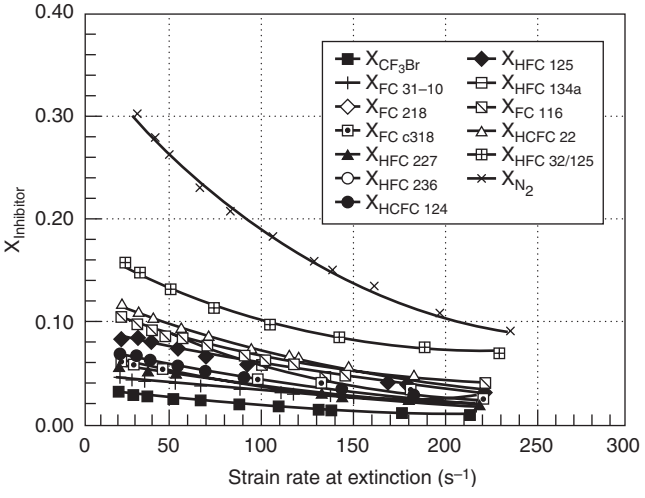

Figure 4-7.2. ***Mole fraction of various suppressants as a function of strain rate at extinction for n-heptane.[3]***

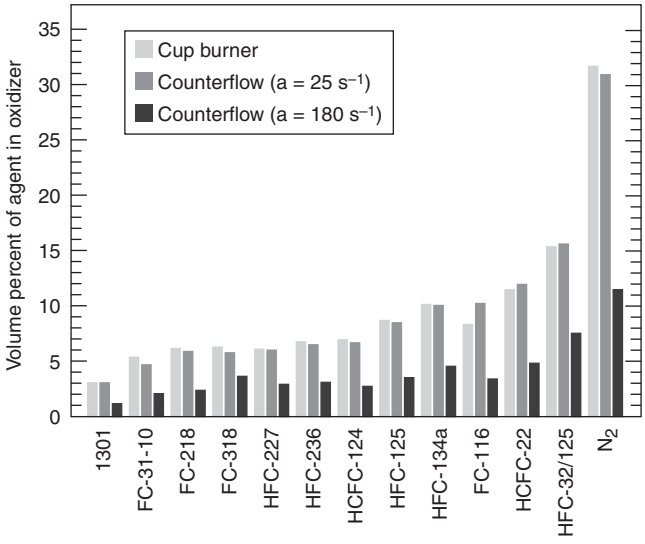

Figure 4-7.3. ***Comparison of n-heptane extinction results for the cup burner and OFDF apparatus at two strain rates.[3]***

Table 4-7.5 ***Inert Gas Extinguishing Concentration Data from VdS[8]***

Extinguishant Gas	Fuel	ISO Cup Burner		VdS Large Cup Burner (percent by volume gas)	Room Fire	
		Fuel Unheated (percent by volume gas)	Fuel Heated (percent by volume gas)		Extinguished (percent by volume gas[a])	Not Extinguished (percent by volume gas[a])
CO_2	Acetone	18.7	19.4	21.4		
	Diethyl ether	—	23.0			
	Ethanol	20.8	23.0			
	n-Heptane	19.6	21.1	23.3	24.1	23.1
	n-Hexane	20.4	21.3			
	Methanol	27.5	28.5	31.3		
	n-Pentane	—	21.6			
	Toluol	15.9	16.7			
	Polypropylene			21.5		
	Polyethylene			20.8		
	Wood crib				26.8	24.4
Argon	Acetone	37.8	38.8	43.7		
	Diethyl ether	—	44.8			
	Ethanol	41.4	44.1			
	n-Heptane	40.9	41.4	45.0	40.8	38.7
	n-Hexane	40.0	41.5			
	Methanol	52.2	55.6	54.5		
	n-Pentane	—	41.7			
	Toluol	32.7	35.5			
	Polypropylene			40.6		
	Polyethylene			37.8		
	Wood crib				30.7	29.0
Inergen	Acetone	29.4	31.7	35.9		
	Diethyl ether	—	35.7			
	Ethanol	32.8	35.5			
	n-Heptane	33.0	33.8	37.2	37.0	33.0
	n-Hexane	31.6	34.8			
	Methanol	41.1	43.8	47.3		
	n-Pentane	—	32.9			
	Toluol	25.7	28.1			
	Polypropylene			35.8		
	Polyethylene			31.3		
	Wood crib				28.1	26.6
Nitrogen	Acetone	28.5	29.9	33.2		
	Diethyl ether	—	33.8			
	Ethanol	32.1	34.5			
	n-Heptane	30.9	32.3	35.6	36.6	33.8
	n-Hexane	30.6	32.6			
	Methanol	38.5	41.2	44.8		
	n-Pentane	—	32.4			
	Toluol	22.2	28.0			
	Polypropylene			34.7		
	Polyethylene			30.8		
	Wood crib				28.6	27.7

[a]Calculated on the basis volume of discharged extinguishant

the cup burner and OFDF apparatus for evaluation of minimum extinguishing concentration.

Extinguishing concentrations for Class A fuels were traditionally developed using wood cribs as part of the equipment listing/approval process. Further, the minimum Class A extinguishing concentration used for design purposes was required to be greater than or equal to the minimum extinguishing concentration for heptane. Recently, additional tests utilizing plastic sheet arrays of polymethylmethacrylate (PMMA), acrylonitrile-butadiene-sytrene (ABS), and polypropylene (PP) have been required.[9,10] Typical results are shown in Figure 4-7.4

Table 4-7.6 ***"Best Values" of Cup Burner Concentrations (vol %)[11]***

Fuel	Halon 1301	FC-3-1-10	FIC-13I1	HCFC Blend A	HCFC-124	HFC-125	HFC-227ea	HFC-23	HFC-236fa	IG-01	IG-100	IG-541	IG-55
70% isopropanol in water													26 (1)
80% methanol/ 20% *n*-heptane	5.8 (1)[a]	5.2 (1)					8.3 (1)[a]						
Acetone				10.0 ± 0.7 (2)[a]			6.8 ± 0.1 (2)[a]			38 (1)	29 (1)	29 ± 0.90 (3)	31 (1)
Acetonitrile				7.0 (1)[a]						33 (1)[a]			16 (1)
Aviation gas, 100 octane, low lead				11.4 ± 0.1 (2)[a]						32 (1)[a]		30 (1)	26 (1)
Benzene	2.4 (1)	3.4 (1)					4.8 (1)	10.6 (1)			31(1)		
n-Butanol				12.2 (1)[a]						36 (1)[a]			33 (1)
n-Butyl acetate				9.8 (1)[a]									36 (1)
Carbon disulfide													49 (1)
Cyclohexane				10.1 ± 0.3 (2)[a]						36 (1)[a]			32 (1)
n-Decane	3.9 (1)										34 (1)		
Diesel					6.8 (1)[a]								
Diesel no. 2				8.9 (1)						27 (1)[a]			26 (1)
Diethyl ether										45 (1)	34 (1)	36 (1)	
n-Dodecane	3.7 (1)										33 (1)		
Ethanol	4.3 ± 0.0 (2)	6.9 ± 0.0 (2)					8.5 ± 0.2 (2)	16.0 ± 0.0 (2)		41 (1)	35 ± 2.7 (3)	35 ± 3.3 (2)	30 (1)
Ethyl acetate				10.6 (1)[a]						35 (1)[a]			30 (1)
Ethylene glycol				11.1 (1)[a]						31 (1)[a]			30 (1)
Exxon Turbo Oil													16 (1)
Gasoline (unleaded)				9.7 (1)[a]	7.5 (1)[a]					37 (1)[a]			26 (1)
Heptane (commercial)	3.2 (1)						6.5 ± 0.2 (1)	12.6 ± 0.5 (2)				32 (1)	
n-Heptane	3.4 ± 0.0 (2)	5.4 ± 0.1 (3)	3.2 (1)[a]	9.9 (1)	6.7 ± 0.3 (3)[a]	8.9 (1)	6.6 ± 0.0 (5)	13.0 ± 0.2 (3)	6.3 ± 0.4 (3)[a]	42 ± 1.4 (3)	33 ± 1.6 (3)	31.2 (5)	35 ± 3.7 (2)
n-Hexane				11.0 ± 0.1 (2)[a]						40 (1)	31 (1)	31 ± 0.4 (2)	29 (1)
Hydraulic oil (Mobil Fluid 350)										26 (1)[a]			21 (1)
Hydrogen				20 (1)[a]									
Isobutanol													29 (1)
Isooctane				9.8 (1)[a]			5.9 (1)	11.3 (1)					
Isopropanol				10.6 (1)[a]			7.2 ± 0.2 (1)			35 (1)[a]		28 (1)	28 (1)
Jet A/JP-5				9.0 (1)[a]	6.9 (1)[a]					32 (1)[a]			26 (1)
JP-4				10.1 (1)[a]						32 (1)[a]			
JP-8				9.7 (1)									
Kerosene	3.4 (1)	5.0 (1)					6.4 (1)	12.5 (1)			30 (1)	31 (1)	
Methane				13.7 (1)[a]						35 (1)[a]			25 (1)
Methanol	7.8 (1)	8.0 (1)		17 (1)			10.2 ± 0.4 (3)	19 (1)	8.0 (1)[a]	52 (1)	41 ± 3.5 (2)	41 (1)	39 (1)
Methyl isobutyl ketone				9.4 (1)[a]									
Morpholine				13.7 (1)[a]						38 (1)[a]			
Natural gas				12.4 (1)[a]									
Nitromethane										34 (1)[a]			32 (1)
n-Octane	3.4 (1)										34 (1)		
n-Pentane											30 (1)[a]		
Propane				12.6 (1)[a]						40 (1)[a]			34 (1)
n-Propanol				10.6 (1)[a]									
Pyrrolidine				10.1 (1)[a]									31 (1)
Tetrahydrofuran				12.0 (1)[a]			4.8 ± 0.3 (4)	9.7 ± 0.0 (2)					32 (1)
Toluene	2.3 ± 0.0 (2)	3.6 ± 0.0 (2)		6.8 (1)			6.6 (1)	12.8 (1)		33 (1)	25 ± 2.0 (3)	25 ± 0.5 (2)	26 (1)
Transformer oil	2.3 (1)	5.4									27 (1)	28 (1)	
n-Undecane			3.8 (1)								33 (1)		
Xylene				8.7 (1)[a]						26 (1)[a]			24 (1)

Number in parentheses indicates the number of different data sources.

[a]Nonstandard cup burner

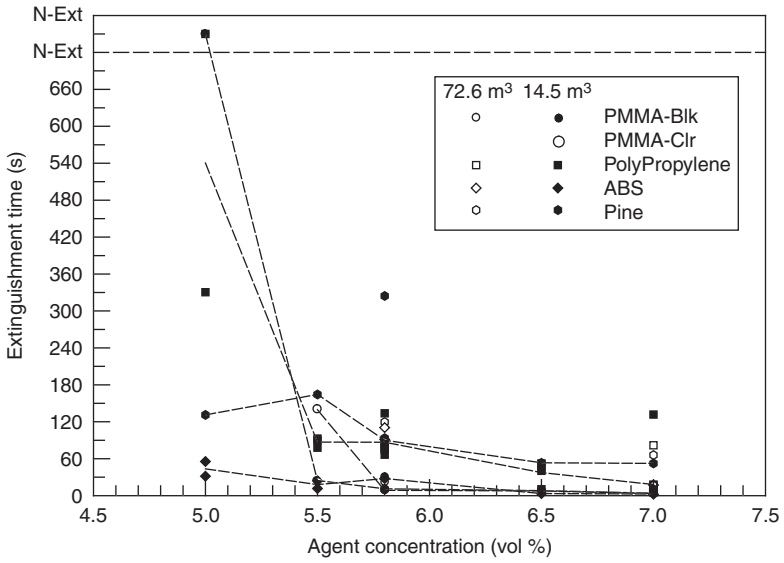

Figure 4-7.4. ***Typical Class A extinguishment results for HFC-227ea.***

for two different room sizes. The results of these tests indicate that for extinguishment times exceeding 3 min, the extinguishing concentrations for these materials are below the heptane cup burner value and in general well above the 10-min extinguishment time value for wood cribs.

Clean agent systems are widely used in electronic equipment areas where fires involving electrically energized cables and equipment are often encountered. Extinguishment tests involving PMMA heated externally with Nichrome wire indicated that agent concentrations substantially higher than those typical for plastic fuels were required. For example, extinguishing concentrations of 9.5, 9, and 20 percent were required for FC-3-1-10, HFC-227ea, and HFC-23, respectively.

Extinguishment tests on actual wire and cable materials were reported by McKenna et al.[12] Three types of tests were conducted: ohmic heating, conductive heating, and printed wiring board arcing. The ohmic heating tests involved deliberate electrical overheating of the conductor. These results are summarized in Table 4-7.7 for HFC-227ea. Note that even under severe overcurrent conditions, all cable assemblies were extinguished at 5.8 percent, a typical Class A extinguishing concentration. The one exception was the 18 AWG polyethylene (PE) coaxial cable, which is generally not used in power applications. The striking difference between these results and those discussed earlier for PMMA probably lies in the fire-retardant nature of real electrical wire and cable assemblies.

Results for cable assemblies heated at the ends by conduction, a situation simulating an overheated connection, showed results similar to the ohmic heating tests for Hypalon and PVC cables.

Tables 4-7.8 and 4-7.9 summarize the fire suppression capability of halon replacement agents relative to Halon 1301 for halocarbon and inert gas agents, respectively. Agent mass and storage volume ratio equivalents for Halon 1301 are given as 1. All comparisons are based on 120 percent of the agent manufacturer's recommended MEC, based on the cup burner. The design values used are as provided by the manufacturer. Design values for HCFC Blend A and Argon are problematic, because these values are below the MEC as measured by the cup burner.

Note that all clean agent alternatives require at least 60 percent more agent by weight and storage volume. This requirement is a consequence of the elimination of bromine in the compounds and subsequent level of catalytic recombination of flame radicals. These data should be taken as representative values, as there are variations between hardware manufacturers.

The storage volume equivalents are based on the maximum fill density permitted in a storage cylinder with a pressure rating as recommended by the manufacturer. The approximate 10 : 1 storage volume requirement for inert gases is a consequence of the inability to liquefy these gases at ambient temperature.

The storage volume equivalent does not translate directly to a required area or volume for storage cylinders. The relative "footprint" of these storage volume equivalents will vary with the volume of the space protected and the maximum storage cylinder size offered by a manufacturer for a particular gas. In general, the floor area required for storage of inert gases exceeds 10 : 1 for large protected volumes.

Explosion Inerting

One of the most important application areas of total flooding fire suppressants is explosion inertion. The inerting concentration of an agent is the concentration required to prevent unacceptable pressure increases in a premixed fuel/air/agent mixture subjected to an ignition source. Inertion concentrations are typically measured in small laboratory-scale spheres, with an electric spark initiator.

The measured inerting concentration of an agent is dependent on the details of the test apparatus used, particularly the ignition source strength and "allowable" pressure rise. The allowable pressure rise is a surrogate

Table 4-7.7 ***Summary of Ohmic Heating Tests with HFC-227ea***

Test	Sample	Current (A)	Orientation	Ignition Source	% C_3HF_7 (FM 200)	Time to Extinguish (s)
EEE035		350	Horizontal	Pilot	5.8	9
EEE036		350	Horizontal	Pilot	5.8	9
EEE046		350	Horizontal	Pilot	5.8	10
EEE049		350	Horizontal	Pilot	5.8	13
EEE037	8 AWG XLPE,	350	Horizontal	Pilot	5.8	13
EEE038	5 wire bundle,	350	Vertical	Pilot	5.8	8
EEE039	center wire energized	350	Vertical	Pilot	5.8	8
EEE054		350	Vertical	Pilot	5.8	10
EEE055		350	Vertical	Pilot	5.8	10
EEE040		350	Vertical	Pilot	5.0	11
EEE047		600	Horizontal	Pilot	5.8	11
EEE050	12 AWG SJTW-A,	600	Horizontal	Pilot	5.8	11
EEE053	6 cable bundle,	600	Horizontal	Pilot	5.8	9
EEE041	4 of 18 conductors	600	Horizontal	Pilot	5.5	9
EEE043	energized	600	Horizontal	Pilot	5.5	8
EEE044		600	Horizontal	Pilot	5.0	11
EEE056	8 AWG PVC,	325	Horizontal	Pilot	5.8	12
EEE059	7 cable bundle,	325	Horizontal	Pilot	5.8	10
EEE062	center wire energized	325	Horizontal	Pilot	5.8	13
EEE068		350	Horizontal	Pilot	6.8	12
EEE069		350	Horizontal	Pilot	6.8	13
EEE071		350	Horizontal	Pilot	6.5	15
EEE075		350	Horizontal	Pilot	6.5	11
EEE079	18 AWG chrome	350	Horizontal	Pilot	6.5	16
EEE076	PVC, over PE,	350	Horizontal	Pilot	6.2	DNE
EEE077	4 cable bundle,	350	Horizontal	Pilot	6.2	15
EEE078	12 conductors	350	Horizontal	Pilot	6.2	DNE
EEE058	energized	350	Horizontal	Pilot	5.8	12
EEE061		350	Horizontal	Pilot	5.8	DNE
EEE065		350	Horizontal	Pilot	5.8	10
EEE066		350	Horizontal	Pilot	5.8	11
EEE067		350	Horizontal	Pilot	5.8	DNE
EEE057	16 AWG neoprene	500	Horizontal	Pilot	5.8	3
EEE060	over rubber, 9 of 12	500	Horizontal	Pilot	5.8	6
EEE064	conductors energized	500	Horizontal	Pilot	5.8	6
EEE031		475	Horizontal	Self-ignited	6.8	14
EEE033		475	Horizontal	Self-ignited	6.8	14
EEE048	18 AWG PE,	475	Horizontal	Self-ignited	6.8	14
EEE029	4 parallel wire array,	475	Horizontal	Self-ignited	6.5	DNE
EEE030	all wires energized	475	Horizontal	Self-ignited	6.5	DNE
EEE028		475	Horizontal	Self-ignited	5.8	DNE
EEE026		475	Horizontal	Self-ignited	5.7	DNE

Time to extinguish is taken from the beginning of discharge.
DNE: did not extinguish

measurement of the distance the flame front travels inside the constant volume sphere prior to suppression. Inerting concentration is not appropriate for use in deflagration or detonation (explosion) suppression.

Small-scale sphere data are used to develop flammability diagrams for various fuel/oxidizer/agent concentrations. Section 2, Chapter 7, which addresses flammability limits, gives an excellent introduction to the subject. There is a wealth of data in the combustion literature on flammability limits for inert gases, such as nitrogen and argon, for a variety of fuels available.

Table 4-7.10 provides inerting concentration data for several agents and fuels, taken from small-scale inertion spheres.[13–15] There are some substantial differences in results. Heinonen[16] has identified both ignition source type and strength as important variables with differences of ±40 percent for Halon 1301 inerting concentrations reported. Figure 4-7.5 shows flammability

Table 4-7.8 ***Weight and Storage Volume Equivalent Data for New Technology Halocarbon Gaseous Alternatives***

Trade Name	Designation	Formula		BP (°C)	Cup Burner (% V/V)[g]	Minimum Design Concentration . (% V/V)	Ratio Agent Mass Required to H 1301[e]	Ratio Agent Storage Volume Required to H 1301[f]	Storage Pressure (psi) 20°C
Halon 1301	Halon 1301	CF_3Br		–58	2.9–3.9	5[d]	1.0	1.0	360
CEA-410	FC-3-1-10	C_4F_{10}		–2	5.0–5.9	6[a,b]	1.9	1.7	360
FM-200	HFC-227ea	C_3F_7H		–16.4	5.8–6.6	7[a,b]	1.7	1.6	360
FE-13	HFC-23	CHF_3		–82.1	12–13	16[a]	1.7	2.2	609
FE-25	HFC-125	H_2HF_5		–48.5	8.1–9.4	10.9[a]	1.9	2.3	166
NAF-S-III	HCFC Blend A	HCFC-22	82%	—	>11	8.6[c]	1.1	1.4	360
		HCFC-123	4.75%						
		HCFC-124	4.5%						
		Organic	3.75%						
CF_3I	Halon 1301	CF_3I		–22.5	2.7–3.2	5.0	~1	~1	—

[a]Based on 120 percent of cup burner value for *n*-heptane

[b]Based on 120 percent of cup burner value verified by listing/approval tests

[c]Based on listing/approval tests

[d]Minimum design concentration per NFPA 12A, *Standard on Halon 1301 Fire Extinguishing Systems,* 1992 edition; cup burner value approximately 3 percent

[e]Ratio of halon design concentration 20.6 lb/ft³ at 70°C to new agent

[f] Ratio of halon storage volume required at minimum design concentration (max. fill density 70 lb/ft³) to new agent

[g]Range of independently established values

Table 4-7.9 ***Agent Weight and Storage Volume Equivalent Data for New Technology Inert Gas Alternatives***

Trade Name	Designation	Formula		Cup Burner (% V/V) (*n*-heptane)	Minimum Design Concentration (% V/V)	Ratio Agent Mass Required to H 1301[b]	Ratio Agent Storage Volume Required to H 1301[d]	Storage Pressure (psi [bar]) 20°C
Halon 1301	Halon 1301	CF_3Br		2.9–3.9[c]	5[a]	1	1	360 (25)
Inergen	IG-541	N_2	52%	29.1[c]	35[f]	2.0	10.0[e]	2180 (150)
		Ar	40%					
Argonite	IG-55	CO_2	8%					
		N_2	50%	30[e]	~36[f]	2.0	10.0[e]	2220 (153)
Argon	IG-01	Ar	50%					
		Ar	100%	30[e]	~36[f]	2.0	8.0[e]	2370 (163)

[a]Minimum design concentration per NFPA 12A, *Standard on Halon 1301 Fire Extinguishing Systems,* 1992 edition; cup burner value approximately 3 percent.

[b]Ratio of halon design concentration 20.6 lb/ft³ at 70°C to new agent.

[c]Range of independently established values.

[d]Ratio of halon storage volume required at minimum design concentration (max. fill density 70 lb/ft³) to new agent.

[e]Manufacturers' values. MEC for argon is approximately 41 percent (see Reference 3).

[f] Based on 120 percent of cup burner value for *n*-heptane.

diagrams derived from small-scale inertion data such as that presented in Table 4-7.10, along with points taken from a large-scale (22.5 m³) explosion vessel. While the small- to large-scale agreement is reasonable, there are scale effects.

Explosion Suppression

Explosion suppression systems employ rapid delivery of agent following very early detection of an ignition. Such systems employ significantly higher agent quantities (than flame suppression or inertion), delivered at higher rates. The total agent delivery time is on the order of 100 milliseconds.

Explosion suppression systems must be specifically designed for a particular application. There are no generic design requirements or standards currently available for such systems.

Senecal[17] and Senecal et al.[18] report on explosion suppression testing in occupied armored fighting vehicles and aerosol filling rooms. Results were obtained on premixed fuel droplet sprays. In contrast to flame suppression or inerting, suppression or deflagration requires significantly more agent. The aerosol filling room tests employed 20 kg of HFC-227ea, FC-3-1-10, and HFC-236fa, and 10 kg of water in a 80-m³ test room to suppress a 90-g propane release in a simulated aerosol filling station. Suppression of the propane-air deflagration was achieved, and the maximum

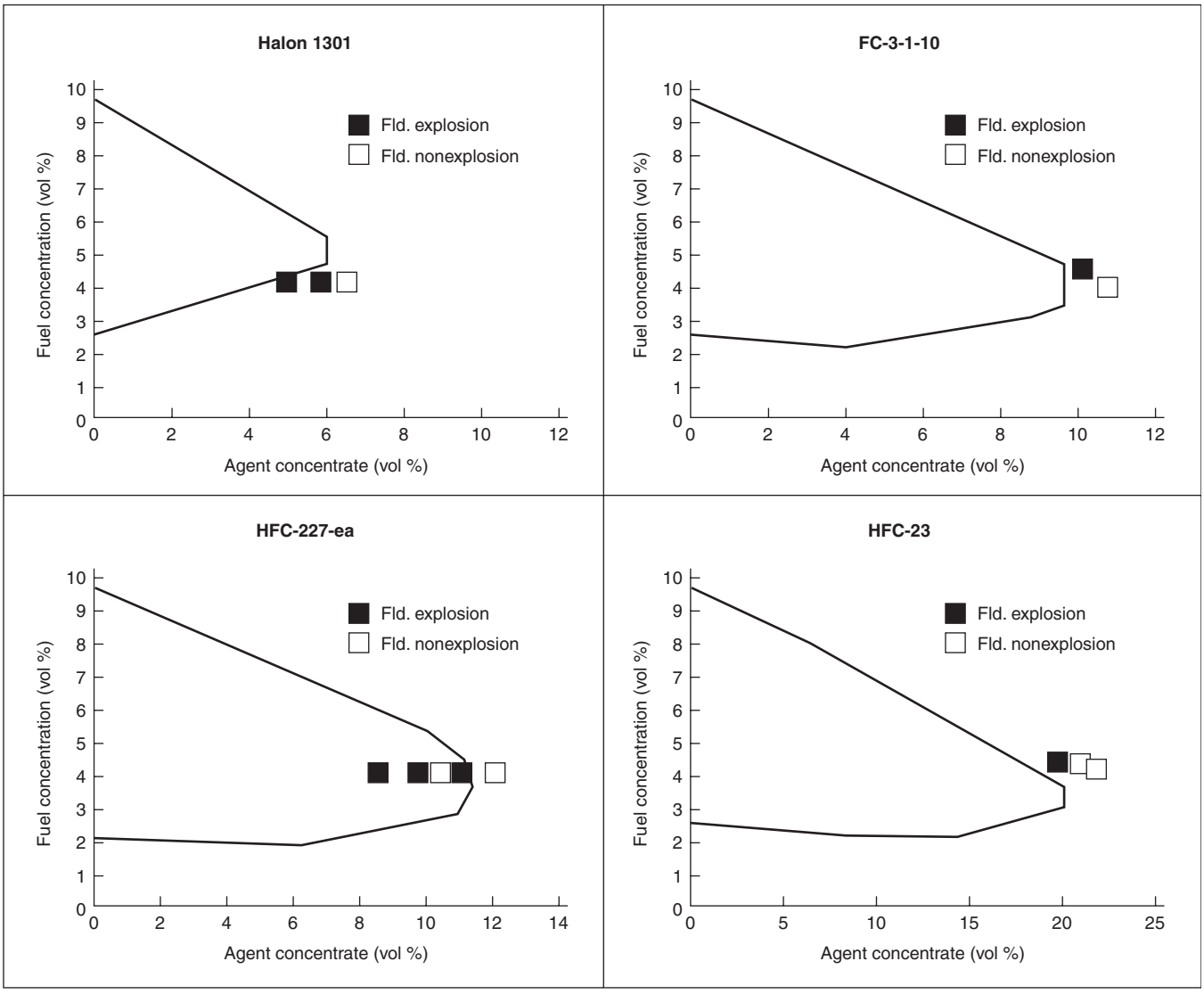

Figure 4-7.5. ***Small-scale flammability diagrams for propane and several replacement agents. Squares denote explosion/nonexplosion points in large-scale 22.5 m³ chamber.[19]***

flame front extension was approximately 4 ft. Suppression tests of heated diesel fuel droplet cloud deflagrations were conducted in simulated armored fighting vehicle crew compartments.

Table 4-7.11 summarizes typical data for flame suppression, inertion, and deflagration suppression concentrations. Note these values are for comparison purposes only. They should not be used in any way for design purposes.

Suppression of detonations requires substantially higher agent concentrations. An excellent discussion is given in Reference 3.

Toxicity

A major factor in the use of a clean agent fire suppressant in a normally occupied area is toxicity. While all halocarbon agents are tested for long-term health hazards, the primary end point is acute or short-term exposure. The primary acute toxicity effects of the halocarbon agents described in this chapter are anesthesia and cardiac sensitization. For inert gases, the primary physiological concern is reduced oxygen concentration.

Halocarbon agents: Cardiac sensitization is the primary short-term toxicity problem for fire suppression applications. Cardiac sensitization is a term describing the sudden onset of cardiac arrhythmia in the presence of a concentration of an agent, caused by sensitization of the heart to epinephrine. The presence of epinephrine is critical to the onset of arrhythmia. This knowledge is important in fire protection applications because production of epinephrine is increased by the body under stress.

Table 4-7.10 ***Explosion Inerting Concentrations, Small-Scale Inertion Sphere***

	Inerting Concentration (vol %) of Fuel			
Agent	Propane	Methane	*i*-Butane	Pentane
FC-3-1-10	10.3[b]	~7.8[d]	—	
	9.5[d]			
HFC-227ea	12.0[d]	8.0[d]	11.3[b]	11.6[a]
	11.6[a]			
HFC-23	20.2[b]	20.2[b]	—	
	19.8[d]	14.0[d]		
IG-541	49.0[c]	43.0[c]	—	
HCFC Blend A	18.0[d]	13.3[d]		

[a]From Reference 4
[b]From Reference 13
[c]From Reference 14
[d]From Reference 15

Table 4-7.11 ***Comparison of Concentrations for Flame Extinguishment, Inertion, and Deflagration Suppression***

	Volume (%)		
Agent	Typical Value Flame Suppression	Inerting Concentration in Propane	Diesel Fuel Droplet Deflagration Suppression
Halon 1301	3	6–7	12
FC-3-1-10	5.5	10.3	8
HFC-227ea	5.8	~12	11
HFC-23	12	20.2	—
IG-541	29	49.0	—

The two toxicity end points used to describe cardiotoxicity and allowable exposure levels are (1) no observed adverse effect level (NOAEL) and (2) the lowest observed adverse effect level (LOAEL). The NOAEL is the highest concentration of an agent at which no "marked" or adverse effect occurred. The LOAEL is the lowest concentration at which an adverse effect was measured.

The procedures used to evaluate cardiac sensitization vary somewhat. The procedure involves intravenous dosing of male beagle hounds with epinephrine for 5 min. Continuous inhalation exposure to the agent follows for 5 min. Following this inhalation exposure, the hound is dosed again with epinephrine and monitored for 5 min to determine the effect of the agent and epinephrine. The protocol is performed at higher doses until an effect occurs.

Effects are monitored by electrocardiograph (EKG) measurements. An adverse effect is generally considered to be the appearance of five or more arrhythmias or ventricular fibrillation. The data from these tests are evaluated by medical experts, and the appropriate NOAEL and LOAEL values are reported by the Environmental Protection Agency (EPA) under the Significant New Alternatives Policy (SNAP) program.

There is no direct correlation between the experimental results from hounds to humans. It is generally accepted, due to the combination of the high doses of epinephrine in the tests and the similarity in cardiovascular function between hounds and humans, that the results can be applied to humans.

In addition to the short-term chronic exposure limits of interest in fire suppression system design, the EPA evaluates longer term inhalation data for these compounds. Table 4-7.12 summarizes NOAEL, LOAEL, and LC_{50} values. Note that the LC_{50} (the concentration lethal to 50 percent of a population) values greatly exceed the NOAEL at typical fire extinguishing concentrations.

Recently, the exposure limits for halocarbon agents have been modified. Physiologically based pharmacokinetic modeling (PBPK) for evaluation of acute exposure to

Table 4-7.12 ***Toxicity Data for Halocarbon Clean Agent Fire Suppressants***

Trade Name	Designation	Formula		NOAEL % V/V[a]	LOAEL % V/V[a]	LC_{50} or ALC[b]
CEA-410	FC-3-1-10	C_4F_{10}		40	>40[c]	>80%
FM-200	HFC-227ea	C_3F_7H		9.0	>10.5	>80%
FE-13	HFC-23	CHF_3		50	>50[c]	>65%
FE-24	HCFC-124	C_2HClF_4		1	2.5	23–29%
FE-25	HFC-125	H_2HF_5		7.5	10.0	>70%
NAF-S-III	HCFC Blend A	HCFC-22	82%	10	>10	64%
		HCFC-123	4.75%			
		HCFC-124	4.5%			
		Organic	3.75%			
CF_3I	Halon 1301	CF_3I		0.2	—	—

[a]From EPA SNAP documents
[b]From NFPA 2001 *Standard on Clean Agent Fire Extinguishing Systems*, 1994 edition
[c]Maximum concentration before oxygen depletion

halocarbon agents has been used to establish alternative exposure limits for halogenated agents.[20] PBPK modeling attempts to account for the time-dependent uptake rate of halocarbons in the body and establishes exposure limits based on the rate of uptake.[21–25] The limits are based on the concentration of agent and the time at which the concentration of agent in the blood equals that of the LOAEL. Typical PBPK results for safe exposure times for HFC-227ea and HFC-125 are given in Table 4-7.13. Note that exposure above the NOAEL limits and up to the LOAEL is permitted.

These limits were derived and supported by the EPA, which has the primary regulatory authority for health and toxicity associated with halon replacements. The use of the PBPK approach partially accounts for the differences between laboratory animal tests and humans. The laboratory results form the basis of the end points (LOAEL) and are still conservative due to the nature of epinephrine dosage used during the animal tests.[26]

Where PBPK modeling data do not exist, the use of halocarbon agents in occupied areas is subject to the constraint that the design concentration must be less than the NOAEL. While it is recommended that all systems employ predischarge alarms and that personnel evacuate prior to system actuation, it is understood that inadvertent discharges and short-term exposures will occur, hence the limitation. It is expected that emergency exposures for up to several minutes at or below the NOAEL are reasonably safe. In no case should systems be designed or installed where intentional exposure of any duration is anticipated.

It has been proposed by the EPA that agents be permitted for use at concentrations up to the LOAEL where evacuation will occur in less than 60 s. This proposal has not been integrated into design standards to date due to the uncertainty of accidental exposure conditions.

Table 4-7.13 ***Exposure Limits Derived from PBPK Modeling for HFC-227ea and HFC-125[20]***

HFC-227ea Concentration			HFC-125 Concentration		
% V/V	ppm	Human Exposure Time (min)	% V/V	ppm	Human Exposure Time (min)
9.0	90,000	5.00	7.5	75,000	5.00
9.5	95,000	5.00	8.0	80,000	5.00
10.0	100,000	5.00	8.5	85,000	5.00
10.5	105,000	5.00	9.0	90,000	5.00
11.0	110,000	1.13	9.5	95,000	5.00
11.5	115,000	0.60	10.0	100,000	5.00
12.0	120,000	0.49	10.5	105,000	5.00
			11.0	110,000	5.00
			11.5	115,000	5.00
			12.0	120,000	1.67
			12.5	125,000	0.59
			13.0	130,000	0.54
			13.5	135,000	0.49

Based on the limitation that the design concentration must be below the NOAEL, it can be seen from Table 4-7.12 that three agents are acceptable for use in normally occupied areas for flame extinguishant purposes: HFC-227ea, HFC-23, and FC-3-1-10.

Inert gas agents: Inert gas agents are, in effect, physiologically inert. The primary physiological problem with these agents is the reduced oxygen concentration caused by the high agent design concentrations. One inert gas blend employs a low concentration of CO_2 (which is not physiologically inert) in order to counter the effects of the reduced oxygen concentration. The mechanism of this effect is discussed in Reference 27.

Current limitations on exposure limits for inert gases are as follows: for gas concentrations up to 43 percent (a residual oxygen concentration of 12 percent), exposure time is limited to 5 min. For agent concentrations between 43 and 52 percent (12 and 10 percent residual oxygen concentration), the exposure time is limited to 3 min. For concentrations greater than 52 percent, exposure time is limited to 30 s.

There is strong indication that small concentrations of CO_2 added to inert gases (such as IG-541) substantially reduce hypoxic effects and improve human performance at low oxygen levels. Regulatory authorities have not yet differentiated between such agents and other inert gases or blends.[27]

Environmental Factors

The evaluation of clean agent fire suppressants includes a consideration of environmental factors. International, national, and local government regulations control the use of any alternatives in this regard. The primary environmental consideration is ozone depletion potential (ODP). ODP is a measure of a chemical's ability to deplete stratospheric ozone, with CFC-12 as a basis with an ODP of 1. All chemicals with non-zero ODP are subject to phaseout under the Montreal Protocol and its amendments. Table 4-7.14 summarizes environmental impact data for halocarbon alternatives. Note that FC and HFC compounds have zero ozone depletion potential. The HCFC compounds have quite low ODP. Other HCFC compounds are widely used as CFC replacements for refrigerants.

Other environmental factors that are potentially important in a regulatory context are global warming potential (GWP) and atmospheric lifetime. GWP is a measure of the contribution of a gas to the so-called greenhouse effect. It is a function of atmospheric lifetime and the ability of the gas to absorb infrared radiation. The evaluation of GWP is an extremely complex issue, and, currently, none of these compounds are regulated on that basis in the United States. Long atmospheric lifetime, a measure of the persistence of a chemical in the atmosphere, is of concern not only as it relates to GWP, but also due to the uncertainty of the effects of chemicals for long time periods in the atmosphere. The EPA currently has use restrictions on FC-3-1-10 based primarily on its long atmospheric lifetime. These restrictions permit the use of this chemical

Table 4-7.14 ***Environmental Factors for Halocarbon Clean Agents***

Trade Name	Designation	Formula		ODP	GWP (100 yr)	Atmospheric Lifetime (yr)
Halon 1301	Halon 1301	CF_3Br		16	5800	100
CEA-410	FC-3-1-10	C_4F_{10}		0	5500	2600
FM-200	HFC-227ea	C_3F_7H		0	2050	31
FE-13	HFC-23	CHF_3		0	9000	280
FE-24	HCFC-124	C_2HClF_4		0.022	440	7
FE-25	HFC-125	H_2HF_5		0	3400	41
NAF-S-III	HCFC Blend A	HCFC-22	82%	0.05	1600	16
		HCFC-123	4.75%			
		HCFC-124	4.5%			
		Organic 3	3.75%			
CF_3I	Halon 1301	CF_3I		<0.2	0	—

in applications where no other alternative is technically feasible.

Thermophysical Properties

Tables 4-7.15 and 4-7.16 give thermophysical properties of clean agent replacements from NFPA 2001,[1] in English and SI units, respectively. Table 4-7.17, extracted from Reference 28, gives independent data and estimates for some thermophysical properties. Additional thermophysical and transport property data can be found in Reference 4 for FM-200, and Reference 28 for a range of halocarbon alternatives.

Isometric diagrams for halocarbon agents HFC-227ea, pressurized at 360 and 600 psig at 70°F with nitrogen, and HFC-23 are given in Figures 4-7.6, 4-7.7, and 4-7.8, respectively. Note that HFC-23 is not pressurized with nitrogen. Figure 4-7.9 gives the pressure/temperature relationship

Table 4-7.15 ***Thermophysical Properties of Clean Halocarbon Agents (English units)***

	Units	FC-3-1-10	HCFC Blend A	HCFC-124	HFC-125	HFC-227ea	HFC-23	IG-541	IG-55	IG-01
Molecular weight	—	238.03	92.90	136.5	120.2	170.03	70.01	34.0	33.95	39.9
Boiling point @ 760 mm Hg	°F	28.4	–37.0	12.2	–55.3	2.6	–115.7	–320	–310.2	–302.6
Freezing point	°F	–198.8	<–161.0	–326.0	–153	–204	–247.4	–109	–327.5	–308.9
Critical temperature	°F	235.8	256.0	252.0	150.8	215.0	78.6	—	–210.5	–188.1
Critical pressure	psia	337	964	524.5	521	422	701	—	602	711
Critical volume	ft^3/lbm	0.0250	0.0280	0.0283	0.0281	0.0258	0.0305	—	—	—
Critical density	lbm/ft^3	39.3	36.00	35.28	35.68	38.76	32.78	—	—	—
Specific heat, liquid @ 77°F	Btu/lb·°F	0.25	0.30	0.270	0.301	0.2831	0.370	—	—	—
Specific heat, vapor @ constant pressure (1 atm) & 77°F	Btu/lb·°F	0.192	0.16	0.177	0.191	0.2054	0.176	0.195	0.187	0.125
Heat of vaporization at boiling point	Btu/lb	41.4	97	83.2	70.8	57.0	103.0	94.7	77.8	70.1
Thermal conductivity of liquid @ 77°F	Btu/h·ft·°F	0.0310	0.052	0.0417	0.0376	0.040	0.0450	—	—	—
Viscosity, liquid @ 77°F	lb/ft·hr	0.783	0.508	0.723	0.351	0.443	0.201	—	—	—
Relative dielectric strength @ 1 atm @ 734 mm Hg 77°F (N_2 = 1.0)	—	5.25	1.32	1.55	0.955 @70°F	2.00	1.04	1.03	1.01	1.01
Solubility of water in agent @ 70°F	—	0.001% by weight	0.12% by weight	0.07% by weight @ 77°F	0.07% by weight @ 77°F	0.06% by weight	500 ppm @ 50°F	0.015%	0.006%	0.006%
Vapor pressure @ 77°F	psi	38.8	1.37	56	199	66.4	686.0	2207	—	—

Table 4-7.16 ***Thermophysical Properties of Clean Halocarbon Agents (SI units)***

	Units	FC-3-1-10	HCFC Blend A	HCFC-124	HFC-125	HFC-227ea	HFC-23	IG-541	IG-55	IG-01
Molecular weight	—	238.03	92.90	136.5	120.2	170.03	70.01	34.0	33.95	39.9
Boiling point @ 760 mm Hg	°C	–2.0	–38.3	–11.0	–48.5	–16.4	–82.1	–196	–190.1	–185.9
Freezing point	°C	–128.2	<–107.2	–198.9	–102.8	–131	–155.2	–78.5	–199.7	–189.4
Critical temperature	°C	113.2	124.4	122.2	66.0	101.7	25.9	—	–134.7	–122.5
Critical pressure	kPa	2323	6647	3614	3595	2912	4836	—	4150	4860
Critical volume	cc/mol	371	162	241.6	210	274	133	—	—	—
Critical density	kg/m³	629	577	565	571	621	525	—	—	—
Specific heat, liquid @ 25°C	kJ/kg°C	1.047	1.256	1.13	1.260	1.184	1.549	—	—	—
Specific heat, vapor @ constant pressure (1 atm) & 25°C	kJ/kg°C	0.804	0.67	0.741	0.800	0.8082	0.737	0.574	0.782	0.523
Heat of vaporization at boiling point	kJ/kg	96.3	225.6	194	164.7	132.6	239.6	220	181	162.2
Thermal conductivity of liquid @ 25°C	W/m°C	0.0537	0.0900	0.0722	0.0651	0.069	0.0779	—	—	—
Viscosity, liquid @ 25°C	centipoise	0.324	0.21	0.299	0.145	0.184	0.083	—	—	—
Relative dielectric strength @ 1 atm @ 734 mm Hg 25°C (N_2 = 1.0)	—	5.25	1.32	1.55	0.955 @ 21°C	2.00	1.04	1.03	1.01	1.01
Solubility of water in agent @ 21°C	—	0.001% by weight	0.12% by weight	0.07% by weight @ 25°C	0.07% by weight @ 25°C	0.06% by weight	500 ppm @ 10°C	0.015%	0.006%	0.006%
Vapor pressure @ 25°C	kPa	267.5	948	386	1371	457.7	4729	15,200	—	—

Table 4-7.17 ***Selected Properties of Agents[28]***

	FC-3-1-10	HFC-227ea	HCFC-124	HFC-125	HFC-23
Boiling point @ 0.101 MPa (°C)	–2.0	–16.4	–13.2	–48.6	–82.1
Critical temperature (°C)	113.2	101.7	122.5	66.3	25.6
Critical pressure (MPa)	2.32	2.9	3.65	3.62	4.82
Vapor pressure @ 25°C (MPa)	0.27	0.47	0.38	1.38	4.73
Liquid density at 25°C (kg/m³)	1497	1395	1401	1245	669
Liquid heat capacity @ boiling point (kJ/kg·K)	0.951	1.074	1.080	1.107	1.269
Liquid heat capacity at 25°C (kJ/kg·K)	1.047	1.184	1.111	1.26	1.55
Latent heat of vaporization at boiling point (kJ/kg)	96	132.6	194	160	240

for inert gases IG-541, IG-55, and IG-01, pressurized to 2175 psig, at 70°F. This display is the pressure/temperature relationship for an ideal gas.

Clean Agent System Design

Once the agent has been selected, the general discussion on clean agent system design presented by Grant in Section 4, Chapter 6 should be reviewed. The basic process is outlined below:

1. Determine the design concentration.
2. Determine the total agent quantity.
3. Establish the maximum discharge time.
4. Select piping material and thickness consistent with pressure rating requirements.
5. Design piping network and select nozzles to deliver required concentration at required discharge time to ensure mixing.
6. Evaluate compartment over/underpressurization and provide venting if required.
7. Establish minimum agent hold requirements and evaluate compartments for leakage.

These attributes apply only to the mechanical design of the system.

The detection and actuation systems are critical and integral parts of a clean agent system design. The detection system should be designed to actuate the system, with ap-

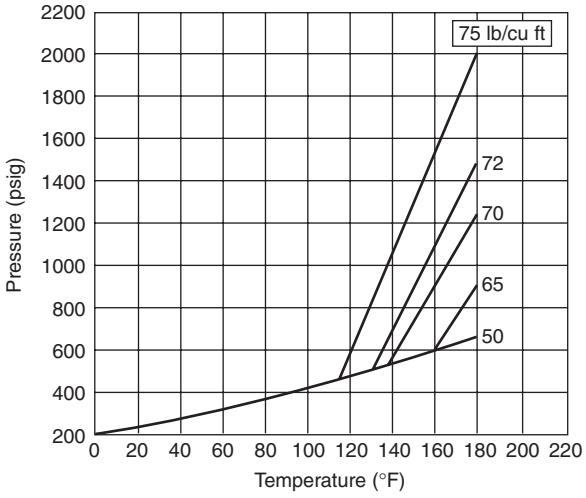

Figure 4-7.6. ***Isometric diagram of HFC-227ea, pressurized to 360 psig with N_2, at 70°F.[4]***

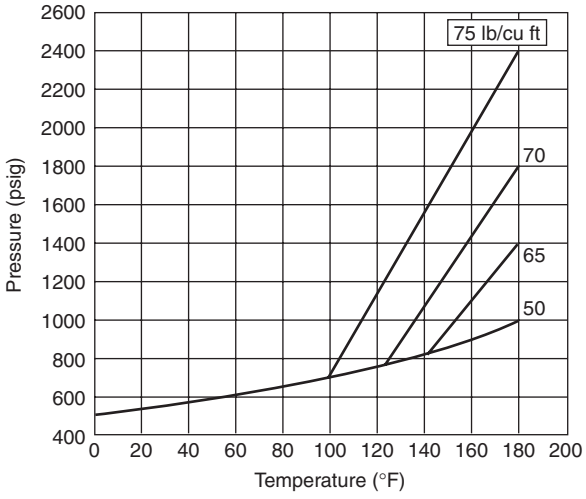

Figure 4-7.7. ***Isometric diagram of HFC-227ea, pressurized to 600 psig with N_2, at 70°F.[4]***

propriate pre-discharge alarms, before unacceptable thermal or nonthermal damage occurs. This aspect is particularly important where the thermal decomposition products of halocarbon clean agents are a concern. Section 4, Chapter 1 provides engineering methods and calculation procedures for this purpose.

In addition to the detection, actuation, and alarm systems, the enclosure itself is critical in the design of any total flooding suppression system. The most important considerations are that the enclosure be of sufficient integrity to (1) prevent preferential agent loss during discharge and (2) prevent excessive agent/air mixture loss after discharge to ensure adequate hold time.

As a general rule, all openings, notably doors and ventilation fans and/or openings, must be secured prior to discharge in conjunction with the detection and alarm

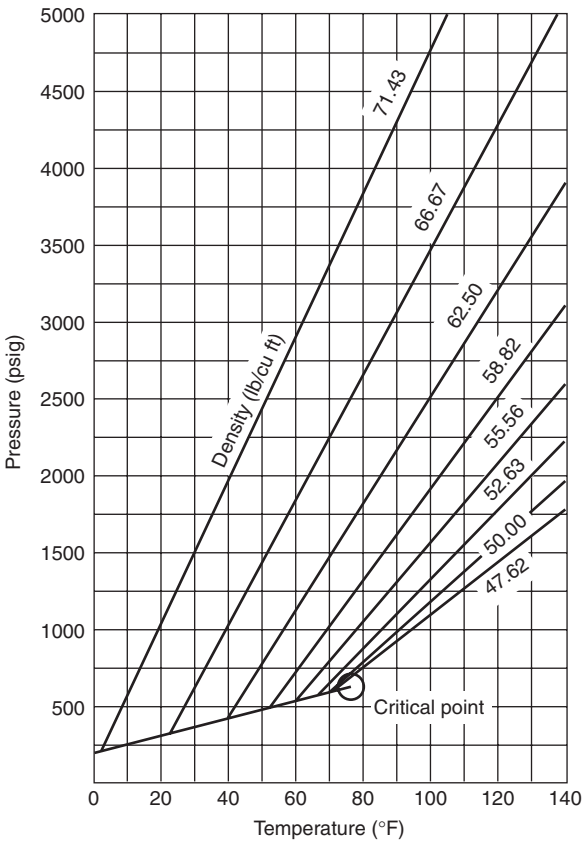

Figure 4-7.8. ***Isometric diagram of HFC-23.[1]***

systems. Agent system installation in rooms with unclosable openings should not be attempted unless sufficient test data are available to ensure adequate concentrations. Some enclosures, such as very tightly sealed low EMF emission electronics spaces, require additional care to avoid compartment damage due to over/underpressurization during agent discharge.

Design Concentration

Flame extinguishment: Design concentrations for various agents and fuel combinations are generally determined by a combination of small-scale testing, large-scale testing, independent laboratory approval of hardware, and addition of design safety factors.

Historically, minimum design concentrations for Halon 1301 were set by the cup burner extinguishing concentration plus a 20 percent safety factor. A minimum Halon 1301 design concentration of 5 percent was also established for all applications. For heptane, the cup burner value was approximately 3 percent; with a 20 percent safety factor, a design concentration of 3.6 percent is obtained. At the minimum design concentration set by NFPA 12A, *Standard on Halon 1301 Fire Extinguishing Systems,* 1992 edition, of 5 percent, a 66 percent safety factor was achieved. For fuels with cup burner extinguishing concentrations greater than 4.2 percent, the safety factor remained at 20 percent.

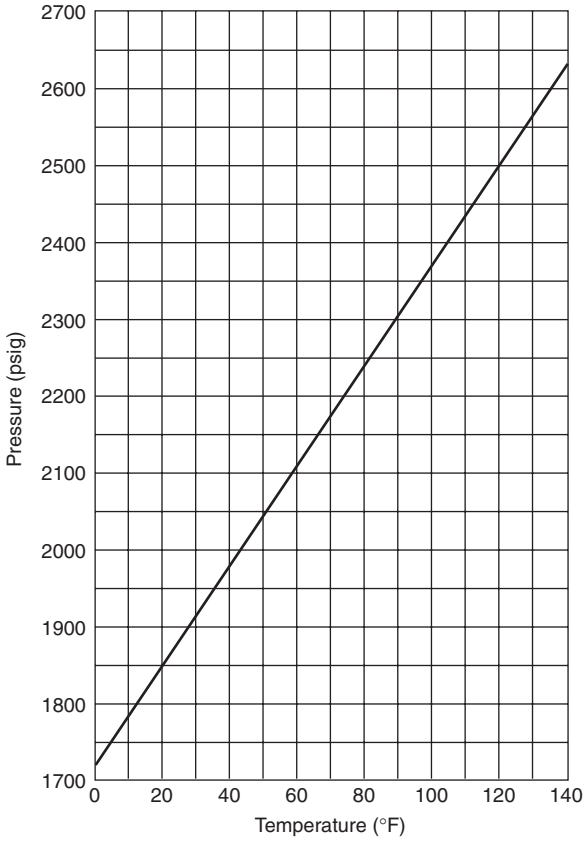

Figure 4-7.9. ***Isometric diagram of inert gases and blends, treated as ideal gases, pressurized to 2175 psig, at 70°F.[1]***

The basic requirement for determining the design concentration of clean agents in NFPA 2001, *Standard on Clean Agent Fire Extinguishing Systems,* 1994 edition, is two-fold. First, the minimum extinguishing concentration as determined by the cup burner must be established. Second, after this minimum is established by the *system* manufacturer, full-scale third-party approval testing is conducted using the manufacturer's hardware on heptane, wood crib, and selected flammable liquids. These tests are performed at the cup burner minimum extinguishing concentration, not the design concentration. Further, they are conducted with flooding factors lower than utilized in design. Hence, the minimum set by the cup burner or equipment manufacturer, whichever is higher, is tested in full scale as part of the approval/listing process for the agent/system combination. Often, hardware manufacturers will establish a minimum concentration greater than the cup burner value to account for nozzle inefficiency.

There has been some full-scale test work that indicates that the 20 percent safety factor may be insufficient. Sheinson et al. noted significant improvement in extinguishing time performance with a safety factor of 40 percent.[29] Brockway noted similar results, with no performance improvement beyond a safety factor of 40 percent.[30]

Analysis by Schlosser[31] indicated that the probability of failure of a system was reduced from approximately 15 to 10 percent when the safety factor increased from 20 to 30 percent. In addition to these data, the variation in cup burner values used as a basis for design concentration was significant due in part to a lack of standardization in the method. Some full-scale test results[32] also indicated a need for higher design concentrations.

Based on these factors, the first edition of ISO 14520-1 required a minimum safety factor of 30 percent.[33] The current edition of NFPA 2001[20] requires a 30 percent safety factor for Class B hazards and for any system actuated by manual means only.

In addition to increased safety factors, the concept of design factors was introduced into the 2000 edition of NFPA 2001. A design factor is used to increase the agent quantity for a specific installation or design that has attributes for which the minimum safety factor may not be sufficient. The only variable for which design factors have been quantified is for systems with multiple flow splits protecting more than four enclosures simultaneously. The motivation for a design factor in these rare cases is the uncertainty in the split of agent mass flow at unbalanced tee junctions and the compound of that uncertainty with more than four tees in series.

It has also been noted by several investigators that higher safety factors result in lower thermal decomposition products.[29,30,34] None of the above referenced investigations utilized listed or approved hardware for the specific agents tested; as in most cases, the tests were performed before such hardware was available.

There is an exception in NFPA 2001, to the general rule that a minimum extinguishing concentration be established by the cup burner method. It was alleged that reliable cup burner data were not available for HCFC Blend A due to the fact that (1) the agent was a blend and (2) one of the blend components heats at a low vapor pressure. In the case of this agent, a minimum extinguishing concentration of 7.2 percent and, hence, a design concentration of 8.6 percent was established through limited full-scale testing. Since at the time insufficient data were available to evaluate the claim, the exception that requires full-scale testing at minimum extinguishing concentration consistent with UL 1058, *Halogenated Agent Extinguishing System Units,*[35] was invoked. Since that time, reliable cup burner data were obtained for the blend from several laboratories. The data are consistent with MEC values for the blend components, primarily HCFC 22. Furthermore, some full-scale testing has indicated that the design concentration of 8.6 percent may be inadequate.[36] This issue is, however, unresolved at the present time.

For Class A fires, NFPA 2001 requires full-scale testing and third-party approval for evaluating design concentration on solid polymeric materials. In many cases, the MEC for heptane is used as a practical minimum.

There has been no systematic evaluation of these agents under so-called "deep-seated" fire scenarios. Part of the problem is the circular definition of deep-seated fires in NFPA 12A. However, the Underwriters Laboratories Inc. (UL) and Factory Mutual Research Corporation (FMRC) listing procedures require testing on wood cribs subsequent to long preburn times (approximately 5 min). Under these tests, surface oxidation and char reactions do occur.

Design concentrations for fire scenarios involving long preburn times in thick arrays of cellulosic fuels will require additional testing. For most applications where incidental quantities of cellulosic materials may be involved and preburn times are relatively short (<5 min) time frames (i.e., automatic actuation), the flame extinguishing concentrations for Class A fuels will be less than, or equal to, that of n-heptane and can be used. Surface oxidation or charring reactions do not occur with most polymers; hence, so-called "deep-seated" fires are not a concern where Class A fuels are involved.

IG-541 is used at 37.5 percent minimum design concentration where Class A materials are involved. Other inert gases should have similar or higher minimum design concentrations.

As previously discussed, the minimum design concentration is a function of the fuel, the agent, and the delivery systems. Design concentrations for specific hazards must be determined in accordance with the system manufacturer's approval or listing.

Agent Quantity

Once the design concentration is established, the quantity of agent necessary to achieve that concentration is determined. The quantity of halocarbon agent necessary is determined by the following equation:

$$w = \frac{V}{S}\left(\frac{C}{100 - C}\right) \tag{1}$$

where

V = net volume of protected space

C = design concentration (%)

w = specific weight of agent required

S = specific volume [ft³/lb (m³/kg)] and is determined by

$$S = k_1 + k_2(T) \tag{2}$$

where T is the minimum ambient temperature of the protected space, and k_1 and k_2 are constants. Values for k_1 and k_2 used in Equation 2 are given in Table 4-7.18.

The flooding factor in Equation 1 [$C/(100 - C)$] implies that the agent/air mixture "lost" during discharge is well mixed and has an agent concentration of C. This formula makes no assumption regarding leakage of the enclosure. During UL/FMRC approval testing, the agent is evaluated with a flooding factor of (C/100), essentially assuming that losses during discharge are 100 percent air.

For inert gases, the following formula is used:

$$X = 2.303\,\frac{V}{S}\log\left(\frac{100}{100 - C}\right)V_s \tag{3}$$

where

X = volume of inert gas required at 70°F

V_s = specific volume at 70°F

V = net protected hazard volume

S = specific volume at ambient temperature in protected volume (from Equation 2) = $k_1 + k_2\,(T)$

Table 4-7.18 ***Specific Volume Constants***

	°F		°C	
Agents	k_1	k_2	k_1	k_2
FC-3–1-10	1.409	0.0031	0.0941	0.0003
HCFC Blend A	3.612	0.0079	0.2413	0.00088
HCFC-124	2.352	0.0057	0.1578	0.0006
HFC-125	2.724	0.0063	0.1701	0.0007
HFC-227ea	1.885	0.0046	0.1269	0.0005
HFC-23	4.731	0.0107	0.2954	0.0012
IG-541	9.7261	0.0211	0.649	0.00237
IG-01	8.514	0.0185	0.5685	0.00208
IG-55	10.0116	0.0217	—	—

The flooding factor used here, $\log [100/(100 - C)]$, is derived assuming that leakage from the compartment during discharge occurs with a varying concentration of agent from zero to C from beginning to the end of discharge. It is identical to the expression used in CO_2 system design. It assumes that the displaced atmosphere is freely vented from the enclosure.

Discharge Time

The maximum discharge time permitted for halocarbon clean agent systems is 10 s. This discharge time is taken to be the moment where all liquid agent has cleared the nozzle. The total discharge time will be longer as agent vapor and nitrogen are expelled from the system.

The 10-s discharge time limitation for halocarbon agents is designed to aid four objectives:

1. Provide high flow rates through nozzles to ensure adequate mixing of agent with air inside the enclosure.
2. Provide sufficient velocity through pipes to ensure homogeneous flow of liquid and vapor.
3. Limit the formation of agent thermal decomposition products.
4. Minimize direct and indirect fire damage, particularly in fast-developing fire scenarios.

The most important of these objectives relative to discharge time is the minimization of agent thermal decomposition product formulation. Items 1 and 2 alone are determined by the piping system design.

The discharge time requirement for inert gases is currently 60 s.[1] Longer discharge times are typically used for these systems in Europe. The two primary reasons to constrain the discharge time of inert gas agents that form no thermal decomposition products are (1) to limit the direct and indirect fire damage and (2) to minimize the length of time that the fire burns in a depleted oxygen atmosphere. As more information is developed on the effect of discharge time on inert gas agent performance, this 60-s limit may be increased for certain applications.

In some applications, such as flammable liquid hazards and explosion inerting, it is necessary to discharge the agent quickly to minimize direct fire damage or to ensure that the agent concentration is achieved prior to the lower explosive limit (LEL) being reached.

Thermal Decomposition Products

All of the halocarbon replacement agents form higher levels of thermal decomposition products than Halon 1301 under similar conditions. For a given fuel, the two primary variables determining the level of decomposition products are (1) the size of the fire at the time of discharge and (2) the time required to reach an extinguishing concentration in the compartment.

The dependence of thermal decomposition product formulation on discharge time and fire size has been extensively evaluated.[29–34,36–39] Figure 4-7.10 from Reference 36 is a plot of peak HF concentration as a function of fire size to room volume ratio. Similar data for 10-min average HF concentrations are given in Figure 4-7.11. Data are given for Halon 1301, HFC-23, HFC-227ea, FC-3-1-10, and HCFC Blend A from three series of fire tests done at different room scales. The data are for a total discharge time of 15 s, which is analogous to a 10-s discharge time based on nozzle liquid runout. The data are for heptane pool or heptane pool and spray fires.

The first observation is that the quantity of HF formed is approximately five to ten times higher for all halocarbon replacements relative to Halon 1301. There may be differences between the various HFC/HCFC compounds tested, but it is not clear from these data whether such differences (1) occur, (2) are attributable to agent mixing and distribution, or (3) are attributable to locally high velocities or concentrations of agent from the nozzle. In all of the data reported, the fire source, that is, heptane pans of varying sizes, was baffled to prevent direct interaction with the agent jet.

These data were taken with an FTIR spectrometer at a location approximately 1 m from the floor, or about mid-flame height, near the wall. The method used was correlated to grab sample and ion-specific electrode (ISE) methods.[37] In all cases, the agreement was good, except for the HCFC blend. In this case, the HF concentration inferred from the treated grab sample was significantly

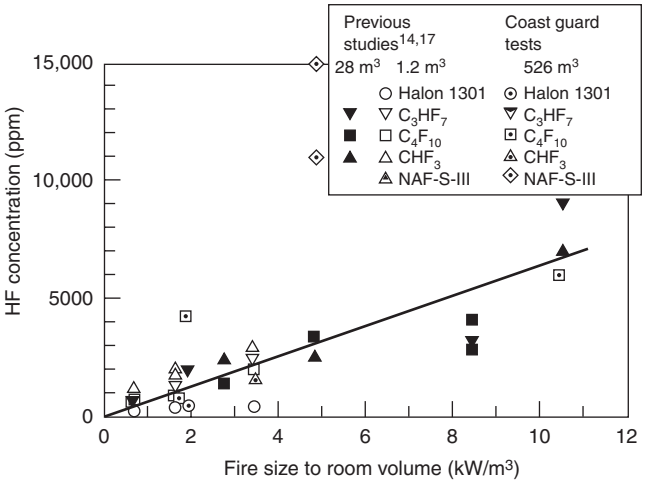

Figure 4-7.10. ***Maximum HF concentration resulting from extinguishment of heptane fires with nominal 10–15 s total discharge times.[36]***

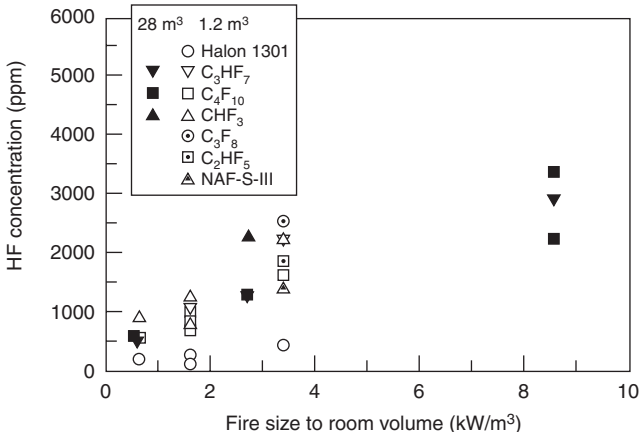

Figure 4-7.11. ***Average HF concentration resulting from extinguishment of heptane pool or heptane pool and spray fires with nominal 15-s total discharge time.[37]***

(>50 percent) higher than that measured using the FTIR. Since the HCFC blend contains an HF "scrubber," it is postulated that treatment of the grab sample with a basic solution, as required for the ISE measurements, caused formation of additional HF by reentry with F loosely bound up by reaction with the scrubber. Hence, the FTIR data presented for HCFC Blend A represent a significantly lower quantity of HF than would actually be expected if the product was hydrolyzed. This condition is also consistent with the fact that the agent was tested at the manufacturer's recommended design concentration, which is approximately 40 percent lower than the basis for all other agents.

The effect of long discharge times or delayed extinguishing times is shown in Figure 4-7.12.[37] The variation between the HFC/HCFC alternatives and Halon 1301, relative to HF production, is approximately the same as that shown in Figure 4-7.11 for different fire sizes.

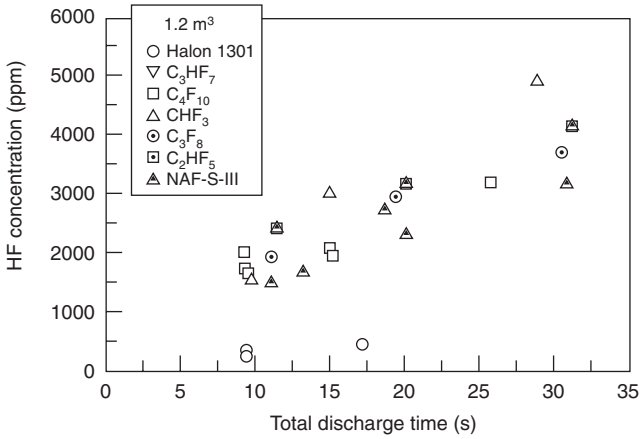

Figure 4-7.12. ***Maximum HF concentration resulting from extinguishment of 4.0-kW heptane fires.[37]***

Although other thermal decomposition products have been identified in some cases, it appears that HF is the primary thermal decomposition product of interest relative to human safety and equipment damage.

HF, like HCl, is an irritant gas, detectable at very low concentrations. For HF there are very large differences between the approximate lethal concentration (ALC) and human detection and severe sensory irritant thresholds (approximately two and three orders of magnitude, respectively).

Fire size necessary to generate short-term lethal concentrations of HF in an enclosure (on the order of >1000 ppm) can, in some cases, pose a greater hazard to personnel in the protected space during a discharge in a fire incident, due to the fire and its effects, than the secondary impact of agent thermal decomposition products. This, however, should be verified for a particular application under a range of fire scenarios, using engineering methods discussed by Hanauska[40] and Hanauska et al.[41]

The production of HF and other agent decomposition products forms a potential hazard for occupants. Table 4–7.19[20] summarizes potential health effects in healthy individuals. Note that exposure above 200 ppm may begin to impair escape particularly at exposure times exceeding 5 min.

Emergency Response Planning Guidelines (ERPG) values, developed by the American Industrial Hygiene Association, for 10-min exposures, are as follows: ERPG-2, a level at which mitigating steps such as evacuation should be taken is 50 ppm, and ERPG-3, the maximum non-lethal exposure concentration for 10 min is 170 ppm. The ERPG values are in contrast to an analysis by Melchrum,[42] which indicates that a dose of 12,000 ppm/min has 1 percent lethality in exposed animals. Additional health-effect and risk-assessment data are given in References 43 to 46.

Table 4-7.19 ***Potential Human Health Effects of Hydrogen Fluoride in Healthy Individuals[20]***

Exposure Time	Hydrogen Fluoride (ppm)	Reaction
2 min	<50	Slight eye and nasal irritation
	50–100	Mild eye and upper respiratory tract irritation
	100–200	Moderate eye and upper respiratory tract irritation, slight skin irritation
	>200	Moderate irritation of all body surfaces, increasing concentration may impair escape
5 min	<50	Mild eye and nasal irritation
	50–100	Increasing eye and nasal irritation, slight skin irritation
	100–200	Moderate irritation of skin, eyes, and respiratory tract
	>200	Definite irritation of tissue surfaces, will impair escape at increased concentrations
10 min	<50	Definite eye, skin, and upper respiratory tract irritation
	50–100	Moderate irritation of all body surfaces
	100–200	Moderate irritation of all body surfaces, escape-impairing effects likely
	>200	Escape-impairing effects will occur, increasing concentrations can be lethal without medical intervention

The impact of thermal decomposition products on electronics equipment is another area of concern. There are not sufficient data at present to predict the effects of a given HF exposure scenario on all electronics equipment. Several evaluations of the impact of HF on electronics equipment have been performed relative to the thermal decomposition of Halon 1301, where decomposition products include HF and HBr. One of the more notable was a NASA study where the shuttle orbital electronics were exposed to 700, 7000, and 70,000 ppm HF and HBr.[40] In these tests, exposures up to 700 ppm HF and HBr caused no failures. At 7000 ppm, severe corrosion was noted; there were some operating failures at this level.

Dumayas exposed IBM-PC-compatible multifunction boards to environments produced by a range of fire sizes as part of an evaluation program on halon alternatives.[47] He found no loss of function of these boards following a 15-min exposure to postfire extinguishment atmosphere up to 5000 ppm HF, with unconditioned samples stored at ambient humidity and temperature conditions for up to 30 days. Forssell et al.[48] exposed multifunction boards for 30 min in the postfire extinguishment environment; no failures were reported up to 90 days posttest. HF concentrations up to 550 ppm were evaluated.

While no generic rule or statement can be made at present, it appears that short-term damage (<90 days) resulting in electronics equipment malfunction is not likely for exposures of between 500 to 1000 ppm HF for up to 30 min. This result, however, is dependent on the characteristics of the equipment exposed, postexposure treatment, exposure to other combustion products, and relative humidity. Important equipment characteristics include its location in the space, existence of equipment enclosures, and the sensitivity of the equipment to damage.

All HCFC and HFC clean agents form more thermal decomposition products than Halon 1301, given similar fire sizes and discharge times. The primary variable controlling the quantity of thermal decomposition products is the size of the fire at the time of agent discharge. Through evaluation of the fire size at the time of system actuation, using engineering methods described in Section 4, Chapter 1, and subsequent design of the detection system, the potential hazard posed can be managed adequately.

Hanauska[40] and Hanauska et al.[41] have indicated that the degree of thermal decomposition products of agents can be managed safely. Full-scale testing with typical Class A fuel packages, in conjunction with typical detection system installation,[48] has shown that the level of thermal decomposition products is acceptable in typical computer/electronics spaces. For installation in hazard areas where very rapidly developing large fires are likely, the degree of thermal decomposition formation should be

evaluated in the context of the hazard posed by the fire and the performance of alternative fire protection systems.

Hydraulic Flow Characteristics

All halocarbon replacement agents exhibit two-phase flow behavior. Since all, except HFC-23, are used in cylinders pressurized to 360 or 600 psig, they are also multiple-component flows. Inert gas mixtures are single-phase gas flows with one or more components. As in the case of engineered Halon 1301 systems, all flow calculation procedures used must be listed or approved by the authority having jurisdiction, and be within the limitations of the flow calculation method determined during the engineered system approval process.

The characteristic that differentiates two-phase pipe flow from incompressible fluid (e.g., water) pipe flow is the existence of gas and liquid phases simultaneously in the pipe network. This aspect, coupled with the relatively short flow times, results in significant challenges to correctly predicting the flow. Among the important factors are the change in density of the fluid with pressure, the release of nitrogen in the cylinder and pipe as the fluid pressure and temperature change, differences in agent mass delivered caused by the flow time imbalances between nozzles, and preferential distribution of phases (and subsequently agent mass) at tee splits.

The need for accurate flow predictions is driven by three design requirements:

1. Control of agent discharge time
2. Maintenance of adequate nozzle flow and pressure to ensure agent distribution and mixing at the listed coverage area
3. Delivery of adequate, but not excessive, agent quantities to different rooms within the same protected area, when such rooms are flooded simultaneously

In addition, agent flow rate and thermodynamic state properties are necessary for estimating compartment pressurization levels during agent discharge.

For pre-engineered systems, limits on discharge time and nozzle pressure are built into the limits on piping system geometry. Agent distribution is handled by constraining pre-engineered systems to balanced flow conditions (i.e., the same agent mass is distributed from each nozzle). For adequate design of engineered systems, accurate methods for predicting these elements are required.

Figure 4-7.13 is an idealized plot of cylinder and nozzle pressure during discharge. Throughout the discharge process the amount of agent vapor and liquid, as well as dissolved and gaseous nitrogen, varies. As the pressure decreases in the cylinder and piping system, more agent is vaporized and nitrogen is released from the solution in the agent. The formation of additional vapor and nitrogen bubbles lowers the average density of the fluid. The rapid vaporization of agent is more pronounced in low boiling point/high vapor pressure agents. The fluid temperature also varies with time and along the length of the piping network. The fluid temperature also impacts the degree of agent vaporization and nitrogen release as well as liquid agent density. The discharge process can be divided into five sections.

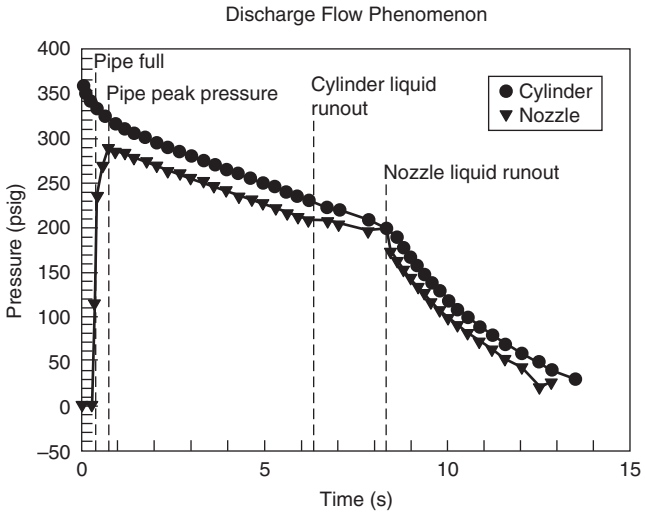

Figure 4-7.13. ***Idealized cylinder and nozzle pressure time curves for halocarbon agents.***

The first is the process of filling the pipe with agent. The rate at which this process occurs is driven by the speed of the agent interface moving through the network. This speed is determined by either the sonic velocity at the agent interface or the discharge of displaced air through the nozzle. This phase determines the time at which the agent discharges from each nozzle. For systems with high degrees of imbalance in terms of flow path length or large pipe volume differences between nozzles, there can be significant delay in agent reaching one nozzle before another. This delay has a dramatic effect on the distribution of mass from each nozzle.

Once the agent reaches the nozzle and is compressed in the pipeline, the so-called nozzle peak pressure is reached. At this moment, agent is discharging from each nozzle.

The next step in the discharge process is the so-called quasi-steady agent flow regime. This step is generally the longest portion of the discharge, particularly for systems with low pipe volume to agent volume ratios. This period of the discharge process is the basis for the simplified pressure drop calculations embodied in NFPA 12A for balanced Halon 1301 systems.

The next milestone during the discharge process is cylinder liquid runout, where no liquid agent remains in the cylinder. At this moment, an interface between liquid agent and nitrogen/agent vapor forms and travels through the network.

When the trailing liquid/vapor interface reaches the first nozzle, nozzle liquid runout occurs. This runout is important in two ways. First, liquid runout occurs at different times during the discharge for each nozzle and can significantly impact the quantity of agent flowing from any given nozzle. Second, it is possible in many circumstances to discharge sufficient vapor/gas mixture from the first nozzle at NLRO (nozzle liquid runout) to reduce the pressure in the piping below that necessary to flow the remaining agent in the network. This aspect is

especially important for low vapor pressure agents and for nozzle designs requiring relatively high minimum operating pressures.

Once all of the nozzles have been cleared of liquid agent, the system is discharging a combination of nitrogen and agent vapor. This regime is usually ignored since most (>95 percent) of the agent has already been delivered through the nozzles.

The importance of the pipe filling and nozzle runout with these alternatives is relatively more critical with low vapor pressure alternatives due to (1) the inability of the agent to deliver significant pressure to the system by boiling and (2) the higher fluid densities that occur in the piping relative to Halon 1301.

Figures 4-7.14(a) through (d) illustrate the stages of the agent discharge network.

Flow regime: If the flow velocity of the agent in the piping is not high enough, the flow may separate into two distinct phases in the piping. This occurrence causes severe problems at tee splits and in evaluating pressure drops. Therefore, minimum flow rates that ensure a homogeneous mixture of agent liquid and vapor/nitrogen bubbles must be maintained. Various flow regimes are illustrated in Figures 4-7.15 and 4-7.16 for horizontal and vertical pipe, respectively. One of the objectives of approval testing of flow calculation procedures is to ensure that homogeneous flow regimes are maintained in the piping throughout the discharge process. In Figures 4-7.15 and 4-7.16, these are denoted as dispersed bubble and bubble flow regimes, respectively.

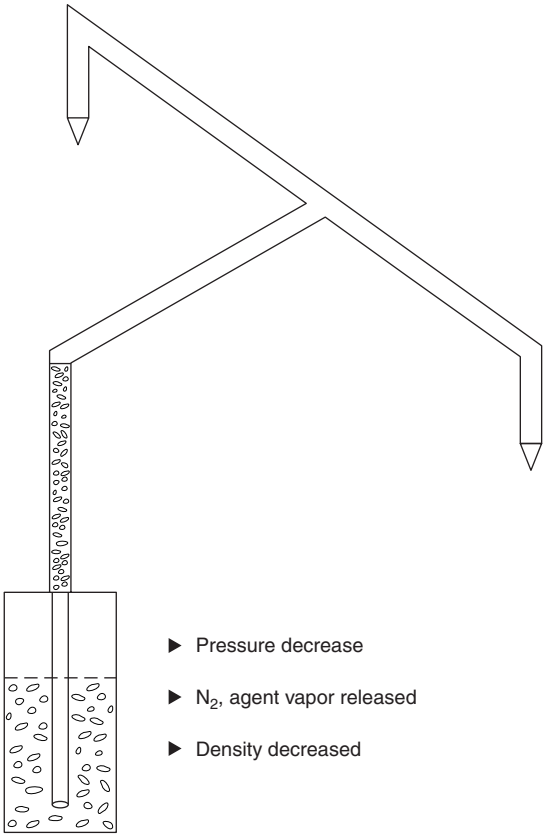

Figure 4-7.14(b). ***Valve open, pipe filling.***

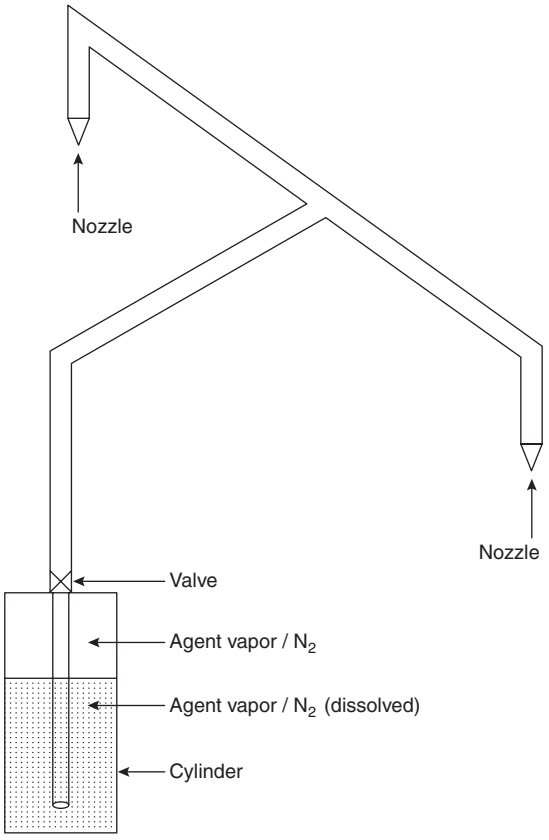

Figure 4-7.14(a). ***Initial conditions.***

Flow division at tees: For a single-component, single-phase flow condition, the flow split at a tee junction is determined by the flow rate of the nozzles downstream of the tee. For two-phase fluids, flow distribution occurs at tees that are sensitive to the velocity of the flow along each branch of the tee, the orientation of the tee, the pressure at the tee, and the phase distribution of the fluid (gas or liquid) entering the tee.

The primary cause of preferential flow splits at tees is the inertia of the liquid versus vapor/gas phase. This condition is most readily envisioned for side-flow tees where one branch of the flow is required to turn 90 degrees. Gas/vapor bubbles with lower momentum relative to the liquid agent will make this change of direction more readily. This change results in relatively less mass flow down the side-flow branch at approximately the same volumetric flow rate or velocity. For bullhead tees, the same problem applies, except that it is more subtle and involves velocity differences through each branch of the tee. For evenly split (50 percent/50 percent) flows, the velocity is identical in both directions, resulting in no flow split correction; as the split becomes greater the velocity

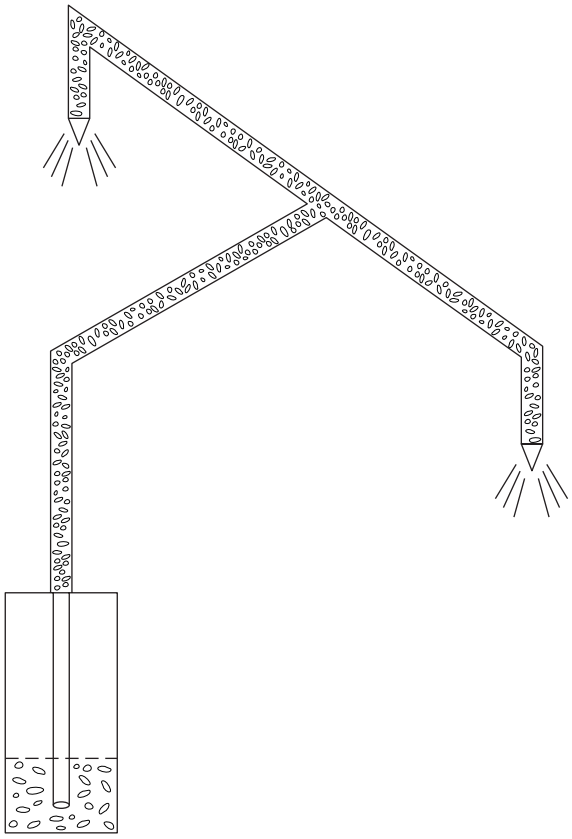

Figure 4-7.14(c). ***Quasi-steady flow, liquid throughout network.***

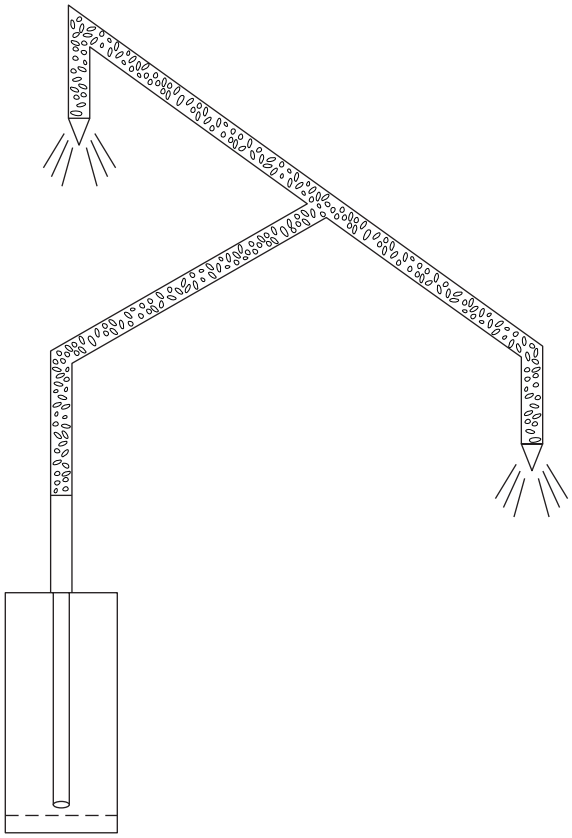

Figure 4-7.14(d). ***Cylinder liquid runout.***

differences are greater, and inertial effects of the gas/vapor relative to the liquid cause significant redistribution of mass through each branch of the tee.

The dependence was understood for Halon 1301 and described in detail by Williamson.[49] Similar processes occur in all two-phase flows including air/water, steam/water, and refrigerant flows. In the context of clean agent system design calculations, this flow distribution is dealt with using empirical factors that redistribute the flow relative to the pure pressure-driven flow distribution which would occur without preferential phase distribution at tees.

Figures 4-7.17 and 4-7.18 illustrate these correction factors for Halon 1301 flows in bullhead and side-flow tees, respectively.[49] All of the halocarbon agent flow predictions require similar treatment. Side-flow tees and bullhead tees require independent empirical correction factors. One of the most important limitations to any flow calculation procedure is the maximum flow split allowed for each type of tee. For a bullhead tee, as one moves farther away from 50 percent/50 percent splits, the correction factor becomes greater, and at some point usually in the range of 80 percent/20 percent, it becomes so large that the prediction becomes unreliable. For side-allowable flow splits, ranges between 75 percent/25 percent and 90 percent/10 percent are typical. This correction of flow splits at tees is one reason that final approval of engineered system designs should be constrained to calculation methods that have undergone testing within the range of flow splits required.

Pressure drop due to friction loss: The pressure drop caused by friction in the pipeline is calculated differently for two-phase fluids. The presence of agent vapor and gas affects the pressure drop per unit length of pipe. There are numerous methods for dealing with two-phase fluid pressure drop.[50,51] Those typically used for fire suppression agent calculations involve either (1) correcting the pressure drop estimated for single-phase fluid as a function of liquid to vapor/gas volume fraction or (2) empirical correlations of the pressure drop to average fluid density. Figure 4-7.19 illustrates the dependence of pressure drop on liquid volume fraction. In all cases for purposes of design of fire protection systems, the pressure drop is calculated on the basis of a homogeneous flow assumption where changes in the liquid fraction are seen as density changes in the homogeneous fluid.

Testing and approval of design methods: The approval or listing of a two-phase flow calculation procedure is part of the approval granted for engineered systems. Since some aspects of two-phase flow calculations are em-

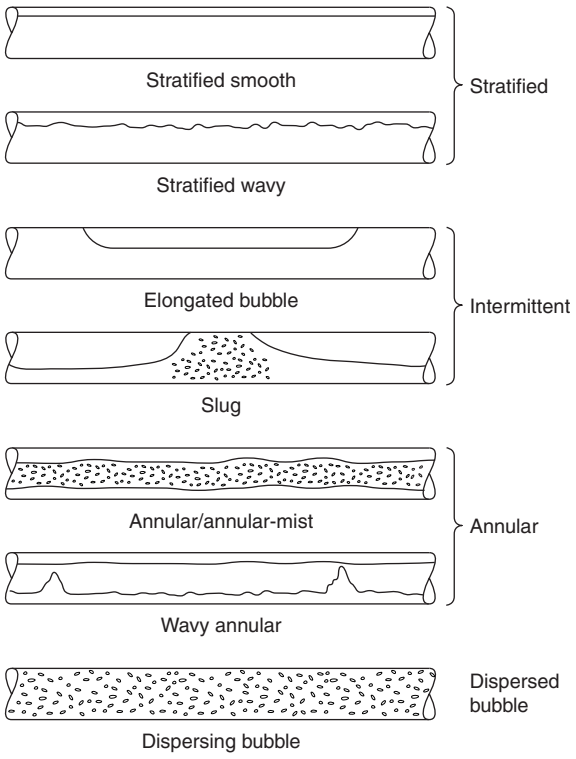

Figure 4-7.15. ***Horizontal pipe flow regimes.[52]***

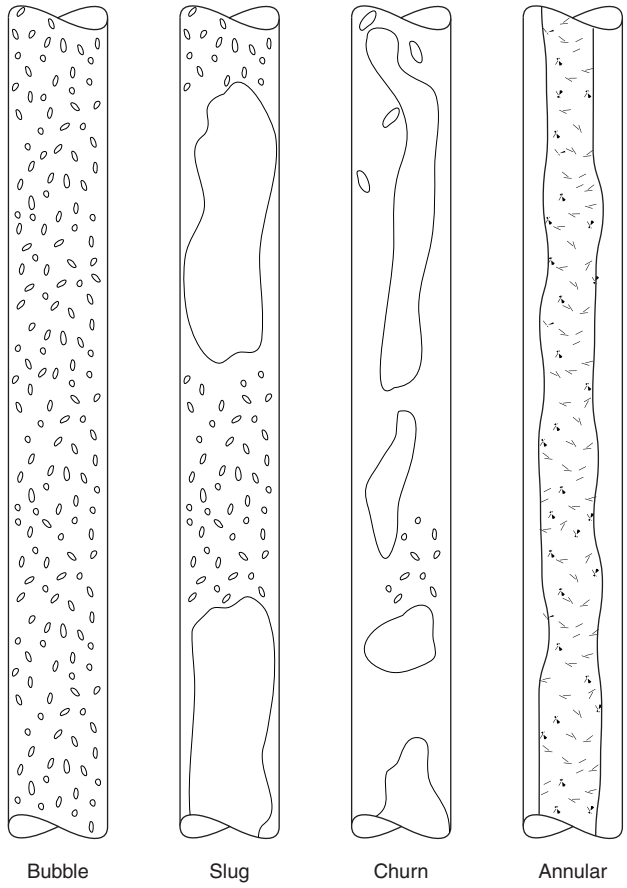

Figure 4-7.16. ***Vertical pipe flow regimes.[52]***

pirically based (e.g., flow regime, pressure drop, and flow splits) and all calculation procedures have some bounds on their validity, testing is performed to verify the predictions and establish the limits of the calculation procedure. These limitations are crucial in helping to ensure that system designs do not exceed verified limits of calculation.

One of the most rigorous approval procedures used in verifying design methods is outlined by Underwriters Laboratories Inc.[35] UL 1058, *Halogenated Agent Extinguishing System Units*, was used for evaluating engineered Halon 1301 systems, but the same approach is taken for all clean agent alternatives. Design method limitations are described by the following ten parameters:

1. Percent of agent in piping (maximum)
2. Minimum and maximum discharge times
3. Minimum pipeline flow rates
4. Variance of piping volume to each nozzle
5. Maximum variance of nozzle pressures within a piping arrangement
6. Maximum ratio of nozzle diameter to inlet pipe diameter
7. Arrangement most likely to exhibit vapor time-imbalance condition at nozzle
8. All types of tee splits, including through tees, bullhead tees, and so forth
9. Minimum and maximum container fill density
10. Minimum and maximum flow split for each type of tee

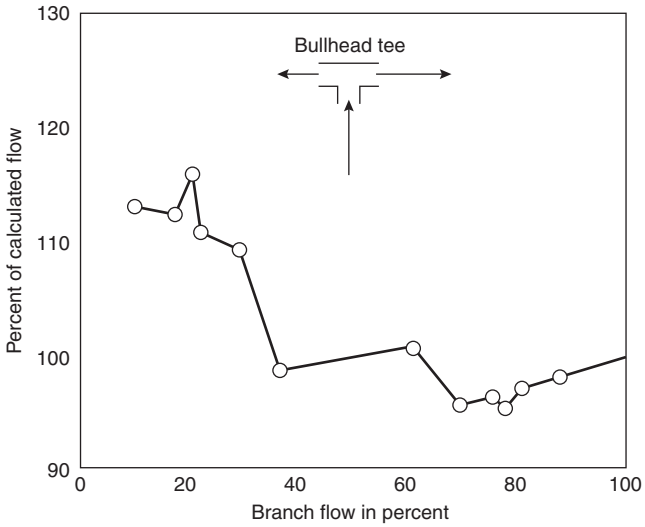

Figure 4-7.17. ***Bullhead-tee-flow split corrections for Halon 1301.[49]***

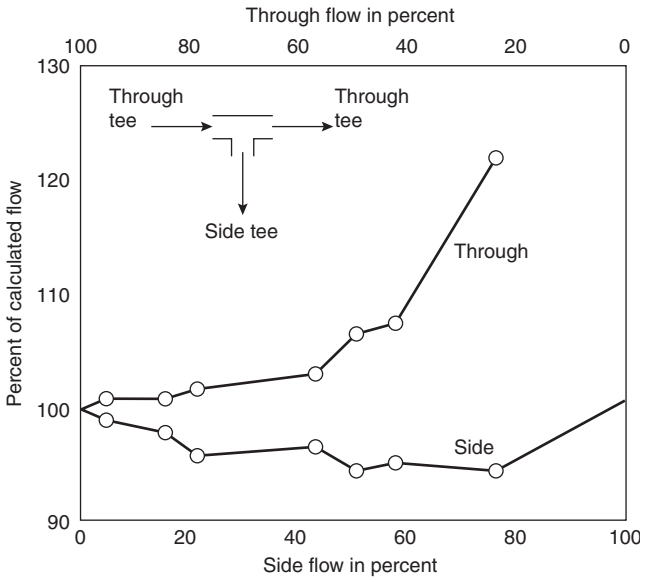

Figure 4-7.18. ***Side- and through tee-flow split corrections for Halon 1301.[49]***

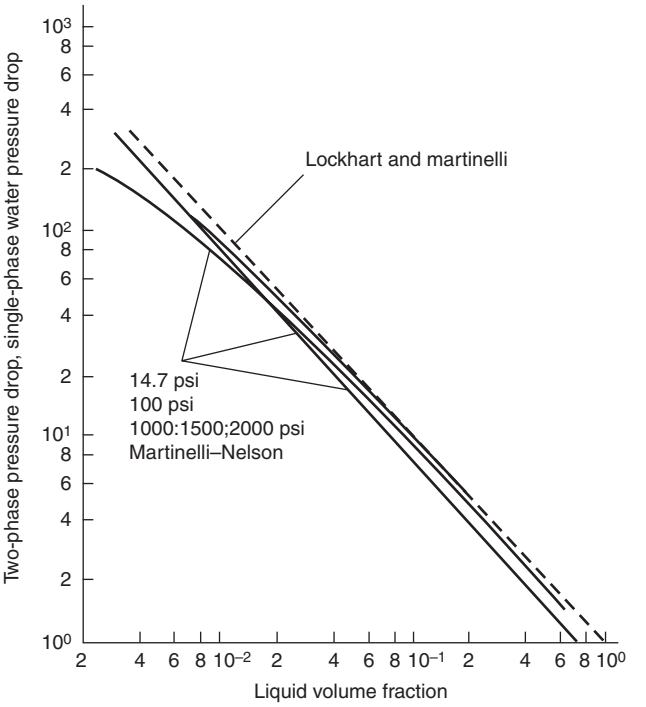

Figure 4-7.19. ***Pressure drop versus liquid volume fraction.[51]***

These parameters are related to the important attributes of the agent discharge process previously discussed. Full-scale testing is performed to evaluate the performance of the design method. The limits on flow calculation method performance are as follows:

1. Actual versus predicted discharge time ±1 s
2. Actual versus predicted nozzle pressure ±10 percent
3. Actual versus predicted mass flow through a nozzle, –5 + 10 percent

Testing in conjunction with a particular manufacturer's hardware is important. Ensuring that pressure drop through a particular valve assembly is calculated properly and nozzle orifice discharge coefficient evaluation are two critical hardware-dependent verifications.

Several generic flow calculation routines have been developed.[37,53–56] Of these, two are directed at single-nozzle systems with very short discharge times[55] or relatively simple balanced networks.[54] It is not recommended that any generic calculation procedure be used for final design purposes, unless it has been tested with the specific hardware to be installed and the system is within the limitations derived by tests.

In order to preserve a 10-s discharge time, the mass flow rate of these clean agents must be higher than Halon 1301. The increased density of some of the alternative agents in the piping, caused by lower vapor pressures and nitrogen solubility differences, may result in high enough mass flow rates to retrofit existing Halon 1301 systems. While agent cylinders and nozzles will require replacement, it is often possible to preserve the existing Halon 1301 pipe network. Preservation often requires the use of lower fill density cylinders to increase the average system pressure throughout the discharge time. Any such retrofit using existing Halon 1301 piping must be carefully evaluated with respect to hydraulic performance, with particular care given to preserving minimum required nozzle pressures and flow divisions at tees.

Nozzle Area Coverage and Height Limitations

One of the most important requirements of a gaseous total flooding fire suppression system is the ability of the system to deliver a uniform concentration of agent throughout the protected enclosure. The nozzle design and minimum nozzle pressure are critical in ensuring this distribution of agent. The performance of the nozzle is evaluated by full-scale approval testing, such as UL 1058.[35] The basic testing performed to evaluate nozzles is as follows:

1. Establish minimum nozzle pressure and maximum nozzle height by ensuring extinguishment of heptane fires located throughout a space with a height equal to the maximum allowable, at the minimum allowable nozzle pressure.
2. Establish maximum nozzle coverage area by extinguishing tests in a plenum at the minimum height (generally less than 0.5 m) at the maximum nozzle coverage area (on the order of 100 m^2) and minimum nozzle operating pressure.

There are substantial differences between hardware manufacturers relative to minimum nozzle pressure, maximum ceiling height, and maximum average coverage. All nozzle orientations should be evaluated. In general, maximum nozzle heights are on the order of 4 to 5 m, nozzle area coverage on the order of 9 to 10 m^2, and minimum nozzle pressure between 3 and 6 bar. It is critical to

ensure that the nozzle spacing, height, and minimum pressure limits are not exceeded for a particular manufacturer's hardware in a specific design.

The flow, mixing, and distribution of an agent from a nozzle into an enclosure can be predicted theoretically for relatively simple nozzle designs using sophisticated computer models.[54] Further development of such methods for complex nozzle designs and compartment geometries may eventually form the basis of a design procedure. At present, however, the primary means of ensuring adequate nozzle performance is the hardware approval process and real-scale testing.

Since many of the halocarbon replacements have lower vapor pressures than Halon 1301, there is often a much higher percentage of liquid at the nozzle. This liquid makes the task of vaporizing and mixing the agent in the compartment more difficult. In general, nozzle designs used for Halon 1301 systems are not adequate for the halocarbon replacement agents. Due to the increased liquid fraction at the nozzle, it is critical to ensure that no unenclosed openings exist along the trajectory of the nozzle orifices. Increased liquid fraction may result in significant preferential loss of agent through these openings. This condition further emphasizes the need for third-party approval testing of nozzle performance. In any retrofit situation, the nozzles will need to be replaced even if the piping is adequately sized to deliver adequate agent flow rates.

Compartment Pressurization

The rapid discharge of agent into a compartment will cause rapid changes in the compartment pressure. Depending on the agent and rate of discharge, the initial pressure change may be negative. Figure 4-7.20 is a plot of compartment pressure versus time for the discharge of HFC-227ea into a 28-m^3 room with a 360-cm^2 (56-$in.^2$) leakage area.[37] Immediately after discharge, the pressure in the compartment drops below ambient to a minimum of −0.3 kPa; at approximately 1.5 s after discharge began, the pressure then begins to increase to a maximum of approximately 0.14 kPa after nozzle liquid runout. Similar results were obtained for FC-3-1-10. HFC-23 discharge exhibited much higher compartment overpressurization, without the marked initial negative pressure. The maximum overpressure for HFC-227ea and FC-3-1-10 discharge was similar to that of Halon 1301.

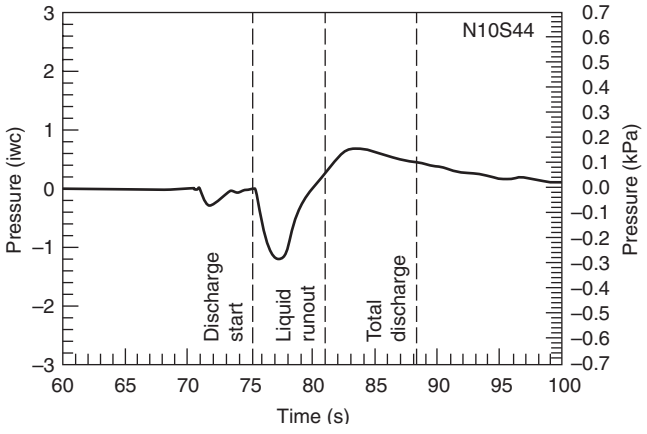

Figure 4-7.20. ***Pressure measured in 28-m^3 enclosure during C_3F_7H discharge, with nominal 15-s discharge time and 5-cm pan of n-heptane.[37]***

As the halocarbon agent is discharged into the space, it vaporizes rapidly, cooling the compartment and lowering the pressure. As the agent/air mixture gains heat from the walls or other objects in the space, the pressure recovers and, as additional agent is added, the pressure increases over ambient as mass is added to the compartment.

The expected maximum and minimum compartment pressure during discharge will be a function of the following:

1. Thermodynamic state of the agent at the nozzle
2. Nozzle design
3. Compartment volume and wall surface area
4. Size of fire
5. Initial conditions in space
6. Leakage area from compartment
7. Agent flow rate

For inert gases, significant compartment overpressurization can occur during discharge, unless adequate free vent area is provided. Calculation of required open area for venting is a part of the design manual for IG-541 systems.[57]

No generalized design procedure for calculating under/overpressurization has been established. Forssell and DiNenno[37] have developed a procedure for estimating the compartment pressure as a function of agent, agent flow rate, agent thermodynamic state at the nozzle, compartment volume, and surface area and leakage area. The method has not been sufficiently tested for general application.

Agent Hold Time and Leakage

Traditionally, total flooding gas systems were required to maintain a minimum concentration for a specified time period (10 to 20 min) after discharge. The minimum required hold time was based on the following:

1. Soak time required for deep-seated Class A fuels
2. Response time of emergency personnel
3. Prevention of reflash due to presence of hot surfaces and other reignition sources, particularly in flammable and combustible liquid applications

Currently, there is no specified minimum hold or soak time for clean agents. The variables described above will vary between installations, and there is no significant database on the performance of these agents on deep-seated fires other than wood cribs. The designer will be required to specify the minimum soak time consistent with the requirements of the hazard being protected.

The ability of a compartment to maintain adequate agent concentrations is a function of the leakage of the compartment. Historically, this was done with Halon 1301 through the use of discharge tests. Discharge testing for

this purpose was rendered unnecessary by the introduction of door fan pressurization leakage tests. Appendix B of NFPA 2001 describes a complete procedure for evaluating agent hold time as a function of compartment leakage measured by the door fan pressurization method.

The only difference between alternative agents and Halon 1301 in this regard is the density of the agent/air mixture, which is the driving force for leakage in quiescent environments. The mixture density can be estimated as follows:[1]

$$\rho_m = V_d \frac{C}{100} + \left[\frac{\rho_a (100 - C)}{100} \right]$$

where

ρ_m = clean agent/air mixture density (kg/m³)
ρ_a = air density (1.202 kg/m³)
C = clean agent concentration (%)
V_d = agent vapor density at 21°C (kg/m³)

Agent vapor densities at 21°C are given below:

FC-3-1-10	9.85 kg/m³ (0.615 lb/ft³)
HBFC-22B1	5.54 kg/m³ (0.346 lb/ft³)
HCFC Blend A	3.84 kg/m³ (0.240 lb/ft³)
HFC-124	5.83 kg/m³ (0.364 lb/ft³)
HFC-125	5.06 kg/m³ (0.316 lb/ft³)
HFC-227ea	7.26 kg/m³ (0.453 lb/ft³)
HFC-23	2.915 kg/m³ (0.182 lb/ft³)
IG-541	1.43 kg/m³ (0.089 lb/ft³)]
Halon 1301	6.283 kg/m³ (0.392 lb/ft³)

All agents, except inert gases, have higher mixture densities than Halon 1301 at 5 percent when used at their design concentrations. This will require slightly more leak-tight enclosures to maintain the same hold time.

Summary

A wide range of inert gas and halocarbon total-flooding clean agents has been introduced over the past several years. More will be commercialized in the near future. The use of an agent must be consistent with applicable environmental regulations. The selection of an agent is driven by its fire performance characteristics, agent and system space and weight concerns, toxicity (particularly for use in occupied areas), and the availability of approved system hardware.

The design of clean agent systems must be carefully done in accordance with third-party listing and approval limitations on both agent and hardware. Given the relative lack of experience with systems employing these new agents, particular care in design, installation, inspection, testing, and maintenance is warranted. Design and installation standards, such as NFPA 2001 form the minimum requirements for these new technologies.

As generalized design methods and more detailed requirements evolve, the ability to design and install systems on a performance basis will increase. A critical part of the installation process is post-installation inspection and testing. NFPA 2001 contains requirements for the approval and post-installation inspection and test of clean agent systems. Bearing in mind the relative complexity of these systems and the importance of the detection system and enclosure integrity, post-installation inspection and testing should be rigorously performed.

References Cited

1. NFPA 2001, *Standard on Clean Agent Fire Extinguishing Systems,* National Fire Protection Association, Quincy, MA, 1994 edition.
2. T.A. Moore, "Cup Burner Analysis," *Halon Substitute Program Review,* (1993).
3. A. Hamins et al., "Flame Suppression Effectiveness," in *Evaluation of Alternative In-Flight Fire Suppressants for Full-Scale Testing in Simulated Aircraft Engine Nacelles and Dry Bays,* NIST SP 861, National Institute of Standards and Technology, Gaithersburg, MD (1994).
4. M.L. Robin, "Properties and Performance of FM-200™," in *Proceedings of the Halon Options Technical Working Conference 1994,* New Mexico Engineering Research Institute, Albuquerque, NM, pp. 531–542 (1994).
5. R. Sheinson et al., "Halon 1301 Total Flooding Fire Testing, Intermediate Scale," in *Proceedings of the Halon Options Technical Working Conference 1994,* New Mexico Engineering Research Institute, Albuquerque, NM, pp. 43–53 (1994).
6. T.A. Moore et al., "Intermediate Scale (645 ft³) Fire Suppression Evaluation of NFPA 2001 Agents," in *Proceedings of the Halon Options Technical Working Conference 1993,* New Mexico Engineering Research Institute, Albuquerque, NM, pp. 115–127 (1993).
7. M.J. Ferreira et al., "Thermal Decomposition Product Results Utilizing PFC-410," in *Proceedings of the Halon Options Technical Working Conference 1992,* New Mexico Engineering Research Institute, Albuquerque, NM (1992).
8. "Extinguishing Behavior of Inert Gases," *Final Report,* VdS, Cologne, Germany (1998).
9. UL 2166, *Halocarbon Clean Agent Extinguishing System Units,* Underwriters Laboratories Inc., Northbrook, IL (1999).
10. UL 2127, *Inert Gas Clean Agent Extinguishing System Units,* Underwriters Laboratories Inc., Northbrook, IL (1999).
11. R.E. Tapscott, "Best Values of Cup Burner Extinguishing Concentration," in *Proceedings of the Halon Technical Options Technical Working Conference 1999,* New Mexico Engineering Research Institute, Albuquerque, NM, pp. 27–29 (1999).
12. L.A. McKenna et al., "Extinguishment Tests of Continuously Energized Class C Fires," in *Halon Options Technical Working Conference 1998,* New Mexico Engineering Research Institute, Albuquerque, NM (1998).
13. J.A. Senecal, "Agent Inerting Concentrations for Fuel-Air Systems," *CRC Technical Note No. 361,* Fenwal Safety Systems, (1992).
14. F. Tamanini, *Determination of Inerting Requirements for Methane/Air and Propane/Air Mixtures by an Ansul Inerting Mixture of Argon, Carbon Dioxide, and Nitrogen,* Factory Mutual Research Corp., Norwood, MA (1992).
15. E. Heinonen, "Laboratory-Scale Inertion Results," *Halon Substitutes Program Review,* (1993).
16. E.W. Heinonen, "The Effect of Ignition Source and Strength on Sphere Inertion Results," in *Proceedings of the Halon Options Technical Working Conference 1993,* Albuquerque, NM, pp. 565–576 (1993).

17. J.A. Senecal, "Explosion Protection in Occupied Spaces: The Status of Suppression and Inertion Using Halon and Its Descendants," in *Proceedings of the 1993 International CFC and Halon Alternatives Conference,* Washington, DC, pp. 767–772 (1993).
18. J.A. Senecal, D.N. Ball, and A. Chattaway, "Explosion Suppression in Occupied Spaces," in *Proceedings of the Halon Options Technical Working Conference 1994,* Albuquerque, NM, pp. 79–86 (1994).
19. T.A. Moore, "Large-Scale Inertion Evaluation of NFPA 2001 Agents," in *Proceedings of the 1993 International CFC and Halon Alternatives Conference,* Washington, DC (1993).
20. NFPA 2001, *Standard on Clean Agent Fire Extinguishing Systems—2000 Edition,* National Fire Protection Association, Quincy, MA, 2000 edition.
21. A. Vinegar and G.W. Jepson, "Cardiac Sensitization Thresholds of Halon Replacement Chemicals Predicted in Humans by Physiologically-Based Pharmacokinetic Modeling," *Risk Analysis,* 16, 4 (1996).
22. A. Vinegar, G.W. Jepson, and J.H. Overton, "PBPK Modeling of Short Term (0 to 5 min) Human Inhalation Exposures to Halogenated Hydrocarbons," *Inhal. Toxicol.,* 10, pp. 411–429 (1998).
23. A. Vinegar, *Performance of Monte Carlo Simulations of Exposure to HFC-227ea,* ManTech Environmental Technology, Inc., Dayton, OH (1999).
24. A. Vinegar, G.W. Jepson, M. Cisneros, R. Rubenstein, and W. J. Brock, "Setting Safe Exposure Limits for Halon Replacement Chemicals Using Phyiologically Based Pharmacokinetic Modeling," *Inhal. Toxicol.* (in press).
25. A. Vinegar, and G. Jepson, "Pharmacokinetic Modeling for Determining Egress from Exposure to Halon Replacement Chemicals," in *Proceedings of Halon Options Technical Working Conference 1998,* New Mexico Engineering Research Institute, Albuquerque, NM (1998).
26. A. Vinegar, and G. Jepson, "Ephinephrine Challenge for Cardiac Sensitization Testing versus Endogenous Ephinephrine," in *Proceedings of the Halon Technical Working Conference 1999,* New Mexico Engineering Research Institute, Albuquerque, NM (1999).
27. "Research Basis for Improvement of Human Tolerance to Hypoxic Atmospheres in Fire Prevention and Extinguishment," *EBRDC Report 10.30.92,* Environmental Biomedical Research Data Center, Institute for Environmental Medicine, University of Pennsylvania, Philadelphia, PA (1992).
28. J.C. Yang and B.D. Bruel, "Thermophysical Properties of Alternative Agents," in *Evaluation of Alternative In-Flight Fire Suppressants for Full-Scale Testing in Simulated Aircraft Engine Nacelles and Dry Bays,* NIST SP 861, National Institute of Standards and Technology, Gaithersburg, MD (1994).
29. R.S. Sheinson et al., "Halon 1301 Replacement Total Flooding Fire Testing, Intermediate Scale," in *Proceedings of Halon Options Technical Working Conference 1994,* New Mexico Engineering Research Institute, Albuquerque, NM, pp. 43–53 (1994).
30. J.C. Brockway, "Recent Findings on Thermal Decomposition Products of Clean Extinguishing Agents," 3M Report presented to NFPA 2001 Committee, Ft. Lauderdale, FL (1994).
31. I. Schlosser, "Reliability and Efficacy of Gas Extinguishing Systems," in *Proceedings of Conference on Fire Extinguishing Systems,* VdS, Cologne, Germany (1998).
32. *Halon Alternatives, A Report on the Fire Extinguishing Performance Characteristics of Some Gaseous Alternatives to Halon 1301, LPR6: July 1996,* Loss Prevention Council, Hertfordshire, UK (1996).
33. ISO 14520-1, *Gaseous Fire Extinguish Systems—Physical Properties and System Design, Part 1: General Requirements,* International Standards Organization, (2000).
34. T.A. Moore et al., "Intermediate Scale (645 ft^3) Fire Suppression Evaluation of NFPA 2001 Agents," in *Proceedings of Halon Options Technical Working Conference 1993,* New Mexico Engineering Research Institute, Albuquerque, NM, pp. 115–128 (1993).
35. UL 1058, *Halogenated Agent Extinguishing System Units,* Underwriters Laboratories Inc., Northbrook, IL (1984).
36. G.G. Back et al., "Draft Report: Full-Scale Machinery Space Testing of Gaseous Halon Alternatives," USCG R&D Center, Groton, CT (1994).
37. E.W. Forssell and P.J. DiNenno, "Evaluation of Alternative Agents for Use in Total Flooding Fire Protection Systems," Contract NAS 10-1181, National Aeronautics and Space Administration, John F. Kennedy Space Center, FL (1994).
38. P.J. DiNenno et al., "Thermal Decomposition Testing of Halon Alternatives," in *Proceedings of the Halon Alternatives Technical Working Conference 1993,* New Mexico Engineering Research Institute, Albuquerque, NM (1993).
39. D.S. Dierdorf et al., "Decomposition Product Analysis During Intermediate Scale (645 ft^3) Testing of NFPA 2001 Agents," in *Proceedings of the Halon Alternatives Technical Working Conference 1993,* New Mexico Engineering Research Institute, Albuquerque, NM (1993).
40. C.P. Hanauska, "Hazard Assessment of HFC Decomposition Products," presented at *1994 International CFC and Halon Alternatives Conference,* Washington, DC (1994).
41. C.P. Hanauska et al., "Hazard Assessment of Thermal Decomposition Products of Halon Alternatives," in *Proceedings of the Halon Alternatives Technical Working Conference 1993,* New Mexico Engineering Research Institute, Albuquerque, NM (1993).
42. M. Meldrum, *Toxicology of Substances in Relation to Major Hazards: Hydrogen Fluoride,* Health and Safety Executive (HSE) Information Centre, Sheffield, England (1993).
43. W. Dalby, *Evaluation of the Toxicity of Hydrogen Fluoride at Short Exposure Times,* Stonybrook Laboratories, Inc., Pennington, NJ, sponsored by the Petroleum Environmental Research Forum (PERF), PERF Project 92–90 (1996).
44. W. Machle and K.R. Kitzmiller, "The Effects of the Inhalation of Hydrogen Fluoride, II. The Response Following Exposure to Low Concentrations," *J. Ind. Hyg. Toxicol.*, 17, pp. 223–229 (1935).
45. W. Machle, F. Tharnann, K.R. Kitzmiller, and J. Cholak, "The Effects of Inhalation of Hydrogen Fluoride, I. The Response Following Exposure to High Concentrations," *J. Ind. Hyg. Toxicol.*, 16, pp. 129–145 (1934).
46. W.J. Brock, "Hydrogen Fluoride: How Toxic is Toxic? (A Hazard and Risk Analysis)," in *Proceedings of the Halon Options Technical Working Conference 1999,* New Mexico Engineering Research Institute, Albuquerque, NM, pp. 27–29 (1999).
47. W.A. Dumayas, "Effect of HF Exposure on PC Multifunction Cards," Senior Research Project, University of Maryland, College Park (1992).
48. E.F. Forssell et al., "Draft Report: Performance of FM-200 on Typical Class A Computer Room Fuel Packages," Hughes Associates, Inc., Columbia, MD (1994).
49. H.V. Williamson, "Halon 1301 Flow in Pipelines," *Fire Technology,* 13, 1, pp. 18–32 (1976).
50. D. Chisholm, "Predicting Two-Phase Flow Pressure Drop," in *Encyclopedia of Fluid Mechanics, Vol. 3 (*N.P. Cheremisinoff, ed.), Gulf Publishing Company, Houston, TX (1986).

51. Y.Y. Hsu and R.W. Graham, *Transport Processes in Boiling and Two-Phase Systems,* Hemisphere Publishing Corporation, Washington, DC (1976).
52. D. Barnea and Y. Taitel, "Flow Pattern Transition in Two-Phase Gas-Liquid Flows," in *Encyclopedia of Fluid Mechanics, Vol. 3 (*N.P. Cheremisinoff, ed.), Gulf Publishing Company, Houston, TX (1986).
53. P.J. DiNenno et al., "Modeling the Flow Properties and Discharges of Halon Replacement Agents," in *Proceedings of the Halon Options Technical Working Conference 1994,* New Mexico Engineering Research Institute, Albuquerque, NM (1994).
54. E.B. Bird et al., "Development of Computer Model to Predict the Transient Discharge Characteristics of Halon Alternatives," in *Proceedings of the Halon Options Technical Working Conference 1994,* New Mexico Engineering Research Institute, Albuquerque, NM (1994).
55. T.G. Cleary et al., "Flow of Alternative Agents in Piping," in *Proceedings of the Halon Options Technical Working Conference 1994,* New Mexico Engineering Research Institute, Albuquerque, NM (1994).
56. W.M. Pitts et al., "Fluid Dynamics of Agent Discharge," in *Evaluation of Alternative In-Flight Fire Suppressants for Full-Scale Testing in Simulated Aircraft Engine Nacelles and Dry Bays, (*Grosshandler et al., eds.), NIST SP 681, National Institute of Standards and Technology, Gaithersburg, MD (1994).
57. Ansul Co., *Inergen System Design Installation and Maintenance Manual,* Ansul Co. (1994).

Additional Readings

P.J. DiNenno, "Content and Relevance of ISO and NFPA Guidelines," in *Proceedings of Conference on Fire Extinguishing Systems,* VdS, Cologne, Germany (1998).

M.R. Driscoll and P.E. Rivers, "Clean Extinguishing Agents and Continuously Energized Circuits: Recent Findings," in *Proceedings of the Halon Options Technical Working Conference 1997,* New Mexico Engineering Research Institute, Albuquerque, NM (1997).

NFPA 12A, *Standard on Halon 1301 Fire Extinguishing Systems,* National Fire Protection Association, Quincy, MA (1992).

R. Nieman, et al., "Evaluation of Selected NFPA 2001 Agents for Suppressing Class 'C' Energized Fires," in *Proceedings of the Halon Options Technical Working Conference 1996,* New Mexico Engineering Research Institute, Albuquerque, NM (1996).

CHAPTER 8

Fire Temperature-Time Relations

T. T. Lie

Introduction

The intensity and duration of fire in buildings can vary in a wide range, and several studies have been carried out to investigate the determining factors. At present it is possible to estimate the temperature course of fire in enclosures under various conditions, provided the values of the parameters that determine it are known.

Several of these parameters, however, such as amount and surface area of the combustible materials, are unpredictable as they change with time and often vary from compartment to compartment in a building. It is not possible, therefore, to know at the time a building is erected the temperature course of a fire to which objects in that building might be exposed during its service life.

It is possible, however, to indicate for any enclosure a temperature-time curve that, with reasonable likelihood, will not be exceeded during the lifetime of the building. Such curves are useful as a basis for the fire-resistive design of buildings. They can also facilitate studies of fire resistance of building components exposed to fires of various intensity and duration.

In this chapter, analytical expressions will be given that describe characteristic temperature curves as a function of the significant parameters for various fire conditions commonly met with in practice.

Expressions will also be given for the standard fire curve used in North America, and for the fire curve adopted by the International Organization for Standardization (ISO).

Fire Temperatures

The temperature course of a fire in an enclosure may be divided into three periods:

1. The growth period
2. The fully developed period
3. The decay period

These periods are illustrated in Figure 4-8.1, where an idealized fire temperature course is shown. During the growth period, heat produced by the burning materials is accumulated in the enclosure. As a result, other materials may be heated so severely that they also ignite. At this stage of the fire, the gas temperatures rise very quickly to high values. The rather sudden ignition of materials in all parts of the room is called *flashover.* After the flashover, the fully developed period starts. Because the temperatures in the enclosure are relatively low in the growth period, their influence on the fire resistance of structural members is negligible. In fire resistance studies, therefore, the growth period can be disregarded. Actual risk of failure of structural members or fire separations begins when the fire reaches the fully developed stage. In this stage, temperatures of about 1000°C or higher can be reached, and the heat transferred from the fire to structural members may substantially reduce their strength. This risk also exists in the decay period.

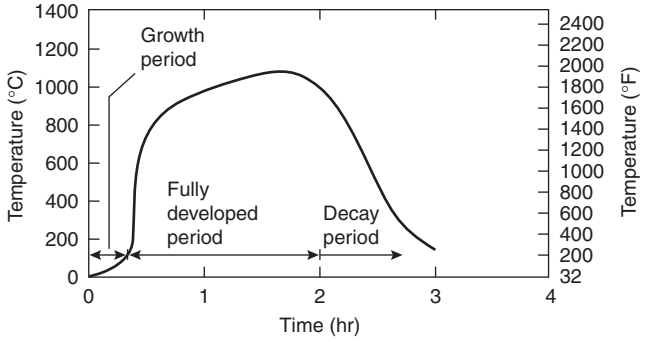

Figure 4-8.1. ***Idealized temperature course of fire.***

Dr. T. T. Lie is a research officer with the Institute for Research in Construction, National Research Council of Canada. He has carried out research related to fire resistance design, which includes evaluation of the fire resistance of building constructions by calculation and testing.

Parameters Determining the Fire Temperature Course

The most important parameters that determine the temperature course of a fire were first shown by Kawagoe and Sekine[1] and by Odeen,[2] who estimated the heat balance for fires in enclosed spaces. Usually part of the heat produced during a fire in an enclosure will be absorbed by the walls and contents, a part by the gases, and a part will be lost by radiation and convection from windows. (See Figure 4-8.2.) There is also loss of chemical energy that could have been released as heat because of outflow of unburned gases, which burn outside the enclosure. In addition, there is loss of unburned particles.

To be able to determine the temperature course, it is necessary to know at each moment during a fire, the rate at which heat is produced and the rate at which heat is lost to exposed materials and surroundings. Several of the parameters that determine heat production and heat losses, such as material properties, room dimensions, wall construction, window area, and emissivity of the flames and exposed materials, can be determined with reasonable accuracy. Others that are known approximately are the amount of gases that burn outside the room, the loss of unburned particles through windows, and the temperature differences in the room.

There are several parameters, however, whose magnitude cannot be predicted. Usually they change with time, and therefore, their value at the time of occurrence of a fire is determined by chance. Such parameters include the amount, surface area, and arrangement of the combustible contents, velocity and direction of wind, and the outside temperature. The influence of wind[3] and that of fire load can be substantial. Surveys show, for instance, that the variability of fire loads in various types of buildings is such that deviations in the order of 50 percent or more from the most probable fire load are common.[4] As a consequence, variability of fire load alone may easily cause deviations from the most probable temperature course of hundreds of degrees centigrade in temperature and 50 percent or more in fire duration.

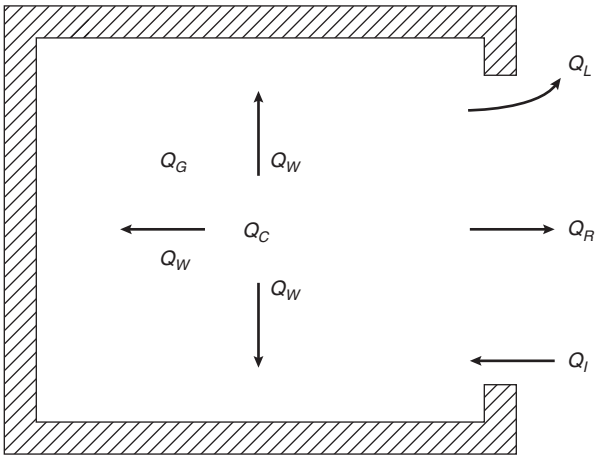

Q_R = Radiation losses
Q_I = Heat content of inflowing air
Q_L = Heat content of outflowing gases
Q_W = Heat losses to the walls
Q_C = Heat produced by combustion
Q_G = Rise of the heat content of the gases in the enclosure

Figure 4-8.2. ***Heat balance for an enclosure during a fire.***

Possible Fire Severities

Owing to the substantial influence of uncertain factors, it is impossible to predict accurately the temperatures to which building components will be exposed during their service life. Even if the analysis to predict fire temperature courses in enclosures is perfect, it is very improbable that a certain predicted temperature course will occur.

The fire temperature to which building components will most likely be exposed during the use of a building is the relatively low temperature of a fire that has been extinguished before it reaches the fully developed stage. There is a small although not insignificant chance of occurrence of a fully developed fire. In this case, and assuming that the fire cannot be influenced by action of the fire brigade, the fire will be controlled either by the surface area of the materials that can participate in the burning or by the rate of air supply through the openings.[2,5]

Whether the fire will be largely controlled by surface area or ventilation depends on the amount of combustible contents. Unless its quantity, surface area, and arrangement are controlled, or the size of the windows and floor area made such that the possibility of a ventilation-controlled fire becomes remote,[6,7] the type of fire that may occur is unpredictable. According to statistical data, combustible contents of 10 to 60 kg per m^2 of floor area are normal, and there is a considerable probability of enclosures having a combustible content of 40 to 100 kg/m^2.[2,4] It is probable that in the latter range, as confirmed by experiments,[5,8] the fire will be mainly ventilation controlled, even when large window openings are present. It is likely that the greater the space behind the windows, or to a certain extent, the deeper the enclosure, the more material or surface area it will contain and therefore the greater will be the probability of a ventilation-controlled fire. Usually a ventilation-controlled fire is the more severe fire, and because of the substantial probability of its occurrence, it is common to base fire resistance requirements for buildings on the assumption that fire severities will be controlled by ventilation.

Characteristic Temperature Curves

It is possible to indicate for any enclosure a characteristic temperature-time curve whose effect, with reasonable likelihood, will not be exceeded during the lifetime of the building. Such curves are useful as a basis for the fire-resistance design of buildings. They can also facilitate studies of fire resistance of building components exposed to fires of different severity.

There are several reports which present the temperature course of fires in fully developed and decay periods.[1,2,7,9,10] In all of these studies a procedure is followed in which the fire temperatures are determined by solving a heat balance for the enclosure under consideration.

For the fully developed period and ventilation-controlled fires, there is reasonable agreement in the temperatures found in the various studies, except for rather shallow rooms of limited size. In the latter case, the amount of combustible gases that burn outside may increase in such a way with increasing ventilation that the temperature decreases.[7]

There is less agreement in the results of the various studies for the decay period, partly due to the complexity of the processes that determine the temperature in that period. So far, rates of decay of temperature can only be established empirically or by making conservative or highly idealized assumptions. Because of the different approaches in deriving the rates of decay, there is a rather wide spread in the results of the various studies. Fortunately the influence of temperature variation in the decay period on the maximum temperatures reached in building components is relatively small.[11] For the purpose of deriving a temperature-time curve that, with reasonable probability, will not be exceeded during the lifetime of the building, it will be sufficient to use a curve that only approximately reflects the effect of heating in the decay period. This approach is further explained in Figure 4-8.3.

In Figure 4-8.3, curve A illustrates a fire temperature curve derived theoretically for a certain building. The probability of occurrence of a fire with a more severe effect than shown by the curve is once in 50 years. Curve B illustrates a fire temperature curve for the same building, but it is assumed that the rate of burning remains constant until all combustible materials are consumed, whereupon the fire temperature drops linearly to room temperature. Although curve B differs in shape from curve A, their heating effect is approximately the same. If curve B is used instead of curve A, the probability of occurrence of a more severe fire than that represented by the relevant curve may change somewhat, for instance, from once in 50 years to somewhat more or less than 50 years. In practice this means that virtually the same fire safety will be provided whether curve A or curve B is used for the fire-resistance design of a building. The use of curve B instead of curve A has the advantage that it is easier to define.

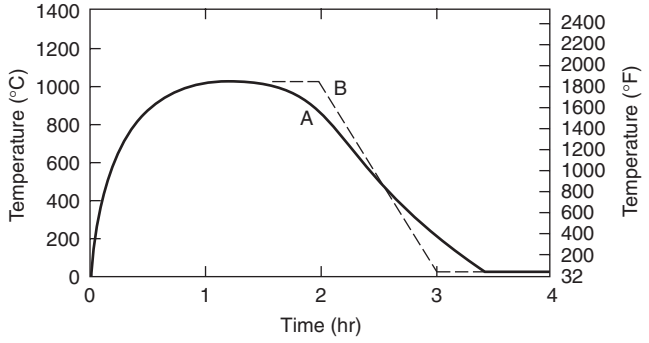

Figure 4-8.3. ***Temperature curves for fire resistance design.***

Expressions for Characteristic Temperature Curves

In the following, analytical expressions are given that describe characteristic temperature curves as a function of the significant parameters for various fire conditions commonly met with in practice. For the fully developed period, the derivation of these curves will be based on the temperature curves for ventilation-controlled fires calculated according to the method described by Kawagoe and Sekine.[1]

The temperatures attained in ventilation-controlled fires are described (in addition to the thermal properties of the material bounding the enclosure) by a parameter, known as the opening factor F

$$F = \frac{A\sqrt{H}}{A_T} \tag{1}$$

where A is area of the openings in the enclosure, H is height of the openings, and A_T is area of the bounding surfaces (walls and floor and ceiling). The method of calculating $A\sqrt{H}$ for openings of unequal height is described in References 9 and 11.

The rate of burning, R, of the combustible materials in the enclosure is given by

$$R = 330A\sqrt{H} \tag{2}$$

and, thus, if Q is the fire load per unit area of the surfaces bounding the enclosure, the duration of the fire, τ, is determined by

$$\tau = \frac{QA_T}{330A\sqrt{H}} = \frac{Q}{330F} \tag{3}$$

For given thermal properties of the material bounding the enclosure, the heat balance can be solved for the temperature as a function of the opening factor F. Besides depending on F, the temperature course is also a function of the thermal properties of the material bounding the enclosure.

In this study, two materials have been chosen as representative bounding materials: one with thermal properties resembling those of a heavy material (high heat capacity and conductivity) and one representing those of a light material (low heat capacity and conductivity). The thermal properties of these materials are given in Table 4-8.1. In practice, materials with a density of approximately 1600 kg/m^2 or more, for example, normal-weight concretes, sand lime brick, and most clay bricks, can be considered as belonging to the group of heavy material. Those with a density of less than 1600 kg/m^2, for example, lightweight and cellular concretes and plasterboard, can be regarded as belonging to the group of light materials.

Using the method described in Reference 11, the temperature course of fires in enclosures has been calculated for the two chosen bounding materials and for various values of the opening factor.[12] The conditions for which the calculations have been performed are shown in Table 4-8.1 and the results of the calculations in Figures 4-8.4 and 4-8.5. The curves in these figures were used as a basis for the derivation of temperature curves for fire-resistance

Table 4-8.1 ***Thermal Properties of the Enclosure***

Factor	Description
k	Thermal conductivity of bounding material: 1.16 W/m·K for a heavy material ($\rho \geq 1600$ kg/m^3), 0.58 W/m·K for a light material ($r < 1600$ kg/m^3)
ρc	Volumetric specific heat of bounding material: 2150×10^3 J/m^3·K for a heavy material ($\rho \geq 1600$ kg/m^3), 1075×10^3 J/m^3·K for a light material ($\rho < 1600$ kg/m^3)
A_T	Total inner surface area bounding the enclosure, including window area: 1000 m^2
H	Window height: 1.8 m
ε	Emissivity for radiation transfer between hot gases and inner bounding surface of the enclosure: 0.7
α_c	Coefficient of heat transfer by convection between fire and inner bounding surface area: 23 W/m^2·K
a_u	Coefficient of heat transfer between outer bounding surface area and surroundings: 23 W/m^2·K
c	Specific heat of combustion gases: 1340 J/N·m^3°C
G	Volume of combustion gas produced by burning 1 kg of wood: 4.9 N·m^3/kg
q	Heat released in the enclosure by burning 1 kg of wood: 10.77×10^6 J/kg
T_0	Initial temperature: 20°C
V	Volume of enclosure:[a] 1000 m^3
Δx	Thickness of elementary layers of bounding material: 0.03 m
Δt	Time increment: 0.0004167 hr
D	Thickness of bounding material: 0.15 m

[a]It can be shown that the influence of the volume of the enclosure on the fire temperature is negligible.

design. It was found that these temperature curves could be reasonably described by the expression

$$T = 250(10F)^{0.1/F^{0.3}} e^{-F^2 t}[3(1 - e^{-0.6t}) - (1 - e^{-3t}) + 4(1 - e^{-12t})] + C\left(\frac{600}{F}\right)^{0.5} \quad (4)$$

where T = the fire temperature in °C, t = time in hr, F = opening factor in m$^{1/2}$, and C = a constant taking into account the influence of the properties of the boundary material on the temperature. $C = 0$ for heavy materials ($\rho \geq 1600$ kg/m^2), and $C = 1$ for light materials ($\rho < 1600$ kg/m).

The expression is valid for

$$t \leq \frac{0.08}{F} + 1 \quad (5)$$

and

$$0.01 \leq F \leq 0.15 \quad (6)$$

If $t > (0.08/F) + 1$, a value of $t = (0.08/F) + 1$ should be used. If $F > 0.15$, a value of $F = 0.15$ should be used.

The temperature-time curves evaluated from Equation 4 and those obtained by solving the heat balance for the enclosure are shown in Figures 4-8.6 and 4-8.7 for various values of the opening factor.

It is seen that with the aid of the analytical expression, temperature curves can be developed that reasonably describe the curves derived from solving the heat balance.

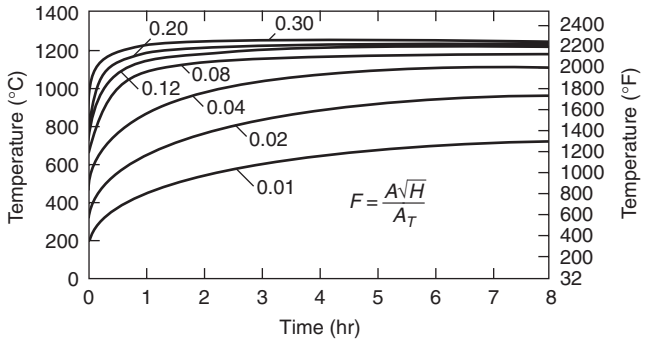

Figure 4-8.4. ***Temperature-time curves for ventilation-controlled fires in enclosures bounded by dominantly heavy materials ($\rho \geq 1600$ kg/m^3), calculated for various opening factors by solving a heat balance for the enclosure.***

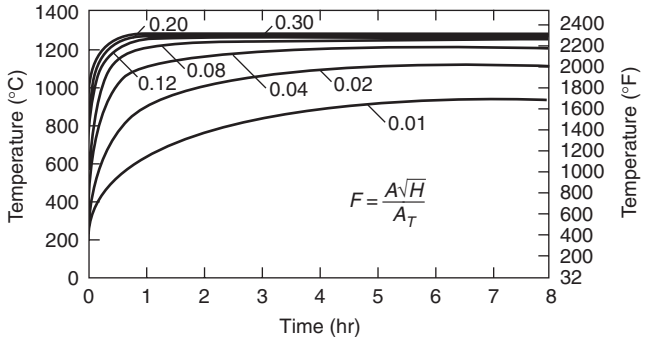

Figure 4-8.5. ***Temperature-time curves for ventilation-controlled fires in enclosures bounded by dominantly light materials ($\rho < 1600$ kg/m^3), calculated for various opening factors by solving a heat balance for the enclosure.***

As discussed previously, the temperatures in the decay period are more difficult to calculate due to the complexity of the processes that determine the temperature in this period. On the other hand, if the temperature variations are not very large, the influence of such variations in the decay period on the temperature attained in exposed building components is in general relatively small. Therefore, describing the temperature course in the decay period by a temperature-time relation that approximately reflects the decrease of temperature in this period is sufficient.

According to experimental data of Kawagoe[8] the rate of temperature decrease of a fire with a fully developed period of less than 1 hr is roughly 10°C per min, and that of a fire with a fully developed period of more than 1 hr is 7°C per min. The Swedish code assumes a rate of decrease of 10°C per min irrespective of the duration of the fully developed period of the fire.[9] A comparison with semi-empirical data developed by Magnusson and Thelandersson[9] shows that the assumption of a rate of decrease of 10°C per min is too fast for fires of long duration and too slow for fires of short duration.

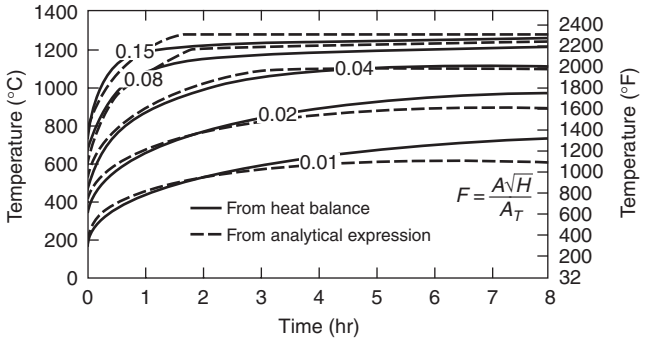

Figure 4-8.6. ***Comparison between temperature-time curves obtained by solving a heat balance and those described by an analytical expression for ventilation-controlled fires in enclosures bounded by dominantly heavy materials (ρ ≥ 1600 kg/m³).***

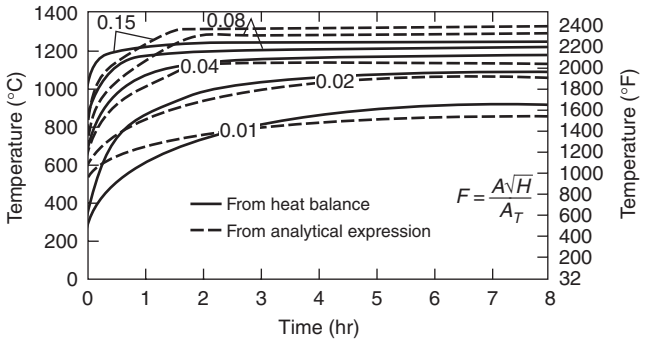

Figure 4-8.7. ***Comparison between temperature-time curves obtained by solving a heat balance and those described by an analytical expression for ventilation-controlled fires in enclosures bounded by dominantly light materials (ρ < 1600 kg/m³).***

According to Harmathy,[7] who studied several experimental fires of relatively short duration,[13,14] the rate of decrease of temperature for such fires is in the order of 15 to 20°C per min.

In general, the longer the duration of the fully developed period, the lower the rate of decrease of temperature. Using this information the following expressions have been derived for the temperature course of fire in the decay period:

$$t = -600\left(\frac{t}{\tau} - 1\right) + T_\tau \qquad (7)$$

with the condition

$$T = 20 \qquad \text{if } T < 20°\text{C} \qquad (8)$$

In the above equations T = fire temperature, τ = time at which the decay starts as given by Equation 3, t = time under consideration ($t > \tau$), and T = temperature given by Equation 4 at the time $t = \tau$.

The temperature curves obtained from Equations 4 and 7 are illustrated in Figure 4-8.8 for various fire loads and an opening factor of 0.05 $m^{1/2}$. In Figure 4-8.9 the influence is shown of the openings on the fire temperature course. It can be seen that the fire load determines the duration of the fire, whereas the openings determine both the duration and the intensity of the fire. In Figure 4-8.10

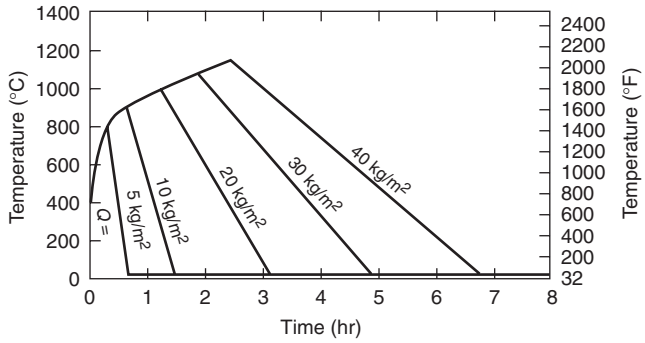

Figure 4-8.8. ***Characteristic temperature curves for various fire loads, Q, (opening factor, F = 0.05 m$^{1/2}$, heavy bounding material).***

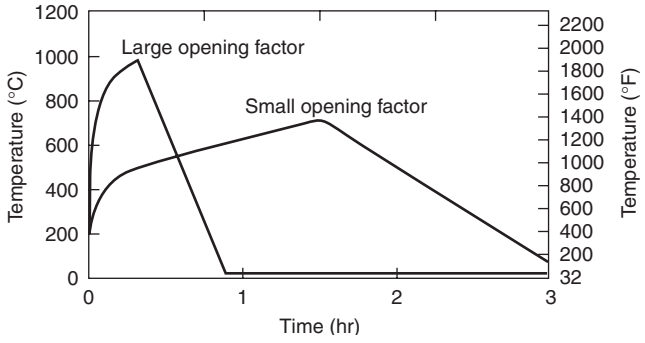

Figure 4-8.9. ***Influence of opening factor on fire temperature course.***

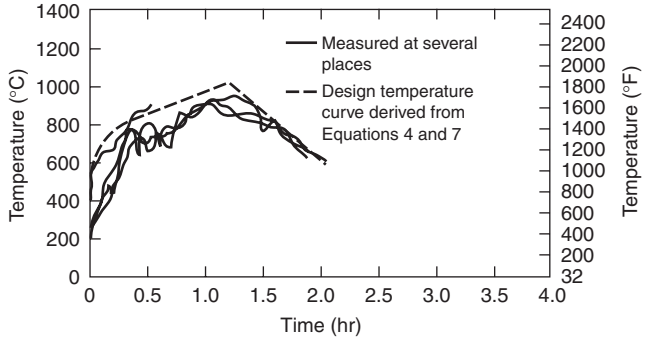

Figure 4-8.10. ***Comparison of design temperature curves derived from analytical expressions with temperatures measured during an experimental fire (fire load per unit internal area of the bounding surfaces Q = 18.75 kg/m³, opening factor F = 0.047 m$^{1/2}$, heavy bounding material).***

a characteristic temperature curve is compared with the temperatures measured at several places in a room during an experimental fire.[1] It is seen that the curve developed from the analytical expression reasonably characterizes the temperatures obtained during the experimental fire. It is somewhat conservative but satisfactory to use as a design curve for fire resistance.

Standard Fire Curve

In studies of fire resistance, it is common to expose building elements to heating in accordance with a standard temperature-time relation. The standard temperature-time curves used in various countries are shown in Figure 4-8.11. It can be seen that there are no significant differences between the various standard curves. The values of the curve adopted by ISO[15] are given in Table 4-8.2. Those used in North America[16] are given in Table 4-8.3.

There are also analytical expressions for several of the standard curves. The expression that describes the ISO curve is

$$T - T_0 = 345 \log_{10}(8t + 1) \quad (9)$$

where

t = time (min)
T = fire temperature (°C)
T_0 = initial temperature (°C)

For the curve used in North America, several analytical expressions exist.[17] One of the expressions is of the form of a sum of exponential functions:

$$T - T_0 = a_1(1 - e^{a_4 t}) + a_2(1 - e^{a_5 t}) + a_3(1 - e^{a_6 t}) \quad (10)$$

where

$a_1 = 532$ for °C, 957 for °F
$a_2 = -186$ for °C, -334 for °F
$a_3 = 820$ for °C, 1476 for °F
$a_4 = -0.6$
$a_5 = -3$
$a_6 = -12$

The extreme deviation from the values given in Table 4-8.2 are −26°C at 45 min, +48°C at 3.5 hr, and −78°C at 8 hr.

Table 4-8.2 ***Standard Temperature-Time Relation According to ISO 834[15]***

Time (hr:min)	Temperature (°F)	Temperature (°C)	Time (hr:min)	Temperature (°F)	Temperature (°C)
0:00	68	20	3:10	1938	1059
0:05	1000	538	3:20	1950	1066
0:10	1300	704	3:30	1962	1072
0:15	1399	760	3:40	1975	1079
0:20	1462	795	3:50	1988	1086
0:25	1510	821	4:00	2000	1093
0:30	1550	843	4:10	2012	1100
0:35	1584	862	4:20	2025	1107
0:40	1613	878	4:30	2038	1114
0:45	1638	892	4:40	2050	1121
0:50	1661	905	4:50	2062	1128
0:55	1681	916	5:00	2075	1135
1:00	1700	927	5:10	2088	1142
1:05	1718	937	5:20	2100	1149
1:10	1735	946	5:30	2112	1156
1:15	1750	955	5:40	2125	1163
1:20	1765	963	5:50	2138	1170
1:25	1779	971	6:00	2150	1177
1:30	1792	978	6:10	2162	1184
1:35	1804	985	6:20	2175	1191
1:40	1815	991	6:30	2188	1198
1:45	1826	996	6:40	2200	1204
1:50	1835	1001	6:50	2212	1211
1:55	1843	1006	7:00	2225	1218
2:00	1850	1010	7:10	2238	1225
2:10	1862	1017	7:20	2250	1232
2:20	1875	1024	7:30	2262	1239
2:30	1888	1031	7:40	2275	1246
2:40	1900	1038	7:50	2288	1253
2:50	1912	1045	8:00	2300	1260
3:00	1925	1052			

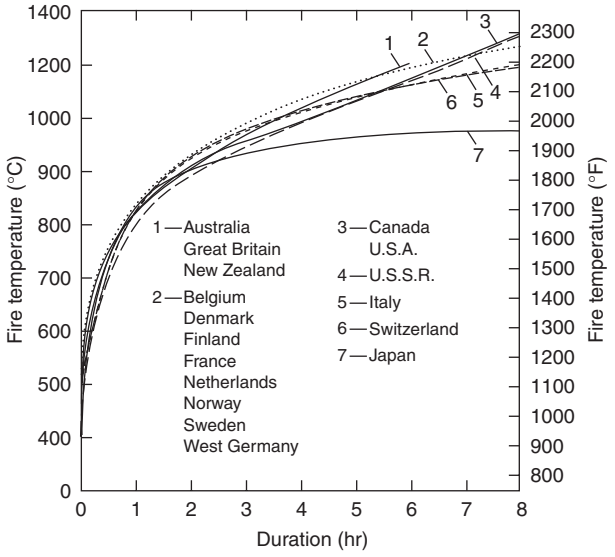

Figure 4-8.11. ***Standard fire temperature-time relations used in various countries for testing of building elements.***

Table 4-8.3 ***Standard Fire Temperature-Time Relation Used in North America (NFPA No. 251)[16]***

Time (min)	Temperature Rise of Fire (°C)
0	0
5	556
10	659
15	718
30	821
60	925
90	986
120	1029
180	1090
240	1133
360	1193

This form is suitable for use in analytical heat flow calculations because when it is used as a boundary condition, the heat transfer equations are integrable.

A set of expressions that more accurately approximate the values given in Table 4-8.2 is

$$T - T_0 = a_1 \tanh a_4 t + a_2 \tanh a_5 t + a_3 \tanh a_6 t, \quad t < 2 \tag{11}$$

$$T - T_0 = 906.7 + 41.67t, \quad t \geq 2 \text{ for °C} \tag{12}$$

$$T - T_0 = 1632 + 75t, \quad t \geq 2 \text{ for °F} \tag{13}$$

where

$a_1 = 580$ for °C, 1044 for °F

$a_2 = -276.8$ for °C, −498.2 for °F

$a_3 = 714.4$ for °C, 1286 for °F

$a_4 = 0.8429$

$a_5 = 0.9736$

$a_6 = 8.910$

The maximum deviation of the temperature after 20 min, given by Equations 11, 12, and 13, from the values tabulated in Table 4-8.2 is −7°C at 40 min.

Another temperature-time relation, given in Reference 18, has the form

$$T - T_0 = a[1 - \exp(-3.79553\sqrt{t})] + b\sqrt{t} \tag{14}$$

where

$a = 750$ for °C, 1350 for °F

$b = 170.41$ for °C, 306.74 for °F

$t =$ time (hr)

This expression is frequently used and is a reasonably accurate approximation of the relation between temperature and time given in Table 4-8.2.

Nomenclature

A	area of the openings in the enclosure (m^2)
A_T	area of the internal bounding surfaces (m^2)
C	constant
F	opening factor ($m^{1/2}$)
H	height of openings in the enclosure (m)
Q	fire load per unit area of the internal bounding surfaces (kg/m^2)
R	rate of burning (kg/hr)
T	fire temperature (°C)
T_τ	fire temperature at the time τ (°C)
t	time (hr)
τ	time at which the temperature starts to decline (hr)

References Cited

1. K. Kawagoe and T. Sekine, "Estimation of Fire Temperature-Time Curve in Rooms," *B.R.I. Occasional Report No. 11,* Building Research Institute, Ministry of Construction, Tokyo (1963).
2. K. Odeen, "Theoretical Study of Fire Characteristics in Enclosed Spaces," *Bulletin 10,* Division of Building Construction, Royal Institute of Technology, Stockholm (1963).
3. P.H. Thomas and A.J.M. Heselden, "Fully Developed Fires in Single Compartments," *Fire Research Note No. 923,* Building Research Establishment, Fire Research Station, Borehamwood, UK (1972).
4. T.T. Lie, *Fire and Buildings,* Applied Science Publishers Limited, London, pp. 19–22 (1972).
5. P.H. Thomas, A.J.M. Heselden, and M. Law, "Fully Developed Compartment Fires; Two Kinds of Behavior," *Fire Research Technical Paper No. 18,* Her Majesty's Stationery Office, London (1967).
6. T.T. Lie, *Fire and Buildings,* Applied Science Publishers Limited, London (1972).

7. T.Z. Harmathy, "A New Look at Compartment Fires, Part I and Part II," *Fire Tech.,* 8, pp. 3–4 (1972).
8. K. Kawagoe, "Fire Behavior in Rooms," *Report No. 27,* Building Research Institute, Ministry of Construction, Tokyo (1958).
9. S.E. Magnusson and S. Thelandersson, "Temperature-Time Curves of Complete Process of Fire Development. Theoretical Study of Wood Fuel Fires in Enclosed Spaces," *Acta Polytechnica Scandinavica,* Civil Engineering and Building Construction Series No. 65, Stockholm (1970).
10. Y. Tsuchiya and K. Sumi, "Computation of the Behavior of Fire in an Enclosure," *Comb. and Flame,* 16 (1971).
11. K. Kawagoe, "Estimation of Fire Temperature-Time Curve in Rooms," *Research Paper No. 29,* Building Research Institute, Japan (1967).
12. T.T. Lie, "Characteristic Temperature Curves for Various Fire Severities," *Fire Tech.,* 10, p. 4 (1974).
13. E.G. Butcher, T.B. Chitty, and L.A. Ashton, "The Temperatures Attained by Steel in Building Fires," *Fire Research Technical Paper No. 14,* Her Majesty's Stationery Office, London (1966).
14. E.G. Butcher, G.K. Bedford, and P.J. Fardell, "Further Experiments on Temperatures Reached by Steel in Buildings," in *Symposium No. 2, Behavior of Structural Steel in Fire, Paper No. 1,* Her Majesty's Stationery Office, London (1968).
15. ISO 834, *Fire Resistance Tests—Elements of Building Construction,* International Standard Organization, Geneva, Switzerland (1975).
16. NFPA 251, *Standard Methods of Fire Tests of Building Construction and Materials,* National Fire Protection Association, Quincy, MA (1990).
17. G. Williams-Leir, "Analytical Equivalents of Standard Fire Temperature Curves," *Fire Tech.,* 9, p. 2 (1973).
18. J.P. Fackler, "Concernant la Resistance au Feu des Elements de Construction," in *Cahier 299,* Centre Scientifique et Technique du Batiment, Paris (1959).

CHAPTER 9

Analytical Methods for Determining Fire Resistance of Steel Members

James A. Milke

Introduction

Traditionally, fire resistance has been evaluated by subjecting a structural member to a standard test for a specified duration.[1] All members performing acceptably are rated and listed for the duration period of the test (e.g., 1 hr, 2 hr). Assemblies not listed are assumed to be unable to meet the test criteria and, thus, have no rating, unless proved otherwise. Providing proof of acceptable performance can be accomplished in one of three manners:

1. Conduct the standard test.[1]
2. Conduct a special experiment.[2]
3. Apply an analytical technique.[3]

The standard test can involve an appreciable turnaround time in order to specify, schedule, and analyze the results of the test. An experimental program can require a substantial amount of effort in order to obtain accurate data. The costs involved in sponsoring a standard test or experimental program can be appreciable. In the case of archaic structural assemblies, materials may no longer be available to reconstruct the design for possible testing.

Because of these drawbacks, calculation methods have been developed to analyze structural designs for fire conditions. The calculation methods have been formulated based on analyses of data from standard tests, experimental programs, and theoretically based investigations.

Analytical methods for fire resistance must consider three basic aspects of the problem:

1. Fire exposure
2. Heat transfer
3. Structural response

The fire exposing the structure must be characterized using methods described in other chapters of this handbook for the case of a real fire, or by assuming the fire exposure specified in the standard test. The thermal response of the structural member can be addressed using principles of heat transfer. Heating within the member is treated by conduction heat transfer analysis (radiation and convection heat transfer may also need to be considered, if voids or porous insulation materials are present within the assembly). Typically, radiative and convective boundary conditions are present. Finally, the structural response is examined by comparing some or all of the following: deflections, strains, and stress levels to established limits.

The following types of calculation methods are available to assess the fire resistance of steel structural members:

1. Empirical correlations
2. Heat transfer analyses
3. Structural analyses

Empirical correlations are based on the analysis of data resulting from performing the standard test numerous times. A limitation of the empirical correlations is that they can only be applied when considering the fire exposure, loading, and span provided in the standard test. If other conditions apply, then another approach is needed.

The second group of calculation methods consists of heat transfer analyses. The heat exposure conditions may be those associated with the standard test or a specified fire. The purpose of the heat transfer analysis is to determine the time required for the structural member to attain a predetermined critical temperature or to provide input to a structural analysis. The temperature endpoint criteria cited by ASTM E119[1] are often accepted as the critical temperatures. Typically, inaccuracies of this method are related to the temperature dependence of the material properties or the description of the heating conditions.

Many of the structural analysis–based calculations are similar to those conducted for structural engineering purposes, except the material properties are evaluated at elevated temperatures and thermal expansion is considered. In structural analyses, the loading and end conditions must be known or assumed. Limitations result from

James A. Milke is an associate professor in the Department of Fire Protection Engineering at the University of Maryland. His recent research activities have included the impact of fires on the structural response of steel and advanced composite members.

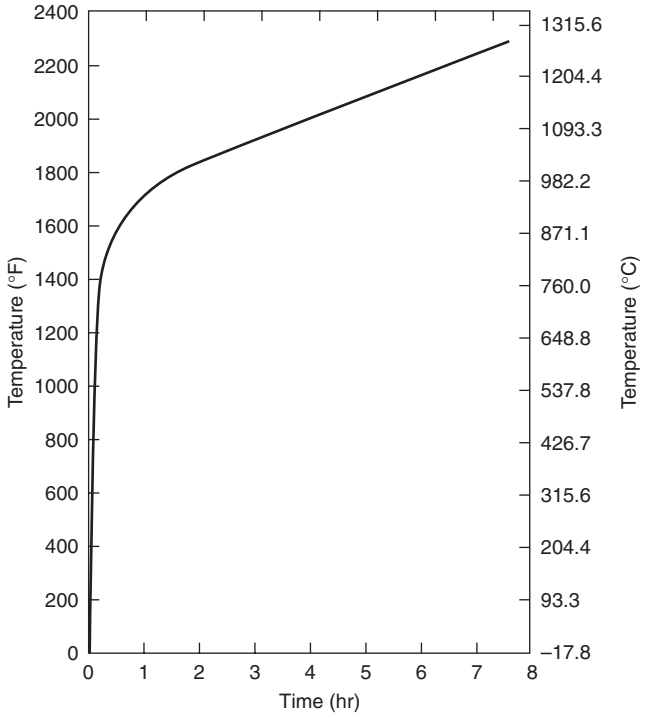

Figure 4-9.1. ***ASTM E119 standard time-temperature curve.[1]***

uncertainties in characterizing the end conditions and the material properties at elevated temperatures.

This chapter provides an overview of the available calculation methods for determining the fire resistance of steel structural members. The basis of each method will be presented along with sample applications.

Standard Test for Fire Resistance of Structural Members

The standard test method in the United States for determining the fire resistance of columns, floor and roof assemblies, and walls is ASTM E119.*[1] Basically, the test involves subjecting the structural component to a heated furnace environment for the desired duration. If the endpoint criteria are not reached prior to the end of the test period, the assembly passes the test and is rated.

Gas burners are used to heat the furnace in testing laboratories throughout North America. The furnace is heated so that the temperature inside the furnace follows the time-temperature curve illustrated in Figure 4-9.1. In principle, the time-temperature curve is intended to relate to a severe exposure from a room fire. Thus, the applicability of the test method to examine the fire resistance of exterior structural members exposed to fires outside of the building is questionable.[4]

Assemblies may be tested with or without load. If tested under load, the assembly is subjected to maximum design stress levels, based on common structural analysis procedures for ambient temperature design. Floor and roof assemblies and bearing walls are always tested under load. Columns are tested with or without a loading. Steel beams and girders may be tested without load if the design loading cannot be achieved in the laboratory.

Structural assemblies may be restrained or unrestrained against thermal expansion. The effect of restraint on the fire resistance of assemblies has been investigated by Bletzacker.[4] The degree of restraint in structural members varies with the geometry, connection method, and framing system, among other factors. The descriptions presented in Table 4-9.1 relate actual construction conditions to the restrained and unrestrained designation noted in the ASTM E119 test method.

The minimum dimensions of the structural components for testing are specified in ASTM E119. A maximum set of dimensions is established by the size of available test furnaces. While the test is large-scale, the test cannot be considered full-scale, given the stipulation of the maximum permissible dimensions. The consequence of not testing full-scale members means that continuous beams, actual floor/roof ASTM assemblies, and long columns are not tested. Consequently, this test is only comparative in nature and cannot be used to assess actual performance.

The ASTM E119 endpoint criteria for building assemblies consider structural integrity, temperature, passage of flame, ignition of cotton waste, and in some cases, response to the hose stream. For the tests without loading, the structural integrity endpoint criterion is relaxed to require that the component only remains in place. The structural integrity criterion addresses the need for members to remain in place (supporting self-weight of member) and to continuously support any applied loads. The ignition-of-cotton-waste endpoint addresses the ability of the structural assembly to prevent the transmission of flame and hot gases to the side not exposed to the furnace fire.

The temperature endpoint criteria are noted in Table 4-9.2. In principle, the endpoint temperatures are based on the maximum allowable reduction in load-bearing capacity of the structural member, based on the reduction in strength experienced at elevated temperature and the maximum permissible loads stipulated by structural design standards.

Fire Resistance of Steel Members

Several calculation techniques are available to determine the fire resistance of steel members, including steel columns, beams in floor and roof assemblies, and trusses.[7–10] Three types of techniques are available: empirically derived correlations, heat transfer analyses, and structural analyses.

The equations and models do not eliminate the need for all future testing. Testing is still required, at least to validate the calculation techniques and assess the interaction and mechanical behavior of the constituents of the assembly, such as the steel structural member, insulating materials, or other components. However, the calculation techniques can be used to extend the application of test results and reduce the number of required tests. In addi-

*Versions of the test method are also published as NFPA 251[5] and UL 263.[6]

Table 4-9.1 ***Restrained and Unrestrained Construction Systems (from ASTM E119 Table X3.1)***[1]

Wall bearing:	
Single span and simply supported end spans of multiple bays:[a]	
Open-web steel joists or steel beams, supporting concrete slab, precast units, or metal decking	unrestrained
Concrete slabs, precast units, or metal decking	unrestrained
Interior spans of multiple bays:	
Open-web steel joists, steel beams or metal decking, supporting continuous concrete slab	restrained
Open-web steel joists or steel beams, supporting precast units or metal decking	unrestrained
Cast-in-place concrete slab systems	restrained
Precast concrete where the potential thermal expansion is resisted by adjacent construction[b]	restrained
Steel framing:	
Steel beams welded, riveted or bolted to the framing members	restrained
All types of cast-in-place floor and roof systems (such as beam-and-slabs, flat slabs, pan joists, and waffle slabs) where the floor or roof system is secured to the framing members	restrained
All types of prefabricated floor or roof systems where the structural members are secured to the framing members and the potential thermal expansion of the floor or roof system is resisted by the framing system or the adjoining floor or roof construction[b]	restrained
Concrete framing:	
Beams securely fastened to the framing members	restrained
All types of cast-in-place floor or roof systems (such as beam-and-slabs, flat slabs, pan joists, and waffle slabs) where the floor system is cast with the framing members	restrained
Interior and exterior spans of precast systems with cast-in-place joints resulting in restraint equivalent to that which would exist in condition III(1)	restrained
All types of prefabricated floor or roof systems where the structural members are secured to such systems and the potential thermal expansion of the floor or roof systems is resisted by the framing system or the adjoining floor or roof construction[b]	restrained
Wood construction:	
All types	unrestrained

[a]Floor and roof systems can be considered restrained when they are tied into walls with or without tie beams, the walls being designed and detailed to resist thermal thrust from the floor or roof system.

[b]For example, resistance to potential thermal expansion is considered to be achieved when:

1. Continuous structural concrete topping is used
2. The space between the ends of precast units or between the ends of units and the vertical face of supports is filled with concrete or mortar, or
3. The space between the ends of precast units, and the vertical faces of supports, or between the ends of solid or hollow core slab units, does not exceed 0.25% of the length for normal-weight concrete members or 0.1% of the length for structural lightweight concrete members.

Table 4-9.2 ***ASTM E119 Temperature Endpoint Criteria***[1]

Structural Member	Location	Maximum Temperature °C (°F)*
Walls/partitions (bearing and nonbearing)	1. Unexposed side	
	Average	139 (250)[a]
	Single point	181 (325)[a]
Steel columns	1. Average	538 (1000)
	Single point	649 (1200)
Floor/Roof assemblies and loaded beams	1. Average	538 (1000)
	Single point	649 (1200)
	1. Unexposed side	
	Average	139 (250)[a]
	Single point	181 (325)[a]
	2. Steel beam	
	Average	593 (1100)
	Single point	704 (1300)
	3. Pre-stressing steel	426 (800)
	4. Reinforcing steel	593 (1100)
	5. Open-web steel joists	593 (1100)
Steel beams/ girders (not loaded)	1. Average	538 (1000)
	Single point	649 (1200)

*Maximum temperature cited refers to the maximum temperature rise above initial conditions

tion, experimental methods are essential in determining the material properties at elevated temperature of the protection materials.

Steel Material Properties

The principal material properties of interest are yield strength, ultimate strength, modulus of elasticity, coefficient of thermal expansion, density, specific heat, and thermal conductivity. The effect of temperature on steel properties has been examined by many researchers.[11] For steel, all of the properties, except for density, are strongly influenced by temperature.

The thermal properties of ASTM A36 steel are provided in the following correlations: [7,12,13,14]

$$k = -0.022T + 48 \quad \text{for } 0 \le T \le 900°\text{C}$$
$$k = 28.2 \quad \text{for } 900°\text{C} < T$$
$$c_s = 0.51T + 420 \quad \text{for } 0 \le T \le 650°\text{C}$$
$$c_s = 8.65T + 4870 \quad \text{for } 650°\text{C} < T \le 725°\text{C}$$
$$c_s = -10.9T + 9340 \quad \text{for } 725°\text{C} < T \le 800°\text{C}$$
$$c_s = 579 \quad \text{for } 800°\text{C} < T$$
$$\rho = 7860 \text{ kg/m}^3$$

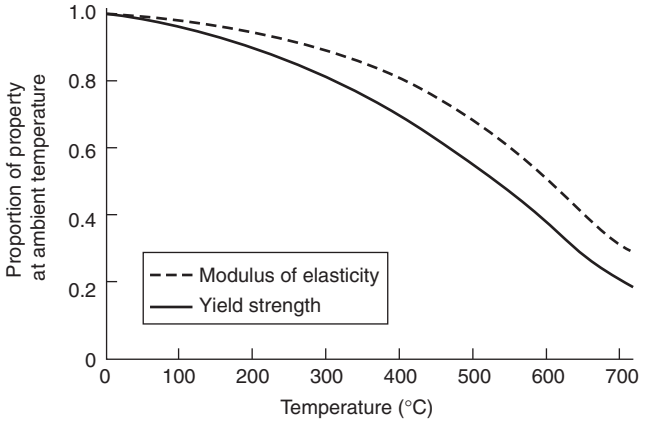

Figure 4-9.2. ***Temperature effects on properties of ASTM A36 steel.***[12,15]

The influence of temperature on the mechanical properties of A36 steel is presented in Figure 4-9.2. At 538°C (1000°F), the yield strength is approximately 60 percent of the value at normal room temperature. The American Institute for Steel Construction's *Specification for the Design, Fabrication, and Erection of Structural Steel for Buildings*[16] limits the maximum permissible design stress to approximately 60 percent of the yield strength. Thus, for structural members at 538°C (1000°F) designed to carry the maximum permissible stress, the applied stress is approximately the same as the strength of the member. It should also be noted that at 538°C (1000°F) the modulus of elasticity has decreased appreciably from the value at normal room temperature.

Mathematical expressions describing the relationship of the yield strength, modulus of elasticity, and coefficient of thermal expansion on temperature are[7,17,18]

For $0 < T \leq 600$°C,

$$\sigma_{yT} = \left[1 + \frac{T}{900 \ln (T/1750)}\right]\sigma_{y0}$$

$$E_T = \left[1 + \frac{T}{2000 \ln (T/1100)}\right]E_0$$

For $T > 600$°C,

$$\sigma_{yT} = \frac{340 - 0.34T}{T - 240}\,\sigma_{y0}$$

$$E_T = \frac{690 - 0.69T}{T - 53.5}\,E_0$$

$$\alpha_T = (0.004T + 12) \times 10^{-6}$$

where

σ_{yT} = yield strength at temperature T (MPa) (psi)
σ_{y0} = yield strength at 20°C (68°F) (MPa) (psi)
E_T = modulus of elasticity at temperature T (MPa) (psi)
E_0 = modulus of elasticity at 20°C (68°F) (MPa) (psi)
α_T = coefficient of thermal expansion at temperature T (m/m°C)
T = steel temperature (°C)

$$\theta = \begin{cases} \dfrac{T' - 68}{1800} & T' \text{ in °F} \\ \dfrac{T' - 20}{1000} & T' \text{ in °C} \end{cases}$$

T' = steel temperature

In addition to the changes in material properties that occur at elevated temperatures, the crystalline structure of steel also changes, as noted in Figure 4-9.3.[19] However, for the low-carbon steels typically used in building construction, significant changes in crystalline structure only begin to occur at temperatures in excess of 650°C (1200°F),[20] above the temperature typically associated with failure.

Creep, the time-dependent deformation of a material, may be significant in structural steel at temperatures in excess of 460°C (860°F).[21] The rate of creep increases approximately 300 times for ASTM A36 structural steel, when the steel temperature is increased from 460 to 520°C (860 to 968°F). Since creep is a complex phenomenon depending on the stress level, rate of heating, and other factors, often it is included implicitly in the mechanical properties to simplify the fire resistance calculations.[15,20] In-depth discussions of creep have been prepared by Harmathy.[22,23]

Methods of Protection

The basic intent of the various methods of protection is to reduce the rate of heat transfer to the structural steel. This is accomplished by using insulation, membranes, flame shielding, and heat sinks.

Insulation

Insulation of the steel is achieved by surrounding the steel with materials that preferably have the following characteristics:[24]

1. Noncombustibility and the added attribute of not producing smoke or toxic gases when subjected to elevated temperatures
2. Thermal protective capability when tested in accordance with the standard fire test ASTM E119
3. Product reliability giving positive assurance of consistent uniform protection characteristics
4. Availability in a form that permits efficient and uniform application
5. Sufficient bond strength and durability to prevent either dislodgement or surface damage during normal construction operations
6. Resistance to weathering or erosion resulting from atmospheric conditions

In addition to the insulating qualities of the protection materials, chemical reactions may occur in the insulation, further reducing the rate of heat transfer. The chemical reactions include calcination, ablation, intumescence, thermal hydrogeneration, and sublimation.

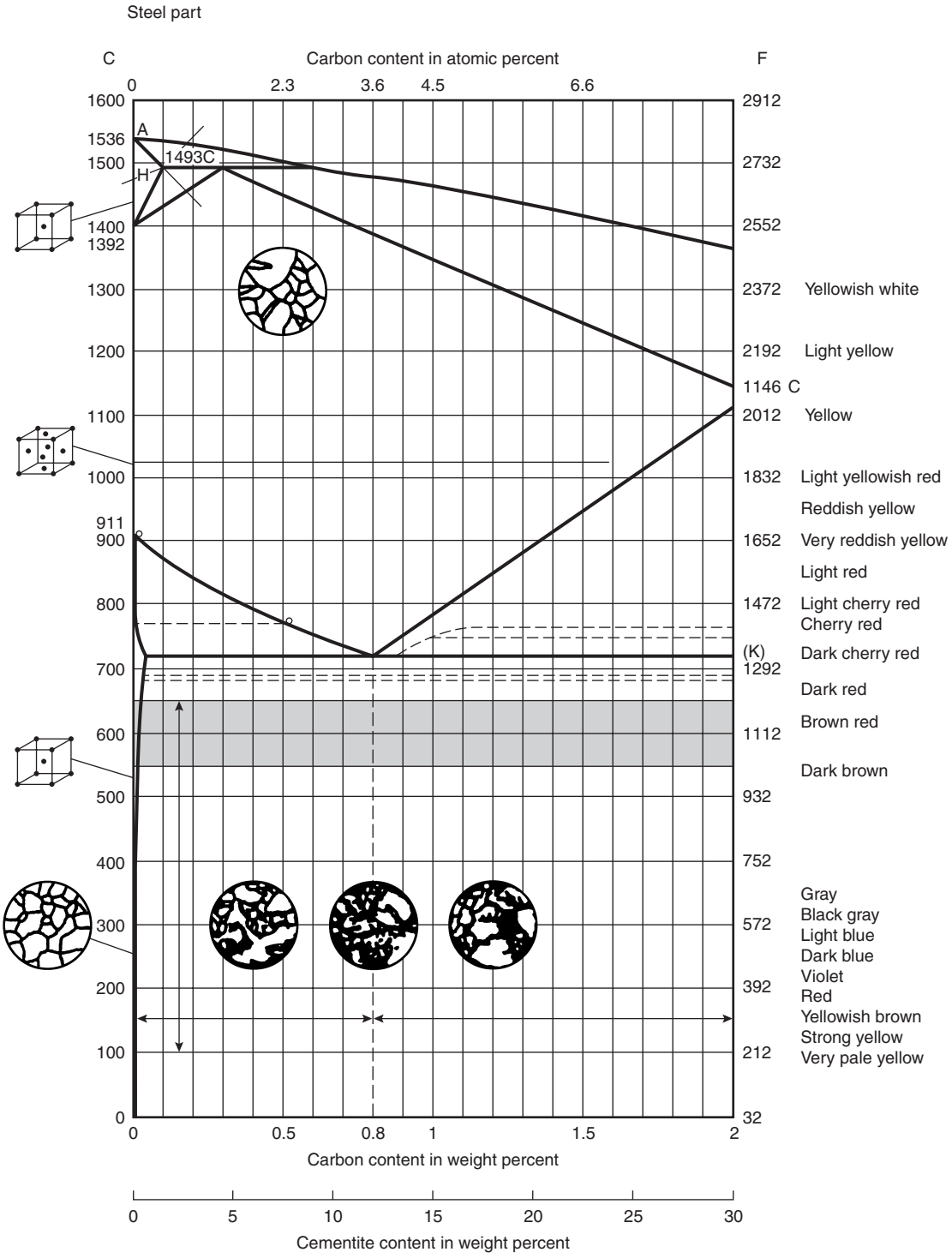

Figure 4-9.3. ***Influence of elevated temperatures versus carbon content in steel.[19]***

Insulating methods include the use of board products, spray-applied materials, and concrete encasement. A brief review of each method is presented below.

Board products: Four types of board products are commonly used to protect structural steel: gypsum board, fiber-reinforced calcium silicate board, vermiculite-sodium silicate board, and mineral fiber board. In each case, the means of attachment of the boards surrounding the steel is a critical parameter affecting the performance of the assembly. Two commonly used methods of attachment of gypsum wallboard with and without steel covers are illustrated in

Figure 4-9.4. Detailed descriptions of the attachment mechanisms for the other board products are provided elsewhere.[25–27] Also, board products can be used in wall assemblies to provide an envelope around steel trusses.

Spray-applied materials: Several types of spray-applied materials are commonly used. These include cementitious plasters, mineral fibers, magnesium oxychloride cements, and intumescents. Sufficient data has been obtained to characterize spray-applied cementitious and mineral fiber materials for the purpose of estimating the fire endurance of structural steel protected with these materials. An illustration of a steel column protected by a spray-applied material is presented in Figure 4-9.5.

Concrete encasement: Concrete encasement of steel members to surround and insulate the steel is illustrated in Figure 4-9.6. As indicated in Figure 4-9.6, the concrete is cast to fill in all re-entrant spaces. Alternatively, concrete column covers may be used, as illustrated in Figure 4-9.7. The concrete is assumed to act only to thermally protect the steel. Some empirical correlations implicitly account for the load-bearing capacity of the concrete and possible steel-concrete composite action.

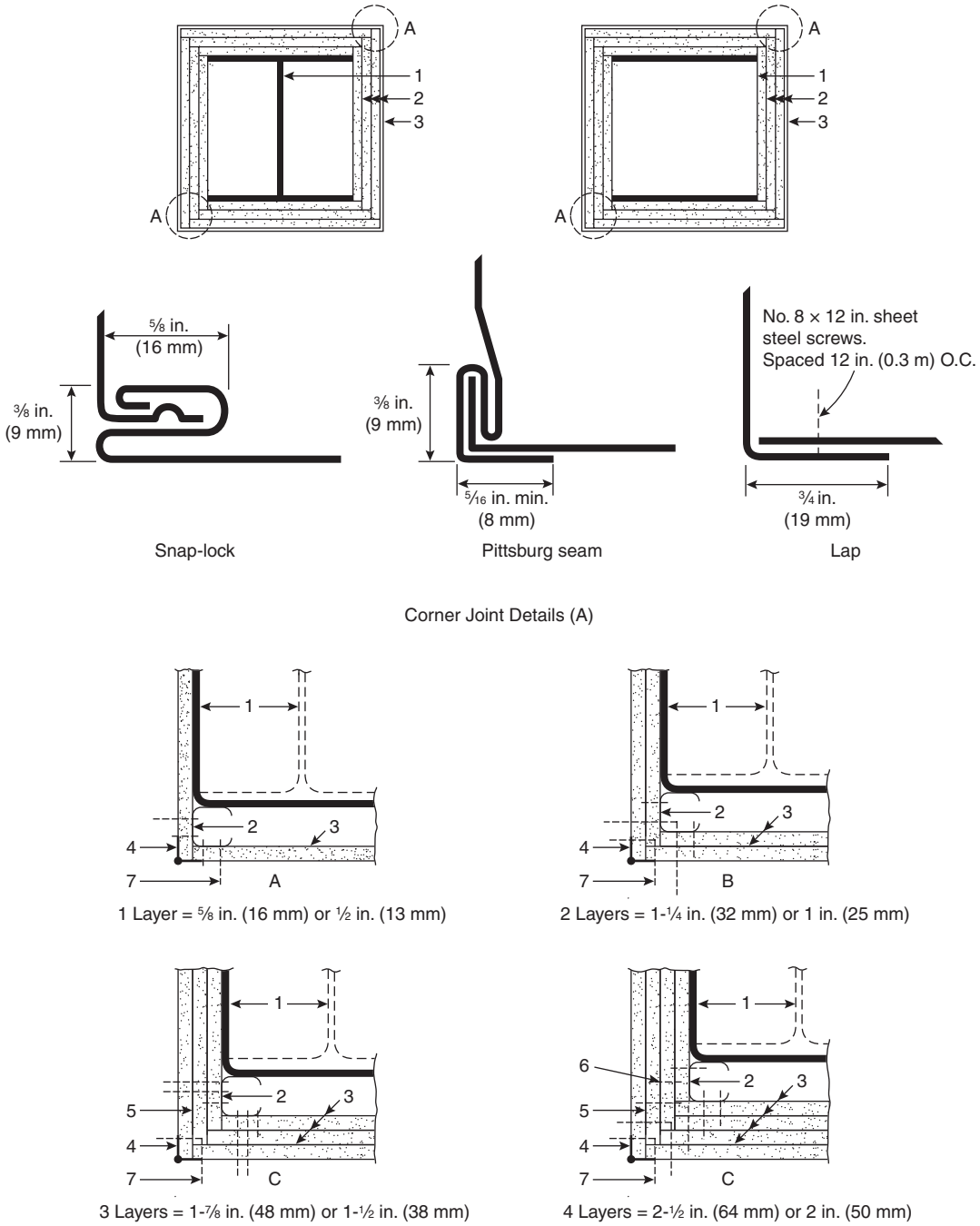

Figure 4-9.4. ***Attachment mechanisms of gypsum wallboard to steel columns.[25]***

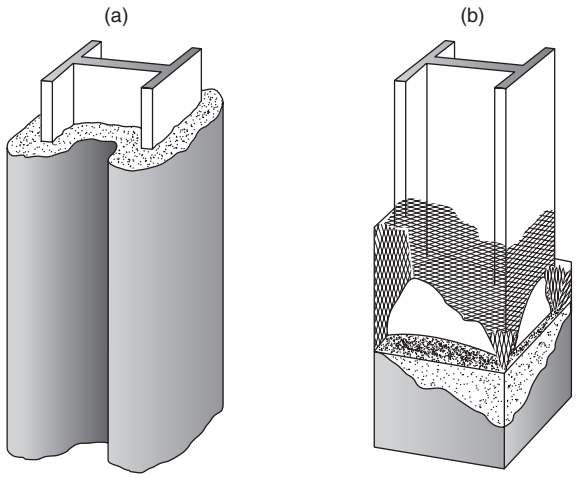

Figure 4-9.5. ***(a) Sprayed insulation; (b) Metal lath and plaster encasement.[24]***

Membrane: Suspended ceiling assemblies are used as membranes to protect structural steel in floor and roof assemblies. The ceiling panels and tiles comprising the ceiling assembly may consist of gypsum, perlite, vermiculite, or mineral fibers.

The membrane method of protection is illustrated in Figure 4-9.8. Heat transfer to the structural steel is reduced due to the air space above the membrane and the insulating characteristics of the membrane. Also, membranes help prevent the direct impingement of flame on the structural steel.

Flame shield: Flame shields are intended to reduce the incident radiant heat flux on the steel by preventing direct flame impingement. The effectiveness of flame shields to protect exposed spandrel beams was first examined by Seigel.[2,28] In this instance, 14-gage sheet steel was used as the flame shield.

Heat sinks: The heat sink approach delays the heating of steel by absorbing heat transferred through the steel. The heat sink approach usually involves liquid- or concrete-filling of the interior of hollow steel members (tubular and pipe sections). Liquid-filling can be used to provide a sufficient level of protection for the columns, without any externally applied coating. The liquid used for protection is an aqueous solution. Additives are provided primarily for antifreeze, corrosion protection, and biological reasons.

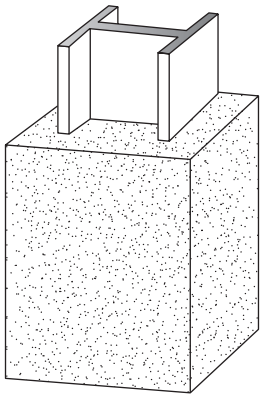

Figure 4-9.6. ***Steel column with concrete encasement.[24]***

A diagram of a typical design for a liquid-filled column fire protection system is presented in Figure 4-9.9. The components of this system include the hollow structural steel columns, piping to connect the columns, a water storage tank, and associated valves.

The system operates on the principle that heat incident on the column is removed by circulation of the liquid. If sufficient heat is delivered to the liquid,boiling can be expected, which enhances the efficiency of the heat-removal process. In many tests with liquid-filling, steel temperatures have been observed to be well below those required for failure, as long as the column remains full of the liquid.

Another heat-sink approach consists of filling the interior of hollow steel columns with concrete. If the concrete is reinforced, load transfer from the steel to the concrete can be expected as the steel weakens with increasing temperature. Calculation methods to determine the fire resistance of concrete-filled steel columns are available.[10,12]

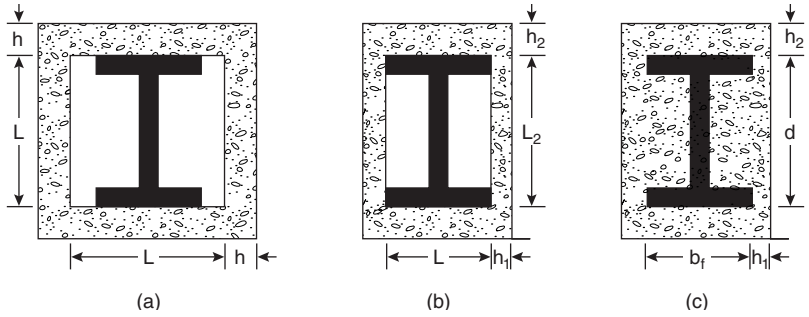

Figure 4-9.7. ***Concrete-protected structural steel columns. (a) Square shape protection with a uniform thickness of concrete cover on all sides; (b) Rectangular shape with varying thickness of concrete cover; and (c) Encasement having all re-entrant spaces filled with concrete.***

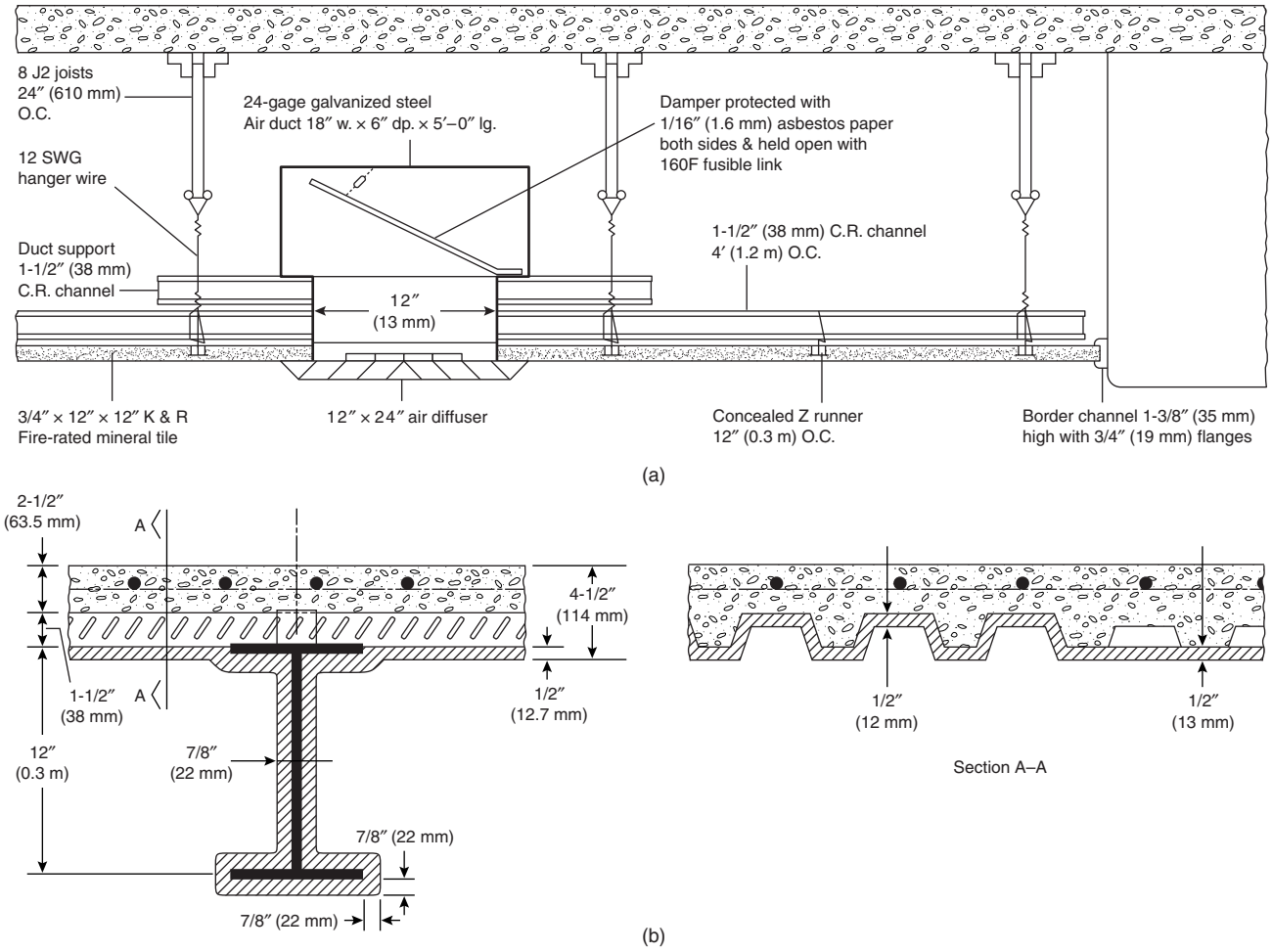

Figure 4-9.8. ***Membrane method of protection,[24] (a) Cross-section of a floor-ceiling system with conventional sheet steel fusible-link damper for protecting typical ceiling outlets in galvanized sheet ducts; (b) Sprayed contact fireproofing applied directly to the underside of formed-steel decking and to a supporting steel beam.***

Empirically Derived Correlations

Numerous, easy-to-use, empirically derived correlations are available to calculate the fire resistance of steel columns, beams, and trusses. The correlations are based on data from performing the standard test numerous times on variations of a particular assembly. Curve-fitting techniques are used to establish the various correlations. In some cases, a best-fit line has been drawn for the data points, whereas in other cases, lines were placed to provide conservative estimates of the fire endurance by connecting the two lowest points.[29]

Steel Columns

The correlations to estimate the fire endurance of unprotected and protected steel columns are given in Table 4-9.3. Present in each of the equations is W/D for wide-flange sections and A/P for hollow sections. The W/D and A/P ratios are comparable. The W/D ratio is the weight per lineal foot to the heated perimeter of the steel at the protection interface (or the perimeter of the steel if unprotected). The A/P ratio is the cross-sectional area divided by the heated perimeter. Essentially, the W/D ratio relates to the product of the density of the steel and the A/P ratio.

The relevance of the W/D and A/P ratios was first noted by Lie and Stanzak.[30] W/D ratios for commonly used wide-flange and tubular shapes for columns and beams are available elsewhere.[25,31,32] The two factors in the W/D ratio that affect the rate of heat transfer to the steel (and consequently the rise in temperature of the steel) are (1) shape of the fire protection system, D, and (2) steel mass per unit of length, W.

The parameter that characterizes the shape of the fire protection system is D, the heated perimeter expressed in inches, which is defined as the inside perimeter of the steel at the fire protection material interface. Figure 4-9.10 illustrates the method for determining D in four typical

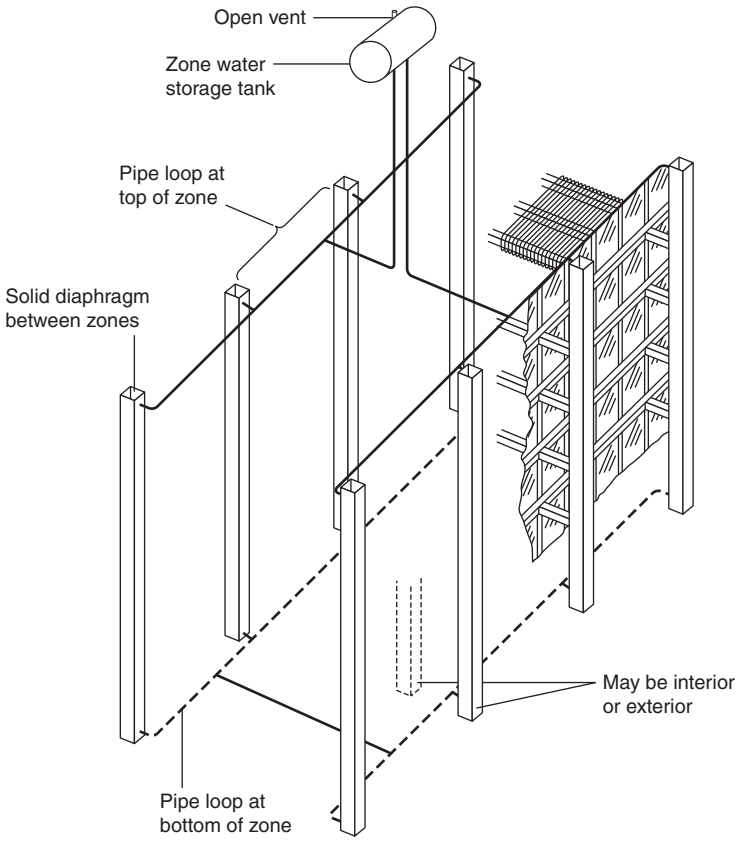

Figure 4-9.9. ***Schematic layout of a typical piping arrangement used in a liquid-filled column fire-protection system.[4]***

cases. As can be seen from the figure, the heated perimeter depends on the size of the column and also on the profile of the protection system. Two different commonly used profiles are: (1) contour profile, where all surfaces of the steel column are in contact with the protection material and (2) box profile, where a rectangular box of protection material is built around the column.

A large value of W refers to a column with a large weight per lineal foot. A given amount of energy will raise the temperature of the massive column to a lesser degree than that of a light column. Less surface area is available for heat transfer if the heated perimeter, D, is small, thereby inhibiting the temperature rise in the steel. The greater the W/D ratio, the greater the inherent fire resistance of the assembly is.

Because steel elements with larger W/D ratios are inherently more fire resistant, substituting shapes with greater W/D ratios for shapes identified in the listed designs in the UL *Fire Resistance Directory*[3] is permitted while maintaining the same thickness of protection. However, such substitution yields inefficient designs, because shapes with large W/D ratios actually require less fire protection material than shapes with small W/D ratios for the same level of fire resistance.

The equation for gypsum wallboard protection is nonlinear. The weight of the gypsum wallboard is included because the heat capacity of gypsum has a considerable

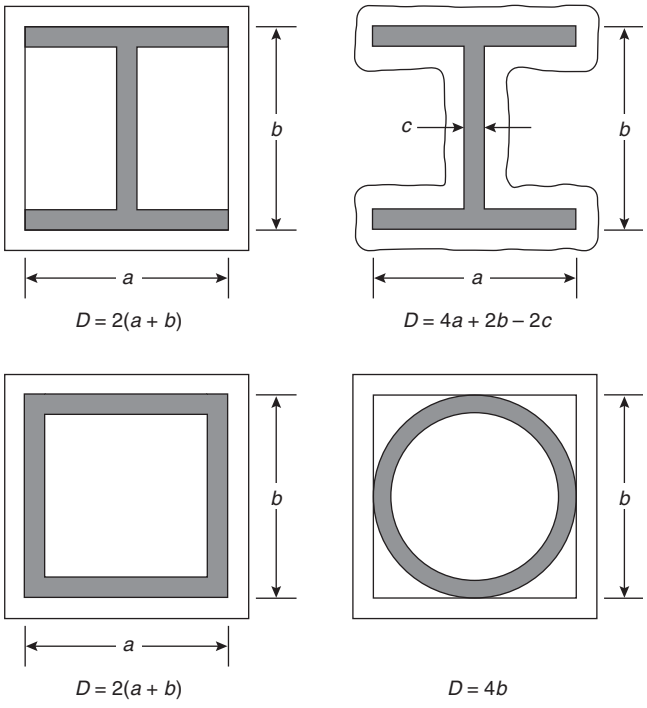

Figure 4-9.10. ***Heated perimeter for steel columns.[25]***

Table 4-9.3 ***Empirical Equations for Steel Columns***[20,26,27]

Member/Protection	Solution	Symbols
Column/Unprotected	$R = 10.3\,(W/D)^{0.7}$, for $W/D < 10$ $R = 8.3\,(W/D)^{0.8}$, for $W/D \geq 10$ (for critical temperature of 1000°F)	R = fire endurance time (min) W = weight of steel section per linear foot (lb/ft) D = heated perimeter (in.)
Column/Gypsum Wallboard	$R = 130\left(\frac{hW'/D}{2}\right)^{0.75}$ where $W' = W + \left(\frac{50hD}{144}\right)$	h = thickness of protection (in.) W' = weight of steel section and gypsum wallboard (lb/ft)
Column/Spray-applied materials and board products—wide flange shapes	$R = [C_1(W/D) + C_2]h$	C_1 & C_2 = constants for specific protection material
Column/Spray-applied materials and board products—hollow sections	$R = C_1\left(\frac{A}{P}\right)h + C_2$	C_1 & C_2 = constants for specific protection material The A/P ratio of a circular pipe is determined by A/P pipe $= \frac{t(d-t)}{d}$ where d = outer diameter of the pipe (in.) t = wall thickness of the pipe (in.) The A/P ratio of a rectangular or square tube is determined by A/P tube $= \frac{t(a+b-2t)}{a+b}$ where a = outer width of the tube (in.) b = outer length of the tube (in.) t = wall thickness of the tube (in.)
Column/Concrete cover	$R = R_0(1 + 0.03m)$ where $R_0 = 10(W/D)^{0.7} + 17\left(\frac{h^{1.6}}{k_c^{0.2}}\right) \cdot \left\{1 + 26\left[\frac{H}{\rho_c c_c h(L+h)}\right]^{0.8}\right\}$ $D = 2(b_f + d)$	R_0 = fire endurance at zero moisture content of concrete (min.) m = equilibrium moisture content of concrete (% by volume) b_f = width of flange (in.) d = depth of section (in.) k_c = thermal conductivity of concrete at ambient temperature (Btu/hr·ft·°F) h = thickness of concrete cover (in.)
Column/Concrete encased	for concrete-encased columns use $H = 0.11W + \frac{\rho_c c_c}{144}(b_f d - A_s)$ $D = 2(b_f + d)$ $L = (b_f + d)/2$	H = thermal capacity of steel section at ambient temperature (= 0.11W Btu/ft·°F) c_c = specific heat of concrete at ambient temperature (Btu/lb·°F) L = inside dimension of one side of *square* concrete box protection (in.) A_s = cross-sectional area of steel column (in.^{2})

impact on the fire resistance of the assembly. The thickness of wallboard required to achieve a particular level of fire resistance as a function of the W/D ratio of the column is presented in Figure 4-9.10.

Based on an elementary heat transfer analysis, Stanzak and Lie conducted a parametric analysis that resulted in correlations of the following form to estimate the thickness of material required to achieve a particular level of fire resistance:[25,27]

$$R = (C_1 W/D + C_2)h$$

where

R = fire endurance (hr)

W= steel weight per lineal foot (lb/ft)

D = heated perimeter of the steel at the insulation interface (in.)

h = thickness of insulation (in.)

The constants C_1 and C_2 need to be determined for each protection material. The constants take into account the thermal conductivity and heat capacity of the insulation material. Constants for some materials are included in listings in the *UL Fire Resistance Directory*.[3]

Considering the equation for the concrete cover column protection method (see Table 4-9.3), R_0 is the fire endurance of the assembly if the concrete has no moisture content. However, because the fire resistance of concrete-cover over steel columns is known to increase by approximately 3 percent for each 1 percent of moisture, R_0 is multiplied by the $(1 + 0.03m)$ factor where m is the equilibrium moisture content of concrete. The parameters h and L noted in the equation are shown in Figure 4-9.7. If the protection thickness or column dimensions are not the same in the vertical and horizontal directions, average values are used for h and L.

The heat capacity of the concrete must be accounted for in the determination of H if all re-entrant spaces are filled. (See Figure 4-9.7.) If specific data on the concrete's thermal properties are not available, values given in Table 4-9.4 may be used. Typical densities for normal-weight and lightweight concrete are 145 and 110 lb/ft^3 (2320 and 1760 kg/m^3). Also, the typical equilibrium moisture content (by volume) for normal-weight concrete is 4 percent and lightweight concrete is 5 percent.

Many of the equations cited in Table 4-9.3 are limited to a range of shapes or protection thickness. Before applying any equation from this table, users should consult the original reference and confirm that the equation is being applied properly.

EXAMPLE 1:

Determine the thickness of spray-applied cementitious material to obtain a 2-hr fire endurance when applied to a $W\,12 \times 106$ column.

SOLUTION:

From UL X772, the applicable equation is

$$R = (63W/D + 36)h$$

Solving for h,

$$h = \frac{R}{63W/D + 36}$$

where

R = 2 hrs = 120 min

W/D = 1.44 lb/ft·in. for a $W\,12 \times 106$ with contour profile protection

Table 4-9.4 ***Thermal Properties of Concrete at 70° F***

	Normal-Weight Concrete	Structural Lightweight Concrete
Thermal conductivity (k)[a]	0.95	0.35
Specific heat (c)[b]	0.20	0.20

[a]Expressed as Btu/hr·ft·°F

[b]Expressed as Btu/lb·°F

Substituting,

$$h = \frac{120}{63 \times 1.44 + 36} = 0.95 \text{ in.}$$

EXAMPLE 2:

Determine the fire endurance of a $W\,8 \times 28$ column encased in lightweight concrete (density of 110 lb/ft^3 [176.2 kg/m^3]) with all re-entrant spaces filled. The concrete cover thickness is 1.25 in. (31.8 mm).

SOLUTION:

From Table 4-9.3, the appropriate equation is

$$R = R_0(1 + 0.03m)$$

where

$$R_0 = 10(W/D)^{0.7} + 17\left(h^{1.6}/k_c^{0.2}\right)\{1 + 26[H/\rho_c c_c h(L + h)]^{0.8}\}$$

Referring to Figure 4-9.7,

$h_2 = h_1 = h = 1.25$ in. (31.8 mm)

$b_f = 6.535$ in. (166 mm)

$d = 8.060$ in. (204.7 mm)

$W/D = 0.67$ lb/ft·in. (39.3 kg/m^2)(contour profile)

$A = 8.25$ in.^{2} (0.0053 m^2)

From Table 4-9.4,

$k_c = 0.35$ Btu/hr·ft·°F

$c_c = 0.20$ Btu/lb·°F

$\rho_c = 110$ lb/ft^3

$$L = \frac{1}{2}(b_f + d) = 7.30 \text{ in.}$$

$$H = 0.11W + \frac{\rho_c c_c}{144}(b_f D - A_s)$$

$$H = 0.11 \times 28 + \frac{110 \times 0.20}{144}(6.535 \times 8.060 - 8.25)$$

$$= 9.87$$

$$R_0 = 10(0.67)^{0.7} + 17\left(\frac{1.25^{1.6}}{0.35^{0.2}}\right) \times \left\{1 + 26\left[\frac{9.87}{110 \times 0.2 \times 1.25(7.30 + 1.25)}\right]^{0.8}\right\}$$

$R_0 = 99$ min

Assuming a moisture content of 5 percent for lightweight concrete,

$$R = 99(1 + 0.03 \times 5) = 114 \text{ min}$$

Steel Beams

As in the case of columns, the W/D ratio is an important parameter affecting the fire resistance of a beam. Beams with larger W/D ratios may be substituted for

beams with lesser W/D ratios for an equivalent rating with no change in the protection thickness. However, as with columns, designs resulting from the direct substitution of larger beams without reducing the protection thickness may be inefficient.

In 1984, an empirically derived correlation was developed to calculate the required thickness of spray-applied material protection.[31] Correlations of the form for steel columns are not possible, given the deck's role as a heat sink. Thus, the thickness of protection for steel beams is determined based on the following scaling relationship:

$$h_1 = \left(\frac{W_2/D_2 + 0.6}{W_1/D_1 + 0.6}\right) h_2 \qquad (1)$$

where

h = thickness of spray-applied fire protection (in.)

W = weight of steel beam (lb/ft)

D = heated perimeter of the steel beam (in.) (See Figure 4-9.11)

and where the subscripts

1 = substitute beam and required protection thickness

2 = the beam and protection thickness specified in the referenced tested design or tested assembly

Limitations of this equation are noted as follows:

1. $W/D \geq 0.37$
2. $h \geq 3/8$ in. (9.5 mm)
3. The unrestrained beam rating in the referenced tested design or tested assembly is at least 1 hr

It should be noted that the above equation only pertains to the determination of the protection thickness for a beam in a floor or roof assembly. All other features of the assembly, including the protection thickness for the deck, must remain unaltered.

EXAMPLE 3:

Calculate the thickness of spray-applied fire protection required to provide a 2-hr fire endurance for a W 12 $\times$ 16 beam to be substituted for a W 8 $\times$ 17 beam requiring 1.44 in. (36.6 mm) of protection for the same rating.

SOLUTION:

The beam substitution correlation, presented as Equation 1, is used.

$$h_1 = \left(\frac{W_2/D_2 + 0.6}{W_1/D_1 + 0.6}\right) h_2$$

where

$$W_2/D_2 = 0.54 \qquad \text{for } W\ 8 \times 17$$
$$W_1/D_1 = 0.45 \qquad \text{for } W\ 12 \times 16$$
$$h_2 = 1.44$$
$$h_1 = \left(\frac{0.54 + 0.6}{0.45 + 0.6}\right) \times 1.44 = 1.6 \text{ in.}$$

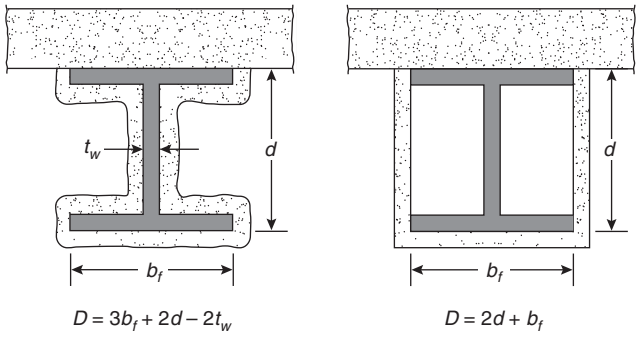

Figure 4-9.11. ***Heated perimeter for steel beams.[31]***

Steel Trusses

There are three types of trusses used in buildings: transfer, staggered, and interstitial trusses. Because of the inherent features of each type of truss, some fire protection systems are more appropriate than others.[33]

A load-transfer truss (see Figure 4-9.12) supports loads from more than one floor. The loads may be suspended

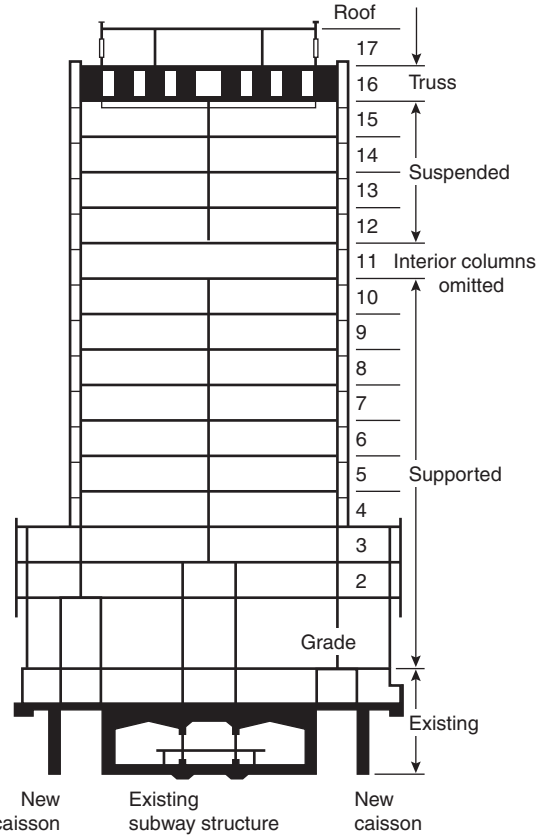

Figure 4-9.12. ***Vierendell truss providing support from above and below.[33]***

from a transfer truss or the transfer truss can be used to eliminate columns on lower floors.

A staggered truss is illustrated in Figure 4-9.13. Generally, staggered trusses are used in residential occupancy buildings. Staggered trusses carry loads from two floors.

Interstitial trusses are used to create deep floor/ceiling concealed spaces containing mechanical and electrical equipment, as shown in Figure 4-9.14. Interstitial trusses support only those loads from the equipment enclosure and the floor above. Interstitial trusses are typically used in health-care facilities with heavy mechanical equipment needs.

Three methods of fire protection are often used for trusses: membrane, envelope, and individual element protection. Some fire protection methods are more appropriate than others for the specific truss types. The fire protection methods typically used for each truss type are indicated in Table 4-9.5. Membrane protection is accomplished through the use of a fire-resistant ceiling assembly. Design parameters for such an assembly can be determined from listings of fire-rated designs.[3,34] No empirical correlations are available to assess the design of membrane protection systems.

The envelope means of protection is illustrated in Figure 4-9.15. The truss is enclosed in layers of a board product, with the number of layers determined by the required fire endurance. Some practical rules of thumb based on test results are noted in Table 4-9.6.

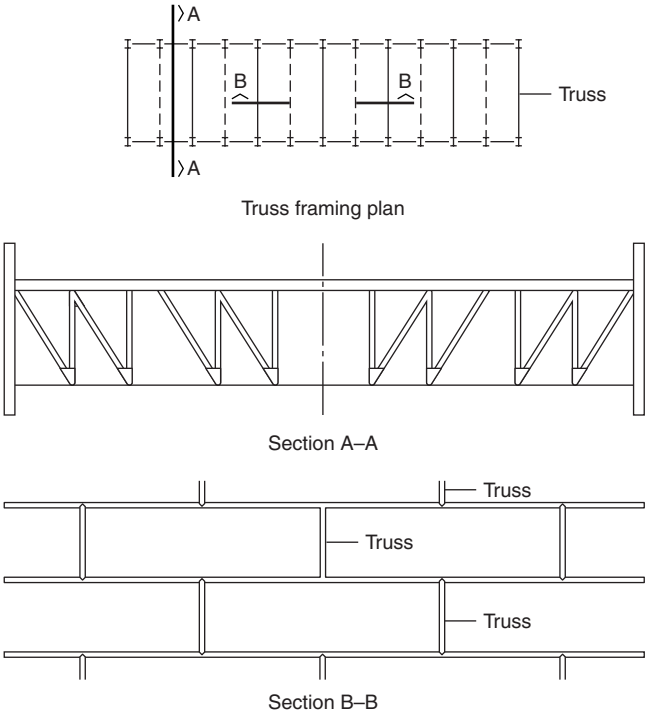

Figure 4-9.13. ***A typical truss and positionings in a staggered truss system.[33]***

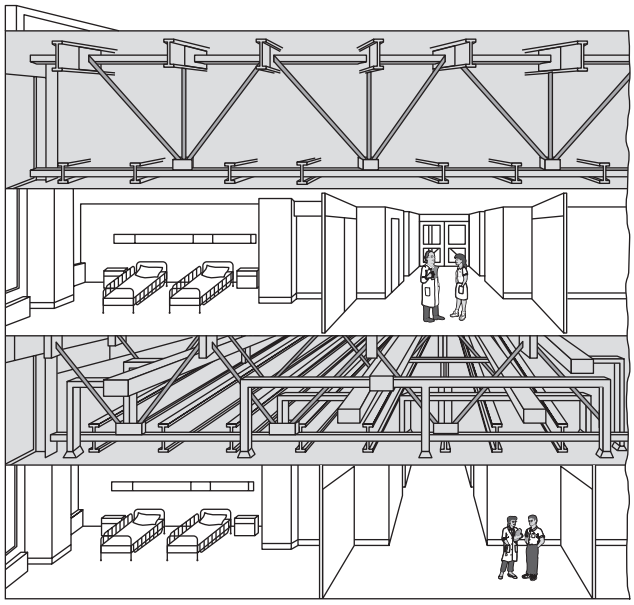

Figure 4-9.14. ***Hospital interstitial truss system.[33]***

Table 4-9.5 ***Typical Fire Protection Methods for Steel Trusses***

	Fire Protection Method		
Truss Type	Membrane	Envelope	Individual Element
Transfer		X	X
Staggered		X	X
Interstitial	X	X	X

Table 4-9.6 ***Practical Guidelines for Thickness of Gypsum Wallboard for Steel Truss Envelope Protection[33]***

Fire Endurance	Gypsum X	Wallboard Type
60	$^5/_8$" (16 mm)	$^5/_8$" (16 mm)
120	$1^1/_4$" (32 mm)	—
180	—	$1^1/_2$" (38 mm)

Individual element protection is generally accomplished using a spray-applied material. Since critical truss elements perform structurally as columns, that is, in tension or compression (as opposed to bending), the applicable equations for determining the thickness of spray-applied material for columns is used. In order to use these equations, the W/D ratio must be calculated for each element. Unlike columns and beams, the ratio may not be readily available. The diagrams in Figure 4-9.16 are provided for assistance in calculating the heated perimeter.

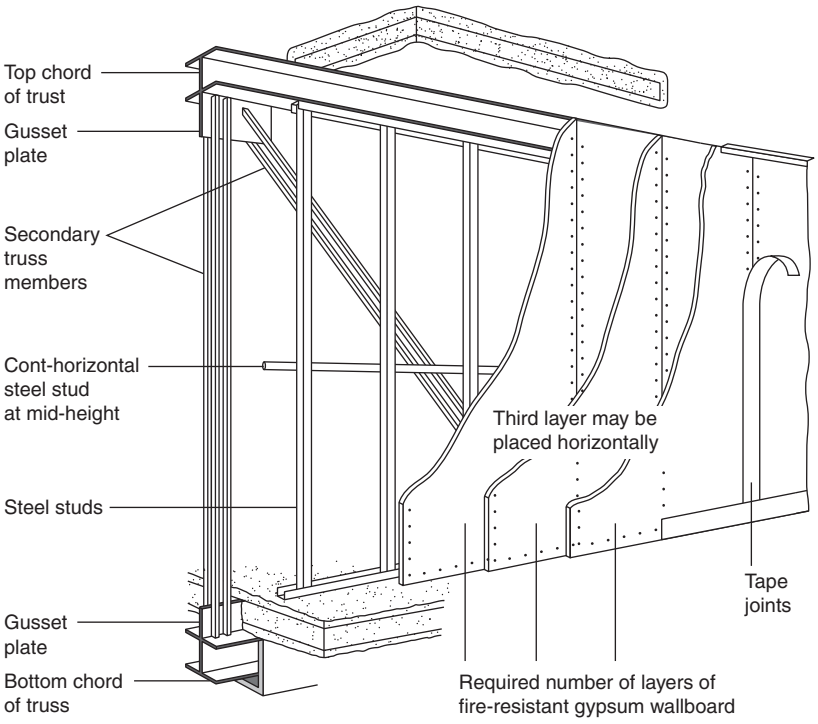

Figure 4-9.15. ***Staggered truss protection with envelope protection.[33]***

Heat Transfer Analyses

Heat transfer analyses are applied to determine the time period required to heat structural members to a specified critical temperature or to provide temperature data as input to the structural analysis of the heated member. The time required to heat the member to a specified critical temperature is often defined as the fire endurance time of the member.

The critical temperature of a structural member can be determined by referring to the temperature endpoint criteria cited in ASTM E119[1] or by a structural assessment, as is discussed later in this chapter.

The available types of heat transfer analyses can be grouped into the following categories:

1. Numerical methods
2. Graphical solutions
3. Computer programs

Numerical Methods

Many numerical methods are available to estimate the temperature rise in steel structural elements. The equations are derived from simplified heat transfer approaches.

Unprotected steel members: The temperature in an unprotected steel member can be calculated using a quasi-steady-state, lumped heat capacity analysis. This method assumes that the steel member is at a uniform temperature. The equation for temperature rise during a short time period, Δt, is[21]

$$\Delta T_s = \frac{\alpha}{c_s(W/D)}(T_f - T_s)\Delta t \qquad (2)$$

where

ΔT_s = temperature rise in steel (°F)(°C)
α = heat transfer coefficient from exposure to steel member (Btu/ft²·s·R)(W/m²·K),
D = heat perimeter (ft)(m) (see Figure 4-9.16)
c_s = steel specific heat (Btu/lb·°F)/(J/kg·°C)
W = steel weight per lineal foot (lb/ft)/(kg/m)
T_f = fire temperature (R)(K)
T_s = steel temperature (R)(K)
Δt = time step (s)

where

$$\alpha = \alpha_r + \alpha_c$$

α_r = radiative portion of heat transfer

$$\alpha_r = \frac{C_1 \varepsilon_f}{T_f - F_s}\left(T_f^4 - T_s^4\right)$$

where $C_1 = 4.76 \times 10^{-13}$ Btu/s·ft²·R⁴ (5.77×10^{-8} W/m³·K⁴) and ε_f, the effective emissivity, can be evaluated from Table 4.97.

α_c = convective portion of heat transfer

9.8×10^{-4} to 1.2×10^{-3} Btu/ft²·s (20 to 25 W/m²·K)

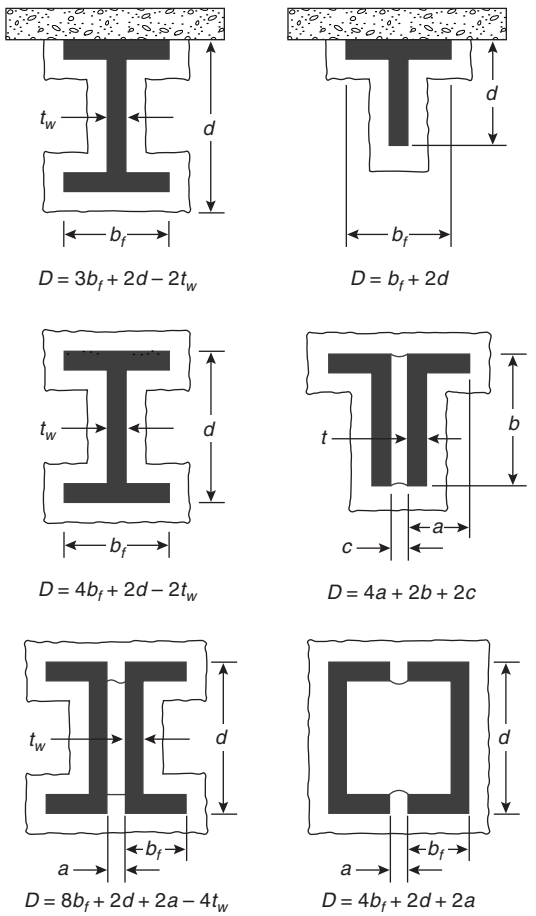

Figure 4-9.16. ***Heated perimeter for steel truss shapes.[33]***

The quasi-steady assumption dictates that the time step should be small, that is, on the order of 10 s.[59]

Equation 2 is successively applied up to the time duration of interest. Correlations for the time-temperature curve associated with standard fire resistance tests are included by Lie, in another chapter of this handbook. For the ISO 834 test, T_f at any time, t, can be estimated by the following expression:[21]

$$T_f = C_T \log_{10}(0.133t + 1) + T_0 \tag{3}$$

where

C_T = 620 with T_f, T_0 in °F
345 with T_f, T_0 in °C

Protected steel members: For protected members, the thermal resistance provided by the insulating material must be considered. If the thermal capacity of the insulation layer is neglected,[21]

$$\Delta T_s = \frac{k_i}{c_s h W/D}(T_f - T_s)\Delta t \tag{4}$$

where all parameters are as defined in Equation 2, and

Table 4-9.7 ***Effective Emissivity[35]***

Type of Construction	Resultant Emissivity
1. Column exposed to fire on all sides	0.7
2. Column outside facade	0.3
3. Floor girder with floor slab of concrete, only the underside of the bottom flange being directly exposed to fire	0.5
4. Floor girder with floor slab on the top flange	
Girder of 1 section for which the width-depth ratio is not less than 0.5	0.5
Girder of 1 section for which the width-depth ratio is less than 0.5	0.7
Box girder and lattice girder	0.7

k_i = thermal conductivity of insulation material (Btu/ft·s·°F) (W/m·°C)

h = protection thickness (ft) (m)

Malhotra suggests that the thermal capacity of the insulation material may be neglected if the following inequality is true (see parameter definitions for Equation 2):[21]

$$c_s W/D > 2c_i \rho_i h$$

If the thermal capacity must be accounted for, as in the case of gypsum and concrete insulating materials, then

$$\Delta T_s = \frac{k_i}{h}\left[\frac{T_f - T_s}{c_s(W/D) + 1/2c_i\rho_i h}\right]\Delta t \tag{5}$$

where all parameters are as defined for Equation 2, and

c_i = specific heat of insulating material (Btu/lb·°F) (J/kg·°C)

ρ_i = density of insulating material (lb/ft^3) (kg/m^3)

An evaluation of the predictive capability of the lumped heat capacity approach using Equation 5 for protected steel sections was conducted by Berger for steel columns protected with a spray-applied cementitious material.[36] The analysis consisted of comparing predicted versus measured temperatures for steel columns exposed to the standard fire exposure. A comparison of the predicted versus measured times for the steel column to reach 538°C is provided in Table 4-9.8. A comparison of the predicted temperature with that measured for one protected steel column assembly is provided in Figure 4-9.17.

Predictions of temperature rise in steel beams by the lumped heat capacity approach are prone to be inherently less accurate than those for steel columns.[37] As noted previously, a steel beam in contact with a slab only has three sides exposed to a fire and also will lose heat to the slab.[38] Consequently, the temperature of a steel beam exposed to fire is likely to vary appreciably from the bottom flange to the top flange, stretching the validity of the uniform temperature assumption. Nonetheless, for many engineering applications, the lumped heat capacity approach can provide a conservative estimate of the average temperature

Table 4-9.8 ***Comparison of Predicted Time from Lumped Heat Capacity Analysis and Measurements for Protected Steel Column to Reach 538° C***

Shape	*h* (cm)	Test (min)	Calc. (min)
W 6 × 16	1.9	58	56
	3.8	112	119
	7.6	210	251
W 8 × 28	3.5	122	121
	8.3	291	298
	9.5	355	352
W 10 × 49	1.9	70	62
	5.6	217	220
W 12 × 106	3.8	200	203
W 14 × 228	1.4	123	140
W 14 × 233	2.9	225	251

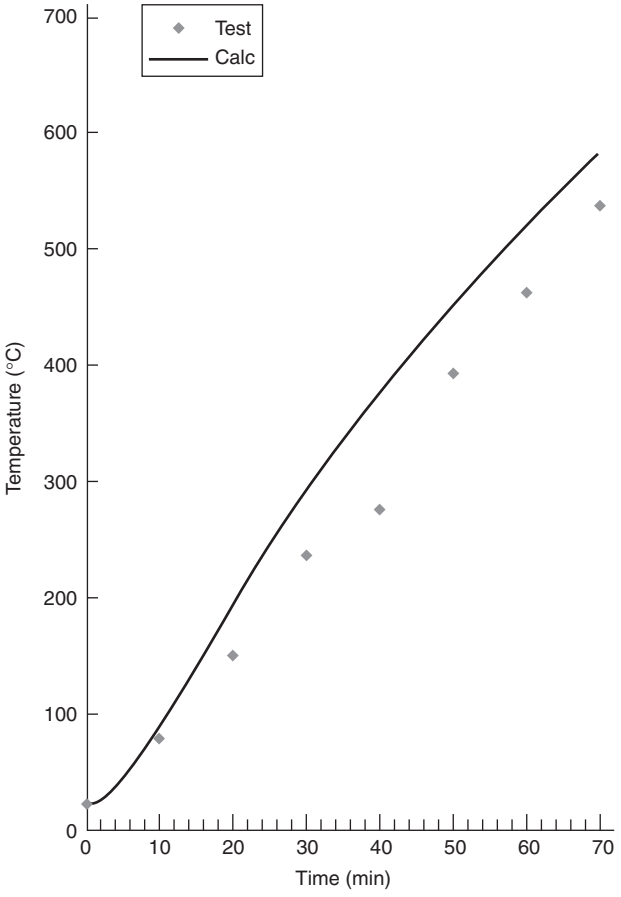

Figure 4-9.17. ***Predicted steel column temperature.[36]***

rise of a steel beam.[39] Heat losses to the slab may be compensated for by reducing the effective flame emissivity to 0.5.[35] However, if the temperature gradient across the beam is important, another analytical approach will need to be applied.[37]

Exterior steel columns and steel spandrel beams: A design guide is available for calculating the exposure of exterior steel columns and steel spandrel beams.[40] The guide is based on research by Law and basic radiation heat transfer principles.[41] A similar calculation procedure is available in the Eurocodes.[9]

The temperature of the steel member is calculated from a steady-state conduction analysis. The exposure boundary conditions consist of radiant heating from a fully developed room fire and flames emitting from windows near the steel member. For this method, a specific design is considered unacceptable if the steel temperature exceeds 1000°F.

Liquid-filled columns: The design calculations for liquid-filled columns are based on the thermal capacity of the liquid. The design of a liquid-filled column fire protection system consists of three major steps:

1. Heat transfer analysis
2. Determination of volume of liquid required
3. Pipe network design

The heat transfer analysis is used to assess the impact of fire exposure on the liquid-filled column. The heat transfer analysis considers radiation and convection heat transfer from the fire to the column surface, conduction through the column wall, and convection with localized boiling into the liquid. Both temperature of the steel column and total amount of heat transferred to the liquid causing evaporation are determined as a result of this analysis.

The liquid volume calculation is important to ensure the column remains full of liquid for the entire fire exposure period. Since heat transferred to the liquid will cause some evaporation, a supplemental amount of liquid must be provided in a storage tank.

The final step in the design method is a hydraulic analysis of the tubular column and pipe network. This analysis assesses the ability of the liquid to circulate based on friction losses, elevation changes, and buoyancy of the heated liquid.

A comprehensive design aid for liquid-filled columns is available.[42] Since the procedure is rather lengthy, it will not be reviewed here.

Graphical Solutions

Because heat transfer analyses can be very tedious and may involve the use of complex computer programs, graphic solutions have been formulated to simplify the estimation of steel temperature. Graphs of the temperature of protected steel members have been developed by Malhotra,[21] Jeanes,[12] Lie,[15] and others.

The series of graphs developed by Malhotra,[21] presented in Figure 4-9.18, for estimating the temperature of steel members exposed to the standard exposure are based on the lumped heat capacity approach described in the previous section. Steel temperatures are plotted versus the D/A ratio (analogous to the inverse of W/D) for selected time periods of exposure and thermal resistances of the insulating material. Time periods of 30 to 120 min are noted in the graphs. The range of thermal resistances of the insulating material covered by these graphs is 0.01 to 0.30 $(W/m^2 \cdot °C)^{-1}$ (0.003 to 0.10) $(Btu/ft^2 \cdot hr \cdot °F)^{-1}$.

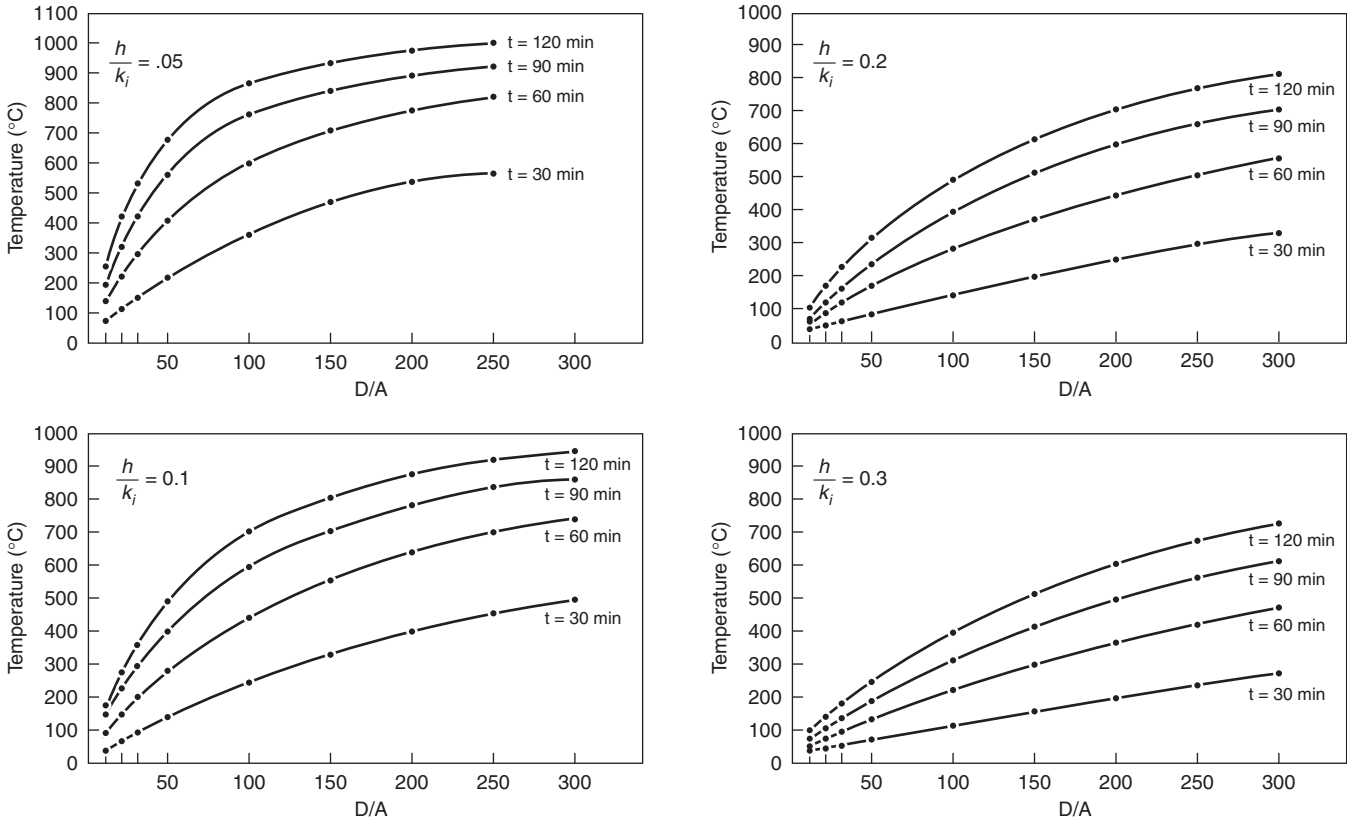

Figure 4-9.18. ***Relationship of heated area to steel weight with temperature.[21]***

Based on the application of FIRES-T3, a heat transfer computer program which will be described in the next section, Jeanes formulated a series of time-temperature graphs of protected steel beams.[12] The steel beams are protected by a proprietary specific spray-applied cementitious material with a range of thicknesses of 0.5 to 1.5 in. (12.7 to 38.1 mm). Graphs are available for a variety of common wide-flange beam shapes.[12] Examples of these graphs are presented in Figure 4-9.19 with graphs addressing the average and single-point steel temperatures relating to the maximum endpoint criteria from ASTM E119.[1] Average and single-point steel temperatures are represented by the dashed lines. These graphs can be used to determine the thickness of protection material required to provide a desired level of fire resistance. Alternatively, the fire endurance can be estimated for a particular steel beam and insulation thickness design which has not been tested.[12]

Information from numerous applications of FIRES-T3 examining the time-temperature response of steel beams protected with a spray-applied cementitious material exposed to the standard fire exposure is summarized in Figure 4-9.20. Using this graph, the fire endurance of protected steel beams with a W/D ratio of 0.4 to 2.5 lb/ft-in. can be determined for thicknesses of the spray-applied protection between 1.3 to 3.8 cm (0.5 to 1.5 in.).

Lie provides graphical representations of the exact solutions of the governing differential equations for the temperature of protected steel members exposed to the standard fire.[15] The heat transfer is assumed to be one-dimensional through the insulation layer. A uniform temperature throughout the steel cross section is assumed. The two graphs presented in Figure 4-9.21 are applicable to a wide range in the Fourier number, Fo, for the insulation layer. In order to use the graphs, the following dimensionless parameters must be defined:

$$\text{Fo} = \frac{\alpha t}{h^2}$$

$$N = \frac{\rho_i c_i h}{c_s (W/D)}$$

$$\theta = \frac{T - T_0}{T_m - T_0}$$

where

α = thermal diffusivity of insulation (ft²/hr) (m²/hr)
t = heating time (hr)
h = thickness of insulation (ft) (m)
ρ_i = density of insulation (lb/ft³) (kg/m³)
c_i = specific heat of insulation (Btu/lb·°F)
cs = specific heat of steel (Btu/lb·°F)
T = temperature of steel at time t (°F) (°C)
T_0 = initial temperature of steel (°F) (°C)
T_m = mean fire temperature (°F) (°C)

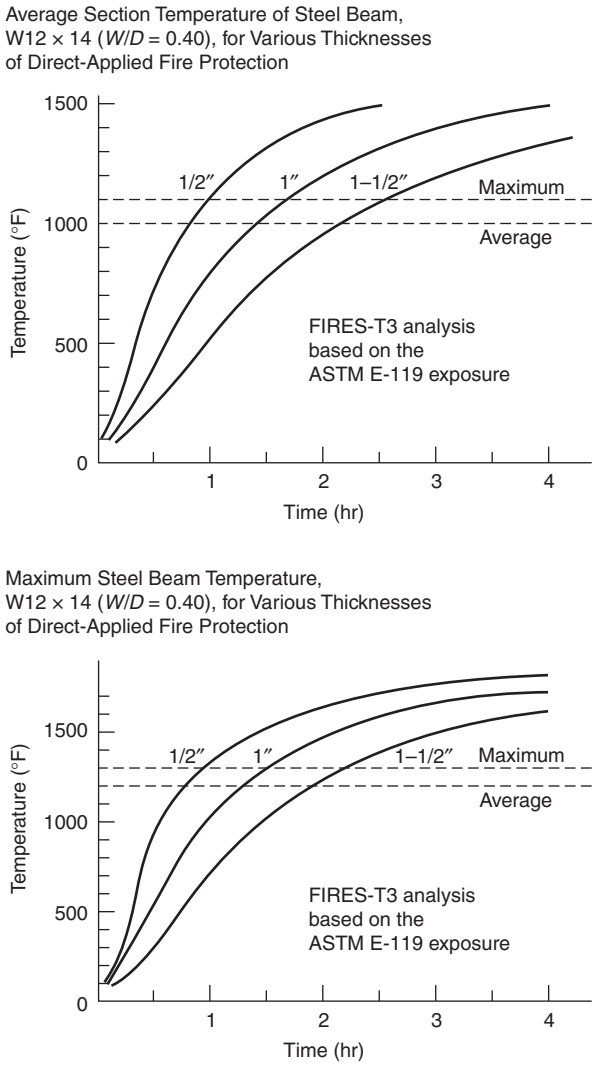

Figure 4-9.19. ***Predicted steel beam temperature by FIRES-T3.[12]***

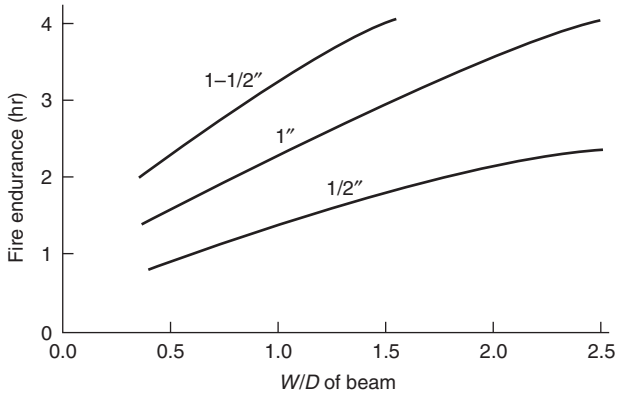

Figure 4-9.20. ***Fire endurance of steel beams versus fire protection thickness for average section temperature of 1000°F (538°C). (Based on FIRES-T3 analysis of ASTM E119 fire exposure.)[12]***

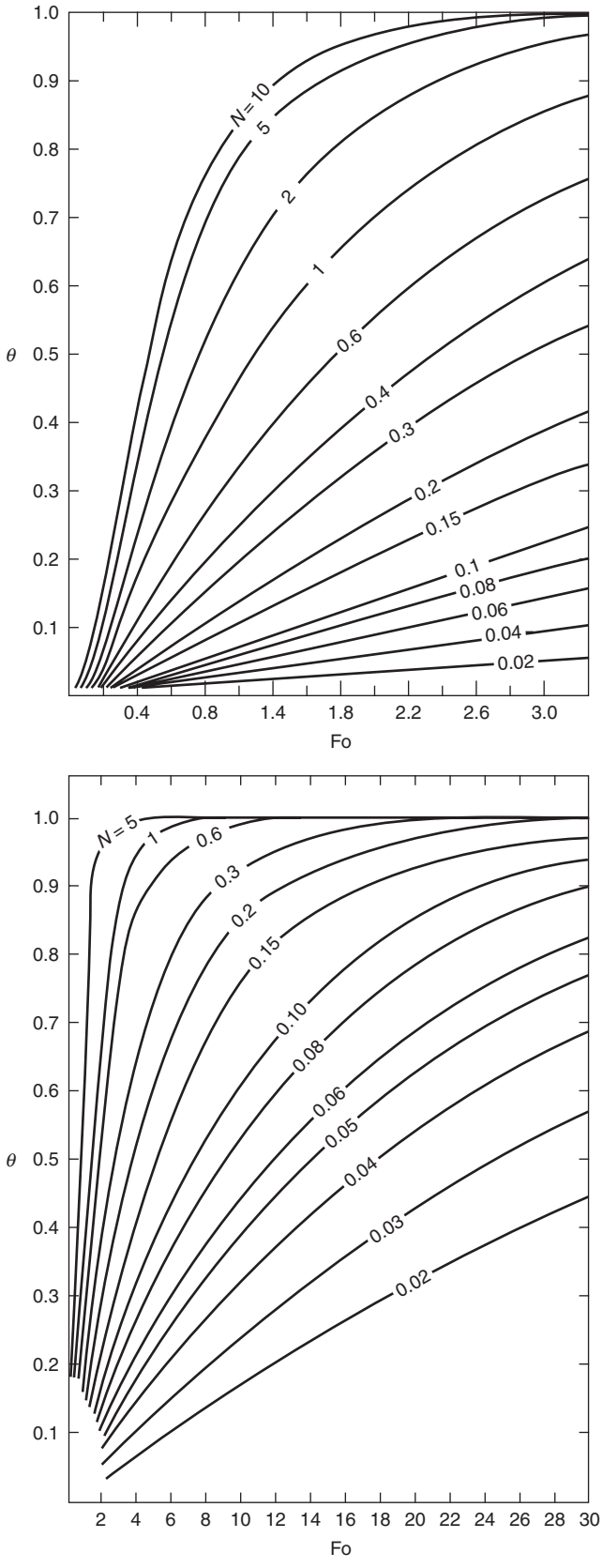

Figure 4-9.21. ***Dimensionless steel temperature versus Fourier numbers.[15]***

The mean fire temperature associated with a heating time, t, for these graphs is calculated from the standard time-temperature curve, where

$$T_m = \begin{cases} 150(\ln 480t - 1) - 30/t, & T°C \\ 270(\ln 480t) - 238 - 54/t, & T°F \end{cases}$$

EXAMPLE 4:

Determine the fire resistance of a W 24 × 76 steel beam based on the temperature endpoint criteria noted in ASTM E119. The beam is protected with 0.50 in. (12.7 mm) of spray-applied cementitious material, by three methods:

1. Graphical approach from Jeanes[12]
2. Graphical approach by Lie[15]
3. Quasi-steady-state approach by Malhotra[21]

SOLUTION:

A W 24 × 76 steel beam has a W/D ratio of 1.03 lb/ft·in. or 12.36 lb/ft². The material properties are evaluated at mean temperatures expected during the exposure. The fire resistance can be assessed using the temperature endpoint criteria in ASTM E119. Mean temperatures of 500°F (260°C) and 750°F (400°C) are selected (arbitrarily) for the steel and insulation, respectively, to determine the thermal properties. The following material property values are assumed:[12]

	Steel	Insulation
Thermal conductivity (Btu/ft·hr·°F)	25.6	0.067
Specific heat (Btu/lb·°F)	0.132	0.304
Density (lb/ft³)	490	15

Jeanes's graph: Using Figure 4-9.21 with a W/D of 1.03 lb/ft·in. and an insulation thickness of 0.50 in. (12.7 mm), the fire endurance is estimated to be 1.33 hr or 80 min.

Lie's graph: Evaluating the dimensionless parameters,

$$\text{Fo} = \frac{\alpha t}{h^2}$$

where

$$\alpha = \frac{k_i}{\rho_i c_i} = \frac{0.067}{15 \times 0.304} = 0.0147 \text{ ft}^2/\text{hr}$$

$$\text{Fo} = \frac{0.0147t}{(0.5/12)^2} = 8.47t \qquad (t \text{ in hr})$$

Referring to Figure 4-9.22 and using a trial and error approach with a critical temperature selected as 1000°F (538°C), the fire endurance time is estimated as approximately 75 min.

Quasi-steady-state approach: First, a check is performed to determine if the thermal capacity of the insulation material must be considered.

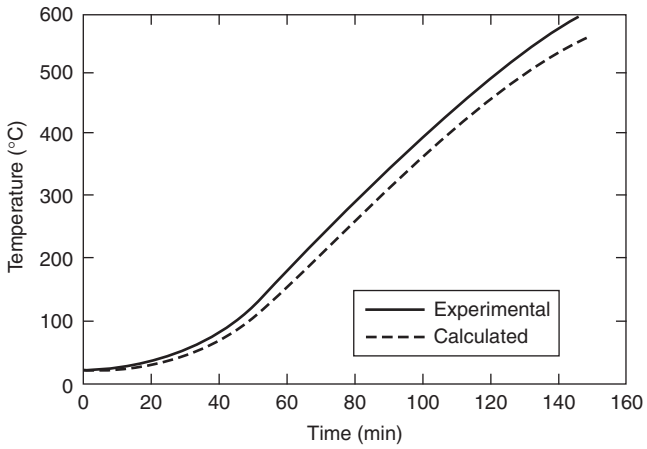

15 × 15 cm steel core, insulated by fire brick

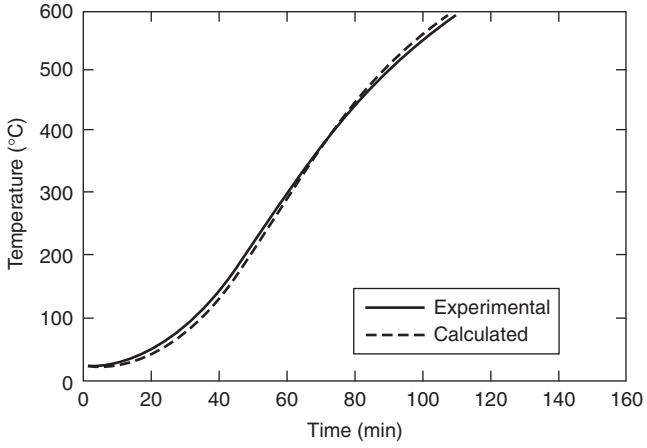

20 × 20 cm steel core, insulated by heavy clay brick

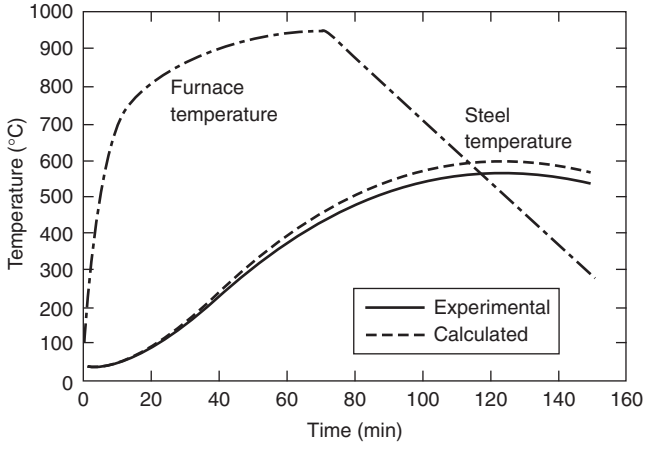

20 × 20 cm steel core, insulated by vermiculite boards

Figure 4-9.22. ***Comparison of calculated and measured steel temperatures.[43]***

$$c_s W/D > 2c_i \rho_i h$$

$$0.132 \times 12.36 > 2 \times 0.304 \times 15 \times 0.50/12$$

$$1.63 > 0.38$$

Disregarding the thermal capacity of the insulation, Equation 4 is used to predict the steel temperature rise for each time step.

$$\Delta T_s = \frac{0.067/3600}{0.0132 \times 0.50/12 \times 12.36}(T_f - T_s)\Delta t$$

$$= 2.74 \times 10^{-4}(T_f - T_s)\Delta t$$

Time	Steel Temperature (°C)	Fire Temperature (°C)	Fire-Steel Temperature (°C)	W/m²·K *k/h*	ΔT_s (°C)
10	20.0	46	26	9.13	0.1
20	20.1	72	51	9.13	0.2
30	20.3	96	76	9.13	0.3
40	20.5	120	99	9.13	0.3
50	20.8	143	122	9.13	0.4
3220	534.2	888	353	9.13	1.2
3230	535.3	888	353	9.13	1.2
3240	536.5	888	352	9.13	1.2
3250	537.7	889	351	9.13	1.2
3260	538.9	889	350	9.13	1.2
3270	540.1	890	350	9.13	1.2
3280	541.2	890	349	9.13	1.2

Thus, the fire endurance is 54 min.

The fire endurances calculated by the three methods can be compared as follows:

Jeanes (FIRES-T3)	80 min
Lie	75 min
Quasi-steady-state	54 min

The agreement between the fire endurance times determined by Jeanes's and Lie's graphs is very good. The significantly reduced fire endurance calculated using the quasi-steady-state approach is attributable to the approximate nature of the lumped heat capacity method assuming an adiabatic surface at the beam–slab interface.

Computer-Based Analyses

Several computer-based analyses are available to estimate the temperature rise of steel members. The analyses range from a spreadsheet procedure to perform the iterative calculations for the quasi-steady-state approach to finite element models.

Spreadsheets are one example of providing a framework to perform the iterative, quasi-steady calculations.[36,37,44] Typically, the spreadsheet procedures mimic the quasi-steady analysis procedure described previously, including the evaluation of material properties at a mid-range temperature for the exposure of interest. Although temperature-dependent material properties can be included within the spreadsheet framework, the accuracy implied by considering temperature-dependent properties is not consistent with the first-order nature of the quasi-steady approach.

Another framework for conducting computer-based analyses includes the numerous mathematical-equation-solver software packages. This software can be used to conduct the iterations associated with the quasi-steady approach or to solve the partial differential equations exactly.

Harmathy and Lie developed a two-dimensional finite difference model to predict the temperature rise in protected steel columns.[43] The two-dimensional network is formulated over the cross-section of the insulation layer, assuming the temperature to be independent of length. The steel is assumed to be a perfect conductor (i.e., the temperature is uniform throughout the steel). Heat transfer via radiation is considered across any air spaces enclosed by the insulation and steel.

The boundary conditions included by Harmathy are those associated with the ASTM E119 test.[1] To simplify the model, convection is disregarded, since convection comprises a minor portion of the heat transfer process in the furnace test. A flame emissivity of 0.9 is selected. A comparison between the calculated and experimental steel temperatures is presented in Figure 4-9.22. As is evident, the agreement is very good for three insulating materials.

Pettersson et al.[35] include a finite difference formulation to predict the temperature rise of steel beams protected with a suspended ceiling exposed to a specified fire. The formulation uses a one-dimensional approximation accounting for conduction through the suspended ceiling and floor slab (above the beam), and radiation and convection in the air space between the slab and beam. The temperature of the steel is assumed to be uniform. The assembly is divided into several elements as depicted in Figure 4-9.23.

A system of simultaneous equations is derived for the temperature rise in each of the assembly elements. A numerical integration technique such as Runge-Kutta is used to obtain the solution. A comparison of the calculated versus experimentally observed temperatures for a steel beam is presented in Figure 4-9.24.

General heat-transfer finite-element programs have been available for many years.[45] FIRES-T3, TASEF-2, SAFIR, and SUPER-TEMPCALC, among others, have been

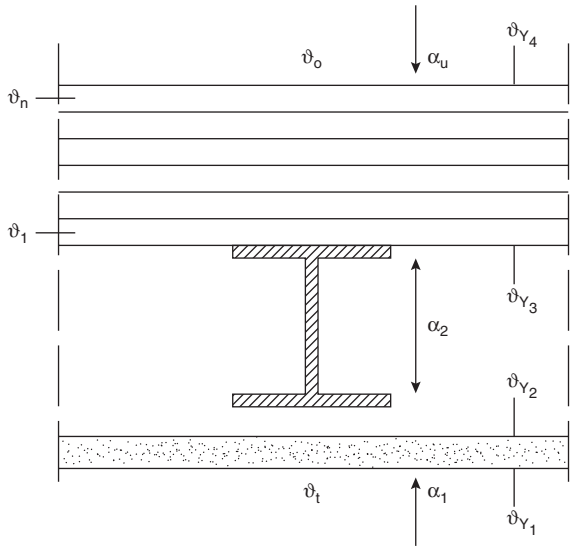

Figure 4-9.23. ***Division of the floor slab into elements.[35]***

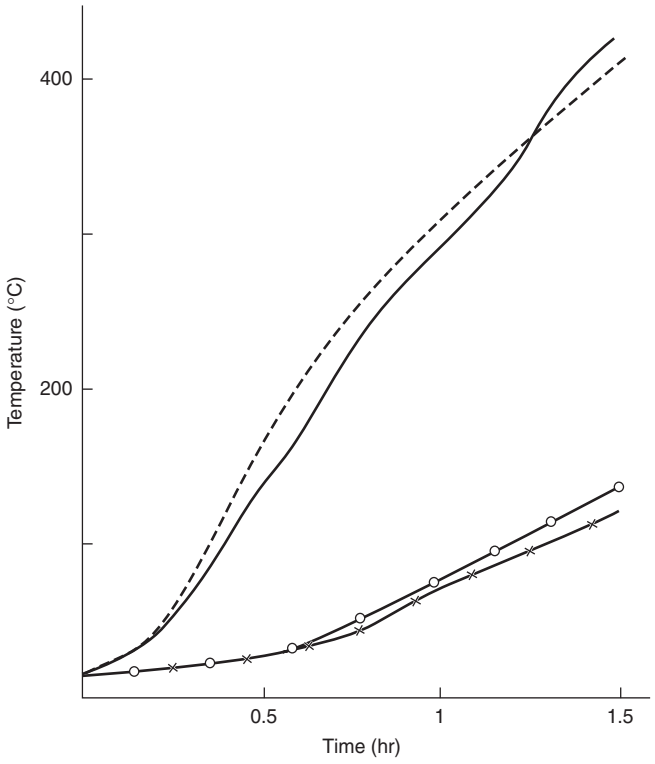

Figure 4-9.24. ***Calculated (--) and measured (—) steel temperature-time (θ_s – t) curve for a floor girder IPE 140 with insulation in the form of a suspended ceiling of 40-mm-thick mineral wool slabs of density γ = 150 kg/m3. The figure also gives the calculated (–∘–) and measured (–x–) temperature-time curve for the top of the 50-mm-thick concrete floor slab.[35]***

developed specifically to address the heating of assemblies with steel structural members exposed to fire conditions.[46–48]

TASEF-2 examines the conduction heat transfer through assemblies.[46] Assemblies may include internal voids, in which convection and radiation heat transfer modes are considered. Two time-temperature curves are available: (1) the ISO 834 standard time-temperature curve and (2) a time-temperature curve from a ventilation-controlled fire.

SUPER-TEMPCALC can also be used to analyze the conduction heat transfer through assemblies with air gaps. Numerous fire curves are included within the software.

FIRES-T3 was specifically developed to examine the heating of structural members exposed to fire conditions.[47] FIRES-T3 has been applied successfully to predict the temperature rise in protected steel beams and columns.[12,49] Almand used a finite-difference heat-transfer model to estimate the protection thickness of spray-applied cementitious material required for tubular steel columns.[50]

The input data requirements for the heat transfer computer models can be grouped into two categories:

1. A description of the assembly
2. A description of the fire exposure

The information necessary to describe the assembly includes geometric factors (dimensions, shape of member) and material property values (thermal conductivity, specific heat, and density). The fire exposure is characterized in terms of the temperature of the surrounding environment and appropriate heat transfer coefficients. The geometry of the assembly is established by formulating an element mesh for the assembly of interest. Required material property data consists of the density, specific heat, and thermal conductivity of the steel and insulation. Material property data is available for a limited number of insulation materials.[12,51] The exposure associated with the ASTM E119 test[1] may be selected as the fire exposure to be simulated by FIRES-T3.[12,49] A pre-processor routine for FIRES-T3 was recently developed by Stubblefield and Edwards.[52] TASEF and SUPER-TEMPCALC also includes a post-processor to generate graphs of the output.

For models using an explicit transient solution technique, such as FIRES-T3, caution must be exercised in selecting the time step and mesh size to obtain correct results that are numerically stable. TASEF-2 internally determines a numerically stable time step. Most heat transfer models do not address the effects of phase changes or chemical reactions that may influence the heating process. Phase changes and chemical reactions have been accounted for by altering the value of the material properties. Milke addressed the evaporization of free water in a spray-applied cementitious material by increasing the specific heat in a narrow temperature region around 100°C (212°F).[49]

Agreement between the predicted and experimental average steel temperatures is quite good in both applications of FIRES-T3 by Jeanes and Milke. A comparison of the temperature history for a steel column protected with a spray-applied cementitious material subjected to the ASTM E119 test is presented in Figure 4-9.25. A similar comparison is presented in Figure 4-9.26 for steel beams protected with the same material.[12]

FIRES-T3 has also been used to conduct a preliminary analysis of the heating of partially protected steel columns (i.e., where a portion of the spray-applied protection is missing).[53] The analysis indicated that even a small portion of missing protection significantly decreased the fire resistance of the column, especially for cases involving small columns. Results of the analysis are indicated in Figure 4-9.27.

Structural Analyses

The structural analysis methods calculate one of three parameters: deflection, critical temperature, or critical load. In several of the methods, all three of the parameters may be considered, since they are interrelated. Algebraic equations, graphs, and computer programs are available to perform a structural analysis for the purpose of addressing fire resistance.

General Discussion of Three Parameters Addressed in Structural Analysis

Deflection: The total deflection and rate of deflection can be calculated for loaded and heated steel beams by

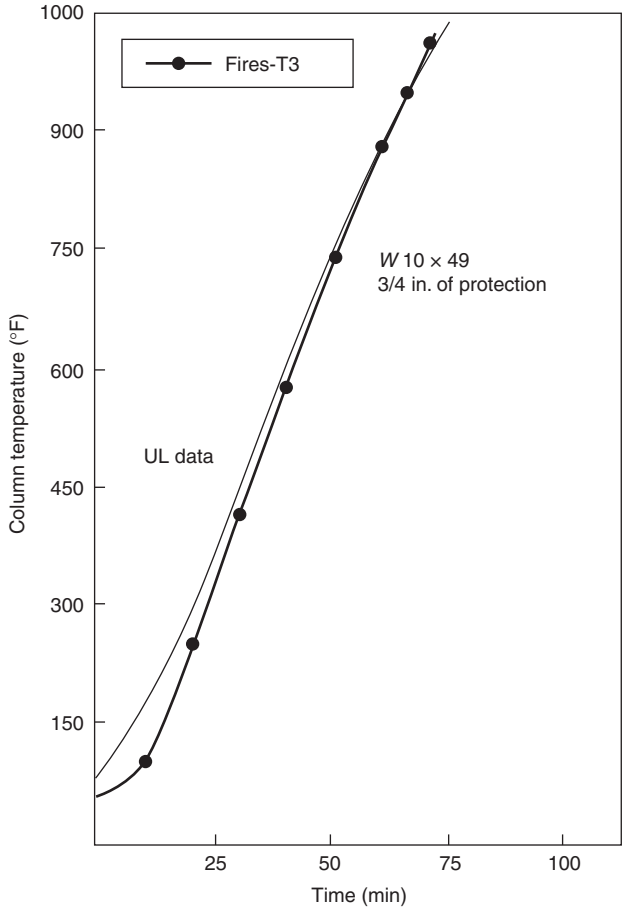

Figure 4-9.25. ***Comparison of predicted and measured average steel column temperature.[47]***

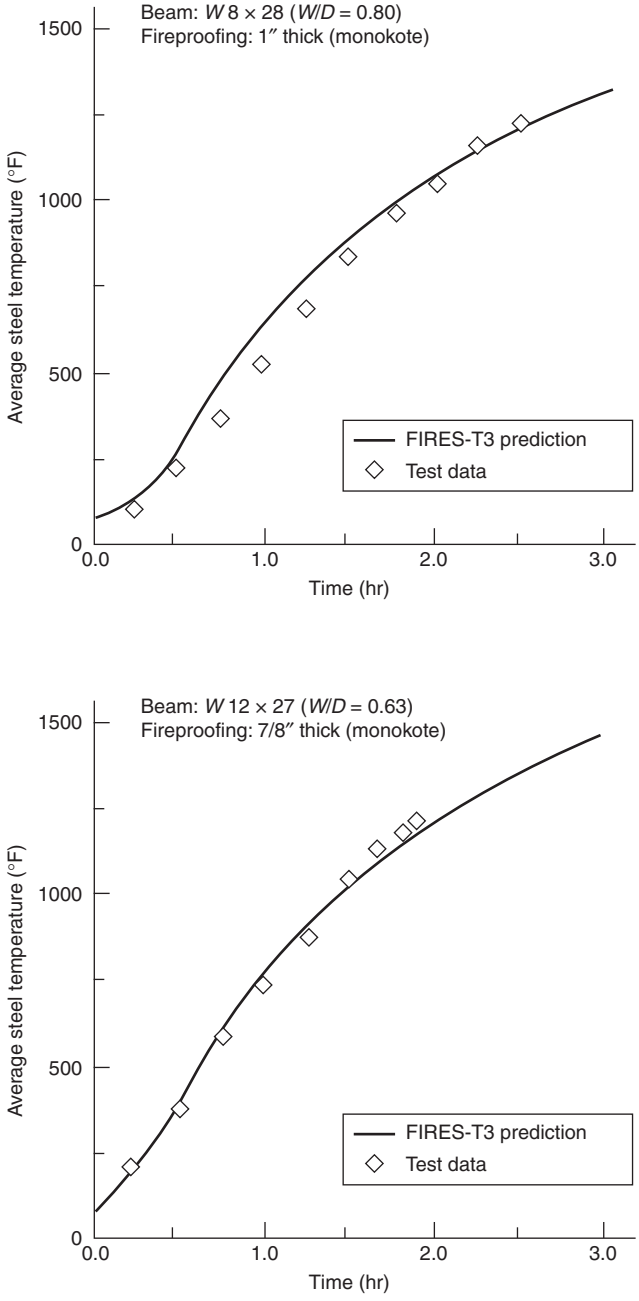

Figure 4-9.26. ***Comparison of experimental data and FIRES-T3 analysis.[12]***

considering all sources of strain. The total strain comprises components of the elastic and plastic strains due to the applied loads, thermal strain (due to thermal expansion), and creep stain.

The calculated deflection and rate of deflection can be compared with established maximum limits of each. The Robertson-Ryan criteria have been widely accepted for this purpose.[20,54,55] However, calculation of the deflection of unheated beams is difficult except for simple loadings, geometries, and end conditions. Adding the thermal expansion and creep components further complicates the calculation, virtually requiring computer solution.

Critical temperature: As mentioned earlier in the chapter, the material properties of steel change with increasing temperature. The most important material properties for critical-temperature calculations are yield strength, ultimate strength, and modulus of elasticity. The critical temperature is defined as the temperature at which the material properties have decreased to the extent that the steel structural member is no longer capable of carrying a specified load or stress level. In this context, the factor of safety of the member is considered to be reduced if the member reaches unacceptable stress levels, buckling becomes imminent, or deflections exceed maximum limits. The critical temperature can be calculated as long as the dependence of the material properties with temperature is known. There are numerous algebraic equations to calculate the critical temperature of steel structural members.[56] Often, the critical temperature is defined based on temperature limits stated in the standard test. However, in recent tests steel members experienced temperatures in excess of 800°C (1470°F) without collapse.[57]

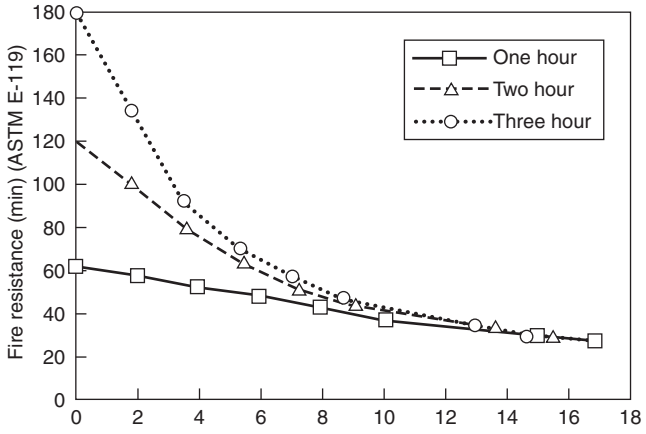

Figure 4-9.27. ***Fire resistance versus percent protection loss for W 10 × 49 column, flange exposure.***

Critical load: The critical load is defined as the minimum applied load that will result in failure if the structural member is heated to a temperature, *T.* The critical load can be expressed as a point load or distributed load. As with critical temperature, the critical load calculation requires the material properties at elevated temperatures. Critical load calculations can be conducted with algebraic equations or with a computer program.

Algebraic Equations: Critical Temperature

Beams

The critical temperature of Grade 250 steel beams with an allowable stress of 20,000 psi (138 Mpa) can be determined using equations by Lie and Stanzak.[30] The Lie and Stanzak equations account for creep strain and assume the beam is simply supported and thermally unrestrained.

Similar approaches have been developed by Malhotra,[21] Vinnakota,[55] and Kruppa.[58] Differences in the percent reduction in yield stress or modulus of elasticity are related to design method (elastic or plastic), factor of safety, and end conditions. Equations for the ratio of yield stress at elevated temperature with yield stress at ordinary room temperature are presented in Table 4-9.9. Typical values of Z/S are between 1.13 and 1.15 for I sections,[21] and 1.5 for rectangular sections.

Another example of the second approach is the analysis of the critical temperature of beams by European Convention for Constructional Steelwork (ECCS).[56,59] The ECCS guide addresses the maximum allowable reduction in yield strength by considering the applied loading, beam geometry, structural end conditions, and whether the applied loading results in stresses in the elastic or plastic range. Critical temperature calculations based on the ECCS analysis are presented in Table 4-9.10.

EXAMPLE 5:

Determine the critical temperature of a simply supported *W* 12 × 26 steel beam supporting a 53-in.- (1.35-m-) thick rectangular slab. The applied moment is 41,750 ft·lb (15,480 N·m). The rectangular slab is 8 ft (2.4 m) wide. The section properties of the beam are

$$Z_e = 33.4 \text{ in.}^3 \ (547 \times 10^3 \text{ mm}^3)$$

$$I = 204 \text{ in.}^4 \ (84.9 \times 10^6 \text{ mm}^4)$$

Assume σ_y = 36,000 psi (248 MPa).

SOLUTION:

Using Lie and Stanzak's equation for a beam,

$$T_{cr} = \frac{70{,}000}{45.62 - 4.23(I_d/I)} - 460$$

$$I_d = \frac{3^3 \times 96}{12} = 216 \text{ in.}^4$$

$$T = \frac{70{,}000}{45.62 - 4.23(216/204)} - 460 = 1{,}240°\text{F}$$

Table 4-9.9 ***Critical Stress Equations[21]***

Design Basics	Critical Yield Stress
Elastic design	$\frac{\sigma_{YT}}{\sigma_Y} = \frac{1}{F_e} \ \frac{Z_e}{Z_p}$
Plastic design	$\frac{\sigma_{YT}}{\sigma_Y} = \frac{1}{F_p}$

where

σ_{YT} = critical yield stress at elevated temperature, T
σ_Y = yield stress at ordinary room temperature
F_e = factor of safety, elastic design
F_p = factor of safety, plastic design
Z_e = elastic section modulus
Z_p = plastic section modulus

Columns. Lie and Stanzak calculated a critical temperature of 941°F (505°C) for slender, axially loaded columns.[30] The calculation was based on the temperature for the onset of elastic buckling for columns under maximum permissible applied stress conditions.

The Euler buckling stress at which elastic buckling is imminent is given by

$$\sigma_{cr} = \frac{\pi^2 E_T}{\lambda^2} \tag{6}$$

where

σ_{cr} = Euler buckling stress (MPa) (psi)
E_T = modulus of elasticity at temperature T (MPa) (psi)
λ = slenderness ratio = Kl/r
r = radius of gyration (ft)(m)
Kl = effective length of column (ft)(m)

Included in the ECCS guide[59] are dimensionless buckling curves for steel columns at elevated temperatures. These curves are presented in Figure 4-9.28.

Table 4-9.10 ***Critical Temperature of Steel Beams[37]***

			factor $\frac{kq^*}{q_e}$ resp. $\frac{kq^*}{q_p}$				
		Static System	0.3	0.4	0.5	0.6	0.7
Base of structural design at room temperature	Theory of plasticity	Statically determinate Statically indeterminate	585	540	490	430	360
	Theory of elasticity	Statically determinate	605	565	525	475	425
		Statically indeterminate					
		Θ = 1.33 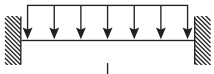	640	605	575	545	510
		Θ = 1.0 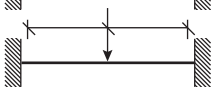	605	565	525	475	425
		Θ = 1.47 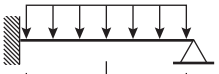	650	615	590	560	535
		Θ = 1.12 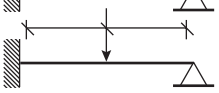	615	580	545	505	465
		Θ = 1.47 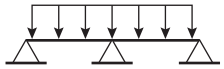	650	615	590	560	535

q_p = Ultimate plastic load
q^* = Applied load
k = Load multiplier
Θ = Factor addressing plastic reserve of beam from redistribution of moments.

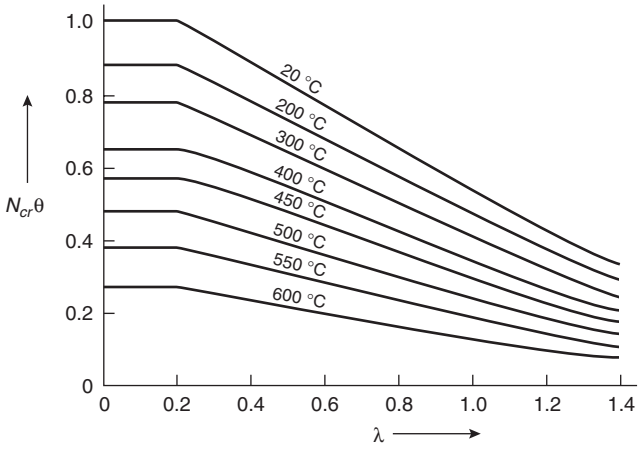

Figure 4-9.28. ***Dimensionless buckling curves for steel columns.[59]***

Equation 6 is only valid for columns that buckle in the elastic range. Generally, slender columns having a slenderness ratio in excess of approximately 90 can be expected to buckle elastically. Buckling stresses for stout columns (slenderness ratio less than 90) are in the plastic range, requiring a more complex analysis. The failure mode for columns with a slenderness ratio between 80 and 100 cannot be reliably predicted.[60] The tangent modulus can be used instead of the modulus of elasticity in Equation 6 for stout columns. However, predictions of the critical temperature using Equation 6 may not be accurate, due to residual stresses from the steel fabrication process.[60] Thus, for stout columns, a conservative estimate for the critical temperature of steel columns may be obtained by determining the temperature at which the yield stress is equal to the applied stress.

General

Malhotra has observed that critical temperatures determined from the structural analysis algebraic equations will be somewhat low when compared to experimental data.[21] Thus, the following correction factors, V, are suggested by Malhotra to improve the prediction capabilities of the approach:

1. Columns: $V = 0.85$
2. Statically determinate beams: $V = 0.77 + 0.15\,\frac{P_s}{P_u}$
3. Statically indeterminate beams: $V = 0.25 + 0.77\,\frac{P_s}{P_u}$

where

P_s = service (applied) load (N or N/m) (lb or lb/ft)
P_u = load to induce ultimate stress at midspan (N or N/m) (lb or lb/ft)

EXAMPLE 6:

Determine if the following steel column is expected to buckle if it achieves an average temperature of 1100°F (593°C). The column is simply supported, 15 ft (4.6 m) long and has an applied load of 12,000 psi (82.8 MPa). Assume the yield stress is 36,000 psi (248.4 MPa) and the modulus of elasticity is 30,000,000 psi. The characteristics of the column are

$A = 8.23$ in.^{2} (5310 mm^2)
$I = 21.6$ in.^{4} (8.99×10^6 mm^2)
$Kl = 180$ in. (4572 mm)

At 1100°F (593°C):

$$E_T = 1 + \frac{T}{2000 \ln (T/1100)}$$
$$E_o = 15.6 \times 10^6$$

SOLUTION:

Calculate the slenderness ratio to determine the failure mode.

$$\lambda = \frac{Kl}{r} = 110$$

Since the slenderness ratio exceeds 90, the column is susceptible to buckling. The buckling stress at 1100°F (595°C) is 12,700 psi (87.6 MPa). Thus, the column does not buckle due to the applied load and elevated temperature.

Critical Stress

Columns: Sample expressions for determining the critical stress for steel columns[30] are noted below.

$$P_{cr}^2 - P_{cr}\left[\sigma_{yT} + \pi^2 E_T\left(4.8 \times 10^{-5} + \frac{1}{\lambda^2}\right)\right] + \sigma_{yT} A \frac{\pi^2 E_t}{\lambda^2} = 0$$

where

P_{cr} = critical point load (N) (lb)
σ_{yT} = yield stress at temperature T (Pa) (psi)
E_T = modulus of elasticity at temperature T (Pa) (psi)
$\lambda = Kl/r$

In order to improve the prediction capabilities of the critical stress approach for slender columns, the modulus of elasticity should be replaced by the reduced modulus of elasticity.[15] The reduced modulus is defined as

$$E_r = \frac{4EE_T}{(\sqrt{E} + \sqrt{E_t})^2}$$

where

E_t = tangent modulus

In addition, the 0.2 percent proof stress may be replaced by the 0.5 percent proof stress in the yield stress parameter.[61]

Results of a buckling analysis on concrete-filled square hollow sections are provided in Figure 4-9.29.

Beams: The expressions for the critical loads for beams assume at failure that the beam is in a state of full plasticity at the location of the maximum moment.[61] Obviously, in order to calculate the critical stress, the material property–temperature relationships must be known.

The critical distributed load for a simply supported beam is[55]

$$q_{cr} = \frac{8\sigma_{yT} Z_P}{L^2}$$

where

q_{cr} = critical distributed load (N/m) (lb/ft)
Z_P = plastic section modulus (m^3) (in.^{3})
L = span of beam (m) (ft)
σ_{yT} = yield stress at elevated temperature (MPa) (psi)

Considering a cantilever beam with a point load applied one-third of the span from the fixed end, plastic hinges can be expected at the point of load application and at the fixed end. The critical load can be determined by

$$p_{cr} \frac{7.5\sigma_{yT} Z}{L}$$

The above equations in this section do not account for creep strain. Based on an analysis of the deflection history of heated, loaded beams, Pettersson et al. include a load ratio, β, to determine the critical distributed stress.[35]

$$q_{cr} = \beta \frac{8\sigma_{yT} Z}{L^2}$$

where the yield stress is evaluated at ordinary room temperature, relaxing the need to know the yield stress–temperature relations. β is defined as the ratio of the load causing a maximum allowable deflection under fire conditions to the load inducing stresses equal to the yield stress at ordinary room temperature. Thus, the parameter β takes into account the dependence of both the yield stress and creep on temperature. Graphs of β are available for a variety of thermal restraint and structural end conditions.

The Eurocodes include a method of analysis using algebraic equations to consider the moment capacity of steel beams which have a temperature gradient through the depth of the beam.[9] The method involves dividing the beam into small isothermal sections and treating these isothermal sections as a composite beam (see Figure 4-9.30). In this case, the moment capacity of the beam is given as

$$M_{cap} = \sum_{i=1}^{n} \sigma_i A_i z_i$$

where

M_{cap} = moment capacity (N·m) (lb·ft)
σ_i = applied stress in isothermal element (Pa) (psi)
A_i = area of isothermal element (m^2) (ft^2)
z_i = distance from neutral axis to centroid of isothermal element (m) (ft)

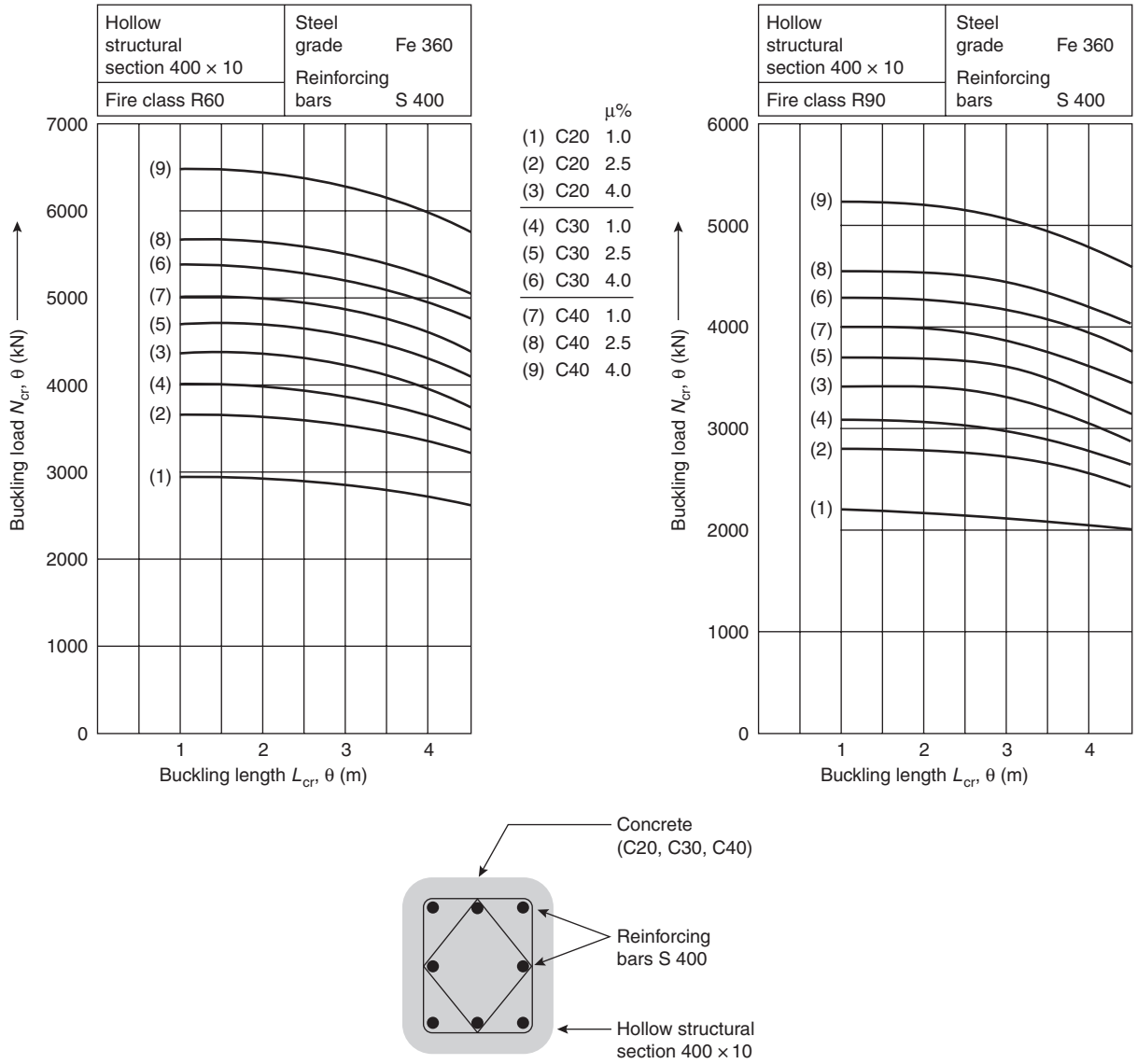

Figure 4-9.29. ***Design graphs for ISO fire resistance requirements R60 and R90. For the concrete-filled square hollow structural section 400 × 10, the axial buckling load is a function of the buckling length, of the concrete quality, and of the percentage μ of reinforcement; this design diagram is based on a simple calculation model.[8]***

Computer Programs

Several finite element computer models are available to assess the structural response of fire-exposed structural members or frames. Sullivan et al. indicate that most of the existing finite element models used for structural fire protection analyses were developed originally for research applications.[62]

FASBUS-II is an example of a finite element model developed in the United States to evaluate the structural response of complex building assemblies such as floor assemblies consisting of a two-way concrete slab, steel deck, and steel beam.[63] Input for FASBUS-II includes the temperature distribution, temperature-dependent mechanical properties, geometry, end conditions, and loading. The output of FASBUS-II includes deflections, rotations,

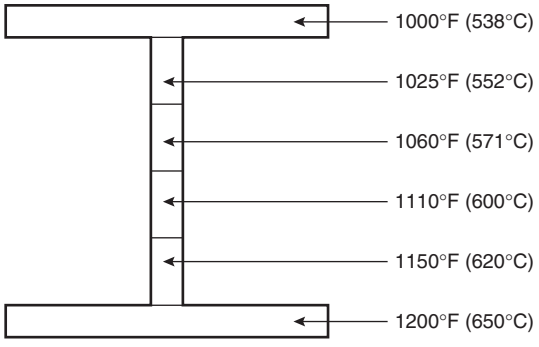

Figure 4-9.30. ***Isothermal sections of beam.***

and stresses in the components of the assembly, which then need to be compared to performance limits.

Sullivan et al. and Franssen et al. provide extensive reviews and comparisons of existing finite element models for structural fire protection applications.[62,64] According to Sullivan et al. all of the models make the following assumptions:

- Plane sections remain plane (Navier-Bernoulli hypothesis).
- Perfect composite action is assumed for steel-concrete assemblies, disregarding any slippage between the steel and concrete.
- Torsion is disregarded.
- Moisture effects are disregarded.
- Large displacements are not accurately modeled.

Traditionally, analysis of the response of the structure exposed to fire has been limited to an analysis of the response of single members. However, in structural frames comprising many members, load transfer or membrane action may occur to permit the steel member to maintain its integrity, despite achieving a temperature in excess of that typically associated with failure.

Load transfer allows stronger members to support additional loads not capable of being carried by heated, weak members. In order to capture this phenomenon, a frame analysis is required.[44] Numerous software packages are available to conduct the frame analysis. Results of a frame analysis are presented in Figures 4-9.31 and 4-9.32.

The frame analyses range from algebraic-equation-based methods to finite element analyses. Pettersson et al.

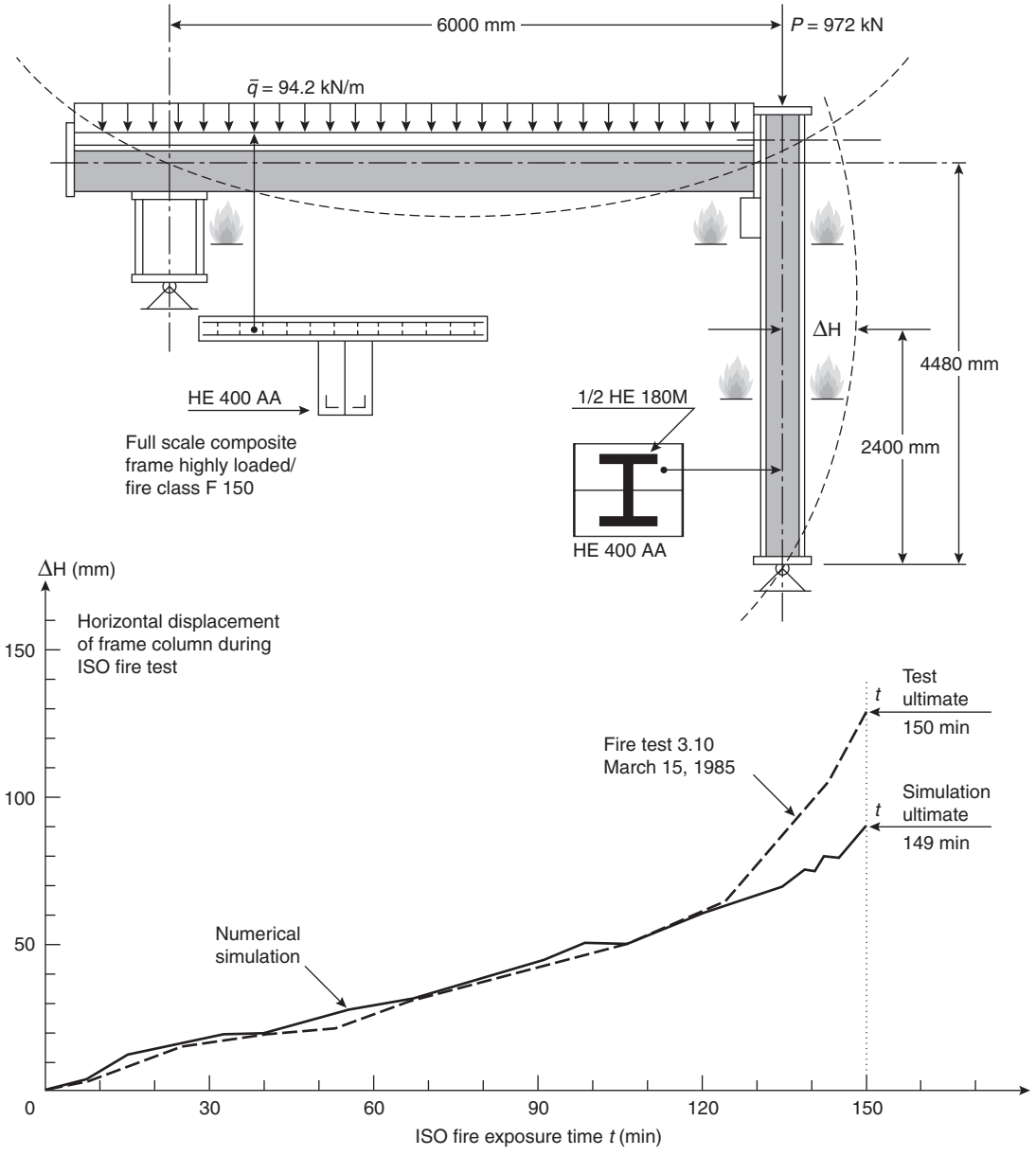

Figure 4-9.31. ***Deformations measured and calculated by a numerical model for a composite frame.[8]***

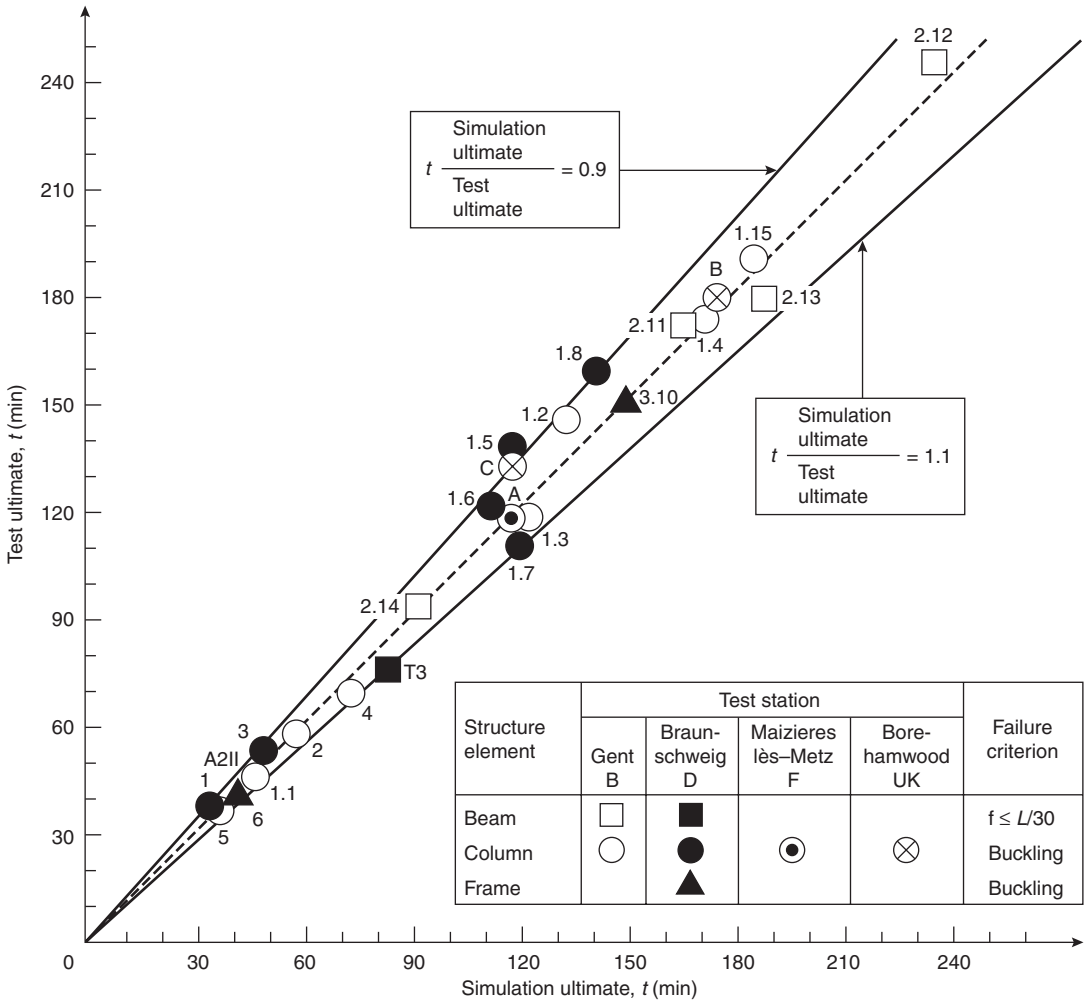

Figure 4-9.32. ***Fire resistance times measured and calculated by a numerical model for columns, beams, or frames of any cross section types (bare steel, protected steel, composite).[6]***

include a frame analysis via algebraic equations used to determine displacement.[35] The frames consist of beams supported by one or two columns at mid-span. The analysis assumes that each beam or column has a uniform temperature (though the temperature of the beam is not required to be that of a column). A pinned connection between the structural members is assumed. The analysis considers the compatibility of the deformation of each member by requiring that the change in length of the column is equal to the beam deflection at the point of contact.

Schleich et al. describe the application of CEFICOSS for a frame analysis.[65,66] The frame consists of a single beam and column, where one end of the column is connected to an end of the beam. Reasonable agreement is indicated between predicted and measured results.

El-Rimavi et al. describe the application of another finite element model, NARR2, for the evaluation of a large building frame involving numerous beams and columns.[67] The large frame is divided into several subframes for computational ease. Good agreement is noted between predictions of deflections and force resultants obtained involving simulations of the full building frame and subframes. Slightly greater failure temperatures were determined for semi-rigid connections as compared to rigid connections.

Nomenclature

a characteristic dimension
A cross-section area of steel tube, steel column
A_s cross-section area of steel column
b characteristic dimension
b_f width of flange
c characteristic dimension
c_c specific heat of concrete
c_i specific heat of protection material
c_s specific heat of steel
C_1 constant

C_2 constant
d outer diameter of steel pipe
d depth of section
D heated perimeter of steel section
E_0 modulus of elasticity at ambient temperature
E_r reduced modulus
E_t tangent modulus
E_T modulus of elasticity at temperature T
F factor of safety
F_e factor of safety, elastic design
F_p factor of safety, plastic design
Fo Fourier number
h thickness of protection material
H thermal capacity of steel section at ambient temperature
k thermal conductivity of steel
k_c thermal conductivity of concrete
k_i thermal conductivity of protection material
K end condition factor
l unsupported length of column
L inside dimension of one side of square concrete box protection
L span of beam
m moisture concrete of concrete
N ratio of thermal capacity of protection material to that of steel
P perimeter of steel tube
P_{cr} critical point load
P_s service (applied) load
P_u ultimate load
q_{cr} critical distributed load
r radius of gyration
R fire resistance
R_0 fire resistance with zero moisture content of concrete
t wall thickness of steel pipe
t time
t_w width of web
Δt time step
T steel temperature
T_f fire temperature
T_m mean fire temperature
T_0 ambient temperature
T_s steel temperature
ΔT_s change in steel temperature
V correction factor
W weight of steel section per unit length
Z_e elastic section modulus
Z_P plastic section modulus

Greek

α thermal diffusivity (when used with Fourier number)
α heat transfer coefficient
α_c convective heat transfer coefficient
α_r radiative heat transfer coefficient
α_T coefficient of thermal expansion at temperature T
β ratio of distributed load causing maximum allowable deflection to distributed load inducing yielding
ε_f fire emissivity
λ slenderness ratio
θ dimensionless temperature
ρ density
ρ_i density of insulation material
σ_{cr} critical stress for buckling
σ_{y0} yield strength at ambient temperature
σ_{yT} yield strength at temperature T

References Cited

1. ASTM-119-98, *Standard Test Methods for Fire Tests of Building Construction and Materials,* American Society for Testing and Materials, Philadelphia (1998).
2. L.G. Seigel, "Fire Test of an Exterior Exposed Steel Spandrel," *Mtls. Res. and Standards,* 10, 2, pp. 10–13 (1970).
3. *Fire Resistance Directory,* Underwriters Laboratories, Northbrook, IL (2000).
4. R.W. Bletzacker, *Effect of Structural Restraint on the Fire Resistance of Protected Steel Beam Floor and Roof Assemblies,* Ohio State University, Columbus, OH (1966).
5. NFPA 251, *Standard Methods of Fire Tests of Building Construction and Materials,* National Fire Protection Association, Quincy, MA (1999).
6. *UL 263, Fire Tests of Building Construction and Materials,* Underwriters Laboratories, Northbrook, IL (1997).
7. T.T. Lie (ed.), *Structural Fire Protection,* American Society of Civil Engineers, New York (1992).
8. *International Fire Engineering Design for Steel Structures: State of the Art,* International Iron and Steel Institute, Brussels, Belgium (1993).
9. *Design of Steel Structures—Part 1–2, General Rules—Structural Fire Design, CEN,* Eurocode 3, Brussels (1995).
10. ASCE/SFPE 29, *Standard Calculation Methods for Structural Fire Protection,* American Society of Civil Engineers (1999).
11. D. Boring, J. Spence, and W. Wells, *Fire Protection through Modern Building Codes,* American Iron and Steel Institute, Washington, DC (1981).
12. D.C. Jeanes, *Technical Report 84-1,* Society of Fire Protection Engineers, Boston (1984).
13. T.Z. Harmathy, *NRCC 20956 (DBR Paper No. 1080),* National Research Council of Canada, Ottawa (1983).
14. M.S. Abrams, *ASTM STP 685,* American Society for Testing and Materials, Philadelphia (1979).
15. T.T. Lie, *Fire and Buildings,* Applied Science, London (1972).
16. *Specification for the Design, Fabrication, and Erection of Structural Steel for Buildings,* American Institute of Steel Construction, New York (1978).
17. T.T. Lie and W.W. Stanzak, "Empirical Method for Calculating Fire Resistance of Protected Steel Columns, *Eng. J.,* 57, 5/6, pp. 73–80 (1974).
18. D.R. Boring, *An Analytical Evaluation of the Structural Response of Simply Supported, Thermally Unrestrained Structural Steel Beams Exposed to the Standard Fire Endurance Test,* master's thesis, Ohio State University, Columbus, OH (1970).

19. R.A. Lindberg, *Processes and Materials of Manufacture,* Allyn and Bacon, Boston (1978).
20. D.C. Jeanes, *Methods of Calculating Fire Resistance of Steel Structures,* Engineering Applications of Fire Technology Workshop, SFPE, Boston (1980).
21. H.L. Malhotra, *Design of Fire-Resisting Structures,* Chapman and Hall, New York (1982).
22. T.Z. Harmathy, "A Comprehensive Creep Model," *ASME J. of Basic Eng.,* 89, pp. 496–502 (1967).
23. T.Z. Harmathy, *ASTM STP 422,* American Society for Testing and Materials, Philadelphia (1967).
24. *Fire Resistant Steel Frame Construction,* American Iron and Steel Institute, Washington, DC (1974).
25. *Designing Fire Protection for Steel Columns,* American Iron and Steel Institute, Washington, DC (1980).
26. W.W. Stanzak and T.T. Lie, *Fire Tests on Protected Steel Columns with Different Cross-Sections,* National Research Council of Canada, Ottawa (1973).
27. PABCO, *Pabco Super Firetemp Fireproofing Board Fire Protection Guide,* Ruston, LA (1984).
28. L.G. Seigel, "Designing for Fire Safety with Exposed Steel," *Fire Tech.,* 6, 4, pp. 269–278 (1970).
29. Standard Building Code Congress, *Southern Standard Building Code,* SSBC, Birmingham, AL (1985).
30. T.T. Lie and W.W. Stanzak, "Fire Resistance of Protected Steel Columns," *Eng. J. Amer. Inst. Steel Const.,* 10, pp. 82–94 (1973).
31. *Designing Fire Protection for Steel Beams,* American Iron and Steel Institute, Washington, DC (1985).
32. *Load and Resistance Factor Design Specification for Structural Steel Buildings,* American Institute of Steel Construction, New York (1993).
33. *Designing Fire Protection for Steel Trusses,* American Iron and Steel Institute, Washington, DC (1980).
34. *Fire Resistance Design Manual,* Gypsum Association, Evanston, IL (1984).
35. O. Pettersson, S. Magnusson, and J. Thor, *Bulletin 52,* Lund Institute of Technology, Lund, Sweden (1976).
36. G. S. Berger, *Estimating the Temperature Response of Wide Flange Steel Columns in the ASTM E119 Test,* Department of Fire Protection Engineering, University of Maryland, College Park (unpublished) (1987).
37. J.A. Milke, "A Simplified Model for Estimating the Thermal Response of Steel Beam/Concrete Slab Ceiling Assemblies," in *ICFRE2,* SFPE, Bethesda, MD (1997).
38. W.W. Stanzak and T.Z. Harmathy, "Effect of Deck on Failure Temperature of Steel Beams," *Fire Tech.,* 4, 4, pp. 265–270 (1968).
39. I.A. Smith and C. Stirland, "Analytical Methods and Design of Fire Safe Steel Structures," in *International Seminar on Three Decades of Structural Fire Safety,* Borehamwood, UK (1983).
40. *Fire-Safe Structural Steel, A Design Guide,* American Iron and Steel Institute, Washington, DC (1979).
41. M. Law, "Prediction of Fire Resistance," *AISC Eng. J.,* pp. 16–29 (1978).
42. G.V.L. Bond, *Fire and Steel Construction—Water Cooled Hollow Columns,* Constrado (1974).
43. T.T. Lie and T.Z. Harmathy, *Fire Study No. 28,* National Research Council of Canada, Ottawa (1972).
44. W.L. Gamble, "Predicting Protected Steel Member Fire Endurance Using Spreadsheet Programs," *Fire Technology,* 25, 3, pp. 256–273 (1989).
45. O.C. Zienkewicz, *The Finite Element Method,* McGraw-Hill, New York (1983).
46. M. Paulsson, *TASEF-2,* Lund Institute of Technology, Lund, Sweden (1983).
47. R.H. Iding, Z. Nizamuddin, and B. Bresler, *UCB FRD 77-15,* University of California, Berkeley (1977).
48. A. Anderberg, *PC-TEMPCALC,* Institutet for Brandtekniska, Fragor, Sweden (1985).
49. J.A. Milke, "Estimating Fire Resistance of Tubular Steel Columns," in *Proceedings of Symposium on Hollow Structural Sections in Building Construction,* ASCE, Chicago (1985).
50. K. Bardell, *ASTM STP 826,* American Society for Testing and Materials, Philadelphia (1983).
51. D. Gross, *NBSIR 85–3223,* National Bureau of Standards, Gaithersburg, MD (1985).
52. R. Stubblefield and M.L. Edwards, *NODES-T3: Making FIRES-T3 a Little Easier,* Department of Fire Protection Engineering, University of Maryland, College Park, MD (unpublished) (1991).
53. D.V. Tomecek and J.A. Milke, "A Study of the Effect of Partial Loss of Protection on the Fire Resistance of Steel Columns," *Fire Technology,* 29, 1, pp. 3–21 (1993).
54. A.F. Robertson and J.V. Ryan, "Proposed Criteria for Defining Load Failure of Beams, Floors, and Roof Constructions during Fire Tests," *J. of Res.,* 63C, 2, pp. 121–124 (1959).
55. S. Vinnkota, *Calculation of the Fire Resistance of Structural Steel Members,* ASCE, p. 105 (1979).
56. ECCS, *Fire Resistance of Steel Structures,* ECCS 89, Brussels, Belgium (1995).
57. B.R. Kirby and D.E. Wainman, *The Behaviour of Structural Steelwork in Natural Fires,* British Steel PLC., Rotherham, England (1997).
58. J. Kruppa, "Collapse Temperature of Steel Structures," *J. of Struc. Div.,* 105, pp. 1769–1788 (1979).
59. European Convention for Constructional Steelwork, Technical Committee 3, *European Recommendations for the Fire Safety of Steel Structures,* Elsevier, Amsterdam (1983).
60. A. Chajes, *Principles of Structural Stability Theory,* Prentice-Hall, Englewood Cliffs, NJ (1974).
61. T.T. Lie and W.W. Stanzak, "Structural Steel and Fire: More Realistic Analyses," *AISC Eng. J.,* 13, 2, pp. 35–42 (1976).
62. P.J.E. Sullivan, M.J. Terro, and W.A. Morris, "Critical Review of Fire Dedicated Thermal and Structural Computer Programs," *J. of Applied Fire Science,* 3, 2, pp. 113–135 (1994).
63. D.C. Jeanes, *F. Safety J.,* 9, 1 (1985)
64. J-M. Franssen, J-B. Schleich, L-G Cajot, D. Talamona, B. Zhao, L. Twilt, and K. Both, "A Comparison Between Five Structural Fire Codes Applied to Steel Elements," in *Proceedings of Fourth International Symposium of Fire Safety Science,* International Association of Fire Safety Science, Ottawa, Canada, pp. 1125–1136 (1994).
65. J.M. Frannsen, *Étude du Comportement au Feu des Structures Mixtes Ancier—Béton (CEFICOSS), A Study of the Behaviour of Composite Steel-Concrete Structures in Fire,* Doctoral Dissertation, Université de Liège, Belgium (1987).
66. J.B. Schleich, J.C. Dotreppe, and J.M. Franssen, "Numerical Simulations of Fire Resistance Tests on Steel and Composite Structural Elements on Frames," in *Proceedings of First International Symposium of Fire Safety Science,* Hemisphere Publishing, Gaithersburg, MD, p. 311 (1986).
67. J.A. El-Rimawi, I.W. Burgess, and R.J. Plank, "Model Studies of Composite Building Frame Behaviour in Fire," in *Proceedings of Fourth International Symposium of Fire Safety Science,* International Association of Fire Safety Science, Ottawa, Canada, pp. 1137–1148 (1994).

CHAPTER 10

Analytical Methods for Determining Fire Resistance of Concrete Members

Charles Fleischmann and Andy Buchanan

Introduction

Concrete structures have a reputation for good behavior in fires. Many reinforced concrete buildings, which have experienced severe fires, have been repaired and put back into use. Concrete is noncombustible and has a low thermal conductivity. Concrete tends to remain in place during a fire, protecting the reinforcing steel, with the cool inner core continuing to carry the load. Catastrophic failures of reinforced concrete structures in fires are rare, but some occasionally occur.[1]

Analytical methods developed to predict the fire resistance of structural assemblies can be divided into two groups: (1) standard and (2) nonstandard fire exposure. For the case of the standard fire exposure, a large database exists from referenced standard tests. The analytical methods use empirically based correlations and minimum dimensions to determine the fire resistance. For nonstandard fire exposure, the analysis is more complicated, requiring both heat transfer and structural analyses. Analytical methods are an alternative to conventional methods that require destructive testing of exemplar systems in accordance with standard testing procedures, for example, ASTM E119 or ISO 834.

Fire resistance calculations typically use the same acceptance criteria specified in standard test methods, that is, heat transmission and structural integrity. The analysis can be broadly divided into two parts: (1) heat transfer and (2) structural analysis. Heat transfer calculations are used to evaluate the unexposed surface temperature and the temperature distribution throughout the member, in order to evaluate material strength. The structural integrity analysis applies the strength theory[2] used to design reinforced concrete members. The reduced strength of the concrete and steel resulting from elevated temperature is taken into account by using experimental results for the compressive and yield strengths as a function of temperature. This procedure is known as the rational design method.

As the fire protection field advances into performance-based engineering, techniques like the rational design method are more likely to be used. In the rational design approach, a design time-temperature curve, based on the expected fire, is specified. The engineer then performs the heat transfer analysis to determine the temperature profile and unexposed surface temperature. Knowing the temperature distribution of the member, a structural analysis is conducted to determine the fire endurance.

This chapter presents an overview of the analytical methods for calculating the fire resistance of concrete structural members and provides a description of the mechanical properties for concrete and steel at elevated temperatures. A brief discussion of heat transfer for a concrete assembly is given, along with temperature profiles from ASTM E119 test results. The structural calculations for simply supported and continuous members are explained. A simple example is shown to further demonstrate the basics of the design concept. Fire resistance for columns and walls is also presented. A more comprehensive discussion of the rational design method can be found elsewhere.[1–5]

Material Properties of Concrete and Steel

Most of the material properties for concrete and steel change significantly at elevated temperatures. In order to accurately predict the structural fire endurance of concrete members, these changes must be taken into account. Temperature-dependent values of strength, modulus of elasticity, and thermal expansion have been presented in a graphical format to aid in the design process. The thermophysical properties required for a heat transfer analysis, that is, thermal conductivity and specific heat, also change

Charles Fleischmann is a senior lecturer in the Department of Civil Engineering, University of Canterbury, in Christchurch, New Zealand.

Andy Buchanan is an associate professor in the Department of Civil Engineering, University of Canterbury, in Christchurch, New Zealand.

significantly. The thermophysical properties have been investigated at elevated temperatures by Harmathy and others.[6–10]

Strength

The strength of the reinforcing steel changes significantly with temperature, and must be taken into account in any structural calculation. Figure 4-10.1 shows the strength-temperature relationship for hot-rolled, cold-drawn, and high-strength alloy steels. Yield strength versus temperature relationship is given for hot-rolled steel, used for reinforcing bars. Tensile strength versus temperature relationship is shown for the cold-drawn steel and high-strength alloy steel, used for prestressing bars, wire, or strands. The change from yield strength to tensile strength for the two steel types relates to the design parameters used for reinforced versus prestressed concrete assemblies.

Like steel, the strength of concrete is also diminished at elevated temperatures. Figure 4-10.2 shows the strength-temperature relationship for carbonate, siliceous, and sand-lightweight aggregate concretes. The compressive strength is not only a function of temperature but is also affected by the applied load.

The results shown in Figure 4-10.2 were obtained from specimens loaded to 40 percent of their compressive strength during the heating process. Once the test temperature of interest was reached, the specimens were loaded to failure. Figure 4-10.2 illustrates that the compressive strength of concrete remains relatively unchanged up to 500°C (900°F). Above 500°C (900°F), the compressive strength of the siliceous aggregate concrete starts to decrease rapidly and is considered ineffective at temperatures above 650°C (1200°F), where the compressive strength has been reduced by approximately 50 percent of the value at normal temperatures. However, for carbonate and lightweight aggregates, compressive strength remains relatively unchanged up to 650°C (1200°F) and is not considered to be ineffective until it reaches a temperature of 650°C (1400°F). The experimental method used may influence the reported compressive strength. Specimens heated without compressive loads and then loaded to failure while hot have lower compressive strengths than those heated while loaded.[4]

Modulus of Elasticity

The modulus of elasticity for steel decreases as the temperature increases, as shown in Figure 4-10.3. Figure 4-10.4 shows the modulus of elasticity-temperature curve for three different concrete aggregates. In each case, the modulus of elasticity of concrete is greatly reduced at elevated temperatures. This large reduction of the elastic modulus is helpful in reducing induced thermal stresses in concrete members due to fire.[4]

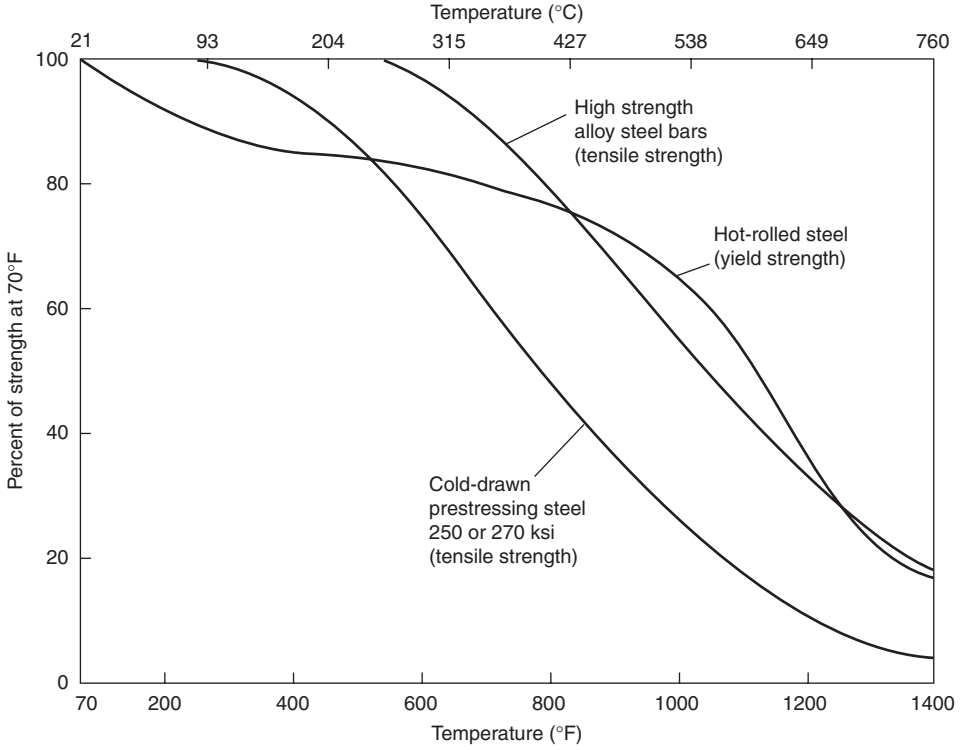

Figure 4-10.1. ***Strength-temperature relationships for hot-rolled, cold-drawn, and high-strength alloy steels.[10–12]***

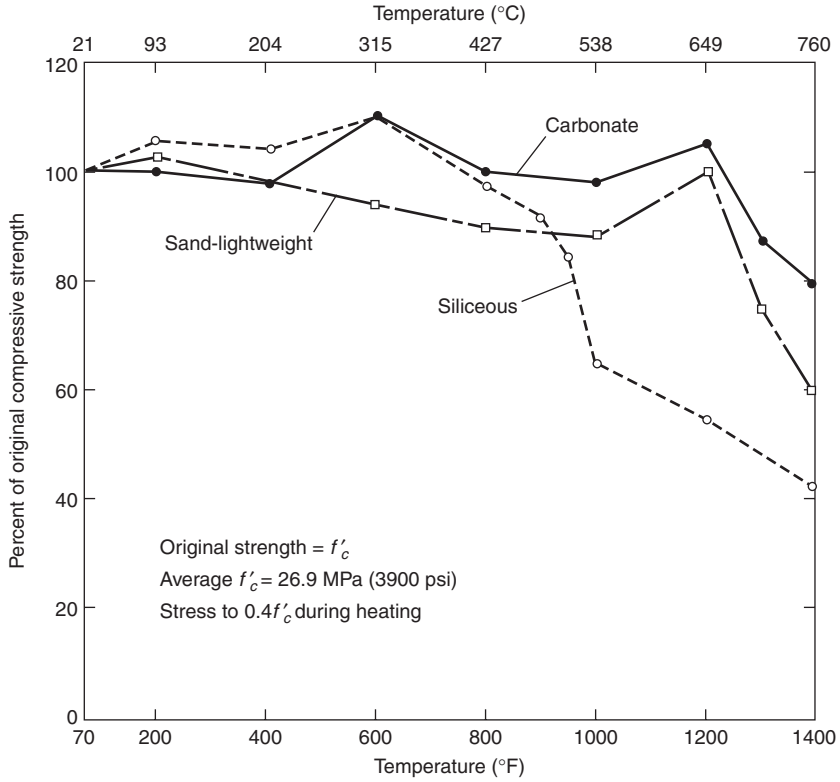

Figure 4-10.2. ***Strength-temperature relationships for carbonate, siliceous, and sand-lightweight aggregate concretes.[13]***

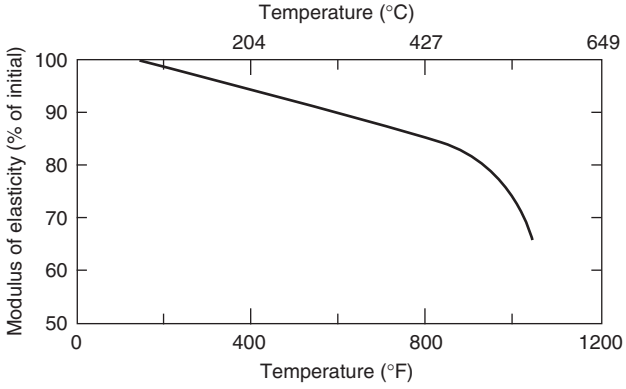

Figure 4-10.3. ***Modulus of elasticity for hot-rolled steel at elevated temperatures.[14]***

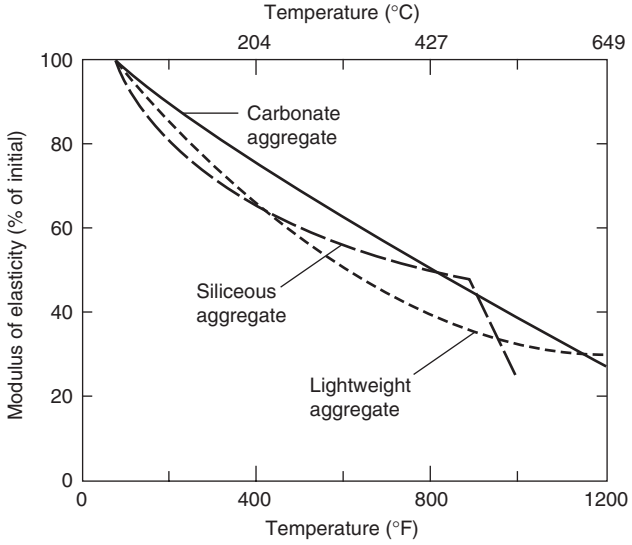

Figure 4-10.4. ***Modulus of elasticity, at elevated temperatures, for carbonate, siliceous, and lightweight concretes.[15]***

Thermal Expansion

Both concrete and steel expand when heated. This thermal expansion can actually increase the fire resistance. The effects of thermal expansion are discussed later in this chapter. Figure 4-10.5 shows the coefficient of thermal expansion for concrete and steel. The values for the steel were calculated using the following equation taken from the *Manual of Steel Construction:*[16]

$$\alpha_C = (11.0 + 0.0062\theta_C) \times 10^{-6}$$
$$\alpha_F = (6.1 + 0.0019\theta_F) \times 10^{-6} \quad (1)$$

where

α = coefficient of thermal expansion (in/in °F) ($\Delta l / l$ °C)
θ_C = temperature (°C)
θ_F = temp

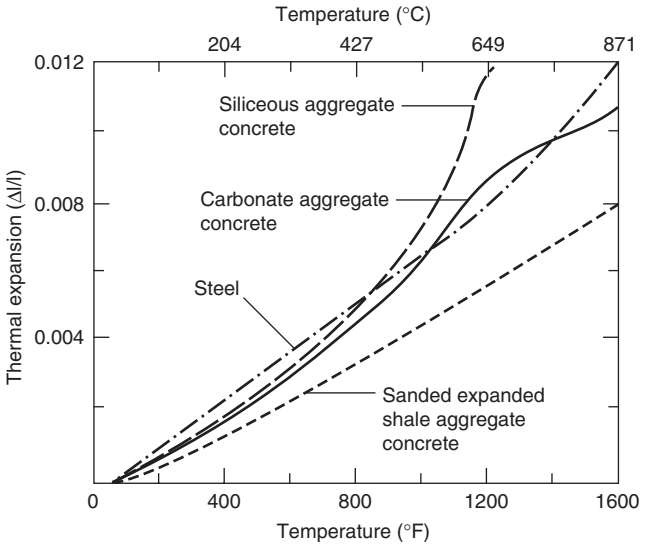

Figure 4-10.5. ***Thermal expansion of concrete and steel at elevated temperatures.[4]***

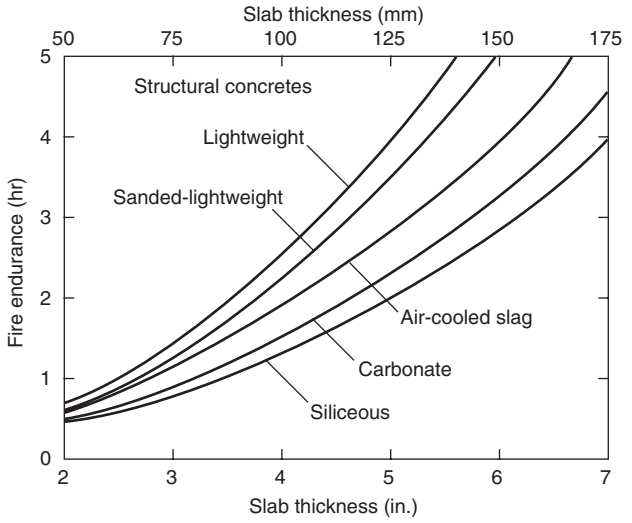

Figure 4-10.6. ***Fire endurance of concrete slabs—effect of thickness and type of aggregate, based on heat transmission.[4]***

Heat Transmission

The temperature of the unexposed side of concrete floors, roofs, and walls are usually limited to prevent ignition of combustibles in contact with the unexposed surface. In ASTM E119 the criteria are 121°C (250°F) average and 163°C (325°F) single-point temperatures. These criteria often govern the fire resistance of the assembly. In addition to the unexposed surface temperature, the temperature distribution throughout the member is required in order to evaluate the material strengths in the structural calculations.

The temperature distribution within concrete slabs exposed to the ASTM E119 time-temperature curve is illustrated in Figures 4-10.8 through 4-10.10. These data apply to any slab thickness, as long as the slab is at least 25 mm (1 in.) thicker than the point in question.

Heat is mainly transferred through a solid concrete member by conduction. The temperature of the unexposed side of the slab is a function of the slab thickness and the type of aggregate used. The fire endurance versus slab thickness is presented in Figure 4-10.6 for three types of concrete typically used in building construction. The data are based on actual fire tests of concrete slabs.[4] For the normal-weight concretes used in the fire tests, the maximum aggregate size was 20 mm (3/4 in.) and the air content was about 6 percent. The maximum aggregate size for the structural lightweight concretes was slightly less than 20 mm (3/4 in.) and the air content was about 7 percent. Although the slab thickness and type of aggregate are the main factors that affect heat transmission through the concrete, other factors do have some impact. These factors include moisture content, unit weight, air content, and maximum aggregate size. Within the usual range of values, water-cement ratio, strengths, and age have been shown to have insignificant effects on the heat transfer process.[4]

Floor and roof slabs are often composites of materials, for example, a concrete base slab with overlays or undercoatings of either insulating materials or other types of concrete. Research has been conducted on two-course composite assemblies. An example of a composite slab of normal and lightweight concrete is shown in Figure 4-10.7. Similar plots for different composite assemblies can be found in Reference 17.

The temperature on the unexposed side is not the only temperature of concern. The temperature distribution within the member is used to determine the temperature of the reinforcing or prestressing steel. The temperature of the reinforcing bars is approximately equal to the temperature of the concrete at the level of the center of the bar;[4] that is, the presence of the steel is neglected in the heat transfer analysis. Thus, temperature distribution is primarily affected by the type of concrete, shape of the member, and exposure conditions. During fire tests, slabs and walls are typically heated on one side only; beams are heated from one, two, or three sides; and columns are heated on all four sides. Data on the temperature distribution within concrete members are available from results of fire tests. Figures 4-10.8, 4-10.9, and 4-10.10 show the temperatures within a slab exposed to the standard ASTM E119 fire for carbonate, siliceous, and sand-lightweight aggregates, respectively.

The temperature distribution within a 150 × 300 mm (6 × 12 in.) rectangular concrete beam exposed to the ASTM E119 standard time-temperature curve is illustrated in Figure 4-10.11. Because the temperature distribution is a function of the beam size, it is not practical to present a complete set of figures. A procedure has been developed in which the temperature distribution can be constructed.[4] With the advent of fast, affordable computers, such empirical techniques are rapidly being

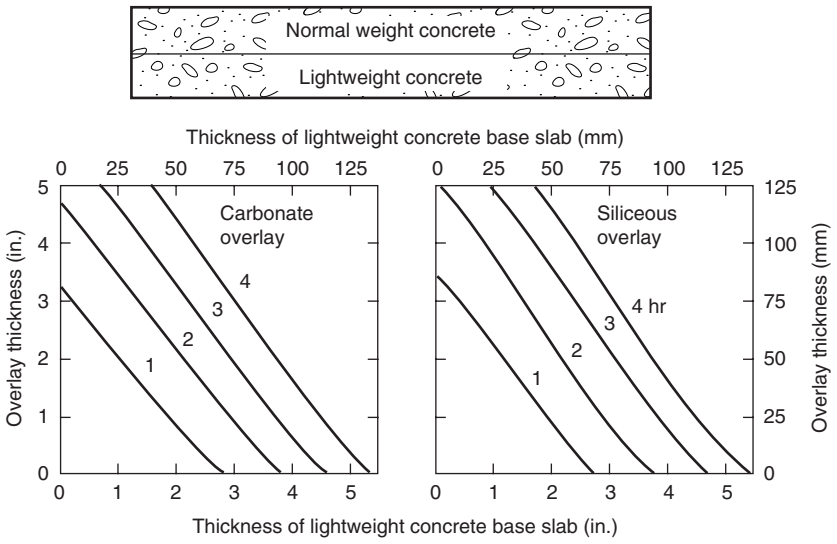

(a) Normal weight concrete overlay on lightweight concrete slab

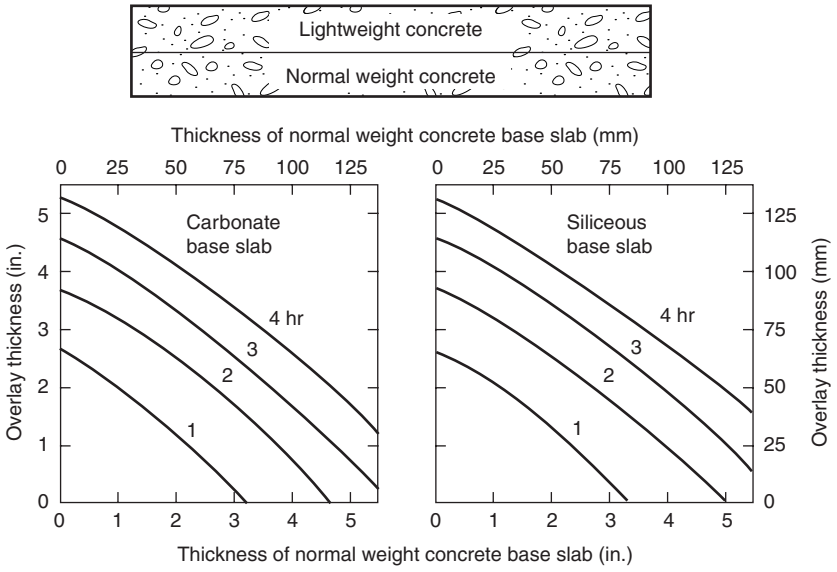

(b) Lightweight concrete overlay on normal weight concrete slab

Figure 4-10.7. ***Fire endurance of base slabs and overlays of normal weight or lightweight concretes, based on heat transmission.[17]***

replaced by complete numerical modeling of the temperature distribution. Computer models such as FIRES T3,[18] TASEF-2,[19] and SAFIR[20] can accurately predict the temperature distribution in various types of concrete members. These models are capable of handling one-, two-, or three-dimensional heat transfer, with time-dependent nonlinear boundary conditions, and temperature dependent thermal properties. None of these models incorporate mass transfer or moisture migration, and thus require modification to the thermal properties to account for latent heat absorption of the water. All three programs use a finite-element technique to solve the energy equation and thus require a skilled operator. Recent improvements to SAFIR include element generation, significantly simplifying the input, and reducing time required. Although these models are not necessary for typical analysis assuming a standard time-temperature curve, with the increased emphasis on performance-based design and more realistic time-temperature curves, the use of such models is likely to increase in the future.

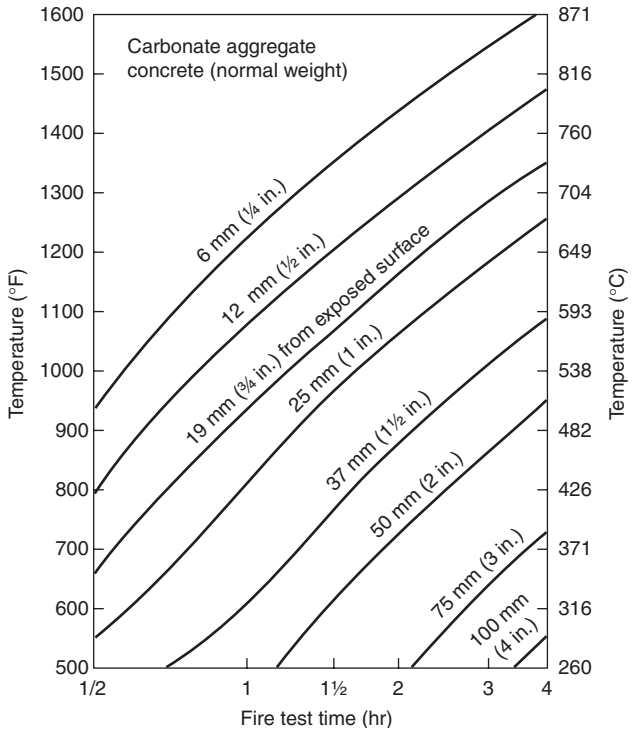

Figure 4-10.8. ***Temperatures within solid or hollow-core concrete slabs during fire tests, carbonate aggregate.[18]***

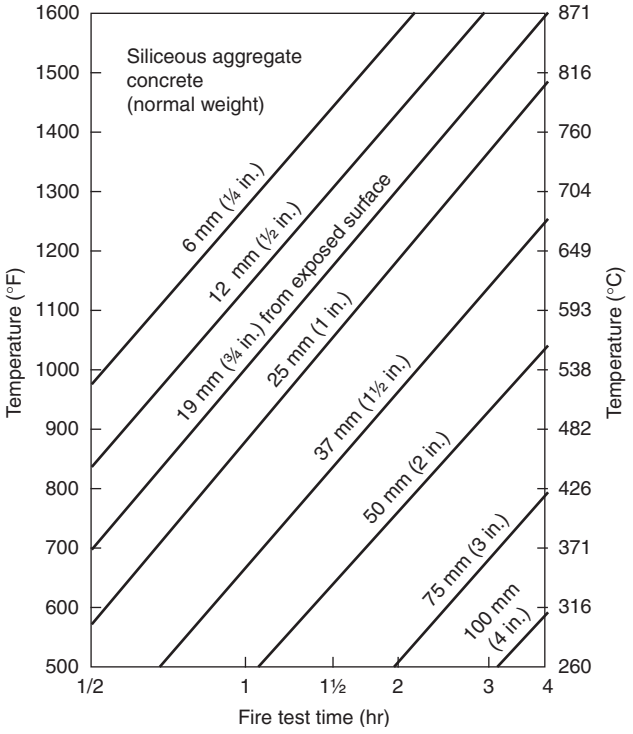

Figure 4-10.9. ***Temperatures within solid or hollow-core concrete slabs during fire tests, siliceous aggregate.[8]***

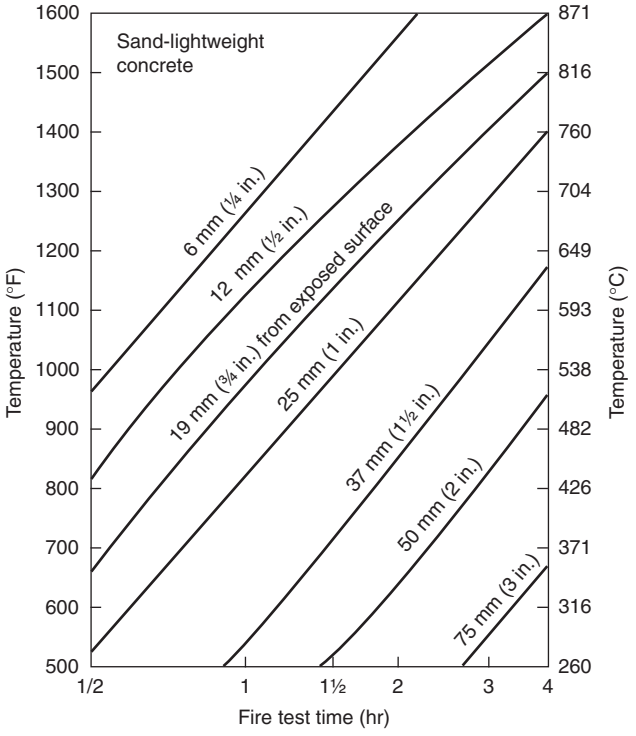

Figure 4-10.10. ***Temperatures within solid or hollow-core slabs during fire tests, sand-lightweight concrete.[18]***

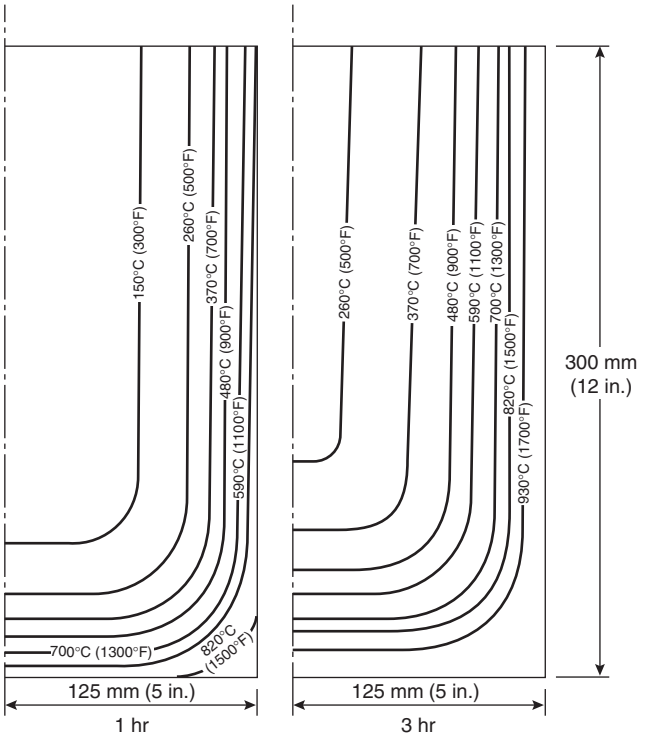

Figure 4-10.11. ***Temperature distribution within a 150- × 300-mm (6- × 12-in.) lightweight concrete beam, 1- and 3-hr exposure time[4]***

Simply Supported Slabs and Beams

Simply supported, unrestrained members are not typically cast in place. However, a discussion of simply supported members will make the discussion of continuous members easier to understand. A simply supported, reinforced concrete slab is illustrated in Figure 4-10.12.

The slab is supported by "frictionless" rollers, so that the slab is free to expand without resistance but should not deflect at the support. The load, w, is evenly distributed over the surface of the slab, and the reinforcing steel runs the entire length of the slab. Considering these conditions without a fire, the moment diagram for the slab is illustrated in Figure 4-10.12(b). The moment strength of the slab will be constant along the entire length:

$$M_n = A_s f_y \left(d - \frac{a}{2}\right) \tag{2}$$

where

A_s = area of the reinforcing steel

f_y = yield stress of the reinforcing steel

d = distance from the extreme compression fiber to the centroid of the reinforcing steel

a = depth of the equivalent rectangular stress block[2]

$$a = \frac{A_s f_y}{0.85 f_c' b} \tag{3}$$

f_c' = compressive strength of the concrete

b = width of the beam or slab

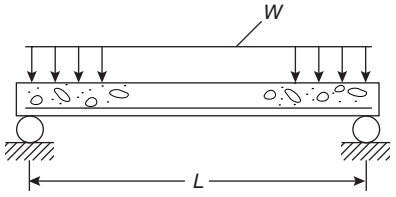

(a) Simply supported one-way slab

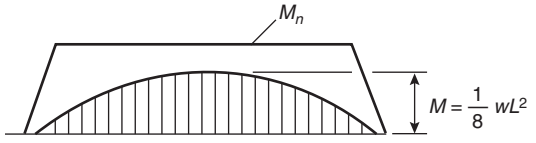

(b) Normal conditions (no fire)

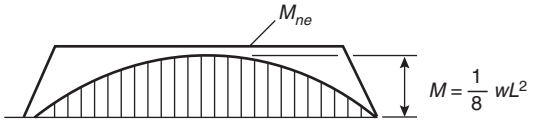

(c) At 2 hr of fire exposure

Figure 4-10.12. ***Applied moments and reduced moment strength diagrams for simply-supported one-way slab.[4]***

During exposure to a fire, the temperature of the reinforcing steel will increase. As the temperature of the steel increases, the yield strength decreases. (See Figure 4-10.12(c).) This reduction in the steel strength causes a reduction of the moment strength of the slab:[4]

$$M_{n\theta} = A_s f_{y\theta} \left(d - \frac{a_\theta}{2}\right) \tag{4}$$

where θ denotes the effects of elevated temperature.

The reduced moment strength diagram is shown in Figure 4-10.12(c).

With a reduction in the yield stress, $f_{y\theta}$, there is a corresponding reduction in the size of the equivalent stress block, a_θ.[4]

$$a_\theta = \frac{A_s f_{y\theta}}{0.85 f_c' b} \tag{5}$$

Typically, the temperature at the top of a slab remains relatively unchanged from normal conditions even after 2 hr of fire exposure, since the concrete is a good insulating medium. (See Figures 4-10.8 through 4-10.10.) Thus, the values for f_c' and d are not affected. However, if the temperatures in the compression zone exceed 480°C (900°F) for a siliceous aggregate or 650°C (1200°F) for a carbonate aggregate, the concrete compressive strength, f_c' should be reduced. (See Figure 4-10.2.)

As previously noted, the compressive strength of concrete is reduced significantly at a critical temperature, selected here as 650°C (1200°F) for a siliceous aggregate or 760°C (1400°F) for a carbonate aggregate. To account for this substantial reduction in strength, regions of concrete in the compression zone at temperatures above the critical temperature are neglected in the design process. As a result, the depth and/or width of the compression zone are reduced by subtracting the area of the concrete, which is heated in excess of the critical temperature.

For a simply supported slab it is unlikely that the compression zone would be heated to above the critical temperature without the steel failing first, but it should be noted that, if the section of concrete is reduced, the value of d in Equation 4 must be adjusted accordingly.

Flexural failure occurs when the moment strength is reduced to the applied service load moment, M, at the center of the span[4]

$$M = \frac{wL^2}{8} \tag{6}$$

where

M = applied service load moment

L = length of the span

w = applied live load plus dead load, with "factor of safety" = 1.0

The factor of safety used in fire endurance calculations is equal to 1.0, which yields the actual applied moment. The factors of safety used in structural design (1.7 live load, 1.4 dead load, etc.) do not apply to fire endurance calculations.[3]

As indicated in Equation 4, the structural fire endurance of a simply supported one-way slab or beam is a function of the load intensity, strength-temperature

characteristics of the reinforcing steel, and the depth of protection given to the reinforcement by the concrete cover. There is no benefit of continuity or restraint of thermal expansion with a simply supported slab, the total slab depth, based on heat transmission, h_t, required to obtain the desired fire rating is probably as small or smaller than the total slab thickness, h_s, required for gravity loads.[4] Therefore, there is no advantage of doing a structural fire endurance analysis for unrestrained, simply supported structural members.[4]

Continuous Unrestrained Flexural Members

Continuous unrestrained members have a considerably longer fire endurance than simply supported members because of their ability to redistribute the applied moments. Figure 4-10.13(a) shows an interior span of a continuous unrestrained slab. The applied moment diagram for a normal condition, with no fire, is shown in Figure 4-10.13(b). The maximum positive moment occurs near the center of the span, and the maximum negative moments are located over the supports.

When the slab is exposed to fire conditions from below, the moments will be redistributed within the slab. This redistribution may be sufficient to cause the negative moment reinforcement to yield. This yielding generally occurs within the first half hour of the fire, based on observation made during standard fire tests.[4] Figure 4-10.13(c) shows the redistribution of moments after 2 hr of fire exposure (2 hr was selected at random). The American Concrete Institute (ACI) warns that increasing the negative reinforcement will increase the attracted negative moment, possibly leading to a compressive failure. It is important that flexural tension governs the design of concrete members. Thus, to avoid compressive failure in the negative moment region, the negative reinforcement should be small enough so that[3]

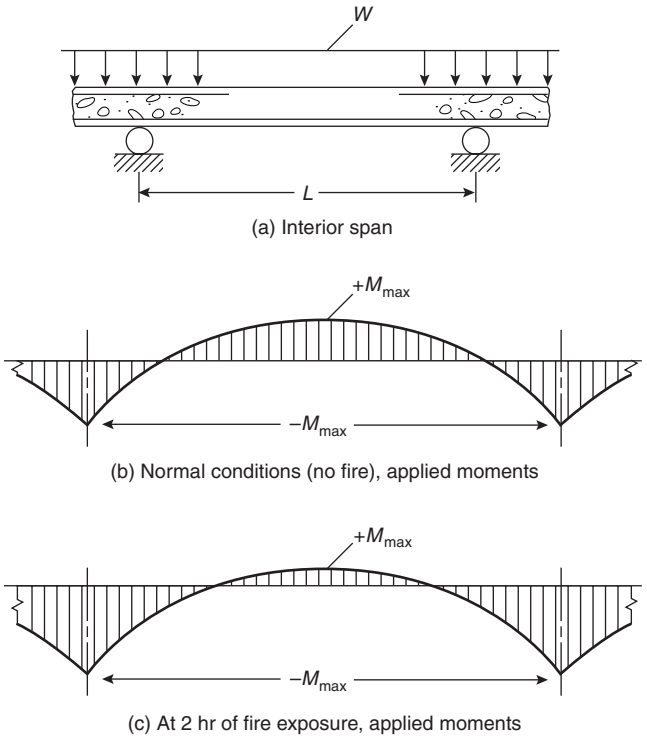

Figure 4-10.13. ***Moment redistribution in interior span of continuous unrestrained one-way slab due to fire exposure.[4]***

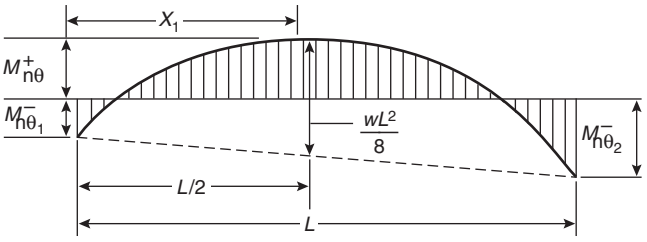

Figure 4-10.14. ***Redistributed applied moment diagram at structural endpoint for span of a uniformly loaded continuous one-way slab or beam with unequal end moments.[4]***

$$\frac{A_s f_{y\theta}}{b_\theta d_\theta f'_{c\theta}} < 0.30 \tag{7}$$

Flexural failure of continuous members occurs when three hinges are formed within a span. One of the hinges will form near the midspan and the other two at the adjacent supports. A hinge is formed at the point where the applied moment is equal to the flexural strength at that point.

The flexural strength at any point can be calculated using Equation 4 for simply supported members. Figure 4-10.14 shows the moment diagram for a one-way span with unequal end moments, that is, when the spans are of unequal lengths. This diagram represents the general case and can be used for other conditions, that is, end spans and slabs with equal spans. The member fails when the sum of the flexural strengths is less than the applied moment, $wL^2/8$. The negative moments are calculated at the supports, and the positive flexural strength is calculated at the center of the span. The negative flexural strength is then used in the following equation for the minimum positive flexural strength:[4]

$$\text{Minimum required } M_{n\theta} = \frac{M^-_{n\theta_1} - M^-_{n\theta_2}}{2wL^2} - \frac{M_{n\theta_1}}{2} - \frac{M_{n\theta_2}}{2} + \frac{wL^2}{8} \tag{8}$$

If the minimum positive flexural strength required is less than the positive flexural strength, the member has the calculated fire endurance. The location of the maximum positive moment, X_1, is calculated from

$$X_1 = \frac{L}{2} + \frac{(M^-_{n\theta_1} - M^-_{n\theta_2})}{wL} \tag{9}$$

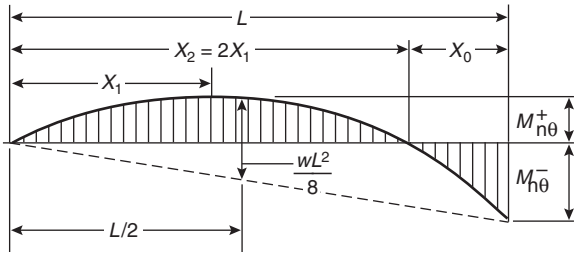

Figure 4-10.15. ***Redistributed applied moment diagram at structural endpoint for end span of a continuous one-way slab or beam.[4]***

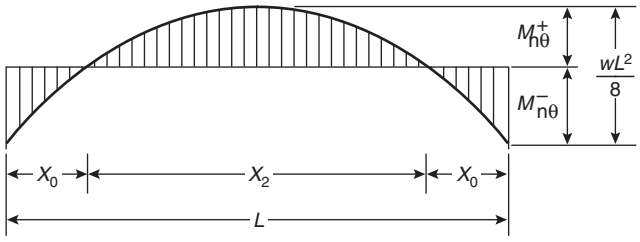

Figure 4-10.16. ***Redistributed applied moment diagram at structural endpoint for symmetrical interior span of a uniformly loaded continuous one-way slab or beam.[4]***

End Span

Equations 8 and 9 can be modified and used for the end span of a continuous member. (See Figure 4-10.15.) For the end span, $M_n = 0$, leaving

$$\text{Minimum required } M^+_{n\theta} = \frac{(M^-_{n\theta})^2}{2wL^2} - \frac{M^-_{n\theta}}{2} + \frac{wL^2}{8} \qquad (10)$$

$$X_1 = \frac{L}{2} - \frac{M^-_{n\theta}}{wL} \qquad (11)$$

Interior Span with Equal End Moments

Equations 8 and 9 can also be modified for spans with equal end moments, as indicated in Figure 4-10.16. For this case, $M^-_{n\theta_1} = M^-_{n\theta_2}$, changing Equation 8 to

$$\text{Minimum required } M^+_{n\theta} = \frac{wL^2}{8} - M^-_{n\theta} \qquad (12)$$

Equation 9 becomes

$$X_1 = \frac{L}{2} \qquad (13)$$

The location of the points of inflection, X_0, is dependent on the magnitude of the negative flexural strengths and can be calculated using

$$X_0 = \frac{L}{2} - \sqrt{\frac{2M^+_{n\theta}}{w}} \qquad (14)$$

The negative moment reinforcement must be extended a sufficient distance beyond the point of inflection to allow the bar strength to become fully developed. Design criteria for the development length are outlined in the ACI *Building Code Requirements for Reinforced Concrete*.[2] It is further recommended that at least 20 percent of the maximum negative moment reinforcement in the span extends throughout the entire length of the span.

Fire Endurance of Concrete Structural Members Restrained against Thermal Expansion

When a fire occurs beneath an interior portion of a floor or roof slab, the heated portion of the slab tends to expand. As this portion of the slab expands, the surrounding cooler portions resist the expansion and exert a resistive force on the heated portion of the slab. This resistive force is referred to as the *thermal thrust force.*

Most U.S. fire tests of floor slabs are conducted with the specimen mounted within a restraining frame which restricts the thermal expansion.[22] The amount of restraining force provided by the restraining frame varies from one laboratory to another, based on factors such as frame design, specimen design, and specimen tightness.

Prior to 1960, no research had been conducted to measure the magnitude of the thermal thrust force. In 1960, the Portland Cement Association (PCA) began operation of its floor furnace.[23] This furnace allowed for both variable and monitored restraint during the fire test. Restraining the slab against expansion greatly affects the thermal thrust, as indicated in Figure 4-10.17. Notice

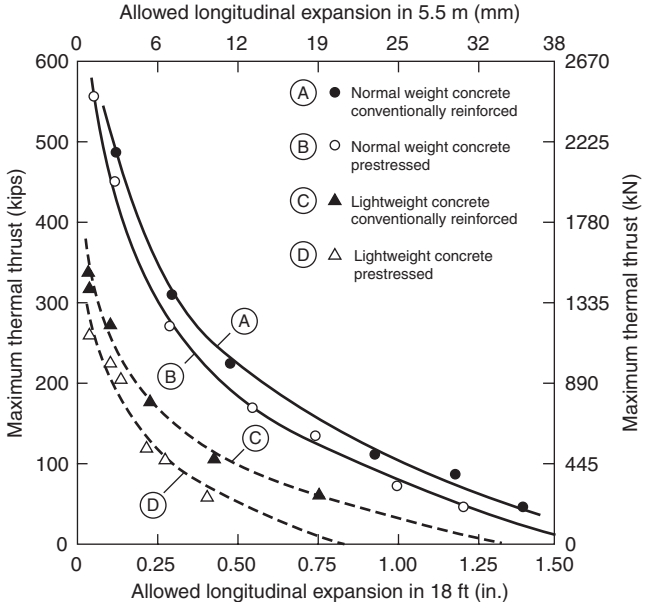

Figure 4-10.17. ***Maximum thrust for allowed expansion of reference specimens.[25]***

that with no expansion allowed, the thermal thrust force would be very high, which would cause compression failure of the concrete. However, with only a slight increase in the allowed expansion, there is a significant decrease in the thermal thrust force. It should also be noted that the thermal thrust force developed in lightweight concrete is considerably less than is developed within normal-weight concrete. This condition is believed to be due to the lower modulus of elasticity and the lower coefficient of expansion of the lightweight concrete.[4]

As a result of the fire research done at PCA, the thermal thrust force was found to vary with the initial modulus of elasticity and the heated perimeter.[24] The heated perimeter, S, is defined as that portion of the perimeter of a section of the specimen, normal to the direction of the thermal thrust, that is exposed to fire. Having assembled a large database of "reference specimens," the thermal thrust from these specimens can be used to predict the thermal thrust within a concrete member:[25]

$$\frac{T_1}{A_1E_1} = \frac{T_0}{A_0E_0}\frac{Z_0}{Z_1} \tag{15}$$

where

$Z_0 = A_0/S_0$

$Z_1 = A_1/S_1$

S_0 = heated perimeter of the reference member

S_1 = heated perimeter of the member in question

T_1 = maximum thermal thrust of the member in question

T_0 = maximum thermal thrust of the reference member

A_0 = cross-sectional area normal to the direction of thermal thrust of the reference member

A_1 = cross-sectional area normal to the direction of thermal thrust of the member in question

E_0 = modulus of elasticity of the member in question

E_1 = modulus of elasticity of the reference member

The parameter $T/(AE)$ is dimensionless, thus the units used for T, A, and E must be consistent.

Nomographs, presented in Figure 4-10.18, are used to solve Equation 15.

For any given partially restrained expansion of a concrete member exposed to fire, there is a compatible thermal thrust developed in the fire-exposed portion. The effect of the thermal thrust on the structural behavior of a reinforced concrete slab is the same as that of a prestressing force along the line of action of the thrust. In structural fire endurance calculations, the flexural strength is the primary interest, for which case the thermal thrust can be considered a "fictitious reinforcement" along the line of an action of the thrust.[26]

The moment due to the thermal thrust, referred to as the thrust moment, is equal to the thrust force multiplied by the distance between the line of action of the thermal thrust and the centroid of the compression block[25]

$$M_T = T\left(d_1 - \Delta - \frac{a_\theta^+}{2}\right) \tag{16}$$

where

$$a_\theta^+ = \frac{T + A_S^+ f_{y\theta}^+}{0.85 f_{c_\theta}' b_\theta} \tag{17}$$

T = magnitude of the thermal thrust

d_t = distance from extreme compression fiber to the line of action of the thermal thrust, T

Δ = deflection of the slab at the point in question

M_T = thrust moment strength

The line of action of the thermal thrust must act below the resultant of the equivalent rectangular stress block in order to contribute to the fire endurance of the slab. Results from fire tests have shown that the line of action for the thermal thrust is near the bottom of the mem-

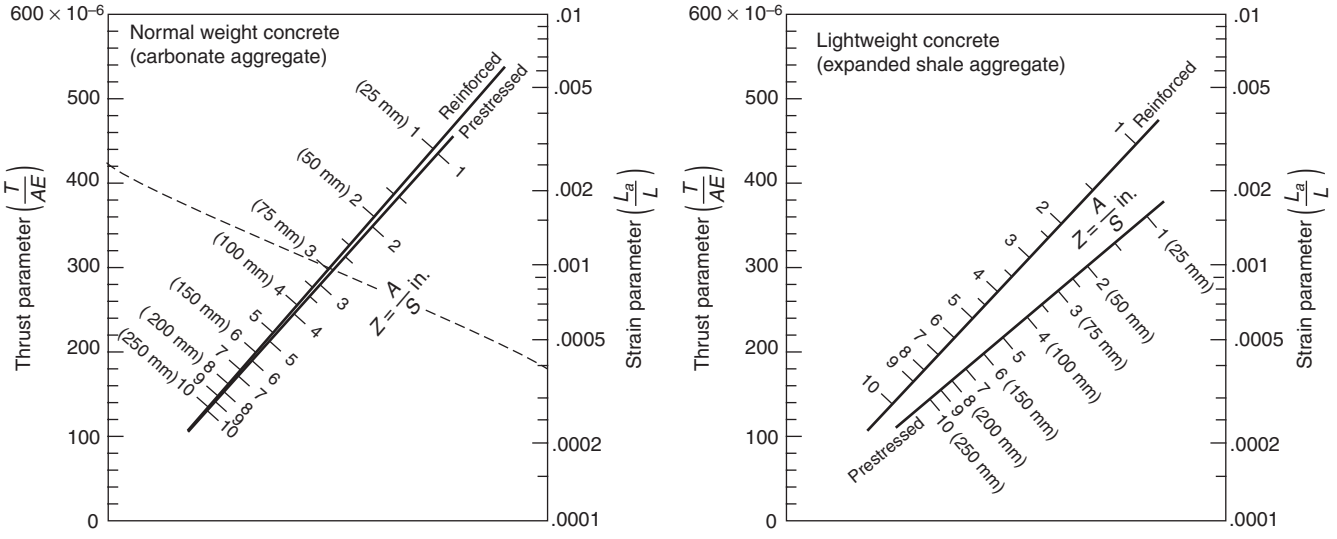

Figure 4-10.18. ***Nomographs relating thrust parameter, strain parameter, and ratio of cross-sectional area to heated perimeter.[25]***

ber throughout the fire test in most cases, particularly when the thrust is small.[25] Although the line of action acts near the bottom, the actual position changes during the fire test. The exact location of the line of action depends on the shape of the member, type of concrete, amount of reinforcement, stiffness of the restraining frame, and the amount of expansion permitted. Table 4-10.1 is used to locate the line of action of the thermal thrust for floor systems developing a minimal restraint to thermal expansion. The guidelines presented in Table 4-10.1 are based on results from standard fire tests.[25]

In order to calculate the thrust moment, the deflection must be estimated. Since the deflections at the supports are assumed to be zero, the only other deflection of interest is at the midspan. The midspan deflection can be approximated using the following equation derived from the deflection equation for simply supported members[25]

$$\Delta_1 = \frac{L_1^2 \Delta_0}{3500 y_{b1}} \tag{18}$$

where

Δ_1 = deflection for the member (in.)

Δ_0 = deflection for the reference member (in.) (see Figure 4-10.19)

L_1 = length of the span of the member (in.)

Table 4-10.1 ***Location of Thermal Thrust Line[3]***

Type of Construction	Fire Exposure (hr)	Location of Thrust Line at Supports[a]
Solid slab	2	25 mm (1 in.)
	3	32 mm (1¼ in.)
	4	38 mm (1½ in.)
Slab-and-joist	≤ 2	0.1*h*
	2–4	0.15*h*

[a]Distance above bottom of member where *h* = overall depth of the joist and slab.

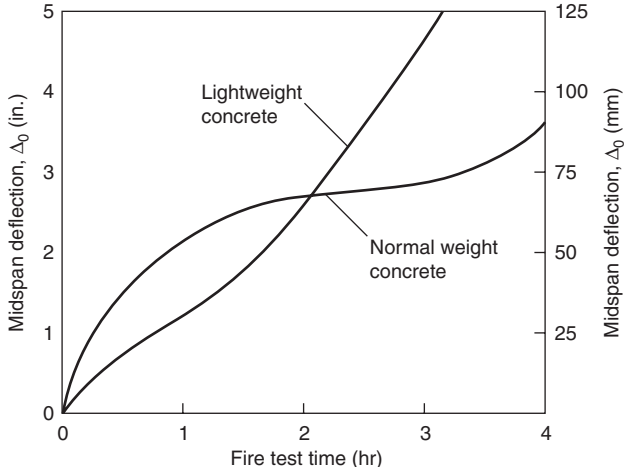

Figure 4-10.19. ***Idealized midspan deflection, Δ_0, of reference specimens with minimal restraint.[4]***

y_{b1} = distance from the centroidal axis to the extreme fiber (in.)

In SI units, Equation 18 becomes

$$\Delta_1 = \frac{L_1 \Delta_0}{88{,}900 y_{b1}}$$

where Δ, L, and y_{b1} are all in mm.

Equation 18 is for members with minimal restraint to thermal expansion. Another equation should be used when the thrust is greater than minimal.[4]

In order to summarize and illustrate how to apply this information to calculate the structural fire endurance for reinforced concrete members, a step-by-step procedure is presented. This procedure was taken from the Concrete Reinforcing Steel Institute (CRSI), *Reinforced Concrete Fire Resistance.* (See Table 4-10.2.)[4]

Example of Continuous One-Way Span

The continuous one-way span example has been included to illustrate the step-by-step procedure for structural analysis for fire endurance that is used. The example problem is for a one-way continuous slab with no thermal restraint assumed. The slab is found to have the desired fire endurance, but the development length of the steel bars required for the negative moment strength is significantly longer than is required for standard gravity loading. The development length is then recalculated assuming minimal thermal restraint.

Given: A one-way, multispan continuous slab supported on beams as shown in Figure 4-10.20. The slab is 100 mm (4 in.) thick with 3.7-m (12-ft) beam spacing. The concrete for the slab is made from siliceous aggregate with a compressive strength of 20.7 MPa (3,000 psi). The slab is subjected to a 3.8 kPa (80 psf) superimposed live load and a 0.25 kPa (5 psf) dead load.

The reinforcement consists of No. 4 bars that meet the requirements of ASTM for A615 Grade 60 (415 MPa). Reinforcing bars are placed in accordance with the 1975 *CRSI Handbook.*[27]

Problem: Determine if the slab has a 2-hr fire endurance.

Step 1: Determine the required fire rating: 2 hr, as stated in the problem.

Step 2: Determine the total depth of the slab, h_t, based on heat transmission: From Figure 4-10.6, h_t = 125 mm (5 in.).

Step 3: Compare h_t vs. h_s: h_t = 125 mm (5 in.) > 100 mm (4 in.) = h_s.

Step 4: In this example, the authority having jurisdiction has waived the requirements for heat transmission, as long as the required structural fire endurance is provided.

Step 5: Because 125 mm (5 in.) > 100 mm (4 in.), the fire endurance for the end span must be computed based on continuity only.

Table 4-10.2 ***Step-by-Step Procedure—Structural Analysis for Fire Endurance***

Step No.	Description
1	From the building code governing the project (model, municipal, state, etc.) look up the required fire ratings.
2	Determine the total depths of slabs, h_t, based on heat transmission to provide the required fire ratings.
3	Compare h_t vs. h_s.
4	If $h_t < h_s$, no further fire endurance considerations are necessary.
4a	If the governing building code permits a reduced fire rating for heat transmission as long as the required structural fire rating is provided, then proceed to Step 5.
5	Only if $h_t > h_s$ (or as in step 4a), compute the structural fire endurance, in hours, based on continuity and/or restraint to thermal expansion.
	STRUCTURAL FIRE ENDURANCE FOR SIMPLY SUPPORTED OR CONTINUOUS SLABS WITH NO AXIAL RESTRAINT
6	*Solid slabs.* Compute the reduced nominal positive and negative flexural strengths, $M_{n\theta}^{+}$ and $M_{n\theta}^{-}$, available at the required fire rating, for example, 3 hr.
7	*Interior spans.* If the absolute sum of available nominal flexural strengths is equal to or greater than the applied moment, that is, if $M_{n\theta}^{+} + M_{n\theta}^{-} \geq wL^2/8$ the fire endurance $\geq$ than the required fire rating.
7a	*Exterior spans.* Using either the reduced nominal negative or positive flexural strength available at the specified fire endurance, compute the minimum required nominal flexural strength.
8	If the nominal flexural strength available $\geq$ minimum required nominal flexural strength, the structural fire endurance is adequate—go to Step 9.
8a	If the nominal flexural strength available $<$ required nominal flexural strength, the structural fire endurance based on continuity only is not sufficient—go to Step 10.
9	If continuity only is considered in the structural fire endurance calculations, and restraint to thermal expansion is neglected, check the lengths of the top reinforcing bars to make sure the bars are long enough to develop the required nominal negative flexural strength.
	The procedure for analyzing continuous beams and joist systems is the same as for the solid slab above, except that isothermal diagrams would be required for determining the available nominal flexural strengths.
	STRUCTURAL FIRE ENDURANCE BASED ON RESTRAINT TO THERMAL EXPANSION
10	Estimate the deflection Δ_1, of the heated bay, assuming minimal restraint occurs.
11	Locate the line of action of the thermal thrust force at the supports.
12	Compute the moment, M_T, which the thermal thrust force has to develop to provide the required additional nominal positive flexural strength for the specified fire endurance. M_T = (Min. req'd $M_{n\theta}^{+}$ – Available $M_{n\theta}^{-}$)
13	Compute the thermal thrust, T_1, required to produce M_T using Equation 16.
14	Compute the thrust parameter, T_1/A_1E_1.
15	Compute the value of $z = A_1/s$.
16	With T_1/A_1E_1 and z, determine the strain parameter.
17	Compute the expansion, ΔL, by multiplying the strain parameter by the heated length, L_h, of the member.
18	Determine if the restraining elements, that is, spandrel or effective edge beams, columns, walls, and so forth, can withstand the thermal thrust, T_1, with a displacement no greater than the expansion, ΔL.

Structural Fire Endurance Based on Continuity Only

Step 6: Compute the reduced positive and negative moment strengths, M_n^+ and M_n^-, respectively, available after 2 hr.

6a: $M_{n\theta}^{+}$ available at 2 hr.

U^+ for bottom bars, $U^+ = 19 + 6 = 25$ mm (1.0 in.) (See Figure 4-10.21.)

At 2 hr, $U^+ = 25$ mm (1.0 in.), $\theta_s^+ = 630$°C (1170°F). (See Figure 4-10.15.)

$f_y = 0.42(60) = 174$ MPa (25.2 ksi). (See Figure 4-10.1.)

Reinforcing is 12.5-mm bars at 215 mm (#4 bars at 9 in.)

$A_s^+ = 570$ mm^2/m (0.27 in.^{2}/ft).

A_s^+ is calculated from the rebar spacing requirements.

$$a_\theta^+ = \frac{A_s f_{y\theta}^+}{0.85 f_c' b} = \frac{570(174)}{0.85(20.7)(1000)} = 5.6 \text{ mm (0.22 in.)}$$

[from Eq. 5]

$$M_{n\theta}^{+} = A_s^+ f_{y\theta}^+ \left(d^+ - \frac{a_\theta^+}{2}\right) = \frac{570(174)(75 - 5.6/2)}{1 \times 10^6}$$

$$= M_{n\theta}^{+} = 7.3 \text{ kN·m/m (1.64 ft·kips/ft)}$$

[from Eq. 4]

6b: $M_{n\theta}^{+}$ available at 2 hr

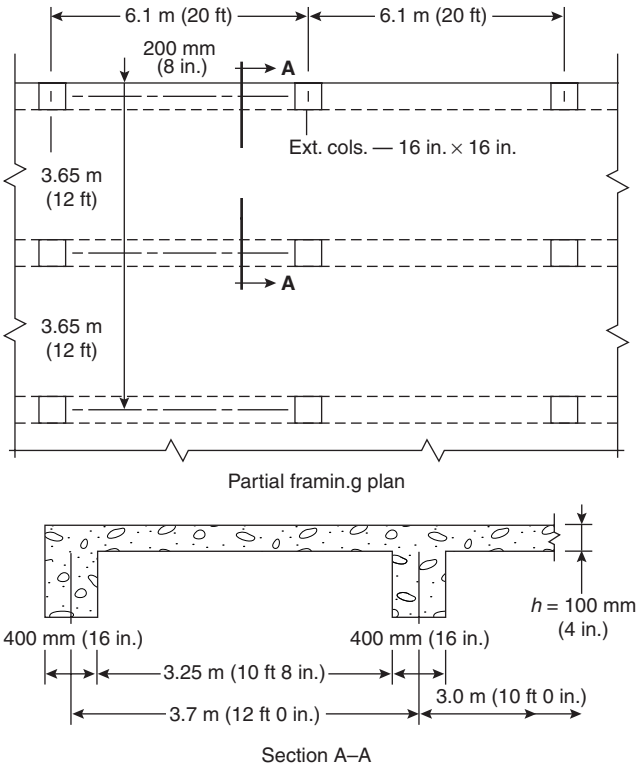

Figure 4-10.20. ***One-way continuous slab, supported on beams.[4]***

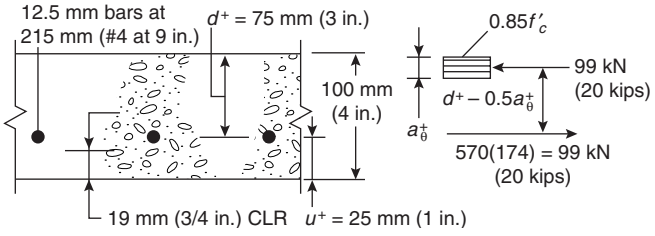

Figure 4-10.21. ***M_n^+ calculation for bottom bars.***

The bottom 1 in. has been neglected, because the concrete temperature is above 650°C (1200°F) with a significantly reduced f_c'.

Top bars, $U^- = 100 - (19 + 6) = 75$ mm (3.0 in.) (See Figure 4-10.22.)

At 2 hr, $U^- = 75$ mm (3.0 in.), $\theta = 270$°C (520°F). (See Figure 4-10.9.)

$f_{y\theta}^- = 0.83\ (60.0) = 344$ MPa (49.8 ksi). (See Figure 4-10.1.) The $f_{y\theta}^-$ stress block, a_θ^-, is estimated to be about 16 mm (5/8 in.) with a temperature ranging from 650 to 480°C (1200 to 900°F).

Temperature values are estimated from Figure 4-10.9. The average temperature is approximately 565°C (1050°F).

$f_c\theta' = 0.65(3) = 13.5$ MPa (1.95 ksi). (See Figure 4-10.2.)

$d_\theta = 4.0 - (0.75 + 0.25 + 1.0) = 50$ mm (2.0 in.)

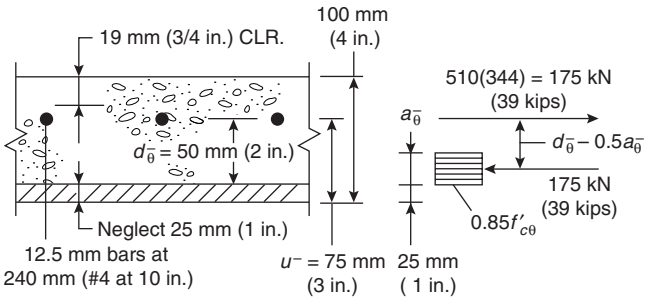

Figure 4-10.22. ***M_n^- calculation for top bars.***

Reinforcing is 12.5-mm bars at 240 mm (#4 at 10 in.)

$$A_s^- = 510 \text{ mm}^2/\text{m}\ (0.24 \text{ in.}^2/\text{ft})$$

$$a_\theta^- = \frac{A_s^- f_{y\theta}^-}{0.85 f_{c\theta}' b} = \frac{510(344)}{0.85(13.5)(1000)} = 15 \text{ mm}\ (0.60 \text{ in.}) \quad \text{[from Eq. 5]}$$

$$\left\{ \begin{aligned} M_n^- = A_s^- f_{y\theta}^- \left(d_\theta^- - \frac{a_\theta}{2} \right) &= \frac{510(344)(50 - 15/2)}{1 \times 10^6} \\ &= Mn_\theta^- = 7.5 \text{ kN·m/m} \\ &\quad (1.69 \text{ ft·kips/ft}) \end{aligned} \right. \quad \text{[from Eq. 4]}$$

Step 7: Calculate the minimum positive moment required at 2 hr.

$$\text{Minimum required } M_{n\theta}^+ = \frac{(M_{n\theta}^-)^2}{2wL^2} - \frac{M_{n\theta}^-}{2} + \frac{wL^2}{8}$$

$$w = 0.1(24) + .25 + 3.8 = 6.45 \text{ kN/m}\ (0.44 \text{ kips/ft})$$

$$\text{Minimum required } M_n^+ = \frac{(7.5)^2}{2(6.45)(3.65)^2} - \frac{7.5}{2} + \frac{6.45(3.65)^2}{8}$$

$$\text{Minimum required } M_n^+ = 7.4 \text{ kN·m/m}\ (1.66 \text{ ft·kips/ft})$$

Step 8: If the positive moment strength available is greater than the required positive moment strength, structural fire endurance is adequate. Because the moment strength available, 7.3 kN·m/m (1.64 ft·kips/ft), is for practical purposes equal to the required moment strength, 7.4 kN·m/m (1.66 ft·kips/ft), the structural fire endurance for the end span is 2 hr.

Step 9: Check the lengths of the top reinforcing bars to make sure the bars are long enough to develop the required negative moment strength. The length of the top bars under normal conditions, considering only gravity loads and no fire, is taken from the *CRSI Handbook*.[27] (See Figure 4-10.23.)

Step 9a: Top bar lengths, at first interior support, neglecting restraint to thermal expansion

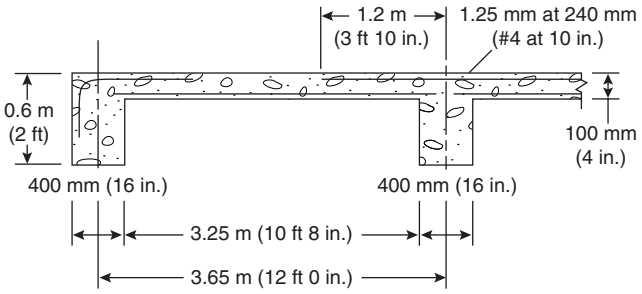

Figure 4-10.23. ***Top bar lengths at 2 hr of fire exposure.***

The distance to the point of inflection at first interior support for structural fire endurance is calculated using

$$X_0 = \frac{2M_{n\theta}^-}{wL}$$

Because the negative reinforcement generally yields early in the fire, as discussed previously, within the first half hour, the value for the negative moment used in Equation 14 should be the maximum negative moment that the beam can support.

$$a = \frac{A_s f_y}{0.85 f_c' b} = \frac{510(415)}{0.85(20.7)(1000)} = 12 \text{ mm (0.47 in.)}$$

$$M_n^- = A_s f_y d - \left(\frac{a}{2}\right) - \frac{510(415)(75 - 12/2)}{1 \times 10^6}$$

$$= M_n^- = 14.6 \text{ kN·m/m (3.28 ft·kips/ft)}$$

The value used for w is left to engineering judgment based on the expected loading during a fire. For this example, the full dead load and one-half the live load is used.

$$w = 0.1(24) + 0.25 + 1.9 = 4.55 \text{ kN/m (0.31 kips/ft)}$$

$$X_0 = \frac{2(14.6)}{4.55 \times 3.65} = 1.75 \text{ m (5 ft 9 in.)}$$

The distance the top bars have to be embedded beyond the point of inflection is given in the ACI *Building Code*.[2] At least one-third of the bars should be embedded 1/16 of the clear span, d, or $12d_b$, whichever is greater. In this example, the 1/16 of the clear span criterion governs (250 mm or 10 in.). Thus, some of the top bars must extend 2.0 m (6 ft 6 in.) into the end span. The length of the top steel, 2.0 m (6 ft 6 in.), is nearly twice the required length for the gravity load (1.2 m or 3 ft 10 in.).The maximum negative moment strength, M_n, used in Equation 14, represents the most severe condition for the development length. However, the assumption of frictionless roller bearing supports used in the above example neglected the restraining force in all calculations. The restraining force, or thermal thrust, T, is developed early in the fire, producing a moment opposite the support moment, which acts to reduce the magnitude of the support moment. The net support moment will then be less than the moment strength, M_n^-, used in the calculation above, thereby overestimating the development length required for the desired fire endurance.[4]

The restraint criteria discussed will be used to determine if there is sufficient restraint developed in the longitudinal direction, to reduce the development lengths to that required for the gravity load.

9b: Top bar lengths, at first interior support, including restraint to thermal expansion

Using X_0 = 1.2 m (3.83 ft), the length required for gravity loading, we can determine the net moment at the support required.

$$X_0 = \frac{2M_n^-}{wL} \tag{19}$$

$$M_n^- = \frac{X_0 wL}{2} = \frac{1.2(4.55)(3.65)}{2}$$

$$= 10 \text{ kN·m/m (2.25 ft·kips/ft)}$$

The thermal thrust must produce a moment equal to

$$M_T = 14.6 - 10.0 = 4.6 \text{ kN·m/m (1.04 ft·kips/ft)}$$

Early in the fire, T will act at or near the bottom of the slab. (See Table 4-10.1.) T is assumed to act 12 mm (1/2 in.) above the bottom of the slab (taking the fire exposure as approximately one-half hour):

$$d_T = 100 - 12 = 88 \text{ mm (3.5 in.)}$$

$$\Delta = 0 \quad \text{at the support}$$

The depth of the stress block, a_θ^+, is assumed initially to be zero because the required thrust is small.

$$T = \frac{M_T}{d_T - \Delta - a_\theta^+} = \frac{4.6(1000)}{88 - 0 - 0} = 52.2 \text{ kN/m (3.6 kips/ft)}$$

Recalculating a_θ^+,

$$a_\theta^+ = \frac{T}{0.85 f_c' b} = \frac{52.2}{0.85(20.7)} = 3 \text{ mm (0.13 in.)}$$

$$T = \frac{1.14(12)}{3.5 - 0 - 0.13/2} = 53.2 \text{ kN/m (3.65 kips/ft)}$$

Compute the expansion, L, that corresponds to

$$T = 53.2 \text{ kN/m (3.65 kips/ft)}$$

$$E_1 = 25{,}000 \text{ MPa } (3.6 \times 10^6 \text{ psi})$$

$$A_1 = 1.0(0.1) = 0.1 \text{ m}^2\text{/m } (48 \text{ in.}^2\text{/ft})$$

$$\frac{T_1}{A_1 E_1} = \frac{53.2}{0.1(25)} = 21 \times 10^{-6}$$

$$Z = \frac{A_1}{s} = \frac{0.1}{1} = 0.1 \text{ m} = 100 \text{ mm (4 in.)}$$

$$\frac{\Delta L}{L_h} = 0.006 \text{ (from Figure 4-10.18)}$$

$$L = 0.006 \times 3650) = 22 \text{ mm (0.86 in.)}$$

In order to maintain equilibrium of the horizontal forces and compatibility of the displacements, the restraining elements must withstand T = 53.2 kN/m (3.65 kips/ft) and not deflect more than ΔL = 22 mm (0.86 in.). The next step would be to check the strength and stiffness of the restraining elements, that is, the exterior spandrel beams and columns of the exterior support and the plane floor area of the first interior support. In this example, it is not necessary to check the strength and stiffness toward the interior of the structure, because there is considerable restraint from the large unheated floor area and many columns to provide the thrust moment at the first interior support.[4] However, the spandrel beams and columns at the exterior support should be checked to ensure that there is sufficient strength and stiffness to resist the thrust moment. Determining the strength and stiffness of the spandrel beams and columns requires a long and complex structural analysis and is not shown here. An explanation of the structural analysis of spandrel beams and columns can be found in the literature.[4]

Assuming there is sufficient restraint in the spandrel beams and columns to resist the thrust moment, the required length of the top bars over the first interior support at 2 hr of fire exposure must be determined. Neglecting restraint to thermal expansion,

$$X_0 = \frac{2M^-_{n\theta}}{wL} = \frac{2(7.5)}{(4.55)(3.65)} = 0.90 \text{ m (2.96 ft)}$$

As previously discussed, at least one-third of the top bars should be embedded 1/16 of the clear span at the point of inflection, X_0, therefore the top steel should extend 1.1 m (3 ft 8 in.) into the end span. This length is less than the top bar length required for gravity loads, so no adjustment in the length of the reinforcement steel is required to obtain the desired fire endurance.

Reinforced Concrete Columns

Throughout the history of concrete construction reinforced concrete columns have performed well when exposed to fire. The reason for this is threefold:

1. Columns are generally large enough to prevent the center core from losing a significant amount of strength even in prolonged fire exposure.
2. Ties or spirals contain the concrete within the core.
3. The vertical reinforcing bars are generally protected by at least 48 mm (1 7/8 in.) of concrete cover, thereby insulating the steel bars.[4]

Most of the building codes in the United States assign 3- and 4-hr fire resistance to reinforced concrete columns larger than 300 mm × 300 mm (12 × 12 in.) for square shapes, or a diameter of at least 300 mm (12 in.) for round columns.

ACI suggests that the information in Table 4-10.3, by Hull and Ingberg,[28] be used for designing reinforced concrete columns for exposure to fire. The information presented in Table 4-10.3 is based on the results of a series of fire tests on concrete columns reported in 1925.[28] More detailed tables are available.[1,44] Detailed assessments of reinforced concrete columns exposed to fires have been made by Anderberg[29] and Lie and Irwin.[30]

Table 4-10.3 ***Fire Endurance Proposed by Hull and Ingberg[8]***

Aggregate Type	Minimum Area of Round or Square Cross Section (cm²)	(sq in.)	Concrete Cover (mm)	(in.)	Fire Endurance Classification (hr)
Siliceous	710	110	38	1 1/2	1 1/2
Siliceous	1,290	200	38	1 1/2	2 1/2
Siliceous	1,290	200[a]	38	1 1/2	3 1/2
Siliceous	1,613	250	64	2 1/2	3
Siliceous	1,613	250[a]	64	2 1/2	6
Traprock & slag[b]	1,290	200	38	1 1/2	4
Carbonate	1,290	200	38	1 1/2	6

[a]Mesh in cover.

[b]Air-cooled slag.

Reinforced Concrete Frames

It is not possible to use simple hand methods for accurate structural design of reinforced concrete frame structures exposed to fires. Individual concrete members can be designed by the methods described above, but for moment-resisting frames, a special purpose computer program is necessary for detailed analysis and design. Available programs include FIRES-RC-II,[31] CONFIRE,[32] and SAFIR.[21]

Reinforced Concrete Walls

Typically, the fire endurance of concrete and concrete masonry walls is determined by heat transmission criteria as opposed to structural performance.[3,4] As a result, estimating the fire resistance of walls can be accomplished using a heat transfer analysis only. For this reason, the discussion of thickness requirements presented in the heat transmission section can be used. The required thickness can be determined graphically or by applying a heat transfer computer model.

The distinction between bearing and nonbearing walls is based on building code structural requirements and not fire endurance. For example, some building codes require bearing walls to be thicker than nonbearing walls. Such a requirement has not been justified by results of a fire test.[4] ASTM E119 requires that a superimposed load be applied and maintained at a constant magnitude throughout the test of a bearing wall. When testing nonbearing walls, there is no applied load; however, the edges of the

walls may be restrained against thermal expansion, in which case a thermally induced load is applied during the fire test. This thermally induced load is of much greater magnitude than the load applied to bearing walls.[4]

Prestressed Concrete Assemblies

Most of this chapter refers to reinforced concrete. The same principles apply to prestressed concrete, which is often more vulnerable in fires for the following reasons: prestressing steels are much more sensitive to elevated temperatures than mild steel reinforcing bars; prestressed concrete is often manufactured in slender components with thin cover concrete; and some failure modes such as debonding, shear, and spalling are more critical in prestressed concrete.

Procedures are also available to calculate the fire resistance of prestressed concrete members. The reader is directed to *Design for Fire Resistance of Precast Prestressed Concrete*.[33]

Composite Steel-Concrete Construction

Composite steel-concrete construction refers to concrete slabs cast on permanent steel-deck formwork and steel beams which act compositely with the concrete slab to resist bending moment, as shown in Figure 4-10.24.

Composite steel-concrete slabs have excellent integrity in fire conditions because even if cracks occur in the concrete slab, the continuous steel deck will prevent any passage of flames or hot gases through the floor. To meet the insulation criterion, it is simply necessary to provide sufficient thickness of slab. A solid slab of uniform thickness requires the same thickness as a normal reinforced concrete slab, but for other profiles it is necessary to evaluate an effective thickness. Generic listings are given in some codes including Eurocode 4,[34] and manufacturers of steel decking have proprietary ratings for their products. It is possible to spray the underside of the steel sheeting with spray-on insulation, but this method is rarely economical.

The strength of composite steel-concrete slabs is severely influenced by fire because the steel sheeting, acting as external reinforcing, loses strength rapidly when exposed to the fire. However, composite slabs can achieve good fire resistance because of three contributing factors: axial restraint, moment redistribution, and fire emergency reinforcement.

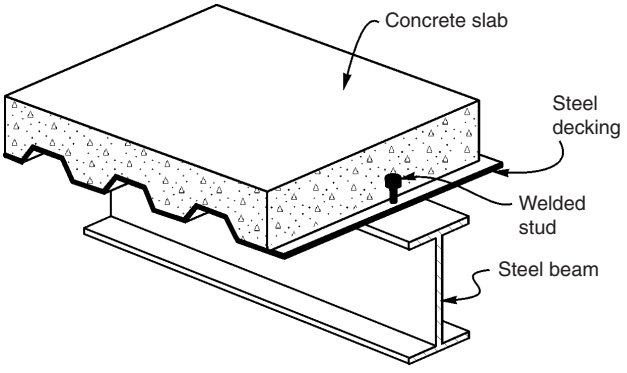

Figure 4-10.24. ***Composite steel-concrete construction.***

Composite slabs often have different fire resistance ratings for restrained and unrestrained conditions.[35] During a fire test, if a composite slab is built into a rigid testing frame which allows almost no axial expansion, the slab can achieve a fire resistance rating with no reinforcing other than the steel sheeting, because of the thermal thrust developed at the supports. Some buildings are sufficiently stiff and strong to provide such restraint to a fire-exposed floor system, but because the amount of restraint is difficult to assess accurately, it is usual to rely on some reinforcing within the slab.

If the nominal reinforcing provided to control shrinkage cracking is placed near the top of the concrete and if the slab is continuous over several supports, it can develop significant negative flexural capacity through moment redistribution and hence retain sufficient load capacity during the fire. If a slab is simply supported, or if moment redistribution is insufficient to resist the applied loads, it is common practice to place *fire emergency reinforcing* in the slab, consisting of steel reinforcing bars in the troughs of the sheeting, with sufficient cover from the bottom surface to control temperatures in the bars. The flexural strength of the slab can be calculated in the usual way using the temperature of the rebars. Further design recommendations are given by ECCS,[36] Lawson,[37] and EC4.[34]

Recent Developments

There is continuing international research on fire performance of reinforced concrete. Several recent developments are described below.

Calculation of Temperatures

Recent publications on thermal and mechanical properties of concrete at high temperatures are given by Harmathy,[38] Schneider,[39] Bazant,[40] and Neville.[41] A simple, approximate formula for calculating internal temperatures in reinforced concrete members exposed to the standard fire has been developed by Wickström.[42] Internal temperatures in concrete slabs and beams exposed to realistic fires are given by Wade.[43]

Eurocodes

The new Eurocodes for structural design have comprehensive chapters on fire design. For reinforced concrete, Eurocode 2[44] gives minimum dimensions and minimum cover necessary to achieve fire resistance ratings for slabs, walls, beams, and columns. It also provides information on thermal and mechanical properties of concrete at high temperatures, with recommended design methods. The Eurocode describes two overall types of design: a "simplified" calculation method and "general" calculation methods. The simplified calculation method is essentially the same as that described in this chapter. The

general calculation methods include those which provide a more realistic analysis of concrete structures exposed to actual fires, based on fundamental physical behavior inluding high temperature effects. Complex structures can only be designed using general methods and computer programs for calculating thermal gradients and analyzing the structure at elevated temperatures, for any type of fire exposure. Design of composite steel-concrete slabs in fire conditions is given in Eurocode 4.[34]

Spalling

The design methods in this chapter are based on the assumption that the concrete remains intact for the duration of the fire. This assumption is invalid if the cover concrete spalls off during the fire, exposing reinforcing steel to the fire temperatures. Experiments and real fire experience have shown that most normal weight concrete members can withstand severe fires without spalling, but spalling does occur sometimes. In some cases spalling is related to the type of aggregate, but it is more often linked to the behavior of the cement paste. It is generally agreed that spalling most often occurs when water vapor is driven from the cement paste during heating, with high pore pressures creating high tensile stresses in the concrete. Susceptibility to spalling results from high moisture content (such as in fresh concrete), rapid rates of heating, slender members, and high stresses at the time of the fire. Recent reviews of concrete spalling are provided by Malhotra[45] and Phan.[46] The most promising new development to reduce spalling is the addition of fine polypropylene fibers to the concrete mix so that the polypropylene melts during fire exposure, leaving cavities through which the water vapor can escape.[47]

High-Strength Concrete

There has been considerable recent interest in high-strength concrete as a construction material. High-strength concrete contains additives such as silica fume and water-reducing admixtures which result in compressive strength in the range 50 to 120 MPa (7000 to 18,000 psi). An extensive survey of high-strength concrete properties at elevated temperatures by Phan[46] shows that they tend to have a higher rate of strength loss than normal concrete at temperatures up to 400°C (750°F), with explosive spalling being a problem in some cases. High-strength concrete is more susceptible to spalling since it has smaller free-pore volume (higher paste density), so that the pores become filled with high pressure water vapor more quickly than in normal weight concrete and the low porosity results in slower diffusion of the water vapor through the concrete. Fire tests on high-strength columns are reported by Aldea et al.[48] and Kodur.[47] Design recommendations are given by Tomasson,[49] who suggests a simple method which ignores concrete above 500°C (950°F) for slabs and beams and above 400°C (750°F) for columns.

Fiber-Reinforced Concrete

Thermal and mechanical properties of steel-fiber reinforced concrete at elevated temperatures are described by Lie and Kodur.[49] They show that the presence of steel fibers increases the ultimate strain and improves the ductility of the concrete during fire exposure.

References Cited

1. A.H. Buchanan, *Structural Design for Fire Safety,* John Wiley and Sons, Chicester, UK (2001).
2. *Building Code Requirements for Reinforced Concrete,* ACI 318-83, American Concrete Institute, Detroit, MI (1983).
3. *Guide for Determining the Fire Endurance of Concrete Elements,* ACI 216-81, American Concrete Institute, Detroit, MI (1982).
4. *Reinforced Concrete Fire Resistance*, Concrete Reinforcing Steel Institute, Chicago (1980).
5. A.H. Gustaferro and T.D. Lin, "Rational Design of Reinforced Concrete Members for Fire Resistance," *Fire Safety Journal,* 11, pp. 85–98 (1986).
6. M.S. Abrams, "Behavior of Inorganic Materials in Fire," *ASTM STP 685,* American Society for Testing and Materials, Philadelphia (1974).
7. T.Z. Harmathy, "Variable-State Methods of Measuring the Thermal Properties of Solids," *Journal of Applied Physics,* 35, p. 4 (1964).
8. T.Z. Harmathy, "Thermal Properties of Concrete at Elevated Temperatures," *Journal of Materials,* 5, p. 4 (1970).
9. T.Z. Harmathy and L.W. Allen, "Thermal Properties of Selected Masonry Unit Concretes," *ACI Journal,* 70, p. 2 (1973).
10. K. Odeen, "Fire Resistance of Prestressed Concrete Double-T Units," *Civil Engineering and Building Construction Series No. 48,* ACTA Polytechnica Scandinavica, Stockholm, Sweden (1968).
11. A.H. Gustaferro et al., "Fire Resistance of Prestressed Concrete Beams; Study C: Structural Behavior During Fire Tests," *PCA Research and Development Bulletin,* RD009.01b, Portland Cement Association, Skokie, IL (1971).
12. M.S. Abrams and C.R. Cruz, "The Behavior at High Temperatures of Steel Strands for Prestressed Concrete," *Journal of the PCA Research and Development Laboratories,* 3, p. 3 (1968).
13. M.S. Abrams, "Compressive Strength of Concrete at Temperatures to 1600°F," *Temperature and Concrete, Special Publication SP-25,* American Concrete Institute, Detroit, MI (1971).
14. R.L. Brockenbrough and B.G. Johnston, *Steel Design Manual,* U.S. Steel Corporation, Pittsburgh, PA (1968).
15. C.R. Cruz, "Elastic Properties of Concrete at High Temperatures," *PCA Research Bulletin, 191,* Portland Cement Association, Skokie, IL (1966).
16. *Manual of Steel Construction,* American Institute of Steel Construction, Chicago (1980).
17. M.S. Abrams and A.H. Gustaferro, "Fire Endurance of Two-Course Floors and Roofs," *Journal of American Concrete Institute,* 66, p. 2 (1969).
18. M.S. Abrams and A.H. Gustaferro, "Fire Endurance of Concrete Slabs as Influenced by Thickness, Aggregate Type, and Moisture," *PCA Research Bulletin,* 223, Portland Cement Association, Skokie, IL (1968).
19. R.H. Iding, Z. Nizamuddin, and B. Bresler, "FIRES T3, A Computer Program for the Fire Response of Structures—Thermal-Three-Dimensional Version," UCB FRG 77-15, University of California, Berkeley (1977).
20. U. Wickstrom, "TASEF-2—A Computer Program for Temperature Analysis of Structures Exposed to Fire," *Report No. 79-2,* Lund Institute of Technology, Lund, Sweden (1979).
21. D.I. Nwosu, V.K.R. Kodur, J.-M. Franssen, and J.K. Hum, "User Manual for SAFIR: A Computer Program for

Analysis of Structures at Elevated Temperature Conditions," *Internal Report 782,* National Research Council of Canada, Ottawa (1999).

22. *Symposium on Fire Resistance of Concrete, ACI Publication SP 5,* American Concrete Institute, Detroit, MI (1962).
23. C.C. Carlson and J.B. Hubbell, "Design and Operation of the PCA Floor Furnace," *PCA Publication RR001,* Portland Cement Association, Skokie, IL.
24. S.L. Selvaggio and C.C. Carlson, "Restraint in Fire Tests of Concrete Floors and Roofs," *ASTM STP 422,* American Society for Testing and Materials, Philadelphia; also *PCA Research Department Bulletin 220,* Portland Cement Association, Skokie, IL (1967).
25. L.A. Issen et al., "Fire Tests of Concrete Members: An Improved Method for Estimating Restraint Forces," *Fire Performance,* ASTM STP 464, American Society for Testing and Materials, Philadelphia.
26. E.A.B. Salse and A.H. Gustaferro, "Structural Capacity of Concrete Beams During Fires as Affected by Restraint and Continuity," in *Proceedings,* 5th CIB Congress, Paris (1971).
27. *CRSI Handbook,* Concrete Reinforcing Steel Institute, Chicago (1975).
28. W.A. Hull and S.H. Ingberg, "Fire Resistance of Concrete Columns," *NBS Technological Papers No. 272,* National Bureau of Standards (1925).
29. Y. Anderberg, "Computer Simulations and a Design Method for Fire Exposed Concrete Columns," *Report 92-50,* Fire Safety Design, Lund, Sweden (1993).
30. T.T. Lie and R.J. Irwin, "Method to Calculate the Fire Resistance of Reinforced Concrete Columns with Rectangular Cross Section," *ACI Structural Journal,* 90, 1, pp. 52–60 (1993).
31. R. Iding, B. Bresler, and Z. Nizamuddin, "FIRES-RC II, A Computer Program for the Fire Response of Structures—Reinforced Concrete Frames," *Fire Research Group Report No. UCB FRG 77-8,* University of California, Berkeley (1977).
32. N.E. Forsen, "A Theoretical Study of the Fire Resistance of Concrete Structures," *FCB-SINTEF Report STF65 A82062,* SINTEF, Trondheim, Norway (1982).
33. *Design for Fire Resistance of Precast Prestressed Concrete,* 2nd ed., Prestressed Concrete Institute, Chicago (1988).
34. EC4, *Eurocode 4: Design of Composite Steel and Concrete Structures. ENV 1993-1-2: General Rules—Structural Fire Design,* European Committee for Standardisation, Brussels, Belgium (1994).
35. UL 1996, *Fire Resistance Directory,* Underwriters Laboratories Inc., Northbrook, IL (1996).
36. ECCS, "Calculation of the Fire Resistance of Composite Concrete Slabs with Profiled Steel Sheet Exposed to the Standard Fire," *Publication No. 32,* European Commission for Constructional Steelwork, Brussels (1983).
37. R.M. Lawson, "Fire Resistance of Ribbed Concrete Floors," *CIRIA Report 107,* Construction Industry Research and Information Association, London (1985).
38. T.Z. Harmathy, *Fire Safety Design and Concrete,* Concrete Design and Construction Series, Longman Scientific and Technical, Harlow, UK (1993).
39. U. Schneider, "Concrete at High Temperatures—A General Review," *Fire Safety Journal,* 13, pp. 55–68 (1988).
40. Z.P. Bazant and M.F. Kaplan, *Concrete at High Temperatures—Material Properties and Mathematical Models,* Concrete Design and Construction Series, Longman Group Ltd, Harlow, UK.
41. A.M. Neville, *Properties of Concrete,* 4th ed., John Wiley and Sons, New York (1997).
42. U. Wickström, "A Very Simple Method for Estimating Temperatures in Fire Exposed Structures," in *New Technology to Reduce Fire Losses and Costs* (S.J. Grayson and D.A. Smith, eds.), Elsevier Applied Science, London, pp. 186–194 (1986).
43. C.A. Wade, "Performance of Concrete Floors Exposed to Real Fires," *Journal of Fire Protection Engineering,* 6, 3, pp. 113–124 (1994).
44. EC2, *Eurocode 2: Design of Concrete Structures–ENU 1992-1-2 General Rules–Structural Fire Design.* European Committee for Standardization, Brussels, Belgium (1993).
45. H.L. Malhotra, "Spalling of Concrete in Fires," *CIRIA Technical Note No. 118,* Construction Industry Research and Information Association, London (1984).
46. L.T. Phan, "Fire Performance of High Strength Concrete: A Report of the State-of-the-Art," *NISTIR 5934,* National Institute of Standards and Technology (1996).
47. V.K.R. Kodur, "Studies on the Fire Resistance of High Strength Concrete at the National Research Council of Canada," in *Proceedings—International Workshop on Fire Performance of High Strength Concrete, NIST Special Publication 919,* National Institute of Standards and Technology, Gaithersburg, MD, pp. 75–86 (1997).
48. C.-M. Aldea, J.-M. Franssen, and J.-C. Dotreppe, "Fire Test on Normal and High Strength Reinforced Concrete Columns," in *Proceedings—International Workshop on Fire Performance of High Strength Concrete, NIST Special Publication 919,* National Institute of Standards and Technology, Gaithersburg, MD (1997).
49. B. Tomasson, "High Performance Concrete—Design Guidelines," Report, Department of Fire Safety Engineering, Lund University, Sweden (1998).
50. T.T. Lie and V.K.R. Kodur, "Thermal and Mechanical Properties of Steel Fibre Reinforced Concrete at Elevated Temperatures," *Canadian Journal of Civil Engineering,* 23, 2, pp. 511–517 (1996).

CHAPTER 11

Analytical Methods for Determining Fire Resistance of Timber Members

Robert H. White

Introduction

The fire resistance ratings of wood members and assemblies, as of other materials, have traditionally been obtained by testing the assembly in a furnace in accordance with American Society for Testing and Materials (ASTM) Standard E119.[1] These ratings are also published in listings, such as the Underwriters Laboratories *Fire Resistance Directory*[2] or the Gypsum Association's *Fire Resistance Design Manual*,[3] and in publications of the model building code organizations. The ratings listed are limited to the actual assembly tested and normally do not permit modifications such as adding insulation, changing member size, changing or adding interior finish, or increasing the spacing between members. Code interpretation of the test results sometimes allows the substitution of larger members, thicker or deeper assemblies, smaller member spacing, and thicker protection layers, without reducing the listed rating. A new ASTM standard[4] provides guidelines on such extension of fire endurance results obtained from the standard ASTM E119 fire test. A fire-endurance design procedure for wood beam and columns and a procedure for wood-frame walls have U.S. and Canadian building code acceptance. In Europe, the new Eurocode 5[5] provides calculation methods at three levels of complexity. In addition, other procedures and models have been proposed or are being developed.

When attention is given to all details, the fire endurance of a wood member or assembly depends on three items:

1. Performance of its protective membrane (if any)
2. Extent of charring of the structural wood element
3. Load-carrying capacity of the remaining uncharred portions of the structural wood elements

Dr. Robert H. White is project leader for wood preservation and fire research at the USDA, Forest Service, Forest Products Laboratory. His research has primarily been in the areas of wood charring and fire endurance of wood assemblies.

The following sections review the methods available for determining the contribution of each item and discuss the major properties of wood that affect the thermal and structural response of wood assemblies or components.

Contribution of the Protective Membrane

Gypsum wallboard and plywood paneling are two common types of protective membrane, which is the first line of resistance to a fire in wood construction. In a protected assembly, the fire resistance rating is largely determined by the type and thickness of the protective membrane. The effects of the protective membrane on the thermal performance of an assembly are included in Harmathy's ten rules of fire endurance rating.[6] These ten rules (Figure 4-11.1) provide guidelines to evaluate the relative effects of changes in materials on the fire resistance rating of an assembly. However, there are exceptions to some of these general rules. The rules apply primarily to the thermal performance of the assembly.

The contribution of the protective membrane to the fire resistance rating of a light-frame assembly is clearly illustrated in the component additive calculation procedure discussed in the following subsection. Brief discussions of direct protection of wood members and numerical heat transfer models are also presented.

Component Additive Method

The Component Additive Method (CAM) is a calculation procedure to determine the fire resistance ratings of light-frame wood floor, roof, and wall assemblies. With this procedure, as with Harmathy's rules 1 and 2, one assumes that times can be assigned to the types and thicknesses of protective membranes and that an assembly with two or more protective membranes has a fire resistance rating at least that of the sum of the times assigned

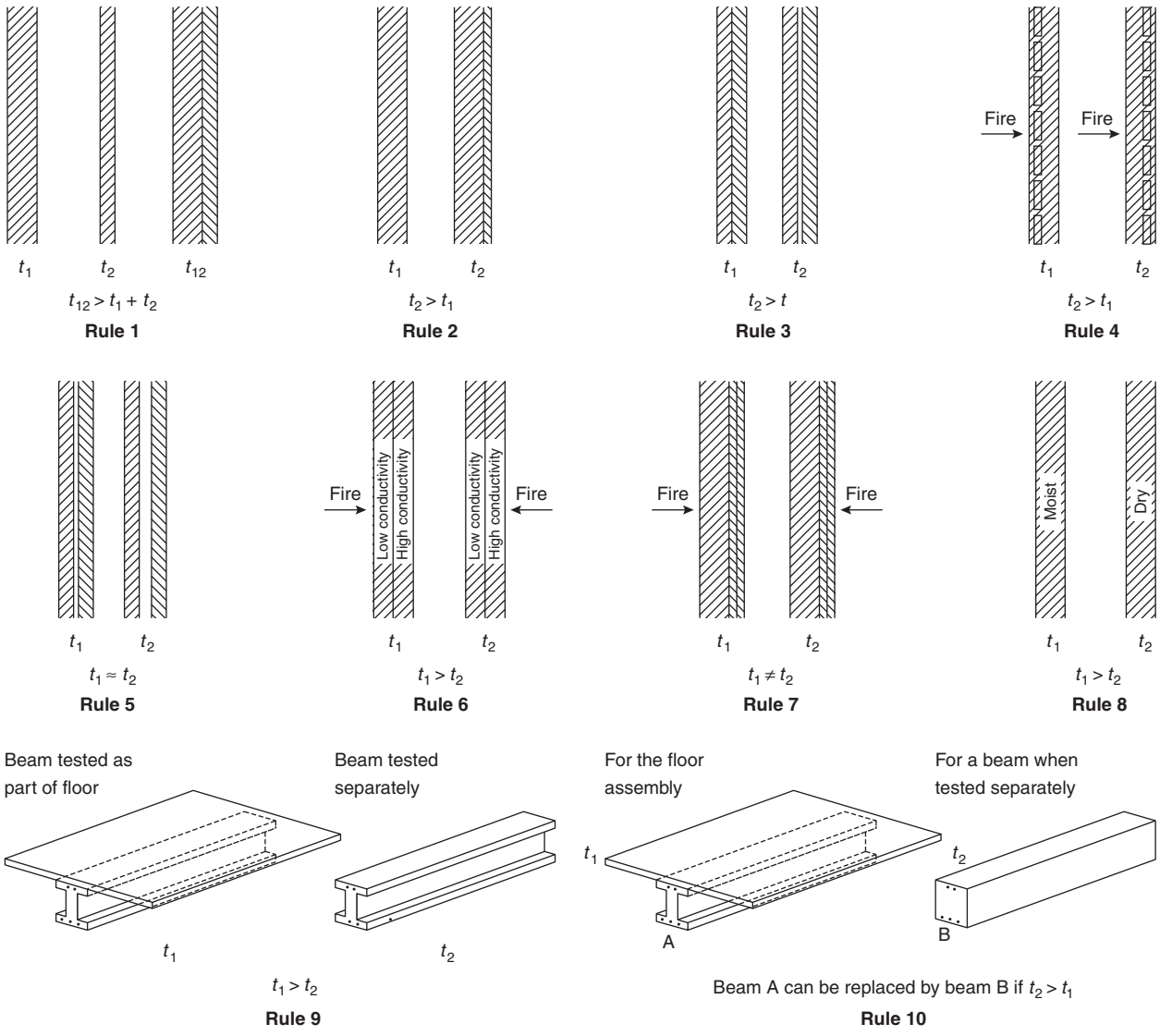

Figure 4-11.1. ***Harmathy's ten rules of fire endurance.***[6]

for the individual layers and the times assigned to the framing. CAM was developed by the National Research Council of Canada (NRCC), and has gained code approval in both the United States and Canada.

The times assigned to the protective membranes (Table 4-11.1), the framing (Table 4-11.2), and other factors are added together to obtain the fire resistance rating for the assembly. The times are based on empirical correlation with actual ASTM E119 tests of assemblies. The ratings obtained in these tests ranged from 20 to 90 min. The times given in Table 4-11.1 are based on the membrane's ability to remain in place during fire tests. The type of fasteners and their spacing on the protective membrane can be critical factors in the performance of the membrane in a fire endurance test. Reference should be made to similar tested assemblies. The addition of insulation to a wall assembly can increase its fire resistance. Adding rock wool

Table 4-11.1 ***Time Assigned to Protective Membranes***[a]

Description of Finish	Time (min)
9.5-mm (3/8-in.) Douglas fir plywood, phenolic bonded	5
13-mm (1/2-in.) Douglas fir plywood, phenolic bonded	10
16-mm (5/8-in.) Douglas fir plywood, phenolic bonded	15
9.5-mm (3/8-in.) gypsum board	10
13-mm (1/2-in.) gypsum board	15
16-mm (5/8-in.) gypsum board	20
13-mm (1/2-in.) type X gypsum board	25
16-mm (5/8-in.) type X gypsum board	40
Double 9.5-mm (3/8-in.) gypsum board	25
13-mm + 9.5-mm (1/2-in. + 3/8-in.) gypsum board	35
Double 13-mm (1/2-in.) gypsum board	40

[a]The applicable building code should be checked for acceptance of, modification to, and limitations on the procedure. There are specific requirements for the installation of some of the membranes.

Table 4-11.2 ***Time Assigned for Contribution of Wood Frame***[a]

Description of Frame	Time (min)
Wood wall studs, 406 mm (16 in.) on center	20
Wood floor and roof joists, 406 mm (16 in.) on center	10

[a]Minimum size for studs is nominal 51 mm by 102 mm (2 in. by 4 in.). Wood joists must not be less than nominal 51 mm (2 in.) in thickness. The spacing between studs or joists cannot exceed 406 mm (16 in.) on center. The applicable building code should be checked for acceptance of, modification to, and limitations on the procedure.

or slag mineral wood insulation batts for additional protection to the wood stud wall generally has an assigned time of 15 minutes, which is added to the times for the framing and for the protective membrane to obtain the rating for the wall assembly. Assigned times, if any, for glass fiber insulation depend on the codes. Adding insulation to a floor or roof assembly can decrease its fire resistance, depending on its location within the assembly and the method of attachment.

For asymmetrical wall assemblies, the rating is based on the side with the lesser fire resistance. For exterior walls rated only from the interior and floor/roof assemblies, there are minimal requirements for the membrane on the side or top of the assembly not exposed to the fire, in order to ensure that the wall or floor/roof assembly does not fail because of fire penetration or heat transfer through the assembly. Specific alternative membranes are identified for the face of wood stud walls not exposed to fire (exterior) and for the flooring or roofing over wood joist framing.

The membrane on the side not exposed to fire (the outside or top) may also be any membrane listed in Table 4-11.1 with an assigned time of 15 min or greater.

The application of the method in the building codes is generally limited to 60 or 90 min. Additional information can be found in publications of the American Forest & Paper Association[7] and the Canadian Wood Council.[8] The applicable building code should be checked for acceptance of, modifications to, and limitations on the procedure. There are differences between the codes in what is accepted.

CAM gives flexibility, for example, in calculations for plywood and gypsum board combined as an interior finish.

EXAMPLE 1:

The calculated fire resistance rating of a wood stud exterior wall (nominal 2-in. × 4-in. [51-mm × 102-mm] studs, 16 in. [406 mm] on center) with 5/8-in. (16-mm) Douglas fir phenolic-bonded plywood over 1/2-in. (13-mm) type X gypsum wallboard on the side exposed to fire is

From Table 4-11.1:	
16-mm (5/8-in.) Douglas fir plywood, phenolic bonded	15 min
13-mm (1/2-in.) type X gypsum board	25 min
From Table 4-11.2:	
Wood stud framing	20 min
Calculated rating (total)	60 min

Mineral wool insulation could be used to increase the fire rating to 75 minutes.

Other Methodologies

The times assigned to the protective membranes in the component additive method are not the "finish ratings" of the material cited in test reports or listings. A finish rating of a protective membrane is generally defined as the time to reach either an average temperature rise of 139°C (250°F) or a maximum rise of 181°C (325°F), as measured on the plane of the wood framing member nearest the fire. Since the charring of wood is associated with a temperature of 300°C (550°F), another method is to assume that the membrane will protect any wood framing for at least the time of the finish rating of the membrane in a test involving wood framing. The fire rating of the entire assembly with the substituted member is assumed to be at least equal to the finish rating of the protective membrane in the test with the solid sawn wood framing. This approach is described as the *onset of char* method in New Zealand publications.[9]

In a Swedish additive method,[10] the fire separation of nonloaded wall assemblies is calculated as the sum of the contribution to fire resistance from each layer of material:

$$b_{tot} = b_1k_1 + b_2k_2 + \cdots = b_nk_n \quad (1)$$

where

b_{tot} = total fire resistance of the wall
b_n = basic fire resistance of layer n
k_n = coefficient of position indicating where the layer is located in relation to the fire

Direct Protection of Wood Members

The steel industry improves the fire endurance of steel members by directly covering them with fire-resistive panels or coatings. Currently, the marketing of fire-resistive coatings for use on wood is very limited or nonexistent. The fire-retardant coatings marketed for wood are only designed and recognized for use to reduce the spread of flames over a surface (flamespread).

Depending upon its thickness and durability under fire exposure, a coating may merely delay ignition of the wood for a few minutes or may provide an effective insulative layer that reduces the rate of charring. For both fire-retardant coatings and fire-resistive coatings, their performance as a fire-resistant membrane on wood has been evaluated.[11–13] In some full-scale testing of beams, those coated with an intumescent fire retardant produced improvements less than that obtained in earlier tests in a small-scale furnace.[14] Bending of the beams during the fire test resulted in adhesion problems. Tests on coated timber members were also reported in Finland and U.S.S.R.[15] There is limited published data on the protection provided by directly covering a wood member with gypsum board or other nonwood panel products. As previously noted, finish ratings listed for panel products used in ASTM E119 tests of assemblies have been used to estimate the delay in the onset of char formation

provided by the panel product. Gardner and Syme[16] found that gypsum board not only delayed the onset of char formation but also reduced the subsequent rate of char formation. In their 2-hour tests, 13-mm- (1/2-in.-) thick gypsum board on wood beams reduced the depth of char by approximately 40 percent. Of the 40 percent, only 17 percent was credited to the initial delay in char formation.

Numerical Heat Transfer Models

The protective membrane contributes to fire resistance by providing thermal protection. Numerical heat transfer methodologies are available to evaluate this thermal protection. Fung[17] developed a one-dimensional finite difference model and computer program for thermal analysis of construction walls. Gammon[18] developed a two-dimensional finite element heat transfer model for wood stud wall assemblies. WALL2D, developed by Forintek Canada,[19,20] is a two-dimensional finite-difference model for predicting heat transfer through wood-stud walls exposed to fire. Difficulties in modeling the charring of wood and the physical deterioration of the panel products complicate these numerical methodologies. Recent research on such models includes activities in Canada,[20] Sweden,[21] New Zealand,[22,23] and Australia.[24] An important application of such models is the determination of the fire endurance of an assembly when the time-temperature curve is a natural or parametric fire exposure. This application is important for performance-based building codes.

Numerical heat transfer models are used not only to model the performance of the protective membranes but also to model the charring of the structural wood members, the second major factor in the fire endurance of a wood member or assembly.

Charring of Wood

Wood undergoes thermal degradation (pyrolysis) when exposed to fire. (See Figure 4-11.2.) The pyrolysis and combustion of wood have been studied extensively. Literature reviews include publications by Browne,[25] Schaffer,[26,27] Hall et al.,[28] and Hadvig.[29] By converting the wood to char and gas, pyrolysis results in a reduction in the wood's density. The pyrolysis gas undergoes flaming combustion as it leaves the charred wood surface. Glowing combustion and mechanical disintegration of the char eventually erode or ablate the outer char layer.

The charring rate generally refers to the linear rate at which wood is converted to char. Under standard fire exposure, the charring rates tend to be fairly constant after a higher initial charring rate.

Establishing the charring rate is critical to evaluating fire resistance, because char has virtually no load-bearing capacity. There is a distinct demarcation between char and uncharred wood. The base of the char layers is wood reaching a temperature of approximately 300°C (550°F). SI conversion of inch-pound units has resulted in 288°C, 290°C, and 300°C being used for 550°F. To determine the charring rate, we use both empirical models based on experimental data and theoretical models based on chemical and physical principles.

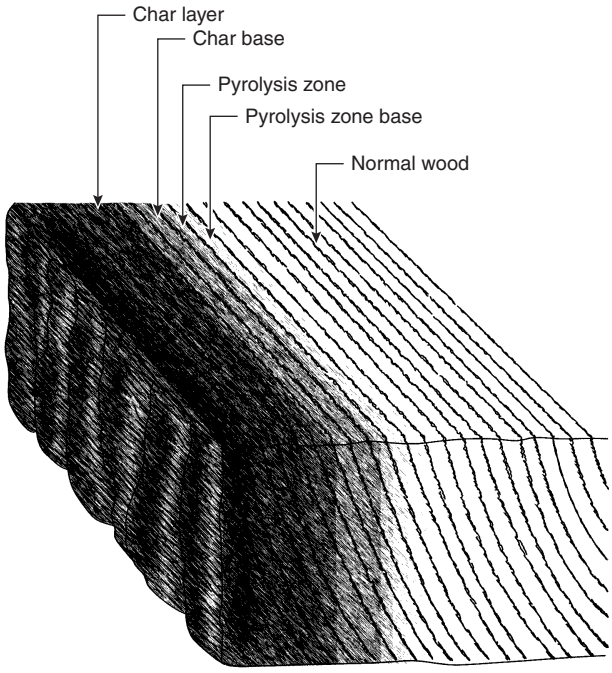

Figure 4-11.2. ***Degradation zones in a wood section.***

Standard ASTM E119 Fire Exposure

Expressions for charring rate in the standard ASTM E119 test are the result of many experimental studies. The empirical model that is most generally used assumes a constant transverse-to-grain char rate of 0.6 mm/min. ($1^1/_2$ in./hr) for all woods, when subjected to the standard fire exposure. There are differences among species associated with their density, chemical composition, and permeability. In addition, the moisture content of the wood affects the charring rate. The charring rate parallel to the grain of wood is approximately twice that transverse to the grain.[28] As a beam or column chars, the corners become rounded. The rounding is generally considered to have a radius equivalent to the char depth on the sides.

Schaffer[30] reported transverse-to-grain charring rates as a function of density and moisture content for Douglas fir, southern pine, and white oak. The regression equations for B (min per mm., the reciprocal of charring rate) were

$$B = (0.002269 + 0.00457u)\rho + 0.331 \text{ for Douglas fir} \quad (2)$$

$$B = (0.000461 + 0.00095u)\rho + 1.016 \text{ for southern pine} \quad (3)$$

$$B = (0.001583 + 0.00318u)\rho + 0.594 \text{ for white oak} \quad (4)$$

where

u = moisture content (fraction of oven-dry mass)

ρ = density (dry mass, volume at moisture content u)

White[31] developed an empirical model based on eight species. The char rate equation was of the form

$$t = mx_c^{1.23} \tag{5}$$

where

t = time (min)
m = char rate coefficient
x_c = char depth (mm)

The char rate coefficients ranged from 0.48 to 0.72 min/mm$^{1.23}$ for the eight species.[31,32] The char rate coefficient could be estimated with the equation

$$m = -0.147 + 0.000564\rho + 1.21u + 0.532f_c \tag{6}$$

where

ρ = oven-dry density (kg/m^3)
u = moisture content (fraction of oven-dry mass)
f_c = char contraction factor (dimensionless)

The char contraction factor was the thickness of the char layer at the end of the fire exposure divided by the original thickness of the wood layer that was charred (char depth). Average values for the char contraction factor were 0.60 for southern pine, 0.83 for western red cedar, 0.86 for redwood, 0.82 for Engelmann spruce, 0.52 for basswood, 0.59 for hard maple, 0.70 for red oak, and 0.67 for yellow poplar. Recent char rate experiments have been reported in Australia,[16] Europe,[33] and New Zealand.[34]

In Eurocode 5,[5] the linear charring rates listed are 0.64 mm/min for glued laminated softwood timber with a characteristic density of 290 kg/m^3, 0.67 for solid softwood timber with a characteristic density of 290 kg/m^3, and 0.54 mm/min for solid or glued laminated hardwood with a characteristic density of 350 kg/m^3. The design values for charring rate depend on the fire endurance methodology being used. The effect of the rounding of the charred member can be taken into account by increasing the values for char rate as is done in Eurocode 5. Eurocode 5 design values for linear charring rate include 0.7 mm/min for glued laminated softwood timber with a characteristic density of 290 kg/m^3, 0.8 for solid softwood timber with a characteristic density of 290 kg/m^3; 0.5 mm/min for solid or glued laminated hardwood with a characteristic density of 450 kg/m^3 and 0.7 mm/min for characteristic density of 290 kg/m^3. Additional design values can be found in the Eurocode 5. Some of the charring rate values for density ρ_o are adjusted for other characteristic densities, ρ_k, with a coefficient, k_ρ, equal to $\sqrt{\rho_o/\rho_k}$ as a multiplier.[5]

Assumption of a constant charring rate is reasonable when the member or panel product is thick enough to be treated as a semi-infinite slab. For smaller dimensions, the charring rate increases once the temperature has risen above the initial temperature at the center of the member or at the unexposed surface of the panel.

Kanury and Holve[35] suggest the model

$$\frac{\ell}{t} \approx \left(\frac{2}{a}\right)\left(1 - \frac{b\ell}{a}\right) \tag{7}$$

where

ℓ = thickness of slab (mm)
t = fire endurance time (min)
a,b = constants

They consider the $2/a$ factor an ideal charring rate and the ratio $b\ell/a$ as a correction factor accounting for thickness and thermal diffusion effects.

Noren and Ostman[36] provided the equation

$$b_m = 1.128t + 0.0088t^2 \tag{8}$$

where

b_m = contribution to fire resistance (min)
t = panel thickness (mm)

The equation is based on data for various wood-based panel products. Differences in the fire resistance at equal thickness depended on panel density, moisture content, type of adhesive, and the structural composition of the panel. The effect of fire-retardant treatment and adhesives on fire resistance depends on the type of adhesive or treatment. Lumber bonded with phenolic or resorcinol adhesives has a charring rate consistent with that of solid wood. Fire-retardant treatments are designed to reduce flamespread. The fire retardant's effect on the charring rate may be to only slightly increase the time until ignition of the wood. Some fire retardants reduce flammability by lowering the temperature at which charring occurs. This may increase the charring rate. However, a few fire retardants have been found to improve charring resistance.[37]

Nonstandard Fire Exposures

The above equations were stated to apply to the standard ASTM E119 fire exposure.[1] Data on charring rates for other fire exposures have been limited. Schaffer[22] provided data for constant temperatures of 538°C (1000°F), 815°C (1500°F), and 927°C (1700°F). Lau and White[38] presented data for constant 500°C and an empirical model for constant or variable temperatures. The charring rate is a function of the external flux. For a range of 20 to 3300 kW/m^2, Butler[39] calculated the char rate (mm/min) to be 0.022 times the irradiance (kW/m^2). Because of increased testing with heat release rate calorimeters, char rate data as a function of external heat flux are becoming more available.[40–45] In tests of spruce, charring rates obtained were 0.56, 0.80, and 1.02 mm/min. for external heat fluxes of 25, 50, and 75 kW/m^2, respectively.[42] In tests of southern pine, the linear charring rate ranged from 0.44 mm/min at 18 kW/m^2 to 0.85 mm/min at 55 kW/m^2.[40,41] Charring rate has been found to be proportional to the ratio of external heat flux over density.[42,44]

Hadvig's Equations for Nonstandard Fire Exposure

Hadvig[29] has developed equations for nonstandard fire exposure. The charring rate in a real fire depends

upon the severity of the fire to which the wood is exposed. The fire severity depends upon such factors as the available combustible material (fire load) and the available air supply (design opening factor).

The design fire load is

$$q = k \cdot \frac{Q}{A_t} \tag{9}$$

where

q = design fire load (MJ/m^2)
k = transfer coefficient (dimensionless)
Q = sum of the products of mass and lower calorific value of materials to be found in the compartment (MJ)
A_t = total internal area of the compartment, including floor, walls, ceiling, windows, and doors (m^2)

The transfer coefficients are given in Table 4-11.3 for different types of compartments and geometrical opening factors. In the case of fire compartments whose bounding structures do not come under any of the types A-H, k is usually determined by a linear interpolation in the table between appropriately chosen types of compartments.

The geometrical opening factor is

$$F' = \frac{A\sqrt{h}}{A_t} \tag{10}$$

where

Table 4-11.3 *The Transfer Coefficient, k*[29,46]

Type of Fire Compartment[a]	Geometrical Opening Factor, F'					
	0.02	0.04	0.06	0.08	0.10	0.12
A	1.0	1.0	1.0	1.0	1.0	1.0
B	0.85	0.85	0.85	0.85	0.85	0.85
C	3.0	3.0	3.0	3.0	3.0	2.5
D	1.35	1.35	1.35	1.50	1.55	1.65
E	1.65	1.50	1.35	1.50	1.75	2.00
F[b]	1.0–0.5	1.0–0.5	0.8–0.5	0.7–0.5	0.7–0.5	0.7–0.5
G	1.50	1.45	1.35	1.25	1.15	1.05
H	3.0	3.0	3.0	3.0	3.0	2.5

[a]A = (Standard fire compartment) The average consisting of brick, concrete, and gas concrete.

B = Concrete, including concrete on the ground

C = Gas concrete (density 500 kg/m^3)

D = 50 percent concrete, 50 percent gas concrete (density 500 kg/m^3)

E = 50 percent gas concrete (density 500 kg/m^3), 33 percent concrete, and 17 percent laminate consisting of (taken from the inside) 13-mm plasterboard (density 500 kg/m^3), 10-cm mineral wool (density 50 kg/m^3), and brick (density 1800 kg/m^3)

F = 80 percent steel plate, 20 percent concrete. The fire compartment is comparable to a storehouse or other building of a similar kind with an uninsulated roof, walls of steel plate, and floor of concrete.

G = 20 percent concrete and 80 percent laminate consisting of a double plasterboard (2 × 13 mm) (density 790 kg/m^3), 10-cm air space, and another double plasterboard (2 × 13 mm) (density 790 kg/m^3)

H = Steel plate on either side of 100-mm mineral wool (density 50 kg/m^3)

[b]The higher values apply to $q < 60$ MJ/m^2; the lower values apply to $q > 500$ MJ/m^2. Intervening values are found by interpolation.

F' = geometrical opening factor (m$^{1/2}$)
A = total area of windows, doors, and other openings in walls (i.e., vertical openings only) (m^2)
h = weighted mean value of the height of vertical openings, weighted against the area of the individual openings (m)

The design opening factor is

$$F = F' \cdot k \cdot f \tag{11}$$

where

F = design opening factor (m$^{1/2}$)
F' = geometrical opening factor (m$^{1/2}$)
k = transfer coefficient of bounding structure (dimensionless)
f = coefficient (dimensionless) to account for horizontal openings

The dimensionless coefficient, f, (Figures 4-11.3 and 4-11.4) increases the opening factors when there are horizontal openings. For only vertical openings, f is equal to 1.

Hadvig's[29] equations are

$$\theta = 0.0175 \frac{q}{F} \tag{12}$$

$$\beta_0 = 1.25 - \frac{0.035}{F + 0.021} \quad \text{for} \quad 0.02 \le F \le 0.30 \tag{13}$$

$$X = \beta_0 \cdot \tau \quad \text{for} \quad 0 \le \tau \le \frac{\theta}{3} \tag{14}$$

$$X = \beta_0 \left(-\frac{1}{12}\theta + \frac{3}{2}\tau - \frac{3}{4}\frac{\tau^2}{\theta} \right) \quad \text{for} \quad \frac{\theta}{3} \le \tau \le \theta \tag{15}$$

where

θ = time at which maximum charring is reached for the values used for F and q (min)
β_0 = initial value of rate of charring (mm/min)
X = charring depth (mm)
F = design opening factor (m$^{1/2}$) (defined in Equation 11)
q = design fire load (MJ/m^2) (defined in Equation 9)
τ = time (min)

These equations are valid for fire exposures less than 120 min. and for a room where the combustible material is wood. Plastic burns more intensely and for a shorter time than wood. When the combustible materials in the room are plastics, Equations 12 and 13 are therefore modified for faster char rate (β_0 is 50 percent higher), shorter time is allowed for maximum charring (θ is cut in half), and Equation 14 is applicable for $\tau < \theta$.[29]

Equations 12 through 15 are for glued timber with a density of 470 kg/m^3 including a moisture content of 10 percent and minimum width of 80 mm or greater or square members of minimum 50 × 50 mm. Equations 14 and 15 are valid only for $0 < X < b/4$, where b is the dimension of the narrow face of a rectangular member. For

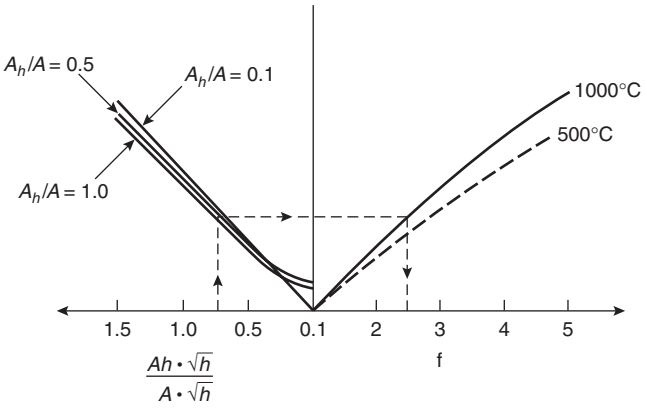

Figure 4-11.3. ***Diagram for the determination of f for fire temperatures of 500°C and 1000°C.***

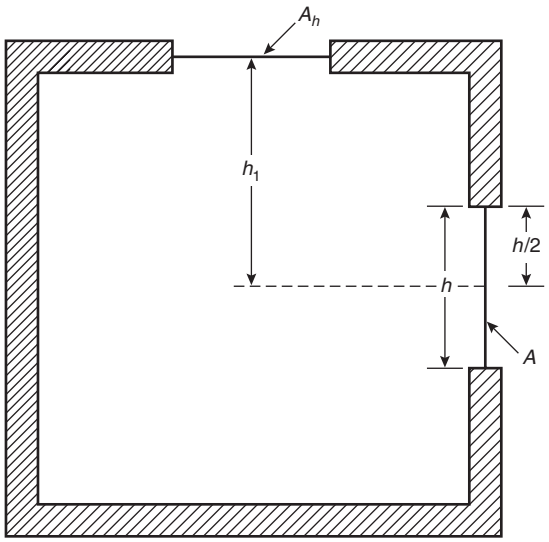

Figure 4-11.4. ***Simplified sketch of vertical cross section of ventilated compartment with notation.[20]***

dimensions of nonsquare cross sections between 30 and 80 mm, the ratio of the original dimensions must be equal to or greater than 1.7, the charring depth perpendicular to the wide face is X, and the charring depth perpendicular to the narrow face is determined by multiplying Equation 14 or 15 by the dimensionless quantity

$$1.35 - 0.0044(b) \qquad (16)$$

where b equals the dimension of the narrow face (mm).

EXAMPLE 2:

The room is a standard fire compartment consisting of brick, concrete, and gas concrete. The floor area is 5×10 m, and the height is 3 m. The openings are one window 1.5 m high and 2 m wide, three windows 1.5 m high and 1 m wide, and one skylight 1.5 m $\times$ 3 m. The skylight is 2 m above the midheight of the windows. The fire load is 6 m^3 of wood.

Assuming a fire temperature of 1000°C, a wood density of 500 kg/m^3, and lower calorific value of 17 MJ/kg, describe the charring of a 38- $\times$ 250-mm wood beam exposed on three sides after 8 min of the fire.

The geometrical opening factor (Equation 10) is

$$F' = \frac{A\sqrt{h}}{A_t} = \frac{[1(1.5 \times 2) + 3(1.5 \times 1)]\sqrt{1.5}}{[2(5 \times 10) + 2(3 \times 5) + 2(3 \times 10)]}$$

$$= \frac{7.5\sqrt{1.5}}{190} = 0.048 \text{ m}^{1/2}$$

The design opening factor (Equation 11) is

$$F = F' \cdot k \cdot f$$

The k is obtained from Table 4-11.3 ($k = 1.0$ for type A, $F' = 0.048$). The f is obtained from Figures 4-11.3 and 4-11.4.

$$\frac{A_h\sqrt{h_1}}{A\sqrt{h}} = \frac{(1.5 \times 3)\sqrt{2}}{7.5\sqrt{1.5}} = \frac{4.5\sqrt{2}}{7.5\sqrt{1.5}} = 0.69$$

$$\frac{A_h}{A} = \frac{4.5}{7.5} = 0.6$$

For $A_h\sqrt{h_1}/A\sqrt{h}$ of 0.69 and A_h/A of 0.6, the f from Figure 4-11.3 is 2.4.

$$F = (0.048)(1.0)(2.4) = 0.115 \text{ m}^{1/2}$$

The design fire load (Equation 9) is

$$q = k \cdot \frac{Q}{A_t} = (1.0)\frac{(6 \times 500 \times 17)}{190} = \frac{51{,}000}{190} = 268 \text{ MJ/m}^2$$

Maximum charring rate will be reached at θ min (Equation 12)

$$\theta = 0.0175\frac{268 \text{ MJ/m}^2}{0.115 \text{ m}^{1/2}} = 41 \text{ min}$$

The initial charring rate (Equation 13) will be

$$\beta_0 = 1.25 - \frac{0.035}{0.115 + 0.021} = 1 \text{ mm/min}$$

At 8 min, the char depth (Equation 14) will be

$$X = 1 \times 8 = 8 \text{ mm} \quad \text{for} \quad 0 \le 8 \le \frac{41}{3}$$

The smaller dimension b of the beam is 38 mm. The charring depth criterion $0 < x < b/4$ is $0 < 8 < 9.5$ mm, so Equations 14 and 15 are valid. The ratio of the original dimensions is 25/3.8 or 6.6. Since 38 mm is less than 80 mm, the multiplying factor (Equation 16) is

$$1.35 - 0.0044(38) = 1.18$$

At 8 min, the uncharred area of the beam will be approximately

$$38 \text{ mm} - 2(8 \text{ mm}) = 22 \text{ mm wide}$$

and

$$250 \text{ mm} - (1.18 \times 8 \text{ mm}) = 240 \text{ mm high}$$

As the charring proceeds after (9.5 mm)/(1 mm/min) or 9.5 min, the $b/4$ criterion of the equations no longer holds. This is because the charring rate increases as the temperature at the center of the beam starts to increase.

Equations for parametric fires are also provided in Eurocode 5. The approach is a simplification of Hadvig's equations. For a period τ_0, the parametric charring rate is

$$\beta_{par} = 1.5\beta_0 \frac{5F - 0.04}{4F + 0.08} \tag{17}$$

where

$F = F'$ of Equation 10

β_0 = design charring rate of Eurocode 5

The time period τ_0 is

$$\tau_0 = 0.006 \frac{q}{F} \tag{18}$$

where q is the total design load of Equation 9.

At τ_0, the char rate decreases to zero at $3\tau_0$. The maximum charring depth during the fire exposure and the subsequent cooling period is $2\beta_0\tau_0$. Equations are valid for F between 0.02 and 0.30 $m^{1/2}$, τ_0 of 40 min or less, and char depths less than one quarter of the dimensions. Oleson and König[47] tested glued-laminated beams and found agreement with Hadvig's equations for the wide vertical side of a member. Oleson and König[47] noted that, compared to conditions at standard exposure, the mechanical behavior at natural fire exposure is different due to the changes of temperature in the residual cross section during the cooling period. The influence of elevated temperature is no longer concentrated to the outer layer of the residual cross section.

For situations for which no empirical models exist, solutions may be found by the use of theoretical models. Most theoretical models have the flexibility to be used for any desired fire exposures.

Theoretical Models

Considerable efforts have gone into developing theoretical models for wood charring. Theoretical models allow calculation of the charring rate for geometries other than a semi-infinite slab and for nonstandard fire exposures. Roberts[48] reviewed the problems associated with the theoretical analysis of the burning of wood, including structural effects and internal heat transfer, kinetics of the pyrolysis reactions, heat of reaction of the pyrolysis reactions, and variations of thermal properties during pyrolysis. He considered the major problems to be in the formulation of a mathematical model for the complex chemical and physical processes occurring and in the acquisition of reliable data for use in the model.

Many models for wood charring are based on the standard conservation of energy equation. The basic differential equation includes a term for each contribution to the internal energy balance. An early model for wood charring was given by Bamford et al.[49] The basic differential equation used by Bamford was

$$c\rho \frac{\partial T}{\partial t} = K \frac{\partial^2 T}{\partial X^2} - q \frac{\partial w}{\partial t} \tag{19}$$

where

K = thermal conductivity

T = temperature (°C)

X = location

w = weight of volatile products per cubic centimeter of wood

t = time

q = heat liberated at constant pressure per gram of volatile material evolved

c = specific heat

ρ = density

In Equation 19, the term on the left side of the equal sign represents the energy stored at a given location as indicated by the increase or decrease of the temperature with time at that location. The first term on the right side of the equal sign represents the thermal conduction of energy away from or into the given location. The second term on the left side represents the energy absorbed (endothermic reaction) or the energy given off (exothermic reaction) as the wood undergoes pyrolysis or thermal degradation. Numerical solutions using computers are normally used to solve these differential equations.

In Bamford's calculations using Equation 19, the rate of decomposition was given by an Arrhenius equation. The heat of decomposition, q, was the difference between the heat of combustion of the wood and that of the products of decomposition. Thermal constants for wood and char were assumed to be the same, and the total thickness of char and wood was assumed to remain constant.

Thomas[50] added a convection term to Bamford's equation to obtain

$$\rho c \frac{\partial T}{\partial t} = K \frac{\partial^2 T}{\partial X^2} + M c_g \frac{\partial T}{\partial X} - q \frac{\partial w}{\partial t} \tag{20}$$

where

M = local mass flow of pyrolysis gases

c_g = specific heat of the gases

The convection term represents the energy transferred in or out of a location due to convection of the pyrolysis gases through a region with a temperature gradient.

The Factory Mutual Research Corporation model (SPYVAP) includes terms for internal convection of volatiles and thermal properties as functions of temperature and density. It was developed by Kung[51] and later revised by Tamanini.[52] Atreya[53] has further revised this model to include moisture absorption. His energy conservation equation is

$$(\rho_a C_{pa} + \rho_c C_{pc} + \rho_m C_{pm}) \frac{\partial T}{\partial t} = \frac{\partial}{\partial X}\left(K \frac{\partial T}{\partial X}\right) + i\left(1 - j \frac{\rho_c}{\rho_f}\right) \cdot M_g \frac{\partial H_g}{\partial X} - \frac{\partial \rho_s}{\partial t}\left[-Q + \left(H_a - H_c \frac{\rho_f}{\rho_w}\right) \Big/ \left(1 - \frac{\rho_s}{\rho_w}\right) - H_g\right] - \frac{\partial \rho_m}{\partial t}(-Q_m + H_m - H_g) \quad (21)$$

where

C_p = specific heat [J/(kgK)]
K = thermal conductivity [W/(m K)]
T = temperature (K)
t = time (s)
X = distance (m)
ρ = density (kg/m^3)
M_g = outward mass flux of volatile gases (kg/m^{2}s)
H = thermal-sensible specific enthalpy (J/kg)
Q = endothermic heat of decomposition of wood for a unit mass of volatiles generated (J/kg at T_∞)
i,j = parameters to simulate cracking, between 0 and 1

Subscripts:

∞ = ambient
w = virgin wood
c = char
g = volatile gases
a = unpyrolyzed active material
m = moisture
f = final value
s = solid wood

Equation 21 is similar to the previous equations except the material has been broken up into its components (wood, water, and char). The parameter j eliminates the convection term if the pyrolysis gases are escaping through cracks or fissures in the wood. The last term represents the heat absorbed with vaporization of the water. The conservation of mass equation is

$$\frac{\partial M_g}{\partial X} = \frac{\partial \rho_s}{\partial t} + \frac{\partial \rho_m}{\partial t} \quad (22)$$

and ensures that the mass of the gases equals the mass loss due to thermal degradation of the wood and vaporization of the moisture.

As noted before, the decomposition kinetics equation for wood is the Arrhenius equation

$$\frac{\partial \rho_s}{\partial t} = -A \frac{(\rho_s - \rho_f)}{(1 - \rho_f/\rho_w)} \exp(-E/RT) \quad (23)$$

where

A = frequency factor (1/s)
E = activation energy (J/mole)
R = gas constant

Atreya[53] uses a moisture desorption kinetics equation for vaporization of the water in the wood, which is

$$\frac{\partial \rho_m}{\partial t} = -A_m \rho_m \exp(-E_m/RT) \quad (24)$$

The CMA model[54] developed for NASA provides good results for oven-dry wood because it includes surface recession. Parker[55] has taken char shrinkage parallel and normal to the surface into account in the model. Parker also includes different Arrhenius equations for each of the three major components of wood: (1) cellulose, (2) hemicelluloses, and (3) lignin. There may be not only moisture desorption but also an increase in moisture content behind the char front caused by moisture movement away from the surface.[56] A model of Fredlund[57] includes mass transfer as well as heat transfer and provides for surface recession due to char oxidation. In a model for wood combustion, Bryden[58] modeled the wood pyrolysis kinetics, including tar decomposition, using three competing primary reactions and two secondary reactions. The surface boundary layer includes both char shrinkage and surface recession due to char combustion.

Kanury and Holve[35] have presented dimensional, phenomenological, approximate analytical, and exact numerical solutions for wood charring. Other models include those of Havens,[59] Knudson and Schniewind,[60] Kansa et al.,[61] Hadvig and Paulsen,[62] and Tinney.[63]

A major issue in the use of the more sophisticated models is the adequacy of the available data to use as input. The thermophysical properties for wood pyrolysis models are discussed by Janssens.[64] While primarily for zone models, there is an ASTM Standard Guide for Data for Fire Models.[65] Wood properties are discussed at the conclusion of this chapter.

Most theoretical models for wood charring not only define the charring rate but also provide results for the temperature gradient. This temperature gradient is important in evaluating the load-carrying capacity of the wood remaining uncharred.

Load-Carrying Capacity of Uncharred Wood

In the standard ASTM E119 test of a wood member, structural failure occurs when the member is no longer capable of supporting its design load. The charring of the wood has reduced the cross-sectional area of the member such that the ultimate capacity of the residual member is exceeded. During the charring of the wood member, the temperature gradient is steep in the wood section remaining uncharred. The temperature at the innermost zone of the char layer is assumed to be 300°C. Because of the low thermal conductivity of wood, the temperature 6 mm inward from the base of the char layer is about 180°C once a quasi-steady-state charring rate has been obtained. Some loss of strength undoubtedly results from elevated temperatures. The peak moisture content occurs where the temperature of the wood is about 100°C, which is about 13 mm from the char base. Schaffer et al.[66] have combined parallel-to-grain strength and stiffness relationships with temperature and moisture content and the gradients of

temperature and moisture content within a fire-exposed slab to obtain graphs of relative modulus of elasticity, compressive strength, and tensile strength as a function of distance below the char layer. (See Figure 4-11.5.) The temperature profile in a semi-infinite wood slab can be expressed as an exponential term or a power term.[67] An equation based on a power term is

$$T = T_i + (300 - T_i)\left(1 - \frac{x}{d}\right)^2 \quad (25)$$

where

T = temperature (°C)
T_i = initial temperature (°C)
x = distance from the char front (mm)
d = thermal penetration depth (mm)

In the tests of White,[31] an average value for the thermal penetration depth was 33.[67] Based on European tests, a more conservative value of 40 was recommended for the thermal penetration depth.[67] The power term does not provide for the plateau in temperatures that often occurs at 100°C in moist wood. The power term has also been used to estimate the temperature profile in wood exposed to a constant heat flux.[41] The theoretical models discussed previously can be used to determine the temperature gradient within the wood remaining uncharred.

There are two approaches to evaluating the load-carrying capacity: to evaluate the remaining section either as a single homogeneous material or as a composite of layers or elements with different properties. In the single homogeneous material approach, one uses either reduced material properties or the room temperature material properties. A greater reduction in cross sectional area is calculated if the material properties are not reduced.

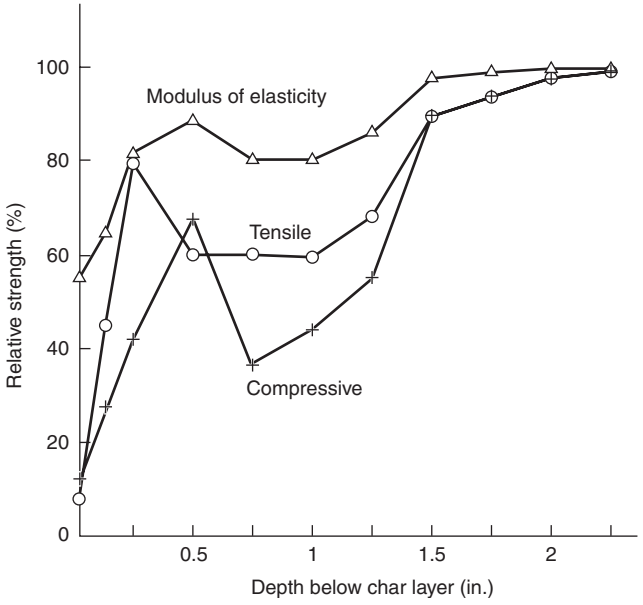

Figure 4-11.5. ***Relative modulus of elasticity and compressive and tensile strength as a function of distance below char layer in softwood section under fire exposures. (Expressed in percent of that at 25°C and initial moisture content of 12 percent). Duration of fire exposure should be equal to or greater than 20 min to apply results of this figure.***

Empirical α Models

One common approach in accounting for the loss in strength in the section remaining uncharred is to assume that the strength and stiffness of the entire uncharred region are fractions α of their room temperature values.

For bending rupture of a beam, an equation of this type would be

$$\frac{M}{S(t)} = \alpha\sigma_0 \quad (26)$$

where

M = applied moment (design load)
S = section modulus of charred member
σ_0 = modulus of rupture at room temperature
t = time

Assuming the residual cross-section is rectangular in shape before and during fire exposure, the section modulus of the charred member is[68]

$$S(t) = \frac{1}{6}\left[(B - 2C_1t)(D - jC_2t)^2\right] \quad (27)$$

where

B = original breadth of beam
D = original depth of beam
C_1 = charring rate in breadth direction
C_2 = charring rate in depth direction
j = 1 for three-sided fire exposure or 2 for four-sided fire exposure (Figure 4-11.6)

Alternative to Equations 22 and 23 are the following, Equations 28 through 30:

$$\frac{k}{\alpha}\frac{B/D}{[d/D - (1 - B/D)]} = \left(\frac{d}{D}\right)^2 \quad (28)$$

for exposure on all four sides,[69] and

$$\frac{k}{\alpha}\frac{B/D}{[B/D - 2(1 - d/D)]} = \left(\frac{d}{D}\right)^2 \quad (29)$$

for exposure on three sides,[70,71]

where

k = load, as fraction of room temperature ultimate load of original member
d = critical depth of the uncharred beam

The fire resistance is equal to the time to reach the critical depth, or

$$t = (D - d)/jC \quad (30)$$

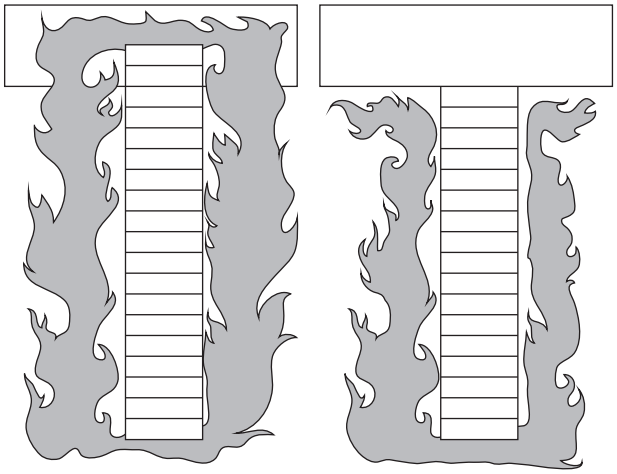

Figure 4-11.6. ***Fire exposure of beams on three or four sides.***

Proposed α values ranged from 0.5 in New Zealand to 0.83 in France.[68] The differences in α values are due to uncertainty, differences in design load, and desired level of safety. The application of the above equations is generally limited to large wood members. In light-frame members, α values would be substantially lower.[72] In Eurocode 5, this approach is called the "reduced strength and stiffness method." The reduction factors are a function of the perimeter of the fire-exposed residual cross section divided by the area of the cross section.

In addition to bending rupture, the fire resistance of a beam may depend on lateral buckling of the beam.[69] Similar expressions can be developed for columns and tension members.[68,70–71,73] Reviews of fire resistance design methodologies for large wood members include those of Schaffer,[68] Pettersson,[74] and Barthelemy and Kruppa.[75] Kirpichenkov and Romanenkov[76] discussed the calculation procedures in the Soviet Union. The fire resistance of wood structures is also briefly discussed by Odeen.[77]

In developing a model for fire-exposed unprotected wood joist floor assemblies, Woeste and Schaffer[78,79] evaluated various time-dependent geometric terms that could be used to modify the strength reduction factor, α. The selected term was

$$\alpha = \frac{1}{1 + (B + 2D/BD)\gamma t_f} \tag{31}$$

where

t_f = failure time

γ = empirical thermal degrade parameter

The model has been experimentally evaluated,[80,81] extended to floor-truss assemblies,[79,82] and used as part of a first-order second-moment reliability analysis of floor assemblies.[78,79] Reliability-based design of the fire endurance of light-frame construction is also discussed by Lau and Barrett.[72] In a model for metal plate–connected wood trusses,[83] the strength degradation factors for the wood are calculated as a function of the duration of exposure and the temperature profile within the wood component.

Effective Cross-Sectional Area Method

For a second approach, an equivalent zero-strength layer, δ, was calculated and the rest of the member is evaluated using room temperature property values. In the model of Schaffer and others[66] for beams, the δ was estimated to be 8 mm (0.3 in. thick). This zero-strength layer, δ, was added to the char depth, βt, to obtain the total zero-strength layer. This zero-strength layer model was incorporated within a reliability-based model to predict the strength of glued-laminated beams with individual laminates of various grades of lumber.[84] This zero-strength layer approach is called the "effective cross-section method" in Eurocode 5. In Eurocode 5, δ is 7 mm after 2 min (linear fraction of 7 mm up to 20 min). In Technical Report 10 of the American Wood Council,[85] a 20 percent increase in the charring rate is used.

Performance of the structural member in a fire will depend on the ratio of the applied load to the ultimate capacity of the residual member. Calculations of the structural capacity of the remaining cross section are normally made using ultimate strength values. Information on obtaining estimates for average ultimate values from allowable design values can be found in Technical Report 10. Examples of the structural calculations and load ratio tables are also provided. Design or characteristic strength values are used in the Eurocode 5 calculations. Design methods account for the various factors affecting performance in different manners. Care must be taken to ensure that all the design values and the methodologies are compatible.

For fire-damaged members, Williamson[86] recommended δ of 6 mm (0.25 in.) for designs controlled by compression (16 mm [0.625 in.] if design is controlled by tension) and the use of 100 percent of the original basic allowable stresses in calculation of load capacity.

Composite Models

The most complex approach to evaluating the fire endurance of a wood member is to assume that the uncharred region consists of layers or elements at different temperatures and moisture contents. The strength and stiffness properties are dependent on the temperature and moisture content profiles. These are referred to as *general calculation methods* in Eurocode 5. In one model with layers, the compressive and tensile strengths and modulus of elasticity of each layer are assumed to be fractions of the room temperature values. Using one 38-mm (1.5-in.) heated layer with reduced properties, Schaffer et al.[66] analyzed a beam using transformed section analysis. In the similar elastic transformed section model of King and Glowinski,[87] the heated zone of the remaining wood section is divided into two layers at elevated temperatures. Transformed section analysis is also used by Lee-Gun Kim and Jun-Jae Lee[88] and by Janssens.[89] A finite difference model for wood beams and columns was developed by Tavakkol-Khah and Klingsch.[90]

Do and Springer[91–93] proposed a fire resistance model for wood beams based on mass loss versus strength data.

The work included a program to predict the temperatures and mass loss within the wood member. The input data came from small-scale tension, compression, and shear tests done on specimens that had previously been heated in a muffle oven.

One-Hour Fire-Resistive Exposed Wood Members

Lie[70] developed simple formulas for calculating the fire resistance of large wood beams and columns based on theoretical studies involving experimental data and equations similar to Equations 26 through 30. These formulas are recognized by the building codes in the United States and Canada. The methodology is discussed in wood industry publications.[94,95] These formulas give the fire resistance time, t, in minutes, of a wood beam or column with minimum nominal dimension of 152 mm (6 in.). The net finish width for a nominal 152-mm (6-in.) glued-laminated member is 130 mm (5 1/8 inches).

For beams, the equations are

$$t = 2.54ZB\left[4 - 2\left(\frac{B}{D}\right)\right] \quad \text{for fire exposure on four sides} \tag{32}$$

$$t = 2.54ZB\left[4 - \left(\frac{B}{D}\right)\right] \quad \text{for fire exposure on three sides} \tag{33}$$

where

B = width (breadth) of a beam before exposure to fire (in.)

D = depth of a beam before exposure to fire (in.)

Z = load factor (See Figure 4-11.7.)

For columns, the equations are

$$t = 2.54ZD\left[3 - \left(\frac{D}{B}\right)\right] \tag{34}$$

for fire exposure on four sides

$$t = 2.54ZD\left[3 - \left(\frac{D}{2B}\right)\right] \tag{35}$$

for fire exposure on three sides

where

B = larger side of a column (in.)

D = smaller side of a column (in.)

The 2.54Z factor in the above equations is 0.10Z for SI units of mm. For columns, the load factor, Z (see Figure 4-11.7) includes the effect of the effective length factor, K_e, (see Figure 4-11.8) and the unsupported length of the column, ℓ. Currently, the codes do not permit the wide side of the column to be the unexposed face (Equation 34). The full dimensions of the column are used even if the column is recessed into a wall.

Connectors and fasteners relating to support of the member must be protected for equivalent fire-resistive construction. Where minimal 1-hr fire endurance is required, connectors and fasteners must be protected from fire exposure by 38 mm (1 1/2 in.) of wood, appropriate thickness of fire rated gypsum board, or any coating approved for a 1-hr rating. The American Forest & Paper Association publication[94] on the procedure includes diagrams giving typical details of such protection. Carling[96] summarized work done in Europe on the fire resistance of joint details in load-bearing wood construction. Eurocode 5 also includes information on calculating the fire endurance of connections and protecting connections in fire-rated timber members.

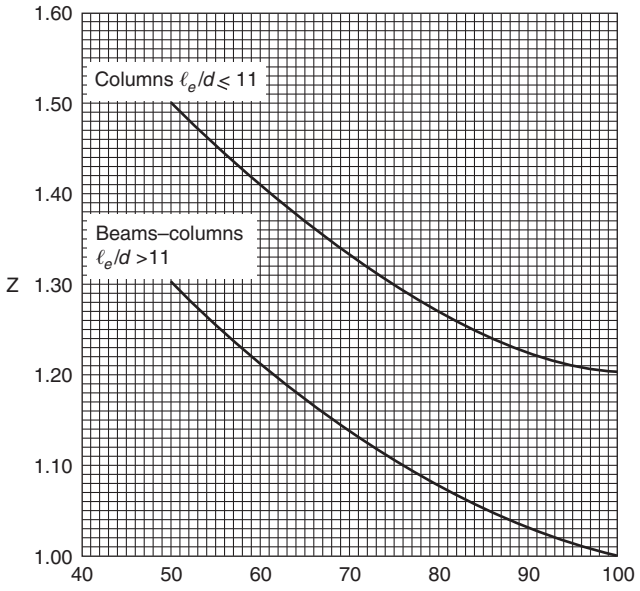

Figure 4-11.7. ***Load factor versus load on member as percent of allowable. (NBCC uses 12 instead of 11 as criterion for two curves.) Effective column length, ℓ_e, is equal to $K_e\ell$ (Fig. 4-11.8) and d is cross-sectional dimension in plane of lateral support.***

There is often a high-strength tension laminate on the bottom of glued-laminated timber beams. As a result, it is required that a core lamination be removed, the tension zone moved inward, and the equivalent of an extra nominal 51-mm- (2-in.-) thick outer tension lamination be added to ensure that there is still a high-strength laminate left after fire exposure.

EXAMPLE 3:

Determine the fire resistance rating for a 5 1/8-in. × 21-in. (130-mm × 533-mm) beam exposed to fire on three sides and loaded to 75 percent of its allowable load.

$$D = 21 \text{ in.}$$

$$B = 5.125 \text{ in.}$$

From Figure 4-11.7, Z for beam loaded to 75 percent of allowable is 1.1. From Equation 33,

$$t = 2.54(1.1)(5.125)([4 - (5.125/21)]$$

$$t = 53.8 \text{ min}$$

The methodology of this section has building code recognition in the United States and Canada but is only applic-

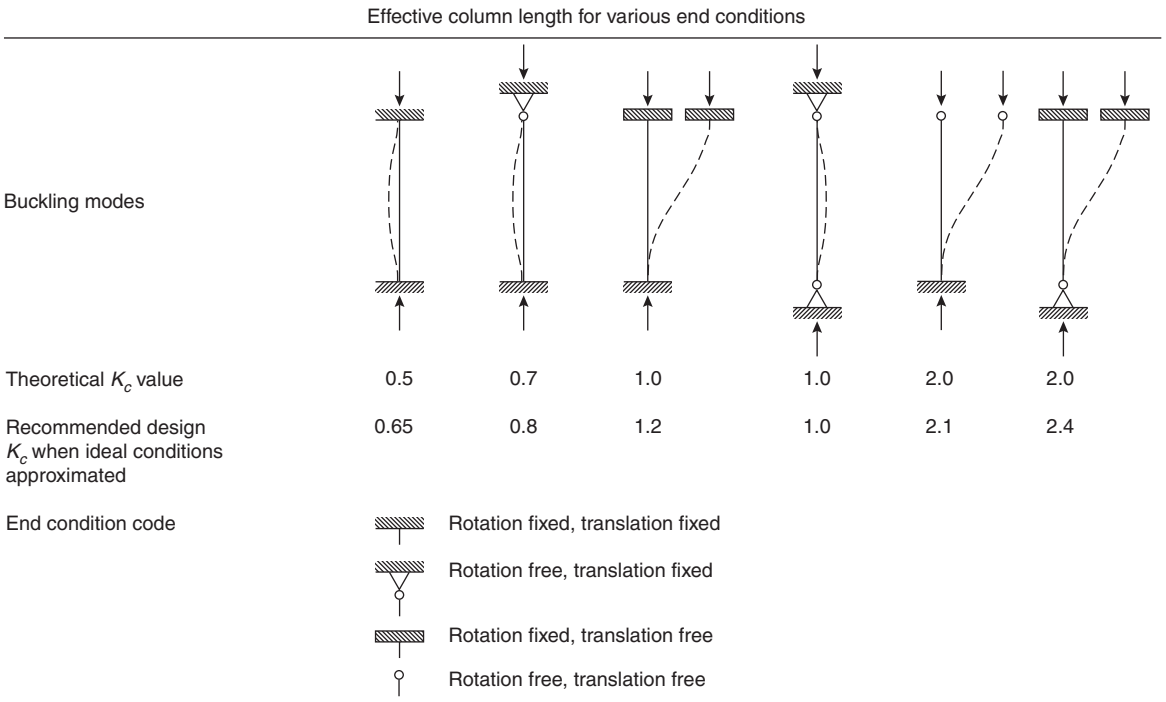

Figure 4-11.8. ***Effective column length.***

able to large wood beams and columns. There is no recognized procedure for solid wood floors or roofs. Possible methodologies for the structural analysis of these timber decks can be found in Technical Report 10,[85] in an article by Janssens,[89] and in Eurocode 5. A methodology for estimating the times for thermal failure is in Eurocode 5. The method is based on the design charring rates and a reduction coefficient for the joints in the timber decks.[89]

Property Data

Proper input data are critical to the use of any model. For the models discussed in this section, property data include strength and stiffness properties and thermal properties. Property data for wood can be found in the various chapters of *Wood Handbook: Wood as an Engineering Material*[32] (available as pdf files from www.fpl.fs.fed.us). A chapter on fire safety is also in the *Wood Handbook.* Equations and graphs of the strength and stiffness of wood as functions of temperature and moisture content are available.[97–99] Recent research in the development of fire endurance models has provided additional data specific for application to such models. An extensive study on fire-exposed wood in tension was done by Lau and Barrett.[100] Thermal properties can also be found in the various references for charring models, Annex E of Eurocode 5, and in other sources.[64,65,101]

While it is often less complicated to assume constant property values, these properties are very often a function of other properties or factors. Most wood properties are functions of density, moisture content, grain orientation, and temperature. Chemical composition may also be a factor. Since an understanding of these factors is important to the application of property data, the factors are defined in the rest of this section.

The oven-dry density of wood can range from 160 kg/m^3 (10 lb/ft^3) to over 1040 kg/m^3 (65 lb/ft^3), but most species are in the 320 to 720 kg/m^3 (20 to 45 lb/ft^3) range.[32] The density of wood relative to the density of water (i.e., specific gravity) is normally based on the oven-dry weight and the volume at some specified moisture content, but in some cases the oven-dry volume is used. As the empirical equations for charring rate show, the materials with higher density have slower char rate.

Wood is a hygroscopic material, which gains or loses moisture depending upon the temperature and relative humidity of the surrounding air. Moisture content of wood is defined as the weight of water in wood divided by the weight of oven-dry wood. Green wood can have moisture content in excess of 100 percent. However, air-dry wood comes to equilibrium at moisture content less than 30 percent. Thirty percent moisture content is also considered the approximate moisture content at which the cell walls are saturated with water but there is no water in the cell lumens. This condition is known as the *fiber saturation point.* At higher moisture contents, water exists in the cell lumens. Many physical and mechanical properties of wood only change with moisture content at moisture contents below the fiber saturation point. Under the conditions stated in ASTM E119 (23°C, 50 percent relative humidity), the equilibrium moisture content is 9 percent. Moisture generally reduces the strength of wood but also reduces the charring rate.

Both density and moisture content affect the thermal conductivity of wood. The average thermal conductivity perpendicular to the grain is[32]

$$k = S(0.0001941 + 0.000004064M) + 0.01864 \quad (36)$$

where

k = thermal conductivity (W/m·K)

S = density based on volume at current moisture content and oven-dry weight (kg/m^3)

M = moisture content (percent)

The above equation is valid for moisture contents of 25 percent or less, densities greater than 300 kg/m^3, and temperature of 24°C. Conductivity increases about 2 to 3 percent per 10°C.[32]

The fiber (grain) orientation is important because wood is an orthotropic material.The longitudinal axis is parallel to the fiber or grain. The two transverse directions (perpendicular to the grain) are the radial and tangential axes. The radial axis is normal to the growth rings, and the tangential axis is tangent to the growth rings. For example, the longitudinal strength properties are usually about 10 times the transverse properties, and the longitudinal thermal conductivity is 1.5 to 2.8 times the transverse property.

In fire-resistance analysis, temperature can have a significant influence on the properties of wood. The preponderance of property data is often limited to temperatures below 100°C. The effect of temperatures on the strength properties of wood is shown in Figures 4-11.9 through 4-11.11. The heat capacity, c_ρ, (kJ/kg·K) of dry wood is approximately related to temperature, t, in K) by[32]

$$c_\rho = 0.1031 + 0.003867t \quad (37)$$

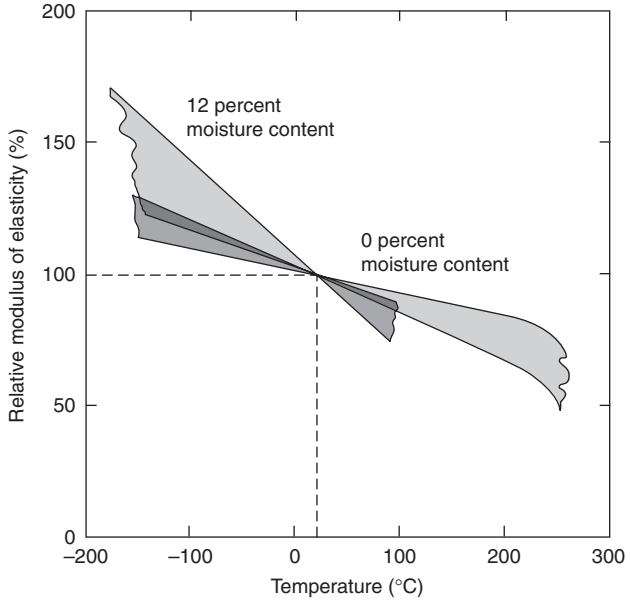

Figure 4-11.9. ***The immediate effect of temperature on modulus of elasticity parallel to the grain at two moisture contents relative to value at 20°C. The plot is a composite of results from several studies. Variability in reported trends is illustrated by the width of bands.[32]***

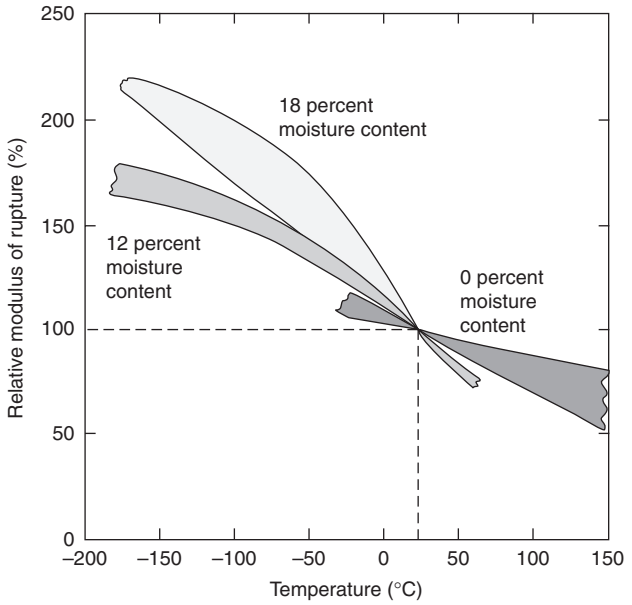

Figure 4-11.10. ***The immediate effect of temperature on modulus of rupture in bending at three moisture contents relative to value at 20°C.[32]***

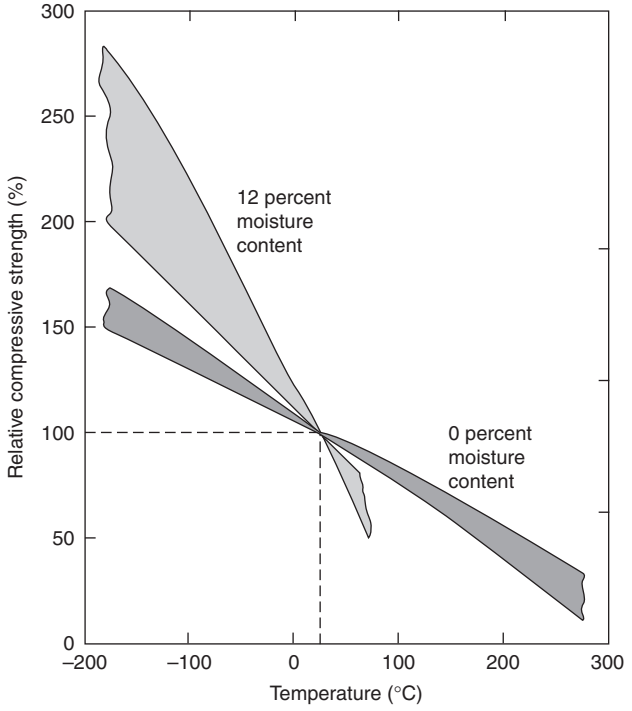

Figure 4-11.11. ***The immediate effect of temperature on compressive strength parallel to the grain at two moisture contents relative to the value at 20°C.***

For moist wood below the fiber saturation point, the heat capacity is the sum of the heat capacity of dry wood and that of water and an additional adjustment factor for the wood–water bond.[32]

The major components of wood are cellulose, lignin, hemicelluloses, extractives, and inorganic materials (ash). Softwoods have lignin contents of 23 to 33 percent, while hardwoods have only 16 to 25 percent. The types and amounts of extractives vary. Cellulose content is generally around 50 percent by weight. The component sugars of the hemicelluloses are different for the hardwood and softwood species. Chemical composition can affect the kinetics of pyrolysis (Equation 23) and the percentage weight of the residual char. In the degradation of wood, higher lignin content results in greater char yield.

References Cited

1. ASTM E119, *Standard Test Methods for Fire Tests of Building Construction and Materials,* American Society for Testing and Materials, West Conshohocken, PA.
2. *Fire Resistance Directory,* Underwriters Laboratories, Northbrook, IL (annual).
3. *Fire Resistance Design Manual,* Gypsum Association, Washington, DC (1997).
4. ASTM E-2032-99, *Standard Guide for Extension of Data from Fire Endurance Tests,* American Society for Testing and Materials, West Conshohocken, PA (1999).
5. ENV 1995-1-2:1994, *Eurocode 5: Design of timber structures—Part 1-2: General rules—Structural design,* European Committee for Standardization, Brussels (1994).
6. T.Z. Harmathy, "Ten Rules of Fire Endurance Rating," *Fire Tech.,* 1, p. 93 (1965).
7. DCA No. 4: *Component Additive Method (CAM) for Calculating and Demonstrating Assembly Fire Endurance,* American Forest & Paper Association, Washington, DC (1991).
8. *Fire Safety Design in Buildings,* Canadian Wood Council, Ottawa (1996).
9. P.C.R. Collier, "Design of Loadbearing Light Timber Frame Walls for Fire Resistance: Part 1," *Study Report No. 36,* Building Research Association of New Zealand, Judgeford (1991).
10. B. Östman, J. König, and J. Norén, "Fire Behaviour of Timber Frame Structures," *Rapport I 9612091,* Trätek, Stockholm (1996).
11. R.H. White, "Use of Coatings to Improve Fire Resistance of Wood," in *ASTM STP 826,* American Society for Testing and Materials, Philadelphia (1983).
12. L.R. Richardson and A.A. Cornelissen, "Fire-Resistant Coatings for Roof/Ceiling Deck Timbers," *Fire and Materials,* 11, p. 191 (1987).
13. R.H. White, "An Empirical Model for Predicting Performance of Fire-Resistive Coatings in Wood Construction," *J. of Test. and Eval.,* 14, p. 97 (1986).
14. Z. Huntierová and G. Wegener, "The Effects of Fire Retardants of the Behaviour of Solid Wood and Glulam Beams Loaded in Bending," in *Proc. Of Wood and Fire Safety Conference,* Technical University Zvolen, Zvolen, Slovak Republic (1996).
15. *Fire Resistance of Wood Structures,* Technical Research Centre of Finland, Helsinki (1980).
16. W.D. Gardner and D.R. Syme, "Charring of Glue-Laminated Australian-Grown Timber Species and the Effect of 13 mm Gypsum Plaster-Board on Their Charring," *Technical Report No. 5,* NSW Timber Advisory Council Ltd., Sydney (1991).
17. F.C.W. Fung, "A Computer Program for the Thermal Analysis of the Fire Endurance of Construction Walls," *NBSIR 77-1260,* National Bureau of Standards, Washington, DC (1977).
18. B.W. Gammon, "Reliability Analysis of Wood-Frame Wall Assemblies Exposed to Fire," Ph.D. Dissertation, University of California, Berkeley (1987).
19. J.R. Mehaffey, P. Cuerrier, and G. Carisse, "A Model for Predicting Heat Transfer through Gypsum-Board/Wood-Stud Walls Exposed to Fire," *Fire and Materials,* 18, p. 297 (1994).
20. H. Takeda and J.R. Mehaffey, "WALL2D: A Model for Predicting Heat Transfer through Wood-Stud Walls Exposed to Fire," *Fire and Materials,* 22, p. 133 (1998).
21. J. König, "Fire Tests of Load-Carrying Timber Frame Assemblies Exposed to Standard and Parameteric Fires," in *Proc. of Fire and Materials '98 Conference,* Interscience Communications Ltd., London (1998).
22. P. Collier, "A Model for Predicting the Fire-Resisting Performance of Small-Scale Cavity Walls in Realistic Fires," *Fire Technology,* 32, 2, p. 120 (1996).
23. A.H. Buchanan and G.C. Thomas, "Predicting the Real Fire Performance of Light Timber Frame Construction," in *Proc. of Wood and Fire Safety Conference,* Technical University Zvolen, Zvolen, Slovak Republic (1996).
24. P. Clancy, "A Model for Predicting the Probability of Failure of Wood Framed Walls and Floors in Real Fire," in *Proc. of Wood and Fire Safety Conference,* Technical University Zvolen, Zvolen, Slovak Republic (1996).
25. F.L Browne, "Theories of the Combustion of Wood and Its Control—A Survey of the Literature," *Report No. 2136,* USDA Forest Service, Forest Product Lab., Madison, WI (1966).
26. E.L. Schaffer, "Review of Information Related to the Charring Rate of Wood," *Res. Note FPL-145,* USDA Forest Service, Forest Product Lab., Madison, WI (1966).
27. E.L. Schaffer, "State of Structural Timber Fire Endurance," *Wood and Fiber,* 9, p. 145 (1977).
28. G.S. Hall, R.G. Saunders, R.T. Allcorn, P.E. Jackman, M.W. Hickey, and R. Fitt, *Fire Performance of Timber—A Literature Survey,* Timber Research and Development Association, High Wycombe, UK (1971).
29. S. Hadvig, *Charring of Wood in Building Fires,* Technical University of Denmark, Lyngby (1981).
30. E.L. Schaffer, "Charring Rate of Selected Woods—Transverse to Grain," *Res. Pap. FPL 69,* USDA Forest Service, Forest Product Lab., Madison, WI (1967).
31. R.H. White and E.V. Nordheim, "Charring Rate of Wood for ASTM E119 Exposure," *Fire Technology,* 28, p. 5 (1992).
32. *Wood Handbook: Wood as an Engineering Material,* Forest Products Society, Madison, WI (1999).
33. M. Lache, *Holz-Zentralblatt,* 117, p. 473 (1991).
34. P.C.R. Collier, "Charring Rates of Timber," *Study Report No. 42,* Building Research Association of New Zealand, Judgeford (1992).
35. A.M. Kanury and D.J. Holve, "A Theoretical Analysis of the ASTM E119 Standard Fire Test of Building Construction and Materials," *NBS-GCR 76-50,* National Bureau of Standards, Washington, DC (1975).
36. B.J. Noren and B.A.-L. Ostman, "Contribution to Fire Resistance from Building Panels," in *Fire Safety Science—Proceedings of the First International Symposium,* Hemisphere, New York (1986).
37. E.L. Schaffer, "Effect of Fire-Retardant Impregnations on Wood Charring Rate," *J. Fire and Flamm.,* 1, p. 96 (1974).
38. P.W.C. Lau, I. Van Zeeland, and R. White, "Modelling the Char Behaviour of Structural Timber," in *Proc. of Fire and Materials '98 Conference,* Interscience Communications Ltd., London (1998).
39. C.P. Butler, "Notes on Charring Rates in Wood," *F.R. Note No. 896,* Joint Fire Research Organization, Borehamwood, UK (1971).
40. H.C. Tran and R.H. White, "Burning Rate of Solid Wood Measured in a Heat Release Rate Calorimeter," *Fire and Materials,* 16, p. 197 (1992).

41. R.H. White and H.C. Tran, "Charring Rate of Wood Exposed to a Constant Flux," in *Proc. of Wood and Fire Safety Conference,* Technical University Zvolen, Zvolen, Slovak Republic (1996).
42. E. Mikkola, "Charring of Wood Based Materials," in *Fire Safety Science—Proceedings of the Third International Symposium,* Elsevier Applied Science, London (1991).
43. T. Harada, "Charring of Wood with Thermal Radiation II," *Mokuzai Gakkaishi,* 42, 2, p. 194 (1996).
44. E. Mikkola, "Charring of Wood," *Research Reports 689,* Technical Research Centre of Finland, Espoo (1990).
45. R.M. Nussbaum, "The Effect of Low Concentration Fire Retardant Impreganations on Wood Charring Rate and Char Yield," *J. Fire Sciences,* 6, p. 290 (1988).
46. O. Pettersson, S.E. Magnusson, and J. Thor, "Fire Engineering Design of Steel Structures," *Publication 50,* Swedish Institute of Steel Construction, Stockholm, Sweden (1976).
47. F.B. Olesen and J. König, "Tests on Glued Laminated Beams in Bending Exposed to Natural Fires," *Report No. I 9210061,* Swedish Institute for Wood Technology Research (Tratek), Stockholm, Sweden (1991).
48. A.F. Roberts, "Problems Associated with the Theoretical Analysis of the Burning of Wood," in *Thirteenth Symposium Int. on Combustion,* Combustion Institute, Pittsburgh, PA (1971).
49. C.H. Bamford, J. Crank, and D.H. Malan, "The Combustion of Wood, Part I," *Proc. of Camb. Phil. Soc.,* 46, p. 166 (1946)
50. P.H. Thomas, "On the Rate of Burning of Wood," *Fire Research Note No. 446,* Fire Research Station, Borehamwood, UK (1960).
51. H. Kung, "A Mathematical Model of Wood Pyrolysis," *Combustion and Flame,* 18, p. 185 (1972).
52. F. Tamanini, "A Numerical Model for One-Dimensional Heat Conduction with Pyrolysis in a Slab of Finite Thickness," in *Appendix A of Factory Mutual Research Corporation Report No. 21011.7,* Factory Mutual Research Corp., Norwood, MA (1976).
53. A. Atreya, *Pyrolysis: Ignition and Fire Spread on Horizontal Surfaces of Wood,* Ph.D. Thesis, Harvard University, Cambridge (1983).
54. R.H. White and E.L. Schaffer, "Application of CMA Program to Wood Charring," *Fire Tech.,* 14, p. 279 (1978).
55. W.J. Parker, "Prediction of the Heat Release Rate of Douglas Fir," in *Fire Safety Science—Proceedings of the Second International Symposium,* Hemisphere, New York (1989).
56. R.H. White and E.L. Schaffer, "Transient Moisture Gradient in Fire-Exposed Wood Slab," *Wood and Fiber,* 13, p. 17 (1981).
57. B. Fredlund, "Modelling of Heat and Mass Transfer in Wood Structures during Fire," *Fire Safety J.,* 20, p. 39 (1993).
58. K.M. Bryden, *Computational Modeling of Wood Combustion,* Ph.D. Dissertation, University of Wisconsin–Madison, Madison, WI (1998).
59. J.A. Havens, *Thermal Decomposition of Wood,* Ph.D. Dissertation, University of Oklahoma, Norman (1969).
60. R.M. Knudson and A.P. Schniewind, "Performance of Structural Wood Members Exposed to Fire," *Forest Prod. J.,* 25, p. 23 (1975).
61. E.J. Kansa, H.E. Perlee, and R.F. Chaiken, "Mathematical Model of Wood Pyrolysis Including Internal Forced Convection," *Comb. And Flame,* 29, p. 311 (1977).
62. S. Hadvig and O.R. Paulsen, "One-Dimensional Charring Rates in Wood," *J. Fire and Flamm.,* 1, p. 433 (1976).
63. E.R. Tinney, "The Combustion of Wood Dowels in Heated Air," in *Tenth Symposium (Int.) on Combustion,* The Combustion Institute, Pittsburgh (1965).
64. M. Janssens, "Thermo-physical Properties for Wood Pyrolysis Models," in *Proc. of Pacific Timber Engineering Conference,* Timber Research and Development Advisory Council, Fortitude Valley MAC, Queensland, Australia (1994).
65. ASTM E-1591-94, *Standard Guide for Data for Fire Models,* American Society for Testing and Materials, West Conshohocken, PA (1994).
66. E.L. Schaffer, C.M. Marx, D.A. Bender, and F.E. Woeste, "Strength Validation and Fire Endurance of Glued-Laminated Timber Beams," *Res. Pap. FPL 467,* USDA Forest Service, Forest Product Lab., Madison, WI (1986).
67. M.L. Janssens and R.H. White, "Short Communication: Temperature Profiles in Wood Members Exposed to Fire," *Fire and Materials,* 18, p. 263 (1994).
68. E.L. Schaffer, "Structural Fire Design: Wood," *Res. Pap FPL 450,* USDA Forest Service, Forest Product Lab., Madison, WI (1984).
69. C. Imaizumi, "Stability in Fire of Protected and Unprotected Glued Laminated Beams," *Norsk Skogind,* 16, p. 140 (1962).
70. T.T. Lie, "A Method for Assessing the Fire Resistance of Laminated Timber Beams and Columns," *Can. J. of Civil Engg.,* 4, p. 161 (1977).
71. K. Odeen, "Fire Resistance of Glued Laminated Timber Structures," in *Fire and Structural Use of Timber in Buildings,* Her Majesty's Stationery Office, London (1970).
72. P.W.C. Lau and J.D. Barrett, "Factors Affecting Reliability of Light-Framing Wood Members Exposed to Fire—A Critical Review," *Fire and Materials,* 18, p. 339 (1994).
73. C. Meyer-Ottens, "Junctions in Wood Structures—Total Construction," in *Three Decades of Structural Fire Safety,* Building Research Establishment, Fire Research Station, Borehamwood, England (1983).
74. O. Pettersson, "Fire Design of Wood Structures," in *Three Decades of Structural Fire Safety,* Building Research Establishment, Borehamwood, UK (1983).
75. B. Barthelemy and J. Kruppa, *Resistance au Leu des Structures,* Editions Eyrolles, Paris (1978).
76. G.M. Kirpichenkov and I.G. Romanenkow, "Basic Principles of Calculating Fire Resistance of Timber Structures," *NBSIR 80-2188,* National Bureau of Standards, Washington, DC pp. 181–189 (1980).
77. K. Odeen, "Fire Resistance of Wood Structures," *Fire Tech.,* 21 p. 34 (1985).
78. F.E. Woeste and E.L. Schaffer, "Second Moment Reliability Analysis of Fire Exposed Wood Joist Floor Assemblies," *Fire and Matls.,* 3, p. 126 (1979).
79. F.E. Woeste and E.L. Schaffer, "Reliability Analysis of Fire Exposed Light-Frame Wood Floor Assemblies," *Res. Pap. FPL 386,* USDA Forest Service, Forest Product Lab., Madison, WI (1981).
80. R.H. White, E.L. Schaffer, and F.E. Woeste, "Replicate Fire Endurance Tests of an Unprotected Wood Joist Floor Assembly," *Wood and Fiber,* 16, p. 374 (1984).
81. E.L. Schaffer and R.H. White, "Fire Endurance Model Validation by Unprotected Joist Floor Fire Testing," in *Proc. 1988 International Conference on Timber Engineering,* Forest Products Research Society, Madison, WI (1988).
82. E.L. Schaffer and F.E. Woeste, "Reliability Analysis of a Fire-Exposed Unprotected Floor Trusses," in *Proceedings, Metal Plate Wood Truss Conference,* Forest Products Research Society, Madison, WI (1985).
83. R.H. White, S.M. Cramer, and D. Shrestha, "Fire Endurance Model for a Metal-Plate-Connected Wood Truss," *Res. Pap. FPL 522,* USDA Forest Service, Forest Products Lab., Madison, WI (1993).

84. D.A. Bender, F.E. Woeste, E.L. Schaffer, and C.M. Marx, "Reliability Formulation for the Strength and Fire Endurance of Glued-Laminated Beams," *Res. Pap. FPL 460,* USDA Forest Service, Forest Prod. Lab., Madison, WI (1985).
85. Technical Report 10, *Calculating the Fire Resistance of Exposed Wood Members,* American Forest & Paper Association, Washington, DC (1999).
86. T.G. Williamson, "Rehabilitation of Fire-Damaged Timber—The Filene Center," in *Evaluation, Maintenance, and Upgrading of Wood Structures,* American Society of Civil Engineers, New York (1982).
87. E.G. King and R.W. Glowinski, "A Rationalized Model for Calculating the Fire Endurance of Wood Beams," *Forest Prod. J.,* 38, 10, p. 31 (1988).
88. Lee-Gun Kim and Jun-Jae Lee, "Studies on Prediction about Behavior of Wood Beam under Standard Fire Condition," *Mokchae Konghak,* 23, 4, p. 10 (1995).
89. M.L. Janssens, "A Method for Calcualting the Fire Resistance of Exposed Timber Decks," in *Fire Safety Science—Proceedings of the Fifth International Symposium,* International Association for Fire Safety Science, Boston (1997).
90. M. Tavakkol-Khah and W. Klingsch, "Calculation Model for Predicting Fire Resistance Time of Timber Members," in *Fire Safety Science—Proceedings of the Fifth International Symposium,* International Association for Fire Safety Science, Boston (1997).
91. M.H. Do and G.S. Springer, "Mass Loss of and Temperature Distribution in Southern Pine and Doublas Fir in the Range 100 to 800°C," *J. of Fire Sci.,* 1, p. 271 (1983).
92. M.H. Do and G.S. Springer, "Model for Predicting Changes in the Strengths and Moduli of Timber Exposed to Elevated Temperatures," *J. of Fire Sci.,* 1, p. 285 (1983).
93. M.H. Do and G.S. Springer, "Failure Time of Loaded Wooden Beams During Fire," *J. of Fire Sci.,* 1, p. 297 (1983).
94. DCA No. 2, *Design of Fire-Resistive Exposed Wood Members,* American Forest & Paper Association, Washington, DC (1985).
95. American Institute of Timber Construction, *Timber Construction Manual,* John Wiley and Sons, New York (1985).
96. O. Carling, "Fire Resistance of Joint Details in Loadbearing Timber Construction—A Literature Survey," *Study Report No. 18,* Building Research Association of New Zealand, Judgeford, NZ (1989).
97. C.C. Gerhards, "Effect of Moisture Content and Temperature on Mechanical Properties of Wood: An Analysis of Immediate Effects," *Wood and Fiber Science,* 14, p. 4 (1982).
98. F.C. Beall, "Effect of Temperature on the Structural Uses of Wood and Wood Products," in *Structural Use of Wood in Adverse Environments,* Van Nostrand Reinhold, New York (1982).
99. B.A.-L. Ostman, "Wood Tensile Strength at Temperature and Moisture Contents Simulating Fire Conditions," *Wood Sci. Tech.,* 19, p. 103 (1985).
100. P.W. Lau and J.D. Barrett, "Modeling Tension Strength Behaviour of Structural Lumber Exposed to Elevated Temperatures," in *Fire Safety Science—Proceedings of the Fifth International Symposium,* International Association for Fire Safety Science, Boston (1997).
101. K.W. Ragland, D.J. Aerts, and A.J. Baker, "Properties of Wood for Combustion Analysis," *Bioresource Technology,* 37, p. 161 (1991).

CHAPTER 12

Smoke Control

John H. Klote

Introduction

In building fires, smoke often flows to locations remote from the fire, threatening life and damaging property. Stairwells and elevators frequently become smoke-logged, thereby blocking and/or inhibiting evacuation. Today smoke is recognized as the major killer in fires.[1]

In the late 1960s, the idea of using pressurization to prevent smoke infiltration of stairwells started to attract attention. This was followed by the idea of the "pressure sandwich," that is, venting or exhausting the fire floor and pressurizing the surrounding floors. Frequently, the building's ventilation system is used for this purpose. The term *smoke control* was coined as a name for such systems that use pressurization produced by mechanical fans to limit smoke movement in fires.

Research in the field of smoke control has been conducted in Australia, Canada, England, France, Japan, the United States, and West Germany. This research has consisted of field tests, full-scale fire tests, and computer simulations. Many buildings have been built with smoke control systems and numerous others have been retrofitted for smoke control.

In this chapter the term *smoke* is defined in accordance with the American Society for Testing and Materials (ASTM)[2] and the National Fire Protection Association (NFPA)[3] definitions that state that smoke consists of the airborne solid and liquid particulates and gases evolved when a material undergoes pyrolysis of combustion.

Smoke Movement

A smoke control system must be designed so that it is not overpowered by the driving forces that cause smoke movement. For this reason, an understanding of the fundamental concepts of smoke movement and of smoke control is a prerequisite to intelligent smoke control design. The major driving forces causing smoke movement are stack effect, buoyancy, expansion, wind, and the heating, ventilating, and air conditioning (HVAC) system. Generally, in a fire, smoke movement will be caused by a combination of these driving forces. The following subsections are a discussion of each driving force as it would act independent of the presence of any other driving force.

Stack Effect

When it is cold outside, there is often an upward movement of air within building shafts such as stairwells, elevator shafts, dumbwaiter shafts, mechanical shafts, or mail chutes. This phenomenon is referred to as a *normal stack effect*. The air in the building has a buoyant force because it is warmer and less dense than the outside air. This buoyant force causes air to rise within the shafts of buildings. The significance of normal stack effect is greater for low outside temperatures and for tall shafts. However, normal stack effect can exist in a one-story building.

When the outside air is warmer than the building air, a downward airflow frequently exists in shafts. This downward airflow is called reverse stack effect. At standard atmospheric pressure, the pressure difference due to either normal or reverse stack effect is expressed as

$$\Delta P = K_s\left(\frac{1}{T_0} - \frac{1}{T_I}\right)h \qquad (1)$$

where

ΔP = pressure difference (in. H_2O [Pa])

T_0 = absolute temperature of outside air (R [K])*

T_I = absolute temperature of air inside shaft (R [K])*

Dr. John H. Klote is a consulting engineer living in McLean, Virginia.

*Because the Fahrenheit and Celsius temperature scales are so commonly used by design engineers, these scales are used exclusively in the discussions in the text and in figures. However, the reader is cautioned to use absolute temperatures in calculations where such temperatures are stipulated.

h = distance above neutral plane, ft (m)*
K_S = coefficient, 7.64 (3460)

For a building 200 ft (60 m) tall, with a neutral plane at the midheight, an outside temperature of 0°F (−18°C) and an inside temperature of 70°F (21°C), the maximum pressure difference due to stack effect would be 0.22 in. H_2O (55 Pa). This means that at the top of the building, a shaft would have a pressure of 0.22 in. H_2O (55 Pa) greater than the outside pressure. At the bottom of the shaft, the shaft would have a pressure of 0.22 in. H_2O (55 Pa) less than the outside pressure. Figure 4-12.1 is a diagram of the pressure difference between a building shaft and the outside. In the diagram, a positive pressure difference indicates that the shaft pressure is higher than the outside pressure, and a negative pressure difference indicates the opposite.

Stack effect is usually thought of as existing between the inside of a building and the outside atmosphere. The air movement in buildings caused by both normal and reverse stack effect is illustrated in Figure 4-12.2. In this case, the pressure difference expressed in Equation 1 would actually refer to the pressure difference between the shaft and the outside of the building.

Figure 4-12.3 can be used to determine the pressure difference due to stack effect. For normal stack effect, the term $\Delta P/h$ is positive, and the pressure difference is positive above the neutral plane and negative below it. For reverse stack effect, the term $\Delta P/h$ is negative, and the pressure difference is negative above the neutral plane and positive below it.

*The neutral plane is the horizontal plane where the hydrostatic pressure inside equals that outside.

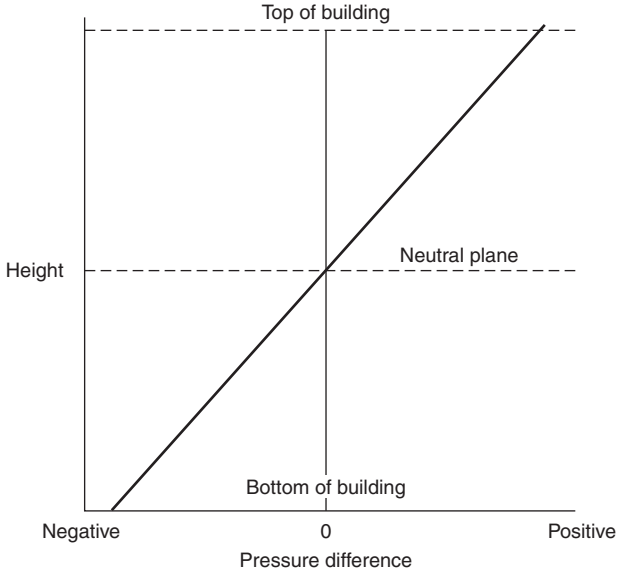

Figure 4-12.1. ***Pressure difference between an inside shaft and the outside due to normal stack effect.***

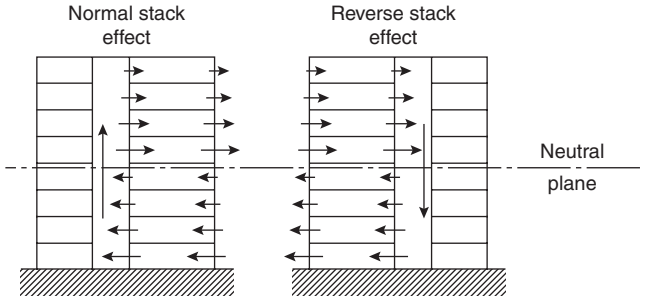

Figure 4-12.2. ***Air movement due to normal (left) and reverse stack effect (right). Note: arrows indicate direction of air movement.***

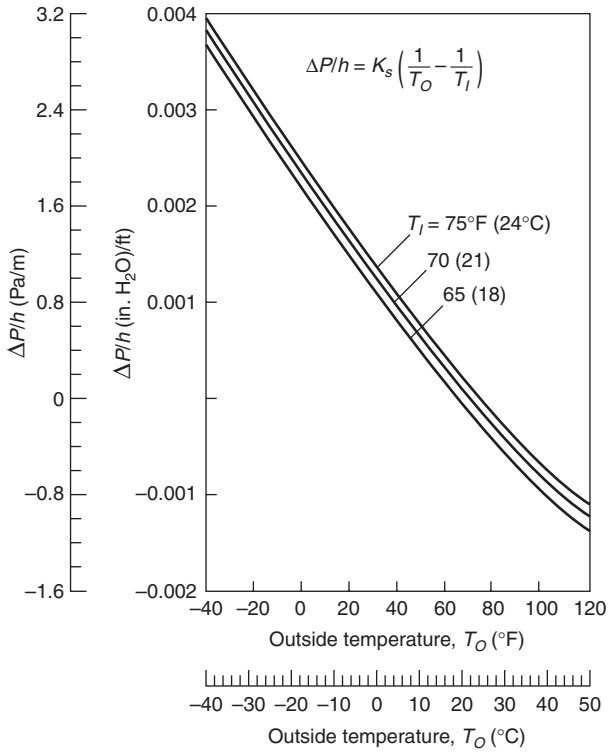

Figure 4-12.3. ***Pressure difference due to stack effect.***

In unusually airtight buildings with exterior stairwells, reverse stack effect has been observed even with low outside air temperatures.[4] In this situation, the exterior stairwell temperature was considerably lower than the building temperature. The stairwell was the cold column of air and other shafts within the building were the warm columns of air.

When considering stack effect, if the air leakage paths between a building and the outside are fairly uniform with height, the neutral plane will be located near the midheight of the building. However, when the leakage paths are not uniform, the location of the neutral plane can vary considerably, as in the case of vented shafts. McGuire

and Tamura[5] provide methods for calculating the location of the neutral plane for some vented conditions.

Smoke movement from a building fire can be dominated by stack effect. In a building with normal stack effect, the existing air currents (as shown in Figure 4-12.2) can move smoke considerable distances from the fire origin. If the fire is below the neutral plane, smoke moves with the building air into and up the shafts. This upward smoke flow is enhanced by any buoyancy forces on the smoke existing due to its temperature. Once above the neutral plane, the smoke flows out of the shafts into the upper floors of the building. If the leakage between floors is negligible, the floors below the neutral plane, except the fire floor, will be relatively smoke free until the quantity of smoke produced is greater than can be handled by stack effect flows.

Smoke from a fire located above the neutral plane is carried by the building airflow to the outside through openings in the exterior of the building. If the leakage between floors is negligible, all floors other than the fire floor will remain relatively smoke-free, again, until the quantity of smoke produced is greater than can be handled by stack effect flows. When the leakage between floors is considerable, there is an upward smoke movement to the floor above the fire floor.

The air currents caused by reverse stack effect are also shown in Figure 4-12.2. These forces tend to affect the movement of relatively cool smoke in the reverse of normal stack effect. In the case of hot smoke, buoyancy forces can be so great that smoke can flow upward even during reverse stack effect conditions.

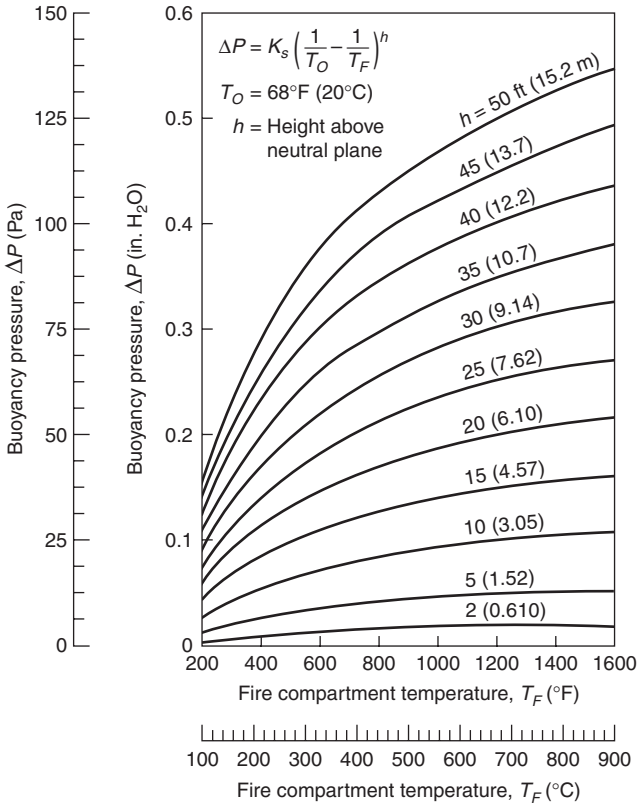

Figure 4-12.4. ***Pressure difference due to buoyancy.***

Buoyancy

High-temperature smoke from a fire has a buoyancy force due to its reduced density. The pressure difference between a fire compartment and its surroundings can be expressed by an equation of the same form as Equation 1.

$$\Delta P = K_s \left(\frac{1}{T_0} - \frac{1}{T_F}\right) h \qquad (2)$$

where

ΔP = pressure difference (in. H_2O [Pa])
T_0 = absolute temperature of the surroundings (R [K])
T_F = absolute temperature of the fire compartment (R [K])
h = distance above the neutral plane (ft [m])
K_s = coefficient (7.64 [3460])

The pressure difference due to buoyancy can be obtained from Figure 4-12.4 for the surroundings at 68°F (20°C). The neutral plane is the plane of equal hydrostatic pressure between the fire compartment and its surroundings. For a fire with a fire compartment temperature of 1470°F (800°C), the pressure difference 5 ft (1.52 m) above the neutral plane is 0.052 in. H_2O (13 Pa). Fang[6] has studied pressures caused by room fires during a series of full-scale fire tests. During these tests, the maximum pressure difference reached was 0.064 in. H_2O (16 Pa) across the burn room wall at the ceiling.

Much larger pressure differences are possible for tall fire compartments where the distance, h, from the neutral plane can be larger. If the fire compartment temperature is 1290°F (700°C), the pressure difference 35 ft (10.7 m) above the neutral plane is 0.35 in. H_2O (88 Pa). This amounts to an extremely large fire, and the pressures produced by it are beyond the state-of-the-art of smoke control. However, the example is included here to illustrate the extent to which Equation 2 can be applied.

In a building with leakage paths in the ceiling of the fire room, this buoyancy-induced pressure causes smoke movement to the floor above the fire floor. In addition, this pressure causes smoke to move through any leakage paths in the walls or around the doors of the fire compartment. As smoke travels away from the fire, its temperature drops due to heat transfer and dilution. Therefore, the effect of buoyancy generally decreases with distance from the fire.

Expansion

In addition to buoyancy, the energy released by a fire can cause smoke movement due to expansion. In a fire compartment with only one opening to the building, building air will flow into the fire compartment and hot smoke will flow out of the fire compartment. Neglecting the added mass of the fuel (which is small compared to

the airflow), the ratio of volumetric flows can simply be expressed as a ratio of absolute temperatures.

$$\frac{Q_{out}}{Q_{in}} = \frac{T_{out}}{T_{in}}$$

where

Q_{out} = volumetric flow rate of smoke out of the fire compartment (cfm [m^3/s])

Q_{in} = volumetric flow rate of air into the fire compartment (cfm [m^3/s])

T_{out} = absolute temperature of smoke leaving fire compartment (R [K])

T_{in} = absolute temperature of air into fire compartment (R [K])

For a smoke temperature of 1290°F (700°C) the ratio of volumetric flows would be 3.32. The reader is reminded to use absolute temperatures for calculation. In such a case, if the air flowing into the fire compartment is 3180 cfm (1.5 m^3/s), then the smoke flowing out of the fire compartment would be 10,600 cfm (4.98 m^3/s). In this case, the gas has expanded to more than three times its original volume.

For a fire compartment with open doors or windows, the pressure difference across these openings due to expansion is negligible. For a tightly sealed fire compartment, however, the pressure differences due to expansion may be important.

Wind

In many instances, wind can have a pronounced effect on smoke movement within a building. The pressure, P_w, that the wind exerts on a surface can be expressed as

$$P_w = \frac{1}{2} C_w \rho_O V^2 \quad (3)$$

where

C_w = dimensionless pressure coefficient

ρ_O = outside air density

V = wind velocity

For an air density of 0.075 lb/ft^3 (1.20 kg/m^3) this relation becomes

$$P_w = C_w K_w V^2 \quad (3a)$$

where

P_w = wind pressure (in. H_2O [Pa])

V = wind velocity (mph [m/s])

K_w = coefficient, 4.82×10^{-4} (0.600)

The pressure coefficients, C_w, are in range of -0.8 to 0.8, with positive values for windward walls and negative values for leeward walls. The pressure coefficient depends on building geometry and varies locally over the wall surface. In general, wind velocity increases with height in the boundary layer nearest the surface of the earth. Detailed information concerning wind velocity variations and pressure coefficients is available from a number of sources.[7–10] Specific information about wind data, with respect to air infiltration in buildings, has been generated by Shaw and Tamura.[11]

A 35 mph (15.6 m/s) wind produces a pressure on a structure of 0.47 in. H_2O (117 Pa) with a pressure coefficient of 0.8. The effect of wind on air movement within tightly constructed buildings with all doors and windows closed is slight. However, the effects of wind can become important for loosely constructed buildings or for buildings with open doors or windows. Usually, the resulting airflows are complicated and, for practical purposes, computer analysis is required.

Frequently in fires, a window breaks in the fire compartment. If the window is on the leeward side of the building, the negative pressure caused by the wind vents the smoke from the fire compartment. This can greatly reduce smoke movement throughout the building. However, if the broken window is on the windward side, the wind forces the smoke throughout the fire floor and even to other floors. This both endangers the lives of building occupants and hampers fire fighting. Pressures induced by the wind in this type of situation can be relatively large and can easily dominate air movement throughout the building.

HVAC Systems

Before the development of the concept of smoke control, HVAC systems were shut down when fires were discovered.

The HVAC system frequently transports smoke during building fires. In the early stages of a fire, the HVAC system can serve as an aid to fire detection. When a fire starts in an unoccupied portion of a building, the HVAC system can transport the smoke to a space where people can smell the smoke and be alerted to the fire. However, as the fire progresses, the HVAC system will transport smoke to every area that it serves, thus endangering life in all those spaces. The HVAC system also supplies air to the fire space, which aids combustion. These are the reasons HVAC systems traditionally have been shut down when fires have been discovered. Although shutting down the HVAC system prevents it from supplying air to the fire, this does not prevent smoke movement through the supply and return air ducts, air shafts, and other building openings due to stack effect, buoyancy, or wind.

Smoke Management

The term *smoke management*, as used in this chapter, includes all methods that can be used independently or in combination to modify smoke movement for the benefit of occupants and fire fighters and for the reduction of property damage. The use of barriers, smoke vents, and smoke shafts are traditional methods of smoke management.

The effectiveness of a barrier in limiting smoke movement depends on the leakage paths in the barrier

and on the pressure difference across the barrier. Holes where pipes penetrate walls or floors, cracks where walls meet floors, and cracks around doors are a few possible leakage paths. The pressure difference across these barriers depends on stack effect, buoyancy, wind, and the HVAC system.

The effectiveness of smoke vents and smoke shafts depends on their proximity to the fire, the buoyancy of the smoke, and the presence of other driving forces. In addition, when smoke is cooled due to sprinklers, the effectiveness of smoke vents and smoke shafts is greatly reduced.

Elevator shafts in buildings have been used as smoke shafts. Unfortunately, this prevents their use for fire evacuation and these shafts frequently distribute smoke to floors far from the fire. Specially designed smoke shafts, which have essentially no leakage on floors other than the fire floor, can be used to prevent the smoke shaft from distributing smoke to nonfire floors.

Principles of Smoke Control

Smoke control uses the barriers (walls, floors, doors, etc.) used in traditional smoke management in conjunction with airflows and pressure differences generated by mechanical fans.

Figure 4-12.5 illustrates a pressure difference across a barrier acting to control smoke movement. Within the barrier is a door, and the high-pressure side of the door can be either a refuge area or an escape route. The low-pressure side is exposed to smoke from a fire. Airflow through the cracks around the door and through other construction cracks prevents smoke infiltration to the high-pressure side.

When the door in the barrier is opened, air flows through the open door. When the air velocity is low, smoke can flow against the airflow into the refuge area or escape route, as shown in Figure 4-12.6. This smoke backflow can be prevented if the air velocity is sufficiently large, as shown in Figure 4-12.7. The magnitude of the velocity necessary to prevent backflow depends on the energy release rate of the fire, as discussed in the section of this chapter regarding airflow.

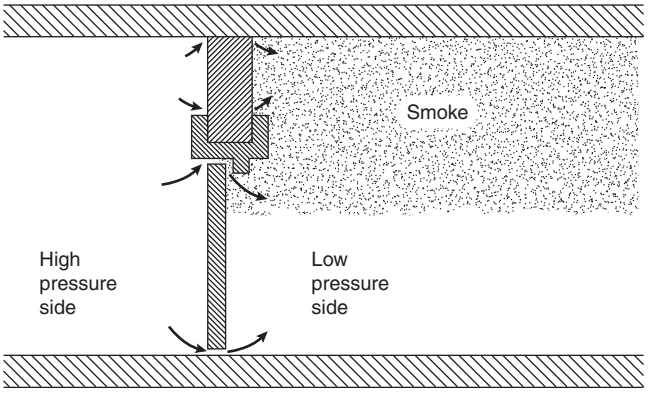

Figure 4-12.5. ***Pressure difference across a barrier of a smoke control system preventing smoke infiltration to the high-pressure side of the barrier.***

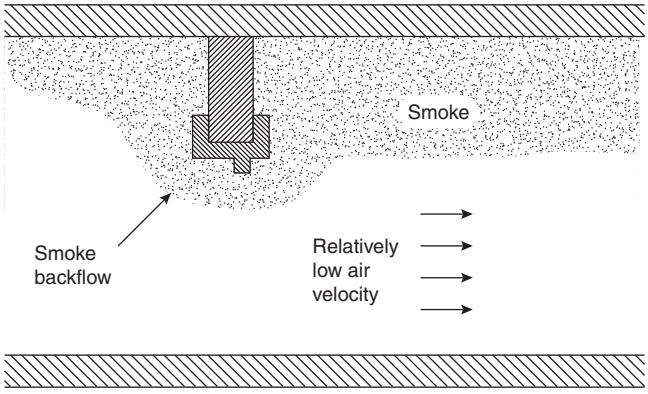

Figure 4-12.6. ***Smoke backflow against low air velocity through an open doorway.***

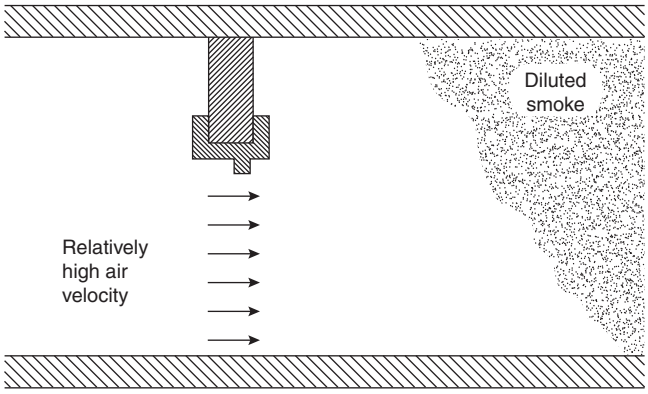

Figure 4-12.7. ***No smoke backflow with high air velocity through an open doorway.***

The two basic principles of smoke control can be stated as follows:

1. Airflow by itself can control smoke movement if the average air velocity is of sufficient magnitude.
2. Air pressure differences across barriers can act to control smoke movement.

The use of air pressure differences across barriers to control smoke is frequently referred to as *pressurization.* Pressurization results in airflows in the small gaps around closed doors and in construction cracks, thereby preventing smoke backflows through these openings. Therefore, in a strict physical sense, the second principle is a special case of the first principle. However, considering the two principles separately is advantageous for smoke control design. For a barrier with one or more large openings, air velocity is the appropriate physical quantity for both design considerations and for acceptance testing. However, when there are only cracks, such as around

closed doors, determination of the velocity is difficult and including it in the design is impractical. In this case, the appropriate physical quantity is pressure difference. Separate consideration of the two principles has the added advantage of emphasizing the different considerations necessary for open and closed doors.

Because smoke control relies on air velocities and pressure differences produced by fans, it has the following three advantages in comparison to the traditional methods of smoke management:

1. Smoke control is less dependent on tight barriers. Allowance can be made in the design for reasonable leakage through barriers.
2. Stack effect, buoyancy, and wind are less likely to overcome smoke control than passive smoke management. In the absence of smoke control, these driving forces cause smoke movement to the extent that leakage paths allow. However, pressure differences and airflows of a smoke control system act to oppose these driving forces.
3. Smoke control can be designed to prevent smoke flow through an open doorway in a barrier by the use of airflow. Doors in barriers are opened during evacuation and are sometimes accidentally left open or propped open throughout fires. In the absence of smoke control, smoke flow through these doors is common.

Smoke control systems should be designed so that a path exists for smoke movement to the outside; such a path acts to relieve pressure of gas expansion due to the fire heat.

The smoke control designer should be cautioned that dilution of smoke in the fire space is not a means of achieving smoke control, that is, smoke movement cannot be controlled by simply supplying and exhausting large quantities of air from the space or zone in which the fire is located. This supplying and exhausting of air is sometimes referred to as *purging the smoke.* Because of the large quantities of smoke produced in a fire, purging cannot assure breathable air in the fire space. In addition, purging in itself cannot control smoke movement, because it does not provide the needed airflows at open doors and the pressure differences across barriers. However, for spaces separated from the fire space by smoke barriers, purging can significantly limit the level of smoke.

Airflow

Theoretically, airflow can be used to stop smoke movement through any space. However, the two places where air velocity is most commonly used to control smoke movement are open doorways and corridors. Thomas[12] has developed an empirical relation for the critical velocity to prevent smoke from flowing upstream in a corridor.

$$V_k = K\left(\frac{gQ}{W\rho cT}\right)^{1/3} \tag{4}$$

where

V_k = critical air velocity to prevent smoke backflow
Q = heat release rate into corridor
W = corridor width
ρ = density of upstream air
c = specific heat of downstream gases
T = absolute temperature of downstream mixture of air and smoke
K = constant of the order of 1
g = gravitational constant

The downstream properties are considered to be taken at a point sufficiently far downstream of the fire for the properties to be uniform across the cross-section. The critical air velocity can be evaluated at $\rho = 0.081$ lb/ft^3 (1.3 kg/m^3), $c = 0.24$ Btu/lb°F (1.005 kJ/kg°C), $T = 81$°F (27°C), and $K = 1$.

$$V_k = K_v\left(\frac{Q}{W}\right)^{1/3} \tag{4a}$$

where

V_k = critical air velocity to prevent smoke backflow (fpm [m/s])
Q = heat release rate into corridor (Btu/s [kW])
W = corridor width (ft [m])
K_v = coefficient, 86.9 (0.292)

This relation can be used when the fire is located in the corridor or when the smoke enters the corridor through an open door, air transfer grille, or other opening. The critical velocities calculated from the above relation are approximate because only an approximate value of K was used. However, critical velocities calculated from this relation are indicative of the type of air velocities required to prevent smoke backflow from fires of different sizes.

Equation 4 is not appropriate for sprinklered fires that have small temperature differences between the upstream air and downstream gases. Shaw and Whyte[13] provide an analysis with experimental verification of a method to determine the velocity needed through an open doorway to prevent backflow of contaminated air. This analysis is specifically for small temperature differences and includes the effects of natural convection. If this method is used for a sprinklered fire where the temperature difference is only 3.6°F (2°C), then an average velocity of 50 fpm (0.25 m/s) would be the minimum velocity needed through a doorway to prevent smoke backflow. This temperature difference is small, and it is possible that larger values may be appropriate in many situations. Further research is needed in this area.

When airflow is used to control smoke, the amount of oxygen supplied to the fire is of concern. Huggett[14] evaluated the oxygen consumed for combustion of numerous natural and synthetic solids. He found that for most materials that are involved in building fires, the energy released per unit of mass of oxygen consumed is approximately 5630 Btu/lb (13.1 MJ/kg). Air is 23.3 percent oxygen by weight. It can be shown that there is sufficient oxygen in 1000 cfm of air at 70°F to support a 1640-Btu/s fire. The equivalent statement in SI units is: There is sufficient oxygen in 1.0 m^3/s of air at 21°C to support a 3660-kW fire.

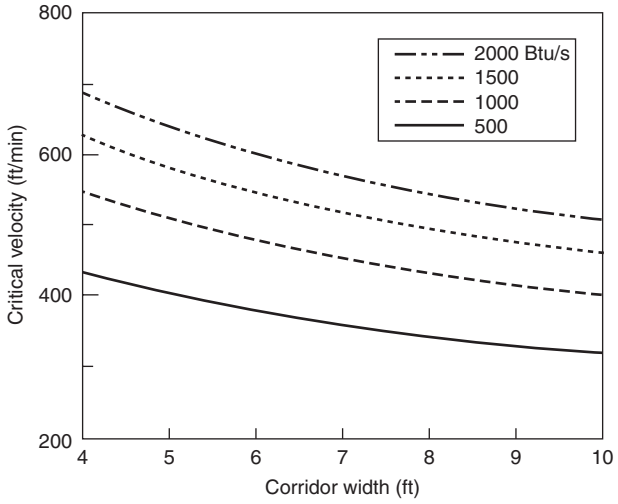

Figure 4-12.8(a). ***Velocity to prevent smoke backflow (English units).***

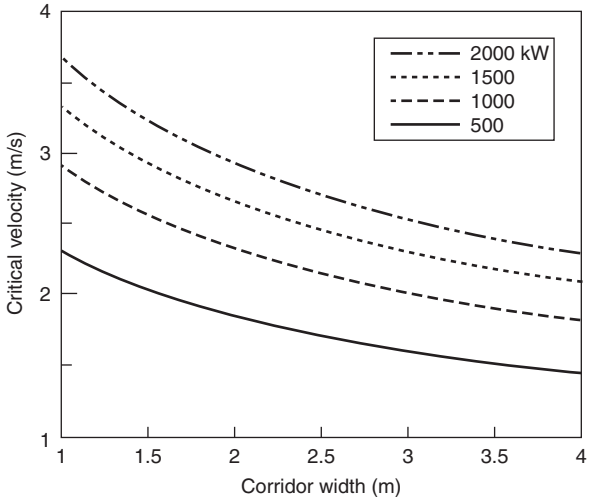

Figure 4-12.8(b). ***Velocity to prevent smoke backflow (SI units).***

Equation 4a can be evaluated from Figures 4-12.8(a) and (b). For example, for a wastebasket fire of 142 Btu/s (150 kW) and a 4.0-ft- (1.22-m-) wide corridor, Equation 4a yields a critical velocity of 286 fpm (1.45 m/s). For a ceiling height of 8 ft, this amounts to a flow of about 9200 cfm (4.3 m^3/s). This is sufficient air to support a 15,000-Btu/s (15,800-kW) fire. Thus the airflow to prevent smoke backflow for this wastebasket fire has sufficient oxygen to support a fire more than 100 times larger than the wastebasket fire. This illustrates the concern of airflow supplying oxygen to the fire, and extreme caution should be exercised when using airflow.

Pressurization

The airflow rate through a construction crack, door gap, or other flow path is proportional to the pressure difference across that path raised to the power n. For a flow path of fixed geometry, n is theoretically in the range of 0.5 to 1. However, for all flow paths except extremely narrow cracks, using $n = 0.5$ is reasonable and the flow can be expressed as

$$\dot{V} = CA\sqrt{\frac{2\Delta P}{\rho}} \tag{5}$$

where

$\dot{V}$ = volumetric airflow rate
C = flow coefficient
A = flow area (also called leakage area)
ΔP = pressure difference across the flow path
ρ = density of air entering the flow path

The flow coefficient depends on the geometry of the flow path as well as on turbulence and friction. In the present context, the flow coefficient is generally in the range of 0.6 to 0.7. For $\rho = 0.075$ lb/ft³ (1.2 kg/m³) and $C = 0.65$, the flow equation above can be expressed as

$$\dot{V} = K_f A\sqrt{\Delta P} \tag{5a}$$

where

$\dot{V}$ = volumetric flow rate (cfm [m^3/s])
A = flow area (ft^2 [m^2])
ΔP = pressure difference across flow path (in. H_2O [Pa])
K_f = coefficient, 2610 (0.839)

Airflow rate can also be determined from Figure 4-12.9. The flow area is frequently the same as the cross-sectional area of the flow path. A closed door with a crack area of 0.11 ft^2 (0.01 m^2) and a pressure difference of

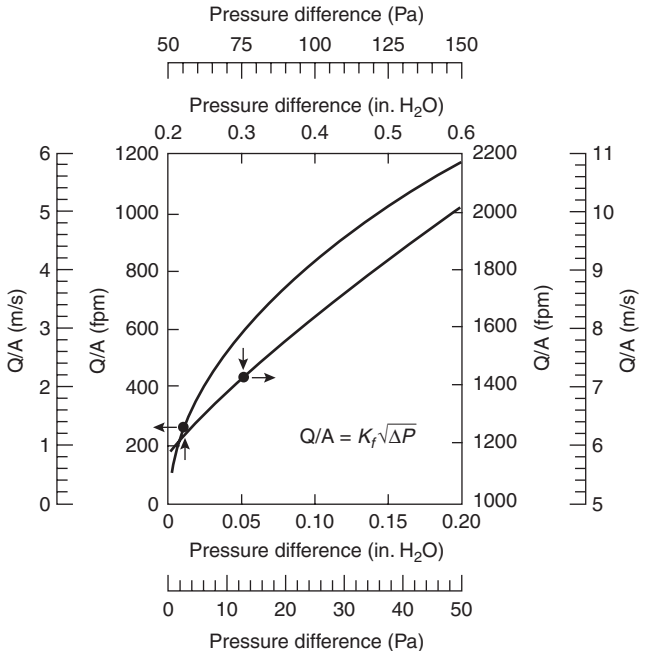

Figure 4-12.9. ***Airflow due to pressure difference.***

0.01 in. H_2O (2.5 Pa) would have an air leakage rate of approximately 29 cfm (0.013 m^3/s). If the pressure difference across the door were increased to 0.30 in. H_2O (75 Pa), then the flow would be 157 cfm (0.073 m^3/s).

In field tests of smoke control systems, pressure differences across partitions or closed doors have frequently fluctuated by as much as 0.02 in. H_2O (5 Pa). These fluctuations have generally been attributed to wind, although they could have been due to the HVAC system or some other source. Pressure fluctuations and the resulting smoke movement are a current topic of research. To control smoke movement, the pressure differences produced by a smoke control system must be sufficiently large so that they are not overcome by pressure fluctuations, stack effect, smoke buoyancy, and the forces of the wind. However, the pressure difference produced by a smoke control system should not be so large that door opening problems result.

Purging

In general, the systems discussed in this chapter are based on the two basic principles of smoke control. However, it is not always possible to maintain sufficiently large airflows through open doors to prevent smoke from infiltrating a space that is intended to be protected. Ideally, such occurrences of open doors will only happen for short periods of time during evacuation. Smoke that has entered such a space can be purged, that is, diluted by supplying outside air to the space.

Consider the case where a compartment is isolated from a fire by smoke barriers and self-closing doors, so that no smoke enters the compartment when the doors are closed. However, when one or more of the doors is open, there is insufficient airflow to prevent smoke backflow into the compartment from the fire space. To facilitate analysis, it is assumed that smoke is of uniform concentration throughout the compartment. When all the doors are closed, the concentration of contaminant in the compartment can be expressed as

$$\frac{C}{C_0} = e^{-at} \tag{6}$$

where

C_0 = initial concentration of contaminant
C = concentration of contaminant at time t
a = purging rate in number of air changes per minute
t = time after doors closed (min)
e = constant, approximately 2.718

The concentrations C_0 and C must both be in the same units, and they can be any units appropriate for the particular contaminant being considered. McGuire, Tamura, and Wilson[15] evaluated the maximum levels of smoke obscuration from a number of tests and a number of proposed criteria for tolerable levels of smoke obscuration. Based on this evaluation, they state that the maximum levels of smoke obscuration are greater by a factor of 100 than those relating to the limit of tolerance. Thus, they indicate that an area can be "reasonably safe" with respect to smoke obscuration if its atmosphere will not be contaminated to an extent greater than 1 percent by the atmosphere prevailing in the immediate fire area. It is obvious that such dilution would also reduce the concentrations of toxic smoke components. Toxicity is a more complicated problem, and no parallel statement has been made regarding the dilution needed to obtain a safe atmosphere with respect to toxic gases.

Equation 6 can be solved for the purging rate as

$$a = \frac{1}{t}\log_e\left(\frac{C_0}{C}\right) \tag{7}$$

For example, if doors are open, the contaminant in a compartment is 20 percent of the burn room concentration and at six minutes after the door is closed the contaminant concentration is 1 percent of the burn room, then Equation 7 indicates that the compartment must be purged at a rate of one air change every two minutes.

In reality, it is impossible to ensure that the concentration of the contaminant is uniform throughout the compartment. Because of buoyancy, it is likely that higher concentrations of contaminant would tend to be near the ceiling. Therefore, an exhaust inlet located near the ceiling and a supply outlet located near the floor would probably purge the smoke even faster than the previous calculations indicate. Caution should be exercised in the location of the supply and exhaust points to prevent the supply air from blowing into the exhaust inlet and thus short-circuiting the purging operation.

Door Opening Forces

The door opening forces resulting from the pressure differences produced by a smoke control system must be considered. Unreasonably high door opening forces can result in occupants having difficulty in, or being unable to open doors to refuge areas or escape routes.

The force required to open a door is the sum of the forces (1) to overcome the pressure difference across the door and (2) to overcome the door closer. This can be expressed as

$$F = F_{dc} + \frac{k_d W A \Delta P}{2(W - d)} \tag{8}$$

where

F = the total door opening force (lb [N])
F_{dc} = the force to overcome the door closer (lb [N])
W = door width (ft [m])
A = door area (ft^2 [m^2])
ΔP = pressure difference across the door (in. H_2O [Pa])
d = distance from the doorknob to the edge of the knob side of the door (ft [m])
K_d = coefficient (5.20 [1.00])

This relation assumes that the door opening force is applied at the knob. Door opening forces due to pressure

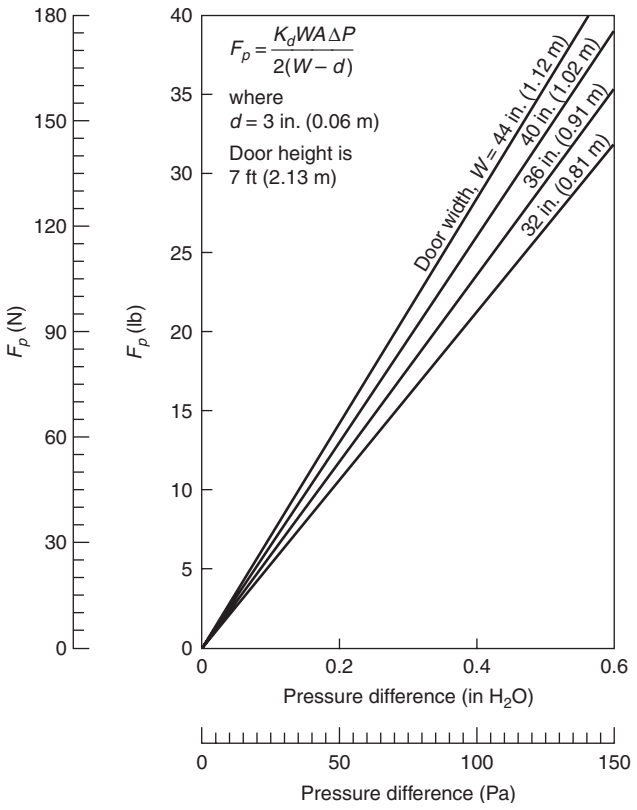

Figure 4-12.10. ***Door opening force due to a pressure difference.***

difference can be determined from Figure 4-12.10. The force to overcome the door closer is usually greater than 3 lb (13 N) and in some cases, can be as large as 20 lb (90 N). For a door that is 7 ft (2.13 m) high and 36 in. (0.91 m) wide, subject to a pressure difference of 0.30 in. H_2O (75 Pa), the total door opening force is 30 lb (133 N), if the force to overcome the door closer is 12 lb (53 N).

Flow Areas

Airflow paths must be identified and evaluated in the design of smoke control systems. Some leakage paths are obvious, such as cracks around closed doors, open doors, elevator doors, windows, and air transfer grilles. Construction cracks in building walls are less obvious but no less important.

The flow area of most large openings, such as open windows, can be calculated easily. However, flow areas of cracks are more difficult to evaluate. The area of these leakage paths depends on workmanship (i.e., how well a door is fitted or how well weatherstripping is installed). A door that is 36 in. by 7 ft (0.9 × 2.1 m) with an average crack width of $\frac{1}{8}$ in. (3.2 mm) has a leakage area of 0.21 ft² (0.020 m²). However, if this door is installed with a $\frac{3}{4}$ in. (19 mm) undercut, the leakage area is 0.32 ft² (0.30 m²). This is a significant difference. The leakage area of elevator doors has been measured in the range of 0.55 to 0.70 ft² (0.051 to 0.065 m²) per door.

For open stairwell doorways, Cresci[16] found that complex flow patterns exist and that the resulting flow through open doorways was considerably below the flow calculated by using the geometric area of the doorway as the flow area in Equation 5a. Based on this research, it is recommended that the flow area of an open stairwell doorway be half that of the geometric area (door height multiplied by width) of the doorway. An alternative approach for open stairwell doorways is to use the geometric area as the flow area and use a reduced flow coefficient. Because it does not allow the direct use of Equation 5a, this alternative approach is not used here.

Typical leakage areas for walls and floors of commercial buildings are tabulated as area ratios in Table 4-12.1. These data are based on a relatively small number of tests performed by the National Research Council of Canada.[17–20] The area ratios are evaluated at typical airflows at 0.30 in. H_2O (75 Pa) for walls, and 0.10 in. H_2O (25 Pa) for floors. It is believed that actual leakage areas are primarily dependent on workmanship rather than construction materials, and in some cases, the flow areas in particular buildings may vary from the values listed. Considerable data concerning leakage through building components are also provided in the *ASHRAE Handbook*.[21]

The determination of the flow area of a vent is not always straightforward, because the vent surface is usually covered by a louver and screen. Thus the flow area is less than the vent area (vent height multiplied by width). Because the slats in louvers are frequently slanted, calculation of the flow area is further complicated. Manufacturers' data should be sought for specific information.

Table 4-12.1 ***Typical Leakage Areas for Walls and Floors of Commercial Buildings***

Construction Element	Wall Tightness	Area Ratio A/A_w
Exterior building walls (includes construction cracks, cracks around windows and doors)	Tight	0.50×10^{-4}
	Average	0.17×10^{-3}
	Loose	0.35×10^{-3}
	Very loose	0.12×10^{-2}
Stairwell walls (includes construction cracks but not cracks around windows or doors)	Tight	0.14×10^{-4}
	Average	0.11×10^{-3}
	Loose	0.35×10^{-3}
Elevator shaft walls (includes construction cracks but not cracks around doors)	Tight	0.18×10^{-3}
	Average	0.84×10^{-3}
	Loose	0.18×10^{-2}
		A/A_F
Floors (includes construction cracks and areas around penetrations)	Tight	0.66×10^{-5}
	Average	0.52×10^{-4}
	Loose	0.17×10^{-3}

A = leakage area; A_W = wall area; A_F = floor area

Effective Flow Areas

The concept of effective flow areas is quite useful for analysis of smoke control systems. The various paths of smoke movement in the system can be parallel with one another, in series, or a combination of parallel and series paths. The effective flow area of a given system of flow paths is the area of a single opening that results in the same flow as the given system when subjected to the same pressure difference over the total system of flow paths. This concept is similar to an effective resistance of a system of electrical resistances.

The effective area, A_e, for the three parallel leakage areas of Figure 4-12.11 is

$$A_e = A_1 + A_2 + A_3 \tag{9}$$

If A_1 is 1.08 ft (0.10 m²) and A_2 and A_3 are 0.54 ft² (0.05 m2) each, then the effective flow area, A_e, is 2.16 ft² (0.20 m²).

Equation 9 can be extended to any number of flow paths in parallel; that is, it can be stated that the effective area is the sum of the individual leakage paths.

$$A_e = \sum_{i=1}^{n} A_i \tag{10}$$

when n is the number of flow areas, A_i, in parallel.

Three leakage areas in series from a pressurized space are illustrated in Figure 4-12.12. The effective flow area of these paths is

$$A_e = \left(\frac{1}{A_1^2} + \frac{1}{A_2^2} + \frac{1}{A_3^2} \right)^{-1/2} \tag{11}$$

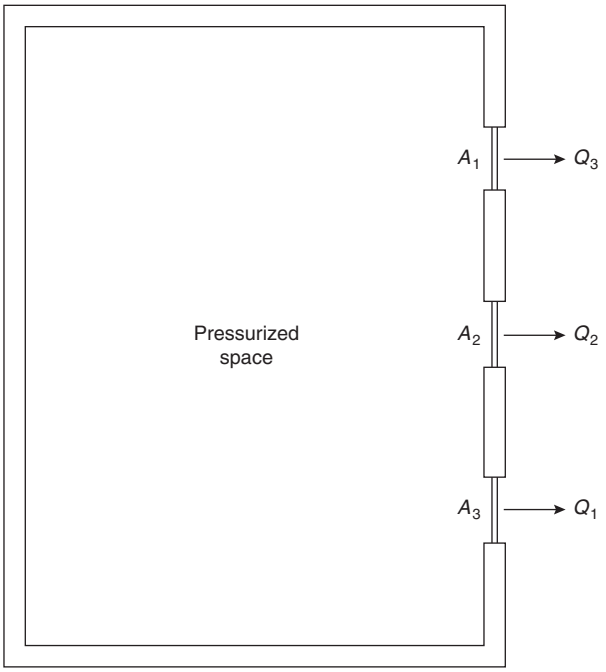

Figure 4-12.11. ***Leakage paths in parallel.***

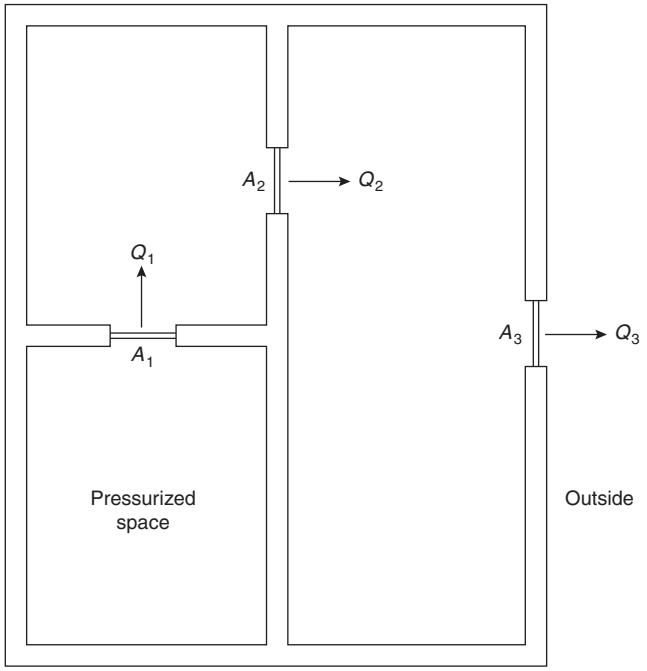

Figure 4-12.12. ***Leakage paths in series.***

The general rule for any number of leakage areas is

$$A_e = \left(\sum_{i=1}^{n} \frac{1}{A_i^2} \right)^{-1/2} \tag{12}$$

where n is the number of leakage areas, A_i, in series. In smoke control analysis, there are frequently only two paths in series. For this case, the effective leakage area is

$$A_e = \frac{A_1 A_2}{\sqrt{A_1^2 + A_2^2}} \tag{13}$$

EXAMPLE 1:

Calculate the effective leakage area of two equal flow paths of 0.2 ft² in series. Let $A = A_1 = A_2 = 0.02$ m².

$$A_e = \frac{A^2}{\sqrt{2A^2}} = \frac{A}{\sqrt{2}} = 0.15 \text{ ft}^2 \quad (0.014 \text{ m}^2)$$

EXAMPLE 2:

Calculate the effective area of two flow paths in series, where $A_1 = 0.22$ ft² (0.22 ft² (0.02 m²) and $A_2 = 2.2$ ft² (0.2 m²).

$$A_e = \frac{A_2 A_2}{\sqrt{A_1^2 + A_2^2}} = 0.219 \text{ ft}^2 \quad (0.0199 \text{ m}^2)$$

Example 2 illustrates that when two areas are in series and one is much larger than the other, the effective area is approximately equal to the smaller area.

The method of developing an effective area for a system of both parallel and series paths is to systemically combine groups of parallel paths and series paths. The system illustrated in Figure 4-12.13 is analyzed as an example.

The figure shows that A_2 and A_3 are in parallel; therefore, their effective area is

$$A_{23_e} = A_2 + A_3$$

Areas A_4, A_5, and A_6 are also in parallel, so their effective area is

$$A_{456_e} = A_4 + A_5 + A_6$$

These two effective areas are in series with A_1. Therefore, the effective flow area of the system is given by

$$A_e = \left(\frac{1}{A_1^2} + \frac{1}{A_{23_e}^2} + \frac{1}{A_{456_e}^2} \right)^{-1/2}$$

EXAMPLE 3:

Calculate the effective area of the system in Figure 4-12.13, if the leakage areas are $A_1 = A_2 = A_3 = 0.22$ ft² (0.02 m²) and $A_4 = A_5 = A_6 = 0.11$ ft² (0.01 m²).

$$A_{23_e} = 0.44 \text{ ft}^2 \quad (0.04 \text{ m}^2)$$
$$A_{456_e} = 0.33 \text{ ft}^2 \quad (0.03 \text{ m}^2)$$
$$A_e = 0.16 \text{ ft}^2 \quad (0.015 \text{ m}^2)$$

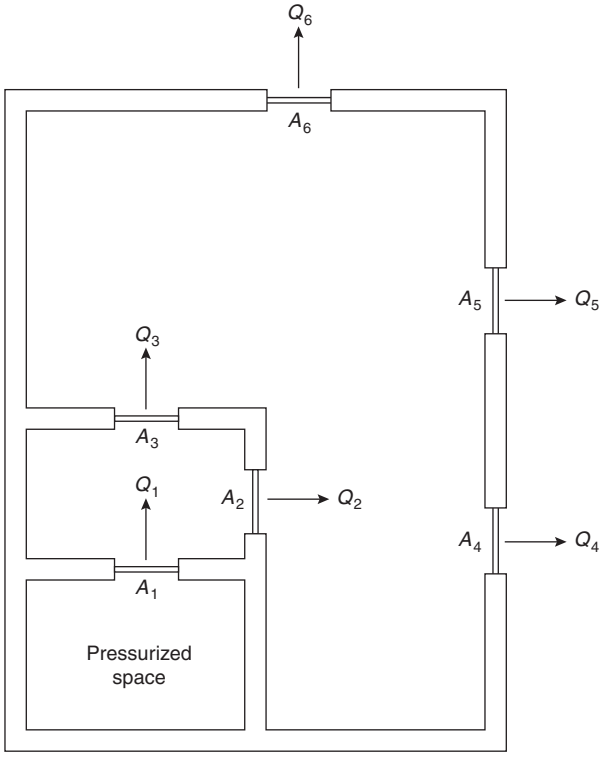

Figure 4-12.13. ***Combination of leakage paths in parallel and series.***

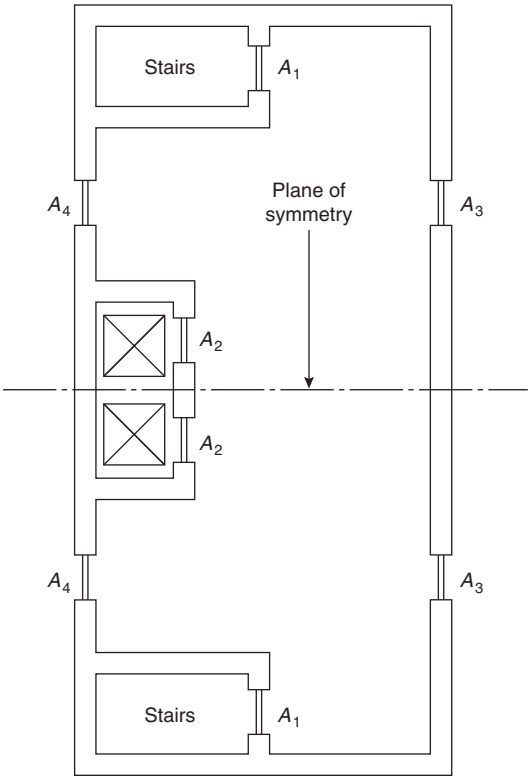

Figure 4-12.14. ***Building floor plan illustrating symmetry concept.***

Symmetry

The concept of symmetry is useful in simplifying problems and thereby easing solutions. Figure 4-12.14 illustrates the floor plan of a multistory building that can be divided in half by a plane of symmetry. Flow areas on one side of the plane of symmetry are equal to corresponding flow areas on the other side. For a building to be so treated, every floor of the building must be such that it can be divided in the same manner by the plane of symmetry. If wind effects are not considered in the analysis or if the wind direction is parallel to the plane of symmetry, then the airflow in only one-half of the building needs be analyzed. It is not necessary that the building be geometrically symmetric, as shown in Figure 4-12.14; it must be symmetric only with respect to flow.

Design Parameters: A General Discussion

Ideally, building and fire codes should contain design parameters leading to the design of functional and economical smoke control systems. Unfortunately, because smoke control is a new field, consensus has not yet been reached as to a definition of reasonable design parameters. Clearly, the designer has an obligation to adhere to any smoke control design criteria existing in appropriate codes or standards, but such criteria should be scrutinized to de-

termine whether they will result in an effective system. If necessary, the designer should seek a waiver of the local codes to ensure an effective smoke control system.

Five areas for which design parameters must be established are (1) leakage areas, (2) weather data, (3) pressure differences, (4) airflow, and (5) number of open doors in the smoke control system.

Leakage areas have already been discussed in this chapter. An additional consideration affecting pressure differences and airflow is whether a window in the fire compartment is broken. This factor is included in the following discussion of these parameters. In the absence of code requirements for specific parameters, the following discussion may be helpful to the designer.

Weather Data

The state-of-the-art of smoke control is such that little consideration has been given to the selection of weather data specifically for the design of smoke control systems. However, design temperatures for heating and cooling during winter and summer are recommended in the *ASHRAE Handbook*.[21] For example, 99 and 97.5 percent winter design temperatures have been provided. These values represent the temperatures that are equaled or exceeded in these portions of the heating season.*

A designer may wish to consider using these design temperatures of smoke control systems. It should be remembered that in a normal winter, there would be approximately 22 hours at or below the 99 percent design value and approximately 54 hours at or below the 97.5 percent design value. Furthermore, extreme temperatures can be considerably lower than the winter design temperatures. For example, the *ASHRAE* 99 percent design temperature for Tallahassee, Florida, is 27°F (−3°C), but the lowest temperature observed there by the National Climatic Center[22] was −2°F (−19°C) on February 13, 1899.

Temperatures are generally below the design values for short periods of time, and because of the thermal lag of building materials, these short intervals of low temperature usually do not result in problems with respect to heating systems. However, the same cannot necessarily be said of a smoke control system. There is no time lag for a smoke control system, that is, a smoke control system is subjected to all the forces of stack effect that exist at the moment the system is being operated. If the outside temperature is below the winter design temperature for which a smoke control system was designed, then problems from stack effect may result. A similar situation can result with respect to summer design temperatures and reverse stack effect.

Wind data are needed for a wind analysis of a smoke control system. ASHRAE[21] provides wind data for smoke control design.

Pressure Differences

It is appropriate to consider both the maximum and minimum allowable pressure differences across the boundaries of smoke control zones. The maximum allowable pressure difference should be a value that does not result in excessive door opening forces, but it is difficult to determine what constitutes excessive door opening forces. Clearly, a person's physical condition is a major factor in determining a reasonable door opening force for that person. NFPA 101®, *Life Safety Code*®,[23] states that the force required to open any door in a means of egress shall not exceed 30 lb (133 N). In the section of this chapter on purging, a method of determining the door opening force is provided.

The criterion used in this chapter for selecting a minimum allowable pressure difference across a boundary of a smoke control system is that no smoke leakage should occur during building evaluation.† In this case, the smoke control system must produce sufficient pressure differences so that it is not overcome by the forces of wind, stack effect, or buoyancy of hot smoke. The pressure differences due to wind and stack effect can become very large in the event of a broken window in the fire compartment. Evaluation of these pressure differences depends on evacuation time, rate of fire growth, building configuration, and the presence of a fire suppression system. In the absence of a formal method of analysis, such evaluation must of necessity be based on experience and engineering judgment.

A method for determining the pressure difference across a smoke barrier resulting from the buoyancy of hot gases is provided in the section of this chapter regarding buoyancy. For a particular application, it may be considered necessary to design a smoke control system to withstand an intense fire next to a door at the boundary of a smoke control zone. Earlier in this chapter it was stated that in a series of full-scale fire tests, the maximum pressure difference reached was 0.064 in. H_2O (16 Pa) across the burn room wall at the ceiling. To prevent smoke infiltration, the smoke control system should be designed to maintain a pressure slightly higher than that generated in fire conditions. A minimum pressure difference in the range of 0.08 to 0.10 in. H_2O (20 to 25 Pa) is suggested.

If a smoke control boundary is exposed to hot smoke from a remote fire, a lower pressure difference due to buoyancy will result. For a smoke temperature of 750°F (400°C), the pressure difference caused by the smoke 5.0 ft (1.53 m) above the neutral plane would be 0.04 in. H_2O (10 Pa). In this situation, it is suggested that the smoke control system be designed to maintain a minimum pressure in the range of 0.06 to 0.08 in. H_2O (15 to 20 Pa).

Water spray from fire sprinklers cools smoke from a building fire and reduces the pressure differences due to buoyancy. In such a case it is probably wise to allow for pressure fluctuations. Accordingly, a minimum pressure difference in the range of 0.02 to 0.04 in. H_2O (5 to 10 Pa) is suggested.

Windows in the fire compartment can break due to exposure to high temperature gases. In such cases, the pressure due to the wind on the building exterior can be

*The heating season usually consists of three winter months. A more exact definition of these temperatures is available in Chapter 26 of the *ASHRAE Handbook—1997 Fundamentals*.[21]

†Other criteria might involve maintaining a number of smoke-free egress routes or preventing smoke infiltration to a refuge area. Discussion of all possible alternatives is beyond the scope of this chapter.

determined from Equation 3. If this window is the only opening to the outside on the fire floor and the window faces into the wind, the boundary of the smoke control system could be subjected to higher pressures. One possible solution is to vent the fire floor on all sides to relieve such pressures. For a building that is much longer than it is wide, it may be necessary to vent only on the two longer sides.

In addition to wind effects, stack effect can be increased in the event of a broken fire compartment window. With a fire on a lower floor during cold weather, stack effect will increase pressures of the fire floor above surrounding spaces. Even though little research has been done on the subject, the chances of a window breaking in the fire compartment are reduced by the operation of fire sprinklers.

Airflow

When the doors in the boundaries of smoke control systems are open, smoke can flow into refuge areas or escape routes unless there is sufficient airflow through the open door to prevent smoke backflow, as discussed in the previous section. One criterion for selecting a design velocity through an open door is that no smoke backflow should occur during building evacuation.* Selection of this velocity depends on evacuation time, rate of fire growth, building configuration, and the presence of a fire suppression system. In the absence of a formal method of analysis, such an evaluation must be based on experience and engineering judgment.

At present, there is still much to be learned about the critical velocity needed to stop smoke backflow through an open door. In the absence of a specific relationship for doorways, the method of analysis presented for corridors in the earlier section regarding airflow can be used to yield approximate results. The width of the doorway may be used in place of the width of the corridor. This technique is based on the assumption that smoke properties are uniform across the cross section. As previously illustrated, for a particular application, it may be considered necessary to design for an intensive fire, such as one with an energy release rate of 8×10^6 Btu/hr (2.4 MW). A critical velocity of approximately 800 fpm (4 m/s) would be required to stop smoke.

In another application, it may be estimated that the building would be subjected to a much less intense fire with an energy release rate of 427,000 Btu/hr (125 kW). To protect against smoke backflow during evacuation, the critical velocity would be 300 fpm (1.5 m/s).

In a sprinklered building, it might be considered that the smoke away from the immediate fire area would be cooled to near ambient temperature by the spray from the sprinklers. In such a case a design velocity in the range of 50 to 250 fpm (0.25 to 1.25 m/s) may be used. Research is needed to fully evaluate the effect of sprinklers on smoke control design parameters.

*Other criteria might include the allowance of limited smoke leakage into areas to be protected. Under such criteria, the toxicity of the smoke is a factor that must be considered.

Number of Open Doors

The need for air velocity through open doors in the perimeter of a smoke control system has been discussed in this chapter. Another design consideration is the number of doors that could be opened simultaneously when the smoke control system is operational. A design that allows for all doors to be opened simultaneously may ensure that the system will always work, but it will probably add to the cost of the system.

Deciding on the number of doors that will be opened simultaneously depends largely on the building occupancy. For example, in a densely populated building, it is very likely that all the doors will be opened simultaneously during evacuation. However, if a staged evacuation plan or refuge area concept is incorporated in the building fire emergency plan, or if the building is sparsely occupied, only a few of the doors may be opened simultaneously during a fire.

Pressurized Stairwells

Many pressurized stairwells have been designed and built with the goal of providing a smoke-free escape route in the event of a building fire. A secondary objective is to provide a smoke-free staging area for fire fighters. On the fire floor, a pressurized stairwell must maintain a positive pressure difference across a closed stairwell door so that smoke infiltration is prevented.

During building fires, some stairwell doors are opened intermittently during evacuation and fire fighting, and some doors may even be blocked open. Ideally, when the stairwell door is opened on the fire floor, there should be sufficient airflow through the door to prevent smoke backflow. Designing such a system is difficult because of the large number of permutations of open stairwell doors and weather conditions that affect the airflow through open doors.

Stairwell pressurization systems are divided into two categories—single and multiple injection systems. A single injection system is one that has pressurized air supplied to the stairwell at one location; the most common injection point is at the top of the stairwell. Associated with this system is the potential for smoke feedback into the pressurized stairwell (i.e., of smoke entering the stairwell through the pressurization fan intake). Therefore, the capability of automatic shutdown in such an event should be considered.

For tall stairwells, single injection systems can fail when a few doors are open near the air supply injection point. All of the pressurized air can be lost through the few open doors, and the system can then fail to maintain positive pressures across doors farther from the injection point. Such a failure mode is especially likely with bottom injection systems when a ground level stairwell door is open.

For tall stairwells, supply air can be supplied at a number of locations over the height of the stairwell. Figures 4-12.15 and 4-12.16 are two examples of many possible multiple injection systems that can be used to overcome the limitations of single injection systems. In these figures the supply duct is shown in a separate shaft, but systems have been built that have eliminated the expense of a separate duct shaft by locating the supply duct in the stairwell itself. Obviously, care must be taken in such a case so that the duct does not become an obstruction to orderly building evacuation.

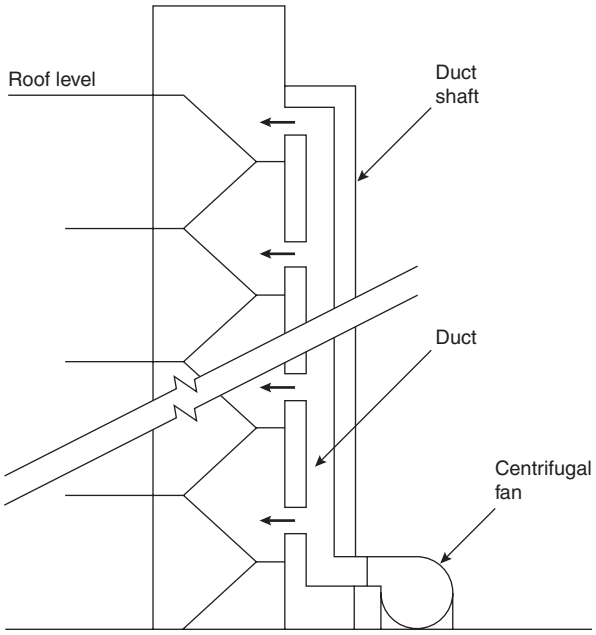

Figure 4-12.15. ***Stairwell pressurization by multiple injection with the fan located at ground level.***

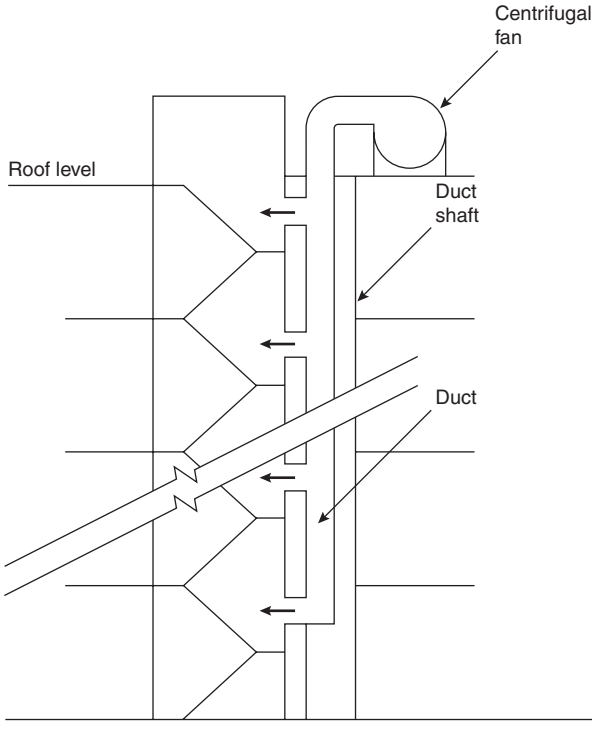

Figure 4-12.16. ***Stairwell pressurization by multiple injection with roof-mounted fan.***

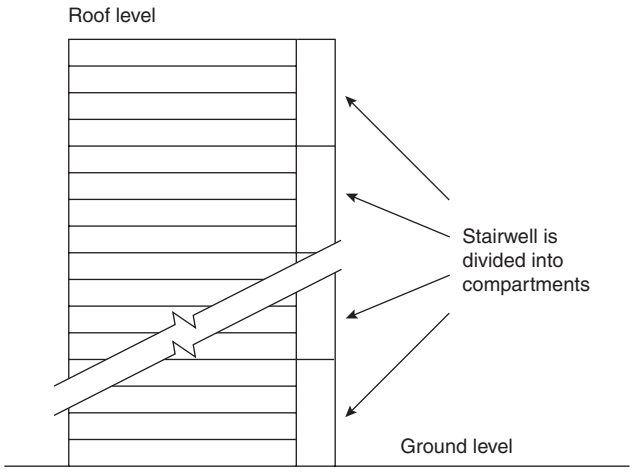

Figure 4-12.17. ***Compartmentation of a pressurized stairwell. Note: each four floor compartment has at least one supply air injection point.***

Stairwell Compartmentation

An alternative to multiple injection is compartmentation of the stairwell into a number of sections, as illustrated in Figure 4-12.17. When the doors between compartments are open, the effect of compartmentation is lost. For this reason, compartmentation is inappropriate for densely populated buildings where total building evacuation by the stairwell is planned in the event of fire. However, when a staged evacuation plan is used and when the system is designed to operate successfully when the maximum number of doors between compartments are open, compartmentation can be an effective means of providing stairwell pressurization for tall stairwells.

Stairwell Analysis

In this section of the chapter, a method of analysis is presented for a pressurized stairwell in a building without vertical leakage. The performance of pressurized stairwells in buildings without elevators may be closely approximated by this method, which is useful for buildings with vertical leakage in that it yields conservative results. Only one stairwell is considered in the building, but the analysis can be extended to any number of stairwells by the concept of symmetry. For evaluation of vertical leakage and open stairwell doors, computer analysis is recommended.

This analysis is for buildings where the leakage areas are the same for each floor of the building and where the only significant driving forces are the stairwell pressurization system and the temperature difference between the indoors and outdoors.

The pressure difference, $\Delta P_S B$, between the stairwell and the building can be expressed as

$$\Delta P_{SB} = \Delta P_{SBb} + \frac{by}{1 + (A_{SB}/A_{BO})^2} \quad (14)$$

where

$\Delta P_{SB}b$ = the pressure difference, P_{SB}, at the stairwell bottom
y = distance above the stairwell bottom
A_{SB} = flow area between the stairwell and the building (per floor)
A_{BO} = flow area between the building and the outside (per floor)

$$b = \frac{gP}{R}\left(\frac{1}{T_O} - \frac{1}{T_S}\right)$$

T_0 = absolute temperature of outside air
T_S = absolute temperature of stairwell air

For a stairwell with no leakage directly to the outside, the flow rate of pressurization air is

$$Q = \frac{2}{3} NCA_{SB}\sqrt{\frac{2}{\rho}}\left(\frac{\Delta P_{SBt}^{3/2} - \Delta P_{SBb}^{3/2}}{\Delta P_{SBt} - \Delta P_{SBb}}\right) \quad (15)$$

where

N = number of floors
C = flow coefficient (See Equation 5)
$\Delta P_{SB}t$ = the pressure difference, ΔP_{SB}, at the stairwell top

EXAMPLE 4:

Each story of a 20-story stairwell is 10.8 ft (3.3 m) in height. The stairwell has a single-leaf door at each floor leading to the occupant space and one ground level door to the outside. The exterior of the building has a wall area of 6030 ft² (560 m²) per floor. The exterior building walls and stairwell walls are of average leakiness. The stairwell wall area is 560 ft² (52 m²) per floor. The area of the gap around each stairwell door to the building is 0.26 ft² (0.024 m²). The exterior door is well gasketed, and its leakage is negligible when it is closed.

For this example, the following design parameters are used: outside design temperatures, T_O = 14°F (−10°C); stairwell temperature, T_S = 70°F (21°C); minimum design pressure differences when all stairwell doors are closed of 0.551 in. H_2O (137 Pa).

SOLUTION:

Using the leakage ratios for an exterior building wall of average tightness from Table 4-12.1, $A_{BO} = 6030 \times (0.21 \times 10^{-3})$ = 1.27 ft² (0.118 m²). Using leakage ratios for a stairwell wall of average tightness from Table 4-12.1, the leakage area of the stairwell wall is $560 \times (0.11 \times 10^{-3})$ = 0.06 ft (0.006 m²). A_{SB} equals the leakage area of the stairwell wall plus the gaps around the closed doors. A_{SB} = 0.06 + 0.26 = 0.32 ft² (0.030 m²). The temperature factor, 6, is calculated at 0.00170 in. H_2O/ft (1.39 Pa/m). The pressure difference at the stairwell bottom is selected as ΔP_{SBb} = 0.080 in. H_2O (20 Pa) to provide an extra degree of protection above the minimum allowable value of 0.052 in. H_2O (13 Pa). The pressure difference, ΔP_{SBt}, is calculated from Equation 14 at 0.426 in. H_2O (106 Pa), using y = 217 ft (66.1 m). Thus, ΔP_{SBt} does not exceed the maximum allowable pressure. The flow rate of pressurization air is calculated from Equation 15 at 8200 cfm (3.9 m³/s).

The flow rate is highly dependent on the leakage area around the closed doors and upon the leakage area that exists in the stairwell walls. In practice, these areas are difficult to evaluate and even more difficult to control. If the flow area, A_{SB}, were 0.54 ft² (0.050 m²) rather than 0.32 ft² (0.030 m²), then a flow rate of pressurization air of 13,800 cfm (6.5 m³/s would have been calculated from Equation 15. A fan with a sheave is one approach to allow adjustment of supply air to offset for variations in actual leakage from the values used in design calculations.

Elevator Smoke Control

Elevator shaft smoke control can prevent smoke spread to floors away from the fire by way of the elevator shaft. The problems that can result from smoke migration through elevator shafts are illustrated by the fire at the MGM Grand Hotel.[24] The fire occurred on the ground floor, but smoke migrated to the upper floors where the majority of the fatalities occurred. The elevators at this hotel did not have any special smoke protection, and they were one of the major paths of smoke migration to the upper floors. This chapter does not address smoke control of elevator systems intended for fire evacuation; however, the topic is addressed by Klote and Milke.[25]

Piston Effect

The transient pressures produced when an elevator car moves in a shaft (i.e., piston effect) affect elevator smoke control. Such piston effect can pull smoke into a normally pressurized elevator lobby or elevator shaft. Klote[26] analyzed air flows and pressures produced by elevator car motion in a pressurized elevator shaft, based on the continuity equation for the contracting control volume in an elevator shaft above a moving elevator car. Piston effect experiments[27] on a hotel elevator in Mississauga, Ontario, Canada, validated the analysis.

From the analysis by Klote, an expression was developed for the critical pressure difference, $\Delta P_{crit,}$ at which piston effect cannot overcome the elevator pressurization system.

$$\Delta P_{crit} = \frac{K_{pe}\rho}{2}\left(\frac{A_s A_e V}{A_a A_{si} C_c}\right)^2 \quad (16)$$

where

ΔP_{crit} = critical pressure difference (in. H_2O [Pa])
ρ = air density in elevator shaft (lb/ft³ [kg/m³])
A_s = cross-sectional area of the elevator shaft (ft² [m²])
A_{si} = leakage area between the lobby and the building (ft² [m²])
A_a = free area around the elevator car (ft² [m²])
A_e = effective area between the elevator shaft and the outside (ft² [m²])
V = elevator car velocity (ft/min [m/s])
C_c = flow coefficient for flow around car, dimensionless
K_{pe} = coefficient, 1.66×10^{-6} (1.00)

The flow coefficient, C_c, was determined experimentally to be about 0.94 for a multiple-car elevator shaft, and about 0.83 for a single-car elevator shaft.[28] Equation 16 is for elevators without enclosed elevator lobbies. The effective area from the elevator to the outside is

$$A_e = \left(\frac{1}{A_{si}^2} + \frac{1}{A_{io}^2} \right)^{-1/2} \quad (17)$$

where A_{io} is the leakage area between the outside and the building, in ft² (m²).

EXAMPLE 5:

An elevator shaft with two cars is pressurized to a minimum of 0.05 in. H_2O (12.4 Pa) from the elevator shaft to the building. This system is to prevent smoke movement through the elevator shaft, and there is no enclosed elevator lobby. The parameters are A_{si} = 1.52 ft² (0.141 m²), A_{io} = 2.26 ft² (0.210 m²), A_s = 121 ft² (11.2 m²), A_a = 80 ft² (7.43 m²), ρ = 0.075 lb/ft³ (1.20 kg/m³), V = 500 ft/min (2.54 m/s), and C_c = 0.94. Is it possible for the pressure difference due to elevator piston effect to pull smoke into the elevator shaft?

SOLUTION:

From Equation 17, A_e = 1.26 ft² (0.117 m²). From Equation 16, ΔP_{crit} = 0.028 in. H_2O (6.9 Pa). The elevator shaft is pressurized at a level above ΔP_{crit}. Therefore, piston effect will not pull smoke into the elevator shaft.

Elevator Shaft Pressurization

These systems supply air to the elevator shaft and can produce a pressure difference sufficient to prevent smoke flow into the elevator shaft in the event of a fire. Upon fire detection, the general procedure is for elevator cars to be taken out of normal service and automatically recalled to the ground floor. A recent modification of this is the capability for recall to an alternative floor in the event of a fire on the ground floor. Two elevator door scenarios can occur: (1) the elevator doors remain open after the car reaches the ground floor or the alternative floor, or (2) the elevator doors close after sufficient time to allow passengers to leave the car. The fire service has elevator keys that enable them to: (1) operate elevators for rescue and (2) transport personnel and equipment to fight the fire.

As with pressurized stairwells, factors that must be considered are shaft friction, outside-to-inside temperature difference, and pressure fluctuations due to doors opening and closing. The analysis of pressurized stairwells can be applied to pressurized elevators by redefining the subscript S in the analysis from stairwell to elevator shaft. This analysis is then applicable to buildings without vertical leakage and to shafts with negligible pressure loss due to friction. This analysis can only be used where the elevator pressurization system is the only system using pressurization or operating in the building. Further, the effect of any exhaust system must be negligible. Computer analysis incorporating shaft friction and more complex building flow paths can be done by the programs cited later in this chapter.

Zone Smoke Control

Pressurized stairwells are intended to prevent smoke infiltration into stairwells. However, in a building that has only stairwell pressurization, smoke can flow through cracks in floors and partitions and through shafts to damage property and threaten life at locations remote from the fire. The concept of zone smoke control is intended to limit such smoke movement.

With this smoke control method, a building is divided into a number of smoke control zones, and each zone is separated from the others by partitions, floors, and doors that can be closed to inhibit the smoke movement. In the event of a fire, pressure differences and airflows produced by mechanical fans are used to limit the smoke spread from the zone in which the fire was initiated. The concentration of smoke in the fire zone is unchecked and, accordingly, it is intended that the building occupants evacuate this zone as soon as possible after fire detection.

Frequently, each floor of a building is chosen to be a separate smoke control zone. However, a smoke control zone can consist of more than one floor, or a floor can be divided into more than one smoke control zone. Some arrangements of smoke control zones are illustrated in Figure 4-12.18. All of the nonsmoke zones in the building may be pressurized. The term *pressure sandwich* is used to describe cases where only zones adjacent to the smoke zone are pressurized as in (b) and (d) of Figure 4-12.18.

The intent of zone smoke control is to limit smoke movement to the smoke zone by use of the two principles of smoke control. Pressure differences in the desired direction across the barriers of a smoke zone can be achieved by either supplying outside (fresh) air to nonsmoke zones, by venting the smoke zone, or by both methods.

Venting of smoke from a smoke zone is important because it prevents significant overpressures that are due to thermal expansion of gases as a result of the fire. However, venting only slightly reduces smoke concentration in the smoke zone. Venting in this zone can be accomplished by exterior wall vents, smoke shafts, and mechanical venting (exhausting).

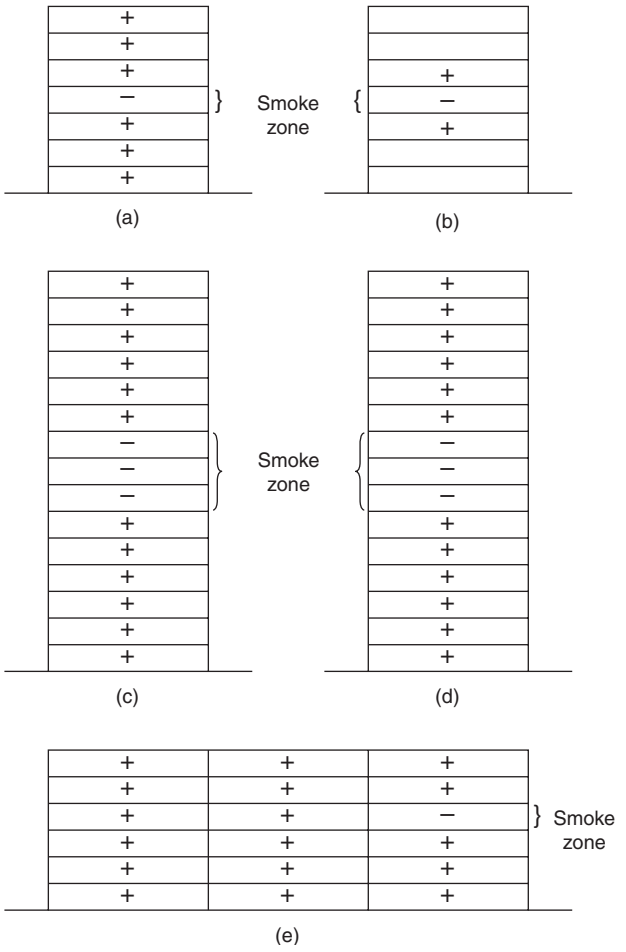

Figure 4-12.18. ***Some arrangements of smoke control zones. The smoke zone is indicated by a minus (–) sign and pressurized spaces are indicated by a (+) sign. Each floor can be a smoke control zone (a, b) or a smoke zone can consist of more than one floor (c, d). All of the nonsmoke zones in a building may be pressurized as in (a) and (c), or only nonsmoke zones adjacent to the smoke zone (b, d). A smoke zone can be limited to a part of a floor (e).***

Computer Analysis

Some design calculations associated with smoke control are appropriate for hand calculation. However, other calculations involve time-consuming, trial-and-error solutions that are more appropriately left to a computer. In 1982, the National Bureau of Standards developed a computer program[29] specifically for analysis of smoke control systems. A number of other programs applicable to smoke control have been developed. Some calculate steady-state airflow and pressures throughout a building;[30,31] other programs go beyond this to calculate the smoke concentrations that would be produced throughout a building in the event of a fire.[32–35]

In 1993, an ASHRAE-sponsored research project evaluated several algorithms for network flow to determine the most appropriate one for smoke control applications.[36] The algorithm selected as the best is the core numerical routine of the public domain computer program CONTAM96.[37] While CONTAM96 was primarily developed for indoor air quality applications, it has been extensively used for smoke control. In addition to fast and reliable numerics, CONTAM96 has a graphical user interface that significantly simplifies data input and reduces the probability of input errors.

Each of these programs differs from the others to some extent but all employ similar basic concepts. A building is represented by a network of spaces, or nodes, each at a specific pressure and temperature. The stairwells and other shafts are modeled by a vertical series of spaces, one for each floor. Air flows through leakage paths from regions of high pressure to regions of low pressure. These leakage paths are doors and windows that may be opened or closed. Leakage can also occur through partitions, floors, and exterior walls and roofs. The airflow through a flow path is a function of the pressure difference across the path as presented in Equation 5.

Air from outside the building can be introduced by a pressurization system into any level of a shaft or even into other building compartments, allowing for simulation of stairwell pressurization. In addition, any building space can be exhausted, allowing simulation of zoned smoke control systems. The pressures throughout the building and flow rates through all the flow paths are obtained by solving the airflow network, including the driving forces such as wind, the pressurization system, or a temperature difference between inside and outside air.

Acceptance Testing

Regardless of the care, skill, and attention to detail with which a smoke control system is designed, an acceptance test is needed to ensure that the system, as built, operates as intended.

An acceptance test should be composed of two levels of testing. The first level is functional, to determine if everything in the system works as it is supposed to work (i.e., an initial check of the system components). The importance of the initial check has become apparent because of the many problems that have been encountered during tests of smoke control systems. These problems include fans operating backward, fans to which no electrical power was supplied, and controls that did not work properly.

The second level of testing is performance oriented, to determine if the system, as a system, performs adequately under all required modes of operation. This testing can consist of measuring pressure differences across barriers under various modes of smoke control system operation. In cases where airflows through open doors are important, these should also be measured. Chemical smoke from smoke candles (sometimes called *smoke bombs*) is not recommended for any performance testing because it normally lacks the buoyancy of hot smoke from a real building fire. Smoke near a flaming fire has a temperature in the range of 1000 to 2000°F (540 to 1100°C). Heating chemical smoke to such temperatures to emulate smoke from a real fire is not recommended unless precau-

tions are taken to protect life and property. These same comments about buoyancy apply to tracer gases. Thus, it seems that pressure difference testing is the most practical performance test.

References Cited

1. W.G. Berl and B.M. Halpin, "Human Fatalities from Unwanted Fires," *J. Hopkins APL Tech. Dig.*, 1, p. 129 (1980).
2. ASTM EL76-80, *Annual Book of ASTM Standards, Part 18,* American Society for Testing and Materials, Philadelphia (1980).
3. NFPA 90A, *Standard for the Installation of Air Conditioning and Ventilating Systems,* National Fire Protection Association, Quincy, MA (1993).
4. J.H. Klote, "Stairwell Pressurization," *ASHRAE Transactions,* 86, p. 604 (1980).
5. J.H. McGuire and G.T. Tamura, "Simple Analysis of Smoke Flow Problems in High Rise Buildings," *Fire Tech.,* 11, p. 15 (1975).
6. J.B. Fang, "Static Pressures Produced by Room Fires," *NBSIR 80-1984,* National Bureau of Standards, Washington, DC (1980).
7. P. Sachs, *Wind Forces in Engineering,* Pergamon, New York (1972)
8. E.L. Houghton and N.B. Carruther, *Wind Forces on Buildings and Structures,* John Wiley and Sons, New York (1976).
9. E. Simiu and R.H. Scanlan, *Wind Effects on Structures: An Introduction to Wind Engineering,* John Wiley & Sons, New York (1978).
10. A.J. MacDonald, *Wind Loading on Buildings,* John Wiley & Sons, New York (1975).
11. C.Y. Shaw and G.T. Tamura, "The Calculation of Air Infiltration Rates Caused by Wind and Stack Action for Tall Buildings," *ASHRAE Transactions,* 83, p. 145 (1977).
12. P.H. Thomas, "Movement of Smoke in Horizontal Corridors Against an Air Flow," *Inst. of Fire Engg. Q.,* 30, p. 45 (1970).
13. B.H. Shaw and W. Whyte, "Air Movement Through Doorways—The Influence of Temperature and Its Control by Forced Air Flow," *Bldg. Serv. Engg.*, 42, p. 210 (1974).
14. C. Huggett, "Estimation of Heat Release by Means of Oxygen Consumption Measurements," *Fire and Materials,* 4, pp. 61–65 (1980).
15. J.H. McGuire, G.T. Tamura, and A.G. Wilson, "Factors in Controlling Smoke in High Buildings," in *Symposium on Fire Hazards in Buildings,* ASHRAE, San Francisco (1970).
16. R.J. Cresci, "Smoke and Fire Control in High-Rise Office Buildings—Part II, Analysis of Stair Pressurization Systems," *Symposium on Experience and Applications on Smoke and Fire Control,* ASHRAE, Atlanta (1973).
17. G.T. Tamura and C.Y. Shaw, "Studies of Exterior Wall Air Tightness and Air Infiltration of Tall Buildings," *ASHRAE Transactions,* 83, p. 122 (1976).
18. G.T. Tamura and A.G. Wilson, "Pressure Differences for a 9-Story Building as a Result of Chimney Effect and Ventilation System Operation," *ASHRAE Transactions,* 72, p. 180 (1966).
19. G.T. Tamura and C.Y. Shaw, "Air Leakage Data for the Design of Elevator and Stair Shaft Pressurization Systems," *ASHRAE Transactions,* 86, p. 54 (1978).
20. G.T. Tamura and C.Y. Shaw, "Experimental Studies of Mechanical Venting for Smoke Control in Tall Office Buildings," *ASHRAE Transaction,* 86, p. 54 (1978).
21. *ASHRAE Handbook—1997 Fundamentals,* Chapter 26—Climatic Design Information American Society of Heating, Refrigerating and Air Conditioning Engineers, Atlanta (1985).
22. *Temperature Extremes in the United States,* National Oceanic and Atmospheric Administration, Ashville, NC (1979).
23. NFPA *101®, Life Safety Code®,* National Fire Protection Association, Quincy, MA (1994).
24. R. Best and D.P. Demers, "Investigation Report on the MGM Grand Hotel Fire—Las Vegas, NV, Nov. 21, 1980," National Fire Protection Association, Quincy, MA (1982).
25. J.K. Klote and J.A. Milke, *Design of Smoke Management Systems,* American Society of Heating, Refrigerating, and Air Conditioning Engineers, Atlanta (1992).
26. J.H. Klote, "An Analysis of the Influence of Piston Effect on Elevator Smoke Control," *NBSIR 88-3751,* U.S. National Bureau of Standards, Gaithersburg, MD (1988).
27. J.H. Klote and G.T. Tamura, "Experiments of Piston Effect on Elevator Smoke Control," *ASHRAE Transactions,* 93, Part 2, pp. 2217–2228 (1987).
28. J.H. Klote and G.T. Tamura, "Elevator Piston Effect and the Smoke Problem," *Fire Safety Journal,* 11, 3, pp. 227–233 (1986).
29. J.H. Klote, "A Computer Program for Analysis of Smoke Control Systems," *NBSIR 82-2512,* National Bureau of Standards, Washington, DC (1982).
30. D.M. Sander, *DBR Computer Program No. 37,* National Research Council of Canada, Ottawa (1974).
31. D.M. Sander and G.T. Tamura, *DBR Computer Program No. 35,* National Research Council of Canada, Ottawa (1973).
32. H. Yoshida, C.Y. Shaw, and G.T. Tamura, *DBR Computer Program No. 45,* National Research Council of Canada, Ottawa (1979).
33. E. Evers and A. Waterhouse, *A Computer Model for Analyzing Smoke Movement in Buildings,* Building Research Establishment, Borehamwood, UK (1978).
34. T. Wakamatsu, "Calculation Methods for Predicting Smoke Movement in Building Fires and Designing Smoke Control Systems, Fire Standards and Safety," *ASTM STP 614,* American Society for Testing and Materials, Philadelphia (1977).
35. J. Rilling, *Smoke Study, 3rd Phase, Method of Calculating the Smoke Movement Between Building Spaces,* Centre Scientifique et Technique du Batiment, Champs Sur Marne, France (1978).
36. C.P. Wray and G.K. Yuill, "An Evaluation of Algorithms for Analyzing Smoke Control Systems," in *ASHRAE Transactions,* 999, Part 1, pp. 160–174 (1993).
37. G.N. Walton, *CONTAM96 User Manual,* National Institute of Standards and Technology, NISTIR 6056 (1997).

CHAPTER 13

Smoke Management in Covered Malls and Atria

James A. Milke

Introduction

The atrium is an architectural construct originating from the era of the Roman Empire.[1] Initially, the atrium was a courtyard bounded by a building, without a roof. During the latter part of this century, a roof or ceiling has been placed over the courtyard, and occasionally bounding walls around the courtyard are removed to provide openings between the courtyard and adjacent spaces.[2] Covered malls are also a relatively recent architectural development. Here, the large-volume structure comprises a pedestrian space, often with large openings into the communicating stores.

Smoke management in large-volume spaces, such as atria and covered malls, poses separate and distinct challenges from well-compartmented spaces. In particular, smoke control strategies using pressure differences and physical barriers described by Klote in Section 4, Chapter 12, and NFPA 92A, *Recommended Practice for Smoke-Control Systems*,[3] are infeasible. Without physical barriers, smoke propagation is unimpeded, spreading easily throughout the entire space. The tall ceiling heights in many large-volume spaces pose additional challenges in terms of substantial quantities of smoke production and delayed detection times. However, on the positive side, the large-volume space and tall ceiling height permit the smoke to become diluted and cooled as it spreads vertically and horizontally. Dilution acts to reduce the level of hazard posed by the smoke.

In atriums, hazard development is moderated by the large volume typically associated with the space. However, there is still a need to ensure that dangerous concentrations of smoke are prevented.

In addition to atria and covered malls, there are many other examples of large-volume spaces, including convention centers, airport terminals, sports arenas, and warehouses. The engineering principles governing the design of smoke management systems for these various large-volume spaces are the same. However, differences in the smoke management system designs for these large-volume spaces may occur as a result of different fire scenarios and design goals reflecting changes in function, shape, and connection to other spaces, among other factors. Given the similarities in engineering principles affecting smoke management system design, the term *atrium* will be used throughout this chapter to refer to all types of large-volume spaces.

The discussion presented in this chapter is divided into two sections. First, conditions within the atrium prior to actuation of a smoke management system are discussed. As part of this discussion, the smoke filling process is described along with the time required for actuation of a smoke management system. The second part includes a description of conditions within the atrium after actuation of the smoke management system.

As a preface to any discussion on smoke management systems, a definition of smoke must be established (NFPA 92B, *Guide for Smoke Management Systems in Malls, Atria, and Large Areas*,[4] Section 1-4):

> The airborne solid and liquid particulates and gases evolved when a material undergoes pyrolysis or combustion, together with the quantity of air that is entrained or otherwise mixed into the mass.

While only the combustion products are visible and potentially toxic, what is visually observed as smoke is a mixture of the combustion products and the entrained air. Air is entrained along the entire height of the smoke plume below a smoke layer. Proportionally, the smoke is mostly entrained air. In the area between the base and tip of the flames, most of the entrained air is not consumed in the combustion process and only dilutes the combustion products. The entrainment of additional air along the plume acts to further dilute the smoke. The smoke be-

James A. Milke is an associate professor in the Department of Fire Protection Engineering at the University of Maryland. His recent research activities have included assessing the performance of smoke management systems and structural members in fires.

comes increasingly more diluted with the increasing height of the plume. Entraining air into the smoke plume also increases the mass flow in the plume to increase the quantity of smoke produced. However, the entrained air also decreases the concentration of combustion gases and cools the smoke. In some cases, the smoke may be sufficiently diluted to mitigate the associated hazards.

Hazard Parameters

Smoke can adversely affect building occupants, fire brigade members, property (including the building structure and contents), and mission continuity. Typically, the threat to people or objects is posed when they come into contact with smoke for a sufficient period of time.

People who become exposed to smoke are generally harmed as a result of the exposure to toxic gases or elevated temperature. The toxic effects of smoke on people are described in Purser (see Section 2, Chapter 6) and Klote and Milke.[5] In addition, smoke may reduce visibility. A reduction of visibility may cause people to become disoriented and can in turn increase the amount of time they are exposed to the smoke.[6] A reduction of visibility may also increase the susceptibility of building occupants to trip over obstructions or even fall over balcony railings.[7]

Building components can be affected by the elevated temperature due to smoke. Building components heated by smoke are considered in fire resistance analyses. In addition, building contents may be affected by exposure to the elevated temperatures, corrosive gases, or particulate matter. Contents exposed to heated smoke may be melted, distorted, or charred, depending on the temperature of the smoke and the degree of exposure. Contents which are submerged in smoke and come into contact with combustion gases and smoke particles may become stained or emit an odor of smoke. Exposure to smoke can damage electronic equipment, especially if restoration activities are not initiated promptly after the fire.[8]

Following a fire, a building or portion thereof may be closed due to restoration, to threaten mission continuity. This results in loss of revenue for the building owner, temporary unemployment of workers in the building, and loss of service of the facility to the community, among other things.

Smoke Layer Interface Position

The smoke layer interface position is located a distance, z, above the top of the fuel, as indicated in Figure 4-13.1. This parameter addresses the danger of people being immersed in a smoke layer. Sole use of this parameter to assess hazard level is conservative by considering any concentration of smoke to be unacceptable. However, even though the physiological effects due to being submerged in "light" smoke levels may be minor, the psychological effects and extended evacuation time may be appreciable. Being surrounded by smoke of any nature may decrease the speed of evacuation, perhaps until the smoke is no longer relatively benign. In terms of property protection issues, any smoke may be unacceptable because of smoke staining or smoke corrosivity.

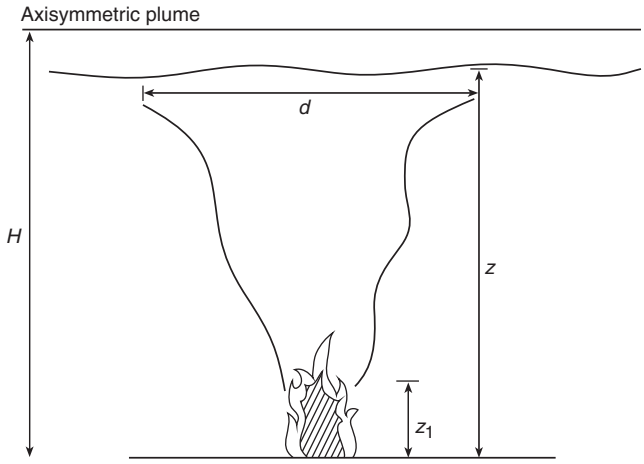

Figure 4-13.1. ***Axisymmetric plume.[4]***

Light Obscuration

As with the smoke layer depth parameter, light obscuration is not lethal by itself.[9] Associated with an increase in light obscuration is a reduction in visibility, which is likely to yield a longer evacuation time and extend exposure to the smoke toxins. In some documented fires, evacuation has been terminated due to a lack of sufficient visibility.[10,11,12] A fire fighter's injury in an atrium fire was attributed to a significant reduction in visibility due to light obscuration.[7] The fire fighter fell from an upper balcony because he could not see the edge.

Limiting values from 0.23 to 1.2 m^{-1} have been suggested for the extinction coefficient.[10,11,12] (See Section 2, Chapter 13.) Alternatively, a critical limit may be based on a preferred minimum visibility distance to a particular target. For example, a limit of light obscuration can be suggested such that occupants can see an illuminated exit sign across a room or at the end of a corridor.

Temperature and Gas Specie Concentration

The final two parameters, elevated temperature of the smoke layer and gas specie concentration (such as CO, CO_2, and HCN), can be directly related to the potential for harm. (See Section 2, Chapter 6.) Critical limits for these two parameters can be suggested based on toxicity studies.

Smoke Management Approaches

The design of a smoke management system for an atrium is influenced by the following three characteristics of the atrium:

1. Geometric shape and dimensions
2. Relative location within the building
3. Separation from communicating spaces

Several approaches are available to achieve smoke management goals in an atrium (e.g., limit the fire size,

provide physical barriers, and provide mechanical or natural ventilation). Selection of the best smoke management approach for a particular atrium should consider the use, size, and arrangement of spaces.

Limiting the fire size can be accomplished by controlling the type, quantity, and arrangement of fuel. In addition, the fire size can be controlled through an automatic suppression system.

Physical barriers limit smoke spread to adjacent spaces. The ability of a physical barrier to limit smoke spread is dependent on the leakage of the barrier and pressure difference across the barrier. The barrier needs to withstand the exposure to smoke and an elevated temperature environment. In an atrium with a tall ceiling, the temperature of the smoke layer in the atrium is likely to be only slightly above ambient conditions.

Mechanical or natural ventilation may be provided to remove smoke from the atrium. Removing smoke from the atrium can limit the accumulation of heat and smoke within the atrium or can arrest the descent of the smoke layer. Mechanical ventilation can be provided in a direction opposite the smoke movement to restrict smoke spread to communicating spaces. Gravity vents may be provided to remove smoke, though their performance may be compromised by environmental factors. Discussions of gravity vents are provided elsewhere.[13] (See Section 3, Chapter 9.)

Analytical Approach

Numerous tools are available to evaluate the adequacy of a smoke management system. The selection of a particular tool is dependent on the accuracy needed for the analysis and the applicability of the analytical tools, given the characteristics of the large space and selected fire scenarios.[14] The principal characteristics that affect applicability are

- Geometry of the large space: variation of horizontal cross-sectional area, sloped versus flat ceiling
- Time period of interest: unsteady versus steady heat release rate, constant operation of smoke management system
- Fire development: heat release rate described by power law
- Environmental effects: stack effect, wind
- Interacting systems: other smoke management systems, HVAC

The range of design tools available to assess the performance of smoke management system designs can be grouped into the following categories:

- Zone model (algebraic equation based)
- Zone model (computer based)
- Field model
- Scale model

The intent of an engineering analysis of smoke conditions in an atrium is to express the level of hazard in terms of physically based parameters, for example, smoke layer interface position, temperature, carbon monoxide concentration, and light obscuration. The magnitude of each of these parameters can be predicted based on engineering principles. In addition to being predictable, critical threshold values are available for the hazard parameters in order to properly assess the severity of the threat. (See Section 2, Chapter 6.) This chapter will concentrate on the life hazards posed by smoke. The hazards smoke poses to contents, property, and mission continuity are described elsewhere.[15,5,8]

Scale Models

Scale models provide physical representations of a space, though in a reduced scale. Scale models are especially useful in examining atria with irregular shapes or numerous projections. A review of applying scale models as a design aid for atrium smoke management systems was provided by Milke and Klote.[14]

Quintiere provided a review of scaling relationships based on preserving the Froude number.[16] The Froude number, Fr, is defined as v/gl.

The scaling relations are

Temperature: $$T_m = T_F \tag{1}$$

Geometric position: $$x_m = x_F \left(\frac{l_m}{l_F}\right) \tag{2}$$

Pressure: $$\Delta p_m = \Delta p_F \left(\frac{l_m}{l_F}\right) \tag{3}$$

Velocity: $$v_m = v_F \left(\frac{l_m}{l_F}\right)^{1/2} \tag{4}$$

Time: $$t_m = t_F \left(\frac{l_m}{l_F}\right)^{1/2} \tag{5}$$

Convective heat release: $$Q_{c,m} = Q_{c,F} \left(\frac{l_m}{l_F}\right)^{5/2} \tag{6}$$

Volumetric flow rate: $$V_{\text{fan},m} = V_{\text{fan},F} \left(\frac{l_m}{l_F}\right)^{5/2} \tag{7}$$

Experiments based on Froude modeling may be done with air at atmospheric pressure. Froude modeling does not preserve the Reynolds number. However, appropriate selection of the size of the model can assure that fully developed flow is achieved to minimize this effect. Because the smoke behavior in only certain areas of the scaled atrium may be of interest, fully developed flow only needs to be achieved in these areas. Often, a scale model with a critical dimension of at least 0.3 m in any areas of interest will be sufficient to achieve fully developed, turbulent flow. As an example, in most shopping centers and atria, the critical dimension in question would be the floor-to-ceiling height of one of the balconies.

In addition, Froude modeling does not preserve the dimensionless parameters concerning heat transfer. Generally, this limitation has little effect because the tempera-

ture is the same for the scale model and the full-scale facility. Froude modeling does not apply to high-temperature locations and low Reynolds locations (e.g., near the flame). However, Froude modeling provides useful information about smoke transport away from the fire.

Some surface effects can be preserved by scaling the thermal properties of the construction materials for the model. The thermal properties can be scaled by

$$\text{Thermal properties:} \quad (k\rho c_p)_{w,m} = (k\rho c_p)_{w,F} \left(\frac{1_m}{1_F}\right)^{0.9} \qquad (8)$$

Because scaling thermal properties has only a secondary effect on fluid flow, considerations of convenient construction and flow visualization may require that some or all surface materials in the model are different from those selected based on thermal property scaling.

EXAMPLE 1:

A scale model is proposed to determine the equilibrium smoke layer position for the atrium depicted in Figure 4-13.2. Because the horizontal cross-sectional area varies with height, algebraic equation and computer-based zone models are of limited value. Assume that the overall height of the atrium is 30.5 m and the design fire is steady with a heat release rate of 5 MW. An exhaust fan capacity of 142 m^3/s is proposed. By applying the scaling relationships to formulate a small-scale model, the basic parameters for the scale model are

- Height: 3.8-m-tall model (1/8 scale)
- Fire size: 28 kW
- Fan capacity: 0.78 m^3/s

Analytical Models

Two categories of analytical models are zone and field models. A description of field models is outside the scope of this chapter. Zone models divide each compartment into a limited number of control volumes, typically an upper and a lower zone. Inherent in the zone approach is the assumption of uniform properties throughout each zone. In spaces with a large floor area, this assumption may be tenuous. Nonetheless, calculations associated with the zone model approach are relatively easy to perform and are often accepted for engineering purposes. Calculations following the zone model approach may be in the form of algebraic equations or a computer algorithm.

The zone approach assumes that smoke from a fire is buoyant, rises to the ceiling, and forms a smoke layer. The buoyant nature of smoke is due to the decreased density of the heated smoke. As smoke rises in a plume, air is entrained to increase the mass flow rate in the plume. A decrease in the velocity and temperature of the smoke plume results from the increase in the plume mass flow rate, as dictated by conservation of momentum and energy. In addition, the entrained air dilutes the combustion products in the plume. The entire smoke layer is assumed to have uniform characteristics. As smoke is supplied to the smoke layer from the plume, the interface between the smoke layer and lower clear air zone descends. The additional smoke supplied by the plume also results in an increase in the smoke layer temperature, carbon monoxide concentration, and light obscuration.

Being a simplification, the zone model approach may not be applicable in some situations. One example includes a scenario with operating sprinklers, which may cool the layer and also entrain smoke from the upper layer into the water spray pattern descending into the lower zone. Another example consists of the case where smoke does not reach the ceiling as a result of a loss of relative buoyancy, where the temperature near the ceiling of the atrium is greater than that near the floor. This situation is discussed in more detail later in this chapter. A third situation involves an atrium with a large cross-sectional area where the horizontal variation in conditions from one portion of the atrium to another is important to the analyst. Where local conditions need to be assessed, field models are more appropriate than zone models.

Two categories of fire scenarios for smoke management design in atria include (1) fires located in the atrium, and (2) fires located in a space adjacent and open to the atrium. This chapter concentrates only on fires within the atrium space. Methods to estimate conditions in any of the adjacent spaces, resulting from fires originating in the atrium or from fires in other adjacent spaces, are addressed elsewhere.[5]

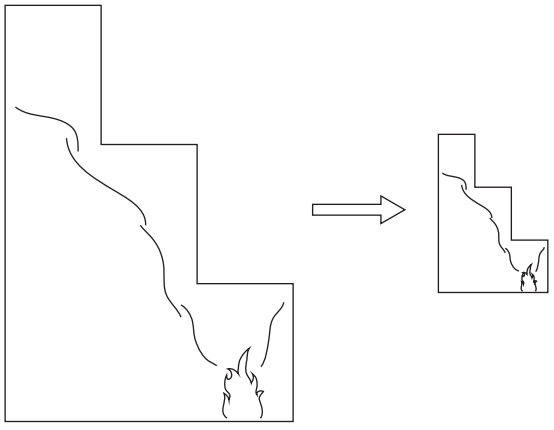

Figure 4-13.2. ***Small-scale model of atrium.***

Smoke Filling Period

A smoke layer is formed once the smoke plume reaches the ceiling and the ceiling jet spreads horizontally to reach the bounding walls of the space. Subsequently, the smoke layer starts to descend in the space. In relatively small spaces with low ceilings, the smoke layer forms almost immediately. However, in large spaces with tall ceilings, the time required to form a smoke layer may be appreciable. The delay in forming a layer is attributable to the transport lag of the smoke. The smoke filling period continues until the smoke exhaust fans are actuated.

Transport Lag

The transport lag is composed of the time for a smoke plume to reach the ceiling (plume transport lag) and the time for the ceiling jet to reach the bounding enclosure (ceiling jet transport lag). These two time periods are depicted in Figure 4-13.3.

Correlations for the plume and ceiling jet transport lag are available in the literature for both steady and t^2 fires.[17,18] Because virtually all fires have a growth period before reaching a steady phase, the transport lag correlations for steady fires have little relevance.

Correlations for the plume transport lag for steady and t^2-fires are

Steady fires: $$t_{pl} = 0.67H^{4/3}/Q^{1/3} \quad (9)$$

t^2 fires: $$t_{pl} = 0.1H^{4/5}t_g^{2/5} \quad (10)$$

Estimates of the plume transport lag from equations 9 and 10 are provided in Figure 4-13.4. As indicated in the figure, even the shortest plume transport lag for t^2 fires, associated with the fast t^2 fire, is greater than that for a modest-size steady fire.

Comparable correlations for the ceiling jet transport lag for steady and t^2 fires are

Steady fires: $$t_{cj} = \frac{r^{11/6}}{1.2\dot{Q}^{1/3}H^{1/2}} \quad (11)$$

t^2 fires: $$t_{cj} = \frac{0.72rt_g^{2/5}}{H^{1/5}} \quad (12)$$

A comparison of the ceiling jet transport lag for a modest-size steady fire and t^2 fires is presented in Figure 4-13.5. Again, the transport lag associated with the steady fire is much less than that associated with any of the t^2 fires.

Smoke Layer Interface Position

Once the smoke layer has formed, the initial rate of descent of the layer is very rapid, slowing as the layer descends. This is attributable to the dependence of the rate of smoke production on the distance from the top of the fuel to the smoke layer.

Both empirical correlations and theoretically based methods are available to address conditions during the smoke filling period using a zone model approach. Theoretically based methods use statements of conservation of mass and energy to determine the volume of the upper layer.[19] Conservation of mass accounts for the smoke mass supplied from the plume to the smoke layer along with any smoke leaving the zone through ventilation openings. Conservation of energy is applied to address the energy being supplied by the plume along with heat losses from the layer.

Generally, predictions of the smoke layer interface position by the two analytical methods differ. The principal reason for the discrepancy is the difference in definitions of the smoke layer interface used by the two

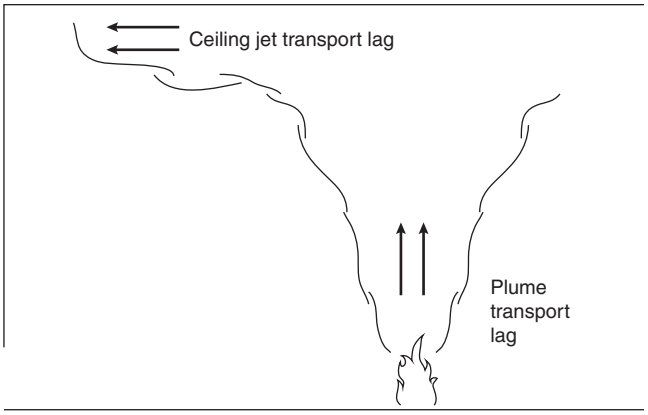

Figure 4-13.3. ***Plume and ceiling jet transport lag.***

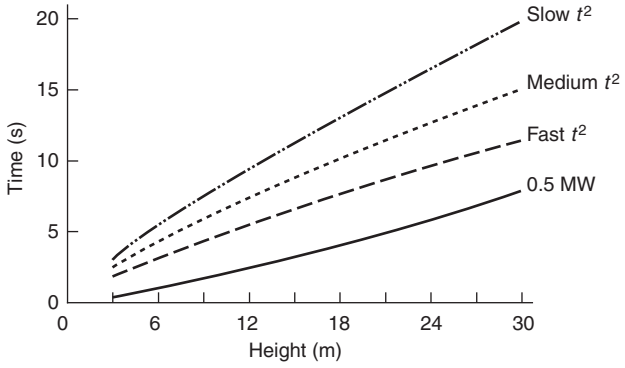

Figure 4-13.4. ***Plume transport lag.***

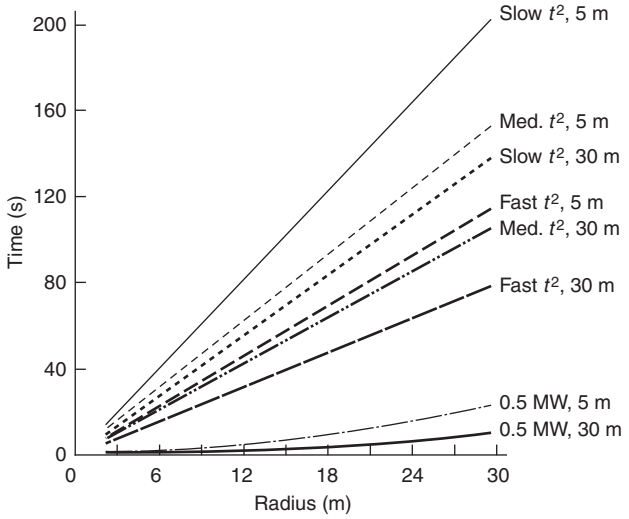

Figure 4-13.5. ***Ceiling jet transport lag.***

methods. The empirical correlations are based on first indications of smoke, either using temperature rise or visual measurements. The theoretically based approach defines the smoke layer position as the demarcation between the upper and lower zones.

Empirical Correlations

Empirical correlations have been developed by Heskestad to determine the smoke layer interface position as a function of time for steady and t^2 fires. These correlations, included in NFPA 92B, *Guide for Smoke Management Systems in Malls, Atria, and Large Areas*,[4] are based on experimental data in large spaces. In the experimental efforts, the smoke layer interface position was established by a variety of means, including visual observations and first change temperature, carbon dioxide concentration, or optical density measurements.

The correlations are simple expressions with easily acquired input and minimal computations. The correlations provide conservative estimates of the smoke layer interface position (i.e., predicting the smoke layer interface to be lower than may be typically expected.)[20] The correlations are applicable to simplified cases related to the fire and geometry of the space. Fire scenarios are either steady or growing and follow a t^2 profile. The assumed geometrical configuration is a space of uniform cross-sectional area (i.e., rectangular or right cylindrical solids). In addition to the noted simplifications, second-order parameters such as environmental factors (e.g., stack effect, wind) and the effect of HVAC systems are neglected.

Steady fires: The position of the smoke layer interface for steady fires can be estimated using Equation 13.[21,22] Equation 13 is based on experimental data from fires in large-volume spaces with A/H^2 of 0.9 to 14.[23–25]

$$\frac{z}{H} = 1.11 - 0.28 \ln\left(\frac{t\dot{Q}^{1/3}H^{-4/3}}{A/H^2}\right) \qquad (13)$$

where $z/H \geq 0.2$.

Equation 13 is presented in nondimensional form. The quantity $t\dot{Q}^{1/3}H^{-4/3}$ represents the normalized time from ignition. The significance of the normalized time parameter is to indicate that the same relative smoke layer position occurs for a long duration, low heat release rate fire in a tall ceiling height atrium, as for a short duration, large fire in an atrium with a short ceiling height. Different atrium geometries are accounted for by the nondimensional shape factor, (A/H^2).[23,24]

The limits noted for A/H^2 reflect the range of shape factors for the facilities in which the experiments were performed.[23,24] Examples of atria within the noted range include atria with a cross-sectional area of 10,000 m^2 and a height of 105 m ($A/H^2 = 0.9$) or a height of 27 m ($A/H^2 = 14$). Comparisons of the predictions from Equation 13 to experimental data from fires in tall spaces are provided in Figure 4-13.6.[25–27]

The initial time period to form a smoke layer is implicitly included in Equation 13. Evidence of this characteristic is obtained for short time durations where the resulting z/H is greater than 1.0 (otherwise $z/H > 1$ would literally mean that the smoke layer interface is *above* the ceiling). The lower limit for z/H of 0.2 relates to the lowest level where data were taken in any of the referenced experiments.

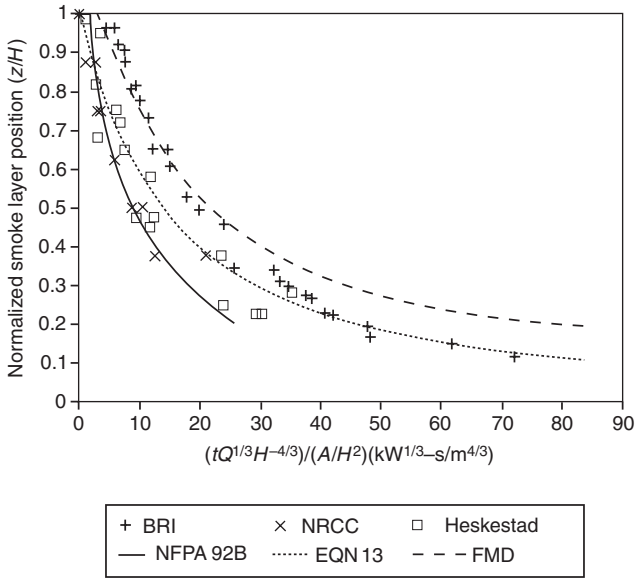

Figure 4-13.6. ***Comparisons of smoke layer position—experimental data versus predictions.***

t^2 fires: Equation 14 provides a correlation of the time-dependent smoke layer interface position for fires following a t^2-type profile.[21,22] Equation 14 is also based on experimental data in spaces with shape factors ranging from 0.9 to 14.[25,28]

$$\frac{z}{H} = 0.91[tt_g^{-2/5}H^{-4/5}(A/H^2)^{-3/5}]^{-1.45} \qquad (14)$$

Equations 13 and 14 both assume that the fire is located near the center of the atrium floor, remote from any walls. Smoke production is greatest for the centered configuration and thereby represents the worst-case condition.

EXAMPLE 2:

For a fast, t^2 fire in an atrium with a cross-sectional area of 800 m^2 and height of 20 m, determine the position of the smoke layer interface after 120 s if the atrium cross-sectional area is 800 m^2.

SOLUTION:

Applying Equation 14 with $A/H = 2.0$ and $t_g = 150$ s, z/H is 0.95 or $z = 19$ m.

EXAMPLE 3:

For a fast, t^2 fire in an atrium with a cross-sectional area of 800 m^2 and height of 20 m, determine the time for the smoke layer interface to reach 15 m above floor level.

SOLUTION:

Re-expressing Equation 14 to solve for t,

$$t = 0.94 t_t^{2/5} H^{4/5} (A/H^2)^{3/5} (z/H)^{-0.69} \quad (15)$$

Applying Equation 15 with $A/H^2 = 2.0$ and $t_g = 150$ s, t is 140 s.

Reviewing the results from Examples 2 and 3, the smoke layer barely descends below the ceiling in the first 120 s. This is indicative of the lag time required for the plume to reach the ceiling and to form a layer. Then, after only another 20 s, the smoke layer descends 4 m, demonstrating the rapid initial descent rate of the smoke layer interface. The rapid descent is attributable to the significant quantity of smoke produced during the early stage of a fire in a tall ceiling space. The trend of rapid filling during the early stage of a fire has been reported by eyewitness accounts from four fires in atria.[7,29–31]

Theoretically Based Approach

Conservation of mass and energy can be applied to provide an estimate for the position of the theoretical smoke layer interface.[19] Equation 16 expresses the conservation of mass, m_u, for the upper smoke layer, assuming no exhaust from the layer

$$\frac{dm_u}{dt} = \dot{m} \quad (16)$$

Approximating the smoke as an ideal gas with properties of heated air, and assuming that the ambient pressure and specific heat are constant, the expression for conservation of energy for the smoke layer is

$$(\rho h)_u \frac{dV_u}{dt} = \dot{Q}_c + \dot{m} h_1 \quad (17)$$

Given the previously assumed conditions, ρh is a constant. Substituting the volumetric flow rate for the mass flow rate and simplifying,

$$\frac{dV_u}{dt} = \frac{\dot{Q}_c}{\rho h} + \dot{V} \quad (18)$$

The growth rate of the upper layer indicated in Equation 18 is dependent on two terms: (1) the volume supplied by the plume and (2) the expansion of the volume due to heating. For the case of an atrium with a constant cross-sectional area, A,

$$\frac{dV_u}{dt} = A \frac{dz_u}{dt} \quad (19)$$

As long as the smoke layer interface is well above the flaming region (see discussion later in this chapter), the plume mass entrainment rate can be estimated from[32]

$$\dot{m} = 0.071 \dot{Q}_c^{1/3} (z - z_o)^{5/3} + 0.002 \dot{Q}_c \quad (20)$$

For large clear heights (i.e., clear heights in excess of 10 m), several simplifications can be made. The clear height is the distance from the top of the fuel to the bottom of the smoke layer. The magnitude of the second term is much less than the first. Generally, z is much greater than z_o. In addition, the volume increase of the upper layer supplied by the plume is appreciably greater than that due to expansion. With these simplifications and by substituting Equations 19 and 20 into Equation 18, an expression for dz_u/dt can be formulated

$$\frac{dz_u}{dt} = \frac{k_v \dot{Q}^{1/3} z^{5/3}}{A} \quad (21)$$

In Equation 21, k_v is the volumetric entrainment constant, defined as

$$k_v = 0.071 \frac{\dot{Q}_c}{\rho \dot{Q}}$$

The convective heat release fraction is the ratio of the convective heat release rate to the total heat release rate and is typically assumed to be on the order of 0.7 to 0.8. Throughout this chapter, a value of 0.7 is selected for the convective heat release fraction.[4] Assuming a plume entrainment constant of 0.071 kg $kW^{-1/3} \cdot m^{-5/3} \cdot s^{-1}$ and the density of ambient air as 1.2 kg/m^3, the volumetric entrainment constant is 0.053 $m^{4/3} kW^{-1/3} s^{-1}$. One difference between Equations 20 and 21 is that the convective portion of the heat release rate is included in Equation 20, whereas the total heat release rate is included in Equation 21.

An expression for the smoke layer position resulting from a steady fire as a function of time can be obtained by integrating Equation 9:

$$\frac{z}{H} = \left[1 + \frac{2 k_v t \dot{Q}^{1/3}}{3 (A/H^2) H^{4/3}} \right]^{-3/2} \quad (22)$$

Alternatively, for a t^2 fire

$$\frac{z}{H} = \left[1 + \frac{4 k_v t (t/t_g)^{2/3}}{(A/H^2) H^{4/3}} \right]^{-3/2} \quad (23)$$

A comparison of the predictions from Equations 13 and 22 is provided in Figure 4-13.6. One principal difference relates to the time delay for the smoke layer to form, i.e., transport lag. Transport lag is included implicitly in Equation 13. Equation 22 assumes that a smoke layer forms immediately. The transport lag can be accounted for separately.[17]

EXAMPLE 4:

For a fast, t^2 fire in an atrium with a cross-sectional area of 800 m^2 and height of 20 m, determine the position of the smoke layer interface after 120 s.

SOLUTION:

Applying Equation 23 with $A/H^2 = 2.0$ and $t_g = 150$ s, z/H is 0.72 or $z = 14.4$ m.

Vented Period

If a smoke management system includes the capability to exhaust smoke, the descent of the smoke layer can

be arrested if the volumetric rate of smoke exhaust from the smoke layer equals the volumetric rate of smoke supplied to the layer. Neglecting the effect of expansion, the layer descent is stopped when the mass exhaust rate is equal to the mass entrainment rate by the plume. Algebraic equations are available to estimate the properties of the smoke layer, including

1. Position of smoke layer interface
2. Temperature of smoke layer
3. Light obscuration in smoke layer and
4. Gas concentration in smoke layer

Equilibrium Smoke Layer Interface Position

The exhaust rate necessary to arrest the descent of the smoke layer can be estimated based on a knowledge of the mass entrainment rate into the plume. The mass entrainment rate depends on the configuration of the plume. Plume configurations reviewed in this chapter are

1. Axisymmetric plume
2. Wall plume
3. Corner plume
4. Balcony spill plume

Axisymmetric plume: Axisymmetric plumes are formed from fires involving fuel packages remote from any walls (i.e., near the center of the atrium floor). Being remote from any walls, air is entrained around all of the plume perimeter along the entire clear height of the plume. The functional relationship of the mass entrainment rate to the heat release rate and clear height is[33]

$$\dot{m} = f(\dot{Q}_c^{1/3} z^{5/3}) \tag{24}$$

The equations for the mass entrainment rate included within NFPA 92B, *Guide for Smoke Management Systems in Malls, Atria, and Large Areas*,[4] were originally derived by Heskestad.[32] One of the equations, previously presented as Equation 20 with z_o set equal to zero, is applicable when the clear height, z, is greater than the limiting height, z_f. The limiting height is defined as the height of the continuous flaming region, (i.e., where flames are present 50 percent of the time). The limiting height may be estimated as[32]

$$z_f = 0.166 \dot{Q}_c^{2/5} \tag{25}$$

The validity of neglecting z_o in Equation 20 is based on the observation that z_o is typically small, compared to z.[4] The location of the virtual origin of an assumed point source can be estimated as[32]

$$z_o = 0.083 \dot{Q}^{2/5} - 1.02 d_o \tag{26}$$

For noncircular fuels, an equivalent diameter needs to be defined. The definition of an equivalent diameter is based on a circle that has an area equal to the floor area covered by the fuel. Considering a wide range of diameters and heat release rates associated with a variety of typical fuel packages, the virtual origin ranges from 0.5 to −5 m. Negative values are obtained when the second term is greater than the first (i.e., for fuel commodities with modest heat release rates spread over a large area).

For clear heights less than the limiting height, the entrainment rate is estimated using Equation 27

$$\dot{m} = 0.032 \dot{Q}_c^{3/5} z \tag{27}$$

Originally, Equations 20 and 27 were developed to describe plumes from horizontal, circular flammable liquid pool fires. However, these equations have been shown to be applicable to more complex fuels, as long as the limiting height is greater than the diameter of the fuel, and the fire only involves the surface of the material (i.e., is not deep-seated).[32]

The mass rate of smoke production estimated by Equations 20 and 27 is independent of the type of materials involved in the fire, other than indirectly in terms of the heat release rate. This is due to the mass rate of entrained air being much greater than the mass rate of combustion products generated, which is true as long as sufficient air is available for combustion. As a result of the fire being approximated as a point source in the entrainment equations, even the shape or form of the fuel is not of primary importance. Thus, the material-related parameters are relegated to a level of secondary importance.

In both Equations 20 and 27, the mass entrainment rate is dependent on the clear height, where the mass entrainment rate increases with increasing values of the clear height. During the early stages of the fire, the clear height has its maximum value to provide the maximum smoke production rate, thereby supporting the eyewitness accounts of the smoke filling process in atria. This is especially true if the flame height is well below the smoke layer, where the smoke production rate is proportional to $z^{5/3}$.

In most engineering applications, the smoke production (or exhaust) rate is expressed in terms of a volumetric rate rather than a mass rate. In order to accommodate this preference, the relationship between the volumetric rate and mass rate is expressed as Equation 28.

$$\dot{V} = \frac{\dot{m}}{\rho} \tag{28}$$

Assuming smoke to have the same properties as air, the density of smoke may be evaluated as the density of air at the temperature of the smoke layer.[5] Graphs relating the volumetric smoke production rate to the clear height for selected total heat release rates ranging from 1000 to 10,000 kW are provided in Figure 4-13.7.

EXAMPLE 5:

A fire has a total heat release rate of 5000 kW and is located at the center of the atrium floor. The smoke layer interface is 35 m above the floor. Determine the mass and volumetric rates of smoke being supplied by the plume to the smoke layer (i.e., at the location of the smoke layer interface).

SOLUTION:

First, the limiting height is evaluated using Equation 25 to determine the applicable equation for the mass rate of entrainment, assuming the convective heat release fraction is 0.7, $z_f = 4.3$ m. Because $z_f < z$, Equation 20 is the

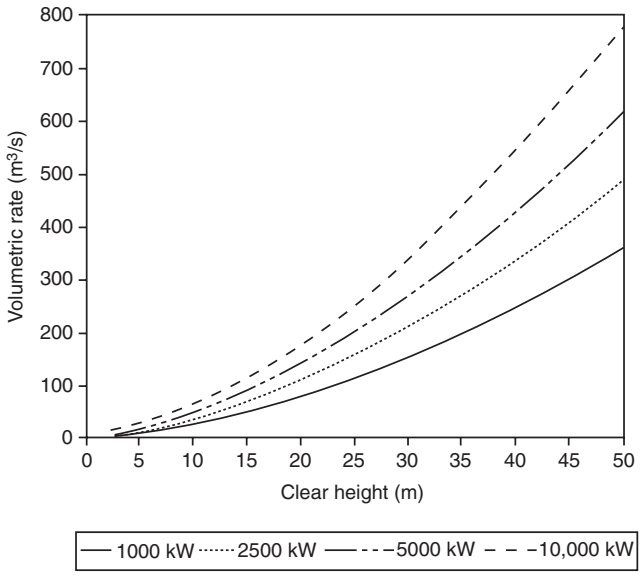

Figure 4-13.7. ***Smoke production rate for axisymmetric plumes.***

applicable equation for determining the mass rate of smoke production. Neglecting z_o, the mass smoke production rate is 410 kg/s. The associated volumetric rate (from Equation 28, assuming standard conditions) is 340 m^3/s.

Wall and corner plumes: Fires located near walls and corners principally entrain air only along the surface of the plume away from the walls or corner. Consequently, the amount of smoke production is reduced for these locations, compared to the axisymmetric plume remotely located from the walls. Using the concept of reflection, the smoke production rate from wall and corner plumes can be estimated.[34,35]

A plume generated by a fire located against a wall only entrains air from approximately half of its perimeter, as indicated in Figure 4-13.8. According to the concept of reflection, the smoke production rate is estimated as half of that from a fire that is twice as large (in terms of heat release rate).

Similarly, a plume generated by a fire located near a corner of a room is referred to as a corner plume. (See Figure 4-13.8.) Using the concept of a reflection, the smoke production rate from corner plumes, where the intersecting walls form a 90-degree angle, is estimated as one-quarter of that from a fire that is four times as large.

EXAMPLE 6:

A fire located on the floor of an atrium has a total heat release rate of 5000 kW. The smoke layer interface is 35 m above the floor. Compare the mass rates of smoke being supplied by the plume to the smoke layer, given an axisymmetric, wall, or corner plume configuration.

SOLUTION:

In Example 5, $z_f = 4.3$ m and the smoke production rate for the axisymmetric plume using Equation 20 is

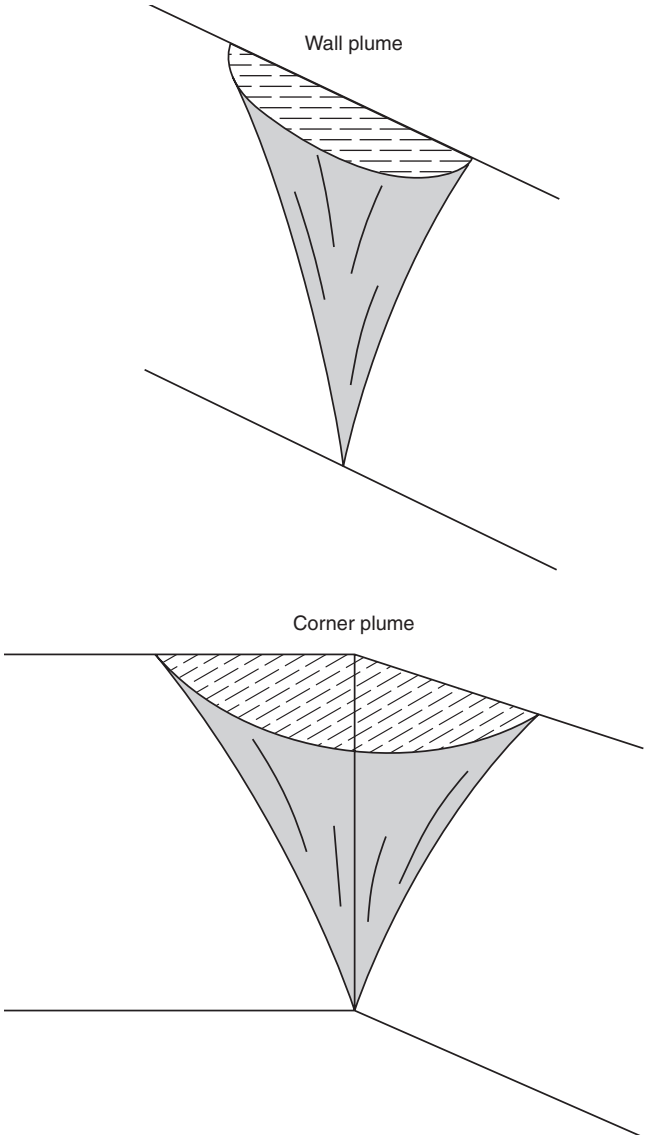

Figure 4-13.8. ***Wall and corner plume diagrams.***

410 kg/s. Applying the same equation for the wall plume, the smoke production rate for a fire size of 10,000 kW is estimated as 520 kg/s. Dividing that rate by two provides the smoke production rate for the wall plume (260 kg/s). Similarly, for the case of the corner plume, the smoke production rate is 170 kg/s (considering one-quarter of the smoke production rate from a 20,000 kW fire).

Comparing the smoke production rates for the three plumes (axisymmetric, wall, and corner plumes), the smoke production rate is greatest for the axisymmetric plume (410 kg/s) compared to 260 and 170 kg/s for the wall and corner plumes, respectively. Thus, conservative hazard assessments should assume an axisymmetric plume is developed from a fire that is located away from the walls, near the center of the space.

Balcony spill plume: A balcony spill plume is generated in cases where smoke reaches an intermediate obstruction, such as a balcony, travels horizontally under the obstruction and then turns and moves vertically. Scenarios with balcony spill plumes involve smoke rising above a fire, reaching a ceiling, balcony, or other significant horizontal projection, then traveling horizontally toward the edge of the balcony. Characteristics of the resulting balcony spill plume depend on characteristics of the fire, width of the spill plume, and height of the ceiling above the fire. In addition, the path of horizontal travel from the plume centerline to the balcony edge is significant.

For situations involving a fire in a communicating space, which is immediately adjacent to the atrium, air entrainment into balcony spill plumes can be estimated using Equation 29. Equation 29 is based on Law's[36] interpretation of small-scale experimental data obtained by Morgan and Marshall.[37] Equation 29 provides an approximation of the mass flow in the plume for a complex situation.

$$\dot{m} = 0.36(QL^2)^{1/3}(z + 0.25H_b) \qquad (29)$$

The small-scale experiments simulated the situation of smoke being generated from a fire in a store, discharging out of the store through a single opening, traveling under a walkway serving the level above, then turning and rising once, reaching the edge of the walkway. The applicability of Equation 29 is questionable as a result of appreciable heat losses from the smoke for situations involving smoke discharging from a space connected to the atrium through a long corridor.

Predictions of the smoke production rate using Equation 29 for the balcony spill plume are included in Figure 4-13.9. The calculations represented in the figure consider a 3-m height to the underside of the balcony.

A comparison of the smoke production rate for axisymmetric and balcony spill plumes is provided in Figure 4-13.10. The heat release rate for both fires is 5000 kW, z_o 30 for the axisymmetric plume, and H_b 33 m for the balcony spill plume. For short heights, the smoke production rate for the balcony spill plume is appreciably greater than that for the axisymmetric plume. However, with increasing height, the smoke production rates from the two plumes become comparable. Eventually, the two curves intersect, suggesting that, at some height, the balcony spill plume behaves the same (i.e., produces the same amount of smoke) as an axisymmetric plume. The point of intersection can be determined by setting Equation 20 equal to Equation 29. For large z and z much greater than H_b, the mass flow rates are equal when z is 12.5 times the width. Consequently, for greater heights the smoke production rate from a balcony spill plume should be estimated using Equation 20 with z evaluated from the balcony to the smoke layer.

The width of the plume, W, can be estimated by considering the presence of any physical vertical barriers attached to the balcony. The barriers act to restrict dispersion of the horizontal flow of smoke under the balcony. However, in the absence of any barriers, an equivalent width can be defined, based on results from visual observations of the width of the balcony spill plume at the balcony edge from the set of small-scale experiments by Morgan and Marshall.[37] The definition of an *equivalent confined plume width* is the width that entrains the same amount of air as an unconfined balcony spill

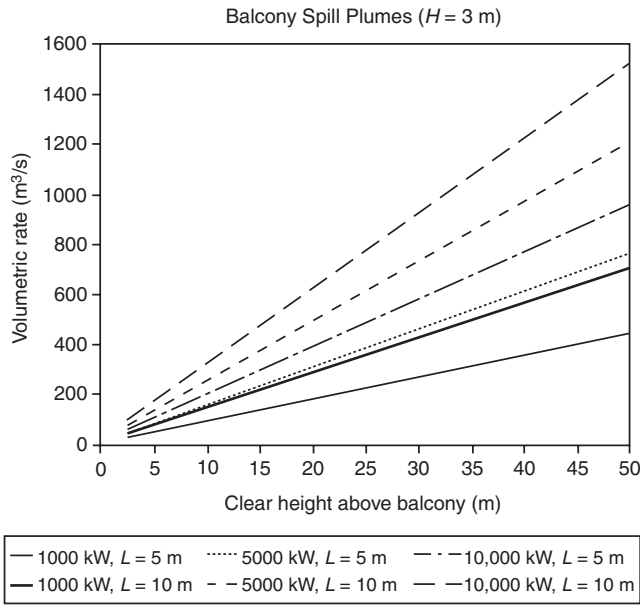

Figure 4-13.9. ***Smoke production rate predictions for balcony spill plumes (H-3m).***

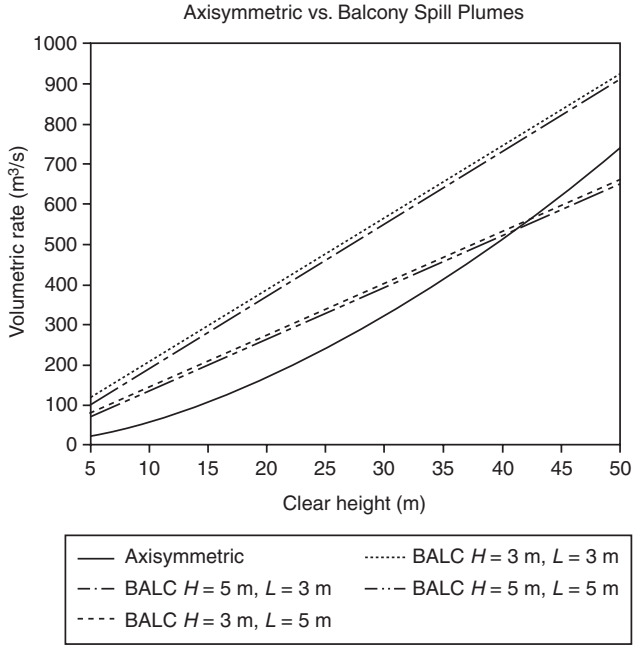

Figure 4-13.10. ***Comparison of smoke production rate for axisymmetric and balcony spill plumes.***

plume. The equivalent width is evaluated using the following expression

$$L = w + b \tag{30}$$

Properties of Smoke Layer

Properties of the smoke layer are of interest both during the filling period of the fire and during the vented period. During the filling period, determination of the smoke layer properties is important to assess the level of hazard prior to actuation of a mechanical smoke management system. During the vented period, smoke layer properties are of interest to assess the level of hazard associated with those cases where occupants are exposed to smoke (i.e., the highest walking level is submerged in the smoke layer). The smoke layer properties of interest include temperature, light obscuration, and gas species concentration.

Temperature rise in smoke layer: The temperature of the smoke layer can be determined based on an energy balance for the volume of the smoke layer. Energy is supplied to the layer by the fire. Energy may be lost from the layer to the enclosure (walls, ceiling) of the space. During the filling period, the resulting expression is[19]

$$T = T_o \exp\left(\frac{(1-\chi_l)Q}{Q_o}\right) \tag{31}$$

Estimates for χ_l vary appreciably. Most of the design guides suggest assuming that the smoke layer is adiabatic (i.e., setting $\chi_l = 0$), in order to be conservative.[4,38] Walton suggested values for χ_l between 0.6 and 0.9 for relatively small spaces of near cubic shape.[39] In many of the large spaces with tall ceiling heights, the temperature rise anticipated for the smoke layer is relatively modest such that convection and radiation heat transfer to an enclosure will also be modest. Consequently, in such applications, the adiabatic assumption will provide reasonable predictions of the temperature rise. However, in low ceiling spaces (under approximately 10 m), the temperature may be significantly overestimated by applying the adiabatic assumption.

Similarly, the equilibrium smoke layer temperature during venting can be approximated by applying an energy balance to the smoke layer. In this case, energy is also lost from the layer due to smoke being exhausted from the atrium.

$$\Delta T = \frac{(1-\chi_l)\dot{Q}_c}{c_p \dot{m}} \tag{32}$$

If the adiabatic assumption is applied, the smoke layer temperature will be overestimated, providing a conservative estimate of the hazard. In reality, some heat is lost from the upper smoke layer to the surrounding walls and ceiling. However, no elementary method is available to estimate the overall proportion of heat that is lost to the surroundings.[40,41] Some zone and field computer fire models account for heat losses to the boundary.[24,42] The adiabatic smoke layer temperature for a range of fire sizes is presented in Figure 4-13.11.

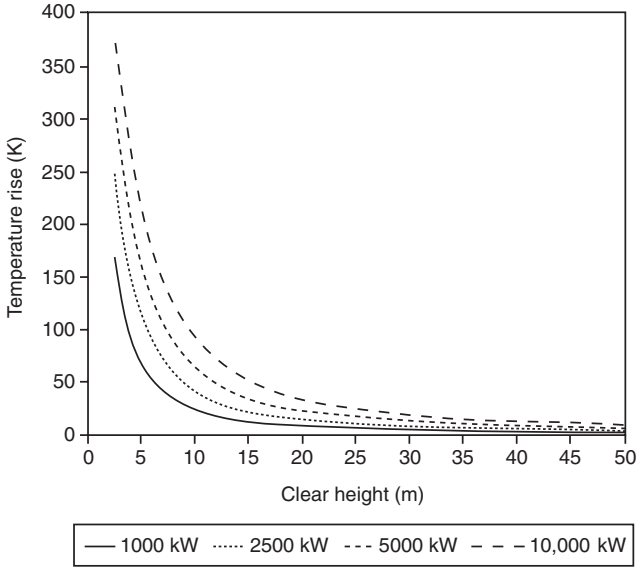

Figure 4-13.11. ***Temperature rise of smoke layer for axisymmetric plumes.***

The degree of overestimation can be assessed by comparing the estimated smoke layer temperature with the plume centerline temperature. For thermodynamic reasons, the smoke layer temperature cannot exceed the plume centerline temperature. The plume centerline temperature, T_c, can be evaluated using Equation 33[43]

$$T_c = 0.08 T_o \dot{Q}_c^{2/3} z^{-5/3} + T_o \tag{33}$$

The volumetric venting rate for other heat release rates or temperature rises may be determined considering that the specific heat is virtually constant for the expected temperature range of interest

$$\frac{\dot{Q}_{c_1}}{\dot{Q}_{c_2}} = \frac{V_1}{V_2}\frac{\Delta T_{\mathrm{ad}_1}}{\Delta T_{\mathrm{ad}_2}}\frac{T_2}{T_1} \tag{34}$$

As can be observed from Equation 34, doubling the volumetric venting rate for the same size fire reduces the temperature rise by approximately 50 percent (the temperature rise is not precisely halved, since the absolute temperature of the smoke layer in both instances is not exactly the same).

Light obscuration: The visibility distance through smoke can be related to the optical density per unit pathlength via empirical correlations.[44,45] (See Section 2, Chapter 13.) The experimental basis for the correlations consists of tests with humans viewing objects through smoke. However, the participants were not directly exposed to the irritating effects of smoke. Consequently, the reported correlations are likely to overestimate the visibility distance.

In addition to the light obscuration quality of the smoke, the visibility of an object is dependent on the light source for the object being viewed as well as ambient lighting conditions.[45,46]

Mulholland provides the following expression to relate visibility to the optical density (see Section 2, Chapter 13):

$$\text{Visibility} = \frac{0.43K}{D} \tag{35}$$

The optical density of the smoke layer can be determined considering that all of the particulates generated by the fire are transported to the layer via the plume and accumulate in the layer. Any deposition on enclosure surfaces is neglected. The resulting expression for the smoke filling and vented periods are provided as Equations 36 and 37.[19]

Smoke filling:
$$D = \frac{D_m Q}{\chi_a H_c A(H - z)} \tag{36}$$

Vented:
$$D = \frac{D_m \dot{Q}}{\chi_a \Delta H_c \dot{m}/\rho} \tag{37}$$

The mass optical density is dependent on the fuel, burning mode, ventilation conditions, and operation of sprinklers. The mass optical density can vary by orders of magnitude for different ventilation conditions.

While a reduction in visibility is not directly life-threatening, it does reduce the walking speed of individuals, thereby increasing the exposure time to toxic gases and elevated temperature. In addition, the reduction in visibility may lead to an increased susceptibility to occupants tripping or falling. The relationship between visibility and movement speed is indicated in Figure 4-13.12.

Carbon monoxide concentration: The concentration of gas species contained in the smoke layer can be determined considering that all of the mass that is supplied to the layer via the plume accumulates in the layer. No absorption by the enclosure is assumed. The resulting expressions for the smoke filling and vented periods are[19]

Smoke filling:
$$Y_i = \frac{f_i Q}{\rho_o \chi_a H_c A(H - z)} \tag{38}$$

Vented:
$$Y_i = \frac{f_i Q}{\dot{m} \chi_a H_c} \tag{39}$$

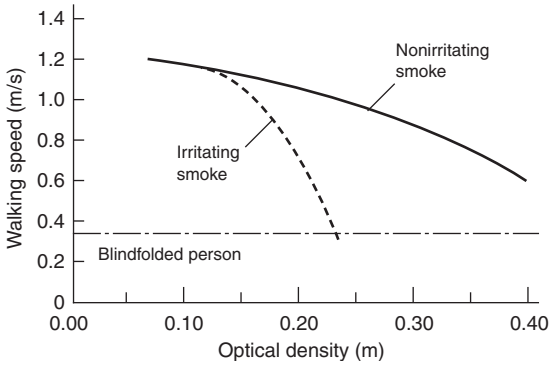

Figure 4-13.12. ***Relationship between visibility through smoke and walking speed.***

In order to express the gas species concentration in units of ppm, Equation 40 needs to be applied

$$ppm_i = \frac{MW_{\text{air}}}{MW_i} Y_i \times 10^6 \tag{40}$$

Input for evaluating the gas species concentration includes the yield fraction and heat of combustion, both of which are fuel dependent parameters. The yield fraction is dependent on the burning mode and oxygen concentration. Most of the information tabulated on the yield fraction, such as that by Tewarson (see Section 3, Chapter 4), assumes well-ventilated, flaming combustion. Most of the fires of interest in large spaces will involve flaming combustion and are likely to be well-ventilated. However, fires in small, connected spaces may become under-ventilated. Caution needs to be exercised in properly identifying ventilation conditions when predicting these parameters because the yield fraction can vary by orders of magnitude for different ventilation conditions. Also, the yield fractions noted by Tewarson are relevant only to cases where sprinklers are not operating.[47]

EXAMPLE 7:

Estimate the steady-state smoke layer properties (temperature, visibility to an internally illuminated exit sign, and CO concentration) during the vented period, given the following situation:

1. The smoke layer interface is maintained 35 m above floor level.
2. The rate of heat release of the flaming fire is 5000 kW.
3. The fuel is comprised principally of polyurethane foam.

SOLUTION:

Smoke Layer Temperature

Equation 32 can be applied to determine the adiabatic smoke layer temperature rise. In Example 5, a mass rate of smoke production of 410 kg/s was determined. Thus, assuming an adiabatic smoke layer, a convective heat release rate fraction of 0.7 and specific heat of air of 1.0 kJ/kg·K, the temperature rise is 8.5°C.

Visibility

Visibility during the vented period is estimated using Equation 37. Fuel-related parameters are obtained in Section 3, Chapter 4 and Section 2, Chapter 13.

$$D_m = 260 \text{ m}^2/\text{kg}$$
$$H_c = 12{,}400 \text{ kJ/kg}$$

Evaluating ρ at the temperature of the smoke layer to be 1.17 kg/m^3, the optical density is 0.32 m^{-1} and the associated visibility is 8.5 m.

CO Concentration

CO concentration for the vented period is estimated using Equations 39 and 40, with the fuel-related properties again evaluated from Section 3, Chapter 4.

$$f_{\text{CO}} \text{ for polyurethane is} \sim 0.030 \text{ kg}_{\text{co}}/\text{kg}_{\text{fuel}}$$

The resulting CO concentration in the smoke layer is 31 ppm.

Special Conditions

There are some aspects of smoke management system design which involve special attention. These aspects, which affect actuation of active smoke management systems and the efficiency of exhaust fans, are

- Intermediate stratification
- Confined flow
- Plugholing
- Make-up air supply

Intermediate Stratification

The upward movement of smoke in the plume is dependent upon the smoke being buoyant relative to the surroundings. Delays in activation may be experienced where ceiling-mounted initiating devices are present if the air near the ceiling is warmer than the rising smoke.[4,48] Dillon[49] reported measurements of the difference in ambient temperature from floor to ceiling to be on the order of 50°C in some atria with glazed ceilings. A prefire, warm air layer may be created due to a solar load where the ceiling contains glazing materials. In such cases, the smoke will stratify below this warm air layer and not reach the ceiling. Early after ignition, the maximum height to which the smoke plume will rise depends on the convective heat release rate and the ambient temperature variation in the open space.

Algebraic correlations may be applied to address two situations (see Figure 4-13.13):

1. The temperature of the ambient air is relatively constant up to a height above which there is a layer of warm air at uniform temperature. This situation may occur if the upper portion of a mall, atrium, or other large space is unoccupied so that the air in that portion is left unconditioned.
2. The ambient interior air within the large space has a constant temperature gradient (temperature change per unit height) from floor level to the ceiling. This case is less likely than the first.

In the first case, where the interior air has a discrete temperature change at some elevation above floor level, then the potential for stratification can be assessed by determining the temperature of the plume at the height associated with the lower edge of the warm air layer. Where the plume centerline temperature is equal to the ambient temperature, the plume is no longer buoyant, loses its ability to rise, and stratifies at that height. One correlation for the plume centerline temperature was presented previously as Equation 23.

In the particular case where the ambient, prefire temperature increases uniformly along the entire height, the maximum plume rise can be determined from[22]

$$z_m = 3.79F^{1/4}G^{-3/8} \tag{41}$$

where

$F = g\dot{Q}_c/(T_o\rho_o c_p)$

$G = -(g/\rho_o)d\rho_o/dz$

Assuming standard conditions and that air is a perfect gas, the expressions for F and G are

$$F = 0.0279\dot{Q}_c$$

$$G = 0.0335\, dT_o/dz$$

Because dT_o/dz is a constant, $\Delta T_o/H$ may be substituted for the derivative. Substituting the simplified expressions for F and G into Equation 41 yields[48]

$$z_m = 5.54\dot{Q}_c^{1/4}(\Delta T_o/H)^{-3.8} \tag{42}$$

By reformulating Equation 42 to solve for $\dot{Q}_c$, a minimum fire size can be determined that is just large enough to force the smoke to the ceiling of an atrium without prematurely stratifying due to the increasing ambient temperature.

$$\dot{Q}_c = 0.00118H^{5/2}\Delta T_o^{3/2} \tag{43}$$

The results of an analysis of intermediate stratification are presented in Figure 4-13.14. In one case, a step function is assumed to provide a 30°C change in temperature 15 m above the floor due to the upper portion of the atrium being unconditioned. For the other case, a tem-

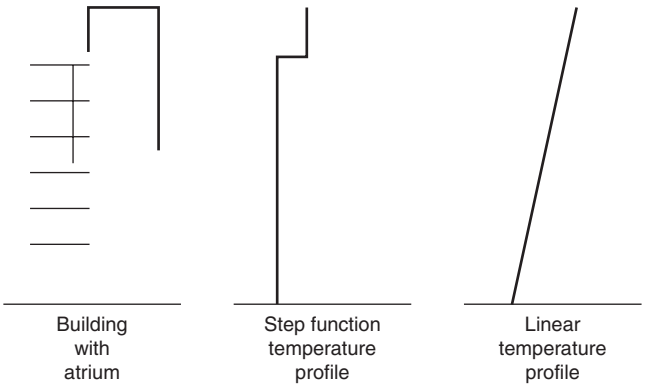

Figure 4-13.13. ***Prefire temperature profiles.***

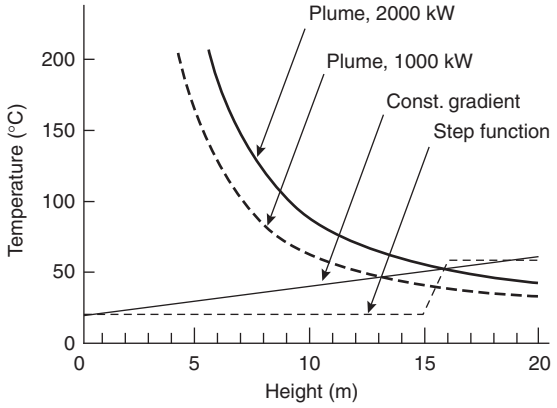

Figure 4-13.14. ***Indoor air and plume temperature profiles with the potential for intermediate stratification.***

perature gradient of 1.5°C/m is arbitrarily assumed in an atrium with a ceiling height of 20 m. Plume centerline temperatures from two size fires are graphed based on Equation 23. As indicated in the figure, for the case with the uniform gradient, smoke is expected to stratify approximately 13 or 15 m above the floor, depending on the fire size. For the case involving the step function change in temperature, the smoke stratifies from both fire sizes at the height of the step change in temperature.

If the smoke is expected to stratify at an intermediate height below the ceiling, then something other than ceiling-mounted detectors (such as projected beam detectors) needs to be considered to initiate the smoke management system. The beam detectors should be placed below the height of stratification to intercept the rising plume. In general, once the smoke management system operates, the warm air layer should be exhausted to permit the smoke to reach the ceiling.

Confined Flow

As a plume rises it also widens, as a result of the entrainment of additional mass into the plume. For tall, narrow spaces, the plume may fill the entire cross section of the atrium prior to reaching the ceiling. Above this position, air entrainment into the plume is greatly reduced due to the limited amount of air available. In such situations, initially the bottom of the smoke layer may be assumed to be located at this point of contact. Following a delay to fill the entire volume above the point of contact, the descent of the smoke layer can be estimated by analogy with the ceiling being moved down to the point of contact. The delay to fill the upper volume can be estimated by assuming duct flow, with the velocity estimated as the plume velocity at the height of contact.

In order to determine the point of contact of the plume with the walls, the plume width must be expressed as a function of height. The width of the plume has been addressed theoretically and also experimentally.

Based on theory (see Section 2, Chapter 1), the plume width is expected to be

$$d = 2.4\alpha z \tag{44}$$

where $\alpha \cong 0.15$

Thus,

$$d = 0.36z \tag{45}$$

Experimentally, the plume width is estimated by examining photographs[50] or the difference between the plume temperature and ambient temperature (i.e., temperature excess at various horizontal distances from the plume centerline).[33] Using temperature measurements, the plume width is defined as the position where the temperature excess is one-half of the value at the centerline.

Handa and Sugawa[50] developed an empirical correlation of the width of the plume determined from photographs of the visual plume from wood crib fires

$$d = d_o z^{1/2} \tag{46}$$

Heskestad[51] noted that the visible plume diameter was greater than that determined from the temperature excess. Consequently, Heskestad estimated the visible plume diameter to be twice that determined by the excess temperature approach. Thus, the plume diameter is estimated as

$$d = 0.48\left(\frac{T_c}{T_o}\right)^{1/2} z \tag{47}$$

The plume centerline temperature, T_c, can be evaluated using Equation 23. As indicated in Equation 23, the plume centerline temperature decreases appreciably with increasing height. Thus, for tall spaces, the plume centerline temperature may be close to ambient. For example, at a height of 30 m with a fire size of 5000 kW and T_o of 293 K, T_c is 312 K. In this case $(T_c/T_o)^{1/2}$ in Equation 47 is only 1.03. Because of the rapid decline in T_c with increasing height, for engineering purposes $(T_c/T_o)^{1/2}$ can be approximated as being 1.0. Consequently, in many cases the total plume diameter may be approximated by considering the plume diameter to be approximately one-half of the height.

Considering the variety of analyses for plume width, the plume width is estimated to be 25 to 50 percent of the height above the top of the fuel package, with the 36 percent proportion from theory being near the middle of the range.

Plugholing

Plugholing occurs when the exhaust capacity at a single point is sufficiently large to draw air from the lower layer in addition to smoke. As such, less smoke is removed by the exhaust fans and a deeper layer results. Because a simple method to estimate the proportion of air drawn in from below the smoke layer by the fans is unavailable, an elementary method of estimating the smoke layer depth during plugholing is not available. As such, simple calculations can only be performed to assess the occurrence of plugholing, not the effect.

The original research on plugholing was done for natural vents (see Section 3, Chapter 9). Recently, Lougheed and Hadjisophocleous demonstrated that the plugholing analysis for natural vents was also applicable to mechanical venting.[52] In order to avoid plugholing, the maximum exhaust capacity at an extract point is

$$\dot{m} = 1.5\left[g(H-z)^5\left(\frac{T_s - T_o}{T_s}\right)\left(\frac{T_o}{T_s}\right)\right]^{1/2} \tag{48}$$

Results of applying Equation 48 are provided in Figure 4-13.15 for a range of temperature rise values of the smoke. Where venting capacities greater than the maximum limit are needed to achieve smoke management objectives, multiple extract points need to be provided to avoid plugholing.

Assuming an axisymmetric plume, $\dot{m}$ can be replaced using Equation 20, and the smoke layer temperature can be replaced using Equation 32 (assuming adiabatic conditions) to express the minimum smoke layer depth in terms of the heat release rate and clear height as indicated in Figure 4-13.16.

For a single extract point, the minimum smoke layer depth is slightly less than 40 percent of the clear height. If numerous extract points are provided, each extracting the same exhaust capacity, the d/z ratio without plugholing can be reduced, as presented in Figure 4-13.17. However,

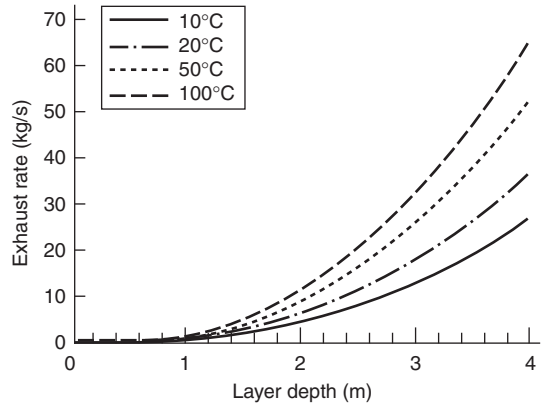

Figure 4-13.15. ***Effect of smoke layer depth and temperature rise on maximum exhaust capacity.***

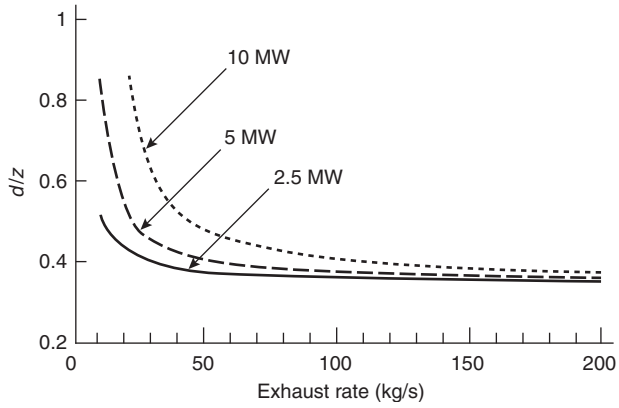

Figure 4-13.16. ***Ratio of smoke layer depth to clear height for single exhaust point.***

the d/z ratio is relatively insensitive to the exhaust rate per fan once if more than 5 exhaust points exist. The d/z ratio approaches an asymptotic value of approximately 0.1. While the legend in the figure indicates that only a heat release rate of 5 MW is considered, the same d/z ratio is obtained for a 5 MW fire with an exhaust per fan of 20 m^3/s as for a 2.5 MW fire with an exhaust rate per fan of 10 m^3/s and a 10 MW fire with an exhaust rate per fan of 40 m^3/s. This trend can be generalized by indicating that the same d/z value is obtained as long as the ratio of the exhaust rate per fan to fire size is maintained constant (in this case 4 m^3/s-MW).

Makeup Air Supply

The makeup air supplied to the atrium should be

- Uncontaminated
- Introduced below the smoke layer
- Introduced at a slow velocity
- Supplied at a rate less than the required exhaust rate

Air that is not contaminated by smoke can be provided by locating intakes for the makeup air remote from

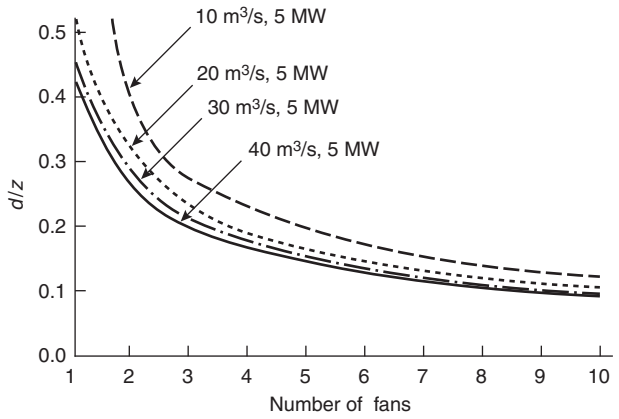

Figure 4-13.17. ***Ratio of smoke layer depth to clear height for multiple exhaust points.***

the smoke exhaust discharge, preventing smoke feedback. In the event that smoke is introduced into the makeup air supply, a smoke detector should be provided to shut down the makeup air supply system. Selection of a smoke detector for this application should consider the operating conditions, range of temperatures, and installation within a duct.

All makeup air should be provided below the smoke layer interface. Any makeup air provided above the smoke layer interface merely adds mass to the smoke layer, which must be added to the required capacity of the smoke exhaust to prevent an increase in the smoke layer depth. If introduced near the smoke layer interface, the makeup air may increase the amount of mixing of clean air with the smoke to further add to the smoke layer.

Makeup air should be provided at a slow velocity so that the plume, fire, and smoke layer are not adversely affected. Makeup air supplied at a rapid velocity near the plume may deflect the plume to enhance the entrainment rate, thereby increasing the rate of smoke production. In addition, the burning rate of the fire may be increased by makeup air provided at an excessive velocity. Because the entrainment process induces an air velocity of approximately 1 m/s, the maximum makeup air velocity in the vicinity of the plume is often recommended to be 1 m/s. Because of the diffusion of air once past the diffuser, the makeup air velocity at the diffuser may be greater than 1 m/s. The relationship of air velocity with distance from the diffuser is outlined elsewhere.[53]

Finally, the mass rate of makeup air supplied must be less than that being exhausted. Failure to follow this guideline may lead to the atrium being pressurized relative to the communicating spaces. Being at a positive pressure, smoke movement will be forced through any unprotected openings in physical barriers into the communicating spaces.

Limited Fuel

In some cases smoke management objectives may be fulfilled without a dedicated smoke management system due to the intrinsic qualities of the atrium. The intrinsic

qualities of the atrium include parameters, such as the composition and quantity of fuel and geometry of the atrium. As an example, a limited amount of fuel may be present that is unable to sustain a fire for a sufficient period of time to create conditions beyond the allowable limits. The amount of fuel consumed during the time period of interest depends on whether the fire is steady or unsteady. In the case of a steady fire, the fuel mass consumed in a given period of time is determined as

$$\dot{m}_f = \frac{\dot{Q}t}{H_c} \tag{49}$$

Alternatively, for an unsteady, t^2 profile fire, the fuel mass consumed during a given period of time is given as

$$\dot{m}_f = 333\,\frac{t^3}{H_c t_g^2} \tag{50}$$

When analyzing the inherent ability of the atrium to fulfill the smoke management design goals, the time period should relate either to the performance of a fire protection system or to the development of smoke layer conditions in excess of acceptable levels. For example, in life safety–oriented designs, the time period may be either that required for evacuation, or for untenable conditions to be generated, whichever is less.

Opposed Airflow

Opposed airflow refers to systems where airflow is provided in a direction opposite to smoke movement. Opposed airflow may be used in lieu of physical barriers to prevent smoke spread from one space to another (i.e., between the communicating space and the atrium). Opposed airflow limits smoke flow by countering the momentum of the smoke attempting to enter the communicating space. A minimum airflow velocity at all points of the opening must be provided in order to prevent smoke migration through the opening. Two empirical correlations to estimate the minimum average velocity for the entire opening are available, based on limited experimental data.[54] The calculated average velocity is greater than the actual minimum velocity required at a point to oppose smoke propagation. The excess velocity is required so that the minimum critical velocity is achieved at all points, considering the effects of turbulence caused by the edges and corners of the opening.

The minimum average velocity to oppose smoke originating in the communicating space is evaluated using Equation 51.

$$v_e = 0.64\sqrt{\frac{gH(T_s - T_o)}{T_s}} \tag{51}$$

Alternatively, if the smoke at the opening is part of a rising plume that is rising along the side of the atrium wall, then Equation 52 is applicable.

$$v_e = 0.057\left(\frac{\dot{Q}}{z}\right)^{1/3} \tag{52}$$

The opposed airflow velocity should not exceed 1 m/s. Above that limit, the airflow velocity may deflect the plume away from the wall, making more plume surface area available for entrainment. The increased area for entrainment will enhance the smoke generation rate. Consequently, the problem of propagation to the communicating space may be solved by an excessive average velocity; however, other problems may be created by the increased smoke production rate and a possible increase in the depth of the smoke layer in the atrium. The volumetric capacity of the mechanical equipment required to deliver the necessary velocity for opposed airflow can be approximated as

$$V_{oa} = A_o v_e \tag{53}$$

If several openings are protected with the opposed airflow approach using the same mechanical equipment, the cross-sectional area should be the sum of the areas for all of the openings. The opposed airflow technique may be infeasible due to the substantial amount of airflow capacity required to protect numerous openings having a large total area.

Where opposed airflow is incorporated to prevent smoke migration into a communicating space from the atrium, the impact of the volume of air being introduced into the atrium must be assessed. Specifically, if smoke exhaust equipment is also provided to maintain a constant position of the smoke layer interface in the atrium, then all of the additional air used for opposed airflow must also be exhausted. The additional air can be accounted for by increasing the required mass rate of exhaust in the atrium by the amount used for the opposed airflow. The additional air being exhausted will also affect the qualities of the smoke layer within the atrium. (See Equations 32, 37, and 39.) The smoke layer temperature, T_s(K), can be determined using Equation 54, based on an analysis included elsewhere.[5]

$$T = 293 + \left[0.0018 + 0.072\dot{Q}_c^{-2/3}z^{5/3} + \frac{712A_o\sqrt{H(T-293)}}{\dot{Q}_c T^{3/2}}\right]^{-1} \tag{54}$$

Equation 54 must be applied iteratively to determine the resulting smoke layer temperature. In cases with large clear heights, the temperature of the air used for the opposed airflow strategy will be virtually equal to the temperature of the smoke layer to permit the addition of volumetric rates of air rather than mass rates.

EXAMPLE 8:

Considering the atrium from Example 5. There are five 5-m-wide × 2.5-m-high openings to the communicating space. The bottoms of the openings are 30 m above the floor of the atrium. Considering a 5000-kW fire in the center of the floor of the atrium, determine the following:

1. Minimum airflow velocity required for opposed airflow
2. Volumetric rate of air supply for opposed airflow
3. Capacity of the exhaust fans in the atrium to maintain the smoke layer interface at an elevation 25 m above floor level and also to accommodate the additional air from the opposed airflow approach

SOLUTION:

The minimum opposed airflow velocity can be determined using Equation 35. However, the temperature of the smoke layer, T, is unknown. Thus, Equation 54 must be applied first. Solving iteratively, T is approximately 305 K. The minimum airflow velocity is 0.20 m/s. The volumetric supply capacity for the opposed airflow strategy for all five openings is 12.5 m^3/s. The associated mass flow rate is 15.0 kg/s.

Without the opposed airflow, the mass rate of smoke exhaust required to maintain the smoke layer interface height in the atrium at a height of 25 m is determined using Equation 20 (neglecting z_o) to be 236 kg/s. Thus, the combined mass exhaust rate necessary is 251 kg/s. This mass flow rate corresponds to a volumetric rate of 209 m^3/s.

As a practical issue, this exhaust rate should be compared to that required to keep the smoke layer interface above the top of the openings (i.e., 32.5 m above floor level). Based on Equations 20 and 28, the required volumetric exhaust rate is 362 kg/s. Thus, in this situation, the combined exhaust rate with the opposed airflow strategy is less than that associated with the strategy to keep the smoke layer interface above the opening.

Nomenclature

A	cross-sectional area of the atrium (m^2)
A_o	cross-sectional area of opening (m^2)
b	distance from the store opening to the balcony edge (m)
C_{CO}	volumetric concentration of carbon monoxide (ppm)
c_p	specific heat (kJ/kg-K)
D	optical density per unit pathlength (m^{-1})
D_m	mass optical density (m^2/kg)
d	plume diameter (based on excess temperature) (m)
d_o	diameter of fire (m)
f_{CO}	yield fraction of CO (kg_{CO}/kg_{fuel})
f_i	yield fraction of species i (kg of species i per kg of fuel consumed)
g	gravitational acceleration (9.8 m/s^2)
H	height of ceiling above top of fuel surface (m)
H_b	height of balcony above top of fuel surface (m)
H_c	heat of combustion (kJ/kg)
$H_{c,conv}$	convective heat of combustion (kJ/kg)
h	enthalpy
K	constant, depending on target being viewed (e.g., = 6 for lighted signs)[5]
k	thermal conductivity (W/m·K)
k_v	volumetric entrainment constant ($0.065\ m^{4/3}kW^{\cdot -1/3}\cdot s^{-1}$)
L	width of balcony spill plume (m)
l	characteristic length (m)
MW_i	molecular weight of species i (kg)
M_{CO}	molecular weight of carbon monoxide (28 kg)
M_{air}	molecular weight of air (29 kg)
m_u	mass of upper smoke layer (kg)
$\dot{m}$	mass entrainment rate in plume (kg/s)
m_f	mass burning rate (kg/s)
Δp	pressure difference (Pa)
r	radius (i.e., horizontal distance from plume centerline (m)
Q	$= \frac{1055}{t_g^2}\frac{t^3}{3}$ for t^2 fires (kJ)
Q	$= \dot{Q}t$ for steady fires (kJ)
Q_o	$= \rho_o c_p T_o A(H - z)$ (kJ)
$\dot{Q}$	heat release rate of fire (kW)
$\dot{Q}_c$	convective portion of heat release rate of fire (kW)
T_c	temperature at plume centerline (K)
T	temperature (K)
ΔT_{ad}	temperature difference between smoke layer and ambient air (°C)
ΔT_o	prefire temperature change from floor to ceiling of the ambient air (°C)
t	time (s)
t_{cj}	ceiling jet transport lag (s)
t_g	growth time (s)
t_{pl}	plume transport lag (s)
$\dot{V}$	volumetric flow rate (m^3/s)
V_{oa}	volumetric capacity required for opposed airflow (m^3/s)
V_u	volume of upper layer (m^3)
v	characteristic velocity (m/s)
v_e	opposed airflow velocity (m/s)
w	width of the store opening from the area of origin (m)
x	position (m)
Y_{CO}	mass fraction of CO (kg of species CO per kg of smoke)
Y_i	mass fraction of gas species i (kg of species i per kg of smoke)
z	clear height, position of smoke layer interface above the top of fuel surface (m)
z_f	limiting height above fuel (m)
z_m	maximum rise of plume (m)
z_o	virtual origin of plume (m)
χ_a	combustion efficiency
χ_1	heat loss fraction from smoke to enclosure
ρ	density (kg/m^3)

Subscripts:

F	full-scale building
m	small-scale model
o	ambient air
w	wall, ceiling, or floor of enclosure

References Cited

1. R. Saxon, *Atrium Buildings, Development and Design,* The Architectural Press, London (1983).
2. P. Robinson, "Atrium Buildings—A Fire Service View," *Fire Surveyor,* 11, pp. 43–47 (1982).
3. NFPA 92A, *Recommended Practice for Smoke-Control Systems,* National Fire Protection Association, Quincy, MA (1993).
4. NFPA 92B, *Guide for Smoke Management Systems in Malls, Atria, and Large Areas,* National Fire Protection Association, Quincy, MA (1991).
5. J.H. Klote and J.A. Milke, *Design of Smoke Management Systems,* ASHRAE, Atlanta (1992).
6. T. Jin, "Irritating Effects of Fire Smoke on Visibility," *Fire Science and Technology,* 5, 1 (1985).
7. J. Morehart, "Sprinklers in the NIH Atrium: How Did They React During the Fire Last May?" *Fire Journal,* 83, pp. 56–57 (1989).
8. NFPA 75, *Standard for the Protection of Electronic Computer/Data Processing Equipment,* National Fire Protection Association, Quincy, MA (1999).
9. G.E. Hartzell, "Criteria and Methods for Evaluation of Toxic Hazard," *Fire Safety J.,* 12, pp. 179–182 (1987).
10. R. D. Peacock and E. Braun, "Fire Tests of Amtrak Passenger Rail Vehicle Interiors," *NBS Technical Note 1193,* National Bureau of Standards, Gaithersburg, MD (1984).
11. V. Babrauskas, "A Laboratory Flammability Test for Institutional Mattresses," *Fire Journal,* 72, 93, pp. 35–40 (1981).
12. S.W. Harpe, T.E. Waterman, and W.S. Christian, "Detector Sensitivity and Siting Requirements for Dwellings, Phase 2, Part 2 'Indiana Dunes Tests,'" Report No. PB-263882, National Bureau of Standards, Gaithersburg, MD (1977).
13. NFPA 204M, *Guide for Smoke and Heat Venting,* National Fire Protection Association, Quincy, MA (1991).
14. J.A. Milke and J.H. Klote, "Smoke Management in Large Spaces in Buildings," Building Control Commission of Victoria and The Broken Hill Proprietary Company Limited, Melbourne, Australia (1998).
15. J.L. Bryan, "Damageability of Buildings, Contents, and Personnel from Exposure to Fire," *Fire Safety J.,* 11, pp. 15–32 (1984).
16. J. G. Quintiere, "Scaling Applications in Fire Research," *Fire Safety J.,* 15, pp. 3–29 (1989).
17. F.W. Mowrer, "Lag Times Associated with Fire Detection and Suppression," *Fire Technology,* 26, 3, pp. 244–265 (1990).
18. J.S. Newman, "Principles for Fire Detection," *Fire Technology,* 24, 2, pp. 116–127. (1988)
19. J.A. Milke and F.W. Mowrer, "A Design Algorithm for Smoke Management Systems in Atria and Covered Malls," *Report FP93-04,* University of Maryland, College Park (1993).
20. J. A. Milke, "Smoke Management for Covered Malls and Atria," *Fire Technology,* 26, 3, pp. 223–243 (1990).
21. G. Heskestad and M.A. Delichatsios, "Environments of Fire Detectors—Phase I: Effect of Fire Size, Ceiling Height, and Materials," *Vol. I—Measurements (NBS-GCR-77-86), Vol. II—Analysis (NBS-GCR-77-95),* National Bureau of Standards, Gaithersburg, MD (1977).
22. B.R. Morton, Sir Geoffrey Taylor, and J.S. Turner, "Turbulent Gravitational Convection from Maintained and Instantaneous Sources," in *Proceedings of Royal Society A,* 234, pp. 1–23, London (1956).
23. G. Mulholland, T. Handa, O. Sugawa, and H. Yamamoto, "Smoke Filling in an Enclosure," *Paper 81-HT-8,* The American Society of Mechanical Engineers, New York (1981).
24. L.Y. Cooper, M. Harkleroad, J. Quintiere, and W. Rinkinen, "An Experimental Study of Upper Hot Layer Stratification in Full-Scale Multiroom Fire Scenarios," *Paper 81-HT-9,* The American Society of Mechanical Engineers, New York (1981).
25. G. Heskestad, Letter to the Editor, *Fire Technology,* 27, 2, pp. 174–185 (1991).
26. T. Yamana and T. Tanaka, "Smoke Control in Large Spaces (Part 2—Smoke Control Experiments in a Large-Scale Space)," *Fire Science and Technology,* 5, 1, pp. 41–54 (1985).
27. G.D. Lougheed, Personal Communication, National Research Council of Canada, (Mar. 20, 1991).
28. S.P. Nowlen, "Enclosure Environment Characterization Testing for the Baseline Validation of Computer Fire Simulation Codes," *NUREG/ CR-4681, SAND 86–1296,* Sandia National Laboratories, Albuquerque, NM (1987).
29. J.A. Sharry, "An Atrium Fire," *Fire Journal,* 67, 6, pp. 39–41 (1973).
30. J. Lathrop, "Atrium Fire Proves Difficult to Ventilate," *Fire Journal,* 73, 1, pp. 30–31 (1979).
31. D.M. McGrail, "Denver's Polo Club Condo Fire: Atrium Turns High-Rise Chimney," *Fire Engineering,* pp. 67–74 (1992).
32. G. Heskestad, "Engineering Relations for Fire Plumes," *SFPE TR 82-8,* Society of Fire Protection Engineers, Boston (1982).
33. C. Beyler, "Fire Plumes and Ceiling Jets," *Fire Safety J.,* 11, pp. 53–76 (1986).
34. R.L. Alpert and E.J. Ward, "Evaluation of Unsprinklered Fire Hazards," *Fire Safety J.,* 7, pp. 127–143 (1984).
35. F.W. Mowrer and B. Williamson, "Estimating Room Temperatures from Fires along Walls and in Corners," *Fire Technology,* 23, 2, pp. 133–145 (1987).
36. M. Law, "A Note on Smoke Plumes from Fires in Multi-Level Shopping Malls," *Fire Safety J.,* 10, pp. 197–202 (1986).
37. H.P. Morgan and N.R. Marshall, "Smoke Control Measures in a Covered Two-Story Shopping Mall Having Balconies and Pedestrian Walkways," *BRE CP11/79,* Fire Research Station, Borehamwood, England (1979).
38. CIBSE, "Relationships for Smoke Control Calculations," *TM 19,* Chartered Institution of Building Services Engineers, London (1995).
39. W.D. Walton, "ASET-B: A Room Fire Program for Personal Computers," *NBSIR 85-3144,* National Bureau of Standards, Gaithersburg, MD (1985).
40. Lincolne Scott Australia Pty Ltd., *Jupiters Casino—Report on Atrium Smoke Tests,* Lincolne Scott Australia Pty Ltd., Toowong, Australia (1986).
41. G.O. Hansell and H.P. Morgan, "Smoke Control in Atrium Buildings Using Depressurization," *PD 66/88,* Fire Research Station, Borehamwood, UK (1988).
42. R.A. Waters, "Stansted Terminal Building and Early Atrium Studies," *J. of Fire Protection Engineering,* 1, 2, pp. 63–76 (1989).
43. G. Heskestad, "Similarity Relations for the Initial Convective Flow Generated by Fire," *Paper 72-WA/HT-17,* American Society of Mechanical Engineers, New York (1972).
44. T. Jin, "Visibility Through Fire Smoke (Part 2)," *Report of the Fire Research Institute of Japan, Nos. 33, 31,* Tokyo (1971).
45. J.G. Quintiere, "An Assessment of Correlations Between Laboratory and Full-Scale Experiments for the FAA Aircraft Fire Safety Program, Part 1: Smoke," *NBSIR 82-2508,* National Bureau of Standards, Gaithersburg, MD (1982).
46. G. Heskestad, "Hazard Evaluation," submitted to NFPA Task Group on Smoke Management of Atria, Covered Malls, and Large Spaces, unpublished manuscript (1988).

47. G.D. Lougheed, "Probability of Occurrence and Expected Size of Shielded Fires in Sprinklered Building; Phase 2, Full-Scale Fire Tests," National Research Council of Canada, Ottawa (1997).
48. G. Heskestad, "Note on Maximum Rise of Fire Plumes in Temperature-Stratified Ambients," *Fire Safety J.,* 15, pp. 271–276 (1989).
49. M. Dillon, "Acceptance Testing and Techniques," presented at *The Roundtable on Fire Safety in Atriums—Are the Codes Meeting the Challenge?,* Washington, DC (1988).
50. T. Handa and O. Sugawa, "Flow Behavior of Plume From Growing Fire Source in High Ceiling Enclosure," *J. of Fire and Flammability,* 12, 1, pp. 31–50 (1981).
51. G. Heskestad, "Fire Plume Entrainment and Related Problems in Venting of Fire and Smoke from Large Open Spaces," submitted to NFPA Task Group on Smoke Management of Atria, Covered Malls, and Large Spaces, unpublished manuscript (1987).
52. G.D. Lougheed and G.V. Hadjisophocleous, "Investigation of Atrium Exhaust Effectiveness," *ASHRAE Transactions,* 103, 2 (1997).
53. American Society of Heating, Refrigerating, and Air-conditioning Engineers, Inc., *1993 ASHRAE Handbook—Fundamentals,* ASHRAE, Atlanta, GA (1993).
54. G. Heskestad, "Inflow of Air Required at Wall and Ceiling Apertures to Prevent Escape of Fire Smoke," *FMRC J. I. OQ4E4.RU,* Factory Mutual Research Corporation, Norwood, MA (1989).

CHAPTER 14

Water Mist Fire Suppression Systems

Jack R. Mawhinney and Gerard G. Back, III

Introduction

This chapter is about the engineering of fixed fire suppression systems that discharge water mist. The term *water mist* as currently understood in the fire protection field relates to fine water sprays with no drops larger than 1.0 mm, or 1000 μm (microns).[1,2] Such sprays are not true mists, however. A *mist* in the scientific sense consists of drops somewhere on a continuum between *aerosol* (particles with diameter ~5 μm) and *fog* (droplet diameters ranging between 10 and 100 μm). Particles less than 20 μm in diameter take a long time to settle out, and hence create what is recognized in both literature and science as a "mist." A water mist as intended for fire protection purposes is a fine water spray consisting of a range of droplet sizes, many of which are in the range of true mist particles and some of which are considerably larger. Water mist nozzles produce sprays that have a higher fraction of very fine droplets, in the range of mist, than is typical of standard sprinklers or water spray nozzles.

Fire suppression research performed in the past 50 years typically referred to "fine water sprays" or "finely divided water sprays" as their subject of study. Remarkable success at cooling and extinguishing diffusion flames was documented using fine water sprays with mean diameters less than 0.3 mm (300 μm).[3,4] The 1950s researchers confirmed the expected improvement in the efficiency of heat absorption due to the increase in surface area available for heat transfer as a spray is divided into smaller and smaller particle sizes. Also, as particles become smaller they settle out less quickly, providing more time for heat absorption and evaporation to take place. More heat is absorbed per unit of mass as the particle size decreases. Thus it was understood that increasing the fraction of very fine water droplets contained in a water spray could reduce the amount of water needed for fire suppression, or in other words, improve the efficiency of application.

The term *water mist* was adopted by the National Fire Protection Association Committee, NFPA 750, *Standard for Water Mist Fire Protection Systems* 2000 edition (current), in the early 1990s as part of the renewed interest in efficient use of water in fire suppression systems. This term distinguishes the technology of NFPA 750 from that of NFPA 15, *Standard for Fixed Water Spray Systems,* 1996 edition[5] and NFPA 13, *Standard for Installation of Sprinkler Systems,* 1999 edition.[6] A more thorough discussion of drop size distribution as a significant spray characteristic is presented later in this chapter.

For technical and economic reasons, the knowledge about the advantages of using fine water sprays for fire suppression did not result in an immediate movement to finer sprays for fire protection. Technical concerns included the negative effects of increasing operating pressures to improve atomization, the potential plugging of small orifices with corrosion products, and doubts about the long-term maintainability of equipment. Economic concerns related to the fact that there were less expensive alternatives: either standard sprinklers or the halogenated hydrocarbons—gaseous agents (halons) such as Halon 1301—could be used. So long as water was cheap and halons were available to handle the special hazards, finer water sprays did not offer enough of a suppression advantage to justify their widespread use.

Jack R. Mawhinney is a senior engineer with Hughes Associates, Inc., in Baltimore. He holds a masters degree (1979) in civil engineering from the University of Alberta. He has 35 years experience in fire protection construction and research, including 11 years with the National Research Council, Canada, Institute for Research in Construction. Mr. Mawhinney is chair of the NFPA 750, Water Mist Systems Committee.

Gerard G. Back, III, is a senior engineer with Hughes Associates, Inc., in Baltimore. He has a bachelor degree (1983) in mechanical engineering and masters in fire protection engineering (1996), both from the University of Maryland. In fifteen years with HAI, Mr. Back has conducted extensive fire testing and analysis of the performance of water mist systems for the U.S. Army, Navy, and Coast Guard research and development programs, and for other international clients.

Three events happened in the 1980s that changed the economic background and revitalized interest in using fine water sprays for fixed fire suppression systems. These were

1. The aviation industry response to the Manchester air crash in 1984
2. The 1987 signing of the Montreal Protocol, an agreement to phase out the use and manufacture of ozone depleting substances (halons)
3. An International Maritime Organization (IMO) ruling that required the installation of marine sprinklers on all existing and new passenger ships capable of carrying more than 35 passengers

The Manchester, England, plane crash in 1984[7] initiated an international effort to develop a fixed water spray system for passenger compartments on aircraft. The SAVE program, as it was called, was funded by the Civil Aviation Authority in England, the Federal Aviation Administration (FAA) in the United States, Transport Canada, and by the major builders of aircraft, such as Boeing and Airbus. The objective of the program was to increase the time available for evacuation of an aircraft passenger compartment exposed to a ground pool fire after a crash landing. Tests were conducted utilizing water spray to prolong the tenability of the space to allow more time for safe evacuation. The SAVE program set well-defined performance objectives relating to tenability.[8] The design was constrained by the need to minimize the weight of the system. The choice of a fine water spray to maximize the effectiveness of a small quantity of water was a natural outcome of the work. A water mist system that exceeded all of the performance objectives was accomplished. The system extended tenability for 7 min, within the weight and volume constraints, using approximately 10 l of water. The SAVE study demonstrated that a fine water mist system using a limited supply of water could be custom designed to meet very specific objectives, within the constraints of the industry. The aviation industry regulatory authorities, however, did not make such systems mandatory on aircraft, on the basis that the cost-per-life-saved was unacceptably high.[7]

The second key event that spurred interest in fine water spray fire suppression systems was the 1987 signing of the Montreal Protocol, an international agreement to reduce the manufacture and use of ozone depleting substances.[9] Widely used halogenated fire suppression gases were discovered to be ozone depleting substances. The threat of a phase-out of halon fire extinguishing agents motivated the release of funds for research into alternative fire suppression agents, water among them. Water at least was not likely to be phased out in the future as an environmentally harmful substance. The high-level research into halon alternatives provided a windfall of improved scientific understanding of the physical and chemical nature of combustion and extinguishment processes. Advances in measurement of suppression phenomena, understanding of fire dynamics, and computer modeling of complex fire scenarios were applicable to the engineering design of innovative fire suppression systems. The loss of halons forced the reexamination of old assumptions about the unsuitability of water for certain types of fires, such as Class B fires in machinery compartments. With improved atomization and reduced flow rates, water could be used where the traditional default had been to use halons. Fine water spray fire suppression systems began to look viable from both performance and economic perspectives as an alternative to gaseous fire suppressants for some applications.

A third congruent event that propelled the use of fine water sprays into the realm of practical fire suppression systems was a move by the International Maritime Organization (IMO) to mandate the installation of sprinkler systems on passenger ships. This very influential rule-making body involves the interests of marine shipping societies, marine regulatory authorities (coast guards), and shipping companies, worldwide. This regulatory action came about as a result of several large life-loss fires on board Scandinavian passenger ferries that occurred in the 1980s.[10] In response, the International Maritime Organization mandated the installation of marine sprinklers on all ships capable of carrying 35 or more passengers, to come into effect in 1995. Marine architects view marine sprinklers as a negative feature in terms of weight, space, and effects on stability. Adding weight to the upper levels of a ship creates potential stability problems, particularly when sprinklers are retrofitted to an existing ship that was not designed to support the additional weight. There were strong economic and technical incentives to develop a system equivalent to sprinklers that would satisfy the intent of the IMO ruling but use less water and weigh less than traditional marine sprinklers. Fine water spray fire suppression systems promised to deliver just that.

Research was conducted to develop performance criteria for fine water spray systems that could be impartially evaluated as equivalent to sprinklers installed on Solas II-2/12.[11,12,13] The Scandinavian countries Sweden, Norway, and Finland performed development testing that laid the foundation for fire test protocols for marine machinery rooms and for accommodations and public spaces on passenger ships. The Swedish National Testing and Research Institute (SP) in Borås, Sweden; SINTEF, the Norwegian fire research institute in Trondheim, Norway; and VTT Building Technology research facility in Espoo, Finland, were the key centers of development for water mist fire testing. Manufacturers who were interested in developing water mist nozzles participated in the development of the tests. The test results were discussed, modified, and eventually accepted as consensus test protocols at meetings of the IMO fire protection subcommittees.

The availability of substantial funding to support research for Halon alternatives, and the creation of a worldwide market for alternatives to marine sprinklers, were the two most important factors that changed the economic viability of using fine water sprays for fire suppression systems. Now there was financial incentive to support the cost of overcoming the engineering challenges involved.

As a result of the two distinct origins of renewed interest, there are two basic domains of application for water mist systems. One area of application is as a replacement for gaseous fire suppressants such as Halon 1301. Thus, in applications involving Class B flammable liquid fuels—or where clean agents were used because of

concern about water damage—water mist is viewed as a halon alternative. For applications where the water mist systems are installed for Class A fuels (ordinary cellulosic combustibles), a water mist system is viewed as a sprinkler equivalent.

Fundamentals of Water Mist Systems

The following review of the fundamentals of water mist system design covers mechanisms of extinguishment and suppression, and spray characteristics.

Mechanisms of Extinguishment and Suppression

Excellent discussions of the extinguishing mechanisms of water mist from an engineering perspective can be found in References 3, 4, and 14. An understanding of the mechanisms of extinguishment associated with water mist (then called "finely divided water spray") was articulated approximately 50 years ago.[3,4] Braidech and Rasbash both concluded that fires were extinguished by dilution of the air (oxygen) with water vapor (steam), resulting from evaporation of water droplets in the area local to the flame. They also concluded that the cooling effects of the water may contribute to the extinguishment of flames.

Mawhinney et al.,[13] describe three primary and two secondary mechanisms associated with extinguishment of hydrocarbon fires. The primary mechanisms are

- Gas phase cooling
- Oxygen depletion and flammable vapor dilution
- Wetting and cooling of the fuel surface

The secondary mechanisms are

- Radiation attenuation
- Kinetic effects

The extinguishing mechanisms apply to extinguishment of Class B liquid fuel fires as well as Class A solid fuels, although with different importance of one mechanism over another. Typically, all mechanisms are involved to some degree in the extinguishment process.

Gas phase cooling: Gas phase cooling refers to the removal of heat from the flame and hot gases, due to evaporation of water. The cooling efficacy of water mist is due to the fact that the water is broken up into many fine droplets, which enhances the evaporation rate. The more water that evaporates, the greater the amount of heat that is extracted from the flame, and the more the temperature of the flame is reduced. If the flame temperature is reduced below the critical value necessary to sustain combustion (limiting adiabatic flame temperature), the flame will be extinguished. The limiting adiabatic flame temperature for diffusion flames is approximately 1600 K (1326°C).[15] The cooling of the flame also reduces the radiation (thermal feedback) to the fuel surface, thus reducing the pyrolysis rate of the fuel. Scientific work involving the extinguishment of methane/air counterflow flames has been conducted that has shown that water mist/vapor is more effective on a mass basis than Halon 1301, if it can be delivered at near 100 percent efficiency.[16,17] The reality is that in full-scale compartment fire suppression, the efficiency of application of water is very much less than 100 percent.

Various attempts have been made to establish a design relationship between the fire size and amount of water needed to extinguish it by gas phase cooling. Wighus[18] defined the term *spray heat absorption ratio* (SHAR), which relates the rate at which heat is absorbed by evaporation of a given mass of water (Q_w), to the rate at which heat is given off by the fire (Q_f).

$$\text{SHAR} = \frac{Q_w}{Q_f}$$

Wighus's experiments showed that, for optimized application of mist to an unconfined propane flame, the heat absorption rate in the water needs to be only a fraction of the heat release rate of the fire, as low as 0.3 under optimum conditions. SHAR values in the range of 0.6 were noted for more realistic machinery space conditions, where small flames can persist in shielded areas to cause re-ignition. (Only enough heat has to be absorbed from the flame to drop the temperature to the limiting adiabatic flame temperature: it is not necessary to drop the temperature to ambient.)

On the surface, it seems promising to use a calculation of the amount of water that must be evaporated to extinguish a fire of a certain heat release rate as a design parameter. In real systems, however, the efficiency of delivery of water mist into flame, hence the rate of evaporation of the droplets in the flame zone, is almost unpredictable, and certainly uncontrollable over the range of conditions encountered in machinery space fires. The SHAR relationship nonetheless holds interesting possibilities for a hydrocarbon extinguishment submodel for use in a computational fluid dynamics (CFD) approach to mist system design.[19,20,21]

Andersson et al.,[21] present the concept of the required extinguishing medium portion (REMP). This is the ratio of the mass application rate of extinguishing agent required (m'_e) to the mass rate of fuel consumed (m'_g). The REMP parameter is similar to the SHAR in that a certain mass of water must be evaporated to extract enough heat to extinguish the flame.

$$\text{REMP} = \frac{m'_e}{m'_g}$$

For propane flames, Andersson et al.[21] measured that the mass application rate of water needed to extinguish a propane flame under laboratory mixing conditions was between 1.2 and 2.2 times the mass burning rate of propane gas. They indicate that this range of REMP values corresponds to a water content volume concentration of 100 to 200 g/m^3—that is, the mass of water mist suspended in a unit volume of air. Note that both the SHAR and REMP values were measured under conditions of ideal interaction of flame and mist: the mist was discharged downward into the upward rising plume. The velocity vectors of mist and flame were opposite, resulting in the maximum degree of turbulent mixing in the collision zone. The mass flow rate of mist estimated from the

REMP values should represent the minimum mass application rate. The mist mass flow rate values for real systems could be expected to be higher, to account for inefficiency in delivery of mist to the flame, and variability in the directional aspects of interaction.

The REMP parameter suggests that the mass application rate of extinguishing agent would have to be set for the largest expected mass burning rate of fuel. This assumption does not take into account the simultaneous action of other extinguishing mechanisms, however. As will be discussed shortly, for fires in enclosures, larger fires can be extinguished using less water than smaller fires, due to the increased efficiency of evaporation attributed to the heat confinement and other phenomena. Thus, one would expect the REMP values to go in opposite directions for enclosed fires versus unenclosed fires.

As was suggested for the SHAR parameter, the REMP parameter is potentially useful in a computer submodel of extinguishment of spray or pool hydrocarbon flames.[20]

A number of researchers have sought to estimate a critical extinguishing concentration (in g/m^3) of water mist surrounding a diffusion flame. Experimental values range from 100 to 200 g/m^3 [21,22,23,24] although values as low as 50 g/m^3 have successfully extinguished heptane flames.[25] Although this appears to be a promising possibility for a universal design parameter, it is difficult to make practical use of this value for selecting spray characteristics or nozzle spacing. It is possible to calculate *nominal* total mass discharge per unit volume values for nozzles discharging into a compartment. It is even possible to measure volume concentrations in g/m^3 of mist at various points in a spray, using a particle size anemometer. On the macroscale of a machinery space, however, it is extremely difficult to predict or control volume concentrations at the point of interaction with flame. There are many randomizing events affecting local concentrations of water mist.

Oxygen depletion and flammable vapor dilution: These mechanisms can occur on either a localized or compartmental scale. On the localized scale, as the water droplets are converted to the vapor phase, the volume occupied by the water increases over three orders of magnitude. If the vaporization of the water occurs in the flame, the volumetric expansion can disrupt the entrainment of air (oxygen) into the flame. On a compartmental scale, the production of steam resulting from mist interactions with the flame, hot gases, and/or hot surfaces can significantly reduce the oxygen concentration in the space.[26] The oxygen available for combustion is a function of the size of the fire, the compartment volume, and the ventilation conditions in the compartment. As the size of the fire increases, the average temperature in the space increases, and the oxygen concentration decreases due to consumption of the oxygen by the fire and dilution of the oxygen by water vapor. If the combined effects of oxygen depletion due to the fire and dilution by water vapor can reduce the oxygen concentration below the critical value necessary to sustain combustion [limiting oxygen concentration (LOC)], the fire will be extinguished.[26] The LOC for most hydrocarbon fuels is approximately 13 percent.[15]

Wetting and cooling of the fuel surface: Wetting/cooling of the fuel surface will be in many cases the dominant extinguishment mechanism for fuels that do not produce combustible mixtures of vapor above the fuel surface at ambient temperatures (i.e., solid fuels, and liquid fuels with flashpoints above normal ambient temperatures). Wetting/cooling of the fuel surface reduces the pyrolysis rate of the fuel. If the vapor/air mixture above the fuel surface is reduced below the lower flammability limit (LFL) of the fuel, the flame will be extinguished.

Radiation attenuation and kinetic effects: Water mist and water vapor measurably reduce radiant heat flux to objects near the fire, which assists in preventing fire spread to unburned fuel. Within the combustion zone, *radiation attenuation* is the result of gas phase cooling and the increase in water vapor concentration between the fuel and the flame. Lowering the flame temperature reduces the radiation feedback to the fuel surface. Also, water vapor in the air above the fuel surfaces acts as a graybody radiator that absorbs radiant energy and reradiates it to the fuel surface at a reduced intensity.[19]

Kinetic effects may contribute either to flame intensification or to extinction. Flame intensification has been measured[14] as a flare-up of a flame upon first contact with mist. Possibly the turbulence and entrainment associated with the rapid evaporation at the flame surface accelerates the burning rate. Kinetic effects may also be involved in flame suppression, the result of both gas phase cooling and oxygen depletion/dilution. When a diluent (in this case water vapor and recycled, vitiated combustion gases) is added in to the combustion reaction, combined with flame cooling, it is expected that reaction rates at the molecular level are changed. The flame speed may be reduced, rendering the combustion reaction susceptible to being blown out by higher-velocity gas streams.

Enclosure effects, turbulent mixing, and cycling: The importance of enclosure effects is described by Mawhinney, Dlugogorski, and Kim[14] and by Liu, Kim, and Su.[27] Enclosure effects maximize the benefits of oxygen depletion and dilution. The hot, vitiated gases collecting in the upper layer of an enclosure are cooled rapidly by the first contact with mist. Vitiated gases plus water vapor are forced down by the spray to the seat of the fire and contribute to extinguishment through oxygen depletion. Depending on the temperature and depth of the hot layer, the rapid cooling results in an instantaneous volume reduction, creating a negative pressure that can suck in the windows or walls of a tight enclosure. If the enclosure had reached flashover temperatures before mist activation, assuming that water could flow through the pipes and mist could be introduced, it is hard to say which phenomenon would dominate, the expansion due to steam generation or contraction due to cooling. At least one manufacturer has investigated a means of allowing an initially small injection of spray to initiate cooling, followed by a gradual increase in flow. Such an approach took the "shock" out of the system. Generally, an automatically activated system will release in the first few minutes of a fire in an enclosure before the upper layer has become too hot and deep. With systems that are man-

ually activated, some thought should be given to the expected effect on introduction of the water mist into a very hot compartment.

Some manufacturers have noticed that turning the spray off momentarily, then on again, can speed up extinguishment in enclosures. The benefits of pulsing, that is, the on/off action of water sprays, also described as cycling, are well described in References 27 and 28. Liu et al.[27] showed that pulsing the injection of water mist into an enclosure resulted in more rapid extinguishment, with less total water usage, than continuous application of mist. It was noted that the compartment temperature rose as the fire regrew during the first off stage, allowing for more evaporation of lingering fine mist. The resurgent fire further reduced the oxygen concentration in the enclosure. The next injection of spray further cooled and mixed the oxygen depleted gases. In this manner, cycling appeared to lead to greater net evaporation and oxygen reduction than with steady injection. Liu et al. attributed the improvement of the efficacy of water mist in fire suppression using cycling discharges to the faster depletion rate of oxygen in the compartment and the recurrent turbulent mixing created by cycling discharge.

In some systems cycling was used to avoid too-rapid cooling of the simulated turbine casing in the FMRC test protocol.[29] That protocol includes a test to ensure that cooling of the turbine casing will not result in damage to the turbine blades. By having spray on for only 50 percent of the time, not only was the cooling test passed, but also the volume of stored water needed for 10 min of protection was significantly reduced. The manufacturer's design criteria therefore incorporated the cycling as an essential element of system performance. Although the repeated off stages in the cycle had been acceptable for purposes of passing the FMRC test protocol, the author notes that cycling may not always be acceptable in installations where the equipment cannot tolerate re-exposure to flame during an extended off cycle. Furthermore, the apparent benefit is likely to be very dependent on the volume of the compartment.

Explosion hazard mitigation with water mist: This section examines a number of practical questions about the possibility of using water mist to mitigate explosion hazards. Water mist systems have been installed to replace Halon 1301 in gas compressor modules on Alaska's North Slope oil fields. The water mist systems were developed and tested for control of liquid fuel or lubricating oil spray or pool fires associated with the turbines that drive the gas compressors. The hazard also involves the potential for a methane gas leak, ignition, and explosion, however. Because the water mist systems are installed for the fire hazard, the question has been raised as to whether water mist could also provide benefits to mitigate the explosion hazard.

A review of experimental work performed over the last 3 decades reveals that there is mixed opinion about "whether application of water spray will quell or invigorate an explosion."[30] It is evident that there were major differences in spray characteristics involved in the various experimental programs, so the data are inconclusive. In general, the literature tends to support the idea that benefits of using water mist to mitigate explosions are substantial, provided attention is paid to the details of application.[31]

Butz et al.[32] investigated the use of water sprays to reduce explosion overpressures from a stoichiometric mixture of hydrogen gas and air released in a test chamber. The test scenario involved creating a mixture of hydrogen and air in a closed chamber, injecting a water spray, and then igniting the mixture. The tests demonstrated that the mist did not stop ignition from occurring, but it required a higher ignition energy than without the mist. The study also indicated that the overpressure generated by the deflagration was reduced by about 15 percent (see Figure 4-14.1). Figure 4-14.1 shows a pressure reduction from 35 to 30 psia "with mist." Butz also measured a significant temperature reduction of the passing flame front, which could reduce the risk of burn injury to personnel who might be exposed to the flash inside a compartment.

Butz concluded that although water mist could not inert the compartment, its use as an explosion hazard mitigant could be justified. The mist concentration required for successful quench (no discernible pressure rise) was found to be 0.7 l/m^3. Cooling in the compartment reduced the likelihood of an ignition source persisting, and the water mist appeared to increase the energy required for ignition.

Much research on explosion hazards on offshore platforms has been conducted at British Gas's (BG) Spadeadam facility in northern United Kingdom as part of a multiyear, multi-industry study aimed at improving the oil industry's confidence in its safety systems with respect to hydrocarbon fires and explosions. The results of almost a decade of testing are reported in the project final report.[33]

In contrast to Butz's results, work done by British Gas of the United Kingdom and by the Christian Mikelson Institute in Norway has shown that water spray augmented the overpressure caused by ignition of a methane-air mixture in a fully enclosed compartment

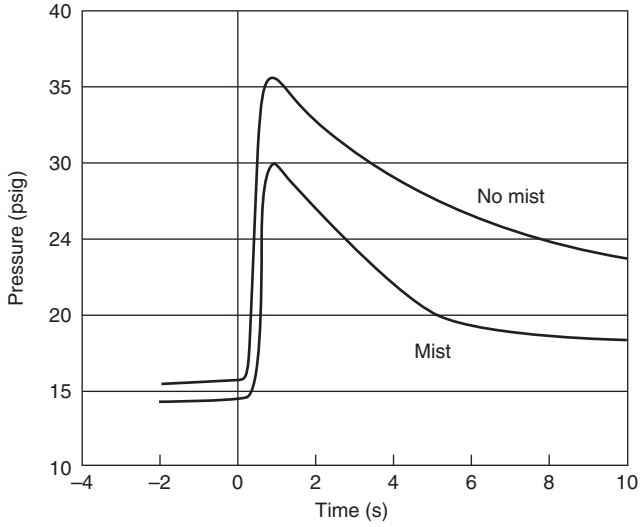

Figure 4-14.1. ***Reduction in explosion chamber overpressure due to presence of water mist.[32]***

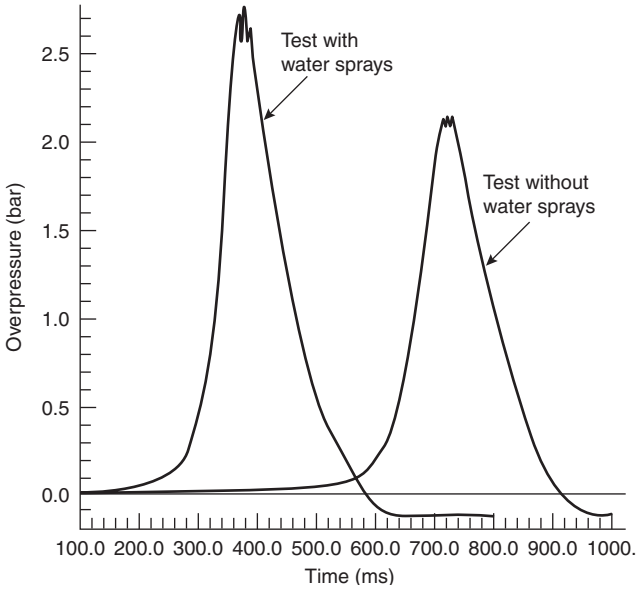

Figure 4-14.2. ***Blast overpressures measured in an enclosure with no open side, with and without water mist, from Selby and Burgan.[33]***

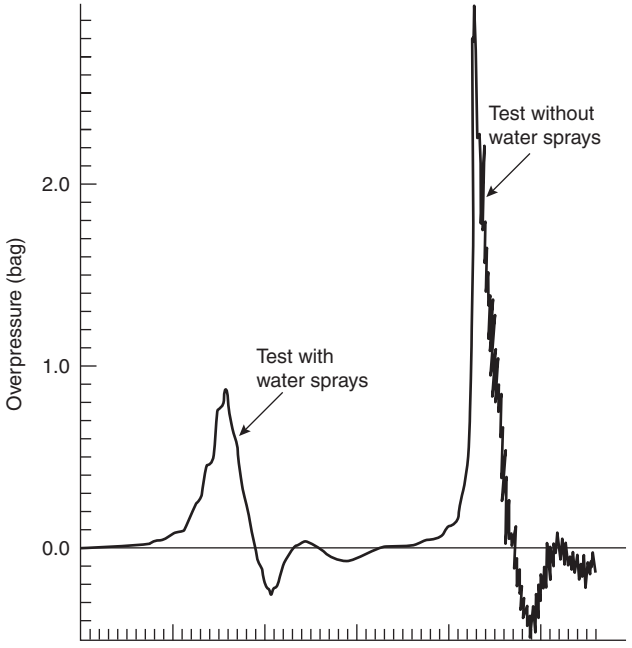

Figure 4-14.3. ***Blast overpressure reduction due to the application of water mist in an enclosure with one open side, from Selby and Burgan.[33]***

(Figure 4-14.2). However, in an open compartment (one wall removed) from the test compartment, a reduction in the overpressure was recorded (Figure 4-14.3), but it was a much greater reduction than the 15 percent measured by Butz. This study also pointed out the role that turbulence plays in accelerating the flame front. Both clutter and the injection of large drop water sprays increase turbulence in the gas/air mixture, and thereby contribute to worsen the deflagration. There were significant differences in the spray characteristics of the nozzles used in Butz's and in British Gas's work. British Gas studies were conducted using a water deluge nozzle typically used on offshore platforms, which probably produces spray much coarser than what we now define as water mist. The editors of the industry report conclude that more work is needed, with focus on working with sprays with finer drop size distributions.

During preparation of the first edition of NFPA 750 (1996), a task group of the committee prepared a review of the literature on fine water spray suppression systems. The literature review was longer than could be accommodated in the space available, so it was not published. The collected material is still on file with the NFPA, however. As part of that work, Robert Zalosh of Worcester Polytechnic Institute (WPI) prepared a review of studies on the use of fine water sprays to mitigate explosion hazards.[34] Several relevant conclusions based on his review are summarized below:

- In an unconfined environment, high-momentum water spray can entrain air into a gas cloud and dilute it below the lower flammable limit.
- Water vapor can slightly narrow the flammability limits for a gas, and it can dilute the gas/air mixture below the flammability limit. At higher temperatures, higher concentrations of water vapor are possible than at lower temperatures, so warm mist is likely to be more effective than cool mist.
- In near-limit gas/air mixtures, the spray/mist can have either a mitigating effect or an exacerbating effect on flame speeds and pressures depending on the turbulence produced by the spray and the characteristic drop size. The mitigating effect has occurred only with gas concentrations only slightly above the lower flammable limit.
- In the case of a very high flame speed with an accompanying shock wave, the spray/mist can reduce deflagration pressures and possibly extinguish the flame because the shock wave breaks up the drops into a micromist with a characteristic drop size on the order of ~1 μm. These tiny drops can evaporate in a sufficiently short time interval to absorb a significant fraction of the combustion energy released during the deflagration.
- The exacerbating effect that occurs in some situations is due to the turbulence produced by the water spray causing the flame speed to increase and/or causing a larger fraction of the flammable gas to burn.
- Generally, drops do not vaporize rapidly enough to absorb the combustion energy before the deflagration is complete, unless they are very small (i.e., on the order of 1 μm).
- More widespread use of water spray systems for deflagration control will depend on the viability of generating a micromist with sufficiently small drop sizes. This will require water mist systems that are different from those being developed commercially for fire suppression applications.

Spray Characteristics

Measuring and understanding the characteristics of sprays produced by different nozzles are prerequisites for understanding differences in performance. To fully characterize a spray requires information about the following elements:

- Drop size distribution (DSD)
- Cone angle
- Velocity of the discharge jet(s)
- Mass flow rate
- Spray momentum (product of velocity and mass)

These spray characteristics potentially determine the nozzle spacing as well as ceiling height limitations.

Drop size distribution: It is difficult to discuss water mist without remarking on its most notable feature, the fact that it is made up of finely divided water drops. Except for computer modeling, the drop size distribution of the spray cannot be used explicitly as a variable in the design of a water mist system. That stage awaits the results of further research work. The value in knowing the drop size distribution (and other characteristics) of a water spray lies in the fact that it relates to system performance, such as the rate of evaporation, how spray is affected by obstructions, and the dynamics of the spray interaction with the fire. If we do not measure the differences in drop size distributions of water sprays, we may never be able to explain the differences in performance between different manufacturers' nozzles. For computer modeling of the dynamics of suppression with water mist, a quantitative measure of the drop size characteristics of the spray is essential.

The term *drop size distribution* refers to the range of drop sizes contained in a representative sample of a spray or mist. There is a distribution of small and large drops, which varies with location in the spray as well as with time. For a continuous discharge, the distribution of drop sizes changes with distance from the source as drops collide, evaporate, or hit surfaces and fall out. For a short burst of spray, the distribution measured at a point in space changes with time as the larger droplets pass through quickly, leaving increasingly finer drops, which take more time to settle.

There are a number of ways to present data about drop size distributions of sprays.[27,28] It is customary in some fields to refer to the size of particles in a spray by a single drop size parameter, such as a Sauter mean diameter (SMD), or volumetric median diameter (VMD). Such single point parameters reveal little about the range of drop sizes in a spray, however. It is important to know about the fraction contained in larger drop sizes and the fraction contained in much smaller drop sizes in a spray, to understand its performance as a fire suppressant.

NFPA 750 has adopted the curve of cumulative percent volume versus diameter to represent the distribution of drop sizes in a water mist. Reasons for this choice are that the cumulative percent volume plot visually reveals the range of sizes, and the volume distribution converts readily to mass distribution, which is the most relevant term for analyzing heat transfer and evaporation rates using computer modeling. The range of drop sizes can be fully described by characteristic parameters such as $D_v0.90$ and $D_v0.50$. The $D_v0.90$ is the drop diameter at which 90 percent of the volume of a sample of the spray is contained in drops of that diameter or smaller. Similarly $D_v0.50$ is the volumetric mean drop diameter, that is, 50 percent of the volume of the spray is contained in drops less than that diameter.

Spray cone angle: Commercially available nozzles typically produce either 90° or 120° spray cones. Other cone angles are possible but not available as listed nozzles. Typically the sprays are solid cones, not hollow cone sprays.

Spray velocity: There are several aspects of spray velocity to consider. First, velocity is a vector quantity—it has both direction and magnitude. The directions of individual jets define the shape of the spray cone. The magnitude of the jet velocity is the velocity at which water emerges from a small orifice and begins to atomize. Second, there is a transfer of the velocity of the individual jets to the surrounding air (through drag effects). It is the overall velocity of the spray from all the jets, combined with the air entrained in the flow, that contributes to the spray momentum, which dictates the overall impact of the spray on a fire plume.

Discharge rate: The mass discharge rate of a nozzle is a function of water pressure and the total area of the orifice(s). Ideally the discharge rate per nozzle could be designed around the SHAR or REMP values—theoretical minimum application rates relative to the amount of heat to be absorbed. In reality, discharge rates vary for different manufacturers for the same fire test scenario.

Spray momentum: Momentum is calculated as mass times velocity. The combination of the mass of water droplets plus the mass of entrained air, multiplied by the velocity of mist particles plus entrained air, constitutes the momentum of a water spray. In general, for a constant mass discharge rate, increasing spray velocity increases the air entrainment rate, which contributes to the spray momentum. Like velocity, momentum is a vector quantity—it has both magnitude and direction—and its direction relative to the fire plume or fuel source has a bearing on its effectiveness. Where the spray direction is opposed to the fire plume direction, there is penetration of the flame by the water mist, and any water vapor created in the flame may be carried to the seat of the fire. In contrast, codirectional flows may not create the turbulent flame/mist mixing needed to enhance evaporation and cooling, and the water vapor formed will be carried away from the fuel surface rather than pushed down to it. Studies to evaluate the relative benefits of using high velocity or low velocity water mist nozzles must include this directional component of the momentum factor, not only the magnitude of jet velocities. Also, since the entrained air forms a significant proportion of the mass flow rate, it contributes to the momentum of the overall spray cone. Two nozzles with similar jet velocities could have very different degrees of air entrainment—hence the spray momentum for each could differ significantly.

As control over the directional aspects of spray application can be a design choice, spray velocity and spray momentum represent potential first-principles design parameters.

Measurement of drop size distributions: Appendix D of NFPA 750 describes a methodology for obtaining a statistically meaningful measurement of the drop size distribution of a water spray. The drop size distribution in a spray is not the same at all locations in the spray cone. A single reading taken at one location may not be representative of the average condition in the spray. It is standard practice in other engineering disciplines in which drop size distribution is of interest (environmental scrubbers for stack emissions, for example) to take a set of readings and combine them into a statistically representative value.[35,36]

Figure 4-14.4 illustrates a setup in which spot readings were taken at 24 different positions in the spray, measured on a plane 1 m below the nozzles. The positions for taking a measurement represent the midpoint of sectors of equal area in the circular cross section of a spray cone. A grid of collector pans is used to collect the flux density at each of the measurement locations. It is assumed that the drop size distributions measured in areas of high flux density are more representative of the overall distribution than measurements taken in areas of low flux density. Thus, Equation 1 is used to calculate a weighted average drop size distribution curve, weighted according to the flux density measurements at each location.

$$R_k = \frac{\sum_i (R_{j,i} \times A_i \times V_i)}{\sum_i (A_i \times V_i)} \quad (1)$$

where

R_k = weighted cumulative volume percent readings for sizes equal to and less than d_{upper}

$R_{j,i}$ = cumulative volume percent readings for sizes equal to and less than d_{upper} at location i

A_i = area centered at location i in which the size distribution is represented by R_k

V_i = water flux density measured at location i

The NFPA 750 appendix method was used to obtain weighted average cumulative percent volume DSD curves for four commercially available water mist nozzles. Figure 4-14.5 compares the weighted cumulative percent volume drop size distribution curves for the four nozzles investigated.[37,38] Nozzles A and B were low-pressure single-fluid nozzles; nozzles C and D were high-pressure single-fluid nozzles. It is interesting to note that even the coarsest spray measured (A) had at least 50 percent of its volume (which equates to its mass) contained in drop sizes smaller than 300 μm. Spray B shows approximately 80 percent of its volume (mass) in drop sizes smaller than 300 μm. However, nozzle B discharged at a

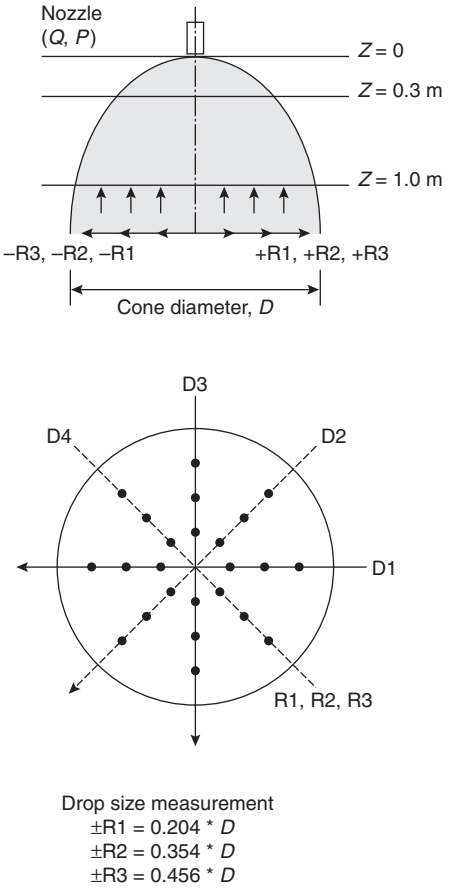

Figure 4-14.4. ***Locations within spray cones for measurement of flux density distribution and drop size distribution. The positions shown are the centroids of segments of equal area.[36]***

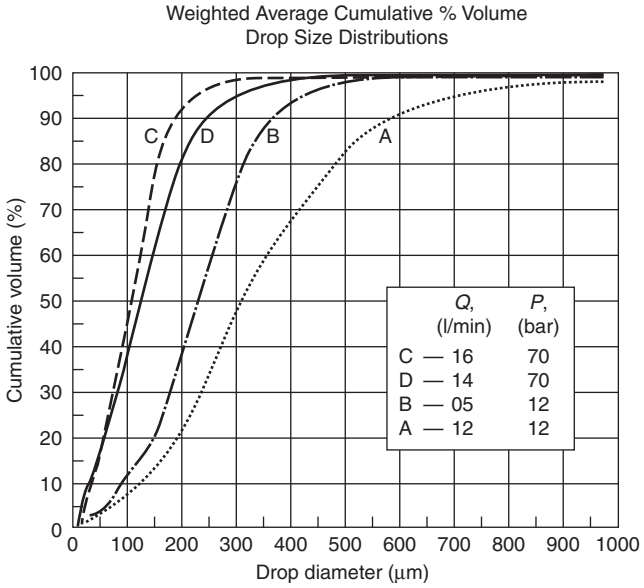

Figure 4-14.5. ***Comparison of statistically weighted cumulative percent volume versus drop size distribution plots for two low-pressure (A and B) and two high-pressure (C and D) water mist nozzles.***

rate of 5 l/min (= kg/min) whereas nozzle A discharged at a rate of 12 kg/min. Therefore nozzle A generated about 6 kg/min of drop sizes below 300 μm, while nozzle B produced only 4 kg/min of sub-300 μm droplets. In terms of potential for heat extraction, one cannot conclude that one spray is "better" than another on the basis of drop-size distribution alone. Factors such as discharge rate, cone angle, and velocity also influence the mixing of mist with fire gases in the compartment.

Spray Velocity

As part of the same study referred to for the drop size distributions shown in Figure 4-14.5, measurements of vertical-downward velocity profiles were taken for two of the nozzles.[37,38] The velocity was measured by placing a vane-type anemometer horizontally in the spray cone at different locations and at two different distances below the nozzle. The anemometer is not measuring the velocity of the spray jets or individual water particles. It measures the vertical component of the velocity of the entrained air plus water drops. Individual drops hitting the rotating vane may either accelerate or decelerate the vane. It was estimated that the effects of individual water drops on the vane speed approximately cancel out, so that the velocity of the entrained air dominates. The measured velocity is then probably less than the velocity of the fastest moving drops, but close to the average velocity of the entrained air.

Figure 4-14.6 compares the downward velocity profiles measured 0.3 m and 1.0 m below a high-pressure (C) and a low-pressure (A) nozzle. These data provide a qualitative means of understanding the difference between how a high-pressure and low-pressure water mist nozzle might interact with the fire plume.

At this time it is not possible to make invariable links between spray drop size distributions, spray velocity, and the suppression efficiencies of different water mist nozzles. However, without a measure by which different nozzles can be compared, we will not be able to analyze the relative importance of different spray characteristics.

Additives and Health Concerns

Low concentrations of additives, such as alkali salts and the surfactants in AFFF solution, improve the extinguishment capabilities of water mist.[39,40] In Class B fires, the surfactant spreads over the liquid pool surface, blocks the generation of fuel vapors, and helps extinguish small flames in hidden corners. Extinguishing the small flames helps break the extinction-reignition cycles that prolong the extinguishment of obstructed pool fires. For enclosed systems, the addition of gaseous additives, such as an inert gas (nitrogen or carbon dioxide) to the mist has been demonstrated to enhance extinguishment by aiding in oxygen depletion.[41] Antifreeze and biocides to prevent algae growth are also potential water mist additives.

The use of additives introduces concern about possible negative effects on human health. The U.S. Environmental Protection Agency (EPA) permits the use of water mist as a halon alternative in occupied spaces only when potable water or normal seawater is used.[42] This permission was based on the response of a panel of toxicity experts convened under the Halon Alternatives Research Corporation (HARC) to questions about the possible adverse health effects of water mist. The report concluded that even the smallest drop sizes in water mist are not present in sufficient quantities to harm humans if breathed into the lungs. However, additives pose a potential threat—if additives are used, the onus is on the proponent of the additive to prove to EPA that it does not pose a health risk.

The report *Water Mist Fire Suppression Systems Health Hazard Evaluation* (1995) was generated by the Halon Alternatives Research Corporation (HARC).[43] Members of the NFPA 750 committee provided technical input to the

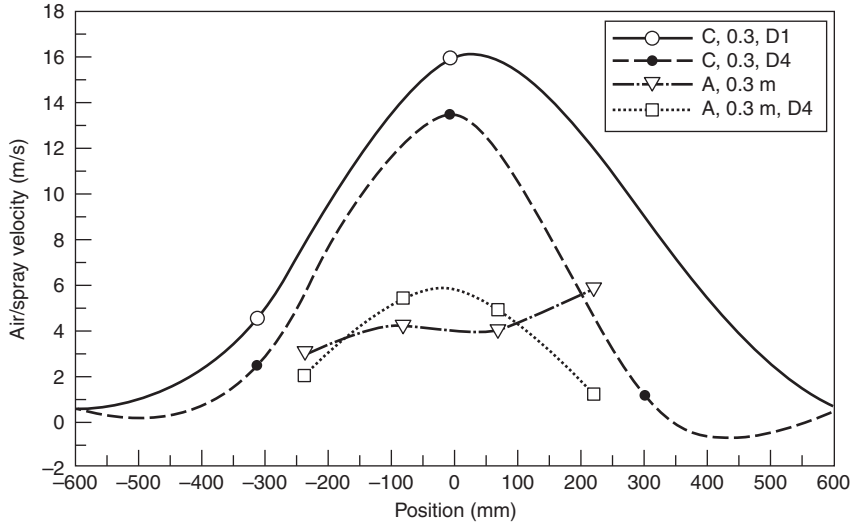

Figure 4-14.6. ***Downward spray velocity profiles, measured 0.3 m and 1.0 m below a high-pressure (C) and a low-pressure (A) water mist nozzle.***

panel of health experts. The report provides a good background for discussion of concerns over water mist and additives to the water. This report includes a section entitled "Toxicity Profile—Water Mist Spray with Additives" that was prepared for the Army Program Executive Office, Armored Systems Modernization group, by the Toxicology Division, U.S. Army Environmental Hygiene Agency. Some highlights from this document are provided below.

There are concerns with storage of water in cylinders for water mist systems for crew compartments in military vehicles. The major concerns range from toxicology of additives used as antifreeze agents or fire retardants, to bacteriological growth in stored water—that is, untreated stored water in which bacteria are present may pose a toxicological hazard as well as water with chemical additives.

The army report summarizes the available toxicity data on water mist and six potential additives. It recommends additives that are the least toxic, and it identifies additional information required for further evaluation of candidate chemicals:

- Propylene and ethylene glycol (antifreeze)—acceptable
- Potassium acetate and calcium chloride (antifreeze plus fire retardant)—acceptable with reservation
- Potassium iodide and lithium chloride—potentially hazardous to humans

The army toxicity profile report notes that its conclusions do not address the matter of how much additive may be present. Is a product safe at 1 percent but unsafe at 5 percent? Some antifreeze solutions may be as high as 30 to 50% by weight. The concentrations needed for bacteria control may be below harmful threshold. One must distinguish between chronic, or long-term exposure, and short-term, low-probability exposure. These matters need to be addressed before the constraints against use of additives in water mist can be relaxed.

In summary, the U.S. Environmental Protection Agency (EPA) states that only "pure" (i.e., potable) water or natural seawater can be used without question for water mist systems in occupied spaces. If additives are considered, the onus is on the proponent to prove that there is no toxicological risk. This ruling raises a difficulty for anyone (within the jurisdiction of the EPA) who proposes to use an additive in a water mist system intended for an occupied space. The only way to prove an additive harmless is to conduct an expensive medical study.

Fire Suppression Modeling

The major difficulties with water mist systems are those associated with design and engineering. These problems arise from the need to generate, distribute, and maintain an adequate concentration of the proper size drops throughout the compartment while gravity and agent deposition losses on surfaces deplete the concentration. There is currently no theoretical basis for designing these parameters. System design parameters are being extrapolated from large-scale test data on a case-by-case basis. This is expensive to the water mist system manufacturers and poses special problems for standards-making and regulating authorities.

An empirical understanding of how water mist systems extinguish a fire is now emerging. This degree of understanding is not yet at the stage where water mist systems can be designed from first principles, though significant progress has been made over the past few years.

A basic understanding of the mechanisms of extinguishment associated with water mist was developed approximately 40 years ago.[3,4] Braidech and Rasbash both concluded that fires were extinguished by dilution of the air (oxygen) with water vapor (steam), resulting from evaporation of water droplets in the area local to the flame. They also concluded that the cooling effects of the water might contribute to the extinguishment process. Research conducted to date has not altered this description. Recent research has, however, identified the primary mechanism(s) associated with extinguishment for a given set of conditions as well as some additional less predominant extinguishment mechanisms.[14]

The mechanisms of extinguishment can be broken down into two basic groups—direct and indirect flame interaction. Direct flame interaction includes gas phase cooling and localized oxygen depletion, and indirect effects include global oxygen depletion and surface wetting/cooling effects.

Direct flame interaction encompasses a broad range of both chemical and thermodynamic relations associated with the release and distribution of energy in the combustion process. Extinguishment by direct flame interaction (primarily gas phase cooling) is basically the removal of energy from the flame and hot gases. As the energy is removed from the flame, the temperature of the flame is reduced. If the flame temperature is reduced below the critical value necessary to sustain combustion (limiting adiabatic flame temperature), the flame will be extinguished. The limiting adiabatic flame temperature for a number of hydrocarbon fuels is approximately 1600 K (1326°C).[15]

Recent investigations have bounded some of the parameters associated with direct flame interaction.[20,22] Numerous research programs have focused on identifying the critical mist concentrations needed to extinguish diffusion flames[17,44,45,46] and to extinguish hydrocarbon pool fires.[22,47] Other research agencies have studied the effects of water vapor as an inerting gas,[48,49] as well as the attenuation of radiation to the fuel surface provided by the mist.[50,51]

The difficulty in predicting extinguishment by direct effects is associated with being able to predict and/or measure the amount of mist reaching the fire. The ability of mist to diffuse into all areas in the space in the same manner as the gaseous agents is significantly limited in the range of drop sizes produced by current commercially available hardware.[47,52] Recent studies have shown that the concentration of mist decreases by more than a factor of two after traveling less than a meter horizontally away from the spray pattern of a nozzle. To compensate for this limitation, the higher performance water mist systems rely on high-velocity sprays to mix the mist throughout the compartment. The fire size (heat release rate) and fire location are also variables that need to be considered. The

fire tends to alter the mist conditions in the compartment by changing the drop size distribution (vaporization and condensation) and affecting the flow patterns throughout the space due to the plume and ceiling jets.

Additional research has bounded the effects of oxygen depletion and dilution (indirect effects) on extinguishment.[18,53,54,55] The production of steam resulting from mist interactions with the flame, hot gases, and/or hot surfaces can significantly reduce the oxygen concentration in the space. The oxygen available for combustion on a compartmental scale is a function of the size of the fire, the compartment volume, and the ventilation conditions in the compartment. As the size of the fire increases, the average temperature in the space increases, and the oxygen concentration decreases due to both the consumption of the oxygen by the fire and dilution of the oxygen by water vapor (steam). If the combined effects of oxygen depletion and dilution can reduce the oxygen concentration below the critical value necessary to sustain combustion [limiting oxygen concentration (LOC)], the fire will be extinguished. The LOC for most hydrocarbon fuels is approximately 13 percent.[56]

Fuel surface effects can be the predominant extinguishment mechanism for fuels that do not produce combustible mixtures of vapor above the fuel surface at ambient temperatures, that is, solid fuels and liquid fuels with high flashpoints (i.e., diesel ≈ 60°C). Wetting/cooling of the fuel surface reduces the pyrolysis rate of the fuel. If the vapor/air mixture above the fuel surface is reduced below the lower flammability limit (LFL), the flame is extinguished. The ability to predict extinguishment based on surface cooling has also been investigated in numerous experimental programs.[57,58,59,60] This information includes both Class A materials as well as high-flashpoint hydrocarbon pool fires.

Typically a combination of mechanisms are involved to some degree in the extinguishment process. In order to accurately predict the conditions required for extinguishment, the combustion chemistry, combined with thermodynamics and fluid dynamics, needs to be covered in detail. These complex relations are best analyzed using computational models that are based on first principles. The current mathematical models used to predict suppression of fires by water mist systems cover the range of approaches from zone fire modeling to computation fluid dynamics (CFD), which are often referred to as field models.

A zone model calculates the fire environment by dividing each compartment into one or two homogeneous zones. The energy balance and conservation of mass equations are solved based on a control volume dictated by the boundaries of the compartment for a single-zone model, or by the zonal boundaries for a two-zone model.

The input requirements for zone models vary depending on the model and the desired output. The compartment geometry and opening dimensions are needed to define the space and the surroundings. The thermal properties of the compartment boundaries are needed to estimate the heat loss through the walls, ceiling, and floor. The fire size must be entered, though the model may modify the heat release rate as the oxygen concentration in the compartment is reduced by the fire. Some zone models account for effects of mechanical ventilation, which means that the fan flow rate and the location of the vent inlets and outlets are required.

CFD models divide the space into a large number of elements and estimate the fire environment in a space by numerically solving the conservation equations (mass, energy, momentum, diffusion, species, etc.) within each element. This is accomplished by using finite difference, finite element, or boundary element methods. The results are three-dimensional in nature and are very refined when compared to a zone-type model. The enormous number of computations performed during these modeling exercises are very time consuming and require powerful computational equipment.

Like zone models, CFD models require a description of the compartment geometry and the openings within the compartment as input. Depending on the sophistication of the extinguishment/fire model, the fire heat release rate may also need to be specified. Heat losses to the compartment boundaries are calculated using the thermal properties of the bounding materials. CFD models maybe used to simulate such phenomena as open plumes (bonfires) and shafts since they are not strictly limited to compartment fire scenarios.

Quasi Steady-State Zone Model

Zone fire suppression models for water mist have been developed by Back et al.,[60] Forssell et al.,[62] and Vaari.[63] All three models assume a single zone and vary in sophistication from steady-state predictions to transient computations.

The quasi steady-state model was developed to predict the effectiveness of water mist systems for extinguishing fuel spray and pool fires in machinery space applications.[64] The model was developed for obstructed fires where extinguishment primarily occurs as a result of a reduction in oxygen concentration (consumption and dilution) and neglects the effects of the interaction of mist with the flame. Consequently, the predictions made by the model serve as the limiting case where obstructions prevent direct spray interactions with the fire. The model is based on conservation of energy and requires the following input parameters: fire size, compartment geometry, vent area, and water flow rate. The steady-state compartment temperatures and oxygen concentrations predicted by the model can be used to determine the smallest fire (critical fire size) that will sufficiently reduce the oxygen concentration to below the LOC of the fuel.

The energy balance used in the model can be expressed by the following equation:

$$\dot{Q}_{Fire} = \dot{Q}_{Boundary} + \dot{Q}_{Vent} + \dot{Q}_{Vapor} + \dot{Q}_{Water} \qquad (2)$$

where

$\dot{Q}_{Fire}$ = heat release rate of the fire
$\dot{Q}_{Boundary}$ = energy lost through the walls, ceiling, and floor
$\dot{Q}_{Vent}$ = energy lost out of the vent opening
$\dot{Q}_{Vapor}$ = heat absorbed by evaporation
$\dot{Q}_{Water}$ = energy absorbed by the mist

The following assumptions were made to simplify the calculation:

- Combustion is complete and takes place entirely within the confines of the compartment (the heat release rate of the fire is a constant).
- The temperature is uniform within the compartment at all times (after discharge), and the gases exhausted are assumed to be at the compartment temperature.
- The exhaust gases and the gases contained in the compartment are assumed to be saturated with water vapor.
- A single surface heat transfer coefficient is used for the entire inner surface of the compartment.
- The heat transfer through the compartment boundaries is unidimensional, that is, corners and edges are ignored and the boundaries are assumed to be infinite slabs.
- Mist droplets are assumed to be heated to the compartment gas temperature.

The individual components of Equation (2) are calculated as follows: The heat release rate of the fire is an input parameter and is calculated based on the known fuel spray or mass burning rate of the fire and the heat of combustion of the fuel. The heat lost through the boundaries of the compartment is determined using an overall heat transfer coefficient developed for preflashover fires. The energy losses by vent gas flow are based on the temperature of the exhaust gases and the exhaust rate determined from a vent flow correlation applicable to well-stirred compartment environments. The heat lost by evaporation is based on achieving the equilibrium vapor pressure (assuming saturation), the vent flow rate, and the heat of vaporation. The heat absorbed by the water is determined from the water mist application rate, assuming all the mist is heated to the compartment temperature.

The computational exercise begins by solving the energy balance to predict the steady-state compartment temperatures in the space and the mass flow rate of air/gases through the vent opening. Once the steady-state temperatures and the mass flow rates are known, the steady-state oxygen concentration is then calculated by first determining the amount of oxygen consumed by the fire and then diluting the remaining oxygen with water vapor until the gases are saturated.

The steady-state oxygen concentrations are then used to predict the critical fire size for the selected compartment configuration and water mist system flow rate. In this context, the critical fire size is defined as the smallest fire that will reduce the oxygen concentration below the LOC of the fuel.

The extinguishment times are predicted using a coupled energy and mass-transfer correlation. The mass transfer is implicit in the following equation, while the energy/temperature dependence is embedded in the volumetric flow rate and predicted steady-state oxygen concentration terms. Assuming that steady-state conditions occur quickly and that the extinguishment of these fires becomes related to the time required to dilute the gases in the compartment, the extinguishment times can be approximated using the following equation:

$$\Delta C_{O_2(t)} = \Delta C_{O_2(ss)}\left(1 - e^{-\dot{v}t/v}\right) \quad (3)$$

where

$C_{O_2(t)}$ = oxygen concentration (percent by volume) in the compartment at time t

$C_{O_2(ss)}$ = predicted steady-state oxygen concentration

v = volume of the compartment

$\dot{v}$ = volumetric flow rate of air/gas through the compartment

The extinguishment times are determined by setting $C_{O_2(t)}$ equal to the LOC of the fuel (14% is typically used during this calculation) and solving Equation (3) for t. This approach is a first-order approximation and is best suited to predict the extinguishment times of large fires. This method loses accuracy as the fire size approaches the critical value. The primary outputs of the model are the extinguishment times for a range of fire sizes for a specific compartment configuration and water mist discharge rate.

The model was developed and validated for hydrocarbon fuel fires (both spray and pan fires). The predictions made by the model compared favorably to the results of four full-scale machinery space investigations conducted for the U.S. Coast Guard. For the range of compartment sizes (100–3000 m^3) and ventilation conditions [closed compartment, naturally ventilated (1.25–5.7 $m^{5/2}$ ventilation factors), and forced ventilation (25 m^3/min)] included in these investigations, the model was able to accurately predict the steady-state compartment temperatures and oxygen concentrations that occurred during the test. In many cases, the larger fires were extinguished before steady-state conditions were reached. This was also predicted by the model. The results of the model were also used to accurately predict the smallest fire (critical fire size) that could be extinguished due to a reduction in oxygen concentration in the space. The model was able to accurately predict the extinguishment times for a wide range of fire sizes, but lost accuracy as the fire approached the critical value.

Although the model shows promise for predicting the steady-state temperatures and oxygen concentrations in an enclosure for a given set of parameters, the limits of the model need to be explored further. The primary assumptions used in the model are that the gases in the compartment are well mixed and saturated with water vapor. The assumption of saturated vapor is a significant limitation, since the model cannot distinguish between water mist systems with similar discharge rates but different spray characteristics. The model also assumes that steady-state conditions are achieved quickly, which may or may not be a good assumption. In order to validate these assumptions, the transient conditions in the space would need to be analyzed. The analysis of these transient conditions significantly increases the complexity of the model.

Transient Zone Models

Two transient zone models that predict the effectiveness of water mist systems to extinguish hydrocarbon fires have also been developed.[62,63] The two models are similar in some respects but different in others.

With respect to similarities, both models solve the conservation of mass and energy equations as a function of time for a given set of conditions. The conservation of mass equations used in the quasi steady-state model have been replaced by conservation of species. The mass/volumetric flow rate of air through the vent is determined using an orifice flow correlation and the pressure in the compartment similar to the quasi steady-state model. The compartment pressure is calculated from the density and gas temperature in the compartment using the equation of state for an ideal gas. The assumption of saturated vapor used in the quasi steady-state model has been replaced by a droplet evaporation algorithm. The method for predicting extinguishment has also been revisited.

The models are different with respect to how they handle boundary losses, handle drop evaporation, and predict extinguishment. The model developed by Vaari neglects all energy losses to the boundaries, whereas the model developed by Forssell includes a lumped mass boundary heat loss algorithm similar to the quasi steady-state model.

The evaporation algorithms differ significantly between the two models. The algorithm developed by Vaari is fairly detailed, as compared to the simplified version developed by Forssell. In the algorithm developed by Vaari, it is assumed that the heat transfer between the gas and liquid phase is infinitely fast, making the two phases identical temperatures. As a result, all of the heat absorbed by the drop is utilized in the evaporation process. The algorithm includes drop concentration and drop size subroutines that include drop agglomeration and terminal velocity predictions. Using the Clausius-Clapeyron equation to calculate the vapor pressure near the drop surface, the mass transfer number (B) for a single drop is determined. This mass transfer number is then used to determine evaporation rate for a single drop, which in turn is applied to the entire spray.

In the algorithm developed by Forssell, the evaporation model has been simplified and incorporates a correlation constant that represents the combination of the mass transfer number (B) and the surface area–to-volume ratio of the droplet. Rather than including a set of subroutines based on a large number of assumptions that need validation, Forssell chose a single empirically fitted correlation constant.

The extinguishment algorithms are also somewhat different in the two models. In the algorithm developed by Vaari, extinguishment is predicted based on a calculated flame temperature determined based on an energy balance conducted in the flame. For this calculation, a limiting flame temperature of 1550 K was selected. This energy balance calculates the temperature of the gases in the flame region by taking into account the species concentrations in the combustion process as well as the mist entrained into the flame. In order to estimate the amount of water droplets entrained into the flame, a simple mist concentration algorithm was developed based on mist discharge rate, terminal drop velocity, and compartment height.

Forssell selects a critical oxygen concentration (14%) to predict extinguishment, similar to the quasi steady-state model. This is basically equivalent to the previous approach with the exception that the entrainment of mist into the flame is not included in the computation.

Both transient models provide as output the gas (species) concentrations and temperature histories in a compartment for a given compartment configuration, ventilation condition, and fire scenario. The advantage of the transient models over a steady-state computation is that they provide the capability to study scenarios that never achieve steady-state conditions. Two examples of these are growing fires (fires with varying heat release rates) and variable flow rate water mist systems. Both transient models include evaporation algorithms, which, in theory, should allow the distinction between two mist systems with similar discharge rates but different spray characteristics. The transient models should also predict extinguishment more accurately than a steady-state model. The limitations are associated with the single zone approximation and the need for experimental data to define the unknown parameters used in the model. The single zone approximation may cause the model to fail if the space is not well mixed or the fire is allowed to burn for a significant duration prior to mist system activation. Neither of the two transient zone models have been thoroughly validated. However, the limited validation data show promise with respect to the accuracy of these models.

CFD Models (Field Models)

CFD models are a level of sophistication above typical zone models and show promise for handling the complex physical and chemical relations required of this application. As stated previously, CFD models divide the computational domain into a large number of small control volumes and solve the conservation equations (Navier-Stokes) in each one simultaneously. CFD models can provide detailed information on the mass/energy transfer between the fire and the water mist, and on the distribution of water spray droplets in the compartment.

Like zone models, CFD models require a description of the compartment geometry and the openings within the compartment as input. Compartment contents and boundary materials must also be specified. The model is run for a specific set of conditions (compartment configuration, fire scenario, and water mist system). The outputs are very detailed in nature and consist of data files containing information pertaining to the conditions (temperature, velocity, mist concentration, gas/species concentrations, etc.) for each element and time step in the computation. This detailed information allows a graphical/visual representation of the conditions in the compartment during selected time intervals. For example, color contour temperature images and velocity fields represented by small arrows, with the magnitude of the velocity indicated by the length of the arrow, are typical outputs for CFD modeling runs. These outputs allow the visualization of the conditions that occur in the compartment during a specific scenario.

Some of the CFD models currently in use include JASMINE, FLOW3D, PHOENICS, SOFIE, TASCFLOW, VULCAN, STAR-CD, and the Fire Dynamics Simulator (FDS), but only a limited number of them have been used to model water mist applications. Many of these models contain variants of the K-Epsilon submodel required to

handle the turbulent conditions produced in this application. K-Epsilon submodels are two additional differential or algebraic equations (where K is turbulence energy and Epsilon is its dissipation rate) that relate turbulent stresses and fluxes to the flow field.

The primary limitations for applying CFD modeling to water mist applications are associated with the lack of knowledge/algorithms to determine fire extinguishment and accurately predict drop transport. Detailed extinguishment algorithms must include an energy balance conducted in the flame and at the fuel surface while completing the combustion process. This combustion process must take into account the following species concentrations: fuel vapor, water vapor, oxygen, nitrogen, combustion gases, and water mist concentration. In most cases, the fuel vapor concentration is driven by the radiation from the flame back to the fuel surface and must be solved simultaneously. The difficulty with drop transport is associated with linking the liquid water droplets to the gas phase domain and showing the influence of one on the other. Recent research has focused on the development of some extinguishment algorithms, but only limited attention has been given to drop transport.

With respect to extinguishment algorithms, the physics and computational issues associated with numerical modeling of fire suppression have been identified.[64,65] Additional studies have focused on specific fire types and scenarios. The National Institute of Standards and Technology (NIST) and the Naval Research Laboratory (NRL) have both recently developed algorithms to predict suppression of opposed flow diffusion flames.[66,67] Limited research has also been conducted on premixed flames as well.[68] On a larger scale, extinguishment algorithms have also been developed for pool fires.[69,70] While these advances are promising, there is still the need to develop an all-encompassing extinguishment algorithm capable of handling a variety of fuel types and configurations to be used with CFD modeling.

The manner in which the spray characteristics of the nozzle affect drop transport and the transport phenomenon in general also needs additional research. Although the effects of fire plumes and ceiling jets on water droplets have been investigated in numerous research efforts,[71,72] the problem lies more on a fundamental level. Drop transport and tracking is currently being performed using either Eulerian or Lagrangian formulations.[73,74] An Eulerian formulation uses a fixed grid and assumes the drops pass through (drops and gases travel at different velocities), whereas the Lagrangian formulation considers the droplets and gases to be a single homogenous mixture. A majority of the water mist modeling has been conducted using the Lagrangian formulation, but the information found throughout the literature is very inconclusive regarding the choice of the appropriate method.[75] The appropriate formulation may depend on the spray characteristics of the nozzle as well as on the application.

A limited number of studies using CFD models for full-scale fire suppression research have been carried out by Hadjisophocleous.[71,76] The research includes the extinguishment of liquid pool fires in both open and closed compartments, and fire suppression in an aircraft cabin. The modeling was performed using the CFD model TASCFLOW with the water spray transport handled using a Lagrangian tracking model. During the initial study,[71] water mist system parameters (the number of nozzles, nozzle locations, spray characteristics, and discharge rate) were systematically varied to determine their effect on the extinguishment process. The predicted results showed reasonably good agreement with corresponding experimental data.

The strengths of CFD modeling are associated with its capabilities to analyze the detailed chemical and thermodynamics processes required of this application. The graphical/visual nature of the output can illustrate the physical phenomena occurring during the event. The limitations are associated with the need to develop and validate algorithms to predict both drop transport and extinguishment. The ability to apply CFD modeling to a specific application (grid selection) is time consuming and requires a certain level of expertise. The licensing of the CFD code and the computing power required to run the model also significantly increases the cost of the effort.

The results obtained using CFD modeling demonstrate that it is a promising tool for analyzing the complex physical and chemical phenomena of fire suppression by water mist. CFD modeling has demonstrated the potential to extend the understanding of the relationships between the water mist systems design parameters and fire suppression. CFD modeling not only has the potential to augment the test and evaluation process, but also shows promise for approving specific designs for actual installations. The potential for CFD modeling as a research and design tool is now being recognized. CFD modeling is already being used as a research tool at NRC Canada, NRL, NIST, SP, SINTEF, and at numerous universities.

Summary

An empirical understanding of how water mist systems extinguish a fire is beginning to emerge. Although progress has beeen made over the past few years, this degree of understanding is not yet at the stage where water mist systems can be designed from first principles, though significant progress has been made over the past few years. In order to accurately predict the conditions required for extinguishment, the combustion chemistry, combined with thermodynamics and fluid dynamics, needs to be covered in detail. These complex relations are best analyzed using computational models. The current mathematical models used to predict suppression of fires by water mist systems cover the range of approaches from zone fire modeling to computation fluid dynamics (CFD), which are often referred to as field models.

Three zone models (one steady-state and two transient) have been developed to predict the effectiveness of water mist systems against hydrocarbon fuel fires (both spray and pan fires). The models appear to make reasonably accurate first-order approximations of the extinguishment of a range of fire sizes for a given compartment configuration and set of mist system characteristics. The strengths of the zone models are their ability to bound the capabilities of a water mist system for a given application. The limitations of these zone models are associated with a general lack of detail incorporated in the computation,

and as a result, these models may lose accuracy when applied to complex configurations (geometries).

CFD modeling has been demonstrated to be a promising tool for analyzing the complex physical and chemical phenomena of fire suppression by water mist. Additional research is required to further develop and validate both the drop transport and extinguishment algorithms used in the CFD codes. The strengths of the CFD models are their ability to expand the understanding of how the water mist system design parameters effect the extinguishment process. The limitations are associated with the high labor and equipment (computer and software) costs required to model a specific application.

In any case, modeling has the potential not only to augment the test and evaluation process, but also to aid in approving specific designs for actual installations.

The Importance of Fire Testing

In the absence of a large empirical database of design criteria and a set of general principles that applies to all water mist hardware, NFPA 750 requires that all water mist system designs be linked to formal fire tests. Testing has shown that the performance of water mist systems is dependent on the specific manufacturer's equipment, particularly the nozzle design. One manufacturer might pass a fire test program at a particular flow rate and nozzle spacing. Another might operate at a lower pressure but have a higher flow rate and closer nozzle spacing to pass the same test. The average flux density for the two systems may differ by a factor of 3! Consequently, it is not yet possible to set generic design criteria (such as nominal flux density for a particular fire scenario) that are independent of the manufacturer's equipment. It appears that barely perceived differences in atomization, spray cone angle, and velocity influence the ability of the spray to mix and cool hot gases and extinguish a fire. The only way to be sure that a particular manufacturer's water mist system will work in a given application is to conduct fire tests.

If a water mist system is "listed" for an application, the system design criteria and performance objectives have been validated through fire tests conducted by a recognized testing laboratory. Table 4-14.1 shows a list of fire test protocols recognized in North America and Europe. Test protocols are intended to test the limits of performance of systems against a realistic range of conditions, including worst-case scenarios, and to establish agreed-upon and measurable performance objectives. Considerable thought and experience go into achieving consensus on the test scenarios. In North America, end users of water mist technology tend to rely on third-party listings by Factory Mutual Research Corporation (FMRC) or Underwriters Laboratories (UL) to confirm suitability. In Europe and Asia, end users are more likely to accept the results of ad hoc testing. Probably the major differences between an ad hoc tests program and a formalized test protocol are the degree of effort put into looking for failure conditions, range of applicability, and breadth of criteria for judging acceptability. Ad hoc tests will be very specific to an application. Ad hoc testing is easier to carry out and less costly than developing a consensus test protocol. Worldwide, many ad hoc water mist test efforts have taken place and continue to take place. Examples include local application systems;[25] high-voltage cable tunnels;[81] railway tunnels;[82,83] heritage properties, libraries, and archival storage on fixed shelving,[84,85] electronic equipment rooms,[86] computer room underfloor areas;[41] aircraft cargo bays,[87] and outdoor transformers.[88] Some of those ad hoc test programs will eventually become formal test protocols. Manufacturers for the most part bear the cost of conducting these tests.

For marine applications, consensus test protocols have been developed through the International Maritime Organization. For land-based industrial applications, formal test protocols have been developed by FMRC for turbine enclosures, machinery spaces, and pump rooms where liquid fuel fire hazards exist (see Table 4-14.1). FMRC has also developed a test protocol for wet benches in clean room environments. Both FMRC and UL have test protocols for light and ordinary hazard applications that are based on the IMO test protocols for crews' quarters and public spaces on ships.

The existence of a listing simplifies the problem of matching a water mist system to a particular hazard. At the same time, complete reliance on a generalized listing, without checking that the performance promised by the listing meets the end-user's actual needs, can be a mistake. The fire protection engineer responsible for the design of a water mist system must confirm that the application is close to the conditions of the listing. He or she must also check that the performance criteria used to judge pass or fail in the test protocol are compatible with the end-user's needs in the actual installation. In some cases the performance requirements of the listing may be lower than what the end-user really needs, so measures to upgrade performance will be required.

Appendix C of NFPA 750[2] describes a number of fire test protocols in detail. Note that the criteria by which systems are deemed acceptable are decided by consensus of a committee. Successful performance does not necessarily mean extinguishment of the fire. For example, the IMO tests for accommodation spaces and public spaces on ships require only that the fire be controlled for a period of ten minutes. At the end of ten minutes, the fire is manually extinguished, and a damage assessment is made. Fire extent and damage to the test materials must be within certain limits. During that ten minutes, the fire continues to burn, and if the water mist system is shut off, the fire will regrow. The IMO machinery space protocol, on the other hand, does require extinguishment of all fires, including small, hidden bilge fires. To achieve extinguishment, the system designers are permitted to utilize combinations of total flooding ceiling nozzles and screening nozzles over the ventilation opening, as well as the addition of surfactants to the water supply. In some cases, separate bilge protection systems are incorporated.

Development of Fire Test Protocols

In the absence of a generalized design method based on engineering first principles, water mist systems must be "listed for specific hazards and protection objectives." It is the intent of NFPA 750 that such listings be obtained

TABLE 4-14.1 ***Fire Test Protocols for Water Mist Fire Protection Systems as of September 1998***

Agency		Water Mist Fire Tests Protocol
1	International Maritime Organization (IMO)	IMO Res. A800 (19): Revised Guidelines for Approval of Sprinkler Systems Equivalent to That Referred to in SOLAS Regulations II-2, Chapter 12[78] • Appendix 1, "Component Manufacturing Standards for Water Mist Nozzles" • Appendix 2, "Fire Test Procedures for Equivalent Sprinkler Systems in Accommodation, Public Space and Service Areas on Passenger Ships," December 1995 IMO MSC/Circular 668: Alternative Arrangements for Halon Fire Extinguishing Systems in Machinery Spaces and Pump Rooms[77] • Appendix A: "Component Manufacturing Standards of Equivalent Water-Based Fire Extinguishing Systems," 1994 • Appendix B: "Interim Test Method for Fire Testing Equivalent Water-Based Fire Extinguishing Systems for Machinery Spaces of Category A and Cargo Pump Rooms," 1994 As amended in MSC/Circ. 728: Amendments to the Test Method for Equivalent Water-Based Fire-Extinguishing Systems for Machinery Spaces of Category A and Cargo Pump-Rooms contained in MSC/Circ. 668, Annex B, June 1996
2	Factory Mutual Research Corporation (FMRC) Norwood, MA, USA	• Draft Protection Requirements for Fine Water Spray Systems for the Protection of Gas Turbines in Enclosures—Class 5560[29] • Draft Performance Requirements for Fine Water Spray Systems for the Protection of Combustion Machinery Spaces and Special Hazard Machinery Spaces—Class 5560 • Proposed Draft Performance Requirements for Fine Water Spray Systems for the Protection of Light Hazard Occupancies • Fire Performance Tests for Fine Water Spray Protection for Wet Benches, 1997
3	Underwriters Laboratories, Inc. (UL) Northbrook, IL	UL 2167, Proposed First Edition of the Standard for Water Mist Nozzles for Fire Protection Service, June 1998[79] • Machinery Spaces • Passenger Cabin Fire Tests • Passenger Cabins Greater than 12 m^2 • Public Space Fire Tests • Residential Area Fire Tests • Light Hazard Area Fire Tests • Ordinary Hazard I and II Tests • Nozzle Construction Design, Marking, and Performance Requirements
4	Verband der Schadenversichen e.V. (VDS) Germany	VDS 2498 Guidelines for Water Extinguishing Systems Requirements and Test Methods for Fine Spray Nozzles, August 1996[80] • Fine Spray Nozzles for Cable Conduits • Fine Spray Nozzles for Engine Test Cell

through full-scale fire tests and system component evaluations conducted by internationally recognized laboratories to demonstrate that reasonable performance objectives can be met. New potential applications of water mist arise continuously, for which ad hoc test procedures must be developed. With respect to fire test protocols, the intent of NFPA 750[2] is as follows:

- The test protocols shall be based on a fire protection engineering evaluation of the fire hazard, the compartment conditions, and the performance objectives for the system.
- The test protocols shall be developed, carried out, and interpreted by recognized fire testing laboratories.

The design of a meaningful fire test scenario includes the following steps:

1. Simulate the compartment conditions and fuel geometry (volume, height, width, and elevation of ventilation and exhaust openings).
2. Be able to vary the ventilation conditions to determine sensitivity of the performance to ventilation factors.
3. Select the fuel arrangement that simulates the expected combustibility and fire growth rate. This may require conducting a review of the end-users' facilities to establish a realistic fuel geometry. Obtain enough fuel packages to do repeatable tests.
4. Establish meaningful and measurable performance objectives, neither too high nor too low.
5. Develop an experiment plan to test the range of parameters for the water mist system design: nozzle selection, cone angle, K-factor, operating pressure (hence, flow rate), nozzle locations, spacing, and orientation.

Test protocols developed in the above manner may eventually be recognized as the basis of a listing. The full listing process culminates in the following outputs:

- A report showing the results of the fire tests
- A report summarizing the results of the component evaluations. This is intended to verify the functional-

ity, durability, corrosion, and environmental resistance of the key components
- A design and installation manual explaining the correct application, installation, and maintenance of the specific equipment. The nozzle characteristics; spacing between nozzles, and maximum distances from walls, ceilings, or obstructions; minimum operating pressures; and water supply requirements are all documented in the manual.

Engineering Details of Water Mist Systems

Design of water mist systems at this stage requires validation through full-scale fire testing. This may be viewed as a negative factor, in that it increases the cost of development of new markets. On the other hand, it creates an opportunity to depart from the constraints of traditional fire protection system design, given that system performance can be validated through testing. If you have to test, why not experiment a little? New ideas have emerged in setting performance objectives for a wide range of fire suppression challenges. There has been much innovation in equipment design. We now have cycled discharge, compressed gas storage, positive displacement high-pressure pumps, and the use of new materials approaches to fire detection and release. New types of nozzles require new types of distribution systems, and new approaches to commissioning and acceptance testing. This section describes a few of the engineering concepts that have been introduced as a result of water mist system research and development.

Types of Water Mist Systems

There are several engineering criteria by which to distinguish one type of a water mist system from another. NFPA 750 refers to three types by *application:* total compartment application, local application, and zoned application systems. Whether a system is a pre-engineered or an engineered system is also discussed under this heading. System types can also be distinguished based on the *method of spray generation:* single-fluid or twin-fluid nozzles. A third division into type is based on the *pressure regime:* low-, intermediate-, or high-pressure systems. This latter division also covers both constant-pressure systems supplied by a pumped source, and declining-pressure systems driven by compressed gas. The following discusses the important engineering features associated with each type of system.

Application systems: As has been noted, water mist systems are most efficient in enclosed compartments where the confinement of water vapor and the normal oxygen depletion caused by the fire can contribute to the extinguishment of even-shielded fires. If the compartment is very large relative to the size of the fire, these enclosure effects are diminished, and more attention must be paid to projecting water mist to the seat of the fire. Thus the approach to setting design criteria will differ depending on the nature of the compartment.

Total compartment application (TCA) systems consist of open nozzles distributed throughout the compartment according to the manufacturer's spacing rules. Open nozzles are used so that water is discharged from all nozzles upon opening of a control valve. TCA systems benefit from enclosure effects (capture of heat, confinement of water vapor, and recirculation of oxygen-depleted gases). TCA systems should not be referred to as "total flooding" systems, because water mist does not extinguish fire in the same manner as a gaseous total flooding agent.[52] Unlike a total flooding gaseous system, it is not enough to inject a fixed quantity of mist into a compartment, close the door, and expect the fire to go out. The amount of time needed to extinguish a fire varies according to the compartment size and size of fire. Therefore, water mist must be injected continuously for a sufficient length of time to bring about control. Gaseous agents require 100 percent integrity of the compartment boundaries to contain the suppression agent, whereas total compartment water mist systems may be effective with fairly large openings in the compartment.[61]

When activated, water is discharged from all nozzles in the manner of a deluge system. It is intended that TCA water mist systems be activated automatically by a separate fire detection and release system. The detection of fire is relatively straightforward since any fire signature picked up anywhere in the compartment initiates release of a single valve. In that case, the fire may be relatively small at the time of activation but may continue to grow for a short period before enclosure effects begin to come into play. In some marine or military applications, however, manual activation of the system is permitted. Some caution should be observed in the design of a system intended to be manually released. If there is a long delay in activation, the combustion gas layer in the compartment may become quite hot and deep. The empty piping and nozzles may become so hot that water will boil explosively, rupturing the piping system. If water reaches the nozzles, the sudden introduction of water mist into the hot gas layer may result in a very rapid cooling, which creates a strong negative pressure in the compartment. During experimental work at the National Fire Laboratories at National Research Council Canada, one wall of a 60-m^3 test enclosure deflected inward and ripped open along the ceiling line when water mist was injected after a 90-s preburn of a 750-kW pan fire. Similar negative pressure spikes were described in Reference 39. The potential for doing damage to the structure upon activation of the mist system in a tight enclosure is not generally noted as a concern in most test protocols, but perhaps it ought to be.

One major drawback to TCA systems is that they demand a lot of water. Many nozzles discharging a small amount of water still adds up to a lot of water! As compartment size increases, there will be a point at which it is unreasonable or unaffordable to discharge water throughout the entire compartment for a fire in a limited area of the compartment. The removal of runoff from a total compartment application system should also be considered as part of the design of the system.

Total compartment systems may be designed for a range of objectives. The IMO machinery space systems

are intended to completely extinguish the fire in a specified period of time. The nozzle spacing and flow rates are designed to meet that challenging objective. On the other extreme, TCA systems have been installed in Norwegian historic wood stave churches to achieve flashover suppression[37,83,84] at much lower flow rates. For flashover supression a fine mist is injected into the upper portion of the compartment to cool the fire gases and reduce thermal feedback to the objects in the compartment, which prevents flashover from occurring. The amount of water that strikes the painted icons on the walls is minimized. Extinguishment of the source fire is achieved by installing nozzles at floor level that discharge water spray at a much higher rate than the ceiling nozzles, without damaging the treasured wall paintings. The lower nozzles are local application nozzles that work in concert with the total compartment system.

Local application (LA) systems are arranged to discharge directly on an object or hazard in an enclosed, partially enclosed, or open outdoor area. Since there may be little confinement of heat, water vapor, or vitiated gases, extinguishment will depend almost entirely on gas phase cooling or wetting of the fuel. To achieve extinguishment will require direct projection of mist to all areas in which fire can persist. Local application systems do not necessarily have to achieve extinguishment. As with the TCA system, it may be sufficient to use the local application system as a screen to block radiant heat from igniting or damaging equipment. Local application systems are considered as necessary subparts of some machinery room systems on ships and in industrial process buildings. Although there must be a TCA system of nozzles installed, the compartment ceiling may be so high that specific equipment must be surrounded with local application mist nozzles to ensure control. Thus a local application system may be installed around specific hazards such as diesel engines, flammable liquid or vapor compressors, or large turbines in an open floor area.

Local application water mist systems may be considered for industrial food processing burners, deep-fat fryers, outdoor transformers, flammable liquid storage racks, and a host of special equipment. As with all water mist systems, NFPA 750 intends that engineering design of local application systems be based on fire testing. There is an FMRC test protocol for a water mist local application system designed for wet benches in clean rooms. VDS in Germany has test protocols for local application systems for engine test cells and electric cable tunnels (see Table 4-14.1). The IMO committees have proposed test protocols for local application system nozzles for marine machinery spaces. One proposed protocol is to mount a single nozzle above a small liquid fuel pan fire, and measure how far to one side it can be moved before it fails to extinguish the fire. This distance is taken to represent one-half the required nozzle spacing. Another proposed test protocol calls for constructing a machinery room mockup with a three-dimensional grid of nozzles surrounding the object. The petroleum industry has examined the use of water mist nozzles around outdoor pumping equipment. The distance of nozzles from the object, spacing between nozzles, height of nozzles above the object, flow rates, and cone angles all must be selected on the basis of ability to meet the test performance criteria. Criteria for judging the performance of the systems must be based on analysis of the specific needs of the application.

As discussed for the total compartment applications, choice of fire detection and release strategy for local application systems is an important part of the design of the system. Some are intended to be manually released, whereas others incorporate special detection systems customized to the application. The detection system, release, and delivery equipment must be carefully matched to the conditions dictated by the hazard.

Zoned application (ZA) systems are designed to protect hazards in a portion of an enclosure, negating the need to fully deluge the entire compartment. The usual incentive for zoning a system is to reduce the overall water flow requirement to a quarter or third of that required by a total compartment application system. The method of extinguishment may be as per a local application system, although enclosure effects may also be contributors. Design of the detection and release system is of critical importance in developing a ZA system. The designer must determine how small to make the zones, how to match the size of the detection zone to the size of the hydraulic system zone, and how many zones must activate to cover the worst-case scenario. A water mist system consisting of individually thermally activated nozzles (as for the marine sprinkler systems) is in essence a zoned application system, in which each nozzle is a combined detector and control valve.

In a proposed water mist system for a 9-km cable tunnel in Auckland, New Zealand, fire testing had established nozzle spacing, positioning, and flow rate.[81] A total compartment application was out of the question. It would not be possible to activate all open nozzles along the 9-km tunnel—the resulting water demand would require very large feed mains and intermediate booster pumps. Also, the cost of pumping all that water out of the tunnel after discharge would be considerable. The use of individually thermally activated nozzles to limit the number of nozzles activated would be defeated by the strong ventilation air movement of 5 m/s, which would carry heat along the tunnel away from the nozzles closest to the fire. The alternative was to release the system in zones that would extend upstream and downstream of the fire source. The difficulty lay in selecting a means of detecting a fire and pinpointing its source so that the nozzles in the immediate vicinity of the fire could be activated.

Often limitations in the detection technology in adverse environments dictate the minimum size of a zone. For the New Zealand tunnel project, the turbulence under normal ventilation mode made smoke and heat detection challenging. Thought must be put into how big a fire is needed to generate sufficient smoke or heat to be detectable, given the turbulent mixing rate. The detectable fire should not be so large that unacceptable fire damage will have already occurred before detection.

As with local application systems, and perhaps more so, the proper integration of the detection system and the hydraulic release system is critical to the performance of ZA water mist systems. The detection system and the hydraulic systems must be tested together. The penalty of failing to accurately locate the fire source and its extent is

that valuable water and pumping energy may be wasted on noninvolved parts of the facility.

It is this author's opinion that the engineering challenges involved in zoning water mist systems present a great opportunity for future innovation and invention. The detection problems require full understanding of the fire dynamics involved. There is great potential for invention in developing piping and valving strategies that are flexible and robust. Increasing the atomization efficiency of nozzles to make smaller drop sizes was only the first stage of the development of water mist technology. The next step is to develop the sophisticated but reliable detection and delivery systems needed to adapt these systems to difficult settings.

Pre-engineered versus engineered systems: A pre-engineered water mist system is one that has been developed for a hazard of a limited size and consistent features defining the compartment. For example, a water mist system may be tested in a mock-up of a turbine or diesel engine enclosure, with specific ceiling height, obstructions, ventilation openings, and fire scenarios. The number of nozzles, their locations, the amount of stored water required for an adequate duration of flow, and the diameters and maximum lengths of pipe or tubing are all pre-engineered. The installer need only stay within the limits stated for pipe diameter and length of run to install the system properly. No engineering calculations are required to ensure that nozzle pressures are adequate and that flow rates and water storage are sufficient for the hazard. Because the compartment conditions are well defined by the test protocol, the detection time and the size of fire upon detection will be predictable for a pre-engineered system. Engineered systems, on the other hand, must adapt basic nozzle spacing rules to a variety of compartments and fire hazards, and then perform the hydraulic calculations to confirm that minimum nozzle pressures and system flow rates are achieved. Not only must the hydraulic performance be calculated, but the implications of increased detection/activation time must also be evaluated.

Where a field application is close to the conditions of the test protocol to which a water mist system was validated, installation of a pre-engineered system is appropriate. In many cases, however, the situation in the field represents the same general fire hazard, but the compartment may be much larger or more cluttered than the test protocol anticipated. Although NFPA 750[2] discourages extrapolation beyond the listing, the reality is that the designer is under pressure to extrapolate from the pre-engineered system to fit the larger application. In some cases that may involve increasing the number of nozzles while maintaining the nozzle spacing, increasing pipe or tubing diameters, and increasing the water storage. Any extrapolation converts the design to an engineered system. It is important that the designer have a broad understanding of the fire dynamics involved and the fire protection engineering issues to be addressed.

Methods of spray generation: Water mist system equipment manufacturers have staked out their preferred means of mist generation. There are numerous ways to generate atomized sprays.[35] Research in the spray and atomization literature uncovers exotic technologies such as electrostatic sprays, nebulizers, and ultrasonic devices. There are techniques that are suitable for atomization in the milligram range, with projection distances measured in millimeters. Spray generation methods more suitable for water mist fire suppression systems must generate mist in industrial quantities. Suitable nozzle types include multi-orifice pressure jet nozzles, impingement nozzles, and twin-fluid nozzles. Mass flow rates are typically measured in the range of 5 to 80 l/min. Cone diameters and projection distances are typically measured in meters. The atomization process must be sustained for tens of minutes in most cases, although explosion suppression systems may complete their discharge in a time scale matched to the velocity of the flame front—several hundred milliseconds. This section will highlight some of the engineering features of importance associated with different methods of generating water mist.

Twin-fluid versus single-fluid nozzles: Twin-fluid nozzles use two streams of fluid, one of water and one of compressed gas, which increases the energy available for the atomizing process. The compressed gas, which is referred to in NFPA 750[1,2] as the "atomizing medium," is injected into the water stream at the nozzle. This discussion regards twin-fluid nozzles as having separate piping for water and compressed gas up to the nozzle. The air-to-liquid ratio (ALR) (ratio of the mass flow rate of air to the mass flow rate of water) at each nozzle can be held approximately constant throughout the discharge. By this definition, systems that inject compressed gas into a single conduit for the supply of water are not twin-fluid systems. Twin-fluid nozzles are used in the HVAC industry for humidity control, and in many other industrial applications for a variety of reasons. They provide a high degree of adjustability between the balance of liquid and gaseous streams—hence they can be easily tuned to maximize the quality of the spray at low water pressures. By utilizing the energy stored in the compressed gas, there is no need to boost water pressure to push water through small-diameter orifices or increase ejection velocity. Hence, twin-fluid nozzles have larger orifices that are less vulnerable to plugging than some single-fluid systems. On the negative side, twin-fluid nozzle systems require storage and delivery of media with distinctly different engineering characteristics. Calculations must be done for both compressible and incompressible fluids in the distribution system. A suggested approach to balancing the distribution of atomizing medium with the water flow is provided in Reference 89.

Single-fluid nozzles use water only. The water is ejected through one or more orifices and either disintegrates into mist due to velocity differences between the water jet and the surrounding air (pressure jet nozzles), or disintegrates into small particles on impact against an impingement surface (impingement nozzles). A more in-depth discussion of how fine water sprays are formed can be found in References 35 and 89. Single-fluid nozzles are more widely used for water mist systems than twin-fluid nozzles.

Manufacturers of nozzles for industrial applications have catalogs filled with different nozzle designs, delivery rates, and cone shapes. They have been manufacturing a

wide range of nozzles for many years. It is surprising therefore how much money and effort has gone into the custom design of water mist nozzles for water mist systems by fire protection specialists. Without exception, the water mist system manufacturers have developed their preferred nozzle design through extensive in-house research and development. Some off-the-shelf commercial nozzles have been adapted for water mist systems, albeit with customized selection of individual orifice sizes.[23,29] The ability to add a thermal release device to a water mist nozzle allows the manufacturer to market its water mist technology in "sprinkler equivalent" systems as approved by IMO test protocols.

Mist generation by flashing of superheated water: Evidence that water mist with sufficiently small drop sizes may quell a dust explosion is found in work conducted at the Irish agricultural research facility involving dusts of dried milk products.[90,91,92] The mist-generating method involves the flashing of superheated water released from a self-pressurized container.[93] Water is superheated to 175°C in a closed container up to 70 l (18.5 gal) in volume. As steam tables indicate, this puts the closed container at a pressure of approximately 10 bar (145 psig). When released to atmospheric pressure, a percentage of the water flashes directly to vapor phase, then condenses into fog-sized particles (<20 μm) as the cloud cools. There is a dynamic release of energy as the liquid flashes, which shatters the remainder of the mass of water into relatively fine spray (D_v 0.90, ~300 μm) (i.e., 90 percent of the volume of the spray as contained in drops less than 300 μm in diameter).[93] The energy exchange also results in intense cooling of the spray, so that 30 cm away from the discharge orifice, the mist temperature may be 35°C or less.[91]

The flashing process does not require a nozzle—simply an open orifice, and it results in a rapid distribution of "mist plus fog" throughout the protected space. The condensed fog is an order of magnitude finer than can be achieved by mechanical generation of spray—a relatively large mass fraction is distributed uniformly throughout the space. Full-scale fire suppression tests carried out by Mawhinney and Taber[91] indicate that the ultrafine mist was not more effective than other mists at extinguishing pool fires in enclosures. It was suggested, however, that its success in dust explosion mitigation may be due to the high mass fraction of very small (~20 μm), closely spaced droplets, suggested by Zalosh[34] to be a prerequisite for explosion mitigation with water mist. Further experimental work is required to validate its potential for vapor/air explosion mitigation.[92]

Pressure regimes: NFPA 750 distinguishes between low-, intermediate-, and high-pressure systems. Low-pressure systems operate at pressures below 12 bar (about 175 psig). In that range, standard sprinkler system installation practices can be followed, and conventional centrifugal fire pumps can be utilized to achieve system pressures. Intermediate-pressure systems have operating pressures that lie between 12 and 34 bar (175 and 500 psig). Pipe fittings and pump selection must be upgraded to handle this above-average pressure range, but in general piping practices are not much different from those of low-pressure systems. High-pressure systems operate above 34 bar (500 psig). Selection of pipe or tubing, installation practices, and the engineering of high-pressure pump systems are quite different from traditional fire protection engineering practices. Twin-fluid systems operate in the low-pressure range, but they require familiarity with high-pressure gas cylinders, gas metering valves, and compressible fluid flow calculations. This section provides information on engineering factors encountered in these different pressure regimes.

There is considerable discussion about whether high-pressure water mist systems are better than low-pressure water mist systems, or vice versa. Proponents of one technology or the other will refer to test results that showed that their system performed better in a given scenario. If the nozzles are not situated or oriented optimally relative to the fire, they won't perform as well as ones that are better oriented, regardless of the pressure regime. It may be that the test results being referenced were optimized for the one pressure regime but not the other. Also, it may be that the difficulty of integrating the water mist systems with existing infrastructure in a facility makes it impractical to choose one pressure regime over the other. It is this author's experience that acceptable fire suppression can be achieved with both high- and low-pressure systems. The engineering and economic issues related to the different technologies will dictate which is the most cost-effective choice for a given application.

On the marketing end, water mist equipment manufacturers are usually committed to a particular technology, hence pressure regime. A manufacturer tooled to produce high-pressure equipment is not going to want to sell low-pressure nozzles, and vice versa. Also, there are engineering aspects of twin-fluid and high-pressure technologies that require specialist expertise with gas cylinders and releasing valves, or high-pressure pumps. It would be challenging for one manufacturer to cover the full range of expertise equally well.

Low- and intermediate-pressure systems: Standard sprinklers are capable of working at end nozzle pressures as low as 0.5 bar (7 psig). It is recognized that the piping system operating pressure will be higher than the minimum nozzle pressure. Therefore, even in sprinkler systems, the operating pressure of the system will typically be between 5 bar to 7 bar, sometimes higher. Pipe fittings will be rated for 8 bar at least, and in many cases 12 bar as standard practice. Some low-pressure water mist nozzles require nozzle pressures of 8 to 12 bar to achieve the desired drop size distribution. With 8- or 12-bar end pressures, the system operating pressure will generally be above 12 bar, that is, in the intermediate-pressure range. Pipe and fittings will have to be rated for the 21-bar range. Many of the low-pressure water mist nozzle manufacturers are edging toward 12- to 20-bar system operating pressures to achieve desired performance. Therefore, not many water mist systems are truly low-pressure systems.

So long as the engineer selects pipe, tubing, valves, and pumps rated for the operating pressure, the design procedures for low- and intermediate-pressure water mist systems do not differ much from standard sprinkler systems.

Some potential water mist system applications cannot support the cost of pumps to boost water pressure out of the low-pressure regime. Examples include heritage buildings, some libraries, and archival storage applications, which often have limited budgets for fire protection. The major advantage that water mist provides over standard sprinklers is that it reduces the water application rate. The end user will be willing to pay additional costs to increase system pressure only if that advantage is valued highly enough. One manufacturer is reported to have conducted tests with nozzle pressure reduced to less than 7 bar for an archival storage facility. However, considering that standard sprinklers can operate comfortably at 1 bar, a minimum nozzle pressure of 7 bar may still mean the existing water supply has to be augmented to meet the water mist system pressure requirement. Thus, even for the low-pressure water mist systems, the cost of increasing system pressure continues to be an economic disadvantage when compared to standard sprinklers.

Low- or intermediate-pressure systems may be connected to a constant pressure water supply, or they may be gas driven, working from a stored volume of water being expelled by a limited supply of compressed gas. The latter are declining pressure systems: the pressure drops continuously throughout the discharge period. The twin-fluid systems also work on a declining pressure principle, unless they are connected to plant air or plant water sources.

The possibility of accommodating larger friction losses in the piping system than normal for sprinkler piping is an incentive to go to higher system operating pressures. If the water mist nozzles use less flow than standard sprinklers, and there is pumping capacity to compensate for relatively high system friction losses, the designer may be able to use smaller diameter pipe or tube in the distribution system than is found in the competing sprinkler system. The designer may be able to extract a compensating advantage from the necessity to operate at a higher pressure range than sprinkler systems. It is not uncommon for a high-pressure system to incorporate head losses of 20 bar between the pump discharge header and the most remote nozzles, without compromising the effectiveness of the system. Generally, the potential to significantly reduce pipe sizes requires a transition into the high-pressure regime.

High-Pressure Systems: NFPA 750 defines high-pressure water mist systems as those that operate above 34 bar. They are installed extensively on passenger cruise ships as equivalents to sprinkler systems. They are also widely used in marine and industrial machinery and equipment spaces. There are two basic types—gas-driven pre-engineered systems for moderate-size compartments, and pump-driven engineered systems for large machinery spaces. Gas-driven systems operate over a declining pressure range, from approximately 140 bar at first release to 30 to 50 bar at the end of a 10-min discharge period. They have FMRC approvals for turbine enclosures, machinery spaces, and special hazard spaces. There is also a gas-driven pump that can extend the operation of a gas-driven high-pressure system for up to 1 hr, without the need for electric-motor or engine-driven pumps.[94]

The design and installation of high-pressure water mist systems involve practices for pipe and tubing systems that until recently were not used in the fire protection field. Stainless steel tubing is used in conformance with the ASME/ANSI B31.1, *Power Piping Code.*[95] Good practices for tube bending, cleaning, and swabbing; supports; and make-up of compression fittings must be applied.

High-pressure water mist systems use motor- or engine-driven, positive displacement (PD) pumps to achieve the high system pressures. This is in contrast to the centrifugal fire pumps traditionally used in fire protection systems. Unlike centrifugal pumps, PD pumps put out a constant Q at a given rotational speed. Fire suppression systems generally have a variable demand, depending on the number of nozzles or groups of nozzles that open. Rather than use one pump driven by one motor for the full range of flows in a facility, as is possible with a centrifugal pump, PD pump systems divide the total load among a number of pumps that can be brought on line as needed to handle increasing load. The total power output of a single motor can be distributed among several small pumps. Then the discharge from each pump can be further split using pressure unloader valves, which divert all or some of the flow to a recirculation line if the pressure rises to its pressure setting. Figure 4-14.7 shows an arrangement in which four motors drive a total of eight pumps. Each motor has enough power to deliver the discharge from both pumps at a low pressure (75 bar), or the discharge from just one of the two pumps at twice that pressure (150 bar). The power requirement of the motor to achieve a particular flow and pressure is calculated as shown in Equation 3.

$$P = Q \times H/600 \times E \tag{3}$$

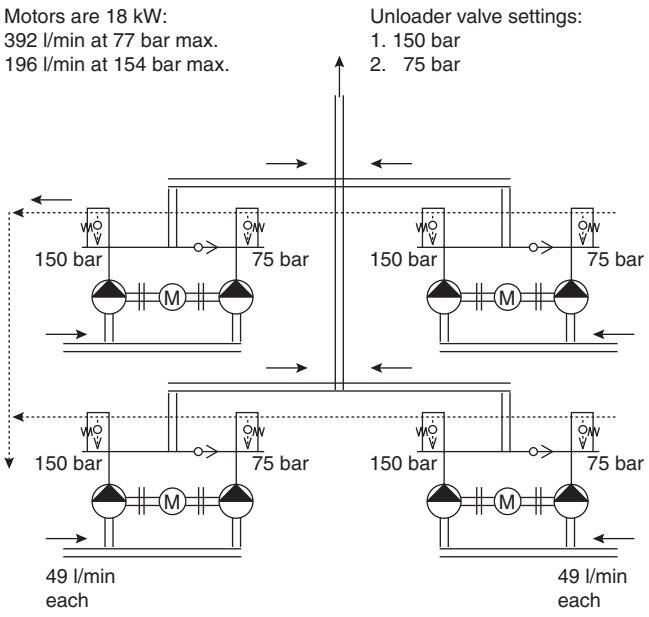

Figure 4-14.7. ***Arrangement of eight positive displacement pumps driven by four electric motors.***

If the power of the motor is known, Equation 4 calculates the maximum possible pressure that the motor could deliver. Equation 4 is used to plot the power limit curve for a given motor-pump combination, as shown in Figure 4-14.8.

$$H = (P \times 600 \times E)/Q \quad (4)$$

where

P = power (kW)

Q = pump discharge (l/min)

H = pump discharge head (bar)

E = combined efficiency of the motor and pumps (ep × em)

Figure 4-14.8 is a graphical means of illustrating the performance of a PD pump arrangement. Each pump motor is set up to drive two pumps. Above the pressure of the lowest unloader setting, the high-pressure side holds the check valve on the low-pressure side closed. The system discharges only the flow from one of the two pumps. The discharge of the second pump is "unloaded" into the recirculation line, and therefore does not draw upon the power resource of the motor. The entire power output can go to increasing the pressure on the pump set for the highest pressure. By distributing the hydraulic demand over several motors, and by using numerous pumps with high and low unloader valve settings, the positive displacement pumping system automatically responds to a variable system demand.

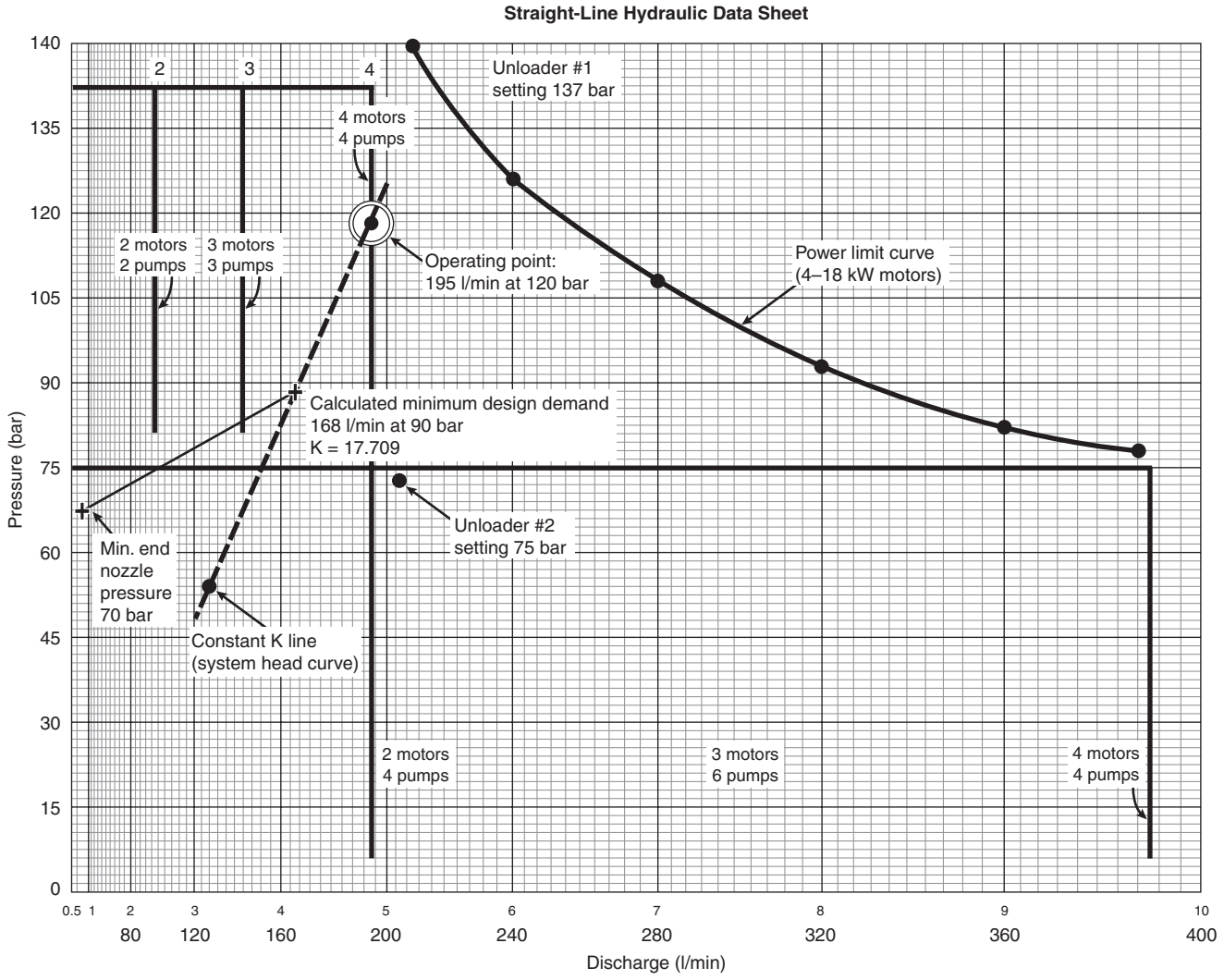

Figure 4-14.8. ***Diagram to predict the operating point of a high-pressure water mist system with multiple positive displacement pumps.***

Figure 4-14.8 illustrates the relationship between the supply provided by the pump(s) and the theoretical system demand as obtained by hydraulic calculations for a hypothetical installation. The calculated minimum demand is not the operating point for the given supply, however. An estimate of the operating point is obtained by extending the constant K line for the calculated system until it intersects the pump supply curve (a vertical line in this case). The K factor for the piping system determines the operating point for the pumping system.

Acceptance Testing of Water Mist Systems

Acceptance testing of twin fluid, declining pressure and pumped high-pressure water mist systems involves engineering analysis that is not typical of traditional sprinkler systems. NFPA 750 recommends that a full system discharge test be conducted if at all possible. This is particularly important for gas-driven, decaying pressure systems. The discharge test is intended to confirm that the operating point (pressure and flow) of the system meets the minimum requirement, and for gas-driven systems to ensure that the supplies of water and compressed gas are sufficient for the discharge duration. Without taking measurements, it is difficult to judge by visual indicators alone whether a system is operating properly.

Visual inspection of the mist conditions during a discharge can confirm only basic aspects of the system performance, such as that valves opened, pipes or nozzles were not plugged, and mist was produced. One can observe that water flows from individual nozzles and that the spray distribution looks acceptable. Only by measuring pressures, however, can one be sure that the system is performing as required, and that the stored quantities of compressed gas and water are adequate.

Figures 4-14.9(a) and 4-14.9(b) are plots of air and water pressure taken during the discharge of a twin fluid system involving cycled flow at the hydraulically most remote nozzle, and at a nozzle very close to the supply tank. The design called for six discharge cycles of 50 s each, with 40-s intervals between them. Air and water pressures at the nozzles should stay between 82 and 66 psig. The timing program in the control panel worked well. From visual and audio observations in the compartment, six discharges occurred. From the pressure traces, however, it was evident that the sixth discharge did not achieve the minimum nozzle pressures, particularly at the most remote nozzle. For the nozzle closest to the supply tank [Figure 4-14.9(b)], the minimum operating air and water pressures were achieved in the fifth, but not the sixth discharge. The differences between pressures at the closest and most remote nozzles indicate that the nozzles closest to the source were discharging considerably more air and water than the remote nozzles.

The recorded pressures of the discharge tests demonstrated that the system exhausted the supply of atomizing medium before the end of the fifth discharge, although not the supply of stored water. Additional cylinders of compressed gas were required to extend the operation for six discharges. A full understanding of the performance of the system and remedies for shortfalls could not have been identified from a partial trip test.

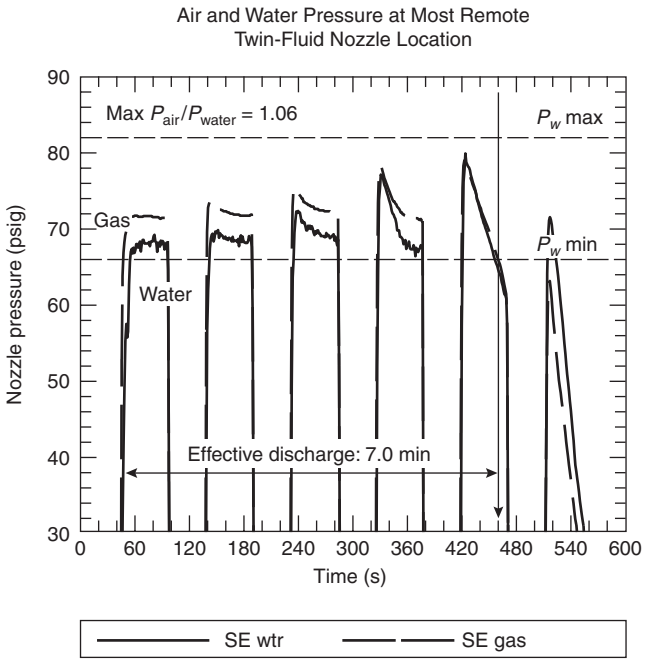

Figure 4-14.9(a). ***Pressure versus time plot of compressed gas and water pressures at the most remote twin-fluid nozzle location. Acceptable operating range is between 66 and 82 psig, with compressed gas pressure required to be approximately the same as the water pressure (P_a/P_w = 1.0).***

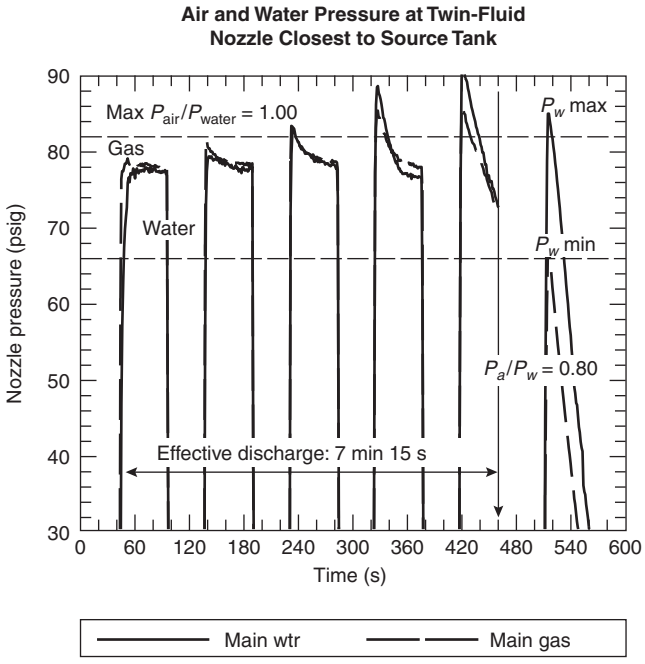

Figure 4-14.9(b). ***Compressed gas and water pressures measured at a nozzle close to the source tank. Acceptable operating range is between 66 and 82 psig, with compressed gas pressure required to be approximately the same as the water pressure (P_a/P_w = 1.0).***

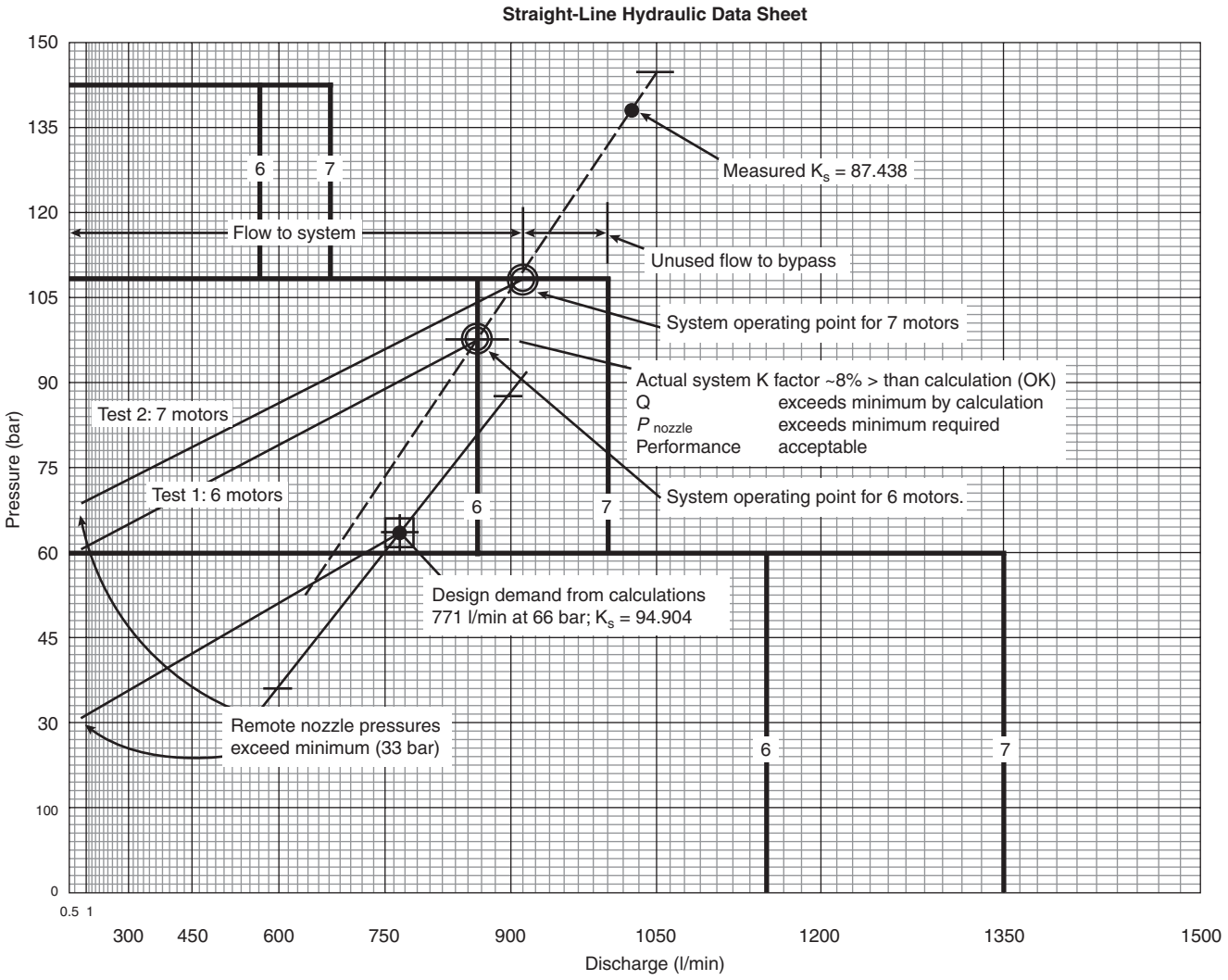

Figure 4-14.10. ***Example of acceptance test results for a high-pressure pumped water mist system.***

Figure 4-14.10 shows data collected during a discharge test of a pumped high-pressure water mist system. The data recorded were the pressure at the pump discharge header, the pressure at the most remote nozzle(s), and confirmation on the number of motors operating. Working on the hydraulic straight-line graph paper, on which the supply curves for different numbers of motors were predrawn, the discharge pressure line was marked. Since it was known that 6 motors were operating, and the pressure reading was between the lowest and highest unloader settings, the system operating point had to lie on the vertical Q line for 6 motors operating, as shown. That operating point defines a K factor for the real system. To judge whether the operating point was "acceptable" or not, it was compared to the theoretical minimum flow condition obtained from hydraulic calculations. Since the calculated demand point was reasonably close to the constant K line determined by the actual operating point, one could conclude (a) that the system was operating above its minimum condition, and (b) that the hydraulic calculations were accurate and reflected the "as-built" piping system.

Conclusions

This chapter has reviewed some of the history behind the evolution of water mist fire suppression systems development over the last decade. The significant studies on how and why finely divided water sprays improved the efficiency of extinguishment had been done years before. Spurred on by the need to find halon alternatives and to develop efficient, lightweight suppression systems for ships, the 1990s saw some new ground broken in fire suppression systems design. Water mist emerged as a viable alternative for a number of halon applications, and the improved efficiency in use of water promised major reductions in the weight and volume of system hardware.

Water mist systems require that full-scale fire suppression testing be done to establish design parameters

for different fire scenarios. Based on the traditional approach to sprinkler systems design, the expectation was that testing would eventually reveal a range of optimum application rates that could be applied to all water mist systems. Interestingly, it was discovered that performance in standard tests differed for different manufacturers' equipment. One water mist system could meet suppression objectives at one flux density (application rate), but a second manufacturer, using a different type of nozzle, would succeed at a lower density. The specific spray characteristics of different nozzles or spray-generation methods have a bearing on the performance. Unfortunately, we cannot (yet) predict exactly what difference a particular change in spray characteristics will make to the suppression outcome. At this stage, the scientific challenge is to at least measure the differences in spray characteristics, in the hope that we will begin to understand the relationships. Thus, there is a need for more theoretical work on the dynamics of the interaction of water sprays and fires in real compartments.

Notwithstanding the limitations in our understanding, water mist system technology has advanced from a promising curiosity in 1990 to a major fire protection market in 2000. The strongest market exists in the international marine sector, where water mist is competitive with the only alternative—marine sprinkler systems. Ship owners are satisfied with the IMO test protocols as an approval base. Penetration of land-based markets has been much slower, particularly in North America, where potential end-users tend to require third-party approvals or listings, such as FMRC or UL, before they will accept the system. The absence of a sufficiently broad base of completed approvals is a major barrier to land-based application of water mist systems in the United States.

There are increasing niche markets for water mist systems in certain land-based sectors, most notably for heavy industry machinery space modules, turbine enclosures, metro-station mechanical rooms, and wet benches in clean rooms. Water mist is viewed as a halon alternative for those applications. Interest in using water mist in place of standard sprinklers in land-based applications is also growing. For example, work began in early 2000 on installation of a water mist system for a large hotel in London. The water mist system is an alternative to standard sprinklers and is reported to be competitive with sprinklers on a cost basis for this application. The water mist system offers the advantages of smaller diameter pipe than in sprinklers (permitting easier retrofit in a heritage building), reduced water demand, plus proof of performance through recent full-scale fire testing. Thus we see the beginnings of an acceleration in the transfer from the marine sector to land-based applications. It is only logical that the burst of innovation in systems design that has accompanied the growth of water mist systems will have benefits for more traditional water-based systems in the next decade.

References Cited

1. NFPA 750, *Standard on Water Mist Fire Suppression Systems,* NFPA, Quincy, MA, 1996 edition.
2. NFPA 750, *Standard on Water Mist Fire Systems,* NFPA, Quincy, MA, 2000 edition.
3. M.M. Braidech, J.A. Neale, A.F. Matson, and, R.E. Dufour, "The Mechanism of Extinguishment of Fire by Finely Divided Water," National Board of Fire Underwriters, New York, p. 73 (1955).
4. D.J. Rasbash, Z.W. Rogowski, and G.W.V. Stark, "Mechanisms of Extinction of Liquid Fuels with Water Sprays," Combustion and Flame, 4, pp. 223–234 (1960).
5. NFPA 15, *Standard for Water Spray Fixed Systems for Fire Protection,* NFPA, Quincy, MA, 1996 edition.
6. NFPA 13, *Standard for the Installation of Sprinkler System,* NFPA, Quincy, MA, 1999 edition.
7. Civil Aviation Authority, "International Cabin Water Spray Research Management Group: Conclusions of Research Programme," *CAA Paper 93012* (1993).
8. R.G. Hill, T.R. Marker, and C.P. Sarkos, "Evaluation and Optimization of an On-Board Water Spray Fire Suppression System in Aircraft," in *Proceedings of Water Mist Fire Suppression Workshop,* NIST, Gaithersburg, MD (1993).
9. The Montreal Protocol on Substances that Deplete the Ozone Layer—Final Act, 1984.
10. D.S. Aldenwinckle and D. Prentice, *The Safety Record and Risk Analysis of Ro-ro Passenger Ferries,* Lloyd's Register Safety Technology Department (1992).
11. Technical Research Centre of Finland (VTT), "Evaluating the Suppression Efficiency of the Hi-Fog Fire Protection System in Accommodation Areas on Passenger Ships According to IMO Res.A.800 (19)," *VTT Test Report No. RTE10320/98,* Espoo, Finland (1998).
12. M. Arvidson, S. Isaksson, and M. Tuomisaari, "Recommended Acceptance Criteria for Sprinkler Systems Equivalent to SOLAS II-2/12," *SP Report 1995:20,* Swedish National Testing and Research Institute, Boras, Sweden (1995).
13. M. Arvidson and S. Isaksson, "Equivalency Sprinkler Fire Tests," *SP Report 1995:19,* Swedish National Testing and Research Institute, Boras, Sweden (1995).
14. J.R. Mawhinney, B.Z. Dlugogorski, A.K. Kim, "A Closer Look at the Extinguishing Properties of Water Mist," in *Proceedings: International Association for Fire Safety Science (IAFSS) Conference,* Ottawa, Ontario (1994).
15. D. Drysdale, *Fire Dynamics,* 2nd edition, John Wiley & Sons, New York (1999).
16. S.P. Fuss, D.J. Dye, B.A. Williams, and J.W. Fleming, "Inhibition of Premixed Methane Air Flames by Mists of Water and Aqueous Sodium Hydroxide," *Halon Options Technical Working Conference,* Albuquerque, NM (2000).
17. E.J.P. Zegers, B.A. Williams, R.S. Sheinson, and J.W. Fleming, "Water Mist Suppression of Methane/Air and Propane/Air Counterflow Flames," *Halon Options Technical Working Conference,* Albuquerque, NM (2000).
18. R. Wighus, "Engineering Relations for Water Mist Fire Suppression Systems," in *Proceedings: Halon Alternatives Technical Working Conference,* Albuquerque, NM, p. 397 (1995).
19. G.V. Hadjisophocleous, A.K. Kim, and K. Knill, "Physical and Numerical Modeling of the Interaction between Watersprays and a Fire Plume," *8th International Symposium on Transport Phenomena in Combustion,* San Francisco, CA, pp. 1–12 (1995).
20. J.R. Mawhinney and G.V. Hadjisophocleous, "The Role of Fire Dynamics in Design of Water Mist Fire Suppression Systems," *Interflam '96,* Cambridge, UK (1996).
21. K. Prasad, C. Li, K. Kailasanath, C. Ndubizu, R. Ananth, and P. Tatem, "Numerical Modeling of Fire Suppression Using Water Mist," *NRL/MR/6410-98-8102,* Naval Research Laboratory, Washington, DC (1998).
22. P. Andersson, M. Arvidson, and G. Holmstedt, "Small Scale Experiments and Theoretical Aspects of Flame Extinguishment with Water Mist," *Report 3080,* Department of Fire Safety Engineering, Lund University, Lund, Sweden (1996).

23. G.G. Back, P.J. DiNenno, J.T. Leonard, and R.L. Darwin, "Full Scale Tests of Water Mist Fire Suppression Systems for Navy Shipboard Machinery Spaces: Part 2, Obstructed Spaces, September 1993-December 1994," *NRL/MR/6180-96-7831,* Hughes Associates, Inc. (1996).
24. G.G. Back, C.L. Beyler, P.J. DiNenno, R. Hansen, and R. Zalosh, "Full-scale Testing of Water Mist Fire Suppression Systems in Machinery Spaces," *Rpt No. CG-D-26-98,* U.S. Coast Guard, Groton, CT (1998).
25. G.G. Back, "Coast Guard Tests for Local Application Protocols," *Rpt No. CG-D-03-99,* U.S. Coast Guard, Groton, CT (1999).
26. G.G. Back III, "A Quasi-Steady State Model for Predicting Fire Suppression in Spaces Protected by Water Mist Systems," Department of Fire Protection Engineering, University of Maryland, College Park, MD (1996).
27. Z. Liu, A. Kim, and J.Z. Su, "Improvement of Efficacy of Water Mist in Fire Suppression by Cycling Discharges," *ICFRE '97,* National Institute of Standards and Technology, Gaithersburg, MD (1997).
28. L. Liu and A.K. Kim, "A Review of Water Mist Fire Suppression Systems—Fundamental Studies," *Journal of Fire Protection Engineering,* 10, 3, pp. 32–50, Bethesda, MD (2000).
29. FMRC, *Draft Protection Requirements for Fire Water Spray Systems for the Protection of Gas Turbines in Enclosures—Class 5560,* Factory Mutual Research Corporation, Norwood, MA.
30. A. Jones and G.O. Thomas, "The Action of Water Sprays on Fires and Explosions," *Process Safety Environment,* 71, 1, pp. 41–49 (1993).
31. J.R. Mawhinney and R.L. Darwin, "Protecting against Vapor Explosions with Water Mist," in *Halon Options Technical Working Conference,* Albuquerque, NM (2000).
32. J.R. Butz, P. French, and M. Plooster, "Application of Fine Water Mists to Hydrogen Delagrations," in *Halon Options Technical Working Conference Proceedings,* Albuquerque, NM, pp. 345–355 (1993).
33. C.A. Selby and B.A. Burgan, eds., *Joint Industry Project on Blast and Fire Engineering for Topside Structures, Phase 2: Final Summary Report,* The Steel Construction Institute, UK (1998).
34. R.G. Zalosh, "Water Mist for Deflagration Control," *NFPA 750 Committee on Water Mist Suppression Systems* (1994).
35. A. Lefebvre, *Atomization and Sprays,* Hemisphere Publishing Corporation, New York (1989).
36. ASTM E 799, *Standard Practice for Determining Data Criteria and Processing for Liquid Drop Size Analysis,* American Society for Testing and Materials (1992).
37. J.R. Mawhinney, P.J. DiNenno, and F.W. Williams, "Using Fine Water Mist for Flashover Suppression on Navy Ships," *Halon Alternatives Technical Working Conference,* Albuquerque, NM (1999).
38. J.R. Mawhinney, P.J. DiNenno, and F.W. Williams, "Water Mist Flashover Suppression and Boundary Cooling System for Integration with DC-ARM: Volume 1: Summary of Testing," *NRL/MR/6180—99-8400 (*1999).
39. J.R. Mawhinney, "Characteristics of Water Mists for Fire Suppression in Enclosures," *Halon Alternatives Technical Working Conference,* Albuquerque, NM (1993).
40. M. Edwards, S. Watkins, and J. Glockling, "Development of Low Pressure Fine Water Spray for the Royal Navy: Additive Concentration and Spray Fire Testing," *Halon Alternatives Technical Working Conference,* Albuquerque, NM (2000).
41. E.W. Forssell, and P.J. DiNenno, "Tests of Marioff Computer Room Fire Protection System," *Client Report,* Hughes Associates, Inc., Baltimore, MD (2000).
42. U.S. Environmental Protection Agency, "Protection of Stratospheric Ozone: Acceptable Substitutes for the Significant New Alternatives Policy (SNAP) Program," *40 CFR Part 82, U.S. Federal Register,* 60, 145, p. 38731 (1995).
43. T.A. Cortina, ed., *Water Mist Fire Suppression Systems Health Hazard Evaluation: Response to Questions Posed by the US Environmental Protection Agency,* Halon Alternative Research Corporation, Washington, DC (1995).
44. A.M. Lentati and H.K. Chelliah, "The Dynamics of Water Droplets in a Counterflow Field and Its Effect on Flame Extinction," in *1996 Proceedings of the Fall Technical Meeting: The Eastern States Section of the Combustion Institute,* Hilton Head, SC, pp. 281–284 (1996).
45. A.K. Lazzarini, R.H. Krauss, H.K. Chelliah, and G.T. Linteris, "Extinction of Counterflow Diffusion Flames with Fine-Water Droplets," in *Proceedings: Halon Alternatives Technical Working Conference,* Albuquerque, NM (2000).
46. S.C. Yang, M.L. Huber, R.A. Bryant, and W.M. Pitts, "Experimental Investigation of Extinguishment of Laminar Diffusion Flames by Thermal Agents," in *Proceedings: Halon Alternatives Technical Working Conference,* Albuquerque, NM (2000).
47. J.T. Leonard, G.G. Back, and P.J. DiNenno, "Small/Intermediate Scale Studies of Water Mist Fire Suppression Systems," *NRL Ltr Rpt 6180/0869.1,* Naval Research Laboratory, Washington, DC (1994).
48. B.Z. Dlugogorski, R.K. Hichens, E.M. Kennedy, and J.W. Bozzelli, "Water Vapour as an Inerting Agent," in *Proceedings: Halon Alternatives Technical Working Conference,* Albuquerque, NM, p. 7 (1997).
49. J. Suh and A. Atreya, "The Effect of Water Vapor on Counterflow Diffusion Flames," *International Conference on Fire Research and Engineering,* Orlando, FL, pp. 103–108 (1995).
50. T.S. Ravigururajan and M.R. Beltran, "A Model for Attenuation of Fire Radiation Through Water Droplets," *Fire Safety Journal,* 15, pp. 171–181 (1989).
51. T. Log, " Flashover Suppression Using Fine Water Spray," *Interflam '96,* Cambridge, UK (1996).
52. P. Andersson and G. Holmstedt, "Limitations of Water Mist as a Total Flooding Agent," *J. of Fire Protection Engineering,* 9, 4, pp 31–50 (1999).
53. R.G. Bill, Jr., R.L. Hansen, and K. Richards, "Fine Spray (Water Mist) Protection of Shipboard Engine Rooms," *Fire Safety Journal,* 29, pp. 317–336 (1997).
54. R.G. Bill, Jr., and E.A. Ural, "Water Mist Protection of Combustion Turbine Enclosures," in *Fire Safety Science—Proceedings of the Sixth International Symposium,* International Association for Fire Safety, Poitiers, France (1999).
55. G.G. Back, C.L. Beyler, and R. Hansen, "The Capabilities and Limitations of Total Flooding Water Mist Fire Suppression Systems In Machinery Space Applications," *Fire Technology,* 36, pp. 8–23 (2000).
56. C. Beyler, "Flammability Limits of Premixed and Diffusion Flames," *The SFPE Handbook of Fire Protection Engineering,* National Fire Protection Association, Quincy, MA, Section 1/Chapter 7 (1988).
57. H.C. Kung and J.P. Hill, "Extinction of Wood Crib and Pallet Fires," *Combustion and Flame,* 24, p. 305 (1975).
58. F. Tamanini, "Application of Water Sprays to the Extinguishment of Crib Fires," *Combustion Science and Technology,* 14, pp. 17–23 (1976).
59. R.S. Magee and R.D. Reitz, "Extinguishment of Radiation Augmented Plastic Fires by Water Sprays," *15th International Symposium on Combustion* (1974).
60. M.B. Kim, Y.J. Jang, and M.O. Yoon, "Extinction Limit of a Pool Fire with a Water Mist," *Fire Safety Journal,* 28, pp. 295–306 (1997).
61. G.G. Back, C.L. Beyler, and R. Hansen, "A Quasi Steady-State Model for Predicting Fire Suppression in Spaces Pro-

tected by Water Mist Systems," *Fire Safety Journal,* 35, Nov 2000, pp. 327–362 (2000).
62. E.W. Forssell, G.G. Back, and Beyler, *A Transient Model for Predicting Fire Suppression in Spaces Protected by Water Mist Systems,* Hughes Associates (1999).
63. J. Vaari, "A Transient One-Zone Computer Model for Total Flooding Water Mist Fire Suppression in Ventilated Enclosures," VTT Rpt FIN-02044 (2000).
64. S.R. Tieszen and A.R. Lopez, "Issues in Numerical Simulation of Fire Suppression," in *Proceedings: Halon Alternatives Technical Working Conference,* Albuquerque, NM (1999).
65. Z. Liu, "The Use of Computer Modeling to Evaluate the Performance of Halon Alternatives—A Literature Review," *Internal Report 738,* National Research Council of Canada, Ottawa (1997).
66. W.M. Pitts and L.G. Blevins, "An Investigation of Extinguishment by Thermal Agents Using Detailed Chemical Modeling of Opposed Flow Diffusion Flames," in *Proceedings: Halon Alternatives Technical Working Conference,* Albuquerque, NM (1999).
67. K. Prasad, C. Li, K. Kailasanath, C. Ndubizu, R. Ananth, and P. Tatem, "Numerical Modeling of Fire Suppression Using Water Mist, 1. Gaseous Methane-Air Diffusion Flames," *NRL/MR/6410-98-8102,* Naval Research Laboratory (1998).
68. R. Srivastava, T. McKinnon, and J.R. Butz, "Modeling Study of the Effect of Fine Water Mists on Premixed CH_4/Air Flame Propagation," in *Proceedings: Halon Alternatives Technical Working Conference,* p. 550 (1997).
69. P.E. DesJardin, L.A. Gritzo, and S.R. Tieszen, "Modeling the Effect of Water Spray Suppression on Large Scale Pool Fires," *Halon Options Technical Working Conference,* Albuquerque, NM (2000).
70. G.V. Hadjisophocleous, A.K. Kim, and K. Knill, "Modeling of a Fine Water Spray Nozzle and Liquid Pool Fire Suppression," *International Conference on Fire Research and Engineering,* Orlando, FL, pp. 1–6 (1995).
71. G.V. Hadjisophocleous and K. Knill, "CFD Modeling of Liquid Pool Fire Suppression Using Fine Water Sprays," *Annual Conference on Fire Research,* Gaithersburg, MD, pp. 71–72 (1994).
72. G.V. Hadjisophocleous, S. Cao, and A.K. Kim, "Modeling the Interaction Between Fine Watersprays and a Fire Plume," *Fourth International Conference on Advanced Computational Methods in Heat Transfer,* Udine, Italy (1996).
73. Adeniji-Fashola and C.P. Chen, "Modeling of Confined Turbulent Fluid-Particle Flows Using Eulerian and Lagrangian Schemes," *Int. J. Heat Transfer,* 33, pp. 691–701 (1990).
74. F. Durst, D. Milijevic, and B. Schonung, "Eulerian and Lagrangian Predictions of Particulate Two-Phase Flows: A Numerical Study," *Appl. Math. Modeling,* 8, pp. 101–115 (1984).
75. M.W. An, A.C.M. Sousa, J.E.S. Venart, "Modeling of Shipboard Waterfog Fire Suppression System," *Contract #991-1042/2045,* National Research Council of Canada (1993).
76. G.V. Hadjisophocleous and S. Cao, "Numerical Simulations of Aircraft Cabin Fire Suppression," *88th Symposium. of the Propulsion and Energetic Panel on Aircraft Fire Safety* (1996).
77. IMO, FTP Code, International Code for Application of Fire Test Procedures (Resolution MSC. 61C67), International Maritime Organization, London, pp. 269–308 (1998).
78. *FTP Code,* "International Code for Application of Fire Test Procedures (Resolution MSC. 61C67)," International Maritime Organization, London, pp. 177–230 (1998).
79. *UL 2167,* "Proposed First Edition of the Standard for Water Mist Nozzles for Fire Protection Service," Underwriters Laboratories, Inc, Northbrook, IL (1998).
80. *VDS 2498,* "Guidelines for Water Extinguishing Systems Requirements and Test Methods for Fine Spray Nozzles," Verbanol der Schadenversichen, Germany (1996).
81. J.R. Mawhinney, "Mercury Energy CBD Tunnel Project, New Zealand—Performance Based Fire Testing of a Water Mist Fire Suppression System." *InterFlam '99,* Edinburgh, UK, pp. 663–673 (1999).
82. P. Southwood and G. Grant, "Eurotunnel's Full-Scale Fire Suppression Test Programme," *International Conference on Tunnel Fires and Escape from Tunnels 5–7,* Lyon, France (1999).
83. G. Grant, and P. Southwood, "Development of an Onboard Fire Suppression System for Eurotunnel HGV Shuttle Trains." *Interflam '99,* Edinburgh, UK, pp. 651–662 (1999).
84. J.R. Mawhinney, "A Linear Water Mist Fire Suppression System for Fixed Shelving in Archival Vaults," Presented at *ICFRE 97,* Gaithersburg, MD.
85. T. Log and P. Cannon-Brookes, "Water Mist for Fire Protection of Historic Buildings and Museums," *Museum Management and Curatorship,* 14, 3, pp. 283–298 (1995).
86. Factory Mutual Research Corporation, "Protecting Telephone Central Offices," *FMRC Update—A Progress Report from the Factory Mutual Research Corporation,* 6, 3, p. 1–4, Norwood, MA (1992).
87. D. Blake, T. Marker, R. Hill, J. Reinhardt, and C. Sarkos, "Cargo Compartment Fire Protection in Large Commercial Transport Aircraft," (1998).
88. M. Tuomisaari and M. Kokkala, "Fire Suppression Tests of a Power Transformer in an Outdoor Installation with a Hi-Fog Fire Protection System," *Research Report No. RTE10607/97,* VTT Building Technology Centre, Espoo, Finland (1997).
89. J.R. Mawhinney and R. Solomon, "Principles of Water Mist Fire Suppression Systems," *NFPA Handbook,* (A. Cote, ed.), National Fire Protection Association, Boston, MA (1996).
90. J. Keary and R. McGovern, "Characterisation of a Heated Water Extinguishing System," Department of Experimental Physics, University College Galway, Galway, Ireland, unpublished manuscript (1994).
91. J.R. Mawhinney, B. Taber, and J.Z. Su, "The Fire Extinguishing Capability of Mists Generated by Flashing of Super-Heated Water," in *Proceedings, American Institute of Chemical Engineers, 1995 Summer National Meeting,* Boston, MA (1995).
92. J.R. Mawhinney and R. Darwin, "Protecting against Vapor Explosions with Water Mist," in *Proceedings, Halon Technical Options Working Conference,* Albuquerque, NM (2000).
93. R. Brown and J.L. York, "Sprays Formed by Flashing Liquid Jets," *American Institute of Chemical Engineers Journal,* 8, 21, pp. 149–153 (1962).
94. Technical Research Centre of Finland (VTT) "Evaluating the Extinguishing Effectiveness of The HI-FOG Fire Protection System in a Class 1 Machinery Space According to IMO MSC/CIRC 668," *VTT Test Report No RTE10310/98,* Espoo, Finland (1998).
95. ASME/ANSI B31.1, *Power Piping Code,* American National Standards Institute, New York (1995).

Section Five
Fire Risk Analysis

Section 5 Fire Risk Analysis

CHAPTER 1

Introduction to Fire Risk Analysis

John M. Watts, Jr. and John R. Hall, Jr.

Introduction

The chapters in this section describe concepts and methods to be used in answering the three questions: What could happen? How bad would it be? How likely is it? This chapter in particular is intended to provide an overview of fire risk analysis as a whole, indicating how the subsequent chapters fit together and how a completed fire risk analysis connects to other evaluative and management activities. The purpose of this introductory chapter is threefold:

1. Introduce some generic terminology and fundamental concepts (building on the three questions raised above)
2. Provide an overview of the other chapters in this section
3. List some broad resources for conducting fire risk analysis (FRA)

What Is Risk?

Risk has always been a part of human endeavor, and for much of human history, the notion that risk could be actively controlled or prevented would have been considered mad or even blasphemous. Even today, when we increasingly expect protection against risk and use codes, regulations, insurance provisions, built-in and planned response mechanisms, and incentives, all to control or reduce risk, very few of our risk reduction and risk management actions proceed from a formal or quantitative risk analysis.

This aspect, too, is changing. Governments around the world are mandating risk analyses in areas of health and safety. Computations of the odds of harm are becoming a powerful force in decisions about activities involving risk.

Every decision related to fire safety is a fire risk decision, whether it is treated as such or not. And so, as our scientific understanding and our suite of quantitative engineering tools have rapidly expanded, we have discovered that we cannot make our fire safety decision-making process more scientific and quantitative unless we first place our new engineering tools into an appropriate fire risk analysis context. To do otherwise is to make many implicit assumptions about patterns of danger and preferences for certainty and for safety versus other human wants and needs.

Basing decisions on fire risk not only requires the challenging technical steps of fire risk estimation but also requires the identification of an acceptable level of risk, which is more a philosophical task than a technical one. Consider, for example, the recent fire loss experience of any country. Does this experience represent a level of fire risk acceptable to the citizens of that country? If the answer is no, then why is there so little attention paid to the problem? If the answer is yes, meaning we accept certain losses, then why is there a great clamor for change following every serious fire?

Accepting a level of risk requires a value judgment, and people have different value judgments. Consider four perspectives on the value of residential sprinklers: technical, societal, enforcer, and managerial.

Technical value judgments are made by experts based on the available technical information and their acquired expertise. Experts pretty much agree that residential sprinklers can significantly reduce the calculated fire risk. The experts most aware of the risk reduction potential of sprinklers are also most likely to evaluate the attractiveness of sprinklers based on that potential, more than on other

Dr. John M. Watts, Jr., holds degrees in fire protection engineering, industrial engineering, and operations research. He is director of the Fire Safety Institute, a not-for-profit information, research, and educational corporation located in Middlebury, Vermont. Dr. Watts also serves as editor of NFPA's *Fire Technology*.

Dr. John R. Hall, Jr., is assistant vice president for fire analysis and research at the National Fire Protection Association. He has been involved in studies of fire experience patterns and trends, models of fire risk, and studies of fire department management experiences since 1974 at NFPA, the National Bureau of Standards, the U.S. Fire Administration, and the Urban Institute.

bases. They may embrace residential sprinklers with great enthusiasm on that basis.

Societal value judgments are the judgments of ordinary people balancing benefits, costs, and risks of the full range of activities and events that affect their daily lives. Their estimation of the benefits and the negative side effects of sprinklers may be based on folklore more than the best thinking of the experts, and they are likely to attach more importance to costs and to other hazards and needs than the experts, having a specific focus, do. Currently, it appears that the reduced fire risk produced by a residential sprinkler system is not valued as highly, by the average citizen, as the increased benefit of a new car.

Enforcer value judgments are the judgments of a few professionals who are asked by society to protect their interests in a specific area. Enforcers are a special group within the larger group of individuals who provide *fire risk management.* An engineer performing a fire risk analysis will usually be working on behalf of a client with fire risk management responsibility, but the engineer cannot base his or her analysis on the values of the client alone. Instead, the fire risk analysis will need to address the client's values and societal values. Enforcers are often seen as the interpreters and guardians of societal values, but at the same time, their technical expertise and focused mission of providing fire safety give them a distinctive set of values. Their estimation of benefits and side effects are likely closer to those of the experts, but their evaluation of those benefits and side effects are likely closer to those of the general public, embodied in societal value judgments. And because they directly incur neither the costs nor the benefits of their decisions, they must factor in some other considerations having to do with when it is acceptable to dictate safety choices to people. Is it equitable to require automatic sprinklers in *all* residences? How can cost be fairly distributed? Who is responsible for system reliability? Should production, installation, and maintenance of sprinklers be regulated?

Managerial value judgments are the judgments of all the other professionals with special responsibilities relevant to fire risk management, which for residential fire sprinklers would include such groups as architects, builders, managers of hardware retail chains, and so forth. Their estimation of the benefits and side effects of sprinklers may be similar to the general public's, their estimation of the costs is probably more accurate than that of any other group, and, most importantly, they themselves are likely to be directly affected by those costs more than by the benefits or side effects. Different information and different goals and values are likely to lead to a different assessment—though still risk based like all the others—of the attractiveness of residential sprinklers.

The chapters of this section are designed to provide the practicing engineer with those contextual tools and supplementary information that will permit him or her to use the knowledge and tools embedded in all the earlier sections and to produce a sound evaluation of alternative choices.

Fire risk estimation is the scientific process of answering three questions: (1) What could happen? (2) How bad would it be if it did happen? (3) How likely is it to happen? Or, to put it another way, risk has two essential components—exposure and undesired consequences. Exposure is a potential risk that becomes real with uncertainty, and so exposure refers to the likelihood or probability of experiencing a destructive event, for example, fire. Undesirable consequences, ranging from deaths or dollars of property damage, to significant intangible losses such as business interruption, mission failure, environmental degradation, and destruction of cultural artifacts, are also potential risks. They become real if exposure occurs. Thus when we speak of fire risk, we are referring to the uncertainty of loss.

Let's return to the three questions that opened this chapter.

What could happen? can refer to a sequence of events ending in a fire loss, the sequence as a whole being called a *scenario,* or to an object or other entity having the potential for a sequence of events ending in a fire loss. A *hazard* is such an object, and *hazard* itself is the potential for loss. *Fire hazard analysis* is a term often used to refer to analyses of what could happen and how bad it would be, without analysis of likelihood.

How bad would it be if it did happen? is often called *consequence* and sometimes called *hazard,* in the sense of a specific measure of potential for loss. The measure of consequence can be direct (e.g., property is damaged) or indirect (e.g., the company is out of business for several days). It can be objective (e.g., replacement cost in monetary units) or subjective (e.g., pain and suffering effects of injury, utility measures of damage).

How likely is it to happen? is usually called *probability.* Probability can be relative (e.g., likelihood of this loss is how much greater or smaller than likelihood of that loss) or absolute (e.g., how many times a year, given a population of people or property). Probability can be regarded as objective and measured objectively (e.g., how many occurrences per year in a recent period of time). It can be regarded as objective but measured subjectively (e.g., how many occurrences do we estimate will occur next year, given data on the number of occurrences last year and impressions on what has changed since last year). It can be regarded as and measured subjectively.

And both consequence and probability can be either explicit in a formal fire risk analysis or implicit and unquantified in a more simplified fire risk analysis (e.g., *fire risk index*).

For purposes of use by fire protection engineers, we assume that fire risk analysis is a scientific process, closely linked to calculations based on proven relationships and the collection and analysis of valid and appropriate data, to describe the form, dimension, and characteristics of the fire risk.

Fire risk analysis can take different approaches depending on the purpose and scope of the analysis or assessment. Some assessments look back to try to infer probabilities and other risk-related measures based on practices and fire loss experience after an event such as the introduction of home smoke alarms. Other assessments look ahead and try to predict what the practices and fire loss experience would be after an event such as legislating residential sprinklers in homes.

The approach taken to fire risk analysis can also differ based on the availability—quantity, quality, and detail—of

data for the purpose. Assessing the fire risk for U.S. residences, for example, one is able to draw on a very large number of documented fire events but with limited detail. Assessing the fire risk for U.S. nuclear power plants, by contrast, has far fewer fire events to draw upon but much more detail on each such event. And assessing the fire risk in any specific existing building will involve very few events in that building and questions of relevance for data from any other building or group of buildings.

In fire safety engineering, risk analysis is most generally used to evaluate fire protection strategies for a particular application or for a class of facility or operation. In other words, there are a sizeable number of buildings and some considerable relevant fire loss history to draw upon.

Terminology and Concepts

The terminology of fire risk analysis is not consistent. For example, a committee of the Society for Risk Analysis identified 17 different definitions of risk.[1] If one considers risk to be the full probability distribution of hazardous events and associated loss consequences associated with a building, product, or other entity to be studied, then all 17 definitions can be seen as alternative summary measures taken from that common distribution. The important point, however, is that for many people, a summary measure is not just a summary measure related to risk, useful for analysis; it *is* the risk.

As another example, the terms *analysis* and *assessment* are often used interchangeably, yet some sources make sharp distinctions. We will provide distinct definitions.

The rest of the chapters in this section also show some inconsistencies in definitions and concepts. These are largely a function of differences in the authors' backgrounds, topics, resources, and intents. In general, the definitions and concepts used are similar, even when they are not identical.

An overview of terms is best presented in the form of a glossary, but the list below is presented in what is meant to be a logical sequence, rather than alphabetically. More extensive glossaries can be found in Grose[2] and Rowe.[3]

Hazard: A hazard is a chemical or physical condition that has the potential for causing damage to people, property, or the environment.[4] Hazard is any situation that has the potential for causing injury to life, or damage to property and the environment.[5]

Risk: Risk is the potential for realization of unwanted, adverse consequences to human life, health, property, or the environment. Estimation of risk (for an event) is usually based on the expected value of the conditional probability of the event occurring times the consequence of the event given that it has occurred.[6] It follows that risk for a building, a product, or some other entity would be the probability distribution of events and associated consequences relevant to that building, product, or entity.

Probability: According to the frequency interpretation, probability is the proportion of the time an event will occur in the long run. According to the subjective interpretation of probability, it is a measure of the strength of a person's belief concerning the occurrence or nonoccurrence of an event.[7] Probabilistic analysis is not well established in fire protection engineering, where empiricism, heuristics, and, more recently, physics-based modeling are principally used to make decisions. Probabilistic analysis is more established in fields such as decision analysis, management science, operations research, industrial and systems engineering, and systems safety. The mathematics of probability allow us to formulate engineering models which recognize uncertainty and deal with it quantitatively and consistently. Probability and statistics are covered in Section 1, Chapters 11 and 12, of this handbook.

Consequence: Consequence is a measure of the expected effects of an incident outcome case.[4]

Perceived risk: Any measure of risk preferences in which the scale is not fully explainable by some objective measure of loss, direct or indirect, may be a measure of perceived risk. Studies of risk perception have identified a number of factors that consistently cause objectively equal risks to be perceived differently, including preferences for more certainty over less certainty (i.e., *risk aversion*), familiar over unfamiliar risks, voluntary over involuntary risks, readily detectable risks over undetectable or hidden risks, and common or ordinary risks over dramatic or memorable risks. The field of *risk communication* is devoted, in part, to finding ways for individuals and groups with differing ways of perceiving risks to communicate effectively, understand one another, and collaborate on mutually acceptable analyses and decisions.

Risk analysis: Risk analysis is the detailed examination, including risk assessment, risk evaluation, and risk management alternatives, performed to understand the nature of unwanted, negative consequences to human life, health, property, or the environment; an analytical process to provide information regarding undesirable events; and the process of quantification of the probabilities and expected consequences for identified risks.[6]

Risk assessment: Risk assessment is the process of establishing information regarding acceptable levels of a risk and/or levels of risk for an individual, group, society, or the environment.[6]

Risk estimation: Risk estimation is the scientific determination of the characteristics of risks, usually in as quantitative a way as possible. These characteristics include the magnitude, spatial scale, duration, and intensity of adverse consequences and their associated probabilities as well as a description of the cause and effect links.[6] One complication is that a totally objective or scientific way to measure fire risk does not exist. Problem identification, data collection and reduction, and integration of information are all replete with subjective evaluations.

Risk evaluation: Risk evaluation is a component of risk assessment in which judgments are made about the significance and acceptability of risk.[6]

Risk identification: Recognizing that a hazard exists and trying to define its characteristics is called risk identification. Often risks exist and are even measured for some time before their adverse consequences are recognized. In other cases, risk identification is a deliberate procedure to review, and, it is hoped, to anticipate possible hazards.[6]

Acceptable risk: A value judgment applied to a particular scale for the measurement of risk yields a definition of acceptable risk. It therefore requires a prior decision on the scale and method used to estimate or measure risk and a second decision on the person or group whose views on acceptability are to be used. For a practicing engineer, acceptable risk is likely to be risk acceptable to the client. For an authority having jurisdiction (AHJ) or anyone answerable to an AHJ, acceptable risk is meant to be acceptable to society in general or to a particular community.

It is an axiom of fire risk analysis that zero risk is not an achievable goal. There are no risk-free alternatives available to individuals or organizations. No technology is 100 percent reliable or totally immune to misuse, and even if technological risk could be eliminated, natural catastrophes such as lightning strikes, wildland fires, earthquakes, and wind storms include the potential for fire loss. An important corollary is that reducing fire risk may increase other forms of risk. An obvious case is the potential damage to the ozone layer from use of halon.

The goal that comes closest to being a practical goal of zero risk is a goal of risk as low as is technically possible. For fire protection engineering, this goal may take the form of accepting the residual risk after all identified risk reduction strategies and choices have been adopted. Or, for individuals with special preferences for particular fire protection strategies (e.g., active systems over product or material requirements, or vice versa, and either over education and training), acceptable risk may be the residual risk after favored choices are in place. One complication is that the residual risk in these cases may be perceived as zero, implying no prior acceptance of the nonzero risk that actually remains.

A universally acceptable level of fire risk does not exist: No matter how one defines the term *acceptable level of fire risk,* it will be dependent on the problem context and on the individual judging acceptability, that is, on the alternatives and objectives. Individuals and organizations are inconsistent in their risk aversion. Surveys show wide variations with respect to factors such as voluntary versus involuntary risk and perceived versus calculated risk.

One contention is that the present public fire risk situation must be acceptable since otherwise there would be greater concern and call for action. This view is not a fully reliable generalization. People may have "accepted" the current risk because they believed it to be lower than it really is, believed no technically feasible alternative existed (which can change because technology changes or because perceptions of technology change), or saw no politically effective way to make their lack of acceptance known. Moreover, the current situation is a compromise among the greatly differing preferences of many individuals and groups, whose relative influence on the process of choice may also change. More elaborate discussion of the issues associated with acceptable risk can be found in Lowrance[8] and Fischoff et al.[9]

Vulnerability: The susceptibility of life, property, and the environment to injury or damage if a hazard manifests its potential is vulnerability.[5]

Methods of Fire Risk Analysis

Fire risk analysis is basically a structured approach to decision making under uncertainty. Within this general structure, there are many techniques or approaches to both qualitative and quantitative fire risk analysis. Each application will want to individually consider the level of mathematical sophistication appropriate to meet objectives.

A generalized concept of fire risk analysis has these components:

1. Identify fire hazards.
2. Quantify consequence and probability of fire hazards.
3. Identify hazard control options.
4. Quantify impact of options on risks of hazards.
5. Select appropriate protection.

At each of the two stages of quantification, there is a wide range of possibilities of depth and detail, and the actual quantification can take place anywhere on a spectrum from a principal basis in hard data and established science to a principal basis in expert judgment.

Fire risk analysis begins—and for some applications may end—with the identification of fire hazards. A preliminary assessment of areas of potential concern in facility design and operational concepts may be organized by location (e.g., area of a plant) or by activity (e.g., manufacturing vs. office functions, wherever they occur). This identification provides a structure for subsequent estimates of the probability of occurrence of the events in each possible accident sequence and thereby of each possible deleterious consequence.

Formal fire risk assessment evolved with the insurance industry in the nineteenth century. Methods of fire risk analysis may be classified into four categories: (1) checklists, (2) narratives, (3) indexing, and (4) probabilistic methods.[10] Checklists and narratives are nonquantitative approaches that may address Steps 1, 3, and 5 above while bypassing Steps 2 and 4. Indexing is a thorough quantification method that is heuristic rather than fundamentally based. Probabilistic methods have grown in use over the last third of a century but remain rare even today.

Checklists are a common accessory of fire safety consisting of a listing of hazards, usually with recommended practices. A checklist is usually less generic than a model code or standard. It may even be so specific that it is intended to apply to a single class of buildings under management of a single owner, reflecting the special concerns of that owner.

A checklist is a practical tool to support analysis of a building relative to a code or standard that forms the basis for the checklist. It is very seldom that all criteria in a code or standard apply to a single building. The fire protection engineer must focus on only those requirements that are applicable to a specific project. A checklist can aid

in this process. It also makes requirements easier to read, understand, and track to compliance.

Checklists face a trade-off between practicality and ease of interpretation. A long checklist might list 50 fire safety factors, with each item described in a manner that is readily visible or measurable, but those 50 items are not all likely to be comparably important. A short checklist, on the other hand, is usually comprised of conceptual features of fire safety, which may all be very important but may all require interpretation to be made measurable.

Moreover, checklists do not capture the interaction of fire risk factors, including the manner in which the importance of one fire risk factor will change as a function of performance on another factor. For example, the relative value of hydrants, sprinklers, and extinguishers is not constant but a function of other features of a structure's form and utility.

Narratives consist of a series of recommendations—things to do and not do—related to fire risk and safety. They are probably the earliest approach to fire risk assessment, stemming from the observation that fire is capable of destroying certain materials, such as wood, fur, and flesh. This realization would have led to a communication from parent to child on the avoidance of these fire dangers. In this earliest form, narratives were much simpler and less finished than checklists. They were not comprehensive with regard to hazards, and so they did not support a thorough review.

As the piecemeal parent's advice format evolved over the years, the narrative approach developed into the present multivolume set of the NFPA *National Fire Codes*® 2000 edition.[11] These contain the bulk of our present-day wisdom on fire safety. The information is presented in the form of descriptions of various hazardous conditions and ways to reduce or eliminate them. In this modern form, narratives are often more finished than checklists, which may be developed as simplified, practical tools to serve the more basic narratives.

Like checklists, narratives do not attempt to evaluate the fire risk quantitatively. A risk is judged acceptable if it is addressed in accordance with published recommendations. The criterion is one of pass or fail, and the residual risk remaining if you pass is never quantified or evaluated. Also like checklists, narratives cannot hope to cover the myriad conditions of human activity. While there is much common ground among different fire hazard situations, there is considerable variation in detail.

Indexing is representative of the quantitative fire risk assessment that originated with the insurance rating schedule. The approach has broadened to include a wide variety of applications. In general, fire risk indexing assigns values to selected variables based on professional judgment and past experience. The selected variables represent both positive and negative fire safety features and the assigned values are then operated on by some combination of arithmetic functions to arrive at a single value. This single value can be compared to other similar assessments or to a standard to rank the fire risk. Section 5, Chapter 10 covers the subject of fire risk indexing.

Some measures used in fire risk analysis, such as *probable maximum loss* (PML), sound more fundamentally grounded than fire risk indexes but may actually be less so. There is no established consensus on how improbable a loss must be to be ineligible as the probable maximum loss, and the designation is sometimes given without benefit of any explicit or formal analysis. The resulting subjectivity of such a determination suggests that this value is more of an ordinal label than a quantitative measure of risk (which is not to say that it does not have usefulness).

Matrices and *contours* are methods that can fall between indexes and full-fledged probabilistic methods. A risk matrix typically provides a discrete partitioning of relative consequences along one dimension and relative likelihood along the other. The entry in each matrix cell may include a description of hazards known or believed to have that combination of consequence severity and likelihood, and may also be used to record judgments on the acceptability of such risks and/or recommendations on steps to take to reduce such risks. A risk contour is a continuous analogue to a risk matrix. Curves are drawn on a two-dimensional graph with one axis for consequence and one for probability, with a curve representing types of hazards or technically achievable states.

Probabilistic methods are the most informative approaches to fire risk assessment in that they produce quantitative values, typically produced by methods that can be traced back through explicit assumptions, data, and mathematical relationships to the underlying risk distribution that all methods are presumably seeking to address. Most of the chapters in this section of the handbook are devoted to engineering methods of use in executing a formal probabilistic analysis of fire risk. Some common, generic methods of fire risk analysis follow.

Event tree: An event tree is a graphical logic model that identifies and quantifies possible outcomes following an initiating event.[4] The tree structure is organized by temporal sequence. Probabilities can be calculated from the tree, and consequences are typically assigned to the end states but may cumulate along the tree.

Fault tree: A fault tree is a method for representing the logical combinations of various system states that leads to a particular outcome.[4] The tree structure is organized by logical dependency. Probabilities can be calculated from the tree. Consequences are typically defined in an either/or form (success or failure) so that the probabilities suffice to calculate the risk, as defined.

Decision tree: A decision tree is a method for representing the possible outcomes following a succession of events, combining points where the ensuing path is subject to choice and points where it is not. The analysis operates similarly to an event or fault tree, and the simplest decision trees consist of a set of initial choices and an event or fault tree associated with each.

Influence diagram: An influence diagram is a graphical representation of the relationship of the decisions and uncertainties in a decision problem.[12,13] The diagram is more flexible and less unidirectional than any type of tree diagram. It is designed to focus more on the elements of decision making and less on relevant underlying physical phenomena.

Overview of the Section

This section of the handbook is organized into three broad areas that progress from the general to the specific. There are some basic tools that most approaches to fire risk analysis should consider if not incorporate. There are some examples of generic models applied to fire safety problems, and there are detailed descriptions of fire risk analysis procedures that have been adopted in several areas of application.

Section 5, Chapters 2 through 7 cover generic tools used in many other disciplines and inherent to fire risk analysis, but not typically included in more traditional approaches to fire protection.

The most common use of fire risk analysis is a basis to make choices. The choice may be between two alternative designs for a building or two alternative formulations for a model code or standard. The choice may be whether to tighten requirements on product type A or product type B. Section 5, Chapter 2 describes *decision analysis,* a generic field on forms of analysis that support this kind of decision making. *Cost-benefit analysis* is a specific type of decision analysis, in which a fire risk analysis provides estimates for some of the benefits, and other analysis quantifies corresponding costs.

Section 5, Chapter 3 addresses *reliability.* Fire risk analysis depends upon many types of probabilities. One is fire scenario probability, the estimation of likelihood for the initial conditions and ensuring major events in fire development. Another group of probabilities might be transitory conditions related to people, such as the locations and capabilities of occupants when a fire begins. A critically important set of probabilities have to do with status and capabilities of fire protection equipment, features, and arrangements. Is the battery working in the smoke alarm? Is the sprinkler valve open or closed? Is the fire door working or blocked open? These are all questions of reliability addressed in Section 5, Chapter 3.

Section 5, Chapter 4 addresses *uncertainty.* Early on, the comment was made that the term *fire risk* refers to the uncertainty of loss. The concept of safety itself is one of uncertainty. There is no such thing as absolute safety; human activity will always and unavoidably involve risks. Section 5, Chapter 4 addresses a narrower definition of uncertainty—not the uncertainty of the potential victim regarding the fact of fire loss but the uncertainty of the engineer or decision maker regarding estimates of the magnitude of fire risk.

Uncertainty may be caused by imprecision or bias in our techniques of observation or calculation, a lack of clarity in our goals, uncontrollable technological variation, or variations of natural phenomena, to name only the major components. The concept of fire is also uncertain. Unwanted combustion is perhaps the least predictable common physical phenomenon. Uncertainty analysis is the scientific calculation procedure that should underpin choices of *safety factors* and *safety margins.* It is central to the valid use of fire risk analysis—or any other form of engineering analysis—for code equivalency, design approval, or any other important decision in the real world.

Section 5, Chapter 5 addresses *data sources* for engineering analysis, particularly data useful for calculating scenario probabilities, reliability probabilities, or any other probabilities needed for fire risk analysis.

Section 5, Chapter 6 addresses the *measurement of consequences in economic terms.* This measurement includes indirect losses, economic measures of the value of a lost life or of an injury, and the use of utility measures to capture people's desire to avoid uncertainty about loss, as well as loss itself, the implications for people's risk aversion for the basic mathematics of insurance, and so on. The common theme is treating consequences comprehensively and in a form that captures people's real preferences and can be readily compared to the costs of alternative choices. Section 5, Chapter 7 addresses *other economic topics* that arise in the practice of engineering analysis, with particular emphasis on monetary valuations over time (e.g., rate of return, interest, discounting).

Section 5, Chapters 8 through 10 describe the use of some examples of generic models of risk analysis and decision making that have been widely adapted and used for fire safety applications. Chapter 8 addresses special topics in the calculation of low probabilities, under the heading of *extreme value theory.* Chapter 9 describes techniques and available models using *computer simulation,* with special emphasis on those having a fire risk analysis basis, such as state-transition models. Chapter 10 describes less-quantified methods of fire risk analysis, involving *fire risk indexing.*

Section 5, Chapters 11 through 15 deal with specific applications of fire risk analysis that have been implemented in the areas of consumer products, buildings, chemical processes, nuclear facilities, and vehicles. Much of the information in these chapters can be extracted and adapted for other areas of application. Of particular note is how the tools in Section 5, Chapters 2 through 10 have been incorporated into the applications in these areas. Chapters 11 and 12, respectively, describe general techniques and available methods for *fire risk analysis of products or buildings.* Chapters 13 and 14 describe the much more specific methods tailored to applications in two industries where the use of fire risk analysis is far more common than in others, namely, *chemical process industries* and *nuclear power plants.* Finally, Chapter 15 describes new methods addressing consequence measurement for *transportation vehicles,* which now exists in a form ready for use in fire risk analysis.

Activities and Resources

Every major group involved in guidance related to fire safety now has a committee or a publication devoted to fire risk analysis, and the emphasis on risk-based or risk-informed approaches to decision making is growing rapidly. Thus, in addition to the many sources of specific models and methods mentioned in the subsequent chapters, there are a growing number of sources for generic work and guidance.

Among the more important activities are the following:

- SFPE addresses the basics of fire risk analysis in its publications on performance-based design. Several of the ongoing task groups of SFPE, intended to add the

next level of detail to already published guidance, are addressing elements of relevance to fire risk analysis.

- NFPA has a new committee, the Technical Committee on Fire Risk Analysis, whose purpose is to provide assistance and guidance to other committees on methods and concepts in fire risk analysis. One of the most widely cited and used fault tree formats in fire risk analysis is NFPA 550, *Guide to the Fire Safety Concepts Tree,* 1995 edition, developed by the now-defunct Systems Concepts Committee and now assigned for maintenance to this new committee. Development of fire risk analysis methods for general and specific purposes has been a recurring emphasis of projects organized by NFPA's Fire Protection Research Foundation.
- ASTM has a Standard E 1766 to guide the writing of fire risk assessment standards for burnable products.
- The International Organization for Standardization (ISO) TC 92 SC 4 has a new Working Group 10 on fire risk analysis. It has just begun to define a work program.
- The Society for Risk Analysis is the principal worldwide professional organization devoted to risk analysis. It devotes comparatively little emphasis to engineering applications and to acute outcomes, instead focusing more on long-term chronic illness consequences.
- The Institute for Operations Research and the Management Sciences (InFORMS) has areas of emphasis in decision analysis and applies and develops risk analysis concepts and methods through that activity.

References Cited

1. *RISK Newsletter,* Society for Risk Analysis, September, p. 5 (1987).
2. V.L. Grose, *Managing Risk,* Prentice Hall, Englewood Cliffs, NJ (1987).
3. W.D. Rowe, *An Anatomy of Risk,* John Wiley and Sons, New York (1977).
4. *Guidelines for Chemical Process Quantitative Risk Analysis,* Center for Chemical Process Safety, American Institute of Chemical Engineers, New York (1989).
5. *Hazardous Materials Emergency Planning Guide,* National Response Team, Washington, DC (1987).
6. Society for Risk Analysis, *Glossary of Risk Analysis Terms,* http://www.sra.org/glossary.htm (2000).
7. J.E. Freund and F.J. Williams, *Dictionary/Outline of Basic Statistics,* McGraw-Hill Book Company, New York (1966).
8. W.W. Lowrance, *Of Acceptable Risk,* William Kaufman, Los Altos, CA (1976).
9. B. Fischoff, S. Lichtenstein, P. Slovic, S.L. Derby, and R.L. Keeney, *Acceptable Risk,* Cambridge University Press, Cambridge (1981).
10. J. Watts, "Systematic Methods of Evaluating Fire Safety: A Review," *Hazard Prevention,* 18, 2, pp. 24–27 (1981).
11. NFPA, *National Fire Codes,* NFPA, Quincy, MA, 2000 edition.
12. R.A. Howard and J.E. Matheson, "Influence Diagrams," in *Readings on the Principles and Applications of Decisions Analysis* (R.A. Howard and J.E. Matheson, eds.), 2, Strategic Decisions Group, Menlo Park, CA, pp. 719–762 (1983).
13. R.A. Howard, "From Influence to Relevance to Knowledge," in *Influence Diagrams, Belief Nets and Decision Analysis* (R.M. Oliver and J.Q. Smith, eds.), John Wiley and Sons, New York, pp. 3–24 (1990).

Additional Reading

ASTM STP762, *Fire Risk Assessment* (G.T. Castino and T.Z. Harmathy, eds.), American Society for Testing and Materials, Philadelphia (1980).

ASTM STP1150, *Fire Hazard and Fire Risk Assessment* (M.M. Hirschler, ed.), American Society for Testing and Materials, Philadelphia (1992).

Center for Chemical Process Safety, *Tools for Making Acute Risk Decisions,* American Institute of Chemical Engineers, New York (1995).

J.N. Dezern, "Risk Assessment and ASTM," *Standardization News,* 16, 2, p. 52 (1988).

Y.Y. Haimes, *Risk Modeling, Assessment, and Management,* John Wiley and Sons, New York (1998).

F. Hakan, *Uncertainty and Risk Analysis in Fire Safety Engineering,* Lund University, Lund, Sweden (1998).

J.R. Hall, Jr. and A. Sekizawa, "Fire Risk Analysis: General Conceptual Framework for Describing Models," *Fire Technology,* 7, 1, pp. 33–53 (1991).

E.J. Henley and H. Kumamoto, *Reliability Engineering and Risk Assessment,* Prentice Hall, Englewood Cliffs, NJ (1981).

N.J. McCormick, *Reliability and Risk Analysis,* Academic Press, New York (1981).

M. Modarres, M. Kaminskiy, and V. Krivtsov, *Reliability Engineering and Risk Analysis, A Practical Guide,* Marcel Decker, New York (1999).

Proceedings—SFPE Symposium on Risk, Uncertainty, and Reliability in Fire Protection Engineering, Society of Fire Protection Engineers, Bethesda, MD (1999).

V. Molak, *Fundamentals of Risk Analysis and Risk Management,* Lewis Publishers, Boca Raton, FL (1997).

CHAPTER 2

Decision Analysis

H. A. Donegan

Introduction

This chapter is devoted to some of the basic elements of decision analysis, a subject that has its roots firmly established in the area of management science, but now enjoys a much wider application. The present article, which is not intended as an exhaustive discussion paper, aims to introduce basic terminology and to illustrate some of the techniques that can be applied to situations in fire protection engineering, one of the many areas of application. The growth in application can be attributed to the significant developments that have taken place within information technology, particularly with regard to the ready availability of user-friendly decision support software. Practitioners interested in particular aspects of the subject and in software will find appropriate references listed in context. The reader should be aware at the outset that decision analysis is more general than risk analysis, which, in terms of fire protection, has its own extensive and highly specialized literature—see, for example, Castino and Harmathy,[1] Gretener,[2] Hall,[3] Hirschler,[4] Watts.[5,6]

The engineering of fire protection necessitates a high degree of decision making at all levels of application, and because of the capricious nature of unwanted fire, it involves a high degree of subjectivity and therefore uncertainty. In practically every aspect of fire protection, the practitioner is faced with choices when presented with options or alternative courses of action, each of which has one or more consequences. If a choice is subjective, then it can be made only when the following pieces of information are known to the decision maker:

1. An understanding of each possible consequence
2. The likelihood of occurrence of each consequence
3. The method for combining values and probabilities of consequences into a meaningful course of action

H.A. (Tony) Donegan is a reader in the Mathematics Division of the Faculty of Informatics at the University of Ulster, Northern Ireland.

Sometimes the sheer number of options will limit the time that can be spent on evaluating each single option, as when one is faced with large product lists—for example, smoke alarms or fire-resistant doors. Or the possible consequences of a course of action are difficult to enumerate, as in the case of increasingly complex new technology. Often the value of a consequence can be estimated only on the basis of sample information, for example, studying a selection of literature. In other cases, the value of a consequence may depend on many dimensions, such as choosing where to live—taxes, transport, amenities, employment, and so on. Or there may be several possible consequences distributed over time, and it is difficult to predict which one of them will occur and at what time—typically when the fire brigade is attempting to suppress a raging fire.

In complex problems, decisions often have to be made when there are several sources of difficulty interacting or competing. For example, deciding whether or not to build a nuclear power plant instead of a conventional alternative in the face of increasing energy demands is perhaps typical. In this situation, the decision makers have to deal with short- and long-term multidimensional consequences; they know that despite extremely low outcome probabilities, a small number of uncertain events could lead to a catastrophe. With the benefit of hindsight, it is a chilling reality that Chernobyl is the epitome of the above scenario and therefore a timely reminder to those engaged in subjective decisions that impact on life safety.

Consequences are often a reflection of the mathematical modeling strategy that underpins many decisions and are therefore only as valid as the appropriateness of the chosen model or, inclusively, the reliability of its input data. Moreover, the fact that much of the data are subjective places the opinion experts at a key point in the chain of responsibility for good decision making (see Winkler and Murphy[7]). In what follows, it is assumed that methodologies under the various decision classifications are supported by the best efforts of practitioners and software designers.

Before proceeding to look at decision classifications, some key words that frequently appear in the literature of decision theory are now discussed. For example, in the above preamble, casual reference was made to the terms *subjectivity* and *uncertainty,* yet these are emotive words with a vast and formal literature—see, for example, Bunn,[8] French,[9,10] Lindley,[11] Raiffa,[12] Viek and Wagenaar.[13]

The concept of probability in decision theory embraces two distinct schools of probabilists—the frequentists and the subjectivists.

The *frequentists* believe that probability can only have meaning in the context of an infinitely repeatable experiment, in which the probability of an event A, namely $P(A)$, is taken to be its long-run relative frequency of occurrence in repeated trials of the experiment—termed *objective probability.* In the reality of risk assessment, approximations called actuarial estimates are used; the relative frequency of the number of times A has previously occurred in some finite experiment is taken as an indication of likely occurrences in the future. For example, if the statistics[14] of residential fire deaths in the sample period (finite experiment) 1983 to 1987 show that on average 47.8 percent of the deaths are identified as occupants aged 65 years and over, then 0.478 is regarded as the probability that a fatal casualty in a residential fire is a person aged 65 or above. Approximations are common in production scenarios. For example, if A represents the event that a sprinkler head is defective, and during the inspection (finite experiment) of a random batch of 240 sprinkler heads 2 are found to be defective, then the chance of picking, at random, a faulty head from the batch is 2 in 240, yet $P(A)$ is stated in general as being 1/120 until revised in another finite experiment.

The *subjectivists* associate probability not with the system under observation, but with the observer of that system identifying probability as the degree or strength of belief that the system will adopt a certain state—termed *subjective probability.* For example, in the modeling of fire spread, the probability of flashover in the room of origin is a measure of opinion relating to the change of state from preflashover to postflashover. It would be decided by the modeler on the basis of experience regarding uncertainties associated with the fire variables in the room of origin. However, such decisions need considerable care; the article by Bunn[8] addresses some of the fundamental issues regarding the assessment of subjective probabilities. A highly pertinent article by Noonan and Fitzgerald[15] discusses the role of subjective probabilities in fire risk management studies.

Developments in artificial intelligence and in expert systems have shown that probability theory in itself is insufficient to cater for the advancement of theories relating to the management of uncertainty in knowledge-based systems. For example, lexical elasticity, which relates to the fuzziness of words in natural language, provides a clear example. A simple relation between X, Y, and Z expressed as

if X is small and Y is very large, then Z is not very small

does not lend itself to a simple interpretation within the field of probability theory. This is by reason of the lexical elasticity of the predicates *large* and *small.*[16] Such developments have inspired the formation a new school of practitioners focused on imprecision rather than uncertainty. The topics are rather specialized and outside the scope of the present article, but the interested reader will find appropriate background reading in Zadeh[17] and in Klir and Folger.[18]

The term *uncertainty* is used prolifically in decision theory, and yet textbooks generally sidestep any attempt at a formal definition. This presentation will not dissent from that established pattern, but will nevertheless construct an interpretation from the axioms of probability. (The subject of probability is discussed elsewhere in this handbook.) The axioms are restated here for convenience:

Axiom 1: *Positiveness*—the probability of an event occurring must be non-negative.

Axiom 2: *Certainty*—the probability of an event that is certain to occur is 1.

Axiom 3: *Addition*—if events A and B are mutually exclusive, then the probability

$$P(A \text{ or } B) = P(A) + P(B)$$

Axioms 1 and 2 imply that the probability of an event occurring must be at least zero and no greater than 1. Hence uncertainty (for the purpose of this discussion) identifies with the probability of an event A such that $0 \leq P(A) < 1$. In a subjective environment, the location of $P(A)$ in the interval [0, 1] lies within a subneighborhood of uncertainty, which is clearly articulated by Bell, Raiffa, and Tversky.[19] They point to the confrontation between abstract theory and realistic behavior, particularly when subjective assessments are required. Real people do not behave like the models say they should. For example,

- Many experts are willing to answer hypothetical questions about uncertain quantities.
- Lay people and indeed experts do not calibrate well. By and large, assessed probability distributions are too tight; people think they know more than they really know and are surprised far too often.
- Some assessment methods lead to less distortion than others.
- It is extremely difficult to assess small probabilities.
- Subjects can learn to calibrate better if they are given systematic feedback.

It is intended that these observations, which are highly pertinent in fire safety, will alert the reader to the realization that decision making is as much an art as it is a science.

Decision Classifications

Broadly speaking, decision classifications can be characterized by the qualitative knowledge spectrum shown in Figure 5-2.1. Given that the spectrum ranges from ambiguous data to well-defined data, in

- Decision making under certainty—the data are known deterministically
- Decision making under risk—the data are described statistically
- Decision making under uncertainty—the data cannot be assigned relevant weights

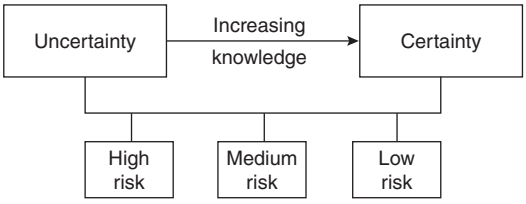

Figure 5-2.1. ***Qualitative knowledge spectrum.***

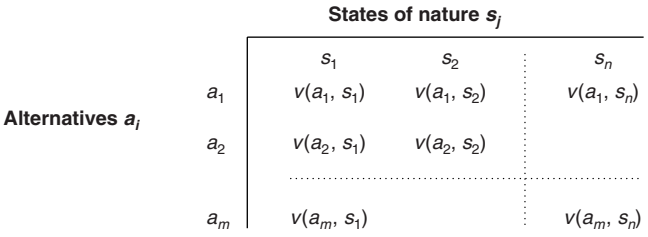

Figure 5-2.2. ***Payoff matrix.***

Decision making under any condition involves alternatives whose payoffs (outcomes) depend on the states of nature, which may be random events. Specifically, the *payoff matrix* of a decision problem with m alternatives and n states of nature can be represented as in Figure 5-2.2. The element a_i represents the alternative i, and the element s_j represents state of nature j. The payoff or outcome associated with a_i and s_j is denoted by $v(a_i, s_j)$.

Decision Making under Certainty

Decision making under certainty means the decision maker knows with certainty the consequence of every alternative or decision choice. For example, a fire engineering consultant with resources to take on a single contract has the choice of two 1-yr guaranteed contracts A and B, each with similar conditions and each capable of being carried out within the consultant's office environment. If the value of A exceeds that of B by \$4,000, then there is certainty that contract A will maximize the consultant's well-being. Of course, there is the classic and perhaps paradoxical phrase that accompanies any certainty, "all other things being equal." The payoff matrix would take the form shown in Figure 5-2.3.

Such matrices are clearly unnecessary for straightforward decision making. However, they offer decision makers a useful structure when the choice of alternative is compounded by more than one state of nature, as in decision making under risk or uncertainty.

Decision Making under Risk

Decision making under risk assumes that the payoff (gain or cost) associated with each alternative, for a given state of nature, has an associated probability. The payoff is usually based on the expected value criterion, which seeks the maximization of expected (average) gain or the minimization of expected cost among the alternatives. The procedure stems from the concept of expectation, perhaps the most important concept in decision theory, which is discussed in elementary textbooks on probability.

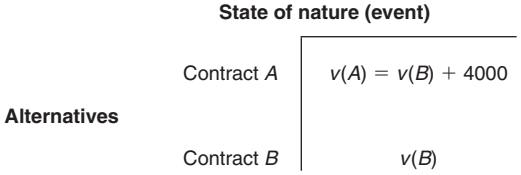

Figure 5-2.3. ***Contract payoff matrix.***

Basically, *expectation* is a weighted average, and to compute its value, one takes the following steps:

1. List all possible alternatives a_i and states of nature (exclusive events) s_j together with the corresponding probabilities $P(s_j)$.
2. Relative to a given fixed state of nature, note the value of each alternative $v(a_i, s_j)$.
3. Calculate $P(s_j) \times v(a_i, s_j)$ as j ranges across all states for each fixed i.
4. Add and note the products for each alternative i.

Consider the situation where a building's lease has just been extended for a 10-yr period, and although the building is fire-safety compliant, the management, in reviewing a number of factors, invite consultants to assess the fire risk with respect to stock. The results of their inquiry are summarized in Table 5-2.1, which reveals pessimistic and optimistic discrete probability distributions for large, medium, and small fires, conditional on there being a fire within the observed stock. The article by Noonan and Fitzgerald[15] discusses such a risk assessment for a warehouse.

The management, who have some understanding of decision theory, agree in the light of the consultant's report to examine the following alternatives:

- Upgrade using a sprinkler system (UUS).
- Upgrade without sprinklers (UWS).
- Retain the existing building (REB).

Increasing the degree of fire protection requires additional investment, and for simplicity it is assumed that a proportion of upgrade costs (dollars) are included in the potential loss values as estimated by management. Also, management, who are neither pessimistic nor optimistic, settle on the following mean probabilities of fire size risk: $P(\textit{large fire}) = 0.5$, $P(\textit{medium fire}) = 0.3$, and $P(\textit{small fire}) = 0.2$. The payoff matrix takes the form shown in Figure 5-2.4.

Hence the expectation for each alternative is given by

$$\text{UUS: } 0.5 \times 24{,}000 + 0.3 \times 16{,}000 + 0.2 \times 8{,}000 = \$18{,}400$$

$$\text{UWS: } 0.5 \times 18{,}000 + 0.3 \times 11{,}000 + 0.2 \times 4{,}000 = \$13{,}100$$

$$\text{REB: } 0.5 \times 30{,}000 + 0.3 \times 15{,}000 + 0.2 \times 5{,}000 = \$20{,}500$$

Table 5-2.1 ***Probability Distribution for a Large, Medium, or Small Fire***

Probability of Fire Type	Large Fire	Medium Fire	Small Fire
Pessimistic case	0.6	0.2	0.2
Optimistic case	0.4	0.4	0.2

		States of nature		
		Large fire	Medium fire	Small fire
		P(*large fire*)	*P*(*medium fire*)	*P*(*small fire*)
		0.5	0.3	0.2
Alternatives	UUS	24,000	16,000	8,000
	UWS	18,000	11,000	4,000
	REB	30,000	15,000	5,000

Figure 5-2.4. ***Payoff matrix showing various outcomes.***

Based on this information, the management would opt for upgrading without sprinklers. The reader should note that the expected value for an alternative is the average cost to the company that would be expected if the decision were repeated a large number of times—it is not the value that would be returned every time. Clearly, if the decision is made only once, the loss could be any of the three values \$18,000, \$11,000, or \$4,000.

Such problems can be represented using a decision tree, as shown in Figure 5-2.5. Taha[20] recommends the following nodal notation—a square (□) to represent a decision point and a circle (○) to represent a chance event. Shields and Silcock[21] offer a tree structure in fire safety terminology. See also the *Guide to Fire Safety Concepts TREE,* NFPA 550.[22]

Decision Making under Uncertainty

Decision making under uncertainty differs from decision making under risk in that in the probability distribution associated with the states of nature, s_j is either unknown or cannot be determined. To overcome this dearth of information, the following models have been developed:

- Laplace paradigm
- Wald (minimax/maximin) paradigm
- Savage paradigm
- Hurwicz paradigm

Each reflects the degree of conservation exhibited by the decision makers in the face of uncertainty.

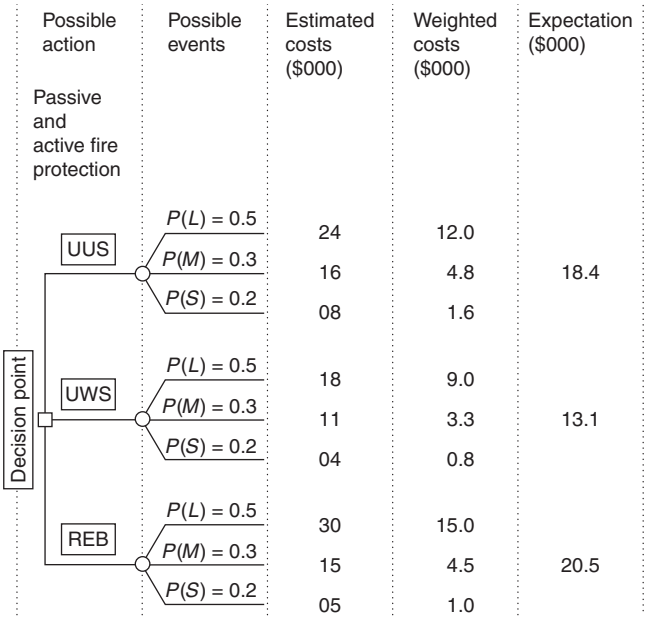

Figure 5-2.5. ***Decision tree to illustrate decision making under risk.***

The Laplace[23] paradigm: This paradigm is based on the principle of insufficient reason.[10] This simply means that, because the probability distribution of the states of nature are not known, there is no reason to believe that they are different. Hence, the j alternatives are evaluated using the optimistic belief that $P(s_j) = 1/n$, where n is the number of states of nature. If the payoff $v(a_i, s_j)$ represents cost (as opposed to gain), then the best alternative is the one that yields

$$\min_{a_i}\left[\frac{1}{n}\sum_{j=1}^{n} v(a_i, s_j)\right]$$

with min changing to max in a gain situation.

The Wald[24] (minimax/maximin) paradigm: The Wald paradigm stems from the conservative attitude of caution—it is a pessimistic criterion of choice in so far as it assumes that the worst will happen. The paradigm aims to get the best out of the worst possible conditions. Given as before, that $v(a_i, s_j)$ is a cost, then the most appropriate alternative selected conforms to

$$\min_{a_i}\left\{\max_{s_j} v(a_i, s_j)\right\}$$

In a gain situation, the operators min and max are transposed.

The Savage[25] paradigm: Often referred to as the Savage regret criterion, the Savage paradigm aims at moderating the pessimistic outlook of Wald's paradigm. Here the payoff matrix $[v(a_i, s_j)]$ is replaced with a regret matrix $[r(a_i, s_j)]$, where the function r is defined as follows:

$$r(a_i, s_j) = \begin{cases} \max\limits_{a_k}[v(a_k, s_j)] - v(a_i, s_j) & \text{if } v \text{ is a gain} \\ v(a_i, s_j) - \min\limits_{a_k}[v(a_k, s_j)] & \text{if } v \text{ is a cost} \end{cases}$$

Regret is the difference between actual outcome and best possible outcome, as in the trivial example of a student who gets 85 percent instead of 100 percent; the student's regret is 15 percent. Likewise, a home owner who pays \$300 for house insurance, when a neighbor insures a similar house with a different company for \$250, experiences a regret of \$50.

The subtlety of moderation in the case of the Savage paradigm over the Wald criterion becomes clear in the following contrived situation. Consider a potential cost matrix where the choice is between a property with smoke

	s_1	s_2	Row max
a_1	90	21,000	$21,000
a_2	20,000	20,000	$20,000 → Minimax

Figure 5-2.6. ***Potential cost matrix.***

	s_1	s_2	Row max
a_1	0	1,000	$1,000 → Minimax
a_2	20,910	0	$20,910

Figure 5-2.7. ***Regret matrix.***

alarms adjacent to the fire brigade (a_1) or one with smoke alarms but 50 miles from the fire brigade (a_2), and the states of nature are s_1 (alarm works) and s_2 (alarm fails) (see Figure 5-2.6). It is clear from the minimax criterion that alternative a_2 with a definite loss of $20,000 is preferable. However, a_1 looks attractive if s_1 is realized with a chance loss of only $90. Clearly, the a_2 alternative is totally conservative.

Now, using Savage's paradigm, the regret matrix in Figure 5-2.7 emerges. The minimax criterion applied to the regret matrix now selects a_1—the less pessimistic option.

The Hurwicz[26] paradigm: This paradigm reflects a range of attitudes from the most optimistic to the most conservative. Letting $v(a_i, s_j)$ represent a cost (or loss), and if t is an index of optimism such that $0 \le t \le 1$, then Hurwicz claims that the most appropriate alternative conforms to

$$\min_{a_i} \left\{ t \min_{s_j} v(a_i, s_j) + (1 - t) \max_{s_j} v(a_i, s_j) \right\}$$

In a gain situation, the operators min and max are interchanged. If $t = 0$, the criterion reduces to the Wald condition, and when $t = 1$, the result is totally optimistic in selecting the best of the best. The decision maker has control over the choice of t, which, in the absence of strong feelings, is taken as 0.5.

Summary Example

The Faculty of Inferno Research Engineers (FIRE) is planning an international conference in Geneva, and FIRE estimates that there are four likely bands of attendance: 150, 200, 250, and 300 attendees. The cost of organization will be a minimum if FIRE can select a venue in Geneva that meets the demand exactly. Clearly, deviations above or below the demand levels incur additional costs resulting from unused seating capacity or lost income opportunities when some of the demand is not satisfied. At the proposed date set for the conference, the organizing committee of FIRE can select one of four appropriate venues that match the corresponding attendance bands. Letting a_1, a_2, a_3, and a_4 represent the alternative venues with respective seating capacities (150, 200, 250, and 300), and letting s_1 through s_4 represent the levels of attendance (150, 200, 250, or 300), the payoff matrix in Figure 5-2.8 summarizes the relative seating and venue costs to FIRE in hundreds of dollars.

The organizing committee applies the above four methods with the results shown below.

- *Laplace paradigm:* If $E(a_i)$ denotes the expectation associated with a_i, then

$$E(a_1) = \tfrac{1}{4}(4 + 9 + 17 + 24) = \$1{,}350$$
$$E(a_2) = \tfrac{1}{4}(7 + 6 + 11 + 22) = \mathbf{\$1{,}150} \quad \text{(Optimum)}$$
$$E(a_3) = \tfrac{1}{4}(20 + 17 + 11 + 20) = \$1{,}700$$
$$E(a_4) = \tfrac{1}{4}(28 + 22 + 18 + 14) = \$2{,}050$$

- *Wald paradigm:* See the matrix in Figure 5-2.9.
- *Savage paradigm:* The regret matrix (See Figure 5-2.10.) is determined by subtracting 4, 6, 11, and 14 from columns 1 through 4, respectively.
- *Hurwicz paradigm:* The data in Table 5-2.2 summarizes the picture for arbitrary t.

		States of nature			
		s_1	s_2	s_3	s_4
Alternatives	a_1	4	9	17	24
	a_2	7	6	11	22
	a_3	20	17	11	20
	a_4	28	22	18	14

Figure 5-2.8. ***Cost payoff matrix.***

	s_1	s_2	s_3	s_4	Row max	
a_1	4	9	17	24	$2,400	
a_2	7	6	11	22	$2,200	
a_3	20	17	11	20	**$2,000**	(Optimum)
a_4	28	22	18	14	$2,800	

Figure 5-2.9. ***Matrix resulting from Wald's paradigm.***

	s_1	s_2	s_3	s_4	Row max	
a_1	0	3	6	10	$1,000	
a_2	3	0	0	8	**$800**	(Optimum)
a_3	16	11	0	6	$1,600	
a_4	24	16	7	0	$2,400	

Figure 5-2.10. ***Regret matrix resulting from the Savage paradigm.***

Table 5-2.2 ***Outcome of the Hurwicz Paradigm***

Alternative	Row min	Row max	t(Row min) + $(1 - t)$(Row max)
a_1	4	24	$24 - 20t$
a_2	6	22	$22 - 16t$
a_3	11	20	$20 - 9t$
a_4	24	28	$28 - 14t$

If you were chairman of FIRE, how would you interpret the above set of results and hence advise your committee on what decision to make?

Multi-Objective Decisions

The above classification examples have one property in common; they all belong to the class of problems where the desired alternative is chosen exclusively on the basis of a single objective—to either minimize cost or maximize gain. When a problem involves two or more objectives, the decision maker must decide on the relative importance of each before analyzing the merits of each alternative. Multiple objectives are often conflicting; for example, a fire authority, in citing a new fire station, might have to balance key objectives such as minimizing cost, minimizing risk, and minimizing travel distance. A problem of this kind never has a correct solution, but the nature of its analysis can offer the stakeholders considerable insight into the quality of any emerging decision.

Terminology

There is a profusion of terminology used in connection with such decision making. For instance, the formal literature uses the terms *multi-attribute decision making, multi-objective decision making,* and *multicriteria decision making* (the terminology preferred by this author) almost interchangeably, and the inexperienced practitioner could well be forgiven for being confused. However, the following definitions should assist the reader who is trying to come to terms with multicriteria decision theory.

Objectives: Objectives are task actions, such as

- To reduce the number of deaths due to unwanted fire
- To improve the level of fire safety in public assembly buildings
- To minimize the number of toxic hazards in the event of a fire
- To maximize the efficiency of fire modeling

French[10] claims that an objective has a dimension together with an indication of the "good" and "bad" ends of the dimension. Thus, to minimize toxic hazards is an objective that indicates that a reduced number of hazards is preferred. This concurs with Keeney and Raiffa,[27] who described an objective as an indication of the preferred direction of change. The performance of a stated objective is measured by its attributes.

Attributes: Synonymous with criteria, attributes are the dimensions of an objective along which alternatives are represented.[10] For example, if alternatives are to be judged against three attributes, picture these as the three axes X, Y, and Z. Then an alternative $\mathbf{a} = (a_1, a_2, a_3)$ is effectively a point in three-dimensional space such that a_1 is in the X dimension, a_2 is in the Y dimension, and a_3 is in the Z dimension. For example, Donegan et al.[28] list the attributes of domestic fire safety evaluation as Occupants, Doors, Communications, Internal Planning, Travel Distance, and Flues/Ducts. In mathematical terms, these represent a six-dimensional attribute space in which, for example, a domestic norm $\mathbf{n} = (n_1, n_2, n_3, n_4, n_5, n_6)$ can be used as a comparator against which to judge the m alternatives $\mathbf{a}^k = (a_1^k, a_2^k, a_3^k, a_4^k, a_5^k, a_6^k)$, where $1 \leq k \leq m$. It is not the intention of this article to dwell on mathematical formalism; the interested reader will find a full axiomatic treatment in French.[10]

Value and utility: For each alternative facing a decision maker, it is conventional to measure the alternative's attractiveness by means of a numerical score aggregated from the attribute scores. If the decisions involve no element of risk or uncertainty, scores are described as *values* of the course of action; otherwise they are known as *utilities* of the course of action. This article, given its introductory status, will restrict its illustrations to the former. For an introduction to utility theory and an excellent account of its application in decision making, with special reference to insurance risk, see Ramachandran.[29]

Weighting: Although the decision maker has chosen, or agreed on, a set of attributes, it does not mean that each attribute has the same merit. Each attribute will rate a degree of importance, but the actual cardinal priority of the attributes is seldom obvious. Although a decision maker familiar with the task in hand might intuitively identify the ordinal priority, it is usually necessary to employ a formal process to arrive at credible weights. Such a process may be as informal as the Delphi method[30] or as formal as the eigenvector technique of the analytic hierarchy process.[31] More will be said of these processes later in this chapter. Figure 5-2.11 summarizes the problem environment.

Dominance: An alternative X is dominated if another alternative Y is "better" in at least one attribute and performs equally with respect to the remaining attributes. This definition permits the initial screening of alternatives in so far as all dominated alternatives are discarded.

Satisficing: The word *satisficing* is probably a contraction of *sufficient to satisfy,*[32] although Watts[33] believes the term was coined by Simon[34] for identifying a solution that is good enough although not necessarily optimal. The method of satisficing, often referred to as the conjunctive method, is purely a screening technique. In order for an alternative to be acceptable, it must exceed stated performance thresholds for all attributes. This compares with the norm strategy used by Shields et al.[35] in their fire safety evaluation of public assembly buildings.

Disjunctive: The term *disjunctive* also applies to screening. Disjunctiveness is the logical complement of satisficing in that an acceptable alternative must exceed a given performance threshold for at least one attribute.

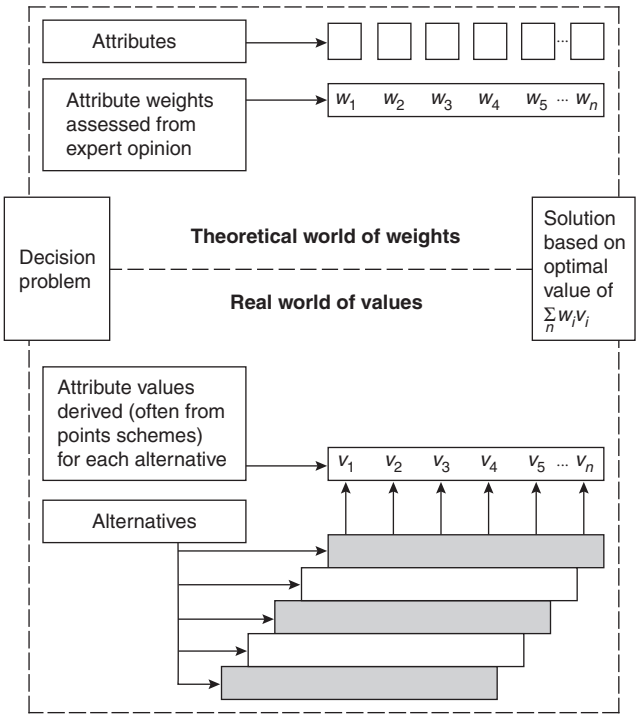

Figure 5-2.11. ***Attributes, values, and weights.***

Additive weighting: The additive weighting method will be demonstrated later in this chapter. Basically, the score attached to an alternative is equal to the weighted sum of its attribute preference valuations (frequently, the generic term *utilities* is used, albeit in the absence of probability distributions). The weights are subjective percentages of importance given to each attribute label. The resulting weighted sums for each alternative can be used to rank, screen, or choose an alternative. It has been shown that, provided trade-offs among the attributes in any subset of the attributes do not depend on the levels of the remaining attributes, the additive weighting model can be applied without reservation. The trade-off proviso is described by Keeney and Raiffa[27] as preferential independence, which is neatly formalized in French.[10]

Simple Multicriteria Illustration

Consider the situation where a new fire station is to be located in a large conurbation offering five potential sites—A, B, C, D, E. Deciding on the most appropriate site is a nontrivial matter, and as with any building project, there are costs and benefits to be considered. This illustration will focus only on the benefits of siting, with considerable simplification to ensure transparency of the methodology. The technique is based on the Simple Multi-Attribute Rating Technique (SMART) of Edwards,[36] and the stages in the process are outlined as follows:

Nominate the decision maker(s) (DM): In this case, an architect is charged with this responsibility. Group decision making is possible (see Goodwin and Wright[37]).

Recognize the alternatives: The alternatives correspond to the siting locations A, B, C, D, E.

Identify the attributes: The attributes are usually finalized with the assistance of a value tree, such as Figure 5-2.12. Here the architect identifies two main predesign attributes, called Site and Situation, and also specifies their subattributes, that is, criteria that can be readily assessed or valued with respect to each site—Spatial Access, Road Infrastructure, Area Fire Statistics, Site Dimensions, Site Bearing Capacity, and Planning Freedom.

Assess each alternative: Using the six attribute labels, the architect assesses each site (alternative) and assigns to it a corresponding attribute value, v_i $(1 \leq i \leq 6)$. The valuation of site attributes can be carried out using direct measurement (if appropriate), a logical points scheme, or, as the architect chose to do in this case, a simple linear rating scale from zero, meaning horrible, to 100, meaning best possible. Attribute valuation using the linear rating scale approach is succinctly discussed in Edwards and Newman.[38] An interesting and instructive observation made by these authors is that a curved (nonlinear) value function almost never makes any difference to the decision. The architect's survey reveals the matrix of values shown in Figure 5-2.13.

Determine a weighting factor w_i(1 ≤ i ≤ 6) for each attribute: The weighting factor could reflect the decision maker's point of view, or a consensus point of view derived from experts. In any event, there are a number of specialized techniques for obtaining such weights, and these will be discussed later in this article. Suffice for the present example that the architect has access to weights. Thus, Spatial Access (26%), Road Infrastructure (34%),

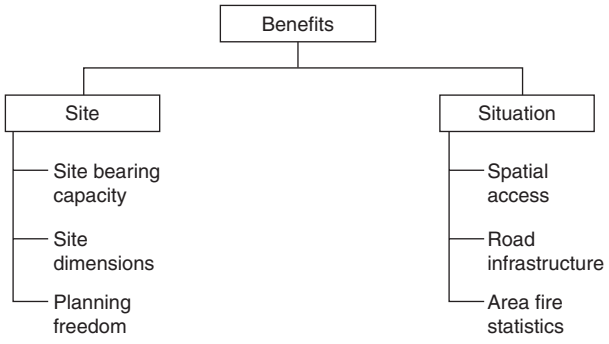

Figure 5-2.12. ***Value tree for fire station location problem.***

	A	*B*	*C*	*D*	*E*
Spatial access	70	75	65	45	55
Road infrastructure	95	15	75	65	35
Area statistics	25	95	05	25	55
Site dimensions	45	25	05	50	95
Bearing capacity	60	05	05	25	85
Planning freedom	70	25	95	85	65

Figure 5-2.13. ***Architect's attribute-scale values.***

Table 5-2.3 ***Values and Weights for Each Site***

Attribute	Weight	Site A	B	C	D	E
Road infrastructure	0.34	95	15	75	65	35
Spatial access	0.26	70	75	65	45	55
Bearing capacity	0.19	60	5	5	25	85
Site dimensions	0.10	45	25	5	50	95
Area statistics	0.08	25	95	5	25	55
Planning freedom	0.03	70	25	95	85	65
Aggregate benefits		70.50	36.4	47.10	48.10	58.20

Area Statistics (8%), Site Dimensions (10%), Bearing Capacity (19%), Planning Freedom (3%). Note that the weights are in percentages, which must sum to 100 percent, or if stated in decimal format, they should sum to 1.

Take a weighted average of the values assigned to each site (alternative): See Table 5-2.3. The weighted average will give the architect a measure of how well a particular site performs over all the attributes. The weighted average (aggregate benefit) is obtained from the sum $\sum_{i=1}^{6} w_i v_i$.

Make a provisional decision: The apparent answer is site A, but the architect must be reassured, and therefore must check the robustness of the results as follows.

Carry out a sensitivity analysis to test the robustness of the decision: The sensitivity analysis is an important aspect of the analysis that is often overlooked in practice, yet it is perhaps the most revealing part of the process and can contribute significantly to the decision maker's understanding of the problem. It is imperative that the procedure not be haphazard. The following strategy is recommended in Goodwin and Wright.[37]

The architect, upon reflecting on the above results, notices that the Situation attribute accounts for 34% + 26% + 8% = 68% of the benefit's weighting, whereas Site features account for the remaining 32%. Accordingly, before giving a formal decision, the architect proceeds to investigate the consequences of varying the weight attached to Situation. Figure 5-2.14 summarizes how the value of benefits for the different sites varies with changes in the Situation weights. The graphical technique is based on the following proposition: If Situation, for example, had a weight of zero, this would imply that the three corresponding attributes (Spatial Access, Road Infrastructure, Area Statistics) would each have zero weights. Correspondingly, the weights of the six lowest attributes would be Spatial Access (0), Road Infrastructure (0), Area Statistics (0), Site Dimensions (10), Bearing Capacity (19), and Planning Freedom (3). When normalized and rounded, these amount to 0, 0, 0, 60, 31, and 9, respectively, as shown in Table 5-2.4. It is not difficult to draw the corresponding graphs for each site, as shown in Figure 5-2.14.

It is evident from the graphs that a zero weighting on Situation would immediately elevate site E to priority status. This status would maintain so long as the weight attached to Situation is less than 48.2 percent. However, this

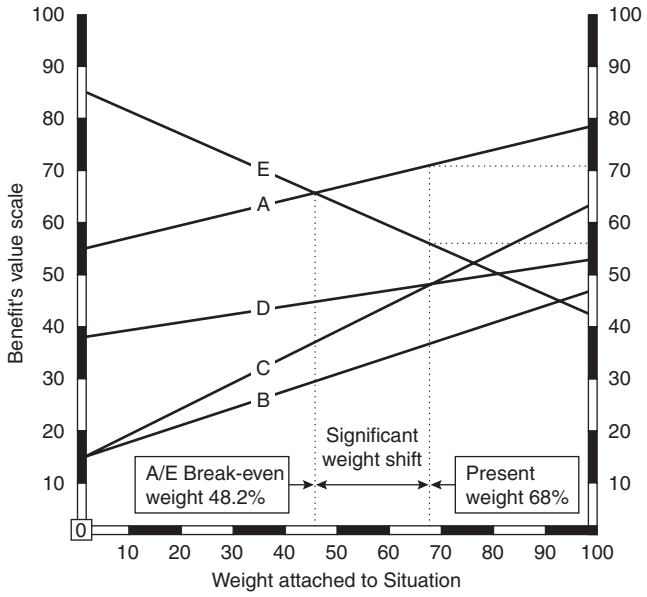

Figure 5-2.14. ***Sensitivity analysis for weight attached to Situation.***

Table 5-2.4 ***Values and Weights When Situation Is Zero Weighted***

Attribute	Weight	Site A	B	C	D	E
Road infrastructure	0.00	95	15	75	65	35
Spatial access	0.00	70	75	65	45	55
Bearing capacity	0.60	60	5	5	25	85
Site dimensions	0.31	45	25	5	50	95
Area statistics	0.00	25	95	5	25	55
Planning freedom	0.09	70	25	95	85	65
Aggregate benefits		56.25	13.00	13.10	38.20	86.30

is clearly significantly lower than the professionally judged figure of 68 percent. The tangibility of the attributes in this example provides little scope for opinion variance, particularly among experts, and therefore it is unlikely that the opinion swing required to put site E in the frontier of consideration is likely to happen. The architect would be justified in the recommendation of site A.

A similar approach could be taken with the lower-level weights. For example, the architect may be instructed to explore the effect of varying the weights attached to Road Infrastructure and Spatial Access while keeping the weight attached to Area Statistics constant. Such in-depth analyses are clearly worthwhile when large amounts of resources are being expended. The reader is reminded that this example dealt only with the multicriteria related to benefits; it did not address the issue of costs and the relationship between costs and benefits. A useful discussion on trade-off between costs and benefits, pitched at the level of this example, can be gleaned from Goodwin and Wright.[37]

Fire Safety Attribute Weighting

Rational solutions for many of today's decision-making problems in fire safety evaluation are difficult to formulate. This is often due not only to the complexity of the problems themselves, but also to the vagueness (also referred to as "fuzziness") of certain concepts. Despite the increased accessibility of modern computing technology, the complexity factor can be handled only by the introduction of a multi-attribute structure into the elements of a problem. Consistent judgments of weight and value must be made on individual fire safety attributes to enable an overall assessment; and it is important to distinguish the tasks involved (see Figure 5-2.11). Finding attribute weights is a theoretical exercise that, for many evaluation problems, reduces to finding a cardinal ranking of criteria (see Watts[6]). On the other hand, finding the corresponding values for each alternative is a real-world exercise, which can involve complex points schemes and specialized economic functional analysis. The buoyant literature devoted to both tasks is conveniently reviewed by Watts.[39] Definitive articles are presented by Nelson and Schibe,[40] Marchant,[41,42] Stollard,[43] Shields et al.,[44] and Dodd and Donegan.[45,46]

The generally accepted attribute levels—objectives, tactics, and components—are shown in Figure 5-2.15, with nomenclature attributed to Marchant.[41] The levels conform to a hierarchical structure with decreasing generality from the apex.

The Hierarchy Philosophy

The example in the preceding section, "Simple Multicriteria Illustration," did not discuss strategies for obtaining the weights of criteria or attributes. These strategies have a vast and specialized literature within the realm of decision theory, but the accepted nature of attribute decomposition within fire safety evaluation has enabled the following distillation of methods.

These all hinge on the structure of a fire safety evaluation hierarchy, shown in Figure 5-2.15. Typically, if the key objective or policy is "fire safety," the next level of the hierarchy lists the secondary, or supporting, objectives—"to save lives" and "to protect property." Sometimes a third objective, "to prevent conflagration," is included, but this will be dictated by the environment of the problem. These objectives are very general, and their balance of importance can be crucial to the ranking outcome of a set of weights (see Dodd and Donegan[45]). The next reduced level of generality comprises the tactics that would be employed by a safety analyst in support of the objectives. For example, "to improve egress capability" or "to facilitate rescue" would be recognized tactics in support of "life safety." At the components level, usually the lowest level, the criteria are chosen to identify with the tactics, but at a much lower level of generality. Each component is seen as a pragmatic dimension to which an engineer can attach a value when surveying an alternative. Most components have long lists of subcomponents, which are useful when seeking an attribute value. The value emerges as a synthesis of scores or points attached in some logical manner to each subcomponent. A typical component could be "doors" and these would be valued on the basis of subcomponents such as "dimensions," "fire resistance," "glazing," or "intumescent stripping."

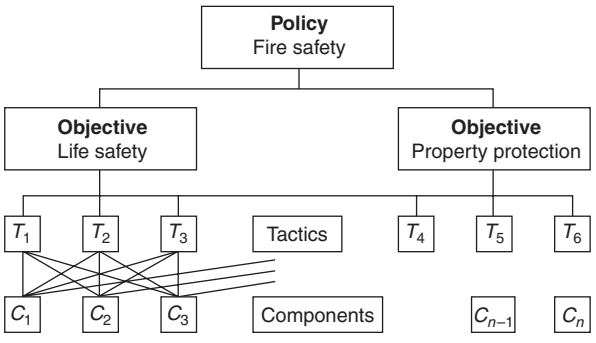

Figure 5-2.15. ***Typical fire safety evaluation hierarchy.***

Effectiveness Matrices

Effectiveness matrices are opinion matrices. (The term *effectiveness matrix* is taken from Lai and Hopkins.[47]) Already, it has been stated that attributes are dimensions along which alternatives can be represented. However, it is possible, as follows, to extrapolate this idea to cater for the cardinal ranking of fire safety components relative to the stated policy. Assume that there are m components, n tactics, and k objectives. A decision maker (DM) can represent each component as a vector of tactics, and, a fortiori, the set of components as an effectiveness matrix $[c_{ij}]_{m\times n}$ in which the rows represent components, and the columns represent tactics. The element c_{ij} is the numerical equivalent of DM's opinion as to the importance of the ith component relative to the jth tactic. Similarly, each tactic can be represented as a vector of objectives, the set of tactics being represented by the effectiveness matrix $[t_{ij}]_{n\times k}$, where t_{ij} represents the importance of the ith tactic relative to the jth objective. Finally, DM declares the importance of each objective relative to the stated policy in the effectiveness matrix $[o_{ij}]_{k\times 1}$ (vector, since there is only a single policy). The product of the three effectiveness matrices,

$$[c_{ij}]_{m\times n} \times [t_{ij}]_{n\times k} \times [o_{ij}]_{k\times 1}$$

yields the components-to-policy vector, which, when linearly normalized gives the required attribute weightings.

The preceding numerical routine is the same for all weighting methods. Any differences in the routine relate to the determination of the effectiveness matrices. These are discussed in the next section using notation that has previously appeared in fire research literature.

Weighting Methods Used in Fire Safety Evaluation

The hierarchical model is amenable to either cross impact analysis or analysis involving pairwise comparisons. These two analysis methods will be discussed in some depth. In either case, the aim is the attachment of subjective weights to all of the objectives, tactics, and components, so that in vector form, components are pri-

oritized with respect to each tactic; tactics are prioritized with respect to each objective, and finally, objectives are prioritized with respect to policy. Ultimately, the decision weight vectors at each level are grouped in matrix format (effectiveness matrices) such that, if they are identified as

C/T—the components-to-tactics matrix
T/O—the tactics-to-objectives matrix
O/P—the objectives-to-policy matrix

then the matrix product **C/T** × **T/O** × **O/P** yields a components-to-policy vector that, when normalized, gives the desired prioritization weights.

Edinburgh Cross-Impact Analysis

This unformalized approach used in the Edinburgh model, attributed in the main to Marchant,[41] is perhaps the most basic form of cross-impact analysis. The decision maker uses a pseudo Likert scale having values from 0 (least important) to 5 (most important). A Likert scale (named after its inventor) is used to measure a respondent's level of agreement on some issue. The values may be considered to be ordinal, ranging from least agreement to most agreement.[48] The decision maker uses the Likert scale to assess the importance of each element on a given hierarchical level relative to each element of the next-highest level, and produces a corresponding effectiveness matrix. When more than one decision maker is involved (as is usually the case), a consensus matrix that summarizes all the decisions can be calculated. The dimensions of all the resulting matrices for the complete hierarchy permit their consecutive multiplication, as shown in the previous section. It is noteworthy that Edwards et al.[49] have shown that judgments of magnitude, while amenable to semantic scaling (classical Likert), "are best when made numerically." This characterizes the pseudo Likert scale (see the discussion in the subsection titled "Interval Scale" later in this chapter).

The simplicity of the cross-impact approach has an obvious appeal because of its acquiescence with intuition. The input data are essentially bias-free, absolute values chosen from a Likert-type scale; there is no limit to the number of elements at a single level, and reasonable precision can be used in determining scores. The lack of uniformity among experts in their perceptions of component independence is accommodated by an *interaction percentage contribution matrix (IPCM).* This is a component-to-component square matrix showing the degree to which the contribution of a component to fire safety is enhanced by the interaction of other components. The reader will find an example in Stollard.[41]

Hierarchical Cross-Impact Analysis (HCIA) Methodology

Hierarchical cross-impact analysis (HCIA) is a multiattribute weighting strategy developed at the University of Ulster using a similar philosophy to the Edinburgh approach. The characterization of HCIA, fully developed by Donegan et al.,[28] addresses the cross-impact approach at two levels—the fundamental level and the pragmatic level. In the *fundamental level*, a pseudo axiomatic approach is taken to

- Define a hierarchy in relation to fire safety
- Explain the meaning of interactive importance
- Propose the notion of a partial impact
- Define a total impact
- Introduce sequential perturbations

In the *pragmatic level*, a modeling approach is taken to

- Maintain the assessment interval through each stage of the quantification
- Stretch the component ranking intervals to enhance the important components and decrease the psychological significance of the less-important components
- Perturb consensus weightings with interaction noise

HCIA methodology formalizes many aspects of the Edinburgh approach. It uses a similar hierarchical cross-impact analysis over the different levels in the system, but allows for interactions between issues at the same level by the use of perturber matrices. Again, it can be used only for hierarchical networks.

Using the attribute terminology outlined above, the partial impact of tactic T_j on component C_i relative to the rth objective O_r is written and defined as

$$\partial I(C_i/T_j)_{O_r} = (C_i/T_j)(T_j/O_r)$$

The total impact of the collection of tactics on C_i relative to O_r is then defined as

$$\sum_{j=1}^{n} \partial I(C_i/T_j)_{O_r} = \sum_{j=1}^{n} t_{ij}\sigma_{jr}$$

which is clearly a matrix product. The elimination of the tactics collection of attributes is completed by defining the interaction

$$C_i/O_r = \sqrt{\frac{1}{n}\sum_{j=1}^{n} t_{ij}\sigma_{jr}}$$

thus giving a components-to-objectives interaction matrix. Similarly, the objectives collection of attributes is eliminated leaving a components-to-policy vector.

The pairwise comparison perturbation matrices, utilized at all the levels in the hierarchy to eliminate the problems of interdependence of issues, are symmetric and generally sparse. These adjust for "noise" in the system resulting from vagueness in the definitions of the attributes at each level.

While the forced stretching of the final vector as described in Donegan et al.[28] was purely subjective and appeared to have some significance at that time, it was recognized that such a strategy was contextually motivated and, unless unanimously adopted by the fire research community, could result in serious obfuscation. Research reported in Dodd and Donegan[45] points to indigenous stretching as a naturally occurring feature of some scales and therefore a factor in scale choice. Although research by Saaty and Vargas[50] illustrates how particular measurement techniques are more appropriate in certain situations, there is the concomitant psychological impact on scoring that results from the manner in which a question is posed—see, for example, the paper by Salo and

Hämäläinen.[51] Insufficient contextual research to date leaves this psychological issue unresolved.

In spite of its formality, HCIA, just like its parent the Edinburgh model, suffers from one serious drawback—the absence of a consistency check. Even in the short time taken to score a set of issues, mood changes, tiredness, or lack of concentration can influence judgment. Short of an alternative to cross-impact analysis, no reliable quality measure has yet been devised to allay this shortcoming. It was this concern that prompted Shields and Silcock[52] to consider using the analytic hierarchy process due to Saaty.[31]

Analytic Hierarchy Process (AHP)

The analytic hierarchy process (AHP) is a procedure that has been widely recognized and used as a method of prioritizing the elemental issues in complex problems in a variety of applications (see, for example, Rahman and Frair,[53] Liu and Xu,[54] and Vachnadze and Markozashvili[55]). Unlike traditional multi-attribute techniques, AHP permits the integration of alternatives into the hierarchy, a merging of the real and theoretical worlds depicted in Figure 5-2.11, though this is not an essential requirement of the process. AHP can also be used as a means of weighting attributes, if desired; it is this latter option that is of concern here. The procedure entails the comparison of all the pairs of individual attributes at each level relative to each attribute in the superior level. The intrinsic complexity of the process prohibits a simple description.

The technique is based on the fact that for a square matrix, **C,** of nonnegative real numbers representing, for example, pairwise comparisons of the importance of component attributes of the hierarchy with respect to one element of the next-higher tactics level, there is a dominant eigenvalue, λ, and a corresponding right eigenvector, **x,** emerging from the characteristic equation $\mathbf{Cx} = \lambda\mathbf{x}$. Given that $\mathbf{C} = (c_{ij})$, where $c_{ij} > 0$ and $i, j = 1, 2, 3, \ldots, m$; and given that $c_{ij} = 1/c_{ji}$ and the consistency condition $c_{ik} = c_{ij} \times c_{jk}$: $i, j = 1, 2, 3, \ldots, m$ holds; then it is easily shown that $\lambda = m$ and, by virtue of the fact that **C** is of unit rank, the remaining $m - 1$ eigenvalues are each zero. For such a matrix, any column is essentially the dominant right eigenvector of priorities (weights). In reality, it is unreasonable to expect decision makers to be perfectly consistent, although a fair degree of consistency is expected. Variations from perfect consistency in **C** perturb the eigenvalues such that $\lambda > m$,[31] the proximity of the maximum eigenvalue to the order of **C** being an indication of the consistency.

The corresponding eigenvector is normalized and the procedure repeated for each tactic in the tactics collection. The set of dominant eigenvectors is considered as an effectiveness matrix of priorities (**C**/**T**) between components and tactics. Similarly, priority effectiveness matrices are established for tactics to objectives (**T**/**O**) and for objectives to policy (**O**/**P**). A combined matrix multiplication (**C**/**T**)(**T**/**O**)(**O**/**P**) yields a component-to-policy priority (weighting) vector. In the calculation of such priorities, the matrix entries are selected from a statistically optimized set of Saaty's weightings:

$$S = \left\{\frac{1}{9}, \frac{1}{8}, \frac{1}{7}, \frac{1}{6}, \frac{1}{5}, \frac{1}{4}, \frac{1}{3}, \frac{1}{2}, 1, 2, 3, 4, 5, 6, 7, 8, 9\right\}$$

Consider, for example, the situation where five components, C_1 to C_5, must be prioritized with respect to, say, tactic T_3. The decision maker indicates the relative importance of C_1 and C_2, C_1 and C_3, C_1 and C_4, and so on, on a scale of 1 to 9. A score of 1 on this scale implies that the two components being compared are "of equal importance," whereas a score of 9 signifies that one of the components is "of absolute importance" relative to the other. The intermediate scores indicate varying degrees of importance between the two extremes. Obviously, the importance of any component relative to itself is unity, and the law of reciprocity holds; that is, if C_1 rates a score of 3 against C_2, then C_2 rates a score of 1/3 against C_1, and so on. Thus, these pairwise criteria comparisons by the decision maker can be incorporated into a "positive reciprocal" (terminology used by Saaty[31]) decision matrix, as shown here.

$$\begin{bmatrix} & C_1 & C_2 & C_3 & C_4 & C_5 \\ C_1 & 1 & 3 & 2 & 2 & 1 \\ C_2 & \frac{1}{3} & 1 & \frac{1}{4} & \frac{1}{4} & 2 \\ C_3 & \frac{1}{2} & 4 & 1 & \frac{1}{2} & 3 \\ C_4 & \frac{1}{2} & 4 & 2 & 1 & \frac{1}{5} \\ C_5 & 1 & \frac{1}{2} & \frac{1}{3} & 5 & 1 \end{bmatrix}$$

Such a matrix is a typical response from a decision maker; if it were perfectly consistent, then the eigenspectrum would be {5,0,0,0}. However, a simple calculation shows the spectrum to have a right dominant eigenvalue, λ, of 6.7 and a corresponding normalized dominant right eigenvector of [0.25, 0.14, 0.19, 0.19, 0.24] in this case. Saaty[31] defines a consistency index,

$$CI = \frac{\lambda - k}{k - 1}$$

where k is the order of the matrix, and a corresponding consistency ratio

$$CR = \frac{CI}{\text{Random consistency number}}$$

Saaty[31] provides a list of random consistency numbers, which are reviewed and updated by Donegan and Dodd.[56]

The consistency check is designed to provoke the decision maker into reconsidering the entries in the decision matrix should the consistency ratio be unacceptable—for example, greater than 10 percent.

Difficulties with AHP: The main user criticism that can be labeled against the procedure is the number of questions that must be posed to busy experts in the exhaustive completion of a questionnaire structured around a given hierarchy. This is particularly frustrating to a research manager who may experience attrition of experts on having to elicit expert opinions on a number of rounds in pursuit of consensus. The availability of convenient AHP

analysis software such as Expert Choice (by Decision Support Software Inc., in Pittsburgh) does not reduce this particular inconvenience at present. Perhaps, with increasing World Wide Web facilities and new methods in survey computing, the problem will not be so manifest. Implicit in this main criticism is the problem associated with obtaining group consensus in AHP. The question of whether to obtain consensus among experts before inputting the data into AHP, or whether to seek vector consensus when each expert's weighting vector has been evaluated, is discussed with an illustration of both methods in Tung.[57]

Criticisms of a theoretical nature continue to be debated in the technical literature stemming from the paper by Dyre,[58] but these are really of academic interest only and should not inhibit the potential user. Perhaps the most abused criticism is that of *rank reversal,* which, among other things, refers to the possibility that ordinal changes can take place in a list of remaining attributes when one is removed from the analysis. The debate is far from being settled, but as AHP was developed by Saaty, it is not unreasonable to quote his view on the concept of rank reversal:[59]

> An important question in decision making is whether adding new alternatives to a decision structure should or should not affect the rank of the old ones. It was once thought that irrelevant alternatives should not affect their rank. But experiments reported in the literature have shown that rank reversal can occur for many different reasons. The decision to preserve rank depends on whether the number of alternatives added, and how good they are, influences preference among the old ones. The AHP has a procedure to preserve rank, as in buying a best computer even if there are many like it, and another to allow rank to change, as in buying a beautiful tie if there are many like it.

The different opinions and complex arguments are beyond the scope of this article, but users of proprietary AHP software will have a mode selection option that will facilitate either rank reversal possibilities or absolute rank preservation.

Measurement

Measurement is defined as the assignation of a number to the entity under consideration in accordance with a rule; this number then reflects the measured property of the entity.[60] In mathematical terminology, the measurement is the image under a *monotonic,* that is, order-preserving, mapping of the dimensional property into a real line. Measurement of the physical entities encountered in experimental work presents a large number of fundamental problems that must be recognized by researchers. For example, the precision of the result cannot exceed the precision of any of the data used in its calculation. Thus, a result to ten significant digits is pointless when even one item of the contributory data is approximated to two significant figures. This is why 10.000 is not the same as 10; the former indicates that the measuring equipment allowed for measurements of three decimal places, and the "correct" result is therefore between 9.9995 and 10.0005, whereas the latter shows much less precision—between 9.5 and 10.5.

Further allowance must be made for experimental error. Many external factors (e.g., heavy road traffic outside the laboratory) can introduce random elements into the measuring process. These factors, however small, must be taken into account in the result. Systematic errors, caused by a bias in the measurement process, assume an even greater significance with the introduction of opinions, which can compromise the work and should be eliminated. The opinion problem is present in most questionnaire design. These opinions, or psychological components, where linearity is less measurable can jeopardize experimental results (see detailed discussion in Viek and Wagenaar[13]).

Scaling

The four types of scale most relevant to fire protection engineering are (1) nominal, (2) ordinal, (3) interval, and (4) ratio. Each scale, in order, represents progressively stronger properties.[61]

Nominal scale: The values on a *nominal scale* classify or categorize the objects represented; in other words, no information on size is implied. For example, the number identifying food items on a menu or the room number in an office block might be regarded as nominal scales. The property common to such items is the *category property.* Many coding systems are nominal scales. For example, the computer system of a car dealer might store car type as a single digit: 01 for Ford, 02 for General Motors, 03 for Lincoln, 04 for Buick, and so on. Such a number does not reflect the size or power of the car; it merely indicates the manufacturer. Similarly, fire extinguishers might be classified by type: 1 for water, 2 for CO_2, 3 for halon, and so on. However, the numbers 1 to 3 have no implications with regard to quality.

Ordinal scale: The *ordinal scale* not only characterizes the entities represented, but also ranks or orders them. However, proportion is not necessarily maintained. This type of scale is exemplified by examination grades: in a descending scale, a grade 2 is better than a grade 3, but one cannot say by how much. Glenburg[61] offers the stripes on military personnel as an ordinal scale: a sergeant (3 stripes) is "superior" to a corporal (2 stripes), but it is nonsense to argue that the sergeant is one and a half times as authoritative. Ordinal scale examples abound in organizations; one example is the ranking of daily tasks in order of priority.

Interval scale: More mathematically tractable and, hence, of greater importance in quantitative assessments, the interval scale is a continuous scale between two points, for example, from 0 to 10, or 1 to 5. Relative difference is maintained; that is, equal intervals of the scale have the same meaning. For example, the effective difference between 1 and 2 is exactly the same as the effective difference between 4 and 5. An example of an interval scale is a ruler or similarly graduated device. Celsius and Fahrenheit temperature scales are interval, and the *equal*

intervals property, or *relative difference property,* is essential when one scale is converted to the other. Arithmetic-based operations involving addition, subtraction, and multiplication by a scalar (a number with no units) can be used on numbers from an interval scale.

Not infrequently, the integer range from 0 to 5 has been used to assign relative values of importance to the attributes of a fire safety hierarchy. The adoption of this numerical range over a spectrum of attributes, described in the literature (e.g., Dunn Rankin[62] and Torgenson[63]) as a Likert-type scale, entails a consideration of its validity in terms of the measurement it achieves. Strictly speaking, the scale is ordinal since it cannot be taken for granted that the distances between attributes are equal. Kumar[64] states that a Likert scale is based on the assumption that each item (attribute) has a priori equal attitudinal value (importance or weight) in terms of reflecting an attitude (from 0 to 5) toward the issue in question, which in the context of fire safety attribute weighting is not the case. Nevertheless, the work of Schiebe et al.[30] has demonstrated that the error in assuming the equal interval property is not significant. Hence, the results obtained from such measurements can be used in combinatorial calculations.

Ratio scale: The *ratio scale* is an interval scale with the *absolute zero property;* in other words, one end is fixed so that the values on it are absolute rather than relative. For example, the Kelvin (K) scale relates temperature to absolute zero temperature, at which all motion ceases. This scale is fundamental to the operation of AHP (see the previous section titled "Analytical Hierarchy Process"), and due consideration must be given to the entity of measurement. For example, a body having a temperature of 40°C indicates twice the temperature of another body at 20°C, but not twice the heat content, which must be referred to the absolute zero of temperature, −273°C.

Panels of Experts

The development of expert systems and case-based reasoning tools implies an underlying assumption as to the meaning of expertness. Consequently the assessment of expert opinion using, for example, a Delphi process, may lead to conclusions that, without some formal insight, could on some occasions be considered ambiguous. A review of Delphi literature (Rowe and Wright[65]) will not solve this problem, since Delphi researchers fail to define the term *expert* as applied to their study. If, in simplistic terms, an expert is regarded as one practiced or skillful within the area of consideration, there is an intuitive extrapolation as to the notion of expertise, and the assessment of expert opinion relies to some extent on a global understanding of this extrapolation. In general, the expert response must conform to some form of measurement criterion in relation to consensus if any conclusion is to be reached on any issue that is the subject of expert opinion.

On the assumption that more heads are better than one in achieving a balanced view, many different forums for assessing group opinion have been utilized over the years (see Schiebe et al.[30]). Some of the most common means of assessing group opinion are discussed as follows.

Committee

The traditional method of forming group opinion is the committee. Under the guidance of a (impartial) chairperson, the issue is isolated (if necessary) and debated, with consensus determined by a majority vote. Besides the obvious discrepancy that a majority and consensus are not synonymous, the recognized difficulties with the method are the existence of one dominant member, and group pressure upon an individual to conform (the herd instinct). Thus, the resultant group pronouncement may not be at all representative of the group.

Nominal Group

A committee is strictly a subgroup of a large organization from which its authority is derived. More relevant to a panel of experts, that is, the pooling of considered opinion, are nominal groups and variations thereof. In this situation, the alternatives are created by the panel members when they are each outside the group context. The individual members' lists, circulated before meetings, are then pooled. Personality issues are reduced, the dominant member should be the member best prepared, authorship of ideas is on record and cannot be disputed, and preconsideration should reduce the herd instinct.

Delphi Panel

Of more rigorous delineation is the Delphi panel (Linstone and Turoff,[66] Render and Stair,[67] Wheelwright and Makridakis,[68] Rowe and Wright[65]), devised as a method of obviating the practical difficulties inherent in the committee concept. In the Delphi panel, the group members never meet physically; all communication is through a group controller or coordinator who selects the members of the panel, presents the basic problem, and informs the individuals in the group of progress to date (feedback). When the atomic or elemental issues that constitute the main problem have been determined (the qualitative phase), consensus is sought on the quantitative value to be ascribed to each of these issues (statistical response).

A series of rounds of voting is held. After each round the group controller returns to each panel member his or her scores together with a measure of the group opinion on each issue. The panel members are then asked if they wish to revise their opinions. The process is repeated until group opinion has converged sufficiently to be described as consensus, or until it is recognized that a consensus is unattainable. Unanimity is less important in the method than the absence of group pressure.

The two essential characteristics in a Delphi panel are (a) the anonymity of panelists and (b) feedback (histograms, measures of central tendency, or analytic consensus). The former eliminates the problem of the dominant member and group pressure to conform. However, a new problem is introduced—a considerable time scale is involved in the sending and receiving of questions and answers. While this (at least) theoretically guarantees a considered opinion, a substantial attrition rate is almost inevitable. Members of the group lose interest, change jobs, or become otherwise indisposed. Also, the group

controller has a role of far greater significance than a committee chairperson; only a high level of awareness on his or her part can prevent the unconscious bias that might be introduced. Other doubts about and difficulties with the method are summarized by Marchant,[69] Shields et al.,[70] Sackman,[71] and Ayton et al.[72]

Computer Conferencing

Modern technology enables remote participation in group discussion. Participants input their views into a computer system, and their views are circulated to the other panelists for comment and reply. A suitable schedule allows either a quick result or a more leisurely, considered process. Anonymity is optional.

This concept can be combined with others, for example, the Delphi method, with a reduction of time scale and consequent diminishing of attrition (i.e., drop-outs). Further, if a computer system for analyzing these data exists, the results may be obtained almost instantaneously. Hence, the group may have access to the consequences of their polling before their views are forgotten. The almost universal availability of the Internet and ISDN developments in survey computing are already having a considerable impact on this type of conferencing.

DACAM Group

A DACAM group[73] is an alternative method of overcoming the problem with committees. Here, the group meets physically but is divided (usually systematically) into subgroups for discussion sessions. Between each session, representatives from the subgroups meet to compare progress and coordinate the agenda for the next session. In this way, the dominant member, being limited to one subgroup, is less influential on the group decision.

While this method guarantees a quick result (e.g., in a day), the facility to organize such a group is dependent on at least substantial goodwill, if not considerable finance.

Consensus

The notion of consensus is very much an intuitive one. In politics, there is "consensus" on a policy that is acceptable to a majority. If no consensus exists, then it can often be achieved by broadening the policy. However, the concept is very largely negative in that the emphasis is on avoidance of what is intolerable to others.

The nature of consensus depends on the context or terms of reference of the problem. For example, the arrangement of a number of options in order of importance or preference (comparative consensus) is essentially different from assessing the importance of a single elemental issue within the problem (definitive consensus).

Definitive Consensus

Definitive consensus involves panel members who assign to each issue a score chosen from a Likert-type scale, that is, a range of values, such as (0,10) or (0,5). For example, one might say that a very definite consensus had been reached if a comfortable majority (say, 60 percent) agreed on an exact value, or if a substantial majority (say, 75 percent) agreed on a small range, or if all agreed to within a slightly larger range. Thus, there is a balance between the number conforming to the view and the range permitted.

The essential problem, however, is finding mechanisms for representing and assessing the opinions on each individual issue for the complete panel, in other words, mechanisms that provide the following for the set of scores for each issue:

- A profile of the scores
- A focal point of agreement (if any)
- A measure of the agreement at that point

Additional problems arise if the panel is divided into several groups, each of which is in internal accord. This is referred to as *split consensus,* or a *multimodal* situation. The interested reader will find a mathematical function (neighborhood consensus) that addresses these issues in Donegan and Dodd.[74]

Traditionally, a histogram was generally used as a profile, and the presence or absence of consensus was determined by a statistical measure of dispersion. Chatterjee and Chaterjee[75] discuss mean- and median-based methods together with the compromises referred to as the trimmed and windsorized means. A *trimmed mean* excludes extreme values, and in a *windsorized mean,* the extreme values are replaced by the second-most extreme values. Some of the assumptions and drawbacks of these measures, for example, the nonrepresentativeness of the mean, the instability of the mode, and the inconsistency and precision-dependence of the median, are described in Dodd and Donegan.[76]

It is worth pointing out here the difference between consensus and compromise. If on a scale of 0 to 5, one half of a group selects 0 and the other half selects 5, then 2.5 is a compromise score. It would be inaccurate, however, to describe 2.5 as a consensus score, since this figure is not representative of any members of the group and, therefore, not a measure of the group itself. There is, in fact, no consensus among the group.

Alternative Stability Approach

A major problem with, for example, Delphi studies is that stability may set in before consensus has been achieved, and the latter might therefore never be reached. When seeking consensus on a large number of issues, this is highly likely for some of the issues and quite consistent with Delphi philosophy, which is more concerned with narrowing the spread of diverse opinions than enforcing an artificial consensus.

It is possible and perhaps simpler to use a definition of stability (based on a comparison of successful rounds) as the termination criterion for a Delphi panel. This would also allow item/individual/tactic/group stability to be considered. The definition of stability might be based on the ratio of total scores for two rounds, for example, the average of the moduli of the differences between the rounds. Linstone and Turoff[66] suggest the quadratic mean as a refinement of this. Alternatively, if

the data were normalized (i.e., translated and magnified to fit a uniform distribution), it might be simpler to use Pearson's correlation coefficient.

The principal advantage of the alternative stability approach is that stability is almost certain to be achieved, and fairly rapidly. It is generally recognized that stability is normally achieved within four polling rounds in most Delphi panels (see Render and Stair[67]).

Comparative Consensus

Comparative consensus involves a panel of individuals who must decide on an arrangement of *n* issues (or objects) in order of importance or merit. For the sake of simplicity, let the issue be a number from 1 to *n.* Each panel member decides on an arrangement that might be expected to differ from the arrangements of others. Two problems can arise—(a) establishing a universally acceptable arrangement, and (b) the amount of agreement among the panel. A typical example of this situation might be the selection of an agreed priority list from 10 independent lists returned by experts whose task is to rank in order of importance the following safety features: fire extinguishers, smoke alarms, sprinklers, flashing lights, and direction signs.

Comparative consensus[77] also involves only the *ranking* of a number of issues (in contrast to the simpler notion of definitive consensus, as described above, in which the agreement of a panel on a single issue is assessed). The obvious question in the situation where several panelists judge several issues is whether (a) it is preferable to determine the agreement on each issue on the basis of scores and then determine rank on the basis of the consensus scores, or whether (b) each panel member should rank all the issues on the basis of his or her scores and subsequently look for consensus on the set of rankings. This has never been satisfactorily resolved.

Compound Consensus

Compound consensus arises when, for example, a panel is required to produce an agreed ranking (with weightings) for a set of issues. This type of consensus can occur when AHP is used by a relatively small panel to produce a set of rankings. The obvious question is whether it is better to (a) find (definitive) consensus among the panel on the issue and then rank the issue for the whole panel, or (b) let each panel member rank the issues and then seek (comparative) consensus on the rankings. Compound consensus allows a weighting of each of the issues to be taken into account.

References Cited

1. G.T. Castino and T.Z. Harmathy, "Fire Risk Assessment," *ASTM (STP) 762,* ASTM, Philadelphia (1982).
2. M. Gretner, *Fire Risk Evaluation,* Association of Cantonal Institutions for Fire Insurance, Society of Engineers and Architects and Fire Prevention Services for Industry and Trade, Zurich (1980).
3. J.R. Hall, "Key Distinctions in and Essential Elements of Fire Risk Analysis," *Fire Safety Science—Proceedings 3rd ISFSS,* Edinburgh, Scotland, pp. 467–474 (1991).
4. M.M. Hirschler, "Fire Hazard and Risk Assessment," *ASTM (STP) 1150,* ASTM, Philadelphia (1992).
5. J.M. Watts, "Dealing with Uncertainty: Some Applications in Fire Protection Engineering," *Fire Safety Journal,* 11, pp. 127–134 (1986).
6. J.M. Watts, "Criteria for Fire Risk Ranking," *Fire Safety Science—Proceedings 3rd ISFSS,* Edinburgh, Scotland, pp. 457–466 (1991).
7. R.L. Winkler and A.H. Murphy, "Good Probability Assessors," *Journal of Applied Meteorology,* 7, pp. 751–758 (1968).
8. D.W. Bunn, *Applied Decision Analysis.* McGraw-Hill, New York (1984).
9. S. French, "On the Axiomatisation of Subjective Probabilities," *Theory and Decision,* 14, pp. 19–33 (1982).
10. S. French, *Decision Theory—An Introduction to the Mathematics of Rationality,* Ellis Horwood, Chichester, UK (1988).
11. D.V. Lindley, *Making Decisions,* Wiley, New York (1971).
12. H. Raiffa, *Decision Analysis,* Addison-Wesley, Glenview, IL (1968).
13. C. Viek and W.A. Wagenaar, *Judgment and Decision Under Uncertainty,* Institute for Experimental Psychology, University of Groningen, The Netherlands. (Reprinted from *Handbook of Psychonomics,* Vol. II., North-Holland Publishing Company, Amsterdam 1979).
14. A. Sekizawa, *Statistical Analyses of Fatalities—Characteristics of Residential Fires,* ISFSS, Edinburgh, Scotland, pp. 475–484 (1991).
15. F. Noonan and R. Fitzgerald, "On the Role of Subjective Probabilities in Fire Risk Management Studies," *Fire Safety Science—Proceedings 3rd ISFSS,* Edinburgh, Scotland, pp. 495–504 (1991).
16. D. Dubois and H. Prade, *Possibility Theory: An Approach to Computerized Processing of Uncertainty,* Plenum, New York (1988).
17. L.A. Zadeh, "The Role of Fuzzy Logic in the Management of Uncertainty in Expert Systems," *Fuzzy Sets and Systems,* 11, pp. 149–184 (1983).
18. G. Klir and T.A. Folger, *Fuzzy Sets, Uncertainty and Information,* Prentice Hall, Upper Saddle River, NJ (1988).
19. D.E. Bell, H. Raiffa, and A. Tversky, "Descriptive, Normative and Prescriptive Interactions in Decision Making," in *Decision Making*: *Descriptive, Normative and Prescriptive Interactions* (D.E. Bell, H. Raiffa, and A. Tversky, eds.), Cambridge University Press, Cambridge, UK, pp. 9–30 (1988).
20. H.A. Taha, *Operations Research,* Prentice Hall, Upper Saddle River, NJ (1997).
21. T.J. Shields and G.W. Silcock, *Buildings and Fire,* Longman Scientific and Technical, Harlow, UK (1987).
22. NFPA 550, *Guide to the Fire Safety Concepts TREE,* NFPA, Quincy, MA (1985).
23. P.S. Laplace, *Essai Philosophique sur les Probabilites,* 5th ed., Paris. Translation by Dover, New York (1952).
24. A. Wald, *Statistical Decision Functions,* Wiley, New York (1950).
25. L.J. Savage, "The Theory of Statistical Decision," *J. Amer. Statist. Assoc.,* 46, pp. 55–67 (1951).
26. L. Hurwicz, "Optimality Criteria for Decision Making Under Ignorance," *Discussion Paper No. 370,* Cowles Commission (1951).
27. R.L. Keeney and H. Raiffa, *Decisions with Multiple Objectives: Preferences and Value Trade-offs,* Wiley, New York (1976).
28. H.A. Donegan, T.J. Shields, and G.W.H. Silcock, "A Mathematical Strategy to Relate Fire Safety Evaluation and Fire Safety Policy Formulation for Buildings," in *Proceedings of the 2nd International Symposium on Fire Safety Science,* Tokyo, pp. 433–441 (1988).

29. G. Ramachandran, *The Economics of Fire Protection,* E & FN Spon, London (1995).
30. M. Schiebe, M. Scutsch, and J. Schofer, "Experiments in Delphi Methodology," in *The Delphi Method: Techniques and Applications* (H.A. Lindstone and M. Turoff, eds.), Addison-Wesley, Glenview, IL, pp. 262–282 (1975).
31. T.L. Saaty, *The Analytical Hierarchy Process,* McGraw-Hill, New York (1980).
32. N.P. Loomba, *Management—A Quantitative Perspective,* Collier Macmillan, Canada (1978).
33. J.M. Watts, personal communication (2000).
34. H.A. Simon, *Administrative Behaviour,* Macmillan, New York (1961).
35. T.J. Shields, G.W. Silcock, and H.A. Donegan, "Towards the Development of a Fire Safety Systems Evaluation for Public Assembly Buildings," *Construction Management and Economics,* 8, pp. 147–158 (1990).
36. W. Edwards, "Social Utilities," *Engineering Economist,* 6, pp. 119–129 (1971).
37. P. Goodwin and G. Wright, *Decision Analysis for Management Judgement,* Wiley, New York (1998).
38. W. Edwards and J.R. Newman, *Multiattribute Evaluation,* Paper No. 26, Sage Publications, London (1982).
39. J.M. Watts, "Fire Risk Ranking," in *SFPE Handbook of Fire Protection Engineering,* 5th ed., NFPA, Quincy, MA, 1995, pp. 5-12–5-26.
40. H.E. Nelson and A.J. Schibe, "A System for Fire Safety Evaluation of Health Care Facilities," *NBSIR 78-1555,* Center for Fire Research, National Bureau of Standards, Washington, DC (1980).
41. E.W. Marchant, *Fire Safety Evaluation (Points) Scheme for Patient Areas within Hospitals: A Report on Its Origins and Development,* University of Edinburgh, Scotland (1982).
42. E.W. Marchant, "Fire Safety Engineering—A Quantified Analysis," *Fire Prevention,* 210, pp. 34–38 (1988).
43. P. Stollard, "The Development of a Points Scheme to Assess Fire Safety in Hospitals," *Fire Safety Journal,* 7, 2, pp. 145–153 (1984).
44. T.J. Shields, G.W. Silcock, and Y. Bell, "Fire Safety Evaluation of Dwellings," *Fire Safety Journal,* 10, 1, pp. 29–36 (1986).
45. F.J. Dodd and H.A. Donegan, "Prioritisation Methodologies in Fire Safety Evaluation," *Fire Technology,* 30, 2 (2nd Quarter), pp. 232–249 (1994).
46. F.J. Dodd and H.A. Donegan, "Some Considerations in the Combination and Use of Expert Opinions in Fire Safety Evaluation," *Fire Safety Journal,* 22, 4, pp. 315–327 (1994).
47. S-K. Lai and L.D. Hopkins, "The Meaning of Trade-Offs in Multiattribute Evaluation Methods: A Comparison," *Environment and Planning B*: *Planning and Design,* 16, pp. 155–170 (1989).
48. R.M. Sirkin, *Statistics for the Social Sciences,* Sage Publications, Thousand Oaks, CA (1995).
49. W. Edwards, M. Guttentag, and K. Snapper, "Effective Evaluation: A Decision Theoretic Approach," in *Evaluation and Experiment: Some Critical Issues in Assessing Social Programmes* (C.A. Bennett and A. Lumsdaine, eds.), Academic, New York (1975).
50. T.L. Saaty and L.G. Vargas, "Experiments on Rank Preservation and Reversal in Relative Measurement," *Mathl. Comput. Modelling,* 17, pp. 13–18 (1993).
51. A.A. Salo and R.P. Hämäläinen, "On the Measurement of Preferences in the Analytic Hierarchy Process," *Journal of Multi-Criteria Decision Analysis,* 6 (1998).
52. T.J. Shields and G.W. Silcock, "An Application of the Analytic Hierarchy Process to Fire Safety Evaluation," *Fire Safety Journal,* 11, 3, pp. 235–242 (1986).
53. S. Rahman and L.C. Frair, "A Hierarchical Approach to Utility Planning," *Energy Research,* 8, pp. 185–196 (1984).
54. B. Liu and S. Xu, "Development of the Theory and Methodology of the Analytic Hierarchy Process and Its Applications in China," *Mathematical Modelling,* 9, 3–5, pp. 179–184 (1987).
55. R.G. Vachnadze and N.I. Markozashvili, "Some Applications of the Analytic Hierarchy Process," *Mathematical Modelling,* 9, 3–5, pp. 185–191 (1987).
56. H.A. Donegan and F.J. Dodd, "A Note on Saaty's Random Indexes," *Mathl. Comput. Modelling,* 15, 10, pp. 135–137 (1991).
57. Y.A. Tung, "Time Complexity and Consistency Issues in Using the AHP for Making Group Decisions," *Journal of Multi-Criteria Decision Analysis,* 7, pp. 144–154 (1998).
58. J. Dyer, "Remarks on the Analytic Hierarchy Process," *Management Science,* 36, 3, pp. 249–258 (1990).
59. T.L. Saaty, *The Analytic Network Process,* RWS Publications, Pittsburgh, PA (1996).
60. N.C. Barford, *Experimental Measurements: Precision, Error, and Truth,* 2nd ed., John Wiley and Sons, New York (1987).
61. A.M. Glenburg, *Learning from Data: An Introduction to Statistical Reasoning,* Harcourt Brace Jovanovich, Orlando (1980).
62. P. Dunn Rankin, *Scaling Methods,* Lawrence Erlbaum Associates, Inc., NJ (1983).
63. W.S. Torgenson, *Theory and Methods of Scaling,* Wiley, New York (1958).
64. R. Kumar, *Research Methodology,* Sage Publications, London (1999).
65. G. Rowe and G. Wright, "The Delphi Technique as a Forecasting Tool: Issues and Analysis," *International Journal of Forecasting,* 15, pp. 353–375 (1999).
66. H.A. Linstone and M. Turoff, *The Delphi Method: Techniques and Applications,* Addison-Wesley, Glenview, IL (1975).
67. B. Render and R.M. Stair, *Quantitative Analysis for Management,* 2nd ed., Allyn and Bacon, Boston (1985).
68. S.C. Wheelwright and S. Makridakis, *Forecasting Methods for Management,* 4th ed., Wiley, New York (1985).
69. E.W. Marchant, "Problems Associated with the Delphi Technique," *Fire Technology,* 24, 1, pp. 59–62 (1989).
70. T.J. Shields, G.W. Silcock, H.A. Donegan, and Y. Bell, "Methodological Problems Associated with the Delphi Technique," *Fire Technology,* 23, 3, pp. 175–185 (1987).
71. H. Sackman, "Delphi Assessment: Expert Opinion, Forecasting and Group Progress," *Paper R-1283-PR,* Rand Corporation, Santa Monica, CA (1974).
72. P. Ayton, W.R. Ferrell, and T.R. Stewart, "Commentaries on 'The Delphi Technique as a Forecasting Tool: Issues and Analysis' by Rowe and Wright," *International Journal of Forecasting,* 15, pp. 377–381 (1999).
73. R.E. Norton, *The DACAM Handbook,* Leadership Series 67, National Center for Research in Vocational Education, Columbus, OH (1987).
74. H.A. Donegan and F.J. Dodd, "An Analytical Approach to Consensus," *Applied Mathematics Letters,* 4, 2, pp. 21–24 (1991).
75. S. Chatterjee and S. Chatterjee, "On Combining Expert Opinions," *Am. Jnl. Math and Mngt. Stud.*, 7, 3 and 4, pp. 271–295 (1987).
76. F.J. Dodd and H.A. Donegan, "The Representation and Combination of Opinions," in *Proceedings of ILIAM,* 6 (H.A. Donegan, ed.), University of Ulster, Belfast, Northern Ireland, pp. 17–29 (1989).
77. F.J. Dodd and H.A. Donegan, "Comparative and Compound Consensus," *Applied Mathematics Letters,* 5, 3, pp. 31–33 (1992).

CHAPTER 3

Reliability

Mohammad Modarres and Francisco Joglar-Billoch

Introduction

Reliability has two connotations. One is probabilistic in nature; the other is deterministic. This chapter generally deals with the probabilistic aspect. First reliability must be defined. The most widely accepted definition of reliability is the *ability of an item (product, system, etc.) to operate under designated operating conditions for a designated period of time or number of cycles.* Consequently, the reliability of systems or components in fire conditions can be expressed as the ability of an item to operate at fire-induced stresses, such as high temperatures and high concentrations of products of combustion. The *ability* of an item to operate can be (1) designated through a probability (the probabilistic connotation) or (2) designated deterministically. The deterministic approach, in essence, deals with understanding how and why an item fails, and how it can be designed and tested to prevent such failures from occurring or recurring. This includes analyses, such as deterministic analysis and review of field failure reports, understanding physics of failure, the role and degree of test and inspection, performance redesign, or performance reconfiguration. In practice, this is an important aspect of reliability analysis.

The probabilistic treatment of an item's reliability according to the definition above can be represented by

$$R(t) = Pr(T \geq t \mid c_1, c_2, \ldots) \tag{1}$$

where

$R(t)$ = reliability of the item

Pr = probability

T = time to failure or cycle to failure of the item

t = designated period of time or cycles for the item's operation (mission time)

$c_1, c_2, \ldots$ = designated conditions, such as environmental conditions

Often, in practice, $c_1, c_2, \ldots$ are implicitly considered in the probabilistic reliability analysis and, thus, Equation 1 reduces to

$$R(t) = Pr(T \geq t) \tag{2}$$

This chapter addresses the basic elements of component and system reliability evaluation, including the classical frequency approach to component reliability, important aspects of component reliability analysis, system reliability models, and logic trees.

Component Reliability

The probabilistic notion is used to quantitatively measure the reliability of an item and treats reliability as the conditional probability of the successful achievement of an item's intended function, given designated conditions. The probabilistic definition of reliability given in Equation 1 is its mathematical representation. The right-hand side of Equation 1 denotes the probability that a specified failure time, T, exceeds a specified mission time, t, given that conditions $c_1, c_2, \ldots$ exist (or are met). Practically, random variable T represents *time-to-failure* of the item, and conditions $c_1, c_2, \ldots$ represent conditions (e.g., design-related conditions) that are required, a priori, for successful performance of the item. Other representations of random variable T include *cycle-to-failure, stress-to-failure,* and so on. In fires different kinds of stresses applied to items are generated. For example, high temperatures and concentrations of combustion products can be considered fire-induced stresses. Although time is an agent of failure in

Dr. Mohammad Modarres is a professor of reliability and of nuclear engineering and a cofounder of the Reliability Engineering Program at the University of Maryland, College Park. He is the director of the Center for Reliability Engineering at the University of Maryland. A consultant to government, industry, and international organizations, he is the author or coauthor of more than 100 professional papers in reliability and risk assessment.

Dr. Francisco Joglar-Billoch is a fire and risk analyst at Science Applications International Corporation (SAIC).

reliability analysis, when fire conditions exist, a different approach should be adopted in order to evaluate an item's reliability. For example, the stress-strength interference model may be introduced to account for the reliability of items subjected to stresses generated by fires. Conditions $c_1, c_2, \ldots$ are often implicitly considered; therefore, Equation 1 is written in a nonconditional form of Equation 2. Equation 2 is used in the remainder of this chapter.

Reliability Function

Time as an Aggregate Agent of Failure

Let's start with the formal definition given in Equation 1. Furthermore, let $f(t)$ denote a probability distribution function representing the random variable T. $f(t)$ is obviously characterized by the design (e.g., strength), operational, and environmental (e.g., stress) effects of the item. The probability of failure of the item as a function of time can be defined by

$$Pr(T \leq t) = \int_0^t f(\theta)\, d\theta = F(t), \quad \text{for } t \geq 0 \tag{3}$$

where $F(t)$ denotes the probability that the item will fail sometime up to time t. Based on Equation 2, Equation 3 is the *unreliability* of the item. Formally, $F(t)$ is called the *unreliability function.* Conversely, one can find the *reliability function* by writing

$$R(t) = 1 - F(t) = \int_t^\infty f(\theta)\, d\theta \tag{4}$$

Provided one can obtain the probability distribution function, $f(\theta)$, one can then obtain $R(t)$. Basic characteristics of the probability distribution function and $R(t)$ can be helpful to create some useful definitions. The *mean time to failure* (MTTF), for example, is defined as the expected value of $f(t)$. This illustrates the expected time during which the item will perform its function successfully (sometimes called *expected life*) as

$$\text{MTTF} = E(t) = \int_0^\infty t f(t)\, dt \tag{5}$$

If $\lim_{t \to \infty} R(t) = 0$, then it is easy to show that a more compact form of Equation 5 is given by

$$E(t) = \int_0^\infty R(t)\, dt \tag{6}$$

MTTF refers to the mean time from first use of a new item to first and only failure. MTTF is different from *mean time between failures* (MTBF), which is the mean time between two consecutive item failures. MTBF includes the time to discover the earlier failure, the time to repair that failure, and the time until it fails again. If discovery and repair are essentially instantaneous and repair is as good as replacement (as with changing a light bulb), then the repaired or replaced item will behave like a new item, and MTBF will equal MTTF. In general, discovery and repair are not instantaneous, repair is not perfect, and MTBF involves very complex modeling.

Stress-Strength Interference Model

During the operation of a system or a component, interactions with its environment effectively subject the system or component to *stress.* While the system is operating successfully, it presents an internal capacity to withstand stress. One form of this capacity is called *strength.* To predict reliability of a system or a component, in which a failure occurs when the stress exceeds the strength, we have to know the nature of both the stress and the strength. If the stress is considered a random variable, and the strength is either a fixed value or another random variable, reliability calculations can be performed.

Random stress and fixed strength: In the case where the stress is a random variable S associated with the probability distribution $f(S)$ and the strength is a fixed value S_0, the reliability is the area in the probability distribution to the left of the strength value. Figure 5-3.1 illustrates this concept. The reliability of the component can be expressed as the probability of S being lower than S_0 or

$$Pr(s < S_0) = \int_{-\infty}^{S_0} f(s)\, ds = 1 - \int_{S_0}^{\infty} f(s)\, ds \tag{7}$$

where $f(S)$ is the probability distribution for the stress random variable. In this approach, the value S_0 can be, for example, the damage temperature of a component and $f(S)$ the distribution for the temperature of the component associated to the impact of the fire.

Random stress and random strength: If the strength is represented by another random variable R associated to a probability distribution $f(R)$, similar to the case presented above, the probability distribution for the strength may be the damage temperature of a component considering uncertainty in the value. The overlapped area between the two distributions will be an indicator of the probability of failure of the component. But the probability of failure is not equal to the common area between the two distributions. Figure 5-3.2 illustrates this concept. The reliability of the system can be expressed as

$$\begin{aligned} R = P(S \leq R) &= \int_0^\infty \int_0^R f(S, R)\, dS\, dR \\ &= \int_0^\infty \int_0^S f(R, S)\, dR\, dS \end{aligned} \tag{8}$$

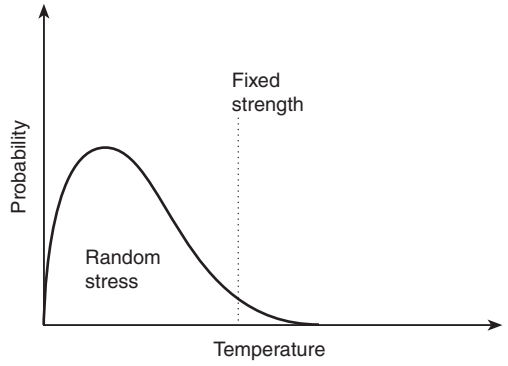

Figure 5-3.1. ***Random stress and fixed strength.***

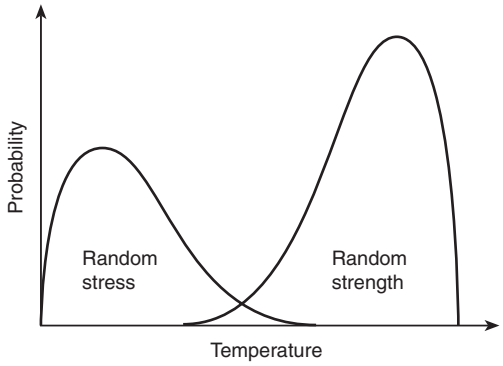

Figure 5-3.2. ***Random stress and random strength.***

where $f(S, R)$ is the joint probability distribution for the two random variables. If S and R are statistically independent random variables, then

$$f(S, R) = f(S) \cdot f(R) \tag{9}$$

Another useful formulation is to define a random variable $Z = R - S$.

$$R = P(S \leq R) = P(Z > 0) = 1 - F_z(0) \tag{10}$$

The cumulative distribution function of Z can be found as follows:

$$\begin{aligned} F_z(Z) &= P(Z \leq z) = P(R - S \leq Z) \\ &= \int_0^\infty \int_0^{S+Z} f(S, R)\, dR\, dS \end{aligned} \tag{11}$$

Finally, differentiating $F_z(z)$, we obtain a simpler expression derived from the joint pdf of s and z.

$$f_z(Z) = \int_0^\infty f_s(S) f_r(S + Z)\, dS \qquad -\infty < Z < \infty \tag{12}$$

$$R = \int_0^\infty f_z(Z)\, dZ = \int_0^\infty \int_0^\infty f_s(S) \cdot f_r(S + Z)\, dS\, dZ \tag{13}$$

Stresses induced by fires usually change with time in the course of the accident. This fact suggests that a probability distribution for stress is not static. For example, if the component temperature changes with time, the probability of failure will also change. In this case we might expect the stress distribution to shift to the right.

EXAMPLE 1:

Find the reliability and the probability of failure of a component subjected to a normally distributed temperature random variable with the mean and standard deviation of 55°C and 10°C, respectively. The component has the capability to withstand temperatures up to a level described by another normally distributed random variable with mean of 60°C and standard deviation of 5°C.

SOLUTION:

First the joint probability density function of the stress and the strength is defined. Assuming both random variables are independent,

$$\begin{aligned} f(R, S) &= f(S) \cdot f(R) \\ &= \frac{1}{\sqrt{2\pi}\sigma_S} e^{-1/2[(S-\mu_S)/\sigma_S]^2} \cdot \frac{1}{\sqrt{2\pi}\sigma_R} e^{-1/2[(S-\mu_R)/\sigma_R]^2} \end{aligned}$$

where

$\mu_R = 60°C$

$\sigma_R = 5°C$

$\mu_S = 55°C$

$\sigma_S = 10°C$

Defining the random variable $Z = R - S$, and using Equation 12

$$\begin{aligned} f_z(Z) &= \int_0^\infty f_S(S) \cdot f_R(S + Z)\, dS \\ &= \frac{1}{2\pi\sigma_R\sigma_S} \int_0^\infty e^{-1/2[(S-\mu_S)/\sigma_S]^2} \cdot e^{-1/2\{[(S+Z)-\mu_R]/\sigma_R\}^2}\, dS \end{aligned}$$

Once an expression for $f_z(Z)$ is obtained, Equation 13 can be used to obtain the reliability.

$$R = \int_0^\infty f_z(Z) = 0.673$$

Therefore, the probability of failure is $1 - R = 0.327$.

Failure Rate and Hazard Rate

Failures can occur due to many physical processes or mechanisms. In probabilistic reliability, all these mechanisms of failure are accounted for through a function called *instantaneous failure rate* or *hazard rate*, $h(t)$. The hazard rate can be interpreted as the probability of the first and only failure of an item in the next instant of time, given that the item is presently operating. Clearly, this only applies to nonrepairable items in which only one failure can occur. For repairable items the most appropriate term is failure rate, or more correctly, the *rate of occurrence of failure*. Hazard rate function is obtained via *life test data*. The rate of failure for a component c is defined as $\lambda = 1/\Delta t$ (probability that c will fail between t and $t + \Delta t$, given that no failure is observed before t). The instantaneous failure rate (hazard rate) for component c is defined as the limit of the rate of failure as the interval Δt approaches zero. $h(t)$ is obtained from

$$h(t) = \frac{f(t)}{R(t)} \tag{14}$$

Here, $f(t)$ represents the time to failure probability distribution function of a component, and $R(t)$is its reliability function. Hazard rate is an important function in reliability analysis, since it shows changes in the probability of failure over the lifetime of a component.

In practice, $h(t)$ often exhibits a bathtub shape and is referred to as a *bathtub curve.* A typical bathtub curve is shown in Figure 5-3.3.

Generally, a bathtub curve can be divided into three regions. The *burn-in failure* region exhibits a *decreasing rate of failure,* characterized by early failures attributable to defects in design, manufacturing, or construction. The *chance failure* region exhibits a reasonably *constant rate of failure,* characterized by random failures of the component. In this period, many mechanisms of failure due to complex underlying physical, chemical, or nuclear phenomena give rise to this approximately constant rate of failure. The third region, called *wear-out failure,* exhibits an *increasing rate of failure,* characterized mainly by complex aging phenomena. Here the component deteriorates (e.g., due to accumulated fatigue) and is more vulnerable to outside shocks. One interesting observation is that these three regions are different for different types of components. Figures 5-3.4 and 5-3.5 show typical bathtub curves for electrical and mechanical devices, respectively. Electrical devices exhibit a relatively higher rate of failure during the chance failure period. Figure 5-3.6 shows the effect of various levels of stress on a device. As stress level increases, the chance failure region decreases, and premature wear-out occurs. Therefore, it is important to minimize stress factors, such as harsh operating environments, to maximize reliability.

Next, the mathematical relationship between $h(t)$ and $R(t)$ needs clarification. Recall that from Equation 4, $R(t) = 1 - F(t)$, or $dR(t) = -dF(t) = -f(t)$. By integrating both sides of Equation 7 from 0 to t,

$$\int_0^t h(x)\,dx = -\ln R(t) + \ln R(0)$$

By assuming that a component is totally reliable at the beginning of life [i.e., $R(0) = 1$)], then

$$\int_0^t h(x)\,dx = -\ln R(t) \tag{15}$$

and

$$R(t) = \exp\left(-\int_0^t h(x)\,dx\right) \tag{16}$$

If the beginning of life is not at $t = 0$, but rather at $t = t_1$, then the integrands of Equation 15 will be between

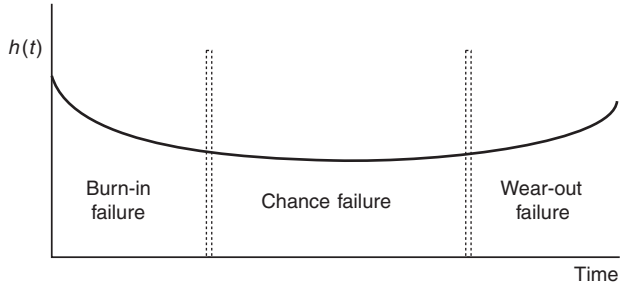

Figure 5-3.3. ***Typical bathtub curve.***

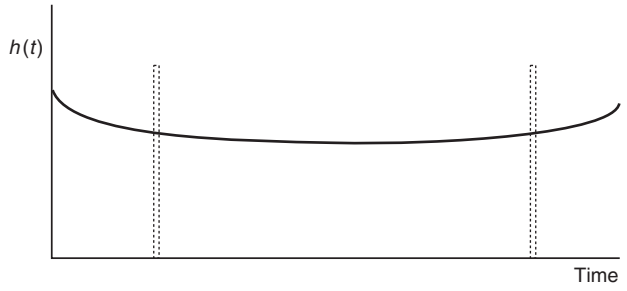

Figure 5-3.4. ***Bathtub curve for typical electrical devices.***

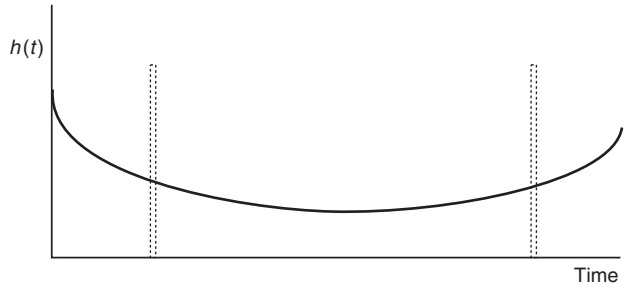

Figure 5-3.5. ***Bathtub curve for typical mechanical devices.***

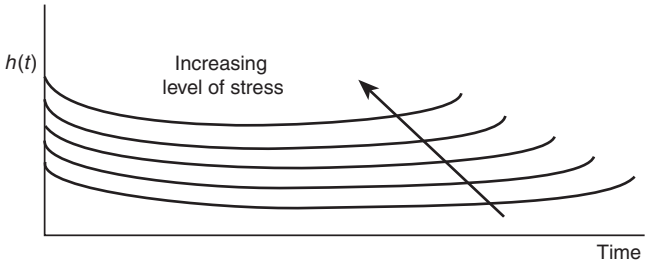

Figure 5-3.6. ***Effect of stress on a typical bathtub curve.***

t_1 and t. If any one of $f(t)$, $h(t)$, or $R(t)$ is known, the other two can be computed by using Equations 14, 15, and 16.

EXAMPLE 2:

A component is known to have an instantaneous failure rate, $h(t)$, as shown below. Determine the probability distribution function and the reliability function.

SOLUTION:

For $0 \le t \le 200$, $h(t) = 5 \times 10^{-6}t^2 - 10^{-3}t + 0.1$

$$\begin{aligned}\int_0^t h(t')\,dt' &= \int_0^t (5 \times 10^{-6}t'^2 - 10^{-3}t' + 0.1)\,dt' \\ &= \left[\left(\frac{5 \times 10^{-6}}{3}\right)t'^3 - \left(\frac{10^{-3}}{2}\right)t'^2 + 0.1t'\right]\Bigg|_0^t \\ &= 1.66 \times 10^{-6}t^3 - 5 \times 10^{-4}t^2 + 0.1t\end{aligned}$$

thus,

$$R(t) = \exp(-1.66 \times 10^{-6}t^3 + 5 \times 10^{-4}t^2 - 0.1t)$$

Using Equation 14,

$$f(t) = (5 \times 10^{-6}t^2 - 10^{-3}t + 0.1) \times \exp(-1.66 \times 10^{-6}t^3 + 5 \times 10^{-4}t^2 - 0.1t)$$

Common Distributions and Parameter Estimation

To represent component failure probabilities as a function of time, the most common distributions are exponential, lognormal, and Weibull probability distribution functions. The exponential distribution is used to model component time to failure when failures have a constant arrival rate. When the mean time to failure of a component is the same, no matter how much time has already passed, the exponential model is reasonable and the parameter estimation should proceed.

The lognormal distribution is useful, in part, because the product of two lognormally distributed variables also has a lognormal distribution. This is useful for a unit whose failure occurs only after the failure of several of its constituent parts. If each part has a lognormal failure probability, then so will the unit. Reflecting this underlying phenomenology, the lognormal distribution can be used for failure probability distributions with very large variances. It is not unusual in such a distribution to see probability values separated by orders of magnitude. The Weibull distribution has three parameters. This creates the greatest challenge but also the greatest flexibility in setting a specific distribution. In particular, the Weibull distribution is flexible enough to depict the distribution for a unit that shows pronounced changes in reliability during the wear-out stage or whose reliability improves over time.

This section introduces common distributions and deals with statistical methods for estimating model parameters, such as λ of the exponential probability distribution function, μ and σ of the lognormal probability distribution functions, and α and β of the Weibull probability distribution function. The objective is to find a *point estimate* and a *confidence interval* for the parameters of interest. It is important to realize why one needs to consider confidence intervals in the estimation process. In essence, this need stems from the fact that there is only a limited amount of information (e.g., times to failure), and thus one cannot state the estimation with certainty. Therefore, the confidence interval is highly influenced by the amount of data available. Of course other factors, such as diversity in the sources of data and accuracy of the selected model and the data sources, also influence the state of uncertainty regarding the estimated parameters.

Exponential Distribution

This distribution is widely used in reliability evaluation to model a random variable representing time to failure of a device (often a device composed of several independent units). The distribution is a one-parameter probability distribution function defined by

$$\begin{aligned} f(t) &= \lambda \exp(-\lambda t) && \lambda,\ t > 0 \\ &= 0, && t \le 0 \end{aligned} \tag{17}$$

It is easy to show that requirements $\int_{\text{all } t} f(t)\,dt = 1$ and $f(t) > 0$ for a valid probability distribution function are met for this distribution. Figure 5-3.7 illustrates the exponential distribution for a value of λ.

EXAMPLE 3:

A component has a constant failure rate of 10^{-3}/hr. What is the probability that this component will fail before $t = 1000$ hrs? Determine the probability that it works for at least 1000 hrs.

SOLUTION:

$$Pr(t < 1000) = \int_0^{1000} \lambda \exp(-\lambda t)\,dt = \exp(-\lambda t)\Big|_0^{1000}$$
$$= 1 - \exp(-1) = 0.632$$
$$Pr(t > 1000) = 1 - Pr(t < 1000) = 0.368$$

Epstein[1] has shown that, if the time to failure is exponentially distributed with parameter λ, the quantity $2r\lambda/\lambda = 2\lambda T$ has a chi-square distribution with $2r$ degrees of freedom for the Type II (failure-terminated) failure data and $(2r + 2)$ degrees of freedom for the Type I (time-terminated) failure data, where r is the number of failures observed, T is the total accumulated operation time, and λ is the point estimator for the parameter λ.

$$\hat{\lambda} = \frac{r}{T} \tag{18}$$

Consequently, for the two-sided confidence interval for the $1 - \alpha/2$ and $\alpha/2$ confidence levels of the chi-square distribution,

$$Pr\left[\chi^2_{\alpha/2}(2r) \le \frac{2r\lambda}{\hat{\lambda}} \le \chi^2_{1-\alpha/2}(2r)\right] = 1 - \alpha \tag{19}$$

By rearranging and using Equation 18,

$$Pr\left[\frac{\chi^2_{\alpha/2}(2r)}{2T} \le \lambda \le \frac{\chi^2_{1-\alpha/2}(2r)}{2T}\right] = 1 - \alpha \tag{20}$$

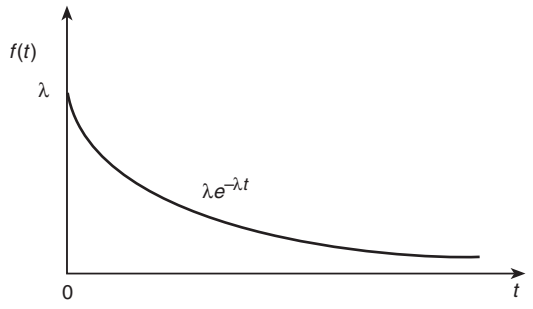

Figure 5-3.7. ***Exponential distribution.***

Equation 20 shows the *two-sided confidence interval* for the true value of λ. Another alternative to Equation 19 is the *one-sided confidence interval*,

$$Pr\left[0 \le \hat{\lambda} \le \frac{\chi^2_{1-\alpha}(2r)}{2T}\right] = 1 - \alpha \tag{21}$$

Accordingly, confidence intervals of MTTF and $R(t)$ at $t = t_0$ can also be obtained for both one-sided and two-sided confidence intervals from Equations 20 and 21.

It is possible to show that the upper confidence limit of λ for the Type I (time-terminated) test is obtained from a chi-square distribution with $(2r + 2)$ degrees of freedom. The lower confidence limit is obtained from the chi-square distribution with $2r$ degrees of freedom. Thus for Type I tests, the two-sided confidence interval is

$$Pr\left[\frac{\chi^2_{\alpha/2}(2r)}{2T} \le \lambda \le \frac{\chi^2_{1-\alpha/2}(2r+2)}{2T}\right] = 1 - \alpha \tag{22}$$

The one-sided confidence interval is

$$Pr\left[0 \le \lambda \le \frac{\chi^2_{1-\alpha/2}(2r+2)}{2T}\right] = 1 - \alpha \tag{23}$$

It should be emphasized here that Equations 19 through 23 apply only when the failure rate is constant. Otherwise, a Weibull model or other appropriate distribution should be used.

If no failure is observed, $\hat{\lambda} = 0$ or MTTF $= \infty$. This cannot realistically be true, since one may have had a small or restricted test. Had the test been continued, eventually a failure would be observed. An upper level estimate for both one-sided and two-sided confidence limits can be obtained with $r = 0$. However, the lower limit for the two-sided confidence limit cannot be obtained with $r = 0$. It is possible to relax this limitation by conservatively assuming that a failure occurs in the very next instant. Then $r = 1$ can be used to evaluate the lower two-sided confidence limit. This conservative modification, although sometimes used to allow a complete statistical analysis, lacks firm statistical basis. Welker and Lipow[2] have shown methods to determine approximate point estimates in these cases.

EXAMPLE 4:

Twenty-five units are subjected to a reliability test that lasts 500 hrs. In this test, eight failures occur at 75, 115, 192, 258, 312, 389, 410, and 496 hrs. The failed units are replaced. Find $\hat{\lambda}$, one-sided and two-sided confidence limits on λ, and MTTF at the 90 percent confidence level, and one-sided and two-sided 90 percent confidence limits on reliability at $t_0 = 1000$ hrs.

SOLUTION:

This is Type I data. The accumulated time T is given by

$$T = 25 \times 500 = 12{,}500 \text{ component hrs.}$$
$$\hat{\lambda} = \frac{8}{12{,}500} = 6.4 \times 10^{-4}\ \text{hr}^{-1}$$

One-sided confidence limits on λ are

$$0 \le \lambda \le \frac{\chi^2(2 \times 8 + 2)}{2 \times 12{,}500}$$
$$\chi^2_{0.9}(18) = 25.99, \qquad 0 \le \lambda \le 1.04 \times 10^{-3}$$

Two-sided confidence limits on λ are

$$\frac{\chi^2_{0.05}(2 \times 8)}{2 \times 12{,}500} \le \lambda \le \frac{\chi^2_{0.95}(2 \times 8 + 2)}{2 \times 12{,}500}$$
$$\chi^2_{0.05}(16) = 7.96, \quad \text{and} \quad \chi^2_{0.95}(18) = 28.87$$

Thus,

$$3.18 \times 10^{-4} \le \lambda \le 1.15 \times 10^{-3}$$

One-sided 90 percent confidence limits on $R(1000)$ are

$$\exp(-1.04 \times 10^{-3} \times 1000) \le R(1000) \le 1,$$

or

$$0.35 \le R(1000) \le 1$$

Two-sided 90 percent confidence limits on $R(t)$ are

$$\exp(-1.15 \times 10^{-3} \times 1000) \le R(1000) \le \exp(-3.18 \times 10^{-4} \times 1000)$$

or

$$0.32 \le R(1000) \le 0.73$$

Lognormal Distribution

A random variable is said to be lognormally distributed if its logarithm is normally distributed. The lognormal distribution has considerable application in engineering. One major application of this distribution is to present random variables that are the result of the product of many independent random variables.

The transformation $T = \ln Y$ or $Y = \exp(T)$ transfers the normal probability distribution function representing random variable T with mean μ_t and standard deviation σ_t to a lognormal probability distribution function.

$$f(y) = \frac{1}{\sigma_t y \sqrt{2\pi}} \exp\left[\frac{-1}{2\sigma_t^2}(\ln y - \mu_t)^2\right] \tag{24}$$
$$y \le 0, \qquad -\infty < \mu_t < \infty, \qquad \sigma_t > 0$$

If μ_t and σ_t are not known, and instead μ and σ of a normal distribution are known, the following equations can be used to obtain μ_t and σ_t:

$$\mu_t = \ln\left(\frac{\mu_y}{(1 + \sigma_y^2/\mu_y^2)^{1/2}}\right) \tag{25}$$

$$\sigma_t = \left[\ln\left(\frac{1 + \sigma_y^2}{\mu_y^2}\right)\right]^{1/2} \tag{26}$$

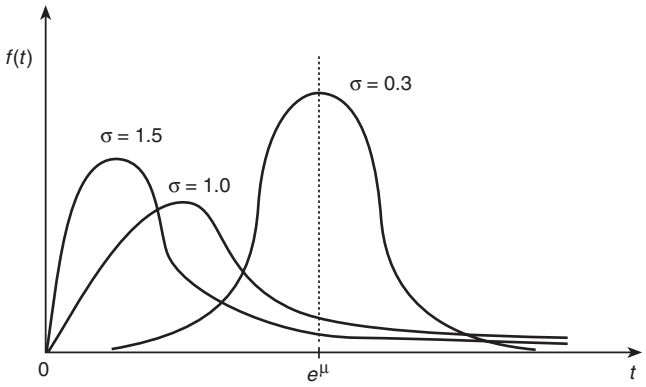

Figure 5-3.8. ***Lognormal distribution.***

Figure 5-3.8 shows the probability distribution function of the lognormal distribution for different values of μ_t and σ_t.

A lognormal distribution is usually used to represent the occurrence of events in time. For example, a random variable representing the length of time required for repair of hardware follows a lognormal distribution. Because the lognormal distribution has two parameters, parameter estimation poses a more challenging problem than for the exponential distribution. It is easy to prove through the maximum likelihood estimation method that point estimators for the two parameters of the lognormal distribution can be obtained from

$$\hat{\mu}_t = \sum_{i=1}^{n} \frac{\ln(t_i)}{n}, \quad \text{and} \quad \hat{\sigma}_t^2 = \frac{\sum_{i=1}^{n} [\ln(t_i) - \hat{\mu}_t]^2}{n-1} \tag{27}$$

where t_i is the time that the ith failure in a set of n failures has occurred. The confidence interval for μ_t is

$$Pr\left[\chi^2_{\alpha/2}(2r) \le \frac{2r\lambda}{\hat{\lambda}} \le \chi^2_{1-\alpha/2}(2r) \right] = 1 - \alpha \tag{28}$$

Similarly, the confidence interval on σ_t is

$$Pr\left[\chi^2_{\alpha/2}(2r) \le \frac{2r\lambda}{\hat{\lambda}} \le \chi^2_{1-\alpha/2}(2r) \right] = 1 - \alpha \tag{29}$$

EXAMPLE 5:

A component fails if its surface temperature reaches 150°C. According to experimental results, a fire can induce surface temperatures in the component between 92°C and 140°C. Assuming these temperature values correspond to the 5th and 95th percentiles of a lognormal distribution, find the mean and standard deviation of the temperature distribution. Calculate the reliability of the component subjected to this condition.

SOLUTION:

In order to solve the first part of this problem, a system of two equations must be solved for the unknown variables μ and σ. The two equations are

$$0.05 = \int_0^{92} \frac{1}{\sqrt{2\pi}\sigma_t T} e^{-1/2\{[\ln(T)-\mu_t]/\sigma_t\}^2} dT \tag{30}$$

$$0.95 = \int_0^{140} \frac{1}{\sqrt{2\pi}\sigma_t T} e^{-1/2\{[\ln(T)-\mu_t]/\sigma_t\}^2} dT \tag{31}$$

An easier way to obtain the values of μ and σ is to use the standardization equation for the normal distribution and use the standard normal percentile table.

For the 5th percentile of a standard normal distribution,

$$-1.64 = \frac{92 - \mu}{\sigma} \tag{32}$$

For the 95th percentile of a standard normal distribution,

$$1.64 = \frac{140 - \mu}{\sigma} \tag{33}$$

Solving these two equations for μ and σ, we obtain the values 116°C and 14.6°C respectively. These values now are transformed to a log scale in order to use them in the lognormal distribution. Using Equations 25 and 26, the following results are obtained: $\mu_t = 4.74$ and $\sigma_t = 0.126$.

Once we have the average and standard deviation of the distribution, the reliability of the component can be found by integrating the lognormal distribution from 0°C to 150°C according to Equation 7. Accordingly, the reliability is found to be 0.983.

Weibull Distribution

The Weibull distribution is widely used to represent the *time to failure* or *life length* of the components in a system, measured from a start time to the time that a component fails. The continuous random variable T representing the time to failure follows a Weibull distribution if

$$f(t) = \frac{\beta(t-\gamma)^{\beta-1}}{\alpha^\beta} \exp\left[-\left(\frac{t-\gamma}{\alpha} \right)^\beta \right] \quad \alpha, \beta > 0;\ t > \gamma \tag{34}$$
$$= 0 \text{ otherwise}$$

The parameter γ serves only to reset the starting time and so is of limited value. The simplified variation of the Weibull distribution used here has $\gamma = 0$.

$$f(t) = \frac{\beta t^{\beta-1}}{\alpha^\beta} \exp\left[-\left(\frac{t}{\alpha} \right)^\beta \right] \quad t, \alpha, \beta > 0 \tag{35}$$
$$= 0 \text{ otherwise}$$

Figure 5-3.9 shows the Weibull distribution for various parameters of α and β. A careful inspection of these graphs reveals that the parameter β has a considerable effect on the shape of the distribution. Therefore, β is referred to as the *shape parameter.* The parameter α, on the other hand, controls the scales of the distribution. For this reason, α is referred to as the *scale parameter.* If $\beta = 1$, the Weibull distribution reduces to an exponential distribution with $\lambda = 1/\alpha$. For values of $\beta > 1$, the distribution becomes bell shaped with some skew.

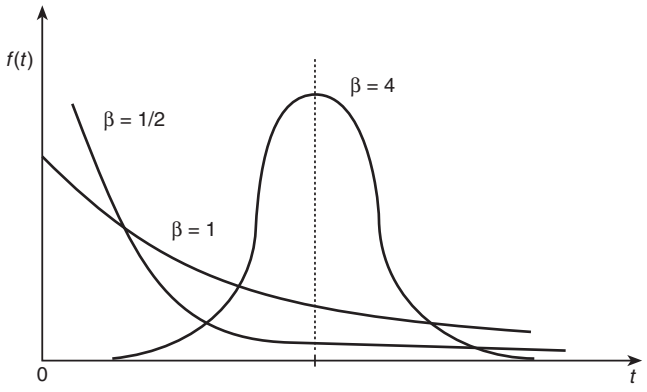

Figure 5-3.9. ***Weibull distribution.***

A Weibull distribution can be used for data believed to have an increasing, decreasing, or constant rate of failure. This distribution is a two-parameter distribution, and estimation of the parameters is rather involved. It can be shown that, under the situation where all n units under test or observation have failed, the maximum likelihood estimates of β and α parameters of the Weibull distribution can be obtained from

$$\frac{\sum_{i=1}^{n}(t_i)^{\hat{\beta}} \ln t_i}{\sum_{i=1}^{n}(t_i)^{\hat{\beta}}} - \frac{1}{\hat{\beta}} = \frac{1}{n}\sum_{i=1}^{n} \ln t_i,$$
$$\hat{\alpha} = \left(\frac{\sum_{i=1}^{n}(t_i)^{\hat{\beta}}}{n}\right)^{1/\hat{\beta}} \tag{36}$$

where t_i is the time that the ith failure in a set of n failures has occurred.

The solution of Equation 36 is not trivial and may require a trial and error process to obtain $\hat{\beta}$. Estimation of the confidence intervals of β and α is very involved. Readers are referred to Bain[3] and Mann et al.[4]

If a lot of failure data is available, the analyst should first fit the data into a distribution that best represents the data. The analyst should then proceed with the estimation of the distribution's parameters. However, when data are not enough, the analyst should check the adequacy of a distribution. Therefore, the exponential, lognormal, or other distribution should only be selected when the adequacy of a distribution fit can be justified. For example, when we have only five sample points for the times required for maintenance, one can theoretically fit these points to several types of distributions. However, we can assume that since the data occur in multiples of time, they can be adequately represented by a lognormal distribution. An accurate representation can only be determined if there are enough data to test the adequacy of the selected model.

System Reliability

Assessment of the reliability of a system from its basic elements is one of the most important aspects of reliability analysis. A system is a collection of items (subsystems, components, units, blocks, etc.) whose proper, coordinated function leads to the proper functioning of the system. In reliability analysis, it is therefore important to model the relationship between various items as well as the reliability of the individual items to determine the reliability of the system as a whole. Previous sections addressed the reliability analysis at a basic item level (one for which enough information is available to predict its reliability). This section addresses methods to model the relationship between system components, which allows the determination of overall system reliability.

The physical configuration of an item that belongs to a system is often used to model system reliability. In some cases, the manner in which an item fails is important for system failure, and should be considered in the system reliability analysis. For example, in a system composed of two parallel electronic units, if a unit fails, the system will fail; but for most other types of failures of the unit, the system will still be functional, since the other unit functions properly.

There are several system modeling schemes for reliability analysis. *Reliability block diagram* methods include series, parallel, standby, shared load, and complex systems. *Logic tree* methods include fault tree and success tree methods, which include the method of construction and evaluation of the tree. *Event tree* methods include modeling of multisystem designs and complex systems whose individual units should work in a chronological or approximately chronological manner to achieve a mission. Failure mode and effect analysis and the master logic diagram (MLD) are also used for reliability analysis.

Reliability Block Diagram Methods

Reliability block diagrams are frequently used to model the effect of items failing (or functioning) on system performance. They often correspond to the physical arrangement of items in the system. However, in certain cases, the arrangement may be different. For instance, when two resistors are in parallel, the system fails if one fails short. Therefore, the reliability block diagram of this system for the "fail short" mode of failure would be composed of two series blocks. However, for other modes of failure of one unit, such as open failure mode, the reliability block diagram is composed of two parallel blocks.

Series systems: A reliability block diagram is in a series configuration when failure of any one item (according to the failure mode of each item, on which the reliability block diagram is based) results in the failure of the system. Accordingly, for functional success of a series system, all of its items must successfully function during the intended mission time of the system. Figure 5-3.10 shows the reliability block diagram of a series system consisting of N units.

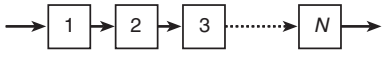

Figure 5-3.10. ***Series system reliability block diagram.***

The reliability of the system in Figure 5-3.10 is the probability that all N units succeed during its intended mission time, t. Thus, probabilistically, the system reliability, $R_s(t)$ for independent units is obtained from

$$R_s(t) = R_1(t) \cdot R_2(t) \cdot \cdots R_N(t) = \prod_{i=1}^{N} R_i(t) \tag{37}$$

where $R_i(t)$ represents the reliability of the ith unit. The hazard rate (instantaneous failure rate) for a series system is also a convenient expression. The hazard rate of the system, $h_s(t)$, is

$$h_s(t) = \sum_{i=1}^{N} h_i(t) \tag{38}$$

Assume a constant hazard rate model for each unit (e.g., assume an exponential time to failure for each unit). Thus, $h_i(t) = \lambda_i$. According to Equation 37, the system constant rate of failure is

$$\lambda_s = \sum_{i=1}^{N} \lambda_i \tag{39}$$

Equation 39 can also be easily obtained from Equation 37 by using the constant failure rate reliability model for each unit, $R_i(t) = \exp(-\lambda_i t)$.

$$R_s(t) = \prod_{i=1}^{N} \exp(-\lambda_i t) = \exp\left(-\sum_{i=1}^{N} \lambda_i\right) t \tag{40}$$

Accordingly, the MTTF of the system (MTTF_s) can be obtained from

$$\text{MTTF}_s = \frac{1}{\lambda_s} = \frac{1}{\sum_{i=1}^{N} \lambda_i} \tag{41}$$

EXAMPLE 6:

A system consists of three units whose reliability block diagram is in a series. The failure rate for each unit is constant, as follows: $\lambda_1 = 4.0 \times 10^{-6}\text{hr}^{-1}$, $\lambda_2 = 3.2 \times 10^{-6}\text{hr}^{-1}$, $\lambda_3 = 9.8 \times 10^{-6}\text{hr}^{-1}$. Determine the following parameters of the system:

1. λ_s
2. R_s (1000 hrs)
3. MTTF_s

SOLUTION:

1. According to Equation 39,

$$\lambda_s = 4.0 \times 10^{-6} + 3.2 \times 10^{-6} + 9.8 \times 10^{-6} = 1.7 \times 10^{-5}\text{hr}^{-1}$$

2. $R_s(t) = \exp(-\lambda_s t) \exp(-1.7 \times 10^{-5} \times 1000) = 0.983$, or unreliability of $F_i(1000) = 0.017$
3. According to Equation 41, $\text{MTTF}_s = 1/\lambda_s = 1/1.7 \times 10^{-5} = 58{,}823.5$ hrs

Parallel systems: A reliability block diagram is in a parallel configuration when the failure of all units in the system results in system failure. Accordingly, for a parallel system, success of only one unit would be sufficient to guarantee the success of the system. Figure 5-3.11 shows a parallel system consisting of N units.

According to the definition of a parallel system, failure of all units results in the failure of the system. Thus, for a set of N independent units,

$$F_s(t) = F_1(t) \cdot F_2(t) \cdot \cdots F_N(t) = \prod_{i=1}^{N} F_i(t) \tag{42}$$

Since $R_i(t) = 1 - F_i(t)$ [i.e., $F_i(t)$ is the unreliability of the units], then

$$R_s(t) = 1 - F_s(t) = 1 - \prod_{i=1}^{N} [1 - R_i(t)] \tag{43}$$

The hazard rate can be determined by using $h(t) = -d \ln R_s(t)/dt$. The resulting form of $h(t)$ is rather complex.

To address various characteristics of system reliability, consider a special case where the instantaneous failure rate is constant for each unit (exponential time-to-failure model), and the system is composed of only two units. Since $R_i(t) = \exp(-\lambda_i t)$, then according to Equation 43,

$$\begin{aligned} R_s(t) &= 1 - [1 - \exp(-\lambda_1 t)][1 - \exp(-\lambda_2 t)] \\ &= \exp(-\lambda_1 t) + \exp(-\lambda_2 t) - \exp[-(\lambda_1 + \lambda_2)t] \end{aligned} \tag{44}$$

Since $h_s(t) = f_s(t)/R_s(t)$ and $f_s(t) = -d[R_s(t)]/dt$, then using Equation 44,

$$h_s(t) = \frac{f_s(t)}{R_s(t)} = \frac{-d[R_s(t)]/dt}{R_s(t)} = \frac{\lambda_1 \exp(-\lambda_1 t) + \lambda_2 \exp(-\lambda_2 t) - (\lambda_1 + \lambda_2) \exp[-(\lambda_1 + \lambda_2)t]}{\exp(-\lambda_1 t) + \exp(-\lambda_2 t) - \exp[-(\lambda_1 + \lambda_2)t]}$$

The MTTF of the system can also be obtained from

$$\begin{aligned} \text{MTTF}_s &= \int_0^\infty R_s(t)\, dt \\ &= \int_0^\infty \{\exp(-\lambda_1 t) + \exp(-\lambda_2 t) \\ &\quad - \exp[-(\lambda_1 + \lambda_2)t]\}\, dt \\ &= \frac{1}{\lambda_1} + \frac{1}{\lambda_2} - \frac{1}{\lambda_1 + \lambda_2} \end{aligned}$$

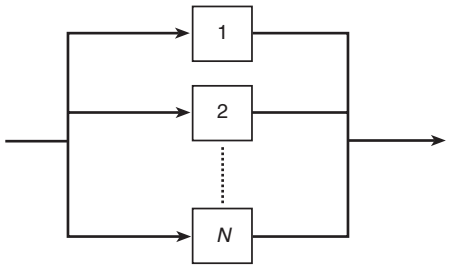

Figure 5-3.11. ***Parallel system block diagram.***

Accordingly, one can use the binomial expansion to derive the MTTF for N parallel units:

$$\begin{aligned}\text{MTTF}_s = &\left(\frac{1}{\lambda_1}+\frac{1}{\lambda_2}+\cdots\frac{1}{\lambda_N}\right)\\ &-\left(\frac{1}{\lambda_1+\lambda_2}+\frac{1}{\lambda_1+\lambda_3}+\cdots+\frac{1}{\lambda_{N-1}+\lambda_N}\right)\\ &+\left(\frac{1}{\lambda_1+\lambda_2+\lambda_3}+\cdots+\frac{1}{\lambda_{N-2}+\lambda_{N-1}+\lambda_N}\right)\cdots\\ &+(-1)^{N+1}\frac{1}{\lambda_1+\lambda_2+\cdots+\lambda_N}\end{aligned} \tag{45}$$

In the special case where all units are identical with a constant failure rate λ (e.g., in an active redundant system), Equation 43 simplifies to the following form

$$R_s(t) = 1-[1-\exp(-\lambda t)]^N \tag{46}$$

and from Equation 45,

$$\text{MTTF}_s = \text{MTTF}\left(1+\frac{1}{2}+\cdots+\frac{1}{N}\right) \tag{47}$$

It can be seen from Equation 47 that, in the design of active redundant systems, the MTTF_s exceeds the MTTF of an individual unit. However, the contribution to the MTTF_s from the second unit, the third unit, and so on would have a diminishing return as N increases. That is, there would be an optimum number of parallel units by which a designer can balance the reliability and the cost of the component in its life cycle.

Consider a more general form of a series and parallel system—the so-called K-out-of-N system. In this type of system, if any combination of K units out of N independent units works, it guarantees the success of the system. For simplicity, assume that all units are identical (which, by the way, is often the case). The binomial distribution can easily represent the probability that the system functions

$$\begin{aligned}R_s(t) &= \sum_{r=K}^{N}\binom{N}{r}[R(t)]^r[1-R(t)]^{N-r}\\ &= 1-\sum_{r=0}^{K-1}\binom{N}{r}[R(t)]^r[1-R(t)]^{N-r}\end{aligned} \tag{48}$$

EXAMPLE 7:

Three sprinkler heads connected in series are the only automatic suppression protection a corridor has. Although the heads are connected in series, the reliability analysis is addressed using a parallel system approach. The corridor will not have automatic suppression protection only if all the heads fail to work. Using the data from example 5, find the unreliability and the MTTF_s of the system.

SOLUTION:

According to Equation 43,

$$\begin{aligned}R_s(t) &= 1-(1-e^{-\lambda_1 t})(1-e^{-\lambda_2 t})(1-e^{\lambda_3 t})\\ F_s(1000) &= 1-R_s(1000)\\ &= 1-(1-e^{-4.0\times10^{-6}\times1000})\\ &\quad\cdot(1-e^{-3.2\times10^{-6}\times1000})(1-e^{-9.8\times10^{-6}\times1000})\\ &= 1.25\times10^{-7}\\ \text{MTTF}_s &= \left(\frac{1}{\lambda_1}+\frac{1}{\lambda_2}+\frac{1}{\lambda_3}\right)\\ &\quad-\left(\frac{1}{\lambda_1+\lambda_2}+\frac{1}{\lambda_1+\lambda_3}+\frac{1}{\lambda_2+\lambda_3}\right)\\ &\quad+\frac{1}{\lambda_1+\lambda_2+\lambda_3} = 4.35\times10^5 \text{ hrs}\end{aligned}$$

EXAMPLE 8:

How many components should be used in an active redundancy design to achieve a reliability of 0.999 such that, for successful system operation, a minimum of two components is required? Assume a mission of $t = 720$ hrs for a set of components that are identical and have a failure rate of 0.00015/hr.

SOLUTION:

For each component $R(t) = \exp(-\lambda t) = \exp(-0.00015 \times 720) = 0.8976$. According to Equation 48,

$$\begin{aligned}0.999 = R_s(t) &= 1-\sum_{r=0}^{1}\binom{N}{r}(0.8976)^r(0.1024)^{N-r}\\ &= 1-(0.1024)^N-N(0.8976)(0.1024)^{N-1}\end{aligned}$$

From the above equation, $N = 5$, which means that at least five components should be used to achieve the desired reliability over the specified mission time.

Standby redundant systems: A system is called a standby redundant system when some of its units remain idle until they are called for service by a sensing and switching device. For simplicity, consider a situation where only one unit operates actively and the others are in standby, as shown in Figure 5-3.12.

In Figure 5-3.12, unit 1 operates constantly until it fails. The sensing and switching device recognizes a unit failure in the system and switches to another unit. This

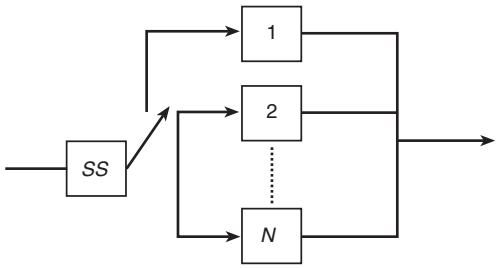

Figure 5-3.12. ***Standby redundant system.***

process continues until all standby units have failed, in which case the system is considered failed. Since units 2 to N do not operate constantly (as is the case in active parallel systems), one would expect them to fail at a much slower rate. This is because the failure rate for components is usually lower when the components are operating than when they are idle or dormant.

It is clear that system reliability is totally dependent on the reliability of the sensing and switching device. The reliability of a redundant standby system is the reliability of unit 1 over the mission time, t (i.e., the probability that it succeeds the whole mission time), plus the probability that unit 1 fails at time t_1 prior to t and the probability that the sensing and switching unit does not fail by t_1 and the probability that standby unit 2 does not fail by t_1 (in the standby mode) and the probability that standby unit 2 successfully functions for the remainder of the mission in an active operation mode, and so on.

Mathematically, the reliability function for a two-unit standby device according to this definition can be obtained from

$$R_s(t) = R_1(t) + \int_0^t f_1(t_1)\,dt_1 \cdot R_{ss}(t_1) \cdot R_2'(t_1) \cdot R_2(t - t_1) \quad (49)$$

where $f_1(t)$ is the probability distribution function for the time to failure of unit 1, $R_{ss}(t_1)$ is the reliability of the sensing and switching device, $R_2'(t)$ is the reliability of unit 2 in the standby mode of operation, and $R_2(t - t_1)$ is the reliability of unit 2 after it started to operate at time t_1.

If all units are identical with perfect switching, then the reliability of the system is

$$R_s(t) = \exp(-\lambda t) + \lambda t \exp(-\lambda t) = (1 + \lambda t)\exp(-\lambda t) \quad (50)$$

Shared load systems: A shared load system refers to a parallel system whose units equally share the system function. For example, if a set of two parallel pumps delivers x gpm of water to a reservoir, each pump delivers $x/2$ gpm. If a minimum of x gpm is required at all times, and one of the pumps fails at a given time t_1, then the other pump's speed should be increased to provide x gpm alone. Other examples of load sharing are multiple load-bearing units (such as those in a bridge), and load-sharing multi-unit electric power plants. In these cases, when one of the units fails, the others should carry its load. Since these other units would then be working under a more stressful condition, they would experience a higher rate of failure.

Assume that two units share a load (i.e., each unit carries half the load), and the time-to-failure distribution for both units to work is $f_h(t)$. When one unit fails (i.e., one unit carries the full load), the time-to-failure distribution is $f_f(t)$. Further, call the corresponding reliability functions during full-load and half-load operation $R_f(t)$ and $R_h(t)$, respectively. The system will succeed if both units carry half the load, or if unit 1 fails at time t_1 and unit 2 carries a full load thereafter, or if unit 2 fails at time t_1 and unit 1 carries the full load thereafter. Accordingly, the system reliability function, $R_s(t)$, can be obtained from

$$R_s(t) = [R_h(t)]^2 + 2\int_0^t f_h(t_1)R_h(t_1)R_i(t - t_1)\,dt_1 \quad (51)$$

In Equation 51, the first term shows the contribution from both units working successfully, with each carrying a half load. The second term represents the two equal probabilities that unit 1 fails first and unit 2 takes the full load at time t_1, or vice versa.

If there are switching or control mechanisms involved to shift the total load to the unfailed unit when one unit fails, then similar to Equation 49, the reliability of the switching mechanism can be incorporated into Equation 51.

In the special situation where an exponential time-to-failure model with failure rates λ_f and λ_h can be used for the two units for full- and half-load cases, respectively, then Equation 38 can be simplified to

$$R_s(t) = \exp(-2\lambda_h t) + \frac{2\lambda_h \exp(-\lambda_f t)}{(2\lambda_h - \lambda_f)}\exp[-(2\lambda_h - \lambda_f)t] \quad (52)$$

Complex systems: Most practical systems are not parallel or series, but exhibit some hybrid combination of the two. These systems are often referred to as *parallel-series systems.* Figure 5-3.13 shows an example of such a system.

A parallel-series system can be analyzed by dividing it into its basic parallel and series modules, and then determining the reliability function for each module separately. The process can be continued until a reliability function for the whole system is determined. Another type of complex system is one that is neither series nor parallel alone, nor parallel-series. Figure 5-3.14 shows an example of such a system.

For the analysis of all types of complex systems, Shooman[5] describes several analytical methods for com-

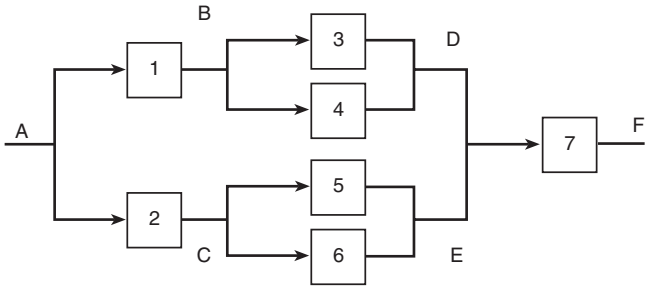

Figure 5-3.13. ***Complex parallel-series system.***

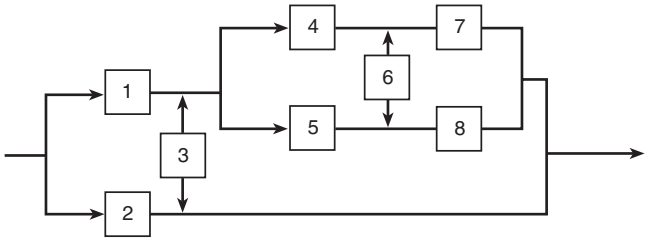

Figure 5-3.14. ***Complex nonparallel-series system.***

plex systems. These are the *inspection method, event space method, path-tracing method,* and *decomposition.* These methods are good only when there are not a lot of units in the system. For analysis of large numbers of units, fault trees would be more appropriate.

A computationally intensive method for determining the reliability of a complex system involves the use of *path set* and *cut set* methods. A path set (or tie set) is a set of units that include a connection between input and output when traversed in the direction of the reliability block diagram arrows. Thus, a path set provides a path through the graph. A minimal path set (or minimal tie set) is a path set that would not provide a connection between the input and output points if any of its units were removed. For example, in Figure 5-3.14, path set $P_1 = (1,3)$ is a minimal path set; but $P_2 = (1,3,6)$ is not, since units 1 and 3 are sufficient to guarantee a path.

A cut set is a set of units that interrupts all possible connections between the input and output points. A *minimal cut set* is the smallest set of units needed to guarantee an interruption of flow. In practice, minimal cut sets show a combination of unit failures that cause a system to fail. For example, in Figure 5-3.14, the minimal path sets are $P_1 = (2)$, $P_2 = (1, 3)$, $P_3 = (1, 4, 7)$, $P_4 = (1, 5, 8)$, $P_5 = (1, 4, 6, 8)$, and $P_6 = (1, 5, 6, 7)$. The minimal cut sets are $C_1 = (1, 2)$, $C_2 = (4, 5, 3, 2)$, $C_3 = (7, 8, 3, 2)$, $C_4 = (4, 6, 8, 3, 2)$, and $C_5 = (5, 6, 7, 3, 2)$. If a system has m minimal path sets denoted by $P_1, P_2, \ldots, P_m$, then the system reliability is given by

$$R_s(t) = \Pr(P_1 \cup P_2 \cup \cdots \cup P_m) \tag{53}$$

where each path set P_i represents the event that units in the path set survive during the mission time, t. This guarantees the success of the system. Since many path sets may exist, the union of all these sets gives all possible events for successful operation of the system. The probability of this union clearly represents the reliability of the system. It should be noted here that, in practice, the path sets, P_is, are not disjoint, which poses a problem for determining the left-hand side of Equation 53. However, a useful upper bound on the system reliability may be obtained by assuming that the P_is are highly disjoint. Thus,

$$R_s(t) \leq \Pr(P_1) + \Pr(P_2) + \cdots + \Pr(P_m) \tag{54}$$

Expression 54 yields better answers when using small reliability values. Since this is not usually the case, Equation 54 is not a good bound for use in practical applications.

Similarly, system reliability can be determined through minimal cut sets. If the system has n minimal cut sets denoted by $C_1, C_2, \ldots, C_n$, then the system reliability is obtained from

$$R_s(t) = 1 - \Pr(C_1 \cup C_2 \cup \cdots \cup C_n) \tag{55}$$

where C_i represents the event that units in the cut set fail sometime before the mission time, t. This guarantees system failure. The term $\Pr(C_1 \cup C_2 \cup \cdots \cup C_n)$, on the right-hand side of Equation 55, shows the probability that at least one of all possible minimal cut sets exists before time t. Thus, it represents the probability that the system fails sometimes before t. By subtracting this probability from 1, the reliability of the system is obtained. Similar to path sets, cut sets are not usually disjoint. Again, Equation 55 can be written in the form of its lower bound, which is a much simpler expression given by

$$R_s(t) \geq 1 - [\Pr(C_1) + \Pr(C_2) + \cdots + \Pr(C_n)] \tag{56}$$

Notice that each element of a path set represents the *success* of a unit, whereas each element of a cut set represents the *failure* of a unit. Thus, for probabilistic evaluations, the reliability function of each unit should be used in connection with path set evaluations (i.e., Equation 54) while the unreliability function should be used in connection with cut set evaluations (i.e., Equation 56).

The bounding technique used in Equation 56, in practice, yields a much better representation of the reliability of the system than Equation 54, because most engineering units have reliabilities greater than 0.9 over their mission time, making the use of Equation 56 appropriate.

In cases that deal with very complex systems that have multiple failure modes for each unit and complex physical and operational interactions, the use of reliability block diagrams is difficult. The method of fault tree and success tree analysis is more appropriate in this context, especially if the role of humans in the operation of the system needs to be modeled.

Logic Tree Methods

Fault tree (FT), success tree (ST), and master plant logic diagram (MLD) are three of the most popular logic tree methods. This section discusses the basic concepts of these logic tree methods by pointing out the differences between them. A simple example (a fire protection system) is discussed for illustration.

Fault tree and success tree: Fault and success trees are deductive processes that have tree-like hierarchical structures. In such a tree-like structure, the basic underlying principles of a complex system are represented. Each node in the tree represents an event (a goal) or a function. As shown in Figure 5-3.15, the top event of system failure or system success can be decomposed to subevents, subgoals, or subfunctions that have, in turn, their own subevents, subgoals, or subfunctions, and so on, until some lowest level of elementary components is reached. A set of symbols similar to the ones shown in Figure 5-3.16 is used to develop a logic tree.

Logically, it must be recognized that logic trees can be developed equally well in success or failure space, so that the tree analysis can proceed with either success or failure orientation. However, experience has shown that success orientation is preferable, since it tends to lead to better and more succinct definition of system functions and operation.

However, when one is attempting to understand the failure characteristics of a piece of equipment or an industrial process, fault descriptions are more easily grasped than the success space descriptions of the system,

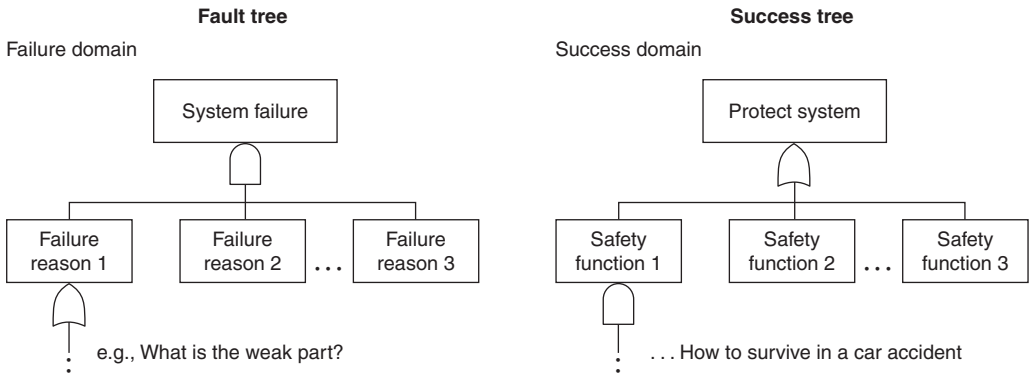

Figure 5-3.15. ***Fault tree vs. success tree.***

because the process is typically being viewed externally, from the perspective that a failure has already occurred. This means that the person is likely to be looking at the system in a deductive manner and tries to find in what way such a failure may occur.

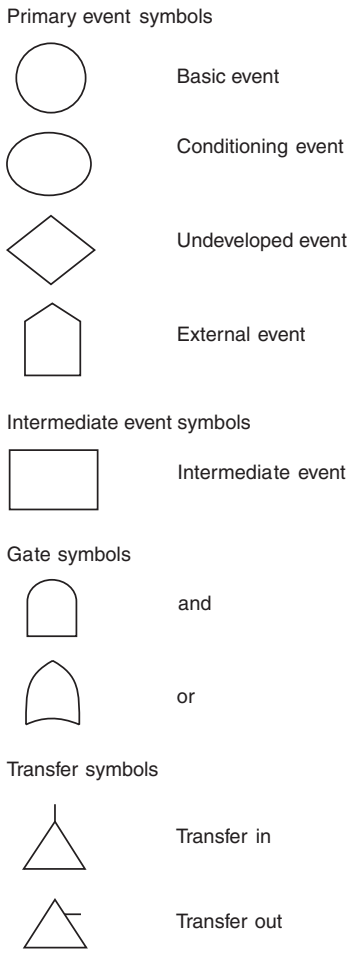

Figure 5-3.16. ***Primary event, gate, and transfer symbols.***

For a more detailed discussion of the construction and evaluation of fault trees, refer to the *Fault Tree Handbook.* The goal tree–success tree structure was initially developed as part of Department of Energy–sponsored research[6] to assess and improve information systems in a nuclear plant. Subsequently, it has been further developed and extended to a number of other applications.[7,8,9]

Master plant logic diagram (MLD): The hardware or human activities in the success tree often are associated with other support equipment, and since more often than not challenges to systems or processes originate from other support equipment, it is important to include these relationships in the success tree. A single visual display of the plant logical relations is represented by an MLD model.[10] This logic diagram shows all of the interrelationships among the so-called front-line systems and support systems. Front-line systems are those that perform main functions of the system or process. Support systems are those that either cool, actuate, power, lubricate, or control the front-line systems. As shown in Figure 5-3.17, the MLD diagram is also developed hierarchically in a top-down manner. Therefore, most of the characteristics of the success tree are equally applicable to this diagram. Computer software called REVEAL_W has been developed to perform the MLD modeling.

EXAMPLE 8:

Consider the fire protection system shown in Figure 5-3.18. This system is designed to extinguish all possible fires in a plant with toxic chemicals. Two physically independent water-extinguishing nozzles are designed such that each is capable of controlling all types of fires in the plant. Extinguishing nozzle 1 is the primary method of injection. Upon receiving a signal from the detector/alarm/actuator device, pump 1 starts automatically, drawing water from the reservoir tank and injecting it into the fire area in the plant. If this pump injection path is not actuated, plant operators can start a second injection path manually. If the second path is not available, the operators will call for help from the local fire department. (The detector also sends a signal to the fire department.) However, due to the delay in the arrival of the local fire de-

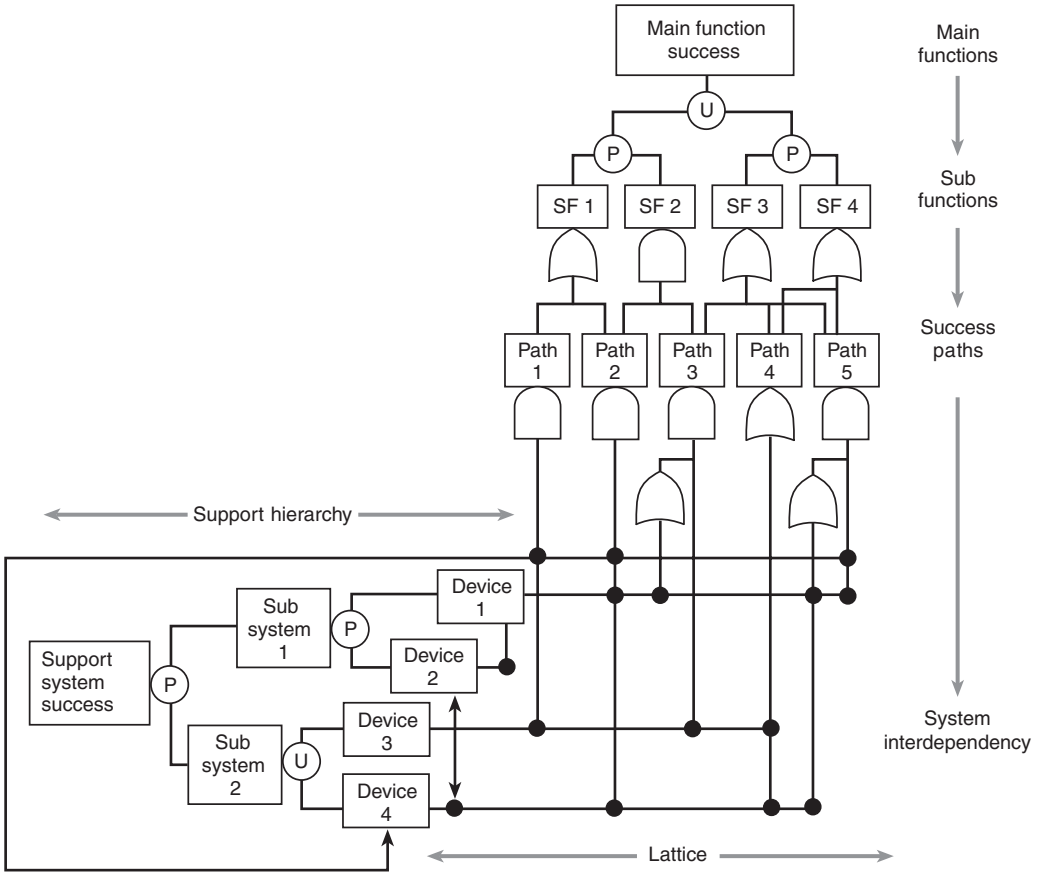

Figure 5-3.17. ***Master logic diagram.***

partment, the magnitude of damage would be higher than it would be if the local fire-extinguishing nozzles were available to extinguish the fire. Under all conditions, if the normal off-site power is not available due to the fire or other reasons, a local generator would provide electric power to the pumps. The power for the detector-alarm-actuator system is provided by batteries, which are constantly charged by the off-site power. Even if the ac power is not available, the dc power provided through the battery is expected to be available at all times. The manual valves on the two sides of pump 1 and pump 2 are normally open, and only remain closed when they are being repaired. The entire fire system and generator are located outside of the reactor compartment, and are therefore not affected by an internal fire.

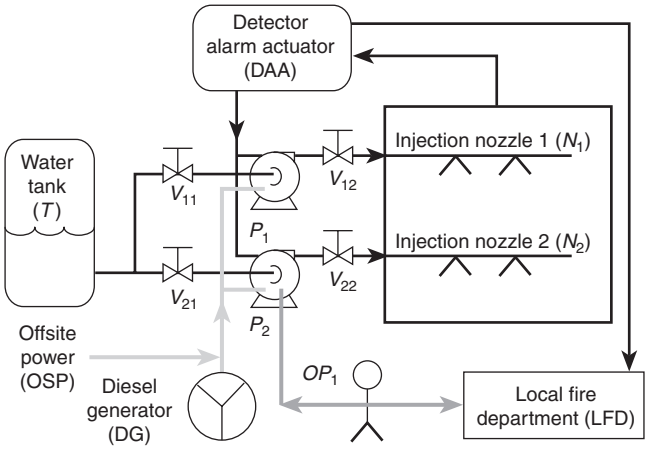

Figure 5-3.18. ***A fire protection system.***

SOLUTION:

For reliability analysis, one should explain the cause and effect relationship between the fire and the progression of events following the fire, and should identify all failures (equipment or human) that lead to failure of the event-tree headings (on-site or off-site protective measures).

For example, Figure 5-3.19 shows the fault tree developed for the on-site fire protection system failure. In this fault tree, all basic events that lead to the failure of the two independent paths are described. Note that MAA, electric power to the pumps, and the water tank are shared by the two paths. Clearly these are considered physical dependencies, which are taken into account in the quantification step of the risk analysis. In this tree, all external event failures and passive failures are neglected.

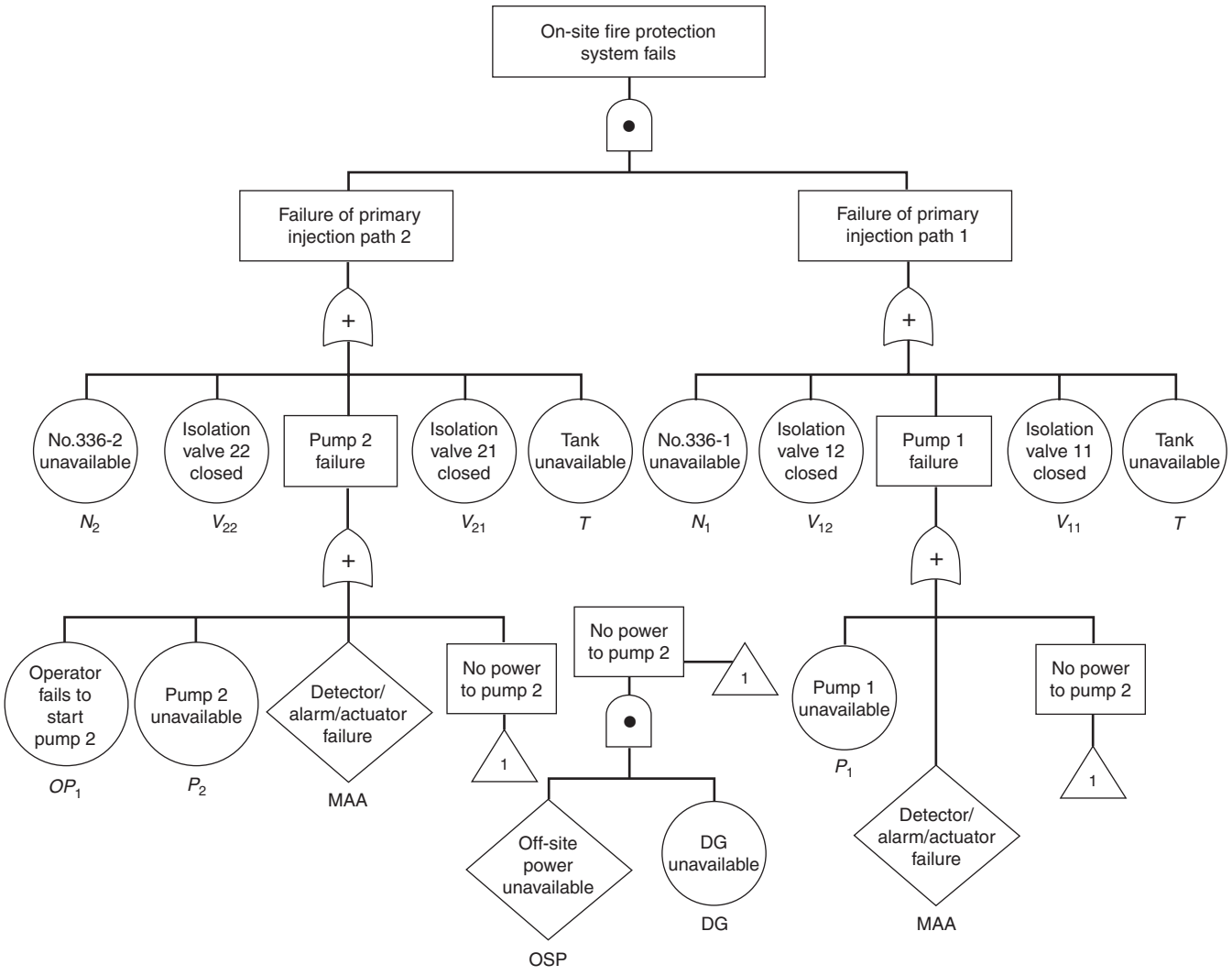

Figure 5-3.19. ***Fault tree for on-site fire protection system failure.***

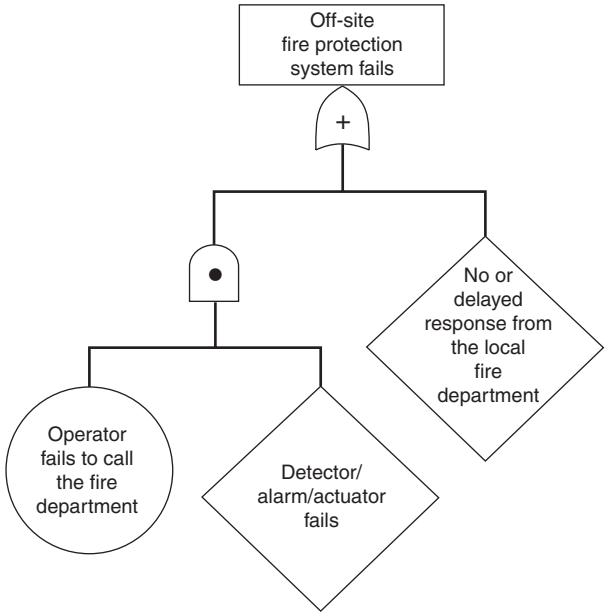

Figure 5-3.20. ***Fault tree for off-site fire protection system failure.***

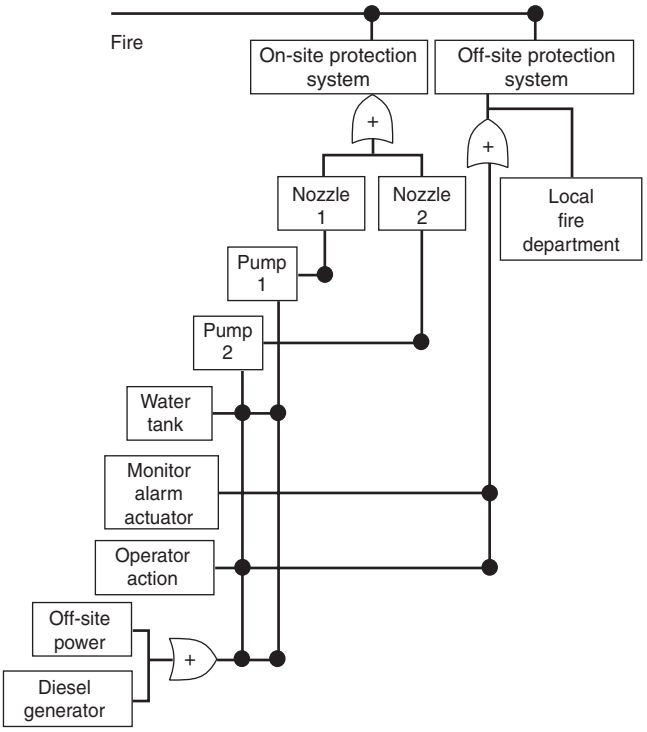

Figure 5-3.21. ***Master logic diagram for fire protection system.***

Figure 5-3.20 shows the fault tree for the off-site fire protection system failure. This tree is simple, since it only includes failures that do not lead to an on-time response from the local fire department. It is also possible to use the MLD for system analysis. An example of the MLD for this problem is shown in Figure 5-3.21.

References Cited

1. B. Epstein, "Estimation from Life Test Data," *Technometrics,* 2, p. 447 (1960).
2. E.L. Welker and M. Lipow, "Estimating the Exponential Failure Rate Dormant Data with No Failure Events," *Proc. Rel. Maint. Sysmp.,* 1, 2, p. 1194 (1974).
3. L.J. Bain, *Statistical Analysis of Reliability and Life-Testing Models: Theory and Methods,* Marcel Dekker, New York (1978).
4. N. Mann, R.E. Schafer, and N.D. Singpurwalla, *Methods for Statistical Analysis of Reliability and Life Data,* John Wiley and Sons, New York (1974).
5. M.L. Shooman, *Probabilistic Reliability: An Engineering Approach,* 2nd ed., Kreiger, Melbourne, FL (1990).
6. R.N. Hunt and M. Modarres, "Integrated Economic Risk Management in a Nuclear Plant," presented at the Annual Meeting of the Society for Risk Analysts (1984).
7. I. Kim and M. Modarres, "Goal Tree–Success Tree Model as the Knowledge-Base of Operator Advisory Systems," *Topical Meeting on Artificial Intelligence and Other Innovative Computer Applications in Nuclear Industry,* Snowbird, UT (1987).
8. L-W. Chen and M. Modarres, "A Hierarchical Decision Process for Fault Administration," *Computers and Chemical Eng. J.,* 16, 5, pp. 425–448 (1992).
9. D. Sebo, D. Marksberry, and M. Modarres, "RSAS: A Reactor Safety Assessment System," in *Proc. of the 7th Power Plant Dynamics, Control and Testing Symposium,* Knoxville, TN (1989).
10. R.N. Hunt and M. Modarres, "Performing a Plant-Specific PRA by Hand—A Practical Reality," presented at the 14th INTER-RAM Conference, Minneapolis (1987).

Additional Reading

U.S. NRC, *Fault Tree Handbook,* U.S. Naval Research Corporation (1981).

CHAPTER 4

Uncertainty

Kathy A. Notarianni

Introduction

The treatment of uncertainty is key to ensuring and maintaining an appropriate level of public safety while allowing the flexibility necessary to reduce costs. This is true for all fire safety engineering calculations whether conducted to meet a performance-based code, to aid in the establishment of a prescriptive requirement, or to compare a performance option to its prescriptive counterpart. However, at present, no method exists for the treatment of uncertainly in a fire safety engineering calculation. Proper treatment of uncertainty will assist engineers and architects in the design process, and assist code officials by increasing confidence in the acceptance of a performance calculation. It will aid researchers in prioritizing enhancements to both the physics and structure of fire models, and aid policymakers by incorporating scientific knowledge and technical predictive abilities in policy decisions.

This chapter is made up of several sections. The first section, Understanding Uncertainty, covers basic concepts of uncertainty and variability in order to develop a common language for discussion among fire safety professionals. It then presents motivating examples that show the importance of dealing with uncertainty in the application of our scientific tools. It is shown how variations in analysis parameters, assumptions, or model inputs can lead to changes in the acceptability of a fire safety design. This is termed *switchover.*[1] A taxonomy is presented in this section that is useful as a framework for understanding, identifying, and investigating uncertainties.

Another section, Treatment of Uncertainty in Design Calculations, discusses the treatment of uncertainty with safety factors as well as quantitative techniques for the treatment of uncertainty in fire protection design calculations. The use of safety factors in both prescriptive and performance-based codes is discussed. Guidance is given on selecting an appropriate factor of safety and on combining safety factors. Quantitative techniques are presented for the treatment of uncertainties in measurement; in analysis parameters, assumptions, and values; and in complex fire models.

A methodology for the application of an uncertainty analysis to a fire safety engineering calculation is suggested. It is shown how results of this type of analysis are used to create distributions of time to untenability, to demonstrate the effect of selecting various sets of performance criteria, to compare two designs, and to provide insight to model development.

The last section of this chapter, Treatment of Uncertainty in Cost-Benefit and Decision Analysis Models, discusses the application of uncertainty analysis to cost-benefit and decision analysis models. An example of a cost-benefit model that incorporates uncertainty is provided.

Understanding Uncertainty

Uncertainty is a broad and general term used to describe a variety of concepts including but not limited to lack of knowledge, variability, randomness, indeterminacy, judgment, approximation, linguistic imprecision, error, and significance. These and many other facets of uncertainty are discussed in more detail in Chapter 4 of the book *Uncertainty.*[1] The variety of types and sources of uncertainty, along with the absence of agreed-upon terminology, generates considerable confusion in the fire protection engineering world. Many facets of uncertainty can be understood through statistical and scientific concepts, some of which are presented below. However, uncertainties in the engineering design process, such as those surrounding the selection of performance criteria, are best understood by their ability to change the accept-

Dr. Kathy A. Notarianni leads the Integrated Performance Assessment Research Group in the Building and Fire Research Laboratory of the National Institute of Standards and Technology in Gaithersburg, Maryland. Her work has focused on topics such as smoke detection, water-based suppression, fire modeling, and uncertainty and performance related to fire regulations.

ability of a design. Finally, to fully understand uncertainty in fire safety engineering, one must be cognizant of the difficulties in conducting a complete uncertainty analysis.

Nature and Sources of Uncertainty

Uncertainty is often discussed as though it was synonymous with measurement uncertainty, that is, doubt about the validity of the result of a measurement. Measurement uncertainties are characterized from both a statistical analysis of a series of observations (to determine the random error) and from systematic effects associated with corrections and reference standards (to determine the systematic error). The total error is defined as a combination of random and systematic errors. Much work has been done to reach an international consensus on the evaluation and expression of measurement uncertainty. General rules for evaluating and expressing uncertainty in measurement are provided in a guide published by the American National Standards Institute and the National Conference of Standards Laboratories.[2] An example of dealing with measurement uncertainty in fire protection engineering is found in a study of the uncertainty surrounding the use of thermocouples to measure temperature.[3]

However, uncertainty also arises from a variety of other sources to which standard techniques for the evaluation and expression of uncertainty do not always apply. Uncertainty can arise from a lack of complete knowledge. What is the heat release rate or radiative fraction of a mixed-fuel package? We have not measured and cannot reliably predict the value of these quantities for all potential fuel packages. Furthermore, the heat-release rate and radiative fraction vary with parameters such as geometry, source and strength of ignition, and ventilation conditions. Uncertainty may arise from *randomness,* such as where and how the fire will start. Uncertainty may arise from *indeterminacy,* defined as the inability to know what will happen in the future. For example, building occupancy and furnishings may differ 10 or 20 years after they were first constructed. Uncertainty may arise due to the unpredictability of human behavior. It is unknown what actions each occupant will take upon discovering a fire or hearing an alarm. Uncertainty can arise because of disagreement between information sources. Rates of generation of products of combustion per gram of fuel burned vary from study to study and even from test to test in the same study using the same instruments.

Uncertainty may arise from difficulties in defining the problem. For example, a goal may be established to provide an equivalent level of fire safety. However, equivalency may be defined as providing the same time available for egress, providing the same level of property protection, providing the same level of fire safety for fire fighters entering the building, or all of the above. Uncertainty may also arise from *linguistic imprecision.* It is difficult to determine exactly what is meant by "flame spread should be limited." Uncertainty often refers to *variability,* for example, the ambient temperature and the total number of deaths from fire. These quantities vary in time by season, month, and day. They also vary in space by region of the country and community size. Even if we had complete information, we may be uncertain because of simplifications and approximations introduced due to computational limitations.

There are also important questions related to understanding uncertainties in perceptions, attitudes, and values toward risk. "In addition to being uncertain about what exists in the external world, we may be uncertain about individual preferences, uncertain about decisions relating to potential solutions, and even uncertain about the level and significance of our uncertainty."[1] Uncertainties inherent in the performance-based analysis and design process are discussed in *Introduction to Performance-Based Fire Safety.*[4]

Understanding the level and significance of our uncertainty is crucial to making good fire safety design decisions. It is therefore important that the fire protection engineering community understands basic concepts of probability and statistics, and that the community agrees on terminology for use in discussing uncertainty.

Terminology for Probability and Statistics

The mathematical concept of probability is used to quantify uncertainty. Elements of probability allow us to quantify the strength of, or confidence in, our conclusions. There are two views of probability, the frequentist (or classical) and the subjectivist (or Bayesian). Each of these are useful in quantifying uncertainties in fire protection engineering. Likewise, inferential statistics has produced an enormous number of analytical tools that allow the engineer or scientist to better understand the systems that generate data. Inferential statistics allows us to go beyond merely reporting data, and enables the drawing of conclusions about the scientific system. Concepts essential to the understanding of uncertainty such as distribution, mean, standard deviation, errors, corrections, correlation, and independence are presented in Section 1 of this handbook. A full treatment of probability concepts is presented in Section 1, Chapter 11, and concepts of statistical analysis are presented in Section 1, Chapter 12.

Probability/frequentist view: The probability of an event's occurring in a particular scenario is defined as the frequency with which it occurred in a long sequence of similar trials. For example, the probability of a fire pump failure may be defined by failure data for that pump in many fires.

Probability/Bayesian view: The probability of an event is the degree of belief that a person has that it will occur, given all relevant information currently known to that person. For example, the probability that a new fire detector will save lives may be based on the judgment of an expert in both fire detection and the nature of fire deaths (who may or may not have frequency data to support such a belief in the classical sense).

Random error and statistical variation: No measurement of an empirical quantity such as the burning rate of jet fuel can be absolutely exact. Imperfections in the measuring instruments and observational technique will inevitably give rise to variations from one observation to

the next. The resulting uncertainty depends on the size of the variations between observations and the number of observations taken. Classical, statistical techniques such as standard deviation, confidence intervals, and others can be used to quantify this uncertainty.

Aleatory uncertainty: Aleatory uncertainty is due to random variations and chance outcomes and has also been referred to as *randomness*,[5] as *stochastic uncertainty*,[6] and as *statistical uncertainty*.[7] In principle, aleatory uncertainty cannot be reduced but can be better characterized through exhaustive study. Stochastic uncertainty has been defined as "the totality of occurrences that can take place in the particular universe under consideration together with a probabilistic characterization of the likelihood of these occurrences."[8]

Epistemic uncertainty: Epistemic uncertainty arises because of lack of knowledge. It has also been referred to as *imprecision*,[5] as *knowledge uncertainty*,[6] as *engineering uncertainty*,[7] and as *subjective uncertainty* because expert judgment is often needed to represent the uncertainty when full knowledge is lacking. In principle, epistemic uncertainty can be reduced through gaining additional information or data. It has been stated that this type of uncertainty often arises due to the uncertainty on the part of the analyst as to how the appropriate values of the quantities should be assigned.[8]

Scientific versus statistical significance: *Statistically significant* refers to a mathematical calculation that verifies that two quantities are likely to be the same or different. *Scientifically significant* refers to whether the difference is large enough to be important.

Uncertainties in the Design Process and the Problem of Switchover

Of practical significance is that direct measurement of the fire safety performance of a building or building system is not usually possible; therefore, we must rely on the technical predictive ability of scientific tools, such as existing fire models. The problem is that the numerous uncertainties in the application of these fire safety design tools often go unrecognized or ignored. Many of these uncertainties are inherent in the design process itself. Variations in analysis parameters, assumptions, or model inputs may cause output criteria to change. *Switchover* occurs when outcome criteria change enough so as to cause a change in the design decision (e.g., the acceptability of a final design). It is critical to know if different sets of reasonable inputs, scenarios, or parameters used in a fire safety engineering design have potential to cause switchover and lead to different acceptable designs.

The Society of Fire Protection Engineers (SFPE) *Engineering Guide to Performance-Based Fire Protection Analysis and Design of Buildings* details several steps in the design process.[9] These are shown in Figure 5-4.1, adapted from the SFPE engineering guide. The stated intent of the guide is to "provide guidance that can be used by both design engineers and approving authorities as a means to determine and *document achievement of agreed upon levels of fire safety* for a particular project" (emphasis added).

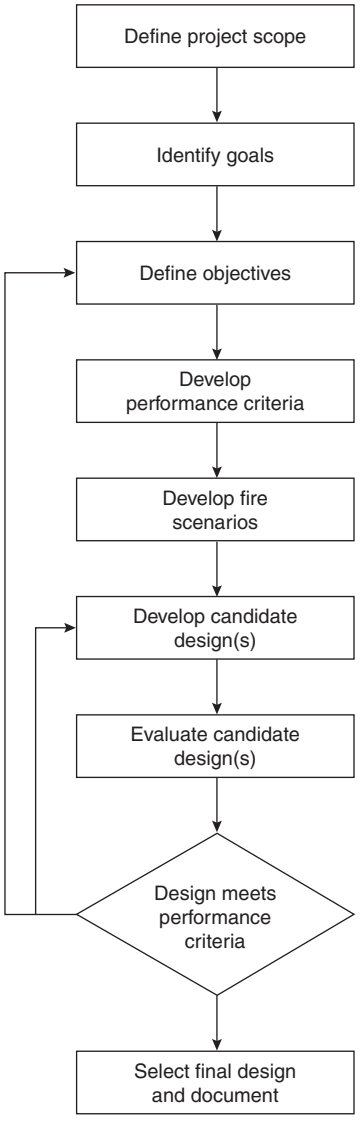

Figure 5-4.1. ***Overview of the performance-based design process.***[9]

A review and analysis of the performance-based design process for fire safety engineering outlined in the guide along with a review of several case studies of performance-based, fire safety engineering designs for actual buildings was conducted.[10] This review uncovered seven major barriers to determining and documenting achievement of agreed-upon levels of fire safety for a particular project. All seven barriers involve various types of uncertainty. Thus, there is a well-defined and strong role for uncertainty analysis in improving the ability to document achievement of agreed-upon levels of fire safety. The seven barriers identified are presented below along with a discussion of how they might lead to switchover of a design from acceptable to unacceptable.

1. Performance criteria are not established or no agreement exists: There is uncertainty in the selection of performance criteria. In fact, performance criteria have not been established or agreed upon by the fire safety community, and current policy allows the stakeholders themselves to select the criteria to be used for each design. Discussions occur around questions such as the following: Is the set of performance criteria sufficient? What do the numerical values actually represent? Should different criteria be used for different subpopulations, such as for people who are sick, elderly, or have disabilities? At one recent international conference, two engineers presented their performance-based case studies conducted for real clients on actual buildings. They had each followed the current design guidelines; however, they had selected very different performance criteria.[11,12] Differences existed on three levels: (1) the parameters included in the set of performance criteria, (2) numerical values selected as the critical or cut-off values for these parameters, and (3) the presence or absence of a time element for reaching the cut-off values. Since predictions of fire models are compared to selected performance/life safety criteria in order to determine if a design is acceptable, variations in criteria can cause the same design to pass or fail.

2. The design fire selection process is unspecified: Design fires are descriptions of fire events (e.g., a grease fire on the stove, a smoldering cigarette fire on the sofa). Along with design fires, several fire scenarios, or descriptions of possible fires that could occur, are developed. For each design fire evaluated, the goal is to provide a fire safety design that would mitigate unwanted fires from developing.

Since it is impossible to evaluate physically the performance of building systems in response to all design fires that might occur, one does not have confidence that design fires and the resulting fire scenarios chosen adequately represent the range of fires that might occur in the building. Usually a designer will try to select worst-case or reasonable worst-case scenarios.* However, it is not always intuitive which scenarios present a worst-case situation or how likely (or unlikely) a particular scenario is. It is debatable whether we should be designing for the one-in-a-million fire and how many design fires and fire scenarios are sufficient. A methodology is needed that would incorporate the likelihood of a design fire and/or associated design fire scenario. It is easy to see how the same design may be deemed acceptable if based on a limited number and type of design fires, or deemed unacceptable if based on an expanded set of scenarios or a different set of scenarios.

3. Assumptions are made about human behaviors during fire: During several critical steps in the design process, assumptions are made about human behaviors during fire. For example, some egress models used by fire protection engineers to predict the time required for safely evacuating a building (or part of a building) make many assumptions about how humans behave. Two assumptions are stated in one internationally used egress model: (1) 100 percent of the occupants are readily mobile and (2) occupants begin leaving the building immediately upon hearing an alarm.[13] Experience demonstrates that this is often not the case.[14,15]

Other behavior assumptions may not be explicitly stated but can be inferred from an analysis of model outputs. For example, results from a recently published study of a performance calculation using the egress model in FASTlite reveal that assumptions are made about human behavior during fires.[13] A decrease in the number of exits by one-third increases the egress time by exactly one-third. This suggests an implied assumption that an equal number of people egress through each available exit. More typically, actual human behavior will be to exit following the path one normally uses to enter and exit the building. Existing egress calculations and models need to be evaluated so that unrecognized and/or unstated uncertainties resulting from assumptions regarding human behavior can be identified. Once revealed, the implications of these assumptions need to be explored quantitatively.

4. Predictive fire models have limitations that are not well documented or widely understood: Fire models and other calculation methodologies are often inappropriately used to develop and evaluate trial designs for buildings and/or scenarios outside of the predictive capabilities of the models. This occurs because limitations of fire models are not well documented or widely understood. For example, computer fire models don't model fire directly and only predict fire effects based on user-selected input data. Because many existing fire model and calculation methodologies were originally developed as research tools, model conditions, defined as "fundamental requirements for the model's validity,"[16] are often unknown or unstated. Estimates provided by a model are technically credible only when model conditions have not been violated.

5. Outputs of fire models are point values that do not directly incorporate uncertainty: Even when the model is used within its intended limitations, fire model outputs are point values that do not reflect inherent input uncertainties (e.g., fire growth rates, initial conditions). Without knowledge of the uncertainty surrounding a prediction, it is impossible to be certain of a design's acceptability. One example is modeling the response of fire protection equipment such as sprinklers, heat detectors, and smoke detectors. Predictions of the time to activation of such devices would specify, for example, 121 s. However, the actual time to activation may be higher or lower depending on uncertain inputs or also on any number of factors not modeled, such as individual detector characteristics and distance below the ceiling.

6. The design process often requires engineers to work beyond their areas of expertise: Problems can also occur when fire protection engineers are required to work in domains outside their expertise. Conservative assumptions

*The term *worst-case scenario* is used in this chapter to represent both worst-case and reasonable worst-case scenarios as understood in the fire protection design field.

made by well-intentioned engineers may not be as conservative as intended. For example, a design engineer intending to be conservative may assume that tenability would be violated if, out of a set of criteria, any one particular criterion, such as temperature or carbon monoxide, exceeded its minimum value. However, toxicity experts might argue that temperature and gas interactions cause tenability to be violated even when every individual species is in acceptable ranges. Likewise, a design engineer may assume that the time needed for a resident to react to an alarm be conservatively set equal to the travel time needed to go from one remote corner of the unit to the other most remote corner of the same unit. However, this may not be that conservative since even a fully ambulatory occupant may stop to gather belongings, rescue a pet, call a neighbor, and so forth.

7. No standardized methods exist to incorporate reliability of systems: The last barrier identified is the uncertainty surrounding both the reliability of a given fire protection device, system, or characteristic and the lack of a standardized method to incorporate reliability into performance-based engineering calculations and decisions based upon these calculations. We may be uncertain about the reliability of a given fire suppression system. Sometimes a fire suppression system is proposed as an alternative to passive fire protection, such as compartmentalization. However, these two alternatives have different reliabilities. There is uncertainty (e.g., no agreement) on how to account for these differences.

These seven barriers to determining and documenting achievement of agreed-upon levels of fire safety for a particular project must be addressed fully in order for all stakeholders to have a known level of confidence in the science-based predictions and the resulting final design. All seven barriers involve various types of uncertainty. Thus, there is a well-defined and important role for uncertainty analysis in fire safety engineering calculations. Although this clear role for uncertainty in improving the development and implementation of performance-based fire safety regulations exists, uncertainty analysis is clearly an uncomfortable topic for many of the stakeholders in the process.

Difficulties with Uncertainty Analysis

Discussion of the proper treatment of uncertainty in a fire safety engineering calculation is difficult for several reasons:

1. *Magnitude of the problem.* It is widely assumed that a mixture of conservative assumptions and factors of safety can be used to explain away uncertainties. However, the magnitude of the problem is not clearly understood. Factors of safety that are applied at various stages of the analysis are not necessarily linearly related to the critical output parameters, potentially resulting in a reduced (or nonexistent) factor of safety in the results.
2. *Uncertainties that go unrecognized or ignored.* These types of uncertainties include those in variables hard-wired in scientific tools, those in tenability/performance criteria, those surrounding the selection of design fires, and those in human behaviors and values.
3. *Effect on the implementation of performance regulations.* It is feared that identification and treatment of uncertainty would show that our current ability to predict the buildup of heat and toxic products of combustion is not accurate enough to judge the acceptability of a proposed design with a high enough confidence level. This would delay implementation of the entire performance process until predictions of critical outcome criteria can be more certain.
4. *Quantitative methodology.* No quantitative methodology exists for treating uncertainty in performance-based designs. A methodology is needed that is both rigorous and user friendly.
5. *Impracticality.* It is feared that the mathematical rigor needed to conduct such an analysis would render the process impractical.
6. *Paucity of data.* To quantify uncertainty adequately, a large quantity of data would be needed to determine ranges of values for input parameters such as heats of combustion, rates of production of various gaseous species, and other important inputs. A large quantity of data would also be needed to validate predicted values with empirical data from real burn scenarios.

It should be pointed out that these are real and valid concerns due to the combination of poorly defined and unstructured problems, and the lack of a user-friendly methodology. Current common practice for conducting uncertainty analyses involves completing a series of single-variable sensitivity studies. Application of these techniques to a complete performance-based design containing hundreds of variables is impractical. The following sections focus on practical ways to identify and account for uncertainties in fire protection engineering design.

Identifying Uncertainties in Fire Protection Engineering

When considering uncertainty in a fire protection engineering calculation, fire protection engineers typically consider first the uncertainties associated with the calculation inputs, usually empirically measured quantities such as heat-release rate. However, there are many other types of uncertainty integral to fire safety engineering design.

In a complete uncertainty analysis, not all uncertain parameters are treated quantitatively, only parameters or combinations of parameters with the potential to cause switchover in the final decision on the acceptability of a design. Others are negligible and best-guess values of these parameters can be used in the calculations. Still others, such as societal values, become policy or regulatory issues, not engineering issues. The intelligent use of safety factors can often cover more than one type of uncertainty. Still, it is useful to first identify sources and types of uncertainty from a broad perspective. Without first adequately identifying the sources of uncertainty, we cannot understand how best to handle them.

This section presents a taxonomy useful in developing a framework for understanding, identifying, and in-

vestigating uncertainties as a function of the steps in a fire safety engineering calculation. The taxonomy builds upon earlier published work.[4,10]

Scientific Uncertainties

Scientific uncertainties are due both to lack of knowledge (e.g., in the underlying physics, chemistry, fluid mechanics, and/or heat transfer of the fire process) and to necessary approximations required for operational practicality of a model or calculation. Of the many types of uncertainty found in performance-based fire safety design calculations, scientific uncertainties are typically the most easily recognizable and quantifiable. The many types of scientific uncertainty can be roughly divided into five subcategories: (1) theory and model uncertainties, (2) data and input uncertainties, (3) calculation limitations, (4) level of detail of the model, and (5) representativeness of the design fire scenarios.

Theory and model uncertainties arise when physical processes are not modeled due to lack of knowledge of how to include them, processes are modeled based on empirically derived correlations, and/or simplifying assumptions are made. These types of uncertainties are present in most compartment fire models, where each of these factors lead to uncertainties in the results. Most compartment fire models are zone models, which make the simplifying assumption that each room can be divided into two volumes or layers, each of which is assumed to be internally uniform and that changes in energy or state are implemented immediately throughout the layers. Current zone models do not contain a combustion model to predict fire growth, forcing the model user to account for any interactions between the fire and the pyrolysis rate. Many compartment fire models also use an empirical correlation to determine the amount of mass moved between the layers.

Data and input uncertainties arise from both lack of knowledge of specific input values and variations in input values as a function of many factors, such as time, temperature, or region of the country. For example, the rate of heat release of a three-cushion upholstered sofa may be uncertain due to lack of available data for sofas with the same dimensions, stuffing, and cover materials. It may also be uncertain because the test method by which the heat-release rate was measured could not specify all combinations of ignition source and strength, and because there are inaccuracies inherent in the instrumentation used in the test. Other inputs such as concentrations of toxic gases produced vary with time as the fire develops and are uncertain. The species production rates used to predict concentrations are a function of the material or combination of materials actually burned. This is unknown a priori at the design stage.

For most fire models and calculation procedures, very different answers can result depending on the calculation limitations, control volume selected for modeling, the level of detail of the model, and the model-domain parameters specified. Model-domain parameters set the scope of the system being modeled and define the model's level of detail and/or baseline properties. Though these parameters or quantities are often ignored during uncertainty analysis, they have the potential for considerable impact.[1] This has been shown for fires in high bay spaces. Differences in the outcome criteria such as maximum temperature, and time to activation of fire detectors and sprinklers are found when a large space is modeled with a simple zone fire model versus a more detailed computational fluid dynamics model.[17] Differences in the outcome criteria are also found when a large space, which is typically subdivided by draft curtains,* is modeled. If a control volume is drawn around a single draft-curtained area (as opposed to drawing the control volume around multiple draft-curtained areas or around the entire building), higher temperatures and faster activation times of installed fire protection devices will be predicted. Also, significant to the uncertainty in the outcome parameters are the index variables of the model. Index variables are used to identify a location in the domain of a model or to make calculations specific to a population, geographic region, and so forth.

Uncertainty arises in both the number and type of design fire scenarios that need to be modeled for a given design/building. There may be significant differences between reality and the design fire scenarios that were used to judge the adequacy of the performance-based design. Variations in the ignition source, rate of growth, and/or the materials burned affect confidence in the results. It is unclear whether all statistically significant fire scenarios must be modeled or whether worst-case or reasonable worst-case scenarios are adequate. Furthermore, a worst-case scenario may be defined in terms of many different variables. A scenario may be worst-case because it is most likely to cause death, because it has potential for large property loss, or for other reasons.

Uncertainties and Variability in Behavior

Human behavioral uncertainties concern both the way in which people act in a fire and how these actions should be considered during steps in the design process (e.g., definition of project goals, selection of performance criteria, and development and evaluation of trial designs). Behavioral scientists tell us that human actions can range from somewhat predictable to unpredictable. Actions are more predictable when choices are limited, procedures are practiced, the situation is not novel, and little chaos is present. Unfortunately, during a typical fire, few if any of these conditions occur. Brannigan discusses what he calls *intentional uncertainty* in relationship to human behavior.[16] Brannigan states, "human decision making does not follow the same kind of well understood rules that control the physical science variables used in models. Human decisions represent intentional uncertainty."

Human behavior in response to a fire alarm must be modeled in terms of time to respond to the alarm and type of response. Does the person immediately begin evacuating the building? Does he/she take the stairs or

*A draft curtain is a barrier that extends a certain vertical distance down from the roof or ceiling. Draft curtains are installed to subdivide a large area with the intent of corralling the heat and smoke.

the elevator? What factors into that choice? Does the person try to fight the fire? Does the person stop to gather personal possessions or call a neighbor? Another area of human behavior relevant to performance-based calculations is behavior during egress. Do people use the best exit or the most familiar one? How long do people take to start to exit?

Human factors also affect the analysis needed for identifying goals and objectives and developing performance criteria. Fire safety goals typically include levels of protection for people, with performance criteria being a further refinement of these objectives. Performance criteria are numerical values to which the expected performance of trial designs can be compared. What range of occupant characteristics, such as age or disability, should be considered? How do human behaviors, for example, during egress, influence the numerical values chosen for performance criteria?

When developing and evaluating trial designs, the efficacy of the proposed fire safety measures mitigating all likely fire scenarios should be determined. This involves varying human behavioral elements. For instance, two very different fire scenarios could develop from the same cooking-initiated design fire: (1) a grease fire from cooking sets off a smoke detector that alerts the occupant who reacts and properly extinguishes the fire while it is still small; or (2) the occupant forgets and leaves a pot simmering on a burner, takes a sleeping aid, and goes to bed. The overheated pot ignites and the fire spreads to one or more adjacent items. The First International Symposium on Human Behaviour in Fire was held in 1998. Proceedings from this conference provide information useful in addressing these issues.[18]

Uncertainties and Variability in Risk Perceptions and Values

There is both variability and uncertainty in the way people perceive and value risk. Capturing differences that people have in their perceptions of risk and values related to risk is a necessary step in the design process. Research has shown that although people typically view consequences from voluntary risks less severely than equal consequences resulting from an unknown and/or involuntary risk, there is variability.[19] For example, while some people would agree that an increase in risk to fire fighters (people who accept risk as part of their job) is justifiable if a corresponding decrease in risk to the public could be achieved, others would not. Few studies have been conducted that clearly demonstrate how society values fire safety risks at the level needed to support performance-based trade-offs. Some work on incorporating risk concepts and identifying levels of acceptable risk is discussed in Section 5, Chapter 12 of this handbook, "Building Fire Risk Analysis." It is important to identify where value judgments enter into a performance-based calculation and to make any assumptions explicit regarding values and the impact of different values on the final design.

Another important factor is the concept of *equivalency.* Equivalency can mean different things to different stakeholders. For example, one person may determine that noncombustible construction is equivalent to an installed sprinkler system if they are both shown to provide time to fully egress the building. Another may argue that they are not equivalent—that the reliability of the sprinkler system is less. Designs may be equivalent in terms of life safety, property protection, business interruption, injuries, and/or prevention of structural collapse, but they are most likely not equivalent in all regards. It is, therefore, important to make explicit the assumptions that equivalency depends on.

Uncertainties Related to the Life-Cycle Use and Safety of Buildings

Many factors change over the lifetime of a building. The uncertainties surrounding future use, occupancy, and other factors contribute to the difficulty in conducting a structured, performance-based design. Even daily fluctuations in these design parameters can affect the safety of a building. For example, a building or area of a building that is normally occupied 24 hours per day may become unoccupied (or occupied by very different people) for extended periods of time due to extraneous factors (e.g., business closing, maintenance, renovation). The characteristics of the different occupants can lead to very different design considerations. Other changes that may affect the life-cycle safety of the building are fire service characteristics such as location, expected response time, and operating procedures and capabilities.

Uncertainties Related to Providing for Equity and Incorporation of Societal Values

Providing for equity and incorporating societal values involves determining what is important to the stakeholders and to what degree protection should be provided. A mechanism should be provided to ensure equal outcomes for subgroups. Since most projects have many stakeholders, such as building owner, design engineer, architect, code official, and the public (users of the building), it is difficult to assign worth to the usefulness or importance of something and apply it across all individual and societal issues. The key here is that decisions that change when a value, attitude, or risk perception varies must be made explicit in the design. Agreement on these key decisions by all stakeholders is critical to the success of a performance-based design.

Relation to Steps in the Design Process

Several types of uncertainty will be encountered at each step in a performance-based design process or during the process of setting a new prescriptive requirement. For example, when developing performance criteria, one will have to deal with scientific uncertainty, such as determining what level of carbon monoxide will cause unacceptable consequences, and how to account scientifically for interactions between products of combustion. One will also have to deal with issues of equity and societal values. At present, performance criteria are not established nor agreed upon. Changes to the set of performance criteria

selected could cause the same design for the same building to be deemed acceptable in one jurisdiction and deemed unacceptable in another jurisdiction. Uncertainties related to life-cycle use and safety of buildings also arise when selecting performance criteria. Over the life cycle of the building, many factors, such as use and occupant characteristics, change.

Nature and Sources of Uncertainty

In conclusion, uncertainty is a broad and general term used to describe a variety of concepts including, but not limited to, lack of knowledge, variability, randomness, indeterminacy, judgment, approximation, linguistic imprecision, error, and significance. Many of these uncertainties are inherent in the design process itself. Variations in analysis parameters, assumptions, or model inputs, may cause output criteria to change. Switchover occurs when outcome criteria change enough so as to cause a change in the design decision (e.g., the acceptability of a final design). It is critical to know whether different sets of reasonable inputs, scenarios, or parameters used in a fire safety engineering design have potential to cause switchover and to lead to different acceptable designs. This section provided an overview of terminology used to describe uncertainty; described aspects of the design process that introduce uncertainty; and presented a taxonomy useful as an aid in identifying uncertainties.

Treatment of Uncertainty

Treatment of Uncertainty with Safety Factors

Safety factor and margin of safety are two commonly used terms in the field of engineering. The dictionary defines factor of safety in terms of stress: "The ratio of the maximum stress that a structural part or other piece of material can withstand to the maximum stress estimated for it in the use for which it is designed." Safety factors do not just apply to stress, however. The idea of a safety factor is that the design values are multiplied by the factor of safety and the design is checked to ensure that the design is safe at the larger value (i.e., the product of the design value and the safety factor). Safety margins are a slightly different concept. A safety margin is additive and not multiplicative. A safety margin is defined as the difference between the design value and the value that would no longer be safe.

Implied versus Explicit Safety Factors

Safety factors are used with both prescriptive and performance codes. These factors of safety can be implied or explicit. Implied safety factors generally are found at various substages or components of a design. Implied safety factors provide for an extra margin of safety simply attributable to the choice of a component of a system. Implied safety factors may also take the form of conservative assumptions or worst-case scenarios. Explicit safety factors are multipliers applied to critical analysis parameters, often (and preferably) the final outcome criteria used to judge the acceptability of a design. Both types of safety factors are used to increase safety by lowering the probability that critical values of analysis parameters will be reached or exceeded.

Use of Safety Factors in Prescriptive and Performance Codes

An example of an implied safety factor in a prescriptive code is use of a pipe material or thickness that exceeds the strength and durability needed to meet the requirements of a sprinkler system. Pipe schedules have implied safety factors. An example of an explicit safety factor incorporated into a prescriptive code provision is a requirement to use a sprinkler flow density 1.5 or some other multiple higher than the minimum shown experimentally to control a given type of fire. In this example, the safety factor is used to cover for uncertainties in the measurement of the needed flow density, variations in the actual fuel package versus the fuel package tested, and uncertainties and variations in geometry, building characteristics, and so forth. An example of an implied safety factor in a performance code is an assumption that the rate of production of carbon monoxide for a given fuel package is equal to the rate of production of the component fuel with the highest production. An example of an explicit factor of safety incorporated into a performance-based design is to directly multiply the time necessary for egress by a factor of 2.

Selecting an Appropriate Factor of Safety

The first step in the use of safety factors is to determine which analysis parameters would be appropriate for the application of a safety factor. When a factor of safety is applied to measures of the final outcome criteria, it is most clear what margin of safety has actually been achieved; however, it is least clear how to alter the design specifications when a higher factor of safety is desired.

Safety factors may also be applied to different analysis parameters at various stages of the analysis. Careful judgment must be used, however, when applying these intermediate safety factors, because the quantity to which they are applied may not be linearly related to the final outcome criteria. Even if the quantity is linearly related to the final outcome criteria, it may not possess a 1 : 1 relationship. Specifically, a 1 : 1 relationship exists when a unit change in the analysis parameter causes a proportional unit change in the outcome criteria. In fire protection engineering calculations, input variables and analysis parameters are not often linearly related to outcome criteria such as upper-layer temperature. Also, they usually do not share common units of measure. In fire protection engineering calculations, time is the only common measure. It is likely that a safety factor of 2 applied to an intermediate quantity will not allow for a safety factor of 2 in the final design. In some cases, a safety factor of 2 applied to an intermediate quantity may not allow for *any* factor of safety design.

This is particularly true for implied factors of safety often found in the form of conservative assumptions. For example, an assumption that a fast growth rate fire is a

worst-case scenario is not true in all cases. A fast-flaming fire may not pose the greatest danger if it activates the sprinkler more quickly. A slower developing fire may be more able to overpower the sprinkler in some circumstances, and a fire originating in an unprotected or shielded space, even though slower growing, may also be more deadly. Therefore, if we wish to provide a safety factor of 2 to the time available to safely egress a building, we cannot assume that doubling the fire size (heat release rate) will achieve this goal. Heat release rate is not linearly related to time to critical temperature.

When an explicit factor of safety is applied, one may chose a value of 1.5, 2, or even higher. How much of a margin of safety is appropriate is as much a function of how much confidence we have in the predictive equations (i.e., are we using a factor of safety as a factor of uncertainty?) used in the calculations as it is of the stakeholders' risk tolerance. It should be noted, however, that increasing the margin of safety usually corresponds to an increase in cost of the project. When historical performance data is available, it can be used to set factors of safety. Otherwise, safety factors are usually set by expert judgment or mandated in policy. Safety factors are set to reflect confidence in the design equations as well as to reflect the stakeholders' acceptable risk tolerance. New specialized methods are being developed for deriving appropriate factors of safety.

Combining Safety Factors

First, it must be stated that there are no official rules, that is, none published and agreed upon by the fire safety community at large, for combining safety factors. The following list of suggestions and potential pitfalls was compiled by the author. After a fairly thorough review of the literature, specific numbers and justifications for safety factors were found lacking. To get good quantitative numbers for safety factors, historical data are needed.

Track the effect of each factor of safety: The effect of each factor of safety on the outcome criteria can be determined by changing the value of the safety factor and observing the net change in the outcome criteria relative to the net change in the safety factor. When the equations are not overly complicated, it may be possible to derive this relationship directly using partial derivatives. For conservative assumptions, the effect of the assumption should be tested by repeat calculations.

Watch for variance: If the normal variation in the population is sufficiently large, a factor of safety applied to the mean will not cover all or even most of the people who will be in the building. For example, if the baseline walking speed is estimated as the walking speed of a young, healthy individual and a safety factor of 2 is used, that would not cover the walking speed of an elderly person or person with physical disabilities if their speed was less than half the average.

Don't assume safety factors are additive: Factors of safety applied to two individual parameters in the analysis will not necessarily provide a total factor of safety equal to the sum of each individual safety factor. The total safety factor could be more or less than the sum of the two individual safety factors. As was discussed earlier, analysis parameters are often not linearly related to outcome criteria. They are most likely in different units of measure, and analysis parameters are likely not linearly related to each other. For these reasons, safety factors cannot be assumed to be additive.

Account for both positive and negative effects on safety: An explicit factor of safety or design assumption may have either a positive or negative contribution towards safety. Careful thought, engineering judgment, and testing using the calculation procedure must be used to test for the effects of each factor of safety and/or design assumption made. For example, doubling the heat of combustion may be conservative in predicting upper-layer temperature whereas doubling the radiative fraction will have the opposite effect.

Evaluate for multiple performance criteria: Also, since most fire safety engineering designs are judged on multiple performance criteria, what might constitute an implied factor of safety for one outcome criterion might constitute a reduction in safety for another parameter. For example, if a soot yield value is conservative for smoke detector activation, then it could not simultaneously be conservative for life safety.[20]

Realize effects may change with time: The relative importance of individual input variables, and thus the factors of safety applied to them, may be a function of time. In particular, variables may be limiting factors in the analysis during the time period of preflashover, and in the postflashover time period have little or no effect. Since in fire protection engineering we often deal with two distinct phases of the fire represented by different physics and mathematics, we must be careful to be aware of changes in the effects of a parameter in these very different phases of fire development.

Derivation of Safety Factors

Researchers at the University of Lund[21,22] have been conducting research on the application of the FOSM (first-order second-moment) methodology for fire safety engineering design. They have applied the FOSM method to derive safety factors for use in fire safety engineering design calculations. The safety index is represented by β, the distance from the origin to a failure line (limit state). β is also referred to as a reliability index where reliability is defined as the probabilistic measure of assurance of performance. β can also be thought of as the overall safety factor for the design.

The overall concept for conducting a design is to specify input data, choose a target reliability index β (they suggest 1.4, which is approximately equivalent to a probability of failure of 8 percent on condition that a fire has started), and vary the design parameters to be determined until the chosen value of β has been obtained. In

this type of analysis, design parameters include design door width and time to detection.[21]

They have also applied the FOSM methodology to derive the safety factor, β, for a design. In this case, design parameters such as door widths and time to detection are already known. An example is worked out for a shopping center.[22] There are some admitted shortcomings to applying this methodology to an actual design problem. First, the importance of the uncertainties in the input parameters needs to be investigated via a sensitivity analysis. A method of incorporating this uncertainty would then need to be standardized.

Techniques for the Quantitative Treatment of Uncertainty

It is important not only to recognize the various types of uncertainty, but also the different types of quantities for which the uncertainty exists, since they need to be treated in different ways. There is a standard procedure for quantifying uncertainty in empirical quantities. This procedure, sometimes referred to as classical uncertainty analysis, is based on the mathematics of probability and statistics. However, as shown by the taxonomy, in any fire safety engineering calculation or decision, there are many nonempirical parameters and assumptions used in the calculations. It is not always appropriate, meaningful, or even possible to treat the uncertainty in these nonempirical parameters by these same probabilistic methods. It has been argued that "probability is an appropriate way to express some of these kinds of uncertainty but not others."[1] The next sections present quantitative methods appropriate for the expression of uncertainty in various types of quantities.

Techniques for Quantifying Measurement Uncertainty

Many calculation and model inputs are empirical in nature. To be empirical, variables must be measurable and have a true value. Empirical quantities in the domain of fire protection engineering include the heat-release rate, the burning rate, and the radiative fraction of a given fuel. Classical uncertainty analysis refers to a statistical method of determining the random and systematic errors (and from them the total error) for a set of measurements. Random error and statistical variation results because no measurement of an empirical quantity can be absolutely exact. Imperfections in the measuring instruments and observational technique will inevitably give rise to variations from one observation to the next. The resulting uncertainty depends on the size of the variations between observations and the number of observations taken.

Classical statistical techniques such as standard deviation, confidence intervals, and others can be used to quantify this uncertainty. These statistical techniques are presented in Section 1, Chapters 11 and 12 on probability and statistics, respectively. A full discussion on uncertainty in measurement is found in the U.S./ISO guide[2] and in the NIST guide.[23] The NIST guide describes two types of evaluations of uncertainty. A Type A evaluation of standard uncertainty may be based on any valid statistical method for treating data. Three examples are (1) calculating the standard deviation of the mean of a series of independent observations; (2) using the method of least squares to fit a curve to data in order to estimate the parameters of the curve and their standard deviations; and (3) carrying out an analysis of variance (ANOVA) in order to identify and quantify random effects in certain kinds of measurements.

A Type B evaluation of standard uncertainty is usually based on scientific judgment using all the relevant information available, which may include previous measurement data, experience, manufacturer's specifications, and calibration reports. There is not always a simple correspondence between the classification of uncertainty components into categories A and B and the commonly used classification of uncertainty components as random and systematic.

The nature of an uncertainty component is conditioned by the use made of the corresponding quantity, that is, on how that quantity appears in the mathematical model that describes the measurement process. When the corresponding quantity is used in a different way, a random component may become a systematic component and vice versa. The NIST guide also differentiates between uncertainty and error. It is assumed that a correction is applied to compensate for each recognized systematic effect that significantly influences the measurement result. The relevant uncertainty to associate with each recognized systematic effect is then the uncertainty of the applied correction.

Techniques for Assessing Uncertainty in Analysis Parameters, Assumptions, and Value Parameters

Probabilistic techniques used to quantify measurement uncertainties are not applicable to uncertainties in establishing performance criteria or uncertainties regarding values such as the value of life. These uncertainties should be evaluated with techniques that make explicit the effect of the uncertainty on the value of all decision variables. Decision variables in fire protection engineering are such things as level of acceptable fire safety and installation of fire protection devices. If a quantity is a decision variable, then by definition it has no absolute, true value. It is up to the decision maker who exercises direct control to decide its value. Morgan and Henrion state that, *"The question of whether a specific quantity is a decision variable, an empirical quantity, or some other type of quantity depends on the context and intent of the model, and particularly who the decision maker is"* (emphasis added).[1] For example, in performance-based design, the minimum, permissible escape time during a fire may be a decision variable for the regulatory body, but it may be an empirical quantity from the viewpoint of the fire protection engineer.

Value parameters represent preferences of individuals. One controversial value parameter is the value of premature death avoided, often referred to as the value of life. Another is risk tolerance or risk preference, a parameter used to specify a degree of risk aversion when comparing

uncertain outcomes. The effect on the outcome of an analysis caused by differences in value parameters should be demonstrated explicitly. This is done by repeating the analysis for a range of possible inputs of the value parameter(s) to determine if a change in the outcome occurs that someone would care about. Several techniques that aid in the evaluation of uncertainty in these types of quantities are presented below. For all these techniques, the effect of various values of analysis parameters, assumptions, and value parameters is made explicit.

Bounding: Evaluating the extremes of the range of possible values of an uncertain quantity. If the extreme values at both ends are acceptable, a more complex and costly analytical uncertainty analysis may be avoided. For example, suppose we bound the ambient room temperature between a low and a high value. If we are trying to predict carbon monoxide buildup in a room, we may find that the results are either not sensitive to ambient temperature, or the range of predicted values of carbon monoxide, based on the range of ambient temperatures, is completely acceptable. We may either eliminate ambient temperature as a variable or set it to our best-guess estimate. We do not need to quantify the uncertainty in the ambient temperature any further.

Sensitivity/sensitivity analysis: Sensitivity of a design to modest variability and uncertainty must be explicitly understood. Sensitivity analysis is useful in assessing the consequences of uncertainty in data and in assumptions. By testing the responsiveness of calculation results to variations in values assigned to different parameters, sensitivity analysis allows the identification of those parameters that are most important to the outcome criteria. It does not tell the decision maker the value that should be used, but it can show the impact of using different values.

Parametric analysis: A parametric analysis is a particular type of sensitivity analysis. In parametric analysis, detailed information is obtained about the effect of a particular input on the value of the outcome criterion. This is done by evaluating and plotting the outcome criterion for a sequence of different values for each input, holding the others constant.

Importance/importance analysis: An importance analysis is a particular type of sensitivity analysis that determines which of the uncertain input variables contributes most to the uncertainty in the outcome variable. The results are used to focus on getting more precise estimates or building a more detailed model for the one or two, or small group of, most important inputs. Importance here is defined as the rank-order correlation between the output value and each uncertain input. Each variable's importance is calculated on a relative scale from 0 to 1. An importance value of 0 indicates that the uncertain input variable has no effect on the uncertainty in the output.

Comparative analysis: Comparative analysis is a technique used to evaluate risks, and the costs to mitigate them, by means of comparison to other similar risks. This technique is useful in evaluating perceptions of risk tolerance. Researchers[24] conducted a comparative analysis of the cost of mandating residential fire sprinklers with the cost of mandating other methods of reducing residential deaths such as radon remediation and ground fault interrupters.

Expert elicitation: Where hard data does not exist and is not possible to create experimentally, an expert elicitation is often conducted in order to obtain expert judgment of an uncertain quantity. An excellent discussion of the techniques for conducting an expert elicitation is provided in Chapter 6 of *Uncertainty.*[1]

Switchover: Variations in analysis parameters, assumptions, or model inputs, will cause output criteria to change. Switchover occurs when outcome criteria change enough so as to cause a change in the design decision (e.g., the acceptability of a final design).

Techniques for Assessing Uncertainty and Sensitivity in Complex Models

Several of the scientific uncertainties discussed in the taxonomy presented above can only be evaluated by examining the structure of the fire model. These include theory and model uncertainties, calculation limitations, and level of detail of the model. Uncertainties arise when physical processes are modeled based on empirically derived correlations, and/or simplifying assumptions are made. Other physical processes are not modeled due to lack of knowledge of how to include them. As stated earlier, most compartment fire models are zone models, which make the simplifying assumption that each room can be divided into two volumes or layers, each of which is assumed to be internally uniform. Current fire models do not contain a combustion model to predict fire growth, and many compartment fire models use an empirical correlation to determine the amount of mass moving between the layers.[25] There are uncertainties introduced by these modeling approximations.

Fire model validation: Fire model validation has become a much-discussed topic since fire models have become relied upon as a means of verifying that a fire safety engineering design meets a set of performance objectives. Work is being done to characterize the additional output uncertainty due to modeling approximations. Part of this work is focused on aiding the user in selecting a model, or set of models, appropriate to the type of prediction(s) needed. Some researchers have suggested a Bayesian framework where each available model is treated as a source of information that can be used in a prediction.[26,27]

In addition, work is ongoing to evaluate computer fire models by comparison of model predictions to predictions of other models or with experimental data. These comparisons are helpful to the user in determining the level of uncertainty likely from a model prediction for a similar set of conditions. However, these comparisons are difficult since they involve comparing two time-series curves, the exper-

imental measurements, and the predicted values. Historically these comparisons have been largely qualitative. The use of a branch of mathematics called functional analysis to make comparisons of these time-series curves is being investigated. This allows lengths, angles, and distances between two arbitrary curves to be defined and quantified.[28] Further validation issues that must be addressed were discussed among various groups of fire safety professionals at the Conference on Fire Safety Design in the Twenty-First Century.[29] Jones discusses issues that must be addressed in a report entitled, "Progress Report on Fire Model Validation."[30] Once a model is selected, it is useful to know the sensitivity of that model's output predictions to the values selected for the inputs.

Sensitivity of output predictions to input values: When selecting and using a fire model, it is important to know the sensitivity of the predicted outcome criteria to the model inputs. In order to facilitate this, several quantitative methods for determining the sensitivity of model predictions to model inputs are described below along with a brief discussion of their positive and negative attributes and limitations of application. These are also discussed in ASTM 1355-92, *Standard Guide for Evaluating Predictive Capability of Computer Fire Models*.[31]

A differential/direct method: For a system of time-dependent, ordinary differential equations, it is possible to solve directly for the partial derivitive of the predicted values with respect to each of the input variables. This set of partial derivatives measures the sensitivity of the solution with respect to changes in the input parameters:

$$Y_I = f_I = (c_1, c_2, \ldots, y_1, y_2, \ldots, t)$$

where c_k are rate parameters.

We simultaneously solve for both y_I and a set of sensitivity functions, $\delta y_i/\delta c_k$, over all times t. These partial derivatives measure the sensitivity of the solution with respect to uncertainties in the parameters c_k and in initial conditions. Often these parameters are not accurately known. Dickson provides an example of a direct solution of a set of ordinary differential equations that composes a large computational model of atmospheric chemical kinetics.[32]

Response surface replacement: Multiple runs, n, of the computer model are made. The model output Y_i and inputs $X_{1i} \ldots, X_{ki}$, $I = 1, \ldots, n$, are used to estimate the parameters of a general linear model of the form:

$$Y = \beta_0 + \sum_j \beta_j X_j$$

The estimated model is known as a fitted response surface, and this response surface is used as a replacement for the computer model. All inferences with respect to uncertainty analysis and sensitivity analysis for the computer model are then derived from this fitted model.[33] Construction of a response surface without specification of the probability distributions for all input variables is discussed by Iman.[34] It is suggested, in fact, that when using certain sampling techniques to build a response surface, it may be desirable to ignore probability distributions and use only the ranges of the variables. Iman provides a good discussion of using a response surface method to conduct a sensitivity analysis and provide a ranking of input variables in a second paper.[35] Beller has discussed the use of response surfaces for modeling upper-layer temperature and layer height.[36]

Monte Carlo sampling: In uncertainty analysis employing Monte Carlo sampling,* it is desired to estimate the distribution function and the variance for the particular output variables under consideration. The uncertainty surrounding each input is represented mathematically and often probabilistically by its individual distribution. When all probability distributions for all uncertain quantities are put together, a simulation model is built that is believed to capture the relevant aspects of the uncertainty in the problem. After running the simulation many times, an approximation of the probability distribution of the output variables is generated. The more simulations that are carried out, the more accurate the approximation becomes.

Advantages and Disadvantages of Each Technique

Iman and Helton state in their paper, "Investigation of Uncertainty and Sensitivity Analysis Techniques for Computer Models," some of the characteristics of large and complex computer models.[33]

- There are many input and output variables.
- The model is time consuming to run on the computer.
- Alterations to the model are difficult and time consuming.
- It is difficult to reduce the model to a single system of equations.
- Discontinuities exist in the behavior of the model.
- Correlations exist among the input variables, and the associated marginal probability distributions are often nonnormal.
- Model predictions are nonlinear, multivariate, time-dependent functions of the input variables.
- The relative importance of the individual input variables is a function of time.

Fire models often posses many and sometimes all of these characteristics. Iman and Helton evaluated the above three techniques as applied to large, complex models having many of the above characteristics. Their evaluation included ease of implementation, flexibility, estimate of the cumulative distribution function (CDF) of the output, and adaptability to different methods of sensitivity (analysis). Their findings clearly show that the technique that had the best overall performance was Monte Carlo sampling. They found that a differential analysis provides good local information about the inputs but does not extend well to a global interpretation. Also, a very real problem with

*There are many sampling techniques. Monte Carlo is one, well-accepted sampling method that has certain statistical advantages but may not be the best choice in all cases.

differential analysis lies in the difficulty of implementation. Response surface replacements were not recommended because the underlying models are often too complex to be adequately represented by a simple function.

The following section describes a methodology for application of uncertainty analysis to fire safety engineering calculations. This methodology employs Monte Carlo sampling. It also incorporates many of the techniques described in previous sections for quantifying measurement uncertainty, and assessing uncertainty in analysis parameters, assumptions, and value parameters.

Application of Uncertainty Analysis to Fire Safety Engineering Calculations

The fire safety community needs to begin to move forward from discussing a set of issues and concerns relating to uncertainty in fire protection engineering to agreeing as a community on practical steps to execute an uncertainty analysis. This section demonstrates a suggested methodology that quantitatively treats variability and uncertainty and applies it to a complex fire protection engineering problem. The methodology suggested is a generic methodology that is applicable to a wide range of fire protection engineering calculations and fire safety design issues. For example, application of the methodology is appropriate for engineering calculations such as those that predict upper-layer temperatures and concentrations of products of combustion. The methodology may also be applied to calculations of time needed to egress. It ties together the issues discussed above regarding uncertainties in the design process and the problem of switchover. Here, a brief introduction to and overview of the methodology is presented. A full description of the methodology and a worked case study of an actual building can be found in Notarianni.[37]

Overview of the Performance-Based Design Process with Uncertainty

The methodology is rigorous but comprehensible. It breaks up the process of conducting an engineering design calculation with uncertainty analysis into identifiable steps, each of which can be expanded or contracted to fit specific design problems. Table 5-4.1 shows the steps in conducting a performance-based fire protection engineering design. The column labeled Performance-Based Design Process lists the steps in the performance-based design process as detailed in the SFPE guide.[11] The right column lists the steps in the performance-based process with uncertainty. Steps or parts of steps in bold signify suggested modifications to the current design process. Steps 1–3 are modified by incorporating treatment of uncertainties noted in parentheses and detailed in the taxonomy presented earlier. The intent of each step does not change; however, the process is made explicit and standardized.

The quantitative methodology for the application of uncertainty analysis is applied throughout Steps 4–8. In Step 4 a probabilistic statement of performance is developed. In Steps 5–7, candidate designs are developed and a process for evaluating these designs through simulation with uncertainty analysis is described. Step 8 now includes a decision of acceptability that makes use of the results of the quantitative uncertainty analysis. Steps 9 and 10 remain the same. It should be noted that performance-based designs may require an iterative process. If in Step 8 the candidate designs are deemed unacceptable, the process returns to Step 6 to develop new candidate designs. If no acceptable design is found to meet the goals and objectives, Steps 1–3 must be revisited.

Steps 1–3: Define Scope, Goals, and Objectives

Many of the types of uncertainties discussed in the taxonomy are important to consider during the process of setting the scope, goals, and objectives of a project. These three steps are described below; for each step, one example of a type of uncertainty to consider is provided.

The first step in the performance-based design process is to define the scope of the project. The project scope is an identification of the boundaries of the performance-based analysis or design. The SFPE guide suggests consideration of several aspects of scope such as occupant and building characteristics and intended use of the building. In the first section of this chapter, indeterminacy was discussed as well as uncertainties related to the life-cycle use and safety of buildings. Indeterminacy affects the scope in that it is impossible to know what the occupancy and furnishings will be in a building at some point in the future. Therefore when assumptions are made regarding occupant and building characteristics, some investigation of the sensitivity of the final design to changes in occupant and building characteristics should be made and documented. If switchover occurs for a particular value of one or a combination of analysis parameters, assumptions, or values, this needs to be made explicit.

The second step in the design process is identifying and documenting fire safety goals of various stakeholders. These include levels of protection for people and property and provide for continuity of operations, historical preservation, and environmental protection. For example, when identifying goals of various stakeholders, a mechanism needs to be provided to ensure equal outcomes for subgroups, including the building owner, design engineer, architect, code official, and the public (end users). Because it is difficult to assign worth in the usefulness or importance of something and apply it across all individual and societal issues, the key here is that decisions that change when a value, attitude, or risk perception varies must be made explicit in the design documentation.

The third step in the design process is the development of objectives, which are essentially the design goals that have been further refined into values quantifiable in engineering terms. Objectives might include mitigating the consequences of a fire expressed in terms of dollar values; loss of life; or maximum, allowable conditions such as the extent of fire spread, temperature, or spread of combustion products. Uncertainties arise here in risk perceptions and values. There is both uncertainty and variability in the way people perceive and value risk.

Capturing differences people have in their perceptions and values related to risk is a necessary step in the design process. For example, it may be a goal of the stake-

Table 5-4.1 ***Steps in the Performance-Based Design Process with and without Uncertainty***

	Performance-Based Design Process[11]		Performance-Based Design Process with Uncertainty[37]
Step 1	Define project scope		Define project scope **(uncertainties related to life-cycle use and safety of buildings)**
Step 2	Identify goals		Identify goals **(uncertainties related to equity and incorporation of societal values)**
Step 3	Define stakeholder and design objectives		Define stakeholder and design objectives **(uncertainties related to risk perception and values)**
Step 4	Develop performance criteria		Develop probabilistic statement of performance **(criteria, threshold, probability, time)**
Step 5	Develop design fire scenarios		**Develop a distribution of design fire scenarios**
		(a)	**Select calculation procedure(s)**
		(b)	**Identify uncertain input parameters**
		(c)	**Generate a distribution of design fire curves**
		(d)	**Define distributions of and model correlations among other input parameters**
		(e)	**Select sampling method and determine number of scenarios**
Step 6	Develop candidate designs		Develop candidate designs
Step 7	Evaluate candidate designs		Evaluate candidate designs
		(a)	**Calculate a set of values for each outcome criteria and create cumulative distribution functions**
		(b)	**Determine sensitivity to elements of probabilistic statement of performance**
		(c)	**Evaluate base case (optional)**
		(d)	**Determine effect of each candidate design on each of the scenarios**
		(e)	**Evaluate uncertainty importance**
Step 8	Design meets performance criteria?		Design meets **all four elements of probabilistic statement of performance?**
Step 9	Select final design		Select final design
Step 10	Prepare design documentation		Prepare design documentation

holders to protect historical features of the building or to protect against business interruption or loss of operating capability. Stakeholders with different values may see these needs differently. It is important to identify where value judgments enter into a performance-based calculation and to make any assumptions explicit regarding values and the impact of different values on the final design.

The following discussion is focused on incorporating uncertainty directly into Steps 4–8. Here, we develop a probabilistic design statement, develop a distribution of statistically significant fire scenarios, calculate a set of values for critical outcome criteria, and evaluate each candidate design to determine whether the design meets the performance criteria within acceptable uncertainty bounds.

Step 4: Develop Probabilistic Statement of Performance

The fourth step in the design process is the development of probabilistic statement(s) of performance, that is, criteria by which to judge the acceptability of the design. These criteria are a further refinement of the design objectives and contain numerical values to which the expected performance of the candidate designs can be compared. Each probabilistic design statement contains a minimum of four elements: probability, time, performance criteria, and threshold value. For example, an objective may be to maintain tenable gas concentrations in the corridor. A corresponding probabilistic design statement for life safety might specify that the design must allow for a 0.9

probability of having 4 min or more before a temperature of 65°C is reached in the corridor. Thus all four elements are included: probability, time, performance criteria, and threshold value. A location is also specified.

There are many issues to be addressed when establishing probabilistic statements of performance. For example, which criterion should one evaluate? One could select, instead of or in addition to temperature, levels of carbon monoxide, heat flux, or obscuration. There is disagreement in the literature as to what values of each of these cause negative consequences. The negative consequences must be defined; that is, should the threshold values represent incapacitation or lethality? Also, the probability element involves determining the level of acceptable risk to the stakeholders, and establishing criteria for time to untenability involves understanding behavioral patterns of people in fire as well as making value judgments as to which subpopulations one is trying to protect. The sensitivity of the design to each element of the probabilistic statement of performance is evaluated in Step 7b.

Based on this type of sensitivity analysis, a two-tiered probablistic statement of performance may be developed based on any of the four elements as well as location. For example, the probabilistic statement of performance may say that the design must allow for a 0.9 probability of having 4 min or more before untenability based on a temperature of 65°C is reached *and* a 0.9 probability of having 6 min or more before 100°C is reached. The design statement may be specified in other ways:

- Include two probability levels, such as the design must have greater than or equal to a 0.95 probability of *X and* less than or equal to a 0.1 or more probability of *Y.*
- Provide a variation such as the design must provide for a 0.9 probability of providing 4 min before 65°C is reached and a 0.9 probability of having 8 min or more before untenable gas conditions are reached.

These are just a few of the possible specification options. Also, the location of evaluation matters. Untenability can be evaluated as a minimum anywhere in any room, including the room of origin, or it can be evaluated along the egress path. These two analyses may give different results in terms of acceptability.

Step 5: Develop a Distribution of Design Fire Scenarios

One of the most important pieces of the methodology is how to generate a set of realistic input scenarios. It is important that this set include a combination of scenarios that represent statistically both the types of fires and the frequency at which they occur in a given occupancy. The input scenario generator should integrate information about the uncertainty, variability, and correlational structure of the input parameters. Using an appropriate sampling method (e.g., Monte Carlo method), a set of any given number of fire scenarios may be constructed. This distribution of scenarios generated will contain the typical cases as well as the worst-case scenarios in the tails of the distribution. The steps involved in developing a distribution of design fire scenarios are (a) selecting a calculation procedure; (b) identifying the uncertain and crucial input parameters; (c) generating a distribution of design fire curves; (d) defining distributions of and modeling correlations among input parameters; and (e) selecting a sampling method and determining the number of scenarios.

Step 5a: Select Calculation Procedure(s)

There are a range of calculation tools and models currently available from which to select the calculation procedure(s) to be used in the performance-based design. The *Fire Protection Handbook* provides a good overview of the various types of fire models.[38] Which model or type of model is selected depends on several factors, including the application of interest. Fire models can be used to predict a hazard, predict a risk, reconstruct a fire, interpolate between or extrapolate beyond test results, or evaluate a parametric variation. The application of fire models for each of these purposes is discussed by Nelson.[39] Each of these applications may have purpose at some stage of the performance-based design process.

Step 5b: Identify Uncertain and Crucial Input Parameters

Once a calculation procedure is chosen and candidate designs have been selected, the input parameters necessary for the calculation are evaluated. Which input parameters will be treated as uncertain must be determined. Ideally, only parameters or combinations of parameters with uncertainty great enough to change decisions regarding the final design are treated as uncertain. These are referred to as the crucial variables. Unfortunately, we do not always know a priori which of the input parameters possess crucial uncertainty. Therefore, we must use a combination of judgment and results of previous analyses. The uncertainty importance of each of the uncertain input parameters is determined so that future analyses may be simplified. Eventually, only a few key parameters may be needed to capture the uncertainty in each calculation.

Step 5c: Generate a Distribution of Design Fires

Design fire scenarios are made up of both possible fire events (heat-release rate curves) and characteristics of the material burning, of the building, and other relevant information such as weather conditions. A set of design fires is established to mimic the type and frequency of fires expected for that occupancy. These design fire curves are based on statistically collected data, judgments, and the goals of the design. Each design fire is assigned a likelihood of occurrence.

Step 5d: Define Distributions of and Correlations among Other Inputs

The uncertainty and variability surrounding each variable must be captured in the mathematical description of that variable. Any and all available knowledge

regarding the value of that parameter should be incorporated into the input scenario generator. This includes empirically measured values, known variations, and statistically compiled data. For example, for a given occupancy type, the NFPA publishes statistical data on the percentage of fires that start in each potential room of fire origin. This information should be incorporated into the random scenario generator so that the generator mimics these statistics. Distributions can be constructed for variables such as temperature, wind, and relative humidity from regional data published by the national weather service data. Methods for quantifying measurement uncertainty[2] are used to capture uncertainty and variability in empirically measured parameters such as rates of production of products of combustion. In many cases, where hard data do not exist and are not possible to create, expert elicitation is needed to quantify the uncertainty.

When two or more variables are correlated, knowledge of the value of one variable tells one something about the value of the other variable(s). Correlation among variables is modeled so that the input scenario generator will not generate unrealistic scenarios. For example, if the design incorporated a weather module, a month of the year would be randomly selected. For that given month, a value is sampled from an outdoor temperature distribution based on National Weather Service data for that region. Outdoor temperature is correlated to external pressure, wind, relative humidity, likelihood of windows/doors being open, indoor temperature and pressure, and initial fuel temperature. This prevents the software from generating, for example, a scenario where there is a fire on a below-freezing day in August, in California, and all the windows are open.

Step 5e: Select Sampling Method and Determine Number of Scenarios

A sampling method, such as Monte Carlo, Latin Hypercube, or quasi-random must be selected. By sampling a single value from each of the distributions in the input scenario generator and combining those numbers with the values of input parameters that are being treated as certain, any number of independent fire scenarios may be generated.

A large number of scenarios increases the statistical significance of the results. However, this relationship is dependent on the sampling method chosen and is not linear. Using 2000 runs may not provide any more insight than using 500. The number of scenarios chosen depends on (1) the number of uncertain input parameters, (2) the average calculation time per scenario for the calculation procedure chosen, and (3) the statistical significance needed. When conducting correlational analyses between inputs and outputs, one obtains importance or correlation coefficients, c, between 0 and 1. Hald provides a formula for determining the relationship between the number of runs, n, and the statistical significance (as measured by a t-test) of the correlation coefficient.[40]

$$t = \frac{c}{\sqrt{1 - c^2}} \left(\sqrt{n - 2}\right)$$

The value for t is related to the confidence level, which is typically chosen as 95 percent.

Step 6: Develop Candidate Designs

The candidate design is intended to meet the project requirements. A candidate design includes proposed fire protection systems, construction features, and operations that are provided in order to meet the performance criteria when evaluated using the design fire scenarios.

Step 7: Evaluating Candidate Designs—Introduction

Each candidate design must be evaluated using each design fire scenario. The evaluations indicate whether the candidate design will meet the elements of the probabilistic statements of performance. Only candidate designs that meet the performance criteria may be considered as final design proposals. Without the quantitative treatment of uncertainties in the design, each calculation will provide a point estimate only of the important outcome criteria. For example the performance criteria for a design may be a 100°C maximum temperature reached in the upper layer. The time to an upper-layer temperature of 100°C may be predicted as 175 s, and the time to activation of a sprinkler may be predicted as 171.2 s by a given computer model. Because the sprinkler is predicted to activate before the performance criteria is exceeded, this would be deemed an acceptable design. However, the uncertainty in the prediction of time to 100°C may be ±20 s. This would mean that the temperature in the room may reach 100°C at 155 s or before activation of the sprinkler. Also, the predicted time to activation of the sprinkler has an uncertainty surrounding it as does the temperature at which untenability might actually occur.

The performance-based design process with uncertainty will aid in the calculation of a range of possible values for each key outcome criterion instead of a single point value. This methodology is useful for and may need to be applied to several parts of the design calculations. For example, it could be applied to the calculation of upper-layer temperatures, to the prediction of time to response of devices, and to the prediction of time needed to egress a building.

Step 7a: Calculate a Set of Values for Each Outcome Criterion

A single value will be determined for each outcome criterion calculated for each design fire scenario run. Much information can be obtained from observation of both the range of values for criteria of interest and from cumulative distribution functions generated from the set of all values.

If criteria are time-series values, each scenario will predict a different curve of the key outcome criteria versus time. For example, if upper-layer temperature is the criterion of interest, four design fire scenarios would produce four curves of upper-layer temperature versus time.

Figure 5-4.2 shows a representative graph of the value of outcome criterion A plotted against time from ignition (in seconds). For any given design, there will be as many curves as there are design fire scenarios calculated. One can see that the curves vary both in the magnitude of the peak value and in the time to the peak value.

The range of values predicted from the set of design fire scenarios represents the uncertainty in the value of the outcome criterion. From the set of predicted values of a single outcome criterion, a cumulative distribution function may be generated. This is done by graphing the value of the criterion against its rank order. For example, for n design fire scenarios, n values of a given criterion are generated. These values are then sorted in descending order. The largest value is graphed versus $1/n$, the second largest against $2/n$,…, and the smallest value against n/n or 1.

An example of a cumulative distribution function (CDF) is shown in Figure 5-4.3. The time to reach a threshold value of 1 or more of the tenability criteria, that is, a value determined to cause injury or death, can be determined from the time-series predictions. The threshold value may be a particular temperature or carbon monoxide level or a parameter used to represent some synergistic effect of a combination of the tenability variables. One value of time to untenability is obtained for each scenario run. The set of all possible values provides a distribution of the outcome criteria.

Figure 5-4.3 shows that for the distribution of design fire scenarios, there is almost a 1.0 probability that the time to a critical value of criterion A is 30 s or more. Likewise, there is a 0.75 probability that the time to this value is 120 s or more, a 0.50 probability that it is 180 s or more, and a 0.1 probability that it is 390 s or more.

Step 7b: Determine Sensitivity of Outcome Criteria to Elements of Probabilistic Statement of Performance

The sensitivity of key outcome criteria to each of the four elements of the probabilistic statement of performance upon which a design is judged must be known before good policy and good design practice can be established. Elements such as criteria, threshold values, probabilities, and times are not mandated nor agreed upon by fire safety and health professionals, nor the public. Therefore, major conclusions of all designs should be checked in order to demonstrate the sensitivity to uncertainty in each of these elements. This might include checking for times to untenable temperature, carbon monoxide, carbon dioxide, and reduction in oxygen. It may include checking for synergistic effects of the presence of these substances. It may also be appropriate to evaluate for heat flux and visibility.

The same design may be judged on two different performance criteria or by two different critical values of the same performance criterion. Figure 5-4.4 shows an example of time to untenability based on different values of upper-layer temperature. This type of presentation could also be used to determine the effect on time to untenability by selecting a group of tenability criteria or by including different sets of components in the specification of tenability criteria.

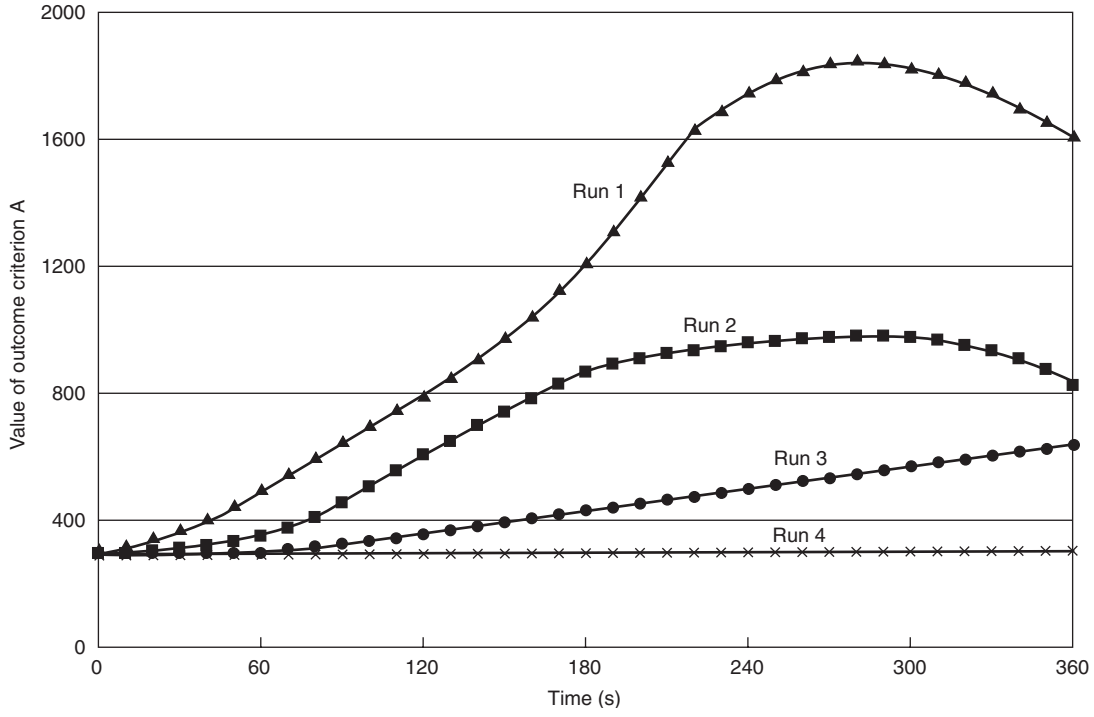

Figure 5-4.2. ***Variation in prediction of time-series values of outcome criterion A.***

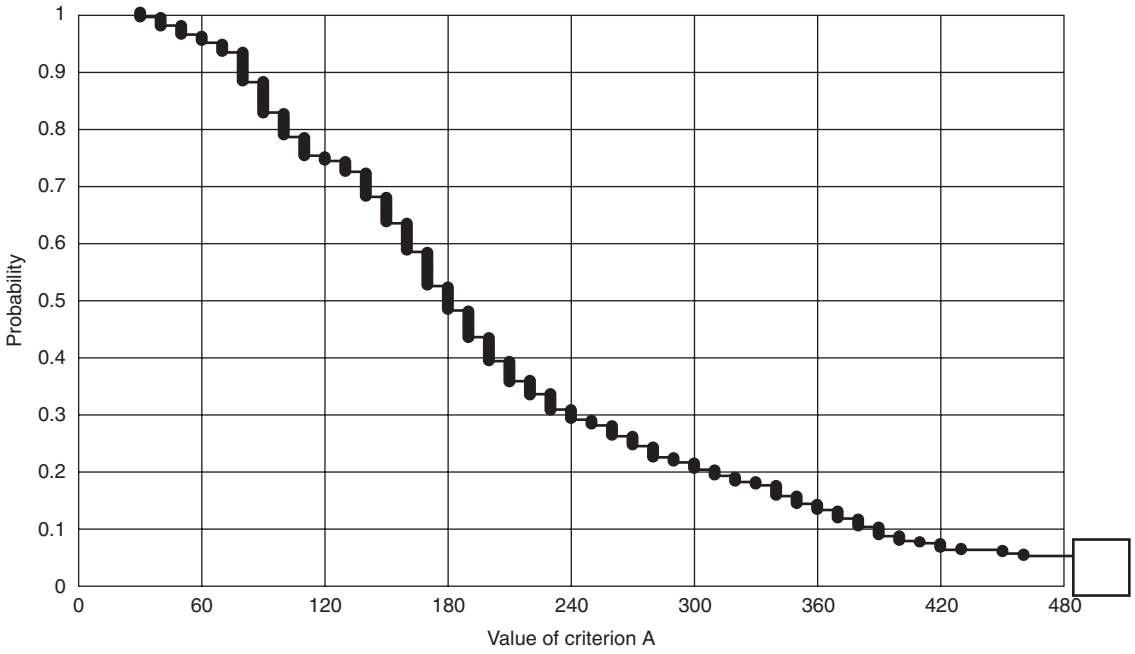

Figure 5-4.3. ***Cumulative distribution function of time to the critical value of criterion A.***

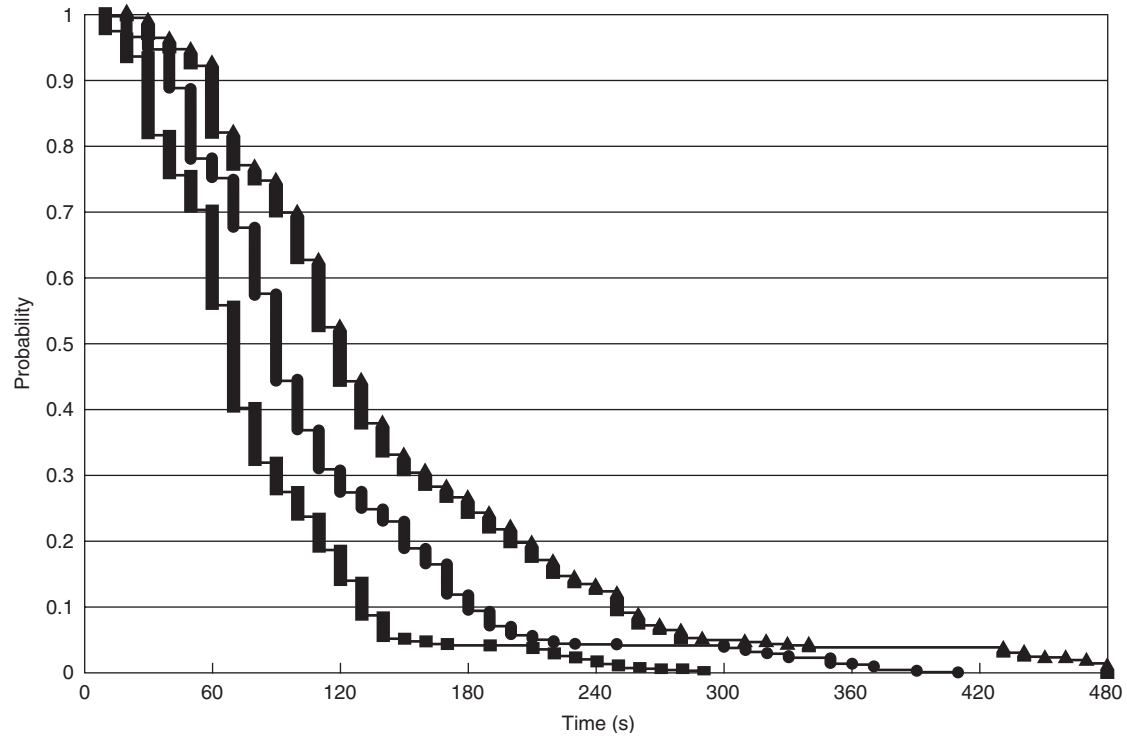

Figure 5-4.4. ***Probability of having X seconds or more before untenable upper-layer temperatures are reached for three different values of untenable temperature.***

This type of evaluation is a good way to focus discussions among stakeholders on deciding which tenability criteria should be included, what effect the selection of different threshold values of tenability criteria has, what probability level is acceptable to the stakeholders, and how to select the final design. At the end of this step, final performance criteria must be selected for use in judging acceptability of designs and choosing a final design.

Step 7c: Evaluate Base Case

Depending upon the needs and the scope of the project, it is helpful to compare a candidate design to a base-case design. The base case can be the design that meets the prescriptive code, the design that includes the fire protection options currently in the building, or the design with no active fire suppression systems. The purpose of having a base case is to benchmark the effects of fire on the building and on the building conditions against each of the designs.

In Figure 5-4.5, the results of multiple scenario runs are used to show the probability of safe egress graphed against the time to untenable conditions for two different designs. Design 1 and Design 2 may represent two different performance designs or a performance design and a prescriptive design. Reiss discusses the need for this comparative approach.[41] The graph shows two design curves that exhibit crossover. Design 1 provides a higher probability of tenability out to 50 s; however, Design 2 provides a higher probability of tenability at longer times.

Another way that the acceptability of a design is judged is by comparison of the level of safety provided to that provided by the corresponding prescriptive design. There is uncertainty associated with the prescriptive design also. The prescriptive code will mandate certain building materials and fire detection and suppression schemes. However, uncertainty and variability remain in the weather, ventilation conditions, human behavioral aspects, and where and how the fire will start. Thus, multiple scenarios can be constructed in a parallel manner to that shown above, holding as constants those factors required by the prescriptive code. Thus, a CDF for the prescriptive code can be generated and compared to the CDF for the performance code.

Step 7d: Determine the Effect of Each Candidate Design on Each of the Scenarios

To compare two different candidate designs, we may want to look at the distribution of differences between the two designs based on the final selected performance criteria. One may consider differences between a design and the reference base case or differences in time to untenability provided by Design 1 versus Design 2. For example, Figure 5-4.6 is a cumulative distribution function of the difference in time to untenability provided by Design 1 minus the time to untenability provided by Design 2.

Figure 5-4.6 shows that there is a 0.25 probability that Design 1 will provide a longer time to untenable conditions than will Design 2. Conversely, there is a 0.75 probability that Design 2 will provide a longer time to untenability than will Design 1 and a 0.25 probability that the difference will be 100 s or more better. In selecting a final design, it may be helpful to investigate what factors might lead to Design 1 providing more time to untenability than Design 2, which could highlight ways to improve the design.

Step 7e: Evaluate Uncertainty Importance

An importance analysis is a particular type of sensitivity analysis that determines which of the uncertain input variables contributes most to the uncertainty in the outcome variable. The results are used to simplify future performance-based designs by identifying the one or two, or small group of, most important inputs. Importance here is measured by the correlation between the output value and each uncertain input. Each variable's importance is calculated on a scale from 0 to 1 (or –1). A correla-

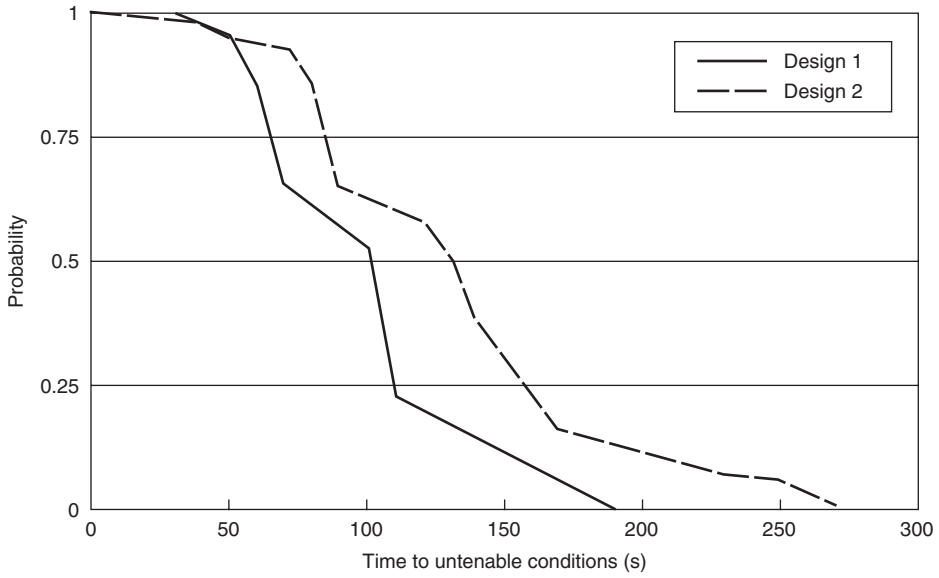

Figure 5-4.5. ***Comparison of cumulative distribution functions of time to untenable conditions for two different designs.***

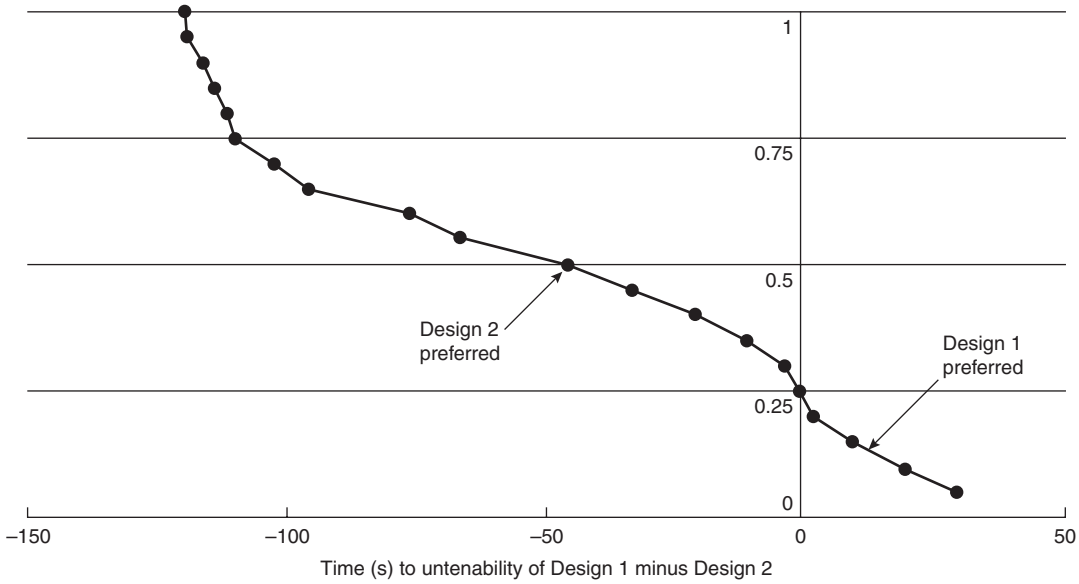

Figure 5-4.6. ***Cumulative distribution function of time to untenability of Design 1 – Design 2.***

tion of 0 indicates that uncertainty in the input variable has no effect on the uncertainty in the output parameter. The input parameters can be correlated to composite or derived outcomes (i.e., an outcome that is not directly an output of the model but one that is derived from the output data). Likewise, input variables can be combined (for example, the volume of a room can be determined from the dimension). Room volume may be correlated with key outcome criteria, for example, peak temperature or time to peak temperature.

Importance analysis can be used to simplify a future uncertainty analysis by determining the input uncertainties that are most crucial. This can simplify the process for a class of buildings and can demonstrate where additional research would be effective in reducing uncertainty and ensuring a safer, more predictable building. It must be remembered, however, that correlation does not equal causation. Thus, any apparent, strong correlation that is counterintuitive should be investigated with good engineering judgment. Also, for each design, the value of the correlation coefficient that is statistically significant will depend on the number of scenarios run and the sampling method used.

Step 8: Judging a Design's Acceptability Based on All Four Elements of Probabilistic Statement of Performance

There are two ways to judge acceptability of a design. The first is based on the minimum time to untenability anywhere in the building, including the room of origin. The second is the time to untenability along the egress path. In general, for both cases, cumulative distribution functions are used to judge acceptability of a design. For example, Figure 5-4.3 is a cumulative distribution function of the time to a specific value of criterion A in the room of origin. If the probabilistic statement of performance required a 0.9 probability of having 30 s or more before reaching this value, it can be determined from the CDF that this criterion is met. In fact, Figure 5-4.3 shows that there is a 0.9 probability of having 80 s or more. However, if the probabilistic statement of performance requires a 1.0 probability of having 50 s or more, Figure 5-4.3 shows that this criterion is not met because the CDF demonstrates a 1.0 probability of having only 30 s or more.

Another way of judging the acceptability of a performance-based design is with a time-to-egress analysis. The time needed to egress a building is often represented in the literature as the time to detect the fire, plus the time to react, plus the time to travel to a safe place. This is represented mathematically as

$$time_{\text{egress}} < time_{\text{untenability}}$$

$$time_{\text{egress}} = time_{\text{detect}} + time_{\text{react}} + time_{\text{travel}}$$

One problem with this approach is that it is very difficult to predict human behavior in terms of reaction time and travel time during a fire. There is both variability due to age and health of the individual and uncertainty as to individual goals and concerns (e.g., will the person try to fight the fire, locate valuables, rescue pets, or notify other occupants about the fire?). The methodology described in this chapter may be applied to egress calculations; however, since these are difficult to predict, it is suggested that perhaps these are best handled as societal and policy decisions. Regulatory decisions may be made as to the available, safe egress time. For example, more time may be mandated for a healthcare facility, where patients may be nonambulatory and/or asleep at the time of the fire, than in an office building where occupants are generally awake and healthy.

Steps 9–10: Select Final Design and Prepare Documentation

Candidate designs that satisfy the probabilistic design statement(s) may be considered for selection as the final design. When more than one candidate design meets all four elements of the probabilistic statement of performance, other factors such as cost and preference are considered. When considering multiple designs or designs with very different features, a multicriteria decision analysis model may be developed to aid in selecting the final design.

Proper documentation of a performance design is critical and should be written so that all parties involved understand what is necessary for the design implementation, maintenance, and continuity of the fire protection design. *The SFPE Engineering Guide to Performance-Based Fire Protection Analysis and Design of Buildings* suggests that the documentation have four parts: the fire protection engineering design brief, the performance design report, the detailed specifications and drawings, and the building operations and maintenance manual.[11] It is important that the performance-based design report convey the expected hazards, risks, and performance over the entire building life. It should include the project scope, goal, and objectives, the probabilistic design statements, a discussion of the design fires and design fire scenarios, and any critical design assumptions.

Treatment of Uncertainty

In conclusion, incorporating uncertainty in a fire safety engineering design calculation aids in ensuring performance. The methodology described in the above section can be used in combination with standard performance-based design procedure. Each step in the methodology may be expanded or contracted to fit the needs of a given calculation. In the future, one may be able to construct libraries of models with families of input scenario generators and develop reusable models for classes of buildings. Ultimately, a fire safety engineering model should be developed that directly incorporates uncertainty.

Application of Uncertainty to Cost-Benefit Models and Decision Analysis Models

Decision Making under Uncertainty

The importance of making good decisions under conditions of uncertainty is becoming better understood in many fields, including fire safety design. The recently released National Science Policy study, "Unlocking Our Future: Toward a New National Science Policy," states that "decision makers must recognize that uncertainty is a fundamental aspect of the scientific process." Good decisions can be made under uncertain conditions; however, one must capture the nature and magnitude of the uncertainty in order to make a good decision.[42]

There is uncertainty involved in deciding among fire safety options, such as whether to install smoke detectors, sprinklers, or both. Another example is deciding whether the cost of redundant pumps or entire redundant systems is justified. These types of decisions are typically modeled using fire safety trees.[43] However, average or best-guess estimates typically are used for parameters in the decision model, and uncertainty and variability in these are rarely considered.

Decisions made by municipalities on whether to mandate fire safety systems, such as residential sprinklers, are likewise often made based on economic analyses using best-guess and national average values. Integration of uncertainty and variability into these types of cost-benefit studies would provide the decision maker more insights into the issues at hand. It would also highlight where engineering technology is able to reduce risks and where regulatory solutions might be more helpful.

This is becoming more complex because implementation of any form of a performance-based standard will require more decisions to be made. These decisions will be more difficult, more complex, and more uncertain than under a prescriptive-based code. Robert Clemen discusses in his book, *Making Hard Decisions,* four reasons why making decisions is so difficult.[44]

- *First, decisions can be difficult simply because of their complexity.* In the case of decisions regarding fire protection features, one must consider the potential for property protection, life safety, injury mitigation, and business continuity. One must also consider the diverse impacts on people with special needs, such as the very young, the elderly, or persons with limited mobility.
- *Second, decisions can be difficult because the decision maker may be working toward multiple or competing objectives.* In fire protection analyses, typically competing objectives are low cost and high level of safety. Progress in one direction, such as installing automatic fire sprinklers for increased fire safety, may impede progress of a competing objective, such as designing an economical building.
- *Third, a problem may be difficult if different perspectives lead to different conclusions.* In a fire protection decision, the perspective of the building owner, designer, and authority having jurisdiction may very well differ.
- *Finally, decisions can also be difficult because of the inherent uncertainty.* Uncertainties may arise in the model physics, the values of the inputs, the reliability of the devices, and the frequency of events. Yet a decision must be made without knowing for sure what these uncertain values will be. In fact, the most important decisions are often those that must be made under the greatest uncertainty, have the highest complexity, and involve multiple perspectives and goods.

The quantitative treatment of variability and uncertainty using the tools and techniques presented earlier in this chapter can help in identifying important sources of uncertainty and representing that uncertainty in a quantitative way.

The following section introduces an analytical approach that allows quantitative models and decisions models to be built with the integrated treatment of uncer-

tainty. The final section demonstrates how these tools were used in a cost-benefit model of the decision to mandate residential fire sprinklers from a municipal standpoint.

Available Software That Incorporates Uncertainty

Decision analysis applications often use generic modeling software such as spreadsheets, statistics packages, and financial modeling languages. Specialized software is also available for modeling decision problems using decision trees, influence diagrams, belief networks, multiattribute utility functions, hierarchical value structures, Monte Carlo simulation, and multicriteria optimization.

Two such pieces of software that allow for direct treatment of uncertainty are Analytica™ by Lumina and @Risk™ by Palisade. These are just two software options. They are described here for informational purposes only, intended to provide the reader with an idea of the capabilities of currently available software. The reader is encouraged to evaluate the full range of available software before selecting a package.

@RISK is a risk analysis and simulation add-in for Microsoft Excel or Lotus 1-2-3. @RISK adds the power of Monte Carlo simulation to your spreadsheet models. It allows the user to replace uncertain values in their spreadsheet with probability functions, which represent a range of possible values. @RISK will recalculate your spreadsheet hundreds or even thousands of times, each time selecting random numbers from the functions entered. The result is distributions of possible outcomes and the probabilities of getting those results. This identifies not only what could happen in a given situation, but how likely it is that it will happen.

Analytica is another program that allows for the direct treatment of uncertainty. A model built in Analytica uses a graphical interface that resembles an influence diagram. This diagram conveys the model structure. A complicated model can be easily organized into a hierarchy of comprehensible and simple modules. The influence diagram format easily distinguishes between decision variables (those you can control), chance variables (uncertain quantities that cannot be controlled), and objectives (criteria to maximize).

Other distinctive features of Analytica are what the company terms *intelligent arrays* and also turn-key importance analysis. With intelligent arrays, data may be entered as an array indexed by several parameters. The software handles operations on these multidimensional values, such as adding, multiplying element by element, or summing over a dimension. Examples of intelligent arrays are presented in the following section.

In Analytica uncertainty can be treated explicitly with probabilities. The user can express uncertainty about any variable, selecting a probability distribution using a graphical browser; propagate uncertainties with the model using Monte Carlo sampling; and display uncertain results as standard statistics, probability bands, probability density functions, or cumulative probability functions. Analytica conducts rank-order and importance analyses. These tools help one decide which uncertainties make a difference to help determine whether getting better data or expanding the model is worthwhile. Analytica also allows for parametric analysis by graphing model behavior as one or more inputs are varied.

Example of Cost-Benefit Model with Variability and Uncertainty

In the United States, approximately 3500 people die each year in residential fires. The number of residential fire deaths, however, varies with the type of housing, area of the country, and community size. The cost of installing residential fire sprinklers varies with areas of the country and house age. Thus, the true cost-benefit will be different for each combination of the above parameters. However, cost-benefit models typically use average costs and probabilities and do not incorporate uncertainty.

A model was built using Analytica that incorporated variability and uncertainty to determine the societal benefits and costs of mandating residential sprinklers. A full description of the mathematical model and the results is beyond the scope of this chapter but can be found in "A Municipal Model of the Cost of Mandating Residential Sprinklers."[45] A brief overview of that study is presented in order to demonstrate the techniques used in the treatment of variability and uncertainty and the implications for fire protection analyses.

Treatment of Variability and Uncertainty

Interyear variability in fire loss statistics: To conduct a cost-benefit study of residential fire sprinkler systems, many fire statistics (e.g., death rates, injury rates, and average direct dollar losses) are needed as inputs. National average values of these numbers are often used in these analyses. For example, the national average value for the residential death rate would be equal to the number of residential fire deaths nationally divided by the number of occupied residential units. The actual fire death rate will vary with a number of parameters.

The U.S. National Fire Protection Association publishes death rates discretized by three of four index variables: region of the country, community size, and house type.[46] The fourth index variable, house age, is accounted for in the cost functions as it is more expensive to retrofit sprinklers than it is to install them during the construction phase. There are four regions of the country, eight community sizes, and three house types. Thus, the death rate used in these calculations is a $4 \times 8 \times 3$ matrix consisting of 96 values for death rate. Two examples would be the death rate in mobile homes in a small community (2500 or less) in the South and the death rate in a one- or two-family dwelling in a community size of 25,000 to 50,000 in the West.

Yearly variability in fire loss statistics: It is important to differentiate between variability and uncertainty. Variability in fire statistics from year to year arises because of the randomness of the occurrence of fires. For instance, in one particular year, several large-loss fires may occur followed by few or none the next year. In this study, since there is an interest in benefits and costs over the life of a fire sprinkler system, mean yearly values were chosen. Yearly variance in deaths, injuries, property loss, and

indirect losses due to fires is thus accounted for by taking mean yearly values over a five-year period. Mean values were calculated from the 1989–1993 data.

Uncertainty in the fire statistics: Uncertainty in fire loss statistics exists due to the impossibility of a full and accurate accounting of all fires and all fire losses. Mathematical techniques are thus used to provide estimates.[47] Uncertainty in the fire data is represented as uncertainty about the mean values. An expert elicitation of the chief statistician of NFPA was conducted to set the uncertainty bands for the fire statistics.[48]

Uncertainty in other (empirical) model inputs: Uncertainty in the cost data and parameters such as the sprinkler reduction factor were determined by bounding. For example, uncertainty in the sprinkler reduction factor arises because of the small number of fires occurring in homes with automatic sprinklers installed. Data from other occupancies were used to bound the uncertainty.

Propagation of uncertainty: Once the uncertainties in the model inputs have been expressed, the question becomes, How can we propagate these uncertainties through the model to discover the uncertainty in the predicted consequences? In this analysis a Monte Carlo simulation was used. A value for each input is randomly selected from its actual probability distribution. From these values, a value for the outcome criteria is calculated. This process is repeated many times, resulting in a probability distribution for each outcome variable.

Value/cost of death averted: For any cost-benefit analysis regarding health and safety, one of the most highly contentious points is setting a value of life. Economists have come up with various ways of estimating the value of a life. These include willingness to pay for safety devices, and income-based estimates.[49] All these methods are highly debated. For this study, the problem of establishing a value of life was avoided by means of careful selection of the outcome criteria. By selecting the outcome criteria to be dollars per premature death averted and dollars per life-year saved, no explicit value of life needs to be specified.

Results—national average calculation versus indexed calculations: When variability due to region, community size, house type, and house age are accounted for, the net cost of residential sprinklers varies tremendously. The net cost for installing residential sprinklers varies by greater than a factor of 35 times. From a low of $1.4 million per premature death averted (for a new mobile home in a small community in the South) to a high of $35.1 million (for a retrofit of a one- and two-family dwelling in a medium-size community in the West). Based on a national average calculation, our model predicts that residential fire sprinklers have a median net cost of $7.3 million dollars per premature death averted.

Comparison to other lifesaving interventions: An article in *Risk Analysis* identified over 500 lifesaving interventions, reporting their net cost in terms of dollars per life-year saved.[50] The accuracy of the results is limited by the accuracy of the data and assumptions in each original analysis, but the results are believable within an order of magnitude. In this study the cost per life-year saved for residential fire sprinklers was compared to the cost per life-year saved for chlorination of drinking water, banning urea-formaldehyde insulation in homes, installing oxygen depletion sensors for gas space heaters, conducting radon remediation, mandating child-resistant cigarette lighters, and installing ground fault interrupters. Figure 5-4.7 below shows this comparison. The heights of the bars represent the relative costs per life-year saved and have all been normalized to the cost of chlorination of drinking water.

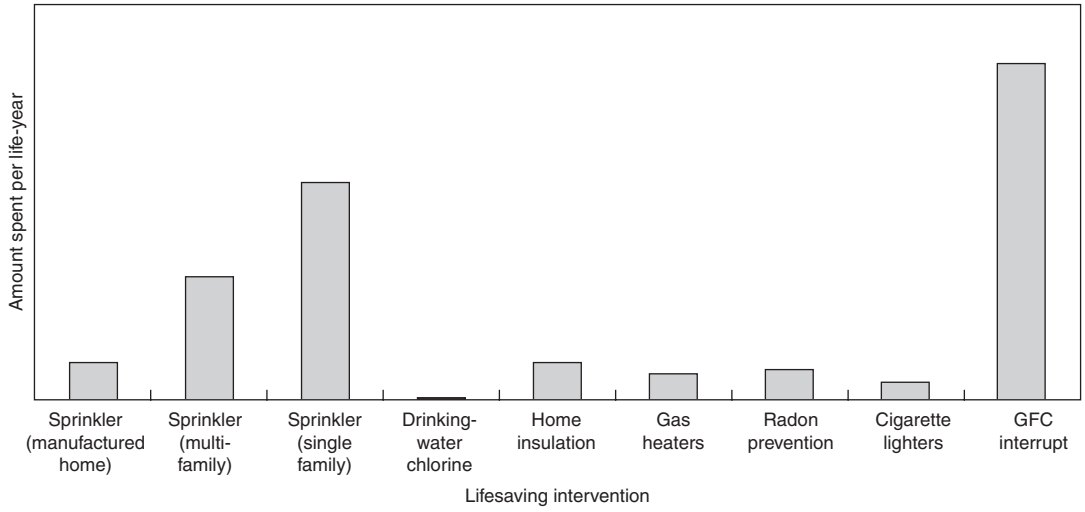

Figure 5-4.7. ***Comparison of net cost of fire sprinklers in manufactured homes with other residential lifesaving interventions.***

Uncertainty in Cost-Benefit and Decision Analysis Models

This example demonstrates how uncertainty and variability may be treated in a cost-benefit or decision analysis model. It also showed that effectively treating variability and uncertainty, and use of tools such as importance analysis and comparative analysis, can lead to greater insights. The cost of mandating residential fire sprinklers in new mobile homes was shown to be as low as five times less than the cost of mandating residential fire sprinklers using national average values for fire risk and costs. The cost of mandating residential fire sprinklers in existing single family homes was shown to be up to five times more than using national average numbers. The comparative analysis provides lawmakers a frame of reference by comparing the cost of mandating residential fire sprinklers to the costs of mandating other residential safety options with lifesaving potential.

Conclusion

The treatment of uncertainty is key to ensuring and maintaining an appropriate level of public safety while allowing the flexibility necessary to reduce costs. This is true for all fire safety engineering calculations, whether conducted to meet a performance-based code, to aid in the establishment of a prescriptive requirement, or to compare a performance option to its prescriptive counterpart. Beyond being just another step in the process of getting a building approved, properly determining and documenting a level of confidence in the design will have numerous benefits. It will facilitate cooperation among stakeholders by increasing the overall understanding of risks and costs.

Distributions of outcomes are a much richer description of what is possible than the typical point value answers. Though stakeholders and/or policy decisions must still determine how much risk to accept, with thorough uncertainty analyses, this decision will be informed and free of the uneasiness that typically surrounds acceptance of a deterministic performance calculation. The information provided in this chapter is intended to help the fire protection community to understand the nature and sources of uncertainty, to aid in the selection of a calculation procedure, to apply a methodology for the treatment of uncertainty, and to incorporate uncertainty into cost-benefit models and decisions.

References Cited

1. G.M. Morgan and M. Henrion, *UNCERTAINTY: A Guide to Dealing with Uncertainty in Quantitative Risk and Policy Analysis,* Cambridge University Press, New York (1990).
2. American National Standards Institute, *U.S. Guide to the Expression of Uncertainty in Measurement,* National Conference of Standards Laboratories, Boulder, CO (1997).
3. W.M. Pitts, E. Braun, R.D. Peacock, H.E. Mitler, E.L. Johnsson, P.A. Reneke, and L.G. Blevins, *Temperature Uncertainties for Bare-Bead and Aspirated Thermocouples Measurements in Fire Environments,* National Institute of Standards and Technology, Gaithersburg, MD (1998).
4. R.L.P. Custer and B.J. Meacham, *Introduction to Performance-Based Fire Safety,* Society of Fire Protection Engineers and National Fire Protection Association, Quincy, MA (1997).
5. J.L. Casti, *Searching for Certainty: What Scientists Can Know about the Future,* William Morrow and Company, New York (1990).
6. S.E. Magnusson, H. Frantzich, and K. Harada, *Fire Safety Design Based on Calculations: Uncertainty Analysis and Safety Verification,* Department of Fire Safety Engineering, Lund University, Lund, Sweden (1995).
7. J. Watts, "Dealing with Uncertainty: Some Applications in Fire Protection Engineering," *Fire Safety Journal,* 11, pp. 127–134 (1986).
8. J. Helton, "Treatment of Uncertainty in Performance Assesments for Complex Systems," *Risk Analysis,* 14, 4, pp. 483–511 (1994).
9. SFPE, *The SFPE Engineering Guide to Performance-Based Fire Protection Analysis and Design of Buildings,* Society of Fire Protection Engineers and National Fire Protection Association, Quincy, MA (2000).
10. K.A. Notarianni and P.S. Fischbeck, "Dealing with Uncertainty to Improve the Regulatory System," in *Fire Safety Design in the Twenty-First Century* (D. Lucht, ed.), Worcester, MA (1999).
11. D.W. Stroup, "Using Performance-Based Design Techniques to Evaluate Fire Safety in Two Government Buildings," in *Second International Conference on Performance-Based Codes and Fire Safety Design Methods,* International Code Council and Society of Fire Protection Engineers, Maui, HI, pp. 429–438 (1998).
12. P.D. Sullivan, "Existing Building Performance-Based Fire Safety Design," in *Second International Conference on Performance-Based Codes and Fire Safety Design Methods,* International Code Council and the Society of Fire Protection Engineers, Maui, HI, pp. 49–60 (1998).
13. R.W. Portier, R.D. Peacock, and P.A. Reneke, *FASTLite: Engineering Tools for Estimation Fire Growth and Smoke Transport,* National Institute of Standards and Technology, Gaithersburg, MD (1996).
14. L. Benthorn and H. Frantzich, "Fire Alarm in a Public Building: How Do People Evaluate Information and Choose Evacuation Exit?" in *Human Behaviour in Fire* (J. Shields, ed.), Fire Safety Engineering Research and Technology Centre, University of Ulster, Belfast, Northern Ireland, pp. 213–222 (1998).
15. G. Proulx, "The Impact of Voice Communication Messages during a Residential Highrise Fire," in *Human Behaviour in Fire* (J. Shields, ed.), Fire Safety Engineering Research and Technology Centre, University of Ulster, Belfast, Northern Ireland, pp. 265–274 (1998).
16. V. Brannigan and C. Smidts, "Performance Based Fire Safety Regulation under Intentional Uncertainty," in *Human Behaviour in Fire: First International Symposium* (J. Shields, ed.), Fire Safety Engineering Research and Technology Centre, University of Ulster, Belfast, Northern Ireland, pp. 411–420 (1998).
17. K.A. Notarianni and W.D. Davis, "The Use of Computer Fire Models to Predict Temperature and Smoke Movement in High-Bay Spaces," *NISTIR 5304,* National Institute of Standards and Technology, Gaithersburg, MD (1993).
18. T.J. Shields, "Human Behaviour in Fire," in *First International Symposium on Human Behaviour in Fire* (T.J. Shields, ed.), University of Ulster, Belfast, Northern Ireland (1998).
19. C. Starr, "Social Benefit vs. Technological Risk," *Science,* 165, pp. 1232–1238 (1969).
20. J. Fleming, "A Code Official's View of Performance-Based Codes," in *Fire Risk and Hazard Assessment Symposium,*

National Fire Protection Research Foundation, San Francisco, pp. 93–117 (1996).

21. H. Frantzich, S.E. Magnusson, B. Holmquist, and J. Ryden, "Derivation of Partial Safety Factors for Fire Safety Evaluation Using the Reliability Index Beta Method," in *Fifth International Symposium on Fire Safety Science,* International Association for Fire Safety Science, Boston, pp. 667–678 (1997).
22. S.E. Magnusson, H. Frantzich, B. Karlsson, and S. Sardqvist, "Determination of Safety Factors in Design Based on Performance," in *Fourth International Symposium on Fire Safety Science,* International Association for Fire Safety Science, Boston, pp. 937–948 (1994).
23. B. Taylor and C. Kuyatt, *Guidelines for Evaluating and Expressing the Uncertainty of NIST Measurement Results,* National Institute of Standards and Technology, Gaithersburg, MD (1994).
24. K.A. Notarianni and P. Fischbeck, "A Methodology for the Quantitative Treatment of Variability and Uncertainty in Performance-Based Engineering Analysis," in *Second International Conference on Performance-Based Codes and Fire Safety Design Methods,* International Code Council and Society of Fire Protection Engineers, Maui, HI, pp. 225–239 (1998).
25. W. Jones, G. Forney, R. Peacock, and P. Reneke, *A Technical Reference for CFAST: An Engineering Tool for Estimating Fire and Smoke Transport,* National Institute of Standards and Technology, Gaithersburg, MD (2000).
26. R. Lantz, "Model Validity Defined and Applied to the Problem of Making Legitimate Predictions from Fire Protection Engineering Models," in *Third International Conference on Performance-Based Codes and Fire Safety Design Methods,* Society of Fire Protection Engineers, Lund, Sweden (2000).
27. N. Siu, E. Droguett, and A. Mosleh, "Model Uncertainty in Fire Risk Assessment," in *SFPE Symposium on Risk, Reliability, and Uncertainty in Fire Protection Engineering,* Society of Fire Protection Engineers, Baltimore (1999).
28. R. Peacock, P. Reneke, W. Davis, and W. Jones, "Quantifying Fire Model Evaluation Using Functional Analysis," *Fire Safety Journal,* 33, pp. 167–184 (1999).
29. D. Lucht, *Strategies for Shaping the Future,* Worcester Polytechnic Institute, Worcester, MA (1991).
30. W. Jones, *Progress Report on Fire Modeling and Validation,* National Institute of Standards and Technology, Gaithersburg, MD (1996).
31. ASTM, *Standard Guide for Evaluating the Predictive Capability of Fire Models,* American Society for Testing and Materials, Philadelphia (1992).
32. R. Dickson, "Sensitivity Analysis of Ordinary Differential Equation Systems—A Direct Method," *Journal of Computational Physics,* 21, pp. 123–143 (1976).
33. R. Iman and J. Helton, "An Investigation of Uncertainty and Sensitivity Analysis Techniques for Computer Models," *Risk Analysis,* 8, 1, pp. 71–90 (1988).
34. R. Iman, "An Approach to Sensitivity Analysis of Computer Models: Part I—Introduction, Input Variable Selection and Preliminary Variable Assessment," *Journal of Quality Technology,* 13, 3, pp. 174–183 (1981).
35. R. Iman, J. Helton, and J. Campbell, "An Approach to Sensitivity Analysis of Computer Models: Part II—Ranking of Input Variables, Response Surface Validation, Distribution Effect and Technique Synopsis," *Journal of Quality Technology,* 13, 4, pp. 232–240 (1981).
36. D. Beller, "Computer Modeling Related to Fire and Decision Support Systems," in *Second International Conference on Performance-Based Codes and Fire Safety Design Methods,* International Code Council and Society of Fire Protection Engineers, Maui, HI (1998).
37. K.A. Notarianni, "The Role of Uncertainty in Improving Fire Protection Regulation," Ph.D. Dissertation, Carnegie Mellon University, Pittsburgh, PA (2000).
38. C. Beyler, "Introduction to Fire Modeling," in *Fire Protection Handbook* (A. Cote, ed.), National Fire Protection Association, Quincy, MA, pp. 10-82–10-85 (1991).
39. H. Nelson, "Application of Fire Growth Models to Fire Protection Problems," in *Fire Protection Handbook* (A. Cote, ed.), National Fire Protection Association, Quincy, MA, pp. 10-109–10-112 (1991).
40. A. Hald, *Statistical Theory with Engineering Applications,* John Wiley and Sons, New York (1952).
41. M. Reiss, "Global Performance-Based Design: Is It the Solution?" in *Second International Conference on Performance-Based Codes and Fire Safety Design Methods,* International Code Council and Society of Fire Protection Engineers, Maui, HI, pp. 191–195 (1998).
42. House Committee on Science, *Unlocking Our Future: Toward a New National Science Policy,* U.S. Congress, Washington, DC (1998).
43. NFPA, *NFPA 550 Guide to the Fire Safety Concepts Tree,* National Fire Protection Association, Quincy, MA (1995).
44. R.T. Clemen, *MAKING HARD DECISIONS: An Introduction to Decision Analysis,* PWS-KENT Publishing Company, Belmont, CA (1990).
45. K. Notarianni, "A Municipal Model of the Cost of Mandating Residential Sprinklers." (1996).
46. M. Karter, *U.S. Fire Experience by Region, 1989–1993,* National Fire Protection Association, Quincy, MA (1995).
47. J. Hall and B. Harwood, "The National Estimates Approach to U.S. Fire Statistics," *Fire Technology,* 26, 2, pp. 99–113 (1989).
48. J. Hall, Personal Communication, Uncertainty Bands (January 1996).
49. W.K. Viscusi, "A Survey of Values of Risk to Life and Health," in *Fatal Tradeoffs: Public and Private Responses to Risk,* Oxford University Press, New York, pp. 51–54 (1992).
50. T.O. Tengs et al., "Five-Hundred Life-Saving Interventions and Their Cost-Effectiveness," *Risk Analysis,* 15, 3 (1995).

CHAPTER 5

Data for Engineering Analysis

John R. Hall, Jr., and Martha J. Ahrens

This chapter addresses sources of input data required for deterministic (e.g., fire hazard) or probabilistic (e.g., fire risk) engineering analysis, such as performance-based design, code change analysis, product evaluation analysis, or major fire reconstruction. An overview of types of analysis engineers may perform, with a brief discussion of the kinds of engineering problems that should be addressed using those kinds of analysis, is given in the list below. Table 5-5.1 then translates each type of analysis into a list of fire or fire-related phenomena that must be characterized to perform the analysis. Each phenomenon is then translated into a list of types of data required to model the phenomenon as part of the analysis.

- (General) fire risk analysis refers to a comprehensive analysis of fire risk associated with a range of situations, whether or not there is a particular focus for the analysis, and is set up in a classic risk analysis format, using scenarios and requiring data on probabilities and consequences for each scenario.
- Fire hazard or risk analysis of a burnable product is needed for evaluation and possibly certification for acceptability (possibly for equivalence to a product regulation) of a product, material, assembly, component, and so on whose role in fire is as something that burns, either the first item ignited or a major fuel source during fire development.
- Fire hazard or risk analysis of a design for an occupiable space is needed for assessment and possibly approval of a design for an entire building (possibly under equivalence or relative to a performance-based code).
- Fire hazard or risk analysis is also appropriate for evaluation and possibly approval of products whose roles in fire are as heat sources that initiate fires.
- Engineering analysis can be appropriately applied to the performance of automatic detection/alarm or suppression systems or of other active fire protection systems.
- Engineering analysis can be appropriately applied to the performance of passive fire protection, such as walls, doors, and structural members.
- Engineering analysis can be appropriately applied to the performance of features designed to ensure safe evacuation of occupants from a building with a developing fire.

As Table 5-5.1 shows, regardless of the type of analysis required, the same generic types of data are typically needed, which may be organized into these few sources:

- Fire incident and field observation (i.e., nonincident event) data
  - Probabilities of ignition or of reliability, given naturally occurring variation in conditions
  - Fire size and consequences, given specified values of certain conditions, factors, or characteristics of interest and naturally occurring variation in all others
  - Characteristics and behavior of people
- Usage or exposure data
  - Denominators for probability calculations from event data (e.g., number of portable electric heaters versus wood stoves in use, to support estimates of fires per year per unit; number of gasoline service stations, to support estimates of probability of fire per service station per year; number of square feet of office space, to support estimates of probability of fire per square foot of office space per year)
- Laboratory test results
  - Fire size (e.g., heat release rate) as a function of time, given planned variation in certain conditions (e.g., fuel load) and unplanned variation in those not recognized or measured (e.g., exact location of fuel items and their proximity to each other)
  - Probabilities of ignition or of reliability, given planned variation in conditions (measured as

Dr. John R. Hall, Jr., is NFPA's assistant vice-president for Fire Analysis and Research.

Martha J. Ahrens is a fire analysis specialist at NFPA.

Table 5-5.1 ***Types of Analysis and Associated Data Needs***

Type of Analysis	Phenomena	Data Needs
General fire risk analysis	Ignition—probability of fire, by scenario	Fire incident data, exposure data
	Consequence—measures of severity of fire, by scenario	Fire incident data, laboratory test results
Burnable product fire hazard or risk analysis	Ignition—probability of fire, by scenario, for different versions of the product	Laboratory test results (related to scenarios, including specific ignition sources), fire incident data, product usage data
	Burning characteristics of product once ignited—time curve for heat release rate, peak heat release rate, flame spread rate, effective heat of combustion, rate of production of smoke or toxic species	Laboratory test results
	Reliability of product—probability, mode or nature, and magnitude of "failure," defined as any deviation from nominal product performance	Field observations (e.g., probability of poor quality control in manufacture of product), usage data (e.g., age effects related to performance, degradation due to wear or vandalism)
	Contribution to harm to people—toxic species production by mass loss ratio or mass loss rate, toxic potency of species, time rate of production of vision-reducing products of combustion	Laboratory test results (of characteristics and effects of fire conditions produced when product burns)
	Contribution to harm to property—mass loss rate by combustion product, corrosivity or other chemical characteristics by combustion product	Laboratory test results (of characteristics and effects of fire conditions produced when product burns)
Design for occupiable space fire hazard or risk analysis	Ignition and burning characteristics	Laboratory test results (related to scenarios, including specific ignition sources), fire incident data, product usage data
	Transition to flashover	Design specifications (e.g., compartment dimensions, thermal properties of compartment surface linings, venting), laboratory test results, other measured or estimated conditions
	Burnout time	Field surveys (fuel load or fuel mass available, compartment geometry, ventilation), laboratory tests (mass burning rate, heat of combustion)
	Space to space fire spread—flame spread rate	Design specifications (e.g., measures of barrier integrity), laboratory test results, other measured or estimated conditions (e.g., paths of fire spread such as HVAC), fire duration (see burnout time)
	Structural performance—collapse or damage making use of building unsafe	Laboratory test results, field observations
	Contribution to harm to people	Same as for burnable product analysis
	Contribution to harm to property	Same as for burnable product analysis
Heat source product fire hazard or risk analysis	Ignition—probability of fire, by scenario, for different versions of the product	Laboratory test results, fire incident data, product usage data
	Reliability of product—probability, nature, and magnitude of deviations from nominal product performance	Field observations (e.g., probability of poor quality control in manufacture of product, testing and maintenance records), usage data (e.g., component failure due to age, degradation due to usage or vandalism)
Active fire protection performance	Time of activation	Laboratory test results (e.g., physical conditions leading to system activation), fire incident data
	System effect—measures of system output (e.g., sound, suppression agent)	Laboratory test results, fire incident data
	Reliability—probability, nature, and magnitude of deviations from nominal system performance	Field observations (e.g., probability of poor quality control in manufacture of product, testing and maintenance records), usage data (e.g., component failure due to age, degradation due to usage or vandalism)
Passive fire protection performance	Time performing function (e.g., time blocking spread of fire, time providing structural integrity while subjected to fire conditions)	Laboratory test results (on passive fire protection element, reflecting materials and type of design or construction), fire incident data, burnout time (see previous reference to burnout time as a phenomenon; it is a calculated time for fire duration exposing passive fire protection element)
	Feature effect—degree to which function is performed (e.g., quantity of fire effects permitted to pass barrier)	Laboratory test results, fire incident data
	Reliability—probability, nature, and magnitude of deviations from nominal feature performance	Field observations (e.g., impairment prior to fire, such as poke-through holes in wall or doors blocked open, probability of poor quality control in manufacture of product), usage data (e.g., component failure due to age, degradation due to usage or vandalism), laboratory test results
Evacuation and other human behavior	Occupant characteristics	Field observations, laboratory test results, design specifications and estimated conditions

numbers of ignitions or numbers of failures divided by numbers of trials, although fire and equipment failure tend to be such rare events that measurement of probabilities in the laboratory can be impractical)

Fire consequences, including specific effects on people (actually data for estimation of effects on people, for example, via animal tests or toxic effects models based on species concentrations and exposure times) or on property, as a function of time and of specified or measured conditions

Discussion of data types and sources will be organized, therefore, around incident data, field observation data, usage or exposure data, and laboratory test results. The last type will be addressed only briefly, as it is the type most familiar already to fire protection engineers and most thoroughly discussed in the other chapters of this handbook.

Incident Data

How often do certain items catch fire, or certain types of equipment start fires, or certain types of occupancies have fires? The first component in all these calculations is data on event frequencies per unit time. If the focus is on products, occupancies, or other subjects of analysis that are well established in widespread use, then fire experience data will include a number of fires involving those items, and those data can be used with usage data to calculate event frequencies.

If the product is new, it will not be reflected in current fire experience data. It may be necessary to use laboratory tests in a full range of relevant scenarios to calibrate the likelihood of ignition for the new product against the likelihood of ignition for a typical established product or mix of products. The performance of the typical product or mix of products indicates the level of performance producing today's product fire problem, which means the degree of difference in the new product's laboratory performance should predict the new product's field performance as a change in the product's fire problem.

There are no standard test protocols for such a calibration and, because ignition is typically a rare event, it may be difficult and expensive to obtain test-based estimates of these relative likelihoods. Subjective estimation and interpretive judgment will likely be required and may in some instances be the only basis available for ignition probability estimates for new products. (For example, experts might agree that a new product will be roughly a third to a half less likely to be involved in fire ignitions than a typical product now in use.)

If fire experience history is relevant, it is important that estimates be drawn from suitable, statistically representative databases and procedures. In the United States, this means starting with national estimates of fire experience using data from the U.S. Fire Administration's National Fire Incident Reporting System (NFIRS) for detail and from the National Fire Protection Association's annual survey of fire departments for projection of NFIRS to national estimates.[1]

NFIRS is the largest and most detailed fire incident database in the world, capturing roughly a million individual fire incidents a year, but it collects only an estimated one-half of the fires reported to U.S. fire departments per year. Historically, since 1980 NFIRS has had participation from some or all communities in roughly 40 of the 50 states, plus the District of Columbia, although not all participating communities have been able to submit data every year. It captures data about the fixed property use or occupancy, the form and type of material first ignited, general type of equipment involved in ignition, form of heat of ignition, ignition factor, and presence of automatic detection and suppression systems.

To project NFIRS results to national estimates, one needs at least an estimate of the NFIRS fires as a fraction of the total so that the fraction can be inverted and used as a multiplier or scaling ratio to generate national estimates from NFIRS data.[2] But NFIRS is a sample from a universe whose size cannot be inferred from NFIRS alone. (*Universe* is the statistical term for the complete set from which a sample is drawn, in this case, the universe of all reported fires.)

Also, participation rates in NFIRS and practices regarding the types and severity of incidents reported are not necessarily uniform across regions and sizes of community. For example, some communities do not report fires with zero property damage. Both region and community size, in turn, are correlated with frequency and severity of fires. This means NFIRS may be susceptible to systematic biases.

No one at present can quantify the size of these deviations from the ideal, representative sample, so no one can say with confidence that they are or are not serious problems. But there is enough reason for concern so that a second database—the NFPA survey—is needed to project NFIRS to national estimates and to project different parts of NFIRS separately. This multiple calibration approach makes use of the annual NFPA survey where its statistical design advantages are strongest. The NFPA survey is a stratified random-sample survey that captures roughly one-tenth of all U.S. fire departments, including most departments protecting a population of at least 100,000. This stratification preserves randomness, hence representativeness, in the sample but reduces total variance, for more precise answers with less sampling uncertainty.

There are separate projection formulas for four major property classes (residential structures, nonresidential structures, vehicles, and other) and for each measure of fire severity (fire incidents, civilian deaths, civilian injuries, and direct property damage).

For example, the scaling ratio for 1996 civilian deaths in residential structures is equal to the total number of 1996 civilian deaths in residential structure fires reported to fire departments, according to the NFPA survey (4080), divided by the total number of 1996 civilian deaths in residential structure fires reported to NFIRS (1504). Therefore, the scaling ratio is $4080/1504 = 2.71$.

The scaling ratios for civilian deaths and injuries and direct property damage are often significantly different from those for fire incidents. Except for fire service injuries, average severity per fire (e.g., average number of deaths per 100 fires, average property damage per fire) is generally higher for NFIRS than for the NFPA survey. Use of different scaling ratios for each measure of severity is equivalent to assuming that these differences are due

either to NFIRS underreporting small fires, resulting in a higher-than-actual loss-per-fire ratio, or possible biases in the NFIRS sample representation by region or size of community, resulting in severity-per-fire ratios characteristic only of the oversampled regions or community sizes.

Most analyses of interest involve the calculation not just of the estimated total number of fires per year within a particular occupancy but more specifically of the estimated number per year of a certain type of fire in the particular occupancy. The types that are most frequently of interest are those defined by some ignition-cause characteristic. The six cause-related characteristics most commonly used to describe fires are two characteristics related to the source of heat of ignition (form of the heat that caused the ignition, equipment involved in ignition), two characteristics related to the first fuel item ignited (form or type of material first ignited), the ignition factor that brought heat source and ignited material together, and area of origin. Other characteristics of interest are victim characteristics, such as ages of persons killed or injured in fire, victim location at ignition, and victim activity at time of injury.

For any characteristic of interest in NFIRS, some reported fires have that characteristic unknown or not reported. If the unknowns are not taken into account, then the propensity to report or not report a characteristic may influence the results far more than the actual patterns on that characteristic. For example, suppose the number of fires remained the same for several consecutive years, but the percentage of fires with cause unreported steadily declined over those years. If the unknown-cause fires were ignored, it would appear as if fires due to every specific cause increased over time while total fires remained unchanged. This, of course, does not make sense.

Consequently, most national estimates analyses allocate unknowns. This is done by using scaling ratios defined by NFPA survey estimates of totals divided by only those NFIRS fires for which the dimension in question was known and reported. This approach is equivalent to assuming that the fires with unreported characteristics, if known, would show the same proportions as the fires with known characteristics. For example, it assumes that the fires with unknown ignition factor contain the same relative shares of child-playing fires, incendiary-cause fires, short-circuit fires, and so forth, as are found in the fires where ignition factor was reported.

It may be useful at this point to summarize sources of error and uncertainty in NFIRS-based national estimates, both those that can be readily quantified and those that cannot:

- Sample-size-based uncertainty—negligible from NFIRS itself because of its enormous size, unless the problem being examined accounts for hundreds of fires per year or less, and modest from the calibrating NFPA survey (about 10% for deaths and much less for other measures of fire loss)
- Sample-bias-based uncertainty—negligible from the NFPA survey because of its design, and unknown for NFIRS, where poorer communities (large or small) are proportionally less well represented but differences in proportional representation appear to be modest; large for any other incident data source, which will tend to be limited to more severe fires and possibly to specially selected victim groups
- Uncertainty due to missing data—the percentage of NFIRS cases with blank or unknown data is addressed, as noted above, by proportional allocation but can also be used to estimate the uncertainty, which in extreme ranges from all the unknowns being relevant to none of the unknowns being relevant
- Uncertainty due to coding inconsistencies—more difficult to address because few coding combinations are truly inconsistent (unusual fires are possible) but can be analyzed as with missing, blank, or unknown data in terms of elimination of a range of suspect cases
- Uncertainty due to error in determining the facts of the case—unmeasureable in the absence of some indicator within the incident record (e.g., inconsistency in coding two or more data elements) or access to a more reliably accurate source of incident data (few incidents have a second source of data, and second sources of data are not necessarily more reliable)

Fire incident commanders provide NFIRS data using a standardized coding system after a fire to complete an incident report. The strengths of the system are also limiting factors. By utilizing a standard classification system to capture the circumstances at all types of fires, data can be captured easily about a wide variety of events. However, the data will not be as detailed as many people would like. The fire service personnel collecting the data are generalists, not specialists. They can usually identify that a particular piece of equipment was the source of ignition, but they are unlikely to know which part of the equipment was involved. Information on brand, model, or component of equipment involved is not coded and typically is not captured. Nor does NFIRS capture very specific types of equipment that are used in only a small number of industries. And even at the level of detail addressed by the database coding, there are many gray areas of interpretation.

To illustrate these points on the limitations and complexities of applying the data to a particular product, consider the steps you might have to go through just to fully capture the detail that is available in NFIRS in order to estimate fires involving a particular type of carpet. Carpet is one of several products that falls within the NFIRS category of floor covering. The NFIRS Form of Material First Ignited code 14 for floor covering includes carpet but also tile, rugs, hardwood flooring, resilient (e.g., vinyl) flooring, and even stairs. The NFIRS database can be checked for number of fires coded as starting with floor covering. However, floor covering will also account for a share (usually estimated as proportional) of fires with Form of Material First Ignited unknown. Floor covering will also account for a share (usually estimated as proportional) of fires under Form of Material First Ignited code 10, which is structural component or finish of unknown type. The standard references on developing national estimates provide guidance on these steps and the specific statistical methods needed to execute them.

To distinguish carpets from other floor coverings, consider the Type of Material First Ignited data. This data

element has codes for several broad categories of fabrics and textiles, including unclassified and unknown types. For carpet constructed from manufactured fabric or fiber (code 71), you might be inclined to consider only those fires and a proportional share of fires coded as Type of Material First Ignited code 70 (unknown-type fabric, textile, fur, or hair) as well as fires coded as totally unknown. This would properly separate carpet fires from hardwood or unfinished floors (Type of Material First Ignited codes in the 60–69 range, which is wood and paper) and from vinyl floor coverings (Type of Material First Ignited codes in the 40–49 range, which is plastics, or perhaps code 81, which is linoleum, or codes 80 and 89, which are unclassified and unknown-type materials compounded with oil). But what about fires coded as cotton or rayon (code 72) or wool (code 73) or fur, silk, or other fabric (code 74)? If each of these possibilities corresponds to another real product—say, a type of rug or another type of carpet—then exclusion of these inappropriate codes makes sense. But any code that does not correspond to another real product is probably a miscoding and so is best treated as another type of partial or complete unknown, to be proportionally allocated and so added to the estimated number of total carpet fires.

For example, one of the most frequently reported Types of Material First Ignited for floor covering fires is gasoline,which clearly refers not to the floor covering but to a substance spilled or poured onto the floor covering. Should such fires be excluded because they clearly do not involve a true floor covering as the first item ignited? Or should they be included on the basis that the gasoline leads to accelerated early involvement of the real floor covering in fire, and so floor covering is the first true product involved in fire? Or should they be excluded on the basis that the burning properties of the floor covering are irrelevant to a fire started with gasoline? Or should they be included on the basis that the relative ability of different floor coverings to absorb gasoline could make a difference in fire development? No matter what the decision, it will not be a simple one.

The gasoline example illustrates another general point. It may be tempting, when constructing national estimates, to exclude certain types of fires as not being fair tests of the product or the building design. This practice is unsound, as all fires involving a product or occupancy are relevant to an overall description of the fire problem associated with it. Factors that make the fire challenge seem unfair can be properly addressed at the stage of analyzing how much fire probabilities can be reduced or interpreting whether a certain fire probability is acceptably low. But exclusions should occur at those points, not at the initial stages of analysis, or else the engineering analysis will be conducted against a misleadingly optimistic view of the size of the problem to be addressed.

At this stage, you may have achieved as detailed and appropriate an estimate of the incident rate as you can derive from NFIRS-based national estimates. It is not possible to ascertain, for example, age, style, specific materials, or specific burning properties of carpet from NFIRS. All types of carpets and rugs may still be inseparably combined in your estimates. In some cases, further refinement is possible based on differential patterns of usage and their implications for areas of origin or for exposure to certain heat sources. For example, the same Equipment Involved in Ignition code is used for irons, hair dryers, and electric blankets. However, these devices are used in very different places and tend to ignite different burnable items because different items are close enough to each type of device to be ignited. Some heuristic estimates could be made. For carpets and rugs, however, there do not seem to be any differences in usage patterns that are clear-cut enough to use in analysis. More detail is needed from another data source.

Further progress depends on inference from a combination of incident data, usage data, and laboratory test data. The inference rules will be discussed after those types of data have been reviewed and discussed individually.

For now, let us return to the earlier statement that valid analysis of incident rates requires the use of a statistically representative database, like NFIRS and the NFPA survey. Many other databases exist that are much more detailed than NFIRS but are either known to be statistically unrepresentative or at best not known to be representative. To see why it is imperative that analysts not sacrifice statistical validity for detail, it may be useful to review a number of half-truths and widely held myths surrounding databases.

Data Half-Truths and Myths

"Someone must collect the data I need": Why? Who would have that much interest? It takes time and resources to collect data. Any organization that collects data will have a reason to do so. And the data they collect will be the data *they* need.

Some databases were developed to serve diverse purposes and constituencies. In 1974, the National Fire Prevention and Control Act, Public Law 93-498, Section 9 established the National Fire Data Center to "provide an accurate, nationwide analysis of the fire problem, identify major problem areas, assist in setting priorities, determine possible solutions to problems, and monitor the effectiveness of programs to reduce fire losses." This act established the U.S. Fire Administration and the National Fire Incident Reporting System (NFIRS).

The U.S. Consumer Product Safety Commission (CPSC) uses data from the sample-based National Electronic Injury Surveillance System (NEISS), which CPSC created, to develop estimates of the number of injuries associated with consumer products and treated at hospital emergency rooms.

NFIRS and NEISS are examples of event databases. Both were designed to help identify a very wide variety of problems and were not designed to "prove" a particular point.

When considering the use of data from a particular source, it is wise to consider why the data collection effort was undertaken in the first place. Who paid for it, and would the sponsors have a vested interest in a particular outcome? In some cases, data may be collected to promote an agenda, and may be virtually useless because of leading questions or other methodological flaws. It is often useful to review the survey instrument or form. Sometimes a data collection effort was designed to answer one

specific question, and the results would not be applicable in other settings. Rural and urban experiences may differ considerably from each other, so, for example, a study of big-city fire problems could not be applied to rural settings without refinement or reconfirmation.

It is not necessary, though, for biases to be inserted deliberately in order for serious biases to arise. Data collection budgets are typically small, and most databases are therefore limited to data that is easy to obtain. Both the accuracy of the data and the representativeness of the incidents captured must be considered highly suspect in any so-called opportunity sample. Even in a well-designed data collection system with no deliberate bias and no special shortage of funds, some biases arise because of the relative difficulty of obtaining reliable information and universal participation. For example, fires in fully sprinklered buildings or buildings with good detection/alarm systems are more likely to be discovered and controlled by on-site resources including the occupants. No data collection system based on third parties, like the fire service, can expect to capture unreported fires. The national estimates of fire problems that are produced by combining NFIRS data and the results of the NFPA survey only reflect data reported to municipal fire departments and exclude those handled by private federal brigades, federal fire-fighting organizations or the occupants themselves. Some occupancies, particularly high-hazard occupancies, are more likely to have fire brigades than others.

Suppose one asked for data on heat-release rates at key points during the fire. No one has the technology to measure or estimate such data outside a laboratory. Suppose one asked for readily observable change points in the fire, such as spread to a new room or floor. No one can expect to be in position to observe such change points at most fires, and fire fighters do not have the discretionary time during a fire to check specific times and record them. When seeking data, it is important to ask how the data collectors would be able to obtain the data and how reliable it would be.

"Anecdotes describe typical incidents": This is often not true. *Anecdotes* are what statisticians call data points from a database that has not been designed to ensure statistical representativeness. The NFPA Fire Analysis and Research Division runs an anecdotal database called the Fire Incident Data Organization (FIDO). A clipping service identifies significant incidents (e.g., large loss, multiple deaths), and additional information is requested from the fire service and other sources. Because serious fires, with multiple deaths or millions of dollars in loss, tend to be widely reported, FIDO's anecdotes can be used as a statistically representative (even complete) database for large fires. However, FIDO also captures well-documented fires on an opportunity basis, and for these fires FIDO is only anecdotal.

From early in the twentieth century until the mid-1970s, NFPA collected information on sprinkler activations.[3] However, over time the easily available data sources became less and less reliable in capturing smaller fires. As FIDO's representativeness for smaller fires declined, so did its representativeness in capturing sprinkler successes. More and more such incidents were missed, and a disproportionate number of captured incidents therefore showed sprinkler problems.

Anecdotal information like that provided by FIDO, NFPA Fire Investigations, or CPSC's In-Depth Investigations file can indicate the range and diversity of fires that *can* happen. Anecdotes cannot be used to estimate incident rates or probabilities.

"A rose is a rose is a rose": Anecdotes are relevant but may not be representative. It is also possible to have representative data that are not relevant, even though they appear to be, because of differing definitions for the same terms. For example, definitions of data elements may differ in different countries or even different data collection systems. In fire incident databases, *space heater* refers to a heater for a relatively small area. The U.S. Department of Energy uses the term *space heater* to describe *all* heating systems, including furnaces and other central heating units. However, the term *heating equipment* in fire incident databases includes not only equipment to heat spaces but also water heaters.

"If data were collected, they must be available": The analyst's life would be easier if this statement were true. Unfortunately, it's not. Some data, such as the detailed information collected by insurance companies, is proprietary and confidential. Corporations may maintain incident records when injuries or mishaps occur, but they are under no obligation to share that information with the general public. Information collected by the government *should* be available. The public can generally obtain copies of reports or files that already exist. However, data may not be kept indefinitely and older data may never have been entered into modern, electronically accessible media. Many computer systems have not been integrated, so analyses that are theoretically quite easy may be impossible without major conversion efforts.

These problems are usually not insurmountable. Some modifications may be needed and sources of uncertainty must be documented. Considerable data is available, as noted, which means estimates of sampling-based uncertainty can be readily constructed.

Field Observation Data

Switching now from fire incident data to other kinds of data based on observations in the field, Table 5-5.1 cites field observation data as relevant to reliability analysis, including instances of unavailability or failures to perform with full effectiveness when needed despite being available, and emergency evacuation analysis.

The chapter on reliability (Section 5, Chapter 3) elsewhere in this handbook provides an overview of issues in and mathematical methods for analyzing reliability. At present, data to support reliability analysis is very scarce. The five types of data sources identified are also relevant to other aspects of engineering analysis:

- Judgments and opinions
- Inspection and testing
- Simulations and laboratory studies
- Incident data
- Product life tracking systems

Judgments and Opinions

In the absence of any type of data from systematic field observations, one can use estimates from individuals whose work experience has provided them with a long period of nonsystematic field observations. There are methods like Delphi panels that try to eliminate bias from the group process of consolidating expert opinions into consensus estimates. (Modified Delphi panels have been used to specify many of the scoring parameters for NFPA 101A, the alternative evaluation scheme to NFPA's *Life Safety Code*.) But shared biases remain and are commonplace. In particular, the mix of observations that occur in the normal course of a job in fire suppression, fire reconstruction, design, and so forth, are subject to many biases that may not be recognized by the experts. (For example, new buildings are more likely to be designed for the affluent end of the general or business population, whereas fires are more likely to occur at the less affluent end, but neither tendency is absolute.)

In addition, there is a tendency for individuals to shade their recollections in favor of a pattern that is simpler than the often complex truth. Thus, a system or feature with relatively high reliability will have its reliability estimated even higher (sometimes called the *halo effect*), while a system or feature with relatively low reliability will have its reliability estimated even lower (sometimes called the *horns effect*).

Inspections and Testing

A program of routine inspection and testing can provide statistically representative data on failure frequencies and severities and is particularly useful for failures that are less than total or that otherwise may not draw attention to themselves when they occur. *Frequency* is how often failure occurs, and *severity* is how damaging failure is when it occurs, so frequency numbers are in fact relative to the level of severity of failure being tallied. However, inspection and testing-based databases are usually proprietary and so not available for routine engineering analysis. And even when available, they are subject to some critical gaps and biases.

First, the inspections that provide this kind of data tend to be part of a very advanced maintenance program, which provides the principal justification for the high cost of frequent inspection and testing. Frequent maintenance and inspection, in turn, are more likely to occur with a better-trained and more safety-conscious workforce, so the human error reliability problems, which tend to dominate mechanical and electrical problems for most systems and features in practice, are likely to be sharply lower. The resulting reliability figures will therefore tend to be much better than those achieved for more typical properties that lack the maintenance to achieve high reliability and the inspections and testing to measure their reliability. This is one reason why estimates of sprinkler reliability in Australia are so much higher than those in the United States.[3] (Another reason is that Australian sprinkler systems are much more likely to have automatic alarm transmittal to the local fire brigades, which means small-fire successes are much more likely to be captured by the same people who create the national fire incident databases.)

Second, this form of data collection can miss transitory failure conditions, such as blocking a door open, or vulnerability to extremely rare external events, such as earthquakes. In both cases, the sampling in time represented by the inspections and tests may not be sufficient to identify an important problem, in the former case because the sampling points are too far apart and in the latter case because the sampling does not (and perhaps could not) cover a sufficiently long period of time.

Finally, the process of inspection and testing is itself subject to error. If inspection is limited to observation only, without more active involvement as with testing, the probability of error in observation can be quite significant. Most databases derived from inspections or tests do not consider this type of error.

Simulations and Laboratory Studies

Exit drills are a form of simulation or laboratory study that provide data on human reliability (and performance) with regard to a range of safety-related behaviors. They illustrate the larger point that simulations and related studies are particularly useful for studying human error reliability, a critical aspect that tends to be less well addressed by other controlled-study data sources.

Simulations may be less than realistic as a result of simplifications done to make the experiment repeatable and manageable, as well as those made to avoid undue risks to participants. A bench-scale fire test cannot be readily scaled up to real-scale fire effects and will avoid the high flux levels of a fully developed fire, in part to avoid harm to operators and equipment, but in so doing may create a misleadingly mild picture of real fire conditions. Even a room-scale test is unlikely to be set up with accelerants, high wind-speed ventilation, conditions promoting backdrafts, or some of the other conditions that can produce the most severe fire conditions. An evacuation drill may avoid bad-weather days to avoid injury to occupants, but this may paint an unrealistically optimistic picture of how slow and how hazardous real evacuations may be.

The field of ergonomics provides design solutions to many of the people-equipment interaction problems that studies and data like these identify.

Incident and Other Field Data on Systems Performance

In theory, the most appropriate database on reliability of a system or feature would be one that captured every naturally occurring test of its availability and performance (i.e., unwanted fires) and every other activation of the system (e.g., nuisance alarms). In practice, this requires constant monitoring, which is almost always too

expensive to be implemented. The attempts to approximate such a database using only fires reported to fire departments or, even worse, fires reported in the media, will miss most incidents and can give a misleadingly pessimistic picture of reliability.

For example, analyses of reported home fires consistently show roughly one-third of smoke alarms are nonoperational,[4] but the last recent study of home installations in general found only one-fifth of smoke alarms are nonoperational.[4] Part of the reason is that occupants who are not careful to maintain smoke alarm operationality are more likely not to be careful to prevent fires. However, analysis of data from unreported fires suggests that a larger reason for the difference is the large number of home smoke alarm successes that keep fires small enough that fire departments are never notified.[4]

A similar story almost certainly applies to sprinklers, where analysis of data from reported fires indicates that sprinklers do not operate in one-sixth to one-fifth of the fires large enough to activate them (manufacturing facilities show only one-tenth).[3] Real reliability, factoring in fires that are controlled so quickly they are never reported, could easily be well over 90 percent and yet be consistent with figures like these 80–86 percent figures derived from reported fires only.[3] NFPA discontinued its sprinkler performance database in 1970 because of problems just like this.

The best databases, therefore, are those maintained by facilities or organizations that are equipped and committed to capture all fires and even all component failures. Such databases exist for process equipment (through the American Institute of Chemical Engineers, Center for Chemical Process Safety), for military equipment (through the Reliability Analysis Center in Rome, New York), and for the nuclear power industry (in documented probabilistic risk assessments for individual plants and through Science Applications International Corporation). (See contact information for some of these groups at the end of this chapter.)

All the databases described here tend to focus on active systems and other equipment. Passive fire protection features, such as fire walls, are less likely to be captured, in part because their failures tend not to be time-specific events (e.g., a smoke alarm has its battery removed, a sprinkler valve is shut off, both events occurring at defined points of time) but rather partial deficiencies in performance (e.g., a door is normally left slightly ajar, a wall has a hole in it). A poke-through hole in a wall, for example, is not a total failure of the wall and does not appear as an event in the course of the fire. Although it may have played a role in extension of the fire, it is unlikely to be identified in a postfire analysis. It also may not fit your definition of a reliability problem, but it is clearly a deviation from intended design that affects and degrades performance. No incident database routinely documents fire development and related factors in enough detail to capture this kind of problem.

Product Life Tracking System

This is the approach to data collection and reliability assurance underlying the extensive component reliability data developed by the military, particularly for aircraft, including their onboard fire protection systems (and available from the Reliability Analysis Center, Rome, New York). It combines the inspection and testing approach with the incident data approach but is also organized by individual component, which supports very specific and targeted analysis, maintenance, redesign, and other uses.

Usage and Exposure Data

Usage and exposure data is necessary at several points in engineering analysis. First, if the analysis addresses fire risk, then usage or exposure data (e.g., number of units of product in use, number of establishments of a particular type, number of people using a product or occupying a building, number of square feet of space devoted to a type of occupancy) is needed to convert incident data to estimates of ignition probability or to convert failure event data to estimates of reliability. Many if not most engineering analyses, however, frame problems in ways that do not require explicit, quantitative treatment of ignition or reliability. Even these analyses still need some usage and exposure data in order to define and specify transitory conditions, such as the numbers, locations, and capabilities of occupants, that affect the achievement of fire safety objectives and so the performance of a design.

For risk calculation, the principal challenge is to find statistically representative data with enough detail and with a structure that matches the structure of the incident or other event data it is meant to be used with. A matrix of different types of home-heating equipment, in the categories for which the U.S. Department of Energy provides usage data, is displayed in Table 5-5.2.

Many, perhaps most, of the "not stated" entries can be reasonably filled in by someone with expert knowledge of available heating technologies, both current and past. However, other studies of usage have indicated significant usage of portable electric heaters for primary heating (which would be concealed here within the category of "other" devices or misclassified as primary heating) and have distinguished wood-burning fireplaces with and without inserts.

Fire incident databases such as NFIRS (through version 4.1) offer these device categories:

- Central heating unit
- Fixed-area space heater
- Portable space heater
- Fireplace
- Chimney
- Chimney connector
- Heat-transfer system
- Other

The last three specific types of equipment are part of distribution and are not linked to the devices they support. How would you apply these categories to a heat pump or a floor, wall, or pipeless gas furnace?

Table 5-5.2 ***Types of Heating Equipment, by Fuel or Power, Local versus Central, Fixed versus Portable, Primary versus Secondary***

Fuel or Power	Type of Device	How Heat Is Distributed	Primary or Secondary Heating?
Natural gas	Central furnace	Forced warm air	Primary or secondary
	Not stated	Steam or hot water	Primary
	Floor, wall, or pipeless furnace	Not stated	Primary
	Room heater or other device	Not stated	Primary or secondary
	Fireplace	Not stated	Secondary
LP-gas	Central furnace	Forced warm air	Primary
	Room heater	Not stated	Primary
	Other	Not stated	Primary
	Not stated	Not stated	Secondary
Fuel oil	Central furnace	Forced warm air	Primary
	Not stated	Steam or hot water	Primary
	Other	Not stated	Primary
	Not stated	Not stated	Secondary
Kerosene	Not stated	Not stated	Primary or secondary
Electricity	Central furnace	Forced warm air	Primary
	Built-in units	Not stated	Primary or secondary
	Heat pump	Not stated	Primary
	Portable heater	Not stated	Secondary
	Other	Not stated	Primary or secondary
Wood	Heating stove	Not stated	Primary or secondary
	Fireplace	Not stated	Secondary
	Other	Not stated	Primary or secondary
Other	Not stated	Not stated	Primary or secondary

Source: A Look at Residential Energy Consumption in 1997, Energy Information Administration, Office of Energy Markets and End Use, U.S. Department of Energy, Washington, DC (November 1999).

For fuel or power, the Form of Heat of Ignition data elements in NFIRS (through version 4.1) will support categories like these:

- Gas-fueled equipment (natural gas and LP-gas not separated)
- Liquid-fueled equipment (fuel oil and kerosene not separated)
- Solid-fueled equipment (wood and coal not separated)
- Electric-powered equipment
- Fueled equipment with no information on type of fuel
- Match, lighter, ember, or other code suggesting fueled rather than electrical equipment but also somewhat incompatible with coding of heating equipment as heat source
- Light bulb or other code suggesting electrical rather than fueled equipment but also somewhat incompatible with coding of heating equipment as heat source
- Fireworks or other codes strongly incompatible with coding of heating equipment or heat source (and, fortunately, almost never used in combination with heating equipment)
- Codes providing no indication of fuel or power source but compatible with coding of heating equipment as heat source

This comparison will suffice to illustrate the point that even modestly detailed incident and usage databases can present a multitude of compatibility problems. Some problems can be solved by one-time special data collection efforts to devise assignment rules for estimation purposes. This is what is typically done to match chimney fires to wood stoves versus fireplaces, for example. Some problems can be solved by examination of the technology alternatives and by asking data collectors what rules they use to resolve questions in the field. Some problems can be addressed by expert judgment. And some problems create limits to the level of detail achievable in the data.

Another example has to do with occupancies. Occupancy refers to the use made of a space, and fixed property use is the NFIRS code that describes the use being made of a fixed property, which is to say a building or part of a building (such as a restaurant in a mall or on the ground floor of a high-rise multiuse building). U.S. Census Bureau codes for establishments are designed to classify the primary activity or line of the business that owns or occupies the building. In pursuit of its primary activity, a business may require and oversee many types of occupancies, from manufacturing to sales to office to storage to public assembly. The codes for businesses also distinguish retail from wholesale sales, whereas the codes for occupancies do not. Is a wholesale sales operation an office building or a mercantile occupancy? Or is it an office occupancy and a storage occupancy sharing a building? (Or the two parts might not be sharing a building.)

There are far more storage occupancies than there are buildings housing businesses whose defining purpose is storage. This means that no matter how one groups fires in storage occupancies, it is not clear that the data will match the data on establishments. Some storage occupancy fires will be in storage businesses, but many, perhaps most, will be in storage buildings associated with a store or a factory, on its complex.

Even when major categorization mismatches are not an issue, minor ones can be. The business codes identify gasoline service stations as a type of retail business. Fire incident database codes identify public service stations, but that category excludes private service stations (which the business codes may not recognize at all, since they classify a building, not the business that owns and runs the activity), excludes marine service stations (which may or may not be included in the business codes), and includes LP-gas dealers (who are probably listed separately under fuel dealers within miscellaneous retail for the business codes).

If all the matching issues are addressed, then one must still consider the measurement scales available. The business code categories are used to count establishments, which is probably the best measure of exposure but also mixes very large and very small buildings without distinction. A better measure for fire risk analysis would probably be square footage, but that data exists only for highly aggregated categories of buildings. Business-coded data also exist on numbers of employees and dollars of payroll, both already related to business size but not clearly relevant to exposure proportional to fire risk.

Current and previous versions of NFIRS (up to Version 4.1) used NFPA 901, *Uniform Coding for Fire Protection,* 1976 edition, as their starting point for data classification. Version 5.0 of NFIRS has reduced the number of fixed-property use codes dramatically. Separate fields are used to identify on-site materials, whether these materials are stored, processed, sold, or repaired at the facility, and building status. We have only begun to consider where and to what degree these extensive changes will make cross-matching business-coded data on establishments with occupancy-coded data on fire incidents more or less difficult.

Now consider occupant characteristics. Engineering analysis is done using scenarios, whether it is done in terms of fire hazard or full analysis of fire risk. Most fire safety objectives trace, directly or indirectly, to a goal of protecting people. Short of a highly conservative (and generally unachievable) objective of preventing any fire effects in any occupied area, engineering analysis will need to address the fates of occupants, explicitly and quantitatively. This, in turn, requires data on the occupants, effective when fire begins. How many are there, where are they, how will they act, and what are they capable of?

A wealth of information exists regarding household structures, which may be useful in defining *occupant sets*—alternative descriptions of occupants for analysis, analogous to fire scenarios—for homes. Information is much less detailed for occupants of any other occupancy, and these will tend to be the types of buildings where engineering analysis is sought. For those properties, one will need to seek data from industry sources and special surveys. Absent such data, it will be tempting, and possibly necessary, to use ad hoc, heuristic methods to shape subjective estimates. Certain cautions must be noted in so doing.

First, occupants do not respond in an ideal or perfectly efficient manner. They do not react immediately to the first cues of fire, they do not evacuate on the basis of perfect knowledge of conditions throughout the building, and they may evacuate in accordance with their normal patterns of movement rather than along rarely used paths best designed for quick, safe evacuation. Occupants may try to defend in place when they should not or try to evacuate when it would be safer to defend in place. None of this is a matter of panic or of irrational behavior or choices. It is not even unusual conservatism. It is simply a realistic view of how people respond to fire. Some evacuation models incorporate best available data on typical behavior and the time it takes. Optimizing models do not.

Second, the places that have fires differ, not in kind but to a significant degree, from the mix of places in general. The former tend to be occupied by people (as residents, guests, workers, shoppers, etc.) who are poorer and less well educated, in buildings whose design, maintenance, and operation tend to be less fire safe, reflecting the limitations of their occupants, managers, and owners. Smokers and consumers of alcohol or other drugs are more likely to be present because their high-risk behavior makes fire more likely, as statistical studies of risk factors repeatedly show.[5,6] There is little data on how best to reflect those patterns, and some of them may be moot for an engineering analysis of a well-designed new building, but analysts are advised to shade their assumptions and parameters toward less capability for occupants than the norm and much less capability than engineers see in their own lives, since engineers, like all professionals, are more affluent and better educated than the national average.

Third, there are far more people with limitations in the general population than ever before, if only because there are far more people in the older age groups. Buildings open to the general public will see more and more occupants with limitations of age. The Americans with Disabilities Act has facilitated access to workplaces and places of assembly for many more physically challenged individuals, while the deinstitutionalization of many people with chronic mental illness decades ago led to a larger share of occupants with mental or emotional limitations. The diversity of physical challenges is also increasingly recognized. Many people have some limitations (wear corrective eyeglasses or contact lenses, for example), and there may be less data with which to model the many moderately limited occupants than there is to model the much fewer severely limited occupants.

Fourth, occupant profiles can often be specified by linkage to time of day.[7] In homes, during the day on weekdays, there will be fewer occupants, and they will represent a different mix of ages and roles than in the evening or at night. In the evening, people will tend to be awake, while at night, most will be asleep. In hotels, different times of day will find different mixes of occupants in the guest rooms, the small meeting rooms, the large function rooms, and the recreational facilities. Overall occupancy is rarely 100 percent, but there is data available to set estimated occupancy.[8] In office buildings, the number, location, and other characteristics of occupants are clearly different during normal working hours than outside them.

Fifth, fire incidence and casualty data can and should be used as input to the process of setting occupant characteristics, but usually that data should not be used directly. For example, suppose you specified a household structure that reflected exactly the age distribution of deaths and injuries in home fires. That specification would not reproduce the observed age distribution of fire deaths and injuries, because the high-risk age groups will be disproportionally likely to suffer death or injury during fire.

On the other hand, it is useful to know that most fire risk in hotels and motels looks like fire risk in homes.[5] It tends to be limited to the person or group in the guest room of origin, and the causes are much the same, after adjusting for the presence or absence of local heating or

cooking equipment. The very large death tolls in some hotel fires justify analysis of a property's vulnerability to extended fire development and smoke spread, but most risk will take place on a different scale and test different aspects of the property's fire safety provisions.

An even larger challenge to what many people may believe is the pattern in fatal office fires. The majority of fatal office fires occur outside business hours, and a large share involve fire spread to or from another occupancy (e.g., to or from an apartment in the same building or complex) or risks associated with dual use of the office property (e.g., the cot in the back room that makes the office into a residential property after hours).[9] The classic concern in office buildings—the ability to safely evacuate large numbers of people faced with the threat of a rapidly growing fire—is almost never a factor in fatal office building fires.[9] This does not mean it should not be part of the evaluation, only that the very different patterns of risk and hazard occurring after-hours or in multiuse properties need to be examined also.

Finally, it is dangerous to limit the challenge posed by occupant characteristics with an assumption of code compliance. The most deadly fires in eating and drinking establishments have involved serious code violations, including severe overcrowding. Many deadly fires have occurred in facilities that were not designed, operated, or licensed to provide health care, but that nevertheless proved to have occupants with severe limitations when a fire occurred.[10] It is unreasonable to expect a building design to protect occupants from fire in the face of pervasive, serious code violations, but it is not unreasonable to conservatively plan for at least occasional, transitory, but possibly significant violations, such as overcrowding or deterioration of occupant capability below the minimum level that allowed them to be admitted for residency. Serious fires do not usually happen where everyone follows all the rules and best practices. A design should be robust enough to protect people even when challenged beyond the strict limits of what is supposed to be possible.

Laboratory Data

For laboratory data on physical properties of fire, products, buildings, and so on, you should start with the other chapters of this handbook, which identify the measures of interest, put them in context, and in many instances provide or reference best available data. Also, read the "Statistics" chapter (Section 1, Chapter 12) for general guidance on handling error and uncertainty in data, and consult. For guidance on error and uncertainty in data from particular test methods, consult precision and bias statements in the standards for those test methods, or consult ASTM E691, *Practice for Conducting an Interlaboratory Study to Determine the Precision of a Test Method.*

On a related point, read the other chapters closely for guidance, specific to each type of data, on what to do if your case does not exactly match the specifications for any available test data. For example:

1. Is it best to choose the closest documented case, or is extrapolation or interpolation better? How do you determine what is the closest? How far outside tested values can you extrapolate with reasonable confidence?
2. What do you do if the tests do not align along any linear scale, making direct interpolation and extrapolation impossible? (For example, there may be one result for each of several materials.) Are there scaled characteristics that can be used as a legitimate, if unproven, basis for interpolation or extrapolation?
3. Is linear interpolation or extrapolation appropriate, or would another functional form be more appropriate?
4. In addition to the characteristics of the object or space for which you need data, are the fire conditions you anticipate the same as those used in the available tests? If not, do the differences matter and can they be adjusted for?
5. Scale matters. Results from bench-scale fire tests cannot be assumed to reflect full-scale performance.
6. Interactions also matter. Fire performance of products that are composites or layered combinations of materials cannot be predicted from test data on their constituent materials.[11]
7. Time and usage change things. Products may change chemically or be altered physically, up to and including vandalism. All such changes may affect the applicability of test data on new products. This is even more true if the laboratory tests were on prototypes—or even prototypes with simplified design features—rather than on actual products ready for use.

In addition to direct use of laboratory test data, such data can be combined with incident data to provide greater detail. Consider the use of laboratory test data to build on the ignition probability estimates developed earlier for a specific product in the carpet and rug class. Under the section headed Incident Data, the discussion showed how to develop floor covering fire estimates, then fabric or textile floor covering fire estimates. Suppose this national estimates approach suffices to provide probabilities of ignition for a product class (e.g., carpet or rug) but not for any type, style, or brand of that product class.

First, the universe of products in use (not the universe of products currently offered for sale) must be divided into a small number of representative pieces such that every variation of product in use is represented by one of these reference pieces. Second, data must be developed on the share of current usage (not the current market share). Then, laboratory tests must be conducted to determine relative ignitability.

Let $i = 1, \ldots, n$ be designations for n different representative pieces. Let u_i be the collective share of total usage accounted for by the ith piece and all the pieces represented by the ith piece. Let p' be the probability of ignition, derived from fire incident national estimates for the product in all its variations. Let p_i be the proportion of laboratory trials of the ith piece in which ignition occurred. Then (all variations of product are represented and none are double-counted)

$$\sum_{i=1}^{n} u_i = 1$$

The usage-weighted average frequency of ignition for the tested pieces is proportional to the experience-derived overall ignition probability for the product class.

$$\sum_{i=1}^{n} u_i p_i \propto p'$$

Therefore, the best estimate of the ignition probability for a piece of type i is

$$\frac{p' u_i p_i}{\sum_{i=1}^{n} u_i p_i}$$

This formula uses the incident data to calibrate the laboratory test data, or it uses the laboratory data to subdivide the ignition probability for the product class into more product-specific ignition probabilities.

Where Can the Data Be Obtained?

It is impossible to list all the data sources that may be useful for engineering analyses. However, a number of principal sources are listed below, and the organizations that provide those databases will often have leads to specialized databases for specific purposes.

Incident or Event Data

National (U.S.) estimates based on NFIRS and the NFPA survey of the frequency and severity of reported fires can be obtained from

One-Stop Data Shop
National Fire Protection Association
1 Batterymarch Park
Quincy, MA 02269-9101
Telephone: (617) 984-7450
Fax: (617) 984-7478
E-mail: osds@nfpa.org
Website: http://www.nfpa.org/Research

The National Fire Incident Reporting System (NFIRS) itself is administered by the U.S. Fire Administration. Specific questions about NFIRS may be addressed to

National Fire Data Center
U.S. Fire Administration
16825 South Seton Avenue
Emmitsburg, MD 21727
Telehone: (301) 447-1000
Fax: (301) 447-1052
Website: http://www.usfa.fema.gov/nfdc

Raw NFIRS data (not calibrated by the NFPA survey or anything else) may be ordered from

National Technical Information Service
Technology Administration
U.S. Department of Commerce
5285 Port Royal Road
Springfield, VA 22161
Telephone: (703) 605-6000 or (800) 553-6847
Website: http://www.ntis.gov/

Fire incident data from the fire brigades of the United Kingdom and results from the British Crime Survey's fire questions (about all fires, not just those that were reported) can be obtained from the address below. The United Kingdom collects information on time before discovery of fire and some other variables not collected by NFIRS.

Home Office
Research and Statistics Directorate
50 Queen Anne's Gate, Room 201
London, SWIH 9AT
United Kingdom
Telephone: 020 7273 2084
E-mail: rds.ho@gtnet.gov.uk
Website: http://www.homeoffice.gov.uk/rds/index.htm

Annual reports of fire losses in Canada may be ordered from

Council of Canadian Fire Marshals and Fire Commissioners
Alberta Labour
Room 601, IBM Building
10808-99th Avenue
Edmonton, Alberta T5K 0G5
Telephone: (403) 427-8392
Fax: (403) 427-5898

Four types of data can be ordered from the National Injury Information Clearinghouse, including

- Sample-based estimates of product-related injuries treated at hospital emergency rooms, from the National Electronic Injury Surveillance System (NEISS)
- Summaries of death certificate data on product-related fatalities
- In-depth investigations of product-related injuries or incidents, from CPSC's special studies and ongoing program of investigations
- Summaries, indexed by product, of CPSC Hotline reports, product-related newspaper accounts and medical examiner reports

The NEISS data and the death certificate data could be used for event data.

National Injury Information Clearinghouse
U.S. Consumer Product Safety Commission (CPSC)
Washington, DC 20207-0001
Telephone: (301) 504-0424
Fax: (301) 504-0025
Website: http://www.cpsc.gov/about/clrnghse.html

Injury data may also be obtained for other countries.

Injury data for the Nordic countries of Denmark, Finland, Iceland, Norway and Sweden can be obtained from

Nordic Medical Statistical Committee
Sejerøgade 11
DK-2100 Copenhagen Ø
Telephone: +45 39 17 39 91
Fax: +45 39 18 51 22
E-mail: nom-nos@inet.uni2.dk
Website: http://www.nom-nos.dk/nomesco.htm

Australian injury data can be obtained from

The National Injury Surveillance and Prevention Project
Research Centre for Injury Studies
Flinders University of South Australia
Mark Oliphant Building
Laffer Drive
Bedford Park, South Australia
Australia
Telephone: +61 8 8374 0970
Fax: +61 8 8374 0702
E-mail: nisu@flinders.edu.au
Website: http://www.nisu.flinders.edu.au

Reliability databases are available from a few sources. Some industries maintain reliability databases of incidents in their own facilities. For example, the American Institute of Chemical Engineers coordinates the Process Equipment Reliability Database for the hydrocarbon and chemical process industries and the Process Safety Incident Database. Participants provide data and share the costs of maintaining the databases. In return, they obtain access to the data. Additional information may be obtained from

Science Applications International Corporation (SAIC)
10260 Campus Point Drive
San Diego, CA 92121
Telephone: (858) 826-6000
Website: http://www.saic.com

Center for Chemical Process Safety
American Institute of Chemical Engineers
3 Park Avenue
New York, NY 10016-5991
Telephone: (212) 591-7319
Fax: (212) 591-8895
E-mail: ccps@aiche.org
Website: http://www.aiche.org/ccps

Reliability Analysis Center
201 Mill Street
Rome, NY 13440-6916
Telephone: (315) 337-0900
Fax: (315) 337-9932
Website: http://rac.iitri.org

H. W. Marryat
Fire: A Century of Automatic Sprinkler Protection in Australia and New Zealand, 1886–1986
Australian Fire Protection Association
Melbourne, Australia

Some data exists from periodic special studies by nationally prominent organizations such as Factory Mutual Global. For example, a June 1992 study (code # FMRC J.I. 0T1R6.RE) displays public-domain failure probability data for automatic fire detection and suppression systems. However, much of the data held by such organizations is proprietary, and the trend has been toward making an even larger share of data and reports proprietary. This reduces the availability of data from this source to the ordinary practicing engineer.

Usage and Exposure Data

Every year, the Bureau of the Census releases an updated *Statistical Abstract of the United States.* This publication contains close to 1500 tables on demographics and economic activity and is a compilation of data collected by the U.S. Census and other entities. Some of the data would help establish usage and exposure. The *State and Metropolitan Area Data Book* and the *County and City Data Book* contain similar data on their respective jurisdictions. All three are available in print and electronically. Ordering information can be obtained from

Customer Services
U.S. Bureau of the Census
Washington, DC 20233
Telephone: (301) 457-4100
Fax: (888) 249-7295 (orders only)
Inquiry Faxes to (301) 457-4714
Website: http://www.census.gov/statab/www

Sources for data in the *Statistical Abstract* are often worth checking for possible additional information that may or may not be published elsewhere.

The Bureau of the Census and the U.S. Department of Housing and Urban Development (HUD) together produce the *American Housing Survey.* Data sets on housing can be obtained from http://huduser.org/datasets/pdrdatas.html.

Demographic and economic (exposure and usage) data from countries in the European Union can be obtained from Eurostat at http://europa.eu.int/comm/eurostat/. The site also has links to other countries' web pages.

The U.S. Department of Energy's Energy Information Administration (EIA) conducts energy consumption surveys of residential, commercial, and industrial users. These surveys provide valuable information on equipment and fuel usage. The EIA will also be conducting surveys on alternative-fueled vehicles. Information can be obtained by contacting the

Energy Information Administration EI30
1000 Independence Avenue, SW
Washington, DC 20585
Telephone: (202) 586-8800
E-mail: infoctr@eia.doe.gov
Website: http://www.eia.doe.gov/emeu/consumption/

Data from more than 100 agencies has been compiled and is accessible through FedStats. Many databases may be downloaded by the user at http://www.fedstats.gov/.

Laboratory Data

The National Institute of Standards and Technology's (NIST's) Building and Fire Research Laboratory (BFRL) maintains the website Fire on the Web at http://fire.nist.gov/. It includes the following resources:

- Data from fire tests on various topics, both from NIST and from industrial donors
- Online BFRL publications

- FireDoc, an online card catalog of NIST fire-related publications
- Fire modeling software

References Cited

1. M. Ahrens, "All Fired Up," *NFPA Journal,* May/June, pp. 80–89 (1998).
2. J.R. Hall, Jr., and Beatrice Harwood, "The National Estimates Approach to U.S. Fire Statistics," *Fire Technology,* May, pp. 99–113 (1989).
3. K.D. Rohr, *U.S. Experience with Sprinklers,* NFPA Fire Analysis & Research Division, Quincy, MA, 2000.
4. M. Ahrens, *U.S. Experience with Smoke Alarms,* NFPA Fire Analysis & Research Division, Quincy, MA, 2000.
5. M. Ahrens, *The U.S. Fire Problem Overview Report,* NFPA Fire Analysis & Research Division, Quincy, MA, 1999.
6. J.R. Hall Jr., *Patterns of Fire Casualties in House Fires by Age and Sex,* NFPA Fire Analysis & Research Division, Quincy, MA, 2000.
7. See, for example, the use of special study data from the U.S. Census Bureau on people's activities by time of day to create occupant set specifications in R.W. Bukowski, F.B. Clarke, J.R. Hall, Jr., and S.W. Stiefel, *Fire Risk Assessment Method: Case Study 1, Upholstered Furniture in Residences,* National Fire Protection Research Foundation, Quincy, MA, 1990.
8. See, for example, the use of industry data on guests to create occupant set specifications in R.W. Bukowski, F.B. Clarke, J.R. Hall, Jr., and S.W. Stiefel, *Fire Risk Assessment Method: Case Study 3, Concealed Combustibles in Hotels,* National Fire Protection Research Foundation, Quincy, MA, 1990.
9. R.W. Bukowski, F.B. Clarke, J.R. Hall, Jr., and S.W. Stiefel, *Fire Risk Assessment Method: Case Study 2, Carpet in Offices,* National Fire Protection Research Foundation, Quincy, MA, 1990.
10. J.R. Hall, Jr., *Special 'Board and Care' Home Analysis,* NFPA Fire Analysis & Research Division, Quincy, MA, 1993.
11. T.Z. Harmathy, "Ten Rules of Fire Endurance Rating," *Fire Technology,* pp. 93–102 (1965).

CHAPTER 6

Measuring Fire Consequences in Economic Terms

G. Ramachandran, Revised by John R. Hall, Jr.

Introduction

In any fire risk analysis or risk-based assessment, valid measurements of the severity of the fire hazard—the consequences of fire, if it occurs—are of paramount importance. Most analyses are limited to simple outcome measures, such as numbers of deaths or injuries or direct property damage, defined as direct harm to property requiring repair or replacement.

Consequences have to be expressed in monetary values if the purpose of the analysis is to permit a decision maker to express and compare all relevant costs and benefits of different choices, in comparable terms that truly capture what is important to the decision maker or the group he or she represents (such as the general public).

The rapidly growing use of performance-based fire protection design is an example in which these advanced methods of consequence measurement are needed at the level of an individual building or product, while the growing number of countries demanding cost-benefit analysis of proposed new national regulations provides an example of the need for these methods of measurement at the level of national policy.

This chapter describes some of the oft-neglected aspects of consequence measurement in support of economic decisions about fire protection engineering choices. Specifically, this chapter offers:

- An overview of the total cost of fire and of efforts to prevent or mitigate fire
- A discussion of how the relevant costs and benefits for the same choices may vary, depending on whether they are analyzed from the point of view of an individual, an organization, or society as a whole
- An overview of the ways in which costs and benefits are treated for insurance purposes
- Methods for translating nonmonetary consequences—notably deaths and injuries—into monetary equivalents for purposes of analysis
- Methods for estimating indirect losses—mainly business interruption costs—caused particularly by large fires
- Utility theory and its role in capturing people's preferences for certainty in outcomes

Principles of life-cycle costing are relevant but are covered at length in this section in Chapter 7, "Engineering Economics." Chapter 7 also provides additional material relevant to many of the subjects covered in this section. A more extensive treatment of the above topics, with a range of examples, can be found in *The Economics of Fire Protection* by G. Ramachandran.[1]

Components of Total National Fire Cost

For more than two decades, the World Fire Statistics Centre (WFSC) has issued periodic studies with comparative statistics from 15–20 countries on the total cost of fire.[2] Their methods are the starting point for most national analyses, including more detailed analyses that have taken place in the United States and Canada.[3] The WFSC methodology tracks deaths and injuries, which are not converted to monetary equivalents, but focuses on four core economic components:

- Damages due to fire, whether reported or unreported (for a fire service database), insured or uninsured (for an insurance database), direct or indirect (where indirect loss includes business interruption losses—also called consequential loss), temporary lodging, missed work, and other costs or lost income associated with recovery from a fire

Dr. G. Ramachandran retired in November 1988 as head of the Operations Research Section at the Fire Research Station, U.K. Since then he has been practicing as a consultant in risk evaluation and insurance. He is a visiting professor at the universities of Manchester and Leeds. His research has focused on statistical and economic problems in fire protection and actuarial techniques in fire insurance.

- Costs of fire-fighting organizations, typically dominated by or limited to the costs of municipal career fire service organizations
- Incremental construction costs for buildings attributable to fire safety requirements or concerns
- Administrative costs of fire insurance, including profits

Table 5-6.1 shows these costs from 1980 through 1997 for the United States.[4] The reports of the World Fire Statistics Centre show comparable figures for many other countries, primarily in Europe but including Japan and Canada. Comparisons are made easier because all loss figures are also shown as percentages of national gross domestic product (GDP). The total U.S. percentage for these core components typically runs about 1 percent of the GDP. The United States tends to have one of the lower percentages for fire damage and fire insurance administration (although the latter is especially hard to calculate and has proven quite volatile from year to year). The United States tends to have one of the higher percentages for costs of fire-fighting organizations and for fire-related costs of building construction (although the latter is a subjective estimate, based on some special studies).

Table 5-6.2 shows the relative importance of the four core components of total cost and how that relative importance has changed over the 18 years studied. The costs of fire-fighting organizations and building construction for fire protection—where the U.S. figures tend to represent one of the higher GDP percentages—are by far the two dominant components of the total cost core, and their dominance has been growing. Not shown in Tables 5-6.1 and 5-6.2 are two other important points. First, in every country except Switzerland providing indirect loss figures, indirect losses tend to be less than 25 percent of direct damages. (The figure for Switzerland is 40 percent.) Second, the U.S. fire death rate, relative to national population, consistently ranks among the highest rates in the countries studied by the World Fire Statistics Centre.

Indirect Loss Estimation—NFPA Approach to U.S. Losses

NFPA did a special study to provide a better basis for calculating indirect loss for properties other than homes. They found that indirect loss varied considerably as a fraction of direct damage, from one type of property to another. Based on their analysis of 109 fires from 1989, indirect losses (principally business interruption costs) add the following amounts to direct loss, based on property class:

- 65 percent for manufacturing and industrial properties
- 25 percent for public assembly, educational, institutional, retail, and office properties
- 10 percent for residential, storage, and special-structure properties
- 0 percent for vehicle and outdoor fires

These percentages may appear low to anyone whose sense of indirect loss is based primarily on a few well-publicized incidents where indirect losses were much larger than direct damages. From a statistical standpoint, however, such incidents are more than offset by the far more numerous incidents where indirect loss is either small or nonexistent.

Table 5-6.1 ***Estimated Core Total Cost of Fire in the United States (in billions of dollars)***

Component of Cost	1980	1981	1982	1983	1984	1985	1986	1987	1988
Economic losses	7.9	8.5	8.1	8.3	8.4	9.1	8.3	8.9	10.5
Reported	6.3	6.7	6.4	6.6	6.7	7.3	6.7	7.2	8.4
Unreported	0.3	0.4	0.3	0.3	0.4	0.4	0.4	0.4	0.4
Indirect	1.3	1.4	1.3	1.4	1.3	1.4	1.2	1.3	1.8
Career fire departments	5.7	6.3	7.0	7.6	8.2	8.5	9.6	10.5	11.8
Net fire insurance	4.1	3.9	4.6	4.8	5.6	4.5	5.0	5.7	4.2
Building construction for fire protection	10.6	11.5	11.6	12.1	14.7	16.9	17.2	17.6	18.4
Total	28.2	30.2	31.3	32.9	36.9	38.9	40.1	42.6	44.9
Component of Cost	1989	1990	1991	1992	1993	1994	1995	1996	1997
Economic losses	11.1	9.6	11.5	10.5	10.5	10.1	11.3	11.5	10.4
Reported	8.7	7.8	9.5	8.3	8.5	8.2	8.9	9.4	8.5
Unreported	0.5	0.4	0.5	0.4	0.5	0.4	0.5	0.5	0.5
Indirect	2.0	1.4	1.5	1.7	1.5	1.5	1.9	1.6	1.5
Career fire departments	11.9	13.2	13.8	14.4	15.4	16.1	17.0	17.7	19.4
Net fire insurance	3.8	4.9	3.1	4.5	4.8	6.7	5.9	6.1	7.0
Building construction for fire protection	20.6	24.0	18.0	17.6	21.1	23.0	24.7	27.4	31.4
Total	47.5	51.7	46.4	47.0	51.8	55.9	58.9	59.0	68.2

Sums may not equal totals because of rounding error. Figures are not adjusted for inflation; they are the figures reported in those years. Some figures for earlier years have been changed from earlier total cost reports to reflect revisions shown in published sources.

Sources: NFPA survey; *Statistical Abstract of the United States*, *Property/Casualty Insurance Facts*, and telephone conversations with their data sources; formulas from special studies.

Table 5-6.2 ***Changes in Components of Core of Total Cost of Fire in the United States, 1980–1997***

Component of Cost	Percent Change 1980–1997	1980 Percent Share	1997 Percent Share
Economic loss	+32	28	16
Career fire departments	+223	20	28
Net fire insurance	+71	14	11
Building construction for fire protection	+181	38	45
Total	+133	100	100
Consumer price index[a]	+95	—	—

[a]In other words, $1.00 in 1980 consumer goods would have cost $1.95 in 1997. The increase in dollars estimated for the core of the total cost of fire is more than the increase due to inflation.

Sums may not equal totals because of rounding error.

Sources: Table 5-6.1; consumer price index data from *U.S. Bureau of the Census, Statistical Abstract of the United States 1999*, Washington, DC (1999).

There remains the problem of quantifying indirect loss associated with properties that never reopen. Here again, the overall pattern is much more modest than some figures that have circulated. Each year, an estimated 2 percent of reported nonresidential structure fires, excluding fires in storage facilities and special structures (e.g., vacant properties, properties under construction, structures that are not buildings), result in business closings. For NFPA's analysis of indirect losses in the United States, a closing is estimated to imply indirect losses equal to four times the reported direct loss in the fire.

These very rough calculations suffice to estimate indirect loss for purposes of a national analysis of total cost from society's point of view. They clearly are not sufficient to produce estimates suitable for insurance purposes or any other decision making at the level of an individual firm. Also, detailed estimates of consequential losses to the national economy should reflect several economic factors, including level of employment or unemployment, level of capacity utilization, volume of exports and imports, exchange rates, and performance of national and international competitors. Due to the interactions of these factors, a detailed evaluation of consequential losses to the national economy is a complex problem requiring the application of econometric models, such as input-output analysis. These national factors do not apply to analysis at the level of an individual firm.

The effects of a fire on the earning capacity of a firm can be measured in terms of loss of profits during the period of interruption following the damage until the resumption of the activity in which the firm was engaged before the fire. Loss of profits is usually expressed as a percentage of loss of turnover. A cover against this loss can be obtained by purchasing a consequential loss insurance policy, the premium for which is a function of the period of indemnity. Loss of profits sustained by a supplier or customer of the firm that suffered the fire (called the "fire-hit firm" from here on) can be covered by a normal consequential loss policy based on reduction in turnover.

The form of insurance policy in more general use in the United States is known as business interruption insurance (BII). BII operates on lines similar to the United Kingdom's contract of consequential loss insurance (CLI) with a turnover specification, though there are some differences. For private sector level insurance firms transacting BII or CLI, there are useful sources of data for estimating consequential losses due to fires in industrial and commercial premises. Organizations such as the Insurance Information Institute in the United States compile consequential loss data furnished by major insurance firms.

Indirect Loss Estimation—Unpublished U.K. Study

Returning to national- and society-level analyses of indirect or consequential loss, some now-old studies done in the United Kingdom illustrate how a more detailed analysis can be done. The U.K. government's Home Office carried out two research studies between 1970 and 1980 on consequential losses to the national economy. The first study adopted an input-output-type model in which all losses were considered output losses.[5] Losses were either (1) losses in the type of output actually hit by fire or (2) losses in some other output, because production factors (e.g., fixed assets, entrepreneurial effort, or labor) have been less effectively employed as a result of the fire. The effects of a fire were assumed to have the most impact on the fire-hit firm, the supplying firm, the purchasing firm, the parallel firm, and the rest of the economy. A fire-hit firm was defined as a compartment of production covering just that type of output that had been hit by a fire and no other output. A parallel firm was defined as the compartment of a firm that produced in parallel to the fire-hit compartment (which might be in the same firm or in another firm). Any effects in a parallel firm or somewhere else in the rest of the economy were assumed to be included in the calculation of the effects in a fire-hit firm, in a supplying firm, or in a purchasing firm.

In this Home Office study, consequential losses were measured by the net present values of streams of annual outputs lost by the fire-hit firm, supplying firms, and purchasing firms. In regard to the fire-hit firm, it was necessary to determine a length of time over which fixed assets destroyed by fire were assumed not to be replaced by extra investment in the economy. This time choice had to depend on a view of the future course of the economy, which depended on unknown events and influences. Hence, alternative calculations were produced that were based on the remaining lives of the assets and on a number of shorter periods. The net present values were corrected for offsetting influences within the fire-hit firm, supplying firms, and purchasing firms. These influences were due to two factors. First, some production factors affected by fire might be used elsewhere in the economy. Second, production factors already employed elsewhere might be used more intensively. The extent to which such offsetting influences would operate would depend largely on the level of employment and the pressure of demand in the economy. Separate calculations were made for three alternative cases—slack, middle, and tight conditions in the economy. Results were given for each of 15

industries, including a factor by which a fixed assets valuation should be multiplied to give the sum of all the corrected output losses.

In order to verify the assumptions employed and results obtained in the study mentioned above, the Home Office commissioned field research aimed at an in-depth investigation of a small sample of fires.[6] This study involved direct contact with fire-hit firms and concentrated on direct, consequential, and, hence, the total loss to the U.K. economy from industrial, distributive, and service sector fires. Consequential losses were considered to arise from loss of exports, extra imports, the diversion of resources from other productive activities, and reduction in the efficiency of resource use following the fire. The study assumed that there was full-capacity utilization of resources and that market values of the resources reflected their true worth. Insurance estimates of losses were used as measures of the assets destroyed in fires. By application of national capital output ratios, these asset losses were translated into losses of output from fire. Allowances were made for the secondary impact on suppliers and customers of fire-hit firms and for the impact of the level of capacity utilization. A correction factor was applied to account for the ability of the economy to "make good" the losses of the fire-hit firm by other firms.

The analysis produced estimates of the ratios of consequential to direct losses to the economy for "off-peak" and "peak" years and for each industry and service sector. The main conclusion was that most fires, except those in chemical and allied industries, produced no consequential losses to the national economy. Only in one sector (chemicals) was evidence found of a statistical link between consequential losses and direct losses. The study failed to estimate this link for other sectors and a number of other possible effects on consequential losses. Note the similarity of this conclusion to the results of the much smaller, rougher, and more recent NFPA study, leading to the indirect loss parameters still used in the United States.

Indirect Loss Estimation—Private Sector Level

A study by Hicks and Liebermann deals with costs and losses from the community and private perspective as they impact the fire victim.[7] The property class categories addressed in this study were commercial occupancies only, separated into four types: (1) mercantile, (2) nonmanufacturing, (3) manufacturing, and (4) warehouses. The authors considered first the following expression, based on a convenient formulation of the Cobb-Douglas production function:[8]

$$IL = ke^{rT}E^{a}X^{1-a} \tag{1}$$

where

IL = indirect loss
k = constant
r, a = regression coefficients
E = expenditure for fire protection (–)
X = number of fires (+)
T = time (surrogate for technological advance) (–)

The signs in parentheses relate to the expected values of the coefficients for the independent variables. The term ke^{rT} is a scalar factor in which r measures increases in fire department efficiency due to technological advances in suppression equipment, training, or facilities as well as altered building codes, smoke alarms, and the like. Equation 1 can be converted to a multiple-regression model by taking logarithms of terms on both sides.

In principle, the parameters r and a can be estimated but, in practice, sufficiently detailed statistics typically are not available. The authors therefore adopted the following, much more simplified, form:

$$IL = c(DL)^{b} \tag{2}$$

where DL is the direct loss and c and b are constants. Equation 2 is based on the assumption that very small fires typically generate small indirect losses while large fires produce larger indirect losses. If $b = 1$, this model reduces to the earlier-cited approach used by NFPA, wherein indirect losses are estimated as proportional to direct damages.

The results obtained by Hicks and Liebermann[6] are given in Table 5-6.3. Note that all values of the parameter b are near 1, which means the deviations from the even simpler model used by NFPA are modest. Statistical tests of significance showed that the regression model fitted well with the data in all the cases except warehouses. Since nationally aggregated data were utilized, it was recommended that the occupancy-specific models be used only at the national level and that any desired analysis of local impacts be accomplished using a local model. The value of parameter b has been estimated to be greater than unity for local and national levels and less than unity for the occupancy levels. For any increase in direct loss, the ratio of indirect to direct loss would increase if $b > 1$, and decrease if $b < 1$. The ratio would be a constant if $b = 1$. From the information given in the study, it was not possible to test whether the value of b was significantly different from unity for any of the six levels.

Indirect Loss—Illustrations from Some Major U.S. Fires

It is not difficult to identify large, well-publicized fires in which the cost of business interruption far exceeds di-

Table 5-6.3 ***Relationship between Direct and Indirect Fire Loss Model Parameters[7]***

	Parameters (from Equation 2)	
Level	c	b
Local	0.203	1.146
National	0.015	1.245
Mercantile	0.109	0.889
Nonmanufacturing	0.069	0.874
Manufacturing	0.135	0.890
Warehouse	0.047	0.804

rect property loss. One type of fire where this can happen involves a property that offers lodging or workspace and suffers so much damage that the slack capacity of the facility or even the community is not sufficient to absorb the displaced demand. An example is the MGM Grand Hotel fire, where the hotel claimed total direct damage and business interruption costs of $211 million, while NFPA's best information placed direct damage at $30–50 million.[9]

Sometimes, though, it can be difficult to determine what the true net loss due to business interruption is—what constitutes an "interruption." Compare two large high-rise office building fires.[10,11] Fire destroyed four floors of the 62-story First Interstate Bank building in Los Angeles in 1988 but also took the entire building out of service for six months—a true business interruption, because the property reopened after repairs.

By contrast, the 1991 One Meridian Plaza fire destroyed more floors in a shorter high-rise office building (38 stories) and the building never reopened. The dozens of firms, occupying nearly a million square feet of office space, had to seek new permanent homes, but the real estate community estimated, a year after the fire, that vacancy rates would still be 11–12 percent *after* every displaced firm had been absorbed.

One Meridian Plaza represented an estimated 2.5 percent of Philadelphia's office space, while the MGM Grand represented a larger share of Las Vegas area hotel rooms. These are all factors in determining how easily a market can compensate for interruption of capacity from one provider. Similar concerns arise for fires in any type of large multiunit residential or health care occupancy.

The most clear-cut examples of widespread vulnerability involve critical elements of the nation's infrastructure. Fears of great damage from a widely distributed computer virus have so far not materialized, and two major interruptions to the northeast electrical power grid in the last third of the twentieth century were not due to fire. However, there have been two fire examples involving telephone exchanges, the more recent in Hinsdale, Illinois, in 1988.[12]

A total of 38,000 customers were served by the Hinsdale office. The majority were still without service five days after the fire, and some did not regain service until nine days after the fire. An estimated 9000 businesses were affected, including a nationwide hotel chain's reservation service, a florist delivery service networked to 12,500 florists around the country, and communications between a Federal Aviation Administration control tower and both of Chicago's major commercial airports. The most conservative estimate of the costs of the associated delays and lost business would exceed the estimated $40–60 million in direct damage.

Economic Costs Not Usually Calculated within the Core

Several cost components have been estimated by Meade but cannot be readily estimated each year.[3] They totaled $27.8 billion in 1991 and consist of the following:

- Costs of meeting fire grade standards in the manufacture of equipment, particularly electrical systems equipment and "smart" equipment with its greater use of computer components ($18.0 billion)
- Costs of fire maintenance, defined to include system maintenance, industrial fire brigades, and training programs for occupational fire protection and fire safety ($6.5 billion)
- Costs of fire retardants and all product testing associated with design for fire safety ($2.5 billion)
- Costs of disaster recovery plans and backups ($0.6 billion)
- Costs of volunteer and paid activities involved in preparing and maintaining codes and standards ($0.2 billion)

The largest piece by far is the first one. Meade's study developed estimates, by industry, firm, or individual making the estimate, that ranged over two orders of magnitude, from 20 to 2000 percent add-on cost. He settled on 30 percent, which seems conservative. However, out of the fraction of equipment that could be affected by these costs, his estimate of the share that is built to these more demanding standards is not conservative. His estimate raises the concern that the fire safety spending habits of industry's most fire-conscious companies have been treated as typical of all industry.

Based on the Consumer Price Index, the $27.8 billion estimated by Meade for 1991 would translate to $32.8 billion in 1997 in the United States.

Costs and Benefits Based on Level

The previous discussion noted that the calculation of indirect loss is done differently if the focus is on an individual firm or on the entire society. Any calculation of costs and benefits associated with fire, fire prevention, or mitigation activities and decisions will show differences based on level, because costs and benefits do not fall equally on all parties.

A fire that interrupts or destroys the ability of a single firm to offer its goods or services to the market results in devastating indirect loss to that firm. Society, however, may experience no discernable effect, provided that

1. The firm represents a small part of its industry, so that neither price nor availability for its products or services is affected by the removal of the firm.
2. The firm represents a small part of the employment opportunities in its community, so that its employees are able to find comparable work and income quickly and easily.

Conversely, a fire that results in little on-site damage but creates devastating environmental damage on the surrounding area, through air or water pollution, may represent a negligible cost to the firm, provided it is able to disown the off-site costs and pay minimal legal costs to do so. Meanwhile, the cost to society is enormous.

The second example cited above involved direct damage to property, and its central premise—that the firm could disavow off-site damages if they were sufficiently difficult to measure and to trace to an event on the firm's site—is probably far-fetched in today's world. The

first example cited above involved a major type of indirect loss, sometimes called business interruption loss or consequential loss, and that example is not at all unusual.

Analysis can be done at many different levels—the individual person, the individual firm, the individual community, the individual industry, the individual state or province, the individual industry plus all industries strongly dependent on it, the individual nation, the entire world—but for purposes of analyzing business interruption or consequential loss, it may be useful to focus on two major levels of economic activity. These are (1) private sector and community level and (2) national and societal level. The first level includes the fire-hit firm and the firms supplying to or purchasing from the fire-hit firm's materials, components, or services. Costs associated with moving, temporary accommodation, and lost profits are valid costs at the private sector level but not at the national level.

At the national level, the loss of a specific unit of productive capacity may be spread among the remaining capacity in the nation such that competitors may seize the opportunity to enter the market and maintain the national rate and volume of manufacture. In such cases, there may be little or no incremental loss to the national economy as a result of a fire in the premises of, for example, a manufacturing firm. Several studies by the now-defunct Insurance Technical Bureau (ITB) in the United Kingdom provide an indication of the various special factors one should consider in the evaluation of consequential losses due to fires and other hazards.

A small number of the total number of production lines in a plant manufacturing pharmaceutical products may generate a very large proportion of total gross profits.[13] Regulatory restrictions may limit possibilities for shifting manufacture to other plants or even to other lines in the same plant. Natural raw materials may be irreplaceable or out of season, creating another source of delay in recovery or another obstacle to meeting demand during the recovery process. Specialized plant equipment (e.g., tailor-made driers or centrifuges) may involve long delays for replacement. Loss of laboratory facilities may seriously interrupt testing and quality control programs.

The aerospace industry is another example where innovation driven by research creates a very short cycle time for the introduction of new products. In such cases there may be little redundancy in the supply of prototypes or other essential elements needed to keep the program on schedule.[14] Examples might include a new aircraft prototype assembly, untried or unproven research and development projects, or specimens for fatigue testing of aircraft structures. Loss of any of the above could result in a significant interruption to the program. In addition, the effect of delays in the development or supply of components or assemblies from specialist equipment manufacturers can be serious. The interactions of the many activities and firms involved in the manufacture of aerospace products makes for involved consequential loss considerations.

An example from the other end of the spectrum of industries would be resin, paint, and ink manufacture, which would not normally be expected to give rise to unduly high consequential loss.[15] Facilities are generally dispersed in small units throughout a given country, and there may be sufficient manufacturing capacity to absorb temporary loss at individual sites. Also few, if any, products are so special that they cannot be made elsewhere in the industry. Consequential loss, therefore, hinges primarily on the time for reinstatement of the plant and the ability of management to arrange for the supply of goods from other sources, pending a return to full production. Loss of raw materials or finished goods normally results in relatively short interruption periods. However, longer periods may be required for the replacement of tanks and pumps destroyed by fires, and for other hazards, such as explosion.

Due to high investment costs, specialized equipment (e.g., electronically or computer-controlled equipment) is generally used at full capacity in some industrial processes. Continuous operation of these processes may reduce the chance of a fire spreading, but provides no scope for making up for lost production following a fire. Specialized equipment, if damaged by fire, cannot be replaced easily or quickly, since either they or spare parts for them may have to be imported. Industries using such equipment are liable to sustain high consequential losses.

Measurement Approaches in the Insurance Industry

Statistical (actuarial) techniques are well developed for calculating the insurance premium for loss of profits due to fire. (For example, see Benckert.[16])

The risk premium is a function of the period of indemnity, and is generally expressed as the product of the loss frequency and the mean amount of loss. The loss frequency is assumed to be independent of the period of indemnity. The frequency function of the period of interruption following a fire has a log-normal distribution.[16,17]

An insurance company generally adds two types of loading to the risk premium to calculate the premium payable by a policyholder. First, a safety loading is added toward chance fluctuations of loss beyond the expected loss. Second, another loading is imposed to cover the insurer's operating costs, which include profits, taxes, and other administrative expenses. A number of texts have been published on different types of insurance and claims concerned with consequential losses. (For example, see Riley.[18])

Monetary Equivalents for Nonmonetary Costs and Consequences

Deaths and Injuries

Damage to life or health in terms of injuries and deaths is an important consequence in fire risk assessment and is usually the first priority consequence cited in national codes or regulations. Its importance is not in question. What is difficult is identifying a valid and acceptable method for estimating and comparing monetary equivalents of consequences of this type with costs and with monetary equivalents of consequences of other

types, such as property damage or indirect/consequential loss.

Insurance claims provide some data for the valuation of injury, though they are likely to be limited to costs mediated by the marketplace, such as treatment costs and the value of work time lost. Other costs, such as pain and suffering, are more difficult to evaluate.

The specification of a dollar equivalent for human losses, particularly for loss of life, remains an extremely controversial subject. It is important to emphasize that no one intends to suggest that there is an acceptable price for losing one's life. Rather, these figures are intended to reflect a social consensus on the value of changes in the risk of death by fire. For example, if most people say they would be willing to pay $1500 to reduce their lifetime risk of dying in a fire from, say, one chance in 500 to one chance in 1000, then a simple way of restating that is that people value a life saved at $1500 for 1/1000 of a life, or $1.5 million per life.

Four approaches to valuing human life have been identified. The first method is concerned with gross output based on goods and services that a person can produce if not deprived, by death, of the opportunity to do so. Sometimes gross productivity is reduced by an amount representing consumption (net output). Discounted values are generally taken to allow for the lag with which the production or consumption occurs. The output approach usually gives a small value for life, especially if discounted consumption is deducted from discounted production. This must be so since the community as a whole consumes most of what it produces. It is argued that when a person dies, although the community loses that person's future output, it also saves concurrent future consumption. The person's own consumption or the utility that would be derived if the person were alive is not counted as a loss. This approach received considerable emphasis, say, 30 years ago, but not today. A variation of this approach is called the "livelihood approach."[19]

The second approach assumes that if an individual has a life insurance policy for x £, then he or she implicitly values his or her life at x £. Collection of necessary data from insurance companies is not a difficult task, and this is the major advantage in adopting the insurance method. There are, however, two drawbacks to this method. First, a decision whether or not to purchase insurance and the amount of insurance is not necessarily made in a manner consistent with one's best judgment of the value of his or her life. This decision depends largely on the premium the insured can bear from his or her income, taking into account family expenditures. Second, purchasing an insurance policy does not affect the mortality risk to an individual. This action is not intended to compensate fully for death or to reduce the risk of accidental death. Hence in insuring life it is not exactly a value tradeoff that is considered between mortality risks and costs.

The third method for assessing value of life involves court awards to heirs of a deceased person as restitution from a party felt to be responsible for the fatality. Here again, collection of necessary data is not a problem. Assessment of values of life could also be expected to be reasonably accurate since lawyers and judges have a massive professional expertise in the ex post analysis of accidents. The object of such an analysis is to discover whether the risk could have been reasonably foreseen and whether the risk was justified or unreasonable.

There are, however, a few problems in using court awards for valuing human life. The court should ideally be concerned with the assessment of suitable sums as compensation for an objective loss (e.g., loss of earnings of the deceased) as well as for a subjective loss (e.g., damages to spouse and children for their bereavement and grief). In some countries damages can include a subjective component for pain and suffering of survivors, but certain courts are generally against such compensation for subjective losses to persons who are not themselves physically injured, believing that bereavement and grief are not losses which deserve substantial compensation. It is also difficult to value the quality of a life that has been lost. People who themselves suffer severe personal injury, of course, qualify for substantial damages for subjective losses. Resource costs such as medical and hospital expenses are significantly higher for obvious reasons in serious injury cases than in fatal cases; hence, awards for subjective losses tend to be much larger and more important in serious nonfatal cases than in fatal cases. Some courts have also limited to very low levels the damages that may be awarded for reductions of life expectancy. Last, in court awards risks to individuals are considered relative to the plaintiff and costs to the defendant. However, value judgments are likely to vary according to whether the individuals making these judgments are associated with the plaintiff, the defendant, or the court.

The fourth approach is the one most widely adopted for valuing life. The willingness to pay is based on the money people are willing to spend to increase their safety or reduce a particular mortality risk.[20,21] It is difficult to differentiate between the benefit from increasing people's feeling of safety and that from reducing the number of deaths. Anxiety is a disbenefit even if the risk is much smaller than believed. Likewise, if a person dies from something of whose risk he or she is unaware, he or she still suffers a loss.

This approach to value of life rests on the principle that living is a generally enjoyable activity for which people would be willing to sacrifice other activities, such as consumption. The implied value of life revealed by a willingness-to-pay criterion would depend on a number of factors. The acceptable expenditure per life saved for involuntary risks is likely to be higher than the acceptable expenditure for voluntary risks, as people are generally less willing to accept involuntarily the same level of risk they will accept voluntarily. The sum people are prepared to pay to reduce a given risk will also depend on the total level of risk, the amount already being spent on safety, and the earnings of the individuals.

The theoretical superiority of the willingness-to-pay method begins with its connection to the principle of consumer sovereignty, which says goods should be valued according to the value individuals put on them. Despite this individual-oriented underpinning, this approach can also be used to develop a general figure for a typical person, based on consensus patterns in the values individuals select. This, in turn, permits analysis of societal decisions using the willingness-to-pay principle.

Surveys have shown variability and inconsistencies in responses, because individuals have difficulty in answering questions involving very small changes in their mortality risks.[22,23,24] Due to insufficient knowledge about the risk, most people find it difficult to accurately quantify the magnitude of a risk. Also, the benefits are often intangible (e.g., enjoyment, peace of mind). It is difficult to put a monetary value on these factors.

Economists therefore use a variety of inferential methods to develop value of life and value of injury averted estimates for purposes of analysis. These include examination of patterns from the other three approaches—foregone future earnings, insurance policy amounts, and especially court judgments. It is also possible to develop an inferred value of life risk reduction from any action that has a cost and achieves such a reduction. Studies have been done of the implied value of life associated with hundreds of safety- and health-related regulatory actions. Studies could be done based on the price and demand curves for safety-oriented products, such as smoke alarms and child-resistant lighters.

It is useful to keep in mind the very wide variation in the estimates and valuations and the implied uncertainty as to what values are reasonable. For example, a landmark 1981 study cited sources for values of statistical life ranging from $50,000 to $8 million.[25] More recent valuations have been higher generally but still vary widely.

Economists at the U.S. Consumer Product Safety Commission have an ongoing program of studies of injury costs. Periodically, they review the literature, including their own studies, and select dollar values for use in policy analysis of fire safety and other product hazard analysis. The NFPA studies of the total cost of fire in the United States use values of $5 million per death and $166,000 per injury as 1993 values, then use the Consumer Price Index to calculate corresponding values for later years *for injuries only,* all in accordance with the practices of CPSC economists.

The total dollar equivalent for reported and unreported fire deaths and injuries in the United States, calculated in this way, was $42.5 billion in 1997.[4]

It is beyond the scope of this chapter or this handbook to review, even briefly, the many nuances, methods, and applications of value of life estimation. For those who wish to pursue the subject in more detail, several listed references are recommended.[26–33]

The Value of Donated Time

In the United States, the largest block of donated time for fire safety consists of the donated time of the roughly 800,000 volunteer fire fighters, who provide municipal fire protection to a sizeable fraction, mostly rural, of the U.S. population. One approach to valuing their donated time is to assume that costs are generated primarily by the workload of responding to fires. (This means assuming fire fighting and response and return involve many more total person-hours for volunteers than do training, maintenance, inspections, fire prevention, etc.)

Fire departments that are (all or mostly) volunteer protect 43 percent of the population, but it is a mostly rural population with a much higher fire rate per capita.[34] Therefore, volunteers respond to the majority of fires. After further allowing for the fact that the U.S. Census Bureau figures for expenditures on local fire protection include nonpersonnel expenditures by both career and volunteer fire departments—which are typically about 13 percent of a career department's total budget—the estimated dollar equivalent for donated volunteer fire fighter time would be roughly the same as the total reported expenditures for local fire protection. (This includes career personnel and nonpersonnel costs for career and volunteer fire departments.)*

This approach ignores services such as response to nonfire emergencies (e.g., medical aid, hazardous materials spill), fire prevention programs, code enforcement and inspection activity, and the like, all of which are more often provided by career than by volunteer fire departments. These services may contribute to costs. Also, this approach ignores differences that may affect the cost of servicing fires, such as special hazards (e.g., large industrial plants, high-rise buildings) that not only require more resources for suppression if fire occurs but also require more equipment and more training to prepare for fires. This approach ignores differences in pay scales and work weeks, which affect the cost of running a fire department. It is not clear whether these factors would tend to raise or lower the average cost of a volunteer fire department that found it had to pay for the time it had previously been given free.

A second approach to valuing time is to assume that costs are generated not so much by the workload of emergencies as by the need to provide coverage and readiness to respond for a certain area, that is, the ability to provide an effective response in a certain response time. If this approach is used, the primary factor in costs would not be workload, but geographical area. The low-density rural areas covered by volunteer fire departments would then require more personnel than would more compact areas of equal population covered by career fire departments.

Communities seeking to set such fire protection coverage at an appropriate level might begin with a response time objective. The part of response time that is most related to resource decisions is travel time, which may be treated as proportional to travel distance. If one thinks of a typical response area as a circle with the fire station in the middle, one can see that travel distance is proportional to the square root of area. For example, if the distance from the fire station to the edge of the response area doubles, that is equivalent to doubling the radius of a circle, whose area then is quadrupled. This also means that if the same population is spread out over an area four times as large, it will need twice as many fire stations to provide equivalent travel times, which means the needed

*Since 1986, the International City Management Association's annual *Municipal Year Book* has included figures on average per capita expenditures on personnel, capital, and other items for municipal fire departments. The sum of these three components is always higher than the indicated total, possibly because of problems with incomplete responses on the survey. Based on comparing the personnel cost to the sum, the personnel share is usually 87 percent, so the rest is usually 13 percent.

number of fire fighters may be treated as inversely proportional to the square root of the population density.

In 1996, the metropolitan statistical areas of the United States had 79.9 percent of U.S. population in 19.9 percent of the area. If one assigns all the remaining area and population to volunteers (which is a rough approximation), then the metropolitan population density (proportional to 79.9 percent divided by 19.9 percent) exceeds the nonmetropolitan population density (proportional to 20.1 percent divided by 80.1 percent) by a factor of 16. The square root is 4.0, which is not too far from the actual ratio in fire fighters (3 : 1 in 1996). (If the figures were more properly adjusted to address career versus volunteer communities and to exclude areas under federal or state jurisdiction, the 4.0 ratio would fall and be even closer to the three-to-one ratio of fire fighters.)

Using the three-to-one to four-to-one ratios for personnel needed, assuming their costs would be the same as in career fire departments, and again adjusting for nonpersonnel costs included in reported local fire expenditures, the result is a range of $48–64 billion in 1997 for the value of time donated by volunteer fire fighters.

If this estimate of the value of donated time by volunteer fire fighters is combined with the earlier estimates of the core components of total cost of fire, the other economic components estimated from data that is not updated yearly, and the estimated monetary equivalent of deaths and injuries associated with fire, the resulting total is $160 to $206 billion for the United States in 1997. This is 2–3 percent of the total U.S. gross domestic product, a figure that fully justifies appeals from the fire protection engineering community for more support for research into ways of reducing the total, either through improved safety or through sustained safety at reduced cost.

Utility Theory

Even after all costs and benefits (e.g., risk reduction) have been converted to monetary equivalents, an important aspect of people's preferences may be overlooked if expected-value techniques are used directly in a cost-benefit analysis of fire safety measures to include the certainty-equivalent of uncertain costs and benefits.

Suppose a person is offered a choice between $5 or a 50/50 coin toss wager between $10 and nothing. The expected values of the two choices are equal, assuming a fair coin. A person who prefers the sure thing is called *risk averse.* Most people are somewhat risk averse in some situations. Just how risk averse a person is can be measured by determining how low the sure-thing offer can be set before the person will choose the wager with the $5 expected value.

Fire loss is never a sure thing, and so people's risk preferences are always relevant to assessing their preferences for choices involving fire risk.

People differ not only in their degree of risk aversion but also as a function of the type of choice being offered. Some people may prefer to take risks in most situations. It also is not unusual to find that a person is a *risk preferer* for ventures involving small losses but a *risk avoider* for those involving large values.

Any pattern of risk preferences can be quantified by the use of *utility functions. Disutility,* the negative counterpart of utility, is the appropriate term in an analysis involving negative outcomes such as fire loss, cost of fire protection, and insurance premiums.

Consider a few more examples based on participation in a game of chance. Suppose a person is offered the following bet on toss of a coin—to win $100 if the coin comes up heads, and lose $75 if the coin comes up tails. If the coin is a fair coin, the probability of heads or tails coming up is one-half. The expected payoff is

$$\frac{1}{2}(\$100) + \frac{1}{2}(-\$75) = \$12.5$$

if the person playing the game takes the bet and $0 if he or she does not take the bet. According to the expected value criterion, the bet should be accepted because its expected value is greater than the expected value of not taking the bet.

Now suppose the amounts involved are $1,000,000 and $750,000 rather than $100 and $75. The expected payoff is now $125,000 if the bet is taken and $0 if the bet is not taken. Every value has been multiplied by 10,000. According to the expected value criterion, the bet should still be taken and is even more attractive. But would you take this bet? Probably not, unless you are wealthy enough that you could afford to lose $750,000. The possible gain of $1,000,000 is tempting, but losing could be devastating or even intolerable.

As another example, consider a choice between two bets. In the first bet, the person playing the game wins $2 million if a coin comes up heads and wins $1 million if the coin comes up tails. In the second bet $8 million can be won if the coin comes up heads, but nothing will be won if the coin comes up tails. The expected payoffs of the two bets are $1.5 and $4 million, respectively. The second bet has a much larger expected payoff than the first, and hence should be chosen on the basis of the expected value criterion. However, many would choose the first bet because they focus on the larger minimum gain—the closest thing to the "sure thing" in a choice between two bets. With the first bet, you are assured of at least $1 million. With the second bet, there is a 50 percent chance of winning nothing.

Consider a third example, defined more directly in terms of fire safety. Suppose the owner of a home or other building faces a probability, p, of fire occurring in the coming year and a loss, L, in the event of a fire. (In this simplified example, only one kind and severity of fire is possible.) The expected annual loss due to fire in that building is pL, and it is a two-outcome bet, like a coin toss.

The sure-thing alternative, from the owner's point of view, can be achieved through insurance. The property owner has two options—to insure or not insure the building. The expected loss (cost) is equal to the insurance premium (call it I) if insured, and pL if not insured.

On the basis of the expected value principle, the owner should choose the insurance option only if I is less than pL. This condition will never be satisfied since an insurance firm would determine the premium, I, for a risk category by adding to the risk premium, pL, two loadings—a safety loading and another loading to cover

the operating costs of the firm which include profits, taxes, and other administrative expenses. From the insurance company's point of view, it should offer the insurance only if I is greater than pL. How is it that insurance even exists under these conditions?

The risk aversion of most people provides the foundation for breaking this dilemma. Based on risk aversion, the building owner will accept a sure-thing loss of I even if I is greater than pL. The difference is typically large enough not only to make a mutually acceptable deal possible, but to allow I to be large enough to cover the two loadings mentioned above.

In practice, many different sizes and severities of fire are possible. For the smallest fires, the building owner's risk aversion will probably be much less pronounced, and insurance may seem unattractive. The creation of a deductible threshold solves that problem by allowing the insurance to be limited to losses large enough for the owner's risk aversion to be strong. If a very large fire occurs, the insurance company may be unable to cover the loss. This leads to reinsurance markets, particularly for properties with the potential for more than one very large loss in a short period of time. For smaller losses, the safety loadings on the risk premium would provide a safety margin for the insurance company, depending on its calculations of the probability distribution for the fire loss. There may also be an upper bound set on the maximum loss the insurance company can cover.

The preference for a small fixed loss over a risk of large loss originates primarily from an aversion to the psychological state of uncertainty. For the reasons mentioned previously, the expected monetary value is not a satisfactory criterion for decisions involving potential losses in ranges where risk aversion is an issue for many people. Note that the ranges of risk aversion can depend on the size of the decision maker's resource base—how large a loss can be sustained at all, and how large a loss can be absorbed without serious inconvenience or harm—and on the number of "bets" undertaken. An insurance purchaser has one bet (at least one per year) going, so he or she is exposed to the full uncertainty of the risk. An insurance company with many customers has many bets going, so the company's annual loss experience will fit a much narrower range around the expected value, except in certain circumstances. If many customers are exposed to a common risk, such as will happen if many customers live in the same hurricane-prone region, the range of probable outcomes for the insurance company will be much wider. If the insurance company's evaluation of the probabilities and consequences is seriously deficient or simply outdated, then its exposure may be quite different than it believes.

Utility and Disutility

For positive outcomes (gains), *utility* means a measurement scale for desirability.[35] It is a number measuring the attractiveness of a consequence—the higher the utility, the more desirable the consequence. A utility function translates monetary consequences into a scale for which expected-value calculations accurately reflect the preferences of an individual, a firm, or a decision maker. For negative outcomes (losses and costs), *disutility* is a measurement scale for undesirability—the higher the disutility, the less desirable the consequence.

The examples given earlier illustrate the fact that, for a specific person, firm, or decision-making entity, the value of gaining x dollars (or consequence of losing x dollars) is not necessarily x multiplied by the value of gaining a single dollar (or consequence of losing a single dollar). Issues of certainty and of the ability to accept loss can cause substantial deviations from the simple multiplicative relationship.

If it were possible to measure the true relative values to the decision maker of the various possible payoffs in a problem of decision making under uncertainty, expected values could be calculated in terms of these true values instead of the monetary values. The theory of utility seeks to develop such values, permitting choices to be analyzed using the decision-making rule—the maximization of expected utility or minimization of expected disutility. Utility theory provides a means of encoding risk preferences in such a way that the risky venture with the highest expected utility or lowest expected disutility is preferred. Symbolically, if the monetary value of the ith outcome is X_i, the utility corresponding to a gain X_i is $U(X_i)$; the disutility corresponding to a loss X_i may be denoted by $D(X_i)$.

Utility Functions

The mathematical structure of the function $U(X)$ is central to the application of utility theory. Figure 5-6.1 graphically shows three typical utility functions that are usually encountered in this analysis.[36] The utility function represented by the straight line A is appropriate for a decision maker operating on an expected monetary value (EMV) basis. This line satisfies the equation $U(X) = X$ and represents risk neutrality. The concave curve B corresponds to a risk-averse (or risk-avoiding) decision maker, and the convex curve C to a risk-prone (or risk-taking) decision maker. For a decision maker who is more risk prone than the EMV individual or who prefers a risk, the utility of a fair game exceeds the utility of not gambling and hence a fair game will always be played. On the other hand a decision maker who is more risk averse than the EMV person is does not like or cannot afford risks and is a risk avoider.

Some individuals could have a sigmoid form of utility function as illustrated by Figure 5-6.2. Such a person is a risk preferer for small values of X but a risk avoider for larger values.

Consider now a game with a 50 percent chance of winning £100 and a 50 percent chance of winning nothing, which has the expected value £50. The expected value line A in Figure 5-6.1 connects the points [0, $u(0)$] and [100, $u(100)$]. To find the utility of the game for the risk avoider (curve B), find the utility value corresponding to the point on the straight line above the expected £50 value of the game. By reading to the left, cutting curve B, this value is equal to U(£20) so that the decision maker's cash equivalent (CE) for the game is £20. He or she would be willing to pay up to £20 to be able to participate in the game. This is still below the EMV of £50 since the utility function B is that of a risk avoider.

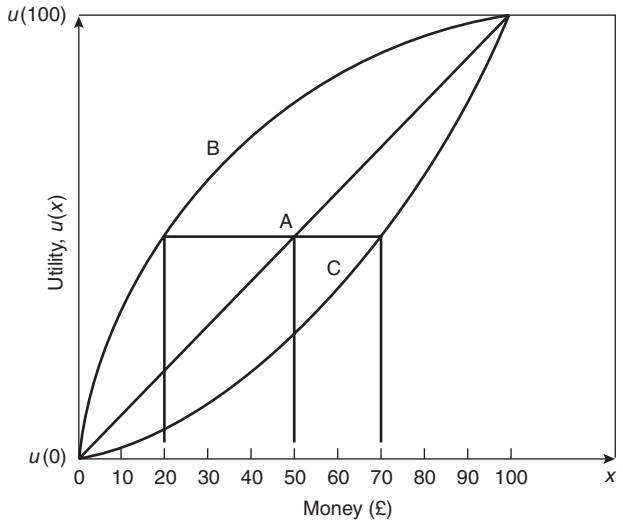

Figure 5-6.1. ***Typical utility functions.***

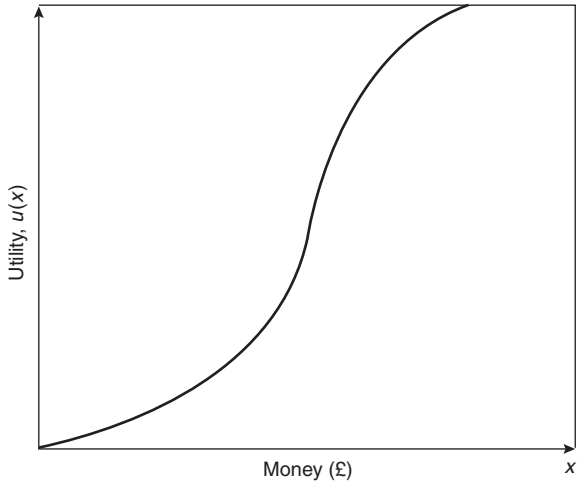

Figure 5-6.2. ***Sigmoid utility function.***

The difference between the EMV and CE is the *risk premium,* which is £30 in this example. The decision maker would be willing to pay £30 to avoid the risk involved in participating in the game.

In the case of the risk taker denoted by curve *C*, the utility of the game is equal to *U*(£70), so £70 is the cash equivalent for the game. Although the expected value is only £50, the risk taker is willing to pay up to £70 to be able to participate in the game. Hence the risk premium is –£20. It is negative because the decision maker, instead of being willing to pay a premium to avoid the risk in the game, is willing to pay a premium (above and beyond the expected value) to be able to participate in the game.

The risk premium, RP, discussed above is the amount which a decision maker, on the basis of his or her utility function, is willing to pay to avoid or participate in a risky activity. For increasing utility functions such as those shown in Figure 5-6.1, the risk premium for any risky venture is defined as

$$\mathrm{RP} = \mathrm{EMV} - \mathrm{CE}\; dx \tag{3}$$

where EMV is the expected monetary value and CE the cash equivalent. The parameter CE is also referred to as *certainty monetary equivalent,* CME, in the literature on utility theory.[37]

For a risk avoider whose increasing utility function is concave, the risk premium RP given by Equation 3, for any situation in which the outcome is uncertain, is positive (EMV is greater than CE). For a risk taker whose increasing utility function is convex, RP is negative. For a risk neutral person whose utility function is linear, RP is always zero (EMV = CE).

The CE is defined mathematically as

$$U(\mathrm{CE}) = E[U(x)] = \overline{U} \tag{4}$$

where the right-hand side is the expected value of the utility over the range of values taken by x. If $x_1, x_2, \ldots, x_n$ are the values (consequences) with probabilities $p_1, p_2, \ldots, p_n$

$$\overline{U} = E[U(x)] = \sum_{i=1}^{n} p_i U(x_i) \tag{5}$$

If x is a continuous variable with probability density function $h(x)$, the expected utility is given by

$$\overline{U} = \int_x U(x)h(x)\,dx \tag{6}$$

The CE or CME of a risky venture, *V,* is an amount, $\hat{x}$, such that the decision maker is indifferent between the risky venture, *V,* and the certain amount, $\hat{x}$. Put another way, $\hat{x}$ is the value for which $U(\hat{x})$, the utility function on $\hat{x}$, is equal to the expected value of the utility function on the full range of possible outcomes.

The expected value of a random variable, x, is given by

$$\overline{x} = E(x_i) = \sum_{i=1}^{n} p_i x_i \tag{7}$$

or by

$$\overline{x} = \int_x xh(x)\,dx \tag{8}$$

in the continuous case.

To illustrate the procedure for calculating a CE or CME, consider, as an example, the specific utility function

$$U(x) = -e^{-cx} \tag{9}$$

Suppose the decision maker is faced with a venture with two possible outcomes: x_1 with probability ½ and x_2 with probability ½. The expected value of the venture is

$$\overline{x} = \frac{x_1 + x_2}{2}$$

The certainty equivalent (CE) is therefore the solution to this equation:

$$U(\hat{x}) = -e^{-c\hat{x}} = -\frac{e^{-cx_1} + e^{-cx_2}}{2}$$

It may be verified that for $c = 1$, $x_1 = 10$ and $x_2 = 20$, the certainty equivalent is

$$\hat{x} = 10.69$$

The expected value is

$$\frac{(10 + 20)}{2} = 15$$

Consider a second example in which the risky venture has a continuous range of outcomes, ranging from 0 to 20, with an exponential probability density function

$$f(x) = e^{-x}$$

The expected value is

$$\bar{x} = \int_0^{20} xe^{-x}\,dx = 1$$

Suppose we further assume a utility function as

$$U(x) = -e^{-2x}$$

The certainty equivalent is given by $\hat{x}$ such that

$$-e^{-2\hat{x}} = -\int_0^{20} e^{-2x}e^{-x}\,dx = -\int_0^{20} e^{-3x}\,dx = -\frac{1}{3} \qquad \hat{x} = 0.55$$

Specific Probability Distributions for Utility Analysis of Fire Safety Choices

Based on the formulations just discussed, a utility analysis requires a probability distribution function for the outcomes of a risky choice and a utility function on those same outcomes. For a risky choice where fire loss is the source of risk, the key variable in differentiating the outcomes is the size of the fire loss (in monetary terms). Let that be defined as x.

Consider a property owner with an asset value of W. If a loss of x is incurred in a fire, the asset value would be reduced to

$$X = W - x \tag{10}$$

The property owner's utility function will be defined in terms of the reduced asset value, rather than the fire loss, because the reduced asset value reflects the owner's wealth and ability to absorb a loss. An appropriate utility function in terms of positive X would be

$$U(X) = -e^{-\theta X}, \quad \theta > 0 \tag{11}$$

which is an increasing risk averse utility function.[39]

Although the extent of risk aversion quantified by θ is constant for all X, this exponential utility function is widely used in view of its computational simplicity.

Next, in order to match the form of the utility function to the form of a distribution on probabilities of fire loss size, Equation 11 should be rewritten as

$$U(x) = -W'e^{\theta x} \tag{12}$$

where $W' = e^{-\theta W}$ and W' is a constant. As discussed earlier, the certainty equivalent $\hat{x}$ is given by solving the following equation for $\hat{x}$:

$$-W'e^{\theta\hat{x}} = -W'\int_x e^{\theta x}v(x)\,dx \tag{13}$$

where $v(x)$ is the probability density function of fire loss, x.

As x increases from zero, $U(x)$ decreases from a value of $-W'$. A larger loss means a lower adjusted asset value and hence lower utility.

According to statistical studies carried out by Ramachandran,[38–40] Shpilberg,[41] and other authors, loss in a fire has a skewed (nonnormal) probability distribution. Ramachandran has concluded that a good fit is obtained from an exponential-type distribution applied to the logarithm, z, of fire loss size, x (i.e., $z = \log x$ follows an exponential distribution). Among distributions of this type, a normal distribution for z or a log-normal distribution for x is commonly used. An exponential distribution for z or a Pareto distribution for x has also been considered by some actuaries.

If the probability distribution function for fire loss is expressed in terms of z (= log x) instead of x, it will be computationally necessary to have a utility function expressed in terms of z as well. Ramachandran[42] has argued that z (= log x) may be used in Equation 12 instead of x so that the utility function is

$$U(z) = -e^{\theta z} \tag{14}$$

which is equivalent to

$$U(x) = -x^{\theta} \tag{15}$$

The utility function in Equation 15 is a decreasing function with $\theta = 1$ representing risk neutrality. The value of θ should be greater than unity to express a risk averse attitude. The degree of risk aversion increases with θ.

Consider a property worth total financial value V belonging to a risk category with fire loss x having a log-normal distribution. If μ and σ are the mean and standard deviation of z (= log x), following the method described by Ramachandran,[1] the certainty equivalent for the range $(0, V)$ is given by

$$\hat{x}^{\theta} = \frac{1}{G(k)}\frac{1}{\sqrt{2\Pi}\sigma}\int_{-\infty}^{\log V} \exp\left[-\frac{1}{2}\left(\frac{z-\mu}{\sigma}\right)^2\right]e^{\theta z} = \frac{G(k-\sigma\theta)}{G(k)}\exp\left(\mu\theta + \frac{\sigma^2\theta^2}{2}\right) \tag{16}$$

where

$$k = (\log_e V - \mu)/\sigma$$

$$G(k) = \frac{1}{\sqrt{2\pi}} \int_{-\infty}^{k} \exp\left(-\frac{t^2}{2}\right)$$

$$G(k - \sigma\theta) = \frac{1}{\sqrt{2\pi}} \int_{-\infty}^{k-\sigma\theta} \exp\left(-\frac{t^2}{2}\right)$$

and $G(t)$ is the standard normal distribution. The expected monetary value of the loss is given by $\theta = 1$ in Equation 16, because risk neutrality means utility is linearly related to loss. For a decreasing utility function (or increasing disutility function) such as Equation 15, the certainty equivalent, CE, is greater than the EMV.

For a property with a given level of fire protection, the CE corresponding to a given degree (θ) of risk averse attitude of the owner is the maximum insurance premium the owner will be willing to pay to meet the uncertain consequences of a fire. The CE will increase with θ; an owner more risk averse than another will be prepared to spend more money on insurance.

Both EMV and CE will decrease with increasing levels of fire protection. Hence, by adopting efficient fire protection measures, a property owner with a given degree of risk aversion can reduce the cost of the insurance premium. He or she can also obtain a further reduction in the premium by taking self-insurance for small losses.

References Cited

1. G. Ramachandran, *The Economics of Fire Protection,* E & FN Spon, London (1998).
2. R.T.D. Wilmot (ed.), *World Fire Statistics Centre Bulletin,* Geneva Association, Geneva, Switzerland (1995).
3. W.P. Meade, "A First Pass at Computing the Cost of Fire Safety in a Modern Society," *NIST-GCR-91-592,* National Institute of Standards and Technology, Building and Fire Research Laboratory, Gaithersburg, MD (1991).
4. J.R. Hall, Jr., *The Total Cost of Fire in the United States,* NFPA Fire Analysis & Research Division, Quincy, MA (2000).
5. "The Economic Cost of Fire," Economist Intelligence Unit Ltd., unpublished report, London (1971).
6. "Investigation of Consequential Losses to the Economy from Fires," PA Management Consultants Ltd., unpublished report, London (1977).
7. H.L. Hicks and R.R. Liebermann, "A Study of Indirect Fire Losses in Non-Residential Properties," *Fou-brand,* 1, pp. 8–15 (1979).
8. J.M. Henderson and R.E. Quandt, *Microeconomic Theory,* Chapter 3, McGraw-Hill, New York (1971).
9. "MGM Fire Litigation," *Business Insurance,* p. 10 (January 2, 1984); and "Fire at the MGM Grand," *Fire Journal,* pp. 19 ff (January 1982).
10. T.J. Klem, "Los Angeles High-Rise Bank Fire," *Fire Journal,* p. 85 (May/June 1989).
11. D.M. Halbfiner, "Incalculable Cost of One Meridian Fire," *Philadelphia Business Journal,* February 24, 1992, pp. 1, 30.
12. M.S. Isner, "Telephone Central Office, Hinsdale, Illinois, May 8, 1988," NFPA Fire Investigation Report, Quincy, MA (1989).
13. *Fire and Explosion Hazards in the UK Pharmaceutical Industry,* The Insurance Technical Bureau, London (1977).
14. *Fire and Explosion Hazards in the UK Aerospace Industry,* The Insurance Technical Bureau, London (1976).
15. *Fire and Explosion Hazards in the UK Paint and Ink Manufacturing Industries,* The Insurance Technical Bureau, London (1978).
16. L.-G. Benckert, "The Premium for Insurance Against Loss of Profit Due to Fire as a Function of the Period of Indemnity," in *Transactions of the 15th International Congress of Actuaries,* New York, pp. 297–305 (1957).
17. D. Flach, J. Schlunz, and J. Straub, "An Analysis of German Fire Loss of Profits Statistics," *Blatter der Deutschen Gesellschaft fur Vesicherungsmathematik,* Vol. X, Part 2 (1971).
18. D. Riley, *Consequential Loss Insurance and Claims,* Sweet and Maxwell Ltd., London (1967).
19. R.F.F. Dawson, "Current Costs of Road Accidents in Great Britain," *Report No. RRLLR 396,* Road Research Laboratory, Crowthorne, UK (1971).
20. J. Linnerooth, "The Evaluation of Life Saving," *Research Report RR-75-21,* International Institute of Applied Systems Analysis, Laxenbury, Austria (1975).
21. S.J. Melinek, "A Method of Evaluating Human Life for Economic Purposes," *Acc. Anal. and Preven.,* 6, p. 103 (1974).
22. J.P. Acton, "Measuring the Social Impact of Heart and Circulatory Disease Programs: Preliminary Framework and Estimates," *Rand R-1697/NHLI,* Rand Corporation, Santa Monica, CA (1975).
23. G.W. Fischer and J.W. Vaupel, "A Lifespan Utility Model; Assessing Preferences for Consumption and Longevity," working paper, Durham, NC (1976).
24. E. Keeler, "Models of Disease Costs and Their Use in Medical Research Resource Allocations," *P-4537,* Rand Corporation, Santa Monica, CA (1970).
25. J.D. Graham and J.W. Vaupel, "Value of a Life: What Difference Does It Make?" *Risk Anal.,* 1, p. 89 (1981).
26. M.W. Jones-Lee (ed.), *The Value of Life and Safety,* Elsevier, North Holland, New York (1982).
27. G. Blomquist, *Estimating the Value of Life and Safety: Recent Developments in the Value of Life and Safety,* North Holland, New York (1982).
28. T.C. Schelling, "The Life You Save May Be Your Own," in *Problems in Public Expenditure Analysis,* Brookings Institution, Washington, DC (1968).
29. G. Maycock, "Accident Modelling and Economic Evaluation," *Acc. Anal. and Preven.,* 18, p. 169 (1986).
30. S.G. Helzer, B. Buchbinder, and F.L. Offensend, "Decision Analysis of Strategies for Reducing Upholstered Furniture Fire Losses," *Technical Note 1101,* National Bureau of Standards, Washington, DC (1979).
31. S.E. Chandler and R. Baldwin, "Furniture and Furnishings in the Home—Some Fire Statistics," *Fire and Matls.,* 7, p. 76 (1976).
32. I.C. Appleton, "A Cost-Benefit Analysis Applied to Foamed Plastics Ceilings," *Current Paper CP 50/77,* Fire Research Station, Borehamwood, UK (1977).
33. M.W. Jones-Lee, *The Value of Life: An Economic Analysis,* Martin Robertson, London (1976).
34. M.J. Karter, Jr., *U.S. Fire Department Profile Through 1997,* NFPA Fire Analysis and Research Division, Quincy, MA (1998).
35. J. von Neumann and O. Morgenstern, *Theory of Games and Economic Behavior,* Princeton Univ. Press, Princeton (1947).
36. P.G. Moore, *Risk in Business Decision,* Longman Group, London (1972).

37. R.L. Keeney and H. Raiffa, *Decisions with Multiple Objectives: Preferences and Value Trade-Offs,* John Wiley and Sons, New York (1976).
38. G. Ramachandran,"Extreme Value Theory and Fire Losses—Further Results," *Fire Research Note No. 910,* Fire Research Station, Borehamwood, UK (1972).
39. G. Ramachandran, "Extreme Value Theory and Large Fire Losses," *ASTIN Bul.,* 7, p. 293 (1974).
40. G. Ramachandran, "Extreme Order Statistics in Large Samples from Exponential Type Distributions and Their Application to Fire Loss," in *Statistical Distributions in Scientific Work,* 355, D. Reidel, Dordrecht, Netherlands (1975).
41. D.C. Shpilberg,"Risk Insurance and Fire Protection; A Systems Approach. Part 1: Modelling the Probability Distribution of Fire Loss Amount," *Technical Report No. 22431,* Factory Mutual Research Corp., Norwood, MA (1974).
42. G. Ramachandran, *The Interaction Between Fire Protection and Insurance,* Seminar, Zurich (1984).

CHAPTER 7

Engineering Economics

John M. Watts, Jr., and Robert E. Chapman

Introduction

Engineering economics is the application of economic techniques to the evaluation of design and engineering alternatives.[1] The role of engineering economics is to assess the appropriateness of a given project, estimate its value, and justify it from an engineering standpoint.

This chapter discusses the time value of money and other cash-flow concepts, such as compound and continuous interest. It continues with economic practices and techniques used to evaluate and optimize decisions on selection of fire safety strategies. The final section expands on the principles of benefit-cost analysis.

An in-depth treatment of the practices and techniques covered in this compilation is available in the ASTM compilation of standards on building economics.[2] The ASTM compilation also includes case illustrations showing how to apply the practices and techniques to investment decisions.

A broader perspective on the application of engineering economics to fire protection engineering can be found in *The Economics of Fire Protection* by Ramachandran.[3] This work is intended as a textbook for fire protection engineers and includes material and references that expand on several other chapters of this section of the SFPE handbook.

Cash-Flow Concepts

Cash flow is the stream of monetary (dollar) values—costs (inputs) and benefits (outputs)—resulting from a project investment.

Dr. John M. Watts, Jr., holds degrees in fire protection engineering, industrial engineering, and operations research. He is director of the Fire Safety Institute, a not-for-profit information, research, and educational corporation located in Middlebury, Vermont. Dr. Watts also serves as editor of NFPA's *Fire Technology*.

Dr. Robert E. Chapman is an economist in the Office of Applied Economics, Building and Fire Research Laboratory, National Institute of Standards and Technology.

Time Value of Money

The following are reasons why $1000 today is "worth" more than $1000 one year from today:

1. Inflation
2. Risk
3. Cost of money

Of these, the cost of money is the most predictable, and, hence, it is the essential component of economic analysis. Cost of money is represented by (1) money paid for the use of borrowed money, or (2) return on investment. Cost of money is determined by an interest rate.

Time value of money is defined as the time-dependent value of money stemming both from changes in the purchasing power of money (inflation or deflation) and from the real earning potential of alternative investments over time.

Cash-Flow Diagrams

It is difficult to solve a problem if you cannot see it. The easiest way to approach problems in economic analysis is to draw a picture. The picture should show three things:

1. A time interval divided into an appropriate number of equal periods
2. All cash outflows (deposits, expenditures, etc.) in each period
3. All cash inflows (withdrawals, income, etc.) for each period

Unless otherwise indicated, all such cash flows are considered to occur at the end of their respective periods.

Figure 5-7.1 is a cash-flow diagram showing an outflow or disbursement of $1000 at the beginning of year 1 and an inflow or return of $2000 at the end of year 5.

Notation

To simplify the subject of economic analysis, symbols are introduced to represent types of cash flows and

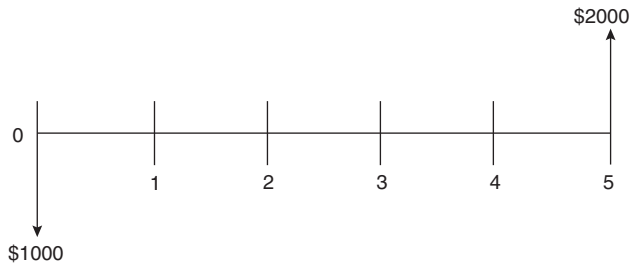

Figure 5-7.1. ***Cash-flow diagram.***

interest factors. The symbols used in this chapter conform to ANSI Z94;[4] however, not all practitioners follow this standard convention, and care must be taken to avoid confusion when reading the literature. The following symbols will be used here:

$P =$ Present sum of money ($)
$F =$ Future sum of money ($)
$N =$ Number of interest periods
$i =$ Interest rate per period (%)

A complete list of the ANSI Z94 symbols is given in Appendix A to this chapter.

Interest Calculations

Interest is the money paid for the use of borrowed money or the return on invested capital. The economic cost of construction, installation, ownership, or operation can be estimated correctly only by including a factor for the economic cost of money.

Simple interest: To illustrate the basic concepts of interest, an additional notation will be used:

$$F(N) = \text{Future sum of money after } N \text{ periods}$$

Then, for simple interest,

$$F(1) = P + (P)(i) = P(1 + i)$$

and

$$F(N) = P + (N)(P)(i) = P(1 + Ni)$$

For example: $100 at 10 percent per year for 5 yr yields

$$\begin{aligned} F(5) &= 100[1 + (5)(0.1)] \\ &= 100(1.5) \\ &= \$150 \end{aligned}$$

However, interest is almost universally compounded to include interest on the interest.

Compound interest

$$F(1) = P + (P)(i) = P(1 + i)$$

is the same as simple interest,

$$F(2) = F(1) + F(1)(i)$$

Interest is applied to the new sum:

$$\begin{aligned} &= (F)(1)(1 + i) = P(1 + i)^2 \\ F(3) &= F(2)(1 + i) = P(1 + i)^3 \end{aligned}$$

and by mathematical induction,

$$F(N) = P(1 + i)^N$$

EXAMPLE:
$100 at 10 percent per year for 5 yr yields

$$\begin{aligned} F(5) &= 100(1 + 0.1)^5 \\ &= 100(1.1)^5 \\ &= 100(1.61051) \\ &= \$161.05 \end{aligned}$$

which is over 7 percent greater than with simple interest.

EXAMPLE:
In 1626 Willem Verhulst bought Manhattan Island from the Canarsie Indians for 60 florins ($24) worth of merchandise (a price of about 0.5 cents per hectare [0.2 cents per acre]). At an average interest rate of 6 percent, what is the present value (2001) of the Canarsies' $24?

$$\begin{aligned} F &= P(1 + i)^N \\ &= \$24(1 + 0.06)^{375} \\ &= \$7.4 \times 10^{10} \end{aligned}$$

Seventy-four billion dollars is a reasonable approximation of the present land value of the island of Manhattan.

Interest Factors

Interest factors are multiplicative numbers calculated from interest formulas for given interest rates and periods. They are used to convert cash flows occurring at different times to a common time. The functional formats used to represent these factors are taken from ANSI Z94, and they are summarized in Appendix B to this chapter.

Compound Amount Factor

In the formula for finding the future value of a sum of money with compound interest, the mathematical expression $(1 + i)^N$ is referred to as the *compound amount factor,* represented by the functional format $(F/P, i, N)$. Thus,

$$F = P(F/P, i, N)$$

Interest tables: Values of the compound amount, present worth, and other factors that will be discussed shortly, are tabulated for a variety of interest rates and number of periods in most texts on engineering economy. Example tables are presented in Appendix C to this chapter. Although calculators and computers have greatly reduced the need for such tables, they are often still useful for interpolations.

Present Worth

Present worth is the value found by discounting future cash flows to the present or base time.

Discounting: The inverse of compounding is determining a present amount which will yield a specified future sum. This process is referred to as discounting. The equation for discounting is found readily by using the compounding equation to solve for P in terms of F:

$$P = F(1 + i)^{-N}$$

EXAMPLE:
What present sum will yield \$1000 in 5 yr at 10 percent?

$$\begin{aligned} P &= 1000(1.1)^{-5} \\ &= 1000(0.62092) \\ &= \$620.92 \end{aligned}$$

This result means that \$620.92 "deposited" today at 10 percent compounded annually will yield \$1000 in 5 yr.

Present worth factor: In the discounting equation, the expression $(1 + i)^{-N}$ is called the *present worth factor* and is represented by the symbol $(P/F, i, N)$. Thus, for the present worth of a future sum at i percent interest for N periods,

$$P = F(P/F, i, N)$$

Note that the present worth factor is the reciprocal of the compound amount factor. Also note that

$$(P/F, i, N) = \frac{1}{(F/P, i, N)}$$

EXAMPLE:
What interest rate is required to triple \$1000 in 10 years?

$$P = \frac{F}{3} = (P/F, i, 10)$$

therefore,

$$(P/F, i, 10) = \frac{1}{3}$$

From Appendix C,

$$(P/F, 10\%, 10) = 0.3855$$

and

$$(P/F, 12\%, 10) = 0.3220$$

By linear interpolation,

$$i = 11.6\%$$

Interest Periods

Normally, but not always, the interest period is taken as 1 yr. There may be subperiods of quarters, months, weeks, and so forth.

Nominal versus effective interest: It is generally assumed that interest is compounded annually. However, interest may be compounded more frequently. When this occurs, there is a *nominal interest* or annual percentage rate and an *effective interest*, which is the figure used in calculations. For example, a savings bank may offer 5 percent interest compounded quarterly, which is not the same as 5 percent per year. A nominal rate of 5 percent compounded quarterly is the same as 1.25 percent every three months or an effective rate of 5.1 percent per year. If

$$r = \text{Nominal interest rate,}$$

and

$$M = \text{Number of subperiods per year}$$

then the effective interest rate is

$$i = \left(1 + \frac{r}{M}\right)^{M} - 1$$

EXAMPLE:
Credit cards usually charge interest at a rate of 1.5 percent per month. This amount is a nominal rate of 18 percent. What is the effective rate?

$$\begin{aligned} i &= (1 + 0.015)^{12} - 1 \\ &= 1.1956 - 1 \\ &= 19.56\% \end{aligned}$$

Continuous interest: A special case of effective interest occurs when the number of periods per year is infinite. This represents a situation of *continuous interest*, also referred to as continuous compounding. Formulas for continuous interest can be derived by examining limits as M approaches infinity. Formulas for interest factors using continuous compounding are included in Appendix B. Continuous interest is compared to monthly interest in Table 5-7.1.

EXAMPLE:
Compare the future amounts obtained under various compounding periods at a nominal interest rate of 12 percent for 5 yr, if P = \$10,000. (See Table 5-7.2.)

Series Payments

Life would be simpler if all financial transactions were in single lump-sum payments, now or at some time in the

Table 5-7.1 ***Continuous Interest (%)***

	Effective	
Nominal %	Monthly	Continuous
5	5.1	5.1
10	10.5	10.5
15	16.1	16.2
20	21.9	22.1

Table 5-7.2 ***Example of Continuous Interest N = 5 yr, r = 12%***

Compounding	*M*	*i*	*NM*	*F/P*	*F*
Annual	1	12.000	5	1.76234	17,623.40
Semi-annual	2	12.360	10	1.79085	17,908.50
Quarterly	4	12.551	20	1.80611	18,061.10
Monthly	12	12.683	60	1.81670	18,167.00
Weekly	52	12.734	260	1.820860	18,208.60
Daily	365	12.747	1825	1.821938	18,219.38
Hourly	8760	12.749	43,800	1.822061	18,220.61
Instantaneously	∞	12.750	∞	1.822119[a]	18,221.19

[a]F/P (instantaneous) $= e^{Ni} = e^{5(0.12)} = e^{0.6}$.

future. However, most situations involve a series of regular payments, for example, car loans and mortgages.

Series compound amount factor: Given a series of regular payments, what will they be worth at some future time?

Let

A = the amount of a regular end-of-period payment

Then, note that each payment, A, is compounded for a different period of time. The first payment will be compounded for $N - 1$ periods (yr):

$$F = A(1 + i)^{N-1}$$

and the second payment for $N - 2$ periods:

$$F = A(1 + i)^{N-2}$$

and so forth. Thus, the total future value is

$$F = A(1 + i)^{N-1} + A(1 + i)^{N-2} + \cdots + A(1 + i) + A$$

or

$$F = \frac{A[(1 + i)^N - 1]}{i}$$

The interest expression in this equation is known as the *series compound amount factor,* $(F/A, i, N)$, thus

$$F = A(F/A, i, N)$$

Sinking fund factor: The process corresponding to the inverse of series compounding is referred to as a *sinking fund;* that is, what size regular series payments are necessary to acquire a given future amount?

Solving the series compound amount equation for A,

$$A = F\left\{\frac{i}{[(1 + i)^N - 1]}\right\}$$

Or, using the symbol $(A/F, i, N)$ for the *sinking fund factor*

$$A = F(A/F, i, N)$$

Here, note that the sinking fund factor is the reciprocal of the series compound amount factor, that is, $(A/F, i, N) = 1/(F/A, i, N)$.

Capital recovery factor: It is also important to be able to relate regular periodic payments to their present worth; for example, what monthly installments will pay for a $10,000 car in 3 yr at 15 percent?

Substituting the compounding equation $F = P(F/P, i, N)$ in the sinking fund equation, $A = F(A/F, i, N)$, yields

$$A = P(F/P, i, N)(A/F, i, N)$$

And, substituting the corresponding interest factors gives

$$A = P\frac{[i(1 + i)^N]}{[(1 + i)^N - 1]}$$

In this equation, the interest expression is known as the *capital recovery factor,* since the equation defines a regular income necessary to recover a capital investment. The symbolic equation is

$$A = P(A/P, i, N)$$

Series present worth factor: As with the other factors, there is a corresponding inverse to the capital recovery factor. The *series present worth* factor is found by solving the capital recovery equation for P.

$$P = A\frac{[(1 + i)^N - 1]}{[i(1 + i)^N]}$$

or, symbolically

$$P = A(P/A, i, N)$$

Other Interest Calculation Concepts

Additional concepts involved in interest calculations include continuous cash flow, capitalized costs, beginning of period payments, and gradients.

Continuous cash flow: Perhaps the most useful function of continuous interest is its application to situations where the flow of money is of a continuous nature. *Continuous cash flow* is representative for

1. A series of regular payments for which the interval between payments is very short
2. A disbursement at some unknown time (which is then considered to be spread out over the economic period)

Factors for calculating present or future worth of a series of annual amounts, representing the total of a continuous cash flow throughout the year, may be derived by integrating corresponding continuous interest factors over the number of years the flow is maintained.

Continuous cash flow is an appropriate way to handle economic evaluations of risk, for example, the present value of an annual expected loss.

Formulas for interest factors representing continuous, uniform cash flows are included in Appendix B.

Capitalized costs: Sometimes there are considerations, such as some public works projects, which are considered to last indefinitely and thereby provide perpetual service. For example, how much should a community be willing to invest in a reservoir which will reduce fire insurance costs by some annual amount, *A?* Taking the limit of the series present worth factor as the number of periods goes to infinity gives the reciprocal of the interest rate. Thus, *capitalized costs* are just the annual amount divided by the interest rate. When expressed as an amount required to produce a fixed yield in perpetuity, it is sometimes referred to as an *annuity.*

Beginning-of-period payments: Most returns on investment (cash inflows) occur at the end of the period during which they accrued. For example, a bank computes and pays interest at the end of the interest period. Accordingly, interest tables, such as those in Appendix C, are computed for end-of-year payments. For example, the values of the capital recovery factor (A/P, i, N) assume that the regular payments, A, occur at the end of each period.

On the other hand, most disbursements (cash outflows) occur at the beginning of the period (e.g., insurance premiums). When dealing with beginning-of-period payments, it is necessary to make adjustments. One method of adjustment for beginning-of-period payments is to calculate a separate set of factors. Another way is to logically interpret the effect of beginning-of-period payments for a particular problem, for example, treating the first payment as a present value. The important thing is to recognize that such variations can affect economic analysis.

Gradients: It occasionally becomes necessary to treat the case of a cash flow which regularly increases or decreases at each period. Such patterned changes in cash flow are called *gradients.* They may be a constant amount (linear or arithmetic progression), or they may be a constant percentage (exponential or geometric progression). Various equations for dealing with gradient series may be found in Appendix B.

Comparison of Alternatives

Most decisions are based on economic criteria. Investments are unattractive, unless it seems likely they will be recovered with interest. Economic decisions can be divided into two classes:

1. Income-expansion—that is, the objective of capitalism
2. Cost-reduction—the basis of profitability

Fire protection engineering economic analysis is primarily concerned with cost-reduction decisions, finding the least expensive way to fulfill certain requirements, or minimizing the sum of expected fire losses plus investment in fire protection.

There are four common methods of comparing alternative investments: (1) present worth, (2) annual cost, (3) rate of return, and (4) benefit-cost analysis. Each of these is dependent on a selected interest rate or discount rate to adjust cash flows at different points in time.

Discount Rate

The term *discount rate* is often used for the interest rate when comparing alternative projects or strategies.

Selection of discount rate: If costs and benefits accrue equally over the life of a project or strategy, the selection of discount rate will have little impact on the estimated benefit-cost ratios. However, most benefits and costs occur at different times over the project life cycle. Thus, costs of constructing a fire-resistive building will be incurred early in contrast to benefits, which will accrue over the life of the building. The discount rate then has a significant impact on measures such as benefit-cost ratios, since the higher the discount rate, the lower the present value of future benefits.

In view of the uncertainty concerning appropriate discount rate, analysts frequently use a range of discount rates. This procedure indicates the sensitivity of the analysis to variations in the discount rate. In some instances, project rankings based on present values may be affected by the discount rate as shown in Figure 5-7.2. Project A is preferred to project B for discount rates below 15 percent, while the converse is true for discount rates greater than 15 percent. In this instance, the decision to adopt project A in preference to project B will reflect the belief that the appropriate discount rate is less than or equal to 15 percent.

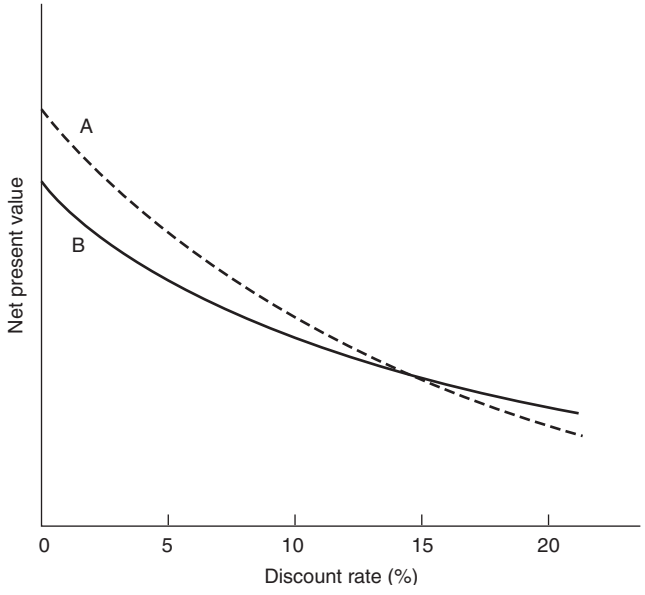

Figure 5-7.2. ***Impact of discount rate on project selection.***

A comparison of benefits and costs may also be used to determine the payback period for a particular project or strategy. However, it is important to discount future costs or benefits in such analyses. For example, an analysis of the Beverly Hills Supper Club fire compared annual savings from a reduction in insurance premiums to the costs of sprinkler installation. Annual savings were estimated at $11,000, while costs of sprinkler installation ranged from $42,000 to $68,000. It was concluded that the installation would have been paid back in four to seven years (depending on the cost of the sprinklers). However, this analysis did not discount future benefits, so that $11,000 received at the end of four years was deemed equivalent to $11,000 received in the first year. Once future benefits are discounted, the payback period ranges from five to eleven years with a discount rate of 10 percent.

Inflation and the discount rate: Provision for inflation may be made in two ways: (1) estimate all future costs and benefits in constant prices, and use a discount rate which represents the opportunity cost of capital in the absence of inflation; or (2) estimate all future benefits and costs in current or inflated prices, and use a discount rate which includes an allowance for inflation. The discount rate in the first instance may be considered the real discount rate, while the discount rate in the second instance is the nominal discount rate. The use of current or inflated prices with the real discount rate, or constant prices with the nominal discount rate, will result in serious distortions in economic analysis.

Present Worth

In a *present worth* comparison of alternatives, the costs associated with each alternative investment are all converted to a present sum of money, and the least of these values represents the best alternative. Annual costs, future payments, and gradients must be brought to the present. Converting all cash flows to present worth is often referred to as *discounting*.

EXAMPLE:

Two alternate plans are available for increasing the capacity of existing water transmission lines between an unlimited source and a reservoir. The unlimited source is at a higher elevation than the reservoir. Plan A calls for the construction of a parallel pipeline and for flow by gravity. Plan B specifies construction of a booster pumping station. Estimated cost data for the two plans are as follows:

	Plan A Pipeline	Plan B Pumping Station
Construction cost	$1,000,000	$200,000
Life	40 years	40 years (structure) 20 years (equipment)
Cost of replacing equipment at the end of 20 yr	0	$75,000
Operating costs	$1000/yr	$50,000/yr

If money is worth 12 percent, which plan is more economical? (Assume annual compounding, zero salvage value, and all other costs equal for both plans.)

$$\text{Present worth (Plan A)} = P + A(P/A, 12\%, 40)$$
$$= \$1{,}000{,}000 + \$1000(8.24378)$$
$$= \$1{,}008{,}244$$

$$\text{Present worth (Plan B)} = P + A(P/A, 12\%, 40) + F(P/F, 12\%, 20)$$
$$= \$200{,}000 + \$50{,}000(8.24378) + \$75{,}000(0.10367)$$
$$= \$619{,}964$$

Thus, plan B is the least-cost alternative.

A significant limitation of present worth analysis is that it cannot be used to compare alternatives with unequal economic lives. That is, a ten-year plan and a twenty-year plan should not be compared by discounting their costs to a present worth. A better method of comparison is annual cost.

Annual Cost

To compare alternatives by annual cost, all cash flows are changed to a series of uniform payments. Current expenditures, future costs or receipts, and gradients must be converted to annual costs. If a lump-sum cash flow occurs at some time other than the beginning or end of the economic life, it must be converted in a two-step process: first moving it to the present and then spreading it uniformly over the life of the project.

Alternatives with unequal economic lives may be compared by assuming replacement in kind at the end of the shorter life, thus maintaining the same level of uniform payment.

	System Cost	Insurance Premium	Life
Partial system	$ 8000	$1000	15 yr
Full system	$15,000	$250	20 yr

EXAMPLE:

Compare the value of a partial or full sprinkler system purchased at 10 percent interest.

$$\text{Annual cost (partial system)} = A + P(A/P, 10\%, 15)$$
$$= \$1000 + \$8000(0.13147)$$
$$= \$2051.75$$

$$\text{Annual cost (full system)} = A + P(A/P, 10\%, 20)$$
$$= \$250 + \$15{,}000(0.11746)$$
$$= \$2011.90$$

The full system is slightly more economically desirable. When costs are this comparable, it is especially important to consider other relevant decision criteria, for example, uninsured losses.

Rate of Return

Rate of return is, by definition, the interest rate at which the present worth of the net cash flow is zero. Computationally, this method is the most complex method of comparison. If more than one interest factor is involved,

the solution is by trial and error. Microcomputer programs are most useful with this method.

The calculated interest rate may be compared to a discount rate identified as the "minimum attractive rate of return" or to the interest rate yielded by alternatives. Rate-of-return analysis is useful when the selection of a number of projects is to be undertaken within a fixed or limited capital budget.

EXAMPLE:

An industrial fire fighting truck costs $100,000. Savings in insurance premiums and uninsured losses from the acquisition and operation of this equipment is estimated at $60,000/yr. Salvage value of the apparatus after 5 yr is expected to be $20,000. A full-time driver during operating hours will accrue an added cost of $10,000/yr. What would the rate of return be on this investment?

@ 40% present worth

$$= P + F(P/F, 40\%, 5) + A(P/A, 40\%, 5)$$
$$= -\$100{,}000 + \$20{,}000(0.18593) + (\$60{,}000 - 10{,}000)(2.0352)$$
$$= \$5{,}478.60$$

@ 50% present worth

$$= P + F(P/F, 50\%, 5) + A(P/A, 50\%, 5)$$
$$= -\$100{,}000 + \$20{,}000(0.13169) + (\$60{,}000 - \$10{,}000)(1.7366)$$
$$= -\$10{,}536.40$$

By linear interpolation, the rate of return is 43 percent.

Benefit-Cost Analysis

Benefit-cost analysis, also referred to as cost-benefit analysis, is a method of comparison in which the consequences of an investment are evaluated in monetary terms and divided into the separate categories of benefits and costs. The amounts are then converted to annual equivalents or present worths for comparison.

The important steps of a benefit-cost analysis are

1. Identification of relevant benefits and costs
2. Measurement of these benefits and costs
3. Selection of best alternative
4. Treatment of uncertainty

Identification of Relevant Benefits and Costs

The identification of benefits and costs depends on the particular project under consideration. Thus, in the case of fire prevention or control activities, the benefits are based on fire losses prior to such activities. Fire losses may be classified as direct or indirect. Direct economic losses are property and contents losses. Indirect losses include such things as the costs of injuries and deaths, costs incurred by business or industry due to business interruption, losses to the community from interruption of services, loss of payroll or taxes, loss of market share, and loss of reputation. The direct costs of fire protection activities include the costs of constructing fire-resistive buildings, installation costs of fire protection systems, and the costs of operating fire departments. Indirect costs are more difficult to measure. They include items such as the constraints on choice due to fire protection requirements by state and local agencies.

A major factor in the identification of relevant benefits and costs pertains to the decision unit involved. Thus, if the decision maker is a property owner, the relevant benefits from fire protection are likely to be the reduction in fire insurance premiums and fire damage or business interruption losses not covered by insurance. In the case of a municipality, relevant benefits are the protection of members of the community, avoidance of tax and payroll losses, and costs associated with assisting fire victims. Potential benefits, in these instances, are considerably greater than those faced by a property owner. However, the community may ignore some external effects of fire incidents. For example, the 1954 automobile transmission plant fire in Livonia, Michigan, affected the automobile industry in Detroit and various automobile dealers throughout the United States. However, there was little incentive for the community to consider such potential losses in their evaluation of fire strategies, since they would pertain to persons outside the community. It might be concluded, therefore, that the more comprehensive the decision unit, the more likely the inclusion of all relevant costs and benefits, in particular, social costs and benefits.

Measurement of Benefits and Costs

Direct losses are measured or estimated statistically or by a priori judgment. Actuarial fire-loss data collected nationally or for a particular industry may be used, providing it is adequately specific and the collection mechanism is reliable. More often, an experienced judgment of potential losses is made, sometimes referred to as the *maximum probable loss* (MPL).

Indirect losses, if considered, are much more difficult to appraise. A percentage or multiple of direct losses is sometimes used. However, when indirect loss is an important decision parameter, a great deal of research into monetary evaluation may be necessary. Procedures for valuing a human life and other indirect losses are discussed in Ramachandran.[3]

In the measurement of benefits, it is appropriate to adjust for utility or disutility which may be associated with a fire loss.

Costs may be divided into two major categories: (1) costs of private fire protection services, and (2) costs of public fire protection services. In either case, cost estimates will reflect the opportunity cost of providing the service. For example, the cost of building a fire-resistive structure is the production foregone due to the diversion of labor and resources to make such a structure. Similarly, the cost of a fire department is the loss of other community services which might have been provided with the resources allocated to the fire department.

Selection of Best Alternative

There are two considerations in determining benefit-cost criteria. The first pertains to project acceptability, while the second pertains to project selection.

Project acceptability may be based on benefit-cost difference or benefit-cost ratio. Benefit-cost ratio is a measure

of project worth in which the monetary equivalent benefits are divided by the monetary equivalent costs. The first criterion requires that the value of benefits less costs be greater than zero, while the second criterion requires that the benefit-cost ratio be greater than one.

The issue is more complicated in the case of project selection, since several alternatives are involved. It is no longer a question of determining the acceptability of a single project, but rather selecting from among alternative projects. Consideration should be given to changes in costs and benefits as various strategies are considered. Project selection decisions are illustrated in Figure 5-7.3. The degree of fire protection is given on the horizontal axis, while the marginal costs and benefits associated with various levels of fire safety are given on the vertical axis. As the diagram indicates, marginal costs are low initially and then increase. Less information is available concerning the marginal benefit curve, and it may, in fact, be horizontal. The economically optimum level of fire protection is given by the intersection of the marginal cost and marginal benefit curves. Beyond this point, benefits from increasing fire protection are exceeded by the costs of providing the additional safety.

A numerical example is given in Table 5-7.3. There are five possible strategies or programs possible. The first strategy, A, represents the initial situation, while the remaining four strategies represent various fire loss reduction activities, each with various costs. Strategies are arranged in ascending order of costs. Fire losses under each of the five strategies are given in the second row, while the sum of fire losses and fire reduction costs for each strategy is given in the third row. The sum of fire losses and fire reduction costs of each strategy is equivalent to the life-cycle cost of that strategy. Life-cycle cost analysis is an alternative to benefit-cost analysis when the outcomes of the investment decision are cost savings rather than benefits per se. Additional information on life-cycle cost analysis is found in Fuller and Petersen.[5]

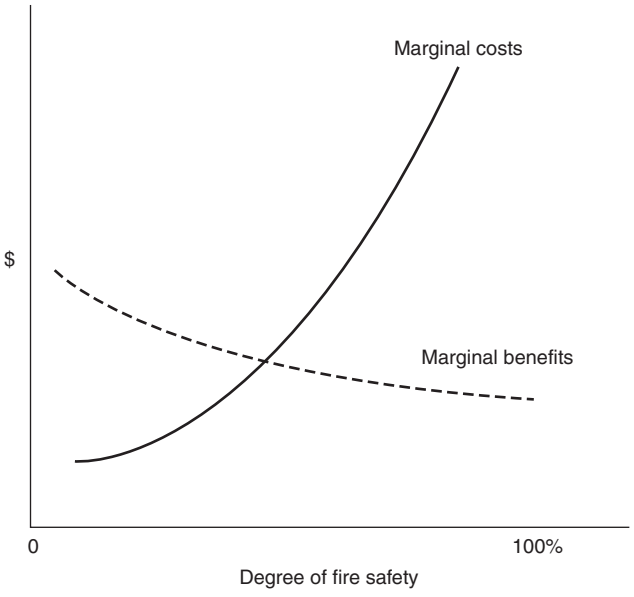

Figure 5-7.3. ***Project selection.***

Table 5-7.3 ***Use of Benefit-Cost Analyses in Strategy Selection***

	Strategy				
Category	A	B	C	D	E
Fire reduction costs	0	10	25	45	70
Fire losses	100	70	50	40	35
Sum of fire reduction costs and fire losses	100	80	75	85	105
Marginal benefits	0	30	20	10	5
Marginal costs	0	10	15	20	25
Marginal benefits minus marginal costs	0	20	5	–10	–20
Marginal benefit-cost ratio	—	3.0	1.33	0.5	0.2

Data in the first two rows may then be used to determine the marginal costs or marginal benefits from the replacement of one strategy by another. Thus, strategy B has a fire loss of $70 compared to $100 for strategy A, so the marginal benefit is $30. Similarly, the marginal benefit from strategy C is the reduction in fire losses from B to C or $20. The associated marginal cost of strategy C is $15. Declining marginal benefits and rising marginal costs result in the selection of strategy C as the optimum strategy. At this point, the difference between marginal benefits and marginal costs is still positive.

Marginal benefit-cost ratios are given in the last row. It is worth noting that, while the highest marginal benefit-cost ratio is reached at activity level B (as is the highest marginal benefit-cost difference), project C is still optimum, since it yields an additional net benefit of $5. This finding is reinforced by examining changes in the sum of fire losses and fire reduction costs (i.e., life-cycle costs). Total cost plus loss first declines, reaching a minimum at point C, and then increases. This pattern is not surprising, since as long as marginal benefits exceed marginal costs, total losses should decrease. Thus, the two criteria—equating marginal costs and benefits, and minimizing the sum of fire losses and fire reduction costs—yield identical outcomes.

Treatment of Uncertainty

A final issue concerns the treatment of uncertainty. One method for explicitly introducing risk considerations is to treat benefits and costs as random variables which may be described by probability distributions. For example, an estimate of fire losses might consider the following events: no fire, minor fire, intermediate fire, and major fire. Each event has a probability of occurrence and an associated damage loss. The total expected loss (EL) is given by

$$EL = \sum_{i=0}^{3} p_i D_i$$

where

p_0 = probability of no fire

p_1 = probability of a minor fire

p_2 = probability of an intermediate fire
p_3 = probability of a major fire
D_n = associated damage loss, n = 0,1,2,3

Expected losses may be computed for different fire protection strategies. Thus, a fire protection strategy that costs C_3 and reduces damage losses of a major fire from D_3 to D_3' will result in an expected loss

$$EL = p_0D_0 + p_1D_1 + p_2D_2 + p_3D_3' + C3$$

Similarly, a fire control strategy that costs C_2 and reduces the probability of an intermediate fire from p_2 to p_2' has an expected loss

$$EL = p_0D_0 + p_1D_1 + p_2'D_2 + p_3D_3 + C_2$$

A comparison of expected losses from alternative strategies may then be used to determine the optimal strategy.

Use of expected value has a limitation in that only the average value of the probability distribution is considered. Discussion of other procedures for evaluating uncertain outcomes is given by Anderson and Settle.[6]

References Cited

1. ASTM E833, *Definitions of Terms Relating to Building Economics,* American Society for Testing and Materials, West Conshohocken, PA (1999).
2. *ASTM Standards on Building Economics,* 4th ed., American Society for Testing and Materials, West Conshohocken, PA (1999).
3. G. Ramachandran, *The Economics of Fire Protection,* E & FN Spon, London (1998).
4. American National Standards Institute Standard Z94.0-1982, "Industrial Engineering Terminology," Chapter 5, *Engineering Economy,* Industrial Engineering and Management Press, Atlanta, GA (1983).
5. S.K. Fuller and S.R. Petersen, "Life-Cycle Costing Manual for the Federal Energy Management Program," *NIST Handbook 135,* National Institute of Standards and Technology, Gaithersburg, MD (1996).
6. L.G. Anderson and R.E. Settle, *Benefit-Cost Analysis: A Practical Guide,* Lexington Books, Lexington, MA (1977).

Additional Readings

R.E. Chapman, "A Cost-Conscious Guide to Fire Safety in Health Care Facilities," *NBSIR 82-2600,* National Bureau of Standards, Washington, DC (1982).

R.E. Chapman and W.G. Hall, "Code Compliance at Lower Costs: A Mathematical Programming Approach," *Fire Technology,* 18, 1, pp. 77–89 (1982).

L.P. Clark, "A Life-Cycle Cost Analysis Methodology for Fire Protection Systems in New Health Care Facilities," *NBSIR 82-2558,* National Bureau of Standards, Washington, DC (1982).

W.J. Fabrycky, G.J. Thuesen, and D. Verma, *Economic Decision Analysis,* 3rd ed., Prentice Hall International, London (1998).

E.L. Grant, W.G. Ireson, and R.S. Leavenworth, *Principles of Engineering Economy,* 8th ed., John Wiley and Sons, New York (1990).

J.S. McConnaughey, "An Economic Analysis of Building Code Impacts: A Suggested Approach," *NBSIR 78-1528,* National Bureau of Standards, Washington, DC (1978).

D.G. Newnan and J.P. Lavelle, *Engineering Economic Analysis,* 7th ed., Engineering Press, Austin, TX (1998).

C.S. Park, *Contemporary Engineering Economics,* 2nd ed., Addison-Wesley, Menlo Park, CA (1997).

J.L. Riggs, D.D. Bedworth, and S.U. Randhawa, *Engineering Economics,* 4th ed., McGraw-Hill, New York (1996).

R.T. Ruegg and H.E. Marshall, *Building Economics: Theory and Practice,* Van Nostrand Reinhold, New York (1990).

R.T. Ruegg and S.K. Fuller, "A Benefit-Cost Model of Residential Fire Sprinkler Systems," *NBS Technical Note 1203,* National Bureau of Standards, Washington, DC (1984).

W.G. Sullivan, J.A. Bontadelli, and E.M. Wicks, *Engineering Economy,* 11th ed., Prentice Hall, Upper Saddle River, NJ (2000).

Appendix A: Symbols and Definitions of Economic Parameters

Symbol	Definition of Parameter
A_j	Cash flow at end of period j
A	End-of-period cash flows (or equivalent end-of-period values) in a uniform series continuing for a specified number of periods
$\bar{A}$	Amount of money (or equivalent value) flowing continuously and uniformly during each period, continuing for a specified number of periods
F	Future sum of money—the letter *F* implies future (or equivalent future value)
G	Uniform period-by-period increase or decrease in cash flows (or equivalent values); the arithmetic gradient
M	Number of compounding periods per interest period[a]
N	Number of compounding periods
P	Present sum of money—the letter "*P*" implies present (or equivalent present value). Sometimes used to indicate initial capital investment.
S	Salvage (residual) value of capital investment
f	Rate of price level increase or decrease per period; an "inflation" of "escalation" rate
g	Uniform *rate* of cash flow increase or decrease from period to period; the geometric gradient
i	Effective interest rate per interest period[a] (discount rate), expressed as a percent or decimal fraction
r	Nominal interest rate per interest period,[a] expressed as a percent or decimal fraction

[a]Normally, but not always, the interest *period* is taken as 1 *yr.*
Subperiods, then, would be quarters, months, weeks, and so forth.

Appendix B: Functional Forms of Compound Interest Factors[a]

Name of Factor	Algebraic Formulation	Functional Format
Group A. All cash flows discrete: end-of-period compounding		
Compound amount (single payment)	$(1 + i)^N$	$(F/P, i, N)$
Present worth (single payment)	$(1 + i)^{-N}$	$(P/F, i, N)$
Sinking fund	$\frac{i}{(1 + i)^N - 1}$	$(A/F, i, N)$
Capital recovery	$\frac{i(1 + i)^N}{(1 + i)^N - 1}$	$(A/P, i, N)$
Compound amount (uniform series)	$\frac{(1 + i)^N - 1}{i}$	$(F/A, i, N)$
Present worth (uniform series)	$\frac{(1 + i)^N - 1}{i(1 + i)^N}$	$(P/A, i, N)$
Arithmetic gradient to uniform series	$\frac{(1 + i)^N - iN - 1}{i(1 + i)^N - i}$	$(A/G, i, N)$
Arithmetic gradient to present worth	$\frac{(1 + i)^N - iN - 1}{i^2(1 + i)^N}$	$(P/G, i, N)$
Group B. All cash flows discrete: continuous compounding at nominal rate r per period		
Continuous compounding compound amount (single payment)	e^{rN}	$(F/P, r, N)$
Continuous compounding present worth (single payment)	e^{-rN}	$(P/F, r, N)$
Continuous compounding present worth (single payment)	$\frac{e^{rN} - 1}{e^{rN}(e^r - 1)}$	$(P/A, r, N)$
Continuous compounding sinking fund	$\frac{e^r - 1}{e^{rN} - 1}$	$(A/F, r, N)$
Continuous compounding capital recovery	$\frac{e^{rN}(e^r - 1)}{e^{rN} - 1}$	$(A/P, r, N)$
Continuous compounding compound amount (uniform series)	$\frac{e^{rN} - 1}{e^r - 1}$	$(F/A, r, N)$
Group C. Continuous, uniform cash flows: continuous compounding		
Continuous compounding sinking fund (continuous, uniform payments)	$\frac{r}{e^{rN} - 1}$	$\bar{A}/F, r, N$
Continuous compounding capital recovery (continuous, uniform payments)	$\frac{re^{rN}}{e^{rN} - 1}$	$\bar{A}/P, r, N$
Continuous compounding compound amount (continuous, uniform payments)	$\frac{e^{rN} - 1}{r}$	$F/\bar{A}, r, N)$
Continuous compounding present worth (continuous, uniform payments)	$\frac{e^{rN} - 1}{re^{rN}}$	$P/\bar{A}, r, N)$

[a]See Appendix A for definitions of symbols used in this table.

Appendix C—Interest Tables

Table C-7.1 ***Present Worth Factor (Changes F to P)***

Yr.	2%	4%	6%	8%	10%	12%	15%	20%	25%	30%	40%	50%
1	.9804	.9615	.9434	.9259	.9091	.8929	.8696	.8333	.8000	.7692	.7143	.6667
2	.9612	.9246	.8900	.8573	.8264	.7972	.7561	.6944	.6400	.5917	.5102	.4444
3	.9423	.8890	.8396	.7938	.7513	.7118	.6575	.5787	.5120	.4552	.3644	.2963
4	.9238	.8548	.7921	.7350	.6830	.6355	.5718	.4823	.4096	.3501	.2603	.1975
5	.9057	.8219	.7473	.6806	.6209	.5674	.4972	.4019	.3277	.2693	.1859	.1317
6	.8880	.7903	.7050	.6302	.5645	.5066	.4323	.3349	.2621	.2072	.1328	.0878
7	.8706	.7599	.6651	.5835	.5132	.4523	.3759	.2791	.2097	.1594	.0949	.0585
8	.8535	.7307	.6274	.5403	.4665	.4039	.3269	.2326	.1678	.1226	.0678	.0390
9	.8368	.7026	.5919	.5002	.4241	.3606	.2843	.1938	.1342	.0943	.0484	.0260
10	.8203	.6756	.5584	.4632	.3855	.3220	.2472	.1615	.1074	.0725	.0346	.0173
11	.8043	.6496	.5268	.4289	.3505	.2875	.2149	.1346	.0859	.0558	.0247	.0116
12	.7885	.6246	.4970	.3971	.3186	.2567	.1869	.1122	.0687	.0429	.0176	.0077
13	.7730	.6006	.4688	.3677	.2897	.2292	.1625	.0935	.0550	.0330	.0126	.0051
14	.7579	.5775	.4423	.3405	.2633	.2046	.1413	.0779	.0440	.0254	.0090	.0034
15	.7430	.5553	.4173	.3152	.2394	.1827	.1229	.0649	.0352	.0195	.0064	.0023
16	.7284	.5339	.3936	.2919	.2176	.1631	.1069	.0541	.0281	.0150	.0046	.0015
17	.7142	.5134	.3714	.2703	.1978	.1456	.0929	.0451	.0225	.0116	.0033	.0010
18	.7002	.4936	.3503	.2502	.1799	.1300	.0808	.0376	.0180	.0089	.0023	.0007
19	.6864	.4746	.3305	.2317	.1635	.1161	.0703	.0313	.0144	.0068	.0017	.0005
20	.6730	.4564	.3118	.2145	.1486	.1037	.0611	.0261	.0115	.0053	.0012	.0003
21	.6698	.4388	.2942	.1987	.1351	.0926	.0531	.0217	.0092	.0040	.0009	
22	.6468	.4220	.2775	.1839	.1228	.0826	.0462	.0181	.0074	.0031	.0006	
23	.6342	.4057	.2618	.1703	.1117	.0738	.0402	.0151	.0059	.0024	.0004	
24	.6217	.3901	.2470	.1577	.1015	.0659	.0349	.0126	.0047	.0018	.0003	
25	.6095	.3751	.2330	.1460	.0923	.0588	.0304	.0105	.0038	.0014	.0002	
30	.5521	.3083	.1741	.0994	.0573	.0334	.0151	.0042	.0012			
35	.5000	.2534	.1301	.0676	.0356	.0189	.0075	.0017	.0004			
40	.4529	.2083	.0972	.0460	.0221	.0107	.0037	.0007	.0001			
45	.4102	.1712	.0727	.0313	.0137	.0061	.0019	.0003				
50	.3715	.1407	.0543	.0213	.0085	.0035	.0009	.0001			$\frac{1}{(1+i)^y}$	
60	.3048	.0951	.0303	.0099	.0033	.0011	.0002					
70	.2500	.0642	.0169	.0046	.0013	.0004						
80	.2051	.0434	.0095	.0021	.0005							
90	.1683	.0293	.0053	.0010	.0002							
100	.1380	.0198	.0030	.0005								

Table C-7.2 ***Capital Recovery Factor (Changes P to A)***

Yr.	2%	4%	6%	8%	10%	12%	15%	20%	25%	30%	40%	50%
1	1.020	1.040	1.060	1.080	1.100	1.120	1.150	1.200	1.250	1.300	1.400	1.500
2	.5150	.5302	.5454	.5608	.5762	.5917	.6151	.6545	.6944	.7348	.8167	.9000
3	.3468	.3603	.3741	.3880	.4021	.4163	.4380	.4747	.5123	.5506	.6294	.7105
4	.2626	.2755	.2886	.3019	.3155	.3292	.3503	.3863	.4234	.4616	.5408	.6231
5	.2122	.2246	.2374	.2505	.2638	.2774	.2983	.3344	.3719	.4106	.4914	.5758
6	.1785	.1908	.2034	.2163	.2296	.2432	.2642	.3007	.3388	.3784	.4613	.5481
7	.1545	.1666	.1791	.1921	.2054	.2191	.2404	.2774	.3163	.3569	.4419	.5311
8	.1365	.1485	.1610	.1740	.1874	.2013	.2229	.2606	.3004	.3419	.4291	.5203
9	.1225	.1345	.1470	.1601	.1736	.1877	.2096	.2481	.2888	.3312	.4203	.5134
10	.1113	.1233	.1359	.1490	.1627	.1770	.1993	.2385	.2801	.3235	.4143	.5088
11	.1022	.1141	.1268	.1401	.1540	.1684	.1911	.2311	.2735	.3177	.4101	.5059
12	.0946	.1066	.1193	.1327	.1468	.1614	.1845	.2253	.2685	.3135	.4072	.5039
13	.0881	.1001	.1130	.1265	.1408	.1557	.1791	.2206	.2645	.3102	.4051	.5026
14	.0826	.0947	.1076	.1213	.1357	.1509	.1747	.2169	.2615	.3078	.4036	.5017
15	.0778	.0899	.1030	.1168	.1315	.1469	.1710	.2139	.2591	.3060	.4026	.5011
16	.0737	.0858	.0990	.1130	.1278	.1434	.1679	.2114	.2572	.3046	.4019	.5008
17	.0700	.0822	.0954	.1096	.1247	.1405	.1654	.2094	.2558	.3035	.4013	.5005
18	.0667	.0790	.0924	.1067	.1219	.1379	.1632	.2078	.2546	.3027	.4009	.5003
19	.0638	.0761	.0896	.1041	.1195	.1358	.1613	.2065	.2537	.3021	.4007	.5002
20	.0611	.0736	.0872	.1019	.1175	.1339	.1598	.2054	.2529	.3016	.4005	.5002
21	.0588	.0713	.0850	.0998	.1156	.1322	.1584	.2044	.2523	.3012	.4003	.5000
22	.0566	.0692	.0830	.0980	.1140	.1308	.1573	.2037	.2519	.3009	.4002	
23	.0547	.0673	.0813	.0964	.1126	.1296	.1563	.2031	.2515	.3007	.4002	
24	.0529	.0656	.0797	.0950	.1113	.1285	.1554	.2025	.2512	.3006	.4001	
25	.0512	.0640	.0782	.0937	.1102	.1275	.1547	.2021	.2510	.3004	.4001	
30	.0446	.0578	.0726	.0888	.1061	.1241	.1523	.2008	.2503	.3001	.4000	
35	.0400	.0536	.0690	.0858	.1037	.1223	.1511	.2003	.2501			
40	.0366	.0505	.0664	.0839	.1023	.1213	.1506	.2001	.2500			
45	.0339	.0483	.0647	.0826	.1014	.1207	.1503	.2001				
50	.0318	.0466	.0634	.0817	.1009	.1204	.1501	.2000				
60	.0288	.0442	.0619	.0808	.1003	.1200	.1500				$\frac{i(1+i)^y}{(1+i)^y-1}$	
70	.0267	.0428	.0610	.0804	.1001							
80	.0252	.0418	.0606	.0802	.1000							
90	.0241	.0412	.0603	.0801								
100	.0232	.0408	.0602	.0800								

CHAPTER 8

Extreme Value Theory

G. Ramachandran

Introduction

The theory of extreme values, as generally known, deals with the statistical properties of the maximum or minimum value of a random variable. The theory has found practical applications in fields such as structural engineering, aeronautics, and meteorology. A comprehensive treatise on the extreme value theory and its applications was presented by Gumbel.[1] Further theoretical developments and applications are contained in *Statistical Extremes and Applications,* edited by Tiago de Oliveira.[2]

Fire protection is one such area, where figures for financial losses are generally available for large fires which, in the United Kingdom, for example, are currently defined as fires costing £50,000 or more in property damage. To make the best use of limited data provided by a small sample of large-loss fires, Ramachandran[3] has developed a general mathematical framework, the extreme order theory, which includes the largest loss as a particular case.

The *object* of this chapter is to explain the basic features of extreme order statistics and show how data on financial losses in large fires can be used for

1. Predicting the behavior of the tail (large losses) of the probability distribution of fire loss
2. Estimating the average loss in all fires, large and small, in a particular building or group of buildings with similar fire risks, and
3. Assessing the probable reduction in loss due to a fire protection measure

A few other possible applications of extreme value theory in the fire protection field are also discussed briefly. These include statistical analysis of test results, fire severity, and fire resistance.

Dr. G. Ramachandran retired in November 1988 as head of the operations research section at the Fire Research Station, United Kingdom. Since then he has been practicing as a consultant in risk evaluation and insurance. He is a visiting professor at the Universities of Manchester and Leeds. His research has focused on statistical and economic problems in fire protection and actuarial techniques in fire insurance. In October 1998 he published a book on the Economics of Fire Protection.

Extreme Order Distributions

The probability distribution of fire loss (x) is skewed, and, in general, the variable z ($= \log x$) has a distribution belonging to the "exponential type." (See Ramachandran[4–6] and Shpilberg.[7]) Among distributions of this type, normal for z (which is the same as log-normal for x) has been recommended widely for modeling fire insurance claims. Exponential for z or Pareto for x has been considered by some actuaries. The (cumulative) distribution function of z may be denoted by $F(z)$ and its density function by $f(z)$.

The logarithms of losses in n fires during a defined period of time constitute a sample of observations generated by the "parent" distribution $F(z)$. If these figures are arranged in decreasing order of magnitude, the mth value in this arrangement may be denoted by $z_{(m)n}$, which is the logarithm of the mth loss $x_{(m)n}$. For the largest value, the subscript m takes the value 1 (first rank).

In a series of samples (periods), each with a large number n of observations (fires), the values pertaining to $z_{(m)n}$ have a probability distribution with density function approximately given by

$$\frac{m^m a_{(m)n}}{(m-1)!} \exp\left[-my_{(m)} - m\exp\left(-y_{(m)}\right)\right] \qquad -\infty \le z_{(m)n} \le \infty \tag{1}$$

$$y_{(m)} = a_{(m)n}[z_{(m)n} - b_{(m)n}] \tag{2}$$

where $a_{(m)n}$ and $b_{(m)n}$ are solutions of

$$F[b_{(m)n}] = 1 - (m/n) \tag{3}$$

$$a_{(m)n} = (n/m)f[b_{(m)n}] \tag{4}$$

The parameter $b_{(m)n}$ is the modal value of $z_{(m)n}$. Ramachandran[3] has discussed different methods of estimating the parameters $a_{(m)n}$ and $b_{(m)n}$.

Behavior of Large Losses

Let $\bar{z}_{(m)n}$ and $s^2_{(m)n}$ be the mean and variance of $z_{(m)n}$, respectively, in N samples. For large N, the values of these two parameters tend to

$$\mu_{(m)z} = b_{(m)n} + \left[\frac{1}{a_{(m)n}}\right]\bar{y}_{(m)} \tag{5}$$

$$\sigma^2_{(m)z} = \frac{\sigma^2_{(m)y}}{a^2_{(m)n}} \tag{6}$$

where

$$\bar{y}_{(m)} = 0.5772 + \log_e m - \sum_{v=1}^{m-1}\left(\frac{1}{v}\right) \tag{7}$$

$$\sigma^2_{(m)y} = 1.6449 - \sum_{v=1}^{m-1}\left(\frac{1}{v^2}\right) \tag{8}$$

The value of $z_{(m)n}$ for any probability level, p, is given by

$$z_{(m)np} = b_{(m)n} + \left[\frac{1}{a_{(m)n}}\right]y_{(m)p} \tag{9}$$

where $y_{(m)p}$ is the value of $y_{(m)}$ corresponding to the probability level, p. The values of $y_{(m)p}$ for selected probability levels have been tabulated by Gumbel.[8]

Consider, as an example, the analysis carried out by Ramachandran[4] using the top 17 fire losses ($m = 1$ to 17) in the U.K. textile industry during the 21-year period ($N = 21$) from 1947 to 1967. The losses (in units of £1000) were first corrected for inflation by adjusting them to 1947 values. Base e was used for calculating the logarithms of losses. The linear method (Ramachandran[3]) was then applied to the logarithms of the corrected losses for estimating the parameters $a_{(m)n}$ and $b_{(m)n}$. Since the number of fires, n, per year varied over the period, the following approximate correction was included in the estimation process:

$$b_{(m)n_j} = b_{(m)n} + \left[\frac{1}{a_{(m)n}}\right]\log_e\left(\frac{n_j}{n}\right) \tag{10}$$

where $b_{(m)n_j}$ is the modal value of $z_{(m)}$ for the year with n_j fires. The results, reproduced in Table 5-8.1, pertain to a sample size of 465 fires, the frequency experienced in the base year 1947.

Figure 5-8.1 has been drawn on a log scale and shows the relationship between the annual frequency of fires in the textile industry and the probable loss, at 1947 prices, of the 1st ($m = 1$), 7th ($m = 7$), and 16th ($m = 16$) largest fires in a year. For each of these three ranks, the modal sizes of the losses are shown with confidence bands. For an estimated number of fires in any year, an ordinate erected at the corresponding point on the x-axis would intersect the upper and lower confidence lines at points giving the corresponding confidence limits. The probability of exceeding the upper or falling short of the lower limit is 0.1. For example, if the number of fires expected in a year in the textile industry is 1000, the most probable value of the largest loss would be £260,000, with upper and lower confidence limits of £700,000 and £180,000; all figures are at 1947 money values.

Table 5-8.1 ***Textile Industry Top Fire Losses from 1947 to 1967, U.K.***

Extreme (m)	$a_{(m)n}$	$b_{(m)n}$
1	2.247	5.214
2	1.785	4.829
3	1.626	4.534
4	1.460	4.327
5	1.387	4.113
6	1.424	3.988
7	1.239	3.749
8	1.163	3.564
9	1.212	3.448
10	1.034	3.259
11	0.973	3.137
12	0.925	2.972
13	0.886	2.832
14	0.924	2.749
15	0.937	2.680
16	0.950	2.583
17	1.002	2.537

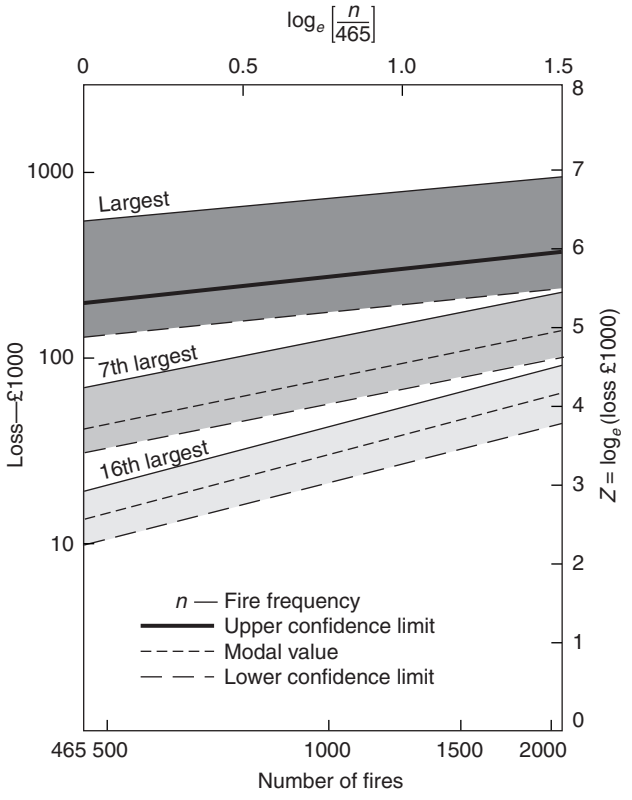

Figure 5-8.1. ***Fire frequency and large losses.***

The confidence lines represent a control chart based on the current trend. The increase in the frequency, n, of fires may be partly due to the inadequacy of fire prevention measures. In addition, if some or all of the actual large losses corrected for inflation exceeded the corresponding upper limits, it may be concluded that general

changes in fire fighting and fire protection methods or in the industrial processes are taking place to alter the picture for the worse. If the losses are less than the lower limits, then the changes are for the better. These arguments and the data on losses and number of fires for the period 1968 to 1978 suggested that protection measures were coping well with fire outbreaks in the U.K. textile industry. (See Ramachandran.[3]) This observation is true to some extent for the later period, as well.

Average Loss

If fire loss, x, is assumed to have a log-normal probability distribution, the expected or average loss is given by

$$\bar{x} = \exp\left(\mu + \frac{\sigma^2}{2}\right)$$

where μ and σ are the mean and standard deviation, respectively, of $z = \log_e x$. Estimation of the parameters μ and σ is a simple statistical problem if loss figures are available for all the n fires in a sample. If loss figures are available only for large losses above a threshold level, extreme value techniques can provide reasonably good estimates of μ and σ. The basic features of these techniques are as follows:

If z (= $\log x$) has a normal distribution, the standard variable

$$t = \frac{(z - \mu)}{\sigma}$$

has also a normal distribution with distribution function $G(t)$ and density function $g(t)$. As defined earlier, if $z_{(m)n}$ is the logarithm of the mth loss $x_{(m)n}$ from the top, the variable

$$t_{(m)n} = \frac{[z_{(m)n} - \mu]}{\sigma} \tag{11}$$

follows the extreme order distribution shown in Equation 1 with

$$y_{(m)} = A_{(m)n}[t_{(m)n} - B_{(m)n}] \tag{12}$$

instead of Equation 2. As in Equations 3 and 4, the parameters $A_{(m)n}$ and $B_{(m)n}$ are given by

$$G[B_{(m)n}] = 1 - \left(\frac{m}{n}\right) \tag{13}$$

$$A_{(m)n} = \left(\frac{n}{m}\right) g[B_{(m)n}] \tag{14}$$

The values of $B_{(m)n}$ for the standard normal distribution have been well tabulated by, for example, Fisher and Yates.[9] The corresponding values of $A_{(m)n}$ can then be obtained for Equation 14. From Equation 12 the expected value of $t_{(m)n}$ is

$$\bar{t}_{(m)n} = B_{(m)n} + \left[\frac{1}{A_{(m)n}}\right] \bar{y}_{(m)} \tag{15}$$

with $\bar{y}_{(m)}$ given by Equation 7. From Equation 11, the expected values of $z_{(m)n}$ is

$$\bar{z}_{(m)n} = \mu + \sigma \bar{t}_{(m)n} \tag{16}$$

The value of $z_{(m)n}$ in a single sample or its mean value over N samples (each with n fires) will provide an estimate of $\bar{z}_{(m)n}$.

If figures for losses are available for, say, r large fires (m = 1 to r), the straight line in Equation 16 can be used to obtain rough estimates of μ and σ by plotting the r pairs of values $[\bar{z}_{(m)n}, \bar{t}_{(m)n}]$ and drawing the best line, or by the method of least squares. However, this method is somewhat imprecise, since the residual errors in Equation 16 arise from ranked variables and, hence, vary with m (not constant) and are correlated (not independent). For dealing with this problem, Ramachandran[3,10] has developed a generalized least squares method that provides the best and unbiased estimates of μ and σ but requires the use of a complex computer program. Ramachandran also described a maximum likelihood method in these studies which involves simple calculations for estimating μ and σ for each sample.

Economic Value of Fire Protection Measures

The economic value of a fire protection measure depends on the reduction in loss that could be expected due to the satisfactory operation of the measure in the event of a fire. This reduction could be assessed in terms of the difference in the expected (average) loss in two groups of buildings with similar fire risks—one group equipped with the fire protection measure and the other not equipped. The reduction in loss or gain is one of the main components in a cost-benefit analysis of a fire protection measure.

Consider, as an example, the investigation carried out by Rogers[11] in regard to the effect of sprinkler protection of buildings. Rogers applied the generalized least square method mentioned in the previous section, assuming specifically that fire loss has a log-normal probability distribution. Table 5-8.2 contains some interesting results obtained by Rogers for average loss in all fires (estimated from large losses). The figures in Table 5-8.2 relate to fires that survived "infant mortality"; very small fires were excluded from the total sample size (n), since their inclusion would distort the shape of the loss distribution, particularly at the upper tail. It is apparent that sprinklers reduce the loss expected in multistory buildings to a considerable extent. Sprinklers also reduce the probability of loss in a fire exceeding a large amount (see Figure 5-8.2), based on the parameters μ and σ estimated from large losses in connection with the results in Table 5-8.2. (The parameters in Figure 5-8.2 pertain to $z = \log_{10} x$.)

Factors Affecting Fire Damage

A full assessment of fire risk ought to consider all the relevant factors affecting fire damage and evaluate their

Table 5-8.2 ***Average Loss per Fire at 1966 Prices (£ × 000)***

	Sprinklered Single Story	Sprinklered Multistory	Nonsprinklered Single Story	Nonsprinklered Multistory
Textiles	2.9	3.5	6.6	25.2
Timber and furniture	1.2	3.2	2.4	6.5
Paper, printing, and publishing	5.2	5.0	7.1	16.2
Chemical and allied	3.6	4.3	4.3	8.2
Wholesale distributive trades	—	4.7	3.8	9.4
Retail distributive trades	—	1.4	0.4	2.4

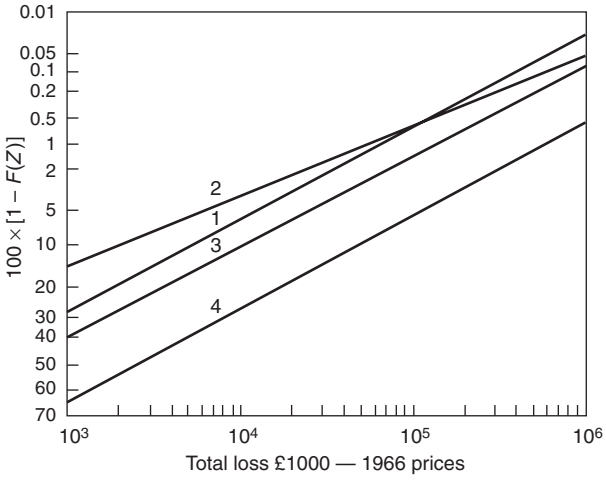

Line	Subpopulation	Parameters
1	Sprinkler/single story	μ = –0.616 σ = 1.024
2	Sprinker/multistory	μ = –1.419 σ = 1.340
3	Nonsprinkler/single story	μ = –0.334 σ = 1.062
4	Nonsprinkler multistory	μ = 0.401 σ = 0.992

$F(Z)$ (cumulative distribution for Z) = probability of loss less than or equal to Z

$V(X)$ (cumulative distribution for X) = probability of loss less than or equal to X

Survivor probability = $1 - F(Z) = 1 - V(X)$ = probability of loss exceeding X or Z

Figure 5-8.2. ***The survivor probability distribution of fire loss for each class in the textile industry.***

independent contribution to the damage. A full assessment is possible by performing a multiple regression analysis. The problem is to estimate the regression parameters, using large observations of the dependent variable, logarithm of loss. (Factors affecting the damage, assigned numerical values, will be independent variables.) For tackling this problem, a multiple regression model, based on extreme order theory, has been developed by Ramachandran.[3,12] Using large losses, this model gives estimates of regression parameters approximately equivalent to estimates that would be obtained if loss figures were available for all the fires and were utilized in the calculations.

Consider, for example, the expected loss which has a "power relationship" with the size of a building such that

$$z = \alpha + \beta \log A \tag{17}$$

where z is the logarithm of loss, and A is the total floor area of a building.

The linear relationship in Equation 17 was incorporated in an investigation concerned with the trade-offs between sprinklers and structural fire resistance (Ramachandran[3]). Based on the information about buildings given in the reports on fires furnished by the fire brigades, industrial buildings were classified into two broad groups—high and low fire resistance. Each of these groups was further divided into single story and multistory and sprinklered and nonsprinklered. The parameters α and β were estimated for each of the eight subgroups and for each industry using large-loss figures. As an example, expected losses for two hypothetical multistory buildings engaged in textile manufacture are given in Table 5-8.3.

Analysis of Test Results

In some fire tests, observations recorded are extreme values (maximum or minimum). In such cases, classical methods of analysis of variance, although normally carried out, are not strictly applicable. Extremes, particularly the maximum and the minimum, have highly skewed

Table 5-8.3 ***Textile Industry, Multistory Buildings Expected Loss (£) at 1978 Prices***

	Floor area (ft²)	
Building Category	100,000	1,000,000
Sprinklered		
High fire resistance	4080	5790
Low fire resistance	6460	23,070
Nonsprinklered		
High fire resistance	19,910	38,260
Low fire resistance	31,510	152,410

probability distributions and, hence, are not normally distributed. In these problems, the following approach may be used to test the difference between two maximum values. (For a similar test for minimum values, see Ramachandran and Rogers.[13])

If the reduced variable of the maximum is written as

$$y_{(1)} = a_{(1)}[z_{(1)} - b_{(1)}] \tag{18}$$

and

$$u_{(1)} = \exp[-y_{(1)}] \tag{19}$$

the variable $2u_{(1)}$ has a chi square distribution with 2 degrees of freedom. It follows, therefore, that $\exp[y_{(1)2} - y_{(1)1}]$ has an "F" distribution with (2, 2) degrees of freedom. The reduced maximums, $y_{(1)1}$ and $y_{(1)2}$, belong to two independent samples from exponential-type parents, with $z_{(1)1}$ and $z_{(1)2}$ as the maximum observations in the samples. From Equation 18

$$y_{(1)1} = a_{(1)1}[z_{(1)1} - b_{(1)1}] \tag{20}$$

$$y_{(1)2} = a_{(1)2}[z_{(1)2} - b_{(1)2}] \tag{21}$$

and from Equation 19

$$u_{(1)1} = \exp[-y_{(1)1}]$$

$$u_{(1)2} = \exp[-y_{(1)2}]$$

As in the "F" test, the values $y_{(1)1}$ and $y_{(1)2}$ should be so denoted that $u_{(1)1}$ is greater than $u_{(1)2}$. The variable

$$z = \frac{1}{2}\log\left[\frac{u_{(1)1}}{u_{(1)2}}\right] = \frac{1}{2}[y_{(1)2} - y_{(1)1}] \tag{22}$$

has the z distribution, the probability points of which have been tabulated by Fisher and Yates.[9] It may be verified that the α percent point of z in this particular case is given by the following formula derived by Ramachandran and Rogers.[13]

$$z = \frac{1}{2}\log_e\left(\frac{1-\alpha}{\alpha}\right) \tag{23}$$

Significant difference in $y_{(1)2} - y_{(1)1}$ at α level would occur if the observed value of z given by Equation 22 is greater than the value of z given by Equation 23.

Consider, as an example, large-scale tests conducted at the Fire Research Station, U.K., to assess the products due to combustion of plastics. The three factors investigated were (1) crib load, (2) weight of the plastic (PVC), and (3) width of ventilation opening. The observations recorded were maximum temperature, maximum concentrations of carbon dioxide and carbon monoxide, and minimum oxygen; a graphic analysis revealed that variables as such (without any log transformation) approximate an exponential-type distribution.

Table 5-8.4 ***Maximum Temperature at Vent Position***

Levels of other factors (kg)		Vent width levels				
		240 mm		700 mm		
Load	PVC	Max Temp.	y	Max Temp.	y	z
120.5	0	870	–0.6533	925	–0.8340	0.0904
120.5	95	950	0.4587	975	–0.1390	0.2989
241	0	960	0.5977	1100	1.5985	0.5004
241	95	1010	1.2927	1020	0.4865	0.4031
103.5 137.5	0	960	0.5977	1070	1.1815	0.2919

For purposes of illustration, the results for maximum temperature at vent position are reproduced in Table 5-8.4. (See Ramachandran and Rogers[13] for full details of the statistical analysis.) It was assumed that the scale parameter $a_{(1)}$ was the same for all the 10 maximum observations arising from 10 independent samples. The standard deviation, σ_z, of these observations was 68.06. According to Gumbel,[1] the standard deviation, σ_y, of $y_{(1)}$ is 0.9497 for $N = 10$. Hence, from Equation 18, an estimated value of $a_{(1)}$ was given by

$$\alpha_{(1)} = \frac{\sigma_y}{\sigma_z} = 0.0139$$

The averages of the maximum temperatures $\bar{z}_{240}$ and $\bar{z}_{700}$ for the two vent width levels were 950 and 1018. For $N = 5$, the mean $[\bar{y}_{(1)}]$ of $y_{(1)}$ was found to be 0.4588. From Equation 18, the values of parameters $b_{(1)}$ were estimated as

$$b_{240} = \bar{z}_{240} - \left[\frac{\bar{y}_{(1)}}{a_{(1)}}\right] = 917$$

$$b_{700} = \bar{z}_{700} - \left[\frac{\bar{y}_{(1)}}{a_{(1)}}\right] = 985$$

For each pair of observations, the y values and the z test statistic were calculated using Equations 20 through 22. From Equation 23, for $\alpha = 0.10$ (10 percent point), the theoretical value of z was 1.0986. In all the five cases, the observed z values in Table 5-8.4 were less than 1.0986. This implied that there was no significant difference between the maximum temperature at the vent position for the two ventilation levels for any fixed level of the other two factors, load and PVC. At present, it is not possible to test the interactions between factors and the differences between overall means, such as $(\bar{z}_{240} - \bar{z}_{700})$.

Fire Severity and Fire Resistance

For the design of a fire-resistant building, knowledge of the expected fire severity is essential. The fire severity in a room will vary with the quantity of combustible material (fire load), the area of ventilation, and the dimensions of the room. Fire severities, however, may differ from room to room in a building, because the furnishings

in a building are seldom everywhere equal and may also change with time. Thus, it is difficult to predict whether a fire in a given building will be ventilation controlled. For the reasons mentioned above, fire severity must be regarded as a random variable with a probability distribution. This distribution can be assumed to be exponential such that the probability of fire severity being greater than S is given by $\exp(-\lambda_s S)$, with the variable S measured in time units, say, minutes. (See, for example, Sara-Coward.[14])

There are no data available at present to estimate the probability distribution of the fire resistance, R, of a room or a complete building. It might be possible to determine this distribution from the fire resistance of structural elements and the plan of a building showing the connections between rooms, corridors, floors, and so forth, using, in addition, data on factors such as doors and windows which affect the fire resistance. Purely from heuristic reasoning, exponential or log-normal distribution has been suggested for the fire resistance of a structural element. Log-normal was assumed in a statistical analysis of fire resistance of laminated timber columns (Ramachandran.[15])

In a fire, failure of the structure of, for example, a room occurs if the fire resistance, R, of the room is less than the fire severity, S, both the variables expressed in units of time. The probability of this failure event can be evaluated from the probability distributions of R and S, if this information is available.

What is ideally required is the probability of minimum fire resistance, R_p, being less than the maximum possible fire severity, S_q. If this probability is denoted by ∂ such that

$$\text{Prob}(R_p < S_q) = \partial \tag{24}$$

then ∂ should be a small value which is allowable or acceptable, depending on the consequences of failure in terms of damage to life and property. From a political point of view, it might be possible to tolerate a certain number of deaths and injuries and a certain amount of property loss resulting from the failure of building structures due to fires. For any type of building, the acceptable level of ∂ depends on the number of buildings of this type at risk and the fire damage (life and property) experienced by these buildings.

It must be recognized that both R_p and S_q are random variables and not constants. Since fire resistance has an exponential-type distribution, the reduced variable

$$y_p = a_p(R_p - b_p) \tag{25}$$

has the probability distribution of the smallest (minimum) value with distribution function

$$1 - \exp[-\exp(y_p)] \tag{26}$$

and density function

$$\exp[y_p - \exp(y_p)] \tag{27}$$

The parameters a_p and b_p can be estimated from the parent distribution of fire resistance, if the exact nature of this distribution is known together with its location and scale parameters. In the case of the minimum, if $U(R)$ is the parent cumulative distribution function,

$$U(b_p) = \frac{1}{n} \tag{28}$$

such that the probability of fire resistance being less than b_p is $(1/n)$. The value of n may be so chosen that Equation 28 gives a small value which is acceptable. The parameter a_p is given by $\nu(b_p)$, where $u(R)$ is the density function corresponding to $U(R)$.

Since fire severity has an exponential-type distribution, the maximum fire severity S_q, with $m = 1$ in Equation 1, has the density function

$$\exp[-y_q - \exp(-y_q)] \tag{29}$$

and distribution function

$$\exp[-\exp(-y_q)] \tag{30}$$

where

$$y_q = a_q(S_q - b_q) \tag{31}$$

If $V(S)$ is the distribution function of fire severity, the parameter b_q, from Equation 3, is given by

$$V(b_q) = 1 - \left(\frac{1}{n}\right) \tag{32}$$

such that the probability of fire severity exceeding b_q is $(1/n)$. Then, from Equation 4, $a_q = nv_{(bq)}$, where $v(s)$ is the density function of fire severity.

Having defined the probability distributions and parameters of minimum fire resistance and maximum fire severity, it follows to study the random behavior of the variable

$$d_{RS} = R_p - S_q \tag{33}$$

which will enable the evaluation of the probability given by Equation 24. This problem is the subject of a current research investigation by the author. In conclusion, the fire resistance of the structural elements of a building should be such that the fire safety level specified in Equation 24 will be satisfied.

References Cited

1. E.J. Gumbel, *Statistics of Extremes,* Columbia Univ. Press, New York (1958).
2. J. Tiago de Oliveira (ed.), *Statistical Extremes and Applications,* D. Reidel, Dordrecht (1984).
3. G. Ramachandran, *F. Safety J.*, 5, p. 59 (1982).

4. G. Ramachandran, *Fire Research Note No. 910,* Fire Research Station, Borehamwood, UK (1972).
5. G. Ramachandran, *ASTIN Bul.,* 7, p. 293 (1974).
6. G. Ramachandran, "Extreme Order Statistics in Large Samples from Exponential-Type Distributions and Their Application to Fire Loss," in *Statistical Distributions in Scientific Work,* 2, p. 335, D. Reidel, Dordrecht (1975).
7. D.C. Shpilberg, *Tech. Rep. 22431,* Factory Mutual Research Corp., Norwood (1974).
8. E.J. Gumbel, *Probability Tables for the Analysis of Extreme Value Data—Applied Mathematics,* National Bureau of Standards, Washington, DC (1953).
9. R.A. Fisher and F. Yates, *Statistical Tables for Biological, Agricultural, and Medical Research,* Oliver and Boyd, London (1953).
10. G. Ramachandran, "Extreme Order Statistics from Exponential-Type Distributions with Applications to Fire Protection and Insurance," Ph.D. Thesis, University of London (1975).
11. F.E. Rogers, *Current Paper CP 9/77,* Building Research Establishment, Borehamwood, UK (1977).
12. G. Ramachandran, *ASTIN Bul.,* 8, p. 229 (1975).
13. G. Ramachandran and F.E. Rogers, "Toxic Gases and Smoke from Polyvinyl Chloride in Fires—Statistical Analysis of Test Results," *Fire Research Note, No. 1021,* Fire Research Station, Borehamwood, UK (1974).
14. K.D. Sara-Coward, *Current Paper CP 31/75,* Building Research Establishment, Borehamwood, UK (1975).
15. G. Ramachandran, *Fire Research Note No. 943,* Fire Research Station, Borehamwood, UK (1972).

CHAPTER 9

Computer Simulation for Fire Protection Engineering

William G. B. Phillips, Revised by Douglas K. Beller and Rita F. Fahy

Introduction

Fire protection engineers are required to deal with a complex fire scenario that includes human reactions and behavior, in addition to the physical and chemical fire processes. Operations research (OR) pioneered the application of the scientific method to the management of organized systems in which human behavior is a key element. Fire protection engineering could be defined as the application of operations research to the fire system.

Systems involving human beings are difficult to study because realistic experiments may be impossible and neither past experience nor the available data provide sufficient insight. Operations research overcomes these difficulties by the use of simulation models. Simulation models are widely used in science, engineering, and mathematics to study problems that involve ordinary and partial differential equations (either overtly or implicitly). In fire science, for example, simulation models have been used to handle phenomena such as smoke movement and absorption of toxic substances. Both computational fluid dynamics (CFD) models and zone models are solved by similar techniques. These matters are dealt with elsewhere in this handbook. This chapter concentrates on the variety of procedural simulation models that may be applied to interdisciplinary systems, specifically those involving human agents and objectives.

Simulation models describe the system under study in terms of individual events of the individual components of the system.[1] In a gross sense, the simulation model of interest to fire protection practitioners can be divided into human (i.e., evacuation or egress) and physics (i.e., fire effects) components. The simulation model then combines these parts in their natural order and allows the computer to present the effect of their interaction on each other.[1] After the model is constructed, it is provided with data and run to simulate the actual operation of the system. Advances in computer software and hardware have greatly reduced the cost and simplified the use of simulation models. Recent developments in virtual reality are expected to facilitate more realistic interaction between the model and its user.

Uncertainty can be handled by introducing stochastic elements into the model. Estimates of risk can be derived from simulation models by the use of Monte Carlo techniques. Regression analysis can be applied to obtain compact expressions that can be used to measure the sensitivity of the output variables to variations in the inputs.

Types of Models

A model can represent a system as a unified and precisely definable whole, all of whose aspects are simultaneously and unambiguously accessible for assessment. Models include pictures, diagrams, and "scale models," as well as mathematical structures.

Models can be classified as descriptive, physical, and symbolic.[2] The *descriptive model* is expressed in ordinary language and is the most common tool for decision making in science, engineering, and everyday life. Descriptive models function like metaphors. For example, the flow of smoke through a vent might be compared to the flow of water in a channel, implying that buoyancy and gravity play a similar role albeit with a reversal of sign.

Physical models include scale models, and examples can range from basic hydraulic models of harbors and estuaries to transparent plastic models to demonstrate the flow of smoke in buildings. They make it possible to try out alternative arrangements in the search for an optimum design or strategy. Analogue models are a special

William G.B. Phillips, BSc (Eng), BSc (Econ), ARSM, MIMM, is a member of the Fire Risk Unit at the Fire Research Station of the Building Research Establishment at Borehamwood, Hertfordshire. His recent research has been mainly concerned with the development of new methods of fire risk assessment based on simulation models.

Douglas K. Beller is a fire modeling specialist.

Rita F. Fahy, PhD, is the manager of fire databases and systems at NFPA.

type of physical model that exploits the isomorphisms that exist between different physical processes. The behavior of voltages, currents, resistance, capacitance, and inductance in an electrical circuit has many analogies with processes in heat and fluid flow and acoustic, electromagnetic, and mechanical systems.

Science and engineering depend heavily on *symbolic models* in which algebraic symbols represent the values of variables and the relationships between them. Once a model has been cast in symbolic form, the whole mathematical apparatus can be deployed to deduce additional relationships and solve equations to find optimal solutions. Symbolic models may be static or dynamic; in the latter case they specifically include a variable representing time. A very important type of dynamic model is formulated in terms of ordinary or partial differential equations. Many problems in fire science lead to models that can be expressed in the form of one or more simultaneous differential equations. Some of these have simple analytic solutions, but many interesting cases do not, for example, the partial differential equations that arise in fluid dynamics (Navier-Stokes equations). Such equations are normally solved on computers by standard numerical methods.

A *simulation model* treats the dynamic relationships that are assumed to exist in the real situation as a series of elementary operations on the appropriate variables. A simulation model is made to predict outcomes by actually executing the procedural steps with appropriate initial data and parameters. All of the components comprising a simulation model need not be contained in a single piece of software. Furthermore, as long as each procedural step is represented in the model, the model need not be entirely computer-based. This is to say that the procedural steps associated with some components of the model may be determined using simple hand calculations. The model user then ensures that the components are constructed in the proper manner to provide the intended output. Running the model creates the prediction. The variables in a simulation may change continuously in value or take on only certain discrete values. These changes may take place at any time or only at certain times, or both. For example, a simulation of a fire incident might handle the flow of hot gases by a differential equation expressed in continuous terms, while the people would be treated as discrete individuals moving at prescribed moments in time. However, since such a model would almost certainly be implemented on a computer, the differential equations would be approximated by a difference equation for the purposes of numerical integration (a computer cannot handle "real" numbers). Therefore, the distinction between continuous simulation models and the dynamic symbolic models discussed in the previous paragraph tends to blur.

Simulation Models

A procedural simulation model is a representation of a dynamic system in which the processes or interactions bear a close resemblance or relationship to those of the specific system being simulated or studied. These models are concrete rather than abstract and may contain approximations and subjective elements. They are amenable to manipulations that would be impossible, too expensive, or impractical to perform on the entity portrayed. The operation of the model can be studied, and properties concerning the behavior of the actual system or its subsystems can be inferred. Manipulation of a procedural model requires the acceptance of inputs and the generation of outputs that are similar or analogous to those of the system represented.

Procedural simulation is essentially a technique that involves setting up a model of a real situation and then performing experiments on the model. The idea that a computer model might partly replace experimentation is both dangerous and attractive. It is, therefore, appropriate to remember a warning given by Ackoff and Beer:[3]

> Often when an operations researcher does not understand a phenomenon which he can nevertheless describe well, he can simulate it on a computer and thus conduct experiments. These are experiments on the model on which the simulation is based, not on the system involved. The fact that a simulation may reproduce history with some accuracy does not by itself establish a correspondence of structure between the model and reality. This is true for the same reason that a straight line may have been generated by a sine function, not one that is linear.

Procedural simulation modeling has been widely applied; examples are Link (aircraft pilot) trainers, military war games, business management games, space exploration, physical models of river basins and estuaries, econometric models, electrical analog devices, and wind-tunnel tests for aircraft. It has proved particularly useful in situations involving human intervention of one kind or another. There are great opportunities for improving the interface between the model and operator, making use of virtual reality techniques. In this way, "realistic experience" of rare events can be acquired without danger and at low cost.

Types of Simulation Models

Simulation models can be classified as either discrete or continuous. In the real world there is no such distinction, yet it is possible to model some real-world systems either discretely or continuously. In both types of simulation what is of concern are the changes in the state of the model. Continuous simulations are analogous to a stream of fluid passing through a pipe. The volume may increase or decrease, but the flow is continuous. Using the pipe analogy for discrete event simulation, the pipe could either be empty or have something traveling through it. Whether anything came out of the pipe would depend on some event occurring at the other end.

Both types of simulation can be applied to fire. As time progresses the state of a building changes continuously as the once small fire becomes larger, overwhelms the building, and eventually dies out as it runs out of fuel. The chemical processes in the fire and the physical processes that mediate the flow of heat and hot gases naturally lend themselves to the continuous type of model.

On the other hand, discrete simulations are more appropriate to the strategies used to fight the fire and evacuate the building. For example, the fire is ignited and detected, fire fighters and equipment arrive, hoses are deployed, water is applied, more equipment may be called in, and so on. Similarly the occupants respond to the alarm, collect their belongings, locate their household members, and go toward the exits in a sequence of clear-cut stages.

In continuous models, changes in the variables are directly based on changes in time. The values of the variables reflect the state of the model at any particular time, and simulated time advances from one step to the next usually in equal increments. In discrete event models, events occur as items move through the simulation. The state of the model changes only when those events occur. Simulated time advances from one event to the next (generally in unequal increments), and the mere passing of time has no direct effect.

Discrete Event Simulation Models

Discrete event simulation models are built up from several different elements. These are given different names in different programming languages. A terminology based on *blocks, items,* and *events* will be used in this discussion. *Items* are characterized by *attributes, priorities,* and *values.*

A *block* is used to represent an action, operation, resource, or process. It is like a block in a block diagram. These blocks are connected in an activity or data flow diagram that represents the system. Information comes into the block and is processed by the program that is in the block. The block then transmits information out of the block to the next block in the simulation. Some blocks may simply represent a source of information that is passed on to other blocks. Other blocks may modify information as it passes through them. Output blocks take information from the simulation and present it to the user in graphic form.

The basic unit passed between the blocks is called an *item.* An item is a data set that carries information about the item's attributes, priorities, and values. In a manufacturing model, an item might be a part on an assembly line; in a network model, an item would be a packet of information; in an evacuation model, an item would be an occupant. Items are generated by special blocks, either according to a fixed schedule or a random distribution.

The model moves items from block to block only when an *event* occurs. Events only occur when specific blocks specify that they should. For example:

1. Blocks that depend on time cause events to happen at an appropriate time. For example, a block representing an activity, for example, the journey from the fire station to the fire location, might introduce a delay of t min into the system representing the duration of the journey. If the alarm was received by the fire station at T min, the block would post an event in the event queue at $T + t$ min.
2. Blocks that have an accumulated demand for inputs cause an event immediately after they receive items. For example, a block representing a parent searching for a child, following a fire alarm, would cause an event when the child is located.
3. Blocks that do not generate events allow the blocks after them to pull items during a single event. Thus, an item can pass through many blocks after a single event if those blocks do not stop it.

Note that every event has the potential to cause every block in a model to move items. Thus, one event may cause many unrelated items to progress in the simulation.

In order to provide true discrete event simulation, the time clock that controls the simulation must move to the exact time of each event. The most common way of doing this is to have an event queue. Each block places the time of its next event in a slot in the event queue. In each cycle the event queue is checked to find the next closest time point; the current time is set to that value, and a "simulate" message is sent to every block. Most blocks ignore these messages unless the message occurs at the event time that was previously posted by the block, or there are items waiting in the block's inputs that can be pulled in. For example, a block representing a queue should pull in an available item whenever it gets a "simulate" message, no matter which block posted the event.

Attributes are an important aspect of discrete event simulation. Attributes are characteristic properties of an item that stay with it as it moves through the simulation. For example, an occupant making an escape from a building might have attributes representing mobility and the amount of carbon monoxide absorbed. *Priorities* specify the relative importance of an item. *Values* allow the model to deal with items that represent groups of identical entities.

Continuous Simulation Models

There is a close similarity between continuous simulation models and the solution of ordinary differential equations by numerical methods. Almost any phenomenon that can be represented by differential equations may be modeled by continuous simulation. This classification includes virtually the whole of classical physics, and the method can easily be extended to chemistry and biology and more speculatively to economics, ecology, and human behavior. The fundamental principle is that the rate of change of certain variables can be expressed as a function of a set of variables (the state variables) that describe the state of the system at a given time. Therefore,

$$\frac{dx_i}{dt} = f(x_1 \ldots x_i \ldots x_n), \quad i = 1 \ldots n$$

The solution to this set of equations is found by integration and yields a function that depends on time, which characterizes the dynamic behavior of the system. For example, suppose the rate at which a chemical reagent is consumed is proportional to the concentration of the reagent. This relationship could be expressed in the form of a differential equation, with the following solution:

$$\frac{dx}{dt} = -kx$$

and, therefore,

$$x = Ae^{-kt}$$

This result can be interpreted to mean that the concentration declines exponentially and tends toward zero as the reaction proceeds. Note that the result is a function of time and not concentration. This example leads to a first order linear differential equation that has an analytic solution. Many systems of interest, however, give rise to higher order nonlinear differential equations, which, in general, do not have analytic solutions or only have solutions if drastic simplifications are imposed. Their solution is normally carried out on computers using one of the standard numerical methods (e.g., Euler, Runge-Kutta). Higher order differential equations can lead to very complex dynamic behavior, for example, various types of oscillation. (It is useful to note that differential equations of an order above the first can always be replaced by one or more first order simultaneous differential equations.)

For a computer to handle a differential equation expressed in continuous terms, the equation has to be replaced by an equivalent difference equation. Consider the following differential equation that shows the rate of change in volume is equal to flow.

$$\frac{d(\text{volume})}{dt} = \text{flow}$$

This equation has an analytic solution that can be found by integration; that is,

$$\text{volume} = \int_{t=\text{start}}^{t=\text{stop}} \text{flow} \cdot dt$$

The original differential equation can be written as a difference equation:

$$\frac{\text{volume}_t - \text{volume}_{t-\Delta t}}{\Delta t} = \text{flow}$$

which can be rearranged to show that

$$\text{volume}_t = \text{volume}_{t-\Delta t} + \Delta t \cdot \text{flow}$$

This equation implies that the value of volume at time t is simply the sum of the value of volume at time $t - \Delta t$ plus the time interval Δt multiplied by flow. This solution (which amounts to Euler's method) can be implemented directly on a computer. Note that the analytic integral solution and the finite difference method will only give the same result if flow is constant. If flow is changing rapidly, the finite difference method will require a large number of iterations (i.e., $\Delta t \rightarrow 0$) to converge to the analytic integral solution.

Continuous simulation models are particularly suited to the analysis of dynamic processes. Frequently the system under examination will display a particular behavior pattern that may be interesting in itself or may be causing a problem. The objective of the model designer is then to construct a model based on differential equations that will reproduce this reference pattern. Decisions need to be made as to which state variables and rates of change are significant. If the model is being used to address some well-understood phenomena, it may be possible to use established relationships that have been tested by experiment. Otherwise, it may be necessary to introduce parameters into the model that lack theoretical backing but enable the model to exhibit the reference behavior either qualitatively or quantitatively.

The overall behavior of the model often depends not as much on the precise value of the parameters and the detailed algebra as on the structure of the model itself. Systems of simultaneous differential equations can usually be shown to be linked together in longer or shorter loops that can be of either positive or negative sign. Positive feedback loops tend to reinforce change and often give rise to exponential growth. Negative feedback loops tend to negate change and are usually associated with goal-seeking activity.

Model building can be thought of as passing through a sequence of iterations in which the model becomes more and more realistic. At each iteration the model designer makes observations, forms hypotheses, carries out tests, modifies the model, and tests the model again. The advantage of working within this framework is that simulation models are objective and explicit rather than subjective and implicit. These characteristics make them particularly valuable for (1) communicating results and (2) acting as a workbench on which alternative solutions to problems can be tested.

Monte Carlo Procedures

Monte Carlo analysis is a simulation technique applicable to problems having a stochastic or probabilistic basis. Two different types of problems give rise to the use of this technique. Firstly, there are those problems that involve some kind of stochastic process. The rate of flame spread and fire growth and the response of individuals to fire alarms are examples of variables that may be considered to be stochastic in nature. In this case, the stochastic element may be introduced at any point in the model run so that the value of a variable at any time depends in some way on its previous value and a random component. Secondly, there are problems in which the process is treated as deterministic, but the starting conditions and model parameters are randomly selected from probability distributions.

The model may be used simply to estimate the value of the endogenous variables at a given location and time. The estimate will, of course, depend on the values of the parameters supplied to the model. However, the exact value of a parameter may not be known, but it might be possible to estimate its mean and variance and the form of its distribution. This information can be encoded as a probability density. A sequence of runs of the model can then be carried out using samples drawn from this distribution. Methods have been developed for generating values from most of the well-known probability distributions as well as any empirical distribution. (For details see Appendix A of this chapter.) It is then possible to estimate probability densities representing, for example, the fire conditions or the number of casualties from the model output. If sensitivity analysis shows that the uncertainty in the input has little effect on the uncertainty in the output, it would not be necessary to go to great expense to refine the value of the input parameter.

Everything said so far about Monte Carlo methods has been on the assumption that there is only one input

variable and one output variable. This assumption can now be relaxed so that all the uncertain input parameters can be treated as random samples from probability densities. The probability density of the output variables is now generated by the probability densities of all the input variables. This function is important because it allows analysis of synergistic effects in which certain combinations of symmetrically distributed input variables can give rise to strongly skewed distributions of the output variables. Distributions of this type are typical of multiplicative stochastic processes. Probability distributions of fire damage are frequently skewed and can often be described by a density of the log-normal variety with a pronounced right-hand tail.[4] This result may be due to the simultaneous occurrence of several adverse factors which tend to reinforce each other due to nonlinearities in the system.

The input parameters can be interpreted as exogenous variables and the model outputs as endogenous variables. This approach suggests that it would be possible to regress the outputs on the inputs using a standard multiple linear regression routine. This method is equivalent to creating a linear model of the nonlinear simulation model. The relationships between the actual fire, the simulation model, and the linear approximation to the simulation model are shown in Figure 5-9.1.[5]

It can be shown[6] that the resulting regression coefficients correspond to the partial differential coefficients (i.e., the rate of change of an endogenous variable, y, with respect to each of the exogenous variables, x).

Applications

There are not many fully developed applications of procedural simulation models to fire protection engineering. For example, CRISP II would certainly qualify, while FIRE STATION is not a complete system model because it ignores the interactions between the fire and the occupants. FIRE STATION might be better described as an OR simulation model. Suites or collections of applications are also available.

CRISP II (Computation of Risk Indices by Simulation Procedures)[7]

Simulation models can be used to compensate for lack of information about "real" fires and to work out the fire risk implications of new materials, building designs, and protection systems. A fire risk assessment model called CRISP II was developed at the Fire Research Station of the United Kingdom to decide priorities for remedial action and to test the validity of new guidelines for building control officers. CRISP II is a Monte Carlo simulation of an entire fire scenario. The model consists essentially of a two-zone model of smoke flow for multiple rooms and a detailed model of human behavior and movement, supervised by a Monte Carlo controller. Its component submodels, which include rooms, doors, windows, detectors and alarms, items of furniture, hot smoke layers and people, run simultaneously so they can continually interact with each other. The model is capable of generating a rich variety of fully interactive behavior patterns. It calculates the fractional effective dose (FED) for occupants as they move through the building and are exposed to smoke. When an occupant's FED reaches 100 percent, that person is considered dead. CRISP II expresses the fire risk of a building design in terms of the number of deaths predicted over a large number of simulations.

FIRE STATION,[8] Optimum Fire Station Location for Minimum Loss of Life and Property

The FIRE STATION model determines the optimum location, among five alternate sites, for an urban fire station in a community of 25 wards. Optimization is the min-

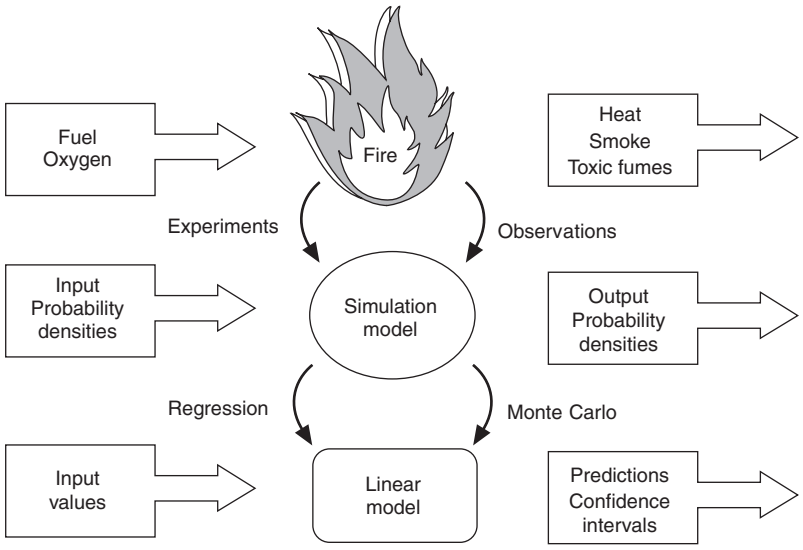

Figure 5-9.1. ***Relationships between observations and models.[5]***

imization of lives lost, building damage, and capital outlay. The model generates a sample population from an observed distribution by ward, structure value, and relative population density. The travel time from the station to the fire is also chosen from an observed distribution. The amount of damage and the number of lives lost is then calculated with reference to the delay in reaching the fire, which depends on the travel time.

Suites or Collections of Fire Protection Computer-Simulated Procedures

Computer models can also be packaged in an integrated set or suite of models that are linked but do not interact as directly as do the modules of CRISP II. Independent models can also be used sequentially, as will be described below. Two examples of integrated suites of computer models are HAZARD I[9] and FiRECAM.[10]

HAZARD I is a fire hazard assessment method that is comprised of four distinct computer models: (1) FAST,[11] a multicompartment energy and mass transport model; (2) DETACT,[12] a detector/sprinkler activation model; (3) EXITT,[13] a human decision/behavior evacuation model; and (4) TENAB,[9] a tenability model which considers incapacitation and lethality from temperature and toxicity. Figure 5-9.2 illustrates how these, and other, software modules are organized. Figure 5-9.2 follows the progress of a hypothetical scenario entitled "CASE" and shows why HAZARD I is a semiautomatic simulation model.

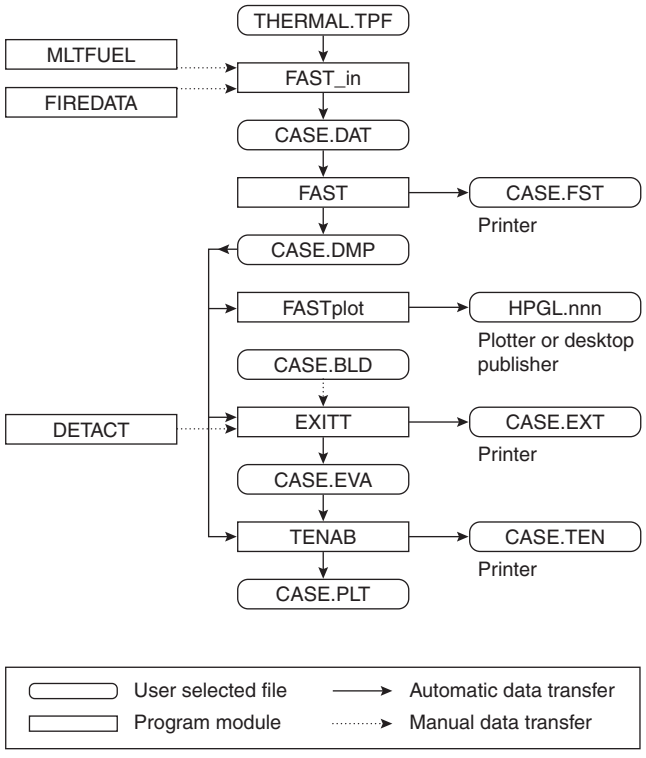

Figure 5-9.2. ***HAZARD I software.***

HAZARD I can model up to six rooms on multiple floors of a building, but data against which its results have been compared are only available for structures of the general dimensions of single-family homes. The method guides the user to identify the fire problems of concern and then to specify representative fire scenarios. The user then employs a computer software package to predict the outcome of each of the identified scenarios in considerable detail. The software predicts over time the temperature, smoke, and fire-gas concentrations in each room of the building; the behavior and movement of the building occupants as they interact with the fire, the building, and each other; and the impact of exposure of each occupant to the fire-generated environment. The occupant exposures are presented as a prediction of successful escape, physical incapacitation, or death along with time, location, and cause. By accounting for the interactions of a large array of factors on the result of a given fire scenario, the method enables the user to analyze the impact of changes in the fire performance of products, building design, and arrangement, or of the inherent capabilities of occupants in the likely outcome of fires. With such information it should be possible to provide better, more cost-effective strategies for reducing fire losses. An overview of the process used by HAZARD I is shown in Figure 5-9.3.

FiRECAM (Fire Risk Evaluation and Cost Assessment Model) consists of submodels that are run in sequence to assess the fire safety performance of a building design in terms of expected risk to life and expected cost of fire. These submodels include a building and risk evaluation model, a fire department response model, a boundary element failure model, an economic model, a design fire model, a fire growth model, a smoke movement model, an occupant response model, a fire department effectiveness model, an evacuation model, a smoke hazard model, a fire spread model, a life loss probability model, a property loss model, an expected number of deaths model, an expected risk to life model, and a fire cost expectation model. FiRECAM can assess whether a proposed design meets the requirements of a performance-based code and can determine if the design is cost effective.

HAZARD I and FiRECAM are examples of methods that link a variety of computer models in such a way that the output from one model can be used directly as the input for the next. It is also possible for the fire protection engineer to use independent models in sequence. There are available collections of programs which cover different aspects of fire technology and science that are components of fire protection simulation models. For example, these collections contain individual programs that predict gas temperatures, heat fluxes on objects, activation of devices, and some aspects of human behavior or evacuation.

These collections do not tend to be comprehensive in nature in that the individual programs are independent of other programs in the collection. Therefore, these programs must be run sequentially and data manually transferred between programs. While less sophisticated and more cumbersome than the integrated simulation models, these models have their uses and may be adequate in some cases. Two advantages of these collections of programs are that they offer the user a significant amount of control over the input to any given component, and they

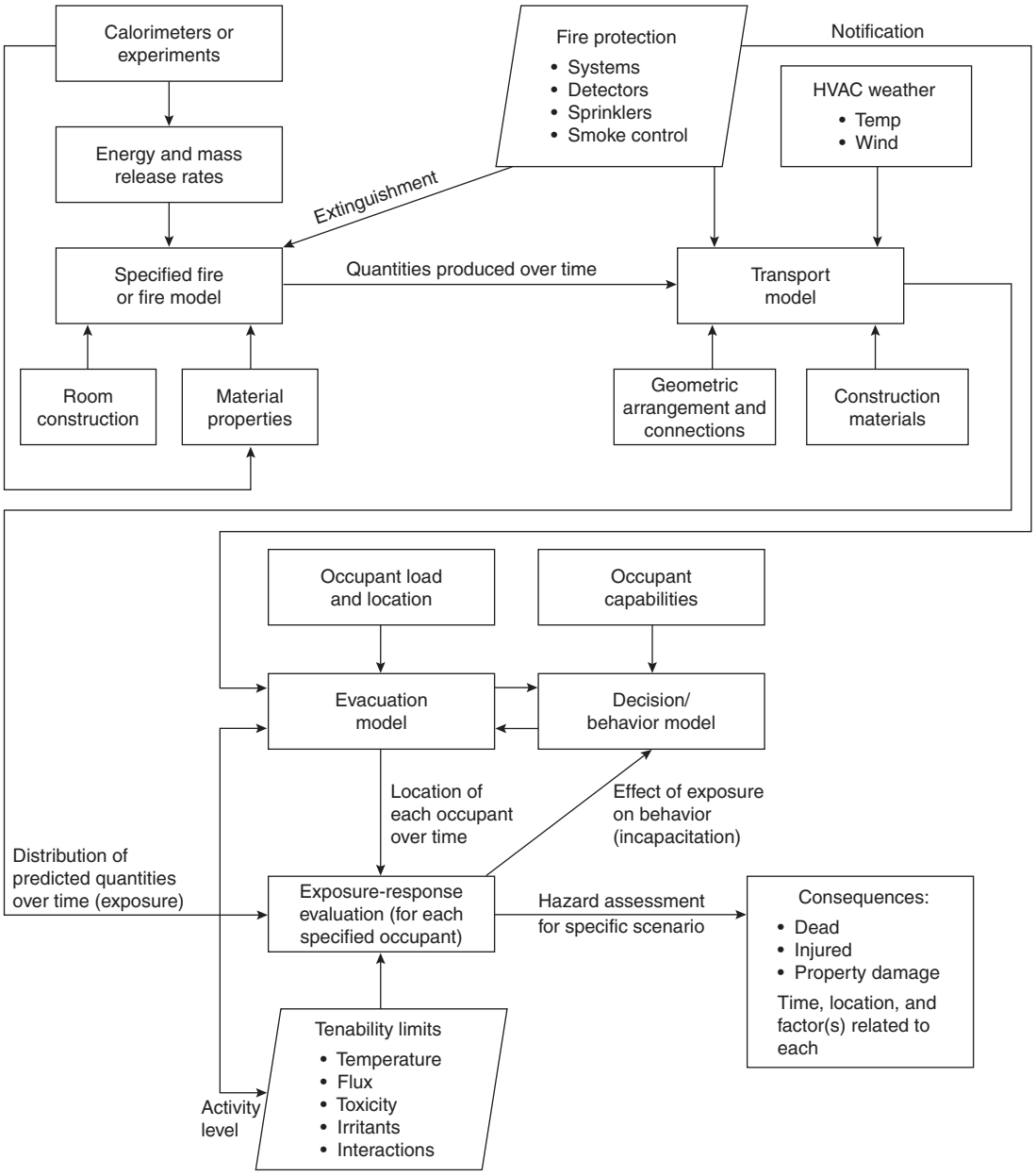

Figure 5-9.3. ***Interrelationships of major components of a fire hazard model.***

lend themselves to being run many times. This latter point is important when the user wishes to characterize a single component. By running the component program many times the user can adequately define the probabilistic nature of the component in question. Examples of these collections include FPEtool,[14] FASTLite,[15] and FireCalc.[16]

The fire protection engineer can also evaluate a design by combining more specialized standalone models of the individual components of interest, for example, a human behavior or egress model with a fire effects model. This approach to simulation modeling, while more cumbersome (since it requires more user intervention), may also be more effective since it allows the user greater control over the process as well as the use of more sophisticated models.

In this approach, the fire effects model would be run independently of the human behavior or egress model. This approach would facilitate analyzing a number of fire scenarios and choosing the ones that most closely reflect the expected conditions. The human behavior or egress model could also be run for a number of conditions and assumptions. The user would then go through the exercise of comparing the predicted output from the two component models and arriving at the final answer.

A number of human behavior or egress models and fire effects models are available that can be used in tan-

dem to perform fire protection simulation modeling. (Space does not permit an attempt to list all models known to the authors, but compendia have been developed[17,18] and are expected to be updated continually to reflect the state of the art.) Given the predicted fire effects obtained from a fire model and the predicted locations of occupants from an evacuation model, the designer or engineer could then use a toxicity model, either a computer model or one of the available calculation methods, to predict the cumulative exposure of the occupants as they move through the modeled fire environment.

Model Validation

Simulation models can never be validated over the whole range of their behavior. However, confidence in the reliability of a model is enhanced if the relationships built into it are based on accepted scientific theory supported by experimental evidence. The model must also stand up to tests designed to show it behaves reasonably in response to exogenous disturbance. The calibrated model should also be able to simulate time-series data from instrumented experimental fires. Finally, the model should be able to mimic the sequence of events recorded by observers at real fires.

Like other models, the validity of simulation models depends on goodness of fit and predictive power. In the fire situation, deterministic predictions are not feasible except in very simple cases. In a typical case, a simulation model would be calibrated to produce an output distribution whose mean and variance were in agreement with an observed distribution. Changes in fire protection strategy would be reflected in the model, which would then be used to generate a new output distribution with a different mean and variance. Comparisons between the output distributions before and after implementing the strategy can be used to calculate confidence intervals for statements such as "if strategy B is preferred to A, casualties will be reduced in x percent of cases." Statistical predictions of this kind are quite sufficient for the purposes of fire protection engineering.

Models undergo limited validation; that is, they are applicable to the experimental results they are based upon and/or the limited set of scenarios to which the model developers compared the model's output. The Society of Fire Protection Engineers has formed a task group to independently evaluate computer models. As of March 2001, they were preparing to finish their first evaluation and had chosen a second model to evaluate. Until more models can be independently evaluated, the model user must rely on the available documentation and previous experience for guidance regarding the appropriate use of a given model. By choosing a specific model, the user is tacitly assuming that the model is valid for the scenario under consideration.

Sensitivity Analysis

Sensitivity analysis can be used to draw useful conclusions to guide decisions on fire safety design and priorities for research. In its simplest form, sensitivity analysis is carried out by varying one of the input parameters in steps over a prescribed range and observing the effect on chosen output parameters, either at the end of the model run or at a set time after the run commences. (Advanced methods of sensitivity analysis are available that allow more than one variable to be varied at a time.) The results of this exercise can then be presented as a table or, more usefully, the output parameter can be regressed against the input parameters to give a simple linear or nonlinear expression that summarizes the results and permits interpolation and extrapolation.

The rate of change of the output parameter, with respect to the input parameter, is defined as the *sensitivity.* In fire safety terms sensitivity might indicate how much the risk is reduced as fire protection measures are improved. If the cost of improved protection is also known, it is possible to estimate the cost of saving a life.

Figure 5-9.4 shows five runs of an evacuation model in which the delay in giving the fire alarm has been increased in steps of 1 min, from 6 min to 10 min. The number of people trapped in a building at, for example, 18 min is represented by the distances between the curves and the horizontal axis. If the number of casualties is regressed against the delay, the results shown in Figure 5-9.5 are obtained. The number of casualties that would occur if the alarm were delayed by t min can be calculated directly from the formula. Conversely, the formula can be used to predict the number of lives that might be saved if the delay were reduced by, for example, an improved alarm system. Note that, in this case, the sensitivity is not a constant, but an exponential function of time.

A similar exercise can be undertaken for fire effects models. Ideally, every input parameter which is based upon an assumption should be the subject of a sensitivity analysis. After establishing a base case, the user should vary the "assumed" input parameter values by ±10 percent and observe what effect this change has on the output variable of interest. If the predicted output varies by

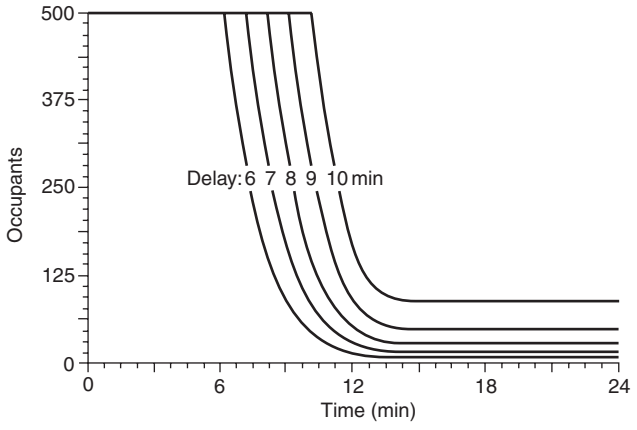

Figure 5-9.4. ***Occupants remaining in a place of assembly if the alarm is delayed for the periods shown.***

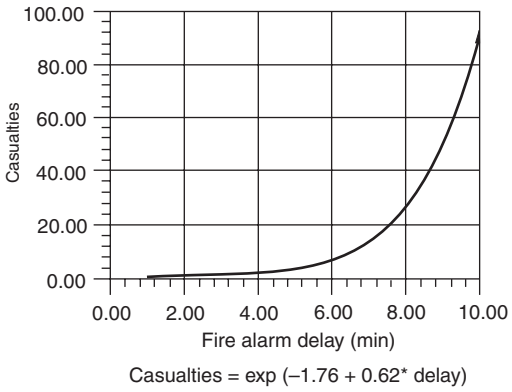

Figure 5-9.5. ***The number of casualties rises exponentially as the delay in giving the signal to evacuate is increased.***

less than ±10 percent, then the output is insensitive to that input variable. Conversely, if the predicted output varies by more than ±10 percent, then the output is sensitive to the input variable in question. The more sensitive input parameters may require further investigation depending on their degree of sensitivity.

The significance of calculations like these is that they enable designers to select those areas where expenditure on fire protection measures would earn the greatest return in terms of lives saved. It also makes it possible to identify those areas where additional expenditure might have little or no effect. This approach is also helpful for making decisions on research priorities. If preliminary calculations indicate that the fire risk can be substantially reduced by a small change in a parameter, it would make sense to put research effort into investigations designed to refine the measurement of that parameter and reduce the level of uncertainty associated with it.

Sensitivity analysis makes it possible to place the tools of fire protection engineering in the hands of designers and other users who might not have the time or the inclination to work directly with a simulation model. The results of the analysis could be published as tables or graphs in manuals for the guidance of draftspersons who would not need to know in detail how the figures were derived. It is vital to ensure that figures are not applied outside their range of application. This criterion implies that the work must be verified by a fully qualified professional who would check that the guidance was appropriate to the circumstances. Similar problems of professional self-regulation have been successfully resolved in other disciplines.

Conclusion

Overall, progress in fire protection engineering is handicapped by data limitations and the difficulty of conducting realistic experiments on complete fire systems involving human behavior, although efforts in the collection of the data on human behavior have intensified over the past several years, particularly in the areas of occupant characteristics and premovement delay times.[19–28] These problems may be overcome by applying a variety of procedural simulation models originally developed in operations research. These models make efficient use of the available data and can be used to test fire protection strategies. They can be complemented by Monte Carlo methods to take account of uncertainty in the data, measure the sensitivity of the casualty rate to fire protection measures, and estimate fire risk.

Appendix A: Handling Uncertainty

Generating Random Numbers

In order to introduce a stochastic element into simulation modeling, a source of random numbers is required. Virtually every computer is equipped with a subroutine that can generate a pseudo-random number in the interval [0, 1] on demand. These are not truly random numbers because they are generated by a deterministic algorithm that will repeat itself cyclically after an interval. The algorithm is designed to make this interval as long as possible given the capacity of the computer. A variety of methods, most of which are based on congruence relationships, are discussed by Naylor et al.[29]

Generating Probability Distributions for Monte Carlo Studies

The generation of simulated statistics is entirely of a numerical nature and is carried out by supplying pseudo-random numbers into the process or system under study and obtaining probability distributions from it as the result. As a rule, statistical simulation involves replacing an actual sample population by some assumed theoretical distribution and then sampling from this theoretical population by means of some type of random number generator. In some cases it may not be possible to find a standard theoretical distribution that describes a particular stochastic process. In these cases the process can be simulated by sampling from an empirical distribution rather than a theoretical one. Naylor et al.[29] provide specific techniques for generating variates from several of the widely used probability distributions as well as general methods for generating variates from empirical distributions.

Inverse transformation method: This method depends on the relationship between the probability density function (pdf) and the cumulative distribution function (cdf). The pdf gives the probability that the variate x lies between x and $x + dx$. The cdf gives the probability that $x \leq x$. The cdf $F(x)$ is obtained from the pdf $f(x)$, by integrating $f(x)\,dx$ over the interval from $-\infty$ to x.

To generate variates x_i from some particular statistical population whose pdf is given by $f(x)$, one must first obtain the cdf $F(x)$. Since $F(x)$ is defined over the range [0, 1], one can generate uniformly distributed random numbers and set $F(x) = r$. It is clear that x is uniquely determined by $r = F(x)$. It follows that for any particular value of r, say r_0, that is generated, it is possible to find the value of

x, in this case x_0 corresponding to r_0 by the inverse function, if it is known. That is,

$$x_0 = F^{-1}(r_0)$$

where $F^{-1}(r)$ is the inverse transformation or mapping of r on the unit interval into the domain of x.

EXAMPLE 1:
Generate variates x with pdf $f(x) = 2x$, $0 \le x \le 1$.

SOLUTION:

$$\begin{aligned} r \quad F(x) &= \int_{-\infty}^{x} f(t)\,dt \\ &= \int_0^x 2t\,dt \quad 0 \le x \le 1 \\ &= x^2 \end{aligned}$$

Then taking the inverse transformation, $F^{-1}(r)$, that is, solving this equation for x, one obtains

$$x = F^{-1}(r) = \sqrt{r} \quad 0 \le r \le 1$$

Therefore, values of x with pdf $f(x) = 2x$ can be generated by taking the square root of random numbers r.

EXAMPLE 2:
Generate a variate x with density function

$$\begin{aligned} f(x) &= \frac{1}{4} \quad 0 \le x \le 1 \\ &= \frac{3}{4} \quad 1 \le x \le 2 \end{aligned}$$

SOLUTION:
The pdf and cdf are illustrated graphically in Figure 5-9.A1. Using the previous results

$$\begin{aligned} r = F(x) &= \int_0^x \frac{1}{4}\,dt \qquad 0 \le x \le 1 \\ &= \frac{x}{4} \\ f = F(x) &= \frac{1}{4} + \int_1^x \frac{3}{4}\,dt \quad 1 \le x \le 2 \\ &= \frac{3}{4}x - \frac{1}{2} \end{aligned}$$

Taking the inverse transformation, that is, solving the above equations for x, one obtains

$$\begin{aligned} x &= 4r \qquad 0 \le r \le \frac{1}{4} \\ x &= \frac{4}{3}r + \frac{2}{3} \qquad \frac{1}{4} \le r \le 1 \end{aligned}$$

The rejection method: In many cases it is either impossible or very difficult to express x in terms of the inverse transformation of the probability distribution, $F^{-1}(r)$. In these cases it is necessary to obtain a numerical approximation to the inverse function, F^{-1}, or make use of the rejection method. The application of the rejection method requires the following steps:

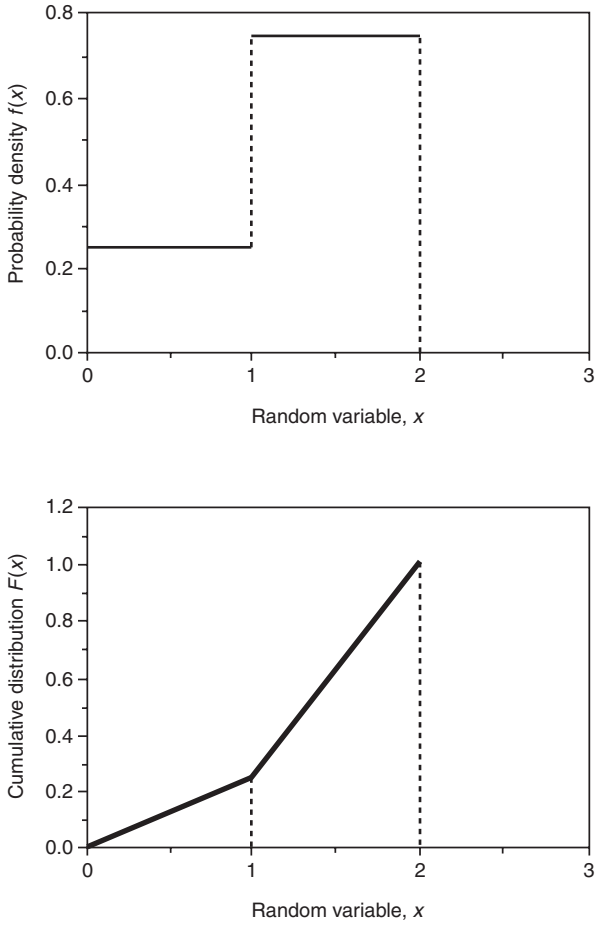

Figure 5-9.A1. ***Probability density function (top) and cumulative distribution (bottom) for empirical data.***

1. Normalize the range of f by a scale factor, c, such that

$$cf(x) \le 1 \qquad a \le x \le b$$

2. Define x as a linear function of r

$$x = a + (b - a)r$$

3. Generate pairs of random numbers (r_1, r_2)
4. Whenever one encounters a pair of random numbers that satisfy the relationship

$$r_2 \le cf[a + (b - a)r_1]$$

then "accept" the pair and use $x = a + (b - a)r_1$ as the variate generated.

The theory behind this method is based on the realization that the probability of r being less than or equal to $cf(x)$ is

$$P[r \le cf(x)] = cf(x)$$

Consequently if x is chosen at random from the range $[a, b]$ according to Step 2 above and then rejected if $r > cf(x)$, the probability density function of accepted x will be exactly $f(x)$. It can be shown[30] that the expected number of trials before a successful pair is found is equal to $1/c$. This result implies that the method may be quite inefficient for certain probability density functions. The rejection method can also be used as a Monte Carlo technique to evaluate definite integrals. This application may be particularly useful for the evaluation of multivariate functions.

EXAMPLE 3:

Use the rejection method to generate variates x with density function $f(x) = 6(x - x^2)$, where $0 \le x \le 1$.

SOLUTION:

Since x was defined over the unit interval, $x = r$. But $f(r) = 6(r - r^2)$ is defined over the interval $0 \le f(r) \le 1.5$. Scaling will transform $f(r)$ to the unit interval if $g(r) = 2/3\, f(r)$, in which case $g(r) = 4(r - r^2)$. The rejection method then consists of the following four steps:

1. Generate r_1 and calculate $g(r_1)$.
2. Generate r_2 and compare with $g(r_1)$.
3. If $r_2 \le g(r_1)$, accept r_1 as x from $f(x)$. If $r_2 > g(r_1)$, then reject r_1 and repeat Step 1.
4. Repeat this procedure until n values of x have been generated.

A comparison between the theoretical distribution and the distribution obtained by using the rejection method is shown in Figure 5-9.A2.

EXAMPLE 4:

Generate a variate with a normal distribution.

SOLUTION:

If a random variable x has a pdf $f(x)$ given as

$$f(x) = \frac{1}{\sigma\sqrt{2\pi}}\, e^{-\frac{1}{2}\left(\frac{x-\mu}{\sigma}\right)^2}, \quad -\infty < x < \infty$$

it is said to have a normal or Gaussian distribution with parameters μ and σ. The graph of this function is the familiar bell-shaped curve. The cdf $F(x)$ does not exist in explicit form and, therefore, the inverse transformation method cannot be applied. There are several ways to avoid this difficulty, which are fully described in the literature. However, it is useful to include here a method for generating variates from a normal distribution, because data with this type of distribution is so widely encountered in practice.

Let r_1 and r_2 be two uniformly distributed random variables defined on the interval [0, 1]. Then

$$x_1 = (-2 \log_e r_1)^{1/2} \cos 2\pi r_2$$
$$x_2 = (-2 \log_e r_1)^{1/2} \sin 2\pi r_2$$

are two variates from a standard normal distribution. This method produces exact results and is quite fast, subject to the efficiency of the special function subroutines.[31]

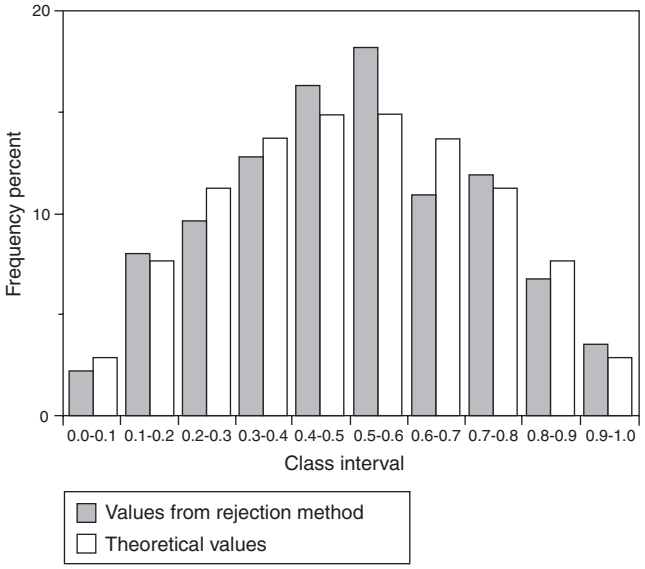

Figure 5-9.A2. ***Generating a sample from a quadratic pdf using the rejection method.***

Appendix B: Analysis of Model Output

Local Linearization

Suppose that at a given time, t, the output variables are dependent on the input variables of the model, according to a set of functions:

$$y_i = f_i(x_1, x_2, \ldots, x_n); \qquad i = 1, \ldots, n$$

Then, in the neighborhood of $x_1, x_2, \ldots, x_n$, one can make a local linear approximation to y_i by expanding $f_i(x_1 + \Delta x_1, x_2 + \Delta x_2, \ldots, x_n + \Delta x_n)$ as a Taylor series about $f_i(x_1, x_2, \ldots, x_n)$, and then truncating all terms after the second. The Taylor series expansion of the ith variable is

$$y_i = f_i(x_1 + \Delta x_1, x_2 + \Delta x_2, \ldots, x_n + \Delta x_n)$$

$$\therefore y_i = f_i(x_1, x_2, \ldots, x_n) + \sum_j \Delta x_j \frac{\partial y_i}{\partial x_j} + \frac{1}{2!}\left(\sum_j \Delta x_j^2 \frac{\partial^2 y_i}{\partial x_j^2} + 2\sum_{j \ne k}\sum_k \Delta x_j \Delta x_k \frac{\partial^2 y_i}{\partial x_j \partial x_k}\right) + \cdots$$

$$\therefore \Delta y_i \cong \sum_j \Delta x_j \frac{\partial y_i}{\partial x_j}; \qquad i = 1, \ldots, n$$

provided that Δx_j is small. It is more convenient to express this in matrix notation:

$$\Delta y = \mathrm{A}\Delta x$$

where A is the Jacobian for the ys, that is,

$$a_{ij} = \frac{\partial y_i}{\partial x_j}$$

Note that, if S is the variance-covariance matrix for the xs, then V is the variance-covariance matrix for the ys and is given by

$$V = A'SA$$

Additivity of Variances

It can often be shown that a model is stable, with respect to variations in any one of its input variables taken one at a time. However, it is possible that, if more than one variable were allowed to change simultaneously, the variance of the sum would be greater than the sum of the variances. This result would imply that the interaction or covariance term could not be ignored. However, if the regression procedure establishes that the linear hypothesis is valid, then the variance of the output is equal to the sum of the variances of the inputs weighted by the squares of the coefficients. Note, however, that the linear hypothesis will probably hold only over a limited range, and can be estimated by examining a plot of the residuals.

If it is established that the linear hypothesis holds over a certain range, that is,

$$y = a_0 + a_1x_1 + a_2x_2 + \cdots + a_nx_n$$

and if $x_1, \ldots, x_n$ are random variables, then

$$\begin{aligned}&\operatorname{var}(a_0 + a_1x_1 + a_2x_2 + \cdots + a_nx_n)\\ &= \sum_i a_i^2 \operatorname{var}(x_i) + \sum_i \sum_j a_i a_j \operatorname{cov}(x_i, x_j)\end{aligned}$$

The variables $x_1, \ldots, x_n$ have been generated so as to be independent, which implies that the covariance term vanishes, and, therefore,

$$\operatorname{var}(y) = \sum_i a_i^2 \operatorname{var}(x_i)$$

The regression model can, therefore, be used to predict the variance of a dependent variable on any assumptions that are chosen about the variances of the independent variables.

If it turned out that the contribution of one variable to the total variance was large, it would be desirable to undertake further studies to establish more exact values for this parameter. A smaller variance could then be assigned to this variable, and one could immediately deduce how much effect this would have on the uncertainty in the dependent variable, without having to carry out any further Monte Carlo runs. Within limits there is no need to be too particular about the variances ascribed to the independent variables in the preliminary studies, since these can be revised at a later date. It is necessary to make a distinction between (1) parameters that have a large variance due to measurement uncertainties (which can be improved), and (2) parameters drawn from populations having a large variance (where further measurement may reduce the uncertainty of the variance but not the variance itself).

References Cited

1. F.S. Hillier and G.J. Lieberman, *Operations Research,* 2nd edition, Holden-Day, Inc., San Francisco (1974).
2. M. Black, *Models and Metaphors,* Cornell University Press, Ithaca, NY.
3. R.L. Ackoff and Stafford Beer, "In Conclusion: Some Beginnings," *Progress in Operations Research* (J.S. Aronofsky, ed.), John Wiley and Sons, New York (1969).
4. G. Ramachandran, "Probabilistic Approach to Fire Risk Evaluation," *Fire Technology,* 24, 3, p. 149 (1988).
5. W.G.B. Phillips, "The Development of a Fire Risk Assessment Model," *BRE Information Paper IP 8/92,* Fire Research Establishment, Borehamwood, UK (1992).
6. W.G.B. Phillips, "Monte Carlo Tests of Conclusion Robustness," in *Proceedings of the Fifth International System Dynamics Conference,* Geilo, Norway, p. 19 (1976).
7. J.N. Fraser-Mitchell, "Risk Assessment of Factors Relating to Fire Protection in Dwellings," in *Fire Safety Science: Proceedings of the 5th International Symposium,* (Y. Hasemi, ed.), International Association for Fire Safety Science, Melbourne, Australia (1997).
8. J. Oberstone, in *Management Science: Concepts and Applications,* West Publishing Company, St. Paul, MN (1990).
9. R.D. Peacock, W.W. Jones, R.W. Bukowski, and C.L. Forney, "Technical Reference Guide for the HAZARD I Fire Hazard Assessment Method," *NIST Handbook 146,* Volume 2, National Institute of Standards and Technology, Gaithersburg, MD (1991).
10. D. Yung et al., "Modelling Concepts for the Risk-cost Assessment Model FIRECAM™ and its Application to a Canadian Government Office Building," in *Proceedings of the Fifth International Symposium on Fire Safety Science* (Y. Hasemi, ed.), International Association for Fire Safety Science, pp. 619–630 (1997).
11. W.W. Jones and R.D. Peacock, "Technical Reference Guide for FAST Version 18," *NIST Technical Note 1262,* National Institute of Standards and Technology, Gaithersburg, MD (1989).
12. D.D. Evans and D.W. Stroup, "Methods to Calculate the Response Time of Heat and Smoke Detectors Installed Below Large Unobstructed Ceilings," *NBSIR 85-3167,* National Bureau of Standards, Gaithersburg, MD (1985).
13. B.M. Levin, "EXITT—A Simulation Model of Occupant Decisions and Actions in Residential Fires: User's Guide and Program Description," *NBSIR 87-3591,* National Bureau of Standards, Gaithersburg, MD (1987).
14. S. Deal, *Technical Reference Guide for FPEtool Version 3.2,* National Institute of Standards and Technology, Gaithersburg, MD (1995).
15. R.W. Portier, R.D. Peacock, and P.A. Reneke, "FASTLite: Engineering Tools for Estimating Fire Growth and Transport," *Special Publication 899,* National Institute of Standards and Technology, Gaithersburg, MD (1996).
16. V.O. Shestopal and S.J. Grubits, "Computer Program for an Uninhibited Smoke Plume and Associated Computer Software," *Fire Technology,* 29, 3, pp. 246–267 (1993).
17. R. Freidman, *Survey of Computer Models for Fire and Smoke,* 2nd ed., Factory Mutual Research Corporation, Norwood, MA (1991).
18. *Computer Software Directory,* Society of Fire Protection Engineers, Bethesda, MD (1994).

19. G. Proulx and R.F. Fahy, "The Time Delay to Start Evacuation: Review of Five Case Studies," in *Proceedings of the Fifth International Symposium on Fire Safety Science (*Y. Hasemi, ed.), International Association for Fire Safety Science, pp. 783–794 (1997).
20. K.E. Boyce, T.J. Shields, and G.W.H. Silcock, "Toward the Characterization of Building Occupancies for Fire Safety Engineering: Prevalence, Type, and Mobility of Disabled People," *Fire Technology,* 35, 1, pp. 35–50 (1999).
21. K.E. Boyce, T.J. Shields, and G.W.H. Silcock, "Toward the Characterization of Building Occupancies for Fire Safety Engineering: Capabilities of Disabled People Moving Horizontally and on an Incline," *Fire Technology,* 35, 1, pp. 51–67 (1999).
22. K.E. Boyce, T.J. Shields, and G.W.H. Silcock, "Toward the Characterization of Building Occupancies for Fire Safety Engineering: Capability of Disabled People to Negotiate Doors," *Fire Technology,* 35, 1, pp. 68–78 (1999).
23. K.E. Boyce, T.J. Shields, and G.W.H. Silcock, "Toward the Characterization of Building Occupancies for Fire Safety Engineering: Capability of People with Disabilities to Read and Locate Exit Signs," *Fire Technology,* 35, 1, pp. 79–86 (1999).
24. G. Proulx, J.C. Latour, J.W. McLaurin, J. Pineau, L.E. Hoffman, and C. Laroche, "Housing Evacuation of Mixed Abilities Occupants in Highrise Buildings," *Internal Report No. 706,* National Research Council of Canada, Ottawa (1995).
25. G. Proulx, "Evacuation Time and Movement in Apartment Buildings," *Fire Safety Journal,* 24, 3 (1995).
26. T.J. Shields, K.E. Boyce, and G.W.H. Silcock, *Unannounced Evacuation of Marks & Spencer Sprucefield Store,* University of Ulster Fire SERT, Carrickfergus, Northern Ireland, unpublished report (1997).
27. G. Proulx, A. Kaufman, and J. Pineau, "Evacuation Time and Movement in Office Buildings," *Internal Report No. 711,* National Research Council of Canada, Ottawa (1996).
28. G. Proulx, J. Latour, and J. MacLaurin, "Housing Evacuation of Mixed Abilities Occupants," *Internal Report No. 661,* National Research Council of Canada, Ottawa (1994).
29. T.H. Naylor, J.L. Balintfy, D.S. Burdick, and K. Chu, *Computer Simulation Techniques,* John Wiley and Sons, New York (1966).
30. K.D. Tocher, *The Art of Simulation,* Van Nostrand Co., New York (1963).
31. Mervin E. Muller, "A Comparison of Methods for Generating Normal Deviates on Digital Computers," *Journal of the Association for Computing Machinery,* 6, pp. 376–383 (1959).

Additional Readings

J. Banks (ed.), *Handbook of Simulation: Principles, Methodology, Advances, Applications, and Practice,* Wiley, New York (1998).

J. Banks, B. Nelson, and J. Carson, *Discrete-Event System Simulation,* 2nd ed. Prentice Hall, Upper Saddle River, NJ (1995).

P. Bratley, B.L. Fox, and L.E. Schrage, *A Guide to Simulation,* 2nd ed., Springer-Verlag, New York (1987).

J.R. Emshoff and R.L. Sisson, *Design and Use of Simulation Models,* Macmillan, New York (1970).

G.S. Fishman, *Principles of Discrete Event Simulation,* Wiley, New York (1973).

J.M. Garrido, *Performance Modeling of Operating Systems Using Object-Oriented Simulation: A Practical Introduction,* Plenum, New York (2000).

S.V. Hoover and R.F. Perry, *Simulation: A Problem Solving Approach,* Addison-Wesley, New York (1989).

A.M. Law, D.W. Kelton, W.D. Kelton, and D.M. Kelton, *Simulation Modeling and Analysis,* 3rd ed. McGraw-Hill, New York (1999).

A.S. Mavor and R.W. Pew (eds.), *Modeling Human and Organizational Behavior: Application to Military Simulations,* National Academy Press, Washington, DC (1999).

J.H. Mize and J. Cox, *Essentials of Simulation,* Prentice Hall, Englewood Cliffs, NJ (1968).

T.H. Naylor, J.L. Balintfy, D.S. Burdick, and K. Chu, *Computer Simulation Techniques,* Wiley, New York (1966).

R.E. Shannon, *Systems Simulation: The Art and Science,* Prentice Hall, Englewood Cliffs, NJ (1975).

R. Suleiman and K.G. Troitzsch (eds.), *Tools and Techniques for Social Science Simulation,* Physica Verlag, Heidelburg, Germany (2000).

B.P. Zeigler, H. Praehofer, and T.G. Kim, *Theory of Modeling and Simulation: Integrating Discrete Event and Continuous Complex Dynamic Systems,* 2nd ed., Academic Press.

G.W. Zobrist and J.V. Leonard (eds.), *Simulation Systems,* Gordon and Breach, Amsterdam (2000).

CHAPTER 10

Fire Risk Indexing

John M. Watts, Jr.

Introduction

Fire risk indexing is a link between fire science and fire safety. As we learn more about the behavior of fire, it is important that we implement new knowledge to meet fire safety goals and objectives. One of the barriers to implementing new technology is the lack of structured fire safety decision making. Fire risk indexing is evolving as a method of evaluating fire safety that is valuable in assimilating research results.

Fire safety decisions often have to be made under conditions where the data are sparse and uncertain. The technical attributes of fire risk are very complex and normally involve a network of interacting components. These interactions are generally nonlinear and multidimensional. However, complexity and sparseness of data do not preclude useful and valid approaches. Such circumstances are not unusual in decision making in business or other risk venues. (The space program illustrates how success can be achieved when there are few relevant data.) However, detailed risk assessment can be an expensive and labor-intensive process, and there is considerable room for improving the presentation of results. Indexing can provide a cost-effective means of risk evaluation that is both useful and valid.

Fire risk indexing systems are heuristic models of fire safety. They constitute various processes of analyzing and scoring hazard and other system attributes to produce a rapid and simple estimate of relative fire risk. They are also known as rating schedules, point schemes, ranking, numerical grading, and scoring. Using professional judgment and past experience, fire risk indexing assigns values to selected variables representing both positive and negative fire safety features. The selected variables and assigned values are then operated on by some combination of arithmetic functions to arrive at a single value, which is then compared to other similar assessments or to a standard.

There are numerous approaches to fire safety evaluation that can be construed as risk indexing. A more general description of this area is presented in Reference 1, while greater detail on the more rigorous application is given in Reference 2.

Dr. John M. Watts, Jr., holds degrees in fire protection engineering, industrial engineering, and operations research. He is director of the Fire Safety Institute, a not-for-profit information, research, and educational corporation located in Middlebury, Vermont. Dr. Watts also serves as editor of NFPA's *Fire Technology.*

Fire Risk Indexing

Quantitative fire risk assessment originated with the insurance rating schedule. The approach has broadened to include a wide variety of applications.[3,4] In general, fire risk rating schedules assign values to selected variables based on professional judgment and past experience. The selected variables represent both positive and negative fire safety features, and the assigned values are then operated on by some combination of arithmetic functions to arrive at a single value. This single value can be compared to other similar assessments or to a standard to rank the fire risk.

A risk index is defined as a single number measure of the risk associated with a facility.[5] Thus, insurance rates are fire risk indices, as are the outputs of other similar schedules or scoring methods. Fire risk indexing, then, is the process of modeling and scoring hazard and exposure attributes to produce a rapid and simple estimate of relative risk. The concept has gained widespread acceptance as a cost-effective prioritization and screening tool for fire risk assessment programs. It is a useful and powerful approach that can provide valuable information on the risks associated with fire.

Figure 5-10.1[6] provides a graphic view of the relative power and limitations of three broad levels of risk quantification. Curves A, B, and C do not represent actual data points but are demonstrative of a continuum of fire risk analysis possibilities.

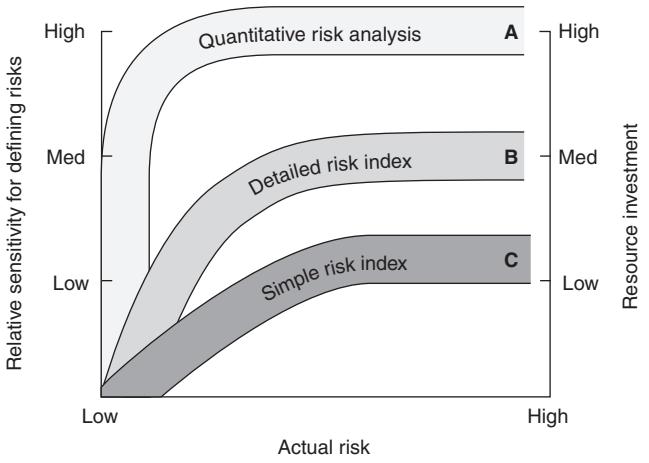

Figure 5-10.1. ***Risk index systems and relative sensitivity for defining actual risk.***[6]

Curve A is representative of a rigorous probabilistic risk analysis where hazard and exposure are analyzed through full quantitative analysis of the hazard and the statistics of exposure. It is clear that this analysis is the most accurate approach to defining risks, especially where the risk is low. However, it is also clear that a large resource investment is necessary to accomplish this task.

Curve C is a simple fire risk indexing that provides the ability to screen for high-risk catastrophic-type situations where the analysis can be consequence oriented. However, for small differences in risk, the ability of the more simplistic screening system to differentiate between two more subtle risks diminishes.

A more complex and accurate assessment model will provide greater differentiation between lesser risks and an improved overall accuracy. The trade-off for this approach is increased time and resources expended for model development, implementation, and data collection.

Applications

Choosing the depth of the risk analysis is a critical decision that depends on such factors as time, resource commitment, and the intended use of the results. Each approach may have certain advantages or trade-offs for specific tasks. A fire risk indexing approach may be appropriate in several situations:

1. Where greater sophistication is not required
2. Where risk screening will be cost-effective
3. Where there is a need for risk communication

The level of accuracy demanded for a fire risk analysis is not typically the same as for other engineering purposes. Often, establishing an order of magnitude will suffice. Time and resource expenditure will increase as the depth of analysis is increased. Where resources are scarce and efficiency is prized, maximizing the utility of the fire risk indexing is clearly desirable.

The principles of fire risk indexing have been applied to a variety of hazard and risk assessment projects to set priorities and help manage resources. Risk assessment can be an expensive and labor-intensive process. Much time and money can be wasted if the products or facilities with the greatest potential for risk and associated liability are not identified and assessed first. Without a prioritization plan, it will not be known whether a risk was worth assessing until after the time and money has been spent.

Fire risk indexing also has appeal to staff charged with risk management decision-making responsibilities and those who may be unfamiliar with the details and mechanics of the risk assessment process. Because fire risk indexing simplifies basic fire risk assessment principles, it can be an effective way to acquire a global grasp of the issues.

Significance

The importance of fire risk indexing has been widely recognized. A working group of educators and researchers addressed the issue of fire risk indexing at the National Academy of Sciences 1987 "Workshop on Analytical Methods for Designing Buildings for Fire Safety."[7] They concluded there is a need for a three-part system of fire safety comprised of (1) codes; (2) the methods of fire risk indexing, referred to as numerical grading systems; and (3) the means of supplying inputs to that system derived, as far as feasible, from basic principles of decision science. The working group went on to state the rationale for its conclusion:

> The advantage of keeping numerical grading systems in the trio is that they provide a coherent structure that still allows some qualitative analysis of fire safety. These systems also readily accept change associated with aspects of operations research, management science, risk analysis, and quantitative analytical solutions or models to the fire safety problem or parts of it.[7]

The importance of scientific rigor in the development of fire risk indexing methods cannot be overemphasized and will be addressed in more detail in a later section of this chapter.

Examples of Approaches to Fire Risk Indexing

It is difficult to describe a typical fire risk indexing method. The practical necessity of trying to assess dozens or hundreds of risks with limited resources has led to the creation of an array of fire risk indexing systems. Approaches to fire risk indexing are virtually limitless in their possible variations. Representative examples of fire risk indexing were selected from the literature and are summarized in the following sections. They provide some idea of the types of variations involved with modeling and quantifying fire risk. Publicly available computer applications of these and other fire risk indexing methods are described in the final section of this chapter.

Insurance Rating

The purpose of risk analysis is to facilitate the process of risk management. One of the most fundamental tools of risk management is the transference of risk by insur-

ance. To be acceptable to an insurer, the risk is rated by actuarial means, applying principles of mathematics to the particular pricing problems of the insurance industry.

Fire insurance rates are promulgated as *class* rates and *specific* rates. Class rates apply to all properties that fall within a given category or classification. The most common example of class rating is for dwellings or residences. When class rates do not apply, specific rates are determined by the application of a schedule or formula designed to measure the relative quantity of fire hazard present. This process, known as *schedule rating,* is typically used for institutions, manufacturing properties, and business establishments.

The two most widely used schedules in the United States are known as the *mercantile schedule* and the *analytic system.*[8] At present, the analytic system is predominantly used throughout the country. It is more generally referred to as the Dean Schedule, named for A.F. Dean, author of the plan.[9] The schedules differ basically in their fundamental analysis of the factors affecting insurance rates, but they are alike in that they establish an arbitrary point from which to build up the rate, based on various physical hazards. A schedule of additions and reductions is computed, and the difference is applied to the arbitrary point of departure.

Schedule rating, then, is a plan by which fire hazards to any particular property are measured. A schedule has been defined as "an empirical standard for the measurement of relative quantity of fire hazard."[10] Schedule rating takes into consideration the various factors contributing to the peril of fire, such as construction and occupancy, and helps determine which features either enhance or minimize the probability of loss. Credits and charges representing departures from standard conditions are incorporated in the schedules. Thus, the schedule rate is typically the sum of all charges less the sum of its credits and constitutes a standard for the measurement of the fire risk.

Specific Commercial Property Evaluation Schedule

The most commonly used insurance rating schedule in the United States is the Insurance Services Office's Specific Commercial Property Evaluation Schedule.[11] For each building, a percentage occupancy charge is determined from tabulated charges for classes of occupancy modified by factors such as the specific hazards of a particular occupancy. The basic building grade is a function of the resistance to fire of structural walls and floor and roof assemblies. The building fire insurance rate is the product of occupancy charges and building grade modified by factors such as the exposure to fire in nearby buildings and protection provided by portable extinguishers, fire alarm systems, and so forth.

An important concept of insurance rating is the use of loss experience. In general, tabulated values and conversion factors are based on actuarial analysis of fire losses paid by insurers and reported to the insurance industry.

Gretener Method

In 1960, Max Gretener of the Swiss Fire Protection Association began to study the possibility of an arithmetical evaluation of fire risk in buildings. His premise was that determining fire risk by statistical methods based on loss experience was no longer adequate for the following reasons:[12]

1. Lack of exchange of loss experience
2. Inadequate analysis with respect to causes and factors determining the size of loss, resulting in distortion of statistical data
3. Rapid technological change altering the credibility of previous experience
4. Different criteria, according to country and company, for data collection and evaluation

As a result of this new approach to schedule rating, the Gretener method has developed into a widely used fire risk index in Switzerland[13] and other European countries.[14,15] The basic idea of the process consists of expressing, in relative, empirically derived numerical values, factors for fire initiation and spread and factors for fire protection. The product of the hazard factors is a value for potential hazard, while the product of the fire protection factors expresses a value for protective measures. The ratio of these products is taken as the measure of expected fire severity.

Of immediate appeal is that the approach begins with the explicit concept of risk as the expectation of loss given by the product of hazard probability and hazard severity:

$$R = A \times B$$

where

R = fire risk

A = probability that a fire will start

B = fire hazard, degree of danger, or probable severity

Thus, the Gretener method is based on these two probabilities and combines them in accordance with probability theory.

A further departure from U.S. schedule rating is the calculation of fire hazard as a ratio rather than a sum:

$$\text{Fire Hazard} = \frac{\text{Potential Hazard}}{\text{Protective Measures}}$$

that is,

$$B = \frac{P}{N \times S \times F}$$

where

B = fire hazard

P = potential hazard

N = standard fire safety measures

S = special measures

F = fire resistance of the building

Potential hazard, P, is the product of hazard elements whose magnitudes are influenced on the one hand by the building contents, that is, materials and merchandise present, and on the other hand, by the building itself.

As with most other schedule approaches, the values for these individual factors are not based on statistics but are empirical figures resulting from a comparison of

analyses of fire risks for which fire protection measures are either common or required by law.

Dow's Fire and Explosion Index

A need for systematic identification of areas with significant loss potential motivated Dow Chemical Company to develop the Fire and Explosion Index and risk guide.[16] The original edition issued in 1964 was a modified version of the Chemical Occupancy Classification rating system developed by Factory Mutual prior to 1957. It has been subsequently improved, enhanced, and simplified, and is now in its seventh edition.[17]

Today there are many risk assessment methods available that can examine a chemical plant in great detail. The Fire and Explosion Index (FEI) remains a valuable screening tool that serves to quantify the expected damage from potential fire, explosion, and reactivity incidents and to identify equipment that could likely contribute to the creation or escalation of an incident.[18] Risks associated with operations where a flammable, combustible, or reactive material is stored, handled, or processed can be evaluated with this system. The guide is intended to provide a direct and logical approach for determining the probable "risk exposure" of a process plant and to suggest approaches to fire protection and loss prevention design. An important application of the FEI is to help decide when a more detailed quantitative risk analysis is warranted, as well as the appropriate depth of such a study.[19] This section will provide an overview of the method. The source document[17] should be consulted for specific application.

The concept of the Fire and Explosion Index (FEI) is to divide a process plant into separate operations or units and consider each of these individually. The key aspect of the method is the identification and assessment of thermodynamic properties of the dominant combustible material in the unit being studied. This basic material factor is then built up with a series of individual features concerning operation of the unit. These potential hazards are based on experience and information from incident records. They are intended to cover the majority of likely abnormal situations leading to fires, explosions, and material releases. Features considered are those upon which all hazard and reliability analyses are based. However, the FEI does not purport to be as comprehensive as a detailed hazard and reliability study. The approach identifies most of the potentially hazardous features of a unit. Quantitative measurements used in the analysis are based on historic loss data, the energy potential of the key material, and the extent to which loss prevention practices are applied.

Index Calculation

The basic procedure for calculation of the Fire and Explosion Index is shown in Figure 5-10.2. The first step is to identify those process units considered pertinent to the process and having the greatest potential impact in the

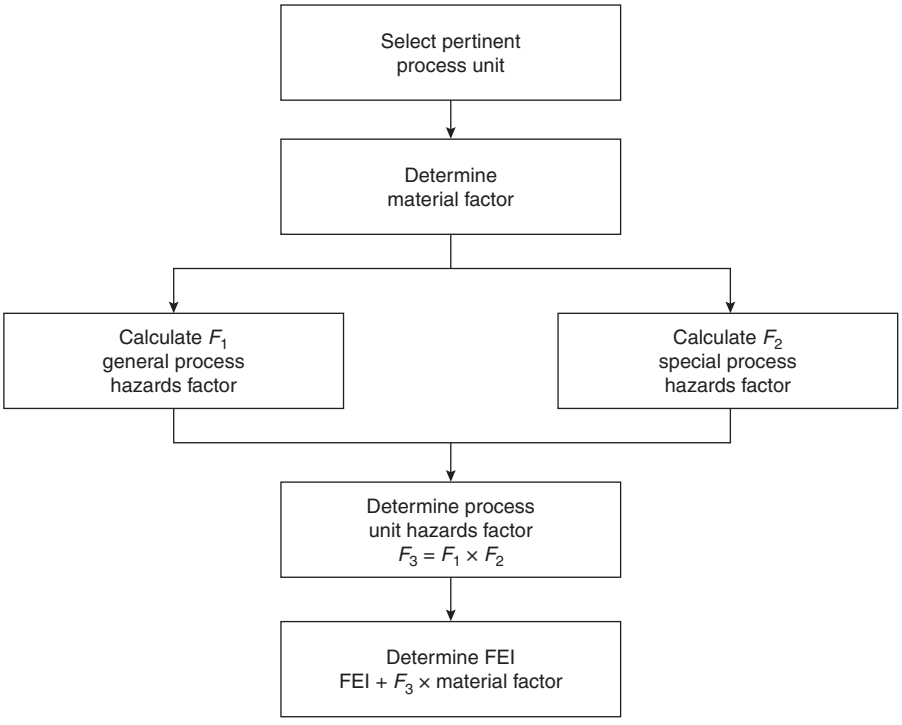

Figure 5-10.2 ***Dow procedure for calculating the Fire and Explosion Index.***

event of loss by fire or explosion. A *unit* is considered to be a part of the plant that can be readily and logically characterized as a separate entity. Generally a unit consists of a segment of the process, such as reactors, blenders, furnaces, storage tanks, and so forth. In some instances, units may be portions of a plant separated from the remainder by distance, fire walls, or other barriers. In other cases, the unit may be an area where a particular hazard exists.

The next step is the determination of the *material factor* for the dominant combustible component of the process unit. The material factor is a measure of intensity of energy release from a chemical compound, mixture of compounds, or substance. It is determined by considering the flammability and reactivity of a material as described in NFPA 704, *Standard System for the Identification of the Fire Hazards of Materials,* 1990 edition;[20] NFPA 49, *Hazardous Chemicals Data,* 1991 edition;[21] and NFPA 325, *Guide to Fire Hazard Properties of Flammable Liquids, Gases, and Volatile Solids,* 1991 edition.[22] Based on these values the material factor is denoted by a number from 1 to 40. This arrangement is an arbitrary ordinal ranking.

Subsequent to selecting the appropriate material factor, penalties for contributing hazards are assessed as indicated by the schedule shown in Figure 5-10.3. Items listed in the schedule are considered contributing factors to an incident that may result in fire or explosion. Not every hazard is applicable to a given process unit; however, all applicable items should be evaluated and an appropriate penalty applied. The list is divided into two parts, "General Process Hazards" and "Special Process Hazards." General process hazards relate to a type of process and represent conditions that may increase the magnitude or severity of an incident. Special process hazards are items that increase the probability of a fire or explosion.

Penalties are summed separately for each class of process hazard. These sums are then multiplied (severity $\times$ probability) to yield a process unit hazards factor. This factor has a numerical range from 1 to 8 and is considered a measure of the probable relative damage exposure magnitude. The Fire and Explosion Index (FEI) is the product of the material factor and the process unit hazards factor.

Risk Analysis

The process unit hazards factor and material factor are also used to derive a damage factor. The damage factor represents the overall effect of fire, plus blast damage resulting from a fire or reactive energy release, caused by the various contributing factors associated with the process unit. It is estimated graphically.

A radius of exposure in feet is estimated as 84 percent of the FEI. The dollar value exposed is the estimated value of all equipment within the circle prescribed by the exposure radius. That is, the defined circular area of exposure indicates those assets that may be exposed to a fire or explosion generated by the process unit being evaluated. The replacement value of equipment in this area multiplied by the damage factor provides the base maximum probable property damage (MPPD), that is, the value at risk times the relative damage potential.

Three categories of loss control features have been assigned credits that can potentially reduce the base MPPD to an actual MPPD: (1) process control, (2) material isolation, and (3) fire protection. Twenty-two potential credit factors are shown in Table 5-10.1. The base MPPD reduced by the loss control credit factor gives the actual MPPD. This value represents the probable resulting loss from an incident of a reasonable magnitude given the proper functioning of protective equipment. Failure of the protective equipment could revert the probable loss to the base MPPD. Final steps include determination of the maximum probable days outage and the business interruption cost. The risk analysis procedure is summarized in Figure 5-10.4.

The most important goal of the FEI analysis is to make the engineer aware of the loss potential of each process area and to help identify ways to lessen the severity and resultant loss of potential incidents. The Dow Chemical Company requires an FEI analysis for existing plants.[18] The requirement for use of the FEI has been adopted into law in the Netherlands.[23] The FEI has been found to be a valuable screening tool that can be used in conjunction with other analyses to help determine the relative risk of process units and to provide valuable guidance to both engineering and management staffs.

Mond Fire, Explosion, and Toxicity Index

The Mond division of Imperial Chemical Industries (ICI), Ltd., identified that the Dow Fire and Explosion Index method had considerable scope for the evaluation of plant hazard potential at the earliest design stages. Following trials with the published Dow method, it was clear that there was a need to extend the method in a number of directions to develop its potential for new project design. The resulting Mond Fire, Explosion, and Toxicity Index[24,25] was developed and has been applied to a range of new projects within ICI.

The main contribution of the Mond method is the inclusion of *offsetting features,* which allow the effect of good design concepts, good management attitudes, and other preventative measures to reduce the overall hazard. An important outcome of using the technique is to raise questions concerning hazard potential at an early enough stage in planning to allow for adequate investigations to be made before the process is in operation. Achieving some measure of hazard early in the planning process provides information that can be used to select appropriate protection features as the planning proceeds. Early assessment of hazards has value in dealing with possible problems in obtaining approval for proposals and in predicting possible delays and problems that are likely to be encountered.

Fire Safety Evaluation System

The Fire Safety Evaluation System (FSES)[26,27] is a risk indexing approach to determining equivalencies to the NFPA *101® Life Safety Code®*, 2000 edition,[28] for certain institutional occupancies. The technique was developed at

FIRE & EXPLOSION INDEX

AREA/COUNTY	DIVISION	LOCATION	DATE
SITE	MANUFACTURING UNIT	PROCESS UNIT	

PREPARED BY:	APPROVED BY: (Superintendent)	BUILDING
REVIEWED BY: (Management)	REVIEWED BY: (Technology Center)	REVIEWED BY: (Safety & Loss Prevention)

MATERIALS IN PROCESS UNIT	
STATE OF OPERATION _____ DESIGN _____ START UP _____ NORMAL OPERATION _____ SHUTDOWN	BASIC MATERIAL(S) FOR MATERIAL FACTOR

MATERIAL FACTOR (See Table 1 or Appendices A or B) Note requirements when unit temperature over 140°F (60°C)

1. GENERAL PROCESS HAZARDS	**Penalty Factor Range**	**Penalty Factor Used** (1)
Base Factor	1.00	1.00
A. Exothermic Chemical Reactions	0.30 to 1.25	
B. Endothermic Processes	0.20 to 0.40	
C. Material Handling and Transfer	0.25 to 1.05	
D. Enclosed or Indoor Process Units	0.25 to 0.90	
E. Access	0.20 to 0.35	
F. Drainage and Spill Control _____ gal or cu.m.	0.25 to 0.50	
General Process Hazards Factor (F_1)		
2. SPECIAL PROCESS HAZARDS		
Base Factor	1.00	1.00
A. Toxic Materials	0.20 to 0.80	
B. Sub-Atmospheric Pressure (<500 mm Hg)	0.50	
C. Operation In or Near Flammable Range _____ Inerted _____ Not Inerted		
1. Tank Farms Storage Flammable Liquids	0.50	
2. Process Upset or Purge Failure	0.30	
3. Always in Flammable Range	0.80	
D. Dust Explosion (See Table 3)	0.25 to 2.00	
E. Pressure (See Figure 2) Operating Pressure _____ psig or kPa gauge Relief Setting _____ psig or kPa gauge		
F. Low Temperature	0.20 to 0.30	
G. Quantity of Flammable/Unstable Material: Quantity _____ lb or kg H_c = _____ BTU/lb or kcal/kg		
1. Liquids or Gases in Process (See Figure 3)		
2. Liquids or Gases in Storage (See Figure 4)		
3. Combustible Solids in Storage, Dust in Process (See Figure 5)		
H. Corrosion and Erosion	0.10 to 0.75	
I. Leakage—Joints and Packing	0.10 to 1.50	
J. Use of Fired Equipment (See Figure 6)		
K. Hot Oil Heat Exchange System (See Table 5)	0.15 to 1.15	
L. Rotating Equipment	0.50	
Special Process Hazards Factor (F_2)		
Process Unit Hazards Factor ($F_1 \times F_2$) = F_3		
Fire and Explosion Index ($F_3 \times MF$ = F&EI)		

Figure 5-10.3. ***Dow Fire and Explosion Index schedule.***

Table 5-10.1 ***Dow Loss Control Credit Factors***

1. Process Control Credit Factor (C_1)

Feature	Credit Factor Range	Credit Factor Used (2)	Feature	Credit Factor Range	Credit Factor Used (2)
a. Emergency power	0.98		f. Inert gas	0.94–0.96	
b. Cooling	0.97–0.99		g. Operating instructions/procedures	0.91–0.99	
c. Explosion control	0.84–0.98		h. Reactive chemical review	0.91–0.98	
d. Emergency shutdown	0.96–0.99		i. Other process hazard analysis	0.91–0.98	
e. Computer control	0.93–0.99				

C_1 Value (3) ☐

2. Material Isolation Credit Factor (C_2)

Feature	Credit Factor Range	Credit Factor Used (2)	Feature	Credit Factor Range	Credit Factor Used (2)
a. Remote control valves	0.96–0.98		c. Drainage	0.91–0.97	
b. Dump/blowdown	0.96–0.98		d. Interlock	0.98	

C_2 Value (3) ☐

3. Fire Protection Credit Factor (C_3)

Feature	Credit Factor Range	Credit Factor Used (2)	Feature	Credit Factor Range	Credit Factor Used (2)
a. Leak detection	0.94–0.98		f. Water curtains	0.97–0.98	
b. Structural steel	0.95–0.98		g. Foam	0.92–0.97	
c. Fire water supply	0.94–0.97		h. Hand extinguishers/monitors	0.93–0.98	
d. Special systems	0.91		i. Cable protection	0.94–0.98	
e. Sprinkler systems	0.74–0.97				

C_3 Value (3) ☐

Loss Control Credit Factor = $C_1 \times C_2 \times C_3$ (3) = ☐

the Center for Fire Research, National Bureau of Standards in cooperation with the U.S. Department of Health and Human Services (formerly Health, Education, and Welfare) in the late 1970s. It was adapted to new editions of the *Life Safety Code* and is presently published in NFPA 101A, *Alternate Approaches to Life Safety*, 2001 edition.[29] (The tables in this section are taken from the worksheets for health care occupancies in Chapter 4 of NFPA 101A.)

Equivalency Concept

In an effort to promote economical upgrading of fire safety, U.S. codes include an equivalency option. This provision allows alternative designs to satisfy regulations if they provide a level of fire safety equivalent to that called for by the regulations. The difficult decision as to what constitutes equivalency has been left to local jurisdictions.

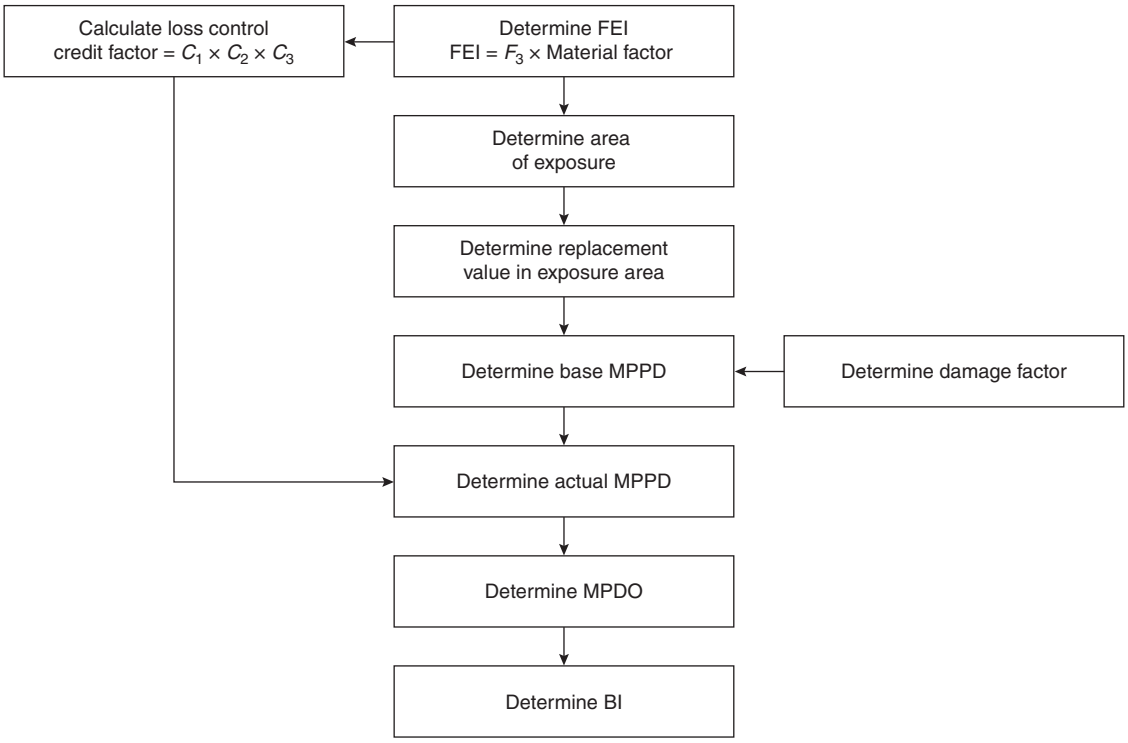

Figure 5-10.4. ***Dow procedure for calculating other risk analysis information.***

Local interpretations lead to a lack of uniformity across the country in terms of what may be waived and what constitutes an adequate alternative to provide the required level of safety. The FSES was developed to provide a uniform method of evaluating health care facilities to determine what fire safety measures would provide a level of fire safety equivalent to that provided by the *Life Safety Code.* The objective was to compile an evaluation system that would be easily workable, presenting useful information for the amount of effort expended.

Fire Zone Concept

Unlike the *Life Safety Code,* the FSES subdivides a building into fire zones for evaluation. A fire zone is defined as a space separated from other parts of the building by floors, fire barriers, or smoke barriers. When fire or smoke barriers do not partition a floor, the entire floor is the fire zone. In application, every zone in the facility should be evaluated. Repetitive arrangements may be evaluated by selection of a typical zone.

Risk

Also unlike the *Life Safety Code,* the FSES begins with a determination of relative risk deriving from characteristics of a health care occupancy. Five occupancy risk parameters are used: (1) patient mobility, (2) patient density, (3) fire zone location, (4) ratio of patients to attendants, and (5) average patient age. Variations of these parameters have been assigned relative weights as indicated in Table 5-10.2. These values were determined from the experienced judgment of a group of fire safety professionals and represent the opinions of that panel of experts. There is no documented process for validating or revising these values.

Occupancy risk factor for a zone is calculated as the product of the assigned values for the five risk parameters. Multiplication implicitly suggests these factors are interdependent. A hardship adjustment for existing buildings is applied to the occupancy risk factor. This adjustment modifies the risk in existing buildings to 60 percent of that for an equivalent new building.

Fire Safety Parameters

Safety features must offset the calculated occupancy risk. Thirteen fire safety parameters were selected. These parameters and their respective ranges of values (shown in Table 5-10.3) were also developed by the same panel of experts. Table 5-10.3 is designed to be used as a survey instrument whereby appropriate values for each safety parameter can be selected by inspection of the fire zone. There is no attempt made to directly correlate these fire safety parameters to the previously defined risk parameters.

Fire Safety Redundancies

An important concept of the FSES is redundancy through simultaneous use of alternative safety strategies. The purpose is to ensure that failure of a single protection device or system will not result in a major fire loss. Three fire safety strategies are identified: (1) containment, (2) ex-

Table 5-10.2 *FSES Occupancy Risk Parameter Factors*

Risk Parameters — Risk Factor Values

1. Patient Mobility (M)

Mobility Status	Mobile	Limited Mobility	Not Mobile	Not Movable
Risk Factor	1.0	1.6	3.2	4.5

2. Patient Density (D)

No. Patients	1–5	6–10	11–30	> 30
Risk Factor	1.0	1.2	1.5	2.0

3. Zone Location (L)

Floor	1st	2nd or 3rd	4th to 6th	7th and Above	Basements
Risk Factor	1.1	1.2	1.4	1.6	1.6

4. Ratio of Patients to Attendants (T)

Patients / Attendant	1–2 / 1	3–5 / 1	6–10 / 1	> 10 / 1	One or More[a] / None
Risk Factor	1.0	1.1	1.2	1.5	4.0

5. Patient Average Age (A)

Age	Under 65 Years and over 1 Year	65 Years and over, 1 Year and Younger
Risk Factor	1.0	1.2

[a]Risk factor of 4.0 is charged to any zone that houses patients without any staff in immediate attendance.

tinguishment, and (3) people movement. Table 5-10.4 indicates the expert panel's opinion of which fire safety parameters apply to each fire safety strategy. Values from Table 5-10.3 are entered in the appropriate places on Table 5-10.4 and summed for each column. The implication of addition is that there is no interaction among the fire safety parameters. The limited value of automatic sprinklers for people movement safety is adjusted for by using one-half of the parameter value in this column. The resulting sums are considered to be the available level of each fire safety strategy.

Equivalency Evaluations

The FSES determines if the fire zone in question possesses a level of fire safety equivalent to that of the *Life Safety Code.* This conclusion is made by comparing the calculated level for each fire safety strategy to stated minimum values. These values for existing buildings range from 100 percent down to 12 percent of those for new buildings. For the column of Table 5-10.4 labeled "General Safety," the sum of all available safety parameter values is compared to the occupancy risk factor calculated from the parameters in Table 5-10.2.

Supplemental Requirements

Because the thirteen selected fire safety parameters were found not to cover all requirements of the *Life Safety Code,* an addendum to the FSES was created. The addendum consists of twelve additional parameters that may be required by the *Life Safety Code.* It should not be implied that these parameters are extraneous to the risk and safety factors of Tables 5-10.2 and 5-10.3 or to the identified fire safety strategies.

Optimization

A distinct advantage of index approaches to fire risk assessment is that they lend themselves to optimization techniques. This characteristic has been exploited for the FSES through incorporation of a linear programming optimization algorithm.[30–35] Linear programming refers to a mathematical model for allocating limited resources among competing activities subject to a set of constraints. The procedure finds the distribution of values that optimizes an objective function.

For a fire risk index, the objective is to minimize cost of fire protection that will meet a prescribed acceptable level. In the FSES, the acceptable levels are given and the variables are the safety parameters that can take on the values indicated in Table 5-10.3. By assigning a cost to each value in Table 5-10.3, an economic optimum can be calculated. A personal computer version of this model is described in the last section of this chapter.

Derivative Applications

NFPA 101A now includes FSESs for health care occupancies, correctional facilities, board and care homes, and

Table 5-10.3 ***FSES Safety Parameter Values***

Parameters	Parameter Values						
1. Construction	Combustible Types III, IV and V				Noncombustible Types I and II		
Floor or Zone	000 (U)	111	200 (U)	211 + 2HH	000 (U)	111	222, 322, 433
First	–2	0	–2	0	0	2	2
Second	–7	–2	–4	–2	–2	2	4
Third	–9	–7	–9	–7	–7	2	4
4th & Above	–13	–7	–13	–7	–9	–7	4

2. Interior Finish (Corridors & Exits)	Class C	Class B	Class A		
	–5 (0)[f]	0 (3)[f]	3		
3. Interior Finish (Rooms)	Class C	Class B	Class A		
	–3 (1)[f]	1 (3)[f]	3		
4. Corridor Partitions/Walls	None or Incomplete	< 1/3 hr	≥ 1/3 < 1 hr	≥ 1 hr	
	–10 (0)[a]	0	1 (0)[a]	2 (0)[a]	
5. Doors to Corridor	No Door	< 20 min fpr	≥ 20 min fpr	≥ 20 min fpr & Auto clos.	
	–10	0	1 (0)[d]	2 (0)[d]	

6. Zone Dimensions	Dead End			No Dead Ends > 30' & Zone Length is:		
	> 100'	>50'–100'	30'–50'	> 150'	100'–150'	<100'
	–6 (0)[b]	–4 (0)[b]	–2 (0)[b]	–2	0	1

7. Vertical Openings	Open 4 or More Floors	Open 2 or 3 Floors	Enclosed With Indicated Fire Resist.		
			< 1 hr	≥ 1 hr < 2 hr	≥ 2 hr
	–14	–10	0	2 (0)[e]	3 (0)[e]
8. Hazardous Areas	Double Deficiency		Single Deficiency		No Deficiencies
	In Zone	Outside Zone	In Zone	In Adjacent Zone	
	–11	–5	–6	–2	0
9. Smoke Control	No Control	Smoke Barrier Serves Zone	Mech. Assisted Systems By Zone		
	–5 (0)[c]	0	3		

10. Emergency Movement Routes	< 2 Routes	Multiple Routes			
		Deficient	w/o Horizontal Exit(s)	Horizontal Exit(s)	Direct Exit(s)
	–8	–2	0	1	5
11. Manual Fire Alarm	No Manual Fire Alarm		Manual Fire Alarm		
			w/o F.D. Conn.	w/F.D. Conn.	
	–4		1	2	
12. Smoke Detection & Alarm	None	Corridor Only	Rooms Only	Corridor & Habit. Space	Total Space in Zone
	0 (3)[g]	2 (3)[g]	3 (3)[g]	4	5
13. Automatic Sprinklers	None	Corridor & Habit. Space	Entire Building		
	0	8	10		

Notes:

[a] Use (0) when Parameter 5 is –10.

[b] Use (0) when Parameter 10 is –8.

[c] Use (0) on floor with less than 31 patients (existing buildings only).

[d] Use (0) when Parameter 4 is –10.

[e] Use (0) when Parameter 1 is based on first floor zone or on an unprotected type of construction (columns marked "U").

[f] Use ( ) if the area of Class B or C interior finish in the corridor and exit or room is protected by automatic sprinklers and Parameter 13 is 0.

[g] Use this value in addition to Parameter 13, Automatic Sprinklers value, if the entire zone is protected with quick-response automatic sprinklers.

Conversion: 1 ft × 0.3048 = m

Table 5-10.4 ***FSES Worksheet for Evaluating Fire Safety Strategies***

Safety Parameters	Containment Safety (S_1)	Extinguishment Safety (S_2)	People Movement Safety (S_3)	General Safety (S_4)
1. Construction				
2. Interior Finish (Corr. & Exit)				
3. Interior Finish (Rooms)				
4. Corridor Partitions/Walls				
5. Doors to Corridor				
6. Zone Dimensions				
7. Vertical Openings				
8. Hazardous Areas				
9. Smoke Control				
10. Emergency Movement Routes				
11. Manual Fire Alarm				
12. Smoke Detection & Alarm				
13. Automatic Sprinklers			÷ 2 =	
Total Value	S_1 =	S_2 =	S_3 =	S_4 =

business occupancies. One of the most widely used of these is Chapter 8, "Fire Safety Evaluation System for Business Occupancies." NFPA 101A classifies the transaction of business other than mercantile, the keeping of accounts and records, and similar purposes, as a business occupancy. Typical examples are professional, financial, and governmental offices. The FSES for business occupancies was derived from a project to appraise the relative level of life safety from fire in existing office buildings and combination office-laboratory buildings of a U.S. government agency.[36] It was based on the approach developed for health care occupancies and was subsequently

incorporated into NFPA 101A. An analysis of the FSES for business occupancies, using the attribute value spread as a measure of importance to rank the fire safety attributes, found a difference between criteria for new and existing buildings of 6 to 10 percent.[37] A PC-based computer program, Enhanced Fire Safety Evaluation System for Business Occupancies (EFSES), is described later in this chapter.

Also derived from the original FSES is Section 3408, "Compliance Alternatives," of the BOCA *National Building Code*®,[38] an indexing system for fire safety in existing buildings. As stated in paragraph 3408.1, the purpose of this section is to maintain or increase safety in existing buildings without full compliance of other chapters of the code. This system allows for older designs to be judged on their performance capabilities rather than forcing the buildings to comply with modern standards for new construction. Originally adopted in the 1985 code, significant changes were effected between the 1993 and 1996 editions. Section 3408 is applicable to all occupancy use groups. For each use group there are separate point values for each safety attribute and separate mandatory values to be considered as criteria for equivalency. This procedure for compliance alternatives has also been adopted as an appendix to Chapter 34 in the International Building Code.[39] A detailed comparison of both qualitative and quantitative aspects of Section 3408 of the BOCA *National Building Code* and Chapter 8 of NFPA 101A shows some significant differences.[40]

Chapter ILHR 70 of the Wisconsin Administrative Code is a building code for historic structures.[41] Its purpose is to provide alternative building standards for preserving or restoring buildings or structures designated as historic. Subchapter IV of the code is a risk indexing system, called the Building Evaluation Method. It assesses life safety for a qualified historic building by comparing seventeen building safety attributes with the requirements of the prevailing code. If a historic building has less of a safety attribute than is required by the prevailing code, a negative number is assigned. If a historic building has more of a safety attribute than is required by the prevailing code, a positive number is assigned. Thus, evaluation is directly related to the prevailing code. If the sum of all the attributes is greater than or equal to zero, the building is compliant. The same trade-offs previously would have been allowed under the variance petition process but are now codified. This system adds a degree of certainty of approval that did not previously exist, often impeding development of historic buildings. Unlike the FSES and BOCA Chapter 34, the Building Evaluation Method has no mandatory scores. If the total safety score is equal to or greater than zero, the building is considered code compliant. Also unlike the FSES and BOCA, Wisconsin Subchapter IV does not vary by occupancy. A table for each attribute gives a set of numerical values, one of which is selected for each evaluation. Criteria for these values refer directly to the prevailing code. The same set of values applies for all nonexcluded building uses and occupancies. This code can be accessed through the State of Wisconsin, Department of Commerce web site http://www.commerce.state.wi.us.

Hierarchical Approach

Development of a hierarchical approach to fire risk ranking was initially undertaken at the University of Edinburgh, sponsored by the U.K. Department of Health and Social Services.[42–44] The objective of this study was to improve the evaluation of fire safety in U.K. hospitals through a systematic method of appraisal. This approach was further developed at the University of Ulster for application to dwelling occupancies.[45,46] It has been refined and implemented for the assessment of fire risk in telecommunications facilities.[47,48]

Defining fire safety is difficult and often results in a listing of factors that together comprise the intent. These factors tend to be of different sorts. For example, fire safety may be defined in terms of goals and aims, such as fire prevention, fire control, occupant protection, and so forth. These broad concepts are usually found in the introductory section of building codes and other fire safety legislation. Or, fire safety may be defined in terms of more specific hardware items, such as combustibility of materials, heat sources, detectors, sprinklers, and so forth. These topics are more akin to items listed in the table of contents of building codes. A meaningful exercise is to construct a matrix of fire safety goals versus more specific fire safety features. This matrix helps to identify the roles of these two concepts, in theory and in practice.

Decision-Making Levels

As a logical extension of a single fire safety matrix, consider that there are more than two categories of fire safety factors. This idea suggests a hierarchy of decision-making levels, or lists denoting things that comprise fire safety. A hierarchy of fire safety decision-making levels is presented in Table 5-10.5.

These represent common levels of fire safety decision making, but there may be more or fewer in a particular

Table 5-10.5 ***Hierarchy of Fire Safety Decision-Making Levels***

Level	Name	Description
1	Policy	Course or general plan of action adopted by an organization to achieve security against fire and its effects
2	Objectives	Specific fire safety goals to be achieved
3	Strategies	Independent fire safety alternatives, each of which contributes wholly or partly to the fulfillment of fire safety objectives
4	Attributes	Components of fire risk that are determinable by direct or indirect measure or estimate
5	Survey items	Measurable feature that serves as a constituent part of a fire safety attribute

application. For example, an even lower level dealing with individual physical items could be added or intermediate levels could be used to better define certain relationships.

This hierarchy of levels of detail of fire safety suggests that a series of matrices is appropriate to model the relationships among various fire safety factors; that is, a matrix of policy versus objectives would define a fire safety policy by identifying the specific objectives that are held most desirable. In turn, a matrix of objectives versus strategies would identify the relationship of these factors, and a matrix of strategies versus attributes would suggest where to use what. Thus, a matrix may be constructed to examine the association of any two adjacent levels in a hierarchy of fire safety factors.

An even more appealing aspect of this approach is that two or more matrices may be combined (multiplied) to produce information on the importance of specific detail of building elements to an overall fire safety policy—information not previously available. This approach is the only such grading of fire safety with an explicitly defined relationship to fire safety goals and objectives.

Generalized Procedure

A generalized procedure for ranking fire safety attributes to determine their relative importance is summarized in the following five steps:

1. Identify hierarchical levels of fire safety specification.
2. Specify items comprising each level.
3. Construct and assign values to matrices of each sequential pair of levels.
4. Combine (multiply) matrices to yield importance ranking of items.
5. Verify the results.

Table 5-10.5 represents an example of Step 1. Step 2 requires that lists of objectives, strategies, attributes, and survey items be developed. A list of fire safety objectives might include statements about life safety, property protection, continuity of operations, environmental protection, and heritage preservation.

No significant work has been done to identify just what it is that fire safety is trying to achieve (i.e., allocation of resources for fire safety is not generally directly associated with a specific corporate objective), so these objectives are a very subjective list. (One benefit of the hierarchical approach is facilitating the incorporation of fire safety into more global organizational objectives.)

In most applications a Delphi process is used to define fire safety policy in terms of the specified list of objectives. That is, a group of experts is asked to rank fire safety objectives with respect to their importance to policy. Each member of the Delphi group receives feedback in the form of response averages, and the process repeats until an acceptable level of consensus is reached. The Delphi exercise yields a vector representing the relative importance of each objective to organizational policy. In some work the more formal Analytical Hierarchy Process (AHP) is used.[49,50] However, this process is unstable when there are more than six or seven factors to be ranked.[2]

The next decision-making level involves fire safety strategies. A list of strategies can be derived by taking a cut set of the NFPA Fire Safety Concepts Tree.[51] Example fire safety strategies are ignition prevention, limitation of combustibles, compartmentation, fire detection and alarm, fire suppression, and protection of exposed people or things.

Now, a matrix of objectives versus strategies can be constructed. Values of the cells are again supplied by Delphi or some other subjective decision-making process. In this case the question to be answered is, how important is each strategy to the achievement of each objective?

In order to facilitate mathematical manipulation, the values of the matrices can be normalized. Then, multiplying the objectives/strategies matrix by the policy vector yields a new vector that shows the relative contribution of each strategy to overall fire safety policy. While this vector is not essential to the fire safety evaluation, it illustrates the matrix manipulation process that is the essence of the hierarchical approach.

Continuing this procedure, the next level of fire safety attributes is considered. The following is a typical list of these attributes:

construction	equipment	fixed suppression
height	special hazards	fire department
compartmentation	detection	egress system
building services	alarm	personnel
furnishings	smoke control	management

A matrix of strategies versus fire safety attributes is then constructed and evaluated. Multiplying this matrix by the previously derived vector yields a new vector that weighs each fire safety attribute according to its relative contribution to organizational fire safety policy. The significance of this vector is that it is the only such weighing of fire safety factors that has an explicit link to fire safety goals and objectives. The matrix manipulation process is summarized in Figure 5-10.5.

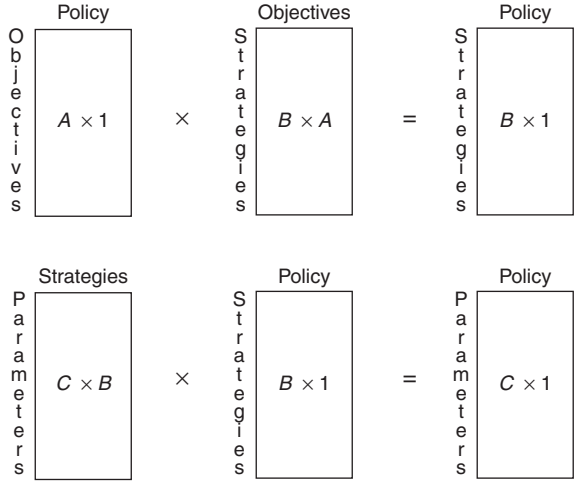

Figure 5-10.5. ***Schematic summary of hierarchical approach.***

Evaluating Attributes

In order to use the resulting vector of attribute weights to develop a fire risk ranking of a building or facility space, the extent to which each attribute is present must be evaluated. That is, a level of functional value of each fire safety attribute must be assessed. These attribute grades may be directly observable or, more often, they are derived from various functions of a lower level of features that includes specific hardware components, for example, fire safety survey items.

Attributes are defined as components of fire risk that are quantitatively determinable by direct or indirect measurement or estimation. They are intended to represent factors that account for an acceptably large portion of the total fire risk. In most cases they are not directly measurable. This case is especially true for existing buildings for which only limited information is readily available.

Each attribute has a specific relative importance that is universal for all facilities within the scope of the assessment method. Individual buildings will vary in the degree to which attributes exist or occur in a space. Attribute grades are a measure of the intensity level or degree of danger or security afforded by the attribute. Partitioning them into measurable constituent parts facilitates grading of attributes. Usually these parts are directly assessable survey items, the next lower level in the decision hierarchy. The determination of attribute grades is dependent on those features of a space identified as survey items.

A survey item is a measurable feature of a space that serves as a constituent part of one or more attributes. In developing means to grade attributes in a given building, each attribute is associated with one or more survey items. These specific features evolve from analysis of the attributes. Items are chosen for contributing significantly to the effectiveness of the irrespective attributes and for being directly measurable. It is, therefore, necessary that survey items be defined in sufficient detail to support these traits. Detailed descriptions of the survey items are required to frame questions that provide input into the decision logic that produces the attribute grades.

In one application, grades were established for each fire risk attribute by associating readily measurable survey items, using logic described by decision tables.[52] Input to these tables included fire test results, fire hazard modeling, field experience from previous fire events, logic diagrams, and professional judgment.

The scalar product of the resulting attribute weights and grades yields a relative measure of fire risk. The result may be used to rank facilities, or it can be compared to a standard value.

Areas of Application

As indicated in the beginning of this section, the hierarchical approach has evolved from applications in the areas of health care facilities, dwellings, and telecommunications central office facilities. Recent applications of this approach to fire risk indexing have developed in many forms and for many uses. In the United States, a Historic Fire Risk Index has been developed that includes an assessment of the cultural significance as a parameter of fire risk.[53,54] In Hong Kong, aspects of fuzzy systems theory have been incorporated into a fire risk indexing technique to evaluate existing high-rise buildings.[55]

While most fire risk indexing methods focus on life safety issues, FireSEPC (fire safety evaluation procedure for the property of parish churches) is insurance motivated and deals with building worth.[56] Using the hierarchical framework, the procedure rates the contribution of eighteen fire safety components and compares the score to a "collated norm" developed from guidance documents.

In Sweden there is a significant program for the development and verification of a fire risk index method for timber-frame, multistory apartment buildings.[57,58] This work is of particular importance due to its comprehensive documentation and validation procedures.

Criteria for Development and Evaluation of Fire Risk Ranking

The fire protection engineering community appears to be largely unconcerned with the proliferation of fire risk ranking and how it is being used. The available literature deals only with development and application of a specific method or general descriptions of several selected approaches. Like any analytical technique, risk ranking methods have their limitations and should not be used uncritically.

The purpose of fire risk ranking is to provide a useful aid to decision making. It must be easy to apply but sophisticated enough to provide a minimum of technical validity. Credibility can also be improved through consistency and transparency. The approach should be systematic, and it should be clear to all interested parties that the relevant technical issues have been appropriately covered. Based on the review of numerous fire risk ranking systems, 10 criteria have been proposed to aid in the development and evaluation of other such systems.[59]

Criterion 1: *Development and implementation of the method should be thoroughly documented according to standard procedures.* One of the hallmarks of professionalism is that, as a study proceeds, a record is made of assumptions, data, attribute estimates and why they were chosen, model structure and details, steps in the analysis, relevant constraints, results, sensitivity tests, validation, and so on. Little of this information is available for most fire risk ranking methods.

In addition to facilitating review, there are three other practical reasons not to slight the documentation: (1) if external validation is to be conducted, adequate documentation will be a prerequisite; (2) during the life cycle of a fire risk ranking system the inescapable changes and adjustments will require appropriate documentation; and (3) clear and complete documentation enhances confidence in the method, while its absence inevitably carries with it the opposite effect.

The value of the documentation will be improved if it follows established guidelines. Standard formats for doc-

umentation are primarily directed at large-scale computer models[60,61] but can be readily adapted in principle to more general applications.

Criterion 2: *Partition the universe rather than select from it.* One of the least well-established procedures in fire risk ranking is the choice of attributes. In following a systemic approach it is best to be comprehensive. Using an exhaustive model of fire safety such as the NFPA Fire Safety Concepts Tree[38] is helpful in being inclusive. This logic tree branches out from the holistic concept of fire safety objectives. A cut set on the tree will then identify a group of attributes that encompasses all possible fire safety features.

Criterion 3: *Attributes should represent the most frequent fire scenarios.* In determining the level of detail of the attributes, it is necessary to look at those factors that are most significant, statistically or by experienced judgment. This criterion may also be used as an alternative to Criterion 2, providing the need for systemic comprehensiveness is satisfied.

Criterion 4: *Provide operational definitions of attributes.* If the methodology is to be used by more than a single individual, it is necessary to ensure precise communication of the intent of key terms. Many fire risk attributes are ambiguous concepts that have a wide variety of interpretation even within the fire community.

Criterion 5: *Elicit subjective values systematically.* Most fire risk ranking methods rely heavily on experienced judgment. The use of formalized, documented procedures, such as the multiattribute utility theory, analytical hierarchy process, and Delphi process, significantly increases credibility of the system. Similarly, use of recognizable scaling techniques will enhance credibility.

Criterion 6: *Attribute values should be maintainable.* One variable that is not explicitly included in fire risk ranking, but which is very important, is time. It influences the fire risk both internally (e.g., deterioration) and externally (e.g., technological developments). In order for a method to have a reasonable useful lifetime, it must be amenable to updating. This requirement implies that the procedure for generating attribute values must be repeatable. Changes over time and new information dictate that the system facilitate revisions.

Criterion 7: *Treat attribute interaction consistently.* In the majority of cases treating attribute interaction consistently will consist of an explicitly stated assumption of no interaction among attributes. Where interactions are considered, it is important that they be dealt with systematically to avoid bias.

Criterion 8: *State the linearity assumption.* While the linearity assumption is universal in fire risk ranking, it is also well known that fire risk variables do not necessarily behave in a linear fashion. It is important to the acceptance of ranking methods and their limitations that such assumptions are understood.

Criterion 9: *Describe fire risk by a single indicator.* The objective of most fire risk ranking methods is to sacrifice details and individual features for the sake of making the assessment easier. Information should be reduced to a single score even in the most complex applications. The results should be presented in a manner that makes their significance clear in a simple and unambiguous way. Unless all those involved can understand and discuss the meaning of the ranking, there will not be general confidence in its adequacy.

Criterion 10: *Evaluate predictive capability.* Some attempt should be made to verify that the method does in fact differentiate between lesser and greater fire risks with sufficient precision. It is not feasible to validate a model per se, but some testing should be documented. Reference 62 gives some guidance on this subject. The level of accuracy demanded here is not the same as for other engineering purposes, and establishing an order of magnitude will generally suffice.

Computer Models for Fire Risk Indexing

In most cases, a fire risk index can be readily implemented on a typical computer spreadsheet. However, several software packages or programs have been developed to facilitate optimization, file management, and extensions of fire risk indexing methods. The following programs are presented as illustrative examples and do not constitute an exhaustive list.

ALARM 1.0 (Alternative Life Safety Analysis for Retrofit Cost Minimization) is a PC software tool that helps decision makers in health care facilities to achieve cost-effective compliance with the *Life Safety Code*.[63,64] The program is based on earlier work by Chapman and Hall.[30–35] It uses a mathematical optimization algorithm called linear programming to quickly evaluate all possible code compliance solutions and identify the least-cost means of achieving compliance. ALARM 1.0 generates a set of options from which the most appropriate code compliance strategy based on cost and design considerations can be selected. Also listed—for both individual zones and the entire building—are up to 20 alternative, low-cost compliance plans and the prescriptive solution for benchmarking purposes. The software includes the integrated code compliance optimizer, full-screen data editor, and file manager. ALARM 1.0 is available from the National Fire Protection Association (www.nfpa.org) through the One-Stop-Data Shop.

COFRA (Central Office Fire Risk Assessment) is a proprietary computer program that assesses risk in telephone central office facilities.[65] Two incidents in the last decade have shown the potential severity of a fire that causes interruption of a telecommunications network. Conformance with fire safety code requirements does not adequately address the susceptibility of critical equipment or service continuity. Initial evaluation of this issue revealed that significant conflicts existed among demands for technical accuracy, ease of use, and implementation cost. This evaluation led to the development of a

fire risk indexing method for the assessment of telecommunications network integrity. The approach uses a multiattribute evaluation model to determine the potential contributions to fire risk from individual fire safety attributes of a facility space.[47,48] Weights for the identified attributes were developed systematically from fire safety policy, objectives, and strategies. Methods were constructed to grade the attributes from onsite survey information. Principles of the Delphi process, decision tables, analytic hierarchy process (AHP), and other techniques of decision analysis were used in the development of attribute weights and grading methods. The scalar product of the attribute weights and grades produces a relative measure of the fire risk to integrity of a communications network. This program is presently an unsupported product of Telcordia Technologies.

EFSES (Enhanced Fire Safety Evaluation System for Business Occupancies)[66,67] is a PC-based computer implementation of Chapter 8 in NFPA 101A and has been adopted as Chapter 9 of NFPA 101A. The PC-based software automates the calculation process and forms generation. Also, it provides the user with guidance and on-line help in making the decisions involved in completing the FSES. The help screens provide background information and reference material to assist the user in choosing attribute values. Another enhancement allows the user to interpolate between attribute values in the worksheet table. The program also allows "refinement calculations" that consider attributes in more depth. For example, the construction refinement calculation uses Law's fire severity calculation to estimate the fire duration in the worstcase space in the building. If this result is less than the fire resistance of the building's structural elements then the attribute value can be increased. The program is distributed through NFPA and can be downloaded and installed from ftp://209.21.183.33/efsesinstall.exe, where the EFSES user manual is on-line in PDF format.

FREM (Fire Risk Evaluation Model) is Windows-based software that calculates a simplified assessment of fire risk associated with a given building.[68,69] FREM follows the general approach of the Gretener method.[13] Developed by National Risk Control Services in Australia, the program was sold to Gallagher Basset Services, Inc., in Itasca, Illinois, in 1996.

RiskPro is another model based on the Gretener method[13] that was also developed in Australia.[70] It incorporates a database of input values for more than 400 typical occupancies.

The software tool **Dow Indices**[71] uses the Dow Fire and Explosion Index[17] in an interactive, computer-based environment to identify hazards associated with the storage and use of flammable and explosive materials in a chemical plant. The program includes a library of chemicals, online help, and a variety of visual tools to determine the dominant contributors to the overall hazard. The Dow Indices tool can be linked to existing chemical process simulators through the Visual Basic programming platform. In addition, the software can be coupled with economic evaluators, such as a cash flow analysis, using the maximum probable property damage and business interruptions loss predicted by the index. The American Institute of Chemical Engineers (AIChE) is currently reviewing the program for marketing opportunities.

References Cited

1. J.M. Watts, Jr., "Index Approach to Quantifying Risk," in *Proceedings—SFPE Symposium on Risk, Uncertainty, and Reliability in Fire Protection Engineering,* Society of Fire Protection Engineers, Bethesda, MD (1999).
2. J.M. Watts, Jr., "Fire Risk Assessment Using Multiattribute Evaluation," in *Fire Safety Science—Proceedings of the Fifth International Symposium,* International Association for Fire Safety Science (1997).
3. H.E. Nelson, "Overview—Numerical Grading Systems," *Report from the 1987 Workshop on Analytical Methods for Designing Buildings for Fire Safety,* Building Research Board, National Academy Press, Washington, DC (1988).
4. J.M. Watts, Jr., "Fire Risk Rating Schedules," in *ASTM STP 1150, Fire Hazard and Fire Risk Assessment* (M.M. Hirschler, ed.), American Society for Testing and Materials, Philadelphia, pp. 24–34 (1992).
5. *Tools for Making Acute Risk Decisions with Chemical Process Safety Applications,* American Institute of Chemical Engineers, New York, p. 35 (1994).
6. G.R. Rosenblum and S.A. Lapp, "The Use of Risk Index Systems to Evaluate Risk," in *Risk Analysis: Setting National Priorities, Proceedings of the Society for Risk Analysis,* Houston, TX (1987).
7. *Report from the 1987 Workshop on Analytical Methods for Designing Buildings for Fire Safety,* Building Research Board, National Academy Press, Washington, DC (1988).
8. J.H. Magee and D.L. Bickelhaupt, *General Insurance,* Richard D. Irwin, Homewood, IL, p. 153 (1964).
9. A.F. Dean, *Analytic System for the Measurement of Relative Fire Hazard,* Western Actuarial Bureau, Chicago (1902).
10. J.S. Glidden, *Analytic System for the Measurement of Relative Fire Hazard, an Explanation,* Western Actuarial Bureau, Chicago, p. 17 (1916).
11. *Specific Commercial Property Evaluation Schedule,* Insurance Services Office, New York (1990).
12. BVD, *Evaluation of Fire Hazard and Determining Protective Measures,* Association of Cantonal Institutions for Fire Insurance (VKF) and Fire Prevention Service for Industry and Trade (BVD), Zurich, Switzerland (1973).
13. M. Fontana, "Swiss Rapid Risk Assessment Method, Institute of Structural Engineering," *SIA 81,* ETH, Zurich, Switzerland (1984).
14. J. Kaiser, "Experiences of the Gretener Method," *Fire Safety Journal,* 2, pp. 213–222 (1980).
15. J.C. Valente, "The Evaluation of the Fire Safety Level in a Historic Centre in Lisbon," in *Proceedings, International Conference on Fire Protection of Cultural Heritage* (K.K. Papaioannou, ed.), Aristotle University of Thessaloniki, Greece, pp. 225–234 (2000).
16. "Process Safety Manual," *Chemical Engineering Progress,* Dow Chemical Company 62, 6 (1966).
17. *Dow's Fire and Explosion Index Hazard Classification Guide,* 7th ed., Dow Chemical Company, American Institute of Chemical Engineers, New York (1994).
18. N.E. Scheffler, "Improved Fire and Explosion Index Hazard Classification," *AICHE Spring National Meeting* (1994).

19. *Guidelines for Chemical Process Quantitative Risk Analysis,* Center for Chemical Process Safety, American Institute of Chemical Engineers, New York, 32 (1989).
20. NFPA 704, *Identification of the Fire Hazards of Materials,* National Fire Protection Association, Quincy, MA, 1996 edition.
21. NFPA 49, *Hazardous Chemicals Data,* National Fire Protection Association, Quincy, MA, 1994 edition.
22. NFPA 325, *Fire Hazard Properties of Flammable Liquids, Gases, and Volatile Solids,* National Fire Protection Association, Quincy, MA, 1994 edition.
23. P172-2E, *Occupational Safety Report Guideline for Compilation,* Directorate-General of Labour of the Ministry of Social Affairs and Employment, Voorburg, The Netherlands (1990).
24. J. Lewis, "The Mond Fire Explosion, and Toxicity Index—A Development of the Dow Index," paper presented at the AIChE Loss Prevention Symposium, Houston, April 1–5, 1979.
25. *The Mond Index,* 2nd ed., Imperial Chemical Industries (ICI) PLC, Explosion Hazards Section, Technical Department, Winnington, UK (1985).
26. I.A. Benjamin, "A Firesafety Evaluation System for Health Care Facilities," *Fire Journal,* 73, 2 (1979).
27. H.E. Nelson and A.J. Shibe, "A System for Fire Safety Evaluation of Health Care Facilities," *NBSIR 78-1555,* Center for Fire Research, National Bureau of Standards, Washington, DC (1980).
28. NFPA *101®, Life Safety Code®,* National Fire Protection Association, Quincy, MA (2000).
29. NFPA 101A, *Alternative Approaches to Life Safety,* National Fire Protection Association, Quincy, MA (2001).
30. R.E. Chapman, "Cost-Effective Methods for Achieving Compliance to Firesafety Codes," *Fire Journal,* 73, pp. 30–39, 123 (1979).
31. R.E. Chapman, W.G. Hall, and P.T. Chen, "Economic Aspects of Fire Safety in Health Care Facilities: Guidelines for Cost-Effective Retrofits," *NBSIR 79-1902,* National Bureau of Standards, Washington, DC (1979).
32. R.E. Chapman, W.G. Hall, and P.T. Chen, "A Computerized Approach for Identifying Cost-Effective Fire Safety Retrofits in Health Care Facilities," *NBSIR 79-1929,* National Bureau of Standards, Washington, DC (1980).
33. R.E. Chapman and W.G. Hall, "Code Compliance at Lower Costs: A Mathematical Programming Approach," *Fire Technology,* 18, 1, pp. 77–89 (1982).
34. R.E. Chapman, and W.G. Hall, "User's Manual for the Fire Safety Evaluation System Cost Minimizer Computer Program," *NBSIR 83-2796,* National Bureau of Standards, Washington, DC (1983).
35. R.E. Chapman, and W.G. Hall, "Programmer's Manual for the Fire Safety Evaluation System Cost Minimizer Computer Program," *NBSIR 83-2749,* National Bureau of Standards, Washington, DC (1983).
36. H.E. Nelson, "Fire Safety Evaluation System for NASA Office/Laboratory Buildings," *NBSIR 86-3404,* National Bureau of Standards, Gaithersburg, MD (1986).
37. J.M. Watts, Jr., "Analysis of the NFPA Fire Safety Evaluation System for Business Occupancies," *Fire Technology,* 33, 3, pp. 276–282 (1997).
38. *The BOCA National Building Code,* Building Officials and Code Administrators International, Country Club Hills, IL (1996).
39. *International Building Code,* International Code Council, Whittier, CA (2000).
40. J.M. Watts, Jr., "Fire Risk Evaluation in the Codes: A Comparative Analysis," in *Proceedings—Second International Conference on Fire Research and Engineering,* Society of Fire Protection Engineers, Bethesda, MD, pp. 226–237 (1998).
41. "Chapter ILHR 70, Historic Buildings," in *Wisconsin Administrative Code,* Department of Industry, Labor, and Human Relations, Madison, WI (1995).
42. *Fire Safety Evaluation (Points) Scheme for Patient Areas Within Hospitals,* Department of Fire Safety Engineering, University of Edinburgh, Scotland (1982).
43. P. Stollard, "The Development of a Points Scheme to Assess Fire Safety in Hospitals," *Fire Safety Journal,* 7, 2, pp. 145–153 (1984).
44. E. Marchant, "Fire Safety Engineering—A Quantified Analysis," *Fire Prevention,* 210, pp. 34–38 (1988).
45. T.J. Shields and G.W. Silcock, "An Application of the Hierarchical Approach to Fire Safety," *Fire Safety Journal,* 11, 3, pp. 235–242 (1986).
46. H.A. Donegan, T.J. Shields, and G.W. Silcock, "A Mathematical Strategy to Relate Fire Safety Evaluation and Fire Safety Policy Formulation for Buildings," in *Fire Safety Science—Proceedings of the Second International Symposium (*Takao Wakamatsu, et al., eds.), Hemisphere, NY, pp. 433–441 (1989).
47. L.L. Parks, B.D. Kushler, M.J. Serapiglia, L.A. McKenna, Jr., E.K. Budnick, and J.M. Watts, Jr., "Fire Risk Assessment for Telecommunications Central Offices," *Fire Technology,* 34, 2, pp. 156–176 (1998).
48. E.K. Budnick, L.A. McKenna, Jr., and J.M. Watts, Jr., "Quantifying Fire Risk for Telecommunications Network Integrity, in *Fire Safety Science—Proceedings of the Fifth International Symposium,* International Association for Fire Safety Science, pp. 691–700 (1997).
49. T.J. Shields, G.W. Silcock, and Y. Bell, "Fire Safety Evaluation of Dwellings," *Fire Safety Journal,* 10, 1, pp. 29–36 (1986).
50. F.J. Dodd and H.A. Donegan, "Prioritization Methodologies in Fire Safety Evaluation," *Fire Technology,* 30, 2, pp. 232–249 (1994).
51. NFPA 550, *Guide to the Fire Safety Concepts Tree,* National Fire Protection Association, Quincy, MA, 1994 edition.
52. J.M. Watts, Jr., E.K. Budnick, and B.D. Kushler, "Using Decision Tables to Quantify Fire Risk Parameters," in *Proceedings, International Conference on Fire Research and Engineering* (D.P. Lund, ed.), Society of Fire Protection Engineers, Boston, pp. 241–246 (1995).
53. J.M. Watts, Jr., and M.E. Kaplan, "Fire Risk Index for Historic Buildings," *Fire Technology,* 37, 1 (2001).
54. M.E. Kaplan and J.M. Watts, Jr., "A Prototypical Fire Risk Index to Evaluate Fire Safety in Historic Buildings," *APT Bulletin,* 30, 2–3, pp. 49–55 (1999).
55. S.M. Lo, "A Fire Safety Assessment System for Existing Buildings," *Fire Technology,* 35, 2, pp. 131–152 (1999).
56. A.G. Copping, "Fire Safety Evaluation Procedure for the Property Protection of English Parish Churches: A Tool to Aid Decision Making," in *Proceedings, International Conference on Fire Protection of Cultural Heritage,* Aristotle University of Thessaloniki, Greece, pp. 255–268 (2000).
57. S.E. Magnusson and T. Rantatalo, "Risk Assessment of Timberframe Multistorey Apartment Buildings: Proposal for a Comprehensive Fire Safety Evaluation Procedure," *IR 7004,* Department of Fire Safety Engineering, Lund University, Sweden (1998).
58. H. Hultquist and B. Karlsson, "Evaluation of a Fire Risk Index Method for Timber-Frame, Multi-Storey Apartment Buildings," *Report 31XX,* Department of Fire Safety Engineering, Lund University, Sweden (2000).

59. J.M. Watts, Jr., "Criteria for Fire Risk Ranking," in *Fire Safety Science—Proceedings of the Third International Symposium* (G. Cox and B. Langford, eds.), Elsevier, London, pp. 457–466 (1991).
60. S.I. Gass, "Documenting a Computer Based Model," *Interfaces,* 14, 3, pp. 84–93 (1984).
61. ASTM E1472, *Documenting Computer Software for Fire Models,* American Society for Testing and Materials, Philadelphia (1998).
62. ASTM E1355, *Evaluating the Predictive Capability of Deterministic Fire Models,* American Society for Testing and Materials, Philadelphia (1992).
63. S.F. Weber, and B.C. Lippiatt, "Cost-Effective Compliance with Life Safety Codes," *Fire Technology,* 32, 4, pp. 291–296 (1996).
64. S.F. Weber and B.C. Lippiatt, "ALARM 1.0, Decision Support Software for Cost-Effective Compliance with Fire Safety Codes," *NISTIR 5554,* National Institute of Standards and Technology, Gaithersburg, MD (1994).
65. L.L. Parks, "COFRA-2: A Tool to Aid in Telecommunications Central Office Fire Risk Assessment," in *Proceedings, Fire Risk and Hazard Assessment Symposium,* National Fire Protection Research Foundation, Quincy, MA, pp. 523–540 (1996).
66. Hughes Associates, Inc., "Fire Safety Evaluation System (FSES) for Business Occupancies Software (ver 1.0 for Windows) User's Manual," *NIST-GCR-96-692,* National Institute of Standards and Technology, Gaithersburg, MD (1996).
67. Hughes Associates, Inc., *Enhanced Fire Safety Evaluation System for Business Occupancies Software,* Version 1.2, Hughes Associates, Inc., Baltimore (1999).
68. *FREM for Windows, User's Manual,* National Risk Control Services Pty. Ltd., Bayswater, Victoria, Australia (1995).
69. J.M. Watts, Jr., "Fire Risk Evaluation Model" (review), *Fire Technology,* 31, 4, pp. 369–371 (1995).
70. *RiskPro,* SimCo Consulting, Wantirna South, Victoria, Australia (2000).
71. P.B. Parikh and D.A. Crowl, "Implementation and Application of the Dow Hazard Evaluation Indices in a Computer-Based Environment," in *Proceedings: International Conference and Workshop on Reliability and Risk Management, San Antonio, TX,* American Institute of Chemical Engineers, New York, pp. 65–83 (1998).

CHAPTER 11

Product Fire Risk

John R. Hall, Jr.

Introduction

In the big picture of fire safety, there are only two ways to make changes—change things or change behavior. Every *thing* you can change could be seen as a product, in that it is a physical object that people buy, for example, from the raw materials that are used to make furniture to the finished furniture, from the components of fire detection and suppression systems to the complete systems, from wood and steel and concrete to whole buildings. That definition of product is too broad for one chapter.

For purposes of this chapter, a product will be a finished product, not raw materials or components in an assembly, but objects in an end-use form. And a product will be something that starts or feeds a fire as either a heat source or a fuel source. Computationally, fuel-source products involve much more elaborate calculations and effects, because the risk of heat-source products is measured solely in terms of whether or not ignition occurs. The treatment in this chapter will reflect that.

The fire risk of a product captures the range of severities of fires associated with the product and the probabilities that fires will occur having those severities. Fire risk is usually measured as expected loss, that is, the sum over all fires of probability times severity, or as the probability of having a fire more severe than a stated threshold. Either way, fire risk analysis relies heavily on fire scenarios, which are used to set up calculations of both probabilities and severities. This is *not* the same as choosing a handful of specific fires and calculating their severities and probabilities. A valid calculation must demonstrate that each specific fire analyzed is representative of a larger class of fires, that probabilities are calculated for the larger classes of fires rather than the specific fires, and that collectively the larger classes include every type of fire there can be.

For additional guidance, examine the sections on fire risk analysis in the two Society of Fire Protection Engineers references on performance-based design.[1,2]

Dr. John R. Hall, Jr., is assistant vice president for Fire Analysis and Research at the National Fire Protection Association. He has been involved in studies of fire experience patterns and trends, models of fire risk, and fire department management experiences since 1974 at NFPA, the National Bureau of Standards, the U.S. Fire Administration, and the Urban Institute.

Steps in a Product Fire Risk Analysis

The steps and sub-steps briefly described below parallel current thinking at U.S. standards-writing organizations, notably the American Society for Testing and Materials (ASTM), and previous global reviews of approaches to this subject, particularly as synthesized by Bukowski and Tanaka.[3] Later sections expand on techniques to be used in executing these steps.

1. **Define the Scope of Products to Be Analyzed, Including Context of Use.**
   a. Define the product or, more typically, the product class to be evaluated.
   b. Specify where and how the product is used. For example, the product class of floor coverings would not include all uses of carpeting, because carpeting is sometimes used as a wall covering. The specification of application will not only limit the range of product characteristics, but also specify or limit the input parameters used to identify fire scenarios in which the product may play a role.
2. **Specify the Class of Properties in Which the Product Will Be Used.** Part of identifying the scope is categorizing and specifying the property in which the product is used. The end-use or principal activity in a property defines it as an *occupancy*, which will imply a variety of characteristics and conditions in the environment of the product. For example, a risk analysis of upholstered furniture in homes will be different from a risk analysis of upholstered furniture in offices, and

both will be different from a risk analysis of upholstered furniture in hotels. The types of pieces used are different, the applicable standards are different, the mix of fires they could be exposed to are different, and the mix of people likely to be present (and their capabilities) are different.

3. **Specify Goals, Objectives, and Measures.**
   a. Specify goals in terms of acceptable target outcomes, usually in terms of types of harm to be prevented, minimized, or otherwise reduced. Life safety, defined in terms of fatal injury or other health effects, is usually the principal goal. Property protection, avoidance of indirect loss, and protection of heritage and the environment are other typical goals.
   b. Specify objectives, which are more specific means to the end, that is, the goals. If objectives are stated in terms of the systems and features that engineers design, they are called *functional* objectives. Alternatively, objectives may be stated in terms of events (e.g., flashover) or other physical conditions of fire.
   c. Specify or quantify goals and objectives in the form of performance criteria or other measures of loss or harm. Some measures, called *end* measures, are meaningful in and of themselves but are very difficult to predict in models or measure in tests (e.g., monetary damages, injuries). Some measures are easily predicted in models or measured in tests, but are not meaningful in themselves (e.g., temperature or toxic gas concentrations or obscuration for particular areas or volumes). Typically, models must be used to convert readily measurable quantities to end measures of loss.
4. **Set Assumptions.** Set assumptions covering all aspects of the building, occupant, system, feature, fuel load, modeling, or other elements affecting the outcomes that are not defined either by the product specifications (for the product being assessed) or by the scenarios, which address factors that vary. Set assumptions in terms of *average* conditions (or, if necessary, *typical* conditions), in order to predict overall risk-severity weighted by probability.
5. **Identify and Specify the Relevant Scenarios.** A scenario is a set of details about the initiating conditions and early growth of a fire that are needed as input conditions to a test method, fire model, or probability or other calculation. This may include
   a. Location and characteristics of the initial fuel and initial heat source. (The product will have the potential to be one or the other, depending on which type of product it is.)
   b. Proximities and characteristics of other fuel packages near the first ignited item. (The product may also belong here, if it is a fuel-source-type product.)
   c. If fire growth or effects beyond the first affected room or area are important to the estimation of the chosen measures of loss, then complete descriptions of those other areas will be needed, including spatial dimensions; fuel load; thermal properties of room linings, barriers, and openings connecting areas; occupants; and damageable property.
   d. Fire protection systems must be specified for any areas to be modeled.
6. **Identify Test Methods, Models, and Other Data Sources and Calculation Procedures.** The models needed will depend, in part, on the scenarios to be addressed, but the models listed below include the major modeling components included in most of the major modeling packages now in use. Each model has implications for data needs, including fire tests and statistical databases. (See Reference 4 for a more detailed review of available models.)
   a. Fire growth model
      i. Model of rate of growth in terms of heat release rate, for example, as a function of fuel load and distances between items
      ii. Horizontal flame spread model
      iii. Barrier failure (e.g., door, ceiling, window)
      iv. Exterior vertical flame spread model
      v. Flame spread model in concealed spaces
      vi. Building-to-building flame spread
   b. Smoke spread model
      i. Model of room filling
      ii. Model of spread between rooms
      iii. Flashover models, including timing of flashover and post-flashover smoke spread
      iv. Model of spread via heating, ventilation, or air conditioning system
   c. Occupant behavior model
      i. Model of automatic detection equipment performance
      ii. Model of how fire is discovered in the absence of automatic detection
      iii. Model of decision-making activities leading to decisions to egress or attempt rescue
      iv. Model of egress and rescue activities
   d. Intervention models
      i. Automatic suppression models, including timing of activation and effects on fire growth
      ii. Model of other suppression or extinguishment efforts and their effects (e.g., whether fire extinguishers will be used and to what effect)
      iii. Fire fighter response models
   e. Fire effects or outcome models
      i. Predicted deaths and injuries due to fire effects in affected areas as a function of time
      ii. Structural damage or failure models
      iii. Predicted extent or monetary value of property damage
   f. Ignition probability models
      i. Fault tree, success tree, or event tree
      ii. Bayesian analysis of test results, historic fire probabilities, and other data

In practice, many of these component models are rarely used. For example, a fire risk assessment of a burnable product may not need an elaborate analysis of intervention strategies, because the dominant scenarios may be those in which no prompt, effective intervention occurs. On the other hand, the modeling components used may identify a need for data for which no standardized source exists (e.g., burning properties of products in post-

flashover environments). It is not unusual, therefore, for the full calculation to require judgments by analysts, which must be checked through sensitivity analyses.

Bukowski and Tanaka[3] have proposed a conceptual scheme for standardizing the role of these expert judgments in fire hazard and risk assessment. Their scheme involves identifying groups of parameters and variables in the models and defining the acceptable sources of data for them, among which could be expert judgments.

Specifying and standardizing needed data sources is an essential part of the process of using fire hazard or risk assessment in a standard. The expectation is that, instead of stating a standard in terms of specifications, the standards-setting process would specify outcome measures, models and other calculation methods, modeling assumptions and input parameters, test methods and other data sources, and possibly the type of expertise required by those who run the models.

Define the Scope of Products to Be Analyzed

The scope definition should define a class of interchangeable items having a common function or application in a specified occupancy and with a range of allowable choices for composition. Specification of the product should be done in a way that facilitates use of existing data, from fire incident data to product test data.

For heat-source products, this means that initial specification of the product by function and construction should be based on the categories defined by NFPA 901, *Uniform Coding for Fire Protection*,[5] 1976 edition, Chapter F, "Equipment Involved in Ignition," and Chapter G, "Form of Heat of Ignition," or directly to categories defined in the National Fire Incident Reporting System (NFIRS) (see Section 5, Chapter 5).

For fuel-source products, this means that initial specification of the product by function should be based on the categories defined by NFPA 901,[5] Chapter I, "Form of Material First Ignited." Initial specification of the product by material composition should be based on the categories defined by NFPA 901,[5] Chapter H, "Type of Material First Ignited" (see Section 5, Chapter 5). A product (e.g., carpet) is defined as a floor covering made of certain materials, chosen to distinguish it from vinyl flooring, wood flooring, concrete slabs, and so forth.

Further specification of the product by function may be needed (e.g., selecting bookcases from the cabinetry group). In such cases, the nationally representative fire incident databases will not be sufficient to estimate probabilities. Other, special fire incident databases and expert judgment will be needed.

When calculating probabilities, be sure to include appropriate shares of fires involving products that were partially or wholly undefined (e.g., upholstered furniture fires should include shares of fires involving unknown-type furniture or unknown-type form of material first ignited, and might include shares of fires involving unclassified furniture or unclassified form of material first ignited).

The range of items defined as examples of the product—which may be referred to as members of the product class—must, for analysis purposes, be reduced to a manageable number of subgroups. Each subgroup will be *defined* by a range of characteristics (e.g., all cellulosic versions of the product) but will be *represented* by one specific set of product fire characteristics. Ordinarily, these product fire characteristics will be identified from review of results of actual fire tests on one or more representatives of the product class.

Specify the Class of Properties

For reasons similar to those already cited for product scope definitions, property classes (i.e., occupancies) should have their primary definitions stated in terms of the categories defined in NFPA 901,[3] Chapter B, "Fixed or Specific Property Use" or in NFIRS. Whenever occupancy scenarios can be defined using nationally representative, valid fire incident data, the analyst will have the strongest possible basis for estimating probabilities. The principal weakness of this data source involves the level of detail of readily available fire incident data, which often falls well short of the detail needed to run the fire hazard analysis portion of the method.

Specify Goals, Objectives, and Measures

Overall goals for fire safety tend to fall into one of the following categories:

- Prevent adverse health effects, particularly fatal injury, to people exposed to fire. Emergency responders are normally addressed separately and may be excluded from consideration.
- Prevent monetary losses due to direct property damage.
- Prevent indirect losses due to fire, such as business interruption, missed work, and temporary housing. The types of indirect losses will differ for residential versus nonresidential occupancies, as will the relative importance of direct damage versus indirect loss.
- Prevent environmental damage. This may be damage due to fire, damage incidental to firefighting or other suppression activities, or damage associated with fire prevention or protection strategies. The negative impact of some fire retardants on recyclability of plastics could be addressed under the latter type of goal.
- Prevent harm to cultural heritage. This refers to historic buildings and similar structures for which fire damage may be more expensive or impossible to repair if historical authenticity is an objective.

The most natural context for fire risk assessment is a whole building, vehicle, or other built environment, because all fire prevention and fire mitigation strategies are available. A fire risk assessment of products can be conducted using the overall goals. It is also possible to use the overall goals for a building or vehicle fire risk or hazard assessment, then to set objectives supporting those goals as functional objectives, defined in terms of the various functions in the building. With such an approach, a product class can be defined as a function having its own objective(s).

The advantage of the functional objective approach is that it does not require the analyst to define scenarios, set assumptions, and model phenomena far away from the product of interest. Instead, it is possible to construct the outcome measures using measurement scales closer to the ones traditionally derived from product fire tests. The disadvantage of the functional objective approach is that it tends to be difficult to execute unless you can specify characteristics at the level of an individual building. If one attempts to use this approach as a basis for qualifying products for an entire class of occupancies, then one is forced to develop all the same information for overall goals, assumptions, scenarios, and models that would have been needed for an assessment at the building level, in order to derive generic functional objectives.

For measures of loss in fire hazard assessment, the measure will be a predicted severity value, such as predicted deaths. For fire risk assessment, both severity and probability are important. Two common summary measures are expected loss (i.e., a sum over all scenarios of scenario probability times predicted scenario hazard) and probability of loss exceeding a certain threshold. Both measures can be calculated directly from nationally representative fire incident databases, without the need for modeling or testing, provided that the product class definition matches the categories used in those databases. For example, a fire risk analysis comparison of the major types of home heating equipment is possible, because each can be identified within the fire incident databases. However, a comparison of different designs for, say, portable electric heaters could not be easily done from statistics alone, because different designs cannot be so distinguished. And for fuel-source products, their role in fire can be identified in statistics only when they are the first item ignited.

For a variety of reasons, therefore, one is usually forced to use test methods and models to develop probability estimates and fire severity estimates more appropriate to the product class and product alternatives of interest. In such cases, much calculation effort can be saved if the problem lends itself to restatement in terms of measures of loss that can be measured in the laboratory and at the fire scene. Three examples are

1. Probability of flashover and/or of flame spread beyond the room of origin
2. Probability of fire ignition
3. Probability that time to flashover exceeds x minutes (where x is chosen to reflect the expected arrival of suppression and rescue forces)

One approach that should usually be avoided is to try to measure loss in terms of the product's share of responsibility for overall fire severity. Such measures tend to be far too subjective and require answers to inherently unanswerable questions. For example, suppose a small trash can fire leads to a large couch fire. If *either* factors in the initial trash ignition or the burning properties of the couch are changed, no large fire would have resulted. How much loss should be assigned to the couch? There is no good answer to that question.

Instead, fire risk analysis should proceed through calculations of differences, that is, fire risk with the product of interest versus fire risk with something else substituted for the product of interest.

From this perspective, one can see how fire risk analyses can be constructed as extensions of past successful applications of fire modeling. For example, one of the earliest practical applications of the Harvard code was to the reconstruction of the 1980 MGM Grand Hotel fire. As suggested above, flashover was used as a well-defined event to focus the analysis, after it was shown that most of the fatal fire victims would have survived if flashover had been prevented. Professor Howard Emmons then used the model to rerun the fire with changes, considered individually, in the room of origin's ceiling covering; its benches and chairs; and the area's heating, ventilating, and air-conditioning (HVAC) arrangements.

If one wished to do a fire risk analysis on, say, benches and chairs for dining areas of hotels, one could define a range of possible fire scenarios, do a similar Harvard code analysis of each, weight the consequences by the scenario probabilities, and thereby calculate an overall probability of flashover with two different choices of benches and chairs. The difference between the two probabilities would be a valid product fire risk measure.

A recent fire hazard analysis of rigid non-metallic conduit in hospital emergency systems, done by Benjamin/Clarke Associates, provides a rare example of circumstances where the product's share of fire loss can be validly used for analysis. Dr. Fred Clarke devised a realistic scenario designed to maximize the likelihood of significant product involvement in fire, by placing the initiating fire directly under the product, which was assumed to be exposed due to missing ceiling tile. From a fire risk analysis perspective, this scenario was designed to put an upper bound on the product's share of fire loss in scenarios with significant loss.

If this upper bound were applied to all scenarios and if it were assumed that a substitute product could eliminate the product's role as a fuel source for the fire, then one would have all the requisite parameters for an upper bound estimate on the fire risk consequences of using that product. This is a one-sided analysis. That is, if the product's fire risk proves to be negligible under these conditions, one knows that the true fire risk is also negligible; but if the product looks bad in this analysis, one does not know whether it would still look bad in a fairer, more representative analysis.

Set Assumptions

Fire risk assessment requires the analyst to make assumptions. Some of the assumptions are embedded in elements of the analysis, such as the zone model's assumption that fire conditions in a room can be reasonably approximated by dividing the room into an upper and a lower layer. Some assumptions set boundaries to the analysis, such as an assumption that an effective local public fire department will respond within five minutes, which permits the designer to track fire development and effects for a limited period of time.

Many assumptions address the building, occupant, fuel load, or system characteristics that do not vary from one scenario to another. These assumptions may be treated

as scenario characteristics in one assessment and as assumptions in the next assessment. Therefore, the more detailed discussion of elements of scenarios, in the next section, also applies to most of the candidate assumptions.

There is a critical difference in the handling of assumptions in fire risk assessment versus fire hazard assessment. In fire risk assessment, the purpose of the calculation is to predict what *will* happen. Challenging, high-severity scenarios must be addressed but given only as much or as little weight as the probabilities of those scenarios would justify. In fire hazard assessment, the purpose of the calculation is to predict what *might* happen for which the designer is responsible. This is where concepts like *probable worst-case scenario* become relevant. Fire hazard assessment needs to address only challenging, high-severity scenarios, and does not discount the scenarios it addresses by their probabilities. But some high-severity scenarios will be declared too challenging for a fire hazard assessment. Thus, fire hazard assessment takes an all-or-nothing approach to scenarios.

Fire risk assessment, for these reasons, will assign more variables to scenarios and fewer to assumptions than will hazard assessment. Fire risk assessment needs to address all possible scenarios. But fire risk assessment will tend to set assumptions in terms of typical or average conditions. This approach better serves the purpose of fire risk assessment, which is to predict what will happen.

Specify Fire Scenarios—Initiating Fire

For every scenario, each aspect of fire initiation and growth must be specified in such a way that (1) one can model, test, or otherwise calculate the fire severity consequences of a fire with those specifications; and (2) one can calculate or estimate the probability of having a fire with those specifications. This process of specification usually requires the analyst to address three stages of fire:

1. *What are the initial heat source, the initial fuel source, and the circumstances that bring them together?* These are the basics of the initiating fire, and they need to be specified so that fire incident databases can be used as a major source for estimating probabilities.
2. *What are the factors that will determine whether, and how quickly, fire will spread from the first item to the product, if they are not the same?*
3. *What are the characteristics of the room or area of origin and its fuel packages and surfaces that will determine how large the fire will grow and whether, and how quickly, it will reach flashover and leave the room?*

These three questions reflect the three stages at which a burnable product may become involved in a fire—as the first item ignited; as a secondary item ignited by exposure to other items ignited earlier; or as part of a room that has gone to flashover, when everything that can burn will burn. (If the product is a heat-source product, the latter two stages are not concerns and the analyst need not address them in as much detail.)

For each scenario characteristic, consider the possibility that the characteristic may need to be handled as a variable. That is, one may need to define a set of scenarios, each having a different value of the scenario characteristic (e.g., a different rate of growth in the rate of heat release for the initial fire growth). Theoretically, of course, one might need to vary this scenario characteristic for every combination of the other scenario characteristics. (For example, varying the rate of growth in the initial rate of heat release would not mean four scenarios instead of one but would mean four times as many total scenarios.) This multiplication of scenarios would quickly become unmanageable.

Two general approaches can be used to set up the model of these stages. One is to use surveys of typical fuel loads, room configurations, and the like. Then, one can run a fire growth model with these specifications. The drawbacks of this approach are that the magnitude of the data requirements is extremely large; that such survey data are very scarce, and, when they exist, almost never capture the variations in practice that produce different probabilities and different fire outcomes; and that the probability of ignition is probably not constant from one configuration to another nor is it susceptible to estimation from any existing fire incident databases. If this approach is used, it will tend to force the analyst away from some of the essentials of fire risk analysis, that is, a suitably diverse set of scenarios and an adequate attention to the role of probabilities.

The other general approach is to infer patterns of fuel loads and room configurations from fire loss experience. The logic used here is as follows: Recent fires were produced by recent fuel load and room layout practices. What would those practices have to be in order to produce the observed fires? A critical element in this approach is data on final extent of flame damage, which are captured in the major fire incident databases, as follows:

- Confined to object of origin
- Confined to area of origin
- Confined to room of origin
- Confined to fire-rated compartment of origin
- Confined to floor of origin
- Confined to building of origin
- Extended beyond building of origin

One can assume that a fire confined to object of origin involved only the first item ignited and that a fire extending beyond the room of origin reached flashover in the room of origin.

If the product was not the first item ignited but the fire spread beyond the object of origin, then the fire could have ignited the product through radiant exposure. What is the best way to estimate the probability that this will occur? The fire risk analysis method FRAMEworks,[6] developed under the auspices of the National Fire Protection Research Foundation, uses the following four elements:

1. For each type of item first ignited (e.g., trash), a set of estimated typical values for mass and burning properties, sufficient to estimate a rate of heat release curve for the product burning alone
2. Ignitability characteristics of the product (i.e., critical radiant flux)
3. For each type of item first ignited, a probability distribution on the distance from the item to the product, as

a function of the type of room, with distributions based on survey data and expert judgment
4. Established mathematical relationships showing the minimum distance at which ignition of a second item will occur, given the first item's burning characteristics and the second item's ignitability characteristics

This second approach still needs the kind of property survey data required by the first approach, but far less of such data because the only geometric information sought is distances between the product and other items. Even so, this is still a data-hungry approach that requires either (1) survey data that may not exist or may be very expensive to collect, or (2) expert judgment that may be especially difficult to make.

As in so many other areas, the temptation will be to reshape the analysis to bypass elements that cannot now be modeled with confidence. However, the analysis must somehow provide a valid basis for combining different product burning properties, and the phenomenon of secondary ignition is central to any evaluation of the product's relative ignitability.

Still other phenomena must be reduced to assumptions for modeling purposes. The following are examples: for a fire that does not reach flashover, what is the physical measure (e.g., temperature) of its peak size? What stops the fire, and what characteristics of fire development (e.g., burning time, detector activation, fire size) triggered fire suppression? (Identifying these characteristics is important in order to know when to stop the fire if the product is changed.) What is the fire's profile after it reaches its peak? Is there an initial smoldering phase, and, if so, how long is it and what is the fire profile during this period? Each of these questions needs to be answered through a crosswalk between the physical parameters measured in tests and used in models and the parameters recorded in fire incident databases, because the latter is always needed to calibrate probability estimation.

Specify Fire Scenarios—The Building Beyond the First Room

The dimensions used to define the different occupancy scenarios need to be dimensions that are relevant to fire development. Most of these dimensions will be one of three types:

1. *Building Dimensions and Geometry.* Dimensions of rooms and other areas in which fire may grow or smoke may spread.
2. *Openings.* Dimensions of openings between rooms and areas relating to paths of flame or smoke spread and sources of air to feed the fire.
3. *Room Linings.* Thermal properties of rooms that may bear on burning at and after flashover.

Building dimensions and geometry: The overall building size and geometry can be structured into a series of questions on which data must be sought and decisions made. The first is the range of variation in the number of floors. After determining this point, the user must specify a number of floors for each occupancy scenario and assign a probability to each.

The second is a room layout for each floor. Room heights and the sizes of openings connecting rooms tend to be standardized by common industry practices, so there may be no need to consider variations. For other factors, (e.g., the number and sizes of rooms) there usually is too much variation in practice and too little data on the relative likelihood of these variations to do much more than (1) estimate one or two values for the number of rooms or the total square feet per floor, and (2) use expert panels to develop detailed layouts for the purposes of modeling and analysis of the rooms or spaces specified in (1).

However, panels of people who are experts on buildings of a certain type are likely to think in terms of the characteristics of the particular buildings they know best. They may therefore give estimates biased toward characteristics of new construction or characteristics of the buildings they live in or frequent. Fires are more likely to occur in smaller, less prestigious units in any property class. The expert panel needs to be continually reminded to adjust their perspective to think in terms of those kinds of buildings.

Openings: There usually will be some information on the sizes of doors and windows, because construction practices are highly standardized even beyond code requirements. However, in a fire, the openings will depend critically on whether and how much key doors and windows are open. There are little or no data on this point for any occupancy. It may be possible to ignore windows, because there are studies indicating that windows affect most fires only after the point in time where fire severity has been determined. (However, the few exceptions will tend to be very large fires, so the reasonableness of an assumption excluding windows will need to be rechecked for any analysis.) How does one set the assumptions for doors, short of large-scale property surveys or special fire data collection projects?

For most fire protection engineering studies, the answer would be to make conservative assumptions, that is, those that present the greatest fire challenge. It is important to understand that this is usually not the right answer for fire risk analysis. If conservative assumptions lead to an overestimate of fire risk, then they may also lead to a gross overestimate or underestimate of the fire risk consequences of particular product choices. There is no substitute for a best estimate, without conservatism, in fire risk analysis.

However, an assumption that might be made in fire hazard analysis because it is conservative may also turn out to be a reasonable best estimate for fire risk analysis, if it reflects a pattern in actual fire experience. If a certain arrangement *could* produce more serious fires, it qualifies as a conservative assumption for fire hazard analysis. If that same arrangement *is producing* more serious fires, then it is more likely that that arrangement is present when a reported fire occurs than that it is present in buildings in general, and one could be justified in assuming that that arrangement is likely, in a fire risk analysis.

However, this line of reasoning has limits. Suppose that open doors is the conservative assumption, but that we know that doors tend to be open only 5 percent of the

time. In that case, the fire risk analysis could reasonably assume that doors are open 10 to 20 percent of the time, reflecting the likelihood that open doors will be more likely in reported fires than in buildings, in general. But the typical situation would still be closed doors.

The analysis would need to have scenarios with open doors and scenarios with closed doors, because neither condition is dominant enough to justify omitting the other condition for a variable (i.e., whether doors are open) that is so influential on final fire size. Or, it might be possible to use one condition, consisting of doors open slightly, trying to seek a single physical condition that will reproduce the appropriate average between fully open and fully closed. Either way, considerable judgment would be needed.

Remember that, if an *average* value is used, the analyst is implicitly assuming that the fire severity associated with that average value is equal to the average of the fire severities associated with all the individual values that occur. In mathematics, this is sometimes called assuming that the average of the function equals the function of the average, and it is not usually the case. The analyst has to make the case that the assumption is reasonable in the situation being analyzed.

Room linings: Linings of rooms and other areas need to be addressed in terms of the thermal properties required for calculations of time to flashover, speed of vertical flame spread, and the like.

Room and area linings for most occupancies are tightly regulated by codes. However, some of the most important occupancies (e.g., dwellings) are not so covered, and even for those that are, one must allow for a significant probability that the codes will not have been in force when fire occurs. Unfortunately, there is little or no data on the probabilities of different combinations of fuels in particular occupancies; and there is only very limited, dated information on typical or average fuel loads and only for some occupancies.

Specifying Fire Scenarios—Exposure of People or Property

In order to translate model or test outputs on the physical characteristics of fire, as a function of location and time, into end-measures of human or property loss, one must address (1) the locations of people or property as a function of time, and (2) the damage or loss consequences to people or property of the different possible physical characteristics of fire, for example, temperature, quantities of toxic gases by type, corrosive properties, and quantities of smoke. The methods for doing this are not extensively developed, except for deaths. Therefore, this section will focus on that outcome.

Occupant exposure depends upon (1) initial locations of the occupants relative to the fire, and (2) their escape behavior. A complete specification of the number of occupants with their initial locations and other characteristics is called an *occupant set.* The user must first define a group of occupant sets that can validly represent all possible combinations of people and their characteristics and locations, and then must estimate probabilities for each. These must then be joined to a model of occupant behavior. (See Reference 2 for a list of evacuation models.)

Occupant behavior models consist of a set of rules for calculating the locations of occupants at a time, *t,* as a function of their locations, other occupant characteristics, and fire characteristics at the time stage just prior to *t.* Some such models track occupants individually; others give only the number of people at each location. Some, but not all, models include interactions among occupants, such as congestion or queuing effects or behavioral rules based on relationships between occupants (e.g., parents who seek to rescue babies). The more comprehensive the model may be in capturing potentially important phenomena, the more computationally demanding it will be and the more data it will demand, possibly including data that are not readily available. As in all other aspects of fire risk analysis, tradeoffs must be made in the modeling.

A brief summary of the steps required is as follows:

- Develop a probability distribution for the number of people present in the building.
- Expand the basic distribution to address relevant characteristics, including ages and relationships of occupants, time of day, and occupant conditions.
- Develop probability distributions for occupant activity as a function of time of day and of occupant characteristics, specified in the previous step.
- Develop probability distributions for occupant location given occupant activity and other occupant characteristics. (If every activity implies a unique location, this will reduce to a crosswalk.)
- Combine all probability distributions to produce a probability distribution for all occupant sets. Merge very similar occupant sets, if needed, for computational simplicity.

Specifying Fire Scenarios—Fire Protection Systems and Features

All significant fires seem to involve a series of failures that set the stage for the event. Thus, it is important to examine the consequences of things not going according to plan. Consider a scenario where automatic systems fail and the fire department does not respond. In a fire hazard assessment, one must ask whether this scenario is so unlikely—or can be made so unlikely through inspection, maintenance, or backups—that the scenario need not be considered. In a fire risk assessment, one must ask whether the scenario's huge severity will be offset by a sufficiently low probability. If nothing else, such scenarios can help to identify the factors that mean the difference between an incidental fire and a major disaster.

The following requirements are straightforward, in principle, but necessary models or data are often sketchy:

- For each type of fire protection system (e.g., detectors, sprinklers, smoke control systems) or feature (e.g., fire doors), identify a range of alternatives. These alternatives must address not only variations in the type and coverage of system or feature used (e.g., quick-response versus conventional sprinkler), but also variations in operational status (e.g., fully operational versus water turned off).

- For each alternative, probabilities will be needed. As in the other parts of the analysis, start with representative national fire incident databases for best estimates, then add needed detail using other databases and expert judgment.
- For each alternative, it will be necessary to specify rules for how the system or feature, under that alternative, will affect the fire development, the evacuation, or other conditions being tracked. Often, this will be fairly simple. One could assume that a fully operational sprinkler system will activate once a specified set of fire conditions are reached and, once activated, will totally and immediately stop the fire, except for certain specified fire scenarios (e.g., fire origin in concealed spaces), when its effect will be only to block fire entry into sprinklered areas. One could assume that a full-coverage automatic detection system will activate once a specified set of smoke or heat conditions is reached and, once activated, will alert everyone in the building to the fire, leading anyone not already in motion in the occupant evacuation model to begin evacuating. In fact, both these examples are oversimplified and possibly dangerously so. A sprinkler's full effect on fire and a detection/alarm system's full effect on occupant behavior will not be instantaneous. The delay may be critical to outcomes and needs to be addressed in the analysis, if only to make explicit what simplifying assumptions have been made.

Identify Test Methods and Models

Analyzing ignition probability: While historic fire data may suffice to estimate ignition probabilities for the mix of existing products, they may not suffice to estimate ignition probabilities for specific existing products, and they will not suffice for new products. The basic approach involves converting laboratory test results to ignition probabilities.

Probabilities of ignition must be estimated from frequencies of ignition in laboratory tests of existing and new products. In essence, it is assumed that, if the new product produces more or fewer ignitions in laboratory tests than the existing products did, then the new product will have a higher or lower probability of ignition, increased or decreased by the same proportion as the ratio of the laboratory ignition frequencies. For fuel-source products, this estimation should be done separately for each of the major classes of heat sources (e.g., flaming versus smoldering), because product ignitability may vary across different heat sources. For heat-source products, it should be done for suitably chosen classes of initial fuel sources.

To prepare a set of laboratory test data for use in these calculations on a fuel-source product, organize the data according to the following terminology:

- Distinguish different versions of the product ($i = 1, 2, \ldots$)
- Distinguish different heat sources ($j = 1, 2, \ldots$)
- Estimate the share of all the product now in use that is version i; call this q_i where $\sum_i q_i = 1$
- Let N_{ij} be the number of times that version i of the product has been tested in the laboratory against heat source j; let n_{ij} be the number of times that ignition occurred; and let $f_{ij} = n_{ij}/N_{ij}$.
- Let p_j be the probability of ignition of the mix of existing product by heat source j, calculated from fire experience data on the occupancy being studied.

  Then assume that p_j (the product's overall probability of ignition) is proportional to $\sum_i q_i f_{ij}$ (the weighted frequency of laboratory ignitions). For a more sophisticated approach, one may wish to use Bayesian analysis, which requires estimating prior probability distributions to which one can apply the lab tests.
- Let f_{Ij} be corresponding values summarizing laboratory tests on new product I against heat source j. Note that every heat source must have its own body of test results.
- Let p_{Ij} refer to the quantities to be estimated, which are the probabilities of ignition of product I by each heat source j. Estimate as follows:

$$p_{Ij} = p_j \left[\frac{f_{Ij}}{\left(\sum_i q_i f_{ij} \right)} \right]$$

In general, the p values will be much smaller than the f values, which is assumed to reflect the fact that the p values incorporate all the probabilities involved in bringing the heat source and the product in contact with one another. This estimation procedure is not so reliable if the f values are equal to, or very near, 0 or 1. Bayesian analysis is definitely required in such cases.

Calibration, sensitivity, and uncertainty analysis: Any fire risk analysis will involve complex calculations, with many unavoidable assumptions. While you should not use a more complex method than necessary, you also should not use a less complex method than is valid. A fire risk analysis model without a long list of stated assumptions is bound to be a model with many hidden assumptions, which are almost certain to be less well-founded, if examined, than a list of shaky but explicit assumptions.

For these reasons, running the calculations in a product fire risk analysis is easier to do well than the blend of science and art required to set up the analysis correctly (e.g., appropriate models, reasonable assumptions, best data) and to interpret the results, which includes calibration and sensitivity analysis.

Every step, starting with framing the problem and choosing the models, tests, and data, is subject to error and uncertainty, and that uncertainty must be examined in any interpretation or evaluation of the analytical conclusions. A design analyzed as having an acceptably low risk may also have enough uncertainty in the analysis to create a significant probability of unacceptably high risk.

The principal rule to remember is that the model is calibrated by assessing how well it reproduces recent fire experience from data on recent product use patterns and other practices. If the model captures the principal aspects of fire risk, then it will predict rates of loss that are very close to those actually experienced in the properties being analyzed. Results should be close not only from an overall perspective, but also for major groups of scenar-

ios. Use the specifics of the scenarios that need better calibration as guides to which assumptions need to be modified. For example, if predictions are poor for fires with long smoldering periods, but good for all other fires, then one might want to adjust the assumptions on length of smoldering period or on fire profiles (e.g., rate of heat release curve) during smoldering periods.

Some options involve changes not just to the parameter values, but to the model structure. Examples include changes that would further multiply scenarios by allowing for multiple values (and associated probabilities) of walking speeds, evacuation decision rules, rules for waking people without detectors, and so forth.

Another approach to calibration is to use the model not to directly predict losses, but to predict percentage changes in losses due to product choices, by major scenario group. The advantage of this approach is that it allows the analyst to use the fire experience statistics to do a great deal of automatic recalibration. The disadvantage is that it does not directly address, or correct, the flawed assumptions and estimates that are preventing the model from producing accurate results without such recalibration.

Most analysts will need to both (1) adjust the structure of the analysis, and (2) use fire statistics to recalibrate.

Identify Data Sources

Product and property survey data: There are many good sources of national data on the characteristics of occupancies or products in general. For occupancies, this kind of data may be obtained from ongoing federal government data collection activities (typified by publications of the U.S. Census Bureau; the General Services Administration, e.g., fuel load per room, by type of room; and the U.S. Departments of Defense and Energy), from major one-time studies, or from industry association surveys (e.g., Building Owners and Managers Association, American Hotel and Motel Association, and American Restaurant Association).

For products, there may exist market surveys on patterns of composition or use. The U.S. Census Bureau and, for certain types of products, the U.S. Departments of Commerce, Energy, Housing and Urban Development, and Health and Human Services are all likely sources of information. Much of the data gathered by the U.S. government can be found in summary form in the *Statistical Abstract of the United States,* with reference to primary sources. Another source of information is the U.S. Consumer Product Safety Commission, which carries out some field surveys of product performance and usage.

Section 5, Chapter 5, gives specific references for these data sources if they are readily accessible. Industry association data are available through the asssociation's periodicals or by special request to the association.

For products, however, often the only source of such information is trade associations of manufacturers and sellers of the product. It is important to recall, however, that some products have a lifetime longer than that of a trade association, which means the association's knowledge of current industry practice, however accurate, may not describe use patterns as a whole. Upholstered furniture, for example, is typically cushioned today with synthetics, with previously used natural materials, such as cotton batting and horsehair, now a rarity. Nevertheless, the lifetime of a piece of furniture can be 30 years or more, during which time it may be re-covered several times and pass through several owners, often of continually diminishing economic station. Therefore, it is reasonable to expect that a substantial fraction of the current furniture inventory retains the burning characteristics of products of a bygone era.

In general, people knowledgeable of today's product will tend to have statistics on, and think in terms of, what is currently being *sold,* not what is currently being *used.* Translating sales data into usage statistics is far from straightforward. Moreover, one might suspect that such products would be found disproportionately where fires are likely to be more common, that is, among people and places at the lower end of the economic spectrum.

For the method to operate, all of these qualitative observations must take a quantitative form, and it is the analyst who must decide how this is to be accomplished.

Always remember that, although data on national practices are more representative of the nation than fire incident data, they are less desirable for that very reason for fire risk analysis, because they do not provide probabilities implicitly weighted by the likelihood of having a fire. For example, if you walked into a randomly selected U.S. home in 1989, the chances were better than 85 percent that you would find a smoke detector present; but if you focused on homes that had fires, the chances would drop below 50 percent. It is the latter probability that is more relevant in determining how risk will develop in home fires. Therefore, when data on national practices are used, it is necessary to review the data for any adjustments that may be needed to better estimate probabilities relevant to fires.

Code requirements: Many relevant building characteristics are covered by provisions of building and fire codes. Some product fire characteristics also are covered by regulations. In the absence of direct data from the field, one may assume that all buildings and products have the characteristics implied by compliance with these codes and regulations. This assumption bypasses the need for probability estimation and usually provides enough detail to permit calculation of the input needs of the fire hazard analysis method.

When this approach is followed, the analyst needs to check a number of points that may undercut the central assumption of the approach, namely, that all buildings and products are as the codes and regulations would have them. In practice, many code provisions are of fairly recent vintage so that they were not in place when many or even most of the buildings and products now in use were put into place. Some jurisdictions do not follow national consensus codes, and many more lack the enforcement apparatus to ensure a high rate of compliance. Buildings and products can be altered or may deteriorate after being built, manufactured, or sold. And some building and product features may be better than code requirements because of marketplace demands.

Putting all this together, it is important that the user verify, through the expertise of people with broad familiarity with the state of old and new buildings and products around the country, that the particular characteristics of interest are ones where the code provisions are good indicators of actual practice in nearly all buildings and products in recent use.

Expert judgment: When all else fails and numbers are needed, there is no alternative but to make the best estimates possible. In some cases, it will be a judgment made by the user alone, but especially in areas where the user is least experienced, one or more true experts should be sought. For example, if the user is a maker or seller of the product, it would be wise to make use of fire scientists for assistance in assigning values to the product's fire properties.

One of the persistent potential pitfalls in the method is the danger that the typical product in use is not the typical product involved in fires. There is no foolproof way to avoid this situation, but one way to address it is to include fire service personnel in drawing up the profile of product characteristics. Fire fighters and fire marshals see the products involved in fires, whether or not they make up a substantial fraction of the statistical profile of the product.

Another pitfall is that, no matter what the expert's area of expertise, he or she may tend to underestimate the (typically) enormous variation in every characteristic of interest. Manufacturers may focus on a few best-selling versions of the product; surveys may focus on a few most widely used versions; and fire officials may focus on a few of the worst, most obsolete versions, seen in the worst (but not necessarily the most) fires. This illustrates the value of (1) a panel of experts, where biases can be balanced, and (2) a facilitator sensitive to the variation in practice, who can steer the group away from premature or overly narrow consensus.

It also suggests that, even when data are available, expert judgment is needed to interpret the data and apply them correctly. Knowledge of common versus uncommon practices, relevant codes and standards, and the length of time they have been in place, are among the kinds of information essential to spot areas of likely bias or critical uncertainty.

For all these reasons, the user can expect to make extensive use of expert judgment and should make sure that the expertise available to the project is both broad and deep.

References Cited

1. Society of Fire Protection Engineers, *SFPE Engineering Guide to Performance-Based Fire Protection: Analysis and Design of Buildings,* National Fire Protection Association, Quincy, MA, and Society of Fire Protection Engineers, Bethesda, MD (2000).
2. R.L.P. Custer and B.J. Meacham, *Introduction to Performance-Based Fire Safety,* Society of Fire Protection Engineers, Bethesda, MD, and National Fire Protection Association, Quincy, MA (1997).
3. R.W. Bukowski and T. Tanaka, "Toward the Goal of a Performance Fire Code," *Fire and Materials,* 15, pp. 175–180 (1991).
4. R. Friedman, "An International Survey of Computer Models for Fire and Smoke," *Journal of Fire Protection Engineering,* 4, 3, pp. 81–92 (1992).
5. NFPA 901, *Uniform Coding for Fire Protection,* NFPA, Quincy, MA (1995).
6. R.W. Bukowski, F.B. Clarke, J.R. Hall, Jr., and S.W. Stiefel, *Fire Risk Assessment Method,* 7 volumes, National Fire Protection Research Foundation, Quincy, MA (1990).

CHAPTER 12

Building Fire Risk Analysis

Brian J. Meacham

Introduction

The aim of building fire risk analysis is to comprehensively understand and characterize fire-related risks to better inform the wide range of decisions that must be made as part of building design, construction, and operation. As used in this chapter, risk is defined as the possibility of an unwanted outcome in an uncertain situation, where the possibility of the unwanted outcome is a function of three factors: loss of or harm to something that is valued, the event or hazard that may occasion the loss or harm, and a judgment about the likelihood that the loss or harm will occur.[1] Specifically, fire risk is the possibility of an unwanted outcome in an uncertain situation, where fire is the hazard that may induce the loss or harm to that which is valued (e.g., life, property, business continuity, heritage, the environment, or some combination of these). Building fire risk analysis, then, is the process of understanding and characterizing the fire hazard(s) in a building, the unwanted outcomes (relevant losses or harm) that may result from a fire, and the likelihood of fire and unwanted outcomes occurring.

Building fire risk analysis must consider several factors. Some of these factors are familiar to fire protection engineers and some perhaps are not. For example, building fire risk analysis should consider (1) what the fire hazards are and how fires might occur; (2) how the unwanted outcomes (consequences) are valued and by whom (including offsetting benefits); (3) what differences in risk perception and valuation exist and how they should be treated (i.e., should high-consequence events be disregarded if the probability of occurrence is very low); (4) if there are any social or cultural issues that may be relevant; (5) if there are different stakeholder views on the likelihood of fire occurrence and of the resulting consequences; and (6) whether uncertainty, variability, and unknowns have been identified and appropriately addressed.

Evaluation of fire hazards is something that fire protection engineers do well, and for which numerous tools and methods exist (e.g., this handbook). The valuation of consequences, however, may not be so familiar to engineers and is typically quite challenging, as it should consider physical, economic, health, environmental, social, cultural, and psychological factors. In valuing life safety consequences, for example, many engineers consider only injury and loss of life to an individual. However, there are also such factors as reduced quality of life, the inability to continue to work, and the impact on family relationships. On property protection, factors such as smoke and water damage should be considered, in addition to thermal damage. On business continuity, there are long-term issues, such as loss of image and market share, in addition to the short-term monetary losses associated with downtime.

Much like the difficulties in valuing consequences, the issue of determining the likelihood of fire occurrence and of resulting consequences is unfamiliar to many fire protection engineers, and is not without its challenges. One issue concerns the differing views on the concept of probability (likelihood): the frequentist view versus the subjectivist view.[1,2] In brief, the frequentist view is held by classical statisticians, who consider probability to be a property of a process that can be determined from an infinite population of data. They believe probability to be a precise value, and that information needed to estimate it can come only from observing the process. (For example, one can only determine the probability of a coin landing with "heads" up or "tails" up by flipping the coin an "infinite" number of times.) The subjectivist view, however, holds that probability has a value at any time that represents the total available knowledge about the process at that particular time. (For example, one can look at a coin

Based in Massachusetts, Brian J. Meacham is a principal risk consultant for Arup and a principal fire engineering consultant for Arup Fire. Brian has over 15 years of professional experience in the United States and in Europe, is a licensed professional engineer (U.S.) and a chartered engineer (U.K.), and holds the degrees of M.S. in fire protection engineering and Ph.D. in risk and public policy. Brian is a fellow of the Society of Fire Protection Engineers.

having a "head" and a "tail," assess whether it is well-balanced, observe a single coin toss, and estimate the probability of getting a "head" or a "tail" if one flips the coin again.)

Regardless of whether one holds the frequentist or subjectivist viewpoint, the availability of information to determine probabilities is critical, as is the applicability of the probability information to the problem at hand. For example, (1) what data are available (e.g., how many fire ignitions have there been in office buildings in the past ten years that did not result in significant fire damage?); (2) how applicable are historical data as an indicator of future events (e.g., were fire loss data from cellulosic materials prior to 1960 an appropriate indicator of fire losses involving synthetic materials after 1960?); and (3) how might changes to the building or its contents in the future impact the likelihood of fire occurrence and/or magnitude and type of consequences?

The above points to a critical factor in building fire risk analysis: there will be uncertainty, variability, and unknowns in any risk problem. How uncertainty, variability, and unknowns are identified and addressed will be critical to the risk analysis, especially with respect to the stakeholders involved in passing judgment on the "acceptability" of the risk. Should point values be used or should distributions? How is the variability in building occupant health and ability addressed in the analysis? These are just a few items that must be addressed.

Building fire risk analysis requires judgments about the likelihood of fires occurring and the consequences that may result. Developing these judgments requires significant information from numerous sources, including objective data (e.g., historical fire loss data), subjective judgment, and input from interested and affected stakeholders. As part of the building fire risk analysis process uncertainty, variability, and unknowns must be identified and appropriately addressed. To help the diversity of stakeholders involved in building fire risk analysis better understand how each view each building fire risk problem, and to address the above issues, an understanding of risk characterization is needed.

Building Fire Risk Characterization

Risk characterization requires a well-defined problem that those involved agree with, a sound scientific base, the proper use of analytical techniques with proper consideration of uncertainties and unknowns, and sufficient discussion and deliberation so that everyone understands all of the issues.[3] The risk characterization process will likely require several iterations, as new information and data become available, and as participants gain better understanding and raise more issues. It needs to be an interactive process, and not one where one group dominates the deliberations and/or analysis and forces a solution.

To help characterize building fire risks, a number of questions need to be asked:[1,3–6]

1. Who or what is exposed?
2. If it is people, what groups are exposed?
3. What is posing the risk?
4. What is the nature of the harm or loss?
5. What qualities of the hazard might affect judgments about the risk?
6. Where is the hazard experience?
7. Where and how do hazards overlap?
8. How adequate are the databases on the risks?
9. How much scientific consensus exists about how to analyze the risks?
10. How much scientific consensus is there likely to be about risk estimates? How much consensus is there among the affected parties about the nature of the risk?
11. Are there omissions from the analysis that are important for decisions?

Various tools and methods exist to help obtain needed information for building fire risk characterization. Several of these are outlined in the following section. Detailed discussion on the above questions can be found in the references.[1,4,5,6]

Methods for Gathering Building Fire Risk Information

To help obtain necessary information regarding what is valued and how, how it may be impacted by fire and fire effects, how particular fire hazard conditions may occur, and the likelihood of losses occurring; several tools, methods, and approaches are available. This section provides a brief overview of various tools, methods, and approaches available to fire protection engineers for the purpose of gathering needed information. This section does not constitute a comprehensive review, and readers are urged to consult the fire and risk literature for more tools, methods, and approaches and for more details on the approaches discussed herein.

As part of a risk analysis effort, one needs to identify what is of value, assess the hazards that may result in harm or loss to that which is valued, and make a judgment regarding the likelihood of the loss occurring. In building fire risk analysis, life safety, property protection, business continuity, the environment, and heritage are the value foci. To determine how they are valued and the associated levels of unacceptable impact (damage, injury, or failure), consequence analysis is used. To determine the extent of exposure from potential hazard situations, fire hazard assessments are undertaken. To complete the risk analysis, judgments concerning the likelihood of hazard events occurring that result in unacceptable or intolerable levels of impact are required.

Consequence Analysis

To determine how a hazard may occasion loss or harm to that which is valued, some form of consequence analysis is required. Consequence analysis, a key component of risk characterization, is concerned with determining the potential impacts of a hazard event without consideration of the likelihood of the consequences occurring. Consequence analysis is more difficult than hazard assessment, in that it may not always be clear in what ways and to what extent something is valued and how the loss should be characterized. Consider life safety. For

some, the line may be drawn simply between life and death. For others, quality of life, pain and suffering, and/or rehabilitation after a fire-induced injury may be critical factors. For property protection, it may not always be clear to the interested and affected parties where, how, and how much damage may occur. Some may not realize that code compliance, for example, can be significantly different than protecting their building, process, contents, or other assets of value. The issues can get even more complex for assessing potential business continuity impacts and damage to historically important buildings or contents. Nonetheless, such differences are important for characterizing risks, determining tolerable impacts, and selecting acceptance (damage, failure) criteria, and are why interested and affected parties must be involved in the process.

The nature of consequence analysis will vary based on the risk problem, with the issues of what is valued and how it is valued being two central foci. Determination of what is valued and how it is valued may require facility surveys, research into the impact of fire effects on that which is valued, an understanding of the state of knowledge for assessing impacts on that which is valued, and discussions with a wide variety of interested and affected parties. Uncertainty, variability, and unknowns will be key factors in many consequence analyses, especially as related to such factors as available data, randomness in affected populations, selection of acceptance criteria, selection of methods for assessing the impacts, and values of the affected and interested parties. (See Section 5, Chapter 4 by Notarianni for discussion on uncertainty, variability, and unknowns.)

In the vernacular of performance-based fire safety design, consequence analysis is often described in terms of establishing fire safety goals, objectives, and criteria; and tools, methods, and approaches to determining fire safety objectives can be found in pertinent references.[7–10] Although such documents contain some guidance on selecting acceptance (performance) criteria, there is often a need to refer to more specific resources for details on particular physiological thresholds, material failure points and related impact-related criteria (e.g., see pertinent chapters in this handbook). For monetary valuation equivalents, guidance can be found elsewhere in this handbook (see Section 5, Chapter 6 by Ramachandran) as well as in the general risk literature.[11–13] It is worth noting, however, that valuation in terms of monetary worth can be difficult to achieve. This is especially true for life safety, where identifying a value for human life can be difficult (if not impossible) and controversial.[14–20] Discussions on monetary valuation for the purpose of insurance/no-insurance tradeoffs can also be found in the literature.[21,22]

Hazard Assessment

The purpose of a fire hazard assessment is to identify possible sources of fire ignition and various conditions that may result from the fire without consideration of the likelihood of occurrence. Fire hazard assessments typically involve surveys of facilities or processes to obtain such information as potential ignition sources, potential fuel sources, arrangement of fuel packages, building and compartment configurations, and presence of fire safety features. Armed with this information, one either assumes ignition or established burning and estimates or predicts the fire growth, spread, and impact under a variety of fuel, compartment, and fire protection systems configurations. Identification of ignition sources requires knowledge of how ignition can occur (see Section 2, Chapter 8 in this handbook) and often involves simply a visual survey. However, visual inspections may be supplemented by general or facility-specific loss data, material hazard data sheets, and other sources of information as appropriate. This latter point is important, as a review of historical loss data can help minimize the chance of focusing too closely on unique hazards, while overlooking more common, but equally important hazards.

There are a number of tools and methods available to the fire protection engineer for the purpose of fire hazard assessment. Checklists are often used as a quick method to verify compliance with codes, standards, or recommended practices. They can be as simple or as detailed as needed, and can provide a good foundation for inexperienced persons to gain an understanding of potential hazards by making them focus on areas of concern. They can be used during design, as part of an approval process, and/or as part of an inspection and maintenance program. A potential downside may exist if the user focuses too much on the checklist and inadvertently ignores other hazards or potentially hazardous conditions. In addition, the user, if inexperienced, may not understand the relative importance of one item on the checklist over another, or how the hazard condition could manifest itself.

Safety reviews are typically performed for existing facilities and involve regularly scheduled visual inspections.[23] The primary purpose is to identify conditions or procedures that could lead to accidents (initiating events), illness, injury, or damage (consequences). As with a checklist, the scope of the review can be as simple or complex as deemed necessary. It may be simply a walk-through, or may require review of material safety data sheets (MSDSs), testing of systems, or other safety-related functions. Checklists and a routine schedule are often helpful components of a safety review.

A "what if" analysis is primarily a mental process used to help identify areas of concern for use in checklists, safety reviews, and the following tools and methods.[23] It involves people asking "what if" about potential situations or scenarios that could arise, such as "what if the pump fails?" or "what if the operator mistakenly activates switch A instead of switch B?" "What if" analysis is typically informal and is used as a basis for initiating more detailed analyses.

Checklists and "what if" analyses can be combined as part of hazard and operability (HazOp) studies.[23] A HazOp study primarily involves taking a checklist, a MSDS, a system flow or operation chart, or other document about a process or system and systematically asking questions aimed at determining outcomes for specific actions. For example, if a valve on a drawing is labeled "flow," the question might be asked, what happens when there is "no flow"? Where the answer is unknown or unsatisfactory, additional analysis is undertaken. As with "what if" analyses, HazOps tend to be more informal than formal.

More formal approaches include failure modes and effects analysis (FMEA) and failure modes and effects and criticality analysis (FMECA).[23] FMEA and FMECA require a tabulation of equipment, components and systems, their failure modes, the effect of the failure, and the criticality of the failure (in a FMECA). These analyses typically focus on single-mode failures, and usually do not include human failure analysis.

If, after application of one of the above methods, a potential failure mode or hazard condition is deemed to require more detailed analysis, fault tree analysis (FTA) or event tree analysis (ETA) is often used.[23] FTA is essentially a "reverse thinking" deductive technique that focuses on one particular event that could (or did) occur (typically an accident) and provides a structure for evaluating the potential causes of the event (e.g., given failure X, what could have been the cause). It does this by providing a structure, in the form of a graphic model, that an analyst uses to display various events, conditions, actions, and outcomes. The output of a FTA is a sequence of events that could lead to (or could have lead to) a failure, and may include component, equipment, system, operating and/or human actions, failures, or errors. Although FTA is primarily a qualitative tool as used in hazard assessment, it can be used as a quantitative risk assessment tool if probabilities are assigned to the various outcomes.

Whereas FTA begins with a failure and provides a structure to look for potential causes, event tree analysis (ETA) provides a structure for postulating an initiating event and analyzing the potential outcomes. The principle tool is a decision tree (as used in decision analysis) with branches for success or failure (yes or no, or other binomial output). The basic approach is to identify an initiating event, identify systems or strategies intended to mitigate the event, and ask the "success or failure" question for each system or strategy, building the tree in the process. As with FTA, ETA is primarily a qualitative tool as used in hazard assessment, but is often used as a quantitative risk assessment tool by assigning probabilities, much the way probabilities are used in a decision tree. (See Section 5, Chapter 13 and other sources.[24–26])

Cause-consequence analysis combines the forward thinking concept of ETA with the reverse thinking concepts of FTA to provide a more broadly encompassing picture of possible sequences of events.[23] Although primarily a qualitative tool as used in hazard assessment, it can be overlaid with frequencies or probabilities where used as a quantitative risk assessment tool.

Human error analysis describes a group of task-analysis-based qualitative techniques used to better understand the types of errors people might make and under what circumstances. Although helpful in better understanding potential sources of error, it has been noted that some such analyses treat human error and reliability in much the same way as mechanical systems, and it is argued that "desirable systems states" may be a more appropriate model.[27] In essence, "desirable systems states" focus on the goals that systems are aiming to achieve; and with why, what, and how questions, focus in on the potential for errors in various states of the system. Where people are part of the system, this approach highlights areas of concern and uncertainty related to human reliability and error.

In addition to the above methods, a variety of analytic tools, such as models, are used to assist in the hazard assessment. As Britter[28] points out, models are useful for a variety of tasks, including

- A means of summarizing extensive analytical and experimental results in order to assist in the transfer of that knowledge and to focus attention on deficiencies in the knowledge base
- A means to provide knowledge in a form accessible to users with varying levels of expertise in the subject area
- A means to highlight the sensitivity of the output to the various input parameters
- Predictive tools for various scenarios of interest that have not, themselves, been tested

As used here, models can be mathematical or physical. Mathematical models include empirical models (based on correlation), models based on fundamental equations, analytical models (exact or approximate solutions to a set of equations in closed form), and numerical models (computational models). Physical models (simulations) rely on actual physical representations, often at a reduced scale (e.g., a wind tunnel), and sometimes with the actual material of concern (e.g., air movement in a wind tunnel), and sometimes with different materials with similar properties. Models are widely used to support fire hazard assessment. Details on fire effects modeling are provided elsewhere in this handbook and can be found throughout the fire literature. It is worth noting here that, regardless of the model one uses for fire hazard assessment or risk analysis, one must understand its uses, applications, and limitations; and appropriately account for the sources of uncertainty and variability that matter. (See Section 5, Chapter 4 by Notarianni for more details.)

Causal Relationship of Initiating Events, Hazards, and Consequences

In addition to being viewed as separate components, consequence analysis and hazard assessment can be thought of as two parts of a process for identifying and evaluating the potential for unwanted consequences (loss or harm of something that is valued) given some initiating event. This definition implies that an event without unwanted consequences does not constitute a hazard and that there is a causal relationship between initiating events and unwanted consequences. One way to assess the potential for some initiating event to result in unwanted consequences is to view the situation in terms of a causal sequence, which looks at the situation as starting with some basic human need and ending in some consequence(s).[29] The basic causal structure is illustrated in Figure 5-12.1.

In brief, there are a variety of basic human needs, such as shelter, companionship, and love, which in turn lead to wants or desires. These wants or desires often result in the application of some technology to address the want. Unfortunately, the choice of technology can result in an out-

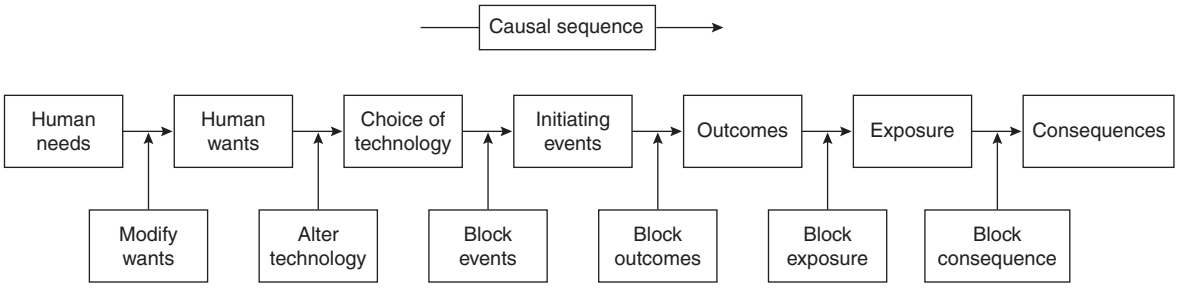

Figure 5-12.1. ***Causal sequence.***[28]

come that exposes someone or something to loss or harm, resulting in some potential for unwanted consequences. To change the potential for unwanted consequences, one can modify the causal sequence by initiating one of six alternatives: modify wants, alter technology, block events, block outcomes, block the exposure, or block the consequence. This can be illustrated by example.

One basic human need is protection from the elements. To address this need, humans want shelters that provide protection from things such as rain, snow, and cold temperatures. To address this want, they may choose to live in structures that provide protection from rain and snow and can be heated to a comfortable temperature. Furthermore, they may choose to build these structures out of wood and to use an open fire as a source of heat. Under "normal" circumstances, everything could work fine, and the choice of technologies would provide the desired benefits. However, there could be some event, such as the blocking of a ventilation opening or too much fuel being put on the fire, that could lead to potentially unwanted outcomes. These outcomes, such as the presence of smoke, CO, or excessive temperatures in the structure, could then lead to exposures to people and property and ultimately result in unwanted consequences. Such a sequence can be illustrated diagrammatically as shown in Figure 5-12.2.

By applying an assessment methodology such as the causal sequence, one is able to visualize events, outcomes, exposures, and consequences in a systematic manner. The application can be as simple or as complex as needed, with the addition of multiple events, outcomes, exposures, and consequences and the addition of feedback loops providing further detail. Furthermore, the approach is compatible with various other hazard assessment techniques, as outlined previously, that may be more focused on specific parts of an overall assessment problem. This is illustrated in Figure 5-12.3.

As can be seen in Figure 5-12.3, numerous methods and approaches can be used for specific hazard assessments. Although some are applicable to a variety of problems, many are intimately associated with specific characteristics of the hazard, the type of risk problem, the

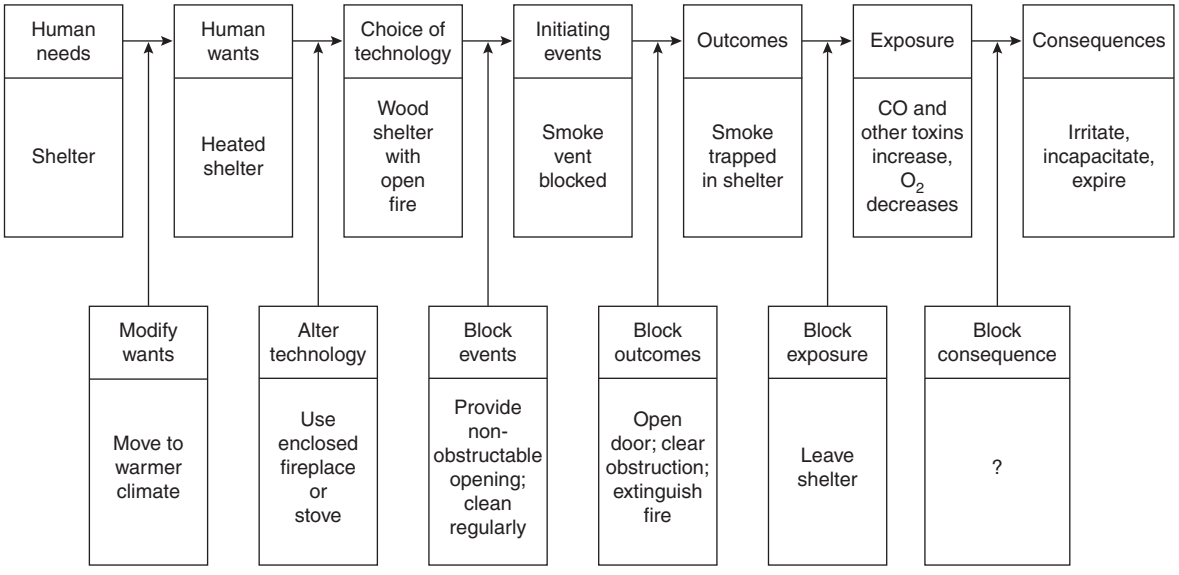

Figure 5-12.2. ***Illustration of potential unwanted fire-related consequences.***

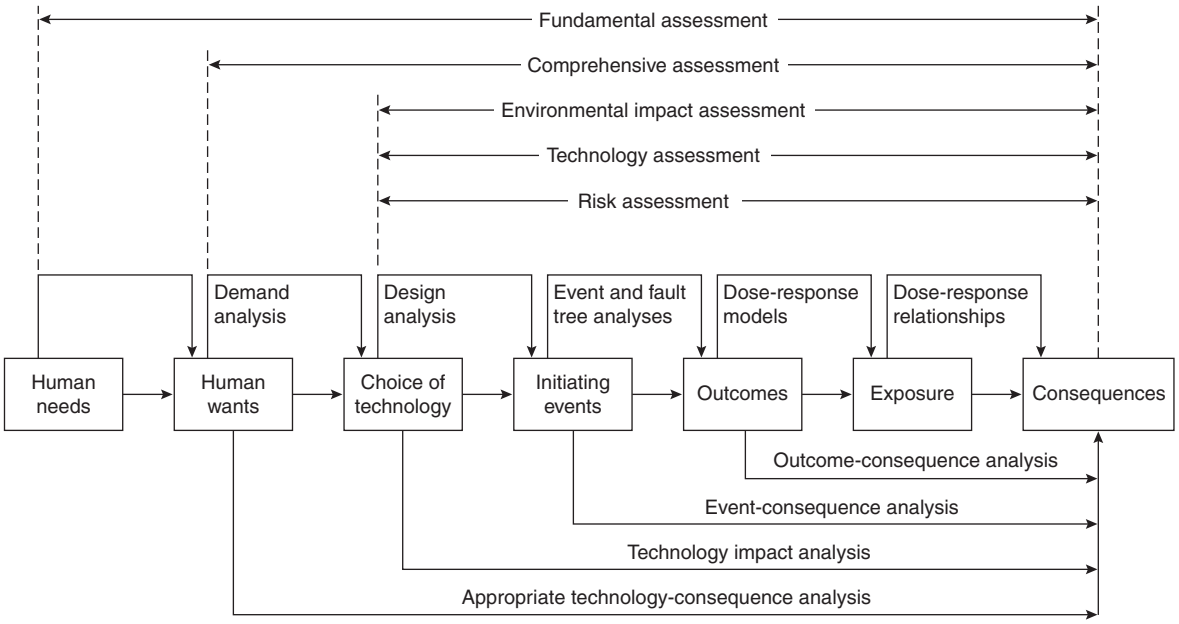

Figure 5-12.3. ***Modes of analysis compatible with the causal structure.[28]***

current state of knowledge, and the available technology. For example, most health hazard and risk assessments (toxicological, physiological, cancer, disease) rely heavily on epidemiological studies and dose-response relationships and models.[30–34] In these cases, a causal relationship is often sought between exposure to a substance and unwanted outcomes (e.g., exposure to asbestos and the causation of cancer). Such approaches may be considered if an incapacitation assessment is being undertaken. For technology-related hazard and risk assessments, the focal point is typically the relationship between initiating events and outcomes (through to consequences). For these analyses, methods such as those outlined previously, like failure mode and effects analyses, fault tree analyses, and event tree analyses are often used.[2,23,35–39]

Fire Safety Concepts Tree

A useful tool for fire hazard and consequence analysis is the *fire safety concepts tree.*[40] The fire safety concepts tree is a graphical representation of the deliberations and professional judgments of the NFPA Technical Committee on Systems Concepts for Fire Protection in Structures, and represents one way in which building fire safety can be viewed.[41] It is divided into two primary branches, "prevent fire ignition" and "manage fire impact," with the concept being that one or the other must be accomplished in order to meet one's fire safety objectives. One can use the tree as a guide to evaluate potential fire impacts in those cases where a building fails to meet the criteria of one or more branches (e.g., if ignition is not prevented, one can evaluate the ability of the building's systems to manage the fire impact). One can also modify the fire safety concepts tree into the form of an event tree or a decision tree for risk analysis.

A portion of the fire concepts tree is provided in Figure 5-12.4, which shows the top-level choices, "prevent ignition" or "manage fire impact." A complete version of the event tree can be found in NFPA 550, *Guide to the Fire Safety Concepts Tree.*[40]

Assessing the Likelihood of Occurrence

Thus far, the risk analysis components of determining what is valued and assessing the hazard conditions that may occasion the loss or harm have been discussed. The final component is concerned with obtaining a judgment on the likelihood of specific losses occurring to what is valued. The concepts of frequency, probability,

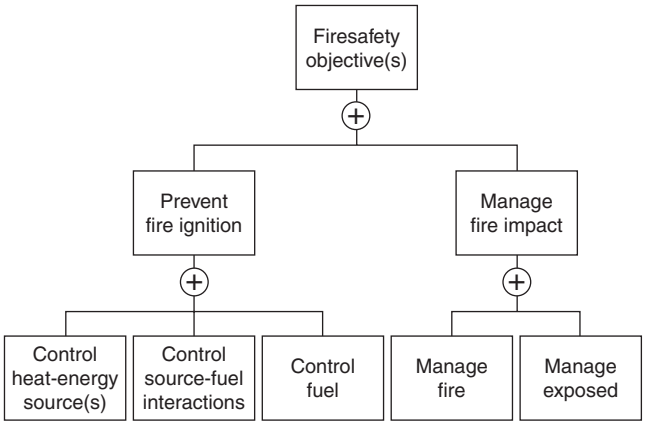

Figure 5-12.4. ***Top branch of the fire concepts tree.[40]***

and the differing views of probability are important to this discussion.

One dictionary defines probability as the likelihood of an occurrence expressed as the ratio of the number of actual occurrences to that of possible occurrences, and frequency as the rate of occurrence.[42] (Inherent in these definitions is the concept of events per unit time.) Thus, a frequency of fire ignitions during a specific period of time, on its own, is not an indication of the probability of fire ignition. To obtain a probability of fire ignition, an estimate of the number of possible occurrences is required as well. For example, a hypothetical statistic of 20 fires per year occurring in toasters as they are switched on is a *frequency.* To estimate the *probability* of a fire in a toaster when it is switched on, one would also need data on the total number of times toasters are switched on per year. If one had data which indicated that toasters are switched on 20 million times per year, one could then estimate the probability of fires in toasters as they are switched on as 20 fires per 20 million toaster starts per year, or one in a million per year.

Probability theory is a branch of mathematics that deals with the modeling of uncertainty through measures of relative likelihood of alternative occurrences.[43] Measuring likelihood is one place where the differing view of frequentists and subjectivists comes into play: the estimation of actual and possible occurrences. As noted earlier in this chapter, frequentist approaches rely heavily on data from observed events whereas subjectivist approaches utilize the current state of knowledge coupled with judgment. This distinction is important to remember because fire is a relatively rare event and thus data are somewhat limited. In addition, people can change the nature of the fire hazard over time (e.g., by reconfiguring buildings, changing contents), and the material composition of building products and contents will likely change, making the ability to predict future hazards or risks, based on past loss experience, challenging at best.

Such conditions provide a strong argument for the use of subjective probability measures over objective measures for building fire risk analysis. Because data are often scarce, and actual occurrences and possible occurrences may not be precisely known, it is often necessary to make estimates. At issue is how one chooses to make the required estimates.[44] For example, whereas one may have frequency data on fire ignitions in a particular class of buildings, a subjective judgment relative to the number of possible future occurrences may be more appropriate than a judgment based on statistical treatment of limited and potentially highly-uncertain data.

Regardless of the differences in philosophy between frequentists and subjectivists, data are needed. Sources of fire loss data, including fire frequency data, can be found in Section 5, Chapter 5 by Hall and Ahrens, as well as in various other publications, including annual[45] and periodic[46,47] journal articles, NFPA reports,[48] government reports,[49] and handbook appendices.[10,50,51] In addition, it should be clear that the concepts of uncertainty, variability, and unknowns, by the nature of the problem, are critical concerns in risk analysis and must be appropriately addressed. (See the following section as well as Section 5, Chapter 4 by Notarianni.)

Uncertainty, Variability, and Unknowns

The amount of literature on the topics of uncertainty, variability, and unknowns indicates that identifying, understanding, and addressing these are clearly critical issues. For example, these issues pervade discussions of acceptable risk,[52–55] risk characterization,[3] risk assessment,[38,56–60] and decision analysis.[11,13,61–64] However, as one can see from a review of the various reference sources, there seems to be little consensus regarding how to treat these factors. There are several reasons for this, many of which impact building fire risk analysis, including

- The risk problem may not be clearly understood or sufficiently well defined.[3,54] Any uncertainty in the problem definition will be propagated throughout the risk assessment and management process. If this uncertainty is large (i.e., if the stakeholders do not agree on key issues or parameters of the problem), the uncertainty in any proposed solution will be some factor greater.
- There are many types of uncertainties that go unrecognized or ignored.[3,54,57,59] These include uncertainties in variables that are built into analytical tools and methods, uncertainties associated with criteria selected for assessing acceptability, and uncertainties in human behavior, attitudes, and values.
- There may be variability that is treated as uncertainty.[32,59,60] If the risk problem relates to the human population, for example, it should be recognized that both uncertainty and variability exist, and that they need to be addressed differently. It may not be known how many people may be exposed (uncertainty), and for any population postulated to be exposed, there will be differences among the individuals (variability). Uncertainty and variability become important when discussing issues such as using the entire population or some subset of sensitive or vulnerable persons, and if the latter is selected, what defines the subset.
- There may be unknowns that are treated as uncertainties.[3,65–67] In some cases, it is impossible to accurately predict some event that may happen far into the future, or to control the circumstances upon which certain assumptions are based. If these indeterminate events are treated as events that can be accurately predicted, the uncertainties in any solution could be significant (see Reference 3).
- There may be disagreement regarding how to address uncertainties of different types. First, the differences between uncertainty, variability, and indeterminacy need to be identified.[60] Then one needs to identify appropriate mechanisms to address the uncertainty, variability, or indeterminacy. For example, Morgan and Henrion[57] argue that the only type of quantities whose uncertainty may be appropriately represented in probabilistic terms are empirical quantities. However, there are other types of quantities, such as model domain parameters, decision variables, and value parameters. For these, parametric or switchover analysis (or other) may be needed.
- There may be disagreement on a quantitative methodology (or set of quantitative methodologies) for treating uncertainty. Even if it is decided to perform a

probabilistic analysis on an empirical quantity, there may be disagreement as to an appropriate approach to apply. For example, probabilistic approaches range from classical, statistical-based analyses to subjective, Bayesian analyses, with other types of quantitative or qualitative analyses scattered in between.[3,44,68,69] To complicate the issue, frequentists often reject the Bayesian approach, and vice versa.

- There is concern that the data, mathematical rigor, and expertise needed to conduct a quantitative uncertainty analysis would render such an analysis impracticable in many situations, and as a result, the analysis would not be undertaken or would be performed incorrectly.[70]

To help people better understand the complex issues surrounding uncertainty, variability, and unknowns (hereafter lumped as uncertainty for convenience), various taxonomies and treatments have been suggested.[3,7,54,57,71,72] Regardless of specific differences, much of the literature identifies the following areas as requiring consideration: scientific uncertainty; human factors uncertainty; uncertainty in risk perceptions, attitudes, and values; and decision-making uncertainty.

Scientific uncertainties result from lack of knowledge (either obtainable through further study or due to random chance and variations) and from necessary approximations. They are often among the most readily recognizable and quantifiable uncertainties, and can be grouped into five subcategories: theory and model uncertainties, data and input uncertainties, calculation limitations, level of detail of the model, and representativeness.[7,28,71,72]

Theory and model uncertainties may arise when physical processes are not modeled due to a lack of knowledge about them or about how to include them, when processes are modeled based on empirically derived correlation, and/or when simplifying assumptions are made. Data and input uncertainties arise from inaccuracies in data collection and reporting, incomplete knowledge of specific input values and variations in those values as a function of confounding factors, and input errors made by the modeler. Calculation limitations encompass such factors as the control volume selected for modeling, the level of detail of the model, and the model-domain parameters specified. Representativeness relates to how well the modeled situation reflects reality.

In considering human factors, uncertainty and variability are present in several modes. There is uncertainty regarding who might be affected and how. That is, it is not always known who will be impacted (uncertainty or indeterminacy), and within the population affected, there will be physiological uncertainties and variability. There are also uncertainties and unknowns related to how people will react in different situations, especially under stress.

As discussed earlier, there can be significant differences in the way people perceive and value risk, as well as in their attitudes about risk. Differing perceptions give rise to both variability and uncertainty, and capturing these differences is important. There will be situations in which age, family, infirmity, or other factors or conditions will impact perceptions of risk. There may be social, economic, philosophical, religious, or cultural differences in people's values systems. In addition, some people are risk tolerant, while others are risk averse. It is important to recognize these differences exist, and thus reduce uncertainty and unknowns, and better understand and address variability where it exists. Also important are the perceptions and issues of equity, efficacy, and fairness—issues of importance in risk characterization and management.[64] Here again, social, economic, or cultural differences of the interested and affected parties may play a major role.

There is also uncertainty in the decision-making process, including uncertainty about how to best define the decision problem, difficulties in assessing the facts of the matter, difficulties in assessing relevant values, uncertainties about the human element in the decision-making process, and difficulties in assessing the quality of the decisions that are produced.[54]

All of these factors should be considered and appropriately accounted for when undertaking a building fire risk analysis. For more details on uncertainty and its treatment, see Section 5, Chapter 4, "Uncertainty," by Notarianni in this Section.

Building Fire Risk Analysis Approaches, Methods, and Models

This section provides a brief overview of various qualitative and quantitative risk analysis approaches, tools, and methods available to fire protection engineers. This section does not constitute a comprehensive review, and readers are urged to consult the fire and risk literature for more approaches to risk analysis and for more details on the approaches discussed herein.

Magnusson[25] suggests that there are two primary approaches to risk analysis: the single scenario, analytic safety index β approach, and the multi-scenario, event-tree approach. In the single scenario, analytic safety index β approach, there is a single-limit state described by an analytical expression developed from physically derived correlation (e.g., mass flow in plumes, smoke-filling times, radiation from flames) or from response surface equations describing output from a computer program. The design problem is formulated in terms of the limit state function, G, as $G(X_1, X_2, \ldots, X_n) = 0$. The parameters X_i are stochastic parameters describing the system, such as fire growth rate and response time of occupants. The goal is to find a solution given the constraint that $P(G < 0) < P_{\text{target}}$.

Challenges and limitations to the use of this approach include difficulty in developing appropriate analytical expressions, difficulty in developing uncertainty factors, and the limitation of being a single-scenario application. Nonetheless, this approach is useful for some applications, and details can be found in the literature.[24–26] Although not developed, it has been suggested that this basic approach can be applied more broadly to the building fire problem as well.[73,74]

Event tree analysis (ETA) is often used to analyze complex situations with several possible scenarios, where several fire or life safety systems are in place or are being

considered. In brief, event trees are developed for a scenario, and probabilities and frequencies for components are applied (see previous discussion on ETA). In the *SFPE Engineering Guide to Performance-Based Fire Protection Analysis and Design*,[10] the method for quantifying fire risk from multiple fire scenarios is given as

$$\text{Risk} = \text{Risk}_i = (\text{Loss}_i < F_i)$$

where

Risk_i = risk associated with scenario i

Loss_i = loss associated with scenario i

F_i = frequency of scenario i occurring

This relationship is similar to the general discussion on engineering risk analysis discussed earlier, but in the case, the term "loss" is used instead of "consequence," and the summation indicates "total" risk from multiple scenarios. This type of risk analysis, commonly referred to as probabilistic risk assessment (PRA), is widely used in the chemical process industry (see Section 5, Chapter 13) and for fire safety assessments of nuclear facilities,[37] and is beginning to see broader application in fire protection engineering applications.[10,24–26,39]

Although ETA-based risk analyses methods are applicable to multi-scenario situations, it does not mean such approaches are necessarily simple. This can be illustrated using a three-room example. Figure 5-12.5 shows an event tree for a three-room building that is compartmented as shown. For this example, the fire scenario frequency, F_i, is assumed to be uniformly distributed across the three rooms, and the consequence of a single room loss is $C/3$ (i.e., the consequence of losing all three rooms to a fire would be C).[10]

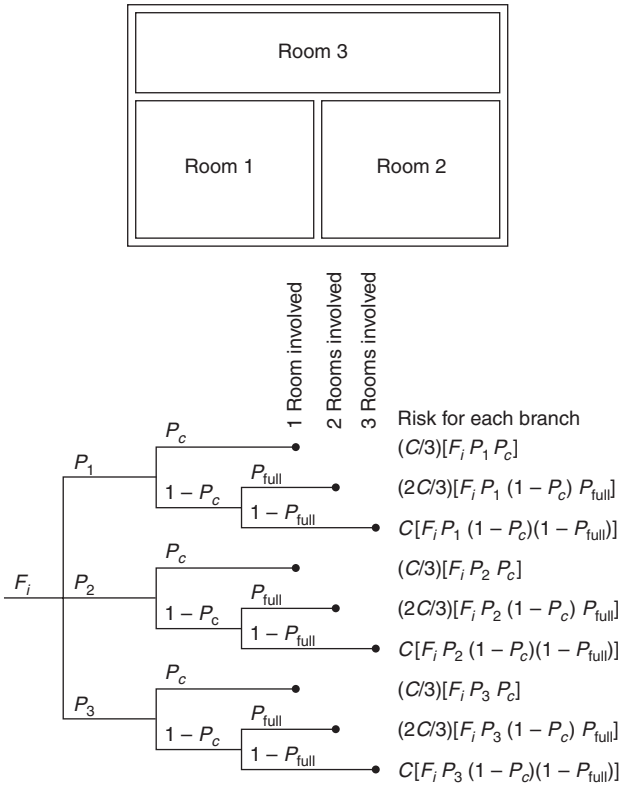

Figure 5-12.5. ***Event tree for three-room fire risk analysis.[10]***

If the probability that the fire will be contained in one room is P_c, and is prevented from propagating to the third is P_f, then the overall risk as shown in Figure 5-12.5 can be estimated as

$$\begin{aligned} R = {} & \frac{C}{3}[F_i P_1 P_c] + \frac{2C}{3}[F_i P_1 (1 - P_c) P_f] \\ & + C[F_i P_1 (1 - P_c)(1 - P_f)] + \frac{C}{3}[F_i P_2 P_c] \\ & + \frac{2C}{3}[F_i P_2 (1 - P_c) P_f] + C[F_i P_2 (1 - P_c)(1 - P_f)] \\ & + \frac{C}{3}[F_i P_3 P_c] + \frac{2C}{3}[F_i P_3 (1 - P_c) P_f] \\ & + C[F_i P_3 (1 - P_c)(1 - P_f)] \end{aligned}$$

where P_1, P_2, and P_3 are the probabilities that a fire will start in room 1, 2, or 3, respectively.

With some mathematical manipulation, the above equation simplifies to the following:

$$R = \frac{CF_i}{3}[3 - 2P_c - P_f + P_c P_f]$$

For this example P_c and P_f can be interpreted as the success probabilities of the fire barriers. To place these results in context, numeric values will be added. If P_c and P_f are both equal to 0.1 (i.e., fire propagates 9 in 10 times), then the *risk* is

$$R = \frac{CF_i}{3}[3 - 2(0.1) - (0.1) + (0.1)(0.1)] = 0.90CF_i$$

If P_c and P_f are both equal to 0.9 (i.e., fire propagates 1 in 10 times), then the *risk* is

$$R = \frac{CF_i}{3}[3 - 2(0.9) - (0.9) + (0.9)(0.9)] = 0.37CF_i$$

If P_c and P_f are set to unity (i.e., fire barriers never fail), then the *risk* is

$$R = \frac{CF_i}{3}[3 - 2(1) - (1) + (1)(1)] = \frac{CF_i}{3} \cup 0.33CF_i$$

Although this example is very simplified, it suggests how complicated a classical ETA-based engineering risk analysis can be. For each fire protection feature considered, the number of branches (i.e., potential outcomes) in the event tree will increase. Given that this increase is usually geometric, the analysis can become quite complex.

The above example also illustrates an important concept in risk-based calculations. The bounding risk for this problem would be CF_i (i.e., complete facility loss). This is the risk if all fire protection features are assumed

to always fail. The risk when the fire protection features are always assumed to work (i.e., the fire barriers never fail, thus P_c and P_f are set to unity) is the lower bound risk. Thus, the potential range for the calculated risk is bounded between $0.33CF_i$ and CF_i. The better the protection, the closer the risk will approach $0.33CF_i$.

The above example can also be used to illustrate the difference between fire scenarios (all possible scenarios that could occur) and design fire scenarios (that subset of fire scenarios selected for design purposes).[10] For example, the total range of fire scenarios for the above example could consider various room-to-room sequences (e.g., starts in room 1, then goes to room 2 and finally to room 3.) If this is done, one finds that there are a total of 15 possible paths of fire propagation:

1. Starts in room 1 and is contained in room 1
2. Starts in room 1 and propagates to room 2, but not to room 3
3. Starts in room 1 and propagates to room 3, but not to room 2
4. Starts in room 1 and propagates to room 2 and then to room 3
5. Starts in room 1 and propagates to room 3 and then to room 2
6. Starts in room 2 and is contained in room 2
7. Starts in room 2 and propagates to room 1, but not to room 3
8. Starts in room 2 and propagates to room 3, but not to room 1
9. Starts in room 2 and propagates to room 1 and then to room 3
10. Starts in room 2 and propagates to room 3 and then to room 1
11. Starts in room 3 and is contained in room 3
12. Starts in room 3 and propagates to room 1, but not to room 2
13. Starts in room 3 and propagates to room 2, but not to room 1
14. Starts in room 3 and propagates to room 1 and then to room 2
15. Starts in room 3 and propagates to room 2 and then to room 1

If simultaneous propagation to the second and third room were considered a significant threat, there would be three additional scenarios. This brings the total scenarios to 18 before considering such details such as doors being open or closed, whether people of various characteristics are in the rooms, and whether they are sleeping.

It is also important to address the fact that fire protection systems may not always be operational. As such, the concepts of availability and reliability should be addressed. A system is considered available when it is ready and able to perform its intended function (e.g., a smoke detection system is installed and working). If a system is taken out of service, even temporarily (e.g., it is undergoing maintenance), it is unavailable. A risk-based approach should consider some probability that a system will be unavailable if it is a possibility. A system that is available but not functional is considered unreliable (e.g., the smoke detection system is installed but the smoke detector opening is blocked with duct tape). Probabilities can be developed for evaluation of system availability and reliability. Availability and reliability are reported or derived as a composite value. (When the latter is the case, it should be made explicit.)

Risk-Cost Assessment Model

Because of the complexity of ETA-based risk analysis, computers are often used to enable multiple scenarios to be evaluated in relatively short timeframes. Two such models, CESARE-Risk and FIRECAM, are based on a fire risk and cost assessment model developed by Beck[75–77] and expanded collaboratively by Beck and Yung.[77,78]

A brief description of the current risk-cost assessment model and its submodels are given in this section.[79] More detailed descriptions are given for the design fire submodel, fire growth submodel, and the smoke movement submodel. As for the other submodels, more details can be found in other publications.[76,78,80–82]

The risk-cost assessment model employs an event-based modeling approach in which events are characterized by discrete times and probability of occurrence. The event-based approach is used to define the outcomes of fire growth and spread scenarios in terms of the times of occurrence of untenable conditions. The consequence of these outcomes is in terms of the number of people exposed to untenable conditions.

The risk-cost assessment model for office and apartment buildings assesses the fire safety performance of a fire protection design in terms of two decision-making parameters: (1) the expected risk-to-life (ERL) and (2) the fire-cost expectation (FCE). The ERL is the expected number of deaths over the lifetime of the building divided by the total population of the building and the design life of the building. The FCE is the total fire cost, which includes the capital cost for the passive and active fire protection systems, the maintenance cost for the active fire protection systems, and the expected losses resulting from fires in the building. The ERL is a quantitative measure of the risk-to-life from all probable fires in the building, whereas the FCE quantifies the fire cost associated with the particular fire safety system design.

To calculate the ERL and FCE values, the risk-cost assessment model considers the dynamic interaction between fire growth, fire spread, smoke movement, human behavior, and the response of fire brigades. These calculations are performed by a number of submodels interacting with each other, as shown in the flowchart in Figure 5-12.6. In Figure 5-12.6, the term "submodel" has been abbreviated as "model."

Design Fire Submodel

The risk-cost assessment model uses six design fires in the room of fire origin, and the subsequent fire and smoke spread, to evaluate life risks and protection costs in office and apartment buildings. The six design fires, representing the wide spectrum of possible fire types, are

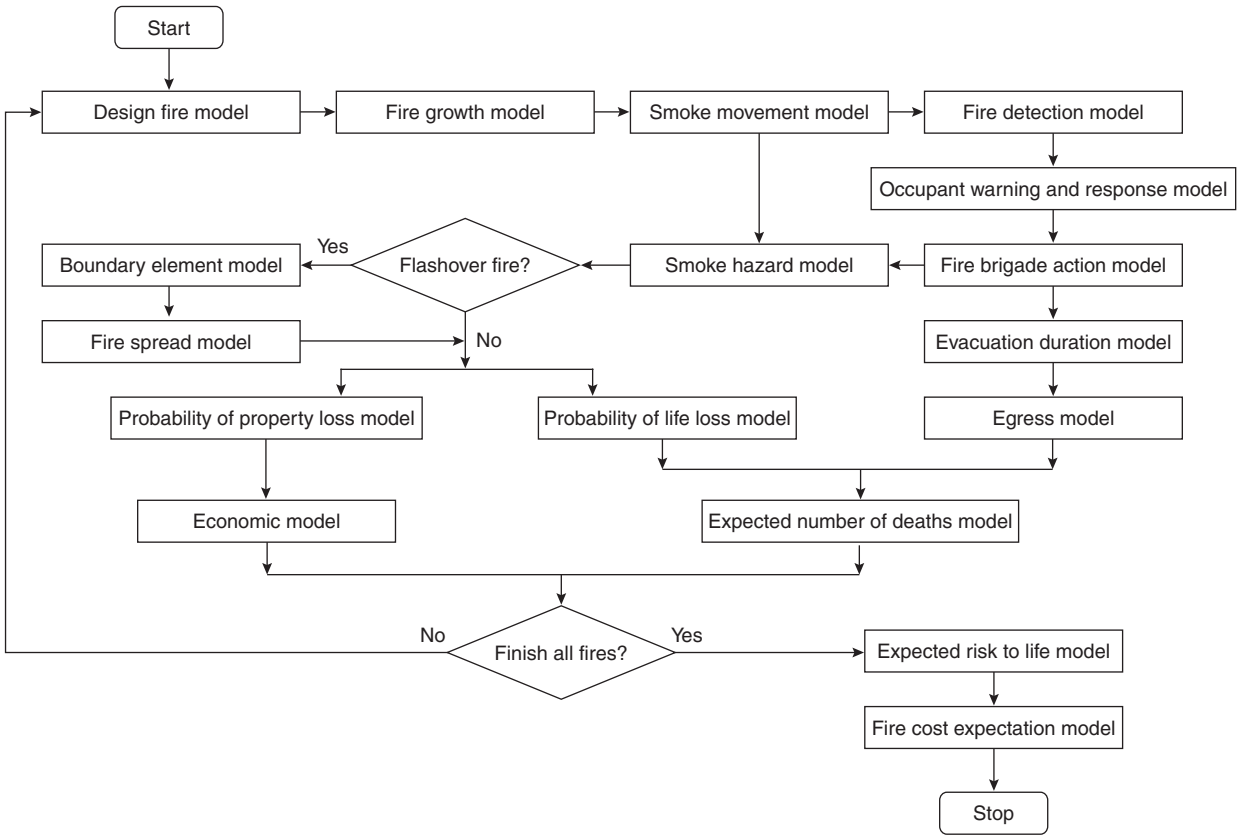

Figure 5-12.6. ***Risk-cost assessment model.***

1. Smoldering fire with room entrance door open
2. Smoldering fire with room entrance door closed
3. Flaming non-flashover fire with room entrance door open
4. Flaming non-flashover fire with room entrance door closed
5. Flashover fire with room entrance door open
6. Flashover fire with room entrance door closed

The probability of occurrence of each design fire, given that a fire has occurred, is based on statistical data. For example, in Canada, statistics show that 18 percent of all apartment fires reach flashover and become fully developed fires, 63 percent are flaming fires that do not reach flashover, and the remaining 19 percent are smoldering fires that do not reach the flaming stage.[83] If sprinklers are installed, the model assumes that some of the flashover and non-flashover fires, depending on the reliability and effectiveness of the sprinkler system, are rendered non-lethal.

The risk-cost assessment model evaluates the effects of various fire scenarios that may occur in the building during its life. For example, in an apartment building, one fire scenario is the fire and smoke spread resulting from one design fire in any one of the apartment units in the building and during a time when the occupants are either awake or asleep. The number of fire scenarios, therefore, is the product of the number of design fires, the number of apartment units, and whether the occupants are awake or asleep.

Fire Growth Submodel

The fire growth submodel[84] predicts the development of the six design fires in the room of fire origin. The submodel calculates the burning rate, room temperature, and the production and concentration of toxic gases as a function of time. With these calculations, the model determines the time of occurrence of five important events: (1) time of fire cue, (2) time of smoke detector activation, (3) time of sprinkler activation, (4) time of flashover, and (5) time of fire burnout. The first three detection times are used by the evacuation duration submodel to estimate the time available for evacuation; the flashover time is used by the fire brigade action submodel, in combination with the arrival time of the fire brigade, to evaluate the effectiveness of fire fighting; and the burnout time is used by the smoke hazard submodel as part of the calculation for the maximum smoke hazard. The submodel also predicts the mass flow rate, the temperature, and the concentrations of CO and CO_2 in the hot gases leaving the fire room. This latter information is used by the smoke movement submodel to calculate the spread of

smoke to different parts of the building as a function of time.

Smoke Movement Submodel

The smoke movement submodel[85] calculates the spread of smoke and toxic gases to different parts of the building as a function of time. The submodel also calculates the critical time when the stairs become untenable, which is considered to be the time when the occupants are trapped in the building. This critical time is used later by the evacuation duration submodel to calculate the time available for evacuation.

Fire Detection Submodel

The fire detection submodel calculates the probabilities of detection at the first three detection times mentioned under the fire growth submodel, based on the probabilities of detection by smoke detectors, sprinklers, and occupants. This information is used by the occupant warning and response submodel to calculate the probabilities of response of the occupants.

Occupant Warning and Response Submodel

The occupant warning and response submodel calculates the probabilities of warning and response at the first three detection times mentioned under the fire growth submodel. This information is used by the fire brigade action submodel to calculate the probability of response of the fire brigade, and by the egress submodel to model the evacuation of the occupants.

Fire Brigade Action Submodel

The fire brigade action submodel calculates the probability and time of arrival of the fire brigade. This submodel also evaluates the effectiveness of fire fighting, based on the flashover time from the fire growth submodel and the arrival time of the fire brigade. The information on arrival and effectiveness of the fire brigade is used by the smoke hazard submodel to calculate the maximum smoke hazard to the occupants, and by the fire spread submodel to calculate the probabilities of fire spread.

Smoke Hazard Submodel

The smoke hazard submodel calculates the maximum smoke hazard to the occupants based on the burnout time from the fire growth submodel and the arrival time and effectiveness of the fire brigade from the fire brigade action submodel. This information is used by the life loss submodel to calculate the probabilities of life loss.

Evacuation Duration Submodel

The evacuation duration submodel uses the three fire detection times from the fire growth submodel and the critical time in the stairs from the smoke movement submodel to calculate three durations available for evacuation. This information is used by the egress submodel to model the evacuation of the occupants.

Egress Submodel

Based on the evacuation time available and the probability of response of the occupants, this submodel calculates the number of occupants who have evacuated the building and the number trapped in the building. This information is used by the expected number of deaths submodel to calculate the expected number of deaths.

Boundary Element Submodel

The boundary element submodel calculates the probabilities of failure of the boundary elements (walls, floors, doors, etc.) when they are subjected to fully developed, realistic fires. The submodel comprises the following probabilistic models: fire severity, temperature distribution, thermo-mechanical material properties, failure performance for each limit state, and overall probability of failure.

Fire Spread Submodel

Based on the probabilities of failure of the boundary elements, this submodel calculates the probabilities of fire spread to each part of the building given a fully developed fire in any enclosure. A probabilistic network of the building is developed where nodes represent building volumes, links represent boundary elements between volumes, and probabilities of failure of the boundary elements are assigned to links. Allowance is made for the effectiveness of the fire brigade. The probability of fire spread information is used by both the property loss submodel and the life loss submodel to estimate fire losses and life loss.

Life Loss Submodel

Based on the probabilities of smoke hazard from the smoke hazard submodel and fire spread from the fire spread submodel, this submodel calculates the probabilities of life loss.

Expected Number of Deaths Submodel

Based on the probabilities of life loss from the life loss submodel and the number of occupants trapped in the building from the egress submodel, this submodel calculates the expected number of deaths in the building.

Property Loss Submodel

Based on the probabilities of fire spread from the fire spread submodel, this submodel calculates the expected property loss.

Economic Submodel

Based on the expected property loss and the capital and maintenance costs of the fire protection systems, this submodel calculates the expected fire costs.

Expected Risk-to-Life Submodel

The expected risk-to-life submodel calculates the overall expected risk to life (ERL) by summing the expected number of deaths in the building for each fire scenario and the probability of each fire scenario.

Fire-Cost Expectation Submodel

The fire-cost expectation submodel calculates the fire-cost expectation (FCE) using the capital and maintenance costs of the fire protection systems, the expected fire loss for each fire scenario, and the probability of each fire scenario.

Assumptions and Limitations

In the risk-cost assessment model, due to the complexity and the lack of sufficient understanding of fire phenomena and human behavior, certain conservative assumptions and approximations were made in the mathematical modeling. In addition, not all aspects of the risk-cost assessment model have been fully verified by full-scale fire experiments or actual fire experience. Only some of the submodels have been verified by experiments or statistical data.

As a result, the predictions made by the model can only be considered as approximate. The model, therefore, should not be used for absolute assessments of life risks and protection costs. For comparative assessments of life risks and protection costs, and for the selection of a cost-effective fire safety system design solution, the model is considered to be reliable.

As in many computer models, the model uses certain input parameters to describe the characteristics of various fire safety designs. These include the fire resistance rating of boundary elements, the reliability of smoke alarms and sprinklers, the probability of doors open or closed, and the response time of fire brigades. The sensitivity of these parameters on the predicted risks have been checked and found to be reasonable.[86]

FRAMEworks

Another computer-based risk assessment model, *FRAMEWorks,* was developed through a collaborative effort between the National Institute of Standards and Technology (NIST), the NFPA Fire Analysis & Research Division, and the private consulting firm of Benjamin/Clarke Associates.[87,88] The goal of this effort was to develop an objective, comprehensive, generally applicable, and widely recognized fire risk assessment methodology for products that go into buildings. The result was a method for quantifying the fire risk associated with a specific class of products in a specified occupancy.

FRAMEworks is similar in many respects to the fire risk and cost assessment model of Beck described above. It combines a quantitative (fire effects modeling) method to evaluate specific products in specific fire scenarios with a statistical method of relating fire deaths to the specific scenarios in order to establish a death rate baseline for the scenarios. The impact of new or replacement products can then be evaluated against the baseline scenarios to determine if the risk is comparatively higher or lower with a change of product(s).

The modeling sequence to compute fire risk in *FRAMEworks* is illustrated in Figure 5-12.7. A more detailed description of the model can be found in the *NFPA Fire Protection Handbook.*[88]

CRISP

A computer-based fire risk assessment model is also under development in the United Kingdom by the Building Research Establishment, Fire Research Station. This model, called CRISP (Computation of Risk Indices by Simulation Procedures), is similar to the Beck model in that it provides a Monte Carlo simulation of entire fire scenarios, but is an object-oriented model as opposed to a state transition model.[89,90] The basic concept of the CRISP approach is that the building-contents-people system is treated as a collection of objects, represented by a section of the program that defines the objects' behavior in response to stimuli (input data). The objects may interact in a number of ways, depending on the information exchanged between them, but data associated with an object cannot be changed by another object (only by changing that object's code). Thus, for any given scenario, the objects will interact with each other, but not change each other, based on the associated object definition and input parameters.

The types of objects modeled include furniture, hot and cold gas layers, vents, walls, rooms, alarms, occupants, and fire fighters.[89] The actions of the objects are governed by physical relationships (e.g., fire growth) and tables of rules (e.g., for people). For each run, various conditions, contents, and occupant characteristics are randomly selected and probabilities are assigned. Once the conditions have been defined, the simulation predicts how a scenario develops with time until the fire is out or the occupants are dead or have escaped.

Thus far, the scope of CRISP runs have been limited to two-story residential occupancies, and have been used to evaluate such tradeoffs as fire detection installation versus the need for additional passive fire protection, and caution has been urged relative to the model's use in more complex buildings.[90]

Hazard and Risk Matrices

In addition to the more complicated single-scenario and ETA-based engineering approaches and computer-based risk modeling, various risk analysis alternatives exist that combine hazard analysis, consequence analysis, and judgments about likelihood of events in less quantitatively rigorous manners. This does not imply the methods

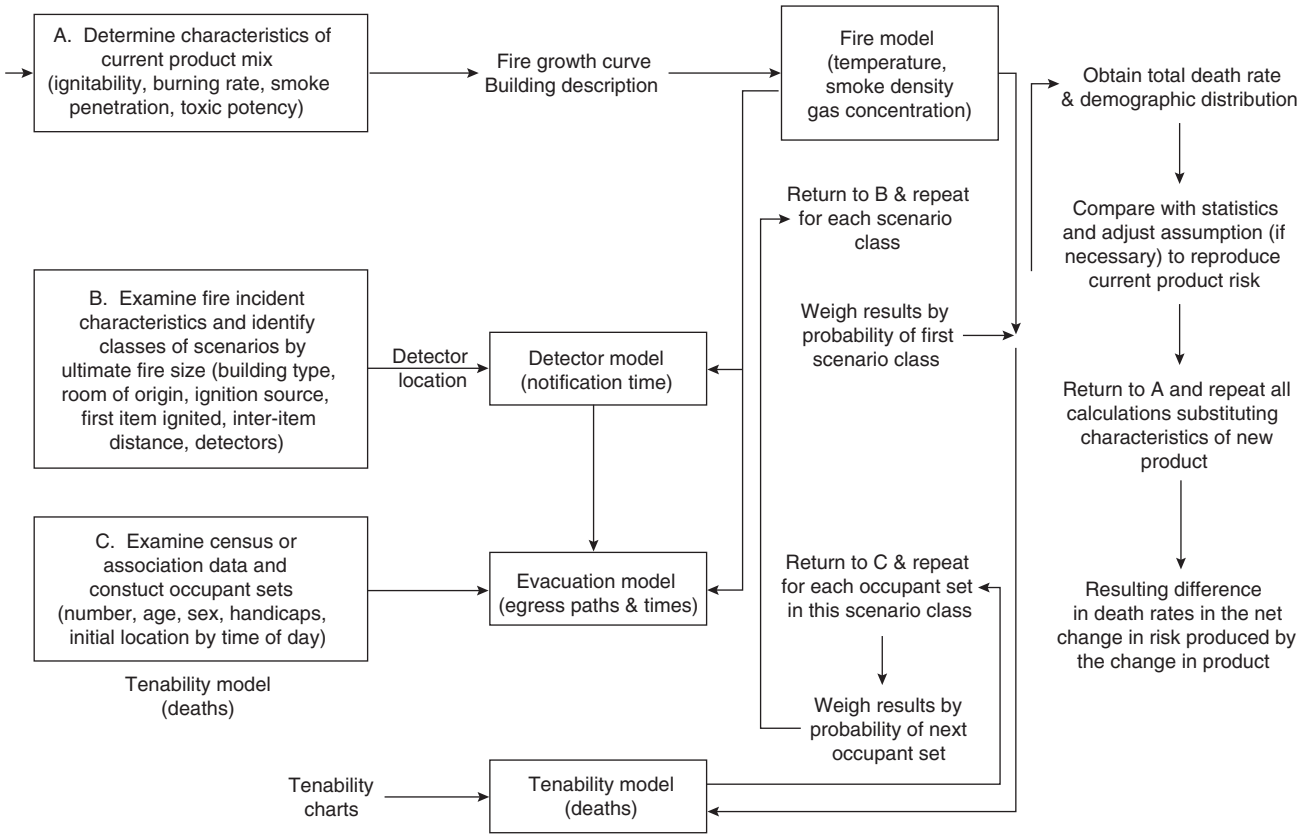

Figure 5-12.7. ***Modeling sequence to compute fire risk in FRAMEworks.[87]***

are less rigorous, or less appropriate, but that they are simply easier to apply. In many cases, such simplified approaches will be more widely accepted by interested and affected parties, as the concepts may be familiar.

One such approach is the hazard matrix,[91] or risk matrix approach.[10,92] This approach is simpler to apply than a classical engineering risk analysis approach, as the importance of identifying all possible outcomes is less critical. In essence, it works by quantifying the consequences of the most severe events anticipated and coupling these with approximate event frequencies. The result is a quantified approximate risk estimate. In this approach, a maximum consequence for each type of loss is identified (life safety, property, business interruption, environmental damage, etc.) that represents the largest realistic event of each type. Each maximum consequence is then ranked. Table 5-12.1 provides an example of possible consequence ranking thresholds (i.e., negligible, low, medium, and high) that may be selected. For these estimates, the consequence predictions should bound all possible event outcomes at the 95th percentile or better.[10] The 95th percentile value is suggested since it has gained ready acceptance in other engineering fields, and by using such a standard value, it may be possible to compare different analyses. If it is desired to use a different bounding level, all stakeholders must agree. An extensive analysis can often be avoided when selecting the maximum consequence if the total replacement costs are assumed to be the maximum consequence.

The frequencies must also be ranked in this type of analysis. Here, the frequencies should be for exceeding a specific loss (i.e., consequence) rather than for a specific scenario, as frequencies based solely on a specific scenario can be misleading. For example, a scenario may have a frequency of 10^{-7} per year, leading one to the conclusion that fire is not a concern. However, the reported fire risk should actually represent the frequency of multiple fire scenarios, so if 30 specific scenarios are developed, each at 10^{-7} fires per year, the net effect is 3×10^{-6} fires per year. Table 5-12.2 provides a specific example for frequency ranking.[10,92] As with consequence ranking, alternate frequency rankings (bins) from those presented in Table 5-12.2 can be developed provided that all interested and affected parties agree. It is also possible to add additional layers of ranking where desirable.

Once the bounding consequences and their respective frequencies have been estimated, they must be converted to an estimate of risk. An estimation is accomplished by plotting the consequence-frequency combination in a matrix as shown in Figure 5-12.8 (the numbers in boxes are for identification purposes and do not imply a ranking). The stakeholders assign each consequence-frequency combination, and the resultant risks are considered bounding risks. After this analysis, events that meet a certain risk cri-

Table 5-12.1 ***Possible Consequence Ranking Criteria[10]***

Consequence Level	Impact on Populace	Impact on Property/Operations
High (*H*)	Immediate fatalities, acute injuries—immediately life threatening or permanently disabling	Damage > \$XX million—building destroyed & surrounding property damaged
Moderate (*M*)	Serious injuries, permanent disabilities, hospitalization required	\$YY < damage < \$XX million—major equipment destroyed, minor impact on surroundings
Low (*L*)	Minor injuries, no permanent disabilities, no hospitalization	Damage < \$YY—reparable damage to building, significant operational downtime, no impact on surroundings
Negligible (*N*)	Negligible injuries	Minor repairs to building required, minimal operational downtime

Table 5-12.2 ***Example Frequency Criteria Used for Probability Ranking[10]***

Acronym	Description	Frequency Level (median time to event)	Description
A	Anticipated, expected	$> 10^{-2}$/yr (<100 years)	Common incidents that may occur several times during the lifetime of the building.
U	Unlikely	$10^{-4} < f < 10^{-2}$/yr (100 to 10,000 years)	Events that are not anticipated to occur during the lifetime of the facility. Natural phenomena of this probability class include: UBC-level earthquake, 100-year flood, maximum wind gust, etc.
EU	Extremely unlikely	$10^{-6} < f < 10^{-4}$/yr (10,000 to 1 million years)	Events that will probably not occur during the life cycle of the building
BEU	Beyond extremely unlikely	$< 10^{-6}$/yr (> 1 million years)	All other accidents

terion may be considered "acceptable" based on the objectives and input from the interested and affected parties (e.g., the interested and affected parties may consider moderate, low, and negligible risk events acceptable).

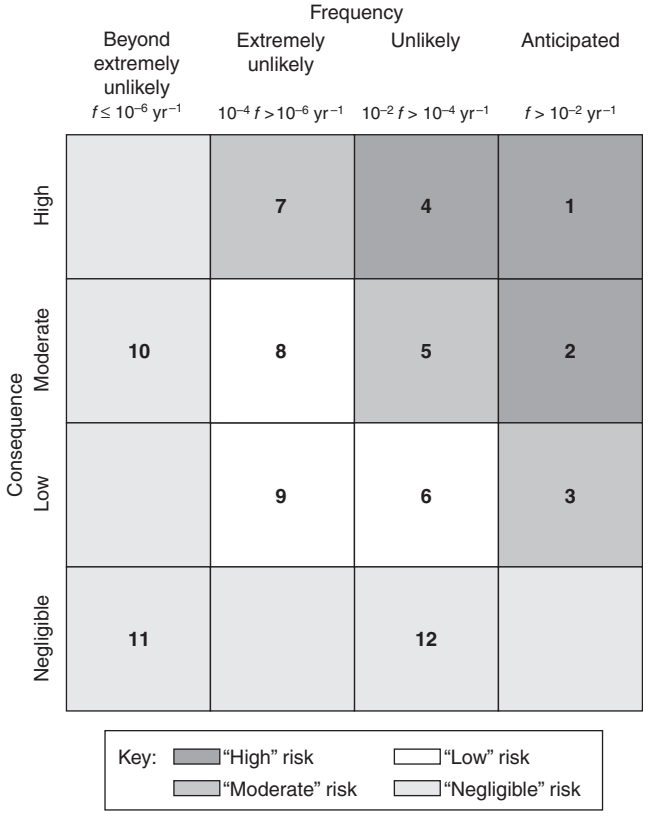

Figure 5-12.8. ***Example risk ranking matrix.[10]***

Performance Matrix

A concept similar to that of the hazard and risk matrices approach described above has been developed for use in building and fire safety regulations.[1,4,5,93–95] This approach establishes a performance matrix that compares performance groups (building types grouped by like performance expectations) by magnitude of design events (probabilistic or deterministic descriptions of hazard event). Within the performance matrix, instead of having risk bins (groups), there are tolerable levels of impact (reflecting the amount of damage expected for buildings within different performance groups given specific magnitudes of design events). As the performance group increases from Group I to Group IV, the level of required performance increases, as do the corresponding levels of tolerable impact. This is illustrated in Figure 5-12.9.

Within the performance matrix, tolerable levels of impacts reflect various limit states of damage, injury, or loss that can be estimated, measured, and/or calculated when subjected to design loads of various magnitudes. As the impacts get larger, it is expected that more damage will occur, unless a higher level of performance is desired. In this manner, the levels of impact are inversely proportional to building performance: less impact means better performance. Establishment of these levels of tolerable impact requires a balance of technical knowledge and ability and societal values. The term *tolerable* is used to reflect the fact that absolute protection is not possible, and

Magnitude of design event (Increasing magnitude of event)	Increasing level of building performance (Performance groups)			
	Performance group I	Performance group II	Performance group III	Performance group IV
Very large (very rare)	Severe	Severe	High	Moderate
Large (rare)	Severe	High	Moderate	Mild
Medium (less frequent)	High	Moderate	Mild	Mild
Small (frequent)	Moderate	Mild	Mild	Mild

Figure 5-12.9. ***Performance matrix.***[1,95]

that some damage, injury, or loss is currently tolerated in structures, especially after a hazard event. The term *impact* is used as a broad descriptor of loss.

If one so chooses, one can overlay probabilities and consequences on the performance matrix in a manner similar to the hazard and risk matrices discussed previously. In the performance matrix (Figure 5-12.9), the magnitudes of design event can be overlaid with probabilities (or frequencies) of event occurrence, from high at the bottom to low at the top. For all high-probability events, the allowable magnitude of impact (consequences) is either mild or moderate depending on the performance group. For low-probability events, the allowable magnitude of impact can be moderate, high, or severe depending on the performance group. This approach allows for decisions to be made on the required level of building performance for low-probability, high-consequence events, based on the performance group to which a building is designated.

Performance groups are simply consolidations of use groups with common performance requirements. They are developed as part of the risk characterization process, considering such issues as numbers of people in a building, sensitive or vulnerable populations, the hazards posed by the building, its contents or processes, and essential facilities and services. The number of performance groups that is required should be based on an analytical-deliberative risk characterization process as described previously. The following definitions of performance groups is one example as used in the International Performance Code for Buildings and Facilities:[95]

Performance Group I is intended to cover those buildings or facilities, such as utility sheds, where the failure of such buildings poses a low risk to human life. Performance Group II is intended to be the minimum for most typical buildings, such as business, mercantile, or storage uses. Performance Group III includes building and facilities with an increased level of societal benefit or importance. These structures and classes of structures require increased levels of performance as they house large numbers of people, vulnerable populations, or occupants with other risk factors; or they fulfill some role of increased importance to the local community or to society in general. Examples include post-disaster command control centers, acute-care hospitals, or a school used as an emergency shelter. Performance Group IV contains building uses or facilities that have an unusually high risk. Such facilities may include nuclear facilities or explosives storage facilities. For specific facilities, for specific jurisdictions, or in countries outside of the United States, other definitions for the performance groups may be appropriate.

Likewise, the number of tolerable levels of impact can be selected based on the level of detail deemed appropriate by interested and affected parties. One possibility is the use of four levels: mild, moderate, high and severe.[95] The definition of each level would reflect the tolerability limits as developed by a risk characterization effort. For example, a moderate level of impact may be defined as follows (remember that levels of impact are inversely proportional to levels of performance, and that these are design goals):

- There is moderate structural damage which is repairable; some delay in reoccupancy can be expected due to structural rehabilitation.
- Nonstructural systems needed for normal building use are fully operational, although some cleanup and repair may be needed. Emergency systems remain fully operational.
- Injuries to building occupants may be locally significant, but generally moderate in numbers and in nature. There is a low likelihood of single life loss and a very low likelihood of multiple life loss.
- Damage to building contents may be locally significant, but is generally moderate in extent and cost.
- Some hazardous materials are released to the environment, but the risk to the community is minimal. No emergency relocation is necessary.

Associated with the tolerable levels of impact is the actual hazard event. One way to look at the hazard event is in terms of its size, or magnitude. The magnitude of a hazard event can be represented deterministically or as a frequency of occurrence. When characterizing the magnitude of hazard events, it is important to remember that (1) they are on a continuum and are compartmentalized for ease of analysis and design; and (2) they should be considered "design loads," and not as a reflection of the actual magnitude of event that could impact a building.

As with tolerable levels of impact, the number of magnitude of event levels can be established by the interested and affected parties. For example, four categories of event magnitude (design loads) can be selected: small (frequent), medium (occasional), large (rare), and very large (very rare). To understand how the magnitudes can be described, consider earthquake loads and fire loads, where earthquake loads are shown in terms of their mean

return period, and fire loads are shown deterministically in terms of extent of flame spread.

Earthquake Loads (mean return period)

Frequent	72 years
Occasional	225 years
Rare	474 years
Very Rare	2475 years

Fire Loads (deterministic)

Small	Contained to object of origin
Medium	Contained to room
Large	Contained to floor
Very Large	Contained to building

There is often correlation between frequent, occasional, rare, and very rare; and small, medium, large, and very large; in that frequent events tend to be small, whereas very large events tend to be very rare. Also, it is often the very large or very rare events that are of particular concern, as it is these events for which providing high levels of protection against is costly and may not be considered reasonable or cost-effective for all buildings.

The Building Fire Safety Evaluation Method (BFSEM)

Another approach to identifying hazards and consequences, and for obtaining judgments on the likelihood of events occurring, is the *building fire evaluation method* (BFSEM).[96–98] The BFSEM is a structured framework for evaluating building fire safety performance that can be used for hazard assessment or risk analysis. With this method, the user can evaluate the likelihood of ignition, fire growth, and fire spread through an existing building or new building for which plans have been developed, focusing on such factors as fuel loading, occupancy characteristics, active fire protection features, and structural features. Using network diagrams, the user evaluates such factors as ignition potential, fire growth potential within the compartment of origin, barrier performance, fire spread beyond the compartment of origin, and occupant safety. The user can assign subjective probabilities, based on experience and engineering judgment, or statistical data when available, to estimate the likelihood of each event occurring (the outcome is the likelihood that any event will or will not occur). Two network diagrams from the BFSEM are shown in Figure 5-12.10.

With the BFSEM, building fire safety performance is evaluated using experience and judgment regarding how fire will develop and spread considering fire-related factors such as fuel load and arrangement, and fire-protection features such as automatic and manual fire detection and suppression, barrier integrity, and emergency systems. When desired or required, experience and judgments can be supported by deterministic calculation methods. In attempting to determine the likelihood of successful control of a fire by sprinkler activation, for example, one must evaluate the ability of the fire to grow to a sufficient size to activate the sprinkler and then evaluate the likelihood that the sprinkler can control the fire. The latter action may involve an evaluation of the sprinkler system (or design), the water supply, and the reliability of the system operation (statistical data, when available, can be added to support this stage of the evaluation).

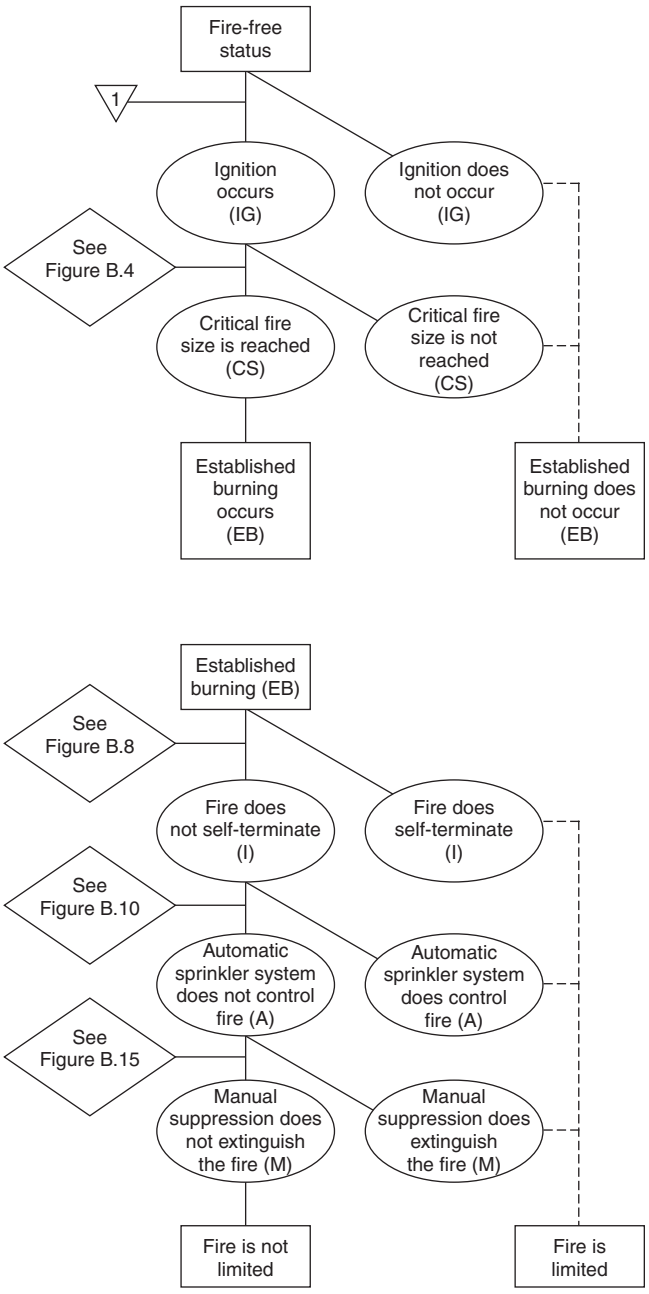

Figure 5-12.10. ***Examples of BFSEM network diagrams.[98]***

In the BFSEM, all buildings are assemblies of spaces and barriers. A clear identification is made for the specific spaces and barriers that are used for a particular building performance analysis. This is defined as *space-barrier organization.* The fire itself is separated into two components: flame/heat and smoke/gas. This is done because each component impacts the building, its occupants, and its contents at different speeds and in different ways.

Within the BFSEM, ignition is defined as self-sustained burning of an item, typically when the first small flame appears (smoldering is defined to occur before ignition). If the ignited material is expected to continue burning (i.e., is not expected to self-terminate), the fire is then classified as having attained *established burning* (i.e., sufficient fuel is present and arranged so as to continue burning if adequate ventilation is present). Assuming no intervention is taken, the fire then grows to full room involvement (i.e., the condition where the surfaces of all combustibles in the room are burning). Full-room involvement can be assumed when flashover occurs. (Flashover is the very rapid ignition of collected fire gases in a room.) After full-room involvement commences, the fire will burn for an extended period of time, until the fuel is nearly consumed or until fire suppression is successful in extinguishing the fire. The literature often describes this stage of the fire as a "post-flashover" or "fully-developed" fire.

In the BFSEM, the term *barrier performance* is used to describe a barrier's ability to prevent fire propagation, where a barrier is defined as any surface that will delay or prevent an ignition into an adjacent space. At any time during the fire, a barrier can be considered as being successful (if it does not permit any ignition to occur in the adjacent space), as having a small failure (e.g., a crack), or as having a massive failure (e.g., door open, large hole, etc.). The *limit of flame movement* is the extent to which the fire spreads before it is terminated. (The term *limit* may be applied to the extent of fire spread either in a space or in a building.)

Evaluation of building performance using the BFSEM is accomplished by applying the above concepts to the following areas: *prevention, flame/heat analysis* (the ability of the building to limit the fire in its spaces and barriers through active and passive fire defenses), *smoke/gas analysis* (the ability of the building to maintain tenable conditions in selected spaces for prescribed time duration), *structural frame analysis* (the ability of the structural frame to avoid unacceptable deformation or collapse for a fire that is not limited), and *people movement analysis* (the time required for building occupants to move within the building or to locations of safety).

Application of the BFSEM provides a comprehensive method for identifying factors that affect the fire safety performance of a building. The method has been widely used and has been adapted by the U.S. Coast Guard to become their ship fire safety engineering methodology (SFSEM).[99]

Summary

Building fire risk analysis is a complex subject. This chapter has provided a brief overview of key issues in the subject area, including discussions on difficulties in defining risk, on risk characterization, on tools and methods to help identify hazards and consequences, and on building fire risk analysis methods. Given the complexities involved in building fire risk analysis, it is intended that this chapter provide a starting point rather than an end point. With this in mind, extensive references and sources for further reading are provided for additional information. A review of other risk-related chapters in this handbook, such as those by Hall, Notarianni, Ramachandran, and Watts is a good place to start. Finally, it is important to remember that when embarking on a building fire risk analysis effort, one should take care to identify and involve the interested and affected stakeholders, carefully consider the range of risk issues involved, and seek the most appropriate approaches, tools, methods, and data for the problem.

References Cited

1. B.J. Meacham, "A Process for Identifying, Characterizing, and Incorporating Risk Concepts into Performance-Based Building and Fire Regulations Development," Ph.D. Dissertation, Clark University, Worcester, MA (2000).
2. N.C. Rassmussen, "The Application of Probabilistic Risk Assessment Techniques to Energy Technologies," in *Readings in Risk* (Glickman and Gough, eds.), Resources for the Future, Washington, DC, pp. 195–206 (1990).
3. P.C. Stern and H.V. Fineburg (eds.), *Understanding Risk: Informing Decisions in a Democratic Society,* National Academy Press, Washington, DC (1996).
4. B.J. Meacham, "Incorporating Risk Concepts into Performance-Based Building and Fire Code Development," in *Proceedings of the Second Conference on Fire Design in the 21st Century,* Worcester, MA (1999).
5. B.J. Meacham, "Incorporating Risk Concepts into Performance-Based Building and Fire Regulation Development," in *Safety Engineering and Risk Analysis,* SERA Volume 9 (J.L. Boccio, ed.), American Society of Mechanical Engineers, New York, pp. 63–70 (1999).
6. B.J. Meacham, "Application of a Decision-Support Tool for Comparing and Ranking Risk Factors for Incorporation into Performance-Based Building Regulations," in *Proceedings of the Third International Conference on Performance-Based Codes and Fire Safety Design Methods,* SFPE, Bethesda, MD (2000).
7. B.J. Meacham and R.L.P. Custer, "Performance-Based Fire Safety Engineering: An Introduction of Basic Concepts," *Journal of Fire Protection Engineering,* 7, 2, pp. 35–54 (1995).
8. R.L.P. Custer and B.J. Meacham, *Introduction to Performance-Based Fire Safety,* NFPA, Quincy, MA (1997).
9. B.J. Meacham, "Assessment of the Technological Requirements for Realization of Performance-Based Fire Safety Design in the United States: Final Report," *NIST GCR 98-763,* NIST, Gaithersburg, MD (1998).
10. *The SFPE Engineering Guide on Performance-Based Fire Safety Analysis and Design of Buildings,* SFPE and NFPA, Quincy, MA (2000).
11. R.L. Keeney and H. Raiffa, *Decisions with Multiple Objectives: Preferences and Value Tradeoffs,* John Wiley and Sons, New York (1976).
12. R.L. Keeney, "Formal Analysis Including Value Judgments and Public Risk," *Toxic Substances Journal,* 3, 1, pp. 8–22 (1981).
13. R.T. Clemen, *Making Hard Decisions: An Introduction to Decision Analysis,* Duxbury Press, Pacific Grove, CA (1996).
14. R. Schwing and W. Albers (eds.), *Societal Risk Assessment: How Safe is Safe Enough?,* Plenum, NY (1980).
15. E. Crouch and R. Wilson, *Risk/Benefit Analysis,* Ballinger Publishing Company, Cambridge, MA (1982).
16. R. Wilson, "Commentary: Risks and Their Acceptability," *Science, Technology and Human Values,* 9, 2, pp. 11–22 (1984).
17. D.J. Alesch and W.J. Petak, *The Politics and Economics of Earthquake Hazard Mitigation: Unreinforced Masonry Buildings in*

Southern California, Institute on Environment and Behavior, University of Colorado, Boulder (1986).
18. S. Kelman, "Cost-Benefit Analysis: An Ethical Critique," in *Readings in Risk* (Glickman and Gough, eds.), Resources for the Future, Washington, DC, pp. 129–137 (1990).
19. S. Breyer, *Breaking the Vicious Circle: Toward Effective Risk Regulation,* Harvard University Press, Cambridge, MA (1993).
20. Tengs et al., "Five Hundred Life-Saving Interventions and Their Cost-Effectiveness," *Risk Analysis,* 15, 3, pp. 369–390 (1995).
21. H. Kunreuther and R.J. Roth, Sr., *Paying the Price: The Status and Role of Insurance Against Natural Disasters in the United States,* Joseph Henry Press, Washington, DC (1998).
22. P.R. Kleindorfer and H.C. Kunreuther, "The Complementary Roles of Mitigation and Insurance in Managing Catastrophic Risks," *Risk Analysis,* 19, 4, pp. 727–738 (1999).
23. *Guidelines for Chemical Process Quantitative Risk Analysis,* American Institute of Chemical Engineers, Center for Chemical Process Safety, New York (1985).
24. S.E. Magnusson, H. Franzich, and K. Harada, "Fire Safety Design Based on Calculations: Uncertainty Analysis and Safety Verification," *Report 3078,* Lund University, Lund, Sweden (1995).
25. S.E. Magnusson, "Risk Assessment," in *Fire Safety Science—Proceedings of the Fifth International Symposium,* IAFSS, pp. 41–58 (1997).
26. H. Frantzich, "Uncertainty and Risk Analysis in Fire Safety Engineering," *Report LUTVDG/(TVBB-1016),* Lund University, Lund, Sweden (1998).
27. N. Groner, "A Critique of Event Modeling as Applied to Human Reliability and a Suggested Alternative," in *Proceedings of the SFPE Symposium on Risk, Uncertainty and Reliability in Fire Protection Engineering,* SFPE, Bethesda, MD, pp. 190–199 (1999).
28. R.E. Britter, "The Evaluation of Technical Models Used for Major-Accident Hazard Installations," *EUR 14774EN,* Commission of the European Communities, Brussels, Belgium (1993).
29. C. Hohenemser, R. Kasperson, and R.W. Kates, "Causal Structure," in *Perilous Progress: Managing the Hazards of Technology (*Kates, Hohenemser, and Kasperson, eds.), Westview Press, Boulder, CO, pp. 25–42 (1985).
30. M.C. White et al., "A Quantitative Estimate of Leukemia Mortality Associated with Occupational Exposure to Benzene," in *Readings in Risk* (Glickman and Gough, eds.), Resources for the Future, Washington, DC, pp. 165–180 (1990).
31. B.N. Ames, R. Magow, and L.S. Gold, "Ranking Possible Carcinogenic Hazards," in *Readings in Risk* (Glickman and Gough, eds.), Resources for the Future, Washington, DC, pp. 76–99 (1990).
32. D. Hattis and D. Kennedy, "Assessing Risks from Health Hazards: An Imperfect Science," in *Readings in Risk* (Glickman and Gough, eds.), Resources for the Future, Washington, DC, pp. 156–163 (1990).
33. B.D. Goldstein, *Issues in Risk Assessment,* National Research Council, National Academy Press, Washington, DC (1993).
34. C.T. Petito and B.D. Beck, "Evaluation of Evidence of Nonlinearities in the Dose-Response Curve for Arsenic Carcinogenesis," *Trace Substances in Environmental Health,* 24, pp. 143–176 (1990).
35. F.P. Lees, *Loss Prevention in the Process Industries,* Butterworths, London (1980).
36. R.L. Keeney et al., "Assessing the Risk of an LNG Terminal," in *Readings in Risk* (Glickman and Gough, eds.), Resources for the Future, Washington, DC, pp. 207–217 (1990).
37. G. Apostolakis, "Fire Risk Assessment and Management in Nuclear Power Plants," *Fire Science and Technology,* 13, Supplement, pp. 12–39 (1993).
38. Y.Y. Haimes, *Risk Modeling, Assessment, and Management,* John Wiley and Sons, New York (1998).
39. *Proceedings of the SFPE Symposium on Risk, Uncertainty and Reliability in Fire Protection Engineering and Joint SFPE/UMD/Clark University Workshop on Encouraging the Use of Risk Concepts in Performance-Based Building and Fire Regulation Development,* SFPE, Bethesda, MD (1999).
40. NFPA 500, *Guide to Systems Concepts for Fire Protection,* National Fire Protection Association, Quincy, MA (1995).
41. J.M. Watts, Jr., "Systems Concepts for Building Fire," in *Fire Protection Handbook,* NFPA, Quincy, MA, pp. 1-34–1-42 (1991).
42. Random House, *The Random House College Dictionary,* Random House, Inc., New York (1980).
43. J.R. Hall, Jr., "Probability Concepts," *SFPE Handbook of Fire Protection Engineering,* SFPE/NFPA, Quincy, MA, Section 1, Chapter 11 (1995).
44. G. Apostolakis, "Probability and Risk Assessment: The Subjectivistic Viewpoint and Some Suggestions," *Nuclear Safety,* 19, 3, pp. 305–315 (1978).
45. M.J. Karter, Jr., "1996 U.S. Fire Loss," *NFPA Journal,* 91, 5, pp. 77–83 (1997).
46. M. Fontana, J.P. Favre, and C. Fetz, "A Survey of 40,000 Building Fires in Switzerland," *Fire Safety Journal,* 32, 2, pp. 137–159 (1999).
47. J. Rahikainen and O. Keski-Rahkonen, "Determination of Ignition Frequency of Fire in Different Premises in Finland," *Fire Engineers Journal,* 58, 197, pp. 33–37 (1998).
48. J.R. Hall, Jr., *The U.S. Fire Problem Overview Report—Leading Causes and Other Patterns and Trends,* National Fire Protection Association, Quincy, MA (1998).
49. *Fire in the United States, 10th Edition, 1986–1995,* National Fire Center, United States Fire Administration, Federal Emergency Management Agency, Emmitsburg, MD (1998).
50. *Fire Safety Engineering in Buildings,* British Standards Institute, DD 240: Parts 1 and 2 (1997).
51. Fire Code Reform Centre, *Fire Engineering Guidelines,* Sydney, Australia (1996).
52. D. Kahneman and A. Tversky, "Judgment Under Uncertainty: Heuristics and Biases," *Science,* 185, pp. 1124–1131 (1974).
53. W.W. Lowrance, *Of Acceptable Risk,* William Kaufmann, Inc., Los Altos, CA (1976).
54. B. Fischhoff et al., *Acceptable Risk,* Cambridge University Press, New York (1981).
55. P. Slovic, "Perception of Risk," *Science,* 236, pp. 280–285 (1987).
56. V.T. Covello, et al. (eds.), *Uncertainty in Risk Assessment, Risk Management, and Decision Making,* Plenum Press, New York (1987).
57. M.G. Morgan and M. Henrion, *Uncertainty: A Guide to Dealing with Uncertainty in Quantitative Risk and Policy Analysis,* Cambridge Press, Cambridge, UK (1990).
58. S.O. Funtowicz and J.R. Ravetz, "Three Types of Risk Assessment and the Emergence of Post-Normal Science," in *Social Theories of Risk* (Krimsky and Golding, eds.), Praeger, Westport, CT, pp. 251–274 (1992).
59. D. Hattis and D.E. Burmaster, "Assessment of Variability and Uncertainty Distributions for Practical Risk Analysis," *Risk Analysis,* 14, 5, pp. 713–730 (1994).
60. F.O. Hoffman and J.S. Hammonds, "Propagation of Uncertainty in Risk Assessment: The Need to Distinguish Between

Uncertainty Due to Lack of Knowledge and Uncertainty Due to Variability," *Risk Analysis,* 14, 5, pp. 707–712 (1994).

61. M.W. Merkhofer, *A Comparative Evaluation of Quantitative Decision-Making Approaches,* SRI International, Menlo Park, CA (1983).
62. M.W. Merkhofer, "Comparative Analysis of Formal Decision-Making Approaches," in *Risk Evaluation and Management* (V.T. Covello et al., eds.), Plenum Press, NY, pp. 183–220 (1986).
63. D.E. Bell, H. Raiffa, and A. Tversky (eds.), *Decision Making: Descriptive, Normative, and Prescriptive Interactions,* Cambridge University Press, Cambridge, UK (1988).
64. D. Hattis and E. Anderson, "What Should Be the Implications of Uncertainty, Variability, and Inherent Biases/Conservatism for Risk Management Decision Making?" Paper presented at *Second Workshop on When and How Can You Specify a Probability Distribution if You Don't Know Much,* University of Virginia, Charlottesville (1997).
65. J.L. Casti, *Searching for Certainty: What Scientists Can Know About the Future,* William Morrow and Company, New York (1990).
66. V. Brannigan et al., "Risk Models Involving Human Decisions: Intentional Uncertainty and the Need for Regulation," *Proceedings of the Second International Conference on Fire Research and Engineering,* SFPE, Bethesda, MD, pp. 252–262 (1998).
67. V.M. Brannigan and C. Smidts, "Performance-Based Fire Safety Regulation Under Intentional Uncertainty," in *Proceedings of the 1st International Symposium on Human Behavior in Fire,* University of Ulster, Jordanstown, Northern Ireland, pp. 411–420 (1998).
68. J.R. Benjamin and C.A. Cornell, *Probabilities, Statistics, and Decision for Civil Engineers,* McGraw-Hill, New York (1970).
69. D. Von Winterfeldt and W. Edwards, *Decision Analysis and Behavioral Research,* Cambridge University Press, Cambridge, UK (1986).
70. G.S. Omenn et al., *Risk Assessment and Risk Management in Regulatory Decision-Making,* Presidential/Congressional Commission on Risk Assessment and Risk Management, Final Report, Volume 2, Washington, DC (1997).
71. K.A. Notarianni and P. Fischbeck, "Dealing with Uncertainty to Improve Regulations," in *Proceedings of the 1999 Conference on Fire Design in the 21st Century,* SFPE and WPI, Worcester, MA (1999).
72. K.A. Notarianni, "The Role of Uncertainty in Improving Fire Protection Regulations," Ph.D. Dissertation, Carnegie Mellon University, Pittsburgh, PA (2000).
73. D.A. Lucht, "Public Policy and Performance-Based Engineering," in *Proceedings of the International Conference on Performance-Based Codes and Fire Safety Design Methods,* SFPE, Bethesda, MD (1997).
74. B.J. Meacham, "Identifying and Addressing Uncertainty in Fire Protection Engineering," in *Proceedings of the 2nd International Conference on Fire Research and Engineering,* SFPE, Bethesda, MD, pp. 238–251 (1998).
75. V.R. Beck, "Cost-Effective Fire Safety and Protection Design Requirements for Buildings," Ph.D. Dissertation, University of New South Wales, Australia (1986).
76. V.R. Beck, "A Cost-Effective Decision-Making Model for Building Fire Safety and Protection," *Fire Safety Journal,* 12, pp. 121–138 (1987).
77. V.R. Beck, "Performance-Based Fire Engineering Design and Its Application in Australia," in *Fire Safety Science—Proceedings of the Fifth International Symposium,* IAFSS, Bethesda, MD, pp. 23–40 (1997).
78. V.R. Beck and D. Yung, "A Cost-Effective Risk Assessment Model for Evaluating Fire Safety and Protection in Canadian Apartment Buildings," *Journal of Fire Protection Engineering,* 2, 3, pp. 65–74 (1990).
79. D. Yung, G.V. Hadjisophocleous, and H. Takeda, "Comparative Risk Assessments of 3-Storey Wood-Frame and Masonry Construction Office Buildings," in *Proceedings of Interflam '93,* Interscience Communications Ltd., London, pp. 499–508 (1993).
80. V.R. Beck and S.L. Poon, "Results from a Cost-Effective Decision-Making Model for Building Fire Safety and Protection," *Fire Safety Journal,* 13, pp. 197–210 (1988).
81. V.R. Beck and D. Yung, "A Cost-Effective Risk Assessment Model for Evaluating Fire Safety and Protection in Canadian Apartment Buildings," *International Fire Protection Engineering Institute, 5th Conference,* Ottawa, Canada (1989).
82. V.R. Beck and D. Yung, "A Risk-Cost Assessment Model for Evaluating Fire Risks and Protection in Apartment Buildings," in *Proceedings of the International Symposium on Fire Engineering for Buildings and Structures,* The Institution of Engineers, Melbourne, Australia (1989).
83. J. Gaskin and D. Yung, "Canadian and U.S.A. Fire Statistics for Use in the Risk-Cost Assessment Model," *IRC Internal Report No. 637,* National Research Council, Ottawa, Canada (1993).
84. H. Takeda and D. Yung, "Simplified Fire Growth Models for Risk-Cost Assessment in Apartment Buildings," *Journal of Fire Protection Engineering,* 4, 2, pp. 53–66 (1992).
85. G.V. Hadjisophocleous and D. Yung, "A Model for Calculating the Probabilities of Smoke Hazard from Fires in Multi-Storey Buildings," *Journal of Fire Protection Engineering,* 4, 2, pp. 67–80 (1992).
86. G.V. Hadjisophocleous and D. Yung, "Parametric Study of the NRCC Fire Risk-Cost Assessment Model for Apartment and Office Buildings," *Proceedings of the 4th International Symposium on Fire Safety Science,* IAFSS, Bethesda, MD, pp. 829–840 (1994).
87. R.W. Bukowski, F.B. Clarke, J.R. Hall, Jr., and S.W. Stiefel, *Fire Risk Assessment Method: Description of Methodology,* National Fire Protection Research Foundation, Quincy, MA (1990).
88. J.R. Hall, Jr., "Product Fire Risk," *Fire Protection Handbook,* 18th ed., NFPA, Quincy, MA (1997).
89. J. Fraser-Mitchell, "An Object-Oriented Simulation (CRISP II) for Fire Risk Assessment," in *Fire Safety Science: Proceedings of the Fourth International Symposium,* IAFSS, Bethesda, MD, pp. 793–803 (1994).
90. J. Fraser-Mitchell, "Risk Assessment of Factors Related to Fire Protection in Dwellings," in *Fire Safety Science: Proceedings of the Fifth International Symposium,* IAFSS, Bethesda, MD, pp. 631–642 (1997).
91. *System Safety Program Requirements, Military Standard 882C,* U.S. Department of Defense, Washington, DC (1993).
92. *Preparation Guide for U.S. Department of Energy Nonreactor Nuclear Facility Safety Analysis Reports, DOE-STD-3009-94,* U.S. Department of Energy, Washington, DC (1994).
93. *IBC Performance Building Code Committee—Interim Committee Report,* International Code Council, Falls Church, VA (1998).
94. *IBC Performance Building Code Committee Draft Report,* International Code Council, Falls Church, VA (1999).
95. *International Performance Code for Buildings and Facilities—Final Committee Report,* International Code Council, Falls Church, VA (2000).
96. R.W. Fitzgerald, "An Engineering Method for Building Fire Safety Analysis," *Fire Safety Journal,* 9, 2, pp. 233–243 (1985).
97. R.W. Fitzgerald, "An Engineering Method for Translating Fire Science into Building Design," in *Proceedings of the CIB W14 International Symposium and Workshops, Engineering Fire*

Safety in the Process of Design: Demonstrating Equivalency, University of Ulster, Jordanstown, Northern Ireland (1993b).

98. R.W. Fitzgerald, *Building Fire Safety Evaluation Method,* Worcester Polytechnic Institute, Worcester, MA (1993).
99. R.W. Fitzgerald, R.C. Richards, and C.L. Beyler, "Fire Analysis of the Polar Icebreaker Replacement Design," *Journal of Fire Protection Engineering,* 3, 4, pp. 137–150 (1991).

Additional Readings

V. Babrauskas, "Ensuring the Public's Right to Adequate Fire Safety Under Performance-Based Building Codes," in *Proceedings of the 1998 Pacific Rim Conference and Second International Conference on Performance-Based Codes and Fire Safety Design Methods,* ICBO and SFPE, Whittier, CA, pp. 239–247 (1998).

M.S. Baram, *Alternatives to Regulation: Managing Risks to Health, Safety and the Environment,* Lexington Books, Lexington, MA (1982).

V. Beck, et al., *Fire Safety and Engineering Project Report,* The Warren Center for Advanced Engineering, Sydney, Australia (1989).

V.R. Beck, et al., "Microeconomic Reform: Fire Regulation," *National Building Fire Safety Systems Code,* in Building Regulation Review Task Force, Department of Industry Technology and Commerce, Canberra, Australia, p. 165 (1991).

V.M. Brannigan and A. Kilpatrick, "Performance-Based Codes: Reengineering the Regulatory System," in *Proceedings of the International Conference on Performance-Based Codes and Fire Safety Design Methods,* SFPE, Bethesda, MD, pp. 139–149 (1997).

H.S. Brown and R.L. Goble, "The Role of Scientists in Risk Assessment," *Risk: Issues in Health and Safety,* 1, 4, pp. 283–311 (1990).

D. Canter (ed.), *Fires and Human Behavior,* 2nd ed., Fulton Publishers, Ltd., London (1990).

R.E. Cheit, *Setting Safety Standards: Regulation in the Public and Private Sectors,* University of California Press, Berkeley, CA (1990).

V.T. Covello et al. (eds.), *The Analysis of Actual versus Perceived Risks,* Plenum Press, New York (1983).

V.T. Covello et al. (eds.), *Risk Evaluation and Management,* Plenum Press, New York (1986).

V.T. Covello and J. Mumpower, "Risk Analysis and Risk Management: A Historical Perspective," in *Risk Evaluation and Management* (V.T. Covello et al., eds.), Plenum Press, New York, pp. 519–540 (1986).

V.T. Covello and M.W. Merkhofer, *Risk Assessment Methods: Approaches for Assessing Health & Environmental Risks,* Plenum Press, New York (1993).

E. Crouch and R. Wilson, *Risk/Benefit Analysis,* Ballinger Publishing Company, Cambridge, MA (1982).

R.E. Donnelly, "Implications of De Minimis Risk Concepts for OSHA," in *De Minimis Risk* (C. Whipple, ed.), Plenum Press, NY, pp. 95–99 (1987).

R.F. Fahy, "Building Fire Simulation Model. An Overview," *Fire Safety Journal,* 9, pp. 189–203 (1985).

A. Finkel, "Comparing Risks Thoughtfully," *Risk: Health, Safety & Environment,* 7, 4, pp. 325–359 (1996).

B. Fischhoff, "Acceptable Risk: A Conceptual Proposal," *Risk: Health, Safety & Environment,* 5, 1, pp. 1–28 (1994).

B. Fischhoff, "Public Values in Risk Research," *The Annals of the American Academy of Political and Social Science,* 545, pp. 75–84 (1996).

B. Fischhoff, "Ranking Risks," *Risk: Health, Safety & Environment,* 6, 3, pp. 191–202 (1996).

B. Fischhoff, P. Slovic, and S. Lichtenstein, "Lay Foibles and Expert Fables in Judgements About Risk," *The American Statistician,* 36, 3, pp. 240–255 (1982).

R.W. Fitzgerald, "Thoughts on Building Codes, Design Standards, and Performance Evaluations for Fire," *Proceedings of the First International Conference on Performance-Based Codes and Fire Safety Design Methods,* SFPE, Bethesda, MD, pp. 127–137 (1997).

W. Freudenburg, "Perceived Risk, Real Risk: Social Science and the Art of PRA," *Science,* 242, pp. 44–49 (1988).

S.O. Funtowicz and J.R. Ravetz, "Three Types of Risk Assessment," in *Risk Analysis in the Private Sector* (Whipple and Covello, eds.), Plenum Press, New York (1985).

B.J. Garrick and W.C. Gekler (eds.), *The Analysis, Communication and Perception of Risk,* Plenum Press, New York (1991).

T.S. Glickman and M. Gough (eds.), *Readings in Risk,* Resources for the Future, Washington, DC (1990).

J.D. Graham, et al. "Science and Analysis: Roles in Risk and Decision Making," in *Risk Evaluation and Management* (V.T. Covello et al., eds.), Plenum Press, New York, pp. 503–518 (1986).

J.R. Hall, Jr., "Societal Issues in Performance-Based Fire Safety Design," in *Proceedings of the Workshop on Performance-Based Fire Safety Design, the Society of Fire Protection Engineers and the Centre for Environmental and Risk Engineering,* Victoria University of Technology, Melbourne, Australia, (1997).

J.R. Hall, Jr., "Using Data for Public Education Decision Making," *Fire Protection Handbook,* 18th ed., NFPA, Quincy, MA pp. 2-12–2-20 (1997a).

J.R. Hall, Jr., and A.E. Cote, "America's Fire Problem and Fire Protection," *Fire Protection Handbook,* 18th ed., NFPA, Quincy, MA, pp. 1-3–1-25 (1997).

Y. Hasemi, "Wooden 3-Storey Apartment Building Shake and Burn Test Report," Building Research Institute, Tsukuba, Japan (1992).

House Committee on Science, *Unlocking Our Future: Toward A New National Science Policy,* Washington, DC (1998).

Health and Safety Executive, *The Tolerability of Risk from Nuclear Power Stations,* HMSO, London (1988).

C.R. Jennings, "Socioeconomic Characteristics and Their Relationship to Fire Incidence: A Review of the Literature," *Fire Technology,* 35, 1, pp. 7–34 (1999).

D. Kahneman and A. Tversky, "The Psychology of Preferences," *Scientific American,* 246, 1, pp. 162–173 (1982).

R.E. Kasperson, "Acceptability of Human Risk," *Environmental Health Perspectives,* 52, pp. 15–20 (1983).

R.E. Kasperson, "Six Propositions for Public Participation and Their Relevance for Risk Communication," *Risk Analysis,* 6, 3, pp. 275–281 (1986).

R.E. Kasperson, "The Social Amplification of Risk: Progress in Developing an Integrative Framework," *Social Theories of Risk* (Krimsky and Golding, eds.), Praeger, Westport, CT, pp. 153–178 (1992).

R.E. Kasperson and J.X. Kasperson, "Determining the Acceptability of Risk: Ethical and Policy Issues," in *Proceedings of Risk: A Symposium on the Assessment and Perception of Risk to Human Health in Canada* (J.T. Rogers and D.V. Bates, eds.), Royal Society of Canada (1982).

R. Kasperson et al., "The Social Amplification of Risk: A Conceptual Framework," *Risk Analysis,* 8, pp. 177–187 (1988).

R.E. Kasperson et al., *Corporate Management of Health & Safety Hazards: A Comparison of Current Practice,* Westview Press, Boulder, CO (1988a).

R.E. Kasperson and I. Palmlund, "Evaluating Risk Communication," in *Effective Risk Communication* (V.T. Covello et al., eds.), Plenum Press, New York, pp. 143–158 (1989).

R.E. Kasperson and J.X. Kasperson, "Hidden Hazards," in *Acceptable Evidence: Science and Values in Hazard Management* (D.C. Mayo and R. Hollander, eds.), Oxford University Press, New York, pp. 9–28 (1990).

R.E. Kasperson and P.J.M. Stallen (eds.), *Communicating Risk to the Public,* Kluwer Academic Publishers, Dordrecht, Netherlands (1991).

R. Kasperson, D. Golding, and S. Tuler, "Social Distrust as a Factor in Siting Hazardous Facilities and Communicating Risks," *Journal of Social Issues,* 48, 4, pp. 167–187 (1992).

R. Kates et al., *Perilous Progress: Managing the Hazards of Technology,* Westview Press, Boulder, CO (1985).

R.L. Keeney, *Value Focused Thinking: A Path to Creative Decision Making,* Harvard University Press, Cambridge, MA (1992).

R.L. Keeney, "The Role of Values in Risk Management," *The Annals of the American Academy of Political and Social Science,* 545, pp. 126–134 (1996).

P.R. Kleindorfer, H.C. Kunreuther, and P.J.H. Schoemaker, *Decision Sciences: An Integrative Perspective,* Cambridge University Press, New York (1993).

M. Kobayashi, "A Methodology for Evaluating Fire/Life Safety Planning of Tall Buildings," in "Evaluation of Fire Safety in Buildings," *Occasional Report of Japanese Association of Fire Science and Engineering* (Nihon Kasaigakka, ed.), 3, pp. 204–214 (1979).

S. Krimsky and D. Golding (eds.), *Social Theories of Risk,* Praeger, Westport, CT (1992).

H. Kunreuther and P. Slovic, "Science, Values, and Risk," in special edition of *The Annals of the American Academy of Political and Social Science* (Kunreuther and Slovic, eds.), 545, pp. 116–125 (1996).

W. Kunreuther and P. Slovic (eds.), "Challenges in Risk Assessment and Risk Management," in special edition of *The Annals of The American Academy of Political and Social Science,* 545 (1996a).

T.T. Lie, "Safety Factors for Fire Loads," *Canadian Journal of Civil Engineering,* 6, pp. 617–628 (1979).

W-C.T. Ling and R.B. Williamson, "Using Fire Tests for Quantitative Risk Analysis," in *ASTM Special Publication STP 762* (G.T. Castino and T.Z. Harmathy, eds.), American Society for Testing and Materials, Philadelphia (1982).

D. Litai, *A Risk Comparison Methodology for the Assessment of Acceptable Risk,* Ph.D. Dissertation, MIT, Cambridge, MA (1980).

D. Litai, D.D. Lanning, and N. Rasmussen, "The Public Perception of Risk," in *The Analysis of Actual Versus Perceived Risks* (V.T. Covello, et al., eds.), Plenum Press, New York, pp. 213–224 (1983).

D.A. Lucht (ed.), *Proceedings of the Conference on Fire Safety Design in the 21st Century,* Worcester, MA (1991).

B.D. McDowell and A.C. Lemer, *Uses of Risk Analysis to Achieve Balanced Safety in Building Design and Operations,* National Academy Press, Washington, DC (1991).

B.J. Meacham, "Risk-Informed Decision-Making in Performance-Based Building and Fire Code Development," in *Proceedings of the NFPRF Fire Risk and Hazard Assessment Research Application Symposium,* NFPRF, Quincy, MA, pp. 62–77 (1998).

B.J. Meacham, "Concepts of a Performance-Based Building Regulatory System for the United States," *NIST GCR 98-762,* NIST, Gaithersburg, MD (1998b).

B.J. Meacham, "The Evolution of Performance-Based Codes and Fire Safety Design Methods," *NIST GCR 98-763,* NIST, Gaithersburg, MD (1998c).

B.J. Meacham, "Integrating Human Factors Issues into Engineered Fire Safety Design," in *Proceedings of the 1st International Symposium on Human Behavior in Fire,* University of Ulster, Northern Ireland, pp. 47–58 (1998d).

B.J. Meacham, "Integrating Human Behavior and Response Issues into Fire Safety Management of Facilities," *Facilities,* 17, 9/10, pp. 303–312 (1999b).

B.J. Meacham, "Integrating Human Factors Issues into Engineered Fire Safety Design," *Fire and Materials,* 23, pp. 273–279 (1999c).

M. Mordarres and Y-S. Hu, "Reliability," *SFPE Handbook of Fire Protection Engineering,* SFPE/NFPA, Quincy, MA (1995).

M.G. Morgan, "Choosing and Managing Technology-Induced Risk," in *Readings in Risk* (Glickman and Gough, eds.), Resources for the Future, Washington, DC, pp. 17–28 (1990).

NFPA, *Fire Protection Handbook,* 18th ed., Quincy, MA (1997).

NFPA 101A, *Guide on Alternative Approaches to Life Safety,* National Fire Protection Association, Quincy, MA (1995).

NIST "1994 Northridge Earthquake: Performance of Structures, Lifelines and Fire Protection Systems," *NIST Special Publication 862* (ICSSC TR14), NIST, Gaithersburg, MD (1994).

NKB "Performance Requirements for Fire Safety and Technical Guide for Verification by Calculation," *NKB Committee and Work Reports, 1994:07 E,* Nordic Committee on Building Regulations (NKB), Fire Safety Committee, Helsinki, Finland (1995).

K.A. Notarianni and P. Fischbeck, "A Methodology for the Quantitative Treatment of Variability and Uncertainty in Performance-Based Engineering Analysis and/or Decision Analysis with a Case Study in Residential Fire Sprinklers," in *Proceedings of the Second International Conference on Performance-Based Codes and Fire Safety Design Methods,* ICBO and SFPE, Whittier, CA, pp. 297–311 (1998).

NRC *Risk Assessment in the Federal Government: Managing the Process,* National Research Council, National Academy Press, Washington, DC (1983).

NRC *Improving Risk Communication,* (J.F. Ahearne et al., eds.), National Research Council, National Academy Press, Washington, DC (1989).

NRC *Science and Judgment in Risk Assessment,* National Academy Press, Washington, DC (1994).

T. O'Riordan, "Approaches to Regulation," in *Regulating Industrial Risks—Science, Hazards and Public Protection* (H. Otway and M. Peltu, eds.), Butterworths, London, pp. 20–39 (1985).

H. Otway "Regulation and Risk Analysis," in *Regulating Industrial Risks—Science, Hazards and Public Protection* (H. Otway and M. Peltu, eds.), Butterworths, London, pp. 1–19 (1985).

H. Otway and D. Von Winterfeldt, "Beyond Acceptable Risk: On Social Acceptability of Technologies," *Policy Sciences,* 14, pp. 247–256 (1982).

H. Otway and M. Peltu (eds.), *Regulating Industrial Risks—Science, Hazards and Public Protection,* Butterworths, London (1985).

H. Otway and B. Wynne, "Risk Communication: Paradigm and Paradox," *Risk Analysis,* 9, 2, pp. 141–145 (1989).

M.E. Pate, "Acceptable Decision Processes and Acceptable Risks in Public Sector Regulations," *IEEE Transactions on Systems, Man, and Cybernetics,* SMC-13, 3, pp. 113–124 (1983).

C. Perrow, *Normal Accidents,* Basic Books, New York (1984).

N. Pidgeon et al., "Risk Perception," *Risk: Analysis, Perception and Management,* Report of the Royal Society, London, pp. 89–134 (1992).

A. Plough and S. Krimsky, "The Emergence of Risk Communication Studies: Social and Political Context," in *Readings in Risk*

(Glickman and Gough, eds.), Resources for the Future, Washington, DC, pp. 223–232 (1990).

M. Pollak, "Public Participation," in *Regulating Industrial Risks—Science, Hazards and Public Protection* (H. Otway and M. Peltu, eds.), Butterworths, London, pp. 76–93 (1985).

R.A. Pollak, "Government Risk Regulation," *The Annals of the American Academy of Political and Social Science,* 545, pp. 25–34 (1996).

D.J. Rasbash, "Criteria for Acceptability for Use with Quantitative Approaches to Fire Safety," *Fire Safety Journal,* 8, pp. 141–158 (1984).

N.C. Rassmussen, *Reactor Safety Study: WASH-1400,* U.S. Nuclear Regulatory Commission, Washington, DC (1975).

O. Renn, "Concepts of Risk: A Classification," in *Social Theories of Risk* (Krimsky and Golding, eds.), Praeger, Westport, CT, pp. 54–79 (1992).

O. Renn and D. Levine, "Credibility and Trust in Risk Communication," in *Communicating Risks to the Public* (R.E. Kasperson and P.M. Stallon, eds.), Kluwer, Dordrecht, Netherlands, pp. 175–218 (1991).

W.D. Rowe, *Anatomy of Risk,* John Wiley and Sons, New York (1977).

W.D. Rowe, "Understanding Uncertainty," *Risk Analysis,* 14, 5, pp. 743–750 (1994).

SFPE *Proceedings of the 1998 International Conference on Performance-Based Codes and Fire Safety Design Methods,* SFPE and ICBO, Bethesda, MD (1998).

T.J. Shields, *A Fire Safety Evaluation Points Scheme for Dwellings,* Ph.D. Dissertation, University of Ulster, Jordanstown, Northern Ireland (1990).

T.J. Shields (ed.), *Proceedings of the 1st International Symposium on Human Behaviour in Fire,* University of Ulster, Antrim, Northern Ireland (1998).

N. Siu and G. Apostolakis, "Uncertain Data and Expert Opinions in the Assessment of the Unavailability of Fire Suppression Systems," *Fire Technology,* 24, pp. 138–162 (1988).

P. Slovic, "Perception of Risk: Reflections on the Psychometric Paradigm," in *Social Theories of Risk* (Krimsky and Golding, eds.), Praeger, Westport, CT (1992).

M.B. Spangler, "A Summary Perspective on NRC's Implicit and Explicit Use of De Minimis Risk Concepts in Regulating for Radiological Protection in the Nuclear Fuel Cycle," in *DeMininis Risk* (C. Whipple, ed.), Plenum Press, New York, pp. 111–143 (1988).

C. Starr, "Societal Benefit vs. Technological Risk," *Science,* 165, pp. 1232–1238 (1969).

C. Starr, "Risk Management, Assessment, and Acceptability," in *Uncertainty in Risk Assessment, Risk Management, and Decision Making* (V.T. Covello et al., eds.), Plenum Press, New York, pp. 63–70 (1986).

I.R. Thomas, I.D. Bennetts, P. Dayawansa, D.J. Proe, and R.R. Lewis, "Fire Tests of the 140 William Street Office Building," Report No. BHPR/ENG/R/92/043/SG2C, BHP Research—Melbourne Laboratories, Australia, Feb. 1992.

W.K. Viscusi, *Regulating Consumer Product Safety,* American Enterprise Institute for Public Policy, Washington, DC (1984).

Warren Centre "Project Report" and "Technical Papers, Books 1 and 2," Fire Safety and Engineering Project, The Warren Centre for Advanced Engineering, the University of Sydney, Australia (1989).

J.M. Watts, Jr., "Dealing With Uncertainty: Some Applications in Fire Protection Engineering," *Fire Safety Journal,* 11, pp. 127–134 (1986).

C. Whipple (ed.), *De Minimis Risk,* Plenum Press, New York (1987).

C.A. Williams and R.M. Heins, *Risk Management and Insurance,* 4th ed., McGraw-Hill, New York (1981).

R. Wilson, "Analyzing the Daily Risks of Life," in *Readings in Risk* (Glickman and Gough, eds.), Resources for the Future, Washington, DC, pp. 55–61 (1990).

A. Wolski, *Addressing Building Fire Safety as an Acceptable Risk Problem: A Guide for Developing Performance-Based Fire Safety Regulations,* Masters Thesis, Worcester Polytechnic Institute, Worcester, MA (1999).

A. Wolski, N. Dembsey, and B. Meacham, "Application of Acceptable Risk Principles to Performance-Based Building and Fire Safety Code Development," in *Proceedings of the 2nd International Conference on Performance-Based Codes and Fire Safety Design Methods,* ICBO and SFPE, Whittier, CA (1998).

A. Wolski, N. Dembsey, and B. Meacham, "Accommodating Perceptions of Risk in Performance-Based Building Fire Safety Code Development," *Fire Safety Journal,* 34, 3, pp. 297–310 (2000).

B. Wynne, "Risk and Social Learning: Reification to Engagement," in *Social Theories of Risk* (Krimsky and Golding, eds.), Praeger, Westport, CT, pp. 275–300 (1992).

D. Yung and G.V. Hadjisophocleous, "The Use of the NRCC Risk-Cost Assessment Model to Apply for Code Changes for 3-Storey Apartment Buildings in Australia," in *Proceedings of the Symposium on Computer Applications in Fire Protection Engineering,* Worcester, MA, pp. 57–62 (1993).

R.J. Zeckhauser and W.K. Viscusi, "The Risk Management Dilemma," in special edition of *The Annals of the American Academy of Political and Social Science* (Kunreuther and Slovic, eds.), 545, pp. 144–154 (1996).

CHAPTER 13

Quantitative Risk Assessment in Chemical Process Industries

Thomas F. Barry

Introduction

Fire and explosion risk, which can involve property damage, business interruptions, life safety, environmental issues, corporate image, and future profitability, presents a major threat to corporate goals and survival.

Quantitative fire and explosion risk assessment offers the capability of being able to identify weak links in loss prevention and protection systems before an accident actually occurs. It also affords the capability of optimizing loss control investments with the greatest allocation going to the area giving rise to the highest risk.

Fire and explosion risk assessment is a function of two parameters: (1) the frequency of occurrence of an undesired loss event, and (2) the consequences resulting from its occurrence.

Risk = Frequency of the Event $\times$ Expected Consequences

This means that in order to reduce the risks from a defined fire or explosion, one can either seek to reduce the frequency of occurrence of the undesired event, the consequences of its occurrence, or both.

The application of quantitative risk assessment (QRA) techniques enforces a disciplined, analytical thinking approach to fire risk problems and provides quantification of key fire safety issues to aid management understanding and decisions. Primary reasons companies utilize risk assessment as decision support include

1. As part of the engineering design process, to reduce risk to acceptable in-house safety standards. Design risks are identified and prioritized to optimize safety investment options.
2. To evaluate code equivalency or the relative risk difference between loss prevention or protection design options. Relative risk reduction assessment is used as an effective cost–benefit analysis tool for establishing the optimum balance between prevention, protection, and emergency response.
3. To demonstrate to the community or to an insurance company that, while the hazard may be large, the risk is small. These studies quantify the probability of the occurrence of extremely severe accidents.
4. To predict gas dispersion, fire radiant heat, and explosion overpressure effect zones, for use in emergency response planning and training.
5. The company is required to develop quantitative risk assessment information by federal, state, or local government agencies.

Environmental Protection Agency (EPA) regulations related to the provisions of the 1990 Clean Air Act Amendments (CAAA) may require facilities with threshold amounts of hazardous materials to develop risk assessment and risk management programs. The prevention (reduction of loss event probabilities) component of the EPA CAAA relates to the Occupational Safety and Health Administration's (OSHA) Process Safety Management (PSM) regulation 1910.119, which focuses on process hazard analysis (PHA) and the documentation, implementation, and monitoring of management loss control programs.

In addition, quantitative risk assessment is increasingly being required by state legislation, such as California's Risk Management and Prevention Program, New Jersey's Toxic Catastrophe Prevention Act, and Delaware's Extremely Hazardous Substances Risk Management Act. The specific objectives of these regulations vary, but the emphasis is on risk reduction and emergency planning.

The hazardous materials specified by EPA, OSHA, and state regulations include many flammable and explo-

Thomas F. Barry, P.E., is director of Risk and Reliability Services at HSB Professional Loss Control, Kingston, TN. He has performed and managed numerous quantitative risk assessments (QRAs) of industrial process hazards at government, chemical, and oil and gas facilities. Tom has a masters degree in fire protection engineering from Worcester Polytechnic Institute.

sive materials. As a result, fire protection engineers will become involved as part of the risk assessment teams responsible for hazard analysis, management programs, and regulatory compliance.

The areas in which fire risk assessment is finding application are rapidly expanding. The credibility of these risk assessment studies in the view of the management decision makers is highly dependent on the personnel, procedures, documentation, and quality assurance controls integrated into the process. The risk assessment process can be broken down into systematic steps, as presented in Figure 5-13.1. The focus of this chapter is to familiarize the reader with risk assessment methods by providing an overview of each of the steps and a discussion of general risk assessment techniques.

Quantitative risk assessment is both an interesting and complex subject. The references listed at the end will supplement and expand on the material summarized in this chapter.

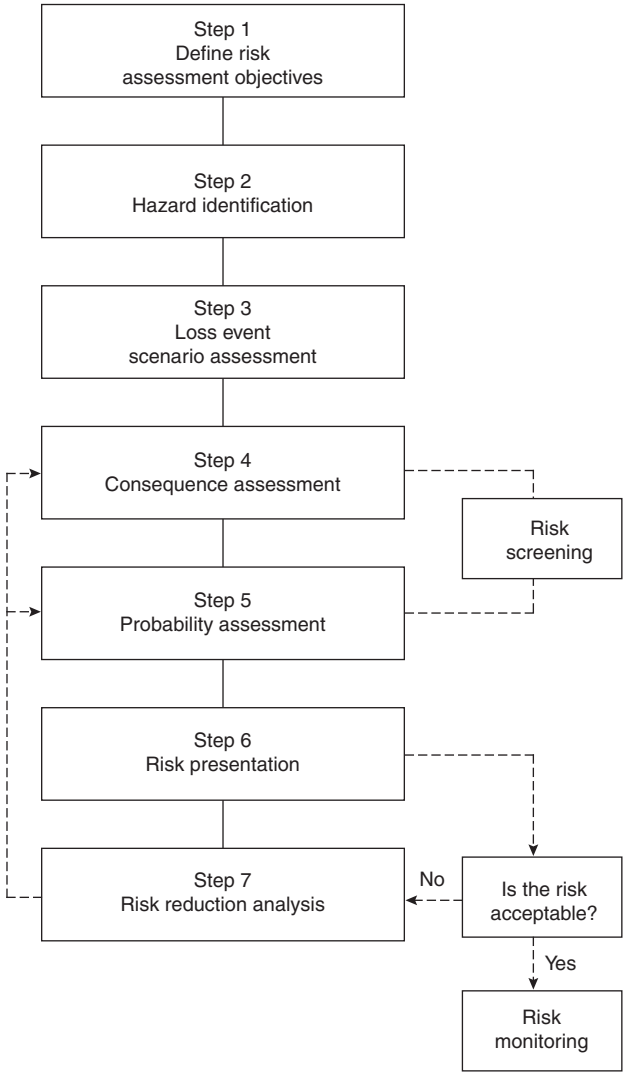

Figure 5-13.1. ***Fire and explosion risk assessment steps.***

The two objectives of this chapter are

1. To familiarize readers with the general process of fire and explosion risk assessment
2. To provide a basis for the readers' future development and involvement in the areas of risk assessment by providing procedural steps and associated references

Step 1: Define Risk Assessment Objectives

Risk assessment is the process by which the results of a risk analysis (i.e., quantitative risk estimates) are used to support risk management decisions through comparison with acceptable risk levels or prioritization of risk reduction strategies. The key term here is *decision support.*

Prior to the start of risk assessment projects it is imperative to have a clear project scope and to explicitly state and agree upon project objectives.

1. What is the decision?
   a. Plant siting
   b. Protection options
   c. Regulatory compliance
2. What is the focus of the assessment?
   a. Casualties or injuries
   b. Property damage
   c. Loss of production or delivery
   d. Health risk to employees, public
   e. Environmental damage
   f. Legal liabilities
3. What is the level of detail?
   a. Relative application of risk assessment
   b. Absolute application of risk assessment
4. What are the acceptable risk limits?
   a. Hazard severity acceptance limits
   b. Event likelihood acceptance limits
   c. Management's risk tolerance profile
5. What are the resources required?
   a. Involvement of plant personnel
   b. Use of experienced risk assessment teams
   c. Quality control procedures and review
   d. Project scheduling and funding

Ten major issues that should be addressed prior to conducting fire and explosion risk assessments are

1. The type of risk profile presentation format that will be used to aid management decision making
2. Establishing management's acceptable risk criteria for risk comparisons
3. Methods for determining the absolute or relative risk levels
4. Models or algorithms for determining the potential sizes of toxic or flammable vapor clouds, overpressure zones from explosions, fire intensities, and so on
5. The weather conditions that will be applied in gas dispersion consequence models
6. Domino effects caused by the initial failure incident
7. Appropriate sources of failure rate and reliability data and selection methods

8. Methods for incorporating loss event time relationships into event tree scenarios
9. Incorporating human error and management factors into failure probability ranges
10. Procedures for conducting uncertainty (sensitivity) analysis and quality control

Step 2: Hazard Identification

Hazard identification is the foundation for conducting credible risk assessment studies. Fire and explosion hazards that are not properly identified and defined in terms of cause and consequences cannot be properly addressed within the risk assessment framework.

The results of the hazard identification should include

1. Identification of the physical and chemical properties of materials processed, stored, or transported on site that can harm employees, the public, property, environment, or other selected risk targets
2. Identification of weaknesses in the design, operation, and protection of facilities that could lead to toxic exposures, fires, or explosions
3. Evaluation of the significance of potential hazardous events associated with a process or activity to allow categorization of the consequences and ranking the risk

The tasks associated with step 2 include

1. Gathering technical information
   a. Plant and process data
   b. Material properties
2. Gathering historical accident data
   a. Facility tour and process review
   b. Plant personnel interviews
   c. Process safety management documentation evaluation
3. Documenting the hazard evaluation(s)
   a. Use of a selected hazard evaluation method (e.g., PHA, HAZOP, FMEA, ETA)

Plant and Process Data

The fire protection risk analyst must understand plant processes, their interdependence, and the inventories and conditions of materials. Plant and process data must describe the plant as it actually operates, which may be different from the original design. The following examples of risk assessment information required may serve as a checklist:

- Material information [material safety data sheets (MSDS)]
- General process chemistry (including side reactions under normal and abnormal conditions)
- Process flow diagrams (including process description and operating parameters such as flow rates, pressures, temperatures, and stream compositions)
- Process design bases (including external events)
- Process utilities (cooling, steam, electricity, instrument, air, and utility backup systems)
- Waste treatment, pollution control systems
- Equipment specifications (including materials of construction)
- Equipment detail drawings
- Piping and instrument diagrams (P&IDs, including utilities and pressure relief systems)
- Plant layout drawings (plant and immediate surroundings, including elevations and potential ignition sources)
- Fire water and drainage system drawings
- Process and equipment modifications
- Control logic (e.g., instrument loopsheets, relay logic diagrams)
- Operating instructions
- Operating philosophy (storage inventory levels, operating schedule, manning, startup and shutdown, operator training, safety policy)
- Protection systems diagrams (fire protection, emergency relief, interlock, and alarm systems; design basis should also be included)
- Historical systems failure incident and maintenance records
- Maintenance philosophy and programs
- Emergency response procedures
- Past hazard identification information (HAZOPs, audits, surveys, etc.)
- Replacement cost estimates (structures, equipment, inventory)
- Production dependency
- Employee distribution by shift in process area and on plant site
- Weather data (e.g., wind rose) and off-site population distribution
- Operational and loss incident history involving fire and explosions
- Process safety management (PSM) documentation

Material Properties

Accurate information concerning material properties, inventories, processing, and storage conditions is required to perform hazard evaluations. Detailed information is needed on both the physical and chemical properties of materials. Some of these data can be obtained from the MSDS. A nonexclusive list of properties includes

1. Thermodynamic data (including vapor pressure, boiling point, freezing point, critical temperature and pressure, specific and latent heats, heats of combustion)
2. Flammability
3. Dust explosion data (for samples reflecting process conditions)
4. Industrial hygiene and toxicity data
5. Shock sensitivity, thermal analysis data from differential scanning calorimetry, accelerating rate calorimetry, vent sizing package
6. Miscellaneous properties (e.g., peroxide-forming materials, susceptibility to spontaneous ignition, ability to hold static charge, effect of contaminants)

Much of the data available in MSDS or other publications are at atmospheric temperature and pressure. Experimental data appropriate to process conditions will sometimes be needed.

Dust explosion data for explosion venting calculations are presented in NFPA 68, *Guide for Venting of Deflagrations,* which includes additional references. A considerable amount of dust explosion data can be obtained from various U.S. Bureau of Mines and National Fire Protection Association (NFPA) publications.

Historical Accident Data

An important part of fire and explosion hazard identification and risk screening is a review of the history of loss incidents similar to the hazard being analyzed. A review of the available information on loss incidents or the available loss trending data provides

1. A relative breakdown of consequential effects, in terms of type of fire or explosion or in terms of resulting damage (can generally be used for estimating conditional event probabilities)
2. Identification of representative or dominant failure modes (equipment related, human error, system(s) related) that have led to fire or explosion accidents
3. Identification of ignition sources and fire propagation contributing factors
4. Information concerning the duration of the fire and the general effect of loss mitigation factors
5. Information to support the generation of credible fire and explosion incident loss scenarios and the structuring of event tree analysis

Databases are the information foundation of hazard analysis. One of the most effective ways to determine whether a system has a fire or explosion potential is to review past loss incident records. Accident data from specific plant operations (if available) is usually the best source and probably more accurate for specific equipment and operations, since the data reflect the operating and maintenance practices of the specific facility. Fire records of NFPA and American Petroleum Institute (API) provide fire loss incident data for a number of processes, plants, and equipment. Federal and state agencies also collect a wide variety of data related to safety and loss prevention issues. A few loss incident data sources are listed in Table 5-13.1.

These kinds of events are sufficiently serious to be reported fairly widely in publicly available sources (e.g., regulatory agencies, research organizations, the media). Data sources can generally be grouped into three categories

1. Failure mechanisms and causes
2. Consequence effects (e.g., downwind gas concentrations, fire radiation levels, explosion overpressures, etc.)
3. Generic frequency categorization of certain types of incidents

Data sources in the first two categories may be helpful in constructing a fault or event tree model or in understanding the consequences of a specific incident. However, they usually do not provide information on the frequency of incidents. Data sources in the third category provide generic frequency information, but should be used with caution. In most cases, frequency data derived from incident reports may not be applicable to the specific risk assessment being conducted. Historical databases are rarely complete. Minor incidents, which could have escalated into major incidents, are sometimes not reported and therefore may not be included in the data. Consequently, the fire and explosion risk analyst must examine sources of data very carefully to determine applicability.

Table 5-13.1 ***Some Sources of Information for Use in Fire Risk Assessments***

Source	Nature of Information
NFPA (National Fire Protection Association)	Fire Incident Data: FIDO (Fire Incident Data Organization) NFIRS (National Fire Incident Reporting System)
DOT (Department of Transportation) NTSB (National Transportation Safety Board), U.S. DOT, Washington, DC	Annual reports on hazardous materials transportation accidents Accident reports: A detailed report is produced for transportation accidents involving hazardous materials Hazardous materials accident spill maps: These maps show the location of the spill, any airborne plume, site of fatalities and/or injured people, at one or more times after the start of the incident
API (American Petroleum Institute) Washington, DC	Annual summaries of petroleum industry loss incidents
Association of American Railroads, Federal Railroad Administration	"Railroad Facts" (annual editions) Accident/incident bulletins (annual)
EPA (Environmental Protection Agency)	Reports on various aspects of hazardous material release incidents
U.S. Department of Transportation, Research and Special Programs Administration, Office of Pipeline Safety Washington, DC	Pipeline leak reports for onshore gas transmission and gathering lines, and liquid lines

Hazard Evaluation

Hazard evaluation techniques include[1]

- Safety review
- Checklist analysis
- Relative ranking indexes
- Preliminary hazard analysis
- "What-if" analysis
- "What-if" checklist analysis
- HAZOP analysis
- FMEA
- Fault tree analysis
- Event tree analysis
- Cause–consequence analysis
- Human reliability analysis

Each technique has specific application benefits, limitations, resource needs (e.g., manpower, time, budget), and documentation requirements. It would be impossible in this chapter to describe each technique. An excellent reference, which addresses those techniques in detail and provides illustrative examples, is the Center for Chemical Process Safety's (CCPS) *Guidelines for Hazard Evaluation Procedures with Examples*.[2]

Documenting Hazard Evaluation

The synonym for hazard evaluation presently in wide use is process hazard analysis (PHA), as this term is used in OSHA's Process Safety Management (PSM) regulation 1910.119.[3]

The OSHA PSM regulation requires an analysis that identifies and evaluates hazards involved in a process, and must include

1. Use of one or more of the following to perform a hazard analysis:
   a. Checklists
   b. "What-if" checklist
   c. Hazard and operability study (HAZOP)
   d. Failure mode and effects analysis (FMEA)
   e. An appropriate equivalent methodology
2. The hazard analysis must address
   a. Process hazards
   b. Engineering and administrative controls
   c. Consequences of failure of controls
   d. Consequence analysis of effects on employees
3. Analysis performance by a team with engineering and operations expertise, including at least one person with knowledge specific to the process
4. Establishment by employer of a system for documenting findings and actions taken, then communicating them to employees
5. Review and update hazard analysis at least once every five years.

It should be noted that OSHA's definition of process includes the storage, handling, processing, and transportation of hazardous chemicals, and flammable and explosive materials.

A broad evaluation of hazards should include the following four general techniques:

1. Safety reviews
2. Checklists
3. Preliminary hazard analysis
4. Relative ranking indexes

However, a detailed analysis of the wide range of hazards during design and operational stages should include the following three fundamental methods:

1. "What-if" checklist analysis
2. HAZOP analysis
3. FMEA

Table 5-13.2 provides a general breakdown of some hazard evaluation techniques in terms of their general capability to provide scenario information and ranking of loss events.[2]

Step 3: Loss Event Scenario Development

Structuring credible fire and explosion loss scenarios is an important aspect of the risk assessment process. The primary components that must be evaluated in the fire and explosion loss scenario development are

1. Initiating failure event(s)
2. Intermediate event(s)
3. Incident outcome(s)

Fire exposure is very time dependent. The most widely used technique in the structure of fire scenarios is the event tree logic, which conveys the initiation, propagation, and consequences of potential fire events for probability versus time assessments.

An event tree provides an inductive, forward logic framework that identifies a failure process, such as fire initiation and propagation. It has a major advantage of being able to incorporate time and sequential conditionality into a scenario. In some cases, it may be weak in identifying specific details that contribute to the consequences. In these cases, fault trees are used to supplement the event tree structure and provide detail to the top events leading to the final consequence.

Risk assessment concerning the release of flammable and explosive materials and expected consequences is a major issue for a fire protection engineer when part of a risk assessment team conducting OSHA and EPA regula-

Table 5-13.2 ***Scenario and Ranking Capabilities of Some Hazard Evaluation Techniques***

Hazard Evaluation Technique	Provides Loss Event Scenario Information?	Loss Event Ranking Possible?
Checklists/Safety reviews	No; specific scenarios usually not identified	No
Dow and Mond indexes	Yes, on a unit or a major system basis	Consequence ranking
Preliminary hazard analysis (PHA)	No; specific scenarios usually not identified	Yes
"What-if" and "what-if"/checklist analysis	No; specific scenarios usually not identified	Consequence ranking
HAZOP analysis	Yes	Consequence ranking
FMEA	Yes	Consequence ranking
Fault tree analysis (FTA)	Yes	Frequency ranking
Event tree analysis (ETA)	Yes	Yes
Cause-consequence analysis	Yes	Yes
Human reliability analysis (HRA)	Yes	Frequency ranking

tory compliance projects and evaluation of risk reduction options.

Figure 5-13.2 presents a breakdown of the general event components from accidental release to consequences.

Initiating Failure Event(s)

Initiating failure events generally include one or a combination of the following:

1. Containment failures
2. Human error
3. Ignitions
4. External exposures (i.e., flooding, earthquake, etc.)

From a review of past fires and explosions associated with the accidental release of flammable liquid or gas, the following causes are evident as major causes of containment failure:[4]

1. Rupture of temporary hose
2. Overfilling of tanks
3. Release from drainage and sampling valves
4. Leaks from gaskets and pump seals
5. Leaks from flanged joints and small pipe connections
6. Piping failures
7. Tank rupture
8. Internal tank overpressures

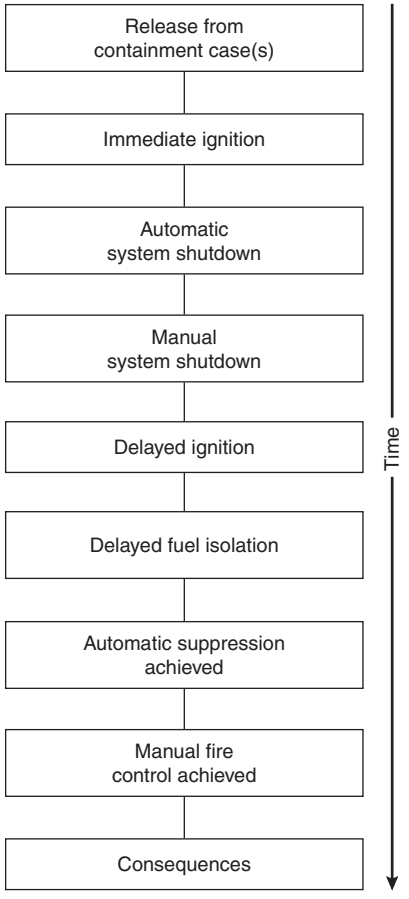

Figure 5-13.2. ***General flammable liquid/gas event sequence.***

Containment failures can be created by equipment malfunctions (mechanical or electrical breakdown, instrumentation failures, etc.), human errors, loss of utilities (electricity or cooling water, etc.), and external events (floods, earthquakes, vandalism, etc.).

Human error analysis [or human reliability analysis (HRA)] generally involves the following evaluations:

1. Describing the characteristics of the personnel, the work environment, and the tasks that are performed
2. Evaluating the human-machine interfaces
3. Performing a task analysis of intended operator functions
4. Performing a human error analysis of intended operator functions to assess human error likelihood

Human error assessment methods and details are related to the process or equipment complexity; the operating environment; human-equipment interface factors; hardware design interfaces for emergency actions; and procedures for operations, maintenance, testing, and training.

Intermediate Event(s)

Intermediate events are events that affect the growth, propagation, and mitigation of the initiating event source. These events are a function of time, which is very important to recognize when addressing the conditional probabilities.

Propagating factors within the fire and explosion development scenario include

1. Process parameter deviations
   a. Pressure
   b. Temperature
   c. Flow rate
   d. Concentration
   e. Phase or state change
2. Material release type
   a. Combustibles
   b. Explosive materials
   c. Toxic materials
   d. Reactive materials
3. Ignition
4. Energy release rate
5. Ventilation or weather effects
6. Operator emergency response errors
7. Domino effects of fires or explosions

Mitigating factors include

1. Safety system responses
   a. Relief valves
   b. Back-up utilities
   c. Back-up components
   d. Back-up systems
2. Barrier effectiveness with time
3. Mitigation system responses
   a. Vents
   b. Dikes
   c. Detection, alarms, shutdown
   d. Fire protection, suppression

4. Control responses and operator responses
   a. Planned
   b. Emergency
5. Contingency operations
   a. Emergency procedures
   b. Personnel safety equipment
   c. Evacuations
   d. Security

Incident Outcome(s)

Potential incidents of primary interest to the fire protection engineer include

1. Radiant heat from a fire
   a. Pool fire
   b. Torch fire
   c. Flash fire
   d. Fire ball [boiling liquid expanding vapor explosion (BLEVE)]
2. Explosion overpressures
   a. Unconfined vapor cloud explosion (UVCE)
   b. Tank or equipment rupture or fragmentation
3. Corrosive smoke or fire products concentration
   a. Toxic gas concentrations

Figure 5-13.3 presents two generic event trees associated with flammable liquid and gas releases developed by The World Bank.[4]

Step 4: Consequence Assessment

Consequence assessment is the estimation of the undesirable result of an accidental fire or explosion exposure to a target, usually measured in terms of health and safety effects to people, loss of property, or business interruption costs.

This assessment involves the evaluation of two issues

1. The susceptibility or vulnerability of people or damage to targets (structures, equipment, etc.) being evaluated in the risk assessment project
2. The rate of development of a hazardous environment (intensity, distance, time) within the boundaries of the predicted hazardous event (gas dispersion, fire, explosion)

When these issues are evaluated quantitatively, they provide estimates of the loss vulnerability to selected targets versus the predicted (distance and time) exposure from the fire or explosion scenario. The analogy within this assessment is one of source → target exposure and vulnerability, as illustrated in Figure 5-13.4. References 4, 5, 6, and 7 provide additional information on this subject.

The steps involved in the quantification of accidental flammable liquid and gas release exposures include

1. Characterizing failure modes
2. Calculating release rates and durations
3. Evaluating ignition scenarios in terms of immediate or delayed ignition times
4. Calculating fire and explosion intensities
5. Estimating the vulnerability to the target(s) of interest
6. Plotting effect distances

Characterizing Failure Modes

Steps 2 and 3 identify failure scenarios. Failure identification, however, must be broken down into potential failure modes to allow quantification of flammable liquid or gas release rates. For example, release from a pipe failure could involve a failure mode stemming from a pinhole leak, to a partial fracture of the pipe, to a full rupture of the pipe. With each failure mode there is associated relative failure probability (e.g., very small leaks are much more likely than major pipe fractures) and a release rate.

To manage failure mode evaluation within a time-constrained risk assessment project, industry risk assessment experts generally focus on three to five failure modes related to the equipment release source being studied.

Figure 5-13.5 provides some general information on some equipment-related failure cases and failure sizes, summarized from The World Bank Technical Paper No. 55, with permission from The World Bank.[4]

Calculating Release Rates and Durations

The release from the failure point may be liquid, gas, or a combination of the two (i.e., two-phase flow). It is beyond the scope of this chapter to discuss the benefits and limitations of various calculation methods (see References 4, 5, and 6 for further information).

When calculating release rates and durations, it is important to document both the physical parameters and assumptions, including

1. The type of release opening (i.e., rectangular or circular, and opening coefficient), the elevation, and size. If using a computer program, these are required input.
2. The effects of containment (diking, curbing) and drainage design reliability.
3. The estimated time to either automatic or manual shutdown to limit the duration of the release. This estimated time will be related to a probability of successful shutdown within the event-free framework.
4. For evaluations involving vapor dispersion (e.g., gas release, liquid pool vaporization), which could lead to flash fires or explosion overpressure effect zones, the topography, selected weather conditions, and any other assumptions (e.g., gas dispersion obstructions or explosion overpressure wave deflections) must be documented.

This step is critical, as the release rate and duration dictate the amount of fuel that can be available in the accident scenario. The methods to actuate the emergency shutdown system (ESS) should be described in detail; this includes gas, flame detection, and emergency isolation valves. The estimated time to shutdown and the residual fuel that can be released following shutdown are important considerations in the justification of the

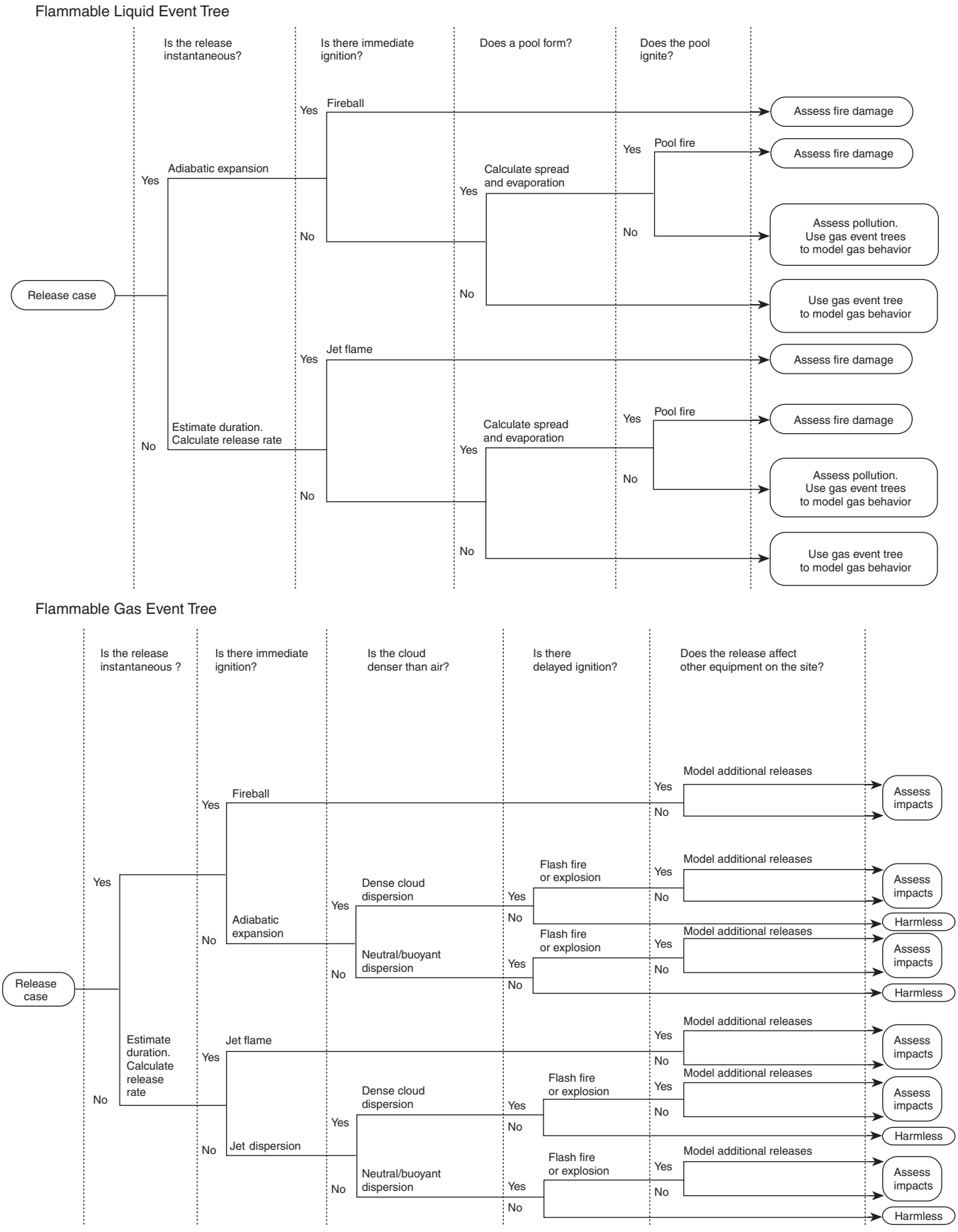

Figure 5-13.3. ***Generic event trees. (Modified from Reference 4.)***

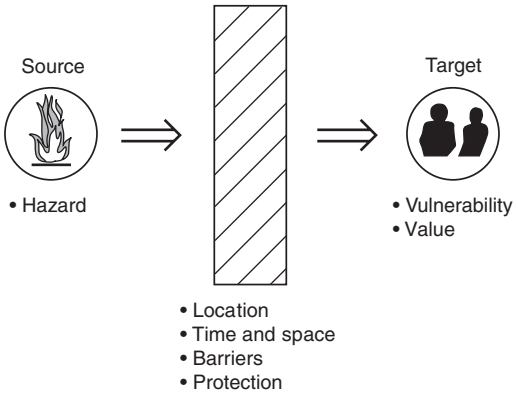

Figure 5-13.4. ***General illustration of source → target concept.***

volume of fuel and the potential duration of exposure if the fuel is ignited.

Isolation of a release: The behavior of a release can be very dependent on its duration. The duration depends on the amount of material available to be released, which in turn depends on the speed and effectiveness of shutdown or isolation. Therefore, isolation can affect the consequences of a release, and it is important to make a realistic estimate of the time required for isolation. This time will depend on the following:

1. *Leak Detection.* It is usual to assume that major ruptures and leaks will be detected quickly, either by process instrumentation or by operators. Smaller leaks may be detected by gas or flame detectors, if installed. The analyst should determine the position, effectiveness, and reliability of such detectors as part of this evaluation.
2. *Shutdown Activation.* The speed of shutdown will depend on whether emergency shutdown actuation is manual or automatic. The response time concerning manual actuation depends on instrumentation and alarm design reliability, operating procedures, and operator emergency response training. Response times of 3 to 15 minutes are typical but must be judged on a plant-specific basis. The analyst should also evaluate the availability and reliability of the shut-down valves and the estimated closing time of the particular emergency shut-down valve design.

Evaluating Ignition Scenarios

Fire and explosion outcomes resulting from the accidental release of flammable liquids or gases can be categorized as follows:[4,5,6,7]

Pool fire: A fire involving a pool of confined or spreading flammable material. This can include both immediate and delayed ignition scenarios creating both near-field and remote damage effects.

Torch fire (or flame jet): A fire extended from a point of release of flammable liquid or gas, which is being discharged under pressure. This is usually associated with an immediate ignition scenario and usually includes near-field damage effects.

BLEVE fireball: BLEVE (boiling liquid expanding vapor explosion) results from the overheating of a pressurized vessel by a primary fire. This overheating raises the internal pressure and weakens the vessel shell, until it bursts open and releases its contents as a large and very intense fireball. This is generally considered a delayed event (8 to 15 minutes of exposure) and can involve both near-field damage effects and remote personnel exposure.

Flash fire: A fire involving the delayed ignition of a dispersed vapor cloud, which does not cause blast damage. That is, the flame speed is not as high as in an unconfined vapor cloud explosion, but the fire spreads quickly throughout the flammable zone of the cloud and is usually associated with near-field damage effects and remote personnel effects.

Unconfined vapor cloud explosion: A release of a large amount of flammable vapors (usually greater than 1 ton), which forms a large vapor cloud and upon delayed ignition explodes, creating an explosion overpressure exposure to the surrounding area, causing both severe near-field damage effects and remote property and personnel exposure.

Calculating Fire and Explosion Intensities

Deterministic models have been developed to support fire and explosion intensities, and more sophisticated models are continuously being refined and validated. Several chapters within this handbook describe fire and explosion modeling methods and available computer programs.

Available consequence computer models generally include the capabilities to[5,7,8]

- Estimate discharge rate of liquid or gas
- Estimate area of liquid pool
- Estimate vaporization rate of liquid pool
- Evaluate toxic vapor dispersion hazards
- Evaluate pool fire radiation hazards
- Evaluate fireball radiation hazards
- Evaluate flame jet hazards
- Evaluate vapor cloud and plume fire hazards
- Evaluate vapor cloud explosion hazards
- Evaluate tank overpressurization rupture and fragmentation hazard
- Evaluate solid and liquid explosion overpressure hazards

In addition, various analytical assessment methods described in this handbook can be applied to consequence and risk assessment studies and include methods for

- Estimating heat release rates and flame heights
- Estimating exposure temperatures from uncontrolled fires using fire plume modeling equations
- Estimating the time to critical damage thresholds for specified targets using heat transfer approaches

Rage tank (ENT conditions)

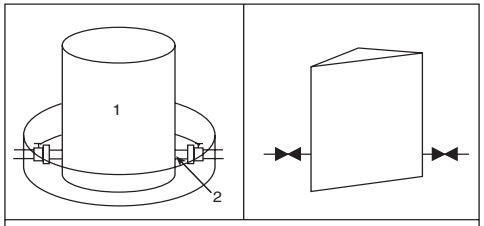

Includes:

All tanks at ambient conditions
(The pipe connections and bund wall are also considered to be part of this component.)

Typical failures	Suggested failure sizes
1. Vessel failure	Total rupture
2. Connection leak	100% and 20% pipe diameter

Storage vessel (pressurized or refrigerated)

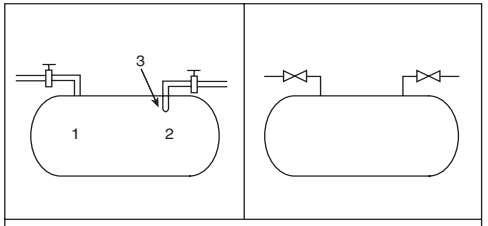

Includes:

Pressurized storage or transport vessels
Refrigerated storage or transport vessels
Buried or non-buried vessels

Typical failures	Suggested failure sizes
1. BLEVE (non-buried case only)	Total rupture (ignited)
2. Rupture	Total rupture
3. Weld failure	100% and 20% pipe diameter

Note: These storage vessels may have bund walls that should be taken into consideration in the analysis.

Flexible connection

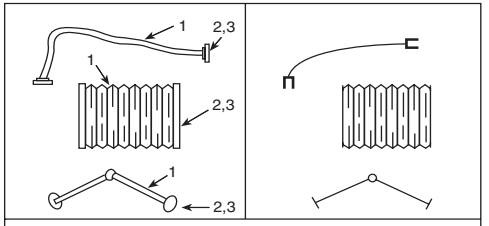

Includes:

Hoses, bellows, articulated arms

Typical failures	Suggested failure sizes
1. Rupture leak	100% and 20% pipe diameter
2. Connection Leak	20% pipe diameter
3. Connection mechanism failure	100% pipe diameter

Pump

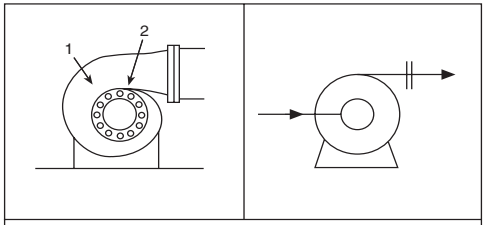

Includes:

Centrifugal pumps, reciprocating pumps

Typical failures	Suggested failure sizes
1. Casing failure	100% and 20% pipe diameter
2. Gland leak	20% pipe diameter

Pressure vessel/process vessel

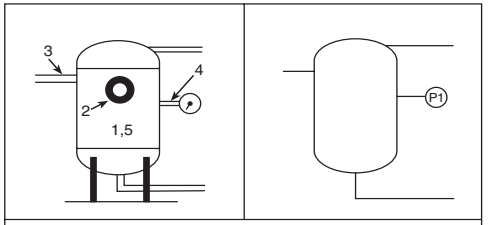

Includes:

Separators, scrubbers, contactors, reactors, heat exchangers, fired heaters, columns, receivers, reboilers

Typical failures	Suggested failure sizes
1. Vessel rupture; vessel leak	Total rupture: 100% pipe diameter of largest pipe
2. Manhole cover leak	20% opening diameter
3. Nozzle failure	100% pipe diameter
4. Instrument line failure	100% and 20% pipe diameter
5. Internal explosion	Total rupture

Pipe

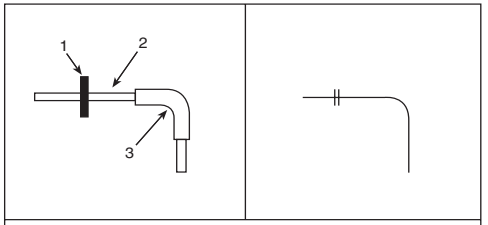

Includes:

Pipes, flanges, welds, elbows

Typical failures	Suggested failure sizes
1. Flange leak	20% pipe diameter
2. Pipe leak	100% and 20% pipe diameter
3. Weld failure	100% and 20% pipe diameter

Figure 5-13.5. ***Suggested failure modes.*** **(*Source:* The World Bank.[4])**

- Estimating the response of existing fire protection or improvement strategies
- Applying the results of fire modeling efforts to support loss estimates and the benefits of recommended fire protection improvements

Target Vulnerability

In evaluating the vulnerability to selected targets, two levels of target vulnerability assessment can be utilized:

1. Use various tables and references that establish generic criteria for damage to people and property from fire and explosion exposures (i.e., radiant heat, explosion overpressures). This level of vulnerability evaluation provides a good first-order review; however, it is weak in terms of specific time relationships. Since time is usually a very uncertain variable, a number of risk assessment projects usually employ generic threshold damage levels.
2. Apply sophisticated heat transfer or structural impact models to support vulnerability assessments where time or specific conditions (design, layout, emergency response) warrant this level of detail, usually termed second-order vulnerability assessment.

Various tables give criteria for damage to people and property from fire, usually expressed in terms of radiation heat intensity. The effect on people is expressed in terms of the likelihood of death and different degrees of injury for different levels of heat radiation. In Table 5-13.3, the radiative incident flux is related to the levels of damage. This table is based on observations of large fires.[4]

Vapor cloud explosion exposures can be generically correlated with the energy of the explosion overpressure. This correlation is used to relate distances to various levels of damage and people exposure. Table 5-13.4 provides a general breakdown of damage threshold levels.[4,7]

Table 5-13.3 ***Damage Caused at Different Incident Levels of Thermal Radiation***

Incident Flux (kW/m^2)	Type of damage caused	
	Damage to Equipment	Exposure to People
37.5	Damage to process equipment	100% lethality in 1 min 1% lethality in 10 s
25.0	Minimum energy to ignite wood at indefinitely long exposure without a flame	100% lethality in 1 min Significant injury in 10 s
12.5	Minimum energy to ignite wood with a flame; melts plastic tubing	1% lethality in 1 min First-degree burns in 10 s
4.0		Causes pain if duration is longer than 20 s, but blistering is unlikely
1.6		Causes no discomfort for long exposure

Table 5-13.4 ***Explosion Overpressure Damage Estimates***

Overpressure (psig)	Characteristic damage	
	To Equipment	To People
2.5–5	Heavy damage to buildings and to process equipment	1% death from lung damage >50% eardrum rupture >50% serious wounds from flying objects
1–2.4	Repairable damage to buildings and damage to the facades of dwellings	1% eardrum rupture 1% serious wounds from flying objects
0.5–1	Glass damage	Injury from flying glass
0.15–0.30	Glass damage to about 10% of panes	Slight injury from flying glass

The general methods for assessing damage and human exposure for flash fires and torch fires is to assume fatalities would occur within the flame envelope of the flash fire or torch fire zone, and to estimate secondary damage potential to equipment or structures within the flame exposure zone.

Plotting Effect Distances

Plotting the results of the fire and explosion consequences associated with defined failure scenarios provides a graphical depiction of potential exposure zones. Figure 5-13.6 provides an illustrative example for plotting effect zones from an uncontrolled liquefied gas release potentially resulting in a torch fire, flash fire, BLEVE, or vapor cloud explosion scenario.

Step 5: Probability Assessment

This section presents an introduction to a complex subject. The mathematics and sensitivity analysis involved in the structuring of detailed event and fault trees is beyond the scope of this section. See References 2, 5, 9, and 10 to gain a more detailed insight into these areas.

Probability assessments must include a team approach. The team assembled to support the fire risk analyst in process risk assessments will generally include members experienced in process design and instrumentation, reliability engineering, safety, and environment issues, as well as team members from the plant knowledgeable in the specific facility hazards and operations. In some cases, the services of a statistician may be required to compile raw plant data from plant insurance reports and OSHA injury logs.

The general structure of the event tree for evaluating the consequences from the release of flammable liquids or gases is presented in Figure 5-13.7.

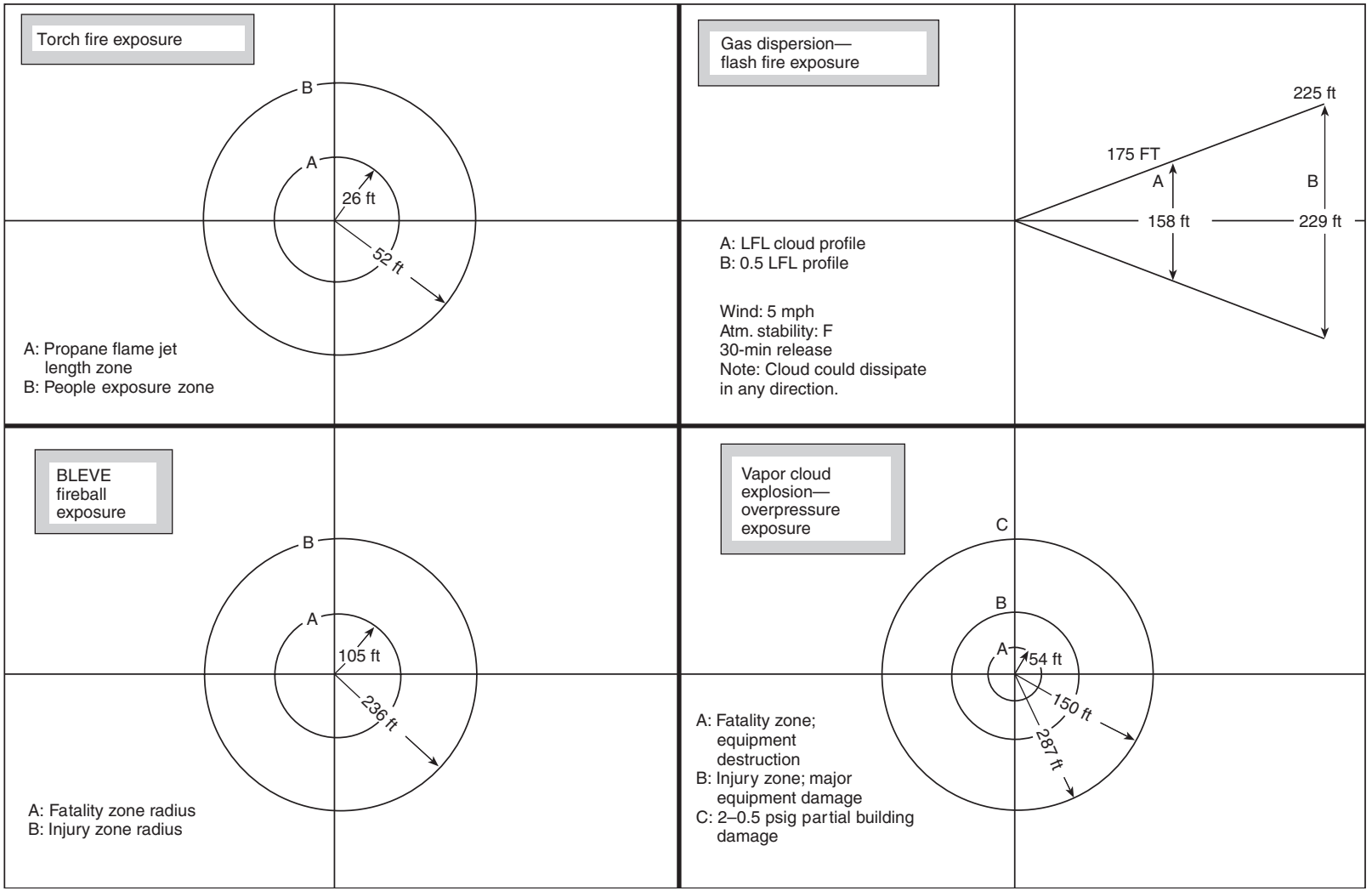

Note: Estimated LPG fire explosion zones for selected baseline scenarios. Calculated using the Archie Computer Model. Distance in feet from point of LPG accidental release origin.

Figure 5-13.6. ***General example of plotting effect zones.***

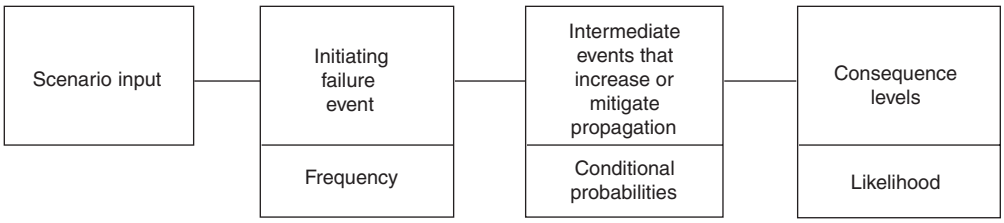

Figure 5-13.7. ***General event tree sequence.***

In mathematical terms, Figure 5-13.7 can be expressed as

$$F_{(\text{Consequences})} = F_{(\text{Initiating events})} \times \sum P_{(\text{Intermediate event probabilities})}$$

Two basic approaches commonly employed in fire and explosion risk assessments to estimate initiating event frequencies and conditional probabilities:

1. Use of relevant historical data
2. Synthesis of event frequencies and probabilities using techniques such as fault trees, human reliability analysis, and expert engineering judgment

In many cases the two approaches are used in a complementary manner to provide an independent check on one another and to increase the validity and confidence in the final results.

The first approach examines (1) relevant historical data in order to assess the frequency with which these events have occurred in the past, and (2) the likelihood of their occurrence in the future. Where sufficient relevant past data are available, historically based frequencies may be adequate in making a reasonable assessment of fire and explosion risks. However, frequencies derived in this way represent only average values and are most applicable to simple systems where there are not a number of variables (i.e., propagation and mitigation factors) that can significantly change the consequential results.

In actual application, assessments of potential fire and explosion risks at a specific facility will usually require adjustments to historical data to reflect the particular facility management and protection deviations. When evaluating the relevance of historical data for use in a specific facility or process risk assessment, the following factors should be taken into account:

1. There are many types of hazardous industrial operations for which historical data are limited or not available to make confident predictions about consequence likelihoods.
2. The general distribution between the primary causes leading to fire explosions shows that human error is the leading cause.[11]
   - Human factors (e.g., management controls, human operator errors): 70 to 85 percent
   - Equipment failures: 10 to 20 percent
   - External factors (e.g., earthquake, floods): 10 to 20 percent

   With the majority of causes being associated with human factors, it would be expected that the majority of risk research would be in this area; however, the quantification of the human element is very difficult, and much research continues in this area.
3. Fire prevention and protection technology is continually being expanded and updated based on new codes, standards, and industry practices that are developed after loss occurrences; and based on continued fire and explosion research efforts.

Considering these factors, the fire risk analyst must take a systematic approach to first determine the best approach for estimating frequencies and probabilities based on available data and specific plant conditions. A general approach is illustrated in Figure 5-13.8.[5]

Risk Assessment Fundamentals

Three primary concerns that the fire risk analyst must address are

1. Integrating failure (equipment, human, external) mechanisms
2. Application of engineering judgment and expert opinion
3. Documentation methods

Integrating failure mechanisms: The method of integrating hardware failures (e.g., equipment, emergency shutdown systems, passive and active protection systems), human errors (e.g., equipment testing and maintenance deficiencies, operational errors), and potential external upsets (e.g., windstorm, flood, earthquake) into top event frequencies must be considered by the risk assessment team. In the majority of fire and explosion risk assessments, top events will have to be supported by fault tree analysis to derive and validate the selected event tree frequencies and conditional probabilities. The general framework is illustrated in Figure 5-13.9.[2] References 5, 9, and 12 provide good information on fault tree structuring, Boolean algebra, cut-sets, and sensitivity analysis.

Engineering judgment and expert opinion: The method for systematic and consistent application of expert engineering judgment and expert opinions within the risk assessment process is a very important consideration.

Many hazardous situations and potential fire events are often encountered where data will be insufficient.

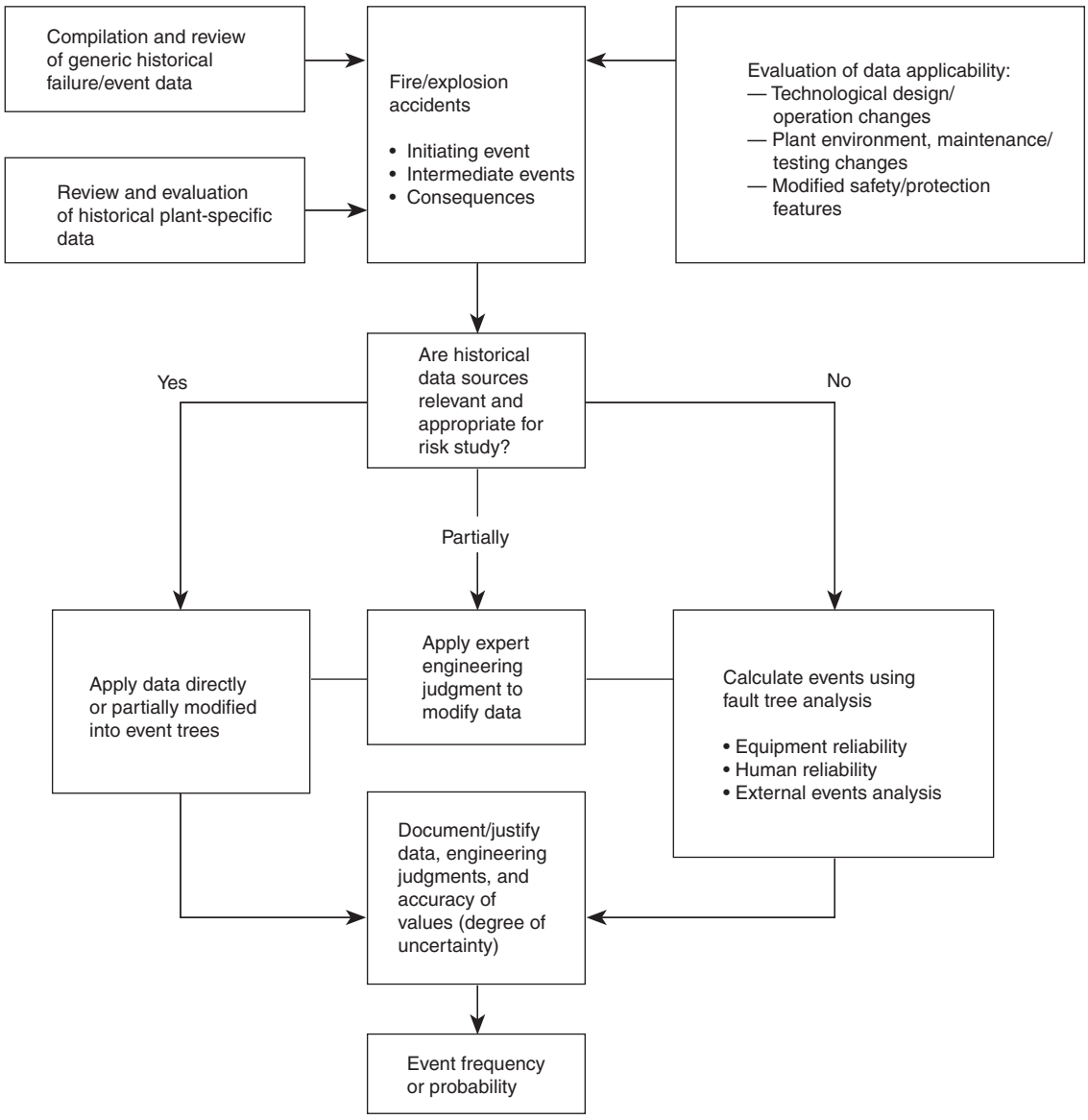

Figure 5-13.8. ***General procedure for estimating event frequency or probability.***

When these situations occur, it is often possible, and many times necessary, to generate data using the engineering judgment and expertise of the risk assessment team and, in some cases, outside experts. Experts, through their past experience with similar hazards or operations, can provide valuable input. Frequency or probability estimates obtained in this manner should combine the judgment and opinions of a group of experts, rather than rely on a single opinion.

Documentation methods: Methods for documenting the frequency and probability selection basis must be determined. To provide documentation, a table is usually constructed for each fire or explosion scenario event tree. Using the event sequences for the release from containment of a flammable liquid or gas, example information is presented in Table 5-13.5. It is essential in all risk assessment projects to document the data selection basis and the associated uncertainties.

Equipment Failure Data Sources

An excellent source for generic equipment failure data is *Guidelines for Process Equipment Reliability Data, with Data Tables,* developed by the CCPS.[13] The failure data can also be obtained as a computerized database on diskette. This book provides a listing and general description of all the data sources used to construct the CCPS generic failure rate database. It is essential for the fire risk analyst to understand the sources of these data, the limitations and applicability to the particular environment, and management controls for the specific facility being

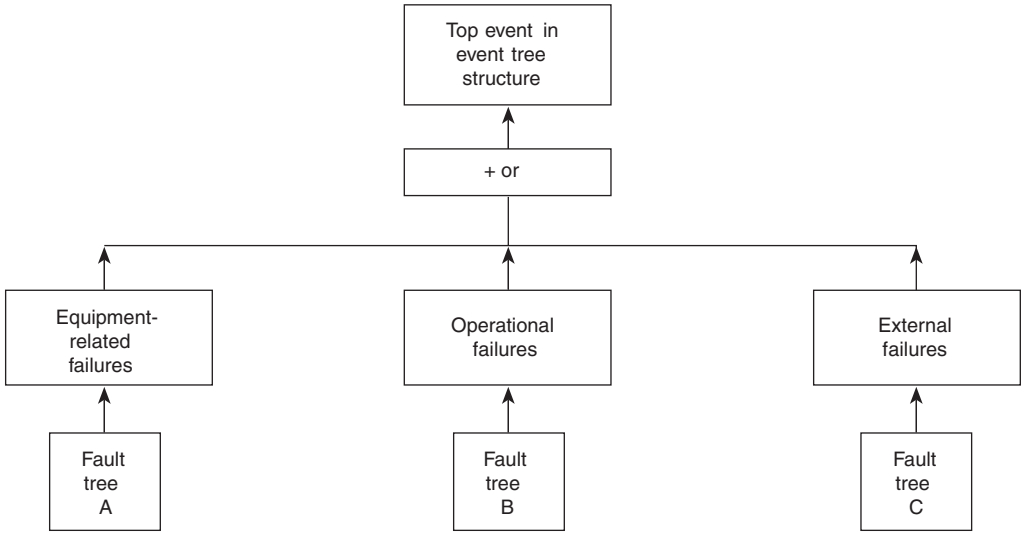

Note: Fault trees A, B, and C are generally required to be developed into separate detailed fault tree models.

Figure 5-13.9. ***General fault tree support framework.***

Table 5-13.5 ***Example of Documentation in Table Format***

Event Tree Designation	Event Description	Frequency (F) or Probability (P) Range	Data Source	Frequency (F) or Probability (P) Assigned to Event	Selection Basis and Comments
Event tree and event branch line identification	Description of event scenario • Release • Ignition • Emergency shutdown • Automatic/manual fire control	Frequency or probability range applied to event	Source of data or method used for establishing range	Assigned frequency or probability within range	Justification of selection • Historical • Records • Fault tree • Engineering judgment • Combination

assessed. This reference provides a good summary of these concerns.

Ignition Likelihood

Ignition likelihood is a measure of the expected ignition occurrence for a defined fire scenario, and may be expressed as

1. Frequency (i.e., number of occurrences per unit of time)
2. Annual probability (i.e., a probability of occurrence during a per-year time interval must be expressed as a number ranging from 0 to 1)
3. Conditional probability of occurrence given that a precursor event has occurred (e.g., release of flammable gas, molten metal spill, etc.)

The objective of ignition likelihood estimation is to estimate, in a systematic and credible manner, the cumulative ignition likelihood from defined fire scenarios. The procedures involved in this method generally require the integration of plant-specific data, deterministic flammable liquid spread, and gas dispersion modeling, as well as engineering judgment. The sources listed in Table 5-13.1 and industrial insurance companies (such as Factory Mutual Research Corporation, Industrial Risk Insurers, etc.) are good sources for obtaining generic ignition data.

Ignition likelihood estimation steps include

1. Characterize and map ignition source potentials in the area(s) being evaluated.
2. Compile available plant-specific ignition–fire data, based on plant records and interviews.
3. Review available historical incident data sources that are similar to hazards being evaluated. (This should be used for reference and comparison.)

Ignition potential area boundaries (i.e., effect zone radius) should include

1. Potential pathway (area of exposure) where a flammable liquid or gas release could exist
2. Potential area that may be affected by a pressured fluid released (e.g., combustible hydraulic fluid, etc.)
3. Potential radiant heat energy effect area from an exposure fire

Figure 5-13.10 provides a general illustration of plotting ignition source distribution within a potential flammable gas dispersion area. Table 5-13.6 provides an example format for estimating cumulative ignition likelihood.

Ignition source potential(s) within the modeled effect zone area should be characterized by

1. Type and location of ignition sources, including fixed point (FP), linear source (LS), and variable point (VP)
2. Continuous (C) or intermittent (I) source
3. Ignition source energy potential [i.e., strong (S), moderate (M), or weak (W)]
4. Ignition source presence, whether (C) continuous or (I) intermittent. This is the estimated percentage (%) of time the ignition source is present
5. Ignition source energy potential. This is in relation to the fuel's ignition sensitivity, and should include chemistry, physical state, surface texture, and moisture content

As a first step in evaluating ignition likelihood, all relevant ignition sources must be identified. Ignition sources usually fall under one of the following categories: fixed point, variable point, or linear sources.

Figures 5-13.11, 5-13.12, and 5-13.13 provide some examples of potential ignition sources.

Ignition is a function of time as well as temperature (i.e., potential fuel subjected to a relatively high temperature for a short period of time may not ignite, while the same fuel can undergo ignition when exposed for a longer duration to a lower temperature). For example, wood has a normal ignition temperature of 400 to 500°F (204 to 260°C), but has been found to ignite when subjected to a heat source of 228°F (109°C) for four days.

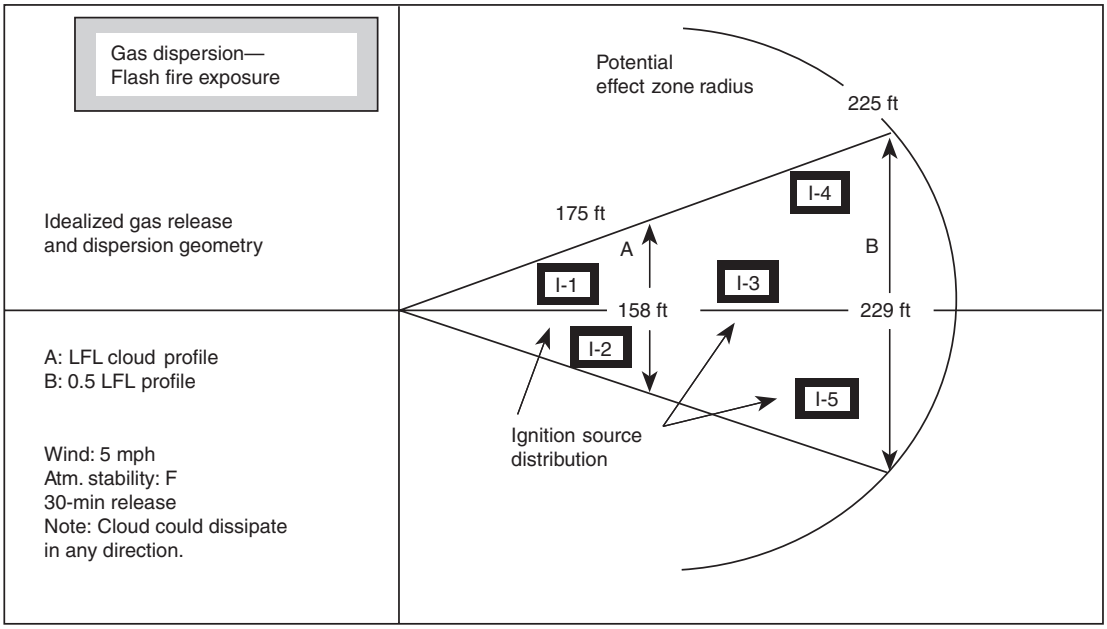

Figure 5-13.10. ***Illustration of plotting an effect zone to evaluate cumulative ignition likelihood. (See Table 5-13.6 for boldfaced box definitions.)***

Table 5-13.6 ***Example of Estimating Cumulative Ignition Likelihood***

(Fig. 5-13.10) Potential Ignition Source(s)	Continuous (C) or Intermittent (I) Ignition Source	Strong (S), Moderate (M), or Weak (W) Ignition Energy Source	Likelihood of Ignition Based on Ignition Source Being Engulfed with Flammable Vapor	If Intermittent Source, Estimated Time (per year) for Which Intermittent Source Is Present and Active	Likelihood of Ignition, Given Release and Flammable Cloud
I–1	I	M	0.06	10%	0.006
I–2	I	S	0.9	15%	0.135
I–3	I	M	0.06	30%	0.018
I–4	C	M	0.06	100%	0.06
I–5	C	S	0.24	100%	0.24
				Cumulative likelihood of ignition:	0.46

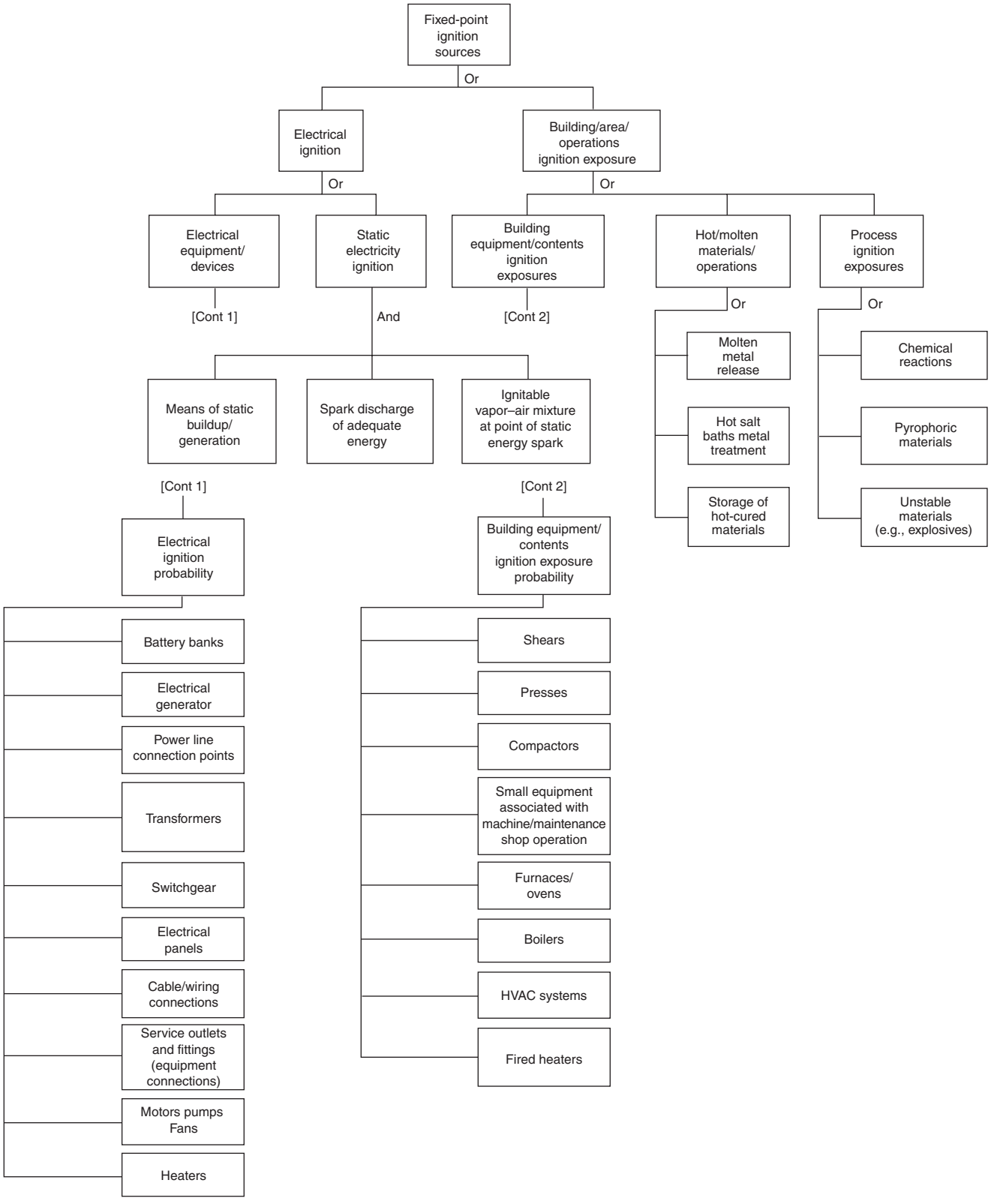

Figure 5-13.11. ***Potential ignition sources—fixed point.***

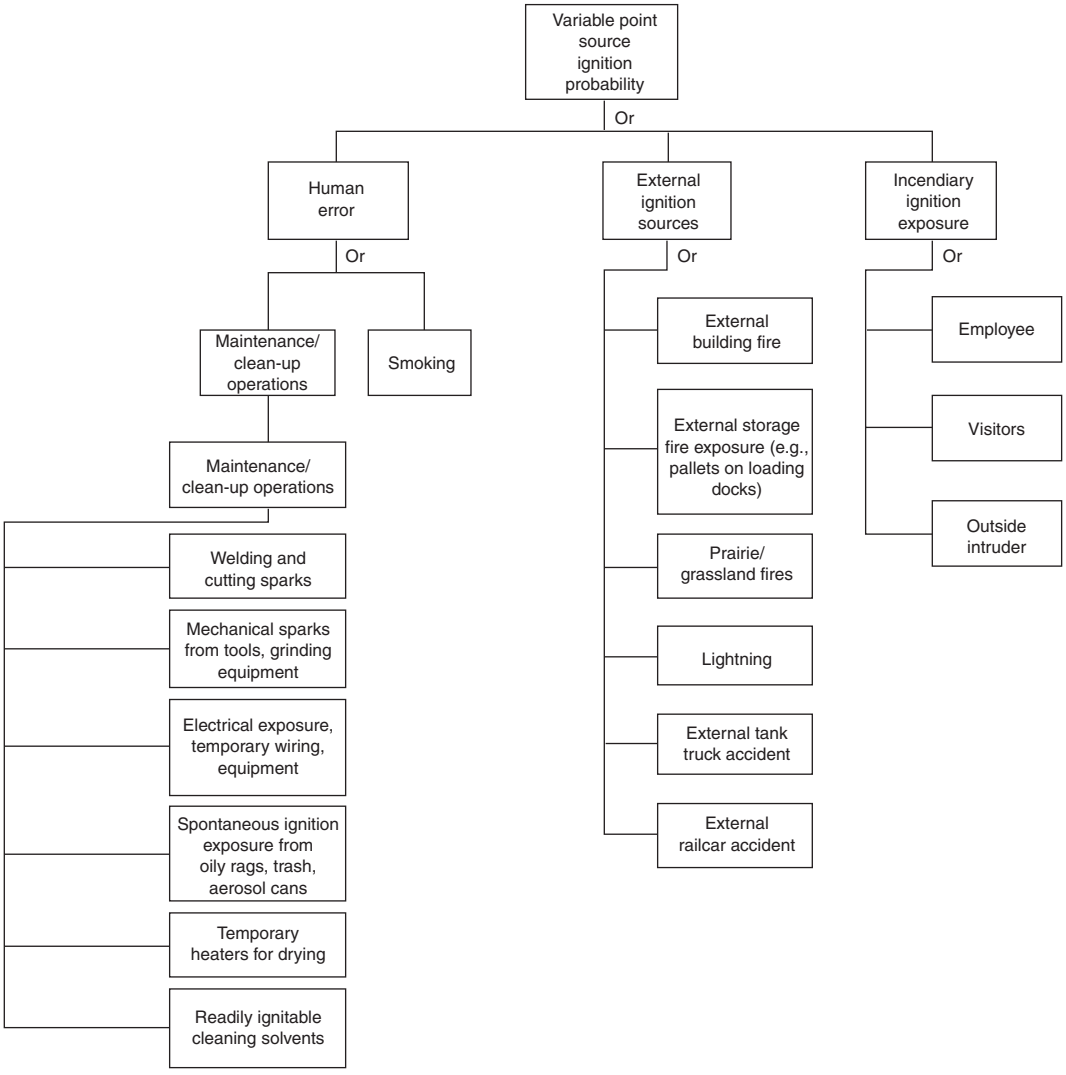

Figure 5-13.12. ***Potential ignition sources—variable point.***

Examples of conditional ignition likelihood ranges for flammable liquid vapors or gases engulfing ignition sources are provided by References 5 and 14.

Qualitative Ranking	Likelihood Range
(*S*) Strong	0.25 to 1
(*M*) Moderate	0.1 to 0.24
(*W*) Weak	0.01 to 0.09

Ignition likelihood estimation provides for the likelihood of ignition, F_{ig}, and is primarily dependent on the following factors:

F_{te} Frequency of time the ignition source exposure is present in the immediate area of the combustible material being examined under defined scenario conditions.

P_{il} Probability the ignition source exposure exceeds the ignition threshold limits (i.e., temperature, energy) for the combustible material being examined under defined scenario conditions. This probability parameter includes both accedence of ignition threshold limits under normal operating conditions and also under fault (e.g., equipment failure that could result in shorting or overheating, thus exceeding the ignition threshold limits of the material being examined).

P_{cf} Probability that the configuration (e.g., unobstructed pathway, positioning) between the ignition source and combustible is conducive to initiating ignition.

P_{ne} Probability the ignition source is *not* eliminated (e.g., automatic, manual shutdown of electrical power, etc.) prior to established ignition.

Therefore, the general sequence of ignition-related events can be represented as

$$F_{ig} = F_{te} \times P_{il} \times P_{cf} \times P_{ne}$$

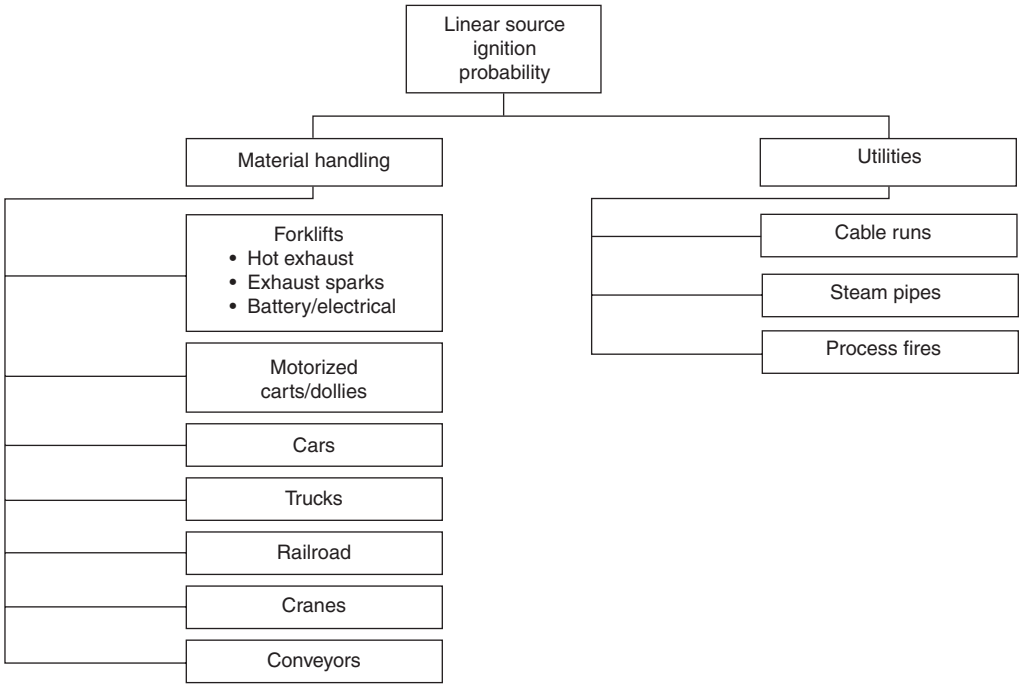

Figure 5-13.13. ***Potential ignition—linear sources.***

Fire Protection System Performance

The following information was extracted from Reference 10 and is based on a methodology applied at industrial process facilities for quantifying the probability of fire protection system (FPS) performance success.

Figure 5-13.14 presents the primary fire protection system of interest in fire risk assessments and includes

- Detection systems
- Emergency control systems
- Automatic suppression systems
- Propagation limiting measures (i.e., fire barriers)
- Manual loss control intervention

Two items to note in Figure 5-13.14 are

1. Fire protection systems performance success is quantified in terms of *conditional probabilities.*
2. The three primary fire protection system performance measures and objectives include
   - Response effectiveness—maximize system response time
   - Online availabilities—minimize system downtime
   - Operational reliability—minimize failure-on-demand probability

For a defined fire protection system under a scenario-specific demand, performance success can be evaluated in terms of performance measures and indicators which are developed from past system failure experience. Figure 5-13.15 provides an example of some primary success measures.

Fire protection system performance success is the product of these three probabilistic success measures:

Primary performance measure	RE Response effectiveness	OLA Online availability	OPR Operational reliability

FPS performance success probability (P_s)

$$P_s = P_{RE} \times P_{OLA} \times P_{OPR}$$

The unique feature in the FPS performance success methodology is that it provides a consistent logical approach towards quantifying performance based on

- Specific scenario input
- Risk tolerance criteria
- Defined performance requirements

The methodology provides a breakdown of experience-based performance success expectation based on response effectiveness (design application bases, system response time), online availability (potential downtime factors), and operational reliability (probability of failure on demand from hidden, and common cause failure potentials).

The methodology allows integration of probabilistic failure of equipment, human error aspects, deterministic modeling to support failure or success probabilities, and

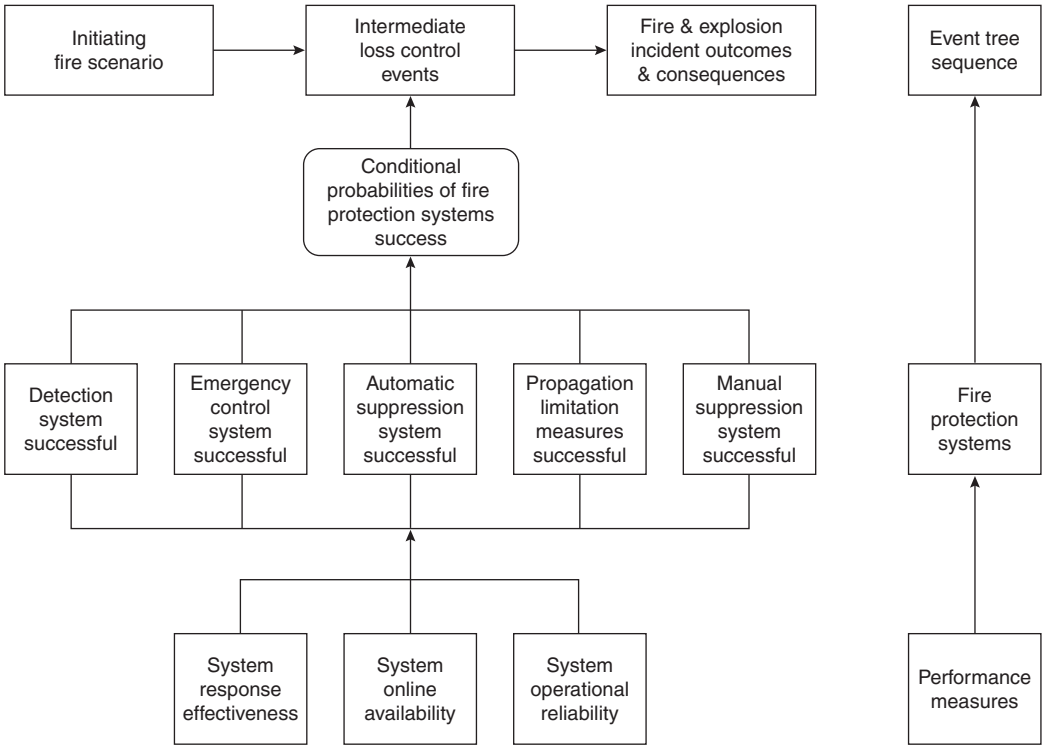

Figure 5-13.14. ***General illustration—loss control systems performance measures.***[10]

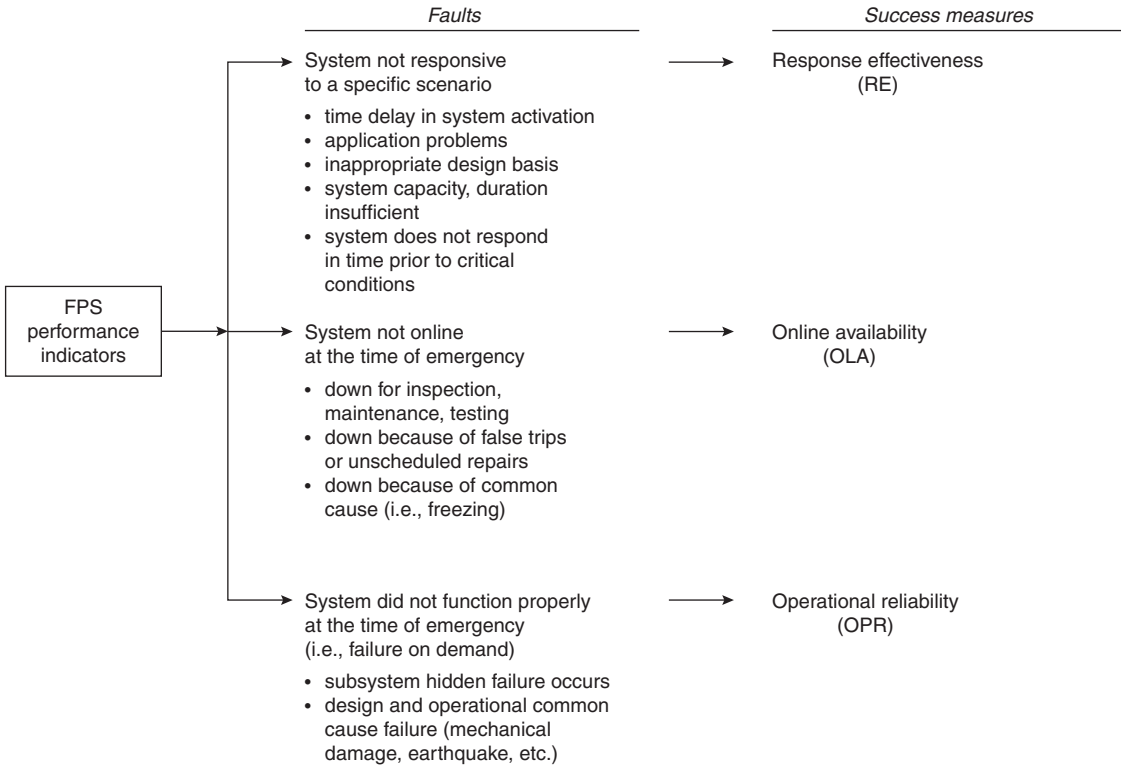

Figure 5-13.15. ***Example of primary FPS success measures.***[10]

incorporation of systematic justification of engineering judgment and expert opinion to support subjective probability (i.e., quality scoring of performance integrity measures). The conditional probabilities of FPS performance success following the defined initiation event are then inserted as top events in the ETA where the time line of sequential events leads to incident outcomes and potential consequence levels.

The methodology can be used to evaluate

- Existing systems
- Modifications/inputs to existing designs
- Newly proposed system design

Figure 5-13.16 presents the general fire protection system success tree logic. This figure highlights the time-related performance factors, which in many cases are very critical factors and which are not well addressed in design standards, such as NFPA standards.

As presented in Figure 5-13.17, the response effectiveness (RE) evaluation is quantified in terms of

- DAB—Design application basis
- SRT—System response time

The following information in this section overviews some of the primary response effectiveness success measures and suggests probability estimation approaches.

DAB evaluation involves

- Identifying DAB success measures
- Probability selection based on functional performance requirements

Figure 5-13.18 provides a listing of the primary DAB success measures, based on past fire protection system faults. These include

- Suitability
- Capacity
- Duration

Figure 5-13.19 illustrates the general DAB success tree framework.

DAB—Suitability

The suitability of the fire protection system must be evaluated in terms of the functional performance requirements, which requires knowledge of the specific scenario input and target threshold damage limits.

Some suitability considerations include

- Is the system actuation device suitable?
- Is the suppression mechanism suitable?
- Will suppression agent create excessive damage?
- Are barriers suitable (i.e., heat, smoke resistance)?

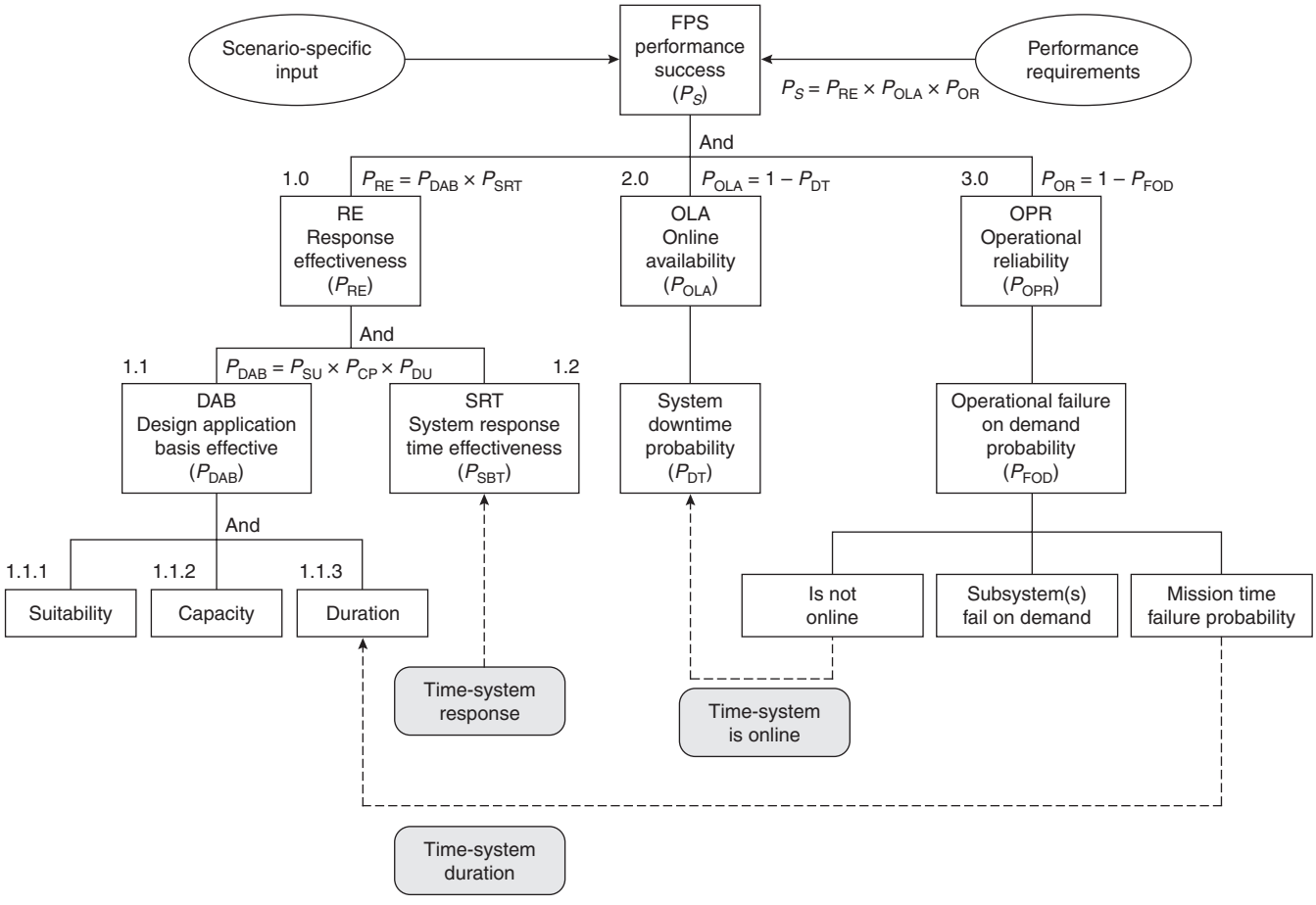

Figure 5-13.16. ***FPS performance success tree framework—highlighting time-related performance factors.***[10]

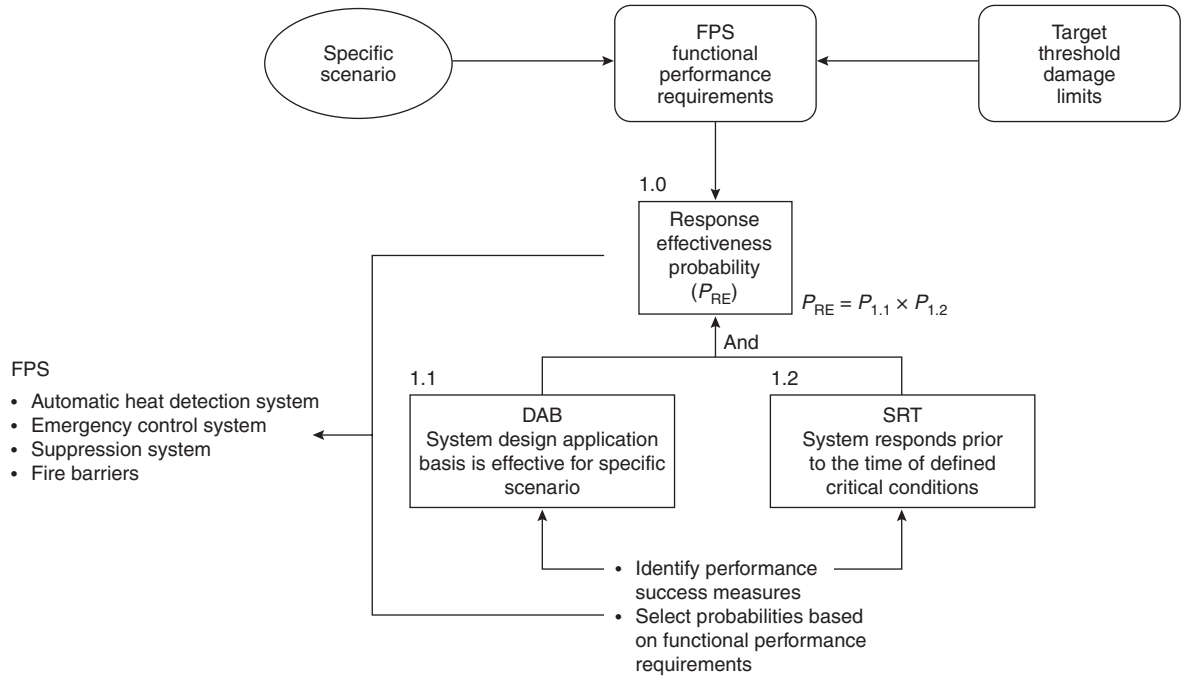

Figure 5-13.17. ***FPS response effectiveness probability as related to functional performance requirements and success measures for FPS under evaluation.[10]***

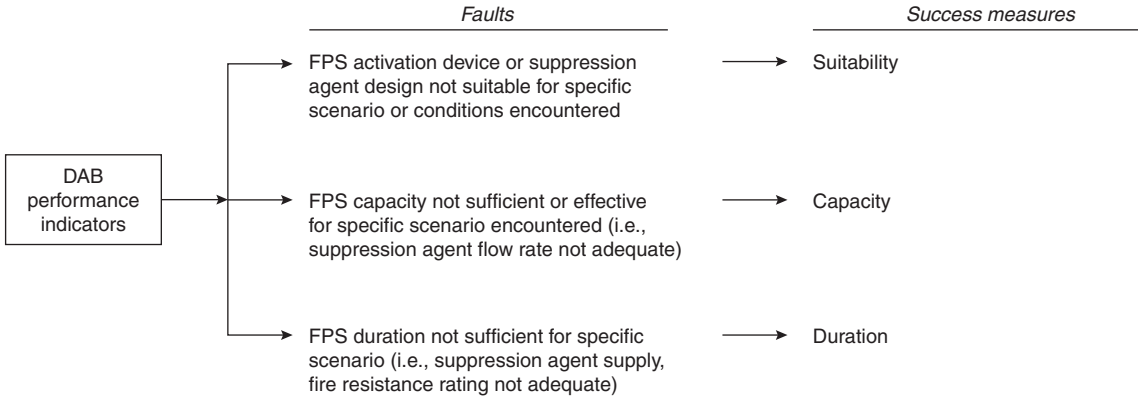

Figure 5-13.18. ***Example of general DAB success measures.[10]***

Suitable means appropriate to a particular situation or condition. Experience is the primary dictator of suitability and can include the following information sources

- Standards, industry practices
- Plant-, industry-specific experience
- Loss incident data
- Research and testing
- Engineering judgment (expert opinion)

Suitability questions whether the fire protection system under evaluation is appropriate to the particular situation, conditions, scenario input, and functional performance requirements. It also should be suitable for the

- Hazard
- Limitation of damage
- Impact on people
- Limitation of production equipment downtime
- Environmental concerns

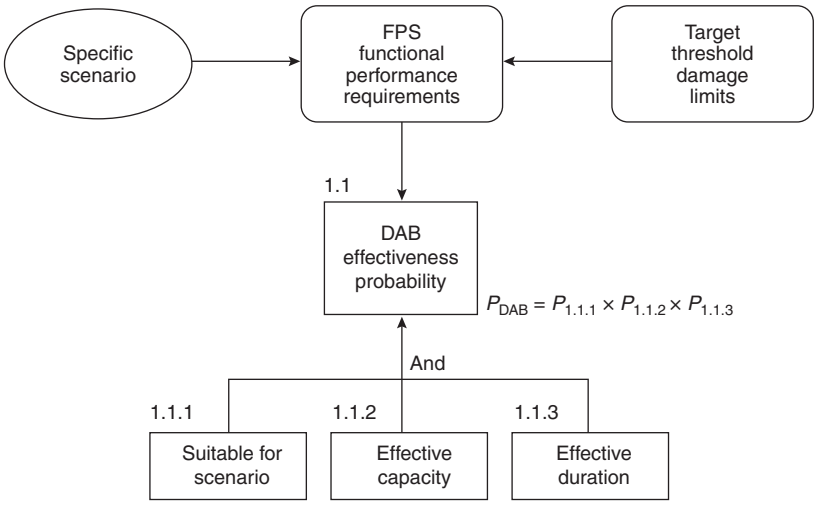

Figure 5-13.19. ***General DAB success tree framework.***[10]

Detection systems functional performance scenario-specific suitability objectives could include detection of

- Smoke (aerosols)
- IR and UV radiant energy (flame)
- Thermal energy (heat, temperature rise)
- Gases [direct releases of flammable, toxic, or corrosive gases or products of fire combustion gases such as carbon monoxide (CO), hydrogen chloride (HCN), etc.]
- Pressure (pressure rise detectors such as those associated with explosion suppression system)

With detection systems, in many cases, there is a relationship between the scenario suitability and response time.

- Emergency control systems (ECS) functional objectives could include
  - Emergency system shutdown of production equipment or utilities (i.e., electrical power, gas lines)
  - Emergency system startup of safety systems
- Emergency system shutdown could include
  - Shutdown flammable liquid pumps
  - Shutdown production equipment
  - Shutdown ventilation systems
  - Shutdown electrical power
- Emergency system operation mechanisms could include
  - Startup ventilation on smoke removal system
  - Startup gas depressurization system
  - Startup/activate suppression systems

The suitability question is whether the existing ECS mechanisms or proposed ECS can meet the defined functional performance requirements. In most cases the focus of ECS evaluation is on the operational reliability. However, ECS such as diking, drainage or containment systems, gas blow down–emergency flare systems, ventilation systems, etc., must first be evaluated from a design application viewpoint.

DAB—Capacity Effectiveness

Capacity can be generally defined as the maximum production, or the output, of an existing FPS or proposed design. Capacity issues are primarily related to suppression systems; however, detection system alarm audibility, emergency control systems (such as drainage systems, gas blow-down systems, etc.) would also be examined in terms of capacity. In most cases, the probability associated with design capacity is fairly straightforward, based on the engineering review.

If for example, the capacity effectiveness is associated with the flow rate or density of a water-based extinguishing system (i.e., sprinkler, water-spray, pumping system, etc.), then based on the functional requirements (i.e., need 0.25 GPM/3000 sq. ft. density), one can determine if this is available using water flow hydraulics modeling.

The most important issue here is to clearly define the functional capacity requirements. When doing a risk-informed evaluation, the focus is on how all the fire protection systems perform in mitigating the initiating scenario in relation to the risk tolerance limit. That means in some cases, only control or suppression, not immediate extinguishment, may be needed to meet risk tolerance.

For example, focusing on a water-based fire protection system, various levels of performance can be achieved based on the defined initiating event, as shown in Figure 5-13.20.

- Fire control
- Fire suppression
- Fire extinguishment

DAB—Duration

As a general definition, duration is the period of time that something lasts as determined by an existing or proposed design. This could be the adequacy of the suppres-

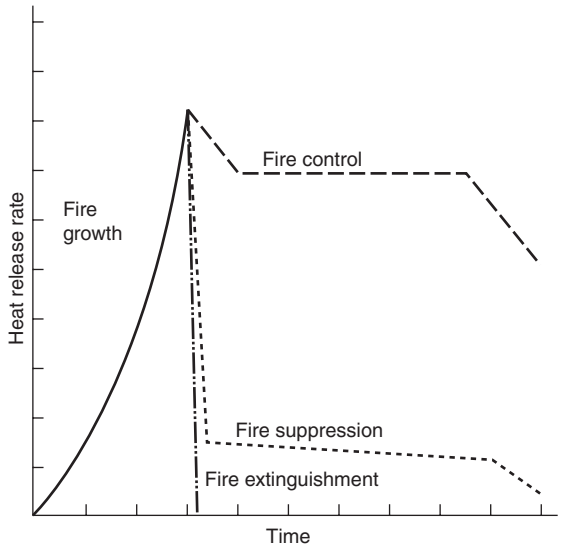

Figure 5-13.20. ***General illustration—control, suppression, extinguishment.***

sion agent supply, the fire resistance rating of a fire barrier wall, and so on.

As with the capacity evaluation, duration effectiveness is evaluated based on our functional performance requirements, not codes. In other words, codes could call for a 2-hour water supply or 2-hour fire wall, while the performance requirement could be 30 min. Or vice versa, the performance requirements could be greater than the codes.

Strongly related to duration is supply redundancy. However, the DAB evaluation is based on the total supply available for use versus performance requirements. The probability that multiple or redundant supplies are available at the time of a fire incident are evaluated as an online availability probability.

DAB—Probability Sources

Primary probability sources for use in evaluating the DAB segment of the system response effectiveness are

1. Experience
   - Standards, industry practices
   - Plant-, industry-specific experience
   - Loss incident data
   - Research and testing
2. Deterministic modeling

   Models to support DAB probability evaluations can include
   - Hydraulic models
   - Heat transfer models
3. Engineering judgment

   In the majority of cases based on items 1 and 2 above, the following probability (P) estimation will be selected:

$P = 1$ DAB is effective
$P = 0$ DAB is not effective

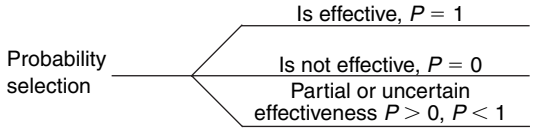

However, in some cases there may be uncertainty due to insufficient knowledge or experience. Engineering judgment usually involves reviewing information obtained from probability sources 1 and 2 and applying expert opinion and team consensus.

System Response Time

SRT evaluation involves

- Identifying success tree indicators
- Relating scenarios to functional performance requirements
- Probability selection

Figure 5-13.21 provides an example of general SRT success measures.

Figure 5-13.22 presents the SRT effectiveness probability related to functional performance requirements and success measures.

Automatic Response Time

Primary considerations include

- Detection unit activation time
- Sprinkler head activation time
- Automatic time delay features
- Barriers—fire resistance integrity times

The scenario-based exposure profile is needed as input to evaluate the time response of fire protection systems. The exposure profile in Figure 5-13.23 provides an example of a critical time line for actuation responses of some fire protection systems, showing the time line at the bottom of the graph and potential target impact levels on the right side of the graph.

Development of the exposure profile and time line is the primary input for evaluating the SRT success probability.

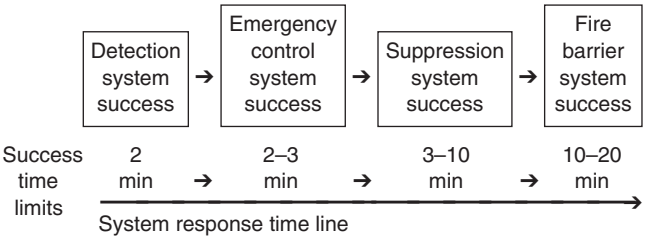

The time limits establish the system response requirements of the evaluation. Remember, even though the FPS may meet the suitability, capacity, and durational measures, if the system cannot respond (i.e., activate, operate) prior to critical conditions at the target, the overall response effectiveness may be severely compromised.

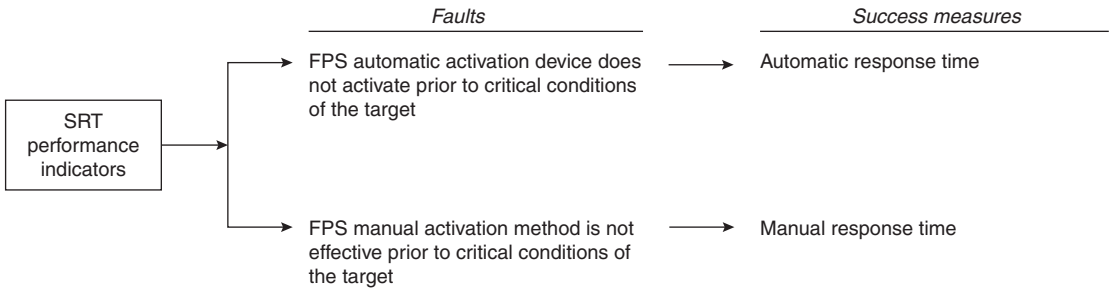

Figure 5-13.21. ***Example general SRT success measures.***[10]

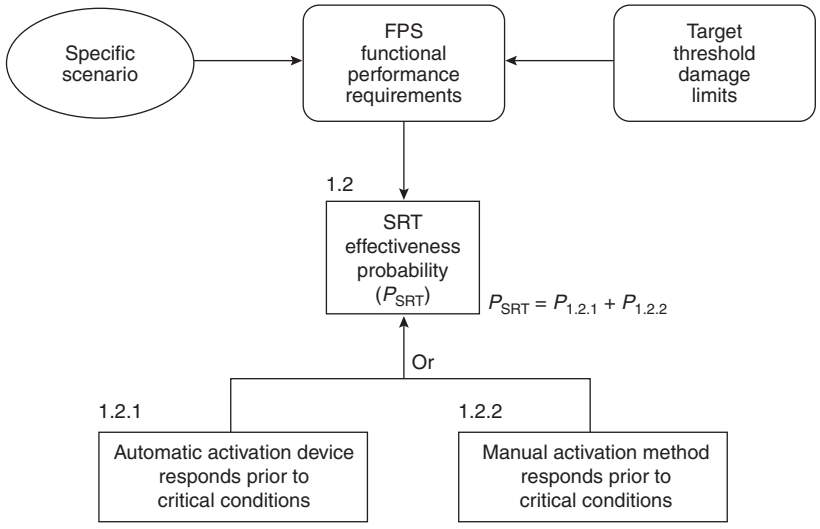

Figure 5-13.22. ***System response time (SRT) effectiveness probability.***[10]

Probability Sources

Probability sources to support SRT evaluation include

- Deterministic modeling
- Manufacturer's information
- Research and testing
- Engineering judgment

Deterministic detector and sprinkler head computerized models can provide support in the selection of probabilistic success estimates. Presently available computer models which estimate detection and sprinkler head response use the concept of a response time index (RTI) as related to the detector or sprinkler head under evaluation. In addition, heat transfer computer models are available to estimate the fire resistance of fire barrier components and assemblies.

Online Availability

If the fire protection system (FPS) is not online during an emergency demand, we have a failure. In our suggested FPS performance evaluation methodology, functional failure potential is broken down as follows:

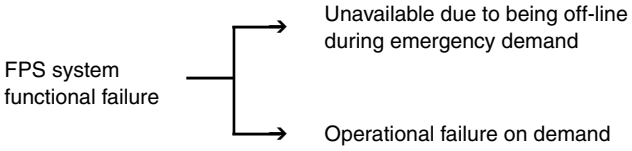

The major difference in this interpretation is that unavailability is primarily related to known or projected downtime potentials, while operational failure on demand is primarily related to hidden failure-on-demand potentials. These are discussed in the next two sections.

In applying performance success tree logic, we have the following correlations:

$$\text{Reliability} = 1 - \text{Functional failure}$$

$$\text{Online availability} = 1 - \text{Unavailability}$$

$$\text{Operational reliability} = 1 - \text{Operational failure on demand}$$

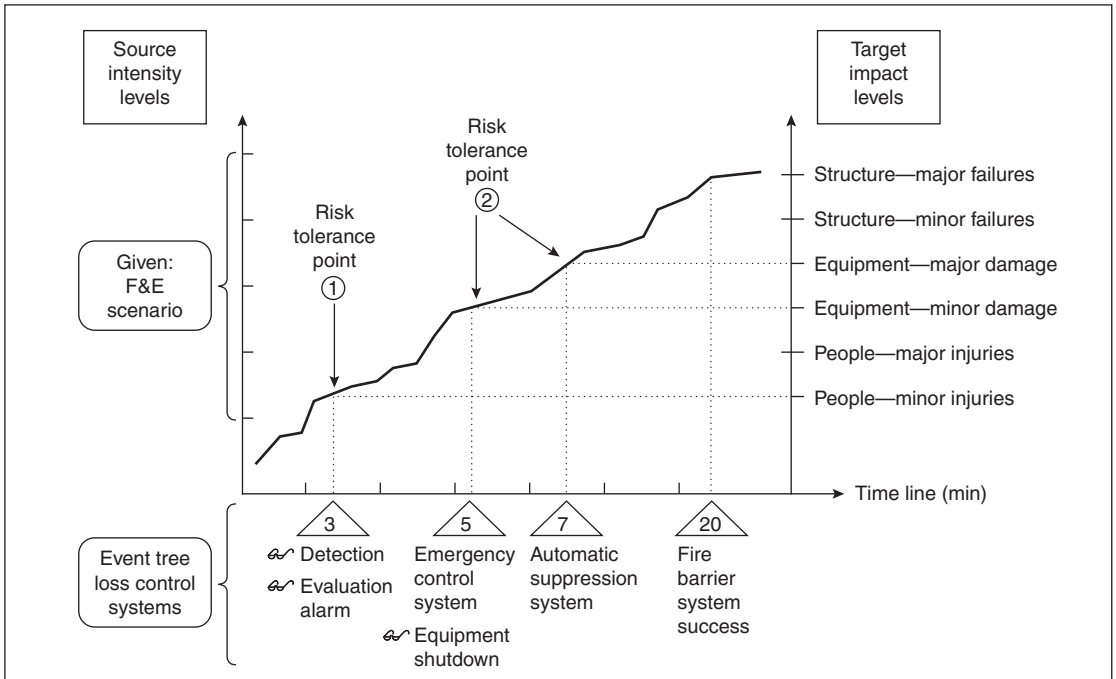

Target risk tolerance points	Estimated time limits	Time line factors			
① People	3 min	Detection time +	Alarm notification time +	Evacuation time	≤ 3 min
② Equipment	5–7 min	Detection time +	ECS operation +	Suppression system operation	≤ 5–7 min

Figure 5-13.23. ***Example scenario-based exposure profile curve with risk tolerance points.***[10]

The benefits of examining online availability (OLA) as an individual reliability-based performance measure are

- Existing systems
  - Allows evaluation of downtime factors based on plant experience
  - Identifies downtime and availability factors related to inspection, maintenance, and testing (IMT) efforts, false system activation problems, and common cause problems such as freezing, flooding, and so on.
- New system designs or modifications
  - Identifies opportunities to minimize potential downtime factors and to maximize availability based on design and recognition of common cause failure potentials.
  - Identifies opportunities to optimize downtime potentials associated with IMT efforts

Presented in Figure 5-13.24 is the logic tree for OLA. As illustrated, a fault tree approach is used to evaluate the downtime probability (note OR gate). This is then converted to success tree logic. The entire logic tree could be handled initially as a success tree; however, this conversion of using fault tree analysis and then converting is generally more efficient because information is usually conveyed in plant records as downtime hours, not as uptime or online hours.

Off-line due to IMT: The primary information sources on downtime associated with FPS system IMT activities are the plant's maintenance logs, records, and interviews with maintenance personnel.

The estimates of this annual probability are derived from the historical or projected time (hours) when the FPS system is not available to perform its intended function, divided by the hours in a year. For example, if the system is taken off-line 80 hours per year to perform IMT efforts, then the annual probability of IMT unavailability is

$$\frac{80 \text{ hr/yr downtime}}{8760 \text{ hr/yr}} = .009$$

Interval unavailability due to periodic IMT is given by

$$\text{Downtime}_{\text{IMT}}(0, T_1) = \frac{t_{\text{TM}}}{T_I}$$

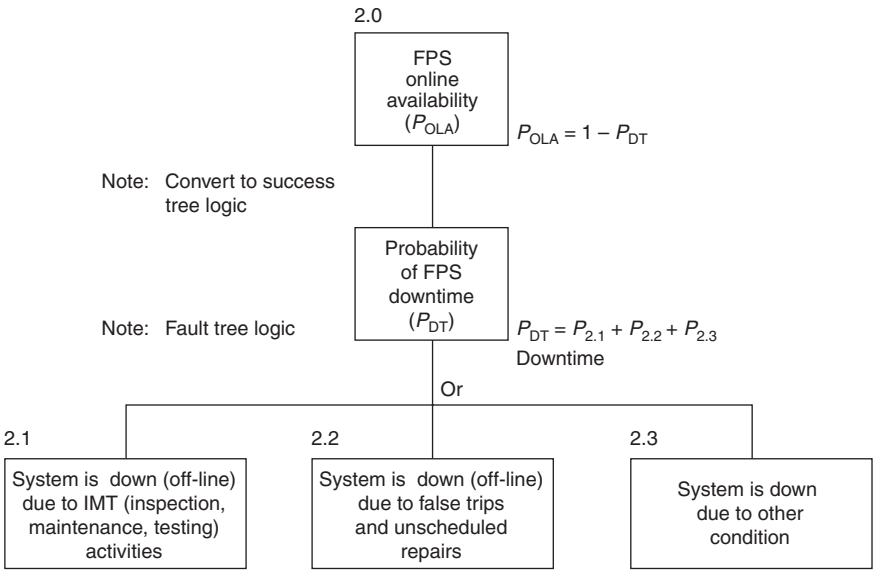

Figure 5-13.24. ***OLA general fault and success tree logic.***[10]

where t_{TM} is the average duration of time the system is out of service for each periodic IMT and T_I is the interval of time between successive IMT efforts. (Note: This unavailability does not include the unavailability due to system failure, which is addressed under operational reliability for hidden failures on demand.)

It should be noted that that IMT activities where systems are taken off-line present a negative effect under online availability evaluation. However, IMT efforts to discover hidden or unrevealed factors in the assessment of operational reliability is a very important factor. An optimized balance between the two needs to be considered when trying to achieve a maximum system performance success probability.

Off-line due to false trips: False trips or activation of FPS, also termed nuisance or spurious trips, create a situation where the system is shut down and taken off-line, so that cause can be investigated and repairs made if necessary.

The problems associated with false trips generally involve

- The system is taken off-line and therefore is not available during a fire.
- When numerous false trips and alarms occur, occupants become complacent, responding slowly or sometimes ignoring alarms—a major problem in the event of a real fire.
- In many cases systems are bypassed and taken off-line for extended periods of time.

Most false trip problems are location and design related.

In many cases, facilities reduce detection-related false alarms by disconnecting or jumpering out the alarm until the problem is resolved. While this reduces false trip errors, it increases the probability of having the detection system unavailable during a fire emergency.

Some other common causes of automatic fire detectors' false activation include

- Insect induced
- Owner induced (lack of maintenance)
- User induced (accidental smoke generation or malicious actuation)
- Serviceman induced (improper testing)
- Environmental effects (lightning)

Unscheduled repairs and external factors: Unscheduled repairs following IMT efforts or external downtime causes can take many forms. Having equipment spares, quick access to repairs versus service contracts, and contingency plans to expedite repair and replacement are very important.

For example, unscheduled repairs for components on fire barriers can represent an availability problem. Forklift damage to fire doors or fire barriers can be a constantly occurring problem. I have reviewed many plans from a design standpoint where, based on a first look, the performance success of the fire barrier walls would be rated high. However, after conducting a field survey, problems identified included damaged fire doors painted links, locks on fire doors, doors wedged open and dampers tied open for ventilation reasons, unsealed cables compromising the fire wall, and so on. Therefore, even if the fire barrier has an appropriate fire resistance design basis, the performance success probability related to scenario-specific performance requirements may be low.

External factors that can cause system downtime include freezing weather, flooding, vehicle damage, and so forth.

For example in one project, based on plant records and interviews, it was identified at one plant that the control valves for a sprinkler protection system over the oil-fired burner system for a boiler were shut off for 4 months a year due to fear of freezing. The corporate safety director was unaware of this practice. The annual downtime probability on this system, which was a critical system from a business interruption standpoint, was equated at

4 months down/12 months =
.33 annual probability of downtime, or .67 availability

As evident, this was a design and communication problem which in overall methodology would severely affect overall system success probability.

Another example was discovered at a chemical plant. Due to flooding, water runoff, and drainage problems, the fire pump house was flooded three times over a 5-year period. When the fire pump house was flooded, the controllers on the fire pumps were shut off, and the average time for cleanup and repair was 32 hours per incident. This equates to fractional downtime probability of .192, or an OLA of .81.

The fire pumps presented a common cause failure to numerous deluge water spray systems at this plant. Recommendations concerning water runoff channeling and drainage in the pump house area were made to improve this situation.

Target availabilities for systems should be in the range of .98 to .999.

Operational Reliability Evaluation Logic

Fire protection system's operational reliability (OPR) is the ability to operate on demand and perform an operational requirement. OPR is a probability to operate on demand, not an OLA probability. For example, if a sprinkler system control valve is shut off to perform maintenance, repair, or testing, this is an unavailability factor. However, if the control valve partially fails or fully fails when placed in an emergency demand state due to a hidden mechanical degradation failure (i.e., gate valve drops causing partial or full obstruction to the water supply to the sprinkler system), this is an operational failure at demand.

Depending on the type of fire protection system, operational function may vary. Therefore, the required operational performance functions of the fire protection system must be defined. For example, a sprinkler system's operational functions may be delivering water from the pumping supply to the sprinkler heads in the area of fire incident. Primary operation on demand contributing factors include the electrical–mechanical subsystem functions needed to make this occur. For example, pump starts, valves open, piping is unobstructed, and sprinkler heads fuse and deliver water to the fire origin. The activation-time response of the sprinkler head(s) and the performance-based water flow capacities and duration would be initially evaluated under the response effectiveness probability prior to this point.

Quantifying the probability of FPS OPR involves an evaluation of

1. Identifying performance success measures
2. Qualitative logic structuring
3. Performance integrity measures
4. Quantification of failure-on-demand probabilities

OPR success measure: Figure 5-13.25 presents some of the primary faults and associated success measures related to FPS operational reliability (OPR).

Figure 5-13.26 provides illustration of the general OPR success tree framework.

The framework for addressing the design application basis and the OLA is very similar for numerous fire protection systems. The evaluation of the subsystem failures which need to be examined as part of the OPR differs. However, there can be a common method for addressing the evaluation structure.

Some of the issues which should be recognized include

- Apply a consistent qualitative logic methodology for FPS system and subsystem breakdown.
- Recognize and integrate manual intervention features if relevant to the evaluation.

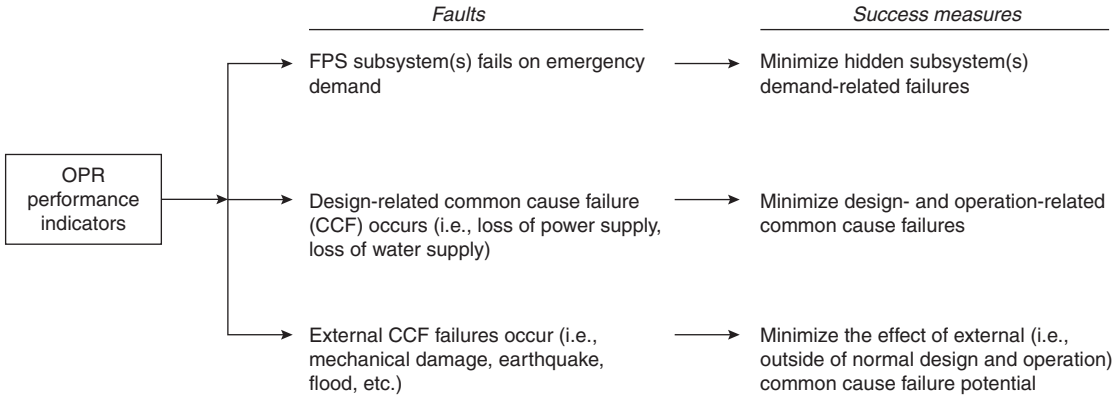

Figure 5-13.25. ***Example of general OPR success measures.***[10]

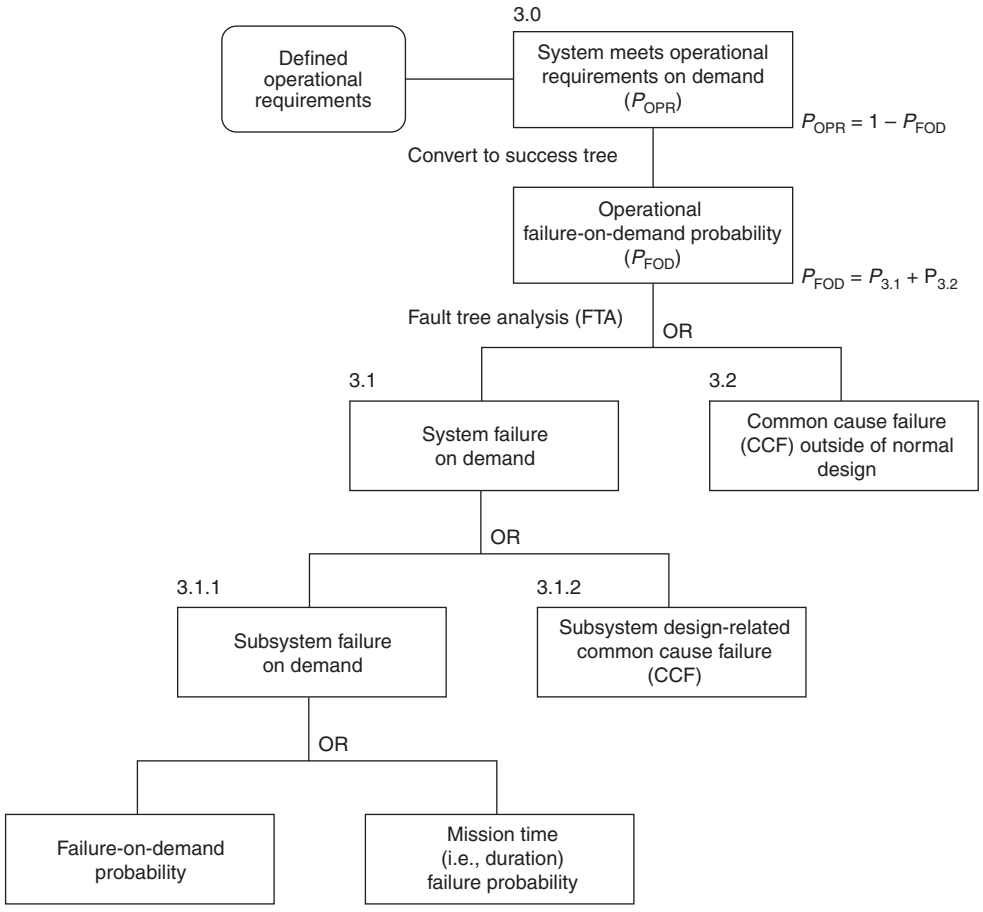

Figure 5-13.26. ***Operational reliability (OPR) success tree framework.***[10]

- Properly address operational requirements versus system redundancy features.
- Document the process and assumptions.

When evaluating operational reliability we are initially concerned with a first-order review. That is, the probability of operational success at demand of the subsystem elements and primary components which significantly contribute to the system level operational requirements.

Figure 5-13.27 provides an example of a first-order breakdown:

- System level
- Subsystems
- Subsystem elements or components
- Evaluation breakdown

Input ➔ control ➔ output: In evaluating FPS system failure on demand potential, one can subdivide the system or subsystem interface into an Input ➔ Control ➔ Output evaluation. Table 5-13.7 summarizes this for some systems.

OPR Quantification

As illustrated in Figure 5-13.28, there can be numerous failure data inputs needed to assess the overall failure-on-demand potential. In many cases the failure data will have to be adjusted or modified based on plant-specific conditions, the quality grading of the performance integrity measures, and engineering judgment.

The failure data sources used in the evaluation should be listed. Remarks might include what failure rate adjustment method was applied if applicable. Some primary failure data sources are listed in Table 5-13.8.

Plant-specific data: Plant data are the best data to compile and apply because they are specific to the process, environment, inspection, and maintenance testing practices.

Drawbacks of this approach are that sufficient plant-specific historical (operational) data may not be available and that available data may not pertain to a specific system but to subsystems or components of different manufacture, design, size, and ratings.

If sufficient operational history pertaining to a particular FPS system or subsystem is available, it may provide accurate estimates of reliability. However, in many situations, the available data may be very limited and the estimation of reliability from such a limited amount of data may be accurate in an order-of-magnitude sense only.

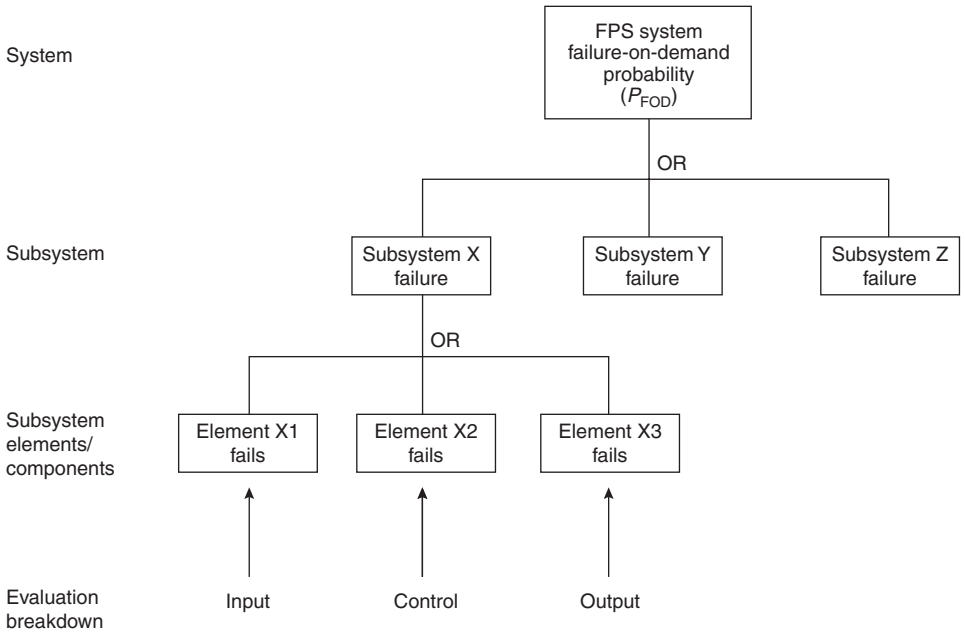

Figure 5-13.27. ***Example of FPS subsystem breakdown.[10]***

Table 5-13.7 ***Example Input → Control → Output[10]***

System	Input	Control	Output
Detection System	Detection Devices	Control Panel	Alarms/Interlocks
Emergency control system	Detection/alarm inputs	Control unit(s) (PLC—programmable logic controller)	Emergency shutdown or startup interlocks
Fire suppression systems (i.e., a sprinkler or water spray system)	Water supply • tanks • pumps	Water distribution • piping • valves • components	Water flow at nozzles • piping • sprinkler heads/water spray nozzles
Fire barrier system	Barrier components • doors • dampers • penetrations	Barrier integrity • components • structural stability of wall	Fire resistance • tightness • duration

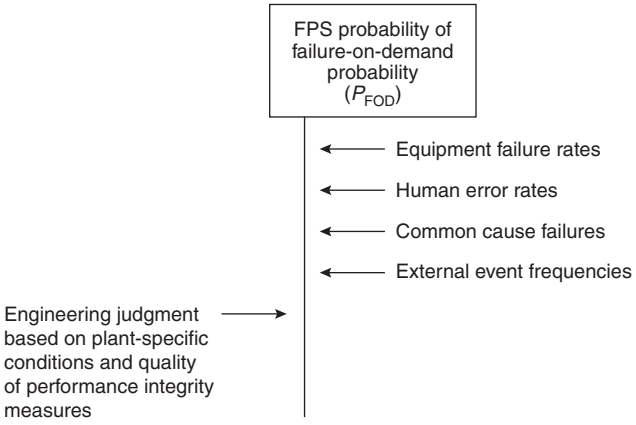

Figure 5-13.28. ***Failure data inputs.***

The advantages of gathering plant-specific data are that they reflect the plant's historical loss profile based on specific

- Design factors
- IMT programs
- Operating procedures
- Management loss control programs

The realities of collecting plant-specific data include

- Many failures and near-loss incidents are not recorded.
- Raw data in maintenance and operation logs may be incomplete and are usually not in a form readily usable for failure and reliability analysis.
- The population or operating time of a facility, process, or equipment may be limited and thus not reflect the long-term failure potential.

Table 5-13.8 ***Some Failure Data Sources***

Data Type	Data Source
Plant-specific data	• Plant records • Plant walkdowns and interviews
Equipment manufacturers' data	• Equipment components—mean time between failure (MTBF) data • System-level reliability data
Relative failure incident data	• Industry associations • Insurance companies
Published failure rate data	• Industry-specific data • Generic failure rate data
Human error data	• Plant records • Generic human reliability data
External event data	• Plant data • Natural event databases
Judgmental data	• Internal expert opinion

Methods that can be applied to compile plant-specific information include

- Conduct structured interviews with plant personnel who have experience in the operations and maintenance of the facility or operation being evaluated, to categorize the potential likelihood of events based on historical experience.
- Compile plant site raw data into a database format.
- Conduct an audit of the plant's management loss control programs. This can be used as input and support for modifying historical failures based on present plant practices.

Published failure rate data: Failure rate data can be preferably extracted from plant-specific data sources. This is the best source of data, and this type of data may be obtained from operational and maintenance logs and records and from numerous interviews conducted with experienced plant personnel. Engineering judgments concerning the use and adjustment of these data can be based on plant surveys, available data, interviews, and experience. Published popular failure rate data sources include the following:

Guidelines for Process Equipment Reliability Data, American Institute of Chemical Engineers, New York (1989).

IEEE Guide to the Collection and Presentation of Electrical, Electronic, Sensing Component, and Mechanical Equipment Reliability Data for Nuclear Power Generating Stations, IEEE Std 500-1984, Institute of Electrical and Electronics Engineers, Inc., New York, NY (1983).

OREDA Participants, *Offshore Reliability Data Handbook,* Penn Well Publishing Company, Hovik, Norway (1984).

Reliability Programs for Nonelectronic Designs, RADC-TR-83-85, Vols. 1 and 2, Rome Air Development Center, Griffiss Air Force Base, NY (1983).

Nonelectronic Parts Reliability Data, NPRD-3, Reliability Analysis Center, Rome Air Development Center, Griffiss Air Force Base, NY (1985).

Nuclear Plant Reliability Data System: Annual Reports of Cumulative System and Component Reliability for Period from July 1, 1974, through December 31, 1982, NPRD AO2/AO3 (INPO 83-034), Institute of Nuclear Power Operations, Atlanta (1983).

Military Handbook for Reliability Prediction of Electronic Equipment, MIL-HDBK- 217E, U.S. Department of Defense, Washington, DC (1986).

Development of an Improved LPG Plant Failure Rate Data Base, Final report GRI-80/0093, Gas Research Institute, Chicago (1981).

Adjustment factor: In evaluating failure rate data from plant-specific records, published failure data, manufacturers' data, expert opinions, and so on, we will develop in most cases a bandwidth in failure rate range:

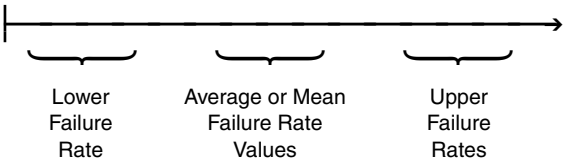

Three basic methods are used toward selecting a point failure rate for the OPR evaluation:

1. Select the mean value.
2. Use engineering judgment and expert opinion to adjust the mean value based on experience and plant-specific knowledge.
3. Use a performance integrity measure (PIM) quality rating (i.e., score card approach) to adjust the failure rate.

Method 3, illustrated in Figure 5-13.29, combines the first two methods and is intended to provide a consistent approach toward failure rate selection and is the preferred method.

The basic equation for estimating a likelihood within an equipment failure rate range is

$$\text{Frequency adjusted} = \text{Frequency historical mean or average} \times \text{MF}_{\text{PIM}} \text{ modification factor via performance integrity measures}$$

Likelihood estimate (i.e., adjusted (frequency)	Data • Plant • Industry • General	Quality grading of • Management factors • Facility, operations, equipment-specific factors

Performance integrity measures provide a set of descriptive measures that provide qualitative and semiquantitative grades of the quality of the FPS system reliability. The term *primary* is intended to indicate that the described set of measures account for greater than 95 percent of the expected reliability performance level.[10]

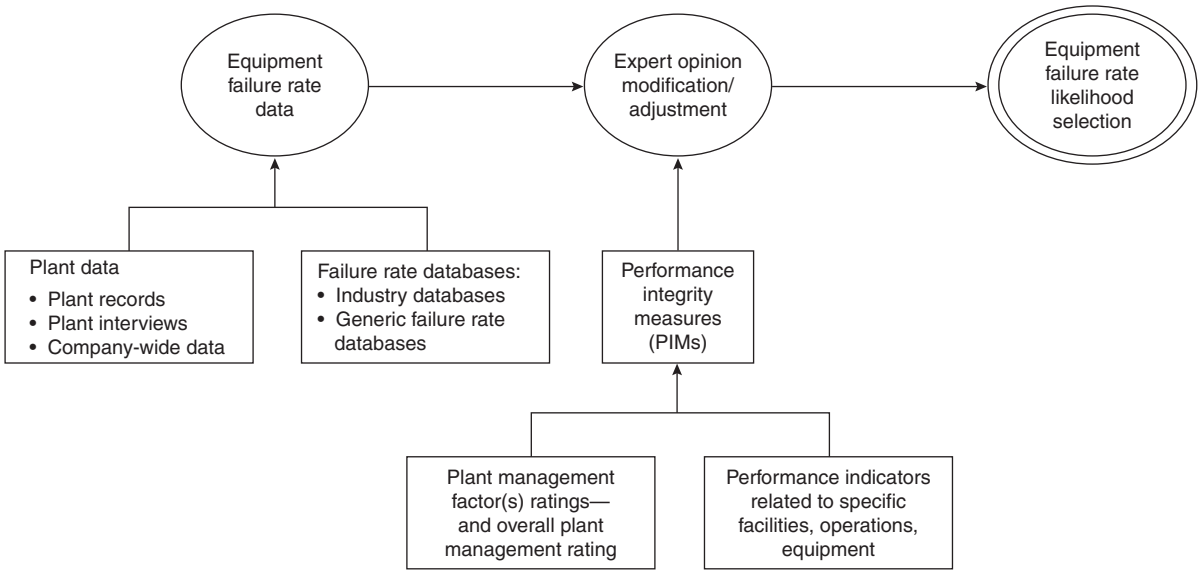

Figure 5-13.29. ***Example of general framework—adjusting historical data for equipment failure rate.[10]***

Some primary measures include

- General design standards
- Life cycle (Age)
- Management of change (MOC) program
- Inspection program
- Maintenance program
- Testing program
- Operating environment (vibration, dust, corrosion, etc.)
- Physical damage exposure (i.e., mechanical damage from equipment, vehicles)
- Redundancy
- Common cause failure potentials

Figure 5-13.30 provides an example of using published failure rate data[13] and applying the performance integrity meaure (PIM) weighted-scoring method[10] as a tool for selecting the most likely failure probability. In this figure, the failure rates are converted to failures per year as follows:

$$0.77 \text{ failures}/1{,}000{,}000 \text{ hr} \times 8760 \text{ hr/yr} = .006 \text{ failure/yr probability}$$

A simplistic linear interpretation of failure range versus PIM score is developed. A low PIM quality score would equate to a higher failure probability, and a high PIM quality score equates to a low failure probability. This method forces identification of factors that contribute to failures and provides a consistant evaluation approach, which includes plant-specific information.

Evaluation of the operational reliability aspect in terms of structuring the fault tree logic of subsystems and equipment components, along with compiling and selecting individual failure-on-demand probability, can be a time-consuming task.

The scope and complexity of the risk-informed, performance-based project that we are undertaking should dictate the level of detail needed and the overall approach. Approaches can include use of one or both of the following:

- Use of quality grading of PIMs in conjunction with engineering judgment and expert opinion to assign a reliability
- Performing fault tree analysis (FTA)

Figure 5-13.31 provides an example of the general framework for using PIMs to support reliability estimates.

As indicated under selection in Figure 5-13.31, the quality scoring or grading of the PIMs can be used in conjunction with engineering judgment and expert opinion to estimate a reliability or probability of failure on demand range. Table 5-13.9 provides on example of establishing this type of relationship.

This approach can be used as a first-order estimate of equipment or system reliability. Other issues which may still need to be addressed include common cause failures (internal and external).

Design standards versus OPR estimates: It would be nice if there were operational reliability ranges associated with full compliance with industry standards and practices, such as NFPA 20, *Standard for the Installation of Stationary Pumps for Fire Protection,* and NFPA 13, *Standard for the Installation of Sprinkler Systems.*

For example, if templates were developed that provided reliability benchmarks or reliability ranges related to meeting levels in design, in the standards, and in IMT frequencies, this would provide valuable input. However, at this writing, fire protection design codes, standards, and guidelines do not provide this type of information. Hopefully in the future, as the use of performance-based standards progresses, design versus quantitative reliability levels will become available for use.

Data on Selected Process Systems and Equipment								
Taxonomy No. 2.2.2				Equipment description ANNUNCIATORS				
Operating mode				Process severity UNKNOWN				
Population	Samples	Aggregated time in service (10^6 hr)			No. of demands			
		Calendar time	Operating time					
Failure mode		Failures (per 10^6 hr)			Failures (per 10^3 demands)			
		Lower	Mean	Upper	Lower	Mean	Upper	
Catastrophic a. Operates spuriously b. Fails to operate on demand		0.0272	0.77	2.90				
Degraded a. Operates at low intensity								
Incipient a. Arcing								

Equipment boundary

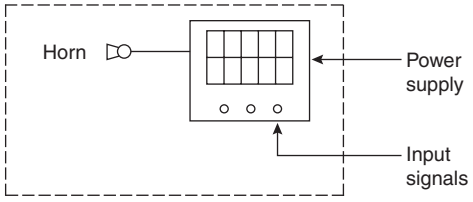

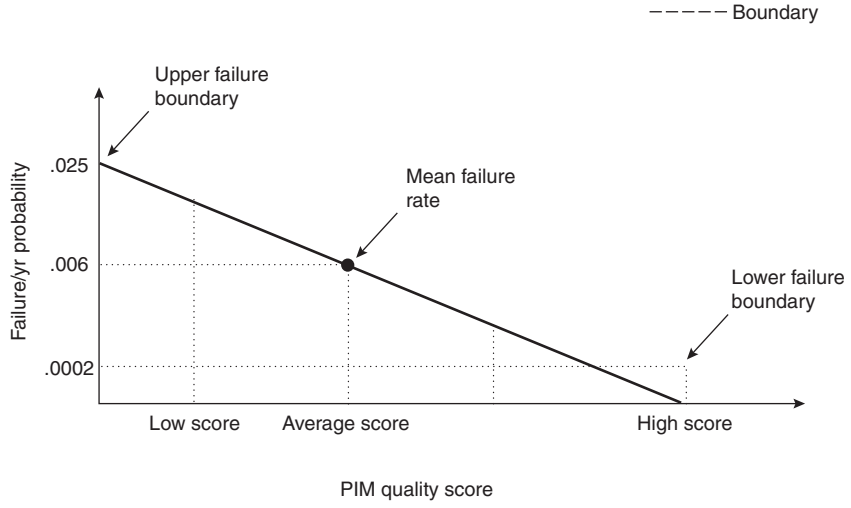

Figure 5-13.30. ***Example of failure rate range using PIM quality score.***[10,13]

Step 6: Risk Presentation

It is very important to integrate the large number of fire and explosion incident frequencies into a presentation format that will be easy to interpret and use by the management decision makers.

The most common risk assessment and presentation method is to multiply the frequency of fire and explosion incidents with the consequences and then sum these products for all scenarios considered in the risk assessment project. The aggregated results can be presented in terms of average exposure values; however, a better ap-

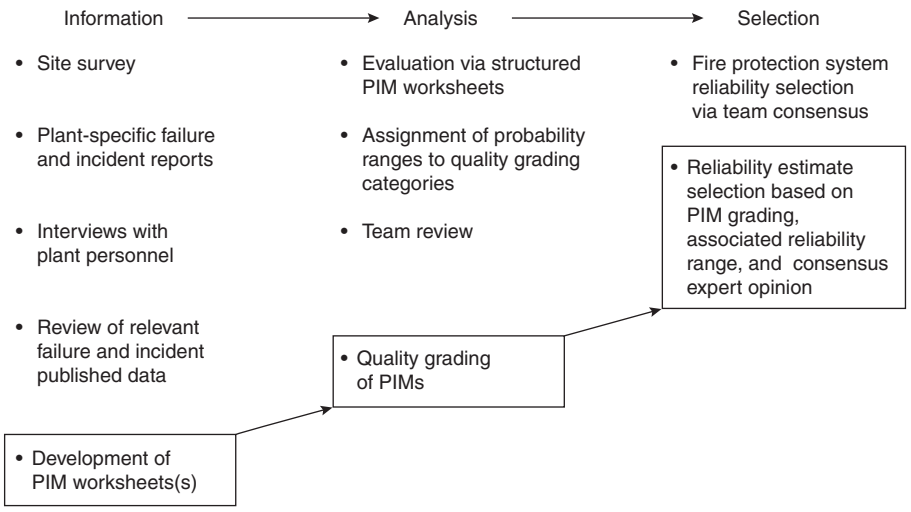

Figure 5-13.31. ***General framework—use of performance integrity measures (PIMs) to support reliability estimates.[10]***

Table 5-13.9 ***Example of Relating PIMs to Reliability Ranges[10]***

Performance Integrity Measure (PIM) Score/Grade	Reliability Range		Probability of Failure on Demand (P_{FOD}) (> 1 – Reliability)	
Very high	Very high	.99–.999	Very low	.01–.001
↓	High	.95 < .99	Low	.05 < .01
	Average	.90 < .95	Average	.10 < .05
	Low	.80 < .90	High	.20 < .10
Very low	Very low	< .80	Very high	> .20

proach is to present the results as a range defined by upper and lower uncertainty bandwidths (confidence limits) that contain the best estimates that can be made.

The objectives of risk presentation are threefold:

1. Provide presentation of estimated risk results in terms of a graphical risk profile or risk contour plot to aid management's understanding of the existing risk to the targets of interest as stated in the risk assessment objectives and acceptable risk limits.
2. Provide a graphical presentation of the differences in risk afforded by various risk reduction strategies to allow further cost–benefit assessment study, which may be a requirement of the specific risk assessment project.
3. Provide an uncertainty bandwidth (i.e., degree of confidence limits) associated with the above two items to allow management the opportunity to evaluate alternative risk management techniques (i.e., risk transfer by insurance). This is especially important for large consequence potentials which may be quantitatively classified as rare events that may also have a high degree of uncertainty in terms of the likelihood of occurrence.

The information provided in this step focuses on item 1 above (i.e., graphical presentation of risk results).

Risk Profiles

Developing a risk profile consists of structuring a graph that portrays the aggregate relationship between the expected frequencies of fire or explosion incidents and their consequences to selected targets. These graphs can be used to present property risk, business interruption risk, and human risk as illustrated in Figure 5-13.32.

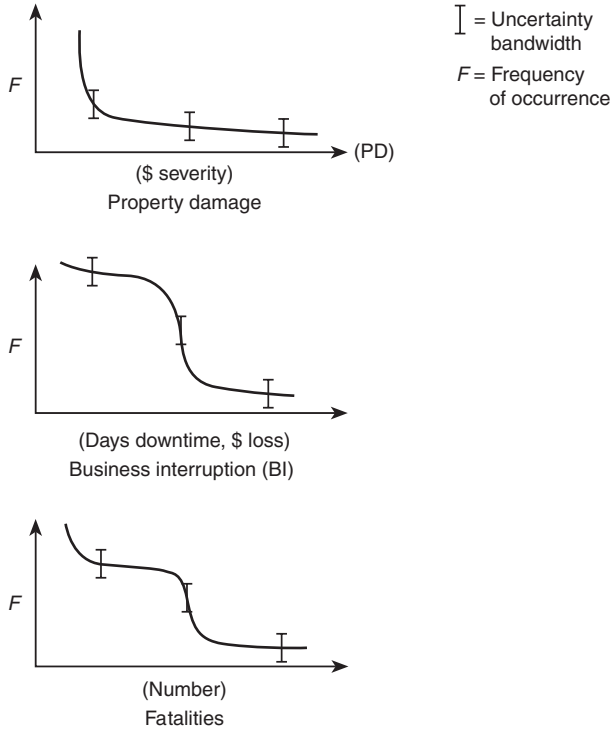

Figure 5-13.32. ***Example of general risk profiles.***

Risk profiles can be used to present the potential degree of individual risk versus distance from the fire or explosive source. Individual risk is the probability of injury or death to a person at a specified location relative to a defined point within the fire or explosion effect zone. An example of an individual risk profile is shown in Figure 5-13.33.

Risk Contours

Individual risk exposure is presented in many risk assessment studies in terms of a risk contour plot. (See Figure 5-13.34.) Developing a risk contour (sometimes called a risk isopleth) consists of structuring a closed line graphical depiction connecting lines of constant potential risk. Points within the contour represent a risk greater than or equal to the risk of the contour edge. Risk contour plots provide a good way of illustrating individual risk versus distance from defined fire or explosion incidents.

Individual risk contours show the geographical distribution of individual risk. The risk contours show the expected frequency of fires or explosions capable of causing a specified level of harm to an individual at a specified location, regardless of whether or not anyone is present at that location to suffer that harm. Reference 5 provides a good discussion on the various measures of individual risk, which includes maximum individual risk and average individual risk.

Societal Risk

Another measure of human risk is societal (sometimes called population) risk, which takes into account the likelihood of multiple casualties resulting from fires or explosions. Societal risk is often presented in the form of *F-N* curves, which are plots of the cumulative frequency (F) of multiple fatalities versus the number (N) of fatalities. Referring to Figure 5-13.35, the left axis is the frequency of exceeding a specified number of fatalities.[5,6]

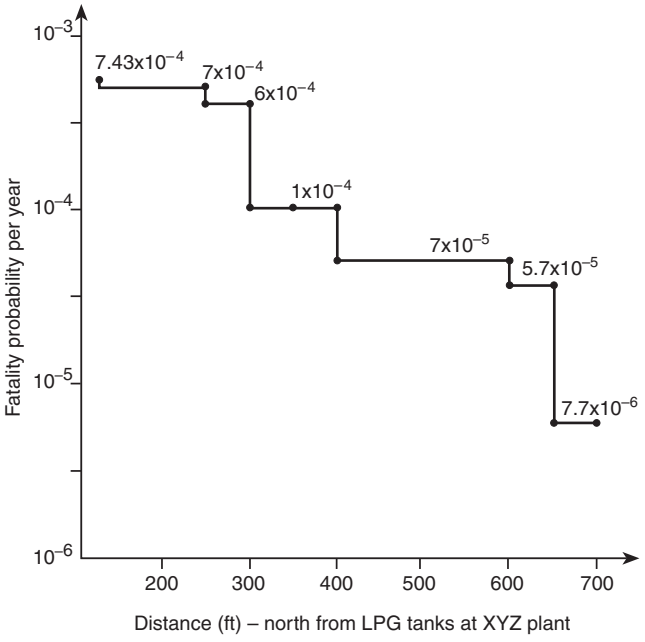

Figure 5-13.33. ***Example of individual risk profile graph.***

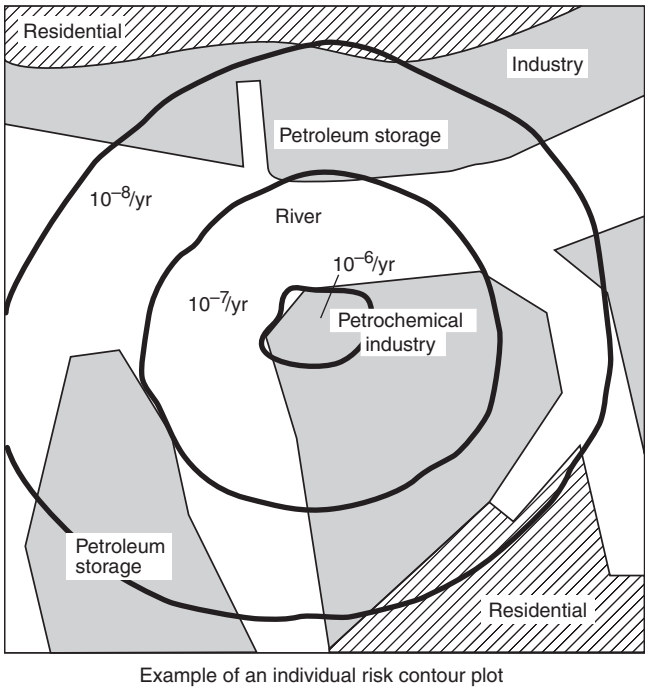

Figure 5-13.34. ***Example of an individual risk contour plot.***

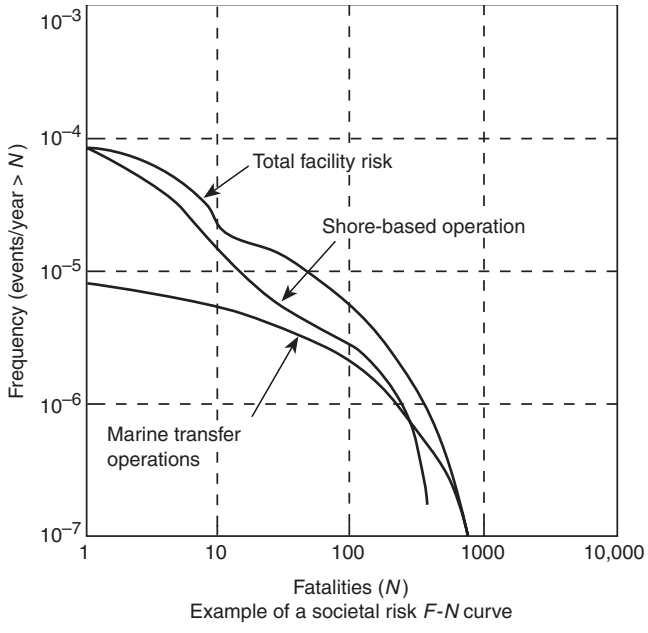

Figure 5-13.35. ***Example of a societal risk F-N curve.***

F-N-type curves can provide useful insight into the degree of risks from a facility or hazardous process to the employees on the plant site and to the community located beyond the plant boundaries. Assessing the risk beyond the plant line boundaries requires a definition of the population at risk (industrial, residential, school, hospital, etc.), likelihood of people being present, and reliability of mitigation factors (people evacuation procedures, etc.).

In constructing *F-N* curves, a logarithmic plot is usually used because the frequency of number of fatalities may range over several orders of magnitude. It is also sometimes useful to identify risk contributors directly in the graph, as illustrated in Figure 5-13.35.

In addition, societal risks can be expressed in the form of various risk indices, which generally provide a summation of risks from each accident and an annual predicted fatality rate. Risk indices usually provide an easily understood, single-value number to present the acute risk and are sometimes quite useful in comparing various engineering design and protection options. A ranking of the events that contribute most to the total risk is also very useful, as this allows the analyst to focus attention on the most critical failures and facilitates efficiency in assessing prevention and mitigation risk reduction options for those events.

Reference 5 provides descriptions of various risk indices and includes

- Fatal accident rate
- Individual hazard index
- Average rate of death
- Equivalent social cost index
- Mortality index
- Economic index

The majority of human risk (i.e., individual risk, societal risk) quantification is conducted on the basis of fatality effects. In evaluating fatal effects, there are uncertainties involved in exactly what constitutes a fatal dose of thermal radiation from a fire, explosion blast effects, or toxic chemicals, and therefore appropriate documentation must be provided for all assumptions and judgments. The same applies when it is desired to estimate potential human injuries in addition to fatalities.

In conducting cost/risk reduction benefit studies, it may be necessary to convert the element of human risk exposure into equivalent monetary terms.

Presentation Format Selection

The specifics of the presentation format should be included in Step 1; that is, define risk assessment objectives. (See Figure 5-13.1.) There is a major time and cost difference between generation of single-point estimates versus detailed generation of a series of risk contours. The following four factors should be considered in deciding which risk presentation forms are chosen:[5]

1. **User Requirements.** The user may have a specific need to see risk estimates in a certain format.
2. **User Knowledge.** Where the user is unfamiliar with presentation formats, sample formats should be presented to and approved by the user before any effort is made to secure approval for the scope of work.
3. **Effectiveness of Communicating Results.** It is vital that the presentation communicate the results in an acceptable fashion. The presentation should be as simple as necessary to ensure comprehension, but not so simple that resolution is lost or that bias is introduced.
4. **Need for Comparative Presentations.** It may be desirable to present comparisons of the results of a study with other risk assessments or risk data. This type of presentation might involve
   a. A comparison of alternate design, operation, or protection options
   b. A comparison of the current risk estimates with risk estimates of other similar systems studied previously, to highlight areas for risk reduction or further study
   c. A comparison of risk estimates with other voluntary and involuntary risks, to rank the current risk estimate among these reference values

Step 7: Risk Reduction Analysis

If the risk is unacceptable or uncertain, then engineering risk reduction analysis can be conducted. Risk reduction can be defined as the identification and selection of cost-effective options for reducing or mitigating unacceptable risks, including technological measures such as fire protection systems, management safety programs such as mechanical integrity programs, loss prevention programs, operator training, and emergency procedures.[5] Risk reduction analysis consists of systematic evaluation of measures to reduce the potential frequency and/or the severity of loss event occurrence.

Frequency Reduction

Incident frequency reduction methods include the following:

- Reduce equipment failure potential
  a. design
  b. testing
  c. preventive maintenance
- Reduce ignition potential
- Reduce human error
  a. operator procedures and training
  b. PSM programs

Severity Reduction

Fire detection and protection features that reduce potential severity levels can include

- Gas and fire detection systems
- Fireproofing structural steel and vessel supports
- Providing automatic or manual water sprays
- Providing monitor nozzles or hand-hose standpipes
- Installing foam protection systems

References Cited

1. *System Safety Analysis Handbook,* System Safety Society, Albuquerque, NM (1993).
2. Center for Chemical Process Safety, *Guidelines for Hazard Evaluation Procedures with Examples,* 2nd ed., American Institute of Chemical Engineers, New York (1992).
3. 29 CFR 1910.119, *Process Safety Management of Highly Hazardous Chemicals,* Occupational Safety and Health Administration, Washington, DC (1992).
4. Technical, Ltd., "Techniques for Assessing Industrial Hazards," *World Bank Technical Paper No. 55,* The World Bank, Washington, DC (1988).
5. Center for Chemical Process Safety, *Guidelines for Chemical Process Quantitative Risk Analysis,* American Institute of Chemical Engineers, New York (1989).
6. J. Whithers, *Major Industrial Hazards: Their Appraisal and Control,* Halsted Press, London (1988).
7. *Handbook of Chemical Hazard Analysis Procedures* (ARCHIE Manual), Federal Emergency Management Agency, Washington, DC (1989).
8. *Chemical Engineering Progress, Software Directory of Hazard and Risk Computer Models,* published annually by the American Institute of Chemical Engineers, New York.
9. D.F. Haasl, et al., *Fault Tree Handbook,* USNRC, *NUREG-0492,* Washington, DC (1981).
10. T.F. Barry, *Risk-Informed Performance-Based Fire Protection,* TFBarry Publications and the PLC Educational Foundation, Knoxville, TN (2001).
11. D.H. Slater, R.M. Pitblado, and J.C. Williams, "Quantitative Assessment of Process Safety Programs," *Plant/Operator Progress,* 9, 3, AIChE, New York (1990).
12. *PRA Procedures Guide: A Guide to the Performance of Probabilistic Risk Assessments for Nuclear Power Plants, NUREG/OR 300* (1983).
13. Center for Chemical Process Safety, *Guidelines for Process Equipment Reliability Data, with Data Tables,* AIChE, New York (1989).
14. M. Considine, G.C. Grint, and P.L. Holden, "Bulk Storage of LPG—Factors Affecting Offsite Risk," *The Assessment of Major Hazards,* American Institute of Chemical Engineers, Pergamon Press, New York (1982).

Additional Readings

American Petroleum Institute, "Management of Process Hazards," Recommended Practice 750, 1st ed., Washington, DC (1990).

G.E. Apostolakis, et al., *Accident Sequence Modeling: Human Actions, System Response, Intelligent Decision Support,* Elsevier Science Publishing Co., Inc., New York (1988).

J. Bond, "The International Safety Rating System or the Five Star Audit System," *Loss Prevention Bulletin No. 80,* UK Institution of Chemical Engineers (1988).

T.A. Braustowski, "Risk Assessment in Large Chemical Energy Projects," in *Technological Risk, Proceedings of a Symposium on Risk in New Technologies, University of Waterloo, Dec. 1981,* University of Waterloo Press, Waterloo, Ontario (1982).

L. Bretherick, *Handbook of Reactive Chemical Hazards,* 4th ed., Butterworth's, London (1990).

Canvey: An Investigation, Health and Safety Executive, Her Majesty's Stationery Office, London (1978).

Canvey: A Second Report, Health and Safety Executive, Her Majesty's Stationery Office, London (1981).

M.L. Casada et al., "Facility Risk Review as an Approach to Prioritizing Loss Prevention Efforts," *Chemical Engineering Progress* (1990).

V.T. Covello et al. (eds.), *The Analysis of Actual Versus Perceived Risks,* Plenum Press, New York (1983).

E.A.C. Crouch and R. Wilson, *Risk/Benefit Analysis,* Ballinger Publishing Company, Cambridge, MA (1982).

Dow Chemical Company, *Fire and Explosion Index Hazard Classification Guide,* 7th ed., American Institute of Chemical Engineers, New York (1989).

J.P. Drago, R.J. Borkowski, D.H. Pike, and F.F. Goldberg, "The In-Plant Reliability Data Base for Nuclear Power Plant Components: Data Collection and Methodology Report," *NUREG/CR-2641, ORNL/TM-9216,* Jan. 1985.

J. Gillett, "Rapid Ranking of Process Hazards," *Process Engineering,* 66, 219 (1985).

H.R. Greenberg and J.J. Cramer (eds.), *Risk Assessment and Risk Management for the Chemical Process Industry,* Van Nostrand Reinhold, New York (1991).

Guide to the Collection and Representation of Electrical, Electronic, Sensing Component, and Mechanical Equipment Reliability Data for Nuclear Generating Stations, IEEE Std. 500-1984, Institute of Electrical and Electronic Engineers, New York (1984).

E.J. Henley and H. Kumamoto, *Reliability Engineering and Risk Assessment,* Prentice Hall, Englewood Cliffs, NJ (1981).

W.G. Johnson, *MORT, The Management Oversight and Risk Tree,* U.S. Atomic Energy Commission, Washington, DC (1983).

T.A. Kletz, *An Engineer's View of Human Error,* The Institution of Chemical Engineers, Warwickshire, UK (1983).

S.A. Lapp, "The Major Risk Index System," *Plant/Operations Progress,* 9, 3 (1990).

F.P. Lees, *Loss Prevention in the Process Industries,* Butterworth's, London (1980).

D.J. Lewis, "Mond Fire, Explosion, and Toxicity Index: A Development of the Dow Index," *13th Annual Loss Prevention Symposium,* Houston, American Institute of Chemical Engineers, New York (1979).

D.K. Lorenzo, *A Manager's Guide to Reducing Human Errors—Improving Human Performance in the Chemical Industry,* Chemical Manufacturers Association, Washington, DC (1990).

W.W. Lowrance, *Of Acceptable Risk,* William Kaufmann, Inc., Los Altos, CA (1976).

A. Mazzocchi and M. Campona, "Risk Analysis of a Large Farm of Liquefied Petroleum Gases," *Reliability Data Collection and Use in Risk and Availability Assessment* (H.J. Wingender, ed.), in *Proceedings of the 5th Euredata Conference,* Heidelberg, Germany, Springer-Verlag Press, New York (1986).

K. Mudan and R. Gustafson, "Ignition Potential Distribution for Heavy Gas Plumes," *International Conference on Vapor Cloud Modeling,* American Institute of Chemical Engineers, New York (1987).

Tools for Making Acute Risk Decisions, Center for Chemical Process Safety (CCPS) of the American Institute of Chemical Engineers, New York (1995).

Offshore Reliability Data Handbook, OREDA-84, Pennwell Publishing Company, Tulsa, OK (1984).

"Procedures for Performing a Failure Mode, Effects, and Criticality Analysis," *MIL-STD-1629A,* Department of Defense, Washington, DC (1980).

R.W. Prugh, "Evaluation of Unconfined Vapor Cloud Explosion Hazards," *International Conference on Vapor Cloud Modeling,*

Cambridge, MA, American Institute of Chemical Engineers, New York (1987).

C.G. Ramsey, R. Evans, and M.A. English, "Siting and Layout of Major Hazardous Installation," *The Assessment of Major Hazards,* Institution of Chemical Engineers, Pergamon Press, New York (1982).

D.J. Rasbash, "Criteria for Acceptability for Use with Quantitative Approaches to Fire Safety, *Fire Safety Journal,* 8 (1984).

"Risk Analysis in the Process Industries," *European Federation of Chemical Engineering Publication No. 45,* The Institution of Chemical Engineers, Rugby, UK (1985).

Risk Analysis of Six Potentially Hazardous Industrial Objects in the Rijnmond Area; A Pilot Study, D. Reidel Publishing Company, Dordrecht, Holland (1982).

W.D. Rowe, *An Anatomy of Risk,* John Wiley and Sons, New York (1977).

J.H. Shortreed and A. Stewart, "Risk Assessment and Legislation," *Journal of Hazardous Materials,* 20, pp. 315–334 (1988).

J. Stephenson, *System Safety 2000—A Practical Guide for Planning, Managing, and Conducting System Safety Programs,* Van Nostrand Reinhold, New York (1991).

The Mond Index, 2nd ed., Imperial Chemical Industries, Winnington, Northwick, Cheshire, UK (1985).

R.A. Waller and V.T. Covello (eds.), *Low-Probability/High-Consequence Risk Analysis,* Plenum Press, New York (1984).

CHAPTER 14

Fire Risk Assessment for Nuclear Power Plants

Nathan Siu

Introduction

Probabilistic risk assessment (PRA), the process of (a) identifying potentially important accident scenarios, (b) determining their consequences, and (c) assessing their likelihood,[1] has been used to evaluate the risk associated with the generation of electric power from nuclear plant operation since the landmark "Reactor Safety Study" (WASH-1400) published in 1975.[2] PRA, also referred to in the literature as probabilistic safety assessment (PSA), provides a systematic approach for assessing plant behavior (including interactions with other systems) under a variety of conditions, sensitivities, and areas of uncertainty and importance. It has proven to be a useful tool for supporting risk management activities by showing where finite resources can be effectively applied to maintain or improve safety.[3,4] PRA studies have been performed for all operating nuclear power plants in the United States and for many plants abroad. Considerable effort has gone not only into the performance of these studies but also into the development of general and application-specific approaches for using the insights and results that are acceptable to the regulators.[5]

Within the framework of nuclear power plant PRA, fire risk assessment for nuclear power plants (henceforth referred to in this chapter as *fire PRA*) is the process used to determine the risk contribution associated with fires starting within the boundaries of a given plant. Thus, a fire PRA identifies potentially important fire-initiated accident scenarios, determines their consequences, and assesses their likelihood. The results of the assessment are typically used to determine if and what changes should be made to a plant's fire protection program. Furthermore, although there are a number of methodological issues concerning the fire PRA state of the art, the results of the assessment are often compared with the results associated with other potential accident initiators (e.g., pipe breaks, losses of off-site power, earthquakes) to support the rational allocation of safety resources across a broad spectrum of hazards.[6]

As will be discussed later in this chapter, the results of numerous fire PRA studies have shown that fire can be a significant or even dominant contributor to the overall risk for a given nuclear power plant. Lessons learned from a number of serious events, including Browns Ferry (United States, 1975),[7] Armenia (Armenia, 1982),[8] Vandellos (Spain, 1989),[9] and Narora (India, 1993),[10] further emphasize fire's potential importance.

Whether or not fire is an important risk contributor at a particular plant is determined by differences in such plant-specific details as the routing of key electrical cables, the separation and orientation of important cable trays, the fire protection scheme used for a particular compartment, and the procedures employed by plant operators in response to a fire. Fire PRA is a quantitative tool for addressing these details and showing how they relate to risk. It provides a systematic framework for addressing the complex phenomenology underlying a fire in an explicit manner. It uses a wide variety of information sources (e.g., model predictions and reported event data), and provides a risk context for discussions of areas with significant controversies and uncertainties.

Numerous papers and reports have been written on fire risk assessment for nuclear power plants. The objective of this chapter is to provide a general review of the subject. The chapter presents some key characteristics of fire PRA, a discussion of the fire PRA methodology employed by most current studies, a summary of the results of a number of analyses, and a brief discussion of current activities and anticipated future developments. The focus is on fire PRA for U.S. plants. Additional details on the topics discussed and on international applications can be

Dr. Nathan O. Siu is a senior technical adviser in the Office of Nuclear Regulatory Research of the U.S. Nuclear Regulatory Commission. His major activities involve the development of improved methods for probabilistic risk assessment, including fire risk assessment.

found in the references and additional reading list provided at the end of the chapter.

Nuclear Plant PRA and Fire PRA

Broadly speaking, fire risk assessment for nuclear power plants (fire PRA) has many of the characteristics of fire risk assessments for nonnuclear industrial facilities (e.g., see Section 5, Chapter 13, "Quantitative Risk Assessment for the Chemical Process Industries"). However, because fire PRA is performed within the context of an overall nuclear power plant PRA and because the latter has evolved a specific structure to support particular decision-making needs, fire PRA has a number of technical characteristics which can distinguish it from fire risk assessments for other applications.

First, as in the overall nuclear power plant PRA, the risk of concern is associated with the health and safety of the general public. (Fire risk assessment methods can be applied to plant worker safety and economic issues, but have not been to date.) One of the conclusions of WASH-1400 was that only accidents involving severe damage to nuclear fuel in the reactor core (i.e., core damage) have the potential for risk-significant radiological releases. Therefore, fire PRA studies focus on accident scenarios that lead to core damage. In particular, because the nuclear fuel is surrounded by cooling water in the most prevalent reactor designs, most studies focus on accident scenarios in which a fire causes a loss of fuel cooling and subsequent core damage. (Note that recent concerns regarding zirconium fires in the spent fuel pools of decommissioning plants have prompted a re-examination of the risk associated with noncore damage events.)

Second, because of the design and operational characteristics of nuclear power plants, the fire PRA studies typically focus on scenarios that involve fire-induced damage to electrical equipment (especially cables) which both initiates and exacerbates an accident scenario. Nuclear power plants are generally designed to spend most of their operating life in a steady-state power-producing mode. The integrity of the reactor core can only be challenged if an upset condition—that is, a plant *transient* (e.g., a loss of normal cooling)—occurs and redundant plant systems provided to mitigate the transient (e.g., by providing emergency cooling) fail to function. Because the independent occurrence of a severe fire, a transient, and the loss of redundant mitigating systems is extremely unlikely, risk-significant fire scenarios typically involve a transient caused by the fire (e.g., a loss of off-site power to plant systems caused by fire-induced damage to equipment, a reactor shutdown performed by plant operators in response to a major fire) and fire-induced loss of some or all of the mitigating systems' functions. In general, the major mechanical components (e.g., pumps, motors, valves) of the mitigating systems are relatively robust with respect to the effects of a distant fire, separated from redundant components by barriers or open space, and located in areas of relatively low fire hazard. The focus, therefore, is on scenarios that involve fire-induced damage to the less robust electrical equipment supporting these components. Electrical cables are particularly important because cables servicing redundant equipment can, in some key areas in some plants, be vulnerable to the effects of a single fire. (Note that cable failures can occur in various ways, e.g., conductor-to-conductor shorts vs. conductor-to-ground shorts. Because these different cable failure modes can have different system impacts, e.g., component spurious actuations vs. loss of component function, they need to be explicitly addressed in fire PRA.) Electrical cabinets are also important for similar reasons.

Third, fire PRA studies generally use the core damage frequency (CDF) as the principal index of scenario risk significance. (As discussed later in this chapter, the CDF is a measure of the likelihood of core damage.) In other words, the studies usually do not directly assess the public health risk associated with fire-initiated accidents. This focus is largely due to the prominence of CDF in past and current approaches to risk-informed decision making.[3–5,11] It should be noted that although the analysis of public health risk is complex and subject to considerable uncertainty (the analysis requires, among other things, assessments of postcore damage accident progression, radiological transport in the environment, and the emergency response of the surrounding population), analyses have been performed for a limited number of plants. However, the analysis is not unique to fire-initiated accidents—fire provides only one of a number of potential mechanisms for core damage.

Fourth, those fire PRA studies that quantitatively treat uncertainties do so within the methodological framework employed by the overall plant PRAs. This framework distinguishes between aleatory (also called random or stochastic) uncertainties and epistemic (also called state of knowledge) uncertainties.[12–15] The former address situations where repeated observations of the variable of interest, under a specified set of conditions, lead to a distribution of outcomes for the variable. This uncertainty is irreducible—until the conditions are more tightly specified. The latter address situations where there is weakness in the state of knowledge of the assessor. These uncertainties can be reduced with additional information (e.g., additional observations). For example, the likelihood of observing a specified number of fire events in a given room over a given time period is typically modeled in fire PRA studies using a Poisson distribution (see the next section for more details). Since the number of fire events is a random variable, this Poisson distribution therefore quantifies aleatory uncertainty. On the other hand, the value of the single parameter which characterizes the Poisson distribution—that is, the room fire frequency—typically is not known with certainty. Since the uncertainties in this parameter can be reduced (with more data for the room or similar rooms), the probability distribution for the room fire frequency quantifies epistemic uncertainty. The distinction between aleatory and epistemic uncertainties is useful for decision making because it helps identify appropriate risk management options (e.g., to reduce uncertainties that are reducible). In addition, it forces a careful consideration of the meaning of the various probability distributions used in a risk assessment.

Finally, fire PRA has not been applied, or has been applied in a very limited fashion, to a number of issues which also have received no or reduced coverage from general PRA studies. These issues include the risk due to accidents during low power and shutdown plant operation modes, the risk due to accidents involving fuel outside of the reactor vessel (e.g., in spent fuel pools), and the risk associated with acts of sabotage. Sabotage is explicitly excluded from the scope of general PRA studies. In fire PRA studies, it is typically assumed that the data used in the analysis are associated with accidental fires. Of course, this assumption will yield conservative predictions concerning accidental fire risk in cases where intentional fires are included in the database.

Fire PRA Structure and Methodology

Overview

Fire risk assessment for commercial nuclear power plants, as it is performed today, is little changed from the analytical process used in the Zion[16] and Indian Point[17] PRA studies of the early 1980s and described by Apostolakis et al.[18,19] and in the PRA Procedures Guide.[20] Weaknesses in the elements of the approach (i.e., the data and tools for specific portions of the analysis) have been identified and progressively addressed in a number of studies.[21,22] Furthermore, a number of remaining weaknesses in these elements (e.g., in the treatment of fire phenomenology) are the subject of discussion and ongoing research, as discussed at the end of this chapter. However, the basic structure of the analysis has remained relatively constant.

In a typical fire PRA, the core damage frequency contribution due to a given fire scenario (where, in this discussion, a fire scenario is defined by the location and burning characteristics of the initiating fire) can be divided into three components:

1. Frequency of the fire scenario
2. Conditional probability of fire-induced damage to critical equipment given the fire
3. Conditional probability of core damage given the specified equipment damage

Formally accounting for the possibility of different levels of equipment damage and different plant responses following fire initiation, the core damage frequency (CDF) is given by

$$\mathrm{CDF} = \sum_i \lambda_i \left[\sum_j p_{\mathrm{ed},j|i} \left(\sum_k p_{\mathrm{CD},k|i,j} \right) \right] \qquad (1)$$

where

λ_i = frequency of fire scenario i

$p_{\mathrm{ed},j|i}$ = conditional probability of damage to critical equipment set j given the occurrence of fire scenario i

$p_{CD,k|i,j}$ = conditional probability of core damage due to plant response scenario k given fire scenario i and damage to critical equipment set j

Note that the second term addresses the issues of fire growth, detection, suppression, and component damageability, and that the third term addresses the unavailability of equipment unaffected by the fire and/or operator failures.

The three-term decomposition of fire risk presented in Equation 1 is not unique—alternate decompositions (often involving more terms) can be found in the literature. From the standpoint of this chapter, however, it is useful because each of the three terms tends to be addressed differently in current fire PRA studies. In particular, the fire frequencies are generally estimated using simple statistical models for fire occurrences, the likelihood of fire damage is estimated using combinations of deterministic and probabilistic models for the physical processes involved, and the likelihood of core damage is estimated using conventional probabilistic risk assessment systems models. The three-term decomposition is also useful because it directly corresponds to the elements of fire protection defense in-depth for nuclear power plants: fire prevention, fire detection and suppression, and fire mitigation.

The general process used to perform the fire PRA involves plant familiarization activities (including design reviews and plant walkdowns) as well as activities to assess each of the terms in Equation 1. The plant familiarization activities are performed to identify and characterize, for each fire area in the plant, potentially important fire initiation scenarios and potentially important target components, including cables. (Note that the term *fire area* is used in this chapter in a generic sense to refer to compartments and fire zones which may not be separated by rated fire barriers, as well as areas which are separated.) Qualitative screening (e.g., using criteria provided in FIVE[23]) is then done to identify areas and scenarios which need not be quantitatively analyzed because they are not expected to contribute to the fire risk. Following qualitative screening, conservative quantitative analyses are usually performed in initial evaluations of Equation 1 to identify additional areas and scenarios which can be screened from detailed analysis. Iterative approaches using progressively more accurate models are then employed to focus analysis resources on those scenarios that contribute most to risk. For example, in many analyses, the term $p_{\mathrm{ed},j|i}$ is initially assumed to be unity; it is only addressed more realistically for those areas where a detailed analysis is needed. The results of the analysis are typically presented on a fire area by fire area basis.

Descriptions of the general fire PRA methodology used in more recent studies can be found in a variety of references. Bohn and Lambright[24] describe the approach used in the NUREG-1150 PRA studies sponsored by the U.S. Nuclear Regulatory Commission (NRC). Guidance developed by the Electric Power Research Institute (EPRI) to address NRC requirements for Individual Plant Examinations of External Events (IPEEEs)[25,26] is presented in the documentation of the Fire-Induced Vulnerability Evaluation (FIVE) methodology[23] and extended by Parkinson et al. in the EPRI Fire PRA Implementation Guide (FPRAIG).[27] A PRA procedures guide, which provides useful information on the interactions between the fire PRA and the overall PRA, has recently been developed to support PRA for Russian reactors.[28] This guidance is generic enough to be applicable

to other reactor types as well. Widely available references documenting plant-specific fire PRA studies (including the study methodologies and data) include the NUREG-1150 studies (e.g., see Bohn et al.[29]), the Risk Methods Integration and Evaluation Program (RMIEP) analysis of the LaSalle plant (see Lambright et al.[22]), and the Surry plant shutdown risk study (see Musicki et al.[30]). More narrowly focused references relevant to specific aspects of the fire PRA methodology are provided in the following discussion of current approaches for performing the analyses underlying the three terms in Equation 1.

Fire Frequency Analysis

A fire frequency analysis involves the definition of representative fire scenarios for the fire area of interest, and the estimation of the frequency (i.e., the quantification) of these scenarios. Depending on the particular objectives of the fire PRA and the potential risk significance of the fire area, the scenarios can be defined in a broad or detailed manner. For example, for areas where a conservative analysis is sufficient, the representative fire scenario can be defined as a fire anywhere in the area. For areas where a more detailed analysis is needed, multiple fire scenarios defined in terms of the precise location and initial magnitude may need to be specified. The quantification process generally involves the statistical analysis of historical data, and the application of judgment.

The statistical analysis is generally done on an area basis or a component basis. The first approach involves the estimation of fire frequencies for different fire areas (e.g., main control room, cable spreading room, switchgear room) or groups of fire areas (e.g., auxiliary building, turbine building). The second approach involves the estimation of fire frequencies for different component types (e.g., pumps, electrical panels, transformers, transient combustibles). In both approaches, it is assumed that fire frequencies are constant over time, that is, that fire occurrences are Poisson events. In other words, the probability of observing N fire scenarios of type i in a time interval of length t is given by the Poisson distribution:

$$P(N \text{ occurrences in time } t) = \frac{(\lambda_i t)^N}{N!} \cdot e^{-\lambda_i t} \qquad (2)$$

where λ_i is, as defined previously, the frequency of fire scenario i (e.g., a fire in the cable spreading room). It can be shown that if t_i represents the time to the first occurrence of fire scenario i, the probability of observing such a scenario before a given time t is given by

$$P(\tau_i < t) = 1 - e^{-\lambda_i t} \approx \lambda_i t \text{ when } \lambda_i t < 0.1 \qquad (3)$$

As λ_i increases, the probability of observing the first occurrence of scenario i by a specified time also increases. It turns out that the average time to the first event is equal to $1/\lambda_i$.

As noted above, a key assumption in the Poisson model for event occurrences is that the characteristic frequency (λ_i in this case) is constant over time. A recent NRC report shows that the frequencies of reported fires in key U.S. nuclear power plant compartments have not changed dramatically when comparing the periods 1965–1985 and 1986–1994, and thereby supports the use of the Poisson model for U.S. nuclear power plant fire occurrences.[31]

In principle, it should be expected that the fire scenario frequencies will vary from plant to plant due to differences in plant design, operation, and maintenance practices. A number of fire PRA studies have developed plant-specific estimates for the λ_i using standard Bayesian procedures.[32] Generic industry data (in the form of n occurrences in time t, grouped by the scenarios defined in the fire PRA, and screened to exclude such events as fires during construction) are used to develop a prior distribution, which is then updated using plant-specific data. A more sophisticated two-stage Bayes approach which statistically accounts for plant-to-plant variability in the generic data, described by Kazarians and Apostolakis,[33] has been used in a few studies. Most studies, however, have used simple point estimates of the fire frequencies based on generic industry data.[23,27] The epistemic uncertainties in the λ_i, which can be considerable, are unquantified in this point estimate approach.

Regarding the role of analyst judgment in fire frequency analysis, it is especially significant when estimating the frequencies of detailed scenarios, for example, fires in a particular portion (location) of a cable spreading room that have a particular severity. Judgment is needed to partition the statistically estimated frequencies (e.g., for cable spreading room fires) when analyzing detailed scenarios because the available fire data are too sparse to allow direct estimation of the frequencies of such potentially challenging fires. In some fire PRA studies, location fractions are employed to reduce plant area–based fire frequencies to account for geometrical factors. Other studies use plant component–based fire frequencies[23,27] for this same purpose. In many others, severity fractions are widely used to address the fraction of fires (in a given compartment or involving a given component) that have the potential to cause significant damage in a relatively short amount of time. Note that the use of severity factors implicitly takes some credit for fire suppression activities. Care must be taken when analyzing fire detection and suppression (as discussed in the following section) to avoid double-counting the effectiveness of detection and suppression.

Equipment Damage Probability

Given a fire in a nuclear power plant compartment, the conditional probability of damage to key equipment (i.e., $p_{\text{ed},j|i}$ needs to be determined. In a detailed fire PRA study, the assessment typically involves the following:

1. A prediction of the fire-induced environmental conditions
2. An assessment of the equipment response to these conditions
3. An assessment of the effectiveness of fire barriers
4. An assessment of the likelihood that the fire will not be detected and suppressed before equipment damage occurs

Regarding the third item, the index j in $p_{\text{ed},j|i}$ accounts for the possibility of multiple equipment damage scenarios due to a single initiating fire scenario. Therefore,

as appropriate, the analysis also needs to consider the effectiveness of fire barriers in preventing fire damage to protected equipment in the room of fire origin and in preventing fire propagation to neighboring compartments.

Based upon the results of the fire environment, equipment response, and suppression analyses, the probability of equipment damage is, in principle, determined using a competing risks model formulated by Apostolakis et al.[18,19] This model states that damage occurs if the time to fire-induced damage is less than the time to fire suppression, that is,

$$p_{\mathrm{ed},j|i} = P(T_{d,j|i} < T_{s|i}) \tag{4}$$

where $T_{d,j|i}$ is the damage time for equipment set j given fire scenario i, and $T_{s|i}$ is the suppression time for fire scenario i.

The elements of the model are represented schematically in Figure 5-14.1. This figure shows model-predicted environment temperatures over time, the resulting time-dependent response of a target (which determines when target damage is predicted to occur), and a stochastic model for the suppression time whose results are compared against the predicted damage time. Note that the presence of barriers will affect the environment seen by the target. Current approaches used to perform these analyses and quantify $p_{\mathrm{ed},j|i}$ are discussed below.

Fire Environment Analysis

Characterization of the fire-induced thermal environment for the purposes of fire PRA requires the estimation of the time-dependent temperature and/or heat fluxes in the neighborhood of the safety equipment of interest (i.e., the targets). This estimation requires the treatment of a variety of phenomena as the fire grows in size and severity. These phenomena include the spread of fire over the initiating component (or fuel), the characteristics of the fire plume and ceiling jet, the spread of the fire to non-contiguous components, the development of a hot gas layer, and the propagation of the hot gas layer or fire to neighboring compartments.

It should be noted that potentially risk-significant nuclear power plant fire scenarios have a number of characteristics which may not be directly addressed by fire models not explicitly designed to model these scenarios. These characteristics include a variety of source fire types (e.g., cable tray, electrical cabinet, liquid pool fires), the possibility of propagation through fuel arrays (e.g., cable tray stacks) prior to flashover, the lack of openings to the environment, the elevated location of many important fuel arrays (note that many plume correlations have been based on experiments where the fire is at ground level) and local obstructions (e.g., cable tray stacks) and barriers. In addition, since the overall concern of this portion of the fire PRA is the fire-induced damage of plant equipment, the analysis needs to address the response of the equipment to the fire. Fire models not designed for fire PRA may not have integrated component response models (discussed in the following subsection), which are convenient for an efficient analysis.

It should also be noted that fire PRA studies often require that fire modeling be done for a number of fire scenarios within a compartment. Different fire scenarios can be defined depending on the number of fixed and transient combustible sources and the variety of ventilation conditions, including possible changes (e.g., the opening of a fire door). Given that multiple compartments may need to be analyzed, the number of scenarios to be mod-

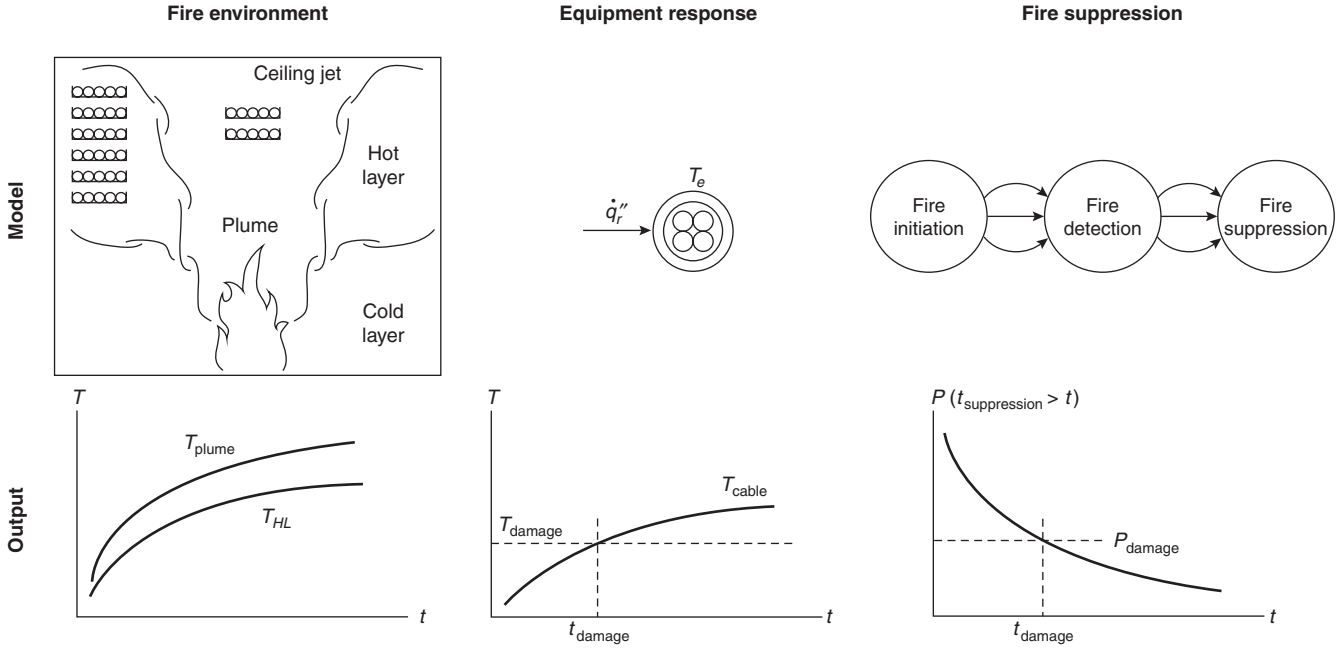

Figure 5-14.1. ***Equipment damage analysis submodels.***

eled can be quite large. Furthermore, in analyses involving formal uncertainty analysis, multiple analyses are required for a single scenario.

A variety of fire-modeling tools have been developed to address the above needs. In U.S. fire PRA studies, including the recent Individual Plant Examinations of External Events (IPEEEs), the most commonly used tools are those provided by the FIVE methodology,[23] COMPBRN IIIe,[34,35] and the methods described in the FPRAIG.[27] The scenarios addressed include cable fires, switchgear fires, oil pool fires, and transient fueled fires.

The FIVE fire models are designed to be used in a vulnerability analysis and are intended to be conservative. They are generally used to determine if, given a specified fire and targets, fire damage is possible. The models consider three key regions within the room: the plume, the ceiling jet, and the hot gas layer. Radiant transfer to targets outside of these regions is also considered. Fire growth is not modeled explicitly; the user is required to specify the physical characteristics (e.g., the location and intensity) of the fire.

The COMPBRN IIIe zone modeling code, similar to its predecessors, is designed to be used as an integrated part of a fire PRA. Thus, one of its key outputs is the predicted time to component damage, which can be compared with the suppression time, as shown in Equation 4. Moreover, recognizing that there are significant uncertainties in the model parameters (e.g., see Brandyberry and Apostolakis[36]), the code uses the distributions quantifying these uncertainties when developing a distribution for the time to damage. (Uncertainties in the model structure are treated separately, as discussed by Siu and Apostolakis[37–38] and Siu et al.[39])

COMPBRN IIIe explicitly addresses fire growth over fuel arrays (including lateral spread over cable trays) and allows for the possibility of growth to noncontiguous fuel cells (which will lead to multiple, interacting fires). It models radiative and convective transfer both inside and outside of the fire plume(s) and hot gas layer. Target heatup is addressed using a one-dimensional transient heat conduction model. The hot gas layer is treated quasistatically (note that it does change as the fire changes). Intercompartment fire spread is not treated.

The COMPBRN series of codes has undergone a limited amount of integral validation. (The code's submodels are largely based on experimental correlations and are therefore individually validated for those situations where the correlations apply.) The 20-ft separation tests documented by Cline et al.[40] have been used to benchmark COMPBRN III (see Ho et al.[41]) and IIIe (see Ho and Apostolakis[34]). The code appears to perform reasonably well, especially regarding the target temperature, which is the principal measure of interest. COMPBRN has also been applied to the Heissdampfreaktor (HDR) tests with mixed results (see Nicolette and Yang[42]). The results of the original version of COMPBRN were compared to data from a variety of fire configurations (including a set of heptane pool fires, a wood crib fire, and a vertical cable tray fire).[43] Finally, COMPBRN IIIe explicitly addresses issues raised in an NRC-sponsored review.[21]

The fire models recommended in the FPRAIG[27] are either based on FIVE (e.g., for the prediction of hot gas layer temperatures) or upon a reinterpretation of existing experimental data (e.g., for the prediction of fire growth through a stack of cable trays). A review of the FPRAIG, including a discussion of the recommended fire models, is provided by Lambright and Kazarians.[44] In response to this review, some of the FPRAIG recommendations concerning fire modeling have been modified or clarified. It is expected that the revised guidance will be published in the near future.

Information relevant to fire modeling for fire PRA, including data on cable properties (e.g., ignition and damage thresholds, mass burning rates, heat release rates), is contained in several reports.[45–50] Other required parameters (e.g., for cable thermal conductivity, specific heat, density) are typically estimated using data for generic materials. Fire spread from other equipment (e.g., major pumps, switchgear) is generally addressed using pool fire models. In some cases (e.g., for pump fires), the pools are taken to represent spilled lubricants, and the properties of the fire are then dictated by the relevant properties of the lubricants. In other cases, the pool is used as a simple representation of the actual fuel source, and the properties of the fire are determined by the assumed flammability properties of the component. Discussions on appropriate heat release rates for electrical cabinet fires, based on experimental data reported by Chavez[51] and Chavez and Nowlen,[52] are provided in the FPRAIG[27] and its review.[44]

Application of fire modeling to scenarios of interest in fire PRA studies has led to a number of general insights. Some key insights are as follows:

1. For many of the configurations analyzed in the fire PRA studies, fairly severe fires (e.g., equivalent to 1-m-diameter oil fires) are needed to cause damage to critical components (primarily cables). Furthermore, if the fire is of sufficient severity to cause damage, it usually is predicted to do so in a fairly short amount of time (on the order of 10 min or less).
2. Due to the sensitivity of model simulation results to initial fire size, more attention needs to be paid to the definition of the initial conditions of the fire scenarios (and their likelihood).
3. It is important to explicitly treat uncertainties. Such an analysis not only can yield useful results (e.g., the probability that a given fire is incapable of causing damage), but also can indicate whether improvements in fire modeling sophistication are likely to change the risk insights for a given scenario.

Regarding the last point, the predictions of fire models are, of course, subject to significant uncertainties. Applications of fire models which neglect these uncertainties (e.g., applications which neglect the possibility of damage to critical cables because they are a few centimeters above the damage height predicted by a given model) can easily lead to nonconservative assessments of fire risk.

The uncertainties in the predictions of the fire models arise from modeling simplifications employed by the analyst or inherent to the modeling tools used, and from a lack of knowledge concerning the values of key model parameters.

The modeling simplifications introduce both conservative and nonconservative biases. As examples of con-

servative simplifications, analyses often ignore (1) the effect of intervening obstacles when calculating heat transfer to a specified target, (2) the heat sink effect of room equipment and the impact of local oxygen starvation on heat release rates, (3) the limiting effect of forced ventilation, and (4) the time required for the fire to reach the "initial" size used to start the fire model simulation. Examples of nonconservative simplifications include the neglect of radiation feedback to the burning fuel in some models, and the common assumption that fires in closed metal cabinets will stay confined within these cabinets. Engineering methods for quantifying fire model uncertainty using integral test data have been developed and applied in a small number of studies.[37–39]

The uncertainty in model parameter values is due to the sparsity of experimental data for some of the parameters (e.g., piloted and nonpiloted ignition temperatures for cables) and the uncertainty as to the applicability of the existing data to the situation in the field (i.e., the particular fire scenario being analyzed). Distributions for a number of parameters have been developed (e.g., see Brandyberry and Apostolakis[36]) and used in a number of fire PRA studies.

Equipment Response Analysis

Given a predicted environment for a piece of equipment, a detailed fire PRA needs to assess the equipment response and determine the likelihood of equipment failure and the mode of failure. Because of the common cause failure potential of cable fires, the key concern is the fragility of electrical cables. However, the fragilities of other potentially vulnerable equipment (e.g., electromechanical and electronic components in electrical cabinets) are also of interest.

Current fire PRA treatments of equipment failure due to heat are very simple. It is generally assumed that damage will occur if a representative temperature (e.g., the surface temperature of a cable) exceeds a threshold value. In some analyses, component damage is also assumed if the incident heat flux exceeds a critical value. When component temperature criteria are used, conservative approaches (e.g., assuming the component is at the local environment temperature) or simple heat transfer models (e.g., lumped capacitance models or one-dimensional transient heat conduction models in the case of cables) are employed. Information relevant to the estimation of thermal fragilities of key equipment is provided in a number of reports.[46–48,50,53–55] Information on the effects of smoke on sensitive equipment is more limited.[56] These effects are not yet explicitly addressed in detailed fire PRA analyses. (The effects of smoke and fire suppressants on sensitive equipment are implicitly addressed in those screening analyses which assume that any fire within a compartment will damage all equipment within that compartment.)

Regarding the treatment of failure modes and their likelihood, all fire PRA studies address fire-induced circuit failures that lead to loss of function. A few also address failures that can lead to spurious actuation of plant equipment. The latter failure mode, typically assumed to be caused by hot shorts (i.e., electrical faults between cable conductors without a loss of conductor integrity or a simultaneous short to ground), has been shown to be an important and sometimes even dominant contributor to fire risk in a number of U.S. studies. The probability of a single hot short is, in many studies, based on a generic probability distribution derived subjectively from a limited amount of information.[57] (The distribution, assumed to be lognormal, has a 5th percentile of 0.01 and a 95th percentile of 0.20; its mean value is 0.07.) In a number of studies, the probability of multiple hot shorts is often obtained by multiplying this probability an appropriate number of times. Note that the latter procedure ignores the potentially significant impact of state-of-knowledge dependencies.

Fire Barrier Analysis

As part of determining the immediate environment of equipment potentially affected by a fire, the fire PRA needs to consider the effectiveness of fire barriers. In the United States, the most extensive investigation of multicompartment fires and the effect of intercompartment barriers was performed by the RMIEP study.[22] In that study, which was intended to extend the PRA state of the art in a number of areas, the possibility of fire propagation across rated fire barriers between up to three fire areas was treated explicitly. Screening analyses using barrier failure probabilities and assuming the loss of all equipment in all affected fire areas were employed to eliminate unimportant combinations of fire areas. (The computer code SETS was used to perform the logic calculations.) More refined analyses which distinguished between active barriers (e.g., doors, dampers) and passive barriers (e.g., penetration seals) and employed less conservative barrier failure probabilities (but still assumed the failure of all equipment in all affected areas) were then performed for the remaining combinations of fire areas. As it turned out, no combinations passed the study's CDF screening criterion of 10^{-8}/yr, and so multiarea fires were determined to be insignificant contributors to fire risk at the LaSalle plant.

More recently, many of the IPEEE studies have investigated the potential for fire vulnerabilities associated with the spread of fire between compartments in a single fire area. (Fire spread between fire areas has not been treated by these studies—it is assumed that the 2- or 3-hr-rated fire barriers generally separating fire areas will contain the fire.) Some of the IPEEEs have used the FIVE methodology,[23] which employs engineering judgment in conjunction with a number of screening criteria. Other IPEEE studies have used the more quantitative procedure described in the EPRI FPRAIG.[27] This procedure addresses fire-modeling concerns (the potential for hot gas layer formation) as well as barrier, fire protection, and safe-shutdown reliability concerns. None of the IPEEE studies investigating multicompartment fires has concluded that these fires are sources of fire risk vulnerabilities, and only a very small number of studies have identified multicompartment scenarios which are potentially visible contributors to fire risk.

Regarding the treatment of local fire barriers (i.e., barriers separating equipment within compartments), the barriers are usually either assumed to be completely reliable or are conservatively neglected. Even when physical models for barrier performance are employed (e.g.,

COMPBRN IIIe provides a one-dimensional steady state heat conduction model[35]), these models do not address such behaviors as gross distortion and mechanical failure of the barrier system. Fire tests have shown that such behaviors are strongly affected by installation practices (e.g., the method of sealing joints). Furthermore, the physical properties of the barriers needed to address such complex issues are not readily available.

Fire Detection and Suppression Analysis

Equation 4 shows that within the context of a fire PRA, the objective of a detection and suppression analysis is to determine the likelihood that a fire will be detected and suppressed before the fire can damage critical equipment. This objective requires an assessment of the performance of automatic systems and of the effectiveness of manual fire-fighting efforts.

Siu and Apostolakis[58] describe a state-transition methodology which assesses the likelihood of multiple detection/suppression scenarios and their associated suppression times using generic fire protection system reliability estimates and detection/suppression time data obtained from nuclear power plant fire events. (A condensed and somewhat simplified version of this methodology which employs data from operational experience has also been developed.[59]) The methodology has been used in a few fire PRA studies (e.g., see Musicki et al.[30]). An alternate methodology which has been used in the RMIEP study of the LaSalle plant,[22] (1) does not explicitly identify different detection and suppression scenarios, (2) uses physical models included in FPETOOL[60] to estimate detector and sprinkler actuation times, and (3) uses expert judgment to estimate other characteristic delay times in the fire detection/suppression process.

Most fire PRA studies have used a simpler detection/suppression model in which automatic systems, if they actuate, are assumed to be immediately effective. (See the guidance provided in the EPRI FPRAIG.[27]) The results of calculations for equipment damage times are sometimes compared with the results of FIVE[23] worksheet calculations for fire detector and sprinkler actuation times to determine if automatic systems should be credited. If automatic suppression is unsuccessful, the likelihood that manual suppression efforts will be effective before equipment damage is then determined. A weakness with many fire PRA studies which model both automatic and manual suppression is that a number of potentially important dependencies between automatic and manual suppression activities (e.g., the reliance on a common fire water supply) are not treated. This deficiency can lead to nonconservative results. Another weakness is that analyses typically neglect delays in fire suppression following fixed-system actuation. However, because the fire growth models used in fire PRA studies do not account for the retarding effects of suppression activities, the risk impact of this neglect is not clear.

Fire Mitigation

For each fire scenario involving damage to a set of equipment, the fire PRA must assess the conditional probability of core damage given that damage. This assessment must address the response of plant hardware and staff under fire conditions. It also must include the possibility of equipment failures and human errors not caused by the fire. (For example, accident mitigating equipment may be undergoing maintenance and may be unavailable at the time of the demand.) Finally, it typically addresses manual recovery actions taken by the plant operators to restore lost equipment functions (e.g., starting a redundant train of cooling when the fire causes the loss of the operating train).

Because fire risk assessment for nuclear power plants is generally performed within the context of an overall PRA and because the overall PRA provides a model for plant behavior under a wide variety of challenges (typically in the form of an event tree/fault tree model, as discussed in the PRA Procedures Guide[20]), the primary concern of the fire PRA analyst is to ensure that the overall PRA model is appropriately modified to address the conditions imposed by the fire scenarios analyzed. Thus, the model needs to be modified to address (a) the failure of plant equipment directly caused by the fire and (b) the effect of the fire on plant operator performance. The former issue is easily accomplished with current PRA software (e.g., SAPHIRE[61]), for example through the use of logical flags to indicate which equipment has been lost. In fact, when such software is used, explicit calculation of the term $p_{CD,k|i,j}$ (commonly referred to as the conditional core damage probability, or CCDP) is generally not required. The latter issue is much more difficult to address. A number of studies increase the PRA base case human error probabilities (HEPs), which can be developed using a number of different methods [e.g., the well-known Technique for Human Error Reliability Prediction (THERP) by Swain[62]] by subjectively determined factors to account for the additional stress induced by the fire. Other studies argue that stress during significant accidents is already high and that additional modifications of the HEPs are not needed. Most studies do not take credit for ex–main control room actions in the affected fire area (because of the heat and smoke present) or for the repair of fire-damaged equipment.

Assembly of Results

Equation 1 shows that, given the evaluation of the terms λ_i, $p_{ed,j|i}$, and $p_{CD,k|i,j}$, the determination of the fire-induced CDF (and other useful intermediate results, such as the CDF associated with a particular fire scenario) is generally a straightforward matter. If standard PRA software tools are used, the calculation (including the propagation of uncertainties) is routine and can be done without the explicit calculation of $p_{CD,k|i,j}$ since this term is implicit in the structure of the PRA event tree/fault tree model. (Most fire PRA studies have calculated this term, since it indicates what the risk consequences of a severe fire might be.) If Equation 1 is evaluated using general purpose software tools (e.g., spreadsheets or equation solvers), some additional work must be done to propagate the uncertainties in the λ_i, $p_{ed,j|i}$, and $p_{CD,k|i,j}$ through the equation. A variety of methods can be used to perform this propagation, but direct Monte Carlo simulation is

perhaps the easiest, given currently available software. It should be noted that this propagation of uncertainties deals with epistemic uncertainties: the PRA model structure accounts for the aleatory uncertainties through the terms λ_i, $p_{\text{ed},j|i}$, and $p_{\text{CD},k|i,j}$ (which are parameters of aleatory distributions, following the discussion in the section on fire frequency analysis).

Fire PRA Results

The earliest fire risk assessment for a nuclear power plant was performed in 1975 as a supplement to WASH-1400 (the Reactor Safety Study[2]). The assessment was aimed at providing a quick estimate of the risk implications of the Browns Ferry cable fire in 1975. The analysis indicated that the CDF associated with that fire was around 10^{-5}/yr, or about 20 percent of the total plant CDF associated with the causes (e.g., pipe break accidents, plant transients) addressed in the main body of the study. It also noted the usefulness of developing a more detailed fire PSA methodology (including improved models and data).

Another early fire PRA was performed in 1979 as part of a PSA for a proposed high-temperature gas-cooled reactor design.[63] The analysis focused on the risk contribution of cable spreading room fires, and it concluded that the core heatup frequency due to such fires was also around 10^{-5}/yr, or about 25 percent of the total core heatup frequency due to all causes.

The first comprehensive, detailed fire PSAs for commercial nuclear power plants were performed in 1981 and 1982 as part of the Zion[16] and Indian Point[17] PRA studies, respectively. A key question addressed by both PRA efforts was if additional accident mitigation systems (e.g., filtered, vented containments) were needed for the two plants. The study results indicated that the fire risk for Zion Units 1 and 2 was relatively small (the mean CDF was about 5×10^{-6}/yr for each unit, about 10 percent of the total mean CDF) and that the fire risk at the Indian Point plants was relatively large. (For example, the mean fire-induced CDF for Unit 2 was about 2×10^{-4}/yr, or about 40 percent of the total mean CDF.) Because the Zion and Indian Point fire PRA studies were performed by the same analysis team using the same analysis methodology and tools, these studies demonstrated how plant-specific features could greatly affect fire risk. More importantly, the studies also identified plant design changes for reducing risk (e.g., fire barriers, a self-contained charging pump, provisions for an alternate power source in the event of damaging fires) that were far more cost-effective than the proposed accident mitigation systems prompting the studies.

Since the Zion and Indian Point studies, a number of fire PRA studies have been performed. Table 5-14.1 summarizes the results from a number of these studies. These results show that fire can be a significant and even dominant contributor to the overall risk for a given plant. A significant number of studies have resulted in estimates of mean fire-induced core damage frequencies (CDF) of 10^{-4}/yr or greater, predicted contributions to total CDF (i.e., CDF from all contributors) of 20 percent or greater, or both.

In 1991, recognizing the value of systematic assessments of fire (and other so-called "external events"), the

Table 5-14.1 ***A Partial List of Fire PRAs for U.S. Nuclear Plants (Not Including IPEEEs)***

Plant	Sponsor	Date	Fire CDF (/yr)	Total CDF (/yr)	Important Contributors[a]
HTGR (design)	USDOE	1979	1.1×10^{-5}[b]	4.1×10^{-5}[b]	CSR (only the CSR was analyzed)
Zion 1/2	Utility	1981	4.6×10^{-6}	4.9×10^{-5}	Electrical equipment room, CSR
Big Rock Point	Utility	1981	2.3×10^{-4}	9.8×10^{-4}	Station power room, cable penetration area
Indian Point 2	Utility	1982	2.0×10^{-4}[c]	4.7×10^{-4}	Electrical tunnels, switchgear room
Indian Point 3	Utility	1982	6.3×10^{-5}[c]	2.3×10^{-4}	Switchgear room, electrical tunnel, CSR
Limerick	Utility	1983	2.3×10^{-5}	1.5×10^{-5}[d]	Equip. rooms, switchgear room, access area, MCR, CSR
Millstone 3	Utility	1983	4.8×10^{-6}	7.2×10^{-5}	MCR, instrument rack room, CSR
Seabrook	Utility	1983	1.7×10^{-5}	2.3×10^{-4}	MCR, CSR
Midland	Utility	1984	2.0×10^{-5}	3.1×10^{-4}	Switchgear room
Oconee	Utility	1984	1.0×10^{-5}	2.5×10^{-4}	
TMI-1	Utility	1987	8.6×10^{-5}	5.5×10^{-4}	Motor control center area, switchgear room, cabinet area
S. Texas Project	Utility	1989	$< 1.2 \times 10^{-6}$[e]	1.7×10^{-4}	MCR
Diablo Canyon 1/2	Utility	1990	2.9×10^{-5}	2.0×10^{-4}	CSR, MCR
Peach Bottom 2	USNRC	1990	2.0×10^{-5}	2.8×10^{-5}[f]	MCR, switchgear rooms, CSR
Surry 1	USNRC	1990	1.1×10^{-5}	7.6×10^{-5}[f]	Switchgear room, MCR, auxiliary building, cable vault/tunnel
La Salle 2	USNRC	1993	3.2×10^{-5}	1.0×10^{-4}	MCR, switchgear rooms, equipment rooms, turbine building, cable shaft
Grand Gulf 1	USNRC	1994	$< 1.0 \times 10^{-8}$[g]	6.7×10^{-5}[f,g]	No areas found to contribute
Surry 1	USNRC	1994	2.7×10^{-4}[g]	4.3×10^{-4}[f,g]	Switchgear room, cable vault/tunnel, containment, MCR

[a]area contribution > 1% total fire CDF; contributing areas prioritized by contribution (most important first); MCR = main control room, CSR = cable spreading room.
[b]frequency of core heatup.
[c]prior to plant modifications identified by risk study.
[d]internal events only.
[e]total contribution from external events.
[f]seismic contribution calculated using EPRI seismicity curve.
[g]shutdown study; results presented for midloop conditions (instantaneous CDF).

NRC issued a requirement that licensees perform Individual Plant Examination of External Events (IPEEE) studies for their plants.[25] The primary goal of the fire risk portion of the IPEEE program was for plant licensees to identify plant-specific vulnerabilities to fire-induced severe accidents that could be fixed with low-cost improvements. Four supporting objectives were for licensees to, with respect to external events, (1) develop an appreciation of severe accident behavior, (2) understand the most likely severe accident sequences that could occur under full-power conditions, (3) gain a qualitative understanding of the overall likelihood of core damage and fission product releases, and (4) reduce, if necessary, the overall likelihood of core damage and radioactive material releases by modifying, where appropriate, hardware and procedures that would help prevent or mitigate severe accidents. Guidance on the performance of an IPEEE analysis is provided by Chen et al.[26]

The results of a preliminary review of the IPEEE submittals are presented by Rubin et al.[64] The results confirm that fire continues to be a significant contributor to overall risk at a number of plants. In addition, they also show that over half of the IPEEE submittals have identified cost-effective improvements. Finally, as discussed earlier in the section on fire modeling, the review process also identified a number of technical issues associated with the guidance provided in the EPRI FPRAIG[27] and led to modifications of that guidance, which are expected to be published in the near future.

Current Activities and Future Directions

In recent years, interest has increased on the parts of both the NRC and industry in the broader use of PRA technology to deal with fire protection issues. This interest, which is consistent with the NRC's policy statement on the use of PRA,[65] is supported by activities in a number of areas. A key activity is the development of a consensus standard, NFPA 805, "Performance-Based Standard for Fire Protection for Light Water Reactor Electric Generating Plants," 1998 edition, which uses risk information in evaluating a plant's fire protection program.[66] As a related activity, the NRC has initiated the development of a risk-informed, performance-based fire protection rule.[67] It is anticipated that the new rule, or regulatory guidance associated with the rule, will indicate how NFPA 805 may be used by licensees in developing or modifying their fire protection programs.

Other notable application activities involving fire PRA or fire PRA methods include the evaluation of the safety significance of exemptions to certain fire protection requirements;[68] the support of fire protection issue identification and prioritization (e.g., the effect of smoke on manual fire-fighting effectiveness); the support of inspection activities (e.g., by identifying areas of focus and evaluating the safety significance of findings); and the development of risk information to support the resolution of generic fire protection issues (e.g., fire-induced circuit failures).

It is important to note that, when the results of PRA studies are used to explicitly support decision making, they are generally not used as the sole basis for the decision making. Other sources of information, including other engineering analyses, are also used to support the decision. In other words, the decision-making process is risk informed, rather than risk based. Under this risk-informed approach, the decisionmaker can make use of information from imperfect or even flawed PRA models, as long as the use of the PRA results and insights improves the non-risk-informed decision-making approach for the problem of interest.

This factor is an important consideration for the use of fire PRAs because the current fire PRA state of the art is not as mature as that for assessing the risk contributions of many other important accident initiators. A review of the fire PRA state of the art by Lambright et al.[21] in 1989 identified a number of methodological weaknesses that are still concerns in many current studies. Reviews of fire PRAs have shown that variations in key analytical assumptions can lead to orders of magnitude variations in estimates of fire-induced CDF and qualitatively different risk insights.

The uncertainties in fire PRA results are not due to the general analytical approach described at the beginning of this chapter. All current nuclear power plant fire PRAs use this approach or some slight variant on it. Rather, a good deal of the uncertainty is due to weaknesses and gaps in the current treatment of a number of application details, and to the assumptions used by analysts when addressing these weaknesses and gaps. Significant uncertainties can arise in the estimation of the likelihood of important fire scenarios (e.g., when addressing the frequency of large, transient-fueled fires or of self-ignited cable fires), the modeling of fire growth and suppression (e.g., when treating fire propagation through a stack of cable trays), the prediction of fire-induced loss of systems (e.g., when quantifying the likelihood of spurious actuations, when addressing the effect of smoke on equipment), and the analysis of plant and operator responses to the fire (e.g., when modeling operator actions during a severe control room fire).[69]

To address these areas, the NRC initiated a fire risk research program in 1998 (see Siu and Woods[70]). The program's technical objectives are aimed at developing the following:

Improved estimates of the frequencies of challenging fires
Improved fire-modeling tools for risk-significant scenarios, including guidance for proper application (accounting for limitations and uncertainties)
Mode-specific thermal fragilities for cables and other key components
Guidance for identifying scenarios for which smoke effects may be risk significant
Improved estimates of the probability of fire and fire effects containment (including active and passive barriers)
Configuration- and condition-sensitive fire protection system reliability estimates, including guidance for application
Improved tools for assessing the risk impact of circuit interactions
Improved understanding of the implications of major fire events for fire PRA

Initial results of the research include an evaluation of experimental data regarding cable failure modes and circuit failures and a review of a number of major fire events.

Concluding Remarks

Fire PRA is a systematic tool for dealing with the complex issues that need to be addressed when assessing fire safety at a nuclear power plant. It is a useful tool for supplementing deterministic analyses on which the reactor design and fire protection are based, as it highlights the strong and weak points of a plant's design and operation with respect to fire hazards. It has proven useful in supporting design, operational, and regulatory decision making, and this use is expected to increase in the coming years as (1) ongoing research and development efforts lead to improvements in the state of the art, and (2) improvements in the application of the state of the art lead to more consistent results.

Acknowledgments

The author gratefully acknowledges the comments of E. Connell of the U.S. Nuclear Regulatory Commission's Office of Nuclear Reactor Regulation and S. Nowlen of Sandia National Laboratories. Portions of this chapter have been adapted from the author's contribution to "Fire Risk Analysis, Fire Simulation, Fire Spreading, and Impact of Smoke and Heat on Instrumentation Electronics," a report recently issued by Principal Working Group 5 of the Organization for Economic Cooperation and Development's Nuclear Energy Agency, Committee for the Safety of Nuclear Installations.

References Cited

1. S. Kaplan and B.J. Garrick, "On the Quantitative Definition of Risk," *Risk Analysis,* 1, pp. 11–27 (1981).
2. "Reactor Safety Study: An Assessment of Accident Risks in U.S. Commercial Nuclear Power Plants," *WASH-1400 (NUREG-75/014),* U.S. Nuclear Regulatory Commission, Washington, DC (1975).
3. N. Rasmussen, "The Application of Probabilistic Risk Assessment Techniques to Energy Technologies," *Annual Review of Energy,* 6, pp. 123–138 (1981).
4. B.J. Garrick, "Lessons Learned from 21 Nuclear Plant PRAs," in *Proceedings of International Topical Conference on Probabilistic Safety Assessment and Management (PSA '87),* Zurich, Switzerland, pp. 369–383 (1987).
5. M.A. Caruso et al., "An Approach for Using Risk Assessment in Risk-Informed Decisions on Plant-Specific Changes to the Licensing Basis," *Reliability Engineering and System Safety,* 63, pp. 231–242 (1999).
6. M. Kazarians, N. Siu, and G. Apostolakis, "Risk Management Application of Fire Risk Analysis," in *Proceedings of the First International Symposium on Fire Safety Science,* Gaithersburg, MD, pp. 1029–1038 (1985).
7. "Recommendations Related to Browns Ferry Fire," *NUREG-0050,* U.S. Nuclear Regulatory Commission, Washington, DC (1976).
8. H. Aulamo, J. Martilla, and H. Reponen, "The Full Stories on Armenia and Beloyarsk," *Nuclear Engineering International,* 40, 492, pp. 32–33 (1995).
9. E. Pla, "Fire at Vandellos 1: Causes, Consequences and Problems Identified," in *Proceedings of Fire Protection and Safety at Nuclear Facilities Conference,* Nuclear Engineering International, Barcelona, Spain (1994).
10. S.A. Bohra, "The Narora Fire and Its Continuing Consequences: Backfitting the Indian PHWRs," in *Proceedings of Fire & Safety 1997: Fire Protection and Prevention in Nuclear Facilities,* London, pp. 219–234 (1997).
11. S.A. Jackson, "Commission Issuance of White Paper on Risk-Informed and Performance-Based Regulation," Memorandum to All NRC 9 Employees, Announcement No. 019, U.S. Nuclear Regulatory Commission (1999).
12. G. Apostolakis, "A Commentary on Model Uncertainty," in *Model Uncertainty: Its Characterization and Quantification* (A. Mosleh, N. Siu, C. Smidts, and C. Lui, eds.), Center for Reliability Engineering, University of Maryland, College Park, MD, pp. 13–22 (1995).
13. G. Apostolakis, "The Concept of Probability in Safety Assessments of Technological Systems," *Science,* 250, pp. 1359–1364 (1990).
14. G.W. Parry, "The Characterization of Uncertainty in Probabilistic Assessments of Complex Systems," *Reliability Engineering and System Safety,* 54, pp. 2–3 (1996).
15. J.C. Helton and D.E. Burmaster (eds.), "Treatment of Aleatory and Epistemic Uncertainty," *Reliability Engineering and System Safety,* 54 (1996).
16. *Zion Probabilistic Safety Study,* Commonwealth Edison Co., Chicago (1981).
17. *Indian Point Probabilistic Safety Study,* Consolidated Edison Company of New York, Inc., and Power Authority of the State of New York, New York (1982).
18. G. Apostolakis, M. Kazarians, and D.C. Bley, "Methodology for Assessing the Risk from Cable Fires," *Nuclear Safety,* 23, pp. 391–407 (1982).
19. M. Kazarians, N. Siu, and G. Apostolakis, "Fire Risk Analysis for Nuclear Power Plants: Methodological Developments and Applications," *Risk Analysis,* 5, pp. 33–51 (1985).
20. American Nuclear Society and the Institute of Electrical and Electronics Engineers, "PRA Procedures Guide: A Guide to the Performance of Probabilistic Risk Assessment for Nuclear Power Plants," *NUREG/CR-2300,* U.S. Nuclear Regulatory Commission (1983).
21. J.A. Lambright, S.P. Nowlen, V.F. Nicolette, and M.P. Bohn, "Fire Risk Scoping Study: Investigation of Nuclear Power Plant Fire Risk, Including Previously Unaddressed Issues," *NUREG/CR-5088,* U.S. Nuclear Regulatory Commission (1989).
22. J.A. Lambright, D.A. Brosseau, A.C. Payne, Jr., and S.L. Daniel, "Analysis of the LaSalle Unit 2 Nuclear Power Plant: Risk Methods Integration and Evaluation Program (RMIEP), Internal Fire Analysis," *NUREG/CR-4832, Vol. 9,* U.S. Nuclear Regulatory Commission (1993).
23. Professional Loss Control, Inc.,"Fire-Induced Vulnerability Evaluation (FIVE)," *TR-100370,* Electric Power Research Institute, Palo Alto, CA (1992).
24. M.P. Bohn and J.A. Lambright, "Procedures for the External Event Core Damage Frequency Analysis for NUREG-1150," *NUREG/CR-4840,* U.S. Nuclear Regulatory Commission (1990).
25. "Individual Plant Examination of External Events (IPEEE) for Severe Accident Vulnerabilities, 10 CFR 50.54(f)," *Generic*

Letter 88-20, Supplement 4, U.S. Nuclear Regulatory Commission (June 28, 1991).

26. J. Chen et al., "Procedural and Submittal Guidance for the Individual Plant Examination of External Events (IPEEE) for Severe Accident Vulnerabilities, Final Report," *NUREG-1407,* U.S. Nuclear Regulatory Commission, Washington, DC (1991).
27. W.J. Parkinson et al., "Fire PRA Implementation Guide," *TR-105928,* Electric Power Research Institute, Palo Alto, CA (1995).
28. "Severe Accident Risks for VVER Reactors: The Kalinin PRA Program," *NUREG/CR-6572, Vol. 3, Part 1,* U.S. Nuclear Regulatory Commission, Washington, DC (1999).
29. M.P. Bohn et al., "Analysis of Core Damage Frequency: Surry Power Station, Unit 1, External Events," *NUREG/CR-4550, Vol. 3, Rev. 1, Part 3,* U.S. Nuclear Regulatory Commission, Washington, DC (1990).
30. Z. Musicki et al., "Evaluation of Potential Severe Accidents During Low Power and Shutdown Operations at Surry, Unit 1: Analysis of Core Damage Frequency from Internal Fires During Mid-Loop Operations," *NUREG/CR-6144, Vol. 3,* U.S. Nuclear Regulatory Commission (1994).
31. J.R. Houghton, "Special Study: Fire Events—Feedback of U.S. Operating Experience," *AEOD/S97-03,* U.S. Nuclear Regulatory Commission Office for Analysis and Evaluation of Operational Data, Washington, DC (1997).
32. N. Siu and D.L. Kelly, "Bayesian Parameter Estimation in Probabilistic Risk Assessment," *Reliability Engineering and System Safety,* 62, pp. 89–116 (1998).
33. M. Kazarians and G. Apostolakis, "Modeling Rare Events: The Frequencies of Fires in Nuclear Power Plants," in *Proceedings of Workshop on Low Probability/High Consequence Risk Analysis,* Society for Risk Analysis, Arlington, VA (1982).
34. V. Ho and G. Apostolakis, "COMPBRN IIIe—A Computer Code For Probabilistic Fire Risk Analysis," *Nuclear Engineering and Design,* 138, pp. 357–373 (1992).
35. V. Ho, S. Chien, and G. Apostolakis, "COMPBRN IIIe: An Interactive Computer Code for Fire Risk Analysis," *EPRI-NP-7282,* Electric Power Research Institute, Palo Alto, CA (1991).
36. M. Brandyberry and G. Apostolakis, "Response Surface Approximation of a Fire Risk Analysis Computer Code," in *Proceedings of International Topical Meeting on Probabilistic Reliability and Safety Assessment (PSA '89),* American Nuclear Society, LaGrange Park, IL (1989).
37. N. Siu and G. Apostolakis, "Probabilistic Models for Cable Tray Fires," *Reliability Engineering,* 3, pp. 213–227 (1982).
38. N. Siu and G. Apostolakis, "On the Quantification of Modeling Uncertainties," in *Transactions of the Eighth International Meeting on Structural Mechanics in Reactor Technology,* Brussels, Belgium, pp. 375–378 (1985).
39. N. Siu, D. Karydas, and J. Temple, "Bayesian Assessment of Modeling Uncertainty: Application to Fire Risk Assessment," in *Analysis and Management of Uncertainty: Theory and Application* (B.M. Ayyub, M.M. Gupta, and L.N. Kanal, eds.), North-Holland, New York, pp. 351–361 (1992).
40. D. Cline, W.A. von Riesemann, and J.M. Chavez, "Investigation of Twenty Foot Separation Distance as a Fire Protection Method as Specified in 10CFR50, Appendix R," *NUREG/CR-3192,* U.S. Nuclear Regulatory Commission, Washington, DC (1983).
41. V. Ho, N. Siu, and G. Apostolakis, "COMPBRN III—A Fire Hazard Model for Risk Analysis," *Fire Safety Journal,* 13, pp. 137–154 (1988).
42. V.F. Nicolette and K.T. Yang, "Fire Modeling of the Heiss Dampf Reaktor Containment," *NUREG/CR-6017,* U.S. Nuclear Regulatory Commission, Washington, DC (1995).
43. N. Siu, "Probabilistic Models for the Behavior of Compartment Fires," *NUREG/CR-2269,* U.S. Nuclear Regulatory Commission, Washington, DC (1981).
44. J. Lambright and M. Kazarians, "Review of the EPRI Fire PRA Implementation Guide," *ERI/NRC 97-501,* U.S. Nuclear Regulatory Commission, Energy Research Inc., Rockville, MD (1997).
45. A. Tewarson, J.L. Lee, and R.F. Pion, "Categorization of Cable Flammability, Part 1: Laboratory Evaluation of Cable Flammability Parameters," *EPRI NP-1200, Part 1,* Electric Power Research Institute, Palo Alto, CA (1979).
46. J.L. Lee, "A Study of Damageability of Electrical Cables in Simulated Fire Environments," *EPRI NP-1767,* Electric Power Research Institute, Palo Alto, CA (1981).
47. L.L. Lukins, "Nuclear Power Plant Electrical Cable Damageability Experiments," *NUREG/CR-2927,* U.S. Nuclear Regulatory Commission, Washington, DC (1982).
48. W.T. Wheelis, "Transient Fire Environment Cable Damageability Test Results: Phase I," *NUREG/CR-4638,* U.S. Nuclear Regulatory Commission, Washington, DC (1986).
49. S.P. Nowlen, "The Impact of Thermal Aging on the Flammability of Electric Cables," *NUREG/CR-5619,* U.S. Nuclear Regulatory Commission, Washington, DC (1991).
50. S.P. Nowlen, "The Impact of Thermal Aging on the Fire Damageability of Electric Cables," *NUREG/CR-5546,* U.S. Nuclear Regulatory Commission, Washington, DC (1991).
51. J.M. Chavez, "An Experimental Investigation of Internally Ignited Fires in Nuclear Power Plant Control Cabinets: Part 1: Cabinet Effects Tests," *NUREG/CR-4527, Vol. 1,* U.S. Nuclear Regulatory Commission, Washington, DC (1987).
52. J.M. Chavez and S.P. Nowlen, "An Experimental Investigation of Internally Ignited Fires in Nuclear Power Plant Control Cabinets: Part II: Cabinet Effects Tests," *NUREG/CR-4527, 2,* U.S. Nuclear Regulatory Commission, Washington, DC (1988).
53. J. Wanless, "Investigation of Potential Fire-Related Damage to Safety-Related Equipment in Nuclear Power Plants," *NUREG/CR-4310,* U.S. Nuclear Regulatory Commission (1985).
54. M.J. Jacobus, "Screening Tests of Representative Nuclear Power Plant Components Exposed to Secondary Fire Environments," *NUREG/CR-4596,* U.S. Nuclear Regulatory Commission (1986).
55. R.A. Vigil and S.P. Nowlen, "An Assessment of Fire Vulnerability for Aged Electrical Relays," *NUREG/CR-6220,* U.S. Nuclear Regulatory Commission (1995).
56. T. Tanaka, S.P. Nowlen, and D.J. Anderson, "Circuit Bridging of Components by Smoke," *NUREG/CR-6476,* U.S. Nuclear Regulatory Commission (1996).
57. M. Kazarians and G. Apostolakis, "Fire Risk Analysis for Nuclear Power Plants," *NUREG/CR-2258,* U.S. Nuclear Regulatory Commission (1981).
58. N. Siu and G. Apostolakis, "A Methodology for Analyzing the Detection and Suppression of Fires in Nuclear Power Plants," *Nuclear Science and Engineering,* 94, pp. 213–226 (1986).
59. N. Siu and G. Apostolakis, "Modeling the Detection and Suppression of Fires in Nuclear Power Plants," in *Proceedings of the International ANS/ENS Topical Meeting on Probabilistic Safety Methods and Applications,* San Francisco, CA, pp. 56-1–56-8 (1985).

60. *FPETOOL 3.0,* U.S. Department of Commerce, National Institute of Standards and Technology (1992).
61. K.D. Russell et al., "Systems Analysis Programs for Hands-on Integrated Reliability Evaluations (SAPHIRE) Version 6.0, System Overview Manual," *NUREG/CR-6532,* U.S. Nuclear Regulatory Commission (1999).
62. A.D. Swain, "Handbook of Human Reliability Analysis with Emphasis on Nuclear Power Plant Applications," *NUREG/CR-1278,* U.S. Nuclear Regulatory Commission, Washington, DC (1983).
63. K.N. Fleming, W.T. Houghton, and F.P. Scaletta, "A Methodology for Risk Assessment of Major Fires and Its Application to an HTGR Plant," *GA-A15402,* General Atomic Company, San Diego, CA (1979).
64. A.M. Rubin et al., "An Update of Preliminary Perspectives Gained from Individual Plant Examination of External Events (IPEEE) Submittal Reviews," *Nuclear Engineering and Design,* 194, pp. 225–250 (1999).
65. U.S. Nuclear Regulatory Commission, "Use of Probabilistic Risk Assessment Methods in Nuclear Activities: Final Policy Statement," *Federal Register, 60,* p. 42622 *(60 FR 42622)* (1995).
66. NFPA 805, "Performance-Based Standard for Fire Protection for Light Water Reactor Electric Generating Plants," NFPA, draft issued for public proposals (1998).
67. "Status of Reactor Fire Protection Projects," *SECY-99-152,* U.S. Nuclear Regulatory Commission, Washington, DC (1999).
68. "Assessment of the Impact of Appendix R Fire Protection Exemptions on Fire Risk," *SECY-99-182,* U.S. Nuclear Regulatory Commission, Washington, DC (1999).
69. N. Siu, J.T. Chen, and E. Chelliah, "Research Needs in Fire Risk Assessment," in *Proceedings of 25th Water Reactor Safety Information Meeting, NUREG/CP-0162,* U.S. Nuclear Regulatory Commission, Washington, DC (1997).
70. N. Siu and H. Woods, "The U.S. Nuclear Regulatory Commission's Fire Risk Research Program—An Overview," in *Proceedings of CSNI Workshop on Fire Risk Assessment,* Helsinki, Finland (1999).

Additional Readings

G. Apostolakis, "Some Probabilistic Aspects of Fire Risk Analysis for Nuclear Power Plants," in *Proceedings of the First International Symposium on Fire Safety Science,* Gaithersburg, MD, p. 1039 (1985).

H.-P. Berg and M. Roewekamp, "Experience from German Reliability Data for Fire Protection Measures in NPPs with Regard to Probabilistic Fire Safety Analyses," in *Proceedings of Fire & Safety 1997: Fire Protection and Prevention in Nuclear Facilities,* London, pp. 63–74 (1997).

D.L. Berry and E.E. Minor, "Nuclear Power Plant Fire Protection, Fire Hazard Analysis," *NUREG/CR-0654,* U.S. Nuclear Regulatory Commission, Washington, DC (1979).

R. Bertrand, F. Bonneval, and P. Lamuth, "Estimation of Fire Frequency from PWR Operating Experience," in *Proceedings of PSA '95, International Conference on Probabilistic Safety Assessment Methodology and Applications,* Seoul, Korea (1995).

R. J. Budnitz et al., "A Methodology for Analyzing Precursors to Earthquake-Initiated and Fire-Initiated Accident Sequences," *NUREG/CR-6544,* U.S. Nuclear Regulatory Commission, Washington, DC (1998).

L.Y. Cooper and K.D. Steckler, "Methodology for Developing and Implementing Alternative Time-Temperature Curves for Testing the Fire Resistance of Barriers for Nuclear Power Plant Applications," *NUREG-1547,* U.S. Nuclear Regulatory Commission, Washington, DC (1996).

"Upgrading of Fire Safety in Nuclear Power Plants," *IAEA-TECDOC-1014,* International Atomic Energy Agency, Vienna, Austria (1998).

J. LaChance, S.P. Nowlen, and F. Wyant, "Cable Hot Shorts and Circuit Analysis in Fire Risk Assessment," in *Proceedings of International Topical Meeting on Probabilistic Reliability and Safety Assessment (PSA '99),* American Nuclear Society, LaGrange Park, IL (1999).

J. Lambright et al., "Evaluation of Generic Issue 57: Effects of Fire Protection System Actuation on Safety-Related Equipment," *NUREG/CR-5580, Vol. 1,* U.S. Nuclear Regulatory Commission, Washington, DC (1992).

P.M. Madden, "Fire Safety Rulemaking Issues Confronting Regulatory Change in the United States," in *Transactions of the Structural Mechanics in Reactor Technology Post-Conference Seminar on Fire Safety in Nuclear Power Plants and Installations,* Lyon, France (1997).

F. Mowrer, "Methods of Quantitative Fire Hazard Analysis," *EPRI TR-100443,* Electric Power Research Institute, Palo Alto, CA (1992).

S.P. Nowlen, "A Summary of Nuclear Power Plant Fire Safety Research At Sandia National Laboratories, 1975–1987," *NUREG/CR-5384,* U.S. Nuclear Regulatory Commission, Washington, DC (1989).

S.P. Nowlen and M. Kazarians, "Risk Insights Gained from Fire Incidents," in *Proceedings of International Topical Meeting on Probabilistic Reliability and Safety Assessment (PSA '99),* American Nuclear Society, LaGrange Park, IL (1999).

"Fire Risk Analysis, Fire Simulation, Fire Spreading, and Impact of Smoke and Heat on Instrumentation Electronics," *NEA/CSNI/R(00),* Organization for Economic Cooperation and Development (2000).

Proceedings of International Workshop on Fire Risk Assessment, Organization for Economic Cooperation and Development, Helsinki, Finland (1999).

M. Roewekamp and H. Liemersdorf, "Analysis of Fire Events in Nuclear Power Plants and Conclusions with Respect to Fundamental Requirements Concerning Fire Safety," in *Proceedings of 3rd International Seminar on Fire Safety of Nuclear Power Plants,* Heidelberg, Germany (1993).

N. Siu, "Physical Models for Compartment Fires," *Reliability Engineering,* 3, pp. 229–252 (1982).

N. Siu, "Modeling Issues in Nuclear Plant Fire Risk Analysis," in *EPRI Workshop on Fire Protection in Nuclear Power Plants, EPRI NP-6476* (J.-P. Sursock, ed.), Electric Power Research Institute, pp. 14-1–14-16 (1989).

N. Siu, E. Droguett, and A. Mosleh, "Model Uncertainty in Fire Risk Assessment," in *Proceedings of SPFE Symposium on Risk, Uncertainty, and Reliability in Fire Protection Engineering,* Baltimore (1999).

CHAPTER 15

Fire Hazard Assessment for Transportation Vehicles

Richard W. Bukowski

Introduction

One of the areas in which fire hazard assessment techniques have been applied within regulation is for transportation vehicles. In particular, commercial aviation and passenger rail have utilized fire hazard assessment as a means to achieve safety goals well before these techniques became common in buildings. This chapter will review the methods employed and the recent evolution of predictive tools specific to transportation. The reader should refer to the general chapter on Fire Hazard Analysis for an introduction to the basic principles. The American Society for Testing and Materials (ASTM) has developed a Standard Guide for Fire Hazard Assessment of Rail Transportation Vehicles, ASTM E2061.[1] This document provides a detailed procedure for the conduct and documentation of a fire hazard assessment including specific design fire scenarios that should be considered.

Current Methods for Regulating Transportation Vehicle Fire Safety

Aviation

The Federal Aviation Administration (FAA) has pioneered the use of fire hazard assessment in the safety regulation of commercial aviation. As with most regulatory systems, the general objective is to protect passengers and crew from unreasonable risk of death or injury in accidents. The issue then becomes to reach some agreement on what is a reasonable or "acceptable" risk. Compared to other transportation modes, and especially private automobiles, the flying public is highly risk (and hazard) averse. Reflecting this concern, commercial aviation is highly regulated and (statistically) the safest mode of transportation.

A review of aviation accidents reveals that most occur on takeoff or landing. From a fire safety viewpoint, in-flight fires are extremely rare, especially in the United States. When fire becomes a threat, it generally involves jet fuel spilled as a result of a crash. Where the crash itself involves high-impact forces, passenger and crew survivability is not possible. This observation led to the early recognition of a specific class of incident known as the "impact survivable, post-crash fire" scenario. This is where most passengers and crew survive the crash and are subsequently capable of escaping the wreckage if given sufficient time.

Research conducted by the FAA on commercial aircraft exposed to an external fuel fire indicated that the time available for passenger egress before flashover occurred in the cabin was approximately 90 s. Thus, the FAA established a regulation that commercial aircraft must be able to demonstrate that a full load of passengers can be evacuated within 90 s. Aircraft materials are tested to demonstrate that they are slow to ignite and burn such that the cabin environment can be kept safe for the 90 s needed for evacuation.

In the 1980s, the FAA promulgated a regulation that required aircraft seats to be protected against fire by a blocking layer between the outer covering and the cushioning. This regulation was supported by a cost-benefit analysis performed by the National Institute of Standards and Technology (NIST).[2] This analysis incorporated the impact of the mitigation strategy on the risk of death of passengers from in-flight, post-crash, and on-ground fires, and included normalization by exposure (in passenger miles) to allow extrapolation to potential future losses accounting for industry growth. The analysis further considered the historical record of aircraft fires as a means to establish current losses and scenarios. Because of the scarcity of incidents, worldwide incidents were included, but only those involving U.S.-built jet aircraft.

Richard W. Bukowski, P.E., is senior research engineer, NIST Building and Fire Research Laboratory, Gaithersburg, MD.

Another interesting approach from this study was the way in which evacuation times were considered. As discussed earlier, FAA regulations require that any aircraft be able to be evacuated within 90 s. But the study needed to determine the value of additional safe egress time provided by seat blocking that delayed flashover. Thus, the authors estimated the passenger evacuation rate from each exit: one per second from main doors (slower if the exit was partially obstructed) and one per 2 s for window exits or fuselage breaks. If a strategy resulted in an additional 4 s of safe egress time and there were two main doors and two window exits available, the strategy was credited with saving 12 passengers.

Rail

While all serious passenger rail accidents are investigated by the National Transportation Safety Board (NTSB), there has not been public pressure for strong safety regulation of rail transportation vehicles until recently. Following the 1996 Silver Spring accident where a Marc commuter train collided with an Amtrak passenger train, resulting in 11 deaths, there was increased interest by the Federal Railroad Administration (FRA) to replace safety guidelines originally issued in 1984 (and slightly revised in 1989) with regulations. These regulations, based on the guidelines but updated with information derived from NIST research, were promulgated in 1999.[3]

The FRA tests and performance criteria cited in the 1999 regulations focus on providing a high level of fire performance for combustible materials found in vehicles. Like aircraft materials, these are to be difficult to ignite and slow burning, producing limited smoke. Unlike aircraft, which suffer severe operational penalties associated with weight, intercity and commuter rail vehicles and rail transit vehicles employ stronger construction, including fire resistance requirements for floors and for roofs when the vehicle is powered from an overhead catenary. Vehicles that make many stops recognize the energy penalties associated with weight, and all involve much lighter construction than intercity passenger trains. The evolution of higher speed trains for intercity applications is bringing the energy issue forward here as well, so weight/cost tradeoffs are becoming more universal. It should be noted that the FRA tests and performance criteria are based on Federal Transit Administration recommended practices for rail transit vehicles published in 1984.

A review of rail accident scenarios reveals that collisions with vehicles at grade crossings or with other trains lead the list. Similar to aircraft, liquid fuel spilled from the vehicle or train is the most common fire exposure. An example is an accident that occurred near Bourbonnais, Illinois, in 1999[4] when a train struck a truck at a grade crossing. Leaking fuel from one of the locomotives ignited and engulfed a sleeping car, where all the deaths occurred. Autopsies showed that four of the victims died due to fire, one died from carbon monoxide poisoning, and six died from physical injuries. Interior fires in moving vehicles are extremely rare, with most such incidents involving small quantities of smoke from malfunctioning/overheating equipment. There was a single fatality involving an Amtrak bi-level sleeping car (cigarette on a mattress) that occurred in 1982 in Gibson, California.[5]

Busses

Busses are covered by only a few fire safety requirements. There are some controls on the flammability of interior linings and seats [Federal Motor Vehicle Safety Standards Section 302 (FMVSS302)],[6] fire resistive barrier around the engine compartment, and recent requirements for physical protection of the fuel tank against penetration. The great majority of bus fires are engine fires, and the barrier provides adequate time to stop the bus and discharge the passengers. Some buses are equipped with fixed extinguishing systems for the engine compartment.

Following a 1988 accident in which a post-crash fire took the lives of 27 persons when a pickup truck struck a church bus in Kentucky, NIST conducted studies of the flammability of bus seats.[7] Similar to the impact survivable post-crash aircraft fire scenario discussed above, this accident involved a leak from the bus fuel tank with fire penetrating through cracks in the floor and impaired exits. The crash destroyed the front door, and the rear emergency exit was blocked by luggage in the aisle and rear seat.

An issue with school buses was the use of extra padding on seat backs and handrails to protect occupants from injury in accidents (required by FMVSS222) because the use of seat belts was considered impractical. This additional padding increased the fuel load and fire development in a post-crash fire. Following the tests of current and potential seating materials in bench- and full-scale, HAZARD I (NIST's fire hazard assessment software) was used to examine the development of fire hazard to occupants from seating fires. The conclusions were that while two seating assemblies developed incapacitating conditions and one lethal condition within 3 min, three other assemblies did not produce untenable conditions within the same time period.[8] In 1993, the FTA published recommended practices for bus materials and engine compartments which cited the same tests and almost the same performance criteria as for rail transit.

Ships

The regulation of commercial vessels is primarily conducted under international law. The International Maritime Organization (IMO) promulgates regulations and test methods for fire resistance and flame spread on interior materials. The U.S. Coast Guard (USCG) enforces these and some other safety and sanitation requirements for foreign flag vessels that operate in U.S. waters.

As a result of U.S. regulatory reform, the USCG initiated and chaired an NFPA technical committee to develop consensus standards as an alternative to the current fire regulations and NVICs.[9] Various NFPA 301, *Code for Safety to Life from Fire on Merchant Vessels,* requirements are described for vessels carrying more than 12 passengers.[10] Materials requirements are similar to the USCG regulations and the NVIC 9-97, with some exceptions. The passenger capacity, type of service (day or overnight), and whether or not the space is protected with automatic

sprinklers determine flame spread limits. NFPA 301 means-of-egress provisions appear to be adapted for the marine environment from NFPA 101®, *Life Safety Code®*,[11] and depend on the number of passengers and whether or not overnight accommodations are provided.

NFPA 301 includes an appendix intended to allow the vessel designer and operator to comply with the Code while accommodating new or unique vessel uses or incorporating new or transfer technology. The appendix provides a standardized hazard analysis and risk assessment methodology to use in demonstrating equivalent safety. The methodology includes a description of several analysis techniques (e.g., preliminary hazard analysis, fault tree analysis, criticality analysis), data inputs (e.g., vessel physical description, design and operating assumptions and conditions), hazard correction measures, and verification and documentation of equivalence.

Application of Fire Hazard Assessment to Transportation

The general process of fire hazard assessment as applied to buildings is also applicable to transportation. In this section the steps for conducting a FHA will be discussed in this context. The steps are

1. Selecting a target outcome
2. Determining the scenarios of concern
3. Selecting design fires
4. Selecting appropriate calculation methods
5. Performing an evacuation calculation
6. Analyzing the impact of exposure
7. Accounting for uncertainty

Selecting a Target Outcome

The objective of safety regulations for transportation is to minimize loss of life and injuries in accidents. Preservation of property, in particular the limitation of damage to the vehicles, is not considered. Thus, regulations focus on vehicle design, material selection, and emergency procedures that would be expected to mitigate human losses in accident scenarios drawn from operating experience. However, since transportation accidents that involve fire are exceedingly rare, hazard scenarios that have been considered include possibilities that may not have actually occurred.

Determining the Scenario(s) of Concern

Scenarios to be evaluated can be drawn from the detailed NTSB accident investigation reports and the operational experience of the industry, but should be supplemented by reasonable scenarios that could result in significant threat to passengers or crew. For example, NIST research conducted for the FRA identified trash bags found on overnight trains as a potentially significant fire exposure (250 kW) to seats and interior materials, even though there are no records of fires involving these trash bags on trains.

Vandalism is a source of fires in subways and commuter rail systems. Scenarios may involve newspapers and small amounts of flammable liquids used to ignite seats that may be slashed to expose interior padding. Some operators require fire testing of seats that have been slashed in an X pattern low on the back and through the upholstery.

Tunnels represent a significant complication in a rail environment. Accidents that may occur in a tunnel pose an additional threat to passengers and crew because the fire effluent is contained around the train where it can continue to expose people who have exited the vehicles. Tunnels, bridges, or other elevated track sections also restrict the ability of people to move to a safe location away from the train. These issues need to be addressed where trains operate in long tunnels or have extended elevated sections.

Selecting the Design Fire(s)

In both the aviation and rail environments, the materials employed for seating and finish are high fire performance materials and systems. Thus, burning rate data on actual materials should be used wherever possible because data on typical materials will not be applicable. Care should be exercised because burning rates may be reported only at higher incident fluxes because the materials do not burn at typical flux levels. The T-squared fire curve still can be used where large-scale burning rate data on actual transportation materials is available and can be shown to correlate to the T-squared growth rate employed.

Selecting Appropriate Methods for Prediction

Particular care should be exercised in the selection of appropriate prediction methods for transportation applications. Planes and trains are spaces with large aspect ratios, so some aspects of zone models may not be appropriate. Aircraft operate under conditions of pressurization to about 8000 ft, so oxygen levels and partial pressures are lower than normal. Their ventilation systems are unique and can have a significant influence on fire development and smoke movement. Train ventilation systems are more like those found in buildings and should not represent special circumstances.

Performing an Evacuation Calculation

In all transportation modes except aircraft, it is necessary to perform an evacuation calculation to estimate the time needed for passengers and crew to move to a safe location. In aviation, passengers and crew must await landing the plane before any egress actions can begin. Once the aircraft comes to a stop, as defined in FAA regulations it can be assumed that everyone can be evacuated within 90 s through half of the available exits. This 90-s emergency evacuation performance is demonstrated for every

commercial aircraft and configuration with a full load of passengers having a distribution of gender and age approximating that of the flying public in order for an aircraft to be certified.

The limitations are that these evacuation certification tests are performed under nearly ideal conditions with the aircraft upright and level and without smoke. Most of the test subjects are employees of the aircraft manufacturer (and as such are usually experienced in emergency evacuation of the aircraft), and none attempt to take carry-on items, as is often reported in actual aircraft evacuations.

In a rail environment, there is no such requirement for evacuation performance and little research or testing from which to obtain details of passenger egress behavior. In trains, passengers are always free to move about, so passengers might be expected to begin egress behavior from one car to another while the train is still moving, although they would have to sit or hold on during any emergency braking. Current emergency procedures for rail vehicles emphasize movement to safe areas in adjacent cars, even when the train is stopped. However, if passengers get off the train, they may be struck by other trains passing on an adjacent track; use of escape windows is only a last resort because many are located too high off the ground. If an emergency occurs while a train is in a tunnel, the train would continue moving until it is clear of the tunnel, if possible. Compared to aircraft usually consisting of a single main cabin and a specified number of flight crew for the number of passengers, a train has many fewer crew per passenger, and passengers may be seated in several separate cars. Train crew would use the public address system to issue emergency instructions but would likely have less direct contact with passengers.

A number of special evacuation characteristics for train cars should be considered in any evacuation calculation. Horizontal travel speeds in a moving train car would be expected to be significantly slower than walking speeds in buildings. Some commuter and intercity trains use bi-level car designs with one or two stairways per car. These stairways are narrower and steeper than building stairs, so travel speeds should be slower. Most such cars have lateral connections on both levels, but there are some notable exceptions—Amtrak double deck sleepers have no lateral connections to adjacent cars on the lower deck. Such details should be accounted for in evacuation calculations.

Analyzing the Impact of Exposure

In any fire hazard assessment, the impact of exposure of people to fire effluent is related to concentration and time. An aircraft experiencing an in-flight fire scenario would be expected to involve a significant exposure time since the typical time to affect an emergency diversion is estimated by the FAA to average about 30 min. Thus, even low concentrations of fire gases can lead to impaired egress performance. For the impact survivable, post-crash fire scenario the exposure time is (by FAA definition) not greater than 90 s, so only thermal threats would be of significance.

In a rail environment, most scenarios of interest would find safe areas in adjacent cars with short movement times to areas of relative safety. Thus, most rail scenarios would involve short exposure times where primary threats would be from thermal insults. One exception is in sleeping cars not equipped with fire detection systems and when the incident occurs in a long tunnel.

Accounting for Uncertainty

One of the more difficult aspects of conducting a fire hazard analysis is the estimation of uncertainty. Where there are data from full-scale tests, these can be used to estimate the uncertainty of a calculation method applied to the same conditions (see following section for an example). In the absence of data, a sensitivity analysis might be performed to quantify the effect of uncertainty on the outcome.

Alternative Uses for Fire Hazard Assessment

The preceding has focused on the use of fire hazard assessment in the evaluation of the performance of a specific transportation system design against the objective of passenger and crew safety. Another application of fire hazard assessment techniques might be to determine the minimum performance level of a major system component necessary to meet the target outcome. An example of such appears in the Phase III report of NIST's research for FRA[12] of passenger rail fire safety, where the hazard assessment supports the regulation of the fire performance of materials in their context of use in the vehicles.

For the car designer or regulator, the objective is to determine the limiting performance level so that the designer has the freedom to use any material in any way that will not violate this bounding condition. Thus, a *fire performance curve* was calculated with NIST's CFAST fire model and applying tenability criteria to obtain time to impaired evacuation and incapacitation as a function of fire growth rate for a typical intercity rail (single deck) coach car. The fire performance curve shows that any fire that does not exceed the medium (*t*-squared) growth rate will not pose a threat to passengers or crew.

Figure 5-15.1 shows the fire performance curve determined from experimental measurements in the gas burner tests along with fire model predicted curves calculated for the test vehicle. For a medium growth rate *t*-squared fire, the time to incapacitation determined from the replicate gas burner tests was (126 Å 7) s. For other growth rate fires, the time to incapacitation ranged from (40 Å 4) s for the ultra-fast growth rate fire to (230 Å 12) s for the slow growth rate fire. On average, the uncertainty of the experimentally determined times to these untenable conditions was less than 7 percent (based on one standard deviation). Once the bounding condition, in this case a medium *t*-squared fire growth rate, is known, the vehicle designer or regulator can use any of several means to assure the limit is not exceeded—including material selection, limiting quantities of combustibles, active

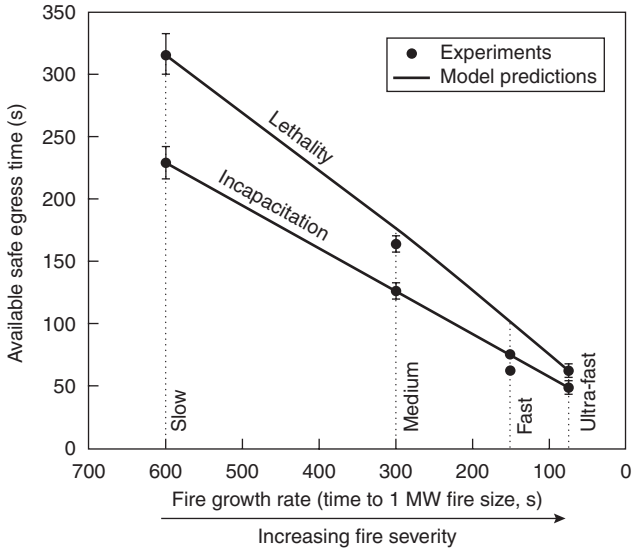

Figure 5-15.1. ***Fire performance curve.***

mitigation strategies such as suppression or smoke venting, and so forth.

Application of Fire Hazard Assessment to Passenger Rail

Recent revisions to 49CFR, Part 238, Section 238-103(d) require that railroad operators conduct a fire safety analysis on all categories of existing passenger railroad equipment and service. The industry, through the American Public Transit Association is developing guidelines for conducting this analysis. The following is intended to demonstrate that process and to produce a recommended practice to guide the industry in meeting the intent of the regulation.

The first issue that needs to be addressed is to understand the intent of the regulation. This is to conduct a systematic analysis of railroad equipment and service that will identify potential fire hazards to passengers and crew and to take steps to mitigate these potential hazards. Where multiple potential hazards are identified, mitigation should be prioritized in order of decreasing risk.

This intent embraces several important concepts. The first is the fire scenario. A *fire scenario* is a description of the sequence of events that must occur to result in an uncontrolled fire. A fire scenario description generally includes an ignition source and an initial item ignited, but may include other special conditions that are required to result in the consequence to be avoided. For example, some fire scenarios may represent a threat to passengers and crew only if they occur in a tunnel that increases the smoke exposure or if the passengers have limited ability to evacuate without assistance.

The second concept is fire hazard assessment. A *fire hazard assessment* is a systematic examination of all potential fire hazards that might occur, resulting in the consequence to be avoided, in this case an injury or fatality to passengers or crew. Note that a fire hazard assessment is not limited to fire hazards that have at some time occurred, but should also consider fire hazard scenarios that are possible, even if they would require several things to go wrong simultaneously.

The third concept is fire risk assessment. A *fire risk assessment* begins with a fire hazard assessment and weights the consequences by the likelihood of the fire scenario. By discounting the consequence by likelihood, the scenario with high consequences and low likelihood and the scenario with low consequences that occurs frequently represent equal risk. Thus, fire risk analysis is a way of normalizing different hazards so that they can be compared or summed to produce a total threat index.

Define Scenarios

The first step in the process is to define the scenarios which could lead to potential injury to passengers and crew. These will include both those fire scenarios that have occurred and those that are possible but have not yet occurred. Traditionally, the former are identified from accident statistics and reports, although, in most cases, the reporting systems have significant shortcomings and the databases are incomplete. Federal regulations (49CFR, Part 225) require that incidents that result in a fatality or injury, or result in damage to property exceeding a threshold ($6700 for 1998) be reported. A recent search of this database identified 156 fire incidents of interest for 1985 to 1998.

Additionally, there are other fire databases that can be examined, such as the National Fire Incident Reporting System (NFIRS). A recent search of NFIRS for passenger rail fire incidents for the 10-year period from 1988 through 1997 identified 71 fires resulting in two civilian deaths and four injuries. Note that such searches should not be limited to those that resulted in fatality or injury because the intent is to identify scenarios that may result in fatality or injury. No scenario should be excluded unless it is determined that it cannot result in harm under any condition.

Defining scenarios that have not occurred requires judgment and experience. They may involve new combinations of ignition sources and fuels, or they may involve new items not previously found in the rail environment. An example would be electronic equipment introduced to entertain passengers or to facilitate work during transit. At this stage, it is best to include everything possible and to cull the list later with justification. Also, since the rail operator is performing the analysis, it should be possible to identify incidents that did not exceed the reporting threshold but are documented internally or in the experience of employees.

Inventory of Equipment—Identification of Hazards

The fire safety analysis will need to be conducted around an inventory of equipment and materials that make up the vehicle. Anything that uses energy or materials that are easily ignited by small sources such as matches or smoking materials should be identified as

potential ignition sources. Any combustible material can be a first item ignited, or a fuel item. The inventory should also identify items in both categories that may be brought aboard by passengers, such as luggage, packages, and even coats and pillows.

Each of these items needs to be characterized in terms useful to the fire safety analysis. Ignition sources are characterized by maximum potential energy; fuel items, by heat release rate (HRR) and yields of smoke and gases, as well as some measure of ignitability.

At the same time, the equipment or design features present that may mitigate hazards or impact on the evolution of hazards should be identified. These vehicle characteristics include number, type, and location of doors and escape windows/hatches; number of levels and stairways; detection, extinguishing, communication, emergency lighting and signage, or smoke management systems.

Analysis of Operating Environment

The operating environment of vehicles has a significant influence on the fire hazards that may be encountered. Operating speeds, grade crossings and their protection, bridges and tunnels, shared right-of-way with freight operations, and even terrain can affect the analysis and should be identified.

Description of Fire Scenarios

Using this inventory, the combination of ignition sources and fuels that can result in a significant fire becomes the basis of a fire scenario description. For example, if a piece of electrical equipment is protected by a fuse so the maximum fault energy is limited, and it is enclosed or separated by a distance from any combustible material so that this maximum fault energy cannot ignite the fuel, then this scenario can be eliminated at this step. Of course, the possibility of the wrong size fuse resulting in a higher fault energy or the presence of combustible materials that are "not supposed to be there" need to be considered as separate scenarios.

Fire Hazard Assessment

For each of the identified fire scenarios, the consequences of the hazards in terms of potential injuries or fatalities to passengers or crew is evaluated. This evaluation is done in any of several ways. First, the judgment of experienced people can be used to determine likely outcomes of some scenarios—especially those for which historical experience exists.

Second, there are various tools to assist in making a determination. These include fault trees such as NFPA550 or simple calculational procedures such as FPEtool. These methods depend on judgment supported by individual calculations to provide quantitative results.

Third, there are more detailed modeling tools, such as HAZARD I, that are increasingly being applied to special areas such as rail. In addition to providing predictions of the outcome of specific scenarios, these tools can be used to estimate general, bounding conditions in the form of fire performance curves as demonstrated in the NIST Phase III report (in press).

The important criterion in the fire hazard assessment is not only to identify conditions or design features that relate to identified hazards, but to determine that the conditions or features actually mitigate the hazard. For example, a fire-rated floor may provide protection against ignition from an overheated wheel, but if combustible lubricants are allowed to build up on the wheel assembly, the overheated wheel may ignite the grease that then may present too great a heat source for the floor to provide adequate protection.

Risk Ranking

Once each of the fire hazard scenarios have been evaluated, those which may potentially result in injury or fatality to passengers or crew and are not already addressed by design or operating procedures will have been identified. Mitigation strategies for each should be suggested and evaluated for effectiveness by rerunning the hazard calculation with the strategy in place. Only where it is not practical to eliminate all identified hazards is it necessary to perform a risk ranking to prioritize those situations to be addressed first.

Here, the likelihood of the remaining scenarios is estimated from historical data or experience. Then this likelihood is used to discount the consequences of each remaining scenario so that the risk of each can be compared. For example, if one scenario is expected to result in 10 passenger injuries and another in 50 passenger injuries, but the first is 10 times more likely, the first is the higher risk and should be addressed first.

Ideally, one would like to be able to define a level of "acceptable risk" below which it is not necessary to take remedial action. Unfortunately this is a very difficult task since risk perception and risk acceptance are quite variable. Normally the "reasonable person" does not expect to be protected from reasonably unexpected hazards or hazards clearly beyond control. An example of the former is to design a train to withstand being struck by a falling airplane. An example of the latter is designing against a terrorist attack.

Beyond these "reasonableness" tests, experience has shown that the public is more hazard averse than risk averse. Transportation accidents resulting in large numbers of fatalities or injuries are considered unacceptable, regardless of a demonstrable low likelihood. Thus, the concept of "acceptable risk" may not be applicable.

Conclusions

Modern fire hazard assessment techniques that are becoming common in the building regulatory arena can be adapted and applied to transportation. While transportation has an excellent fire safety record, these new techniques are desirable because they provide increased design flexibility particularly with respect to the introduction of innovative materials.

Recent research into fire hazard assessment for passenger rail has resulted in the promulgation of regulations and the development of procedures that can be used

by the industry for compliance. These techniques also have application to other transportation sectors such as transit and may be adapted for use there in the future.

References Cited

1. ASTM E2061, *Standard Guide for Fire Hazard Assessment of Rail Transportation Vehicles,* American Society for Testing and Materials, Philadelphia (2000).
2. J.R. Hall and S.W. Stiefel, "Decision Analysis Model for Passenger-Aircraft Fire Safety with Application to Fire Blocking of Seats," *NBSIR 84-2817,* National Institute of Standards and Technology, Gaithersburg, MD (1984).
3. Federal Railroad Administration (FRA), *49 CFR, Transportation,* Parts 216, 223, 229, 231, and 238, "Passenger Equipment Safety Standards, Final Rule," *Federal Register,* 64, 91, USDOT, National Archives and Records Administration, Washington, DC (1999).
4. Washington Post, A1–A3, March 17, 1999.
5. National Transportation Safety Board (NTSB), "Railroad Accident Report—Fire Onboard Amtrak Passenger Train No. 11, the Coast Starlight, Gibson, California, June 23, 1982," *Report No. NTSB/RAR-83/03,* Washington, DC (1983).
6. National Highway Traffic Safety Administration (NHTSA), *49 CFR, Transportation,* Part 571, "Federal Motor Vehicle Safety Standards," Subpart 571.302, "Flammability of Interior Materials—Passenger Cars, Multi-Purpose Passenger Vehicles, Trucks, and Buses," National Archives and Records Administration, Washington, DC (1996).
7. E. Braun, S. Davis, J. Klote, B. Levin, and M. Paabo, "Assessment of the Fire Performance of School Bus Interior Components," *NISTIR 4347,* National Institute of Standards and Technology, Gaithersburg, MD (1990).
8. E. Braun, J. Klote, S. Davis, B. Levin, M. Paabo, and R. Gann, "Performance of School Bus Seats: A Fire Hazard Assessment," in *FRCA Conference Proceedings—Fire Safety Developments and Testing, Oct 21–24, 1990,* Fire Retardant Chemicals Association, Lancaster, PA, pp. 105–125 (1990).
9. J. Snyder, "Fire Safety, New U.S. Vessel Fire Code Set for Comment," *Marine Log* (1997).
10. NFPA, *Code for Safety of Life from Fire on Merchant Vessels, NFPA 301,* National Fire Protection Association, Quincy, MA (1998).
11. *NFPA 101®, Life Safety Code®,* National Fire Protection Association, Quincy, MA (2000).
12. R.D. Peacock, J.D. Averill, D. Madrzykowski, D.W. Stroup, and R.W. Bukowski, "Fire Safety of Passenger Trains, Phase III: Evaluation of Fire Hazard Analysis Using Real-Scale Tests," National Institute of Standards and Technology, Gaithersburg, MD (2001).

Appendices

Contents

References Cited

1. E.A. Mechtly, "The International System of Units, Physical Constants and Conversion Factors," 2nd revision, National Aeronautics and Space Administration, Washington, DC (1973).
2. B.N. Taylor, W.H. Parker, and D.N. Langenberg, "Determination of e/h, QED, and the Fundamental Constants," *Reviews of Modern Physics,* 41 (1969).
3. B.D. Tapley and T.R. Poston (eds.), *Eshbach's Handbook of Engineering Fundamentals,* 4th ed., John Wiley and Sons, New York (1990).
4. E.R.G. Eckert and R.M. Drake, *Analysis of Heat and Mass Transfer,* McGraw-Hill, New York (1972).
5. J.P. Holman, *Heat Transfer,* McGraw-Hill, New York (1986).
6. A.M. Kanury, *Introduction to Combustion Phenomena,* Gordon and Breach Science Publishers, New York (1975).
7. V. Babrauskas, "Tables and Charts," *Fire Protection Handbook,* 17th ed. (A.E. Cote and J. Linville, eds.), National Fire Protection Association, Quincy, MA (1991).
8. P. Blackshear (ed.), *Heat Transfer in Fires,* Scripta Book Company, Washington, DC (1974).
9. R. Siegel and J.R. Howell, *Thermal Radiation Heat Transfer,* 3rd ed., Taylor & Francis, Washington, DC (1992).
10. R.H. Perry and C.H. Chilton (eds.), *Chemical Engineers Handbook,* McGraw-Hill, New York (1973).

APPENDIX A

Conversion Factors

Table A.1 ***Names and Symbols of SI Units[1]***

Quantity	Name of Unit	Symbol	
	SI BASE UNITS		
Length	Meter	m	
Mass	Kilogram	kg	
Time	Second	s	
Electric current	Ampere	A	
Thermodynamic temperature	Kelvin	K	
Luminous intensity	Candela	cd	
Amount of substance	Mole	mol	
	SI-DERIVED UNITS		
Area	Square meter	m^2	
Volume	Cubic meter	m^3	
Frequency	Hertz	Hz	s^{-1}
Mass density (density)	Kilogram per cubic meter	kg/m^3	
Speed, velocity	Meter per second	m/s	
Angular velocity	Radian per second	rad/s	
Acceleration	Meter per second squared	m/s^2	
Angular acceleration	Radian per second squared	rad/s^2	
Force	Newton	N	$kg \cdot m/s^2$
Pressure (mechanical stress)	Pascal	Pa	N/m^2
Kinematic viscosity	Square meter per second	m^2/s	
Dynamic viscosity	Newton-second per square meter	$N \cdot s/m^2$	
Work, energy, quantity of heat	Joule	J	$N \cdot m$
Power	Watt	W	J/s
Quantity of electricity	Coulomb	C	$A \cdot s$
Potential difference, electromotive force	Volt	V	W/A
Electric field strength	Volt per meter	V/m	
Electric resistance	Ohm	Ω	V/A
Capacitance	Farad	F	$A \cdot s/V$
Magnetic flux	Weber	Wb	$V \cdot s$
Inductance	Henry	H	$V \cdot s/A$
Magnetic flux density	Tesla	T	Wb/m^2
Magnetic field strength	Ampere per meter	A/m	
Magnetomotive force	Ampere	A	
Luminous flux	Lumen	lm	$cd \cdot sr$
Luminance	Candela per square meter	cd/m^2	
Illuminance	Lux	lx	lm/m^2
Wave number	1 per meter	m^{-1}	
Entropy	Joule per kelvin	J/K	
Specific heat capacity	Joule per kilogram kelvin	$J/(kg \cdot K)$	
Thermal conductivity	Watt per meter kelvin	$W/(m \cdot K)$	
Radiant intensity	Watt per steradian	W/sr	
Activity (or a radioactive source)	1 per second	s^{-1}	
	SI SUPPLEMENTARY UNITS		
Plane angle	Radian	rad	
Solid angle	Steradian	sr	

Table A.2 ***Definitions of SI Units***[1]

Meter (m)	The *meter* is the length equal to 1 650 763.73 wavelengths in vacuum of the radiation corresponding to the transition between the levels 2 p_{10} and 5 d_s of the krypton-86 atom.
Kilogram (kg)	The *kilogram* is the unit of mass; it is equal to the mass of the international prototype of the kilogram. (The international prototype of the kilogram is a particular cylinder of platinum-iridium alloy that is preserved in a vault at Sèvres, France, by the International Bureau of Weights and Measures.)
Second (s)	The *second* is the duration of 9 192 631 770 periods of the radiation corresponding to the transition between the two hyperfine levels of the ground state of the cesium-133 atom.
Ampere (A)	The *ampere* is that constant current, which, if maintained in two straight parallel conductors of infinite length, of negligible circular cross section, and placed 1 meter apart in a vacuum, would produce between these conductors a force equal to 2×10^{-7} newton per meter of length.
Kelvin (K)	The *kelvin,* unit of thermodynamic temperature, is the fraction 1/273.16 of the thermodynamic temperature of the triple point of water.
Candela (cd)	The *candela* is the luminous intensity, in the perpendicular direction, of a surface of 1/600 000 square meter of a blackbody at the temperature of freezing platinum under a pressure of 101 325 newtons per square meter.
Mole (mol)	The *mole* is the amount of substance of a system that contains as many elementary entities as there are carbon atoms in 0.012 kg of carbon 12. The elementary entities must be specified and may be atoms, molecules, ions, electrons, other particles, or specified groups of such particles.
Newton (N)	The *newton* is that force that gives to a mass of 1 kilogram an acceleration of 1 meter per second per second.
Joule (J)	The *joule* is the work done when the point of application of 1 newton is displaced a distance of 1 meter in the direction of the force.
Watt (W)	The *watt* is the power that gives rise to the production of energy at the rate of 1 joule per second.
Volt (V)	The *volt* is the difference of electric potential between two points of a conducting wire carrying a constant current of 1 ampere, when the power dissipated between these points is equal to 1 watt.
Ohm (Ω)	The *ohm* is the electric resistance between two points of a conductor when a constant difference of potential of 1 volt, applied between these two points, produces in this conductor a current of 1 ampere, this conductor not being the source of any electromotive force.
Coulomb (C)	The *coulomb* is the quantity of electricity transported in 1 second by a current of 1 ampere.
Farad (F)	The *farad* is the capacitance of a capacitor between the plates of which there appears a difference of potential of 1 volt when it is charged by a quantity of electricity equal to 1 coulomb.
Henry (H)	The *henry* is the inductance of a closed circuit in which an electromotive force of 1 volt is produced when the electric current in the circuit varies uniformly at a rate of 1 ampere per second.
Weber (Wb)	The *weber* is the magnetic flux that, linking a circuit of one turn, produces in it an electromotive force of 1 volt as it is reduced to zero at a uniform rate in 1 second.
Lumen (lm)	The *lumen* is the luminous flux emitted in a solid angle of 1 steradian by a uniform point source having an intensity of 1 candela.
Radian (rad)	The *radian* is the plane angle between two radii of a circle that cut off on the circumference an arc equal in length to the radius.
Steradian (sr)	The *steradian* is the solid angle that, having its vertex in the center of a sphere, cuts off an area of the surface of the sphere equal to that of a square with sides of length equal to the radius of the sphere.

The names of multiples and submultiples of SI units can be formed by application of the prefixes in Table A.3. The International Organization for Standardization (ISO) recommends the following rules for the use of SI prefixes:

1. Prefix symbols are printed in roman (upright) type without spacing between the prefix symbol and the unit symbol.
2. An exponent affixed to a symbol containing a prefix indicates that the multiple or submultiple of the unit is raised to the power expressed by the exponent.

Example: $1\ cm^3 = 10^{-6}\ m^3$
$1\ cm^{-1} = 10^2\ m^{-1}$

3. Compound prefixes, formed by the juxtaposition of two or more SI prefixes, are not to be used.

Example: 1 nm *but not:* 1 mμm

ISO has issued additional recommendations with the aim of securing uniformity in the use of units. According to these recommendations,

1. The product of two or more units is preferably indicated by a dot. The dot may be dispensed with when there is no risk of confusion with another unit symbol.

Example: N·m or Nm *but not:* mN

2. A solidus (oblique stroke, /), a horizontal line, or negative powers may be used to express a derived unit formed from two others by division.

Example: m/s, $\frac{m}{s}$, or $m \cdot s^{-1}$

3. The solidus must not be repeated on the same line unless ambiguity is avoided by parentheses. In complicated cases negative powers or parentheses should be used.

Example: m/s^2 or $m \cdot s^{-2}$ *but not:* m/s/s
$m \cdot kg/(s^3 \cdot A)$ or $m \cdot kg \cdot s^{-3} \cdot A^{-1}$
but not: $m \cdot kg/s^3/A$

Table A.3 ***SI Prefixes[1]***

Factor by Which Unit Is Multiplied	Prefix	Symbol
10^{12}	Tera	T
10^9	Giga	G
10^6	Mega	M
10^3	Kilo	k
10^2	Hecto	h
10	Deka	da
10^{-1}	Deci	d
10^{-2}	Centi	c
10^{-3}	Milli	m
10^{-6}	Micro	μ
10^{-9}	Nano	n
10^{-12}	Pico	p
10^{-15}	Femto	f
10^{-18}	Atto	a

Table A.4 lists physical constants from the work of B. N. Taylor, W. H. Parker, and D. N. Langenberg.[2] Their least-squares adjustment of values of the constants depends strongly on a highly accurate (2.4 ppm) determination of e/h from the ac Josephson effect in superconductors, and is believed to be more accurate than the 1963 adjustment, which appears to suffer from the use of an incorrect value of the fine structure constant as an input datum. See also *NBS Special Publication 344,* issued March 1971.

Table A.4 ***Physical Constants[2]***

Quantity	Symbol	Value	Error (ppm)	Prefix	Unit
Speed of light in vacuum	c	2. 997 925 0	0.33	$\times 10^{8}$	$m \cdot s^{-1}$
Gravitational constant	G	6. 673 2	460	10^{-11}	$N \cdot m^{2} \cdot kg^{-2}$
Avogadro constant	N_A	6. 022 169	6.6	10^{26}	$kmol^{-1}$
Boltzmann constant	k	1. 380 622	43	10^{-23}	$J \cdot K^{-1}$
Gas constant	R	8. 314 34	42	10^{3}	$J \cdot kmol^{-1} \cdot K^{-1}$
Volume of ideal gas, standard conditions	V_0	2. 241 36	—	10^{1}	$m^{3} \cdot kmol^{-1}$
Farady constant	F	9. 648 670	5.5	10^{7}	$C \cdot kmol^{-1}$
Unified atomic mass unit	u	1. 660 531	6.6	10^{-27}	kg
Planck constant	h	6. 626 196	7.6	10^{-34}	J·s
	$h/2\pi$	1. 054 591 9	7.6	10^{-34}	J·s
Electron charge	e	1. 602 191 7	4.4	10^{-19}	C
Electron rest mass	m_e	9. 109 558	6.0	10^{-31}	kg
		5. 485 930	6.2	10^{-4}	u
Proton rest mass	m_p	1. 672 614	6.6	10^{-27}	kg
		1. 007 276 61	0.08	—	u
Neutron rest mass	m_n	1. 674 920	6.6	10^{-27}	kg
		1. 008 665 20	0.10	—	u
Electron charge to mass ratio	e/m_e	1. 758 802 8	3.1	10^{11}	$C \cdot kg^{-1}$
Stefan-Boltzmann constant	σ	5. 669 61	170	10^{-8}	$W \cdot m^{-2} \cdot K^{-4}$
First radiation constant	$2\pi hc^2$	3. 741 844	7.6	10^{-16}	$W \cdot m^{2}$
Second radiation constant	hc/k	1. 438 833	43	10^{-2}	m·K
Rydberg constant	R_∞	1. 097 373 12	0.10	10^{7}	m^{-1}
Fine structure constant	α	7. 297 351	1.5	10^{-3}	
	α^{-1}	1. 370 360 2	1.5	10^{2}	
Bohr radius	a_0	5. 291 771 5	1.5	10^{-11}	m
Classical electron radius	r_e	2. 817 939	4.6	10^{-15}	m
Compton wavelength of electron	λ_C	2. 426 309 6	3.1	10^{-12}	m
	$\lambda_C/2\pi$	3. 861 592	3.1	10^{-13}	m
Compton wavelength of proton	$\lambda_{C,p}$	1. 321 440 9	6.8	10^{-15}	m
	$\lambda_{C,p}/2\pi$	2. 103 139	6.8	10^{-16}	m
Compton wavelength of neutron	$\lambda_{C,n}$	1. 319 621 7	6.8	10^{-15}	m
	$\lambda_{C,n}/2\pi$	2. 100 243	6.8	10^{-16}	m
Electron magnetic moment	μ_e	9. 284 851	7.0	10^{-24}	$J \cdot T^{-1}$
Proton magnetic moment	μ_p	1. 410 620 3	7.0	10^{-26}	$J \cdot T^{-1}$
Bohr magneton	μ_B	9. 274 096	7.0	10^{-24}	$J \cdot T^{-1}$
Nuclear magneton	μ_n	5. 050 951	10	10^{-27}	$J \cdot T^{-1}$
Gyromagnetic ratio of protons in H_2O	γ'_p	2. 675 127 0	3.1	10^{8}	$rad \cdot s^{-1} T^{-1}$
	$\gamma'_p/2\pi$	4. 257 597	3.1	10^{7}	$Hz \cdot T^{-1}$
Gyromagnetic ratio of protons in H_2O	γ'_p	2. 675 196 5	3.1	10^{8}	$rad \cdot s^{-1} T^{-1}$
Corrected for diamagnetism of H_2O	$\gamma'_p/2\pi$	4. 257 707	3.1	10^{7}	$Hz \cdot T^{-1}$
Magnetic flux quantum	Φ_0	2. 067 853 8	3.3	10^{-15}	Wb
Quantum of circulation	$h/2m_e$	3. 636 947	3.1	10^{-4}	$J \cdot s \cdot kg^{-1}$
	h/m_e	7. 273 894	3.1	10^{-4}	$J \cdot s \cdot kg^{-1}$

Table A.4 ***(Continued)***

Unitless Numerical Ratios		Value	Error (ppm)	Prefix
(c^2)	kg/eV	5. 609 538	4.4	10^{35}
(c^2)	u/eV	9. 314 812	5.5	10^{8}
	u/kg	1. 660 531	6.6	10^{-27}
(c^2)	m_c/eV	5. 110 041	3.1	10^{5}
(c^2)	m_p/eV	9. 382 592	5.5	10^{8}
(c^2)	m_n/eV	9. 395 527	5.5	10^{8}
	eV/J	1. 602 191 7	4.4	10^{-19}
(h^{-1})	eV/Hz	2. 417 965 9	3.3	10^{14}
(hc^{-1})	eVm	8. 065 465	3.3	10^{5}
(k^{-1})	eV/K	1. 160 485	42	10^{4}
(hc)	$(\text{eVm})^{-1}$	1. 239 854 1	3.3	10^{-6}
(hc)	R_∞/J	2. 179 914	7.6	10^{-18}
(hc)	R_∞/eV	1. 360 582 6	3.3	10^{1}
(c)	R_∞/Hz	3. 289 842 3	0.35	10^{15}
(hc/k)	R_∞/K	1. 578 936	43	10^{5}
	m_p/m_e	1. 836 109	6.2	10^{3}
	μ_e/μ_B	1. 001 159 638 9	0.0031	
	μ'_p/μ_B	1. 520 993 12	0.066	10^{-3}
	μ_p/μ_B	1. 521 032 64	0.30	10^{-3}
	μ'_p/μ_n	2. 792 709	6.2	
	μ_p/μ_n	2. 792 782	6.2	

Other Important Constants
$\pi = 33.141\ 592\ 653\ 589$
$e = 2.718\ 281\ 828\ 459$
$\mu_0 = 4\pi \times 10^{-7}$ H/m (exact), permeability of free space
$= 1.256\ 637\ 061 \times 10^{-6}$ H/m
$\varepsilon_0 = \mu_0^{-1} c^{-2}$ F/m, permittivity of free space
$= 8.854\ 185 \times 10^{-12}$ F/m

The following tables express the definitions of miscellaneous units of measure as exact numerical multiples of coherent SI units, and provide multiplying factors for converting numbers and miscellaneous units to corresponding new numbers and SI units.

The first two digits of each numerical entry represents a power of 10. An asterisk following a number expresses an exact definition. For example, the entry –02 2.54* expresses the fact that 1 inch $= 2.54 \times 10^{-2}$ meter, exactly, by definition. Most of the definitions are extracted from National Bureau of Standards (NBS) documents. Numbers not followed by an asterisk are only approximate representations of definitions, or are the results of physical measurements.

The conversion factors are listed alphabetically in Table A.5 and by physical quantity in Table A.6. The listing by physical quantity (Table A.6) includes only relationships that are frequently encountered, and deliberately omits the great multiplicity of combinations of units that are used for more specialized purposes. Conversion factors for combinations of units are easily generated from numbers given in the alphabetical listing (Table A.5) by the technique of direct substitution or by other well-known rules for manipulating units. These rules are adequately discussed in many science and engineering textbooks and are not repeated here.

Table A.5 ***Alphabetical Listing of Conversion Factors[1]***

To Convert from	to	Multiply by
Abampere	Ampere	+01 1.00*
Abcoulomb	Coulomb	+01 1.00*
Abfarad	Farad	+09 1.00*
Abhenry	Henry	−09 1.00*
Abmho	Siemens	+09 1.00*
Abohm	Ohm	−09 1.00*
Abvolt	Volt	−08 1.00*
Acre	Meter^2	+03 4.046 856 422 4*
Angstrom	Meter	−10 1.00*

Table A.5 ***(Continued)***

To Convert from	to	Multiply by
Are	$Meter^2$	+02 1.00*
Astronomical unit (IAU)	Meter	+11 1.496 00
Astronomical unit (radio)	Meter	+11 1.495 978 9
Atmosphere	$Newton/meter^2$	+05 1.013 25*
Bar	$Newton/meter^2$	+05 1.00*
Barn	$Meter^2$	−28 1.00*
Barrel (petroleum, 42 gallons)	$Meter^3$	−01 1.589 873
Barye	$Newton/meter^2$	−01 1.00*
Board foot (1' × 1' × 1")	$Meter^3$	−03 2.359 737 216*
British thermal unit		
IST before 1956	Joule	+03 1.055 04
IST after 1956	Joule	+03 1.055 056
British thermal unit (mean)	Joule	+03 1.055 87
British thermal unit (thermochemical)	Joule	+03 1.054 350
British thermal unit (39°F)	Joule	+03 1.059 67
British thermal unit (60°F)	Joule	+03 1.054 68
Bushel (U.S.)	$Meter^3$	−02 3.523 907 016 688*
Cable	Meter	+02 2.194 56*
Caliber	Meter	−04 2.54*
Calorie (International Steam Table)	Joule	+00 4.1868
Calorie (mean)	Joule	+00 4.190 02
Calorie (thermochemical)	Joule	+00 4.184*
Calorie (15°C)	Joule	+00 4.185 80
Calorie (20°C)	Joule	+00 4.181 90
Calorie (kilogram, International Steam Table)	Joule	+03 4.1868
Calorie (kilogram, mean)	Joule	+03 4.190 02
Calorie (kilogram, thermochemical)	Joule	+03 4.184*
Carat (metric)	Kilogram	−04 2.00*
Celsius (temperature)	Kelvin	$t_K = t_c + 273.15$
Centimeter of mercury (0°C)	$Newton/meter^2$	+03 1.333 22
Centimeter of water (4°C)	$Newton/meter^2$	+01 9.806 38
Chain (engineer or ramden)	Meter	+01 3.048*
Chain (surveyor or gunter)	Meter	+01 2.011 68*
Circular mil	$Meter^2$	−10 5.067 074 8
Cord	$Meter^3$	+00 3.624 556 3
Cubit	Meter	−01 4.572*
Cup	$Meter^3$	−04 2.365 882 365*
Curie	Disintegration/second	+10 3.70*
Day (mean solar)	Second (mean solar)	+04 8.64*
Day (sidereal)	Second (mean solar)	+04 8.616 409 0
Degree (angle)	Radian	−02 1.745 329 251 994 3
Denier (international)	Kilogram/meter	−07 1.00*
Dram (avoirdupois)	Kilogram	−03 1.771 845 195 312 5*
Dram (troy or apothecary)	Kilogram	−03 3.887 934 6*
Dram (U.S. fluid)	$Meter^3$	−06 3.696 691 195 312 5*
Dyne	Newton	−05 1.00*
Electron volt	Joule	−19 1.602 191 7
Erg	Joule	−07 1.00*
Fahrenheit (temperature)	Kelvin	$t_K = (5/9)(t_F + 459.67)$
Fahrenheit (temperature)	Celsius	$t_c = (5/9)(t_F - 32)$
Faraday (based on carbon 12)	Coulomb	+04 9.68 70
Faraday (chemical)	Coulomb	+04 9.649 57
Faraday (physical)	Coulomb	+04 9.652 19
Fathom	Meter	+00 1.828 8*
Fermi (femtometer)	Meter	+15 1.00*
Fluid ounce (U.S.)	$Meter^3$	−05 2.957 352 967 25*
Foot	Meter	−01 3.048*
Foot (U.S. survey)	Meter	+00 1200/3937*

Table A.5 ***(Continued)***

To Convert from	to	Multiply by
Foot (U.S. survey)	Meter	−01 3.048 006 096
Foot of water (39.2°F)	Newton/meter^2	+03 2.988 98
Footcandle	Lumen/meter^2	+01 1.076 391 0
Footlambert	Candela/meter^2	+00 3.426 259
Free fall, standard	Meter/second^2	+00 9.806 65*
Furlong	Meter	+02 2.011 68*
Gal (galileo)	Meter/second^2	−02 1.00*
Gallon (U.K. liquid)	Meter^3	−03 4.546 087
Gallon (U.S. dry)	Meter^3	−03 4.404 883 770 86*
Gallon (U.S. liquid)	Meter^3	−03 3.785 411 784*
Gamma	Tesla	−09 1.00*
Gauss	Tesla	−04 1.00*
Gilbert	Ampere turn	−01 7.957 747 2
Gill (U.K.)	Meter^3	−04 1.420 652
Gill (U.S.)	Meter^3	−04 1.182 941 2
Grad	Degree (angular)	−01 .900*
Grad	Radian	−02 1.570 796 3
Grain	Kilogram	−05 6.479 891*
Gram	Kilogram	−03 1.00*
Hand	Meter	−01 1.016*
Hectare	Meter^3	+04 1.00*
Hogshead (U.S.)	Meter^3	−01 2.384 809 423 92*
Horsepower (550 ft·lbf/second)	Watt	+02 7.456 998 7
Horsepower (boiler)	Watt	+03 9.809 50
Horsepower (electric)	Watt	+02 7.46*
Horsepower (metric)	Watt	+02 7.354 99
Horsepower (U.K.)	Watt	+02 7.457
Horsepower (water)	Watt	+02 7.460 73
Hour (mean solar)	Second (mean solar)	+03 3.60*
Hour (sidereal)	Second (mean solar)	+03 3.590 170 4
Hundredweight (long)	Kilogram	+01 5.080 234 544*
Hundredweight (short)	Kilogram	+01 4.535 923 7*
Inch	Meter	−02 2.54*
Inch of mercury (32°F)	Newton/meter^2	+03 3.386 389
Inch of mercury (60°F)	Newton/meter^2	+03 3.375 85
Inch of water (39.2°F)	Newton/meter^2	+02 2.490 82
Inch of water (60°F)	Newton/meter^2	+02 2.4884
Kayser	1/meter	+02 1.00*
Kilocalorie (International Steam Table)	Joule	+03 4.186 8
Kilocalorie (mean)	Joule	+03 4.190 02
Kilocalorie (thermochemical)	Joule	+03 4.184*
Kilogram mass	Kilogram	+00 1.00*
Kilogram force (kgf)	Newton	+00 9.806 65*
Kilopound force	Newton	+00 9.806 65*
Kip	Newton	+03 4.448 221 615 260 5*
Knot (international)	Meter/second	−01 5.144 444 444
Lambert	Candela/meter^2	+04 1/π*
Lambert	Candela/meter^2	+03. 3.183 098 8
Langley	Joule/meter^2	+04 4.184*
Lbf (pound force, avoirdupois)	Newton	+00 4.448 221 615 260 5*
Lbm (pound mass, avoirdupois)	Kilogram	−01 4.535 923 7*
League (U.K. nautical)	Meter	+03 5.559 552*
League (international nautical)	Meter	+03 5.556
League (statute)	Meter	+03 4.828 032*
Light-year	Meter	+15 9.460 55
Link (engineer or ramden)	Meter	−01 3.048*
Link (surveyor or gunter)	Meter	−01 2.011 68*
Liter	Meter^3	−03 1.00*

Table A.5 ***(Continued)***

To Convert from	to	Multiply by
Lux	Lumen/meter^2	+00 1.00*
Maxwell	Weber	−08 1.00*
Meter	Wavelengths Kr 86	+06 1.650 763 73*
Micron	Meter	−06 1.00*
Mil	Meter	−05 2.54*
Mile (U.S. statute)	Meter	+03 1.609 344*
Mile (U.K. nautical)	Meter	+03 1.853 184*
Mile (international nautical)	Meter	+03 1.852*
Mile (U.S. nautical)	Meter	+03 1.852*
Millibar	Newton/meter^2	+02 1.00*
Millimeter of mercury (0°C)	Newton/meter^2	+02 1.333 224
Minute (angle)	Radian	−04 2.908 882 086 66
Minute (mean solar)	Second (mean solar)	+01 6.00*
Minute (sidereal)	Second (mean solar)	+01 5.983 617 4
Month (mean calendar)	Second (mean solar)	+06 2.628*
Nautical mile (international)	Meter	+03 1.852*
Nautical mile (U.S.)	Meter	+03 1.852*
Nautical mile (U.K.)	Meter	+03 1.853 184*
Oersted	Ampere/meter	+01 7.957 747 2
Ounce force (avoirdupois)	Newton	−01 2.780 138 5
Ounce mass (avoirdupois)	Kilogram	−02 2.834 952 312 5*
Ounce mass (troy or apothecary)	Kilogram	−02 3.110 347 68*
Ounce (U.S. fluid)	Meter^3	−05 2.957 352 956 25*
Pace	Meter	−01 7.62*
Parsec (IAU)	Meter	+16 3.085 7
Pascal	Newton/meter^2	+00 1.00*
Peck (U.S.)	Meter^3	−03 8.809 767 541 72*
Pennyweight	Kilogram	−03 1.555 173 84*
Perch	Meter	+00 5.0292*
Phot	Lumen/meter^3	+04 1.00
Pica (printers)	Meter	−03 4.217 517 6*
Pint (U.S. dry)	Meter^3	−04 5.506 104 713 575*
Pint (U.S. liquid)	Meter^3	−04 4.731 764 73*
Point (printers)	Meter	−04 3.514 598*
Poise	Newton second/meter^2	−01 1.00*
Pole	Meter	+00 5.0292*
Pound force (lbf avoirdupois)	Newton	+00 4.448 221 615 260 5*
Pound mass (lbm avoirdupois)	Kilogram	−01 4.535 923 7*
Pound mass (troy or apothecary)	Kilogram	−01 3.732 417 216*
Poundal	Newton	−01 1.382 549 543 76*
Quart (U.S. dry)	Meter^3	−03 1.101 220 942 715*
Quart (U.S. liquid)	Meter^3	−04 9.463 592 5
Rad (radiation dose absorbed)	Joule/kilogram	−02 1.00*
Rankine (temperature)	Kelvin	$t_K = (5/9)t_R$
Rayleigh (rate of photon emission)	1/second meter^2	+10 1.00*
Rhe	Meter^2/newton second	+01 1.00*
Rod	Meter	+00 5.0292*
Roentgen	Coulomb/kilogram	−04 2.579 76*
Rutherford	Disintegration/second	+06 1.00*
Second (angle)	Radian	−06 4.848 136 811
Second (ephemeris)	Second	+00 1.000 000 000
Second (mean solar)	Second (ephemeris)	Consult American Ephemeris and Nautical Almanac
Second (sidereal)	Second (mean solar)	−01 9.972 695 7
Section	Meter^2	+06 2.589 988 110 336*
Scruple (apothecary)	Kilogram	−03 1.295 978 2*

Table A.5 ***(Continued)***

To Convert from	to	Multiply by
Shake	Second	−08 1.00
Skein	Meter	+02 1.097 28*
Slug	Kilogram	+01 1.459 390 29
Span	Meter	−01 2.286*
Statampere	Ampere	−10 3.335 640
Statcoulomb	Coulomb	−10 3.335 640
Statfarad	Farad	−12 1.112 650
Stathenry	Henry	+11 8.987 554
Statohm	Ohm	+11 8.987 554
Statute mile (U.S.)	Meter	+03 1.609 344*
Statvolt	Volt	+02 2.997 925
Stere	$Meter^3$	+00 1.00*
Stilb	$Candela/meter^2$	+04 1.00
Stoke	$Meter^2/second$	−04 1.00*
Tablespoon	$Meter^3$	−05 1.478 676 478 125*
Teaspoon	$Meter^3$	−06 4.928 921 593 75*
Ton (assay)	Kilogram	−02 2.196 666 6
Ton (long)	Kilogram	+03 1.016 046 908 8*
Ton (metric)	Kilogram	+03 1.00*
Ton (nuclear equivalent of TNT)	Joule	+09 4.20
Ton (register)	$Meter^3$	+00 2.831 684 659 2*
Ton (short, 2000 pound)	Kilogram	+02 9.071 847 4*
Tonne	Kilogram	+03 1.00*
Torr (0°C)	$Newton/meter^2$	+02 1.333 22
Township	$Meter^2$	+07 9.323 957 2
Unit pole	Weber	−07 1.256 637
Yard	Meter	−01 9.144*
Year (calendar)	Second (mean solar)	+07 3.1536*
Year (sidereal)	Second (mean solar)	+07 3.155 815 0
Year (tropical)	Second (mean solar)	+07 3.155 692 6
Year 1900, tropical, Jan., day 0, hour 12	Second (ephemeris)	+07 3.155 692 597 47*
Year 1900, tropical, Jan., day 0, hour 12	Second	+07 3.155 692 597 47*

Table A.6 ***Listing Conversion Factors by Physical Quantity[1]***

To Convert from	to	Multiply by
	ACCELERATION	
$Foot/second^2$	$Meter/second^2$	−01 3.048*
Free fall, standard	$Meter/second^2$	+00 9.806 65*
Gal (galileo)	$Meter/second^2$	−02 1.00*
$Inch/second^2$	$Meter/second^2$	−02 2.54*
	AREA	
Acre	$Meter^2$	+03 4.046 856 422 4*
Are	$Meter^2$	+02 1.00*
Barn	$Meter^2$	−28 1.00*
Circular mil	$Meter^2$	−10 5.067 074 8
$Foot^2$	$Meter^2$	−02 9.290 304*
Hectare	$Meter^2$	+04 1.00*
$Inch^2$	$Meter^2$	−04 6.4516*
$Mile^2$ (U.S. statute)	$Meter^2$	+06 2.589 988 110 336*
Section	$Meter^2$	+06 2.589 988 110 336*
Township	$Meter^2$	+07 9.323 957 2
$Yard^2$	$Meter^2$	−01 8.361 273 6*

Table A.6 ***(Continued)***

To Convert from	to	Multiply by
	DENSITY	
Gram/centimeter^3	Kilogram/meter^3	−03 1.00*
Lbm/inch^3	Kilogram/meter^3	+04 2.767 990 5
Lbm/foot^3	Kilogram/meter^3	+01 1.601 846 3
Slug/foot^3	Kilogram/meter^3	+02 5.153 79
	ENERGY	
British thermal unit		
IST before 1956	Joule	+03 1.055 04
IST after 1956	Joule	+03 1.055 056
British thermal unit (mean)	Joule	+03 1.055 87
British thermal unit (thermochemical)	Joule	+03 1.054 350
British thermal unit (39°F)	Joule	+03 1.059 67
British thermal unit (60°F)	Joule	+03 1.054 68
Calorie (International Steam Table)	Joule	+00 4.1868
Calorie (mean)	Joule	+00 4.190 02
Calorie (thermochemical)	Joule	+00 4.184*
Calorie (15°C)	Joule	+00 4.185 80
Calorie (20°C)	Joule	+00 4.181 90
Calorie (kilogram, International Steam Table)	Joule	+03 4.1868
Calorie (kilogram, mean)	Joule	+03 4.190 02
Calorie (kilogram, thermochemical)	Joule	+03 4.184*
Electron volt	Joule	−19 1.602 191 7
Erg	Joule	−07 1.00*
Foot lbf	Joule	+03 1.355 817 9
Foot poundal	Joule	−02 4.214 011 0
Joule (international of 1948)	Joule	+00 1.000 165
Kilocalorie (International Steam Table)	Joule	+03 4.1868
Kilocalorie (mean)	Joule	+03 4.190 02
Kilocalorie (thermochemical)	Joule	+03 4.184*
Kilowatt hour	Joule	+06 3.60*
Kilowatt hour (international of 1948)	Joule	+06 3.600 59
Ton (nuclear equivalent of TNT)	Joule	+09 4.20
Watt hour	Joule	+03 3.60*
	ENERGY/AREA TIME	
Btu (thermochemical)/foot^2 second	Watt/meter^2	+04 1.134 893 1
Btu (thermochemical)/foot^2 minute	Watt/meter^2	+02 1.891 488 5
Btu (thermochemical)/foot^2 hour	Watt/meter^2	+00 3.152 480 8
Btu (thermochemical)/inch^2 second	Watt/meter^2	+06 1.634 246 2
Calorie (thermochemical)/cm^2 minute	Watt/meter^2	+02 6.973 333 3
Erg/centimeter^2 second	Watt/meter^2	−03 1.00*
Watt/centimeter^2	Watt/meter^2	+04 1.00*
	FORCE	
Dyne	Newton	−05 1.00*
Kilogram force (kgf)	Newton	+00 9.806 65*
Kilopound force	Newton	+00 9.806 65*
Kip	Newton	+03 4.448 221 615 260 5*
Lbf (pound force, avoirdupois)	Newton	+00 4.448 221 615 260 5*
Ounce force (avoirdupois)	Newton	+01 2.780 138 5
Pound force, lbf (avoirdupois)	newton	+00 4.448 221 615 260 5*
Poundal	Newton	−01 1.382 549 543 76*
	LENGTH	
Angstrom	Meter	−10 1.00*
Astronomical unit (IAU)	Meter	+11 1.496 00
Astronomical unit (radio)	Meter	+11 1.495 978 9
Cable	Meter	+02 2.194 56*
Caliber	Meter	−04 2.54*
Chain (surveyor or gunter)	Meter	+01 2.011 68*

Table A.6 *(Continued)*

To Convert from	to	Multiply by
	LENGTH *(continued)*	
Chain (engineer or ramden)	Meter	+01 3.048*
Cubit	Meter	−01 4.572*
Fathom	Meter	+00 1.8288*
Fermi (femtometer)	Meter	−15 1.00*
Foot	Meter	−01 3.048*
Foot (U.S. survey)	Meter	+00 1200/3937*
Foot (U.S. survey)	Meter	−01 3.048 006 096
Furlong	Meter	+02 2.011 68*
Hand	Meter	−01 1.016*
Inch	Meter	−02 2.54*
League (U.K. nautical)	Meter	+03 5.559 552*
League (international nautical)	Meter	+03 5.556*
League (statute)	Meter	+03 4.828 032*
Light-year	Meter	+15 9.460 55
Link (engineer or ramden)	Meter	−01 3.048*
Link (surveyor or gunter)	Meter	−01 2.011 68*
Meter	Wavelengths Kr 86	+06 1.650 763 73*
Micron	Meter	−06 1.00*
Mil	Meter	−05 2.54*
Mile (U.S. statute)	Meter	+03 1.609 344*
Mile (U.K. nautical)	Meter	+03 1.853 184*
Mile (international nautical)	Meter	+03 1.852*
Mile (U.S. nautical)	Meter	+03 1.852*
Nautical mile (U.K.)	Meter	+03 1.853 184*
Nautical mile (international)	Meter	+03 1.852*
Nautical mile (U.S.)	Meter	+03 1.852*
Pace	Meter	−01 7.62*
Parsec (IAU)	Meter	+16 3.085 7
Perch	Meter	+00 5.0292*
Pica (printers)	Meter	−03 4.217 517 6*
Point (printers)	Meter	−04 3.514 598*
Pole	Meter	+00 5.0292*
Rod	Meter	+00 5.0292*
Skein	Meter	+02 1.097 28*
Span	Meter	−01 2.286*
Statute mile (U.S.)	Meter	+03 1.609 344*
Yard	Meter	−01 9.144*
	MASS	
Carat (metric)	Kilogram	−04 2.00*
Gram (avoirdupois)	Kilogram	−03 1.771 845 195 312 5*
Gram (troy or apothecary)	Kilogram	−03 3.887 934 6*
Grain	Kilogram	−05 6.479 891*
Gram	Kilogram	−03 1.00*
Hundredweight (long)	Kilogram	+01 5.080 234 544*
Hundredweight (short)	Kilogram	+01 4.535 923 7*
Kgf second^2 meter (mass)	Kilogram	+00 9.806 65*
Kilogram mass	Kilogram	+00 1.00*
Lbm (pound mass, avoirdupois)	Kilogram	−01 4.535 923 7*
Ounce mass (avoirdupois)	Kilogram	−02 2.834 952 312 5*
Ounce mass (troy or apothecary)	Kilogram	−02 3.110 347 68*
Pennyweight	Kilogram	−03 1.555 173 84*
Pound mass, lbm (avoirdupois)	Kilogram	−01 4.535 923 7*
Pound mass (troy or apothecary)	Kilogram	−01 3.732 417 216*
Scruple (apothecary)	Kilogram	−03 1.295 978 2*
Slug	Kilogram	+01 1.459 390 29
Ton (assay)	Kilogram	−02 2.196 666 6
Ton (long)	Kilogram	+03 1.016 046 908 8*
Ton (metric)	Kilogram	+03 1.00*
Ton (short, 2000 pound)	Kilogram	+02 9.071 847 4*
Tonne	Kilogram	+03 1.00*

Table A.6 ***(Continued)***

To Convert from	to	Multiply by
	POWER	
Btu (thermochemical)/second	Watt	+03 1.054 350 264 488
Btu (thermochemical)/minute	Watt	+01 1.757 250 4
Calorie (thermochemical)/second	Watt	+00 4.184*
Calorie (thermochemical)/minute	Watt	−02 6.973 333 3
Foot lbf/hour	Watt	−04 3.766 161 0
Foot lbf/minute	Watt	−02 2.259 696 6
Foot lbf/second	Watt	+00 1.355 817 9
Horsepower (550 ft·lbf/second)	Watt	+02 7.456 998 7
Horsepower (boiler)	Watt	+03 9.809 50
Horsepower (electric)	Watt	+02 7.46*
Horsepower (metric)	Watt	+02 7.354 99
Horsepower (U.K.)	Watt	+02 7.457
Horsepower (water)	Watt	+02 7.460 43
Kilocalorie (thermochemical)/minute	Watt	+01 6.973 333 3
Kilocalorie (thermochemical)/second	Watt	+03 4.184*
Watt (international of 1948)	Watt	+00 1.000 165
	PRESSURE	
Atmosphere	Newton/meter^2	+05 1.013 25*
Bar	Newton/meter^2	+05 1.00*
Barye	Newton/meter^2	−01 1.00*
Centimeter of mercury (0°C)	Newton/meter^2	+03 1.333 22
Centimeter of water (4°C)	Newton/meter^2	+01 9.806 38
Dyne/centimeter^2	Newton/meter^2	−01 1.00*
Foot of water (39.2°F)	Newton/meter^2	+03 2.988 988
Inch of mercury (32°F)	Newton/meter^2	+03 3.386 389
Inch of mercury (60°F)	Newton/meter^2	+03 3.376 85
Inch of water (39.2°F)	Newton/meter^2	+02 2.480 82
Inch of water (60°F)	Newton/meter^2	+02 2.4884
Kgf/centimeter^2	Newton/meter^2	+04 9.806 65*
Kgf/meter^2	Newton/meter^2	+00 9.806 65*
Lbf/foot^2	Newton/meter^2	+01 4.788 025 8
Lbf/inch^2 (psi)	Newton/meter^2	+03 6.894 757 2
Millibar	Newton/meter^2	+02 1.00*
Millimeter of mercury (0°C)	Newton/meter^2	+02 1.333 224
Pascal	Newton/meter^2	+00 1.00*
Psi (lbf/inch^2)	Newton/meter^2	+03 6.894 757 2
Torr (0°C)	Newton/meter^2	+02 1.333 22
	SPEED	
Foot/hour	Meter/second	−05 8.466 666 6
Foot/minute	Meter/second	−03 5.08*
Foot/second	Meter/second	−01 3.048*
Inch/second	Meter/second	−02 2.54*
Kilometer/hour	Meter/second	−01 2.777 777 8
Knot (international)	Meter/second	−01 5.144 444 444
Mile/hour (U.S. statute)	Meter/second	−01 4.4704*
Mile/minute (U.S. statute)	Meter/second	+01 2.682 24*
Mile/second (U.S. statute)	Meter/second	+03 1.609 344*
	TEMPERATURE	
Celsius	Kelvin	$t_K = t_C + 273.15$
Fahrenheit	Kelvin	$t_K = (5/9)(t_F + 459.67)$
Fahrenheit	Celsius	$t_C = (5/9)(t_F - 32)$
Rankine	Kelvin	$t_K = (5/9)t_R$

Table A.6 ***(Continued)***

To Convert from	to	Multiply by
	TIME	
Day (mean solar)	Second (mean solar)	+04 8.64*
Day (sidereal)	Second (mean solar)	+04 8.616 409 0
Hour (mean solar)	Second (mean solar)	+03 3.60*
Hour (sidereal)	Second (mean solar)	+03 3.590 170 4
Minute (mean solar)	Second (mean solar)	+01 6.00*
Minute (sidereal)	Second (mean solar)	+01 5.983 617 4
Month (mean calendar)	Second (mean solar)	+06 2.628*
Second (ephemeris)	Second	+00 1.000 000 000
Second (mean solar)	Second (ephemeris)	Consult American Ephemeris and Nautical Almanac
Second (sidereal)	Second (mean solar)	−01 9.972 695 7
Year (calendar)	Second (mean solar)	+07 3.1536*
Year (sidereal)	Second (mean solar)	+07 3.155 815 0
Year (tropical)	Second (mean solar)	+07 3.155 692 6
Year 1900, tropical, Jan., day 0, hour 12	Second (ephemeris)	+07 3.155 692 597 47*
Year 1900, tropical, Jan., day 0, hour 12	Second	+07 3.155 692 597 47
	VISCOSITY	
Centistoke	$Meter^2$/second	−06 1.00*
Stoke	$Meter^2$/second	−04 1.00*
$Foot^2$/second	$Meter^2$/second	−02 9.290 304*
Centipoise	Newton second/$meter^2$	−03 1.00*
Lbm/foot second	Newton second/$meter^2$	+00 1.488 163 9
Lbf·second/$foot^2$	Newton second/$meter^2$	+01 4.788 025 8
Poise	Newton second/$meter^2$	−01 1.00*
Poundal second/$foot^2$	Newton second/$meter^2$	+00 1.488 163 9
Slug/foot second	Newton second/$meter^2$	+01 4.788 025 8
Rhe	$Meter^2$/newton second	+01 1.00*
	VOLUME	
Acre foot	$Meter^3$	+03 1.233 481 837 547 52*
Barrel (petroleum, 42 gallons)	$Meter^3$	−01 1.589 873
Board foot	$Meter^3$	−03 2.359 737 216*
Bushel (U.S.)	$Meter^3$	−02 3.523 907 016 688*
Cord	$Meter^3$	+00 3.624 556 3
Cup	$Meter^3$	−04 2.365 882 365*
Dram (U.S. fluid)	$Meter^3$	−06 3.696 691 195 312 5*
Fluid ounce (U.S.)	$Meter^3$	−05 2.957 352 946 25*
$Foot^3$	$Meter^3$	−02 2.831 684 659 2*
Gallon (U.K. liquid)	$Meter^3$	−03 4.546 087
Gallon (U.S. dry)	$Meter^3$	−03 4.404 883 770 86*
Gallon (U.S. liquid)	$Meter^3$	−03 3.785 411 784*
Gill (U.K.)	$Meter^3$	−04 1.420 652
Gill (U.S.)	$Meter^3$	−04 1.182 941 2
Hogshead (U.S.)	$Meter^3$	−01 2.384 809 423 92*
$Inch^3$	$Meter^3$	−05 1.638 706 4*
Liter	$Meter^3$	−03 1.00*
Ounce (U.S. fluid)	$Meter^3$	−05 2.957 352 956 25*
Peck (U.S.)	$Meter^3$	−03 8.809 767 541 72*
Pint (U.S. dry)	$Meter^3$	−04 5.506 104 713 575*
Pint (U.S. liquid)	$Meter^3$	−04 4.731 764 73*
Quart (U.S. dry)	$Meter^3$	−03 1.101 220 942 715*
Quart (U.S. liquid)	$Meter^3$	−04 9.463 592 5
Stere	$Meter^3$	+00 1.00*
Tablespoon	$Meter^3$	−05 1.478 676 478 125*
Teaspoon	$Meter^3$	−06 4.928 921 593 75*
Ton (register)	$Meter^3$	+00 2.831 684 659 2*
$Yard^3$	$Meter^3$	−01 7.645 548 579 84*

Conversion Factor Tables[3]

Table A.7 ***Length (L)***

Multiply Number of → / to Obtain ↓ (by ↘)	Centimeters	Feet	Inches	Kilometers	Nautical Miles	Meters	Mils	Miles	Millimeters	Yards
Centimeters	1	30.48	2.540	10^5	1.853 $\times 10^5$	100	2.540 $\times 10^{-3}$	1.609 $\times 10^5$	0.1	91.44
Feet	3.281 $\times 10^{-2}$	1	8.333 $\times 10^{-2}$	3281	6080.27	3.281	8.333 $\times 10^{-5}$	5280	3.281 $\times 10^{-3}$	3
Inches	0.3937	12	1	3.937 $\times 10^4$	7.296 $\times 10^4$	39.37	0.001	6.336 $\times 10^4$	3.937 $\times 10^{-2}$	36
Kilometers	10^{-5}	3.048 $\times 10^{-4}$	2.540 $\times 10^{-5}$	1	1.853	0.001	2.540 $\times 10^{-8}$	1.609	10^{-6}	9.144 $\times 10^{-4}$
Nautical miles		1.645 $\times 10^{-4}$		0.5396	1	5.396 $\times 10^{-4}$		0.8684		4.934 $\times 10^{-4}$
Meters	0.01	0.3048	2.540 $\times 10^{-2}$	1000	1853	1		1609	0.001	0.9144
Mils	393.7	1.2 $\times 10^4$	1000	3.937 $\times 10^7$		3.937 $\times 10^4$	1		39.37	3.6 $\times 10^4$
Miles	6.214 $\times 10^{-6}$	1.894 $\times 10^{-4}$	1.578 $\times 10^{-5}$	0.6214	1.1516	6.214 $\times 10^{-4}$		1	6.214 $\times 10^{-7}$	5.682 $\times 10^{-4}$
Millimeters	10	304.8	25.40	10^6		1000	2.540 $\times 10^{-2}$		1	914.4
Yards	1.094 $\times 10^{-2}$	0.3333	2.778 $\times 10^{-2}$	1094	2027	1.094	2.778 $\times 10^{-5}$	1760	1.094 $\times 10^{-3}$	1

Table A.8 ***Area (L^2)***

Multiply Number of → / to Obtain ↓ (by →)	Acres	Circular Mils	Square Centimeters	Square Feet	Square Inches	Square Kilometers	Square Meters	Square Miles	Square Millimeters	Square Yards
Acres	1			2.296×10^{-5}		247.1	2.471×10^{-4}	640		2.066×10^{-4}
Circular mils		1	1.973×10^{5}	1.833×10^{8}	1.273×10^{6}		1.973×10^{9}		1973	
Square centimeters		5.067×10^{-6}	1	929.0	6.452	10^{10}	10^{4}	2.590×10^{10}	0.01	8361
Square feet	4.356×10^{4}		1.076×10^{-3}	1	6.944×10^{-3}	1.076×10^{7}	10.76	2.788×10^{7}	1.076×10^{-5}	9
Square inches	6,272,640	7.854×10^{-7}	0.1550	144	1	1.550×10^{9}	1550	4.015×10^{9}	1.550×10^{-3}	1296
Square kilometers	4.047×10^{-3}		10^{-10}	9.290×10^{-8}	6.452×10^{-10}	1	10^{-6}	2.590	10^{-12}	8.361×10^{-7}
Square meters	4047		0.0001	9.290×10^{-2}	6.452×10^{-4}	10^{6}	1	2.590×10^{6}	10^{-6}	0.8361
Square miles	1.562×10^{-3}		3.861×10^{-11}	3.587×10^{-8}		0.3861	3.861×10^{-7}	1	3.861×10^{-13}	3.228×10^{-7}
Square millimeters		5.067×10^{-4}	100	9.290×10^{4}	645.2	10^{12}	10^{6}		1	8.361×10^{5}
Square yards	4840		1.196×10^{-4}	0.1111	7.716×10^{-4}	1.196×10^{6}	1.196	3.098×10^{6}	1.196×10^{-6}	1

Table A.9 ***Volume (L^3)***

Multiply Number of → / to Obtain ↓ (by →)	Bushels (dry)	Cubic Centimeters	Cubic Feet	Cubic Inches	Cubic Meters	Cubic Yards	Gallons (liquid)	Liters	Pints (liquid)	Quarts (liquid)
Bushels (dry)	1		0.8036	4.651×10^{-4}	28.38			2.838×10^{-2}		
Cubic centimeters	3.524×10^{4}	1	2.832×10^{4}	16.39	10^{6}	7.646×10^{5}	3785	1000	473.2	946.4
Cubic feet	1.2445	3.531×10^{-5}	1	5.787×10^{-4}	35.31	27	0.1337	3.531×10^{-2}	1.671×10^{-2}	3.342×10^{-2}
Cubic inches	2150.4	6.102×10^{-2}	1728	1	6.102×10^{4}	46,656	231	61.02	28.87	57.75
Cubic meters	3.524×10^{-2}	10^{-6}	2.832×10^{-2}	1.639×10^{-5}	1	0.7646	3.785×10^{-3}	0.001	4.732×10^{-4}	9.464×10^{-4}
Cubic yards		1.308×10^{-6}	3.704×10^{-2}	2.143×10^{-5}	1.308	1	4.951×10^{-3}	1.308×10^{-3}	6.189×10^{-4}	1.238×10^{-3}
Gallons (liquid)		2.642×10^{-4}	7.481	4.329×10^{-3}	264.2	202.0	1	0.2642	0.125	0.25
Liters	35.24	0.001	28.32	1.639×10^{-2}	1000	764.6	3.785	1	0.4732	0.9464
Pints (liquid)		2.113×10^{-3}	59.84	3.463×10^{-2}	2113	1616	8	2.113	1	2
Quarts (liquid)		1.057×10^{-3}	29.92	1.732×10^{-2}	1057	807.9	4	1.057	0.5	1

Table A.10 ***Plane Angle (no dimensions)***

Multiply Number of → / by → / to Obtain ↓	Degrees	Minutes	Quadrants	Radians	Revolutions[a] (circumferences)	Seconds
Degrees	1	1.667×10^{-2}	90	57.30	360	2.778×10^{-4}
Minutes	60	1	5400	3438	2.16×10^{4}	1.667×10^{-2}
Quadrants	1.111×10^{-2}	1.852×10^{-4}	1	0.6366	4	3.087×10^{-6}
Radians[a]	1.745×10^{-2}	2.909×10^{-4}	1.571	1	6.283	4.848×10^{-6}
Revolutions[a] (circumferences)	2.788×10^{-3}	4.630×10^{-5}	0.25	0.1591	1	7.716×10^{-7}
Seconds	3600	60	3.24×10^{5}	2.063×10^{5}	1.296×10^{6}	1

[a]2π rad = 1 circumference = 360 degrees by definition.

Table A.11 ***Linear Velocity (LT^{-1})***

Multiply Number of → / by → / to Obtain ↓	Centimeters per Second	Feet per Minute	Feet per Second	Kilometers per Hour	Kilometers per Minute	Knots[a]	Meters per Minute	Meters per Second	Miles per Hour	Miles per Minute
Centimeters per second	1	0.5080	30.48	27.78	1667	51.48	1.667	100	44.70	2682
Feet per minute	1.969	1	60	54.68	3281	101.3	3.281	196.8	88	5280
Feet per second	3.281×10^{-2}	1.667×10^{-2}	1	0.9113	54.68	1.689	5.468×10^{-2}	3.281	1.467	88
Kilometers per hour	0.036	1.829×10^{-2}	1.097	1	60	1.853	0.06	3.6	1.609	96.54
Kilometers per minute	0.0006	3.048×10^{-4}	1.829×10^{-2}	1.667×10^{-2}	1	3.088×10^{-2}	0.001	0.06	2.682×10^{-2}	1.609
Knots[a]	1.943×10^{-2}	9.868×10^{-3}	0.5921	0.5396	32.38	1	3.238×10^{-2}	1.943	0.8684	52.10
Meters per minute	0.6	0.3048	18.29	16.67	1000	30.88	1	60	26.82	1609
Meters per second	0.01	5.080×10^{-3}	0.3048	0.2778	16.67	0.5148	1.667×10^{-2}	1	0.4470	26.82
Miles per hour	2.237×10^{-2}	1.136×10^{-2}	0.6818	0.6214	37.28	1.152	3.728×10^{-2}	2.237	1	60
Miles per minute	3.728×10^{-4}	1.892×10^{-4}	1.136×10^{-2}	1.036×10^{-2}	0.6214	1.919×10^{-2}	6.214×10^{-4}	3.728×10^{-2}	1.667×10^{-2}	1

[a]Nautical miles per hour.

Table A.12 ***Linear Acceleration (LT^{-2})***

Multiply Number of → / by → / to Obtain ↓	Centimeters per Second per Second	Feet per Second per Second	Kilometers per Hour per Second	Meters per Second per Second	Miles per Hour per Second
Centimeters per Second per Second	1	30.48	27.78	100	44.70
Feet per Second per Second	3.281×10^{-2}	1	0.9113	3.281	1.467
Kilometers per Hour per Second	0.036	1.097	1	3.6	1.609
Meters per Second per Second	0.01	0.3048	0.2778	1	0.4470
Miles per Hour per Second	2.237×10^{-2}	0.6818	0.6214	2.237	1

The (standard) acceleration due to gravity (g_0) = 908.7 cm/s² = 32.17 ft/s² = 35.30 km/h·s = 9.807 m/s² = 21.94 mph/s.

Table A.13 ***Mass (M) and Weight****

Multiply Number of → / by → / to Obtain ↓	Grains	Grams	Kilograms	Milligrams	Ounces†	Pounds†	Tons (long)	Tons (metric)	Tons (short)
Grains	1	15.43	1.543×10^{4}	1.543×10^{-2}	437.5	7000			
Grams	6.481×10^{-2}	1	1000	0.001	28.35	453.6	1.016×10^{6}	$\times 10^{6}$	9.072×10^{5}
Kilograms	6.481×10^{-5}	0.001	1	10^{-6}	2.835×10^{-2}	0.4536	1016	1000	907.2
Milligrams	64.81	1000	10^{6}	1	2.835×10^{4}	4.536×10^{5}	1.016×10^{9}	10^{9}	9.072×10^{8}
Ounces	2.286×10^{-3}	3.527×10^{-2}	35.27	3.527×10^{-5}	1	16	3.584×10^{4}	3.527×10^{4}	3.2×10^{4}
Pounds	1.429×10^{-4}	2.205×10^{-3}	2.205	2.205×10^{-6}	6.250×10^{-2}	1	2240	2205	2000
Tons (long)		9.842×10^{-7}	9.842×10^{-4}	9.842×10^{-10}	2.790×10^{-5}	4.464×10^{-4}	1	0.9842	0.8929
Tons (metric)		10^{-6}	0.001	10^{-9}	2.835×10^{-5}	4.536×10^{-4}	1.016	1	0.9072
Tons (short)		1.102×10^{-6}	1.102×10^{-3}	1.102×10^{-9}	3.125×10^{-5}	0.0005	1.120	1.102	1

*These conversion factors apply to the gravitational units of force having the corresponding names.

†Avoirdupois pounds and ounces.

Table A.14 ***Density or Mass per Unit Volume (ML^{-3})***

Multiply Number of → / by → / to Obtain ↓	Grams per Cubic Centimeter	Kilograms per Cubic Meter	Pounds per Cubic Foot	Pounds per Cubic Inch
Grams per cubic centimeter	1	0.001	1.602×10^{-2}	27.68
Kilograms per cubic meter	1000	1	16.02	2.768×10^{4}
Pounds per cubic foot	62.43	6.243×10^{-2}	1	1728
Pounds per cubic inch	3.613×10^{-2}	3.613×10^{-5}	5.787×10^{-4}	1
Pounds per mil foot[a]	3.405×10^{-7}	3.405×10^{-10}	5.456×10^{-9}	9.425×10^{-6}

[a]Unit of volume is a volume one foot long and one circular mil in cross-section area.

Table A.15 ***Force (MLT^{-2}) or (F)***

Multiply Number of → / by → / to Obtain ↓	Dynes	Grams	Joules per Centimeter	Newtons or Joules per Meter	Kilograms	Pounds	Poundals
Dynes	1	980.7	10^{7}	10^{5}	9.807×10^{5}	4.448×10^{5}	1.383×10^{4}
Grams	1.020×10^{-3}	1	1.020×10^{4}	102.0	1000	453.6	14.10
Joules per centimeter	10^{-7}	9.807×10^{-5}	1	0.01	9.807×10^{-2}	4.448×10^{-2}	1.383×10^{-3}
Newtons or joules per meter	10^{-5}	9.807×10^{-3}	100	1	9.807	4.448	0.1383
Kilograms	1.020×10^{-6}	0.001	10.20	0.1020	1	0.4536	1.410×10^{-2}
Pounds	2.248×10^{-6}	2.205×10^{-3}	22.48	0.2248	2.205	1	3.108×10^{-2}
Poundals	7.233×10^{-5}	7.093×10^{-2}	723.3	7.233	70.93	32.17	1

Conversion factors between absolute and gravitational units apply only under standard acceleration due to gravity conditions.

Table A.16 ***Pressure or Force per Unit Area ($ML^{-1}T^{-2}$) or (FL^{-2})***

Multiply Number of → / by → / to Obtain ↓	Atmospheres[a]	Baryes or Dynes per Square Centimeter	Centimeters of Mercury at 0°C[b]	Inches of Mercury at 0°C[b]	Inches of Water at 4°C	Kilograms per Square Meter[c]	Pounds per Square Foot	Pounds per Square Inch	Tons (short) per Square Foot	Pascal
Atmospheres[a]	1	9.869×10^{-7}	1.316×10^{-2}	3.342×10^{-2}	2.458×10^{-3}	9.678×10^{-5}	4.725×10^{-4}	6.804×10^{-2}	0.9450	9.689×10^{-6}
Baryes or dynes per square centimeter	1.013×10^{6}	1	1.333×10^{4}	3.386×10^{4}	2.491×10^{-3}	98.07	478.8	6.895×10^{4}	9.576×10^{5}	10
Centimeters of mercury at 0°C[b]	76.00	7.501×10^{-5}	1	2.540	0.1868	7.356×10^{-3}	3.591×10^{-2}	5.171	71.83	7.501×10^{-4}
Inches of mercury at 0°C[b]	29.92	2.953×10^{-5}	0.3937	1	7.355×10^{-2}	2.896×10^{-3}	1.414×10^{-2}	2.036	28.28	2.953×10^{-4}
Inches of water at 4°C	406.8	4.015×10^{-4}	5.354	13.60	1	3.937×10^{-2}	0.1922	27.68	384.5	4.015×10^{-3}
Kilograms per square meter[c]	1.033×10^{4}	1.020×10^{-2}	136.0	345.3	25.40	1	4.882	703.1	9765	0.1020
Pounds per square foot	2117	2.089×10^{-3}	27.85	70.73	5.204	0.2048	1	144	2000	2.089×10^{-2}
Pounds per square inch	14.70	1.450×10^{-5}	0.1934	0.4912	3.613×10^{-2}	1.422×10^{-3}	6.944×10^{-3}	1	13.89	1.450×10^{-4}
Tons (short) per square foot	1.058	1.044×10^{-6}	1.392×10^{-2}	3.536×10^{-2}	2.601×10^{-3}	1.024×10^{-4}	0.0005	0.072	1	1.044×10^{-5}
Pascal	1.013×10^{5}	10^{-1}	1.333×10^{3}	3.386×10^{3}	2.49×10^{2}	9.807	47.88	6.895×10^{3}	9.576×10^{4}	1

[a]Definition: One atmosphere (standard) = 76 cm of mercury at 0°C.

[b]To convert height h of a column of mercury at t degrees centigrade to the equivalent height h_0 at 0°C, use $h_0 = h[1 - (m - l)t/(1 + mt)]$ where $m = 0.0001818$ and $l = 18.4 \times 10^{-6}$ if the scale is engraved on brass; $l = 8.5 \times 10^{-6}$ if on glass. This assumes the scale is correct at 0°C; for other cases (any liquid) see *International Critical Tables,* Vol. 1 (1968).

[c]1 g/cm^2 = 10 kg/m^2.

Table A.17 ***Energy, Work, and Heat (ML^2T^{-2}) or (FL)***

Multiply Number of → / by → / to Obtain ↓	British Thermal Units[a]	Centimeter Grams	Ergs or Centimeter Dynes	Foot Pounds	Horsepower Hours	Joules[b] or Watt Seconds	Kilogram Calories[a]	Kilowatt Hours	Meter Kilograms	Watt Hours
British thermal units[a]	1	9.297×10^{-8}	9.480×10^{-11}	1.285×10^{-3}	2545	9.480×10^{-4}	3.969	3413	9.297×10^{-3}	3.413
Centimeter grams	1.076×10^{7}	1	1.020×10^{-3}	1.383×10^{4}	2.737×10^{10}	1.020×10^{4}	4.269×10^{7}	3.671×10^{10}	10^{5}	3.671×10^{7}
Ergs or centimeter dynes	1.055×10^{10}	980.7	1	1.356×10^{7}	2.684×10^{12}	10^{7}	4.186×10^{10}	3.6×10^{13}	9.807×10^{7}	3.6×10^{10}
Foot pounds	778.0	7.233×10^{-5}	7.367×10^{-8}	1	1.98×10^{6}	0.7376	3087	2.655×10^{6}	7.233	2655
Horsepower hours	3.929×10^{-4}	3.654×10^{-11}	3.722×10^{-14}	5.050×10^{-7}	1	3.722×10^{-7}	1.559×10^{-3}	1.341	3.653×10^{-6}	1.341×10^{-3}
Joules[b] or watt seconds	1054.8	9.807×10^{-5}	10^{-7}	1.356	2.684×10^{6}	1	4186	3.6×10^{6}	9.807	3600
Kilogram calories[a]	0.2520	2.343×10^{-8}	2.389×10^{-11}	3.239×10^{-4}	641.3	2.389×10^{-4}	1	860.0	2.343×10^{-3}	0.8600
Kilowatt hours	2.930×10^{-4}	2.724×10^{-11}	2.778×10^{-14}	3.766×10^{-7}	0.7457	2.788×10^{-7}	1.163×10^{-3}	1	2.724×10^{-6}	0.001
Meter kilograms	107.6	10^{-5}	1.020×10^{-8}	0.1383	2.737×10^{5}	0.1020	426.9	3.671×10^{5}	1	367.1
Watt hours	0.2930	2.724×10^{-8}	2.778×10^{-11}	3.766×10^{-4}	745.7	2.778×10^{-4}	1.163	1000	2.724×10^{-3}	1

The *horsepower* used in Tables A.17 and A.18 is equal to 550 foot pounds per second by definition. Other definitions are one horsepower equals 746 watts (U.S. and Great Britain) and one horsepower equals 736 watts (continental Europe). Neither of these latter definitions is equivalent to the first; the *horsepowers* defined in these latter definitions are widely used in the rating of electrical machinery.

[a]Mean calorie and Btu used throughout. One gram-calorie = 0.001 kilogram-calorie; one Ostwald calorie = 0.1 kilogram-calorie.The IT cal, 1000 international steam table calories, has been defined as the 1/860th part of the international kilowatt-hour (see *Mechanical Engineering,* Nov., 1935, p. 710). Its value is very nearly equal to the mean kilogram-calorie, 1 IT cal-1.00037 kilogram-calories (mean). 1 Btu = 251.996 IT cal.

[b]Absolute joule, defined as 10^7 ergs. The international joule, based on the international ohm and ampere, equals 1.0003 absolute joules.

Table A.18 ***Power or Rate of Doing Work (ML^2T^{-3}) or (FLT^{-1})***

Multiply Number of → / by → / to Obtain ↓	British Thermal Units per Minute	Ergs per Second	Foot Pounds per Minute	Foot Pounds per Second	Horsepower	Kilogram Calories per Minute	Kilowatts	Metric Horsepower	Watts
British thermal units per minute	1	5.689×10^{-9}	1.285×10^{-3}	7.712×10^{-2}	42.41	3.969	56.89	41.83	5.689×10^{-2}
Ergs per second	1.758×10^{8}	1	2.259×10^{5}	1.356×10^{7}	7.457×10^{9}	6.977×10^{8}	10^{10}	7.355×10^{9}	10^{7}
Foot pounds per minute	778.0	4.426×10^{-6}	1	60	3.3×10^{4}	3087	4.426×10^{4}	3.255×10^{4}	44.26
Foot pounds per second	12.97	7.376×10^{-8}	1.667×10^{-2}	1	550	51.44	737.6	542.5	0.7376
Horsepower	2.357×10^{-2}	1.341×10^{-10}	3.030×10^{-5}	1.818×10^{-3}	1	9.355×10^{-2}	1.341	0.9863	1.341×10^{-3}
Kilogram calories per minute	0.2520	1.433×10^{-9}	3.239×10^{-4}	1.943×10^{-2}	10.69	1	14.33	10.54	1.433×10^{-2}
Kilowatts	0.01758	10^{-10}	2.260×10^{-5}	1.356×10^{-3}	0.7457	0.06977×10^{-2}	1	0.7355	0.001
Metric horsepower	2.390×10^{-2}	1.360×10^{-10}	3.072×10^{-5}	1.843×10^{-3}	1.014	9.485×10^{-2}	1.360	1	1.360×10^{-3}
Watts	17.58	10^{-7}	2.260×10^{-2}	1.356	745.7	69.77	1000	735.5	1

1 Cheval vapeur = 75 kilogram meters per second
1 Poncelet = 100 kilogram meters per second

See general note to Table A.17.

Table A.19 ***Heat Flux (power/area)***

From → / Multiply by → / to Obtain ↓	Btu/(min·ft²)	Btu/(s·ft²)	kW/m²	W/m²	W/cm²
Btu/(min·ft²)	1	1.6×10^{-2}	5.28	5.2×10^{-3}	5.2×10^{-1}
Btu/(s·ft²)	60	1	6.81×10^{-2}	8.8×10^{-5}	8.8×10^{-3}
kW/m²	0.18923	11.3565	1	10^{-3}	10^{-1}
W/m²	189.273	1.1356×10^{4}	10^{3}	1	10^{4}
W/cm²	1.89273	1.1356×10^{2}	10	10^{-4}	1
kg-cal/s·m²	6.135×10^{-6}	1.02×10^{-7}	8.60400×10^{5}	8.6×10^{2}	8.604×10^{4}
kg-cal/s·m²	3.681×10^{-4}	6.07×10^{-6}	1.434×10^{4}	1.4341×10^{1}	1.434×10^{3}

Table A.20 ***Specific Heat ($L^2T^{-2}t^{-1}$, t = temperature)***

To change specific heat in gram calories per gram per degree centigrade to the units given in any line of the following table, multiply by the factor in the last column.

Unit of Heat or Energy	Unit of Mass	Temperature Scale[a]	Factor
Gram calories	Gram	Centigrade	1
Kilogram calories	Kilogram	Centigrade	1
British thermal units	Pound	Centigrade	1.800
British thermal units	Pound	Fahrenheit	1.000
Joules	Gram	Centigrade	4.186
Joules	Pound	Fahrenheit	1055
Joules	Kilogram	Kelvin	4.187×10^{3}
Kilowatt hours	Kilogram	Centigrade	1.163×10^{-3}
Kilowatt hours	Pound	Fahrenheit	2.930×10^{-4}

[a]Temperature conversion formulae:

t_C = temperature in centigrade degrees
t_f = temperature in Fahrenheit degrees
t_K = temperature in kelvin degrees

$1°F = \frac{5}{9}°C$

$1\ K = 1°C$

$t_C = \frac{5}{9}(t_f - 32)$

$t_f = \frac{9}{5}t_C + 32$

$t_K = t_C + 273$

Table A.21 ***Thermal Conductivity ($LMT^{-3}t^{-1}$)***

From → / Multiply by → / to Obtain ↓	Btu·ft per h·ft²·°F	Btu·in. per h·ft²·°F	Btu·in. per s·ft²·°F	Joules per m·s·°C	Kcal per m·h·°C	Erg per cm·s ·°C	Kcal per m·s·°C	Cal per cm·s·°C	W per ft·°C	W per m·K
Btu·ft per h·ft²·°F	1	8.333×10^{-2}	3.0×10^{2}	5.778×10^{-1}	6.720×10^{-1}	5.778×10^{-6}	2.419×10^{3}	2.419×10^{2}	1.895	5.778×10^{-1}
Btu·in. per h·ft²·°F	12	1	3.6×10^{3}	6.933	8.064	6.933×10^{-5}	2.903×10^{4}	2.903×10^{3}	2.275×10^{1}	6.933
Btu·in. per s·ft²·°F	3.333×10^{-3}	2.778×10^{-4}	1	1.926×10^{-3}	2.240×10^{-3}	1.926×10^{-8}	8.064	8.064×10^{-1}	6.319×10^{-3}	1.926×10^{-3}
Joules per m·s·°C	1.731	1.442×10^{-1}	5.192×10^{2}	1	1.163	1.000×10^{-5}	4.187×10^{3}	4.187×10^{2}	3.281	1.0
Kcal per m·h·°C	1.483	1.240×10^{-1}	4.465×10^{2}	8.599×10^{-1}	1	8.599×10^{-6}	3.6×10^{3}	3.6×10^{2}	2.821	8.599×10^{-1}
Erg per cm·s·°C	1.731×10^{5}	1.442×10^{4}	5.192×10^{7}	1.0×10^{5}	1.163×10^{5}	1	4.187×10^{8}	4.187×10^{7}	3.281×10^{5}	1.0×10^{5}
Kcal per m·s·°C	4.134×10^{-4}	3.445×10^{-5}	1.240×10^{-1}	2.388×10^{-4}	2.778×10^{-4}	2.388×10^{-9}	1	1.0×10^{-1}	7.835×10^{-4}	2.388×10^{-4}
Cal per cm·s·°C	4.134×10^{-3}	3.445×10^{-4}	1.240	2.388×10^{-3}	2.778×10^{-3}	2.388×10^{-8}	10	1	7.835×10^{-3}	2.388×10^{-3}
W per ft·°C	5.276×10^{-1}	4.395×10^{-2}	1.582×10^{2}	3.048×10^{-1}	3.545×10^{-1}	3.048×10^{-6}	1.276×10^{3}	1.276×10^{2}	1	3.048×10^{-1}
W per m·K	1.731	1.442×10^{-1}	5.192×10^{2}	1.0	1.163	1.00×10^{-5}	4.187×10^{3}	4.187×10^{2}	3.281	1

International Table Btu = 1.055056×10^{3} joules; and International Table cal = 4.1868 joules are used throughout.

APPENDIX B

Thermophysical Property Data

Table B.1 ***Approximate Properties of Common Gases[3]***

	Engineering Gas Constant, R (ft-lb/slug·R)	Universal Gas Constant, $\mathcal{R} = mR$ (ft-lb/slug·R)	Adiabatic Exponent, k	Specific Heat at Constant Pressure, c_p (ft-lb/slug·R)	Viscosity at 68°F (20°C), $\mu \times 10^5$ (lb-s/ft^2)
English (FSS) Units					
Carbon dioxide	1,123	49,419	1.28	5,132	0.0307
Oxygen	1,554	49,741	1.40	5,437	0.0419
Air	1,715	49,709	1.40	6,000	0.0377
Nitrogen	1,773	49,644	1.40	6,210	0.0368
Methane	3,098	49,644	1.31	13,095	0.028
Helium	12,419	49,677	1.66	31,235	0.0411
Hydrogen	24,677	49,741	1.40	86,387	0.0189
	R (J/kg·K)	$\mathcal{R} = mR$ (J/kg·K)	k	c_p (J/kg·K)	$\mu \times 10^5$ (Pa·s)
SI Units					
Carbon dioxide	187.8	8,264	1.28	858.2	1.47
Oxygen	259.9	8,318	1.40	909.2	2.01
Air	286.8	8,313	1.40	1,003	1.81
Nitrogen	296.5	8,302	1.40	1,038	1.76
Methane	518.1	8,302	1.31	2,190	1.34
Helium	2,076.8	8,307	1.66	5,223	1.97
Hydrogen	4,126.6	8,318	1.40	14,446	0.90

Table B.2 ***Thermophysical Property Values for Gases at Standard Atmospheric Pressure[4]***

T (K)	ρ (kg/m^3)	c_p (Ws/kg·K)	μ (kg/ms)	ν (m^2/s)	k (W/m·K)	α (m^2/s)	Pr
Air							
100	3.6010	1.0266×10^3	0.6924×10^{-5}	1.923×10^{-6}	0.009246	0.0250×10^{-4}	0.768
150	2.3675	1.0099	1.0283	4.343	0.013735	0.0574	0.756
200	1.7684	1.0061	1.3289	7.514	0.01809	0.1016	0.739
250	1.4128	1.0053	1.488	10.53	0.02227	0.1568	0.722
300	1.1774	1.0057	1.983	16.84	0.02624	0.2216	0.708
350	0.9980	1.0090	2.075	20.76	0.03003	0.2983	0.697
400	0.8826	1.0140	2.286	25.90	0.03365	0.3760	0.689
450	0.7833	1.0207	2.484	31.71	0.03707	0.4636	0.683
500	0.7048	1.0295	2.671	37.90	0.04038	0.5564	0.680
550	0.6423	1.0392	2.848	44.27	0.04360	0.6532	0.680
600	0.5879	1.0551	3.018	51.34	0.04659	0.7512	0.682
650	0.5430	1.0635	3.177	58.51	0.04953	0.8578	0.682
700	0.5030	1.0752	3.332	66.25	0.05230	0.9672	0.684

Table B.2 ***(Continued)***

T (K)	ρ (kg/m^3)	c_p (Ws/kg·K)	μ (kg/ms)	ν (m^2/s)	k (W/m·K)	α (m^2/s)	Pr
			Air *(Continued)*				
750	0.4709	1.0856	3.481	73.91	0.05509	1.0774	0.686
800	0.4405	1.0978	3.625	82.29	0.05779	1.1951	0.689
850	0.4149	1.1095	3.765	90.75	0.06028	1.3097	0.692
900	0.3925	1.1212	3.899	99.3	0.06279	1.4271	0.696
950	0.3716	1.1321	4.023	108.2	0.06525	1.5510	0.699
1000	0.3524	1.1417	4.152	117.8	0.06752	1.6779	0.702
1100	0.3204	1.160	4.44	138.6	0.0732	1.969	0.704
1200	0.2947	1.179	4.69	159.1	0.0782	2.251	0.707
1300	0.2707	1.197	4.93	182.1	0.0837	2.583	0.705
1400	0.2515	1.214	5.17	205.5	0.0891	2.920	0.705
1500	0.2355	1.230	5.40	229.1	0.0946	3.266	0.705
1600	0.2211	1.248	5.63	254.5	0.100	3.624	0.705
1700	0.2082	1.267	5.85	280.9	0.105	3.977	0.705
1800	0.1970	1.287	6.07	308.1	0.111	4.379	0.704
1900	0.1858	1.309	6.29	338.5	0.117	4.811	0.704
2000	0.1762	1.338	6.50	369.0	0.124	5.260	0.702
2100	0.1682	1.372	6.72	399.6	0.131	5.680	0.703
2200	0.1602	1.419	6.93	432.6	0.139	6.115	0.707
2300	0.1538	1.482	7.14	464.0	0.149	6.537	0.710
2400	0.1458	1.574	7.35	504.0	0.161	7.016	0.718
2500	0.1394	1.688	7.57	543.0	0.175	7.437	0.730
			Helium				
144	0.3379	5.200	125.5×10^{-7}	37.11×10^{-6}	0.0928	0.5275×10^{-4}	0.70
200	0.2435	5.200	156.6	64.38	0.1177	0.9288	0.694
255	0.1906	5.200	181.7	95.50	0.1357	1.3675	0.70
366	0.13280	5.200	230.5	173.6	0.1691	2.449	0.71
477	0.10204	5.200	275.0	269.3	0.197	3.716	0.72
589	0.08282	5.200	311.3	375.8	0.225	5.215	0.72
700	0.07032	5.200	347.5	494.2	0.251	6.661	0.72
800	0.06023	5.200	381.7	634.1	0.275	8.774	0.72
			Hydrogen				
150	0.16371	12.602	5.595×10^{-6}	34.18×10^{-5}	0.0981	0.475×10^{-4}	0.718
200	0.12270	13.540	6.813	55.53	0.1282	0.772	0.719
250	0.09819	14.059	7.919	80.64	0.1561	1.130	0.713
300	0.08185	14.314	8.963	109.5	0.182	1.554	0.706
350	0.07016	14.436	9.954	141.9	0.206	2.031	0.697
400	0.06135	14.491	10.864	177.1	0.228	2.568	0.690
450	0.05462	14.499	11.779	215.6	0.251	3.164	0.682
500	0.04918	14.507	12.636	257.0	0.272	3.817	0.675
550	0.04469	14.532	13.475	301.6	0.292	4.516	0.668
600	0.04085	14.537	14.285	349.7	0.315	5.306	0.664
700	0.03492	14.574	15.89	455.1	0.351	6.903	0.659
800	0.03060	14.675	17.40	569	0.384	8.563	0.664
900	0.02723	14.821	18.78	690	0.412	10.217	0.676
			Oxygen				
150	2.6190	0.9178	11.490×10^{-6}	4.387×10^{-6}	0.01367	0.05688×10^{-4}	0.773
200	1.9559	0.9131	14.850	7.593	0.01824	0.10214	0.745
250	1.5618	0.9157	17.87	11.45	0.02259	0.15794	0.725
300	1.3007	0.9203	20.63	15.86	0.02676	0.22353	0.709
350	1.1133	0.9291	23.16	20.80	0.03070	0.2968	0.702
400	0.9755	0.9420	25.54	26.18	0.03461	0.3768	0.695
450	0.8682	0.9567	27.77	31.99	0.03828	0.4609	0.694
500	0.7801	0.9722	29.91	38.34	0.04173	0.5502	0.697
550	0.7096	0.9881	31.97	45.05	0.04517	0.6441	0.700

Table B.2 ***(Continued)***

T (K)	ρ (kg/m^3)	c_p, (Ws/kg·K)	μ (kg/ms)	ν (m^2/s)	k (W/m·K)	α (m^2/s)	Pr
			Nitrogen				
200	1.7108	1.0429	12.947×10^{-6}	7.568×10^{-6}	0.01824	0.10224×10^{-4}	0.747
300	1.1421	1.0408	17.84	15.63	0.02620	0.22044	0.713
400	0.8538	1.0459	21.98	25.74	0.03335	0.3734	0.691
500	0.6824	1.0555	25.70	37.66	0.03984	0.5530	0.684
600	0.5687	1.0756	29.11	51.19	0.04580	0.7486	0.686
700	0.4934	1.0969	32.13	65.13	0.05123	0.9466	0.691
800	0.4277	1.1225	34.84	81.46	0.05609	1.1685	0.700
900	0.3796	1.1464	37.49	91.06	0.06070	1.3946	0.711
1000	0.3412	1.1677	40.00	117.2	0.06475	1.6250	0.724
1100	0.3108	1.1857	42.28	136.0	0.06850	1.8591	0.736
1200	0.2851	1.2037	44.50	156.1	0.07184	2.0932	0.748
			Carbon dioxide				
220	2.4733	0.783	11.105×10^{-6}	4.490×10^{-6}	0.010805	0.05920×10^{-4}	0.818
250	2.1657	0.804	12.590	5.813	0.012884	0.07401	0.793
300	1.7973	0.871	14.958	8.321	0.016572	0.10588	0.770
350	1.5362	0.900	17.205	11.19	0.02047	0.14808	0.755
400	1.3424	0.942	19.32	14.39	0.02461	0.19463	0.738
450	1.1918	0.980	21.34	17.90	0.02897	0.24813	0.721
500	1.0732	1.013	23.26	21.67	0.03352	0.3084	0.702
550	0.9739	1.047	25.08	25.74	0.03821	0.3750	0.685
600	0.8938	1.076	26.83	30.02	0.04311	0.4483	0.668
			Ammonia, NH3				
273	0.7929	2.177	9.353×10^{-6}	1.18×10^{-5}	0.0220	0.1308×10^{-4}	0.90
323	0.6487	2.177	11.035	1.70	0.0270	0.1920	0.88
373	0.5590	2.236	12.886	2.30	0.0327	0.2619	0.87
423	0.4934	2.315	14.672	2.97	0.0391	0.3432	0.87
473	0.4405	2.395	16.49	3.74	0.0467	0.4421	0.84
			Water vapor				
380	0.5863	2.060	12.71×10^{-6}	2.16×10^{-5}	0.0246	0.2036×10^{-4}	1.060
400	0.5542	2.014	13.44	2.42	0.0261	0.2338	1.040
450	0.4902	1.980	15.25	3.11	0.0299	0.307	1.010
500	0.4405	1.985	17.04	3.86	0.0339	0.387	0.996
550	0.4005	1.997	18.84	4.70	0.0379	0.475	0.991
600	0.3652	2.026	20.67	5.66	0.0422	0.573	0.986
650	0.3380	2.056	22.47	6.64	0.0464	0.666	0.995
700	0.3140	2.085	24.26	7.72	0.0505	0.772	1.000
750	0.2931	2.119	26.04	8.88	0.0549	0.883	1.005
800	0.2739	2.152	27.86	10.20	0.0592	1.004	1.010
850	0.2579	2.186	29.69	11.52	0.0637	1.130	1.019

Table B.3 ***Approximate Properties of Common Liquids at Standard Atmospheric Pressure[3]***

	English (FSS) Units						
	Temperature, T (°F)	Density, ρ (slug/ft^3)	Specific Gravity, s.g.	Modulus of Elasticity, K (psi)	Viscosity, $\mu \times 10^5$ (lb-s/ft^2)	Surface Tension, σ (lb/ft)	Vapor Pressure, ρ_v (psia)
Benzene	68	1.70	0.88	150,000	1.37	0.0020	1.45
Carbon tetrachloride	68	3.08	1.59	160,000	2.035	0.0018	1.90
Crude oil	68	1.66	0.86	—	15.0	0.002	—
Ethyl alcohol	68	1.53	0.79	175,000	2.51	0.0015	0.85
Freon-12	60	2.61	1.35	—	3.10	—	—
	–30	2.91	—	—	3.82	—	—
Gasoline	68	1.32	0.68	—	0.61	—	8.0
Glycerin	68	2.44	1.26	630,000	3,120	0.0043	0.000002
Hydrogen	–431	0.143	—	—	0.0435	0.0002	3.1
Jet fuel (JP-4)	60	1.50	0.77	—	1.82	0.002	1.3
Mercury	60	26.3	13.57	3,800,000	3.26	0.035	0.000025
	600	24.9	12.8	—	1.88	—	6.85
Oxygen	–320	2.34	—	—	0.58	0.001	3.1
Sodium	600	1.70	—	—	0.690	—	—
	1000	1.60	—	—	0.472	—	—
Water	68	1.936	1.00	318,000	2.10	0.0050	0.34
	SI Units						
	T (°C)	ρ (kg/m^3)	s.g.	K (kPa)	$\mu \times 10^4$ (Pa·s)	σ (N/m)	ρ_v (kPa)
Benzene	20	876.2	0.88	1,034,250	6.56	0.029	10.0
Carbon tetrachloride	20	1,587.4	1.59	1,103,200	9.74	0.026	13.1
Crude oil	20	855.6	0.86	—	71.8	0.03	—
Ethyl alcohol	20	788.6	0.79	1,206,625	12.0	0.022	5.86
Freon-12	15.6	1,345.2	1.35	—	14.8	—	—
	–34.4	1,499.8	—	—	18.3	—	—
Gasoline	20	680.3	0.68	—	2.9	—	55.2
Glycerin	20	1,257.6	1.26	4,343,850	14,939	0.063	0.000014
Hydrogen	–257.2	73.7	—	—	0.21	0.0029	21.4
Jet fuel (JP-4)	15.6	773.1	0.77	—	8.7	0.029	8.96
Mercury	15.6	13,555	13.57	26,201,000	15.6	0.51	0.00017
	315.6	12,833	12.8	—	9.0	—	47.2
Oxygen	–195.6	1,206.0	—	—	2.78	0.015	21.4
Sodium	315.6	876.2	—	—	3.30	—	—
	537.8	824.6	—	—	2.26	—	—
Water	20	998.2	1.00	2,170,500	10.0	0.073	2.34

Table B.4 ***Properties of Water***[5]

T (°F)	T (°C)	c_p (kJ/kg·°C)	ρ (kg/m³)	μ (kg/m·s)	k (W/m·°C)	Pr	$\frac{g\beta\rho^2 c_p}{\mu k}$[a] (1/m³·°C)
32	0	4.225	999.8	1.79×10^{-3}	0.566	13.25	1.91×10^{9}
40	4.44	4.208	999.8	1.55	0.575	11.35	6.34×10^{9}
50	10	4.195	999.2	1.31	0.585	9.40	1.08×10^{10}
60	15.56	4.186	998.6	1.12	0.595	7.88	1.46×10^{10}
70	21.11	4.179	997.4	9.8×10^{-4}	0.604	6.78	1.91×10^{10}
80	26.67	4.179	995.8	8.6	0.614	5.85	2.48×10^{10}
90	32.22	4.174	994.9	7.65	0.623	5.12	3.3×10^{10}
100	37.78	4.174	993.0	6.82	0.630	4.53	4.19×10^{10}
110	43.33	4.174	990.6	6.16	0.637	4.04	4.89×10^{10}
120	48.89	4.174	988.8	5.62	0.644	3.64	5.66×10^{10}
130	54.44	4.179	985.7	5.13	0.649	3.30	6.48×10^{10}
140	60	4.179	983.3	4.71	0.654	3.01	7.62×10^{10}
150	65.55	4.183	980.3	4.3	0.659	2.73	8.84×10^{10}
160	71.11	4.186	977.3	4.01	0.665	2.53	9.85×10^{10}
170	76.67	4.191	973.7	3.72	0.668	2.33	1.09×10^{11}
180	82.22	4.195	970.2	3.47	0.673	2.16	
190	87.78	4.199	966.7	3.27	0.675	2.03	
200	93.33	4.204	963.2	3.06	0.678	1.90	
220	104.4	4.216	955.1	2.67	0.684	1.66	
240	115.6	4.229	946.7	2.44	0.685	1.51	
260	126.7	4.250	937.2	2.19	0.685	1.36	
280	137.8	4.271	928.1	1.98	0.685	1.24	
300	148.9	4.296	918.0	1.86	0.684	1.17	
350	176.7	4.371	890.4	1.57	0.677	1.02	
400	204.4	4.467	859.4	1.36	0.665	1.00	
450	232.2	4.585	825.7	1.20	0.646	0.85	
500	260	4.731	785.2	1.07	0.616	0.83	
550	287.7	5.024	735.5	9.51×10^{-5}			
600	315.6	5.703	678.7	8.68			

[a] $\mathrm{Gr}_x\mathrm{Pr} = \left(\frac{g\beta\rho^2 c_p}{\mu k}\right)\Delta T$

Table B.5 ***Properties of Saturated Liquids[4]***

t (°C)	ρ (kg/m³)	c_p (kJ/kg·°C)	ν (m²/s)	k (W/m·°C)	α (m²/s)	Pr	β (K^{-1})
			Ammonia, NH_3				
–50	703.69	4.463	0.435×10^{-6}	0.547	1.742×10^{-7}	2.60	
–40	691.68	4.467	0.406	0.547	1.775	2.28	
–30	679.34	4.476	0.387	0.549	1.801	2.15	
–20	666.69	4.509	0.381	0.547	1.819	2.09	
–10	653.55	4.564	0.378	0.543	1.825	2.07	
0	640.10	4.635	0.373	0.540	1.819	2.05	
10	626.16	4.714	0.368	0.531	1.801	2.04	
20	611.75	4.798	0.359	0.521	1.775	2.02	2.45×10^{-3}
30	596.37	4.890	0.349	0.507	1.742	2.01	
40	580.99	4.999	0.340	0.493	1.701	2.00	
50	564.33	5.116	0.330	0.476	1.654	1.99	
			Carbon dioxide, CO_2				
–50	1,156.34	1.84	0.119×10^{-6}	0.0855	0.4021×10^{-7}	2.96	
–40	1,117.77	1.88	0.118	0.1011	0.4810	2.46	
–30	1,076.76	1.97	0.117	0.1116	0.5272	2.22	
–20	1,032.39	2.05	0.115	0.1151	0.5445	2.12	
–10	983.38	2.18	0.113	0.1099	0.5133	2.20	
0	926.99	2.47	0.108	0.1045	0.4578	2.38	
10	860.03	3.14	0.101	0.0971	0.3608	2.80	
20	772.57	5.0	0.091	0.0872	0.2219	4.10	14.00×10^{-3}
30	597.81	36.4	0.080	0.0703	0.279	28.7	
			Sulfur dioxide, SO_2				
–50	1,560.84	1.3595	0.484×10^{-6}	0.242	1.141×10^{-7}	4.24	
–40	1,536.81	1.3607	0.424	0.235	1.130	3.74	
–30	1,520.64	1.3616	0.371	0.230	1.117	3.31	
–20	1,488.60	1.3624	0.324	0.225	1.107	2.93	
–10	1,463.61	1.3628	0.288	0.218	1.097	2.62	
0	1,438.46	1.3636	0.257	0.211	1.081	2.38	
10	1,412.51	1.3645	0.232	0.204	1.066	2.18	
20	1,386.40	1.3653	0.210	0.199	1.050	2.00	1.94×10^{-3}
30	1,359.33	1.3662	0.190	0.192	1.035	1.83	
40	1,329.22	1.3674	0.173	0.185	1.019	1.70	
50	1,299.10	1.3683	0.162	0.177	0.999	1.61	
			Dichlorodifluoromethane (freon), CCl_2F_2				
–50	1,546.75	0.8750	0.310×10^{-6}	0.067	0.501×10^{-7}	6.2	2.63×10^{-3}
–40	1,518.71	0.8847	0.279	0.069	0.514	5.4	
–30	1,489.56	0.8956	0.253	0.069	0.526	4.8	
–20	1,460.57	0.9073	0.235	0.071	0.539	4.4	
–10	1,429.49	0.9203	0.221	0.073	0.550	4.0	
0	1,397.45	0.9345	0.214	0.073	0.557	3.8	
10	1,364.30	0.9496	0.203	0.073	0.560	3.6	
20	1,330.18	0.9659	0.198	0.073	0.560	3.5	
30	1,295.10	0.9835	0.194	0.071	0.560	3.5	
40	1,257.13	1.0019	0.191	0.069	0.555	3.5	
50	1,215.96	1.0216	0.190	0.067	0.545	3.5	
			Glycerin, $C_3H_5(OH)_3$				
0	1,276.03	2.261	0.00831	0.282	0.983×10^{-7}	84.7×10^3	
10	1,270.11	2.319	0.00300	0.284	0.965	31.0	
20	1,264.02	2.386	0.00118	0.286	0.947	12.5	0.50×10^{-3}
30	1,258.09	2.445	0.00050	0.286	0.929	5.38	
40	1,252.01	2.512	0.00022	0.286	0.914	2.45	
50	1,244.96	2.583	0.00015	0.287	0.893	1.63	

Table B.5 ***(Continued)***

t (°C)	ρ (kg/m³)	c_p (kJ/kg·°C)	ν (m²/s)	k (W/m·°C)	α (m²/s)	Pr	β (K^{-1})
			Ethylene glycol, $C_2H_4(OH)_2$				
0	1,130.75	2.294	57.53×10^{-6}	0.242	0.934×10^{-7}	615	
20	1,116.65	2.382	19.18	0.249	0.939	204	0.65×10^{-3}
40	1,101.43	2.474	8.69	0.256	0.939	93	
60	1,087.66	2.562	4.75	0.260	0.932	51	
80	1,077.56	2.650	2.98	0.261	0.921	32.4	
100	1,058.50	2.742	2.03	0.263	0.908	22.4	
			Engine oil (unused)				
0	899.12	1.796	0.00428	0.147	0.911×10^{-7}	47,100	
20	888.23	1.880	0.00090	0.145	0.872	10,400	0.70×10^{-3}
40	876.05	1.964	0.00024	0.144	0.834	2,870	
60	864.04	2.047	0.839×10^{-4}	0.140	0.800	1,050	
80	852.02	2.131	0.375	0.138	0.769	490	
100	840.01	2.219	0.203	0.137	0.738	276	
120	828.96	2.307	0.124	0.135	0.710	175	
140	816.94	2.395	0.080	0.133	0.686	116	
160	805.89	2.483	0.056	0.132	0.663	84	
			Mercury, Hg				
0	13,628.22	0.1403	0.124×10^{-6}	8.20	42.99×10^{-7}	0.0288	
20	13,579.04	0.1394	0.114	8.69	46.06	0.0249	1.82×10^{-4}
50	13,505.84	0.1386	0.104	9.40	50.22	0.0207	
100	13,384.58	0.1373	0.0928	10.51	57.16	0.0162	
150	13,264.28	0.1365	0.0853	11.49	63.54	0.0134	
200	13,144.94	0.1570	0.0802	12.34	69.08	0.0116	
250	13,025.60	0.1357	0.0765	13.07	74.06	0.0103	
315.5	12,847	0.134	0.0673	14.02	81.5	0.0083	
			Water, H_2O				
0	1,002.28	4.2178×10^3	1.788×10^{-6}	0.552	1.308×10^{-7}	13.6	0.18×10^{-3}
20	1,000.52	4.1818	1.006	0.597	1.430	7.02	
40	994.59	4.1784	0.658	0.628	1.512	4.34	
60	985.46	4.1843	0.478	0.651	1.554	3.02	
80	974.08	4.1964	0.364	0.668	1.636	2.22	
100	960.63	4.2161	0.294	0.680	1.680	1.74	
120	945.25	4.250	0.247	0.685	1.708	1.446	
140	928.27	4.283	0.214	0.684	1.724	1.241	
160	909.69	4.342	0.190	0.680	1.729	1.099	
180	889.03	4.417	0.173	0.675	1.724	1.004	
200	866.76	4.505	0.160	0.665	1.706	0.937	
220	842.41	4.610	0.150	0.652	1.680	0.891	
240	815.66	4.756	0.143	0.635	1.639	0.871	
260	785.87	4.949	0.137	0.611	1.577	0.874	
280.6	752.55	5.208	0.135	0.580	1.481	0.910	
300	714.26	5.728	0.135	0.540	1.324	1.019	

Table B.6 ***Properties of Metals[4]***

Metal	Properties at 20°C				Thermal Conductivity k (W/m·°C)									
	ρ (kg/m^3)	c_p (kJ/kg·°C)	k (W/m·°C)	α (m^2/s $\times$ 10^5)	–100°C –148°F	0°C 32°F	100°C 212°F	200°C 392°F	300°C 572°F	400°C 752°F	600°C 1112°F	800°C 1472°F	1000°C 1832°F	1200°C 2192°F
Aluminum														
Pure	2,707	0.896	204	8.418	215	202	206	215	228	249				
Al-Cu (Duralumin) 94–96% Al, 3–5% CU, trace Mg	2,787	0.883	164	6.676	126	159	182	194						
Al-Si (Silumin, copper bearing) 86.5% Al, 1% Cu	2,659	0.867	137	5.933	119	137	144	152	161					
Al-Si (Alusil) 78–80% Al, 20–22% Si	2,627	0.854	161	7.172	144	157	168	175	178					
Al-Mg-Si 97% Al, 1% Mg, 1% Si, 1% Mn	2,707	0.892	177	7.311		175	189	204						
Lead	11,373	0.130	35	2.343	36.9	35.1	33.4	31.5	29.8					
Iron														
Pure	7,897	0.452	73	2.034	87	73	67	62	55	48	40	36	35	36
Wrought iron 0.5% C	7,849	0.46	59	1.626		59	57	52	48	45	36	33	33	33
Steel (C max ≈ 1.5%): Carbon steel														
C ≈ 0.5%	7,833	0.465	54	1.474		55	52	48	45	42	35	31	29	31
1.0%	7,801	0.473	43	1.172		43	43	42	40	36	33	29	28	29
1.5%	7,753	0.486	36	0.970		36	36	36	35	33	31	28	28	29
Nickel steel														
Ni ≈ 0%	7,897	0.452	73	2.026										
20%	7,933	0.46	19	0.526										
40%	8,169	0.46	10	0.279										
80%	8,618	0.46	35	0.872										
Invar 36% Ni	8,137	0.46	10.7	0.286										
Chrome steel														
Cr = 0%	7,897	0.452	73	2.026	87	73	67	62	55	48	40	36	35	36
1%	7,865	0.46	61	1.665		62	55	52	47	42	36	33	33	
5%	7,833	0.46	40	1.110		40	38	36	36	33	29	29	29	
20%	7,689	0.46	22	0.635		22	22	22	22	24	24	26	29	
Cr-Ni, chrome-nickel 15% Cr, 10% Ni	7,865	0.46	19	0.526										
18% Cr, 8% Ni (V2A)	7,817	0.46	16.3	0.444		16.3	17	17	19	19	22	26	31	
20% Cr, 15% Ni	7,833	0.46	15.1	0.415										
25% Cr, 20% Ni	7,865	0.46	12.8	0.361										
Tungsten steel														
W = 0%	7,897	0.452	73	2.026										
1%	7,913	0.448	66	1.858										
5%	8,073	0.435	54	1.525										
10%	8,314	0.419	48	1.391										

Table B.6 ***(Continued)***

Metal	Properties at 20°C				Thermal Conductivity k (W/m·°C)									
	ρ (kg/m^3)	c_p (kJ/kg·°C)	k (W/m·°C)	α (m^2/s × 10^5)	–100°C –148°F	0°C 32°F	100°C 212°F	200°C 392°F	300°C 572°F	400°C 752°F	600°C 1112°F	800°C 1472°F	1000°C 1832°F	1200°C 2192°F
Copper														
Pure	8,954	0.3831	386	11.234	407	386	379	374	369	363	353			
Aluminum bronze 95% Cu, 5% Al	8,666	0.410	83	2.330										
Bronze 75% Cu, 25% Sn	8,666	0.343	26	0.859										
Red brass 85% Cu, 9% Sn, 6% Zn	8,714	0.385	61	1.804		59	71							
Brass 70% Cu, 30% Zn	8,522	0.385	111	3.412	88		128	144	147	147				
German silver 62% Cu, 15% Ni, 22% Zn	8,618	0.394	24.9	0.733	19.2		31	40	45	48				
Constantan 60% Cu, 40% Ni	8,922	0.410	22.7	0.612	21		22.2	26						
Magnesium														
Pure	1,746	1.013	171	9.708	178	171	168	163	157					
Mg-Al (electrolytic) 6–8% Al, 1–2% Zn	1,810	1.00	66	3.605	138	52	62	74	83					
Molybdenum	10,220	0.251	123	4.790		125	118	114	111	109	106	102	99	92
Nickel														
Pure (99.9%)	8,906	0.4459	90	2.266	104	93	83	73	64	59				
Ni-Cr 90% Ni, 10% Cr	8,666	0.444	17	0.444		17.1	18.9	20.9	22.8	24.6				
80% Ni, 20% Cr	8,314	0.444	12.6	0.343		12.3	13.8	15.6	17.1	18.0	22.5			
Silver														
Purest	10,524	0.2340	419	17.004	419	417	415	412						
Pure (99.9%)	10,524	0.2340	407	16.563	419	410	415	374	362	360				
Tin, pure	7,304	0.2265	64	3.884	74	65.9	59	57						
Tungsten	19,350	0.1344	163	6.271		166	151	142	133	126	112	76		
Zinc, pure	7,144	0.3843	112.2	4.106	114	112	109	106	100	93				

Table B.7 ***Properties of Nonmetals***[5]

Substance	Temperature (°C)	k (W/m·°C)	ρ (kg/m³)	C (kJ/kg·°C)	α (m²/s × 10⁷)
Insulating material					
Asbestos					
Loosely packed	–45	0.149	470–570	0.816	3.3–4
	0	0.154			
	100	0.161			
Asbestos-cement boards	20	0.74			
Sheets	51	0.166			
Felt, 40 laminations/in.	38	0.057			
	150	0.069			
	260	0.083			
20 laminations/in.	38	0.078			
	150	0.095			
	260	0.112			
Corrugated, 4 plies/in.	38	0.087			
	93	0.100			
	150	0.119			
Asbestos cement	—	2.08			
Balsam wool, 2.2 lb/ft³	32	0.04	35		
Cardboard, corrugated	—	0.064			
Celotex	32	0.048			
Corkboard, 10 lb/ft³	30	0.043	160		
Cork, regranulated	32	0.045	45–120	1.88	2–5.3
Ground	32	0.043	150		
Diatomaceous earth (Sil-o-cel)	0	0.061	320		
Felt, hair	30	0.036	130–200		
Wool	30	0.052	330		
Fiber, insulating board	20	0.048	240		
Glass wool, 1.5 lb/ft³	23	0.038	24	0.7	22.6
Insulex, dry	32	0.064			
		0.144			
Kapok	30	0.035			
Magnesia, 85%	38	0.067	270		
	93	0.071			
	150	0.074			
	204	0.080			
Rock wool, 10 lb/ft³	32	0.040	160		
Loosely packed	150	0.067	64		
	260	0.087			
Sawdust	23	0.059			
Silica aerogel	32	0.024	140		
Wood shavings	23	0.059			
Structural and heat-resistant materials					
Asphalt	20–55	0.74–0.76			
Brick					
Building brick, common	20	0.69	1600	0.84	5.2
face		1.32	2000		
Carborundum brick	600	18.5			
	1400	11.1			
Chrome brick	200	2.32	3000	0.84	9.2
	550	2.47			9.8
	900	1.99			7.9
Diatomaceous earth, molded and fired	200	0.24			
	870	0.31			
Fireclay brick, burnt 2426°F	500	1.04	2000	0.96	5.4
	800	1.07			
	1100	1.09			

Table B.7 ***(Continued)***

Substance	Temperature (°C)	k (W/m·°C)	ρ (kg/m^3)	C (kJ/kg·°C)	α (m^2/s $\times$ 10^7)
		Insulating material			
Brick, continued					
Fireclay brick, burnt 2642°F	500	1.28	2300	0.96	5.8
	800	1.37			
	1100	1.40			
Missouri	200	1.00	2600	0.96	4.0
	600	1.47			
	1400	1.77			
Magnesite	200	3.81		1.13	
	650	2.77			
	1200	1.90			
Cement, portland		0.29	1500		
Mortar	23	1.16			
Concrete, cinder	23	0.76			
Stone 1-2-4 mix	20	1.37	1900–2300	0.88	8.2–6.8
Glass, window	20	0.78 (avg)	2700	0.84	3.4
Corosilicate	30–75	1.09	2200		
Plaster, gypsum	20	0.48	1440	0.84	4.0
Metal lath	20	0.47			
Wood lath	20	0.28			
Stone					
Granite		1.73–3.98	2640	0.82	8–18
Limestone	100–300	1.26–1.33	2500	0.90	5.6–5.9
Marble		2.07–2.94	2500–2700	0.80	10–13.6
Sandstone	40	1.83	2160–2300	0.71	11.2–11.9
Wood (across the grain)					
Balsa 8.8 lb/ft^3	30	0.055	140		
Cypress	30	0.097	460		
Fir	23	0.11	420	2.72	0.96
Maple or oak	30	0.166	540	2.4	1.28
Yellow pine	23	0.147	640	2.8	0.82
White pine	30	0.112	430		

APPENDIX C

Fuel Properties and Combustion Data

Table C.1 ***Physical and Combustion Properties of Selected Fuels in Air[6]***

Fuel	Mol. wt.	Spec. grav.	T_{Boil} (°C)	Heat of vap. (kJ/kg)	Heat of comb. (mJ/kg)	Stoichiometry		Flammability Limits (% stoichio.)		Spont. Ign. Temp. (°C)	Fuel for Max. Flame Speed (% stoichio.)	Max. Flame Speed (cm/s)	Flame Temp. at Max. Fl. Speed K	Ign. Energy		Quenching Dist.	
						% Vol.	f^a	Lean	Rich					Stoich. (10^{-5} cal.)	Min. (10^{-5} cal.)	Stoich. (mm)	Min. (mm)
Acetaldehyde	44.1	0.783	–56.7	569.4	—	0.0772	0.1280	—	—	—	—	—	—	8.99	—	2.29	—
Acetone	58.1	0.792	56.7	523.0	30.8	0.0497	0.1054	59	233	561.1	131	50.18	2121	27.48	—	3.81	—
Acetylene	26.0	0.621	–83.9	—	48.2	0.0772	0.0755	31	—	305.0	133	155.25	—	0.72	—	0.76	—
Acrolein	56.1	0.841	52.8	—	—	0.0564	0.1163	48	752	277.8	100	61.75	—	4.18	—	1.52	—
Acrylonitrile	53.1	0.797	78.3	—	—	0.0528	0.1028	87	—	481.1	105	46.75	2461	8.60	3.82	2.29	1.52
Ammonia	17.0	0.817	–33.3	1373.6	—	0.2181	0.1645	—	—	651.1	—	—	2600	—	—	—	—
Aniline	93.1	1.022	184.4	432.6	—	0.0263	0.0872	—	—	593.3	—	—	—	—	—	—	—
Benzene	78.1	0.885	80.0	431.8	39.9	0.0277	0.0755	43	336	591.7	108	44.60	2365	13.15	5.38	2.79	1.78
Benzyl alcohol	108.1	1.050	205.0	—	—	0.0240	0.0923	—	—	427.8	—	—	—	—	—	—	—
1,2-Butadiene (methylallene)	54.1	0.658	11.1	—	45.5	0.0366	0.0714	—	—	—	117	63.90	2419	5.60	—	1.30	—
n-Butane	58.1	0.584	–0.5	385.8	45.7	0.0312	0.0649	54	330	430.6	113	41.60	2256	18.16	6.21	3.05	1.78
Butanone (methylethyl ketone)	72.1	0.805	79.4	—	—	0.0366	0.0951	—	—	—	100	39.45	—	12.67	6.69	2.54	2.03
1-Butene	56.1	0.601	–6.1	443.9	45.3	0.0377	0.0678	53	353	443.3	116	47.60	2319	—	—	—	—
d-Camphor	152.2	0.990	203.4	—	—	0.0153	0.0818	—	—	466.1	—	—	—	—	—	—	—
Carbon disulfide	76.1	1.263	46.1	351.0	—	0.0652	0.1841	18	1120	120.0	102	54.46	—	0.36	—	0.51	—
Carbon monoxide	28.0	—	–190.0	211.7	—	0.2950	0.4064	34	676	608.9	170	42.88	—	—	—	—	—
Cyclobutane	56.1	0.703	12.8	—	—	0.0377	0.0678	—	—	—	115	62.18	2308	—	—	—	—
Cyclohexane	84.2	0.783	80.6	258.1	43.8	0.0227	0.0678	48	401	270.0	117	42.46	2250	32.98	5.33	4.06	1.78
Cyclohexene	82.1	0.810	82.8	—	—	0.0240	0.0701	—	—	—	—	44.17	—	20.55	—	3.30	—
Cyclopentane	70.1	0.751	49.4	388.3	44.2	0.0271	0.0678	—	—	385.0	117	41.17	2264	19.84	—	3.30	—
Cyclopropane	42.1	0.720	–34.4	—	—	0.0444	0.0678	58	276	497.8	113	52.32	2328	5.74	5.50	1.78	1.78
trans-Decalin	138.2	0.874	187.2	—	—	0.0142	0.0692	—	—	271.7	109	33.88	2222	—	—	—	—
n-Decane	142.3	0.734	174.0	359.8	44.2	0.0133	0.0666	45	356	231.7	105	40.31	2286	—	—	2.06	—
Diethyl ether	74.1	0.714	34.4	351.6	—	0.0337	0.0896	55	2640	185.6	115	43.74	2253	11.71	6.69	2.54	2.03
Ethane	30.1	—	–88.9	488.3	47.4	0.0564	0.0624	50	272	472.2	112	44.17	2244	10.04	5.74	2.29	1.78
Ethyl acetate	88.1	0.901	77.2	—	—	0.0402	0.1279	61	236	486.1	100	35.59	—	33.94	11.47	4.32	2.54
Ethanol	46.1	0.789	78.5	836.8	26.8	0.0652	0.1115	—	—	392.2	—	—	—	—	—	—	—
Ethylamine	45.1	0.706	16.7	611.3	—	0.0528	0.0873	—	—	—	—	—	—	57.36	—	5.33	—
Ethylene oxide	44.1	1.965	10.6	581.1	—	0.0772	0.1280	—	—	428.9	125	11.35	2411	2.51	1.48	1.27	1.02
Furan	68.1	0.936	32.2	400.0	—	0.0444	0.1098	—	—	—	—	—	—	5.40	—	1.78	—
n-Heptane	100.2	0.688	98.5	364.9	44.4	0.0187	0.0661	53	450	247.2	122	42.46	2214	27.49	5.74	3.81	1.78
n-Hexane	86.2	0.664	68.0	364.9	44.7	0.0216	0.0659	51	400	260.6	117	42.46	2239	22.71	5.50	3.56	1.78
Hydrogen	2.0	—	–252.7	451.0	119.9	0.2950	0.0290	—	—	571.1	170	291.19	2380	0.36	0.36	0.51	0.51
iso-Propanol	60.1	0.785	82.2	664.8	—	0.0444	0.0969	—	—	455.6	100	38.16	—	15.54	—	2.79	—
Kerosene	154.0	0.825	250.0	290.8	43.1	—	—	—	—	—	—	—	—	—	—	—	—
Methane	16.0	—	–161.7	509.2	50.0	0.0947	0.0581	46	164	632.2	106	37.31	2236	7.89	6.93	2.54	2.03
Methanol	32.0	0.793	64.5	1100.9	19.8	0.1224	0.1548	48	408	470.0	101	52.32	—	5.14	3.35	1.78	1.52
Methyl formate	60.1	0.975	31.7	472.0	—	0.0947	0.2181	—	—	—	—	—	—	14.82	—	2.79	—
n-Nonane	128.3	0.772	150.6	288.3	44.6	0.0147	0.0665	47	434	238.9	—	—	—	—	—	—	—

Table C.1 ***(Continued)***

Fuel	Mol. wt.	Spec. grav.	T_{Boil} (°C)	Heat of vap. (kJ/kg)	Heat of comb. (mJ/kg)	Stoichiometry		Flammability Limits (% stoichio.)		Spont. Ign. Temp. (°C)	Fuel for Max. Flame Speed (% stoichio.)	Max. Flame Speed (cm/s)	Flame Temp. at Max. Fl. Speed K	Ign. Energy		Quenching Dist.	
						% Vol.	f^a	Lean	Rich					Stoich. (10^{-5} cal.)	Min.	Stoich. (mm)	Min.
n-Octane	114.2	0.707	125.6	300.0	44.8	0.0165	0.0633	51	425	240.0	—	—	2251	—	—	—	—
n-Pentane	72.1	0.631	36.0	364.4	45.3	0.0255	0.0654	54	359	284.4	115	42.46	2250	19.60	5.26	3.30	1.78
1-Pentene	70.1	0.646	30.0	—	45.0	0.0271	0.0678	47	370	298.3	114	46.75	2314	—	—	—	—
Propane	44.1	0.508	–42.2	425.5	46.3	0.0402	0.0640	51	283	504.4	114	42.89	2250	7.29	—	2.03	1.78
Propene	42.1	0.522	–47.7	437.2	45.8	0.0444	0.0678	48	272	557.8	114	48.03	2339	6.74	—	2.03	—
n-Propanol	60.1	0.804	97.2	685.8	—	0.0444	0.0969	—	—	433.3	—	—	—	—	—	—	—
Toulene	92.1	0.872	110.6	362.8	40.9	0.0227	0.0743	43	322	567.8	105	38.60	2344	—	—	—	—
Triethylamine	101.2	0.723	89.4	—	—	0.0210	0.0753	—	—	—	—	—	—	27.48	—	3.81	—
Turpentine	—	—	—	—	—	—	—	—	—	252.2	—	—	—	—	—	—	—
Xylene	106.0	0.870	130.0	334.7	43.1	—	—	—	—	—	—	—	—	—	—	—	—
Gasoline 73 octane	120.0	0.720	155.0	338.9	44.1	—	—	—	—	298.9	—	—	—	—	—	—	—
Gasoline 100 octane	—	—	—	—	—	—	—	—	—	468.3	106	37.74	—	—	—	—	—
Jet fuel JP1	150.0	0.810	—	—	43.0	0.0130	0.0680	—	—	248.9	107	36.88	—	—	—	—	—
JP3	112.0	0.760	—	—	43.5	0.0170	0.0680	—	—	—	—	—	—	—	—	—	—
JP4	126.0	0.780	—	—	43.5	0.0150	0.0680	—	—	261.1	107	38.17	—	—	—	—	—
JP5	170.0	0.830	—	—	43.0	0.0110	0.0690	—	—	242.2	—	—	—	—	—	—	—

[a] f is the stoichiometric air/fuel ratio; i.e., $f = 1/r$.

Table C.2 ***Heats of Combustion and Related Properties of Pure Substances[7]***

Material	Composition	Molecular Weight, W	Gross, Δh_c^u (MJ/kg)	Net, Δh_c^l (MJ/kg)	$\Delta h_c^l / r_o$ (MJ/kg O_2)	Oxygen Fuel Mass Ratio, r_o	Boiling Temp., T_b (°C)	Latent Heat of Vaporization, Δh_v (kJ/kg)	Liquid Heat Capacity, C_{pl} (kJ/kg·°C)	Vapor Heat Capacity, C_{pv} (kJ/kg·°C)
Acetaldehyde	C_2H_4O	44.05	27.07	25.07	13.81	1.816	20.8	—	1.94	1.24
Acetic acid	$C_2H_4O_2$	60.05	14.56	13.09	12.28	1.066	118.1	395		1.11
Acetone	C_3H_6O	58.08	30.83	28.56	12.96	2.204	56.5	501	2.12	1.29
Acetylene	C_2H_2	26.04	49.91	48.22	15.70	3.072	–84.0	—	—	1.69
Acrolein	C_3H_4O	56.06	29.08	27.51	13.77	1.998	52.5	505	—	1.17
Acrylonitrile	C_3H_3N	53.06	33.16	31.92	14.11	2.262	77.3	615	2.10	1.20
(Allene) → propadiene										
Ammonium perchlorate[a]	NH_4ClO_4	117.49	2.35	2.16	3.97	0.545	—	—	—	
iso-Amyl alcohol	$C_5H_{12}O$	88.15	37.48	34.49	12.67	2.723	132.0	501	2.90	1.50
Aniline	C_6H_7N	93.12	36.44	34.79	13.06	2.663	184.4	478	2.08	1.16
Benzaldehyde	C_7H_6O	106.12	33.25	32.01	13.27	2.412	179.2	385	1.61	
Benzene	C_6H_6	78.11	41.83	40.14	13.06	3.073	80.1	389	1.72	1.05
Benzoic acid[a]	$C_7H_6O_2$	122.12	26.43	25.35	12.90	1.965	250.8	415	—	0.85
Benzyl alcohol	C_7H_8O	108.13	34.56	32.93	13.09	2.515	205.7	467	2.00	1.19
Bicyclohexyl	$C_{12}H_{22}$	166.30	45.35	42.44	12.61	3.367	236.0	263		
1,2-Butadiene	C_4H_6	54.09	47.95	45.51	13.99	3.254	10.8	—	—	1.48
1,3-Butadiene	C_4H_6	54.09	46.99	44.55	13.69	3.254	–4.4	—	—	1.47
(1,3-Butadiyne) → diacetylene										
n-Butane	C_4H_{10}	58.12	49.50	45.72	12.77	3.579	–0.5	—	2.30	1.68
iso-Butane	C_4H_{10}	58.12	48.95	45.17	12.62	3.579	–11.8	—	—	1.67
1-Butene	C_4H_8	56.10	48.44	45.31	13.24	3.422	–6.2	—	—	1.53
n-Butylamine	$C_4H_{11}N$	73.14	41.75	38.45	12.84	2.994	77.8	372	2.57	1.62
d-Camphor[a]	$C_{10}H_{16}O$	152.23	38.75	36.44	12.84	2.838	203.4	—	—	0.82
Carbon[a]	C	12.01	32.80	32.80	12.31	2.664	4200.0	—	—	0.71
Carbon disulfide	CS_2	76.13	6.34	6.34	5.03	1.261	46.5	351	1.00	0.60
Carbon monoxide	CO	28.01	10.10	10.10	17.69	0.571	–191.3	—	—	1.04
Cellulose[a]	$C_6H_{10}O_5$	162.14	17.47	16.12	13.61	1.184	—	—	1.16	—
(Chloroethylene) → vinyl chloride										
(Chloroform) → trichloromethane										
Chlorotrifluoroethylene	C_2F_3Cl	116.47	2.00	2.00	3.64	0.549	–28.3	188	1.34	0.72
m-Cresol	C_7H_8O	108.13	34.26	32.64	12.98	2.515	202.2	399	2.00	1.13
Cumene	C_9H_{12}	120.19	43.40	41.20	12.90	3.195	152.3	312	1.77	1.26
Cyanogen	C_2N_2	52.04	21.06	21.06	17.12	1.230	–21.2	—	—	1.12
Cyclobutane	C_4H_8	56.10	48.91	45.77	13.38	3.422	12.9	—	—	1.29
Cyclohexane	C_6H_{12}	84.16	46.58	43.45	12.70	3.422	80.7	357	1.84	1.26
Cyclohexene	C_6H_{10}	82.14	45.67	42.99	12.99	3.311	82.8	371	1.80	1.28
Cyclohexylamine	$C_6H_{13}N$	99.18	41.05	38.17	12.79	2.984	134.5			
Cyclopentane	C_5H_{10}	70.13	46.93	43.80	12.80	3.422	49.3	389	2.23	1.18
Cyclopropane	C_3H_6	42.08	49.70	46.57	13.61	3.422	–32.9	—	1.92	1.33
(Decahydronaphthalene) → *cis*-decalin										
cis-Decalin	$C_{10}H_{18}$	138.24	45.49	42.63	12.70	3.356	195.8	309	1.67	1.21
n-Decane	$C_{10}H_{22}$	142.28	47.64	44.24	12.69	3.486	174.1	276	2.19	1.85
Diacetylene	C_4H_2	50.06	46.60	45.72	15.89	2.877	10.3	—	—	1.47
(Diamine) → hydrazine										
Diborane	H_6B_2	27.69	79.80	79.80	23.02	3.467	–92.5	—	—	1.75
Dichloromethane	CH_2Cl_2	84.94	6.54	6.02	10.65	0.565	39.7	330	1.18	0.80
Diethyl cyclohexane	$C_{10}H_{20}$	140.26	46.30	43.17	12.58	3.422	174.0		1.87	
Diethyl ether	$C_4H_{10}O$	74.12	36.75	33.79	13.04	2.590	34.6	360	2.34	1.52
(2,4 Diisocyanotoulene) → toluene diisocyanate										
(Diisopropyl ether) → *iso*-propyl ether										
Dimethylamine	C_2H_7N	45.08	38.66	35.25	13.24	2.662	6.9	—	—	1.80
(Dimethyl aniline) → xylidene										
Dimethyldecalin	$C_{12}H_{22}$	166.30	45.70	42.79	13.15	3.254	220.0	260		
(Dimethyl ether) → methyl ether										
1,1-Dimethylhydrazine (UDMH)	$C_2H_8N_2$	60.10	32.95	30.03	14.10	2.130	25.0	578	2.73	
Dimethyl sulfoxide	C_2H_6SO	78.13	29.88	28.19	15.30	1.843	189.0	677	1.89	1.14
1,3 Dioxane	$C_4H_8O_2$	88.10	26.57	24.58	9.66	2.543	105.0	404		

Table C.2 ***(Continued)***

Material	Composition	Molecular Weight, W	Gross, Δh_c^u (MJ/kg)	Net, Δh_c^l (MJ/kg)	$\Delta h_c^l / r_o$ (MJ/kg O_2)	Oxygen Fuel Mass Ratio, r_o	Boiling Temp., T_b (°C)	Latent Heat of Vaporization, Δh_v (kJ/kg)	Liquid Heat Capacity, C_{pl} (kJ/kg·°C)	Vapor Heat Capacity, C_{pv} (kJ/kg·°C)
1,4 Dioxane	$C_4H_8O_2$	88.10	26.83	24.84	9.77	2.543	101.1	406	1.74	1.07
Ethane	C_2H_6	30.07	51.87	47.49	12.75	3.725	–88.6	—	—	1.75
Ethanol	C_2H_6O	46.07	29.67	26.81	12.87	2.084	78.5	837	2.43	1.42
(Ethene) → ethylene										
Ethyl acetate	$C_4H_8O_2$	88.10	25.41	23.41	12.89	1.816	77.2	367	1.94	1.29
Ethyl acrylate	$C_5H_8O_2$	100.12	27.44	25.69	13.39	1.918	100.0	290		1.14
Ethylamine	C_2H_7N	45.08	38.63	35.22	13.23	2.662	16.5	—	2.89	1.61
Ethyl benzene	C_8H_{10}	106.16	43.00	40.93	12.93	3.165	136.1	339	1.75	1.21
Ethylene	C_2H_4	28.05	50.30	47.17	13.78	3.422	–103.9	—	2.38	1.56
Ethylene glycol	$C_2H_6O_2$	62.07	19.17	17.05	13.22	1.289	197.5	800	2.43	1.56
Ethylene oxide	C_2H_4O	44.05	29.65	27.65	15.23	1.816	10.7	—	1.97	1.10
(Ethylene trichloride) → trichloroethylene										
(Ethyl ether) → diethyl ether										
Formaldehyde	CH_2O	30.03	18.76	17.30	16.23	1.066	–19.3	—	—	1.18
Formic acid	CH_2O_2	46.03	5.53	4.58	13.15	0.348	100.5	476	2.15	0.98
Furan	C_4H_4O	68.07	30.61	29.32	13.86	2.115	31.4	398	1.69	0.96
a-D-glucose[a]	$C_6H_{12}O_6$	180.16	15.55	14.08	13.21	1.066	—	—	—	—
(Glycerine) → glycerol										
Glycerol	$C_3H_8O_3$	92.10	17.95	16.04	13.19	1.216	290.0	800	2.42	1.25
(Glycerol trinitrate) → nitroglycerin										
n-Heptane	C_7H_{16}	100.20	48.07	44.56	12.68	3.513	98.4	316	2.20	1.66
n-Heptene	C_7H_{14}	98.18	47.44	44.31	12.95	3.422	93.6	317	2.17	1.58
Hexadecane	$C_{16}H_{34}$	226.43	47.25	43.95	12.70	3.462	286.7	226	2.22	1.64
Hexamethyldisiloxane	$C_6H_{18}Si_2O$	162.38	38.30	35.80	15.16	2.364	100.1	192	2.01	—
(Hexamethylenetetramine) → methenamine										
n-Hexane	C_6H_{14}	86.17	48.31	44.74	12.68	3.528	68.7	335	2.24	1.66
n-Hexene	C_6H_{12}	84.16	47.57	44.44	12.99	3.422	63.5	333	2.18	1.57
Hydrazine	H_4N_2	32.05	52.08	49.34	49.40	0.998	113.5	1180	3.08	1.65
Hydrazoic acid	HN_3	43.02	15.28	14.77	79.40	0.186	35.7	690	—	1.02
Hydrogen	H_2	2.00	141.79	130.80	16.35	8.000	–252.7	—	—	14.42
(Hydrogen azide) → hydrazoic acid										—
Hydrogen cyanide	HCN	27.03	13.86	13.05	8.82	1.480	25.7	933	2.61	1.33
Hydrogen sulfide	H_2S	34.08	48.54	47.25	16.77	2.817	–60.3	548	—	1.00
Maleic anhydride[a]	$C_4H_2O_3$	74.04	18.77	18.17	14.01	1.297	202.0	—	—	—
Melamine[a]	$C_3H_6N_6$	126.13	15.58	14.54	12.73	1.142	—	—	—	—
Methane	CH_4	16.04	55.50	50.03	12.51	4.000	–161.5	—	—	2.23
Methanol	CH_4O	32.04	22.68	19.94	13.29	1.500	64.8	1101	2.37	1.37
Methenamine[a]	$C_6H_{12}N_4$	140.19	29.97	28.08	13.67	2.054	—	—	—	—
2-Methoxyethanol	$C_3H_8O_2$	76.09	24.23	21.92	13.03	1.682	124.4	583	2.23	—
Methylamine	CH_5N	31.06	34.16	30.62	13.21	2.318	–6.3	—	—	1.61
(2-Methyl 1-butanol) → *iso*-amyl alcohol										
(Methyl chloride) → dichloromethane										
Methyl ether	C_2H_6O	46.07	31.70	28.84	13.84	2.084	–24.9	—	—	1.43
Methyl ethyl ketone	C_4H_8O	72.10	33.90	31.46	12.89	2.441	79.6	434	2.30	1.43
1-Methylnaphthalene	$C_{11}H_{10}$	142.19	40.88	39.33	12.95	3.038	244.7	323	1.58	1.12
Methyl methacrylate	$C_5H_8O_2$	100.11	27.37	25.61	12.33	2.078	101.0	360	1.91	—
Methyl nitrate	CH_3NO_3	77.04	8.67	7.81	75.10	0.104	64.6	409	2.04	0.99
2-Methyl propane) → *iso*-butane										
Naphthalene[a]	$C_{10}H_8$	128.16	40.21	38.84	12.96	2.996	217.9	—	1.18	1.03
Nitrobenzene	$C_6H_5NO_2$	123.11	25.11	24.22	14.90	1.625	210.7	330	1.52	—
Nitroglycerin	$C_3H_5N_3O_9$	227.09	6.82	6.34	—	—	Unstable	462	1.49	—
Nitromethane	CH_3NO_2	61.04	11.62	10.54	15.08	0.699	101.1	567	1.74	0.94
n-Nonane	C_9H_{20}	128.25	47.76	44.33	12.69	3.493	150.6	295	2.10	1.65
Octamethyl-cyclotetrasiloxane	$C_8H_{24}Si_4O_4$	296.62	26.90	25.10	14.56	1.725	175.0	127	1.88	—
n-Octane	C_8H_{18}	114.22	47.90	44.44	12.69	3.502	125.6	301	2.20	1.65
iso-Octane	C_8H_{18}	114.22	47.77	44.31	12.65	3.502	117.7	272	2.15	1.65
1-Octene	C_8H_{10}	112.21	47.33	44.20	12.92	3.422	121.3	301	2.19	1.59

Table C.2 ***(Continued)***

Material	Composition	Molecular Weight, W	Gross, Δh_c^g (MJ/kg)	Net, Δh_c^l (MJ/kg)	$\Delta h_c^l / r_o$ (MJ/kg O_2)	Oxygen Fuel Mass Ratio, r_o	Boiling Temp., T_b (°C)	Latent Heat of Vaporization Δh_v (kJ/kg)	Liquid Heat Capacity, C_{pl} (kJ/kg·°C)	Vapor Heat Capacity, C_{pv} (kJ/kg·°C)
(1-Octylene) → 1-octene										
1,2-Pentadiene	C_5H_8	68.11	47.31	44.71	13.60	3.288	44.9	405	2.21	1.55
n-Pentane	C_5H_{12}	72.15	48.64	44.98	12.68	3.548	36.0	357	2.33	1.67
1-Pentene	C_5H_{10}	70.13	47.77	44.64	13.04	3.422	30.0	359	2.16	1.56
Phenol[a]	C_6H_6O	94.11	32.45	31.05	13.05	2.380	181.8	433	1.43	1.10
Phosgene	$COCl_2$	98.92	1.74	1.74	10.74	0.162	8.3	247	1.02	0.58
Propadiene	C_3H_4	40.06	48.54	46.35	14.51	3.195	–34.6	—	—	1.44
Propane	C_3H_8	44.09	50.35	46.36	12.78	3.629	–42.2	—	2.23	1.67
n-Propanol	C_3H_8O	60.09	33.61	30.68	12.81	2.396	97.2	686	2.50	1.45
iso-Propanol	C_3H_8O	60.09	33.38	30.45	12.71	2.396	80.3	663	2.42	1.48
Propene	C_3H_6	42.08	48.92	45.79	13.38	3.422	–47.7	—	—	1.52
(*iso*-Propylbenzene) → cumene										
(Propylene) → propene										
iso-Propyl ether	$C_6H_{14}O$	102.17	39.26	36.25	12.86	2.819	67.8	286	2.14	1.55
Propyne	C_3H_4	40.06	48.36	46.17	14.45	3.195	–23.3	—	—	1.51
Styrene	C_8H_8	104.14	42.21	40.52	13.19	3.073	145.2	356	1.76	1.17
Sucrose[a]	$C_{12}H_{22}O_{11}$	342.30	16.49	15.08	13.44	1.122	—	—	1.24	—
1,2,3,4-Tetrahydronaphthalene) → tetralin										
Tetralin	$C_{10}H_{12}$	132.20	42.60	40.60	12.90	3.147	207.0	425	1.64	1.19
Tetranitromethane	CN_4O_8	196.04	2.20	2.20	—	—	125.7	196	—	—
Toluene	C_7H_8	92.13	42.43	40.52	12.97	3.126	110.4	360	1.67	1.12
Toluene diisocyanate	$C_9H_6N_2O_2$	174.16	24.32	23.56	13.50	1.746	120.0	—	1.65	—
Triethanolamine	$C_6H_{15}NO_3$	149.19	29.29	27.08	15.30	1.770	360.0	—	—	—
Triethylamine	$C_6H_{15}N$	101.19	43.19	39.93	12.95	3.083	89.5	303	2.22	1.59
1,1,2-Trichloroethane	$C_2H_3Cl_3$	133.42	7.77	7.28	11.02	0.660	114.0	260	1.11	0.67
Trichloroethylene	C_2HCl_3	131.40	6.77	6.60	12.05	0.548	86.9	245	1.07	0.61
Trichloromethane	$CHCl_3$	119.39	3.39	3.21	9.60	0.335	61.7	249	0.97	0.55
Trinitromethane	CHN_3O_6	151.04	3.41	3.25	—	—	Unstable	—	—	—
Trinitrotoluene[a]	$C_7H_5N_3O_6$	227.13	15.12	14.64	19.80	0.740	240.0	322	1.40	—
Trioxane	$C_3H_6O_3$	90.08	16.57	15.11	14.17	1.066	114.5	450	—	—
Urea[a]	CH_4ON_2	60.06	10.52	9.06	11.34	0.799	—	—	—	1.55
Vinyl acetate	$C_4H_6O_2$	86.09	24.18	22.65	13.54	1.673	72.5	167	2.00	1.05
Vinyl acetylene	C_4H_4	52.07	47.05	45.36	14.76	3.073	5.1	—	—	1.41
Vinyl bromide	C_2H_3Br	106.96	12.10	11.48	13.95	0.823	15.6	—	2.42	0.53
Vinyl chloride	C_2H_3Cl	62.50	20.02	16.86	11.97	1.408	–13.8	—	—	0.86
(Vinyl trichloride) → 1,1,2-trichlorolthane										
Xylenes	C_8H_{10}	106.16	42.89	40.82	12.90	3.165	138–144	343	1.72	1.21
Xylidene	$C_8H_{11}N$	121.22	38.28	36.29	12.79	2.838	192.7	366	1.77	—

[a]Denotes substance in crystalline solid form; otherwise, liquid if $T_b > 25°C$, gaseous if $T_b > 25°C$.

Table C.3 ***Heats of Combustion and Related Properties of Plastics[7]***

Material	Unit Composition	Molecular Weight, W	Gross, Δh_c^u (MJ/kg)	Net, Δh_c^l (MJ/kg)	$\Delta h_c^l / r_o$ (MJ/kg O_2)	Oxygen Fuel Mass Ratio, r_o	Heat Capacity Solid, C_{ps} (kJ/kg·°C)
Acrylonitrile-butadiene styrene copolymer	—	—	35.25	33.75			1.41–1.59
Bisphenol A epoxy	$C_{11.85}H_{20.37}O_{2.83}N_{0.3}$	212.10	33.53	31.42	13.41	2.343	
Butadiene-acrylonitrile 37% copolymer	—	—	39.94				
Butadiene/styrene 8.58% copolymer	$C_{4.18}H_{6.09}$	56.30	44.84	42.49	13.11	3.241	1.94
Butadiene/styrene 25.5% copolymer	$C_{4.60}H_{6.29}$	61.55	44.19	41.95	13.07	3.209	1.82
Cellulose acetate (triacetate)	$C_{12}H_{16}O_8$	288.14	18.88	17.66	13.25	1.333	1.34
Cellulose acetate-butyrate	$C_{12}H_{18}O_7$	274.27	23.70	22.3	14.67	1.517	1.70
Epoxy, unhardened	$C_{31}H_{36}O_{5.5}$	496.63	32.92	31.32	13.05	2.400	
Epoxy, hardened	$C_{39}H_{40}O_{8.5}$	644.74	30.27	28.90	13.01	2.221	
Melamine formaldehyde (Formica™)	$C_6H_6N_6$	162.08	19.33	18.52	12.51	1.481	1.46
Nylon 6	$C_6H_{11}NO$	113.08	30.1–31.7	28.0–29.6	12.30	2.335	1.52
Nylon 6,6	$C_{12}H_{22}N_2O_2$	226.16	31.6–31.7	29.5–29.6	12.30	2.405	1.70
Nylon 11 (Rilsan)	$C_{11}H_{21}NO$	183.14	36.99	34.47	12.33	2.796	1.70–2.30
Phenol formaldehyde foam	$C_{15}H_{12}O_2$	224.17	27.9–31.6 21.6–27.4	26.7–30.4 20.2–26.2	11.80	2.427	1.70
Polyacenaphthalene	$C_{12}H_8$	152.14	39.23	38.14	12.95	2.945	
Polyacrylonitrile	C_3H_3N	53.04	32.22	30.98	13.70	2.262	1.50
Polyallylphthalate (Polyamides) → nylon	$C_{14}H_{14}O$	198.17	27.74	26.19	9.54	2.745	
Poly-1,4-butadiene	C_4H_6	54.05	45.19	42.75	13.13	3.256	
Poly-1-butene	C_4H_8	56.05	46.48	43.35	12.65	3.426	1.88
Polycarbonate	$C_{16}H_{14}O_3$	254.19	30.99	29.78	13.14	2.266	1.26
Polycarbon suboxide	C_3O_2	68.03	13.78	13.78	14.64	0.941	
Polychlorotrifluorethylene	C_2F_3Cl	116.47	1.12	1.12	2.04	0.549	0.92
Polydiphenylbutadiene	$C_{16}H_{10}$	202.18	39.30	38.2	13.05	2.928	
Polyester, unsaturated	$C_{5.77}H_{6.25}O_{1.63}$	101.60	21.6–29.8	20.3–28.5	11.90	2.053	1.20–2.30
Polyether, chlorinated	$C_5H_8OCl_2$	154.97	17.84	16.71	12.45	1.342	
Polyethylene	C_2H_4	28.03	46.2–46.5	43.1–43.4	12.63	3.425	1.83–2.30
Polyethylene oxide	C_2H_4O	44.02	26.65	24.66	13.57	1.817	
Polyethylene terephthalate	$C_{10}H_8O_4$	192.11	22.18	21.27	12.77	1.666	1.00
Polyformaldehyde	CH_2O	30.01	16.93	15.86	14.88	1.066	1.46
Poly-1-hexene sulfone	$C_6H_{12}SO_2$	148.13	29.78	28.00	14.40	1.944	
Polyhydrocyanic acid (Polyisobutylene) → poly-1-butene	HCN	27.02	23.26	22.45	15.17	1.480	
Polyisocyanurate foam	—		26.3	22.2–26.2			
Polyisoprene	C_5H_8	68.06	44.90	42.30	12.90	3.291	
Poly-3-methyl-1-butene	C_5H_{10}	70.06	46.55	43.42	12.67	3.426	
Polymethyl methacrylate	$C_5H_8O_2$	100.06	26.64	24.88	12.97	1.919	1.44
Poly-4-methyl-1-pentene	C_6H_{12}	84.08	46.52	43.39	12.67	3.425	2.18
Poly-α-methylstyrene	C_9H_{10}	118.11	42.31	40.45	13.00	3.116	
Polynitroethylene	$C_2H_3O_2N$	73.03	15.96	15.06	19.64	0.767	
Polyoxymethylene	CH_2O	30.01	16.93	15.65	14.68	1.066	
Polyoxytrimethylene	C_3H_6O	58.04	31.52	29.25	13.27	2.205	
Poly-1-pentene	C_5H_{10}	70.06	45.58	42.45	12.39	3.426	
Polyphenylacetylene	C_8H_6	102.09	40.00	38.70	13.00	2.978	
Polyphenylene oxide	C_8H_8O	120.09	34.59	33.13	13.09	2.531	1.34
Polypropene sulfone	$C_3H_6SO_2$	106.10	23.82	22.58	16.64	1.357	
Poly-β-propiolactone	$C_3H_4O_2$	72.14	19.35	18.13	13.62	1.331	
Polypropylene	C_3H_6	42.04	46.37	43.23	12.62	3.824	2.10

Table C.3 ***(Continued)***

Material	Unit Composition	Molecular Weight, W	Gross, Δh_c^u (MJ/kg)	Net, Δh_c^l (MJ/kg)	$\Delta h_c^l / r_o$ (MJ/kg O_2)	Oxygen Fuel Mass Ratio, r_o	Heat Capacity Solid, C_{ps} (kJ/kg·°C)
Polypropylene oxide	C_3H_6O	58.04	31.17	28.90	13.11	2.205	
Polystyrene	C_8H_8	104.10	41.4–42.5	39.7–39.8	12.93	3.074	1.40
Polystyrene-foam	—		39.7	35.6–40.8			
Polystyrene-foam, FR	—		41.2–42.9				
Polysulfones, butene	$C_4H_8SO_2$	120.11	24.04–26.47	22.25–25.01	14.79	1.598	1.30
Polysulfur	S	32.06	9.72	9.72	9.74	0.998	
Polytetrafluoroethylene	C_2F_4	100.02	5.00	5.00	7.81	0.640	1.02
Polytetrahydrofuran	C_4H_8O	72.05	34.39	31.85	13.04	2.443	
Polyurea	$C_{15}H_{18}O_4N_4$	318.20	24.91	23.67	13.45	1.760	
Polyurethane	$C_{6.3}H_{7.1}NO_{2.1}$	130.30	23.90	22.70	13.16	1.725	1.75–1.84
Polyurethane-foam	—		26.1–31.6	23.2–28.0			
Polyurethane-foam, FR	—		24.0–25.0				
Polyvinyl acetate	$C_4H_6O_2$	86.05	23.04	21.51	12.86	1.673	
Polyvinyl alcohol	C_2H_4	44.03	25.00	23.01	12.66	1.817	1.70
Polyvinyl butyral	$C_8H_{14}O_2$	142.10	32.90	30.70	13.00	2.365	
Polyvinyl chloride	C_2H_3Cl	62.48	17.95	16.90	12.00	1.408	0.90–1.20
Polyvinyl-foam	—		22.83				1.30–2.10
Polyvinyl fluoride	C_2H_3F	46.02	21.70	20.27	10.60	1.912	
Polyvinylidene chloride	$C_2H_2Cl_2$	96.93	10.52	10.07	12.21	0.825	1.34
Polyvinylidene fluoride	$C_2H_2F_2$	64.02	14.77	14.08	11.26	1.250	1.38
Urea formaldehyde	$C_3H_6O_2N_2$	102.05	15.90	14.61	13.31	1.098	1.60–2.10
Urea formaldehyde-foam	—	—	14.80				

Table C.4 ***Heats of Combustion of Miscellaneous Materials[7]***

Material	Gross, Δh_c^u (MJ/kg)	Net, Δh_c^l (MJ/kg)
Acetate (see cellulose acetate)		
Acrylic fiber	30.6–30.8	
Blasting powder	2.1–2.4	
Butter	38.5	
Celluloid (cellulose nitrate and camphor)	17.5–20.6	16.4–19.2
Cellulose acetate fiber, $C_8H_{12}O_6$	17.8–18.4	16.4–17.0
Cellulose diacetate fiber, $C_{10}H_{14}O_7$	18.7	
Cellulose nitrate, $C_6H_9N_1O_7/C_6H_8N_2O_9/C_6H_7N_3O_{11}$	9.11–13.48	
Cellulose triacetate fiber, $C_{12}H_{16}O_8$	18.8	17.6
Charcoal	33.7–34.7	33.2–34.2
Coal—anthracite	30.9–34.6	30.5–34.2
—bituminous	24.7–36.3	23.6–35.2
Coke	28.0–31.0	28.0–31.0
Cork	26.1	
Cotton	16.5–20.4	
Dynamite	5.4	
Epoxy, $C_{11.9}H_{20.4}O_{2.8}N_{0.3}/C_{6.064}H_{7.550}O_{1.222}$	32.8–33.5	31.1–31.4
Fat, animal	39.8	
Flint powder	3.0–3.1	
Fuel oil—No. 1	46.1	
—No. 6	42.5	
Gasketing—chlorosulfonated polyethylene (Hypalon)	28.5	
—vinylidene fluoride/ hexafluoropropylene (Fluorel, Viton A)	14.0–15.1	

Table C.4 ***(Continued)***

Material	Gross, Δh_c^u (MJ/kg)	Net, Δh_c^l (MJ/kg)
Gasoline	46.8	43.7
Jet fuel—JP1		43.0
—JP3		43.5
—JP4	46.6	43.5
—JP5	45.9	43.0
Kerosene (jet fuel A)	46.4	43.3
Lanolin (wool fat)	40.8	
Lard	40.1	
Leather	18.2–19.8	
Lignin, $C_{2.6}H_3O$	24.7–26.4	23.4–25.1
Lignite	22.4–33.3	
Modacrylic fiber	24.7	
Naphtha	43.0–47.1	40.9–43.9
Neoprene, C_5H_5Cl—gum	24.3	
—foam	9.7–26.8	
Nomex™ (polymethaphenylene isophthalamide) fiber, $C_{14}H_{10}O_2N_2$	27.0–28.7	
Oil—castor	37.1	
—linseed	39.2–39.4	
—mineral	45.8–46.0	
—olive	39.6	
—solar	41.8	
Paper—brown	16.3–17.9	
—magazine	12.7	
—newsprint	19.7	
—wax	21.5	
Paraffin wax	46.2	43.1
Peat	16.7–21.6	
Petroleum jelly ($C_{7.118}H_{12.957}O_{0.091}$)	45.9	
Rayon fiber	13.6–19.5	
Rubber—buna N	34.7–35.6	
—butyl	45.8	
—isoprene (natural) C_5H_8	44.9	42.3
—latex foam	33.9–40.6	
—GRS	44.2	
—tire, auto	32.6	
Silicone rubber (SiC_2H_6O)	15.5–16.8	
—foam	14.0–19.5	
Sisal	15.9	
Spandex fiber	31.4	
Starch	17.6	16.2
Straw	15.6	
Sulfur—rhombic		9.28
—monoclinic		9.29
Tobacco	15.8	
Wheat	15.0	
Wood—beech	20.0	18.7
—birch	20.0	18.7
—douglas fir	21.0	19.6
—maple	19.1	17.8
—red oak	20.2	18.7
—spruce	21.8	20.4
—white pine	19.2	17.8
—hardboard	19.9	
Woodflour	19.8	
Wool	20.7–26.6	

APPENDIX D

Configuration Factors

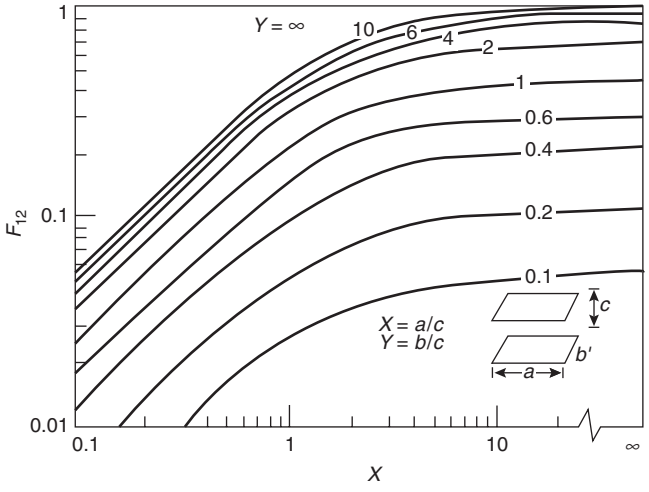

Figure D-1. ***View factor for parallel, rectangular plates.[8]***

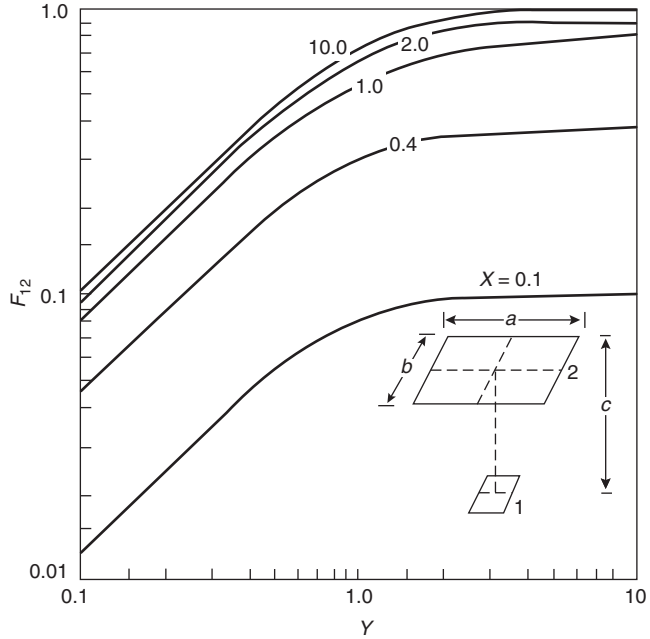

$$F_{12} = \frac{2}{\pi}\left[\frac{X}{\sqrt{1+X^2}}\tan^{-1}\frac{Y}{\sqrt{1+X^2}} + \frac{Y}{\sqrt{1+Y^2}}\tan^{-1}\frac{X}{\sqrt{1+Y^2}}\right]$$

$$X = \frac{A}{C}$$

$$Y = \frac{B}{C}$$

Figure D-2. ***View factor for parallel, rectangular radiator.[8]***

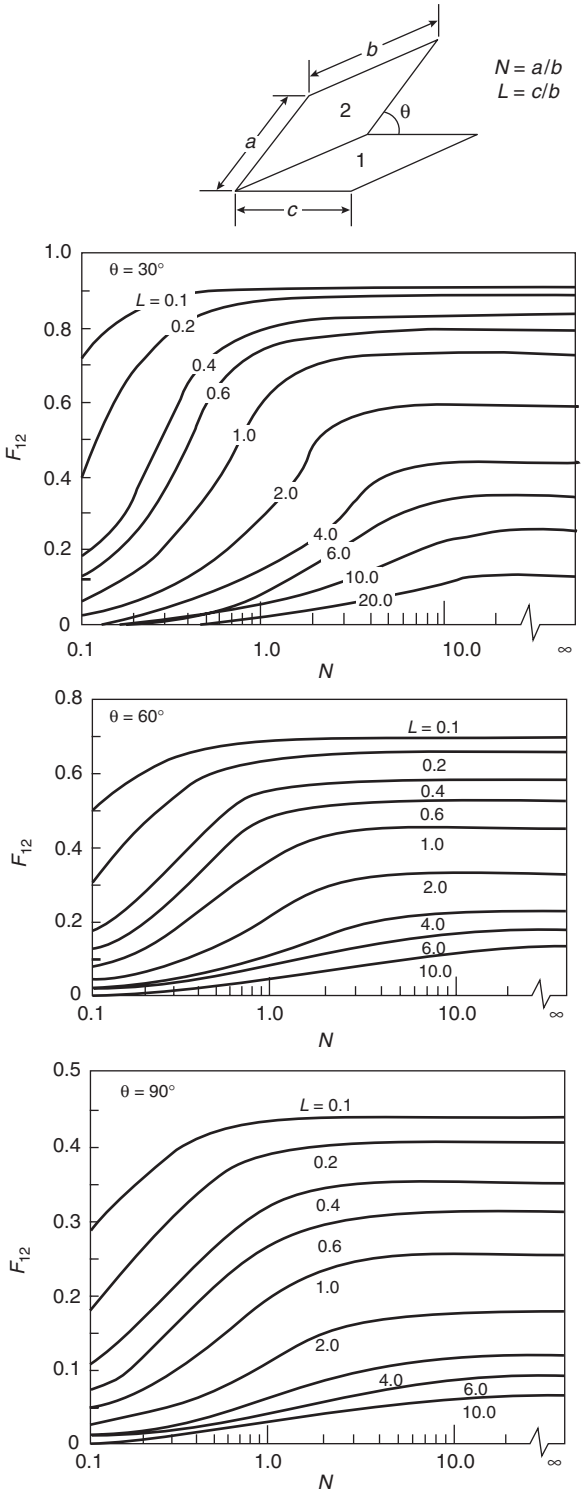

Figure D-3. ***View factor for rectangular plates at various angles.[8]***

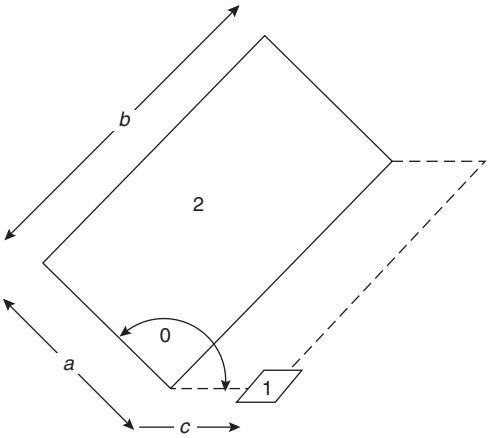

$$F_{12} = \frac{1}{2\pi}\left\{\begin{array}{l}\tan^{-1}\left(\frac{1}{L}\right) + V\,(N\cos\phi - \phi\,L)\tan^{-1}V \\ + \frac{\cos\phi}{W}\left[\tan^{-1}\left(\frac{N - L\cos\phi}{W}\right) + \tan^{-1}\left(\frac{L\cos\phi}{W}\right)\right]\end{array}\right\}$$

$$V = \frac{1}{\sqrt{N^2 + L^2 - 2NL\cos\phi}}$$

$$W = \sqrt{1 + L^2\sin^2\phi}$$

$$N = \frac{a}{b}$$

$$L = \frac{c}{b}$$

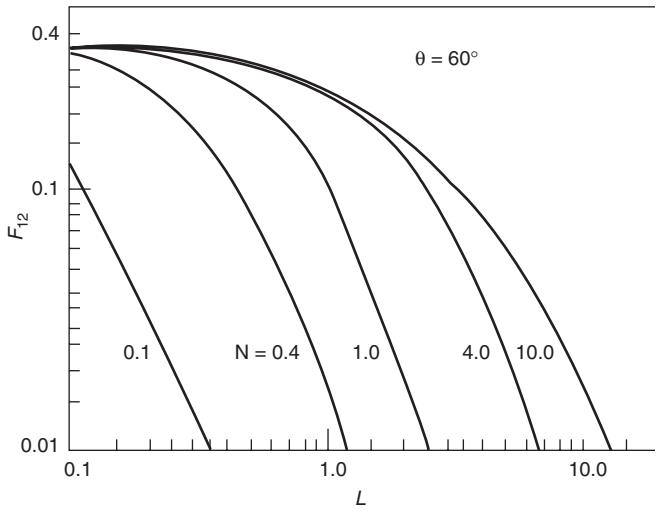

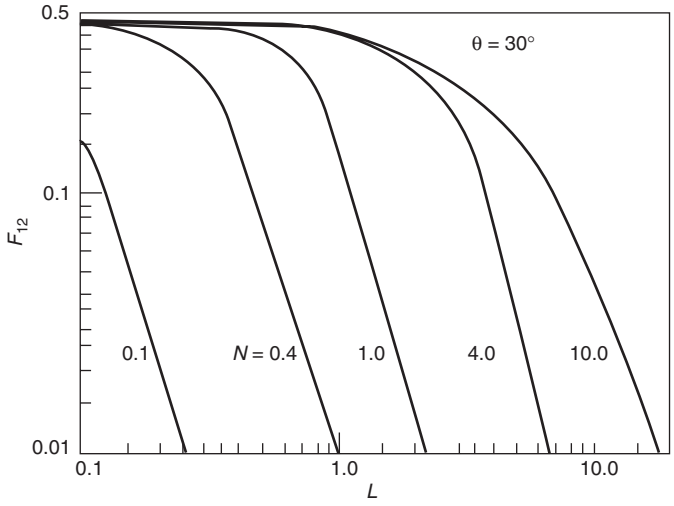

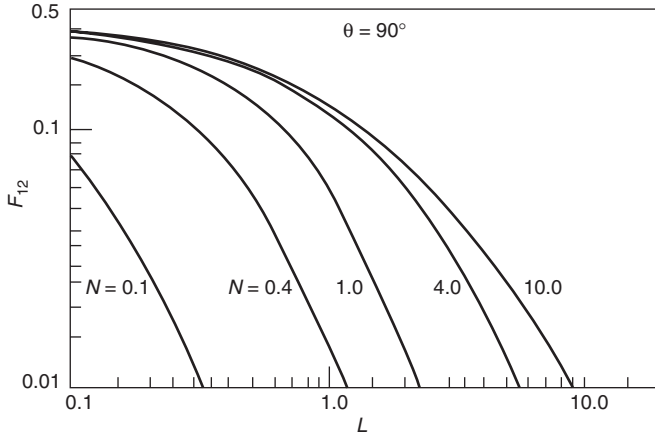

Figure D-4. ***View factor for rectangular radiator to differential area at various angles.[8]***

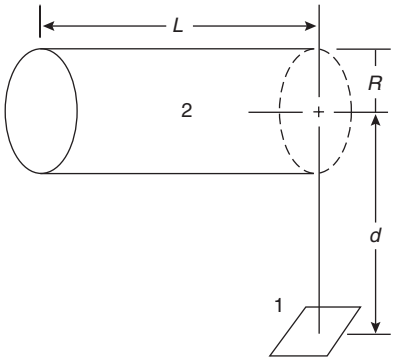

$$F_{12} = \frac{1}{\pi D}\ \tan^{-1}\left(\frac{L}{\sqrt{D^2-1}}\right) + \frac{L}{\pi}\left[\frac{A-2D}{D\sqrt{AB}}\tan^{-1}\sqrt{\frac{A(D-1)}{B(D+1)}} - \frac{1}{D}\tan^{-1}\sqrt{\frac{D-1}{D+1}}\right]$$

$$D = \frac{d}{r} \qquad L = \frac{L}{R}$$

$$A = (D+1)^2 + L^2 \qquad B = (D-1)^2 + L^2$$

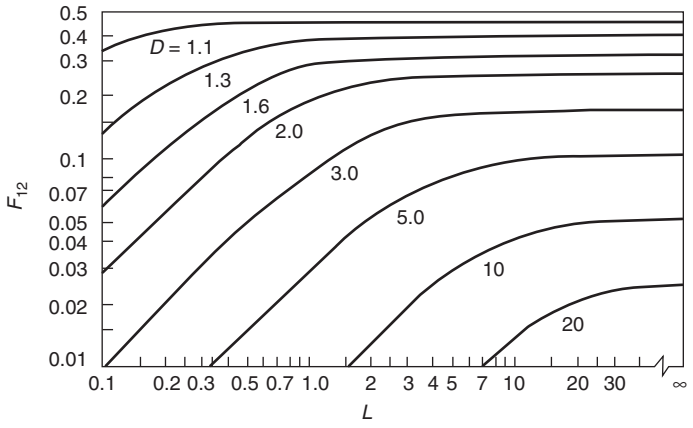

Figure D-5. ***Cylindrical radiator to parallel receiver.[8]***

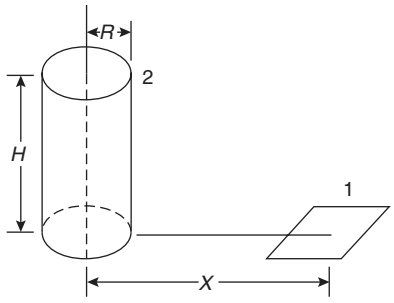

$$F_{12} = \frac{1}{\pi}\left[\tan^{-1}\sqrt{\frac{X'+R'}{X'-R'}} - \frac{(1.0+X'^2-R'^2)}{(1.0+X'^2+R'^2)}\tan^{-1}\sqrt{\frac{X'+R'}{X'-R'}}\right]$$

$$X' = \frac{X}{H}$$

$$R' = \frac{R}{H}$$

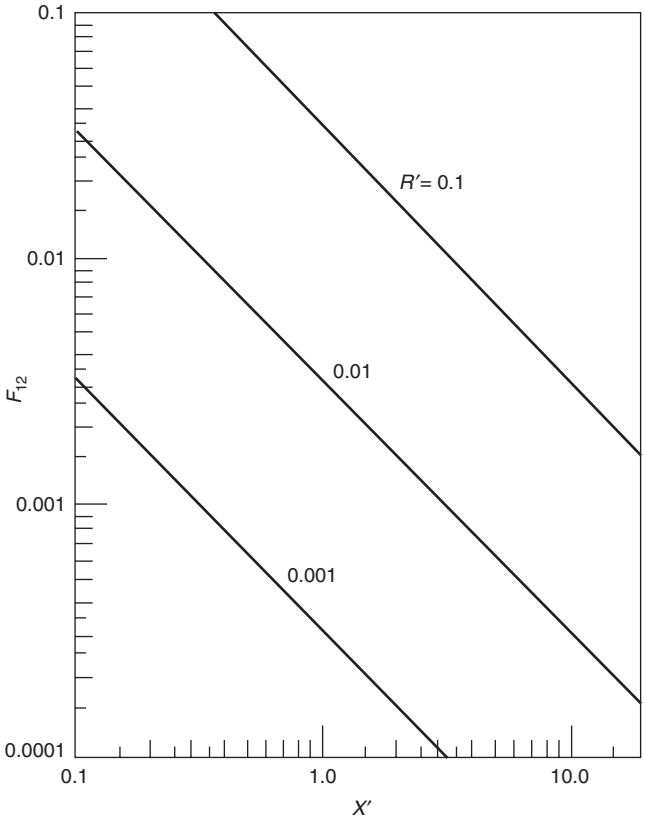

Figure D-6. ***View factor for cylindrical radiator to normal target.[8]***

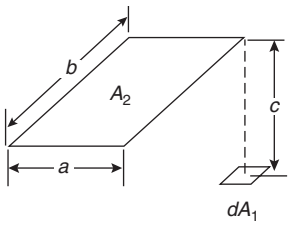

Plane element dA_1 to plane parallel rectangle; normal to element passes through corner of rectangle.

$$X = \frac{a}{c} \qquad Y = \frac{b}{c}$$

$$F_{d1-2} = \frac{1}{2\pi}\left(\frac{X}{\sqrt{1+X^2}}\tan^{-1}\frac{Y}{\sqrt{1+X^2}} + \frac{X}{\sqrt{1+Y^2}}\tan^{-1}\frac{X}{\sqrt{1+Y^2}}\right)$$

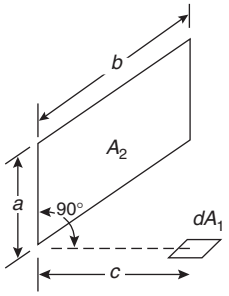

Plane element dA_1 to rectangle in plane 90° to plane of element

$$X = \frac{a}{b} \qquad Y = \frac{c}{b}$$

$$F_{d1-2} = \frac{1}{2\pi}\left(\tan^{-1}\frac{1}{Y} - \frac{Y}{\sqrt{X^2+Y^2}}\tan^{-1}\frac{1}{\sqrt{X^2+Y^2}}\right)$$

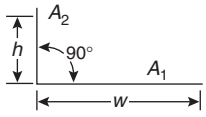

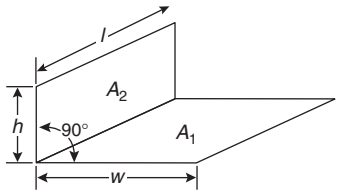

$$F_{1-2} = \frac{1}{\pi W}\left(W\tan^{-1}\frac{1}{W} + H\tan^{-1}\frac{1}{H} - \sqrt{H^2+W^2}\tan^{-1}\frac{1}{\sqrt{H^2+W^2}} + \frac{1}{4}\ln\left\{\frac{(1+W^2)(1+H^2)}{1-W^2+H^2}\left[\frac{W^2(1+W^2+H^2)}{(1+W^2)(W^2+H^2)}\right]^{W^2}\left[\frac{H^2(1+H^2+W^2)}{(1+H^2)(H^2+W^2)}\right]^{H^2}\right\}\right)$$

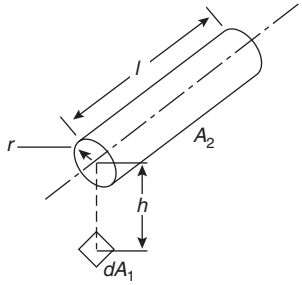

Plane element dA_1 to right circular cylinder of finite length l and radius r; normal to element passes through one end of cylinder and is perpendicular to cylinder axis

$$L = \frac{l}{r} \qquad H = \frac{h}{r}$$

$$X = (1+H)^2 + L^2$$
$$Y = (1-H)^2 + L^2$$

$$F_{d1-2} = \frac{1}{\pi H}\tan^{-1}\frac{1}{\sqrt{H^2-1}} + \frac{L}{\pi}\left[\frac{X-2H}{H\sqrt{XY}}\tan^{-1}\sqrt{\frac{X(H-1)}{Y(H+1)}} - \frac{1}{H}\tan^{-1}\sqrt{\frac{(H-1)}{(H+1)}}\right]$$

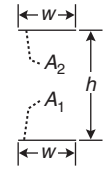

Two infinitely long, directly opposed parallel plates of the same finite width

$$H = \frac{h}{w}$$

$$F_{1-2} = F_{2-1} = \sqrt{1+H^2} - H$$

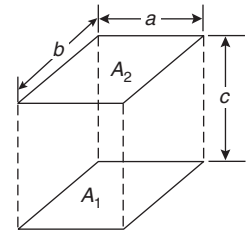

Identical, parallel, directly opposed rectangles.

$$Y = \frac{a}{c} \qquad Y = \frac{b}{c}$$

$$F_{1-2} = \frac{2}{\pi XY}\left\{\ln\left[\frac{(1+X^2)(1+Y^2)}{1+X^2+Y^2}\right]^{1/2} + X\sqrt{1+Y^2}\tan^{-1}\frac{X}{\sqrt{1+Y^2}} + Y\sqrt{1+X^2}\tan^{-1}\frac{Y}{\sqrt{1+X^2}} - X\tan^{-1}X - Y\tan^{-1}Y\right\}$$

Two infinitely long plates of unequal widths h and w, having one common edge and having an angle of 90° to each other

$$H = \frac{h}{w}$$

$$F_{1-2} = \frac{1}{2}\left(1 + H - \sqrt{1+H^2}\right)$$

Two finite rectangles of same length, having one common edge and having an angle of 90° to each other

$$H = \frac{h}{l} \qquad H = \frac{w}{l}$$

Figure D-7. ***View factor equations for various geometries.[9]***

APPENDIX E

Piping Properties

Table E.1 ***Properties of Steel Pipe[10]***

Nominal Pipe Size (in.)	Outside Diam. (in.)	Schedule No.	Wall Thickness (in.)	Inside Diam. (in.)	Cross-Sectional Area		Circumference (ft) or Surface (sq ft/ft of length)		Capacity at Velocity (1 ft/s)		Weight of Plain-End Pipe (lb/ft)
					Metal (sq in.)	Flow (sq ft)	Outside	Inside	U.S. gal/ min	Water (lb/hr)	
1/8	0.405	10S	0.049	0.307	0.055	0.00051	0.106	0.0804	0.231	115.5	0.19
		40ST, 40S	0.068	0.269	0.072	0.00040	0.106	0.0705	0.179	89.5	0.24
		80XS, 80S	0.095	0.215	0.093	0.00025	0.106	0.0563	0.113	56.5	0.31
1/4	0.540	10S	0.065	0.410	0.097	0.00092	0.141	0.107	0.412	206.5	0.33
		40ST, 40S	0.088	0.364	0.125	0.00072	0.141	0.095	0.323	161.5	0.42
		80XS, 80S	0.119	0.302	0.157	0.00050	0.141	0.079	0.224	112.0	0.54
3/8	0.675	10S	0.065	0.545	0.125	0.00162	0.177	0.143	0.727	363.5	0.42
		40ST, 40S	0.091	0.493	0.167	0.00133	0.177	0.129	0.596	298.0	0.57
		80XS, 80S	0.126	0.423	0.217	0.00098	0.177	0.111	0.440	220.0	0.74
1/2	0.840	5S	0.065	0.710	0.158	0.00275	0.220	0.186	1.234	617.0	0.54
		10S	0.083	0.674	0.197	0.00248	0.220	0.176	1.112	556.0	0.67
		40ST, 40S	0.109	0.622	0.250	0.00211	0.220	0.163	0.945	472.0	0.85
		80XS, 80S	0.147	0.546	0.320	0.00163	0.220	0.143	0.730	365.0	1.09
		160	0.188	0.464	0.385	0.00117	0.220	0.122	0.527	263.5	1.31
		XX	0.294	0.252	0.504	0.00035	0.220	0.066	0.155	77.5	1.71
3/4	1.050	5S	0.065	0.920	0.201	0.00461	0.275	0.241	2.072	1036.0	0.69
		10S	0.083	0.884	0.252	0.00426	0.275	0.231	1.903	951.5	0.86
		40ST, 40S	0.113	0.824	0.333	0.00371	0.275	0.216	1.665	832.5	1.13
		80XS, 80S	0.154	0.742	0.433	0.00300	0.275	0.194	1.345	672.5	1.47
		160	0.219	0.612	0.572	0.00204	0.275	0.160	0.917	458.5	1.94
		XX	0.308	0.434	0.718	0.00103	0.275	0.114	0.461	230.5	2.44
1	1.315	5S	0.065	1.185	0.255	0.00768	0.344	0.310	3.449	1725	0.87
		10S	0.109	1.097	0.413	0.00656	0.344	0.287	2.946	1473	1.40
		40ST, 40S	0.133	1.049	0.494	0.00600	0.344	0.275	2.690	1345	1.68
		80XS, 80S	0.179	0.957	0.639	0.00499	0.344	0.250	2.240	1120	2.17
		160	0.250	0.815	0.836	0.00362	0.344	0.213	1.625	812.5	2.84
		XX	0.358	0.599	1.076	0.00196	0.344	0.157	0.878	439.0	3.66
1 1/4	1.660	5S	0.065	1.530	0.326	0.01277	0.435	0.401	5.73	2865	1.11
		10S	0.109	1.442	0.531	0.01134	0.435	0.378	5.09	2545	1.81
		40ST, 40S	0.140	1.380	0.668	0.01040	0.435	0.361	4.57	2285	2.27
		80XS, 80S	0.191	1.278	0.881	0.00891	0.435	0.335	3.99	1995	3.00
		160	0.250	1.160	1.107	0.00734	0.435	0.304	3.29	1645	3.76
		XX	0.382	0.896	1.534	0.00438	0.435	0.235	1.97	985	5.21
1 1/2	1.900	5S	0.065	1.770	0.375	0.01709	0.497	0.463	7.67	3835	1.28
		10S	0.109	1.682	0.614	0.01543	0.497	0.440	6.94	3465	2.09
		40ST, 40S	0.145	1.610	0.800	0.01414	0.497	0.421	6.34	3170	2.72
		80XS, 80S	0.200	1.500	1.069	0.01225	0.497	0.393	5.49	2745	3.63
		160	0.281	1.338	1.429	0.00976	0.497	0.350	4.38	2190	4.86
		XX	0.400	1.100	1.885	0.00660	0.497	0.288	2.96	1480	6.41
2	2.375	5S	0.065	2.245	0.472	0.02749	0.622	0.588	12.34	6170	1.61
		10S	0.109	2.157	0.776	0.02538	0.622	0.565	11.39	5695	2.64
		40ST, 40S	0.154	2.067	1.075	0.02330	0.622	0.541	10.45	5225	3.65
		80ST, 80S	0.218	1.939	1.477	0.02050	0.622	0.508	9.20	4600	5.02
		160	0.344	1.687	2.195	0.01552	0.622	0.436	6.97	3485	7.46
		XX	0.436	1.503	2.656	0.01232	0.622	0.393	5.53	2765	9.03

Table E.1 ***(Continued)***

Nominal Pipe Size (in.)	Outside Diam. (in.)	Schedule No.	Wall Thickness (in.)	Inside Diam. (in.)	Cross-Sectional Area		Circumference (ft) or Surface (sq ft/ft of length)		Capacity at Velocity (1 ft/s)		Weight of Plain-End Pipe (lb/ft)
					Metal (sq in.)	Flow (sq ft)	Outside	Inside	U.S. gal/ min	Water (lb/hr)	
$2^1/_2$	2.875	5S	0.083	2.709	0.728	0.04003	0.753	0.709	17.97	8985	2.48
		10S	0.120	2.635	1.039	0.03787	0.753	0.690	17.00	8500	3.53
		40ST, 40S	0.203	2.469	1.704	0.03322	0.753	0.647	14.92	7460	5.79
		80XS, 80S	0.276	2.323	2.254	0.02942	0.753	0.608	13.20	6600	7.66
		160	0.375	2.125	2.945	0.02463	0.753	0.556	11.07	5535	10.01
		XX	0.552	1.771	4.028	0.01711	0.753	0.464	7.68	3840	13.70
3	3.500	5S	0.083	3.334	0.891	0.06063	0.916	0.873	27.21	13,605	3.03
		10S	0.120	3.260	1.274	0.05796	0.916	0.853	26.02	13,010	4.33
		40ST, 40S	0.216	3.068	2.228	0.05130	0.916	0.803	23.00	11,500	7.58
		80XS, 80S	0.300	2.900	3.016	0.04587	0.916	0.759	20.55	10,275	10.25
		160	0.438	2.624	4.213	0.03755	0.916	0.687	16.86	8430	14.31
		XX	0.600	2.300	5.466	0.02885	0.916	0.602	12.95	6475	18.58
$3^1/_2$	4.0	5S	0.083	3.834	1.021	0.08017	1.047	1.004	35.98	17,990	3.48
		10S	0.120	3.760	1.463	0.07711	1.047	0.984	34.61	17,305	4.97
		40ST, 40S	0.226	3.548	2.680	0.06870	1.047	0.929	30.80	15,400	9.11
		80XS, 80S	0.318	3.364	3.678	0.06170	1.047	0.881	27.70	13,850	12.51
4	4.5	5S	0.083	4.334	1.152	0.10245	1.178	1.135	46.0	23,000	3.92
		10S	0.120	4.260	1.651	0.09898	1.178	1.115	44.4	22,200	5.61
		40ST, 40S	0.237	4.026	3.17	0.08840	1.178	1.054	39.6	19,800	10.79
		80XS, 80S	0.337	3.826	4.41	0.07986	1.178	1.002	35.8	17,900	14.98
		120	0.438	3.624	5.58	0.07170	1.178	0.949	32.2	16,100	18.98
		160	0.531	3.438	6.62	0.06647	1.178	0.900	28.9	14,450	22.52
		XX	0.674	3.152	8.10	0.05419	1.178	0.825	24.3	12,150	27.54
5	5.563	5S	0.109	5.345	1.87	0.1558	1.456	1.399	69.9	34,950	6.36
		10S	0.134	5.295	2.29	0.1529	1.456	1.386	68.6	34,300	7.77
		40ST, 40S	0.258	5.047	4.30	0.1390	1.456	1.321	62.3	31,150	14.62
		80XS, 80S	0.375	4.813	6.11	0.1263	1.456	1.260	57.7	28,850	20.78
		120	0.500	4.563	7.95	0.1136	1.456	1.195	51.0	25,500	27.04
		160	0.625	4.313	9.70	0.1015	1.456	1.129	45.5	22,750	32.96
		XX	0.750	4.063	11.34	0.0900	1.456	1.064	40.4	20,200	38.55
6	6.625	5S	0.109	6.407	2.23	0.2239	1.734	1.677	100.5	50,250	7.60
		10S	0.134	6.357	2.73	0.2204	1.734	1.664	98.9	49,450	9.29
		40ST, 40S	0.280	6.065	5.58	0.2006	1.734	1.588	90.0	45,000	18.97
		80XS, 80S	0.432	5.761	8.40	0.1810	1.734	1.508	81.1	40,550	28.57
		120	0.562	5.501	10.70	0.1650	1.734	1.440	73.9	36,950	36.42
		160	0.719	5.187	13.34	0.1467	1.734	1.358	65.9	32,950	45.34
		XX	0.864	4.897	15.64	0.1308	1.734	1.282	58.7	29,350	53.16
8	8.625	5S	0.109	8.407	2.915	0.3855	2.258	2.201	173.0	86,500	9.93
		10S	0.148	8.329	3.941	0.3784	2.258	2.180	169.8	84,900	13.40
		20	0.250	8.125	6.578	0.3601	2.258	2.127	161.5	80,750	22.36
		30	0.277	8.071	7.265	0.3553	2.258	2.113	159.4	79,700	24.70
		40ST, 40S	0.322	7.981	8.399	0.3474	2.258	2.089	155.7	77,850	28.55
		60	0.406	7.813	10.48	0.3329	2.258	2.045	149.4	74,700	35.66
		80XS, 80S	0.500	7.625	12.76	0.3171	2.258	1.996	142.3	71,150	43.39
		100	0.594	7.437	14.99	0.3017	2.258	1.947	135.4	67,700	50.93
		120	0.719	7.187	17.86	0.2817	2.258	1.882	126.4	63,200	60.69
		140	0.812	7.001	19.93	0.2673	2.258	1.833	120.0	60,000	67.79
		XX	0.875	6.875	21.30	0.2578	2.258	1.800	115.7	57,850	72.42
		160	0.906	6.813	21.97	0.2532	2.258	1.784	113.5	56,750	74.71

Table E.1 ***(Continued)***

Nominal Pipe Size (in.)	Outside Diam. (in.)	Schedule No.	Wall Thickness (in.)	Inside Diam. (in.)	Cross-Sectional Area		Circumference (ft) or Surface (sq ft/ft of length)		Capacity at Velocity (1 ft/s)		Weight of Plain-End Pipe (lb/ft)
					Metal (sq in.)	Flow (sq ft)	Outside	Inside	U.S. gal/ min	Water (lb/hr)	
10	10.75	5S	0.134	10.842	4.47	0.5993	2.814	2.744	269.0	134,500	15.19
		10S	0.165	10.420	5.49	0.5922	2.814	2.728	265.8	132,900	18.65
		20	0.250	10.250	8.25	0.5731	2.814	2.685	257.0	128,500	28.04
		30	0.307	10.136	10.07	0.5603	2.814	2.655	252.0	126,000	34.24
		40ST, 40S	0.365	10.020	11.91	0.5475	2.814	2.620	246.0	123,000	40.48
		80S, 60XS	0.500	9.750	16.10	0.5185	2.814	2.550	233.0	116,500	54.74
		80	0.594	9.562	18.95	0.4987	2.814	2.503	233.4	111,700	64.40
		100	0.719	9.312	22.66	0.4729	2.814	2.438	212.3	106,150	77.00
		120	0.844	9.062	26.27	0.4479	2.814	2.372	201.0	100,500	89.27
		140, XX	1.000	8.750	30.63	0.4176	2.814	2.291	188.0	94,000	104.13
		160	1.125	8.500	34.02	0.3941	2.814	2.225	177.0	88,500	115.65
12	12.75	5S	0.156	12.438	6.17	0.8438	3.338	3.26	378.7	189,350	20.98
		10S	0.180	12.390	7.11	0.8373	3.338	3.24	275.8	187,900	24.17
		20	0.250	12.250	9.82	0.8185	3.338	3.21	367.0	183,500	33.38
		30	0.330	12.090	12.88	0.7972	3.338	3.17	358.0	179,000	43.77
		ST, 40S	0.375	12.000	14.58	0.7854	3.338	3.14	352.5	176,250	49.56
		40	0.406	11.938	15.74	0.7773	3.338	3.13	349.0	174,500	54.56
		XS, 80S	0.500	11.750	19.24	0.7530	3.338	3.08	338.0	169,000	65.42
		60	0.562	11.626	21.52	0.7372	3.338	3.04	331.0	165,500	73.72
		80	0.688	11.374	26.07	0.7056	3.338	2.98	316.7	158,350	88.57
		100	0.844	11.062	31.57	0.6674	3.338	2.90	299.6	149,800	107.29
		120, XX	1.000	10.750	36.91	0.6303	3.338	2.81	283.0	141,500	125.49
		140	1.125	10.500	41.09	0.6013	3.338	2.75	270.0	135,000	139.68
		160	1.312	10.126	47.14	0.5592	3.338	2.65	251.0	125,500	160.33
14	14	5S	0.156	13.688	6.78	1.0219	3.665	3.58	459	229,500	23.07
		10S	0.188	13.624	8.16	1.0125	3.665	3.57	454	227,000	27.73
		10	0.250	13.500	10.80	0.9940	3.665	3.53	446	223,000	36.71
		20	0.312	13.376	13.42	0.9750	3.665	3.50	438	219,000	45.68
		30, ST	0.375	13.250	16.05	0.9575	3.665	3.47	430	215,000	54.57
		40	0.438	13.124	18.66	0.9397	3.665	3.44	422	211,000	63.37
		XS	0.500	13.000	21.21	0.9218	3.665	3.40	414	207,000	72.09
		60	0.594	12.812	25.02	0.8957	3.665	3.35	402	201,000	85.01
		80	0.750	12.500	31.22	0.8522	3.665	3.27	382	191,000	106.13
		100	0.938	12.124	38.49	0.8017	3.665	3.17	360	180,000	130.79
		120	1.094	11.812	44.36	0.7610	3.665	3.09	342	171,000	150.76
		140	1.250	11.500	50.07	0.7213	3.665	3.01	324	162,000	170.22
		160	1.406	11.188	55.63	0.6827	3.665	2.93	306	153,000	189.15
16	16	5S	0.165	15.670	8.21	1.3393	4.189	4.10	601	300,500	27.90
		10S	0.188	15.624	9.34	1.3314	4.189	4.09	598	299,000	31.75
		10	0.250	15.500	12.37	1.3104	4.189	4.06	587	293,500	42.05
		20	0.312	15.376	15.38	1.2985	4.189	4.03	578	289,000	52.36
		30, ST	0.375	15.250	18.41	1.2680	4.189	3.99	568	284,000	62.58
		40, XS	0.500	15.000	24.35	1.2272	4.189	3.93	550	275,000	82.77
		60	0.656	14.688	31.62	1.1766	4.189	3.85	528	264,000	107.54
		80	0.844	14.312	40.19	1.1171	4.189	3.75	501	250,500	136.58
		100	1.031	13.938	48.48	1.0596	4.189	3.65	474	237,000	164.86
		120	1.219	13.562	56.61	1.0032	4.189	3.55	450	225,000	192.40
		140	1.438	13.124	65.79	0.9394	4.189	3.44	422	211,000	223.57
		160	1.594	12.812	72.14	0.8953	4.189	3.35	402	201,000	245.22

Table E.1 ***(Continued)***

Nominal Pipe Size (in.)	Outside Diam. (in.)	Schedule No.	Wall Thickness (in.)	Inside Diam. (in.)	Cross-Sectional Area		Circumference (ft) or Surface (sq ft/ft of length)		Capacity at Velocity (1 ft/s)		Weight of Plain-End Pipe (lb/ft)
					Metal (sq in.)	Flow (sq ft)	Outside	Inside	U.S. gal/ min	Water (lb/hr)	
18	18	5S	0.165	17.670	9.25	1.7029	4.712	4.63	764	382,000	31.43
		10S	0.188	17.624	10.52	1.6941	4.712	4.61	760	379,400	35.76
		10	0.250	17.500	13.94	1.6703	4.712	4.58	750	375,000	47.39
		20	0.312	17.376	17.34	1.6468	4.712	4.55	739	369,500	59.03
		ST	0.375	17.250	20.76	1.6230	4.712	4.52	728	364,000	70.59
		30	0.438	17.124	24.16	1.5993	4.712	4.48	718	359,000	82.06
		XS	0.500	17.000	27.49	1.5763	4.712	4.45	707	353,500	93.45
		40	0.562	16.876	30.79	1.5533	4.712	4.42	697	348,500	104.76
		60	0.750	16.500	40.64	1.4849	4.712	4.32	666	333,000	138.17
		80	0.938	16.124	50.28	1.4180	4.712	4.22	636	318,000	170.84
		100	1.156	15.688	61.17	1.3423	4.712	4.11	602	301,000	208.00
		120	1.375	15.250	71.82	1.2684	4.712	3.99	569	284,500	244.14
		140	1.562	14.876	80.66	1.2070	4.712	3.89	540	270,000	274.30
		160	1.781	14.438	90.75	1.1370	4.712	3.78	510	255,000	308.55
20	20	5S	0.188	19.624	11.70	2.1004	5.236	5.14	943	471,500	39.78
		10S	0.218	19.564	13.55	2.0878	5.236	5.12	937	467,500	46.06
		10	0.250	19.500	15.51	2.0740	5.236	5.11	930	465,500	52.73
		20, ST	0.375	19.250	23.12	2.0211	5.236	5.04	902	451,000	78.60
		30, XS	0.500	19.000	30.63	1.9689	5.236	4.97	883	441,500	104.13
		40	0.594	18.812	36.21	1.9302	5.236	4.92	866	433,000	123.06
		60	0.812	18.376	48.95	1.8417	5.236	4.81	826	413,000	166.50
		80	1.031	17.938	61.44	1.7550	5.236	4.70	787	393,500	208.92
		100	1.281	17.438	75.33	1.6585	5.236	4.57	744	372,000	256.15
		120	1.500	17.000	87.18	1.5763	5.236	4.45	707	353,500	296.37
		140	1.750	16.500	100.3	1.4849	5.236	4.32	665	332,500	341.10
		160	1.969	16.062	111.5	1.4071	5.236	4.21	632	316,000	379.14
24	24	5S	0.218	23.564	16.29	3.0285	6.283	6.17	1359	679,500	55.37
		10, 10S	0.250	23.500	18.65	3.012	6.283	6.15	1350	675,000	63.41
		20, ST	0.375	23.250	27.83	2.948	6.283	6.09	1325	662,500	94.62
		XS	0.500	23.000	36.90	2.885	6.283	6.02	1295	642,500	125.49
		30	0.562	22.876	41.39	2.854	6.283	5.99	1281	640,500	140.80
		40	0.688	22.624	50.39	2.792	6.283	5.92	1253	626,500	171.17
		60	0.969	22.062	70.11	2.655	6.283	5.78	1192	596,000	238.29
		80	1.219	21.562	87.24	2.536	6.283	5.64	1138	569,000	296.53
		100	1.531	20.938	108.1	2.391	6.283	5.48	1073	536,500	367.45
		120	1.812	20.376	126.3	2.264	6.283	5.33	1016	508,000	429.50
		140	2.062	19.876	142.1	2.155	6.283	5.20	965	482,500	483.24
		160	2.344	19.312	159.5	2.034	6.283	5.06	913	456,500	542.09
30	30	5S	0.250	29.500	23.37	4.746	7.854	7.72	2130	1,065,000	79.43
		10, 10S	0.312	29.376	29.10	4.707	7.854	7.69	2110	1,055,000	98.93
		ST	0.375	29.250	34.90	4.666	7.854	7.66	2094	1,048,000	118.65
		20, XS	0.500	29.000	46.34	4.587	7.854	7.59	2055	1,027,500	157.53
		30	0.625	28.750	57.68	4.508	7.854	7.53	2020	1,010,000	196.08

Table E.2 ***Properties of Copper Water Tube, Types K, L, M***

Nominal Size	Actual Outside Diam. (in.)	Mean Outside Diam. Tolerances (in.)		Wall Thickness (in.)						Theoretical Weight (lb/ft)		
				Type K		Type L		Type M				
		Soft Annealed	Hard Drawn	Nominal	Tolerance	Nominal	Tolerance	Nominal	Tolerance	Type K	Type L	Type M
1/4	0.375	0.002	0.001	0.035	0.004	0.030	0.0035	—	—	0.145	0.126	
3/8	0.500	0.0025	0.001	0.049	0.004	0.035	0.0035	0.025	0.0025	0.269	0.198	0.145
1/2	0.625	0.0025	0.001	0.049	0.004	0.040	0.0035	0.028	0.0025	0.344	0.285	0.204
5/8	0.750	0.0025	0.001	0.049	0.004	0.042	0.0035	—	—	0.418	0.362	
3/4	0.875	0.003	0.001	0.065	0.0045	0.045	0.004	0.032	0.003	0.641	0.455	0.328
1	1.125	0.0035	0.0015	0.065	0.0045	0.050	0.004	0.035	0.0035	0.839	0.655	0.465
1 1/4	1.375	0.004	0.0015	0.065	0.0045	0.055	0.0045	0.042	0.0035	1.04	0.884	0.682
1 1/2	1.625	0.0045	0.002	0.072	0.005	0.060	0.0045	0.049	0.004	1.36	1.14	0.940
2	2.125	0.005	0.002	0.083	0.007	0.070	0.006	0.058	0.006	2.06	1.75	1.46
2 1/2	2.625	0.005	0.002	0.095	0.007	0.080	0.006	0.065	0.006	2.93	2.48	2.03
3	3.125	0.005	0.002	0.109	0.007	0.090	0.007	0.072	0.006	4.00	3.33	2.68
3 1/2	3.625	0.005	0.002	0.120	0.008	0.100	0.007	0.083	0.007	5.12	4.29	3.58
4	4.125	0.005	0.002	0.134	0.010	0.110	0.009	0.095	0.009	6.51	5.36	4.66
5	5.125	0.005	0.002	0.160	0.010	0.125	0.010	0.109	0.009	9.67	7.61	6.66
6	6.125	0.005	0.002	0.192	0.012	0.140	0.011	0.122	0.010	13.9	10.2	8.92
			+ −									
8	8.125	0.006	0.002 0.004	0.271	0.016	0.200	0.014	0.170	0.014	25.9	19.3	16.5

Table E.3 ***Properties of Copper and Red Brass Pipe***

A. Dimensions and Weights of Regular Pipe

Nominal Pipe Size (in.)	Nominal Dimensions (in.)			Cross-Sectional Area of Bore (sq in.)	lb/ft		Nominal Pipe Size (in.)	Nominal Dimensions (in.)			Cross-Sectional Area of Bore (sq in.)	lb/ft	
	Outside Diam.	Inside Diam.	Wall Thickness		Red Brass	Copper		Outside Diam.	Inside Diam.	Wall Thickness		Red Brass	Copper
1/8	0.405	0.281	0.062	0.062	0.253	0.259	2 1/2	2.875	2.501	0.187	4.91	5.99	6.12
1/4	0.540	0.376	0.082	0.110	0.447	0.457	3	3.500	3.062	0.219	7.37	8.56	8.75
3/8	0.675	0.495	0.090	0.192	0.627	0.641	3 1/2	4.000	3.500	0.250	9.62	11.2	11.4
1/2	0.840	0.626	0.107	0.307	0.934	0.955	4	4.500	4.000	0.250	12.6	12.7	12.9
3/4	1.050	0.822	0.114	0.531	1.27	1.30	5	5.562	5.062	0.250	20.1	15.8	16.2
1	1.315	1.063	0.126	0.887	1.78	1.82	6	6.625	6.125	0.250	29.5	19.0	19.4
1 1/4	1.660	1.368	0.146	1.47	2.63	2.69	8	8.625	8.001	0.312	50.3	30.9	31.6
1 1/2	1.900	1.600	0.150	2.01	3.13	3.20	10	10.750	10.020	0.365	78.8	45.2	46.2
2	2.375	2.063	0.156	3.34	4.12	4.22	12	12.750	12.000	0.375	113.0	55.3	56.5

B. Dimensions and Weights of Extra-Strong Pipe

Nominal Pipe Size (in.)	Nominal Dimensions (in.)			Cross-Sectional Area of Bore (sq in.)	lb/ft		Nominal Pipe Size (in.)	Nominal Dimensions (in.)			Cross-Sectional Area of Bore (sq in.)	lb/ft	
	Outside Diam.	Inside Diam.	Wall Thickness		Red Brass	Copper		Outside Diam.	Inside Diam.	Wall Thickness		Red Brass	Copper
1/8	0.405	0.205	0.100	0.033	0.363	0.371	2 1/2	2.875	2.315	0.280	4.21	8.66	8.85
1/4	0.540	0.294	0.123	0.068	0.611	0.625	3	3.500	2.892	0.304	6.57	11.6	11.8
3/8	0.675	0.421	0.127	0.139	0.829	0.847	3 1/2	4.000	3.358	0.321	8.86	14.1	14.4
1/2	0.840	0.542	0.149	0.231	1.23	1.25	4	4.500	3.818	0.341	11.5	16.9	17.3
3/4	1.050	0.736	0.157	0.425	1.67	1.71	5	5.562	4.812	0.375	18.2	23.2	23.7
1	1.315	0.951	0.182	0.710	2.46	2.51	6	6.625	5.751	0.437	26.0	32.2	32.9
1 1/4	1.660	1.272	0.194	1.27	3.39	3.46	8	8.625	7.625	0.500	45.7	48.4	49.5
1 1/2	1.900	1.494	0.203	1.75	4.10	4.19	10	10.750	9.750	0.500	74.7	61.1	62.4
2	2.375	1.933	0.221	2.94	5.67	5.80							

Index

C

D

E

I

J

K

L

M

Q

R

T

X

Y

Z